Pergamon

S0277-5387(96)00190-8

Polyhedron Vol. 16, No. 1, pp. 1–17, 1997
Copyright © 1996 Elsevier Science Ltd
Printed in Great Britain. All rights reserved
0277-5387/97 $15.00+0.00

POLYHEDRON REPORT NO. 63

Metal–metal bond formation in the oxidative addition to dinuclear gold(I) species. Implications from dinuclear and trinuclear gold chemistry for the oxidative addition process generally

John P. Fackler, Jr

Laboratory for Molecular Structure and Bonding, Department of Chemistry, Texas A&M University, College Station, TX 77843-3255, U.S.A.

CONTENTS

1. INTRODUCTION TO THE GENERAL CONCEPTS OF DINUCLEAR OXIDATIVE ADDITION 1

2. GENERAL FEATURES OF THE OXIDATIVE ADDITION PROCESS 2

3. OXIDATIVE ADDITION IN DINUCLEAR AND POLYMETALLIC SYSTEMS . . 4

4. OXIDATIVE ADDITION TO DINUCLEAR GOLD(I) COMPLEXES 4

5. DOES THE INITIAL OXIDATIVE ADDITION INVOLVE BOTH METAL CENTRES? 6

6. EVIDENCE THAT OXIDATIVE ADDITION DOES NOT FIRST FORM A MIXED-VALENCE Au^{III}/Au^{I} SPECIES 7

7. RADICAL INTERMEDIATES 9

8. OXIDATIVE ADDITION OBSERVATIONS WITH OTHER DINUCLEAR GOLD(I) COMPLEXES 10

9. IMPLICATIONS OF THE GODDARD–LOW OXIDATIVE ADDITION CONCEPT TO THE DINUCLEAR GOLD(I) CHEMISTRY 10

10. OXIDATIVE ADDITION TO LINEAR TRINUCLEAR SPECIES 12

11. SUMMARY 14

1. INTRODUCTION TO THE GENERAL CONCEPTS OF DINUCLEAR OXIDATIVE ADDITION

Malcolm Chisholm stated some years ago,[1] "What one metal can do, two metals can do better". There is considerable evidence that chemistry associated with multinuclear metal species[2] can be significantly different from the chemistry that occurs with molecules containing only a single metal atom. In their book, Collman, Hegedus, Norton and Finke have described[3] some very interesting examples involving two metal atoms. Chisholm,[4a] Balch,[4b,4c] Cowie[4d] and our group[4i,5d] have discussed results involving metal–metal bond formation and rupture with di- and trinuclear species. Bosnich[4e] demonstrated with dinuclear Pd, Rh and Ir complexes that proximity factors can nega-

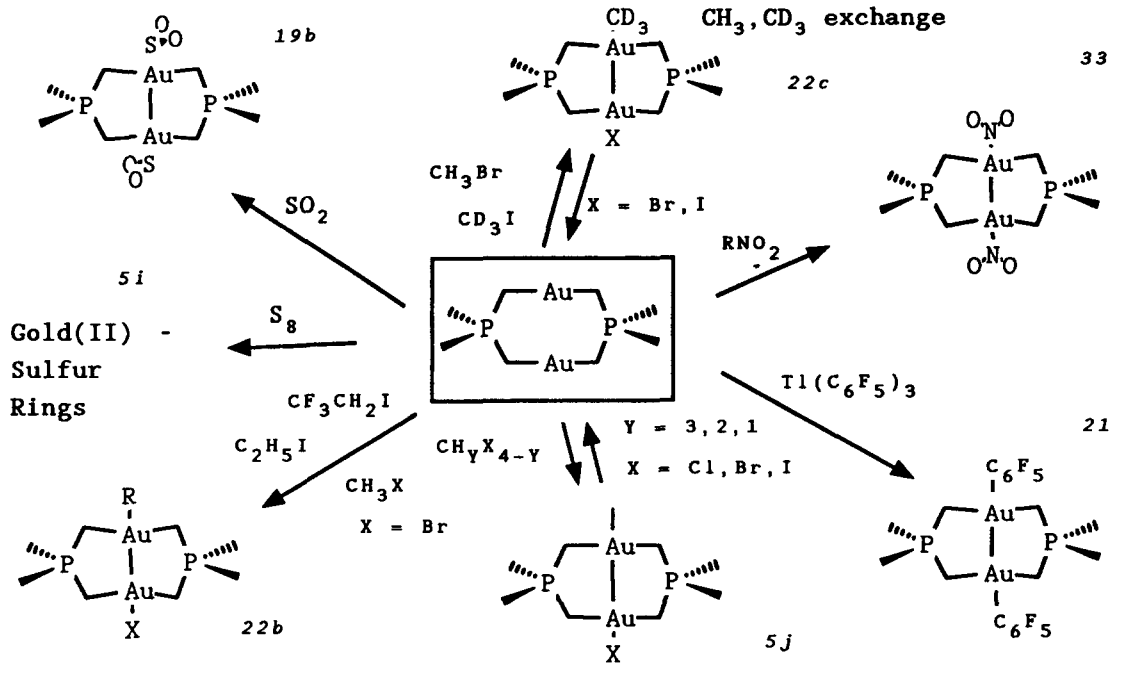


Fig. 1. Reactions of dinuclear gold(I) ylides with various small molecules. A lead paper describing the chemistry is listed in italics.

tively influence oxidative addition in dinuclear systems in which the metal atoms "were within a cooperative distance", but not capable of metal–metal bond formation. Stobart[4f] examined the oxidative addition of alkyl halides and halogens to $[Ir(\mu\text{-pz})L_2]_2$, pz = pyrazoyl and L = CO, cyclooctadiene or PPh_3, CO mixtures. These reactions produce a two-centre two-electron addition with the formation of a metal–metal bond. However, with alkyl- and arylamido ligands, Ahmed[4h] showed that CH_3I addition to $[IrB(CO)_2]_2$ (B = NHR^- or NH_2^-) produces a Ir^{III}–Ir^{I} complex, while I_2 gives the metal–metal bonded Ir^{II}–Ir^{II} species. Also the oxidative addition chemistry at dinuclear Pt centres has been described recently in a review by Anderson.[4g]

One of the important aspects of dinuclear systems is the ability of the two metal atoms to form a metal–metal bond, thereby stabilizing a reactant, a product or an intermediate. Alternatively, the second metal atom may inhibit[4e] the reaction of a normally reactive centre, either through steric or electronic properties or both. Studies in this area with dinuclear gold(I) complexes were pioneered by Schmidbaur and expanded by ourselves and others.[5] They have demonstrated a rich reaction chemistry with this element (Fig. 1), a chemistry which depends upon the ability of the two (or more) metal atoms to interact with each other. The implications of this chemistry for the understanding of oxidative addition processes[4i,6] in dinuclear and polynuclear complexes is the focus of this report. A very well presented description of the recent organometallic chemistry of gold by Grohmann and Schmidbaur should be consulted for more general information than is contained in this report.[5l]

2. GENERAL FEATURES OF THE OXIDATIVE ADDITION PROCESS

Oxidative addition at a single metal centre is described as a one- or two-electron exchange between the metal atom and the molecule being added.[3] The one-electron process is "radical" in character, while the two electron exchange most often is described in terms of nucleophilic substitution, S_N2.

In dinuclear compounds the distance between these metal atoms can influence the oxidative addition chemistry. The metal atoms may be held close by bridging ligands or by other bonding interactions. The specific electronic properties of both of the metal atoms, therefore, can influence the observed chemistry. Widely separated metal atoms are expected to behave relatively independently (Fig. 2), but if the metal atoms are close, factors related to the extent of metal–metal interactions and the electronic properties of the metal atoms as adjusted by the ligands must be considered.

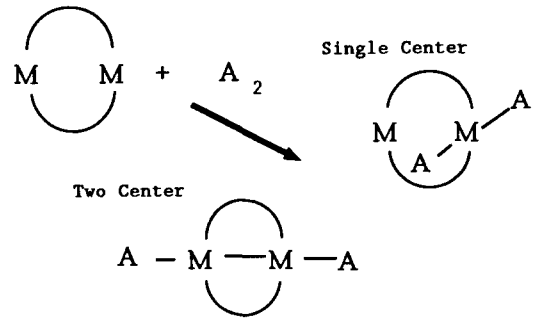


Fig. 2. Oxidative addition to dinuclear complex.[5d]

Goddard and Low[6] have discussed the role of electronic structure in oxidative addition. They suggest that an electronic promotion occurs at the metal centre undergoing "oxidation". The promotion is considered from a closed or pseudo-closed-shell ground state configuration to an open-shell configuration, which can be associated with a (excited state) configuration suitable for bonding to the molecule being added. In the case of the closed shell d^{10} complexes such as Au^{I} or Pt^{0} this open-shell configuration is $d^{9}s^{1}$. Hence, the greater the energy separation between the d^{10} and $d^{9}s^{1}$ configurations, the more difficult the oxidative addition process. Table 1 lists the closed-shell to open-shell (HOMO–LUMO) energy separation[7] for ions of interest to this report. In the Goddard–Low model,[6] excitation to the open-shell configuration, *not oxidation* (ionization), is the key to understanding the reactivity.

Although there are obvious features in common between the oxidative addition studies described in this report and studies involving open-shell ions such as Ir^{I} or Pt^{II}, the specific influence of completely filled electronic levels at the metal atom is different enough from system to system that electronic generalizations become less reliable. Hence, this report will focus on the oxidative addition of closed-shell metal species, with one important exception on which calculations have been performed.[4i] For closed-shell d^{10} metal atoms or ions, the experimentally observed pattern of closed-shell to open-shell energy separation determined from spectroscopic data[7] parallels the oxidative addition process. For the ions important to this report the energy separation pattern is: $Hg^{II} > Ag^{I} \gg Au^{I} > Pd^{0} > Pt^{0}$. The greater the energy separation, the more difficult it is to achieve oxidative addition. Conversely, the smaller the energy separation between the closed- and open-shell configurations, the easier the addition. This concept is very similar to the idea of Chatt,[8] who stated that the stability of organometallic compounds closely follows their HOMO–LUMO

Table 1. Promotion energies ("HOMO–LUMO gap separations") and ionization potentials for some ions important to oxidative addition reactions (eV)

Ion	HOMO–LUMO gap (eV)[a]	Ionization potential (eV)
Cu^{I}	2.715	20.292
Ag^{I}	4.959	21.49
Au^{I}	1.859	20.52
Pt^{0}	0.744	9.00
Pd^{0}	0.814	8.337
Tl^{I}	6.137	20.4
Pb^{II}	7.488	15.03
Hg^{II}	5.306	34.2

[a] The energy separation between the closed-shell atomic configuration and the lowest open-shell configuration.

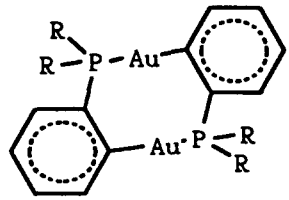
separation. Changing the HOMO–LUMO separation by using different co-ligands at the metal centre changes the reactivity of the complex, a concept widely utilized in organometallic syntheses.

3. OXIDATIVE ADDITION IN DINUCLEAR AND POLYMETALLIC SYSTEMS

With dimetallic and polymetallic systems, the excited-state energy as well as the ground-state energy will be influenced by the close proximity of another metal atom. Spectroscopic evidence suggests that metal–metal bond formation[9] contributes to the description of the excited state with some of these species. Obviously, metal–metal bond formation makes the "open-shell" excited state more accessible relative to the case in which no metal–metal bond can form, for example, when the metal atoms are well separated.

Electron-accepting metal centres or ligands adjacent to the metal atom undergoing the initial attack during the oxidative addition can be expected to stabilize the HOMO or "closed-shell" ground state through electron exchange. This increases the HOMO–LUMO separation, thereby making oxidative addition less favourable. Similarly, cation charge and pi-bonding from adjacent metal atoms or ligands also can be expected to increase the HOMO–LUMO separation, diminishing the tendency for oxidative addition, relative to uncharged or electron-rich anionic complexes or those complexes with strongly donating ligands.

Experimental differences are observed in the ease of small molecule oxidative addition to various dinuclear gold(I) complexes having different charges or ligand atoms on the metal centres. For example, with $[Au_2(diphos)_2]^{2+}$, diphos = $Ph_2PCH_2PPh_2$, a cationic complex with pi-accepting phosphorus ligands, halogen addition does not occur,[10] even with very strong oxidants such as Cl_2. However, with the neutral complex $[Au_2(o\text{-}PC)_2]$, o-PC = $Ph_2P—C_6H_4$,



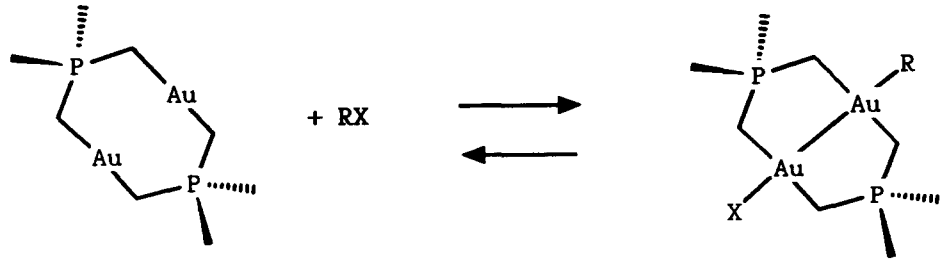
containing the strongly basic phenyl ligands, iodine readily adds.[11] In both types of compound, the Au···Au distance is *ca* 3.0 Å. Several dinuclear gold complexes with C—Au—S and S—Au—S coordination[12] also exist with Au···Au separations of *ca* 3.0 Å and are known to add halogens (see below), but less readily than the ylide complexes of Fig. 1.

Accumulated data regarding the reactivity of dinuclear and polynuclear metal complexes is consistent with the idea that neighbouring metal atoms and coordinated ligands influence the oxidative addition process both positively and negatively.

Methyl iodide oxidative addition across two metal atoms with metal–metal bond formation was first reported in 1975 by Schmidbaur[13a,13b] for a dinuclear gold(I) ylide complex and shortly thereafter by Gray[14] for the $[Rh_2(bridge)_2]^{2+}$, bridge = $NCCH_2CH_2CN$. X-ray structural results were not easily obtained for either complex. The gold complex is photosensitive and easily decomposes into the metal–metal bonded diiodide product. However, Basil successfully crystallized this complex, which has the structure we reported[15] in 1982. Structures also have been reported for products having CH_3Br and CH_3I across metal–metal Rh—Rh[16] and Pd—Pd[17] bonds, but these adducts had been obtained by protonation of methylene bridged A-frame intermediates.

4. OXIDATIVE ADDITION TO DINUCLEAR GOLD(I) COMPLEXES

In general, alkyl halide oxidative addition reactions that have been studied with dinuclear gold ylide complexes follow the kinetic and thermodynamic patterns expected for S_N2-type nucleophilic



Equilibrium: CF_3CH_2I >> CH_3CH_2I

Kinetics: $PhCH_2Br$ (120) >> CH_3Br (20) >> $(CH_3)_3SiCH_2Br$ (1)

Fig. 3. Alkyl halide oxidative addition, thermodynamics and rates with relative rates in parentheses.

reactions[18] summarized in Fig. 3. The Au^I centres have been established to be nucleophilic through structural characterization of the SO_2 adduct.[19] The reactions with methyl halides are chemically reversible in solution and also in the solid state.

Not only do dinuclear Au^I ylide complexes undergo a two-electron oxidative addition with metal–metal bond formation, but oxidation by four electrons also can occur, producing products which can be isolated and structurally characterized.[20] Since the four-electron oxidation proceeds through a metal–metal bonded Au^{II} intermediate, this metal–metal bond must be broken while producing the Au^{III} products. A number of these reactions have produced well characterized products (Fig. 4). We also have observed ligand exchange to occur at the Au^{II} centres without oxidation.[21] However, oxidative addition to the dinuclear Au^{II} complexes often gives radical products. Except for the CH_2 insertion reactions into the metal–metal bond using diazomethane and the known two-step addition of dihalomethanes to the dinuclear ylide complexes, which also apparently involve a CH_2 insertion,[5e] it is not known what role metal–metal bonding interactions play in influencing the course of these reactions. Therefore, detailed consideration will not be given in this report to the four-electron

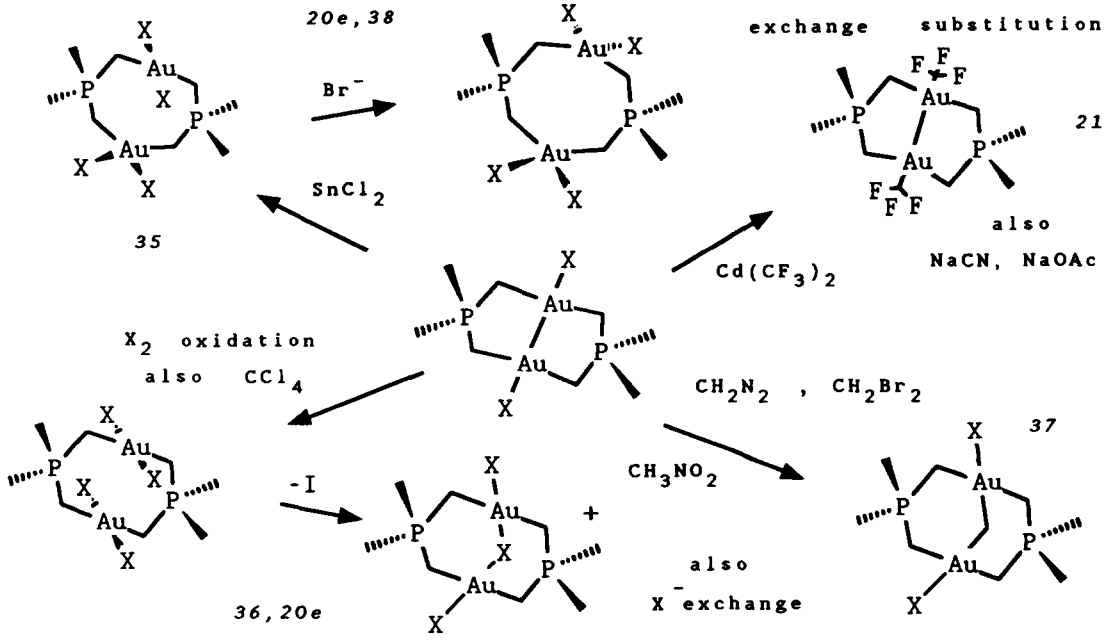


Fig. 4. Reactions of dinuclear gold(II) complexes.

oxidative addition process, the radical oxidative additions or oxidative additions from dinuclear Au^{II} to Au^{III} species, although some dinuclear Au^{II}/Au^{III} chemistry will be described.

5. DOES THE INITIAL OXIDATIVE ADDITION INVOLVE BOTH METAL CENTRES?

The oxidative addition scheme proposed for the dinuclear Au^{I} complexes (Fig. 5) suggests that metal–metal bonding promotes the formation of an ionic intermediate. While a cationic product of this type has not been characterized structurally, a related species has been characterized by Uson, Laguna and Laguna.[22a] This dicationic species has a short, 3.6 Å, metal–metal bond. Thus cationic Au—Au bonded intermediates are very reasonable intermediates in the dinuclear oxidative addition process. Comparative structural data for the CH_3CH_2I and CF_3CH_2I adducts suggests ionization of the I^- in the ethyl adduct is more facile than in the case of the thermodynamically more stable trifluoroethyl iodide adduct.[22b] Furthermore, halide exchange at the Au^{II} centres is known to be rapid.[22c] How certain are we that metal–metal bond formation occurs in the initial oxidation step? After all, a mixed-valent Au^{I}/Au^{III} intermediate could be formed initially and then rapidly rearrange to the observed products. More will written on this point.

The best evidence we have that nucleophilic attack by a Au^{I} centre on the addend molecule involves metal–metal bond formation originates from the structural results obtained with the SO_2 adduct.[19] In addition to establishing the nucleophilicity of the Au^{I}, which produces a pyramidal geometry about the S atom,[39] The $Au^{I} \cdots Au^{I}$ distance shortens to 2.838 from 2.976 Å. The donation of electron density from gold to the SO_2 is accompanied by increased metal–metal bonding. Although formal "oxidation" does not occur with SO_2, the process is similar to what is expected in a Goddard–Low[6] oxidative addition, but with incomplete electron transfer to the ligand centres. There is an overall two-electron deficiency for the formation of three sigma bonds along the S—Au—Au—S axis. (The SO_2 contributes no electrons to the addition while each Au^{I} atom contributes two electrons to the axial sigma bonds.) Alternatively, it may be argued that the shortened gold distance has resulted from the removal of repulsive electron density at the Au^{I} centres by the SO_2. Notably, the Au^{I} atoms in this complex are coordinated by four ligand atoms in an approximate plane, a rare occurrence with Au^{I}. The author is aware of only three other examples, a pentanuclear gold complex reported by Uson,[22] the SO_2 adduct to the trinuclear [Au···Pt···Au] complex described below[19] and a recently characterized tetranuclear complex,[23] in which $[Au(TPA)_3]^+$, TPA = 1,3,5-triaza-7-phosphoraadamantane, coordinates through Au^{I} to $[Au_2\ (i\text{-MNT})_2]^{2+}$, i-MNT = $[S_2CC(CN)_2]^{2+}$.

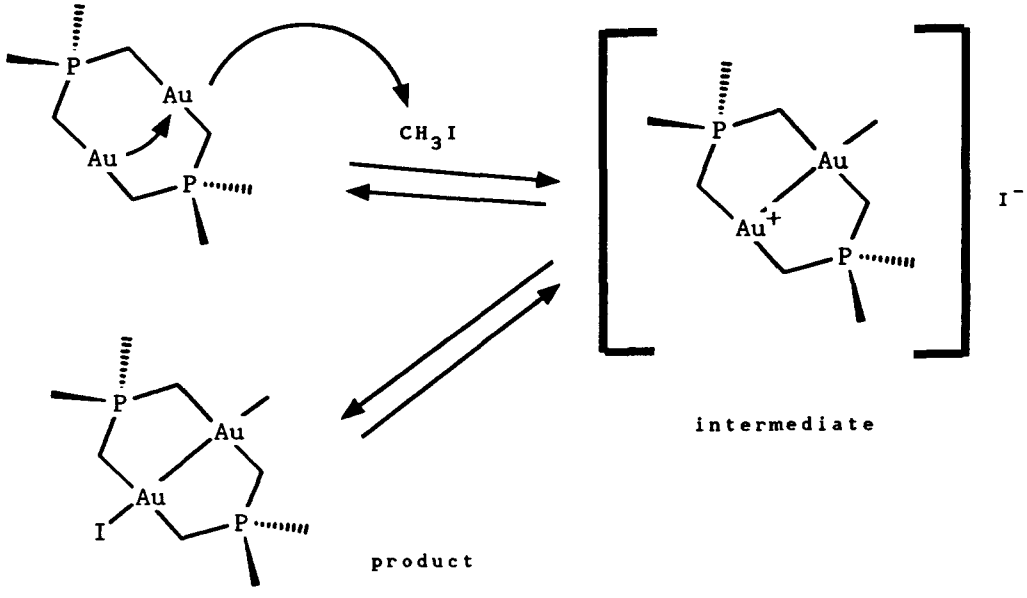
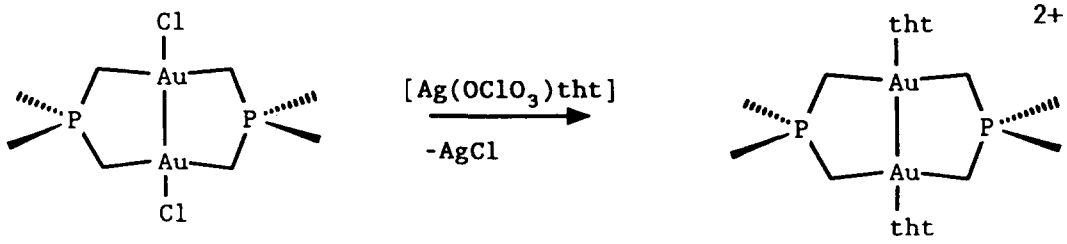
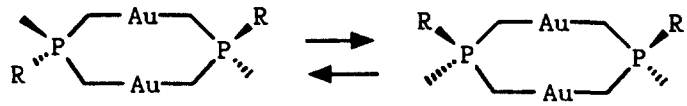


Fig. 5. Anchimerically assisted nucleophilic addition.



There is related evidence that metal–metal bonding accompanies the donation of electron density to small molecules interacting with the Au^{I} atoms. Several years ago, Schmidbaur and his students[24] recognized that a mixture of different dinuclear ylide complexes exchanged ligands slowly enough that the various isomers could be separated on a column. This observation requires that Au—C bond rupture occur, a process likely to be influenced by either by intermolecular Au · · · Au interactions, or by solvent effects, since ring opening would leave a Au^{I} centre coordinated only to one C atom. In our effort to synthesize the dinuclear ylide complex of $[(CH_2)_2P(CH_3)C_6H_5]^-$ to examine the question of Au—C bond lability, it was discovered[19b] that the standard basic conditions for synthesis led to the crystallization of only the *trans* isomer. This isomer rearranged in solution, slowly forming an approximately 53 : 46 mixture of the *trans* and *cis* forms. The *cis* form has not been structurally characterized, but is clearly identified in the NMR patterns obtained. Oxidative addition of halogens or other oxidants leads to crystallization of *trans* dinuclear Au^{II} products which do not undergo further rearrangement.[25]

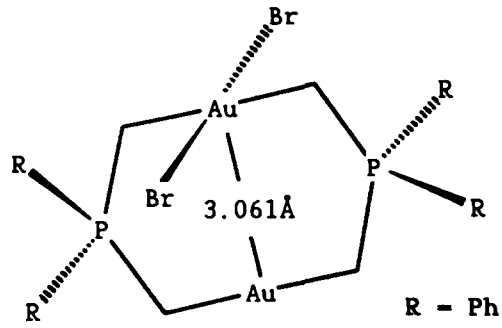


trans *cis*

The *trans* to *cis*/*trans* rearrangement was found to be general acid catalysed. Strong protonic acids such as HCl are known to symmetrically cleave[26] the eight-membered ring, with deuterium incorporation into the ylide using DCl. However, CD_3COOD catalyses the isomerization without introducing D into the complex. Since SO_2, Ph_3PAuCl and other Lewis acids also catalyse the isomerization, it was suggested[19b] that rearrangement occurs via the formation of an adduct such as the structurally characterized SO_2 adduct with its shortened Au · · · Au interaction, an adduct of a type similar to the initial electrophilic interaction suggested for small molecules undergoing oxidative addition at the Au^{I} centre.

6. EVIDENCE THAT OXIDATIVE ADDITION DOES NOT FIRST FORM A MIXED-VALENCE Au^{III}/Au^{I} SPECIES

Although the SO_2 studies are consistent with a nucleophilic attack by a Au^{I} centre on the adduct, which is assisted by metal–metal bond formation, it remained plausible that the addition occurs first at one centre to form a Au^{III} species, followed by a rapid rearrangement to the dinuclear Au^{II} product observed. Structural data for the addition of I_2 to $[Au(MTP)]_2$ clearly established that both the homovalent and the mixed-valent species were formed with this halogen.[27] However, ligand rearrangement also occurs causing the Au^{III} centre to have *trans*-AuC_2I_2 coordination. The dinuclear MTP species with added Cl_2 or Br_2 crystallize as Au^{II} products,[28] but the C_s-$[Au^{I}Au^{III}(MTP)_2Cl_2]$ could be formed starting with the $Au^{III}(MTP)_2Cl$.[20a] Thus, a synthesis of the mixed-valent ylide complex with Cl or Br ligands seemed reasonable, especially if these materials were not intermediate in the formation of the homovalent Au^{II} products. Furthermore, Schmidbaur had previously demonstrated that the dimethyl product is C_s-$\{Au^{I}Au^{III}[(CH_2)_2PPh_2]_2Me_2\}$, at least in solution,[29] Uson *et al.*[30] had demonstrated that the dinuclear complex $R_2Au_2[(\mu\text{-}PPh_2)_2NH]$, $R = C_6F_5$, was oxidized to a metal–metal bonded Au^{II} species, which then rearranged in polar solvents to a mixed-valent Au^{III}/Au^{I} product, a rearrangement we also reported[40] for the dinuclear ylide complexes.



The synthesis of C_s-$\{Au^{I}Au^{III}[\mu\text{-}(CH_2)_2PPh_2]_2Br_2\}$, was accomplished[20b,20e] by oxidizing $\{Au^{II}[\mu\text{-}(CH_2)_2PPh_2]CN\}_2$ with excess Br_2 in CH_2Cl_2 or by reducing the *trans,trans*-tetrabromide with AgCN in CH_2Cl_2. Both this material and the chloride analogue [Au···Au, 3.052(2) Å] were insufficiently soluble as the CH_2Cl_2 solvates to perform solution NMR studies of the rate of rearrangement to the Au^{II}/Au^{II} product. If the material was heated in contact with the solvent, the product formed from the resulting solution is largely the Au^{II}/Au^{II} species.

This data appears to mitigate strongly against a mixed-valent Au^{III}/Au^{I} species being formed first in the oxidative addition process. However, this assumes that the initial oxidative addition product is a mixed-valent species, in which the halide atoms are *trans* to each other on the Au^{III} centre. Since dinuclear Au^{III}/Au^{III} species had been synthesized and characterized, in which the halides (or sulfur-containing ligands) were *cis* on both centres and also species *cis* on one centre and *trans* on the other,[20e] the possibility remained that oxidative addition involves *cis* addition at one centre followed by rearrangement to the stable Au^{II}/Au^{II} product. Schmidbaur had reported the formation of *trans* asymmetric Au^{III}/Au^{I} cations from the reaction of $\{Au[\mu\text{-}CH_2)PPh_2]X\}_2$ (X = Br, Cl or I), with neutral ylides, $CH_2 = PR_3$ (R_3 = Me_3, $MePh_2$ or Ph_3). These complexes had been characterized by NMR and ^{197}Au Mössbauer spectroscopies.[32]

The reaction of BrCN with $Au_2[\mu\text{-}(CH_2)_2PPh_2]_2$ leads to three products, as determined from the ^{1}H NMR patterns and by crystallographic characterization of isolated products. The Au^{I}/Au^{III} dibromide product found (Fig. 6) in the *cis* form was isolated from the mixture of products after dissolution in CH_2Cl_2 and layering with benzene or hexane, while being exposed to sunlight or a UV source.[41] Unfortunately, overexposure produces gold mirrors, but defining the conditions for "overexposure" have not yet been achieved. The formation of the *cis* Au^{I}/Au^{III} product was reproduced, however, and the material was characterized by X-ray crystallography. With regard to the topic of this report, the *cis* adduct at the Au^{III} centre does not undergo transformation into the

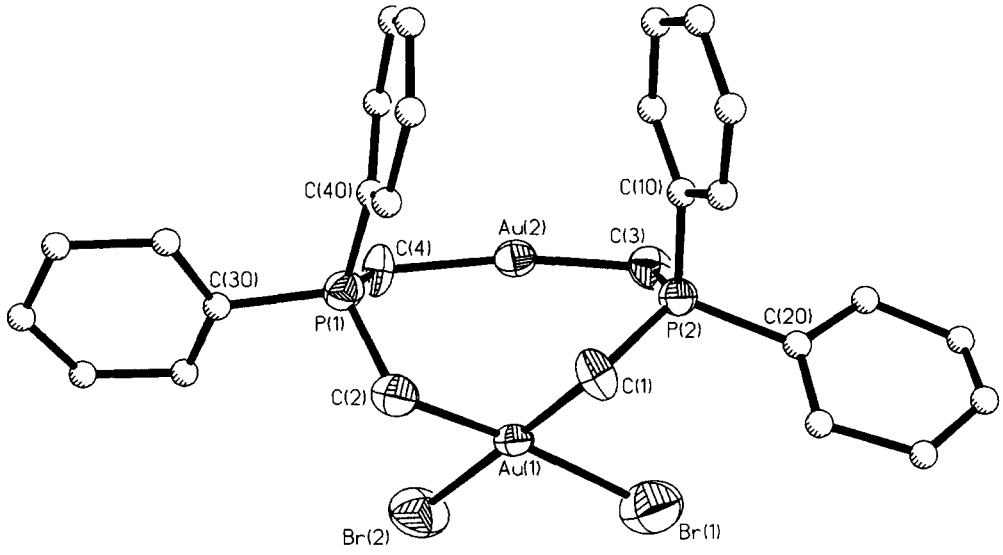


Fig. 6. Thermal ellipsoid drawing of the structure of the *cis*-Au^{I} $Au^{III}[\mu\text{-}(CH_2)_2PPh_2]Br_2$.

symmetrical Au^{II} material. Thus, *cis* oxidative addition at one centre followed by rearrangement cannot be important to the oxidative addition process itself.

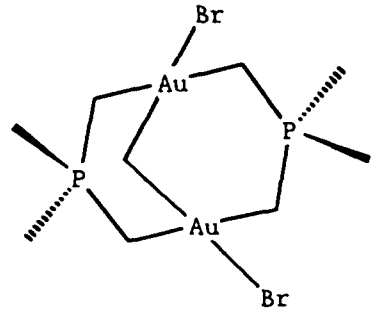
While oxidative addition of symmetrical oxidants invariably leads [5d] to symmetrically ligated (*trans*) metallocycles, $\{Au[\mu\text{-}(CH_2)PPh_2]X\}_2$ (X = Br, Cl, CN,[37] OOCPh,[42] NO_3[33] and C_6F_5[21]) and metathesis can be used to produce new symmetrically ligated complexes (X = CF_3[21]), asymmetrically ligated species also $\{Au[\mu\text{-}(CH_2)PPh_2]XY\}_2$ have been synthesized from the oxidative addition of alkyl halide reagents: X = Br, Y = Me, CH_2Ph, $CH_2C(O)Ph$,[43] CH_2CN, $CHCl_2$; X = Cl, Y = CCl_3;[36] X = I, Y = Me,[15] CH_2CH_3,[44] CH_2CF_3,[44] CH_2SiMe_3,[5d] CH_2Cl.[46] In fact, the kinetics of the alkylhalide addition follows a pattern typically expected[5d] for S_N2 processes. The addition furthermore was shown to be reversible with the addition product stability greatly dependent[44] on the presence of electron-withdrawing groups on the alkyl moiety.

7. RADICAL INTERMEDIATES

Nitroalkanes oxidatively add to $[Au(ylide)]_2$ to produce NO_2 coordination and carbon-based radical products.[33] While the initial step may be a non-radical oxidative addition for this system, as suggested for the alkyl halides, followed by rapid homolytic Au—C bond cleavage induced by the strong *trans*-labilizing effect of the NO_2, this reaction is sufficiently complicated that further study is essential to determine what bearing it has, if any, on binuclear oxidative addition. Radical coupling of the THF solvent is known to occur. The addition of CH_3NO_2 to the Au^{II} species, $Au_2(ylide)_2(OBz)_2$, OBz = benzoate, causes insertion of $CHNO_2$ into the Au—Au bond.[33] Radical processes also appear to be involved in the formation of the products in these systems.

Although strong evidence exists in many oxidative addition reactions[45] that a one-electron first step can occur in oxidative addition (electron transfer to the addend) to form a metal-based cation radical, evidence for such radical intermediates with the dinuclear gold compounds appears limited and is greatest in systems involving the addition of nitroalkanes,[33] disulfides[19b,47] or diselenides,[48] sulfur[49] and the addition of strong oxidants, which have sterically blocked C centres such as[36] CCl_4 or centres which are only weakly aurophilic such as in benzoylperoxide.[42] While no Au^I/Au^{II} radical intermediates have been characterized, nor have they been observed from ESR studies, uncharacterized "blue" intermediates sometimes are observed. Evidence for radicals was found with the CCl_4 addition, in which there was the formation of sufficient $HCCl_3$ in THF to account for the Au^{II} and Au^{III} products isolated. However, even with CCl_4, a metal–metal bonded Cl—Au(μ-ylide)$_2$Au—CCl_3 adduct could be isolated and structurally characterized.[36] Metal–metal interactions also could promote an electron-transfer first step in the oxidative addition process.

The oxidative addition of small molecules to the dinuclear Au^{II} species also can occur by one-electron steps or a two-electron process. Structural evidence,[5e] although weakened by a crystallographic disorder, suggests that the second step in the formation of μ-methylene Au^{III} derivatives



formed from the addition of CH_2Br_2 and its analogues to the dinuclear Au^I complexes occurs by insertion of CH_2 into the Au—Au bond. Diazomethane also adds across the Au—Au bond in dinuclear Au^{II} species.[50]

In general, the formation of the dinuclear Au^{III} species (Fig. 4) must be accompanied by metal–metal bond rupture of Au^{II} products. Direct oxidation to Au^{III} species does not occur with weakly oxidizing species such as alkyl monohalides. since the Au^{II} centres are considerably less nucleophilic in the dinuclear Au^{II} species than in the dinuclear Au^I complexes, electron-transfer and radical

intermediates are likely to be more important in the oxidation of Au^{II} species than the Au^{I} compounds. The HOMO in the Au^{II} species is metal–metal bonding and metal–halide antibonding, giving rise to a strong transannular influence of the alkyl group on the metal–halide distance. This lengthening of the Au–halide bond compared with similar bonds in mononuclear sigma-bonded compounds has been described as an *amplified* structural *trans* influence.[5d]

Although the dinuclear Au^{III} complexes rapidly react with the dinuclear Au^{I} ylide dimers to form Au^{II} products, only symmetrical Au^{II} products have been isolated to date by this route. Furthermore, kinetic and mechanistic studies designed to determine whether this reaction follows atom-transfer or electron-transfer dynamics have not been performed. The lability of the Au^{II}-halide bond in the presence of the dinuclear Au^{I} species may impede the development of meaningful mechanistic studies.

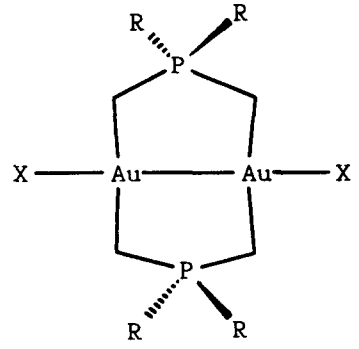
8. OXIDATIVE ADDITION OBSERVATIONS WITH OTHER DINUCLEAR GOLD(I) COMPLEXES

The fact that dinuclear diphos complexes of Au^{I} do not oxidatively add small molecules prompted us to examine the possibility of addition to other dinuclear Au^{I} species. Isolated, characterized products have been obtained by us and others for the species listed in Fig. 7. As stated above, the iodide products undergo rearrangement to mixtures which contain Au^{I}/Au^{III} products. The $[Au_2(i\text{-}MNT)_2X_2]^{2-}$ species are compounds which slowly rearrange[51] in solution to Au^{III} and Au^{I} products. This rearrangement has been studied kinetically and is found to be first order in added halide. Thus, the presence of free halide nucleophiles presumably impacts upon the product distributions found in the oxidative additions to dinuclear Au^{I} species, such as reactions observed with $Au_2(MTP)_2$ and even the ylide complexes. Qualitatively, rearrangement to Au^{I}/Au^{III} products appears to be associated with the electrophilic nature of the Au^{II} centres in the oxidative addition product. With P—Au—C, S—Au—C or S—Au—S coordination at the Au^{II} centres, halide exchange is facile and the metal centres are sufficiently electrophilic so that rearrangements are found. Burmeister suggested[52] that even the well-known $Au_2(dtc)_2$, dtc = dialkyldithiocarbamate, forms a symmetric Au^{II} product when oxidized with halogens. However, the material was found to be too unstable to isolate at room temperature. The anionic charge associated with the *i*-MNT complex, in which the Au^{I} product has a nearly identical coordination structure to that of the Au^{I} dithiocarbamate, appears to give the Au^{II} species, $[Au_2(i\text{-}MNT)_2X_2]^{2-}$, greatly increased stability. The fact that the stability of these species in solution changes in the order $Cl^- > Br^- > I^-$ follows closely the increased nucleophilicity of any halide freed by ionization. This observation may account for some of the difficulty our group had initially[13] in reproducing Schmidbaur's observation of CH_3I addition to the ylide complex, although the primary problem was the sensitivity of the complex to UV light.[5d]

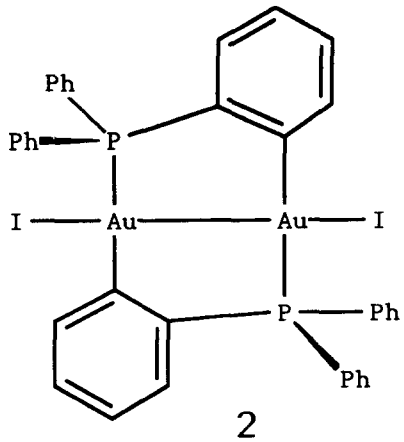
9. IMPLICATIONS OF THE GODDARD–LOW OXIDATIVE ADDITION CONCEPT TO THE DINUCLEAR GOLD(I) CHEMISTRY

The oxidative addition chemistry described above follows nicely the Goddard–Low concepts. Basic ligands attached to the Au^{I} centres enhance the ease of closed-shell to open-shell formation. The open-shell configuration on the Au^{I} centre to which the small molecule is initially added involves a *d*-orbital perpendicular to the axis of ligand coordination to the Au^{I} and directed, at least partially, toward the adjacent Au^{I} centre. As long as this distance is around 3.0 Å or less, an Au—Au bond can form, leaving the second metal atom "open". With alkyl halides, nucleophilic attack by the Au^{I} on the C atom with metal–metal bond formation and heterolytic C-halide bond rupture (Fig. 5) leaves the second gold centre coordinately unsaturated and the overall charge of the complex cationic. Hence, the reaction pattern is the same as observed for oxidative addition to square planar complexes, but gives a product with the addition across the Au—Au bond. The fact that the cationic $[Au_2(diphos)_2]^{2+}$ complexes do not oxidatively add small molecules or otherwise easily oxidize appears directly related to the apparent increase in the energy required to obtain the open-shell configuration with phosphine ligand coordination and the positive charge on the complex.

The presence of another metal ion centre such as Hg^{2+} or Tl^{+} adjacent to the Au^{I} in dinuclear MTP complexes also prevents the oxidative addition.[53] While the charge may be important with

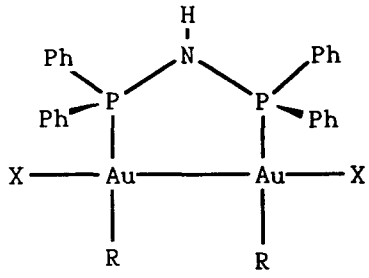


1

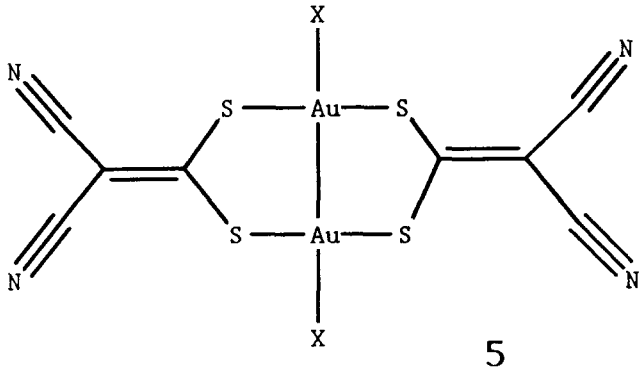


2

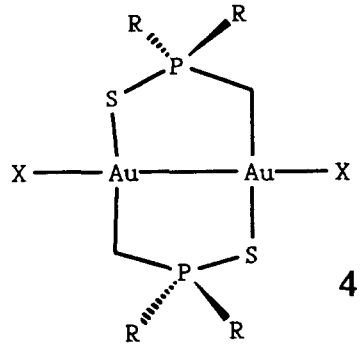
3



2-



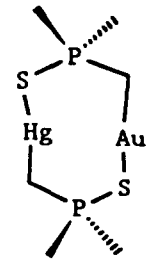
5



4

Fig. 7. General classes of structurally characterized dinuclear Au^{II} compounds: **1**[5m] $[Au_2(\mu\text{-}(CH_2)_2PR_2)_2X_2]$; **2**[11] $[Au_2(o\text{-}PC)_2I_2]$; **3**[30] $R_2Au_2[\mu\text{-}PPh_2)_2NH]$; **4**[12b] $[Au_2(MTP)_2X_2]$; **5**[51] $[Au_2(i\text{-}MNT)_2X_2]^{2-}$, X is generally a halide but also may be a variety of other anions.

Hg^{2+}, the neighbouring group influence is most likely to be the failure of the two adjacent metal atoms to be able to form a good electron pair bond.



+

PF_6^- or BPh_4^-

Yet, with all of the studies performed to date with dinuclear Au^I complexes, some uncertainty still remains regarding the specific role the adjacent metal atom plays in electronically influencing the oxidative addition. While the Goddard–Low concept appears to explain the results observed

for dinuclear oxidative addition, a clearer understanding of the impact of the electronic properties of the adjacent metal center comes from studies of the chemistry of linear trinuclear species.

10. OXIDATIVE ADDITION TO LINEAR TRINUCLEAR SPECIES

Direct evidence for a positive electronic influence of a neighbouring metal atom on the oxidative addition process, with a resultant metal–metal bond formation, can be observed in the chemistry of linear trimetallic species. The process that leads to "terminal addition" (Fig. 8) is a typical two-electron oxidative addition. This product is the expected product as long as the metal atom in the middle of the linear array, M, allows addition to take place. The two-electron oxidative addition which produces the four sigma bonds, the "*trans* addition", cannot occur with metal–metal bond formation unless M contributes electrons and orbitals to the process. Four sigma bonds cannot form from a two-electron oxidative addition event.

The Goddard–Low concept of oxidative addition pinpoints the metal atoms, M, for which the *trans* addition might become possible. Assuming that the unoxidized species has M in planar coordination, a filled orbital near the HOMO and an empty orbital near the LUMO in energy must be found which can be involved in the bonding. To form metal–metal bonds, these orbitals must be directed largely along the metal–metal axis. Open-shell formation at M′ can induce bonding to M, but it also must promote an electron into an empty orbital at M. This orbital becomes an open-shell orbital which allows bonding to the other M′. Consequently, A_2 adds across the three-metal-atom array. Should M not have available orbitals for bonding to M′ nor two electrons to contribute to the bonding process, single centre oxidative addition might occur providing the neighbouring metal atom did not inhibit addition totally as observed in many dinuclear systems.

Single-centre oxidative addition has been observed with the trinuclear pyrazolate (pyra) species tris-(μ-3,5-triphenylpyrazolato)trigold(I). When the planar complex $[Au^{I}(pyra)]_3$ is oxidized with halogens or even with *aqua regia* the mixed-valent product $[Au^{III}Cl_2Au_2(I)(pyra)_3)]$ is obtained, which has been structurally characterized (Fig. 9). The distance between gold atoms is *ca* 3.3 Å in the unoxidized and oxidized materials.

The MTP ligand furnished us with an opportunity to synthesize linear trinuclear species in which the oxidative addition process could be tested.[54] By reacting [PPN][Au(MTP)$_2$] with K_2PtCl_4 the product *trans*-$[Au^{II}(\mu\text{-MTP})_2Pt(\mu\text{-MTP})_2Au^{II}]Cl_2$ was obtained and studied structurally (Fig. 10). The unoxidized precursor $[Au^{I}(\mu\text{-MTP})_2Pt(\mu\text{-MTP})_2Au^{I}]$ was formed from [PPN][Au(MTP)$_2$] by reaction with *cis*-$PtCl_2(SEt_2)_2$. Oxidation with halogens or with $PhICl_2$ cleanly forms the Au^{II} product, which can be reduced back to the Au^{I} material with $LiCH_3$. Oxidation shortens the Au—Pt distance from 3.03 to 2.66 Å. In these complexes the Pt atom is planar and four-coordinate to the S atoms of the bridging MTP ligands. Aside from the formation of the terminal metal–halide bonds and the shortening of the Au—Pt distance, the geometric changes found upon oxidation of the complex are small.

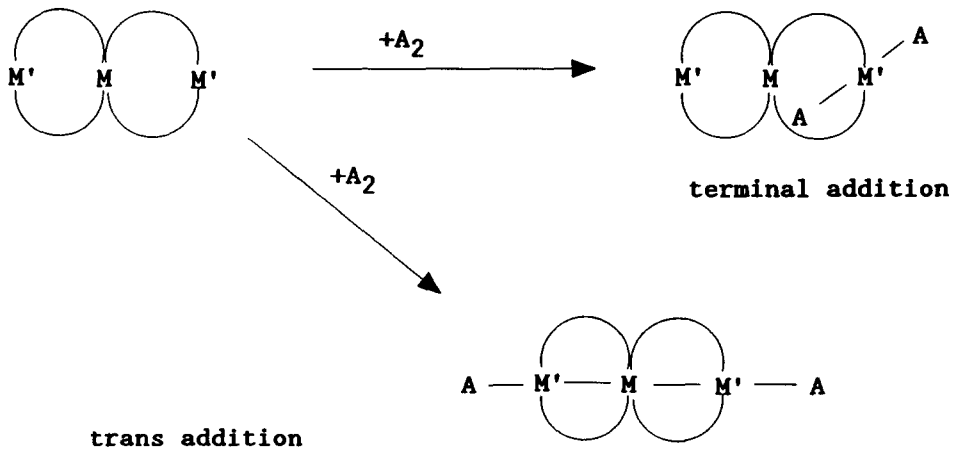


Fig. 8. Oxidative addition to linear trinuclear species.

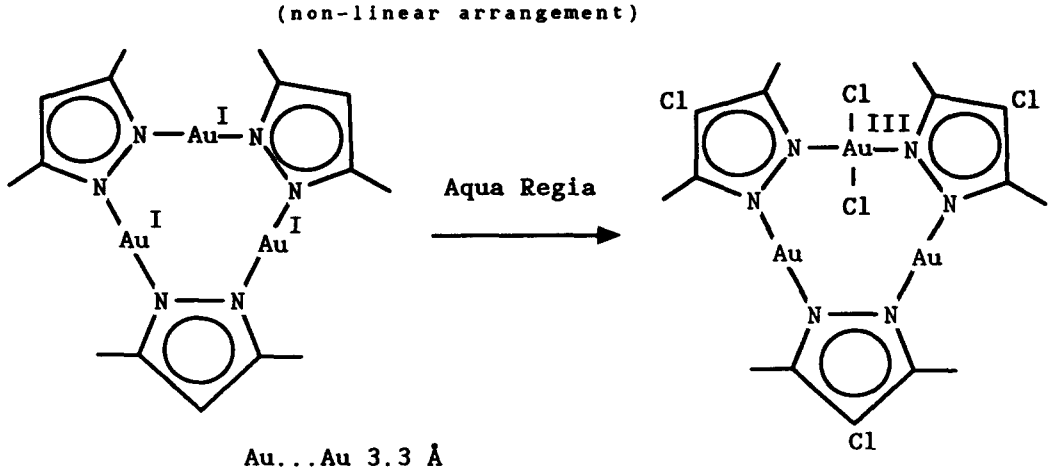


Fig. 9. Oxidation of tris-(μ-3,5-triphenylpyrazolato)trigold(I) with *aqua regia*.

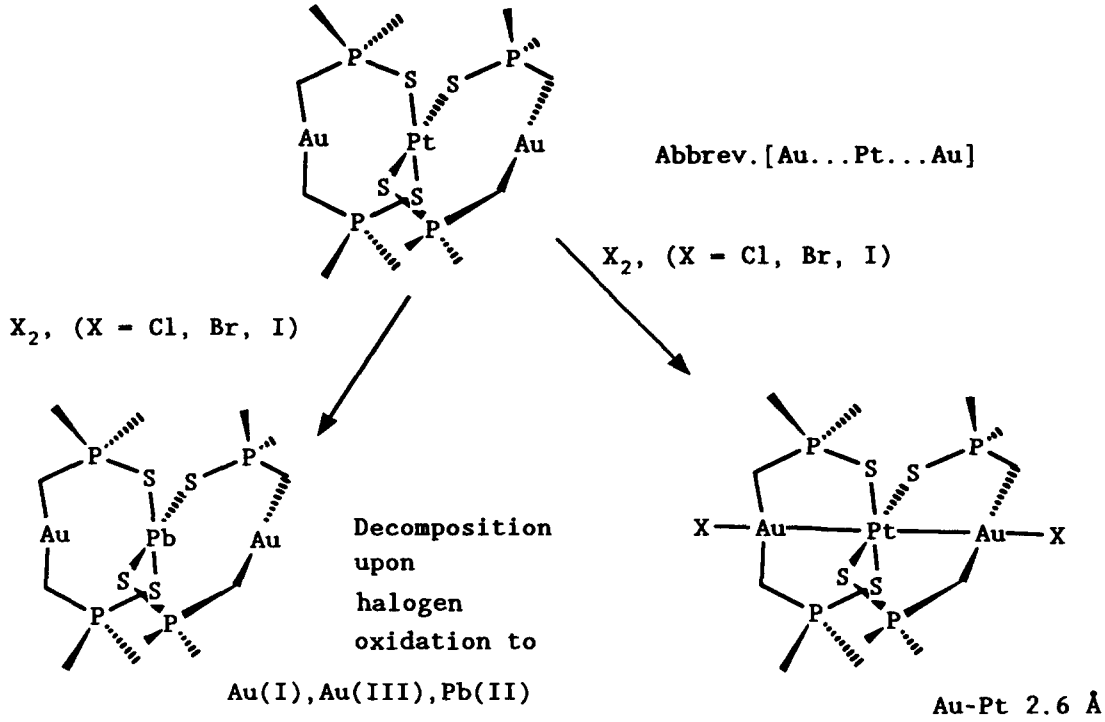


Fig. 10. Linear trinuclear [Au···Pt···Au] and [Au···Pb···Au] complexes with the ligand MTP.

As in the dinuclear gold ylide complexes, SO_2(g) also adds[19a] to the [Au^I(μ-MTP)$_2$Pt(μ-MTP)$_2$Au^I]. The shortening of the Au—Pt distance to 2.868 Å and the pyramidal geometry about the coordinated S atom bonded to the Au entirely parallels the observations made with the SO_2 addition to the dinuclear ylide complex. Thus, the nucleophilic interaction of the gold centres with the SO_2 leads to partial "oxidation" of the complex, with full oxidative addition occurring upon halogen addition.

Fenske–Hall calculations[4i] show that the HOMO in the linear trinuclear complex [Au···Pt···Au] is antibonding with respect to the metal–metal interaction along the linear metal axis. Oxidation results in the formation of a bonding HOMO along this axis. While it is convenient to describe the gold atoms as the atoms being oxidized, the correct description is that a [Au—Pt—Au]$^{2+}$ moiety bridged by the MTP and coordinated to the halides is formed.

A Goddard–Low description of this trinuclear oxidative addition process implies that the closed-shell d^{10} Au^{I} centre becomes an open-shell species upon interaction with the oxidant and induces an "excitation" of the Pt^{II} in the middle of the complex. The unoxidized complex has a typical, well-studied PtS_4 coordination with a HOMO involving significant d_{z^2} character and a LUMO with substantial p_z character. The filled d_{z^2} orbital falls along the metal–metal axis. Promotion of an electron from this orbital to the p_z orbital produces an "open-shell" configuration, which induces the formation of the open-shell configuration for the second gold atom. Electron pair bonds are formed between the gold and platinum atoms.

The Goddard–Low description of the oxidative addition process for the trinuclear species suggests that the metal atom in the middle of the complex must have electrons to contribute to the bonding and low-lying "open-shell" excited state. Several metal ions in addition to Pt^{II} are reasonable candidates such as Ir^{I} or Pd^{II}, but to date trinuclear MTP species with these ions as the metal in the middle have not been characterized. However, Pb^{II} in the complex $[Au^{I}(\mu\text{-MTP})_2Pb(\mu\text{-MTP})_2Au^{I}]$ does occupy essentially the same coordination position as Pt^{II}, Fig. 10.[55] The geometry is not rigorously square planar about the Pb^{II} as it is with the Pt^{II}, but the tetrahedral distortion is very small. The $Au^{I}\cdots Pb^{II}$ distance is about the same as $Au^{I}\cdots Pt^{II}$ distance, 3.0 Å. Oxidation of this complex with $PhICl_2$ or halogens leads to decomposition. Stoichiometric studies with $PhICl_2$ indicate that the oxidation produces approximately equal molar quantities of Au^{I}, Au^{III} and Pb^{II} species. There appears to be no stability to any oxidized trinuclear product.

Since the four coordinate Pb^{II} in the centre of the trinuclear $(Au\cdots Pb\cdots Au)$ complex contains no low-lying empty orbitals, promotion from the s^2 configuration of the ion must be into antibonding Pb—S orbitals. In fact, Fenske–Hall calculations[55] indicate that the HOMO in this system is largely Pb(6*S*) in character, with bonding and antibonding contributions from the Au atoms. The SHOMO is bonding in character, making oxidation considerably more difficult than with the Pt complex where the HOMO is antibonding. Promotion to the LUMO produces no net metal–metal bonding as apparently occurs with $[Au\cdots Pt\cdots Au]$ (Fig. 11).

The chemistry of a third linear trinuclear MTP complex[4i] further relates to the Goddard–Low model of oxidative addition. This cation $[Hg_2Pt(MTP)_4]^{2+}$ (Fig. 12) is exactly isoelectronic with the $[Au\cdots Pt\cdots Au]$ species. However, it undergoes no oxidation chemistry with mild halogenation. Various salts of the cation have been characterized, but chemical oxidative addition has not been achieved in any case. In this system which is structurally similar to the other complexes, the HOMO has no Hg—Pt character and is largely associated with the Pt—S coordination. The LUMO does have Pt—Hg bonding associated with it. However, promotion of the closed-shell Hg^{2+} to its open-shell configuration is very difficult energetically. It appears to be a "dead" system to oxidative addition.

11. SUMMARY

The oxidation or attempted oxidation by small-molecule oxidants of the linear $[Au\cdots Pt\cdots Au]$, $[Au\cdots Pb\cdots Au]$ and $[Hg\cdots Pt\cdots Hg]^{2+}$ require us to acknowledge that neighbouring-atom electronic features can both inhibit and promote the oxidative addition process. A similar type of electronic influence appears prevalent in the oxidative addition to dinuclear Au^{I} complexes and probably exists whenever the Goddard–Low concept of oxidative addition can involve both metal atoms in the process. Metal–metal bond formation accompanying the oxidative addition stabilizes intermediates which lead to the formation of products in which the addend adds across the metal–metal bond(s). The promotion of the oxidative addition will depend on the ease of closed-shell to open-shell promotion of the neighbouring atom as well as the atom to which the adduct initially interacts. Such behaviour presumably exists in many systems wherein bimetallic heterogeneous catalysis is more effective than in the monometallic system.

Acknowledgements—The author thanks the large number of students and postdoctorals who have contributed to the studies described in this report. Their names are in the references. Three postdoctoral colleagues stand out for their special contributions, H. H. Murray, III, Suning Wang and Richard J. Staples. The National Science Foundation and The Welch Foundation made our studies possible. The author also thanks the Penguin Foundation for support with a Wilhelm Manchot Research Professorship at the Technical University of Munich and to numerous excellent discussions with Professor Hubert Schmidbaur of that institution and Professor F. A. Cotton and Michael B. Hall of Texas A&M University.

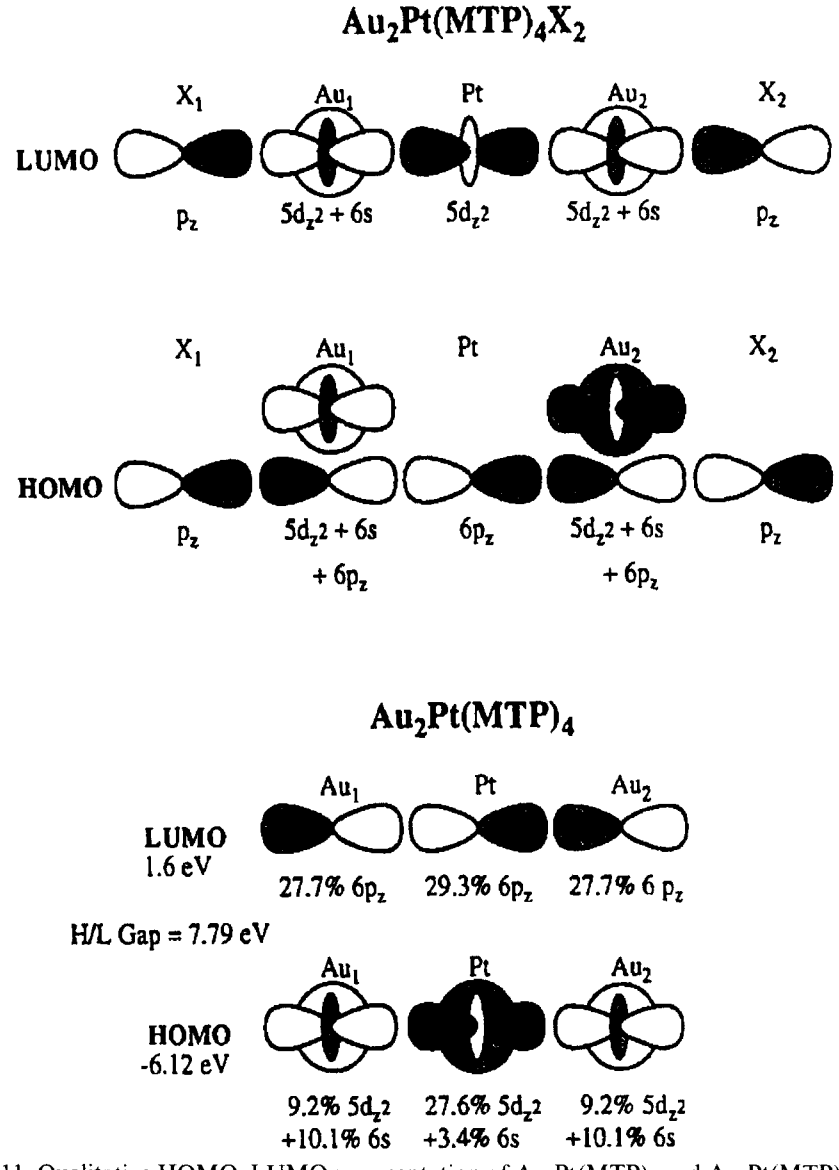


Fig. 11. Qualitative HOMO–LUMO representation of $Au_2Pt(MTP)_4$ and $Au_2Pt(MTP)_4X_2$.[57]

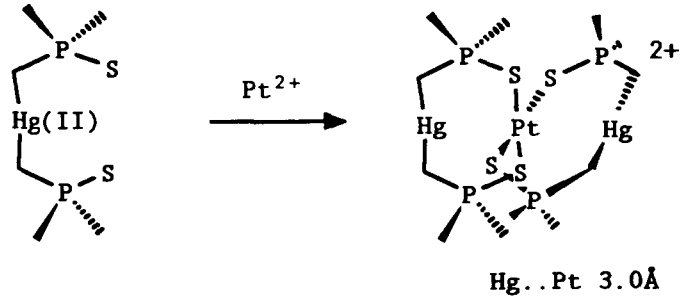


Fig. 12. Synthesis and structure of the cation $[Hg_2Pt(MTP)_4]^{2+}$, which is isoelectronic with [Au···Pt···Au].

REFERENCES

1. M. Chisholm, *Reactivity of Metal–Metal Bonds* (edited by M. Chisholm). ACS Symposium Series, American Chemical Society, (1981).
2. (a) F. A. Cotton and R. A. Walton, *Multiple Bonds Between Metal Atoms*. John Wiley and Sons, New York, (1982); (b) R. Adams and I. T. Horvath, *Prog. Inorg. Chem.* 1985, **33**, 127; (c) J. H. Sinfelt, *Accts Chem. Res.* 1977, **10**, 15.
3. J. P. Collman, L. S. Hegedus, J. Norton and R. Finke, *Principles and Applications of Organotransition Metal Chemistry* 2nd edn. University Science Books, Mill Valley, California (1987).
4. (a) M. Chisholm, *Metal–Metal Bonds in Clusters and Catalysis* (edited by J. P. Fackler Jr). Plenum Publishing Co., New York (1990); (b) A. L. Balch, *Metal–Metal Bonds in Clusters and Catalysis* (edited by J. P. Fackler Jr). Plenum Publishing Co., New York (1990); (c) A. L. Balch, B. C. Noll, M. M. Olmstead and D. V. Toronto, *Inorg. Chem.* 1992, **31**, 5226; (d) F. Antwi-Nsiah and M. Cowie, *Organometallics* 1992, **11**, 3157; (e) T. G. Schenck, C. R. C. Milne, J. F. Sawyer and B. Bosnich, *Inorg. Chem.* 1988, **24**, 2388; (f) R. D. Brost and S. R. Stobart, *Inorg. Chem.* 1989, **28**, 4307, and refs therein; (g) G. K. Anderson, *Adv. Organomet. Chem.* 1993, **35**, 1; (h) M. K. Kolel-Veetil, A. Rheingold and K. J. Ahmed, *Organometallics* 1993, **12**, 3439; (i) T. G. Carlson, J. P. Fackler Jr, R. J. Staples and R. E. P. Winpenny, *Inorg. Chem.* 1995, **34**, 426; (j) R. G. Pearson and W. R. Muir, *J. Am. Chem. Soc.* 1970, **92**, 5519.
5. (a) R. Uson and A. Laguna, *Coord. Chem. Rev.* 1986, **70**, 1; (b) R. J. Puddephatt, *The Chemistry of Gold*. Elsevier, Amsterdam (1978); (c) H. Schmidbaur, *Organogold Compounds*, Gmelin Handbook of Inorganic Chemistry, Springer-Verlag, Berlin, (1980); (d) J. D. Basil, H. H. Murray III, J. P. Fackler Jr, J. Tocher, A. M. Mazany, B. Trzcinska-Bancroft, H. Knachel, D. Dudis, T. J. DeLord and D. O. Marler, *J. Am. Chem. Soc.* 1985, **107**, 6908; (e) H. H. Murray III, J. P. Fackler Jr and D. A. Tocher, *J. Chem. Soc. Chem. Commun.* 1985, 1278; (f) F. A. Cotton and G. Wilkinson, *Advanced Inorganic Chemistry*, 5th edn, p. 950. John Wiley & Sons, New York (1988); (g) H. Schmidbaur, *Gold Bull.* 1990, **23**, 11, and references therein; (h) C. E. Housecroft, *Chem. Soc. Ann. Rep.* 1991 (Gold literature for 1990); (i) L. C. Porter and J. P. Fackler Jr, *J. Am. Chem. Soc.* 1986, **108**, 2750; (j) H. H. Murray III and John P. Fackler Jr, *Inorg. Chim. Acta* 1986, 115; (k) L. G. Kuz'mina, *Organomet. Chem. U.S.S.R.* 1992, **5**, 358; (l) A. Grohmann and H. Schmidbaur, *Comprehensive Organometallic Chemistry II* (edited by J. Wardell, E. W. Abel, F. G. A. Stone and G. Wilkinson) Vol. 3, Pergamon Press, Oxford (1995).
6. J. J. Low and W. Goddard III, *J. Am. Chem. Soc.* 1984, **106**, 6928; J. J. Low and W. Goddard III, *Organometallics* 1986, **5**, 609; J. L. Low and W. Goddard III, *J. Am. Chem. Soc.* 1986, **108**, 6115.
7. C. E. Moore, *Atomic Energy Levels*, Circular of the National Bureau of Standards 467 (1949).
8. J. E. Chatt, *Accad. Nazionale Dei Lincei.* IV Curso Estivo di Chimica, 7 October (1959).
9. (a) P. D. Harvey and H. B. Gray, *J. Am. Chem. Soc.* 1988, **110**, 2145; (b) H.-R. Jaw, M. M. Savas, R. D. Rogers and W. R. Mason, *Inorg. Chem.* 1989, **28**, 1028; (c) C.-M. Che, H.-L. Kwong, V. W.-W. Yam and K.-C. H. Cho, *J. Chem. Soc, Chem. Commun.* 1989, 885.
10. J. Shain and J. P. Fackler Jr, *Inorg. Chim. Acta* 1987, **131**, 157.
11. M. A. Bennett, S. K. Bhargawa, K. D. Griffiths, G. B. Robertson, W. A. Wickramasinghe and A. C. Willis, *Angew. Chem.* 1987, **99**, 261. A mixed valent $Me_2Au^{III}Au^{I}[\mu\text{-}(o\text{-}PC)]_2$ derivative (private communication) also has been structurally characterized by Bennett.
12. (a) M. N. I. Khan, S. Wang and J. P. Fackler Jr, *Inorg. Chem.* 1989, **28**, 3579; (b) A. M. Mazany and J. P. Fackler Jr, *J. Am. Chem. Soc.* 1984, **106**, 801.
13. (a) H. Schmidbaur and R. Franke, *Inorg. Chim. Acta* 1975, **13**, 85; (b) J. P. Fackler Jr and J. D. Basil, Inorganic Chemistry,: Toward the 21st Century (edited by M. H. Chisolm), pp. 201–208. No. 211, Am. Chem. Soc., Symposium Series (1983).
14. N. S. Lewis, K. R. Mann, G. Gordon II and H. B. Gray, *J. Am. Chem. Soc.* 1976, **98**, 7461.
15. J. P. Fackler Jr and J. D. Basil, *Organometallics* 1982, **1**, 871.
16. W. A. Herrmann, J. Plank, M. L. Ziegler and B. Balbach, *J. Am. Chem. Soc.* 1980, **102**, 5908.
17. A. L. Balch, C. T. Hunt, C.-L. Lee, M. Olmstead and J. P. Farr, *J. Am. Chem. Soc.* 1981, **103**, 3764.
18. F. Basolo and R. G. Pearson, *Mechanisms of Inorganic Reactions. A Study of Metal Complexes in Solution*. John Wiley & Sons, Inc., New York (1967).
19. (a) C. King, D. D. Heinrich, G. Garzon, J.-C. Wang and J. P. Fackler Jr, *J. Am. Chem. Soc.* 1989, **111**, 2300; (b) D. D. Heinrich, R. J. Staples and J. P. Fackler Jr, *Inorg. Chim. Acta* 1995, **229**, 61.
20. (a) H. H. Murray, G. Garzon, R. G. Raptis, A. M. Mazany, L. C. Porter and J. P. Fackler Jr, *Inorg. Chem.* 1988, *27*, 836; (b) R. G. Raptis, L. C. Porter, R. J. Emrich, H. H. Murray and J. P. Fackler Jr, *Inorg. Chem.* 1990, **29**, 4408; (c) R. G. Raptis, J. P. Fackler Jr, J. D. Basil and D. S. Dudis, *Inorg. Chem.* 1991, **30**, 3072; (d) D. D. Heinrich and J. P. Fackler Jr, *Inorg. Chem.* 1990, **29**, 4402; (e) R. G. Raptis, H. H. Murray, R. J. Staples, L. C. Porter and J. P. Fackler Jr, *Inorg. Chem.* 1993, **32**, 5576, and refs therein.
21. H. H. Murray, J. P. Fackler Jr, L. C. Porter, D. A. Briggs, M. A. Guerra and R. J. Lagow, *Inorg. Chem.* 1987, **26**, 357.

22. (a) R. Uson, A. Laguna, M. Laguna, J. Jimenez and P. G. Jones, *J. Chem. Soc., Dalton Trans.* 1991, 1361; R. Uson, A. Laguna, M. Laguna, J. Jimenez and P. G. Jones, *Angew Chem. Int. Edn Engl.* 1991, **30**, 198; (b) H. H. Murray, J. P. Fackler Jr and B. Trzcinska-Bancroft, Organometallics 1985, **4**, 1633; (c) J. P. Fackler Jr and H. H. Murray, *Organometallics* 1984, **3**, 821.
23. J. P. Fackler Jr, R. J. Staples and Z. Assefa, *J. Chem. Soc., Chem. Commun.* 1994, 431.
24. P. Jandik and H. Schmidbaur, *J. Chromatogr.* 1981, 47.
25. D. W. Heinrich, Ph.D. thesis, Texas A&M University (1987).
26. H. C. Knachel, C. A. Dettorre, H. J. Galaska and T. A. Salupo, *Inorg. Chim. Acta* 1987, **126**, 7.
27. A. M. Mazany and J. P. Fackler Jr, *J. Am. Chem. Soc.* 1984, **106**, 801.
28. L. C. Porter and J. P. Fackler Jr, *Acta Cryst.* 1987, **C43**, 587, and refs therein.
29. H. Schmidbaur and R. Franke, *Inorg. Chim. Acta* 1975, **13**, 85.
30. R. Uson, A. Laguna, M. Laguna, M. N. Fraile, P. G. Jones and G. M. Sheldrick, *J. Chem. Soc., Dalton Trans.* 1986, 291; L. S. Moore, R. V. Parish, R. Uson, A. Laguna, M. Laguna and M. N. Fraile, *J. Chem. Soc., Dalton Trans.* 1988, 23.
31. R. G. Raptis, L. C. Porter, R. J. Emerich, H. H. Murray and J. P. Fackler Jr, *Inorg. Chem.* 1990, **29**, 4408.
32. H. Schmidbaur, C. Hartman, G. Reber and G. Müller, *Angew. Chem, Int. Edn Engl.* 1987, **26**, 1146.
33. B. Trzcinska-Bancroft, M. N. I. Khan and J. P. Fackler Jr, *Organometallics* 1988, **7**, 993.
34. H. C. Knachel, D. S. Dudis and J. P. Fackler Jr, *Organometallics* 1984, **3**, 1312.
35. D. S. Dudis and J. P. Fackler Jr, *Inorg. Chem.* 1985, **24**, 3758.
36. H. H. Murray III, J. P. Fackler Jr, L. C. Porter and A. M. Mazany, *J. Chem. Soc., Chem. Commun.* 1986, 321.
37. H. H. Murray III, A. M. Mazany and J. P. Fackler Jr, *Organometallics* 1985, **4**, 154.
38. R. G. Raptis, J. P. Fackler Jr, J. D. Basil and D. S. Dudis, *Inorg. Chem.* 1991, **30**, 3072.
39. R. R. Ryan, G. J. Kubas, D. C. Moody and P. G. Eller, *Struct. Bonding (Berlin)* 1982, **46**, 47.
40. J. P. Fackler Jr and B. Trzcinska-Bancroft, *Organometallics* 1985, **4**, 1891.
41. D. C. Neitling, M.Sc. dissertation, Texas A&M University (1995).
42. L. C. Porter and J. P. Fackler Jr, *Acta Cryst.* 1986, **C42**, 1128.
43. H. H. Murray, J. P. Fackler Jr, A. M. Mazany, L. C. Porter, J. Shain and L. R. Falvello, *Inorg. Chim. Acta* 1986, **116**, 171.
44. H. H. Murray, J. P. Fackler Jr and B. Trzcinska-Bancroft, *Organometallics* 1985, **4**, 1633.
45. J. K. Kochi, *Organometallic Mechanisms and Catalysis.* Academic Press, New York (1978).
46. H. H. Murray, J. P. Fackler Jr and A. M. Mazany, *Organometallics* 1984, **3**, 1310.
47. D. D. Heinrich and J. P. Fackler Jr, *J. Chem. Soc., Chem. Commun.* 1987, 1260.
48. L. C. Porter and J. P. Fackler Jr, *Acta Cryst.* 1987, **C43**, 29.
49. L. C. Porter and J. P. Fackler Jr, *Acta Cryst.* 1991, **C47**, 1180; J. P. Fackler Jr and L. C. Porter, *J. Am. Chem. Soc.* 1986, **108**, 2750.
50. J. P. Fackler Jr, unpublished observation, S. Wang and J. P. Fackler Jr, *Organometallics* 1989, **8**, 1578.
51. M. N. I. Khan, J. P. Fackler Jr, C. King, J. C. Wang and S. Wang, *Inorg. Chem.* 1988, **27**, 1672; M. N. I. Khan, S. Wang and J. P. Fackler Jr, *Inorg. Chem.* 1989, **28**, 3579.
52. D. C. Calabro, B. A. Harrison, G. T. Palmer, M. K. Moguel, R. L. Rebbert and J. L. Burmeister, *Inorg. Chem.* 1981, **11**, 227.
53. S. Wang, *Organometallics* 1988, **7**, 2415; S. Wang and J. P. Fackler Jr, *Organometallics* 1990, **111**.
54. H. H. Murray, D. A. Briggs, G. Garzon, R. Raptis, L. C. Porter and J. P. Fackler Jr, *Organometallics* 1987, **6**, 1992.
55. S. Wang, G. Garzon, C. King, J.-C. Wang and J. P. Fackler Jr, *Inorg. Chem.* 1989, **28**, 4623.
56. S. Wang, J. P. Fackler Jr, C. King and J.-C. Wang, *J. Am. Chem. Soc.* 1988, **110**, 3308.
57. T. F. Carlson, Ph.D. thesis, Texas A&M University (1993).

Pergamon

S0277-5387(96)00275-6

Polyhedron Vol. 16, No. 1, pp. 19–23, 1997
Copyright © 1996 Elsevier Science Ltd
Printed in Great Britain. All rights reserved
0277-5387/97 $15.00+0.00

The structure of hydrated lead(II) dimethylacetate, $[Pb_6(O_2CCH(CH_3)_2)_{12}]$ $4H_2O$: a hexanuclear carboxylate

G. D. Fallon, L. Spiccia, B. O. West* and Q. Zhang

Centre for Chemical Synthesis and Department of Chemistry, Monash University, Clayton, Victoria, 3168, Australia

(Received 30 April 1996; accepted 28 May 1996)

Abstract—Hydrated lead(II) dimethylacetate forms hexanuclear units $[Pb_6(O_2CCH(CH_3)_2)_{12}]4H_2O$ in the solid state consisting of a ring of four lead atoms linked by oxygen atoms belonging to chelated carboxylates, with two further lead atoms linked to the ring by bridging carboxylate oxygens. Water molecules are coordinated to four lead atoms. There are pairs of Pb atoms with 7, 6 and 5-fold coordination in the molecular unit. The hexanuclear molecularity is retained in solution but Pb^{207} NMR measurements indicate different 5-coordinate sites are formed. Copyright © 1996 Elsevier Science Ltd

Keywords: lead(II); dimethylacetate; carboxylate; structure; Pb^{207} NMR.

As an aid to synthetic studies of the reactions of lead carboxylates with metal alkoxides in organic solvents [1] we have required a lead carboxylate which is reasonably soluble either in simple alcohols or toluene, preferably in both. Such a compound is lead dimethylacetate which, when isolated in a hydrated form, is readily soluble in a number of common organic solvents including ethanol, both iso- and normal propanols and benzene or toluene. This behaviour contrasts with that of the acetate which is sparingly soluble in alcohols and does not dissolve in benzene or toluene. We present the results of an X-ray structural study of the dimethylacetate compound which has disclosed the existence of hexanuclear molecular units in the solid state rather than the polymeric form of the acetate and other characterized lead carboxylates [2].

EXPERIMENTAL

Molecular weights were obtained using a Knauer Type II vapour phase osomometer (VPO) in benzene solution at 60°C using benzil as standard. Pb^{207} NMR measurements were performed on a Bruker AM-300 instrument. Chemical shifts were measured in ppm with $PbMe_4$ as an external standard for Pb^{207} NMR spectra. The latter measurements were converted to values relative to $Pb(NO_3)_2$ by adding 2961 [3]. Microanalysis was by CMAS (Melbourne).

Lead dimethylacetate hydrate

Dimethylacetic acid (Me_2CHCO_2H) (2.32 cm^3, 24.9 mmol) was dissolved in toluene (20 cm^3) and yellow PbO (2.78 g, 12.5 mmol) added to the solution. The mixture was refluxed until all but a trace of the solid had dissolved. The solution was filtered hot and crystals formed as the filtrate cooled. The solid was filtered and dried by pumping under reduced pressure (10^{-2} Torr). Yield: 95%. M.pt. 96–97°C. Found: C, 24.6; H, 4.1. Calc. for $C_{48}H_{92}O_{28}Pb_6$: C, 24.4; H, 3.9%. Mol. wt. (VPO) (benzene, 60°C) 2400 ± 50 (theor. for $C_{48}H_{92}O_{28}Pb_6$, 2360). Pb^{207} NMR spectrum (toluene) 300 K: δ = 1667, 2170, 2661, 2709 ppm.

Crystallographic study of $[Pb(O_2CCH(CH_3)_2)_2]_6 \cdot 4H_2O$

A sample of the compound was recrystallized from toluene and a representative clear tabular crystal from the batch of approximate dimensions 0.25 ×

* Author to whom correspondence should be addressed.

Table 1. Crystallographic data for $[Pb_6(O_2CCH(CH_3)_2)_{12}]4H_2O$

Compound	$C_{48}H_{92}O_{28}Pb_6$
Formula weight	2360
Crystal system	Monoclinic
Space group	$P2_1/n$
a (Å)	12.770(4)
b (Å)	20.479(6)
c (Å)	14.407(5)
α (°)	90
β (°)	110.82(3)
γ (°)	90
V (Å^3)	3522(2)
Density calc. (g cm^{-3})	2.23
Z	2
T (°C)	−80(1)
λ (Mo-K_α) (Å)	0.71073
μ (Mo-K_α) (mm^{-1})	14.47
F(000)	2192
Scan mode	w, 1.40° range
2θ range (°)	3.5–55.0
Scan rate (° min^{-1})	2.49–10.19
Data collected	8007
Data used [$F \geqslant 6s(F)$]	3477
$R(wR)$	0.071 (0.092)

0.24×0.15 mm was used for data collection. Intensity measurements were made on a Nicolet R3m/V diffractometer using graphite monochromated Mo-K_α radiation. Relevant crystallographic data are collected in Table 1. Three standard reflections monitored every 197 reflections showed no significant variation in intensity over the data collection period. Intensity data were corrected for Lorentz and polarization effects. A face indexed numerical absorption correction was applied on seven crystal faces, the maximum and minimum transmission factors being 0.040 and 0.153 respectively. Atomic scattering factors for neutral atoms were taken from literature values [4] and corrected for anomalous dispersion. All calculations were performed on a MicroVAX 2000 computer. The program for least squares refinement was that of Sheldrick [5]. The structure was solved by conventional Patterson and Fourier methods. Final refinement was by full matrix least squares employing anisotropic thermal parameters for Pb and isotropic thermal parameters for all other non-hydrogen atoms. Hydrogen atoms were positioned in geometrically idealized positions (C—H 0.96 Å) and given a single isotropic thermal parameter, fixed at 0.08 Å^2. At convergence (190 variables, 3477 observed data) R was 0.071 and wR, 0.092, where $wR = \Sigma(|F_o - F_c|)w^{1/2}/\Sigma|F_o|w^{1/2}$ and $w = [s^2(F_o) + 0.0084F_o^2]^{-1}$. The goodness-of-fit value $(\Sigma w(|F_o| - |F_c|)^2/(N_{observns} - N_{params})]^{1/2}$ was 0.87. The highest peak in the difference-Fourier synthesis was 4.6 e Å^{-3}.

RESULTS AND DISCUSSION

Properties of lead dimethylacetate

The reaction between PbO and dimethylacetate acid in undried toluene proved to be a convenient method of synthesis for the lead salt. The compound was isolated as a hydrate readily soluble in toluene and a variety of other solvents. Its molecular weight in benzene, determined by vapour phase osmometry, indicated a considerable degree of association corresponding to the presence of hexanuclear species. Its Pb^{207} NMR spectrum showed four resonances, two having equivalent intensities at 1667 and 2170 ppm and a further two of approximately half the intensity of the first two were observed close together at 2661 and 2709 ppm.

The structure of $[Pb(O_2CCH(CH_3)_2)_2]_6 \cdot 4H_2O$

Previous X-ray crystal studies of lead carboxylates have shown them to be polymeric because of carboxylate bridging. The carboxylate group may bridge between two metal atoms with an oxygen bonded to each as in the sparingly water soluble, anhydrous lead(II) formate [2] which has a three dimensional structure solely defined by such non-chelating, carboxylate bridges. Alternatively the group can be a chelating ligand to one metal atom and may also bridge through one or both of its oxygen atoms to neighbouring metal atoms. This mode of coordination is found in lead(II) acetate trihydrate [2, 6, 7] and the pentafluorobenzoate [2]. Both carboxylate groups are chelated to each lead atom in these compounds while one or both carboxylate groups are further coordinated to neighbouring lead atoms through carboxylato oxygen leading to chain structures for these species. Water molecules are also coordinated to each lead in the case of the acetate and contribute to the chain formation by hydrogen bonding contacts. A chain structure has also been observed for the crotonate [8] while in addition to single and bridging chelated groups, hydrogen bonding between carboxyl and hydroxyl groups causes a three dimensional structure to be formed by the glycollate [9]. Such structural features no doubt contribute to the low solubility of lead carboxylates in weakly solvating solvents such as alcohols and their general insolubility in non-polar solvents.

In hydrated lead(II) dimethylacetate, each lead atom is chelated by two carboxylate groups, at least one of which is coordinated to a neighbouring Pb atom. This basic "building block" format is similar to that leading to the polymeric structures of the acetate, pentafluorobenzoate and crotonate. However it is likely that the bulkiness of the $CH(CH_3)_2$ group prevents an infinite chain structure being formed and leads to the form of the present compound. Crystals of hydrated lead dimethylacetate contain hexanuclear

units consisting of a ring of four Pb atoms linked by single oxygen bridges from chelated carboxyls with a further two "terminal" lead atoms each linked to a ring-lead atom by two oxygen bridges derived from their chelated carboxyl groups (Fig. 1). Indeed the structure can be alternatively viewed as forming by the dimerization of two short Pb_3 chains. There are chelating, "non-bridging" carboxylate groups attached to each of the terminal and two of the ring Pb atoms. The Pb—O distances show marked asymmetry in the "non bridging" chelated carboxylates attached to the terminal Pb atoms (Pb(1)—O(1) 2.710 Å, Pb(1)—O(2) 2.368 Å) whereas there is virtually symmetric bonding of the analogous "non bridging" carboxylate groups to Pb atoms in the ring (Pb(3)—O(11) 2.510 Å, Pb(3)—O(12) 2.507 Å).

Single water molecules are coordinated to the two "terminal" Pb atoms and the ring Pb atoms to which they are bridged. These variations in coordination behaviour lead to the existence of three, differently coordinated Pb atoms in the hexanuclear units. Using an arbitrary length of approximately 2.8 Å to define maximum bonding interactions (this being the sum of the two ionic radii [10]), data in Table 2 show that Pb(1) may be considered as 6-coordinate, Pb(2) 7-coordinate and Pb(3) 5-coordinate. This contrasts with the Pb atoms in the acetate, formate and pentafluorobenzoate where 8-fold coordination is found. Longer range contacts between Pb(3) and O(10) at 2.832(20) Å and the inter-molecular contact with O(3) at 2.899(2) Å may contribute further bonding interactions, increasing local coordination numbers to 6 or 7.

The molecule in solution

The molecular weight data shows that the hexanuclear structure of the compound is essentially retained in benzene solution. However four sharp Pb^{207} resonances are observed with two well spaced chemical shifts of 1167, 2170, and two close together at 2661 and 2709 ppm instead of the three expected on the basis of the crystal structure. The peaks are in the ratio 2 : 2 : 1 : 1. There is relatively little information at present correlating chemical shift with coordination number among metal-organic lead(II) compounds, nevertheless some conclusions can be drawn from existing data. Table 3 lists Pb^{207} chemical shifts for compounds whose solid state structures have been determined or for which a comparable derivative has been studied and for which solution molecular weight measurements have indicated that the solid state molecularity has at least been retained. Coordination number 4 appears associated with shifts in the range 4152–5032 ppm while 5-coordinate compounds show values in the range 2558–3883 ppm. In this connection, the compound $[Pb_2Ti_2(\mu\text{-}O)(OAc)_2(OPr^i)_8]$, which has been shown by structural analysis to contain both 4 and 5-coordinate Pb in the crystal [14] has been found by us [1] to show two Pb^{207}

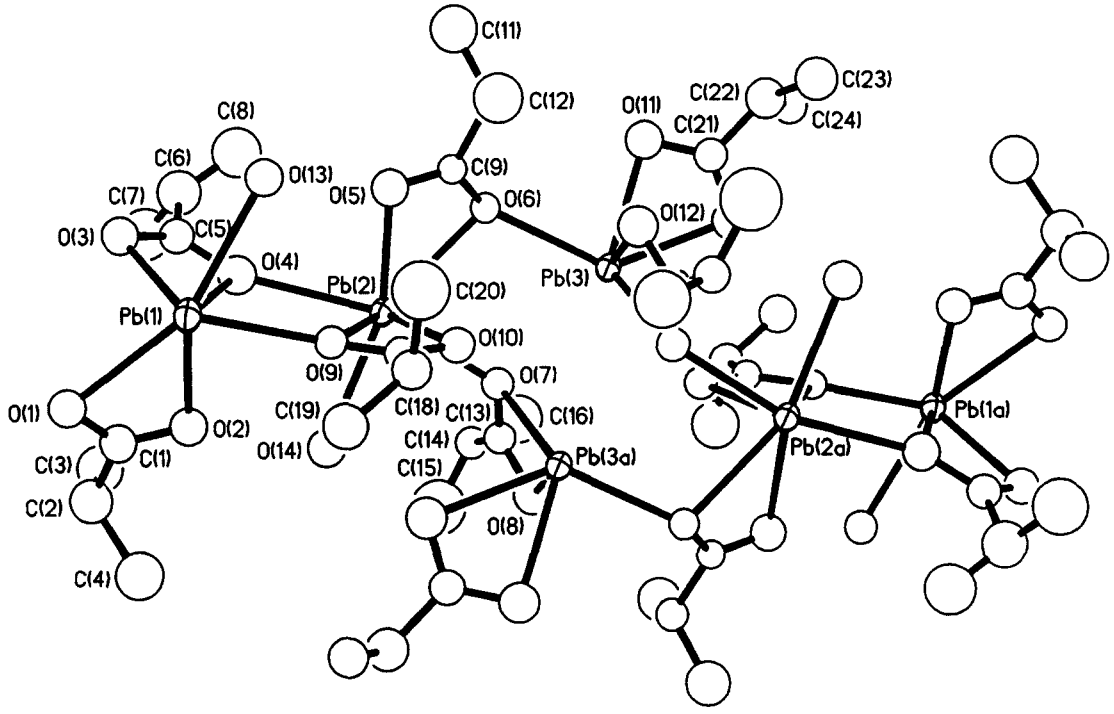


Fig. 1. Molecular structure diagram of $[Pb_6(O_2CCH(CH_3)_2)_{12}] \cdot 4H_2O$ showing the atom labelling scheme. Thermal ellipsoids at 50% probability.

Table 2. Selected bond lengths (Å) and angles (°)

Pb(1)—O(1)	2.710(22)	Pb(2)—O(4)	2.728(20)	Pb(3)—O(6)	2.552(11)
Pb(1)—O(2)	2.368(24)	Pb(2)—O(5)	2.528(24)	Pb(3)—O(7a)	2.720(18)
Pb(1)—O(3)	2.488(20)	Pb(2)—O(6)	2.671(17)	Pb(3)—O(8a)	2.381(26)
Pb(1)—O(4)	2.397(20)	Pb(2)—O(7)	2.578(18)	Pb(3)—O(11)	2.510(22)
Pb(1)—O(9)	2.499(16)	Pb(2)—O(9)	2.568(16)	Pb(3)—O(12)	2.507(21)
Pb(1)—O(13)	2.696(22)	Pb(2)—O(10)	2.462(20)		
		Pb(2)—O(14)	2.683(22)		

O(1)—Pb(1)—O(2)	50.3(6)	O(14)—Pb(2)—O(4)	81.7(7)
O(1)—Pb(1)—O(3)	77.5(6)	O(14)—Pb(2)—O(9)	70.8(7)
O(3)—Pb(1)—O(4)	53.7(7)	O(14)—Pb(2)—O(6)	157.2(6)
O(4)—Pb(1)—O(9)	68.2(6)	O(14)—Pb(2)—O(7)	80.8(6)
O(4)—Pb(1)—O(13)	75.8(7)	O(6)—Pb(3)—O(11)	82.9(6)
O(9)—Pb(1)—O(13)	72.7(6)	O(6)—Pb(3)—O(12)	134.5(7)
O(4)—Pb(2)—O(9)	62.4(6)	O(6)—Pb(3)—O(7a)	115.2(5)
O(5)—Pb(2)—O(6)	50.5(5)	O(6)—Pb(3)—O(8a)	82.5(7)
O(6)—Pb(2)—O(7)	76.8(6)	O(7a)—Pb(3)—O(8a)	50.0(7)
O(7)—Pb(2)—O(9)	111.5(5)	O(7a)—Pb(3)—O(11)	119.4(7)
O(9)—Pb(2)—O(10)	52.4(6)	O(7a)—Pb(3)—O(12)	83.7(6)
		Pb(1)—O(4)—Pb(2)	113.5(8)
		Pb(1)—O(9)—Pb(2)	115.6(7)
		Pb(2)—O(6)—Pb(3)	110.1(6)
		Pb(2)—O(7)—Pb(3a)	113.7(6)

Table 3. Structure-chemical shift data correlations for Pb(II) metal-organic compounds

Compound	$^{207}Pb^{a}$ (ppm)	Reference
Coordination No. 4[b]		
$Pb_4(\mu\text{-}O)(OBu^t)_6$	5032	[13]
$Pb_4(\mu\text{-}O)(OPr^i)_6$	4982	[13]
$Pb_4(\mu\text{-}O)(OEt)_6$	4977	[13]
$Pb_6(\mu\text{-}O)_4(OPr^i)_4$	4985	[13]
$Pb_6(\mu\text{-}O)_4(OEt)_4$	5019	[13]
Coordination No. 5[c]		
$PbZr_3(\mu\text{-}O)(OAc)_2(OPr^i)_{10}$ [14]	2558	[14]
$Pb_2Ti_2(\mu\text{-}O)(OPr^i)_{10}$ [15]	3016	[15]
$Pb_2Ti_2(\beta\text{-}O)(acac)_2(OPr^i)_8$	3883	[15]
$Pb_2Ti_2(\mu\text{-}O)(OAc)_2(OPr^i)_8$ [14]	2824, 2447	[1]
	3016	[14]
$Pb_2Ti_4(\mu\text{-}O)_2(OAc)_2(OEt)_{14}$ [1, 16]	2868	[1]
	2900	[14]

[a] Measurements in toluene or d^7-toluene.

[b] Coordination No. 4 based on structures of $Pb_4(\mu\text{-}O)(OSiPh_3)_6$ [11] and $Pb_6(\mu\text{-}O)_4(OPr^i)_4$ [12].

[c] Coordination No. 5 based on structures of compounds listed below.

resonances* both considerably moved upfield from the 4–5000 ppm range suggested to indicate 4-coordinate Pb(II) and being within or close to the range indicated for other 5-coordinate Pb compounds. This suggests the possibility that in solution the Pb/Ti compound undergoes a structural readjustment such that each Pb atom becomes 5-coordinate.

There do not appear to be other appropriate compounds with X-ray structurally defined 6 or 7 coordination for Pb^{II} for which Pb^{207} NMR data are also available to be used for comparison. However, one may conclude that increased coordination around a Pb atom will lead to increased shielding, resulting in an upfield shift of the corresponding Pb^{207} resonance. Therefore it can be anticipated that Pb atoms with coordination numbers of 6 and higher should display chemical shifts at successively higher fields than for 4 and 5-coordinate compounds. Thus in the case of Pb dimethylacetate, the resonance at 1667 ppm is assigned to the 7-coordinate Pb(2) and (2a) atoms and that at 2170 ppm to the 6-coordiate atoms Pb(1) and (1a). The remaining resonances, found close together at 2661 and 2709 ppm, are within the range for 5-coordinate Pb^{II} as defined above. The crystal structure data do not show any obvious differences between the ligand arrangements or Pb—O bond lengths at the 5-coordinate Pb(3) and Pb(3a) sites which could lead to different Pb^{207} resonances being observed for the two atoms. It can only be concluded therefore that some relaxation of the coordination arrangements existing in the crystal at Pb(3) and Pb(3a) occurs in solution, such as the lengthening of one or more Pb—O bonds, which allows the essential 5-coordinate form to be retained but causes a distinct structural difference to exist between the sites.

* An earlier report [14] mentioned only a single resonance at 3016 ppm with the comment that the molecule is fluxional.

Acknowledgements—This work was supported in part by

the Australian Research Council and a Generic Industrial Research and Development Grant (to L.S. and B.O.W.) and a Monash Departmental Scholarship (to Q.Z.).

REFERENCES

1. J. Bates, Q. Zhang, L. Spiccia and B. O. West, *J. Sol-Gel Sci. Technol.* 1994, **2,** 29; Q. Zhang, L. Spiccia and B. O. West, in preparation.
2. P. G. Harrison and A. T. Steel, *J. Organometal. Chem.* 1982, **239,** 105.
3. J. J. Dechter, *Prog. Inorg. Chem.* 1982, **29,** 285; R. K. Harris, J. J. Kennedy and W. McFarland, *NMR and the Periodic Table* (Edited by R. K. Harris and B. E. Mann). Academic Press, New York (1978).
4. J. A. Ibers and W. C. Hamilton (Editors), *International Tables for X-ray Crystallography*, Vol. IV. Kynoch Press, Birmingham (1974).
5. G. M. Sheldrick, *SHELXTL PLUS, Revision* 4.11. Siemens Analytical X-ray Instruments Inc., Madison, Wisconsin, USA (1990).
6. R. K. Rajaram and J. K. Mohana Rao, *Z. Kristallogr.* 1982, **160,** 225.
7. R. G. Bryant, V. P. Chacko and M. C. Etter, *Inorg. Chem.* 1984, **23,** 3580.
8. W. Clegg, I. R. Little and B. P. Straughan, *Acta Cryst.* 1986, **C42,** 1319.
9. C. D. Chandler, M. J. Hampden-Smith and E. N. Duester, *Inorg. Chem.* 1992, **31,** 4891.
10. R. D. Shannon, *Acta Cryst.* 1976, **A32,** 751.
11. C. Gaffney, P. G. Harrison and T. J. Key, *J. Chem. Soc., Chem. Commun.* 1980, 12.
12. A. I. Yanovskii, N. Ya. Turova and E. P. Turevskaya, *Koord. Khim.* 1982, **8,** 153 (Engl. Trans., Plenum Pub. Co.).
13. R. Papiernik, L. G. Hubert-Pfalzgraf and M. C. Massiani, *Polyhedron* 1991, **10,** 1657.
14. L. G. Hubert-Pfalzgraf, *Polyhedron* 1994, **13,** 1181.
15. S. Daniele, R. Papiernik and L. G. Hubert-Pfalzgraf, *Inorg. Chem.* 1995, **34,** 628.
16. H. K. Chae, D. A. Payne, Z. Xu and L. Ma, *Chem. Mater.* 1994, **6,** 1589.

Pergamon

S0277-5387(96)00272-0

Polyhedron Vol. 16, No. 1, pp. 25–31, 1997
Copyright © 1996 Elsevier Science Ltd
Printed in Great Britain. All rights reserved
0277-5387/97 $15.00 + 0.00

Coordination modes of the cyanoacetate ion; silver(I) and bis(η-cyclopentadienyl)titanium(IV) cyanoacetates. X-ray crystal structures of $[Ag(NCCH_2CO_2)]$ and $[TiCp_2(NCCH_2CO_2)_2]$

Dennis A. Edwards,* Mary F. Mahon and Timothy J. Paget

School of Chemistry, University of Bath, Bath BA2 7AY, U.K.

(Received 17 April 1996; accepted 28 May 1996)

Abstract—Polymeric silver(I) cyanoacetate contains the classical bis(carboxylato-*O*,*O*′) bridged metal dimer arrays in which each pair of adjacent metal atoms is doubly bridged by co-planar carboxylate groups in the *syn-syn* conformation. These dimeric units are extended into a polymeric chain by terminal linkage of all cyano-nitrogen atoms to silver atoms of adjacent dimer units. In this manner, an individual cyanoacetate anion is *O*,*O*′,*N*-bonded to three different silver centres. EHMO calculations suggest weak direct metal–metal interactions can result from the mixing of metal *s* and *p* orbitals into the d^{10} shells. Reactions of silver(I) or sodium cyanoacetates with $[(\eta\text{-}C_5H_5)_2TiCl_2]$ afford the bis(cyanoacetato) complex $[(\eta\text{-}C_5H_5)_2Ti(O_2CCH_2CN)_2]$ which has a solid state structure involving *O*-unidentate carboxylate groups, the cyano-nitrogen atoms not being bonded to a metal. This compound can also be prepared from $[(\eta\text{-}C_5H_5)_2Ti(CH_3)_2]$ and cyanoacetic acid.
Copyright © 1996 Elsevier Science Ltd

Keywords: carboxylate; cyanoacetate; cyclopentadienyl; silver; structure; titanium.

Although metal carboxylates are probably the most important and ubiquitous group of compounds with metal–oxygen–carbon bonds, few metal cyanoacetates have been investigated, particularly from a structural standpoint. The small number that have been studied show sufficient structural differences to suggest a rich variety of potential coordination modes in further examples. Thus both *O*-unidentate and *O*,*O*′;*O*-chelating and bridging cyanoacetate ligands are found [1] in $\{[Nd(O_2CCH_2CN)_3(DMF)(H_2O)]\cdot H_2O\}_n$ whereas in $[Fe_3(\mu_3\text{-}O)(O_2CCH_2CN)_6(H_2O)_3]$ the cyanoacetate groups are all *O*,*O*′-bridging bidentate [2]. Cadmium cyanoacetate contains [3] equal numbers of *O*,*O*′;*O*-bridging bidentate and *O*,*O*′;*N*-bridging tridentate cyanoacetate ligands. Finally, the copper(I) compounds $[Cu(O_2CCH_2CN)(PCy_3)_2]$, $[Cu(O_2CCH_2CN)(PPh_3)_2]_2$ and $[Cu(O_2CCH_2CN)_2H(PPh_3)_2]$ involve *O*-unidentate, *O*,*N*-bridging bidentate and, remarkably, *N*-unidentate cyanoacetate groups, respectively [4, 5]. In the light of these established coordination motifs, we have determined the structure of silver(I) cyanoacetate, this example being chosen because of the current interest [6] by several research groups in the structural chemistry of silver(I) carboxylates as a class of compounds.

Although a few silver(I) carboxylates, e.g. the 2,4-dichlorophenoxyacetate [7], contain mononuclear silver(I) units extended into oligomeric or polymeric structures by bridging carboxylate ligands, the basic unit found in the majority of silver(I) carboxylates is that of a bis(carboxylato-*O*,*O*′)disilver(I) dimer. Compounds containing this unit have been sub-divided [8], into four major types, A–D. Using this categorisation, the structure of the previously unreported cyanoacetate is shown here to be a new example of type B. It has also been used to synthesise $[(\eta\text{-}C_5H_5)_2Ti(O_2CCH_2CN)_2]$, the structure of which shows it to be a metal cyanoacetate containing solely unidentate *O*-cyanoacetato ligands.

EXPERIMENTAL

Unless otherwise stated, all reactions and operations were carried out under dry nitrogen gas.

* Author to whom correspondence should be addressed.

Cyanoacetic acid and bis(η-cyclopentadienyl) titanium dichloride (Aldrich Chemicals Co.) were used without further purification. Bis(η-cyclopentadienyl)dimethyltitanium was prepared from the dichloride and methyllithium in diethyl ether. Tetrahydrofuran and diethyl ether were purified prior to use by distillation over sodium benzophenone. Other solvents were stored over molecular sieves for several days before use. Infrared spectra were recorded on a Nicolet 510P FTIR spectrophotometer as Nujol or hexachlorobutadiene mulls. ^{1}H and ^{13}C NMR spectra were recorded on Jeol JNM GX270 and EX400 spectrometers.

Preparation of silver(I) cyanoacetate

A solution of silver nitrate (1.91 g, 11.3 mmol) in water (10 cm^3) was added dropwise to a stirred solution of cyanoacetic acid (0.96 g, 11.3 mmol) and sodium hydroxide (0.45 g, 11.3 mmol) in water (50 cm^3). After 20 min the resulting white precipitate was filtered, washed with portions of water, ethanol and diethyl ether and dried *in vacuo*, all operations being carried out in subdued light with final storage in the dark. Yield: 1.56 g, 72%. (Found: C, 18.8; H, 1.0; N, 7.4. $C_3H_2AgNO_2$ requires C, 18.8; H, 1.0; N, 7.3%). IR: 2953 m, 2923 m [ν(CH$_2$)]; 2269 m, [ν(CN)]; 1608 sh, 1566 s, [ν_{asym}(CO$_2$)]; 1456 s, 1400 s, [ν_{sym}(CO$_2$)]; 1366 m, [CH$_2$ scissors]; 1273 ms, [CH$_2$ wag]; 1208 mw, [CH$_2$ twist]; 963 m, [CH$_2$ rock]; 928 m, [ν(C—CN)]; 912 w, [ν(CC)]; 721 m, br [CO$_2$ scissors] cm^{-1}. ^{1}H NMR (D_2O, 270 MHz), δ 3.47 (s, CH$_2$); ^{13}C NMR (D_2O, 67.8 MHz), δ 169.3 (CO$_2$), 117.5 (CN), 26.0 (CH$_2$).

The crystal used in the structure determination was selected from a crop grown from the filtrate of the above reaction after storage in the absence of light for two months.

Preparation of bis(cyanoacetato)bis(η-cyclopentadienyl)titanium(IV)

Method A. Bis(η-cyclopentadienyl)titanium dichloride (0.50 g, 2.0 mmol) and sodium cyanoacetate (0.56 g, 5.2 mmol) were placed in a flame-dried flask fitted with a reflux condenser and stirrer and freshly distilled tetrahydrofuran (25 cm^3) added. The solvent was refluxed under nitrogen for 1 h after which time the orange solution produced was cooled, filtered and evaporated to dryness to give a bright orange solid. Yield: 0.46 g, 66%.

Blood-red octrahedra suitable for single crystal X-ray crystallography were obtained by slow evaporation of a chloroform solution under nitrogen. (Found: C, 55.4; H, 4.0; N, 8.0. $C_{16}H_{14}N_2O_4Ti$ requires C, 55.5; H, 4.1; N, 8.1%). IR: 2255 m, [ν(CN)]; 1666 vs, [ν_{asym}(CO$_2$)]; 1308 vs, [ν_{sym}(CO$_2$)]; C_5H_5 vibrations at 3110, 3098, 1447, 1019 and 826 cm^{-1}. ^{1}H NMR ($CDCl_3$, 270 MHz), δ 3.47 (s, 4H, CH$_2$); 6.63 (s, 10H, C_5H_5); ^{13}C, δ 26.9 (CH$_2$); 115.2 (CN); 119.4 (C_5H_5); 167.2 (CO$_2$).

Method B. Bis(η-cyclopentadienyl)titanium dichloride (0.50 g, 2.0 mmol) was dissolved in degassed water (40 cm^3) by stirring for 2 h. A solution of sodium cyanoacetate (1.00 g, 9.3 mmol) in water (10 cm^3) was then added and stirring continued for a further hour at room temperature. The product was obtained by extraction from the aqueous phase using three 50 cm^3 portions of dichloromethane which were then dried over $MgSO_4$. Slow evaporation of this solution gave, after filtration, red crystals. Yield: 0.53 g, 75%.

Method C. Chloroform (40 cm^3) was added to a mixture of bis(η-cyclopentadienyl)titanium dichloride (0.50 g, 2.0 mmol) and silver cyanoacetate (1.15 g, 6.0 mmol) and the reactants stirred in the dark for 1 h at room temperature. Filtration to remove silver chloride followed by evaporation of the orange chloroform solution produced a red crystalline solid. Yield: 0.56 g, 81%.

Method D. A solution of bis(η-cyclopentadienyl)dimethyltitanium (50 mg, 0.24 mmol) in freshly distilled tetrahydrofuran (3 cm^3) was added with stirring to a solution of cyanoacetic acid (41 mg, 0.48 mmol) in tetrahydrofuran (2 cm^3). Methane was evolved and the solution darkened from a pale to a deep orange colour. Evaporation of the solvent *in vacuo* gave a bright red crystalline solid. Yield: 69 mg, 83%.

Products from methods B–D gave good C, H and N analyses and identical NMR spectra to those given above in Method A.

X-ray crystallography

Crystal data, data collection and refinement details for both compounds are given in Table 1 and selected bond lengths and angles in Tables 2 and 3. Additional material for each structure is available from the Cambridge Crystallographic Data Centre and comprises final fractional atomic coordinates, thermal parameters, hydrogen atom coordinates and further bond lengths and angles. The asymmetric unit of silver cyanoacetate produced using ORTEX [9] is shown in Fig. 1 along with the labelling scheme, the polymeric arrangement being depicted in Fig. 2. The asymmetric unit of the titanium compound is shown in Fig. 4.

Data were collected at room temperature on a CAD-4 automatic four-circle diffractometer using Mo-K_α radiation. The diffraction intensities were corrected for Lorentz and polarisation effects but not for absorption. The silver structure was solved by direct methods [10,11], using SHELX86 and refined using SHELX93. The titanium structure was solved [12] by Patterson methods, and refined using SHELX76. In the final least squares cycles all atoms were allowed to vibrate anisotropically. In the silver structure hydrogen atoms were included at calculated positions where relevant, whereas in the titanium structure hydrogens were included at calculated positions on the cyclo-

Table 1. Crystal data and data collection details for silver(I) cyanoacetate and for bis(cyanoacetato)bis(η-cyclopentadienyl)titanium(IV)

Formula	$C_3H_2AgNO_2$	$C_{16}H_{14}N_2O_4Ti$
Formula weight	191.93	346.2
Crystal System	triclinic	triclinic
Space Group	$P\bar{1}$	$P\bar{1}$
a (Å)	4.6920(6)	8.231(1)
b (Å)	7.053(1)	9.850(1)
c (Å)	7.292(1)	10.537(2)
α (°)	111.00(2)	93.46(1)
β (°)	103.88(2)	108.57(1)
γ (°)	94.82(1)	99.42(1)
V (Å^3)	214.82	793.1
Z	2	2
D_c (g cm^{-3})	2.967	1.45
μ (mm^{-1})	4.544	0.56
$F(000)$	180	356
Crystal dimensions (mm)	$0.2 \times 0.2 \times 0.2$	$0.4 \times 0.4 \times 0.5$
Measured reflections	761	2658
Unique reflections [$I > 2\sigma(I)$]	669	2063
$R1$, $wR2$	0.0490, 0.1250	0.0354, 0.0401[a]
Weighting scheme, w	$1/[\sigma^2(F_o^2)+(0.1000P)^2]$ where $P=(F_o^2+2F_c^2)/3$	$2.4649/[\sigma^2(F)+0.000448(F)^2]$
Largest residuals (e Å^{-3})	2.060, −2.005	0.12, −0.12

[a] R, R_w for the Ti compound.

Table 2. Selected bond lengths (Å) and angles (°) for silver(I) cyanoacetate

Ag(1)—O(1)	2.198(5)	Ag(1)—O(2)	2.187(4)
Ag(1)—N(1b)	2.370(6)	Ag(1)—Ag(1a)	2.8939(12)
C(1)—O(1)	1.242(8)	C(1)—O(2a)	1.263(8)
C(1)—C(2)	1.523(8)	C(2)—C(3)	1.426(8)
C(3)—N(1)	1.157(10)		

O(1)—Ag(1)—O(2)	162.6(2)	O(1)—Ag(1)—N(1b)	97.7(2)
O(2)—Ag(1)—N(1b)	99.6(2)	O(1)—Ag(1)—Ag(1a)	81.94(14)
O(2)—Ag(1)—Ag(1a)	80.97(13)	N(1b)—Ag(1)—Ag(1a)	171.2(2)
C(1)—O(1)—Ag(1)	123.9(5)	C(1a)—O(2)—Ag(1)	125.4(4)
C(3)—N(1)—Ag(1a)	154.4(5)	O(1)—C(1)—O(2a)	127.4(7)
O(1)—C(1)—C(2)	117.2(6)	O(2a)—C(1)—C(2)	115.4(5)
C(1)—C(2)—C(3)	113.9(5)	C(2)—C(3)—N(1)	177.3(6)

pentadienyl rings but located and positionally refined in the cyanoacetate ligand.

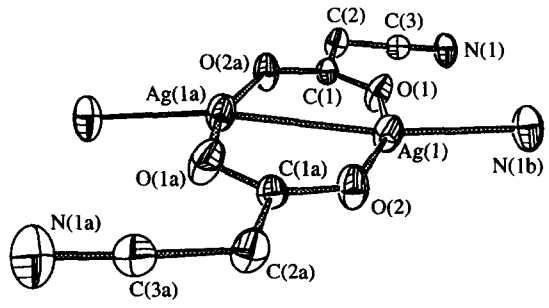


Fig. 1. The asymmetric unit of silver(I) cyanoacetate with atom labelling. Thermal ellipsoids are represented at the 30% probability level.

M.O. calculations

Calculations on metal–metal interactions in silver(I) cyanoacetate were of the extended Hückel type [13] using the CACAO suite of programs [14]. The parameters used were taken from [15] and [16].

RESULTS AND DISCUSSION

Silver(I) cyanoacetate

This compound has been prepared in good yield from the aqueous reaction of silver nitrate with sodium cyanoacetate, the latter being generated *in situ* from the carboxylic acid and sodium hydroxide. The ^1H and ^{13}C NMR spectroscopic data (see Exper-

Table 3. Selected bond lengths (Å) and angles (°) for bis(cyanoacetato)bis(cyclopentadienyl)titanium(IV)

Ti(1)—O(1)	1.963(4)	Ti(1)—O(3)	1.966(4)
Ti(1)—C(1)	2.340(5)	Ti(1)—C(6)	2.358(5)
Ti(1)—C(2)	2.360(5)	Ti(1)—C(7)	2.362(5)
Ti(1)—C(3)	2.330(5)	Ti(1)—C(8)	2.385(5)
Ti(1)—C(4)	2.348(6)	Ti(1)—C(9)	2.389(5)
Ti(1)—C(5)	2.360(6)	Ti(1)—C(10)	2.391(5)
O(1)—C(11)	1.282(4)	O(3)—C(14)	1.284(4)
O(2)—C(11)	1.202(4)	O(4)—C(14)	1.195(4)
N(1)—C(13)	1.137(5)	N(2)—C(16)	1.140(5)
C(11)—C(12)	1.518(6)	C(14)—C(15)	1.527(6)
C(12)—C(13)	1.457(5)	C(15)—C(16)	1.450(6)

Average C—C in cyclopentadienyl rings: C(1)—C(5) 1.338(8); C(6)—C(10) 1.366(6)

O(1)—Ti(1)—O(3)	89.3(2)		
Ti(1)—O(1)—C(11)	143.5(2)	Ti(1)—O(3)—C(14)	147.4(2)
O(1)—C(11)—O(2)	126.4(4)	O(3)—C(14)—O(4)	126.6(4)
O(1)—C(11)—C(12)	111.7(3)	O(3)—C(14)—C(15)	114.6(3)
O(2)—C(11)—C(12)	121.9(3)	O(4)—C(14)—C(15)	118.8(4)
C(11)—C(12)—C(13)	113.1(3)	C(14)—C(15)—C(16)	114.4(3)
C(12)—C(13)—N(1)	178.4(4)	C(15)—C(16)—N(2)	179.7(2)

Average C—C—C angles in cyclopentadienyl rings: C(1)—C(5) 108.0(5), C(6)—C(10) 108.0(4)

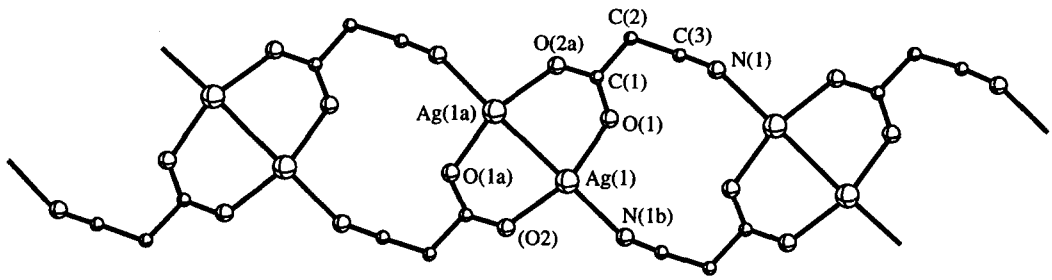


Fig. 2. The polymeric form of silver(I) cyanoacetate.

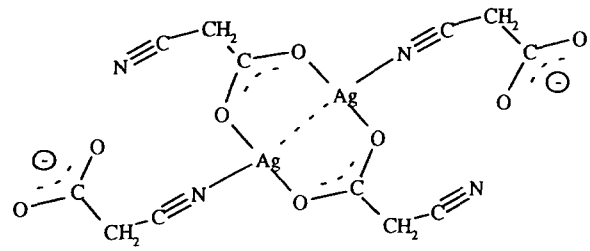


Fig. 3. A portion of the silver(I) cyanoacetate structure as used in the EHMO calculation.

imental) in D_2O and the infrared data are in accord with the structure determined by X-ray diffraction. For example, the differences of 150–160 cm^{-1} between the infrared symmetric and asymmetric CO_2 stretches are in accord with the *syn–syn* bridging mode of the carboxylate ligands.

The type B structure [8] of silver(I) cyanoacetate (Fig. 2) is that of an infinite sheet polymer based on a bis(carboxylato-*O*,*O'*) bridged Ag_2L_2 dimer with an Ag–Ag distance of 2.894(1) Å. This distance, which is exactly that found in the metal itself, is very similar to the Ag–Ag bond length in other silver carboxylate structures based on dimeric units (range from 2.778 Å in the 3-hydroxy-4-phenyl-2,2,3-trimethylcyclohexanecarboxylate [17] to 3.005 Å in the maleate [6a]). Distances in this range have often been regarded

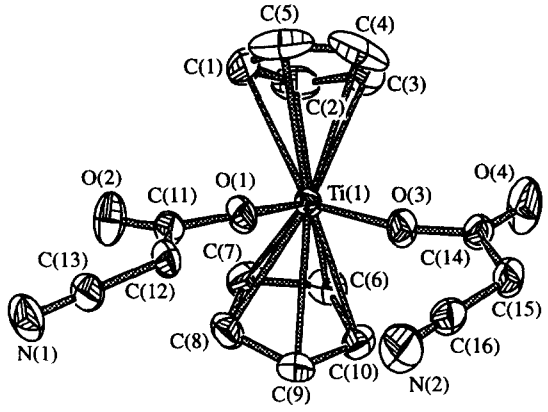


Fig. 4. The asymmetric unit of bis(cyanoacetato)bis(cyclopentadienyl)titanium(IV) with atom labelling. Thermal ellipsoids are represented at the 30% probability level.

as indicative of direct metal–metal interaction [8]. However, others have taken the view that short metal–metal distances in dimers of this type do not necessarily imply bonding [18]. This facet is explored later.

Within the eight-membered centrosymmetric dimers, the silver atoms are bridged by co-planar carboxylato-*O,O'* ligands in the *syn–syn* conformation. The Ag—O distances [2.187(4), 2.198(5) Å] and O—Ag—O angle, 162.6(2)° are comparable to those of other dimeric silver carboxylates (Ag—O distances range from 2.158(3) Å [19] to 2.387(3) Å [6a] and O—Ag—O angles from 155.8(1)° [8] to the exceptional 171.8(1)° [19]). The dimers are extended into a polymeric sheet-like structure (Fig. 2) by the formation of silver-cyano nitrogen bonds positioned axially with respect to the Ag_2 units. As a result, each eight-membered Ag_2L_2 ring is adjoined to a twelve-membered $AgOCCH_2CNAgOCCH_2CN$ ring with Ag—N distances of 2.370(6) Å. Although the C—C—N angle of the cyanomethyl moiety is close to 180° [177.3(6)°], the C—N—Ag angle shows a considerable departure from linearity [154.4(5)°]. This non-linearity is also apparent in the structures of $[Cd(O_2CCH_2CN)_2]$ [3], [C—N—Cd, 164.3(5)° where the cyanoacetate groups are *N*-bonded in addition to *O,O'*-chelated to cadmium atoms], in $[Cu(O_2CCH_2CN)_2H(PPh_3)_2]$ [5] with a C—N—Cu angle of 153.3(3)° and in $[Cu(O_2CCH_2CN)(PPh_3)_2]_2$ [4] with a C—N—Cu angle of 162.0(4)°.

As a result, the silver atoms in the compound are coordinated by two carboxylato-oxygen atoms and a cyano-nitrogen atom in a T-shaped array [O—Ag—N, 99.6(2), 97.7(2)°] thus rendering a tridentate cyanoacetate. If an additional bond is considered between Ag(1) and Ag(1a), (related by the operator $-x, 1-y, -z$), then the coordination at each metal can be regarded as distorted square planar [Ag—Ag—O, 81.94(14), 80.97(13)°]. The supramolecular packing arrangement is such that the separations between successive infinite polymer sheets precludes any significant inter-sheet associations, e.g. the shortest Ag · · · Ag distance (generated by the operator $-x+1, -y+1, -z$) is 3.273(1)Å.

Within the individual *O,O'*-bridging carboxylate groups, the C—O, C—CH_2, C—CN and C—N bond lengths and related angles are very much in accord with those previously reported for $[Fe_3(\mu_3\text{-}O)(O_2CCH_2CN)_6(H_2O)_3]$ [2] and $[Cd(O_2CCH_2CN)_2]$ [3]. The C≡N cyano-bond length, 1.157(10) Å, is slightly longer than that in the iron trimer [2] where there is no *N*-donation to a further metal. In the cadmium salt [3] there is little apparent difference between *N*-bonded and free cyano bond lengths at 1.139(9) and 1.132(10) Å, respectively.

Returning to the question of direct metal–metal bonding in the silver cyanoacetate, we have examined the molecule using an EHMO approach, the aims being to estimate the Ag—Ag bond strength and to evaluate the effect that the ligand set has on such a bond. The approach closely follows that used previously by Hoffmann [16] when investigating d^{10}–d^{10} interactions between copper(I) centres.

A portion of the solid state structure (Fig. 3) having an Ag_2^{2+} core surrounded by four cyanoacetate ligands, two of which were *O,O'*-bonded and two *N*-bonded to Ag with a consequent overall charge of −2, was taken as the basis for the calculations. This portion was treated as two fragments, the Ag_2^{2+} core and the four $NCCH_2CO_2^-$ groups, to allow comparison of any Ag—Ag bonding in an isolated Ag_2^{2+} cation with that in the whole complex. An interaction diagram for an Ag_2^{2+} cation with a separation of 2.894 Å (as found crystallographically), constructed using only the 4*d* orbitals on silver, indicates a repulsive interaction (positive binding energy of +0.019 eV and an overlap population of −0.001 electrons) relative to two isolated Ag^+ centres. However, by including silver 5*s* and 5*p* orbitals in the calculation the interaction becomes more attractive (negative binding energy of −0.163 eV and an overlap population of +0.053 electrons) than two isolated Ag^+ centres. These results bear close similarity with those of Hoffmann [16] for Cu_2^{2+}, who showed that the favourable interaction arose primarily from *s*, p_z and d_{z^2} orbital mixing, resulting in an increase in the bonding character of the σ-orbital and a reduction in the antibonding character of the σ* orbital. Using the parameters obtained from the crystal structure, we have also looked at the effect of the cyanoacetate groups, arranged as in Fig. 3, on the Ag—Ag bond. Introduction of the ligand set generates an enhanced attractive Ag—Ag interaction, the Ag—Ag orbital overlap population increasing from +0.051 electrons to +0.062 electrons. The Ag—N and Ag—O overlap populations of +0.22 and +0.20 electrons are similar to that found for adsorbed atomic oxygen on a silver (110) surface [15].

A more detailed consideration of the gross atomic orbital populations shows that in comparison to the isolated Ag_2^{2+} cation, the *d–d* population in the com-

plex decreases from 9.97 to 9.93 whereas the *s* and *p* populations increase to a greater extent (from 0.026 to 0.422) for the 5*s* and from 0.009 to 0.297 for the 5*p* orbitals, respectively) giving an overall increase in the Ag–Ag orbital overlap population. Introducing the cyanoacetate groups seems to increase *s*, *p* and *d* orbital mixing, enhancing the *s* and *p* orbital contributions to the Ag–Ag interaction relative to the isolated Ag_2^{2+} cation i.e. moving towards a $d^9s^np^{1-n}$ electron configuration. These calculations therefore consolidate the view expressed by others of the existence of a positive Ag–Ag interaction promoting the stabilisation of dinuclear silver(I) carboxylates.

Bis(cyanoacetato)bis(η-cyclopentadienyl)titanium(IV)

This compound has been prepared in good yield from reactions of the dichloride with sodium cyanoacetate in either tetrahydrofuran or water, the dichloride with silver cyanoacetate in chloroform or the dimethyl with cyanoacetic acid in tetrahydrofuran. Infrared bands assigned to the asymmetric and symmetric carboxyl stretches differ in frequency by 358 cm^{-1} indicative of unidentate carboxylate bonding, as confirmed (Fig. 4) by the single-crystal X-ray structure determination. The two non-coordinated oxygen atoms O(2) and O(4) are well beyond possible bonding distances to titanium (3.598 and 3.657 Å). Unidentate carboxylate coordination has been previously established for the bis(η-cyclopentadienyl)titanium(IV) benzoate, (both monoclinic (α) [20] and orthorhombic (β) [21] modifications), the *m*-methoxybenzoate [22], the *o*-methoxybenzoate [23] and the trifluoroacetate [24]. On occasions [25] infrared data have been interpreted as indicating the presence of bidentate chelating carboxylate groups in various bis(η-cyclopentadienyl)titanium(IV) carboxylates but such an arrangement has not been confirmed to date by crystallography.

Consideration of the bond lengths and angles of the two cyanoacetate groups show that differences between them are rather insignificant, a situation quite unlike that of the orthorhombic form of the benzoate [21] and the *m*-methoxybenzoate [22] where the two carboxylate ligands are distinctly different (e.g. benzoate [21]: Ti—O—C angles of 135.2(3) and 168.7(3)°, Ti—O bond lengths of 1.894(4) and 1.995(3) Å and C—O bond lengths of 1.275(5) and 1.300(4) Å; *cf.* cyanoacetate Ti—O—C angles of 147.4(2) and 143.5(2)°, Ti—O bond lengths of 1.966(4) and 1.963(4) Å and C—O bond lengths of 1.284(4) and 1.282(4) Å). For the benzoate, the shorter Ti—O bond lengths and larger Ti—O—C bond angles have been rationalised [21] as indicating the presence of a strong Ti—O π-interaction supplementing the σ-bonding for *one* of the benzoate groups only, this allowing achievement of an effective 18-electron configuration rather than a formal count of 16 valence electrons. Conversely, the monoclinic form of the benzoate [20] and, clearly, the cyanoacetate have near-equivalent carboxylate groups with unexpectedly large Ti—O—C angles (when compared with typical M—O—C angles in unidentate carboxylate complexes) and short Ti—O bond lengths implying the attainment of an effective 18-electron configuration by additional Ti—O π-bonding for *both* carboxylate groups. This proposal is supported by some EHMO calculations of Hoffmann *et al.* [20] on the model compound $[(\eta\text{-}C_5H_5)_2Ti(O_2CH)_2]$.

Bond lengths and angles within the cyanoacetate ligands, Table 3, show the expected features such as C—C—N angles close to 180° and C≡N bond lengths (1.137(5) and 1.140(5) Å) slightly shorter than those of, for example, the silver salt (1.157(10) Å) where the cyano-group is *N*-bonded to a further metal atom. As expected, for unidentate carboxylate coordination there is a significant difference in the C—O bond lengths depending on whether the oxygen atom is coordinated to titanium (1.282(4) and 1.284(4) Å) or not (1.202(4) and 1.195(4) Å).

For the cyclopentadienyl ligands, the average C—C bond length of 1.366(6) Å and the average C—C—C bond angles of 108.0(4)° are in line with values from other $[(\eta\text{-}C_5H_5)_2TiX_2]$ structure determinations ([20] and references therein). The centroids of the cyclopentadienyl ligands, Z, and the two bonded oxygen atoms define a much distorted tetrahedral array around the metal with a Z—Ti—Z angle of 131.5(2)° and an O—Ti—O angle of 89.3(2)°. The distances from the metal atom to the centroids of the cyclopentadienyl rings (Ti—Z) of 2.053 and 2.061 Å and Ti—C bond lengths of between 2.330(5) and 2.391(5) Å (average 2.362 Å) are again in excellent agreement with comparable distances in other bis(η-cyclopentadienyl)titanium(IV) compounds [20].

There are several contacts between cyclopentadienyl carbons on different rings which are less than the van der Waals contact between two aromatic rings of 3.4 Å indicative of crowding around the metal resulting from the presence of ten carbon and two oxygen atoms.

Acknowledgement—We thank EPSRC for a studentship to T.J.P.

REFERENCES

1. P. Starynowicz, *Acta Cryst., Sect. C* 1993, **49**, 1621.
2. T. Nakamoto, M. Katada, S. Kawata, S. Kitagawa, K. Kikuchi, I. Ikemoto, K. Endo and H. Sano, *Chem. Lett.* 1993, 1463.
3. M. L. Post and J. Trotter, *J. Chem. Soc., Dalton Trans.* 1974, 285.
4. D. J. Darensbourg, E. M. Longridge, M. W. Holtcamp, K. K. Klausmeyer and J. H. Reibenspies, *J. Am. Chem. Soc.* 1993, **115**, 8839; D. J. Darensbourg, M. W. Holtcamp, E. M. Long-

ridge, B. Khandelwal, K. K. Klausmeyer and J. H. Reibenspies, *ibid.* 1995, **117,** 318.
5. D. J. Darensbourg, E. M. Longridge, E. V. Atnip and J. H. Reibenspies, *Inorg. Chem.* 1991, **30,** 357.
6. See for example: (a) G. Smith, D. S. Sagatys, C. Dahlgren, D. E. Lynch, R. C. Bott, K. A. Byriel and C. H. L. Kennard, *Z. Kristallographie* 1995, **210,** 44; (b) A. Michaelides, S. Skoulika, V. Kiritsis and A. Aubry, *J. Chem. Soc., Chem. Commun.* 1995, 1415; (c) T. C. W. Mak, W.-H. Yip and X. M. Chen, *Inorg. Chim. Acta* 1993, **203,** 97; (d) T. C. W. Mak, G. Smith and C. H. L. Kennard, *Z. Kristallographie* 1993, **207,** 33; (e) F. Jaber, F. Charbonnier, R. Faure and K. Gebicki, *Acta Cryst., Sect. C* 1994, **50,** 1444 and references therein.
7. T. C. W. Mak, W.-H. Yip, C. H. L. Kennard, G. Smith and E. J. O'Reilly, *J. Chem. Soc., Dalton Trans.* 1988, 2353.
8. T. C. W. Mak, W.-H. Yip, C. H. L. Kennard, G. Smith and E. J. O'Reilly, *Austral. J. Chem.* 1986, **39,** 541.
9. P. McArdle, *J. Appl. Cryst.* 1994, **27,** 438.
10. G. M. Sheldrick, SHELX86, A computer program for crystal structure solution, *Acta Cryst., Sect. A* 1990, **46,** 467.
11. G. M. Sheldrick, SHELX93, A computer program for crystal structure refinement, University of Göttingen (1993).
12. G. M. Sheldrick, SHELX76, *A Computer Program for Crystal Structure Refinement.* University of Cambridge (1976).
13. R. Hoffmann, *J. Chem. Phys.* 1963, **39,** 1397; R. Hoffmann and W. N. Lipscomb, *ibid.* 1962, **36,** 2179, 3489; **37,** 2872.
14. C. Mealli and D. M. Proserpio, *J. Chem. Educ.* 1990, **67,** 399.
15. K. A. Jorgensen and R. Hoffmann, *J. Phys. Chem.* 1990, **94,** 3046.
16. P. K. Mehrotra and R. Hoffmann, *Inorg. Chem.* 1978, **17,** 2187; K. M. Merz and R. Hoffmann, *ibid.* 1988, **27,** 2120.
17. P. Coggon and A. T. McPhail, *J. Chem. Soc., Chem. Commun.* 1972, 91.
18. G. W. Hunt, T. C. Lee and E. L. Amma, *Inorg. Nuclear Chem. Lett.* 1974, **10,** 909.
19. G. Smith, D. S. Sagatys, C. A. Campbell, D. E. Lynch and C. H. L. Kennard, *Austral. J. Chem.* 1990, **43,** 1707.
20. D. M. Hoffmann, N. D. Chester and R. C. Fay, *Organometallics* 1983, **2,** 48.
21. K. Doppert, H.-P. Klein and U. Thewalt, *J. Organomet. Chem.* 1986, **303,** 205; C. R. Lucas, E. J. Gabe and F. L. Lee, *Can. J. Chem.* 1988, **66,** 429.
22. B. Bracke, Y. Dang, A. T. H. Lenstra and H. J. Geise, *Acta Cryst., Sect. C* 1991, **47,** 2043.
23. Y.-K. Zhou, Z.-Q. Wang and Y. Zhou, *Polyhedron* 1990, **9,** 783.
24. G. S. Herrmann, G. H. Alt and U. Thewalt, *J. Organomet. Chem.* 1990, **393,** 83.
25. Y. Dang, *Coord. Chem. Rev.* 1994, **135,** 93.

Pergamon

S0277-5387(96)00262-8

Polyhedron Vol. 16, No. 1, pp. 33–37, 1997
Copyright © 1996 Elsevier Science Ltd
Printed in Great Britain. All rights reserved
0277-5387/97 $15.00+0.00

Asymmetric diorganotellurides containing substituted pyridyl groups—synthesis and ligation with palladium(II) and platinum(II). Crystal structure of $[Pd\{4\text{-}MeC_6H_4TeCH_2CH_2\text{-}2\text{-}(C_5H_4N)\}Cl_2]\cdot 2CHCl_3$

Abu Khalid and Ajai K. Singh*

Department of Chemistry, Indian Institute of Technology, New Delhi-110016, India

(Received 3 April 1996; accepted 20 May 1996)

Abstract—A (N,Te,N) ligand 2-(2-pyridoethyletelluro)ethylpyridine (**1**) has been synthesized by reacting *in situ* generated Na_2Te with 2-(2-chloroethyl)pyridine. The Pd^{II} and Pt^{II} complexes of stoichiometry $[MCl\cdot\mathbf{1}]Cl$ have been studied. The deshielding of *ortho* protons of pyridine and CH_2Te signal (up to 0.5 ppm) indicate that **1** ligates in a tridentate mode. The red shift (20–25 cm^{-1}) in ν(Te—C(alkyl)) supports the involvement of Te in coordination. Molecular weights and Λ_M values of these complexes support their ionic nature (1 : 1 electrolyte). The reactions of 2-(chloromethyl)pyridine and 2,6-bis(chloromethyl)pyridine with ArTeNa (Ar = 4-$MeOC_6H_4$) could not produce (N,Te) and (Te,N,Te) ligands comprising pyridyl groups. The $CHCl_3$ present as a solvent in these reactions reacted with ArTeNa resulting in $(ArTe)_2CH_2$. To understand the behaviour of Te donor site *vis-à-vis* pyridyl group the single crystal structure of $Pd\{4\text{-}MeC_6H_4TeCH_2CH_2\text{-}2\text{-}(C_5H_4N)\}Cl_2\cdot 2CHCl_3$ was solved. An *endo*, puckered chelate ring is formed by (N,Te) ligand. The *trans* influence of the pyridyl group appears to be lower or comparable to that of tellurium. Copyright © 1996 Elsevier Science Ltd

Keywords: diorganotelluride; palladium; platinum; synthesis; complexation; structure.

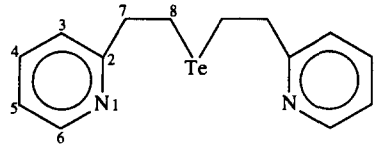
The ligation of asymmetric diorganotellurides has received attention in the recent past [1,2]. Some neutral ligands having "hard" donor centres *viz.*, N and O along with "soft" donor tellurium have been synthesized and explored for their ligation behaviour. Most of the ligands containing Te and N atom as donor atoms [3] have amino nitrogen. A few ligands having a donor set of pyridine nitrogen and tellurium have also been studied [4–6]. Since the pyridine nitrogen has good coordinating capability, it was thought worthwhile to design new hybrid telluroether ligands containing pyridine nitrogen as a donor. In the present paper the synthesis of a (N,Te,N) ligand, its complexation with Pd^{II} and Pt^{II}, the results of attempted synthesis of **2** and **3** and as a consequence of these attempts the resulted novel synthesis of $(ArTe)_2CH_2$ and crystal structure of palladium(II) complex of **4** are reported.

EXPERIMENTAL

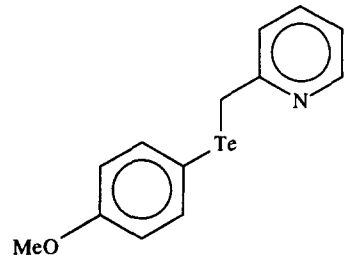
The synthesis of $(4\text{-}MeOC_6H_4)_2Te_2$ [7] and the ligand **4** [6] were carried out by published methods. 2-(2-Chloroethyl)pyridine, 2-(chloromethyl)pyridine and 2,6-bis(chloromethyl)pyridine were synthesized by chlorination [8] of the corresponding alcohols.

IR spectra in the range 200–4000 cm^{-1} were recorded on a Nicolet 5DX FT-IR spectrometer in KBr/CsI pellets and far-IR spectra in the range 30–700 cm^{-1} were recorded in polyethylene on a Perkin-Elmer 1700X FT-IR spectrometer. ^1H and $^{13}C\{^1H\}$ NMR spectra were recorded on a JEOL FX100 FT-NMR spectrometer at 99.5 and 25 MHz respectively using Me_4Si as an internal standard. UV-visible spectrophotometer of Hitachi model 330 was used to rec-

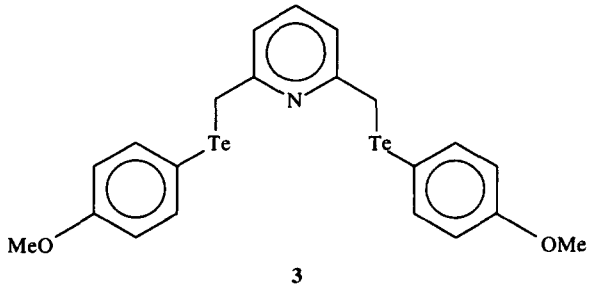
* To whom correspondence should be addressed.



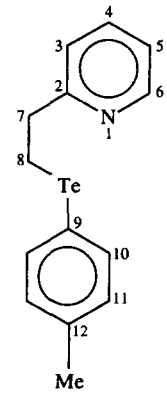
1



2



3



4

ord electronic spectra. Conductance measurements were made on *ca* 1 mM solution using the Metrohm 660 conductometer and molecular weights were determined using a Knauer vapour pressure osmometer. Elemental analyses were performed on a Perkin-Elmer elemental analyzer 240C. $^{125}Te\{^1H\}$ NMR spectra were recorded at 126 MHz (using $(CH_3)_2Te$ as an external standard) on a Bruker AMX-400 FT-NMR spectrometer.

Single crystal structure of $[PdCl_2 \cdot 4]$

The X-ray diffraction data of crystals of $[PdCl_2 \cdot 4]$ grown from chloroform solution were collected on an Enraf-Nonius CAD-4 diffractometer using nickel filtered Cu-K_α radiation ($\lambda = 1.518$ Å). The intensities were measured at azimuth position corresponding to minimum absorption using an imaginary crystal with infinitely small thickness but infinitely large surface area (flat psi mode). The ω-2θ scan mode was used. The $2\theta_{max}$ was 152° and h, k, l ranges were 0 to +10, −9 to +9 and −11 to +11, respectively. Of the 3594 reflections collected, 3357 were unique and out of which 3069 were with $I \geqslant 3\sigma$. The intensities were corrected for Lorentz and polarization effects. The semi-empirical absorption corrections were also applied.

The initial coordinates of Pd, Pt and Te were determined using SHELXS 86 [9(a)]. The remaining atoms were located from successive difference Fourier maps. The refinement was carried out by full-matrix least-squares procedures using SHELX 76 [9(b)] for positional parameters and initially isotropic and finally anisotropic temperature factors for all the non-hydrogen atoms. The atomic scattering factors were taken from the literature [10]. All the calculations were performed on a Microvax II computer using SDF plus V.30 system of crystallographic program. The crystallographic data are given in Table 1.

Table 1. Crystallographic data of $[PdCl_2 \cdot 4]$

Formula	$C_{14}H_{15}NTePdCl_2 \cdot 2CHCl_3$
Crystal size (mm)	$0.7 \times 0.2 \times 0.2$
Crystal system	triclinic
Space group	$P\bar{1}$
a(Å)	9.175(1)
b(Å)	10.498(2)
c(Å)	12.928(1)
α(°)	95.80(1)
β(°)	96.25(2)
γ(°)	90.68(1)
V, Å^3	1231.7(2)
D_c(g cm^{-3})	2.021
Z	2
F(000)	704
μ(cm^{-1})	226.67
R	0.061
R_w	0.061
S	3.159
Weighing scheme	Constant weights

Synthesis of 2-(2-*pyridoethyltelluro*)*ethylpyridine*(**1**)

Tellurium powder (2 g, 16 mmol) and sodium borohydride (5 g dissolved in 10 cm^3 of 10% NaOH) were refluxed in water (50 cm^3) till a colourless solution of Na_2Te was obtained. 2-(2-Chloroethyl) pyridine (4.2 g, 32 mmol) dissolved in 5 cm^3 of ethanol was added drop-wise to the solution of Na_2Te and the mixture was refluxed for 2 h with vigorous stirring. The ligand thus formed was extracted into chloroform (250 cm^3). The extract was washed with water and dried over anhydrous sodium sulfate. On removing chloroform under reduced pressure the red liquid was obtained. Yield: 91%, b.p. 134°C. Mol. wt.: Found (Calc.): 320 (307). Analyses: Found (Calc.): Te, 40.9(41.6)% NMR (^1H, $CDCl_3$, 25°C) δ: 3.3(t, 4H, H_7+H_8) 7.39(m, 4H, H_3+H_5), 7.58 (m, 2H, H_4), 8.55 (d, 2H, H_6); ($^{13}C\{^1H\}$, $CDCl_3$, 25°C) δ: 2.2(C_8), 40.3(C_7), 120.2(C_3), 122.3(C_5), 135.6(C_4), 136.5(C_2), 148.2(C_6); ($^{125}Te\{^1H\}$ $CDCl_3$, 25°C) δ: 167. IR (cm^{-1}): 495 [ν(Te—C (alkyl))], 408 (δ(N—C)).

Synthesis of [PdCl · **1**]Cl *and* [PtCl · **1**]Cl

Potassium tetrachloropalladate(II) or platinate(II) (0.15 or 0.20 g, 0.5 mmol) was dissolved in 5 cm^3 of water. A solution of ligand **1** (0.17 g, 0.5 mmol) in 5 cm^3 of acetone was added to it with rapid stirring at room temperature. The stirring was continued further for 15 min. The precipitate was filtered immediately, washed with water and hexane successively and dried *in vacuo*. The results of elemental analyses and spectral data are given below.

[PdCl · **1**]Cl: Yield: 68.5%. Mol. wt.: Found (Calc.): 270(517), m.p. 100°C (d). Analyses: Found (Calc.): C, 32.9 (33.5); H, 3.2 (3.1); N, 5.1 (5.5)%. NMR(^1H, $CDCl_3$, 25°C) δ: 3.33–3.91(m, 8H, H_7+H_8), 7.42–7.72 (m, 6H, $H_3+H_4+H_5$), 8.88 (d, 2H, H_6). IR(cm^{-1}): 469[ν(Te—C(alkyl)], 424 (δ(C—N), 295(ν(Pd—Cl)).

[PtCl · **1**]Cl: Yield: 82%. Mol. wt.: Found (Calc.) 320(606), m.p. 112°C (d). Analyses: Found (Calc.): C, 27.5 (27.7); H, 2.5 (2.6); N, 4.7 (4.6)%. NMR(^1H, $CDCl_3$, 25°C)δ, 3.09–3.58(m, 8H, H_7+H_8), 7.42–7.72(m, 6H, $H_3+H_4+H_5$) 9.05(d, 2H, H_6); ($^{125}Te\{^1H\}$, DMSO-d_6: 25°C) δ 515. IR (cm^{-1}): 474[ν(Te—C(alkyl))], 425 (δ(C—N)), 335(ν (Pt—Cl)).

Synthesis of **2** and **3**

The sodium 4-metoxyphenyltellurolate was reacted with 2-(chloromethyl)/2,6-bis(dichloromethyl)pyridine by the procedure described for the synthesis of **4** earlier [6]. However, in both the cases ditelluride was recovered. On carrying out the reactions in the presence of $CHCl_3$ bis(4-methoxyphenyltelluro) methane resulted. The reaction of chloroform with [NaTeAr] separately also resulted in the same product. The synthesis procedure is given below:

Synthesis of bis(4-*methoxyphenyltelluro*)*methane*

The solution of sodium 4-methoxyphenyltellurolate generated *in situ* by borohydride reduction of bis(4-methoxyphenyl)ditelluride (1.88 g, 4 mmol in 50 cm^3 of ethanol), was mixed with chloroform (5 cm^3, 10 mmol) in one lot, under refluxing condition. The reaction mixture was further refluxed for 30 min. On cooling to 0°C, crystals separated out which were washed successively with water, ethanol and hexane and dried *in vacuo*. Yield: 85%, m.p. 98°C (lit. value 99–102°C) [16]. Found (Calc.): C, 37.1(37.2); H, 3.3(3.3)%.

Synthesis of [$PdCl_2$ · 4]

Potassium tetrachloropalladate (0.15 g, 0.5 mmol) was dissolved in 7 cm^3 of water. A solution of **4** (0.5 mmol) made in 5 cm^3 of methanol was added dropwise to palladium(II) solution with stirring at room temperature. The mixture was further stirred at room temperature for 1 h. The resulting orange precipitate was filtered, washed twice with water and diethyl ether and recrystallized from chloroform. Yield: 72%, m.p. 118°C(d), Mol. wt.: Found (Calc.): 510(502). Analyses: Found (Calc.): C, 33.0(33.5) H, 3.1(3.0); N, 2.9(2.8)%. NMR (^1H, DMSO-d_6, 25°C)δ: 2.31–4.20 (m, 7H, $H_7+H_8+CH_3$), 6.94–7.78(m, 8H, Ar + pyridine protons) 9.00 (d, 1H, H_6). IR (cm^{-1}): 460 [ν(Te—C(alkyl))], 424(δ(C—N)), 329, 295 (ν(Pd—Cl)).

RESULTS AND DISCUSSION

The ligand **1** has been synthesized by the reaction of eq. 1. The synthesis

$$Te \xrightarrow{NaBH_4} Na_2Te + 2ClCH_2CH_2 2\text{-}(C_5H_4N) \qquad (1)$$

of **2** and **3** by reacting the appropriate halide with [4-$MeOC_6H_4TeNa$] did not succeed. On attempting the reaction by taking [ArTeNa] in aqueous phase and 2-(chloromethyl)/2,6-bis(dichloromethyl)pyridine in chloroform the product was bis(4-methoxyphenyltelluro)methane. On reacting chloroform separately with the tellurolate in the presence of base $NaBH_4$, bis(4-methoxyphenyltelluro)methane was formed in good yield (>80%) which is the highest compared to other synthetic routs reported earlier [11–16]. Moreover, the chloroform based present synthetic route is less time-consuming and free from the requirements of special techniques. The most plausible mechanism of the synthesis of $(4\text{-}MeOC_6H_4Te)_2CH_2$ from $CHCl_3$ seems to be the following (eq. (2)),

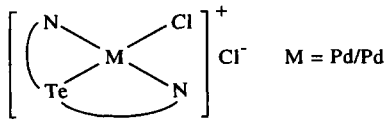
$$CHCl_3 \xrightarrow{OH^-} CCl_3^- \rightarrow :CCl_2 \xrightarrow{ArTe^-}$$

$$(ArTe)_2C: \xrightarrow{BH_4^-} (ArTe)_2CH^- \xrightarrow[solvent]{H^+} (ArTe)_2CH_2. \quad (2)$$

The **1** and its Pd^{II} and Pt^{II} complexes have been authenticated by elemental analyses and spectral data given in the experimental section.

The ^1H NMR spectrum of **1** shows multiplets for H_7 and H_8 rather than two triplets as observed in the spectrum of its precursor 2-(2-chloroethyl)pyridine at 3.9 and 3.2 ppm respectively. The upfield shift (0.7 ppm) of H_8 in the spectrum of ligand **1** with respect to its precursor may be due to replacement of chlorine atoms by the less electronegative tellurium. This shielding of H_8 results in its merger with the H_7 signals. The signal due to H_6 appears downfield as compared to other ring protons of pyridine because the electronegative nitrogen deshields the *ortho* carbon and hydrogen linked to it. The assignments of H_4, H_3 and H_5 protons in ^1H NMR spectrum of **1** are in agreement with those of alkyl pyridines.[17].

The molecular weights of [PdCl·**1**]Cl and [PtCl·**1**]Cl indicate that in solution they behave as a 1 : 1 electrolyte, which is supported by their Λ_M values (135 and 129 ohm^{-1} cm^2 mol^{-1}, respectively). The comparison of ^1H NMR spectrum of **1** with those of [PdCl·**1**]Cl and [PtCl·**1**]Cl reveals that signal of H_6 (proton *ortho* to pyridine nitrogen) undergoes deshielding (0.33/0.50 ppm) and signals having contribution from H_8 are also affected similarly. This indicates that **1** acts as a tridentate ligand coordinating with Pd and Pt in these complexes through Te and two pyridine nitrogen atoms. In the $^{125}Te\{^1H\}$ NMR spectrum of **1** the lone signal was observed at 167 ppm which is in agreement with the ^{125}Te NMR signals of other dialkyl tellurides [15]. The ^{125}Te NMR, spectrum of [PtCl·**1**]Cl shows a signal highly deshielded with respect to that of **1** (even after taking into account the solvent effect) which indicates that in this complex **1** ligates through tellurium. The coupling satellites were not observed due to the low solubility of the complex. The red shifted (20–25 cm^{-1}) ν(Te—C(alkyl)) appearing in the IR spectra of Pd/Pt complexes with respect to that of **1** further supports the ligation of **1** through tellurium. The electronic spectra of both the complexes exhibit three bands around 25, 30 and 42 kK. The first one of these bands seems to arise from $^1A_{ig} \rightarrow {}^1B_{ig}$ transition of complexed Pd/Pt having square planar coordination geometry. The other two bands seem to originate from intraligand transitions. Thus the following structure seems to be most plausible for both the complexes.



M = Pd/Pd

Neither [PdCl·**1**]Cl nor [PtCl·**1**]Cl gave crystals suitable for X-ray diffraction, therefore to understand the Pd—Te bond in conjunction with the Pd—N(pyridine) bond the crystal structure of [$PdCl_2$·**4**], a closely related complex, was explored.

Crystal structure [$PdCl_2$·**4**]

The structure of [$PdCl_2$·**4**] in the solid state consists of discrete molecules. For each complex molecule two molecules of $CHCl_3$ are present, in their crystal. The molecular structure of the complex and a packing diagram are shown in Figs 1 and 2 respectively. Selected bond lengths and bond angles are given in Table 2. The chelate ring (Fig. 1) adopts an *endo*-puckered conformation with respect to C(2) and Pd. The aromatic ring makes an angle of 110.3° with respect to the square planar geometry while the pyridine ring is

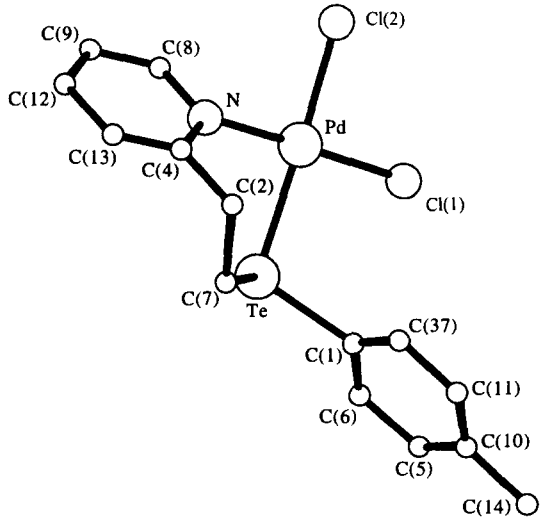


Fig. 1. Molecular structure of [$PdCl_2$·**4**].

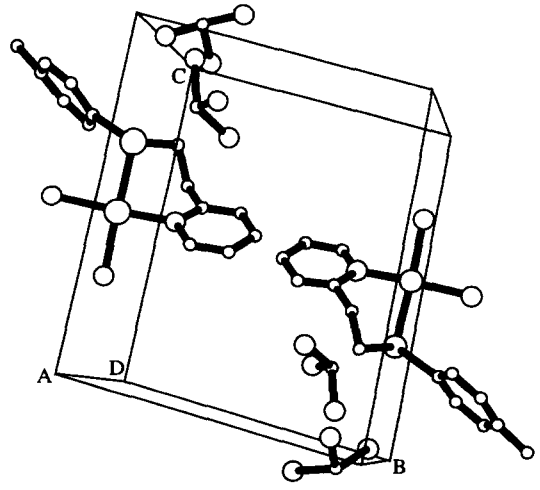


Fig. 2. Unit cell packing of [$PdCl_2$·**4**].

Table 2. Selected bond lengths (Å) and bond angles (°)

Te—Pd	2.517(1)
Pd—Cl(1)	2.287(3)
Pd—Cl(2)	2.352(3)
Pd—N	2.041(10)
Te—C(1)	2.118(12)
Te—C(7)	2.165(14)
C(2)—C(7)	1.505(19)
C(4)—(N)	1.356(17)
Cl(1)—Pd—Te	88.7(1)
Cl(2)—Pd—Te	177.8(1)
Cl(2)—Pd—Cl(1)	92.4(1)
N—Pd—Te	88.0(3)
N—Pd—Cl(1)	175.9(3)
N—Pd—Cl(2)	90.8(3)
C(1)—Te—Pd	107.2(3)
C(7)—Te—Pd	96.8(3)
C(7)—Te—C(1)	95.8(5)
C(4)—N—Pd	123.8(8)
C(7)—Te—Pd	96.8(3)
C(2)—C(4)—N	118.3(10)
C(2)—C(7)—Te	111.9(9)
C(4)—C(2)—C(7)	111.5(12)

inclined to it by 55.2°. The Pd—Te bond length in the present structure is slightly shorter than the value 2.525(1) Å observed in the crystal structure of [Pd{*meso*-PhTe$(CH_2)_3$TePh}Br_2] [18]. The Te-C(7) bond length is compatible with earlier reported Te—C(alkyl)bond distances. The Pd—N bond length in the present structure is somewhat shorter than the earlier reports on Pd—N(pyridine) bond lengths [19]. This is probably caused by steric influence of the large tellurium on the six membered chelate ring. The Pd—Cl bond *trans* to tellurium is longer than the other. This in conjunction with a similar observation made earlier for the Pt^{II} complex of a (Te, S) ligand [20] indicates that the *trans* influence of Te should not be underestimated and lability originating due to this is worth exploring. The C—C bond lengths of benzene ring are between 1.358(16) and 1.434(18) Å and their C—C—C bond angles are between 115.1(13) and 123.3(12)° as expected. Similarly the pyridine ring bond length and bond angles are normal [C—C bond length 1.377(19) to 1.419(23) Å, C—N bond length ~ 1.356(18) Å and C—C—C/C—C—N/C—N—C bond angles 117.4(12)–123.4(13)°].

Acknowledgements—The authors thank Professor T. P. Singh, Biophysics Department, All India Institute of Medical Science for crystal data. DST and UGC (India) are acknowledged by authors A.K.S. and A.K., respectively for financial support.

REFERENCES

1. A. K. Singh and V. Srivastava, *J. Coord. Chem.* 1992, **27,** 237.
2. E. G. Hope and W. Levason, *Coord. Chem. Rev.* 1993, **122,** 109.
3. V. Srivastava, R. Batheja and A. K. Singh, *J. Organomet. Chem.* 1994, **484,** 93.
4. M. R. Greaves, T. A. Hamor, B. L. Howlin, T. S. Lobana, S. A. Mbogo, W. R. McWhinnie and D. C. Povey, *J. Organomet. Chem.* 1991, **420,** 327.
5. S. A. Mbogo, W. R. McWhinnie and T. S. Lobana *Inorg. Chim. Acta* 1992, **193,** 5.
6. A. Khalid, B. L. Khandelwal, A. K. Singh, T. P. Singh and B. Padmanabham, *J. Coord. Chem.* 1994, **31,** 19.
7. K. J. Irgolic and R. A. Zingaro, in *Organometallic Reactions* (Edited by E. Becker and M. Tsutsui), Vol. 2, p. 275. John Wiley and Sons, New York (1971).
8. S. Okio and Y. Noike, *J. Pharm. Sci., Japan* 1952, **72,** 490.
9. (a) G. M. Sheldrick, *SHELXS* 86, *A Programme for Crystal Structure Determination.* Anorganisch Chemisches Institüt der Univ., Gottingen, Germany (1986); (b) G. M. Sheldrick, *SHELX* 76, *A Program for Crystal Structure Determination.* Anorganisch Chemisches Institüt der Univ., Gottingen, Germany (1976).
10. D. T. Cromer and J. B. Mann, *Acta Cryst.* 1968, **24A,** 321; D. T. Cromer and D. Liberman, *J. Chem. Phys.* 1970, **53,** 1891.
11. G. Petragnani and G. Schill, *Chem. Ber.* 1971, **103,** 2271.
12. D. Seeback and A. K. Beck, *Chem. Ber.* 1975, **108,** 314.
13. L. Engman and M. P. Cava, *Organometallics* 1982, **1,** 470.
14. L. Torres, C. *J. Organomet. Chem.* 1990, **381,** 69.
15. E. G. Hope, T. Kemmitt and W. Levason, *Organometallics* 1987, **6,** 207; 1988, **7,** 78.
16. H. M. K. K. Pathirana and W. R. McWhinnie, *J. Chem. Soc., Dalton Trans.* 1986, 2003.
17. R. M. Silverstein, G. C. Bassler and T. C. Morrill, *Spectrometric Identification of Organic Compounds,* 5th Ed. John Wiley and Sons, New York (1991).
18. T. Kemmitt, W. Levason and M. Webstar, *Inorg. Chem.* 1989, **28,** 692.
19. R. E. Rulke, D. Kliphuis, C. S. Elsevier, J. Fraanje, K. Goubitz, P. W. N. M. Van Leeuwen and K. Vrieze, *J. Chem. Soc., Chem. Commun.* 1994, 1817.
20. A. K. Singh, V. Srivastava, S. K. Dhingra, J. E. Drake and J. H. E. Bailey, *Acta Cryst.* 1992, **C48,** 655.

Pergamon

S0277-5387(96)00254-9

Polyhedron Vol. 16, No. 1, pp. 39–45, 1997
Copyright © 1996 Elsevier Science Ltd
Printed in Great Britain. All rights reserved
0277-5387/97 $15.00+0.00

Syntheses of $[Ni_2(dien)_2(NCS)_4(H_2O)]$ and $[Ni(aepn)(NCS)_2]_n$ (dien = bis(2-aminoethyl)amine and aepn = *N*-(2-aminoethyl)-1,3-propanediamine): single crystal structure analysis and thermal behaviour in the solid state

Arunendu Mondal,[a] Chandi Pariya,[a] Nirmalendu Ray Chaudhuri,[a]* Nirmalya Prasun Nayak,[b] Alok K. Mukherjee[b] and Ashutosh Ghosh[c]

[a]Department of Inorganic Chemistry, Indian Association for the Cultivation of Science, Calcutta 700 032, India

[b]Department of Physics, Jadavpur University, Calcutta 700 032, India

[c]Department of Chemistry, Jhargram Raj College, Jhargram 721 507, West Bengal, India

(Received 20 March 1996; accepted 22 May 1996)

Abstract—$[Ni_2(dien)_2(NCS)_4(H_2O)]$ (**1**) and $[Ni(aepn)(NCS)_2]_n$ (**2**) (where dien = bis(2-aminoethyl)amine and aepn = *N*-(2-aminoethyl)-1,3-propanediamine) have been synthesised from solution. Single crystal X-ray structure analyses of **1** and **2** reveal that the metal atoms in both the complexes display distorted octahedral geometry with the triamine coordinating facially in **1** and meridionally in **2**. The dinuclear $[Ni_2(dien)_2(NCS)_4(H_2O)]$ unit in **1** is bridged *via* a thiocyanate moiety while in **2** the nickel(II) octahedra form a polymeric chain. The species **1** on deaquation at ~165°C followed by cooling yields a conglomerated mass (**1a**). The species **2** melts at ~230°C which on cooling yields conglomerated mass (**2a**). Both **1a** and **2a** are amorphous; the former reverts to **1** in a humid atmosphere. Copyright © 1996 Elsevier Science Ltd

Keywords: nickel(II) thiocyanate; bis(2-aminoethyl)amine; *N*-(2-aminoethyl)-1,3-propanediamine; thermal analysis; single crystal structure; triamine.

Curtis *et al.* [1] reported the syntheses of $NiL(SCN)_2$ (where L = bis(2-aminoethyl)amine (dien) and bis(3-aminopropyl)amine (dpt)) and proposed structures with one bridging thiocyanate and one N-bonded terminal thiocyanate in *cis* position on the basis of IR spectroscopy. For the corresponding anhydrous and hydrated chloro complexes, it was suggested that the terminal chlorine atoms (in the anhydrous form) or the water molecules (in the hydrated form) are in the *trans* position. Cannas *et al.* [2] reported the X-ray crystal structures of $CdLCl_2$ [(where L = dien, dpt and *N*-(2-aminoethyl)-1,3-propanediamine (aepn)] and observed noticeable differences in the structures on increasing the chain length of the triamine; i.e. $Cd(dien)Cl_2$ is polymeric while $Cd(aepn)Cl_2$ and $Cd(dpt)Cl_2$ are dimeric with *cis* and *trans* configuration, respectively. This led us to assume that the corresponding nickel(II) complexes with several counter anions (Cl^-, Br^- and NCS^- etc.) should also show structural differences. Starting with the $Ni(NCS)_2$ salt of three triamines (dien, aepn and dpt) we have been able to synthesise the single crystals of dien and aepn complexes. The present paper reports the syntheses and X-ray structure analyses of $[Ni_2(dien)_2(NCS)_4(H_2O)]$ and $[Ni(aepn)(NCS)_2]_n$ along with their thermal properties in the solid state.

* Author to whom correspondence should be addressed.

EXPERIMENTAL

Materials

Bis(2-aminoethyl)amine (dien) and *N*-(2-aminoethyl)-1,3-propanediamine (aepn) was purchased from the Aldrich Chemical Company Inc. and used as received. Nickel(II) thiocyanate was prepared by the standard procedure as reported by Sarma and Poddar [3]. All other chemicals used were of AR grade.

Physical measurements

The thermal analysis (TG-DTA) was carried out on a Shimadzu DT-30 thermal analyser in dynamic atmosphere of dinitrogen (flow rate: 30 cm^3 min^{-1}). The sample (particle size within 150–200 mesh) was heated in a platinum crucible at a rate of 10°C min^{-1} with inert alumina as reference. The enthalpy change of phase transition was calculated using a Perkin–Elmer DSC-2 differential scanning calorimeter, with indium metal as calibrant (rate of heating 10°C min^{-1}). The instruments used for recording the IR spectra (KBr disc at ambient), electronic spectra (nujol mull), elemental analyses and effective magnetic moments at ambient temperature (22°C) were as reported earlier [4].

Preparation of $[Ni_2(dien)_2(NCS)_4(H_2O)]$ (**1**)

The triamine(dien) (1 mmol) was added dropwise to nickel(II) thiocyanate (1 mmol) dissolved in ethanol (10 cm^3). The resulting blue solution was kept in a desiccator. After a few days fine blue crystals were separated out, filtered, washed with ethanol and dried in a desiccator. Found: C, 25.0; H, 4.8; N, 24.4; Ni, 20.3. Calc. for $C_{12}H_{28}N_{10}Ni_2OS_4$ (**1**): C, 25.0; H, 4.8; N, 24.4; Ni, 20.4%. μ_{eff} = 3.1 B.M.;* λ_{max} = 807, 540 and 360 nm.

Preparation of $[Ni(aepn)(NCS)_2]_n$ (**2**)

The triamine (aepn) (1 mmol) was added dropwise to nickel(II) thiocyanate (1 mmol) dissolved in ethanol (10 cm^3). The resulting bluish pink solution on slow evaporation in a desiccator yielded the desired bluish pink coloured crystalline complex. The crystals were separated, washed with ethanol and dried in a desiccator. Found; C, 28.7; H, 5.0; N, 23.8; Ni, 20.0. Calc. for $C_7H_{15}N_5S_2Ni$ (**2**): C, 28.7; H, 5.1; N, 23.9; Ni, 20.1%. μ_{eff} = 3.1 B.M.; λ_{max} = 827, 781, 556 and 369 nm.

* Non-S.I. Unit employed: B.M. 9.27×10^{-24} Am^2.

X-ray diffraction structural study

Single crystals suitable for X-ray analysis were obtained by recrystallization of **1** and **2** from acetonitrile–methanol mixture (1:1) and acetonitrile respectively.

A single crystal of complex **1** was mounted on a Nicolet R3m/V diffractometer, while the crystal of complex **2** was mounted on an Enraf-Nonius CAD4 diffractometer. Lattice constants, orientation matrices were determined by least-squares refinement of the angular settings of 25 well-centred reflections. Crystal data collection and structure solution parameters for complexes are summarised in Table 1.

Intensity data were collected using Mo-K_α radiation (λ = 0.71073 Å) for complex **1** and Cu-K_α radiation (λ = 1.5418 Å) for complex **2** with ω-2θ scan technique. Three control reflections monitored at regular intervals during the X-ray exposures indicated no significant variation in the intensities. All data were corrected for Lorentz and polarisation effects. An empirical absorption correction [5] based on ψ-scan was applied to both the cases. The structures were solved by Patterson techniques followed by Fourier syntheses and refined through full-matrix least-squares calculations. Anisotropic refinements were carried out for the non-hydrogen atoms. The hydrogen atoms were introduced in the final structure-factor calculations at idealized positions with fixed isotropic thermal parameters. Complex neutral-atom scattering factors [6] were used throughout. Calculations were carried out using SHELXS 86 [7], SHELXL 93 [8], PARST [9] and ORTEPII [10] programs. Selected bond lengths and angles of complexes **1** and **2** are listed in Table 2.

RESULTS AND DISCUSSION

Following the method of preparation of Curtis *et al.* it was observed from the TG-curve and elemental analysis that $Ni(dien)(NCS)_2$ is always associated with 0.5 molecule of water. This is also true when **1** is synthesised by adding the ligand (dien) straight to $Ni(NCS)_2$ in aqueous solution (*viz.* experimental). IR, electronic spectra, magnetic susceptibility and conductance data are similar to those reported earlier [1] and corroborate the six-coordinated structure of the complex. The mono triamine complexes can exist in *fac*- and *mer*-isomeric forms and can be distinguished by the inspection of IR spectra [11,12] in the region 1500–1400 cm^{-1}, ~1250 cm^{-1} and 850–700 cm^{-1} for —CH_2 bending, —NH wagging and —NH_2 rocking respectively. In the present case the compound possesses CH_2-bending at 1430 cm^{-1}, 1440 cm^{-1}, 1460 cm^{-1} and 1480 cm^{-1}, NH_2-rocking at 770 cm^{-1}, 790 cm^{-1}, 810 cm^{-1} but no NH-wagging at 1250 cm^{-1}, which are compatible with the *fac* isomer. From the IR spectra it is not clear whether the water molecule is coordinated to nickel(II) or not. It has been found

Table 1. Crystal data for complexes **1** and **2**

	1	**2**
Formula	$C_{12}H_{28}N_{10}Ni_2OS_4$	$C_7H_{15}N_5S_2Ni$
Colour	blue	bluish-pink
Formula weight	574.10	292.07
Crystal system	Orthorhombic	Orthorhombic
Space group	$P2_12_12_1$	$P2_12_12_1$
a (Å)	10.835(7)	7.366(1)
b (Å)	14.037(7)	11.647(2)
c (Å)	15.527(8)	14.832(3)
V (Å^3)	2362(2)	1272.5(4)
Z	4	4
Radiation (λ, Å)	Mo-K_α (0.71073)	Cu-K_α (1.5418)
F (000)	1192	608
μ (mm^{-1})	1.974	5.094
D_c (g cm^{-3})	1.615	1.525
D_x (g cm^{-3})	1.630	1.520
Crystal size (mm)	$0.6 \times 0.4 \times 0.2$	$0.5 \times 0.3 \times 0.2$
θ range (°)	$1.5 < \theta < 22.5$	$3 < \theta < 75$
Unique reflections	1728	1369
Observed reflections $[I > 2\sigma(I)]$	1552	1362
$R1^a$, $WR2^b$	0.0315, 0.0798	0.0659, 0.1008
Weighting parameters (A, B)	0.0562, 0.0	0.2273, 0.96
Goodness-of-fit (^{d}S)	0.988	2.268
Maximum Δ/e.s.d.	0.152	0.204
Final $\Delta\rho$, max/min (eÅ^{-3})	0.29/−0.49	0.57/−0.78

^{a} $R1 = \Sigma\|F_o| - |F_c\|/\Sigma|F_o|$.
^{b} $WR2 = [\Sigma\{w(F_o^2 - F_c^2)^2\}/\Sigma\{w(F_o^2)^2\}]^{1/2}$.
^{c} $W = 1/[\sigma^2(F_o^2) + (AP)^2 + BP]$, where $P = (F_o^2 + 2F_c^2)/3$.
^{d} $S = [\Sigma\{w(F_o^2 - F_c^2)^2\}/(N\text{-}P)]^{1/2}$, where N is the number of data and P is the total number of parameters refined.

from simultaneous TG-DTA analysis that the elimination of water takes place at relatively high temperature (~165°C) indicating that the water molecule is likely to be coordinated to nickel(II).

Although Curtis *et al.* reported the syntheses of $NiL(NCS)_2$ (where L = dien and dpt) but no such mono complex of $Ni(NCS)_2$ with aepn ligand has been reported so far. We have synthesised $Ni(aepn)(NCS)_2$ and its electronic spectra and magnetic susceptibility measurement indicate that $Ni(aepn)(NCS)_2$ possesses six-coordinated octahedral geometry. The conductivity measurement (Λ_m = 57 ohm^{-1} cm^2 mol^{-1} in methanol) indicates that both the thiocyanate ions are coordinated to nickel(II) centre. The IR spectrum shows that aepn is chelated. This complex may also exist in two isomeric forms i.e. *fac-* and *mer-* like its dien analogue. However, it is not possible to distinguish between the isomers from the IR spectra due to lack of similar reports in literature. Assuming tridentacy of aepn, to satisfy six-coordinated octahedral geometry in $Ni(aepn)(NCS)_2$, one of the thiocyanate ions is expected to be bridged. The bridging thiocyanate usually shows the ν_{CN} band well above 2100 cm^{-1} [13]. But the ν_{CN} frequency of this complex is at 2090 cm^{-1}. Thus bridging of thiocyanate can not be ascertained.

Description of structures of $[Ni_2(dien)_2(NCS)_4(H_2O)]$ (**1**) *and* $[Ni(aepn)(NCS)_2]_n$ (**2**)

ORTEP views of the complexes **1** and **2** with atom labelling scheme are shown in Figs 1 and 2. Complex **1** consists of neutral dinuclear $[Ni_2(dien)_2(NCS)_4(H_2O)]$ units in *cis* configuration bridged *via* thiocyanates. The coordination polyhedra around the two metal centres in complex **1** are best described as distorted octahedrons with N_5O and N_5S chromophores, respectively. The distortions from ideal octahedral geometry are due to the asymmetric nature of the binding ligands and are refined in the deviations of the angles formed at the metal centres (Table 2) from 90°. Three ligand nitrogen atoms, N(2), N(4), N(5) and the aqua O atom, O(1), around Ni(1) define an equatorial plane and the remaining two N atoms [N(1), N(3)] are in axial positions; Ni(1) being displaced by 0.095(3) Å towards N(1). The corresponding equatorial plane about Ni(2) is defined by S(2) (sulfur atom of bridging NCS moiety), N(7), N(9) and N(10) [Ni(2) is deviated by 0.004(3) Å towards N(6)]; N(6) and N(8) occupying the axial sites. The dihedral angle between the two equatorial planes is 44.3(2)°. The two five-membered chelate rings associated with each metal centre display envelope conformations and are approxi-

Table 2. Selected bond distances (Å) and angles (°) in complexes **1** and **2**

	$[Ni_2(dien)_2(NCS)_4(H_2O)]$ **1**	$[Ni(aepn)(NCS)_2]_n$ **2**
Ni(1)—N(1)	2.054(6)	2.051(3)
Ni(1)—N(2)	2.090(6)	2.081(3)
Ni(1)—N(3)	2.137(6)	2.101(2)
Ni(1)—N(4)	2.107(6)	2.104(3)
Ni(1)—N(5)	2.084(7)	2.073(3)
Ni(1)—O(1)	2.176(5)	
Ni(1)—S(2)[a]		2.632(1)
Ni(2)—N(6)	2.058(7)	
Ni(2)—N(7)	2.093(6)	
Ni(2)—N(8)	2.096(6)	
Ni(2)—N(9)	2.062(7)	
Ni(2)—N(10)	2.087(6)	
Ni(2)—S(2)	2.573(2)	
N(1)—C(1)	1.130(9)	1.166(5)
N(2)—C(2)	1.473(10)	1.464(5)
N(3)—C(3)	1.489(9)	1.456(4)
N(3)—C(4)	1.482(9)	1.473(3)
N(4)—C(5)	1.482(10)	
N(4)—C(6)		1.481(4)
N(5)—C(6)	1.140(9)	
N(5)—C(7)		1.142(5)
N(6)—C(7)	1.147(9)	
N(7)—C(8)	1.445(10)	
N(8)—C(11)	1.459(9)	
N(9)—C(12)	1.151(9)	
N(10)—C(9)	1.491(10)	
N(10)—C(10)	1.513(9)	
S(1)—C(1)	1.641(8)	1.629(3)
S(2)—C(6)	1.669(9)	
S(2)—C(7)		1.645(3)
S(3)—C(7)	1.632(8)	
S(4)—C(12)	1.641(8)	
C(2)—C(3)	1.503(11)	1.528(5)
C(4)—C(5)	1.504(11)	1.521(5)
C(5)—C(6)		1.517(6)
C(8)—C(9)	1.501(13)	
C(10)—C(11)	1.490(11)	
N(1)—Ni(1)—N(2)	94.8(2)	95.0(1)
N(1)—Ni(1)—N(3)	171.7(2)	177.7(1)
N(1)—Ni(1)—N(4)	91.6(3)	90.7(1)
N(1)—Ni(1)—N(5)	95.2(3)	91.9(1)
N(1)—Ni(1)—O(1)	88.4(2)	
N(1)—Ni(1)—S(2)[a]		83.6(1)
N(2)—Ni(1)—N(3)	81.8(2)	83.1(1)
N(2)—Ni(1)—N(4)	99.4(2)	172.4(1)
N(2)—Ni(1)—N(5)	90.6(2)	91.2(1)
N(2)—Ni(1)—O(1)	174.6(2)	
N(2)—Ni(1)—S(2)[a]		87.5(1)
N(3)—Ni(1)—N(4)	81.5(2)	91.0(1)
N(3)—Ni(1)—N(5)	92.4(2)	89.6(1)
N(3)—Ni(1)—O(1)	95.6(2)	
N(3)—Ni(1)—S(2)[a]		94.9(1)
N(4)—Ni(1)—N(5)	167.4(2)	93.5(1)
N(4)—Ni(1)—O(1)	84.8(2)	
N(4)—Ni(1)—S(2)[a]		88.3(1)
N(5)—Ni(1)—O(1)	84.8(2)	
N(5)—Ni(1)—S(2)[a]		175.2(1)
N(6)—Ni(2)—N(7)	89.1(3)	
N(6)—Ni(2)—N(8)	171.0(2)	
N(6)—Ni(2)—N(9)	87.7(3)	
N(6)—Ni(2)—N(10)	90.9(2)	

Table 2. *Continued*

	$[Ni_2(dien)_2(NCS)_4(H_2O)]$ **1**	$[Ni(aepn)(NCS)_2]_n$ **2**
N(6)—Ni(2)—S(2)	92.6(2)	
N(7)—Ni(2)—N(8)	95.1(3)	
N(7)—Ni(2)—N(9)	176.7(3)	
N(7)—Ni(2)—N(10)	82.4(3)	
N(7)—Ni(2)—S(2)	87.3(2)	
N(8)—Ni(2)—N(9)	88.1(3)	
N(8)—Ni(2)—N(10)	81.8(2)	
N(8)—Ni(2)—S(2)	95.5(2)	
N(9)—Ni(2)—N(10)	98.2(3)	
N(9)—Ni(2)—S(2)	92.3(2)	
N(10)—Ni(2)—S(2)	169.0(2)	
Ni(1)—N(1)—C(1)	173.4(7)	172.6(3)
Ni(1)—N(5)—C(6)	173.1(6)	
Ni(1)—N(5)—C(7)		170.8(3)
Ni(2)—N(6)—C(7)	175.6(6)	
Ni(2)—N(9)—C(12)	156.0(6)	
Ni(2)—S(2)—C(6)	103.1(2)	
N(1)—C(1)—S(1)	178.6(7)	178.7(3)
N(5)—C(6)—S(2)	177.6(7)	
N(5)—C(7)—S(2)		177.6(3)
N(6)—C(7)—S(3)	177.7(7)	
N(9)—C(12)—S(4)	178.1(7)	

[a] $-x+1, y+1/2, -z+3/2$

mately orthogonal to each other. The dihedral angles between the planar parts of the chelate rings at Ni(1) [Ni(1), N(2), N(3), C(2) and Ni(1), N(3), N(4), C(5)] and Ni(2) [Ni(2), N(7), N(10), C(8) and Ni(2), N(8), N(10), C(10)] are 82.1(2) and 84.2(2)° respectively.

The molecular structure of complex **2** consists of polymeric chains of nickel octahedra. In each monomeric unit of $Ni(aepn)(NCS)_2$ in *trans* configuration the metal atom is bonded to five ligand nitrogen atoms and a sulfur atom of one of the symmetry related thiocyanate groups (Ni—S(2)^i 2.632(1) Å, $i = -x+1, y+1/2, -z+3/2$) completes the distorted octahedron.

The six-membered chelate ring in complex **2** displays a chair conformation with C(5) 0.708(6) Å above and Ni 0.866(4) Å below the least-square plane through the remaining endocyclic atom while the five-membered ring adopts an open envelope form with C(3) atom, on the flap, 0.582(5) Å away from the least-squares plane defined by the other four ring atoms. The dihedral angle between the planar parts of the two chelate rings is 33.2(1)°. The Ni—N dis-

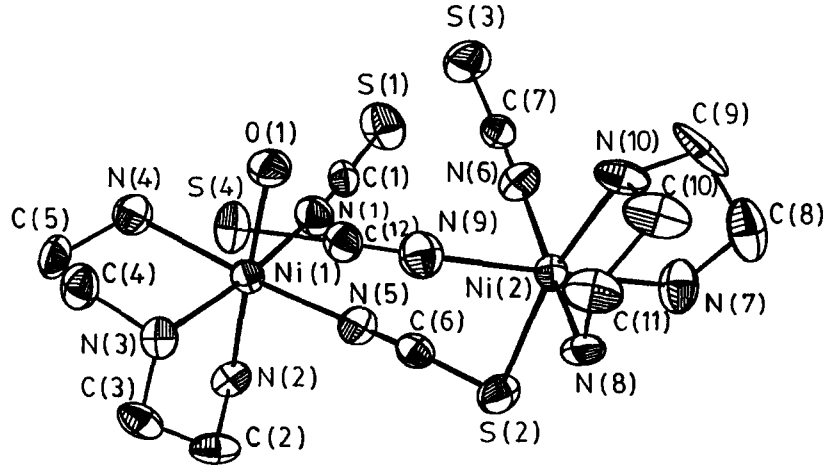


Fig. 1. ORTEP-plot of $[Ni_2(dien)_2(NCS)_4(H_2O)]$ (**1**) with atom numbering scheme.

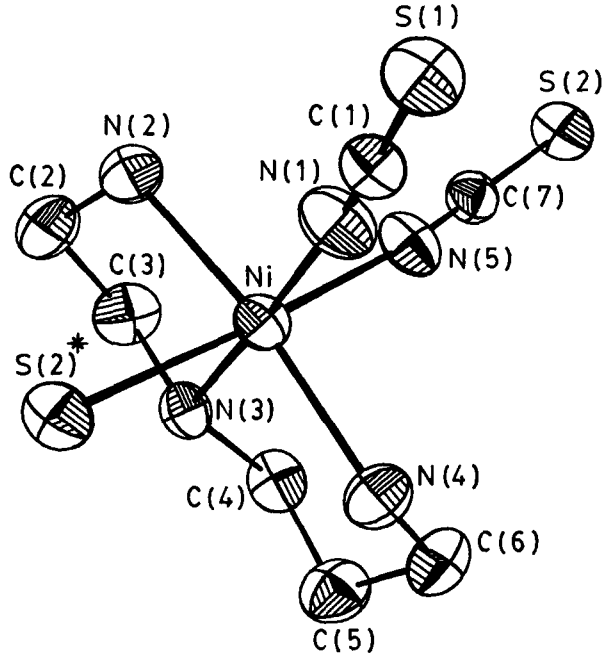


Fig. 2. ORTEP-plot of [Ni(aepn)(NCS)$_2$] (**2**) with atom numbering scheme.

tance in both the complexes, in the range 2.051(3)–2.137(6) Å, are consistent with the corresponding values for nickel(II)–triamine systems with octahedral metal coordination (Table 3).

Thermal analysis

$Ni_2(dien)_2(NCS)_4(H_2O)$ (**1**) (blue) upon heating starts to lose water at 110°C and becomes dehydrated at 165°C showing an endothermic peak at 150°C (ΔH = 46.7 kJ mol^{-1}) in its DTA curve. The dehydrated species (**1a**) (deep blue) is found to be conglomerated. When cooled to ambient temperature and powdered, **1a** transforms to $Ni_2(dien)_2(NCS)_4H_2O$ (**1**) on keeping in a humid atmosphere for about 12 h. But it is stable in a desiccator. Ni(aepn)$(NCS)_2$ (**2**) (blue) upon heating melts (230°C, ΔH = 53.3 kJ mol^{-1}) which on cooling yields a conglomerated mass (**2a**) which is stable in the open atmosphere.

Magnetic moment and electronic spectra (μ_{eff} = 3.0 B.M., λ_{max} = 575 and 400 nm for **1a**; μ_{eff} = 3.0 B.M., λ_{max} = 560 and 380 nm for **2a**) of both **1a** and **2a** are typical of octahedral nickel(II). The IR spectra of both the species are broad in comparison to the spectra of the parent species. The X-ray powder diffraction patterns show that the species (**1a** and **2a**) are amorphous although the hydrated species **1** and **2** are crystalline in nature.

Acknowledgements—The authors are grateful to the National Single Crystal Diffractometer Facilities at the Indian Association for the Cultivation of Science, Calcutta, and All India Institute of Medical Sciences, New Delhi, for providing diffractometer data for complexes **1** and **2**, respectively. Funding for the work described was provided by the Council

Table 3. A comparison of Ni—N(primary/secondary) distances (Å) and N(primary)—Ni—N(primary) bond angles (°) in octahedral nickel(II)-triamine complexes

	Ni—N(Pr)	Ni—N(sec)	N(pr)—Ni—N(pr)	Reference
$[Ni_2(dien)_2(NCS)_4(H_2O)]$	2.090(6)–2.107(6)	2.087(6)–2.137(6)	95.1(3)–99.4(2)	This work
$[Ni(aepn)(NCS)_2]_n$	2.081(3)–2.104(3)	2.101(2)	172.4(1)	This work
$[Ni(dpt)_2](ClO_4)_2$	2.12(2)–2.17(2)	2.22(2)–2.23(2)	175.5(3)–176.9(3)	[14]
$[Ni(dpt)(H_2O)_2(SO_4)]H_2O$	2.084(2)–2.099(3)	2.088(2)	170.0(1)	[15]
$[Ni_2(N_3)_3(dpt)_2]ClO_4$	2.059(5)–2.076(4)	2.117(4)	171.4(2)	[16]
$[Ni(dien)_2](NCS)_2$	2.096(1)–2.134(1)	2.110(1)	92.6(1)	[17]
$[Ni(NCO)_2(terpy)(H_2O)]$	2.152(2)–2.165(2)	2.074(3)	154.8(1)	[18]
$[Ni(bamp)_2]Cl_21.67H_2O$	2.128(3)–2.168(3)	2.001(3)–2.025(3)	157.1(1)–159.1(1)	[19]

terpy = 2,2′ : 6,2″-terpyridine.
bamp = 2,6-bis(aminomethyl)pyridine,

of Scientific and Industrial Research (New Delhi) Grants Scheme and is gratefully acknowledged.

REFERENCES

1. N. F. Curtis and Y. M. Curtis, *Aust. J. Chem.* 1996, **19,** 1423.
2. M. Cannas, G. Marongieu and S, Saba, *J. Chem. Soc., Dalton Trans.* 1908, 2090.
3. K. P. Sarma and R. K. Poddar, *Trans. Met. Chem.* 1984, **9,** 135.
4. C. Pariya, A. Ghosh, N. Ray Chaudhuri, S. Ghosh, M. Mukherjee and A. K. Mukherjee, *Polyhedron* 1996, **15,** 1643 and refs. therein.
5. A. C. T. North, D. C. Philips and F. S. Mathews, *Acta Cryst., Sect. A* 1968, **24,** 351.
6. International Tables for Crystallography, Vol. C, Tables 4.2.6.8 and 6.1.1.4 (1992).
7. G. M. Sheldrick, *SHELXS* 86. *Program for the Solution of Crystal Structures.* University of Gottingen, Germany (1985).
8. G. M. Sheldrick, *SHELXL* 93, *Program for the Solution of Crystal Structure.* University of Gottingen, Germany (1993).
9. M. Nardelli, *Comput. Chem.* 1983, **7,** 1995.
10. C. K. Johnson, ORTEP II, Report ORNL-5138. Oak Ridge National Laboratory, Tennessee (1976).
11. G. H. Searle and D. A. House, *Aust. J. Chem.* 1987, **40,** 361.
12. P. Paoletti, S. Biazini and M. Cannas, *Chem. Commun.* 1969, 513.
13. K. Nakamoto, *Infrared and Raman Spectra of Inorganic and Coordination Compounds*, 3rd edn, p. 275. Wiley-Interscience, New York (1978).
14. S. Biagini and M. Cannas, *J. Chem. Soc. A* 1970, 2398.
15. M. Mukherjee, A. K. Mukherjee, C. Pariya and N. Ray Chaudhuri, *Acta Cryst., Sect. C* 1995, **51,** 1543.
16. R. Vicente, A. Escuer, J. Ribas and X. Solans, *Inorg. Chem.* 1992, **31,** 1726.
17. A. K. Mukherjee, S. Koner, A. Ghosh, N. Ray Chaudhuri, M. Mukherjee and A. J. Welch, *J. Chem. Soc., Dalton Trans.* 1994, 2367.
18. R. Cortes, M. I. Arriortua, T. Rojo, J. L. Mesa, X. Solans and D. Beltran, *Acta Cryst., Sect. C* 1988, **44,** 986.
19. P. Bonhote, M. Ferigo, H. Stoeckli-Evans and W. Marty, *Acta Cryst., Sect. C* 1993, **49,** 2102.

Pergamon

S0277-5387(96)00255-0

Polyhedron Vol. 16, No. 1, pp. 47–55, 1997
Copyright © 1996 Elsevier Science Ltd
Printed in Great Britain. All rights reserved
0277-5387/97 $15.00+0.00

Complete spin crossover in tris(pyridylbenzimidazole) iron(II)

Roman Boča,[a]* Peter Baran,[a] L'ubor Dlháň,[a] Jozef Šima,[a] Günther Wiesinger,[b] Franz Renz,[b] Usama El-Ayaan[b] and Wolfgang Linert[b]*

[a]Department of Inorganic Chemistry, Slovak Technical University, SK-812 37 Bratislava, Slovakia

[b]Institute of Inorganic Chemistry, Institute of Experimental Physics, Vienna University of Technology, A-1060 Vienna, Austria

(Received 19 March 1996; accepted 22 May 1996)

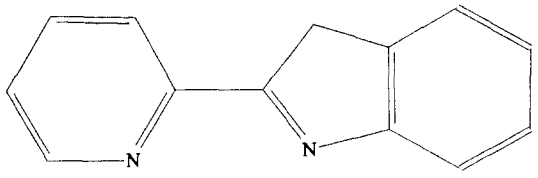
Abstract—The magnetic properties of a hexacoordinated iron(II) complex with the bidentate ligand pyridylbenzimidazole (pybzim), $[Fe(pybzim)_3](ClO_4)_2 \cdot H_2O$, (**1**), have been investigated by AC susceptometry, ^{57}Fe-Mössbauer, ESR and NMR spectroscopy. The temperature dependence of the AC magnetic susceptibility for a powder sample showed essentially diamagnetic behaviour below 85 K and paramagnetism (μ_{eff}/μ_B = 4.5–5.3, $S = 2$) above 160 K, obeying the Curie–Weiss law. Spin crossover behaviour can be found within the temperature range 90–160 K; it is centered at 141 K. The Mössbauer spectra confirm the susceptibility measurements: the area fraction of the high-spin quadrupole doublet plotted against temperature shows a curve similar to that deduced from susceptibility measurements. The complex is ESR silent in the X-band mode: neither the powder sample (77 K and 300 K) nor a methanolic solution exhibit an ESR signal. NMR measurements in methanol, acetone, nitromethane, acetonitrile and dimethylsulfoxide show an increasing magnetic moment μ_{eff}/μ_B from 1.6 (220 K, acetone) to 5.2 (325 K, DMSO), respectively. The spin-crossover transition of a freshly prepared powder sample is complete. However, time evolution causes (within months) an increasing admixture of iron(III), which was proved by magnetic susceptibility measurement, ^{57}Fe-Mössbauer, ESR and electronic spectra of the complex. Copyright © 1996 Elsevier Science Ltd

Keywords: spin-crossover; iron(II); magnetic susceptibility; Mössbauer spectra; NMR spectra; ESR spectra.

Spin-crossover phenomena ($S = 0$ to $S = 2$ transition) are well documented for various Fe^{II} complexes [1, 2]. Among them $[Fe(phen)_2(NCS)_2]$, $[Fe(phen)_2(NCSe)_2]$ and $[Fe(bpy)_2(NCS)_2]$ represent prototypes for broad studies using different experimental techniques. It should be pointed out that $[Fe(phen)_3]X_2 \cdot nH_2O$ complexes keep their spin state unchanged under temperature variation: they are either low-spin, $^1A_1$ ($S = 0$), intermediate spin, $^3T_1$ ($S = 1$) or high-spin, $^5T_2$ ($S = 2$) [3]. Generally, some asymmetry in the ligand sphere can produce an appropriate balance between the ligand field strength and the spin pairing energy leading thus to the conditions necessary for the spin crossover.

In this context it is interesting that $[Fe(pybzim)_3]X_2 \cdot nH_2O$ is a spin crossover system, which has been studied already by various techniques (pybzim = 2-(2′-pyridyl) benzimidazole, see Chart 1) [4–8]. In the solid state, however, the actual behaviour varies with the counter anion, e.g., X = BPh_4^-, BF_4^-, PF_6^-, NO_3^-, Br^-, I^- and ClO_4^- [9–12]. Also the conditions of the preparation may cause different magnetic properties [13]. Additionally, in solution the nature of the solvent affects the spin transition [14].

The perchlorate complex was prepared as a monohydrate as well as a dihydrate exhibiting different magnetic properties [11]. The monohydrate is interesting because its spin transition is rather sharp



* Authors to whom correspondence should be addressed.

and apparently complete at room temperature. This may allow industrial applications using the spin-switching technique of the monohydrate complex.

However, oxidation of iron(II) to iron(III) may occur depending on time and sample handling, and these traces may interfere with quantitative analysis of magnetic data, but are usually not accounted for. Therefore we prepared $Fe(pybzim)_3(ClO_4)_2 \cdot H_2O$ complex which was subjected to a detailed magnetochemical investigation using powder sample AC (alternating current) magnetic susceptibility measurements, Mössbauer and ESR spectroscopy. NMR and electronic spectra in solution were recorded and analyzed.

EXPERIMENTAL

Synthesis

The iron(II) salt, $Fe(ClO_4)_2 \cdot 6H_2O$, was of reagent grade (Merck). Ethanol (96%) was used as received. The ligand 2-(2′-pyridyl)benzimidazole (pybzim) was prepared according to the method of Addison [15]. A solution of $Fe(ClO_4)_2 \cdot 6H_2O$ (1 mmol, 0.363 g) in ethanol (10 cm^3) was added to a hot solution of the ligand (3 mmol, 0.586 g) in ethanol (35 cm^3). The transparent red solution was heated under stirring for approx. 30 min, then allowed to cool and crystallize. The dark Bordeaux-red solid was filtered off, washed with a small amount of ethanol and dried at 60°C. The Bordeaux-red adduct changed during drying to a pale red polycrystalline solid. Yield: 78%. Found: C, 51.1; H, 3.5; N, 14.7. Calc. for $[C_{36}H_{27}Cl_2FeN_9O_8] \cdot H_2O$: C, 50.4, H, 3.4; N, 14.7%.

IR spectra

The IR spectra were taken at room temperature in Nujol suspension using a FTIR spectrometer (Philips, model PU9800). Peaks at 3576 and 3495 cm^{-1} confirm the presence of water in the sample. No such peaks occur in pure Nujol and for the free ligand, respectively.

TGA and DSC measurements

Thermal properties were investigated by thermogravimetric (Shimadzu, model TGA-50) and calorimetric (Shimadzu, model DSC-50) measurements within the range of room temperature to 400°C (sample mass 0.70 mg). Decomposition starts at 248°C with a mass loss of 22%; the TGA curve reaches a plateau at 300°C and the decomposition continues (at 400°C with increasing temperature the mass loss is 48%). The DSC curve exhibits a sharp exothermic peak centered at 250°C indicating "an explosion" of the perchlorate. Thus no liberation of crystal water was observed.

Electronic spectroscopy

Electronic spectra were recorded at room temperature using a UV spectrometer (Carl Zeiss, model M40). As the iron(II) may be oxidized to Fe^{III}, the spectroscopic determination of the Fe^{III}/Fe^{II} ratio was based on the following principles.

(i) Phosphato ions can bind Fe^{III} into thermodynamically stable, nearly colourless phosphato-Fe^{III} complexes.
(ii) Ascorbic acid is able to reduce quantitatively Fe^{III} to Fe^{II} complexes.
(iii) The spectral characteristics of the complex $[Fe(phen)_3]^{2+}$ are well known ($\lambda_{max} = 510$ nm; $\varepsilon_{510} = 1.12$ M^{-1} μm^{-1}) and this complex is redox stable relative to oxygen.

In a methanolic solution of **1** the eventual Fe^{III} portion was first trapped by phosphoric acid. Then the content of Fe^{II} was determined by addition of an excess of solid 1,10-phenantroline and measuring the absorbance at 510 nm. Then phosphato–Fe^{III} complexes were reduced by adding solid ascorbic acid leading to the formation of $[Fe(phen)_3]^{2+}$ and the total amount of Fe^{II} was determined as above. From the difference the content of Fe^{III} results.

Magnetic susceptibility measurements

Temperature variation of the magnetic susceptibility was recorded with an AC susceptometer [16] (LakeShore, models 7221 and 7130). The experimental parameters were: $f = 666.7$ Hz, $H_{AC} = 320$ Am^{-1}, $m = 0.09405$ g, 105 data points between 77–300 K. The recorded voltage was corrected to the signal of the free sample holder (an evacuated nylon made container) positioned at the same level within the detecting coils as the sample. The measurements were done several times and they were averaged to eliminate the data scattering for these low signals.

^{57}Fe-*Mössbauer spectra*

The Mössbauer spectra were taken (4.2 K–300 K) using a conventional transmission spectrometer [17]. ^{57}Co(Rh) was used as a source and the isomer shift data are given relative to α-Fe at room temperature. The sample was measured over a period of four months and the data were analyzed by a least squares fit routine assuming Lorentzian lines.

ESR spectra

The ESR data were recorded using an X-band spectrometer (Bruker, ER 200D SRC) at room temperature as well as at 77 K.

NMR spectra

Proton NMR spectra in different solvents were recorded using a 250 MHz spectrometer (Bruker, AC 250 FT) and analyzed by the Evans method as described elsewhere [18].

RESULTS

Characterization of a freshly prepared sample

Based on the unchanged absorbance of the Fe^{II} phenanthroline complex (within experimental error $\pm 1\%$) we found that there is no detectable amount of Fe^{III} present in the freshly prepared sample.

Analogously, the absence of an ESR signal at room temperature and 77 K brings evidence that neither iron(III) nor any free radicals are present in the freshly prepared sample.

Susceptibility measurements

The recorded mass susceptibility has been converted to molar susceptibility and corrected for underlying diamagnetism with $\alpha_{dia} = -5.66 \times 10^{-9}$ m^3 mol^{-1} [19]. The molar magnetic susceptibility χ'_{mol} shows a paramagnetic ($S = 2$) behaviour of the complex from 300 to 160 K. Below 160 K, spin crossover transition occurs, leading to a reduction of χ'_{mol} (μ_{eff}) nearly to the zero at 85 K (Fig. 1). The low-temperature data (below 85 K) indicate diamagnetism ($S = 0$) within experimental error.

No hysteresis was observed in the χ'_{mol} *vs* T curve on heating/cooling within the experimental error. It can be concluded that the spin crossover in the given sample falls into "class I" of a complete and sharp interconversion [2].

The effective magnetic moment was evaluated as $\mu_{eff}/\mu_B = 798(\chi'_{mol}\ T)^{1/2}$ in SI units. Its room temperature value is calculated as $\mu_{eff}/\mu_B = 5.20$ and decreases according to a straight line down to $\mu_{eff}/\mu_B = 4.70$ at 160 K. The spin only value is $\mu_{eff}/\mu_B = 4.90$.

In order to analyze the magnetic data quantitatively three models were applied to describe the temperature dependent part of the magnetic susceptibility.

The well-known Curie–Weiss law (the model **1**) is presented in the form

$$\chi'_{mol} = C_0 g_{av}^2 [S(S+1)/3]/(T-\theta) \qquad (1)$$

where $C_0 = N_A \mu_0 \mu_B^2/k$ comprises fundamental physical constants, $S = 2$ is the spin number of the complex, θ the Weiss constant and g_{av} is the isotropic magnetogyric factor.

An application of the zero-field splitting (the model **2**) is based on the spin Hamiltonian in the form

$$\hat{H}_a = \mu_B B g_a \hat{S}_a + D[\hat{S}_z^2 - S(S+1)/3] + E(\hat{S}_x^2 - \hat{S}_y^2) \qquad (2)$$

for $a = x, y, z$. The basis set consists of five spin functions ($S = 2$). Here D represents the axial zero-field splitting parameter, which accounts for magnetic asymmetry of systems with $S > 1/2$. This causes a splitting of the spin quintet state into three sublevels: a singlet ($M_S = 0$), and two Kramers doublets ($M_S = \pm 2$) separated by D and $4D$, respectively. The rhombic zero-field splitting parameter E is usually neglected. Using this approximation the magnetic sus-

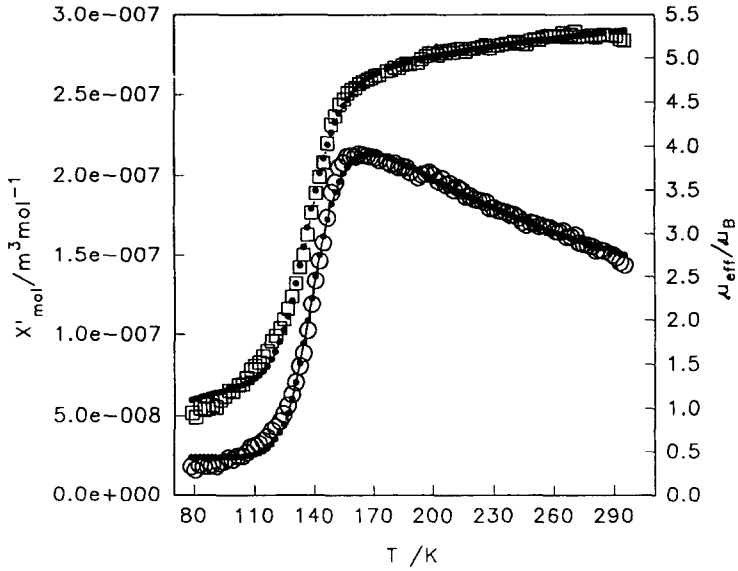


Fig. 1. Temperature variation of the molar magnetic susceptibility (χ'_{mol}, circles) and the effective magnetic moment (μ_{eff}/μ_B, squares) for **1**. Full points, theoretical fit (see text).

ceptibility components can be expressed in terms of analytic functions

$$\chi_{\parallel} = (C_0 g_{\parallel}^2/T)(2e^{-x}+8e^{-4x})/(1+2e^{-x}+2e^{-4x}) \tag{3}$$

$$\chi_{\perp} = (C_0 g_{\perp}^2/T)[(6/x)(1-e^{-x}) + (4/3x)(e^{-x}-e^{-4x})]/(1+2e^{-x}+2e^{-4x}) \tag{4}$$

with $x = D/kT$. The magnetogyric factor, in principle, is anisotropic. The average molar paramagnetic susceptibility is given by

$$\chi_{hs} = (\chi_{\parallel}+2\chi_{\perp})/3 \tag{5}$$

The last model (the model **3**) assumes a combined effect of the axial distortion due to the ligand field and spin-orbit coupling within the $^5T_2$ term with the Hamiltonian

$$\hat{H}_a = \mu_B B[G\hat{L}_a + g_a\hat{S}_a] + J_\lambda \hat{L}\cdot\hat{S} + \Delta[\hat{L}_z^2 - L(L+1)/3] \tag{6}$$

Here $G = -k$ accounts for the orbital reduction factor and its sign is given by the isomorphism between $^5T_2$ and ^5P terms [20]. The coupling parameter $J_\lambda = -k\lambda = k\xi/2S$ contains the (positive) spin-orbit coupling constant ($\xi_0 = 400$ cm^{-1} for Fe^{2+}); Δ is the axial crystal field splitting parameter. The basis set contains 15 functions as they result from the direct product of three orbital functions ($L = 1$) and five spin functions ($S = 2$). Due to the axial symmetry, two directions (a parallel, $\hat{H}_x$, and perpendicular, $\hat{H}_x = \hat{H}_y$) should be distinguished.

Attempts to reproduce the recorded susceptibility curve over the whole temperature interval were successful when the following function was considered

$$\chi'_{mol} = c_{hs}(\chi_{hs}+\alpha_{hs}) + (1-c_{hs})\alpha_{ls} \tag{7}$$

The expression $c_{hs} = f(T)$ gives the molar fraction of the high-spin complex (see later) and α_{hs} represents its temperature-independent paramagnetism. The susceptibility of the low-spin complex is expected to be positive and temperature independent, given by α_{ls} term. The temperature independent term increases with presence of low-lying excited states and therefore we assume that α_{ls} is substantial (the low-spin state has thermally accessible excited states).

Using the recorded χ'_{mol} *vs* T data the molar fraction of the high-spin complex is readily calculated as

$$c_{hs} = (\chi'_{mol}T - \chi_{ls}T)/(\chi_{hs}T - \chi_{ls}T) \tag{8}$$

with $\chi_{ls}T = 1.3\times10^{-6}$ m^3 mol^{-1} K^{-1} and $\chi_{hs}T = 44.14\times10^{-6}$ m^3 mol^{-1} K^{-1} as maximum value.

In order to fit the c_{hs} values to a smooth curve the domain model has been assumed. Although it has limitations it is probably effective in this particular case when no hysteresis is observed. The theoretical curve then becomes [21]

$$c_{hs} = 1/\{1+\exp[(n\Delta H/R)(1/T-1/T_C)]\} \tag{9}$$

Here n is the averaged number of magnetic active entities within the domain, ΔH the enthalpy and T_C the temperature of the transition, respectively.

The actual fitting procedure contains six free parameters: g_{av}, θ, $h = n\Delta H/R$, T_C, α_{hs} and α_{ls} when the Curie–Weiss law for the paramagnetic part is applied. For the zero-field splitting model we have $g_\perp$, $g_\parallel$, D, h, T_C, α_{hs} and α_{ls}. However, the g-tensor components taken as free parameters were found effectively dependent and thus we returned back to g_{av}. For the model **3** there were seven free parameters: G, J_λ, Δ, h, T_C, α_{hs} and α_{ls} (the electronic magnetogyric factor $g_{av} = 2$ was frozen). The error function to be minimized was

$$F = \sum_i (\chi_i^c - \chi_i^o)^2 \tag{10}$$

The quality of the regression was expressed by the agreement factor

$$R = \frac{\sum_i [(\chi_i^o)^2 - (\chi_i^c)^2]}{\sum_i (\chi_i^o)^2} \tag{11}$$

The final set of magnetic parameters is collected in Table 1. It should be noted that α_{hs} is determined accurately from precise high-temperature data. On the other hand, the D-parameter of the zero-field splitting at low temperature disappears, due to the spin switch to $S = 0$. Therefore, these parameters should be considered only as the first estimates. The quality of the fit is quite good for higher temperature and the deviations of theoretical and experimental data below 100 K is not critical (see Fig. 1).

The fitted high-spin molar fraction function (9), i.e. the domain model, compared with the experimental c_{hs} function (8) show limited degree of agreement (Fig. 2). Evidently, for a better description there is required a more flexible theoretical function.

As the sample under investigation was measured several times over months, a small increase in the susceptibility below 80 K was observed. Therefore, a reinvestigation of the same sample encapsulated in the sample holder for six months with temperatures down to 20 K was performed. While cooling down the susceptibility passed through a minimum and then increased like a typical paramagnet. This shows that a paramagnetic impurity (PI) gains significance with time. However, even a small paramagnetic admixture has dramatic consequences to the effective magnetic moment at low temperature, which increases considerably. This point will be discussed later.

The content of the PI has been estimated as follows. For a Curie paramagnet the plot χ'_{mol} *vs* $(1/T)$ is a straight line. Based on low temperature data only the slope of the regression line determines the Curie constant C_{mol}. This obeys the relationship

$$C_{mol} = C_0 g^2 [S(S+1)/3]\rho \tag{12}$$

where measured $C_{mol} = 1.7762\times10^{-6}$ m^3 mol^{-1} K,

Table 1. Final set of magnetic parameters

Parameter	Model-1 C-W	Model-2 ZFS	Model-3 T_{2g}+SOI+CF
g_{av}	2.039±0.004	1.951±0.004	2.000
θ K	−26.7±0.2		
D cm^{-1}		−72.8±0.2	
J, cm^{-1}			74.2
G			−0.80
Δ cm^{-1}			−617
T_C K	141.5±0.2	141.5±0.2	140.9
h K	2405±45	2399±45	2561
α_{hs} 10^{-9} m^3 mol^{-1}	27.0±0.2	30.6±0.2	37.1
α_{ls} 10^{-9} m^3 mol^{-1}	23.3±0.2	23.2±0.2	24.0
R %	2.40	2.40	2.38

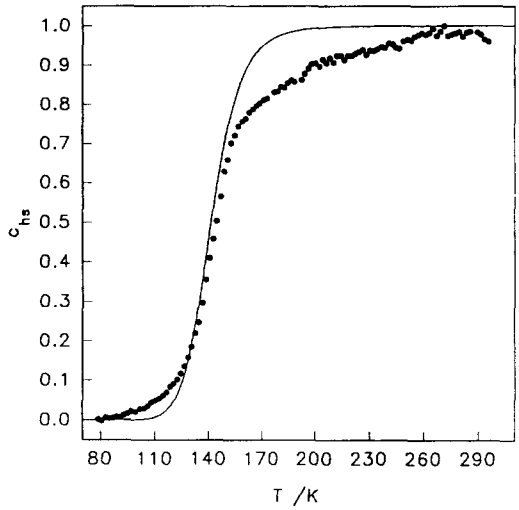


Fig. 2. Temperature variation of the molar fraction of the high-spin complex (c_{hs}, points) and the theoretical curve according to the domain model.

known $C_0 = 4.714 \times 10^{-6}$ m^3 mol^{-1} K and estimated $g = 2$ and $S = 5/2$ for the high-spin Fe^{III} evaluates the molar fraction of PI to $\rho = 0.032$.

ESR measurements

For a freshly prepared sample no ESR absorption signal was observed either at 77 K or at 300 K. This may result from rapid spin-lattice relaxation effects characteristic for Fe^{II} complexes. Also a methanolic solution of the complex is ESR silent, which may follow from the zero-field splitting: the spin quintet ($S = 2$) is split into a singlet ($M_S = 0$) and a pair of Kramers doublets ($M_S = \pm 1$ and $M_S = \pm 2$). Since the selection rule $\Delta M_S = \pm 1$ restricts the allowed transitions, the $M_S = 0$ to -1 transition is observable only at high fields or high microwave frequencies when the zero-field splitting $|D|$ is high.

Characterization of a half-year old sample

A six-month old sample was remeasured by ESR and no signal was evident at room temperature. At 77 K, however, a very broad absorption maximum appeared with the centre at $g_{eff} = 5.95$. This indicates the presence of iron(III) in the sample.

In order to determine the content of iron(III) quantitatively, the electron spectroscopic determination was repeated and 5.2% of Fe^{III} was found.

Mössbauer measurements

The Mössbauer spectra of a three and a six month old sample respectively were measured within a temperature range 4.2–295 K. They exhibit two quadrupole doublets: the former (small splitting) is associated with the $S = 0$ state whereas the latter (large splitting) corresponds to $S = 2$ (Fig. 3).

Since the intensities of the resonance lines depend upon the Debye–Waller factors for the states involved, it is difficult to measure quantitatively the fractions of the $^1A_1$ and $^5T_2$ species present at any given temperature. If we assume the two different states to have the same Debye–Waller factors, the ratio of the area under the $^5T_2$ lines to the total spectra area will give an approximate measure of the high spin species. The area fraction associated with the high-spin complex, P_{hs}, is plotted *vs* temperature (Fig. 4). The data derived from a computer fit are collected in Table 2. The spin crossover is sharp and centered at 140 K. The application of the domain model (8) to fit the P_{hs} *vs* T data yields $n\Delta H/R = 1123$ K and $T_C = 141$ K, which is in good agreement with the AC susceptibility data.

From a chemical point of view, the *s*-electrons should give the dominant contribution to the isomer shift and the *d*- and *p*-electrons to the quadrupole splitting [22]. The isomer shift of the high spin complex is more positive than that of the low spin counterpart. This can be interpreted due to different symmetry

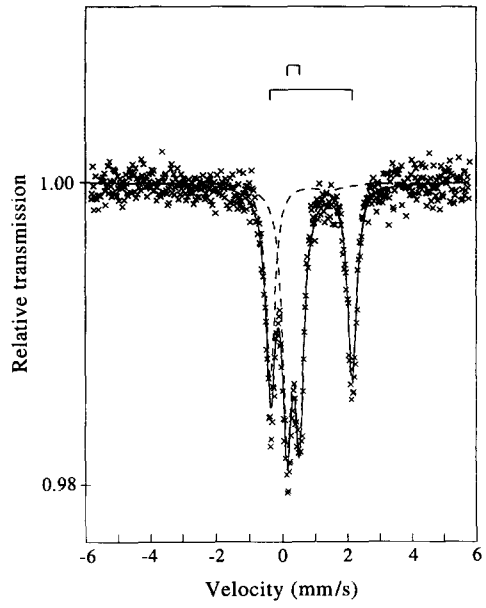


Fig. 3. Representative Mössbauer spectrum of **1** at 140 K.

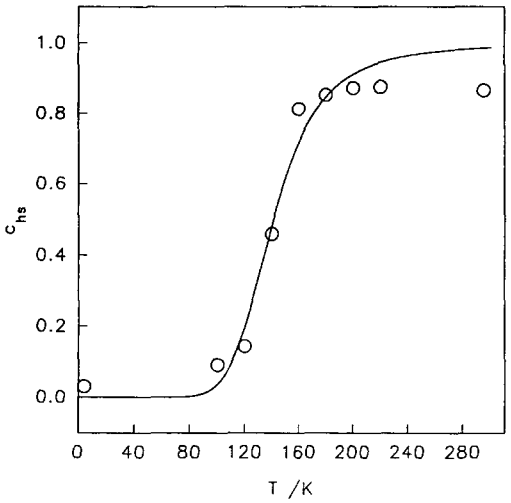


Fig. 4. Temperature dependence of the Mössbauer area fraction of the high-spin quadrupole doublet for **1**. Solid, domain model theoretical curve.

of the *d*-electrons, where asymmetry in the high spin ($^5T_2$) compared to the low spin ($^1A_1$) causes a change in the electric field gradient, i.e. decreasing *s*-electron density at the iron nucleus. This is in good agreement with known measurements.

Fe^{III} admixtures can be observed in Mössbauer experiments in concentrations at least higher than 5%. In addition, the range of isomer shift and quadrupole splitting in Fe^{II} low spin is overlapping with Fe^{III} high spin. Nevertheless, Fe^{III} high spin can be determined, because it looks like a time dependent hs/ls ratio. Remeasuring of the six months old sample allowed to estimate 6% of Fe^{III} with an isomer shift of 0.02 mm s^{-1}.

Table 2. Mössbauer data[a]

T K	ΔE_Q(hs)	ΔE_Q(ls)	δ_{hs}	δ_{ls}	P_{hs}	P_{ls}
4.2	2.44	0.43	0.93	0.38	3.0	97.0
100	2.48	0.42	0.94	0.37	9.0	91.0
120	2.55	0.41	0.95	0.36	14.3	85.7
140	2.52	0.39	0.90	0.34	45.9	54.1
160	2.45	0.83	0.96	0.03	81.3	18.7
180	2.42	0.62	0.92	0.12	85.2	14.8
200	2.30	0.28	0.88	0.33	87.2	12.8
220	2.23	0.34	0.87	0.19	87.5	12.5
295	1.96	0.32	0.83	0.15	86.5	13.5

[a] Quadrupole splitting (ΔE_Q) and isomer shift (δ, relative to Fe in Rh) in mm s^{-1} (accuracy ± 0.01 from 4.2 to 140 K, at higher temperatures ± 0.05); *P*, area fraction.

NMR measurements

NMR measurements were performed in solution, using methanol (MeOH), acetone (Ac), nitromethane (NM), acetonitrile (AN) and dimethylsulfoxide (DMSO) as solvents, at temperatures limited by solvent properties (Table 3). The temperature variation of the effective magnetic moment (evaluated by means of the Evans method) allows the conclusion that spin crossover occurs also in solution. In contrast to the solid state, the spin transition in solutions is a gradual process belonging to the "Group II" [23].

The solution measurements are complicated by two effects: (i) ligand dissociation at higher temperature, and (ii) deprotonation of the acidic imidazole N—H group. Products of the ligand dissociation, the solvated complexes of $[Fe(pybzim)_2L_2]^{2+}$, $[Fe(pybzim)L_4]^{2+}$ and $[FeL_6]^{2+}$ type possess a decreased ligand field strength manifesting itself in the stabilization of the high-spin state. A three step deprotonation will increase the electron density at the donor nitrogen atom of the imidazole ligand. This is reflected

Table 3. Magnetic moments obtained from NMR using Evans method for various solvents on $[Fe(pybzim)_3](ClO_4)_2$

T K	MeOH μ_{eff}/μ_B	Ac μ_{eff}/μ_B	AN μ_{eff}/μ_B	NM μ_{eff}/μ_B	DMSO μ_{eff}/μ_B
325					5.37
320	4.74	4.96	3.56	4.76	5.33
315					5.29
310	4.83	4.95	3.24	4.69	5.24
300	4.90	4.87	3.19	4.44	
290	4.80	4.79	3.13	4.36	
280	4.68	4.71	3.08	3.94	
270	4.57	4.46	3.02	3.88	
260	4.45	4.20			
250	4.19	3.56			
240	3.92	2.85			
230	3.64	1.97			
220	3.21	1.60			

in the strengthening of the Fe—N bond and consequently the ligand field splitting increases. The greater the ligand field strength, the better the stabilization of the low-spin rate.

In methanol the spin transition is already observable at 220 K and culminates at 300 K. Even better resolution of the spin crossover is seen in acetone (Fig. 5). In contrast, in acetonitrile only a small variation of the effective magnetic moment is seen within 270 to 320 K. In nitromethane and dimethylsulfoxide only the high-spin state is stabilized within the accessible temperature range.

DISCUSSION

As already mentioned, the complex under investigation has been characterized as a spin crossover system by several groups [9–11, 13]. An inspection of Table 4 shows that the published data differ each from other and also our set of characteristics is different. The particular factors associated with the composition and/or structure of the complex which may affect the spin-crossover are as follows:

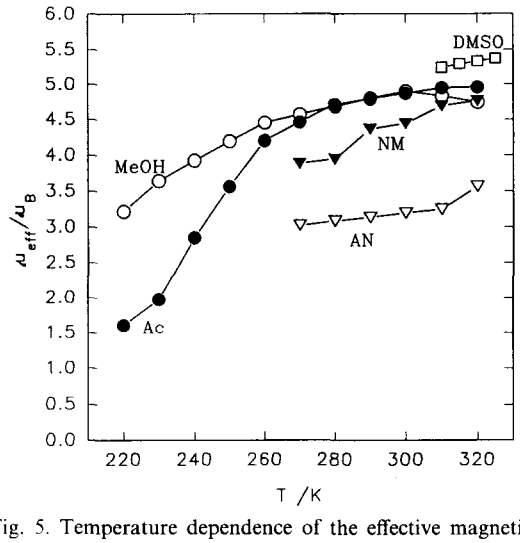


Fig. 5. Temperature dependence of the effective magnetic moment in solutions.

(i) the way of preparation, at least the presence of acidic media, can alter the acidity of the hydrogen atom associated with the imidazole nitrogen;
(ii) the variable content of water, particularly a reversible aquation and/or liberation of a second crystalline water molecule;
(iii) possible stabilization of either *mer*-, *fac*-, or both isomers of $[Fe(pybzim)_3]^{2+}$ complex;
(iv) the possible presence of Fe^{III} impurities can alter the magnetic data and their interpretation as well;
(v) the published susceptibilities correspond to the thermal equilibrium (thermal susceptibilities in the static magnetic field) as opposed to the AC susceptibility, which is a frequency (f) dependent quantity (adiabatic magnetic susceptibility) deviating from the thermal limit ($f \rightarrow 0$). To our knowledge the AC magnetic susceptibilities are always lower than their thermal equilibrium counterparts.

The arguments leading us to consider a simple zero-field splitting model (the model **2**) can be summarized as follows. The ground electronic state of the hexacoordinate Fe^{II} high-spin complexes is $^5T_{2g}$. The asymmetry of the pybzim ligand allows, in principle, the existence of two geometrical isomers; the *mer*- and *fac*-isomers having C_{2v} and C_{3v} symmetry, respectively. The magnetic-perturbation Mössbauer spectra indicate that there it is the *mer*-isomer which is present [11]. Therefore within the C_{2v} symmetry only an orbital singlet is possible so that the basis set consists of five spin functions only. The value of $D = -73$ cm^{-1} indicates a considerable zero-field splitting, consistent in sign with the negative Weiss constant for the model **1**.

The model **3** is approximately of the same quality but the parameters received have a different meaning. The most important finding is a rather high axial crystal field splitting $\Delta = -617\ cm^{-1}$ which may have a consequence that in the temperature interval concerned only the lowest (of 15) states are effectively populated. This might be a basis for the justification

Table 4. Results of various investigations on $[Fe(pybzim)_3](ClO_4)_2 \cdot nH_2O$[a]

No.	T (K)	μ_{eff}/μ_B	T (K)	μ_{eff}/μ_B	Technique	Ref.	n
1	295	5.2	90	1.3	m	[9]	m
2	298.5	5.25	85.9	3.41	torsion balance	[13]	$n = 1$
3	284.4	5.44	90.7	2.05	Gouy balance	[11]	$n = 1$
4[b]	295.2	5.20	90.6	1.01	AC susceptometer	This work	$n = 1$
5[c]	293.7	5.52	m	m	Faraday balance	This work	$n = 1$
6	m	m	80	1.3	Gouy balance	[10]	$n = 2$
7	290.3	5.23	95.0	1.29	Gouy balance	[11]	$n = 2$

[a] m, missing data.
[b] Freshly prepared sample.
[c] One year old sample.

of the model **2**. The orbital reduction factor $k = 0.8$ and the spin-orbit coupling constant $\xi = 371$ cm^{-1} (evaluated from G and J_λ values) sound very reasonable.

The temperature independent paramagnetism for the high-spin complex, however, is much higher than that expected for Fe^{II} complexes. This may have roots in the presence of an undetermined amount of a paramagnetic impurity of Fe^{III} with $S = 5/2$ which apparently raises the measured data over the whole temperature interval.

A one-year-old sample was remeasured on Faraday type balances (field $B = 1.5$ T, $T = 294$ K) and $\mu_{eff}/\mu_B = 5.52$ was found.

Despite the minor effect of different diamagnetic corrections that may have been applied for recorded susceptibility data we plotted the published susceptibility data *vs* temperature together with our data set (Fig. 6).

On first sight it is evident that the published data exhibit a minimum followed by a susceptibility increase on cooling typical for the presence of a paramagnetic impurity (PI) manifesting itself at low temperature. Having different amounts of PI, the differences in displayed magnetic moments are not surprising (Fig. 7).

The content of PI was estimated as described above: $\rho^{(13)} = 0.129$ and $\rho^{(11)} = 0.0525$ are calculated for data according to refs 13 and 11, respectively.

Thus we can conclude, that the system under study, when freshly prepared, exhibits a rather sharp spin crossover centered at 140 K, which is almost complete above 160 K. Below 100 K some residual paramagnetism remains, which can be interpreted as the temperature independent paramagnetic contribution for the low-spin state. A paramagnetic impurity represented by iron(III) appears over a period of time which enhances the paramagnetism of the sample also at low temperature and apparently increases the effective magnetic moment.

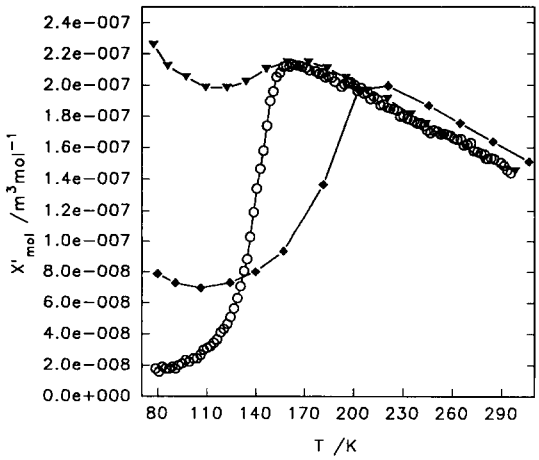


Fig. 6. Comparison of recorded molar paramagnetic susceptibilities: circles, this work (fresh sample); diamonds, according to ref. 11; triangles, ref. 13.

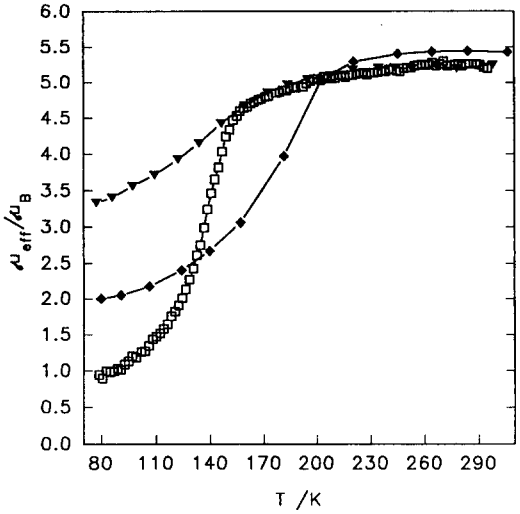


Fig. 7. Comparison of effective magnetic moments: squares, this work; diamonds, ref. 11; triangles, ref. 13.

Acknowledgements—Drs Marián Valko, Róbert Klement and Milan Mazúr (Department of Physical Chemistry, Slovak Technical University, Bratislava) are acknowledged for measurements of the ESR data. Miss Maria Attanasopoulou (Institute of Physical Chemistry, Technical University Darmstadt, FRG) is acknowledged for performing a Faraday balance measurement. The authors are grateful to the "Fond zur Förderung der wissenschaftlichen Forschung in Österreich" (project 10818), Slovak Grant Agency and to exchange program between Austria and Slovakia (project 2ÖS11) and the "Hochschuljubiläumsstiftung der Gemeinde Wien" for financial support.

REFERENCES

1. P. Gütlich, A. Hauser and H. Spiering, *Angew. Chem.* 1994, **106,** 2109.
2. E. König, *Struct. Bonding* 1991, **76,** 51.
3. P. Gütlich, *Struct. Bonding* 1981, **44,** 83.
4. J. K. Beattie and K. J. McMahon, *Aust. J. Chem.* 1988, **41,** 1315.
5. J. J. McGarvey and I. Lawthers, *J. Chem. Soc., Chem. Commun.* 1982, 906.
6. J. J. McGarvey, I. Lawthers, K. Heremans and H. Toftlund, *Inorg. Chem.* 1990, **29,** 252.
7. E. V. Dose, M. A. Hoselton, N. Sutin, M. F. Tweedle and L. J. Wilson, *J. Am. Chem. Soc.* 1978, **100,** 1141.
8. J. DiBenedetto, V. Arkle, H. A. Goodwin and P. C. Ford, *Inorg. Chem.* 1985, **24,** 455.
9. D. M. L. Goodgame, *Bull. Soc. Chim. Fr.* 1972, 3.
10. J. R. Sams, J. C. Scott and T. B. Tsin, *Chem. Phys. Lett.* 1973, **18,** 451.
11. J. R. Sams and T. B. Tsin, *J. Chem. Soc., Dalton Trans.* 1976, 488.
12. A. W. Addison, S. Burman, C. G. Wahlgren, O.

A. Rajan, T. M. Rowe and E. Sinn, *J. Chem. Soc., Dalton Trans.* 1987, 2621.
13. Y. Sasaki and T. Shigematsu, *Bull. Chem. Soc. Jpn* 1973, **46,** 3438.
14. K. A. Reeder, E. V. Dose and L. J. Wilson, *Inorg. Chem.* 1978, **17,** 1071.
15. A. W. Addison, *J. Heterocyclic Chem.* 1983, **20,** 1481.
16. R. Roča, P. Baran and L'. Dlháň, *Chem. Papers* 1994, **48,** 177.
17. W. Linert, V. Gutmann, O. Baumgartner, G. Wiesinger and H. Kirchmayer, *Inorg. Chim. Acta* 1983, **74,** 123.
18. W. Linert, M. Konecny and F. Renz, *J. Chem. Soc., Dalton Trans.* 1994, 1523.
19. E. König, in *Landolt-Börstain*, Neue Serie, Vol. 2, pp. 1–16. Springer, Berlin (1966).
20. J. S. Griffith, *The Theory of Transition-Metal Ions*, pp. 238, 356. University Press, Cambridge (1964).
21. O. Kahn, *Molecular Magnetism*, p. 67. VCH, New York (1993).
22. P. Gütlich, R. Link, A. X. Trautwein ; *Mössbauer Spectroscopy and Transition Metal Chemistry*. Springer, Berlin, Heidelberg, New York (1978).
23. E. König and S. Kremer, *Theoret. Chim. Acta* 1971, **20,** 143.

Pergamon

S0277-5387(96)00253-7

Polyhedron Vol. 16, No. 1, pp. 57–59, 1997
Copyright © 1996 Published by Elsevier Science Ltd
Printed in Great Britain. All rights reserved
0277-5387/97 $15.00+0.00

Synthesis and X-ray crystal structure of 1,2-diaminepropane platinum(II) cantharidinate

Yun-Hua Wang,[a] Zhong-Xian Huang[a]* and Guang Wu[b]

[a]Department of Chemistry, Fudan University, Shanghai 200433, P.R. China

[b]Center of Analysis and Measurement, Fudan University, Shanghai 200433, P.R. China

(Received 13 March 1996; accepted 22 May 1996)

Abstract—The 1,2-diaminepropane platinum(II) cantharidinate was synthesized by reacting sodium cantharidinate with 1,2-diaminepropane diiodo platinum(II) in aqueous solution. The crystal structure of the platinum complex was determined by X-ray diffraction. The complex is a binuclear molecule, in which each platinum ion is coordinated by two carboxylic oxygen atoms from two different cantharidinates and two amine nitrogen atoms from the same 1,2-diaminepropane molecule. The platinum(II) ion takes a typical square planar configuration. Copyright © 1996 Published by Elsevier Science Ltd

Keywords: platinum complex; cantharidine; synthesis; structure determination.

The success of cisplatin has stimulated widespread searching for more effective and lower toxicity antitumor platinum complexes [1]. By introducing an O-donor ligand as the leaving group, a series of new platinum complexes, so-called second generation anticancer drugs, have been developed. Among others the diamineplatinum(II) cyclobutyl 1,1-dicarboxylate, (carboplatin, JM-8) is the most outstanding one [2–4]. Meanwhile, if some antitumor drug can be combined into these platinum complexes as a ligand, it might produce unexpected results. Cantharidine has long been used as a Chinese medicine [5]. In the past three decades several studies showed that cantharidine and its derivatives present potential antitumor capability against lung, colon and breast cancer [6–8]. A number of platinum cantharidine complexes have been synthesized. Here we wish to report the synthesis and crystal structure of 1,2-diaminepropane platinum(II)-2,3-dimethyl-7-oxobicyclo-[2,2,1]-heptane-2,3-bicarboxylate (cantharidinate).

EXPERIMENTAL

Preparation and analysis of the complex

The title complex was prepared according to the following reactions:

$$K_2PtCl_4 + 4KI \rightarrow K_2PtI_4 + 4KCl \quad (1)$$

$$K_2PtI_4 + NH_2CH_2CH(NH_2)CH_3 \rightarrow Pt[NH_2CH_2CH(NH_2)CH_3]I_2 + 2KI \quad (2)$$

$$Pt[NH_2CH_2CH(NH_2)CH_3]I_2 + 2AgNO_3 + H_2O \rightarrow [Pt(NH_2CH_2CH(NH_2)CH_3)(H_2O)_2](NO_3)_2 + 2AgI\downarrow \quad (3)$$

$$[Pt(NH_2CH_2CH(NH_2)CH_3)(H_2O)_2](NO_3)_2 + C_6H_6O(CH_3)_2(COONa)_2 \rightarrow [Pt(NH_2CH_2CH(NH_2)CH_3)(C_6H_6O(CH_3)_2(COO)_2)] + NaNO_3. \quad (4)$$

The hydrolysis of $Pt[NH_2CH_2CH(NH_2)CH_3]I_2$ was employed in the dark for 24 h. The appropriate ligand was dissolved in NaOH with vigorous stirring; the final pH of the solution was about 6.8. The solution was stirred at 4°C and finally the pale yellowish crystal collected. Found: C, 27.7; H, 3.8; N, 5.9; Calc: 27.4; H, 4.7; N, 6.2%. $\nu_{(C=O)}$ 1600 cm^{-1}, $\nu_{(C\ O\ C)}$ 990, 920 cm^{-1}, $\nu_{(NH)}$ 3400 cm^{-1}, $\nu_{(Pt-N)}$ 410, 422 cm^{-1}.

Crystallography

$[C_{26}H_{38}N_5O_{10}NaPt_2][4H_2O]$, fw = 1065.85, monoclinic, a = 13.297(3), b = 19.089(4), c = 15.999(2) Å,

*Author to whom correspondence should be addressed.

$\beta = 103.29(2)°$, $V = 3952.2$ Å^3, space group $P2_1/a$, $Z = 4$, $D_c = 1.791$ g/cm^3, μ (M_o-K_α) = 72.16 cm^{-1}, $\lambda = 0.71073$ Å.

Data collection and processing

Data were collected on an Enraf–Nonius CAD4 diffractometer on the ω-2θ scan mode ($0 \leqslant \theta \leqslant 25°$) with graphite-monochromated M_o-K_α radiation, 5528 reflections were measured, of which 3574 reflections with $I \geqslant 3\sigma(I)$ were considered to be observed and used in the refinement. The data were corrected for Lorentz and polarization factors.

Structure analysis and refinement

The structure was solved by the heavy-atom method. The position of platinum was obtained from the Patterson function. The difference electron density map revealed all the non-hydrogen atoms. All atoms except hydrogen were refined anisotropically with full-matrix least-squares. The hydrogen atoms were assigned a common refined isotropic thermal parameter and allowed to ride on their parent atoms. The final values of R and R_w are 0.053 and 0.068, respectively.

RESULTS AND DISCUSSION

The crystal structure of the title complex is shown in Fig. 1. Selected bond lengths and bond angles are listed in Table 1. Interestingly, this is a binuclear molecule of platinum. Each platinum is coordinated by two nitrogen atoms of 1,2-diaminepropane and two oxygen atoms of carboyxlates, each one from different cantharidinate molecules. Two Pt(2)—N bond lengths are 2.073 and 2.100 Å respectively, then the Pt(2)—O bonds have almost identical lengths (2.056 and 2.052 Å). The central platinum atoms are both coordinated by two nitrogen and two oxygen atoms with essentially a square planar coordination configuration, but the two PtN_2O_2 geometries are not really identical and show different tetrahedral distortions from the normal square planar geometry. The Pt(1) plane has a square pyramidal pattern, on the other hand, the geometry around Pt(2) is very slightly puckered; the N(2′) and O(3′) atoms are above the mean $Pt(2)N_2O_2$ plane, whilst N(2′) and O(3′) lie below it (see the Table of Least-Squares Planes). The O(3′)—Pt(2)—N(2′) groups [176.2(3)°] are essentially linear. It is noteworthy that the bridging oxo-oxygen atom on the cantharidinate molecule did not participate in the coordination to the platinum ion, instead it binds to sodium, and thus strengthens the

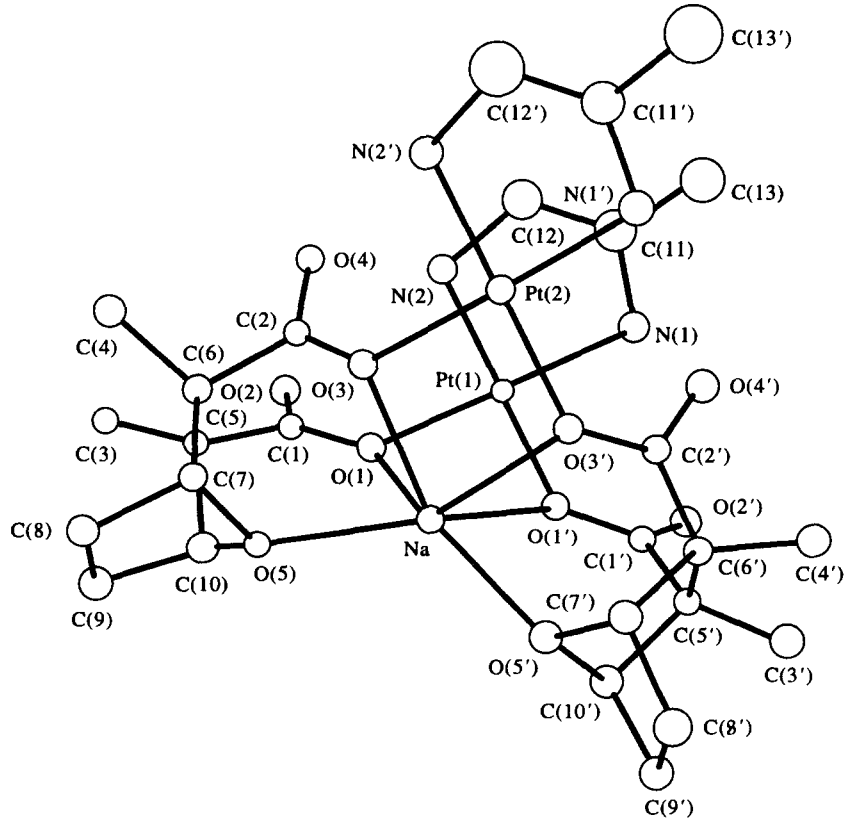


Fig. 1. View of 1,2-diaminepropane platinum(II) cantharidinate with atomic numbering.

Table 1. Selected bond lengths (Å) and angles ( )

Pt(1)—N(1)	2.085(7)	Pt(2)—N(1′)	2.100(8)
Pt(1)—N(2)	2.046(7)	Pt(2)—N(2′)	2.073(8)
Pt(1)—O(1)	2.044(5)	Pt(2)—O(3)	2.056(6)
Pt(1)—O(1′)	2.022(5)	Pt(2)—O(3′)	2.052(5)
		Na—O(1)	2.368(6)
		Na—O(1′)	2.370(6)
		Na—O(3)	2.402(6)
		Na—O(3′)	2.442(7)
		Na—O(5)	2.292(6)
		Na—O(5′)	2.301(6)
N(1)—Pt(1)—N(2)	85.6(3)	N(1′)—Pt(2)—N(2′)	86.0(3)
O(1)—Pt(1)—O(1′)	81.7(2)	O(3)—Pt(2)—O(3′)	86.0(3)
O(1)—Pt(1)—N(1)	174.2(2)	O(3)—Pt(2)—N(1′)	173.7(3)
O(1′)—Pt(1)—N(1)	96.6(2)	O(3′)—Pt(2)—N(1′)	95.4(3)
O(1)—Pt(1)—N(2)	95.5(2)	O(3)—Pt(2)—N(2′)	92.1(3)
O(1′)—Pt(1)—N(2)	173.3(2)	O(3′)—Pt(2)—N(2′)	176.2(3)
O(1)—Na—O(1′)	68.3(2)	O(1′)—Na—O(3′)	76.9(2)
O(3)—Na—O(3′)	70.7(2)	O(1′)—Na—O(3)	114.5(3)
O(5)—Na—O(5′)	121.0(2)	O(1′)—Na—O(5)	75.6(2)
O(1)—Na—O(3)	77.0(2)	O(1′)—Na—O(5)	136.8(2)
O(1)—Na—O(3′)	115.5(3)	O(3)—Na—O(5)	77.7(2)
O(1)—Na—O(5)	75.4(2)	O(3)—Na—O(5′)	142.6(2)
O(1)—Na—O(5′)	136.3(2)	O(3′)—Na—O(5′)	77.5(2)
		O(3)—Na—O(5)	142.3(2)

Na—O (carboxylate) coordination. This behaviour is different from that in the Cu-cantharidinate structure, where the bridging oxo atom is directly bound to the copper(I) ion [9].

Acknowledgement—This project is supported by the National Medicine and Drug Bureau of China.

REFERENCES

1. O. J. Vaughan, *Platinum Metals Rev.* 1993, **37,** 212.
2. L. C. Chen and Z. X. Huang, *Acta Pharmaceutica Sinica* 1989, **24,** 234.
3. L. R. Kelland, S. J. Clarke and M. J. McKeage, *Platinum Metals Rev.* 1992, **36,** 178.
4. C. F. J. Barton. *Platinum Metals Rev.* 1995, **39,** 63.
5. S. Z. Li, *Encyclopedia of Chinese Medical Herbs*, Vol. 40, p. 1528. Peoples Hygiene Press, Beijing (1957).
6. Z. Y. Cui, S. Y. Xu, S. Q. Wang, D. T. Huang and G. S. Wang, *Chinese Pharm. Bull.* 1984, **19,** 567.
7. D. H. Li, N. K. Li, S. K. Chang, X. G. Hao, R. Zhen, K. S. Ma and Z. L. Wang, *National Med. J. China* 1984, **18,** 785.
8. I. R. Shimi, Z. Zaki, S. Shoukry and A. M. Medhat, *Eur. J. Cancer Clin. Oncol.* 1982, **18,** 785.
9. Z. X. Huang, L. W. Yang, M. Q. Chen and G. Wu, *J. Mol. Sci.* 1990, **6,** 29.

Pergamon

S0277-5387(96)00268-9

Polyhedron Vol. 16, No. 1, pp. 61–65, 1997
Copyright © 1996 Elsevier Science Ltd
Printed in Great Britain. All rights reserved
0277-5387/97 $15.00+0.00

Synthesis and structures of paramagnetic organo titanium fluoride clusters†

Feng-Quan Liu,[a] Antje Künzel,[a] Axel Herzog,[a] Herbert W. Roesky,[a]* Mathias Noltemeyer,[a] Roland Fleischer[b] and Dietmar Stalke[b]*

[a]Institut für Anorganische Chemie der Universität Göttingen, Tammannstr. 4, D-37077 Göttingen, Germany

[b]Institut für Anorganische Chemie der Universität Würzburg, Am Hubland, D-97074 Würzburg, Germany

(Received 7 May 1996; accepted 20 May 1996)

Abstract—The organo titanium(IV)trifluoride $[C_5H_4(SiMe_3)]TiF_3$, **2**, has been reduced with zinc and manganese, respectively. As an intermediate product from these reactions the tetra-nuclear Ti^{III} cluster $\{[C_5H_4(SiMe_3)]_2TiF_2\}_3Ti$, **3**, has been obtained. By oxidative fluorination using AgF complex **3** was converted to the titanium(IV) complex $[C_5H_4(SiMe_3)]_2TiF_2$. Reduction of $(C_5H_5)_2TiF_2$ with gallium led to the formation of $[(C_5H_5)_2TiF_2]_3Ga$, **7**. Copyright © 1996 Elsevier Science Ltd

Keywords: organometallic; titanium; cluster; fluoride.

Recently, the reduction of cyclopentadienyl substituted titanium trifluorides has been carried out for the first time. In contrast to the analogous reduction of the corresponding titanium chlorides reaction intermediates were isolated and have been characterised by X-ray structural analysis. The use of activated alkali- and alkaline earth metals in the reaction using $Cp'TiF_3$ ($Cp' = C_5H_4(SiMe_3)$, C_5H_4Me, C_5H_5) leads to the formation of clusters with varying molecular size [1, 2]. The clusters possess $Cp'TiF_2$ units which are connected by alkali- and alkaline earth fluorides. The molecules demonstrate that molecular solids such as NaF, MgF_2 and CaF_2 can be used as ligands in organometallic chemistry. However, the reduction of titanocene difluoride using aluminium resulted in the generation of the complex $[(C_5H_5)_2TiF_2]_3Al$, **1** [3]. This result demonstrates that the number of organic substituents at the titanium center can act as a tuning factor in determining the size of the clusters. Herein we report on the reduction of the half-sandwich fluorides of titanium using transition metals and the reaction of titanocene difluoride with gallium.

RESULTS AND DISCUSSION

As described previously the reaction of $HgCl_2$ activated zinc with $(C_5Me_5)TiCl_3$ leads exclusively to the titanium(III) complex $(C_5Me_5)TiCl_2$ [4, 5]. In contrast to this result we found that no reaction takes place using the corresponding titanium fluoride $(C_5Me_5)TiF_3$ and zinc under the same reaction conditions. Obviously $(C_5Me_5)TiF_3$ has a higher reduction potential compared to the chloro derivative and hence cannot be reduced by zinc. The reducing potential can be altered by changing the coordinated ligand ($C_5Me_5 \rightarrow C_5H_4(SiMe_3)$). Indeed, $[C_5H_4(SiMe_3)]TiF_3$, **2**, and an excess of zinc in THF react within 2 days to give a green–blue solution from which blue crystals were obtained after condensing a small amount of hexane onto the reaction mixture. Unexpectedly the mass spectrum of the blue crystals showed fragments for $[C_5H_4(SiMe_3)]_2TiF$ (341, 64%) and $[C_5H_4(SiMe_3)]_2TiF$ minus methyl (326) as the base peak indicating that these titanocene(III) fluoride moieties are the building blocks of the product. Accordingly,

* Authors to whom correspondence should be addressed.

† Dedicated to Professor Erwin Weiß on the occasion of his 70th birthday.

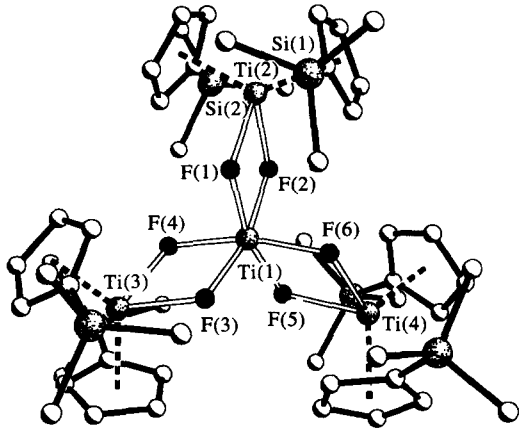


Fig. 1. Molecular structure of $\{[C_5H_4(SiMe_3)]_2TiF_2\}_3Ti$, **3**, average bond length (Å) and angles (°) (Cp′ = $C_5H_4(SiMe_3)$-centroid): Ti(1)—F 1.974(2), Ti(2),(3),(4)—F 2.097(2), Ti—Cp′ 2.045(2); F—Ti(1)—F (inside the Ti_2F_2 kite shaped four-membered rings) 75.6(1), F(equatorial)—Ti(1)—F (equatorial) 95.3(1), F(axial)—Ti(1)—F(axial) 165.0(1), F—Ti(2),(3),(4)—F 70.5, Cp′—Ti—Cp′ 133.9(1).

$[C_5H_4(SiMe_3)]_2TiF_2$ could be obtained after oxidative fluorination using AgF. The sublimation point as well as the mass, ^1H and ^{19}F NMR spectroscopic data of $[C_5H_4(SiMe_3)]_2TiF_2$ are in agreement with those given in the literature [6].

The X-ray structural analysis of the blue crystals reveals three $[C_5H_4(SiMe_3)]_2TiF_2$ moieties arranged around a central titanium atom (Ti(1)) in a propeller blade geometry (Fig. 1).

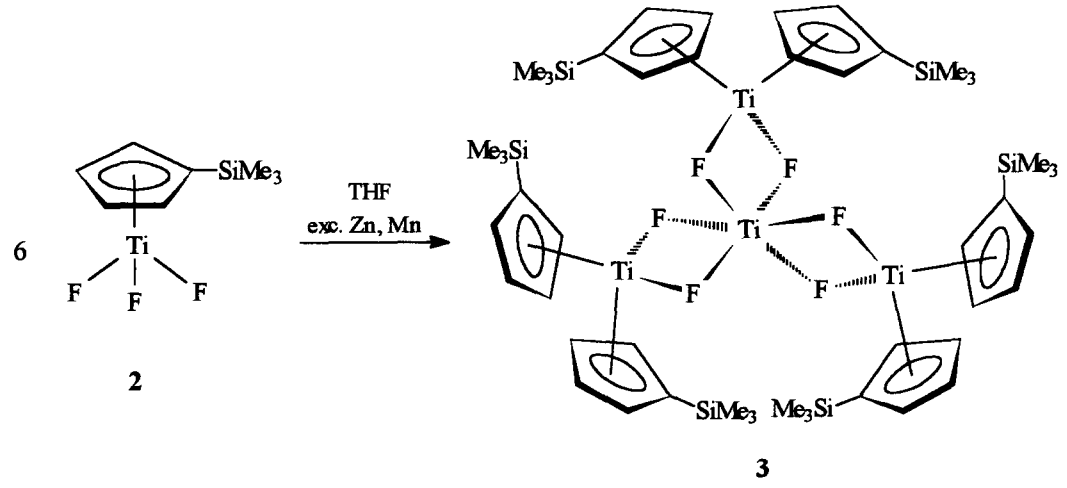
The central Ti(1) atom in $\{[C_5H_4(SiMe_3)]_2TiF_2\}_3Ti$, **3**, is coordinated to six μ_2 bridging fluorine atoms to give a distorted octahedral TiF_6 polyhedron. **3** is isotype to $[(C_5H_5)_2TiF_2]_3Ti$, **4**, although C_3 symmetry is prevented due to the trimethylsilyl substituents at the C_5 perimeter of the cyclopentadienyl ligand. **4** can be obtained in the reaction of $(C_5H_5)_2TiF_2$, **5**, with $(C_5H_5)_2Ti(CO)_2$ in the molar ratio of 1 : 1 [3]. Remarkably, the central Ti(1)—F bonds are 0.12 Å (av. 1.974(2)) shorter than the Ti—F bonds in the periphery (av. Ti(2),(3),(4)—F 2.097(2)), although one might have expected the opposite because of sterical crowding. However, both values are in good accordance with the related distances in **4**. The mean "propeller blade angle" in **3** (the intersection angle of the orthogonals of the best Ti_2F_2 planes) of 82.7° is very similar to that in **4** (86.5°).

Complex **3** can also be obtained when **2** is reacted with activated manganese under the same reaction conditions as those used for the reduction of **2** with zinc.

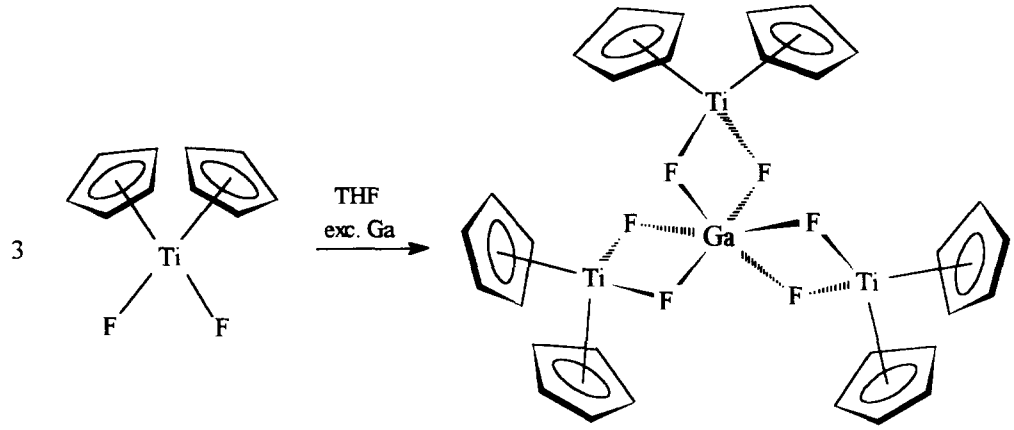
To the best of our knowledge the migration of the $C_5H_4(SiMe_3)$ substituent to a metal center of a half sandwich complex forming a metallocene unit is reported herein for the first time. The opposite case, the detachment of one of the C_5H_5 rings of metallocenes in redox processes is well known, e.g. in the formation of mono cyclopentadienyl substituted titanium oxygen and sulfur clusters from the oxidation reactions of $(C_5H_5)_2Ti(CO)_2$ with H_2O [7, 8] and H_2S, respectively [9].

It is noteworthy that the direct synthesis of **3** from the reduction of $[C_5H_4(SiMe_3)]_2TiF_2$ using activated titanium fails. On the other hand, the reduction of $(C_5H_5)_2TiF_2$, **5**, and $(C_5H_4Me)_2TiF_2$ with activated aluminium leads to complexes **1** and $[(C_5H_4Me)_2TiF_2]_3Al$, **6**, respectively [3]. The single crystal structure analysis reveals **6** to be similar to the structure determined for **3** and **4**: the TiF_6 octahedron is replaced by an AlF_6 octahedron. Obviously, the driving force for the formation of **6** is the excess of heat of formation energy resulting from the formation of the aluminium–fluorine bonds. This way of stabilisation is in contrast to that observed for the formation of the reduction product when zinc and manganese were used as reducing agents.

In order to achieve the minimum energy of the metal–fluorine bond which is necessary to incorporate



Scheme 1.



5 7

Scheme 2.

a certain metal into the complex we aimed at reacting gallium and indium with **5**. While gallium metal reacts with **5** to give the expected product $[(C_5H_5)_2TiF_2]_3Ga$, **7**, the reducing power of elemental indium apparently is not high enough to promote the related reaction.

Single crystals of **7** suitable for X-ray diffraction were obtained from n-hexane/THF solution. **7** crystallises in the space group $R\bar{3}c$ with the central gallium atom on the $\bar{3}$ axis. This axis can be regarded as the shaft of the propeller molecule. The structure of **7** in the solid state is analogous to that of **1** revealing the distorted GaF_6 octahedron as the central unit (Fig. 2).

The gallium–fluorine distances are about 0.10 Å longer than the related aluminum–fluorine bonds in **1** while the titanium–fluorine distances in both complexes **1** (mean 2.095 Å) and **7** (2.106 Å) differ only marginally. The distances of the titanium atoms in **3** and **7** to the center of the C_5 perimeters are almost identical, and hence not affected by the presence of silyl substituents. The planes of the three four-membered GaF_2Ti propeller blades intersect at an angle of 85.3°.

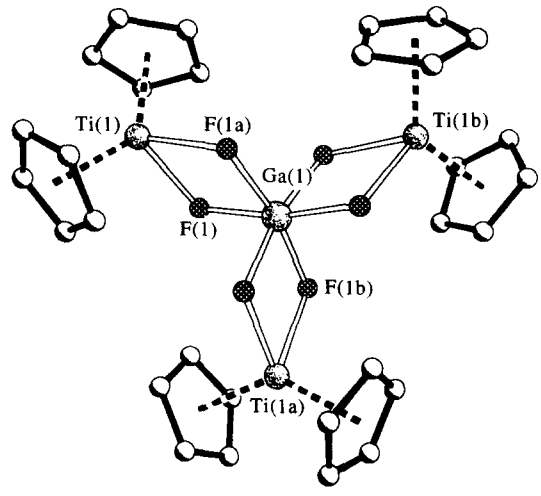


Fig. 2. Molecular structure of $[(C_5H_5)_2TiF_2]_3Ga$, **7**, bond length (Å) and angles (°) (Cp = C_5H_5-centroid): av. Ga(1)—F 1.912(2), Ti(1)—F(1) 2.106(2), Ti(1)—Cp 2.052(1); F(1)—Ga(1)—F(1a) (inside the GaF_2Ti kite-shaped four-membered rings) 78.4(1), F(equatorial)—Ga(1)—F(equatorial) 94.1(1), F(axial)—Ga(1)—F(axial) 168.7(1), F(1)—Ti(1)—F(1a) 70.0(1), Cp—Ti—Cp 134.5(1).

In spite of the fact that these complexes are paramagnetic, (as can be verified from their ESR signals [10]) reasonably sharp resonances (especially **3**) in the ^1H and ^{19}F NMR experiment were obtained. The chemical shifts are within the expected regions. However, for **7** just a broad singlet in the ^{19}F NMR spectrum could be detected. Related NMR measurements for the previously discussed complexes **4** and **6** have not been carried out. The result leads to the conclusion that the mean electron contribution at the titanium centers in **3** need to be unsymmetric.

EXPERIMENTAL

Materials and measurements

All manipulations were carried out under argon using standard Schlenk techniques. Elemental zinc, manganese and gallium as well as mercury(II)chloride and silver fluoride were used as purchased (Aldrich). $[C_5H_4(SiMe_3)]TiF_3$, **2** [11], and $(C_5H_5)_2TiF_2$, **5** [11], were prepared according to literature methods. IR spectra were obtained on a Perkin–Elmer Bio-Rad FTS-7 spectrophotometer as Nujol mulls between KBr plates, NMR spectra on Bruker AM 250 and WP 80 SY, mass spectra on Finnigan MAT 8230 and Varian MAT CH 5. Micro analyses were performed at the analytical laboratory of the Institut für Anorganische Chemie Göttingen and the Mikroanalytisches Laboratorium Beller, Göttingen.

Synthesis of $\{[C_5H_4(SiMe_3)]_2TiF_2\}_3Ti$, **3**

A solution of $[C_5H_4(SiMe_3)]TiF_3$ (0.97 g, 4.0 mmol) in THF (40 cm^3) was added to zinc and manganese powder (about 8.0 mmol), respectively, which has been activated by stirring with $HgCl_2$ (2 mg) for several hours in THF (20 cm^3). The mixture was stirred for 2 days at ambient temperature. During this time the colour of the solution changed from yellow–orange to blue. The solution was concentrated to 20 cm^3 and, after addition of n-hexane (60 cm^3), filtered through celite. The filtrate was concentrated again to 30 cm^3 and kept at 0°C for 2 days to afford the product as blue crystals. Yield: 50% (Zn), 80% (Mn). M.p. 335°C (decomp). Found: C, 51.0; H, 7.0; F, 9.9. $C_{48}H_{78}F_6Si_6Ti_4$ requires: C, 51.1; H, 6.9; F, 10.1%. IR: 3043 m, 1248 s, 1176 s, 1058 s, 906 s, 873 s, 813 s, 756 s, 492 s, 403 s cm^{-1}. MS (EI): 360 $\{[C_5H_4(SiMe_3)]_2TiF_2$, 8%$\}$, 341 $\{[C_5H_4(SiMe_3)]_2TiF$, 64%$\}$, 326 $\{[C_5H_4(SiMe_3)]_2$ TiF—Me, 100%$\}$. ^1H NMR ($CDCl_3$, TMS): 6.55–6.44 (m, 4H), 0.21 (s, 9H) ppm. ^{19}F NMR ($CDCl_3$, $CFCl_3$): 72 ppm.

Synthesis of $[(C_5H_5)_2TiF_2]_3Ga$, **7**

A suspension of $(C_5H_5)_2TiF_2$ (0.50 g, 2.3 mmol) in THF (30 cm^3) was added to a mixture of gallium (0.56 g, 8.0 mmol) and $HgCl_2$ (2 mg) in THF (30 cm^3) which has been stirred for activation for several hours. The reaction mixture was stirred for 3 days during which time the colour of the solution turned from yellow to blue. The solution was separated from surplus gallium by filtration through celite and concentrated to 20 cm^3. Blue crystals of the product are formed when n-hexane (20 cm^3) was condensed slowly to the solution. Yield: 0.65 g (39%). M.p. 335°C (decomp). Found: C, 49.2; H, 4.8; F, 16.5. $C_{30}H_{30}F_6Ti_4Ga$ requires: C, 50.1; H, 4.2; F, 15.9%. IR: 3110 m, 1013 m, 805 s, 489 s, 404 s, 379 m, 354 m cm^{-1}. MS (EI): 216 $[(C_5H_5)_2TiF_2$, 52%$]$, 197 $[(C_5H_5)_2TiF_2$—F, 100%$]$. ^{19}F NMR ($CDCl_3$, $CFCl_3$): 92 (broad) ppm.

X-ray data collection, structure solution and refinement

Intensities for all structures were collected on a Stoe-Siemens-AED instrument with graphite-monochromated Mo-K_α radiation (λ = 71.073 pm). Data were collected from oil-coated rapidly cooled crystals [12] at low temperatures with a profile-fitted method [13]. The structures were solved by direct methods with SHELXS-90 [14]. All structures were refined by full-matrix least-squares procedures on F^2, using SHELXL-96 [15]. The hydrogen atoms were geometrically idealized and refined using a riding model. The disorder of one of the six Me_3Si- groups present in **3** over two positions was refined by using distance similarity restraints. Relevant crystallographic data for **3** and **7** are listed in Table 1. Further details on the crystal structure analysis are available on request from the Director of the Cambridge Crystallographic Data Centre, 12 Union Road, Cambridge CB2 1EZ, U.K. by quoting the full journal citation.

Table 1. Crystallographic data for **3** and **7**

	3	**7**
Formula	$C_{48}H_{78}F_6Si_6Ti_4$	$C_{36}H_{30}F_6GaTi_3$
fw	1129.24	790.02
Temperature (K)	193(2)	153(2)
Crystal size (mm)	0.5 × 0.4 × 0.4	0.5 × 0.5 × 0.4
Space group	$P\bar{1}$	$R\bar{3}c$
a (Å)	12.094(1)	16.242(1)
b (Å)	12.665(1)	16.242(1)
c (Å)	20.358(2)	21.308(3)
α (°)	77.442(6)	90
β (°)	84.082(7)	90
γ (°)	74.291(7)	120
V (nm^3)	2.9268(5)	4.8680(8)
Z	2	6
ρ_c (Mg m^{-3})	1.281	1.617
μ (mm^{-1})	0.698	1.593
F (000)	1184	2382
2θ range (°)	8–45	8–45
No. of measured reflections	14040	3169
No. of unique reflections	7655	716
$R1(I > 2\sigma(I))$	0.033	0.027
$wR2^a$ (all data)	0.080	0.077
g1/g2^b	0.0323/1.9015	0.0300/19.5000
Ref. parameters/ restraints	608/72	83/0
Max. dif. peak/hole (e nm^{-3})	286/−265	360/−510

$^a wR2 = \{[\Sigma w(F_c^2 - F_o^2)]^2/[\Sigma w(F_o^2)^2]\}^{1/2}$.
$^b w^{-1} = \sigma^2(F_o^2) + (g1 \times P)^2 + g2 \times P$; $= [F_o^2 + 2F_c^2]/3$.

Acknowledgements—Financial support from the Bundesministerium für Bildung und Forschung (BMBF), the Deutsche Forschungsgemeinschaft (DFG), the Fonds der Chemischen Industrie, the Volkswagen-Stiftung Niedersachsen and the Hoechst AG is gratefully acknowledged.

REFERENCES

1. F.-Q. Liu, A. Kuhn, R. Herbst-Irmer, D. Stalke and H. W. Roesky, *Angew. Chem.* 1994, **106**, 577; *Angew. Chem. Int. Ed. Engl.* 1994, **33**, 555.
2. F.-Q. Liu, D. Stalke and H. W. Roesky, *Angew. Chem.* 1995, **107**, 2004; *Angew. Chem. Int. Ed. Engl.* 1995, **34**, 1872.
3. F.-Q. Liu, H. Gornitzka, D. Stalke and H. W. Roesky, *Angew. Chem.* 1993, **105**, 447; *Angew. Chem. Int. Ed. Engl.* 1993, **32**, 441.

4. C. R. Lucas and M. L. H. Green, *Inorg. Chem.* 1976, **16**, 237.
5. J. Nieman, J. W. Pattiasina and J. H. Teuben, *J. Organomet. Chem.* 1984, **262**, 157.
6. H. Köpf and N. Klouras, *Chemica Scripta* 1982, **19**, 122.
7. J. C. Huffman, J. G. Stone, W. C. Krusell and K. G. Caulton, *J. Am. Chem. Soc.* 1977, **99**, 5829.
8. F. Bottomley, D. F. Drummond, G. O. Egharevba and P. S. White, *Organometallics* 1986, **5**, 1620.
9. F. Bottomley, G. O. Egharevba and P. S. White, *J. Am. Chem. Soc.* 1985, **107**, 4353.
10. We thank Dr D. Marsh, Max-Planck-Institut für Biophysikalische Chemie, Göttingen, for recording the ESR specta.
11. A. Herzog, F.-Q. Liu, H. W. Roesky, A. Demsar, K. Keller, M. Noltemeyer and F. Pauer, *Organometallics* 1994, **13**, 1251.
12. T. Kottke and D. Stalke, *J. Appl. Crystallogr.* 1993, **26**, 615.
13. W. Clegg, *Acta Cryst. Sect. A* 1981, **37**, 22.
14. G. M. Sheldrick, *Acta Cryst. Sect. A* 1990, **46**, 467.
15. G. M. Sheldrick, *SHELXL-96 Program for Crystal Refinement*. University of Göttingen, Germany (1996).

Pergamon

S0277-5387(96)00266-5

Polyhedron Vol. 16, No. 1, pp. 67–70, 1997
Copyright © 1996 Elsevier Science Ltd
Printed in Great Britain. All rights reserved
0277-5387/97 $15.00+0.00

Structure and ^{1}H NMR study of copper(I) complex with ethylene and tetramethylethylenediamine

Yusaku Suenaga,[a]* Liang Ping Wu,[a] Takayoshi Kuroda-sowa,[a] Megumu Munakata[a]* and Masahiko Maekawa[b]

[a]Department of Chemistry, Kinki University, Kowakae, Higashi-Osaka, Osaka 577, Japan

[b]Research Institute for Science and Technology, Kinki University, Kowakae, Higashi-Osaka, Osaka 577, Japan

(Received 19 April 1996; accepted 20 May 1996)

Abstract—A ternary copper(I) complex with ethylene and tetramethylethylenediamine(tmen) has been prepared and the structure characterized by the single crystal X-ray method. The copper atom is coordinated to two nitrogen atoms of tmen and an ethylene molecule in a trigonal-planar arrangement. The C=C bond distance of 1.36(1) Å is slightly longer than that of the free ethylene (1.335 Å). In the ^{1}H NMR study, chemical shifts of ethylene protons at 5.46 ppm move upfield (4.16 ppm) upon coordination to copper(I). This indicates that the π back donation from copper to the ethylene is rather weak compared with other metal–ethylene systems. Copyright © 1996 Elsevier Science Ltd

Keywords: crystal structure; copper(I) complex; copper(I)-ethylene bonding; tetramethylethylenediamine; ^{1}H NMR.

The nature of metal-olefin bonding has been the subject of numerous theoretical studies [1–3]. The Dewar–Chatt–Duncanson concept [4] regarding olefins as σ donors and π acceptors has been used to explain most of the features observed in olefin bondings and shown to be readily applicable to the bonding of other types of unsaturated molecules.

We are interested in whether σ donation or π back-donation is dominant in the olefin complexes of copper(I) from its bonding difference with aromatic N-ligand and aliphatic N-ligand [5]. Some ethylene complexes of copper(I) with aromatic N-ligand have been characterized by the single crystal X-ray method [6] but no aliphatic N-ligand. It has been reported that π back-donation in the Cu–ethylene bond of ternary copper(I) complexes $[Cu(biL)(C_2H_4)]^+$ is promoted with increasing basicity of biL, where biL is 1,10-phenanthroline or its derivatives [5]. In this paper, we report the synthesis and structure of a copper(I) ethylene complex with an aliphatic N-ligand tetramethylenediamine(tmen), $[Cu(tmen)(C_2H_4)]ClO_4$. The nature of the copper(I) ethylene bonding is also discussed.

EXPERIMENTAL

General

The preparation was carried out under dry, purified nitrogen and ethylene by using the standard Schlenk or vacuum line technique. Tetrakis(acetonitrile) copper(I) perchlorate was prepared according to the literature procedures [8]. Ethanol treated with Mg/I_2 was refluxed for 5 h. Acetonitrile was purified according to the literature procedure [9]. Reagent grade tetramethylethylenediamine(tmen) was obtained from Wako Pure Chemical, Inc. All other chemicals were of reagent grade and used without further purification.

Synthesis of $[Cu(tmen)(C_2H_4)]ClO_4$

Tmen (22.5 cm^3, 30 mmol) was added to a solution of tetrakis(acetonitrile)copper(I) perchlorate (55.9 mg,

* Authors to whom correspondence should be addressed.

Table 1. Crystallographic data for $[Cu(tmen)(C_2H_4)]ClO_4$

Empirical formula	$C_8H_{20}N_2CuClO_4$
Formula weight	307.26
Color; habit	colorless brick
Crystal size (mm)	$0.30 \times 0.30 \times 0.25$
Crystal system	monoclinic
Space group	$C2$
a (Å)	14.753(4)
b (Å)	7.151(4)
c (Å)	14.132(5)
β (°)	112.03(2)
V (Å^3)	1382(2)
Z	4
Density (calc.) (g cm^{-3})	1.477
F (000)	640
λ (Å)	0.71069 (Mo-K_α)
μ (cm^{-1})	17.79 (Mo-K_α)
Scan method	ω-2θ
Scan speed (° min)	8
2θ range (°)	$1.73+0.30\tan\theta$
No. reflections measured	1216 (total), 1158 (unique)
No. observed reflections	1021 ($I = 3\sigma(I)$)
R	0.039
R_w	0.049

30 mmol) in ethanol (5.0 cm^3) under ethylene at 0°C. The colorless solution was sealed in a glass tube and left standing at 5°C. After 2 days, colorless crystals of the complex suitable for X-ray diffraction studies were obtained which were filtered off and dried under ethylene gas. Found: C, 31.4; H, 6.2; N, 9.3. Calc. for $C_8H_{20}N_2CuClO_4$: C, 31.3; H, 6.6; N, 9.1%.

X-ray structure analysis

A crystal was coated with paraffin to avoid decomposition in the air. Diffraction data were obtained on a Rigaku AFC-6S four-circle diffractometer. Crystal data and details of measurements for the compound are summarized in Table 1. Three standard reflections were monitored every 100 measurements, and the decay of their intensities was within 5%. Reflection data were corrected for Lorentz and polarization effects. Empirical absorption corrections were applied.

The structure was solved by the heavy-atom method and refined anisotropically for non-hydrogen atoms by full-matrix least-squares calculations. Reliability factors are defined as $R = \Sigma(|F_o| - |F_c|)/\Sigma(|F_o|)$ and $R_w = \{\Sigma w(|F_o| - |F_c|)^2/\Sigma w|F_c|^2\}^{1/2}$. All hydrogen atoms were placed in calculated positions, but their parameters were not refined.

Atomic scattering factors and anomalous dispersion terms were taken from the usual sources. The calculations were performed on the FACOM M 780 computer at Data Processing Center of Kyoto University by using the programme system TEXSAN.

Selected bond distances and angles are listed in Table 2.

^{1}H NMR spectroscopy

^{1}H NMR spectra were obtained in $(CD_3)_2CO$ at 200 MHz with a JEOL FX-200 NMR spectrometer, and chemical shifts are given in ppm relative to tetramethylsilane as an internal reference.

RESULTS AND DISCUSSION

Molecular structure

The molecular structure of $[Cu(tmen)(C_2H_4)]ClO_4$ together with the atomic numbering scheme is given in Fig. 1. The structure consists of a discrete monomeric $[Cu(tmen)(C_2H_4)]^+$ cation and an uncoordinated perchlorate anion. Each copper(I) ion involves a trigonal planar coordination environment comprising two N atoms of tmen and one molecule of ethylene. The perchlorate anion is not coordinated to the copper atom as the closest contact between its oxygen and the metal centre is 3.124(9) Å. The averaged Cu—C(olefin) distances of 1.96 Å is in the range of 1.93–2.07 Å observed in the previously reported ternary copper(I) complexes Cu(biL) $(C_2H_4)ClO_4$ where biL is an aromatic nitrogenous ligand such as 2,2′-dipyridine, or 1,10-phenanthroline [7].

The C=C distance of 1.36(1) Å found in [Cu

Table 2. Selected bond lengths (Å) and bond angles (°) for $[Cu(tmen)(C_2H_4)]ClO_4$

Cu(1)—C(7)	1.95(1)	Cu(1)—C(3)	1.969(9)
Cu(1)—N(1)	2.010(6)	Cu(1)—N(2)	2.037(7)
C(2)—C(1)	1.38(2)	C(1)—N(1)	1.44(2)
C(2)—N(2)	1.44(1)	C(8)—N(1)	1.49(2)
C(4)—N(1)	1.49(1)	C(6)—N(2)	1.46(1)
C(5)—N(2)	1.50(1)	C(7)—C(3)	1.36(1)
C(7)—Cu(1)—C(3)	40.6(4)	C(7)—Cu(1)—N(1)	116.1(4)
C(7)—Cu(1)—N(2)	155.2(4)	C(3)—Cu(1)—N(1)	156.7(4)
C(3)—Cu(1)—N(2)	114.6(4)	N(1)—Cu(1)—N(2)	88.7(3)

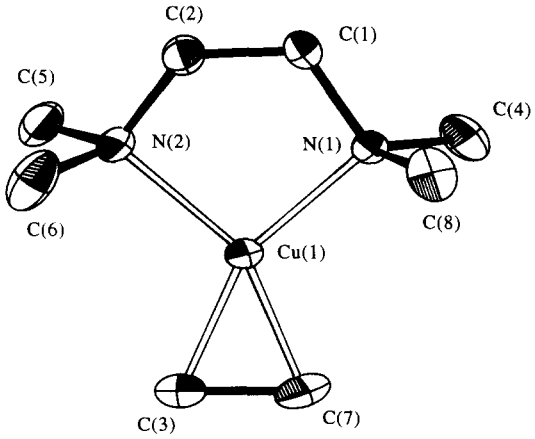


Fig. 1. Molecular structure of $[Cu(tmen)(C_2H_4)]^+$.

$(tmen)(C_2H_4)]ClO_4$ is slightly longer than that for the free ethylene molecule (1.335 Å (average)), but compares well with those in $[Cu(bpy)(C_2H_4)]ClO_4$ (1.346–1.360 Å), [7], and $[Cu(phen)(C_2H_4)]ClO_4$ (1.361 Å) [7]. Ethylene exhibits a C=C stretching frequency coupled with $\delta_s(CH_2)$ at 1623 cm^{-1}, whereas the copper(I) ethylene complex with tmen shows the stretching frequency at 1525 cm^{-1} upon coordination. The decreasing of the C=C stretching frequency is thought to correspond roughly to the increase in the π character of the double bond [10], which will be discussed in the following section.

^1H *NMR spectra*

^1H NMR spectra of tmen, ethylene, and $[Cu(tmen)(C_2H_4)]^+$ at −90°C are shown in Fig. 2. The resonances of free tmen at 2.29 ppm(1-H) and 3.83 ppm(2-H) shifted to 2.73 ppm and 3.78 ppm in the ethylene complex, respectively. Such a downfield shift of the resonances of tmen is generally observed with coordination to a metal ion [5,11,16]. In contrast, the resonance of the olefinic protons of ethylene at 5.43 ppm moves upfield (to 4.16 ppm) upon coordination. This agrees with the trend that olefin π complexation for most transition metals results in shielding of the olefinic protons. The ^1H NMR chemical shifts of the olefinic protons with the other ternary Cu^I complexes of aromatic nitrogenous ligands are 4.84 ppm for $[Cu(bpy)(C_2H_4)]^+$, 5.02 ppm for $[Cu(phen)(C_2H_4)]^+$ [5,11]. The ^1H NMR spectra of the present complex demonstrate the formation of the ternary copper(I) complex with ethylene and tmen in solution.

The ^1H NMR resonances of the olefinic protons in these ternary systems shifting upfield is due to increased shielding of the protons caused by the π back-donation. The magnitude of this shift is dependent on basicity of the N-ligands (aromatic) as described above [5]. It is expected from this fact that the upfield shifts in ternary Cu^I ethylene complexes with aliphatic N-ligand tmen should be larger compared with the aromatic N-ligands, because the pK_a value (basicity) for tmen ($pK_{a1} = 9.15$, $pK_{a2} = 5.91$, the average value = 7.53) is generally higher than that for phen and its derivatives ($pK_a = 4.10$–6.58). In fact the chemical shift for the former indicates a larger upfield shift (4.16 ppm) than for the latter (4.72–5.34 ppm). The results clearly indicate that the σ donation of the tmen nitrogens to copper(I) is enhanced as the nitrogen basicity increases and the resulting electron-rich copper promotes π back-donation in the copper–ethylene bonding.

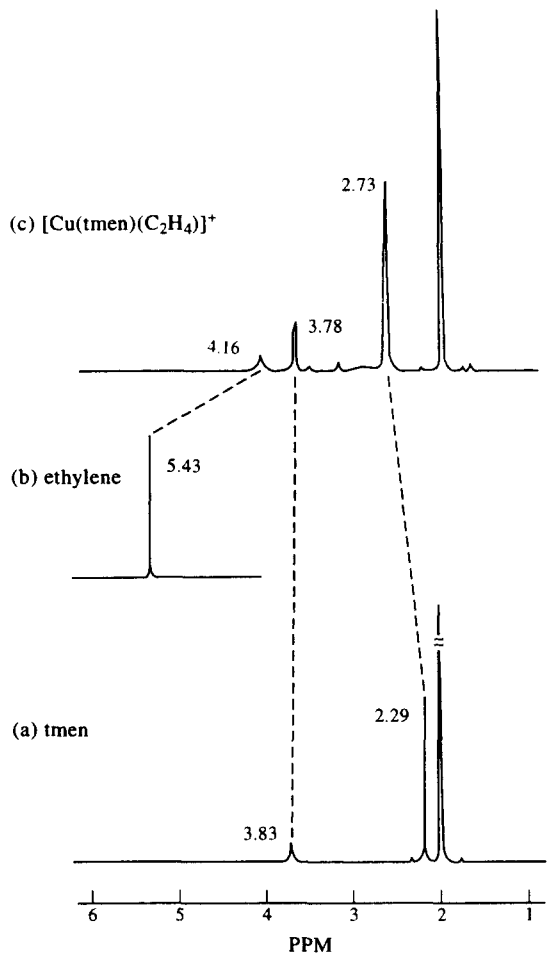


Fig. 2. ^1H NMR spectra of (a) tmen, (b) ethylene, (c) $[Cu(tmen)(C_2H_4)]^+$ in acetone-d_6 at −90°C.

It is worth noting that a linear relationship between C=C distances and ^1H NMR chemical shifts of the ethylene for the metal–ethylene complexes is shown in Fig. 3 with data referring to Table 3, indicating that the metal–ethylene bonding can be correlated with the ^1H NMR chemical shifts. All copper(I) ethylene complexes exhibit shielding of olefinic protons, similar to the ethylene complexes of rhodium (3.1 ppm), [12] platinum (2.0 ppm [13], and nickel (1.9 ppm) [12b, 14]. In contrast, only the silver(I) ethylene complex exhibits deshielding (5.7 ppm) [12b]. A delicate difference in metal–olefin bonding nature can be quali-

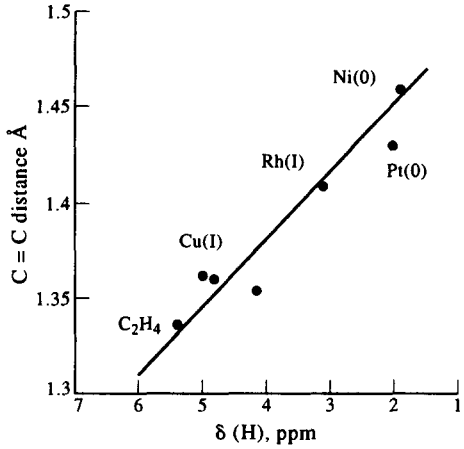


Fig. 3. Plot of ^{1}H NMR chemical shifts of the olefinic protons of ethylene in $[Cu(tmen)(C_2H_4)]^+$ at −90°C against C=C distances of ethylene.

Table 3. C=C distances and ^{1}H NMR chemical shifts of ethylene metal complexes

	C=C distances (Å)	$\delta(^1H)$ (ppm)	Reference
C_2H_4	1.337	5.4	[5]
$Cu(tmen)(C_2H_4)$	1.354	4.16	This work
$Cu(bpy)(C_2H_4)$	1.353	4.84	[5]
$Cu(phen)(C_2H_4)$	1.361	5.02	[5]
$Rh(acac)(C_2H_4)$	1.41	3.1	[17]
$Pt(PPh_3)_2(C_2H_4)$	1.43	2.0	[17]
$Ni(PR_3)_2(C_2H_4)$	1.46	1.9	[15]
$Ag(C_2H_4)$		5.7	[17]

tatively distinguished from the ^{1}H NMR chemical shifts of olefin protons rather than the C=C bond distances, because the small difference in the distances is generally within the standard deviation.

SUPPLEMENTARY MATERIAL

Fractional coordinates of all atoms, anisotropic thermal parameters, all bond distances and angles, and observed and calculated structure factors are available from the authors on request.

Acknowledgements—This work was partially supported by a Grant-in-Aid for Science Research (Nos. 0723226 and 07241260) from the Ministry of Education, Science and Culture in Japan. The authors are also grateful to Kinki University for the financial support (GG1100). The authors thank Ms. T. Tsujikawa and Ms. M. Tsujigami for their assistance.

REFERENCES

1. (a) T. Ziegler and A. Rauk, *Inorg. Chem.* 1979, **18**, 1558; (b) R. J. Cramer, *J. Am. Chem. Soc.* 1964, **86**, 217; (c) T. A. Albright, R. Hoffmann, J. C. Thibeault and D. L. Thorn, *J. Am. Chem.* 1979, **101**, 3801; (d) B. F. G. Johnson and J. A. Segel, *J. Chem. Soc., Chem. Commun.* 1972, 1312.
2. (a) B. Akermark, M. Almemark, J. F. Almlof, J. E. Backvall, B. Roos and A. Stogard, *J. Am. Chem. Soc.* 1977, **99**, 4617; (b) R. M. Pitzer and H. F. Schaefer, *J. Am. Chem. Soc.* 1979, **101**, 7176; (c) N. Rosch and R. Hoffmann, *Inorg. Chem.* 1974, **13**, 2656; (d) T. H. Upton and W. A. Goddard, *J. Am. Chem. Soc.* 1978, **100**, 321; (e) C. Bachmann, J. Demuynck and A. Veillard, *J. Am. Chem. Soc.* 1978, **100**, 236.
3. (a) P. J. Hay, *J. Am. Chem. Soc.* 1981, **103**, 1390; (b) F. U. Axe and D. S. Marynick, *J. Am. Chem. Soc.* 1984, **106**, 6230.
4. (a) M. J. S. Dewar, *Bull. Soc. Chim. Fr.* 1951, **18**, C79; (b) J. Chatt and L. A. Duncanson, *J. Chem. Soc.* 1953, 2939.
5. M. Munakata, S. Kitagawa, S. Kosome and A. Asahara, *Inorg. Chem.* 1986, **25**, 2622.
6. (a) J. S. Thompson, R. L. Harlow and J. F. Whitney, *J. Am. Chem. Soc.* 1983, **105**, 3522; (b) J. F. Thompson and J. F. Whitney, *J. Am. Chem. Soc.* 1983, **105**, 5488.
7. H. Masuda, N. Yamamoto, T. Taga, K. Machida, S. Kitagawa and M. Munakata, *J. Organometallic Chem.* 1987, **322**, 121.
8. P. Hemmerich and C. Sigwart, *Experientia* 1963, **15**, 488.
9. J. F. Coetzee, *Pure Appl. Chem.* 1966, **13**, 429.
10. W. Partenheimer and B. Durham, *J. Am. Chem. Soc.* 1974, **96**, 3800.
11. J. S. Thompson and R. M. Swiatek, *Inorg. Chem.* 1985, **24**, 110.
12. (a) R. J. Cramer, *J. Am. Chem. Soc.* 1964, **86**, 217; (b) C. A. Tolman, A. D. English and L. E. Manzer, *Inorg. Chem.* 1975, **14**, 2353.
13. P. T. Cheng, C. D. Cook, S. C. Nyburg and K. Y. Wan, *Inorg. Chem.* 1971, **10**, 2210.
14. W. C. Seidel and C. A. Tolman, *Inorg. Chem.* 1970, **9**, 2354.
15. L. J. Guggenberger, *Inorg. Chem.* 1973, **21**, 499.
16. (a) S. Kitagawa and M. Munakata, *Inorg. Chem.* 1981, **20**, 2261; (b) S. Kitagawa, M. Munakata and N. Miyaji, *Inorg. Chem.* 1982, **21**, 3842.
17. C. A. Tolman and W. C. Seidel, *J. Am. Chem. Soc.* 1974, **96**, 2774.

Pergamon

S0277-5387(96)00263-X

Polyhedron Vol. 16, No. 1, pp. 71–73, 1997
Copyright © 1996 Elsevier Science Ltd
Printed in Great Britain. All rights reserved
0277-5387/97 $15.00+0.00

Synthesis and crystal structure of bis(acetylacetonato)(isonicotinato) monoaquamanganese(III) dihydrate

Duanjun Xu,[a]* Cungen Zhang,[a] Yuanzhi Xu[a] and Xiaoying Huang[b]

[a]Department of Chemistry, Zhejiang University, Hangzhou 310027, P.R. China

[b]Fujian Institute of Research on the Structure of Matter, Fuzhou 350002, P.R. China

(Received 10 April 1996; accepted 20 May 1996)

Abstract—The title complex was synthesized by reaction of sodium isonicotinate with manganese(III) acetylacetonate. The single crystal structure of the complex was determined by X-ray diffraction. Around the Mn^{III} atom the octahedral coordination polyhedron is tetragonally elongated. An isonicotinate anion coordinates to the Mn^{III} atom through the pyridine nitrogen atom in the axial direction with a Mn—N bond of 2.293(3) Å, while two acetylacetonate anions chelate to Mn^{III} in the equatorial plane with average Mn—O length of 1.91 Å. Copyright © 1996 Elsevier Science Ltd

Keywords: isonicotinato; acetylacetonato; manganese(III) complex; synthesis; crystal structure; Jahn–Teller distortion.

Manganese chemistry has been receiving a great deal of attention. Manganese ions are found to play an important role in some biological enzymes such as manganese superoxide dismutase (SOD), non-heme catalases and photosystem-II. This stimulated a desire to understand the structural chemistry of Mn in different oxidation states [1–3]. Octahedral complexes of high-spin Mn^{III} are also expected to be susceptible to Jahn–Teller distortions [4–7] causing them to deviate from identical Oh symmetry by either a trigonal distortion or a tetragonal elongation or compression. The studies on manganese ions chelated by biochemical reagents have been ongoing in our laboratory with the aim of mimicking the chemical environment of manganese enzymes. As a part of our study we report here the synthesis and structure of $[Mn(acac)_2(i\text{-}nic)(H_2O)]$.

EXPERIMENTAL

Synthesis

To an aqueous solution of $MnAc_2 \cdot 4H_2O$ (1.98 g, 8 mmol in 20 cm^3) acetylacetone (2 g, 20 mmol) was added, followed by dropwise addition of an aqueous solution of $KMnO_4$ (0.216 g, 2 mmol in 10 cm^3). After stirring for about 15 min at room temperature, the sodium isonicotinate solution prepared previously (10 mmol in 20 cm^3) was added with continuous stirring for 30 min. After filtering and standing the solution for several days, the well-shaped crystals of the title complex were obtained from the filtrate.

X-ray structure analysis

Preliminary examination of the crystal and data collection were performed on an Enraf-Nonius CAD-4 diffractometer. Intensity data were collected by ω-2θ scans using graphite monochromated Mo-K_α radiation. A total of 1856 independent reflections were measured with 2θ up to 50°, of which 1490 observed reflections [$I > 3\sigma(I)$] were employed in the structure refinements. Both Lp correction and empirical absorption correction were applied. The structure was solved by the Patterson method followed by Fourier syntheses. The crystallographic parameters are summarized in Table 1.

RESULTS AND DISCUSSION

Synthesis

The described synthetic procedures offer convenient routes for the preparation of the title complex. The

* Author to whom correspondence should be addressed.

Table 1. Crystal structure parameters for $[Mn(acac)_2(i\text{-nic})(H_2O)]$

Formula	$MnO_9NC_{16}H_{24}$
Molecular weight	429.3
Crystal system	Monoclinic
Space group	$C2/c$
a (Å)	14.544(3)
b (Å)	13.648(4)
c (Å)	10.971(5)
β (°)	111.77(3)
V (Å^3)	2022(2)
Z	4
D_{calc} (g cm^{-3})	1.41
$F(000)$	896
μ(cm^{-1})	6.69
Temperature (°C)	23
No. of observations (I) > $3\sigma(I)$	1490
No. of variables	125
R	0.042
Rw	0.054
Goodness of fit indicator	1.49
Max. shift in final cycle	0.03
Largest peak in final diff. map (e Å^{-3})	0.42

$MnAc_2 \cdot 4H_2O$ can be substituted by either $MnCl_2 \cdot 4H_2O$ or $MnSO_4 \cdot H_2O$. But the dark brown title complex is always accompanied by a white crystalline compound, which was found to be an Mn^{II} complex, bis(isonicotinato)tetraaquamanganese(II), by the later X-ray structure analysis.

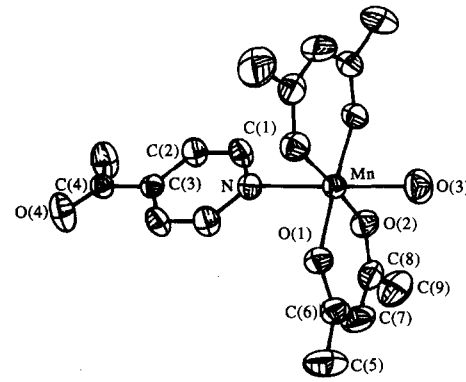


Fig. 1. ORTEP drawing (50% probability thermal ellipsoids) and labelling scheme for the non-hydrogen atoms of $[Mn(acac)_2(i\text{-nic})]$.

Structure

The molecular structure of the title complex is shown in Fig. 1. In the crystal the molecule is located about the twofold axis. The Mn^{III} atom has an elongated octahedral coordination geometry as shown in Table 2. The axial Mn—O(H_2O) bond is about 0.2 Å longer than the Mn—O(acac) bond in the equatorial plane. The axial Mn—N(i-nic) bond distance is about 0.3 Å longer than the Mn—N bond in the equatorial plane found in $[Mn(phen)_2Cl_2]NO3$ [9], and comparable to those in the axial direction of reported Mn^{III} complexes, for example in $Mn(acac)_2(NCS)$ [4], $Mn(acac)_2(N_3)$ [6], Mn(TPP)(N_3) [8], Mn(TPP)(NCS)(py) [4] and Mn(TPP)(Cl)(py) [10]. These

Table 2. Selected bond distances (Å) and angles (°) with e.s.d.s in parentheses

Mn—O(1)	1.892(2)	N—C(1)	1.335(3)
Mn—O(2)	1.932(2)	C(1)—C(2)	1.372(4)
Mn—O(3)	2.143(3)	C(3)—C(4)	1.521(5)
Mn—N	2.293(3)	C(5)—C(6)	1.498(5)
O(1)—C(6)	1.283(4)	C(6)—C(7)	1.375(5)
O(2)—C(8)	1.266(4)	C(7)—C(8)	1.397(5)
O(4)—C(4)	1.235(3)	C(8)—C(9)	1.499(5)
C(2)—C(3)	1.389(4)		

O(1*)—Mn—O(1)	175.3(1)	C(1)—N—Mn	121.6(2)
O(1)—Mn—O(2)	91.8(1)	N—C(1)—C(2)	123.5(3)
O(1*)—Mn—O(2)	88.4(1)	C(1)—C(2)—C(3)	119.9(3)
O(1)—Mn—O(3)	87.64(6)	C(2*)—C(3)—C(2)	116.4(4)
O(1)—Mn—N	92.36(6)	C(2)—C(3)—C(4)	121.8(2)
O(1*)—Mn—O(3)	87.68(6)	O(4)—C(4)—C(3)	116.5(2)
O(1*)—Mn—N	92.32(6)	O(1)—C(6)—C(7)	124.4(3)
O(2)—Mn—O(3)	92.36(7)	O(1)—C(6)—C(5)	121.5(3)
O(2*)—Mn—O(3)	92.38(7)	C(6)—C(7)—C(8)	124.7(3)
O(2*)—Mn—N	87.62(7)	O(2)—C(8)—C(7)	123.8(3)
O(3)—Mn—N	180.00	O(2)—C(8)—C(9)	115.9(3)
C(6)—O(1)—Mn	127.3(2)	C(7)—C(8)—C(9)	120.2(3)

Symmetry code: *1 $-x$, y, 1/2 $-z$.

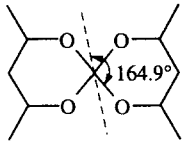


Fig. 2. Orientation of the pyridine plane with respect to the equatorial ligands (acac).

observations are consistent with a Mn^{III} in the high-spin state. Both the C3—C4 bond length of 1.521(5) Å and the dihedral angle of 9.6° between the carboxyl group and the pyridine plane suggest no conjugation between the pyridine ring and the carboxyl group. This agrees with nicotinate complexes reported previously [11]. The acac ligand is highly coplanar but not perpendicular to the twofold axis. The dihedral angle between two acac ligands, related by a twofold axis, is 170.4°. The torsional angles of O1—Mn—N—C1* [15.1°] and O1—Mn—N—Cl [164.9°] indicate that the pyridine ring does not bisect the dihedral angle between acac ligands (see Fig. 2). The short non-bonded O1—C1 atomic separation of 3.184 Å implies van der Waals contact between the pyridine ring and the acac ligand. This is also comparable to a previous report [12]. In the unit cell, the extensive hydrogen-bonding network exists among carboxyl O atoms, coordinated and uncoordinated water molecules. The crystal packing is mainly through hydrogen bonding. Van der Waals forces also contribute to the crystal packing.

Acknowledgement—This project was supported by The Natural Science Foundation of Zhejiang Province.

REFERENCES

1. V. L. Pecoraro, M. J. Baldwin and A. Gelasco, *Chem. Rev.* 1994, **94**, 807 and references therein.
2. W. M. Coleman and L. T. Taylor, *Coord. Chem. Rev.* 1980, **32**, 1.
3. K. Wieshardt, *Angew. Chem. Int. Ed. Engl.* 1989, **28**, 1153.
4. B. R. Stults, R. O. Day, R. S. Marianelli and V. W. Day, *Inorg. Chem.* 1979, **18**, 1847.
5. B. R. Stults, R. S. Marianelli and V. W. Day, *Inorg. Chem.* 1979, **18**, 1853.
6. B. R. Stults, R. S. Marianelli and V. W. Day, *Inorg. Chem.* 1975, **14**, 722.
7. V. W. Day, B. R. Stults, E. L. Tasset, R. O. Day and R. S. Marianelli, *J. Am. Chem. Soc.* 1974, **96**, 2650.
8. V. W. Day, B. R. Stults, E. L. Tasset, R. S. Marianelli and L. J. Boucher, *Inorg. Nucl. Chem. Lett.* 1975, **11**, 505.
9. K. R. Reddy and M. V. Rajasekharan, *Polyhedron* 1994, **13**, 765.
10. J. F. Kirner and W. R. Scheidt, *Inorg. Chem.* 1975, **14**, 2081.
11. C. Zhang, D. Xu, Y. Xu and X. Huang, *Acta Cryst.* 1996, **C52**, 591.
12. P. J. Toscano, P. T. Dimauro, S. Geremia, L. Randaccio and E. Zanggrando, *Inorg. Chim. Acta* 1994, **217**, 195.

Pergamon

S0277-5387(96)00260-4

Polyhedron Vol. 16, No. 1, pp. 75–79, 1997
Copyright © 1996 Elsevier Science Ltd
Printed in Great Britain. All rights reserved
0277-5387/97 $15.00+0.00

Molybdenum(VI) complex with citric acid: synthesis and structural characterization of 1:1 ratio citrato molybdate $K_2Na_4[(MoO_2)_2O(cit)_2]\cdot 5H_2O$

Zhao-Hui Zhou,* Hui-Lin Wan and Khi-Rui Tsai

Department of Chemistry and State Key Laboratory for Physical Chemistry of Solid Surface, Xiamen University, Xiamen 361005, P.R. China

(Received 2 April 1996; accepted 17 May 1996)

Abstract—Sodium potassium citrato molybdate $K_2Na_4[(MoO_2)_2O(cit)_2]\cdot 5H_2O$ has been prepared by the reaction of potassium trihydrogen citrate and sodium molybdate. Analysis of the crystal structure reveals that the anion of the complex contains a bent $(MoO_2)O(MoO_2)$ core with an Mo—O—Mo angle 142°. Each molybdenum has a distorted octahedral coordination and citrato ligands are tridentate to the two molybdenum atoms via the deprotonated hydroxy-, α- and β-carboxyl groups. Principal dimensions are: $[Mo{=}O(t)]_{av}$, 1.706(4); $[Mo{-}O(b)]_{av}$, 1.899(3); $[Mo{-}O(hydroxy)]_{av}$, 1.944(3); $[Mo{-}O(\alpha\text{-carboxy})]_{av}$, 2.207(3), and $[Mo{-}O(\beta\text{-carboxy})]_{av}$, 2.264(3) Å. The IR, ^1H and ^{13}C NMR spectra are in agreement with this structure.
Copyright © 1996 Elsevier Science Ltd

Keywords: oxomolybdenum(VI); molybdate(VI); citric acid citrate; nitrogenase; crystal structure.

Molybdenum is a trace element which plays an important role in different living plants and animal organisms [1]. It is known that some types of small biomolecules such as hydroxycarboxylic acids are strong molybdenum binders. Recent studies on the nitrogenase enzyme revealed its active site as a cage-like $MoFe_7S_9$ homocitrate cluster, in which the octahedral coordination sphere of the Mo within the cluster consists of three sulfides, a nitrogen atom from the imidazole group of a histidine residue, and two oxygen atoms from the hydroxy group and α-carboxyl moiety of homocitric acid [2], alternative polycarboxylic acids including citric, malic and citramalic by *in vitro* syntheses of the FeMo-co displayed N_2 reduction activity well above the background limits [3]. This prompted an investigation of the coordination chemistry of oxomolybdenum citrato complexes.

Citric acid (H_4cit) has been found to act usually as a polydentate ligand, generally involving the central hydroxy and carboxyl group [4]. Of the four ionizable protons, three or four usually dissociate upon coordination, and a citrate with the charge −2 is less common. Its complexes with oxomolybdenum have been studied in the solid and in solution [5–13]. The first well characterized citrato molybdate was reported as $[Me_3N(CH_2)_6NMe_3]_2[Mo_4O_{11}(Hcit)_2]\cdot 12H_2O$ [8], and later a similar Mo:cit ratio 2:1 compound was prepared as $K_4[Mo_4O_{11}(Hcit)_2]\cdot 6H_2O$ [10]. Formation of 1:1 ratio complex was obtained as early as $K_2[MoO_3(OH)(H_3cit)]\cdot 2H_2O$ and $K_3[MoO_4(H_3cit)]\cdot 2H_2O$ [9], later $K_4[(MoO_2)_2O(Hcit)_2]\cdot 5H_2O$, $K_6[(MoO_2)_2O(cit)_2]\cdot 7H_2O$ and $K_4[MoO_3(cit)H_2O]$ [12] were obtained by precipitation from aqueous solution at pH 4–8. These complexes have been characterized by a variety of methods, however, the isolation of molybdenum(VI) citrate complexes in crystalline form suitable for X-ray structural analysis has been quite difficult [13]. The present X-ray analysis of the title compound shows that potassium trihydrogen citrate reacts with sodium molybdate to give the sodium potassium oxocitrato molybdate(VI) dimer, which shows a bent $(MoO_2)O(MoO_2)$ core configuration, and the molybdenum(VI) atoms are coordinated tridentately by the oxygen atoms of hydroxy- and carboxylate of quadridentate citrate anion. The

* Author to whom correspondence should be addressed.

^1H and ^{13}C NMR spectroscopy suggest this dimeric structure also exists in solution.

EXPERIMENTAL

All reagents are commercially available. Potassium trihydrogen citrate was prepared from the reaction of equimolar citric acid and sodium hydroxide. Infrared spectra were recorded as Nujol mulls between KBr plates using a Nicolet 740 FT-IR spectrometer. The ^1H and ^{13}C NMR spectra were recorded on a Varian UNITY 500 NMR spectrometer.

Preparation of sodium potassium citrato molybdate $K_2Na_4[(MoO_2)_2O(cit)_2]\cdot 5H_2O$

Sodium molybdate (20 mmol) was reacted with an excess potassium trihydrogen citrate in a water bath. The resulting mixture was filtered, cooled and crystallized. The solid was collected and washed to give a white solid (6.0 g, 66%). Found: C, 15.4; H, 1.9. Calc. for $C_{12}H_{18}O_{24}Na_4K_2Mo_2$: C, 15.9; H, 2.0%; IR(KBr): ν_{asym} (C=O) 1644 vs, 1588 s; ν_{sym} (C=O) 1398 vs, ν (Mo=O) 950 s, 902 s, ν (Mo—O_b) 715 s, cm^{-1}, ^1H NMR δ_H (500 MHz, D_2O) ppm: 2.714 (4H, J_{AB} 16.0 Hz, CH_{2B}), 2.516 (4H, J_{AB} 16.5 Hz, CH_{2A}); ^{13}C NMR (500 MHz, D_2O) ppm: 186.111, 185.490 $(CO_2)\alpha$, 178.372, 178.323, 178.275, 178.111 $(CO_2)_\beta$, 85.738, 84.843 (≡C—O), 46.131, 45.834, 45.119, 44.791, 44.085, 43.788 ppm (=CH_2).

Crystals of suitable quality for the subsequent X-ray diffraction studies were obtained as transparent plates by slow evaporation of a related solution of the title compound at room temperature. The resulting crystals were sealed to prevent loss of water molecules.

X-ray data collection, structure solution and refinement

Crystallographic data for the citratomolybdate are summarized in Table 1. Diffraction data were collected on an Enraf-Nonius CAD-4 diffractometer with graphite monochromated Mo-K_α radiation at 296 K. Lp factor, anisotropic decay and empirical absorption corrections were applied. The structure was solved by heavy atom methods and refined by full-matrix least-squares procedures with anisotropic thermal parameters for all the non-hydrogen atoms. All H atoms were located on a difference Fourier map and refined isotropically. All calculations were performed on a 486 DX2/66 microcomputer using MoLEN software package.

Table 1. Crystal data and summaries of intensity data collection and structure refinement

Compound	$K_2Na_4[(MoO_2)_2O(cit)_2]\cdot 5H_2O$
Color/shape	colorless, plate
Formula weight	908.31
Space group	$P2_1/n$
Temp. (°C)	23
Cell constants[a]	
a (Å)	10.036(2)
b (Å)	13.408(2)
c (Å)	19.816(3)
α (°)	
β (°)	90.41(1)
γ (°)	
Cell volume (Å^3)	2666(1)
Formula units/unit cell	4
D_{calc} (g cm^3)	2.263
μ_{calc} (cm^{-1})	13.948
Diffractometer/scan	Enraf-Nonius CAD-4/ω-2θ
Radiation, graphite monochromator	Mo-K_α (λ = 0.71073 Å)
Max. crystal dimension, mm	0.15 × 0.20 × 0.25
Scan width	0.45 + 0.35 tan θ
Standard reflections	221; 438
Decay of standards	±2%
Reflections measured	5367
2θ range (°)	2 ⩽ 2θ ⩽ 52
Range of h, k, l	±12, −16, −24
Reflections observed [$F_o \leqslant 3\sigma(F_o)$][b]	4672
Computer programs[c]	MoLEN
Structure solution	MoLEN
No. of parameters varied	470
Weight	$[\sigma(F_o)^2 + 0.0001F_o^2 + 1]^{-1}$
GOF	0.81
$R = \Sigma\|\|F_o\| - \|F_o\|\|/\Sigma\|F_o\|$	0.033
R_w	0.037
Largest feature final diff. map	1.0 e$^-$ Å^3

[a] Least-squares refinement of $[(\sin\theta)/\lambda]^2$ values for 25 reflections $\theta > 20°$.

[b] Corrections: Lorentz-polarization.

[c] Neutral scattering factors and anomalous dispersion corrections.

RESULTS AND DISCUSSION

The title compound was prepared by the reactions of sodium molybdate and excess potassium trihydrogen citrate (KH_3cit). Note a similar reaction of sodium tungstate or ammonium metavanadate with citric acid has been reported [14,15]. However, the pH values in the reactions are controlled easily by citrate anions acting as both reactant and buffer agent. The loss of protons suggest the reaction (1), which corresponds to $[(MoO_4)_p(Hcit)_q(H^+)_r]^{(2p+3q-r)-}$ stoichiometry of 2:2:4 showed in potentiometry, spectrophotometry, differential pulse polarography and calorimetry [13].

$$2MoO_4^{2-} + 2H_3cit^- \rightarrow [(MoO_2)_2O(cit)_2]^{6-} + 3H_2O \quad (1)$$

Similarly, good yield of citrato tungstate could be obtained by the reaction of sodium tungstate with sodium trihydrogen citrate as reaction (2).

$$2WO_4^{2-} + 2H_3cit^- \rightarrow [(WO_2)_2O(cit)_2]^{6-} + 3H_2O \quad (2)$$

This is also true for the reaction of ammonium metavanadate with potassium dihydrogen citrate as (3).

$$2VO_3^- + 2H_2cit^{2-} \rightarrow [VO_2(cit)]_2^{6-} + 2H_2O \quad (3)$$

The complex crystallizes in the space group $P2_1/n$. Its structure is depicted in Fig. 1. Selected atomic distances and bond angles are given in Table 2.

The dimeric anion consists of the common oxo-bridged $[Mo_2O_5]^{2+}$ entity which is noncentrosymmetric. The angle of Mo—O—Mo is 144.7(2)°, which is intermediate between the values of strictly 180° in $[(MoO_2)_2O(C_2O_4)_2(H_2O)_2]^{2-}$ and 136° in $[(MoO)_2O(O_2)_4(H_2O)_4]^{2-}$ [16,17]. The two terminal oxo groups are in a *cis*-configuration. Each molybdenum atom is six-coordinate with approximately octahedral geometry. The terminal and bridging oxo-groups adopt a *fac*-stereochemistry. The *trans* positions are occupied by a fully deprotonated tridentate citrate. The coordination mode is similar to the proposed structure of citrato cubane $MoFe_3S_4$ cluster $(Et_4N)_2[MoFe_3S_4Cl_3(H_2cit)]$, and probably the hydroxy group in the cubane should be deprotonated [18].

Although no symmetry is imposed upon the molecule, there is a pseudo-twofold axis that passes through the bridging oxygen, which is perpendicular to the Mo—Mo vector. The lists of chemically equi-

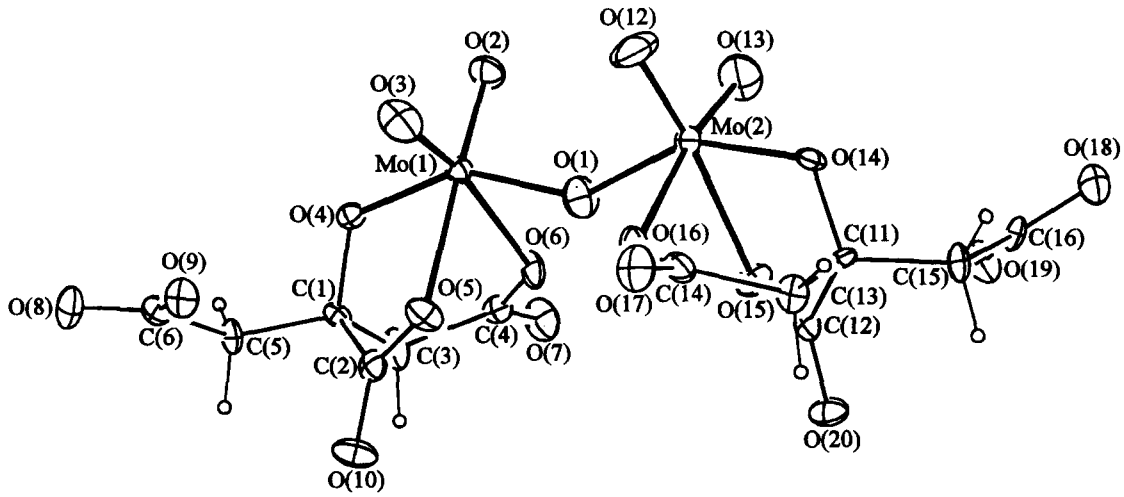


Fig. 1. Perspective view of the anion structure of citratomolybdate.

Table 2. Selected bond lengths (Å) and angles (°) of $Na_4K_2[(MoO_2)_2O(cit)_2] \cdot 5H_2O$

Mo(1)—O(1)	1.916(3)	Mo(2)—O(14)	1.958(3)	O(10)—C(2)	1.226(5)	C(1)—C(3)	1.533(6)
Mo(1)—O(2)	1.706(4)	Mo(2)—O(15)	2.196(4)	O(14)—C(11)	1.425(4)	C(1)—C(5)	1.516(5)
Mo(1)—O(3)	1.709(3)	Mo(2)—O(16)	2.278(3)	O(15)—C(12)	1.281(5)	C(3)—C(4)	1.511(6)
Mo(1)—O(4)	1.930(3)	O(4)—C(1)	1.413(5)	O(16)—C(14)	1.282(5)	C(5)—C(6)	1.526(6)
Mo(1)—O(5)	2.217(3)	O(5)—C(2)	1.273(5)	O(17)—C(14)	1.234(5)	C(11)—C(12)	1.533(5)
Mo(1)—O(6)	2.250(3)	O(6)—C(4)	1.274(5)	O(18)—C(16)	1.251(5)	C(11)—C(13)	1.527(5)
Mo(2)—O(1)	1.882(3)	O(7)—C(4)	1.228(5)	O(19)—C(16)	1.250(6)	C(11)—C(15)	1.530(5)
Mo(2)—O(12)	1.713(4)	O(8)—C(6)	1.258(5)	O(20)—C(12)	1.228(5)	C(13)—C(14)	1.515(6)
Mo(2)—O(13)	1.694(4)	O(9)—C(6)	1.241(5)	C(1)—C(2)	1.532(5)	C(15)—C(16)	1.526(5)

O(1)—Mo(1)—O(2)	102.1(1)	O(1)—Mo(1)—O(3)	96.4(2)	O(1)—Mo(1)—O(4)	148.9(1)
O(1)—Mo(1)—O(5)	80.7(1)	O(1)—Mo(1)—O(6)	76.6(1)	O(2)—Mo(1)—O(3)	104.2(2)
O(2)—Mo(1)—O(4)	97.8(1)	O(2)—Mo(1)—O(5)	168.5(1)	O(2)—Mo(1)—O(6)	91.9(1)
O(3)—Mo(1)—O(4)	101.7(1)	O(3)—Mo(1)—O(5)	86.6(1)	O(3)—Mo(1)—O(6)	163.6(1)
O(4)—Mo(1)—O(5)	75.3(2)	O(4)—Mo(1)—O(6)	79.0(2)	O(5)—Mo(1)—O(6)	77.7(2)
O(1)—Mo(2)—O(12)	101.8(2)	O(1)—Mo(2)—O(13)	101.1(2)	O(1)—Mo(2)—O(14)	148.6(1)
O(1)—Mo(2)—O(15)	79.4(1)	O(1)—Mo(2)—O(16)	79.2(1)	O(12)—Mo(2)—O(13)	102.7(2)
O(12)—Mo(2)—O(14)	98.6(2)	O(12)—Mo(2)—O(15)	163.4(1)	O(12)—Mo(2)—O(16)	85.9(2)
O(13)—Mo(2)—O(14)	97.4(1)	O(13)—Mo(2)—O(15)	93.2(2)	O(13)—Mo(2)—O(16)	171.0(2)
O(14)—Mo(2)—O(15)	74.4(2)	O(14)—Mo(2)—O(16)	78.7(2)	O(15)—Mo(2)—O(16)	78.0(1)
Mo(1)—O(1)—Mo(2)	144.7(2)				

Table 3. Comparisons of the M—O bonds(Å) in malato or citrato complexes

Complex	Mo—O(hydroxy)	M—O(α-carboxy)	M—O(β-carboxy)	Ref.
$Cs_2[MoO_2(Hmal)_2]\cdot H_2O$, $K_2[MoO_2(Hmal)_2]\cdot H_2O$	1.939(8)	2.243(9)		[20]
$(NH_4)_4[(MoO_2)_2O_3(R\text{-mal})_2]\cdot 6H_2O$	1.925(5)	2.235(5)	2.296(5)	[22]
$K_2[MoO(O_2)_2(H_2cit)]\cdot 1/2H_2O_2\cdot 6H_2O$	2.011(7)	2.220(8)		[21]
$[Me_3N(CH_2)_6NMe_3]_2[(MoO_2)_4O_3(Hcit)_2]\cdot 12H_2O$, $K_4[(MoO_2)_4O_3(Hcit)_2]\cdot 6H_2O$	1.976(5), 1.968(5)	2.185(5), 2.211(5)	2.318(5) av	[8]
$K_2Na_4[(MoO_2)_2O(cit)_2]\cdot 5H_2O$	1.929(3), 1.958(3)	2.218(3), 2.197(4)	2.264(3) av	This work
$Na_6[(WO_2)_2O(cit)_2]\cdot 10H_2O$	1.958(2)	2.195(3)	2.289(2)	[14]
$K_2(NH_4)_4[VO_2(cit)]_2\cdot 6H_2O$	1.961(2), 2.005(2)	1.981(3)		[15]
$K_2[VO_2(H_2cit)]_2\cdot 4H_2O$	1.961(3), 2.010(4)	1.980(3)		[23]

valent bond distances and angles (Table 2) illustrate the approximately twofold symmetry. The configuration is consistent with one of the proposed structures of 1 : 1 dinuclear complex of molybdenum(VI) and citrate [7, 12, 13]. The Mo—O distances can be classified into three types with the order Mo=O (unshared oxygen) (1.694 ~ 1.713 Å) < Mo—O (bridging oxo group) (1.882 ~ 1.916 Å) ≈ Mo—O(hydroxy) (1.930 ~ 1.958 Å) < Mo—O(α-carboxy) (2.196 ~ 2.217 Å) ≈ Mo—O(β-carboxy) (2.250 ~ 2.278 Å). The Mo(1,2)—O(1) distances (av. 1.899 Å) are very close to those in $[(MoO_2)_2O(C_2O_4)_2(H_2O)_2]^{2-}$ (1.876 Å) [16] and $[(MoO_2)_2O(Hnta)_2]^{2-}$ [1.880 Å, $H_3nta = N(CH_2CO_2H)_3$] [19]. The Mo(VI)—O(hydroxy) distances (av. 1.944 Å) are similar to those in $[MoO_2(Hmal)_2]^{2-}$ (H_3mal = malic acid) (1.939 Å) [20] and $[MoO(O_2)_2(H_2cit)]^{2-}$ (2.011 Å) [21]. The Mo—O (α-carboxy) distances (av. 2.207 Å) and the longest Mo—O (β-carboxy) (av. 2.264 Å) show weak coordination of the carboxyl group with Mo^{VI}. The Mo—O (β-carboxy) is shorter than those already reported tetramers $[(MoO_2)_4O_3(Hcit)_2]^{4-}$ (2.323 Å) [14] and $[(MoO_2)_4O_3(R\text{-mal})_2]^{4-}$ (2.296 Å) [22] (Table 3).

Due to the Mo—O single bond which exists in the dimer and the existence of the monomer in narrow pH range [12], the equilibrium for the dimerization reaction might proceed easily as follows:

$$2[MoO_3(Hcit)(H_2O)]^{3-} \rightleftharpoons [Mo_2O_5(cit)_2]^{6-} + 2H_2O$$

Moreover, like the citratovanadates, the protonation and deprotonation of citratomolybdate might have less influence on the dimeric structure [23]. This means the different p, q, r in $[(MoO_4)_p(Hcit)_q(H^+)_r]^{(2p+3q-r)-}$ like [2, 2, 4], [2, 2, 5], [2, 2, 6] can be transformed in solution without changing the dimeric structure of citratomolybdate as following:

$$[Mo_2O_5(cit)_2]^{6-}$$

$$\rightleftharpoons [Mo_2O_5(Hcit)(cit)]^{5-} \rightleftharpoons [Mo_2O_5(Hcit)_2]^{4-}$$

The crystal structure comprises discrete $[(MoO_2)_2O(cit)_2]^{6-}$ anions, sodium or potassium cations and water molecules. Waters of crystallization are distributed throughout the cell and together with various of the anion oxygens, make the sodium or potassium cations six-coordinate.

Moreover, the complex exhibits the following infrared absorption bands: ν_{asym} (COO): 1644 vs, 1588 s, ν_{sym} (COO): 1398 vs, ν (Mo=O): 950 s, 902 s cm^{-1}, and ν (Mo—O_b—Mo): 715 s. The separation (Δ) between ν_{asym} and ν_{sym} is 246 and 190 cm^{-1}, which is greater than the value of 150 cm^{-1} for uncomplexed sodium citrate salt, implying the presence of free or unidentately coordinated carboxyl groups. The strong band at 715 cm^{-1} is assigned to the symmetric Mo—O—Mo stretch in agreement with previous studies. There is no other band at higher energy that can be assigned to asym stretching consistent with a bent disposition of the bridge. The Mo=O bands give rise to two major bands around 900 cm^{-1}, characteristic of the symmetric and asymmetric stretches of the *cis*-dioxo groups.

In the ^1H NMR spectra the methylene protons of citric acid give rise to an AB quartet which shifts with pH [24]. Complexation with molybdenum(VI) leads to a slightly distorted AB quartet with $\delta q = 2.714$, 2.516 ppm respectively, indicating that both CH_2CO_2 arms are almost equivalent [12]. The shifts of the ^{13}C resonances (in comparison with those for citrate) [12, 24] of the alcoholic and α-carboxylic function show that the citrate is coordinated through these two groups, while the β-carboxylic region only a small shift is observed, indicating that the bonding to molybdenum is weak.

Acknowledgements—Financial support by the National Science Foundation of China (No. 29503021) and the State Science and Technology Committee is gratefully acknowledged.

REFERENCES

1. E. I. Stiefel, *Molybdenum Enzymes, Cofactors and*

Model Systems. p. 1, American Chemical Society, Washington, DC (1993).
2. (a) J. Kim and D. C. Rees, *Science* 1992, **257,** 2677; (b) M. K. Chan, J. Kim and D. C. Rees, *Science* 1993, **260,** 792.
3. M. S. Madden, T. D. Paustian, P. W. Ludden and V. K. Shah, *J. Bacteriol.* 1991, **173,** 5403.
4. J. P. Glusker, *Acc. Chem. Res.* 1980, **13,** 345.
5. J. D. Jesus and M. D. Farropas, *Trans. Met. Chem.* 1983, **8,** 193.
6. J. J. Cruywagen and R. F. Van de Water, *Polyhedron* 1986, **5,** 521.
7. M. Bartusek, J. Havel and D. Matula, *Collect. Czech. Chem. Commun.* 1986, **51,** 2702.
8. L. R. Nassimbeni, M. L. Niven, J. J. Cruywagen and J. B. B. Heyns, *J. Crystallogr. Spectrosc. Res.* 1987, **17,** 373.
9. M. Dudek, E. Hodorowicz, A. Kanas, A. Samotus, B. Sieklucka, J. Szklarzewicz and E. Beltowska-Lehman, *Proc. 11th Conf. Coord. Chem.*, p. 57. Smolenice, Czechoslovakia.
10. N. W. Alcock, M. Dudek, R. Grybos, E. Hodorowicz, A. Kanas and A. Samotus, *J. Chem. Soc., Dalton Trans.* 1990, 707.
11. D. O. Martire, M. R. Feliz and A. L. Capparelli, *Phys. Chem. Leipzig.* 1989, **270,** 951.
12. A. Samotus, A. Kanas, M. Dudek, R. Grybos and E. Hodorowicz, *Trans. Met. Chem.* 1991, **16,** 495.
13. J. J. Cruywagen, E. A. Rohwer and G. F. S. Wessels, *Polyhedron* 1995, **14,** 3481.
14. (a) J. J. Cruywagen, L. J. Saayman and M. L. Niven, *J. Crystallogr. Spectrosc. Res.* 1992, **22,** 737; (b) E. Llopis, J. A. Ramirez, A. Domenech and A. Cervilla, *J. Chem. Soc., Dalton Trans.* 1993, 1121.
15. (a) Z. H. Zhou, H. L. Wan and K. R. Tsai, *Chinese Sci. Bull.* 1995, **40,** 749; (b) Z. H. Zhou, H. L. Wan, S. Z. Hu and K. R. Tsai, *Inorg. Chim. Acta* 1995, **237,** 193.
16. F. A. Cotton, S. M. Morehause and S. J. Wood, *Inorg. Chem.* 1964, **3,** 1603.
17. R. Stomberg, *Acta Chem. Scand.* 1968, **22,** 1076.
18. K. D. Demadis and D. Coucouvanis, *Inorg. Chem.* 1995, **34,** 436.
19. C. Knobler, B. R. Penfold, W. T. Robinson, C. J. Wilkins and S. H. Yong, *J. Chem. Soc., Dalton Trans.* 1980, 248.
20. (a) C. B. Knobler, A. J. Wilson, R. N. Hider, I. W. Jensen, B. R. Penfold, W. T. Robinson and C. J. Wilkins, *J. Chem. Soc., Dalton Trans.* 1983, 1299; (b) R. Stomberg and S. Olson, *Acta Chem. Scand., Ser. A* 1985, **39,** 79.
21. J. Flanagan, W. P. Griffith, A. C. Skapski and R. W. Wiggins, *Inorg. Chim. Acta* 1985, **96,** L23.
22. (a) J. E. Berg, S. Brandange, L. Lindbolm and P. E. Werner, *Acta Chem. Scand., Ser. A* 1977, **31,** 325; (b) M. A. Porai-Koshits, L. A. Aslanov, G. V. Ivanova and T. N. Polinova, *J. Struc. Chem.* (Eng. Transl.) 1968, **9,** 401; (c) Z. H. Zhou, W. B. Yan, H. L. Wan and K. R. Tsai, *Chinese J. Struc. Chem.* 1995, **14,** 255.
23. Z. H. Zhou, W. B. Yan, H. L. Wan, K. R. Tsai, J. Z. Wang and S. Z. Hu, *J. Chem. Crystallogr.* 1995, **25,** 807; (b) D. W. Wright, P. A. Humiston, W. H. Orme-Johnson and W. H. Davis, *Inorg. Chem.* 1995, **34,** 4194.
24. (a) A. Loewenstein and J. D. Roberts, *J. Chem. Soc.* 1960, **82,** 2705; (b) A. Cervilla, J. A. Ramirez and E. Llopis, *Trans. Met. Chem.* 1986, **11,** 186.

Pergamon

S0277-5387(96)00251-3

Polyhedron Vol. 16, No. 1, pp. 81–87, 1997
Copyright © 1996 Elsevier Science Ltd
Printed in Great Britain. All rights reserved
0277-5387/97 $15.00+0.00

Synthesis, characterization, redox properties and reactivities of a group of phenolato complexes of ruthenium(III)

Prasanta Kumar Sinha, Joydip Chakravarty and Samaresh Bhattacharya*

Department of Chemistry, Inorganic Chemistry Section, Jadavpur University, Calcutta 700 032, India

(Received 13 February 1996; accepted 16 May 1996)

Abstract—Seven complexes of the type $[Ru^{III}(PPh_3)_2(L)Cl_2]$ (where L = 8-quinolinolate, 4-methyl-2-(phenylazo)phenolate and salicylal-diminate anion) have been synthesized by the reaction of $[Ru(PPh_3)_3Cl_2]$ with HL. These complexes are one-electron paramagnetic and show rhombic ESR spectra in 1 : 1 dichloromethane-toluene at 77 K. In CH_2Cl_2 solution, these complexes show intense LMCT transitions in the visible region together with weak ligand-field transitions at lower energies. Each of these complexes shows a ruthenium(III)–ruthenium(II) reduction (−0.12 to −0.40 V *vs* SCE) and a ruthenium(III)–ruthenium(IV) oxidation (0.78–0.88 V *vs* SCE) in acetonitrile solution. The potentials of the ruthenium(III)–ruthenium(II) reduction vary linearly with the nature of substituent in L. The $[Ru^{III}(PPh_3)_2(L)Cl_2]$ complexes react with bidentate chelating ligands (L′ = 8-quinolinolate anion, 2,2′-bipyridine, 1,10-phenanthroline) to afford complexes of type $[Ru(PPh_3)_2(L)(L')]^{n+}$. These complexes are diamagnetic and show intense MLCT transitions in the visible region. The potential of the ruthenium(II)–ruthenium(III) couple in these complexes depend on the nature of both L and L′. Copyright © 1996 Elsevier Science Ltd

Keywords: ruthenium phenolates; synthesis; characterization; redox properties.

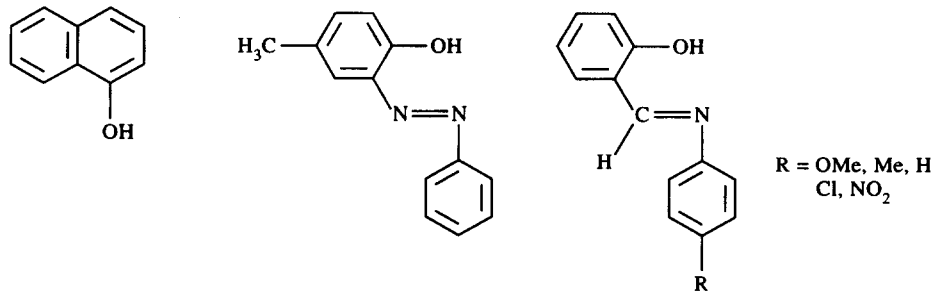
The present work has developed from our interest in the chemistry of ruthenium in different coordination spheres [1]. We have observed that coordination of ruthenium by phenolate oxygen is very effective in stabilizing the higher oxidation states of this metal [2]. In this study, phenolic ligands of three different types have been used, which are 8-quinolinol (HQ, **1**), 4-methyl-2-(phenylazo)phenol (Hap, **2**) and salicylaldimine (Hsal-R, **3**). All these ligands (abbreviated in general as HL, where H stands for the acidic hydrogen) bind to a metal ion as bidentate N,O-coordinator *via* dissociation of the phenolic proton. It may be noted here that the ruthenium chemistry of these ligands has received relatively little attention [3–5]. Herein we report the synthesis and characterization of a group of complexes of type $[Ru^{III}(PPh_3)_2(L)Cl_2]$ and their spectroscopic and electron-transfer properties. Reactivity studies, involving the dissociation of Ru—Cl bonds, are also described.

* Author to whom correspondence should be addressed.

EXPERIMENTAL

Materials

Commercial ruthenium trichloride, purchased from Arora Matthey, Calcutta, India was converted to $RuCl_3 \cdot 3H_2O$ by repeated evaporation with concentrated hydrochloric acid. Triphenylphosphine (PPh_3), triethylamine (Et_3N), 2,2′-bipyridine (bpy), 1,10-phenanthroline (phen) and 8-quinolinol (HQ) were purchased from SD Fine Chemicals, Bombay, India. $[Ru(PPh_3)_3Cl_2]$ was prepared by following a reported procedure [6]. The salicylaldimine ligands were prepared by reacting equimolar amounts of salicylaldehyde and the respective amine in hot ethanol. The 4-methyl-2-(phenylazo)phenol ligand was prepared by coupling diazotized aniline with *p*-cresol. Purification of acetonitrile and dichloromethane and preparation of tetraethylammonium perchlorate (TEAP) for electrochemical work were performed as reported earlier [1a]. All other chemicals and solvents were reagent grade commercial materials and were used as received.



HQ Hap H sal-R

1 2 3

Preparation of complexes

The seven $[Ru(PPh_3)_2(L)Cl_2]$ complexes were synthesized by using a general procedure. Yields varied in the range 80–90%. Specific details are given for one complex.

$[Ru(PPh_3)_2(Q)Cl_2]$. To a mixture of $[Ru(PPh_3)_3Cl_2]$ (100 mg, 0.10 mmol) and 8-quinolinol (15 mg, 0.10 mmol) was added dichloromethane (40 cm^3). The resulting solution was stirred for 30 min. The volume of the solvent was reduced by evaporation and hexane was added to it upon which $[Ru^{III}(PPh_3)_2(Q)Cl_2]$ started separating out as a dark-coloured solid. This was collected by filtration, washed thoroughly with hexane and dried in air. The yield was 70 mg, 83%.

$[Ru(PPh_3)_2(Q)_2]$. To a solution of $[Ru(PPh_3)_2(Q)Cl_2]$ (100 mg, 0.12 mmol) and 8-quinolinol (17 mg, 0.12 mmol) in acetonitrile (40 cm^3) was added triethylamine (24 mg, 0.24 mmol). The resulting solution was refluxed for 1 h upon which the colour of the solution changed from green to yellowish red. The solution was cooled and concentrated by evaporation. Ether was then added to the solution and $[Ru(PPh_3)_2(Q_2)]$ separated out as a brown microcrystalline solid. It was filtered, washed with water and ethanol and dried in air. The yield was 95 mg, 87%.

$[Ru(PPh_3)_2(ap)(phen)]ClO_4$. To a solution of $[Ru^{III}(PPh_3)_2(ap)Cl_2]$ (100 mg, 0.11 mmol) and 1,10-phenanthroline (22 mg, 0.11 mmol) in acetonitrile (40 cm^3) was added triethylamine (22 mg, 0.22 mmol). The colour of the solution changed from green to yellowish red upon refluxing the solution for 1 h. The solution was then cooled to room temperature and a saturated aqueous solution of $NaClO_4$ (10 cm^3) was added to it. $[Ru^{III}(PPh_3)_2(ap)(phen)]ClO_4$ precipitated as a dark solid, which was collected by filtration, washed with ice-cold water and dried *in vacuo* over P_4O_{10}. Recrystallization of this crude product from acetonitrile–toluene solution gave $[Ru(PPh_3)_2(ap)(phen)]ClO_4$ in the pure state. The yield was 75 mg, 60%.

$[Ru(PPh_3)_2(sal\text{-}H)(bpy)]ClO_4$. This was prepared by following the same above procedure using $[Ru(PPh_3)_2(sal\text{-}H)Cl_2]$ and bpy instead of $[Ru(PPh_3)_2(ap)Cl_2]$ and phen, respectively.

Physical measurements

As described earlier [1a].

RESULTS AND DISCUSSION

Synthesis and characterization

The reaction of $[Ru(PPh_3)_3Cl_2]$ with an equimolar quantity of HL in dichloromethane solution at ambient temperature afforded the $[Ru(PPh_3)_2(L)Cl_2]$ complexes [eq. (1)] in good yields. In total seven complexes have been prepared using different phenolic ligands.

$$[Ru^{II}(PPh_3)_3Cl_2] + HL \rightarrow [Ru^{III}(PPh_3)_2(L)Cl_2] + H^+ + e^- \quad (1)$$

It is interesting to note here that during the course of this synthetic reaction ruthenium undergoes a one-electron oxidation. In view of the low ruthenium(III)–ruthenium(II) reduction potential in these complexes (*vide infra*) oxygen in the air appears to be the probable oxidant [7].

Elemental (C, H, N) analytical data (Table 1) confirm the compositions of these complexes. Magnetic susceptibility measurements show that these complexes are one-electron paramagnetic (Table 1), as expected for complexes of ruthenium(III) (low-spin d^5, $S = 1/2$). The infrared spectra of these complexes contain many sharp bands of different intensities due to vibrations arising from the coordinated PPh_3, L and Cl^- and are therefore complex in nature. No attempt has been made to assign individual bands. However, comparison of the IR spectra of these $[Ru(PPh_3)_2(L)Cl_2]$ complexes with that of $[Ru(PPh_3)_3Cl_2]$ shows that besides small shifts in frequencies, some vibrations are common in both the spectra (e.g. vibrations near 520, 540, 690 and 740 cm^{-1}) which are due to the common PPh_3 ligand. Some additional bands are observed in the spectra of the $[Ru(PPh_3)_2(L)Cl_2]$ complexes which are obviously due to the coordinated phenolic ligand L. Two sharp bands of medium intensity, observed in all the com-

Table 1. Microanalytical, magnetic moment, electronic spectral and cyclic voltammetric data

Compound	Analytical data[a] %C	%H	%N	μeff (BM)	Electronic spectral data[b] λ_{max}, nm (ε, M^{-1} cm^{-1})	Cyclic-voltammetric data[c] E^0_{298}, $V(\Delta E_p$, mV) $Ru^{II/III}$	$Ru^{III/IV}$
$[Ru(PPh_3)_2(Q)Cl_2]$	64.2	4.1	1.6	1.85	1800(42), 760(625)	−0.40[e]	0.85[f]
	(64.3)	(4.3)	(1.7)		425[d](3550), 390(4200)		
$[Ru(PPh_3)_2(ap)Cl_2]$	64.6	4.5	3.0	1.92	1400(80), 625(370),	−0.22(120)	0.78[f]
	(64.8)	(4.5)	(3.1)		420(9400)		
$[Ru(PPh_3)_2(sal\text{-}OMe)Cl_2]$	65.1	4.4	1.5	1.95	667(2190), 515(3210)	−0.34(70)	0.84[f]
	(65.1)	(4.6)	(1.5)				
$[Ru(PPh_3)_2(sal\text{-}Me)Cl_2]$	66.0	4.4	1.5	1.89	600(2530), 400[d](5170)	−0.30(60)	0.86[f]
	(66.2)	(4.6)	(1.6)				
$[Ru(PPh_3)_2(sal\text{-}H)Cl_2]$	65.7	4.4	1.6	1.84	1600[d](70), 660(2650),	−0.27(60)	0.85[f]
	(65.9)	(4.5)	(1.6)		390[d](5400), 340(6600)		
$[Ru(PPh_3)_2(sal\text{-}Cl)Cl_2]$	63.4	4.0	1.5	1.90	600(2950), 375(7570)	−0.24(70)	0.88[f]
	(63.5)	(4.2)	(1.5)				
$[Ru(PPh_3)_2(sal\text{-}NO_2)Cl_2]$	62.6	4.2	1.4	1.83	550(3230), 435(6900),	−0.12(70)	0.86[f]
	(62.8)	(4.2)	(1.5)		340(17575)		
$[Ru(PPh_3)_2(sal\text{-}H)(bpy)]ClO_4$[g]	65.7	4.4	3.8	—	600[d](840), 425[d](2050)	0.72(80)	—
	(65.8)	(4.5)	(3.9)				
$[Ru(PPh_3)_2(ap)(phen)]ClO_4$[g]	65.5	4.3	4.9	—	575[d](1580), 410(2950)	0.76(80)	—
	(65.6)	(4.4)	(5.0)				

[a] Calculated values are given in parentheses.

[b] In dichloromethane solution.

[c] Supporting electrolyte, TEAP (0.1 M); reference electrode, SCE; $E^0_{298} = 0.5\ (E_{pa} + E_{pc})$, where E_{pa} and E_{pc} are anodic and cathodic peak potentials; $\Delta E_p = E_{pa} - E_{pc}$; scan rate, 50 mV s^{-1}; solvent acetonitrole.

[d] Shoulder.

[e] E_{pc} value.

[f] E_{pa} value.

[g] Electronic spectra recorded in acetonitrile solution.

plexes near 315 cm^{-1} and 330 cm^{-1}, have been attributed to the ν(Ru—Cl) stretching mode [8]. The infrared spectral data are therefore in good agreement with the compositions of these complexes.

The $[Ru(PPh_3)_2(L)Cl_2]$ complexes may exist in four geometrical isomeric forms. However, it is well known that complexes containing the $Ru^{III}(PPh_3)_2$ moiety prefers the *trans* geometry [3b, 9] and hence we assume a similar structure, with the two PPh_3 ligands *trans* to each other, for these $[Ru(PPh_3)_2(L)Cl_2]$ complexes. In this geometry the two Ru—Cl bonds are non-equivalent and hence are expected to vibrate at different energies, as actually observed in the infrared spectra (*vide supra*). The $[Ru(PPh_3)_2(L)Cl_2]$ complexes are soluble in acetonitrile and dichloromethane producing green solutions. Conductivity studies in acetonitrile show that these complexes behave as non-electrolytes in solution, indicating that the chloride ligands do not dissociate in solution. Electronic spectra of these complexes have been recorded in dichlormethane solution. Spectral data are presented in Table 1 and selected spectra are shown in Fig. 1. All the seven complexes display two or three intense absorptions, one of which appears in the visible region while the others extend into the UV region. These are probably due to allowed metal-to-ligand charge-transfer transitions. A low-intensity absorption at lower energy is also displayed by all these complexes which is discussed below.

ESR spectra of three representative complexes, *viz.*, $[Ru^{III}(PPh_3)_2(Q)Cl_2]$, $[Ru^{III}(PPh_3)_2(sal\text{-}H)Cl_2]$ and $[Ru^{III}(PPh_3)_2(ap)Cl_2]$ have been recorded in 1 : 1 dichloromethane–toluene solution at 77 K. A selected spectrum is shown in Fig. 2 and the g-values are given in Table 2. All the three complexes show rhombic spectra with three distinct g-values. The rhombicity of the spectra reflects the asymmetry of electronic environments around ruthenium in these complexes. Under the combined influence of this low-symmetry and spin-orbit coupling, the three t_2-levels get well separated. Hence two electronic transitions (transition energies ΔE_1 and ΔE_2; $\Delta E_1 < \Delta E_2$) within these three levels are probable. These transition energies have been computed (Table 2) using the observed g-values: the g-tensor theory of low-spin d^5 complexes [10] and a reported method [11]. The ΔE_2 transitions in all these three complexes have indeed been observed close to the theoretically predicted values as a low-intensity absorption (Table 1, Fig. 1) whereas the ΔE_1 transitions fall in the IR region and could not be detected. The ESR spectral data therefore show that these ruthenium(III) complexes are significantly distorted

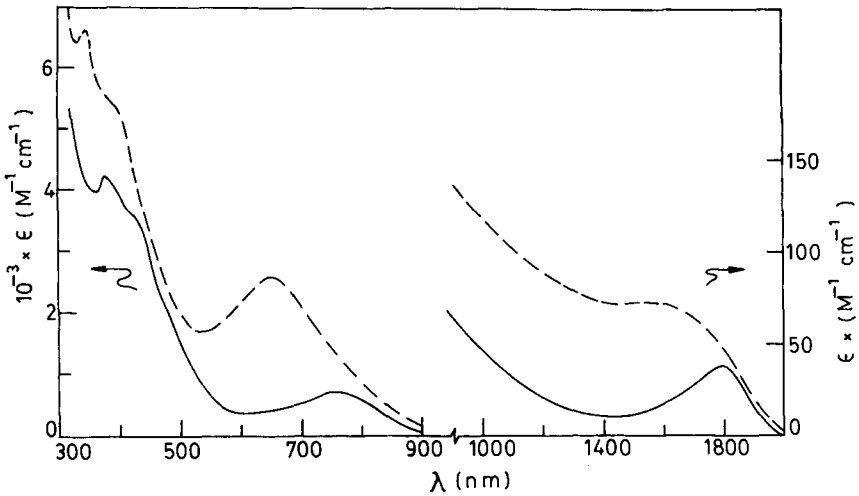


Fig. 1. Electronic spectra of $[Ru(PPh_3)_2(Q)Cl_2]$ (——) and $[Ru(PPh_3)_2(sal\text{-}H)Cl_2]$ (– – –) in dichloromethane solution.

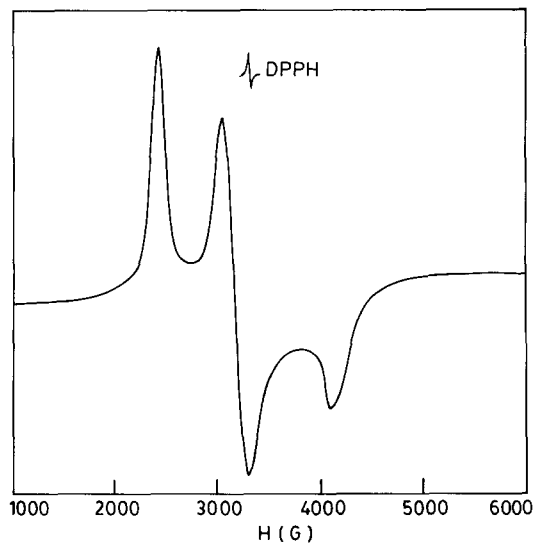


Fig. 2. ESR spectrum of $[Ru(PPh_3)_2(Q)Cl_2]$ in 1 : 1 dichloromethane–toluene at 77K.

from ideal octahedral geometry, which is understandable by simple examination of the coordination sphere consisting of three different P—Ru—P, N—Ru—Cl and O—Ru—Cl axes.

Cyclic voltammetric studies

Electron-transfer properties of the $[Ru(PPh_3)_2(L)Cl_2]$ complexes have been studied in acetonitrile solution (0.1 M TEAP) by cyclic voltammetry. A selected voltammogram is shown in Fig. 3

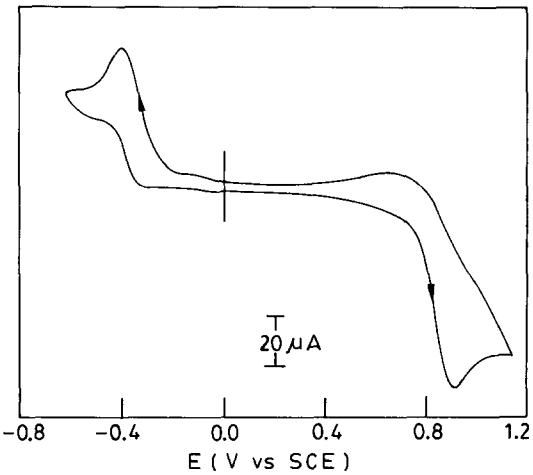


Fig. 3. Cyclic voltammogram of $[Ru(PPh_3)_2(Q)Cl_2]$ in acetonitrile solution (0.1 M TEAP) at a scan rate of 50 mV s^{-1}. The solute concentration was 10^{-3} M.

Table 2. ESR g values and derived energy parameters of ruthenium(III) complexes

Compound	g values[a]			Derived energy parameters (cm^{-1})	
	g_1	g_2	g_3	ΔE_1	ΔE_2
$[Ru(PPh_3)_2(Q)Cl_2]$	2.7263	2.0985	1.6225	2300	5700
$[Ru(PPh_3)_2(sal\text{-}H)Cl_2]$	2.4508	2.2265	1.8424	3800	6400
$[Ru(PPh_3)_2(ap)Cl_2]$	2.3862	2.1962	1.8695	4100	6800

[a] ESR spectra recorded in 1 : 1 dichloromethane–toluene at 77 K.

and voltammetric data are given in Table 1. All these complexes show a ruthenium(III)–ruthenium(II) reduction [eq. (2)] on the negative side of SCE and a ruthenium(III)–ruthenium(IV) oxidation [eq. (3)] on the positive side.

$$[Ru^{III}(PPh_3)_2(L)Cl_2 + e^- \rightleftharpoons [Ru^{II}(PPh_3)_2(L)Cl_2]^- \quad (2)$$

$$[Ru^{III}(PPh_3)_2(L)Cl_2] \rightleftharpoons [Ru^{IV}(PPh_3)_2(L)Cl_2]^+ + e^- \quad (3)$$

In $[Ru(PPh_3)_2(Q)Cl_2]$ both electron-transfer processes take place irreversibly at -0.40 V and 0.85 V, respectively, which indicates that in the NOP_2Cl_2 coordination sphere the $+3$ state of ruthenium is stable while the $+2$ and $+4$ states are not. The ruthenium(III)–ruthenium(II) potential in this complex is 430 mV less than that in $[Ru(PPh_3)_2(bpy)Cl_2]$ (0.39 V) [1a] which indicates that relative to bpy, 8-quinolinolate is a much better stabilizer of ruthenium(III). This is due to the recognized ability of phenolate oxygen to stabilize the higher oxidation states of ruthenium. In $[Ru(PPh_3)_2(ap)Cl_2]$, the ruthenium(III)–ruthenium(II) reduction and ruthenium(III)–ruthenium (IV) oxidation are observed at -0.22 V and 0.78 V respectively. In $[Ru(PPh_3)_2(sal\text{-}R)Cl_2]$ complexes the irreversible ruthenium(III)–ruthenium(IV) oxidation is observed near 0.85 V and remains virtually insensitive to the substituent R. However, the ruthenium(III)–ruthenium(II) reduction potential varies as R is varied. The plot of this reduction potential *vs* the Hammett substituent constant [12] of R is linear (Fig. 4) with $\rho = 0.20$ V [13]. This shows that ruthenium(III)–ruthenium(II) reduction potential in the $[Ru(PPh_3)_2(sal\text{-}R)Cl_2]$ complexes can be finetuned by varying R in the salicylaldiminate ligand.

Reactivities

Solution electrical conductivity studies have shown (*vide supra*) that the chloride ligands of the $[Ru(PPh_3)_2(L)Cl_2]$ complexes do not dissociate in solution. This indicates the strong bonding between trivalent ruthenium and chloride ion. However, both the chloride ligands can be displaced from the coordination sphere under mild condition by bidentate chelating ligands (L′). Such reactivity studies have been restricted to only three representative complexes, *viz.* $[Ru(PPh_3)_2(Q)Cl_2]$, $[Ru(PPh_3)_2(sal\text{-}H)Cl_2]$ and $[Ru(PPh_3)_2(ap)Cl_2]$. Reaction of these complexes with another ligand (L′) in the presence of NEt_3 affords new complexes of the type $[Ru(PPh_3)_2(L)(L')]^+$ [eq. (4)] in decent yields. Two types of L′, monoanionic (8-quinolinolate anion, Q) and neutral (2,2′-bipyridine, bpy; 1,10-phenanthroline, phen) have been used and three complexes [L = L′ = Q; L = sal-H, L′ = bpy and L = ap, L′ = phen] have been synthesized. Triethylamine primarily serves the function of a reducing agent for the ruthenium(III) complexes thereby facilitating the dissociation of the Ru(II)—Cl bond (formed due to the reduction) followed by the subsequent incorporation of the L′ ligand. It is interesting to note here that ruthenium undergoes a one-electron reduction during the course of the synthetic reaction [eq. (4)].

$$[Ru^{III}(PPh_3)_2(L)Cl_2] \xrightarrow[EtOH/reflux]{Et_3N,L'} [Ru^{II}(PPh_3)_2(L)(L')]^+ \quad (4)$$

The characterization data of these $[Ru(PPh_3)_2(L)(L')]^+$ complexes [14] are given in Table 1. Microanalytical data agree well with the compositions of these complexes. All the three complexes are diamagnetic, confirming the $+2$ oxidation state of ruthenium (low-spin d^6, $S = 0$) in these complexes. IR spectra of the $[Ru(PPh_3)_2(L)(L')]^+$ complexes show many vibrations, some of which are also observed in the spectra of their respective precursors. Some additional bands are observed in the fingerprint region of the spectra of $[Ru(PPh_3)_2(L)(L')]^+$, which are obviously due to the new coordinated ligand L′. The ν(Ru—Cl) vibrations observed in the spectra of the precursor complexes, are absent as expected. Intense bands are observed near 1100 cm^{-1} and 620 cm^{-1} in the spectra of $[Ru(PPh_3)_2(sal\text{-}H)(bpy)]ClO_4$ and $[Ru(PPh_3)_2(ap)(phen)]ClO_4$ due to the presence of ClO_4^-.

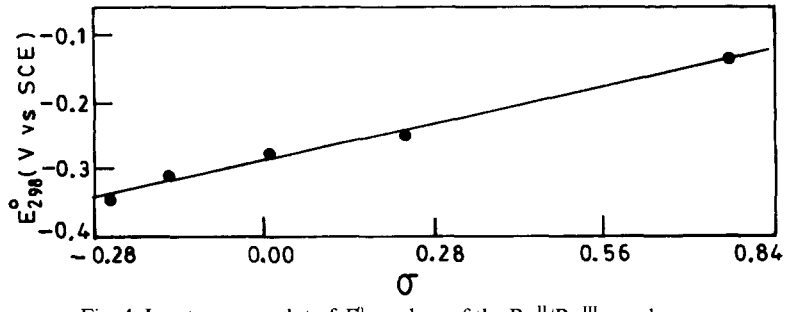


Fig. 4. Least-squares plot of E^0_{298} values of the Ru^{II}/Ru^{III} couple *vs* σ.

The spectral and cyclic voltammetric properties of $[Ru(PPh_3)_2(Q)_2]$, synthesized by us from $[Ru(PPh_3)_2(Q)Cl_2]$, are virtually identical to those of the *trans–trans–trans* isomer of this complex reported earlier [3b]. Hence $[Ru(PPh_3)_2(Q)_2]$, synthesized by us, is assumed to have the completely *trans* geometry. The $[Ru(PPh_3)_2(sal\text{-}H)(bpy)]^+$ and $[Ru(PPh_3)_2(ap)(phen)]^+$ complexes can exist in only one geometrical isomeric form provided the two PPh_3 ligands are *trans*, as assumed in their respective precursors. The displacement of the two chloride ions from $[Ru(PPh_3)_2(L)Cl_2]$ by L′ [eq. (4)] therefore takes place without any gross change of stereochemistry.

All the three $[Ru(PPh_3)_2(L)(L')]^+$ complexes are soluble in acetonitrile. Conductivity measurements show that in solution $[Ru(PPh_3)_2(sal\text{-}H)(bpy)]ClO_4$ and $[Ru(PPh_3)_2(ap)(phen)]ClO_4$ complexes behave as 1 : 1 electrolytes (Λ_M = 140 and 155 ohm^{-1} cm^2 M^{-1} respectively) while $[Ru(PPh_3)_2(Q)_2]$ is a non-electrolyte, as expected. Electronic spectra of these three complexes have been recorded in acetonitrile solution (Table 1). Each complex shows several intense absorptions in the visible region which are probably due to allowed metal-to-ligand charge-transfer transitions.

Redox properties of the $[Ru(PPh_3)_2(L)(L')]^+$ complexes have been studied in acetonitrile solution (0.1 M TEAP) by cyclic voltammetry. Voltammetric data are given in Table 1. A reversible ruthenium(II)–ruthenium(III) oxidation is displayed by all three complexes, the potential of which varies as L and L′ are varied. In $[Ru(PPh_3)_2(sal\text{-}H)(bpy)]^+$, this oxidation takes place at 0.72 V, which is approximately 1 V more positive than that of the ruthenium(II)–ruthenium(III) couple in $[Ru(PPh_3)_2(sal\text{-}H)Cl_2]$. This shows that replacement of two chloride ions by one bpy stabilizes the bivalent state of ruthenium to a great extent. A similar shift in the ruthenium(II)–ruthenium(III) potential was observed in the pair: $[Ru(bpy)_2Cl_2]$, (0.30 V) [15] and $[Ru(bpy)_3]^{2+}$, (1.30 V) [16]. One quasi-reversible one-electron reduction is observed in $[Ru(PPh_3)_2(sal\text{-}H)(bpy)]^+$ at -1.39 V, which is assigned to the reduction of the coordinated bpy. Each bpy is expected to show two one-electron reductions [17]. The second one-electron reduction of bpy, which is expected to occur at much more negative potential, has not been observed due to solvent cut-off. In $[Ru(PPh_3)_2(ap)(phen)]^+$, the ruthenium(II)–ruthenium(III) couple appears at 0.76 V, which is again $\sim$1 V more positive than that in $[Ru(PPh_3)_2(ap)Cl_2]$, as in the previous case. The one-electron reduction of phen is observed as a quasi-reversible process in $[Ru(PPh_3)_2(ap)(phen)]^+$ at -1.43 V.

Acknowledgements—Financial assistance received from the Department of Science and Technology (SR/OY/C-08/93), New Delhi, is gratefully acknowledged. One of us (J.C.) thanks the Council of Scientific and Industrial Research, New Delhi, for his fellowship. We thank Professor A. Chakravorty and Professor K. Nag of the Indian Association for the Cultivation of Science, Calcutta and Professor R. G. Bhattacharyya and Professor M. K. Das of Jadavpur University, Calcutta for their help.

REFERENCES

1. (a) J. Chakravarty and S. Bhattacharya, *Polyhedron* 1994, **13,** 2671; (b) N. Ghatak and S. Bhattacharya, *Polyhedron* 1994, **13,** 2999; (c) N. Ghatak, J. Chakravarty and S. Bhattacharya, *Trans. Met. Chem.* 1995, **20,** 138; (d) N. Ghatak, J. Chakravarty and S. Bhattacharya, *Polyhedron* 1995, **14,** 3591; (e) J. Chakravarty and S. Bhattacharya, *Proc. Indian Acad. Sci. (Chem. Sci.)* 1995, **107,** 361; (f) N. Ghatak and S. Bhattacharya, *Trans. Met. Chem.* 1996, **21,** 158.
2. (a) S. Bhattacharya, *Polyhedron* 1993, **12,** 235; (b) S. Bhattacharya, *Polyhedron* 1994, **13,** 451; (c) J. Chakravarty and S. Bhattacharya, *Polyhedron* 1996, **15,** 257; (d) J. Chakravarty and S. Bhattacharya, *Polyhedron* 1996, **15,** 1047; (e) P. K. Sinha, J. Chakravarty and S. Bhattacharya, *Polyhedron* 1996, **15,** 2931.
3. (a) G. K. Lahiri, S. Bhattacharya, B. K. Ghosh and A. Chakravorty, *Inorg. Chem.* 1987, **26,** 4324 and references therein; (b) M. Menon, A. Pramanik, N. Bag and A. Chakravorty, *J. Chem. Soc., Dalton Trans.* 1995, 1417.
4. (a) E. P. Benson and J. I. Legg, *Inorg. Chem.* 1981, **20,** 2504; (b) G. K. Lahiri, S. Bhattacharya, M. Mukherjee, A. K. Mukherjee and A. Chakravorty, *Inorg. Chem.* 1987, **26,** 3359.
5. (a) A. M. El-Hendawy, A. El-Ghany El-Kourashy and M. M. Shanab, *Polyhedron* 1992, **11,** 523; (b) A. M. El-Hendawy, A. H. Alkubaisi, A. El-Ghany El-Kourashy and M. M. Shanab, *Polyhedron* 1993, **12,** 2343.
6. T. A. Stephenson and G. Wilkinson, *J. Inorg. Nucl. Chem.* 1966, **28,** 945.
7. S. F. Colson and S. D. Robinson, *Polyhedron* 1989, **8,** 2179.
8. S. Choudhury, M. Kakoti, A. K. Deb and S. Goswami, *Polyhedron* 1992, **11,** 3183.
9. (a) S. Chattopadhyay, N. Bag, P. Basu, G. K. Lahiri and A. Chakravorty, *J. Chem. Soc., Dalton Trans.* 1990, 3389; (b) S. Bhattacharya and C. G. Pierpont, *Inorg. Chem.* 1991, **30,** 1511.
10. (a) B. Bleany and M. C. M. O'Brien, *Proc. Phys. Soc. Lond. Sect. B* 1956, **69,** 1216; (b) J. S. Griffith, *The Theory of Transition Metal Ions*, p. 364. Cambridge University Press, Cambridge (1961).
11. S. Bhattacharya and A. Chakravorty, *Proc. Indian Acad. Sci., Chem. Sci.* 1985, **95,** 159.
12. (a) L. P. Hammett, *Physical Organic Chemistry*, 2nd edn. McGraw-Hill, New York (1970); (b) The σ values used are: OMe = -0.27, Me = -0.17, H = 0.00, Cl = 0.23 and NO_2 = 0.78.
13. R. N. Mukherjee, O. A. Rajan and A. Chakravorty, *Inorg. Chem.* 1982, **21,** 785.

14. Characterization data of $[Ru(PPh_3)_2(Q)_2]$ are neither given in Table 1 nor discussed in the text as they are identical to those reported in reference [3b].
15. E. C. Johnson, B. P. Sullivan, D. J. Salmon, S. A. Adeyemi and T. J. Meyer, *Inorg. Chem.* 1987, **17,** 2211.
16. N. E. Tokel-Takvorian, R. E. Hemingway and A. J. Bird, *J. Am. Chem. Soc.* 1973, **95,** 6582.
17. A. A. Vlcek, *Coord. Chem. Rev.* 1982, **43,** 39.

Pergamon

S0277-5387(96)00242-2

Polyhedron Vol. 16, No. 1, pp. 89–93, 1997
Copyright © 1996 Elsevier Science Ltd
Printed in Great Britain. All rights reserved
0277-5387/97 $15.00+0.00

Spectroscopic properties and electronic states of five-coordinate copper(II) complexes with linear pentadentate ligands containing two amide groups

Tasuku Murakami,* Takaaki Takei and Yuichiro Ishikawa

Faculty of Education, Iwate University, Morioka 020, Japan

(Received 3 April 1996; accepted 9 May 1996)

Abstract—The geometry and electronic states of five-coordinate copper(II) complexes, [Cu(dgepH$_{-2}$)] and [Cu(pcepH$_{-2}$)], are discussed on the basis of the absorption and ESR(X- and Q-band) spectra in solid and solution states, where dgepH$_{-2}$ and pcepH$_{-2}$ represent the divalent anion of 1,8-di(dimethylglycinoyl)-1,4,8-triazaoctane and 1,8-dipicolinoyl-1,4,8-triazaoctane, respectively. These complexes exhibit the spectral features of the intermediate geometries between square pyramidal(SP) and trigonal bipyramidal(TBP). The magnitude of distortion from TBP to SP was estimated by utilizing the vibronic-coupling treatment of the electronic states. Copyright © 1996 Elsevier Science Ltd

Keywords: five-coordinate copper(II) complex; electronic spectra; ESR; geometry; square pyramid; trigonal bipyramid.

For the copper(II) ion, which usually forms complexes with four nearby donor atoms arranged approximately in a plane with the possibility of one or two more distant axial donors, five-coordinate complexes with a variety of donor groups have become of considerable interest stereochemically or spectrochemically, as well as biologically.[1,2] The stereochemistry of five-coordinate copper(II) complexes has been reviewed and discussed comprehensively by Hathaway.[3] Most adopting geometries are intermediate between square pyramidal(SP) and trigonal bipyramidal(TBP). Reinen *et al.* have discussed the electronic states of the intermediate geometry by the vibronic-coupling treatment.[4–6]

This paper reports the spectroscopic properties of copper(II) complexes of dgep (1,8-di(dimethylglycinoyl)-1,4,8-triazaoctane) and pcep (1,8-dipicolinoyl-1,4,8-triazaoctane). These ligands are linear unsymmetrical pentadentate which could form a 5,5,6,5-membered tetra-fused chelate, and they have two amide groups in inner parts and two dimethyl-substituted amino groups or two pyridyl groups as the terminal donor groups. For the pyridyl-terminal ligand, pcep, the preparation and the absorption spectra of its copper(II) complex have been already reported.[7] Here the geometry and the electronic states of these copper(II) complexes will be discussed on the basis of the absorption and X- and Q-band ESR spectra in solid and solution states.

EXPERIMENTAL

Preparations

The ligand, dgep, was synthesized by refluxing a methanolic mixture of N,N-dimethyl glycine methyl ester and N-(2-aminoethyl)-1,3-propanediamine according to the method similar to that for pcep.[7] From the aqueous solution containing equimolar amounts of copper(II) hydroxide and dgep, a non-ionic complex, [Cu(dgepH$_{-2}$)], was isolated as dark-blue plates, which was ascertained by elementary analyses and IR spectral measurements (dgepH$_{-2}$ represents the divalent anion of dgep). Found: C, 44.4; H, 8.0; N, 19.9. Calc. for $CuC_{13}H_{27}N_5O_2$: C, 44.8; H, 7.8; N, 20.1%. The IR spectrum of the isolated

* Author to whom correspondence should be addressed.

complex shows a strong band around 1590 cm^{-1}, but no band in the region of 1620–1650 cm^{-1}, which indicates that the two amide groups are deprotonated and coordinate to copper(II) ion through the negative amide nitrogens.[8] The complex of pcep, [Cu(pcepH$_{-2}$)], was also prepared according to the literature.[7]

Spectral measurements

Solution and solid-state electronic absorption spectra were measured with a Hitachi U-3400 spectrophotometer at room temperature. The solid-state spectra were obtained by means of the Nujol mull technique. Solution and powder ESR spectra (X- and Q-bands) were recorded on a JES-FE3XG spectrometer at room and liquid-nitrogen temperatures. DPPH was used as standard (g = 2.003$_7$). Infrared spectra were recorded on a Jasco A-3 spectrophotometer as KBr pellets.

RESULTS AND DISCUSSIONS

Figure 1 shows the visible absorption spectra of [Cu(dgepH$_{-2}$)] in the solid-state (a) and methanol solution (b), together with those of [Cu(pcepH$_{-2}$)]. The solid-state (powder in Nujol mull) spectrum of [Cu(dgepH$_{-2}$)] exhibits two peaks at 14,300 and 17,200 cm^{-1}: the low-energy band is more intense and accompanied by a shoulder around 12,800 cm^{-1}. This spectral pattern is typical of a five-coordinate copper(II) complex with a TBP-based geometry.[3,9] The bands of 14,300 and 17,200 cm^{-1} are tentatively assigned to the symmetry-allowed $A_1' \rightarrow E'$ and forbidden $A_1' \rightarrow E''$ transitions, respectively, in D_{3h} symmetry.[5,9] In Fig. 2 are illustrated the qualitative term diagrams for Cu^{2+} ion in ligand fields of D_{3h} (TBP), C_{4v} (SP) and intermediate C_{2v} symmetry.[5] The shoulder band around 12,800 cm^{-1} suggests the splitting of the E′ state due to the geometric distortion of D_{3h} to C_{2v}. The split of the TBP E″ state, however, will not be observed as distinct bands, because its splitting energy is rather small.[9]

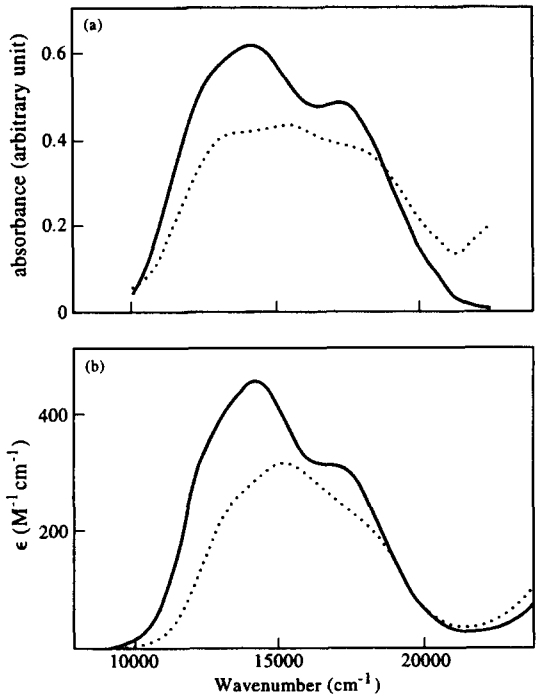
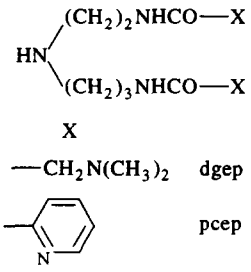


Fig. 1. Powder ((a): mull transmittance) and solutions ((b): methanol) absorption spectra of [Cu(dgepH$_{-2}$)] (——) and [Cu(pcepH$_{-2}$)] (– – –).



Scheme 1.

A methanol solution of [Cu(dgepH$_{-2}$)] exhibits a very similar spectrum to that seen in the solid-state, indicating that the TBP-based geometry is basically maintained also in methanol. Another remarkable feature of this solution spectrum is its extremely intense magnitude with an ε_{max} (molar absorptivity) value over 450 M^{-1} cm^{-1}; this spectrum is probably the most intense ever observed for the *d–d* transitions of discrete copper(II) complexes. The corresponding complex of pcep, [Cu(pcepH$_{-2}$)], also shows a considerably intense absorption bands (ε_{max} = 310 M^{-1} cm^{-1}). Therefore, the linkage of the donor groups, common in dgepH$_{-2}$ and pcepH$_{-2}$, will bring about the large geometrical distortions around the CuN_5 chromophore which serve to break the orbital-forbidden character of the *d–d* transitions a great deal. The bulkiness of the terminal dimethyl-substituted amino groups of dgep would play an additional role to the distortion.

The X-band ESR spectrum (Fig. 3) of [Cu(dgepH$_{-2}$)] in methanol at liq. N_2 temperature was entirely different from those usually observed for ordinary tetragonal copper(II) complexes. The *g* values, which are very helpful in determining the geometry of five-coordinate copper(II) complexes, were hard to evaluate from this spectrum due to the signal-overlapping. Then, the Q-band ESR of the methanol solution sample was measured at liq. N_2 temperature (Fig. 4a). The Q-band spectrum obtained clearly displayed three different *g* tensors with well-resolved hyperfine structures in the g_z and g_x signals, which strongly indicates a rhombic ligand field.[3] The *g* values observed for its powder samples at room temperature were almost the same as those for the frozen methanolic sample (Fig. 4b), which suggests

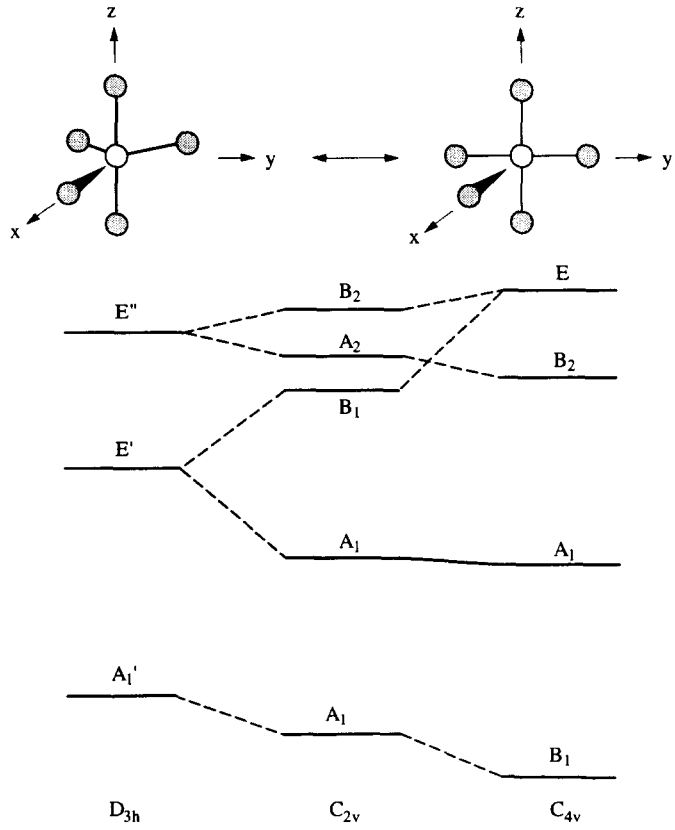


Fig. 2. Term diagrams for copper(II) ion in the ligand fields of D_{3h} (TBP), C_{4v} (SP) and intermediate C_{2v} symmetry.[5]

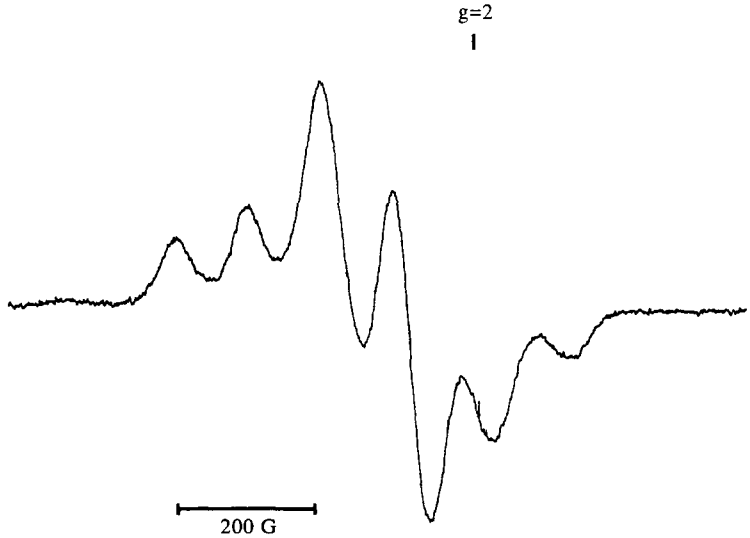


Fig. 3. X-Band ESR spectrum of [Cu(dgepH$_{-2}$)] in methanol at liq. N_2 temperature.

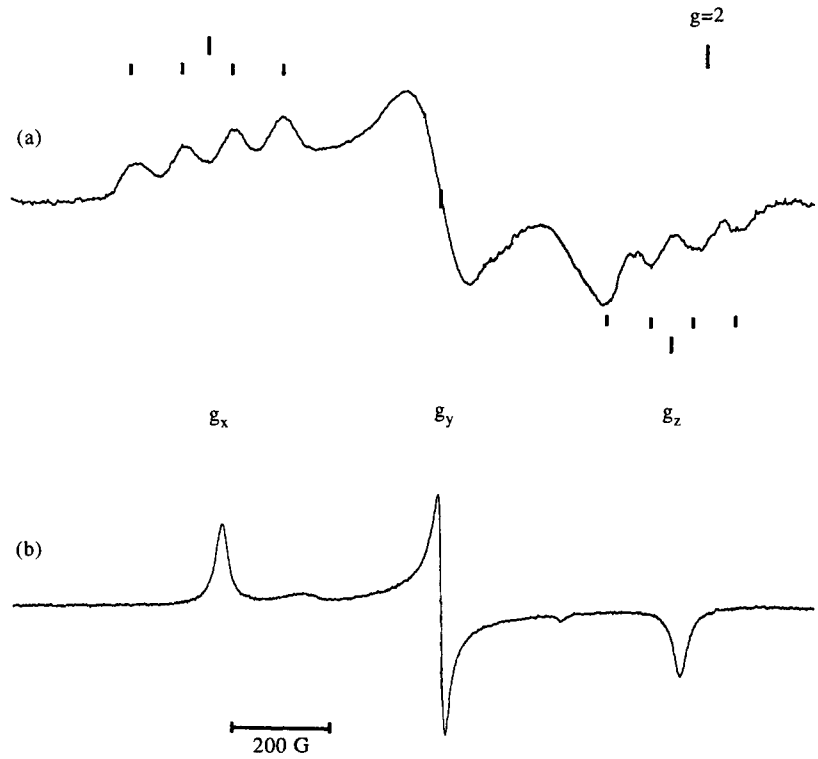


Fig. 4. Q-Band ESR spectra of [Cu(dgepH$_{-2}$)]; (a): in methanol at liq. N_2 temperature, (b): powder at room temperature.

that the powder g tensors also equate with the g values of the local molecular structure with no exchange between neighbouring copper(II) chromophores.

The ligand-field absorption and ESR spectral parameters found for [Cu(dgepH$_{-2}$)] and [Cu(pcepH$_{-2}$)] are summarized in Table 1, together with those of some related complexes with CuN_5 chromophores. The CuN_5 geometries of these related complexes have been determined by X-ray crystal analyses; $[Cu(NH_3)(tren)](ClO_4)_2$[10] and $[Cu(en)(dien)](ClO_4)_2$[11] are nearly regular TBP and SP, respectively, while $[Cu(NH_3)(bpy)_2](BF_4)_2$[12] and [Cu(SS-chxn)(pmdt)]$(ClO_4)_2$[13] are intermediate between TBP and SP. From the comparison of these spectral data, it seems reasonable to conclude that [Cu(dgepH$_{-2}$)] and [Cu(pcepH$_{-2}$)] take on the intermediate geometries.

The ground-state wave function of a five-coordinate copper(II) complex with an intermediate geometry (C_{2v}) between TBP(D_{3h}) and SP(C_{4v}), which has been derived by Reinen *et al.*,[4-6] is expressed by

$$\varphi_g = (1+c^2)^{-1/2}\{d_{z^2} + cd_{x^2-y^2}\}, \qquad (1)$$

where the coordinate system is defined as that shown in the top of Fig. 2. The mixing coefficient is $c = 0$ for TBP(d_{z^2} ground state) and $c = 1/3^{1/2}$ for SP ($d_{z^2-y^2}$ ground state). The g values are expressed as follows, according to this ground state function,[5]

$$g_z = g_0 + \frac{8c^2}{1+c^2}u_z,$$

$$g_y = g_0 + \frac{2c^2}{1+c^2}\left(1-\frac{\sqrt{3}}{c}\right)^2 u_y,$$

$$g_x = g_0 + \frac{2c^2}{1+c^2}\left(1+\frac{\sqrt{3}}{c}\right)^2 u_x, \qquad (2)$$

where g_0 is a value for a free ion (2.0023). The orbital contributions u_i are defined as

$$u_i = \frac{k_i^2\zeta_0}{\Delta E_i}\ (i = z, y, x), \qquad (3)$$

where k_i and ζ_0 ($=830$ cm^{-1}) are covalency factors and the spin–orbit coupling parameter of the free Cu^{2+} ion, respectively. the ΔE_i energies refer to the d–d transitions ΔE_i ($i = z, y, x$): $A_1 \rightarrow B_1$, B_2, A_2 in C_{2v} symmetry (Fig. 2).

By use of the observed ΔE_i energies, the mixing coefficient c and covalency factors k_i can be so estimated as to reproduce the experimental g values. For [Cu(dgepH$_{-2}$)], for example, the two absorption bands at 14,300 and 17,200 cm^{-1} (Table 1) are assigned to $A_1 \rightarrow B_1$ and to the unresolved $A_1 \rightarrow A_2$, B_2, respectively, in C_{2v} symmetry as mentioned above. With these transition energies, a set of $c = 0.2$–0.25 and $k_{av}(=k_z \approx k_y \approx k_x) \approx 0.70$ can reproduce best the

Table 1. Electronic absorption and ESR spectral data for a selection of copper(II) complexes with the CuN_5 geometry

Complex	Solvent	Absorption υ_{max} (ε)[a]	Condition[b]	ESR g_z	g_y	g_x
[Cu(dgepH$_{-2}$)]	mull	12.8sh, 14.3, 17.2sh	powder(rt)	2.015	2.098	2.183
	CH_3OH	12.8sh, 14.3(452), 17.0sh	CH_3OH(lnt)	2.019 ($A_z = 89$)[c]	2.101	2.188 ($A_x = 104$)[c]
[Cu(pcepH$_{-2}$)]	mull	13.4sh, 15.5, 17.9sh	powder(rt)	2.015	2.085	2.180
	CH_3OH	13.6sh, 15.2(310), 17.7sh	CH_3OH(lnt)	2.020 ($A_z = 65$)[c]	2.080	2.182 ($A_x = 135$)[c]
$[Cu(NH_3)(bpy)_2](BF_4)_2$[e]	reflectance[d]	10.9, 12.8, 15.5sh	powder(rt)	2.011	2.137	2.210
[Cu(SS-chxn)(pmdt)] $(ClO_4)_2$[f]	mull	11.5sh, 15br	powder(rt)	2.032	2.093	2.213
$[Cu(en)(dien)](ClO_4)_2$[g]	reflectance	11.6sh, 16.6	powder(rt)	$g_\parallel$ 2.209		$g_\perp$ 2.045
$[Cu(NH_3)(tren)](ClO_4)_2$[h]	mull	10.5sh, 12.3, 15.4sh	H_2O/CH_3OH(lnt)	g 2.003		$g_\perp$ 2.170
	CH_3CN	11sh, 12.7(141), 15.4sh		($A_\parallel = 60$)[c]		($A_\perp = 118$)[c]

[a] υ in 10^3 cm^{-1} (ε in mol^{-1} dm^3 cm^{-1}).
[b] rt = room temperature, lnt = liquid nitrogen temperature.
[c] A in 10^{-4} cm^{-1}
[d] at 5K.
[e] ref. 12.
[f] ref. 13.
[g] ref. 11.
[h] ref. 10.

experimental g values. This implies that the CuN_5 chromophore is considerably distorted to SP: $c = 0$ for regular TBP and $c = 0.577$ for regular SP. Similarly, for [Cu(pcepH$_{-2}$)] (the transition energies: 15,500 cm^{-1} for $A_1 \rightarrow B_1$ and 17,900 cm^{-1} for $A_1 \rightarrow A_2$, B_2) the values of $c = 0.3$–0.35 and $k_{av} \approx 0.72$ are derived. The larger c value indicates that the degree of distortion from TBP to SP is larger. The small difference in the covalency factor k_{av}, which is used as an empirical parameter, between these two complexes probably reflects the variation of the terminal donor groups, dimethylamino compared to pyridyl.

For the X-ray analyzed complexes cited in Table 1, $[Cu(NH_3)(bpy)_2](BF_2)_2$ and [Cu(SS-chxn)(pmdt)] $(ClO_4)_2$, such estimations of the c and k parameters are also performed. With the transition energies of 12,800 cm^{-1} ($A_1 \rightarrow B_1$) and 15,500 cm^{-1} ($A_1 \rightarrow A_2$, B_2) of the former, a set of $c = 0.15$–0.2 and $k_{av} \approx 0.74$ can best reproduce the observed g values. For the latter complex, the broad band around 15,000 cm^{-1} is tentatively assigned to the unresolved $A_1 \rightarrow B_1$, B_2, A_2 and the shoulder at 11,500 cm^{-1} assigned to $A_1 \rightarrow A_1$ in C_{2v} symmetry (Fig. 2). Therefore, with the same energy (15,000 cm^{-1}) to the transitions of $A_1 \rightarrow B_1$, A_2, B_2, the parameters are refined; $c \approx 0.35$ and $k_{av} \approx 0.70$ are the best set. These parameter values indicate that the CuN_5 geometry of $[Cu(NH_3)(bpy)_2](BF_4)_2$ is less distorted to SP from TBP than that of [Cu(SS-chxn)(pmdt)]$(ClO_4)_2$, in good agreement with the magnitude of distortion calculated by using the bond angles (the τ-values of 77% TBP for the former and 57% TBP for the latter).[12,13]

REFERENCES

1. N. Wei, N. N. Murthy and K. D. Karlin, *Inorg. Chem.* 1994, **33**, 6093 and references cited therein.
2. G. A. McLachlan, G. D. Fallon, R. L. Martin and L. Spiccia, *Inorg. Chem.* 1995, **34**, 254.
3. B. J. Hathaway, in Comprehensive Coordination Chemistry (Edited by G. Wilkinson, R. D. Gillard and J. A. McCleverty), vol. 5, p. 533, Pergamon, Oxford (1987).
4. M. I. Arriortua, J. L. Mesa, T. Rojo, T. Debaerdemaeker, D. B.-Porter, H. Stratemeier and D. Reinen, *Inorg. Chem.* 1988, **27**, 2976.
5. D. Reinen and M. Atanasov, *Chem. Phys.* 1989, **136**, 27.
6. D. Reinen and M. Atanasov, *Magn. Resonance Rev.* 1991, **15**, 167.
7. N. Iwasaki, K. Sone and H. Ojima, *Bull. Chem. Soc. Jpn* 1975, **48**, 2279.
8. A. E. Martell and M. K. Kim, *J. Coord. Chem.* 1974, **4**, 9.
9. C. Su, W. Lu, T. Hui, T. Chang, S. Wang, and F. Liao, *Polyhedron* 1993, **12**, 2249 and references cited therein.
10. M. Duggan, N. Ray, B. J. Hathaway, G. Tomlinson, P. Brint and K. Pelin, *J. Chem. Soc. Dalton Trans.* 1980, 1342.
11. M. J. Bew, B. J. Hathaway, and R. J. Fereday, *J. Chem. Soc. Dalton Trans.* 1972, 1229.
12. S. Tyagi, B. J. Hathaway, S. Kremer, H. Stratemeier, and D. Reinen, *J. Chem. Soc. Dalton Trans.* 1984, 2087.
13. T. Murakami, T. Takei, and Y. Ishikawa, *Polyhedron* in preparation.

Pergamon

S0277-5387(96)00236-7

Polyhedron Vol. 16, No. 1, pp. 95–102, 1997
Copyright © 1996 Elsevier Science Ltd
Printed in Great Britain. All rights reserved
0277-5387/97 $15.00+0.00

Synthesis, physical properties and X-ray crystal structure of $[(DMNP)_2(MNP)_2SiMo_{12}O_{40}\cdot 2DMF]$ a charge-transfer salt between organic donor and polyoxometalate acceptor

Xiao-Min Zhang, Bao-Zhen Shan and Xiao-Zeng You*

Coordination Chemistry Institute, State Key Laboratory of Coordination Chemistry, Nanjing University, Centre for Advanced Studies and Technology of Microstructures, Nanjing 210093, P.R. China

and

Hoong-Kun Fun

X-ray Crystallography Unit, School of Physics, Universiti Sains Malaysia, 11800, USM, Penang, Malaysia

(Received 6 February 1996; accepted 7 May 1996)

Abstract—The title complex $[(DMNP)_2(MNP)_2SiMo_{12}O_{40}\cdot 2DMF]$ (where DMNP is $MeNC_5H_4NMe_2$, MNP is $MeNC_5H_4NHMe$ and DMF is N,N-dimethyl formamide) has been synthesized and characterized by elemental analysis, XPS, ESR and IR spectra studies. The X-ray crystal structure revealed that the title complex possesses a noncentrosymmetrical arrangement in the unit cell.

Keywords: crystal structure; charge-transfer; donor; acceptor; polyoxometalate; Keggin structure.

In the last few years there has been a rapidly growing number of reports in the literature addressing the use of polyoxometalates (POM) in many fields of research such as catalysis, biology, medicine and materials science.[1–3] Numerous heteropoly anions can be reversibly reduced to mixed-valence species (heteropoly "blues" and "browns") by addition of various specific numbers of electrons, which are delocalized over a significantly large number of atoms of the heteropoly framework, retaining the gross structure of the oxidized anions.[4] The above property of polyoxoanions makes them attractive precursors for the preparation of charge-transfer hybrid salts made up of organic donors and inorganic acceptors derived from the polyoxometalates.[5] By use of the special properties of the polyoxoanion such as Keggin structures $M_{12}O_{40}^{n-}$ ($M = Mo$, W; $n = 3$–4), our aim is to design and synthesize molecular materials with the applications in non-linear optics, photorefractive effect and magnetism.

Here, we report the preparation of a charge-transfer salt by use of the organic donor DMNP and inorganic acceptors $(TBA)_4SiMo_{12}O_{40}$ (TBA = tetrabutylamino). The compound was characterized by IR, UV–Vis spectra, ESR measurements. The X-ray structure determination reveals that the title complex has non-centrosymmetric character, and probably possesses non-linear optical properties. The lost methyl of the N atom may be catalyzed by the polyoxometalate. Further related work is being done.

EXPERIMENTAL

All chemicals were reagent grade and used without further purification. The polyoxometalate $(TBA)_4$

* Author to whom correspondence should be addressed

$SiMo_{12}O_{40}$ was synthesized according to the procedure described earlier.[6] The DMNP was obtained by the literature method.[7]

Preparation of $(DMNP)_2(MNP)_2SiMo_{12}O_{40} \cdot 2DMF$

To a solution of $(TBA)_4SiMo_{12}O_{40}$ (0.3 mmol, 0.69 g) in 50 cm^3 acetonitrile, the DMNP-iodide (1.2 mmol, 0.422 g) was added. The mixture was refluxed for 2 h. After cooling to room temperature, the green precipitate was filtered by suction and washed three times with acetonitrile. Yield: 0.63 g, 90%. The green crystals of the title complex were obtained from DMF solution by diffusion of ether. Found: C, 17.8; H, 2.9; N, 6.0. Calc. for $C_{36}H_{62}Mo_{12}N_{10}O_{42}Si$: C, 17.6; H, 2.8; N, 5.7%.

Physical measurements

Elemental analysis was performed on a Perkin–Elmer 240C analytical instrument. The IR spectrum was recorded on a Nicolet FT–IR 170SX spectrophotometer with KBr pellet in the range of 4000–400 cm^{-1}. The solid state reflectance spectrum was recorded on a Shimadzu UV–240 spectrophotometer. Electronic spectra was obtained on a Shimadzu UV–3100 spectrometer in solution. The powder ESR spectrum was carried out using a Bruker 2000–SRC spectrometer at 110K. XPS was performed on a VG ESCALAB MK-II.

X-ray structure determination of the complex

A green prism crystal of size $0.30 \times 0.32 \times 0.60$ mm was used for data collection. The data were collected using a Siemens P4 four-circle diffractometer with graphite monochromated Mo-K_α radiation (λ = 0.71073 Å) using $\theta/2\theta$ scan mode. Intensities were measured for 9717 reflections of which 8695 independent reflections, and the 8692 observed reflections ($I > 2.0\sigma(I)$) were used for further computation. The data were corrected for Lorentz and polarization effects during data reduction using XSCANS.[8]

Structure solution and refinement

The structure was solved by direct methods using SHELXL86[9] and refined on F^2 by Full-matrix least-squares methods using SHELXL93.[10] All non-hydrogen atoms were refined anisotropically, but the hydrogen atoms were refined isotropically. The final reliability factor was R = 0.0517. All computations were performed on an IBM compatible 486/DX2 personal computer. The crystal data and the parameters of data collection and refinement are listed in Table 1. The final atomic coordinates, the thermal parameters, together with observed and calculated structure factors, have been deposited as supplementary material with the Editor, from whom copies are available on request.

Table 1. Crystallography data for $[C_8H_{13}N_2]_2[C_7H_{11}N_2]_2[C_3H_7NO]_2[Mo_{12}O_{40}Si]$

Molecular formula	$C_{36}H_{62}Mo_{12}N_{10}O_{42}Si$
Formula weight	2486.33
Colour	green
Crystal size (mm)	$0.30 \times 0.32 \times 0.60$
Crystal system	monoclinic
Space group	$P2_1$
Unit cell	
a (Å)	14.294(4)
b (Å)	14.245(1)
c (Å)	16.709(1)
β (°)	94.26(1)
V (Å^3)	3392.9(10)
Z	2
μ (mm^{-1})	2.259
F (000)	2404
D_x (Mg/m^3)	2.434
R_{int}	0.021
Collection range	h: −1 to 18, k: −1 to 18, l; −21 to 21 $2\theta_{max} = 55°$
Reflections collected	9171
Independent reflections	8695
Reflections on refinement with $I > 2.0\sigma(I)$	8692
F^2_{Gof}	1.048
R	0.0517
Residual extrema in final difference map	+1.303 to −1.385 eÅ^3

RESULTS AND DISCUSSION

IR spectrum

Comparing the IR spectra of the title compound with the IR spectra of $(TBA)_4SiMo_{12}O_{40}$, the vibrational band of Mo=O_d band of the title compound has a red shift from 954(s) cm^{-1} to 946(s) cm^{-1}. The bands of Mo–O_b–Mo and Mo–O_c–Mo both have red shifts from 890(w) cm^{-1}, 797(vs) cm^{-1} to 880(w) cm^{-1} and 787(vs) cm^{-1}, respectively,[11] due to the presence of partial charge transfer between the organic donor and polyoxometalate acceptor. This has been verified by the later ESR spectra and the central SiO_4 tetrahedron has been little influenced by the electron transfer, so the vibrational frequency of the Si–O bond remains unchanged at 900(vs) cm^{-1}. The band at 1655(vs) cm^{-1} is due to the C=O vibration from DMF molecule of the compound. The υ(N–H) vibration appears at 3046 cm^{-1}, which provides evidence of the loss of a methyl group from DMNP to give MNP.

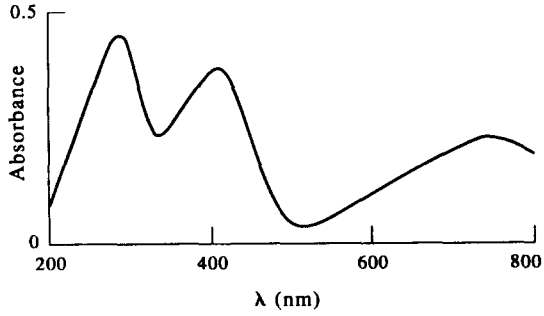


Fig. 1.

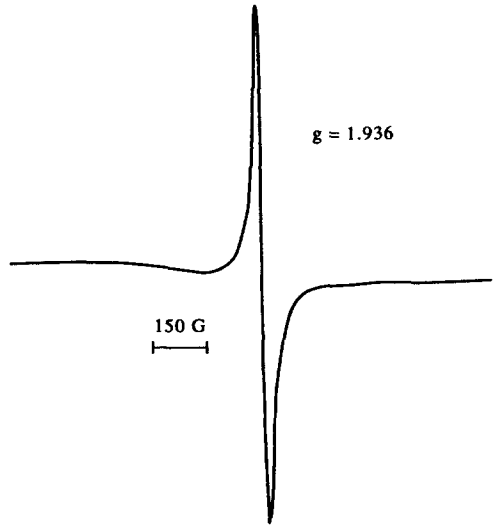


Fig. 3.

Electronic spectra

Figure 1 shows the reflectance electronic spectra of the title compound. The bands are 282 nm and 418 nm belong to O → Mo and *d–d* transition of MoO_6 octahedra, respectively.[12] The band at 740 nm is assigned to intervalence charge transfer ($Mo^{5+} \rightarrow Mo^{6+}$) IVCT band of $[SiMo_{12}O_{40}]^{5-}$, which indicates that electron transfer occurs between the organic substrate and polyoxoanion, converting $[SiMo_{12}O_{40}]^{4-}$ to the heteropoly blue $[SiMo_{12}O_{40}]^{5-}$.

Figure 2 compares the UV spectra of the title compound with the $(TBA)_4SiMo_{12}O_{40}$ dissolved in DMF. The title compound has a broad band at 790 nm similar to that of the solid, which is assigned to an $Mo^{5+} \rightarrow Mo^{6+}$ IVCT band. The solution of $(TBA)_4SiMo_{12}O_{40}$ has very weak absorption that can be omitted in the wavelength range. The above results indicate that the charge-transfer of the polyoxometalate anion is obviously influenced by the presence of DMNP.

ESR spectra

The ESR spectrum of the title complex at 110K is shown in Fig. 3. The spectrum reveals the presence of a single isotropic signal g = 1.936, which is ascribed to the Mo^{5+}, which is close to those observed in similar polyoxoanions containing Mo^{5+} (S = 5/2) species.[6,13] No hyperfine splitting of the ESR signal of Mo^{5+} of the complex has been observed due to the rapid intra-ionic hopping of the unpaired electron being comparable with the ESR time-scale.[4]

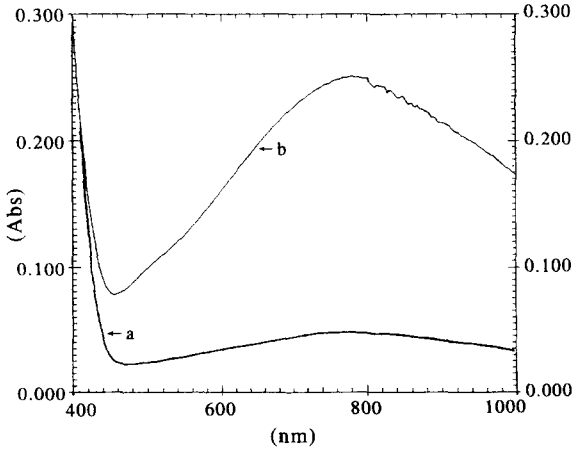


Fig. 2.

XPS study

X-ray photoelectron spectroscopy provides useful information on the oxidation state of the metal ion in the polyoxometalates, and can assess the stoichiometric ratio of the elements present in the compounds. The binding energies of $Mo3d_{5/2}$ in the title compound and tetraalkylammonium polyoxomolybdenum(VI) are 232.4ev and 232.3ev respectively. The binding energy of O_{1s} in the title compound is 530.5ev, which is also close to that of $(TBA)_4SiMo_{12}O_{40}$ (530.2ev). The above effects are due to the fact that the molybdenum atoms are all equivalent and the value of the binding energy is quite close to the value found for the completely oxidised anion. The existence of reduced molybdenum in the polyoxoanion cannot be ruled out as this is of class IIIA of the Robin and Day scheme.[14] In this case, the shift in energy would be very small as the extra electron is delocalized over all the molybdenum atoms.

X-ray crystal structure

The bond distances and angles of the title complex are listed in Tables 2 and 3, respectively. The crystal structure of the polyoxoanion and a stereoview of the molecular packing are shown in Figs 4 and 5, respectively. The analysis of the crystal structure reveals that the compound possesses the $P2_1$ space group, which is non-centrosymmetric. There exists the

Table 2. Selected bond lengths (Å)

Mo(1)—O(26)	1.683(9)	Mo(7)—O(33)	1.871(11)
Mo(1)—O(13)	1.823(9)	Mo(7)—O(18)	1.951(13)
Mo(1)—O(14)	1.828(11)	Mo(7)—O(28)	1.961(11)
Mo(1)—O(23)	1.942(10)	Mo(7)—O(10)	2.360(8)
Mo(1)—O(33)	1.988(13)	Mo(8)—O(4)	1.675(12)
Mo(1)—O(10)	2.377(8)	Mo(8)—O(25)	1.828(11)
Mo(2)—O(32)	1.652(10)	Mo(8)—O(37)	1.838(12)
Mo(2)—O(38)	1.885(14)	Mo(8)—O(21)	1.987(11)
Mo(2)—O(9)	1.924(11)	Mo(8)—O(27)	2.025(13)
Mo(2)—O(25)	1.941(12)	Mo(8)—O(40)	2.335(9)
Mo(2)—O(34)	1.952(11)	Mo(9)—O(39)	1.677(12)
Mo(2)—O(3)	2.336(7)	Mo(9)—O(17)	1.798(10)
Mo(3)—O(31)	1.642(13)	Mo(9)—O(16)	1.947(9)
Mo(3)—O(16)	1.831(9)	Mo(9)—O(34)	1.962(11)
Mo(3)—O(18)	1.877(14)	Mo(9)—O(24)	2.051(11)
Mo(3)—O(1)	1.951(9)	Mo(9)—O(3)	2.400(8)
Mo(3)—O(14)	2.016(10)	Mo(10)—O(29)	1.636(13)
Mo(3)—O(10)	2.414(9)	Mo(10)—O(1)	1.800(9)
Mo(4)—O(8)	1.670(11)	Mo(10)—O(5)	1.844(12)
Mo(4)—O(28)	1.821(12)	Mo(10)—O(17)	1.984(10)
Mo(4)—O(24)	1.872(10)	Mo(10)—O(37)	2.038(13)
Mo(4)—O(20)	1.99(2)	Mo(10)—O(40)	2.428(10)
Mo(4)—O(9)	2.062(10)	Mo(11)—O(30)	1.666(13)
Mo(4)—O(3)	2.349(9)	Mo(11)—O(20)	1.79(2)
Mo(5)—O(11)	1.673(11)	Mo(11)—O(2)	1.926(10)
Mo(5)—O(27)	1.805(13)	Mo(11)—O(12)	1.959(12)
Mo(5)—O(15)	1.902(9)	Mo(11)—O(19)	2.034(10)
Mo(5)—O(38)	1.905(13)	Mo(11)—O(35)	2.347(8)
Mo(5)—O(2)	2.081(10)	Mo(12)—O(36)	1.649(11)
Mo(5)—O(35)	2.319(8)	Mo(12)—O(23)	1.825(9)
Mo(6)—O(6)	1.654(9)	Mo(12)—O(19)	1.894(10)
Mo(6)—O(22)	1.842(11)	Mo(12)—O(22)	1.938(11)
Mo(6)—O(21)	1.912(13)	Mo(12)—O(15)	2.016(9)
Mo(6)—O(13)	1.937(9)	Mo(12)—O(35)	2.364(9)
Mo(6)—O(5)	1.970(13)	Si—O(40)	1.580(9)
Mo(6)—O(40)	2.395(9)	Si—O(10)	1.591(9)
Mo(7)—O(7)	1.676(10)	Si—O(3)	1.638(9)
Mo(7)—O(12)	1.825(12)	Si—O(35)	1.683(10)

Table 3. Selected bond angles (°)

O(26)—Mo(1)—O(13)	106.1(5)	O(8)—Mo(4)—O(3)	163.9(5)
O(26)—Mo(1)—O(14)	100.1(7)	O(28)—Mo(4)—O(3)	91.1(5)
O(13)—Mo(1)—O(14)	93.2(5)	O(24)—Mo(4)—O(3)	74.9(4)
O(26)—Mo(1)—O(23)	103.5(7)	O(20)—Mo(4)—O(3)	85.7(6)
O(13)—Mo(1)—O(23)	87.6(4)	O(9)—Mo(4)—O(3)	71.3(4)
O(14)—Mo(1)—O(23)	155.1(4)	O(11)—Mo(5)—O(27)	102.7(6)
O(26)—Mo(1)—O(33)	97.1(5)	O(11)—Mo(5)—O(15)	96.3(6)
O(13)—Mo(1)—O(33)	156.0(5)	O(27)—Mo(5)—O(15)	96.6(5)
O(14)—Mo(1)—O(33)	88.8(5)	O(11)—Mo(5)—O(38)	101.8(6)
O(23)—Mo(1)—O(33)	80.8(5)	O(27)—Mo(5)—O(38)	89.9(6)
O(26)—Mo(1)—O(10)	164.5(5)	O(15)—Mo(5)—O(38)	158.9(5)
O(13)—Mo(1)—O(10)	88.4(4)	O(11)—Mo(5)—O(2)	91.8(5)
O(14)—Mo(1)—O(10)	72.8(4)	O(27)—Mo(5)—O(2)	165.3(5)
O(23)—Mo(1)—O(10)	82.4(4)	O(15)—Mo(5)—O(2)	84.4(4)
O(33)—Mo(1)—O(10)	69.4(4)	O(38)—Mo(5)—O(2)	84.4(5)
O(32)—Mo(2)—O(38)	103.4(7)	O(11)—Mo(5)—O(35)	161.8(5)
O(32)—Mo(2)—O(9)	96.4(5)	O(27)—Mo(5)—O(35)	94.0(5)
O(38)—Mo(2)—O(9)	93.3(6)	O(15)—Mo(5)—M(35)	74.3(4)
O(32)—Mo(2)—O(25)	100.5(6)	O(38)—Mo(5)—O(35)	85.3(5)
O(38)—Mo(2)—O(25)	85.8(6)	O(2)—Mo(5)—O(35)	72.1(3)
O(9)—Mo(2)—O(25)	162.8(5)	O(6)—Mo(6)—O(22)	108.6(7)
O(32)—Mo(2)—O(34)	94.4(6)	O(6)—Mo(6)—O(21)	98.6(5)
O(38)—Mo(2)—O(34)	161.9(5)	O(22)—Mo(6)—O(21)	92.7(5)
O(9)—Mo(2)—O(34)	87.9(5)	O(6)—Mo(6)—O(13)	103.9(5)
O(25)—Mo(2)—O(34)	87.8(5)	O(22)—Mo(6)—O(13)	87.6(4)
O(32)—Mo(2)—O(3)	165.3(6)	O(21)—Mo(6)—O(13)	156.2(5)
O(38)—Mo(2)—O(3)	88.4(5)	O(6)—Mo(6)—O(5)	96.5(8)
O(9)—Mo(2)—O(3)	73.9(4)	O(22)—Mo(6)—O(5)	154.1(6)
O(25)—Mo(2)—O(3)	88.9(5)	O(21)—Mo(6)—O(5)	89.6(6)
O(34)—Mo(2)—O(3)	74.5(4)	O(13)—Mo(6)—O(5)	80.2(6)
O(31)—Mo(3)—O(16)	109.3(6)	O(6)—Mo(6)—O(40)	163.0(6)
O(31)—Mo(3)—O(18)	101.8(7)	O(22)—Mo(6)—O(40)	86.1(4)
O(16)—Mo(3)—O(18)	91.2(5)	O(21)—Mo(6)—O(40)	71.6(4)
O(31)—Mo(3)—O(1)	104.1(6)	O(13)—Mo(6)—O(40)	84.7(4)
O(16)—Mo(3)—O(1)	87.1(4)	O(5)—Mo(6)—O(40)	70.2(4)
O(18)—Mo(3)—O(1)	153.1(5)	O(7)—Mo(7)—o(12)	102.7(7)
O(31)—Mo(3)—O(14)	97.1(6)	O(7)—Mo(7)—O(33)	101.5(6)
O(16)—Mo(3)—O(14)	153.1(4)	O(12)—Mo(7)—O(33)	94.2(5)
O(18)—Mo(3)—O(14)	88.2(5)	O(7)—Mo(7)—O(18)	99.5(7)
O(1)—Mo(3)—O(14)	81.5(5)	O(12)—Mo(7)—O(18)	156.4(6)
O(31)—Mo(3)—O(10)	163.6(5)	O(33)—Mo(7)—O(18)	89.3(5)
O(16)—Mo(3)—O(10)	85.4(4)	O(7)—Mo(7)—O(28)	100.4(6)
O(18)—Mo(3)—O(10)	69.9(5)	O(12)—Mo(7)—O(28)	85.8(5)
O(1)—Mo(3)—O(10)	83.2(4)	O(33)—Mo(7)—O(28)	157.5(6)
O(14)—Mo(3)—O(10)	69.1(4)	O(18)—Mo(7)—O(28)	82.2(5)
O(8)—Mo(4)—O(28)	104.1(6)	O(7)—Mo(7)—O(10)	167.1(6)
O(8)—Mo(4)—O(24)	97.3(7)	O(12)—Mo(7)—O(10)	88.9(5)
O(28)—Mo(4)—O(24)	98.4(5)	O(33)—Mo(7)—O(10)	71.5(5)
O(8)—Mo(4)—O(20)	100.8(7)	O(18)—Mo(7)—O(10)	70.1(5)
O(28)—Mo(4)—O(20)	84.1(6)	O(28)—Mo(7)—O(10)	86.0(5)
O(24)—Mo(4)—O(20)	160.5(7)	O(4)—Mo(8)—O(25)	101.4(6)
O(8)—Mo(4)—O(9)	94.5(5)	O(4)—Mo(8)—O(37)	99.8(7)
O(28)—Mo(4)—O(9)	159.7(5)	O(25)—Mo(8)—O(37)	95.7(5)
O(24)—Mo(4)—O(9)	87.2(5)	O(4)—Mo(8)—O(21)	97.0(6)
O(20)—Mo(4)—O(9)	84.4(6)	O(25)—Mo(8)—O(21)	159.0(6)

continued over

Table 3.—Continued.

O(37)—Mo(8)—O(21)	91.0(5)	O(23)—Mo(12)—O(15)	158.3(5)
O(4)—Mo(8)—O(27)	98.9(6)	O(19)—Mo(12)—O(15)	87.3(4)
O(25)—Mo(8)—O(27)	85.8(5)	O(22)—Mo(12)—O(15)	83.3(4)
O(37)—Mo(8)—O(27)	160.5(6)	O(36)—Mo(12)—O(35)	163.2(4)
O(21)—Mo(8)—O(27)	81.5(5)	O(23)—Mo(12)—O(35)	88.5(4)
O(4)—Mo(8)—O(40)	167.0(5)	O(19)—Mo(12)—O(35)	73.8(4)
O(25)—Mo(8)—O(40)	90.8(5)	O(22)—Mo(12)—O(35)	84.2(4)
O(37)—Mo(8)—O(40)	74.4(5)	O(15)—Mo(12)—O(35)	71.3(3)
O(21)—Mo(8)—O(40)	71.8(5)	O(40)—Si—O(10)	114.2(5)
O(27)—Mo(8)—O(40)	86.2(5)	O(40)—Si—O(3)	110.4(5)
O(39)—Mo(9)—O(17)	108.0(7)	O(10)—Si—O(3)	110.4(5)
O(39)—Mo(9)—O(16)	104.9(5)	O(40)—Si—O(35)	107.8(5)
O(17)—Mo(9)—O(16)	88.7(4)	O(10)—Si—O(35)	108.5(5)
O(39)—Mo(9)—O(34)	97.9(5)	O(3)—Si—O(35)	105.2(5)
O(17)—Mo(9)—O(34)	94.7(4)	Mo(10)—O(1)—Mo(3)	151.8(6)
O(16)—Mo(9)—O(34)	154.7(4)	Mo(11)—O(2)—Mo(5)	118.5(5)
O(39)—Mo(9)—O(24)	94.5(6)	Si—O(3)—Mo(2)	124.2(5)
O(17)—Mo(9)—O(24)	157.3(5)	Si—O(3)—Mo(4)	124.9(5)
O(16)—Mo(9)—O(24)	82.6(4)	Mo(2)—O(3)—Mo(4)	94.8(3)
O(34)—Mo(9)—O(24)	84.8(4)	Si—O(3)—Mo(9)	119.9(5)
O(39)—Mo(9)—O(3)	163.0(6)	Mo(2)—O(3)—Mo(9)	91.8(3)
O(17)—Mo(9)—O(3)	87.3(4)	Mo(4)—O(3)—Mo(9)	92.4(3)
O(16)—Mo(9)—O(3)	82.3(3)	Mo(10)—O(5)—Mo(6)	127.9(7)
O(34)—Mo(9)—O(3)	72.8(4)	Mo(2)—O(9)—Mo(4)	119.8(5)
O(24)—Mo(9)—O(3)	70.8(4)	Si—O(10)—Mo(7)	126.3(5)
O(29)—Mo(10)—O(1)	108.9(7)	Si—O(10)—Mo(1)	123.3(5)
O(29)—Mo(10)—O(5)	99.9(7)	Mo(7)—O(10)—Mo(1)	93.1(3)
O(1)—Mo(10)—O(5)	92.4(6)	Si—O(10)—Mo(3)	121.2(5)
O(29)—Mo(10)—O(17)	106.4(6)	Mo(7)—O(10)—Mo(3)	92.1(3)
O(1)—Mo(10)—O(17)	87.5(4)	Mo(1)—O(10)—Mo(3)	91.5(3)
O(5)—Mo(10)—O(17)	152.2(5)	Mo(7)—O(12)—Mo(11)	148.6(7)
O(29)—Mo(10)—O(37)	96.0(7)	Mo(1)—O(13)—Mo(6)	149.3(6)
O(1)—Mo(10)—O(37)	154.2(5)	Mo(1)—O(14)—Mo(3)	126.5(5)
O(5)—Mo(10)—O(37)	90.2(6)	Mo(5)—O(15)—Mo(12)	120.9(5)
O(17)—Mo(10)—O(37)	78.5(5)	Mo(3)—O(16)—Mo(9)	150.4(5)
O(29)—Mo(10)—O(40)	162.1(7)	Mo(9)—O(17)—Mo(10)	149.4(5)
O(1)—Mo(10)—O(40)	87.5(4)	Mo(3)—O(18)—Mo(7)	127.8(8)
O(5)—Mo(10)—O(40)	71.3(5)	Mo(12)—O(19)—Mo(11)	121.1(5)
O(17)—Mo(10)—O(40)	81.0(4)	Mo(11)—O(20)—Mo(4)	149.2(8)
O(37)—Mo(10)—O(40)	69.1(4)	Mo(6)—O(21)—Mo(8)	123.4(7)
O(30)—Mo(11)—O(20)	103.7(7)	Mo(6)—O(22)—Mo(12)	149.9(6)
O(30)—Mo(11)—O(2)	95.8(5)	Mo(12)—O(23)—Mo(1)	150.4(6)
O(20)—Mo(11)—O(2)	100.7(6)	Mo(4)—O(24)—Mo(9)	121.7(5)
O(30)—Mo(11)—O(12)	101.3(6)	Mo(8)—O(25)—Mo(2)	148.1(8)
O(20)—Mo(11)—O(12)	84.2(6)	Mo(5)—O(27)—Mo(8)	142.9(8)
O(2)—Mo(11)—O(12)	160.5(5)	Mo(4)—O(28)—Mo(7)	148.1(8)
O(30)—Mo(11)—O(19)	94.1(6)	Mo(7)—O(33)—Mo(1)	125.9(7)
O(20)—Mo(11)—O(19)	160.4(5)	Mo(2)—O(34)—Mo(9)	120.7(5)
O(2)—Mo(11)—O(19)	85.3(4)	Si—O(35)—Mo(5)	123.4(5)
O(12)—Mo(11)—O(19)	84.4(4)	Si—O(35)—Mo(11)	123.1(5)
O(30)—Mo(11)—O(35)	163.1(6)	Mo(5)—O(35)—Mo(11)	95.2(3)
O(20)—Mo(11)—O(35)	91.6(6)	Si—O(35)—Mo(12)	120.8(4)
O(2)—Mo(11)—O(35)	74.1(4)	Mo(5)—O(35)—Mo(12)	93.4(3)
O(12)—Mo(11)—O(35)	87.0(5)	Mo(11)—O(35)—Mo(12)	93.1(3)
O(19)—Mo(11)—O(35)	71.9(4)	Mo(8)—O(37)—Mo(10)	124.3(7)
O(36)—Mo(12)—O(23)	106.8(5)	Mo(2)—O(38)—Mo(5)	146.7(7)
O(36)—Mo(12)—O(19)	97.6(5)	Si—O(40)—Mo(8)	127.5(5)
O(23)—Mo(12)—O(19)	94.4(4)	Si—O(40)—Mo(6)	123.1(5)
O(36)—Mo(12)—O(22)	102.9(5)	Mo(8)—O(40)—Mo(6)	93.0(3)
O(23)—Mo(12)—O(22)	86.8(4)	Si—O(40)—Mo(10)	120.9(5)
O(19)—Mo(12)—O(22)	157.9(4)	Mo(8)—O(40)—Mo(10)	92.0(3)
O(36)—Mo(12)—O(15)	94.2(5)	Mo(6)—O(40)—Mo(10)	90.5(3)

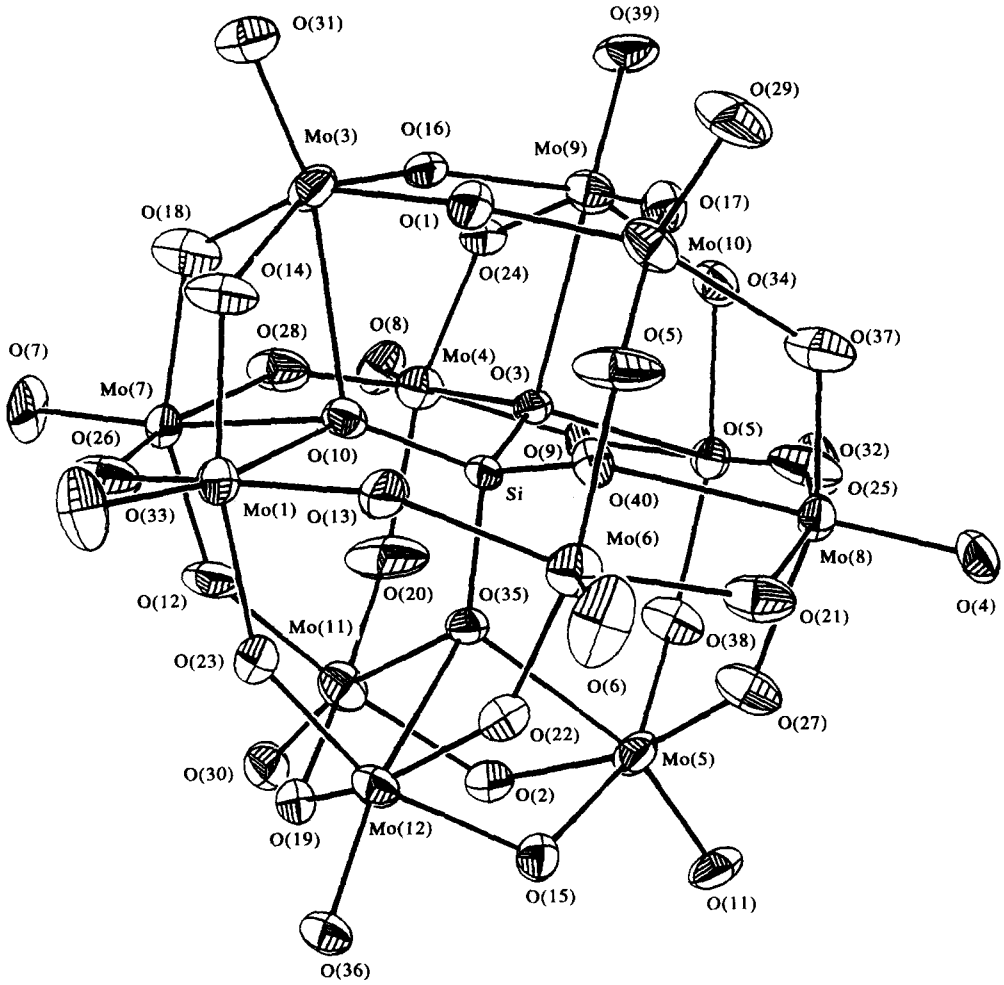


Fig. 4.

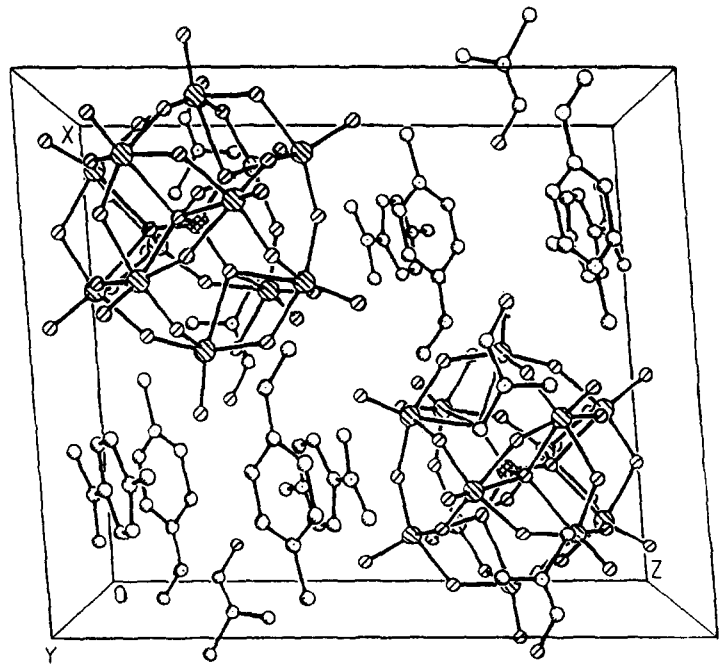


Fig. 5. Crystal packing of the title compound viewed down the *Y* axis.

Keggin structure of the $[SiMo_{12}O_{40}]^{4-}$ anion built up of four Mo_3O_{13} groups which result from the association of three edge-sharing MoO_6 octahedra. The four Mo_3O_{13} groups tetrahedrally surround the central Si heteroatom in such a way that the full unit has T_d symmetry.[4] This situation is rare in salts containing $XM_{12}O_{40}$ which form easily a disordered pseudo-Keggin polyoxoanion.[15] The polyanion has four kinds of oxygen atoms. O_a (the oxygen atoms in SiO_4 tetrahedra), O_b (the bridging oxygen atoms within one triplet group of MoO_6 octahedra), O_c (the bridging oxygen atoms between two triplet groups of MoO_6 octahedra) and O_d (the terminal oxygen atoms).

The sets of Mo–O bond lengths corresponding to the four types of oxygen atoms, central tetrahedron Mo–O_a 2.319(8)–2.428(10) Å, bridging Mo–$O_{b,c}$ 1.800(9)–2.081(10) Å, and terminal Mo–O_d 1.636(13)–1.683(9) Å are in the expected range.[16] The Si–O_a distances are in the range of 1.580(9)–1.683(10) Å. The organic cations of the title complex can be divided into two types DMNP and MNP. From the least-squares planes in the compound, the two types organic cation are planar. The counterpart dihedral angle between the two planes of DMNP and MNP is in the range of 17.37(0.59)–19.81° (0.54) in the unit cell. The shortest distances between polyoxoanion and organic donor is 3.00 Å[N(4B)···O(21)], and 3.08 Å[C(14A)···O(34)], which is shorter than the Van der Waals distance (3.20 Å). This may explain why charge transfer occurs between the polyanion and organic cation. The relevant bond distances and angles of the organic cations are in the range of related compounds,[17,18] and are not discussed further here.

Acknowledgements—The authors would like to thank the State Science Technology Commission and the National Nature Science Foundation of China for a major key research project and the Malaysia Government and Universiti Sains Malaysia for research grant RD No. 123–4317–2201.

REFERENCES

1. M. T. Pope and A. Muller, *Agnew. Chem. Int.* Ed. Engl. 1991, **30**, 34 and refs therein.
2. M. T. Pope and A. Muller, *Polyoxometalates: from platonic solids to Antiretroviral Activity*. Kluwer Acad. Pub., Dordrecht, The Netherlands. (1994).
3. E. Coronado and C. J. Gomez-Garcia, *Comments Inorg. Chem.* 1995, **17**, 255 and refs therein.
4. M. T. Pope, *Heteropoly and Isopoly Oxometalates*. Springer-Verlag; Berlin, (1983).
5. L. Ouahab, M. Bencharif, A. Mhanni, D. Pelloquin, J. F. Halet, O. Pena, J. Padion and D. Grandjean, *Chem. Mater.* 1992, **4**, 666.
6. C. Sanchez, J. Livage, J. P. Launay, M. Fournier and Y. Jeannin, *J. Am. Chem. Soc.* 1982, **104**, 3194.
7. A. P. Phillips, *J. Org. Chem.* 1948, **13**, 302 and refs therein.
8. Siemens, *XSCANS (Version 2.1) User Manual*. Siemens Analytical X-ray Instruments Inc., Madison, USA (1994).
9. G. M. Sheldrick, *Acta Cryst.* 1990, **A46**, 467.
10. G. M. Sheldrick, *SHELXL93. Program for Crystal Structure Refinement*. University of Gottingen, Germany (1993).
11. C. Rocchiccioli-Deltcheff, M. Fournier, R. Franck and R. Thouvenot, *Inorg. Chem* 1983, **22**, 207.
12. B. Z. Wan, J. H. Lunsford, *Inorg. Chim. Acta* 1982, **65**, L29.
13. L. Ouahab, M. Bencharif, A. Mhanni, D. Pelloquin, J.-F. Halet, O. Pena, J. Padion and D. Grandjean, *Chem. Mater.* 1992, **4**, 666.
14. M. B. Robin and P. Day, *Adv. Inorg. Chem. and Radiochem.* 1967, **10**, 247.
15. H. T. Jr. Evans and M. T. Pope, *Inorg. Chem.* 1984, **23**, 501.
16. L. Yu, J. Wang and H. Chen, *J. Solid State Chem.* 1992, **97**, 239.
17. X. Xue-Xiang, Y. Xiao-Zeng and H. Xiao-Ying, *Polyhedron* 1995, **14**, 1815.
18. F. Hoong-Kun, S. Kandasamy, Y. Boon-Chuan, T. Yu-Peng, D. Chun-Ying, L. Zhong-Lin and Y. Xiao-Zeng, *Acta Cryst.* 1995, **C51**, 2080.

Pergamon

S0277-5387(96)00232-X

Polyhedron Vol. 16, No. 1, pp. 103–107, 1997
Copyright © 1996 Elsevier Science Ltd
Printed in Great Britain. All rights reserved
0277–5387/97 $15.00+0.00

Synthesis, characterization and luminiscent DNA-binding study of a series of ruthenium complexes containing 2-arylimidazo[f]1,10-phenanthroline

Jian-Zhong Wu, Lin Li, Tian-Xian Zeng and Liang-Nian Ji*

Department of Chemistry, Zhongshan University, Guangzhou 510275, P.R. China

and

Jian-Ying Zhou, Ting Luo and Run-Hua Li

State Key Laboratory of Ultrafast Laser Spectroscopy, Zhongshan University, Guangzhou 510275, P.R. China

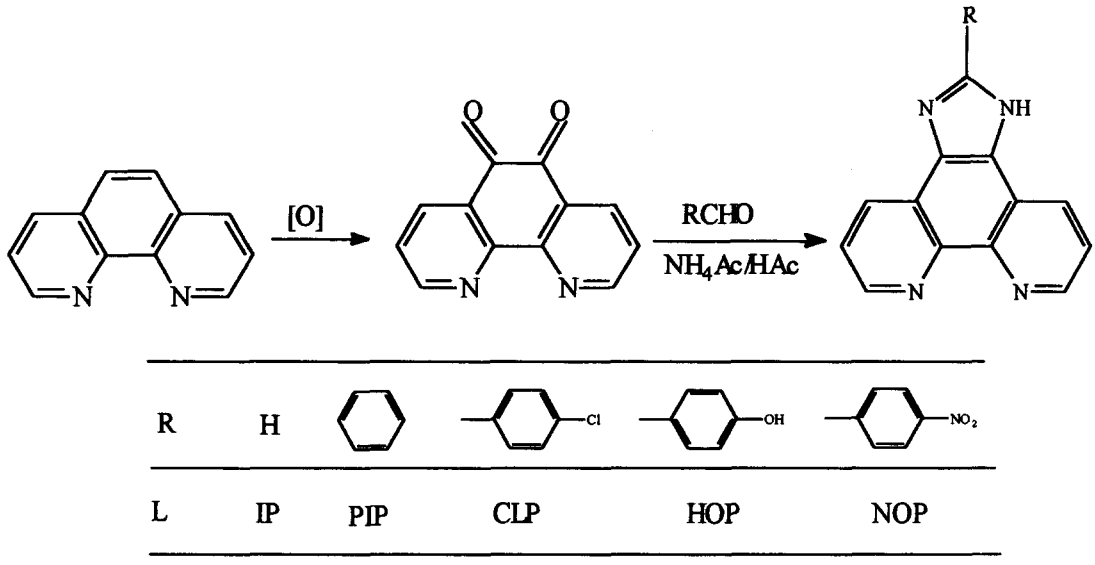
(Received 21 November 1995; accepted 3 May 1996)

Abstract—Starting from 1,10-phenanthroline, a series of novel ligands(L), imidazo[f]1,10-phenanthroline (IP), 2-phenylimidazo[f]1,10-phenanthroline (PIP) and the derivatives, and their complexes $[Ru(bpy)_2L]^{2+}$ have been synthesized and characterized. The effects of different electron donor and acceptor groups on the ^1H NMR, electronic absorption and emission spectra were studied. Time-resolved luminescence studies revealed that the addition of calf thymus DNA into the complex solution results in increases for both the emissive intensities and excited state lifetimes, and indicates that the electron group on L has no significant effect on the intercalation binding mode between DNA and the complexes. Copyright © 1996 Elsevier Science Ltd

Ruthenium(II) polypyridine complexes have received great interest for their unique combination of chemical stabilities, redox properties, luminescence emission and excited state lifetimes.[1] Recently a great deal of attention has been attracted to the recognition of DNA secondary structure with octahedral ruthenium(II) complexes, which is an important issue of biochemistry and biophysics.[2,3,4] It has been shown experimentally that the size and the shape of the ligand affected the interaction of the complex with DNA. However, the effect of an electron donor or acceptor group in the potential intercalating ligand, or in other words, the hydrogen bonding ability of the ligand on the interaction has not yet been studied systematically to our knowledge.

In our previous letters,[5,6,7] we reported the synthesis of the first two novel ligands, imidazo[f]1,10-phenanthroline (IP) and 2-phenylimidazo[f]1,10-phenanthroline (PIP), and their ruthenium complexes, and we studied the DNA-binding properties of $[RuL'L]^{2+}$ (L′ = 2,2′-bipyridine(bpy) or 1,10-phenanthroline(phen); L = IP or PIP) using electronic absorption, circular dichroism and steady state emission spectroscopy. The experiments showed that IP and PIP can intercalate into DNA base pairs. In this paper, we report the synthesis of three derivatives of PIP, 2-(4′-chlorophenyl)imidazo[f]1,10-phenanthroline(CLP), 2-(4′-hydroxyphenyl)imidazo[f]1,10-phenanthroline (HOP) and 2-(4′-nitrophenyl)imidazo [f]1,10-phenanthroline (NOP) (shown in Scheme 1), and studies on the emission properties of $[Ru(bpy)_2L]^{2+}$ (L = IP, PIP, CLP, HOP, NOP) bound to DNA using transient luminescent spectroscopy. Because bpy has no or very weak intercalating ability to DNA base pairs,[8] the DNA–Ru intercalating behavior is ligand L dependent.

* Author to whom correspondence should be addressed.



Scheme 1.

EXPERIMENTAL

All starting materials were commercially available and of analytical grade quality. Calf thymus DNA was dissolved in doubly distilled water containing 5 mM tris(hydroxymethyl)aminomethane (tris), 50 mM NaCl and pH = 7.2. DNA concentration was determined by $\varepsilon_{260} = 6600\ M^{-1}\ cm^{-1}$ ($\varepsilon_{260}/\varepsilon_{280} > 1.9$).

Elemental analyses were carried out using a Perkin–Elmer 240 analyser. The ^1H NMR spectra were recorded on a JEOL FX90Q spectrometer (90 MHz) using $CDCl_3/d_6$–DMSO as solvent and Me_4Si as internal reference. The UV–vis spectra were obtained on a Shimadzu MPS-2000 spectrophotometer. The emission experiment was conducted with an excimer laser (Lambda Physik EMG 201 MSC) pumped dye laser (Lambda Physics model FL2002) system. The nominal pulse width and the linewidth of the dye laser output is 10 ns and 0.18 cm^{-1}, respectively. Fluorescence of the sample is collected by two lenses into a monochromator and detected by a photomultiplier and processed by a Boxcar Averager (EG&G model 162) and a microcomputer. The dye laser emission was at 450 nm, about the absorption maximum of metal to ligand charge transfer (MLCT) complexes. The concentration of ruthenium complex and DNA was 1×10^{-5} and 4.7×10^{-4} M, respectively.

Synthesis of ligands (L)

Scheme 1 shows the two-step synthetic procedure. First, 1,10-phenanthroline was oxidized to 1,10-phenanthroline-5,6-dione according to literature[9] except for using methanol as recrystallization solvent instead of methylbenzene. Then, an imidazole ring preparation method established by Steck and Day[10] was applied to produce the ligands. The crude products were separated by 60–100 mesh silica gel with ethanol as eluent and recrystallized from aqueous ethanol to get yellow crystals. Their melting points are all above 310°C. The data of elemental analyses and ^1H NMR spectra are given in Table 1.

Synthesis of complexes $[Ru(bpy)_2L]^{2+}$

The mixture of 0.5 mmol of cis-$[Ru(bpy)_2Cl_2]\cdot 2H_2O$[11] and the equivalent L in 20 cm^3 of methane and 10 cm^3 of water was refluxed under argon for 2 hours and then most of methanol was evaporated withdrawing the condenser. The red solution was chromatographically separated by SP-Sephadex C-25 with 0.1 M NaCl of 4 : 1 acetone/water solution as eluent. The saturated solution of sodium perchlorate was added dropwise to precipitate the complex microcrystal. The composition and analyses are shown in Table 2.

RESULTS AND DISCUSSION

^1H *NMR spectra*

For all the five ligands, a broad peak appears at 13–14 ppm, which is assigned to the imidazole ring H–N since it conforms basically to the description for benzoimidazole.[12] That is to say, the above proton quickly exchanges between the two nitrogens of the imidazole ring. So the molecules of all the ligands show C_{2v} symmetry in solutions, leading to that the protons H-1 and H-2 (positions 1 and 2, see Table 1), H-3 and H-4, H-5 and H-6, H-9 and H-10, H-11 and H-12 are chemically equivalent, respectively.

Comparing the ^1H spectra of PIP, CLP, HOP and NOP, we can find the influence of substituents Cl,

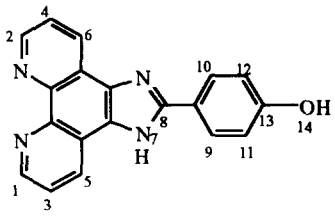
Table 1. Data of elemental analyses and ^{1}H NMR of ligands

Compound	Analyse(%)[a]	Chemical shift[b,c]
IP	C70.6	13.54, br., 1H, H-7
	(70.9)	9.05, dd, H-5, H-6
	H3.6	8.79, d, 2H, H-1, H-2
	(3.7)	8.30, s, 1H, H-8
	N25.2	7.75, dd, 2H, H-3, H-4
	(25.4)	
PIP·C_2H_5OH	C73.3	13.48, br., 1H, H-7
	(73.7)	9.04, dd, 2H, H-5, H-6
	H5.2	8.90, d, 2H, H-1, H-2
	(5.3)	8.31, d, 2H, H-9, H-10
	N16.5	8.23, t, 1H, H-13
	(16.4)	7.70, dd, 2H, H-3, H-4
		7.49, dd, 2H, H-11, H-12
CLP·1.5H_2O	C63.6	13.49, br.s, 1H, H-7
	(63.7)	9.06, dd, 2H, H-5, H-6
	H3.8	8.92, d, 2H, H-1, H-2
	(3.9)	8.27, d, 2H, H-9, H-10
	N15.6	7.72, dd, 2H, H-3, H-4
	(15.6)	7.53, d, 2H, H-11, H-12
HOP·C_2H_5OH	C70.1	13.31, br.s, 1H, H-7
	(70.0)	9.72, s, 1H, H-14
	H5.0	9.05, d, 2H, H-5, H-6
	(5.0)	8.92, d, 2H, H-1, H-2
	N15.8	8.13, d, 2H, H-9, H-10
	(15.6)	7.73, dd, 2H, H-3, H-4
		6.97, d, 2H, H-11, H-12
NOP·0.5H_2O	C65.3	13.92, br.s, 1H, H-7
	(65.1)	9.07, d, 2H, H-5, H-6
	H3.3	8.94, d, 2H, H-1, H-2
	(3.5)	8.53, d, 2H, H-11, H-12
	N20.2	8.39, d, 2H, H-9, H-10
	(20.0)	7.78, dd, 2H, H-3, H-4

[a] Calculated values are given in parentheses.

[b] The chemical shifts lower than 5 due to crystal ethanol or water are omitted.

[c] The numbering of positions related to hydrogen atoms is shown below for HOP as an example:



–OH and $-NO_2$ on the chemical shifts of their nearby protons. The group $-NO_2$ has strong electron accepting ability so it makes the chemical shifts of H-11(12), H-9(10) and even H-7 of NOP move downfield significantly relative to those of PIP. As the opposite, the electron donating property of –OH creates the upfield of H-11(12), H-9(10) and H-7 of HOP relative to PIP. Whereas the electron attracting by induction and the electron repelling by conjugation seem to be offset, so the values of δ(H-11, 12), δ(H-9, 10) and δ(H-7) are almost identical for CLP and PIP, respectively.

Electronic spectra

The wavelengths (λ_{max}) and the extinction coefficients (ε_{max}) of the absorption maxima of the ligands and the complexes are summarized in Table 3. The electronic spectra of the ligands are illustrated in Fig. 1. The spectrum of NOP appears obviously different from the others. A new peak at 372 nm emerges due to the chromophoric effect of $-NO_2$, and the ε_{max}'s of NOP decrease, probably because the electron transfer involved with $-NO_2$ contains some composition of $n \rightarrow \pi^*$ forbidden transfer.

The electronic spectra of the complexes are quite similar to that of $[Ru(bpy)_3]^{2+}$. Those of $[Ru(bpy)_2(PIP)]^{2+}$, $[Ru(bpy)_2(CLP)]^{2+}$ and $[Ru(bpy)_2(HOP)]^{2+}$ are almost identical. Along with the expansion of π delocallization from IP to PIP to NOP, the MLCT band of the corresponding complex shifts red from 455 to 458 to 461 nm.

Two characteristics of $[Ru(bpy)_2(NOP)]^{2+}$ are worthy of note. First, the band of NOP at 372 nm shifts blue to 360 nm in $[Ru(bpy)_2(NOP)]^{2+}$, owing to the coordination of NOP to Ru. Second, the absorption of the MLCT band of $[Ru(bpy)_2(NOP)]^{2+}$ is stronger than that of the other four complexes. It appears that the electron accepting property of $-NO_2$ makes the MLCT more easily occur.

Emission properties

The emission properties of the complexes themselves and in the presence of calf thymus DNA in Tris buffer at ambient temperature were studied by time-

Table 2. Data of elemental analyses of complexes

Complex	%Found(%Calc.)		
	C	H	N
$[Ru(bpy)_2(IP)](ClO_4)_2 \cdot 1.5H_2O$	46.1 (46.1)	3.2 (3.2)	13.2 (13.0)
$[Ru(bpy)_2(PIP)](ClO_4)_2 \cdot 2H_2O$	51.3 (52.0)	2.8 (3.2)	11.5 (11.3)
$[Ru(bpy)_2(CLP)](ClO_4)_2 \cdot 3H_2O$	46.5 (46.9)	2.7 (3.1)	11.3 (11.2)
$[Ru(bpy)_2(HOP)](ClO_4)_2 \cdot 2.5H_2O$	48.1 (48.3)	2.9 (3.4)	11.6 (11.6)
$[Ru(bpy)_2(NOP)](ClO_4)_2 \cdot 3H_2O$	46.2 (46.5)	2.8 (3.3)	12.6 (12.5)

Table 3. UV–vis spectra data of ligands and complexes

Compound[a]	λ_{max} (nm)	ε_{max} (M^{-1} cm^{-1})
IP	282(sharp)	14,900
	248	23,000
	242	22,400
	203	18,800
PIP	288	29,100
	273	32,300
	222	24,500
	195	28,800
CLP	320(shoulder)	22,300
	303(shoulder)	23,400
	276(shoulder)	30,700
	226	26,800
	203	32,960
HOP	279(shoulder)	23,900
	224	19,750
	198	28,160
NOP	372(wide)	7,850
	256(shoulder)	11,710
	228	7,520
$[Ru(bpy)_2(IP)]^{2+}$	455(shoulder)	16,200
	280(sharp)	79,900
	250	55,500
$[Ru(bpy)_2(PIP)]^{2+}$	458(shoulder)	17,600
	283(sharp)	100,100
	253(shoulder)	34,700
	244(shoulder)	35,500
$[Ru(bpy)_2(CLP)]^{2+}$	458(shoulder)	17,400
	284(sharp)	100,000
	253(shoulder)	32,000
	244(shoulder)	33,000
$[Ru(bpy)_2(HOP)]^{2+}$	459(shoulder)	18,100
	285(sharp)	103,300
	254(shoulder)	32,200
	242(shoulder)	33,400
$[Ru(bpy)_2(NOP)]^{2+}$	461(shoulder)	26,900
	360(wide)	29,100
	285(sharp)	91,100
	254(shoulder)	46,300

[a] The solvent is ethanol for all ligands and water for all complexes.

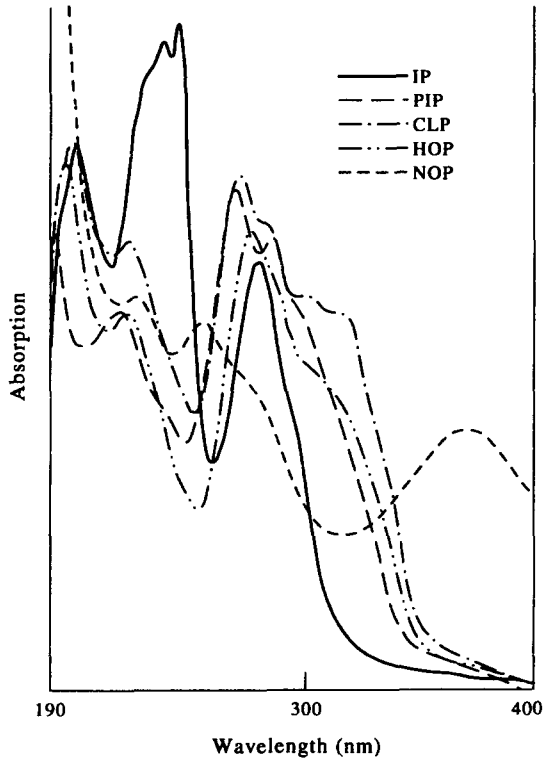


Fig. 1. Electronic spectra of ligands (——) IP, (— — —) PIP, (—·—·—) CLP, (—··—··—) HOP, (– – –) NOP.

resolved emission spectroscopy. The relevant data are collected in Table 4. We observe the relatively strong photoluminescence of $[Ru(bpy)_2L]^{2+}$ (L = IP, PIP, CLP and HOP) compared to that of $[Ru(bpy)_3]^{2+}$ but no emission of $[Ru(bpy)_2(NOP)]^{2+}$. The strong electron accepting group $-NO_2$ seems to have emission quenching ability. This could be explained in terms of the photo excited electron being captured by the end $-NO_2$ group and being unable to give emission to return to the ground state.

In fact, the different influences of substituents, Cl, –OH and $-NO_2$ on the MLCT based electron transfer have been observed in the electronic spectra of the complexes as discussed above. The conclusions derived from the absorption and emission spectra are quite coincident.

The intensity and lifetime of $[Ru(bpy)_3]^{2+}$ remains constant no matter whether DNA is present. But those of $[Ru(bpy)_2L]^{2+}$ (L = IP, PIP, CLP and HOP) increase significantly when bound to DNA. These kinds of increase have been demonstrated by most researchers as proofs that the potential intercalation ligand penetrates into the DNA base pairs thus the complex gets into a hydrophobic environment and avoids the quenching effect of solvent water molecules. So $[Ru(bpy)_3]^{2+}$ does not bind to calf thymus DNA by intercalation, which is consistent with the previous report.[8] Whereas the intercalation mode exists between $[Ru(bpy)_2L]^{2+}$ (L = IP, PIP, CLP and HOP) and calf thymus DNA. Our previous studies using other photophysical measurement have shown the intercalation of $[Ru(bpy)_2(IP)]^{2+}$ and $[Ru(bpy)_2(PIP)]^{2+}$ into calf thymus DNA.[6] So it can be concluded that the substituents Cl, –OH on the PIP ligand do not change the binding mode and the potential hydrogen bonding abilities of Cl and –OH seem to give no contribution.

Table 4. Emission properties of $[Ru(bpy)_2L]^{2+}$

L	bpy	IP	PIP	CLP	HOP	NOP
λ_{max}(nm)	617	625	615	616	606	—
I_0[b]	1	2.62	2.64	2.27	3.02	—
τ_0(ns)	410	556	462	585	450	—
I_D[b]	1.09	5.14	5.99	5.55	5.94	—
τ_D(ns)	418	1383	1456	1586	975	—

[a] I_0 and τ_0, I_D and τ_D denote the integrated luminescence intensity and lifetime at emission maximum (λ_{max}) with DNA ([DNA]/[Ru] = 47) and without DNA, respectively

[b] The values of I_0 and I_D are ratios to that of $[Ru(bpy)_3]^{2+}$ by assuming I_0 of the latter in the abscence of DNA as 1.

For the complex $[Ru(bpy)_2NOP]^{2+}$ we detected no photoluminescence both in the absence and the presence of calf thymus DNA. Barton *et al.*, have discovered a 'light switch' complex $[Ru(bpy)_2(dppz)]^{2+}$ (dppz is dipyrido[3,2–a : 2′,3′-c]phenanzine),[13] which displays no detectable luminescence in aqueous solution, but intense luminescence in the presence of double helical DNA to which it binds avidly by intercalation. This was due to the extreme sensitivity of the excited state to quenching by water; in DNA, the complex into the helix was protected from the aqueous solvent, thereby preserving the luminescence. But for $[Ru(bpy)_2NOP]^{2+}$, the 'quenching' of emission is caused by the electron acceptor group $-NO_2$ in the complex structure itself, so it is not sensitive to the environment. Therefore, the non-emissive behaviour of $[Ru(bpy)_2NOP]^{2+}$ does not imply that it cannot interact with DNA by intercalation.

Acknowledgements—We gratefully acknowledge the State Scientific and Technological Committee of China, the Lanzhou Institute of Chemical Physics of Chinese Academy of Sciences and the Royal Society of Chemistry Research Fund 1995 for the support of the project. JYZ is supported by a transcentury training program for young talents under the Chinese State Educational Committee.

REFERENCES

1. A. Juris, V. Balzani, F. Barigelletti, S. Campagna, P. Belser and A. von Zelewsky, *Coord. Chem. Rev.* 1988, **84**, 85.
2. A. M. Pyle and J. K. Barton, *Prog. Inorg. Chem.* 1990, **38**, 413 and references therein.
3. R. T. Morgan, S. Chaterjee, A. D. Baker and T. C. Stekas, *Inorg. Chem.* 1991, **30**, 2687.
4. M. Eriksson, M. Leijon, C. Hiort, B. Norden and A. Graslund, *J. Am. Chem. Soc.* 1992, **114**, 4933.
5. J.-Z. Wu, L. Wang, G. Yang, T.-X. Zeng and L.-N. Ji, *Chinese Chem. Lett.* 1995, **6**, 893.
6. J.-Z. Wu, L. Wang, G. Yang, T.-X. Zeng and L.-N. Ji, *Chinese Chem. Lett.* 1995, **6**, 999.
7. L. Wang, J.-Z. Wu, G. Yang, T.-X. Zeng, H.-Y. Yang and L.-N. Ji, *J. Inorg. Biochem.* 1995, **59**, 174.
8. C. V. Kumar, J. K. Barton and N. J. Turro, *J. Am. Chem. Soc.* 1985, **107**, 5518.
9. C. Hiort, P. Lincoln and B. Norden, *J. Am. Chem. Soc.* 1993, **115**, 3448.
10. E. A. Steck and A. R. Day, *J. Am. Chem. Soc.* 1943, 452.
11. B. P. Sullivan, D. J. Salmon and T. J. Meyer, *Inorg. Chem.* 1978, **17**, 3334.
12. Sadtler Research Laboratories, *The Sadtler Guide to NMR Spectra*, No. 463.
13. A. E. Friedman, J.-C. Chambron, J.-P. Sauvage, N. J. Turro and J. K. Barton, *J. Am. Chem. Soc.* 1990, **112**, 4960.

Pergamon

S0277-5387(96)00238-0

Polyhedron Vol. 16, No. 1, pp. 109–112, 1997
Copyright © 1996 Elsevier Science Ltd
Printed in Great Britain. All rights reserved
0277-5387/97 $15.00+0.00

Active site model of carbonic anhydrase: synthesis and crystal structure of the functional tetrahedral zinc complex with hydrotris(3-phenyl-5-methylpyrazolyl-1-yl)borate

Ke-Wu Yang, Yong-Zhen Wang and Zhong-Xian Huang*

Department of Chemistry, Fudan University, Shanghai 200433, P.R. China

and

Jie Sun

Shanghai Institute of Organic Chemistry, Academic Sinica, Shanghai 200032, P.R. China

(Received 14 March 1996; accepted 1 May 1996)

Abstract—Potassium hydrotris(3-phenyl-5-methylpyrazol-l-yl) borate and the zinc complex, [η^3-HB(3-Ph-5-Mepz)$_3$Zn(NO$_3$)], were synthesized and characterized by elemental analysis and ^{1}H NMR. Crystal structure determination shows that the coordination environment about the Zn centre is distorted tetrahedral. Copyright © 1996 Elsevier Science Ltd

Keywords: model compound; synthesis; characterization; crystal structure.

In the active center of zinc-containing enzymes, the zinc ion is almost always coordinated in a tetrahedral fashion.[1] Three of the four coordination sites are occupied by amino acid side chains while the fourth coordination site is occupied by a "functional" group OH or a water molecule. This basic L_3ZnX arrangement has been found in several metalloprotein crystal structure determinations,[2] and various model studies have applied it.[3–5] Because of the lability of zinc complexes and their diverse coordination possibilities, it is difficult to obtain this simple coordination pattern in model complexes. Thus, the work on models of zinc-containing enzymes has centred on the design of chelating ligand that approximates the distorted four-coordination active site, and one way of obtaining functional model compounds of this type is the use of tridentate ligands, which provide an appropriate set of donor atoms and a favourable stereochemical configuration.

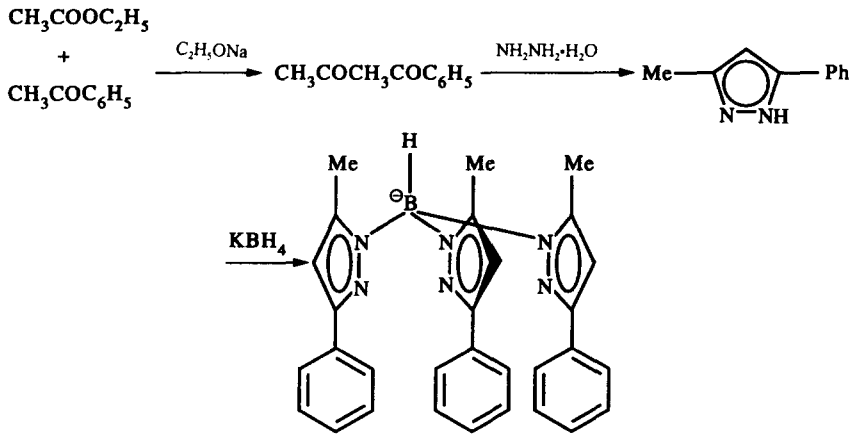
Recently, we reported substituted hydrotris(pyrazolyl)borate ligands (*e.g.* 3,5-dimethyl or 3-phenyl) and their stable tetrahedral complexes L_3MX (M = Cu[6], X = PPh_3; M = Zn,[7] X = Br)$_4$. In particular, zinc complexes of the latter ligand imitate structurally the active site of the carbonic anhydrase. In order to obtain a series of functional tetrahedral L_3ZnX species and study their structure–function relationship, in this paper we report the synthesis, characterization and the crystal structure of zinc complex with (3-phenyl-5-methylpyrazol-l-yl)borate ligand.

EXPERIMENTAL

Preparation and analyses of the complex

All chemicals were of reagent grade. C, H, N were determined by a Carbo Erba 1106 Elemental Analyzer, ^{1}H NMR spectra were obtained on a Bruker MSL 300MHz spectrometer using $CDCl_3$ as solvent and TMS as an internal reference. The synthetic route of the ligand, potassium hydrotris(3-phenyl-5-methylpyrazol-l-yl)borate, KHB(3-Ph-5-Mepz)$_3$, is shown in Scheme 1, and the synthesis method refers to the published procedure.[8] Zinc nitrate (2 mmol) was added to 20 cm^3 of methanol, and to this stirred solu-

* To whom correspondence should be addressed.



Scheme 1.

tion was added all at once a THF solution of the crude ligand (2 mmol), and some white solid material was separated. Water (100 cm^3) was added into the solution, then a white precipitate was filtered and washed thoroughly with hot water and then with methanol. The white solid was recrystallized from toluene and dried in a vacuum desiccator. Found: C, 59.4; N, 15.7; H, 4.6%. Calc. for $C_{30}H_{28}O_3N_7BZn$ (611): C, 59.0; N, 16.1; H, 4.6%. ^1H NMR ($CDCl_3$) δ ppm 2.32 (s, 9H, Me), 6.35 (m, 3H, pz), 7.3–7.7 (m, 15H, Ph).

Crystal structure determination

Crystals of the title compound were obtained by slowly cooling the hot toluene solution to room temperature, and a colourless platelet of 0.20 × 0.20 × 0.30 mm was chosen for the X-ray structural measurement. All crystallographic data were collected with a Rigaku AFC7R diffractometer using Mo-K_α radiation (λ = 0.71069 Å) in the ω-2θ scan mode. 3231 reflections were independent, and 2433 reflections with $I > 3.00\sigma(I)$ were used for the calculations after an empirical absorption correction based on ψ scans. The structure was solved by direct methods. The non-hydrogen atoms were refined anisotropically. The final cycle of full matrix least-squares refinement was converged with $R = 0.039$, $Rw = 0.047$ (unweighted and weighted agreement factors resp.).

Table 1. Crystallographic data for the complex

Formula	$C_{30}H_{28}O_3N_7BZn$
Formula weight	610.79
Crystal system	Triclinic
Space group	$P\bar{1}$
a (Å)	12.079(2)
b (Å)	12.467(2)
c (Å)	11.999(2)
α (°)	109.18(1)
β (°)	98.20(1)
γ (°)	115.76(1)
V (Å^3)	7487(3)
Z	2
Dc (g cm^{-3})	1.401
$F_{(000)}$	632.00
μ (MoK_α) (cm^{-1})	8.93
Temperature	20 ± 1°C
Scan type	ω-2θ
Data collection range	$6.0 < 2\theta < 45.0°$
No. of reflections measured	
Total/Unique	3443/3231
No. variables	379
R, R_w	0.039, 0.047

RESULTS AND DISCUSSION

The compound [η^3-HB(3-Ph-5-Mepz)$_3$Zn(NO_3)] was synthesized and characterized by spectroscopy and an X-ray crystal structure determination. The crystallographic data are listed in Table 1, bond distances and angles are listed in Tables 2 and 3. An ORTEP plot and a unit cell packing diagram are presented in Figs 1 and 2, respectively.

The crystal structure analysis clearly shows that three phenyl rings form a cage-like pocket, the zinc ion is coordinated by three pyrazole nitrogen atoms and a nitrato oxygen atom, and the coordination environment about the zinc centre is distorted tetrahedral with the O(1)—Zn—N (120.8–130.3°) and the N—Zn—N angle (90.4–98.8°). The Zn—N bond distance (2.04 Å) falls into the range for normal zinc complexes with the tris(pyrazolyl)hydroborato ligand, while the Zn—O bond distance (1.94 Å) is slightly longer than the value of 1.85 Å found in [η^3-HB(3-Bu^t-5-Mepz)$_3$ZnOH].[9] This coordination environment around zinc in the title complex also compares

Table 2. Selected bond lengths (Å) for [η^3-HB(3-Ph-5-Mepz)$_3$Zn(NO_3)]

Zn—O(1)	1.945(4)	Zn—N(2)	2.033(4)
Zn—N(5)	2.027(4)	Zn—N(7)	2.048(4)
N(2)—N(3)	1.375(5)	N(4)—N(5)	1.376(6)
N(6)—N(7)	1.373(5)	N(3)—B	1.554(8)
N(4)—B	1.542(8)	N(6)—B	1.557(8)

Table 3. Selected bond angles ( ) for [η^3-HB(3-Ph-5-Mepz)$_3$Zn(NO$_3$)]

O(1)—Zn—N(2)	130.3(2)	O(1)—Zn—N(5)	120.8(2)
O(1)—Zn—N(7)	113.4(2)	N(2)—Zn—N(5)	98.8(2)
N(2)—Zn—N(7)	93.4(2)	N(5)—Zn—N(7)	90.4(2)
Zn—N(2)—N(3)	110.5(3)	Zn—N(5)—N(4)	108.9(3)
Zn—N(7)—N(6)	110.5(3)	N(2)—N(3)—B	120.9(4)
N(5)—N(4)—B	120.4(4)	N(7)—N(6)—B	120.7(4)
N(3)—B—N(4)	108.6(5)	N(3)—B—N(6)	107.7(5)
N(4)—B—N(6)	109.5(4)	N(2)—C(7)—C(6)	123.4(5)
N(5)—C(17)—C(16)	122.0(5)	N(7)—C(27)—C(26)	122.1(5)

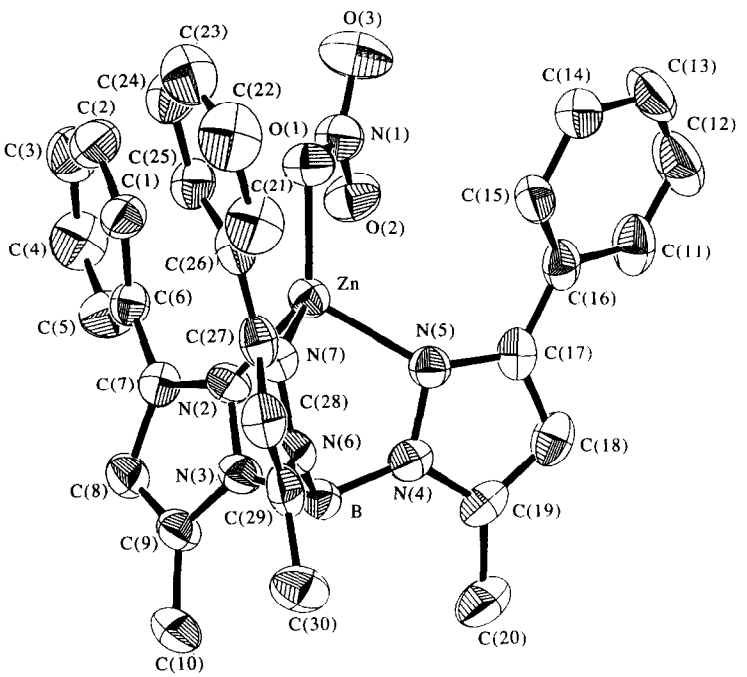


Fig. 1. The structure of [η^3-HB(3-Ph-5-Mepz)$_3$Zn(NO$_3$)].

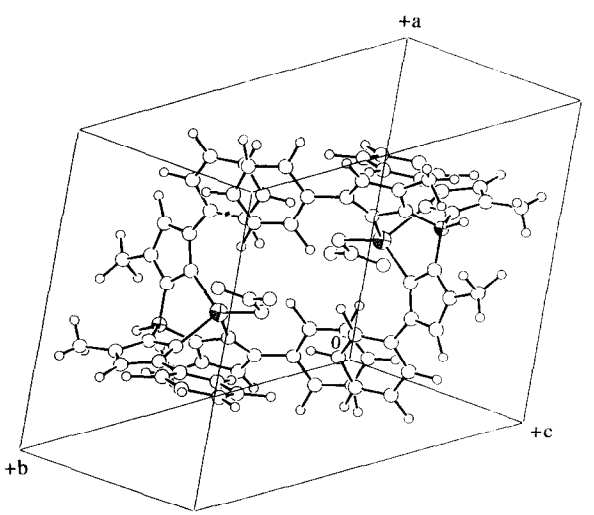


Fig. 2. Unit cell packing diagram for [η^3-HB(3-Ph-5-Mepz)$_3$Zn(NO$_3$)].

reasonably well with the theoretical calculation for the active site of carbonic anhydrase with bond lengths with angles of Zn—O = 1.96 Å, Zn—N = 2.10 Å, and O—Zn—N = 117.6°.[10] The B—N bond lengths (av. 1.55 Å) and N—B—N angles (av. 108.6°) correspond to the normal value for other metal complexes with pyrazolylborate ligand.[11] The title compound is an interesting active site model of carbonic anhydrase in three respects: first, the pocket around zinc in L_3ZnX has enough room for a monodentate X or a small ligand as substrate; second, the zinc ion in the complex has the same (N, N, N, O) donor set as in carbonic anhydrase; third, the nitrato ligand is isoelectronic with hydrogen carbonate, the substrate of carbonic anhydrase.

Acknowledgements——This work was supported by the Postdoctoral Science Foundation of China, Postdoctoral Science Foundation of Shanghai City and National Nature Science Foundation of China.

REFERENCES

1. T. G. Spiro (Ed), *Zinc, Enzymes*. Wiley, New York, (1983).
2. H. Sigel (Ed), *Metal Ions in Biological Systems, Vol.* 15, *Zinc and its Role in Biology and Nutrition*. Marcel Dekker, New York (1983).
3. D. Qiu, L. T. Kilpatrick, N. Kitajima, T. G. Spiro, *J. Am. Chem. Soc.* 1994, **116**, 2585.
4. A. Abufarag, H. Vahrenkamp, *Inorg. Chem.* 1995, **34**, 2207.
5. A. Abufarag, H. Vahrenkamp, *Inorg. Chem.* 1995, **34**, 3279.
6. K. W. Yang, Y. Q. Yin, D. S. Jin, *Chinese Chem. Lett.*, 1994, **5**, 341.
7. K. W. Yang, Y. Q. Yin, D. S. Jin, *Polyhedron*, 1995, **14**, 1021.
8. S. Trofimenko, J. C. Calabrese, and J. S. Thompson, *Inorg. Chem.* 1987, **26**, 1507.
9. R. Alsfasser, S. Trofimenko, A. Looney, G. Parkin, and H. Vahrenkamp, *Inorg. Chem.* 1991, **30**, 4098.
10. M. M. Kenneth, R. Hoffman, and M. J. S. Dewar, *J. Am. Chem. Soc.* 1989, **111**, 5636.
11. S. Trofimenko, J. C. Calabrese, P. J. Domaille, and J. S. Thompson, *Inorg. Chem.* 1989, **28**, 1091.

Pergamon

Polyhedron Vol. 16, No. 1, pp. 113–117, 1997
Copyright © 1996 Published by Elsevier Science Ltd
Printed in Great Britain. All rights reserved
0277-5387/97 $15.00+0.00

S0277-5387(96)00235-5

Synthesis and characterization of novel phthalocyanines peripherally fused to four 20-membered tetraaza-dioxamacro cycles

Yasar Gok* and S. Zeki Yildiz

Department of Chemistry, Karadeniz Technical University, 61080 Trabzon-Turkey

(Received 31 January 1996; accepted 1 May 1996)

Abstract—New metal-free **3** and metallophthalocyanines **4–5** (M = Ni or Zn) substituted with four 20-membered tetraaza-dioxa macrocycles from 21,22-dicyano-2,8,11,17-tetra-(toluene-p-sulfonyl)-1,2,3,4,5,6,7,8,9,10,11,12,13,14,15,16,17,18-octadecahydrox[*l*] [2,8,11,17]tetraaza [4,13]dioxadicontine (**2**) are described. Cyclotetramerization of the substituted phthalonitrile (**2**) leads to a product very soluble in common organic solvents. The characterization of the compounds was accomplished by elemental analysis, ^1H, ^{13}C NMR, IR, UV–vis and MS spectral data. Copyright © 1996 Published by Elsevier Science Ltd

The phthalocyanine macrocycles are of considerable interest owing to their fascinating electronic and optical properties. In recent years, a large number of phthalocyanine derivatives has been prepared to facilitate the exploitation of these properties such as gas sensors, electrophotography, fuel cells, solar energy conversion, non-linear optics, catalysis and the photodynamic therapy of cancer.[1] The attractive and challenging characteristics of the phthalocyanines are their great variety, chemical stability, the relative ease with which they can be synthesized and the strong dependence of their properties on peripheral and axial substitution patterns.[2] In this context, substitution on the aromatic groups of phthalocyanine by various groups such as crown ether, thiacrown or mixed donor macrocycle leads to new products having additional functionalities or properties.[3] Among these are supramolecular systems which consist of two identical molecular entities coexisting together without the assistance of covalent binding.[4] The notable feature of these compounds is that they exhibit spectral properties different from those of the individual molecular units.

Phthalocyanine-bridged tetrakis(benzocrown ether)s include crown ether-substituted phthalocyanines and tetrakis(benzocrown ether) containing phthalocyanines. These polytopic ligands consist of a phthalocyanine core to which four benzocrown ether moieties are attached. Attachment of crown ether units to the phthalocyanine ring significantly increases the solubility of phthalocyanine in many organic solvents leading to significant advances in research such as biological modelling, homogeneous catalysis, alkaline or earth alkaline and lanthanide metal extractions.[5] Although incorporation of macrocyclic groups such as crown ethers, tetraaza, diazatrioxa or diza-dioxa macrocycles onto the periphery of phthalocyanine are well known and continue to be the subject of increasing research activity, tetraazadioxa macrocycles which contain a larger cavity than the usual crown or mixed donor macrocycles are relatively few.[6] For this reason, attention has been focused on their synthesis and characterization with new substituents.

Recently, activity in our laboratory has focused upon synthesizing and understanding the properties of novel types of aza-oxa mixed macrocycle or ionophore substituted metal-free and transition metal phthalocyanines.[6] The present paper reports the synthesis of free and transition metal-complexed phthalocyanines containing four 20-membered teraaza-dioxa macrocyclic moieties in the molecule. The major opportunities offered by these novel phthalocyanines are the capability of binding five cations.

RESULTS AND DISCUSSION

21,22-Dicyano-2,8,11,17-tetra(toluene-p-sulfonyl)-1,2,3,4,5,6,7,8,9,10,11,12,13,14,15,16,17,18-octadecahydrobenzo[*l*] [1,7,10,16]tetraaza[4,13]-dioxacyclodicontine (**2**) was obtained from the dibromo derivative by refluxing in DMF with 3 equi-

* Author to whom correspondence should be addressed.

valents of CuCN.[7] The free phthalocyanine was obtained by heating a mixture of dicyano substituted tetraaza-dioxa macrocycle with hydroquinone in a sealed tube.[8] The metallophthalocyanines were prepared from the dicyano derivative of the macrocycle and the corresponding metal salts in high-boiling anhydrous solvents (*e.g.* dimethylformamide or quinoline). The yields were satisfactory and depended upon the transition metal ion.

The most obvious feature of free phthalocyanine and metallophthalocyanines is their extensive solubility in common organic solvents such as, chloroform, dichloromethane, dimethylformamide and dimethylsulfoxide. The solubilities in chloroform or dichloromethane are higher than those of similar complexes containing only crown ether[9] or tetraaza macrocyclic substituents. The unusual solubilities of these compounds are due to the bulky group substitution.[10]

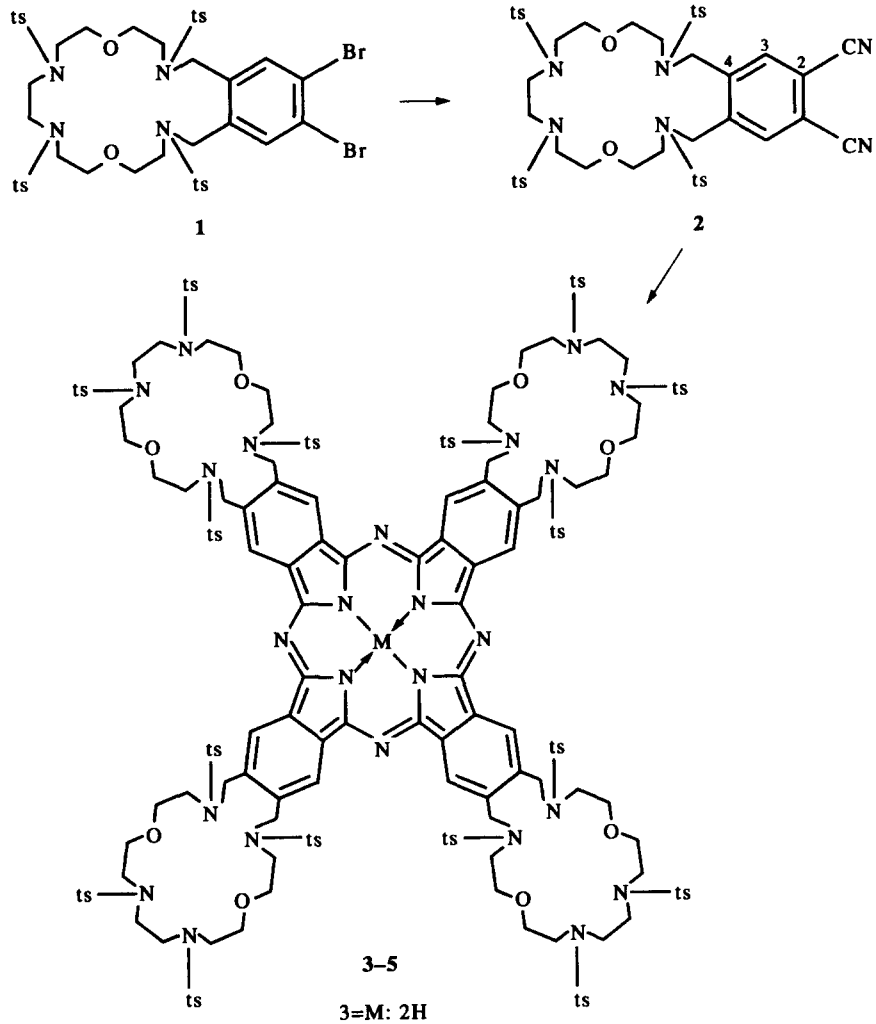
Elemental analyses, IR, ^{1}H and ^{13}C NMR, MS and UV–vis spectra confirm the proposed structures of the compounds. The preparation of **2** has been accomplished in a 78% yield by the reaction of **1** with CuCN in dry DMF. In the IR spectrum of **2**, the intense absorption band at 2222 cm^{-1} corresponds to the C≡N groups. The C—Br stretching vibration observed at 645 cm^{-1}, belonging to **1**, disappears after the conversion into the dicyano derivative. The rest of the spectrum is closely similar to that of **1** including the characteristic vibrations of tosyl and ether groups. This spectrum exhibits characteristic frequencies at 3029 (Ar–H), 2962–2860 (C–H), 1345 and 1148 (SO_2) cm^{-1}. In the ^{1}H NMR spectrum of **2**, the singlet at $\delta = 2.42$ ppm and multiplets at $\delta = 7.78$–7.61, 7.38–7.23 correspond to methyl and aromatic protons. The chemical shifts belonging to methylene protons connecting nitrogen and oxygen show different values at $\delta = 3.45$–3.36 ppm (CH_2–O) and at $\delta = 3.25$–2.94 ppm (CH_2–N) as expected. The other methylene chemical shift which is connected to the phenyl ring was observed at $\delta = 4.45$ ppm as a singlet. The proton-decoupled ^{13}C NMR spectral data given below are also in accord with the expected structure. The carbon resonances of the *p*-tolylsulfonyl groups appear at $\delta = 143.72$, 135.72, 129.89, 128.12, 127.08 and 126.88 ppm. The other chemical shifts belonging to aromatic, methyl, nitrile and aza-oxa crown carbons appear at $\delta = 141.72$ (C_4), 134.88 (C_3), 113.88 (C_2) ppm (aromatic), at $\delta = 116.08$ ppm (C≡N), at $\delta = 49.49$–46.65 ppm (N–CH_2), at $\delta = 69.93$–68.11 ppm (O–CH_2) and at $\delta = 21.33$ (Ar–CH_3) ppm. The fast atom bombardment mass spectrum (FAB-positive) of **2** shows the expected molecular ion peak at $m/z = 1003$ $[M+1]^+$.

The metal free phthalocyanine **3** was synthesized by heating a mixture of dicyano derivative of tetraza-dioxa macrocycle (**2**) with hydroquinone in a Schlenk system. Metal free phthalocyanine (**3**) was obtained 38% yield. The IR spectra of **3** is very similar to that of **2**. A diagnostic feature of the phthalocyanine formation from dicyano derivative (**2**) is the disappearance of the C≡N stretching vibration at 2222 cm^{-1} of the precursor compound. Another difference is the presence of N–H stretching and bending vibrations assigned to bands at 3305 and 1028 cm^{-1}, respectively.[8] The ^{1}H NMR spectrum of **3** indicates aromatic protons at $\delta = 7.85$–7.22 ppm, aliphatic ether protons at $\delta = 3.77$–3.48 (CH_2–O) and nitrogen connected CH_2 groups at $\delta = 3.40$–3.18 ppm. A common feature of these spectra of metal-free phthalocyanines is the broad absorptions probably caused by the aggregation of phthalocyanine. Also the NH protons of this compound (**3**) could not be observed due to this phenomenon. Because of the distinct ring current of the 18π electron system of the inner phthalocyanine core, the protons are characteristically shifted to low or high field.[11] The molecular ion species in the FAB mass spectrum which is analyzed as solution in chloroform are observed in accord with calculated value. The molecular mass fragment ions corresponding to the molecular ion and cleavage of the two tosyl groups from **3** appear at $m/z = 4011$ $[M+1]^+$ and 3700, respectively.

In order to obtain the metallophthalocyanine **4–5**, the dinitrile derivative **2** was directly treated with the anhydrous transition metal salts [$NiCl_2$ or $Zn(O_2CMe)_2$]. The yields obtained were satisfactory although the workup conditions were cumbersome. The metallophthalocyanine **4** was obtained in 46.8% yield and the other compound **5** was obtained in 60% yield. The intense green products are very soluble in a number of solvents such as dichloromethane, chloroform, carbon tetrachloride, tetrahydrofuran, dimethyl formamide and dimethyl sulfoxide.

Elemental analyses, ^{1}H NMR, IR, MS and UV-vis spectra confirm the proposed structures of the metallophthalocyanines. In the IR spectrum of **2**, the intense absorption vibrations at 2222 cm^{-1} corresponding to the C≡N groups disappear after their conversion into the metallophthalocyanines (**4–5**). The rest of the IR spectra are very similar to those of **2** including the characteristic vibrations of tosyl, crown and aza-crown groups. In the ^{1}H NMR spectrum of **4** and **5**, the chemical shifts belonging to aromatic, crown and aza-crown groups at $\delta = 7.93$–7.27, 7.88–7.16, 3.92–3.63, 3.89–3.57, 3.44–3.07 and 3.36–2.97 ppm were observed after the cyclotetramerization, respectively. Broad NMR absorptions were observed for nickel(II) and zinc(II) phthalocyanines possibly due to aggregation. The mass spectrum (FAB positive) of **4** [$m/z = 4067$ $(M+1)^+$] supports the structure of nickel(II) phthalocyanine. The fast atom bombardment mass spectrum of **5** shows the molecular ion peak at 4074 $[M+1]^+$ and another peak at 3454 attributed to the loss of four tosyl groups [M-4Ts].

The phthalocyanines **3–5** show typical electronic spectra with two strong absorption regions, one of them in the UV region at about 240–345 nm (B band) and the other in the visible part of the spectrum at



Scheme 1.

670–700 nm (Q band). In extremely dilute solutions (*ca* 10^{-6} M), the metal-free or metallophthalocyanines behave as monomers in organohalide solution.[11] Increasing the concentration leads to aggregation which is easily observed by the values of the Q bands which shift to higher energies and by the decrease in the molar absorption coefficient. While the N-tosylated phthalocyanines are soluble in chloroform, their spectra in this solvent exhibit an intense Q band at the lowest energy region at 686, (**3**), 677 (**4**) and 691 nm (**5**) which the sharp band or shoulder around 630 nm [627 (**3**), 617 (**4**) and 629 (**5**)] can be attributed to aggregation.[12] On the other hand, while the monomeric species, in extremely dilute chloroform solution, with D_{2h} symmetry (metal-free derivative) shows two intense absorptions around 690 nm, that having D_{4h} symmetry gives only a single band in this region.[13]

EXPERIMENTAL

^{1}H and ^{13}C NMR spectra were recorded on a Varian XL-300 NMR spectrometer. IR and UV-vis recorded on a ATIunicam FT-IR in KBr pellets and a GBC 911 UV-vis spectrophotometer, respectively. Fast atom bombardment (FAB positive, matrix: *m*-nitro benzyl alcohol) mass spectra were measured on a VG Auto-Spec from VG Analytical. The elemental analyses were determined by a Hewlett–Packard 185 analyzer. 21,22-Dibromo-2,8,11,17-tetra(toluene-p-sulfonyl)-1,2,3,4,5,6,7,8,9,10,11,12,13,14,15,16,17,18-octadecahydrobenzo[*l*] [1,7,10,16]tetraaza[4,13]dioxacyclodicontine (**1**) was prepared according to the reported procedure.[6] Commercially available pure grade CuCN, $NiCl_2$, $Zn(O_2CMe)_2$ and solvent dried and purified by conventional procedures,[14] were used.

21,22-*Dicyano*-2,8,11,17-*tetra*(*toluene*-*p*-*sulfonyl*)-1,2,3,4,5,6,7,8,9,10,11,12,13,14,15,16,17,18-*octadecahydrobenzo*[*l*] [1,7,10,16]*tetraaza*[4,13]*dioxacyclodicontine* (**2**)

A two-necked round-bottom flask fitted with a condenser was evacuated, refilled three times with argon and then flamed under high vacuum. Under argon, the flask was charged with CuCN (1.2 g, 13.5 mmol), argon saturated anhydrous dimethyl formamide (25 cm^3) and the dibromo derivative of tetraaza-dioxa macrocycle (5 g, 4.5 mmol) (**1**) and the mixture was heated gradually to 175°C. It was then kept at this temperature for 12 h. During this time, the resulting solution became dark brown. Then the heating was stopped and the reaction mixture was allowed to cool to room temperature, opened to air and diluted with aqueous NH_4OH (57 cm^3) and air was passed through the solution for 24 h. The end of this period, the solution became dark blue and a green precipitate formed. The reaction mixture was filtered through Celite and washed with dilute NH_4OH (10%) and water, until the filtrate was neutral. This crude precipitate was then dried and extracted with chloroform and then dried with $NaSO_4$. This mixture was filtered and the filtrate evaporated to dryness. The oily product obtained was refluxed in ethanol (75 cm^3) for 4 h and cooled to room temperature. To this solution n-hexane was added gradually until the precipitation was completed then the product was isolated as a tannish powder by stirring in n-hexane (150 cm^3) for 2 days. The powder was collected by filtration, washed with cold ethanol and n-hexane and then dried *in vacuo*. Yield 3.5 g (78%), m.p. 105°C. ^1H NMR ($CDCl_3$): δ 7.78–7.61 (m, 10H, Ar–H), 7.38–7.23 (m, 8H, Ar–H), 4.45 (s, 4H, CH_2–Ar), 3.45–3.36 (m, 8H, O–CH_2), 3.25–2.94 (m, 12H, N–CH_2), 2.42 (s, 12H, CH_3) ppm. ^{13}C NMR ($CDCl_3$): δ 143.72 (Ts–Ar), 141.75 (C_4), 135.74 (Ts–Ar), 134.88 (C_3), 129.89 (Ts–Ar), 128.12 (Ts–Ar), 127.08 (Ts–Ar), 126.88 (Ts–Ar), 116.08 (C≡N), 113.88 (C_2), 69.93–68.11 (O–CH_2), 49.49–46.65 (N–CH_2), 21.33 (Ar–CH_3) ppm. IR (KBr): 3029 (Ar–H), 2962–2860 (C–H), 2222 (C≡N), 1605, 1451, 1345 (SO_2), 1148, 1136, 1076, 995, 821, 695 cm^{-1}. Mass spectrum (FAB positive): m/z 1003 $[M+1]^+$. Found: C, 57.3; H, 5.2; N, 8.2; Calc. for $C_{48}H_{54}N_6O_{10}S_4$: C, 57.5; H, 5.4; N, 8.4%.

Metal-free [*hexadecakis*(N-*p*-*tosyl*)-*tetrakis*-*macrocyclophthalocyanine*], **3**

A mixture of dicyano derivative of macrocycle (**2**) (0.80 g, 0.8 mmol) and hydroquinone (0.09 g, 0.8 mmol; purified by sublimation) was placed in a Schlenk tube under argon, gently heated, and subsequently heated at 200°C for 10 h. After cooling to room temperature a dark green product was obtained. The crude product was dissolved in chloroform, washed with water and filtered and then dried over anhydrous $MgSO_4$. The green solution was concentrated *in vacuo* and n-hexane was added dropwise into this solution to obtain dark-green metal-free phthalocyanine. The resulting dark green precipitate was filtered off, washed with n-hexane and then with diethyl ether and dried *in vacuo*. Yield 0.30 g (38%). ^1H NMR ($CDCl_3$): δ 7.85–7.22 (m, 72H, Ar–H), 4.49 (s, 16H, Ar–CH_2), 3.77–3.48 (m, 32H, OCH_2), 3.40–3.18 (m, 48H, NCH_2), 2.47 (s, 48H, CH_3). IR (KBr): 3305, 3033 (Ar–H), 2950–2848 (C–H), 1638, 1597, 1462, 1352 (SO_2), 1173, 1028, 1007, 839, 711 cm^{-1}. UV-vis λ_{max} · (log ε) (in $CHCl_3$, 10^{-4} M): 686sh (5.86), 627, (4.09), 338 sh (4.98), 288 (4.71), 263 (5.24), UV-vis λ_{max} · (log ε) (in $CHCl_3$, 10^{-6} M): 695 (6.32), 635sh (4.31), 342 (5.19), 294 (5.04), 270 (5.37). Mass spectrum (FAB positive): m/z 4011 $[M+1]^+$, 3700 [M-2Ts]. Found: C, 57.3; H, 5.3; N, 8.2. Calc. for $C_{192}H_{218}N_{24}O_{40}S_{16}$: C, 57.4; H, 5.4; N, 8.4%.

[*Hexadecakis*(N-*p*-*tosyl*)-*tetrakis*-*macrocyclephthalocyaninato*]*nickel*(II), **4**

Compound **2** (0.5 g, 0.5 mmol), anhydrous $NiCl_2$ (0.016 g, 0.125 mmol) and anhydrous dimethyl formamide (1 cm^3) were mixed in a Schlenk tube under argon and then the mixture was heated and stirred at 165°C for 36 h under inert atmosphere. After cooling to room temperature, the dark blue mixture was diluted with methanol (50 cm^3) until the crude product precipitated. It was filtered off and washed with hot ethanol. The precipitate was dissolved in chloroform (12 cm^3) and then reprecipitated by adding methanol. In order to obtain metallophthalocyanine and to remove unreacted organic material, the crude product was dissolved in 1,1,2,2-tetrachloroethane (4 cm^3) and reprecipitated with hexane. The precipitate was filtered off, washed with methanol and diethyl ether and then dried *in vacuo*. Yield 0.24 g (46.8%). ^1H NMR ($CDCl_3$): δ 7.93–7.27 (m, 72H, Ar–H), 4.45 (s, 16H, AR–CH_2), 3.92–3.63 (m, 32H, OCH_2), 3.44–3.07 (m, 48H, NCH_2, 2.53 (s, 48H, CH_3). IR (KBr): 3042 (Ar–H), 2943–2859 (C—H), 1642, 1447, 1339 (SO_2), 1150, 1083, 1001, 833, 702 cm^{-1}. UV-vis λ_{max} · (log ε) in $CDCl_3$, 10^{-4} M): 677 (5.61), 617sh (3.52), 338 (5.17), 300sh (4.06), 273 (4.14), 244 (5.12). UV-vis λ_{max} · (log ε) (in $CDCl_3$, 10^{-6} M): 684 (5.88), 629sh (3.74), 345 (5.32), 310sh (4.27), 276 (4.27), 250 (5.29). Mass spectrum (FAB positive): m/z 4067 $[M+1]^+$. Found: C, 56.3; H, 5.1; N, 8.0. Calc. for $C_{192}H_{216}N_{24}O_{40}S_{16}Ni$: C, 56.6; H, 5.3; N, 8.3%.

[*Hexadecakis*(N-*p*-*tosyl*)-*tetrakis*-*macrocyclephthalocyaninato*]*zinc*(II), **5**

A mixture of **2** (0.50 g, 0.5 mmol), anhydrous $Zn(O_2CMe)_2$ (0.034 g, 0.18 mmol) and anhydrous quinoline (1 cm^3) was placed in Schlenk tube and heated to 195–200°C under argon with stirring and held at this temperature for 10 h. After cooling to room temperature the dark blue mixture was diluted with ethanol (5 cm^3) and filtered. The crude product

was dissolved in chloroform, washed with water and then dried over anhydrous $MgSO_4$. After filtration, the filtrate was concentrated (10 cm^3) and ethanol was added dropwise to this solution with stirring. The precipitate formed was filtered off, washed with ethanol then with diethyl ether and dried *in vacuo*. Yield 0.30 g (60%). ^1H NMR ($CDCl_3$): δ 7.88–7.16 (m, 72H, Ar–H), 4.47 (s, 16H, Ar–CH_2), 3.89–3.57 (m, 32H, OCH_2), 3.36–2.97 (m, 48H, NCH_2), 2.55 (s, 48H, CH_3). IR (KBr): 3036 (Ar–H), 2949–2867 (C–H), 1636, 1603, 1443, 1341, (SO_2), 1163, 1123, 1092, 1000, 829, 724 cm^{-1}. UV-vis λ_{max} · (log ε) (in $CDCl_3$, 10^{-4} M): 691sh (4.78), 629 (4.11), 342sh (4.20), 275 (4.49), 246 (5.26). UV-vis λ_{max} · (log ε) (in $CDCl_3$ 10^{-6} M): 697 (4.96), 636sh (4.34), 347 (4.36), 278 (4.63), 254 (5.41). Mass spectrum (FAB positive): *m/z* 4074 $[M+1]^+$, 3454 [M-4Ts+1]. Found: C, 56.4; H, 5.2; N, 8.0. Calc. for $C_{192}H_{216}N_{24}O_{40}S_{16}Zn$: C, 56.6; H 5.3; N, 8.2%.

Acknowledgements—We are indebted to the Research Fund of Karadeniz Technical University for supporting this study.

REFERENCES

1. G. L. Clarkson, N. B. McKeown and K. E. Treacher, *Chem. Soc., Perkin Trans.* I 1995, 1817; C. C. Leznoff, A. P. B. Lever, *Phthalocyanines: Properties and Applications*, VCH, New York (1993).
2. S. Dabak, A. Gul and O. Bekaroglu, *Chem. Ber.* 1994, **127**, 2009; H. Schulz, H. Lehman, M. Rein and M. Hanack, *Struct. Bonding.* 1991, **74**, 41.
3. A. R. Koray, V. Ahsen and O. Bekaroglu, *J. Chem. Soc., Chem. Commun.* 1986, 932; A. G. Gurek and O. Bekaroglu, *Helv. Chim. Acta.* 1991, **77**, 1616; E. Hamuryudan and O. Bekaroglu, *J. Chem. Res. (S).* 1993, 460.
4. A. G. Gurek, V. Ahsen, A. Gul and O. Bekaroglu, *J. Chem. Soc., Dalton Trans.* 1991, 33; C. Piechocki, J. Simon, *Nouv. J. Chem.* 1985, **9**, 159.
5. A. An, J. S. Bradshaw, R. M. Izatt and Z. Yan, *Chem. Rev.* 1994, **94**, 939; O. E. Sielcken, J. Schram, R. J. M. Nolte, J. Schoonman and W. Drenth, *J. Chem. Soc., Chem. Commun.* 1988, 108; E. Musluoglu, V. Ahsen, A. Gul and O. Bekaroglu, *Chem. Ber.* 1991, **124**, 2531.
6. Y. Gok and S. Z. Yildiz, *J. Coord. Chem.* 1995, **36**, 175; Y. Gok, S. Z. Yildiz, to be submitted for publication (1996).
7. S. Sarýgul and O. Bekaroglu, *Chem. Ber.* 1989, **122**, 291.
8. A. W. Snow and N. L. Jarvis, *J. Am. Chem. Soc.* 1984, **106**, 4706.
9. V. Ahsen, E. Yýlmazer, M. Erdas and O. Bekaroglu, *J. Chem. Soc., Dalton Trans.* 1988, 401.
10. M. Kocak, A. Cihan, A. I. Okur and O. Bekaroglu, *J. Chem. Soc., Chem. Commun.* 1991, 578.
11. G. Gumus, Z. Z. Ozturk, V. Ahsen, A. Gul and O. Bekaroglu, *J. Chem. Soc., Dalton Trans.* 1992; 2585; A. Hirsch and M. Nanack, *Chem. Ber.* 1991, **124**, 833.
12. M. Kocak, A. G. Gurek and O. Bekaroglu, *Chem. Ber.* 1994, **127**, 355.
13. A. G. Gurek and O. Bekaroglu, *J. Chem. Soc., Dalton Trans.* 1994, 1419.
14 D. D. Perrin and W. L. F. Armarego, *Purification of Laboratory Chemicals*, 3rd edn. Pergamon Press, Oxford (1988).

Pergamon

S0277-5387(96)00216-1

Polyhedron Vol. 16, No. 1, pp. 119–123, 1997
Copyright © 1996 Elsevier Science Ltd
Printed in Great Britain. All rights reserved
0277-5387/97 $15.00+0.00

A novel, more vivid Cu_2Zn_2SOD model: crystal structure and some properties of the Schiff base copper(II) complex: $[Cu(appn)](ClO_4)_2 \cdot H_2O$

Cai-Ming Liu, Ren-Gen Xiong and Xiao-Zeng You*

Coordination Chemistry Institute, State Key Laboratory of Coordination Chemistry, Centre for Advanced Studies in Science and Technology of Microstructure, Nanjing University, Nanjing 210093, P.R. China

and

Hoong-Kun Fun and Kandasamy Sivakumar

X-ray Crystallography Unit, School of Physics, Universiti Sains Malaysia, 11800 Penang, Malaysia

(Received 13 February 1996; accepted 29 April 1996)

Abstract—The novel Cu_2Zn_2 superoxide dismutase (Cu_2Zn_2SOD) mimic compound $[Cu(appn)](ClO_4)_2 \cdot H_2O$ [where appn = N,N′-propylenebis(2-actoylpyridineiminato)] has been prepared. Single-crystal X-ray analysis revealed that the copper(II) ion has a distorted square-pyramidal environment very similar to that of Cu_2Zn_2SOD: the basal positions are occupied by four nitrogen atoms from the Schiff base ligand and the apical position by an oxygen atom of a hydrate molecule. The Cu—N and Cu—O bond lengths are 1.972(2)···2.029(2) and 2.326(2) Å, respectively. Copyright © 1996 Elsevier Science Ltd

The coordination chemistry of Schiff base ligands derived from 2-pyridyl ketones has found more and more applications in biological modelling of Cu_2Zn_2 superoxide dismutase (Cu_2Zn_2SOD) recently.[1–4] Up to now several Cu_2Zn_2SOD mimic complexes have been synthesized and identified structurally, such as [N,N′-butylenebis(2-acetylpyridineiminato)]copper(II)diperchlorate[2] $[Cu(apy)L](ClO_4)_2$ (apy = 2-acetylpyridine and L = N-ethylene(2-acetylpyridineimine)],[3] [N,N′-bis(2-pyridyl-phenyl)menthylene-1,4-butanediamine]-(N,N′,N″,N‴)-copper(II). However, their coordination environments are not very similar to that of Cu_2Zn_2SOD due in part to there being no coordinated hydrate occupying the apical position of the pyramid, while the copper atom in Cu_2Zn_2SOD is located in the centre of a distorted square pyramidal of five coordinating atoms [four nitrogen atoms of four histidylimidazolate residues (his-44,46,61,118) form the base and the water molecule occupies the apical site, Fig. 1]. In our previous work $\{[Cu(bppn)](ClO_4)_2\}_2 \cdot H_2O$ [bppn = N,N′-propylenebis(2-benzoylpyridineiminato)] was prepared and crystallized, but the hydrate is not coordinated

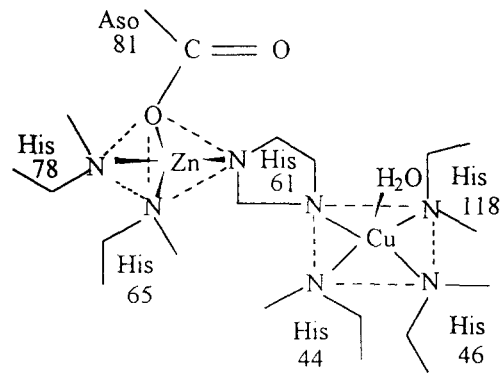


Fig. 1. The active site of Cu_2Zn_2 superoxide dismutase.

* Author to whom correspondence should be addressed.

and the copper(II) ions have distorted tetrahedronal coordination environment. As a continuation of this work, we have prepared a new Cu_2Zn_2SOD mimic complex, $[Cu(appn)](ClO_4)_2 \cdot H_2O$; its crystal structure showed that the copper(II) atom has a coordination geometry very similar to that of Cu_2Zn_2SOD.

EXPERIMENTAL

Preparation of $\{[Cu(bppn)](ClO_4)_2\}_2 \cdot H_2O$

All chemicals were commercial materials and were used without further purification.

To 30 cm^3 methanolic solution containing both $Cu(ClO_4)_2 \cdot 6H_2O$ (0.76 g, 2.07 mmol) and 2-acetylpyridine (0.5 g, 4.13 mmol), a solution of 1,3-propane diamine in MeOH (10 cm^3) was added dropwise while stirring. The solution was refluxed and stirred for 1 h, then the reaction mixture turned into a deeply blue colour. The blue block crystals were formed when the solution was cooled to room temperature. The crystals were separated and washed with ethanol, yield 45.8%. A single crystal suitable for X-ray determination was obtained from recrystallization in acetonitrile. Found: C, 36.3; H, 3.9; N, 9.9. Calc. for $C_{17}H_{22}CuCl_2N_4O_9$: C, 36.4; H, 3.9; N, 10.0%.

Measurements

C, H and N analyses were performed on a Perkin–Elmer 240 elemental analyser; IR and far-IR spectra were recorded on a Nicolet FTIR 170SX spectrophotometer with KBr discs in the 4000–400 and 500–100 cm^{-1} regions, respectively. Electronic spectra were recorded on a Shimadzu-UV 3100 spectrometer in a solution of acetonitrile at a concentration of 3.0×10^{-3} M. EPR was obtained on a Brucker ER 200D-SRC spectrometer at 120 K. Cyclic voltammetry was measured on a PARC M273 electrochemical analyser at a complex concentration of 1×10^{-3} M in twice distilled water with 0.08 M KCl (A.R. recrystallized before use) as the supporting electrolyte. A platinum wire working electrode, a platinum plate auxiliary electrode and a saturated calomel electrode (S.C.E.) reference electrode were employed.

Data collection and structure solution

Diffraction data were collected on a Siemens P4 diffractometer using graphite-monochromated Mo-K_α radiation ($\lambda = 0.71073$ Å). The scan mode was $\theta/2\theta$. 6500 reflections were measured ($1.85 \leqslant \theta \leqslant 27.51°$, $-1 \leqslant h \leqslant 11$, $-1 \leqslant k \leqslant 23$, $-18 \leqslant l \leqslant 18$), of which 5145 were unique [R(int) = 0.0328] and used in the structure refinement.

Crystal data. $C_{17}H_{22}N_4CuCl_2O_9$, $M = 560.83$, monoclinic, space group $P2_1/c$, $a = 9.021(3)$, $b = 17.780(3)$, $c = 14.082(3)$ Å, $\beta = 92.00(1)°$, $V = 2257.3(1.0)$ Å^3, $Z = 4$, $D_c = 1.650$ g cm^{-3}, $\mu = 12.61$ cm^{-1}, $F(000) = 1148$.

The structure was solved by direct methods using SHELXS86[9] and refined using SHELXL93.[10] The coordinates and the anisotropic thermal parameters for the non-hydrogen atoms were refined by full-matrix least-squares on F^2. The hydrogen atoms of the methylene and methyl groups were placed in calculated positions (two H atoms in the water molecule were not included) and refined using a riding model (C—H = 0.96, N—H = 0.90 Å; $U_{iso} = 0.08$), the other hydrogen atoms were located from ΔF maps and refined isotropically. All non-hydrogen atoms were refined with anisotropic thermal parameters. Calculations were carried out on a PC. The final cycle of refinement on $|F|^2$ included 468 variable parameters and converged with $R = 0.0411$, $R_w = 0.1169$ [$I > 2\sigma(I)$], S = 1.051, final difference-Fourier synthesis: $-0.364 \leqslant \Delta\rho \leqslant 0.530$ e Å^{-3}. The atomic coordinates, thermal parameters and structure factors have been deposited with the Editor as supplementary data.

RESULTS AND DISCUSSION

Description of the crystal structure

Selected bond distances and bond angles of the title complex are listed in Table 1. Figures 2 and 3 show the cation configuration and the molecular arrangement of $[Cu(appn)](ClO_4)_2 \cdot H_2O$ in the unit cell, respectively. The coordination geometry of the copper(II) atom closely resembles that of Cu_2Zn_2SOD. A distorted square-pyramid configuration is formed with four nitrogen atoms from the Schiff base ligand as the base and the oxygen atom of water molecule occupying the apical site, while the copper(II) atom is located approximately in the centre of the pyramid base. $[Cu(apy)L](ClO_4)_2$ or $CuPuPhePy(ClO_4)_2$ as previously reported[3,4] have a similar distorted square-pyramidal geometry, but the oxygen atom in the apical position is from the 2-acetylpyridine ligand or perchlorate ion rather than the hydrate molecule, which makes it more difficult for the complexes to change their configurations. The Cu—N bond distances [1.979(2)–2.029(2) Å] of $[Cu(appn)](ClO_4)_2 \cdot H_2O$ are normal coordination bonds and are in good agreement with those found in other mimic copper(II) complexes derived from the 2-pyridal ketones.[2–5] The Cu—O bond length is 2.326(2) Å and shorter than that in SOD (2.80 Å), while the Cu—N bond distances of the title complex are shorter than those in SOD (2.04–2.14 Å), suggesting the present complex possesses lower activity than SOD.

The dihedral angle between the two pyridine ring planes I [N(1), C(1), C(2), C(3), C(4), C(5)] and II [N(4), C(13), C(14), C(15), C(16), C(17)] is 30.49°. Cu^{II} and four N atoms composed are approximate planar square, but the coplanarity is poor. The structure of CuN_4 is obviously distorted towards a tetra-

Table 1. Selected bond distances (Å) and angles (°) for the cations of $[Cu(appn)](ClO_4)_2 \cdot H_2O$

Cu(1)—N(1)	2.029(2)	N(3)—C(10)	1.472(4)
Cu(1)—N(2)	1.992(2)	C(8)—C(9A)	1.476(6)
Cu(1)—N(3)	1.979(2)	C(8)—C(9B)	1.476(6)
Cu(1)—N(4)	1.991(2)	C(9A)—C(10)	1.476(6)
Cu(1)—O(9)	2.326(2)	C(9B)—C(10)	1.475(6)
N(2)—C(6)	1.269(4)	C(12)—C(13)	1.482(4)
N(3)—C(12)	1.266(4)	C(5)—C(6)	1.488(4)
N(3)—Cu(1)—N(4)	80.89(9)	N(2)—Cu(1)—O(9)	91.17(10)
N(3)—Cu(1)—N(2)	96.14(10)	N(1)—Cu(1)—O(9)	95.81(10)
N(4)—Cu(1)—N(2)	172.56(9)	C(8)—C(9A)—C(10)	117.2(4)
N(3)—Cu(1)—N(1)	158.89(10)	C(8)—C(9B)—C(10)	117.2(4)
N(4)—Cu(1)—N(1)	104.64(8)	N(3)—C(10)—C(9B)	123.0(9)
N(2)—Cu(1)—N(1)	80.58(9)	N(3)—C(10)—C(9A)	109.5(3)
N(3)—Cu(1)—O(9)	105.12(11)	N(2)—C(8)—C(9A)	113.4(3)
N(4)—Cu(1)—O(9)	83.08(9)	N(2)—C(8)—C(9B)	108.5(10)

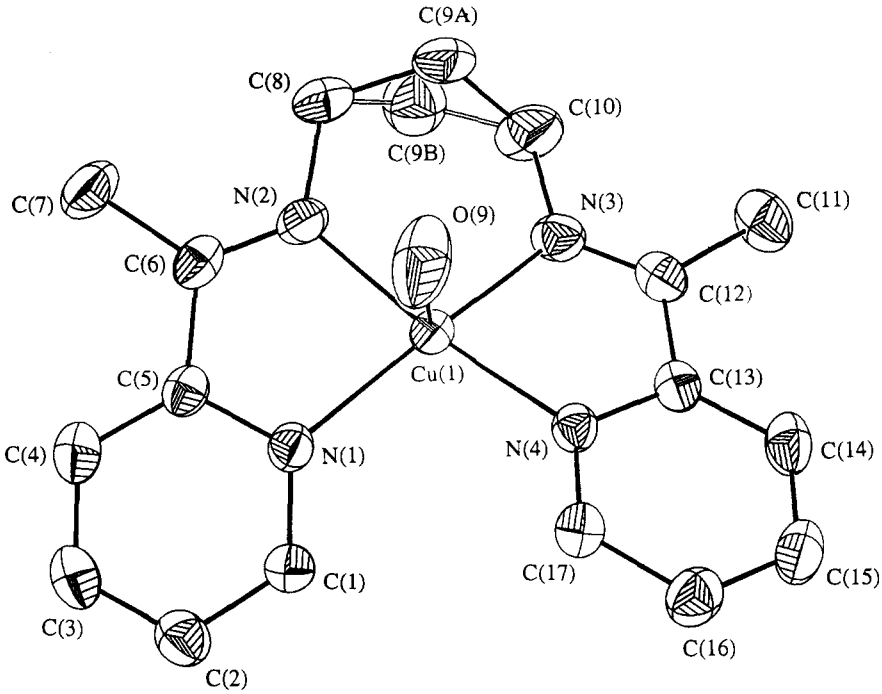


Fig. 2. Perspective view of the complex cation with the atomic numbering scheme.

hedron. Similar trends were observed in previously reported mimic compounds such as [N,N′-butylenebis(2-acetylpyridineiminato)] copper(II) diperchlorate,[2] $[Cu(apy)L](ClO_4)_2$ (apy = 2-acetylpyridine and L = N-ethylene(2-acetylpyridineimine)],[3] [N,N′-bis(2-pyridyl-phenyl)menthylene-1,4-butanediamine]-(N,N′,N″,N‴)-copper(II).[4]

The coordinated water molecule is hydrogen-bonded with perchlorate ions (Table 2). The H—O—H···O contacts range from 2.802(0.020) to 2.97(0.011) Å, indicating the hydrogen bonds are of medium strength.[11] Furthermore, extensive hydrogen bonds involve the perchlorate oxygen atoms [O(1), O(2), O(4), O(6), O(7), O(8)], pyridine ring and carbon chain, and the C···O contacts vary from 3.100(0.018) to 3.358(0.027) Å, suggesting the hydrogen bond strength is weaker than those of the former.

IR, EPR and electronic spectra

In the $\nu(O—H)_{water}$ region of the IR spectrum, $[Cu(appn)](ClO_4)_2 \cdot H_2O$ shows at least two strong and sharp bands around 3519 and 3467 cm^{-1}, mainly attributed to the presence of coordinated water.[10] The medium band at 1631 cm^{-1} was assigned to the C=N stretching vibration of the Schiff's base linkages. A strong and broad band at 1093 cm^{-1} was assigned to be typical of the uncoordinated perchlorate. The strong band at 622 cm^{-1} and weak band at 413 cm^{-1} could be assigned to the in-plane and out-of-plane

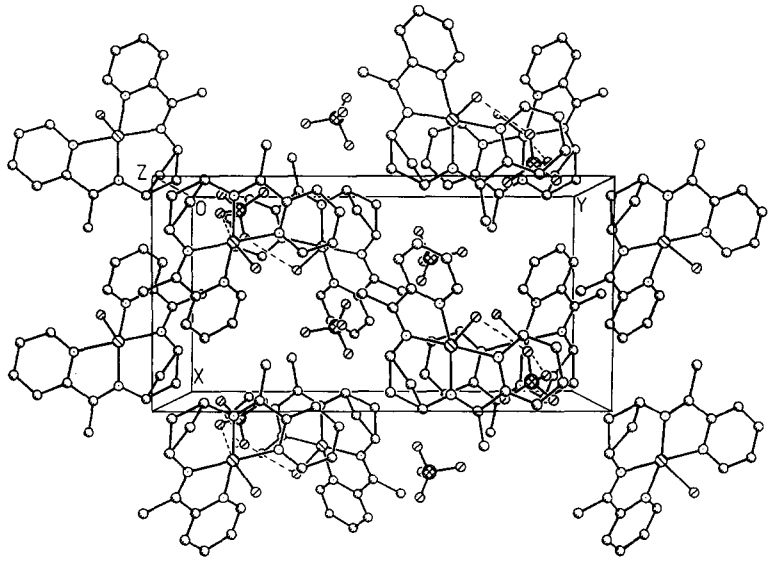


Fig. 3. Unit cell packing diagram.

Table 2. Hydrogen bond distances (Å) of $[Cu(appn)](ClO_4)_2 \cdot H_2O$

C(8)···O(1)[a]	3.358(0.016)	C(11)···O(7A)[a]	3.341(0.012)
O(9)···O(7)[a]	2.877(0.013)	O(9)···O(6A)[a]	2.974(0.011)
C(10)···O(2)[b]	3.100(0.018)	C(8)···O(6)[c]	3.381(0.015)
O(9)···O(3B)[d]	2.802(0.020)	O(9)···O(1A)[d]	2.803(0.021)
O(9)···O(3)[d]	2.987(0.017)	C(16)···O(4A)[e]	3.254(0.016)
C(17)···O(2A)[c]	3.226(0.013)	C(17)···O(2B)[e]	3.103(0.028)
C(2)···O(7A)[f]	3.335(0.009)	C(4)···O(8A)[g]	3.410(0.012)
C(11)···O(2B)[h]	3.358(0.027)		

Symmetry code: [a] x, y, z; [b] $-x, -y, -z+2$; [c] $-x, +y-1/2, -z+1/2+1$; [d] $-x+1, -y, -z+2$; [e] $-x+1, +y+1/2, -z+1/2+1$; [f] $x+1, -y+1/2, +z-1/2$; [g] $-x+1, +y-1/2, -z+1/2+1$; [h] $-x, +y+1/2, -z+1/2+1$.

pyridine ring deformation vibrations, respectively, as previously suggested.[5,8] Other far-IR spectra bands at 386(m), 305(m), 322(m) and at 249(w), 263(w), 241(w), 208(s) cm^{-1} may be assigned to $\nu(Cu—N_{Schiff})$ and $\nu(Cu—N_{ring})$, respectively. Because metal–nitrogen stretching vibrations are often coupled with other normal modes of vibration of the same symmetry, especially ring vibrations.[12] The above attribution of the Cu—N stretching vibrations are only approximate. In addition, the appearance of a new medium band at 397 cm^{-1} is assigned to $\nu(Cu—O_{water})$.[13]

$[Cu(appn)](ClO_4)_4 \cdot H_2O$ displays an electronic spectra band at 626.0 nm (110 $M^{-1}\,cm^{-1}$) in MeCN. It is typical of *d–d* transitions of Cu^{II} in a weak tetragonal field and in accord with those reported for SOD mimic compounds.[4]

The EPR spectrum of the title complex consists of only a quasisymmetric signal centred at $g = 2.076$, which is quite unusual and very different from those of other mimic complexes. The latter always exhibit anisotropic features; the main cause is probably due to the presence of extensive disorder in the structure.

Electrochemistry

The cyclic voltammogram of $[Cu(appn)](ClO_4)_2 \cdot H_2O$ was measured in aqueous solution in the range 2.0 to −2.2 V. The complex is electrochemically active and displays an irreversible one-electron ($i_{pa}/i_{pc} = 1.0$; $E_{pa} = -0.26$ V; $E_{pc} = -0.460$ V; $\Delta E_p = 200$ mV) reduction wave at −0.36 V versus SCE, which is assigned to Cu^{II}/Cu^{I}. The value of $E_{1/2}$ is comparable to those reported SOD mimic compounds (from −0.264 to −0.504 V) and exhibits more positive reduction potential than that of another similar Schiff base mimic complex derived from propane diamine-1,2: $[Cu(appn)](ClO_4)_2$ (reduction potential −0.472 V).[1] The former researchers indicated that the more positive the reduction potential of the mimic compound, the higher its relative activity,[1] suggesting the $[Cu(appn)](ClO_4)_2 \cdot H_2O$ should give better result in simulating superoxide dismutase than the previously reported $[Cu(appn)](ClO_4)_2$.

Acknowledgements—This work was financially supported by

a major project from the State Science and Technology Commission and The National Nature Science Foundation of China. HKF and KS would like to thank the Malaysian government and Universiti Sains Malaysia for research grant R & D No. 123-3417-2201.

REFERENCES

1. Q. Lu, C.-Y. Shen and Q.-H. Luo, *Polyhedron* 1993, **12**, 2005.
2. Q.-H. Luo, Q. Lu, A.-B. Dai and L.-R. Huang, *Inorg. Biochem.* 1993, **51**, 655.
3. Q.-H. Luo, L. Kong, C.-Y. Shen, S.-Y. Yu and Q. Lu, *Trans. Met. Chem.* 1993, **18**, 583.
4. J. Müller, K. Felix, C. Maichle, E. Lengfelder, J. Strähle and U. Weser, *Inorg. Chim. Acta.* 1995, **233**, 11.
5. C.-M. Liu, R.-G. Xiong, X.-Z. You, Y.-J. Liu and K.-K. Cheung, *Polyhedron*, in press.
6. G. M. Sheldrick, SHELXS86, *Acta Cryst.* 1990, **A46**, 47.
7. G. M. Sheldrick, SHELXL93. *Program for Crystal Structure Refinement*. University of Göttingen, Germany (1993).
8. C.-M. Liu, R.-G. Xiong, J.-L. Zuo, X.-Z. You and X.-Y. Huang, *Polyhedron* 1996, **15**, 2051.
9. M. Liness and U. Weser, *Inorg. Chim. Acta* 1986, **125**, 117.
10. L. S. Gelfand, F. J. Iaconianni, L. L. Pytlewski, A. N. Speca, C. M. Mikulski and N. M. Karayannis, *J. Inorg. Nucl. Chem.* 1980, **42**, 377.
11. F. A. Cotton and G. Wilkinson, *Advanced Inorganic Chemistry*, 5th edn, p. 93. Wiley, New York (1988).
12. A. B. P. Lever and E. Mantovani, *Inorg. Chem.* 1971, **10**, 817.
13. K. Nakamoto, *Infrared and Raman Spectra of Inorganic and Coordination Compounds*, 4th edn. Wiley, New York (1986).

Pergamon

S0277-5387(96)00219-7

Polyhedron Vol. 16, No. 1, pp. 125–132, 1997
Copyright © 1996 Elsevier Science Ltd
Printed in Great Britain. All rights reserved
0277-5387/97 $15.00+0.00

Synthesis and spectroscopic characterization of (trialkyl/triaryl)-phosphine gold(I) thiocyanate complexes

M. Naseem Akhtar, Anvarhusein A. Isab,* A. R. Al-Arfaj and M. Sakhawat Hussain

Department of Chemistry, King Fahd University of Petroleum and Minerals, Dhahran 31261, Saudi Arabia

(Received 19 April 1996; accepted 26 April 1996)

Abstract—$R_3PAuS^{13}C^{15}N$ (where R_3P = Me_3P, Et_3P, *i*-Pr_3P, *p*-$TolPh_2P$, Ph_3P and cyanoethylphosphine CEP) complexes have been prepared. The Au—NCS/Au—SCN ratios for these complexes have been determined, using IR spectroscopy (ν_{CN} integrated absorption intensity ratios). The observation that the Au—NCS/Au—SCN ratio increases as the *trans* influence of the phosphine ligand increases is completely in agreement with the trend predicted by the antisymbiotic *trans* influence theory. In the solid state only the S-bonded isomer of each complex is observed. The ^{13}C, ^{15}N and ^{31}P NMR chemical shifts of these complexes were also measured and are compared with $R_3PAu^{13}C^{15}N$ complexes. The results show that unlike $R_3PAu^{13}C^{15}N$ complexes, which undergo disproportionation in solution, the $R_3PAuS^{13}C^{15}N$ complexes do not undergo disproportionation. Copyright © 1996 Elsevier Science Ltd

Gold(I) has a strong tendency to form linear two-coordinate complexes of the type L—Au—X, where "L" is a neutral Lewis base (e.g. phosphines, thioethers, etc.) and "X" is a halide, pseudohalide, aryl or alkyl group.[1–3] These complexes are usually formulated as neutral complexes, but since gold(I) is generally labile, there exists the possibility of ligand redistribution in solution to form the symmetrically substituted complexes of the type $[AuL_2]^+$ and $[AuX_2]^-$, as shown in eq. (1).

$$2L—Au—X \rightleftharpoons [AuL_2]^+ + [AuX_2]^- . \quad (1)$$

It has been reported[4] that anionic cyano(thiolato)gold(I) complexes, $[RSAuCN]^-$, are in equilibrium with substantial concentrations of $[Au(CN)_2]^-$ and $[Au(SR)_2]^-$ in aqueous solution. This ligand redistribution reaction is also observed in cyano (alkyl,aryl)phosphinegold(I) complexes.[2,5,6]

The thiocyanate is an ambidentate ligand, which can bind to the central metal via "S" or "N" atom. Thus, L—Au—SCN linear complexes appeared to be an ideal system to study the antisymbolic *trans* effect in class (b) metals, because there is no effect of steric hinderance since the ligands are present on opposite sides of the molecule and also due to the neutral nature of the complexes they are not susceptible to the counter-ion effect. Moreover, the IR spectra become very simple to analyse due to the presence of only two ligands.

The concept of antisymbiotic *trans* influence predicts that the site *trans* to a strong *trans* directing ligand will become harder in complexes of class (b) metals. It has been found[7,8] that in the solid state, thiocyanate is bonded only via "S" to the gold atom. However, Burmeister and Melpolder[9,10] have observed this antisymbiotic trend in a series of solutions of linear L—Au—SCN complexes using IR; the L—Au—NCS/L—Au—SCN ratio increases as the *trans* effect of the "L" phosphine ligand increases.

In the present study we have prepared a series of doubly labelled $R_3PAuS^{13}C^{15}N$ (where R_3P = Me_3P, Et_3P, *i*-Pr_3P, *p*-$TolPh_2P$, Ph_3P and cyanoethylphosphine CEP) complexes to see whether ligand redistribution reactions and the antisymbiotic *trans* effect is observed in these types of gold(I) complexes using ^{13}C, ^{31}P, ^{15}N NMR and IR spectroscopy.

* Author to whom correspondence should be addressed.

EXPERIMENTAL

Reagents

$KS^{13}C^{15}N$ (50%) was purchased from Merck Sharp and Dohme, Canada. Sodium tetrachloroaurate dihydrate, phosphine ligands (trimethyl, triethyl, tiphenyl, tri-isopropyl, triscyanoethyl and paratollyldiphenyl) were obtained from Stream Chemical Co., U.S.A.; CD_3OD and dichloromethane were obtained from Fluka Chemical Co.

R_3PAuCl

The R_3PAuCl complexes were prepared by the addition of phosphine ligands to the ethanolic solution of $NaAuCl_4$, as described in the literature.[11,12]

$R_3PAuS^{13}C^{15}N$

R_3PAuCl was dissolved in acetone and 1 equiv. of $AgNO_3$ was added to produce R_3PAuNO_3 in solution by precipitation of AgCl[7]. Then 1 equiv. of an aqueous solution of $KS^{13}C^{15}N$ (50% labelled) was added to the solution of R_3PAuNO_3 and was stirred for 1 h. The solution was then placed under vacuum to remove the solvent. Finally, a white crystalline solid was recovered, which was washed several times with deionized water to remove KNO_3, then with ethanol and ether. The elemental analysis, melting points and % yield for $R_3PAuSCN$ complexes are given in Table 1.

IR spectroscopy

The solid-state IR spectra of $R_3PAuS^{13}C^{15}N$ complexes were recorded on a Perkin–Elmer IR 180 spectrophotometer using KBr pellets. While a Perkin–Elmer 1600 FT series was used to measure solution IR spectra in the ν_{CN} region.

The ratios of the ν_{CN} integrated absorption intensities of N-bonded/S-bonded thiocyanates were calculated as follows.[10] The IR stretching region was recorded using the linear absorbance mode rather than the linear transmittance mode. The low-energy tail of the high-energy absorption band was drawn in (an estimate) and the resulting envelops were traced on paper, which were carefully cut out and weighed on a Mettler balance. The weight of the N-bonded band was divided by that of S-bonded band giving an N-bonded/S-bonded ratio.

^{13}C, ^{15}N *and* ^{31}P *NMR spectroscopy*

The ^{13}C NMR spectra were measured at 50.30 MHz on a Varian XL-200 spectrometer operating in the pulsed Fourier transform mode. The ^{13}C NMR measurements were made with broad-band ^1H decoupling.

The ^{15}N NMR spectra were obtained at 20.28 MHz on a Varian XL-200 spectrometer using CD_3OD solutions at the probe temperature of 297 K. The chemical shift for ^{15}N NMR spectra were measured using sealed $NH_4^{15}NO_3$ as an external reference, which has a resonance at 375.11 ppm relative to pure CH_3NO_2, 380.2 ppm.[13,14] We did not measure the T_1 values of any resonance. The spectral conditions were: 5.0 s delay time, 16 K data points, spectral width 10 000 Hz, pulse width 6.0 μs (20°), and 10 mm multinuclear probe. Approximately 60 000 scans were accumulated for each sample.

The ^{31}P NMR spectra were obtained at 80.98 MHz on a Varian XL-200 spectrometer using the above solutions at the probe temperature 297 K. The ^{31}P NMR chemical shifts were measured from external reference 1% TMP.[16] The spectral conditions were: 1.0 s delay time, 32 K data points, spectral width 4000 Hz, pulse width 5.0 μs, 10 mm multinuclear probe. Approximately 10 000 scans were accumulated for each sample.

The ^{13}C, ^{15}N and ^{31}P NMR chemical shifts for various $R_3PAuS^{13}C^{15}N$ complexes are given in Tables 2 and 3.

RESULTS AND DISCUSSION

The ^{31}P-$\{^1H\}$ NMR spectra of $R_3PAuS^{13}C^{15}N$ (where R_3P = Me_3P, Et_3P, *i*-Pr_3P, *p*-$TolPh_2P$, Ph_3P and cyanoethylphosphine CEP) complexes were measured in their methanolic solution. In each case a single sharp resonance was observed. There was no splitting due to $^3J(^{31}P—^{13}C)$ or $^4J(^{31}P—^{15}N)$. The ^{31}P chemical shifts for all $R_3PAuS^{13}C^{15}N$ complexes are given in Table 2.

The ^{13}C-$\{^1H\}$ NMR spectra of $R_3PAuS^{13}C^{15}N$ complexes were recorded with the same solutions used for ^{31}P NMR studies. Two broad resonances were observed in low-field region of $Me_3PAuS^{13}C^{15}N$, $Et_3PAuS^{13}C^{15}N$,

Table 1. The elemental analysis, melting points and % yield of $R_3PAuS^{13}C^{15}N$ complexes

$R_3PAuS^{13}C^{15}N$	Found (Calc.) % C	H	N	S	M.p.	% Yield
i-$Pr_3PAuS^{13}C^{15}N$	28.0(29.0)	5.0(5.0)	3.1(3.5)	7.4(7.7)	72	56
$Et_3PAuS^{13}C^{15}N$	21.2(22.6)	3.9(4.0)	3.6(3.9)	8.7(8.6)	50[8]	65
$Me_3PAuS^{13}C^{15}N$	14.6(14.6)	2.6(2.7)	3.9(4.4)	9.6(9.6)	123–125	70
p-$TolPh_2PAuS^{13}C^{15}N$	46.9(47.2)	3.7(3.8)	2.4(2.6)	5.8(5.7)	50–52	75
$Ph_3PAuS^{13}C^{15}N$	43.2(44.1)	2.8(2.9)	2.8(2.8)	5.9(6.2)	165[7]	65
$CEPAuS^{13}C^{15}N$	26.7(26.8)	2.7(2.7)	12.9(12.6)	7.2(7.1)	124–126	55

Table 2. The ^{13}C, ^{15}N and ^{31}P NMR chemical shifts and ν_{CO} for $R_3PAuS^{13}C^{15}N$ complexes

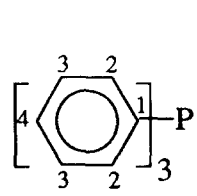
$R_3PAuS^{13}C^{15}N$	$\delta(^{31}P)$	$\delta(^{13}C)$ of S-bonded	$\delta(^{13}C)$ of N-bonded	$\delta(^{15}N)$	ν_{CO}[a]
i-$Pr_3PAuS^{13}C^{15}N$	68.14	119.42	119.14	233	2059.2
$Et_3PAuS^{13}C^{15}N$	36.37	119.89	119.61	232	2061.7
$Me_3PAuS^{13}C^{15}N$	−4.64	120.28	120.01	231	2064.1
p-$TolPh_2PAuS^{13}C^{15}N$	30.54	124.83	124.76	—	2068.2
$Ph_3PAuS^{13}C^{15}N$	35.00	126.48	126.48	—	2068.9
$CEPAuS^{13}C^{15}N$	47.54	129.53	129.30	—	2077.9

[a] Taken from reference 18 for $[R_3PNi(CO)_3]$.

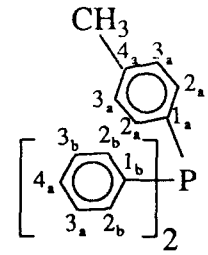
Table 3. The ^{13}C chemical shifts of $R_3PAuS^{13}C^{15}N$ complexes

$R_3PAuS^{13}C^{15}N$	δ_{C_1} (ppm)	δ_{C_2} (ppm)	δ_{C_3} (ppm)	δ_{C_4} (ppm)	δ_{SCN} (ppm)	$^1J_{PC}$ (Hz)
i-$Pr_3PAuS^{13}C^{15}N$	24.93	20.70	—	—	119.28	30.8
$Et_3PAuS^{13}C^{15}N$	18.60	9.51	—	—	119.75	35.7
$Me_3PAuS^{13}C^{15}N$	15.22	—	—	—	120.15	38.8
$Ph_3PAuS^{13}C^{15}N$	135.20	133.45	130.74	130.64	126.48	—
$CEPAuS^{13}C^{15}N$	24.09	10.08	124.00	—	129.42	—
p-$TolPh_2PAuS^{13}C^{15}N$	δ_{CH_3} 21.44	$\delta_{C_{1a}}$ 135.29	$\delta_{C_{2a}}$ 133.36	$\delta_{C_{1a}}$ 130.66	$\delta_{C_{4a}}$ 135.02	$\delta_{C_{1b}}$ 135.09
	$\delta_{C_{2b}}$ 133.36	$\delta_{C_{3b}}$ 129.94	$\delta_{C_{4b}}$ 129.70	δ_{SCN} 124.83	—	—

Where R_3P are $(^1CH_3)_3P$, $(^2CH_3—^1CH_2)_3P$, $[(^2CH_3)_2^1CH]_3P$, $(^3CN—^2CH_2—^1CH_2)_3P$,



,



i-$Pr_3PAuS^{13}C^{15}N$ and $CEPAuS^{13}C^{15}N$ complexes for $—AuS^{13}C^{15}N$ and $—Au^{15}N^{13}CS$ linkage isomers. The $^1J(^{13}C—^{15}N)$ was not resolved in these complexes due to exchange between S-bonded and N-bonded isomers. The resonance due to S-bonded isomer was more intense and was at low field compared with the N-bonded isomer. In the case of p-$TolPh_2PAuS^{13}C^{15}N$ the two resonances for S-bonded and N-bonded isomers were resolved as doublets, while in the case of the $Ph_3PAuS^{13}C^{15}N$ complex only one broad resonance was resolved for both linkage isomers. The ^{13}C chemical shifts for all $R_3PAuS^{13}C^{15}N$ complexes are given in Tables 2 and 3.

The $^{15}N[^1H]$ NMR spectra of some solutions of $R_3PAuS^{13}C^{15}N$ complexes were also recorded, but due to the low sensitivity of the instrument, low solubility of the complexes and only 50% labelled ^{15}N, the signal-to-noise ratio was very poor. We were able to obtain the resonances for i-$Pr_3PAuS^{13}C^{15}N$, $Et_3PAuS^{13}C^{15}N$ and $Me_3PAuS^{13}C^{15}N$ complexes only, in the region 231–233 ppm. In the case of i-$Pr_3PAuS^{13}C^{15}N$ two broad resonances were resolved for S-bonded and N-bonded linkage isomers. The $^1J(^{13}C—^{15}N)$ was not resolved due to exchange between linkage isomers, while in the other complexes only one broad resonance was resolved without any splitting for both isomers. The ^{15}N chemical shifts for $R_3PAuS^{13}C^{15}N$ complexes are given in Table 2. The typical ^{31}P, ^{13}C and ^{15}N NMR spectra of i-$Pr_3PAuS^{13}C^{15}N$ are shown in Fig. 1.

The solution IR spectra of all $R_3PAuSCN$ complexes, except CEPAuSCN, in dichloromethane yielded two separate absorption bands in the region 2122–2129 cm^{-1} for the S-bonded isomer, while the other in the region 2082–2091 cm^{-1} for N-bonded isomer,[10] which are given in Table 4. In the case of CEPAuSCN due to very low solubility, the solution IR spectrum was not very good and two separate absorption bands were not resolved. A typical solution IR spectrum of i-$Pr_3PAuSCN$ in the ν_{CN} region is shown in Fig. 2. It was observed that the N-bonded isomer was a minor component in all $R_3PAuSCN$ complexes, since the integrated absorption intensity of the ν_{CN} band of an N-bonded thiocyanate is generally an order of magnitude larger[5] than that of an S-bonded thiocyanate. However, it is clear that the proportion of N-bonded isomer increases as the *trans* influence of the phosphine ligand increases. If the assumption is made that the intensity of the N-bonded

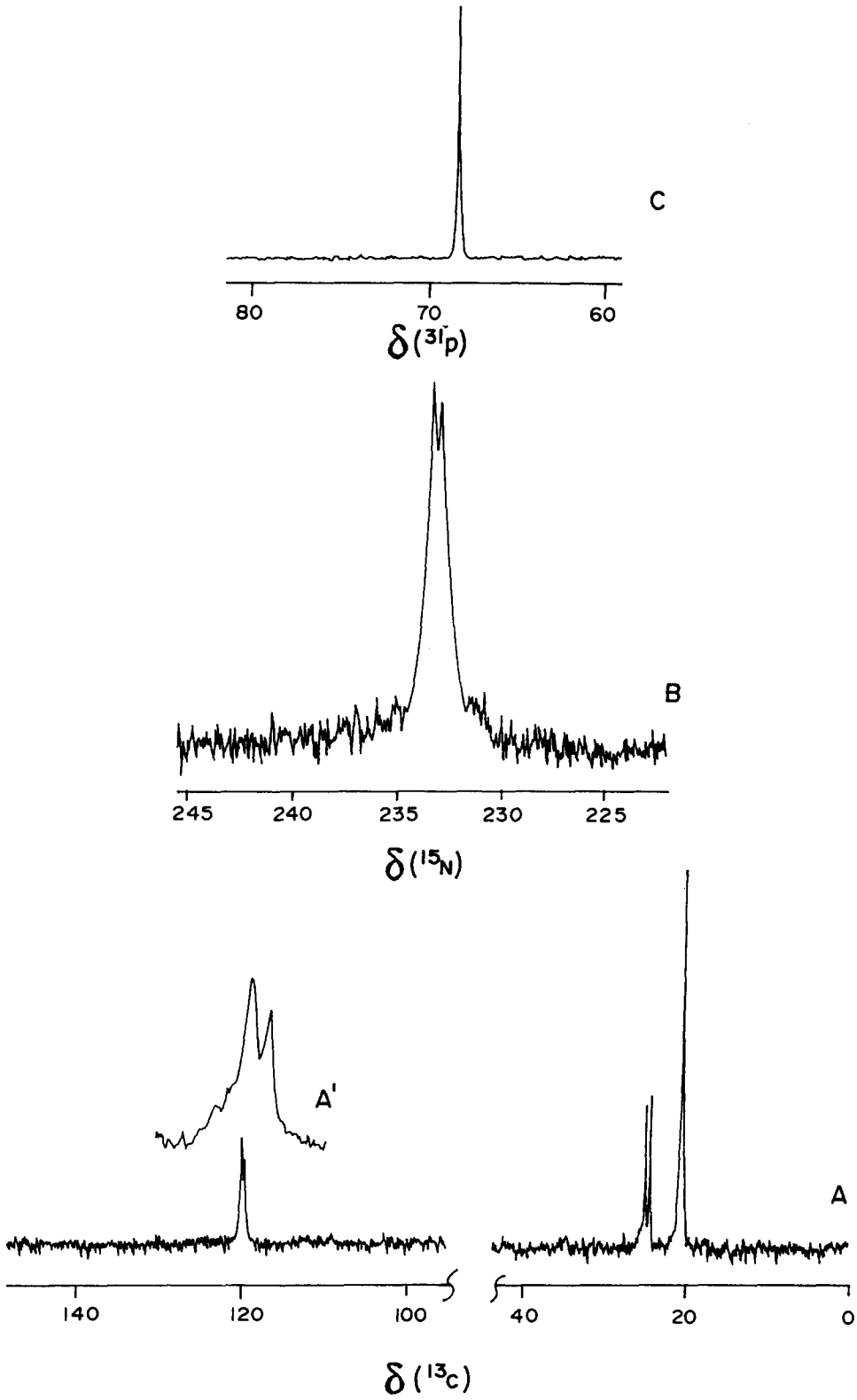


Fig. 1. NMR spectra of 0.45 M *i*-$Pr_3PAuS^{13}C^{15}N$ in CD_3OD: (A) ^{13}C NMR; (A′) expansion of ^{13}C NMR spectrum in "SCN" region; (B) ^{15}N NMR and (C) ^{31}P NMR spectra.

Table 4. ν_{SCN}, ν_{NCS}, Au—NCS/Au—SCN ratio and % N-bonded isomer in $R_3PAuSCN$ complexes from their solution IR spectra

$R_3AuS^{13}C^{15}N$	ν_{SCN} (cm^{-1})	ν_{NCS} (cm^{-1})	Au—NCS/Au—SCN	%N-bonded isomer
i-$Pr_3PAuS^{13}C^{15}N$	2124.7	2085.7	0.224	2.2
$Et_3AuS^{13}C^{15}N$	2126.0	2084.3	1.570	5.7
$Me_3PAuS^{13}C^{15}N$	2122.0	2091.7	1.112	10.0
$Ph_3PAuS^{13}C^{15}N$	2129.5[10]	2082.7	0.470	4.5[10]
$CEPAuS^{13}C^{15}N$	2125.8	—	—	—
p-Tol · $Ph_2PAuS^{13}C^{15}N$	2125.9	20.89.5	1.851	15.6

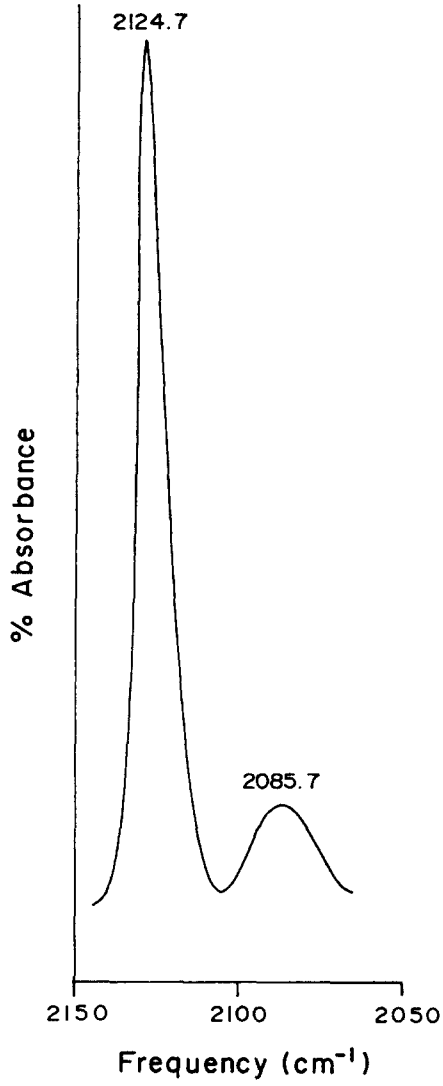


Fig. 2. The IR spectrum of 0.50 M Pri-$_3PAuS^{13}C^{15}N$ in dichloromethane in the absorption mode for the "SCN" group.

isomer is exactly 10 times that of the S-bonded isomer, then the per cent of N-bonded isomer present at equilibrium can be calculated[10] as follows: $10X(1-X)$ = Au—NCS/Au—SCN ratio; $10X$ is the per cent of N-bonded isomer present in the solution.

The ratios of integrated absorption intensities of ν_{CN} IR absorption bands and per cent of N-bonded isomer present in the solution of all $R_3PAuSCN$ complexes are given in Table 4. The solid-state IR spectra of all $R_3PAuSCN$ complexes showed that only the S-bonded isomer is present in the solid form. Apparently the crystal packing favours the geometry of this isomer.

The ^{31}P NMR spectra of R_3PAuCN complexes gave[5,6] two separate resonances for $[(R_3P)_2Au]^+$ and R_3PAuCN species due to ligand redistribution reactions. However, in the present studies for all $R_3PAuS^{13}C^{15}N$ complexes only one resonance is observed, which indicates that there is no ligand redistribution reaction in $R_3PAuS^{13}C^{15}N$ complexes or that it is so fast that it cannot be resolved on the NMR time scale. In the case of $R_3PAu^{13}C^{15}N$ complexes we have measured $^2J(^{31}P—^{13}C)$ and $^3J(^{31}P—^{15}N)$ coupling constants, but in this case we were unable to find any splitting due to $^3J(^{31}P—^{13}C)$ or $^4J(^{31}P—^{15}N)$, which means that in $R_3PAuS^{13}C^{15}N$ complexes the exchange between "S"-bonded and "N"-bonded SCN is so fast that this splitting is not resolved.

The ^{13}C-$\{^1H\}$ NMR studies are also consistent with the observations of ^{31}P NMR studies. The ^{13}C NMR gave rise to two broad resonances for linkage isomers, but the resonance due to $[Au(S^{13}C^{15}N)_2]^-$ was not observed, which indicates that there is no ligand redistribution reaction as shown in eq. (1). While in the case of $R_3PAu^{13}C^{15}N$ complexes two separate resonances were observed[6] for $R_3PAu^{13}C^{15}N$ and $[Au(^{13}C^{15}N)_2]^-$ species due to ligand redistribution reactions.

The ^{15}N NMR spectra of $R_3PAuS^{13}C^{15}N$ complexes was considered to be the most important technique to probe the S-bonded and N-bonded "SCN" ligand in this series of complexes. However, due to low sensitivity of the instrument only one broad resonance was resolved in the region 231–233 ppm for both S-bonded and N-bonded linkage isomers. However, a single resonance in the ^{15}N NMR spectra of $R_3PAuS^{13}C^{15}N$ complexes supports the results of ^{13}C and ^{31}P NMR studies that ligand redistribution reactions do not occur in this series of complexes, otherwise ^{15}N resonances due to $R_3PAuS^{13}C^{15}N$ and $[Au(S^{13}C^{15}N)_2]^-$ species would have been observed as shown in eq. (1).

The formation constants ($\log\beta_2$) for $[Au(CN)_2]^-$ and $[Au(SCN)_2]^-$ are reported[17] to be 39.0 and 17.0, respectively. The R_3PAuCN complexes readily undergo ligand redistribution reactions as shown in eq. (1) due to the large formation constant of $[Au(CN)_2]^-$, while this ligand redistribution reaction is not favourable in $R_3PAuSCN$ complexes due to the small formation constant of $[Au(SCN)_2]^-$.

A correlation that is frequently used to determine the relative basicity of phosphines is the electronic parameter ν_{CO} for $[R_3PNi(CO)_3]$ complexes (values tabulated by Tolman[18]). A decrease in the ν_{CO} value indicates a net increase in the electron-donating ability of a phosphine. Figure 3 shows an opposite behaviour of dependence of $\delta(^{13}C)$ of CN and SCN groups of $R_3PAu^{13}C^{15}N$ and $R_3PAuS^{13}C^{15}N$, respectively, on ν_{CO} values of different phosphines. In $R_3PAu^{13}C^{15}N$ complexes $\delta(^{13}C)$ decreases with an increase in the ν_{CO} value of phosphines due to the involvement of π-bonding between gold(I) and the —CN group.[6] While in $R_3PAuS^{13}C^{15}N$ complexes there is no π-bonding between gold(I) and the —SCN group, therefore, the basicity of the phosphine is effecting $\delta(^{13}C)$ directly, i.e. an increase in the basicity of phosphine causes more donation of electron towards gold(I), which in turn increases the effective nuclear charge on the "C" atom causing an upfield shift of $\delta(^{13}C)$.

The solution IR spectroscopy has been observed to be the most successful technique for the study of antisymbiotic *trans*-effect in $R_3PAuSCN$ complexes. Figure 4 shows a linear relationship between the *trans* effect (basicity) of phosphines and the % N-bonded isomer in all complexes, except that of $Ph_3PAuSCN$. As the *trans* effect of phosphines increases (basicity

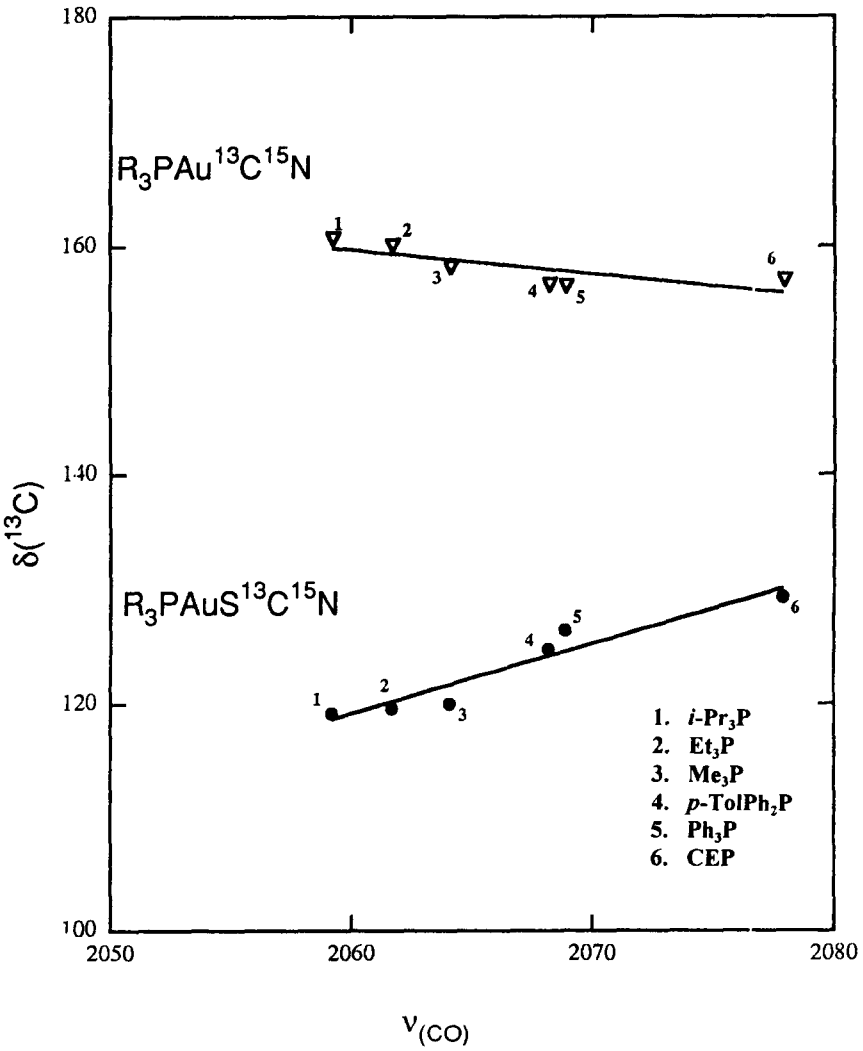


Fig. 3. Plot of ^{13}C NMR chemical shifts of $R_3PAu^{13}C^{15}N$ and $R_3PAuS^{13}C^{15}N$ complexes versus ν_{CO}. The solid lines are regression lines. The ^{13}C NMR chemical shift values for $R_3PAu^{13}C^{15}N$ complexes are taken from reference 5.

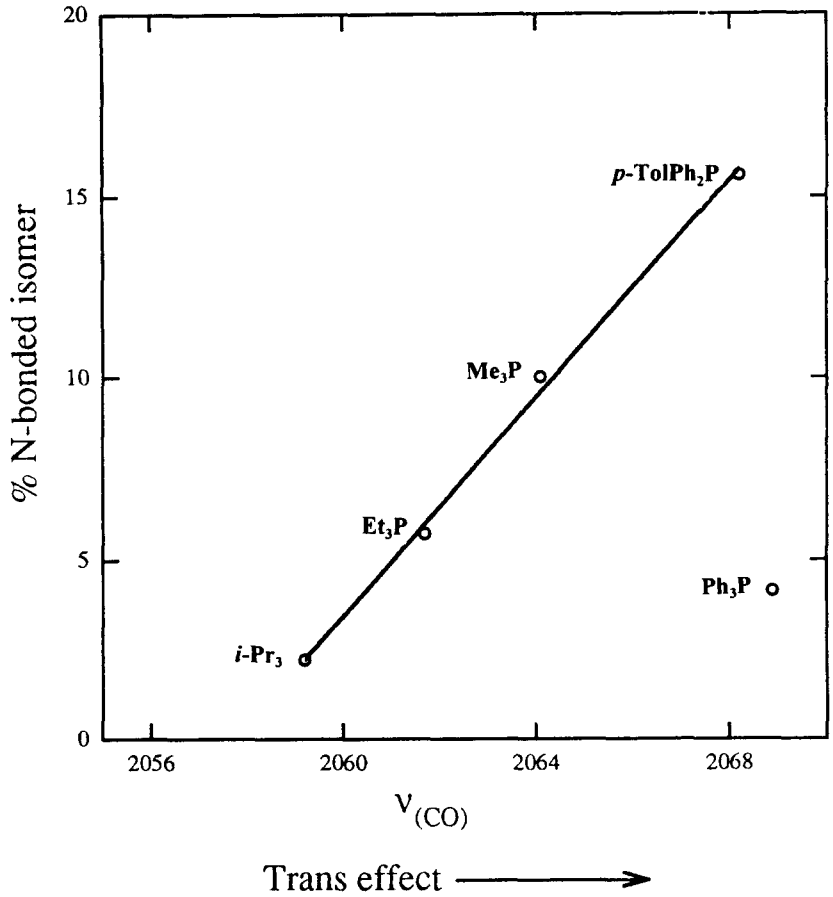


Fig. 4. Plot of % N-bonded isomer in $R_3PAuS^{13}C^{15}N$ complexes versus ν_{CO} of the phosphines. The solid line is regression line. Note: The value of $Ph_3PAuS^{13}C^{15}N$ is not included in the regression.

decreases) it causes decrease in the strength of the "Au—P" bond, which in turn favours the "NCS"-bonded isomer.[10]

This linkage isomerism can be explained on the basis of bridging of the "SCN" group between two gold species. The "—Au—SCN" bond undergoes cleavage and a new "—Au—NCS" bond with an "SCN" group of other species is formed. In this way $R_3PAuSCN$ complexes do not undergo disproportionation during linkage isomerism as is observed in R_3PAuCN complexes.

CONCLUSION

The results of this study follow the results exhibited by other class (b) metal systems[15] and add further support to the concept of the antisymbiotic *trans* influence[9,10,19] as being the primary electronic effect which causes certain coordination sites on class (b) metals to exhibit class (a) behaviour. When a soft ligand is placed *trans* to thiocyanate, as in LAuSCN, the stronger the *trans* director L becomes, the more N-bonding is observed, which is exactly what would be expected. In this case steric control of the bonding mode of the thiocyanate does not interfere with the interpretation of the results. The ^{13}C, ^{31}P and ^{15}N NMR spectroscopy shows that these complexes do not undergo ligand redistribution reactions as in the case of R_3PAuCN complexes.

Acknowledgements—We are thankful to Mr Khurshid Aalam from the Research Institute KFUPM for running IR spectra of the complexes. This research was supported by the King Fahd University of Petroleum and Minerals Research Committee under project No. CY/CYANIDE/175.

REFERENCES

1. P. L. Bellon, M. Manassero and M. Sansoni, *Ric. Sci.* 1969, **39**, 173.
2. A. L. Hormann, C. F. Shaw III, D. W. Bennett and W. M. Reiff, *Inorg. Chem.* 1986, **25**, 3953.
3. P. Jones and J. Lautner, *Acta Cryst.* 1988, **C44**, 2091.
4. G. Lewis and C. F. Shaw III, *Inorg. Chem.* 1986, **25**, 58.
5. A. L. Hormann-Arendt and C. F. Shaw III, *Inorg. Chem.* 1990, **29**, 4683.
6. M. N. Akhtar, I. H. Ghazi, A. A. Isab, A. R. Al-Arfaj, M. I. M. Wazeer and M. S. Hussain, *J. Coord. Chem.* 1995, **36**, 149.
7. N. J. DeStefano and J. L. Burmeister, *Inorg. Chem.* 1971, **10**, 998.

8. M. M. El-Etri and W. M. Scovell, *Inorg. Chem.* 1990, **29**, 480.
9. J. L. Burmeister and J. B. Melpolder, *J. Chem. Soc., Chem. Commun.* 1973, 613.
10. J. B. Melpolder and J. L. Burmeister, *Inorg. Chim. Acta* 1981, **49**, 115.
11. D. A. Duddell, P. L. Goggin, R. J. Goodfellow, M. G. Norton and J. G. Smith, *J. Chem. Soc. (A)* 1970, 545.
12. F. G. Mann, A. F. Wells and D. Purdie, *J. Chem. Soc.* 1937, 1828.
13. A. A. Isab, I. H. Ghazi, M. I. M. Wazeer and H. P. Perzanowski, *J. Inorg. Biochem.* 1993, **50**, 299.
14. P. R. Srinivasan and R. L. Lichter, *J. Magn. Reson.* 1977, **28**, 227.
15. J. L. Burmeister, *The Chemistry and Biochemistry of Thiocyanic Acid and its Derivatives* (Edited by A. A. Newman), pp. 68–130. Academic Press, New York.
16. A. A. Isab, C. F. Shaw III, J. D. Hoeschele and J. Locke, *Inorg. Chem.* 1988, **27**, 3588.
17. P. N. Dickson, A. Wehlri and G. Geier, *Inorg. Chem.* 1988, **27**, 2921.
18. C. A. Tolman, *Chem. Rev.* 1977, **77**, 313.
19. R. G. Pearson, *Inorg. Chem.* 1973, **12**, 712.

Pergamon

S0277-5387(96)00206-9

Polyhedron Vol. 16, No. 1, pp. 133–141, 1997
Copyright © 1996 Elsevier Science Ltd
Printed in Great Britain. All rights reserved
0277-5387/97 $15.00+0.00

Divalent metal chloride amidine complexes—2. Compounds of Mn, Co and Ni

Deirdre I. Arnold, F. Albert Cotton,* David J. Maloney and John H. Matonic

Department of Chemistry and Laboratory for Molecular Structure and Bonding, Texas A&M University, College Station, TX 77843, U.S.A.

and

Carlos A. Murillo*

Department of Chemistry and Laboratory for Molecular Structure and Bonding, Texas A&M University, College Station, TX 77843, U.S.A. and Department of Chemistry, University of Costa Rica, Ciudad Universitaria, Costa Rica

(Received 12 March 1996; accepted 23 April 1996)

Abstract—A series of compounds of the type $[MCl_2(amidine)_2]_n$, M = Mn, Co and Ni, has been prepared in high purity and yield by solubilizing otherwise insoluble metal chlorides in the presence of neutral amidines in refluxing toluene. As crystalline solids, they are stable in air for several days. The compounds are excellent starting materials for the formation of dinuclear compounds. A complete chemical and structural characterization is provided for the penta-coordinated dimanganese compound $[MnCl_2(HDPhF)_2]_2$, **I** (DPhF = diphenylformamidinato), the mononuclear compounds $CoCl_2(HDPhBz)_2$, **II** (DPhBz = diphenylbenzamidinato), and $NiCl_2(HDTolF)_2$, **III** (DTolF = di-*p*-tolylformamidinato). The HDPhF analogue of **III** reacts with a strong base to give the dinuclear species $Ni_2(DPhF)_4$ (**IV**), the structure of which is also reported here. Copyright © 1996 Elsevier Science Ltd

The use of amidinato ligands of the type $RNC(R')NR^-$ has met with considerable success for the preparation of transition metal complexes, especially of the dinuclear type.[1] In part 1[2] of this two-part report, the synthesis and structural characterization of a series of divalent metal chloride formamidines, M^{II} = Fe, Co and Pt was described.

At the time, we indicated that "the facility with which they form and the high purity in which they are isolated, as well as their favourable solubility characteristics, make them attractive starting materials for the preparation of other formamidinato complexes". In this paper we will show that our predictions were correct and will present the synthesis and characterization of new $MCl_2(amidine)_2$ compounds for M = Mn, Co and Ni as well as that of the dinuclear compound $Ni_2(DPhF)_4$.

EXPERIMENTAL

Materials and methods

All manipulations were performed under an atmosphere of nitrogen using standard Schlenk techniques. Samples for spectroscopic characterization were prepared in a Vacuum Atmospheres drybox under an atmosphere of argon. Toluene, THF and hexanes were purified by conventional methods and were freshly distilled from Na/K alloy under nitrogen immediately prior to use. $MnCl_2$, $CoCl_2$ and $NiCl_2$ were purchased from Aesar. Both

* Author to whom correspondence should be addressed.

$CoCl_2$ and $NiCl_2$ were refluxed for 20 min with thionylchloride (obtained from Fisher Scientific), then dried under vacuum prior to use. Celite 545 (not acid washed) was purchased from Spectrum Chemical; *n*-butyllithium (1.6 M solution in hexanes) and HDPhF were purchased from Aldrich Chemical Co.; HDTolF was prepared according to a slight modification of a published procedure,[3] HDPhBz was prepared by a literature method.[4] Elemental analyses were provided by Canadian Microanalytical Service Ltd. IR spectra were obtained as Nujol mulls between CsI plates on a Perkin–Elmer 16PC FT-IR spectrophotometer and magnetic susceptibility measurements were made using in a Johnson–Matthey MSB-1 balance.

$[MnCl_2(HDPhF)_2]_2$ (I)

$MnCl_2$ (1.00 g, 7.94 mmol) was refluxed in THF for 2 h and the solvent was then eliminated under vacuum. To the activated solid was added HDPhF (3.01 g, 15.9 mmol). Warm toluene (50 cm^3) was then added to the mixture which was refluxed for 30 min while stirring. The yellowish solution was quickly filtered while hot and left undisturbed for 1 day in a Dewar flask. Many single crystals of the compound were collected by filtration and washed with hexanes (2×10 cm^3). Yield: 3.00 g (76%). Found: C, 60.6; H, 4.8; N, 10.8. Calc. for $C_{52}H_{48}Cl_4Mn_2N_8$: C, 60.2; H, 4.7; N, 10.8%. IR (Nujol, cm^{-1}): 3340(s), 3185(m), 3109(m), 2723(w), 1639(s), 1601(s, sh), 1586(s), 1377(s), 1320(s), 1205(s), 1179(m), 1072(w), 1027(w), 975(w), 895(m), 753(s), 696(s), 630(s). The magnetic susceptibility corresponded to a magnetic moment of 5.88 BM per $MnCl_2(HDPhF)_2$ unit.

$CoCl_2(HDPhBz)_2$ (II)

$CoCl_2$ (0.13 g, 1.0 mmol) and HDPhBz (0.50 g, 1.84 mmol) were stirred together in toluene (15 cm^3) and heated overnight. The mixture was then filtered through Celite to remove excess $CoCl_2$. The filtrate was layered with hexanes (20 cm^3) and allowed to stand at room temperature for 24 h, then placed in a freezer at $-20°C$ for another 24 h. Crystals of the compound, some of which were suitable for X-ray diffraction, were collected by filtration and washed with hexanes (2×10 cm^3). Yield: 0.48 g (70%). Found: C, 62.7; H, 5.2; N, 7.2. Calc. for $C_{38}H_{32}Cl_2CoN_4$: C, 62.2; H, 4.4; N, 7.6%. IR (Nujol, cm^{-1}): 3155(w), 3100(w), 2854(s), 1622(m), 1607(s), 1583(s), 1565(s), 1411(s), 1377(s), 1239(w), 1205(m), 1073(w), 1026(w), 830(m), 789(s), 772(s), 703(m). The magnetic susceptibility corresponded to a magnetic moment of 4.40 BM.

$NiCl_2(HDTolF)_2$ (III)

$NiCl_2$ (0.39 g, 3.0 mmol) and HDTolF (0.90 g, 4.0 mmol) were stirred together in toluene (20 cm^3) and warmed to 100°C as the colour changed from pale yellow to green. After about 1 h the mixture was dried *in vacuo* and hexanes (20 cm^3) were added. The mixture was heated and quickly filtered to remove any unreacted ligand. The remaining dark green solid was redissolved in toluene (10 cm^3) and filtered to remove the excess $NiCl_2$. The yield after drying was 0.70 g (61%). Crystals suitable for study by X-ray diffraction were obtained by dissolving 0.05 g of the green solid in toluene (5 cm^3), layering with hexanes and cooling the solution to $-20°C$. Large green block-shaped crystals formed within 48 h. IR (Nujol, cm^{-1}): 3188(m), 3100(m), 1651(s), 1607(m), 1589(m), 1520(m), 1505(s), 1377(m), 1312(s, br), 1221(m), 1201(m), 1018(w), 989(m), 808(m), 753(w), 720(w), 571(w), 506(m), 496(w). The magnetic susceptibility corresponded to a magnetic moment of 3.54 BM.

$Ni_2(DPhF)_4$ (IV)

A solution of $NiCl_2(HDPhF)_2$ (0.10 g, 0.19 mmol), synthesized in the same manner as $NiCl_2(HDTolF)_2$, in toluene (15 cm^3) was prepared and cooled to $-78°C$. $NaEt_3BH$ (0.1 cm^3, 0.10 mmol) was added to the stirring solution and the resultant dark green–brown mixture was stirred and kept at $-78°C$. After 1 h, *n*-butyllithium (0.24 cm^3, 0.38 mmol) was slowly added and the mixture immediately changed to a deep brown colour. After the mixture had warmed to room temperature, it was filtered through Celite and the filtrate was layered with hexanes (20 cm^3) and stored at $-20°C$. Within 2 days, dark brown crystals had formed at the bottom of the tube. The yield of this reaction was not optimized.

Structure determinations

Geometric and intensity data for **I** were collected at room temperature on a Rigaku AFC5R rotating Cu anode diffractometer, data for **II**, **III** and **IV** were gathered at $-60°C$ on an Enraf–Nonius FAST area detector system, utilizing the software program MADNES.[5] Detailed procedures have previously been described.[6]

Unit-cell refinement for **I** utilized 25 reflections in the range $35 \leqslant 2\theta \leqslant 50°C$. For **II**, **III** and **IV** indexing was performed on 50 reflections taken

from three 10° ω-rotations in the range $0 \leqslant \omega \leqslant 100°$ and unit-cell refinement used 250 reflections in the range $20 \leqslant 2\theta \leqslant 32°$. In each case, the cell dimensions and Laue group were confirmed with axial images. All data were corrected for Lorentz and polarization effects. Three strong reflections measured periodically throughout the data collection for **I** showed no significant decay. An empirical absorption correction based on six ψ-scans was applied for **I**. Data were processed into SHELX format using the program TEXSAN[7] and ABSURD[8] for **I**, **II**, **III** and **IV**, respectively.

In all structures, the positions of heavy atoms were found in direct methods E-maps using the software solution program in SHELXTL.[9] Subsequent cycles of least-squares refinement followed by difference-Fourier synthesis produced the positions of the remaining non-hydrogen atoms. For purposes of structure factor calculations, hydrogen atoms were placed in idealized positions. Details of data collection and refinement are given in Table 1. Selected bond distances and angles for **I**, **II**, **III** and **IV** are listed in Tables 2, 3, 4 and 5, respectively. Supplementary data for **I**, **II**, **III** and **IV** have been deposited with the Cambridge Crystallographic Data Centre.

RESULTS AND DISCUSSION

$[MnCl_2(HDPhF)_2]_2$

The best way to prepare **I** is to start with finely divided $MnCl_2$ prepared by eliminating THF from $Mn(THF)_2Cl_2$[10] and then refluxing it with HDPhF in toluene. A brief refluxing time and the filtration of the hot reaction mixture are crucial steps to obtain good yields of the pure and homogeneous crystalline product.

The molecular structure of **I** is shown in Fig. 1. In the solid state the compound is composed of discrete dinuclear molecules. Each molecule possesses crystallographically imposed C_i symmetry. The manganese atoms are bound to five groups, namely two neutral HDPhF molecules, one terminal and two bridging chloride ions. A long metal–metal separation [3.798(2) Å] and a magnetic moment which corresponds to five unpaired electrons precludes the existence of any type of manganese–manganese bond. The dinuclear molecule is internally stabilized by the presence of short (3.11 Å) contacts between N(4) and Cl(2) due to an intramolecular hydrogen bond.

As seen in Table 2, the distribution of atoms about the manganese atom, as well as the bond distances, is very irregular. The Mn—N(3) bond, where N(3) is almost *trans* to Cl(1A), is 0.12 Å longer than the Mn—N(1) bond. The bond asymmetry is also observed for the bridging chloride ions. The Mn—Cl(1) bond distance is *ca* 0.26 Å shorter than that of Mn(1A)—Cl(1). As it is frequently encountered in compounds which contain both terminal and bridging groups, the former bond is slightly shorter.

$CoCl_2(HDPhBz)_2$

In our earlier study[2] we prepared $CoCl_2(HDTolF)_2$ by a melt reaction using $CoCl_2$ and HDTolF. We have found that such reactions sometimes yield a product that is slightly oily and, therefore, further purification steps are sometimes needed. If the reagents are refluxed in toluene the reaction preceeds more cleanly and in higher yields. We suggest the latter procedure as well as the use of an excess of $CoCl_2$ for the preparation of **II**. $CoCl_2(HDPhBz)_2$ displays the characteristic blue colour of tetrahedral Co^{II} compounds. Its reactivity is similar to that of its HDPhF analogue. The structure is illustrated in Fig. 2 and is very similar to the previously described $CoCl_2(HDPhF)_2$. The two chloride ions and a nitrogen atom of each HDPhBz group complete the pseudo-tetrahedral coordination sphere. As with all other known tetrahedral $MCl_2(amidine)_2$ compounds, there are N—N···Cl hydrogen bonds which help stabilize the molecules. In **II**, Cl(1) and N(4), and Cl(2) and N(2) have separations of 3.25 and 3.19 Å, respectively. Presumably the presence of hydrogen bonds contributes significantly to the observed chemical stability of the crystalline samples of $MCl_2(amidine)_2$, M = Mn, Fe, Co and Ni, as well as to the facility with which they are crystallized.

$NiCl_2(HDTolF]_2$ (**III**)

While the synthesis of this compound proceeds quite poorly as a melt reaction, it goes smoothly by refluxing in toluene, occurring in a fashion similar to the preparations of **I** and **II**. It is important to note, however, that the reflux reaction must be stopped after a relatively short time, otherwise a flocculent white solid precipitates from the reaction mixture. This solid renders the reaction mixture difficult to filter and its production dramatically lowers the yield of **III**. The white solid has not been characterized, but based on its colour and insolubility may be an oligomeric or polymeric Ni^{II} octahedral species. It is also very important to use strictly anhydrous $NiCl_2$. The magnetic susceptibility of **III** (3.54 BM) falls within the range expected for tetrahedral Ni^{II} complexes.[11]

The structure of **III** is shown in Fig. 3. The aver-

Table 1. Crystal data for $[MnCl_2(HDPhF)_2]_2$ (**I**), $CoCl_2(HDPhBz)_2$ (**II**), $NiCl_2(HDTolF)_2$ (**III**) and $Ni_2(DPhF)_4$ (**IV**)

	I	**II**	**III**	**IV**
Formula	$C_{52}H_{48}Cl_4Mn_2N_8$	$C_{38}H_{32}Cl_2CoN_4$	$C_{30}H_{32}Cl_2N_4Ni$	$C_{52}H_{44}N_8Ni_2$
Formula weight	1036.66	674.51	578.21	898.37
Space group	$P2_1/c$	$P\bar{1}$	$P2_1/c$	$C2/c$
a (Å)	13.106(1)	10.4516(6)	10.222(4)	13.841(4)
b (Å)	10.210(1)	17.292(2)	14.965(9)	13.665(9)
c (Å)	19.226(1)	10.384(3)	19.450(8)	22.792(8)
α (°)	90	105.33(1)	90	90
β (°)	108.362(6)	112.91(1)	100.23(3)	91.03(6)
γ(°)	90	88.15(1)	90	90
V (Å^3)	2441.7(3)	1661.9(5)	2928(2)	4310(3)
Z	2	2	4	4
d_{calc} (g cm^{-3})	1.410	1.348	1.312	1.384
Crystal size (mm^3)	$0.35 \times 0.27 \times 0.25$	$0.35 \times 0.20 \times 0.20$	$0.20 \times 0.30 \times 0.40$	$0.30 \times 0.10 \times 0.10$
Absorption coefficient (mm^{-1})	6.573	0.710	0.870	0.921
Data collection instrument	Rigaku AFC5R	FAST	FAST	FAST
Radiation (monochromated in incident beam)	Cu-K_α(λ_α = 1.54184 Å)	Mo-K_α(λ_α = 0.71073 Å)	Mo-K_α(λ_α = 0.71073 Å)	Mo-K_α(λ_α = 0.71073 Å)
Temperature (°C)	20(2)	−60(2)	−60(2)	−60(2)
Data collection range, θ (°)	3.55–60.11	2.21–22.5	2.44–22.50	2.27–21.00
Number of unique data, total with $F_o^2 > 2\sigma(F_o^2)$	3640	3728	3690	2021
Number of parameters refined	298	534	418	280
Transmission factors, min., max.	0.4865, 0.9995	—	—	—
R_w^a	0.044	0.053	0.066	0.089
wR_2^b	0.105	0.110	0.134	0.164
Quality-of-fit indicator	1.032	1.122	1.180	1.190

[a] $R_w = [\Sigma w(F_o - F_c)^2/\Sigma wF_o^2]^{1/2}$.

[b] $wR_2 = [\Sigma w(F_o^2 - F_c^2)^2/\Sigma w(F_o^2)^2]^{1/2}$, $w = 1[\sigma^2(F_o^2) + (ap)^2 + bp$, $p = \max(F_o^2 \text{ or } 0) + 2(F_c^2)]/3$. $a = 0.0499$ and $b = 2.3830$ for **I**, $a = 0.0322$, $b = 4.657$ for **II**; $a = 0.0454$ and $b = 6.0556$ for **III**; $a = 0.0242$ and $b = 75.843$ for **IV**.

Table 2. Selected bond lengths (Å) and angles (°) for $[MnCl_2(HDPhF)_2]_2$ (**I**)[a]

Mn···Mn	3.798(1)	N(1)—C(1)	1.298(5)
Mn(1)—N(1)	2.181(3)	N(1)—C(10)	1.439(5)
Mn(1)—N(3)	2.302(4)	N(2)—C(1)	1.350(6)
Mn(1)—Cl(2)	2.350(1)	N(2)—C(20)	1.426(5)
Mn(1)—Cl(1)	2.408(1)	N(3)—C(2)	1.297(5)
Mn(1)—Cl(1A)	2.665(1)	N(3)—C(30)	1.438(5)
Cl(1)—Mn(1A)	2.665(1)	N(4)—C(2)	1.349(6)
		N(4)—C(40)	1.431(6)
N(1)—Mn(1)—N(3)	86.7(1)	C(1)—N(1)—C(10)	114.8(3)
N(1)—Mn(1)—Cl(2)	121.2(1)	C(1)—N(1)—Mn(1)	125.5(3)
N(3)—Mn(1)—Cl(2)	99.81(9)	C(10)—N(1)—Mn(1)	119.6(3)
N(1)—Mn(1)—Cl(1)	129.2(1)	C(1)—N(2)—C(20)	123.9(4)
N(3)—Mn(1)—Cl(1)	94.45(9)	C(2)—N(3)—C(30)	114.6(4)
Cl(2)—Mn(1)—Cl(1)	108.71(6)	C(2)—N(3)—Mn(1)	130.8(3)
N(1)—Mn(1)—Cl(1A)	84.52(9)	C(30)—N(3)—Mn(1)	114.2(3)
N(3)—Mn(1)—Cl(1A)	166.4(1)	C(2)—N(4)—C(40)	125.6(4)
Cl(2)—Mn(1)—Cl(1A)	93.60(5)	N(1)—C(1)—N(2)	122.5(4)
Cl(1)—Mn(1)—Cl(1A)	83.18(4)	N(3)—C(2)—N(4)	120.0(4)
Mn(1)—Cl(1)—Mn(1A)	96.82(4)		

[a] Atoms labelled with an "A" are related by an inversion centre.

Table 3. Selected bond lengths (Å) and angles (°) for $CoCl_2(HDPhBz)_2$ (**II**)

Co(1)—Cl(1)	2.270(2)	N(2)—C(1)	1.350(6)
Co(1)—Cl(2)	2.265(2)	N(2)—C(20)	1.419(6)
Co(1)—N(1)	2.033(4)	N(3)—C(2)	1.302(6)
Co(1)—N(3)	2.041(4)	N(3)—C(30)	1.438(6)
N(1)—C(1)	1.317(6)	N(4)—C(2)	1.356(6)
N(1)—C(10)	1.450(6)	N(4)—C(40)	1.420(7)
Cl(1)—Co(1)—Cl(2)	111.06(6)	Co(1)—N(1)—C(1)	127.4(3)
Cl(1)—Co(1)—N(1)	108.5(1)	Co(1)—N(1)—C(10)	113.3(3)
Cl(1)—Co(1)—N(3)	109.6(1)	Co(1)—N(3)—C(2)	124.2(3)
Cl(2)—Co(1)—N(1)	111.3(1)	Co(1)—N(3)—C(30)	116.0(3)
Cl(2)—Co(1)—N(3)	103.5(1)	N(1)—C(1)—N(2)	117.9(5)
N(1)—Co(1)—N(3)	112.8(2)	N(3)—C(2)—N(4)	117.2(4)

Table 4. Selected bond lengths (Å) and angles (°) for $NiCl_2(HDTolF)_2$ (**III**)

Ni(1)—Cl(1)	2.250(2)	N(2)—C(1)	1.322(7)
Ni(1)—Cl(2)	2.247(2)	N(2)—C(10)	1.426(7)
Ni(1)—N(1)	2.004(5)	N(3)—C(2)	1.310(7)
Ni(1)—N(3)	2.006(4)	N(4)—C(2)	1.331(7)
N(1)—C(1)	1.298(7)	N(4)—C(24)	1.412(7)
N(3)—C(17)	1.436(7)		
Cl(1)—Ni—Cl(2)	120.33(8)	Ni—N(1)—C(1)	130.0(4)
Cl(1)—Ni—N(1)	105.2(1)	Ni—N(1)—C(3)	116.0(3)
Cl(1)—Ni—N(3)	106.3(1)	Ni—N(3)—C(2)	125.8(4)
Cl(2)—Ni—N(1)	108.2(2)	Ni—N(3)—C(17)	119.5(3)
Cl(2)—Ni—N(3)	115.5(1)	N(1)—C(1)—N(2)	123.3(6)
N(1)—Ni—N(3)	98.7(2)	N(3)—C(2)—N(4)	123.8(6)

Table 5. Selected bond lengths (Å) and angles (°) for $Ni_2(DPhF)_4$ (**IV**)[a]

Ni—Ni(A)	2.490(3)	N(1)—C(1)	1.31(1)
Ni—N(1)	1.922(9)	N(2)—C(2)	1.33(1)
Ni—N(2)	1.899(9)	N(3)—C(1A)	1.31(1)
Ni—N(3)	1.93(1)	N(4)—C(2A)	1.32(1)
Ni—N(4)	1.90(1)		
N(1)—Ni—N(2)	174.5(4)	N(3)—Ni—N(4)	172.5(4)
N(1)—Ni—N(3)	89.4(4)	N(1)—C(1)—N(3A)	125(1)
N(1)—Ni—N(4)	89.4(4)	N(2)—C(2)—N(4A)	123(1)
N(2)—Ni—N(3)	89.9(4)	N(1)—Ni—Ni(A)—N(3A)	14.5(4)
N(2)—Ni—N(4)	90.6(4)	N(2)—Ni—Ni(A)—N(4A)	14.9(4)

[a] Atoms labelled with an "A" are related by a two-fold axis.

age Ni—Cl and Ni—N bond lengths are 2.249(2) and 2.005(1) Å, respectively. Short distances between the chloride ions and the protonated nitrogen atoms of the HDTolF molecules are a clear indication of the presence of hydrogen bonds. The Cl(1)—N(4) distance is 3.11 Å and the Cl(2)—N(2) separation is 3.20 Å.

In general, the trend of slightly shorter C—N (imido) as compared with C—N(amine) bond distances observed in other complexed and uncomplexed neutral amidines[12] is also seen here. Surprisingly, only a few tetrahedral Ni^{II} species containing an N_2Cl_2 donor ligand set have been characterized by X-ray crystallography. When the nitrogen donor ligand is 3,4-dihydro-1-phenyl-1H-[1,4]-oxazino[4,3-a]-benzimidazole, average Ni—Cl and Ni—N distances are reported as 2.23(1) and 2.00(5) Å, respectively.[13] The crystal structure of dichlorobis [2,4-bis(isopropylamino)-6-methoxy-1,3,5-triazene] nickel(II) has also been reported,[14] in which the Ni^{II} centre exists in a distorted tetrahedral environment and also has two long [2.700(7) Å] contacts with oxygen atoms of the ligands. Average Ni—Cl and Ni—N bond lengths for this compound are 2.281(2) and 2.017(8) Å, respectively.

$Ni_2(DPhF)_4$ (**IV**)

The action of a strong base on the HDPhF analogue of **III** yields crystal of $Ni_2(DPhF)_4$, which is in all important respects identical with the previously reported $Ni_2(DTolF)_4$.[15] Its molecular structure is

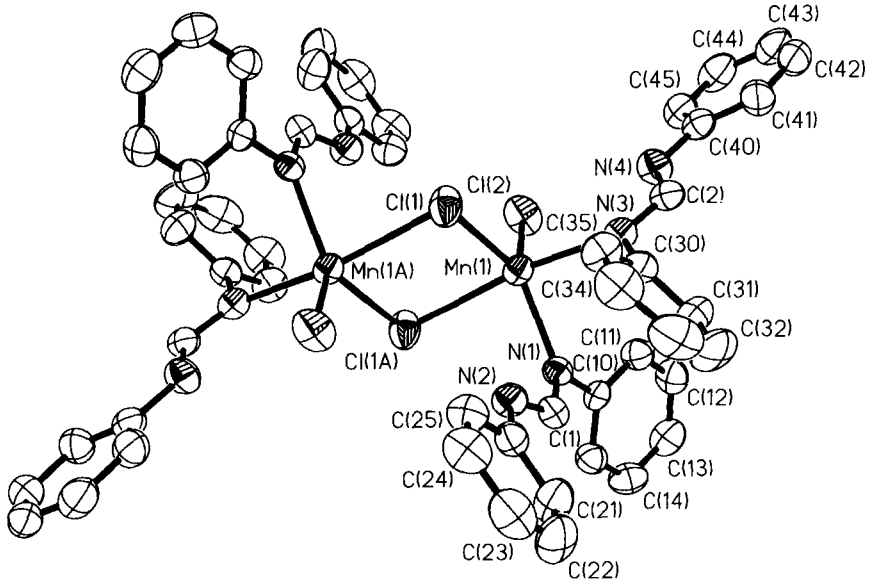


Fig. 1. Thermal ellipsoid plot of the dinuclear compound $[MnCl_2(HDPhF)_2]_2$. Atoms are represented by their 50% probability ellipsoids.

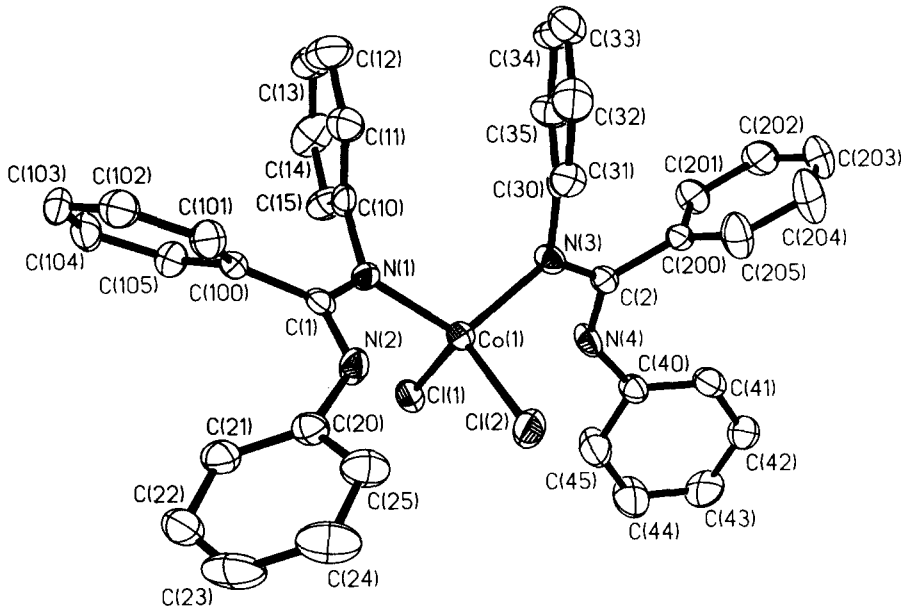


Fig. 2. Structural representation of $CoCl_2(HDPhBz)_2$. Atoms are represented by their 50% probability ellipsoids.

shown in Fig. 4. The long Ni—Ni separation [2.490(3) Å] is consistent with the absence of a bond. Four amidinato groups form bridges between the metal atoms, which have an essentially square planar coordination.

The main interest in the preparation of **IV** was to show that there exists a general pathway to the synthesis of dinuclear amidinato compounds from species of the type $MCl_2(amidine)_2$. Table 6 contains a listing of several compounds of the types $M_2(amidinato)_3$ and $M_2(amidinato)_4$. Some of them have been made exclusively from mononuclear $MCl_2(amidine)_2$ compounds; those of the types $Fe_2(amidinato)_4$, $Fe_2(amidinato)_3$ and $Co_2(amidinato)_3$ cannot be made using other classical synthetic pathways.

We have now been able to prepare various $MCl_2(amidine)_2$ compounds for M = Mn, Fe, Co, Ni and Pt. Except for the latter, our present results indicate that their preparation and purification is best accomplished if the reaction of the corresponding finely divided anhydrous metal dichloride and the amidine is carried out in a toluene solution. The fact that the stoichiometry is correct to produce the corresponding tetrabridged dimetal(II) species of elimination of 2 equiv. of HCl indicates that their use will probably produce a significant number of metal–metal bonded compounds, especially those of the post-chromium elements of the first transition series, which until now have been very difficult to synthesize.

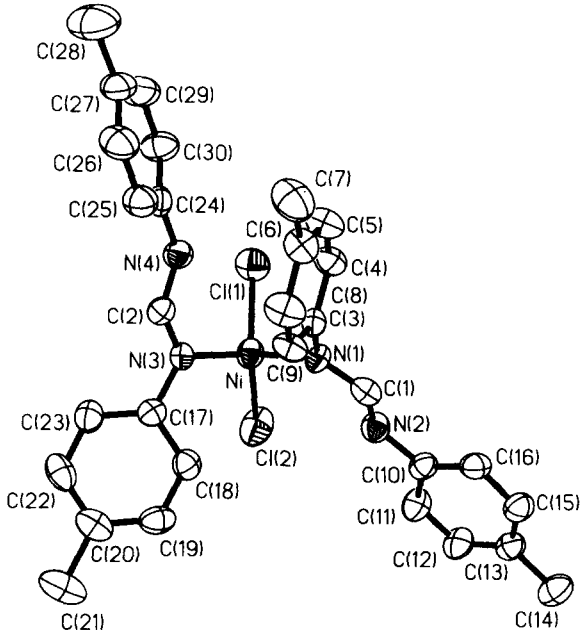


Fig. 3. A plot of the molecular structure of $NiCl_2(HDTolF)_2$. Atoms are represented by their 50% probability ellipsoids.

Acknowledgements—We are grateful to the Vicerrectoría de Investigación U. C. R. (Project 115-87-516) and the Department of Chemistry for support of work at the Univeristy of Costa Rica and to the National Science Foundation for support of work at Texas A&M University. We also thank Dr L. M. Daniels for crystallographic advice.

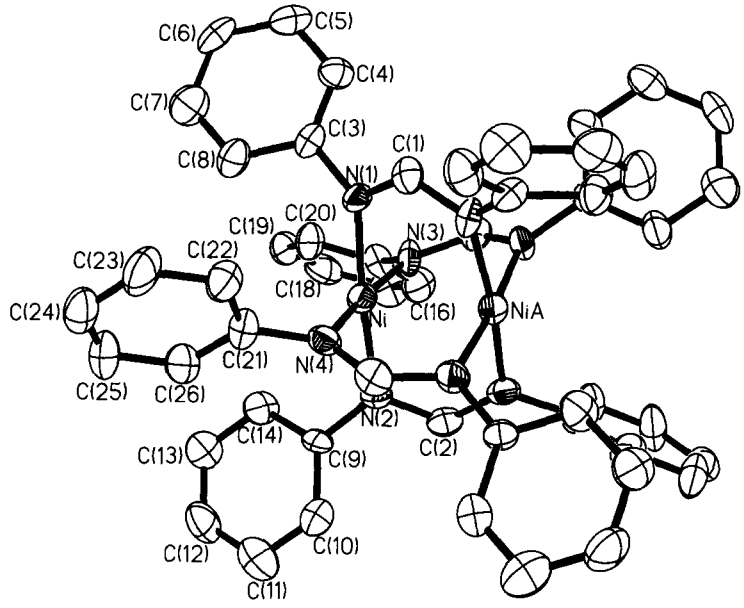


Fig. 4. A drawing and labelling scheme of the molecular structure of $Ni_2(DPhF)_4$. Non-hydrogen atoms are shown as 50% probability ellipsoids.

Table 6. Some dinuclear compounds prepared from $MCl_2(amidine)_2$ starting materials

Starting material	Dinuclear compound formed	Metal–metal separation (Å)	Reference
$[MnCl_2(HDPhF)_2]_2$	—	—	Work in progress
$FeCl_2(HDPhF)_2$	$Fe_2(DPhF)_3$	2.2318(8)	16
	$Fe_2(DPhF)_4$	2.462(2)	17
$FeCl_2(HDPhBz)_2$	$Fe_2(\mu\text{-}DPhBz)_2(\eta^2\text{-}DPhBz)_2$	3.124(1)	18
$CoCl_2(HDPhF)_2$	$Co_2(DPhF)_3$	2.385(1)	19
	$Co_2(DPhF)_4$	2.3735(9)	20
$CoCl_2(HDPhBz)_2$	$Co_2(DPhBz)_3$	2.320(1)	19
	$Co_2(DPhBz)_4$	2.298(2)	20
$NiCl_2(HDPhF)_2$	$Ni_2(DPhF)_4$	2.490(3)	This work
trans-$PtCl_2(HDPhF)_2$	$Pt_2(\mu\text{-}DPhF)_2(\eta^2\text{-}DPhF)_2$	2.9128(9)	21
	$Pt_2(\mu\text{-}DPhF)_4$	2.649(2)	21

REFERENCES

1. See for example, F. A. Cotton, L. M. Daniels and C. A. Murillo, *Inorg. Chem.* 1993, **32**, 2881, and refs therein.
2. F. A. Cotton, L. M. Daniels, D. J. Maloney, J. H. Matonic and C. A. Murillo, *Polyhedron* 1994, **13**, 815.
3. R. M. Roberts, *J. Org. Chem.* 1949, **14**, 277.
4. A. C. Houtz and E. C. Wagner, *Organic Synthesis*, Collective Vol. 4, p. 383. John Wiley & Sons, New York.
5. J. Pflugrath, A. Messerschmitt MADNES, Munich Area Detector (New EEC) System, Version EEC 11/1/89, with enhancements by Enraf–Nonius Corporation, Delft, The Netherlands. A description of MADNES appears in: A. Messerschmitt and J. Pflugrath, *J. Appl. Cryst.* 1987, **20**, 30.
6. (a) J. C. Bryan, F. A. Cotton, L. M. Daniels, S. C. Haefner and A. P. Sattelberger, *Inorg. Chem.* 1995, **34**, 1875; (b) W. R. Scheidt and I. Turowska-Turk, *Inorg. Chem.* 1994, **33**, 1314.
7. TEXSAN–TEXRAY. *Structure Analysis Package*. Molecular Structure Corporation (1985).
8. P. R. Evans, ABSURD. *Absorption Correction Program for the Area Detector*. MRC Laboratory of

Molecular Biology, Hills Road, Cambridge, U.K. (1990).
9. SHELXTL, Version 5.03. Siemens Industrial Automation Inc, Madison, Wisconsin, U.S.A.
10. A. Hosseiny, C. A. McAuliffe, K. Minten, M. J. Parrott, R. Pritchard and J. Tames, *Inorg. Chim. Acta* 1980, **39**, 227.
11. L. Sacconi, F. Mani and A. Bencini, *Comprehensive Coordination Chemistry* (Edited by G. Wilkinson, R. D. Gillard and J. A. McCleverty), Vol. 4, Ch. 50, p. 54. Pergamon Press, Oxford, U.K. (1987).
12. F. A. Cotton, S. C. Haefner, J. H. Matonic, C. A. Murillo and X. Wang, *Polyhedron*, in press.
13. B. Piggott and A. C. Skapsi, *Inorg. Chim. Acta* 1983, **77**, L171.
14. G. Reck, A. Kircheiss, R. Bauwe and H. Schrauber, *Cryst. Struct. Commun.* 1982, **11**, 1147.
15. F. A. Cotton, M. Matusz, R. Poli and X. Feng, *J. Am. Chem. Soc.* 1988, **110**, 1144.
16. F. A. Cotton, L. M. Daniels, L. R. Falvello and C. A. Murillo, *Inorg. Chim. Acta* 1994, **219**, 7.
17. F. A. Cotton, L. M. Daniels and C. A. Murillo, *Inorg. Chim. Acta* 1994, **224**, 5.
18. F. A. Cotton, J. H. Matonic and C. A. Murillo, unpublished results.
19. F. A. Cotton, L. M. Daniels, D. J. Maloney and C. A. Murillo, *Inorg. Chim. Acta* 1996, **249**, 9.
20. F. A. Cotton, L. M. Daniels, X. Feng, D. J. Maloney, J. H. Matonic and C. A. Murillo, *Inorg. Chim. Acta*, accepted.
21. F. A. Cotton, J. H. Matonic and C. A. Murillo, *Inorg. Chem.* 1996, **35**, 498.

Pergamon

S0277-5387(96)00194-5

Polyhedron Vol. 16, No. 1, pp. 143–152, 1997
Copyright © 1996 Elsevier Science Ltd
Printed in Great Britain. All rights reserved
0277-5387/97 $15.00+0.00

Ruthenium(II) complexes with two N–S donors: 2-(2-pyridyl)benzothiazoline and 2-methyl-2-(2-pyridyl)benzothiazoline: synthesis, reactivity and electrochemistry

Mosarraf Hossain, Shyamal Kumar Chattopadhyay* and Saktiprosad Ghosh†

Department of Inorganic Chemistry, Indian Association for the Cultivation of Science, Calcutta 700 032, India

(Received 21 November 1995; accepted 17 April 1996)

Abstract—An interesting array of Ru^{II} complexes of the two NNS chelating ligands 2-(2-pyridyl)benzothiazoline ($\mathbf{L_1H}$) and its methyl analogue 2-methyl-2-(2-pyridyl) benzothiazoline ($\mathbf{L_2H}$) have been synthesized and characterized. Diverse coordination behaviour of the ligand ($\mathbf{L_1H}$) encompassing its (a) neutral bidentate, (b) monoacid tridentate and (c) monoacid bidentate character are amply illustrated in this study. However, $\mathbf{L_2H}$ was found to behave only in the tridentate fashion. The complexes synthesized were of the type $Ru_2(L)_2X_2$ [where L = L_1, X = Cl (**1**); Br (**2**); and L = L_2, X = Cl (**6**); Br (**7**)], *trans* and *cis* $[Ru(L_1H)_2Cl_2]\cdot 2H_2O$ [(**3**) and (**5**)], $[Ru(L_1H)_2(H_2O)Cl]ClO_4$ (**4**) and $Ru(L_1)(L_1H)Cl$ (**8**). Several mixed-ligand complexes containing substituted imidazoles and bipyridine were also isolated and in some of them the ligand is found to be coordinated as a neutral bidentate NS chelating agent. The chemical and electrochemical reactivity patterns of these complexes were explored. Plausible structural representation of the reported complexes are proposed from the analysis of spectroscopic and cyclic voltammetric data. Copyright © 1996 Elsevier Science Ltd

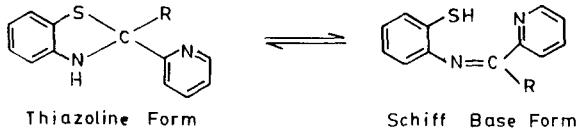
Keywords: ruthenium complexes; diverse coordination behaviour; chemical reactivity; N–S donor ligands; mixed ligand complexes.

Sulfur and nitrogen-coordinated transition-metal ions are found to constitute the active centres of several oxidoreductases such as hydrogenase, xanthine oxidase and nitrogenase.[1,2] Studies on the structure and reactivity of transition-metal complexes of N–S donor ligands are, therefore, expected to make a valuable contribution to the understanding of the functions of these enzymes at the molecular level.[1]

The sulfur atom present in such ligands is also known to stabilize uncommon oxidation states of the coordinated metal ions,[3–8] to generate uncommon coordination numbers in the resultant complexes[6–9] and to participate in a variety of interesting redox reactions.[10–12] In contrast to the detailed studies of the chemistry of N–S donor complexes of other transition metals, the chemistry of ruthenium ligated to such donors has been rather ill-explored. We have previously reported the synthesis of ruthenium complexes of biologically relevant N-S donor ligands such as thiosemicarbazides[13] and thiosemicarbazones.[14] It has been observed that 2-(2-pyridyl)-benzothiazoline ($\mathbf{L_1H}$), which itself is not a Schiff base ligand, is known to form the corresponding classical Schiff base (Fig. 1) complexes with mainly first transition ions.[15] In this paper we report the synthesis, reactivity and electrochemistry of a series of mono- and binuclear Ru^{II} complexes of 2-(2-pyridyl)-benzothiazoline ($\mathbf{L_1H}$) and its methyl analogue 2-methyl-2-(2-pyridyl)benzothiazoline ($\mathbf{L_2H}$). Our recent work revealing the antitumour properties of ruthenium complexes of some selected

* Permanent address: Department of Chemistry, Bengal Engineering College (Deemed University), Howrah 711 103, West Bengal, India.

† Author to whom correspondence should be addressed.



L_1H : R = H; L_2H : R = CH_3

Fig. 1.

N–S donor ligands[16] has enhanced our interest in the redox chemistry of the reported ruthenium complexes.

EXPERIMENTAL

Ruthenium trichloride received from Arora-Matthey, India, was converted to $RuCl_3 \cdot 3H_2O$ by repeated evaporation to dryness with concentrated hydrochloric acid. The ligand (2-(2-pyridyl) benzothiazoline ($\mathbf{L_1H}$) was prepared by a reported procedure.[8] The ligand 2-methyl-2-(2-pyridyl) benzothiazoline ($\mathbf{L_2H}$) was synthesized following a similar procedure using 2-acetyl pyridine in place of pyridin-2-carboxaldehyde. All other chemicals used for preparative work were of reagent grade and were used without further purification. Reagent-grade solvents were dried and distilled by the usual methods.[17] The solvents were stored over molecular sieves (4 Å). Commercial tetraethylammonium bromide was converted to pure tetraethyl ammonium perchlorate (TEAP) by the reported procedure.[16] Dinitrogen gas was purified by successively bubbling it through alkaline dithionite and concentrated sulfuric acid.

Preparation of the complexes

All operations were carried out under dinitrogen using deaerated dry solvents.

$Ru_2(L_1)_2Cl_2$ (**1**) *and* $Ru_2(L_1)Br_2 \cdot 2H_2O$ (**2**). Ruthenium chloride (130 mg, 0.5 mmol) was dissolved in degassed methanol (30 cm^3) and the ligand (L_1H 214 mg, 1 mmol) in degassed methanol (30 cm^3) was added, drop by drop, over a period of 3 h with constant stirring. The mixture was stirred for further 3 h and the resultant precipitate was filtered, washed with methanol and dried *in vacuo* over fused $CaCl_2$. The analytical results pointed to a polymeric composition such as $Ru_3(C_{12}N_2H_9S)_2Cl_4$ and the product was rejected.

The violet filtrate (pH = 3) was concentrated to half of its original volume in a rotaevaporator. Excess degassed diethylether was then added when a violet compound precipitated out. It was filtered, washed thoroughly with diethylether and dried over fused $CaCl_2$. Analytical results indicated the composition $Ru_2(C_{12}N_2H_9S)_2Cl_2$.

The compound $Ru_2(L_1)_2Br_2 \cdot 2H_2O$ (**2**) was obtained by a similar procedure except $RuBr_3$ was generated *in situ* by refluxing ruthenium chloride (130 mg) with 5 equiv. of LiBr in methanol for 45 mins. The resultant solution was cooled and reacted with the ligand. The first polymeric residue was rejected and the expected compound was isolated from the mother liquor (pH 3) by the method described earlier. The compound analysed as $Ru_2(C_{12}N_2H_9S)_2Br_2 \cdot 2H_2O$.

trans-$[Ru(L_1H)_2Cl_2] \cdot 2H_2O$ (**3**). To a solution of the ligand (214 mg, 1 mmol) in degassed methanol (20 cm^3) ruthenium chloride (130 mg, 0.5 mmol) in degassed methanol (30 cm^3) was added slowly and the reaction mixture was stirred for 4 h. The residue produced was filtered off and rejected. The light violet filtrate (pH 6) was concentrated to one third of its original volume in a rotaevaporator and excess diethylether was added. The precipitated complex was filtered, washed with deaerated Et_2O and dried *in vacuo* over fused $CaCl_2$. The dark violet compound analysed as $Ru(C_{12}N_2H_{10}S)_2Cl_2 \cdot 2H_2O$.

$[Ru(L_1H)_2(H_2O)Cl]ClO_4$ (**4**). This complex was prepared by a method similar to that employed for complex **3**. The final isolation was carried out in the following way: To the concentrated (in a rotaevaporator) filtrate excess deaerated aqueous $NaClO_4$ solution was added and it was allowed to stand in a refrigerator. The precipitated compound was filtered and washed thoroughly with deaerated water. It was dried and analysed as $[Ru(C_{12}N_2H_{10}S)_2(H_2O)Cl]ClO_4$.

cis-$[Ru(L_1H)_2Cl_2]$ (**5**). Solid $Ru_2(L_1)_2Cl_2$ (**1**; *ca* 100 mg) was stirred continuously in degassed dichloromethane (100 cm^3), over 12 h under nitrogen. The solid compound dissolved slowly and the resultant blue solution was filtered and the residue was rejected. The CH_2Cl_2 solution was slowly evaporated at room temperature when a brown complex was obtained. The compound analysed as $Ru(C_{12}N_2H_{10}S)_2Cl_2$.

$Ru_2(L_2)_2Cl_2 \cdot 2H_2O$ (**6**) *and* $Ru_2(L_2)_2Br_2$ (**7**). These compounds were prepared by following the same procedure used for the preparation of $Ru_2(L_1)Cl_2$ (**1**) and $Ru_2(L_1)_2Br \cdot 2H_2O$ (**2**), except that the ligand $\mathbf{L_2H}$ was used in place of $\mathbf{L_1H}$. The compounds isolated from the filtrate (pH = 4) were analysed as $Ru_2(C_{13}N_2H_{12}S)_2Cl_2 \cdot 2H_2O$ and $Ru_2(C_{13}N_2H_{12}S)_2Br_2$.

$Ru(L_1)(L_1H)Cl$ (**8**) *and* $[Ru(L_1)(L_1H)(1\text{-Meimz})]ClO_4 \cdot CH_2Cl_2$ (**9**). $Ru_2(L_1)_2Cl_2$ (**1**, 100 mg) was taken in a conical flask and CH_2Cl_2 (15 cm^3) was added. The mixture was stirred for 15–20 min under nitrogen. 1-Methylimidazole (1-Meimz; *ca* 1

cm^3) was added and the solution was stirred for 20 h. The resultant dark blue–violet solution was filtered and was evaporated nearly to dryness. Deaerated water (20 cm^3) was then added with stirring. The mixture was allowed to stand for 5 min and then filtered through a sintered glass crucible. The solid residue was recrystallized from CH_2Cl_2. It analysed as $Ru(C_{12}N_2H_9S)(C_{12}N_2H_{10}S)Cl$.

To the filtrate (blue–violet) excess deaerated aqueous $NaClO_4$ solution was added and allowed to stand in a refrigerator. The separated solid was filtered, washed thoroughly with deaerated water and dried over fused $CaCl_2$. It was recrystallized from dichloromethane. The recrystallized product was analysed as $Ru(C_{12}N_2H_9S)(C_{12}N_2H_{10}S)(C_4N_2H_6)ClO_4 \cdot CH_2Cl_2$.

$[Ru(L_2)(1\text{-Meimz})(H_2O)_2]ClO_4$ (**10**). Solid $Ru_2(L_2)_2Cl_2 \cdot 2H_2O$ (**6**; 240 mg) and 1-Meimz (2.5 cm^3) in methanol (50 cm^3) was stirred for 24 h under nitrogen. The solution was filtered and the volume of the filtrate was reduced in a rotaevaporator to *ca* 10 cm^3. Excess deaerated aqueous $LiClO_4$ solution was added to this concentrated solution and the resultant precipitate was allowed to settle in a refrigerator. It was filtered and washed thoroughly with deaerated water. The compound was recrystallized from CH_2Cl_2 and dry CH_3OH mixture. It analysed as $[Ru(C_{13}N_2H_{11}S)(C_4N_2H_6)(H_2O)_2]ClO_4$.

$[Ru(L_1)(bpy)ClO_4] \cdot H_2O$ (**11**). $Ru_2(L_1)_2Cl_2$ (**1**; 175 mg, 0.25 mmol) was taken in CH_3CN (15 cm^3). To it 2,2′-bipyridine (bpy; 80 mg, 0.5 mmol) was added followed by CH_3CN (25 cm^3). The mixture was refluxed under nitrogen for 30 h. The residue was filtered and rejected. The volume of the filtrate was reduced in a rotaevaporator and excess deaerated aqueous $LiClO_4$ solution was added. The precipitate formed was allowed to settle in a refrigerator (0.5 h), filtered and washed with deaerated water and Et_2O. The dried compound was recrystallized from CH_2Cl_2 and analysed as $[Ru(C_{12}N_2H_9S)(C_{10}N_2H_8)ClO_4] \cdot H_2O$.

$[Ru(L_2)(bpy)(H_2O)]ClO_4$ (**12**). This compound was prepared by a method similar to that of complex **11** using $Ru_2(L_2)_2Cl_2 \cdot 2H_2O$ (**6**) as the starting material. The dried compound was recrystallized from CH_2Cl_2 and analysed as $Ru(C_{13}N_2H_{11}S)(C_{10}N_2H_8)(H_2O)ClO_4$.

Physical measurements

Carbon, hydrogen and nitrogen were analysed in a Perkin–Elmer 240 C,H,N analyser. IR spectra were recorded as KBr pellets using a Perkin–Elmer 783 spectrophotometer. Solution electrical conductivity was measured with a Philips PR-9500 conductivity bridge fitted with a dip-type cell calibrated with 0.02 M KCl solution. Static susceptibility measurements at room temperature were made using a Princeton Applied Research Model 155 vibrating sample magnetometer using Hg[Co $(SCN)_4$] as the calibrant. ^1H NMR spectra were recorded with a Varian XL100 FT-NMR spectrometer using TMS as the reference. Electronic spectra were recorded using a Shimadzu Model UV-2100 spectrophotometer. EPR spectra were recorded on a Varian E-4 X-band EPR spectrometer using dpph as the internal field marker. Cyclic voltammetric studies were carried out with a Bioanalytical system CV-27 Electrochemical analyser and a BAS X-Y recorder at 298 K. The experiments were performed in a one-compartment cell equipped with a platinum working electrode (BAS), a platinum auxiliary electrode and a standard calomel electrode (SCE) as the reference which was separated by a salt bridge connected to the solvent through a glass frit tip. Electrochemical measurements in CH_3CN were made by employing 0.1 M tetraethylammonium perchlorate (TEAP) as the supporting electrolyte. Under these experimental conditions the ferricenium–ferrocene couple was located at 0.42 V versus SCE.

RESULTS AND DISCUSSION

The ruthenium compounds reported in this study are sufficiently pure and gave satisfactory analytical results, as listed in Table 1. The conductance data (Table 1) also support the proposed formulation of the compounds. Diamagnetic nature of all the complexes suggests the presence of +2 oxidation state of ruthenium. The IR and UV–vis spectral data are listed in Table 2 and Table 3, respectively. The redox behaviour of all the complexes has been examined in acetonitrile (0.1 M TEAP) at a platinum working electrode using cyclic voltammetry (Table 4).

We have chosen the novel N–S donor system 2-(2-pyridyl)benzothiazoline (**L_1H**), which (a) reduces the Ru^{III} starting materials ($RuCl_3$ or $RuBr_3$) to Ru^{II} and (b) coordinates as a bidentate N–S donor in the thiazoline form as well as the NNS^- donor Schiff base form generated through a metal-induced ring opening process. Although **L_1H** is found to be coordinated in either tridentate or bidentate manner, **L_2H** is found to behave only in a tridentate fashion. However, the products obtained are highly dependent on experimental conditions such as medium of the reaction, order of addition of reactants, etc.

It has been observed that 2-(2-pyridyl)-benzothiazoline, which is not itself a Schiff base ligand, forms classical Schiff base complexes with many

Table 1. Analytical and physical data for the ruthenium complexes

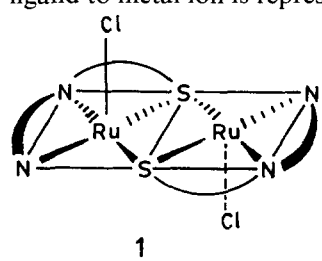
Complex	Analysis Found (Calc.)% C	N	H	Cl	Conductance (ohm^{-1} cm^2 mol^{-1})
$Zn(L_2)_2$	59.0 (60.1)	10.1 (10.1)	3.9 (4.1)	—	
$Ru_2(L_1)_2Cl_2$ (**1**)	41.5 (41.2)	8.0 (8.0)	2.7 (2.6)	10.8 (10.2)	33[a]
$Ru_2(L_1)_2Br_2 \cdot 2H_2O$ (**2**)	35.8 (35.0)	7.0 (6.8)	2.6 (2.7)	—	41[a]
trans-$Ru(L_1H)_2Cl_2 \cdot 2H_2O$ (**3**)	45.2 (45.3)	8.2 (8.8)	3.1 (3.8)	11.6 (11.2)	94[b]
$[Ru(L_1H)_2Cl(H_2O)]ClO_4$	42.6 (42.2)	8.1 (8.2)	2.7 (3.2)	—	56[a]
cis-$Ru(L_1H)_2Cl_2$ (**5**)	48.6 (48.0)	9.4 (9.3)	2.9 (3.3)	12.2 (11.8)	34[b]
$Ru_2(L_2)_2Cl_2 \cdot 2H_2O$ (**6**)	40.2 (40.9)	7.3 (7.3)	3.1 (3.4)	9.9 (9.3)	55[b]
$Ru_2(L_2)_2Br_2$ (**7**)	38.8 (38.2)	6.2 (6.9)	2.6 (2.7)	—	101[b]
$Ru(L_1)(L_1H)Cl$ (**8**)	51.9 (51.1)	10.0 (9.9)	3.8 (3.4)	6.9 (6.3)	19[a]
$[Ru(L_1)(L_1H)(1\text{-Meimz})ClO_4 \cdot CH_2Cl_2$ (**9**)	44.1 (43.8)	10.1 (10.6)	3.1 (3.4)	—	72[a]
$[Ru(L_2)(1\text{-Meimz})(H_2O)_2]ClO_4$ (**10**)	37.0 (37.4)	10.5 (10.3)	3.5 (3.8)	—	68[a]
$Ru(L_1)(bpy)ClO_4 \cdot H_2O$ (**11**)	45.3 (44.9)	9.2 (9.5)	2.8 (3.2)	—	84[a]
$[Ru(L_2)(bpy)(H_2O)]ClO_4$ (**12**)	46.5 (45.9)	8.6 (9.3)	3.5 (3.5)	—	63[a]

[a] DMF.
[b] MeCN.

metal ions.[15] Later, Que *et al.* reported[18] that the Schiff base derived from the condensation of saclicylaldehyde and bis(2-aminophenyl)disulfide can undergo ring closure leading to the formation of thiazole ring when reacted with $FeCl_3 \cdot 6H_2O$ in hot MeOH and allowed to stand for several weeks. The thiazole derivative formed *in situ* is found to act as a bidentate ligand coordinating through the thiazole nitrogen and the deprotonated phenolic oxygen of the salicylaldehyde moiety.

So, it is quite possible that the Schiff base from one of the NSS^- donor of $\mathbf{L_1H}$ can undergo cyclization during its reaction with $RuCl_3$ and subsequent crystallization of the product leads to the formation of the corresponding thiazoline form coordinating preferably through the thiazoline sulfur and the pyridine ring nitrogen; the N–S coordination is preferred to the N–N mode because the acceptor centre Ru^{II} is a second-row transition-metal ion and a reasonably soft acceptor. Thus, both the ring opening of 2-(2-pyridyl)-benzothiazoline ($\mathbf{L_1H}$) leading to the formation of the NNS tridentate donor Schiff base N-2-mercaptophenyl(2′-pyridyl)-methylenimine and the ring closure of the coordinated Schiff base to the corresponding thiazoline derivative behaving as a bidentate NS donor can take place. The recyclization of the coordinated Schiff base form is probably promoted by bringing the thiolato sulfur and the carbon atom of the C=N moiety in the Ru^{II} complex in an appropriate position required for such a ring closure.

The compound $Ru_2(L_1)_2Cl_2$ (**1**) obtained by the addition of ligand to metal ion is represented as:



1

Table 2. Important IR bands (cm^{-1}) for the compounds

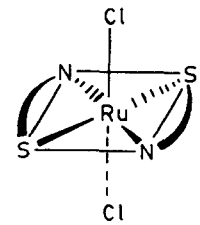
Compound	$\nu_{C=N}+\nu_{C=C}$	ν_{CS}	Other characteristic vibrations
L_1H	1585, 1570	750(s)	620, 490, 420, 405
L_2H	1580, 1570, 1560	740(s)	620, 595(s), 525(s), 430, 405
$Zn(L_1)_2$	1572, 1560, 1545, 1522	740(s)	625, 575(s), 495, 430
$Zn(L_2)_2$	1570, 1522	750(s)	625, 570, 425
$Ru_2(L_1)_2Cl_2$ (**1**)	1620, 1595	765(s)	615, 575, 515, 455, 320
$Ru_2(L_1)_2Br_2 \cdot 2H_2O$ (**2**)	1615, 1590	765(s)	610, 580, 520, 475
trans-$Ru(L_1H)_2Cl_2 \cdot 2H_2O$ (**3**)	1610, 1590, 1550	765(s)	610, 570, 550, 510, 440, 315
$[Ru(L_1H)_2Cl(H_2O)]ClO_4$ (**4**)	1610, 1595, 1578, 1550	765(s)	630, 570, 520, 440, 320, 1090(b,s)[a]
cis-$Ru(L_1H)_2Cl_2$ (**5**)	1615, 1585, 1575, 1550	765(s)	625, 590, 550, 525, 460, 325, 310
$Ru_2(L_2)_2Cl_2 \cdot 2H_2O$ (**6**)	1615, 1590	770(s)	610, 555, 500, 455, 310
$Ru_2(L_2)_2Br_2$ (**7**)	1615, 1585	770(s)	605, 550, 500, 410
$Ru(L_1)(L_1H)Cl$ (**8**)	1610(sh), 1575, 1550, 1500	765(s)	620, 570, 520, 450, 320
$Ru(L_1)(L_1H)(1\text{-Meimz})ClO_4 \cdot CH_2Cl_2$ (**9**)	1610, 1585, 1550, 1525	765(s)	625(s), 570, 520, 455, 1100(b,s)[a]
$[Ru(L_2)(1\text{-Meimz})(H_2O)_2]ClO_4$ (**10**)	1615, 1585	765(s)	630(s), 525, 460, 1100(b,s)[a]
$Ru(L_1)(bpy)ClO_4 \cdot H_2O$ (**11**)	1625, 1600, 1585(sh), 1560	770(s)	640(s),[a] 630(s), 1090(s),[a] 1120(s),[a] 1150(s)[a]
$[Ru(L_2)(bpy)(H_2O)]ClO_4$ (**12**)	1610, 1580	760(s)	622(s), 570, 490, 455, 1090(b,s)[a]

sh = shoulder, s = strong, b = broad.

[a] $\nu_{ClO_4^-}$.

In this proposed dimeric formulation both the ligands are present in the deprotonated Schiff base form acting in a monoanionic NNS^- tridentate manner, dimerization taking place through thiolate sulfur bridging. In the Schiff base all the atoms are in conjugation and hence all the N-S donor atoms are planar.[19] The presence of two ruthenium(II) centres are indicated by two successive one-electron oxidations of **1** corresponding to two Ru^{II}/Ru^{III} oxidations commonly observed for the related type of binuclear Ru^{II} complexes. The presence of only one ν(Ru—Cl) mode in the IR spectrum of **1** along with its non-electrolyte nature in solution and the results of elemental analysis support the proposed formulation. The corresponding data for **6** suggests the same type of sulfur-bridged dimeric formulation. Reasons for ruling out the alternative chloro-bridged structure is included in the discussion on the electrochemistry of the complexes. The corresponding bromide containing complexes **2** and **7**, quite logically, should have a similar formulation, the chlorides being replaced by the bromide ions. The ^1H NMR spectra of the ligand L_1H and L_2H exhibit signals at δ 5.12 and δ 5.63 ppm, which are assigned to the N—H proton and confirmed by D_2O exchange experiment. The absence of such N—H proton signals in complexes **1**, **2**, **6** and **7** indicates that the Schiff base form of ligand is present in them. These results endorse the proposed structural representation of the compounds **1**, **2**, **6** and **7**.

The δ 4.51 ppm signal observed in the ^1H NMR spectrum of **3** is assigned to the N—H proton and is confirmed by the D_2O exchange experiment. This points to the presence of the benzothiazoline form of the ligand in **3** which may be represented as:



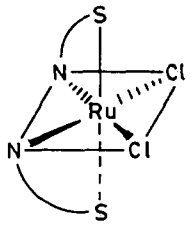
3

The *trans* disposition of the two coordinated chloride is evident from the non-electrolyte nature of **3** and the presence of only one ν(Ru—Cl) band in its IR spectrum.

Compound **4**, prepared by treating a solution of **3** in methanol with aqueous $NaClO_4$ solution, obviously, has a structure similar to that of **3**, with one of the two coordinated halogens of **3** replaced by one water molecule. This is corroborated by the uni-univalent electrolytic nature of **4** in solution.

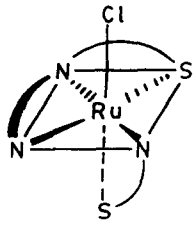
When **1** is stirred in CH_2Cl_2, it dissolved partly forming a blue solution from which the compound **5** was isolated. Compound **5** is found to be a non-electrolyte and its analytical results point to the composition $Ru(L_1H)_2Cl_2$. Compound **5** is EPR

silent even at 77 K, corroborating the proposed formulation. The presence of two different ν(Ru—Cl) bands in its IR spectrum clearly indicates the *cis*-disposition of the two coordinated chlorides, both the ligands being present in the thiazoline form. The sulfur bridges appear to become disrupted in CH_2Cl_2 solution and the effectively 1 : 1 binuclear complex **1** experiences ligand disproportionation or metal disproportionation to yield a 1 : 2 metal: ligand chelate, the ligand moieties undergoing cyclization simultaneously. This dissolution in CH_2Cl_2 leads to the generation of 1 : 2 species in solution is an acceptable proposition because a series of complexes containing two L_1H ligands and other co-ligands are obtained by treating the CH_2Cl_2 solution of complex **1** with different reagents. However, complex **1** behaves differently when it is dissolved in acetonitrile, because compound **11** is isolated from this solution. Thus, compound **5** may be represented as:



5

Treatment of a CH_2Cl_2 solution of **1** with excess 1-methylimidazole followed by the addition of water leads to the formation of $Ru(L_1H)(L_1)Cl$ (**8**). It is proposed to have the structure:



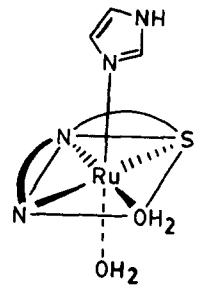
8

which is arrived at from its analytical data, non-conducting nature in solution and the single ν(Ru—Cl) bands in its IR spectrum.

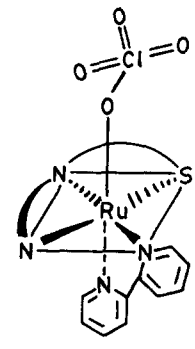
When the CH_2Cl_2 solution of **1** is treated with excess 1-Meimz followed by a concentrated aqueous ClO_4^- solution, **9** is produced. Elemental analysis, the uni-univalent electrolytic nature in solution and the single CH_3 proton signal in NMR spectrum indicates that its formulation should be similar to that of **8**, with the coordinated Cl^- being replaced by a 1-Meimz moiety. The EPR inactivity even at 77 K also corroborated the proposed formula of the compounds **8** and **9**.

Compound **11** was prepared by treating the acetonitrile solution of **1** by bipyridine in 1 : 1 molar proportion, followed by excess aqueous ClO_4^- solution. The proposed structure was arrived at from elemental analysis and IR spectral characteristics (*vide infra*), which showed the ClO_4^- ion to be coordinated to the ruthenium acceptor centre. However, as this compound exhibits a uni-univalent electrolytic behaviour on dissolution in acetonitrile, the ClO_4^- moiety is rather weakly coordinated. Compound **12**, in the L_2H series, appears to have a similar structure, the only difference being the presence of a coordinated H_2O in place of the coordinated ClO_4.

Elemental analysis data of compound **10**, obtained by treating **6** first with excess 1-Meimz and then with aqueous ClO_4^- solution, may be assigned the formulation $[Ru(L_2)(1\text{-Meimz})(H_2O)_2]ClO_4$. It behaves as 1 : 1 electrolyte in solution and its IR spectra indicates the presence of ionic perchlorate. These observations point to the following probable structure for **10**.



10



11

IR spectra

The important IR bands of the ligands L_1H and L_2H and their metal complexes are listed in Table 2. All chloro complexes exhibit a medium intensity band at $\sim$320 cm^{-1} due to the ν_{Ru-Cl} vibration. However, the ν_{Ru-Br} signal could not be detected because it is beyond the detection limit of our instrument. The absence of any band at 2400–2500 cm^{-1} corresponding to ν_{S-H} points to the absence

Table 3. Electronic spectral data for the ruthenium complexes

Complex	Bands λ_{max} (nm) [ε, M^{-1} cm^{-1}) Solvent CH_3CN	Bands λ_{max} (nm) CH_2Cl_2
$Ru_2(L_1)_2Cl_2$ (**1**)	578 (1452), 315 (9197), 250(sh) (8175), 217 (15,853)	755(sh)(>860), 588 (>3825), 523(sh)(>3001), 394(sh) (>3825), 346 (sh) (>13,268), 325(b) (>23,170), 316 (>23,627), 252 (>18,594), 231 (>27,122)
$Ru_2(L_1)_2Br_2 \cdot 2H_2O$ (**2**)	517 (2000), 312 (12,738), 253 (11,349), 212 (27,129)	747(sh) (>273), 573(b) (>1347), 516(b) (>1231), 343(sh) (>5905), 328(sh) (>3365), 313 (>10,040), 252(sh) (>8746), 230 (>13,078)
trans-$Ru(L_1H)_2Cl_2 \cdot 2H_2O$ (**3**)	565 (2308), 395 (3749), 310 (20,888), 253 (21,366), 212 (45,609)	584(b) (>4605), 522(sh) (>2747), 397(sh) (>4932), 320 (>26,760), 251(sh) (>23,163), 229 (>33,000)
$[Ru(L_1H)_2Cl(H_2O)]ClO_4$ (**4**)	576 (3796), 527 (3976), 324 (27,657), 313 (28,850), 251(sh) (25,618), 219 (45,119)	575(sh) (>2870), 530(sh) (>3226), 484(sh) (>3510), 442(sh) (>3383), 352 (>12,250), 328(sh) (>9365), 320 (>20,438), 252(sh) (>16,797), 229 (>24,300)
cis-$Ru(L_1H)_2Cl_2$ (**5**)		583 (4348), 522 (3282), 395 (3552), 319 (24,715), 251 (19,241), 216 (37,207)
		755(sh) (1134), 589(b) (5147), 525(sh) (3695), 395(sh) (4262), 350(sh) (18,361), 324(b) (29,787), 315(b) (29,147), 250 (22,409), 229 (31,344)
$Ru_2(L_2)_2Cl_2 \cdot 2H_2O$ (**6**)	556 (1676), 318 (7055), 253 (10,528), 212 (21,380)	536(b) (>963), 324(sh) (>3834), 307(sh) (>4019), 255(sh) (>5892), 228 (>8304)
$Ru_2(L_2)_2Br_2$ (**7**)	561 (2640), 477 (2985), 309 (13,870), 253 (16,071), 211 (36,922)	557(b) (>11,655), 326(sh) (>19,775), 310(>62,747), 295(sh) (>23,610), 252(sh) (>74,026), 230 (>100,493)
$Ru(L_1)(L_1H)Cl$ (**8**)	577 (1832), 396(sh) (1923), 311 (13,636), 249 (10,340), 212 (22,525)	576, 395, 315, 250
$Ru(L_1)(L_1H)$(1-Meimz)$ClO_4 \cdot CH_2Cl_2$ (**9**)	561 (4229), 489 (4601), 316 (21,771), 253 (21,186), 212 (43,284)	554, 495(sh), 350(sh), 320, 255, 230
$[Ru(L_2)$(1-Meimz)$(H_2O)_2]ClO_4$ (**10**)	566 (3196), 315 (8696), 253 (12,092), 213 (22,619)	575(sh), 300(sh), 250(sh), 230
$Ru(L_1)(bpy)ClO_4 \cdot H_2O$ (**11**)	589 (2934), 462 (4392), 311 (23,837), 294 (24,132), 253 (20,573), 212 (40,208)	567, 488(sh), 428(b), 350(sh), 335, 310(sh), 291, 255(sh)
$[Ru(L_2)(bpy)(H_2O)]ClO_4$ (**12**)	540 (4023), 324 (13,008), 286 (20,000), 212 (36,719)	536, 286, 255, 245, 205

b = broad, sh = shoulder

of the free S–H moiety in all the complexes.[20] The overlapping $\nu_{C=N}$ and $\nu_{C=C}$ mode present in the free ligand around 1570 cm^{-1} suffer a positive shift of ~40 cm^{-1}, indicating coordination of the ligand through its pyridine nitrogen[21] and this is corroborated by the shift of pyridine ring vibrations (at 620 and 420 cm^{-1}) in all the complexes. The ligand band around 750 cm^{-1}, assigned to the ν_{CS} vibration, suffers a positive shift of 15–20 cm^{-1} on complexation[22] and is symptomatic of metal–sulphur bond formation. The presence of a broad band in the 1030–1140 cm^{-1} range in all perchlorate-containing complexes is an indication of the non-participation of ClO_4^- in coordination,[14] the only exception being complex **11**, in which this broad band is split into sharp bands at 1090, 1120

Table 4. Cyclic voltammetric results[a,b] for Ru^{II} complexes at 298 in CH_3CN

Complex	$E_{1/2}$, V (ΔE_p, mV)
$Ru_2(L_1)_2Cl_2$ (**1**)	0.44(100), E_{pa} = 1.01
$Ru_2(L_1)_2Br_2 \cdot 2H_2O$ (**2**)	0.58(100), 0.84(120)
trans-$Ru(L_1H)_2Cl_2 \cdot 2H_2O$ (**3**)	0.42(80), 0.71(100), E_{pa} = 1.00
$[Ru(L_1H)_2Cl(H_2O)]ClO_4$ (**4**)	0.43(100)
cis-$Ru(L_1H)_2Cl_2$ (**5**)	0.39(100)
$Ru_2(L_2)_2Cl_2 \cdot 2H_2O$ (**6**)	0.69(70), E_{pa} = 0.93
$Ru_2(L_2)_2Br_2$ (**7**)	0.57(100), 0.95(120)
$Ru(L_1)(L_1H)Cl$ (**8**)	0.39(90)
$Ru(L_1)(L_1H)$(1-Meimz)$ClO_4 \cdot CH_2Cl_2$ (**9**)	0.67(80)
$[Ru(L_2)$(1-Meimz)$(H_2O)_2]ClO_4$ (**10**)	E_{pa} = 1.0
$Ru(L_1)(bpy)ClO_4 \cdot H_2O$ (**11**)	0.87(60)
$[Ru(L_2)(bpy)(H_2O)]ClO_4$ (**12**)	E_{pa} = 0.82

[a] Working electrode platinum; reference electrode SCE; $E_{1/2} = 0.5\ (E_{pa} + E_{pc})$; $\Delta E_p = E_{pc} - E_{pa}$, where E_{pc} and E_{pa} are cathodic and anodic peak potentials, respectively.

[b] Supporting electrolyte 0.1 M TEAP, solute concentration 10^{-3} M. Scan rate 50 mV s^{-1}.

and 1150 cm^{-1}. This is indicative of the presence of coordinated perchlorate[23] in complex **11**. New bands of weak to medium intensity lying below 500 cm^{-1} are assigned to the coupled ν(M—N) and ν(M—S)[24] vibrations.

Electrochemistry

Dimeric complexes (**1**, **2**, **6**, *and* **7**). The redox behaviour of the compounds has been examined in CH_3CN (0.1 M TEAP) at a platinum working electrode using cyclic voltammetry. All potentials are referenced to SCE. Results are given in Table 4. All the complexes exhibit two successive reversible to irreversible oxidative couples at positive potentials. The complexes $Zn(L_1)_2$ and $Zn(L_2)_2$ do not show any such reversible couple in the potential range studied and this precludes oxidation of the coordinated ligands under the present experimental conditions. The electrochemical behaviour of these complexes can be logically interpreted in terms of the sulfur-bridged dimeric structure (**1**), the observed difference of $E_{1/2}$ (**2**) and $E_{1/2}$ (**1**) being a common feature of such binuclear species.[6,25] The two distinct oxidative peaks indicate two $Ru^{II/III}$ couples, which corresponds to the process (1).

$$[Ru_2(L)_2X_2] \xrightarrow{-e} [Ru_2(L)_2X_2]^{+}$$

$$[Ru_2(L)_2X_2]^{+} \xrightarrow{-e} [Ru_2(L)_2X_2]^{+2}$$

where

$$L = L_1/L_2\ ;\quad X = Cl^-/Br^-. \qquad (1)$$

At slow scan rate (v = 50 mV s^{-1}) the peak-to-peak separation, ΔE_p, is found to be 70–100 mV, showing that the process is almost reversible and the current heights for both the couples correspond to one-electron transfer processes. The observed ΔE_p values are larger than the ideal Nernstian value of 59 mV as is observed for other binuclear complexes[26] and are possibly due to uncompensated solution resistance.[27] It has also been suggested that the large ΔE_p values could result from the close proximity of the two waves.[27]

The alternative chloro-bridged structure can be easily excluded by comparing the potential differences of the two successive oxidations observed here with those reported for sulfur-bridged and chloro-bridged dimeric five-coordinated complexes.[6,7] Thus, the proposed formulation for the dimeric sulfur-bridged penta-coordinated complexes is quite logical.

Monomeric complexes. The electron-transfer behaviour of the monomeric complexes has been examined in CH_3CN by cyclic voltammetry at a platinum electrode. The mononuclear complex **3** exhibits two reversible peaks at 0.42 and 0.71 V and an irreversible peak at 1.03 V. The one-electron change responsible for the peak at 0.42 V was checked coulometrically. The i_{pa}/i_{pc} of **1** indicated its reversible nature. On repeated scanning the wave retains its original shape, pointing to the high reversibility of the electrode reaction. The appreciable conductance value of **3** in acetonitrile in comparison to that of compound **5** with a similar formula indicated partial dissociation of the halides from the coordination sphere of the metal ion in complex **3**. This is also supported by the formation of the complex **4** from **3** replacing one Cl^- by a ClO_4^-. Therefore, the entire electrochemical process can be rationalized in terms of the process (2).

$$\textit{trans}\text{-}[Ru^{II}(L_1H)_2Cl_2] \xrightarrow[E_{1/2}=0.42\,V]{-e} [Ru^{III}(L_1H)_2Cl_2]^{+1}$$

$$\textit{trans}\text{-}[Ru^{II}(L_1H)_2Cl_2 \xrightarrow{CH_3CN} [Ru^{II}(L_1H)_2Cl \cdot CH_3CN]^{+}Cl^-$$

$$[Ru^{II}(L_1H)_2Cl \cdot CH_3CN]^{+} \xrightarrow[E_{1/2}=0.71\,V]{} [Ru^{III}(L_1H)_2Cl \cdot CH_3CN]^{2+}. \qquad (2)$$

An irreversible anodic wave at $E_{pa} = 1.0$ V observed in the cyclic voltammogram of the compound **3** probably corresponds to the process (**3**).

$$[(CH_3CN)Ru(L_1H)_2Cl]^+Cl^- \xrightarrow[E_{pa}=1.0\,V]{-e} [(CH_3CN)Ru(L_1H)_2Cl]^+ + Cl. \quad (3)$$

The process (**3**) actually corresponds to the oxidation of Cl^- to a chlorine radical,[28] the oxidation of chloride from KCl in CH_3CN being known to occur at the same potential.

The mononuclear compounds **4**, **5** and **8** exhibit a reversible couple at 0.40 V due to the Ru^{II}/Ru^{III} oxidation, as observed in the case of **3**.

In the case of monocationic complexes **9–12**, the $E_{1/2}$ values are more positive compared with those of the neutral complexes due to the electrostatic effect. The one-electron oxidation of all these complexes are assigned to Ru^{II} to Ru^{III} oxidation. Thus, the above electrochemical results corroborated the proposed dimeric and monomeric formulations for the complexes.

Electronic spectra

All the complexes exhibit highly rich electronic spectra (Table 3). Most of them exhibit two low-energy bands in the visible region, which probably correspond to an electronic excitation from a metal *d* level to the π^* level of the ligand. When the spectra of **3** and **5** are compared, compound **3** is found to exhibit MLCT bands at 565 and 395 nm, whereas in compound **5** three MLCT bands are located at 583, 522 and 395 nm. This observation is compatible with the proposed *trans–cis* structure.[14,29] Moreover the only MLCT band in the spectra of the complexes **1**, **2** and **6** is in good agreement with the proposed symmetric dimeric structure. Some additional bands are present in the different mixed chelate complexes, the nature and position of which are found to be dependent on the nature of coligands present.

The higher energy band of all the complexes at 315, 250 and 216 nm are due to intra-ligand transitions. The band at 290 nm in compounds **11** and **12** corresponds to the presence of bipy, as observed in other bipyridyl complexes.[30,31]

CONCLUSION

This study adequately illustrates the diverse ligational behaviour of the ligands 2-(2-pyridyl) benzothiazoline and 2-methyl-2-(2-pyridyl) benzothiazoline towards the Ru^{II} acceptor centre. The profound influence of the reaction conditions (nature of the solvents, order of addition of reactants, presence of the coligands and their nature, etc.) on the nature of the products isolated is strikingly exposed. The spectroscopic and electrochemical data have contributed significantly towards the proposed structural representation of the reported complexes.

Acknowledgement—Financial assistance from DST, Govt of India, New Delhi, is gratefully accepted.

REFERENCES

1. A. Muller and B. Krebs, *Sulfur, its Significance for Chemistry, for the Geo- and Cosmosphere and Technology*; Studies in Inorganic Chemistry 5. Elsevier Science Publishers, Amsterdam, (1984).
2. S. D. Conradsson, B. K. Burgess, W. W. Newton, K. O. Hodgson, J. W. McDonald, J. F. Rubinson, S. F. Gheller, L. E. Mortenson, M. W. W. Adams, P. K. Mascharek, W. A. Armstrong and R. H. Holm, *J. Am. Chem. Soc.* 1985, **107**, 7935.
3. S. A. Koch, *J. Am. Chem. Soc.* 1983, **105**, 3362.
4. H. J. Kruger and R. H. Holm, *Inorg. Chem.* 1989, **28**, 1148.
5. H. J. Kruger, G. Peng and R. H. Holm, *Inorg. Chem.* 1991, **30**, 734.
6. A. P. Koley, S. Purohit, S. Ghosh, L. S. Prasad and P. T. Manoharan, *J. Chem. Soc., Dalton Trans.* 1988, 2607.
7. A. P. Koley, S. Purohit, S. Ghosh, L. S. Prasad and P. T. Manoharan, *Inorg. Chem.* 1992, **31**, 305.
8. A. P. Koley, R. Nirmala, S. Ghosh, L. S. Prasad and P. T. Manoharan, *Inorg. Chem.* 1992, **31**, 1764.
9. D. Sellmann, W. Ludwig, G. Hutner and L. Zsolnai, *J. Organomet. Chem.* 1985, **294**, 199.
10. C. E. Forbes, A. Gold and R. H. Holm, *Inorg. Chem.* 1971, **10**, 2479.
11. S. I. Shupack, E. Billig, R. J. H. Clark, R. Williams and H. B. Gray, *J. Am. Chem. Soc.* 1964, **86**, 4594.
12. S. Purohit, A. P. Koley, L. S. Prasad, P. T. Manoharn and S. Ghosh, *Inorg. Chem.* 1989, **28**, 3735.
13. S. K. Chattopadhyay and S. Ghosh, *Inorg. Chim. Acta* 1987, **131**, 15.
14. S. K. Chattopadhyay and S. Ghosh, *Inorg. Chim. Acta* 1989, **163**, 245.
15. M. Akbar Ali and S. E. Ligingstone, *Coord. Chem. Rev.* 1974, **13**, 101.
16. F. Bregant, S. Pacor, S. Ghosh, S. K. Chattopadhyay and G. Sava, *Anticancer Res.* 1993, **13**, 1007.
17. D. T. Sawyer and J. L. Roberts, *Experimental Electrochemistry for Chemists*, p. 167. Wiley, New York (1971).
18. J. W. Pyrz, X. Pan, D. Britton and L. Que Jr, *Inorg. Chem.* 1991, **30**, 3461.
19. L. F. Lindoy and S. E. Livingstone, *Inorg. Chem.* 1968, **7**, 1149.

20. N. B. Colthup, L. H. Daly and S. E. Wiberley, *Introduction to Infrared and Raman Spectroscopy*. Academic Press, New York (1964).
21. M. J. Campbell, R. Grzeskowiak and R. Thomas, *Spectrochim. Acta* 1976, **32A**, 556.
22. G. J. Sutton, *Aust. J. Chem.* 1963, **16**, 1137.
23. K. Nakamoto, *Infrared and Raman Spectra of Inorganic and Coordination Compounds*. John Wiley, New York (1978).
24. H. K. Gupta and S. K. Dikshit, *Polyhedron* 1987, **6**, 1009.
25. M. Haga, T. M.-Inoue and S. Yamabe, *Inorg. Chem.* 1987, **26**, 4148.
26. R. W. Callahan, F. R. Keene, T. J. Meyer and D. J. Salmon, *J. Chem. Soc.* 1977, **99**, 1064.
27. G. M. Brown, Ph.D. dissertation, University of North Carolina, Chapel Hill (1974).
28. S. H. Wheeler, B. M. Mattson, G. L. Miessler and L. H. Pignolet, *Inorg. Chem.* 1978, **17**, 340.
29. A. M. Zwickel and C. Creutz, *Inorg. Chem.* 1971, **10**, 2396.
30. H. Masui, A. B. P. Lever and P. R. Auburn, *Inorg. Chem.* 1991, **30**, 2402.
31. G. Juriga, M. Scattgast and M. E. MeGuire, *Inorg. Chim. Acta* 1991, **183**, 39.

Pergamon

S0277-5387(96)00228-8

Polyhedron Vol. 16, No. 1, pp. 153–160, 1997
Copyright © 1996 Elsevier Science Ltd
Printed in Great Britain. All rights reserved
0277-5387/97 $15.00+0.00

Preparation and crystal structures of two polymeric silver(I) complexes of betaine derivatives

Ping-Rong Wei,* Qi Li, Bo-Mu Wu† and Thomas C. W. Mak‡

Department of Chemistry, The Chinese University of Hong Kong, Shatin, New Territories, Hong Kong

(Received 1 April 1996; accepted 15 April 1996)

Abstract—Polymeric silver(I) complexes of two betaine derivatives, namely $[\{Ag_2(L^1)_2(NO_3)(H_2O)\}_n](NO_3)_n$ (**1**) and $[\{Ag_4(L^2)_3\}_n](ClO_4)_{4n}\cdot 3nH_2O$ (**2**) [L^1 = 4-dimethylaminopyridinioacetate, *p*-$Me_2NC_5H_4N^+CH_2CO_2^-$; L^2 = 1,4-diazoniabicyclo[2.2.2]octane-1,4-dipropionate; $^-O_2C(CH_2)_2N^+(CH_2CH_2)_3N^+(CH_2)_2CO_2^-$], have been prepared and characterized by X-ray crystallography. Complex **1** exhibits a zigzag chain structure *via* comparatively weak metal–carboxylate linkages between adjacent bis(carboxylato-*0,0′*)-bridged dimers, in which the coordination spheres of two independent Ag^I atoms are each completed by an unidentate nitrate or aqua ligand at a much longer contact. Complex **2** consists of three independent infinite zigzag chains running parallel to the *b* direction, in which the Ag^I atoms are cross-linked by double betaine ligands in the end-to-end mode. The Ag···Ag separation [2.750(2) Å] in one infinite chain based on bis(carboxylato-*0,0′*)-bridged centrosymmetric dimeric units is the shortest one hitherto found among silver(I) complexes and hence indicative of a significantly stronger metal–metal interaction. Copyright © 1996 Elsevier Science Ltd

Keywords: silver(I) complex; betaine; 1,4-diazoniabicyclo[2.2.2]octane-1,4-dipropionate; coordination polymer; carboxylate; dimeric complex.

The poor solubility and light-sensitive nature of silver(I) carboxylates present practical difficulties in their structural characterization.[1] The reported crystal structures of silver(I) carboxylates consist mostly of discrete dimers or polymeric chains/networks constructed by the linkage of dimeric subunits and the structures have been classified into four principle types.[2] Type A contains discrete [Ag_2(carboxylate-*0,0′*)$_2$] dimers without any axial ligand;[3] B and C have similar dimeric structures with the axial sites occupied by one and two ligands, respectively, and they are commonly polymeric species,[2,4] and D comprises dimeric subunits that are extended into a step polymer through the linkage of each metal centre to a carboxylate group of an adjacent dimer,[5,6] while the modified type D has an additional axial ligand attached to each metal atom.[7,8] The unusual polymeric structure of $[Ag_3(Me_2N^+(CH_2CO_2^-)CH_2CO_2^-)_2\}_n](ClO_4)_n$ that is based on trimeric units has been reported.[9]

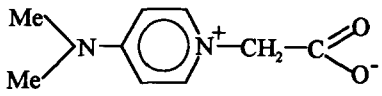
By virtue of their overall charge neutrality, betaine ($Me_3N^+CH_2CO_2^-$, IUPAC name: trimethylammonioacetate) and its derivatives can be used to prepare soluble metal complexes in which the metal centre may bear additional anionic ligands. In view of this, the use of betaine ligands provides a ready synthetic access to new polymeric silver(I) complexes. In our latest studies we have determined the crystal structures of several silver(I) complexes of betaines[10] and established some new structural types.[9]

* On sabbatical leave from the Department of Chemistry, Zhengzhou University, Zhengzhou 450052, P.R. China.

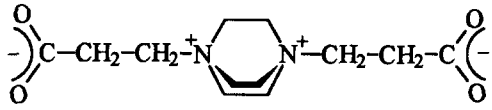
† On sabbatical leave from the Institute of Biophysics, Beijing 100101, P.R. China.

‡ Author to whom correspondence should be addressed.

As a sequel to this work, the present report describes the preparation and X-ray analysis of two new polymeric silver(I) complexes, namely $[\{Ag_2(L^1)_2(NO_3)(H_2O)\}_n](NO_3)_n$ (**1**) and $[\{Ag_4(L^2)_3\}_n](ClO_4)_{4n}\cdot 3nH_2O$ (**2**) [L^1 = 4-dimethylaminopyridinioacetate, p-$Me_2NC_5H_4N^+CH_2CO_2^-$, L^2 = 1,4-diazoniabicyclo [2.2.2]octane-1,4-dipropionate, $^-O_2C(CH_2)_2N^+(CH_2CH_2)_3N^+(CH_2)_2CO_2^-$].



L^1



L^2

EXPERIMENTAL

Preparation

Silver(I) nitrate and silver(I) perchlorate were purchased from BDH. The betaines L^1 and L^2 were synthesized as described previously.[11,12] IR spectra were recorded from KBr pellets in the range of 4000–400 cm^{-1} on a Perkin–Elmer 1600 FT-IR spectrometer.

$[\{Ag_2(L^1)_2(NO_3)(H_2O)\}_n](NO_3)_n$ (**1**). Solutions of $AgNO_3$ (85 mg, 0.5 mmol) and L^1 (180 mg, 1.0 mmol) in distilled water (3.0 cm^3 each) were mixed at *ca* 60°C with stirring and then ethanol was diffused into the resulting solution for a week to give colourless needle-like crystals of **1**. IR data (KBr): 3381.3(s), 3262.4(s), 3078.7(m), 2945.4(w), 1658.9(vs), 1621.3(s), 1568.1(s), 1542.1(w), 1383.6(s), 1300.4(m), 1211.8(m), 1185.4(w), 1130.4(w), 1070.4(w), 1034.7(w), 947.2(w), 903.2(w), 826.4(m), 751.6(m), 682.1(m), 589.8(w) cm^{-1}.

$[\{Ag_4(L^2)_3\}_n](ClO_4)_{4n}\cdot 3nH_2O$ (**2**). A solution of $AgClO_4$ (104 mg, 0.5 mmol) dissolved in distilled water (3.0 cm^3) was added to a solution of L^2 (256 mg, 1.0 mmol) in distilled water (3.0 cm^3) at *ca* 60°C with stirring. After the resulting clear solution was cooled to room temperature and allowed to stand at room temperature for several days, colourless crystals of **2** were formed. IR data (KBr): 3460.8(s), 3007.8(m), 2963.8(w), 1592.1(s), 1540.0(w), 1463.7(w), 1416.0(w), 1384.6(s), 1319.4(w), 1281.1(w), 1113.9(s), 1086.5(s), 923.4(w), 846.4(w), 825.4(w), 743.1(w), 626.2(m) cm^{-1}.

X-ray crystallography

Data processing parameters and details of the structural analysis are summarized in Table 1. The intensity data of complex **1** were measured on a Siemens R3m/V diffractometer according to established procedures.[13] The raw data were processed with the learnt-profile procedure[14] and absorption corrections were applied by fitting a pseudo-ellipsoid to the ψ-scan data of selected strong reflections over a range of 2θ angles.[15] The intensity data of complex **2** were measured on a MSC/Rigaku RAXIS-IIC imaging plate system with a rotating anode Mo K_α X-ray source (λ = 0.71073 Å, 50 kV, 150 mA)[16] and corrected for absorption through correlation of symmetry-equivalent reflections using the REQAB program.[17] The direct method yielded all the non-hydrogen atoms and the hydrogen atoms of the double betaine ligands were generated geometrically (C—H = 0.96 Å) and allowed to ride on their respective parent carbon atoms. The nitrate group and perchlorate group exhibit disorder and distance restraints of N—O = 1.22±0.010, O···O = 2.11±0.020 and Cl—O = 1.41±0.010, O···O = 2.13±0.020 Å, respectively, were applied. The final refinement cycles were performed by full-matrix least-squares with anisotropic thermal parameters for all non-hydrogen atoms and assigned isotropic thermal parameters for hydrogen atoms. All computations were performed on a PC-486 computer with the SHELXTL-PLUS program package.[18] Analytic expressions of neutral-atom scattering factors were employed and anomalous-dispersion corrections were incorporated.[19(a)] Selected bond distances and bond angles are listed in Table 2. Supplementary materials comprising atomic coordinates and thermal parameters have been deposited at the Cambridge Crystallographic Data Center and observed and calculated structure factors are available from the corresponding author on request.

RESULTS AND DISCUSSION

$[\{Ag_2(L^1)_2(NO_3)(H_2O)\}_n](NO_3)_n$ (**1**).

Complex **1** is a coordination polymer based on bis(carboxylate-*0,0′*)-bridged dimers containing two crystallographically independent silver(I) atoms in different coordination geometries (Fig. 1), with the carboxylate group of L^1 acting in the *syn–syn* bridging mode [C(1)—O(1) 1.229(2) Å, O(1)—C(1)—O(2) 128.1(4)°, C(1)—O(2) 1.236(5) Å, O(3)—C(10)—O(4) 128.3(4)°, C(10)—O(3) 1.233(3), C(10)—O(4) 1.254(5) Å]. The intra-dimer Ag···Ag separation [2.881(2) Å] is slightly smaller than that (2.89 Å) in metallic silver[19(b)] and thus suggestive of a comparable extent of metal–metal interaction. The intra-dimer Ag—O distances and O—Ag—O angles are in the range 2.203(4)–2.270(4) Å and 169.8(1)–153.0(1)°, respectively, being comparable to those

Table 1. Crystallographic data for complexes **1** and **2**

Complex	**1**	**2**
Formula	$C_{18}H_{26}N_6O_{11}Ag_2$	$C_{36}H_{66}N_6O_{31}Cl_4Ag_4$
Formula weight	718.2	1652.2
Colour; habit	Colourless needle	Colourless plate
Crystal size (mm^3)	$0.10\times0.12\times0.35$	$0.08\times0.15\times0.18$
a (Å)	14.944(2)	15.162(1)
b (Å)	5.121(3)	15.290(1)
c (Å)	15.683(2)	23.067(1)
β(°)	95.41(1)	
V (Å^3)	1195.0(5)	5348(3)
Z	2	4
Space group	*Pc*(No. 7)	*Pnma* (No. 62)
F(000)	716	3312
ρ(calc.) (g cm^{-3})	1.996	2.052
μ (mm^{-1})	1.710	1.745
Transmission factors (relative)	0.7483/0.8492	0.7390/1.2421
Collection range, $2\theta_{max}$ (°)	17, 5, ±17; 48	19, ±17, ±29; 48
Unique data measured	1949	5554
Observed data, n	1655 [$F > 4\sigma(F)$]	4153 [$F > 6\sigma(F)$]
No. of variables, p	329	413
R^a	0.041	0.063
R_g	0.047	0.084
S(GOF)	1.14	1.64

^{a} $R = \Sigma\Delta/\Sigma|F_o|$, $R_g = [\Sigma\omega\Delta^2/\Sigma\omega|F_o|^2]^{1/2}$ and $S = [\Sigma\omega\Delta^2/(n\text{-}p)]^{1/2}$, where $\omega = [\sigma^2(F_o)+K|F_o|^2]^{-1}$, $\Delta = ||F_o|-|F_c||$; $K\times10^4 = 6$ and 0.5 for complexes **1** and **2**, respectively.

found in the dimeric structures of several known silver(I) carboxylates.[10(c),(d)] As illustrated in Fig. 2, the present structure is extended into a stairs-like polymer running parallel to the *b* axis via comparatively weak metal–carboxylate linkages [Ag(1)—O(2b) 2.611(4), Ag(2)—O(4a) 2.665(4) Å] between adjacent dimers, generating rhombic Ag_2O_2 units as found in the type D and modified type D structures. A similar example has recently been found in a tetranuclear silver(I) carboxylate, $[\{Ag_2(4\text{-}FC_6H_4CH_2CO_2)_2(H_2O)_2\}_2]$,[20] in which a pair of Ag_2(carboxylate-*0,0′*)$_2$ dimers are linked together through weak axial metal–carboxylate bonds [2.498(4) Å], resulting in a centrosymmetric rhombic Ag_2O_2 unit. The coordination spheres of silver atoms Ag(1) and Ag(2) are completed by an unidentate nitrate ligand [2.501(4) Å] and an aqua ligand [O(1w)] of much longer contact [2.660(4) Å], respectively, at the axial site. It is noteworthy that the axial nitrate and aqua ligands lie on opposite sides if the mean plane of the bridged dimeric unit, giving a new modified type D structure different from that found in $[\{Ag_2(Me_3N^+CH_2CH_2CO_2^-)_2(NO_3)_2\}_n]$, where the axial nitrate ligands lie on the same side of the dimeric Ag_2(carboxylate-*0,0′*)$_2$ plane.[10(c)] The molecular skeleton of L^1 in complex **1** possesses approximate C_s symmetry, as the mean deviations of two sets of atoms O(1), O(2), C(1), C(2), N(1), C(5), N(2) and O(3), O(4), C(10), C(11), N(3), C(14), N(4) to their least-squares planes are 0.030 and 0.010 Å, respectively. The carboxymethyl groups are nearly perpendicular to the dimethylaminopyridinio skeletons, the relevant torsion angles C(1)—C(2)—N(1)—C(7) and C(10)—C(11)—N(3)—C(16) being 86.4 and −90.4°, respectively. The conformation of the L^1 ligand is thus similar to that in its hydrate form.[11]

$[\{Ag_4(L^2)_3\}_n](ClO_4)_{4n}\cdot 3nH_2O$ (**2**)

The structure of complex **2** comprises cationic polymeric chains and discrete perchlorate anions plus lattice water molecules (Fig. 3). There are three crystallographically independent silver(I) atoms with different coordination environments in the asymmetric unit. Atoms Ag(1) and Ag(2), located at Wyckoff position 4(*c*) of symmetry *m*, are bonded nearly linearly to two unidentate carboxylate groups from different double betaine ligands [Ag(1)—O(1) 2.142(2), Ag(2)—O(4) 2.160(2) Å, O(1)—Ag(1)—O(1b) 165.3(1), O(4)—Ag(2)—O(4b) 167.7(1)°] in a manner similar to that in [(4-chloro-2-methylphenoxy)ethanoato-0,0′]silver(I).[21] The most notable structural feature is that the pair of unidentate carboxylate groups attached to atoms Ag(1) and Ag(2) [Ag(1)—O(1)—C(1) 108.8(2), Ag(2)—O(4)—C(7) 110.6(2)°] bear a *syn* relationship with dihedral angles between them of 21.2 and 14.8°, respectively. The coordination geometry about the Ag(3) atom is based on the usual type A bis(carboxylate-*0,0′*)-bridged centrosymmetric dimeric subunit [Ag(3a)—O(5)—C(13) 120.0(2), Ag(3)—O(6)—C(13) 126.6(2)°], in which the Ag···Ag separation [2.750(2) Å] is even smaller than the shortest one [2.778(5) Å] hitherto reported in a binuclear silver(I) carboxylate, namely bis(3-hydroxy-2,2,3-trimethyl-4-phenylcyclohexanecarboxylato-*0,0′*)disilver(I) dihydrate[22] and hence indicative of a metal–metal inter-

Table 2. Selected bond lengths (Å) and bond angles (°)

$[\{Ag_2(L^1)_2(NO_3)(H_2O)\}_n](NO_3)_n$ (1)			
Ag(1)—O(1)	2.213(4)	Ag(1)—O(4)	2.203(4)
Ag(2)—O(2)	2.256(4)	Ag(2)—O(3)	2.270(4)
Ag(2)—O(6)	2.501(4)	O(1)—C(1)	1.229(2)
O(2)—C(1)	1.236(5)	C(1)—C(2)	1.510(5)
C(2)—N(1)	1.502(5)	N(1)—C(3)	1.354(6)
N(1)—C(7)	1.328(5)	C(3)—C(4)	1.338(5)
C(4)—C(5)	1.403(5)	C(5)—C(6)	1.417(6)
C(5)—N(2)	1.332(4)	C(6)—C(7)	1.366(5)
N(2)—C(8)	1.430(5)	N(2)—C(9)	1.471(6)
O(3)—C(10)	1.233(3)	O(4)—C(10)	1.254(5)
C(10)—C(11)	1.539(5)	C(11)—N(3)	1.462(5)
N(3)—C(12)	1.319(6)	N(3)—C(16)	1.361(5)
C(12)—C(13)	1.363(5)	C(13)—C(14)	1.421(5)
C(14)—C(150	1.408(6)	C(14)—N(4)	1.363(5)
C(15)—C(16)	1.354(5)	N(4)—C(17)	1.472(6)
N(4)—C(18)	1.445(5)	Ag(1)···Ag(2)	2.881(2)
Ag(1)···O(1w)	2.660(4)	Ag(1)···O(2b)	2.611(4)
Ag(2)···O(2a)	2.665(4)	Ag(1a)···Ag(2)	3.414(4)
Ag(2)···Ag(1)—O(1)	82.0(1)	Ag(2)···Ag(1)—O(4)	88.5(1)
O(1)—Ag(1)—O(4)	169.8(1)	Ag(1)···Ag(2)—O(2)	79.9(1)
Ag(1)···Ag(2)—O(3)	75.0(1)	O(2)—Ag(2)—O(3)	153.0(1)
Ag(1)···Ag(2)—O(6)	162.5(1)	O(2)—Ag(2)—O(6)	108.3(1)
O(3)—Ag(2)—O(6)	98.5(1)	Ag(1)—O(1)—C(1)	122.5(3)
Ag(2)—O(2)—C(1)	124.1(2)	O(1)—C(1)—O(2)	128.1(4)
O(1)—C(1)—C(2)	117.4(4)	O(2)—C(1)—C(2)	114.5(2)
C(1)—C(2)—N(1)	111.9(2)	C(2)—N(1)—C(3)	119.7(3)
C(2)—N(1)—C(7)	119.4(4)	C(3)—N(1)—C(7)	119.4(3)
N(1)—C(3)—C(4)	121.7(3)	C(3)—C(4)—C(5)	121.3(4)
C(4)—C(5)—C(6)	115.6(3)	C(4)—C(5)—N(2)	124.6(4)
C(6)—C(5)—N(2)	119.6(3)	C(5)—C(6)—C(7)	120.0(3)
N(1)—C(7)—C(6)	121.9(4)	C(5)—N(2)—C(8)	124.1(4)
C(5)—N(2)—C(9)	120.6(3)	C(8)—N(2)—C(9)	114.3(3)
Ag(2)—O(3)—C(10)	130.5(3)	Ag(1)—O(4)—C(10)	116.5(2)
O(3)—C(10)—O(4)	128.3(4)	O(3)—C(10)—C(11)	117.9(4)
O(4)—C(10)—C911)	113.8(2)	C(10)—C(11)—N(3)	109.9(2)
C(11)—N(3)—C(12)	121.1(3)	C(11)—N(3)—C(16)	119.4(4)
C(12)—N(3)—C(16)	119.2(3)	N(3)—C(12)—C(13)	123.8(3)
C(12)—C(13)—C(14)	118.7(4)	C(13)—C(14)—C(15)	115.8(3)
C(13)—C(14)—N(4)	121.3(4)	C(15)—C(14)—N(4)	122.9(3)
C(14)—C(15)—C(16)	121.8(3)	N(3)—C(16)—C(15)	120.4(4)
C(14)—N(4)—C(17)	122.9(3)	C(14)—N(4)—C(18)	118.7(4)
C(17)—N(4)—C(18)	118.2(3)	Ag(2)—O(6)—N(5)	127.4(3)
$[\{Ag_4(L^2)_3\}_n](ClO_4)_{4n}\cdot 3nH_2O$ (2)			
Ag(1)—O(1)	2.142(2)	Ag(1)—O(1b)	2.142(2)
O(1)—C(1)	1.250(4)	O(2)—C(1)	1.225(4)
C(1)—C(2)	1.525(4)	C(2)—C(3)	1.503(4)
C(3)—N(1)	1.520(3)	N(1)—C(4)	1.511(4)
N(1)—C(5)	1.500(4)	N(1)—C(6)	1.503(4)
C(4)—C(4c)	1.497(5)	C(5)—C(5c)	1.502(5)
C(6)—C(6c)	1.494(5)	Ag(2)—O(4)	2.160(2)
Ag(2)—O(4b)	2.160(2)	O(3)—C(7)	1.222(4)
O(4)—C(7)	1.260(4)	C(7)—C(8)	1.510(4)
C(8)—C(9)	1.522(4)	C(9)—N(2)	1.501(3)
N(2)—C(10)	1.506(4)	N(2)—C(11)	1.508(4)
N(2)—C(12)	1.501(4)	C(10)—C(10c)	1.519(5)
C(11)—C(11c)	1.488(5)	C(12)—C(12c)	1.494(5)
Ag(3)—O(6)	2.187(3)	Ag(3)···Ag(3a)	2.750(2)
Ag(3)—O(5a)	2.196(3)	O(5)—C(13)	1.257(5)
O(6)—C(13)	1.244(5)	C(13)—C(14)	1.531(4)
C(14)—C(15)	1.519(5)	C(15)—N(3)	1.510(4)
N(3)—C(16)	1.507(5)	N(3)—C(17)	1.502(4)
N(3)—C(18)	1.513(4)	C(16)—C(16b)	1.491(5)
C(17)—C(17b)	1.524(5)	C(18)—C(18b)	1.502(5)

Table 2.—*Continued.*

O(1)—Ag(1)—O(1b)	165.3(1)	Ag(1)—O(1)—C(1)	108.8(2)
O(1)—C(1)—O(2)	125.7(3)	O(1)—C(1)—C(2)	114.6(2)
O(2)—C(1)—C(2)	119.7(2)	C(1)—C(2)—C(3)	111.7(2)
C(2)—C(3)—N(1)	114.0(2)	C(3)—N(1)—C(4)	111.9(2)
C(3)—N(1)—C(5)	107.9(2)	C(4)—N(1)—C(5)	109.3(2)
C(3)—N(1)—C(6)	112.3(2)	C(4)—N(1)—C(6)	107.0(2)
C(5)—N(1)—C(6)	108.3(2)	N(1)—C(4)—C(4c)	110.6(1)
N(1)—C(5)—C(5c)	110.7(1)	N(1)—C(6)—C(6c)	110.8(1)
O(4)—Ag(2)—O(4b)	167.7(1)	Ag(2)—O(4)—C(7)	110.6(2)
O(3)—C(7)—O(4)	126.4(3)	O(3)—C(7)—C(8)	118.3(3)
O(4)—C(7)—C(8)	115.3(2)	C(7)—C(8)—C(9)	112.0(2)
C(8)—C(9)—N(2)	113.6(2)	C(9)—N(2)—C(10)	107.7(2)
C(9)—N(2)—C(11)	113.2(2)	C(10)—N(2)—C(11)	107.5(2)
C(9)—N(2)—C(12)	112.2(2)	C(10)—N(2)—C(12)	108.5(2)
C(11)—N(2)—C(12)	107.6(2)	N(2)—C(10)—C(10c)	110.6(1)
N(2)—C(11)—C(11c)	111.2(1)	N(2)—C(12)—C(12c)	111.2(1)
O(6)—Ag(3)···Ag(3a)	80.6(1)	O(6)—Ag(3)—O(5a)	165.6(1)
Ag(3a)···Ag(3)—O(5a)	85.6(1)	C(13)—O(5)—Ag(3a)	120.0(2)
Ag(3)—O(6)—C(13)	126.6(2)	O(5)—C(13)—O(6)	126.0(3)
O(5)—C(13)—C(14)	117.7(3)	O(6)—C(13)—C(14)	116.2(3)
C(13)—C(14)—C(15)	116.9(3)	C(14)—C(15)—N(3)	114.9(3)
C(15)—N(3)—C(16)	109.2(3)	C(15)—N(3)—C(17)	112.3(2)
C(16)—N(3)—C(17)	107.4(2)	C(15)—N(3)—C(18)	112.2(2)
C(16)—N(3)—C(18)	107.8(2)	C(17)—N(3)—C(18)	107.8(2)
N(3)—C(16)—C(16b)	111.5(1)	N(3)—C(17)—C(17b)	110.9(1)
N(3)—C(18)—C(18b)	111.2(1)		
Hydrogen bonding			
O(1W)···O(3)	2.805(4)	O(1W)···O(3b)	2.805(4)

Symmetry codes for **1**: (a) $x, -1+y, z$; (b) $x, 1+y, z$. Symmetry codes for **2**: (a) $1-x, 1-y, -z$; (b) $x, 1.5-y, z$; (c) $x, 0.5-y, z$.

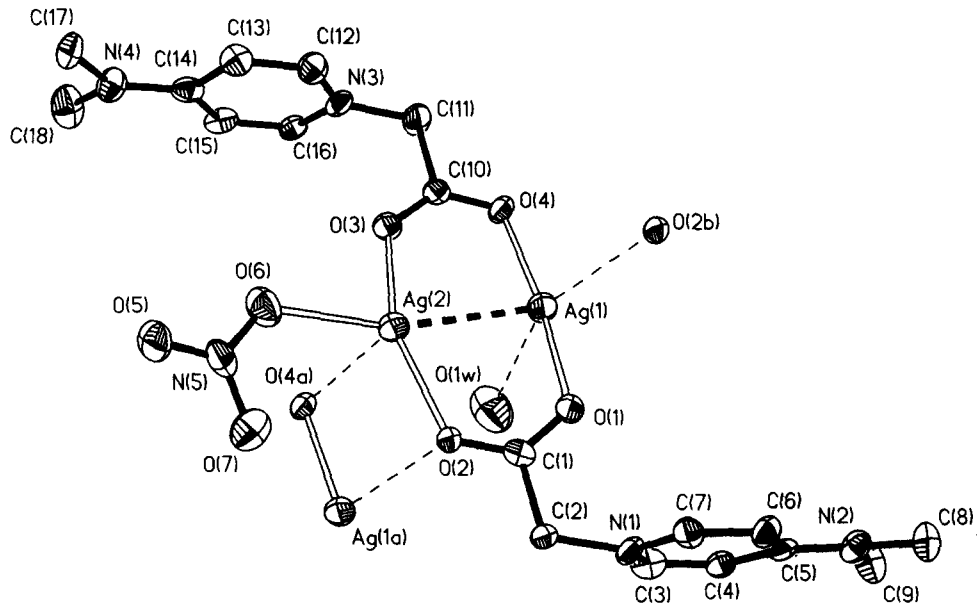


Fig. 1. Perspective view (35% thermal ellipsoids) showing the coordination environment of the independent silver(I) atoms in **1** and the atom labelling scheme. Symmetry codes are given in Table 2.

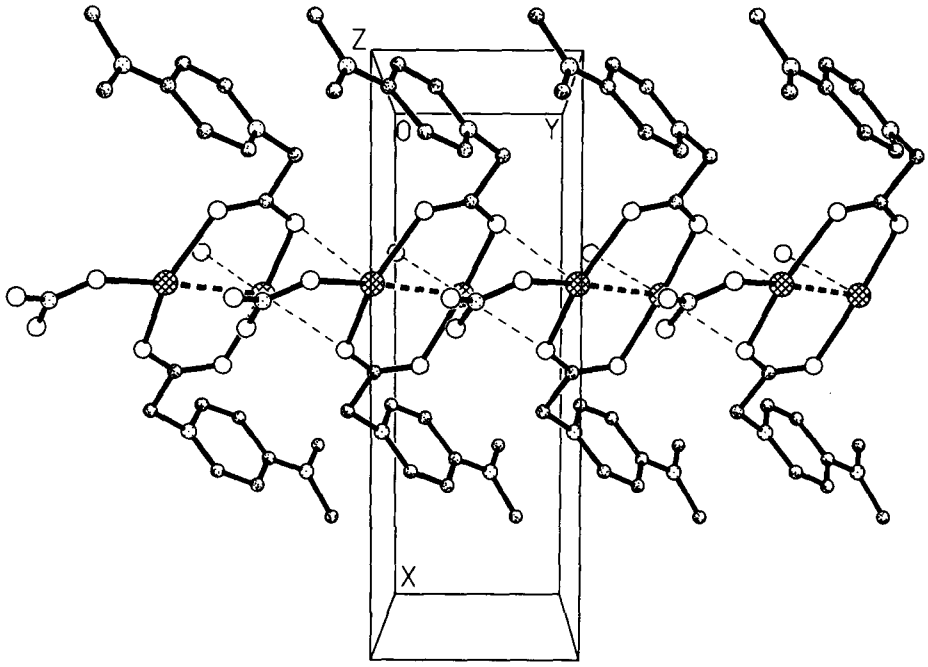


Fig. 2. Projection of the crystal structure of **1** along the *c* axis, showing the one-dimensional polymeric chain structure running parallel to the *b* axis.

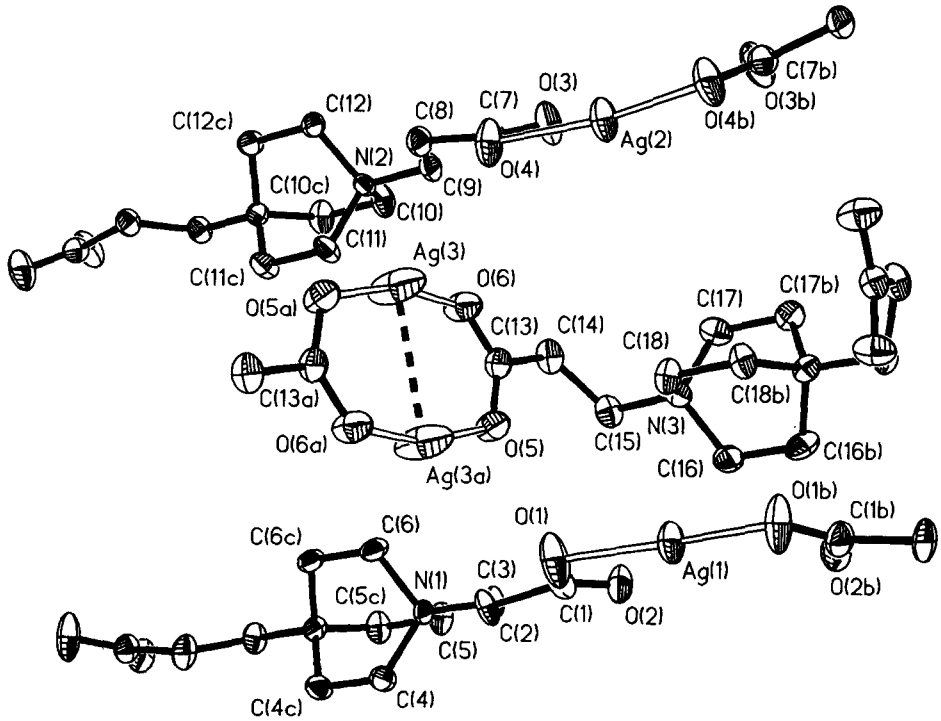


Fig. 3. Perspective view (35% thermal ellipsoids) showing the coordination environment of the three independent silver(I) atoms in **2** and the atom labelling scheme. Symmetry codes are given in Table 2.

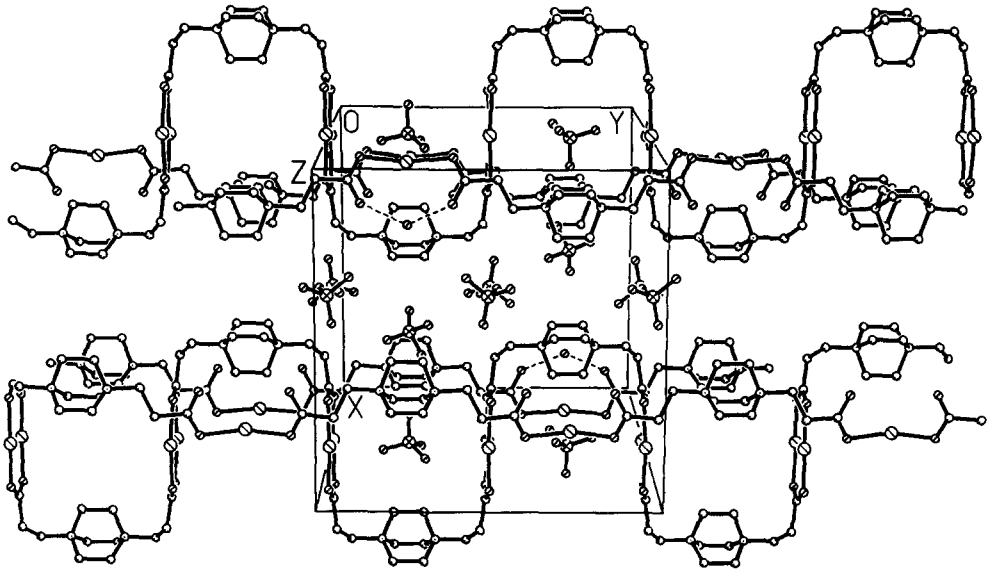


Fig. 4. Projection of the crystal structure of **2** along the *c* axis showing the one-dimensional polymeric chain structure running parallel to the *b* axis.

action even stronger than that (2.89 Å) in metallic silver.[19(b)] The intra-dimer Ag—O distances [2.187 (3)–2.196(3) Å] and O—Ag—O angle [165.6(1) °] are comparable to those in complex **1**. There are three half molecules of L^2 in the asymmetric unit of complex **2**. Ligand L^2 has symmetry *m* bisecting all three CH_2—CH_2 bonds of the central cage with pairs of carboxylato groups oriented nearly parallel to each other, being conformationally quite different from that in $[\{Zn(L^2)_2\}_n](ClO_4)_{2n}$,[12] in which the molecular skeleton of the double betaine ligand L^2 exhibits C_2 symmetry with one carboxylato group nearly perpendicular to the other.

In the crystal structure of complex **2**, as illustrated in Fig. 4, the double betaine ligand L^2 coordinates the silver(I) atoms in the end-to-end mode to form three independent infinite zigzag chains running parallel to the *b* direction; note that the infinite chain composed of dimeric subunits takes the shape of a square wave. The lattice water molecule [O(1w)] forms donor hydrogen bonds [O(1w)···O(3) 2.805 Å] with an uncoordinated carboxylato oxygen atom [O(3)] and its symmetry equivalent. The perchlorate groups, one of which exhibits orientional disorder, are packed in the (200) family of planes. The crystal structure is built up from a stacking of these chains such that the inter-chain interactions are mainly of the van der Waals type.

Acknowledgement—This work is supported by Hong Kong Research Grants Council Earmarked Grant CUHK 89/93E.

REFERENCES

1. R. J. Lancashire, *Comprehensive Coordination Chemistry* (Edited by G. Wilkinson, R. D. Gillard and J. A. McCleverty), Ch. 54, p. 808. Vol. V, Pergamon Press, Oxford (1987).
2. T. C. W. Mak, W.-H. Yip, C. H. L. Kennard, G. Smith and E. J. O'Reilly, *Aust. J. Chem.* 1986, **39**, 541.
3. (a)G. Smith, C. H. L. Kennard, and T. C. W. Mak, *Z. Kristallogr.* 1988, **184**, 275; (b)B. T. Usubaliev, E. M. Movsumov, I. R. Amiraslanov, A. I. Akhmedov, A. A. Musaev and Kh. S. Mameov, *Zh. Strukt. Khim.* 1981, **22**, 98.
4. J. K. M. Rao and M. A. Viswamitra, *Acta Cryst.* 1972, **B28**, 1484.
5. R. G. Griffith, J. D. Ellett, M. Mehring, J. G. Bullitt and J. S. Waugh, *J. Chem. Phys.* 1972, **57**, 2147.
6. M. E. Kamwaya, E. Papavinasam, S. G. Teoh, and R. K. Rajaram, *Acta Cryst.* 1984, **C40**, 1318.
7. X.-M. Chen and T. C. W. Mak. *J. Chem. Soc., Dalton Trans.* 1991, 1219.
8. M. Hedrich and H. Hartl, *Acta Cryst.* 1983, **C39**, 533.
9. P.-R. Wei, D.-D. Wu and T. C. W. Mak, *Inorg. Chim. Acta* 1996, in press.
10. (a) W.-Y. Huang, L. Lu, X.-M. Chen and T. C. W. Mak, *Polyhedron* 1991, **10**, 2687; (b) X.-M. Chen and T. C. W. Mak, *Polyhedron* 1991, **10**, 1723; (c) X.-M. Chen and T. C. W. Mak, *J. Chem. Soc., Dalton Trans.* 1991, 1219; 3253; (d) D.-D. Wu and T. C. W. Mak, *J. Chem. Soc., Dalton Trans.* 1995, 2671.
11. P.-R. Wei, Q. Li and T. C. W. Mak, *J. Chem. Crystallogr.* 1996, **26**, 133.
12. P.-R. Wei, B.-M. Wu, W. P. Leung and T. C. W. Mak, *Polyhedron* 1996, **15**, 4041.
13. R. A. Sparks, *Crystallographic Computing Techniques* (Edited by F. R. Ahmed), p. 452. Munksgaard, Copenhagen (1976).
14. R. Diamond, *Acta Cryst.* 1969, **A27**, 43.
15. G. Kopfmann and R. Huber, *Acta Cryst.* 1968, **A24**, 348.
16. (a) K. L. Krause and G. N. Phillips Jr, *J. Appl. Cryst.* 1992, **25**, 146; (b) M. Sato, M. Yamamoto, K. Imada, Y. Katsube, N. Tanaka and T. Higashi, *J. Appl. Cryst.* 1992, **25**, 348; (c) J. Tanner and K. L. Krause, *The Rigaku J.* 1994, **11**, 4.

17. L. L. Miller and R. A. Jacobson, *Comput. Chem.* 1989, **13**, 1.
18. (a) G. M. Sheldrick, SHELXTL-PC. *Program Package for X-ray Crystal Structure Determination.* Siemens Analytical Instruments Inc., Karlsruhe (1990); (b) G. M. Sheldrick, *Computational Crystallography* (Edited by D. Sayre), p. 506. Oxford University Press, New York (1982); (c) G. M. Sheldrick, *Crystallographic Computing* 3: *Data Collection, Structure Determination, Proteins and Databases* (Edited by G. M. Sheldrick, C. Krüger and R. Goddard), p. 175. Oxford University Press, New York (1985).
19. *International Tables for X-ray Crystallography* (Edited by J. A. Ibers and W. C. Hamilton) (a) Vol. IV. pp. 55, 99, 149; (b) Vol. IV. p. 278. Kynoch Press, Birmingham (1974). Now distributed by Kluwer Academic Publishers, Dordecht.
20. G. Smith, D. S. Sagatys, C. A. Campbell, D. E. Lynch and C. H. L. Kennard, *Aust. J. Chem.* 1990, **43**, 1707.
21. T. C. W. Mak, W.-H. Wip, C. H. L. Kennard, G. Smith and E. J. O'Reilly, *J. Chem. Soc., Dalton Trans.* 1988, 2353.
22. P. Coggon and A. T. McPhail, *J. Chem. Soc., Chem. Commun.* 1972, 91.

Pergamon

S0277-5387(96)00224-0

Polyhedron Vol. 16, No. 1, pp. 161–163, 1997
Copyright © 1996 Elsevier Science Ltd
Printed in Great Britain. All rights reserved
0277-5387/97 $15.00+0.00

Direct synthesis and crystal structure of a mixed-valence copper complex

Larisa A. Kovbasyuk, Olga A. Babich and Vladimir N. Kokozay*

Department of Chemistry, Kiev Shevchenko University, 252033 Kiev, Ukraine

(Received 21 March 1996; accepted 15 April 1996)

Abstract—The mixed-valence complex $[Cu^{II}(DMF)_4][Cu^{I}_4(SCN)_4(CN)_2]$ (DMF = N,N-dimethylformamide) has been synthesized using a direct method of interaction and characterized by X-ray crystallography. The complex consists of layers formed by polymeric $[Cu^{I}_4(SCN)_4(CN)_2]^{2-}_n$ anions and the $[Cu^{II}(DMF)_4]^{2+}$ cations disposed between anionic layers.
Copyright © 1996 Elsevier Science Ltd

Keywords: mixed-valence complex; copper; direct synthesis; X-ray structure.

Staged oxidation of copper metal to copper(II) in the non-aqueous solutions of complexing agents[1] reveals a possibility of the direct synthesis[2] of mixed-valence complexes. The search for suitable conditions and systems showed that the presence of thiocyanate ions in the reaction mixture promotes formation of the above-mentioned complexes.

Under interaction of copper powder with N,N-dimethylformamide solutions of methyl-, dimethyl-, trimethylammonium thiocyanate or with ammonium thiocyanate in the presence of aminoacetic acid the formation of mixed-valence complexes $[Cu^{II}(DMF)_4][Cu^{I}_4(SCN)_4(CN)_2]$ has been discovered. The presence of cyano groups in the compound composition can be explained by the hydrolysis of dithiocyan[3] formed from ammonium or alkylammonium salts:

$$3(SCN)_2 + 4H_2O \rightarrow 5HNCS + H_2SO_4 + HCN$$

The presence of sulfate ions in the reaction mixture has been confirmed by analytical tests.

EXPERIMENTAL

All chemicals were commercial products of reagent grade, used without further purification. Methyl-, dimethyl- and trimethylammonium thiocyanate were synthesized from the corresponding alkylammonium chlorides and potassium thiocyanate in acetone solution under an exchange reaction. All experiments were carried out in air.

Synthesis of $[Cu^{II}(DMF)_4][Cu^{I}_4(SCN)_4(CN)_2]$

For the preparation of the complex the following method was used: Cu (0.63 g, 10 mmol), $(CH_3)_2$ NH*HSCN (1.55 g, 15 mmol) and N,N-dimethylformamide (20 cm^3) were placed in a flask in the above order. The mixture was heated to 50–60°C and stirred until the complete dissolution of copper (30–40 min). The resulting dark green solution was cooled and then isopropanol (15 cm^3) was added. The crystals were separated over 2 weeks and dried *in vacuo*; yield 1.4 g (80%). Found: C, 23.7; H, 3.0; N, 15.5; Cu, 34.6. Calc. for $Cu_5C_{18}H_{28}H_{10}O_4S_4$: C, 24.2; H, 3.2; N, 15.7; Cu, 35.5%.

Crystal structure determination

Crystallographic measurements were obtained at 20°C using an Enraf–Nonius CAD-4 diffractometer operating in the ω-2θ scan mode (the ratio of the scanning rates was $\omega/\theta = 1.2$). The intensity data were collected within the range $4.68 \leqslant \theta \leqslant 55.95°$ using graphite-monochromated Mo-K_α radiation. Accurate unit-cell parameters and the orientation matrix for data collection were obtained from least-squares refinement, using the setting angles of 24 reflections in the range $13 < \theta < 15°$. The structure was solved by direct methods and refined by full-matrix least-squares techniques in the anisotropic approximation using SHELXL-93.[4] The positions of the hydrogen atoms were idealized and included in the calculations of the structure factors as the fixed contributions. The crystallographic data are summarized in Table 1.

* Author to whom correspondence should be addressed.

Table 1. Crystal data and summary of intensity data collection and refinement

Compound	$[Cu^{II}(DMF)_4][Cu^{I}_4(SCN)_4 \cdot (CN)_2]$
Colour	Light brown
Formula weight	894.44
Space group	$P\bar{1}$
a(Å)	9.325(9)
b(Å)	9.468(3)
c(Å)	9.810(5)
α(°)	76.01(3)
β(°)	79.14(6)
γ(°)	69.99(4)
Cell volume (Å^3)	784.4(9)
Formula units	1
T(K)	293
D_{calc}(g cm^{-3})	1.894
Radiation (Å)	Mo-K_α (λ = 0.71073)
F(000)	447
Number of unique data	2192
Data used in refinement	2038 [$I > 2\sigma(I)$]
Refinement method	Full matrix least-squares on F^2
Software	SHELX-93 [4]
R	0.0552 (wR_2 = 0.1580)
GOF	1.121

Table 2. Selected bond lengths (Å) and angles (°) for $[Cu^{II}(DMF)_4][Cu^{I}_4(SCN)_4(CN)_2]$

Cu(1)—O(1)	1.946(3)
Cu(1)—O(2)	1.941(3)
Cu(2)—S(1)	2.376(2)
Cu(2)—S(1b)	2.729(3)
Cu(2)—C(3)	1.892(5)
Cu(2)—N(2)	1.949(5)
Cu(3)—S(2d)	2.352(2)
Cu(3)—S(2b)	2.829(3)
Cu(3)—N(1)	1.940(5)
Cu(3)—N(3c)	1.914(6)
N(2)—C(2)	1.151(7)
O(1)—C(4)	1.249(6)
N(4)—C(4)	1.299(7)
N(4)—C(5)	1.456(7)
N(4)—C(6)	1.448(7)
O(1)—Cu(1)—O(1a)	180.0
O(1)—Cu(1)—O(2)	90.5(1)
O(1a)—Cu(1)—O(2)	89.5(1)
N(2)—Cu(2)—S(1)	106.9(2)
N(2)—Cu(2)—S(1b)	98.7(1)
C(3)—Cu(2)—N(2)	123.0(2)
C(3)—Cu(2)—S(1)	119.5(2)
C(3)—Cu(2)—S(1b)	108.8(2)
Cu(2)—S(1)—Cu(2b)	86.33(8)
S(1)—Cu(2)—S(1b)	93.67(8)
Cu(2)—N(2)—C(2)	169.1(4)
Cu(2)—C(3)—N(3)	177.2(5)
Cu(1)—O(1)—C(4)	124.9(3)
Cu(1)—O(2)—C(7)	127.9(3)
C(4)—N(4)—C(5)	120.1(5)
C(4)—N(4)—C(6)	121.2(4)
C(6)—N(4)—C(5)	118.4(5)

Symmetry transformations used to generate equivalent atoms: (a) $\{-x+1, -y, -z\}$; (b) $\{-x, -y, -z\}$; (c) $\{-x, -y+1, -z\}$; (d) $\{x, y+1, z-1\}$.

Convergence was reached at the agreement factor listed in Table 1.

DISCUSSION

A fragment of the crystal structure of the complex with the atomic labelling schemes and a perspective view of the packing in the unit cell are shown in Fig. 1. Selected bond distances and angles are given in Table 2. The Cu(1) atom of $[Cu^{II}(DMF)_4][Cu^{I}_4(SCN)_4(CN)_2]$ occupies a special (1/2, 0, 0) position, while the other atoms are located in general positions.

The polymeric anion is formed by infinite $\{—Cu—SCN—\}_n$ chains stretching along $y0z$ plane. These chains are linked in pairs by contacts between copper(I) and sulfur atoms of the thiocyanate groups with the formation of the planar four membered Cu_2S_2 cycles. The angles at the copper(I) and sulfur atoms in the Cu_2S_2 cycle are approximately 94 and 86°, respectively. The similar chain and cyclic structural fragments are known;[5,6] however, it is necessary to note non-equivalent Cu^I—S— bonds in the examined structure. Thus, the interatomic Cu^I—S distance in the $\{—Cu—SCN—\}_n$ chains is *ca* 2.36(4) Å (e.g. d[Cu(2)—S(1)] = 2.376(2) Å; d[Cu(3)—S(2) < x, $y+1, z>$] = 2.352(2) Å, which allows the postulation of covalent bonds; whereas the Cu^I—S bond length which links $\{—Cu—SCN—\}_n$ chains in pairs is *ca* 2.78(3) Å (e.g. d[Cu(3)—S(2b) < $-x, -y, -z>$] = 2.829(3), d[Cu(3)—S(2b) < $-x, -y, -z>$ = 2.729(3) Å]; which is essentially more than the sum of ionic radii of copper(I) and sulfur atoms.[7] The angles between least-squares planes of CuNCSCu′ N′C′S′ atoms (the mean deviation from planarity is 0.0225 Å) and CuSCu′S′ atoms is 70°.

The twin chains formed are linked in a layer by bridging cyanide groups (Fig. 2). Thus, the anionic layer comprises two crystallographically independent copper(I) atoms. Both copper(I) atoms have a distorted tetrahedral environment [angles at the copper(I) atom range from 108 to 123°], but Cu(2) is bonded to two sulfur and one nitrogen atom of the thiocyanate group and a carbon atom of the cyanide group, whereas the environment of the Cu(3) is completed by the nitrogen atom of the cyanide group. The values of interatomic distances Cu(I)—N and Cu(I)—C agree well with reported ones for known mixed-valence compounds.[8]

The complex cations $[Cu^{II}(DMF)_4]^{2+}$ are disposed between anionic layers. The Cu^{II} atoms are covalently linked with four oxygen atoms of DMF [d(Cu—O) *ca* 1.94(3) Å, O—Cu—O = 180°]. Weak Cu···S contacts [d Cu(1)—S(1)] = 3.047 Å; S(1)—Cu—S(1a) < $1-x, -y, -z>$ = 180°] with each second sulfur atom in twin $\{—Cu—SCN—\}$ chains (Fig. 1) provide total electroneutrality of the complex. Taking into consideration these contacts, the coordination environment of the Cu^{II} possesses tetragonal bipyramidal geometry. The DMF molecules are struc-

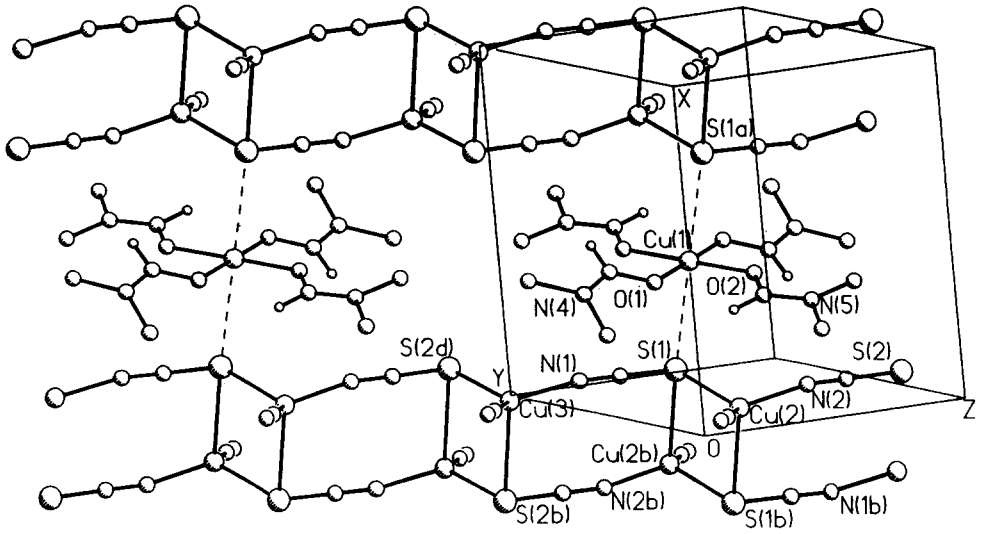


Fig. 1. Crystal structure of $[Cu^{II}(DMF)_4][Cu^{I}_4(SCN)_4(CN)_2]$ [(a), (b) and (d) refer to the following equivalent positions relative to the $<x,y,z>$ sets: $\{-x+1,-y,-z\}$, $\{-x,-y,-z\}$ and $\{x,y+1,z-1\}$, respectively].

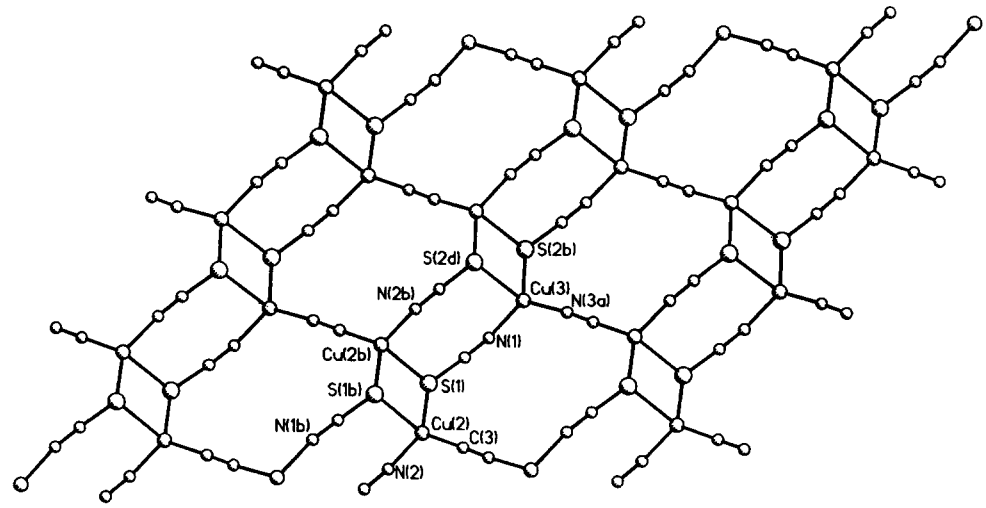


Fig. 2. View of the structure of $[Cu^{I}_4(SCN)_4(CN)_2]^{2-}_n$ anionic layer [(a), (b) and (d) refer to the following equivalent positions relative to the $<x,y,z>$ sets: $\{-x+1,-y,-z\}$, $\{-x,-y,-z\}$ and $\{x,y+1,z-1\}$, respectively].

turally normal and deviate slightly from a planar structure. The angle between the least-squares planes of the atoms of neighbouring DMF molecules is 27°. Such mutual disposition can be explained by steric hindrances which arise as a result of repulsion of bulky methyl radicals in an idealized planar $[Cu^{II}(DMF)_4]^{2+}$ cation.

REFERENCES

1. O. U. Vasilieva and V. N. Kokozay, *Ukr. Khim. Zh.* (*Russ. Ed.*) 1993, **59**, 176.
2. V. V. Skopenko, V. N. Kokozay and V. A. Pavlenko, *Ukr. Khim. Zh.* (*Russ. Ed.*) 1993, **59**, 485.
3. A. M. Golub and H. Kohler, *Chemie der Pseudohalogenide*, p. 161. VEB Deutscher Verlag der Wissenschaften, Berlin (1979).
4. G. M. Sheldrick, SHELX93. *A System of Computer Programs for X-ray Structure Determination*. University of Göttingen, Germany (1993).
5. C. Raston, B. Walter and A. White, *Aust. J. Chem.* 1979, **32**, 2757.
6. A. Wells, *Structural Inorganic Chemistry*. Clarendon Press, Oxford (1986).
7. S. Batsanov, *Zh. Neorg. Khim.* 1991, **36**, 3015.
8. M. Dunaj-Jurco, G. Ondrejovic and M. Melnik, *Coord. Chem. Rev.* 1988, **83**, 19.
9. P. G. Harrison, *Comprehensive Coordination Chemistry* (Edited by G. Wilkinson, R. D. Gillard and J. A. McCleverty), Vol. 2, p. 491, Pergamon Press, Oxford (1987).

Pergamon

S0277-5387(96)00227-6

Polyhedron Vol. 16, No. 1, pp. 165–169, 1997
Copyright © 1996 Elsevier Science Ltd
Printed in Great Britain. All rights reserved
0277-5387/97 $15.00+0.00

Synthesis and structure of $[Mo_2(NR)_2(\eta^2\text{-}S_2CNEt_2)_2(\mu\text{-}S)(\mu\text{-}\eta^2\text{-}\eta^2\text{-}S_2)]$ ($R = 2,6\text{-}Pr^i_2C_6H_3$): a molecular model for molybdenum trisulphide?

Thérèse A. Coffey and Graeme Hogarth†

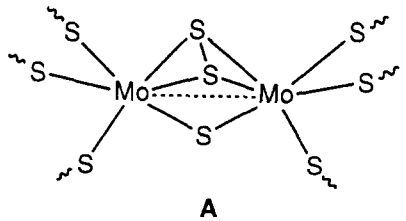
Chemistry Department, University College London, 20 Gordon Street, London WC1H 0AJ, U.K.

(Received 23 February 1996; accepted 15 April 1996)

Abstract—Reaction of the bis(imido) complex $[Mo(NR)_2(\eta^2\text{-}S_2CNEt_2)_2]$ ($R = 2,6\text{-}Pr^i_2C_6H_3$) with excess hydrogen sulfide leads to the low yield formation of $[Mo_2(NR)_2(\eta^2\text{-}S_2CNEt_2)_2(\mu\text{-}S)(\mu\text{-}\eta^2\text{-}\eta^2\text{-}S_2)]$, shown by crystallography to contain both μ-S and $\mu\text{-}\eta^2\text{-}\eta^2\text{-}S_2$ ligands bridging the molybdenum–molybdenum vector [2.797(2) Å], features which have recently been ascribed to MoS_3 and $MoS_3 \cdot nH_2O$. Copyright © 1996 Elsevier Science Ltd

Keywords: molybdenum; sulfide; dithiocarbamate; imido reduction; dimeric.

Molybdenum trisulfide (MoS_3) and other group 6 trichalcogenides were first prepared at the beginning of the last century,[1] yet somewhat surprisingly, and despite a large number of studies, their structures are still not well understood. The local structure has been postulated to be based on chains of face-sharing MoS_6 octahedra with alternating long and short molybdenum–molybdenum distances,[2,3] or trimolybdenum units,[4] the latter being inferred from reactivity studies. Recently, on the basis of molybdenum K-edge EXAFS measurements of MoS_3 and $MoS_3 \cdot nH_2O$, Hibble *et al.* have proposed that the layers consist of Mo_2S_9 building blocks linked by vertex or edge-sharing of octahedra (**A**).[5] The molybdenum atoms are in close proximity (2.76 Å), being bridged by both sulfido and disulfide ligands, the overall formulation being described as $Mo(S^{2-})_2(S_2^{2-})_{0.5}$. This then provides an oxidation state of +5 for each metal centre, the observed diamagnetism being ascribed to the presence of a metal–metal bond.



A

† Author to whom correspondence should be addressed.

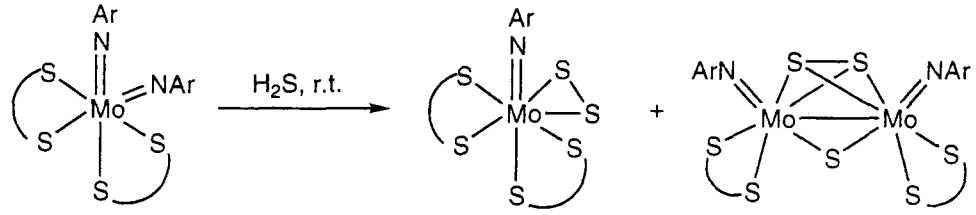
At a molecular level, a large range of sulfur-containing dimolybdenum complexes have been prepared and characterized.[6] For example, addition of sulfur to $[Cp^*Mo(CO)_2]_2$ affords three such complexes, namely $[Cp^*_2Mo_2(\mu\text{-}\eta^2\text{-}\eta^2\text{-}S_2)(S)_2]$, $[Cp^*_2Mo_2(\mu\text{-}\eta^2\text{-}\eta^2\text{-}S_2)(\mu\text{-}S)_2]$ and *trans*-$[Cp^*MoS(\mu\text{-}S)_2]$,[7] while sulfur-rich $[Cp^*_2Mo_2(\eta^2\text{-}S_2)(\mu\text{-}\eta^1\text{-}\eta^1\text{-}S_2)(\mu\text{-}\eta^1\text{-}\eta^1\text{-}S_2)_2]$ has also been prepared.[8] Despite this wide-range of dimolybdenum complexes with a variety of sulfur ligands,[6] as far as we are aware, no molecular dimolybdenum complex has previously been prepared which contains the essential features of the dimolybdenum building blocks proposed by Hibble *et al.*,[5] namely, bridging S^{2-} and $\eta^2\text{-}\eta^2\text{-}S_2^{2-}$ ligands, two molybdenum (V) centres in close proximity and an octahedral coordination geometry at each of these centres.

During recent studies of molybdenum imido complexes we have prepared a number of sulfido-bridged dimolybdenum complexes,[9] together with mononuclear bis(imido) complexes of the type $[Mo(NR)_2(\eta^2\text{-}S_2CNEt_2)_2]$.[10] While carrying out reactivity studies of the latter, we sought to replace one of the imido ligands with a disulfide moiety and found that addition of excess hydrogen sulfide was a successful strategy.[11] In the case of the bulky imido complex $[Mo(N\text{-}2,6\text{-}Pr^i_2C_6H_3)_2(\eta^2\text{-}S_2CNEt_2)_2]$ (**1**), however, as well as isolating high yields of the desired disulfide complex $[Mo(N\text{-}2,6\text{-}Pr^i_2C_6H_3)(\eta^2\text{-}S_2)(\eta^2\text{-}S_2CNEt_2)_2]$ (**2**), a further low-yield dimolybdenum product was isolated which displays *all* of the structural features of the Mo_2S_9 building-blocks proposed by Hibble *et al.*, together with a weak intramolecular

interaction which may model the interactions between chains.

RESULTS AND DISCUSSION

Purging a dichloromethane solution of [Mo(N-2,6-$Pr^i_2C_6H_3$)$_2$(η^2-S_2CNEt_2)$_2$] (**1**) with hydrogen sulfide resulted in a slow reaction over 2 days to afford, after chromatography, the known disulfide complex [Mo(N-2,6-$Pr^i_2C_6H_3$)(η^2-S_2CNEt_2)$_2$] (**2**), 68%,[12] together with the new dimolybdenum complex [Mo_2(N-2,6-$Pr^i_2C_6H_3$)$_2$(η^2-S_2CNEt_2)$_2$(μ-S)(μ-η^2-S_2)] (**3**) in 13% yield. The latter is an air-stable, diamagnetic, pale orange crystalline solid and single crystals were grown upon slow diffusion of methanol into a dichloromethane solution. Characterization was made on the basis of analytical and spectroscopic data, while in order to elucidate the precise nature of the structure a crystallographic study was carried out the results of which are summarized in Fig. 1 and Table 1.



1 **2** **3**

As can be clearly seen, the molecule contains all the essential features of the proposed Mo_2S_9 unit in molybdenum trisulfide. It consists of equivalent molybdenum(V) centres separated by 2.797(2) Å and spanned approximately symmetrically by a sulfido [Mo(1)—S(1) 2.349(3), Mo(2)—S(1) 2.337(3) Å] and somewhat more asymmetrically by a disulfide ligand. Each molybdenum centre also carries both a dithiocarbamate and an imido ligand, such that there is a *cis* relative configuration at adjacent centres. The molybdenum–imido bonds [Mo(1)—N(3) 1.74(1), Mo(2)—N(4) 1.716(9) Å] are within the range associated with molybdenum(V) and molybdenum(VI)[9,13] complexes of this ligand, for example, the molybdenum–nitrogen bond in **2** is 1.734(3) Å.[12] Ignoring the metal–metal bond, the coordination geometry about each molybdenum(V) centre can be described as approximately octahedral, albeit with considerable distortions.

In light of comparisons with molybdenum trisulfide and related compounds, it is worth considering the central core of the molecule in more detail. The two ends of the disulfide ligand have quite different coordination environments. For example, while S(3) lies approximately *trans* to the imido ligands [N(3)—Mo(1)—S(3) 151.5(3), N(4)—Mo(2)—S(3)

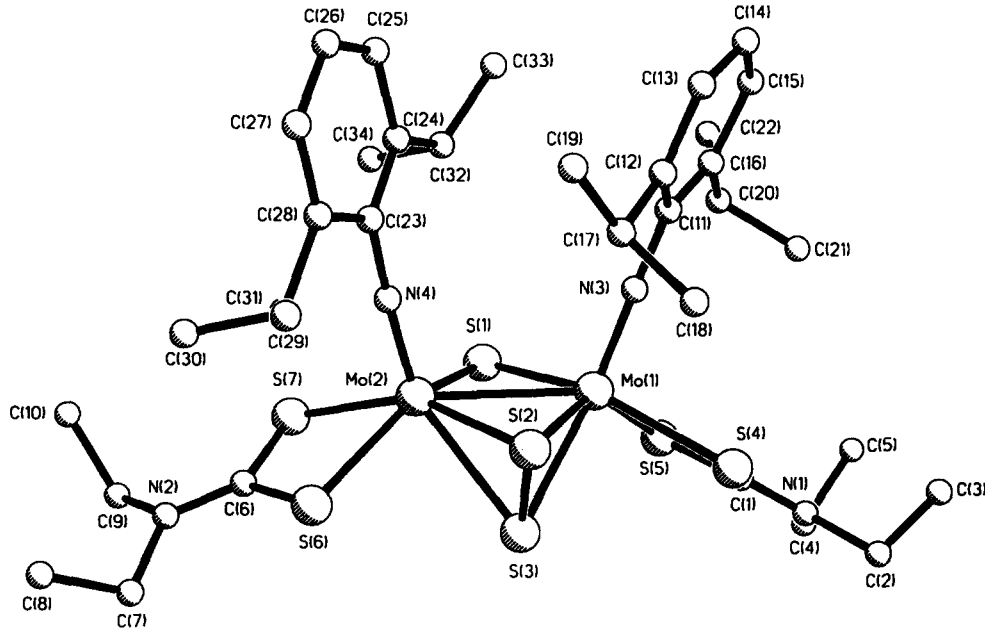


Fig. 1. Molecular structure of **3**.

Table 1. Selected bond lengths (Å) and angles (°) for **3**

Mo(1)—Mo(2)	2.797(2)	Mo(1)—S(1)	2.349(3)
Mo(1)—S(2)	2.370(4)	Mo(1)—S(3)	2.551(5)
Mo(2)—S(1)	2.337(3)	Mo(2)—S(2)	2.383(4)
Mo(2)—S(3)	2.657(5)	Mo(1)—N(3)	1.74 (1)
Mo(2)—N(4)	1.716(9)	S(2)—S(3)	1.936(6)
Mo(1)—S(1)—Mo(2)	73.3(1)	Mo(1)—S(2)—Mo(2)	72.1(1)
Mo(1)—S(3)—Mo(2)	64.9(1)	Mo(1)—N(3)—C(11)	177.0(9)
Mo(2)—N(4)—C(23)	174.4(9)		

145.2(3)°], S(2) is *cis* to both [N(3)—Mo(1)—S(2) 105.4(3), N(4)—Mo(2)—S(2) 100.4(3)°]. A further major difference is their relative orientations with respect to the sulfido-bridge, with S(2) lying approximately in the $Mo_2S(1)$ plane (0.034 Å), while S(3) lies some 2.00 Å from this plane. This difference in sulfur environments is manifested in the very different metal–sulfur bond lengths. Thus, S(2) lies significantly closer to the binuclear metal centre [Mo(1)—S(2) 2.370(4), Mo(2)—S(2) 2.383(4) Å] than S(3) [Mo(1)—S(3) 2.551(5), Mo(2)—S(3) 2.657(5) Å], while the binding of the latter is quite asymmetric. It is interesting to compare this highly asymmetric disulfide unit with respect to the highly symmetric arrangement the same ligand adopts in the molybdenum(IV) dimer $[Cp^*_2Mo_2(\mu\text{-}\eta^2\text{-}\eta^2\text{-}S_2)(\mu\text{-}S)_2]$, where the four molybdenum–sulfur bonds vary only by 0.006 Å (average 2.446 Å).[7] The origin of the pronounced lengthening of the bonds to S(3) is probably the strong *trans* influence of the imido ligands,[13] however, it may in part be due to the *trans* influence of the bridging sulfido ligand. The sulfur–sulfur bond within the disulfide unit of 1.936(6) Å is also elongated somewhat with respect to related dimolybdenum complexes[6] and again is probably also a result of the movement of S(3) away from the binuclear centre. Thus, the central core of **3** closely resembles the proposed Mo_2S_9 layer forming units in molybdenum trisulfide.

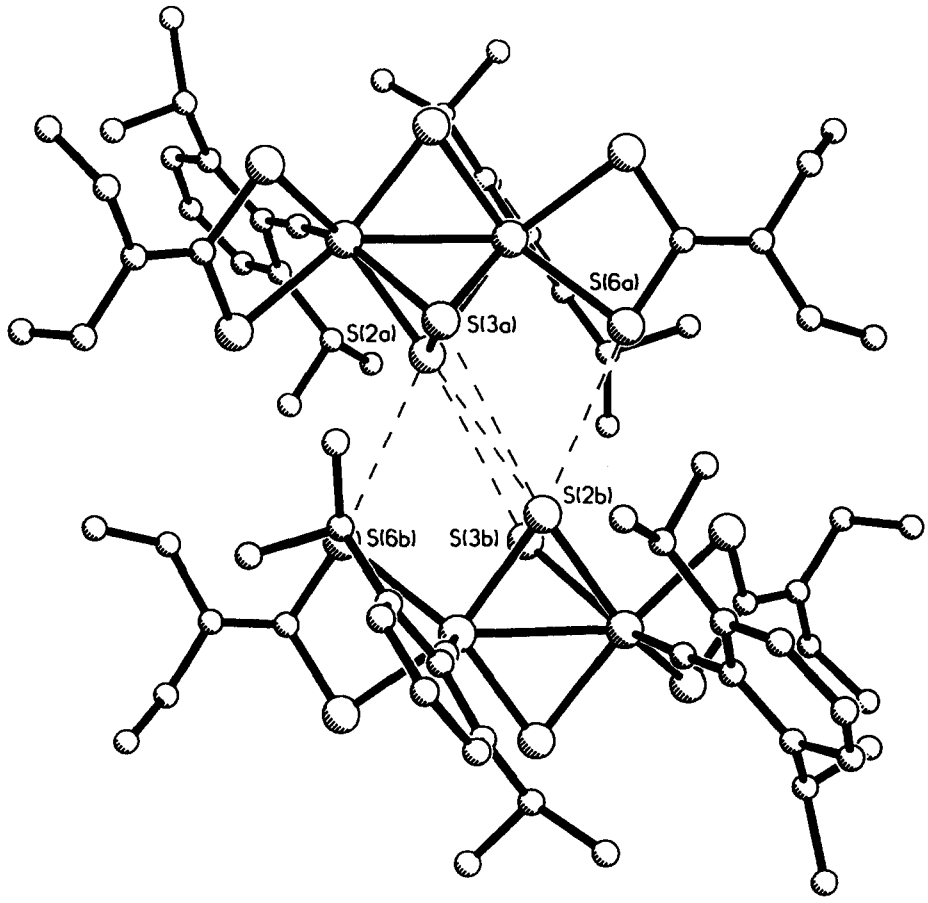


Fig. 2. Part of the packing diagram for **3** showing the association of two dinuclear units.

While these features have not previously been observed at a dimolybdenum centre, a number of complexes have been prepared that are related to **3**. These include the mixed-valence complex $[(Me_2S)_2Cl_2Mo(\mu\text{-}\eta^2\text{-}\eta^2\text{-}S_2)(\mu\text{-}S)MoCl_3(SMe_2)]$[14] and the ditungsten selenide complex $[W_2Cl_8(\mu\text{-}Se)(\mu\text{-}\eta^2\text{-}\eta^2\text{-}Se_2)]^{2-}$,[15] however, in both of these the dichalcogenide bridges the dinuclear centre in an approximately symmetrical manner.

The polymeric chains which are believed to make up the structure of molybdenum trisulfide must be held together via weak long-range interactions. Examination of a packing diagram of **3** reveals the presence of weakly bound dimeric units, as shown in Fig. 2. These are held together primarily by long-range interactions between the disulfide moieties [S(2a)—S(2b) 3.483, S(2a)—S(3b) 3.566 Å] and the disulfide and one of the dithiocarbamate ligands [S(2a)—S(6b) 3.458 Å], the former providing some clue as to the nature of the interchain interactions in molybdenum trisulfide and related chalcogenides.

The mode of formation of **3** is as yet unknown, however, the mononuclear disulfide **2** is not an intermediate. We have previously prepared related dithiocarbamate-stabilized bis(sulfido)-bridged dimolybdenum(V) complexes, which contain a puckered $Mo_2(\mu\text{-}S)_2$ core[9] and the formation of **3** can be envisaged to result from further sulfur addition to the latter, that is at the position occupied by S(3).

Table 2. Crystallographic data for **3**

Formula	$Mo_2C_{34}H_{54}N_4S_7$
Colour	Orange
Crystal size (mm)	$0.42 \times 0.28 \times 0.08$
Crystal system	Monoclinic
Space group	$P2_1/n$
a(Å)	17.824(5)
b(Å)	10.981(4)
c(Å)	22.497(4)
α(°)	90
β(°)	102.72(2)
γ(°)	90
V (Å^3)	4296(2)
Z	4
F(000)	1928
d_{calc}(g cm^{-3})	1.45
μ(Mo-K_α)(cm^{-1})	9.24
Radiation	Mo-K_α(λ = 0.71073)
Orientation reflections: no.; range	25; $16 \leqslant 2\theta \leqslant 26$
Temperature (°C)	19
Data measured	6182
Unique data	5415
No. of unique with $I \geqslant 3.0\sigma(I)$	3489
No. of parameters	442
R^a	0.058
$R_w{}^b$	0.058
Weighting scheme	$w^{-1} = \sigma^2(F) + 0.000381F^2$
Largest shift/e.s.d., final cycle	0.04
Largest peak (eÅ^{-3})	0.70

$^aR = \Sigma[|F_o| - |F_c|]/\Sigma|F_o|$
$^bR_w = \Sigma w^{1/2}[|F_o| - |F_c|]/\Sigma w^{1/2}|F_o|$

EXPERIMENTAL

General procedures[9] and the synthesis of **1**[10] were as previously described.

Synthesis of $[Mo_2(N\text{-}2,6\text{-}Pr^i_2C_6H_3)_2(\mu^2\text{-}S_2CNEt_2)_2(\mu\text{-}S)(\mu\text{-}\eta^2\text{-}\eta^2\text{-}S_2)]$ **(3)**

A dichloromethane (20 cm^3) solution of **1** (0.25 g, 0.34 mmol) was purged with H_2S for approximately 5 min to obtain a saturated solution and then left to stir for 3 days. The solution was purged with nitrogen to remove excess H_2S and the solvent was removed under vacuum. The solid residue was absorbed onto alumina and purified by chromatography on deactivated alumina. Elution with dichloromethane–light petroleum (b.pt 40–60°C) (1:4) afforded a brown band which yielded unreacted **1** (0.06 g); elution with dichloromethane: light petroleum (3:7) afforded an orange band, which yielded **3** (0.04 g, 13%); elution with dichloromethane: light petroleum (2:3) afforded a purple band which yielded **2** (0.11 g, 68%). Recrystallization of **3** was effected upon slow mixing of dichloromethane solutions with methanol. Data for **3**: ^{1}H NMR ($CDCl_3$): δ 6.84 (t, 1H, J = 7.5 Hz), 6.81 (t, 1H, J = 7.5 Hz), 6.72 (d, 2H, J = 7.6 Hz), 6.68 (d, 2H, J = 7.6 Hz), 4.04–3.88 (m, 4H, CH_2), 3.79 (sept, 1H, J = 6.8 Hz, C*H*Me$_2$), 3.66 (sept, 1H, J = 6.8 Hz, C*H*Me$_2$), 3.43–3.29 (m, 4H, CH_2), 1.34–1.28 (tx4, 12H, J = 7.1 Hz, CH_2CH_3), 0.97–0.91 (dx4, 24H, J = 6.8 Hz, CH*Me*$_2$); ^{13}C NMR ($CDCl_3$): δ 207.7, 206.1 (S_2CN), 153.7, 152.1 (*ipso*), 147.9, 146.3 (*o*-C_6H_3), 126.6–121.3 (m, aromatic), 45.7–44.5 (m, CH_2), 28.9–27.4 (m, *C*HMe$_2$), 23.7–23.0 (m, CH*Me*$_2$), 12.9–12.3 (m, CH_2CH_3). We ascribe the complex nature of these spectra to the restricted rotation about the N—C bond of the imido ligands. IR (KBr): 1510m, 1459m, 1438m, 1384m, 1262s, 1096s, 1021s, 803s, 669w, 549w, 468w and 454w cm^{-1}. Found: C, 43.9; H, 5.8; N, 5.7. $C_{34}H_{54}N_4S_7Mo_2$ requires: C, 43.7; H, 5.8; N, 6.0%.

Single-crystal X-ray structure determination of **3**

Intensity data were collected on a crystal of dimensions $0.42 \times 0.28 \times 0.08$ mm mounted on a Nicolet R3mV diffractometer, by the ω scan technique ($5 \leqslant 2\theta \leqslant 45°$). From the 6182 measured data (5415 unique measurements), 3489 with $I \geqslant 3\sigma(I)$ were considered observed. The structure was solved via direct methods and refined by full-matrix least squares to R and R' values of 0.058 and 0.058. Structure solution utilized the SHELXTL PLUS program[16] on a Micro Vax II computer. All non-hydrogen atoms were refined anisotropically. Hydrogen atoms were placed in idealized positions (C—H 0.96 Å) and assigned a common isotropic thermal parameter (U = 0.08 Å^2). Three standards showed no drop in intensity during data collection. A summary of the crystal data, structure solution and refinement parameters is given in

Table 2. Atomic coordinates, thermal parameters and bond lengths and angles have been deposited at the Cambridge Crystallographic Data Centre.

Acknowledgements—We thank the EPSRC for the provision of a studentship to T.A.C.

REFERENCES

1. J. W. Mellor, *A Comprehensive Treatise on Inorganic and Theoretical Chemistry*, Vol. 11, p. 1437, Longman, London (1931).
2. S. P. Cramer, K. S. Liang, A. J. Jacobson, C. H. Chang and R. R. Chianelli, *Inorg. Chem.* 1984, **23**, 1215.
3. F. Z. Chien, S. C. Moss, K. S. Liang and R. R. Chianelli, *Phys. Rev.* 1984, **B29**, 4606.
4. A. Müller, V. Fedin, K. Hegetschweiler and W. Amrein, *J. Chem. Soc., Chem. Commun.* 1992, 1795.
5. S. J. Hibble, D. A. Rice, D. M. Pickup and M. P. Beer, *Inorg. Chem.* 1995, **34**, 5109.
6. T. Shibahara, *Coord. Chem. Rev.* 1993, **123**, 73.
7. H. Brunner, W. Meier, J. Wachter, E. Guggoiz, T. Zahn and M. L. Zeigler, *Organometallics* 1982, **1**, 1107.
8. M. Rakowski DuBois, D. L. DuBois, M. C. VanDerveer and R. C. Haltiwanger, *Inorg. Chem.* 1981, **20**, 3064.
9. T. A. Coffey, G. D. Forster and G. Hogarth, *J. Chem. Soc., Dalton Trans.* 1995, 2337.
10. T. A. Coffey, G. D. Forster, G. Hogarth and A. Sella, *Polyhedron* 1993, **12**, 2741; T. A. Coffey, G. D. Forster and G. Hogarth, unpublished results.
11. T. A. Coffey and G. Hogarth, unpublished results.
12. T. A. Coffey, G. D. Forster and G. Hogarth, *J. Chem. Soc., Chem. Commun.* 1993, 1524; T. A. Coffey, G. D. Forster and G. Hogarth, *J. Chem. Soc., Dalton Trans.* 1996, 183.
13. W. A. Nugent and J. M. Mayer, *Metal–Ligand Multiple Bonds*, Wiley, New York (1988).
14. D. L. Hughes, J. D. Lane, R. L. Richards and C. Shortman, *J. Chem. Soc., Dalton Trans.* 1994, 621.
15. M. G. B. Drew, G. W. A. Fowles, E. M. Page and D. A. Rice, *J. Am. Chem. Soc.* 1979, **101**, 5827.
16. G. M. Sheldrick, SHELXTL-PLUS, *Program Package for Structure Solution and Refinement*, Version 4.2. Siemens Analytical Instruments Inc., Madison, Wisconsin (1990).

Pergamon

S0277-5387(96)00229-X

Polyhedron Vol. 16, No. 1, pp. 171–177, 1997
Copyright © 1996 Elsevier Science Ltd
Printed in Great Britain. All rights reserved
0277-5387/97 $15.00+0.00

Thermal behaviour of heterobimetallic compounds of the type $dppfMCl_2$ [dppf = 1,1-bis(diphenylphosphino)ferrocene and M = Ni, Pd, Pt] in an oxidizing atmosphere and characterization of the final decomposition products

O. L. Casagrande Jr,* A. E. Gerbase, F. C. Stedile and F. O. V. da Cunha

Grupo de Catálise, Instituto de Química, UFRGS, Av. Bento Gonçalves, 9500, 91501–970 Porto Alegre, RS, Brazil

and

L. Amaral and I. J. R. Baumvol

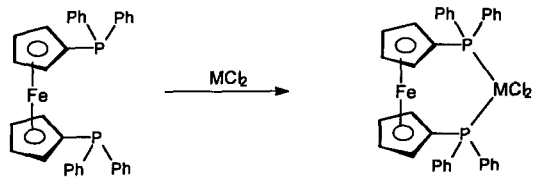
Instituto de Física, UFRGS, Av. Bento Gonçalves, 9500, 91501–970 Porto Alegre, RS, Brazil

(Received 31 January 1996; accepted 10 April 1996)

Abstract—The thermal behaviour of dppf [dppf = 1,1bis(diphenylphosphino)ferrocene] and $dppfMCl_2$ [M = Ni, Pd, Pt] in dry air has been investigated by thermal analysis and the final decomposition products were characterized by Rutherford backscattering spectrometry, infrared spectroscopy, Mössbauer spectroscopy and X-ray powder diffractometry. Thermal decomposition mechanisms, the thermal stability as well as the composition and final residues are influenced by the MCl_2 fragments. The thermal stability decreases in the order dppf > $dppfNiCl_2$ > $dppfPtCl_2$ > $dppfPdCl_2$. The analysis of the RBS spectra of the final decomposition products shows that the phosphorus atoms are not lost during the heating, while all the chlorine has evolved as Cl_2 gas. The Mössbauer and X-ray results show the formation of several iron phosphates besides nickel metaphosphate, nickel oxide, metallic Pd and Pt. Copyright © 1996 Elsevier Science Ltd

The chemistry of organometallic compounds represents an important branch of chemistry, particularly because of the use of these compounds as homogeneous catalysts[1] and as precursors to heterogeneous catalysts.[2] The heterogeneous catalysts are used in various important catalytic reactions such as oxidation,[3] metathesis,[4] olefin polymerization[5] and hydrogenation.[6] In particular, heterogeneous catalysts containing metallic Pd, Pt or NiO have received special attention, for example, in the oxidation of carbon monoxide,[7] naphtha reforming,[8] paraffin dehydrogenation[8] and conversion of benzoic acid to phenol.[9] However, the heterogeneous catalytic systems present some disadvantages related essentially with regio- and stereo-selectivity and for these reasons several trials to develop synthetic routes to prepare compounds that present higher selectivity and activity have been performed.[10] Among the synthetic routes used, one process resides in the thermal decomposition of organometallic compounds. For that, thermal analysis has become in recent years an important tool for providing information about the thermal decomposition mechanism and for the production of heterogenous materials which can be used as catalysts.[11] The use of heterobimetallic compounds as precursors to obtain new heterogeneous materials seems to be very attractive since they have two different metallic species not

* Author to whom correspondence should be addressed.



1

2 : M = Ni
3 : M = Pd
4 : M = Pt

Scheme 1.

directly bonded but close enough to interact and produce synergic effects which can result in interesting catalytic properties.

In this context, the present work reports on the thermal behaviour of heterobimetallic compounds of the type $dppfMCl_2$ [dppf = 1,1-bis(diphenylphosphino) ferrocene and M = Ni, Pd, Pt] (see Scheme 1) and the characterization of the final decomposition products by Rutherford backscattering spectrometry, infrared spectroscopy, Mössbauer spectroscopy and X-ray powder diffractometry.

EXPERIMENTAL

Starting materials and instrumental

All the syntheses were carried out under purified argon in a Schlenk apparatus. Solvents were purified and dried by specific methods.[12] $PdCl_2$, $PtCl_2$, $NiCl_2 \cdot 6H_2O$ and dppf were purchased from Aldrich Chemicals and used without further purification. The compounds $dppfMCl_2$ [dppf = 1,1-bis(diphenylphosphino)ferrocene and M = Ni,Pd,Pt] were prepared by methods described in the literature.[13–15]

Thermogravimetric analysis

Thermogravimetric analyses (TG) were carried out under dynamic flow of dry synthetic air (25 cm^3 min^{-1}) and a heating rate of 20°C.min^{-1} using a TGS-2 Perkin–Elmer Thermoanalyser.

Rutherford backscattering spectrometry

The Rutherford Backscattering Spectrometry (RBS) spectra were obtained using the 4 MV Van de Graaff Accelerator of the Physics Department, at PUC-RJ, in Rio de Janeiro. The principle of RBS was presented in ref. 16. The calculations of the stoichiometric ratios of the decomposition products were performed using the full expression for the differential scattering cross-section.[16] The errors involved in the detection, counting and calculation of the stoichiometric ratios lead to an overall error of 10%.

Infrared spectrometry

Infrared spectra (IR) were recorded on a Mattson 3020 FTIR spectrophotometer in the range 4000–400 cm^{-1} with the samples in the form of potassium bromide pellets at room temperature.

Mössbauer spectroscopy

The Mössbauer spectra were recorded at room temperature on a conventional constant acceleration Mössbauer spectrometer using the standard transmission geometry. The employed source was ^{57}Co in a rhodium matrix. The experimental data were fitted by simple least-squares procedures in a IBM/PC® compatible microcomputer, using special software.[17] Typical errors for the Mössbauer areal fraction are smaller than 3%.

X-ray diffractometry

X-ray diffractograms were obtained with a Kristalloflex 810 Siemens diffractometer with a step $2\theta = 0.05°$ and using Cu K_α radiation (1.542 Å). The peaks were identified using the ASTM data cards.[18]

RESULTS AND DISCUSSION

Organometallic compounds decompose when submitted to high temperatures, usually generating as final products metallic oxides, pure metal particles or inorganic salts. The composition of the final products, however, depend on several variables such as the decomposition atmosphere (oxidising, reducing or inert), the heating rate, the organic ligands and metal centers present in the organometallic compounds. In the present work, the thermal decomposition of dppf and some of its derivatives containing group 10 metals was performed. The purpose of this study was, on the one hand, to reveal the influence of the MCl_2 moiety (M = Ni, Pd, Pt) on the initial decomposition temperature of the precursors using thermogravimetric analysis and, on the other hand, to characterize the final decomposition products using several techniques (RBS, IR, Mössbauer spectroscopy and X-ray diffractometry). The results obtained and some discussion based on them will be presented hereafter.

Thermogravimetric analysis

The TG curves of the compounds **1–4** performed under dry synthetic air are shown in Fig. 1, while their corresponding data are displayed in Table 1.

The decomposition of **1** starts above 376°C with an abrupt mass loss. The TG curve shows two steps in the temperature range 376–788°C which were attributed to the pyrolysis and oxidation of the phosphorus ligands. The final deep grey residue was identified as a mixture of compounds formed mainly

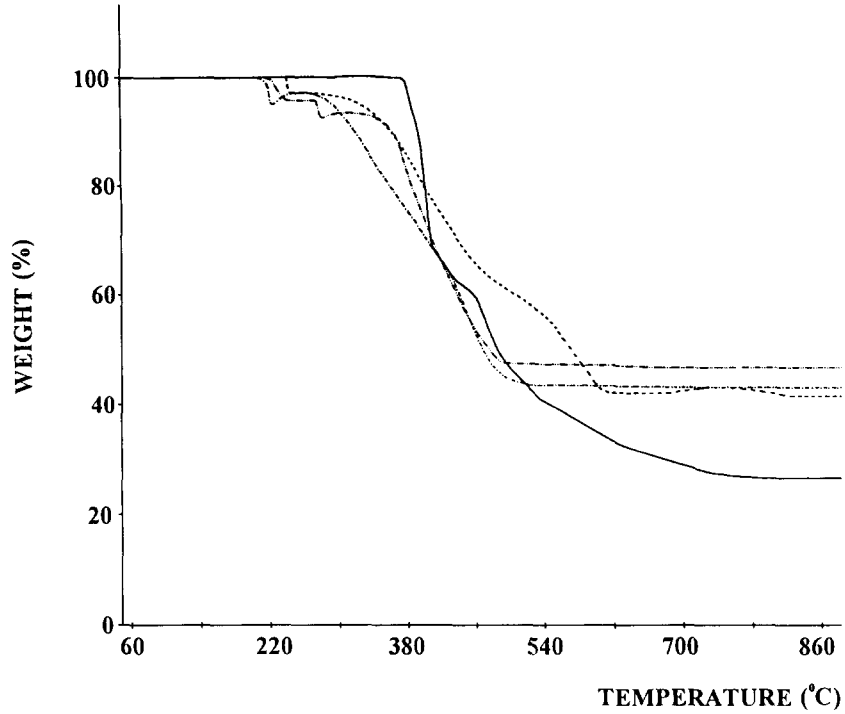


Fig. 1 TG curve of dppf (—), dppfNiCl$_2$ (– – –), dppfPdCl$_2$ (– · – · –) and dppfPtCl$_2$ (– · · – · · –) in dry air.

Table 1. Thermal analysis data for compounds **1–4**

Compound	Step	T_i (°C)	T_f (°C)	Δm (%)
dppf	1	376	458	40.90
	2	458	788	32.90
				(73.80)
dppfNiCl$_2$	1	240	246	2.22
	2	246	460	30.67
	3	460	543	7.55
	4	543	606	13.33
				(53.77)
dppfPdCl$_2$	1	215	224	4.44
	2	224	242	−2.22
	3	268	486	51.11
				(53.33)
dppfPtCl$_2$	1	220	239	3.73
	2	274	279	3.46
	3	279	300	−0.88
	4	322	487	45.33
				(51.64)

T_i = initial temperature; T_f = final temperature; Δm = mass variation; Total percentual mass losses are showed in parentheses for each compound.

by iron phosphates (see Mössbauer and X-ray results).

The TG curve of **2** shows that its thermal degradation starts above 240°C. The first decomposition step suggests, by mass calculation, the loss of Cl_2 and the uptake of O_2. This first step is followed by mass losses associated with the combustion of the organic ligands. In the range 685–819°C a small mass gain is observed, probably due to the sample oxidation, followed by an additional small mass loss attributed to the conversion of these compounds into less oxygenated ones. A constant mass was reached at 819°C and the pale yellow residue was identified as a mixture of iron and nickel phosphates and nickel oxide (see Mössbauer and X-ray results).

The thermal decomposition of **3** starts at 215°C with a mass loss attributable to, as observed for **2**, the loss of Cl_2 and the uptake of O_2. In the second step (224–242°C) a consumption of O_2, associated with a mass gain occurs, followed by a third step associated with the pyrolysis of the organic ligands. A constant mass was reached at 486°C and the deep grey residue was identified as a mixture of Pd(0) and iron phosphates (see Mössbauer and X-ray results).

The TG curve of compound **4** shows that its thermal degradation starts above 220°C. At somewhat higher temperatures, two steps probably associated with the loss of chlorine and the uptake of O_2 take place. Between 322 and 487°C, a mass loss occurs which was attributed to the pyrolysis and breakdown of the $CpPPh_2$ fragments. A constant mass was reached at 487°C and the final grey residue was identified as a mixture of Pt(0) and iron phosphates (see Mössbauer and X-ray results).

Summarizing the above results it was seen that the complexes **2–4** liberate Cl_2 at the beginning of the decomposition process. All complexes are oxidized but the thermal processes themselves and the composition of the final residues are influenced by the nature of the group 10 metal. The initial decomposition temperatures of **2–4** are lower than that of its

precursor **1**, probably due to the coordination of metallic centres to organic ligands, *via* the formation of M–P bonds (see Scheme 1), destabilizing the heterobimetallic compounds. A thermal destabilization was also seen to occur when sulfur or oxygen were bonded to $CpPPh_2$ fragments.[19]

RBS spectra

RBS was used to determine the stoichiometric ratio among the various elements of the samples after their thermal decomposition. The RBS spectra were obtained using α-particle beams and the geometry described in the caption of Fig. 2, which is sketched in the top of this figure. The samples were homogeneous tablets made from a randomly oriented powder of the thermal decomposition products with a certain amount of BN, used as an inert load. The spectrum of the decomposition products of dppf is shown in Fig. 2a, while in Fig. 2b is shown the spectrum of the decomposition products of $dppfPdCl_2$. From the relative intensities of the signals, the atomic ratio between two given elements could be calculated. The main results obtained from the analysis of the spectra were: (i) P was not lost during the thermal decomposition process. The P/Fe ratio in the case of the compounds **1**, **3** and **4** remained equal to 2 before and after decomposition. In the case of $dppfNiCl_2$ a ratio P/(Fe+Ni) = 1 was found. In this last case a direct P/Fe ratio could not be determined. Ni and Fe have very similar masses and, for that, their signals cannot be resolved by RBS even at 2 MeV (the greater the incident energy the greater will be the mass resolution) and in the spectrum they appear superimposed. However, if the assumption that Fe/Ni = 1 is considered (Fe/Pd and Fe/Pt ratios equal to 1 were found for the other compounds), a P/Fe = 2 will be found, meaning that neither Ni nor P are lost during the thermal

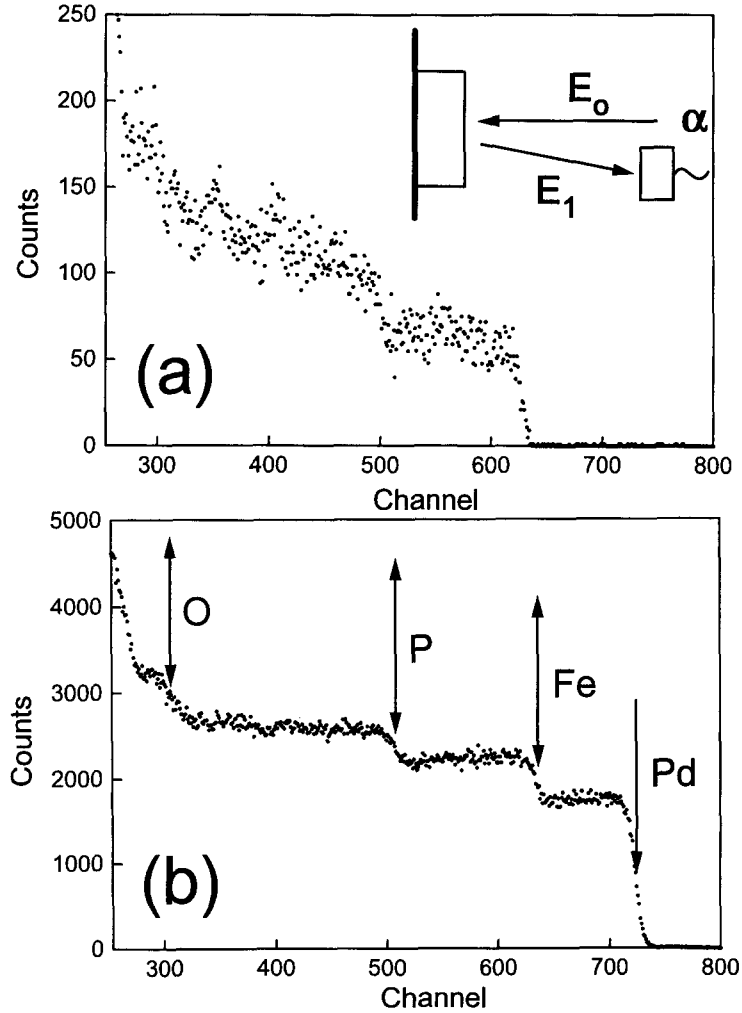


Fig. 2 Rutherford Backscattering spectra obtained from the final decomposition products of dppf (a) and $dppfPdCl_2$ (b). The energy of the incident α-particle beam was 2.0 MeV. The incidence angle was 0° with the sample normal, and the detection angle was 165° with respect to the incidence direction of the beam. A scheme of this geometry, showing also the sample and the detector, is sketched in the top of Fig. 2a. The arrows in spectrum 2b indicate the outermost position of the respective elements in the samples.

decomposition process; (ii) A great amount of O, an element that was not present in the molecules before thermal treatment, was found in the samples after it. The ratio O/Fe varied from sample to sample, indicating the presence of different oxygenated compounds. Nevertheless, the O/P ratio was found to be between **4** and **5** in all cases, indicating the presence of, for example, a phosphate (PO_4) and an oxide. These results were confirmed by Mössbauer spectroscopy and X-ray diffractometry (see other results below); (iii) The amount of C was seen to remain roughly (the C signal was somewhat hidden by the N signal coming from the BN) about 60% in the case of the dppf decomposed sample but in a much smaller amount, around 30%, in the case of the bimetallic samples; (iv) Cl must have been almost or completely transformed into a gas, since in the RBS spectra no traces of it were found. This fact coincides with the observation from the TG that during the first heating steps Cl_2 was released.

Infrared spectra

The IR spectra of the final decomposition compounds are very similar. In the range 3100–2990 cm^{-1}, no stretching bands corresponding to $\nu_{C\,H}$ were observed, indicating that the organic molecules were decomposed during the heating process, as expected. Several strong superimposed bands were found, however, in the region of 1350–900 cm^{-1}, which were attributed to the $\nu_{P\,O}$ modes[20] and indicate the formation of phosphates. These results agree with those obtained from RBS spectra and also with those from Mössbauer spectroscopy and X-ray diffraction which will be presented below.

Mössbauer spectra

The Mössbauer spectrum of the decomposition products of dppf (Fig. 3A) could be fitted with four doublets corresponding to two Fe^{2+} sites (I and II), and two Fe^{3+} sites (III and IV) (see Table 2). The site I was assigned to $Fe_3(PO_4)_2$[21] while the site II could not be assigned to any particular compound, but its large δ and Δ characterizes an Fe^{2+} compound. The two Fe^{3+} compounds have parameters very close to the ones observed for iron (III) phosphates.[21–23] From this fitting, a $Fe^{2+}:Fe^{3+}$ proportion of 58:42 was found. Looking closer at this Mössbauer spectrum it is evident that other iron compounds are present that were not identified but the presence of iron carbides, α-FeOOH and Fe_2O_3 was ruled out.[21,24–25]

The Mössbauer spectrum of the decomposition products of **2** (Fig. 3B) could be fitted with three sites (V, VI, and VII in Table 2). Site V corresponds to an Fe^{2+} compound present in a small amount (4%). Sites VI and VII have hyperfine parameters characteristic of Fe^{3+} compounds which are very close to the ones observed for iron phosphates.[21–23] These compounds correspond to 96% of the total amount of iron present

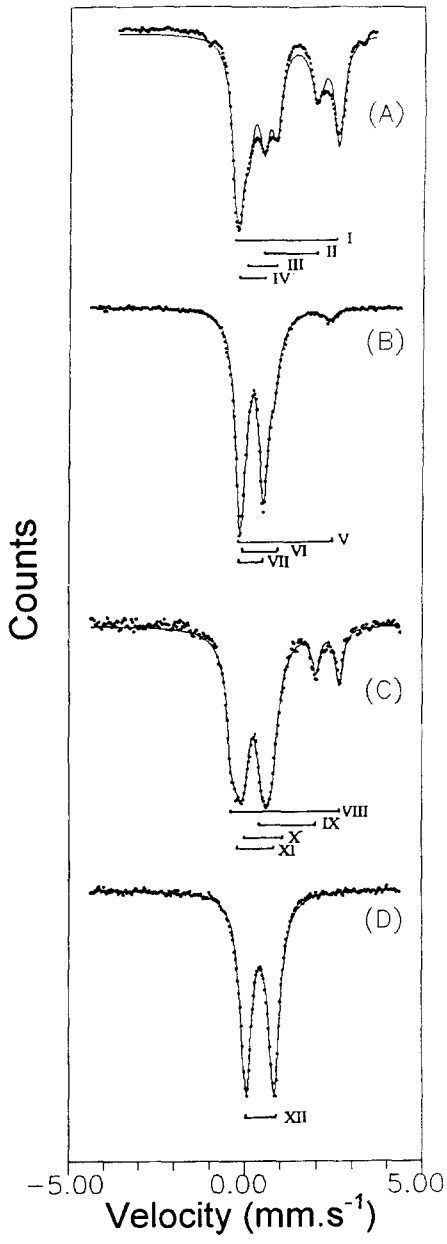


Fig. 3. Mössbauer spectra of the final decomposition products of compounds **1**–**4**: (A) dppf; (B) dppfNiCl_2; (C) dppfPdCl_2; (D) dppfPtCl_2.

in the sample. The presence of the magnetic compound $NiFe_2O_4$ in the final decomposition residue of **2** could be excluded since there is no evidence of the presence of any magnetic compound even in a Mössbauer spectrum obtained with a maximum velocity of 12.25 mm/s.[26]

The Mössbauer spectrum of the decomposition products of **3** (Fig. 3C) shows, as in the case of complex **2**, that a high proportion of Fe^{3+} compounds is present in the sample ($Fe^{2+}:Fe^{3+}$ = 23:77). The data could be well fitted with four doublets, two corresponding to Fe^{2+} compounds (VIII and IX in Table

Table 2. Mössbauer parameters for final decomposition products

Decomposition products of	Site	Proportion (%)	Oxidation state	δ (mm/s)	Δ (mm/s)	Γ (mm/s)
dppf	I	34	Fe^{2+}	1.23	2.88	0.33
	II	24	Fe^{2+}	1.31	1.50	0.42
	III	30	Fe^{3+}	0.54	0.78	0.33
	IV	12	Fe^{3+}	0.28	0.66	0.26
$dppfNiCl_2$	V	4	Fe^{2+}	1.24	2.45	0.34
	VI	24	Fe^{3+}	0.49	0.84	0.37
	VII	72	Fe^{3+}	0.28	0.67	0.32
$dppfPdCl_2$	VIII	13	Fe^{2+}	1.24	3.02	0.26
	IX	10	Fe^{2+}	1.33	1.51	0.27
	X	41	Fe^{3+}	0.48	0.80	0.46
	XI	36	Fe^{3+}	0.28	0.80	0.45
$dppfPtCl_2$	XII	100	Fe^{3+}	0.55	0.78	0.39

δ = Isomer shift referred to metallic iron at room temperature (zero shift); Δ = Quadrupole splitting; Γ = Linewidth. Typical standard deviations of these parameters were 0.01 mm/s.

2) and two having hyperfine parameters characteristic of Fe^{3+} compounds (X and XI).

The Mössbauer spectrum of the decomposition products of complex **4** (Fig. 3D) was the simplest one. It shows the presence of only one doublet (site XII in Table 2) whose hyperfine parameters are characteristic of an Fe^{3+} compound. Since only iron(III) metaphosphate was identified in the X-ray diffractogram (see below), the doublet was assigned to this compound.

The above results show a great tendency to the dppf and its derivatives, when submitted to thermal treatment under specific conditions (see experimental section), to form various iron phosphates. It is interesting to note that another iron phosphine derivative, $[Fe(CO)_3(PPh_3)_3]$, when submitted to thermal decomposition under the same conditions, produced only $FePO_4$ and Fe_2O_3.[27] These results indicate that the organic ligands present in the organometallic compound influence its thermal behaviour and the composition of the final products after thermal treatment.

The Mössbauer results also show that the presence of a second transition metal coordinated to dppf decreased the Fe^{2+}/Fe^{3+} ratio. In the case of the thermal decomposition of **4**, an extreme case was reached where 100% of Fe^{3+} was found.

The Mössbauer spectroscopy is a useful technique to characterize the final decomposition products. However, it is limited in the sense that, in the present work, only iron compounds can be detected by it. In order to have a more thorough idea of all the present compounds, a complementary technique had to be used. In the present case, X-ray diffraction was chosen to further clarify the decomposition process products.

X-ray diffractograms

The X-ray diffractogram of the decomposition products of **1** (Fig. 4A) was a very complex one. However, compounds such as iron(II) pyrophosphate, $Fe_4(P_2O_7)$ (ASTM card file 24-526),[17]

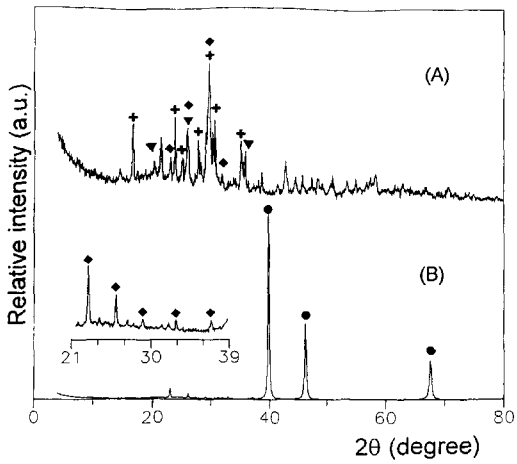


Fig. 4. X-ray diffractograms of the final decomposition products of the compounds: (A) dppf and (B) $dppfPtCl_2$. The crystalline phases identified in the samples are: (◆) $Fe(PO_3)_3$; (●) Pt; (▼) $FePO_4$; (+) $Fe_4(P_2O_7)$.

iron(III) metaphosphate, $Fe(PO_3)_3$ (ASTM 7-184)[17] and iron(III) phosphate, $FePO_4$ quartz like phase (ASTM card file 17-837)[17] could be identified. The peaks of the $Fe_3(PO_4)_2$, if present were hidden by the amorphous baseline or by other peaks. This amorphous feature was partially assigned to the formation of amorphous carbon, since the RBS spectrum indicated a high amount of carbon and neither iron carbonates nor iron carbides were identified in the Mössbauer spectrum. There was also no evidence of the presence of iron oxides, at least as major products.

In the X-ray diffractograms of the final decomposition products of the heterobimetallic compounds, the decrease in the number of phases present was noticeable. In the diffractogram of the final decomposition products of **2** it was possible to assign peaks to the presence of NiO (ASTM card file 22-1189)[17], $Ni(PO_3)_3$ (ASTM card file 28-708)[17] and $FePO_4$ quartz like phase (ASTM card file 17-837), while in the case

of the final decomposition products of **3**, the X-ray diffractogram showed the formation of metallic palladium (ASTM card file 5-0686)[17] as the major product, besides other iron compounds such as $Fe(PO_3)_3$. The presence of palladium oxide was expected thermodynamically ($\Delta H_f^0 = -20\,kcal/mol$; $T_{decomp} = 877°C$) during the thermal treatment of **3** under an oxidizing atmosphere. Nevertheless the presence of PdO in the final decomposition product was ruled out, suggesting that the presence of the iron atom in the organometallic compound makes the reduction of the Pd atom easier. This unexpected behaviour contrasts with the results obtained from the thermal decomposition of other palladium complexes, which do not contain iron and produce palladium oxide as the major product.[28-29] It must be mentioned that due to the complexity of the decomposition products diffractograms of the Ni and Pd bimetallic compounds some peaks could not be assigned to any of the probable phases in the JCPDS files. On the other hand, the final decomposition products of **4** (Fig. 4B) were fully identified. The X-ray diffractogram showed the presence of metallic platinum (ASTM card file 4-802)[17] and $Fe(PO_3)_3$ (ASTM 7-184). Platinum oxide was not observed, as expected from its thermodynamic data ($\Delta H_f^0 = 41\,kcal/mol$; $T_{decomp} = 507°C$).

In conclusion, the results of the present work have demonstrated that the coordination of the group 10 metals of dppf promotes the thermal destabilization of the heterobimetallic complexes. The final decomposition products consist on a mixture of inorganic compounds, containing O and P but not Cl. Their composition and proportion depend on the MCl_2 moiety. It was also seen that the presence of the second transition metal coordinated to dppf promotes the formation of the Fe phosphates in their higher oxidised state (Fe^{3+}). Current studies are under way to investigate the thermal decomposition of other organometallic compounds and the catalytic application of their final decomposition products.

Acknowledgement—This work was supported in part by CNPq, FAPERGS and FINEP (Brazil).

REFERENCES

1. G. W. Parshall and S. D. Ittel (Eds), *Homogeneous Catalysts*. John Wiley, New York (1992); J. A. Moulijn, P. W. N. M. van Leeuwen and R. A. van Santen (Eds), *Catalysts*, Vol. 79, Elsevier Science, Amsterdam (1993).
2. *Catalysts by Supported Complexes* (Edited by Y. I. Yermakov, B. N. Kuznetsov and V. A. Zalcharov), Elsevier Science Publishers, Amsterdam (1981); D. C. Bailey and S. H. Langer, *Chem. Rev.* 1981, **81**, 109.
3. R. A. van Santen, and H. P. C. E. Kuipers, *Adv. Catal.* 1987, **35**, 265.
4. W. A. Hermann, W. Wagner, U. N. Flessner, V. Volkhardt and H. Komber, *Angew. Chem. Int. Ed. Engl.* 1991, **30**, 1636.
5. M. P. McDaniel, *Adv. Catal.* 1985, **33**, 47; F. J. Karol, *Catal. Rev.-Sci. Eng.* 1984, **26**, 557.
6. P. Rylander, *Catalytic Hydrogenation in Organic Syntheses*. Academic Press, London (1979).
7. S. Imamura, Y. Tsuji, Y. Miyake and T. Ito, *J. Catal.* 1995, **151**, 279; Y. F. Yu Yao, *J. Catal.* 1984, **87**, 152.
8. E. E. Davies, J. S. Elkins and R. Ch. Pitkethly, *US Patent* 3,759,823 1971; F. M. Dautzenberg, *German Offen.* 2,121,765 (1971); F. C. Wilhelm (UOP) *US Patent* 3,844,938. (1974); S. M. Davis, F. Zaera and G. A. Somorjai, *J. Catal.* 1982, **77**, 439.
9. J. Miki, M. Asanuma, Y. Tachibana and T. Shikada, *J. Catal.* 1995, **151**, 323.
10. G. A. Somorjai, *Introduction to Surface Chemistry and Catalysis*, Ch. 7, pp. 400–595, John Wiley, New York (1994).
11. P. A. Chaloner, *Coord. Chem. Rev.* 1990, **101**, 1.
12. R. M. V. Assumpção and T. Morita (Eds), *Manual de Soluções, Reagentes e Solventes*, Edgar Buncher, São Paulo (1968).
13. I. R. Butler, W. R. Cullen, T. J. Kim, S. J. Rettig and J. Trotter, *Organometallics* 1985, **4**, 972.
14. B. Corain, B. Longato, G. Favero, D. Ajò, U. Russo and F. R. Kreissl, *Inorg. Chim. Acta* 1989, **157**, 259.
15. D. A. Clemente, G. Pilloni,. B. Corain, B. Longato and M. Tripicchio-Camellini, *Inorg. Chim. Acta* 1986, **115**, L9.
16. W. K. Chu, J. W. Mayer and M. A. Nicolet (Eds), *Backscattering Spectrometry*. Academic Press, New York (1963); W. K. Chu, J. W. Mayer , M. A. Nicolet, T. M. Buck, G. Amsel and F. Esien, *Thin Solid Film* 1973, **17**, 1.
17. *Notes from the Mössbauer Laboratory*, Physics Institute of Federal University of Rio Grande do Sul, Porto Alegre (1984).
18. *Powder Diffraction File of the Joint Committee on Power Diffraction Standards*, International Center of Diffraction Data, Swarthmore, PA 19081 (1982).
19. T. S. Andy Hor, Z.-G. Fang, Y.-S. Wen, L.-K. Liu and T. C. W. Mark, *Polyhedron* 1995, **14**, 2403.
20. K. Nakamoto, *Infrared and Raman Spectra of Inorganic and Coordination Compounds*, Third Edition, John Wiley, New York (1978).
21. E. Fluck, W. Kerler and W. Neuwirth, *Angew. Chem. Int. Ed. Engl.* 1963, **2**, 277.
22. I. N. Rabinowitz, F. F. Davis and R. H. Herber, *J. Am. Chem. Soc.* 1966, **88**, 4346.
23. A. R. Champion, R. W. Vaughan and H. G. Drickamer, *J. Chem. Phys.* 1967, **467**, 2583.
24. I. M. Baibich, A. E. Gerbase, R. G. da Rosa, L. Amaral and A. Vasquez, *Spectrochim. Acta* Part A 1989, **45**, 933.
25. G. B. Raupp and W. N. Delgass, *J. Catal.* 1979, **58**, 348.
26. D. Kedem and T. Rothem, *Phys. Rev. Lett.* 1967, **18**, 165.
27. O. L. Casagrande Jr, *Ph.D thesis*, Universidade Estadual Paulista-UNESP (1991).
28. P. Román, J. I. Beitia, A. Luque and C. Guzmán-Miralles, *Polyhedron* 1994, **13**, 2819.
29. O. L. Casagrande Jr and J. Dupont, unpublished results.

Pergamon

S0277-5387(96)00230-6

Polyhedron Vol. 16, No. 1, pp. 179–185, 1997
Copyright © 1996 Elsevier Science Ltd
Printed in Great Britain. All rights reserved
0277-5387/97 $15.00+0.00

Crystal structure and properties of the nickel(II) complex of a dioxo[13]aneN$_4$ ligand bearing quinoline pendants. Striking differences between the nickel(II) and copper(II) analogues of (dioxo[13]aneN$_4$ = 1,4,7,10-tetraazacyclotridecane-11,13-dione)

Xian He Bu, Dao Li An, Zhi Ang Zhu* and Yun Ti Chen

Department of Chemistry, Nankai University, Tianjin 300071, P.R. China

and

M. Shionoya and E. Kimura

Department of Medicinal Chemistry, School of Medicine, Hiroshima University, Hiroshima 734, Japan

(Received 8 January 1996; accepted 10 April 1996)

Abstract—The Ni(II) complex of dioxo[13]aneN$_4$ ligand bearing two 8-methylquinoline as additional donor pendants (H_2L) has been prepared and its crystal structure and properties studied. The Ni^{II} atom is in square-planar coordination whilst the two 8-methylquinoline pendants are not coordinated. In contrast, in the Cu(II) analogue CuL(2), the Cu(II) atom is five coordinate and forms a distorted square-pyramidal configuration with one of the quinoline pendants coordinated. Electrochemical studies of 1 in aqueous solution revealed that L can further stabilize the trivalent state of nickel [$E_{1/2}(+2 \rightarrow +3) = 0.60$ V versus SCE] compared with unsubstituted L° [$E_{1/2}(+2 \rightarrow +3) = 0.92$ V versus SCE]. This behaviour is also in contrast with that observed for CuL under the same conditions. An unusual red-shift was observed for the maximum absorption band of the electronic spectrum of NiL in comparison to that of NiL°. Copyright © 1996 Elsevier Science Ltd

Keywords: crystal structure; electrochemical; nickel complex; dioxo[13]aneN$_4$; 8-methylquinoline.

The chemistry of macrocyclic dioxotetraamines has attracted much interest and has been extensively studied in recent years.[1–5] Such compounds are unique chelators for some transition metal ions, *eg.*, they can selectively coordinate Cu^{2+}, Ni^{2+}, Co^{2+}, Pt^{2+}, etc., with simultaneous dissociation of two protons from the amido groups, giving neutral complexes designated as MLH_{-2}.[1,2] They bear the dual features of macrocyclic tetraamines and oligo-peptides, and have many interesting functions and biological relevance.[1,4] Their transition metal complexes have shown some interesting properties and function as important models for metalloproteins and oxygen carriers.[4] Macrocyclic oxotetraamines can stabilize the trivalent state of Cu and Ni in aqueous solution,[5] and may be used as effective oxidants and redox catalysts.[6] Such compounds can also serve as models for galactose oxidase.[7] Furthermore, some of these compounds may function as powerful chelating agents.[8]

However, up to now, most of the reported studies have been concerned with their chemistry in solution since it is difficult to obtain single crystals of macrocyclic dioxotetraamine complexes for structural studies.[9] Herein, we report the crystal structure and

* Author to whom correspondence should be addressed.

properties of the nickel complex of a dioxo[13]aneN$_4$ (dioxo[13]aneN$_4$ = 1,4,7,10 - tetraazacyclotridecane-11,13-dione) ligand bearing two 8-methylquinoline as additional donor pendants (Scheme 1). Striking differences have been found to exist between the nickel and copper complexes of this ligand. To our knowledge, this is the first example of the crystal structure for the nickel complex with dioxo[13]aneN$_4$ ligand.

EXPERIMENTAL

Materials

All the starting materials and solvents for synthesis were obtained commercially and purified by standard method prior to use. Dioxo[13]aneN$_4$ (H_2L°, 1,4,7,10-tetraazacyclotridecane-11,13-dione) was prepared according to a modified literature method.[10] The procedure for the synthesis of H_2L has been described elsewhere.[11] All the other reagents for syntheses and analyses were of analytical grade. FT-IR spectra were taken on a 170SX (Nicolet) spectrometer. Elemental analysis was performed on a P–E 240C analyzer.

Preparation of NiL · 3H$_2$O(1)

For complex 1, a single crystal suitable for X-ray analysis was obtained by mixing a 1 : 1 molar ratio of Ni(CH$_3$COO)$_2$ and L in deoxygenated H$_2$O. A NaOH solution was used to adjust the pH to ~9. The solution was heated to ~60°C for ~15 min. The yellow reaction mixture was filtered and the filtrate was allowed to stand. A single crystal suitable for X-ray analysis was obtained by slow evaporation of the solvent. Found: C, 57.0; H, 6.1; N, 13.5 Calc for $C_{29}H_{36}NiN_6O_5$: C, 57.3; H, 6.0; N, 13.8%. IR(KBr pellet): 807, 840, 1038, 1281, 1385, 1458, 1496, 1546, 1579 (C=O), 2855, 2952, 3400 cm^{-1}.

Electrochemical studies

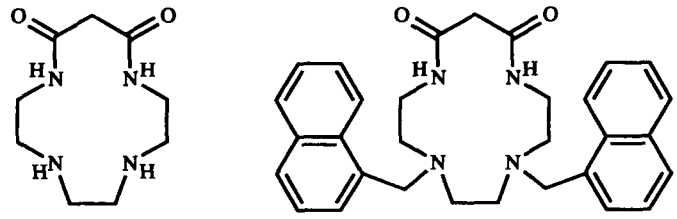
Cyclic voltammetric measurements were performed with a PARC Model 273 electrochemical apparatus in aqueous solution at 25 ± 0.05°C with 0.50 mol/dm^3 sodium sulfate (Na$_2$SO$_4$) as supporting electrolyte and the solution was bubbled with pure Ar gas. The concentration of the complexes of L° or L was kept at 2×10^{-3} mol · dm^{-3} (1 : 1 ligand and nickel or copper sulfate aqueous solution). The pH was adjusted with concentrated NaOH or H_2SO_4 solution. The cyclic voltammograms, with scan rates of 100 or 200 mV/sec, were evaluated graphically. A three-electrode system was employed; glassy carbon as working electrode, saturated calomel electrode (SCE) as reference and Pt coil as counter electrode.

Spectroscopic studies

Electronic spectra were recorded on a Shimadzu UV-240 spectrophotometer. The solution was prepared by mixing 1 : 1 molar ratio of ligand and metal acetate in methanol solution at 25°C. The pH value of the solution was adjusted by concentrated NaOH methanol solution.

X-ray structural determinations

A crystal (approximately 0.15 × 0.2 × 0.2 mm) was mounted on an Enraf-Nonius CAD-4 diffractometer equipped with a graphite crystal monochromator for data collection. The determination of unit cell parameters and the data collection were carried out with MoKα radiation (λ = 0.71073 Å). Unit cell dimensions were obtained by least-square refinement of the setting angles of 25 reflections. The intensities of reflections were measured with the ω-2θ scan mode in the range of $2 < \theta < 25°$ at room temperature. A total of 4358 independent reflections were collected and 1630 reflections with $I > 3\sigma(I)$ were considered to be observed and used in the subsequent refinement. Corrections for LP factors were applied to the data, and the structures were solved by direct method (MULTAN 82). Most of the atoms were located from an E-map. The other non-hydrogen atoms were determined with successive differential Fourier syntheses. Final refinement by full matrix least-squares methods was carried out with anisotropic thermal parameters for non-hydrogen atoms. Convergence resulted in unweighted and weighted (unit weights for all observed reflections) agreement factors of 0.063 and 0.067. The highest peak in the final difference Fourier map had a height of 0.67 e/Å^3. The hydrogen atoms were treated as "riding" on their attached atoms, and refined isotropically. All the calculations were per-



H_2L^0 H_2L

Scheme 1.

formed on a PDP11/44 computer, using the SDP-PLUS program package.

RESULTS AND DISCUSSION

Crystal structure

Figure 1 shows an ORTEP drawing of NiL(1) with 35% probability thermal ellipsoids. Crystallographic and data collection parameters are displayed in Table 1. Selected bond distances and bond angles are listed in Table 2.

The square-planar N_4 coordination of four nitrogens with Ni^{II} is evident with the dioxo[13]aneN$_4$ moiety composed of two NH's and two deprotonated amide N^-'s. These four donor atoms, N(1), N(2), N(3) and N(4), are nearly coplanar. The two quinoline pendants remained uncoordinated to Ni(II). In contrast, in the analogous copper(II) complex CuL (Fig. 3), Cu(II) is five coordinate, forming a distorted pyramidal configuration in which one of the pendant quinolines coordinates to Cu(II) from the apical position. The apical Cu(II)–N(II) distance of 2.240(5) Å is longer than those of the basal Cu–N distances, suggesting the weaker coordination of the pendant nitrogen due to the Jahn–Teller effect. In NiL, the two quinoline pendants are on different sides of the plane of the macrocycle and the macrocycle takes a *trans* conformation, whereas in the analogue CuL(2), the two quinoline pendants are on the same side of the plane of the dioxo[13]aneN$_4$ and the macrocycle takes a *cis* conformation.[11]

As anticipated, the two deprotonated amide nitrogens [N(3) and N(4)] have stronger coordination bonds [Ni–N^- bond average 1.847(4) Å] than those for tertiary amines [N(1) and N(2)] (1.915(4) Å). Different molecules of the complex in the unit cell link each other with water molecules *via* hydrogen bonds and the structure is thus stabilized (see Fig. 2).

The different coordination configurations between NiL(1) and CuL(2) may partly be due to the fact that the ionic radius of nickel(II) is smaller than that of Cu(II).[3b] The cavity of the 13-membered ring is about right for Ni(II) but too small for Cu(II). Thus, the Ni(II) ion can completely fall into the least-square plane of dioxo[13]aneN$_4$, preventing the quinoline pendant from coordinating to Ni^{II} due to steric constraints. Whereas, the Cu(II) ion cannot completely fall into the tight cavity of dioxo[13]aneN$_4$ and this allows the quinoline pendant to coordinate easily to Cu(II). Furthermore, Ni(II) ions (with d^8 electronic configuration) usually assume square-planar coordination in strong ligand fields (as L').

Electrochemical studies

The electrochemical data of the nickel(II) complexes of ligands L' and L studied in aqueous solution (0.5 mol/L Na_2SO_4 at 25°C), are summarized in Table 3. All the cyclic voltammograms showed one quasi-

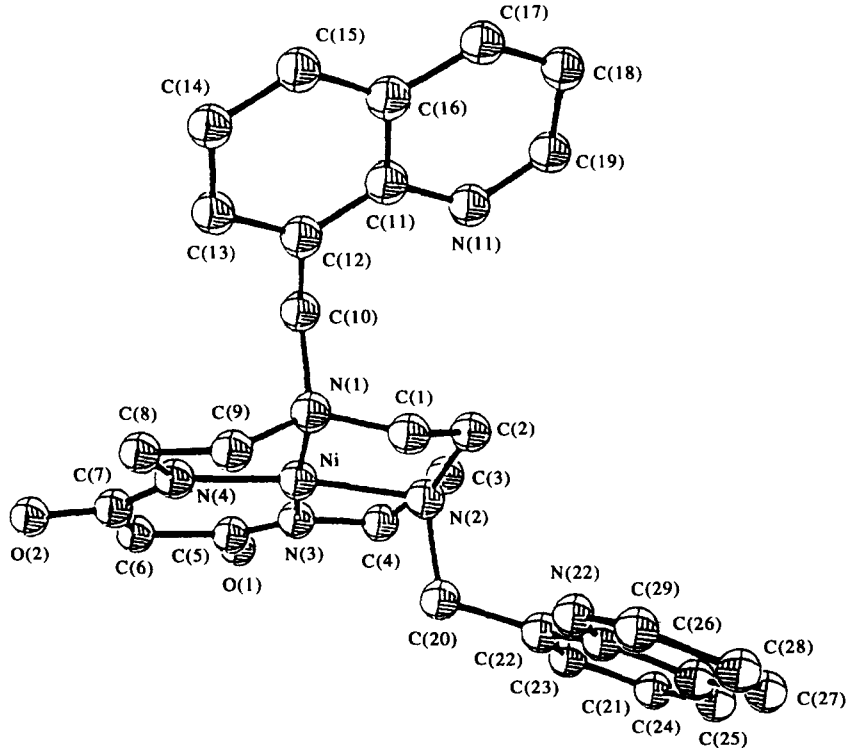


Fig. 1. ORTEP drawing of complex 1 with atom-numbering scheme. All atoms are represented by 35% thermal ellipsoids.

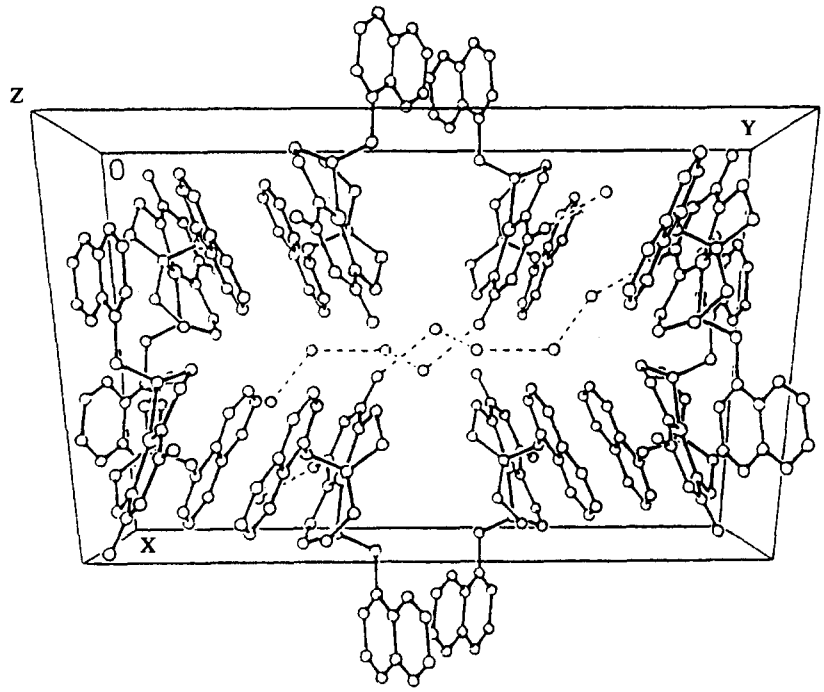


Fig. 2. ORTEP packing diagrams of the unit cell of complex 1.

Table 1. Crystal data and collection summary for complex 1

	1
Formula	$NiC_{29}H_{30}N_6O_2 \cdot 3H_2O$
Mr	607.36
Crystal colour	yellow
Crystal system	monoclinic
Space group	C2/c
Cell diminsions	
a, Å	17.858(5)
b, Å	24.083(7)
c, Å	15.587(6)
β, deg	124.83(2)
V Å^3	5502(7)
Z	8
Calcd density, g/cm^3	1.466
μ, cm^{-1}	7.558
F(000)	2560
Cryst. dimens., mm	$0.15 \times 0.2 \times 0.2$
Radiation	MoKα
λ, Å	0.71073
Temperature (K)	299 ± 1
Max. 2θ (deg)	50
Scan speed (°/min)	0.92–5.49
No. of indep. reflcns	4358 ($R_{int} = 0.21$)
No. of unique reflcns ($I > 3\sigma(I)$)	1630
absorption correction	Empirical absorption corrections[13]
R	0.063
Rw	0.067
Maximum Δ/σ	0.10
GOF	6.107
Max. residual peak (e/A^3)	0.67

Table 2. Selected bond lengths (Å), bond angles (deg) and torsion angles (deg) for complex 1 with e.s.d.s in parentheses

		bond distance (Å)	
Ni—N(1)	1.917(4)	N(2)—C(2)	1.536(5)
Ni—N(2)	1.913(4)	N(2)—C(3)	1.495(6)
Ni—N(3)	1.852(5)	N(2)—C(20)	1.535(6)
Ni—N(4)	1.842(4)	N(3)—C(4)	1.493(6)
O(1)—C(5)	1.262(6)	N(3)—C(5)	1.314(7)
O(2)—C(7)	1.274(7)	N(4)—C(7)	1.343(6)
N(1)—C(1)	1.506(5)	N(4)—C(8)	1.493(6)
N(1)—C(9)	1.516(6)	C(6)—C(7)	1.538(8)
N(1)—C(10)	1.518(6)	C(5)—C(6)	1.555(8)
		bond angle (deg)	
N(1)—Ni—N(2)	90.0(2)	Ni—N(2)—C(2)	106.0(3)
N(1)—Ni—N(3)	168.2(2)	Ni—N(2)—C(3)	104.5(3)
N(1)—Ni—N(4)	86.6(2)	Ni—N(2)—C(20)	104.8(4)
N(2)—Ni—N(3)	86.8(2)	Ni—N(3)—C(4)	114.2(3)
N(2)—Ni—N(4)	168.5(2)	Ni—N(3)—C(5)	128.0(4)
N(3)—Ni—N(4)	98.6(2)	Ni—N(4)—C(7)	126.0(4)
Ni—N(1)—C(1)	107.1(3)	Ni—N(4)—C(8)	115.5(3)
Ni—N(1)—C(9)	104.5(4)	C(5)—C(6)—C(7)	116.9(5)
Ni—N(1)—C(10)	105.2(4)		
		torsion angle (deg)	
N(1)—C(1)—C(2)—N(2)	−54.81(1.08)	C(5)—C(6)—C(7)—O(2)	−174.21(1.20)
C(1)—C(2)—N(2)—C(3)	154.72(0.92)	C(5)—C(6)—C(7)—N(4)	5.15(2.03)
C(2)—N(2)—C(3)—N(4)	−163.09(0.96)	C(6)—C(7)—N(4)—C(8)	179.80(1.22)
N(2)—C(3)—C(4)—N(3)	38.46(1.29)	C(7)—N(4)—C(8)—C(9)	162.46(1.13)
C(3)—C(4)—N(3)—C(5)	163.11(1.12)	N(4)—C(8)—C(9)—N(1)	37.11(1.31)
C(4)—N(3)—C(5)—O(1)	−2.21(1.95)	N(1)—Ni—N(2)—C(2)	−14.28(0.74)
C(4)—N(3)—C(5)—C(6)	−179.74(1.21)	N(1)—Ni—N(3)—C(4)	60.67(2.30)
N(3)—C(5)—C(6)—C(7)	3.08(2.01)	N(1)—Ni—N(4)—C(8)	−14.56(0.90)
O(1)—C(5)—C(6)—C(7)	−174.67(1.22)		

reversible oxidation wave. The $Ni^{III/II}$ potential of complex 1, 0.60 V *vs* SCE, is lowered by 0.32 V as compared to that of NiL° complex under similar conditions ($E_{1/2}$ = 0.92 V *vs* SEC),[1a] implying that the quinoline N-substituted L ligand can further stabilize the trivalent oxidation state of Ni compared with unsubstituted L°. This behaviour is also in contrast to that observed for the analogous CuL (see Table 3). The displacement of Na_2SO_4 for $NaClO_4$ as supporting electrolyte did not significantly alter the $E_{1/2}$ values of the above mentioned complexes.

This fact can be interpreted in terms of more or less favourable fitting of Cu(II)/Cu(III) and Ni(II)/Ni(III) ions in the macrocyclic cavity and the different electronic configurations of the two metal ions. The change from Cu(II) into Cu(III) state (d^8 low spin) involves a drastic reduction of the metal ion radius. In the case of the square-planar complex of Cu(III) with a deprotonated tripeptide, a Cu(III)-N(deprotonated amido) distance of 1.80 Å and a Cu(III)-N(amino) distance of 1.90 Å have been found.[12] Such distances fit quite well with the 13-membered cavity. So in CuL, when Cu(II) is oxidized to Cu(III), the smaller Cu(III) ion would fall into the least-squares plane of the basal four nitrogens. This causes the coordination of the pendant N(11) to Cu(III) to become quite difficult or impossible due to steric constraints. Since the N-substitution increases the steric constraint of the macrocycle ring and lowers the coordinative ability of the macrocycle, the Cu(III) ion in CuL is therefore not as stable as in unsubstituted L°. Whereas in the case of nickel, the change from low spin Ni(II) to high spin Ni(III) involves an increase of the ionic radius.[3b] When Ni(II) is oxidized to Ni(III) in NiL, the larger Ni(III) ion will rise out from the least-squares plane of dioxo[13]aneN$_4$ (like that for Cu(II) in CuL) and it becomes possible for the quinoline pendant to coordinate to it. Ni(III) is thus stabilized in NiL.

Spectroscopic studies

The absorption maxima data of the present Ni complexes in MeOH solution are listed in Table 3. The *d–d* transition band of the nickel(II) of NiL significantly shifts to higher wavelength than that of NiL° (from 415 nm of NiL° to ~470 nm of NiL, shifted by *ca* 50 nm). This fact indicates that the in-plane bonding in NiL was lowered due to the N-substitution by the quinoline pendants. This behaviour is similar to that observed for CuL.[11]

Supplementary material available

Full details of the crystal data and crystallographic data collections, thermal parameters, bond distances and angles, mean planes and dihedral angles between the planes, listings of observed and calculated struc-

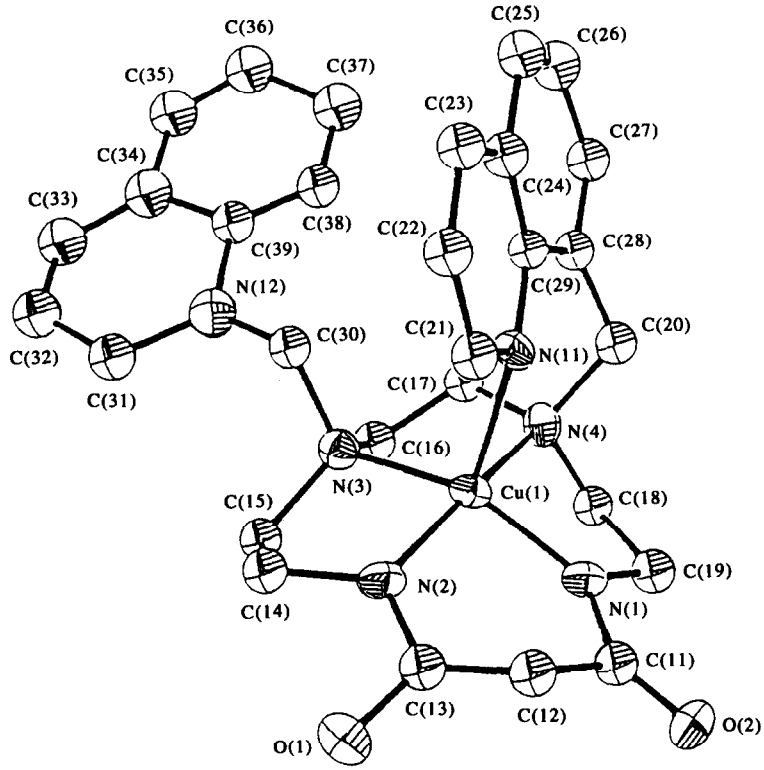


Fig. 3. ORTEP drawing of CuL complex with atom-numbering scheme. All atoms are represented by 35% thermal ellipsoids.

Table 3. Physical properties of the Ni(II) and Cu(II) complexes of L° and L

Complex		NiL°	NiL	CuL°	CuL[11]
CV[a,b]	SR, mV/S	200	200	100	200
	pH	~8	~8	~6	~5
	$E_{1/2}$, V	0.92	0.60	0.58	0.84
UV–vis[c]	Solvent	MeOH	MeOH	MeOH	MeOH
	pH	~9	~9	~8	~8
	$\lambda_{max,nm}(\varepsilon)$	415(100)	470(100)	516(100)	600(230)

[a] In H_2O at 25°C, V *vs* SCE.
[b] The concentration of the complexes of L° and L was kept at 2×10^{-3} mol·dm^{-3} and $\sim 1 \times 10^{-3}$ mol·dm^{-3}
[c] At 25°C.

tural factors for complex 1 are available from the author.

Acknowledgements—We gratefully acknowledge the financial support from the National Natural Science Foundation of China, and a fundation from the State Education Commission of China for X. H. Bu. This work was also partially supported by the State Key Lab of Coord. Chem. of Nanjing University.

REFERENCES

1. (a) E. Kiumura, *J. Coord. Chem.* 1986, **15**, 1; (b) E. Kimura, *Pure & Appl. Chem.* 1986, **58**, 1461; (c) E. Kimura, in *Crown Compounds Toward Future Applications* (Edited by S. R. Cooper), 6. VCH, New York (1992).
2. (a) M. Kodama, and E. Kimura, *J. Chem. Soc., Dalton Trans.* 1979, 325; (b) M. Kodama, E. Kimura, *ibid.* 1979, 1783; (c) M. Kodama, and E. Kimura, *ibid.* 1981, 694; (d) K. Ishizu, J. Hirai, M. Kodama, E. Kimura, *Chem. Lett.* 1979, 1045; (e) R. Machida, E. Kimura, M. Kodama, *Inorg. Chem.* 1983, **22**, 2055; (f) E. Kimura, T. Koike, R. Machida, R. Nagai, and M. Kodama, *Inorg. Chem.* 1984, **23**, 4181; (g) E. Kimura, C. A. Dalimunte, A. Yamashita, and R. Machida, *J. Chem. Soc., Chem. Commun.* 1985, 1041; (h) E. Kimura, Y. Lin, R. Machida and H. Zenda, *ibid.* 1986, 1020; (i) E. Kimura, S. Korenali, M. Shionoya and M. Shiro, *ibid.* 1988, 1166; (j) E. Kimura, M. Shionoya, M. Okamoto and H. Nada,

J. Am. Chem. Soc. 1988, **110**, 3679; (k) M. Shionoya, E. Kimura and Y. Iitaka, *ibid.* 1990, **112**, 9237.

3. (a) R. W. Hay, M. P. Pujari and F. Mclaren, *Inorg. Chem.* 1984, **23**, 3033; (b) L. Fabbrizzi, *Comments Inorg. Chem.*, 1985, **4**, 33; (c) L. C. Siegfried and T. A. Kaden, *J. Phy. Org. Chem.* 1992, 549; (d) L. Fabbrizzi, A. Perotti, A. Profumo, and T. Soldi, *Inorg. Chem.* 1986, **25**, 4256; (e) L. Fabbrizzi, F. Forlini, A. Perotti, and B. Seghi, *Inorg. Chem.* 1984, **23**, 807; (f) L. Fabbrizzi, T. A. Kaden, A. Perotti, B. Seghi and L. Siegfried, *Inorg. Chem.* 1986, **25**, 321; (g) G. D. Santis, L. Fabbrizzi, M. Licchelli, and P. Pallavicini, *Coord. Chem. Rew.* 1992, **120**, 237.
4. (a) F. Kimura, H. Nada, *Tanpaku-Kakusan-Koso* 1988, **16**, 2914; (b) R. Machida, E. Kimura and M. Kodama, *Inorg. Chem.* 1983, **22**, 2055; (c) E. Kimura, R. Machida, *Yuki Gosei Kagaku* 1984, **42**, 407.
5. (a) L. Fabbrizzi, A. Poggi, *J. Chen. Soc., Chem. Commun.* 1980, 646; (b) L. Fabbrizzi, A. Perotti, and A. Poggi, *Inorg. Chem.* 1983, **22**, 1411; **25**, 4256; (d) R. Hay, R. Rembi and W. Sommerville, *Inorg. Chim. Acta* 1982, **59**, 147; (e) Y. D. Lampeka and S. P. Gavrish, *J. Coord. Chem.* 1990, **21**, 351.
6. (a) D. W. Margerum and G. D. Oven, in *Metal Ions in Biological Systems* (Edited by H. Sigel). Vol. 12, p. 75, Marcel Dekker, New York (1981), (b) T. R. Wagner and C. J. Burrows, *Tetrahedron Lett.* 1988, **29**, 5091; (c) T. R. Wagner, Y. Fang and C. J. Burrows, *J. Org. Chem.* 1989, **54**, 1584.
7. B. J. Hathaway, in *Comprehensive Coordination Chemistry*, (Edited by G. Wilkinson), Vol. 5, p. 533, Pergamon Press (1987).
8. (a) J. M. Lehn, *Angew. Chem. Int. Ed. Engl.* 1988, **27**, 89; (b) J. M. Lehn, *ibid.* 1990, **29**, 1304.
9. (a) E. Kimura, T. Koike, R. Machida, R. Nagai and M. Kodama, *Inorg. Chem.* 1984, **23**, 4181; (b) E. Kimura, T. Koike, H. Nada and Y. Iitaka *Inorg. Chem.* 1988, **27**, 1036; (c) E. Kimura, S. Korenali, M. Shionoya, and M. Shiro, *J. Chem. Soc., Chem. Commun.* 1988, 1166; (d) S. Zhu, H. Lin and Y. T. Chen, *Inorg. Chim. Acta* 1995, **228**, 225.
10. I. Tabushi, H. Okino, and Y. Kuroda, *Tetrahedron Lett.* 1976, 4339.
11. X. H. Bu, D. L. An, Y. T. Chen, M. Shionoya and E. Kimura, *J. Chem. Soc. Dalton Trans.* 1995, 2289.
12. L. Y. Martin, L. J. DeHayes, L. J. Zompa, D. H. Busch, *J. Am. Chem. Soc.* 1974, **96**, 4046.
13. N. Walker and D. Stuart, *Acta Cryst.* 1983, **A39**, 159.

Pergamon

S0277-5387(96)00175-1

Polyhedron Vol. 16, No. 1, pp. 187–194, 1997
Copyright © 1996 Elsevier Science Ltd
Printed in Great Britain. All rights reserved
0277-5387/97 $15.00+0.00

Synthesis, characterization and crystal structure of a novel tris(2-aminoethyl) amine copper(II) complex with an asymmetric coordinated 4,5-diazafluorene-9-hydrazine

Zhong-Lin Lu, Chun-Ying Duan, Yu-Peng Tian and Xiao-Zeng You*

Coordination Chemistry Institute, The State Key Laboratory of Coordination Chemistry, Nanjing University, The Center for Advanced Studies in Science and Technology of Microstructure, Nanjing, 210093, P.R. China

and

Hoong-Kun Fun and Boon-Chuan Yip

X-ray Crystallography Unit, School of Physics, Universiti Sains Malaysia, 11800 Penang, Malaysia

and

Eric Hovestreydt

Siemens, AG, X-ray Analytical Systems, Department Aut 37 PM, D76181 Karlsruhe, Germany

(Received 17 October 1995; accepted 9 April 1996)

Abstract—The compound, tris(2-aminoethyl)amine-4,5-diazafluorene-9-hydrazine copper(II) perchlorate complex, $[Cu(C_6H_{18}N_4)(C_{11}H_8N_4)](ClO_4)_2$ (**1**), has been designed, synthesized and characterized. The X-ray analysis reveals that the copper(II) is coordinated by four nitrogen atoms from tris(2-aminoethyl)amine (tren) and two nitrogen atoms from 4,5-diazafluorene-9-hydrazine (dzfh) to form an unusual (4+1+1′) six-coordinate geometry. This structure is very rare, and to our knowledge, is a unique example of a tripodal copper(II) complex with an asymmetric bidentate phenanthroline derivative. The 110 K ESR and electronic reflectance spectra studies demonstrate that the coordinated geometry of copper(II) is quite similar to square-based pyramidal stereochemistry, instead of the trigonal bipyramidal stereochemistry, which is the common structure for $[Cu(tren)L]^{2+}$ (L = monodentate ligand) complexes. The electronic and variable-temperature ESR spectra in absolute DMF suggest that the two nitrogen atoms of the dzfh coordinate to the copper(II) ion in the two-dimensional fluxional model. For comparison, the complex, $Cu(tren)(Py)(ClO_4)_2$ (Py is pyridine) (**2**), was also synthesized and characterized. Copyright © 1996 Elsevier Science Ltd

Keywords: crystal structure; tris(2-aminoethyl)amine; copper(II) complexes; two-dimensional fluxional model; variable-temperature ESR spectra; associative complex.

Tripodal complexes have attracted much attention because of their importance in biochemistry.[1,2,3] These compounds provide adequate model systems for enzymes in some cases. Five-coordinate tripodal copper(II) complexes are quite common, but no six-coordinate ones have been reported so far. On the other hand, the associative mechanism has been

* Author to whom correspondence should be addressed.

suggested for the ligand-exchange and ligand-substitution reactions for $[Cu(tren)L]^{2+}$ [where tren is tris(2-aminoethyl)amine, L is a monodentate ligand],[4,5] the structure of the associative complex in the reaction has not been determined, and no associative complex has been observed owing to its instability.

In our laboratory, $[Cu(tren)(L\text{–}L)]^{2+}$ complexes have been designed and synthesized, where L–L is a strong chelated ligand, such as 2,2′-bipyridine, 1,10-phenanthroline and their derivatives.[6] This idea comes from: (i) the strong chelated ligand, such as 2,2′-bipyridine, should make the $[Cu(tren)(L\text{–}L)]^{2+}$ cation form a six-coordinate stereochemistry, which has the same coordination number as the associative complex; (ii) the relatively rigid tripodal construction of tren has a strong tendency to form five-coordinated complexes of copper(II). These two strongly differing tendencies should make the $[Cu(tren)(L\text{–}L)]^{2+}$ cation form an unusual $(4+1+1')$ structure, in which the complex has five stronger coordinated atoms and a weak semi-coordinated atom. The structure of these new kind of tripodal copper(II) complexes should be similar to that of the associative complex in the ligand-substitution reaction of $[Cu(tren)L]^{2+}$.

We report here the synthesis, characterization and crystal structure of one such complex, $[Cu(C_6H_{18}N_4)(C_{11}H_8N_4)](ClO_4)_2$ (**1**), where $C_6H_{18}N_4$ is tris (2-aminoethyl)amine (tren) and $C_{11}H_8N_4$ is 4,5-diazafluorene-9-hydrazine (dzfh).

For comparison the five-coordinated complex, $[Cu(tren)(Py)](ClO_4)_2$ (**2**), was also synthesized and characterized (Py is pyridine).

EXPERIMENTAL

CAUTION! Perchlorate salts of metal complexes with organic ligands are potentially explosive, only small amounts of material should be handled.

Materials and preparations

All chemicals were reagent grade and used without further purification. 4,5-Diazafluorene-9-hydrazine was prepared using the literature method.[7] The complex of $[Cu(tren)](ClO_4)_2$ was synthesized according to the procedure described earlier,[8] but using $Cu(OAc)_2 \cdot H_2O$ and $NaClO_4$ instead of $CuCl_2 \cdot 2H_2O$ and KSCN.

$[(tren)Cu(dzfh)]ClO_4)_2$ (**1**). To a solution of $[Cu(tren)](ClO_4)_2$ (1 mmol, 0.408 g) in ethanol/acetonitrile (1 : 1) (30 cm^{-3}) was added 4,5-diazafluorene-9-hydrazine (1 mmol, 0.196 g). The mixture was refluxed for 3 h. After cooling to room temperature, the precipitate was filtered by suction and dried *in vacuo* over silica. Yield: 0.483 g, 80%, m.p. 237°C (decomp.). Λ_M (DMF, 1.03×10^{-3} mol dm^{-3}, 20°C): 156 Ω^{-1} cm^2 mol^{-1}. Magnetic moment: $\mu_{eff} = 1.98$ B.M. IR (cm^{-1}): ν(N—H) 3418s, 3332s, 3280s; ν(C=N) 1644s, 1579s; ν(Cl—O) 1090vs, 993s, 623m; ν(Cu—N(3°)] 525s. Found: C, 34.2; H, 4.1; N, 19.3. Calc. for $C_{17}H_{26}Cl_2CuN_8O_8$: C, 33.8; H, 4.3; N, 18.8%.

$[(tren)Cu(Py)](ClO_4)_2$ (**2**).[9] The complex was obtained as blue needle crystals in a similar manner to **1**. Yield: 85%, m.p. 217°C (decomp.). Λ_M (DMF, 1.53×10^{-3} mol dm^{-3}, 20°C); 140 Ω^{-1} cm^2 mol^{-1}. Magnetic moment: $\mu_{eff} = 2.08$ B.M. IR (cm^{-1}): ν(N—H) 3339s, 3287s; ν(C=N) 1608s; ν(Cl—O) 1091vs, 995s, 623m; ν[Cu—N(3)] 530s. Found: C, 26.7; H, 4.6; N, 13.9. Calc. for $C_{11}H_{23}Cl_2CuN_5O_8$: C, 27.1; H, 4.8; N, 14.4%.

Physical measurements

Elemental analyses were performed on a Perkin–Elmer 240C analytical instrument. Molar conductances were measured at 25°C in DMF solutions on a DDS-11A conductometer. Magnetic measurement on a powder sample was carried out with a CAHN 2000 Faraday-type magnetometer at 293K. IR spectra were recorded on a Nicolet 170SX FT spectrophotometer as KBr pellets in the range 4000–500 cm^{-1}. The far-IR spectra (500–100 cm^{-1}) were recorded as Nujol mulls between polyethylene sheet. Electronic reflectance spectra were recorded on a Shimadzu 240 spectrophotometer. Electronic spectra in absolute DMF were performed on a Shimadzu 310 spectrophotometer. The 110 K ESR spectra of complexes, and the variable-temperature ESR spectra of **1** in absolute DMF solutions, were measured using a Bruker 200D-SRC spectrometer.

Crystallography

Data collection. A prismatic crystal of **1**, of size $0.20 \times 0.04 \times 0.03$ mm, was obtained by slow evaporation of its ethanol/acetonitrile (5 : 1) solution at room temperature. We had some difficulties finding a good crystal. Attempts to improve the size of the crystals by many recrystallizations were unsuccessful. The data were collected using a Siemens SMART CCD system with monochromated Mo-K_α ($\lambda = 0.71073$ Å) radiation. The data were corrected for Lorentz and polarization effects during data reduction using SHELXTL5.[10] From a total of 9127 reflections measured for $2\theta \leqslant 46.6°$ ($11 \leqslant h \leqslant 11$, $-16 \leqslant k \leqslant 11$, $-16 \leqslant k \leqslant 16$), 3435 were independent and 2678 reflections were considered observed using the criteria $I > 2\sigma(I)$.

Table 1. Crystallographic parameters for complex **1**

Formula	$C_{17}H_{26}C_{12}CuN_8O_8$
Fw	604.90
Crystal dimensions (mm)	$0.20 \times 0.04 \times 0.03$
Crystal system	Monoclinic
Space group	*P*21/c
a (Å)	10.699(4)
b (Å)	15.005(6)
c (Å)	14.942(6)
β(°)	95.310(10)
V (Å)^3	2389(2)
Z	4
μ (mm^{-1})	1.200
F(000)	1244
Dx (Mg m^{-3})	1.68

Structure solution and refinement. The structure was solved by direct methods using SHELXS86[11] and refined on F^2 by full-matrix least-squares methods using SHELXL93.[12] All non-hydrogen atoms were refined anisotropically. All the hydrogen atoms were generated geometrically and refined using the riding model with the isotropic thermal parameters set to 1.2 times of the atom they ride on. Final conventional $R(F) = 0.1072$ and $wR(F^2) = 0.1886$ for $I > 2\sigma(I)$ with weighting scheme, $w = 1/[\sigma^2(F^2) + (0.0093P)^2 + 19.4233P]$ where $P = (F_0^2 + 2F_c^2)/3$. The maximum and minimum residual electron densities of the difference Fourier map are 0.627 and -0.547 eÅ^{-3}. The molecular graphics were plotted using SHELXTL/PC.[13] All computations were performed on an IBM compatible 486/DX2 personal computer. The crystal data are summarized in Table 1. Supplementary crystallographic data have been deposited at the Cambridge Crystallographic Data Centre.

RESULTS AND DISCUSSION

Crystal structure

For comparison, the main bond distances and bond angles of complexes **1** and **2** are listed in Table 2 and the labelled ORTEP plot of the molecular cation structures are shown in Figs 1 and 2, respectively. The copper(II) ion in complex **1** is coordinated by four nitrogen atoms from tren and one nitrogen atom from dzfh, to form a distorted square-based pyramidal geometry (the geometric parameter τ is 0.43),[14] with the sixth, potentially bonding position occupied by N(5) at 2.956(9) Å from the copper, a distance that is considered as weak "semi-coordination".[15] The crystal structure of complex **2** has been published elsewhere.[9] The copper(II) ion in complex **2** is coordinated by four nitrogen atoms from tren and one nitrogen atom from Py to form a regular trigonal-bipyramidal geometry (the geometric parameter τ is 0.95). It can be seen that the structure of complex **1** is very different from that of complex **2** and the general $[Cu(tren)L]^{2+}$ system (the τ value is often close to 1.0[14]).

It is very important to note that the dzfh acts as an asymmetric bidentate ligand in complex **1**. The

Table 2. Selected bond distances and bond angles for complex **1** and **2**

1		**2**	
Cu—N(1)	2.043(9)	Cu—N(1)	2.038(6)
Cu—N(2)	2.017(8)	Cu—N(2)	1.995(6)
Cu—N(73)	2.023(9)	Cu—N(73)	2.065(6)
Cu—N(83)	2.017(9)	Cu—N(83)	2.065(6)
Cu—N(93)	2.251(9)	Cu—N(93)	2.083(7)
Cu—N(5)	2.956(9)		
N(1)—Cu—N(2)	174.8(4)	N(1)—Cu—N(2)	178.2(2)
N(1)—Cu—N(73)	84.0(4)	N(1)—Cu—N(73)	83.7(2)
N(1)—Cu—N(83)	84.3(4)	N(1)—Cu—N(83)	83.7(2)
N(1)—Cu—N(93)	82.6(4)	N(1)—Cu—N(93)	89.9(3)
N(2)—Cu—N(73)	94.5(3)	N(2)—Cu—N(73)	95.5(2)
N(2)—Cu—N(83)	94.6(3)	N(2)—Cu—N(83)	95.5(2)
N(2)—Cu—N(93)	102.5(3)	N(2)—Cu—N(4)	97.9(3)
N(73)—Cu—N(83)	149.0(4)	N(73)—Cu—N(83)	121.5(6)
N(73)—Cu—N(93)	102.9(4)	N(73)—Cu—N(93)	117.5(3)
N(83)—Cu—N(93)	103.9(4)	N(83)—Cu—N(93)	117.5(3)

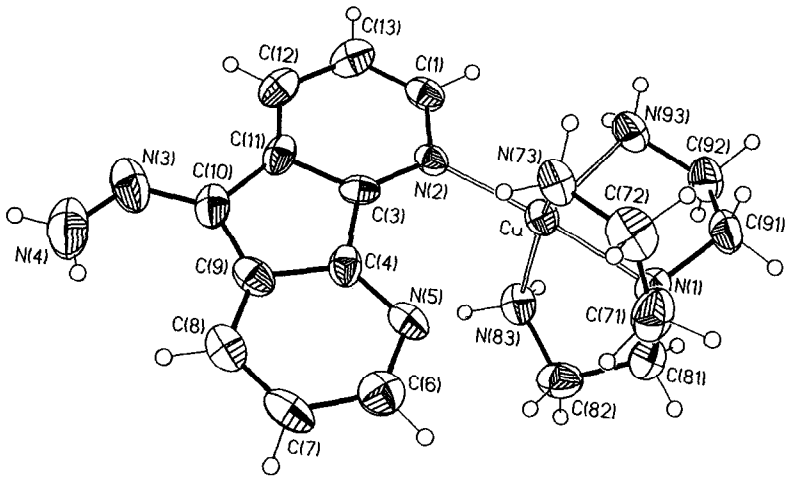


Fig. 1. The ORTEP plots of the cation of complex **1**: $[(C_6H_{18}N_4)Cu(C_{11}H_8N_4)]^{2+}$.

high complexation of dzfh and the relatively rigid tripodal construction of tren, which often enforces a five-coordination on copper(II) ion,[16] make this unusual coordinated structure quite stable. The best evidence for the very weak coordination of Cu—N(5) is the unusual trigonally distorted square-based pyramidal stereochemistry, which can be thought of as six coordinate $(4+1+1')$.[15,17] The atoms N(2), N(83) and N(1) from the equatorial plane, and the atoms N(5) and N(93) are in the axial positions. This may be confirmed by the bond length data that the Cu—N(93) is 0.23 Å longer than the other four Cu—N bonds. In fact, the axial bonds of most six-coordinate copper(II) complexes are often elongated as a result of the Jahn–Teller effect. Because of the relatively rigid geometry of tren, the Cu—N(93) bond is shorter than the usual axial Cu—N bond in the elongated octahedral geometry,[15,18] and this may be one of the reasons that the other axial Cu—N bond [Cu—N(5)] is longer than the usual axial Cu—N bond. This structure is very rare, and to our knowledge, it is a unique example of a tripodal copper(II) complex with an asymmetric bidentate phenanthroline derivative.

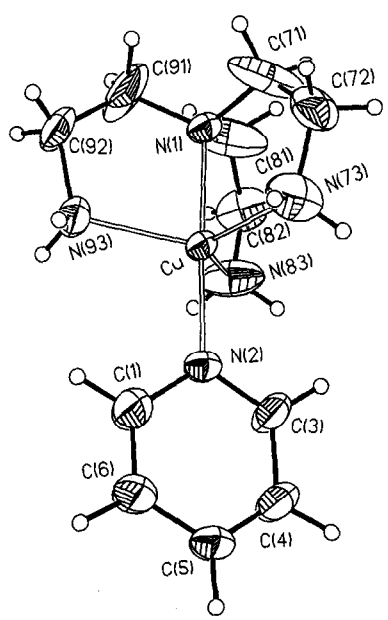


Fig. 2. The ORTEP plots of the cation of complex **2**:[9] $[(C_6H_{18}N_4)Cu(C_5H_5N)]^{2+}$.

Electronic spectra

(*a*) *Electronic reflectance spectra.* Figure 3 shows the electronic reflectance spectra of complexes **1** and **2**. The spectral data are summarized in Table 3. The complexes absorb light in the same region of the visible spectrum; yet their spectra are quite different. Complex **1** has a band maximum at 15,600 cm^{-1} and a lower energy shoulder at 11,900 cm^{-1};

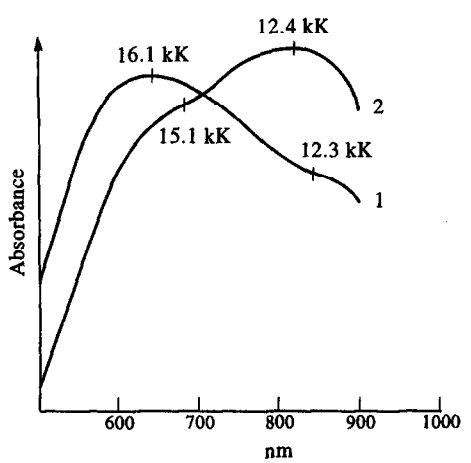


Fig. 3. Electronic reflectance spectra of **1** and **2**.

Table 3. Electronic spectral data for **1** and **2** (cm^{-1}).

Complex	Bands (cm^{-1}) (ε_{max})[a]	
1		
(in DMF)	13,500(100)	11,900(112)
(Gaussion analysis	I 15,000, II 12,400	III 11,000, IV 9700
(reflectance of solid)	15,600	11,900
2		
(in DMF)	14,300(95)	12,300(141)
(reflectance of solid)	14,700	12,200

[a] ε_{max} in units of M^{-1} cm^{-1}.

while complex **2** has a maximum at 12,200 cm^{-1} and a high-energy shoulder at 14,700 cm^{-1}. Both spectra agree with those previously reported for $[Cu(NH_3)5]^{2+}$[19] and $[Cu(tren)(NH_3)]^{2+}$,[20] respectively. This result may demonstrate that complex **1** has a distorted square-based pyramidal geometry, instead of the trigonal bipyramidal stereochemistry which is very common in five coordinated tris(2-aminoethyl)amine copper(II) complexes. The assignment of the electronic reflectance spectra of copper(II) has been extensively discussed in the literature.[15] It would be reasonable to assign the intense band of complex **1** at 15,600 cm^{-1} as the d_{xz}, $d_{yz} \rightarrow d_{x^2-y^2}$ transition and the shoulder at 11,900 cm^{-1} as the $d_{z^2} \rightarrow d_{x^2-y^2}$ transition with the $d_{xy} \rightarrow d_{x^2-y^2}$ transition at $\approx$14,000 cm^{-1} in the Gaussian analysis.[21] This assignment is in agreement with that suggested for other square-based pyramidal copper(II) complexes.[14,15,20]

A tentative assignment of the electronic reflectance spectra of the $[Cu(tren)L]^{2+}$ cations has been suggested; namely the band maximum at 12,200 cm^{-1} of complex **2** as the d_{xy}, $d_{x^2-y^2} \rightarrow d_{z^2}$ transition, the less intense shoulder at 14,700 cm^{-1} as the d_{xy}, $d_{yz} \rightarrow d_{z^2}$ transition. This shows the characteristics of the trigonal-bipyramidal stereochemistry.[9,15,20,21]

(*b*) *Solution electronic spectra.* Figure 4 shows the electronic spectra of complex **1** and **2** in DMF at room temperature. It is obvious that the electronic spectrum of complex **1** is quite different to that in the solid state, which indicates that the stereochemistry of complex **1** has changed in solution. Variable-solvent spectra show that the electronic spectrum of complex **1** has no visible change in different organic solvent, such as acetonitrile and DMF. Therefore, the equilibrium

$$Cu(tren)(dzfh)^{2+} + S \rightarrow Cu(tren)(S)^{2+} + dzfh$$

(where S represents solvents) does not exist in solution. Considering the asymmetric coordination of the dzfh ligand, the different stereochemistries in

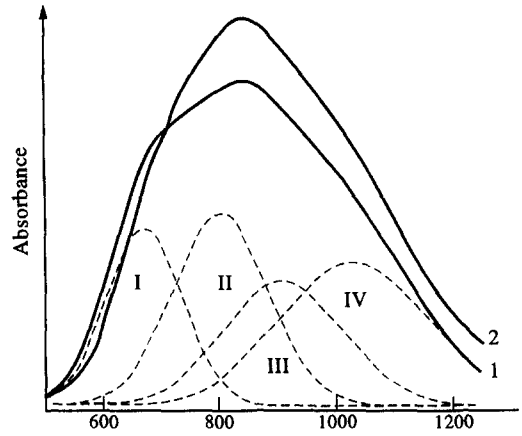


Fig. 4. The electronic spectra in absolute DMF solutions of complexes **1** and **2**.

the solid state and in solution may be attributed to the transformation of the two nitrogen atoms of dzfh in solution. If the sum of Gaussian-shaped bands corresponding to the different types of transition are reproduced with good accuracy,[22,23] four bands can be observed. Bands I and III are quite similar to those of the solid state, which can be assigned as d_{xy}, $d_{yz} \rightarrow d_{x^2-y^2}$ and $d_{z^2} \rightarrow d_{x^2-y^2}$ of the square-based pyramidal complex; while bands II and IV are quite similar to those of the solid state spectrum of the *cis* distorted octahedral copper(II) complex[24] in which two nitrogen atoms of dzfh coordinate to the copper(II) ion in the two-dimensional fluxional model and can be assigned as d_{yz}, $d_{x^2-y^2}$, $d_{xz} \rightarrow d_{z^2}$ and $d_{xy} \rightarrow d_{z^2}$. These results may demonstrate that not only does the square-pyramidal stereochemistry exist which has the lowest potential wells I and II (Fig. 5) in the solution, but also that the *cis* distorted octahedral stereochemistries with different Cu—N(2) and Cu—N(5) bond distances exist, which have a higher potential energy than those of wells I and II. The populations of the different stereochemistries may be controlled

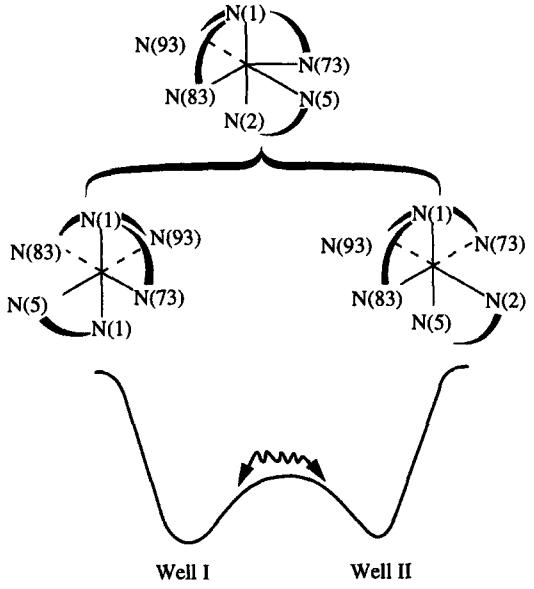


Fig. 5. The two-dimensional fluxional disorder model of the pseudo *cis* distorted octahedral geometry with qualitative potential energy wells diagram.

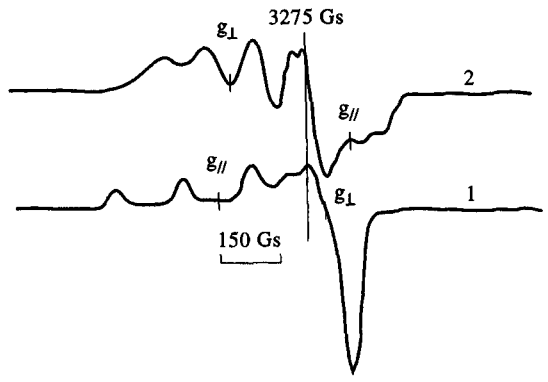


Fig. 6. ESR spectra of the complexes **1** and **2** in frozen absolute DMF solutions.

by temperature and potential energy of the chromophore CuN_4NN'.

ESR spectra

(*a*) 110 *K ESR spectra.* The ESR spectra of complexes **1** and **2** are shown in Fig. 6, the data for the ESR spectra are summarized in Table 4. The spectrum of **1** involves an intense $g_\parallel$ signal with clear resolution of the four copper hyperfine lines, $g_\parallel = 2.228$, $A_\parallel = 16.82 \times 10^{-3}$ cm^{-1} and a very intense $g_\perp$ signal with $g_\perp = 2.021$, $A_\perp = 13.02 \times 10^{-3}$ cm^{-1}. The fact that $g_\parallel > g_\perp$ confirms a square-based pyramidal stereochemistry in complex **1**.[14,15] While the spectrum of **2** shows a line shape characteristic of a complex with two different g-values, but the reverse of that of complex **1**, with $g_\parallel = 1.992$, $A_\parallel = 7.41 \times 10^{-3}$ cm^{-1} and $g_\perp = 2.182$, $A_\perp = 11.86 \times 10^{-3}$ cm^{-1}. This fact, $g_\perp > g_\parallel$, agrees with the trigonal bipyramidal stereochemistry established for the $[Cu(tren)L]^{2+}$ system.[9,15,20,21]

(*b*) *Variable-temperature ESR of* **1** *in DMF solution.* In order to obtain further insight into the coordination geometry of complex **1** in solution, the variable-temperature ESR spectra were observed (Fig. 7). It can be seen that the solution coordination of complex **1** is significantly temperature dependent. The $d_{x^2-y^2}$ ground state in the frozen solution (200, 160 and 110 K) shows a dominant tetragonal component in the solution stereochemistry. The ESR spectra in solution (290 and 240 K) show the isotropic spectra of the copper(II) ion. From the g-value of the solution stereochemistry, which is bigger than that of the frozen state, we can suggest that there exist other stereochemistries with bigger g-values, except the square-based pyramidal stereochemistry. Considering the asymmetric coordination of dzfh and the electronic spectrum, the stereochemistries with bigger g-values

Table 4. ESR spectral data for complex **1** and **2** in absolute DMF.

Complex	Temperature	$g_\parallel$	$A_\parallel$[a]	$g_\perp$	$A_\perp$	g_{iso}
1	287K					2.133
	240K					2.103
	200K	2.228	16.83	2.026	10.26	2.093
	160K	2.228	16.83	2.023	12.44	2.091
	110K	2.228	16.82	2.021	13.02	2.090
2	110K	1.992	7.41	2.182	11.86	2.119

[a]A values are $\times 10^3$ cm^{-1}.

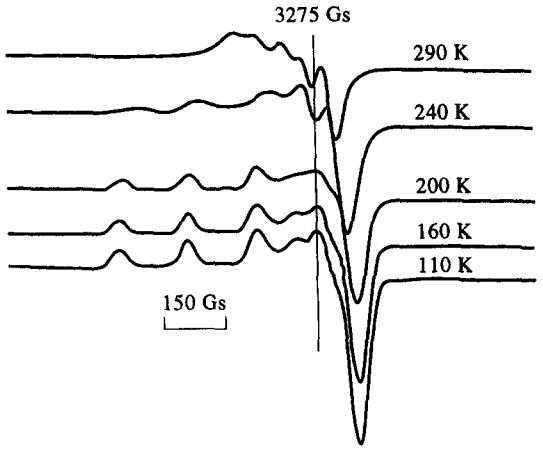


Fig. 7. The variable-temperature ESR spectra of complex **1** in absolute DMF solution.

are best referred to the pseudo *cis* distorted octahedral stereochemistries, in which the two nitrogen atoms of dzfh coordinate to the copper(II) ion in the two-dimensional fluxional model.[25,26]

Consequently, the electronic and variable-temperature ESR spectra suggest that the structure of complex **1** in solution is not the genuine stereochemistry of the copper(II) ion, but arises as a consequence of the pseudo-dynamic Jahn–Teller effect[27] generating a two-dimensional fluxional model involving a static distorted square-based pyramidal (4+1+1′) structure, with nearly equal thermal population of the two lowest potential wells I and II corresponding to the square-base pyramidal geometry and a higher potential barrier corresponding to the *cis* distorted octahedral stereochemistry, with a different bond distance ratio of Cu—N(2) : Cu—N(5) from 0.68 to 1.47. The highest potential barrier corresponds to the *cis* distorted octahedral stereochemistry with two equal Cu—N(2) and Cu—N(5) bond distances.

It is very interesting to speculate on the significance of the structure of complex **1** for the model associative complex in the associative mechanism for the ligand-exchange and ligand-substitution reactions of $[Cu(tren)L]^{2+}$, owing to their importance in studying the elementary steps in the catalytic cycles of enzymes, such as Cu—Zn SOD, involving substitution reactions at the copper sites.[28,29]

Acknowledgements—This work was supported by a major research project from the State Science and Technology Commission and National Nature Science Foundation of China and the research grant R&D No. 123-3417-2201 from the Malaysian Government and Universiti Sains Malaysia.

REFERENCES

1. S. H. Gou, X. Z. You, K. B. Yu and J. P. Lu, *Inorg. Chem.* 1993, **32**, 1883.
2. Z. W. Mao, D. Cheng, W. X. Tang, K. B. Yu and L. Liu, *Polyhedron* 1992, **11**, 191.
3. K. Wieghardt, *Angew. Chem.* 1989, **28**, 1153.
4. G. R. Cayley, I. D. Kelly, P. F. Knowles and K. D. S. Yadav, *J. Chem. Soc., Dalton Trans.* 1981, 2370.
5. D. H. Powell, A. E. Merbach, I. Fábián, S. Schindler and R. van Eldik, *Inorg. Chem.* 1994, **32**, 4468.
6. Z. L. Lu, C. Y. Duan, Y. P. Tian, X. Z. You and X. Y. Huang, *Inorg. Chem.* 1996, **35**, 2253.
7. J. Molochoski and Z. Szule, *Pol. J. Chem.* 1983, **67**, 33.
8. K. N. Raymond and F. Basolo, *Inorg. Chem.* 1966, **5**, 1632.
9. H. K. Fun, K. Sivakumar, Z. L. Lu, C. Y. Duan, Y. P. Tian and X. Z. You. *Acta Cryst., Sect. C* 1995, (in press).
10. G. M. Sheldrick, SHELXTL5, *The Complete Software Package for Single Crystal Structure Determination*, Siemens, AG, Analytical System Aut37, D76181 Karlsruhe 21, Germany (1995).
11. G. M. Sheldrick, *Acta Cryst., Sect. A* 1969, **46**, 467.
12. G. M. Sheldrick, SHELXL93. *Program for Crystal Structure Refinement*, University of Gottingen, Germany (1993).
13. G. M. Sheldrick, SHELXTL-PC, *Structure Determination Software Programs*, Siemens Analytical X-ray Instruments Inc., Madison, Wisconsin, USA (1990).
14. A. W. Addison, T. N. Rao, J. Reedijk, J. V. Rijn and G. C. Verschoor, *J. Chem. Soc., Dalton Trans.* 1984, 1349.
15. B. J. Hathaway and A. A. G. Tomlinson, *Coord. Chem. Rev.* 1970, **5**, 1.
16. E. J. Laskowski, D. M. Duggen and D. N. Henderson, *Inorg. Chem.* 1975, **4**, 2449.
17. W. D. Harrison and B. J. Hathaway, *Acta Cryst., Sect. B* 1980, **36**, 1069.
18. T. Dister and P. A. Vagham, *Inorg. Chem.* 1967, **6**, 126.
19. B. J. Hathaway and A. A. G. Tomlinson, *J. Chem. Soc. (A)* 1968, 1695.
20. M. Duggen, N. Ray, B. J. Hathaway, G. Tomlinson, P. Brint and K. Pelin, *J. Chem. Soc., Dalton Trans.* 1980, 1342.
21. R. J. Dudley, B. J. Hathaway, P. G. Power and D. J. Loose, *J. Chem. Soc., Dalton Trans.* 1974, 1005.
22. All bands in the spectra are assumed to have a Guassian shape, with the relevant band parameters defined by $f(\nu) = \varepsilon_{max}\exp(-[(\nu-\nu_{max})/0.060(\nu_{1/2})]^2)$. The actual spectrum of every single species can be reproduced in the spectra range of interest as a sum of individual bands to a precision of $\pm 5\%$.
23. C. A. Bignozzi, C. Paradisi, S. Roffia and F. Scandola, *Inorg. Chem.* 1988, **27**, 408.
24. B. J. Hathaway, I. M. Procter, R. C. Slade and A. A. G. Tomlinson, *J. Chem. Soc. (A)* 1969, 2219.
25. W. Fitzgerald, B. Murphy, S. Tyagi, B. Walsh, A.

Walsh and B. J. Hathaway, *J. Chem. Soc., Dalton Trans* 1981, 2271.
26. B. J. Hathaway, M. Duggan, A. Murphy, J. Mullane, C. Power, A. Walsh and B. Walsh, *Coord. Chem. Rev.* 1981, **36**, 267.
27. I. B. Bersuker, *Coord. Chem. Rev.* 1975, **14**, 357.
28. G. Cayley, D. Cross and P. F. Knowles, *J. Chem. Soc., Chem. Commun.* 1976, 837.
29. I. Bertini, L. Banci and M. Piccioli, *Coord. Chem. Rev.* 1990, **100**, 67.

Pergamon

S0277-5387(96)00167-2

Polyhedron Vol. 16, No. 1, pp. 195–198, 1997
Copyright © 1996 Elsevier Science Ltd
Printed in Great Britain. All rights reserved
0277-5387/97 $15.00+0.00

COMMUNICATION

Synthetic and structural studies on substituted cyclopentadienyl titanium(III) complexes with intramolecular amino group coordination

Yanlong Qian,* Rongwei Guo† and Jiling Huang

East China University of Science and Technology, Laboratory of Organometallic Chemistry, Meilong Road 130, Shanghai 200237, P.R. China

and

Qingchun Yang

Institute of Physical Chemistry, Beijing University, Beijing 100871, P.R. China

(Received 16 January 1996; accepted 19 March 1996)

Abstract—Three substituted cyclopentadienyl titanium(III) complexes with intramolecular amino group coordination have been prepared and the crystal structure of $(C_5H_4CH_2CH_2NMo_2)_2TiCl$(**1**) has been determined.

In recent years there has been considerable interest in metallocycles which are often involved in a number of significant catalytic reactions, such as olefin polymerization[1] and isomerization.[2] Previous studies in our group have focused on the chemistry of substituted cyclopentadienyl titanium complexes, their syntheses, structure and catalytic reactions.[3] We are now interested in investigating terminal amino group coordinated titanium complexes, specially in the low valent state. Such coordination may provide a model for studying the mechanism of Ziegler–Natta polymerization of olefin with titanocene complexes as catalysts. Here we report the syntheses and structural studies of three terminal amino substituted cyclopentadienyl titanium (III) complexes. The synthetic route is shown in Scheme 1.

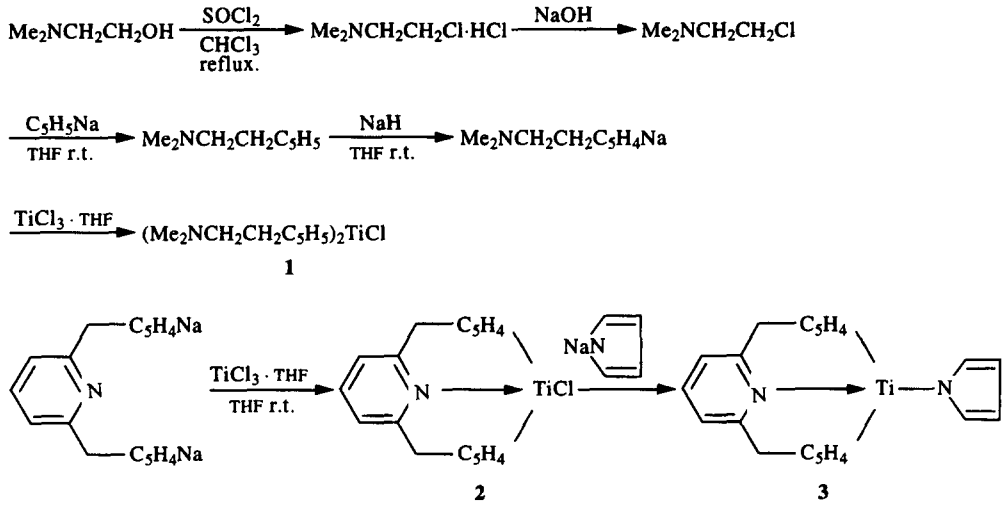
Compounds **1–3** have been characterized by ^{1}H-NMR, MS, IR and elemental analysis and provided satisfactory spectroscopic and analytical data. The crystal structure of **1** has been determined and is shown in Fig. 1.

The structure of **1** reveals that there is only one atom of nitrogen in the side chain coordinated to titanium atom with a N—Ti bond length 2.428 Å, and the other nitrogen is not coordinated to the metal. We have also determined the X-ray photoelectron spectrometry (XPS) of compounds **1–3** and compared them with their analogues. The results are shown in Table 1.

Compared with the analogous complex, the N1*s* binding energy (B.E.) in complex **1** is increased 1.9 eV and Ti $2p_{3/2}$ of that is decreased 0.2 eV. The results show that there is a N → Ti coordination bond which is consistent with the molecular structure. Similarly, the changes of N1*s* and Ti $2p_{3/2}$ binding energies in complex **2** are +0.8 eV and −0.4 eV respectively. It also gives evidence of N → Ti coordination in complex **2**. The same coordination exists in complex **3** supposedly.

* Author to whom correspondence should be addressed.

† Present address: Central China Normal University, Wuhan 430070, Hubei, China



Scheme 1.

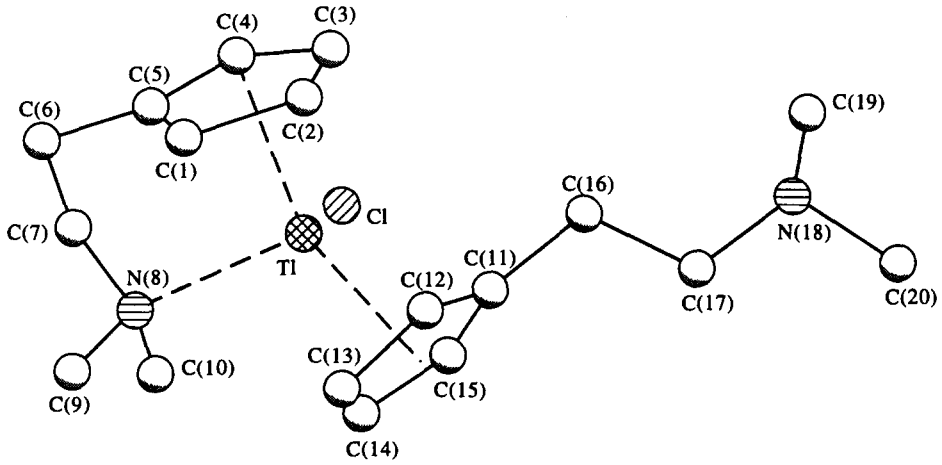
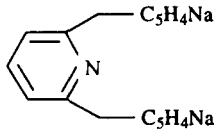
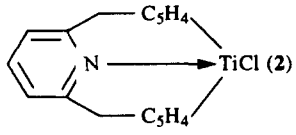


Fig. 1. Molecular structure for Compound **1**, selected bond distance (Å) and angles (°): Ti—Cl: 2.483(4); Ti—C(2): 2.366(14); Ti—C(4): 2.415(14); Ti—N(8): 2.428(9); Ti—C(12): 2.386(14); Ti—C(14): 2.382(14); Cl—Ti—C(1): 135.2(3); Cl—Ti—C(4): 78.6(3); Cl—Ti—N(8): 85.5(3); Cl—Ti—C(13): 130.6(4); Cl—Ti—C(14): 98.1(4).

Table 1. XPS data (eV)

Complexes	N1*s* B.E.	N1*s* ΔE	Ti $2p_{3/2}$ B.E.	Ti $2p_{3/2}$ ΔE
$(C_5H_5)_2TiCl$				458.0
$(Me_2NCH_2CH_2C_5H_4)_2TiCl_2$	400.6			
$(Me_2NCH_2CH_2C_5H_4)_2TiCl$ (**1**)	402.5	+1.9	−0.2	457.8
	398.6			
	399.4	+0.8	−0.4	457.6

Acknolwedgements—We thank the National Natural Science Foundation of China for financial support. This project is also supported by Union Laboratory of Asymmetric Synthesis (Chengdu Institute of Organic Chemistry, Academia sinica; Hong Kong Polytechnic University; Kuo Ching Chemical Co., Ltd), and State Key Laboratory of Coordination Chemistry, Nanjing University.

REFERENCES

1. (a) You-Xian Che, M. D. Rausch and J. C. W. Chien, *Organometallics* 1994, **13**, 748; (b) W. Spaleck, F. Küber, A. Wintyer, J. Rohrmann, B. Bachmann, M. Antberg, V. Dolle and E. F. Paulus, *Organometallics*, 1994, **13**, 954; (c) U. Steling, J. Diebold, R. Kirsten, W. Röll, H.-H. Brintzinger, S. Jüngling, R. Mülhaput

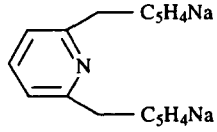
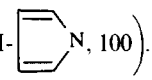
Footnotes

1. All new compounds provided satisfactory analytical and spectroscopic data.

The typical synthetic procedure and selected analytical data for compounds **1–3** are as follows.

1. A solution of $(CH_3)_2NCH_2CH_2CpNa$ (10.02 mmol) in THF was added dropwise to a solution of $TiCl_3 \cdot 3THF$ (1.86 g, 5.01 mmol) in THF. It was stirred for 6 h. The solvent was removed. The residue was extracted and a blue green powder 1.23 g (Yield 69%) was obtained. m.p. 130–132°C, MS (*m*/*z*): 355 (M^+, 21); 320 (M—Cl, 27).

2. By using the same procedure as the complex **1**, it gave dark blue solid, yield 81.6%. MS (*m*/*z*): 316 (M^+, 100); 280 (M—Cl—H, 96).

3. After the reaction of  and $TiCl_3 \cdot 3THF$ was completed,  was added. The solvent was removed, the residue was extracted, and a dark blue crystal was obtained. MS (*m*/*z*): 347(M^+, 43); 281  .

2. Crystal data for Compound **1**: $C_{18}H_{28}ClN_2Ti$. Molecular Weight: 355.77; Data collection was made on a Siemens R 3m/v Diffractometer using Mo-K_α radiation and a highly orientated graphite crystal monochromator. The crystal structure was solved by direct methods using a Siemens SHELXTL PLUS (VMS) System and refined by full-matrix least-squares. Crystal size 0.15 × 0.15 × 0.25 mm; green blue prism, orthorhombic; space group: $P2_12_12_1$; a = 9.190(5), b = 10.814(7), c = 18.410(13), V = 1830(2) Å^3, Z = 4, D_c = 1.292 g cm^{-1}; $F(000)$ = 756; *Mo*-K_α (λ = 0.71073); 2θ Range: 3.0 to 50.0°; reflections collected: 3630; independent reflection: 3235 (R_{int} = 3.20%), observed reflections: 1398 ($P > 5.0s(f)$); R = 0.0687, $R\omega$ = 0.0558. Atomic coordinates, bond lengths and angles, anisotropic displacement coefficients, H-atom coordinates and isotropic displacement coefficients have been deposited with the Editor.

and F. Langhauser, *Organometallics* 1994, **13**, 964; (d) J. C. Flores, J. C. W. Chien and M. D. Rausch, *Organometallics* 1994, **13**, 4140.

2. Y. Qian, G. Li, Y. He, W. Chen, B. Li and S. Chen, *J. Mol. Catal.* 1990, **60**, 19.
3. (a) Q. Huang, Y. Qian, W. Xu, M. Shao and Y. Tang, *Wuji Huaxue* (*Chin. J. Inorg. Chem.*) 1986, **1**, 166; (b) Y. Qian, J. Lu and W. Xu, *J. Mol. Catal.* 1986, **34**, 31; (c) Y. Qian, J. Zhuang, J. Lu, Q. Huang, W. Xu and S. Chen, *J. Mol. Catal.* 1986, **38**, 331; (d) B. He, Y. Qian and S. Chen, *J. Organomet. Chem.* 1987, **320**, 27; (e) Q. Huang and Y. Qian, *Synthesis* 1987, 910; (f) Q. Huang, Y. Qian and Y. Tang, *J. Organomet. Chem.*, 1989, **368**, 277; (g) Q. Huang, Y. Qian and Y. Tang, *Trans. Met. Chem.* 1989, **14**, 315; (h) Y. Qian, G. Li, W. Chen, B. Li and X. Jin, *J. Organomet. Chem.* 1989, **373**, 185; (i) Y. Qian, G. Li, W. Chen, B. Li and X. Jin, *Trans. Met. Chem.* 1990, **15**, 478; (j) Q. Huang, Y. Qian, G. Li and Y. Tang, *Trans. Met. Chem.* 1990, **15**, 483; (k) G. Li, Y. Qian, Y. Huang and S. Chen, *J. Mol. Catal.* 1992, **72**, L15; (l) Y. Qian and G. Li, *Polyhedron* 1993, **12**, 967; (m) Y. Qian, J. Huang, X. Chen, G. Li, W. Chen, B. Li, X. Jin and Q. Yang, *Polyhedron* 1994, **13**, 1105.

Pergamon

S0277-5387(96)00292-6

Polyhedron Vol. 16, No. 2, pp. 199–205, 1997
Copyright © 1996 Elsevier Science Ltd
Printed in Great Britain. All rights reserved
0277-5387/97 $15.00+0.00

Mononuclear cadmium(II) halide complexes of triphenylphosphoniobutyrate, $[CdCl_2L_2 \cdot H_2O]$ and $[CdX_2L_2]$ (X = Br, I)(L = $Ph_3P^+(CH_2)_3CO_2^-$)

Song-Lin Li and Thomas C. W. Mak*

Department of Chemistry, The Chinese University of Hong Kong, Shatin, New Territories, Hong Kong

(Received 1 April 1996; accepted 13 June 1996)

Abstract—Three mononuclear cadmium(II) complexes containing the tertiary phosphine betaine ligand triphenylphosphoniobutyrate, $Ph_3P^+(CH_2)_3CO_2^-$, (L) have been synthesized and characterized by single crystal X-ray analysis. In $CdCl_2L_2 \cdot H_2O$ (**1**) the cadmium(II) atom is coordinated by pairs of unidentate betaine ligands and chloro ligands in a tetrahedral environment, and the primarily discrete species are joined by donor hydrogen bonds from the solvated water molecules to the pendant oxygen atom of the betaine ligands to form a dimer. In $CdBr_2L_2$ (**2**) the cadmium(II) atom is coordinated in a similar manner, but one Cd—Br distance is so long that it may be considered as a weak interaction. In CdI_2L_2 (**3**) the betaine ligands act differently in the bidentate chelate and unidentate modes. Copyright © 1996 Elsevier Science Ltd

Keywords: mononuclear complex; triphenylphosphoniobutyrate; cadmium(II) halide; crystal structure.

The coordination chemistry of cadmium in both the non-biological and biological areas has attracted the interest of many researchers [1]. Recently, the ^{113}Cd nucleus has been utilized as an excellent metallobioprobe owing to its favorable NMR properties as compared to some native metal ions, e.g. Zn^{II}, Ca^{II} and MG^{II} [2–6].

In the coordination chemistry of cadmium(II), complexes with carboxylic acid or carboxylic acid-like ligands figure prominently [1–7]. This is ascribed to two factors. First of all, cadmium(II) has a d^{10} electron configuration which rules out ligand–field stabilization in its complexes and, as a consequence, adapts well to a variety of stereochemical environments. A recent statistical survey of 200 crystal structures of cadmium(II) complexes of low molecular weight showed that cadmium(II) has coordination numbers of 4, 5 and 6 in about 19, 8 and 56%, respectively [8]. Another statistical study on the structural aspects of metal ion–carboxylate interactions showed that the maximum deviation of the cadmium(II) atom from the carboxylate plane can reach up to ~1.5 Å, but for most transition metal ions such as manganese(II, III), cobalt(II, III), nickel(II), iron(II, III), copper(I, II) and zinc(II), they tend to lie in the carboxylate plane [9]. This means the cadmium(II) ion is more accommodating to the arrangement of carboxylate ligands in its coordination sphere. Secondly, the carboxylato group has a π-conjugated system with two lone pairs on each oxygen atom, which facilitate a variety of coordination modes to metal ions [10–18]. These two factors are also responsible for the relative scarceness of cadmium(II) carboxylates containing both monomeric and discrete oligomeric units.

Recently, we studied the interaction of a tertiary phosphine betaine triphenylphosphoniopropionate, $Ph_3P^+(CH_2)_2CO_2^-$, with various cadmium(II) salts, and a series of tetrakis-μ-carboxylato-*O*,*O*′dicadmium(II) complexes were synthesized and fully characterized by single crystal X-ray analysis. It has been suggested that the occurrence of these complexes can be attributed to the steric effect of the bulky Ph_3P group [19]. A subsequent investigation of the reaction of $Ph_3P^+(CH_2)_2CO_2^-$ with cadmium(II) salts led to the formation of mono-, bi-, tri- and tetranuclear cadmium(II) complexes containing discrete units [20]. In the present paper, we report the reaction of CdX_2 (X = Cl, Br, I) with triphenylphosphoniobutyrate, $Ph_3P^+(CH_2)_3CO_2^-$, which has one more —CH_2— spacer than $Ph_3P^+(CH_2)_2CO_2^-$, and three new mononuclear cadmium(II) complexes have been syn-

* Author to whom correspondence should be addressed.

thesized and characterized by single crystal X-ray analysis.

EXPERIMENTAL

Synthesis

$Ph_3P^+(CH_2)_3CO_2^-$ was synthesized by a literature method [21]. Solvents and other chemicals were used as purchased.

All three complexes $[CdCl_2\{Ph_3P(CH_2)_3CO_2\}_2]\cdot H_2O$ (**1**), $[CdBr_2\{Ph_3P(CH_2)_3CO_2\}_2]$ (**2**) and $[CdI_2\{Ph_3P(CH_2)_3CO_2\}_2]$ (**3**) were prepared by the same procedure. To a mixture of $Ph_3P^+(CH_2)_3CO_2^-$ (340 mg, 1.0 mmol) and cadmium(II) halide [$CdCl_2\cdot 2H_2O$ (115 mg, 0.5 mmol), $CdBr_2$ (130 mg, 0.5 mmol), or CdI_2 (175 mg, 0.5 mmol)] was added distilled water (*ca* 5 cm^3), and a white precipitate formed immediately. After the slurry was stirred for about 5 min at *ca* 60°C, dimethylformamide (dmf) was added until the precipitate dissolved completely. Colorless prismatic crystals of **1–3** were obtained after the solutions were allowed to stand for two days at ambient temperature (yield: 280 mg, 62% for **1**; 250 mg, 52% for **2**; 310 mg, 58% for **3**).

X-ray data collection and structure refinement

Information concerning X-ray data collection and structure refinement is summarized in Table 1. The intensities for complexes **1–3** were collected at 290 K in the ω-scan mode [22] on a Nicolet R3m/V (for **2** and **3**) and a Siemens P4/PC (for **1**) diffractometer using Mo-K_α radiation ($\lambda = 0.71073$ Å), respectively. Unit-cell parameters were calculated from least-squares fitting of the 2θ angles for 25 selected strong reflections. Crystal stability was monitored by recording three check reflections at intervals of 120 data measurements, and no significant variation was detected. Empirical absorption correction based on azimuthal scans was applied to the intensity data processing for **1** and **3**.

The crystal structures of all three complexes were solved by direct methods. All non-hydrogen atoms were refined anisotropically by full-matrix least squares. The hydrogen atoms of the ligands were placed in their calculated positions with C—H = 0.96 Å, assigned fixed isotropic thermal parameters, and allowed to ride on their respective parent carbon atoms. These hydrogen atoms were included in the structure factor calculations, but their positions were not varied.

All calculations were carried out on a PC 486 using the SHELXTL-PLUS program package [23]. Analytical expressions of neutral-atom scattering factors were employed, and anomalous dispersion corrections were incorporated [24]. The selected bond lengths and angles for **1–2** are listed in Table 2.

RESULTS AND DISCUSSION

Structures of $[CdCl_2\{Ph_3P(CH_2)_3CO_2\}_2]\cdot H_2O$ (**1**) *and* $[CdBr_2\{Ph_3P(CH_2)_3CO_2\}_2]$ (**2**)

Complex **1** crystallizes with a packing of discrete $[CdCl_2\{Ph_3P(CH_2)_3CO_2\}_2]$ molecules and lattice water molecules, while complex **2** consists of discrete $[CdBr_2\{Ph_3P(CH_2)_3CO_2\}_2]$ molecules only. As illustrated in Figs 1 and 2, the structures of both complexes are very similar. The cadmium(II) atom is coordinated by two unidentate $Ph_3P^+(CH_2)_3CO_2^-$ ligands [Cd—O = 2.232(4) and 2.213(2) Å for **1**, 2.148(7) and 2.037(7) Å for **2**, respectively; Cd···O (pendant = 2.809(2) and 2.981(2) Å for **1**, 2.826(7) and 2.847(7) Å for **2**) and two halo ligands [Cd—Cl = 2.463(1) and 2.469(1) Å for **1**, Cd—Br = 2.580(2) and 2.926(2) Å for **2**] in a slightly distorted tetrahedral environment (the bond angles around the cadmium(II) atom lies in the range of 98.6(1)–128.2(1)° for **1** and 92.2(2)–127.0(3)° for **2**].

The two Cd—O bonds in **1** are nearly identical and similar to those found in tetrakiscarboxylato-*O*,*O*′-bridged dicadmium(II) anions $[Cd_2X_2\{Ph_3P(CH_2)_2CO_2\}_4]^{2+}$ (X = Cl, NO_3) [2.236(7)–2.251(6) Å] [19] in which the carboxylate groups act in a *syn–syn* bidentate bridging mode. The Cd—Cl bond lengths in **1** are well within the Cd—Cl(terminal) bond lengths [2.436–2.458 Å] [25a] found in four-coordinated cadmium(II) complexes. The torsion angles Cd(1)—O(1)—C(22)—O(2) at −9.3° and Cd(1)—O(3)—C(44)—O(4) at 7.1° indicate that the cadmium(II) atom nearly lies in the plane of each of the carboxylate groups. On the other hand, the two carboxylate groups are approximately mutually perpendicular with a dihedral angle of 99.9°. Two monomeric molecules are bridged by donor hydrogen bonds from the lattice water molecule to the pendant oxygen atoms of the betaine ligands[O(1W)···O(4) = 2.899(4) and O(1W)···O(2a) = 2.858(4) Å, O(4)···O(1W)···O(2a) = 126.7°] to form a dimeric structure.

For complex **2**, the two Cd—O bond lengths are markedly different and significantly shorter than those in **1**. In addition, one Cd—Br bond is well comparable to the average Cd—Br(terminal) bond length of 2.588 Å [25b] in four-coordinated cadmium(II) complexes and is much shorter than the other Cd—Br bond. The Cd—Br(2) bond length of 2.926(2) Å is so long that it may be considered as a secondary interaction between the Cd^{II} atom and the Br atom, so that the coordination environment about the cadmium(II) atom in **2** is better described as distorted pyramidal rather than distorted tetrahedral, and the change of coordination geometry may be responsible for the shorter Cd—O distances in **2** than in **1**. However, the torsion angles Cd(1)—O(1)—C(22)—O(2) and Cd(1)—O(3)—C(44)—O(4) [−8.2 and 10.7°] and the dihedral angle between the two carboxylate groups [81.3°] are similar to those in complex **1**.

Table 1. Crystallographic data for compounds **1**–**3** (L = $Ph_3P^+(CH_2)_3CO_2^-$)

Formula	$[CdCl_2L_2]\cdot H_2O$ **1**	$[CdBr_2L_2]$ **2**	$[CdBr_2L_2]$ **3**
M	898.0	968.9	1062.9
Crystal system	Triclinic	Triclinic	Triclinic
Space group	$P\bar{1}$	$P\bar{1}$	$P\bar{1}$
Crystal size (mm)	$0.28\times0.30\times0.34$	$0.18\times0.20\times0.34$	$0.12\times0.36\times0.40$
a (Å)	12.102(1)	10.711(2)	10.785(7)
b (Å)	13.909(4)	10.754(2)	11.076(8)
c (Å)	14.218(2)	19.019(4)	18.817(9)
α (°)	98.55(1)	105.54(3)	96.09(5)
β (°)	111.89(1)	93.80(3)	104.72(5)
γ (°)	106.32(1)	101.15(3)	99.67(5)
V (Å^3)	2042(1)	2055(1)	2117(2)
Z	2	2	2
D_c (g cm^{-3})	1.461	1.566	1.668
$F(000)$	920	960	1044
Transmission coefficients	0.873–0.918	—	0.430–0.532
μ (cm^{-1})	7.89	25.95	20.90
2θ range (°)	2–50	3–48	3–48
No. of data independent	6679	6488	6683
No. of data used, n	5263[$>4\sigma(F)$]	3630[$>4\sigma(F)$]	3946[$>4\sigma(F)$]
No. of variables, p	488	479	479
R	0.032	0.061	0.057
R'	0.042	0.064	0.067
S	0.99	1.25	1.26

$R = \Sigma\Delta/\Sigma|F_o|$, $R' = [\Sigma w\Delta^2/\Sigma|F_o|^2]^{1/2}$ and $S = [w\Delta^2/(n-p)]^{1/2}$ where $w = [\sigma^2F_o)+K|F_o|^2]^{-1}$, $\Delta = ||F_o|-|F_c||$; 10^4 K = 80, 100 and 100 for complexes **1**, **2** and **3**, respectively. Extinction parameter χ = 0.00036, 0.00147 and 0.00008 for complexes **1**, **2** and **3**, respectively where the "corrected" calculated structural factor $F_{corr} = F_c(1+0.002\chi F_c^2/\sin 2\theta)^{-1/4}$.

Crystal structure of $[CdI_2\{Ph_3P(CH_2)_3CO_2\}_2]$ (**3**)

Complex **3** also comprises discrete molecules $[CdI_2\{Ph_3P(CH_2)_3CO_2\}_2]$ packed in the crystal lattice. However, unlike **1** and **2** the cadmium(II) atom in **3** is five-coordinated in a distorted square-pyramidal geometry (Fig. 3) with the oxygen atoms of both $Ph_3P^+(CH_2)_3CO_2^-$ ligands and one iodo ligand forming the base, and the other iodo ligand occupying the axial position. The most distorted bond angle is O(1)—Cd(1)—O(2) = 54.4(4)°. Of the two betaine ligands, one acts in the asymmetric bidentate chelate mode [Cd—O = 2.238(10) and 2.497(10) Å, Δ(Cd—O) = 0.259 Å] and the other in the unidentate mode [Cd—O = 2.232(8) Å]. The Cd—O(unidentate) bond length is comparable with those in $[Cd\{Ph_3P(CH_2)_2CO_2\}_4(H_2O)_2](ClO_4)_2\cdot 2H_2O$ [Cd—O = 2.219(5) and 2.231(4) Å [20] in which the cadmium(II) atom is coordinated by four unidentate $Ph_3P^+(CH_2)_2CO_2^-$ betaine ligands. The two Cd—I bond lengths of 2.809(2) and 2.844(3) Å are significantly longer than the average Cd—I bond length of 2.750 Å [25c] and those [2.701(1) and 2.706(1) Å] found in $[CdI_2\{Ph_3P(CH_2)_2CO_2\}]$ [20] in which the Cd^{II} atom is also penta-coordinated but in a very different coordination geometry. The dihedral angle between the two carboxylate groups of 84.8° is comparable to those in **1** and **2**. In addition, the dihedral angle between the plane CdI(1)I(2) and O(3)C(44)O(4) of 89.4° indicates that the orientation of the pendant oxygen atom of the carboxylate group C(44)O(3)O(4) is dictated by the repulsive interaction between it and the two iodo ligands.

The bidentate chelate mode is found in cadmium(II) complexes of many carboxylic acids, such as $[Cd(PA)_2(H_2O)_2]$ (PAH = phenoxyacetic acid) in which the cadmium(II) atom is six-coordinated with two symmetrically chelated carboxylato groups lying in the equatorial plane [Cd—O = 2.363(4) and 2.365(4) Å] [26]. It also occurs commonly in cadmium(II) complexes of amino acids, such as aqua(L-glutamato)dicadmium(II) hydrate [Cd—O = 2.317(5), 2.458(5) Å] in which the cadmium(II) atom is six-coordinated, triaquabis(L-glutomato) cadmium(II) hydrate [Cd—O = 2.361(5), 2.502(5) and 2.368(5), 2.499(5) Å] and aqua(glycyl-L-glutamato) cadmium(II) hydrate [Cd—O = 2.277(5), 2.867(5) and 2.331(5), 2.435(5) Å] in each of which the cadmium(II) atom is seven-coordinated with two carboxylato groups acting in the bidentate chelate mode [27], as well as dichlorobis (glycylglycine) cadmium(II) [Cd—O = 2.255(5), 2.602(5) Å] in which

Table 2. Selected bond lengths (Å) and angles (°) for complexes **1–3**

Complex **1**			
Cd(1)—Cl(1)	2.469(1)	Cd(1)—Cl(2)	2.463(1)
Cd(1)—O(1)	2.232(4)	Cd(1)—O(3)	2.213(2)
C(22)—O(1)	1.260(5)	C(22)—O(2)	1.241(5)
C(44)—O(3)	1.266(5)	C(44)—O(4)	1.245(5)
Cl(1)—Cd(1)—Cl(2)	106.1(1)	Cl(1)—Cd(1)—O(1)	98.6(1)
Cl(2)—Cd(1)—O(1)	110.0(1)	Cl(1)—Cd(1)—O(3)	109.9(1)
Cl(2)—Cd(1)—O(3)	128.2(1)	O(1)—Cd(1)—O(3)	100.2(1)
C(21)—C(22)—O(1)	116.2(3)	C(21)—C(22)—O(2)	119.2(4)
O(1)—C(22)—O(2)	124.6(4)	Cd(1)—O(1)—C(22)	111.4(3)
C(43)—C(44)—O(3)	118.7(3)	C(43)—C(44)—O(4)	118.1(3)
O(3)—C(44)—O(4)	123.1(3)	Cd(1)—O(3)—C(44)	106.9(2)
Complex **2**			
Cd(1)—Br(1)	2.926(2)	Cd(1)—Br(2)	2.580(2)
Cd(1)—O(1)	2.148(7)	Cd(1)—O(3)	2.037(7)
C(22)—O(1)	1.39(1)	C(22)—O(2)	1.09(1)
C(44)—O(3)	1.26(1)	C(44)—O(4)	1.12(1)
Br(1)—Cd(1)—Br(2)	107.6(1)	Br(1)—Cd(1)—O(1)	109.9(3)
Br(2)—Cd(1)—O(1)	109.2(2)	Br(1)—Cd(1)—O(3)	92.2(2)
Br(2)—Cd(1)—O(3)	108.6(2)	O(1)—Cd(1)—O(3)	127.0(3)
O(1)—C(22)—O(2)	120.2(9)	Cd(1)—O(1)—C(22)	107.8(6)
O(3)—C(44)—O(4)	125.4(9)	Cd(1)—O(3)—C(44)	112.6(7)
Complex **3**			
Cd(1)—I(1)	2.809(2)	Cd(1)—I(2)	2.844(3)
Cd(1)—O(1)	2.24(1)	Cd(1)—O(2)	2.50(1)
Cd(1)—O(3)	2.232(8)	C(22)—O(1)	1.26(2)
C(22)—O(2)	1.24(2)	C(44)—O(3)	1.26(2)
C(44)—O(4)	1.24(2)		
I(1)—Cd(1)—I(2)	110.2(1)	I(1)—Cd(1)—O(1)	114.6(2)
I(2)—Cd(1)—O(1)	97.9(3)	I(1)—Cd(1)—O(2)	92.0(2)
I(2)—Cd(1)—O(2)	150.8(3)	C(22)—Cd(1)—O(2)	27.2(4)
O(1)—Cd(1)—O(2)	54.4(4)	I(1)—Cd(1)—O(3)	102.5(2)
I(2)—Cd(1)—O(3)	96.9(2)	C(22)—Cd(1)—O(3)	114.5(3)
O(1)—Cd(1)—O(3)	131.9(3)	O(2)—Cd(1)—O(3)	96.6(3)
C(21)—C(22)—O(1)	118(1)	Cd(1)—C(22)—O(2)	66.8(7)
O(1)—C(22)—O(2)	121(1)	Cd(1)—O(1)—C(22)	97.8(9)
Cd(1)—O(2)—C(22)	86.0(8)	C(43)—C(44)—O(3)	117(1)
C(43)—C(44)—O(4)	119(1)	O(3)—C(44)—O(4)	124(1)
Cd(1)—O(3)—C(44)	107.1(8)		

the cadmium(II) atom is six-coordinated [27]. Betaine ligands exhibiting the bidentate chelate mode are found in $[Cd(Et_3BET)(\mu\text{-}Cl)_2]_n$ ($Et_3BET = Et_3N^+(CH_2)_2CO_2^-$) [Cd—O = 2.407(2), 2.435(2) Å] in which the cadmium(II) atom is six-coordinated [28], in $[CdCl_2\{Ph_3P(CH_2)_2CO_2\}_2]\cdot 7H_2O$ [Cd—O = 2.306 (9), 2.567(9) and 2.287(8), 2.576(8) Å] in which the cadmium(II) atom is six-coordinated with a pair of chelated carboxylato groups [20], in *trans*-$Cd(H_2O)_4[Cl_2Cd(\mu\text{-}Cl)\{Ph_3P(CH_2)_2CO_2\}]_2\cdot 4H_2O$ [Cd—O = 2.290(6), 2.541(7) Å] in which the cadmium(II) atom is five-coordinated [20]. In all these examples the Δ(Cd—O) value lies in a wide range of 0.002–0.590 Å which indicates that the steric strain imposed by the formation of a four-membered chelate ring can be released by having one carboxylato oxygen atom strongly coordinating to the cadmium(II) and the other loosely bound. It should be noted that in many cadmium(II) carboxylates the center of mass of the pair of oxygen atoms of a chelated carboxylato group can be taken as a ligand site in considering the corresponding idealized polyhedral geometry [20,29]. In complex **3** the angles between the vectors from cadmium(II) to the midpoint of a line linking O(1) with O(2), and to O(3), I(1) and I(2) vary in the range 96.9–126.2°, which lie within ± 17% of the ideal tetrahedral

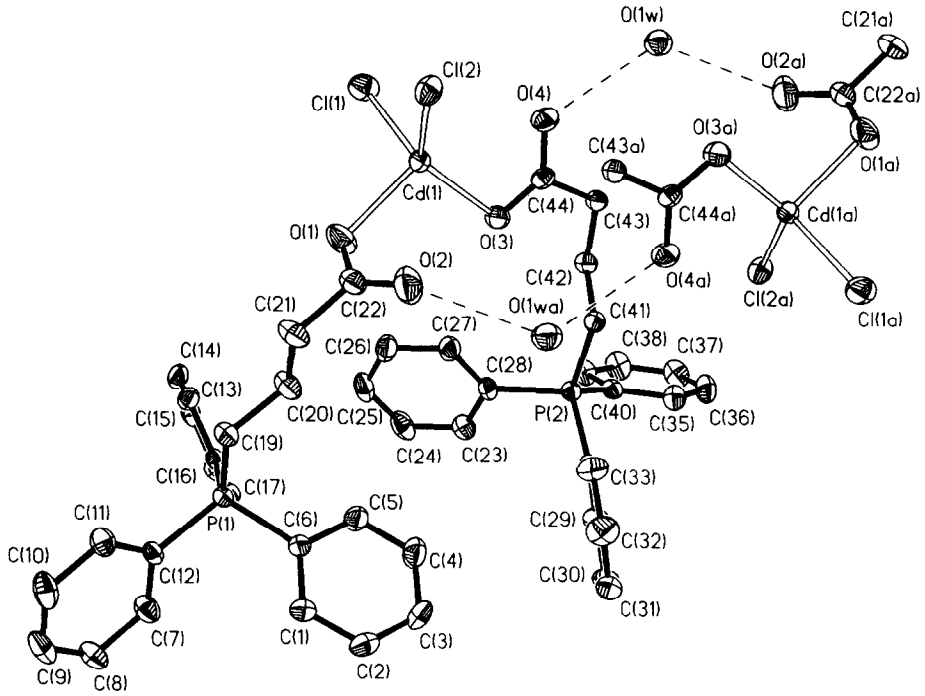


Fig. 1. Molecular structure and atom numbering of $[CdCl_2\{Ph_3P(CH_2)_3CO_2\}_2]\cdot H_2O$ **1**. Hydrogen atoms are omitted for clarity, and hydrogen bonds are indicated by broken lines. The thermal ellipsoids are drawn at the 35% probability level.

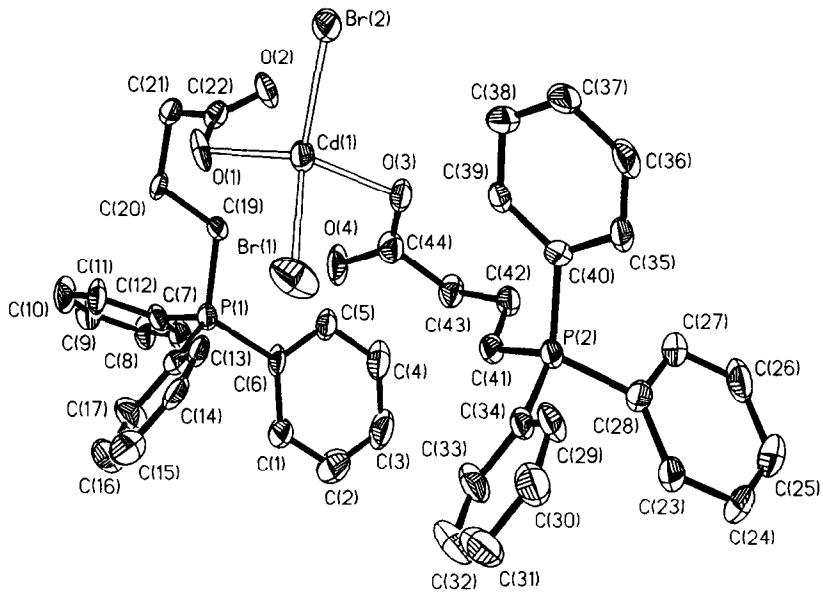


Fig. 2. Molecular structure and atom number of $[CdBr_2\{Ph_3P(CH_2)_3CO_2\}_2]$ **2**. Hydrogen atoms are omitted for clarity. The thermal ellipsoids are drawn at the 35% probability level.

bond angle. This suggests that the Δ(Cd—O) value is mainly influenced by the coordination geometry around the cadmium(II) atom.

Although the unidentate coordination mode commonly exists in zinc(II) carboxylates such as $[Zn(H_2O)_4L_2]$ and $[Zn(H_2O)_2L_2]$ (HL = 2,4-dichlorophenoxyacetic acid) [30], as well as zinc(II) complexes of tertiary amine betaines such as $[Zn(pyBET)(H_2O)Cl_2]$, $[Zn(pyBET)_2Cl_2]$ (pyBET = $C_5H_5N^+CH_2CO_2^-$), $[Zn(BET)_2Cl_2]\cdot H_2O$ (BET =

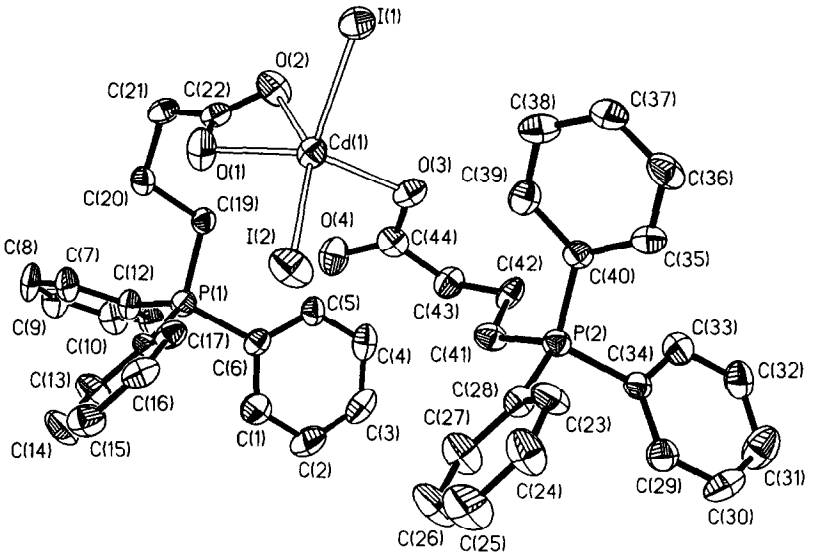


Fig. 3. Molecular structure and atom numbering of $[CdI_2\{Ph_3P(CH_2)_3CO_2\}_2]$ **3**. Hydrogen atoms are omitted for clarity. The thermal ellipsoids are drawn at the 35% probability level.

$Me_3N^+CH_2CO_2^-$) [31] and $[Zn(ppBET)_2Cl_2]$ [32] (ppBET = $C_5H_5N^+(CH_2)_2CO_2^-$), it is relatively rare in cadmium(II) carboxylates owing to the much larger radius of Cd^{II} as compared with Zn^{II} and the tendency of Cd^{II} to form polymeric species with neighboring Cd^{II} atoms through μ-*O,O'*-bridging by carboxylate groups. A plausible reason for the ease of the $Ph_3P^+(CH_2)_3CO_2^-$ betaine ligand to act in the unidentate mode to yield monomeric metal complexes is that its flexible alkyl chain enables the bulky Ph_3P group to be positioned close to the metal center and thus hinder the approach of another mononuclear species.

Acknowledgement—This work was supported by Hong Kong Research Grants Council Earmarked Grant CUHK 89/93E.

REFERENCES

1. R. H. Prince, *Comprehensive Coordination Chemistry* (Edited by G. Wilkinson, R. D. Gillard and J. A. McCleverty), Vol. 5, p. 968. Pergmon Press, Oxford (1987).
2. E. Rivera, M. A. Kennedy, R. D. Adams and P. D. Ellis, *J. Am. Chem. Soc.* 1990, **112,** 1400.
3. (a) R. S. Honkonen, F. D. Doty and P. D. Ellis, *J. Am. Chem. Soc.* 1983, **105,** 4163; (b) R. S. Honkonen, P. S. Machetti and P. D. Ellis, *J. Am. Chem. Soc.* 1984, **106,** 5488; (c) R. S. Honkonen and P. D. Ellis, *J. Am. Chem. Soc.* 1986, **108,** 912.
4. M. A. Kennedy and P. D. Ellis, *Inorg. Chem.* 1990, **29,** 541.
5. M. F. Summers, *Coord. Chem. Rev.* 1988, **86,** 43.
6. P. D. Ellis, *Science* 1983, **221,** 1141.
7. G. B. Deacon and R. J. Phillips, *Coord. Chem. Rev.* 1980, **33,** 227.
8. H. Sigel and R. B. Martin, *Chem. Soc. Rev.* 1994, **23,** 83.
9. J. Christopher, H. L. Carrell, J. Erlebacher and J. P. Glusker, *J. Am. Chem. Soc.* 1988, **110,** 8651.
10. R. C. Mehrotra and R. Bohra, *Metal Carboxylates*. Academic Press, New York (1983).
11. G. Webber, *Acta Cryst., Sect. B* 1980, **36,** 1947.
12. N. C. Charles, E. A. H. Griffith, P. F. Rodesiler and E. L. Amma, *Inorg. Chem.* 1983, **22,** 2717.
13. D. Dakternieks, *Coord. Chem. Rev.* 1985, **63,** 1.
14. M. L. Post and J. Trotter, *J. Chem. Soc., Dalton Trans.* 1974, 285.
15. J. P. Deloume and H. Loiseleur, *Acta Cryst., Sect. B* 1974, **30,** 607.
16. Y. Yukawa, Y. Inomata, T. Takeuchi, M. Shimoi and A. Ouchi, *Bull. Chem. Soc. Jpn* 1982, **55,** 3135.
17. Y. Yukawa, Y. Inomata and T. Takeuchi, *Bull. Chem. Soc. Jpn* 1983, **56,** 2125.
18. M.-Y. Chow, X.-M. Chen and T. C. W. Mak, *J. Chem. Soc., Dalton Trans.* 1993, 3413.
19. S.-L. Li and T. C. W. Mak, *J. Chem. Soc., Dalton Trans.* 1995, 1519.
20. S.-L. Li and T. C. W. Mak, *Inorg. Chim. Acta*, accepted.
21. D. B. Denney and L. C. Smith, *J. Org. Chem.* 1962, **27,** 3404.
22. R. A. Sparks, *Crystallographic Computing Techniques* (Edited by R. F. Ahmed), p. 452, Munksgaard, Copenhagen (1971).
23. G. M. Sheldrick, *Computational Crystallography* (Edited by D. Sayre), pp. 506–514. Oxford University Press, New York (1982).
24. *International Tables for X-Ray Crystallography* vol. 4, pp. 55, 99, 149. Kynoch Press, Birmingham (now distributed by Kluwer Academic Press, Dordrecht) (1974).
25. (a) A. G. Orpen, L. Brammer, F. H. Allen, O. Kennard, D. G. Watson and R. Taylor, *J. Chem.*

Soc., Dalton Trans. 1989, S66; (b) *ibid.* S69; (c) *ibid.* S70.
26. T. C. W. Mak, W.-H. Yip, E. J. O'Reilly, G. Smith and C. H. L. Kennard, *Inorg. Chim. Acta* 1985, **100,** 267.
27. R. J. Flook, H. C. Freeman, C. J. Moore and M. L. Scudder, *J. Chem. Soc., Chem. Commun.* 1973, 753.
28. M. L. Post and J. Trotter, *J. Chem. Soc., Dalton Trans.* 1974, 674.
29. X.-M. Chen and T. C. W. Mak, *Acta Cryst.* 1992, **C48,** 57.
30. C. H. L. Kennard, G. Smith, E. J. O'Reily, K. M. Stadnicka and B. J. Oleksyn, *Inorg. Chim. Acta* 1982, **59,** 241.
31. X.-M. Chen and T. C. W. Mak, *Inorg. Chim. Acta* 1991, **182,** 139.
32. X.-M. Chen and T. C. W. Mak, *Jiegou Huaxue* (*Chinese J. Struct. Chem.*) 1993, **12,** 56.

Pergamon

S0277-5387(96)00284-7

Polyhedron Vol. 16, No. 2, pp. 207–215, 1997
Copyright © 1996 Elsevier Science Ltd
Printed in Great Britain. All rights reserved
0277-5387/97 $15.00 + 0.00

Synthesis and characterization of copper(I) derivatives with *N*-donor ligands—IV.† Poly(1*H*-pyrazol-1-yl)borates cyclohexylphosphine Cu^{I}, the X-ray crystal structures of $[HB\text{-}(\mu\text{-}pz)_3\text{-}CuP(Cy)_3]$ and $[HB\text{-}(\mu\text{-}3,5\ Me_2pz)_3\text{-}CuP(Cy)_3]$

Giancarlo Gioia Lobbia,[a]‡ Claudio Pettinari,[a] Carlo Santini,[a] Marcello Colapietro[b] and Patrizio Cecchi[c]

[a]Dipartimento di Scienze Chimiche, Università di Camerino, Via S. Agostino 1, I-62032 Camerino, Italy

[b]Dipartimento di Chimica, Università di Roma "La Sapienza" P. le A. Moro, 8, 00100 Roma, Italy

[c]Dipartimento di Agrobiologia ed Agrochimica, Università della Tuscia, Via S. C. De Lellis, I-01100 Viterbo, Italy

(Received 29 February 1996; accepted 5 June 1996)

Abstract—The binding abilities of several polypyrazolylborato ligands ($Tp^{\#}$) toward nitrato bis(cyclohexylphosphine)Cu^{I} have been investigated. Complexes of empirical formula $(Cy_3P)_2Cu \cdot Tp^{\#}$ ($Tp^{\#}$ = Bp or pzTp) and $(Cy_3P)Cu \cdot Tp^{\#}$ ($Tp^{\#}$ = Tp, Tp^{Me}, Tp* or Tp^{*Cl}) have been synthesized and characterized through analytical and spectral (IR, ^{1}H, ^{13}C and ^{31}P NMR) measurements. The compound $(Cy_3P)_2Cu \cdot pzTp$ is fluxional at room temperature. In the crystal structure of the title compounds the copper atom is found in a strongly distorted tetrahedral coordination (the N—Cu—N and N—Cu—P angles range from 87.5(1) to 90.8(1)° and from 120.8(1) to 130.3(1)°, respectively. Comparison is made with related phosphino copper(I) derivatives.
Copyright © 1996 Elsevier Science Ltd

Keywords: polypyrazol-1-ylborates; cyclohexylphosphine Cu^{I}; X-ray; ^{31}P; synthesis; derivatives of copper(I).

Metal derivatives containing poly(pyrazolyl)borato ligands have been widely investigated by inorganic, organometallic and bioinorganic chemists [1,2]. Recently, the tris(pyrazolyl)borato ligand system [$Tp^{\#}$] has found widespread use in the study of copper chemistry, a metal which plays a relevant role in the synthesis of catalytic systems [3,4] and models for biomimetic studies [4–8]. Phosphino-copper(I) derivatives have also potential applications in microelectronic technology [9].

In previous papers, the synthesis and characterization of bis(triarylphosphine)copper(I) derivatives with bis(azolyl)alkanes [10] and bis-, tris- and tetrakis(pyrazolyl)borato ligands have been described [11,12]. Now, we have extended our studies to the interaction of poly(pyrazolyl)borato ligands Bp, $Tp^{\#}$ ($Tp^{\#}$ = Tp, Tp^{Me}, Tp*, Tp^{*Cl}) and pzTp (Fig. 1) with a more sterically hindered Cu^{I} acceptor as $(Cy_3P)_2Cu^{I}$.

In this paper we describe the synthesis and spectroscopic characterization of six new Cu^{I} derivatives and also the solid state structural study of two of them, namely $[HB\text{-}(\mu\text{-}pz)_3\text{-}CuP(Cy)_3]$ and $[HB\text{-}(\mu\text{-}3,5\text{-}Me_2pz)_3\text{-}CuP(Cy)_3]$. We have observed that the diversity of stoichiometries and geometries in these kind of complexes is strongly dependent on the steric and electronic requirements of the donors employed. The factors affecting the stoichiometry and the coordination number are here discussed and rationalized

† Part III is Reference 12.

‡ Author to whom correspondence should be addressed.

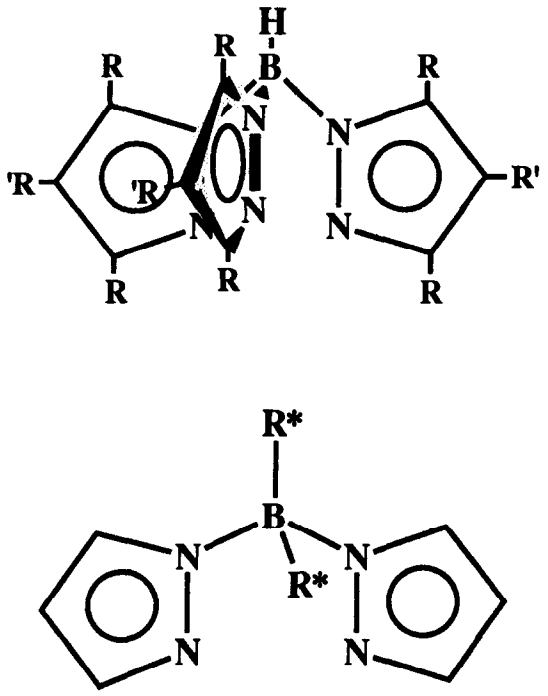


Fig. 1. Structure of the poly(pyrazol-1-yl)borato ligands employed in this work.

on the basis of steric and electronic arguments (for example Tolman's cone angle [13]).

EXPERIMENTAL

All solvents were dried by standard techniques. The reagents were obtained from Aldrich Chemical Co. and from Alfa. The samples were dried *in vacuo* to constant weight (20°C, *ca* 0.1 Torr). Concentration was always carried out under reduced pressure (water aspirator). Elemental analyses were carried out in-house with a Fisons Instruments 1108 CHNS-O Elemental analyzer. IR spectra from 4000 to 100 cm^{-1} were recorded with a Perkin-Elmer System 2000 FT-IR, instrument. ^1H, ^{13}C and ^{31}P NMR spectra were recorded on a VX-300 Varian spectrometer operating at room temperature (300 for ^1H, 75 for ^{13}C and 121.4 MHz for ^{31}P) or on a Varian Gemini-200 (200 MHz for ^1H, 50 MHz for ^{13}C). Melting points were taken on an IA 8100 Electrothermal instrument. The electrical resistances of solutions were measured with a Crison CDTM 522 conductimeter at room temperature.

All manipulations of Cu^I complexes were executed under dinitrogen to avoid any oxidation to Cu^{II}.

Synthesis of the donors

The donors Bp, Tp, Tp^{Me}, Tp*, Tp^{*Cl} and pzTp were prepared by published methods [14].

Synthesis of nitrato[bis{tricyclohexylphosphine}copper(I)]

The starting compound $\{(Cy_3P)_2CuNO_3\}$ was prepared according to the literature [15].

[Bis(tricyclohexylphosphine)copper(I)dihydridobis(pyrazol-1-yl)borato] (1)

A dichloromethane solution (25 cm^3) of bis(tricyclohexylphosphine) copper(I)nitrate (680 mg, 1.0 mmol) was added to a stirred dichloromethane suspension (30 cm^3) of potassium dihydrobis(1*H*-pyrazol-1-yl)borate (186 mg, 1 mmol) under a stream of N_2. After 3 h stirring the solid (KNO_3) was filtered and washed with dichloromethane (20 cm^3). The filtered solution was evaporated to dryness; the residue was purified from dichloromethane–heptane affording product **1** (460 mg, 0.6 mmol). Compound **2** was obtained similarly.

[(Tricyclohexylphosphine)copper(I)hydridotris(1H-pyrazol-1-yl)borato] (3)

A dichloromethane solution (25 cm^3) of bis(tricyclohexylphosphine)copper(I)nitrate (680 mg, 1.0 mmol) was added to a stirred dichloromethane suspension (30 cm^3) of potassium hydridotris(1H-pyrazol-1-yl)borate (250 mg, 1.0 mmol) under a stream of N_2. After 3 h stirring the solid (KNO_3) was filtered and washed with dichloromethane (20 cm^3). After slow evaporation of the solvent, the residue was recrystallized from acetonitrile-Et_2O, affording complex **3** (410 mg, 0.74 mmol). Compounds **4–6** were prepared similarly.

X-ray crystallography

Crystals and experimental data are summarized in Table 1. Colourless crystals of compound $Cy_3PCu \cdot Tp$ (**3**) were obtained from an acetonitrile/diethyl ether solution. For data collection one sample was used of approximate dimensions $0.2 \times 0.2 \times 0.3$ mm. The cell parameters were refined by least squares from angular position of 12 reflections in the range $7 < 2\theta < 26°$.

Colourless crystals of compound $Cy_3PCu \cdot Tp^* \cdot CH_3CN$ (**5A**) were obtained from an acetonitrile/diethyl ether solution and the data were collected from a crystal of about $0.15 \times 0.15 \times 0.2$ mm. The cell parameters were refined by least squares from angular positions of 14 reflections in the range $7 < 2\theta < 18°$.

Both crystals were mounted on a CS automatic four-circle diffractometer equipped with a Huber goniometer [16] using graphite monochromatized Mo-K_α radiation ($\lambda = 0.710689$ Å). The data were

Table 1. Crystallographic data

Compound	**3**	**5A**
Formula	$C_{27}H_{43}BCuN_6P$	$C_{33}H_{55}BCuN_6P \cdot CH_3CN$
Formula weight	557.1	682.2
Crystal system	monoclinic	orthorhombic
Space group	$P2_1/n$	$Pna2_1$
a (Å)	8.519(2)	20.475(4)
b (Å)	18.939(4)	12.470(2)
c (Å)	18.541(4)	14.663(3)
β (°)	103.27(3)	
V (Å^3)	2911.6(15)	3744(2)
Z	4	4
D_c (g cm^{-3})	1.271	1.210
μ (cm^{-1})	8.31	6.59
$F(000)$	1184	1464
No. of measured reflections	8454	4100
No. of unique reflections	8454	3564
No. of observed reflections	4187	3350
	$\lvert F_o\rvert > 2\sigma\lvert F_o\rvert$	$\lvert F_o\rvert > 6\sigma\lvert F_o\rvert$
Function minimized	$\Sigma w(\lvert F_o\rvert - \lvert F_c\rvert)^2$	
Variables refined	325	424
$R = \Sigma(\lvert F_o\rvert^2 - \lvert F_c\rvert)^2/\Sigma F_o^2$	0.029	0.039
$R_w = \Sigma_w(\lvert F_o\rvert - \lvert F_c\rvert)^2/\Sigma_w F_o^2$	0.049	0.057
$w^{-1} = \sigma^2(F_o) + KF_o^2$	$K = 0.0025$	$K = 0.0030$

collected at room temperature for $3 < 2\theta < 60°$ using an ω scan technique with a $\Delta\omega = 1°$. The scan rate was automatically chosen according to the peak intensity in the range 2.0–30.0° min^{-1}. Background counts were taken with stationary crystal with an offset of 0.5° at each end of the scan, and a total background to scan time ratio of 0.5. The intensities of three standard reflections were monitored every 97 reflections during the data collections in order to evaluate the decay. Data were corrected for Lorentz and polarization effects and for decay, but not for absorption.

Both of the structures were solved by direct methods by using SIR 92 structure determination package [17]. All the non-hydrogen atoms were refined by full-matrix least-squares methods with anisotropic thermal parameters. For the compound $Cy_3PCu \cdot Tp$ (**3**) the hydrogen atoms were introduced in the final refinement in idealized positions (C—H = 0.96 Å). Each hydrogen atom was assigned arbitrarily the equivalent isotropic temperature factor of the parent carbon atom and allowed to ride on it.

For the compound $Cy_3PCu \cdot Tp^* \cdot CH_3CN$ (**5A**), which crystallizes with a molecule of solvent in the asymmetric unit, the hydrogen atoms of the methyl groups, which are affected by large amplitude thermal motion, were introduced in calculated positions for the two more-populated conformations revealed by the Fourier difference. Their occupancy factor was kept fixed during the final refinement to 0.5. Otherwise each hydrogen atom was treated as described previously for the compound $Cy_3PCu \cdot Tp$ (**3**).

All calculations were carried out on a PC using the SIR CAOS [18] and SHELXTL [19] packages.

RESULTS AND DISCUSSION

The copper(I)polypyrazolylborato complexes **1**–**6** were synthesized from the interaction of bis(cyclohexylphosphine)copper(I)nitrato with potassium salts of the ligands, in dichloromethane suspension in accordance with the following equations:

$$(Cy_3P)_2CuNO_3 + KTp^{\#} \rightarrow KNO_3 + (Cy_3P)_2Cu \cdot Tp^{\#} \quad (I)$$

($Tp^{\#}$ = Bp, pzTp)

$$(Cy_3P)_2CuNO_3 + KTp^{\#} \rightarrow KNO_3 + Cy_3P + (Cy_3P)Cu \cdot Tp^{\#} \quad (II)$$

($Tp^{\#}$ = Tp, Tp^{Me}, Tp*, Tp^{*Cl})

All reactions resulted in the formation of the desired products in fair yields.

The complexes were generally purified from acetonitrile/Et_2O: $Cy_3PCu \cdot Tp^*$ (**5**) crystallizes also with a molecule of CH_3CN (compound **5A**). It is worth noting that the ligand pzTp, even if it is more sterically hindered with respect to Tp, is not able to act as tridentate donor by displacing a phosphine group.

The compounds **1**–**6** gave satisfactory elemental analyses. They are soluble in CH_2Cl_2, $CHCl_3$, DMSO and acetone. In the last solvent they are non-electrolytes (Table 2). This is in reasonable agreement with the neutral structures proposed in Fig. 2. In $CHCl_3$ (concentration in the range $1.0–2.0 \times 10^{-2}$ m), the ratio r between the vaporimetric molecular weight

Table 2. Yields, analyses, and physical properties of compounds **1–6**

	Compound[a]	M.p.	Yield	Elemental Analysis (Found/Calc.) (%) C	H	N	Λ^b
1	$[(Cy)_3\text{-P}]_2Cu \cdot Bp$	114–116	61	65.6	9.6	7.2	6.3
				65.4	9.7	7.3	(1.0)
2	$[(Cy)_3\text{-P}]_2Cu \cdot pzTp$	155–157	79	63.7	8.8	12.6	7.8
				63.8	8.7	12.4	(1.0)
3	$[(Cy)_3\text{-P}]Cu\text{-}Tp$	88–90	74	58.4	7.9	14.9	6.7
				58.2	7.8	15.1	(1.1)
4	$[(Cy)_3\text{-P}]Cu\text{-}Tp^{Me}$	194–196[c]	68	60.5	8.0	13.8	6.4
				60.2	8.2	14.0	(1.0)
5	$[(Cy)_3\text{-P}]Cu\text{-}Tp^*$	179–181[c]	70	62.0	8.8	12.9	7.5
				61.8	8.7	13.1	(0.9)
5A	$[(Cy)_3\text{-P}]Cu\text{-}Tp^* \cdot CH_3CN$	179–181[c]	15	61.8	8.8	13.9	7.2
				61.6	8.6	14.4	(0.9)
6	$[(Cy)_3\text{-P}]Cu\text{-}Tp^{*Cl}$	206–208[c]	62	53.6	6.9	11.1	8.7
				53.2	7.0	11.3	(1.0)

[a] Bp is dihydridobis(1*H*-pyrazol-1-yl)borate, $C_6H_8N_4B$; pzTp is tetrakis(1*H*-pyrazol-1-yl)borate, $C_{12}H_{12}N_8B$; Tp is hydridotris(1*H*-pyrazol-1-yl)borate, $C_9H_{10}N_6B$; Tp^{Me} is hydridotris(3-Me-1*H*-pyrazol-1-yl)borate, $C_{12}H_{16}N_6B$; Tp* is hydridotris(3,5Me_2-1*H*-pyrazol-1-yl)borate, $C_{15}H_{22}N_6B$; Tp^{*Cl} is hydridotris(3,5-Me_2,4-Cl-1*H*-pyrazol-1-yl)borate, $C_{15}H_{19}Cl_3N_6B$.

[b] Specific conductivity in acetone solution (ohm^{-1} cm^2 mol^{-1}) at room temperature and the molar concentration $\times 10^{-3}$ indicated in parentheses in the lower line.

[c] Melting with decomposition.

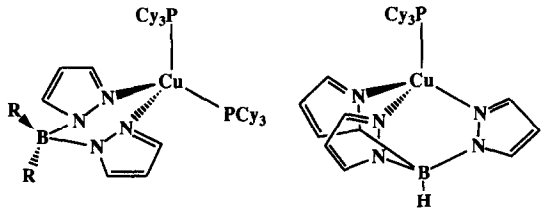


Fig. 2. Structures of the copper(I) derivatives.

and the formula weight for compound **1** lies in the range 0.70–0.80 and indicates that this complex presumably dissociates partly in this solvent in accordance with eq. III:

$$(Cy_3P)_2Cu \cdot Bp \rightleftharpoons (Cy_3P)Cu \cdot Bp + Cy_3P \quad \text{(III)}$$

All the complexes **1–6** were characterized through infrared (Nujol mull and chloroform solution) (Table 3) and ^1H, ^{13}C, and ^{31}P NMR spectra (Tables 4–5).

Infrared data

The IR spectra (Table 3) show several bands which may be taken as diagnostic of the poly(pyrazol-1-yl)borato ligands: weak and medium vibrations at about 3100 cm^{-1} due to C—H stretching in the pyrazolic ring, several more intense absorptions between 1600 and 1500 cm^{-1} typical of ring breathing [20] and finally in the derivatives **1** and **3–6,** one or two weak bands due to B—H stretching, generally unchanged with respect to those observed in the spectra of potassium salts of the ligands [21]. In the far-IR region the weak bands in the range 400–380 cm^{-1} are likely due to P—C stretching modes [22], whereas some weak absorptions at *ca* 300 cm^{-1}, absent in the spectra of both the starting copper(I) derivative and poly(pyrazolyl)borato ligands, are tentatively assigned to Cu—N stretching modes, also on the basis of previous reports in literature [23].

No significant differences were observed between the spectra in Nujol mull and those recorded in chloroform solution.

We have observed that the bis(tricyclohexyl-phosphine)derivatives **1–6** were more oxygen sensitive than the previously reported triphenylphosphine analogues [11,12]. Indeed, when the compounds **1–6** were dissolved in chloroform and exposed to air, their solutions turned deep green or blue, two characteristic colours of copper(II) derivatives.

^1H, ^{31}P and ^{13}C-NMR spectra

The ^1H and ^{13}C-NMR spectra (Tables 4 and 5) show the signals due to ligand moieties in the expected position and multiplicity [14] (e.g. for ^1H: two doublets and a pseudo-triplet for the derivatives of Bp, pzTp and Tp, two doublets for the Tp^{Me} pyrazole ring protons, together with a Me singlet, a singlet for 4-H and two singlets for the 3- and -5-Me in the Tp* derivative, and finally two Me singlets for Tp^{*Cl}). On comparison between the chemical shift related to the same type of proton in the starting potassium poly-

Table 3. Selected IR data (cm^{-1})[a]

Compound	No.	>3000	1600–1500	<650	ν(B—H)
$[(Cy_3P)_2Cu \cdot Bp]$	**1**	3109w	1502w, 1499w	520w, 510m, 490m, 470m, 396w, 386w, 351w, 325w, 306w, 279w, 247w, 224w	2446m, 2390w
$[(Cy_3P)_2Cu \cdot pzTp]$	**2**	3172w, 3148w	1508m, 1499m	519m, 474w, 462w, 420w, 395w, 386w, 360m, 346w, 280w, 247w	
$[(Cy_3P)Cu \cdot Tp]$	**3**	3115w, 3089w, 3134w	1589w, 1050sh, 1496m	520br, 473m, 460sh, 418w, 385w, 333m, 303w, 280w, 247w, 225w	2458m, 2403w
$[(Cy_3P)Cu \cdot Tp^{Me}]$	**4**	3179w, 3115w	1576w, 1506m	520m, 492w, 473w, 395w, 380w, 346w, 326w, 280m, 247w, 212w, 203w	2458w, 2405w
$[(Cy_3P)Cu \cdot Tp^*]$	**5**	3115w	1541m	513m, 483m, 469w, 460w, 396w, 383w, 352w, 326w, 303w, 280m, 254m, 247m	2516w
$[(Cy_3P)Cu \cdot Tp^*] \cdot CH_3CN$	**5A**	3115w	1541m	513m, 483m, 469w, 460w, 396w, 383w, 352w, 326w, 303w, 280m, 254m, 247m	2516w
$[(Cy_3P)Cu \cdot Tp^{*Cl}]$	**6**	3174w	1538m, 1522w, 1505sh	538w, 519m, 490w, 481w, 470w, 426w, 383w, 326vw, 279m, 247w, 226m	2458w, 2405w

[a] Nujol mull and/or $CHCl_3$ solution.

Table 4. ^1H and ^{31}P NMR data[a]

No.	Compound[b]	3- or 5-H		4-H	3- or 5-pz-Me		Cy groups	^{31}P
1	$[(Cy)_3P]_2Cu \cdot Bp$	7.59 d	7.48 d	6.16 t	—	—	1.90–1.72 m, br 1.42–1.20 m, br	17.92
2	$[(Cy)_3P]_2Cu \cdot pzTp$	7.65 d	7.07 d	6.22 t	—	—	1.80 m, br; 1.25 m, br	25.62
3	$[(Cy)_3P]Cu \cdot Tp$	7.62 d	7.47 d	6.10 t	—	—	2.08–1.72 m, br 1.52–1.25 m, br	22.37[c]
4	$[(Cy)_3P]_2Cu \cdot Tp^{Me}$	7.42 d	—	5.90 d	2.28	—	1.86–1.64 m, br 1.42–1.20 m, br	21.21
5	$[(Cy)_3P]_2Cu \cdot Tp^*$	—	—	5.66 s	2.34	2.20	1.89–1.70 m, br 1.45–1.22 m, br	26.34[c]
5A	$[(Cy)_3P]_2Cu \cdot Tp^* \cdot CH_3CN$	—	—	5.68 s	2.34	2.22	1.89–1.70 m, br 1.45–1.22 m, br	
6	$[(Cy)_3P]_2Cu \cdot Tp^{*Cl}$	—	—	—	2.32	2.20	1.90–1.74 m, br 1.56–1.24 m, br	24.44

[a] $CDCl_3$ solutions, δ in ppm from Me_4Si, calibration from internal deuterium solvent lock.
[b] The NMR data of potassium salts of bis-, tris- and tetrakis(pyrazolyl)borates are in [14].
[c] Recorded at −45°C.

Table 5. ^{13}C NMR data[a]

No.	Compound[b]	3- or 5-C		4-C	Cy	*pz*-Me
1	$[(Cy)_3Pl_2Cu \cdot Bp$	140.5	135.4	103.9	Cy: 32.6 d, 31.4 s, 28.0 d, 26.9 s	
2	$[(Cy)_3P]_2Cu \cdot pzTp$	141.6	134.9	104.6	Cy: 32.1 d, 30.7 d, 27.3d, 26.1 s	
3	$[(Cy)_3P]Cu \cdot Tp$	140.1	134.3	103.9	Cy: 32.8 br, 31.4 s, 28.1 d, 26.9 s	
4	$[(Cy)_3P]Cu \cdot Tp^{Me}$	149.1	135.8	102.2	Cy: 33.0 d, br, 31.9 s, 28.0 d, 26.4 s	Me: 15.1
5	$[(Cy)_3P]Cu \cdot Tp^*$	147.1	143.2	104.6	Cy: 33.8 d, 30.9 s, 27.9 d, 26.4 d	Me: 14.8, 12.9
6	$[(Cy)_3P]Cu \cdot Tp^{*Cl}$	145.2	140.4	108.4	Cy: 34.2 d, 32.7 d, 28.4 d, 26.7 s	Me: 13.2, 11.4

[a] $CDCl_3$ solutions, δ in ppm from Me_4Si, calibration from internal deuterium solvent lock.
[b] NMR data of potassium tris(pyrazolyl)borates are in [14].

(pyrazol-1-yl)borates and in the corresponding phosphinocopper(I) derivatives **1–6**, generally we have found downfield resonances in the case of H(5), CH_3—C(5) and CH_3—C(3) and upfield resonances in the case of H(4), whereas only a negligible shift was detected in the case of H(3). This is likely due to change in electron density of azole ring upon coordination of the donor to copper ion. Differences in chemical shifts of the cyclohexyl protons with respect to the starting $(Cy_3P)_2CuNO_3$ [15] are not significant. In all the ^1H and ^{13}C we observed one set of signals for each magnetically equivalent nucleus. Assuming that a tetrahedral coordination, similar to that found in the crystal structures of derivatives **3** and **5A**, is operating in solution also in the case of derivative **2**, we hypothesized a fluxional behaviour of this compound which likely requires a fast concomitant breaking and formation of the Cu—N bond. This behaviour is analogous to those observed in the corresponding $(Ar_3)_2Cu(I)\cdot pzTp$ [12]. In the ^{13}C-NMR spectra we found a pattern of chemical shifts in keeping with what has been previously described [14].

The ^{31}P NMR spectra of complexes **1–6** are reported in Table 4. In all the cases we observed only a single resonance. This is due to a fluxional behaviour of these complexes. The signal observed for the (pyrazol-1-yl)boratocopper(I) derivatives **1–6** appears downfield with respect to those observed for the free tricyclohexylphosphine signal (11.8 ppm). $\Delta\delta^{31}P = \delta^{31}P_{complex} - \delta^{31}P_{ligand}$, the difference in shift between the free phosphine and copper(I) complexes is in the order of 6–14 ppm. The shift is smaller than those observed in platinum and gold complexes [24]. These acceptors are more electronegative than phosphorus and inductively they withdraw electron density from the phosphorus atom which experiences a greater net magnetic field. In the ^{31}P NMR spectrum of the derivative **1** we found a broad signal upfield shifted with respect to those reported for derivatives **2–6**. This is likely due to instability of complex **1** in solution which undergoes rapid ligand exchange in accordance with equilibrium III.

Description of the molecular structures of $Cy_3PCu\cdot Tp$ (**3**) *and* $Cy_3PCu\cdot Tp^*\cdot CH_3CN$ (**5A**)

Perspective drawings of $Cy_3PCu\cdot Tp$ (**3**) and $Cy_3PCu\cdot Tp^*\cdot CH_3CN$ (**5A**) are shown in Figs 3 and 4 together with the numbering scheme. Selected interatomic distances and angles are reported in Tables 6 and 7. In both derivatives the copper atom is tetracoordinate, being bonded to one phosphorus atom of Cy_3P and three nitrogen atoms of the tridentate Tp and Tp*. The copper atom is in a strongly distorted tetrahedral environment: the N—Cu—N and N—Cu—P angles are in the range 87.5(1)–90.8(1)° and 120.8(1)–130.3(1)°, respectively. This finding is probably due to remarkable steric hindrance of the tricyclohexylphosphine [13] and Tp ligands. The

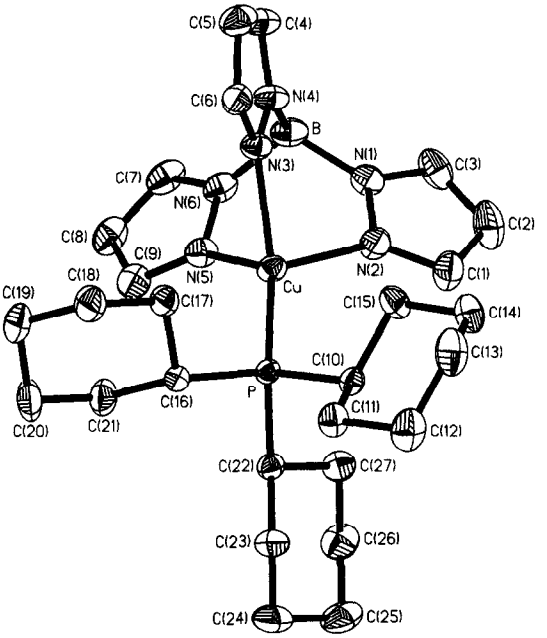


Fig. 3. Molecular structure and labelling scheme for $[(Cy)_3P]_2Cu\cdot Tp$ **3**.

Table 6. Selected bond lengths (Å)

Compound	**3**	**5A**
Cu—P	2.170(1)	2.207(1)
Cu—N(2)	2.104(2)	2.133(2)
Cu—N(3)	2.095(2)	2.106(2)
Cu—N(5)	2.093(2)	2.147(2)
P—C(10)	1.864(2)	1.852(5)
P—C(16)	1.847(2)	1.860(5)
P—C(22)	1.860(2)	1.867(4)
N(1)—N(2)	1.361(3)	1.369(5)
N(1)—C(3)	1.338(4)	1.352(6)
N(2)—C(1)	1.332(3)	1.326(6)
N(3)—N(4)	1.364(3)	1.374(4)
N(3)—C(6)	1.326(3)	1.330(5)
N(4)—C(4)	1.334(3)	1.358(5)
N(5)—N(6)	1.351(3)	1.388(5)
N(5)—C(9)	1.325(3)	1.312(6)
N(6)—C(7)	1.350(3)	1.340(6)
C(1)—C(2)	1.385(5)	1.379(7)
C(2)—C(3)	1.351(5)	1.386(7)
C(4)—C(5)	1.376(4)	1.376(6)
C(5)—C(6)	1.379(4)	1.393(6)
C(7)—C(8)	1.354(4)	1.396(7)
C(8)—C(9)	1.383(4)	1.375(6)
C(1)—C(28)		1.504(7)
C(3)—C(29)		1.492(6)
C(4)—C(30)		1.494(6)
C(6)—C(31)		1.510(6)
C(7)—C(32)		1.484(7)
C(9)—C(33)		1.496(1)
N(90)—C(91)		1.086(13)
C(91)—C(92)		1.459(12)

Table 7. Selected bond angles (°)

Compound	3	5A
P—Cu—N(2)	120.8(1)	125.4(1)
P—Cu—N(3)	130.3(1)	126.9(1)
P—Cu—N(5)	125.5(1)	124.1(1)
N(2)—Cu—N(3)	90.8(1)	90.2(1)
N(3)—Cu—N(5)	87.5(1)	89.5(1)
N(2)—Cu—N(5)	90.6(1)	89.5(1)
Cu—P—C(10)	116.0(1)	112.4(2)
Cu—P—C(16)	114.6(1)	113.2(2)
Cu—P—C(22)	111.5(1)	112.0(1)
N(2)—N(1)—C(3)	109.9(2)	110.1(4)
N(1)—N(2)—C(1)	105.8(2)	106.3(4)
N(4)—N(3)—C(6)	106.0(2)	106.1(3)
N(3)—N(4)—C(4)	109.9(2)	110.6(3)
N(6)—N(5)—C(9)	106.1(2)	106.0(3)
N(5)—N(6)—C(7)	109.6(2)	109.8(3)
N(2)—C(1)—C(2)	110.3(3)	110.8(4)
C(1)—C(2)—C(3)	105.5(3)	105.9(5)
N(1)—C(3)—C(2)	108.6(3)	106.9(4)
N(4)—C(4)—C(5)	108.3(3)	106.5(3)
C(4)—C(5)—C(6)	104.8(2)	106.7(3)
N(3)—C(6)—C(5)	111.1(2)	110.1(3)
N(6)—C(7)—C(8)	108.4(2)	107.2(4)
C(7)—C(8)—C(9)	105.0(2)	105.3(4)
N(5)—C(9)—C(8)	110.9(2)	111.7(4)
N(2)—C(1)—C(28)		121.6(4)
C(2)—C(1)—C(28)		127.7(5)
N(1)—C(3)—C(29)		123.2(4)
C(2)—C(3)—C(29)		129.9(5)
C(5)—C(4)—C(30)		130.8(4)
N(4)—C(4)—C(30)		122.8(4)
C(5)—C(6)—C(31)		128.3(4)
N(3)—C(6)—C(31)		121.5(3)
N(6)—C(7)—C(32)		123.8(5)
C(8)—C(7)—C(32)		129.0(5)
N(5)—C(9)—C(33)		121.6(4)
C(8)—C(9)—C(33)		126.8(5)
N(90)—C(91)—C(92)		178.3(12)

Cu—N bond lengths [**3**: 2.093(2), 2.095(2) and 2.104(2) Å; **5A**: 2.106(2), 2.133 and 2.147(2) Å] are somewhat longer than those observed previously in other copper(I)-azole compounds [25], suggesting a weak bonding interaction between the poly(pyrazol-1-yl)borate and the copper(I) acceptor.

Interesting features involving the metal coordination environment are recognizable comparing the structures of the compounds through some characteristic parameters such as those reported in Table 8. While the bond distances Cu(I)—N and Cu(I)—P are greater in **5A** than in **3**, the mean N—Cu—N (bite angles) and N—Cu—P angles in **5A** and in **3** are similar. In the phosphorus environment, besides the already cited lengthening of the Cu—P bond in **5A**, the C(ipso)—P mean bond distance is slightly greater in **5A** than in **3**, the angles C(ipso)—P—C(ipso) are significantly wider in **5A** than in **3**. Substitution of Me for hydrogen in position 3 of the pyrazole rings clearly makes the Tp$^{\#}$ sterically more demanding. Indeed, methyls show close contacts with the cyclohexyl groups whose shortest values range from 3.868 to 3.723 Å. The widening of C—P—C angles in **5A** at P are a consequence of the longer distance from Cu and are reflected, in part, in the enlarged C(ipso)—P distances.

Comparing the Cu—P bond lengths in the complexes **3** and **5A** with the corresponding ones in the precursors Cy_3P—$CuNO_3$ [15] or Cy_3P—$CuClO_4$ [26] a contraction of such bonds is observed on complex formation. This is to be expected on the basis of the actual oxidation state of Cu. In the precursors the phosphine is bonded to an essentially ionic metal centre, while in the complexes they are bonded to a nearly neutral one. This makes the retrodonation of electron density, from Cu to P low-lying antibonding orbitals, more effective and so the bond is stronger and shorter.

The greater value of Cu—P bond length in **5A** with respect to **3** may indicate that the overall donating power of Tp* is here lower than that of Tp for steric reasons. Since Tp* is known to be a better donor to non-hindered centres (in particular to the proton) this behaviour is likely due to steric hindrance. Indeed, recalling that the Cu—N bond lengths are greater in **5A** than in **3** as well, it may be concluded that the Me substituted ligand Tp* is here somewhat prevented from an approach so close to the bulky metal moiety as that of unsubstituted Tp.

It is also of interest to compare the present structure of **3** with the previously obtained one of $Ph_3PCu \cdot Tp$ [12] besides the N—Cu—N, N—Cu—P, and C—P—C angles which are similar and underscore the homogeneity of the complexes, the Cu—N and Cu—P bond lengths are greater in **3** than in $Ph_3PCu \cdot Tp$. This offers the chance to compare the Cu moieties (instead of the ligand ones, *vide supra*) in their contribution to steric hindrance. Here again the lengthenings observed in **3** (*vs* $Ph_3PCu \cdot Tp$) are accounted for by the same motivations as above. The P—C lengths are not comparable in this case since the carbon atoms have different hybridizations. Although the differences in the angles are slight it may be noted that the increase in N—Cu—P value for **3** is consistent with a consequent decrease of the N—Cu—N one. This, taken together with the C—P—C increase, depict a situation in which the bulky Cy_3PCu moiety demands more space and slightly compresses the Tp moiety.

Supplementary material available

Full tables of bond lengths and angles, tables of atomic coordinates and equivalent displacement coefficients, tables of observed and calculated structural factors, anisotropic thermal parameters for non-H atoms as well as hydrogen atom parameters are available as supplementary material.

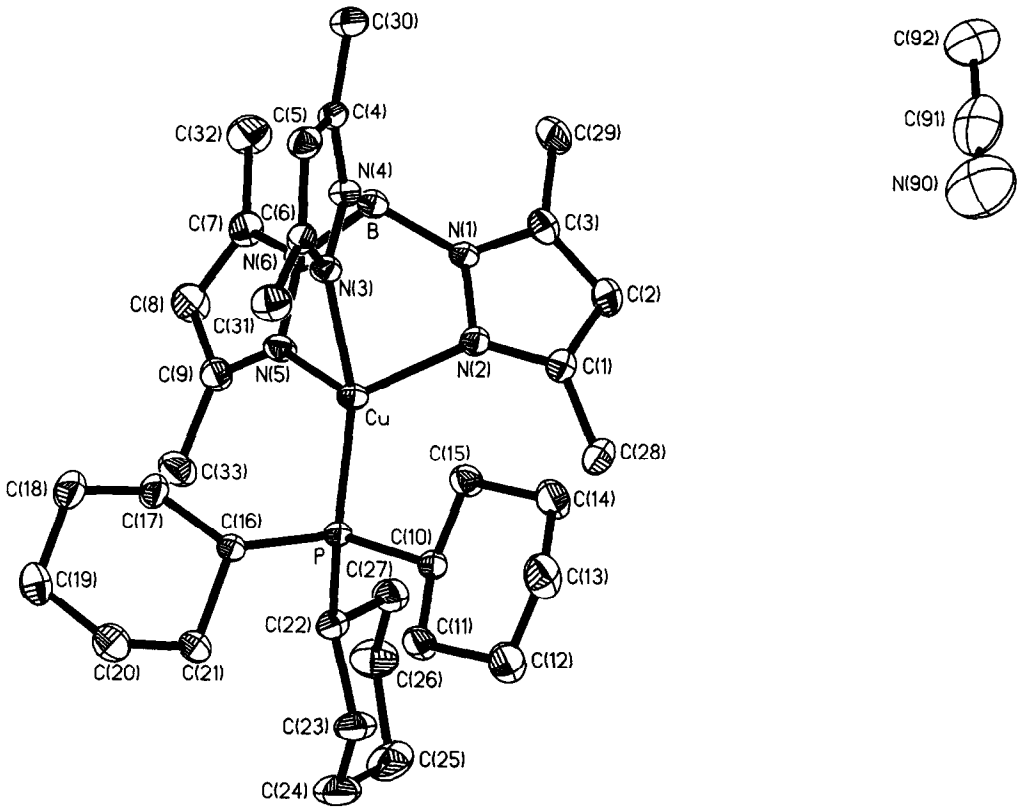


Fig. 4. Molecular structure and labelling scheme for $[(Cy)_3P]_2Cu \cdot Tp^* \cdot CH_3CN$ **5A**.

Table 8. Comparison of significant structural parameters

Compound	Cu—N[a]	Cu—P[a]	P—C[a]	N—Cu—N[b]	N—Cu—P[b]	C—P—C[b]	Reference
$Cy_3PCu \cdot Tp$ (3)	2.097	2.170	1.857	89.63	125.53	104.50	—
$Ph_3PCu \cdot Tp$	2.076	2.153	1.829	90.40	125.00	103.70	12
$(Ph_3P)_2Cu \cdot pzTp$	2.069	2.316	1.823	92.60	[d]	102.43	11
$Cy_3PCu \cdot Tp^*$ (**5A**)[c]	2.128	2.207	1.860	89.73	125.47	106.23	—

[a] In Å.
[b] In degrees.
[c] $+CH_3CN$.
[d] There are two different mean values according to the presence of two phosphines: 117.84 and 102.13°.

Acknowledgements—Financial support from the Ministero dell'Università e della Ricerca Scientifica e Tecnologica (MURST) and the Consiglio Nazionale delle Recerche (C.N.R.-Rome) is gratefully acknowledged. The authors would also like to acknowledge Dr Fabio Marchetti (Università di Camerino) for helpful discussion and Professor M. Bonamico (CNR-Montelibretti) for the help in the refinement of complex **5A**.

REFERENCES

1. S. Trofimenko, *Chem. Rev.* 1993, **93,** 943.
2. S. Trofimenko, *Prog. Inorg. Chem.* 1989, **34,** 115.
3. (a) M. R. Churchill, B. G. DeBoer, F. J. Rotella, O. M. Abu Salah and M. I. Bruce, *Inorg. Chem.* 1975, **14,** 2051; (b) M. I. Bruce and A. P. P. Ostazewsky, *J. Chem. Soc., Dalton Trans.* 1973, 2433.
4. (a) C. E. Ruggiero, S. M. Carrier, W. E. Antholine, J. W. Whitaker, C. J. Cramer and W. B. Tolman, *J. Am. Chem. Soc.* 1993, **115,** 11285; (b) S. M. Carrier, C. E. Ruggiero and W. B. Tolman, *J. Am. Chem. Soc.* 1992, **114,** 4407.
5. C. E. Ruggiero, S. M. Carrier and W. B. Tolman, *Angew. Chem., Int. Edn. Engl.* 1994, **33,** 895.
6. C. Mealli, C. S. Arcus, J. L. Wilkinson, T. J. Marks and J. A. Ibers, *J. Am. Chem. Soc.* 1976, **98,** 711.
7. (a) N. Kitajima, S. Hikichi, M. Tanaka and Y. Moro-Oka, *J. Am. Chem. Soc.* 1993, **115,** 5496; (b) N. Kitajima, K. Fujisawa, C. Fujimoto, Y.

Moro-oka, S. Hashimoto, T. Kitagawa, K. Toriumi, K. Tatsumi and A. Nakamura, *J. Am. Chem. Soc.* 1992, **114,** 1277; (c) N. Kitajima, *Adv. Inorg. Chem.* 1992, **39,** 1; (d) N. Kitajima, T. Koda, S. Hashimoto, T. Kitagawa and Y. Moro-oka, *J. Am. Chem. Soc.* 1991, **113,** 6554; (e) N. Kitajima, H. Fukui, Y. Moro-oka, H. Mizutani and T. Kitagawa, *J. Am. Chem. Soc.* 1990, **112,** 6402; *idem, ibidem* 1990, **112,** 3210; (f) N. Kitajima, H. Fukui and Y. Moro-oka, *Inorg. Chem.* 1990, **29,** 357.

8. W. B. Tolman, *Inorg. Chem.* 1991, **30,** 4877.
9. (a) D. Temple and A. Reisman, *J. Electrochem. Soc.* 1989, **136,** 3525; (b) Y. Arita, *Mater. Res. Soc. Symp. Proc.* VLSI V, p. 335 (1990); (c) A. E. Kaloyeros, A. Feng, J. Garhat, K. C. Brooks, S. K. Gosh, A. N. Saxena and F. Luethers, *J. Electron. Mater.* 1991, **19,** 271; (d) W. G. Lai, Y. Xie and G. L. Griffin, *J. Electrochem. Soc.* 1989, **138,** 3449.
10. C. Pettinari, G. Gioia Lobbia, G. Sclavi, D. Leonesi, M. Colapietro, and G. Portalone, *Polyhedron* 1995, **14,** 1709.
11. P. Cecchi, B. Bovio, G. Gioia Lobbia, C. Pettinari and D. Leonesi, *Polyhedron* 1995, **14,** 2441.
12. G. Gioia Lobbia, C. Pettinari, F. Marchetti, B. Bovio and P. Cecchi, *Polyhedron* 1996, **15,** 881.
13. C. A. Tolman, *J. Am. Chem. Soc.* 1970, **92,** 2956; *Chem. Rev.* 1977, **77,** 313.
14. G. Gioia Lobbia, F. Bonati, P. Cecchi, A. Lorenzotti and C. Pettinari, *J. Organomet. Chem.* 1991, **405,** 317; G. Gioia Lobbia, P. Cecchi, R. Spagna, M. Colapietro, A. Pifferi and C. Pettinari, *J. Organomet. Chem.* 1995, **485,** 45.
15. W. A. Anderson, A. J. Carty, G. J. Palenik and G. Schreiber, *Can. J. Chem.* 1971, **49,** 761 and references therein.
16. M. Colapietro, G. Cappuccio, C. Marciante, A. Pifferi, R. Spagna and J. R. Helliwell, *J. Appl. Crystallogr.* 1994, **27,** 435.
17. A. Altomare, G. Cascarano, C. Giacovazzo, A. Guagliardi, M. C. Burla, G. Polidori and M. Camalli, *J. Appl. Crystallogr.* 1992, **25,** 192.
18. M. Camalli, D. Capitani, G. Cascarano, S. Cerrini, C. Giacovazzo and R. Spagna, Italian Patent No 35403c186. SirCAOS USERGUIDE, Istituto di Strutturistica Chimica CNR.
19. SHELXTL: P.C. Siemens Analytical X-ray Instruments Inc., Madison, W.I. (1990).
20. G. Nieuwpoort, J. G. Vos and W. L. Groeneveld, *Inorg. Chim. Acta* 1978, **29,** 117.
21. S. Trofimenko, *J. Am. Chem. Soc.* 1967, **89,** 3170.
22. K. Nakamoto, *Infrared and Raman Spectra of Inorganic and Coordination Compounds*, 4th edn, p. 338. Wiley Interscience, New York (1986).
23. B. C. Cornilsen and K. Nakamoto, *J. Inorg. Nucl. Chem.* 1974, **36,** 2467.
24. S. Attar and J. Malito, *Polyhedron* 1992, **11,** 2409.
25. T. N. Sorrell and D. J. Jameson, *J. Am. Chem. Soc.* 1983, **105,** 6013; L. M. Engelhardt, C. Pakawatchai, A. H. White and P. C. Healy, *J. Chem. Soc., Dalton Trans.* 1985, 125.
26. J. R. Restivo, A. Costin, G. Ferguson, A. J. Carty, *Can. J. Chem.* 1975, **51,** 1949.

Pergamon

S0277-5387(96)00280-X

Polyhedron Vol. 16, No. 2, pp. 217–222, 1997
Copyright © 1996 Elsevier Science Ltd
Printed in Great Britain. All rights reserved
0277-5387/97 $15.00 + 0.00

Syntheses, characterizations and structures of a novel double-chain polymeric cluster complex $[WS_4Ag \cdot NH_3C(CH_2OH)_3 \cdot H_2O]_n$ and its precursory single-chain complex $[WS_4Ag \cdot NH_3C(CH_2OH)_3 \cdot 2DMF]_n$

Qun Huang, Xintao Wu,* Tianlu Sheng, Quanming Wang and Jiaxi Lu

State Key Laboratory of Structural Chemistry, Fujian Institute of Research on Structure of Matter, Chinese Academy of Sciences, Fuzhou, Fujian 350002, P.R. China

(Received 10 April 1996, accepted 3 June 1996)

Abstract—The title single chain complex **1** was obtained from reaction of ammonium tetrathiotungstate, silver nitrate and tris(hydroxy-methyl)-amino-methane in DMF, and the title double-chain complex **2** from the recrystallization of **1** in ethanol and a little amount of water. The anionic structure of **1** is a $[WAgS_4]_n$ linear chain, and that of **2** is a $[WAgS_4]_n$ double chain which can be viewed as two zigzag —SWSAg— chains bridged by μ_2-S atoms. In **2**, H_2O molecules and $NH_3C(CH_2OH)_3^+$ cations interact with each other through hydrogen bonding and form a two-dimensional network supramolecular structure. The inversion of configurations from **1** to **2** by re-self-assembly of $[WAgS_4]$ fragments, as well as IR spectra of both complexes, is described.
Copyright © 1996 Elsevier Science Ltd

Keywords: chalcogenides; clusters; silver compounds; tungsten compounds; polymeric tungsten–silver–sulfur complexes; structures.

The chemistry of compounds containing thiotungstate and thiomolybdate has developed rapidly in recent years because of the following main factors [1]: (1) interest in the various geometric structural types; (2) their relevance to Mo—Cu antagonism and the core structure of nitrogenase; (3) research on non-linear optical properties on some of such compounds [2]. Recently, a series of compounds with several novel structural types has been synthesized in our laboratory, using thiotungstate and thiomolybdate as reactants, such as $\{M_4Cu_4S_{12}\}$ [3], $\{M_4Cu_8S_{12}\}$ [3], $\{M_2CuS_4\}$ [4], $\{M_2Cu_2S_4\}$ [5], $\{M_2M'_6S_6(SCMe_3)_2\}$ [6] (M = Mo, W; M′ = Cu, Ag) and $\{(\mu_6\text{-S})Cu_6S_6(S_2)_6Mo_6O_6\}$ [7].

Polymeric transition metal chalcogenides have attracted much attention because they have many useful properties that are derived from the low-dimensional solid state structure [8]. In the tungsten(molybdenum)–silver–sulfur system, the general configuration of polymeric chalcogenides is linear chain [9], such as $[(PPh_4)\cdot(AgMoS_4)]_n$ [9a, b], $[(AgMS_4)\cdot(4\text{-MePyH})]_n$ [9c] $[(tmenH_2)\cdot(W_2Ag_2S_8)\cdot(tmen)\cdot(H_2O)]_n$ [9d] and $[(AgWS_4)\cdot(HNEt_3)\cdot(DMF)]_n$ [9e] (M = Mo, W; tmen = *N,N,N′,N′*-tetramethylethylenediamine). Herein, the detailed syntheses, characterization and structures of briefly-reported $[WS_4Ag\cdot NH_3C(CH_2OH)_3\cdot H_2O]_n$ (double-chain) **2** with novel one-dimensional polymeric cluster anions and two-dimensional network hydrogen-bonding cations and its precursor $[WS_4Ag\cdot NH_3C(CH_2OH)_3\cdot 2DMF]_n$ (single-chain) **1** are reported [10], additionally, the inversion of configuration from **1** to **2** is described.

EXPERIMENTAL

All manipulations were carried out in air. $(NH_4)_2WS_4$ was synthesized according to the literature [11]. The other chemicals were used as purchased. Elemental analyses were performed by the Elemental

* Author to whom correspondence should be addressed.

Analysis Laboratories of our Institute. IR spectra were recorded on a Nicolet Magna 750 FT-IR spectrometer.

Preparation of $[WS_4Ag \cdot NH_3C(CH_2OH)_3 \cdot 2DMF]_n$ **(1)**

$AgNO_3$ (0.34 g, 2 mmol) and $NH_2C(CH_2OH)_3$ (0.12 g, 1 mmol) were dissolved in 10 cm^3 of DMF. To this solution was added a solution of $(NH_4)_2WS_4$ (0.35 g, 1 mmol) in 10 cm^3 of DMF, and then the dark precipitate was filtered off. After 3 days, 0.39 g of orange crystals of **1** were obtained by allowing Et_2O vapor to diffuse into the orange–red filtrate. Found: C, 17.9; H, 3.9; N, 6.3; S, 18.4; W, 26.4. Calc: C, 17.5; H, 3.8; N, 6.1; S, 18.6; W, 26.7%. IR (KBr pellet, cm^{-1}), W-μ_2-S 439.7.

Preparation of $[WS_4Ag \cdot NH_3C(CH_2OH)_3 \cdot H_2O]_n$ **(2)**

The complex **2** was the only product of recrystallization of **1** in EtOH containing a little water. Several drops of water were added to a solution of **1** (0.40 g, 0.58 mmol) in 20 cm^3 of EtOH. Dark-red crystals of **2** (0.27 g, 0.48 mmol) were obtained by allowing the solution to stand in air for 3 days. Found: C, 8.7; H, 2.6; N, 2.4; S, 22.5; W, 32.5. Calc: C, 8.6; H, 2.5; N, 2.5; S, 22.9; W, 32.8%. IR (KBr pellet, cm^{-1}), W-μ_2-S 445.5 and 476.4.

Crystal structure determination

Crystals of **1** were selected and enveloped with epoxide resin, and as with the selected crystals of **2** were mounted on glass fibers for single-crystal X-ray diffraction experiments. The crystallographic and machine data are given in Table 1. Diffraction data were collected on a RIGAKU AFC-5R diffractometer for both complexes by use of Mo-K_α radiation ($\lambda = 0.71069$ Å) at room temperature. Cell constants and orientation matrices were obtained from least-squares by using setting angles of 20 reflections for **1** and **2** in the range $12 < 2\theta < 50°$. Intensities were corrected for polarization and Lorentz factors and for absorption by using empirical psi-scan data and the method of Walker and Stuart (DIFABS) [12].

The structures were solved by direct method using MULTAN, and the positions of two heavy atoms were obtained from E-map. The remaining non-hydrogen atoms were located from difference Fourier map. No attempt was made to locate hydrogen atoms for either structural determination. In complex **1**, oxygen atoms of two DMF groups are disordered, and these two DMF groups and the $NH_3C(CH_2OH)_3^+$ cation were rigidly refined. The direction of the polar axis (z) was determined using the Rogers method for **1** [13]. The refinement of structures of both complexes was performed by full-matrix least-squares techniques using the MolEN program package [14]. Metal and sulfur atoms were refined anistropically for both complexes. All calculations were carried out on a COMPAQ PROLINEA 4/50 computer. Atomic scattering factors were taken from [15].

RESULTS AND DISCUSSION

The reactions involved in the synthesis of **1** have shown that tris(hydroxy-methyl)-amino-methane can somewhat retard the formation of the dark precipitate of AgS and can be conducive to the stability of the linear chain $[WAgS_4]_n$.

The inversion of configuration between two polymeric chalcogenides is very rare. Hydrogen bonding is undoubtedly the driving force of the inversion of configuration from **1** to **2** (see Scheme 1). When water was added to the solution of **1** in EtOH, strong hydrogen-bonding interaction occurred between H_2O molecules and $NH_3C(CH_2OH)_3^+$ cations. Water and this hydrogen-bonding interaction can cause the linear chains $[WAgS_4]_n$ to be decomposed into $[WAgS_4]^-$ fragments. The supramolecular cationic structure formed through hydrogen bonding can affect a re-self-assembly of these anionic fragments, on the other hand, the latter can also drive the former to transform from the disordered state to the ordered state. Both of them interact with each other; finally, the novel double-chain polymeric cluster anions, as well as two-dimensional network hydrogen-bonding cations, were formed and crystallized from the solution. The attempt to synthesize the isomorphous molybdenum complex of **2** was unsuccessful.

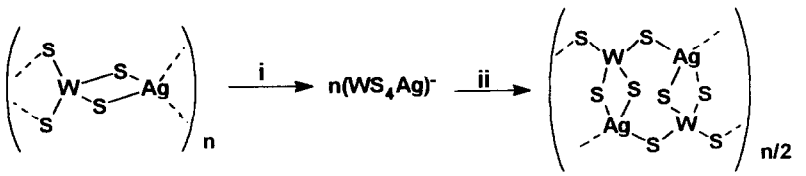
The structure of a portion of the anion of **1** is shown in Fig. 1. Selected geometric parameters of **1** are listed in Table 2. In this linear anion chain, the arrangement of the metal atoms (W, Ag) is almost linear with the bond angles of W—Ag—W(c) and Ag—W—Ag(a) being 176.4(5) and 176.4(3)°, respectively. The W atom retains its tetrahedral coordination by four sulfur atoms as in WS_4^{2-}. The Ag atom attached to the WS_4 moiety displays a distorted tetrahedron [94.1(4)–119.1(9)°]. The AgS_2W units are planar, and neighboring ones perpendicular to each other along this polymeric chain. The average W—Ag distance of 2.931 Å in complex **1** is shorter than the corresponding values in discrete molecules, such as 2.971 Å in $[WS_4Ag_2(PPh_3)_3 \cdot 0.8CH_2Cl_2]$ [16], 2.997 Å in $[Ag_4W_2S_8(PPh_3)_4]$ [17] and 3.080 Å in $[WS_4Ag_3(PPh_3)_3(S_2P(OCH_2CH_3)_2]$ [18], and also shorter than the value in a similar polymeric linear-chain complex $[AgWS_4 \cdot 4\text{-MePyH}]_n$ [9c] (2.949 Å).

As shown in Fig. 2, the anionic structure of **2** can be viewed as two zigzag —SWSAg— chains bridged by μ_2-S atoms. Selected geometric parameters of **2** are listed in Table 3. Each metal atom is coordinated by four μ_2-S atoms with an approximate tetrahedral geometry, but the coordination geometry of Ag atoms is more distorted with bond angles varying from

Table 1. Crystal data and experimental details

Compound	$[WS_4Ag \cdot NH_3C(CH_2OH)_3 \cdot 2DMF]_n$ (**1**)	$[WS_4Ag \cdot NH_3C(CH_2OH)_3 \cdot H_2O]_n$ (**2**)
Formula	$C_{10}H_{26}N_3O_5S_4Ag_1W_1$	$C_4H_{14}N_1O_4S_4Ag_1W_1$
M_r	688.31	560.14
Crystal dimension (mm)	$0.60 \times 0.10 \times 0.10$	$0.30 \times 0.15 \times 0.15$
Crystal appearance	Orange, rectangular	Dark-red, rectangular
Crystal system	Orthorhombic	Monoclinic
Space group	$P\,mn2_1$	$P2_1/n$ (alt. $P2_1/c$, No. 14)
a (Å)	8.708 (5)	9.461(2)
b (Å)	5.859(2)	7.381(1)
c (Å)	25.559(13)	19.023(5)
β ( )		101.96(2)
V (Å^3)	1304(1)	1299.5(5)
Z	2	4
D_c(g cm^{-3})	1.75	2.86
μ(Mo-K_α (cm^{-1})	55.7	111.4
F(000)	664	1048
Scan type	2θ-ω	2θ-ω
Scan rate (min^{-1})	16	16
Scan width	$0.9+0.350$ tan (θ)	$1.6+0.350$ tan (θ)
2θ(max)( )	50	50
h, k, l ranges	0–10, 0–7, 0–30	0–11, 0–9, −23–23
R_{int}		0.048
Measured reflections	1394	2648
Unique reflections	1392	2490
Obs. reflections [$I > 3\sigma(I)$]	627	1340
Minimum, maximum transmission coefficients	0.86, 1.12	0.95, 1.14
No. of parameters	53	91
R^a	0.078	0.049
R'^b	0.086	0.066
Goodness of fit	1.85	1.74
Maximum (Δ/σ)	0.53	0.01
Maximum, minimum ($\Delta\rho$/e Å^{-3})	1.79, −1.59	1.78, −1.56

$^a R = \Sigma(|F_o| - |F_c|)/\Sigma|F_o|$.
$^b R' = [\Sigma w(|F_o| - |F_c|)^2/\Sigma w|F_o|^2]^{1/2}$, $w = [\sigma^2(|F_o|^2) + (0.020 \times |F_o|)^2 + 1.000]^{-1}$.



i. decomposition

ii. re-self-assembly

Scheme 1. The inversion of configurations from **1** to **2**.

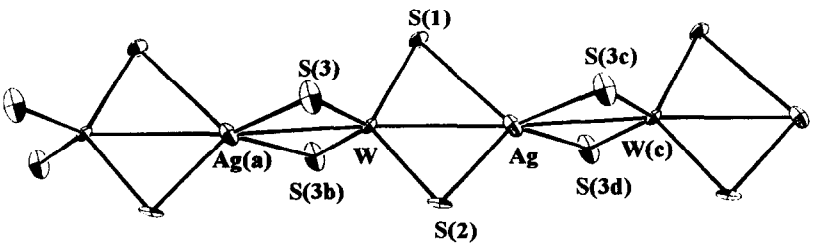


Fig. 1. Structure of a portion of the anion of **1**.

Table 2. Selected bond distances (Å) and angles (°) in $[WS_4Ag \cdot NH_3C(CH_2OH)_3 \cdot 2DMF]_n$ (**1**)

W—Ag	2.947(6)	W—S(3b)	2.21(1)
W—Ag(a)	2.915(6)	Ag—S(1)	2.75(2)
W—S(1)	2.21(3)	Ag—S(2)	2.29(2)
W—S(2)	2.25(2)	Ag—S(3c)	2.53(1)
W—S(3)	2.21(1)	Ag—S(3d)	2.53(1)
Ag—W—Ag(a)	176.4(3)	S(1)—Ag—S(3c)	116.1(9)
S(1)—W—S(2)	112.8(8)	S(1)—Ag—S(3d)	116.1(9)
S(1)—W—S(3)	106.7(9)	S(2)—Ag—S(3c)	119.1(9)
S(1)—W—S(3b)	106.7(9)	S(2)—Ag—S(3d)	119.1(9)
S(2)—W—S(3)	109.1(9)	S(3c)—Ag—S(3d)	94.1(4)
S(2)—W—S(3b)	109.1(9)	W—S(1)—Ag	72.0(6)
S(3)—W—S(3b)	114.5(4)	W—S(2)—Ag	81.0(6)
S(1)—Ag—S(2)	94.3(7)	W—S(3)—Ag(a)	75.8(4)
W—Ag—W(c)	176.4(5)		

a: $(x, y+1, z)$; b: $(1-x, y, z)$; c: $(x, y-1, z)$; d: $(1-x, y-1, z)$.

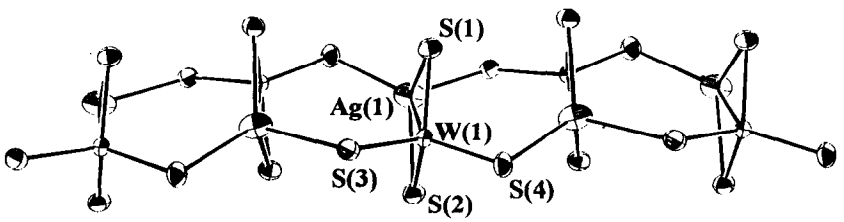


Fig. 2. Structure of a portion of the anion of **2**.

92.1(2) to 126.7(2)°. The average W—S and Ag—S distances are 2.204 and 2.565 Å, respectively, similar to those in other complexes, such as 2.22 and 2.52 Å in **1** and 2.206 and 2.533 Å in $[AgWS_4 \cdot 4\text{-MePyH}]_n$ [9c], the W—Ag distance of 2.980(2) Å can be comparable with those of 2.971 Å in $[(PPh_3)_3Ag_2WS_4 \cdot 0.8CH_2Cl_2]$ [16], 2.997 Å in $[Ag_4W_2S_8(PPh_3)_4]$ [17] and 3.080 Å in $[WS_4Ag_3(PPh_3)_3(S_2P(OCH_2CH_3)_2$ [18], but longer than those values found in linear chain polymeric complexes, such as 2.931 Å in **1** and 2.949 Å in $[AgWS_4 \cdot 4\text{-MePyH}]_n$ [9c]. The crystal structure determination shows that μ_2-S atoms in complex **2** are in two different environments, this is also reflected in the split of the ν(W-μ_2-S) IR stretching vibration peak (IR spectrum: ν(W—μ_2-S) 476.4 and 445.5 cm^{-1}).

A portion of the two-dimensional network hydro-

Table 3. Selected bond distances (Å) and angles (°) in $[WS_4Ag \cdot NH_3C(CH_2OH)_3 \cdot H_2O]_n$ (**2**)

W—Ag	2.980(2)	Ag—S(1)	2.546(6)
W—S(1)	2.187(5)	Ag—S(2)	2.563(6)
W—S(2)	2.217(5)	Ag—S(3a)	2.613(8)
W—S(3)	2.213(8)	Ag—S(4b)	2.538(8)
W—S(4)	2.197(7)		
S(1)—W—S(2)	113.2(3)	S(1)—Ag—S(4b)	115.2(2)
S(1)—W—S(3)	107.3(2)	S(2)—Ag—S(3a)	116.0(2)
S(1)—W—S(4)	110.0(3)	S(2)—Ag—S(4b)	126.7(2)
S(2)—W—S(3)	110.9(3)	S(3a)—Ag—S(4b)	98.6(3)
S(2)—W—S(4)	108.9(3)	W—S(1)—Ag	77.6(2)
S(3)—W—S(4)	106.3(2)	W—S(2)—Ag	76.7(2)
S(1)—Ag—S(2)	92.1(2)	W—S(3)—Ag(b)	106.3(3)
S(1)—Ag—S(3a)	107.9(2)	W—S(4)—Ag(a)	97.5(3)

a: $(1/2—x, -1/2+y, 3/2-z)$; b: $(1/2-x, 1/2+y, 3/2-z)$.

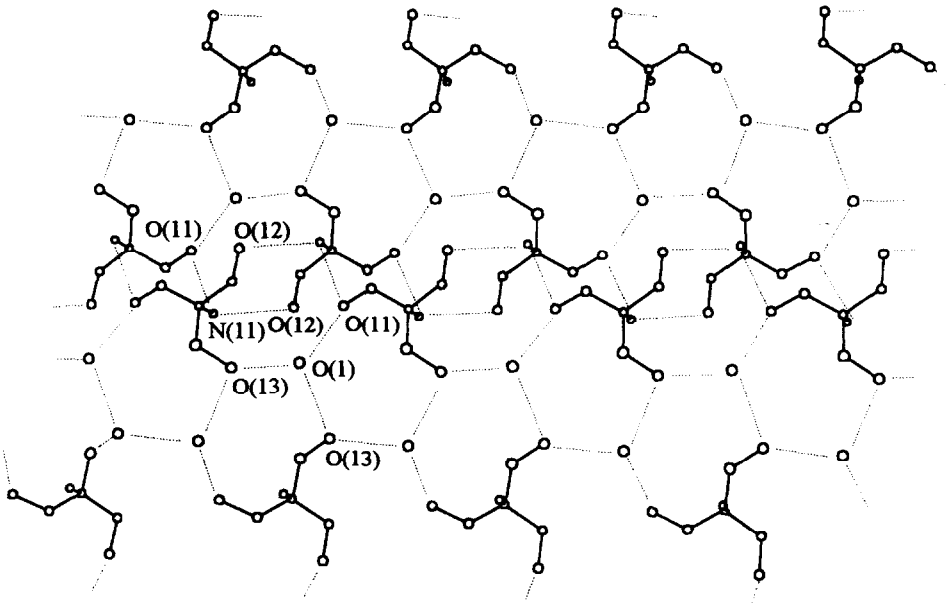


Fig. 3. A portion of two-dimensional network hydrogen-bonding cationic structure of **2**.

gen-bonding supramolecular cationic structure is shown in Fig. 3. Corresponding with the synthetic phenomena, water molecules play a crucial role in the network hydrogen-bonding structure. Hydrogen bond distances and angles are listed in Table 4. Through hydrogen bonding, H_2O groups bridge three neighboring $NH_3C(CH_2OH)_3^+$ cations. The distances of O(1)···O(11), O(1)···O(13a) and O(1)···O(13b) are 2.70, 2.73 and 2.83 Å, respectively, and the angles of O(11)···O(1)···O(13a), O(11)···O(1)···O(13b) and O(13b)···O(1)···O(13b) are 108, 119 and 106°, respectively. Similarly, a $NH_3C(CH_2OH)_3^+$ cation, acts as a μ_2 bridge between two neighboring $NH_3C(CH_2OH)_3^+$ cations. The distances of N(11)···O(11c) and N(11)···O(12d) are both 2.86 Å, and the angles of O(11c)···N(11)···O(12d) is 96°. This kind of hydrogen bonding structure is conducive to the stability of the complex **2**. The packing drawing of complex **2** is shown in Fig. 4. The polymeric double-chain cluster anions are arrayed between two cationic hydrogen-bonding "walls".

In the 3000–3500 cm^{-1} region of the IR spectra, both complexes display complicated absorption bands of N—H and O—H stretching vibrations. The very strong absorption bands in the spectra of **1** at 1668 and 1645 cm^{-1} are dominated by C=O double-bond stretching vibration; additionally, the strong single absorption peak at 440 cm^{-1} can be attributed to W—μ_2—S absorption vibration. Although sulfur atoms of complex **2** are all μ_2-S atoms, they are in two different environments according to the crystal structure determinations; so the W—μ_2—S absorption vibration of **2** appears in two different positions, 476 and 445 cm^{-1}.

Table 4. Hydrogen bond distances (Å) and angles (°) in $[WS_4Ag \cdot NH_3C(CH_2OH)_3 \cdot H_2O]_n$ (**2**)

O(1)···O(11)	2.70(2)	N(11)···O(11c)	2.86(2)
O(1)···O(13a)	2.73(2)	N(11)···O(12d)	2.86(2)
O(1)···O(13b)	2.83(2)		
O(11)···O(1)···O(13a)	108(2)	O(13a)···O(1)···O(13b)	106(2)
O(11)···O(1)···O(13b)	119(2)	O(11c)···N(11)···O(12d)	96(2)

a: $(x, 1+y, z)$; b: $(3/2-x, 1/2+y, 3/2-z)$; c: $(1-x, -y, 1-z)$; d: $(1-x, -1-y, 1-z)$.

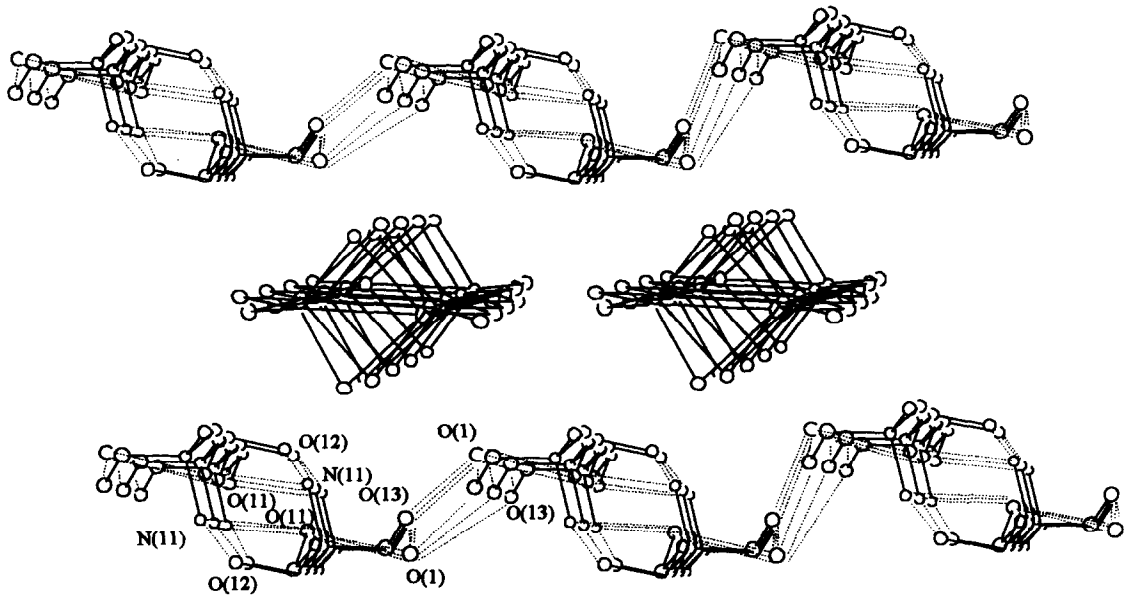


Fig. 4. Packing drawing of complex **2**.

Acknowledgements—This research was supported by grants from the State Key Laboratory of Structural Chemistry, Fujian Institute of Research on Structure of Matter, Chinese Academy of Sciences, the National Science Foundations of China, and the Provincial Science Foundations of Fujian.

REFERENCES

1. (a) A. Müller, E. Diemann, R. Jostes and H. Bögge, *Angew. Chem. Int. Ed. Engl.* 1981, **20,** 934; (b) C. E. Holloway and M. Melnik, *Rev. Inorg. Chem.* 1993, **13,** 233; (c) X. T. Wu, P. C. Chen, S. W. Du, N. Y. Zhu and J.-X. Lu, *J. Clust. Sci.* 1994, **5,** 265.
2. (a) S. Shi, W. Ji, J. P. Lang and X. Q. Xin, *J. Am. Chem. Soc.* 1994, **116,** 3615; (b) S. Shi, W. Ji, J. P. Lang and X. Q. Xin, *J. Phys. Chem.* 1994, **98,** 3570; (c) H. W. Hou, X. Q. Xin, J. Liu, M. Q. Chen and S. Shi, *J. Chem. Soc., Dalton Trans.* 1994, 3211; (d) S. Shi, W. Ji, and X. Q. Xin, *J. Phys. Chem.* 1995, **99,** 894.
3. Q. Huang, X. T. Wu, Q. M. Wang, T. L. Sheng and J. X. Lu, *Inorg. Chem.* 1996, **35,** 893.
4. N. Y. Zhu, Y. F. Zheng and X. T. Wu, *Inorg. Chem.* 1990, **29,** 2705.
5. N. Y. Zhu, Y. F. Zheng and X. T. Wu, *J. Chem. Soc., Chem. Commun.* 1990, 780.
6. S. W. Du, N. Y. Zhu, P. C. Chen and X. T. Wu, *Angew. Chem. Int. Ed. Engl.* 1992, **8,** 31.
7. X. T. Wu, B. Wang, Y. F. Zheng and J. X. Lu, *Jiegou Huaxue* (*Chinese J. of Struct. Chem.*) 1988, **71,** 47.
8. (a) D. D. Christio, S. Subramanian, L. K. Thompson and M. J. Zaworotko, *J. Chem. Soc., Chem. Commun.* 1994, 2563; (b) A. McAuley, S. Subramanian and M. J. Zaworotko, *J. Chem. Soc., Chem. Commun.* 1992, 1321; (c) V. H. Houlding and V. M. Miskowski, *Coord. Chem. Rev.* 1991, **111,** 145.
9. (a) A. Müller, W. Hellmann, J. Schneider, U. Schimanski, U. Demmer, A. Trautwein and U. Bender, *Inorg. Chim. Acta* 1982, **65,** L41; (b) A Müller and W. Hellmann, *Spectrochim. Acta* 1985, **41A,** 359; (c) J. P. Lang, J. G. Li, S. Bao and X. Q. Xin, *Polyhedron* 1993, **12,** 801; (d) Q. Huang, X. T. Wu, T. L. Sheng and Q. M. Wang, *Acta Cryst.* 1996, **C52,** 29; (e) Q. Huang, X. T. Wu, T. L. Sheng and Q. M. Wang, *Acta Cryst.* 1996, **C52,** 795.
10. Q. Huang, X.-T. Wu, T. L. Sheng and Q. M. Wang, *Inorg. Chem.* 1995, **34,** 4931.
11. J. W. McDonald, G. D. Friesen, L. D. RosenHein and W. E. Newton, *Inorg. Chim. Acta* 1983, **72,** 205.
12. N. Walker and D. Stuart, *Acta Cryst.* 1983, **A39,** 158.
13. D. Rogers, *Acta Cryst.* 1981, **A37,** 734.
14. MolEN, *An Interactive Intelligent System for Crystal Structure Analysis.* Enraf-Nonius, Delft, The Netherlands (1990).
15. D. T. Cromer and J. T. Waber, *International Tables for X-ray Crystallography*, Vol. 4. Tables 2.2a, 2.3.1. Kynoch Press, Birmingham, England (1974).
16. A. Müller, H. Bögge, E. Koniger-Ahlborn, *Z. Naturforsh* 1979, **34b,** 1698.
17. A. Müller, H. Bögge, E. Koniger-Ahlborn, *J. Chem. Soc., Chem. Commun.* 1978, 739.
18. S. W. Du, N. Y. Zhu, P. C. Chen and X. T. Wu, *J. Mol. Struct.* 1993, **291,** 167.

Pergamon

S0277-5387(96)00279-3

Polyhedron Vol. 16, No. 2, pp. 223–227, 1997
Copyright © 1996 Elsevier Science Ltd
Printed in Great Britain. All rights reserved
0277-5387/97 $15.00 + 0.00

Synthesis and crystal structure of a new phenoxy oxygen bridged binuclear cadmium(II) polyaza cryptate

Xin-You Xu,[a] Jian-Ling Chen,[a] Qin-Hui Luo,[a]* Meng-Chang Shen,[a] Xiao-Yun Huang and Quiang-Jin Wu[b]

[a]Coordination Chemistry Institute, Coordination Chemistry State Key Laboratory, Nanjing University, Nanjing 210093, P.R. China

[b]Fuzhou State Key Laboratory of Structure Chemistry, Fuzhou 350002, P.R. China

(Received 13 February 1996; accepted 3 June 1996)

Abstract—A new tris(phenoxy oxygen) bridged bicadmium(II) polyaza cryptate has been synthesized by [2 + 3] Schiff-base condensation of tris(3-aminopropyl)amine with sodium 2,6-diformyl-4-methylphenolate in the presence of $Cd(ClO_4)_2 \cdot 6H_2O$. The crystal structure, characterization of spectra and molar conductivity shows that two cadmium(II) atoms were bridged by three phenoxy oxygen atoms. Each cadmium(II) located in a seven coordination environment (N_4O_3). The coordination geometry around the Cd^{II} is a capped distorted octahedron. Copyright © 1996 Elsevier Science Ltd

Keywords: cadmium(II); cryptate; crystal structure; polyaza; binuclear; phenoxy oxygen bridge.

Pilkington and Robson [1] obtained a new kind of macrocyclic ligand in 1970 by template condensation of 2,6-diformyl-4-methylphenol with diamines. They have strong donors, namely, phenoxy oxygen atoms as well as amine nitrogen atoms, therefore they played excellent roles in catalysis and biological simulation [2,6] for their special coordination ability with transition metal ions. Recently Gagne [7], Nelson [8] and others [9] synthesized successfully several transition metal cryptates with interesting structures by [2 + 3] Schiff base condensation of tris(3-aminoethyl)amine (tren) with 2,6-diformyl-4-methylphenol (dmp). But so far few reports have been made of cryptates synthesized by condensation of corresponding aldehydes with tris(3-aminopropyl)amine (trpn, the analogue of tren). The cryptates synthesized by using trpn are expected to be more versatile in host–guest properties for flexible long chain of trpn. We have obtained the first penta-nuclear silver(I) cluster [10] by condensation of trpn with dmp in the presence of silver(I). In this paper we report the synthesis, characterization and X-ray crystal structure of the μ-oxo ligand binuclear cadmium(II) cryptate (Fig. 1).

* Author to whom correspondence should be addressed.

EXPERIMENTAL

Materials

2,6-Diformyl-4-methylphenol (dmp) was prepared using the method described by literature [11]. Sodium 2,6-diformyl-4-methylphenolate was obtained by mixing equimolar amounts of dmp and NaOH in ethanol. Tris(3-aminopropyl)amine was prepared by a modified literature method [12] with a purity of over 99%. All starting materials were of chemical purity.

Physical measurements

Solution electrical conductivity was measured by a BDS-A numerical conductometer (Jiangsu, China) with solution concentrations of $\sim 10^{-4}$ mol dm^{-3} in acetonitrile. IR spectra were measured as KBr discs using a Nicolet 5DX FT-IR spectrophotometer. Electronic spectra were recorded on a Shimadzu UV-240 spectrophotometer.

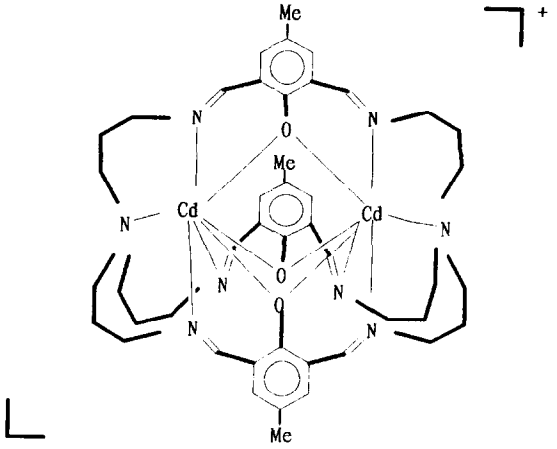


Fig. 1. The structure of the cryptate cation $[Cd_2H_{-3}L]^+$.

Preparation of cryptate

$[Cd_2H_{-3}L]ClO_4 \cdot 2CH_3OH$. To a stirred solution of sodium 2,6-diformyl-4-methylphenolate (0.1395 g, 0.75 mmol) and $Cd(ClO_4) \cdot 6H_2O$ (0.262 g, 0.625 mmol) in 30 cm^3 absolute methanol was added dropwise a solution of tris(3-aminopropyl)amine (0.094 g, 0.5 mmol) in 15 cm^3 absolute methanol at 0°C. After stirring for 2 h at 35°C, the yellowish microcrystals were precipitated and filtered off, washed with methanol and dried *in vacuo*, yield 65%. Found: C, 49.7; H, 5.3; N, 9.6; Cd, 19.3. Calc. for $C_{47}H_{65}N_8O_9ClCd_2$: C, 49.2; H, 5.7; N, 9.8; Cd, 19.6%. IR (cm^{-1}, KBr): 3452(br, ν(OH)(CH_3OH)); 1631(s, ν(C=N)); 1539(s, ν(Ar·O)); 1089(ClO_4). UV–vis (λ_{max}(nm), CH_3CN) 240(28000 mol^{-1} dm^3 cm^{-1}); 430(1×10^5). Λ_M(CH_3CN, 301 K) 100 S cm^2 mol^{-1}. The yellowish crystals $[Cd_2(H_{-3}L)]ClO_4$ suitable for X-ray structure determination were obtained by slow evaporation of the mother liquor at ambient temperature.

CAUTION. Perchlorate salts of metal complexes with organic ligands are potentially explosive. Only small amounts of material should be prepared, and these should be handled with caution. The complexes described in this report have, so far, been found to be safe when used in small quantities.

X-ray crystal structure determination of $[Cd_2(H_{-3}L)]ClO_4$

Crystal data

$C_{45}H_{57}N_8O_7ClCd_2$, M = 1082.27, yellowish plate crystal, dimensions $0.9 \times 0.15 \times 0.05$ mm, monoclinic, space group $P2_1/n$(#14), a = 15.847(0), b = 15.891(0), c = 18.058(0) Å, β = 95.24(0)°, V = 4528.41(0) Å^3, F(000) = 2220, Z = 4, D_c = 1.59 g cm^{-3}, T = 296 K, μ = 10.52 cm^{-1}.

Data collection and refinement of the crystal structure

A single crystal of dimensions $0.9 \times 0.15 \times 0.05$ mm was mounted on a glass fibre. The diffraction data were collected on an Enraf-Nonius CAD4 four-cycle diffractometer with graphite-monochromated Mo-K_α radiation (λ = 71069 Å) using an ω-2θ scan mode with ω scan width $0.65 + 0.350 \tan\theta$, scan rate 5.49° min^{-1}; a total of 7459 independent reflections were collected in the range $2 < 2\theta < 48°$, of which 4245 reflections with $I > 3\sigma(I)$ were used in the structure determination and refinement after Lp corrections. The structure was solved by the directed methods program MITHRIL. The remaining non-hydrogen atoms were located from a difference Fourier map. Hydrogen atoms were introduced in calculated position but not refined. The final least-square cycle gave R = 0.068, Rw = 0.078 ($w = 1/\sigma^2(F_o)$). The maximum and minimum residuals had heights of 1.08 e Å^{-3} and −1.34 e Å^{-3}. All calculations were performed using the programs contained in the TEXSAN package.

RESULTS AND DISCUSSION

Characterization of the cryptate

In the infrared spectrum a strong peak appears at 1630 cm^{-1} corresponding to the stretching vibration of imino C=N bonds, but shows no symmetric or unsymmetric stretching frequencies (3280 and 3330 cm^{-1}) for the NH_2 groups, nor of the strong peaks at 1650–1700 cm^{-1} for the carbonyl groups. This means that all the NH_2 and CO groups have been condensed into C=N bonds. A broad band at *ca* 3400 cm^{-1} characteristic of the OH group of CH_3OH showed that methanol molecules exist in the crystal of the cryptate, in agreement with elemental analysis, but are lost during the growth of the single crystal for X-ray structure determination. The strong peak at 1090 cm^{-1} without splitting showed that ClO_4^- does not take part in coordination with the Cd^{II} atom. This is also confirmed by molar conductivity of the cryptate (Λ_M = 100 S cm^2 mol^{-1}) which is attributable to 1 : 1 electrolyte. Two intense absorptions in electronic spectrum of the cryptate are designated to π–π^* transitions of the K band of the benzene rings and of C=N groups.

Description of the structure of $[Cd_2H_{-3}L]ClO_4$

A perspective view of cation $[Cd_2H_{-3}L]^+$ and a packing diagram are displayed in Figs 2 and 3, respectively. The selected bond distances and bond angles are given in Tables 1 and 2, respectively.

Figures 2 and 3 show that each unit cell contains four molecules of cryptates and each molecule of cryptate consists of complex cation $[Cd_2H_{-3}L]^+$ and one

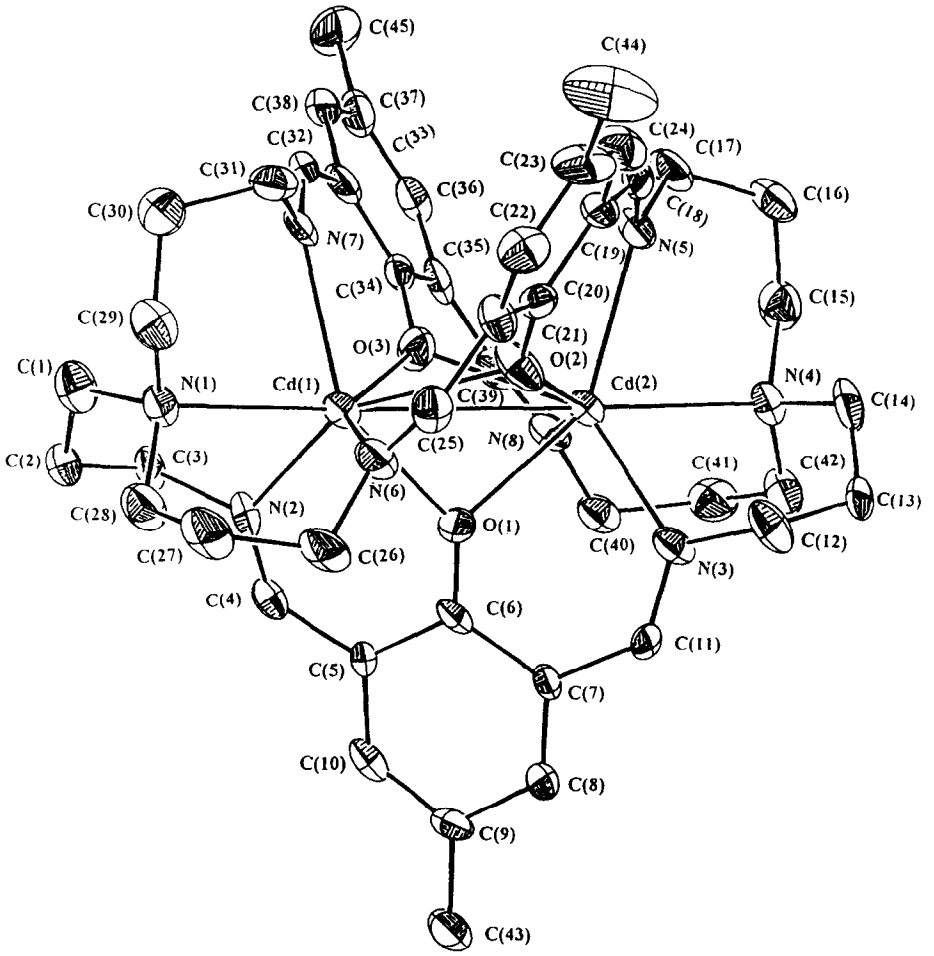


Fig. 2. The crystal structure of the cryptate cation $[Cd_2H_{-3}L]^+$ with the atom numbering scheme.

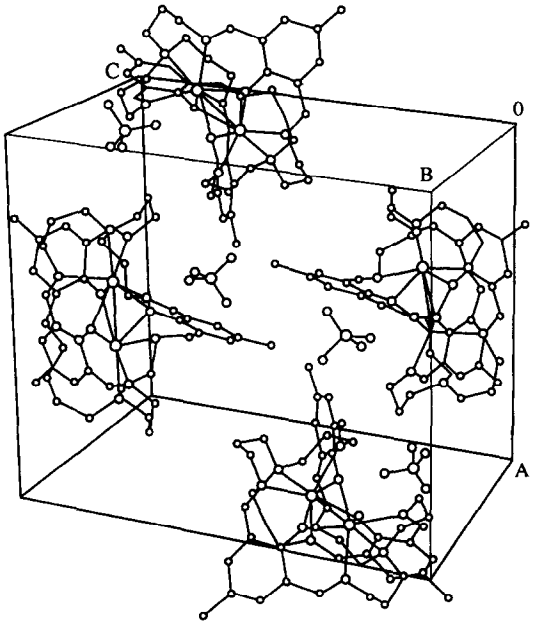


Fig. 3. A packing diagram of the cryptate $[Cd_2H_{-3}L]ClO_4$.

Table 1. Selected bond distances (Å) of the cryptate

Cd(1)—Cd(2)	3.472(1)	Cd(2)—O(1)	2.404(8)
Cd(1)—O(1)	2.247(9)	Cd(2)—O(2)	2.274(8)
Cd(1)—O(2)	2.405(8)	Cd(2)—O(3)	2.341(9)
Cd(1)—O(3)	2.286(8)	Cd(2)—N(3)	2.32(1)
Cd(1)—N(6)	2.37(1)	Cd(2)—N(5)	2.41(1)
Cd(1)—N(7)	2.37(1)	Cd(2)—N(8)	2.38(1)
Cd(1)—N(2)	2.377(9)	Cd(2)—N(4)	2.65(1)
Cd(1)—N(1)	2.60(1)	N(1)—N(4)	8.71(2)

anion. The structure of complex cation has crystallographic C_2 symmetry. Each cadmium atom is located in the centre of a capped octahedron with coordination number seven. For the Cd(1)— center, the two imine nitrogen atoms N(2), N(3) and two phenoxy oxygen atoms O(2), O(3) are all located at equatorial positions, another imine nitrogen atom N(7) and another phenoxy oxygen atom O(1) are located respectively at two axial sites. The bridgehead

Table 2. Selected bond angles (°) of the cryptate

O(1)—Cd(1)—O(3)	71.9(3)	O(1)—Cd(2)—N(5)	138.2(3)
O(1)—Cd(1)—N(6)	89.4(4)	O(1)—Cd(2)—N(4)	141.1(3)
O(1)—Cd(1)—N(7)	143.9(3)	O(3)—Cd(1)—N(6)	144.2(3)
O(1)—Cd(1)—N(2)	75.1(3)	O(3)—Cd(1)—N(7)	75.9(3)
O(1)—Cd(1)—O(2)	66.8(3)	O(3)—Cd(1)—N(2)	83.6(3)
O(1)—Cd(1)—N(1)	138.2(3)	O(3)—Cd(1)—O(2)	73.4(3)
O(1)—Cd(1)—Cd(2)	43.5(2)	O(3)—Cd(1)—N(1)	137.6(3)
O(1)—Cd(2)—Cd(1)	40.0(2)	O(3)—Cd(1)—Cd(2)	42.0(2)
O(2)—Cd(1)—N(1)	138.3(3)	O(3)—Cd(2)—N(8)	71.7(3)
O(2)—Cd(1)—Cd(2)	40.7(2)	O(3)—Cd(2)—O(1)	68.2(3)
O(2)—Cd(2)—N(3)	92.1(4)	O(3)—Cd(2)—N(5)	89.0(3)
O(2)—Cd(2)—O(3)	74.8(3)	O(3)—Cd(2)—N(4)	137.2(3)
O(2)—Cd(2)—N(8)	146.1(4)	O(3)—Cd(2)—Cd(1)	40.8(2)
O(2)—Cd(2)—O(1)	66.5(3)	N(1)—Cd(1)—Cd(2)	178.3(2)
O(2)—Cd(2)—N(5)	74.1(3)	N(4)—Cd(2)—Cd(1)	178.0(2)
O(2)—Cd(2)—N(4)	137.6(3)	N(2)—Cd(1)—O(2)	139.9(3)
O(2)—Cd(2)—Cd(1)	43.6(2)	N(2)—Cd(1)—N(1)	79.8(3)
N(6)—Cd(1)—N(7)	108.2(4)	N(2)—Cd(1)—Cd(2)	101.5(2)
N(6)—Cd(1)—N(2)	121.5(3)	N(3)—Cd(2)—O(3)	141.0(3)
N(6)—Cd(1)—O(2)	71.2(3)	N(3)—Cd(2)—N(8)	110.8(4)
N(6)—Cd(1)—N(1)	76.0(3)	N(3)—Cd(2)—O(1)	72.8(3)
N(6)—Cd(1)—Cd(2)	104.0(3)	N(3)—Cd(2)—N(5)	123.1(3)
N(7)—Cd(1)—N(2)	117.2(4)	N(3)—Cd(2)—Cd(1)	106.1(2)
N(7)—Cd(1)—O(2)	88.8(3)	N(8)—Cd(2)—O(1)	95.9(3)
N(7)—Cd(1)—N(1)	77.6(3)	N(8)—Cd(2)—N(5)	110.0(4)
N(7)—Cd(1)—Cd(2)	100.8(2)	N(8)—Cd(2)—N(4)	74.3(3)
N(8)—Cd(2)—Cd(1)	104.2(3)		

amine nitrogen N(1) is the capping atom. Three phenoxy oxygen atoms act as the bridges between Cd(1) and Cd(2). The least square planes 1, 2 or 3 consist of Cd(1), Cd(2) and O(1), O(2) or O(3), respectively. The dihedral angles between planes 1 and 2, 1 and 3 or 2 and 3 are 110.51, 119.85 and 129.64°, respectively. Cd(2) is similar to Cd(1) in coordination environment but slightly different to Cd(1) in distortion degree of the capped octahedron. The bond distances of Cd(1)—N(imine) and Cd(2)—N(imine) are in the range of 2.32–2.41 Å. Six bond distances between two Cd atoms and three phenoxy oxygen atoms are in the range of 2.25–2.40 Å, among them the bond distances of Cd(1) are approximate to those of Cd(2). This range of the bond lengths of Cd—μ—Oph is close to those reported by Drew *et al.* [8]. The bond distances of Cd(1)—N(1) and of Cd(2)—N(4) are 2.60 and 2.65 Å, respectively, implying weak interaction between Cd atoms and bridgehead nitrogen atoms. But in a similar cadmium cryptate synthesized by condensation of tren with dmp, the corresponding bond distance of Cd—N (bridgehead) is 2.787 Å [8], quite larger than that reported in this paper. In addition, the distance between Cd(1) and Cd(2), 3.472 Å, is larger than that of corresponding cryptate of tren (3.436 Å), this is due to the lengthening of carbon chain enlarging the cavity of the cryptate. However the flexibility of carbon chain strengthens the coordination ability of bridgehead nitrogen atoms and thus stabilizes the structure of cryptate.

Acknowledgements—The project was supported by the Natural Science Foundation of China and Fuzhou State Key Laboratory of Structure Chemistry.

REFERENCES

1. N. H. Pilkington and R. Robson, *Aust. J. Chem.* 1970, **23,** 2225.
2. P. Zanello, S. Tamburini, P. A. Vigato and G. A. Mazzochim, *Coord. Chem. Rev.* 1987, **77,** 165.
3. P. A. Vigato, S. Tamburini and D. E. Fenton, *Coord. Chem. Rev.* 1990, **106,** 105.
4. R. Menif, A. E. Martell, P. J. Squattrito and A. Clearfield, *Inorg. Chem.* 1990, **29,** 4723.
5. Cheng-Yu Shen, Ming-Fei Hu, Qin-Hui Luo, Meng-Chang Shen, *Trans. Met. Chem.* 1995, **20,** 634.
6. V. McKee and S. S. Tandon, *J. Chem. Soc., Chem. Commun.* 1988, 1334.
7. M. D. Timken, W. A. Marrit, D. N. Hendrickson, R. A. Gagne and E. Sin, *Inorg. Chem.* 1985, **24,** 4202.
8. M. G. B. Drew, O. W. Howart, G. G. Morgan and J. Nelson, *J. Chem. Soc., Dalton Trans.* 1994, 3149.
9. P. Chakraborty and S. K. Chandra, *Polyhedron* 1994, **13,** 683.

10. Jun Wang, Qin-Hui Luo, Meng-Chang Shen, Xiao-Yun Huang and Quiang-Jing Wu, *J. Chem. Soc., Chem. Commun.* 1995, 2373.
11. S. Taniguchi, *Bull. Chem. Soc. Jpn* 1984, **57,** 268.
12. J. Chin, M. Banaszczyk, V. Jubian and X. Zou, *J. Am. Chem. Soc.* 1989, **111,** 186.

Pergamon

S0277-5387(96)00278-1

Polyhedron Vol. 16, No. 2, pp. 229–233, 1997
Copyright © 1996 Elsevier Science Ltd
Printed in Great Britain. All rights reserved
0277-5387/97 $15.00 + 0.00

A novel structure arrangement of molybdenum dimethylglyoxime complexes. Compounds with $MoON_2C_2$ six-membered rings

R. M. Ramadan,* M. S. A. Hamza and A. S. Attia

Chemistry Department, Faculty of Science, Ain Shams University, Cairo, Egypt

(Received 2 February 1996; accepted 3 June 1996)

Abstract—Thermal reactions of $Mo(CO)_6$ with dimethylglyoxime (H_2DMG) in THF solutions, either in vacuum or under atmospheric pressure, gave three compounds with formulae $Mo(H_2DMG)_3$, **I**, $Mo_2O_6(H_2DMG)_2$, **II** and $Mo_2O_4(CO)_2(H_2DMG)_2$ **III**. Spectroscopic studies of these complexes revealed that H_2DMG is bonded to the molybdenum through the nitrogen atom of one oxime moiety and the oxygen of the other moiety. The hydrogen atom of the latter oxime was transferred to the nitrogen of the same group to form an NH group. ^1H NMR studies of compounds **II** and **III** at various temperatures showed that the hydrogen atom of this NH group was rigid on the NMR time scale while the hydrogen atom of the other oxime was fluxional. A mechanism involving terminal-bridge CO and O exchange was proposed to explain the stereochemical nonrigidity of these complexes. Appearance of a resonance at about 7.1 ppm in the ^1H NMR spectra of **II** and **III** due to a deshielded CH proton suggested some sort of aromaticity in these six membered chelates. Copyright © 1996 Elsevier Science Ltd

Keywords: dimethylglyoxime; molybdenum; coordination isomers; stereochemical nonrigidity; spectra; ligands.

Trans-bis (dimethylglyoximato) metal complexes have been known for many years [1]. They presented excellent models for many important species in biology [2]. However, investigation of other dimethylglyoxime complexes such as tris(dimethylglyoximates) and dinuclear metal complexes were not performed until recently [3–5]. Our interest in the chemistry of molybdenum complexes containing chelates with oxygen and nitrogen donors [6,7] has prompted us to investigate the reactions of molybdenum hexacarbonyl with dimethylglyoxime. It was expected that dimethylglyoxime would bind to the molybdenum atom from the two nitrogen atoms of the oxime moieties. However, different structural features were observed in this study. Also, the complexes reported here represent unique examples of the stereochemical non-rigidity of the —NOH proton.

* Author to whom correspondence should be addressed.

EXPERIMENTAL

Materials

Molybdenum hexacarbonyl, $Mo(CO)_6$ and dimethylglyoxime (H_2DMG) were supplied from Aldrich Chemical Co., Inc.

Complex syntheses

$Mo_2O_4(CO)_2(H_2DMG)_2$. $Mo(CO)_6$ (0.1 g, 0.38 mmol) and H_2DMG (0.05 g, 0.43 mmol) were mixed together in a sealed tube containing ~20 cm^3 of tetrahydrofuran solvent. The mixture was degassed with one freeze–thaw cycle and then heated for 24 h at 80°C. The colour of the solution was changed to brown. The reaction mixture was cooled and the solvent was removed on a vacuum line. The brown residue left was washed several times with boiling petroleum ether (60–80). The complex was then recrystallized from THF to yield brown crystals (yield

56%). The complex was left to dry *in vacuo* for ~3 h. The compound was found to be air stable.

$Mo(H_2DMG)_3$ *and* $Mo_2O_6(H_2DMG)_2$. A mixture of $Mo(CO)_6$ (0.13 g, 0.49 mmol) and H_2DMG (0.08 g, 0.69 mmol) in about 30 cm^3 THF was heated to reflux under atmospheric pressure for 2 days. The colour of the reaction mixture was changed to brown and a dark brown solid was isolated. The reaction mixture was then cooled and the dark brown precipitate was separated by filtration. The isolated residue was purified by boiling it several times with tetrahydrofuran followed by washing with hot petroleum ether. The complex was recrystallized from dimethylformamide to give the dark brown compound $Mo_2O_6(H_2DMG)_2$. The complex was left to dry on a vacuum line (yield 38%) and it was found to be air stable.

From the brown filtrate of the reaction mixture, the solvent was removed on a vacuum line to yield a brown residue. The residue was washed several times with boiling petroleum ether and then recrystallized from THF. The brown crystals, $Mo(H_2DMG)_3$, were dried on a vacuum line. The complex (yield 46%) was found to be air stable.

Physical measurements

The IR measurements were carried out on a Unicam-Mattson 1000 FT-IR spectrometer with the use of KBr discs. UV–vis measurements were performed on a Perkin-Elmer Lambda 4β spectrophotometer with the use of 10 mm quartz cells. Samples of concentrations *ca* 1×10^{-6} M in dimethylsulfoxide (DMSO) were measured against the solvent in the reference cell. NMR measurements were performed on a Bruker AC300 MHz spectrometer. The samples were dissolved in DMSO-d_6 using tetramethylsilane (TMS) as internal reference. Besides the spectroscopic studies, all the complexes were characterized by elemental analysis and mass spectroscopy. The data are given in Tables 1–3.

RESULTS AND DISCUSSION

Reaction of molybdenum hexacarbonyl with dimethylglyoxime under atmospheric pressure, yielded the tris-derivative $Mo(H_2DMG)_3$ as well as the dinuclear complex $Mo_2O_6(H_2DMG)_2$ (eq. (1)). On the other hand, reaction of $Mo(CO)_6$ and H_2DMG *in vacuo* resulted in the formation of only one product, $Mo_2O_4(CO)_2(H_2DMG)_2$ (eq. (2)).

$$Mo(CO)_6 + H_2DMG \xrightarrow{\text{reflux in air}} \underset{\mathbf{I}}{Mo(H_2DMG)_3} + \underset{\mathbf{II}}{Mo_2O_6(H_2DMG)_2} \quad (1)$$

$$Mo(CO)_6 + H_2DMG \xrightarrow{\text{vacuum}} \underset{\mathbf{III}}{Mo_2O_4(CO)_2(H_2DMG)_2} \quad (2)$$

Table 1. Elemental analysis and mass spectroscopic data for the molybdenum dimethylglyoxime complexes

Complex	Elemental analysis %C Calc.	%C Found	%H Calc.	%H Found	%N Calc.	%N Found	Mass spectrometry Mol. Wt.	Mass spectrometry $m/z(p^+)$
$Mo(H_2DMG)_3$	32.4	32.1	5.4	5.9	18.9	18.3	444.31	445
$Mo_2O_6(H_2DMG)_2$	18.5	18.2	3.1	3.5	10.8	10.2	520.12	521
$Mo_2O_4(CO)_2(H_2DMG)_2$	22.1	21.7	3.0	3.3	10.3	10.6	544.14	545

Table 2. The important IR and NMR data for the molybdenum dimethylglyoxime complexes

Complex	IR data (cm^{-1})[a] ν_{NH}	ν_{OH}	ν_{CO}	$\nu_{Mo=O}$	$\nu_{Mo-O-Mo}$	NMR data (ppm)[b]
$Mo(H_2DMG)_3$	3119 (m)	3212 (s) 3328 (m)	—	—	—	1.93 (s), 3.36 (s), 11.37 (s)
$Mo_2O_6(H_2DMG)_2$	3128 (s)	3186 (vs) 3423 (s)	—	903 (vs)	708 (s)	1.92 (s), 3.36 (s), 7.27 (b), 11.37 (b)
$Mo_2O_4(CO)_2(H_2DMG)_2$	3125 (s)	3214 (vs) 3304 (s)	2018 (w) 1933 (m) 1887 (s) 1807 (w)	904 (vs)	707 (m) 653 (m)	1.92 (s), 3.36 (s), 7.02 (b), 11.37 (s), 12.06 (s)

[a] w, weak; m, medium; s, strong; vs, very strong.
[b] s, singlet; b, broad.

Table 3. The UV–vis data for dimethylglyoxime and its molybdenum complexes in dimethylsulfoxide solvent

Compound	λ (nm)
H_2DMG	270
$Mo(H_2DMG)_3$	271, 483[a]
$Mo_2O_6(H_2DMG)_2$	263, 528[a]
$Mo_2O_4(CO)_2(H_2DMG)_2$	264, 300, 385, 459

[a] Broad.

Dimethylglyoxime exists in isomeric oxime and nitroso forms. Thus, its IR spectrum shows stretching frequencies due to free and bonding OH, NH and N=O bonds. The IR spectrum of the tris product, $Mo(H_2DMG)_3$, shows an almost identical pattern as that of dimethylglyoxime itself (Fig. 1). On the other hand, the vibrational spectra of $Mo_2O_6(H_2DMG)_2$ and $Mo_2O_4(CO)_2(H_2DMG)_2$ complexes are completely different from that of H_2DMG (Fig. 2). However, it is interesting that all the three molybdenum complexes display frequencies in the IR

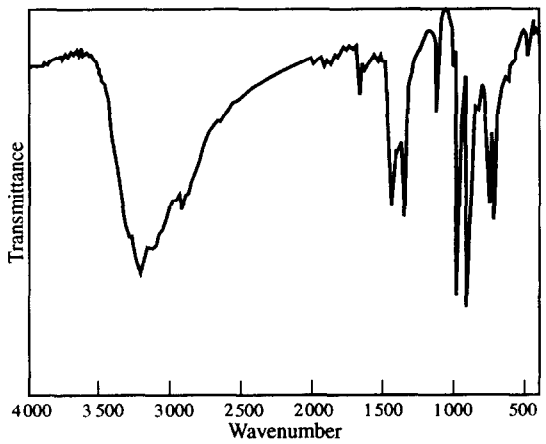


Fig. 1. The IR spectrum of $Mo(H_2DMG)_3$ complex.

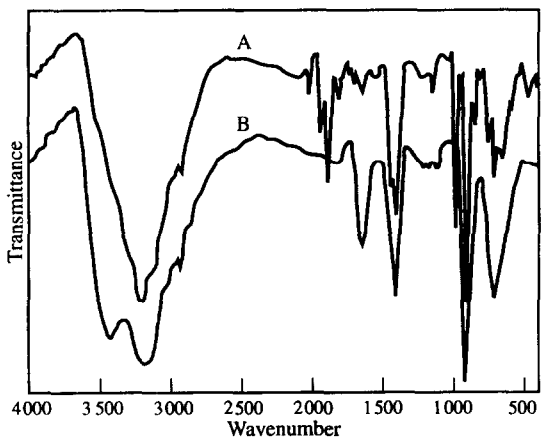
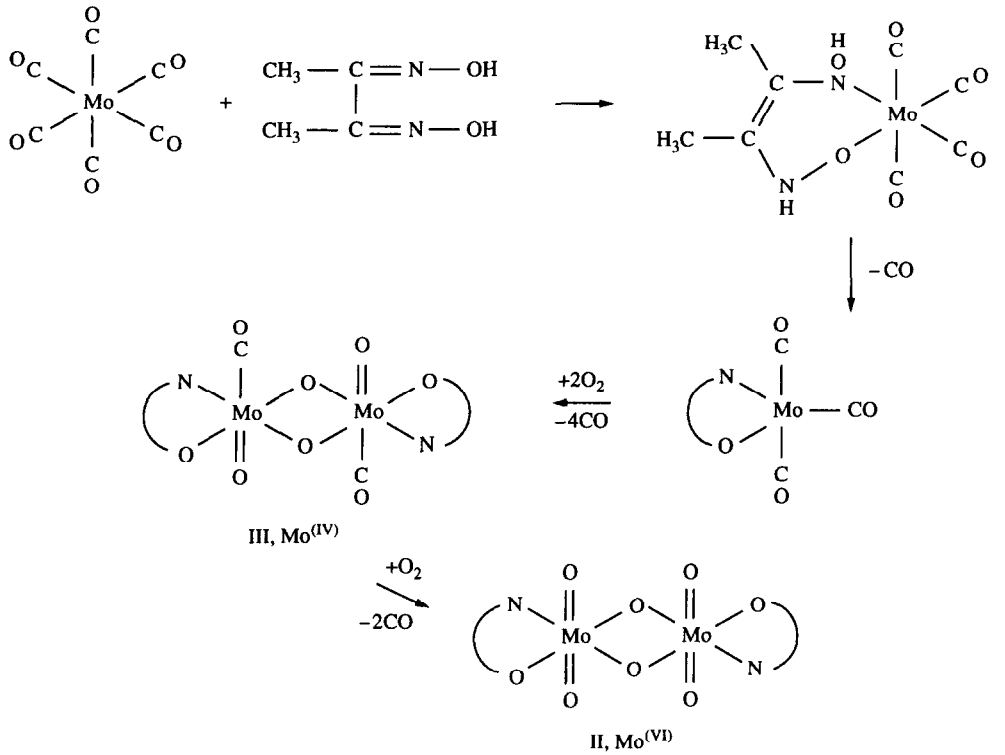


Fig. 2. The IR spectrum of (A) $Mo_2O_4(CO)_2(H_2DMG)_2$ complex, and (B) $Mo_2O_6(H_2DMG)_2$ complex.

spectra due to ν_{NH} bonds (Table 2). It was expected that this ν_{NH} band of H_2DMG would disappear from the spectra of the complexes. Therefore, the presence of these NH bands, which are also confirmed by ^1H NMR (*vide infra*), suggests that the bonding between the molybdenum atom and H_2DMG is from a nitrogen atom of one oxime group and the oxygen atom of the other group to form a chelate of a six membered ring. This unusual bonding for dimethylglyoxime was only observed previously in the dinuclear copper complex $Cu_2(DMG)(HDMG)(H_2DMG)$ where the dimethylglyoximato (DMG) moiety bridged the two copper atoms from an oxygen atom [5]. On the contrary, the crystal structure of the *tris*-(dimethylglyoxime)ruthenium(II) dichloride has shown that the ruthenium atom is bonded to H_2DMG from the two nitrogen atoms [6]. However, the unusual bonding observed here may be attributed to the larger size of the molybdenum with respect to that of ruthenium. Dimethylglyoxime as well as its three molybdenum complexes all showed bands due to free and bonded OH groups (Table 2). Also, the $Mo_2O_4(CO)_2(H_2DMG)_2$ showed four CO frequencies in the terminal and bridging metal carbonyl regions confirming the presence of the complex in two isomeric forms with terminal and bridged CO groups. We were unable to separate these two isomers. They may exist in equilibrium even in the solid state. Some bands due to terminal Mo=O and bridged Mo—O—Mo bonds were detected from the IR spectra of the two complexes $Mo_2O_6(H_2DMG)_2$ and $Mo_2O_4(CO)_2(H_2DMG)_2$, Table 2. It is interesting to speculate that the latter two complexes were prepared through the intermediate $Mo(CO)_3(H_2DMG)$. Reaction of oxygen with such intermediate would result in the formation of the products [6], Scheme 1.

Investigation of the molybdenum dimethylglyoxime complexes by ^1H NMR showed dramatic changes in the spectra. The ^1H NMR spectrum of $Mo(H_2DMG)_3$ in DMSO-d_6 displayed, besides the resonance of the methyl groups, two singlets at 3.36 and 11.37 ppm due to the protons of the NH and OH groups. The signal due to NH group was slightly broadened which is usual for a hydrogen atom bonded to a nitrogen atom (^{14}N, $I = 1$). The resonance of OH was sharp and occurred within the range for partially hydrogen-bonded OH of aromatic systems [8]. The proton NMR spectra of both $Mo_2O_6(H_2DMG)_2$ and $Mo_2O_4(CO)_2(H_2DMG)_2$ showed in addition to those signals, a broad signal at about 7.2 ppm. The $Mo_2O_4(CO)_2(H_2DMG)_2$ also showed a singlet due to a free OH at 12.06 ppm with a ratio of 1 : 5 to that of the 11.37 ppm signal (Fig. 3). This set of signals of free and bonded OH groups suggested the existence of two isomers for this complex in solution with the one having free OH groups representing about 20% abundance. Interestingly, heating the solutions of either $Mo_2O_6(H_2DMG)_2$ or $Mo_2O_4(CO)_2(H_2DMG)_2$ at 75°C resulted in broadening of all the signals. Further heating to 125°C led the signals at 12.06, 7.02 and



Scheme 1

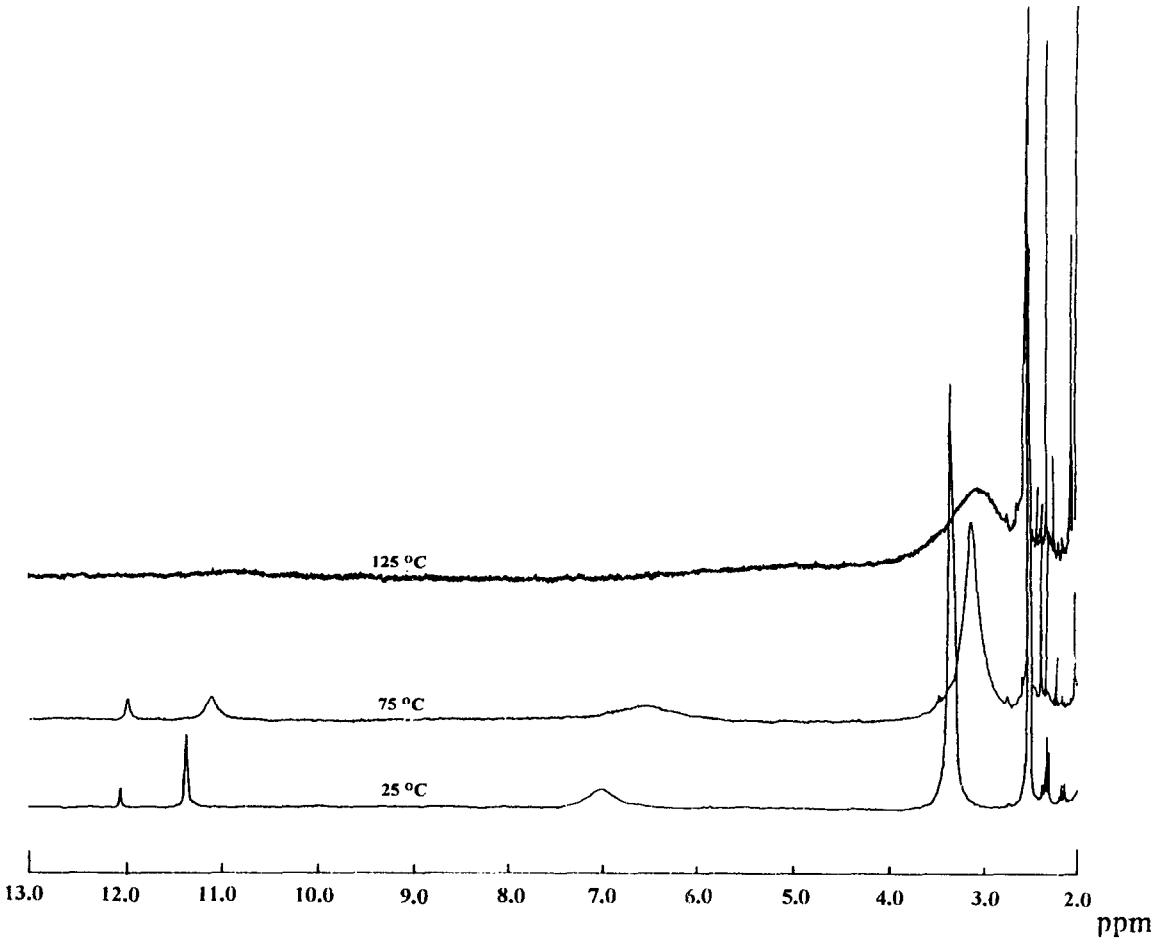
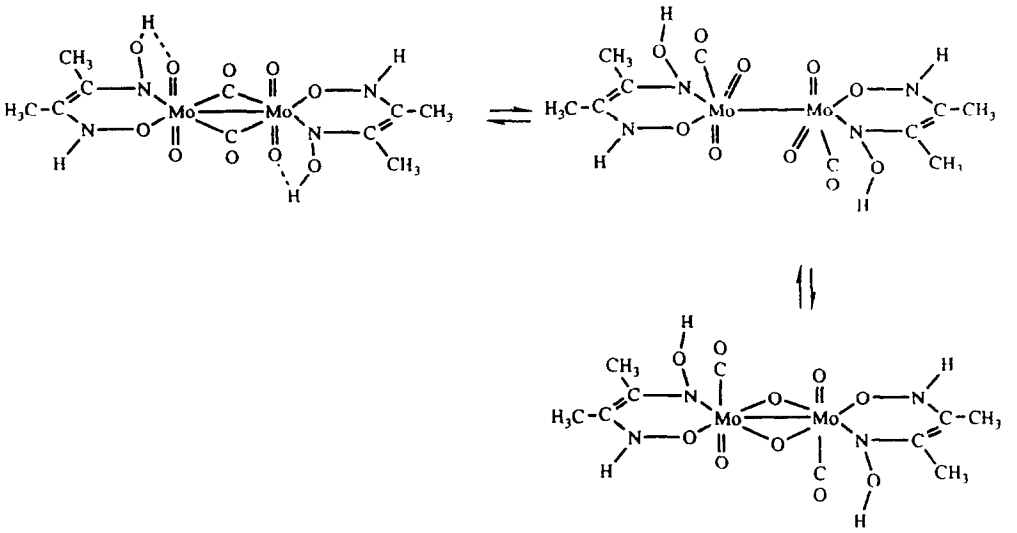


Fig. 3. The ^{1}H NMR spectra of $Mo_2O_4(CO)_2(H_2DMG)_2$ at various temperatures.



Scheme 2

11.37 ppm of the $Mo_2O_4(CO)_2(H_2DMG)_2$ to collapse into the base line (Fig. 3). It is noteworthy that the signal at 3.34 ppm due to the proton of NH group was still present in the spectrum. Thus, the proton of this group was rigid at this temperature on the NMR time scale. Unfortunately, we could not obtain ^1H NMR spectra at higher temperatures to detect the average signal due to decomposition of the complexes. Therefore, this fluxional behaviour of these two complexes indicated that the protons of the free and bonded OH groups were exchangeable. Also, the presence of a broad band around 7.1 ppm (a strong deshielded CH proton) may indicate that the OH proton transferred to one of the carbon atoms in the six membered chelate. The presence of such signal as well as the appearance of the OH signals around 11.3–12.0 ppm may imply aromaticity in the six membered ring formed. Contribution of the lone pairs of the nitrogen and oxygen atoms with the odd electron in the p_z of each carbon atom along with an appropriate $d\pi$ orbital from the molybdenum atom may be responsible for such aromaticity [9].

A mechanism is proposed to explain the stereochemical non-rigidity of these complexes, Scheme 2. Such a mechanism has several attractive features: it permits the other ligands such as O or CO to be involved in the exchange. Such an intermediate could allow carbonyl exchange to occur by a terminal-bridge mechanism. It also provides a pathway by which the OH proton can transfer to a carbon atom of the six membered ring.

The electronic absorption spectrum of dimethylglyoxime in DMSO showed only a single absorption band in the UV range at 270 nm. This band hardly changed in the case of the tris derivative $Mo(H_2DMG)_3$. However, hypsochromic shifts of this band were observed in the spectra of the other two complexes, $Mo_2O_6(H_2DMG)_2$ and $Mo_2O_4(CO)_2(H_2DMG)_2$, (Table 3). In addition, the UV–vis spectra of all the three complexes displayed visible bands due to the n–π^* transitions. Furthermore, the $Mo_2O_4(CO)_2(H_2DMG)_2$ complex illustrated another visible band confirmed the existence of this complex in two isomeric forms (Table 3).

REFERENCES

1. A. Chakravorty, *Coord. Chem. Rev.* 1974, **13**, 1.
2. J. J. R. Frausto da Silva and R. J. P. Williams, *The Biological Chemistry of the Elements*. Clarendon Press, Oxford (1991).
3. M. M. Taqui Khan, K. Venkatasubramanian, S. H. R. Abdi, M. M. Bhadbhade and B. Tyagi, *Acta Cryst.* 1992, **48**, 1402.
4. R. Ruiz, J. Sanz, B. Cervera, F. Lloret, M. Julve, C. Bois, J. Faus and M. C. Munoz, *J. Chem. Soc., Dalton Trans.* 1993, 1623.
5. R. Ruiz, J. Sanz, B. Cervera, F. Lloret, M. Julve, J. Faus, C. Bois and M. C. Munoz, *J. Chem. Soc., Dalton Trans.* 1993, 3035.
6. R. M. Ramadan, A. S. Attia and M. F. El-Shahat, *Polyhedron* 1996, **15**, 301.
7. R. M. Ramadan, M. F. El-Shahat and A. S. Attia, *Polyhedron* 1996, **15**, 2545.
8. R. M. Silverstein, G. C. Bassler and T. C. Morrill, *Spectrometric Identification of Organic Compounds*. 4th ed., Wiley, New York (1981).
9. H. G. Heal, *The Inorganic Heterocyclic Chemistry of Sulfur, Nitrogen and Phosphorus*. Academic Press, London (1980).

Pergamon

S0277-5387(96)00274-4

Polyhedron Vol. 16, No. 2, pp. 235–242, 1997
Copyright © 1996 Elsevier Science Ltd
Printed in Great Britain. All rights reserved
0277-5387/97 $15.00+0.00

Polymeric complexes of cadmium(II) bridged simultaneously by tetradentate picolinato and μ(1,1)-azido or μ(N,S)-thiocyanato anions. Synthesis and structural characterization of $[Cd(picolinato)(N_3)]_n$ and $[Cd(picolinato)(NCS)]_n$

Franz A. Mautner,[a]* Morsy A. M. Abu-Youssef[b] and Mohamed A. S. Goher[c]*

[a]Institut für Physikalische und Theoretische Chemie, Technische Universität Graz, A-8010 Graz, Austria

[b]Department of Chemistry, Faculty of Science, Alexandria University, Alexandria 21321, Egypt

[c]Department of Chemistry, Faculty of Science, Kuwait University, P.O. Box 5969 Safat, 13060 Kuwait

(Received 25 April 1996; accepted 28 May 1996)

Abstract—Two mixed ligand complexes of picolinic acid and cadmium(II) azide or thiocyanate, namely catena-μ(1,1)-azido-μ(N,O,O,O′-picolinato)cadmium(II) (**1**) and catena μ(N,S)-thiocyanato-μ(N,O,O,O′-picolinato)cadmium(II) (**2**) have been prepared and characterized by spectroscopic and X-ray crystallographic methods. The coordination environment of the cadmium(II) atom in complex **1** is a distorted octahedron. Each metal atom is chelated by a picolinato anion via its ring nitrogen N(1) [Cd—N = 2.356(6) Å] and a carboxylate oxygen atom O(1). O(1) is further coordinated to another cadmium atom to form cyclic Cd_2O_2 units [Cd—O = 2.327(5) and 2.459(5) Å]. O(2) links a third metal centre. The cyclic Cd_2O_2 units are connected by μ(1,1) bridging azido groups to form sheets of polyhedra which are arranged normal to the long *c*-axis of the unit cell. Complex **2** features distorted octahedral cadmium atoms, N,O,O,O′-tetradentate chelating bridging picolinato anions, μ(N,S) bridging thiocyanato ligands and one-dimensional chains of polyhedra which are oriented along the *b*-axis of the monoclinic unit cell. The IR and Raman spectra are also reported and correlated with the structures of the complexes. The vibrational bands of diagnostic value are compared to the values of the free acid. Copyright © 1996 Elsevier Science Ltd

Keywords: cadmium complexes; X-ray structure analysis; thiocyanate; azide; picolinato complexes; vibrational spectroscopy.

Picolinic acid (pic-H), also called pyridine-2-carboxylic acid, and its derivatives have a broad spectrum of physiological effects on the activity functions of both animal and plant organisms which are attributed to their ability to form complexes with transition metals [1]. This acid may function as a neutral ligand as found in the structures of $[K(pic\text{-}H)_2(H_2O)_2][AuBr_4]\cdot(pic\text{-}H)_2$ [2], and $Ag(C_5H_4NCO_2H_{1/2})\cdot H_2O$ [3], or as a picolinate anion [4–9]. The picolinate anion may act as a N,O-bidentate chelating ligand as found in the structure of $[Mg(pic)_2(H_2O)_2]\cdot 2H_2O$ [6] or as a N,O,O′-tridentate chelating bridging ligand, coordinating *via* the ring nitrogen and the two carboxylate oxygen atoms as in the structure of $[Cu(pic)_2]\cdot 2H_2O$ [10].

Recently we established that picolinic acid coexists as neutral and anionic N,O-bidentate ligands in $[Mn(pic)(pic\text{-}H)(Cl)]_2$ [11], as N,O,O-tridentate chelating bridge ligand in $[Mn(pic)(N_3)(H_2O)]_n$ [12] and as N,O,O,O′-tetradentate ligand in the structure of $[Cu(pic)Cl]_n$ [13]. Thus a substitution of one of the two picolinato anions in the parent $[M(pic)_2]$ complex by other anions, e.g. Cl^- or N_3^-, leads to new modes

* Authors to whom correspondence should be addressed.

of bonding of the picolinato anion. As the azide and thiocyanate anions are versatile ligands that can bind metals atoms in a variable manner [14–20], we used both anions to replace one of the two picolinate anions in the parent complex $[Cd(pic)_2]_n$ [7], in order to appraise the influence of these anions on the mode of bonding of each other. The synthesis and structural characterizations of the title complexes, as elucidated by spectroscopic and X-ray crystallographic methods are the subject of this paper.

EXPERIMENTAL

Picolinic acid was obtained from Aldrich and the other chemicals were of analytical grade quality.

Preparation of $[Cd(picolinato)(N_3)]_n$ *complex* (**1**)

Complex **1** was prepared by mixing 4 cm^3 of an aqueous solution of $CdCl_2$ (0.2 g, 1 mmol) and picolinic acid (0.3 g, 2.5 mmol) in 3 cm^3 ethanol. To this clear solution an aqueous solution of NaN_3 (0.13 g, 2 mmol) in 2 cm^3 distilled water was added dropwise and the solution was shaken thoroughly after each addition. The clear solution, was allowed to stand over several days to produce colourless crystals. The crystals were filtered, washed with a very little amount of ethanol, air dried and stored in a desiccator. Found: C, 26.0; H, 1.6; N, 20.4; Cd, 40.5. Calc.: C, 26.1; H, 1.5; N, 20.3; Cd, 40.6%.
CAUTION: Cadmium azides can be explosive under grinding or heating!

Preparation of $[Cd(picolinato)(NCS)]_n$ *complex* (**2**)

Complex **2** was prepared by mixing 4 cm^3 of an aqueous solution of $CdCl_2$ (0.2 g, 1 mmol) and picolinic acid (0.3 g, 2.5 mmol) in 8 cm^3 ethanol/water (1 : 1). To this clear solution an aqueous solution of KSCN (0.2 g, 2 mmol) in 3 cm^3 distilled water was added dropwise with thorough shaking. The clear solution was allowed to stand over 10 days to produce colourless crystals. Found: C, 28.8; H, 1.4; N, 9.5; Cd, 38.3. Calc.: C, 28.7; H, 1.4; N, 9.6; Cd, 38.4%.

Physical measurements

Procedures and instruments used for other physical measurements are as described previously [11].

X-ray crystallography

A modified STOE four circle diffractometer was used for single crystal X-ray measurements. Orientation matrix and lattice parameters were obtained by least-squares refinement of the diffraction data from 20 (compound **1**) and 31 (compound **2**) reflections in the 2θ range 13–25°. Intensity data were collected at 298(1) K using graphite crystal-monochromatized Mo-K_α radiation ($\lambda = 0.71069$ Å) and processed in the usual way (corrections: LP factor, absorption [21] for compound **2**, no extinction correction).

The structures were solved *via* the heavy-atom procedures and Fourier syntheses (following full-matrix least-squares, with scattering factors calculated using the data from [22]). All non-hydrogen atoms were refined with anisotropic displacement factors. Hydrogen atoms were identified in difference maps and included in the refinements with isotropic U values, but with constraints applied to the positional parameters. The programs DIFABS [21] SHELX-76 [23], SHELXS-86 [24], PLATON [25] and THE XRAY SYSTEM [26] were used for computations. Crystallographic data and processing parameters are given in Table 1, selected bond distances and bond angles in Table 2. Positional parameters, anisotropic displacement parameters, hydrogen atom coordinates, a full list of bond lengths and angles and observed and calculated structure factors have been deposited with the Editor as supplementary material; copies are available on request.

RESULTS AND DISCUSSION

The interaction between cadmium(II) ions and picolinic acid in ethanolic solution, in the presence of sodium azide or thiocyanate afforded colourless complexes (**1**) and (**2**). Both complexes have the same general formula Cd(picolinato)X, and are insoluble in many polar and non-polar solvents indicating their polymeric nature.

Figure 1 illustrates the principal structural features of the Cd(picolinato)(N_3) complex (**1**). Each cadmium atom is six-coordinated in a distorted octahedron geometry. The picolinate anion chelates a cadmium atom, Cd(1), *via* its ring nitrogen atom N(1) and a carboxylate oxygen atom O(1) to form a five-membered ring. The chelate ring deviates only 0.12 Å from planarity, the distance N(1)···O(1) is 2.719(8) Å. The oxygen atom O(1) is further coordinated to another cadmium centre, Cd(1c), to form cyclic Cd_2O_2 units. The second oxygen atom O(2) of the carboxylate group bridges a third cadmium atom Cd(1d). Thus the picolinato anion behaves as a N,O,O,O′-tetradentate chelating bridging ligand in this complex. The centrosymmetric dimeric Cd_2O_2 units are connected by $\mu(1,1)$ bridging azido groups to form sheets of polyhedra. These sheets of polyhedra are arranged normal to the long c-axis of the unit cell (Fig. 2). Conforming to the general characteristics of coordinated azides [14, 15], the $\mu(1,1)$ azido group is linear and asymmetric [angle N—N—N = 179.1(10) and N(11)—N(12) = 1.209(10)°, N(12)—N(13) = 1.132 (11) Å]. The di-$\mu(1,1)$ mode of bridging azide has previously been found in the structures of $[Cu_2(t\text{-Bupy})_4(N_3)_2]^{2+}$ [27], $[(CO)_3Mn(N_3)_3Mn(CO)_3]^-$ [28], $[Cu(2\text{-ampy})(N_3)_2(H_2O)]_2$ [29], $[Pd_2(N_3)_6]^{2-}$ [30],

Table 1. Crystallographic data and processing parameters

Compound	(1)	(2)
Molecular formula	$C_6H_4CdN_4O_2$	$C_7H_4CdSN_2O_2$
Molecular weight	276.53	292.59
Crystal system	Orthorhombic	Monoclinic
a (Å)	9.860(3)	17.454(4)
b (Å)	6.648(2)	5.879(2)
c (Å)	24.229(8)	18.200(5)
α ( )	90	90
β ( )	90	105.51(3)
γ ( )	90	90
V (Å^3)	1588.2(9)	1799.5(9)
Space group	*Pbca* (No. 61)	*I2/a* (No. 15)
Z	8	8
$F(000)$	1056	1120
μ(Mo-K_α) (mm^{-1})	2.71	2.61
D_{calc}/D_{obs} (Mg m^{-3})	2.313/2.30(3)	2/160/2.17(3)
Approx. crystal size (mm)	$0.35 \times 0.15 \times 0.13$	$0.60 \times 0.25 \times 0.15$
Data collection limits	h, k, l; $2\theta < 53^\circ$	$\pm h, k, l$; $2\theta < 52^\circ$
Scan mode	ω-scan, $\Delta\omega = 1.50$	ω-scan, $\Delta\omega = 1.75$
$F_o > 3\sigma(F_o)$	947	1421
Least squares parameters	122	122
R	0.033	0.027
R_w	0.033	0.028
Weighting scheme	$1.199\sigma^2(F_o)$	$1.255\sigma^2(F_o)$
Residual extrema in final difference map (e Å^{-3})	+0.91/−0.79	+0.40/−0.69

[Cu(2-Bzpy)$(N_3)_2$]$_2$ [17], and [Cu(3-pic)$(N_3)_2$]$_n$ [31]. The structure of the title complex is, however, novel in that the μ(1,1) azido bridging occurs between a pair of Cd_2O_2 units rather than simply between a pair of metal atoms. The Cd—N(N_3) bond distances given in Table 2 are slightly shorter than corresponding values [2.340 to 2.350 Å] found in the structure of Cd (pyridine)$(N_3)_2$ containing only μ(1,3) bridging azides [15]. The average Cd—N(N_3) distances in previously reported crystal structures of $K_2Cd(N_3)_4$ and $KCd(N_3)_3 \cdot H_2O$ [32] are 2.37 Å; a corresponding value of 2.35(4) Å has been observed in the structure of $Tl_8Cd_3(N_3)_{14}$ [33]. All cadmium(II) centres of the latter three compounds are six-coordinated with distorted octahedral geometries.

The most notable feature of the present structure is the coordination mode of the picolinato anion. To our knowledge this type of bonding has been observed only once in the structure of [Cu(picolinato)Cl]$_n$ [13]. In this latter complex each picolinate anion serves as a tetradentate ligand: N(1) and O(2) are coordinated to the same Cu^{II} centre whereas O(1) is bonded to a neighbouring Cu(1c) centre and each O(2) is further bonded to the latter Cu(1c) giving rise to distorted tetragonal bipyramidal environments around the copper atoms.

The present structure of complex **1** differs from that found for the complex [Mn(picolinato)$(N_3(H_2O)]_n$ (**3**), although **3** contains centrosymmetric dimeric units Mn_2O_2 and distorted octahedron manganese atoms [12]. In this manganese complex the picolinate anion acts as a N,O,O-tridentate chelating bridging ligand. The dimeric units, however, are connected by μ(1,3) bridging azido ligands to form a two-dimensional layer structure along the *ab*-plane of the unit cell.

The principal structural features of complex **2** are given in Fig. 3. As in the structure of the azido complex **1**, each cadmium atom is distorted octahedrally coordinated and the picolinato anions serve as a N,O,O,O′-tetradentate chelating bridging ligand but behaving in a different manner. Whereas in complex **1** the picolinato anion is coordinated to three different cadmium centres, in complex **2** the picolinato anion is coordinated *via* N(1) and O(1) to Cd(1) forming also a chelating five-membered ring. The chelate five-membered ring deviates only 0.09 Å from planarity and the N(1)···O(1) distance is 2.679(5) Å. O(1) and O(2) are further coordinated to the Cd(1c) centre forming an additional chelating four-membered ring [deviation from planarity = 0.05 Å, O(1)···O(2) = 2.200(4) Å]. As a consequence the cadmium atoms and O(1) atoms of the picolinate anions are forming the back-bone of a zigzag chain structure oriented along the short *b*-axis of the monoclinic unit cell.

The thiocyanato groups are functioning in the μ(N,S) mode to bridge each cadmium atom with its second nearest cadmium neighbour within the zigzag chain: i.e.: Cd(1)···Cd(1b), Cd(1c)···Cd(1d), and so on (Figs 3 and 4). Two of the Cd—O bond lengths

Table 2. Selected bond distances (Å) and bond angles (°)

(a) [Cd(picolinato)$(N_3)]_n$ (**1**)

Cd(1)···Cd(1c)	3.756(1)	Cd(1)···Cd(1a)	4.008(2)
Cd(1)···Cd(1d)	5.496(2)	Cd(1)—N(1)	2.356(6)
Cd(1)—N(11)	2.258(7)	Cd(1)—N(11b)	2.335(6)
Cd(1)—O(1c)	2.459(5)	Cd(1)—O(2e)	2.247(5)
Cd(1)—O(1)	2.327(5)	O(1)—C(6)	1.280(8)
O(2)—C(6)	1.254(8)	N(1)—C(1)	1.353(9)
N(1)—C(5)	1.322(10)	N(11)—N(12)	1.209(10)
N(12)—N(13)	1.132(11)	C(1)—C(2)	1.385(11)
C(1)—C(6)	1.510(10)	C(2)—C(3)	1.406(11)
C(3)—C(4)	1.369(12)	C(4)—C(5)	1.392(11)
O(1)—Cd(1)—N(1)	71.0(2)	O(1)—Cd(1)—N(11)	151.1(2)
O(1)—Cd(1)—N(11b)	103.4(2)	O(1)—Cd(1)—O(1c)	76.7(2)
O(1)—Cd(1)—O(2e)	91.1(2)	N(1)—Cd(1)—N(11)	94.4(2)
N(1)—Cd(1)—N(11b)	84.8(2)	N(1)—Cd(1)—O(1c)	104.1(2)
N(1)—Cd(1)—O(2e)	159.9(2)	N(11)—Cd(1)—N(11b)	99.8(2)
N(11)—Cd(1)—O(1c)	83.4(2)	N(11)—Cd(1)—O(2e)	105.7(2)
Cd(1)—O(1)—C(6)	116.6(4)	Cd(1)—O(1)—Cd(1c)	103.3(2)
C(6)—O(1)—Cd(1c)	114.4(4)	C(6)—O(2)—Cd(1d)	119.9(4)
Cd(1)—N(1)—C(1)	114.2(5)	Cd(1)—N(1)—C(5)	125.6(5)
C(1)—N(1)—C(5)	118.6(6)	Cd(1)—N(11)—N(12)	117.3(5)
Cd(1)—N(11)—Cd(1a)	121.6(3)	N(12)—N(11)—Cd(1a)	121.2(5)
N(11)—N(12)—N(13)	179.1(10)	O(1)—C(6)—O(2)	125.2(6)
O(1)—C(6)—C(1)	118.3(6)	O(2)—C(6)—C(1)	116.5(6)

Symmetry code: (a) $1/2-x, -1/2+y, z$; (b) $1/2-x, 1/2+y, z$; (c) $-x, -y, -z$; (d) $-1/2+x, 1/2-y, -z$; (e) $1/2+x, 1/2-y, -z$.

(b) [Cd(picolinato)(NCS)]$_n$ (**2**):

Cd(1)···Cd(1c)	4.461(2)	Cd(1)···Cd(1b)	5.879(2)
Cd(1)—O(1)	2.293(3)	Cd(1)—N(1)	2.315(4)
Cd(1)—N(2)	2.275(4)	Cd(1)—S(1a)	2.594(2)
Cd(1)—O(1d)	2.355(3)	Cd(1)—O(2d)	2.453(3)
S(1)—C(7)	1.646(4)	O(1)—C(6)	1.266(5)
O(2)—C(6)	1.239(5)	N(1)—C(1)	1.346(6)
N(1)—C(5)	1.336(6)	N(2)—C(7)	1.148(6)
C(1)—C(2)	1.387(6)	C(1)—C(6)	1.513(6)
C(2)—C(3)	1.372(7)	C(3)—C(4)	1.373(8)
C(4)—C(5)	1.382(7)		
O(1)—Cd(1)—N(1)	71.7(1)	O(1)—Cd(1)—N(2)	163.1(2)
O(1)—Cd(1)—S(1a)	101.3(1)	O(1)—Cd(1)—O(1d)	86.7(1)
O(1)—Cd(1)—O(2d)	87.1(1)	N(1)—Cd(1)—N(2)	95.8(2)
N(1)—Cd(1)—S(1a)	101.3(1)	N(1)—Cd(1)—O(1d)	107.5(1)
N(1)—Cd(1)—O(2d)	153.6(1)	N(2)—Cd(1)—S(1a)	92.2(1)
N(2)—Cd(1)—O(1d)	86.4(1)	N(2)—Cd(1)—O(2d)	101.3(2)
C(7)—S(1)—Cd(1b)	97.9(2)	Cd(1)—O(1)—C(6)	118.3(3)
Cd(1)—O(1)—Cd(1c)	147.4(1)	C(6)—O(1)—Cd(1c)	93.0(2)
C(6)—O(2)—Cd(1c)	89.2(3)	Cd(1)—N(1)—C(1)	114.8(3)
Cd(1)—N(1)—C(5)	125.3(3)	Cd(1)—N(2)—C(7)	165.4(4)
O(1)—C(6)—O(2)	122.9(4)	O(1)—C(6)—C(1)	117.5(4)
O(2)—C(6)—C(1)	119.5(4)	S(1)—C(7)—N(2)	178.8(4)
O(1)—Cd(1c)—O(2)	54.4(1)		

Symmetry code: (a) $x, -1+y, z$; (b) $x, 1+y, z$; (c) $-x, -1/2+y, 1/2-z$; (d) $-x, 1/2+y, 1/2-z$.

[2.355(3) and 2.293(3) Å] in complex **2** are slightly longer than corresponding values [2.327(5) and 2.247(5) Å] in complex **1**. The Cd···Cd distances in complex 2 are 4.461(2) and 5.879(2) Å, whereas Cd···Cd distances of 3.756(1), 4.008(2) and 5.496(2) Å have been observed in complex **1**. The Cd—N(pic) distance of 2.315(6) Å in complex **2** is shorter than the Cd—N(pic) bond length [2.356(6) Å] in complex **1**. The thiocyanato ligand is linear [<NCS = 178.8(4)°]. The C—S bond length of 1.646(4) Å found in the present complex is larger than, whereas the N—C distance of 1.148(6) Å is equal to

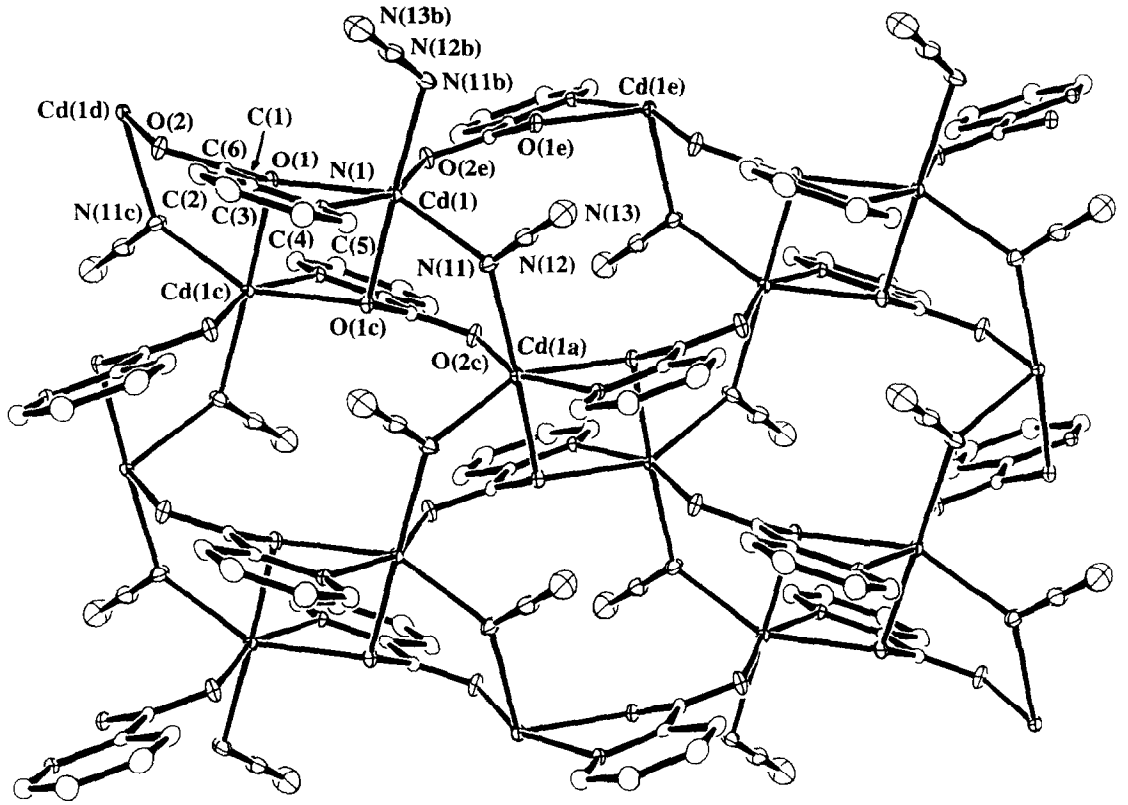


Fig. 1. The molecular geometry and atom numbering scheme of $[Cd(picolinato)(N_3)]_n$ (**1**). Symmetry code according to Table 2a.

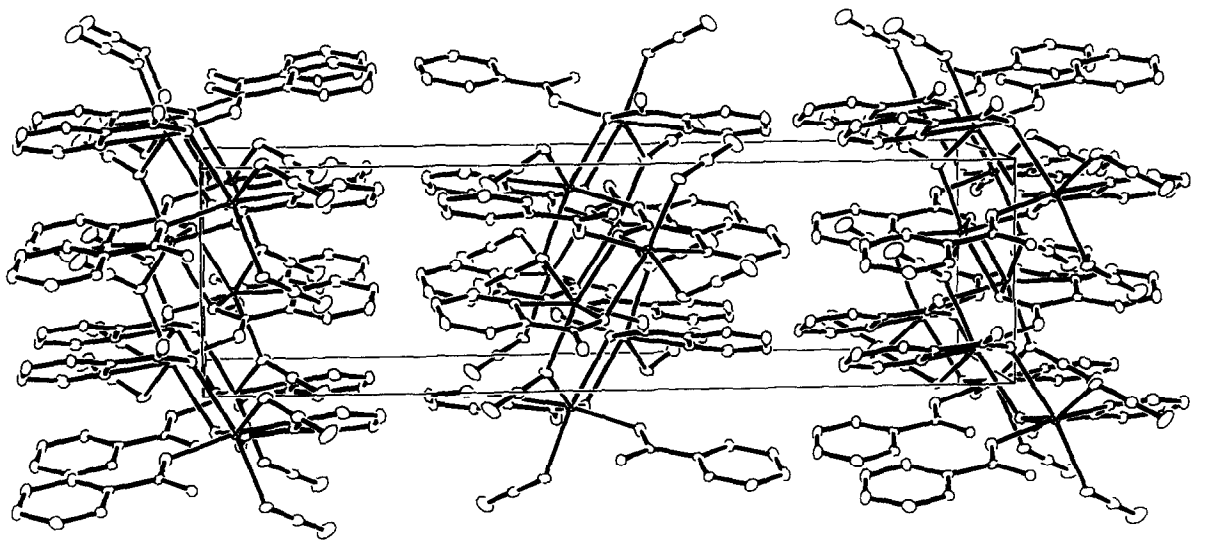


Fig. 2. Packing plot of $[Cd(picolinato)(N_3)]_n$, (**1**), viewed along the *a*-axis of the unit cell.

corresponding values [1.626(9) for S—C and 1.140(11) Å for N—C] found in [Mn(H-quin)(quin)(NCS)$(H_2O)_2$] complex (H-quin is quinaldic acid) with terminal nitrogen bonded thiocyanato ligands [34].

The structure of complexes **1** and **2** differ from that of the parent complex $[Cd(picolinato)_2]_n$ (**4**), although it contains octahedrally coordinated cadmium atoms and centrosymmetric dimeric units Cd_2O_2. Complex **4**, however, contains two independent chelating picolinato anions; in one the chelating carboxylate oxygen atom bridges the second cadmium centre of the dimer, whereas in the other the non-chelating carboxylate oxygen atom bridges a neighbouring dimer

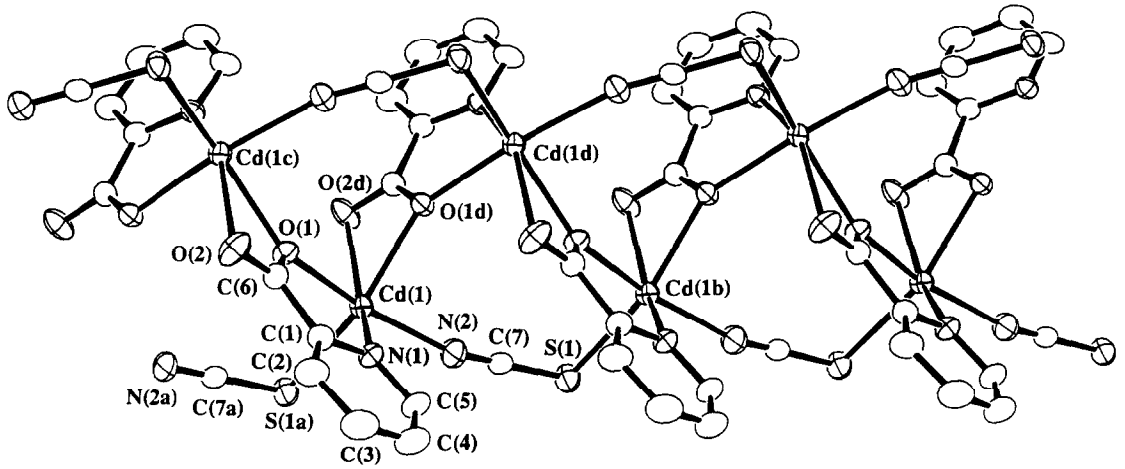


Fig. 3. The molecular geometry and atom numbering scheme of [Cd(picolinato)(NCS)]$_n$ (**2**). Symmetry code according Table 2b.

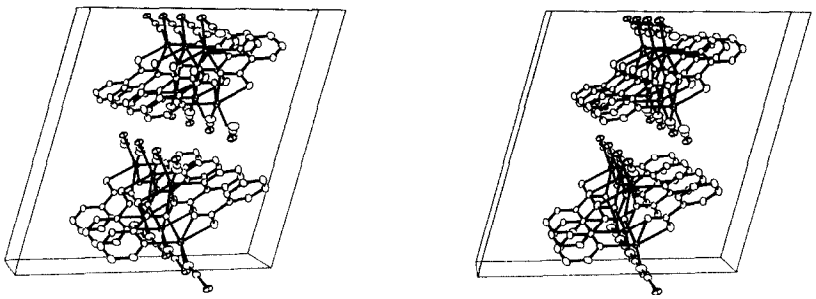


Fig. 4. Packing plot (stereo) of [Cd(picolinato)(NCS)]$_n$, (**2**), viewed along the *b*-axis of the unit cell.

[7]. Picolinato anion was found to coexist as bi- and tetradentate ligands in the structure of the complex $[Na_2Co(pic)_2(N_3)_2(H_2O)_6][Co(pic)_2(N_3)_2]\cdot 2H_2O$ [35]. The complex anion $[Co(pic)_2(N_3)_2]^-$ contains a bidentate picolinato anion whereas the picolinate ligands in the complex cation serve as tetradentate ligands. The tetradentate picolinato anions, however, link the cobalt(II) and sodium centres, rather than two metal centres of the same type.

The room temperature IR and Raman spectra of the crystalline picolinic acid and its cadmium(II) azido and thiocyanato complexes, (**1**) and (**2**), together with tentative assignments of the bands are given in Table 3.

In the high frequency region of the spectrum of free acid where hydrogen bonding of the type (O—H···O) involving the carboxylic acid group, very broad bands centered around 3400 cm^{-1}, and hydrogen bonding of the type (O—H···N) is indicated by the presence of broad, medium strong bands near 2560, 2150 and 2050 cm^{-1}. These bands are completely absent in the spectra of both complexes. The IR and Raman spectra of free picolinic acid exhibit the following bands (cm^{-1}): 1719, 1655 (IR), 1691, 1655 (R) as [ν_{as} (COO^-)], 1307 (IR), 1302 (R) as [$\nu_s(COO^-)$], 1410 (IR), 1410 (R) as [δ(OH) in plane], 966 (IR) as [δ(OH) out of plane], 688, 680 (IR), 676 (R) as [δ(COO)] in accordance with earlier work [36,37]. Compared to the free acid, both complexes show a substantial decrease of the ν_{as}(COO) to 1635–1630 (IR) and 1635–1638 (R) and a consequent increase of the ν_s(COO) to around 1380 (IR) and 1400 (R), which are characteristic of bonding type (II) rather than (I) [38].

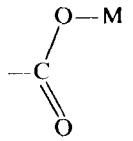
The vibrations related to the pyridine moiety spread over all the spectra are broad, similar to those of the pyridine itself and slightly shifted to higher wave numbers in the solid complexes. The bands at 364 and 334 cm^{-1} which appeared in the Raman spectrum of complex **1** are tentatively assigned to the ν[Cd—N(N_3)], as these bands are absent in the spectra of free acid and complex **2**. The bands around 240–200 cm^{-1} (R) are assigned to ν(Cd—N(pic)] in both complexes.

Complex **1** contains asymmetric azido groups as revealed by X-ray crystallography. As a consequence, the three vibration modes of the azide are both infrared and Raman active. The results given in Table 3 agree well with this expectation. The ν_{as} which is Raman-inactive in the symmetric azide, appears as a split band of medium intensity at 2085, 2070 cm^{-1} (R) and 2080 cm^{-1} vs, (IR), whereas the ν_s mode appears at 1340 sh, 1287 cm^{-1}, s (IR) and 1300 cm^{-1}, ms (R). The appearance of this latter mode in the IR and the former in the Raman spectrum strongly support the

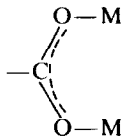
Table 3. Infrared and Raman spectral data (cm^{-1})

Pic—H		$[Cd(pic)(N_3)]_n$		$[Cd(pic)(NCS)]_n$		
IR	Raman	IR	Raman	IR	Raman	Assignments
		2080 s*	2085 m	2080 s*	2125 vs	$\nu_{as}(N_3)$ or
			2070 wm		2085 w	ν(CN)
1719 vs	1691 wm					ν_{as}(COOH) and/
1655 ms	1655 w	1635 s	1638 w	1630 m	1635 wm	or ν_{as} (COO^-)
1608 vs	1610 w	1616 vs	1610 wm	1618 vs	1608 m	4×405
1595 m	1546 s	1587 vs	1588 s	1590 s	1592 s	pyridine
1573 s						
1542 s	1573 ms	1561 vs	1586 wm	1562 ms	1566 ms	pyridine
1455 vs	1487 w	1472 ms	1486 wm	1470 wm	1486 wm	pyridine
1439 s	1440 w	1440 ms	1442 ms	1440 wm	1444 m	pyridine
1410 wm	1410 w					δ(OH) in plane
1372 sh	1377 m	1420 w		1415 wm		pyridine
1343 vs	1355 wm	1388 sh	1410 vw	1385 sh		pyridine
1307 vs	1302 w	1380 vs	1400 s	1378 vs	1390 s	$\nu_s(COO^-)$
		1340 sh	1356 s			$\nu_s(N_3)$
1294 vs	1296 vw	1305 sh		1300 sh		pyridine
1252 s	1258 vw	1287 s	1300 s	1280 w	1290 vw	$2\times630+\nu_s(N_3)$
1198 s	1263 w	1240 m	1260 w	1260 wm	1260 w	pyridine
1170 s	1170 wm	1168 m	1176 wm	1168 wm	1173 wm	
1159 s	1150 wm	1150 m	1152 m	1150 wm	1156 wm	pyridine
1088 s	1088 w	1095 m	1090 w	1095 wm	1092 w	pyridine
1048 s	1038 m	1044 ms	1056 ms	1046 m	1054 m	pyridine
1010 s	1011 s	1018 s	1020 vs	1018 m	1022 vs	pyridine
995 s	997 s	998 wm	1005 wm	998 w	1008 wm	pyridine
966						δ(OH) out
						of plane
838 ms	841 ms	852 s	850 m	856 ms	860 wm	pyridine
820 ms	823 wm	834 m	836 w	835 wm	833 w	405+420
752 vs	775 w	760 vs	764 w	764 ms	766 wm	pyr.+2×370
698 m	696 w	700 s	705 w	705 m	705 wm	pyridine
680 vs	667 w					δ(COO)
618 m	616 wm	638 s	642 wm	640 w	642 vs	pyr.+$\delta(N_3)$
		600 wm				$\delta(N_3)$
500 s	520 w		520 w			
420 s	420 m	458 m	448 wm	448 w	448 w	pyridine
405 s	405 m	403 m	436 w	425 wm	430 wm	pyridine
			364 w		366 vw	Cd-O(pic)
			334 wm			Cd-N(N_3)
			306 m			Cd-N(N_3)
			240 m		230 m	Cd-N(pic)
			195 s		205 m	

v = very, w = weak, m = medium, s = strong, br = broad, sh = shoulder, ν_{as} = asymmetric vibration, ν_s = symmetric vibration, * = split band.



(I)



(II)

asymmetric nature of the azide ligand in complex **1**. The infrared spectrum of the thiocyanato complex **2** shows a strong band at 2080 cm^{-1} due to ν(C—N) mode suggesting N-bonded thiocyanate. This result is not consistent with the X-ray structure of this complex with ν(N,S)-thiocyanate and hence two bands, above and below 2000 cm^{-1}, are expected [39]. The Raman spectrum of **2**, however, exhibits two peaks at 2125 and 2085 cm^{-1} as expected from the crystallographic result.

Acknowledgement—The authors thank Professor Ch. Kratky for the use of experimental equipment.

REFERENCES

1. B. A. Bovikin, A. M. Omel'chenko, R. N. Sharonina and I. A. Zanina, *Abstracts of Proceedings*,

15th All-Union Chugaevskii Conference on the Chemistry of Complex Compounds, Ukraine, Vol. I, p. 229 (1985).
2. M. A. S. Goher, A. E. H. Abdou, W.-H. Yip and T. C. W. Mak, *Polyhedron* 1993, **12,** 1879.
3. P. J.-P. Deloume, R. Faure and H. Loiseleur, *Acta Cryst.* 1977, **B33,** 2709.
4. A. Anagnostopoulos, R. A. Matthews and R. A. Walton, *Can. J. Chem.* 1972, **50,** 1307.
5. G. W. A. Fowles, R. A. Matthews and R. A. Walton, *J. Chem. Soc. (A)* 1968, 1108.
6. P. J.-P. Deloume, H. Loiseleur and G. Thomas, *Acta Cryst.* 1973, **B29,** 668.
7. P. J.-P. Deloume and H. Loiseleur, *Acta Cryst.* 1974, **B30,** 607.
8. S. C. Chang, J. K. H. Ma, J. S. Wang and N. C. Li, *J. Coord. Chem.* 1972, **2,** 31.
9. A. Kleinstein and G. A. Webb, *J. Inorg. Nucl. Chem.* 1971, **33,** 405.
10. A. Takenaka, N. Utsumi, T. Yamamoto and I. Nita, *Nippon Kagaku Zsashi* 1970, **91,** 928.
11. M. A. S. Goher, M. A. M. Abu-Youssef, F. A. Mautner and A. Popitsch, *Polyhedron* 1993, **12,** 1751.
12. M. A. S. Goher, M. A. M. Abu-Youssef, F. A. Mautner and A. Popitsch, *Polyhedron* 1992, **11,** 2137.
13. M. A. S. Goher, A. K. Hafez, M. A. M. Abu-Youssef, A. Popitsch, H. P. Fritzer and F. A. Mautner, *Monatsh. Chem.* 1994, **125,** 833.
14. Z. Dori and R. F. Ziolo, *Chem. Rev.* 1973, **73,** 247.
15. I. Agrell, *Acta Chem. Scand.* 1970, **24,** 3575; *ibid.* 1967, **21,** 2647.
16. M. A. S. Goher and T. C. W. Mak, *Inorg. Chim. Acta* 1985, **99,** 223.
17. T. C. W. Mak and M. A. S. Goher, *Inorg. Chim. Acta* 1986, **115,** 17.
18. Y. Agnus, R. Louis and R. Weiss, *J. Am. Chem. Soc.* 1979, **101,** 3381.
19. D. C. Foyt, T. W. Siddal, H. C. J. Alexander and M. Good, *Inorg. Chem.* 1974, **13,** 1793.
20. R. A. Bailey, S. L. Kozak, T. W. Michelson and W. N. Mills, *Coord. Chem. Rev.* 1971, **6,** 407.
21. N. Walker and D. Stuart, *Acta Cryst.* 1983, **A39,** 158.
22. *International Tables for X-Ray Crystallography*, Vol. IV, pp. 99 and 149. Kynoch Press, Birmingham (1974).
23. G. M. Sheldrick, *SHELX*-76, *A Program for Crystal Structure Determination.* University Chemical Laboratory, Cambridge (1976).
24. G. M. Sheldrick, *SHELXS*-86. Universität Göttingen, F. R. G. (1986).
25. A. L. Spek, in *Computational Crystallography* (Edited by D. Sayre), p. 528. Clarendon Press, Oxford (1982).
26. J. M. Stuart, *The X-RAY SYSTEM, version of* 1976, Technical Report TR-466. University of Maryland, College Park (1976).
27. S. Sikorav, I. Bkouche-Waksman and O. Kahn, *Inorg. Chem.* 1984, **23,** 490.
28. R. Mason, G. A. Rusholme, W. Beck, H. Engelmann, K. Joos, B. Indenberg and H. S. Smedal, *Chem. Commun.* 1971, 496.
29. M. A. S. Goher and T. C. W. Mak, *Inorg. Chim. Acta* 1984, **85,** 117.
30. W. P. Fehlhammer and L. F. Dahl, *J. Am. Chem. Soc.* 1972, **94,** 3377.
31. M. A. S. Goher and T. C. W. Mak, *Inorg. Chim. Acta* 1984, **89,** 119.
32. W. Clegg, H. Krischner, A. I. Saracoglu and G. M. Sheldrick, *Z. Kristallogr.* 1982, **161,** 307.
33. H. Krischner, Ch. Kratky and H. E. Maier, *Z. Kristallogr.* 1982, **161,** 225.
34. M. A. S. Goher and F. A. Mautner, *Polyhedron*, 1993, **12,** 1863.
35. M. A. S. Goher, M. A. M. Abu-Youssef and F. A. Mautner, *Z. Naturforsch.* 1993, **48b,** 1795.
36. S. Yoshida, M. Asai, *Chem. Pharm. Bull. (Japan)* 1959, **7,** 162.
37. I. Nakagawa and T. Shimanouchi, *Spectrochim. Acta* 1964, **20,** 429.
38. A. B. P. Lever, J. Lewis and R. S. Nyholm, *J. Chem. Soc.* 1962, 5262.
39. M. A. S. Goher, *Coll. Czech. Chem. Commun.* 1977, **42,** 1478, and references therein.

Pergamon

S0277-5387(96)00271-9

Polyhedron Vol. 16, No. 2, pp. 243–251, 1997
Copyright © 1996 Elsevier Science Ltd
Printed in Great Britain. All rights reserved
0277-5387/97 $15.00+0.00

Molybdenum(VI) complex formation. Equilibria and thermodynamic quantities for the reactions with malate

J. J. Cruywagen,* E. A. Rohwer and R. F. van de Water†

Department of Chemistry, University of Stellenbosch, Stellenbosch 7600, South Africa

(Received 3 April 1996; accepted 28 May 1996)

Abstract—Complex formation between molybdate and malate has been investigated in the pH range 1.5–7.5 by potentiometric, spectrophotometric and enthalpimetric titrations at 25°C in 1.0 mol dm^{-3} (Na)Cl. The "best" reaction model comprises mononuclear, dinuclear and tetranuclear complexes. The formation constants of the complexes, denoted by β_{pqr}, where the subscripts p, q, and r refer to the stoichiometric coefficients in the general formula $[(MoO_4)_p(mal)_qH_r]$, have the values: log $\beta_{111} = 7.47$, log $\beta_{112} = 13.23$, log $\beta_{113} = 15.87$, log $\beta_{122} = 15.48$, log $\beta_{123} = 20.13$, log $\beta_{124} = 24.14$, log $\beta_{213} = 20.10$, log $\beta_{214} = 24.35$, log $\beta_{224} = 28.06$, log $\beta_{225} = 32.01$, log $\beta_{428} = 52.92$, log $\beta_{429} = 54.35$, log $\beta_{4210} = 55.27$, and log $\beta_{4411} = 69.92$. Enthalpy and entropy changes for complexes occurring in sufficiently high concentrations were calculated from the calorimetric data using these formation constants. $\Delta H^\circ_{111} = -47.9$, $\Delta H^\circ_{112} = -55.5$, $\Delta H^\circ_{113} = -57$, $\Delta H^\circ_{122} = -77.0$, $\Delta H^\circ_{123} = -83$, $\Delta H^\circ_{124} = -85.6$, $\Delta H^\circ_{213} = -75$, $\Delta H^\circ_{224} = -85$, $\Delta H^\circ_{225} = -85$, $\Delta H^\circ_{428} = -232$, $\Delta H^\circ_{429} = -214$, $\Delta H^\circ_{4210} = -197$, and $\Delta H^\circ_{4411} = -221$ kJ mol^{-1}. Thermodynamic parameters for the protonation of malate in 1.0 mol dm^{-3} (Na)Cl have also been determined: log $\beta_{011} = 4.44$ and log $\beta_{012} = 7.57$; $\Delta H^\circ_{011} = -2.0$, and $\Delta H^\circ_{012} = -6.5$ kJ mol^{-1}. Copyright © 1996 Elsevier Science Ltd

Keywords: molybdate; molybdenum(VI); complexation; thermodynamic quantities; malic acid.

Previous studies of the complexation of molybdate with malate [malic acid, $H_3mal = CH(OH)(COOH)CH_2COOH$)] revealed the existence of a number of complexes in solution [1–9]. Although some typical stoichiometries such as 1:1, 1:2, and 2:1 for the molybdate to malate ratio have been proposed, the composition and stability of most complexes are still uncertain. Some contradictory reports seem to be the result of different conditions used in experiments as well as problems with the unequivocal interpretation of data pertaining to solutions containing various combinations of complex ions [4,7,8]. A thorough NMR study [7] showed the existence of four complexes in the pH range 4–7.5, namely a 2:1 (presumably 4:2), a 1:1 and also two 1:2 species which appeared to be geometrical isomers. A comprehensive polarimetric investigation by Beltrán *et al.* [8] over a wider pH range, 1–8, indicated the existence of six different complexes which for brevity are herein represented by the stoichiometric coefficients of the reactants molybdate, malate and protons: $[1,1,1]^{3-}$, $[1,1,2]^{2-}$, $[1,2,2]^{4-}$, $[2,2,4]^{4-}$, $[2,2,5]^{3-}$ and $[4,2,8]^{4-}$. Formation constants for three of these species were calculated using straight line extrapolation methods. These authors differ from some others in that both mono- and dinuclear complexes of a 1:1 molybdate to malate stoichiometry are proposed.

Examples of salts of complex ions that have been crystallized and of which the structures have been determined by X-ray analysis are $[NH_4]_4[Mo_4O_{11}(mal)_2]\cdot H_2O$ [6], $[NH_4]_4[Mo_4O_{11}(mal)_2]\cdot 6H_2O$ [10] and $Cs_2[MoO_2(Hmal)_2]\cdot H_2O$ [11]. The existence of these compounds is strong evidence for the occurrence in solution of the complex ions $[4,2,8]^{4-}$ and $[1,2,4]^{2-}$. Other compounds which have been prepared and chemically analyzed [11] are the salts of the complex ions $[1,2,2]^{4-}$ and $[1,2,3]^{3-}$, namely $Cs_4[MoO_2(mal)_2]\cdot 3H_2O$ and $(NH_4)_3[MoO_2H(mal)_2]\cdot H_2O$.

The occurrence of protonated forms of different types of complexes can lead, depending on the con-

* Author to whom correspondence should be addressed
† Present address: Department of Chemistry, Mangosutho Technikon, Durban, R.S.A.

ditions, to strong overlap of their stability regions. Knowledge about species distributions, based on reliable formation constants for all complexes, is therefore essential and ought to provide the necessary insight to resolve conflicting interpretations of experimental results obtained under diverse conditions.

In this paper we report the results of a potentiometric, spectrophotometric and enthalpimetric investigation of the complexation of molybdate with malate. A reaction model and set of equilibrium constants have been established which give a satisfactory description of the complexation behaviour under different conditions. Not only could these results be used for a meaningful evaluation of some previous research work, but also served as basis for a calorimetric investigation of the system and the determination of enthalpy and entropy changes of all but the very minor complexes. By comparing these thermodynamic quantities with those determined previously for other α-hydroxy-carboxylates a consistent and coherent picture of the complexation behaviour of molybdenum(VI) with this type of ligand was established.

EXPERIMENTAL

Reagents and solutions

All reagents were of analytical grade (Merck, BDH, Aldrich) and solutions were prepared with water obtained from a Millipore Milli-Q system. Sodium molybdate stock solution was prepared from the recrystallized salt $[Na_2MoO_4]\cdot 2H_2O$ and standardized gravimetrically as described previously [12]. Hydrochloric acid was standardized indirectly against potassium hydrogenphthalate by titration with sodium hydroxide. Sodium chloride was purified as described previously [12]. Malic acid was used as received but its purity was checked by titration with sodium hydroxide. Malate solutions were prepared by accurate neutralization of malic acid.

Potentiometric titrations

Mixtures of sodium molybdate and sodium malate (80 cm^3) were titrated with hydrochloric acid at 25°C using either a Metrohm 636 Titroprocessor or a Metrohm Dosimat. All solutions were made 1.0 mol dm^{-3} with respect to chloride ions by addition of the appropriate amount of recrystallized sodium chloride. To exclude carbon dioxide from the system a stream of purified nitrogen was passed through 1.0 mol dm^{-3} NaCl and then bubbled slowly through the titration solution. The initial concentrations (mol dm^{-3}) of molybdate and malate were as follows: 0.005, 0.005; 0.01, 0.01; 0.05, 0.05; 0.02, 0.01; 0.01, 0.005; 0.01, 0.02 and 0.025, 0.10, thus obtaining solutions with equal concentrations of molybdate and malate or an excess of one of these reactants. The pH_c range covered was 7.5–1.5. In the final computer treatment of the data some of the duplicate titrations were left out in order to limit the data to 600 points. The protonation constants of malate were determined by potentiometric titration of solutions (80 cm^3 0.05 mol dm^{-3}) with 1.0 mol dm^{-3} hydrochloric acid.

The free hydrogen ion concentration, h, was determined by measuring the potential, E^0, to ±0.2 mV using a Ross combination electrode (Orion) with a 3.0 mol dm^{-3} KCl bridge solution. Equation (1) was used to calculate h from the measured potential at each titration point:

$$E = E^0 + 59.16 \log h + E_j \qquad (1)$$

Values for E^0 and E_j (the liquid junction potential) were determined from titrations of 1.0 mol dm^{-3} NaCl with HCl as described by Rossotti [13]. For brevity $-\log h$ is denoted by pH_c.

Spectrophotometric titrations

A GBC 920 UV/VIS double beam spectrophotometer equipped with a Peltier thermocell was used for absorption measurements. The solution in the titration cell, kept in a thermostatted water-bath at 25°C, was stirred with a non-electric immersion magnetic stirrer. Absorbances were measured in the wavelength range 206–320 nm with intervals of 3 nm using quartz cuvettes of pathlength 1.0 cm; the composition of the reference solution was that of the ionic medium, i.e. 1.0 mol dm^{-3} NaCl. The concentration of both molybdate and malate in the reaction vessel was 1.0×10^{-4} mol dm^{-3}. The titrant solution contained in addition to hydrochloric acid and sodium chloride (0.1 and 0.9 mol dm^{-3}) also molybdate and malate at the same concentration as the test solution. The hydrogen ion concentration was measured as described for the potentiometric titrations. Twenty-one spectra were recorded at pH_c intervals of ~ 0.2 in the range 5.6–1.5. A similar titration of malate (1.6×10^{-3}) with hydrochloric acid was carried out from which the protonation constants of malate as well as the individual spectra of $Hmal^-$ and H_2mal were calculated using the program SQUAD [14]. The spectra were supplied to the program for the treatment of the absorption data pertaining to complexation. In the wavelength range used the absorption of malate species is very small compared to that of molybdate.

Calorimetric titrations

An isothermal calorimeter, Tronac model 1250, was used for the enthalpy measurements. Solutions containing molybdate and malate (25.0 cm^3) were titrated with 1.0 mol dm^{-3} hydrochloric acid from a precision microburette (2.5 cm^3). The initial concentrations (mol dm^{-3}) of molybdate and malate were as follows: 0.01, 0.04; 0.03, 0.03; 0.03, 0.05 and 0.05, 0.20. The

data were collected automatically by means of a personal computer using software supplied by Tronac. Separate titrations of malate (0.02 mol dm^{-3}) with hydrochloric acid (1.0 mol dm^{-3}) were performed to determine the enthalpy involved in the protonation of malate. Again, all solutions were made 1.0 mol dm^{-3} with respect to chloride by addition of the appropriate amount of recrystallized sodium chloride. Titrations were carried out in duplicate. The data were corrected for the endothermic heat of dilution of hydrochloric acid titrated into sodium chloride by using results of previous blank titrations [15].

RESULTS AND DISCUSSION

Potentiometric investigation

The various protonation, condensation and complexation reactions that can take place when a solution containing molybdate and malate is acidified are represented by the general equation (2).

$$p\mathrm{MoO_4^{2-}} + q\mathrm{Hmal^{2-}} + r\mathrm{H^+} \rightleftharpoons [\mathrm{COMPLEX}]^{(2p+2q-r)-} \quad (2)$$

The malate anion is formulated as $\mathrm{Hmal^{2-}}$ to show the proton of the α-hydroxyl group which (in the pH range in question) is released only when complexation takes place. Overall formation constants are denoted by $\beta_{p,q,r}$ in accordance with the description of species in terms of the stoichiometric coefficients of the reactants, for example, [0, 1, 2] for malic acid.

The results of some representative titrations of malate and of mixtures of molybdate and malate with hydrochloric acid are shown in Fig. 1 as plots of F against pH_c. The function F (eq. 3) represents the fraction of the total negative charge neutralized due to protonation where H, B and C are the analytical concentrations of acid, molybdate and malate, respectively.

$$F = (H-h)/(2B+2C) \quad (3)$$

An F value of 1.0 therefore indicates an average charge of zero for the species in solution. For a solution containing only malate species $F \simeq 0.98$ at $pH_c \sim 1.5$ indicating almost complete protonation to H_3mal (Fig. 1). For mixtures of molybdate and malate at the same pH_c the much lower value of $F = 0.8$ shows that protonation of the complexes are more difficult than protonation of malate itself. However, in the region of higher pH_c the curves show that significant complexation already occurs before malate is protonated.

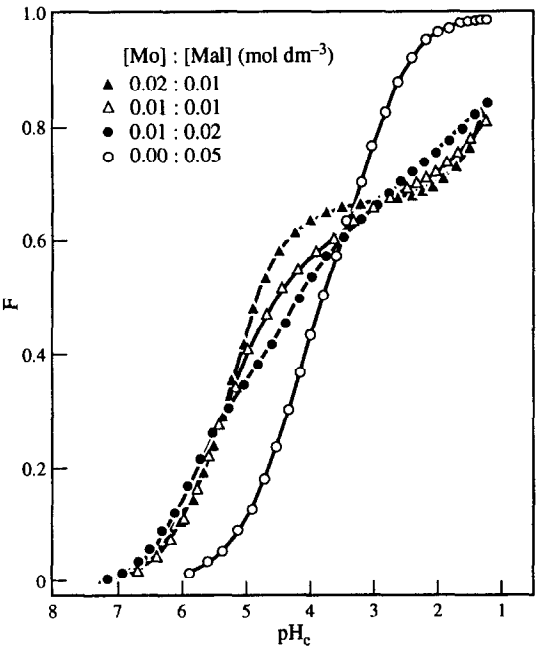


Fig. 1. Plots of function F versus pH_c for some representative potentiometric titrations.

To create conditions that would be favourable for the formation of complexes with stoichiometry other than a 1 : 1 ratio of molybdate to malate an excess of either molybdate or malate was used. In the treatment of the data it was therefore important to consider all side-reactions of uncomplexed molybdate and malate with protons. The molybdate species $[HMoO_4]^-$, $[MoO_3(OH_2)_3]$, $[MoO_2(OH)(OH_2)_3]^+$, $[HMo_2O_7]^-$, $[Mo_7O_{24}]^{6-}$, $[HMo_7O_{24}]^{5-}$, $[H_2Mo_7O_{24}]^{4-}$, $[H_3Mo_7O_{24}]^{3-}$, $[Mo_8O_{26}]^{4-}$ and $[HMo_2O_6]^+$ were taken into account using previously determined equilibrium constants pertaining to 1.0 mol dm^{-3} NaCl medium at 25°C [16–18]. In the final calculations (limited to data at $pH_c > 1.5$) however, it turned out that only four of these species were really necessary to account for uncomplexed molybdate, namely $[MoO_3(OH_2)_3]$, $[Mo_7O_{24}]^{6-}$, $[HMo_7O_{24}]^{5-}$ and $[H_3Mo_7O_{24}]^{3-}$. Due to the formation of complexes having a 2 : 1 molybdate to malate stoichiometry the amount of uncomplexed molybdate was relatively small. The calculation of stability constants and model testing were performed with the computer program SUPERQUAD [19].

The protonation constants of malate in 1.0 mol dm^{-3} NaCl were determined in separate titrations. The values obtained, $\log \beta_{011} = 4.44$ and $\log \beta_{012} = 7.57$ are the same as the literature values at this ionic strength [20].

On account of our previous experience with systems of this type all possible complex species with $p = 1$–4 and having reasonable q and r values have been considered in the calculations to find the "best" reaction model. SUPERQUAD automatically rejects species for which the relative standard deviation of the formation constant is greater than 33% (or $3\sigma > 0.43$ log units). The final model comprises fourteen species of which only the $[2, 1, 4]^{2-}$ has a standard deviation of greater than 7%, actually 16%, and its existence is therefore much less certain than that of the other species. A value for $s = 0.97$ (sample standard deviation) [19] based on errors of 0.01 cm^3 in the volume and 0.002 in the pH_c implies a very good fit. Although the fit could be improved marginally by the addition

of some very minor species, these species were not included in the best model. For example, inclusion of a $[4,4,9]^{7-}$ species for which a relatively large standard deviation of 18% in the value of the formation constant was calculated caused a lowering of s from 0.97 to 0.95. The distribution of the complexes as a function of pH_c at concentrations chosen to illustrate the stability regions are shown in Figs 2 and 3.

The molybdenum–malate stoichiometry of the complexes is typical of those previously observed for other comparable molybdenum ligand systems [21]. In particular, the model is very similar to that obtained for molybdenum(VI) with citrate as ligand. The difference between citrate and malate is the extra carboxylate group of citrate which remains uncoordinated and therefore affords additional protonation possibilities for a particular complex. Accordingly, analogues of protonated citrate complexes, such as the $[1,1,4]^{-}$, $[2,1,5]^{2-}$ and $[2,2,6]^{4-}$ do not occur in the molybdenum–malate system. In general the malate complexes are a little less stable than the analogous citrate complexes, e.g. the formation constant of the $[1,1,1]^{3-}$ malate complex is about one log unit smaller than that of the $[1,1,1]^{4-}$ citrate complex.

Classified in terms of molybdenum–malate stoichiometry there are six different types of complexes protonated to various degrees. With the exception of the 4:4 type, salts of all types have been isolated in the solid state either as malate or citrate complexes. Thus, salts of the $[1,2,2]^{4-}$, $[1,2,3]^{3-}$, $[1,2,4]^{2-}$ and $[4,2,8]^{4-}$ malate complexes have been prepared, e.g. $Cs_4[MoO_2(mal)_2]\cdot 2.5H_2O$ [11], $[NH_4]_3[MoO_2H(mal)_2]\cdot H_2O$ [11], $Cs_2[MoO_2(Hmal)_2]\cdot H_2O$ [11] and $[NH_4]_4[Mo_4O_{11}(mal)_2]\cdot 6H_2O$ [6,10]. Citrate analogues of the latter complex are also known and have been structurally characterized by X-ray analysis, e.g. $[Me_3N(CH_2)_{6NMe3})]_2[Mo_4O_{11}(Hcit)_2]\cdot 12H_2O$ [22]. Other citrate complexes [23] of molybdenum which have been obtained by precipitation from aqueous solution and have stoichiometries which correspond with those of malate complexes now identified are potassium salts of $[1,1,1]^{4-}$, $[2,2,4]^{6-}$ and $[2,2,6]^{4-}$. These complexes have been characterized by chemical analysis and various other methods. A complex of composition $M_2[Mo_2O_5(OH)H_2O(Hcit)]\cdot 0.5H_2O$ where M^+ is K^+ or NH_4^+ and which corresponds to $[2,1,5]^{2-}$ has also been reported [24].

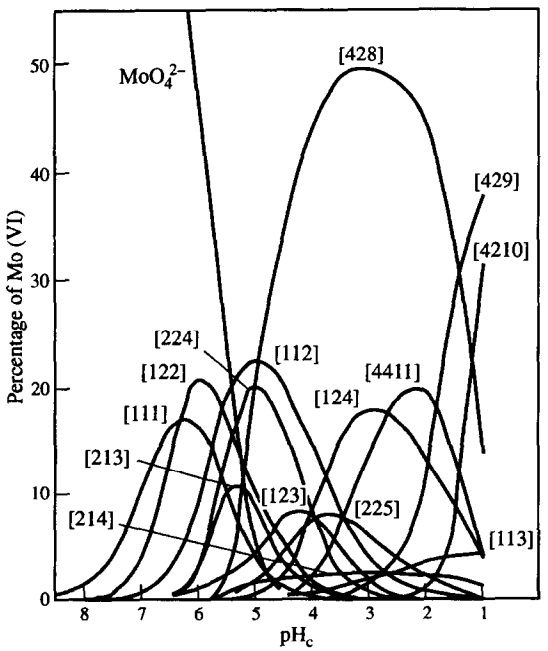


Fig. 2. Distribution of species in the molybdenum(VI) malate system as a function of pH_c for an equimolar solution of 0.05 M.

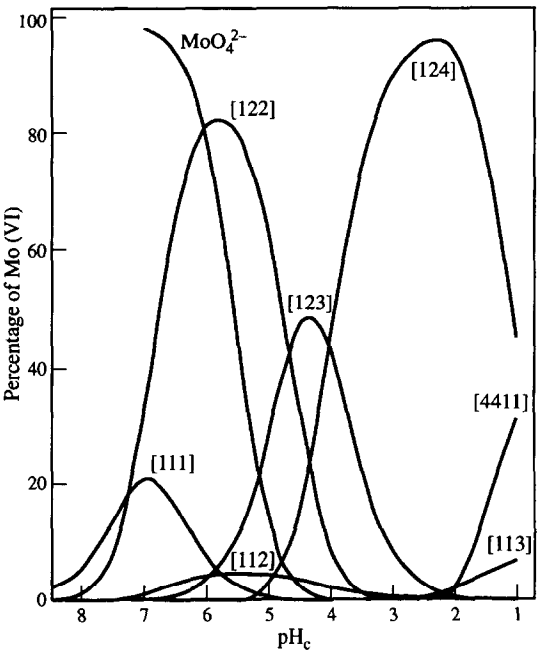


Fig. 3. Distribution of species in the molybdenum(VI) malate system as a function of pH_c. Total concentrations of molybdate and malate are 0.05 M and 0.20 M, respectively.

If tridentate coordination of malate, similar to that of citrate [21], is assumed, structures with five- and six-membered rings with molybdenum will be formed as shown in Fig. 4 for the 1:1 and 2:2 type of complexes. Tridentate coordination is expected to have a stabilizing effect on these complexes affording them to compete successfully with the $[1,2,r]$ complexes under suitable conditions. The typical behaviour of α-hydroxycarboxylic acids towards molybdenum(VI) and tungsten(VI) is to form particularly stable 1:2 rather than 1:1 and 2:2 complexes (*cf.* last section).

The reaction model established and the available formation constants can now be employed to calculate species distributions pertaining to conditions of previous investigations. For example the distribution of the $[4,2,8]^{4-}$ and $[2,2,4]^{4-}$ complexes correlate well

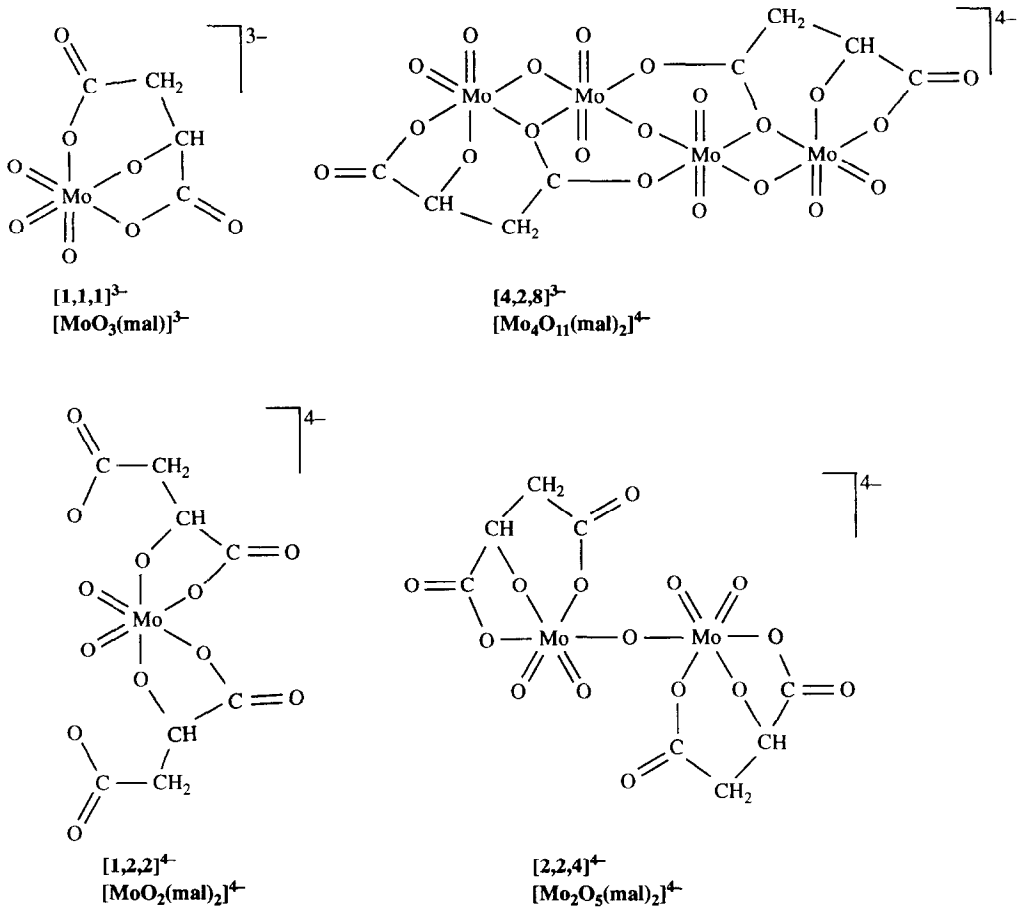


Fig. 4. Known and proposed structures for mononuclear [11], dinuclear and tetranuclear [6, 10] complexes of molybdenum(VI) with malate.

with the Job curves constructed from NMR data by Caldeira *et al.* [7]. As pointed out by these authors inherent limitations of Job's method prevented firm conclusions about the 2 : 1 and 1 : 1 stoichiometries proposed for the first two complexes. The calculated distribution curves, taking into account all complexes as well as side-equilibria of uncomplexed molybdate and malate, clearly show that the maxima of the Job curves for the $[4,2,8]^{4-}$ and $[2,2,4]^{4-}$ complexes (at pH = 5 and 1 mol dm^{-3} solution) would occur at a mole ratios of smaller than 2 : 1 and 1 : 1, respectively as was observed by these authors. Further, the Job curves for their complexes *b* and *a*, identified as 1 : 2 species, tally with distribution curves for the $[1,2,2]^{4-}$ and $[1,2,3]^{3-}$ complexes. However, the distinct NMR spectra observed for these two complexes showed that they cannot just differ in the degree of protonation and geometrical isomers were suggested [7].

The results of the present investigation also concur with the conclusions of a polarimetric study [8] regarding the stoichiometry and approximate stability regions of the six complexes $[111]^{3-}$, $[112]^{2-}$, $[1,2,2]^{4-}$, $[2,2,4]^{4-}$, $[2,2,5]^{3-}$ and $[4,2,8]^{4-}$. In particular, there is a close correlation between the change in rotatory power and the distribution curve of the $[4,2,8]^{4-}$ complex with the change in malic acid/molybdate ratio at constant pH values 3 and 4. The values obtained by graphical extrapolation for the formation constants of three complexes namely, log $\beta_{111} = 8.2$ (7.47), log $\beta_{122} = 13.9$ (15.48) and log $\beta_{224} = 22.6$ (28.06) differ appreciably from those now determined (shown in parentheses). However, considering the complexity of the system, the extrapolated values should be regarded as reasonable approximations.

Spectrophotometric investigation

First the individual spectra of the malate species have been determined from 17 experimental spectra in the pH_c range 5.7–1.3. Compared to the spectra of the molybdate species the absorption of the malic acid species is almost negligible (Fig. 5). The values calculated for the protonation constants using the program SQUAD [14] agreed very well with those obtained by potentiometry, shown in parentheses, log $\beta_{011} = 4.43 \pm 0.02$ (4.44), log $\beta_{012} = 7.59 \pm 0.06$ (7.57).

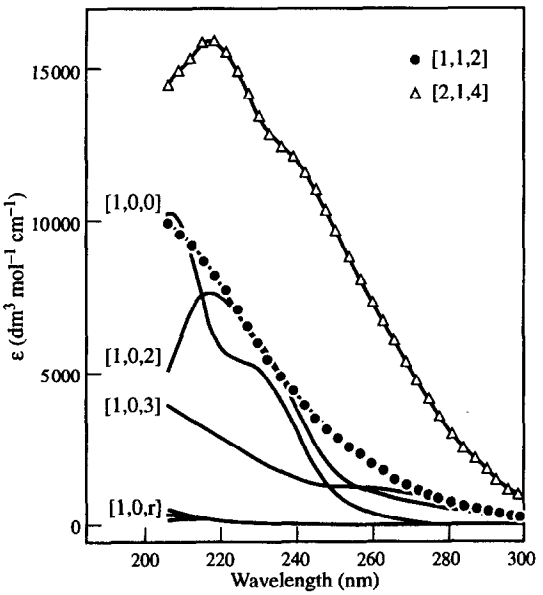


Fig. 5. Calculated molar absorption spectra of the [1, 1, 2] and [2, 1, 4] complexes and of the various malate species, [0, 1, *r*]. The spectra of the uncomplexed molybdenum(VI) monomers are also shown.

Complexation was then investigated by measuring the absorption of solutions of molybdate and malate at very low concentration (1×10^{-4} mol dm^{-3} in the pH_c range 5.6–1.5. Under these conditions the system is only just simple enough to extract useful formation constants and absorption spectra of two complexes, namely the $[1, 1, 2]^{2-}$ and $[2, 1, 4]^{2-}$. The expected maximum percentage concentrations of these complexes (based on the potentiometric results) were 50 and 20%, respectively. The $[1, 1, 3]^{-}$ complex reaches a maximum concentration of $\simeq$ 5%. Rather than neglecting it in the calculations its formation constant was supplied to the program and the calculations carried out on the basis that is has the same spectrum as the $[1, 1, 2]^{2-}$ complex. The known protonation constants and spectra of the malate species were supplied to the program. Also given were the protonation constants of monomeric molybdate β_{101}, β_{102} and β_{103} and the spectrum of $[HMoO_4]^-$ [16,25,26]. The values obtained for the formation constants were as follows: $\log \beta_{112} = 13.34$ (13.23) and $\log \beta_{214} = 24.33$ (24.35). The agreement with the values determined by potentiometry, given in parentheses, is better than what one would expect considering the uncertainties involved in the method. Reassuring also, is the good agreement between the spectra now calculated for the [102] and $[103]^+$ species and those previously determined [26]. As noted in the previous section the greatest uncertainty was associated with the $[2, 1, 4]^{2-}$ complex. Having provided additional evidence for its existence and also verifying the value of the formation constant of the $[1, 1, 2]^{2-}$ complex the reaction model could be accepted with confidence to be used as a basis for an enthalpimetric study.

Enthalpimetric investigation

The results obtained in some of the enthalpimetric titrations are shown in Fig. 6 where the total amount of heat measured, Q, is plotted against the molar ratio of acid added to molybdate. (The curves do not start at the origin because the enthalpy of the first few data points, before a steady state is reached, are not included.) The different shapes of the two curves (b) and (c) at the same molybdate concentration but with different malate concentrations reflect the change in relative concentrations of the complexes. Above a 1 : 1 mole ratio of acid to molybdate more heat is developed for the solution having an excess of malate because of the higher percentage of [1, 2, *r*] complexes. For the solution with a four fold excess of malate the [1, 2, *r*] species dominate (*cf* Fig. 3) and in keeping with this complete conversion to the $[1, 2, 2]^{4-}$ complex is indicated by a distinct break in the curve occurring at a 2 : 1 mole ratio of acid to molybdate (Fig. 6).

The enthalpy changes for the formation of the complexes were calculated from the measured heat, Q, corrected for dilution effects,

$$Q = \Sigma n_{pqr} \Delta H^{\circ}_{pqr} \qquad (4)$$

where n_{pqr} is the number of moles formed and ΔH°_{pqr} the molar enthalpy change of a given species [*p*, *q*, *r*]

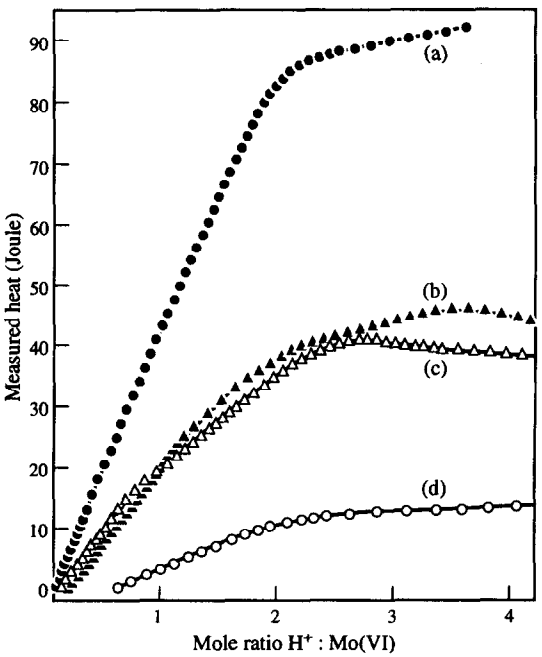


Fig. 6. Measured heat as a function of the molar ratio of acid to molybdate for titrations of the following solutions ([Mo] : [mal]) with hydrochloric acid: (a) 0.05 M : 0.20 M; (b) 0.03 M : 0.05 M; (c) 0.03 M : 0.03 M; and (d) 0.01 M : 0.04 M.

at 25°C in 1.0 mol dm^{-3} (Na)Cl medium. The set of linear equations obtained from corresponding Q and n_{pqr} values were solved for the unknown ΔH°_{pqr} parameters using a BMDP least squares program [27].

The n_{pqr} values at each titration point were calculated, in a subroutine supplied to the BMDP program, from the concentrations of the species obtained by simultaneous solution of the three mass-balance equations (5)–(7)

$$B = b + \Sigma p\beta_{pqr} b^p c^q h^r \quad (5)$$

$$C = c + \Sigma q\beta_{pqr} b^p c^q h^r \quad (6)$$

$$H = h + \Sigma r\beta_{pqr} b^p c^q h^r \quad (7)$$

where b, c, and h are the equilibrium concentrations of $[MoO_4]^{2-}$, $Hmal^{2-}$ and H^+, respectively.

The enthalpy changes for the protonation of $Hmal^{2-}$ in 1 mol dm^{-3} NaCl, $\Delta H^{\circ}_{011} = -2.0$ kJ mol^{-1} and $\Delta H^{\circ}_{012} = -6.5$ kJ mol^{-1} were determined in separate titrations and treated as fixed parameters in the calculation of the ΔH°_{pqr} values of the complexes. The small enthalpy changes are typical for this type of protonation reaction which is normally entropy driven [28]. The enthalpy changes for the protonation of malate can be compared with those of citrate in the same ionic medium, i.e. $\Delta H^{\circ}_{011} = -1.3$ kJ mol^{-1} and $\Delta H^{\circ}_{012} = -5.8$ kJ mol^{-1}. Literature values for malate [20] pertaining to ionic strength 0.1 mol dm^{-3} are $\Delta H^{\circ}_{011} = 0.59$ kJ mol^{-1} and $\Delta H^{\circ}_{012} = -2.84$ kJ mol^{-1}.

The ΔH° values calculated for the various complexes are listed in Table 1. Because the maximum percentage concentration of the $[2,1,4]^{3-}$ complex under the experimental conditions never exceeded 5% a realistic value for its enthalpy change could not be evaluated from the data. Rather than neglecting this complex, the quite reasonable approximation, based on results of this and previous investigations [21], was made that the enthalpy change for a complex and its protonated form has about the same value. The data were therefore treated on the assumption that $\Delta H_{213} = \Delta H^{\circ}_{214}$. Since ΔH°_{213} could be calculated with reasonable accuracy the approximation only affected the value of ΔH°_{214}.

The quite favourable enthalpy change for complexation is typical for molybdate and is the result of an increase in coordination number of molybdenum from four to six. The enthalpy changes determined for the formation of mononuclear molybdenum–malate complexes of the type $[1,1,r]$ concur with values previously reported for other α-hydroxycarboxylate ligands which are typically about −50 to −60 kJ mol^{-1} [21]. The agreement between the enthalpy changes for comparable malate and citrate complexes reflects the similarity in their structures. The enthalpy change for the $[Mo_4O_{11}(mal)_2]^{4-}$ and $[Mo_4O_{11}(Hcit)_2]^{4-}$, for example, are −232 and −251 kJ mol^{-1}, respectively. The more favourable entropy change for the citrate complex [21] ($T\Delta S = 118$) compared with that of the malate complex ($T\Delta S^{\circ} = 70$) is in keeping with the two extra protons involved in its formation; the increase in $T\Delta S$ per protonation is typically 20–25 kJ mol^{-1} and it is also seen that the value of $T\Delta S^{\circ}$ for $[Mo_4O_{11}(Hmal)_2]^{2-}$ is

Table 1. Values of the formation constants and other thermodynamic quantities for molybdenum(VI) malate complexes. The value in parentheses is approximate; see text

Complex $[p,q,r]$	$\log\beta \pm 3\sigma$	ΔG° kJ/mol	ΔH kJ/mol	$T\Delta S^{\circ}$ kJ/mol
$[1,1,1]^{3-}$	7.47±0.01	−42.64	−47.9±0.4	−5.3
$[1,1,2]^{2-}$	13.23±0.01	−75.52	−55.5±1.2	20
	13.34±0.10[a]			
$[1,1,3]^{-}$	15.87±0.08	−90.59	−57±4	33
$[1,2,2]^{4-}$	15.48±0.01	−88.36	−77.0±0.2	11.4
$[1,2,3]^{3-}$	20.13±0.01	−114.9	−83±1	32
$[1,2,4]^{2-}$	24.14±0.01	−137.8	−85.6±0.8	52
$[4,2,8]^{4-}$	52.92±0.03	−302.1	−232±5	70
$[4,2,9]^{3-}$	54.35±0.05	−310.2	−214±15	96
$[4,2,10]^{2-}$	55.27±0.09	−315.5	−197±21	118
$[2,1,3]^{3-}$	20.10±0.04	−114.7	−75±4	40
$[2,1,4]^{2-}$	24.35±0.24	−139.0	(−75)	64
	24.33±0.40[a]			
$[2,2,4]^{4-}$	28.06±0.03	−160.2	−85±10	75
$[2,2,5]^{3-}$	32.01±0.07	−182.7	−85±8	98
$[4,4,11]^{5-}$	69.92±0.09	−399.1	−221±14	178
$[0,1,1]^{-}$	4.44±0.01	−25.3	−2.0±0.1	23.3
	4.43±0.03[a]			
$[0,1,2]$	7.57±0.01	−43.2	−6.5±0.1	36.7
	7.59±0.03[a]			

[a] Spectrophotometric values.

the same as that of $[Mo_4O_{11}(Hcit)_2]^{4-}$. The tetranuclear complex $[Mo_4O_{11}(mal)_2]^{4-}$ is an important species even at relatively low concentrations because compared to most of the mono- and dinuclear complexes occurring in the same pH_c region it has a very favourable ΔH° ($\sim$ 60 kJ mol^{-1} per Mo atom or per mal^{3-}). Assuming that it has the same structure in solution as in the solid state, the extra stability is most likely due to the manner in which the malate ligands are utilized in connecting the two dimeric $Mo_2O_5^{2+}$ units. Both oxygen atoms of each of the β-carboxylate groups are coordinated to molybdenum which implies a more favourable enthalpy change per malate because of the extra bond energy. Further, due to the absence of free carboxylate groups and the unavailability of negatively charged (formally) oxygens the enthalpy change for the protonation of the $[4,2,8]^{4-}$ complex is positive resulting in rather small protonation constants.

Noteworthy is the very favourable enthalpy change for the $[1,2,2]^{4-}$ complex (about -80 kJ mol^{-1} per Mo atom) and which explains its greater stability compared to other complexes occurring in the same pH region. When compared with the $[1,1,1]^{3-}$ complex, for example, it gains in stability because of the formation of two stable five-membered rings as against one five- and one six-membered ring in the $[1,1,1]^{3-}$ complex. Also to be considered is the enthalpy cost involved in the ionization of the alcoholic proton in the formation of the 1 : 1 complex, but which can be regained (with profit) *via* a water molecule when two ligands are coordinated to form the $[1,2,2]^{4-}$ complex. The prominence of 1 : 2 complexes in the case of α-hydroxycarboxylic acids has been noted in previous papers and especially for monocarboxylates such as lactate and madelate [29, 30].

CONCLUSION

Depending on the concentration of molybdate and malate several complexes occur in varying quantities in the pH_c range 1.5–7.5. Complexes with six different stoichiometric ratios of molybdate to malate have been identified, namely 1 : 1, 1 : 2, 2 : 2, 2 : 1, 4 : 2 and 4 : 4. The stoichiometry of these complexes are the same as those of molybdenum citrate complexes except that citrate complexes afford additional protonation possibilities because of the extra uncoordinated carboxylate group. The complexes can be described as follows: the mononuclear complexes $[MoO_3(mal)]^{3-}$ and $[MoO_2(mal)_2]^{4-}$ and their protonated forms, the dinuclear complexes $[Mo_2O_5(mal)_2]^{4-}$ and $[Mo_2O_6(mal)(H_2O)_2]^{3-}$ and their protonated forms, and finally the tetranuclear complexes $[Mo_4O_{11}(mal)_2]^{4-}$ and $[Mo_4O_{10}(OH)(Hmal)_4]^{5-}$ of which the latter has no protonated forms in the pH_c range in question. Thermodynamic quantities for the complexes have been determined and compared with those previously reported for molybdenum–citrate complexes.

Acknowledgements—Financial support by the Foundation of Research Development and the University of Stellenbosch is gratefully acknowledged.

REFERENCES

1. E. Richardson, *J. Inorg. Nucl. Chem.* 1960, **13,** 84.
2. M. J. Baillie and D. H. Brown, *J. Chem. Soc.* 1961, 3691.
3. S. Prasad and L. P. Pandey, *J. Indian Chem. Soc.* 1965, **42,** 783.
4. M. Cadiot and B. Viossat, *Rev. Chim. Minèrale* 1969, **6,** 727.
5. E. Mikanová and M. Bartušek, *Scripta Fac. Sci. Nat. Univ. Purk. Brun.* 1981, **11,** 439.
6. J.-E. Berg, S. Brandänge, L. Lindblom and P.-E. Werner, *Acta Chem. Scand.* 1977, **A31,** 325.
7. M. M. Caldeira, M. E. T. L. Saraiva and V. M. S. Gil, *Inorg. Nucl. Chem. Letts* 1981, **17,** 295 and references therein.
8. A. Beltrán, A. C. Avalos and J. Beltrán, *J. Inorg. Nucl. Chem.* 1981, **43,** 1337.
9. D. O. Mărtine, M. R. Fĕliz and A. L. Capparelli, *Polyhedron* 1988, **7,** 2709.
10. M. A. Porai-Koshits, L. A. Aslanov, G. V. Ivanova and T. V. Polynova, *J. Struct. Chem. (Engl. Trans.)* 1968, **9,** 401.
11. C. B. Knobler, A. G. Wilson, R. N. Hider, I. W. Jensen, B. R. Penfold, W. T. Robinson and C. J. Wilkins, *J. Chem. Soc., Dalton Trans.* 1983, 1299.
12. J. J. Cruywagen, J. B. Heyns and R. F. van de Water, *J. Chem. Soc., Dalton Trans.* 1986, 1857.
13. H. S. Rossotti, *Talanta* 1974, **21,** 809.
14. D. J. Legget, in *Computational Methods for the Determination of Formation Constants* (Edited by D. J. Legget), p. 221. Plenum Press, New York (1985).
15. J. J. Cruywagen, J. B. B. Heyns and E. A. Rohwer, *J. Chem. Soc., Dalton Trans.* 1990, 1951.
16. J. J. Cruywagen, J. B. B. Heyns and E. F. C. H. Rohwer, *J. Inorg. Nucl. Chem.* 1978, **40,** 53.
17. K. H. Tytko, B. Baethe and J. J. Cruywagen, *Inorg. Chem.* 1985, **24,** 3132.
18. J. J. Cruywagen and E. A. Rohwer, unpublished work.
19. P. Gans, A. Sabatini and A. Vacca, *J. Chem. Soc., Dalton Trans.* 1985, 1195.
20. R. M. Smith and A. E. Martell, *Critical Stability Constants* Vol. 6: 2nd Suppl, p. 339. Plenum Press, New York (1989).
21. J. J. Cruywagen, E. A. Rohwer and G. F. S. Wessels, *Polyhedron* 1995, **14,** 3481 and references therein.
22. L. R. Nassimbeni, M. L. Niven, J. J. Cruywagen and J. B. B. Heyns, *J. Crystallogr. Spectrosc. Res.* 1987, **17,** 373.
23. A. Samotus, A. Kanas, M. Dudek, R. Grybos and E. Hodorowicz, *Trans. Met. Chem.* 1991, **16,** 495.
24. J. D. Pedrosa de Jesus, M. de D. Farropas, P.

O'Brien, R. D. Gillard and P. A. Williams, *Trans. Met. Chem.* 1983, **8,** 193.
25. J. J. Cruywagen and J. B. B. Heyns, *Inorg. Chem.* 1987, **26,** 2569.
26. J. J. Cruywagen, J. B. B. Heyns and E. F. C. H. Rohwer, *J. Inorg. Nucl. Chem.* 1976, **38,** 2033.
27. W. J. Dixon (Editor), *BMDP Statistical Software.* University of California Press, Berkeley, CA (1981).
28. J. J. Christensen, R. M. Izatt and L. D. Hansen, *J. Am. Chem. Soc.* 1967, **89,** 213.
29. J. J. Cruywagen and E. A. Rohwer, *J. Chem. Soc., Dalton Trans.* 1995, 3433.
30. V. M. S. Gil, *Pure Appl. Chem.* 1989, **61,** 841.

Pergamon

S0277-5387(96)00270-7

Polyhedron Vol. 16, No. 2, pp. 253–258, 1997
Copyright © 1996 Elsevier Science Ltd
Printed in Great Britain. All rights reserved
0277-5387/97 $15.00 + 0.00

Template synthesis of asymmetrical nickel(II) of substitute mono-benzo-N_4 and effect of substitute for methine sites in their complexes

Yu-Chul Park,* Seong-Su Kim,† Dong-Cheol Lee and Chul-Hyeon An

Department of Chemistry, Kyungpook National University, Taegu 702-701, Korea

(Received 7 May 1996; accepted 22 May 1996)

Abstract—Reaction of a 1 : 1 mixture of the appropriate phenylenediamine (e.g. 4-methyl-1,2-phenylenediamine 4-chloro-1,2-phenylenediamine) and alkylenediamine (e.g. ethylenediamine and propylenediamine) with 2,4-pentanedione in presence of nickel(II) salt gave a series of asymmetrical nickel(II) complexes of the $[Me_4\text{-}RBzo[X]tetraeneN_4]^{2-}$ ligand (where R = CH_3 or Cl; X = 14 or 15). These complexes were investigated by means of mass, infrared, NMR and electronic spectra. Hammett plots of the ^{13}C NMR resonances of methine carbons for $[Ni\text{-}(Me_4\text{-}RBzo[X]tetraeneN_4]$ complexes (where R = CH_3, H, Cl or NO_2; X = 14 or 15) *vs* σ_p were linear and had slopes of 2.97 and 2.63 for 14-membered and 15-membered complexes, respectively.
Copyright © 1996 Elsevier Science Ltd

Keywords: template synthesis; asymmetrical nickel(II) macrocycle.

Studies of tetraaza[14]annulene nickel(II) complex, which was obtained by the template condensation of 1,2-phenylenediamine with 2,4-phentanedione in the presence of nickel(II) ion as first described by Jäger [1], have been widely investigated on account of their structural features in common with the porphyrin [2, 3]. However, most macrocyclic complexes [4–7] obtained by the Jäger method were symmetrical complexes and examples of asymmetrical complexes synthesized by this method are rare.

In a previous paper [8], we reported that the asymmetrical nickel(II) complexes with tetraaza[X]benzo macrocycles, $[Ni(Me_4\text{-}Bzo[14]tetraeneN_4)]$ (**14H**), $[Ni(Me_4\text{-}NO_2Bzo[14]tetraeneN_4]$ (**14NO$_2$**), $[Ni(Me_4\text{-}Bzo[15]tetraeneN_4)]$ (**15H**) and $[Ni(Me_4\text{-}NO_2Bzo[15]tetraeneN_4)]$ (**15NO$_2$**), could be obtained by the reaction of a 1 : 1 mixture of the appropriate phenylenediamine (e.g. 1,2-phenylenediamine and 4-nitro-1,2-phenylenediamine) and alkylenediamine (e.g. ethylenediamine and propylenediamine) with 2,4-pentanedione in the presence of a nickel(II) salt.

This paper describes the synthesis of the new asymmetrical nickel(II) macrocycles, $[Ni(Me_4\text{-}CH_3Bzo[14]tetraeneN_4)]$ (**14CH$_3$**), $[Ni(Me_4\text{-}ClBzo[14]tetraeneN_4]$ (**14Cl**), $[Ni(Me_4\text{-}CH_3Bzo[15]tetraeneN_4)]$ (**15CH$_3$**), $[Ni(Me_4\text{-}ClBzo[14]tetraeneN_4)]$ (**15Cl**) by a procedure similar to that described for the complexes mentioned above. Also, we have studied the effect of varying the substituent R groups (R = CH_3, H, Cl and NO_2) in $[Ni(Me_4\text{-}RBzo[14]tetraeneN_4)]$ (X = 14 and 15) using ^1H and ^{13}C NMR spectra.

EXPERIMENTAL

Physical measurements

The EI mass spectra for **14CH$_3$**, **14Cl**, **15CH$_3$** and **15Cl** were determined with a JEOL MS-DX 300 gas chromatograph mass spectrometer at 70 eV using a direct inlet system. The infrared spectra in the area of the 400–4000 cm^{-1} were obtained as disks in KBr on a Perkin-Elmer 1430 IR spectrophotometer. UV–vis electronic absorption spectra were recorded on a Shimadzu UV-265 double beam spectrophotometer for chloroform solutions at room temperature. ^1H (300 MHz) and ^{13}C (75.5 MHz) NMR spectra were recorded on a Bruker instrument in $CDCl_3$ at room temperature and the chemical shifts were given in ppm

* Author to whom correspondence should be addressed.
† Department of Chemistry, Michigan State University, East Lansing, MI 48824, U.S.A.

relative to tetramethylsilane as an internal reference standard. Elemental analyses of the new complexes were performed at the Kolon R&D Center.

Preparation of the new complexes

All reagents and solvents used were of analytical grade.

[Ni(Me_4-CH_3Bzo[14]tetraeneN_4)], **14CH$_3$**. Under a N_2 atmosphere, 0.04 mol (4g) of 2,4-pentanedione was added to the methanol (50 cm^3) solution of nickel(II) acetate tetrahydrate (5 g, 0.02 mol). To the hot (60°C) mixture were added 4-methyl-1,2-phenylenediamine (2.5 g, 0.02 mol) and ethylenediamine (1.2 g, 0.02 mol). The solution was refluxed until precipitation of the product was complete. The hot solution was filtered, washed with hot methanol, and air-dried. The product was recrystallized from dichloromethane–methanol (1 : 1) mixture. Yield: 30%. Found: C, 62.6; H, 6.5; N, 15.4. Calc. for $C_{19}H_{24}N_4Ni$: C, 62.2; H, 6.6; N, 15.3%; IR(KBr disc): ν(C=C) and ν(C=N) 1528, 1482, 1420; ν(aromatic) 750 cm^{-1}; UV–vis, (ε) in $CHCl_3$, nm: 548 (2680), 376 (24960); EIMS: m/z (relative intensity) 368 (43.9), 367 (32.2), 366 (100), 365 (35.2).

[Ni(Me_4-ClBzo[14]tetraeneN_4)], **14Cl**. This was prepared from 2,4-pentanedione (4 g, 0.04 mol), nickel(II) acetate tetrahydrate (5 g, 0.02 mol), 4-chloro-1,2-phenylenediamine (2.9 g, 0.02 mol), ethylenediamine (1.2 g, 0.02 mol) and methanol (50 cm^3), following the above procedure. Yield: 31%. Found: C, 55.5; H, 5.2; N, 14.3. Calc. for $C_{18}H_2N_4ClNi$: C, 55.8; H, 5.5; N, 14.5%; IR(KBr disc): ν(C=C) and ν(C=N) 1526, 1472, 1420; ν(aromatic) 768 cm^{-1}; UV–vis, (ε) in $CHCl_3$, nm: 547 (3140), 381 (25470); EIMS: m/z (relative intensity) 388 (61.1), 387 (31.1), 386 (100), 385 (22.4).

[Ni(Me_4-CH_3Bzo[15]tetraeneN_4)]. **15CH$_3$**. This was prepared from 2,4-pentanedione (4 g, 0.04 mol), nickel(II) acetate tetrahydrate (5 g, 0.02 mol), 4-methyl-1,2-phenylenediamine (2.5 g, 0.02 mol), propylenediamine (1.5 g, 0.02 mol) and methanol (50 cm^3), following the above procedure. Yield: 55%. Found: C, 62.9; H, 6.8; N, 14.8. Calc. for $C_{20}H_{26}N_4Ni$: C, 63.0; H, 6.9; N, 14.5%; IR(KBr disc): ν(C=C) and ν(C=N) 1526, 1472, 1420; ν(aromatic) 758 cm^{-1}; UV–vis (ε) in $CHCl_3$, nm: 559 (2100), 385 (21800); EIMS: m/z (relative intensity) 382 (37.5), 381 (22.8), 380 (100).

[Ni(Me_4-ClBzo[15]tetraeneN_4)], **15Cl**. This was prepared from 2,4-pentanedione (4 g, 0.04 mol), nickel(II) acetate tetrahydrate (5 g, 0.02 mol), 4-chloro-1,2-phenylenediamine (2.9 g, 0.02 mol), propylenediamine (1.5 g, 0.02 mol) and methanol (50 cm^3), as described above. Yield: 55%. Found: C, 56.4; H, 5.6; N, 13.7. Calc. for $C_{19}H_{23}N_4ClNi$: C, 56.8; H, 5.8; N, 14.0%; IR(KBr disc): ν(C=C) and ν(C=N) 1553, 1472, 1414. ν(aromatic) 747 cm^{-1}; UV–vis (ε) in $CHCl_3$, nm: 569 (2590), 385 (24,540). EIMS: m/z (relative intensity (402 (58.2), 401 (24.2), 400 (94.1), 387 (66.7), 386 (21.7), 385 (100).

RESULTS AND DISCUSSION

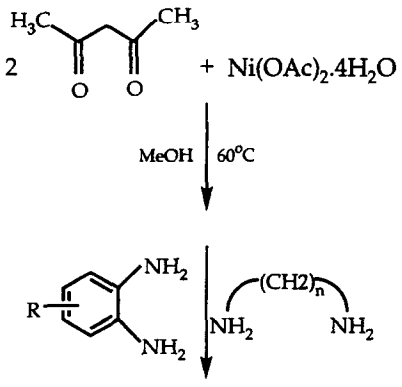
Synthesis of the asymmetric macrocyclic complexes

The asymmetrical macrocyclic complexes of **14R** and **15R** series were prepared following the synthetic route shown in Scheme 1. The initial step in the synthesis involves the formation of a nickel(II) acetylacetonate complex that functioned as a template for condensation of a 1 : 1 mixture of appropriate 1,2-phenylenediamine and alkylenediamine to produce the desired macrocycles. Also, we attempted to prepare the other similar **16R** series such as **16CH$_3$**, **16H**, **16Cl** and **16NO$_2$** from the reaction of the appropriate phenylenediamine and butylenediamine with 2,4-pentanedione in the presence of nickel(II) salt. However, these complexes were not produced. Elemental analyses of **14CH$_3$**, **14Cl**, **15CH$_3$** and **15Cl** given in the Experimental section are consistent with these formulations.

Mass, IR and electronic spectra of the new complexes

The mass spectral data of **14CH$_3$**, **14Cl**, **15CH$_3$** and **15Cl** are given in the Experimental Section. The EI mass spectra for **14CH$_3$**, **14Cl** and **15CH$_3$** show the presence of a molecular ion M^+ at m/z 366 (^{58}Ni), 386 (^{35}Cl, ^{58}Ni) and 380 (^{58}Ni), respectively. These peaks are the base peaks in each mass spectrum. While **15Cl** exhibits a molecular ion M^+ at m/z 400 (^{35}Cl, ^{58}Ni) which is not a base peak. All complexes show masses of the major fragment $[M\text{-}CH_3]^+$ at m/z 351, 371, 365 and 385, respectively. The masses of the fragment at m/z 351 and 365 for **14Cl** and **15Cl** corresponds to $[M\text{-}Cl]^+$, but the relative intensities are very small.

The characteristic IR bands of the four complexes display strong bands around 1550–1520, 1480 and



[Ni(Me_4-RBzo[X]tetraeneN_4)]

Scheme 1.

1420 assignable to ν(C=C) and ν(C=N). This observation indicates the formation of the conjugated six membered chelate ring in the reaction [9]. The aromatic bands of these complexes also occur at around 750 cm^{-1}.

The electronic absorption spectral data for **14CH$_3$**, **14Cl**, **15CH$_3$** and **15Cl** are given in the Experimental section. The absorption bands ranging from 370 to 570 nm are reasonably attributed to $\pi \rightarrow \pi^*$ transitions within the ligand molecular and charge transfer (CT) transitions from metal to ligand since the molar extinction coefficients of the bands (2100–25,470 M^{-1} cm^{-1}) are much larger than those commonly assigned to ligand-field bands which were obscured by intense $\pi \rightarrow \pi^*$ and CT transition bands [10]. These results are supported by similar observations with tetraaza [14]annulene nickel(II), **14R** and **15R** (where R = H or NO_2) reported earlier [4,8].

^{1}H *NMR spectra*

Consistent with a diamagnetism of the new macrocyclic nickel(II) complexes, **14CH$_3$**, **14Cl**, **15CH$_3$** and **15Cl** gave well-resolved ^{1}H NMR spectra. The assignments were made by the comparisons of the spectra with those of other macrocyclic nickel(II) complexes reported earlier [5,11]. ^{1}H NMR chemical shifts and their assignments for the complexes, **14CH$_3$**, **14Cl**, **15CH$_3$** and **15Cl** are listed in Table 1. The δ-carbon sites of the diiminate framework of the tetraaza [14] annulene nickel(II) complex have been found to be a reactive nucleophilic center named the methine site. Thus, the chemical shift values in NMR spectra of the methine sites for **14R** and **15R** series are worth special mention. The methine proton peaks (H′ and H″) for **14CH$_3$** and **15CH$_3$** with a methyl substituent and those for **14Cl** and **15Cl** with a chloro substituent on the phenyl ring are nonequivalent and show two singlets, respectively (see Table 1). These peaks of **14CH$_3$** and **15CH$_3$** show slight upfield shifts (about 0.02–0.04 and 0.02–0.03 ppm) relative to the 5.03 and 4.88 ppm of **14H** and **15H** with no substituent on the phenyl ring, respectively. On the other hand, the peaks of **14Cl** and **15Cl** show slight downfield shifts (0.02–0.03 and 0.01–0.02 ppm) relative to **14H** and **15H** [12]. The results are attributed to the shielding and deshielding effect of the substituents on the phenyl ring.

^{13}C *NMR spectra and Hammett plot*

^{13}C NMR data and their assignments for **14CH$_3$**, **14Cl**, **15CH$_3$** and **15Cl** are presented in Table 2 and the resonances of methine carbons for **14R** and **15R** series shown in Fig. 2. The resonances of methine carbons for **14CH$_3$**, **14Cl**, **15CH$_3$** and **15Cl** are also shifted upfield or downfield relative to **14H** and **15H** which are in agreement with the corresponding ^{1}H NMR spectral behavior. The **14R** and **15R** series contains macrocycles with various electron donor and withdrawing groups that have different σ_p values [13]. The effect of the substituents on the resonances of methine carbons for these complexes was examined by means of a Hammett plot. Figure 3 shows that the relationship between $\Delta\delta$ [15] and σ_p is linear with a slope of 2.97 (a correlation coefficient of 0.99) for the **14R** series and with a slope of 2.63 (a correlation coefficient of 0.99) for the **15R** series, respectively. In view of the similarity of structures of **14R** and **15R** series, the difference in their slopes seems unexpectedly great. When intramolecular repulsion of chelate ring alkylene groups and diiminate framework are considered, the positional changes seem rational. This difference between the **14R** and **15R** series in the repul-

Table 1. ^{1}H NMR spectra of **14CH$_3$**, **14Cl**, **15CH$_3$** and **15Cl**[a]

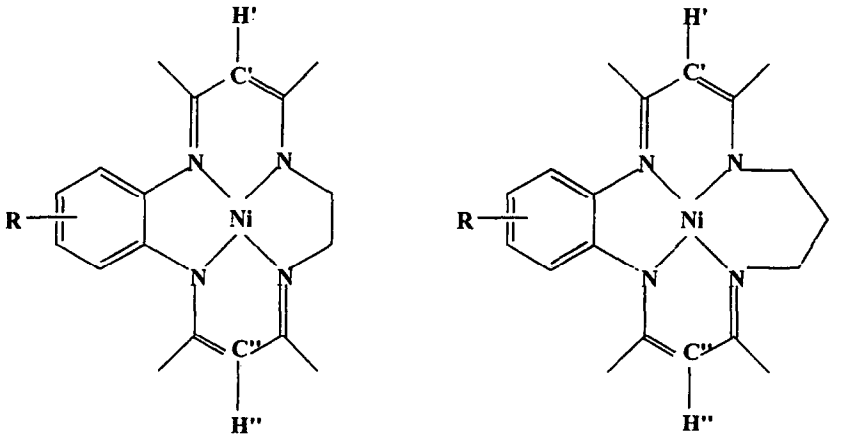
Compound	Methyl	Toulene Methyl	Ethylene N—CH_2	Propylene —CH_2—, —N—CH_2—		Methine	Aromatic
14CH$_3$	2.05(s) 2.37(s) 2.38(s)	2.27(s)	3.35(s)			4.99(s) 5.02(s)	6.49–7.06(m)
14Cl	2.07(s) 2.35(s) 2.37(s)		3.37(s)			5.05(s) 5.06(s)	6.64–7.12(m)
15CH$_3$	1.92(s) 2.08(s) 2.10(s)	2.22(s)		2.32(m)	2.81(m)	4.85(s) 4.86(s)	6.43–6.74(m)
15Cl	1.95(s) 1.96(s) 2.11(s) 2.14(s)			2.33(m)	2.95(m)	4.93(s) 5.05(s)	6.78–7.68(m)

[a] Chemical shifts in ppm from internal TMS. Measured in $CDCl_3$ solutions at 300 MHz. Multiplicity of a proton signal is given in parentheses after δ-value: s = singlet, m = multiplet.

Table 2. ^{13}C NMR spectra of **14CH$_3$**, **14Cl**, **15CH$_3$** and **15Cl**[a]

Compound	Methyl	Toluene Methyl	Ethylene N—*C*—	Propylene C—*C*—C	Propylene N—C	Methine	Aromatic	Diiminate
14CH$_3$	20.23	21.20	52.78			103.33	119.62	154.61
	20.31		52.50			103.81	120.12	154.72
	23.11						120.70	157.64
	23.13						129.03	157.74
							143.10	
							145.28	
14Cl	20.37[b]		52.64			104.16	118.62	154.42
	22.98		52.78			104.63	119.44	154.45
	23.00						119.98	158.23
							124.14	158.48
							143.90	
							146.07	
15CH$_3$	20.02	21.12		31.91	50.84	103.48	120.02	154.91[b]
	20.98				50.95	103.96	120.52	160.14
	21.21						121.20	160.38
	21.25						129.60	
							143.88	
							145.99	
15Cl	20.85			31.79	50.89	104.23	119.32	154.61
	20.90				51.01	104.68	120.14	154.73
	21.32[b]						120.55	160.78
							124.47	161.09
							144.90	
							147.03	

[a] Chemical shifts in ppm from internal TMS. Measured in $CDCl_3$ at 75.5 MHz.
[b] One peak of two carbons.



14R series

14CH$_3$: R= CH$_3$
14H: R= H
14Cl: R= Cl
14NO$_2$: R= NO$_2$

15R series

15CH$_3$: R= CH$_3$
15H: R= H
15Cl: R= Cl
15NO$_2$: R= NO$_2$

Fig. 1. Chemical structures of asymmetrical N_4 macrocycles with substituent and the corresponding ones with no substituent on phenyl ring.

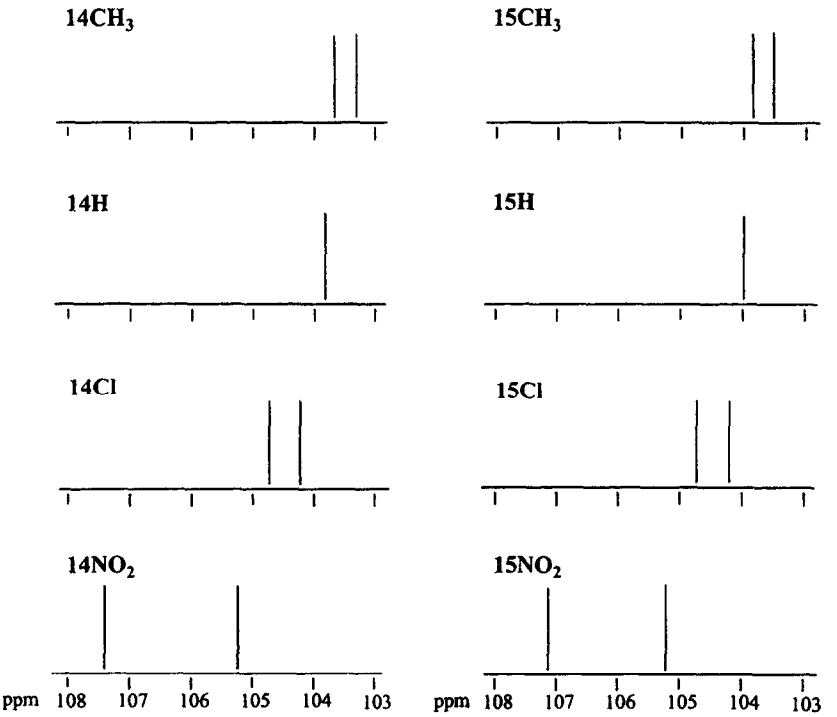


Fig. 2. The ^{13}C NMR spectra of the resonances of methine carbons for **14R** and **15R** series. Those of **14H**, **14NO$_2$**, **15H** and **15NO$_2$** are referred to in ref. 8.

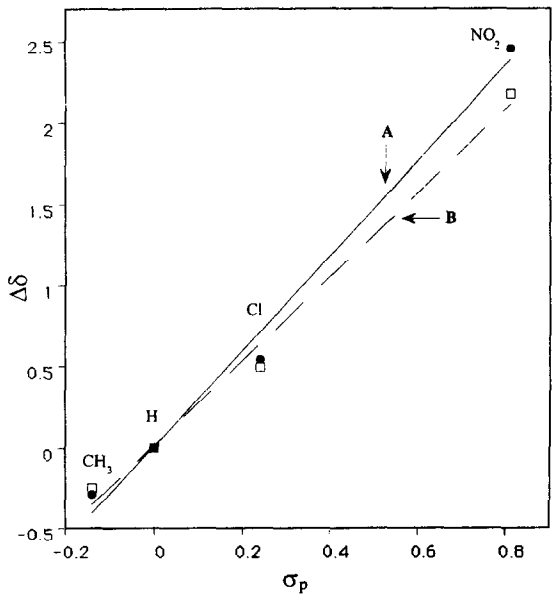


Fig. 3. Hammett plot of $\Delta\delta$ *vs* σ_p. A, **14R** series (corr = 0.99, slope = 2.97); B, **15R** series (corr = 0.99, slope = 2.63). $\Delta\delta$ = the average values of the resonances of methine carbons for complexes with substituent − the resonance of methine carbons corresponding to those with no substituent.

sion are exhibited in the Hammet plot as slope difference of 0.34. Interestingly, these slopes are similar to those of the oxidation potentials for metalloporphyrins with β substituents located on the pyrrole residues of the porphyrin ligand [16,17].

The resonances of the methine carbon for the 14R and 15R series are significantly affected by substituents on the phenyl ring.

Acknowledgements—This work was supported by a grant from the Korea Science and Engineering Foundation (93-0500-08-01-3) and the Basic Science Research Program (BSKI-94-3404), the Ministry of Education, Korea.

REFERENCES

1. E. G. Jäger, *Z. Chem.* 1964, **4,** 437.
2. W. H. Woodruff, R. W. Pastor and J. C. Dabrowiak, *J. Am. Chem. Soc.* 1976, **98,** 8014.
3. D. R. Neves and J. C. Dabrowiak, *Inorg. Chem.* 1976, **15,** 129.
4. C. L. Bailey, R. D. Bereman, D. P. Rillema and R. Nowak, *Inorg. Chem.* 1984, **23,** 3956.
5. K. Sakata, H. Tagami and M. J. Hashimoto, *J. Heterocyclic Chem.* 1989, **26,** 805.
6. M. Hashimoto, H. Tagami and K. Sakata, *J. Heterocyclic Chem.* 1990, **27,** 1265.
7. K. Sakata, M. Hashimoto, T. Hamada and S. Matsuno, *Polyhedron* 1996, **15,** 967.
8. Y. C. Park, Z. U. Bae, S. S. Kim and S. K. Baek, *Bull. Korean Chem. Soc.* 1995, **16,** 287.
9. J. G. Martin and S. C. Cummings, *Inorg. Chem.* 1973, **12,** 1477.
10. A. B. D. Lever, *Introduction to Ligand Fields*, 2nd Ed. Elsevier, Amsterdam (1984).
11. A. L. Cutler, C. S. Alleyne and D. Dolphin, *Inorg. Chem.* 1985, **24,** 2276.
12. Although the magnitudes of these shifts are very

small, they are proportional to the magnitude of the Hammett parameter of substituents. This is supported by a downfield shifts in ref. 8 about 0.13–0.21 and 0.05–0.17 ppms for **14NO$_2$** and **15NO$_2$** relative to **14H** and **15H,** respectively.

13. As pointed out elegantly by Kadish *et al.* in Ref. 14, the exact choice of which Hammett parameter to use, i.e. σ_p, σ^+, σ^-, etc., is not clear. We have chosen σ_p because the correlations are linear and it offers comparisons to the widest range of literature data.

14. T. Malinshi, D. Chang, L. A. Bottomley and K. M. Kadish, *Inorg. Chem.* 1982, **21,** 4248.
15. We have chosen the average values of the resonances of methine carbons for the complexes with substituent on the phenyl ring because it is difficult to distinguish those of the complexes on the basis of ^{1}H and ^{13}C NMR spectra only.
16. A. Giraudeau, H. J. Callot and M. Gross, *Inorg. Chem.* 1979, **18,** 201.
17. A. Giraudeau, H. Callot, J. Jordon, I. Ezhar and M. Gross, *J. Am. Chem. Soc.* 1979, **101,** 3857.

Pergamon

S0277-5387(96)00259-8

Polyhedron Vol. 16, No. 2, pp. 259–261, 1997
Copyright © 1996 Elsevier Science Ltd
Printed in Great Britain. All rights reserved
0277-5387/97 $15.00 + 0.00

Synthesis and structure of a novel dinuclear copper(II) complex containing 1,4,7-triazacyclododecane: $[Cu_2(HO)(MeCO_2)(tacd)_2](ClO_4)_2$

Xiao-Ming Chen,[a]* Xiao-Lan Yu,[a] Yu-Xing Yao[a] and Xiao-Ying Huang[b]

[a]Department of Chemistry, Zhongshan University, Guangzhou 510275, P.R. China

[b]State Key Laboratory of Structural Chemistry, Fujian Institute of Research on the Structure of Matter, Chinese Academy of Sciences, Fuzhou 350002, P.R. China

(Received 2 April 1996; accepted 22 May 1996)

Abstract—The novel dinuclear copper(II) complex has been prepared by reaction of tacd with $Cu(MeCO_2)_2 \cdot H_2O$ in ethanolic solution. The crystal structure shows that a pair of copper(II) atoms separated at 3.288(1) Å are bridged by a μ_2-HO^- and a μ_2-carboxylato-*O*,*O*′ group into a dinuclear structure in which each copper(II) atom is capped by a tacd ligand, resulting in a distorted trigonal-bipyramidal N_3O_2 coordination environment about the copper(II) atom with the Cu—N bonds at 2.040(5)–2.144(4) Å, Cu—O bonds at 1.895(2)–1.970(3) Å. Copyright © 1996 Elsevier Science Ltd

Keywords: copper(II); triazacyclodecane; carboxylate; hydroxide; synthesis; crystal structure.

Macrocyclic triamines are of current interest in the synthesis of metal complexes of biological significance. A large number of metal complexes containing this kind of tripodal ligand, especially the derivatives of nine-membered triazacyclonane and 12-membered triazacyclododecane, have been synthesized and their structures and properties studied [1–5]. We have used the less well known 10-membered macrocycle triazacyclodecane (tacd) to synthesize two monomeric complexes, $[M(tacd)_2]^{2+}$ ($M = Cu^{2+}, Zn^{2+}$) [6], and two chloro-bridged dimeric complexes $[M_2(tacd)_2Cl_2]^{2+}$ ($M = Cu^{2+}, Zn^{2+}$) [7], and the structural investigations demonstrated that the 10-membered ring is more flexible in coordination to metal ions. We now report the preparation and structural characterization of a novel (μ_2-hydroxo-μ_2-carboxylato-*O*,*O*′)-bridged dinuclear copper(II) complex with tacd, namely $[Cu(HO)(MeCO_2)(tacd)_2](ClO_4)_2$ (**1**).

EXPERIMENTAL

Preparation

The ligand tacd was synthesized by a modification of the literature method [8], and complex **1** was prepared as follows: To an aqueous ethanolic solution (80%, 15 cm^3) of $Cu(MeCO_2)_2 \cdot H_2O$ (0.1 g, 0.5 mmol) was added tacd (0.07 g, 0.5 mmol), and the mixture was stirred for 20 min at 60°C, followed with addition of an aqueous solution (3 cm^3) containing $NaClO_4$ (0.07 g). The pH value of the resulting solution was adjusted to *ca* 6. After slow evaporation of the blue solution, blue polyhedral crystals of complex **1** were deposited. Found, C 27.7, H 5.7, N 12.0. Calc. for $C_{16}H_{38}Cl_2Cu_2N_6O_{11}$: C 27.9, H 5.6, N 12.2%. IR data

* Author to whom correspondence should be addressed.

(cm^{-1}): 3402 m(br), 3295 m, 3205 s, 2931 m, 2882 m, 2853 m, 1581 s, 1447 m, 1418 s, 1370 w, 1314 w, 1264 w, 1096 vs(br), 997 m, 948 m, 885 m, 842 m, 800 w, 632 s.

Crystallography

$C_{16}H_{38}Cl_2Cu_2N_6O_{11}$, mol. wt. 688.50, orthorhombic, space group *Pnma* (no. 62), $a = 13.309(3)$, $b = 12.754(3)$, $c = 16.432(3)$ Å, $V = 2789.2(10)$ Å^3, $Z = 4$, $D_c = 1.640$ Mg m^{-3} $F(000) = 1424$, Mo-K_α($\lambda = 0.71069$ Å), $\mu = 17.88$ cm^{-1}.

Intensity data (crystal size $0.2 \times 0.2 \times 0.3$ mm; $2\theta_{max} = 50°$, 2564 unique (data) were collected at 21°C on an Enraf-Nonius CAD4 diffractometer using the ω-2θ scan mode. An empirical absorption correction was applied to the data. The structure was solved with direct methods using SAPI-91 program [9], and full-matrix least-squares refinement was performed with SHELXL-93 program [10]. The non-hydrogen atoms were refined anisotropically. Hydrogen atoms of the organic ligands were generated geometrically (C—H = 0.96 Å), assigned isotropic temperature factors and included in the structure-factor calculations. Analytical expressions of neutral-atom scattering factors were employed, and anomalous dispersion corrections were incorporated [11]. The final $R_1(R_{w2})$ value was 0.083 (0.260) for 181 parameters and 152 observed reflections with $I \geqslant 2\sigma(I)$. The high values reflect the poor quality of the crystal. No improvement in the structure could be achieved by using the space group $Pn2_1a$. The selected interatomic distances and bond angles are listed in Table 1. Supplementary materials including non-hydrogen and hydrogen atomic coordinates, and thermal parameters have been deposited at the Cambridge Crystallographic Data Centre.

RESULTS AND DISCUSSION

The crystal structure of complex **1** consists of discrete $[Cu_2(HO)(MeCO_2)(tacd)_2]^{2+}$ cations and perchlorate anions. As illustrated in Fig. 1, a pair of Cu^{II} atoms separated at a non-bonding distance of 3.288(1) Å are bridged by a μ_2-hydroxo and a μ_2-carboxylato-*O*,*O*′ group into a dinuclear unit, in which each Cu^{II} atom is capped with the tripodal tacd ligand. A crystallographic mirror plane bisects the dinuclear unit through the acetate carbon atoms and the hydroxo oxygen atom. The Cu^{II} atom is coordinated by three nitrogen atoms of the tacd ligand, one oxygen atom of the hydroxo group and one oxygen atom of the carboxylato group, resulting in a distorted trigonal-bipyramidal N_3O_2 environment with the axial positions occupied by the N(1) and O(2) atoms. The most distorted bond angle of the polyhedron is N(2)—Cu(1)—N(3) at 82.3(2)°. The Cu—N bond lengths fall in range of 2.040(5)—2.144(4) Å, which are slightly shorter than those found for the octahedral $[Cu(tacd)_2]^{2+}$ cations [6]. The hydroxo Cu(1)—O(1) bonds (1.895(2) Å) are significantly shorter than the carboxylato Cu(1)—O(2) bond (1.970(3) Å). The Cu—O—Cu bond angle is at 120.2(3)°, indicative of sp^2 hybridization.

It is noteworthy to mention that dinuclear complexes comprising analogous μ_2-hydroxo-μ_2-carboxylato bridge or μ_2-alkoxo-$\mu_2$carboxylato bridge are not commonly observed, and only two examples have previously been reported [12,13]. Moreover, similar dinuclear structures have been uncovered in some metalloenzymes, such as the zinc enzyme phospholipase-C and the iron enzyme ribonucleotide reductase [14,15], where the Zn···Zn and Fe···Fe distances are 3.30 Å and 3.20 Å, respectively, being strikingly similar to the Cu···Cu distance in complex **1**. Hence further exploration of analogous complexes containing zinc or iron ions will be of interest.

Acknowledgement—This work was supported by NSFC and the State Education Commission of China.

Table 1. Selected interatomic distances (Å) and bond angles (°)

Cu(1)—O(1)	1.895(2)	Cu(1)—O(2)	1.970(3)
Cu(1)—N(1)	2.040(5)	Cu(1)—N(2)	2.111(5)
Cu(1)—N(3)	2.144(4)	Cu(1)···Cu(1a)	3.288(1)
O(1)—Cu(1)—O(2)	96.0(1)	O(1)—Cu(1)—N(1)	88.4(2)
O(2)—Cu(1)—N(1)	175.6(1)	O(1)—Cu(1)—N(2)	127.1(2)
O(2)—Cu(1)—N(2)	95.1(1)	N(1)—Cu(1)—N(2)	81.9(2)
O(1)—Cu(1)—N(3)	150.1(2)	O(2)—Cu(1)—N(3)	85.5(2)
N(1)—Cu(1)—N(3)	90.0(2)	N(2)—Cu(1)—N(3)	82.3(2)
Cu(1a)—O(1)—Cu(1)	120.2(3)	C(1)—O(2)—Cu(1)	133.4(3)
O(2)—C(1)—O(2a)	125.9(5)	C(3)—N(1)—Cu(1)	114.1(4)
C(3)—N(1)—C(9)	117.1(4)	C(9)—N(1)—Cu(1)	108.3(5)
C(5)—N(2)—Cu(1)	108.0(3)	C(4)—N(2)—Cu(1)	106.2(4)
C(7)—N(3)—Cu(1)	111.7(4)	C(6)—N(3)—Cu(1)	108.5(4)

Symmetry code: (a) x, $1/2-y$, z

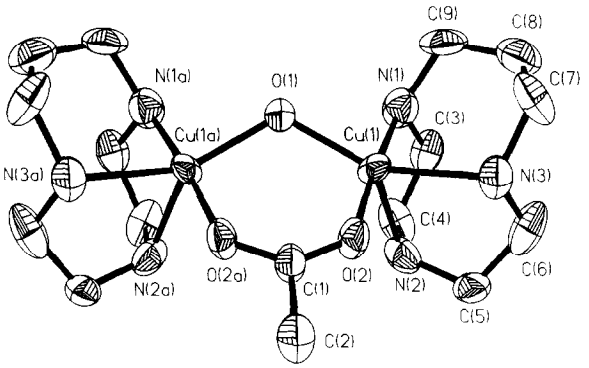


Fig. 1. Structure of the $[Cu_2(\mu_2\text{-}OH)(\mu_2\text{-}MeCO_2)(tacd)_2]^{2+}$ cation with the atom-numbering scheme. Symmetry code: (a) x, $1.2-y, z$.

REFERENCES

1. P. Chaudhuri and K. Wieghardt, *Prog. Inorg. Chem.* 1987, **35,** 329.
2. R. Hotzelmann, K. Wieghardt, U. Flörke, H.-J. Haupt, D. C. Weatherburn, J. Bonvoisin, G. Blondin and J.-J. Girerd, *J. Am. Chem. Soc.* 1992, **114,** 1681.
3. P. Chaudhuri, C. Stockheim, K. Wieghardt, W. Deck, R. Gregorzik, H. Vahrenkamp, B. Nuber and J. Weiss, *Inorg. Chem.* 1992, **31,** 1451.
4. E. Kimura, T. Shiota, T. Koike, M. Shiro and M. Kodama, *J. Am. Chem. Soc.* 1990, **112,** 5805.
5. V. McKee, *Adv. Inorg. Chem.* 1994, **40,** 323.
6. X.-M. Chen, Y.-X. Yao, K.-L Shi and T. C. W. Mak, *Aust. J. Chem.* 1995, **48,** 139.
7. X.-M. Chen, Y.-X. Yao, Z.-T. Xu, K.-L. Shi and Y.-J. Xu, *Polyhedron* 1995, **14,** 1195.
8. Y.-X, Yao, M.Sc. thesis, Department of Chemistry, Zhongshan University (1994).
9. H.-F. Fan, J.-X. Yao, C.-D. Zheng, Y.-X. Gu and J.-Z. Qian, SAPI-91, *Structure Analysis Program with Intelligence.* Institute of Physics, Academia Sinica, Beijing, China (1991).
10. G. M. Sheldrick, *SHELXL-93, Program for X-ray Crystal Structure Refinement.* University of Göttingen, Germany (1993).
11. *International Tables for X-ray Crystallography,* Vol. C, Tables 4.2.6.8 and 6.1.1.4. Kluwer Academic Publisher, Dordrecht (1992).
12. W. B. Tolman, R. L. Rardin and S. J. Lippard, *J. Am. Chem. Soc.* 1989, **111,** 4532.
13. V. McKee, M. Zvagulis, J. V. Dagdigian, M. G. Patch and C. A. Reed, *J. Am. Chem. Soc.* 1984, **106,** 4765.
14. E. Hough, K. L. Hansen, B. Birkness, K. Jynge, S. Hansen, A. Hardvick, C. Little, E. Dodson, Z. Derewenda, *Nature* 1989, **338,** 357.
15. R. G. Wilkins, *J. Chem. Soc., Dalton Trans.* 1992, 171.

Pergamon

S0277-5387(96)00257-4

Polyhedron Vol. 16, No. 2, pp. 263–266, 1997
Copyright © 1996 Elsevier Science Ltd
Printed in Great Britain. All rights reserved
0277–5387/97 $15.00 + 0.00

A new copper(II)lead(II) heterotetranuclear complex containing 2-dimethylaminoethanol: direct synthesis and structure

Olga Yu. Vassilyeva,* Vladimir N. Kokozay, Nadezhda A. Zhukova and Larisa A. Kovbasyuk

Department of Inorganic Chemistry, Kiev Shevchenko University, Volodimirska st., 64, Kiev 252033, Ukraine

(Received 26 March 1996; accepted 22 May 1996)

Abstract—The heterotetranuclear $Cu^{II}Pb^{II}$ complex containing 2-dimethylaminoethanol has been synthesized using copper powder and PbI_2 as starting materials and characterized by X-ray crystallography. The crystal comprises dimeric centrosymmetric molecules $\{Cu_2Pb_2[(CH_3)_2NCH_2CH_2O]_4I_4(DMSO)_2\}$ bridged by oxygen atoms of chelated 2-dimethylaminoethoxo groups, and DMSO molecules of crystallization. The nearest copper coordination environment has a somewhat distorted square planar geometry. The coordination geometry around the Pb atom is a highly distorted octahedron. The bridging oxygen atoms arrange a strictly planar central Pb_2O_2 rhombus in the structure of the complex. Copyright © 1996 Elsevier Science Ltd

Keywords: heteronuclear complexes; crystal structure; direct synthesis.

Exploring a new structural class of coordination compounds, namely heteronuclear complexes, may allow the discovery of agents that possess biological properties quite different from those of mononuclear complexes. The design of heteronuclear complexes is of importance in investigations concerning the mutual influences of several metal centers on the electronic, magnetic and electrochemical properties of such heteronuclear systems. Many heteronuclear compounds, especially ones containing copper and lead, have been obtained as complexes of binucleating macrocycles. The binucleating macrocycle derived from the 2:2 condensation of 2,6-diformyl-4-methylphenol and propane-1,3-diamine and related macrocycles have been extensively used for studies on homo- and heterobinuclear complexes and the synthetic work is rather complicated [1–3]. Our aim in this study was to establish an efficient synthetic method to obtain desirable heteronuclear complexes, first of all containing simpler ligands (e.g. aminoalcohols). In our previous study direct synthesis was successfully applied for the preparation of numerous homonuclear complexes and some of them possess unusual crystal structures and indicate biological activity [4–9]. Direct synthesis and the structural features of the heteronuclear $Cu^{II}Pb^{II}$ complex containing the 2-dimethylaminoethoxo ligand are reported.

EXPERIMENTAL

All chemicals were commercial products of reagent grade, used without further purification.

Synthesis of $\{Cu_2Pb_2[(CH_3)_2NCH_2CH_2O]_4I_4(DMSO)_2\} \cdot 2DMSO$

For the preparation of the compound the following method was used: copper powder (0.32 g, 5 mmol) PbI_2 (2.31 g, 5 mmol), DMSO (5 cm^3) and 2-dimethylaminoethanol (1.5 cm^3, 15 mmol) were placed in a flask in the above order. The mixture was heated in air up to 60°C and stirred until total dissolution of Cu and PbI_2 was observed (40–50 min). The clear green solution obtained was allowed to stand at room temperature for 2 h; then crystals separated from the solution. The crystals were filtered, washed with i-PrOH, and finally dried *in vacuo* at room temperature; yield 3.04 g (71%). Found: H, 3.7; C, 16.9; N, 3.2;

* Author to whom correspondence should be addressed.

I, 30.1; Cu, 7.4; Pb, 24.3. Calc. for $C_{12}H_{32}CuI_2N_2O_4PbS_2$: H, 3.8; C, 16.8; N, 3.3; I, 29.6; Cu, 7.4; Pb, 24.2%.

Determination of the structure

Crystallographic measurements were made at 293 K using an Enraf-Nonius CAD-4 diffractometer operating in the ω-2θ scan mode (the ratio of the scanning rates was ω-θ = 1.2). The intensity data were collected within the range $1.6 \leqslant \theta \leqslant 23°$ using graphite-monochromated Mo-K_α radiation. The accurate unit cell parameters and the orientation matrix for data collection were obtained from least-squares refinement, using the setting angles of 24 reflections in the range $13 < \theta < 15°$. Crystal data, details of data collection and structure refinement parameters are summarized in Table 1. The structure was solved by direct methods and refined by full-matrix least-squares computations in the anisotropic approximation. The positions of the hydrogen atoms were idealized and included in the calculations of the structure factors as the fixed contributions. Convergence was reached at the agreement factors listed in Table 1; largest peak in final difference map 1.732 e/Å^3 at a distance from the lead atom of 1.15(1) Å. Corrections for the Lorentz and polarization effects as well as an empirical correction for absorption using the DIFABS [12] were applied. Observed and calculated structure factors, anisotropic thermal parameters, atomic coordinates, full lists of interatomic distances, bond angles and torsion angles are given in the supplementary material.

Table 1. Crystallographic data

Formula	$C_{12}H_{32}CuI_2N_2O_4PbS_2$
Formula weight	857.07
Colour	green
Crystal size (mm)	$0.05 \times 0.05 \times 0.1$
Habit	prismatic
Crystal system	triclinic
Space group	$P\bar{1}$
a (Å)	8.305(3)
b (Å)	12.132(3)
c (Å)	12.755(3)
α (°)	84.86(2)
β (°)	80.79(3)
γ (°)	73.26(3)
V (Å^3)	1213.5(6)
Z	2
D_{calc} (g cm^{-3})	2.345
μ(Mo-K_α) (cm^{-1})	105.36
Radiation (Å)	Mo-K_α (0.71073)
F(000)	798
Number of unique data	3052
Data used in refinement [$I > 2\sigma(I)$]	2359
Refinement method	full matrix least-squares on F^2
R	0.0438
$wR2$	0.1150
Goodness of fit	1.027
Software	SHELX-93 [10, 11]

The structure of the complex $\{Cu_2Pb_2[(CH_3)_2NCH_2CH_2O]_4I_4(DMSO)_2\} \cdot 2DMSO$ with the atomic labelling scheme and the perspective view of the unit cell packing are shown in Figs 1 and 2. Selected bond lengths and bond angles are contained in Table 2.

RESULTS AND DISCUSSION

The crystal comprises dimeric centrosymmetric molecules $\{Cu_2Pb_2[(CH_3)_2NCH_2CH_2O]_4I_4(DMSO)_2\}$ bridged by oxygen atoms of chelated 2-dimethylaminoethoxo groups, and DMSO molecules of crystallization in the lattice cavities (Figs 1 and 2). The S atom in the last-mentioned molecules is disordered and has partial occupancy of 0.8 and 0.2 in two positions: S(21) and S(22), respectively.

The two oxygen, O(1) and O(2), and two nitrogen atoms, N(1) and N(2) of the two coordinated 2-dimethylaminoethoxo groups form the copper coordination environment, which has a somewhat distorted square planar geometry. The values of interatomic distances Cu—N, Cu—O and angles at the copper atom O—Cu—N (Table 2) agree well with reported ones for copper complexes containing aminoalcohols [13]. The maximum deviation of oxygen and nitrogen atoms from the least-squares plane is 0.13(1) Å, while the copper atom is shifted from this plane by approximately 0.20(1) Å towards the iodine atom I(2) $\{1-x, 1-y, -z\}$. The interatomic separation d[Cu···I(2) $\{1-x, 1-y, -z\}$] = 3.167(2) Å is too long for a covalent interaction [13–15], but is significantly less than the sum of the van der Waals radii of the named atoms [r(Cu) 1.9, r(I) 2.1 Å] [13–15], to all appearances this is evidence of a peculiar interatomic interaction [14].

The close lead atom coordination environment is formed by three oxygen atoms of 2-dimethylaminoethoxo groups, O(1), O(2) and O(2) $\{1-x, 1-y, -z\}$ and an oxygen atom of a coordinated DMSO molecule, O(3); appropriate bond distances are 2.343(7)–2.601(7) Å (Table 2). The remote iodine atoms, I(1) and I(2), located at a distance from the lead atom of 3.285(1)–3.390(1) Å, complete the coordination of lead to give a highly distorted octahedral configuration. The lead–iodine interatomic distances exceed the average length of the covalent bond of these atoms and, therefore, these contacts have very little covalent character [13, 15]. The Pb···I(2) distance is elongated compared with Pb···I(1) one (Table 2) probably because of the bridging of the I(2) to the copper atom. It should be noted that Pb···Cu and Pb···Cu $\{1-x, 1-y, -z\}$ separations (3.394(2) and 3.634(2) Å, respectively) are similar to those of $Cu^{II}Pb^{II}$ complexes of macrocycles (3.344(3)–3.577(2)

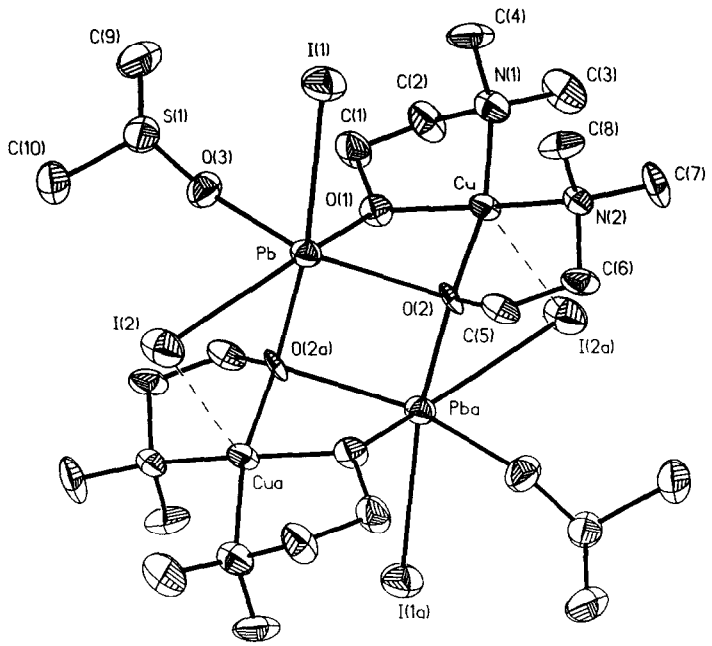


Fig. 1. Perspective view of the $\{Cu_2Pb_2[(CH_3)_2NCH_2CH_2O]_4I_4(DMSO)_2\}$ complex with 40% probability of thermal ellipsoids ("a" denotes the equivalent positions $\{1-x, 1-y, -z\}$; hydrogen atoms are omitted; the additional interaction is shown as dashes).

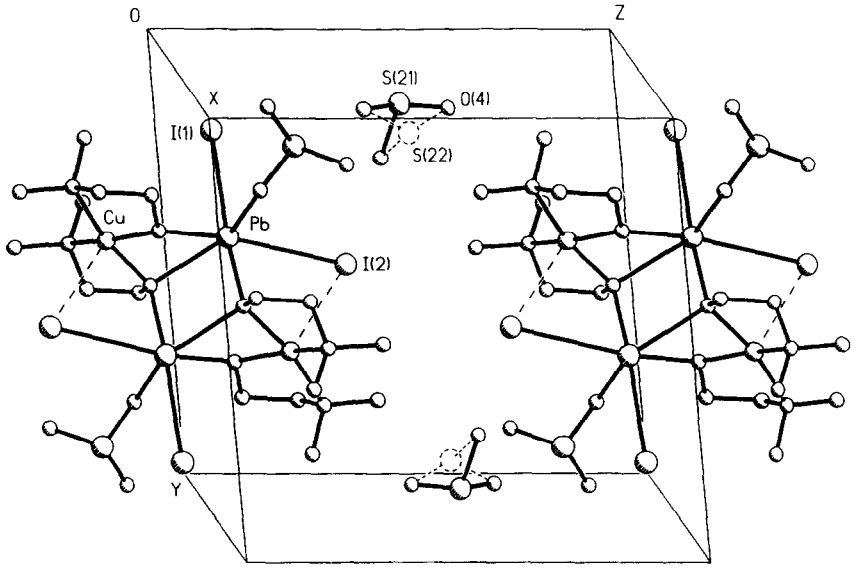


Fig. 2. A fragment of the $\{Cu_2Pb_2[(CH_3)_2NCH_2CH_2O]_4I_4(DMSO)_2\} \cdot 2DMSO$ crystal structure (the minor component of the disordered sulfur atoms are shown as dotted circles).

Å) [1–3]. Another common feature is the existence of oxygen atoms bridging both metal centers: phenolic ones and oxygen atoms of acetate groups in the case of $Cu^{II}Pb^{II}$ complexes of macrocycles and oxygen atoms of 2-dimethylaminoethoxo groups in the case of the complex under consideration. This leads to the arrangement of a strictly planar central Pb_2O_2 rhombus in the structure of $\{Cu_2Pb_2[(CH_3)_2NCH_2CH_2O]_4I_4(DMSO)_2\} \cdot 2DMSO$.

The 2-dimethylaminoethoxo groups are structurally normal [d(O—C) *ca* 1.42(2), d(C—C) *ca* 1.48(2)–1.51(2), d(C—N) *ca* 1.48(2)–1.49(2), d(N—C(terminal) *ca* 1.45(2)–1.51(2) Å) and are coordinated to copper *via* oxygen and nitrogen atoms, forming five-membered puckered rings with the *gauche* configuration [the torsion N—C—C—O angles are *ca* 49(2)–52(1)°]. The coordinated DMSO molecules [d(O—S) 1.508(9), d(S—C) *ca* 1.75(2)–1.76(2) Å, O—S—C 105.1(7) and C—S—C 98.3(9)°] are structurally normal [13].

Table 2. Selected bond lengths (Å) and angles (°) for $\{Cu_2Pb_2[(CH_3)_2N\text{-}CH_2CH_2O]_4I_4(DMSO)_2\}\cdot 2DMSO$

Lead environment			
Pb···Cu	3.394(2)	Pb—O(2a)	2.473(8)
Pb···Cu(a)[a]	3.634(2)	Pb—O(2)	2.601(7)
Pb—O(1)	2.343(7)	Pb—I(1)	3.285(1)
Pb—O(3)	2.384(9)	Pb—I(2)	3.390(1)
O(1)—Pb—O(3)	79.4(3)	O(3)—Pb—I(1)	85.5(2)
O(1)—Pb—O(2a)	81.3(3)	O(2a)—Pb—I(1)	168.4(2)
O(3)—Pb—O(2a)	83.1(3)	O(2)—Pb—I(1)	103.3(2)
O(1)—Pb—O(2)	61.0(3)	O(1)—Pb—I(2)	156.0(2)
O(3)—Pb—O(2)	139.8(3)	O(3)—Pb—I(2)	86.4(2)
O(2a)—Pb—O(2)	84.2(2)	O(2a)—Pb—I(2)	77.9(2)
O(1)—Pb—I(1)	94.5(2)	O(2)—Pb—I(2)	127.7(2)
		I(1)—Pb—I(2)	103.59(3)
Copper environment			
Cu—O(1)	1.914(8)	Cu—N(2)	2.07(1)
Cu—O(2)	1.941(7)	Cu—I(2a)	3.167(2)
Cu—N(1)	2.06(1)		
O(1)—Cu—O(2)	81.6(3)	N(1)—Cu—N(2)	105.2(4)
O(1)—Cu—N(1)	85.7(4)	O(1)—Cu—I(2a)	102.1(3)
O(2)—Cu—N(1)	166.9(4)	O(2)—Cu—I(2a)	91.4(2)
O(1)—Cu—N(2)	157.6(4)	N(1)—Cu—I(2a)	94.3(3)
O(2)—Cu—N(2)	85.8(4)	N(2)—Cu—I(2a)	96.6(3)

[a] "a" refers to the $\{-x+1, -y+1, -z\}$ equivalent positions.

REFERENCES

1. M. Tadokoro, H. Okawa, N. Matsumoto, M. Koikawa and S. Kida, *J. Chem. Soc., Dalton Trans.* 1991, 1657.
2. M. Tadokoro, H. Sakiyama, N. Matsumoto, M. Kodera, H. Okawa and S. Kida, *J. Chem. Soc., Dalton Trans.* 1992, 313.
3. H. Okawa, J. Nishio, M. Ohba, M. Tadokoro, N. Matsumoto, M. Koikawa, S. Kida and D. E. Fenton, *Inorg. Chem.* 1993, **32,** 2949.
4. V. V. Skopenko, V. N. Kokozay and V. A. Pavlenko, *Ukr. Khim. Zh.* (*Russ. Ed.*) 1993, **59,** 485.
5. V. V. Skopenko, V. N. Kokozay, V. R. Polyakov and A. V. Sienkiewicz, *Polyhedron* 1994, **13,** 15.
6. V. N. Kokozay and A. V. Sienkiewicz, *Polyhedron* 1994, **13,** 1439.
7. V. N. Kokozay and A. V. Sienkiewicz, *Polyhedron* 1995, **14,** 1547.
8. V. A. Schlyakhovenko, V. N. Kokozay and O. Yu. Vassilyeva, *Experimentalnaya onkologiya* 1991, **13,** 22.
9. V. A. Schlyakhovenko, V. N. Kokozay and S. R. Petrusenko, *Experimentalnaya onkologiya* 1994, **16,** 210.
10. G. M. Sheldrick, *Acta Cryst.* 1990, **A46,** 467.
11. G. M. Sheldrick, *SHELX*93, *A System of Computer Programs for X-ray Structure Determination.* Gottingen, Germany (1993).
12. N. Walker and D. Stuart, *Acta Cryst.* 1983, **A39,** 158.
13. A. F. Wells, *Structural Inorganic Chemistry.* Clarendon Press, Oxford (1986).
14. P. G. Harrison, in *Comprehensive Coordination Chemistry*: *The Synthesis, Reaction, Properties & Applications of Coordination Compounds*, Eds G. Wilkinson, R. D. Gillard and J. A. McCleverty, vol. 3, ch. 26, p. 183. Pergamon Press, Oxford (1987).
15. S. S. Batsanov, *Zh. Neorg. Khim.* (*Russ. Ed.*) 1991, **36,** 3015.

Pergamon

S0277-5387(96)00256-2

Polyhedron Vol. 16, No. 2, pp. 267–274, 1997
Copyright © 1996 Elsevier Science Ltd
Printed in Great Britain. All rights reserved
0277-5387/97 $15.00 + 0.00

Direct synthesis and crystal structure of zinc thiocyanate complexes with 1,4-diazabicyclo(2,2,2)octane

Svitlana R. Petrusenko, Vladimir N. Kokozay* and Igor O. Fritsky

Department of Chemistry, Kyiv Shevchenko University, 252033 Kyiv, Vladimirska st. 64, Ukraine

(Received 21 March 1996; accepted 22 May 1996)

Abstract—A direct method of synthesis of zinc thiocyanate complexes with 1,4-diazabicyclo(2,2,2)octane (or triethylenediamine, Ten) is reported. The main peculiarities of interaction of zinc oxide with non-aqueous (methanol, acetonitrile, *N*,*N*-dimethylformamide = DMF, dimethylsulfoxide = DMSO) solutions of ammonium thiocyanate in the presence of Ten were investigated. The crystal structures of the compounds $[Zn_2(NCS)_4(NH_3)_2Ten]$ (**I**), $(HTen)_2[Zn(NCS)_4]$ (**II**) and $[Zn(NCS)_2(Ten)DMSO]$ (**III**) were determined by X-ray diffraction. The complexes contain four (**I**) and five (**III**) coordinate zinc atoms linked by μ_2-bridging nitrogen atoms of Ten forming the dimeric and polymeric molecules respectively; the complex (**II**) has an ionic-type crystal lattice with $(HTen)^+$ cations and $[Zn(NCS)_4]^{2-}$ anions. Copyright © 1996 Elsevier Science Ltd

Keywords: direct synthesis; zinc(II); methylenediamine; X-ray structure; thiocyanate; 1,4-diazabicyclo(2,2,2)-octane.

Previously, nickel(II) thiocyanate complexes with triethylenediamine of original crystal structure have been synthesized by the direct (one-stage) method based on reaction of metal powder with a solution of an ammonium salt and an appropriate ligand [1,2]. In continuation of the elaboration of direct methods for synthesis of coordination compounds with bioactive ligands we studied the interaction of zinc oxide with non-aqueous (methanol, acetonitrile, DMF, DMSO) solutions of ammonium thiocyanate in the presence of Ten and herein report the main results of these investigations, including details of the preparation and the structural features of several complexes.

EXPERIMENTAL

Synthesis and analytical data

All chemicals were commercial products of reagent grade, used without further purification; all experiments were carried out in air. Examples of the preparation of the complexes are presented below.

Synthesis of $(HTen)_2[Zn(NCS)_4]$

Zinc oxide (0.41 g; 0.005 M) ammonium thiocyanate (1.42 g; 0.02 M) and triethylenediamine (1.12 g; 0.01 M) were placed into the reactor and then 20 cm^3 of acetonitrile was added. The reaction mixture was heated to boiling and stirred for 2–3 min to complete the solution of the oxide. Yield: 2.2 g (83%).

Synthesis of $[Zn(NCS)_2(Ten)DMSO]$

Zinc oxide (0.41 g; 0.005 M) ammonium thiocyanate (0.76 g; 0.01 M) and triethylenediamine (0.56 g; 0.005 M) were placed into the reactor and then 20 cm^3 of DMSO was added. The reaction mixture was heated upon constant stirring during 1 h. Undissolved residue of zinc oxide was filtered off, the solution obtained was cooled. Yield: 0.6 g (32%).

Synthesis of $[Zn_2(NCS)_4(NH_3)_2Ten]$

Zinc oxide (0.41 g; 0.005 M) ammonium thiocyanate (1.42 g; 0.02 M) and triethylenediamine

* Author to whom correspondence should be addressed.

Table 1. Investigated systems and complexes obtained

System	Results of analysis, % Found (Calc) Zn	NCS	N	C	H	Compound
ZnO-NH_4NCS-Ten-CH_3OH	25.7	45.2	19.6	21.9	3.4	$Zn_2(NCS)_4(NH_3)_2$Ten
	(25.7	45.6	22.0	23.6	3.6)	(**I**)
ZnO-NH_4NCS-Ten-CH_3CN	12.6	44.5	22.1	35.9	4.9	$(HTen)_2Zn(NCS)_4$
	(12.5	44.3	21.4	36.7	5.0)	(**II**)
ZnO-2NH_4NCS-Ten-DMSO	17.7	30.5	15.1	31.3	4.4	$Zn(NCS)_2$(DMSO)Ten
	(17.6	31.2	15.1	32.3	4.9)	(**III**)
ZnO-2NH_4NCS-Ten-DMF	15.5	27.5	21.1	41.3	6.4	$Zn(NCS)_2(Ten)_2 \cdot 0.5$DMF
	(15.3	27.2	21.3	43.6	6.5)	(**IV**)
ZnO-4NH_4NCS-Ten-DMF,DMSO	14.1	36.5	21.5	37.3	5.4	$Zn(HTen)(Ten)(NCS)_3$
	(14.1	37.5	21.1	38.7	5.4)	(**V**)

(0.56 g; 0.005 M) were placed into the reactor and then 20 cm^3 of methanol was added. The oxide dissolution proceeds spontaneously for 2–3 min. In 10–15 min formation of the crystalline precipitate from the solution was observed. Yield: 0.3 g (24%). The rest of the product could be isolated as the amorphous residue by precipitation of the filtered solution.

All complexes prepared were characterized by elemental analysis (Table 1) and infrared spectra (4000–400 cm^{-1}, KBr). The identification and investigation methods are analogous to those described previously [3]. The compounds $[Zn_2(NCS)_4(NH_3)_2Ten]$, $[Zn(NCS)_2(Ten)DMSO]$ and $(HTen)_2[Zn(NCS)_4]$ were studied by X-ray diffraction.

Crystal structure determination

Crystallographic data, parameters of data collection and refinement are listed in Table 2. X-ray data were collected on an Enraf Nonius CAD-4 diffractometer (graphite-monochromatized radiation) operating in the $w/2\theta$ scan mode with a ratio of the scanning rates of $w/\theta = 1/2$. The geometrical corrections were taken into account upon reducing the intensities to the structure amplitudes.

The structures were solved by the heavy atom method, the zinc atoms were located from the Patterson maps. The refinements were carried out anisotropically for non-hydrogen atoms and isotropically for H-atoms using SHELXS-93 [4,5].

Selected bond distances and angles are presented in Tables 3–5. Lists of atomic coordinates, observed and calculated structure factors, anisotropic thermal parameters and all bond distances and angles have been deposited as "Supplementary material".

RESULTS AND DISCUSSION

One can see in Table 1 that the composition of the synthesized complexes depends to a large extent on the nature of the solvent, and in the case of DMF and DMSO on the molar ratio ZnO : NH_4NCS as well. Note that the excess of the ammonium salt influences significantly the reaction rate and the degree of conversion of the oxide. For example, the complete dissolution of the zinc oxide proceeds in 3–5 min in all the solvents upon four-fold excess of ammonium thiocyanate, whereas it does not occur completely in the case of ZnO : NH_4NCS = 1 : 2 ratio even upon heating (up to 50–90°C) for 1.5 h.

The crystalline complexes were formed by cooling the reaction mixture, or in the case of DMF solutions by precipitation with the isopropanol–ether mixture.

All compounds obtained are colourless and have low solubilities in water.

In the IR spectra of the synthesized complexes only the ν(CN) vibration of the thiocyanate group (2070 and 2090 cm^{-1}) coordinated *via* the nitrogen atom can be identified easily. The bands corresponding to ν(CO) = 1670 and ν(SO) = 1020 cm^{-1} vibrations of the coordinated DMF and DMSO, respectively, were observed in the spectra of compounds III and IV [6, 7].

The crystal structure of compound **I** consists of molecular dimeric centrosymmetric complexes $[(SCN)_2(NH_3)Zn{-}(\mu_2\text{-Ten}){-}Zn(NH_3)(NCS)_2]$ (Fig. 1) which are linked by van der Waals interactions ($S \cdots S$ = 3.39–3.62 Å; $S \cdots N(NH_3)$ = 3.04–3.29 Å) [10]. The complex molecules form columns along the z direction, so that the $Zn(1) \cdots Zn(2)$ line is perpendicular to this direction (Fig. 2). The columns are related between themselves by 2_1 screw axes and the symmetry centres. The Zn(1) and Zn(2) atoms are in a distorted tetrahedral environment of four nitrogen atoms belonging to two thiocyanate groups, the ammonia molecule and the bridging Ten molecule. The differences in Zn—N distances are rather considerable: the largest is Zn—$N(NH_3)$ ($\approx$1.99 Å); the Zn—N(Ten) ($\approx$1.94 Å) are somewhat shorter and the Zn—N(NCS) ($\approx$1.85 Å) are the shortest. The Zn(1) and Zn(2) polyhedra differ noticeably by two Zn—N(NCS) bond distances: for the Zn(1) polyhedron this difference is 0.07 Å, for Zn(2) it is 0.19 Å. Significant deviations of the bond angles from tetra-

Table 2. Crystallographic data

Compound	I	II	III
Formula weight	509.30	524.06	371.83
Crystal system	orthorhombic	monoclinic	orthorhombic
Space group	$Pna2_1$	$P2_1/n$	Pmmn
a(Å)	16.677(3)	9.695(2)	12.069(2)
b(Å)	10.442(2)	13.995(3)	7.200(1)
c(Å)	9.730(2)	17.920(4)	8.920(2)
α(°)	90	90	90
β(°)	90	94.66(3)	90
γ(°)	90	90	90
Volume (Å^3)	1694.4(6)	2423.4(9)	775.1(2)
Z	4	4	2
T(K)	293(2)	293(2)	293(2)
D_{calc} (g cm^{-3})	1.997	1.436	1.593
Irradiation	Cu-K_α	Cu-K_α	Mo-K_α
Wavelength (Å)	1.54178	1.54178	0.71073
μ (cm^{-1})	82.05	47.88	19.85
F(000)	1032	1088	384
θ range (°)	5.00–87.21	4.01–55.94	2.28–24.96
Index ranges	$0 \leqslant h \leqslant 21$	$0 \leqslant h \leqslant 10$	$0 \leqslant h \leqslant 14$
	$0 \leqslant k \leqslant 11$	$0 \leqslant k \leqslant 15$	$0 \leqslant k \leqslant 8$
	$0 \leqslant l \leqslant 10$	$-19 \leqslant l \leqslant 19$	$0 \leqslant l \leqslant 10$
Independent data	1571	3377	780
Observed data	1488	3157	685
Discrimination	26	26	26
Parameters refined	228	271	72
$R1$	0.032	0.037	0.039
$wR2$	0.095	0.105	0.108
Goodness-of-fit on F^2	1.196	0.999	0.826
Abs. struc. parameter	0.01(5)	—	—

Table 3. Bond lengths (Å) and angles (°) for $[Zn_2(NCS)_4(NH_3)_2Ten]$

Zn(1)—N(1)	1.791(7)	N(1)—Zn(1)—N(2)	111.4(3)
Zn(1)—N(2)	1.863(7)	N(1)—Zn(1)—N(5)	98.3(3)
Zn(1)—N(5)	1.939(5)	N(2)—Zn(1)—N(5)	114.5(3)
Zn(1)—N(7)	1.985(8)	N(1)—Zn(1)—N(7)	121.5(3)
Zn(2)—N(3)	1.754(6)	N(2)—Zn(1)—N(7)	103.4(3)
Zn(2)—N(6)	1.930(5)	N(5)—Zn(1)—N(7)	108.3(3)
Zn(2)—N(4)	1.946(8)	N(3)—Zn(2)—N(6)	93.9(3)
Zn(2)—N(8)	1.993(7)	N(3)—Zn(2)—N(4)	115.2(3)
Zn(2)—C(8)	2.589(7)	N(6)—Zn(2)—N(4)	101.5(3)
S(1)—C(1)	1.528(8)	N(3)—Zn(2)—N(8)	111.7(3)
S(2)—C(2)	1.564(7)	N(6)—Zn(2)—N(8)	113.1(2)
S(3)—C(3)	1.426(7)	N(4)—Zn(2)—N(8)	118.3(3)
S(4)—C(4)	1.586(8)	C(1)—N(1)—Zn(1)	166.8(7)
N(1)—C(1)	1.09(1)	C(2)—N(2)—Zn(1)	168.1(7)
N(2)—C(2)	1.14(1)	C(3)—N(3)—Zn(2)	171.9(7)
N(3)—C(3)	1.031(9)	C(4)—N(4)—Zn(2)	164.3(6)
N(4)—C(4)	1.14(1)		

Table 4. Bond lengths (Å) and angles (°) for $[Zn(NCS)_2(Ten)DMSO]$

Zn—N(1)	1.968(4)	N(1A)—Zn—N(1)	123.5(3)[a]
Zn—O	1.976(5)	N(1)—Zn—O	118.3(2)
Zn—N(2)	2.299(3)	N(1)—Zn—N(2)	90.22(4)
S(1)—C(1)	1.593(5)	O—Zn—N(2)	89.53(7)
S(2)—O	1.363(5)	N(2A)—Zn—N(2)	179.1(2)
N(1)—C(1)	1.153(7)	S(2)—O—Zn	153.4(1)
N(2)—C(2)	1.476(4)	C(1)—N(1)—Zn	177.4(5)
N(2)—C(3)	1.475(5)		

[a] A = $-x+1/2, -y+1/2, z$

hedral are noted: 98.3–121.5° for Zn(1) and 93.9–118.3° for Zn(2). The non-equivalent character of the thiocyanate groups is reflected in different values of the bond angles Zn—N—C which vary in the range of 164.3–171.9°. However, there is no correlation between these angles and the corresponding Zn—N distances. At the same time one can notice the correlation between the Zn—NCS distances and N—C and C—S distances in the corresponding thiocyanate groups: the shortened N—C and C—S distances correspond to shorter Zn—N bonds. For example, Zn(2)—N(3) = 1.754(6); N(3)—C(3) = 1.031(9); C(3)—S(3) = 1.426(7) Å; Zn(2)—N(4) = 1.946(8); N(4)—C(4) = 1.140(4); C(4)—S(4) = 1.586(8) Å.

The geometrical parameters of the Ten molecule are close to those normally observed. The torsion angles along the C—C bond for the NCCN fragments are -5.4–(-7.0)° which reflect their gauche-conformation with a low degree of deviation from the

Table 5. Bond lengths (Å) and angles (°) for $(HTen)_2[Zn(NCS)_4]$

Zn—N(1)	1.944(4)	N(3)—Zn—N(1)	115.3(2)
Zn—N(2)	1.970(4)	N(3)—Zn—N(2)	110.3(2)
Zn—N(3)	1.935(4)	N(1)—Zn—N(2)	109.2(2)
Zn—N(4)	1.977(5)	N(3)—Zn—N(4)	106.9(2)
		N(1)—Zn—N(4)	108.1(2)
S(1)—C(1)	1.609(6)	N(2)—Zn—N(4)	106.6(2)
S(2)—C(2)	1.619(5)		
S(3)—C(3)	1.598(5)	C(1)—N(1)—Zn	172.1(4)
S(4)—C(4)	1.619(6)	C(2)—N(2)—Zn	173.2(4)
		C(3)—N(3)—Zn	166.3(4)
N(1)—C(1)	1.152(6)	C(4)—N(4)—Zn	172.2(4)
N(2)—C(2)	1.150(5)		
N(3)—C(3)	1.163(6)	N(1)—C(1)—S(1)	178.7(4)
N(4)—C(4)	1.153(6)	N(2)—C(2)—S(2)	178.7(4)
		N(3)—C(3)—S(3)	179.8(3)
		N(4)—C(4)—S(4)	179.8(5)

planar conformation. The deviations found take intermediate values between the corresponding values observed in the structures of $Ni(HTen)_2(NCS)_4$ (13.8–15.8°) [1] and $HTen(NCS)\cdot 0.5H_2O$ (1–2°) [8].

In the compound **III** the bridging function of Ten is realized as well (Fig. 3) which leads, unlike the compound **I**, to the formation of polymeric chains. Those chains are packed along the y direction of the crystal (Fig. 4), and are linked by van der Waals interactions. The monodentate thiocyanate groups and the DMSO molecules are oriented approximately perpendicular to the chain direction. The coordination environment of the zinc atom is an elongated trigonal bipyramid formed by two donor nitrogen atoms of the bridging Ten molecules, two nitrogen atoms of the terminal thiocyanate groups and the oxygen atom of the DMSO molecule. As the N(1), N(1a) and N(2), N(2a) atoms are symmetrically related, the linear and angular distortions of the polyhedron are not significant. They are characterized by elongated axial Zn—N(Ten) distances and small deviations of the bond angles near the zinc atom in the equatorial plane (118 and 123°). The Zn—N(Ten) distances in **III** are found to be significantly longer than the corresponding distances in structure **I** (Tables 2, 3).

The NCCN fragments in the Ten molecules are observed to be planar.

In contrast to **I** and **III**, the compound **II** is ionic and consists of complex anions $[Zn(NCS)_4]^{2-}$ and $(HTen)^+$ cations which are linked into polymeric chains by means of hydrogen bonds N(7)—H···N(6) and N(5)—H···N(8) (Fig. 5A) [11]. The H-bonds parameters NH···N between the protonated Ten molecules are: d(N(7)···N(6)) = 2.82, d(N(7)···H) = 0.91, d(H···N(6)) = 1.92 Å, <N(7)NH(6) = 172.5°; d(N(5)···N(8) $(-0.5+x,\ 0.5-y,\ 0.5+z)$) = 2.78, d(N(5)—H) = 0.85, d(H···N(8) $(-0.5+x,\ 0.5-y,\ 0.5+z)$) = 1.94 Å, <N(5)HN(8) $(-0.5+x,\ 0.5-y,\ 0.5+z)$) = 168.6°. Unlike the related compound $(H_2Ten)[ZnCl_4]$, which has a similar structure, the isolated two-fold protonated cations $(H_2Ten)^{2+}$ are present [9]. In the analogous complex $Ni(HTen)_2(NCS)_4$ reported earlier [1] the protonated Ten molecules are coordinated to the central atom.

The complex cation $[Zn(NCS)_4]^{2-}$ is a distorted tetrahedron: the Zn—N bond lengths are in the range 1.94–1.98 Å; deviations of values from tetrahedral of the bond angles at the central atom are 0.3–5.8°. The ZnNC angle values vary from 166.3 to 173.2° (Table 5, Fig. 5B). The coordinated thiocyanate groups are in fact linear.

The conformation of NCCN fragments in $(HTen)^+$ cations is slightly different from that in the planar neutral ligand: the corresponding torsion angles do not exceed 3.3°.

In the crystal packing the complex anions form a

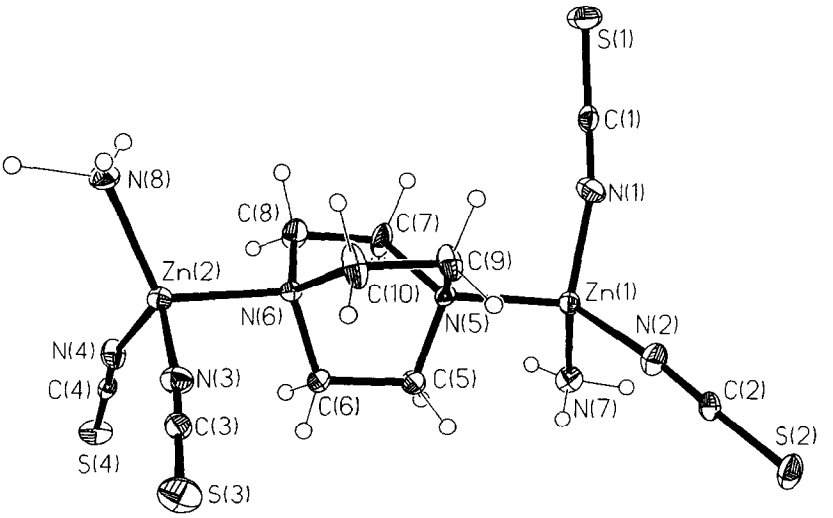


Fig. 1. The molecular structure of $[Zn_2(NCS)_4(NH_3)_2Ten]$ (hydrogen atoms are unlabelled for clarity).

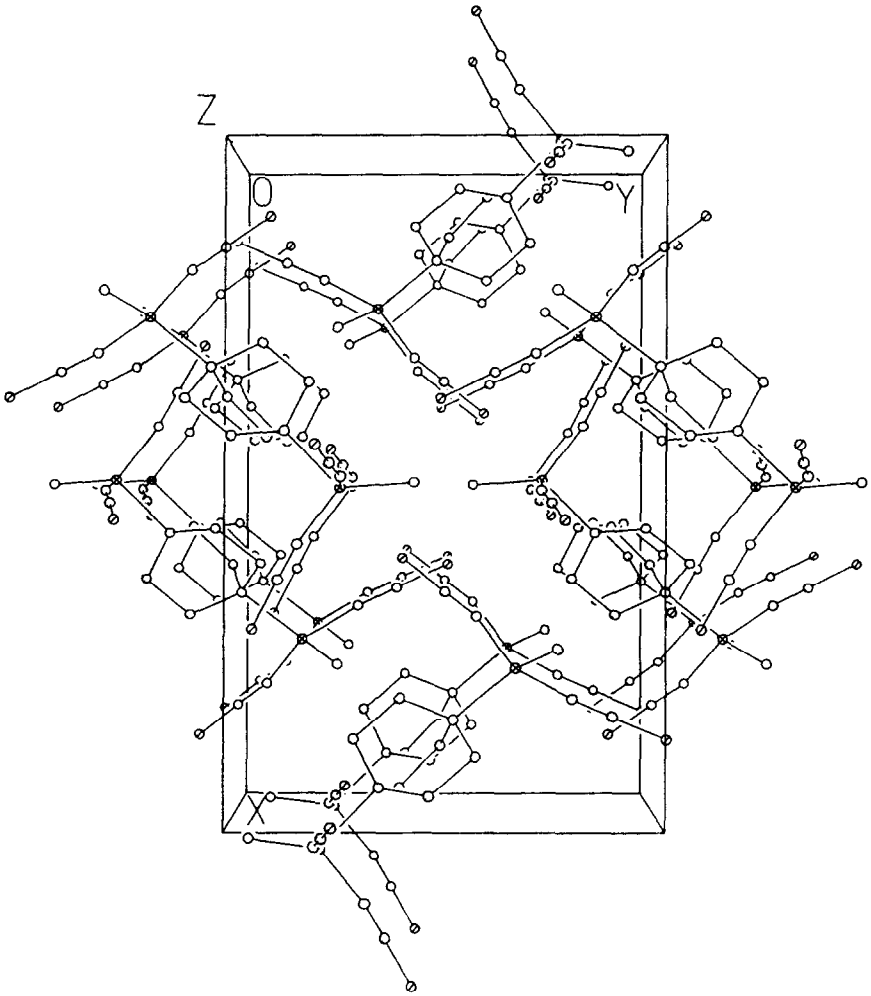


Fig. 2. Perspective view of the unit cell packing for $[Zn_2(NCS)_4(NH_3)_2Ten]$.

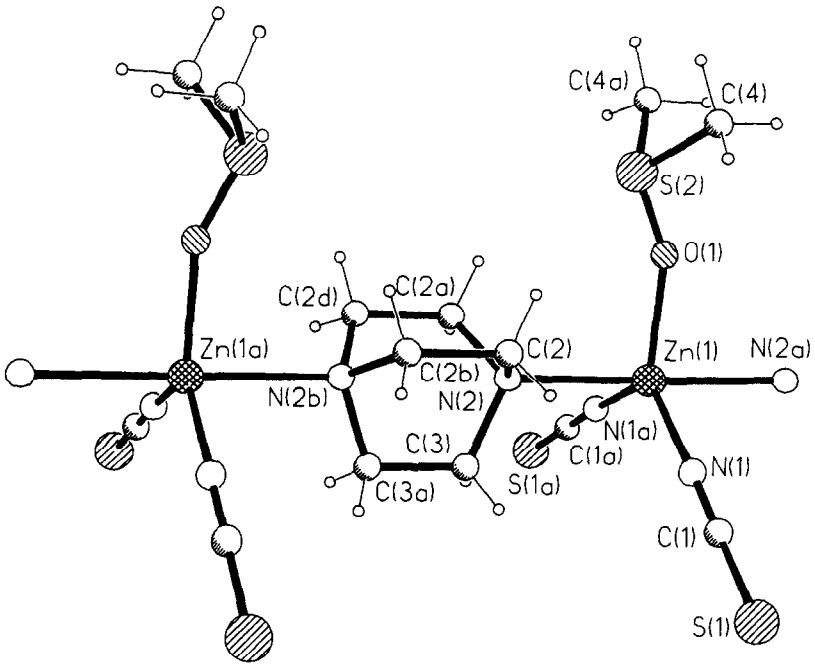


Fig. 3. A fragment of the crystal structure of $Zn(NCS)_2(Ten)DMSO$ ("a", "b", "d" refer to atoms related by the symmetry operations $0.5-x, y, z$; $x, -0.5-y, z$ and $0.5-x, -0.5-y, z$, respectively; (hydrogen atoms are unlabelled for clarity).

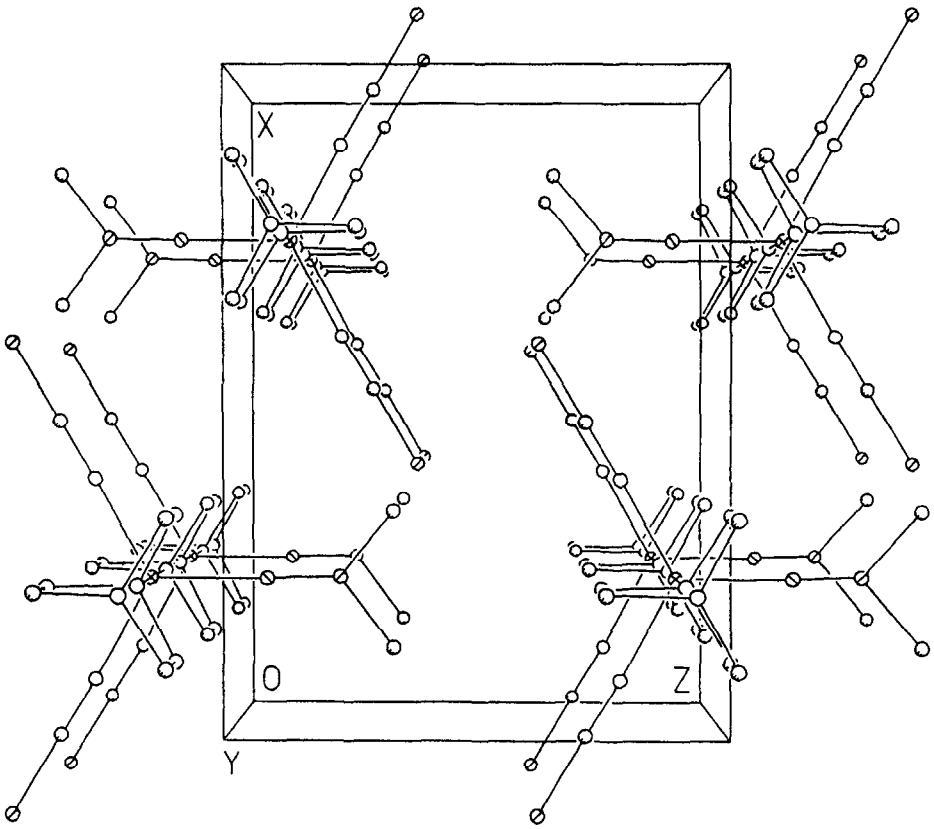


Fig. 4. Perspective view of the unit cell packing for $[Zn(NCS)_2(Ten)DMSO]$.

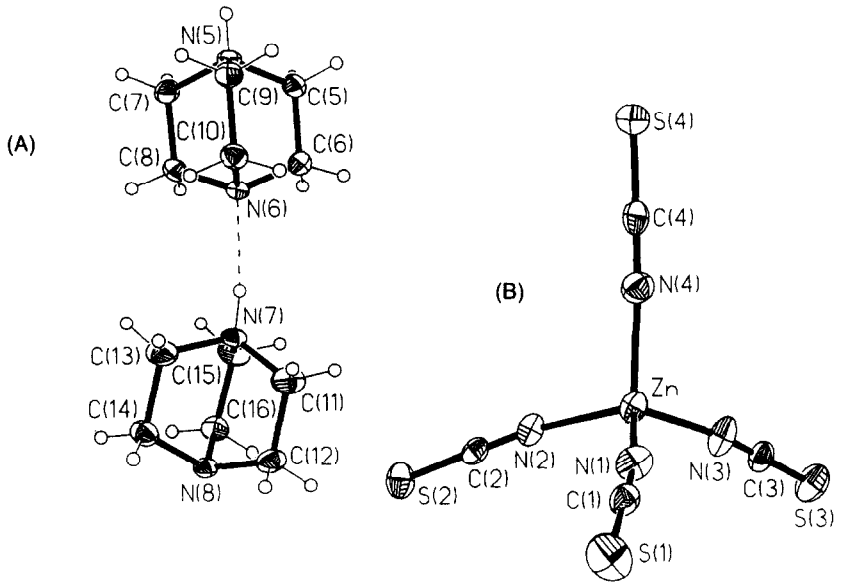


Fig. 5. The structure of $HTen^{+}$ {A} and $[Zn(NCS)_4]^{2-}$ {B} ions (hydrogen atoms are unlabelled for clarity).

framework with hexagonal channels which are filled by polymeric chains of the $(HTen)^{+}$ cations arranged parallel to the *xz* plane (Fig. 6).

In all the structures determined the significant deviations of the geometrical parameters of the coordination polyhedra from regularity are observed as probably connected with the rigid conformation ability of the bicyclic ligand.

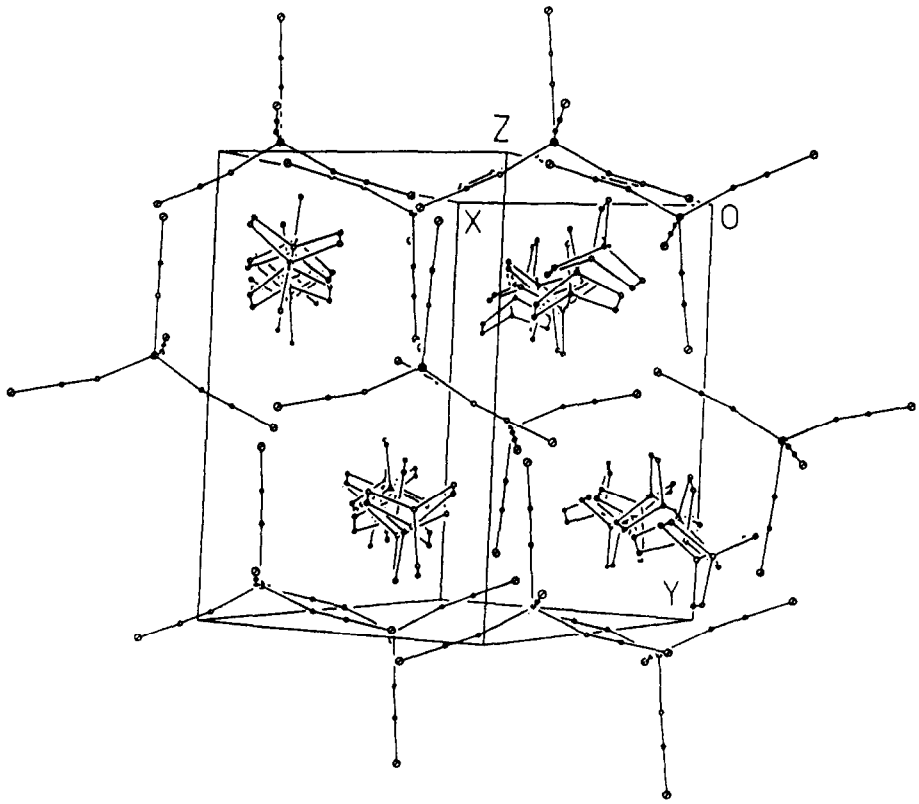


Fig. 6. Perspective view of the unit cell packing for $(HTen)_2[Zn(NCS)_4]$.

Acknowledgements—This work has been partly financed by the International Soros Program of support of education in the field of natural sciences (ISSEP), grant No PSU053098.

REFERENCES

1. V. Kokozay, Yu. Simonov, S. Petrusenko and A. Dvorkin, *Zh. Neorg. Khim.* 1990, **35,** 2839.
2. Yu. Simonov, V. Skopenko, V. Kokozay, S. Petrusenko and A. Dvorkin, *Zh. Neorg. Khim.* 1991, **36,** 625.
3. O. Vassilyeva, V. Kokozay and V. Skopenko, *Dokl. Akad. Nauk UkSSR* 1990, 35.
4. *G. M. Sheldrick, SHELX, Acta Cryst.* 1990, **A46,** 467.
5. G. M. Sheldrick, *SHELX*93, *A System of Computer Programs for X-Ray Structure Determination.* Gottingen, Germany (1993).
6. A. Golub, H. Kohler, V. Skopenko (Eds), *Chemistry of Pseudohalides.* Elsevier, Amsterdam (1986).
7. K. Nakamoto, *Infrared and Raman Spectra of Inorganic and Coordination Compounds*, 4th edn. Wiley-Interscience, (1986).
8. V. Kokozay, S. Petrusenko, A. Sienkiewicz and A. Dvorkin, *Ukr. Khim. Zh.* 1992, **58,** 527.
9. B. Viossat, P. Khodadad and N. Rodier, *Bull. Soc. Chim. Fr.* 1984, 214.
10. S. Batsanov, *Zh. Neorg. Khim.* 1991, **36,** 3015.
11. A. Wells, *Structural Inorganic Chemistry*, 5th edn. Clarendon Press, Oxford (1986).

Pergamon

S0277-5387(96)00249-5

Polyhedron Vol. 16, No. 2, pp. 275–279, 1997
Copyright © 1996 Elsevier Science Ltd
Printed in Great Britain. All rights reserved
0277-5387/97 $15.00 + 0.00

Dithiolene-like nickel and platinum complexes of methyl 3-(4′-methoxy) and 3-(4′-nitro) phenyl dithiocarbazate

Lucantonio Petrilli, Franco Tarli,* Gianni Chiozzini and Cristina Riccucci

Istituto di Chimica dei Materiali del C.N.R. Area della Ricerca di Roma, C.P. 10, via Salaria Km 29.500, 00016 Monterotondo Stazione, Roma, Italy

(Received 21 December 1995; accepted 22 May 1996)

Abstract—The spectroscopic and electrochemical properties of the complexes $[M\{NRNC(S)SMe\}_2]$ (M = Ni or Pt; R = C_6H_4OMe-4 or $C_6H_4NO_2$-4) and of the anionic derivatives $[AsPh_4]$ $[M\{N(C_6H_4NO_2\text{-}4)NC(S)SMe\}_2]$ (M = Ni or Pt) were investigated. Heating of $[Ni\{NC_6H_4OMe\text{-}4)NC(S)SMe\}_2]$ led to [Ni{N[4-MeOPhN(4-MeO)C_6H_3]NC(S)SMe}(NCS)]. Copyright © 1996 Elsevier Science Ltd

Keywords: complexes; nickel; platinum; methyldithiocarbazates; dithiolene-like; electron-transfer.

We have previously investigated the coordination properties of methyldithiocarbarzate $NH_2NHC(S)SMe$ and its 3-substituted derivatives in platinum [1], nickel [2], copper [3] and palladium [4] complexes prepared under different chemical conditions. The ligands are generally coordinated through thiono sulfur and terminal nitrogen atoms in neutral or anionic deprotonated form; the deep coloured complexes containing the doubly deprotonated ligands are dithiolene-like and belong to electron-transfer series. These compounds show similarities with complexes of dithiosemicarbazides, containing doubly deprotonated ligands, which are known to be deeply coloured and to belong to electron-transfer series [5, 6]. We have observed that the properties and reactivity of the complexes of N(3) substituted dithiocarbazic esters strongly depend on the substituent and on the metal. Here we report an extention of our researches on dithiolene-like complexes of nickel and platinum with $NH(4\text{-}MeOC_6H_4)NHC(S)SMe$ and $NH(4\text{-}O_2NC_6H_4)NHC(S)SMe$, containing electron-releasing and electron-attracting substituents on N(3), respectively.

* Author to whom correspondence should be addressed.

EXPERIMENTAL

Materials

The chemicals were commercial analytical grade reagents and used without further purification, except for the solvents employed for electrochemical measurements which were purified as described in ref. [7]. Nitrogen gas was an ultra-high purity commercial product. All the compounds were dried *in vacuo* (1 torr) over P_4O_{10}, unless otherwise stated.

Preparation of the ligands

The compounds NHRNHC(S)SMe (R = 4-$MeOC_6H_4$ or 4-$O_2NC_6H_4$) were prepared following the methods reported in Ref. [4].

Preparation of the complexes

$[Ni\{N(C_6H_4OMe\text{-}4)NC(S)SMe\}_2]$**1a**. A solution of $NiCl_2 \cdot 6H_2O$ (5.50 mmol) in water (30 cm^3) was added to a solution of $NH(C_6H_4OMe\text{-}4)NHC(S)SMe$ (1.1 mmol) in EtOH (40 cm^3). Ammonium hydroxide (1 mol dm^{-3}) was added until pH 9. After 12 h stirring

in an open vessel the product was filtered off and dried. Yield 73%.

$[Ni\{N(C_6H_4NO_2\text{-}4)NC(S)SMe\}_2]$ **1b**. This complex was prepared as above starting from solutions of $NiCl_2 \cdot 6H_2O$ (1.0 mmol in 20 cm^3 of water) and $NH(C_6H_4NO_2\text{-}4)NHC(S)SMe$ (2.0 mmol in 80 cm^3 of EtOH). After addition of ammonium hydroxide stirring was continued for 12 h. Yield 61%.

$[AsPh_4]$ $[Ni\{N(C_6H_4NO_2\text{-}4)NC(S)SMe\}_2]$ **1c**. The compound $NH_2NH_2 \cdot H_2O$ (10 cm^3) was added to a stirred and heated suspension of **1b** (24.0 mmol) in EtOH (40 cm^3). After formation of a dark-red solution the heating was stopped. At room temperature a solution of $AsPh_4 \cdot H_2O$ (24.0 mmol) in H_2O (20 cm^3) was added. After 45 min of stirring the dark-violet compound was filtered off, washed with water and dried. Yield 74%.

$[Ni\{N[C_6H_3(OMe\text{-}4)NC_6H_4(OMe\text{-}4)]NC(S)SMe\}(NCS)]$ **1d**. A solution of **1a** (2.0 mmol) in CS_2 (100 cm^3) was boiled for 1 h. The solution was left at $-40°C$ for 12 h and the separated product was filtered off and dried. Yield 40%.

$[Pt\{N(C_6H_4OMe\text{-}4)NC(S)SMe\}_2]$ **2a**, $[Pt\{N(C_6H_4NO_2\text{-}4)NC(S)SMe\}_2]$ **2b** and $[AsPh_4][Pt\{N(C_6H_4NO_2\text{-}4)NC(S)SMe\}_2]$ **2c** were prepared as reported for the compounds **1a**, **1b** and **1c**, respectively, starting from solutions of $K_2[PtCl_4]$. Yields: **2a** 30%, **2b** 70%, **2c** 84%.

Physical measurements

Analytical data for the complexes are given in Table 1. Microanalyses were performed by Microanalytical Service of the Area della Ricerca di Roma del CNR. The UV/VIS reflectance spectra of the finely powdered solids were obtained on a Cary 5 spectrophotometer fitted with a standard reflectance attachment and MgO in the reference beam. Solution spectra were recorded at room temperature on Perkin-Elmer 330 spectrophotometer (10^{-3} mol dm^{-3}). Infrared spectra were determined (200–4000 cm^{-1}) on a Perkin-Elmer 16FPC FT-IR spectrophotometer as Nujol or poly(chlorotrifluoroethylene) mulls. Magnetic measurements were performed on solid samples with a Gouy balance calibrated with $HgCo(SCN)_4$.

Table 1. Analytical data for nickel and platinum complexes

Compound	Colour	Analysis (%)[a] C	H	N	S
1a	Dark brown	42.6 (42.3)	3.9 (3.9)	10.8 (11.0)	23.6 (25.1)
1b	Dark green	35.8 (35.5)	2.4 (2.6)	15.3 (15.5)	23.2 (23.7)
1c	Dark violet	52.2 (51.9)	4.0 (3.7)	9.0 (9.0)	13.6 (13.9)
1d	Black	43.7 (43.9)	3.7 (4.0)	11.8 (12.1)	20.5 (20.8)
2a	Green	33.1 (33.4)	2.8 (3.1)	8.4 (8.7)	19.5 (19.8)
2b	Green	28.6 (28.4)	1.9 (2.1)	12.3 (12.4)	18.7 (18.9)
2c	Dark green	45.0 (45.3)	3.0 (3.2)	8.2 (7.9)	12.4 (12.1)

[a]Required values are given in parentheses.

Electrochemical measurements

D.C. polarography and cyclovoltammetry were performed, as reported in Ref. [7], with an Amel model 471 three-electrode multifunctional assembly. The working electrode was a standard Amel pulsing or stationary electrode and the counter electrode was a platinum wire. A $Hg|Hg_2Cl_2$, NaCl (saturated, aq)|agar-NaCl (aq)|agar (1.5%, w/v)-dmf-water (40%, v/v)-NEt_4ClO_4 (saturated)|methyl cellulose (5%, w/v)-dmf-NEt_4ClO_4 (saturated) sintered-glass disc (dmf = dimethylformamide) served as reference electrode. Its potential was 2.2 mV *vs* an aqueous saturated calomel electrode (SCE), the liquid junction potential being included. All potentials reported in Tables 3 and 4 are quoted with respect to the reference electrode with an accuracy of ± 5 mV.

RESULTS AND DISCUSSION

Preparation and properties of nickel and platinum complexes

The compounds $NHRNHC(S)SMe$ ($R = C_6H_4OMe\text{-}4$ or $C_6H_4NO_2\text{-}4$) reacted readily with K_2PtCl_4 or $NiCl_2$ in aqueous ethanol. If the medium is made strongly basic, crystalline, intensely coloured, diamagnetic compounds **1a, 1b, 2a** and **2b**, which contain doubly deprotonated ligands, are formed. We assume that there is a progressive deprotonation of the ligands, in accord with reports on dithiolene-like complexes of thiosemicarbazides [5,6] and with our reports on the reactions of $NH_2NHC(S)SMe$ and its 3-substituted derivatives with K_2PtCl_4 [1], $NiCl_2$ [2], $CuCl_2$ [3] and $K_2[PdCl_4]$ [4]. The complexes are soluble in most organic solvents, showing differences depending on the substituent in the phenyl ring. The NO_2-substituted compounds are the least soluble. The complexes can be electrochemically reduced giving anionic complexes whereas only some of them can be oxidized giving cationic complexes. They can be easily reduced by $NH_2NH_2 \cdot H_2O$ to monoanionic complexes. We have isolated and characterized $[AsPh_4][Ni\{N(C_6H_4NO_2\text{-}4)NC(S)SMe\}_2]$ **1c** and $[AsPh_4][Pt\{N(C_6H_4NO_2\text{-}4)NC(S)SMe\}_2]$ **2c**. The complex $[Ni\{N(C_6H_4OMe\text{-}4)NC(S)SMe\}_2]$ **1a** shows peculiar behaviour when crystallized from boiling CS_2. The complex formally loses one mole of MeSH giving the new compound $[Ni\{N[4\text{-}MeOPhN(4\text{-}MeO)C_6H_3]NC(S)SMe\}(NCS)]$. We already observed simi-

lar behaviour for the complexes [Ni{NPhNC(S)SMe}$_2$] [2], [Pd{NPhNC(S)SMe}$_2$] [4] and [Pd{N(C_6H_4OMe-4)NC(S)SMe}$_2$] [4] which gave rise to the complexes [Ni{$PhNC_6H_4$NNC(S)SMe}(NCS)], [Pd {N(C_6H_4NPh-2)NC(S)SMe}(NCS)]·0.5C_6H_6, [Pd{N[C_6H_3(OMe-4)NC_6H_4(OMe-4)]NC(S)SMe}(SCN)]·0.5C_6H_6, respectively. The complexes obtained show structural differences and we note that the reaction does not take place when the metal is platinum and when NO_2 groups are present in the ligands.

Infrared spectra

The absorption bands, which in the spectra of the ligands NHRNHC(S)SMe are attributed to ν(N—H) (3199 and 3103 cm^{-1} for R = C_6H_4OMe-4, 3281 and 3115 cm^{-1} for R = $C_6H_2NO_2$-4) [4] are no longer present in the spectra of the corresponding nickel and platinum complexes [M{NRNC(S)SMe}$_2$] **1a, 1b, 2a** and **2b** confirming that both N atoms of the ligands are deprotonated. Moreover the spectra show bands attributable to ν(M—N) and to ν(M—S) in the ranges 490–405 and 393–303 cm^{-1}, respectively, supporting N—S chelation of the ligands. In the spectrum of [Ni{N[4-MeOPhN(4-MeO)C_6H_3]NC(S)SMe}(NCS)] a sharp absorption at 2100 cm^{-1} is assigned to ν(C≡N) of the isothiocyanato group, as found in [Ni{NCC_6H_4Ph-2)NC(S)SMe}(NCS)] [2].

Electronic spectra

Data are given in Table 2. The electronic spectra of the complexes **1a, 1b, 2a** and **2b** are very similar and show features common to dithiolene-like complexes with electron-transfer properties (see Figs 1 and 2). The prominent strong bands in the range 11,000–13,000 cm^{-1} are assigned to ligand-to-metal c.t. absorptions in accord with our previous reports on similar complexes of platinum [1], nickel [2], copper [3] and platinum [4]. The spectrum of **1d** (see Fig. 3) shows very similar features to the spectra of [Ni{N-[$PhNC_6H_4$]NC(S)SMe}(NCS)] and [Pd{N[4-MeO PhN(4-MeO)C_6H_3]NC(S)SMe}(SCN)]·0.5C_6H_6, as we have already reported [2,4].

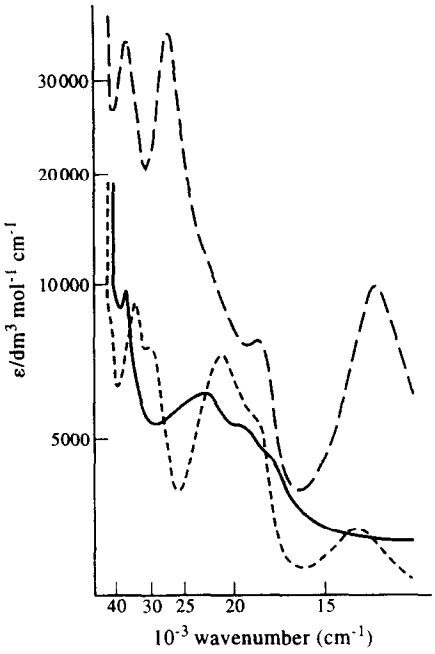


Fig. 1. Electronic spectra in CH_2Cl_2 of complexes **1a** (– – –), **1b** (— — —) and **1c** (— · —).

Electrochemical measurements

Cyclovoltammetric and polarographic data are reported in Tables 3 and 4. The voltage range 0 to +1.5 V was explored in the oxidation mode and the range 0 to −1.5 V in the reduction mode. The data concerning the compounds with doubly deprotonated ligands show that the nickel and platinum complexes belong to electron-transfer series as is usual for dithi-

Table 2. Electronic solution (CH_2Cl_2) spectra of the nickel and platinum complexes

Compound	Chromophore	$10^3\,\nu^a$/cm^{-1}
Ni{NPhNC(S)NEt_2}$_2$ [8]	*trans*NiN_2S_2	11.9 (3.37), 17.4 (4.07), [19.6] (3.90), 23.5 (4.08), 31.3 (4.43), [33.9] (4.34)
1a		11.9 (3.69), 17.1 (4.13), 20.0 (4.27), [31.0] (4.28), 34.3 (4.36), [44.4] (4.33)
1b		11.4 (3.89), 17.4 (3.79), 26.3 (4.42), 36.0 (44.1)
1c		[15.9] (3.92),^{b} 18.3 (4.05),^{b} 21.7 (4.13),^{b} 38.0 (4.32)^b
1d		17.3 (3.87),^{b} 22.3 (4.29),^{b} [40.08] (4.43)^b
Pt{NPhNC(S)SMe}$_2$ [9]	*trans*PtN_2S_2	13.6 (4.43), 2.20 (sh) (3.37), 24.0 (3.82), 31.5 (4.18), 40.0 (sh) (4.23), 45.7 (4.10)
2a		13.2 (4.24), 19.7 (3.94), 30.3 (3.94), [39.0] (4.10)
2b		12.9 (3.73), 26.4 (3.70), 38.0 (3.90)
2c		9.0 (4.05),^{b} 14.8 (3.80),^{b} 22.1 (4.29),^{b} [26.9] (3.98),^{b} [37.6] (4.29)^b

^{a}log (ε/dm^3 mol^{-1} cm^{-1}) in parentheses, shoulders in square brackets.
^{b}Very dilute solution (10^{-5} mol dm^{-3}).

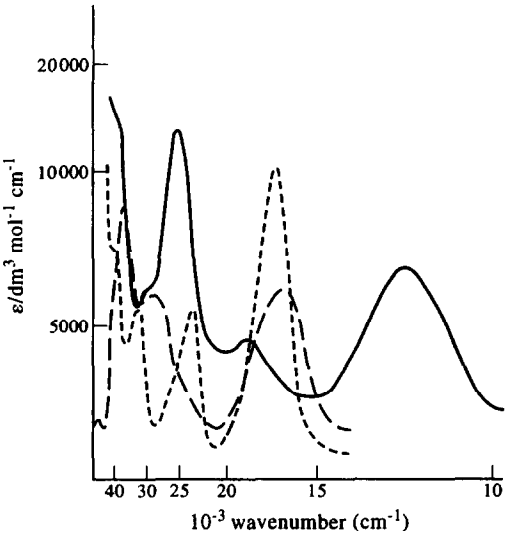


Fig. 2. Electronic spectra in CH_2Cl_2 of complexes **2a** (– – –), **2b** (— — —) and **1c** (——).

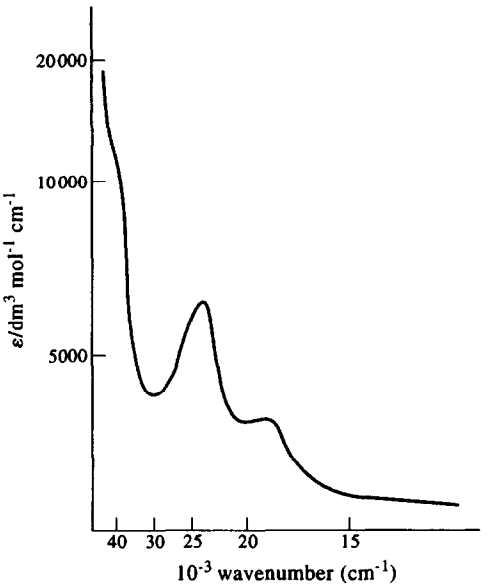


Fig. 3. Electronic spectrum in CH_2Cl_2 of complex **1d**.

olene and dithiolene-like complexes with five-membered delocalized chelate rings (Scheme 1).

The nickel and platinum complexes show well-defined waves corresponding to one-electron quasi-reversible processes as inferred from the values of $E_{3/4}-E_{1/4}$ in d.c. voltammetry (slopes in Tables 3 and 4) and from the cyclicvoltammetric anodic/cathodic or cathodic/anodic current ratios, which are close to the theoretical value for a one-electron reversible process. The complexes **1a** and **2a** show oxidation and reduction waves corresponding to processes leading to the formation of the cations 1 and 2 and the anions

$$[Pd(N_2S_2)]^{2+} \underset{-1e}{\overset{+1e}{\rightleftarrows}} [Pd(N_2S_2)]^{1+} \underset{-1e}{\overset{+1e}{\rightleftarrows}} [Pd(N_2S_2)] \underset{-1e}{\overset{+1e}{\rightleftarrows}} [Pd(N_2S_2)]^{1-} \underset{-1e}{\overset{+1e}{\rightleftarrows}} [Pd(N_2S_2)]^{2-}$$

1 2 3 4 5

Scheme 1.

Table 3. Electrochemical data for the oxidation of nickel and platinum complexes in CH_2Cl_2 solution (1×10^{-3} mol dm^{-3})[a]

	Cyclic voltammetry[b]								
Compound	E_p^1(an)/V	E_p^2(an)/V	E_p^3(an)/V	ΔE_p^{1c}/V	ΔE_p^{2c}/V	ΔE_p^{3c}/V	i^1(an)/i^1(cat)	i^2(an)/i^2(cat)	i^3(an)/i^3(cat)
1c			+0.216			0.080			1.0
2c			+0.116			0.085			1.0

	D.c. voltammetry at a pulsing platinum electrode[d]								
	$E_{1/2}^1$/V	$E_{1/2}^2$/V	$E_{1/2}^3$/V	i^1/μA	i^2/μA	i^3/μA	Slope[1e]/V	Slope[2e]/V	Slope[3e]/V
1a		0.805			1.64			0.070	
1c			+0.195			2.96			0.075
2a	1.240	1.035		1.48	1.48		0.070	0.060	
2c			+0.106			3.76			0.070

[a]Containing 0.1 mol dm^{-3} NBu_4BF_4, 20°C, all potentials *vs* SCE.
[b]Scan rate 200 mV s^{-1}.
[c]Anodic to cathodic peak potential separation.
[d]Pulsing time $t_p = 2$ s.
[e]Calculated using $E_{3/4}-E_{1/4}$.

Table 4. Electrochemical data for the reduction of nickel and platinum complexes in CH_2Cl_2 solution (1×10^{-3} mol dm^{-3})[a]

	Cyclic voltammetry[b]					
Compound	E_p^4(cat)/V	E_p^5(cat)/V	ΔE_p^{4c}/V	ΔE_p^{5c}/V	i^4(cat)/i^4(an)	i^5(cat)/i^5(an)
1a	−0.425	−0.980	0.100	0.100	0.9	1.0
1c		−0.274		0.080		0.9
1d	−0.199	−0.855	0.090	0.110	1.1	1.1
2a	−0.405	−1.080	0.085	0.080	1.0	1.0
2c		−0.274		0.095		1.0

	D.c. voltammetry at a pulsing platinum electrode[d]					
	$E_{1/2}^4$/V	$E_{1/2}^5$/V	i^4/μV	i^5/μV	Slope^{4e}/V	Slope^{5e}/V
1a	−0.390	−0.980	1.84	1.92	0.070	0.070
1c		−0.259		2.24		0.050
1d	−0.205	−0.850	1.24	1.60	0.070	0.070
2a	−0.390	−1.025	1.44	1.44	0.070	0.080
2c		−0.254		3.92		0.060

[a]Containing 0.1 mol dm^{-3} NBu_4BF_4, 20°C, all potentials *vs* SCE.
[b]Scan rate 200 mV s^{-1}.
[c]Cathodic to anodic peak potential separation.
[d]Pulsing time $t_p = 2$ s.
[e]Calculated using $E_{3/4}$–$E_{1/4}$.

4 and 5. The complexes **1c** and **2c**, corresponding to the anions 4, were studied instead of the neutral complexes because their low solubility prevented electrochemical measurements. They show oxidation waves corresponding to the processes leading to formation of the neutral complexes 3 and reduction waves corresponding to the processes leading to the anions 5. The complex **1d** containing isothiocyanate anion shows two reduction waves corresponding to processes leading to mono- and di-anionic forms. We note that the reduction potentials of the complexes containing NO_2 group are at lower values with respect to the values we found for dithiolene-like complexes of nickel and platinum with other 3-substituted dithiocarbazic esters [1, 2, 3, 4], according to the strong electron-attracting effect of the group.

Acknowledgement—The authors wish to thank Mr F. Dianetti for microanalysis.

REFERENCES

1. M. Bonamico, V. Fares, P. Imperatori, L. Suber and F. Tarli, *J. Chem. Soc., Dalton Trans.* 1990, 931 and references therein.
2. D. Attanasio, V. Fares, P. Imperatori, G. Mattogno and F. Tarli, *J. Chem. Soc., Dalton Trans.* 1988, 1217.
3. L. Petrilli and F. Tarli, *Polyhedron* 1990, **9**, 1457.
4. M. Bonamico, V. Fares, L. Petrilli, F. Tarli, G. Chiozzini and C. Riccucci, *J. Chem. Soc., Dalton Trans.* 1994, 3349.
5. C. E. Forbes, A. Gold, and R. H. Holm, *Inorg. Chem.* 1971, **10**, 2479.
6. K. A. Jensen, K. Bechgaard and C. T. Pedersen, *Acta Chem. Scand.* 1972, **26**, 2913.
7. R. Andruzzi, and A. Trazza, *J. Electroanal. Chem.* 1978, **86**, 201.
8. K. Bechgaard, *Acta Chem. Scand., Sect. A* 1974, **28**, 1985.
9. C. Battistoni, A. M. Giuliani, E. Paparazzo and F. Tarli, *J. Chem. Soc., Dalton Trans.* 1984, 1293.

Pergamon

S0277-5387(96)00265-3

Polyhedron Vol. 16, No. 2, pp. 281-289, 1997
Copyright © 1996 Elsevier Science Ltd
Printed in Great Britain. All rights reserved
0277-5387/97 $15.00+0.00

Dinuclear copper(II) complexes containing nitroso-oximato bridges: two different copper(II)-bridging entities from the same precursor

Jose M. Dominguez-Vera,[a] Enrique Colacio,[a]* Albert Escuer,[b]* Martti Klinga,[c] Raikko Kivekäs[c] and Antonio Romerosa[d]

[a] Departamento de Química Inorgánica, Facultad de Ciencias, Universidad de Granada, 18071 Granada, Spain

[b] Department de Química Inorgánica, Universitat de Barcelona, Diagonal 647, 08028 Barcelona, Spain

[c] Division of Inorganic Chemistry, University of Helsinki, Vuorikatu 20, SF 00100 Helsinki, Finland

[d] Departamento de Química Inorgánica, Facultad de Ciencias Experimentales, Universidad de Almeria, 04071 Almeria, Spain

(Received 12 April 1996; accepted 20 May 1996)

Abstract—The complexes $[Cu(\mu\text{-L})Cu(bipy)(EtOH)](ClO_4)_2$ **2a** and $[Cu(\mu\text{-}^1L)Cu(bipy)(H_2O)](ClO_4)_2 \cdot H_2O$ **2b** [where H_2L = *N,N'*-bis(1,3-dimethyl-5-nitrosopyrimidine-2,4-(1H,3H)-dion-6-yl)propylenediamine; H_2^1L arises from H_2L by elimination of a CO molecule from one of the pyrimidine rings] have been obtained from the reaction of the precursor $[Cu(\mu\text{-HL})Cu(H_2O)_2(CH_3CH_2OH)](ClO_4)_3$ **1** with bipy and $Cu(ClO_4)_2 \cdot 6H_2O$, respectively. The structures of **2a** and **2b** have been solved by X-ray crystallographic methods. The structure of **2a** is made up of $[Cu(\mu\text{-L})Cu(bipy)(EtOH)]^{2+}$ cations and two semi coordinated perchlorate anions. The [Cu(1)L] fragment coordinates to the external Cu(2) ion through the two deprotonated oximate oxygens to afford a dinuclear structure with double *syn-syn* nitroso-oximate bridge and an intramolecular Cu–Cu distance of 3.731(1) Å. The Cu(1) exhibits a CuN_4O_2 pseudooctahedral coordination polyhedron whereas the geometry around the Cu(2) ion is distorted square-pyramidal CuN_2O_2O. The structure of **2b** consists of $[Cu(\mu\text{-}^1L)Cu(bipy)(H_2O)]^{2+}$ cations, two perchlorate anions and one lattice water molecule. The coordination of the $[Cu(^1L)]$ unit to the external Cu(2) ion takes place through the two nitroso-oximate groups, one of them disordered on two sets of crystallographic positions, one with a 63% occupancy and the other with a 37% occupancy. The intramolecular Cu(1)—Cu(2) distance is 3.655(3) Å. The Cu(1) occupying the inner site of the $^1L^{2-}$ ligand exhibits a 4+1 CuN_4O (63%) $[CuN_3O_2$ (37%)] coordination environment whereas the Cu(2) atom is in a distorted square-pyramidal CuN_2O_3 (63%) $[CuN_3O_2$ (37%)] environment. The dinuclear fragments of **2a** and **2b** are almost planar with dihedral angles between the mean basal coordination planes of 4.1(2)° and 4.6°, respectively. Both **2a** and **2b** are diamagnetic at room temperature, so that $J < -1000$ cm^{-1}. The structural and magnetic data for these complexes have been compared with those of similar compounds, but no correlation between the magnitude of the exchange interaction and the degree of deviation from planarity is evident. In view of this and to rationalize the influence of the distortion from planarity on the magnetic properties in oximate-bridged complexes, MO Extended Hückel calculations have been performed. Copyright © 1996 Elsevier Science Ltd

Keywords: oximato; copper(II); dinuclear; complexes; magnetism; X-ray structures.

* Author to whom correspondence should be addressed.

Magnetostructural studies on polynuclear metal complexes are of continuing interest for coordination chemists since they can provide the understanding of fundamental factors governing their magnetic properties. This knowledge can be applicable for the design and preparation of new molecular materials exhibiting expected magnetic properties such as molecular-based magnets [1], or to deduce the structure of active sites in metalloproteins with interacting paramagnetic centers [2].

To design and synthesize polynuclear metal complexes, one of the best and common strategies is the use of mononuclear complexes as ligands. These complexes must contain donor groups for another metal ion or metal complex with empty coordination sites. Typical examples of this class of mononuclear precursors are the oximato copper(II) complexes [3], which can coordinate another metal ion through the deprotonated oximate oxygens, leading to oximate-bridged homo- and heteropolynuclear metal complexes [4,5]. Previously, we reported the synthesis and characterization of a dinuclear copper(II) complex of formula $[Cu(\mu\text{-HL})Cu(H_2O)_2(CH_3CH_2OH)](ClO_4)_3$ **1**, which was obtained by the reaction of the multidentate dioxime ligand *N,N'*-bis(1,3-dimethyl-5-nitroso pyrimidine-2,4-(1H,3H)-dion-6-yl)propylenediamine, H_2L, with an excess of Cu^{2+} [4h]. In this complex, the copper(II) ion occupying the external site must be coordinated by the nitroso-oximate oxygens atoms and by labile ligands (CH_3OH or H_2O), which can be easily replaced by a chelate ligand. This route allowed us to obtain a series of new dinuclear complexes with different "end-cap" ligands. In the present paper we report on the structures and magnetic properties of two oximate-bridged dinuclear copper(II) complexes, both containing 2,2'-bipyridyl (bipy) as "end-cap" ligand, which were obtained from the same precursor **1**.

EXPERIMENTAL

The ligand *N,N'*-bis(1,3-dimethyl-5-nitroso-pyrimidine-2,4-(1H,3H)-dion-6-yl) propylenediamine (H_2L) and the complex $[Cu(\mu\text{-HL})Cu(H_2O)_2(CH_3CH_2OH)](ClO_4)_3$ **1** were prepared as previously described [4h,5g].

Synthesis of the complexes

CAUTION! Perchlorate salts of metal complexes are potentially explosive. Only a small amount of material should be prepared, and it should be handled with caution.

$[Cu(\mu\text{-L})Cu(bipy)(EtOH)](ClO_4)_2$ **2a**. 2,2'-bipyridyl (0.23 g, 1.5 mmol) was added to a suspension of **1** (0.46 g, 0.5 mmol) in 50 cm^3 of ethanol/water/acetonitrile (10 : 1 : 1). After a few minutes at 60°C, a black solution was obtained, which was filtered to remove any amount of insoluble material. Suitable black crystals for X-ray analysis were obtained by evaporation of the solution at room temperature. Yield: 72%. Found: C, 34.6; H, 3.6; N, 15.0; Cl, 7.9; Cu, 13.3. Calc. for $C_{27}H_{32}N_{10}O_{15}Cl_2Cu_2$: C, 34.7; H, 3.4; N, 15.0; Cl, 7.6; Cu, 13.6%.

$[Cu(\mu\text{-}^1L)Cu(bipy)(H_2O)](ClO_4)_2 \cdot H_2O$ **2b**. Copper(II) perchlorate (0.30 g, 0.8 mmol) and bipyridyl (0.12 g, 0.8 mmol) were successively added to a stirred suspension of **1** (0.46 g, 0.5 mmol) in 50 cm^3 of ethanol/water (10 : 1) and the mixture was refluxed for one hour. From the resulting solution, black crystals of **2b** were separated by slow evaporation at room temperature. Yield: 31%. Found: C, 32.0; H, 3.5; N, 15.3; Cl, 7.7; Cu, 14.0. Calc. for $C_{24}H_{30}N_{10}O_{15}Cl_2Cu_2$: C, 32.1; H, 3.3; N, 15.6; Cl, 7.9; Cu, 14.2%.

Physical measurements

Microanalysis and magnetic susceptibility data were obtained as already described [5g].

X-ray data collection and structure determination of the compounds

Single-crystal data collection of **2a** was performed at 296 K with a Nicolet P3F diffractometer using monochromized Mo-K_α radiation. The unit cell parameters were determined by least-squares refinement of 25 carefully centered reflections. The data obtained were correct for Lorentz and polarization effects and for dispersion. Also, a correction for empirical absorption (Ψ scan) was applied. The space group, $P2_1/c$, was confirmed by systematic absences and structure analysis. The structure was solved by Patterson method [6] and successive Fourier maps. The solvent ethanol molecule coordinated to Cu(2) is partly disordered with the oxygen atom O(30) occupying two positions, and refinements yielded site occupation parameter 0.441(8) for O(30A) and 0.559(8) for O(30B). In the final refinements the non-hydrogen atoms of the disordered ethanol molecule were refined isotropically. The methyl groups were refined as rigid groups with group isotropic displacement parameters. The rest of the non-hydrogen atoms were refined with anisotropic displacement parameters. The hydrogen atoms were placed at their calculated positions (C—H = 0.96 Å and U(H) equal to U of bonded atom), except those of the disordered ethanol molecule, which were not positioned. All refinements were performed using XTAL3.0 program system [7], which minimized the function $\Sigma w(|F_o| - |F_c|)^2$, where $w = 1/\sigma F^2$.

Single-crystal data collection of **2b** was performed at 193 K with a Rigaku AFC-7S diffractometer using graphite monochromatized Mo-K_α radiation and MSC/AFC Diffractometer Control Software (Molecular Structure Corporation, 1993) [8]. Data were corrected for Lorentz and polarization effects. The structure was solved by direct methods and refined by

full-matrix least-squares using programs in SHELXTL/PC package [9]. One nitroso-oximate group is disordered with site occupancy factor of 0.63(4) for atoms labelled N(14A) and O(14A) and 0.37(4) for N(14B) and O(14B). H atoms were placed on calculated positions (C—H = 0.96 Å) except those of the water molecules, that were refined as a rigid group (O—H = 0.85 Å), all with fixed isotropic temperature factor of 0.08 Å^2.

Crystal data and details of data collections of the **2a** and **2b** complexes are listed in Table 1.

RESULTS AND DISCUSSION

On treating H_2L with an excess of copper(II) perchlorate hexahydrate in ethanol, the complex with the empirical formula $[Cu(\mu\text{-}HL)Cu(H_2O)_2(CH_3CH_2OH)](ClO_4)_3$ **1** was obtained [4h]. This dinuclear complex can react with 2,2′-bipyridyl to afford the complex $[Cu(\mu\text{-}L)Cu(bipy)(EtOH)](ClO_4)_2$ **2a**, in which bipy has replaced the labile ligands coordinated to the external copper(II) in **1**. However, when $[Cu(bipy)]^{2+}$ was used instead of bipy as counterpart, the dinuclear $[Cu(\mu\text{-}^1L)Cu(bipy)(H_2O)](ClO_4)_2 \cdot H_2O$ **2b** complex was isolated. $(^1L)^{2-}$ is obtained from L^{2-} by elimination of one CO molecule from one of the pyrimidine rings, leading to an imidazole ring.

Crystal structure of **2a**

The structure of complex **2a** consists of dinuclear $[Cu(\mu\text{-}L)Cu(bipy)(EtOH)]^{2+}$ cations and two semi-coordinated perchlorate atoms. A perspective view of the dinuclear copper(II) cation with the atom-labelling scheme is given in Fig. 1. Selected bonds lengths and angles are listed in Table 2.

As expected, the external copper(II) ion, Cu(2), is coordinated by the unit [Cu(1)L] through the two diatomic *syn-syn* nitroso-oximate groups to afford a dinuclear complex with Cu(1)—Cu(2) distance of 3.731(1) Å.

The Cu(1) ion occupies the inner site of the double deprotonated ligand L^{2-} exhibiting a pseudo-octahedral coordination. Four short bonds of *ca* 1.98 Å are formed with N(5), N(6), N(15) and N(16), that are practically coplanar (deviations from the least-square plane lower than 0.044 Å). The Cu(1) ion is lifted 0.103(1) Å from the N_4 mean basal plane toward the oxygen atom O(33) belonging to a perchlorate anion, which occupies one of the axial positions at a distance of 2.404(5) Å. The other axial position is occupied by the oxygen atom O(37) of the second perchlorate anion with a Cu(1)—O(37) distance of 2.660(7) Å.

Within the [Cu(1)L] fragment, the bond lengths and angles do not significantly differ from those observed in the complex $[CuL(H_2O] \cdot 3H_2O$ [5g].

Table 1. Summary of crystal data, intensity data collection and structure refinements for complexes **2a** and **2b**

	2a	**2b**
Formula	$C_{27}H_{32}N_{10}O_{15}Cl_2Cu_2$	$C_{24}H_{30}N_{10}O_{15}Cl_2Cu_2$
fw	934.6	896.6
Cryst. syst	Monoclinic	Monoclinic
Space group	$p2_1/c$	$P2_1/c$
a (Å)	11.158(2)	10.249(6)
b (Å)	8.023(1)	10.582(9)
c (Å)	38.861(9)	30.608(7)
γ (°)	94.25(2)	92.29(4)
V (Å^3)	3469(1)	3317(2)
Z	4	4
ρ_{calcd} (g cm^{-3})	1.789	1.795
μ (mm^{-1})	1.47	1.53
Crystal size (mm)	0.25 × 0.35 × 0.28	0.30 × 0.20 × 0.15
θ_{max} (°)	26.5	26.5
T (°C)	23	−77
No. of measured reflections	8127	6508
No. of unique reflections [$\|F_o\| > 4\sigma\|F_o\|$]	4467	2633
No. of refined parameters	488	489
Weighting scheme ($w =$)	$1/\sigma^2(F)$	$1/\sigma^2(F)$
Maximum, minimum residual Electron density (eÅ^{-3})	−0.7–0.9	−0.6–0.7
$R(F)^a$	0.062	0.077
$Rw(F)^a$	0.054	0.078

^{a} $R = \Sigma\|\|F_o\| - |F_c\|\|/\Sigma|F_o|$ and $Rw = [\Sigma w(|F_o| - |F_c|)^2/\Sigma w|F_o|^2]^{1/2}$.

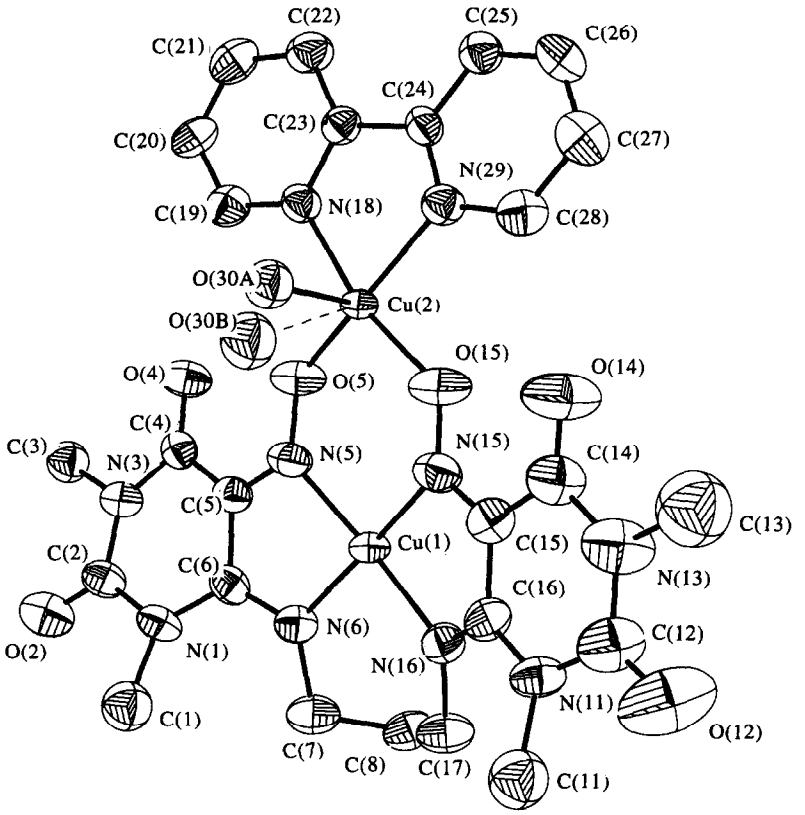


Fig. 1. Perspective view of the cation $[Cu(\mu\text{-L})Cu(bipy)(EtOH)]^{2+}$ **2a**. For clarity, only the coordinated oxygen atom of the ethanol molecule is shown.

Table 2. Selected bond distances (Å) and angles (°) for the complex **2a**

Cu(1)—N(5)	2.007(5)	Cu(1)—N(6)	1.957(5)
Cu(1)—N(15)	1.979(5)	Cu(1)—N(16)	1.967(5)
Cu(1)—O(33)	2.404(5)	Cu(1)—O(37)	2.660(7)
Cu(2)—O(5)	1.927(4)	Cu(2)—O(15)	1.918(4)
Cu(2)—N(18)	1.992(5)	Cu(2)—(29)	2.008(5)
Cu(2)—O(30A)	2.31(1)	Cu(2)—O(30B)	2.274(9)
O(4)—C(4)	1.216(7)	O(14)—C(14)	1.215(7)
O(5)—N(5)	1.287(6)		
O(15)—N(15)	1.285(6)		

N(5)—Cu(1)—N(6)	81.4(2)	N(5)—Cu(1)—N(15)	100.3(2)
N(5)—Cu(1)—N(16)	175.6(2)	N(5)—Cu(1)—O(33)	90.0(2)
N(5)—Cu(1)—O(37)	89.6(2)	N(6)—Cu(1)—N(15)	171.3(2)
N(6)—Cu(1)—N(16)	95.9(2)	N(6)—Cu(1)—O(33)	103.8(2)
N(6)—Cu(1)—O(37)	89.3(2)	N(15)—Cu(1)—N(16)	81.8(2)
N(15)—Cu(1)—O(33)	84.8(2)	N(15)—Cu(1)—O(37)	82.3(2)
N(16)—Cu(1)—O(33)	94.1(2)	N(16)—Cu(1)—O(37)	86.9(2)
O(33)—Cu(1)—O(37)	166.8(2)	O(5)—Cu(2)—O(15)	103.3(2)
O(5)—Cu(2)—N(18)	87.8(2)	O(5)—Cu(2)—N(29)	156.8(2)
O(5)—Cu(2)—O(30A)	107.7(3)	O(5)—Cu(2)—O(30B)	85.7(2)
O(15)—Cu(2)—N(18)	166.9(2)	O(15)—Cu(2)—N(29)	86.9(2)
O(15)—Cu(2)—O(30A)	93.5(3)	O(15)—Cu(2)—O(30B)	90.2(3)
N(18)—Cu(2)—N(29)	80.3(2)	N(18)—Cu(2)—O(30A)	89.5(3)
N(18)—Cu(2)—O(30B)	97.6(3)	N(29)—Cu(2)—O(30A)	92.1(3)
N(29)—Cu(2)—O(30B)	115.4(2)	O(30A)—Cu(2)—O(30B)	23.7(3)
Cu(2)—O(5)—N(5)	127.1(3)	Cu(1)—N(5)—O(5)	127.2(4)
Cu(2)—O(15)—N(15)	128.7(4)	Cu(1)—N(15)—O(15)	128.0(4)

The coordination geometry around the Cu(2) ion is distorted square pyramidal, CuN_2O_2O. The basal plane is defined by the two nitroso-oximate O(5) and O(15), and the two bipyridyl N(18) and N(29) atoms with distances of about 1.92 and 2.00 Å, for Cu—O and Cu—N, respectively. The fifth position is occupied at a longer distance of about 2.29 Å by a disordered oxygen atom O(30) from the molecule of ethanol, with occupancy factor of 0.441(8) and 0.559(8) for O(30A) and O(30B), respectively.

Bipy coordinates to Cu(2) in a bidentate fashion. As usual, the N(18)—Cu(2)—N(29) angle is significantly smaller than 90° (80.3(2)°) as consequence of the geometric constraints of the bipyridyl ring system. The equatorial atoms are not coplanar but pair-wise distorted, so that O(15) and N(18) are lifted 0.118(6) and 0.143(6) Å, respectively, above the mean basal plane whereas O(5) and N(29) are located 0.106(6) and 0.158(6) Å, respectively, below the plane. The Cu(2) atom sticks out from the mean basal plane N_2O_2 by 0.213(1) Å toward the axially-bonded ethanol molecule.

The dinuclear fragment $[Cu(\mu\text{-L})Cu(bipy)]^{2+}$ cation is practically planar. Thus, the dihedral angle between the plane defined by Cu(1)N(5)N(15)O(5)O(15) and Cu(2)O(5)O(15)N(18)N(29) is 4.1(2)°.

Crystal structure of **2b**

The asymmetric unit of **2b** contains one $[Cu(\mu\text{-}^1L)Cu(bipy)(H_2O)]^{2+}$ cation, two perchlorate anions, one of them semi-coordinated, and one lattice water molecule. A perspective view of the dinuclear cation with the atom-labelling scheme can be observed in Fig. 2. Selected bond lengths and angles are listed in Table 3.

The most interesting feature of the structure results from the elimination of one CO molecule of one pyrimidine ring in L^{2-} leading to an imidazole ring. It is interesting to note that a similar decarbonilation process has been observed for the same ligand L^{2-} in the complex $[Cu(ClO_4)(\mu\text{-}^1L)Ni(Me_3[12]N_3)](ClO_4)\cdot H_2O$ [5g], and other uracil derivatives. For instance, when an aqueous solution of 1,3-dimethyl-5,6-diaminouracil is treated with ferric chloride, 1,3-dimethyl-2,4,5-imidazolinetrione is obtained in good yield [10].

As can be seen in Fig. 2, the coordination of the $[Cu(1)^1L]$ unit to the external copper(II) ion, Cu(2), takes place through the two NO groups, giving rise to a dinuclear copper(II) complex with a Cu(1)—Cu(2) distance of 3.655(3) Å. One of the NO groups, the N(14)—O(14), is disordered, exhibiting two different bridging conformations. The first one (0.63(4) occupancy factor) is of *syn* type, like that of the non-disordered NO group, whereas the second one (0.37(4) occupancy factor) is *O*-monoatomic with a Cu(1)—O(14B)—Cu(2) angle of 128(1)°. This last conformation of the NO group is rather uncommon and it has been only observed in the complexes $[Cu(ClO_4)(\mu\text{-}^1L)Ni(Me_3[12]N_3)](ClO_4)\cdot H_2O$ [5g] and $\{[Cu_2(dmg)(Hdmg)(H_2dmg)]_2(SO_4)\}$ $2.5H_2O$ [4f]. It seems that the elimination of the CO molecule from one of the pyrimidine rings of H_2^1L enables the *O*-monoatomic bridging mode of the NO group bonded to the imidazole ring.

The Cu(1) ion occupying the internal site of the $^1L^{2-}$ ligand exhibits a 4 + 1 coordination environment. Four short bonds of *ca* 1.98 Å are formed with N(5), N(6), N(10), and with either N(14A) (63%) or O(14B) (37%). The fifth position is occupied at a longer distance of 2.47(1) Å by an oxygen atom, O(31) from a perchlorate anion. The copper(II) ion is lifted 0.077(4) and 0.089(4) Å toward the apical positions from the N_3O and N_4 mean basal planes, respectively.

The coordination of the ligand to Cu(1) results in the formation of two five- and one six-membered chelate ring in the case of the Cu(1)—N(14A)—O(14A)—Cu(2) bridging conformation, and two six- and one five-membered chelate ring for the Cu(1)—O(14B)—Cu(2) conformation.

The copper atom Cu(2) is in a distorted square-pyramidal environment. The four nearest neighbours at about 2.0 Å are the O(5), either O(14A) or N(14B) from the unit $[Cu(1)^1L]$, and the N(18) and N(29) belonging to the terminal ligand bipy. The fifth position is occupied by the O(30) atom belonging to a water molecule. The deviations of the Cu(2) from the basal planes N(18)N(29)O(5)O(14A) and N(18)N(29)O(5)O(14B) are 0.194(4) and 0.183(4) Å, respectively.

As in **2a,** the dinuclear fragment is almost planar, with a dihedral angle between the coordination planes of 4.6(1)°. Bond lengths and angles of bipy in **2a** and **2b** are very close and similar to those found for other 2,2′-bypyridyl containing complexes.

Magnetic properties

Both **2a** and **2b** complexes are diamagnetic at room temperature. This diamagnetism reveals a strong antiferromagnetic coupling between copper(II) ions, so that the only state thermally populated, even at room temperature, is the $S = 0$. In accordance with this, the polycrystalline EPR spectra of both complexes show no signal at this temperature.

These data can only give an estimation of the lower limit of the exchange coupling parameter J, which must be placed at $J < -1000\ cm^{-1}$. This magnetic behaviour is not unexpected in view of the remarkable ability of the oximato bridge to mediate strong antiferromagnetic exchange interactions between paramagnetic centers, either in *syn*, *anti* or *o*-monoatomic conformation [4]. It must be pointed out that, in spite of the numerous examples of oximato-bridged copper(II) complexes reported so far, no clear magnetostructural correlations have been established.

Table 3. Selected bond distances (Å) and angles (°) for the complex **2b**

Cu(1)—N(5)	1.99(1)	Cu(1)—N(6)	1.98(1)
Cu(1)—N(10)	1.97(1)	Cu(1)—N(14A)	1.99(2)
Cu(1)—O(14B)	1.98(2)	Cu(1)—O(31)	2.47(1)
Cu(2)—O(5)	1.93(1)	Cu(2)—O(14A)	1.94(2)
Cu(2)—O(14B)	2.06(2)	Cu(2)—N(18)	2.02(1)
Cu(2)—N(29)	2.02(1)	Cu(2)—O(30)	2.21(1)
C(4)—O(4)	1.20(2)	N(5)—O(5)	1.30(1)
N(10)—C(10)	1.26(2)	C(10)—N(11)	1.38(2)
C(10)—C(14)	1.44(2)	N(11)—C(12)	1.39(2)
C(12)—O(12)	1.19(2)	C(12)—N(13)	1.39(2)
N(13)—C(14)	1.46(2)	C(14)—N(14A)	1.29(3)
C(14)—N(14B)	1.39(4)	N(14A)—O(14A)	1.30(3)
N(14B)—O(14B)	1.44(4)		

N(5)—Cu(1)—N(6)	80.9(4)	N(5)—Cu(1)—N(10)	174.9(5)
N(6)—Cu(1)—N(10)	96.0(5)	N(5)—Cu(1)—N(14A)	105.7(7)
N(6)—Cu(1)—N(14A)	170.9(6)	N(10)—Cu(1)—N(14A)	76.9(7)
N(5)—Cu(1)—O(14B)	79.4(8)	N(6)—Cu(1)—O(14B)	159.9(8)
N(10)—Cu(1)—O(14B)	103.3(8)	N(14A)—Cu(1)—O(14B)	26(1)
N(5)—Cu(1)—O(31)	91.4(4)	N(6)—Cu(1)—O(31)	101.6(4)
N(10)—Cu(1)—O(31)	93.2(5)	N(14A)—Cu(1)—O(31)	84.8(6)
O(14B)—Cu(1)—O(31)	83.1(8)	O(5)—Cu(2)—O(14A)	107.1(6)
O(5)—Cu(2)—O(14B)	78.7(8)	O(14A)—Cu(2)—O(14B)	28.7(9)
O(5)—Cu(2)—N(18)	84.9(5)	O(14A)—Cu(2)—N(18)	162.3(7)
O(14B)—Cu(2)—N(18)	161.4(8)	O(5)—Cu(2)—N(29)	162.4(5)
O(14A)—Cu(2)—N(29)	85.5(7)	O(14B)—Cu(2)—N(29)	114.1(8)
N(18)—Cu(2)—N(29)	80.3(5)	O(5)—Cu(2)—O(30)	100.5(4)
O(14A)—Cu(2)—O(30)	93.4(6)	O(14B)—Cu(2)—O(30)	94.4(7)
N(18)—Cu(2)—O(30)	97.2(4)	N(29)—Cu(2)—O(30)	90.8(5)
Cu(1)—N(5)—O(5)	124.6(8)	Cu(2)—O(5)—N(5)	127.5(8)
C(1)—N(11)—C(12)	113(1)	N(11)—C(12)—N(13)	106(1)
C(12)—N(13)—C(14)	109(1)	C(10)—C(14)—N(13)	106(1)
Cu(1)—N(14A)—O(14A)	125(2)	Cu(1)—N(14A)—O(14B)	76(2)
Cu(2)—O(14A)—N(14A)	127(2)	Cu(2)—O(14A)—N(14B)	175(3)
Cu(1)—O(14B)—Cu(2)	128(1)	Cu(1)—O(14B)—N(14A)	77(2)
Cu(2)—O(14B)—N(14A)	154(3)	Cu(1)—O(14B)—O(14A)	162(3)
Cu(2)—O(14B)—O(14A)	69(2)	Cu(1)—O(14B)—N(14B)	125(2)
Cu(2)—O(14B)—N(14B)	106(2)		

Nevertheless, from the magnetic data of centrosymmetric oximate-bridged dicopper systems (compounds **a–d** in Table 4), some general conclusions can be drawn: (i) The bond lengths Cu—N_{oxime}, Cu—O_{oxime}, N_{oxime}—O_{oxime} and the Cu—Cu distance do not show any kind of correlation with the magnetic properties; (ii) compounds with planar or nearly planar $Cu(NO)_2Cu$ skeleton are always perfectly coupled even at room temperature. Although the same general trends seem to be followed for the large number of well characterized trinuclear and non-centrosymmetric dinuclear copper(II) complexes reported in the recent past years, no correlation between the magnitude of the exchange coupling and the degree of deviation from planarity is evident (see Table 4). Thus, for instance, the di- and trinuclear compounds (**i**) and (**m**) given in Table 4 are practically coupled at room temperature despite their high deviations from planarity. In view of this, a rationalization of these apparently contradictory results is needed.

In order to evaluate the influence of some structural parameters, connected with the distortion from planarity, on the magnetic properties MO Extended-Huckel calculations have been performed by means of the CACAO program. [16]. The parameters used were the standard of the program, and the oximate system modelized. The bond parameters used were Cu—NH_3, 2.10 Å; Cu—O and Cu—N, 1.95 Å; N—O, 1.32 Å; C—N, 1.30 Å; NH_3—Cu—NH_3, 80°; N—Cu—O, 106° and C—N—O, 115°. From this basic scheme, calculations have been performed for the following geometries: square-planar, 4+1 planar and 4+1 coordination with the copper atom lifted 0.5 Å toward the apical position and finally for the chair distortion with dihedral angle of 30°. The σ^* molecular orbitals ϕ_g and ϕ_u are obtained from the

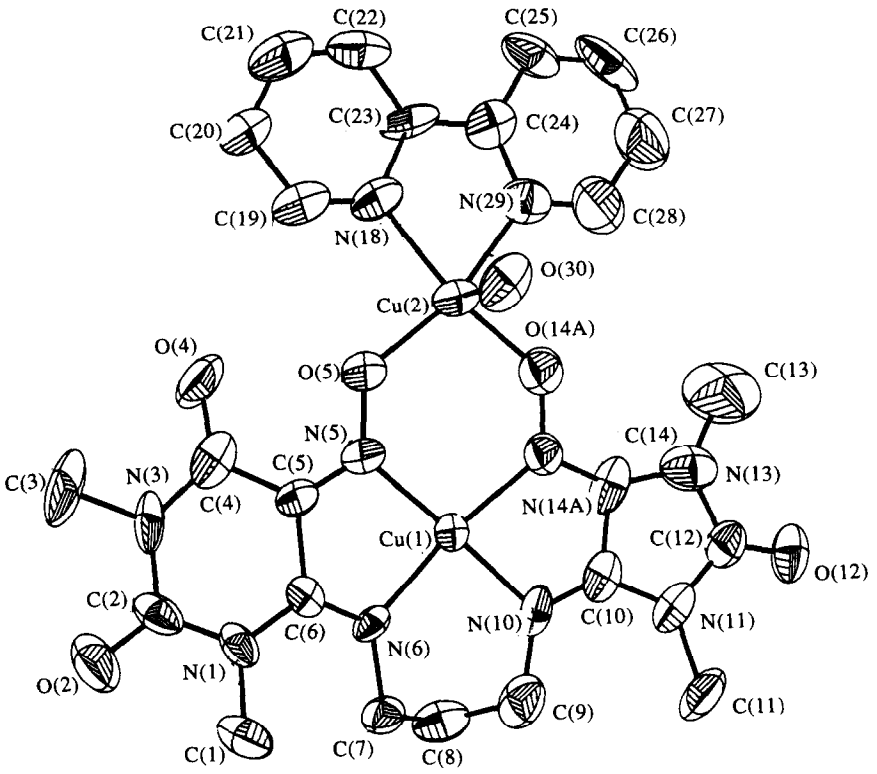


Fig. 2. Perspective view of the cation $[Cu(\mu\text{-}L^1)Cu(bipy)(H_2O)]^{2+}$ **2b**.

interaction of the symmetrical and antisymmetrical combinations of the copper d_{xy} orbitals and the similar combinations of the oximato ligands. In the ϕ_u orbital the interaction between $2p$ oxygen and nitrogen orbitals of the oximato bridge is bonding in character whereas in ϕ_g is of antibonding type and therefore, ϕ_g is much higher in energy than ϕ_u. The value of the energy gap $\Delta = \phi_g - \phi_u$ (0.205 eV) which, according to the Hoffmann's model, is the determining factor for the antiferromagnetic contribution to J (singlet–triplet energy difference), is in agreement with the large triplet–singlet energy difference observed for planar oximate-bridged copper(II) complexes. In addition, the results of these calculations show that the HOMO-LUMO energy gap is practically not affected by the apical coordination to copper(II), and moreover, either the displacement of the copper atom out of the coordination basal plane or the dihedral angle between the basal and oximate planes only decrease moderately the energy gap (about 10%) for the extremely large values of those parameters used in the calculations. This result is not unexpected in view of the pseudospherical symmetry of the lobes of the oximato MO involved in the superexchange pathway. This symmetry allows a considerable deviation from planarity of the $Cu(NO)_2Cu$ core without a significant decrease of the overlap between the interacting orbitals. From these results it should be concluded that the superexchange coupling in copper-oximato systems is very strong but a simple relation between planarity and J parameter is not consistent. We feel that other factors, such as the nature of oximate ligand itself and the nature of the "end-cap" ligands, may be, at least, as important in determining the exchange interactions as the structural parameters in the bridging fragment. In fact, all the dinuclear and trinuclear copper complexes containing the dimethyglyoxime ligand are coupled at room temperature even though some of them exhibit considerable distortions from planarity (compounds **i** and **m**). Moreover, the complexes $[Cu(L^7)Cu(phen)(H_2O)_2](ClO_4)_2$ [4c] and $[Cu(L^6)Cu(bipy)(H_2O)](ClO_4)_2 \cdot H_2O$ [4g] containing the same dioximate ligand (L^6 is 3,3′-aminopropylenedinytrilobis(2-butanoneoximate)) but different "end-cap" ligands (phen or bipy), have quite separate $2J$ values of -866 and -674 cm^{-1}, respectively, in spite of the fact that both exhibit similar deviations from planarity (the dihedral angles in the $Cu(NO)_2Cu$ cores are 29 and 26.7°, respectively). In order to gain insight into this subject, more examples of oximate-bridged complexes are needed, preferably closely related ones displaying variation over only one of the structural parameters.

Acknowledgements—E.C., J.M.D.-V. and A.R. are grateful to the Dirección General de Investigación Científica y Técnica for the Project of Investigation PB91-0725 and to the Junta de Andalucía for financial support. R.K. thanks Suomen Kulttuurirahasto for grants.

Table 4. Structural and magnetic parameters for some dinuclear and trinuclear oximate-bridged copper(II) complexes

Compound	Magnetic data	Deviation of copper from the mean basal plane (Å)	Dihedral angle (°) between mean coordination planes	Reference
$[Cu(L)Cu(bipy)(EtOH)](ClO_4)_2$	f.c.r.t.	0.103, 0.203	4.1	This work
$[Cu(^1L)Cu(bipy)(H_2O)](ClO_4)_2 \cdot H_2O$	f.c.r.t.	0.077–0.089 0.183–0.194	4.6	This work
$[Cu_2(L^2)_2(ClO_4)_2(H_2O)_2]$ (**a**)	f.c.r.t.	0.066	0	[11]
$[Cu_2(L^3)_2(CH_3CN)_2](ClO_4)_2$ (**b**)	μeff(r.t.) = 0.66	0.31	32	[12]
$[Cu_2(L^4)_2(ClO_4)_2]$ (**c**)	f.c.r.t.	0.038	0	[13]
$[Cu_2(L^4)_2(CH_3OH)_2]$ (**d**)	f.c.r.t.	0.055	0	[13]
$[Cu_2(L^5)](BF_4)_2$ (**e**)	μeff(r.t.) = 0.6	0.195, 0.186	10.4	[14]
$[Cu_2L^6)_2](ClO_4)_2$ (**f**)	$2J = -545$ cm^{-1}	0.123	24.4	[15]
$[Cu_2(L^7)Cu(phen)(H_2O)_2](ClO_4)_2$ (**g**)	$2J = -866$ cm^{-1}	0.120, 0.168	26.7[a]	[4c]
$[Cu_2(L^7)Cu(bipy)(H_2O)_2](ClO_4)_2$ (**h**)	$2J = -674$ cm^{-1}	0.170, 0.166	29.0[a]	[4g]
$[Cu_2(HL^8)(H_2L^8)(H_2O)_2](ClO_4)_2$ (**i**)	f.c.r.t. $2J = 1000$ cm^{-1}	0.240 0.158	26.1	[4e]
$[Cu_3(L^8)(bipy)_2(CH_3OH)_2](NO_3)_2$ (**j**)	f.c.r.t. $2J < -600$ cm^{-1}	0.176	7.5	[4a]
$[Cu_3(L^9)(bipy)_2(CH_3OH)_2](NO_3)_2$ (**k**)	f.c.r.t. $2J < -600$ cm^{-1}	0.183	14.5	[4a]
$[Cu\{Cu(L^6)\}_2](ClO_4)_2$ (**l**)	$2J = -580$ cm^{-1}	0.145	55.9[a]	[4b]
$[(TACN)_2Cu_2(L^8)_2CuBr]ClO_4$ (**m**)	f.c.r.t. $2J < -600$ cm^{-1}	0.40	55.2[a]	[4d]
$[\{Cu(HL)Cu(H_2O)Cu(L)\}(Cl)](ClO_4)_2$ (**n**)	$2J = -378$ cm^{-1}	0.054, 0.215	64	[4g]

[a] Bending angle of the $Cu(NO)_2Cu$ core. f.c.r.t. = fully coupled at room temperature. HL^2 = 2-(2-hydroxyethyl)imino-3-oximobutane. HL^3 = 2-[2(pyridyl)ethyl]imino-3-butaneoxime. HL^4 = 1-(*N*,*N*-dimethyl-2-aminoethyl)-1-phenyl-2-oximopropane. HL^5 = 2,6-diacetylpyridinedioxime. HL^6 = 2-(*N*-(2-hydroxyethyl)-2-aminoethyl)imino-3-butanoneoximato. HL^7 = 3,3′-aminopropylenedinitrilbis(2-butanoneoxime). HL^8 = dimethylglyoxime. HL^9 = diphenylglyoxime. TACN = 1,4,7-trimethyl-1,4,7-triazacyclononane.

REFERENCES

1. D. Gatteschi, O. Kahn, J. S. Miller and F. Palacio, NATO ASI Series E, 198, 35–52. Kluwer Academic Publishers, Dordrecht, The Netherlands (1991).
2. *Metal Clusters in Proteins.* Edited by L. Que Jr. ASC Symposium Series 372, American Chemical Society, Washington D.C. (1988).
3. A. Chakravorty, *Coord. Chem. Rev.* 1974, **13,** 1.
4. (a) H. Okawa, M. Koikawa, S. Kida, D. Luneau and H. Oshio, *J. Chem. Soc., Dalton Trans.* 1990, 469; (b) D. Luneau, H. Oshio, H. Okawa and S. Kida, *J. Chem. Soc., Dalton Trans.* 1990, 2283; (c) D. Luneau, H. Oshio, H. Okawa, M. Koikawa and S. Kida, *Bull. Chem. Soc. Jpn.* 1990, **63,** 2212; (d) P. Chaudhuri, M. Winter, B. P. C. Della Vedova, E. Bill, A. Trautwein, S. Gehring, P. Fleischauer, B. Nuber and J. Weiss, *Inorg. Chem.* 1991, **30,** 2148; (e) R. Ruiz, J. Sanz, B. Cervera, F. Lloret, M. Julve, C. Bois, J. Faus and M. C. Muñoz, *J. Chem. Soc., Dalton Trans.* 1991, 1623; (f) R. Ruiz, J. Sanz, F. Lloret, M. Julve, J. Faus, C. Bois and M. C. Muñoz, *J. Chem. Soc., Dalton Trans.* 1993, 3035; (g) R. Ruiz, F. Lloret, M. Julve, M. C. Muñoz and C. Bois, *Inorg. Chim. Acta* 1994, **219,** 179; (h) E. Colacio, J. M. Dominguez-Vera, A. Escuer, M. Klinga, R. Kivekas and A. Romerosa, *J. Chem. Soc., Dalton Trans.* 1995, 343.
5. (a) P. Chaudhuri, M. Winter, P. Fleischauer, W. Haase, U. Florke and J. Haupt, *J. Chem. Soc., Chem. Commun.* 1990, 1728; (b) P. Basu, S. Pal, A. Chakravorty, *J. Chem. Soc., Dalton Trans.* 1991, 3217; (c) S. Pal, R. Mukherjee, M. Tomas, L. R. Falvello and A. Chakravorty, *Inorg. Chem.* 1986, **25,** 200; (d) Z. J. Zhong, H. Okawa, N. Matsumoto, H. Sakiyama and S. Kid, *J. Chem. Soc., Dalton Trans.* 1991, 497; (e) F. Lloret, R. Ruiz, M. Julve, J. Faus, Y. Yournaux, I. Castro and M. Verdaguer, *Chem. Mat.* 1992, **4,** 1150; (f) F. Birkelbach, M. Winter, U. Flörke, H. J. Haupt, C. Butzlaff, M. Leugen, E. Bill, A. X. Trautwein, K. Wieghart and P. Chaudhuri, *Inorg. Chem.* 1994, **33,** 3390; (g) E. Colacio, J. M. Dominguez-Vera, A. Escuer, R. Kivekas and A. Romerosa, *Inorg. Chem.* 1994, **33,** 3914; (h) F. Lloret, R. Ruiz, B. Cervera, I. Castro, M. Julve, J. A. Real, F. Sapiña, Y. Journaux, J. C. Colin and M. Verdaguer, *J. Chem. Soc. Chem. Commun.* 1994, 2615.
6. G. M. Sheldrick, *SHELXS86. Program for the solution of crystal structures.* Univ. of Gottingen, Germany (1986).
7. S. R. Hall and J. M. Stewart (Editors), *XTAL* 3.0 *Reference Manual.* Universities of Western Australia, Australia, and Maryland, U.S.A. (1990).
8. Molecular Structure Corporation. MSC/AFC Diffractometer Control Software. MSC Research

Forest Drive, The Woodlands, TX77381, U.S.A. (1993).
9. G. M. Sheldrick, *SHELXTXTL/PC. Release* 4.1. Siemens Analytical X-ray Instruments Inc., Madison, Wisconsin, U.S.A. (1990).
10. Y. Okamoto, K. Ogura, Y. Kurasawa and T. Kinoshita, *Heterocycles* 1984, **22,** 1231.
11. J. A. Bertrand, J. S. Smith and P. G. Eller, *Inorg. Chem.* 1974, **13,** 1649.
12. J. A. Bertrand, J. S. Smith and D. G. vanDerveer, *Inorg. Chem.* 1977, **16,** 1477.
13. R. J. Butcher, C. J. O'Connor and E. Sinn, *Inorg. Chem.* 1979, **18,** 1913.
14. G. A. Nicholson, J. L. Petersen and B. J. McCormick, *Inorg. Chem.* 1980, **19,** 195.
15. M. Näsäkkälä, H. Saarinen, J. Korvenranta and E. Näsäkkälä, *Acta Chem. Scand.* 1981, **35,** 569.
16. C. Mealli, D. M. Proserpio, Computer Aided Composition of Atomic Orbitals (CACAO Program) (1992), *J. Chem. Educ.* 1990, **67,** 399.

Pergamon

S0277-5387(96)00261-6

Polyhedron Vol. 16, No. 2, pp. 291–295, 1997
Copyright © 1996 Elsevier Science Ltd
Printed in Great Britain. All rights reserved
0277-5387/97 $15.00 + 0.00

Synthesis and structure of new 2,6-(diphenylphosphinomethyl)pyridine ruthenium(II) complexes

Laurent Barloy,[a] Swee Y. Ku,[a] John A. Osborn,[a]* André De Cian[b] and Jean Fischer[b]

[a]Laboratoire de Chimie des Métaux de Transition et de Catalyse, URA 424 CNRS, Institut Le Bel, Université Louis Pasteur, 4 rue Blaise Pascal, 67070 Strasbourg Cedex, France

[b]Laboratoire de Cristallochimie et Chimie Structurale, URA 424 CNRS, Institut Le Bel, Université Louis Pasteur, 4 rue Blaise Pascal, 67070 Strasbourg Cedex, France

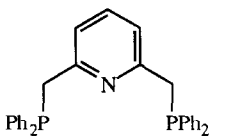
(Received 4 April 1996; accepted 17 May 1996)

Abstract—The reaction of the tridentate rigid ligand PNP (2,6-bis(diphenylphosphinomethyl)pyridine) with $RuCl_2(PPh_3)_3$ led to the formation of two new ruthenium(II) complexes, $RuCl_2(PNP)(PPh_3)$ (**1**) and $[RuCl(MeCN)(PNP)(PPh_3)]Cl$ (**2**), which were analytically and spectroscopically characterized. The X-ray diffraction study of **1** shows that the PNP ligand coordinates Ru in a meridional mode, and reveals some steric congestion within the complex. Copyright © 1996 Elsevier Science Ltd

Keywords: ruthenium(II) complexes; tridentate ligands; X-ray analysis.

Homogeneous catalysis by transition metal complexes provides mild and selective routes to various chemicals of industrial importance [1] and the search for new efficient catalysts remains an important objective.

Ruthenium complexes have received considerable interest as catalysts for the hydrogenation of various substrates, particularly in the enantioselective reduction of ketones and alkenes [2]. We have been interested in the use of tridentate ligands for such catalytic reactions and have reported recently the synthesis of a family of C_2-symmetric chiral tridentate diphosphine ligands [3]. The coordination chemistry of the simplest achiral member of this family, 2,6-(diphenylphosphinomethyl)pyridine (hereafter designated PNP), has been well studied, but with few applications of the obtained complexes in catalysis [4–7]. As a result of the rigid backbone and fused five membered ring chelation about the metal centre, this PNP ligand should in preference form meridional rather than facial complexes. This is noteworthy because when the chiral C_2-symmetric ligand analogues are used, the C_2 axis can be preserved in the *mer* but not in the *fac* arrangement. This will be important in enantioselective reactions, as the number of diastereoisomeric forms of catalytic intermediates will thus be limited and permit greater stereocontrol of the reaction [8].



PNP

We report here the synthesis and characterization of two new ruthenium(II) complexes bearing the PNP ligand, including a structure analysis by X-ray diffraction methods.

EXPERIMENTAL

General

All experiments were carried out under a nitrogen or argon atmosphere, using a vacuum line or Vacuum Atmospheres glovebox equipped with Dri-Train HE-493 inert gas purifier. Conductivity measurements were performed with a WTW LF535 apparatus. ^1H (300 MHz) and $^{31}P\{^1H\}$ (121.5 MHz, broadband

* Author to whom correspondence should be addressed.

decoupled) NMR spectra were recorded in $CDCl_3$ on a Bruker AC300 instrument and referenced to Me_4Si and 85% aqueous H_3PO_4, respectively. FT-IR spectra were recorded on a Perkin-Elmer 1600 Series spectrometer on KBr pellets. FAB MS spectra and elemental analyses were carried out by the corresponding facilities at the Centre de Recherche de Chimie, Université Louis Pasteur, Strasbourg. Methylene chloride and acetonitrile were distilled under nitrogen over calcium hydride, and pentane over sodium. PNP [4] and $RuCl_2(PPh_3)_3$ [9] were prepared following literature methods.

Preparation of $RuCl_2(PNP)(PPh_3)$ (**1**)

A solution of PNP (100 mg, 0.210 mmol) and $RuCl_2(PPh_3)_3$ (210 mg, 0.219 mmol) in 20 cm^3 CH_2Cl_2 was refluxed for 15 min. The orange solution obtained was left at 0°C for 24 h, and **1** precipitated as orange crystals that were collected by filtration, washed with pentane and dried *in vacuo*. Yield: 94%. FAB MS *m/z* (assignment, relative intensity): 909.0 (M^+, 66%), 874.0 ([M—Cl]$^+$, 45%), 838.1 [M—2Cl—H]$^+$, 28%), 647.0 ([M—PPh_3]$^+$, 100%), 612.0 ([M—Cl—PPh_3]$^+$, 59%), 576.0 ([M—2Cl—H—PPh_3]$^+$, 72%). ^1H NMR δ (ppm): 7.57–7.00 and 6.90–6.83 (m, 38 H, $H_{arom.}$), 4.54 (t, 4H, CH_2).

Preparation of [RuCl(MeCN)(PNP)PPh_3)]Cl (**2**)

A solution of PNP (100 mg, 0.210 mmol) and $RuCl_2(PPh_3)_3$ (210 mg, 0.219 mmol) in 20 cm^3 CH_3CN was refluxed for 30 min. The dark yellow solution obtained was left at 0°C for 24 h, and a small crop of crystals of **1** precipitated. After filtration, the filtrate was concentrated and left again for 24 h at 0°C. Fine yellow crystals were collected by filtration, washed with pentane and dried *in vacuo*. Yield: 85%. Found: C, 64.2; H, 4.6; N, 2.8. Calc. for $C_{51}H_{45}N_2P_3Cl_2Ru$: C, 64.4; H, 4.8; N, 2.9%. FAB MS *m/z* (assignment, relative intensity): 915.1 [M—Cl]$^+$, 19%), 874.1 ([M—Cl—CH_3CN]$^+$, 100%), 838.1 ([M—H—2Cl—CH_3CN]$^+$, 46%), 612.0 ([M—Cl—CH_3CN—PPh_3]$^+$, 73%), 576.0 ([M—H—2Cl—CH_3CN—PPh_3]$^+$, 87%). ^1H NMR δ (ppm): 7.75–7.09 and 6.90–6.84 (m, 38 H, $H_{arom.}$), 4.86 and 4.53 (2dt, 2 × 2H, CH_2), 1.73 (s, 3H, CH_3CN).

RESULTS AND DISCUSSION

The reaction of PNP with a slight excess of $RuCl_2(PPh_3)_3$ in refluxing methylene chloride leads to the neutral complex $RuCl_2(PNP)(PPh_3)$ (**1**) as an orange, air-stable, diamagnetic crystalline solid in excellent yield. Two IR bands (KBr pellet) are observed at 1599 and 1565 cm^{-1} which are characteristic of a coordinated pyridine [4]. In addition, a weak band at 328 cm^{-1} is indicative of two mutually *trans* chlorides, according to the interpretation given by Bianchini and coworkers for an analogous ruthenium complex [10]. The $^{31}P\{^1H\}$ NMR spectrum of **1** in $CDCl_3$ exhibits a doublet at 35.3 ppm and a triplet at 41.8 ppm ($^2J_{PP}$ = 28.6 Hz), these chemical shifts falling in the range expected for coordinated PNP and PPh_3 ligands [7,11]. The two PNP phosphorus atoms are thus chemically equivalent and coupled to the phosphorus of a triphenylphosphine located in a *cis* position, as indicated by the magnitude of the coupling constant.

The ^1H NMR spectrum shows a triplet at 4.54 ppm attributed to the methylene protons (Fig. 1(a)). This is typical of an $A_2A'_2XX'$ system where each proton is virtually coupled to the two equivalent phosphorus nuclei ($|{}^2J_{HP}+{}^4J_{HP'}| = 9.7$ Hz). Such a situation has been frequently described in the literature concerning other PNP coordination compounds [6, 7] and is characteristic of a meridional coordination, where the two protons of each CH_2 moiety are chemically equivalent. Therefore the molecule possesses a plane of symmetry that comprises the three donor atoms of PNP, so that PPh_3 necessarily lies *trans* to the pyridine nitrogen.

The X-ray diffraction study of **1** · CH_3CN confirms this interpretation (Fig. 2) [12]. Selected bond distances and angles are given in Table 1. **1** appears as a monomeric complex with a somewhat distorted octahedral geometry around the ruthenium. Importantly, it is confirmed that the PNP ligand coordinates the metallic center in a tridentate meridional mode, with the triphenylphosphine ligand *trans* to pyridine. It is probable that the alternative *cis* configuration would be unstable because of an increased steric hindrance between the phenyl groups on the three phosphorus atoms.

All Ru—P (2.340–2.368 Å), Ru—Cl (2.412, 2.426 Å) and Ru—N (2.168(2) Å) distances lie within the normal range [13]; in particular, the ruthenium–phosphorus and ruthenium–chloride bond lengths compare well with the corresponding bond lengths observed by Bianchini *et al.* in the closely related complex *mer*-$RuCl_2[nPrN(CH_2CH_2PPh_2)_2](PPh_3)$ [14]. The values of the P(1)—Ru—N and P(2)—Ru—N bond angles (78.60, 79.31°) are also very close to Bianchini's data (79.45, 80.69°), or to the value of 80.3(1)° found by DuBois *et al.* [7] for the N—Pd—P angle in the cationic complex $[Pd(PNP)(PEt_3)]^{2+}$. The ruthenium atom lies approximately in the plane defined by the nitrogen and the three phosphorus atoms, with a deviation of only 0.018 Å. The four ligands *cis* to PPh_3 are all bent away from PPh_3, as illustrated by the reduced Cl(1)—Ru—Cl(2) angle (171.81(3)°) and the even smaller P(1)—Ru—P(2) angle (157.90(3)°). A large Cl(2)—Ru—P(2) angle of 95.49(3)° is observed, while the Cl(1)—Ru—P(2) angle is normal (88.17(3)°). The reason for this is probably that Cl(2) is sterically hindered by C(49) and therefore bent away from P(2). These considerations of the bond distances and angles in $RuCl_2(PNP)(PPh_3)$ show that the molecule is sterically congested, as seven phenyl groups and two chlorides are forced together in close proximity. In comparison, the $RuCl_2[nPrN(CH_2CH_2PPh_2)_2](PPh_3)$ and $[Pd(PNP)(PEt_3)]^{2+}$ complexes suffer less steric

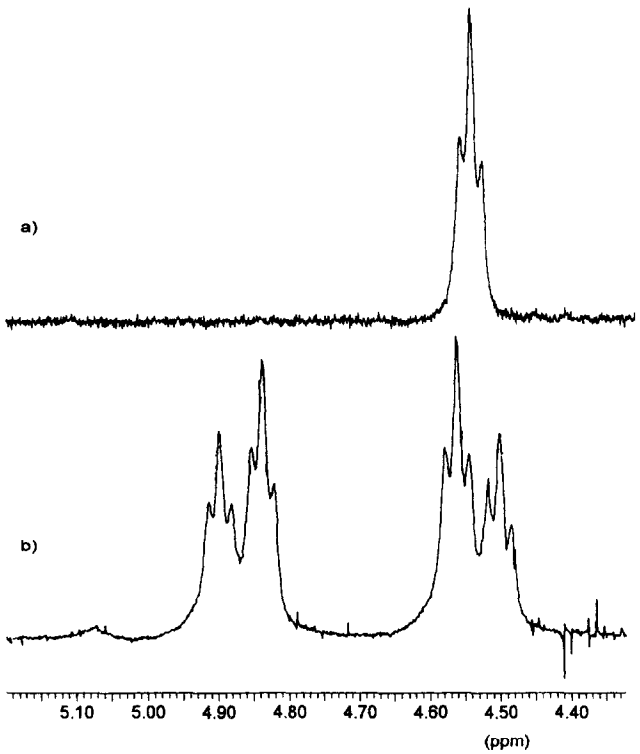


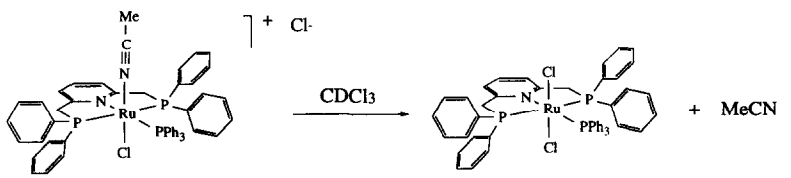
Fig. 1. ^{1}H NMR signals of the PNP methylene protons in $CDCl_3$; (a) complex **1**; (b) complex **2**.

hindrance, probably because in the first case nPrN($CH_2CH_2PPh_2$)$_2$ is more flexible than PNP, and in the second PEt_3 is less bulky than PPh_3 and further, the complex bears no axial ligand.

When the reaction of PNP on $RuCl_2(PPh_3)_3$ is performed in acetonitrile instead of methylene chloride and at higher temperature (MeCN reflux), yellow crystals of **2** are obtained in good yield, **1** now being present as a by-product. Like **1**, **2** is diamagnetic and stable in the air. Its elemental analysis is consistent with the formula $RuCl_2(MeCN)(PNP)(PPh_3)$. The value of the molar conductivity of **2** in acetonitrile is 106 Ω^{-1} cm^2 mol^{-1} at a 2×10^{-3} M concentration, which falls within the expected range (92–199 Ω^{-1} cm^2 mol^{-1}) for a 1:1 electrolyte in this solvent [15]. The FAB-MS spectrum of **2** (NBA matrix) exhibits a signal at m/z 915.1; this value and the isotope profile structure fit a molecular peak [M—Cl]$^+$ formulated as $RuCl(MeCN)(PNP)(PPh_3)^+$. The IR spectrum of **2** shows two bands at 2276 and 2351 cm^{-1} characteristic of an end-on coordination of the acetonitrile ligand [7, 16]. Further, the bands in the 1500 1600 cm^{-1} region are very similar to those displayed in the spectrum of **1** (1598 and 1562 cm^{-1}), indicative of a coordination of Ru^{II} by the central pyridine moiety.

The $^{31}P\{^1H\}$ NMR spectrum of **2** resembles very much that of **1** (doublet at 31.3 ppm and triplet at 42.0 ppm; $^2J_{PP}$ = 26.5 Hz). However the PNP methylene signals now appear in the ^{1}H NMR spectrum as a set of two doublets of triplets centered at 4.53 ppm and 4.86 ppm, corresponding to an AA′BB′XX′ system [6a] (Fig. 1(b)). The two methylene protons borne by each carbon are no longer equivalent, and a *gem* coupling constant of 16.9 Hz is observed. Each of them is virtually coupled to the phosporus atoms, with slightly different coupling constants ($|^2J_{HP}+{}^4J_{HP'}| = 8.9$ and 9.4 Hz). The plane of symmetry observed for **1** (*vide supra*) is lost, indicating the presence of two different axial ligands.

When **2** is allowed to stand in $CDCl_3$ for 24 h, the solution turns from yellow to orange and orange crystals form. ^{31}P and ^{1}H NMR analyses indicate that the totality of **2** has been converted into **1**:



2
(hypothetical structure)

1

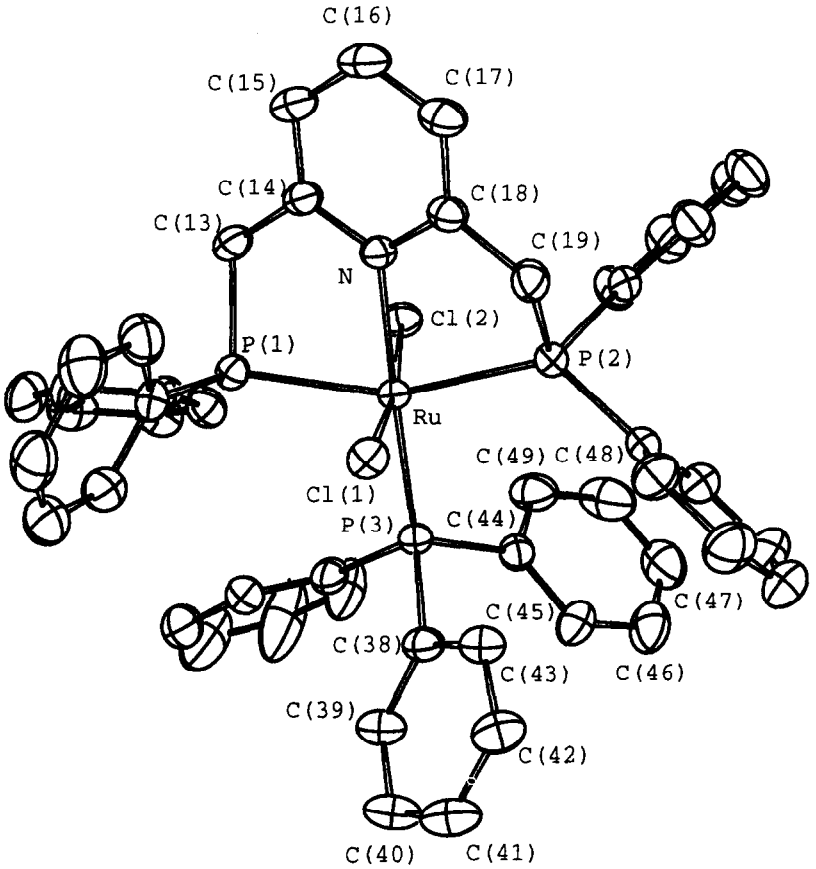


Fig. 2. ORTEP drawing of $RuCl_2(PNP)(PPh_3) \cdot CH_3CN$ showing 30% probability thermal ellipsoids and the atom-numbering scheme. MeCN and hydrogen atoms are omitted for clarity.

Table 1. Selected bond distances (Å) and bond angles (°) for $\mathbf{1} \cdot CH_3CN$

Ru—Cl(1)	2.4122(7)	Ru—N	2.168(2)
Ru—Cl(2)	2.4263(7)	P(1)—C(13)	1.842(3)
Ru—P(1)	2.3682(7)	C(14)—N	1.360(3)
Ru—P(2)	2.3641(7)	N—C(18)	1.355(3)
Ru—P(3)	2.3401(7)	C(19)—P(2)	1.835(3)
Cl(1)—Ru—Cl(2)	171.81(3)	N—Ru—P(2)	78.60(6)
Cl(1)—Ru—P(1)	89.65(3)	N—Ru—P(3)	177.62(6)
Cl(1)—Ru—N	86.24(6)	P(2)—Ru—P(3)	99.17(2)
Cl(1)—Ru—P(2)	88.17(3)	Ru—P(1)—C(13)	98.21(8)
Cl(1)—Ru—P(3)	92.88(2)	Ru—N—C(18)	120.4(2)
Cl(2)—Ru—P(1)	84.20(3)	Ru—P(2)—C(19)	97.32(8)
Cl(2)—Ru—N	87.31(6)	Ru—P(3)—C(38)	118.98(9)
Cl(2)—Ru—P(2)	95.49(3)	P(1)—C(13)—C(14)	112.0(2)
Cl(2)—Ru—P(3)	93.76(3)	C(18)—C(19)—P(2)	108.4(2)
P(1)—Ru—N	79.31(6)	C(13)—C(14)—N	117.0(2)
P(1)—Ru—P(2)	157.90(3)	N—C(18)—C(19)	116.7(2)
P(1)—Ru—P(3)	102.90(2)	C(14)—N—C(18)	118.4(2)

A straightforward interpretation of this observation is that the chloride anion and the acetonitrile compete as a ligand for ruthenium, the competition being in favour of MeCN when it is used as the solvent, and in favour of Cl^- in a solvent of low polarity such as chloroform.

CONCLUSION

We have prepared and characterized two new ruthenium(II) complexes with the PNP ligand where it is found to be bound in a meridional way to the metal. An X-ray crystallographic study has shown

that the presence of triphenylphosphine as an ancillary ligand induces important steric constraints in these complexes. Experiments are under way in our laboratory to study the catalytic properties of these and similar complexes and in particular those of the chiral analogues of the PNP for asymmetric catalysis. It will be of interest to compare our findings with the closely related results reported by Zhang *et al.* in a publication that appeared during the preparation of this manuscript [17].

Acknowledgements—We are indebted to Rafaël Sablong, Claire Newton and Marie-Thérèse Youinou for helpful discussions, David J. Taylor for technical assistance, and Nathalie Kyritsakas for X-ray analysis. We thank the Erasmus program for the support of S.Y.K. We also thank the CNRS for financial support.

REFERENCES

1. J. M. Brown, *Chem. Soc. Rev.* 1993, **22,** 25.
2. (a) M. A. Bennett and T. W. Matheson, in *Comprehensive Organometallic Chemistry* (Edited by G. Wilkinson, F. G. A. Stone, E. W. Abel), vol. 4, 931 Pergamon Press, Oxford (1986); (b) A. Spencer, in *Comprehensive Coordination Chemistry* (Edited by G. Wilkinson, R. D. Gillard and J. A. McCleverty), vol. 6, p. 229, Pergamon Press, Oxford (1987); (c) R. Noyori, *Asymmetric Catalysis In Organic Synthesis*, J. Wiley & Sons, New York (1994); (d) D. Rose, J. D. Gillett, R. P. Richardson and G. Wilkinson, *J. Chem. Soc.* (*A*) 1969, 2610.
3. (a) R. Sablong, C. Newton, P. Dierkes and J. A. Osborn, *Tetrahedron Lett.* 1996, **37,** 4933; (b) R. Sablong and J. A. Osborn, *Tetrahedron Lett.* 1996, **37,** 4937.
4. W. V. Dahlhoff and S. M. Nelson, *J. Chem. Soc.* (*A*) 1971, 2184.
5. (a) P. Giannoccaro, G. Vasapollo and A. Sacco, *J. Chem. Soc., Chem. Commun.* 1980, 1136; (b) G. Vasapollo, P. Giannoccaro, C. F. Nobile and A. Sacco, *Inorg. Chim. Acta* 1981, **48,** 125; (c) P. Giannoccaro, G. Vasapollo, C. F. Nobile and A. Sacco, *Inorg. Chim. Acta* 1982, **61,** 69; (d) A. Sacco, P. Giannoccaro and G. Vasapollo, *Inorg. Chim. Acta* 1984, **83,** 125.
6. (a) G. Vasapollo, C. F. Nobile and A. Sacco, *J. Organomet. Chem.* 1985, **296,** 435; (b) A. Sacco, G. Vasapollo, C. F. Nobile, A. Piergiovanni, M. A. Pellinghelli and M. Lanfranchi, *J. Organomet. Chem.* 1988, **356,** 397.
7. B. D. Steffey, A. Miedaner, M. L. Maciejewski-Farmer, P. R. Bernatis, A. M. Herring, V. S. Allured, V. Carperos and D. L. DuBois, *Organometallics* 1994, **13,** 4844.
8. (a) C. Newton, Doctorate Thesis, Université Louis Pasteur, Strasbourg, France (1995); (b) J. K. Whitesell, *Chem. Rev.* 1989, **89,** 1581.
9. P. S. Hallman, T. A. Stephenson and G. Wilkinson, *Inorg. Synth.* 1970, **12,** 238.
10. C. Bianchini, P. Innocenti, D. Masi, M. Peruzzini and F. Zanobini, *Gazz. Chim. Ital.* 1992, **122,** 461.
11. J. F. Nixon and A. Pidcock, *Annual Review of NMR Spectroscopy* (Edited by E. F. Mooney), vol. 2, 345. Academic Press, London (1969).
12. Crystal data for $\mathbf{1}\cdot CH_3CN$: $C_{51}H_{45}N_2P_3Cl_2Ru$, $M = 950.8$, triclinic, space group $P\text{-}1$, $a = 10.663$ (3), $b = 13.710$ (4), $c = 17.300$ (5) Å, $\alpha = 68.26$ (2), $\beta = 87.05$ (2), $\gamma = 71.70$ (2)°, $V = 2224.4$ Å^3, $Z = 2$, $r_{calcd} = 1.420$ g cm^{-3}. A total of $10225 + h \pm k \pm l$ reflections was collected on an orange crystal of dimensions $0.40 \times 0.38 \times 0.20$ mm^3, using a Nonius CAD4-F diffractometer, graphite monochromated Mo-K_α ($\lambda = 0.7107$ Å), $\mu = 6.091$ cm^{-1}, $2 < \theta < 26$°, room temperature. 7188 unique reflections having $I > 3\sigma(I)$ were used to determine (heavy atom method) and refine the structure (refinements against $|F|$). Hydrogen atoms were introduced as fixed contributors, C—H = 0.95 Å, B(H) = 1.3*Beqv(C) Å^2. 532 parameters. Final results: $R(F) = 0.030$, $Rw(F) = 0.044$, GOF = 1.084, maximum residual electronic density = 0.14 eÅ^{-3}. For all computations the Enraf-Nonius MolEN (C.K. Fair in *MolEN: An Interactive Intelligent System for Crystal Structure Analysis*. Nonius, Delft, The Netherlands (1990)) package was used running on a DEC Alpha3600S computer. Further details of the crystal structure investigation are available on request from the Director of Cambridge Crystallographic Data Center, 12 Union Road, GB-Cambridge CB2 1EZ (U.K.), on quoting the full journal citation. Complete listings of crystal data, atomic coordinates, thermal parameters, bond distances and angles have been deposited with the Cambridge Crystallographic Data Center.
13. A. G. Orpen, L. Brammer, F. H. Allen, O. Kennard, D. G. Watson and R. Taylor, *J. Chem. Soc., Dalton Trans.* 1989, S1.
14. C. Bianchini, D. Masi, M. Peruzzini, A. Romerosa and F. Zanobini, *Acta Cryst.* 1995, **C15,** 2514.
15. W. J. Geary, *Coord. Chem. Rev.* 1971, **7,** 81.
16. (a) K. Nakamoto, *Infrared and Raman Spectra of Inorganic and Coordination Compounds*, 4th edn, p. 280. J. Wiley & Sons, New York (1986); (b) B. N. Storhoff and H. C. Lewis, *Coord. Chem. Rev.* 1977, **23,** 1.
17. Q. Jiang, D. Van Plew, S. Murtuza and X. Zhang, *Tetrahedron Lett.* 1996, **37,** 797.

Pergamon

S0277-5387(96)00258-6

Polyhedron Vol. 16, No. 2, pp. 297–305, 1997
Copyright © 1996 Elsevier Science Ltd
Printed in Great Britain. All rights reserved
0277-5387/97 $15.00 + 0.00

The coordination chemistry of (2-thiazolin-2-yl)hydrazine hydrochloride (TzHyHCl)—II. Study of its interaction with zinc(II) and cadmium(II)

A. Bernalte-García,[a]* M. A. Díaz-Díez,[a] F. J. García-Barros,[a] F. J. Higes-Rolando,[a] A. M. Pizarro-Galán,[a] J. D. Martín-Ramos[b] and C. Valenzuela-Calahorro[c]

[a]Departamento de Química Inorgánica, Facultad de Ciencias, Universidad de Extremadura, 06071 Badajoz, Spain

[b]Departamento de Mineralogía y Petrología, Facultad de Ciencias, Universidad de Granada, 18071 Granada, Spain

[c]Departamento de Química Inorgánica, Facultad de Farmacia, Universidad de Granada, 18071 Granada, Spain

(Received 1 April 1996; accepted 17 May 1996)

Abstract—The complexation equilibria of (2-thiazolin-2-yl)hydrazine hydrochloride (TzHyHCl) with zinc(II) and cadmium(II) have been studied in aqueous solution at 298 K and 0.1 M ionic strength in $NaClO_4$. The formation constants were determined and are discussed in terms of the characteristics of the ligand. The compounds $[ZnCl(TzHy)_2]Cl$ and $[Cd(TzHy)(\mu\text{-}Cl)_2]_n \cdot nH_2O$ have been isolated and their crystal structures determined. In the Zn^{II} compound, the geometry around the central atom is a distorted trigonal-bipyramid composed of four nitrogen atoms from two TzHy ligands and one chlorine. The Cd^{II} complex is polymeric, with octahedrally coordinated cadmium linked into infinite chains by double (μ-chloro) bridges. The coordination sphere around each cadmium center is completed by two nitrogen atoms from a TzHy ligand. In both cases, the crystal structure is stabilized by an extensive hydrogen-bond network. Copyright © 1996 Elsevier Science Ltd

Keywords: zinc(II) complex; cadmium(II) complex; thiazoline; hydrazine.

In a previous paper [1], we have described the crystal structure of (2-thiazolin-2-yl)hydrazine hydrochloride (TzHyHCl) together with its coordination behaviour and equilibria study with nickel(II) in aqueous solution as well as the isolation and crystal structure of the compound diaquabis[(2-thiazolin-2-yl)hydrazine]nickell(II) chloride dihydrate. In this paper we report our investigations of the coordination behaviour of TzHyHCl with Zn^{II} and Cd^{II} in aqueous solution. Likewise, the solid phase obtained by the reaction between the ligand and the aforementioned divalent cations have been characterized by elemental analysis, and X-ray diffraction.

EXPERIMENTAL

Reagents

The ligand (2-thiazolin-2-yl)hydrazine hydrochloride (TzHyHCl) was prepared according to a reported procedure [2], taking into account published modifications [3] and recrystallized from ethanol.

Zinc(II), and cadmium(II) stock solutions were prepared and standardized as usual [4]. The ionic strength of the solutions was adjusted to a perchlorate con-

* Author to whom correspondence should be addressed.

centration of 0.1 M by addition of sodium perchlorate. Sodium hydroxide stock solutions were prepared by dilution of a concentrated solution of sodium hydroxide, according to Kolthoff *et al.* [5]. These solutions were kept under CO_2-free atmosphere and standardized by titration against potassium hydrogen phthalate. All other chemicals were AR grade and used without further purification.

Preparation of the complexes

The crystals of Zn^{II} and Cd^{II} complexes were prepared, in the same manner as analogous nickel ones, by evaporation of relevant water solutions, as described elsewhere [1]. Found: C, 19.7; H, 3.7; N, 22.7; S, 17.2; Zn, 17.4. Calc. for $C_6H_{14}Cl_2N_6S_2Zn$: C, 19.4; H, 3.8; N, 22.7; S, 17.3; Zn, 17.6%. Found: C, 11.5; H, 2.7; N, 13.1; S, 9.0; Cd, 34.2. Calc. for $C_3H_9Cl_2N_3OSCd$: C, 11.3; H, 2.8; N, 13.2; S, 10.0; Cd, 35.3%.

Instrumental procedures

Chemical analyses of carbon, hydrogen, nitrogen and sulfur were performed by means of microanalytical methods using a Perkin–Elmer 240C microanalyser. In both complexes, the metal content was estimated by thermogravimetry as oxide for the Zn^{II} and as sulfide in the case of Cd^{II}. IR spectra were recorded on a Perkin–Elmer FT-IR 1720 spectrophotometer, using KBr as dispersing agent. TG studies were carried out on a Mettler TA-4000 instrument. The procedures and apparatus used for potentiometric measurements were described in detail previously [1]. Briefly, measurements were made at 25 ± 0.1°C and 0.1 M ($NaClO_4$) ionic strength. The electrode system was calibrated in terms of hydrogen ion concentration by performing strong acid versus strong base titrations [6]. Concentration of ligand in the experimental solutions was always 2×10^{-3} mol dm^{-3}, and successive 1:1, 2:1 and 3:1 ligand-to-metal ratios were investigated. The numerical analysis of all the experimental e.m.f. data were carried out with the computer program SUPERQUAD [7]. All calculations were performed on an IBM RS/6000 computer (Computer Center, University of Extremadura). X-ray powder diffraction was obtained through a Philips PW-1700 diffractometer using Cu-K_α radiation.

Crystal structure determinations

Crystal data, data collection and refinement details for $[ZnCl(TzHy)_2]Cl$ and $[Cd(TzHy)(\mu\text{-}Cl)_2]_n \cdot nH_2O$ are given in Table 1. Examination of three standard reflections, monitored after 97 scans, showed no sign of crystal deterioration. The data were corrected for Lorentz and polarization effects, and were also corrected for absorption effects using an empirical method based on azimuthal scan data. The structures were solved by direct methods and subsequent Fourier differences using the SHELXTL-IRIS program [8] and refined by full-matrix least-squares. The H-atoms were located from a differential Fourier synthesis, and included in the calculation with estimated isotropic displacement parameters without refinement (riding model). All calculations were performed with a Silicon Graphics Iris Indigo XS24.

Thermal parameters and atom coordinates have been deposited with the Cambridge Crystallographic Data Centre.

RESULTS AND DISCUSSION

The analytical results agree with the molecular formulae $C_6H_{14}Cl_2N_6S_2Zn$ and $C_3H_9Cl_2N_3OSCd$ for the colourless Zn^{II} and Cd^{II} complexes, respectively.

Potentiometric studies

The final stoichiometries and formation constants of the complexes formed were determined by means of the computer program SUPERQUAD [7] to identify that which, according to χ^2, best fitted the experimental data. The chemical models yielding the best fits between the measured and calculated titration curves, together with the refined formation constants, and statistical parameters (SIGMA and χ^2), are compiled in Table 2. Metal hydrolysis reactions of the sort described by Baes and Mesmer [9] were incorporated into every chemical model tried. It was verified that all the proposed species (denoted as $M_p(TzHy)_qH_r$) existed in significant concentrations over a reasonable data range.

It can be seen that for the $TzHyHCl/Zn^{II}$ system while in the titration curve with a relation ligand: metal of 1:1, the apparently simple model of 111 satisfied the experimental data; in the titration curve 2:1 the combination of complexes 111 and 122 gave the best agreement. With respect to the relation ligand: metal of 3:1, the model chosen, formed by 122 and 133, resulted in a satisfactory numerical and graphical fitting. With respect to the $TzHyHCl/Cd^{II}$ system, it can also be seen from the aforementioned Table 2 that all titration curves contain the complex 133. In addition to this species the existing experimental evidence was sufficient to determine with accuracy that the 111 complex is present in the titrations with relative ligand: metal of 1:1 and 2:1. The experimental results show that in all $M_p(TzHy)_qH_r$ complexes detected q has the same value as that of r, which may be taken as evidence that in the $TzHyHCl/Zn^{II}$

Table 1. Crystal data, data collection and refinement details for $[ZnCl(TzHy)_2]Cl$ and $[Cd(TzHy)(\mu\text{-}Cl)_2]_n \cdot nH_2O$

	$[ZnCl(TzHy)_2]Cl$	$[Cd(TzHy)(\mu\text{-}Cl)_2]_n \cdot nH_2O$
Crystal shape	Pyramidal	Prismatic
Size (mm)	$0.40 \times 0.22 \times 0.20$	$0.50 \times 0.45 \times 0.35$
Chemical formula	$C_6H_{14}Cl_2N_6S_2Zn$	$C_3H_9Cl_2N_3OSCd$
Formula weight	370.6	318.5
Crystal system	Orthorhombic	Monoclinic
Space group	$Pna2_1$	$P2_1/c$
a (Å)	9.242(1)	13.244(2)
b (Å)	10.180(1)	10.349(1)
c (Å)	14.636(2)	7.086(1)
β (°)		102.84(1)
Cell volume (Å^3)	1377.0(4)	946.9(4)
Z	4	4
D_x (g cm^{-3})	1.788	2.234
μ (cm^{-1})	24.62	30.41
F (000)	752	616
Diffractometer	Siemens P4	Siemens P4
Radiation	Mo-K_α ($\lambda = 0.71073$ Å)	Mo-K_α ($\lambda = 0.71073$ Å)
Collection method	2θ-θ	2θ-θ
2θ range	2.0–55.0	2.0–60.0
Index ranges	$-1 \leqslant h \leqslant 12$; $-1 \leqslant k \leqslant 13$ $-1 \leqslant l \leqslant 18$	$-18 \leqslant h \leqslant 18$; $-14 \leqslant k \leqslant 1$ $1 \leqslant l \leqslant 9$
Independent reflections	1747	2732
Observed reflections	1623 [$F > 2\sigma(F)$]	2516 [$F > 2\sigma(F)$]
No. of refined parameters	153	100
R	0.038	0.027
R_w	0.048	0.036
w	$1/[\sigma^2(F) + 0.0006\ F^2]$	$1/[\sigma^2(F) + 0.0005\ F^2]$
GOF	1.26	1.09
ρ_{max}, ρ_{min} (e Å^{-3})	0.50, −0.43	0.57, −0.55

Table 2. Formation constants (log β) at 25 °C and $I = 0.1$ mol dm^{-3}

System	Species	log β	χ^2	Σ
$TzHyH^+/Zn^{2+}$ (1/1)	$[Zn(TzHyH)]^{3+}$	9.80(1)	10.00	2.9
$TzHyH^+/Zn^{2+}$ (2/1)	$[Zn(TzHyH)]^{3+}$	9.85(1)	9.33	1.7
	$[Zn(TzHyH)_2]^{4+}$	20.69(2)		
$TzHyH^+/Zn^{2+}$ (3/1)	$[Zn(TzHyH)_2]^{4+}$	20.65(1)	8.67	1.4
	$[Zn(TzHyH)_3]^{5+}$	28.78(2)		
$TzHyH^+/Cd^{2+}$ (1/1)	$[Cd(TzHyH)]^{3+}$	10.51(1)	3.53	3.1
	$[Cd(TzHyH)_3]^{5+}$	30.32(8)		
$TzHyH^+/Cd^{2+}$ (2/1)	$[Cd(TzHyH)]^{3+}$	10.90(3)	10.57	0.9
	$[Cd(TzHyH)_3]^{5+}$	31.35(1)		
$TzHyH^+/Cd^{2+}$ (3/1)	$[Cd(TzHyH)_3]^{5+}$	31.84(1)	11.20	1.6

and $TzHyHCl/Cd^{II}$ systems only the species $(TzHyH)^+$ acts as ligand.

Description of the structures

The structure of $[ZnCl(TzHy)_2]Cl$ consists of $[ZnCl(TzHy)_2]^+$ cations and chloride anions. Figure 1 shows the molecular structure of the cation complex and the atom numbering system used. Selected bond lengths, angles and the hydrogen contacts are listed in Table 3. Within the cation, the geometry around the zinc atom may be described as a distorted trigonal-bipyramid, according to the value of 0.84 found for the index of trigonality $\tau[\tau = (\beta - \alpha)/60$, where α and β are the N(6)—Zn—N(3) and N(4)—Zn—N(1) bond angles, respectively] [10]. The coordination polyhedron comprises one chlorine atom [Cl(1)] and two thiazolinic nitrogens [N(1), N(4)] in the equatorial positions, and two terminal hydrazinic nitrogens [N(3), N(6)] in axial positions. The zinc atom lies 0.034 Å out of the plane of the N(1), N(4) and Cl(1) atoms toward the N(3) atom. The whole molecule

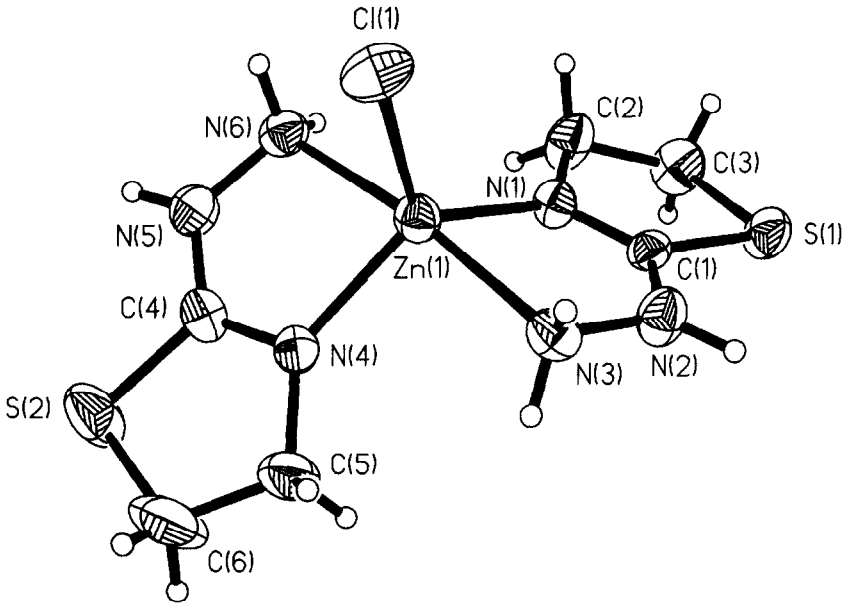


Fig. 1. Molecular structure of the $[ZnCl(TzHy)_2]^+$ cation, showing the atom-numbering scheme. The thermal ellipsoids are drawn at a 50% level.

Table 3. Selected bond lengths (Å), angles (°) and hydrogen bonds for $[ZnCl(TzHy)_2]Cl$

Zn—Cl(1)	2.271(2)	Zn—N(4)	2.046(6)
Zn—N(1)	2.010(5)	Zn—N(6)	2.312(6)
Zn—N(3)	2.231(5)	S(1)—C(1)	1.745(6)
S(1)—C(3)	1.824(8)	S(2)—C(4)	1.736(7)
S(2)—C(6)	1.772(11)	N(4)—C(4)	1.296(8)
N(4)—C(5)	1.457(9)	N(1)—C(2)	1.458(8)
N(1)—C(1)	1.291(8)	N(6)—N(5)	1.407(8)
N(3)—N(2)	1.423(7)	N(5)—C(4)	1.337(8)
C(2)—C(3)	1.523(9)	N(2)—C(1)	1.331(7)
C(5)—C(6)	1.472(15)		
Cl(1)—Zn—N(4)	117.6(2)	Cl(1)—Zn—N(1)	121.0(1)
N(4)—Zn—N(1)	121.3(2)	Cl(1)—Zn—N(6)	90.9(1)
N(4)—Zn—N(6)	76.2(2)	N(1)—Zn—N(6)	99.8(2)
Cl(1)—Zn—N(3)	97.0(1)	N(4)—Zn—N(3)	97.1(2)
N(1)—Zn—N(3)	79.1(2)	N(6)—Zn—N(3)	171.4(2)
C(1)—S(1)—C(3)	89.6(3)	C(4)—S(2)—C(6)	89.6(4)
Zn—N(4)—C(4)	116.1(4)	Zn—N(4)—C(5)	131.8(5)
C(4)—N(4)—C(5)	111.6(6)	Zn—N(1)—C(2)	132.4(4)
Zn—N(1)—C(1)	114.3(4)	C(2)—N(1)—C(1)	112.6(5)
Zn—N(6)—N(5)	106.1(3)	Zn—N(3)—N(2)	105.3(3)
N(6)—N(5)—C(4)	117.5(5)	N(1)—C(2)—C(3)	110.5(5)
N(3)—N(2)—C(1)	117.4(5)	S(1)—C(1)—N(1)	118.4(4)
S(1)—C(1)—N(2)	118.1(4)	N(1)—C(1)—N(2)	123.5(5)
S(2)—C(4)—N(4)	117.7(5)	S(2)—C(4)—N(5)	119.3(5)
N(4)—C(4)—N(5)	123.0(6)	S(1)—C(3)—C(2)	106.6(5)
N(4)—C(5)—C(6)	110.7(7)	S(2)—C(6)—C(5)	109.0(6)

Bond A...H—D	Position of D	A...D (Å)	A...H—D (°)
Cl(2)...H(14)—N(6)	$1/2-x, 1/2+y, 1/2+z$	3.249(5)	162.9(1)
Cl(2)...H(6)—N(3)	$x, y, 1+z$	3.242(6)	163.4(1)
Cl(2)...H(13)—N(6)	$-x, -y, 1/2+z$	3.302(5)	129.2(1)
Cl(2)...H(5)—N(2)	$-1/2+x, 1/2-y, 1+z$	3.234(6)	178.0(1)
Cl(1)...H(7)—N(3)	$-1/2+x, 1/2-y, z$	3.492(5)	139.2(1)
Cl(1)...H(12)—N(5)	$-x, -y, -1/2+z$	3.581(6)	159.0(1)

exhibits pseudo-C_2 symmetry with the C_2 axis passing through the Zn—Cl(1) bond.

The Zn—Cl(1) distance of 2.271(2) Å is comparable to the value observed for other five-coordinate zinc(II) complexes [11]. The Zn—N(axial) distances [2.231(5) Å and 2.312(6) Å] are appreciably longer than the Zn—N(equatorial) distances [2.010(5) Å and 2.046(6) Å]. Several molecular orbital treatments of trigonal-bipyramidal coordination have predicted contradictory results about the relative strength of axial *vs* equatorial bonds for $(n-1)d^{10}$ systems. In this sense, Herlinger *et al.* [12] have pointed out that the crystal packaging effects could play an important role in the nonequivalency of the bond lengths. According to the above, and neglecting the electronic factors due to the central atom, our data can be explained by the result of two contributions: one is the different hybridation of the nitrogen atoms in the hydrazine

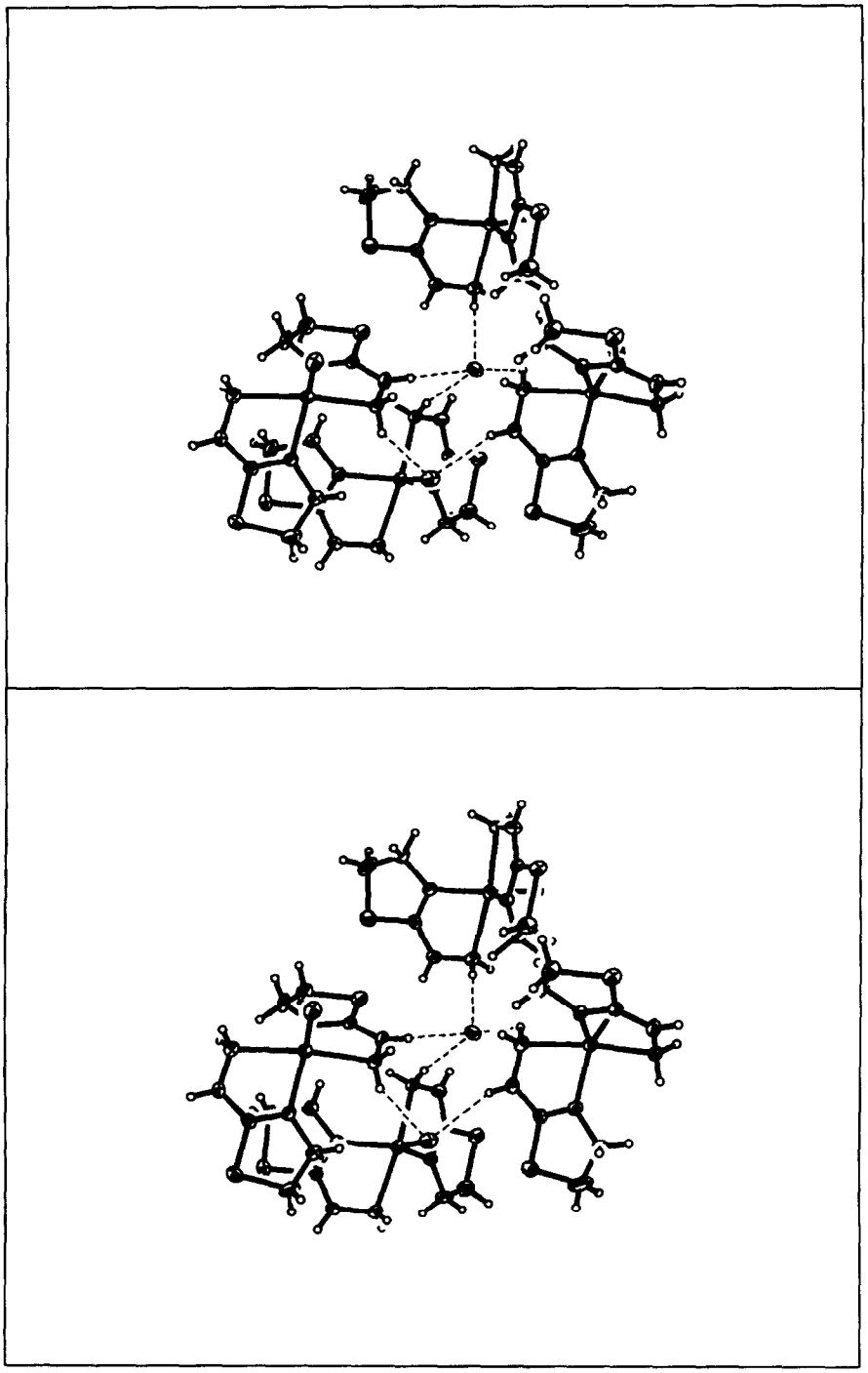


Fig. 2. Stereoscopic view of the hydrogen bond network of $[ZnCl(TzHy)_2]Cl$.

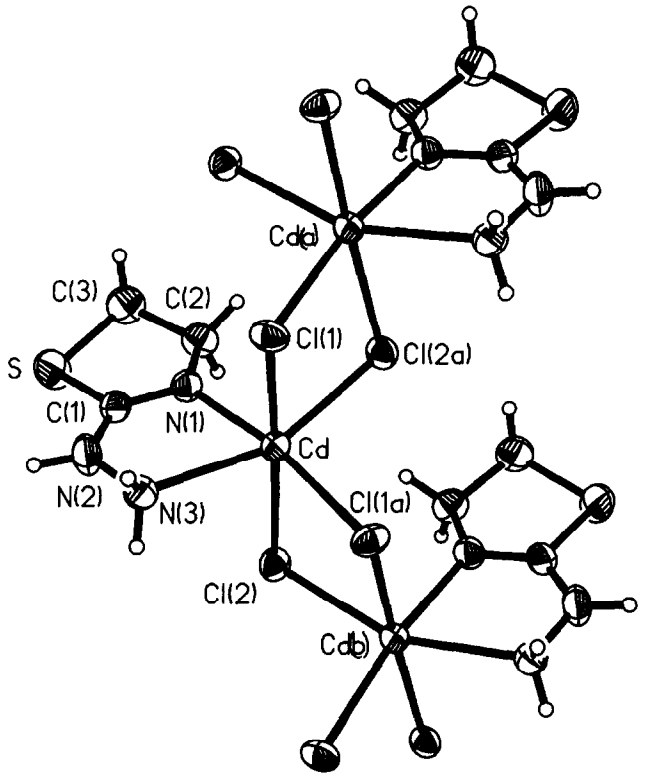


Fig. 3. View of the polymeric chain in $[Cd(TzHy)(\mu\text{-}Cl)_2]_n \cdot nH_2O$, showing the atom-numbering scheme. The thermal ellipsoids are drawn at a 50% level.

($\sim sp^3$) and in the thiazoline ($\sim sp^2$) which leads to a decrease of the covalent radius of nitrogen. The other is the different behaviour of these atoms in the formation of hydrogen bonds. Thus, N(1) and N(4) do not participate in hydrogen bonding, whereas N(6) forms two strong hydrogen bonds and N(3) is involved in one weak and one strong hydrogen bond.

The two five-membered chelate rings are essentially planar, with maximum mean-plane deviations observed for the thiazolinic nitrogens [N(1) 0.046 Å, N(4) 0.076 Å]; the angle between the normals to the best chelate planes is 53.2°. Bonds lengths and angles in the organic ligands are similar to those obtained in TzHyHCl and $[Ni(TzHy)_2(H_2O)_2]Cl_2 \cdot 2H_2O$ [1] and indicate that the organic moiety preserves the thiazoline-hydrazine form. The puckering parameters for the S(1)—C(1)—N(1)—C(2)—C(3) thiazoline ring ($q_2 = 0.150$ Å and $\phi_2 = 135.1°$) describe a slightly distorted form intermediate between envelope and half-chair conformations [13]. For the other thiazoline ring, with $q_2 = 0.117$ Å and $\phi_2 = 139.4°$, the value is close to the value (144°) appropriate to one envelope conformation with apex at C(6).

As pointed out above, the crystal packaging is determined by a network of hydrogen bonds in which all hydrazinic nitrogen atoms act as hydrogen donors, while the chloride anion [Cl(2)] and coordinated chlorine [Cl(1)] act as acceptors. A stereoscopic view showing this network is given in Fig. 2.

The cadmium compound contains water molecules of crystallization and polymeric $[CdCl_2(TzHy)]_n$ chains in which the units are linked by double (μ-chloro) bridges. The chains run along the crystallographic *c* axis. A view of one segment of the polymer is given in Fig. 3. Selected bond lengths, angles and the hydrogen contacts are listed in Table 4. The octahedral coordination sphere of Cd^{II} is completed by two *cis* nitrogen atoms from the TzHy ligand which acts as didentate. The octahedron is appreciably distorted with the ligand–metal–ligand bite angles varying between 104.6(1)° and 72.2(1)°.

The chlorine bridges are very asymmetric; while the Cd—Cl(1a) [2.556(1) Å] and Cd—Cl(2a) [2.605(1) Å] distances are similar to those found in several compounds involving chlorine bonded to two cadmium atoms [14–17], the Cd—Cl(1) [2.745(1) Å] and Cd—Cl(2) [2.719(1) Å] distances are significantly greater and are comparable with the distances found for chlorine atoms bonded to three cadmium atoms [17–20]. In similar form to that observed in the zinc(II) complex, and for analogous reasons, the metal–hydrazinic nitrogen bond Cd—N(3) [2.449(2) Å] is longer than the metal–thiazolinic nitrogen bond Cd—N(1) [2.241(2) Å].

Likewise in the zinc(II) complex, the chelate ring is planar, with maximum mean-plane deviation for the thiazolinic nitrogen N(1) [0.042 Å]. Complexation to the metal does not dramatically affect the geometry

Table 4. Selected bond lengths (Å), angles (°) and hydrogen bonds for $[Cd(TzHy)(\mu\text{-}Cl)_2]_n \cdot nH_2O$

Cd—N(3)	2.449(2)	Cd—Cl(1)	2.745(1)
Cd—Cl(2)	2.719(1)	Cd—N(1)	2.241(2)
Cd—Cl(1a)	2.566(1)	Cd—Cl(2a)	2.605(1)
S—C(1)	1.756(3)	S—C(3)	1.808(4)
N(3)—N(2)	1.421(3)	C(1)—N(2)	1.330(4)
C(1)—N(1)	1.287(3)	C(2)—C(3)	1.520(5)
C(2)—N(1)	1.471(3)	Cl(1)—Cd(a)	2.556(1)
Cl(2)—Cd(b)	2.605(1)		
N(3)—Cd—Cl(1)	86.9(1)	N(3)—Cd—Cl(2)	87.2(1)
Cl(1)—Cd—Cl(2)	170.8(1)	N(3)—Cd—N(1)	72.2(1)
Cl(1)—Cd—N(1)	95.6(1)	Cl(2)—Cd—N(1)	89.3(1)
N(3)—Cd—Cl(1a)	101.8(1)	Cl(1)—Cd—Cl(1a)	89.8(1)
Cl(2)—Cd—Cl(1a)	84.5(1)	N(1)—Cd—Cl(1a)	171.6(1)
N(3)—Cd—Cl(2a)	158.4(1)	Cl(1)—Cd—Cl(2a)	83.2(1)
Cl(2)—Cd—Cl(2a)	104.6(1)	N(1)—Cd—Cl(2a)	89.6(1)
Cl(1a)—Cd—Cl(2a)	97.4(1)	C(1)—S—C(3)	89.2(1)
Cd—N(3)—N(2)	107.0(2)	S—C(1)—N(2)	118.7(2)
S—C(1)—N(1)	116.6(2)	N(2)—C(1)—N(1)	124.6(3)
C(3)—C(2)—N(1)	107.9(2)	S—C(3)—C(2)	105.3(2)
N(3)—N(2)—C(1)	119.6(2)	Cd—Cl(1)—Cd(a)	94.5(1)
Cd—Cl(2)—Cd(b)	94.2(1)	Cd—N(1)—C(1)	116.2(2)
Cd—N(1)—C(2)	129.9(2)	C(1)—N(1)—C(2)	112.6(2)

Bond A...H—D	Position of D	A...D (Å)	A...H—D (°)
O...H(5)—N(2)	$1-x, 1/2+y, 1/2-z$	2.890(3)	173.1(1)
O...H(6)—N(3)	$1-x, -y, -z$	3.042(3)	159.7(1)
Cl(1)...H(7)—N(3)	$1-x, -y, 1-z$	3.452(2)	145.8(0)
Cl(1)...H(2W)—O	x, y, z	3.275(3)	127.8(1)
Cl(2)...H(1W)—O	$1-x, -y, -z$	3.206(2)	162.1(1)

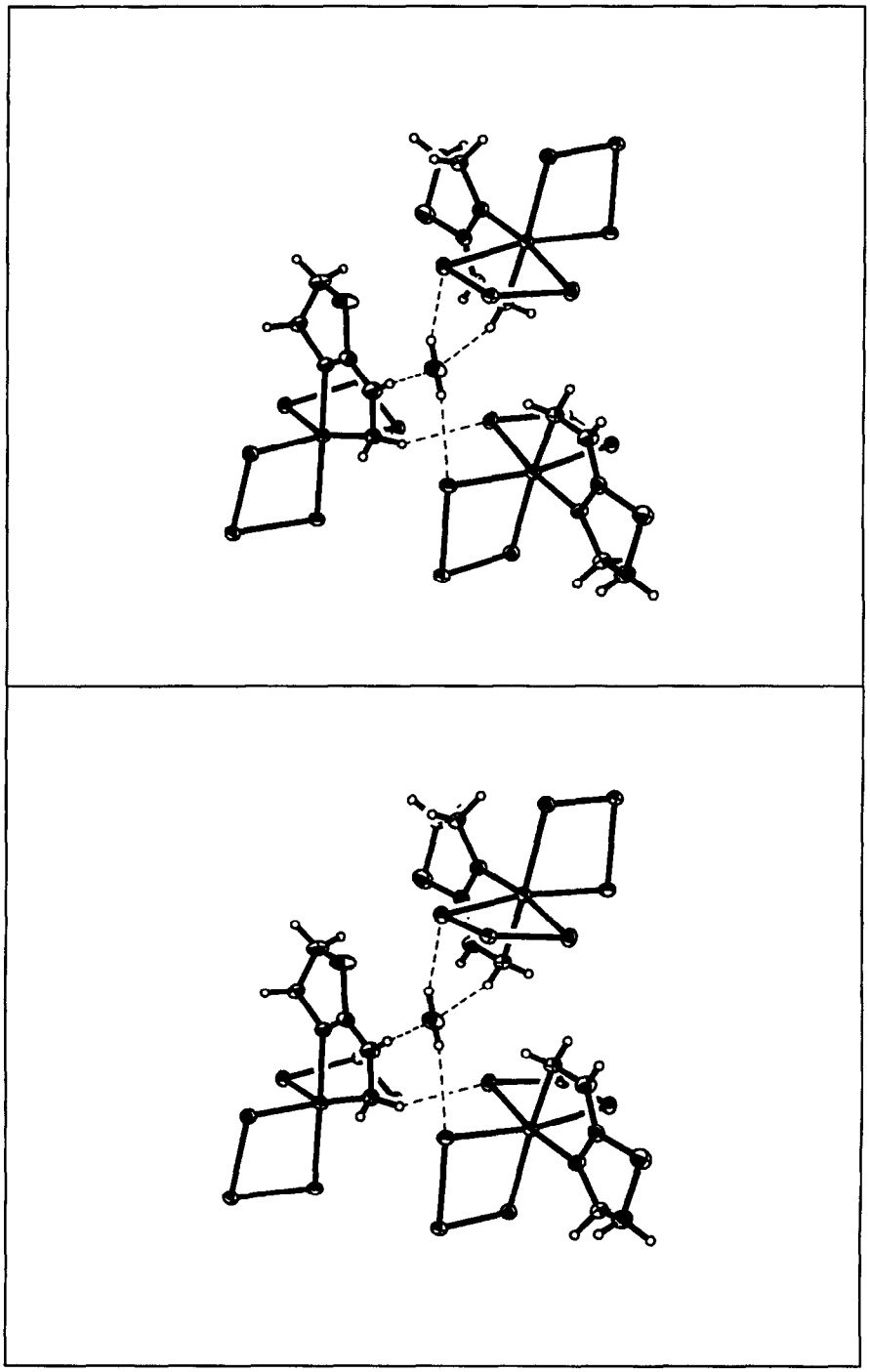


Fig. 4. Stereoscopic view of the hydrogen bond network of $[Cd(TzHy)(\mu\text{-}Cl)_2]_n \cdot nH_2O$.

of the organic ligand, although the thiazoline ring is here more puckered than in the other compounds containing the TzHy moiety [1]. The puckering parameters for the thiazoline ring ($q_2 = 0.293$ Å and $\phi_2 = 137.7°$) indicate a conformation near to envelope with apex at C(3) [13].

Into the chains, the Cd···Cd separations 3.901(1) Å (x, $0.5-y$, $-0.5+z$ and x, $0.5-y$, $0.5+z$) are in good agreement with values obtained in ammonium cadmium chloride [21] and related complexes. The shortest Cd···Cd separation intra chains is 6.643(1) Å ($1-x$, $-y$, $-z$).

Besides normal van der Waals interactions, the structure is stabilized by a complicated hydrogen-bond network (Fig. 4) in which each water molecule participates in four hydrogen bonds, acting as bridge between three adjacent chains. Moreover, contact between neighbouring chains is reinforced by direct

hydrogen bonds involving terminal hydrazinic nitrogen N(3) as donors and Cl(1) as acceptors.

REFERENCES

1. A. Bernalte, M. A. Díaz, F. J. G. Barros, F. J. Higes, A. M. Pizarro, J. Romero and C. Valenzuela, *Polyhedron* 1996, **15,** 1691.
2. M. F. Ansell (Ed.), *Rodd's Chemistry of Carbon Compounds. Heterocyclic compounds*, Vol. 4 C. Elsevier (1986).
3. M. Ávalos, R. Babiano, P. Cintas, J. L. Jiménez and J. C. Palacios, *Heterocycles* 1992, **33,** 973.
4. F. Bermejo and A. Prieto, *Aplicaciones Analíticas del AEDT y Análogos*. Ser. Publ. Univ., Santiago de Compostela (1960).
5. I. M. Kolthoff, E. B. Sandell, E. J. Meehan and S. Bruckenstein, *Quantitative Chemical Analysis*. The Macmillan Company, Collier–Macmillan Canada Ltd., Toronto (1969).
6. P. W. Linder, R. G. Torrington and D. R. Williams, *Analysis Using Glass Electrodes*. Open University Press, Milton Keynes (1984).
7. P. Gans, A. Sabatini and A. Vacca, *J. Chem. Soc., Dalton Trans.* 1985, 1195.
8. G. M. Sheldrick, *SHELXTL-IRIS. Release* 4.2. Siemens Analytical X-ray Instruments Inc., Madison, Wisconsin, U.S.A. (1991).
9. C. F. Baes Jr and R.E. Mesmer, *The Hydrolysis of Cations*. John Wiley & Sons, New York (1976).
10. A. W. Addison, T. N. Rao, J. Reedijk, J. van Rijn and G. C. Verschoor, *J. Chem. Soc., Dalton Trans.* 1984, 1349.
11. A. G. Orpen, L. Brammer, F. H. Allen, O. Kennard, D. G. Watson and R. Taylor, *J. Chem. Soc., Dalton Trans.* 1989, S1.
12. A. W. Herlinger, J. N. Brown, M. A. Dwyer and S. F. Pavkovic, *Inorg. Chem.* 1981 **20,** 2366.
13. D. Cremer and J. A. Pople, *J. Am. Chem. Soc.* 1975, **97,** 1354.
14. G. De Munno, S. Mauro, T. Pizzino and D. Viterbo, *J. Chem. Soc., Dalton Trans.* 1993, 1113.
15. M. Cannas, G. Marongiu and G. Saba, *J. Chem. Soc., Dalton Trans.* 1980, 2090.
16. R. Bonomo, F. Bottino, F. R. Fronczek, A. Mamo and S. Pappalardo, *Inorg. Chem.* 1989, **28,** 4593.
17. M. Kubiak and T. Głowiak, *Acta Cryst.* 1985, **C41,** 1580.
18. L. R. Nassimberi and A. L. Rodgers, *Acta Cryst.* 1976, **B32,** 257.
19. M. M. Rolies and C. J. de Ranter, *Acta Cryst.* 1978, **B34,** 3216.
20. M. Kubiak, T. Głowiak and H. Kozolwski, *Acta Cryst.* 1983, **C39,** 1637.
21. M. M. Rolies and C. J. de Ranter, *Acta Cryst.* 1978, **B34,** 3057.

Pergamon

S0277-5387(96)00252-5

Polyhedron Vol. 16, No. 2, pp. 307–313, 1997
Copyright © 1996 Elsevier Science Ltd
Printed in Great Britain. All rights reserved
0277 5387/97 $15.00 + 0.00

Rhodium complexes with diacetyl monoxime ligands; crystal structure of [Rh*cis*-$(C_4H_6NO)_2$*cis*-$(PPh_3)_2$]$ClO_4 \cdot CHCl_3$

M. Moszner,[a]* T. Glowiak,[a] M. Kubiak,[a] J. J. Ziólkowski,[a] G. Costa[b] and C. Tavagnacco[b]

[a]Faculty of Chemistry, University of Wrocław, 14 F. Joliot-Curie Str, 50-383 Wrocław, Poland

[b]Dipartimento di Scienze Chimiche, Universita degli Studi di Trieste, Via Giorgieri 1, 34-127 Trieste, Italy

(Received 12 March 1996; accepted 17 May 1996)

Abstract—The reaction of $RhCl_3 \cdot 3H_2O$ with Hdamo and PPh_3 (Hdamo = diacetyl monoxime = C_4H_7NO), both in the absence (**1**) and in the presence of $HClO_4$ (**2**) afforded the complex Rh(damo)$(PPh_3)_2Cl_2$. The reaction of the acidic water/ethanolic solution of $[Rh(H_2O)_6]^{3+}$ with Hdamo and PPh_3 (**3**) gave the mixture of the isomers of the compound $[Rh(damo)_2(PPh_3)_2]ClO_4$ (**3A** and **3B**). A similar mixture of isomers was formed when $[Rh(H_2O)_6]^{3+}$ reacted with H_2dopn (H_2dopn = 3,9-dimethyl-4,8-diazaundeca-3,8-diene-2,10-dione dioxime) and PPh_3 (**4**). Two isomers (**4A** = **3B**) and [Rh*cis*-$(damo)_2$*cis*-$(PPh_3)_2$]$ClO_4 \cdot CHCl_3$ (**4B**) have been isolated. All the compounds were characterized by elemental analysis NMR and IR spectroscopy. Single-crystal X-ray diffraction studies were carried out on the complex **4B**. In this compound the coordination environment around rhodium(III) is pseudooctahedral composed of two *cis*-oxime nitrogen atoms [av. Rh—N = 2.031(3) Å], two *trans*-oxime oxygen atoms [av. Rh—O = 2.026(2) Å] and two *cis*-phosphine phosphorus atoms [av. Rh—P = 2.403(1) Å]. Copyright © 1996 Elsevier Science Ltd

Keywords: rhodium complexes; rhodoxime complexes; monoxime complexes; crystal structure.

Until recently the chemistry of rhodium compounds with bidentate oximato ligands was by and large limited to the presence of two dioximato groups, coordinated to a metal center through four nitrogen atoms. For these substances ligands in the equatorial plane are equivalent and perturbations were largely the result of varying the axial ligands or the nature of the R group of the dioximato ligands [1–6].

There are no reports of rhodium complexes containing monoximato ligands (Fig. 1) with donor atoms other than nitrogen. An exception is the complex of rhodium(III) with the 3-methoxy-3-methyl-2-butanone oxime [7]. The starting material used for syntheses of most rhodium compounds with dioximes is $RhCl_3 \cdot 3H_2O$. Very recently studies on a reaction between $[Rh(H_2O_6]^{3+}$, H_2dmg (H_2dmg = dimethylglyoxime) and $[Rh(H_2O)_6]^{3+}$, H_2dmg and PPh_3 resulted in isolation of complexes [Rh $(dmgH)_2(L)_2]ClO_4$, (L = H_2O, PPh_3) [8], which are impossible to obtain in syntheses using the former starting material. This prompted us to carry out the reactions in a few different systems:

(**1**) $RhCl_3 \cdot 3H_2O + Hdamo + PPh_3$
→ Rh(damo)$(PPh_3)_2Cl_2$

(**2**) $RhCl_3 \cdot 3H_2O + Hdamo + PPh_3/HClO_4$
→ Rh(damo)$(PPh_3)_2Cl_2$

(**3**) $[Rh(H_2O)_6]^{3+} + Hdamo + PPh_3/HClO_4$
→ $[Rh(damo)_2(PPh_3)_2]ClO_4$
3A and/or **3B**

(**4**) $[Rh(H_2O)_6]^{3+} + H_2dopn + PPh_3/HClO_4$
→ $[Rh(damo)_2(PPh_3)_2]ClO_4$
4A and/or **4B**

The complex containing one $damo^-$ anion [Rh (damo)$(PPh_3)_2Cl_2$] has been found as the product of the reactions (**1**) and (**2**) whereas three isomeric forms of the compound $[Rh(damo)_2(PPh_3)_2]ClO_4$ with two coordinated $damo^-$ ions have been identified as the

* Author to whom correspondence should be addressed.

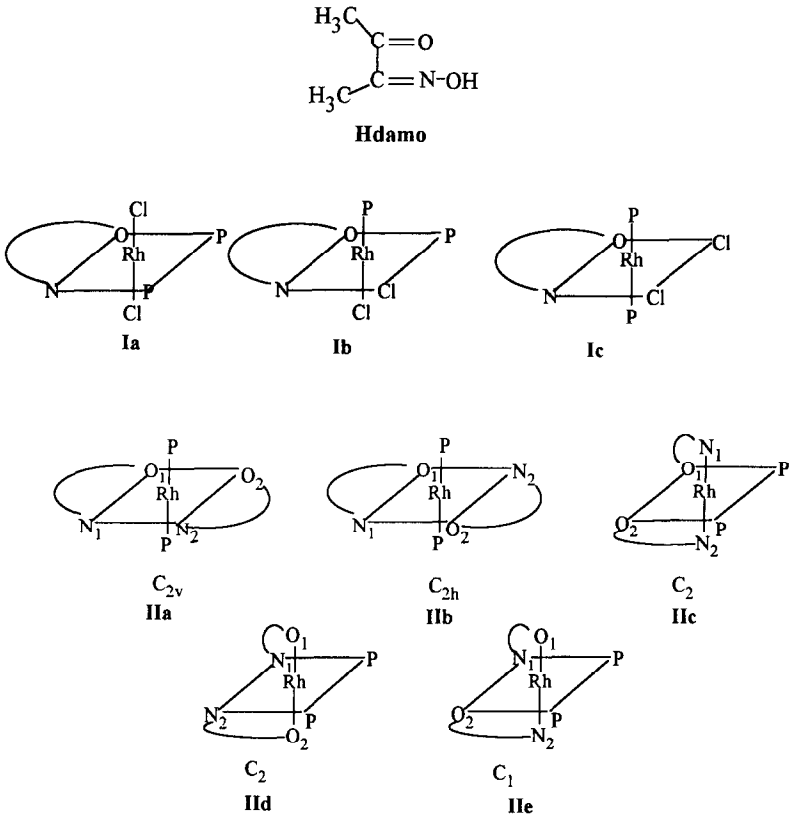


Fig. 1. Possible substitution products for compounds of general formula (I) $Rh(damo)L_2Cl_2$ and (II) $[Rh(damo)_2L_2]ClO_4$, (L = PPh_3 = P).

products of the reactions (**3**) and (**4**). Complexes containing mixed hetero donor atoms in the basal plane are far more complex with respect to their electronic and/or structural effects than rhodium dioximates. The effect of such changes is bound to reflect on the electronic structure of the rhodium center as well as on potential chemistry that may occur in the axial and/or equatorial direction of a given isomer.

As seen in Fig. 1, there are few possible geometrical isomers for compounds of general formula [Rh (damo)L_2Cl_2] (L = PPh_3) and $[Rh(damo)_2L_2]ClO_4$, (L = PPh_3) for five-membered N,O-chelation which is common for most metal complexes with oximes, although six-membered O,O-chelation cannot be excluded [9].

As far as we are aware complexes presented in this paper are the first examples of rhodium compounds containing diacetyl monoximato ligands.

EXPERIMENTAL

Physical measurements

UV–vis spectra were monitored on a Hewlett-Packard 8452A rapid scan dioda-array spectrometer. The NMR spectra were recorded on a Bruker spectrometer (^1H at 300.13 MHz, ^{13}C at 75.47 MHz, ^{31}P at 121.496 MHz) with solvent signals being used as internal standards for ^1H and ^{13}C, and external 85% H_3PO_4 for ^{31}P. Infrared spectra were measured in the range 4000–400 cm^{-1} as KBr disks on a Nicolet FTIR spectrophotometer.

Materials

$RhCl_3 \cdot H_2O$ was purchased from Aldrich. The compound $[Rh(H_2O)_6]ClO_4$ was synthetized according to the method of Ayres and Forrester in the reaction of $RhCl_3 \cdot 3H_2O$ with concentrated perchloric acid. Solutions were standardized spectrophotometrically by using the known absorption spectrum of $[Rh(H_2O)_6]^{3+}$, with peaks at 311 (ε = 67.4 M^{-1} cm^{-1}) and 396 nm (ε = 62) [10]. H_2Dopn was prepared by literature method [11]. All other chemicals were of reagent grade and were used as commercially obtained.

CAUTION! Perchlorate salts of metal complexes are potentially explosive. Only a small amount of material should be prepared, and it should be handled with caution.

Synthesis of $Rh(damo)(PPh_3)_2Cl_2$ (*Reaction* **1**). Hdamo ligand (0.082 g, 0.81 mmol) dissolved in 10 cm^3 of hot ethanol was combined with $RhCl_3 \cdot 3H_2O$ (0.104, 0.4 mmol) in 3 cm^3 of warm ethanol. The solution was refluxed for 5 min. PPh_3 (0.209 g, 0.8 mmol) dissolved in 10 cm^3 of hot EtOH was next

added and the solution was heated under reflux for 15 min. The initial red colour of the solution turned to dark yellow, and was filtered while hot. Upon standing at ambient temperature, the mixture deposited the yellow microcrystalline product which was filtered off, washed with small portions of ethanol, diethyl ether, and air-dried. Yield: 0.25 g (79%). Found: C, 60.0; H, 4.3; N, 1.7. Calc. for $RhC_{40}H_{36}N_1P_2O_2Cl_2$: C 60.2; H, 4.5; N, 1.7%. NMR spectra ($CDCl_3$), δ (ppm): ^1H: 1.054(s) (CH_3(CO)) (3H), 1.42(s) (CH_3(CN)) (3H), 7.28–7.75(m) aromatic (30H); ^{31}P: 18.56(d), ^1J(Rh,P) = 91.9 Hz.

Reaction **2**. A hot ethanolic solution (10 cm^3) of Hdamo (0.083 g, 0.82 mmol) was added to a 3 mol dm^{-3} $HClO_4$ solution in water (10 cm^3) containing $RhCl_3 \cdot 3H_2O$ (0.104, 0.4 mmol). The resulting solution was kept under reflux for 2 h. PPh_3 (0.215 g, 0.82 mmol) dissolved in 20 cm^3 of hot ethanol was added to the reaction mixture. After 1 h heating the solution was filtered and left to stand at room temperature. The yellow microcrystalline product was filtered off, washed with ethanol, diethyl ether and air-dried. Yield: 0.18 g (57%). Found: C, 59.9; H, 4.43; N, 1.70. Calc. for $RhC_{40}H_{36}N_1P_2O_2Cl_2$: C, 60.2; H, 4.5; N, 1.7%. NMR spectra ($CDCl_3$), δ (ppm): ^1H: 1.054(s) (CH_3(CO)) (3H), 1.42(s) (CH_3(CN)) (3H), 7.28–7.75(m) aromatic (30H); ^{31}P: 18.55(d) ^1J(Rh—P) = 91.9 Hz; ^{13}C: 12.36 (CH_3(C—N)), 23.05 (CH_3(CO)), 128.43 (P(m-C_6H_5)$_3$), 129.14(vt) (P(i-C_6H_5)$_3$), 131.02 (P(p-C_6H_5)$_3$), 135.67(P(o-C_6H_5)$_3$), 152.26 (C—N), 200.27 (C—O). No IR bands due to the ClO_4^- anion were detected.

Synthesis of $[Rh(damo)_2(PPh_3)_2]ClO_4$ (*Reaction* **3**). To a solution of $[Rh(H_2O)_6]^{3+}$ (1.02 mmol) in 3 mol dm^{-3} $HClO_4$, Hdamo (0.204 g, 2.04 mmol) in 15 cm^3 of hot ethanol was added and the resulting mixture refluxed for 2 h. PPh_3 (0.46 g, 2.04 mmol) dissolved in 20 cm^3 of hot EtOH was added and reaction mixture heated under reflux for 20 min. After filtration while hot the solution was cooled to room temperature. The product crystallized out as pale yellow microcrystals, which were filtered off, washed with ethanol and diethyl ether and air-dried. Yield: 0.37 g (40%). Found: C, 56.9; H, 4.4; N, 3.0. Calc. for $RhC_{44}H_{42}N_2P_2O_8Cl$: C, 57.0, H, 4.6; N, 3.0%. IR (as KBr pallets): medium band at 623 cm^{-1} due to $\nu(ClO_4^-)$. NMR spectra of the isolated precipitate indicated two components: **3A** and **3B**.

3A. NMR spectra, δ (pm): ^1H ($CDCl_3$) 0.92 s (CH_3(CO)) (6H), 1.59 s (CH_3(CN)) (6H), 7.4–7.59 (aromatic) (30H); (CD_2Cl_2): 0.88 s (6H), 1.55 s (6H), 7.57–7.49 m (30H), ^{31}P ($CDCl_3$): 21.2 d ^1J(Rh,P) = 97.2 Hz; (CD_2Cl_2): 21.42 ^{1}J(Rh,P) = 97.6 Hz, ^{13}C (CD_2Cl_2): 11.63 (CH_3(CN)), 23.82 (CH_3(CO), 125.6 d (P(i-C_6H_5)$_3$), 129.1 vt (P(m-C_6H_5), 132.4 s (P(p-C_6H_5), 134.6 vt (P(o-C_6H_5)$_3$), 157.4 (C—N), 204. (C—O).

3B. NMR spectra, δ (ppm): ^1H ($CDCl_3$): 0.96 s (CH_3(CO)) (6H), 1.55 s (CH_3(CN)) (6H), 7.37–7.48 m (aromatic) (30H), (CD_2Cl_2): 0.93 s (6H), 1.48 s (6H), 7.38–7.55 (m) (30H), ^{31}P ($CDCl_3$): 20.62 d ^1J(Rh,P) = 92.9 Hz; (CD_2Cl_2): 20.82 d ^1J(Rh,P) = 92.9 Hz, ^{13}C (CD_2Cl_2): 10.71 (CH_3(CN)), 23.3 (CH_3(CO), 125 d (P(i-C_6H_5)$_3$), 129.1 vt (P(m-C_6H_5), 132.4 s (P(p-C_6H_5), 134.3 vt (P(o-C_6H_5)$_3$), 153.1 (C—N), 202.7 (C—O).

Reaction **4**. The solution of $[Rh(H_2O)_6]^{3+}$ (1.1 mmol) in 3 mol dm^{-3} $HClO_4$ was combined with the hot ethanolic solution in H_2Dopn (0.227 g, 1.2 mmol). The solution was refluxed for 2 h; during this time a brown–yellow solution with a concomitant formation of a white solid resulted. After reduction of the solution volume down to 3–5 cm^3, the white precipitate was filtered off, washed with a small amount of ethanol, ethyl ether and air dried. Yield: 0.285 g (90%). Found: C, 13.3; H, 4.5; N, 10.2. Calc. for $C_3H_{12}N_2O_8Cl_2$: C, 13.1; H, 4.4; N, 10.2%. IR (as KBr disk): 629 cm^{-1} due to ν (ClO_4^-). NMR spectra (D_2O): ^1H: 2.11 CH_2 (2), 3.15 CH_2 (4). The clear brown–yellow filtrate was next charged with 0.61 g (2.3 mmol) of PPh_3 dissolved in warm ethanol. After 1 h of heating the solution was cooled to room temperature. The brownish–golden precipitate (**4A**) deposited as a first crop was filtered off, washed with ethanol, diethyl ether and air-dried. Yield: 0.31 g (30%). Found: C, 57.0; H, 4.6; N, 2.9. Calc. for $RhC_{44}H_{42}N_2P_2O_8Cl$: C, 57.0; H, 4.6; N, 3.0%. IR (as KBr disc): 625 cm^{-1}, ν (ClO_4^-). NMR spectra, δ (ppm): ^1H ($CDCl_3$): 0.96 s (CH_3(CO)) (6H), 1.55 s (CH_3(CN)) (6H), 7.4–7.6 m (aromatic) (30H); (CD_2Cl_2): 0.93 s (6H), 1.48 s (6H), 7.38–7.55 m (30H): (dmso-d_6): 0.89 s (6H), 1.57 s (6H), 7.3–7.65 m (30H); ^{31}P ($CDCl_3$): 20.6 d ^1J(Rh,P) = 93 Hz); (CD_2Cl_2): 20.8 d ^1J(Rh,P) = 93 Hz; ^{13}C (CD_2Cl_2): 10.81 (CH_3(C—N)), 23.34 (CH_3(C—O)), 125.23 (vt) (P(i-C_6H_5)$_3$), 129.22 vt (P(m-C_6H_5), 132.52 s (P(p-C_6H_5), 134.69 vt (P(o-C_6H_5)$_3$), 157.5 (C—N), 204.1 (C—O).

When the solution was allowed to stand overnight, the second crop **4B** crystallized out as the yellow microcrystals, which after filtration and washing with ethanol and diethyl ether were air-dried. Dark yellow single crystals [Rh*cis*-(damo)$_2$*cis*-$(PPh_3)_2$]$ClO_4 \cdot CHCl_3$ were obtained by slow evaporation in a refrigerator from a $CHCl_3$/EtOH solution of the crop **4B**. Yield: 0.25 g (25%). Found: C, 51.4; H, 4.2; N, 2.6. Calc. for $RhC_{45}H_{43}N_2P_2O_8Cl_4$: C, 51.6; H, 4.1; N, 2.7%. IR (as KBr disc): 625 cm^{-1}, ν (ClO_4^-). NMR spectra ($CDCl_3$), δ (ppm): ^1H: 1.33 s (CH_3(CO)) (6H), 2.36 s (CH_3(CN)) (6H), 7.3–7.5 (m) aromatic (30H); ^{31}P: 17.2 d ^1J(Rh,P) = 103.9 Hz; ^{13}C: 12.16 (CH_3(C—N)), 26.05 (CH_3(C—O)), 125.65 vt, (P(i-C_6H_5)$_3$), 129.4 (P(m-C_6H_5)$_3$), 132.2 (P(p-C_6H_5)$_3$), 134.6 (P(o-C_6H_5)$_3$), 153.2 (C—N), 209.83 (C—O).

X-ray diffraction

Preliminary examination of the crystal of [Rh*cis*-(damo)$_2$*cis*-$(PPh_3)_2$]$ClO_4 \cdot CHCl_3$ by Weissenberg photographs indicated the triclinic system. Data were

collected on a Kuma KM-4 κ-axis diffractometer with graphite-monochromated Mo-K_α radiation using the ω-2θ scan mode. 6427 independent reflections measured were observed ($F > 4\sigma(F)$). Three standard reflections showed no variation. Data were corrected for Lorentz and polarization effects. Experimental details are given in Table 1. The structure was solved using SHELXS-86 [12] and refined by full-matrix least-square methods using SHELXL-93 [13] with anisotropic thermal parameters for non-H atoms. In the final cycles of the refinement H-atom parameters were included. Scattering factors were those incorporated in the SHELXL-93 program.

RESULTS AND DISCUSSION

X-ray studies of [Rhcis-(damo)$_2$cis-(PPh$_3$)$_2$]ClO$_4$·CHCl$_3$

The crystal structure consists of [Rh(damo)$_2$(PPh$_3$)$_2$]$^+$ cations, ClO$_4^-$ anions and solvate CHCl$_3$ molecules, held together by electrostatic and van der Waals interactions, Fig. 2. Bond lengths and angles are given in Tables 2 and 3, respectively. The complex cations contain a pseudooctahedral arrangement of two PPh$_3$ ligands *cis*- to each other, and two bidentate damo$^-$ anions. The latter coordinate to the rhodium(III) ions in a chelating fashion through the oxime nitrogens and carbonyl oxygen atoms, forming five membered rings which remain planar. The complex cations have nearly C_2 symmetry. The rhodium atom is displaced out of the plane defined by two *cis*-oxime nitrogen and two *cis*-phosphorus atoms of PPh$_3$ by 0.0107(3) Å towards the O(4) oxime atom. The P(1)-Rh-P(2) angle, 98.42(4)°, is somewhat greater than the ideal angle of 90°. The angles: O(2)—Rh—O(4), 168.8(1)°, N(1)—Rh—P(1), 172.8(1)° and N(2)—Rh—P(2), 171.96(9)° are not strictly *trans*. This decrease is attributable to the presence of two bulky PPh$_3$ ligands in the *cis* position. The bite angles of the two chelates: O(2)—Rh—N(1) and O(4)—Rh—N(2) are similar, 78.7(1) and 79.1(1)° respectively. The Rh—P bonds, 2.401(1) and 2.406(1) Å, are slightly shorter than 2.447(1) in [Rh(dmgH)$_2$(PPh$_3$)(C$_2$H$_3$)] [17] and 2.461(2) Å in [Rh(dmgH)$_2$(PPh$_3$)(C$_2$H$_5$)] [18] but longer than 2.327(1) Å in Rh(dmgH)$_2$(PPh$_3$)Cl [19]. The average Rh—N distance 2.031(3) Å is long compared to the known rhodium(III) complexes containing the dmgH ligands in the equatorial plane, as well as to the compound of formula [Rh(ether oxime)$_2$Cl$_2$] [7]. In Rh(dmgH)$_2$(PPh$_3$)Cl, [Rh(dmgH)$_2$(PPh$_3$)(C$_2$H$_3$)], [Rh(dmgH)$_2$(PPh$_3$)(C$_2$H$_5$)] and [Rh(ether oxime)$_2$Cl$_2$], the average Rh—N bond lengths are 1.992(4), 1.957(2), 1.948(6) and 1.958(3) Å, respectively. The torsion angles N(1)—C(1)—C(2)—O(2) and N(2)—C(5)—C(6)—O(4) are 2.40(5) and 2.08(5)° respectively. The dihedral angle between these planes is 109.5(5)°. The N—C—C—O planes are perpendicular to the N(1)N(2)P(1)P(2) coordination plane. The rhodium atom is displaced 0.252(3) Å from the N(1)C(1)C(2)O(2) plane, and 0.197(3) Å from the N(2)C(5)C(6)O(4) plane. The O(1) and O(3) atoms are displaced 0.043(3) Å and −0.043(3) Å, respectively from these damo planes. The C(1)—C(2) and C(5)—C(6) bond lengths average 1.407(5) Å, and are in good agreement with a C(sp^2)—C(sp^2) double bond value for carbon in trigonal hybridization. As far as the carbon–oxygen and nitrogen–oxygen bonds are concerned, the average values 1.270(4) Å and 1.247(4) Å respectively, reveal a significant percentage of double-bond character in both ligands. Finally the carbon–nitrogen bond, 1.337(5) Å is in good agreement with single bond values. Of special note is the mutual position of rings C$_{21}$—C$_{26}$ and C$_{41}$—O$_{46}$ bound to the two different phosphorus atoms of the PPh$_3$ ligands, P$_1$ and P$_2$, respectively. The angle between these planes is 3.5°, indicating them to be almost parallel.

Table 1. Crystal data and structure refinement

Empirical formula	$C_{45}H_{42}C_{14}N_2O_8P_2Rh$
Formula weight	1045.46
Crystal size (mm)	0.07 × 0.09 × 0.15
Temperature (K)	293(2)
Wavelength (Å)	0.71069
Crystal system	triclinic
Space group	$P\bar{1}$
Unit cell dimensions	
a (Å)	11.402(2)
b (Å)	13.109(3)
c (Å)	16.191(3)
α (°)	91.83(3)
β (°)	102.26(3)
γ (°)	95.71(3)
V (Å^3)	2349.6(8)
Z	2
Density (calculated) (mg m^3)	1.478
Density (measured) (mg m^3)	1.48
Absorption coefficient (mm^{-1})	0.712
F(000)	1066
Theta range (°)	2.00 to 25.00
Scan ranges:	$0 \leqslant h \leqslant 13$, $-15 \leqslant k \leqslant 15$, $-19 \leqslant l \leqslant 18$
Measured reflections	6427
Independent reflections	6427
Data/restraints/parameters	6427/0/559
Goodness-of-fit	1.088
R	0.0350
wR	0.1013
Largest diff. peak and hold	0.613 and −0.582 e Å^{-3}

Studies of reactions

Reactions **1** *and* **2**. Reaction of RhCl$_3$·3H$_2$O with Hdamo (**1**) gave the yellow product of formula [Rh(damo)(PPh$_3$)$_2$Cl$_2$]. The same compound was obtained

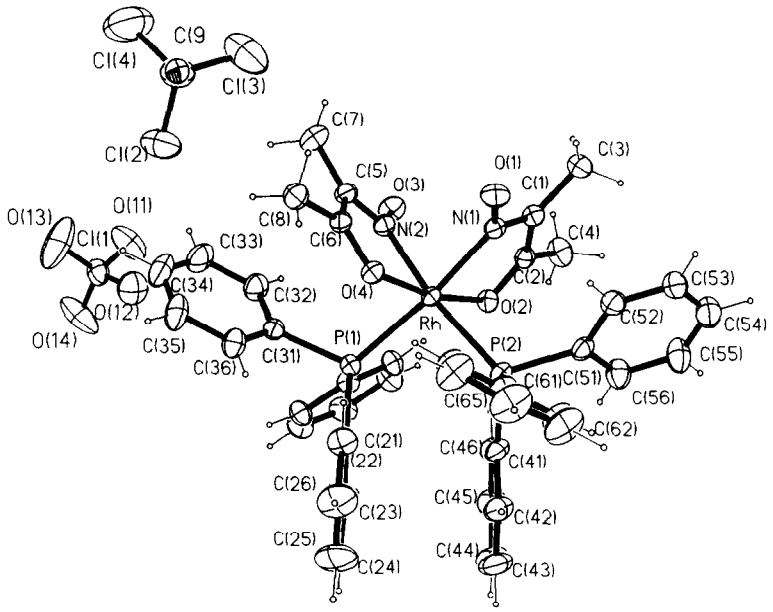


Fig. 2. Molecular structure with labelling scheme for non-hydrogen atoms of [Rh*cis*-(damo)$_2$*cis*-(PPh$_3$)$_2$]ClO$_4$·CHCl$_3$.

Table 2. Selected bond lengths [Å] for [Rh*cis*-(damo)$_2$*cis*-(PPh$_3$)$_2$]ClO$_4$·CHCl$_3$

Rh—N(1)	2.034(3)
Rh—N(2)	2.027(3)
Rh—O(2)	2.028(2)
Rh—O(4)	2.023(2)
Rh—P(1)	2.406(1)
Rh—P(2)	2.401(1)
O(1)—N(1)	1.241(4)
O(2)—C(2)	1.264(4)
N(1)—C(1)	1.337(5)
C(1)—C(2)	1.409(5)
C(1)—C(3)	1.473(5)
C(2)—C(4)	1.488(5)
O(3)—N(2)	1.253(4)
O(4)—C(6)	1.277(4)
N(2)—C(5)	1.337(5)
C(5)—C(6)	1.404(5)
C(5)—C(7)	1.481(5)
C(6)—C(8)	1.490(5)
P(1)—C(21)	1.815(4)
P(1)—C(11)	1.820(4)
P(1)—C(31)	1.841(4)
P(2)—C(61)	1.822(4)
P(2)—C(51)	1.823(4)
P(2)—C(41)	1.823(4)
Cl(1)—O(11)	1.400(4)
Cl(1)—O(12)	1.450(4)
Cl(1)—O(13)	1.355(5)
Cl(1)—O(14)	1.384(5)
Cl(2)—C(9)	1.739(6)
Cl(3)—C(9)	1.744(7)
Cl(4)—C(9)	1.696(7)

in the reaction (**2**), carried out in the presence of the perchloric acid. No IR bands due to the ClO_4 anion were detected in the isolated complex and its composition has been revealed to be like that of the reaction (**1**), on the basis of elemental analysis and NMR data. The formation of the complex is evidenced by the movement of the 1.87 and 2.31 ppm methyl protons for the Hdamo ligand to higher field upon coordination to the rhodium(III) centre in the compound being discussed. The ^{31}P NMR spectra show one doublet at 18.55 ppm with the ^1J(Rh,P) coupling constant of 92 Hz. Very similar values have been found for the complexes: Rh(dmgH)$_2$(PPh$_3$)$_2$Cl (92 Hz) [2] and [Rh(dmgH)$_2$(PPh$_3$)$_2$]ClO$_4$ (91 Hz) [8] for phosphorus atoms *trans* to each other. This suggests that the substitution reactions of $RhCl_3 \cdot 3H_2O$ with the diacetyl monoxime led to the mononuclear complex having one damo$^-$ anion and two Cl^- ions in the equatorial plane and two PPh_3 ligands in *trans* axial arrangement, independently of the reaction conditions used, Fig. 1, Ib and/or Ic.

Reaction **3**. Compounds of a general formula [Rh(damo)$_2$(PPh$_3$)$_2$]ClO$_4$ have been found to be the products of the reaction between $[Rh(H_2O)_6]^{3+}$ and Hdamo. The ^1H, ^{31}P and ^{13}C NMR spectra showed the formation of two geometrical isomers: **3A** and **3B**. These isomers have always been found to coprecipitate together. In the ^1H spectra of the isomer **3A**, the methyl resonances are observed at 0.92 and 1.59 ppm, whereas for **3B** at 0.96 and 1.55 ppm (in $CDCl_3$). The ^{31}P spectra show the doublets at 21.2 ppm (^1JRh,P = 97 Hz) and 20.6 ppm (^1JRh,P = 93 Hz) for the isomers **3A** and **3B**, respectively. We postulate the structures IIa and IIb with two *trans* PPh_3 groups

Table 3. Selected angles (°) for [Rh*cis*-(damo)$_2$*cis*-(PPh$_3$)$_2$]ClO$_4$ · CHCl$_3$

O(2)—Rh—N(1)	78.67(11)
O(2)—Rh—P(1)	101.61(7)
O(2)—Rh—P(2)	85.22(8)
O(4)—Rh—N(1)	93.12(11)
O(4)—Rh—N(2)	79.11(11)
O(4)—Rh—O(2)	168.80(9)
O(4)—Rh—P(1)	85.57(7)
O(4)—Rh—P(2)	102.37(8)
N(1)—Rh—P(1)	172.77(8)
N(1)—Rh—P(2)	88.80(8)
N(2)—Rh—O(2)	92.24(11)
N(2)—Rh—N(1)	83.21(12)
N(2)—Rh—P(1)	89.56(9)
N(2)—Rh—P(2)	171.96(9)
P(2)—Rh—P(1)	98.42(4)
C(11)—P(1)—Rh	117.16(12)
C(21)—P(1)—Rh	115.40(13)
C(31)—P(1)—Rh	110.31(12)
C(41)—P(2)—Rh	114.21(12)
C(51)—P(2)—Rh	110.00(12)
C(61)—P(2)—Rh	119.28(13)
C(2)—O(2)—Rh	112.4(2)
C(6)—O(4)—Rh	112.3(2)
O(1)—N(1)—Rh	123.3(2)
C(1)—N(1)—Rh	114.3(2)
O(3)—N(2)—Rh	123.4(2)
C(5)—N(2)—Rh	114.3(2)
O(1)—N(1)—C(1)	122.3(3)
O(2)—C(2)—C(4)	117.6(3)
O(2)—C(2)—C(1)	121.1(3)
N(1)—C(1)—C(2)	112.3(3)
N(1)—C(1)—C(3)	120.9(3)
C(1)—C(2)—C(4)	121.3(3)
C(2)—C(1)—C(3)	126.8(3)
O(3)—N(2)—C(5)	122.1(3)
O(4)—C(6)—C(5)	121.0(3)
O(4)—C(6)—C(8)	116.3(3)
N(2)—C(5)—C(6)	112.5(3)
N(2)—C(5)—C(7)	120.1(3)
C(5)—C(6)—C(8)	122.6(3)
C(6)—C(5)—C(7)	127.4(4)
C(11)—P(1)—C(31)	101.4(2)
C(21)—P(1)—C(11)	106.4(2)
C(21)—P(1)—C(31)	104.5(2)
C(61)—P(2)—C(51)	100.3(2)
C(61)—P(2)—C(41)	108.1(2)
C(51)—P(2)—C(41)	102.9(2)
O(13)—Cl(1)—O(14)	111.3(5)
O(13)—Cl(1)—O(11)	111.8(5)
O(14)—Cl(1)—O(11)	109.1(3)
O(13)—Cl(1)—O(12)	107.4(4)
O(14)—Cl(1)—O(12)	110.3(4)
O(11)—Cl(1)—O(12)	106.9(3)
Cl(4)—C(9)—Cl(2)	109.8(4)
Cl(4)—C(9)—Cl(3)	108.3(4)
Cl(2)—C(9)—Cl(3)	110.3(3)

in axial positions (Fig. 1) for the products being described, on the base of the ^1J(Rh,P) coupling constants registered for these species, literature data as well as for a *cis, cis* isomer determined both by the X-ray (*vide supra*) and the NMR measurements (*vide infra*). However, X-ray structures of single crystals are needed to distinguish the isomers.

Reaction **4**. A condensation product of the diacethyl monoxime and a diaminopropane is 3.9-dimethyl-4,8-diazaundeca - 3,8 - diene - 2,10 - dione dioxime H_2dopn [11]. Syntheses of many cobalt compounds with this ligand resulted in the description of very interesting Costa-type complexes, models of Vit.B_{12} [14–16]. Attempts to synthesise the rhodium analgoues using $RhCl_3 \cdot 3H_2O$ as starting reagent failed to yield the desired species. The reaction between $[Rh(H_2O_6)]^{3+}$ and H_2dopn confirmed the instability of this ligand in the presence of water and acid [11]. The elemental analyses of these reaction products gave excellent agreement with calculated values for the complex of formula $[Rh(damo)_2(PPh_3)_2]ClO_4$ and the species $[(H_2N)_2C_3H_6] \cdot 2HClO_4$, the second decomposition product of H_2dopn. The formation of the latter was also confirmed by the IR and NMR spectra measurements. Fractional crystallisation of the reaction mixture allowed the separation of two different complexes of rhodium(III). The first crystallised product (**4A**) appeared to have identical ^1H, ^{31}P and ^{13}C NMR spectra with those of the isomer **3B** described above. The second rhodium(III) species (**4B**), characterised both spectroscopically and crystallographically, has been proved to be the isomer with two Rh—N bonds of the monoxime and two Rh—P bonds of the PPh_3 molecules on the rhodium ion *cis* to their own kind, and two Rh—O bonds in the *trans* arrangement (Fig. 2, IId.) In the ^1H NMR spectrum the CH_3 groups protons are shifted downfield whereas the PPh_3 groups in the ^{31}P spectrum are shifted upfield in comparison with the complexes having the triphenylphosphine ligands in the *trans* position to each other. Simultaneously the ^1J(Rh,P) coupling constant has been demonstrated to be *ca.* 10 Hz higher for the former. This suggests the metal to phosphine π-donation to be more effective in the *cis* stereochemistry than in the *trans* arrangement.

These compounds are stable to air as solids when kept in the dark. However, in contrast to the well-known stability of dioximato rhodium(III) complexes, the monoximato derivatives are labile both in solution and when exposed to light.

Results described in this paper raise interesting questions with respect to the factors that determine the isomer distribution for these reaction systems. This is probably related to the reaction conditions, e.g. pH, thermodynamic preference and the mechanism of the exchange process. More detailed kinetics and thermodynamic studies are needed before we can solve these problems. The different substrates used in the syntheses clearly demonstrate the effect of the ligands (Cl^-, H_2O) coordinated to the rhodium center on the

nature of the substitution products. To our knowledge no rhodium(III) complexes with the monoxime ligands have hitherto been reported. Thus the syntheses of rhodium compounds with hetero donor molecules like Hdamo opens new ways for the study of rhodium oximato species.

REFERENCES

1. N. Bresciani Pahor, R. Dreos-Garlatti, S. Geremia and L. Randaccio, *Inorg. Chem.* 1990, **29**, 3437.
2. F. Asaro, R. Dreos-Garlatti, G. Pellizer and G. Tauzher, *Inorg. Chim. Acta* 1993, **211**, 27.
3. B. Giese, J. Hartung, C. Kesselheim, H. J. Lindner and I. Svoboda, *Chem. Ber.* 1993, **126**, 1193.
4. S. Geremia, R. Dreos, L. Randaccio and G. Tauzher, *Inorg. Chim. Acta* 1994, **216**, 125.
5. R. Dreos, G. Tauzher, S. Geremia, L. Randaccio, F. Asaro, G. Pellizer, C. Tavagnacco and G. Costa, *Inorg. Chem.* 1994, **33**, 5404.
6. M. Kubiak, T. Głowiak, M. Moszner, J. J. Ziółkowski, F. Asaro, G. Costa, G. Pellizer and C. Tavagnacco, *Inorg. Chim. Acta*, 1995, **236**, 141.
7. G. Ergun Efe and E. O. Schlemper, *Polyhedron* 1991, **14**, 1611.
8. M. Moszner, F. Asaro, S. Geremia, G. Pellizer and C. Tavagnacco, *Inorg. Chim. Acta*, to be published.
9. A. Nakamura, A. Konishi and S. Otsuka, *J. Chem. Soc., Dalton Trans.* 1979, 488.
10. G. H. Ayres and J. S. Forester, *J. Inorg. Nucl. Chem.* 1957, **3**, 365.
11. E. Uhlig and M. Fridrich, *Z. Anorg. Allg. Chem.* 1966, **343**, 299.
12. G. M. Sheldrick, *Acta Cryst., Sect. A.* 1990, **46**, 467.
13. G. M. Sheldrick, *SHELXL* 93, *program for the refinement of crystal structures*. University of Göttingen, Germany (1994).
14. G. Pellizer, G. R. Tauszik, G. Tauzher and G. Costa, *Inorg. Chim. Acta* 1973, **7**, 60.
15. G. R. Tauszik, G. Pellizer and G. Costa, *J. Inorg. Nucl. Chem.* 1975, **37**, 1532.
16. A. Gerli and L. G. Marzilli, *Inorg. Chem.* 1992, **31**, 1152.
17. M. Dunaj-Jurčo, V. Kettmann, D. Steinborn and M. Ludwig, *Acta Cryst.* 1994, **C50**, 1427.
18. V. Kettmann, M. Dunaj-Jurčo, D. Steinborn and M. Ludwig, *Acta Cryst.* 1994, **C50**, 1239.
19. F. A. Cotton and J. G. Norman, Jr, *J. Am Chem. Soc.* 1971, **93**, 80.

Pergamon

S0277-5387(96)00246-X

Polyhedron Vol. 16, No. 2, pp. 315–320, 1997
Copyright © 1996 Elsevier Science Ltd
Printed in Great Britain. All rights reserved
0277-5387/97 $15.00+0.00

Mesomorphic dithiocarbamate complexes

Daniel J. Price, Michael A. Wali and Duncan W. Bruce*

Department of Chemistry, University of Exeter, Stocker Road, Exeter EX4 4QD, U.K.

(Received 3 April 1996; accepted 13 May 1996)

Abstract—Complexes of 4-(4′-alkyloxyphenylethyl)piperidine dithiocarbamates with nickel, palladium, copper and zinc have been formed. The nickel and copper complexes are mesomorphic showing smectic phases S_C and crystal B mesophases. Copyright © 1996 Elsevier Science Ltd

Keywords: metallomesogens; dithiocarbamates.

Metal-containing liquid crystals are of great interest [1]. With such systems it is possible to introduce desirable properties inherent in metal complexes, such as high electronic polarisability, colour and paramagnetism, into liquid crystalline systems. This combination of novel electronic and magnetic molecular properties with the macroscopic supramolecular ordering of a mesophase is likely to lead to a variety of new and interesting effects. Many such modifications to these physical properties would be extremely difficult to achieve in purely organic materials.

Although the first metallomesogens were reported over 80 years ago [2] it is only recently that this field has attracted more serious and systematic study. The advent of this more focused research followed reports of the now classic nickel dithiolene complexes of Giroud and Mueller-Westerhoff (Fig. 1) [3]. Since these first compounds, relatively few liquid-crystalline sulfur coordination complexes have been synthesised and studied. Ohta [4] and ourselves [5] have reported the liquid crystalline behaviour of some 4-alkyloxydithiobenzoate complexes (Fig. 2), while Ohta also reported derivatives of the dithiolenes above (Fig. 3) which showed columnar mesophases [6]. More recently, Hoshino-Miyajima [7] demonstrated for the first time mesomorphism in complexes of piperazine dithiocarbamates (Fig. 4).

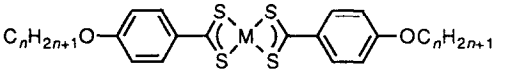


Fig. 2. Mesomorphic dithiobenzoates.

We too have turned our attention to 1,1-dithiolato systems. Simple dithiocarbamate complexes have been extensively studied [8] and thus have a well-developed chemistry, offering great synthetic flexibility. We report here on the synthesis and characterisation of some new piperidine dithiocarbamate complexes of nickel, palladium, copper and zinc. We describe the observed mesomorphism and try to rationalise this behaviour with respect to the ligand and to the effect of the metal centre. In-mesophase EPR studies of these complexes have already been reported [9].

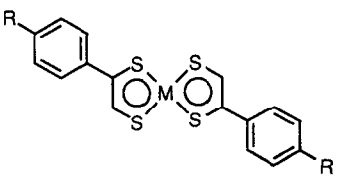


Fig. 1. Mesomorphic dithiolenes.

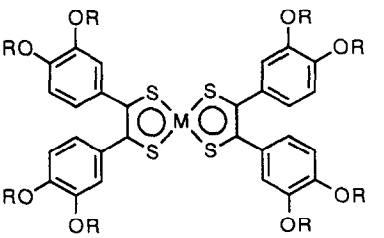


Fig. 3. Columnar dithiolenes.

* Author to whom correspondence should be addressed.

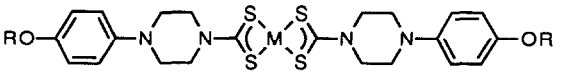


Fig. 4. Hoshino-Miyajima's mesomorphic dithiocarbamates.

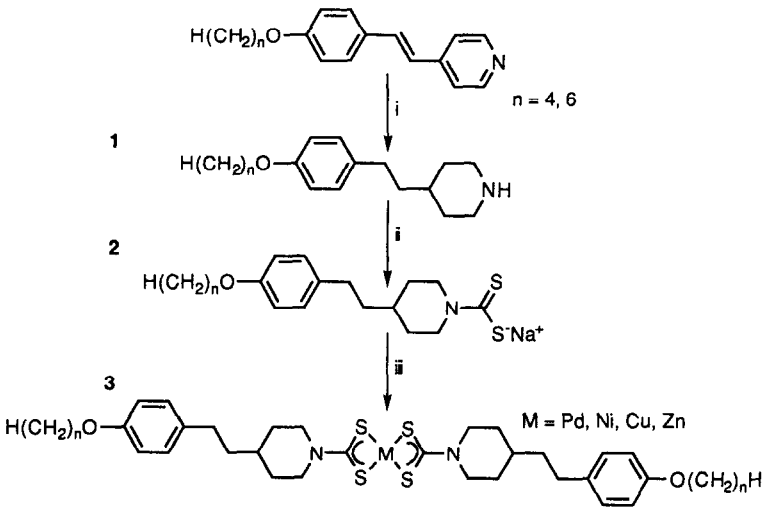
RESULTS AND DISCUSSION

The mesogenic complexes, **3**, were prepared by the multistep synthesis outlined in Scheme 1. The 4-alkyloxy-4′-stilbazoles are mesomorphic, and were synthesised by a procedure we have described previously [10]. Catalytic hydrogenation of the butyloxy and hexyloxy stilbazole derivatives with platinum(IV) oxide (Adams catalyst) gave the 4-substituted piperidine (**1**; $n = 4, 6$). Deprotonation of these secondary amines and subsequent reaction with carbon disulfide gave the sodium salt of the dithiocarbamate ligand (**2**; $n = 4, 6$), the reaction of which with an appropriate divalent metal salt yielded the complexes (**3**; M = Ni, Pd, Cu, Zn; $n = 4, 6$). These complexes were sparingly soluble in most organic solvents and the palladium derivatives tended to decompose in chlorinated solvents. By analogous synthetic procedures, we have also made a variety of other simple piperidine dithiocarbamate complexes (Fig. 5) **4**–**7** (the unsubstituted piperidine derivative), **5** (4-phenylpiperidine), **6** (4-nonylpiperidine) and **7** (3-octyloxypiperidine). We include these non-mesomorphic materials because they make for a useful comparison with our mesomorphic complexes, **3**, and those complexes of Hoshino-Miyajima [7]. They also give an indication of the large differences in melting points that simple structural modifications of dithiocarbamate metal complexes can afford.

The mesomorphism of these materials was studied by optical microscopy and differential scanning calorimetry. The phases and the transition temperatures were assigned on the basis of the microscopy and are given in Table 1.

The simple piperidine derivative, **4** melted at 306°C with decomposition. Addition of the phenyl group in the 4-position, **5**, raised the melting point to 333°C (with decomposition), while further substitution by a nonyl group in the 4-position of the phenyl ring, **6**, decreased the melting point to 238°C. However, most impressive was the reduction in the melting point to 68°C if 3-octyloxy substitution was employed. (This material, **7**, is not strictly comparable, because it is a mixture of two enantiomers and another diasterioisomer; consequently there may be a considerable depression in melting point with respect to a single, pure component.) That simple substitution gives such a large range of crystal stabilities suggests that with suitable molecular design, mesomorphic behaviour may be attainable.

An interesting comparison can be made between our nickel complex **6** (m.p. 238°C) and a similar compound of Hoshino-Miyajima [7], namely the bis(4-octylpiperazine-1-dithiocarbamato) complex of palladium(II). This complex exhibited an enantiotropic nematic phase, melting at 209°C and clearing at 237°C. Since palladium derivatives tend to melt at a few degrees above their nickel congeners, we attribute this difference in phase behaviour to the difference in the ring structures. Our piperidine derivative is rigid, and inversion of the nitrogen in the 1-position is not possible since it is conjugated through the sulfur to the metal. This rigidity of the piperidine ring is supported by the NMR data for all our substituted



Scheme 1. Reagents and conditions: (i) H_2, PtO_2 in AcOH; (ii) NaOH, CS_2 in EtOH; (iii) $Pd_3(AcO)_6$ $NiCl_2 \cdot 6H_2O$, $CuSO_4 \cdot 5H_2O$ or $Zn(AcO)_2$ all in EtOH and H_2O.

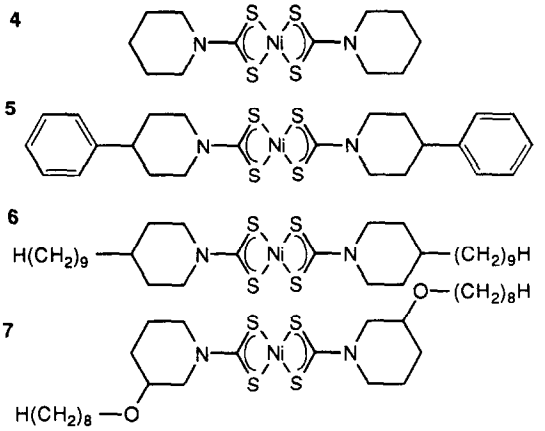


Fig. 5. Non-mesomorphic dithiocarbamate nickel complexes.

Table 1. The mesomorphism of the dithiocarbamate complexes: Transition temperatures are given in °C. Enthalpies, ΔH, in parentheses, are given in kJ mol^{-1}; monotropic phase transitions are indicated in parentheses; [a] signifies the transition was accompanied by thermal decomposition

Complex	Phases and Transition Temperatures						
	K	K′	K″	K‴	B	S_C	I
3 Ni4	• 110 {9.2}	• 303[a] {46.8}				•	
3 Ni6	• 65 {7.5}	• 148 {7.1}	• 241 {13.7}	• 256 {15.6}	• 291[a] {15.9}	• 295[a] {24.7}	•
3 Pd4	• 75	• 321[a]					•
3 Cu4	• 155 {16.5}	• 244 {29.5}			• (242)	• 248[a]	•
3 Cu6	• 145 {4.6}	• 216 {27.6}			• (201)	• 241[a]	•
3 Zn6	• 203 {62.9}						•
4 Ni	• 306[a]						•
5 Ni ph	• 225	• 333[a] {32.9}					•
6 Ni9	• 110	• 238 {43.0}					•
7 Ni8	• 68 {37.5}						•

derivatives, in which axial and equatorial protons are non-equivalent and the couplings are well resolved. However, Hoshino-Miyajima reported the piperazine derivatives in solution and at room temperature to have equivalent axial and equatorial protons. The mechanism for this is quite clearly rapid inversion of the nitrogen in the 4-position, on an NMR timescale, causing a conformational interconversion between chair forms, in which the 4-substituent always remains equatorial. It is this inversion that destabilizes the crystal and does not appear to be detrimental to the mesomorphism, revealing a nematic phase which cannot be seen in the more rigid piperidine complex [6].

Of the mesogenic complexes, **3**, only the nickel and copper derivatives showed liquid-crystalline behaviour, the palladium and zinc complexes being non-mesomorphic. Both the nickel and copper complexes (**3**; M = Ni, Cu; $n = 6$) showed similar phase behaviour. On cooling from the isotropic liquid (**3**; M = Ni, Cu; $n = 6$) a highly birefringent, schlieren texture of a S_C phase was observed. This phase was quite viscous and cohesive and no two brush schlieren could be seen. Further cooling saw a transition to a crystal B phase, in which a mosaic texture and a few focal conic domains were observed. That it was possible to focus well on the texture would seem to preclude the possibility of identification as an S_I phase.

This similarity in phase behaviour of the nickel and copper derivatives is not wholly unsurprising, as typically they adopt essentially isostructural square planar geometries. However, in the solid state, the copper dithiocarbamates tend to associate as weakly bound

dimers, so as to give each of the copper centres a square pyramidal geometry. That this is a weak interaction is indicated by the fact that dissolution in polar solvents invariably generates the monomeric species. We envisage that at the temperatures of the mesophase there is more than sufficient energy to break the dimer, and this is supported by the remarkable similarity to the mesomorphism of monomeric nickel derivative. This square planar geometry, leaves large uncoordinated areas above and below the plane, which are potentially free for dynamic, lateral intermolecular metal/ligand (sulfur) and metal/metal interactions. Originally we had considered the possibility that such interactions might promote the formation of the observed smectic phases, however the observation of a nematic phase in the dithiocarbamate complexes of Hoshino-Miyajima [7] means that this cannot be the case. Thus, the observed smectic behaviour is more likely to be due simply to the alternate areas of high and low polarisability present in the structure.

The palladium derivative (**3**; M = Pd; $n = 4$) was expected to adopt a similar structure to the nickel congener. However that no mesomorphism was observed was probably due simply to the alkyl chain not being sufficiently long to depress the melting point sufficiently to uncover the phase behaviour. No monotropic phases were observed as upon melting, thermal and chemical decomposition occurred. In the zinc derivative (**3**; M = Zn, $n = 6$), no mesomorphism was observed, rather a simple melting into an isotropic state. Simple zinc dithiocarbamates have a great propensity to form dimers in the solid state, which at least in the case of the dithiobenzoate complexes which we studied, persist into the mesophase. Thus, it is not entirely clear why these systems are not mesomorphic.

EXPERIMENTAL

Microanalyses were performed at the Universities of Sheffield and Leeds. IR spectra were recorded as KBr discs on a Perkin–Elmer 1600 Series FTIR. UV spectra were recorded on a Philips PU 8720 UV–vis scanning spectrophotometer. Proton NMR were recorded on a Bruker ACL250 spectrometer; proton chemical shifts are quoted relative to internal $CDCl_3$ or CD_2Cl_2, all proton couplings are in Hz; for structural assignments refer to Fig. 2. Mass spectra were recorded on a Kratos MS25 instrument with a DS55 data system. The mesomorphism was studied by polarising optical microscopy using a Carl Zeiss Labpol microscope equipped with a Linkam TH600 hot stage and a PR600 temperature controller, and by differential scanning callorimitry with a Perkin–Elmer DSC7 instrument. The transition temperatures and phase types were assigned on the basis of the microscopy studies. All chemicals were used as received unless otherwise specified.

4-(4′-Butyloxyphenethyl)piperidine (**1**; $n = 4$)

To a solution of *trans*-4-butyloxy-4′-stilbazole (1.51 g, 5.95×10^{-3} mol), in glacial acetic acid (100 cm^3), platinum(IV) oxide (147 mg, 6.48×10^{-4} mol) was added. The mixture was placed under a hydrogen atmosphere, stirred vigorously and the uptake of hydrogen monitored. After 4 equivalents of hydrogen had reacted, the reaction was stopped. The acetic acid was distilled off under high vacuum, the residue was taken into dichloromethane (150 cm^3), washed with water (5×30 cm^3), and saturated brine solution (1×20 cm^3). The organic phase was dried over anhydrous magnesium sulphate, filtered and the solvent removed under reduced pressure. Crystallisation from methanol gave the colourless, crystalline product 4-(4′-butyloxyphenethyl)-piperidine (0.307 g, 21%). m.p. 91.6°C; (Found: C, 77.7; H, 10.4; N, 5.1. $C_{17}H_{27}ON$ requires C, 78.1; H, 10.4; N, 5.4%); δ_H (250 MHz; $CDCl_3$) 0.97 (3H, t, $^3J_{AB}$ 7.3, H^A), 1.10–1.30 (4H, m br, H^{Ja} and H^B), 1.40–1.60 (4H, m br, H^{Je} and H^H), 1.60–1.80 (3H, m, H^C and H^J), 1.91 (2H, t br, $^2J_{KaKe} = {}^3J_{KaJa}$ 11, H^{Ka}), 2.55 (2H, m, H^G), 2.90 (1H, s, H^L), 2.97 (2H, d, $^2J_{KeKa}$ 11, H^{Ke}), 3.93 (2H, t, $^3J_{DC}$ 6.5, H^D), 6.81 (2H, AA′XX′, $^3J_{FE}$ 8.5, J 2.5, H^E), 7.07 (2H, AA′XX′, $^3J_{EF}$ 8.5, J 2.5, H^F).

Sodium 4-(4′-butyloxyphenethyl)piperidine dithiocarbamate (**2**; $n = 4$)

4-(4′-Butyloxyphenylethyl)piperidine (150 mg, 5.74×10^{-4} mol) and sodium hydroxide (34.2 mg, 8.55×10^{-4} mol) were dissolved in ethanol (10 cm^3) and heated under reflux for 30 mins. Carbon disulfide (5.0×10^{-2} cm^3, 8.5×10^{-4} mol) was added. This solution was cooled to room temperature over a period of 1 h. The product, sodium (4(4′-butyloxyphenethyl) piperidine dithiocarbamate was not isolated but was used *in situ*.

Bis-[4-4′-butyloxyphenethyl)piperidine dithiocarbamatol nickel (II) (**3**; M = Ni; $n = 4$)

To the solution of sodium 4-(4′-butyloxyphenylethyl)piperidine dithiocarbamate (2.8×10^{-4} mol) in ethanol (10 cm^3), a solution of nickel (II) chloride hexahydrate (33 mg, 1.4×10^{-4} mol) in water (2 cm^3) was added. The green product precipitated immediately. The mixture was stirred for 1 hour, filtered, and the crude product washed with water, methanol, ethanol, pentane and hot acetone. Recrystallisation from dichloromethane yielded the product, bis[4-(4′-*n*-butyloxyphenethyl)piperidine dithiocarbamato] nickel (II), (39 mg, 42%). (Found: C, 59.0; H, 7.2; N, 3.8. $C_{36}H_{52}O_2N_2S_4Ni$ requires C, 59.1; H, 7.26; N, 3.8%); δ_H (250 MHz; $CDCl_3$) 0.96 (6H, t, $^3J_{AB}$ 7.2, H^A), 1.20 (4H, quart, $^2J_{JaJe} = {}^3J_{JaKa} = {}^3J_{JaI}$ 12.5, H^{Ja}), 1.35–1.70 (10H, m br, H^B, H^H and H^I), 1.73 (4H, quin, $^3J_{CD} = {}^3J_{CB}$ 7.0, H^C), 1.83 (4H, d br, $^2J_{JeJa}$ 12.5, H^{Je}),

2.50 (4H, t br, $^3J_{GH}$ 8.1, H^G), 2.92 (4H, d*t*, $^2J_{KaKe}$ = $^3J_{KaJa}$ 13, $^3J_{KaJe}$ 3, H^{Ka}), 3.92 (4H, *t*, $^3J_{DC}$ 6.6, H^D), 4.48 (4H, d br, $^2J_{KeKa}$ 13, H^{Ke}), 6.78 (4H, AA′XX′, $^3J_{FE}$ 8.5, H^F), 7.07 (4H, AA′XX′,$^3J_{EF}$ 8.5, H^E).

The synthesis of all other derivatives was carried out in a similar manner to that described above.

4-(4′-*Hexyloxyphenethyl*)*piperidine* (**1**; n = 6)

δ_H (250MHz; $CDCl_3$) 0.90 (3H, t, $^3J_{AB}$ 9.5, H^A), 1.15–1.37 (8H, m br, H^{Ja} and H^B), 1.37–1.58 (4H, m br, H^{Je} and H^H), 1.58–1.83 (3H, m, H^C and H^I), 1.91 (2H, t br, $^2J_{KaKe}$ = $^3J_{KaJa}$ 10.4, H^{Ka}), 2.55 (2H, m, H^G), 2.88 (1H, s, H^L), 2.97 (2H, d, $^2J_{KeKa}$ 10.4, H^{Ke}), 3.92 (2H, t, $^3J_{DC}$ 6.5, H^D), 6.81 (2H, AA′XX′, $^3J_{FE}$ 8.4, J 2.5, H^E), 7.07 (2H, AA′XX′, $^3J_{EF}$ 8.4, J 2.5, H^E).

Bis [4-(4′-*hexyloxyphenethyl*)*piperidine dithiocarbamato*] *nickel* (II) (**3**; M = Ni; n = 6)

Analytical data: Found: C, 60.9; H, 7.6; N, 3.5. $C_{40}H_{60}O_2N_2S_4Ni$ requires C, 61.0; H, 7.7; N, 3.6%; NMR data as for the homologue above.

Bis [4-(4′-*butyloxyphenethyl*)*piperidine dithiocarbamato*] *palladium* (II) (**3**; M = Pd; n = 4)

Analytical data: Found: C, 55.2; H, 6.7; N, 3.55. $C_{36}H_{52}O_2N_2S_4Pd$ requires C, 55.47; H, 6.72; N, 3.59%; NMR data as for the homologue above.

Bis [4-(4′-*butyloxyphenethyl*)*piperidine dithiocarbamato*] *copper* (II) (**3**; M = Cu; n = 4)

Analytical data: Found: C, 58.6; H, 7.2; N, 3.7. $C_{36}H_{52}O_2N_2S_4Cu$ requires C, 58.7; H, 7.1; N, 3.8%; λ_{max} (CH_2Cl_2)/nm 230 (ε/dm^3 mol^{-1} cm^{-1} 27,500), 274 (43,300), 437 (14,000), 508sh (3800) and 610 (1200).

Bis [4-(4′-*hexyloxyphenethyl*)*piperidine dithiocarbamato*] *copper* (II) (**3**; M = Cu; n = 6)

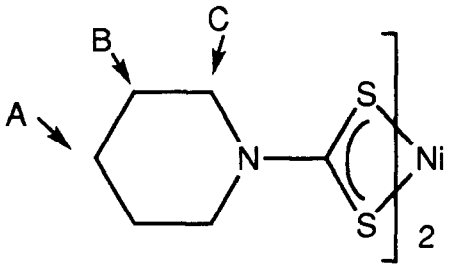
Analytical data: Found: C, 60.5; H, 7.3; N, 3.6; S, 15.8. $C_{40}H_{60}O_2N_2S_4Cu$ requires C, 60.6; H, 7.6; N, 3.5; S, 16.2%; λ_{max} (CH_2Cl_2)/nm 232 (ε/dm^3 mol^{-1} cm^{-1} 23,800), 274 (44,500), 436 (14,100), 442sh (13,800), 505sh (4300) and 607sh (1300).

Bis [4-(4′-*hexyloxyphenethyl*)*piperidine dithiocarbamato*] *zinc* (II) (**3**; M = Zn; n = 6)

Analytical data: Found: C, 60.6; H, 7.5; N, 3.6; S, 16.2. $C_{40}H_{60}O_2N_2S_4Zn$ requires C, 60.5; H, 7.6; N, 3.5; S 16.1%; δ_H (250MHz; $CDCl_3$) 0.90 (6H, t, $^3J_{AB}$ 7.3, H^A), 1.25–1.65 (22H, m br, H^{Ja}, H^B, H^H and H^J), 1.77 (4H, quin, $^3J_{CD}$ = $^3J_{CB}$ 7.0, H^C), 1.88 (4H, d br, $^2J_{JeJa}$ 13, H^{Je}), 2.59 (4H, t br, $^3J_{GH}$ 7.5, H^G), 3.11 (4H, d*t* $^2J_{KaKe}$ = $^3J_{KaJa}$ 13, $^3J_{KaJe}$ 2.3, H^{Ka}), 3.92 (4H, t, $^3J_{DC}$ 6.5, H^D), 4.98 (4H, d br, $^2J_{KeKa}$ 13, H^{Ke}), 6.82 (4H, AA′XX′, $^3J_{FE}$ 8.4, J 2.5, H^F), 7.07 (4H, AA′XX′,$^3J_{EF}$ 8.4, J 2.5, H^E); FAB mass spectrum *m/z* 736 (M^+, 25%), 459 (9), 306 (100), 288 (52), 273 (5), 241 (8) and 195 (9).

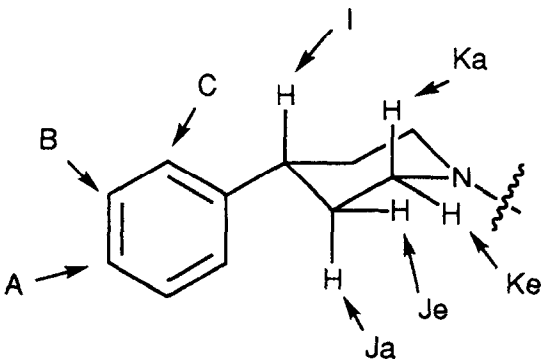
Bis [*piperidine dithiocarbamato*] *nickel* (II) (**4**; M = Ni)

Analytical data: Found : C, 37.9; H, 5.4; N, 7.4; S, 33.4. $C_{12}H_{20}N_2S_4Ni$ requires C, 38.0; H, 5.3; N, 7.4; S, 33.4%; δ_H (250MHz; $CDCl_3$) 1.65 (12H, br m, H^B and H^C), 3.71 (8H, br t, H^A).



Bis [4-*phenylpiperidine dithiocarbamato*] *nickel* (II) (**5**; M = Ni; n = Ph)

Analytical data: Found: C, 54.1; H, 5.5; N, 5.2; S, 23.7. $C_{24}H_{30}N_2S_4Ni$ requires C, 54.2; H, 5.3; N, 5.3; S, 24.1%; δ_H (250MHz, $CDCl_3$) 1.74 (4H, d quart, $^2J_{JaJe}$ = $^3J_{JaI}$ = $^3J_{JaKa}$ 13, $^3J_{JaKe}$ 5, H^{Ja}), 1.98 (4H, br d, $^2J_{JeJa}$ 14, H^{Je}), 2.85 (2H, t t, $^3J_{IJa}$ 15, $^3J_{IJe}$ 3.4, H^I), 3.03 (4H, d t, $^2J_{KaKe}$ = $^3J_{KaJa}$ 13, $^3J_{KaJe}$ 3, H^{Ka}), 4.74 (4H, br d, $^2J_{KeKa}$ 14, H^{Ke}), 7.20–7.35 (6H, m, H^A, H^B and H^C).



Bis [4-*nonylpiperidine dithiocarbamato*] *nickel* (II) (**6**; M = Ni; n = 9)

Analytical data: found: C, 57.0; H, 8.8; N, 4.5; S, 20.2. $C_{30}H_{56}N_2S_4Ni$ requires C, 57.0; H, 8.9; N, 4.4; S, 20.3%; λ_{max} (CH_2Cl_2)/nm 244 (ε/dm^3 mol^{-1} cm^{-1} 37,800), 328 (37,600), 383sh (6500), 394 (6900), 429sh

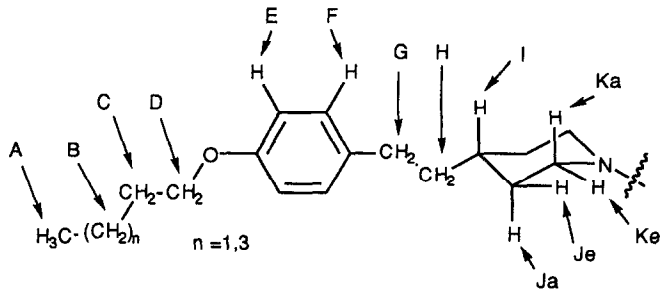


Fig. 6. The assignment of protons for the NMR of **1**; $n = 4$, 6, and **3**; M = Ni, Pd, Zn; $n = 4$, 6.

(1400) and 476sh (200); δ_H (250MHz; $CDCl_3$) 0.88 (6H, t, $^2J_{AB}$ 6, H^A), 1.07–1.40 (16H, br m, H^B and H^{Ja}), 1.55 (2H, m, H^I), 1.78 (4H, br d, $^2J_{JeJa}$ 14, H^{Je}), 2.89 (4H, d t, $^2J_{KaKe} = {}^3J_{KaJa}$ 13, $^3J_{KaJe}$ 3.8 H^{Ka}), 4.52 (4H, br d, $^2J_{KeKa}$ 13, H^{Ke}).

Acknowledgements—Finally, we would like to thank SERC for support (DJP, MAW) and Johnson Matthey for loans of palladium salts.

REFERENCES

1. D. W. Bruce in *Inorganic Materials* (Edited by D. W. Bruce and D. O'Hare), p. 405, Wiley, Chichester (1992); D. W. Bruce, *J. Chem. Soc., Dalton Trans.* 1993, 2983; P. Espinet, M. A. Esteruelas, L. A. Oro, J. L. Serrano and E. Sola, *Coord. Chem. Rev.* 1992, **117,** 215; A.-M. Giroud-Godquin and P. M. Maitlis, *Angew. Chem., Int. Ed. Engl.* 1991, **30,** 375; S. A. Hudson and P. M. Maitlis, *Chem. Rev.* 1993, **93,** 861.
2. D. Vorländer, *Ber. Dt. Chem. Ges.* 1910, **43,** 3130.
3. A.-M. Giroud and U. T. Mueller-Westerhoff, *Mol. Cryst., Liq. Cryst.*, 1977, **41,** 11.
4. K. Ohta, H. Ema, Y. Morizumi, T. Watanabe, T. Fujimoto and I. Yamamoto, *Liq. Cryst.* 1990, **8,** 311.
5. H. Adams, A. C. Albeniz, N. A. Bailey, D. W. Bruce, A. S. Cherodian, R. Dhillon, D. A. Dunmur, P. Espinet, J. L. Feijoo, E. Lalinde, P. M. Maitlis, R. M. Richardson and G. Ungar, *J. Mater. Chem.* 1991, **1,** 843.
6. K. Ohta, H. Hasebe, H. Ema, T. Fujimoto and I. Yamamoto, *J. Chem. Soc. Chem. Commun.* 1989, 1610.
7. N. Hoshino-Miyajima, *J. Chem. Soc., Chem. Commun.* 1993, 1442.
8. R. Eisenberg, *Prog. Inorg. Chem.* 1970, **12,** 295; D. Coucouvanis, *Prog. Inorg. Chem.* 1970, **11,** 233.
9. J. L. Martinez, D. W. Bruce, D. J. Price and P. J. Alonso, *Liq Cryst* 1995, **19,** 127.
10. D. W. Bruce, D. A. Dunmur, E. Lalinde, P. M. Maitlis and P. Styring, *Liq. Cryst.* 1988, **3,** 385.

Pergamon

S0277-5387(96)00237-9

Polyhedron Vol. 16, No. 2, pp. 321 325, 1997
Copyright © 1996 Elsevier Science Ltd
Printed in Great Britain. All rights reserved
0277-5387/97 $15.00+0.00

Synthesis and crystal structure of the cryptate complex $[Gd(L)(DMF)] \cdot KSCN \cdot CH_3CN \cdot 3H_2O$ (L is a deprotonated phenol-based N_8O_3 cryptand)

Shu-Yan Yu,[a] Quan-Ming Wang,[a] Biao Wu,[a] Xin-Tao Wu,[a]* Huai-Ming Hu,[b] Liu-Fang Wang[c] and An-Xin Wu[c]

[a]State Key Laboratory of Structural Chemistry, Fujian Institute of Research on the Structure of Matter, Chinese Academy of Sciences, Fuzhou, Fujian 350002, P.R. China

[b]State Key Laboratory of Coordination Chemistry, Nanjing University, Nanjing 210093, P.R. China

[c]Department of Chemistry, Lanzhou University, Lanzhou 730000, P.R. China

(Received 23 February 1996; accepted 1 May 1996)

Abstract—The cryptate complex $[Gd(L)(DMF)] \cdot KSCN \cdot CH_3CN \cdot 3H_2O$ has been synthesized by the reaction of gadolinium isothiocyanate and potassium thiocyanate with cryptate $[Na(H_2L)]$, which was prepared by a (2+3) Schiff-base condensation of tris(2-aminoethyl)amine and 2,6-diformyl-4-methoxyphenol in the presence of NaOH. The Gd atom is encapsulated in the cryptand with an unsymmetric eight-coordinate environment. Copyright © 1996 Elsevier Science Ltd

Keywords: gadolinium; cryptate; complex; cryptand; synthesis; structure.

Much current attention has been devoted to the design and synthesis of lanthanide complexes of macrocyclic ligands [1]. Their studies are extensively correlated with many emerging fields of application, such as supramolecular devices [2–4], luminescent labels and fluorescent probes in biological and medical applications [5], magnetic resonance imaging [6] and catalytic cleavage of RNA [7], etc. The lanthanide complexes of phenol-based two-dimensional macrocyclic ligands have been extensively studied up to 1995. Drew [8] reported several kinetically stable lanthanide complexes of phenol-based protonated cryptands (three-dimensional macrobicyclic ligands). Recently, we synthesized a series of lanthanide cryptates with deprotonated analogous cryptands. Herein we describe the synthesis and crystal structure of $[Gd(L)(DMF)] \cdot KSCN \cdot CH_3CN \cdot 3H_2O$. Owing to the compartment coordination, the cryptate possesses an unsymmetrical mononuclear eight-coordinate conformation.

* Author to whom correspondence should be addressed.

EXPERIMENTAL

Gadolinium isothiocyanate was prepared from the reaction of gadolinium chloride (99.9%, China) and potassium thiocyanate. Tris(2-aminoethyl)amine and 2,6-diformyl-4-methoxyphenol were prepared by the modified methods according to Kimura [9] and Hu [10], respectively. Elemental analysis was carried out by the analytical division of the State Key Laboratory of Structural Chemistry. NMR, IR and UV-vis spectra were recorded on Varian Unity 500, Perkin–Elmer 577 and Shimadzu UV-3000 instruments, respectively.

Synthesis of $[Na(H_2L)]$

To a stirred suspension of NaOH (0.060 g, 1.5 mmol) and 2,6-diformyl-4-methoxyphenol (0.270 g, 1.5 mmol) in anhydrous methanol (50 cm^3) was added dropwise an anhydrous methanol solution (50 cm^3) of tren (0.146 g, 1 mmol) at room temperature over 1 h. The resulting orange precipitate was filtered off and recrystalized from chloroform, yield 71%. Found: C,

62.6; H, 6.5; N, 15.2. Calc. for $C_{39}H_{47}N_8O_6Na$: C, 62.7, N, 15.0%. ^1H NMR (d_6-DMSO, TMS): δ 13.78 (s(br), 2H, ph-OH), 8.45 (s(br), 6H, imino-CH), 6.94 (s(br), 6H, ph-H), 3.67 (s, 9H, OCH_3), 3.59, 3.55 (d, 12H, H_2C—N (imino)), 2.81 (s(br), 12H, H_2C—N (bridgehead)). IR (cm^{-1}, KBr disc.): 3543w (υ_{OH}), 3411, 3244, 3012, 2995, 2939, 2906, 2842, 2810, 1643s ($\upsilon_{C=N}$), 1597, 1460, 1317, 1259, 1155, 1051, 960, 815, 754. UV–vis spectrum (CH_3CH): 258 (ε_{mol} 14900 dm^3 cm^{-1} mol^{-1}), 370 nm (10000).

Synthesis of [Gd(L)(DMF)]·KSCN·CH_3CN·$3H_2O$

A mixture of [Na(H_2L)] (0.149 g, 0.2 mmol) in acetonitrile (20 cm^3) and aqueous gadolinium isothiocyanate (0.176 g, 0.4 mmol) and potassium thiocyanate (0.02 g, 0.2 mmol) in ethanol (30 cm^3) was stirred and heated for 0.5 h. The reaction solution was filtered and the yellow filtrate stood for several minutes, yellow microcrystals were isolated. The crude product is redissolved into DMF by slow diffusion of ether over a week, yellow crystals suitable for X-ray structure determination were obtained, yield 75%. Found: C, 47.4; H, 5.1; N, 13.7. Calc. for $C_{45}H_{61}N_{11}O_{10}SGdK$: C, 47.2; H, 5.4; N, 13.5%. IR (cm^{-1}, KBr disc.): 3420w (υ_{OH}), 2056s (υ_{SCN}), 1652s ($\upsilon_{C=N}$), 1636sh, 1604, 1545, 1470, 1345, 1295, 1220, 1037, 796. UV–vis spectrum (CH_3CN): 260 (ε_{mol} 14300), 475 nm (11800).

X-ray crystal structure determination of [Gd(L)(DMF)]·KSCN CH_3CN·$3H_2O$

A yellow block crystal encapsulated with gel possessing approximate dimensions $0.35 \times 0.25 \times 0.25$ mm was mounted on a glass fibre in a random orientation. The unit cell parameters were determined from least-squares refinement of the setting angle ($12 < \theta < 14°$), for 19 reflections. Intensity data were recorded on an Enraf–Nonius CAD4 diffractometer at 23°C, using graphite-monochromated Mo-K_α radiation ($\lambda = 0.71073$ Å). A total of 9640 reflections were measured, of which 9207 were unique and 5963 with $\imath > 3.0\ \sigma\ (\imath)$ were used in the refinement (ω-2θ scan type, $2\theta_{max} = 50°$, scan rate 1–7° min^{-1} in ω). Three representative reflections were measured every 120 mins, no significant decay was observed. Lorentz-polarization and empirical absorption corrections were applied. Intensities of equivalent reflections were averaged. The structure was solved by Patterson heavy-atom method using MolEN [11] program, which revealed the coordinates of the Gd atom. The remaining non-hydrogen atoms were located in succeeding difference Fourier syntheses. Hydrogen atoms were located theoretically and not refined. The K atom is disordered. All calculations were performed on a COMPAQ PL4/50 computer. See details in Table 1.

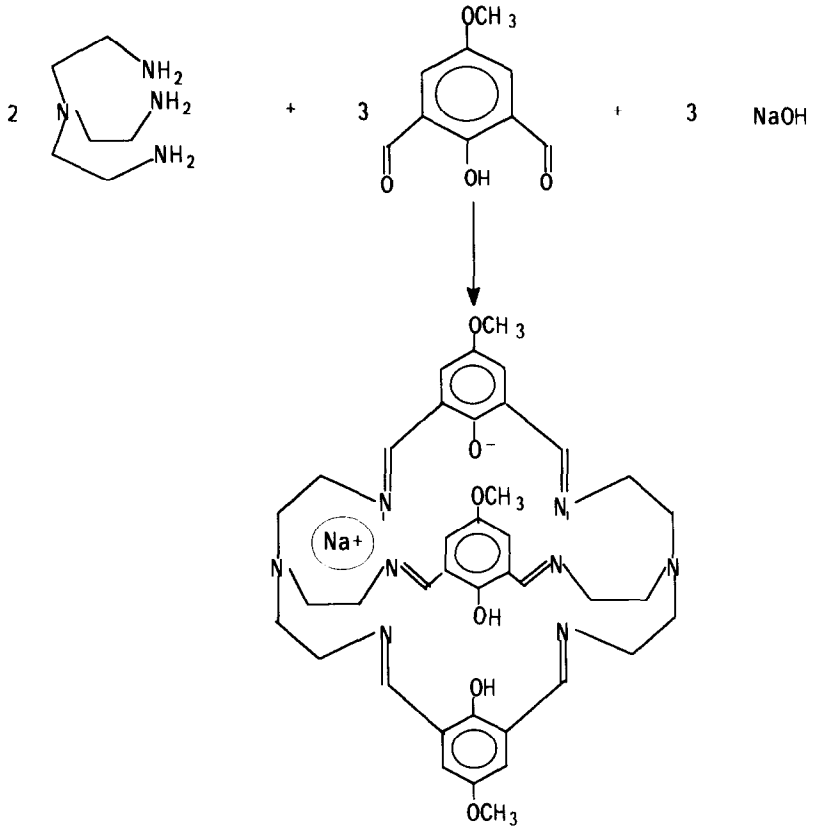
Table 1. Crystal data for [Gd(L)(DMF)]·KSCN·CH_3CN·$3H_2O$

Formula	$C_{45}H_{61}N_{11}O_{10}SGdK$
F.W.	1144.47
$F(000)$	1174
Crystal dimensions	$0.35 \times 0.25 \times 0.25$ mm
Radiation	Mo-Kα($\lambda = 0.71073$ Å)
Temperature (°C)	23
Crystal system	triclinic
Space group	P-1
a (Å)	13.354(3)
b (Å)	13.674(5)
c (Å	15.777(2)
α (°)	89.04(2)
β (°)	93.51(1)
γ (°)	114.20(3)
V (Å^3)	2622(1)
Z	2
D_{calc} (g cm^{-3})	1.45
μ (cm^{-1})	14.5
Scan type	ω-2θ
Scan rate (° min^{-1} in ω)	1–7
Maximum 2θ (°)	50.0
Range of h, k, l	0–15, −16–16, −18–18
Refl. measured	9640 total, 9207 unique
R_{int}	0.053
T_{max} and T_{min}	0.998, 0.845
Least-squares weights	1.0 if $F_0 < 56.5$ $(56.5/F_0)^2$ if $F_0 \geqslant 56.5$
Reflections included	5963 with $\imath > 3.0\ \sigma\ (\imath)$
Parameters refined	561
R	0.073
R_w	0.086
Goodness-of-fit	1.04
Largest shift	0.05
High and Low peak in final map (e Å)	1.93, −0.19

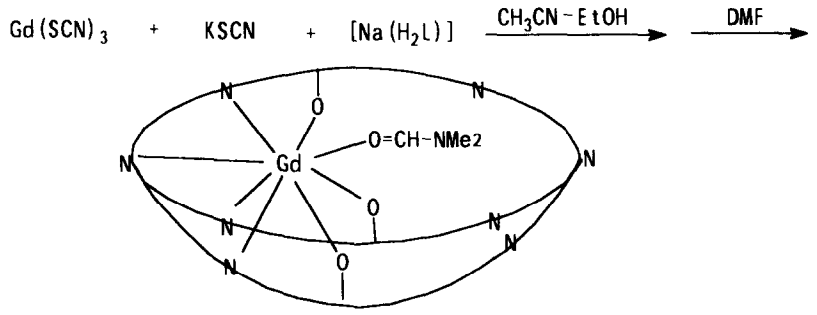
RESULTS AND DISCUSSION

Cryptate [Na(H_2L)] was synthesized by a facile sodium template reaction as shown in Scheme 1.

Only one phenolic proton was replaced by NaOH in the formation of the cryptand, resulting in a mono sodium cryptate. This template effect is different from the sodium template synthesis of phenol-based two-dimensional macrocycles [12]. The cavity size plays an important role in synthesis of the sodium cryptate. The IR spectra show no bands with the characteristic stretching frequency of the carbonyl groups and the primary amine groups. However, the cryptate possesses a very strong absorption band at 1643 cm^{-1}, assigned to the imino stretching mode, supporting the Schiff-base linkage. There are some broad peaks in its ^1H NMR spectra, perhaps resulting from a rapid conformational exchange. At room temperature, distinguishable NMR splitting similar to the unsymmetric sodium mononuclear cryptates described by Nelson *et al.* [13–14] was not observed.



Scheme 1.



Scheme 2.

The complex $[Gd(L)(DMF)]\cdot KSCN\cdot CH_3CN\cdot 3H_2O$ was synthesized as shown in Scheme 2.

The crude product isolated from CH_3CN—EtOH is difficult to dissolve in normal solvents. Thus the pure thiocyanate coordinate cryptate failed to be obtained. When redissolved in DMF, the crystals composed of a Gd cryptate [Gd(L)(DMF)] and a KSCN were obtained. In the IR spectra, the very strong vibration absorption of SCN is observed at 2056 cm^{-1}. The crystal structure of [Gd(L)(DMF)] is illustrated as Fig. 1.

The Gd^{III} ion is linked to one bridgehead nitrogen (N1) and three imino-nitrogen atoms (N(11), N(21) and N(31)) as well as three phenol-oxygen atoms (O(1), O(2) and O(3)), forming a $N_4(O\text{-})_3$ coordination inside the cryptand. DMF acts as another O donor to the Gd atom. The other nitrogen donors of the cryptand (N(2), N(12), N(22) and N(32)) are not bonded to the Gd atom. The cryptand gives three coordinated imino N donors (N(11), N(21), N(31)) at one side, and three uncoordinated imino N atoms (N(12), N(22), N(32)) at another side. Thus, the metal ion is eight-coordinate and is unsymmetrically encapsulated in the cryptand. The coordination geometry about the Gd atom can be considered as a distorted dodecahedron, being isostructural with the complexes of the neutral cryptand [8]. This unsymmetric conformation was also observed in mononuclear Na^+, Zn^2, Pb^{2+} and Cd^{2+} complexes of neutral phenol-based cryptands [13, 14]. Selected bond lengths (Å) and angles (°) are shown in Table 2.

The average Gd—O (phenol) distance is 2.316 Å,

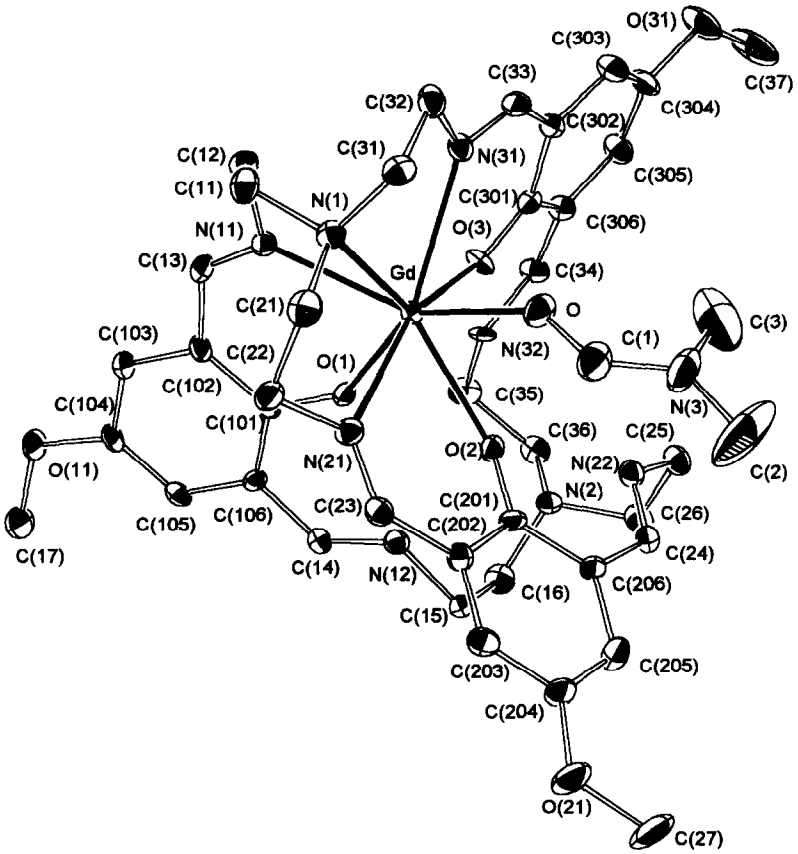


Fig. 1. Structure of cryptate [Gd(L)(DMF)].

Table 2. Selected bond lengths (Å) and angles (°) with e.s.d.s in parentheses

Gd—O	2.354(9)	N(21)—C(23)	1.27(2)
Gd—O(1)	2.311(8)	N(31)—C(33)	1.26(2)
Gd—O(2)	2.376(9)	N(12)—C(14)	1.32(2)
Gd—O(3)	2.260(8)	H(22)—C(24)	1.29(1)
Gd—N(1)	2.64(1)	N(32)—C(34)	1.34(2)
Gd—N(11)	2.50(1)	Gd···N(2)	5.74(1)
Gd—N(21)	2.497(9)	Gd···N(12)	4.47(1)
Gd—N(31)	2.59(2)	Gd···N(22)	4.52(1)
N(11)—C(13)	1.28(2)	Gd···N(32)	4.45(1)

O—Gd—O(1)	143.0(3)	O(2)—Gd—N(1)	133.9(3)
O—Gd—O(2)	72.3(3)	O(2)—Gd—N(11)	140.4(3)
O—Gd—O(3)	98.1(3)	O(2)—Gd—N(21)	71.7(3)
O—Gd—N(1)	81.4(4)	O(2)—Gd—N(31)	133.4(3)
O—Gd—N(11)	145.3(4)	O(3)—Gd—N(1)	135.1(3)
O—Gd—N(21)	84.2(3)	O(3)—Gd—N(11)	95.6(4)
O—Gd—N(31)	70.6(4)	O(3)—Gd—N(21)	156.4(4)
O(1)—Gd—O(2)	70.7(3)	O(3)—Gd—N(31)	71.9(3)
O(1)—Gd—O(3)	78.6(3)	N(1)—Gd—N(11)	66.6(3)
O(1)—Gd—N(1)	126.7(3)	N(1)—Gd—N(21)	68.4(3)
O(1)—Gd—N(11)	71.0(3)	N(1)—Gd—N(31)	65.6(3)
O(1)—Gd—N(21)	85.6(3)	N(11)—Gd—N(21)	95.6(3)
O(1)—Gd—N(31)	138.9(2)	N(11)—Gd—N(31)	83.8(3)
O(2)—Gd—O(3)	86.5(3)	N(21)—Gd—N(31)	130.0(3)

consistent with the range in the complexes of phenol-based cryptands [8] and macrocyclic [15] as well as tripodal hemi-cage ligands [16,17]. The average Gd—N (imino) bond distance is 2.529 Å, being shorter by 0.1 Å than that in the normal macrocyclic complexes [1]. Comparing the bond lengths of C=N, we can see that the average distance of coordinated imino groups is shorter by 0.05 Å than that of uncoordinated ones, showing that coordination caused π electron of bis(iminophenol) moieties of the cryptand to be transferred to the metal ion. The distances of Gd···N (uncoordinated) are in the range of 4.45(1)-5.74(1) Å. This size may be expected to provide coordination to a second metal ion, but the second lanthanide or sodium ion failed to be encapsulated possibly owing to their high coordination numbers or large radii. In other words, this compartment cryptand only recognizes selectively one lanthanide(II) ion or sodium ion.

Acknowledgements—We thank the State Key Laboratories of Structural Chemistry and Coordination Chemistry of China as well as the Chinese Postdoctoral Science Foundation for support.

REFERENCES

1. V. Alexander, *Chem. Rev.* 1995, **95**, 273.
2. J.-M. Lehn, *Angew. Chem., Int. Ed. Engl.* 1988, **27**, 89.
3. V. Balzani and F. Scandola, *Supramolecular Photochemistry*. Horwood, Chichester, U.K. (1991).
4. N. Sabbatini and M. Guardigli, *Mater. Chem. Phys.* 1992, **31**, 13.
5. J.-C. G. Bunzli, in *Lanthanide probes in Life, Medical and Environment Sciences* (Edited by G. R. Choppin and J.-C. G. Bunzli), chap. 7. Elsevier, Amsterdam, The Netherlands (1989).
6. K. Kumar and M. F. Tweedle, *Pure Appl. Chem.* 1993, **65**, 515.
7. R. Breslow and D.-L. Hunang, *Proc. Natl Acad. Sci. U.S.A.* 1991, **88**, 4080.
8. M. G. B. Drew, O. W. Howarth, C. J Harding, N. Martin and J. Nelson, *J. Chem. Soc., Chem. Commun.* 1995, **8**, 903.
9. E. Kimura, S. Young and J. P. Collman, *Inorg. Chem.* 1990, **9**, 1183.
10. Y. Hu and H. Hu, *Chem. J. Chin. Univ.* 1986, **7**, 132.
11. MolEN, *An Interactive Structure Solution Procedure*. Enrad-Nonius, Delft, The Netherlands (1990).
12. S. Gou and D. E. Fenton, *Inorg. Chim. Acta.* 1994, **223**, 169.
13. M. G. B. Drew, O. W. Howarth, G. G. Morgan and J. Nelson, *Chem. Soc., Chem. Commun.* 1994, **21**, 3149.
14. V. McKee, M. Dorrity, J. Malone, D. J. Marrs and J. Nelson, *J. Chem. Soc., Chem. Commun.* 1992, **4**, 383.
15. I. A. Kahwa, S. Folkes, D. J. Williams, S. V. Ley, C. A. O'Mahoney and G. L. McPherson, *J. Chem. Soc., Chem. Commun.* 1989, **20**, 1531.
16. S. Liu, L. Gelmini, S. J. Rettig, R.-C. Thompson and C. Orvig, *J. Am. Chem. Soc.* 1992, **114**, 6081.
17. S. Liu, L.-W. Yang, S. J. Rettig, and C. Orvig, *Inorg. Chem.* 1993, **32**, 2773.

Pergamon

S0277-5387(96)00215-X

Polyhedron Vol. 16, No. 2, pp. 327–334, 1997
Copyright © 1996 Elsevier Science Ltd
Printed in Great Britain. All rights reserved
0277-5387/97 $15.00+0.00

Reaction mechanism of copper(I) catalysed head-to-head dimerization of 1-alkynes: an experimental and theoretical study

Nurettin Balcioğlu,* İnci Uraz (Ünalan), Cetin Bozkurt and Fatma Sevin

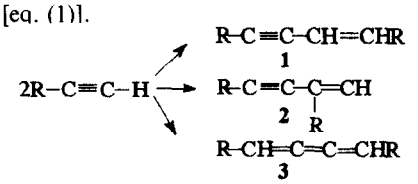
Department of Chemistry, Hacettepe University, Beytepe 06532, Ankara, Turkey

(Received 8 February 1996; accepted 26 April 1996)

Abstract—The Strauss reaction is regioselective and unique for the head-to-head coupling of terminal acetylenes. For the success of the catalytic conversion, the presence of copper(I) carboxylate is necessary. The corresponding carboxylic acid may be used pure, as solvent, or diluted in non-nucleophilic solvents. However, its presence in excess is also necessary. The formation of the product, 1,4-dialkylenynes, shows some stereoselectivity. The *E* isomer is always dominant in the mixture, but the *E*/*Z* ratio may be manipulated by the steric effects of the R groups of the carboxylic acid and of the monomers as well. The nucleophilic solvents such as H_2O, ROH and phosphine ligands inhibit the catalytic reaction. The isolated products are the copper acetylides or its phosphine complexes, respectively. Mesitylacetylene and *p*-nitrophenylacetylene do not undergo the catalytic conversion. However, the former gives the cross-product with phenylacetylene. The possible mechanism of the reaction is discussed and the suggested pathway is supported with computational calculations. Copyright © 1996 Elsevier Science Ltd

Seeking simple synthetic routes to enynes becomes extremely important since these compounds not only appear in natural products, but can also be used as building blocks for more complex hydrocarbon structures.

1-Alkynes dimerize in different ways producing head-to-head **1**, head-to-tail **2** and cumulene **3** products [eq. (1)].



(1)

Dimerization of 1-alkynes has been extensively studied with a variety of transition-metal catalysts. $[Cr(O\text{-}Bu\text{-}n)4]/ZnEt_2$,[1] $[RhCl(PPh_3)]_3$,[2] $Pd(OAc)_2$/tris(2,6-dimethoxyphenyl-phosphine),[3] $[Rh(PMe_3)_2Cl]_2$[4] and $(\eta^5\text{-}C_6Me_5)_2TiCl_2/RMgX$[5] are representative catalysts for head-to-tail dimerization of 1-alkynes to convert them to **2**.

Cationic Lewis-base free zirconocene complexes such as $\{Zr(C_5Me_5)_2Me\{B(4\text{-}C_6H_4F)_4\}$ also form **2**. However, this catalyst is particularly efficient for the oligomerization of terminal acetylenes.[6] Strauss coupling, the non-oxidative head-to-head coupling of terminal alkynes produces both the *Z* and the *E* isomers of the corresponding enynes **1**.[7] Similar head-to-head couplings with yields up to 21% of the (*Z*)-enyne is observed when phenylacetylene is heated with the catalytic amount of cationic hydride of ruthenium. $[Ru(CO)H(CN\text{-}Bu^t)(C_5H_5N)(PPh_3)_2]\cdot PF_6$ catalyses the dimerization of phenylacetylene in ethanol giving an *E* and *Z* mixture of 1,4-diphenylbuten-3-ynes.[8] Ruthenium complexes, such as [Ru(cod)(cot)] (cod = 1,5-cyclooctadiene, cot = cyclooctatriene) and $[Ru(CO)(PPh_3)_3(H)_2]$, are unique catalysts to convert 1-alkynes to cumulene derivatives **3**.[9] A similar reaction takes place with trimethysilyl[10] or with *t*-butylacetylene.[11] In all these cases 1,3-enynes appear to be the by-products of the reaction.

Mechanisms of Ti-, Rh- and Ru^{II}-catalysed dimerization reactions have been analysed in great detail.[4,5,8] However, not much is known about the mechanism of Cu^I-catalysed dimerization of 1-alkynes.

In this work we report our investigation of the mechanism of copper-mediated head-to-head dimer-

* Author to whom correspondence should be addressed.

ization of 1-alkynes by analysing the effects of different parameters on the progress of this convenient reaction.

RESULTS

The standard Strauss reaction was carried out by refluxing alkylacetylenes and Cu_2O in glacial acetic acid under nitrogen. A mixture of (*Z*)- and (*E*)-1,4-dialkyl butenyne was obtained. A small amount (~%1) of 1,4-dialkyl butadiyne was also formed. The progress of the reaction was followed by the colour of the mixture. The brick red colour of the initial solution was changed in about 1 h over yellow to blue–green, accompanied by the separation of metallic copper. The orange and blue–green colour of the solution results from the formation of the intermediates such as alkylacetylide and $Cu(OAc)_2$ sequentially.

The progress and yield distribution of the reaction was affected by the variations of the solvents, catalyst components, alkyl groups of the monomers as well as upon the addition of the secondary ligands, such as PR_3, ROH and H_2O, to the reaction mixture.

Variation of the catalyst components

It was attempted to catalyse the reaction by sequentially replacing the metallic and anionic part of the catalyst. In the presence of the acetates of the monovalent and divalent main group elements such as Na^I, Li^I and Mg^{II}, the dimerization did not occur. The starting compounds were completely recovered. The same experiments with the acetates of the d^{10} transition metals Ag^I and Hg^{II} resulted in the corresponding acetylide formation in stoichiometric amounts. The d^8, d^6 and d^5 complexes Ni^{II}, Cr^{III} and Fe^{III} are totally inactive under the applied standard reaction conditions. A d^9 complex, the copper(II) acetate, also catalysed the dimerization of the terminal acetylenes, giving a similar product distribution as the Cu^I-catalysed reactions. It is shown, however, that the real catalyst here is again the Cu^I species, which is formed by the disproportionation of the initial Cu^{II} complexes.[12]

The anionic part of the catalyst is also very important. As with Cu^I, the presence of the carboxylate is also necessary for the success of the catalytic Strauss reaction. It may be introduced directly as copper(I) acetate or may be produced in the reaction mixture over the precursors such as the oxide or acetylides of Cu^I when the carboxylic acids are used as solvents [eqs (2) and (3)].

$$Cu_2O + CH_3COOH \rightarrow 2CuOAc + H_2O \quad (2)$$

$$R{-}C{\equiv}Cu + CH_3COOH \rightleftharpoons CuOAc + R{-}C{\equiv}C{-}H. \quad (3)$$

The conjugate bases of strong inorganic acids like the halides are not suitable as catalyst components. The existence of the equilibrium in eq. (3) has been proven by deuterium exchange.[12]

Solvent and ligand effects

The Strauss reaction succeeds only in the presence of excess carboxylic acids. Carboxylic acids may be used as solvents in pure or in diluted form. In the repeated experiments using Cu^IOAc, in the absence of simple carboxylic acids, using either excess of the monomer or different solvents such as *n*-decane, nitrobenzene, *n*-butanol and dichloroacetic acid, the dimerization did not occur.[13] The reaction was stopped at the acetylide formation step, except in dichloroacetic acid. In this solvent the acetylide formation was not observed. A 1 : 1 mixture of the carboxylic acid with the above-mentioned solvents gave different results. In the presence of nitrobenzene the reaction was complete, as in the standard condition, in *ca* 1 h with the same product distribution. The presence of *n*-decane reduced the rate of the reaction significantly. Here, the reaction terminated in 3 h, with the same product composition. In the presence of *n*-butanol the dimerization failed. Only Cu^Iacetylide was isolated from the reaction mixture. Similar results were obtained when the reaction was repeated in aqueous acetic acid (90%). The reaction was stopped at the acetylide formation step. The addition of an equivalent amount of the trialkyl phosphine resulted in the formation of the corresponding Cu^Ialkylacetylide trialkyl phosphine complex, without the formation of the expected enynes.

Substituent effects

The progress and product distribution of the Strauss reaction depends strongly on the nature of the alkyl groups of the monomer and of the carboxylic acids used as solvents.

The results of the experiments concerning the latter effect are given in Table 1, with the steric parameters, *V*, of the alkyl groups, evaluated from the van der

Table 1. Product distribution of the phenylacetylene dimerization depending on the steric effects of the alkyl groups of the carboxylic acid used as solvents

R	*Z*, 1 (%)	*E*, 2 (%)	Diyne (%)	*E*/*Z*	V
Me	17.6	80.5	1	4.6	0.52
Et	22.5	74.0	1	3.3	0.56
Pr-n	28.3	70.9	1.1	2.5	0.68
Pr-i	32.0	47.5	1.5	1.5	0.76
Bu-i	37.5	53.8	2.6	1.4	0.98
n-Pentyl	20.3	40.6	1.0	2.0	0.68
3-Heptyl	2.7	3.5	1.3	1.3	1.02

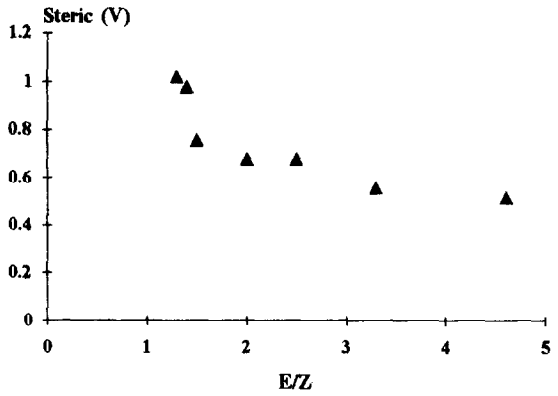
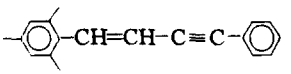


Fig. 1. Correlation between the E/Z ratio and steric parameters of the substituents.

Waals radius.[14] Steric parameters roughly correlate with the E/Z ratio (Fig. 1).

Comparative experiments in glacial acetic acid, using phenylacetylene and 1-hexyne, gave a different product distribution. The E/Z ratio was changed from 4.6 to 1.7 when the phenyl group was replaced by the *n*-butyl group. The attempted dimerization of the *p*-nitrophenylacetylene and mesitylacetylene failed. Only their copper(I) acetylide complexes were isolated.

Cross-dimerization of *p*-nitrophenylacetylene with the mesityl and phenylacetylene compounds also failed. The copper(I) *p*-nitrophenylacetylide complex was formed if mesitylacetylene was used as the reaction partner. In the presence of phenylacetylene, only the corresponding dimer of phenylacetylene with an E/Z ratio of 2.5 was formed. Cross-dimerization of phenyl and mesitylacetylenes was successfully accomplished. Approximately 23% of the homodimer of phenylacetylene (E/Z: 3.1) and 13% of the cross-dimer (E/Z: 3.3) were formed. The formation of the cross-dimer was regioselective. In the isolated product, while the phenyl group is attached to the acetylenic end, the mesityl group is connected to the olefinic end of the molecule.[15]



In the MS spectra of both isomers the characteristic peak of mesitylacetylide was not observed, the most eminent peak, m/z: 101, corresponding to phenylacetylide fragment.

DISCUSSION

It can be concluded from the foregoing experimental facts that there are four significant steps in the catalytic dimerization of the terminal acetylenes:

(i) the acetylide formation from the monomer;
(ii) C—C bond formation;
(iii) the protonation of the intermediate to give the free dimer and to regenerate the catalyst;
(iv) termination of the catalytic cycle.

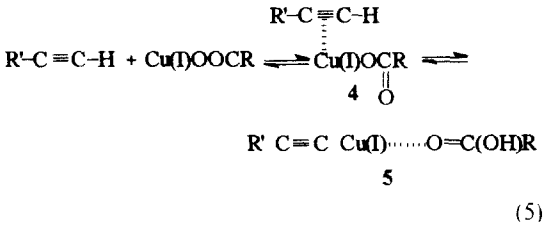
For the sake of clarity each step will be discussed separately.

(i) *Formation of the acetylide*

As mentioned above, the presence of the carboxylate anions is essential for the formation of the corresponding acetylides, which are the real intermediates of the Strauss reaction. The carboxylate anion might be introduced directly as metal salts or may be generated *in situ* in carboxylic acid solvents using suitable precursors [eq. (4)].

$$Cu_2O + 2RCOOH \rightarrow 2CuOCOR + H_2O. \quad (4)$$

However, the formation of the carboxylates is not sufficient for the acetylide formation. Also the presence of strong π-bonding transition metals is necessary. Obviously, the terminal acetylenes are sufficiently activated upon complexation with the d^{10} transition metals, such as Cu^{I}, Ag^{I} and Hg^{II}, to donate the acetylenic proton to a weak base such as the carboxylate anions [eq. (5)].



(5)

Complexes **4** and **5** are not isolated. However the structure of the related phosphine complexes are known.[16] Furthermore the properties of the corresponding $Ag^{I}OTf$ complex have been studied and it has been shown that the deuterium exchange rate of the terminal acetylenes increased more than 10^5 upon complexation. In the suggested mechanism the incorporation of the silver acetylide formation was excluded.[17] In our labelling experiment we have also observed a fast deuterium exchange under the standard Strauss reaction conditions. We believe, however, that in the presence of a relatively strong base, such as the carboxylate anion, the loss of deuterium from the penylacetylene-1-D should involve the intermediate acetylide formation.

Failure of the acetylide formation, in the experiments using dichloroacetic acid as solvent, might be attributed to the weakness of the conjugate base of the dichloroacetic acids. The basicity of dichloroacetates is *ca* 3.5×10^3-fold lower than the simple alkyl carboxylates in aqueous solution. In order to obtain an idea about the degree of activation by complex formation, we have calculated the theoretical acidities of the terminal acetylenes and of some acidic solvents used in this study. The semiempirical method,

PM3, was used to calculate the AH and A^- values in eq. (6). The experimental heat of formation of H^+ (366.05 kcal mol^{-1}) was used in the calculation of the AH value.

$$AH \rightleftharpoons A^- + H^+$$

$$\Delta H_A = H_f^{A^-} + H_f^{H^+} - H_f^{AH}. \quad (6)$$

In Table 2 along with the theoretical acidities and heat of formation, H_f, HOMO and LUMO energy levels of the monomers and its conjugate bases calculated using the PM3 and EHM methods are given as well as the results of the similar calculation for acetic acid and dichloroacetic acid used as solvent given together. According to these calculations, in the presence of the acetate anion, the acidity of the phenylacetylene should be increased by *ca* 30 kcal mol^{-1} for the generation of a significant amount of phenylacetylide in the equilibrium. On the other side, generation of the same moiety by the dichloroacetate anion required much higher energy, *ca* 45 kcal mol^{-1}. Another interesting feature concerning the dichloroacetic acid is its relatively low ionization potential. The HOMO of this molecule corresponds mainly to the lone-pair electrons of the chlorine atom. So, the dichloroacetic acid may compete with the acetylenic compounds for the complexation with Cu^I and restrict the above-suggested activation. Results of the EHM calculations indicate a considerable amount of bonding interaction between the copper and chlorine atoms, the overlap population being 0.165.[18] Probably both effects are responsible for the failure of the acetylide formation in dichloroacetic acid.

Concluded from the MO calculations and in terms of the hard–soft interaction, the rate of formation of the intermediate **4** should increase in the following sequence:

mesitylacetylene > phenylacetylene > 1-hexyne > *p*-nitrophenylacetylene

Hence, the substrate-selective formation of the *p*-nitrophenylacetylide in the cross-coupling experiments should be thermodynamic controlled formation of the intermediate complex **5**. Although it is expected that in the first stage of the reaction, electron-rich monomers should be preferentially complexed.

(ii) C—C *bond formation*

The next step of the coupling reaction is the coordination of another monomer to the sphere of Cu^I acetylide to give the HOMO- or cross-coupling products [eq. (7)]:

$$R'—C{\equiv}C—Cu + R''C{\equiv}C—H \rightleftharpoons \begin{matrix} H—C{\equiv}C—R'' \\ \vdots \\ R'C{\equiv}C—Cu \end{matrix} \rightleftharpoons \underset{\mathbf{6}}{\begin{matrix} \\ \\ \\ \end{matrix}}$$

$$R'—C{\equiv}C—CH{=}C(Cu)R'' \quad (7)$$

7

There is no direct experimental evidence for the formation of complex **6**. All attempts to isolate the olefinic complex by quenching experiments failed. The study isolable compound was the copper(I) alkylacetylide. Inhibition of the catalytic cycle, in the presence of sigma-electron-donating ligands such as H_2O and R—O—H, indicates the instability of this intermediate. However, a structurally similar phosphine complex, $PhC{\equiv}CCuPPh_3$, was isolated by trapping experiments and is strong evidence for its formation. This isolated phosphine complex may be accepted as a good model for the proposed intermediate **6**. The structure of the phosphine complex, $Ph—C{\equiv}C—CuP(CH_3)_3$ was resolved by X-ray diffraction analysis.[19] The complex contains tetrameric units in an orthombic cell formally built up from $[(Me_3P)_2Cu]^+$ and $[(Ph—C{\equiv}C)_2Cu]^-$ units. The copper which coordinates the phosphine molecules interacts with the ethynyl groups of the $(Ph—C{\equiv}C)_2Cu$ units to give a tetrahedral structure,

Table 2. Calculated values of the used monomers, acid solvents and their conjugate bases: heat of formation (H_f) in kcal mol^{-1}; energies of frontier orbitals (HOMO–LUMO) in eV (EHM values in parenthesis); acidity (H_A) in kcal mol^{-1}

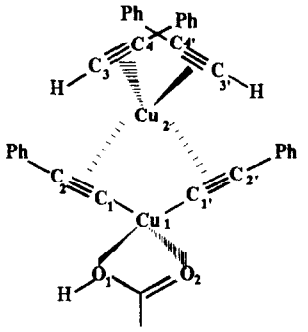
AH	H_f^{AH}	$H_f^{A^-}$	H_A	AH HOMO	AH LUMO	A^- HOMO	A^- LUMO
$C_4H_9C{\equiv}CH$	−47.42	−24.84	388.63	−10.765 (−12.963)	1.884 (−6.793)	−3.743 (−12.816)	6.542 (−12.559)
$C_6H_5—C{\equiv}CH$	−86.77	−74.66	378.16	−9.894 (−12.419)	1.884 (−8.917)	−3.988 (−12.298)	4.257 (−9.308)
$(CH_3)_3C_6H_2C{\equiv}CH$	−60.55	−48.91	377.69	−9.016 (−12.239)	−0.030 (−8.510)	−3.947 (−12.130)	4.140 (−9.005)
p-$NO_2—C_6H_4—C{\equiv}CH$	−60.12	−66.04	360.13	−10.302 (−12.569)	−1.377 (−10.537)	−4.976 (−12.341)	2.419 (−10.587)
CH_3COOH	−101.90	−119.64	348.31	−11.434 (−13.752)	0.930 (−8.543)	3.927 (−13.595)	8.120 (−8.447)
$CHCl_2COOH$	−102.46	−134.89	333.62	−10.870 (−12.493)	−0.133 (−8.392)	−4.784 (−12.534)	4.685 (−8.320)

whereas the copper bearing the ethynyl groups interacts with the triple bond of another ethynyl in the unit, giving a trigonal structure. Unlike the polymeric copper(I) acetylides, the phosphine complexes have rather good solubilities. It is known that 1 : 1 acetylide/phosphine complexes are dimeric in nitrobenzene and rather more associated in benzene.[20]

The formation of complex **6** should be substrate-selective and electron-rich monomers should be preferred. So a high percentage of the cross-product should be expected from the mesityl/*p*-nitrophenylacetylene mixture. However, neither HOMO- nor cross-coupling products were formed from these monomers. In the case of mesitylacetylene the steric effect of the *ortho*-methyl groups must be the probable reason for the failure of the HOMO-coupling products, since it has a comparable acidity with the phenylacetylene and more suitable HOMO–LUMO energy levels of a soft–soft type interaction. Indeed it gives the expected cross-product with phenylacetylene [R′ = mesityl in eq. (7)]. The reason for the failure of coupling in the experiments involving *p*-nitrophenylacetylene may be due to the low nucleophilicity of the generated acetylides as the PM3-method predicted charge densities implies.

The Strauss reaction shows high regioselectivity, leading to head-to-head coupling product formation. The observed regioselectivity might be explained by considering the possible structure of the intermediate **6**. Probably it is a dinuclear complex, similar to the isolated phosphine complex, with only one coordination site available for olefinic ligands for each copper atom. As mentioned above, the equivalent amounts of the secondary ligands are sufficient to stop the catalytic reaction. The possibility of the formation of a mononuclear complex as an active catalyst is excluded since it should have more than one available coordination site. To visualize the possible structure of the intermediates we have undertaken molecular mechanics (MMX) calculations. Calculations with a dinuclear complex, taking the structure of the phosphine complex as the model, indicates that in the most stable structure, the coordinated terminal acetylenes are oriented opposite the acetylide groups to minimize the repulsive interaction (Fig. 2). In this structure the C(1), C(3), C(4) and Cu(2) atoms are almost in the same plane and in suitable positions for head-to-head coupling. Overall, it is a type of *cis*-addition with the formation of the alkenyl copper complex with an *E* configuration in the double bond. The same complex might be generated upon interaction of the C(1), C(3′), C(4′) and Cu(2) atoms, although they are not in the same plane. An alternative head-to-tail coupling is less possible from the estimated structure.

As mentioned above with silver(I) salts the acetylide formation was observed, but the reaction was not catalysed, probably due to structural reasons. Unlike copper(I), the triphenyl phosphine complexes of silver(I) acetylide has a linear chain structure.[21]



Cu_1 - C_1 : 1.83	Cu_2 - C_1 : 2.13
Cu_1 - C_3 : 3.14	Cu_2 - C_3 : 2.09
Cu_1 - C_4 : 3.94	Cu_2 - C_4 : 2.32
Cu_1 - $C_{3'}$: 3.20	Cu_2 - $C_{4'}$: 2.27
Cu_1 - $C_{4'}$: 3.54	Cu_1 - C_2 : 2.65

$C_1Cu_1C_{1'}$: 104°
$Cu_1C_1Cu_2$: -12°

Fig. 2. Estimated structure of the intermediate acetylenic copper acetylide complex.

(iii) *Protonation of intermediate alkenyl-copper compound* **7**

Following the foregoing discussion, only the formation of the *E* isomer of the 1,4-dialkylenyne should be expected, if the protonation of the intermediate alkenyl copper is stereospecific. Indeed it has been observed that the hydrolysis of the simple alkenyl copper compounds proceeds with retention of the stereochemistry.[22] In our experiments, however, we have obtained a mixture of the *E*/*Z* isomer in a ratio depending on the nature of the alkyl group of the carboxylic acid used as solvent. In separate experiments it was shown that both isomers are configurationally stable under the applied reaction conditions. Variation of the product composition is mainly affected by steric factors. The solvents have approximately the same pK_a values, but different steric effects. The *E*/*Z* ratio shows a linear dependency with the steric substituent parameters of the alkyl groups (Fig. 1).

Hence, the product composition is determined by the kinetics of the reaction. The carboxylic acid molecules should be incorporated in the structure of the activated complex in this step. A similar observation was made on the hydrolysis of (*E*)-1,2-diarylpropenylcopper. Here, depending on the hydrolysing agent and the solvent, a mixture of the *E*/*Z* isomers of the product was obtained.[23] Primary electrophilic attack of the H^+ on the alpha carbon atom followed by free-rotation of the Cα—Cβ bond was suggested to explain the observed isomerization. The suggested mechanism, however, cannot explain the observed steric effects on the product composition of the Strauss reaction. The following mechanistic

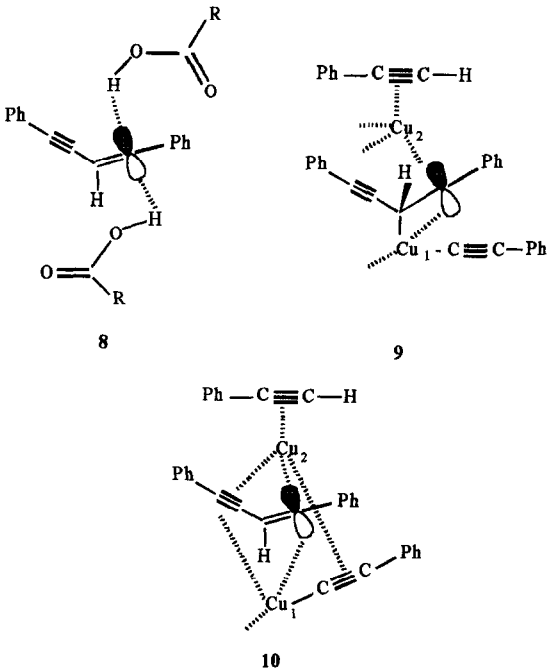
possibilities may give a better explanation for this experimental fact:

(a) Considering the relatively high thermal conditions of the Strauss reactions and the thermal instability of the vinyl-copper compounds, the formation and release of a vinyl carbanion from the intermediate may be expected. The resonance-stabilized molecule should have a V-shaped intermediate **8** (given in Scheme 1), resulting in an unsymmetrical environment on the *sp*-hybridized carbanion centre.

This geometry facilitates the attack of the bulky carboxylic acid from the less hindered side, thus leading to the formation of the less stable *Z* isomer in increasing amounts.

(b) Displacement of the sigma bonds between the two copper atoms, leading to the formation of a carbene-like structure, **9** (given in Scheme 1) stabilized from both sides by copper atoms, would generate again an unsymmetrical structure. The attack of the carboxylic acids, coordinated on both copper atoms or in the free form, would again be facilitated from the less hindered side leading to *Z* isomer formation.

(c) As a combination of both of the two suggestions above, it is imaginable that the generated carbanion remains within the copper complex and is stabilized equally well by both copper atoms. In the above estimated structure **10** of the intermediate given in Scheme 1, the anionic carbon is almost equidistant to both copper atoms. The distance between the copper atoms is smaller than the initial complex. All these imply a three-centre bond formation. Again, in this structure the attack of the carboxylic acid leading to the formation of the *Z* isomer is facilitated. Further calculations are necessary to make a decision among the suggested pathways.



8 **9** **10**

Scheme 1.

(iv) *Termination of the catalytic cycle*

It has been shown experimentally that when no more monomer is left in the reaction medium, copper(I) alkyl acetylide disporportionates to copper(II) and metallic copper [eq. (8)] with the formation of a small amount of diyne. This has been monitored by the formation of the blue colour of copper(II) salts and separation of metallic copper from the reaction mixture.

$$(R{-}C{\equiv}C{-}Cu)_4 \xrightarrow{-2Cu} [(RC{\equiv}C)_2Cu]_2 \longrightarrow$$
$$R{-}C{\equiv}C{-}C{\equiv}C{-}R + (R{-}C{\equiv}C{-}Cu)_2. \quad (8)$$

METHODS

The theoretical calculations were carried out on a 486-IBM compatible PC, by using the standard PM3 procedure with the normal (RHF) version as implemented in the MOPAC (6.version) program, the FORTICON8 program for performing extended Huckel calculations (QCPE 344) and the PCMODEL PI(89.0) Serena software for MMX calculations. All geometries were found by minimizing the energy without making any assumptions.

EXPERIMENTAL

All reactions were carried out under nitrogen. Solvents were dried over suitable reagents and freshly distilled under nitrogen before use. Copper(I) oxide, copper(II) oxide, copper(II) chloride and magnesium(II) acetate were Analar grade. Copper(II) acetate, nickel(II) acetate, lithium(I) acetate, mercury(II) acetate, iron(II) nitrate and chromium(II) acetate were obtained from BDH. Copper(I) acetate,[21] copper(I) phenylacetylide,[22] *cis*-1,4-diphenylbutenyne,[23] *trans*-1,4-diphenylbutenyne[24] and 1,4-diphenylbutadiyne[25] were prepared by known procedures. Ph—C≡C—D was synthesized by heating Ph—C≡C—H with D_2O at 40° for 24 h in the presence of CaO.[26] ^1H NMR showed that the product was 80% deuterated. Na(1) acetate was from Fisher. All the acetylenic compounds, tri-*n*-butylphosphine and triphenylphosphine, were purchased from Aldrich.

IR spectra were recorded on a Perkin–Elmer SP 1200 spectrophotometer (only characteristic bands are given). ^1H NMR spectra were recorded on Varian H A 100 spectrometers with $CDCl_3$ solutions containing tetramethylsilane as an internal standard. Mass spectra were determined using a Varian CH 8 mass spectrometer. For analytical GLC a Packard Becker 409 gas chromatograph was used with 1.8 M 5% SE 30 on Gas Chrom Q using benzene as internal standard. To analyse the products obtained from cross-dimerization reactions a Perkin–Elmer F2 gas

chromatograph was used with a column packed with 30 M SE 54. The *trans*-stilbene was used as an internal standard. GC-MS analysis was carried out with Finigan MAT model 3620 instrument.

Strauss coupling of phenylacetylene

Cu_2O (0.52 g, 0.0036 mol) was added to glacial acetic acid (100 cm^3) boiling under nitrogen. To this Ph—C≡C—H (5 cm^3, 0.045 mol) was added. After 1 h the colour of the solution became green. The solution was cooled, then extracted with ether. The ether phase was neutralized by concentrated $NaHCO_3$ solution. Then washed with H_2O. The organic layer was dried over $MgSO_4$ and ether was evaporated. The crude product was dissolved in benzene and analysed by GC.

The same procedure has been used in other coupling reactions, where different 1-alkynes, catalysts and solvents have been used, respectively.

Isolation of trialkylphosphine copper(I) acetylide complex

Copper(I) acetylide (1.5 g, 0.01 mol) was added to glacial acetic acid (120 cm^3) boiling under nitrogen. When the salt dissolved, the colour of the solution became orange–red. To this triphenylphosphine (25 g, 0.01 mol) was added. The colour of the solution disappeared. The clear solution was heated at 114°C for 1 h and glacial acetic acid was removed *in vacuo*. The crude product crystallized from alcohol and petroleum ether mixture. The IR spectrum of the product was the same as that of Ph—C≡C—Cu(PPh_3) given in the literature.[20] IR (cm^{-1}): ν(C≡C) 2043, ν(monosubstituted benzene) 680, 750, 1580, 1470, 1430. The same procedure was used for isolation of the tri-n-butylphosphine copper(I) phenylacetylide complex. IR (cm^{-1}): ν(C≡C) 2020, ν(C—H aromatic) 2950, 2890.

The quenching experiment

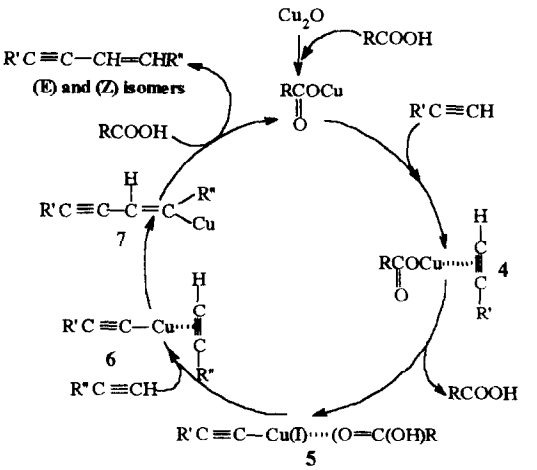
Cu_2O (0.52 g, 0.0036 mol) was added to glacial acetic acid (100 cm^3) boiling under nitrogen atmosphere. To this Ph—C≡C—H (5 cm^3, 0.45 mol) was added. As soon as the colour of the mixture turned orange–red, the reaction was stopped. The mixture was cooled to room temperature. The quantitative analyses of copper was made on the sample of crude product. The sample (0.3 g) was heated with dilute HNO_3 (15 cm^3). The solution was heated vigorously. The yellow solution was extracted with ether and H_2SO_4 was added to the aqueous layer. The solution was evaporated to 5 cm^3 and reheated to evaporate HNO_3. To the resulting solution Na_2CO_3 was added at room temperature and its pH adjusted to 4. Then KI (10 g) was added to the solution, which was kept in the dark for 10 min and then titrated with 0.1 N $Na_2S_2O_3$. Starch solution was used as an indicator. The sample contained 38.6% copper.

The cross-Strauss coupling of mesitylacetylene and phenylacetylene

Glacial acetic acid (5 cm^3) was boiled under nitrogen for 30 min. To this *trans*-stilbene (0.1 g used as internal standard), Cu_2O (10.4 mg, 7.8×10^{-5} mol) and mesitylacetylene (0.14 cm^3, 9.7×10^{-4} mol) were added. A yellow suspension formed. The colour of the suspension became more yellow after the gradual addition of Ph—C≡C—H (0.1 cm^3, 9.8×10^{-4} mol). The mixture was heated under reflux for 3 h, H_2O (20 cm^3) was added and the mixture was filtered. The filtrate was then extracted with ether. The ether extracts were neutralized with Na_2CO_3, then washed with H_2O. The ether phase was dried over $MgSO_4$, filtered and concentrated to 5 cm^3. The crude products were characterized by comparison of the GC retention times of the authentic samples and by means of GC-MS analysis.

CONCLUSION

The Strauss reaction is unique for the head-to-head coupling of terminal acetylenes. Although it has been known for more than 90 years, and a version of which has found industrial application, there are still some questions about the mechanism of this reaction. In Scheme 2, a catalytic cycle of the dimerization is given depending on the experimental facts and on the foregoing discussions. In this scheme the active complex **5** has been shown as monocentric, for the sake of clarity. However, it is most likely for this expected intermediate to have a dinuclear structure. Further experimental and theoretical information is needed to clarify the dependency of the product composition and to explain the failure of the catalytic conversion under certain conditions.



Scheme 2.

REFERENCES

1. N. Hagihara, M. Tamura, H. Yamazaki and M. Fujiwara, *Bull. Chem. Soc. Jpn* 1961, **34**, 892.
2. L. Carlton and G. Read, *J. Chem. Soc., Perkin Trans.* 1 1978, 1631.
3. B. M. Trost, C. Chan and G. Ruther, *J. Am. Chem. Soc.* 1987, **109**, 3486.
4. W. T. Boese and A. S. Goldman, *Organometallics* 1991, **10**, 782.
5. M. Akita, H. Yasuda and A. Nakamura, *Bull. Chem. Soc. Jpn* 1984, **57**, 480.
6. A. D. Horton, *J. Chem. Soc., Chem. Commun.* 1992, 185.
7. (a) F. Strauss, *Annalen* 1905, **342**, 190; (b) M. Akhtar and B. C. L. Weedon, *Proc. Chem. Soc.* 1958, 303; (c) M. Akhtar, T. A. Richards and B. C. L. Weedon, *J. Chem. Soc.* 1959, 933.
8. A. M. Echavarren, J. Lopez, A. Santos and J. Montoya, *J. Organomet. Chem.* 1991, **414**, 393.
9. Y. Wakasuki, H. Yamazaki, N. Kumegawa, T. Satoh and J. Y. Satoh, *J. Am. Chem. Soc.* 1991, **113**, 9604.
10. H. Yamazaki, *J. Chem. Soc., Chem. Commun.* 1976, 841.
11. Y. Wakasuki, H. Yamazaki, N. Kumegawa and P. S. Johar, *Bull. Chem. Soc. Jpn* 1993, **66**, 987.
12. İ. Ünalan (Uraz). Ph.D. thesis, Hacettepe University (1980).
13. Ç. Bozkurt. Ms. thesis, Hacettepe University (1983).
14. M. Charton, *J. Am. Chem. Soc.* 1975, **97**, 1552.
15. F. Sevin. Ms. thesis, Hacettepe University (1989).
16. M. G. B. Drew, A. Hamid Bin Othman, D. A. Edwards and R. Richards, *Acta Cryst.* 1975, **B31**, 2695.
17. G. L. Lewandos, J. W. Maki and J. P. Ginnebaugh, *Organometallics* 1982, **1**, 1700.
18. MMX optimized geometry of the complex $Cu(OOCCCl_2H)(HCl_2CCOOH)$ was used in the EHM calculations.
19. P. W. R. Corfield and H. M. M. Shearer, *Acta Cryst.* 1966, **21**, 757.
20. G. E. Coates and C. Parkin, *J. Inorg. Nucl. Chem.* 1961, **22**, 59.
21. P. W. Corfield and H. M. M. Shearer, *Acta Cryst.* 1966, **20**, 502.
22. J. F. Normant, G. Cahiez, C. Chuit and J. Villieras, *J. Organomet. Chem.* 1974, **77**, 269.
23. R. W. M. ten Hoedt, G. Van Koten and J. G. Noltes, *J. Organomet. Chem.* 1980, **201**, 327.
24. J. Burdon, P. L. Coe, C. R. Marsh and J. C. Tatlow, *J. Chem. Soc., Chem. Commun.* 1967, 1259.
25. I. D. Campbell and G. E. Eglinton, *Org. Synth.* 1965, **45**, 39.
26. J. E. Baldwin and J. A. Kapecki, *J. Am. Chem. Soc.* 1970, **92**, 4874.

Pergamon

S0277-5387(96)00101-5

Polyhedron Vol. 16, No. 2, pp. 335–339, 1997
Copyright © 1996 Elsevier Science Ltd
Printed in Great Britain. All rights reserved
0277-5387/97 $15.00 + 0.00

Synthesis and stereochemistry of bis(cyclopalladium) complexes of 1,1′-bis[1-(arylimino)ethyl]ferrocenes

Yang Jie Wu* and Yuan Hong Liu

Department of Chemistry, Zhengzhou University, Zhengzhou 450052, P.R. China

and

Li Yang and Qixiu Zhu

National Laboratory of Applied Organic Chemistry, Lanzhou University, Lanzhou 730000, P. R. China

(Received 18 January 1996; accepted 7 February 1996)

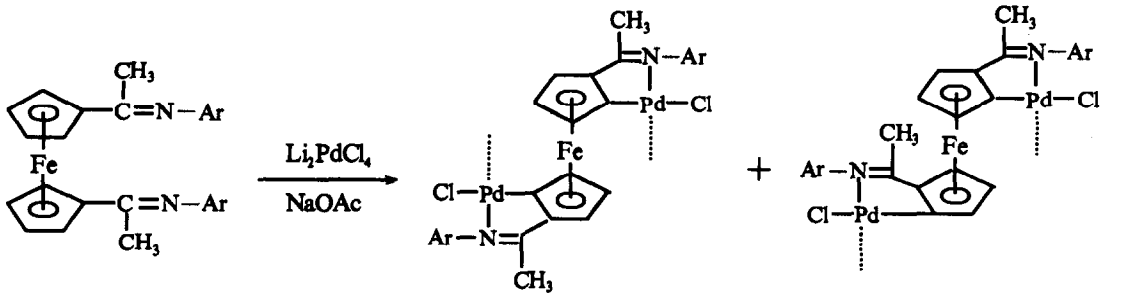
Abstract—Double cyclopalladation of 1,1′-bis[(arylimino)ethyl]ferrocenes with Li_2PdCl_4 followed by treatment with PPh_3 afforded *meso* and *dl* stereoisomers of bis(palladium) complexes and the individual stereoisomers were isolated successfully by column chromatography. The composition and the structure of the metallocycles were characterized by elemental analysis, IR and ^1H NMR spectroscopy. A mechanism for the formation of stereoisomers in the cyclopalladation reaction was suggested. Copyright © 1996 Elsevier Science Ltd

The chemistry of cyclometalated compounds, especially those containing N-donor ligands and palladium is one of the most advanced areas of modern organometallic chemistry. These cyclopalladated compounds have been successfully used in organic syntheses, catalysis, asymmetric synthesis, photochemistry, and as potential biologically active materials.[1] More recently, the cyclopalladation of some ferrocenylimines has been reported by López's and our laboratories. It was found that the reaction occurred predominantly at the *ortho* position of the substituted Cp ring to afford the corresponding cyclopalladated derivatives.[2,3] But double cyclopalladation of 1,1′-disubstituted ferrocene is scarce, only the double cyclopalladations of 1,1′-diacetylferrocene bis (acetylhydrazone)[4] and N,N,N′,N′-tetramethylferrocene-1,1′-dicarbothioamide[5] have been reported in the literature. In the present paper, we report our studies on the synthesis and characterization of the stereoisomers of bis[palladium(II)] complexes of 1,1′-bis[(arylimino)ethyl]ferrocenes.

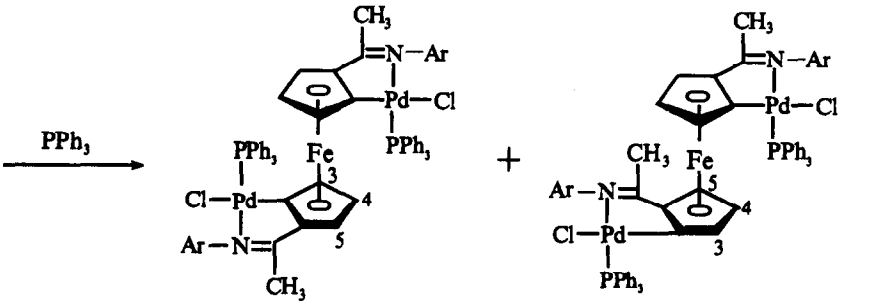
RESULTS AND DISCUSSION

The novel bisferrocenylimines [(η^5—C_5H_4 CMe=NAr)$_2$Fe] designated as bis (FKM)] were synthesized by the reaction of bis-acetylferrocene with the corresponding amine in the presence of freshly activated Al_2O_3.[6] The cyclopalladation reaction was carried out with bis(FKM) **1** and two mole equivalents of Li_2PdCl_4 and anhydrous sodium acetate in CH_2Cl_2—MeOH mixed solvent at room temperature for about 20 h, then the solvent was evaporated *in vacuo* to give a brown–red solid which was tentatively assigned to be a polymeric or dimeric dipalladio derivative **2**. Given the high solubility of **2** in chloroform, dichloromethane etc., the formation of the dimeric form is highly possible. Owing to the inevitable contamination by the bis adducts of $PdCl_2$ with ligand **1** formed in the cyclopalladation reaction and the decomposition of the products during purification by column chromato-

* Author to whom correspondence should be addressed.



1 **2(*meso*)** **2(*dl*)**



3(*meso*) **3(*dl*)**

Ar = *p*-$CH_3OC_6H_4$ (**a**), *p*-$CH_3C_6H_4$ (**b**), C_6H_5 (**c**), *p*-ClC_6H_4 (**d**), *p*-BrC_6H_4 (**e**), *p*-$NO_2C_6H_4$ (**f**), *m*-$CH_3C_6H_4$ (**g**), *m*-ClC_6H_4 (**h**), *m*-BrC_6H_4 (**i**).

graphy on silica gel, a pure sample of **2** was not isolated. The brown–red solid was directly subjected to bridge-splitting reaction with ligand triphenylphosphine to produce the *meso* and *dl* monomeric stereoisomers (the total yields of *meso* and *dl* isomers are 15–46%), which is a typical reaction of a chlorine-bridged binuclear complex of palladium.[7] What is most interesting is that the *meso* and *dl* isomers can be separated successfully by silica gel column chromatography except for **3a** and **3b**, which provided the key to an interpretation of the spectra. The homoannular ring formed by chelation of a ferrocenylimine ligand to Pd^{II} also displays stereoisomerism arising from planar chirality. All the new compounds **3** are air stable powders, and very soluble in chloroform, dichloromethane, and slightly soluble in methanol. The yields, analytical data and IR data of the compounds are shown in Table 1, and the ^1H NMR data in Table 2. The compounds **3** melt at high temperature (>200°C) and with decomposition.

The IR spectral features of *meso* and *dl* isomers are very similar to each other. No absorption bands can be found at 1000 cm $^{-1}$ and 1100 cm^{-1}, which indicated the substitution of two cyclopentadienyl rings.[8] The C=N absorptions (~1570 cm^{-1}) in **3** are shifted to lower energy by ~50 cm^{-1} in comparison with those of the corresponding bis(FKM), indicating the coordination of nitrogen to palladium through its lone pair of electrons.[9] The strong absorption at about 745 cm^{-1} and 690 cm^{-1} observed in **3**, being the feature of monosubstituted phenyl ring, are assigned to the δ(CH) of PPh_3.

The assignments of the signals of the Cp ring protons in ^1H NMR spectra of two isomers are similar to the mono (palladium) complex $[PdCl\{(\eta^5\text{—}C_5H_5)Fe(\eta^5\text{—}C_5H_3CMe{=}NAr)\}(PPh_3)]$. The chemical shifts are different between the isomers because the Cp ring protons are in different magnetic environments. The pair of the proton signals for Cp rings and C-methyl group for the individual stereoisomers, *meso*-3c and *dl*-3c, occur at 3.09, 4.15, 4.16, 1.62 and 2.84, 3.98, 4.23, 2.10 ppm, respectively, compared with 3.37, 4.11, 4.45, 2.06 ppm for the mono (palladium) analogue. It seems impossible that the cyclopentadiene rings of the ferrocene moiety in the two isomers could adopt the eclipsed configuration, because of the significant steric interactions between the cyclopentadienyl substituents, although it is recognized[10] that the balance between intramolecular ring interactions and intermolecular packing forces usually

Table 1. Yields, analytical data and IR data of **3**

Compound		Empirical formula	Yield (%)	Elemental analyses[a] C	H	N	IR data (cm^{-1})		
3a		$C_{64}H_{56}Cl_2FeN_2O_2P_2Pd_2$	32	59.6	4.7	2.5	1570	1500	1435
				(59.7)	(4.4)	(2.2)	1248	820	750
3b		$C_{64}H_{56}Cl_2FeN_2P_2Pd_2$	46	61.2	4.7	2.3	1571	1437	818
				(61.3)	(4.5)	(2.2)	748	695	
3c	*meso*	$C_{62}H_{52}Cl_2FeN_2P_2Pd_2$	17	60.3	4.2	2.4	1570	1433	740
	dl		26	60.4	4.1	2.4	690		
				(60.7)	(4.3)	(2.3)			
3d	*meso*	$C_{62}H_{50}Cl_4FeN_2P_2Pd_2$	10	57.1	4.2	2.2	1575	1438	820
	dl		17	57.3	4.2	2.3	749	698	
				(57.5)	(3.9)	(2.2)			
3e	*meso*	$C_{62}H_{50}Br_2Cl_2FeN_2P_2Pd_2$	7	54.1	4.1	2.2	1568	1432	817
	dl		13	54.3	4.2	2.2	740	690	
				(53.8)	(3.6)	(2.0)			
3f	*meso*	$C_{62}H_{50}Cl_2FeN_4O_4P_2Pd_2$	13	55.9	3.4	4.2	1570	1433	1340
	dl		16	55.9	3.5	4.0	825	746	690
				(56.6)	(3.8)	(4.3)			
3g	*meso*	$C_{64}H_{56}Cl_2FeN_2P_2Pd_2$	11	61.0	4.8	2.2	1570	1433	748
	dl		14	60.9	4.8	2.2	692		
				(61.3)	(4.5)	(2.2)			
3h	*meso*	$C_{62}H_{50}Cl_4FeN_2P_2Pd_2$	13	57.5	4.1	2.2	1570	1431	745
	dl		14	57.5	4.2	2.2	690		
				(57.5)	(3.9)	(2.2)			
3i	*meso*	$C_{62}H_{50}Br_2Cl_2FeN_2P_2Pd_2$	13	53.7	3.9	2.1	1565	1431	742
	dl		23	53.7	4.1	2.4	690		
				(53.8)	(3.6)	(2.0)			

[a] Calculated values in parentheses.

Table 2. ^{1}H NMR data of compds. **3**[a] (1.00–6.00 ppm)

Compound		3	4	5	Others	
3a	*meso*	3.07bs	4.14bs	4.16bs	1.63s	3.77s
	dl	2.83bs	3.80bs	4.23bs	2.12s	3.74s
3b	*meso*	3.06bs	4.15bs	4.17bs	1.62s	2.32s
3c	*meso*	3.09bs	4.15bs	4.16bs	1.62s	
	dl	2.84bs	3.98bs	4.23bs	2.10s	
3d	*meso*	3.10bs	4.14bs	4.18bs	1.63s	
	dl	2.86bs	3.93bs	4.16bs	2.11s	
3e	*meso*	3.10bs	4.14bs	4.17bs	1.62s	
	dl	2.86bs	3.93bs	4.16bs	2.03s	
3f	*meso*	3.20bs	4.18bs	4.25bs	1.65s	
	dl	2.92bs	4.08bs	4.27bs	2.11s	
3g	*meso*	3.21bs	4.15bs	4.20bs	1.60s	2.37s
	dl	2.86bs	3.98bs	4.23bs	2.11s	2.31s
3h	*meso*	3.09bs	4.16bs	4.16bs	1.63s	
	dl	2.87bs	4.03bs	4.22bs	2.10s	
3i	*meso*	3.09bs	4.15bs	4.23bs	1.63s	
	dl	2.88bs	4.03bs	4.22bs	2.12s	

[a] Chemical shifts in ppm, TMS as the internal standard.

results in a preference for an eclipsed conformation of the cyclopentadiene rings. In the *dl* configuration, protons 3-H can be shielded by two PPh_3 groups, whereas in the *meso* configuration protons 3-H are shielded only by one PPh_3 group. According to ^{1}H NMR study of the mono(palladium) complex one can conclude that the shielding effect of the PPh_3 group is very large. For example, in comparison with the di-μ-chloro-bridged cyclopalladated complex [{Pd[(η^5—C_5H_5)Fe(η^5—C_5H_3CMe = NAr)] (μ—Cl)}$_2$] (Ar = *p*—$C_6H_{13}OC_6H_4$, *p*—$C_{12}H_{25}OC_6H_4$ and *p*—$C_{16}H_{33}OC_6H_4$), the resonance of the substituted Cp protons 3-H, 4-H, 5-H and unsubstituted Cp ring protons in their corresponding monomeric cyclopalladated triphenylphosphine derivatives shifts to upfield significantly by *ca* 0.48, 0.16, 0.20, 0.47 ppm, respectively.[11] So in the present cases, the signals of protons 3-H in *dl* form should appear at upfield by comparison with those in *meso* form. Thus we suggest that in each separation, the band possessing the highest R_f value contains the *meso* form and the second band contains *dl* form. In general, the chemical

shifts of protons in Cp ring show no dependence on substituents in the N—phenyl ring, this may be due to the nonplanarity between the ferrocenyl ring and the N—phenyl ring, which can influence the transmission of the electronic effects of the substituents in the phenyl ring through the C=N bond to the ferrocenyl moiety.

A proposed explanation for the formation of stereoisomers in cyclopalladation reactions of a bis(palladium) complex is shown in Scheme 1. The bis(FKM) may exist in the forms of conformer-I and conformer-II; double cyclopalladation of I and II affords the corresponding *dl* and *meso* isomers, respectively, which in *meso* product, the sites of electrophilic attack are at 2- and 2′-positions whereas attack on the 2- and diametrically opposite side 5′-position leads to the *dl* form. After the two chelate rings are formed, interconversion of the stereoisomers is not possible without breaking the σPd—C bond of one chelate ring.

EXPERIMENTAL

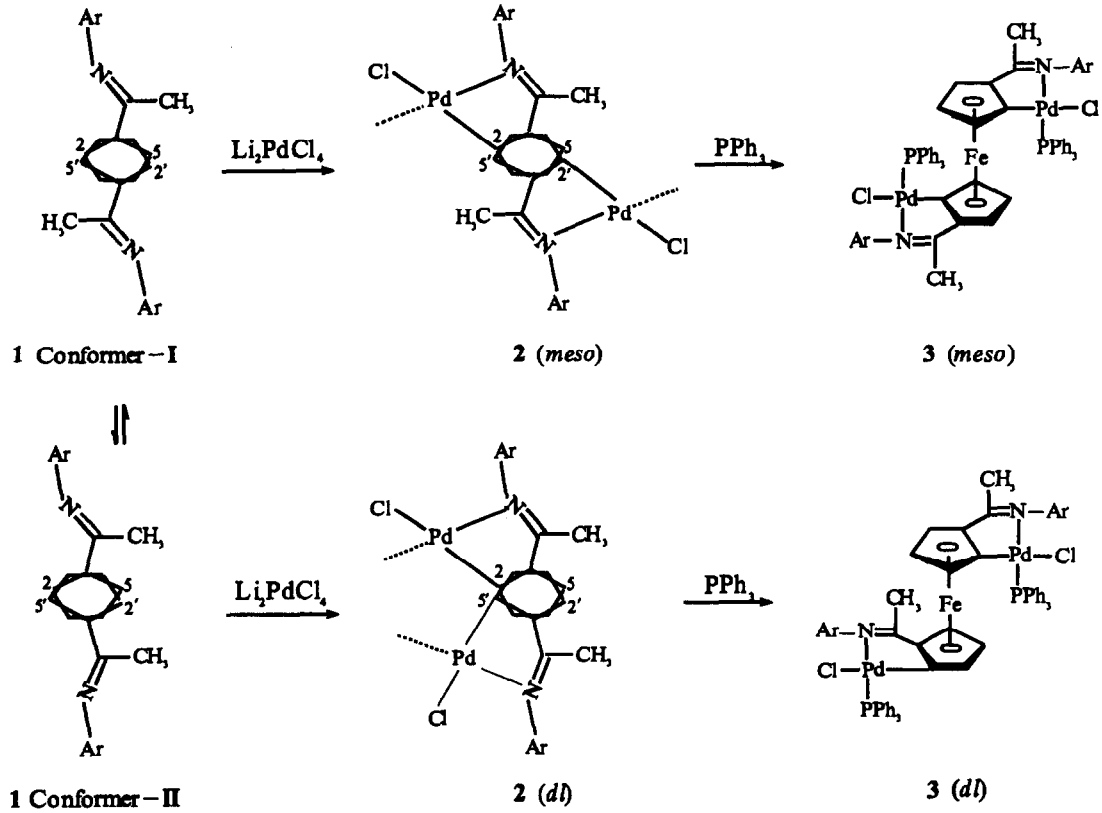
Materials and instruments

^{1}H NMR spectra were recorded on a Bruker AM 400 spectrometer, using $CDCl_3$ as the solvent and tetramethylsilane as an internal standard. IR spectra were recorded on a Perkin-Elmer FTIR 1750 spectrophotometer. Elemental analyses were determined with a Carlo Erba 1106 elemental analyser. Chromatographic work was carried out using silica gel under reduced pressure.

A lithium tetrachloropalladate(II) solution in methanol (0.1 M) was prepared by stirring two equivalents of anhydrous lithium chloride and one equivalent of anhydrous palladium chloride in methanol until a homogeneous solution was formed. The novel bisferrocenylimines were synthesized by the reaction of bis-acetyl-ferrocene with the corresponding amine in the presence of freshly activated Al_2O_3.[6]

General procedure for the double cyclopalladation of **1**

A solution of lithium tetrachloropalladate(II) in 5 cm^3 of methanol (0.13 g of Li_2PdCl_4, 0.5 mmol) was added to a solution of bisferrocenylimines (0.25 mmol) and anhydrous sodium acetate (41 mg, 0.5 mmol) in 16 cm^3 of dichloromethane/methanol (8 : 1, v/v). The mixture was stirred at room temperature for about 20 h, then the solvent evaporated *in vacuo* until a brown–red solid formed. The crude brown–red product was washed several times with



Scheme 1.

a small amount of methanol, then without further purification, it was treated with PPh_3 (0.13 g, 0.5 mmol) in CH_2Cl_2 at room temperature for 0.5 h. The product was separated by passing through a short silica gel column with CH_2Cl_2 as eluent, which the first band (the highest R_f value) contained the *meso* form and the second band contained the *dl* form. After the evaporation of the solvent, the residue was recrystallized from dichloromethane–petroleum ether (60–90°C) to give *meso*-**3** and *dl*-**3** with the yields shown in Table 1.

Acknowledgements—We are grateful to the National Natural Science Foundation of China and the Natural Science Foundation of Henan Province for financial support of this work.

REFERENCES

1. (a) A. D. Ryabov, *Synthesis* 1985, 233, and the references therein; (b) G. R. Newkome, W. E. Puckett, W. K. Gupta and G. E. Kiefer, *Chem. Rev.* 1986, **86**, 451; (c) I. Omae, *Coord. Chem. Rev.* 1988, **83**, 137; (d) V. V. Danina, O. A. Zalevzkyaya and V. M. Potatov, *Russ. Chem. Rev.* 1988, **57**, 250; (e) A. D. Ryabov, *Chem. Rev.* 1990, **90**, 403.
2. (a) C. López, J. Sales, X. Solans and R. Zquiak, *J. Chem. Soc., Dalton Trans.* 1992, 2321; (b) R. Bósque, C. López, J. Sales and X. Solans, *J. Organomet. Chem.* 1994, **483**, 61.
3. (a) S. Q. Huo, Y. J. Wu, C. X. Du, Y. Zhu, H. Z. Yuan and X. A. Mao, *J. Organomet. Chem.* 1994, **483**, 139, (b) Y. J. Wu, Y. H. Liu, K. L. Ding, H. Z. Yuan and X. A. Mao, *J. Organomet. Chem.* 1995, **505**, 37.
4. M. Sugimoto and M. Nonoyama, *Inorg. Nucl. Chem. Lett.* 1979, **15**, 405.
5. K. Hamamura, M. Kita, M. Nonoyama and J. Fujita, *J. Organomet. Chem.* 1993, **463**, 169.
6. Y. H. Liu, Y. J. Wu, H. Y. Yun, L. Yang and Q. X. Zhu, *Chem. J. Chinese Univ.* 1996, **17**, 1225.
7. M. Orchin and P. L. Schimdt, *Coord. Chem. Rev.* 1968, **2**, 345.
8. M. Rosenblum and R. B. Woodward, *J. Am. Chem. Soc.* 1958, **80**, 5443.
9. (a) M. Orchin and P. L. Schimdt, *Coord. Chem. Rev.* 1968, **2**, 345. (b) M. Onoue, K. Minami and K. Nakagawa, *Bull. Chem. Soc. Jpn* 1970, **43**, 3480.
10. M. F. Daniel, A. J. Leadbetter, M. A. Mazid and J. Piper, *J. Chem. Soc., Faraday Trans.* 2, 1983, **79**, 1663.

Pergamon

S0277-5387(96)00289-6

Polyhedron Vol. 16, No. 2, pp. 341–343, 1997
Copyright © 1996 Elsevier Science Ltd
Printed in Great Britain. All rights reserved
0277-5387/97 $15.00+0.00

COMMUNICATION

Iridium complexes with secondary phosphines: synthesis and X-ray crystal structure of $[IrCl(Bu^t_2PH)_3]$

H.-C. Böttcher,* Marion Graf and Kurt Merzweiler

Department of Chemistry, Martin Luther University, Halle-Wittenberg, Kurt-Mothes-Str. 2, D-06120 Halle/Saale, Germany

(Received 24 May 1996; accepted 13 June 1996)

Abstract—The reaction of $[\{IrCl(COE)_2\}_2]$ (**1**) (COE = cyclooctene) with Bu^t_2PH in hexane at room temperature gave the complex $[IrCl(Bu^t_2PH)_3]$ (**2**) which has been fully characterized by both spectroscopic and crystallographic methods. **1** reacts with carbon monoxide to give the Vaska-type complex *trans*-$[IrCl(CO)(Bu^t_2PH)_2]$ (**3**). Copyright © 1996 Elsevier Science Ltd

Keywords: iridium; complex; mononuclear; secondary phosphines; crystal structure.

Recently we reported the synthesis and X-ray crystal structures of the new phosphido-bridged heterobimetallic complexes $[FeIr(CO)_5(\mu\text{-}PBu^t_2)(Bu^t_2PH)]$ and $[CoIr(CO)_5(\mu\text{-}H)(\mu\text{-}PBu^t_2)(Bu^t_2PH)]$ by reaction of $[IrCl(Bu^t_2PH)_3]$ (**2**) with $[Fe(CO)_5]$ and $K[Co(CO)_4]$/$AgPF_6$, respectively [1]. In view of **2** we have to remark that the number of reports on the synthesis of low-valent mononuclear complexes containing late transition metals with secondary phosphines as ligands is notably low [2]. The analogous complex to **2**, namely $[RhCl(Bu^t_2PH)_3]$, was described by Masters and Shaw [3]. Concerning the chemistry of $[\{RhCl(Bu^t_2PH)_2\}_2]$ [4] we were interested in the synthesis of the corresponding iridium analogue. As starting material we used $[\{IrCl(COE)_2\}_2]$ (**1**) [5], which was often applied in syntheses of iridium–chloro complexes containing phosphines, for instance $[IrCl(PPr^i_3)_2]$ [6–8], and also other authors used the latter species prepared *in situ* in the same way [9,10]. Furthermore, reactions of **1** with some secondary phosphines (in excess) in alcoholic medium in the presence of perchlorate or tetraphenylborate were described, yielding four-coordinate complexes $[Ir(R_2PH)_4]^+$ [11]. Bennett and Latten reported the synthesis of $[IrCl(PPh_3)_3]$ by reaction of **1** with an excess of the phosphine in petroleum ether [12]. In accordance with these observations we found that reaction of **1** with Bu^t_2PH in hexane at room temperature during 2 h (even under various molar ratios) yielded exclusively the complex $[IrCl(Bu^t_2PH)_3]$ (**2**) isolated in *ca* 95%.† At present we have no evidence for species with the formula $[IrCl(COE)L_2]$ (L = PPr^i_3, [7]; L = PF_3, [13]) or $[IrCl(COE)L_3]$ (L = PMe_3, [14]). In the ^1H NMR spectrum (C_6D_6) of **2** the presence of three chemically inequivalent phosphine ligands in the molecule is

* Author to whom correspondence should be addressed.

† Analytical and spectroscopic data for **2**. Found: C, 43.1; H, 8.2; Cl, 5.3. Calc. for $C_{24}H_{57}ClIrP_3$: C, 43.2; H, 8.6; Cl, 5.2%. IR (KBr): 2983 (s), 2940 (vs), 2890 (vs), 2859 (s), 2323 (m), 2295 (m), 2250 (m), 1472 (s), 1448 (m), 1387 (m), 1361 (s), 1177 (m), 1023 (m), 935 (m), 911 (w), 879 (s), 812 (s), 572 (m), 467 (m), 426 (w); (CsBr): ν(Ir—Cl) 289 cm^{-1}. ^1H NMR (C_6D_6): δ 1.34 (d, $^3J_{PH}$ = 13.1 Hz, 18H, PBu^t_2), 1.57 (d, $^3J_{PH}$ = 13.1 Hz, 18H, PBu^t_2), 1.63 (d, $^3J_{PH}$ = 13.1 Hz, 18H, PBu^t_2) 3.96 (dd, J_{PH} = 312.2 Hz, $^3J_{PH}$ = 18.5 Hz, 1H, Bu^t_2PH), 4.62 (dd, J_{PH} = 336.2 Hz, $^3J_{PH}$ = 7.9 Hz, 1H, Bu^t_2PH), 4.68 (dd, J_{PH} = 325.0 Hz, $^3J_{PH}$ = 7.6 Hz, 1H, Bu^t_2PH); $^{31}P\{^1H\}$ NMR (THF/D_2O-cap.): spin system AMX, δ 21.92 (dd, J_{PP} = 339.5 Hz, J_{PP} = 19.5 Hz, P_A), δ 49.06 (dd, J_{PP} = 19.5 Hz, J_{PP} = 19.6, P_X), 58.56 (dd, J_{PP} = 339.5 Hz, J_{PP} = 19.6 Hz, P_M); MS: 666, M^+, 520 $[M-Bu^t_2PH]^+$; 484 $[M\text{-}Bu^t_2PH, \text{-}Cl]^+$; 374 $[M-2Bu^t_2PH]^+$.

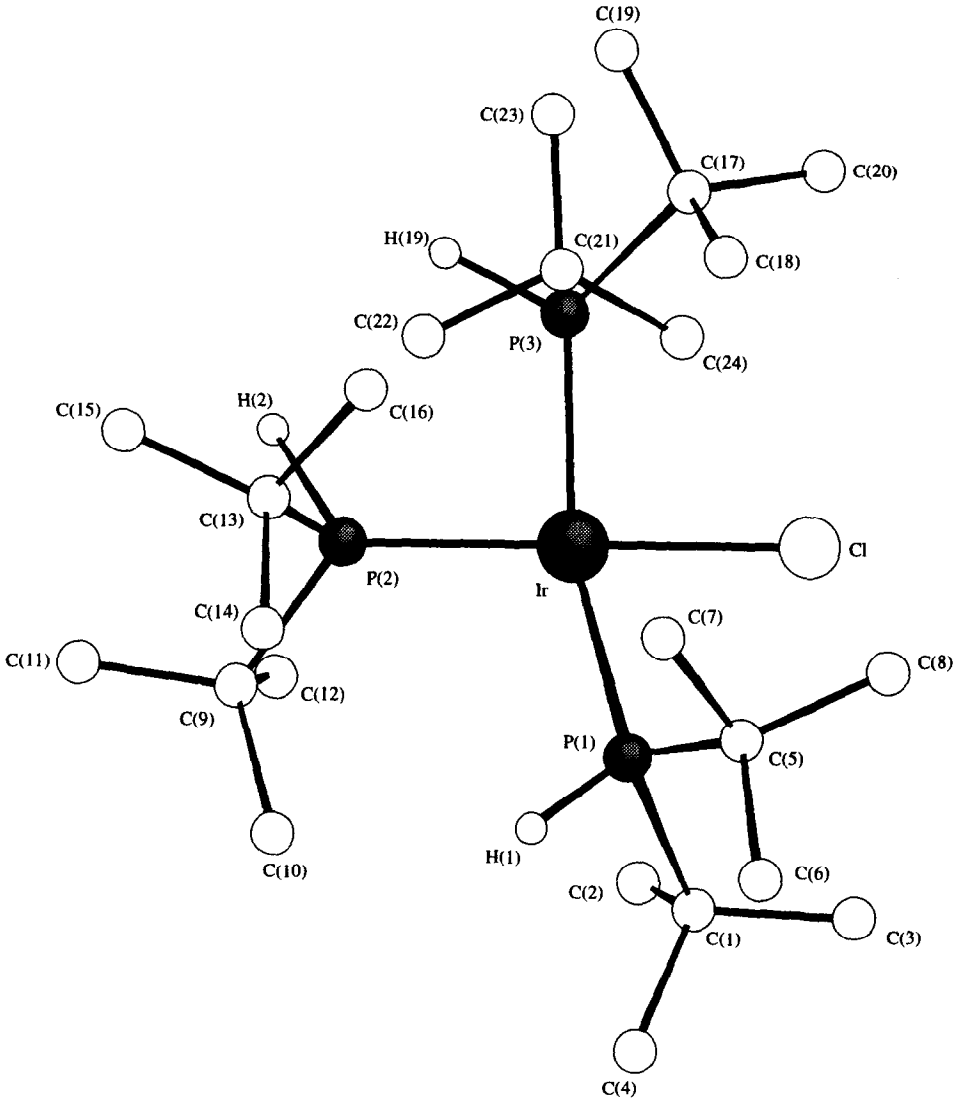


Fig. 1. Molecular structure of $[IrCl(Bu^t_2PH)_3]$ (**2**). Selected bond lengths (Å) and angles (°): Ir—Cl 2.396(1), Ir—P(1) 2.319(1), Ir—P(2) 2.231(1), Ir—P(3) 2.299(1), P(1)—C(1) 1.918(5), P(2)—C(9), 1.897(5), P(3)—C(21) 1.888(5); P(1)—Ir—Cl 84.9(1), P(1)—Ir—P(2) 100.0(1), P(2)—Ir—Cl 169.9(1), P(2)—Ir—P(3) 90.0(1), P(3)—Ir—Cl 87.1(1), P(3)—Ir—P(1) 164.7(1).

clearly indicated. This fact is also confirmed by the $^{31}P\{^1H\}$NMR data, an AMX spin system is observed with a large *trans* coupling (J_{PP} = 339.5 Hz) and the corresponding *cis* couplings of 19.5 and 19.6 Hz, respectively. As observed for similar constituted complexes this effect could be assigned to slowing rotation about the P—Ir and P—(*t*-Bu) bonds [15]. In contrast to **2** for $[IrCl(PPh_3)_3]$ in the $^{31}P\{^1H\}$NMR spectrum an A_2B (almost A_2X) pattern was observed [12].

Complex **2** has been structurally characterized by single crystal X-ray crystallography.* The molecular structure is shown in Fig. 1. The angle P(3)—Ir—P(1) is 164.7(1)° and the P(2)—Ir—Cl angle is 169.9(1)°, therefore the coordination geometry around the iridium atom can be described as a distorted square-planar arrangement. This configuration is forced on the molecule by the bulk of the phosphine ligands. The Ir—Cl distance was found to be 2.396(1) Å and is slightly longer than expected probably also by reason of the sterical hindrance of the bulky ligands. The iridium–phosphorus bond lengths Ir—P(1) with 2.319(1) and Ir—P(3) 2.299(1) Å lie in the usual range observed for phosphines in *trans* position to each other. The ligand P(2) is situated in *trans* position to the chloride ligand and the Ir—P(2) distance is with 2.231(1) Å in the average by 0.08 Å shorter than Ir—P(1) and Ir—P(3). Such an effect was also observed in the molecule $[Ir(C_6F_5)(PEt_3)_2(PEt_2F)]$, for instance [16]. In this case the two Ir—P distances in *trans* position to each other are longer than the third Ir—P bond (av. 0.1 Å).

*Crystal data for $C_{24}H_{57}ClIrP_3$, **2**: M = 666.26, monoclinic, space group $P2_1/n$, a = 8.738(1), b = 20.813(4), c = 16.961(1) Å, α = 90.00, β = 96.49(1), γ = 90.00°, V = 3064.9(7) Å^3, Z = 4, D_c = 1.444 mg m^{-3}, Mo-K_α radiation, λ = 0.71073 Å, μ(Mo-K_α) = 4.610 mm^{-1}, F(000) = 1360, T = 220 K, orange plate. The crystal used for data collection had the dimensions 0.2 × 0.2 × 0.1 mm. 5603 intensity data were collected on a Stoe STADI-4 diffractometer using graphite monochromated Mo-K_α radiation (range $1.55 \leqslant \theta$ 25.01°; $-10 \leqslant h \leqslant 10$, $0 \leqslant k \leqslant 24$, $-14 \leqslant l \leqslant 20$), 5402 independent reflections (R_{int} = 0.0607). The structure was solved by direct methods using SHELXS-86 and refined by full-matrix least-squares on F^2 (all non-hydrogen atoms anisotropic) using SHELXL-93 [17]. Final R_1 = 0.0287, [$I > 2\sigma(I)$], wR_2 = 0.0695 (all data). Full details of the structure determination have been deposited at the Fachinformationszentrum Karlsruhe, Gesellschaft für wissenschaftlich-technische Information mbH, D-76344 Eggenstein-Leopoldshafen, Germany, from where this material may be ordered on quoting the full literature citation and the reference number CSD 5933.

The reactivity of compound **2** towards small molecules such as carbon monoxide and ethylene was investigated. **2** was quickly transformed in hexane under a slow stream of carbon monoxide into the Vaska-type complex *trans*-$[IrCl(CO)(Bu^t_2PH)_2]$ (**3**) in nearly quantitative yield. **3** was characterized by the known spectroscopic data [15]. With ethylene (hexane, 4 h) no reaction was observed, and therefore these results resemble the corresponding reactions of $[IrCl(PPh_3)_3]$ [12].

Acknowledgements—We thank the Deutsche Forschungsgemeinschaft and the Fonds der Chemischen Industrie for financial support.

REFERENCES

1. H.-C. Böttcher, M. Graf and K. Merzweiler, *J. Organomet. Chem.*, in press.
2. P. Leoni, *Organometallics* 1993, **12,** 2432 and references cited therein.
3. C. Masters and B. L. Shaw, *J. Chem. Soc.* 1971, 3679.
4. B. Walther, H.-C. Böttcher, M. Scheer, G. Fischer, D. Fenske and G. Süss-Fink, *J. Organomet. Chem.* 1992, **437,** 307.
5. A. van der Ent and A. L. Onderdelinden, *Inorg. Synth.* 1990, **28,** 90.
6. A. Höhn, H. Otto, M. Dziallas and H. Werner, *J. Chem. Soc., Chem. Commun.* 1987, 852.
7. H. Werner, A. Höhn and M. Schulz, *J. Chem. Soc., Dalton Trans.* 1991, 777.
8. R. W. Lass, P. Steinert, J. Wolf and H. Werner, *Chem. Eur. J.* 1996, **2,** 19.
9. D. B. Grotjahn and H. C. Lo, *J. Am. Chem. Soc.* 1996, **118,** 2097.
10. D. B. Grotjahn and H. C. Lo, *Organometallics* 1995, **14,** 5463.
11. P. Rigo and M. Bressan, *Inorg. Chem.* 1976, **15,** 220.
12. M. A. Bennett and J. L. Latten, *Inorg. Synth.* 1989, **26,** 200.
13. M. A. Bennett and D. J. Patmore, *Inorg. Chem.* 1971, **10,** 2387.
14. T. Herskovitz and L. J. Guggenberger, *J. Am. Chem. Soc.* 1976, **98,** 1615.
15. C. H. Bushweller, C. D. Rithner and D. J. Butcher, *Inorg. Chem.* 1986, **25,** 1610 and references cited therein.
16. O. Blum, F. Frolow and D. Milstein, *J. Chem. Soc., Chem. Commun.* 1991, 258.
17. G. M. Sheldrick, SHELXS-86, SHELXL-93, *Programs for Crystal Structure Determination.* University of Göttingen (1986), 1993.

Pergamon

S0277-5387(96)00281-1

Polyhedron Vol. 16, No. 2, pp. 345–347. 1997
Copyright © 1996 Elsevier Science Ltd
Printed in Great Britain. All rights reserved
0277 5387/97 $15.00+0.00

COMMUNICATION

Synthesis and X-ray crystal structure of $[Li(C_4H_8O)_4][Yb(NPh_2)_4]$

Wai-Kwok Wong,[a]* Lilu Zhang,[a] Feng Xue[b] and Thomas C. W. Mak[b]

[a]Department of Chemistry, Hong Kong Baptist University, 224 Waterloo Road, Kowloon, Hong Kong

[b]Department of Chemistry, The Chinese University of Hong Kong, Shatin, N.T., Hong Kong

(Received 25 April 1996; accepted 5 June 1996)

Abstract—The interaction of $Yb(NPh_2)_2Cl$ with one equivalent of $Li[(CH_2)(CH_2)PPh_2]$ in tetrahydrofuran gave the unexpected dark red complex $[Li(C_4H_8O)_4][Yb(NPh_2)_4]$ (**1**) in 30% yield. An X-ray diffraction study reveals that the lanthanide–amide *ate* complex is composed of a discrete cation $[Li(C_4H_8O)_4]^+$ and a discrete homoleptic tetrahedral Yb-amide anion $[Yb(NPh_2)_4]^-$. Copyright © 1996 Elsevier Science Ltd

Keywords: ytterbium(III); structure; discrete homoleptic amide anion; diphenylamide; homoleptic amide complex; lanthanide–amide *ate* complex.

Lanthanide amide complexes are excellent synthetic precursors for lanthanide-alkoxides [1], phosphides [2] and thiolates [3] which can be prepared *via* protonolysis of the lanthanide–amide bond with alcohols, phosphines and thiols, respectively. Homoleptic three-coordinate lanthanide amide complexes had been known for some time [4], however, it was not until recently that homoleptic tetra-coordinate lanthanide amide *ate* complexes had been reported [5,6]. There are relatively few structural characterization studies on lanthanide–amide *ate* complexes [6,7], particularly those containing a discrete homoleptic tetra-coordinate lanthanide–amide *ate* anion. In this communication, we report the X-ray crystal structure of a Yb-amide complex with a discrete homoleptic tetra-coordinate Yb-amide *ate* moiety.

The interaction of $Yb(NPh_2)_2Cl$ with one equivalent of $Li[(CH_2)(CH_2)PPh_2]$ in tetrahydrofuran for 16 h, work up gave the unexpected dark red crystals of stoichiometry $[Li(C_4H_8O)_4][Yb(NPh_2)_4]$† (**1**) in 30% yield after recrystallization from a toluene solution. The structure of **1** was established by an X-ray diffraction study.‡ A perspective drawing of **1** is shown in Fig. 1; and selected bond lengths and bond angles are given in the caption.

The crystal structure analysis revealed that **1** is composed of a discrete cation and a discrete anion. In

* Author to whom correspondence should be addressed.

† $[Li(C_4H_8O)_4][Yb(NPh_2)_4]$: Dark red crystals, m.p. 188–190°C dec. Found: C, 66.8; H, 6.0; N, 4.9. Calc. for $C_{64}H_{72}LiN_4O_4Yb$: C, 67.3; H, 6.3; N, 4.9%. IR (cm^{-1}, in KBr): 3038 w, 1596 vs, 1520 vs, 1495 vs, 1458 s, 1418 s, 1320 vs, 1240 w, 1173 m, 1080 w, 1031 w, 991 w, 877 m, 745 vs, 701 m, 690 vs, 504 w, 431 w. ^1H NMR (C_6D_6): δ 7.23 (16 H, br, s), 6.92 (8H, br, s), 4.90 (8H, br, s), 4.43 (16 H, br, s), 2.21 (8H, br, s), 1.36 (8H, br, m), 1.02 (8H, br, s) ppm.

‡ Crystal data for $[Li(C_4H_8O)_4][Yb(NPh_2)_4]$: $F_w = 1141.24$, monoclinic, $P2_1$ (No. 4), $a = 10.914$ (2), $b = 14.094$ (3), $c = 19.330$ (4) Å, $\beta = 96.66$ (3)°, $V = 2953$ (1) Å^3, $Z = 2$, $F(000) = 1178$, $D_c = 1.283$ g cm^{-3}, $\mu = 16.31$ cm^{-1}. Crystal dimensions: $0.60 \times 0.20 \times 0.20$ mm. Intensity data were collected on a Rigaku AFC7R diffractometer, using Mo-K_α radiation ($\lambda = 0.71073$ Å) at 293 K. Unit cell parameters were calculated from least-squares fitting of the

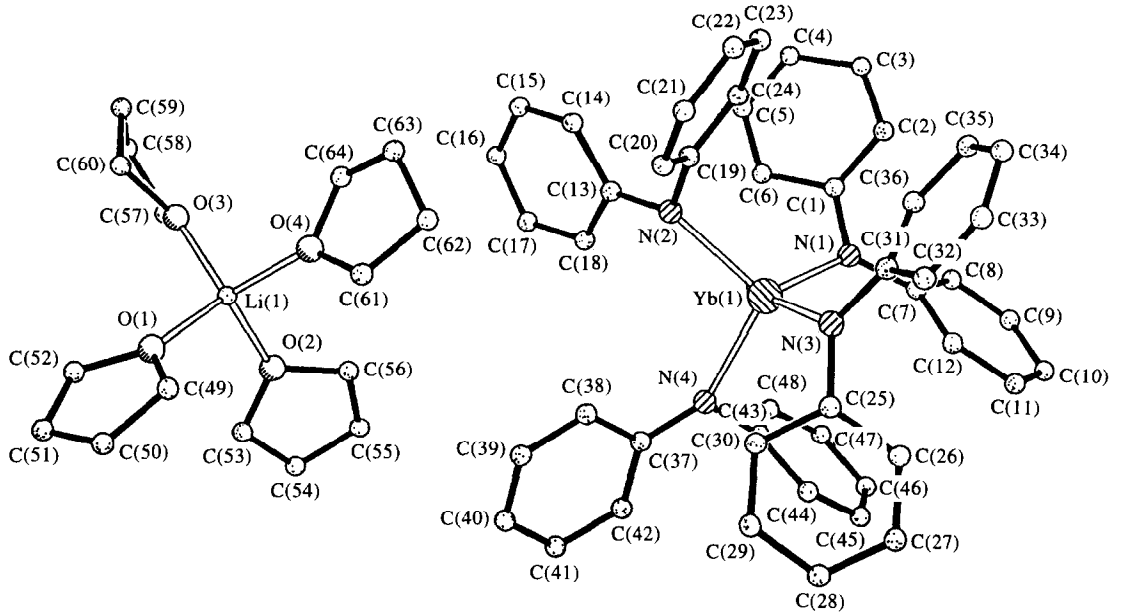


Fig. 1. A perspective view of the molecular structure of $[Li(C_4H_8O)_4][Yb(NPh_2)_4]$. Selected bond lengths (Å) and bond angles (°): Yb(1)—N(1), 2.201(9); Yb(1)—N(2), 2.216(9); Yb(1)—N(3), 2.188(9); Yb(1)—N(4), 2.241(9); N(1)—C(1), 1.398(12); N(1)—C(7), 1.391(12); N(2)—C(13), 1.388(12); N(2)—C(19), 1.417(12); N(3)—C(25), 1.395(12); N(3)—C(31), 1.388(12); N(4)—C(37), 1.382(13); N(4)—C(43), 1.412(13); Li(1)—O(1), 1.90(2); Li(1)—O(2), 1.88(2); Li(1)—O(3), 1.90(2); Li(1)—O(4), 1.91(2); N(1)—Yb(1)—N(2), 112.8(3); N(1)—Yb(1)—N(3), 106.7(4); N(1)—Yb(1)—N(4), 110.9(4); N(2)—Yb(1)—N(3), 111.7(3); N(2)—Yb(1)—N(4), 104.0(4); N(3)—Yb(1)—N(4), 110.8(3); C(1)—N(1)—C(7), 116.0(9); C(13)—N(2)—C(19), 115.0(9); C(25)—N(3)—C(31), 118.2(9); C(37)—N(4)—C(43), 119.9(9).

$[Li(C_4H_8O)_4]^+$, the Li atom adopts a tetrahedral geometry with four molecules of tetrahydrofuran coordinated to the Li atom *via* the oxygen atoms. The Li—O distances and the O—Li—O angles are normal and lie in the range 1.88 (2)–1.91 (2) Å and 108.1 (10)–111.3 (11)°, respectively. The anion $[Yb(NPh_2)_4]^-$ can be described as a distorted tetrahedron with the Yb atom coordinated by four terminal NPh_2 groups. The Yb—N distances ranging from 2.188 (9)–2.241 (9) Å are longer than the terminal Yb—N(silylamide) bonds of the three-coordinate $Yb[N(SiMe_3)_2]_3$ complex [2.158(13) Å] [8] and shorter than the terminal Yb—N(silylamide) bond of the five-coordinate $Yb[OC(CMe_3)(2\text{-}CH_2NC_5H_3Me\text{-}6)_2]_2[N(SiMe_3)_2]$ complex [2.260 (5) Å] [9]. The N—Yb—N angles ranging from 104.0(4)–112.8 (3)° are typical of a slightly distorted tetrahedron. The N atoms of the amide groups adopt a planar geometry with C—N—C angles ranging from 115.0(9)–119.9(9)° and can be considered as sp^2 hybridized. Lanthanide *ate* complexes with homoleptic NR_2 groups have been structurally characterized recently [6,7]. However, in all of them the cation and the anion moieties of the complexes are linked together *via* two bridging amide groups. Notably **1** is the first structurally characterized lanthanide amide *ate* complex to comprise a discrete cation and a discrete homoleptic tetra-coordinate lanthanide–amide anion.

2θ angles for 25 selected strong reflections. Crystal stability was monitored by recording three check reflections at intervals of 150 data measurements, and no significant variation was detected. An empirical absorption correction based on Ψ-scans was applied, resulting in relative transmission factors ranging from 0.880 to 1.035 [10]. A total of 5416 unique reflections ($4° \leqslant 2\theta \leqslant 50°$) were measured and 3224 reflections have $I \geqslant 2\sigma(I)$. The structure was solved by the direct method using SHELXTL-PLUS [11] and refined against F^2 using SHELXL-93 [12]. Non-hydrogen atoms were refined anistropically by full-matrix least-squares. Hydrogen atoms were placed in their calculated positions (C—H bond fixed at 0.96 Å) and allowed to ride on their respective parent carbon atoms. Analytical expressions of neutral-atom scattering factors were employed, and anomalous dispersion corrections were incorporated [13]. The final *R*, *Rw* values were 0.048, 0.112.

Acknowledgements—This work is supported by the Hong Kong Research Grants Council Earmarked Grant HKBU/94-95/II-74-P (W.-K. W.) and CUHK 89/93E (T.C.W.M.).

REFERENCES

1. M. F. Lappert, A. Singh and R. G. Smith, *Inorg. Synth.* 1990, **27**, 164.
2. H. C. Aspinall, D. C. Bradley and K. D. Sales, *J. Chem. Soc., Dalton Trans.* 1988, 2211.

3. H. C. Aspinall, D. C. Bradley, M. B. Hursthouse, K. D. Sales and N. P. C. Walker, *J. Chem. Soc., Chem. Commun.* 1985, 1585.
4. (a) D. C. Bradley, J. S. Ghotra and F. A. Hart, *J. Chem. Soc., Dalton Trans.* 1973, 1021; (b) D. C. Bradley, J. S. Ghotra and F. A. Hart, *Inorg. Nucl. Chem. Lett.* 1976, **12,** 735.
5. H. C. Aspinall and M. R. Tillotson, *Polyhedron* 1994, **13,** 3229.
6. W. J. Evans, R. Anwander, J. W. Ziller and S. I. Khan, *Inorg. Chem.* 1995, **34,** 5927.
7. H. Schumann, P. R. Lee and J. Loebel, *Chem. Ber.* 1989, **122,** 1897.
8. P. G. Eller, D. C. Bradley, M. B. Hursthouse and D. W. Meek, *Coord. Chem. Rev.* 1977, **24,** 1.
9. W. J. Evans, R. Anwander, U. H. Berlekamp and J. W. Ziller, *Inorg. Chem.* 1995, **34,** 3583.
10. G. Kopfmann and R. Huber, *Acta Cryst., Sect. A*, 1968, **24,** 348.
11. (a) G. M. Sheldrick, *Computational Crystallography* Edited by D. Sayre, p. 506. Oxford University Press, New York (1982); (b) G. M. Sheldrick, *Crystallographic Computing* 3: *Data Collection, Structure Determination, Proteins, and Databases*, Edited by G. M. Sheldrick, C. Kruger and R. Goddard, p. 175. Oxford University Press, New York (1985).
12. (a) G. M. Sheldrick, *SHELXL*-93, *Program for Crystal Structure Refinement*, University of Göttingen, Germany 1993; (b) G. M. Sheldrick, *Crystallographic Computing* 6: *A Window on Modern Crystallography*, Edited by H. D. Flack, L. Párkányi and K. Simon. Oxford University Press, New York (1993).
13. J. A. Ibers and W. C. Hamilton, *International Tables for X-ray Crystallography* (a) Vol. 4, pp. 55, 99 and 149; (b) Vol. 3, p. 278. Kynoch Press, Birmingham (1974).

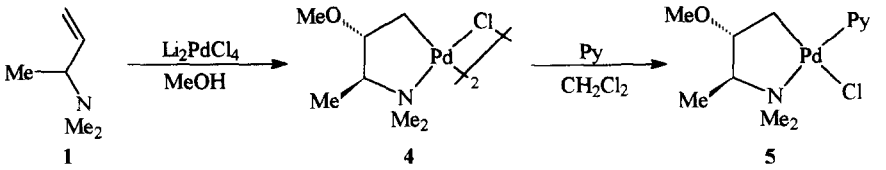
Pergamon

Polyhedron Vol. 16, No. 2, p. 349, 1997
Elsevier Science Ltd. Printed in Great Britain

ERRATUM

Methoxy-palladation of allylamines: a facile synthesis of chiral cyclopalladated compounds. X-ray crystal structure of *trans*-[Pd($CH_2CH(OMe)CH(Me)NMe_2$)(Cl)(Py)]. J. Dupont, R. A. P. Halfen, R. Schenato, A. Berger, M. Horner, A. Bortoluzzi and C. Maichle-Mössmer (*Polyhedron*, Vol. 15, No. 20, pp. 3465–3468 (1996)).

The figures in Scheme 2 have been erroneously substituted by those of Scheme 1. The correct version of Scheme 2 should have appeared as follows:



1 4 5

Scheme. 2.

Pergamon

PII: S0277-5387(96)00314-2

Polyhedron Vol. 16, No. 3, pp. 351–353, 1997
Copyright © 1996 Elsevier Science Ltd
Printed in Great Britain. All rights reserved
0277-5387/97 $17.00+0.00

Structural characterization of the acetonitrile complex $NbCl_5(MeCN)$

Gerald R. Willey,[a]* Timothy J. Woodman[a] and Michael G. B. Drew[b]

[a]Department of Chemistry, University of Warwick, Coventry CV4 7AL, U.K.

[b]Department of Chemistry, University of Reading, Whiteknights, Reading RG6 2AD, U.K.

(Received 30 April 1996; accepted 27 June 1996)

Abstract—The monosolvate (MeCN) of niobium(V) chloride has been structurally characterized. The metal is six coordinate with a somewhat distorted octahedral geometry in which the four equatorial chlorine atoms are coplanar but are clearly bent towards the bound axial acetonitrile ligand, mean N_{ax}—Nb—Cl_{eq} 83.62(12)°. The Nb—Cl bond distances lie in the range 2.249(2)–2.319(2) Å and the metal to ligand distance, Nb—N, is 2.236(4) Å. Copyright © 1996 Elsevier Science Ltd

Keywords: structure; niobium(V); acetonitrile; adduct; octahedral.

Niobium(V) and tantalum(V) chlorides, which enjoy a common dimeric halogen-bridged structure [1], are conveniently soluble in Lewis donor solvents such as alkyl cyanides [2], ethers and thioethers [3] to give mononuclear adducts that can be used as suitable precursors for a wide range of metal(V) complexes *via* ligand exchange reactions. However, with nitrogen donor ligands such as pyridine, trimethylamine, γ-picoline, bipyridyl and 1,10-phenanthroline there is an attendant problem, *viz.*, reduction to the +4 oxidation state is commonplace [4].

In this paper we report the salient structural features of the acetonitrile solvate $NbCl_5(MeCN)$ following room temperature X-ray diffraction studies.

EXPERIMENTAL

All manipulations were carried out under argon using standard Schlenk vacuum-line techniques. Acetonitrile was purified following the recommended procedure [5], stored over P_4O_{10} and distilled under argon prior to use. $NbCl_5$ was used as supplied commercially (Aldrich).

Preparation of $NbCl_5(MeCN)$

$NbCl_5$ (6.0 g, 22.2 mmol) was placed in a dried thimble and extracted (Soxhlet) with acetonitrile (100 cm^3) over a period of 4 h. On cooling the resulting yellow solution (0°C) a large crop of yellow, barrel-shaped crystals separated out. These were collected, washed with n-hexane (2 × 20 cm^3) and pumped to dryness *in vacuo* at room temperature. (Yield 5.2 g, 16.8 mmol). Found: C, 7.7; H, 0.9; N, 4.5; Nb, 29.7; Cl, 56.8. Calc. for $C_2H_3NNbCl_5$: C, 7.7; H, 1.0; N, 4.5; Nb, 29.8; Cl, 57.0%.

X-ray crystallography

Crystal data are given in Table 1, together with refinement details. Data were collected with Mo-K_α radiation using the MARresearch Image Plate System. The crystal was positioned at 75 mm from the image plate. A total of 95 frames were measured at 2° intervals with a counting time of 2 min. Data analysis was carried out with the XDS program [6]. The structure was solved by heavy atom methods. The non-hydrogen atoms were refined with anisotropic thermal parameters. The hydrogen atoms were included in geometric positions and given thermal parameters equivalent to 1.2 times the carbon atom to which they were attached. The structure was refined using SHELXL [7]. All calculations were carried out on a Silicon Graphics R4000 workstation at the University of Reading. A complete listing of bond distances and angles is given in Table 2. Supplementary material including atomic coordinates, tables of thermal par-

* Author to whom correspondence should be addressed.

Table 1. Crystal data and structure refinement for $NbCl_5(MeCN)$

Formula	$NbCl_5(MeCN)$
Empirical formula	$C_2H_3Cl_5NNb$
Formula weight	311.21
Temperature (K)	293 (2)
Wavelength (Å)	0.71073
Crystal system	monoclinic
Space group	$P2_1/c$
Unit-cell dimensions (Å, °)	a 6.013(8)
	b 9.942(7)
	c 15.600(10)
	β 97.13(1)
Volume (Å^3)	925.4
Z	4
Density (calculated) (Mg/m^3)	2.234
Absorption coefficient (mm^{-1})	2.665
$F(000)$	592
Crystal size (mm)	$0.23 \times 0.25 \times 0.30$
θ range for data collection (°)	3.98–24.86
Index ranges	$0 \leqslant h \leqslant 6$,
	$-11 \leqslant k \leqslant 11$,
	$-18 \leqslant l \leqslant 18$
Reflections collected	2673
Independent reflections	1473[R(int) = 0.0374]
Weighting scheme (a,b)[a]	0.04, 2.67
Data/parameters	1473/84
Goodness-of-fit on F^2	1.105
Final R indices [$I > 2\sigma(I)$]	$R_1 = 0.0363$,
	$wR_2 = 0.0937$
R indices (all data)	$R_1 = 0.0399$
	$wR_2 = 0.0962$
Largest diff. peak and hole (e Å^{-3})	0.513, −0.942

[a]Weight = $1/[\sigma^2(F_0^2) + (aP)^2 + bP]$, where $P = (\max(F_0^2, 0) + 2F_c^2)/3$.

Table 2. Bond lengths (Å) and angles (°) for $NbCl_5(MeCN)$

Nb—N(1)	2.236(4)
Nb—Cl(1)	2.249(2)
Nb—Cl(2)	2.317(1)
Nb—Cl(3)	2.293(1)
Nb—Cl(4)	2.286(2)
Nb—Cl(5)	2.319(2)
N(1)—C(2)	1.115(6)
C(2)—C(3)	1.455(7)

N(1)—Nb—Cl(1)	177.92(12)
N(1)—Nb—Cl(4)	83.22(12)
Cl(1)—Nb—Cl(4)	97.30(7)
N(1)—Nb—Cl(3)	85.30(12)
Cl(1)—Nb—Cl(3)	96.70(6)
Cl(4)—Nb—Cl(3)	90.33(6)
N(1)—Nb—Cl(2)	84.00(12)
Cl(1)—Nb—Cl(2)	93.98(6)
Cl(4)—Nb—Cl(2)	89.97(6)
Cl(3)—Nb—Cl(2)	169.18(6)
N(1)—Nb—Cl(5)	81.94(13)
Cl(1)—Nb—Cl(5)	97.53(8)
Cl(4)—Nb—Cl(5)	165.15(7)
Cl(3)—Nb—Cl(5)	88.49(6)
Cl(2)—Nb—Cl(5)	88.46(6)
C(2)—N(1)—Nb	178.4(5)
N(1)—C(2)—C(3)	179.5(6)

ameters, hydrogen atom coordinates and observed and calculated structure factors is available from the authors on request.

RESULTS AND DISCUSSION

$NbCl_5(MeCN)$ was obtained as yellow, barrel-shaped crystals from direct Soxhlet extraction of niobium(V) chloride with acetonitrile. The product shows rapid hydrolysis/decomposition on the slightest exposure to the atmosphere but individual crystals can be easily manipulated into Lindemann tubes under argon.

The crystal and molecular structure of this mono-solvate $NbCl_5(MeCN)$ shows a six-coordinate, essentially octahedral, metal geometry with acetonitrile acting as a conventional σ-donor ligand. See Fig. 1 for the atom numbering scheme.

For $NbCl_5(MeCN)$ the observed metal–chlorine bond distances lie in the range 2.249(2)–2.319(2) Å with a mean value of 2.293 Å. Terminal Nb—Cl bond lengths that can be cited for comparison include: the parent halide $(NbCl_5)_2$ 2.25 Å [1]; $CpNbCl_4(PMePh_2)$ 2.4127(8), 2.3965(8), 2.4168(8), 2.4315(9) Å [8]; $Cp^*NbCl_4(CN\text{-}2,6\text{-}Me_2C_6H_3)$ 2.396(3)–2.435(3) Å [9]; $[Cp_2NbCl_2][SbF_6]$ mean 2.341 Å [10]; $[Cp_2Nb(CH_2SiMe_3)Cl][PF_6]$ 2.362(3) Å [11]; $[Cp_2NbCl_2][BF_4]\cdot CH_3CN$ 2.343(1) Å [12]; $[NbCl_4(O)(THF)]^-$ 2.378(4), 2.387(4), 2.376(4) Å [13]; Cp_2NbCl_2 2.464(5), 2.475(4) Å [14]; $CpNbCl_3(dppe)\cdot C_6H_5CH_3$ 2.479(3), 2.460(5), 2.473(6) Å [15]; *cis*-$NbCl_4(MeCN)_2$ 2.328(7), 2.343(6), 2.349(4) Å [16]; *trans*-$NbCl_4L_2$, where

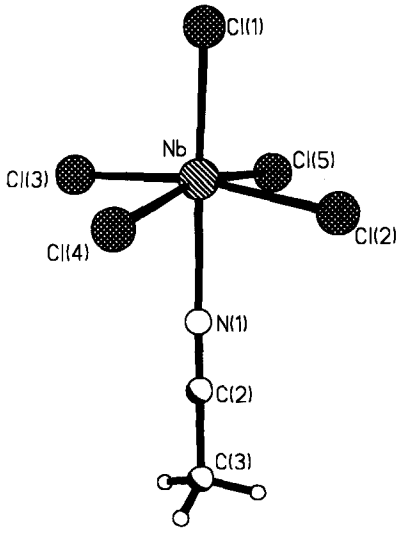


Fig. 1. The molecular structure of $NbCl_5(MeCN)$ including the atomic numbering.

L = PEt_3 2.357(3), 2.374(4) Å and L = PPh_2Et 2.401(1), 2.333(1) Å [17]; $[CpNb(CNCMe_3)_4Cl]^+$ 2.505(4) Å [13]; $[Cp^*NbCl_2[CN\text{-}2,6\text{-}Me_2C_6H_3]_3]$ 2.575(2), 2.546(2) Å [9]. These values are in accord with a perceptible lengthening in Nb—Cl bond length as the metal oxidation state decreases from +5 to +4 to +3, as might be anticipated; no such variation with metal oxidation state is observed for the Nb—N linkage, i.e. $NbCl_5(MeCN)$ (this study) 2.236(4) Å and *cis*-$NbCl_4(MeCN)_2$ 2.220(13) Å [16]. The binding of the acetonitrile (solvent) molecule is linear Nb—N—C 178.4(5), N—C—C 179.5(6)°. The arrangement of the five chlorine atoms around the central metal is slightly distorted from the ideal octahedral geometry. The four equatorial chlorine atoms are coplanar within experimental error, but are clearly bent back towards the coordinated acetonitrile molecule and away from the remaining axial chlorine atom. The metal is displaced from this plane by 0.22 Å and the resulting N_{ax}—Nb—Cl_{eq} angles lie in the range 81.94(13)–85.30(12)° mean 83.62(12)°. These deviations most probably originate from intramolecular steric/packing requirements rather than any intermolecular forces, and are seen to reflect the larger steric bulk of Cl_{ax} versus N_{ax}, especially since this axial chlorine has the shortest of the metal–chlorine bonds, at 2.249(2) Å.

Following the same approach we have isolated $TaCl_5(MeCN)$ as small white flakes. Found: C, 6.0; H, 0.7; N, 3.5; Ta, 45.2; Cl, 44.3. Calc. for C_2H_3N $TaCl_5$: C, 6.0; H, 0.8; N, 3.5; Ta, 45.3; Cl, 44.4%. The compound is isomorphous with its Nb^V counterpart as confirmed by X-ray diffraction studies. Cell data: monoclinic, space group $P2_1/c$, $a = 6.115(8)$, $b = 10.193(9)$, $c = 15.878(12)$ Å, $\beta = 97.08(1)°$. Data were collected and the structure proved to be similar to that of the Nb analogue but the determination was of insufficient quality to report here.

Acknowledgements—We thank the University of Warwick for a postgraduate studentship award (to T.J.W.). Financial support by the EPSRC and the University of Reading for the image plate system is gratefully acknowledged and we thank Mr A. W. Johans for technical assistance with the X-ray crystallographic studies.

REFERENCES

1. F. A. Cotton and G. Wilkinson, *Advanced Inorganic Chemistry*, 5th edn, pp. 787–804. Wiley Interscience, New York (1988); A. F. Wells, *Structural Inorganic Chemistry*, 5th edn, pp. 427, 444. Clarendon Press, Oxford (1986).
2. K. Feenan and G. W. A. Fowles, *J. Chem. Soc.* 1964, 2842.
3. K. Feenan and G. W. A. Fowles, *J. Chem. Soc.* 1965, 2449; J. D. Wilkins, *J. Inorg. Nucl. Chem.* 1975, **37**, 2095.
4. See for example, G. W. A. Fowles and C. M. Pleass, *J. Chem. Soc.* 1957, 2078; P. J. H. Carnell and G. W. A. Fowles, *J. Chem. Soc.* 1959, 4113; P. J. H. Carnell and G. W. A. Fowles, *J. Less-Comm. Met.* 1962, **4**, 40; R. E. McCarley, B. G. Hughes, J. C. Boatman and B. A. Torp, *Adv. Chem. Ser.* 1963, **37**, 243; M. Allbutt, K. Feenan and G. W. A. Fowles, *J. Less-Comm. Met.* 1964, **6**, 299.
5. M. Walter and L. Ramaley, *Annal. Chem.* 1973, **45**, 165.
6. W. Kabsch, *J. Appl. Cryst.* 1988, **21**, 916.
7. G. M. Sheldrick, *SHELXL93, Program for crystal structure refinement*. University of Gottingen, Germany (1993).
8. J. C. Fettinger, D. W. Keogh and R. Poli, *Inorg. Chem.* 1995, **34**, 2343.
9. M. I. Alcalde, J. de la Mata, M. Gómez, P. Royo, M. A. Pellinghelli and A. Tiripicchio, *Organometallics* 1994, **13**, 462.
10. P. Gowik, T. Klapötke and J. Pickardt, *Organometallics* 1989, **8**, 2953.
11. J. Arnold, T. D. Tilley, A. L. Rheingold and S. J. Geib, *Organometallics* 1987, **6**, 473.
12. K.-H. Thiele, W. Kubak, J. Sieler, H. Borrmann and A. Simon, *Z. Anorg. Allg. Chem.* 1990, **587**, 80.
13. H. C. Aspinall, M. M. Roberts and S. J. Lippard, *Inorg. Chem.* 1984, **23**, 1782.
14. K. Prout, T. S. Cameron and R. A. Forder, *Acta Cryst.* 1974, **B30**, 2290.
15. J. C. Daran, K. Prout, A. De Cian, M. L. H. Green and N. Siganporia, *J. Organomet. Chem.* 1977, **136**, C4.
16. A. J. Benton, M. G. B. Drew, R. J. Hobson and D. A. Rice, *J. Chem. Soc., Dalton Trans.* 1981, 1304.
17. F. A. Cotton, S. A. Duraj and W. J. Roth, *Inorg. Chem.* 1984, **23**, 3592.

Pergamon

PII: S0277-5387(96)00313-0

Polyhedron Vol. 16, No. 3, pp. 355–362, 1997
Copyright © 1996 Elsevier Science Ltd
Printed in Great Britain. All rights reserved
0277-5387/97 $17.00+0.00

The first X-ray crystallographic characterization of a dialkylaminomethylenephosphonic acid: synthesis of crystalline *N,N'*-diethylaminomethylenephosphonic acid, its protonation equilibria, and the stabilities of its complexes with lead(II)

Nick Choi, Maria Constantinou, David Hyatt, Ray W. Matthews,* Mary McPartlin and Ian J. Scowen

School of Applied Chemistry, University of North London, Holloway Road, London N7 8DB, U.K.

(Received 2 February 1996; accepted 27 June 1996)

Abstract—The X-ray crystal structure of *N,N'*-diethylaminomethlenephosphonic acid (LH_2) shows the molecule to be present as the N-protonated zwitterion. The unusually large P—C—N angle [120.1(3)°] is apparently owing to steric factors arising from the "eclipsed" conformation of the ethyl methylene carbon atoms and phosphonate oxygen atoms. Potentiometric titration and determination of the pH dependence of δ^{31} (P) were used to elucidate the protonation equilibria for LH_2. Stoichiometric stability constants for complexes of LH_2 with lead(II) provide evidence that LH_2 is selective for lead(II) over most transition metal ions [$\log \beta_{PbLH}$(PbLH): 11.55±0.12(011); 16.92±0.15(012); 18.3±0.5(013); 7.45±0.18(110); 14.81±0.35(111); −0.49±0.33(01-1)]. Copyright © 1996 Elsevier Science Ltd

Keywords: 1-aminophosphonic acid; *N,N'*-diethylaminomethylenephosphonic acid; protonation; stability constants; lead complexes; X-ray structure.

A large number of recent patent applications demonstrate the importance of 1-aminoalkylphosphonic acids in industry [1], and their potential in medical applications has been indicated [2]. Among the most widely used is diethylenetriamine-*N,N,N',N'',N''*-pentamethylenephosphonic acid; available under various trade names such as "DEQUEST" and "BRIQUEST", its detergent and metal ion-complexing abilities are utilized in textile and paper processing. The wide applicability of such compounds provides the stimulus for current interest in studies of their protonation equilibria and of their complicated complexing behaviour towards metal ions [3]. Such studies on the larger polymethylenephosphonates are, however, limited by the plethora of protonation and coordination sites [4]. Simpler aminomethylenephosphonic acids, e.g. *N,N'*-diethylaminomethylenephosphonic acid (LH_2), the subject of the present study, serve as models for understanding the behaviour of more complex systems. Work of this type is often limited by the difficulties experienced in isolating 1-aminoalkylphosphonic acids [5] from the Moedritzer–Irani reaction [6], the most commonly used method of preparation, a problem particularly manifest for aminomethylenephosphonic acids derived from secondary amines [6]. Previous investigations by Carter *et al.* [7] and Wozniak and Nowogrocki [8] of the protonation equilibria of LH_2 yielded pK_a values of $[LH]^-$ and $[LH_2]$ only. Stoichiometric stability constants for complexes of LH_2 with Mg^{II}, Ca^{II} [7] and Cu^{II} [8] were also determined. Protonation equilibria and the stabilities of complexes with a range of metal ions have been studied for a number of simple 1-aminomethylenephosphonic acids closely related to LH_2, e.g. $R_nN(CH_2PO_3H_2)_{3-n}$ (R = Me, [7,9] Et; [7,10] n = 0, 1 or 2), $R'HNCH_2PO_3H_2$ (R' = H [10,11], Me, Et [8]). For the series of 1-aminomethylenephosphonic acids

* Author to whom correspondence should be addressed.

$Et_nN(CH_2PO_3H_2)_{3-n}$ ($n = 0$, 1 or 2), X-ray crystal structure determinations have been reported only for the compounds with $n = 0$ [12] and 1 [13].

We have developed a method for obtaining LH_2 in pure form, allowing the first solid state characterization of a l-aminomethylenephosphonic acid derived from a secondary amine, and demonstrating that the molecule is present as the N-protonated zwitterion. A detailed study of its protonation equilibria has provided a value for the pK_a of $[LH_3]^+$ for the first time, together with those for LH_2 and $[LH]^-$. Stoichiometric stability constants for complexes with lead(II) over the pH range 4.6–8.7 show that the complex species formed at low pH is predominantly $[PbLH]^+$ and that this, with increasing pH, deprotonates to give PbL and, ultimately, $[PbL(OH)]^-$. There is evidence that the ligand is selective for lead (II) over most first row transition metals, indicating a potential use for ligands of this type in the removal of this toxic metal.

EXPERIMENTAL

Preparation of N,N′-*diethylaminomethylenephosphonic acid* (LH_2)

The compound LH_2 was prepared using a method developed from the general procedure described by Moedritzer and Irani [6] for the synthesis of l-aminomethylenephosphonic acids.

Aqueous diethylamine (70%, 23.3 g, 0.25 mol) was dissolved in a mixture of ice and water (250 cm^3) and treated with aqueous hydrochloric acid (6 mol dm^{-3}, 40 cm^3) in portions while stirring and cooling. Phosphorous acid (16.4 g, 0.20 mol) was added and the mixture was brought to reflux. Aqueous formaldehyde (40%, 22 cm^3, 0.30 mol) was added to the refluxing mixture over 60 min and refluxing was continued for a further 8 h. The reaction mixture was concentrated under reduced pressure and then treated with propylene oxide (*ca* 50% excess) at 40°C. Further concentration under reduced pressure yielded a pale yellow oil which was treated with an equal volume of ethanol/acetone (*ca* 3 : 1 v/v). After storage in a stoppered vessel for three months, the mixture yielded a white crystalline solid which was isolated by filtration, washed with cold ethanol and desiccated *in vacuo* over phosphorus pentoxide for 24 h. [Yield: 13.2 g (40%). M.p. 195–197°C). Found: C, 36.6; H, 8.7; N, 8.5. Calc. for $C_5H_{14}NO_3P$: C, 35.9; H, 8.4; N, 8.4%.]

Crystals suitable for X-ray diffraction studies were obtained from a mixture of LH_2 (0.30 g, 0.002 mol) and a solution of n-butylstannoic acid (0.40 g, 0.002 mol) in toluene (100 cm^3). The mixture was heated under reflux for 6 h using a Dean–Stark trap, and then left to stand overnight at room temperature before being filtered. Square crystals were isolated from the filtrate after storage in a stoppered container for four months. [Recovery: 0.27 g (87%). M.p. 210–212.1°C. Found: C, 35.8; H, 8.5; N, 8.3%]. IR (16 mm KBr disc): $\bar{\nu}_{max}/cm^{-1}$: *ca* 3420br, 2964m, 2935m, 2873m, 2758w, 2660w, 1636m, 1468m, 1124s br, 1005 s, 878w, 772w, 686w, 576m, 513s. ^1H NMR (D_2O): δ 3.37 (approx. quintet, CH_3CH_2), 3.28 [d, CH_2-P, $^2J(HP) = 13.0$ Hz], 1.31 [t, CH_3, $^3J(HH) = 7.3$ Hz]. ^{13}C NMR (D_2O): δ 52.39 [d, CH_3CH_2, $^3J(CP) = 4.4$ Hz], 51.44 [d, CH_2-P, $^1J(CP) = 136.8$ Hz], 11.15 (CH_3). ^{31}P NMR (D_2O): δ 8.45 [t, $^2J(PH) = 13.0$ Hz].

Crystal structure determination

Crystal data. $C_5H_{14}NO_3P$, $M = 167.15$, monoclinic, space group $P2_1/n$ (non-standard setting of No. 14), $a = 7.708(2)$, $b = 11.398(3)$, $c = 9.435(2)$ Å, $\beta = 105.3(2)°$, $U = 799.54$ Å^3, $Z = 4$, $F(000) = 360$, $D_c = 1.389$ g cm^{-3}, μ(Mo-K_α) = 2.9 cm^{-1}.

Data collection. X-ray intensity data were collected on a colourless translucent crystal of dimensions $0.20 \times 0.20 \times 0.15$ mm^3, using a Philips PW1100 four-circle diffractometer with Mo-K_α radiation ($\lambda = 0.71069$ Å) from a graphite monochromator, in the θ-range $3 \leqslant \theta \leqslant 25°$ and with a scan width of 0.90°, as described previously [14]. A total of 1582 reflections were scanned and equivalent reflections were merged to give 843 unique reflections with $I/\sigma(I) > 3$.

Structural solution and refinement [15]. The coordinates of the phosphorus and oxygen atoms were located by direct methods. The positions of the remaining non-hydrogen atoms were found from successive difference Fourier maps. A difference Fourier synthesis calculated using data with $\sin\theta < 0.35$ revealed the positions of the acidic protons, and all the carbon-bonded hydrogen atoms were included in idealized positions (C—H 1.08 Å) with their thermal parameters fixed at 0.08 Å^2. In the final cycles of full-matrix least-squares refinement all non-hydrogen atoms were assigned anisotropic thermal parameters and converged at $R = 0.0469$ and $R_w = 0.0486$ with weights of $1/\sigma^2(F)$ assigned to individual reflections. The final difference Fourier synthesis showed no residual maximum greater than 0.3 eÅ^{-3}.

Potentiometric measurements

Potentiometric titrations were carried out in aqueous solution, under an atmosphere of water-saturated, CO_2-free nitrogen, using a purpose-built automated titration apparatus [16]. All reagents used were of analytical grade (e.g. BDH AnalaR) or better (e.g. BDH ARISTAR); water was deionized by reverse osmosis (to BS3978 grade 1 specification) and degassed, as appropriate, by refluxing under nitrogen. Solution potential was measured using a glass electrode referenced to a large calomel electrode *via* a salt bridge. The titration environment was maintained at 25.0 ± 0.1°C by water circulating through jackets sur-

rounding both the titration cell and the calomel electrode. Data for each point in the titration were recorded when the averages of two successive sets of potential measurements (typically 60 in each set) were stable to within 0.05 mV. All titrations were carried out at constant ionic strength (0.1 mol dm^{-3}) provided by KNO_3 as the supporting electrolyte. Aqueous HNO_3/KNO_3 (0.004 mol dm^{-3} and 0.096 mol dm^{-3}, respectively; 25 cm^3) in the titration cell was titrated against carbonate-free aqueous KOH (0.1 mol dm^{-3}) to determine the cell calibration constants E_0 and pK_w. Similar titrations with (a) added LH_2 (*ca* 1×10^{-3} mol dm^{-3}) and (b) LH_2 (*ca* 1×10^{-3} mol dm^{-3}) and the appropriate metal nitrate salt ([M]:[L] *ca* 1:1, 1:2 or 1:3) gave data for determination of, respectively, pK_a values and stability constants for the metal complexes. Metal ion concentrations in stock solutions were determined by titration with aqueous EDTA solution [17].

Typically, 200 data points were collected for each titration in the pH range *ca* 2.5–11.0. Three titrations were performed for the free ligand, three for the ligand/Pb^{II} system, and at least two for each ligand/M^{II} system (M = Co, Ni, Cu, Zn and Cd). Using the program SUPERQUAD [18], variously 128–195 titration points were used in data analyses to obtain pK_a values and 29–36 points were used to determine log K values for the Pb^{II} complexes.

NMR spectra

The pH dependence of the ^{31}P NMR spectrum for LH_2 was determined by monitoring $\delta(^{31}P)$ during titration of a solution of LH_2 (*ca* 0.02 mol dm^{-3}) in an initially acid H_2O/D_2O medium at constant ionic strength ($[HNO_3] = 0.04$ mol dm^{-1}, $[KNO_3] = 0.96$ mol dm^{-3}, 10% D_2O v/v, $I = 1.0$ mol dm^{-3}) against aqueous KOH (1.0 mol dm^{-3}) in an NMR tube (o.d. 10 mm). All reagents were of purities that matched those used in the potentiometric measurements. Aliquots of base (normally 0.012 cm^3, but 0.006 cm^3 near 'end-point' regions) were delivered from a motorized piston burette (Metrohm Dosimat 655). After addition of each aliquot, the pH of the solution was determined in the NMR tube using a thin stem combination electrode (Russell) linked to a Corning 150 pH/ion meter and calibrated against potassium hydrogen phthalate (pH *ca* 4.0) and phosphate (pH *ca* 6.9) buffers [17]. Thereafter, the $^{31}P\{^1H\}$ broad band decoupled NMR spectrum was obtained on the spinning sample at 32.29 MHz on a Bruker WP80 NMR spectrometer.

Chemical shifts were referenced to external 85% H_3PO_4 by sample substitution. The reference was contained in a 5 mm (o.d.) coaxial tube within a 10 mm (o.d.) NMR tube containing a solution of LH_2 identical to that used at the start of the titration. Reference signals were recorded after every five data points and showed variations of <0.05 ppm. At the end of the titration, a volume of base solution, equal to the total delivered in the titration, was added to the solution surrounding the aqueous H_3PO_4 reference tube. Subsequent determination of the ^{31}P NMR spectrum showed the position of the reference signal to be independent of the pH of the solution providing the lock signal. A satisfactory spectrum was obtained at each titration point with *ca* 100 transients, pulse length 1.0 μs, delay 3.0 s, spectral width 1602 Hz and 16 K data points.

Routine ^1H, ^{13}C and ^{31}P NMR spectra were obtained on a Bruker AM250 spectrometer using TSP-d_4 (^1H, ^{13}C) and external aqueous H_3PO_4 (^{31}P) as references.

RESULTS AND DISCUSSION

The syrupy ligands resulting from evaporation of the reaction mixtures in the preparation of 1-aminoalkylphosphonic acids from secondary amines by the Moedritzer–Irani reaction retain significant amounts of hydrochloric acid which cannot be easily removed [6]. Removal of hydrochloric acid may be important in overcoming the reluctance of these liquids to crystallize, so, in the synthesis of LH_2, the syrup was treated with propylene oxide at 40 °C [19]; both the oxide and its addition product with HCl were removed under reduced pressure. The pure aminophosphonic acid was obtained in good yield, although crystallization was a very lengthy process. This allowed the first X-ray crystallographic determination of LH_2. Isolation of the anion $[LH]^-$ as the K^+ salt has been previously reported [7].

Full characterization of LH_2 was carried out on the recrystallized sample, which was also used for X-ray diffraction studies. A notable feature of the ^1H NMR spectrum obtained at 250 MHz in D_2O is the slightly broadened "quintet" [$^3J(HH) \approx 7.6$ Hz] assigned to $-CH_2CH_3$. Aside from the expected coupling to the methyl protons, further coupling to phosphorus [$^4J(HP)$] is ruled out by the expected magnitude of such long-range coupling (<1 Hz) and the absence of the appropriate pattern in the ^{31}P NMR spectrum. We conclude that these methylene protons are rendered anisochronous by the prochiral nitrogen atoms, the normally fast nitrogen inversion process being sufficiently slowed by protonation of the nitrogen atoms in the zwitterionic species which are exclusively present below pH *ca* 9 (*vide infra*). The "quintet" pattern can be accounted for by overlap of the quartets arising from the anisochronous methylene protons with a chemical shift difference of *ca* 0.03 ppm. At 80 MHz, the multiplet becomes a broad "quartet" and a simulation indicates the geminal coupling to be *ca* -2 Hz.

Protonation equilibria

Values of protonation constants for LH_2 determined as the mean of several independent refinements

Table 1. Protonation constants for LH_2 and stability constants for complexes of LH_2 with Pb^{II}[a]

mlh	$\log \beta_{mlh}$[b]	$\log K_{mlh}$
011	11.55±0.12	11.55±0.12[c]
	(11.81±0.03) [8]	(12.32±0.19) [7]
012	16.92±0.15	5.37±0.03[c]
	(17.09±0.03) [8]	(5.79±0.11) [7]
013	18.3±0.5	1.4±0.4[c]
110	7.45±0.18	7.45±0.18
111	14.81±0.35	7.36±0.17
11−1	−0.49±0.33[d]	−7.94±0.51[e]

[a] Data obtained at constant ionic strength, $I = 0.1$ mol dm^{-3}, KNO_3; 25.0±0.1 °C. Convention β_{mlh} for $M_mL_lH_h$; $L = Et_2NCH_2PO_3^{2-}$. Values of $\log \beta_{mlh}$ and $\log K_{mlh}$ are unweighted means of values obtained for each satisfactory refinement of each titration data set; error limits encompass the range of values obtained for each $\log \beta_{mlh}$ (and $\log K_{mlh}$).

[b] $\beta_{mlh} = [M_mL_lH_h]/[M]^m[L]^l[H]^h$. Values obtained by previous workers are given in the parentheses.

[c] $K_{0lh} = [LH_h]/[LH_{h-1}][H]$.

[d] $\{Pb(H_2O)_n\}^{2+} + L \rightleftharpoons \{Pb(L)(H_2O)_{n-1}(OH)\}^- + H^+$; $\beta_{11-1} = [\{Pb(L)(H_2O)_{n-1}(OH)\}^-][H^+]/[\{Pb(H_2O)_n\}^{2+}][L]$.

[e] $\{Pb(L)(H_2O)_n\} \rightleftharpoons \{Pb(L)(H_2O)_{n-1}(OH)\}^- + H^+$; $K_{11-1} = [\{Pb(L)(H_2O)_{n-1}(OH)\}^-][H^+]/[\{Pb(L)(H_2O)_n\}]$; $\log K_{11-1} = \log \beta_{11-1} - \log \beta_{110}$.

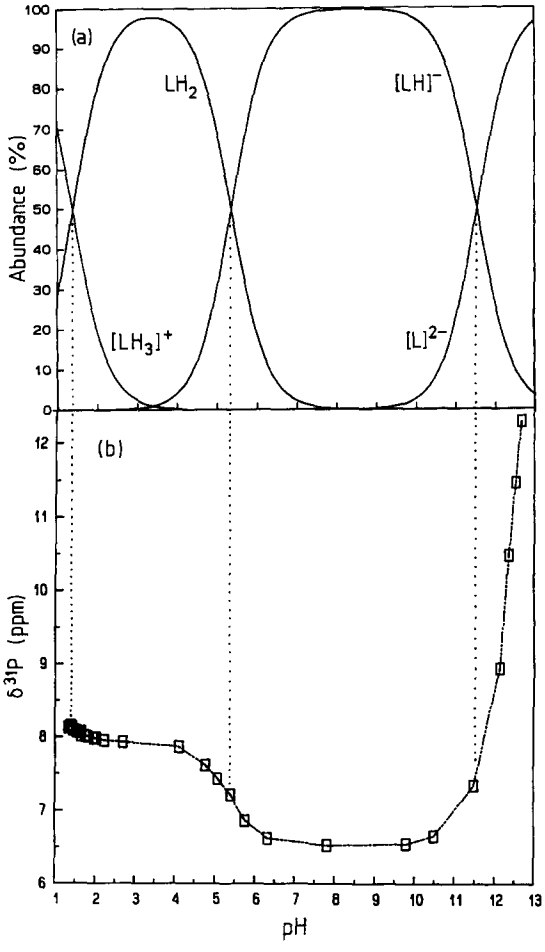


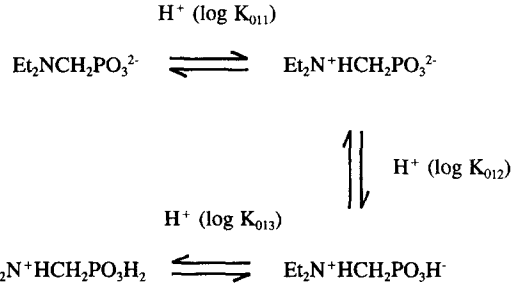
Fig. 1. (a) Distribution of ligand species derived from LH_2 as a function of pH calculated [20] using values of $\log \beta_{0lh}$ determined in aqueous KNO_3 ($I = 0.1$ mol dm^{-3} KNO_3) (this work); (b) pH dependence of $\delta(^{31}P)$ for LH_2 in aqueous KNO_3 ($I = 1.0$ mol dm^{-3}). Dotted lines indicate correlation between 'half-neutralization' points in (a) and inflections on curves in (b).

of the data from three titrations are given in Table 1. Relatively large intratitration (different refinements on the same data set) and intertitration variations in the value of $\log \beta_{013}$ were found (evident in the error limits on this value) and presumably arise because of the low abundance of the tri-prontonated ligand (<10% at pH 2.4; see Fig. 1a).

Previous potentiometric investigations by Wozniak and Nowogrocki [8] of the protonation equilibria of LH_2 yielded pK_a values of $[LH]^-$ and LH_2 only. The present study (Table 1) yielded, additionally, a pK_a value for $[LH_3]^+$. The results for $[LH]^-$ and LH_2 agree most closely with the values obtained by Wozniak and Nowogrocki under similar conditions ($I = 0.1$ mol dm^{-3}, KNO_3), and less so with those reported by Carter *et al.* [7] from solutions of higher ionic strength [$I = 1.0$ mol dm^{-3}, (KNO_3)]. The latter authors point out that complexation of K^+ by the ligand may significantly affect the magnitude of $\log K_{011}$ in these experiments.

The first protonation step has been assigned [7] to protonation of the nitrogen on the basis of ^1H and ^{31}P NMR spectra obtained for solutions of LH_2 with the addition of, respectively, 0, 1, 2 and 3 equivalents of NaOD. The protonation scheme (Scheme 1) implied by these results was confirmed in the present study by comparison of a detailed investigation of the pH dependence of the ^{31}P NMR spectrum for LH_2 with the species distribution plot (Fig. 1).

The empirical utility of ^{31}P shielding/deshielding effects in determining the protonation sequence for 1-aminomethylenephosphonic acids has been firmly established; deprotonation of the phosphonic acid function shielding the ^{31}P nucleus [7, 21–25] and deprotonation of amine sites causing deshielding [7, 23, 25]. Two inflections are apparent below pH 7 and both are in regions of the curve where the ^{31}P NMR signal moves to higher field with increasing pH. This



Scheme 1.

is consistent with stepwise deprotonation of the phosphonic acid function $[LH_3]^+$. Larger changes in $\delta(^{31}P)$ above pH 10, but this time to lower field with increasing pH, correlate with increasing abundance of the fully deprotonated form of LH_2 and are characteristic of amine deprotonation. Intrinsic ^{31}P chemical shifts for $[LH]^-$ and for the zwitterion LH_2 are determined, by inspection, as δ 6.5 and 7.9.

Crystal structure of LH_2

The molecular structure of LH_2 in the solid state is shown in Fig. 2a and selected bond lengths and angles for are given in Table 2. All the acidic hydrogen atoms were located directly; LH_2 is zwitterionic with the nitrogen atom and one phosphonate oxygen atom each being protonated. Neglecting the proton on the phosphonate oxygen atom, the molecule has, overall, virtual C_s symmetry about the plane containing the nitrogen–carbon–phosphorus linkage.

The angle subtended by the nitrogen and phosphorus atoms at C(1) is extremely large [N(1)—C(1)—P 120.1(3)], and significantly greater than the corresponding values (110.9–117.9°) found for other 1-aminomethylenephosphonic acids [12, 13, 25–28]. This marked distortion from an approximately tetrahedral environment for the methylenephosphonate carbon appears to be caused by steric factors arising indirectly from the staggered conformation about the P—C(1) bond (Fig. 2b) which results in the ethyl carbon atoms, C(21) and C(31), being "eclipsed" by the phosphonate oxygen atoms O(2) and O(1), respectively, so that very short contact distances result [H(21b)···O(2) 2.48 and H(31b)···O(1) 2.39 Å]. Attempts to minimize these interactions can also be seen in enlargement of the angles at nitrogen involving the ethyl and methylenephosphonate carbon atoms [C(21)—N(1)—C(1) 113.7(3) and C(31)—N(1)—C(1) 114.0(3)] relative to the angle between the two ethyl groups [C(21)—N(1)—C(31) 110.2(3)]. It appears that repulsion between the phosphonate and ethyl groups causes the latter to be 'pushed' away from the phosphonate and towards each other. Steric factors appear to be less important in the other two members of the series $Et_nN(CH_2PO_3H_2)_{3-n}$, compared with the diethyl derivative LH_2. Where either the ethyl group is absent ($n = 0$), or only one is present ($n = 1$), the C—N—C angles are fairly close in value, being within the narrow range 112.2–113.1° [12, 13].

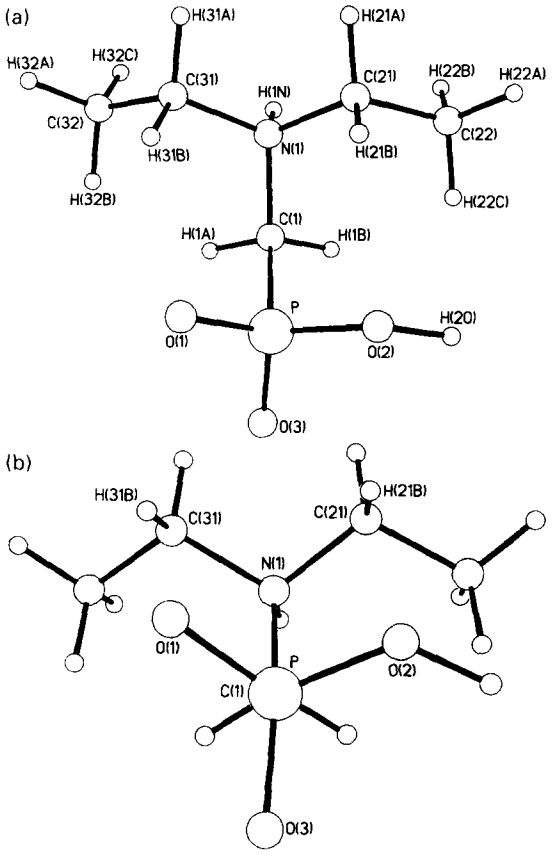


Fig. 2. Molecular structure of LH_2; (a) general view; (b) viewed along the P—C(1) bond to show the 'eclipsed' conformation of phosphonate oxygen and methylene carbon atoms.

The geometry around the phosphorus atom is substantially distorted from tetrahedral. Two patterns of P—O bond lengths are commonly found for 1-aminoalkylphosphonic acids: (a) two long P—O(H) distances in the range 1.548–1.527 Å and one shorter P=O distance (1.492–1.465 Å) corresponding to the doubly protonated group [12, 25, 27, 29]; (b) one long P—O(H) distance (1.578–1.538 Å) and two shorter P=O distances (1.514–1.486 Å) for monoprotonated groups [12, 13, 25–27, 29, 30]. The P—O distances in LH_2 most closely match pattern (b), although the longer of the two 'short' distances [P—O(3) = 1.520(3) Å] is at the upper end of the range, presumably owing to the involvement of O(3) in strong intermolecular hydrogen bonding (Fig. 3). Assignment of partial double bond character to the bonds from the non-protonated oxygen atoms [O(1) and O(3)] is supported by the angular deviations from tetrahedral geometry at phosphorus; the repulsion between these bonds results in the angle between them [114.3(2)] being significantly larger than the other O—P—O angles [111.6(2) and 111.7(2)].

Hydrogen bonds between the protonated nitrogen atoms and the non-protonated oxygen atoms [O(1′)] in molecules related by the 2_1 screw axis result in an infinite helical chain of molecules along the *b*-axis direction (Fig. 3). A second, stronger, intermolecular hydrogen bond gives rise to "dimer" bridge units by linking the protonated oxygen atom, O(2), and the non-protonated oxygen atom, O(3′), of centrosymmetrically related molecules. Therefore, adjacent helical chains are linked through these dimer bridges to form a two-dimensional hydrogen-bonded sheet.

Table 2. Selected bond lengths (Å) and angles (°) for $[LH_2]$

P—O(1)	1.487(3)	P—O(2)	1.543(3)
P—O(3)	1.520(3)	P—C(1)	1.821(4)
C(1)—N(1)	1.489(5)	N(1)—C(21)	1.493(5)
N(1)—C(31)	1.506(5)	C(21)—C(22)	1.517(7)
C(31)—C(32)	1.488(7)	O(2)—H(20)	1.23(6)
N(1)—H(1N)	0.97(6)		

O(2)—P—O(1)	111.6(2)	O(3)—P—O(1)	114.3(2)
O(3)—P—O(2)	111.7(2)	C(1)—P—O(1)	109.9(2)
C(1)—P—O(2)	106.8(2)	C(1)—P—O(3)	101.8(2)
N(1)—C(1)—P	120.1(3)	C(21)—N(1)—C(1)	113.7(3)
C(31)—N(1)—C(1)	114.0(3)	C(31)—N(1)—C(21)	110.2(3)
C(22)—C(21)—N(1)	111.1(4)	C(32)—C(31)—N(1)	111.5(4)
H(20)—O(2)—P	123(2)	H(1N)—N(1)—C(1)	101(3)
H(1N)—N(1)—C(21)	110(3)	H(1N)—N(1)—C(31)	107(3)

Complex formation

An investigation of complex formation between LH_2 and a range of metal ions (M^{II}; M = Co, Ni, Cu, Zn, Cd, Pb) was attempted using the potentiometric titration technique. For each metal ion, at least two titrations, each at different [M] : [L] ratios, were carried out. However, only titrations of LH_2 in the presence of Pb^{II} yielded results from which reliable $\log\beta$ values could be calculated. For all the other metal ions investigated, precipitation occurred at higher pH and, with the exception of Cu^{II}, there was no evidence of complex formation at low pH; this is consistent with $\log\beta$ values for Mg^{II} and Ca^{II} previously reported [7]. In the case of Cu^{II}, titration curves indicated appreciable complex formation, but at pH values too close to the point of precipitation to allow reliable refinement, although stability constants for some Cu^{II} complexes have been reported by Wozniak and Nowogrocki [8]. The precipitates observed during our titrations are ascribed to hydrolysis products; the potentiometric titration curve for $Co(NO_3)_2$ in the absence of LH_2 shows irregularities at pH *ca* 8.5 which mimic those observed for titrations in the presence of LH_2.

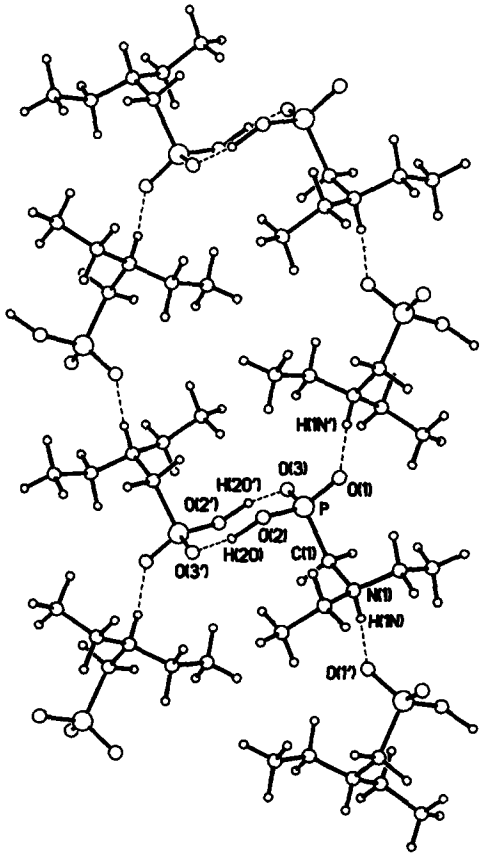


Fig. 3. Two-dimensional hydrogen-bonded sheet of molecules of LH_2. Intermolecular distances (Å): N(1)···O(1′) 2.67, O(2)···O(3′) 2.54.

In contrast, the titration curves for LH_2 in the presence of Pb^{II} were smooth and showed no evidence of precipitation. Analysis of titrations at [M] : [L] ratios of *ca* 1 : 1, 1 : 2 and 1 : 3, respectively, gave the stability constants (Table 1) for the species [PbL], $[PbLH]^+$ and $[PbL(OH)]^-$ and showed no evidence for the species $[PbL_2]^{2-}$, $[Pb(OH)]^+$ or $[PbLH_2]^{2+}$. Comparison of the distribution diagram for LH_2 (Fig. 1a) with those for the system with $[Pb^{II}]/[LH_2] = 1$ over a range of Pb^{II} concentrations showed that, in the pH range 4.6–8.7 and for $[Pb^{II}] > ca\ 0.005$ mol dm^{-3} (e.g. Fig. 4), the species $[LH]^-$, which dominates the proton equilibria, is largely replaced by the protonated complex $[PbLH]^+$, which, as the pH is increased, deprotonates to give PbL. The latter complex is presumably aquated and itself deprotonates to yield $[PbL(OH)]^-$.

The stability constants for complexes of metal ions with LH_2 are evidently much lower than for those with *N*-ethyliminobis(methylenephosphonic acid), $EtN(CH_2PO_3)_2$ (L^1H_4); e.g. $\log\beta_{11h}$ ($h = 0, 1$) values for Cu^{II} with LH_2 (7.46 and 14.12, respectively [8]) are substantially lower than those for Cu^{II} with L^1H_4 (13.5 and 18.1, respectively [31]). This also applies to

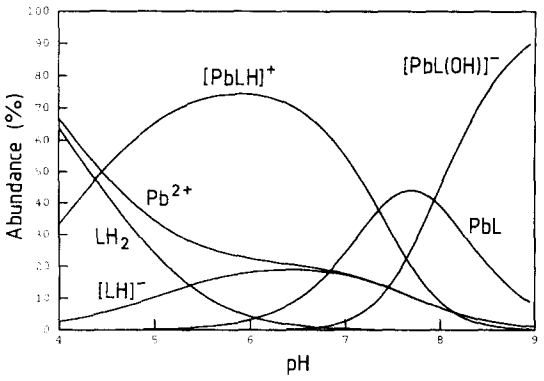


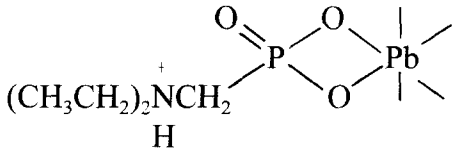
Fig. 4. Species distribution diagram for complexes of LH_2 with Pb^{II} calculated [20] for $[Pb^{II}] = [LH_2] = 0.01$ mol dm^{-3}.

complexes with Pb^{II} (for L^1H_4, $\log\beta_{110} = 11.18$ and $\log\beta_{111} = 17.73$ [31]). These results are consistent with the stability constants determined by Sawada *et al.* [9] for the methyl analogues of LH_2 and L^1H_4, and reflect the enhanced basicity of the ligands containing two (rather than one) methylenephosphonic acid functions.

The rather high values of $\log\beta_{110}$ found for Pb^{II} complexes with LH_2 and L^1H_4 are similar to those found for Cu^{II} [8,31], the transition metal ion expected to form the most stable complexes according to the Irving–Williams series [32]. Enhanced stability for complexes of Pb^{II} with some other l-aminoalkylphosphonic acids has also been observed [11, 33] suggesting that l-aminoalkylphosphonic acids may offer reagents for selective complexation of this toxic heavy metal.

It is likely that, in all of the three Pb^{II} complexes with LH_2, the lead atom is coordinated to at least one phosphonate oxygen atom. Although only a few crystal structures of metal complexes with aminoalkylphosphonic acids have been reported [28,34–38], all show this coordination mode. In only three cases has additional N-coordination being demonstrated [35–37]. Excluding the N-coordinated complexes, a characteristic feature of the solid state structures of these complexes is their polymeric nature [28,34–39]; however, it is unlikely that such structures would be present to any significant extent in solution.

While the question of whether there is a Pb—N bond in the species PbL remains unresolved, the stability constants provide information about the structure of the monoprotonated complex, $[PbLH]^+$. The first protonation constant ($\log K_{111}$) of the complex [PbL] is *ca* 2 log units larger than the second protonation constant ($\log K_{012}$) of the ligand. Since K_{012} characterizes the first protonation of the phosphonate group, it follows [9] that [PbL] is protonated at the nitrogen atom, reflecting the high proton affinity of the nitrogen atom of aminoalkylphophonates (e.g. refs [8, 9]). A possible structure of $[PbLH]^+$, consistent with these observations, is represented by **I**.



It is worth noting that structure **I** includes a bidentate, chelating phosphonate group. This arrangement has not been observed in solid state structures of l-aminoalkylphosphonic acid complexes with metal ions [28,34–39] with ionic radii up to and including that of Cd^{2+} (1.09 Å) [40]. However, chelating phosphonate groups have been found for the Ca^{II} complex of *N*-phosphonomethylglycine [41] and in the structure of the Pb^{II} complex of piperazine-1,4-diylbis-(methylene)-bis(phosphonic acid) [39]; it may be that the larger Ca^{2+} and Pb^{2+} ions (ionic radii, 1.20 and 1.33 Å [40], respectively) are required to accommodate the small angle (O—P—O) subtended at the ligand by the donor oxygen atoms.

Acknowledgements—We gratefully acknowledge funding for Research Studentships from the National Advisory Board (to N.C.) and the EPSRC (to M.C. and I.J.S.), and for development of the potentiometric titration apparatus from the EPSRC and Zeneca Specialities (Cooperative Research Grant).

REFERENCES

1. For example, M. Ishida, H. Kanazawa and M. Hida, Jpn. Kokai Tokkyo Koho JP 03,193,357, 1991, *Chem. Abstr.* **115,** 258475e; K. J. Radimer, Eur. Pat. Appl. EP 97,305, 1984, *Chem. Abstr.* **100,** 123537w; Y. Riad, H. M. El-Nahas and H. M. Hamza, *J. Soc. Dyers Colour* 1991, **107,** 1447; J. P. Terry and O. W. May, U.S. US 4,671,934, 1987, *Chem. Abstr.*, **107,** 119312w.
2. For example, S.-W. A. Bligh, C. T. Harding, A. B. McEwen and P. J. Sadler, *Polyhedron* 1994, **13,** 1937; V. V. Fedurov, A. A. Orlovskii, A. V. Alistratov, V. A. Solodenko, G. N. Kasheva, O. I. Kolodyazhnyi and V. P. Kukhar, *Dokl. Akad. Nauk Ukr. SSSR* 1991, 154; Y. Isomura, M. Takeuchi, S. Sakamoto and T. Abe, Eur. Pat. Appl. EP 325,482, 1989, *Chem. Abstr.*, **112,** 21140s.
3. For example, K. Sawada, T. Araki, T. Suzuki and K. Doi, *Inorg. Chem.* 1989, **28,** 2687; R. R. Amirov, L. A. Demidova and Z. A. Saprykova, *Koord. Khim.* 1990, **16,** 834; C. F. G. C. Geraldes, A. D. Sherry and G. E. Kiefer, *J. Magn. Reson.* 1992, **97,** 290.
4. R. D. Gillard, P. D. Newman and J. D. Collins, *Polyhedron* 1989, **8,** 2077.
5. P. B. Iveson, M. P. Lowe and J. C. Lockhart, *Polyhedron* 1993, **12,** 2313.
6. K. Moedritzer and R. R. Irani, *J. Org. Chem.* 1966, **31,** 1603.
7. R. P. Carter, R. L. Carroll and R. R. Irani, *Inorg. Chem.* 1967, **6,** 939.

8. M. Wozniak and G. Nowogrocki, *Talanta* 1979, **26,** 1135.
9. K. Sawada, T. Kanda, Y. Naganuma and T. Suzuki, *J. Chem. Soc., Dalton Trans.* 1993, 2557.
10. F. I. Bel'skii, I. B. Goryunova, P. V. Petrovskii, T. Ya. Medved' and M. I. Kabacknik, *Izv. Akad. Nauk SSSR. Ser. Khim.* 1982, 103.
11. R. J. Motekaitis and A. E. Martell, *J. Coord. Chem.* 1985, **14,** 139.
12. J. J. Daly and P. J. Wheatley, *J. Chem. Soc. A* 1967, 212.
13. B. I. Makaranets, T. N. Polynova, V. K. Bel'skii, S. A. Il'ichev and M. A. Porai-Koshits, *Zh. Strukt. Khim.* 1985, **26,** 131.
14. M. K. Cooper, P. J. Guerney, H. J. Goodwin and M. McPartlin, *J. Chem. Soc., Dalton Trans.* 1982, 757.
15. G. M. Sheldrick, *SHELX* 76, University of Cambridge (1976); *SHELX* 86, University of Cambridge (1986).
16. P. Biggins, S. Edwards, D. Hyatt, T. Lucas, R. W. Matthews, I. J. Scowen and C. J. L. Silwood, unpublished work.
17. *Vogel's textbook of Quantitative Inorganic Analysis*, 4th edn. Longmans, London (1978).
18. P. Gans, A. Sabatini and A. Vacca, *J. Chem. Soc., Dalton Trans.* 1985, 1195.
19. D. G. Cameron, H. R. Hudson and M. Pianka, *Phosphorus, Sulfur, and Silicon* 1993, **83,** 21.
20. R. J. Motekaitis, FORTRAN 77 program SPE, 1987, in *The Determination and Use of Stability Constants*, (Edited by A. E. Martell and R. J. Motekaitis). VCH, Weinheim (1988); C. Crees, *TURBO-C program SPECIES*, unpublished work (1990); C. J. L. Silwood, *GW-BASIC program HPPLOT*, unpublished work (1990).
21. K. Moedritzer, *Inorg. Chem.* 1967, **6,** 936.
22. R. J. Grabenstetter, O. T. Quimby and T. J. Flautt, *J. Phys. Chem.* 1967, **71,** 4194.
23. T. G. Appleton, J. R. Hall, A. D. Harris, H. A. Kimlin and I. J. McMahon, *Aust. J. Chem.* 1984, **37,** 1833; T. G. Appleton, J. R. Hall and I. J. McMahon, *Inorg. Chem.* 1986, **25,** 726; K. Sawada, T. Araki and T. Suzuki, *Inorg. Chem.* 1987, **26,** 1199; C. F. G. C. Geraldes, A. D. Sherry and W. P. Cacheris, *Inorg. Chem.* 1989, **28,** 3336; A. E. Martell and B. Szpoganicz, *Inorg. Chem.* 1989, **28,** 4199.
24. Z. Glowacki, M. Hoffmann, M. Topolski and J. Rachon, *Phosphorus, Sulfur and Silicon* 1991, **60,** 67.
25. W. Clegg, P. B. Iveson and J. C. Lockhart, *J. Chem. Soc., Dalton Trans.* 1992, 3291.
26. L. M. Shkol'nikova, G. V. Polyanchuk, V. E. Zavodnik, M. V. Rudomino, S. A. Pisareva, N. M. Dyatlova and I. A. Polyvakova, *Zh. Strukt. Khim.* 1987, **28,** 124; P.M. Darriet, J. Darriet, A. Cassaigne and E. Neuzil, *Acta Cryst.* 1975, **B31,** 469.
27. G. V. Polyanchuk, L. M. Shkol'nikova, M. V. Rudomino, N. M. Dyatlova and S. S. Makarevich, *Zh. Strukt. Khim.* 1985, **26,** 109; L. M. Shkol'nikova, G. V. Polyanchuk, N. M. Dyatlova, T. Ya. Medved, I. B. Goryunova and M. I. Kabachnik, *Izv. Akad. Nauk SSSR, Ser. Khim.* 1985, 1035.
28. N. Choi, I. Khan, R. W. Matthews, M. McPartlin and B. P. Murphy, *Polyhedron* 1994, **13,** 847.
29. I. Lázár, D. C. Hrncir, W.-D. Kim, G. E. Kiefer and A. D. Sherry, *Inorg. Chem.* 1992, **31,** 4422.
30. J. Kowalik, W. Sawka-Dobrowolska and T. Glowiak, *J. Chem. Soc., Chem. Commun.* 1984, 446; W. Sawka-Dobrowolska, *Acta Cryst.* 1985, **C41,** 84; W. Sawka-Dobrowolska and J. Kowalik, *Acta Cryst.* 1988, **C44,** 1624.
31. M. Constantinou, R. W. Matthews and I. J. Scowen, unpublished work.
32. H. Irving and R. J. P. Williams, *J. Chem. Soc.* 1952, 3192.
33. M. I. Kabachnik, T. Ya. Medved, N. M. Dyatlova, M. N. Rusina and M. V. Rudomino, *Izv. Akad. Nauk SSSR, Ser. Khim.* 1967, 1501.
34. Y. Ortiz-Avila, P. R. Rudolf and A. Clearfield, *J. Coord. Chem.* 1989, **20,** 109; P. Fenot, J. Darriet, C. Garrigou-Lagrange and A. Cassaigne, *J. Mol. Struct.* 1978, **43,** 49; T. Glowiak, W. Sawka-Dobrowolska, B. Jeżowska-Trzebiatowska and A. Antonow, *J. Cryst. Mol. Struct.* 1980, **10,** 1.
35. M. I. Kabachnik, M. Yu. Antipin, B. K. Shcherbakov, A. P. Baranov, Yu. T. Struchkov, T. Ya. Medved' and Yu. M. Polikarpov, *Koord. Khim.* 1988, **14,** 536.
36. M. Yu. Antipin, A. P. Baranov, M. I. Kabachnik, T. Ya. Medved', Yu. M. Polikarpov, Yu. M. Struchkov and B. K. Shcherbakov, *Dokl. Akad. Nauk SSSR* 1986, **287,** 130.
37. L. M. Shkol'nikova, A. L. Poznyak, V. K.Bel'skii, M. V. Rudomin and N. M. Dyatlova, *Koord. Khim.* 1986, **12,** 981.
38. T. Glowiak, W. Sawka-Dobrowolska, B. Jeżowska-Trzebiatowska and A. Antonow, *Inorg. Chim. Acta* 1980, **45,** 105.
39. N. Choi, I. Khan, R. W. Matthews and M. McPartlin, unpublished work.
40. R. D. Shannon, *Acta Cryst.*, 1976, **A32,** 751.
41. P. R. Rudolf, E. T. Clarke, A. E. Martell and A. Clearfield, *Acta Cryst.*, 1988, **C44,** 796.

Pergamon

PII: S0277-5387(96)00302-6

Polyhedron Vol. 16, No. 3, pp. 363–368, 1997
Copyright © 1996 Elsevier Science Ltd
Printed in Great Britain. All rights reserved
0277-5387/97 $17.00+0.00

Complexations of 13-group metals^{III} with 7-[(2-hydroxy-5-chlorophenyl)azo]-8-hydroxyquinoline-5-sulfonate

Longhe Piao, Fumiaki Kai* and Masaaki Hirohata

Department of Chemistry, Faculty of Science, Kumamoto University, Kurokami, Kumamoto 860, Japan

(Received 3 April 1996; accepted 24 June 1996)

Abstract—The complexations of the 13-group metals (Ga^{III}, In^{III} and Tl^{III}) with 7-[(2-hydroxy-5-chlorophenyl)azo]-8-hydroxyquinoline-5-sulfonate(hpaq) were studied. In Ga^{III}-complexation, hpaq coordinates to Ga^{III} to form a yellow complex through a fast process and then this yellow complex slowly changes to a red complex. The rate constant of the slow process is independent of the experimental Ga^{III} concentration, indicating the presence of a linkage isomerism. In the cases of In^{III}- and Tl^{III}-complexations, no linkage isomerism was observed. Copyright © 1996 Elsevier Science Ltd

Keywords: complexation; multidentate ligand; 13-group metal; Ga^{III}; linkage isomerism; kinetics.

In the course of the studies on the coordination selectivities of the azo system multidentate ligands toward various metal ions [1–10], the evidence for linkage isomerism in the complexation between Al^{III}, one of the 13-group elements, and hpaq has been reported in detail [11].

Afterwards, it was found that Ga^{III} also showed similar linkage isomerism in the complexation with hpaq [11], but not in the cases of the In^{III}- and Tl^{III}-hpaq complexations, because the 13-group elements in the trivalent state is basically a consequence of the systematical increase in softness and ionic radius in the order $Al^{III} < Ga^{III} < In^{III} < Tl^{III}$.

This paper describes an investigation of the complexation equilibria, kinetics and reaction mechanisms of the hpaq-complexations with Ga^{III}, In^{III} and Tl^{III}.

EXPERIMENTAL

Ligands and metal ion source

The preparation of hpaq has been described elsewhere [11]. All the metallic ions M^{III} were prepared as aqueous perchlorate solutions from metallic Ga (Wako, 99.99%), $In(OH)_3$ (Aldrich) and Tl_2O_3 (Wako), respectively.

Measurements

All the measurements (except polarograms) are the same as those reported in the previous paper [11]. Polarograms were recorded on a Yanaco Polarographic Analyzer P-1100 in an aqueous solution containing 0.1 mol dm^{-3} KNO_3 as the supporting electrolyte, and 0.01% gelatin as the maximum suppressor. A three-electrode cell was used for measurements, in which the working electrode was a dropping mercury electrode (DME); the auxiliary electrode was a platinum coil. The DME had the following characteristics: $m = 2.02$ mg s^{-1}, $t = 1.00$ s/drop at -0.5 V versus SCE, in electrolytic solution at $-\log[H^+] = 7.0$.

The observed rate constant, k_{obs}, was calculated from the gradient of the linear relation of logarithmic absorbance change versus t on the basis of eq. (1):

$$\ln[(A_i - A_\infty)/(A_t - A_\infty)] = k_{obs}t \qquad (1)$$

where A_i, A_t, and A_∞ refer to the absorbances at the initial state, at time t, and at the infinite equilibrium state of the kinetic process, respectively. For the Ga^{III}-complexation, $k_{obs(fast)}$ and $k_{obs(slow)}$ of the first(fast) and second(slow) steps were calculated independently

*Author to whom all correspondence should be addressed.

according to eq. (1), because the two steps took place with different time scales. All the pH were corrected by using the activity coefficient $f_{H^+} = 0.83$ at 25°C [12].

RESULTS AND DISCUSSION

Electronic absorption spectra of complexes

In Fig. 1 the spectral changes for the slow process of the Ga^{III}-hpaq complexation from 0 min (a), corresponding to the yellow complex $Ga(Hhpaq)^+$-N,O, to 80 min (b), corresponding to the red complex Ga (hpaq)-O,N,O are shown. In this period the colour of the solution changes gradually from yellow to red. The spectra have two clear isosbestic points at 17.5×10^3 and 20.9×10^3 cm^{-1}; this finding means that the yellow complex [spectrum (a)] changes quantitatively to the red complex [spectrum (b)]. As shown below in the kinetics discussion, this spectral change was not influenced by the initial Ga^{III} concentration, suggesting an intramolecular rearrangement of coordination sites, from N,O-bidentate to O,N,O-tridentate complexes.

Polarograms

In addition to the reasoning for the coordination sites from the above electronic spectra, a mutual comparison of reduction potentials between the azo group in free hpaq and in the metal complexes provides direct information to judge whether or not the azo N-atom coordinates to metal ions.

In comparison with the relation between $-\log[H^+]$ and reduction potentials ($E_{1/2}$) of the azo group in free hpaq ($E_{1/2} = 0.038 + 0.058 \log[H^+]$, $r = 0.999$), the potentials for the Ga^{III}-hpaq complex between $-\log[H^+] = 2$–8, which were measured after the yellow complex was completely converted to the red complex, are shifted negatively by about 160 mV, then at $-\log[H^+] > 8$ the potentials lie on the same reduction potentials of free hpaq because of a hydrolysis of the complex, showing a stabilization by a negative shift effect [13,14]. In other words, one of the N-atoms in the azo group coordinates evidently to Ga^{III}. For the In^{III}-hpaq set, on the other hand, the potentials are almost the same as those of free hpaq. This result shows that an N-atom in the azo group does not coordinate to In^{III}, showing the coordination at only 8-hydroxyquinoline moiety as N,O-bonding.

In this polarographic study, reduction potentials of a Tl^{III}-complex were not obtained because Tl^{III} is reduced (at +0.72 V) prior to the reduction of the azo group.

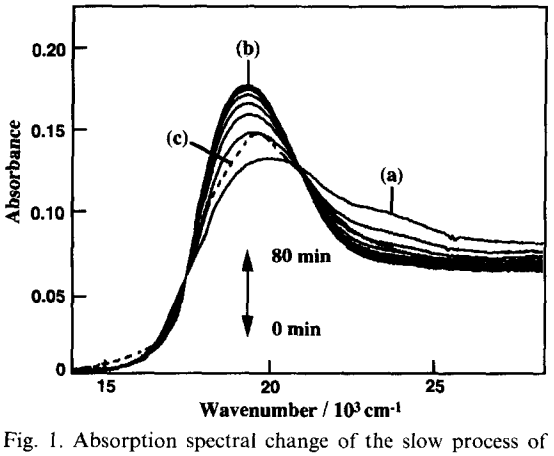


Fig. 1. Absorption spectral change of the slow process of Ga^{III}-hpaq complex from 0 (a) to 80 min (b) at $-\log[H^+]$ 1.95. Spectrum (c): free H_2hpaq^- at $-\log[H^+]$ 5.50. Other spectra show intermediate complex from yellow to red. $[Ga^{III}] = 3.00 \times 10^{-4}$ mol dm^{-3}, [hpaq] = 2.00×10^{-5} mol dm^{-3}.

Complexation equilibria and stability constants

Complexation equilibria are summarized in Table 1, in which the pH ranges, where complexations occur, to judge a reacting hpaq species, the maximum wavenumbers (with molar absorptivities), and the stability constants calculated from the equations described below are listed. All of the compositions of the complexes were determined by the continuous variation method. A sharp and single maximum at the hpaq (or metal) mole fraction of 0.5 was obtained for all the M^{III}-hpaq sets, indicating clearly the presence of 1 : 1 complexes as listed in Table 1. It is necessary to discuss the stability constants and kinetic consideration to take into account such species as $[M(OH)(H_2O)_5]^{2+}$ besides $[M(H_2O)_6]^{3+}$ (hereafter, abbreviated as MOH^{2+} for the former and M^{3+} for the latter, respectively).

On the basis of the characteristic spectral features of the complexes and the $-\log[H^+]$ ranges where the complexations occur, and thus the equilibration modes listed in Table 1, all of the complexation equilibria may be represented as follows:

$$M^{3+} + H_2hpaq^- = M(hpaq) + 2H^+$$

Accordingly, stability constants $\beta_{M(hpaq)}$ can be calculated from eq. (2),

$$\begin{aligned}\log \beta_{M(hpaq)} &= \log\{[M(hpaq)]/[M^{3+}][hpaq^{3-}]\} \\ &= \log\{[M(hpaq)]/[H_2hpaq^-]\} \\ &\quad + 2\log[H^+] - \log[M^{3+}] \\ &\quad + \log K_{(hqOH)} K_{(phOH)} + \log(\alpha_M \alpha_L), \end{aligned} \quad (2)$$

where, $[M^{3+}]$ refers to experimental initial concentration (all the mixtures are composed of $[M^{3+}] \gg [hpaq]$ as experimental conditions, *ca* 10–50 : 1). The protonation constants [11], $K_{(hqOH)} = 10^{7.04}$ and $K_{(phOH)} = 10^{10.30}$, are used for the calculation. α_M

Table 1. Complexing pH range, equilibrium mode, maximum wavenumber (molar absorptivity), and stability constants for metal-complexes

Ligand	pH Range	Equilibrium	$\nu_{max}/10^3(\varepsilon_{max}/10^4)$	$\log\beta_{ML}$
hpaq	0.58–1.66	$Ga^{3+}+H_2hpaq^- \Leftrightarrow Ga(hpaq)\text{-}O,N,O+2H^+$	17.9(0.85)	33.9_2
hpaq	2.27–3.00	$In^{3+}+H_2hpaq^- \Leftrightarrow In(hpaq)\text{-}N,O+2H^+$	21.7(0.62)	18.6_2
hpaq	2.06–3.01	$Tl^{3+}+H_2hpaq^- \Leftrightarrow Tl(hpaq)\text{-}N,O+2H^+$	21.7(0.79)	25.4_6
baq[a]	0.16–2.68	$Ga^{3+}+H_2baq \Leftrightarrow Ga(baq)^+\text{-}N,O+2H^+$	25.0(4.25)	18.1_3

[a] baq = 7-[(4-chlorophenyl)azo]-8-hydroxyquinoline-5-sulfonate.

$(=1+K_{MOH}/[H^+])$ is side reaction coefficients by monohydroxo complexes MOH^{2+}, in which $K_{MOH}=[MOH^{2+}][H^+]/[M^{3+}]=10^{-3.10}$ for Ga^{3+}, $10^{-3.50}$ for In^{3+}, and $10^{-1.20}$ mol dm^{-3} for Tl^{3+} are used for the correction [15]. And, α_L $(=1+K_{(hqNH)}K_{(hqOH)}K_{(phOH)}[H^+]^3+K_{(hqOH)}K_{(phOH)}[H^+]^2+K_{(phOH)}[H^+])$ is also side reaction coefficient by the protonation of hpaq, in which the value [11] $K_{(hqNH)}=10^{2.98}$ was used for the correction. All the stability constants $\log\beta_{M(hpaq)}$ were calculated by finding a $-\log[H^+]$ value at $\log[M(hpaq)]/[H_2hpaq^-]=0$ from a straight line with a gradient *ca* 2. The stability constants obtained are listed in Table 1 with an indication of coordinating donor atoms.

Kinetics of fast process for Ga^{III}*-hpaq complexation*

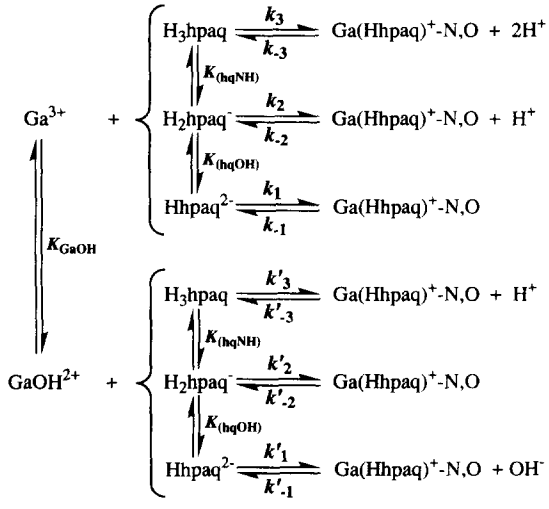
The Ga^{III}-hpaq complexation can be treated in terms of two consecutive reactions with different time scales: fast complexation to form the yellow complex $Ga(Hhpaq)^+$-N,O ($k_{obs(fast)}$), followed by a slow intramolecular change to the red complex Ga(hpaq)-O,N,O ($k_{obs(slow)}$). Each reaction step obeyed the first-order kinetics. By eq. (1), a fine linear relation was obtained between the logarithmic absorbance change with time for more than half-life periods at 19.8×10^3 cm^{-1}. By taking into consideration the protonation constants of hpaq, the hydrolysis constants of Ga^{III}, the stability constants of the 1:1 complex, and the more rapid attainment of equilibria for the protolytic process [16], the fast formation of the complex $Ga(Hhpaq)^+$-N,O is considered to proceed as shown in Scheme 1. Here, six possible reaction pathways are proposed with their rate equations by using the steady state approximation:

$$\begin{aligned}
&d[Ga(Hhpaq)^+\text{-}N,O]/dt\\
&=[Ga^{3+}]\{k_3[H_3hpaq]+k_2[H_2hpaq^-]\\
&\quad+k_1[Hhpaq^{2-}]\}+[GaOH^{2+}]\{k'_3[H_3hpaq]\\
&\quad+k'_2[H_2hpaq^-]+k'_1[Hhpaq^{2-}]\}\\
&\quad-[Ga(Hhpaq)^+-N,O]\{k_{-3}[H^+]^2\\
&\quad+(k_{-2}+k'_{-3})[H^+]+k'_{-1}[OH^-]+(k_{-1}+k'_{-2})\}.
\end{aligned}\tag{3}$$

Here, k_i and k'_i denote the rate constants for the forward reactions concerning $[Ga^{3+}]$ and $[GaOH^{2+}]$, and k_{-i} and k'_{-i} those for the backward reactions related to $[Ga(Hhpaq)^+\text{-}N,O]$, respectively. Under the pseudo-first-order kinetic conditions with respect to Ga^{III} concentration, the forward rate constant k_i can therefore be obtained from the experimental relation of $k'_{obs(fast)}$ as a function of $[H^+]$, as eqs (4) and (5).

$$\begin{aligned}
&k'_{obs(fast)}\\
&=([H_ihpaq^{(3-i)-}]/[Hhpaq^{2-}])\\
&\quad\times\left\{\sum_{i=1}^{3}(k_i+k'_i[GaOH^{2+}]/[Ga^{3+}])\right\}\\
&=k_3K_{(hqNH)}K_{(hqOH)}[H^+]^2+(k_2K_{(hqOH)}\\
&\quad+k'_3K_{(hqNH)}K_{(hqOH)}K_{GaOH})[H^+]\\
&\quad+k'_1K_{GaOH}[H^-]^{-1}+(k_1+k'_2K_{(hqOH)}K_{GaOH}).
\end{aligned}\tag{4}$$

$$\begin{aligned}
k'_{obs(fast)}=k_{obs(fast)}/\{&1/\beta'_{Ga(Hhpaq)\text{-}N,O}\\
&+C_{Ga}/(K_{(hqNH)}K_{(hqOH)}[H^+]^2\\
&+K_{(hqOH)}[H^+]+1)(1+K_{GaOH}[H^+]^{-1})\},
\end{aligned}\tag{5}$$



Scheme 1. Possible pathways of fast Ga^{III}-hpaq complexations.

where, $\beta'_{Ga(Hhpaq)\text{-}N,O} = [Ga(Hhpaq)^+\text{-}N,O]/[Ga^{3+}][Hhpaq^{2-}]$. However, no real value of $\beta'_{Ga(Hhpaq)\text{-}N,O}$ could be obtained directly in this study, accordingly, the value $\beta_{Ga(baq)\text{-}N,O} = 10^{18.1}$, which was calculated separately (see Table 1), was tentatively used for the calculation. C_{Ga} corresponds to an experimental Ga^{III} concentration ($= [Ga(Hhpaq)^+\text{-}N,O] + [Ga^{3+}] + [GaOH^{2+}]$). From eq. (4), it was found that the experimental data plots of $k'_{obs(fast)}$ are proportional only to the $[H^+]^{-1}$ term with a zero intercept [Fig. 2(a)], from which it has become apparent that the formation of complex $Ga(Hhpaq)^+$-N,O proceeds *via* reaction pathway, $GaOH^{2+} + Hhpaq^{2-} \rightarrow Ga(Hhpaq)^+\text{-}N,O + OH^-$.

Kinetics of slow process for Ga^{III}*-hpaq complexation*

In the slow process, the observed rate constant, $k_{obs(slow)}$, does not depend on C_{Ga} at a constant $[H^+]$. This fact, once again, indicates evidently that the slow process corresponds to an intramolecular rearrangement of the Ga^{III}-hpaq complex between two possible coordination modes. Scheme 2 shows the equilibria among four possible species of the Ga^{III}-hpaq complexes. Therefore the formation of the red complex, Ga(hpaq)-O,N,O, can be expected to proceed *via* four reaction pathways, with rate equations as given in eq. (6).

$$\begin{aligned} &d[Ga(hpaq)\text{-}O,N,O]/dt \\ &\quad = -d[Ga(Hhpaq)^+\text{-}N,O]/dt \\ &\quad = (k_A[A] + k_B[B] + k_C[C] + k_D[D]) \\ &\qquad - [Ga(hpaq)\text{-}O,N,O]\{k_{-A}[H^+] \\ &\qquad + (k_{-B} + k_{-C}) + k_{-D}[OH^-]\}, \end{aligned} \tag{6}$$

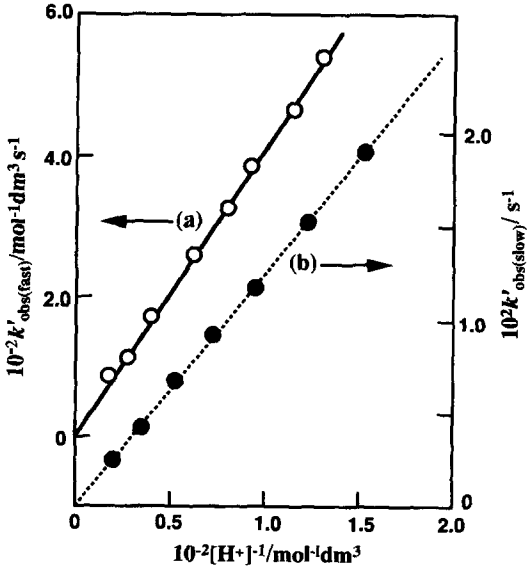
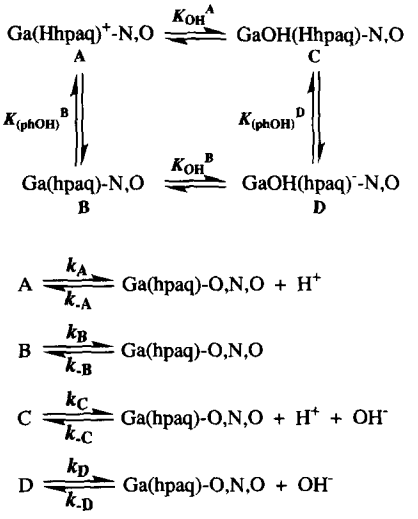


Fig. 2. Plots of (a) $k'_{obs(fast)}$ and (b) $k'_{obs(slow)}$ *vs* $[H^+]^{-1}$ of Ga^{III}-hpaq complexes. $[Ga^{III}] = 2.00 \times 10^{-4}$ mol dm^{-3}, [hpaq] $= 2.00 \times 10^{-5}$ mol dm^{-3}, absorbance at 530 nm.



Scheme 2. Pathways of slow Ga^{III}-hpaq complexations.

where k_i and k_{-i} are the rate constants for the forward and reverse pathways of the slow reaction step related to the complex species i, respectively. By defining the modified rate constant, $k'_{obs(slow)}$, which can be defined by the use of eq. (7) from the $k_{obs(slow)}$ value determined experimentally:

$$k'_{obs(slow)} = k_{obs(slow)}/\{1/\beta_{Ga(hpaq)\text{-}O,N,O} + 1/(1 + K_{(phOH)}[H^+])(1 + K_{GaOH}/[H^+])\}, \tag{7}$$

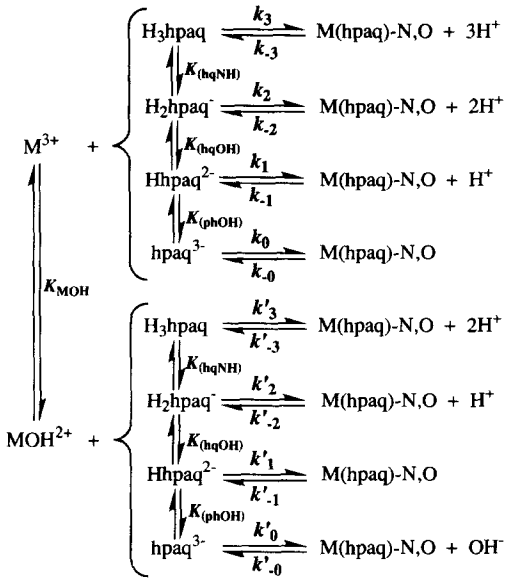
where, $\beta_{Ga(hpaq)\text{-}O,N,O}$ is the stability constant of the complex $[Ga(hpaq)\text{-}O,N,O]/[Ga^{3+}][hpaq^{3-}]$, eq. (8) can then be derived from Scheme 2:

$$k'_{obs(slow)} = k_A K^B_{(phOH)}[H^+] + (k_B + k_C K^D_{(phOH)} K^A_{OH}) + k_D K^B_{OH}[H^+]^{-1}. \tag{8}$$

Here, $K^B_{(phOH)}$ and $K^D_{(phOH)}$ refer to the protonation constants of the species B and D, and K^A_{OH} and K^B_{OH}, to the hydrolysis constants of Ga^{III} in the species A and B, respectively. However, since we have not obtained these constants directly, in the following treatment, $K^A_{(phOH)}$ and $K^D_{(phOH)}$ were approximated to $K_{(phOH)}$ ($= 10^{10.30}$), K^A_{OH} and K^B_{OH} to K_{GaOH} ($= 10^{-3.10}$), respectively. From eq. (8), only the plots of $k'_{obs(slow)}$ *vs* $[H^+]^{-1}$ show a linear relation with a zero intercept [Fig. 2(b)]. This result strongly indicates that the intramolecular rearrangement takes place through the pathway of the complex species D, $GaOH(hpaq)^-$-N,O.

Kinetics of In^{III}*- and* Tl^{III}*-complexations*

The kinetics of the In^{III}- and Tl^{III}-complexations were also studied, for comparison, under pseudo-first-order kinetic conditions with respect to M^{III} concentrations. The results showed that linkage isom-



$M^{3+} = In^{III}$ and Tl^{III}

Scheme 3. Possible pathways of In^{III}- and Tl^{III}-hpaq complexations.

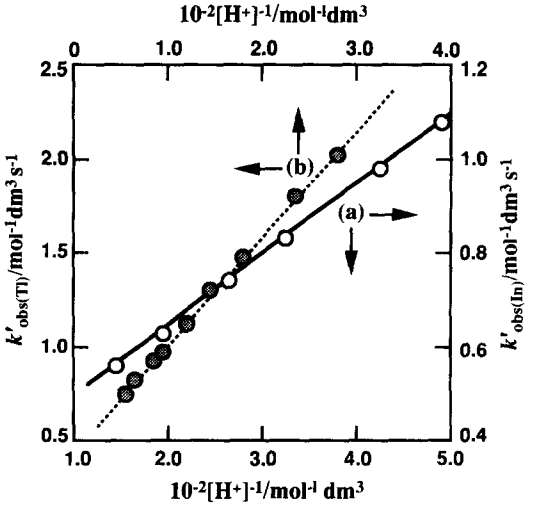


Fig. 3. Plots of (a) $k'_{obs(In)}$ and (b) $k'_{obs(Tl)}$ *vs* $[H^+]^{-1}$ of hpaq-complexation. $[M^{III}] = 2.00 \times 10^{-4}$ mol dm^{-3}, [hpaq] $= 2.00 \times 10^{-5}$ mol dm^{-3}, absorbance at 570 nm for In^{III}-complexation and 550 nm for Tl^{III}-complexation, respectively.

erism for the complexations of In^{III} and Tl^{III} with hpaq was not observed, and these reactions were slow, just as in the case of the second step of the Ga^{III}-hpaq complexation.

The eight possible pathways of both complexations through a wide $-\log[H^+]$ range are shown in Scheme 3. By the same kinetic treatments from Scheme 3 as those for the fast Ga^{III}-complexation, the modified rate constant, k'_{obs}, is also expressed as a function of $[H^+]$ as eq. (9).

$$k'_{obs} = ([H_i hpaq^{(3-i)-}]/[hpaq^{3-}]) \times \left\{ \sum_{i=0}^{3} (k_i + k'_i[MOH^{2+}]/[M^{3+}]) \right\}$$

$$= k_3 K_{(hqNH)} K_{(hqOH)} K_{(phOH)} [H^+]^3 + (k_2 K_{(hqOH)} K_{(phOH)} + k'_3 K_{(hqNH)} K_{(hqOH)} K_{(phOH)} K_{MOH})[H^+]^2 + (k_1 K_{(phOH)} + k'_2 K_{(hqOH)} K_{(phOH)} K_{MOH})[H^+] + k'_0 K_{MOH}[H^+]^{-1} + (k_0 + k'_1 K_{(phOH)} K_{MOH}), \quad (9)$$

where K_{MOH} denotes K_{InOH} and K_{TlOH}. According to eq. (9), only the plots of k'_{obs} *vs* $[H^+]^{-1}$ show linear relation with zero intercept as shown in Fig. 3. This means that both reactions of In^{III} and Tl^{III} with hpaq proceed *via* $MOH^{2+} + hpaq^{3-} \rightarrow M(hpaq)\text{-}N,O + OH^-$. The various rate constants obtained are summarized in Table 2 together with those of the Al^{III}-complexation [11] for comparison.

The rate constant of the fast process to form $Ga(Hhpaq)^+$-N,O ($k'_1 = 5.2 \times 10^3$ mol^{-1} dm^3 s^{-1}) is somewhat larger than that for $Al(Hhpaq)^+$-N,O ($k'_1 = 5.4 \times 10^2$ mol^{-1} dm^3 s^{-1}). This may be explained in terms of the complexity of the Al^{III}-hydroxo system involving dimeric and polymeric structures etc. [17], it requires longer time to form the reacting monohydroxo species, $AlOH^{2+}$, compared with that for $GaOH^{2+}$.

Table 2. Kinetic parameters of M^{III}-complexations (with Al^{III}-complexations [11]) at $\mu = 0.10(KNO_3)$, 25.0 ± 0.5 C

Pathway	Rate constant/mol^{-1} dm^3 s^{-1}	Remark
$GaOH^{2+} + Hhpaq^{2-}$	$k'_1 = (5.2 \pm 0.3) \times 10^3$	fast step, $K_{GaOH} = 10^{3.10}$
$Ga(Hhpaq)^+$-N,O(OH)	$k_D = (1.5 \pm 0.4) \times 10^{-1}$	slow step, k_D/s^{-1}
$InOH^{2+} + Hhpaq^{2-}$	$k'_0 = (4.7 \pm 0.3) \times 10^0$	$K_{InOH} = 10^{-3.50}$
$TlOH^{2+} + Hhpaq^{2-}$	$k'_0 = (9.1 \pm 0.3) \times 10^{-2}$	$K_{TlOH} = 10^{1.20}$
$AlOH^{2+} + Hhpaq^{2-}$	$k'_1 = (5.4 \pm 0.3) \times 10^2$	fast step, $K_{AlOH} = 10^{4.49}$
$Al(Hhpaq)^+$-N,O(OH)	$k_D = (4.8 \pm 0.4) \times 10^{-3}$	slow step, k_D/s^{-1}

All of the pathways involve monohydroxo complexes MOH^{2+}; this finding seems to be reasonable from the pH ranges where the complexations occur (Table 1), judging from the K_{MOH} values described above. A sequence of the rate constants for the reactions of $MOH^{2+} + Hhpaq^{2-}$ (k'_1, for $M = Ga^{III}$, and k'_0 for $M = In^{III}$ and Tl^{III}) is in the order $Ga^{III} > In^{III} > Tl^{III}$. This sequence may be a reflection of an increase of softness through Ga^{III} to Tl^{III}.

Finally, the linkage isomerism is observed only in the sets of Al^{III}- and Ga^{III}-hpaq, but not in those of In^{III} and Tl^{III}. A molecular model of these sets clearly shows that, in case of the In^{III} and Tl^{III}-sets, the O,N,O-tridentate chelate rings are scarcely formed due to the large ionic radii of In^{III} and Tl^{III}.

REFERENCES

1. H. Huang, H. Chikushi, M. Nakamura and F. Kai, *Bull. Chem. Soc. Jpn* 1990, **63,** 1985.
2. H. Huang, Y. Asai, M. Hirohata, M. Nakamura and F. Kai, *Nippon Kagaku Kaishi* 1990, 1348.
3. H. Huang, F. Kai, Y. Asai, M. Hirohata and M. Nakamura, *Chem. Lett.* 1991, 65.
4. H. Huang, F. Kai, C. Uragami, M. Hirohata, H. Chikushi, H. Yanaka, M. Honda and M. Nakamura, *Bull. Chem. Soc. Jpn* 1991, **64,** 1982.
5. H. Huang, F. Kai, Y. Asai, M. Hirohata and M. Nakamura, *Bull. Chem. Soc. Jpn* 1991, **64,** 2464.
6. H. Huang, F. Kai, Y. Asai, M. Hirohata and M. Nakamura, *J. Coord. Chem.* 1992, **25,** 357.
7. H. Huang, F. Kai, T. Shoda and M. Nakamura, *J. Coord. Chem.* 1993, **28,** 155.
8. H. Huang, F. Kai, M. Hirohata, M. Nakamura, S. Matsuzaki, K. Komori and Y. Tsunematsu, *J. Coord. Chem.* 1993, **30,** 131.
9. M. Hirohata, F. Kai, K. Kurosawa, H. Huang, K. Ishii, Y. Matsuoka, K. Komori and M. Nakamura, *J. Coord. Chem.* 1993, **30,** 379.
10. M. Hirohata, F. Kai, L. Piao, K. Komori, Y. Matsuoka and H. Huang, *J. Coord. Chem.* 1994, **31,** 237.
11. L. Piao, F. Kai, M. Hirohata, Y. Matsuoka and H. Huang, *Polyhedron* 1996, **15,** 3107.
12. J. Kielland, *J. Am. Chem. Soc.* 1937, **59,** 1675.
13. G. W. Latimer, Jr, *Talanta Review* 1968, **15,** 1.
14. L. Holleck, J. M. Abd El Kader and A. M. Shams El Din, *J. Electroanal. Chem.* 1969, **20,** 287.
15. A. E. Martell and R. M. Smith, *Critical Stability Constants* Vol. 23. Plenum Press, New York (1989); L. G. Sillen and A. E. Martell, *Stability Constants, Special Publication* No. 17. The Chemical Soc., London (1964).
16. M. Eigen, *Pure Appl. Chem.* 1963, **6,** 97; Protolytic reactions for both metal and ligand species are assumed to be always at equilibrium since they are generally very fast compared with the complex formation process.
17. F. A. Cotton and G. Wilkinson, *Advanced Inorganic Chemistry—A Comprehensive Text*, p. 333. John Wiley & Sons, Inc., New York (1980).

Pergamon

PII: S0277-5387(96)00303-8

Polyhedron Vol. 16, No. 3, pp. 369–375, 1997
Copyright © 1996 Elsevier Science Ltd
Printed in Great Britain. All rights reserved
0277-5387/97 $17.00+0.00

Palladium complexes with simultaneous O : S coordination, syntheses, structures and characterization of complexes with 2-mercaptophenol or 2-mercaptopyridine N-oxide

Ji-Cheng Shi,[a]* Ting-Bin Wen,[a] Yu Zheng,[a] Shi-Jun Zhong,[a] Da-Xu Wu,[a] Qiu-Tian Liu,[a] Bei-Sheng Kang,[b]* Bo-Mu Wu[c] and Thomas C. W. Mak[c]

[a]State Key Laboratory of Structural Chemistry and Fujian Institute of Research on the Structure of Matter, Chinese Academy of Sciences, Fuzhou, Fujian 350002, P.R. China

[b]Department of Chemistry, Zhongshan University, Guangzhou, Guandong 510275, P.R. China

[c]Department of Chemistry, The Chinese University of Hong Kong, Shatin, New Territories, Hong Kong

(Received 7 May 1996; accepted 22 June 1996)

Abstract—Complexes $(Et_4N)_2[Pd_2(mp)_2(Hmp)_2]$ (**1**) and $[Pd(mpo)_2]$ (**2**) synthesized from the reactions of palladium chloride with 2-mercaptophenol (H_2mp) and 2-mercaptopyridine N-oxide (Hmpo) or 2,2′-dithiobis(pyridine N-oxide) (dtpo), respectively, have been characterized by X-ray diffraction analyses and studied by IR, Raman, ^1H and ^{13}C NMR, and EI-MS techniques. The palladium atoms in the two compounds are in square planar environments. The average Pd—O distances are 2.009 Å and 2.043 Å for **1** and **2**, respectively. The results of EHMO calculations show that the Pd—O bonds are weaker than the Pd—S bonds in both compounds and large delocalized π bonds extend in the $(mp)_2Pd_2S_2$ plane in **1** and in the $Pd(mpo)_2$ plane in **2**. The reaction of $[Ni(mpo)_2]$ with $[Pd(COD)Cl_2]$ led to the formation of **2** also, which implies that the bidentate O : S ligand mpo readily transfers from the Ni^{II} to the Pd^{II} ion. Copyright © 1996 Elsevier Science Ltd

Keywords: palladium complexes; 2R; Raman; NMR; EI-MS; X-ray crystal structures.

Interest in the coordination chemistry of thiolato transition-metal complexes arises in part from the fact that the thiolato group mimics the ligation of cysteinyl residues in proteins [1]. We have studied a series of transition metal complexes with 1,2-bidentate sulfur-containing ligands such as 2-mercaptophenol (H_2mp) [2–7] and 2-mercaptopyridine N-oxide (Hmpo) [8–10], of which H_2mp has been found to be a multifunctional ligand in its ligation to transition metal atoms with versatile coordination modes. Recently Zhu *et al.* [11–14] have found that some simple metal complexes, particularly those of palladium complexes containing sulfur ligands, possess the ability of selective-hydrolytic cleavage of proteins and peptides. The regioselectivities of these hydrolyses vary with substrate. The mechanisms are complicated and it is not clear whether the palladium(II) may activate the C—N bond, or deliver H_2O. Also, since characterized structures with both Pd—S and Pd—O bonds in the same molecule are rare, it is necessary to study complexes with S and O ligations in detail in order to elucidate the reaction mechanism. This contribution reports the syntheses and physicochemical characterizations of $(Et_4N)_2[Pd_2(mp)_2(Hmp)_2]$ [15] (**1**) and $[Pd(mpo)_2]$ (**2**). EHMO calculations have been carried out, indicating large delocalized π bonds extending in the $(mp)_2Pd_2S_2$ plane in **1** and in the $Pd(mpo)_2$ plane in **2**.

EXPERIMENTAL

Air-sensitive manipulations were carried out under dry dinitrogen. Standard Schlenk-tube, vacuum-line and syringe techniques were utilized. Solvents were

* Authors to whom correspondence should be addressed.

dried by standard methods and redistilled before use. 2-Mercaptophenol (H_2mp), sodium 2-mercaptopyridine N-oxide (Nampo), 2,2′-dithiobis(pyridine N-oxide) (dtpo) and palladium chloride were all commercially available and used without further purification. [Pd(COD)Cl2] [16] (COD = 1,5-cyclooctanediene) and [Ni(mpo)$_2$] [8] were prepared by literature methods.

Physical measurements and instrumentation

Elemental analyses were performed by the analytical laboratory of this Institute. Infrared spectra were measured on a Nicolet Magna-750 FT-IR or a Bio-Rad FTS-40 spectrometer, in KBr discs. Raman spectra were recorded on a Nicolet 910 FT-Raman spectrometer using Raman 1064 nm laser source at a resolution of 2 cm^{-1} with 200–400 scans. NMR spectra were measured in DMSO-d_6 solutions on a varian Unity-500 spectrometer operating at 499.98 MHz for ^{1}H, and 124.71 MHz for ^{13}C; the internal reference was $SiMe_4$ in all cases (ppm). Mass spectra were obtained at 70 eV on a Finnigan Mat 312 GC-MS spectrometer by the direct inlet method.

Preparation of $(Et_4N)_2[Pd_2(mp)_2(Hmp)_2]$ (**1**)

To a solution of Na_2mp (0.80 g, 5.0 mmol) in absolute EtOH (20 cm^3) was added a solution of [$PdCl_2$] (0.34 g, 2.0 mmol) in MeCN (30 cm^3) within 10 min at room temperature. After stirring for 30 min until the color no longer changed, the brown solution was filtered and combined with Et_4NCl (0.50 g, 3.0 mmol) in EtOH (10 cm^3). Brown precipitates formed immediately and the solution was kept at 5°C for a few hours and then filtered. The crude product was recrystallized from DMF/MeCN (5 : 1, v/v) to give 0.8 g of brown needle crystals (yield 41%). Found: C, 49.1; H, 5.9; N, 2.6; S, 12.5. Calc. for $C_{40}H_{58}N_2O_4Pd_2S_4$: C, 49.4; H, 6.0; N. 2.9; S, 13.2%. ^{1}H NMR: 11.02 (s, *HO*), 8.79 (dd, $^3J_{16,15}$ = 8.0 Hz, $^4J_{16,14}$ = 1.5 Hz, H16), 6.92 (dt, $^3J_{14,13}$ = 6.5 Hz, $^3J_{14,15}$ = 7.7 Hz, $^4J_{14,16}$ = 1.5 Hz, H14), 6.83 (dt, $^3J_{26,25}$ = 7.2 Hz, $^4J_{26,24}$ = 1.0 Hz, H26), 6.60 (dd, $^3J_{13,14}$ = 6.5 Hz, $^4J_{13,15}$ = 1.5 Hz, H13), 6.58 (dt, $^3J_{24,23}$ = 7.7 Hz, $^3J_{24,25}$ = 7.5 Hz, $^4J_{24,26}$ = 1.0 Hz, H24), 6.55 (dd, $^3J_{15,14}$ = 7.7 Hz, $^3J_{15,16}$ = 8.0 Hz, $^4J_{15,13}$ = 1.5 Hz, H15), 6.31 (dd, $^3J_{23,24}$ = 7.7 Hz, $^4J_{23,25}$ = 1.0 Hz, H23), and 6.29 (dt, $^3J_{25,24}$ = 7.5 Hz, $^3J_{25,26}$ = 7.2 Hz, $^4J_{25,23}$ = 1.0 Hz, H25). ^{13}C NMR: 167.0 (C22), 158.4 (C12), 137.1 (C16), 134.6 (C21), 127.2 (C26), 126.3 (C11, C14), 121.7 (C24), 119.3 (C15), 117.8 (C13), 115.3 (C23, C25). IR (CsI, cm^{-1}): ν(OH) 3452(w), ν(aryl-H) 3047(m), ν(C=C) 1556(s), ν(C—O) 1230(vs), 1171(s), ν(C—S) 1056(m), 1026(m), ν(Pd—O) 379(m), ν(Pd—S) 313(w), 297(m), 295(m).

Preparation of [Pd(mpo)$_2$] (**2**)

Route (a): To a suspension of dtpo (0.38 g, 1.5 mmol) and NaOMe (0.10 g, 1.85 mmol) in MeOH/MeCN (50 cm^3, 1 : 1, v/v) was added [$PdCl_2$] (0.18 g, 1.0 mmol). After stirring for 20 h at room temperature, the solution developed a brown color and was filtered. The filtrate gave deep brown prismatic crystals of **2** (yield 60%) on standing at 5°C, which were collected by filtration. Found: C, 33.4; H, 2.1; N, 7.7; S, 17.7. Calc. for $C_{10}H_8N_2O_2PdS_2$: C, 33.5; H, 2.2; N, 7.8; S, 17.9%. ^{1}H NMR: 8.41 (dd, $^3J_{1,2}$ = 6.7 Hz, $^4J_{1,3}$ = 1.2 Hz, H1), 7.62 (dd, $^3J_{4,3}$ = 8.4 Hz, $^4J_{4,2}$ = 1.8 Hz, H4), 7.46 (dt, $^3J_{3,2}$ = 7.2 Hz, $^3J_{3,4}$ = 8.4 Hz, $^4J_{3,1}$ = 1.2 Hz, H3), and 7.18 (dt, $^3J_{2,3}$ = 7.2 Hz, $^3J_{2,1}$ = 6.7 Hz, $^4J_{2,4}$ = 1.8 Hz, H2). ^{13}C NMR: 156.4 (C5, C10), 138.0 (C1, C6), 130.9 (C3, C8), 127.8 (C2, C7), 119.5 (C4, C9). IR (CsI, cm^{-1}): ν(aryl-H) 3094(m), 3067(m), ν(C=C) 1547(vs), ν(N—O) 1246(vs), ν(C—S) 1042(m), ν(Pd—O) 392(m), ν(Pd—S) 338(w), 315(w), 294(w), 248(m).

Route (b): A mixture of [$PdCl_2$] (0.18 g, 1.0 mmol) and Nampo (0.60 g, 4.0 mmol) in MeOH/MeCN (80 cm^3, 1 : 1, v/v) was stirred for 2 h and filtered. The precipitate was recrystallized from DMF to give brown plate crystals of **2** (yield 72%). The IR spectrum and crystal parameters are identical to that obtained by route (a).

Route (c): To a solution of Ni(mpo)$_2$ (0.08 g, 0.26 mmol) in CH_2Cl_2 (10 cm^3) was added a solution of [Pd(COD)Cl_2] (0.074 g, 0.26 mmol) in CH_2Cl_2 (10 cm^3). A yellow precipitate formed immediately and the product **2** was recrystallized from DMF (5 cm^3) (yield 65%). The IR spectrum and crystal parameters are identical to that obtained by route (a) or (b).

Crystallography

Intensity data for single crystals of $(Et_4N)_2$ $[Pd_2(mp)_2(Hmp)_2]$ **1** and [Pd(mpo)$_2$] **2** were collected at room temperature with Mo-K_α radiation (graphite monochromator), λ = 0.71073 Å. The data sets were corrected for Lorentz and polarization effects and for absorption employing an analytical procedure. Crystal data are compiled in Table 1.

The structures were solved by the Patterson method and refined by a full-matrix least-squares procedure based on *F*. Final refinement details are also given in Table 1. The maximum residual electron density peaks in the final difference maps are 1.03 e Å^{-3} for **1** and 0.57 e Å^{-3} for **2**, located in the vicinity of the Pd atoms.

Molecular orbital calculations

Extended-Hückel molecular orbital (EHMO) calculations with charge iteration (sense* charge dependence) and weighted H_{ij} were carried out by using the

Table 1. Crystallographic data and data collection parameters for $(Et_4N)_2[Pd_2(mp)_2(Hmp)_2]$ **1** and $[Pd(mpo)_2]$ **2**

	$(Et_4N)_2[Pd_2(mp)_2(Hmp)_2]$	$[Pd(mpo)_2]$
Formula	$C_{40}H_{58}N_2O_4Pd_2S_4$	$C_{10}H_8N_2O_2PdS_2$
Colour	Brown plate	Brown plate
M	971.95	358.7
Crystal system	Monoclinic	Monoclinic
Space group	$P2_1/n$	$P2_1/n$
a (Å)	9.088(1)	8.709(1)
b (Å)	17.851(4)	14.060(2)
c (Å)	12.932(1)	10.025(1)
β (°)	93.21(1)	96.79(1)
V (Å^3)	2094.7(7)	1218.9(6)
Z	2	4
D_c (g cm^{-3})	1.54	1.955
μ (mm^{-1})	1.08	1.845
Crystal size (mm^3)	$0.35 \times 0.26 \times 0.18$	$0.15 \times 0.20 \times 0.30$
$F(000)$	1000	704
Diffractometer	Enraf-Nonius CAD4	Rigaku RAXIS
Temperature (K)	296	293
Scan type	2θ	[a]
2θ range (°)	49.9	[a]
No. of unique reflections	3096($I \geq 3\sigma(I)$)	2128
Weighting scheme	$w = 1/\sigma^2(F)$	$w = [\sigma^2 F_o + 0.0010 F_o^2]^{-1}$
R, R	0.044, 0.055	0.045, 0.070

[a] Take oscillation IP photos; 20 frames in total, $\phi = 0$–180°, $\Delta = 9°$, 15 mins per frame.

ICON 8 version. A total of 164 and 81 valence orbitals involving five d orbitals of Pd were employed for **1** and **2**, respectively. The parameters of Pd atom were taken from [17].

RESULTS AND DISCUSSION

Syntheses

Excess of mp is necessary to obtain the compound $(Et_4N)_2[Pd_2(mp)_2(Hmp)_2]$ **1**. If the molar ratio of mp : $[PdCl_2]$ is decreased from 2.5 : 1 to 2.0 : 1, a highly air-sensitive crystalline product was isolated, which cannot be identified under present conditions. Treatment of $[PdCl_2]$ with Nampo (route (b)) or with the organic disulphide dtpo under strongly basic condition (route (a)) gave the compound $[Pd(mpo)_2]$ **2**. In the attempt to use the S donor in $[Ni(mpo)_2]$ to coordinate further, it is interesting to find that compound **2** was obtained from the reaction of $[Ni(mpo)_2]$ with $[Pd(COD)Cl_2]$ (eq. 1). This reaction suggests that the bidentate-O : S ligand mpo has transferred from Ni^{II} to Pd^{II}, in contrast with bidentate-N : S ligand aminoethanethiolate which transferred from Pd^{II} to Ni^{II} [18].

$$Pd(COD)Cl_2 + Ni(mpo)_2 \rightarrow Pd(mpo)_2 + NiCl_2 + COD \quad (1)$$

Molecular vibration spectra

The IR and Raman (see Fig. 1) spectra of complex **1** showed the vibrations of C—S bonds appearing at 1056 and 1026 cm^{-1} as two peaks while only one peak at 1042 cm^{-1} was present in **2**. The typical absorptions of C—O bonds for **1** appear at 1230 and 1171 cm^{-1}. It is interesting to note that the absorption peaks of the N—O bonds of **2** are both very strong at 1246 cm^{-1} for the IR and Raman spectra and the N—O bending vibration is at 416 cm^{-1}. The stretching vibrations of Pd—O bonds have been observed at 378 (IR) and 399, 385 and 366 cm^{-1} (Raman) for **1** and

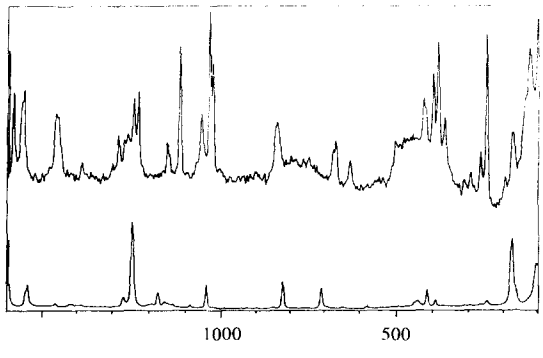


Fig. 1. Raman spectra of compounds **1** (upper) and **2** (lower).

391 cm^{-1} (IR and Raman) for **2**, which are comparable to the values of 395–340 cm^{-1} in triangulo-hexa-μ-acetatopalladium(II) [19] and are lower than that of 464 cm^{-1} in acetylactonatopalladium(II) [20]. The Pd—S stretching vibrations are in the range of 313–295 cm^{-1} for both **1** and **2** in their molecular vibration spectra, consistent with ν(Pd—S) (388–240 cm^{-1}) [21,22]. It also seems reasonable to assign bands in the range of 100–140 cm^{-1} to O—Pd—S bending vibrations.

EI-MS characterization

The molecular ion peak of **1** in a positive EI-MS spectrum was not observed, but the fragment $[Pd(Hmp)_2]^+$ peak with low abundance (2%) appeared and decomposed to produce the ions $[Pd(Hmp)_2—O]^+$ (45%), $[Pd(Hmp)_2—CO]^+$ (3%) and $[Pd(Hmp)_2—Cs]^+$ (4%). Ions $[PdO(S)]^+$ (100%) and $[PdS]^+$ (29%) were also observed together with one of the major ions $[Hmp]^+$ (56%). The MS spectrum of $[Pd(mpo)_2]$ **2** is similar to the other complexes containing mpo ligand [23] with the ions: M^+ (100%), $[M^+—O]$ (5%), $[M^+—2O$ or $S]$ (9%), $[M^+—SC]$ (85), $[M^+—2S]$ (2%), $[M^+—2O—2S]$ (6%), $[M^+—mpo]$ (3%), $[M^+—mpo—O]$ (20%), $[M^+—mpo—S]$ (8%), $[M^+—mpo—CS]$ (88%), $[M^+—mpo—S—O]$ (25%), $[PdO(S)]^+$ (5%), $[mpo]^+$ (4%) and $[mpo—O]^+$ (6%).

NMR spectra

The ^1H and ^{13}C NMR spectra of complex **2** are easy to assign, however, those of the dinuclear anion of **1** cannot be analyzed simply owing to the fact that the mp ligands is of the ABCD system and in the two kinds of terminal and bridging coordination modes. The ^1H signals overlap in the region of 6–7 ppm, and only ten ^{13}C signals appear in its ^{13}C NMR spectrum although there should be twelve inequivalent carbons, in which the signals at 126.3 and 115.3 ppm may be the overlapped peaks estimated roughly from their intensity. Consequently, some 2D NMR techniques have been applied to assign the NMR spectra.

The signal at 11.03 ppm comes from the hydroxy proton of the bridging mp ligand which forms a strong intermolecular hydrogen bond with the oxygen atoms of the terminal mp ligand [O(1)···O(2*), 2.596 Å]. This fact indicates clearly that the dinuclear anion also exists in the DMF solution. The other ^1H signals in the region of 6–9 ppm can be assigned into two groups: 8.79 [H(16)], 6.92 [H(14)], 6.60 [H(13)], and 6.55 [H(15)]; 6.83 [H(26)], 6.58 [H(24)], 6.31 [H(23)], and 6.29 [H(25)], by the ^1H–^1H COSY and simulated spectra. However, which group of signals are contributed by the bridging or terminal mp ligand cannot be assigned. Then the ^1H–^{13}C HMBC (Heteronuclear Multiple Bond Connectivity) spectrum was recorded [24]. The ^1H signal at 11.03 ppm of hydroxy proton correlates to the ^{13}C one at 117.8 ppm [C(13)] in ^1H–^{13}C HMBC spectrum, and the C(13) signal also correlates to the signal at 6.60 [H(13)] ppm in the ^1H–^{13}C HMQC spectrum (Fig. 2), suggesting that the former group signals should be ascribed to the protons of the bridging mp ligand and the latter group to the terminal mp ligand.

The ^{13}C signal at 115.3 ppm correlates to both H(23) and H(25) in the HMQC spectrum, implying that the 115.3 ppm signal is contributed from both C(23) and C(25). Accordingly, the C(13) (117.8), C(14) (126.3), C(15) (119.3), C(16) (137.1), C(24) (121.7), and C(26) (127.2) were assigned. In the HMBC spectrum, the ^{13}C signal at 126.3 ppm [contributed partially from C(14)], not only correlates to H(16) owing to the result of C(14), but also to H(13) and H(15), demonstrating that the 126.3 ppm signal is also contributed from C(11). The last three signals: 167.0 ppm correlating to H(26) and H(24), 158.5 to H(16) and H(14), and 134.6 ppm to H(25) and H(23) in the HMBC spectrum, indicate that they are C(22), C(12), and C(21), respectively.

Description of the structures

The molecular structures of the anion $[Pd_2(mp)_2(Hmp)_2]^{2-}$ of **1** and the compound $[Pd(mpo)_2]$ **2** are illustrated in Figs 3 and 4, respectively. Selected structural parameters are listed in Tables 2 and 3.

The dinuclear anion of **1** consists of two equivalent molecular fragments related by a crystallographic inversion center. The two Pd, four S, two O atoms and the two phenyl rings in the terminal ligands are essentially coplanar, while the planes of the two phenyl rings in the bridging ligands are tilted by 68.6° from the $mp_2Pd_2S_2$ plane. The structure is quite similar to that reported for $(Et_4N)_2[Ni_2(mp)_2(Hmp)_2]$ [2].

The molecule of **2**, which is also quite similar to that of $[Ni(mpo)_2]$ [8], has a palladium atom in the centre of the nearly square planar PdS_2O_2 unit with the two mpo ligands in the *cis* configuration. The whole molecule exhibits a *pseudo*-C_{2v} symmetry with

Table 2. Selected atomic diatances (Å) and bond angles (°) for the anion $[Pd_2(mp)_2(Hmp)_2]^{2-}$ of **1**

Pd—O(2)	2.009(3)	Pd—S(2)	2.280(1)
Pd—S(1)	2.295(1)	Pd—S(1*)	2.349(1)
S(1)—C(11)	1.796(5)	S(2)—C(21)	1.773(5)
O(1)—C(12)	1.353(7)	O(2)—C(22)	1.358(6)
O(2)—Pd—S(2)	86.6(1)	O(2)—Pd—S(1)	176.7(1)
O(2)—Pd—S(1*)	91.4(1)	S(2)—Pd—S(1)	96.30(5)
S(2)—Pd—S(1*)	177.99(6)	S(1)—Pd—S(1*)	85.72(5)
C(11)—S(1)—Pd	107.9(2)	C(11)—S(1)—Pd(*)	105.4(2)
Pd—S(1)—Pd(*)	94.28(5)	C(21)—S(2)—Pd	96.8(2)
C(22)—O(2)—Pd	118.0		

Symmetry operator: *, $1-x$, $-y$, $1-z$.

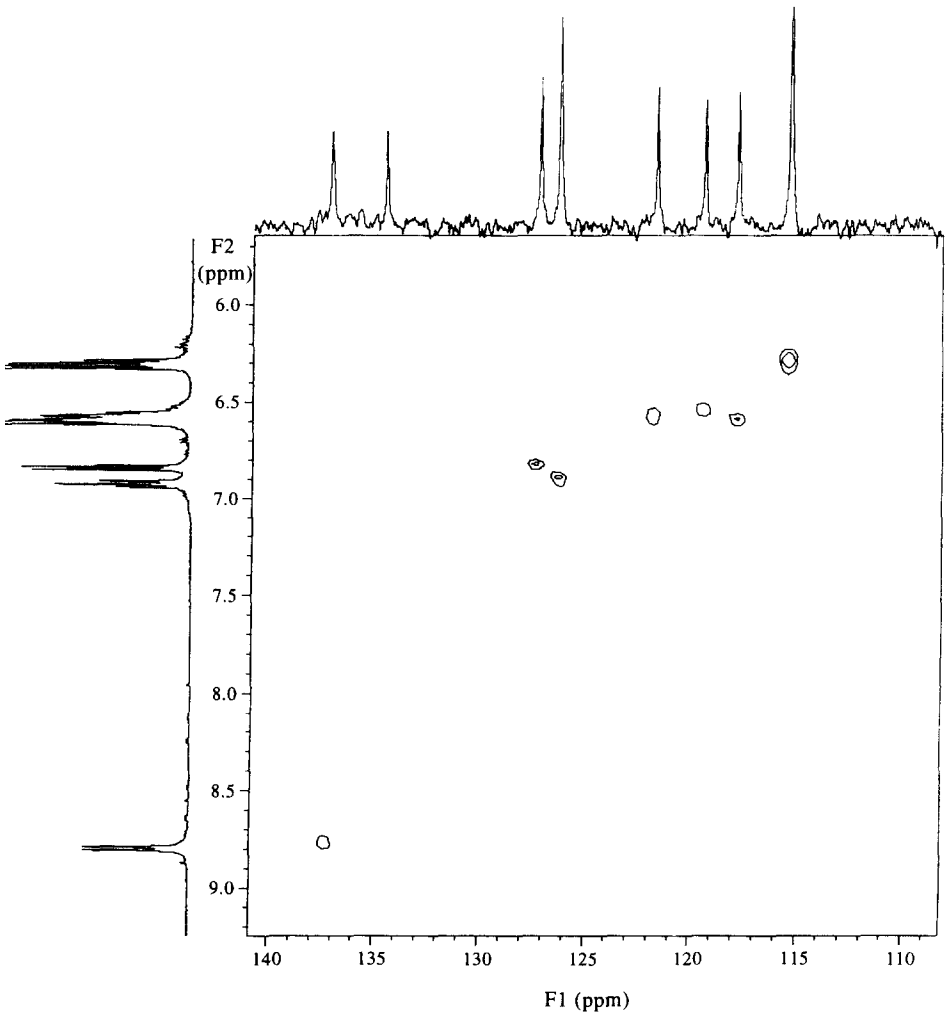


Fig. 2. ^{1}H–^{13}C HMQC spectrum of **1**.

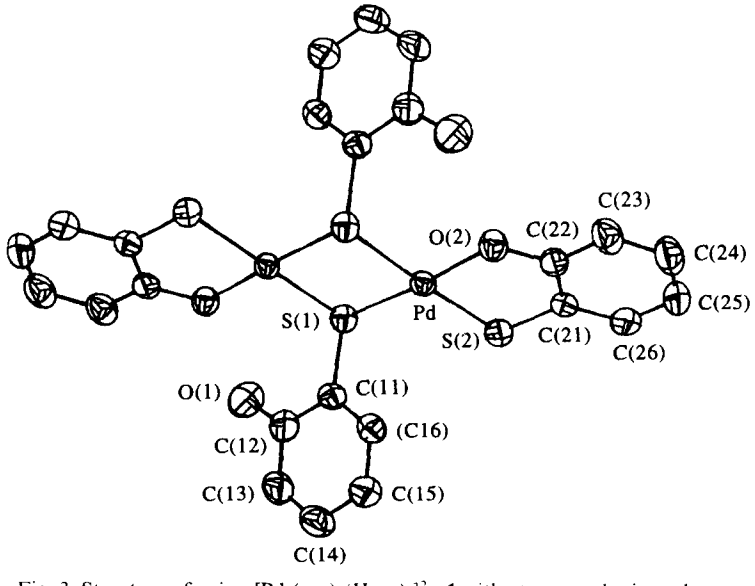


Fig. 3. Structure of anion $[Pd_2(mp)_2(Hmp)_2]^{2-}$ **1** with atom numbering scheme.

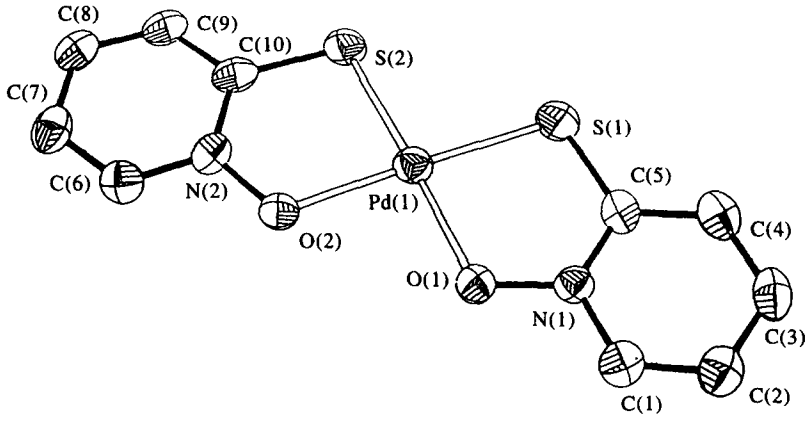


Fig. 4. Structure of $[Pd(mpo)_2]$ **2** with atom numbering scheme.

the C_2 axis passing through the palladium atom and the mid-points of S(1)···S(2) and O(1)···O(2).

The Pd—S bond length of av. 2.412 Å of **2** are somewhat longer than those terminal (2.280 Å) and bridging (av. 2.322 Å) Pd—S bonds of **1**, and than that reported (2.296 Å) [25]. The Pd—O bond of av. 2.043 Å in **2** is also slightly longer than that in **1** (2.009 Å) and that in the tetrachlorocatechol complex $[Pd(C_6Cl_4O_2)(PPh_3)_2]$ (av. 2.033 Å) [26], and than the values reported for $[Pd\{PhC(O)CC(O)Me\}_2]$ (1.98 Å) [27]. The long Pd···Pd* distance of 3.404(1) Å indicates that a Pd···Pd* bonding interaction seems unlikely. The relatively short C—S distances (av. 1.73 Å) in **2** show partial double bond character as they are nearly 0.1 Å shorter than the normal covalent distance (1.81 Å) [28] for a C—S single bond, and also definitely shorter by 0.04–0.05 Å than that in **1**. This feature results in the fact that complexes with mpo ligands have little ability to bridge another metal ion through the sulfur atom to form polynuclear complexes. The bite angles O—Pd—S of **2** (85.6°) are smaller than that in **1** (86.6°). The Pd—S—C angle of 96.8° for **1** of the terminal ligand, and of 98.0° (average) for **2** show the bonding orbital of the chelating sulfur atoms are mainly of *p* character, and the oxygen atom of Pd—O—C (118.0°) in **1** and of Pd—O—N (115.8°) in **2** show more of sp^2 character.

Table 3. Selected atomic distances (Å) and bond angles (°) for $[Pd(mpo)_2]$, **2**

Pd—S(1)	2.241(2)	Pd—O(1)	2.042(4)
Pd—S(2)	2.243(2)	Pd—O(2)	2.045(5)
S(1)—C(5)	1.741(6)	O(1)—N(1)	1.351(7)
S(2)—C(10)	1.720(7)	O(2)—N(2)	1.356(7)
N(1)—C(1)	1.353(8)	N(1)—C(5)	1.339(7)
S(1)—Pd—O(1)	85.6(1)	S(1)—Pd—S(2)	95.8(1)
O(1)—Pd—S(2)	178.4(1)	S(1)—Pd—O(2)	178.0(1)
O(1)—Pd—O(2)	92.5(2)	S(2)—Pd—O(2)	86.1(1)
Pd—S(1)—C(5)	97.9(2)	Pd—O(1)—N(1)	115.8(3)
Pd—S(2)—C(10)	98.2(2)	Pd—O(2)—N(2)	115.8(3)

Theoretical calculations

The Pd—O bonds with the average bond order 0.275 and 0.277 for **1** and **2**, respectively, are a lot weaker than the Pd—S bonds (av. 0.458 and 0.408 for **1** and **2**, respectively).

The HOMO at −10.806 eV of the anion of **1** consisting of the atomic orbital: Pd(1.4%), O(3.4%), S(17.6%) and C(74.8%), shows that the HOMO involves 23% *d-p* π component and 77% C—C π component. The LUMO at −9.469 eV contains the atomic orbital: Pd(36.9%), O(23.6%) and S(37.2%), in which *d-p* π* character is obvious.

The HOMO at −11.380 eV of **2** contains: Pd(3.9%), O(33.1%), S(24.4%) and C(34.9%), involving 63.7% *d-p* π and 36.3% C—C π components. Similar to that of **1**, the LUMO at −9.466 eV consisting of the atomic orbitals: Pd(33.8%), O(16.5%) and S(42.3%), shows also significant *d-p* π* character.

The facts mentioned above indicate that there are some large delocalized π bonds extending in the $(mp)_2Pd_2S_2$ plane in **1** and in the $Pd(mpo)_2$ plane in **2**. The energy gap (1.915 eV) between LUMO and HOMO in the anion of **1** is larger than that of **2** (1.337 eV), which suggests that the mixing of the *d-p* π with π of the phenyl ring is better in **1** than in **2**.

Acknowledgements—This work was supported by the Climbing Program-State key Project for Fundamental Research, the National Natural Science Foundation of China and the Hong Kong Research Grants Council Earmarked Grant No. CUHK 311/949.

REFERENCES

1. B. S. Kang, Q. T. Liu, and J. X. Lu, *Nitrogen Fixation Research in China* (Edited by G. F.

Hong) Ch. 6, p. 151. Springer–Verlag, Heidelberg (1992).
2. B. S. Kang, L. H. Weng, D. X. Wu, F. Wang, Z. Guo and H. Q. Liu, *Inorg. Chem.* 1988, **27,** 1128.
3. B. S. Kang, L. H. Weng, D. X. Wu, L. R. Huang, F. Wang, Z. Guo and H. Q. Liu, *Inorg. Chim. Acta* 1988, **148,** 147.
4. B. S. Kang, L. H. Weng, H. Q. Liu, L. R. Huang, D. X. Wu, C. Z. Lu, J. H. Cai, X. T. Chen and J. X. Lu, *Inorg. Chem.* 1990, **29,** 4873.
5. X. T. Chen, H. Q. Liu, L. H. Weng, L. R. Huang, D. X. Wu, X. J. Lei and B. S. Kang, *J. Coord. Chem.* 1991, **22,** 109.
6. B. S. Kang, X. T. Chen, L. H. Weng, L. R. Huang, C. Z. Lu and J. X. Lu, *Science in China (chi.) Ser. B* 1991, 18.
7. B. S. Kang, Y. J. Xu, X. L. Xie, C. N. Chen, Q. T. Liu and J. X. Lu, *Inorg. Chem.* 1994, **33,** 3770.
8. X. T. Chen, Y. H. Hu, D. X. Wu, L. H. Weng and B. S. Kang, *Polyhedron* 1991, **10,** 2651.
9. Y. H. Hu, L. H. Weng, L. R. Huang, X. T. Chen, D. X. Wu and B. S. Kang, *Acta Cryst., Sect. C* 1991, **47,** 2655.
10. B. S. Kang, Y. J. Xu, J. H. Peng, D. X. Wu, X. T. Chen, Y. H. Hu, M. C. Hong and J. X. Lu, *Polyhedron* 1993, **12,** 871.
11. L. Zhu and N. M. Kostic, *Inorg. Chem.* 1992, **31,** 3994.
12. L. Zhu and N. M. Kostic, *J. Am. Chem. Soc.* 1993, **115,** 4539.
13. L. Zhu and N. M. Kostic, *J. Am. Chem. Soc.* 1994, **116,** 5218.
14. L. Zhu and N. M. Kostic, *Inorg. Chim. Acta* 1994, **217,** 21.
15. Structural data has already been communicated: J. S. Shi, X. Y. Huang, T. B. Wen, Y. H. Deng, C. N. Chen, Q. T. Liu and B. S. Kang, *Jiegou Huaxue* 1995, **14,** 293.
16. R. Ros, G. Garturan and G. Mauro, *Trans. Met. Chem.* 1976, **1,** 13.
17. J. K. Burdett and T. Hughbarks, *J. Am. Chem. Soc.* 1984, **106,** 3101.
18. T. Konno, K. Yonenobu, J. Hidaka and K. Okamoto, *Inorg. Chem.* 1994, **33,** 861.
19. L. Soptrajanova and B. Soptrajanov, *Spectroscopy Lett.* 1992, **25,** 1131.
20. M. Mikami, I. Nakagawa and T. Shimanouchi, *Spectrochim. Acta* 1968, **24A,** 1291.
21. J. Sola and R. Yaner, *J. Chem. Soc., Dalton Trans.* 1986, 2021.
22. D. M. Roundhill, *Inorg. Chem.* 1980, **19,** 557.
23. Y. H. Hu, X. T. Chen, L. Dai, L. H. Weng and B. S. Kang, *Jiegou Huaxue* 1993, **12,** 38.
24. D. X. Wu, J. C. Shi and B. S. Kang, *Chinese J. Magnetic Resonance* 1996, **13,** 377.
25. J. P. Beale and N. C. Stephenson, *Acta Cryst. Sect. B* 1972, **28,** 557.
26. C. G. Pierpoint and H. H. Downs, *Inorg. Chem.* 1975, **14,** 343.
27. S. Okeya, S. Oci, K. Matsumoto and Y. Nakamura, *Bull. Chem. Soc. Jpn.* 1981, **54,** 1085.
28. J. D. Lydon, R. C. Elder and E. Deutsch, *Inorg. Chem.* 1982, **21,** 3168.

Pergamon

PII: S0277-5387(96)00308-7

Polyhedron Vol. 16, No. 3, pp. 377–382, 1997
Copyright © 1996 Elsevier Science Ltd
Printed in Great Britain. All rights reserved
0277-5387/97 $17.00+0.00

Stabilization of a Y-shaped Cu^{I} coordination in $[CuPt_2(PPh_3)_5(\mu_3\text{-}S)_2]PF_6$ by $Pt_2(PPh_3)_4(\mu\text{-}S)_2$ and its expansion to a pentanuclear aggregate $[Cu\{Pt_2(PPh_3)_4(\mu_3\text{-}S)_2\}_2]PF_6$. X-ray crystal structure of $[CuPt_2(PPh_3)_5(\mu_3\text{-}S)_2]PF_6$

Huang Liu,[a] Agnes L. Tan,[b] Yan Xu,[c] K. F. Mok[a]* and T. S. Andy Hor[a]*

[a] Department of Chemistry, National University of Singapore, Kent Ridge, Singapore 119260

[b] Department of Computational Science, National University of Singapore, Kent Ridge, Singapore 119260

[c] Division of Chemistry, National Institute of Education, Nanyang Technological University, 469 Bukit Timah Road, Singapore 259756

(Received 24 May 1996; accepted 19 June 1996)

Abstract—Addition of $Pt_2(PPh_3)_4(\mu\text{-}S)_2$, **1**, to an equimolar quantity of $Cu(NO_3)(PPh_3)_2$ gave $[CuPt_2(PPh_3)_5(\mu_3\text{-}S)_2]NO_3$, **2a**, which readily reacted with NH_4PF_6 giving $[CuPt_2(PPh_3)_5(\mu_3\text{-}S)_2]PF_6$, **2b**. Further addition of a molar equivalent of **1** to **2b** gave rise to a pentanuclear $\{CuPt_4\}$ complex of $[Cu\{Pt_2(PPh_3)_4(\mu_3\text{-}S)_2\}_2]PF_6$, **3**. Complex **3** was also obtained from the direct 2 : 1 addition of **1** to $[Cu(CH_3CN)_4]PF_6$. Complexes **2** and **3** have been characterized by IR and $^{31}P\text{-}\{^1H\}$ NMR spectroscopy and in the case of **2b** single crystal X-ray crystallography. The geometry of Cu^{I} in **2b** is three-coordinate and Y-shaped. It represents the first crystallographically characterized mixed-metal complex of **1** with a trigonal-planar heterometal. The unexpectedly short non-bonding Cu—Pt distances (av. 2.869(4) Å) are associated with a more open $\{Pt_2S_2\}$ butterfly core (θ 137.5(5)°). Some theoretical aspects of these geometric peculiarities are discussed. Copyright © 1996 Elsevier Science Ltd

Keywords: copper; platinum; sulfide; aggregate; crystal structure; phosphine.

Designed syntheses of heterometallic platinum sulfide complexes have been established with the use of $Pt_2(PPh_3)_4(\mu\text{-}S)_2$, **1**, as a versatile metalloligand [1–10]. With appropriate Lewis acids, polynuclear aggregates with 3 [1–8], 4 [8], 5 [9], and 6 [10] metal centres can be assembled. The butterfly-shape of the dithiol ligand with a changeable bite angle and a flexible hinge angle stabilizes a variety of geometries of the heterometal (M) (e.g. linear [8], angular [4], T-shaped [10], tetrahedral [5, 6, 9], square-planar [1, 2, 9], square pyramidal [6], trigonal bipyramidal [7] etc.). Its ability to function as a unidentate [8], bridging [10] and chelating ligand [1–7, 9], coupled with an adjustable flow of electron donation/acceptance of the phosphines and thiol centres [11] further makes this one of the most powerful metalloligands known to date.

All the polyheterometallics assembled from **1** do not show active metal–metal interaction (hence the term "aggregates" [1a]), with $[Ag_2\{Pt_2(PPh_3)_4(\mu_3\text{-}S)_2\}_2]^{2+}$ [10] as the only notable exception (Ag—Ag 2.815(4) Å). The metal centres are generally brought to vicinity ($\geq$3.0 Å) by capping sulfur ligands. In this paper, we report the activity of **1** towards Cu^{I} to give $[CuPt_2(PPh_3)_5(\mu_3\text{-}S)_2]^+$, **2**, which captures another molecule of **1** in an aggregate expansion reaction to give $[Cu\{Pt_2(PPh_3)_4(\mu_3\text{-}S)_2\}_2]^+$, **3**. There is no crystallographic report in the literature that **1** can function

* Authors to whom correspondence should be addressed.

as a chelating ligand on a metal which favors a trigonal-planar geometry. The bite angle of **1** among the aggregates is found to be largest in $[GaPt_2Cl_2(PPh_3)_4(\mu_3\text{-}S)_2]^+$ (83.9(1)°) [6], which is still significantly smaller than the ideal trigonal-planar angle of 120°. The inter-relationship of the chelate bite, dihedral angle of the $\{Pt_2S_2\}$ butterfly, and the metal–metal distance is discussed in this paper.

RESULTS AND DISCUSSION

Mixing of $Cu(NO_3)(PPh_3)_2$ with **1** (1 : 1 molar ratio) in MeOH gives an addition compound $[CuPt_2(PPh_3)_5(\mu_3\text{-}S)_2]NO_3$, **2a**. The product shows typical (1 : 1) ionic behavior in MeOH and the ionic nitrate group is verified by a strong IR band at 1384 cm^{-1}. The intensity ratio of the Cu- and Pt-coordinated phosphines is approximately 1 : 4 in the $^{31}P\text{-}\{^1H\}$ NMR spectrum. Complex **2a** undergoes metathesis easily with NH_4PF_6 to give $[CuPt_2(PPh_3)_5(\mu_3\text{-}S)_2]PF_6$, **2b**. Both **2a** and **2b** slowly decompose in solution (e.g. in THF and CH_2Cl_2) in air to give an unknown deep-blue complex, presumably a Cu^{II} species. This decomposition is probably facilitated by phosphine dissociation as it is inhibited by doping of the solution with excess PPh_3. There is, however, no evidence for phosphine addition to **2**. The complex is also inert to displacement of PPh_3 by a bidentate phosphine such as dppe or dppf (dppf = 1,1′-bis(diphenylphosphino) ferrocene). However, displacement by an additional molar equivalent of **1** rapidly occurs to give $[Cu\{Pt_2(PPh_3)_4(\mu_3\text{-}S)_2\}_2]^+$, **3**. Such rapid displacement of a good σ-donor such as PPh_3 was not expected. The chelating ability of **1** on Cu^I appears to provide some stability to **3**. Similar pentametallic complexes with two chelating ligands of **1** coordinated to a central metal have been reported for Ni^{II}, Hg^{II}, and Pd^{II} [9, 12]. They are almost invariably synthesized from a Lewis acid with good labile ligands such as PhCN or Me_2S. Complex **3** can also be obtained from the reaction of **1** with $[Cu(CH_3CN)_4]^+$ in 2 : 1 molar ratio.

A single-crystal X-ray diffraction study was carried out on **2b**. Data collection and refinement are summarized in Table 1. Selected bond lengths and angles are listed in Tables 2 and 3, respectively. The structure shows a near-symmetrical chelation of the dithiol ligand **1** on a Cu^I centre with PPh_3 completing a trigonal planar configuration (Fig. 1). With an acute bite angle ∠S(1)—Cu—S(2) of 84.6(2)° and two similar but significantly larger angles ∠P(3)—Cu—S (139.4(2) and 135.7(2)°), the local geometry is best described as "Y-shaped". Such geometry (trigonal planar or Y-shaped) has not been found among the vast variety of mixed-metal aggregates formed from **1**. Similar complexes formed from AuCl and $AuCl(PPh_3)$ give two-coordinate linear Au^I or a distorted linear geometry with Au strongly bonded to one sulfur and weakly to the other [8]. On the contrary, the heterometal atom, *viz.* Cu in **2b** is approximately equidistant to both sulfur atoms (Cu—(μ_3-S) 2.269(5) and 2.303(5) Å). These lengths (av. 2.286(5) Å) are marginally longer than those of Cu—(μ_3-S) in $[PPh_4]_2[Cu_3WCl_3(\mu\text{-}S)_2(\mu_3\text{-}S)_2]$ [13] (ranging from 2.247(5) to 2.279(5) Å) and those in $[Cu(SP(CH_3)_3)Cl]_3$ [14] (av. 2.265(1) Å), but significantly shorter than those in $[Et_4N][(Ph_3P)_2Cu(\mu\text{-}S)_2W(\mu\text{-}S)_2FeCl_2]$ [15] (av. 2.374(2) Å).

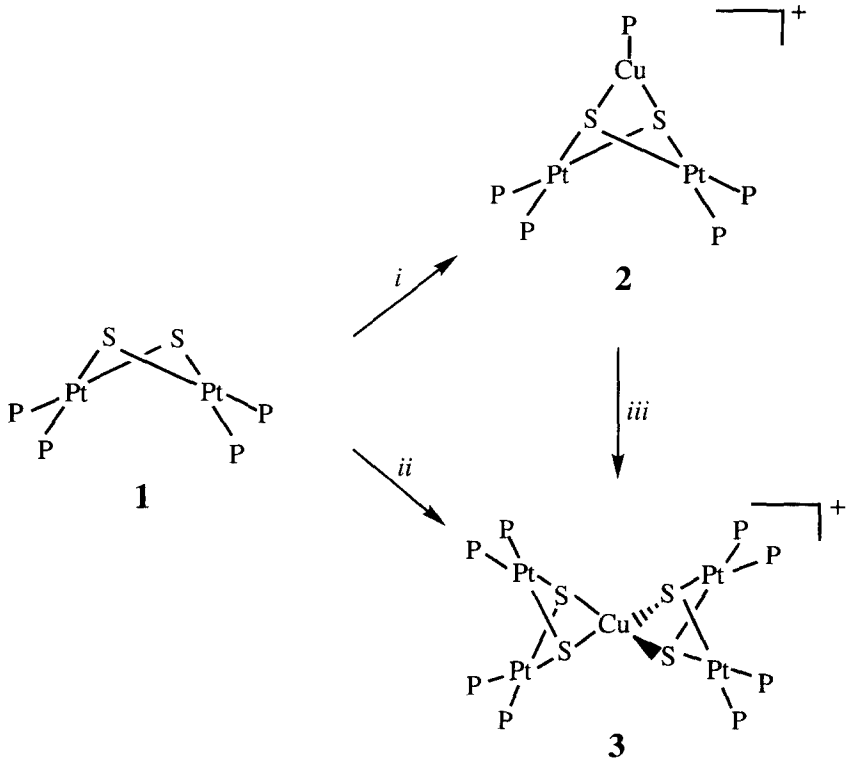
Table 1. Summary of crystal data collection and refinement parameters

Chemical formula	$C_{90}H_{75}CuF_6P_6Pt_2S_2$
Formula weight	1974
Crystal system	Orthorhombic
Lattice parameters	
a (Å)	14.261(3)
b (Å)	18.878(5)
c (Å)	29.831(8)
V (Å^3)	8031(4)
Space group	$P2_12_12_1$
Z	4
D_{calc} (g cm^{-3})	1.633
μ (mm^{-1})	3.969
θ range for data collection (°)	1.58 to 25.05
$h\ k\ l$ range	0 to 16, 0 to 22 and 0 to 35
No. of unique data	7794
No. of observations [$I > 2\sigma(I)$]	5909
No. variables	966
Residuals: R, R_w	0.0555, 0.1106
Goodness of fit: S	1.186
$(\Delta/\sigma)_{max}$	0.0016
$(\Delta\rho)_{max}$, $(\Delta\rho)_{min}$ (e Å^{-3})	1.345, −1.002

Other bonding features of **2b** are comparable to those found in the other heterometallics except that the non-bonding distances of Cu···Pt is unexpectedly short (av. 2.869(2) Å). This distance is significantly shorter than the Co—Pt distances (3.066(4) Å) in the related $[CoPt_2Cl_2(PPh_3)_4(\mu_3\text{-}S)_2]$ [5] although the atomic size of Co (1.28 Å) and Cu (1.3 Å) are similar [16]. The shorter Cu···Pt separation is especially peculiar when one considers that the oxidization state of Cu^I is lower than that of Co^{II}. Other similar aggregates invariably show typical non-bonding M···Pt separations, e.g. Ag···Pt distances in $[Ag_2\{Pt_2(PPh_3)_4(\mu_3\text{-}S)_2\}_2][PF_6]_2$ [10] range from 3.450(3) to 3.905(3) Å. Nevertheless, with a triangular core comprising 16-

Table 2. Selected bond lengths (Å) for $[CuPt_2(PPh_3)_5(\mu_3\text{-}S)_2]PF_6$, **2b**

Cu(3)—P(3)	2.174(5)	Cu(3)—S(1)	2.303(5)
Cu(3)—S(2)	2.269(5)	Pt(1)—P(1A)	2.305(5)
Pt(1)—P(1B)	2.284(5)	Pt(2)—P(2A)	2.305(5)
Pt(2)—P(2B)	2.288(5)	Pt(1)—S(1)	2.342(5)
Pt(1)—S(2)	2.366(5)	Pt(2)—S(1)	2.366(5)
Pt(2)—S(2)	2.350(5)	Pt(1)···Cu(3)	2.875(2)
Pt(2)···Cu(3)	2.864(2)		



Scheme 1. Addition reaction of $Pt_2(PPh_3)_4(\mu\text{-}S)_2$ with Cu^I. (*i*) $Cu(NO_3)(PPh_3)_2$ (1 : 1 molar ratio to **1**); (*ii*) $[Cu(CH_3CN)_4]PF_6$ (1 : 2 molar ratio to **1**); (*iii*) **1**; P = PPh_3.

electron sq-planar Pt^{II} and trigonal-planar Cu^I, no Pt—Pt or Cu—Pt bond is envisaged.

Another peculiar feature is the large hinge angle of the $\{Pt_2S_2\}$ butterfly core along the S···S axis. This angle is a subject of our recent discussion; it shows a linear relationship with the atomic radii of the heteroatoms [11]. With Cu (At. Rad. 1.28, Cov. Rad. 1.38 Å) and Ga (At. Rad. 1.4, Cov. Rad. 1.26 Å) [17] being similar in size, it is surprising that the $\{Pt_2S_2\}$ hinge angle in **2b** (137.5(5)°) is significantly larger than that in $[GaPt_2Cl_2(PPh_3)_4(\mu_3\text{-}S)_2]^+$ (123.1(2)°) [6].

In an attempt to gain insight into some structural aspects of the molecule, notably the short Cu···Pt distances and the unexpectedly large $\{Pt_2S_2\}$ dihedral angle, we have performed Fenske–Hall MO calculations [18]. The calculated overlap populations indicate no bonds between the Cu and Pt atoms. It may thus be inferred that the short distances are due to the Cu—S bonds and the large dihedral angle.

Why then is the dihedral angle larger than expected, and does it not follow the trend of the angle increasing with the size of the heterometal? A clue can be found in the high percentage of sulfur p_z orbital (see details of alignment [19]) used in Cu—S bonding (78.0 and 75.6% compared to 54.6 and 56.3% for the $GaCl_2^+$ adduct [6], in which the M—S bond lengths are about the same, 2.296 and 2.292 Å; in both cases the dihedral angle was set at 123.1°). It has been shown [11] that the percentage of sulfur p_z in the lone pair orbital used to interact with the heterometal increases with the size of the dihedral angle. Thus, the large dihedral angle in **2b** is consistent with the higher percentage of sulfur p_z needed to bind to Cu.

The question then naturally arises as to possible reasons for the latter. A compelling reason is that unlike all the other compounds considered in the past, Cu has a ligand coordinated along the z-axis.* Good σ- and moderate π-interaction between Cu and PPh_3, along with the fact that the S—Cu—S angle is extremely small for a trigonal planar geometry, suggest that the Cu p_z orbital is more involved in bonding to PPh_3 (Table 4), at the expense of the Cu—S bonds, which could also use some interaction involving Cu p_z. (This may account for the weak Cu—S bonds). The Cu p_y orbital, on the other hand, is relatively available; from geometrical considerations, this orbital alone interacts best with the sulfur p_z orbitals, hence the increased use of the latter. In support of the foregoing argument, the ratio of the partial heterometal p_z/p_y to sulfur overlap populations is 0.52 on average for **2b** (dihedral angle adjusted to 123.1°), while for the Ga compound the ratio is 0.62.

Another relevant observation is that, in all the compounds considered in the past (including a $CoCl_2$ adduct [5]), the heterometal uses its d_{yz} orbitals, in

* Also, PPh_3 is neutral and not negative like the ligands in the other compounds; at this point the authors are unsure about the effects of ligand charge.

Table 3. Selected bond angles (°) for $[CuPt_2(PPh_3)_5(\mu_3\text{-}S)_2]PF_6$, **2b**

P(3)—Cu(3)—S(1)	135.7(2)	P(3)—Cu(3)—S(2)	139.4(4)
S(2)—Cu(3)—S(1)	84.6(2)	Cu(3)—S(1)—Pt(1)	76.5(2)
Cu(3)—S(1)—Pt(2)	75.6(2)	Cu(3)—S(2)—Pt(1)	76.6(2)
Cu(3)—S(2)—Pt(2)	76.6(2)	P(1A)—Pt(1)—S(1)	169.1(2)
P(1A)—Pt(1)—S(2)	87.4(2)	P(1B)—Pt(1)—S(1)	90.8(2)
P(1B)—Pt(1)—S(2)	172.1(2)	P(2A)—Pt(2)—S(1)	86.3(2)
P(2A)—Pt(2)—S(2)	166.6(2)	P(2B)—Pt(2)—S(1)	171.5(2)
P(2B)—Pt(2)—S(2)	90.2(2)	S(1)—Pt(1)—S(2)	81.6(2)
S(2)—Pt(2)—S(1)	81.5(2)	P(1B)—Pt(1)—P(1A)	100.1(2)
P(2B)—Pt(2)—P(2A)	101.9(2)	Pt(1)—S(1)—Pt(2)	89.9(2)
Pt(2)—S(2)—Pt(1)	89.7(2)		

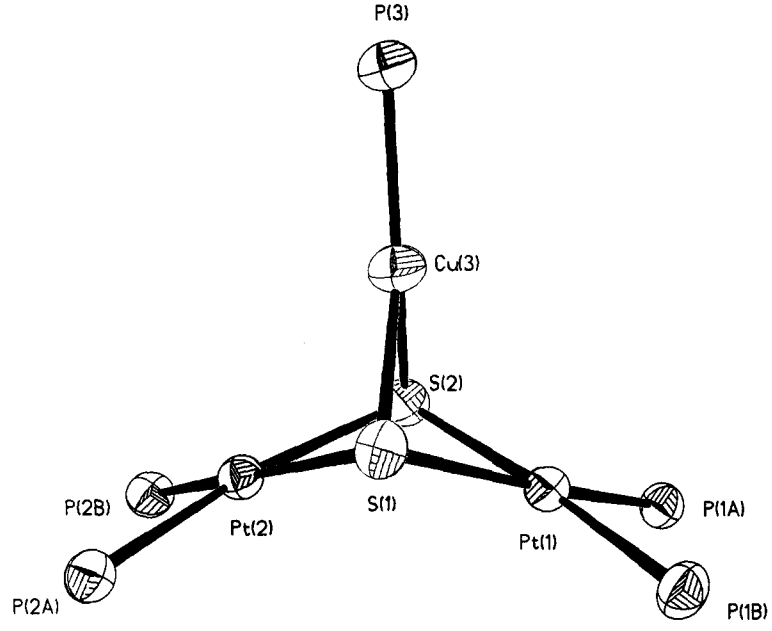


Fig. 1. ORTEP plot of the structure of the molecular cation in $[CuPt_2(PPh_3)_5(\mu_3\text{-}S)_2]PF_6$, **2b** (phenyl groups omitted for clarity).

addition to its *s* and *p* orbitals, to bind to sulfur. Note that this is possible for d^7 Co^{II} since the d_{yz} orbital is less than half-filled. (The d_{xz} orbital, which is Co—Cl antibonding and mixes a little with the d_{yz} orbital, is empty.) In contrast, all the *d* orbitals in Cu^I are filled, and thus cannot be used for σ-bonding. Use of the d_{yz} orbital may result in a high percentage of sulfur p_y.

Recent theoretical work [20] by Capdevila *et al.* on $Pt_2(PPh_3)_4(\mu\text{-}S)_2$ and its alkyl adducts demonstrated that the energetic cost of varying the dihedral angle is relatively small. From our experience in dealing with adducts of $Pt_2(PPh_3)_4(\mu\text{-}S)_2$ in which the heterometal caps the two sulfur ligands, we have found quite generally [21] that as the dihedral angle decreases, the Pt—S overlap populations decrease, whilst those between the heterometal and sulfur increase. This observation, which holds true for this work (see Cu—S overlap population in Table 4), could account for the shorter Pt—S bonds in **2b** than in the $GaCl_2^+$ adduct (average 2.388 Å). It also implies that the Cu—S bonds are relatively weak, thus offering an additional explanation for the easy decomposition of **2** in solution.

In a $BiCl_3$ adduct studied earlier, it was found that the Bi—Cl bonds became stronger as the dihedral angle increases* [21]. In contrast, the Cu—P overlap population decreases (see Table 4); this is partly due to the increased use of the Cu p_z orbital to bind to the S p_y orbitals. The latter are made more available

* We have not calculated this for the other compounds.

Table 4. Relevant overlap populations for $[CuPt_2(PPh_3)_5(\mu_3\text{-}S)_2]^+$, with $\{Pt_2S_2\}$ dihedral angle at 137.5° (experimental value) and 123.1° (angle for $[GaPt_2Cl_2(PPh_3)_4(\mu_3\text{-}S)_2]^+$ in which the M—S bond lengths are about the same as in the present case). Calculations for an intermediate value are consistent with the trend

Dihedral angle	137.5	123.1
Cu—P	0.3931	0.3912
Cu p_z—P	0.2394	0.2379
Cu—S	0.1760	0.1833
	0.2014	0.2078
Cu—S p_y	0.0381	0.0432
	0.0409	0.0458
Cu—S p_z	0.1429	0.1429
	0.1579	0.157
Cu p_y—S	0.0732	0.0733
	0.0746	0.0736
Cu p_z—S	0.0302	0.0334
	0.0397	0.0430

because of less utilization in binding to Pt when the dihedral angle decreases. It is likely that the opening up of the dihedral angle is due to an effort to optimize the Cu—P interaction, which, from Table 4, appears to be significantly stronger than the Cu—S bonds.

EXPERIMENTAL

Materials and Methods

All reactions were performed in air. All solvents were analytical grade and were used without further purification. $Pt_2(PPh_3)_4(\mu\text{-}S)_2$ [22], $Cu(NO_3)(PPh_3)_2$ [23] and $[Cu(CH_3CN)_4]PF_6$ [24] were synthesized according to literature methods. Elemental analyses were conducted in the Microanalytical Laboratory in our department. $^{31}P\text{-}\{^1H\}$ NMR spectra were run on a Bruker ACF 300 spectrometer with H_3PO_4 as external reference at 298 K. Infrared spectra were taken in KBr disc on a Perkin-Elmer 1600 FT-IR spectrophotometer. Conductivity was measured by using a STEM Conductivity 1000 meter.

Synthesis of $[CuPt_2(PPh_3)_5(\mu_3\text{-}S)_2]X$ (X = NO_3^-, **2a**, PF_6^-, **2b**)

$Pt_2(PPh_3)_4(\mu\text{-}S)_2$ (0.15 g, 0.1 mmol) was added to the solution of $Cu(NO_3)(PPh_3)_2$ (0.066 g, 0.1 mmol) in MeOH (10 cm^3). The orange suspension was stirred for a few min to give a clear orange solution. After stirring further for 30 min to ensure complete reaction, the solution was filtered and the filtrate was evaporated to dryness *in vacuo* to obtain a crude orange product. This product was purified by recrystallization from CH_2Cl_2/hexane to yield **2a** (0.151 g, 70%). (Found: C 56.2; H 4.0; Cu 3.2; N 0.8; P 7.7; Pt 19.1; S 3.6. Calc. for $C_{90}H_{75}CuNO_3P_5Pt_2S_2$: C 57.2; H 4.0; Cu 3.4; N 0.7; P 8.2; Pt 20.6; S 3.4%). $\nu(NO_3^-)$ 1384s cm^{-1}. Λ_m (10^{-3} M, MeOH) 76 ohm^{-1} cm^2 mol^{-1}. δp ($CDCl_3$) 20.7 (4P, t, ^1J(P—Pt) = 3104 Hz, ^3J(P—Pt) = 22 Hz) and 1.9 (1P, s).

$[CuPt_2(PPh_3)_5(\mu_3\text{-}S)_2]PF_6$, **2b** was prepared by treating **2a** with NH_4PF_6 in MeOH. (Found: C 54.8; H 3.7; P 10.2; S 3.3. Calc. for $C_{90}H_{75}CuF_6P_6Pt_2S_2$: C 54.8; H 3.8; P 9.5; S 3.2%). $\nu(PF_6^-)$ 839 vs cm^{-1}.

Synthesis of $[Cu\{Pt_2(PPh_3)_4(\mu_3\text{-}S)_2\}_2]PF_6$, **3**

To a suspension of **1** (0.15 g, 0.1 mmol) in CH_3CN (20 cm^3) was added with stirring $[Cu(CH_3CN)_4]PF_6$ (0.019 g, 0.05 mmol). The orange suspension turned dark-blue immediately. After the mixture was stirred for 10 min, the suspension dissolved completely to result in a red-brown solution. Further stirring for 2 h was followed by filtration, after which the filtrate was concentrated *in vacuo* to *ca* 10 cm^3. Addition of Et_2O gave rise to a red–brown precipitate which was isolated and purified by recrystallization from CH_2Cl_2/hexane to yield **3** (0.101 g, 60%). (Found: C 53.4; H 3.7; Cu 1.9; P 8.4; Pt, 21.5; S 4.2. Calc. for $C_{144}H_{120}CuF_6P_9Pt_4S_4$: C 53.8; H 3.7; Cu 2.0; P 8.7; Pt, 24.3; S 4.0%). δp ($CDCl_3$) 5.81 (t, ^1J(P—Pt) = 4023 Hz), $\nu(PF_6^-)$ 839 vs cm^{-1}.

Complex **3** could be similarly obtained by stirring **1** (0.075 g, 0.05 mmol) with **2b** (0.098 g, 0.05 mmol) in THF (15 cm^3) for 1 h. The resultant clear red-brown solution was similarly treated to obtain **3** (0.070 g, 41%).

X-ray crystallography of complex **2b**

Orange single crystals of **2b** were obtained by slow evaporation of a sample solution in CH_2Cl_2/MeOH (1:3) in air. A crystal with approximate dimensions of 0.13 × 0.20 × 0.32 mm was used for structure determination. Data collection was performed at 293(2) K with Mo-K_α radiation (λ = 0.71073 Å) on a Siemens R3m/v diffractometer equipped with a graphite monochromator and ω-2θ scan mode. Unit cell parameters were determined using 20 reflections obtained from a random search routine. Two intensity standards were measured every 98 reflections; no significant variation of intensity was observed. The data were corrected for Lorentz and polarization effects; semi-empirical absorption correction was also applied.

The structure was solved by direct methods and difference Fourier maps. Full-matrix least-squares refinement was carried out with anisotropic temperature factor for all non-hydrogen atoms. Hydrogen atoms were placed on calculated positions (C—H 0.96 Å) and assigned isotropic thermal parameters riding on their parent atoms. Initial calculations were carried out on a PC using SHELXTL PC software package; SHELXL-93 [25] was used for the final refinement.

Acknowledgements—This work was supported by the National University of Singapore (NUS) (RP 950695). H. L. thanks NUS for the award of a research studentship. A. L. T. is grateful to the National Science and Technology Board for a postdoctoral fellowship award, and the National Supercomputing Research Centre for use of its computing facilities and software.

REFERENCES

1. (a) C. E. Briant, D. I. Gilmour, M. A. Luke and D. M. P. Mingos, *J. Chem. Soc., Dalton Trans.* 1985, 851; (b) D. I. Gilmour, M. A. Luke and D. M. P. Mingos, *J. Chem. Soc., Dalton Trans.* 1987, 335.
2. B. H. Aw, K. K. Looh, H. S. O. Chan, K. L. Tan and T. S. A. Hor, *J. Chem. Soc., Dalton Trans* 1994, 3177.
3. M. Zhou, Y. Xu, C.-F. Lam, L.-L. Koh, K. F. Mok, P.-H. Leung and T. S. A. Hor, *Inorg. Chem.* 1993, **32,** 4660.
4. M. Zhou, Y. Xu, L.-L. Koh, K. F. Mok, P.-H. Leung and T. S. A. Hor, *Inorg. Chem.* 1993, **32,** 1875.
5. H. Liu, A. L. Tan, K. F. Mok and T. S. A. Hor, *J. Chem. Soc., Dalton Trans* 1996, in press.
6. M. Zhou, Y. Xu, C.-F. Lam, P.-H. Leung, L.-L. Koh, K. F. Mok and T. S. A. Hor, *Inorg Chem.* 1994, **33,** 1572.
7. M. Zhou, P.-H. Leung, K. F. Mok and T. S. A. Hor, *Polyhedron* 1996, **15,** 1737.
8. W. Bos, J. J. Bour, P. P. J. Schlebos, P. Hageman, W. P. Bosman, J. M. M. Smits, J. A. C. van Wietmarschen and P. T. Beurskens, *Inorg. Chim. Acta* 1986, **119,** 141.
9. C. E. Briant, T. S. A. Hor, N. D. Howells and D. M. P. Mingos, *J. Chem. Soc., Chem. Commun.* 1983, 1118.
10. C. E. Briant, T. S. A. Hor, N. D. Howells and D. M. P. Mingos, *J. Organomet. Chem.* 1983, **256,** C15.
11. A. L. Tan, M. L. Chiew and T. S. A. Hor, *J. Molec. Struct. (TheoChem.)*, 1996, in press.
12. T. S. A. Hor, D. Phil. Thesis. University of Oxford (1983).
13. J. M. Manoli, C. Potvin and F. Secheresse, *J. Chem. Soc., Chem. Commun.* 1982, 1159.
14. J. A. Tiethof, J. K. Stalick and D. W. Meek, *Inorg. Chem.* 1973, **12,** 1170.
15. T.-L. Sheng, S.-W. Du and X.-T. Wu, *J Cluster Sci.* 1993, **4,** 89.
16. L. Pauling, *The Nature of the Chemical Bond*, 3rd edn p. 403. Cornell University Press, Ithaca, N.Y. (1960).
17. A. J. Gordon and R. A. Ford, The Chemist Companion. pp. 82–83. Wiley, N.Y. (1972).
18. M. B. Hall and R. F. Fenske, *Inorg. Chem.* 1972, **11,** 768.
19. *Details of calculations*— The models of the molecules used for the calculations are based on their crystal structures. All phenyl rings on phosphines were replaced by hydrogen atoms. The molecule was aligned such that the S···S line is along the *yz*-axis and CuS_2 in the *y*-plane such that the Pt···Pt line is approximately parallel to the *x*-axis. Calculations were performed using the self-consistent Fenske–Hall approximate molecular orbital method. The basis functions were obtained by fitting the results of $X\alpha$ (Herman–Skillman) [26] calculations to Slater orbital [27], double-ζ functions were used for transition metal *d* orbital and main group *p* orbital. An exponent of 1.2 was used for hydrogen. Mulliken populations analyses [28] were employed to calculate atomic charges and overlap populations. All calculations were performed on a SGI Onyx computer using MDSI Cerius2 software.
20. M. Capdevila, W. Clegg, P. González-Duarte, A. Jarid and A. Lledós, *Inorg. Chem.* 1996, **35,** 490.
21. M. Zhou, Y. Xu, C.-F. Lam, P.-H. Leung, K. F. Mok, A. L. Tan, L.-L. Koh and T. S. A. Hor, unpublished works.
22. R. Ugo, G. La Monica, S. Cenini, A. Serge and F. Conti, *J. Chem. Soc., A* 1971, 522.
23. H. J. Gysling and G. J. Kubas, *Inorg. Synth.* 1979, **19,** 93.
24. G. J. Kubas, B. Monzyk and L. Crumbliss, *Inorg. Synth.* 1979, **19,** 90.
25. G. M. Sheldrick, *SHELXL*-93, *Program for Crystal Structure Refinement*. University of Göttingen, Germany (1993).
26. F. Herman and S. Skillman, *Atomic Structure Calculations*. Prentice-Hall, Englewood Cliffs, N.J. (1963).
27. B. E. Bursten, R. J. Jensen and R. F. Fenske, *J. Chem. Phys.* 1978, **68,** 3320.
28. R. S. Mulliken, *J. Chem. Phys.* 1955, **23,** 1841.

Pergamon

PII: S0277-5387(96)00309-9

Polyhedron Vol. 16, No. 3, pp. 383–392, 1997
Copyright © 1996 Elsevier Science Ltd
Printed in Great Britain. All rights reserved
0277-5387/97 $17.00+0.00

Electronic and bonding properties of mixed-ligand copper(II) complexes of *N*-(2-picolyl)picolinamide (pmpa). X-ray crystal structures of [Cu(pmpa)(4-methylimidazole)(H_2O)](H_2O)(ClO_4) and [Cu(pmpa)(4-methylpyridine)(H_2O)](H_2O)(ClO_4)

Chiou-Yuh Wu and Chan-Cheng Su*

Department of Chemistry, National Taiwan Normal University, Taipei 11718, Taiwan, R.O.C.

(Received 24 May 1996; accepted 19 June 1996)

Abstract—Mixed-ligand *N*-(2-picolyl)picolinamidocopper(II) complexes, [Cu(pmpa)(L)(X)·nH_2O] [pmpa = *N*-(2-picolyl)picolinamide anion; L = imidazole (n = 0, 1 or 2), *N*-methylimidazole (n = 0 or 1), 4-methylimidazole (4MImH) (n = 0 or 2), pyridine (n = 0), 2-methylpyridine (n = 0), 3-methylpyridine (n = 0), 4-methylpyridine (4Mpy) (n = 2), and NH_3 (n = 2); X = ClO_4^- or BF_4^-], have been synthesized and characterized by elemental analyses, and electronic, vibrational, and EPR spectroscopic measurements. Molecular structures of [Cu(pmpa)(4MImH)(H_2O)](H_2O)(ClO_4) (**1**) and [Cu(pmpa)(4Mpy)(H_2O)](H_2O)(ClO_4) (**2**) have been determined by X-ray diffraction methods. Both complexes are square pyramidal with the pmpa and the heterocyclic unidentate ligands forming the basal plane and a H_2O molecule on the apical position. The dihedral angles of the heterocyclic unidentate nucleus and the CuN_4 basal plane are 79.3° for **1** and 74.5° for **2**. The structures of other pmpa complexes are suggested to be square pyramidal or square planar based on their spectroscopic data. The sequence of d orbitals is assigned as $d_{x^2-y^2} \gg d_{z^2} > d_{yz} > d_{xy} > d_{xz}$ for the square pyramidal complexes and $d_{x^2-y^2} \gg d_{yz} > d_{xy} > d_{xz} > d_{z^2}$ for the square planar complexes. The significant rise in energy of the d_{yz} orbital suggests that the central amido of the pmpa ligand is a strong π-donor. Copyright © 1996 Elsevier Science Ltd

Keywords: *N*-(2-picolyl)picolinamidocopper(II) complexes; X-ray structures; visible spectra; EPR spectra; bonding; Gaussian analysis.

In the course of our studies on copper(II)—N bonding properties in mixed-ligand copper(II) complexes containing a tridentate and a heterocyclic unidentate ligand, we have found that the structures of these complexes and the orientations of the heterocyclic nuclei vary depending on the bonding abilities of the tridentate ligands. Thus, the diethylenetriamine (dien) complex, [Cu(dien)(4-methylimidazole)(ClO_4)$_2$] [1], has an elongated octahedral structure with the heterocyclic ring of the unidentate ligand tilted by 41.2° from the CuN_4 coordination plane, whereas the elongated octahedral terpyridine (terpy) complex, [Cu(terpy)(4-methylimidazole)(H_2O)(BF_4)](BF_4) [2], and the square pyramidal glycylglycinato (glygly) complex, [Cu(glygly)(acetylhistamine)] [3], have the corresponding imidazole nucleus lying nearly perpendicular and parallel, respectively, to the [Cu(tridentate)(heterocyclic unidentate)] coordination plane. The variation in orientation of the unidentate heterocyclic nuclei has been ascribed to the π-bonding abilities of the tridentate ligands, specifically, the central donating moieties *trans* to the unidentate ligand. Based on the Gaussian resolved d–d spectra, the central pyridine of terpyridine is suggested a π-acceptor and the central amido of glycylglycinate is a π-donor.

* Author to whom correspondence should be addressed.

Recently, we have found that the dianionic dipicolinato (dipic) complex, [Cu(dipic)(*N*-methylimidazole)] [4], has a square planar structure with the imidazole ring coplanar with the coordination plane. The dipicolinate has been suggested to be a π-donor. Since pyridine type ligands are potential π-acceptors [5, 6], the drastic change in the π-bonding capability has been attributed to the ionic bonding in the dipicolinato complex.

Because of the importance of peptide complexes in biological systems, studies have been focused on the bonding properties of the anionic amido moiety to reveal the origin of its π-donating ability. Herein, we report the structures and spectroscopic properties of mixed-ligand *N*-(2-picolyl)picolinamidocopper(II) complexes and elucidate their electronic structures and bonding properties.

EXPERIMENTAL

Materials and preparations

Picolinic acid (Aldrich), 2-(aminomethyl)pyridine (Aldrich), *N*-methylimidazole (Aldrich), 4-methylimidazole (Merck), imidazole (Merck), 2-methylpyridine (TCI), 3-methylpyridine (TCI), 4-methylpyridine (TCI), pyridine (Merck), $POCl_3$ (Merck), $Cu(ClO_4)_2 \cdot 6H_2O$ (Aldrich), and organic solvents were used as received. $Cu(BF_4)_2 \cdot 6H_2O$ was prepared from CuO and HBF_4.

N-(2-picolyl)picolinamide [7] was prepared as follows: to an anhydrous dichloromethane (100 cm^3) solution of picolinic acid (6.16 g, 0.05 mole), triethylamine (5.05 g, 0.05 mole) and 2-(aminomethyl)pyridine (5.40 g, 0.05 mole), phosphorus oxychloride (7.67 g, 0.05 mole) in dichloromethane (40 cm^3) was added dropwise with constant stirring at 0°C. An additional amount of triethylamine (10.1 g, 0.1 mole) was added. After reaction at 0°C for 1.5 h and at room temperature for an additional 1 h, the contents were neutralized with aqueous sodium bicarbonate. The organic layer was separated and evaporated to give a viscous residue. Yield, 7.65 g (72%).

The pmpa complexes were prepared by the following general procedure: To a CH_3OH solution (10 cm^3) of $Cu(ClO_4)_2 \cdot 6H_2O$ (0.37 g, 1 mmol) and the unidentate ligand (2 mmol), *N*-(2-picolyl)picolinamide (0.21 g, 1 mmol) in CH_3OH (5 cm^3) was added. After reaction for 2 h, the solution was stored overnight to yield crystalline products, which were filtered and washed with ether and dried *in vacuo* over P_4O_{10}.

[Cu(pmpa)(py)(ClO_4)]. Purple. Yield 82%. M.p. 210°C (dec). IR (cm^{-1}): ν (amido) 1640 s, 1609 s, 1601 s; ν (ClO_4) 1094 vs, 932 m, 623 s; δ (py) 432 m; ν [Cu—N(pmpa)] 359 m, 284 m, 255 m; ν [Cu—N(py)] 318 m. Found: C, 44.2; H, 3.3; N, 11.9. Calc. for $C_{17}H_{15}N_4O_5ClCu$: C, 44.9; H, 3.3; N, 11.3%. Molar conductivity: 97 S cm^2 mol^{-1} in CH_3OH; 137 S cm^2 mol^{-1} in CH_3CN.

[Cu(pmpa)(2Mpy)(ClO_4)]. Blue. Yield 44%. M.p. 310°C(dec). IR (cm^{-1}): ν (amido) 1628 s, 1613 s, 1599 s; ν (ClO_4) 1092 vs, 623 s, δ (py) 430 mw; ν [Cu—N(pmpa)] 351 m, 280 m, 249 m; ν [Cu—N(py)] 320 m. Found: C, 45.5; H, 3.9; N, 11.5. Calc. for $C_{18}H_{17}N_4O_5ClCu$: C,46.2; H, 3.7; N, 12.0%. Molar conductivity: 80 S cm^2 mol^{-1} in CH_3OH; 120 S cm^2 mol^{-1} in CH_3CN.

[Cu(pmpa)(3Mpy)(ClO_4)]. Blue. Yield 92%. M.p. 188°C(dec). IR (cm^{-1}): ν (amido) 1636 s, 1611 s, 1599 s; ν (ClO_4) 1094 vs, 930 m, 621 s; δ (py) 415 m; ν [Cu—N(pmpa)] 359 m, 284 m, 245 ms; ν [Cu—N(py)] 320 m. Found: C, 45.8; H, 3.6; N, 11.8. Calc. for $C_{18}N_{17}N_4O_5ClCu$: C, 46.2; H, 3.7; N, 12.0%. Molar conductivity: 105 S cm^2 mol^{-1} in CH_3OH; 138 S cm^2 mol^{-1} in CH_3CN.

[Cu(pmpa)(4Mpy)(ClO_4)(H_2O)$_2$]. The blue tetragonal lamellar crystals obtained were suitable for X-ray structure determination. Yield. 79%. M.p. 200°C(dec). IR (cm^{-1}): ν (O—H) 3580 s, 3488 s, 3260 s, br; ν (amido) 1636 s, 1599 s; ν (ClO_4) 1090 vs, 623 s; δ (py) 455 mw; ν [Cu—N(pmpa)] 353 m, 284 m, 259 m; ν [Cu—N(py)] 324 m. Found: C, 42.6; H, 4.1; N, 10.9. Calc. for $C_{18}H_{21}N_4O_7ClCu$: C, 42.9; H, 4.2; N, 11.1%. Molar conductivity: 90 S cm^2 mol^{-1} in CH_3OH; 127 S cm^2 mol^{-1} in CH_3CN.

[Cu(pmpa)(ImH)(ClO_4)]. Purple-blue. Yield 68%. M.p. 198°C(dec). IR (cm^{-1}): ν (N—H) 3290 m; ν (amido) 1622 s, 1587 s; ν (ClO_4) 1110 vs, 931 m, 625 s; ν [Cu—N(pmpa)] 363 m, 287 m, 249 m; ν [Cu—N(ImH)] 324 m. Found: C, 40.2; H, 3.1; N, 15.4. Calc. for $C_{15}H_{14}N_5O_5ClCu$: C, 40.6; H, 3.2; N, 15.8%. The filtrate was stored for 3 days to yield deep-blue [Cu(pmpa)(ImH)(ClO_4)(H_2O)]. Yield 7%. M.p. 210°C(dec). IR (cm^{-1}): ν (O—H) 3500 ms; ν [N—H(ImH)] 3250 s, br; ν (amido) 1630 s, 1601 s; ν (ClO_4) 1128 vs, 623 s; ν [Cu—N(pmpa)] 355 m, 280 m, 255 m; ν [Cu—N(ImH)] 324 m. Found: C, 39.0; H, 3.4; N, 15.0; Calc. for $C_{15}H_{16}N_5O_6ClCu$: C, 39.1; H, 3.5; N, 15.2%. Molar conductivity: 80 S cm^2 mol^{-1} in CH_3OH; 132 S cm^2 mol^{-1} in CH_3CN.

[Cu(pmpa)(NMIm)(ClO_4)]. Purple-blue. Yield 67%. M.p. 240°C(dec). IR (cm^{-1}): ν (amido) 1631 s, 1601 s; ν (ClO_4) 1109 vs, 932 mw, 623 s; ν [Cu—N(pmpa)] 359 m, 287 m, 249 m; ν [Cu—N(NMIm)] 320 m. Found: C, 41.5; H, 3.4; N, 15.2. Calc. for $C_{16}H_{16}N_5O_5ClCu$: C, 42.0; H, 3.5; N, 15.3%. The filtrate was stored for 3 days to yield blue [Cu(pmpa)(NMIm)(ClO_4)(H_2O)]. IR (cm^{-1}): ν (O—H) 3320 m, br; ν (amido) 1632s, 1599 s; ν (ClO_4) 1192 vs, 1063 vs, 932 w, 621 s; ν [Cu—N(pmpa)] 361 m, 287 m, 260 m; ν [Cu—N(NMIm)] 320 m. Found: C, 40.1; H, 3.6; N, 15.4. Calc. for $C_{16}H_{18}N_5O_6ClCu$: C, 40.4; H, 3.8; N, 14.7%. Molar conductivity: 87 S cm^2 mol^{-1} in CH_3OH; 118 S cm^2 mol^{-1} in CH_3CN.

[Cu(pmpa)(4MImH)(ClO_4)]. Yield 67%. M.p. 196°C(dec). IR (cm^{-1}): ν (N—H) 3300 m, br; ν (amido) 1626 s, 1612 s, 1599 s; ν (ClO_4) 1094 vs, 621 s; ν [Cu—N(pmpa)] 372 m, 282 m, 239 m; ν [Cu—N(4MImH)] 328 m. Found: C, 41.5; H, 3.5;

N, 15.2. Calc. for $C_{16}H_{16}N_5O_5ClCu$: C, 42.0; H, 3.5; N, 15.2%. The filtrate was stored for 3 days to yield the blue lamellar crystals [Cu(pmpa)(4MImH)(ClO_4)(H_2O)$_2$], which were suitable for X-ray structure determination. IR (cm^{-1}): ν (O—H) 3602 m, 3522 m; ν (N—H) 3289 ms, br; ν (amido) 1632 s, 1600 s; ν (ClO_4) 1109 s, 1075 s, 621 m; ν [Cu—N(pmpa)] 359 m, 283 m, 267 m; ν [Cu—N(4MImH)] 325 mw. Found: C, 39.0; H, 4.1; N, 14.2. Calc. for $C_{16}H_{20}N_5O_7ClCu$: C, 39.0; H, 3.9; N, 13.6%. Molar conductivity: 83 S cm^2 mol^{-1} in CH_3OH; 139 S cm^2 mol^{-1} in CH_3CN.

[Cu(pmpa)(NH_3)(ClO_4)(H_2O)$_2$]. Yield 11%. M.p. 288 C(dec). IR (cm^{-1}): ν (O—H+N—H) 3341 m, 3295 m, 3255 m, br, 3160 m, br; ν (amido) 1644 ms, 1612 ms, 1595 s; ν (ClO_4) 1085 vs, br, 931 w, 623; ν [Cu—N(pmpa)] 338 m, 272 m, 238 m; ν [Cu—N(NH_3)] 415 m. Found: C, 32.7; H, 3.2; N, 13.1. Calc. for $C_{12}H_{17}N_4O_7ClCu$: C, 33.7; H, 4.0; N, 13.1%. Molar conductivity: 85 S cm^2 mol^{-1} in CH_3OH; 163 S cm^2 mol^{-1} in CH_3CN.

[Cu(pmpa)(py)(BF_4)]. This purple-blue complex was prepared as described above, but by using $Cu(BF_4)_2 \cdot 6H_2O$. Yield 57%. M.p. 243°C(dec). IR (cm^{-1}): ν (amido) 1641 s, 1609 s, 1603 s; ν (BF_4) 1070 vs, br; δ (py) 432 s; ν [Cu—N(pmpa)] 359 m, 284 m, 255 m; ν [Cu—N(py)] 320 m. Found: C, 47.5; H, 3.4; N, 12.3. Calc. for $C_{17}H_{15}N_4OBF_4Cu$: C, 47.9; H, 3.5; N, 13.2%. Molar conductivity: 67 S cm^2 mol^{-1} in CH_3OH; 145 S cm^2 mol^{-1} in CH_3CN.

[Cu(pmpa)(ImH)(BF_4)(H_2O)$_2$]. Blue. Yield 86%. M.p. 198 C(dec). IR (cm^{-1}): ν (O—H) 3545 ms; ν (N—H) 3337 s, br; ν (amido) 1630 s, 1601 s; ν (BF_4) 1078 vs, br; ν [Cu—N(pmpa)] 355 m, 280 m, 255 m; ν [Cu—N(ImH)] 326 mw. Found: C, 38.7; H, 3.6; N, 15.0. Calc. for $C_{15}H_{18}N_5O_9BF_4Cu$: C, 38.6; H, 3.9; N, 15.0%. Molar conductivity: 109 S cm^2 mol^{-1} in CH_3OH; 175 S cm^2 mol^{-1} in CH_3CN.

Physical measurements

IR spectra were recorded as Nujol mulls or KBr pellets on a BIO-RAD FTS-40 FTIR spectrometer. GBC 914 and Hitachi U-3501 spectrophotometers were used for electronic spectra measurement. Solid samples were recorded as Nujol mulls on Whatman No. 1 filter paper. EPR spectra were obtained by using a Bruker ER 200D spectrometer and calibrated with DPPH ($g = 2.0037$). A VAX 3300 computer-controlled Enraf-Nonius CAD-4 diffractometer was used for crystal data collection. Elemental analyses were carried out by the microanalysis laboratories of Taiwan University, Taipei.

Structure determination and refinement

Details of crystal data and processing parameters are summarized in Table 1. Twenty-five independent reflections with $12.26 \leqslant 2\theta \leqslant 28.44°$ for **1** and $21.46 \leqslant 2\theta \leqslant 30.46$ for **2** were used for least-squares determination of the crystal systems and the cell constants. Diffractometer examination of the reciprocal lattice showed the space group to be $P\bar{1}$ for both complexes. Intensity data (ω-θ scan, $2\theta \leqslant 50$) were collected at 298 K for four octants of the sphere ($0 \leqslant h \leqslant 8$, $-12 \leqslant k \leqslant 12$, $-15 \leqslant l \leqslant 16$ for **1**; $0 \leqslant h \leqslant 8$, $-12 \leqslant k \leqslant 12$, $-15 \leqslant l \leqslant 15$ for **2**), and corrected for Lorentz and polarization effects, but not for absorption. Three standard reflections were monitored every 2 h and showed no signs of crystal deterioration. The structures were solved by direct methods using Personal SDP software incorporated SIR for **1** and SHELXS for **2** [8-10] and refined by full-matrix least-squares on F values. Scattering factors and anomalous dispersion correction terms were taken from the *International Tables for X-ray Crys-*

Table 1. Summary of crystal data and processing parameters for [Cu(pmpa)(4MImH)(H_2O)](H_2O)(ClO_4) (**1**) and [Cu(pmpa)(4Mpy)(H_2O)](H_2O)(ClO_4) (**2**)

	$C_{16}H_{20}N_5O_7ClCu$ (**1**)	$C_{18}H_{21}N_4O_7ClCu$ (**2**)
fw	493.36	504.38
Crystal size (mm)	$0.15 \times 0.28 \times 0.37$	$0.08 \times 0.35 \times 0.40$
Space group	$P\bar{1}$	$P\bar{1}$
a (Å); α ( )	7.536(1); 75.09(1)	7.704(1); 79.98(2)
b (Å); β ( )	10.269(1); 76.48(1)	10.457(4); 75.81(1)
c (Å); γ ( )	14.113(3); 88.45(1)	13.917(2); 87.33(2)
V (Å^3)	1025.7	1070.3
Z	2	2
D_{calc} (g cm^{-3})	1.597	1.565
μ (mm^{-1})	1.24	1.19
Radiation (λ, Å)	Mo-K_α (0.71073)	Mo-K_α (0.71073)
Independent reflection	3597[2461 $\geqslant 3.0\,\sigma(I)$]	3761[2738 $\geqslant 3.0\,\sigma(I)$]
Final R, R_w	0.056, 0.062	0.051, 0.055
Largest shift Δ/σ	<0.01	<0.01
Largest difference peak (e Å^{-3})	0.60	0.85

tallography [11]. The hydrogen atoms included in the refinement were located in succeeding difference Fourier syntheses after the non-hydrogen atoms were refined anisotropically. All calculations were done on a 80486/33 PC. Additional material deposited comprises structure factors, atomic coordinates, anisotropic thermal parameters, and a full list of bond lengths and angles.

RESULTS AND DISCUSSION

Description of structures

The molecular structures of the 4-methylimidazole complex **1** and the 4-methylpyridine complex **2** are shown in Figs 1 and 2, respectively. Selected bond lengths and angles are listed in Table 2. Their structures are very similar. The copper(II) ions are bound by the tridentate anionic pmpa and a unidentate N-donor ligand forming a basal plane and a H_2O on the z axis to complete a [4 + 1] elongated square pyramidal structure. The copper(II) ions are slightly above the CuN_4 plane in both complexes. The deviations from the least-squares plane through the CuN_4 atoms are N(1) −0.0029, N(2) −0.0557, N(3) −0.0044, N(4) −0.0554 and Cu 0.1184 Å for **1** and N(1) −0.0384, N(2) −0.0208, N(3) −0.0390, N(4) −0.0310 and Cu 0.1293 Å for **2**. Their Cu—N bond lengths of *ca* 2.0 Å for the two terminal pyridines of pmpa are comparable to the usual Cu—N(py) bond lengths [12–15], but the Cu—N(amido) distances of 1.910(4) Å for **1** and 1.904(4) Å for **2** are short. The bite angles of the pmpa ligand are *ca* 81°. The unidentate N-donor ligands of both complexes are bound somewhat tightly [1.960(4) Å for **1** and 1.986(4) Å for **2**] and are nearly perpendicular to the CuN_4 plane [dihedral angle 79.3° for **1** and 74.5° for **2**]. There are hydrogen bonds between the H_2O molecules, O(6)—O(7), 2.875 Å for **1** and 2.686 Å for **2**, and between the perchlorate and the imidazole ligand, N(5)—O(5) 2.955 Å, in complex **1**. The bond lengths and angles of the ligands are in the normal ranges. It is noteworthy that the amide C=O of 1.26 Å and C—N of 1.31 Å are the same as those observed in [Cu(glygly)(acetylhistamine)] (C=O, 1.257(7) Å; C—N, 1.310(7) Å) [3]. This is a good indication of π-delocalization through the N—C—O amide skeleton for these complexes. Moreover, the very short Cu—N(amido) distances in these three complexes strongly imply the analogy in their bonding modes. The dimensions of the perchlorate anions are also normal, but the thermal vibrations are large for the perchlorate in complex **2**.

Spectroscopic studies

The visible and EPR spectroscopic data for the pmpa copper(II) complexes are listed in Table 3. The complexes exhibiting a single broad band in their solid state mull spectra can be divided into two groups: one with the λ_{max} at 581 to 606 nm and the other at 554 to 574 nm. Both complexes **1** and **2** belong to the former group suggesting that the structures of these complexes are square pyramidal. The apical H_2O molecule

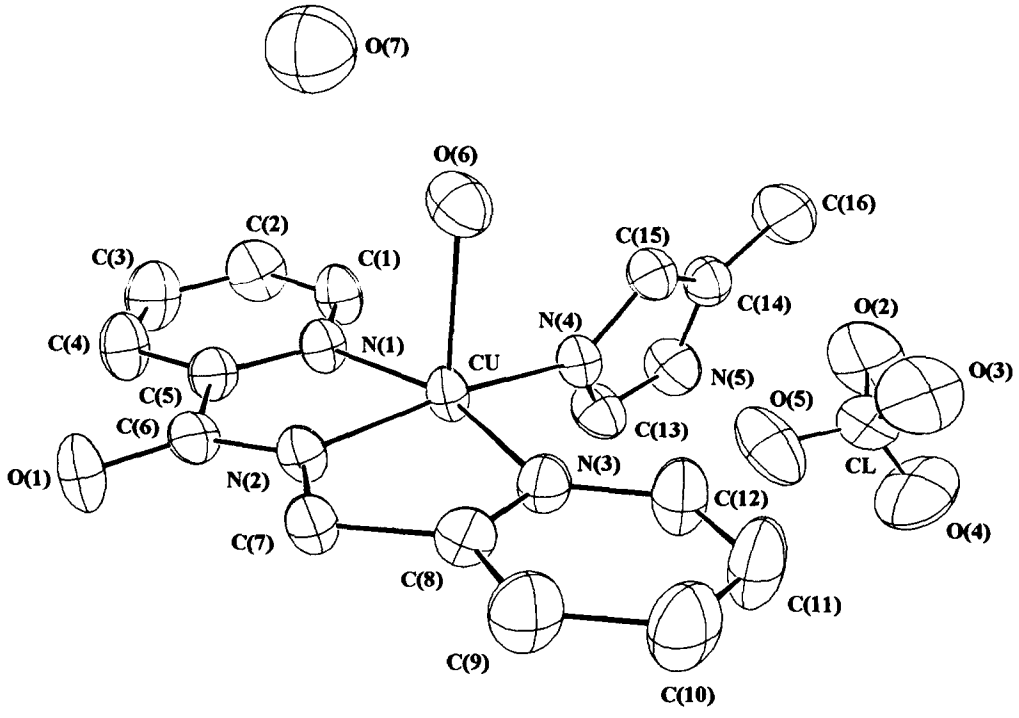


Fig. 1. Molecular structure of [Cu(pmpa)(4MImH)(H_2O)](H_2O)(ClO_4) (**1**) with numbering scheme.

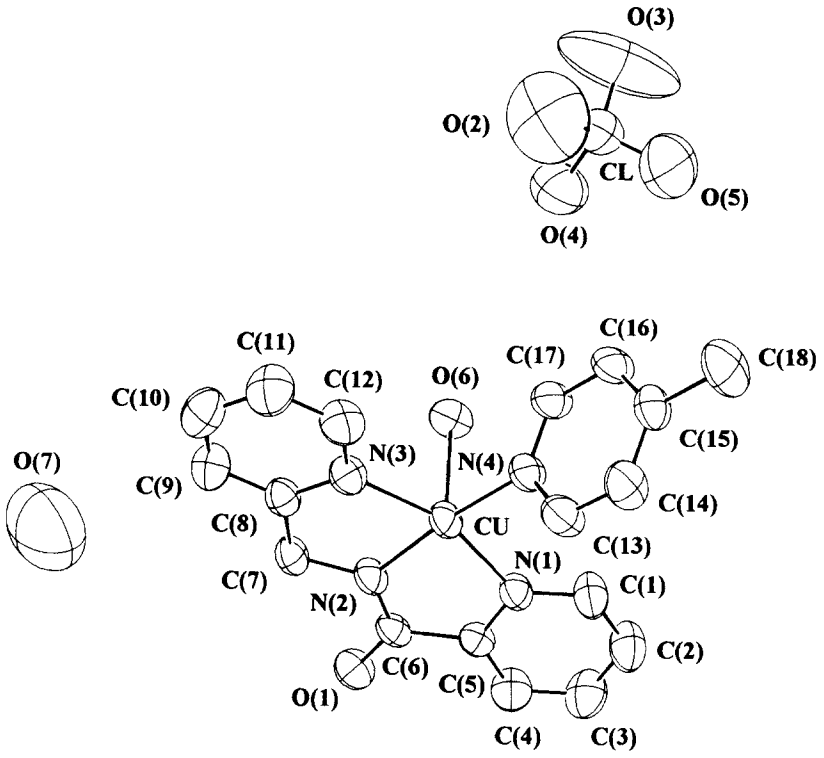


Fig. 2. Molecular structure of [Cu(pmpa)(4Mpy)(H_2O)](H_2O)(ClO_4) (**2**) with numbering scheme.

Table 2. Bond lengths (Å) and angles (°) for [Cu(pmpa)(4MImH)(H_2O)](H_2O)(ClO_4) (**1**) and [Cu(pmpa)(4Mpy)(H_2O)](H_2O)(ClO_4) (**2**)

[Cu(pmpa)(4MImH)(H_2O)](H_2O)(ClO_4) (**1**)			
Cu—N(1)	2.034(6)	Cu—N(2)	1.910(4)
Cu—N(3)	2.022(6)	Cu—N(4)	1.960(4)
Cu—O(6)	2.380(5)	C(6)—O(1)	1.257(7)
C(6)—N(2)	1.309(8)	C(7)—N(2)	1.440(8)
N(1)—Cu—N(2)	81.2(2)	N(1)—Cu—N(3)	161.4(2)
N(1)—Cu—N(4)	96.6(2)	N(2)—Cu—N(3)	81.0(2)
N(2)—Cu—N(4)	169.6(2)	N(3)—Cu—N(4)	100.0(2)
O(6)—Cu—N(1)	93.1(2)	O(6)—Cu—N(2)	97.3(2)
O(6)—Cu—N(3)	94.4(2)	O(6)—Cu—N(4)	93.0(2)
C(5)—C(6)—O(1)	120.7(6)	N(2)—C(6)—O(1)	127.1(6)
C(5)—C(6)—N(2)	112.2(5)	C(6)—N(2)—C(7)	121.4(4)
[Cu(pmpa)(4Mpy)(H_2O)](H_2O)(ClO_4) (**2**)			
Cu—N(1)	2.023(4)	Cu—N(2)	1.904(4)
Cu—N(3)	2.020(5)	Cu—N(4)	1.986(4)
Cu—O(6)	2.368(4)	C(6)—O(1)	1.258(6)
C(6)—N(2)	1.308(7)	C(7)—N(2)	1.443(6)
N(1)—Cu—N(2)	81.6(2)	N(1)—Cu—N(3)	161.2(2)
N(1)—Cu—N(4)	96.6(2)	N(2)—Cu—N(3)	81.5(2)
N(2)—Cu—N(4)	170.8(2)	N(3)—Cu—N(4)	98.7(2)
O(6)—Cu—N(1)	98.7(2)	O(6)—Cu—N(2)	96.3(2)
O(6)—Cu—N(3)	91.3(2)	O(6)—Cu—N(4)	92.9(2)
C(5)—C(6)—O(1)	119.9(5)	N(2)—C(6)—O(1)	127.6(5)
C(5)—C(6)—N(2)	112.5(4)	C(6)—N(2)—C(7)	122.7(4)

of the water containing complexes of the first group can be identified by the appearance of one or two sharp OH stretching peaks in the 3500 cm^{-1} region. The latter group, consisting of complexes mainly with a pmpa and a unidentate ligand, is likely of square planar structure in agreement with the strong ligand field strengths. The structure of [Cu(pmpa)(2Mpy)(ClO_4)], however, is believed to be square pyramidal due to its λ_{max} at 601 nm. The complexes, [Cu(pmpa)(NMIm)](ClO_4)(H_2O) and [Cu(pmpa)(NH_3)](ClO_4)(H_2O)$_2$, are also square planar because of their high ligand field strengths. In addition, the water molecules are probably not bound to the central copper, because no sharp O—H stretching peaks appear in the 3500 cm^{-1} region. In methanol solution, all of the complexes show λ_{max} in the 600 nm region indicating coordination of solvent molecules to give square pyramidal structures.

The powder EPR spectra are generally of axial type [16], namely, $g_\parallel > g_\perp > 2$. Some square planar complexes showed exchange coupling. The spectra in methanol glass matrix exhibit the fine structures of rhombic spectral features. There are six superhyperfine components with relative intensities close to the values of 1 : 2 : 3 : 3 : 2 : 1 for the $A_\parallel$(Cu) and $A_\parallel$(N) and followed by another set of five components of 1 : 2 : 3 : 2 : 1 for the $A_\perp$(N) as illustrated in Fig. 3. It is proper to designate the y axis along the Cu—N

Table 3. Visible and EPR spectral data for pmpa-Cu^{II} complexes

Compound[a]	LF bands[b] $\lambda_{max}(\varepsilon)$, nm	EPR[c] g_z	g_y	g_x	A_z(Cu)	A_y(Cu)	A_y(N)	A_x(N)
[Cu(pmpa)(ImH)(H_2O)](BF_4)	606/mull	(2.216	2.061)					
(H_2O)	602(102)/CH_3OH	2.228	2.059	2.021	171	~12	~12	~12
[Cu(pmpa)(ImH)(H_2O)](ClO_4)	606/mull	(2.217	2.064)					
	592(126)/CH_3OH	2.226	2.059	2.022	175	~13	~13	~12
[Cu(pmpa)(4MImH)(H_2O)]	594/mull							
(ClO_4)(H_2O)	592(113)/CH_3OH	2.219	2.059	2.021	176	~13	~13	~12
[Cu(pmpa)(4Mpy)(H_2O)]	581/mull	(2.241	2.066)					
(ClO_4)(H_2O)	604(112)/CH_3OH	2.219	2.059	2.021	178	~12	~12	~12
[Cu(pmpa)(2Mpy)](ClO_4)	601/mull	([d]	2.079)					
	617(126)/CH_3OH	2.208	—	—	186	—	—	—
[Cu(pmpa)(ImH)](ClO_4)	565/mull	[e]						
	600(121)/CH_3OH	2.218	2.059	2.025	172	~12	~12	~12
[Cu(pmpa)(NMIm)](ClO_4)	563/mull	(2.121	2.064)					
	600(123)/CH_3OH	2.219	2.060	2.022	176	~12	~12	~12
[Cu(pmpa)(NMIm)](ClO_4)(H_2O)	565/mull	([d]	2.069)					
	604(172)/CH_3OH	2.221	2.067	2.029	174	~12	~12	~12
[Cu(pmpa)(4MImH)](ClO_4)	567/mull	(2.194	2.056)					
	599(115)/CH_3OH	2.219	2.059	2.021	176	~13	~13	~12
[Cu(pmpa)(py)](BF_4)	554/mull	[e]						
	613(107)/CH_3OH	2.217	2.059	2.021	181	~12	~12	~12
[Cu(pmpa)(py)](ClO_4)	558/mull	[e]						
	617(125)/CH_3OH	2.218	2.060	2.021	180	~12	~12	~12
[Cu(pmpa)(3Mpy)](ClO_4)	555/mull	([d]	2.060)					
	608(117)/CH_3OH	2.217	2.059	2.021	178	~12	~12	~12
[Cu(pmpa)(NH_3)](ClO_4)(H_2O)$_2$	574/mull	(2.202	2.054)					
	612(285)/CH_3OH	2.170	—	—	178	—	—	—

[a] pmpa = *N*-(2-picolyl)picolamido; ImH = imidazole; 4MImH = 4-methylimidazole; NMIm = *N*-methylimidazole; py = pyridine; 2Mpy = 2-methylpyridine; 3Mpy = 3-methylpyridine; 4Mpy = 4-methylpyridine.

[b] ε in M^{-1} cm^{-1}.

[c] X-band EPR spectra measured at 77 K in CH_3OH matrix with hyperfine coupling constants in 10^{-4} cm^{-1}. Powder data in parentheses.

[d] Not observed.

[e] Exchange coupling.

(amido) in the CuN_4 plane and the x axis parallel to the direction of the two copper-pyridine (pmpa) bonds. Apparently, the bonding strengths along the x and y directions are different. The energy levels of d_{yz} and d_{xz} are, therefore, non-degenerate. For the NH_3 complex, the superhyperfine coupling is not obvious. Two sets of rhombic spectra were observed for the 2-methylpyridine complex. All of the g_z and A_z values are not much varied, suggesting that these complexes comprise a very similar CuN_4 square plane very much similar to those observed in complexes **1** and **2**.

The infrared spectra data for the pmpa complexes are given in the Experimental section. There are usually two relatively sharp O—H stretching absorptions in the 3500 cm^{-1} region assignable for H_2O molecule bound directly to the central copper ion analogous to the structures of complexes **1** and **2**. The amide CO and CN stretching peaks are lowered by *ca* 30–40 cm^{-1} as compared with those of the free ligand. The Cu—N (pmpa) stretches were tentatively assigned at *ca* 350, 280 and 250 cm^{-1} and the Cu—N stretches for the unidentate ligands at *ca* 320 cm^{-1}.

Electronic structures and bonding properties

The *d–d* spectra of the complexes were deconvoluted into Gaussian component bands. Starting from a set of four trial peaks, computer iteration processes for curve fitting were carried out until a minimum value of the reliability factor, R (see Table 4), was reached. Each of the complexes had an excellent fit with $R <$ *ca* 0.5% and showed a resulting set comprising four Gaussian peaks. Representative examples are shown in Fig. 4. The peak positions are presented in Table 4 along with their half-height widths and relative peak areas. Attempts to fit with three component peaks were less satisfactory; the R values were

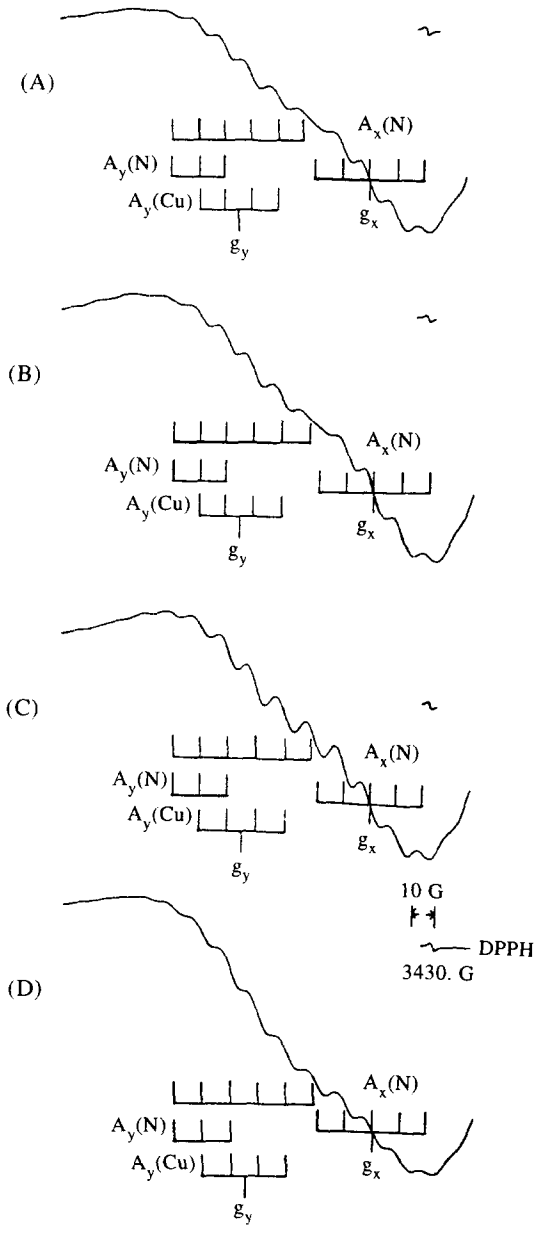


Fig. 3. The high field region of X-band EPR spectra measured at 77 K in MeOH matrix for (A) [Cu(pmpa)(4Mpy)(H_2O)](ClO_4)(H_2O); (B) [Cu(pmpa)(py)](ClO_4); (C) [Cu(pmpa)(4MImH)(H_2O)](ClO_4)(H_2O); (D) [Cu(pmpa)(ImH)](ClO_4).

higher. In addition, the rhombic EPR spectroscopic data of these complexes suggest nondegeneracy for the d_{xz} and d_{yz} orbitals.

Because the complexes consist of a common tridentate pmpa and a unidentate ligand in the coordination plane, the following effects are anticipate: first, the $d_{x^2-y^2}$ level, being most involved in the copper-unidentate ligand bonding, will be considerably varied in energy due to the bonding capabilities of the unidentate ligands in the xy plane, resulting in shifts for all of the d–d transitions; secondly, defining the y axis along the Cu—N(2) bond, the d_{yz} level will not be affected by changing the unidentate ligand and the shift in the $d_{yz} \rightarrow d_{x^2-y^2}$ will mainly reflect the varying of the $d_{x^2-y^2}$ level; thirdly, the d_{xz} level will virtually not be affected, because the two coordinated groups of the terminal pyridine moieties are alike in the x direction. The shift in the $d_{xz} \rightarrow d_{x^2-y^2}$ transition will again reflect the variation of the $d_{x^2-y^2}$ level; finally, the d_{xy} level may be affected by changing the unidentate ligands and the shift in the $d_{xy} \rightarrow d_{x^2-y^2}$ transition will reflect the variation of the π-bonding capabilities of the unidentate ligands.

In this context, the energy difference between the d_{xz} and d_{yz} levels is expected to be nearly constant for these mixed-ligand pmpa copper(II) complexes. Inspecting the Gaussian component peaks, the lowest energy peak in the square pyramidal complexes, and the highest energy peak in the square planar complexes, both having the smallest intensity, can be assigned as $d_{z^2} \rightarrow d_{x^2-y^2}$ transition as reported in many square pyramidal copper(II) complexes [16–19], and in square planar copper(II) complexes [4]. The energy differences between the highest and the lowest peaks of the remaining three peaks are 3.5 ± 0.1 kK. The sequence of the d orbitals is therefore designated as $d_{x^2-y^2} \gg d_{z^2} > d_{yz} > d_{xy} > d_{xz}$ for the square pyramidal complexes and as $d_{x^2-y^2} \gg d_{xz} > d_{xy} > d_{yz} > d_{z^2}$ for the square planar complexes. Although the energy differences between the d_{xy} and d_{xz} orbitals are also nearly constant (1.8 ± 0.1 kK), an alternative assignment is less likely. Because the bonding capabilities of the anionic amido are very similar for the pmpa and the glygly ligands (*vide supra*), a difference of 3.5 kK is reasonably in agreement with the value observed for the glygly complexes [3]. Strong π-interactions along the y axis are in accordance with the very short Cu—N(2) bonds.

Because the d_{xz} level is raised relative to the d_{yz} orbital, we conclude that the central amido moiety of the pmpa ligand is a strong π-donor in these complexes. This is analogous to the central amido moiety of the glycylglycinate ligand. But unlike the glygly complexes, the unidentate heterocyclic ligands in the pmpa complexes are nearly perpendicular to the equatorial coordination plane. Obviously, steric hindrance is the major factor preventing the heterocyclic nucleus from lying coplanarly with the equatorial coordination plane. Another difference is that preparation of glygly complexes containing pyridine type ligands, except 4-dimethylaminopyridine, has failed. It is likely that a π-donating ligand is required by the *trans* amido of glygly ligand. However, this is not the case in the present study. We suspect that the dianionic nature of the glygly ligand has important effects on the bondings. Further studies in this direction are in progress.

Acknowledgements—Financial support from the National Science Council of the Republic of China (NSC85-2113-M-003-001) is gratefully acknowledged.

Table 4. Gaussian component bands for the visible spectra of pmpa-Cu^{II} complexes

Band	ν(kK)	Area[a]	$\delta_{1/2}$[b]	Assignment
[Cu(pmpa)(ImH)(H_2O)](BF_4)(H_2O)/mull (R = 0.34%)[c]				
I	13.0	0.84	2.90	d_{z^2}
II	15.1	2.08	2.99	d_{yz}
III	16.7	3.03	3.52	d_{xy}
IV	18.5	4.05	4.53	d_{xz}
[Cu(pmpa)(ImH)(H_2O)](ClO_4)/mull (R = 0.38%)[c]				
I	12.8	0.47	2.34	d_{z^2}
II	14.7	2.13	2.88	d_{yz}
III	16.3	3.12	3.08	d_{xy}
IV	18.2	4.28	3.74	d_{xz}
[Cu(pmpa)(4MImH)(H_2O)](ClO_4)(H_2O)/mull (R = 0.42%)[c]				
I	13.7	0.63	2.73	d_{z^2}
II	15.7	3.65	3.15	d_{yz}
III	17.4	3.47	3.18	d_{xy}
IV	19.3	2.25	3.15	d_{xz}
[Cu(pmpa)(4Mpy)(H_2O)](ClO_4)(H_2O)/mull (R = 0.26%)[c]				
I	13.7	1.19	3.02	d_{z^2}
II	15.8	2.77	2.90	d_{yz}
III	17.5	2.78	2.97	d_{xy}
IV	19.3	3.26	3.64	d_{xz}
[Cu(pmpa)(2Mpy)](ClO_4)/mull (R = 0.50%)[c]				
I	13.4	0.63	2.26	d_{z^2}
II	15.4	3.63	2.80	d_{yz}
III	17.2	3.21	2.62	d_{xy}
IV	19.0	2.53	2.85	d_{xz}
[Cu(pmpa)(ImH)](ClO_4)/mull (R = 0.31%)[c]				
I	15.8	2.08	2.80	d_{yz}
II	17.4	3.22	2.96	d_{xy}
III	19.2	3.71	3.40	d_{xz}
IV	21.2	0.99	3.23	d_{z^2}
[Cu(pmpa)(NMIm)](ClO_4)/mull (R = 0.27%)[c]				
I	16.0	1.96	2.85	d_{yz}
II	17.6	3.43	2.98	d_{xy}
III	19.4	3.47	3.47	d_{xz}
IV	21.5	1.14	3.47	d_{z^2}
[Cu(pmpa)(NMIm)](ClO_4)(H_2O)/mull (R = 0.41%)[c]				
I	15.9	1.95	4.52	d_{yz}
II	17.0	3.31	3.33	d_{xy}
III	19.2	3.59	3.43	d_{xz}
IV	21.7	1.15	3.00	d_{z^2}
[Cu(pmpa)(4MImH)](ClO_4)/mull (R = 0.32%)[c]				
I	15.6	2.83	2.92	d_{yz}
II	17.4	2.70	2.72	d_{xy}
III	19.2	3.09	2.96	d_{xz}
IV	21.3	1.38	2.85	d_{z^2}
[Cu(pmpa)(py)](BF_4)/mull (R = 0.44%)[c]				
I	15.9	2.21	3.06	d_{yz}
II	17.6	2.99	2.95	d_{xy}
III	19.4	4.14	3.41	d_{xz}
IV	21.6	0.66	2.89	d_{z^2}
[Cu(pmpa)(py)](ClO_4)/mull (R = 0.27%)[c]				
I	15.6	2.51	3.70	d_{yz}
II	17.4	2.47	3.14	d_{xy}
III	19.1	3.27	3.51	d_{xz}
IV	21.2	1.75	3.85	d_{z^2}
[Cu(pmpa)(3Mpy)](ClO_4)/mull (R = 0.33%)[c]				
I	15.8	2.57	3.90	d_{yz}
II	17.5	3.06	3.10	d_{xy}
III	19.3	2.96	3.01	d_{xz}
IV	21.2	1.41	2.86	d_{z^2}
[Cu(pmpa)(NH_3)](ClO_4)(H_2O)$_2$/mull (R = 0.44%)[c]				
I	14.8	2.28	3.25	d_{yz}
II	16.8	3.23	3.18	d_{xy}
III	18.6	3.28	3.27	d_{xz}
IV	20.5	1.21	3.25	d_{z^2}

[a] Relative peak area in arbitrary scale based on a sum of 10.
[b] Half-width at $\varepsilon_{max}/2$.

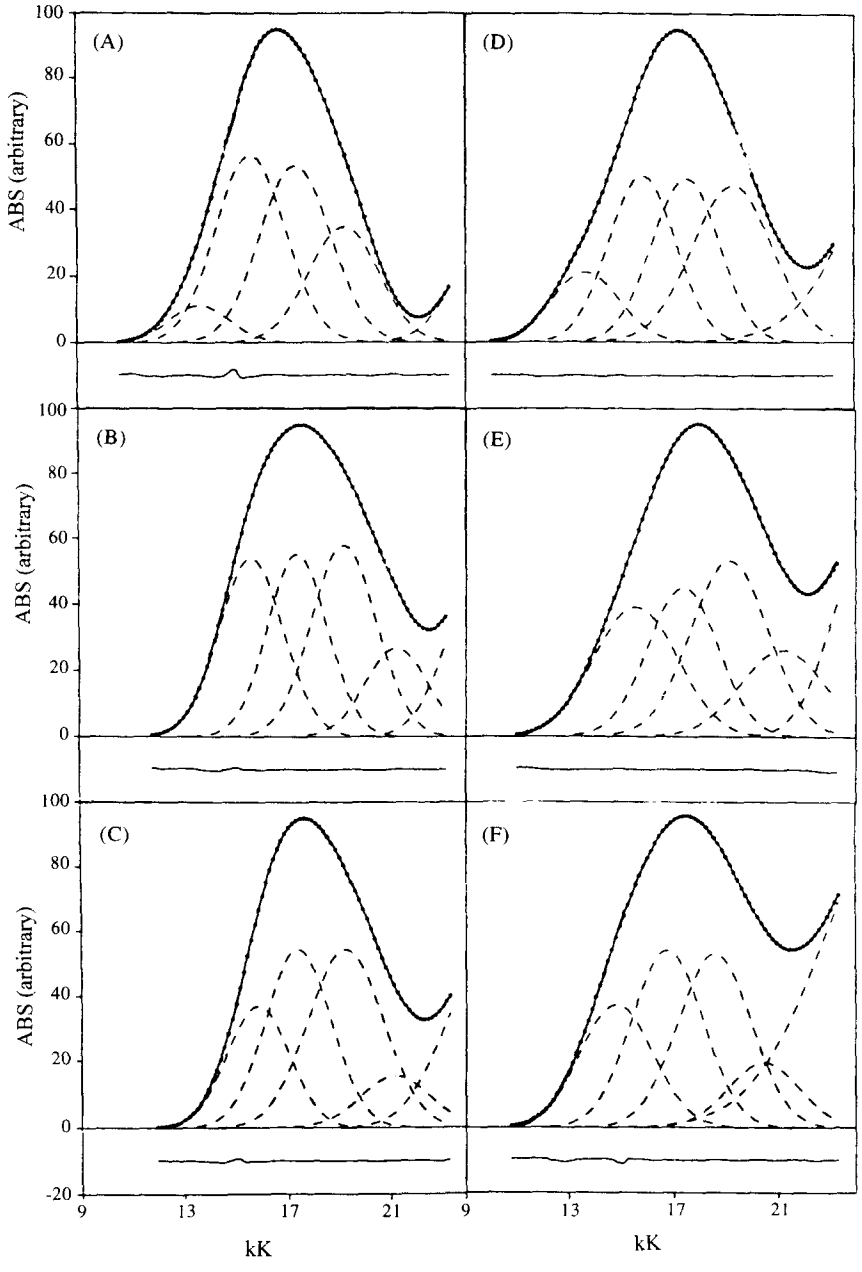


Fig. 4. Visible spectra and Gaussian line-shape analysis with difference plots of (A) [Cu(pmpa)(4MImH)(H_2O)](ClO_4)(H_2O), $R = 0.42\%$; (B) [Cu(pmpa)(4MImH)](ClO_4), $R = 0.32\%$; (C) [Cu(pmpa)(ImH)](ClO_4), $R = 0.31\%$; (D) [Cu(pmpa)(4Mpy)(H_2O)](ClO_4)(H_2O), $R = 0.26\%$; (E) [Cu(pmpa)(py)](ClO_4), $R = 0.27\%$; (F) [Cu(pmpa)(NH_3)](ClO_4)(H_2O)$_2$, $R = 0.44\%$. (—), observed spectrum; (...), Gaussian components; (*) profile-fitting points.

REFERENCES

1. C.-C. Su and C.-Y. Wu, *J. Coord. Chem.* 1994, **33,** 1.
2. C.-C. Su and C.-B. Li, *Polyhedron* 1994, **13,** 825.
3. H.-J. Chiu, C.-C. Su, S.-L. Wang and F.-L. Liao, *Trans. Met. Chem.* 1994, **19,** 413.
4. C.-C. Su and S.-Y. Chiu, *Polyhedron* 1996, **15,** 2623.
5. H. Sigel, P. R. Huber, R. Griesser and B. Prijs, *Inorg. Chem.* 1973, **12,** 1198.
6. B. E. Fischer and H. Sigel, *Inorg. Chem.* 1979, **18,** 425.
7. O. P. Vig, I. R. Trehan, G. L. Kad and J. Ghose, *Indian J. Chem.* 1992, **21B,** 748.
8. B. Frenz, *Personal SDP Reference Manual.* B. A. Frenz and Associates Inc., Houston, TX (1992).
9. G. M. Sheldrick, *SHELXS86 Program for the Solution of Crystal Structures.* University of Gottingen, Germany (1985).
10. M. C. Burla, M. Camalli, G. Cascarano, C. Giacovazzo, G. Polidori, R. Spangna and D. Viterbo, *J. Appl. Cryst.* 1989, **22,** 389.
11. *International Tables for X-ray Crystallography*, Vol. 4. Kynoch, Birmingham (1974).

12. C.-C. Su, Y.-L. Lin, S.-L. Wang and W.-C. Chou, *Trans. Met. Chem.* 1993, **18,** 113.
13. D. D. Swank and R. D. Willett, *Inorg. Chem.* 1980, **19,** 2321.
14. B. A. Cartwright, L. Couchman and A. C. Skapski, *Acta Cryst.* 1979, **B35,** 824.
15. J. Pradilla-Sorzano, H. W. Chen, F. W. Koknat and J. P. Fackler, Jr, *Inorg. Chem.* 1979, **18,** 3519.
16. B. J. Hathaway and A. A. G. Tomlison, *Coord. Chem. Rev.* 1970, **5,** 1.
17. B. J. Hathaway and D. E. Billing, *Coord. Chem. Rev.* 1970, **5,** 143.
18. A. A. G. Tomlison and B. J. Hathaway, *J. Chem. Soc.*(*A*) 1968, 1685.
19. C.-C. Su, J.-S. Lin, Y.-L. Lin, S.-L. Wang and F.-L. Liao, *J. Coord. Chem.* 1993, **30,** 91.

Pergamon

PII: S0277-5387(96)00310-5

Polyhedron Vol. 16, No. 3, pp. 393–401, 1997
Copyright © 1996 Elsevier Science Ltd
Printed in Great Britain. All rights reserved
0277-5387/97 $17.00+0.00

Structural characterisation of Ru^{II} [9]aneS_3 polypyridyl complexes by NMR spectroscopy and single crystal X-ray diffraction

Brian J. Goodfellow,[a,c]* Victor Félix,[b,c]* Sara M. D. Pacheco,[c] Júlio Pedrosa de Jesus[c] and Michael G. B. Drew[d]*

[a] Departamento de Química (and Centro de Química Fina e Biotecnologia), Faculdade de Ciências e Tecnologia, Universidade Nova de Lisboa, 2825 Monte de Caparica, Portugal

[b] Instituto de Tecnologia Química e Biológica, Rua da Quinta Grande 6, 2780 Oeiras, Portugal

[c] Departamento de Química, Universidade de Aveiro, 3800 Aveiro, Portugal

[d] Department of Chemistry, The University, Whiteknights, Reading RG6 6AD, U.K.

(Received 24 May 1996; accepted 18 June 1996)

Abstract—The synthesis of a series of Ru^{II} complexes with the thioether ligand [9]aneS_3 and various polypyridyl ligands was carried out using $[Ru(dmso)_4Cl_2]$ as a starting material. The first synthetic step involved the introduction of the thioether ligand and the isolation of the compound $[Ru([9]aneS_3)(dmso)Cl_2]$. The polypyridyl ligands were then exchanged to give a series of complexes $[Ru([9]aneS_3)(X)(Cl)]^+$ (X = 1,10-phenanthroline (phen), 2,2′-bipyridyl (bpy), 4,4′-diphenyl-2,2′,-bipyridyl (dbp) and 4,7′-diphenyl-1,10-phenanthroline (dip)). These complexes were characterised by NMR and UV spectra. The complexes with X = phen and bpy were crystallised and single crystal X-ray diffraction studies carried out. Distorted octahedral coordination geometry was observed for both complexes. The equatorial planes are formed by two macrocyclic sulfur donor atoms and two nitrogen atoms from polypyridyl ligands (bpy or phen). The hexa-co-ordination is achieved *via* a chlorine and the remaining sulfur, macrocyclic atom. The [9]aneS_3 macrocyclic ligand adopts a [333] facial arrangement. The results from NMR studies for $[Ru([9]aneS_3)(phen)Cl]^+$ and $[Ru([9]aneS_3)(bpy)Cl]^+$ indicate that both complexes exist as two forms in solution with C_S symmetry consistent with a [333] facial arrangement. Copyright © 1996 Elsevier Science Ltd

Keywords: Ru^{II}; [9]aneS_3 complexes; polypyridyl ligands; crystal structures; NMR.

The interaction of ruthenium based compounds with DNA has seen much work over the last five years. Ruthenium polypyridyl complexes have been extensively studied following the work of Barton *et al.* [1] where the interaction of the two isomers of $[Ru(1,10\text{-phenanthroline})_2Cl_2]$ with B-DNA was explored. These studies [1–12] have found that there are a number of possible modes of interaction of Ru complexes with DNA, these include: intercalation, whereby the polypyridyl ligand is inserted (fully or partially) between the stacked bases of the DNA double helix, surface binding, within one of the DNA grooves, and covalent binding where ligands in the Ru complex are replaced by heteroatoms of the DNA bases (normally the nitrogen of guanine) [2]. Spectroscopic studies have proved to be especially useful in probing the interactions between the Ru complexes and DNA.

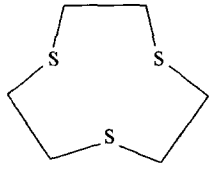
Following the work of Rosenberg *et al.* [13] in 1969 with *cis*-platin the search to find similar anti-tumor agents has been ceaseless. In the last few years, following the studies of Barton *et al.* a number of possible compounds of Ru have been discovered; Alessio *et al.* [14] found that *trans*-$[Ru(dmso)_4Cl_2]$ showed promising anti-tumor activity with adjacent guanines being the preferred interaction site on DNA while Keppler *et al.* [15] Carried out an extensive study of various Ru complexes finding that $[Ru(Im)_2Cl_4]$(ImH) and $[Ru(Ind)_2Cl_4](IndH)$, where Im = imidazole and Ind = indazole, show anti-tumor activity.

* Authors to whom correspondence should be addressed.

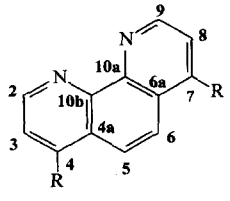
These *in vitro* studies of Ru complexes have shown that the number and type of polypyridyl, and ancillary ligands have a profound effect on the manner and type of interaction with biomolecules. Factors such as the ability of the ligands to form H-bonds or favourable VDW interactions with the functional groups of the DNA bases have been found to play a determining role in binding. A first step in the design of Ru complexes with selective DNA binding characteristics is the choice of a suitable ligand followed by the structural characterisation of the complex.

The use of macrocyclic polyamines and polythioethers in transition metal chemistry has been considerable as these ligands are thermodynamically and kinetically inert and also have the ability to stabilise unusual oxidation states (e.g. Rh^{II}) [16]. Krotz *et al.* [17] synthesised a series of Rh^{III} complexes with cyclic polyamines or [12]aneS_4 and a 9,10-diaminophenanthrene ligand in order to probe specific binding interactions to DNA. A systematic variation of thioether-polypyridyl ligands complexed to Ru^{II} would allow conclusions to be drawn as to the structural characteristics of these compounds and the role these play in DNA binding,the goal being the design of a complex with specific DNA binding characteristics. The first step in this process is, therefore, the synthesis and characterisation of the Ru^{II} based complexes followed by the determination of their three dimensional structure.

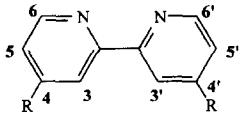
In this paper the synthesis (from $[Ru(dmso)_4Cl_2]$) of a number of $[Ru([9]aneS_3)(X)Cl]$ complexes (X = 1,10-phenanthroline (phen), 2,2′-bipyridyl (bpy), 4,4′-diphenyl-2,2′-bipyridyl (dbp) and 4,7′-diphenyl-1,10-phenanthroline (dip)) is reported along with their spectroscopic characterisation. The structures of $[Ru([9]aneS_3)(1,10\text{-phenanthroline})Cl]^+$ and $[Ru([9]aneS_3)(2,2'\text{-bipyridyl})Cl]^+$ are compared in solution by NMR and in the solid state by X-ray crystallography.



[9]aneS_3



phen R = H
dip R = Ph



bpy R = H
dbp R = Ph

Scheme 1.

RESULTS AND DISCUSSION

The NMR characterisation of these complexes in solution show a number of interesting aspects. Compounds **1** and **2** seem to exist in solution in 2 forms. The ^1H spectrum for the aromatic region of complex **1** is shown in Fig. 1. In a symmetric complex with C_{2v} symmetry a 1,10-phenanthroline ligand would be expected to have 4 groups of resonances from the protons at positions ; 9/2, 8/3, 7/4 and 6/5 (see diagram 1). Complex **1** shows 8 groups of peaks suggesting that 2 forms exist in solution in the ratio 3 : 1. The peaks at 9.19(d, 5.2 Hz), 8.30(d, 8.2 Hz), 7.72(d of d, 8.4 and 5.2 Hz) and 7.62(s) ppm are from the 9/2, 7/4, 8/3 and 6/5 protons of the major form. The minor form has peaks at 9.34 (d, 5.2 Hz), 8.58(d, 8.3 Hz), 7.99(s) and 7.86(d of d, 8.2 and 5.2 Hz) ppm. The peaks from the macrocyclic ring are second order, therefore it is difficult to determine whether there are 2 sets of peaks for the thioether ligand. The ^{13}C spectra for the aromatic region and the macrocyclic region for complex **1** are shown in Figs 2a and 2b. The aromatic region shows 6 sets of peaks for the major form ; 152.8 (C9/C2), 146.9 (C10a/C10b), 137.2 (C7/C4), 130.2 (C4a/C6a), 127.1 and 125.5 (C8/C3 or C6/C5) ppm. The minor form has peaks at ; 153.6 (C9/C2), 147.4 (C10a/C10b), 138.3 (C7/C4), 130.6 (C4a/C6a), 127.5 and 125.8 (C8/C3 or C6/C5) ppm. The ^{13}C peaks of the thioether ligand also show 2 forms. The major form has peaks at 34.1, 32.1 and 31.3 ppm and the minor at 33.6, 31.6 and 31.1 ppm. Again the ratio is around 3 : 1. It is clear from the ^{13}C data that the complex has 2 forms in solution and that the thioether ligand has 2 sets of peaks. A 2D NOESY spectrum of complex **1** was recorded to check the assignment and through space connectivities for the 2 forms. Cross peaks were observed between the thioether protons and the H-9/H-2 proton on the phenanthroline ring for both forms indicating the minor set of peaks arise from a complexed form of phenanthroline and not from the free ligand.

The NMR data for complex **2** also suggests two forms in solution. The ^1H spectrum of the aromatic region for complex **2** is shown in Fig. 3. Resonances at 9.01(d, 5.6 Hz) (H-6/6′), 8.38(d, 8.1 Hz) (H-4/4′), 8.06(m) (H-5/5′) and 7.56(m) (H-3/3′) ppm are from the major form. The minor form has peaks at 9.11(d, 5.6 Hz), 8.47(d, 8.2 Hz), 8.17(m) and 7.66(m) ppm. The ratio between the forms is 3 : 1. The ^{13}C spectrum of complex **2** is shown in Fig. 4. The aromatic peaks for the major form are at 156.4 (C2/2′), 152.8 (C6/6′), 138.4 (C4/4′), 127.2 (C5/5′) and 123.6 (C3/3′) ppm. The minor form has peaks at 156.9, 153.3, 139.3, 127.5 and 123.8 ppm. The thioether ligand for complex **2** has peaks at 34.3, 32.1 and 31.1 ppm for the major form and at 33.8, 31.7 and 31.3 ppm for the minor form.

The fact that two sets of resonances are seen for the polypyridyl and thioether ligands in complexes **1** and **2** in solution is most probably a result of the thioether

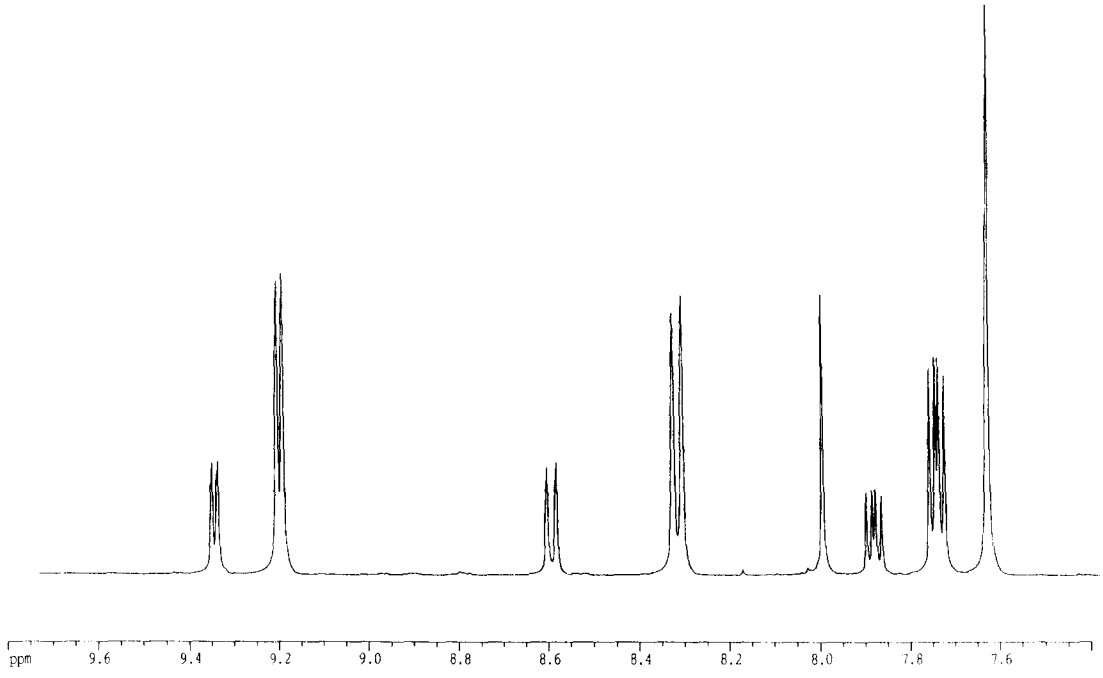


Fig. 1. The aromatic region of the ^1H spectrum of complex **1** in D_2O at 303 K.

Table 1. Selected bond lengths (Å), angles and endocyclic torsion anglers ( ) for complexes **1** and **2**

Complex	1	2
Ru(1)—N(1)	2.091(5)	2.099(6)
Ru(1)—N(2)	2.087(5)	2.112(5)
Ru(1)—S(1)	2.291(2)	2.320(2)
Ru(1)—S(2)	2.284(2)	2.316(2)
Ru(1)—S(3)	2.272(2)	2.287(2)
Ru(1)—Cl	2.438(2)	2.476(2)
N(2)—Ru(1)—N(1)	78.8(2)	78.0(2)
N(1)—Ru(1)—S(1)	174.4(1)	175.7(2)
N(2)—Ru(1)—S(1)	96.4(1)	97.8(2)
N(1)—Ru(1)—S(2)	96.8(1)	96.5(2)
N(2)—Ru(1)—S(2)	174.8(1)	174.3(2)
N(1)—Ru(1)—S(3)	94.6(1)	92.7(2)
N(2)—Ru(1)—S(3)	94.6(1)	90.2(2)
N(1)—Ru(1)—Cl	86.2(1)	88.4(2)
N(2)—Ru(1)—Cl	86.7(1)	90.2(2)
S(1)—Ru(1)—Cl	90.8(1)	90.50(8)
S(2)—Ru(1)—Cl	90.2(1)	91.24(7)
S(3)—Ru(1)—Cl	178.6(1)	178.8(1)
S(2)—Ru(1)—S(1)	87.9(1)	87.7(1)
S(3)—Ru(1)—S(1)	88.5(1)	88.4(1)
S(3)—Ru(1)—S(2)	88.5(1)	88.6(1)
S(3)—C(5)—C(6)—S(1)	−46.0(7)	−46.9(8)
C(5)—C(6)—S(1)—C(1)	135.5(5)	135.2(7)
C(6)—S(1)—C(1)—C(2)	−66.6(6)	−68.6(8)
S(1)—C(1)—C(2)—S(2)	−44.7(7)	−43.5(9)
C(1)—C(2)—S(2)—C(3)	132.1(6)	130.8(8)
C(2)—S(2)—C(3)—C(4)	−72.8(6)	70.4(7)
S(2)—C(3)—C(4)—S(3)	−41.4(8)	−45.0(9)
C(3)—C(4)—S(3)—C(5)	130.6(6)	134.1(8)
C(4)—S(3)—C(5)—C(6)	−68.9(6)	−66.1(7)

ring having 2 different conformations in solution when complexed. As only three ^{13}C peaks are seen for the [9]aneS$_3$ ligand for each form (Fig. 2b) the ligand must adopt conformations where a plane of symmetry runs through the Ru, Cl and one sulfur atom and bisects the angle N—Ru—N for the polypyridyl ligand. Therefore both forms must have C_S symmetry.

The single crystal X-ray diffraction studies of complexes [Ru([9]aneS$_3$)(phen)Cl]Cl·3H$_2$O and [Ru([9]aneS$_3$)(bpy)Cl]Cl·3H$_2$O indicate hexa-coordination for the Ru centres. Molecular diagrams with corresponding atomic labelling schemes are shown in Figs 5 and 6 for cations [Ru([9]aneS$_3$)(phen)Cl]$^+$ and [Ru([9]aneS$_3$)(bpy)Cl]$^+$, respectively. The selected bond lengths, angles and endocyclic torsion angles are listed in Table 1. The structural parameters associated with the Ru coordination spheres show distorted octahedral geometry for both complex cations. The equatorial planes are formed by two macrocyclic sulfur donor atoms and two nitrogen atoms from polypyridyl ligands (bpy or phen). The hexa-coordination is achieved *via* a chlorine and the remaining sulfur macrocyclic atom.

In complex **1**, the axial Ru—S bond length [Ru—S(3) = 2.272(2) Å] is shorter than equatorial bond lengths [Ru—S(1) = 2.291(2) and Ru—S(2) = 2.284(2) Å]. A more pronounced differential *trans* influence is observed for complex **2**, where the Ru—S(3) bond length is 2.287(2) and the Ru—S(2) and Ru—S(1) bonds are 2.316(2) and 2.320(2) Å respectively. These facts suggest that in addition to a σ-*trans* effect, the competitive π acceptance of polypyridyl ligands plays an important role in determining

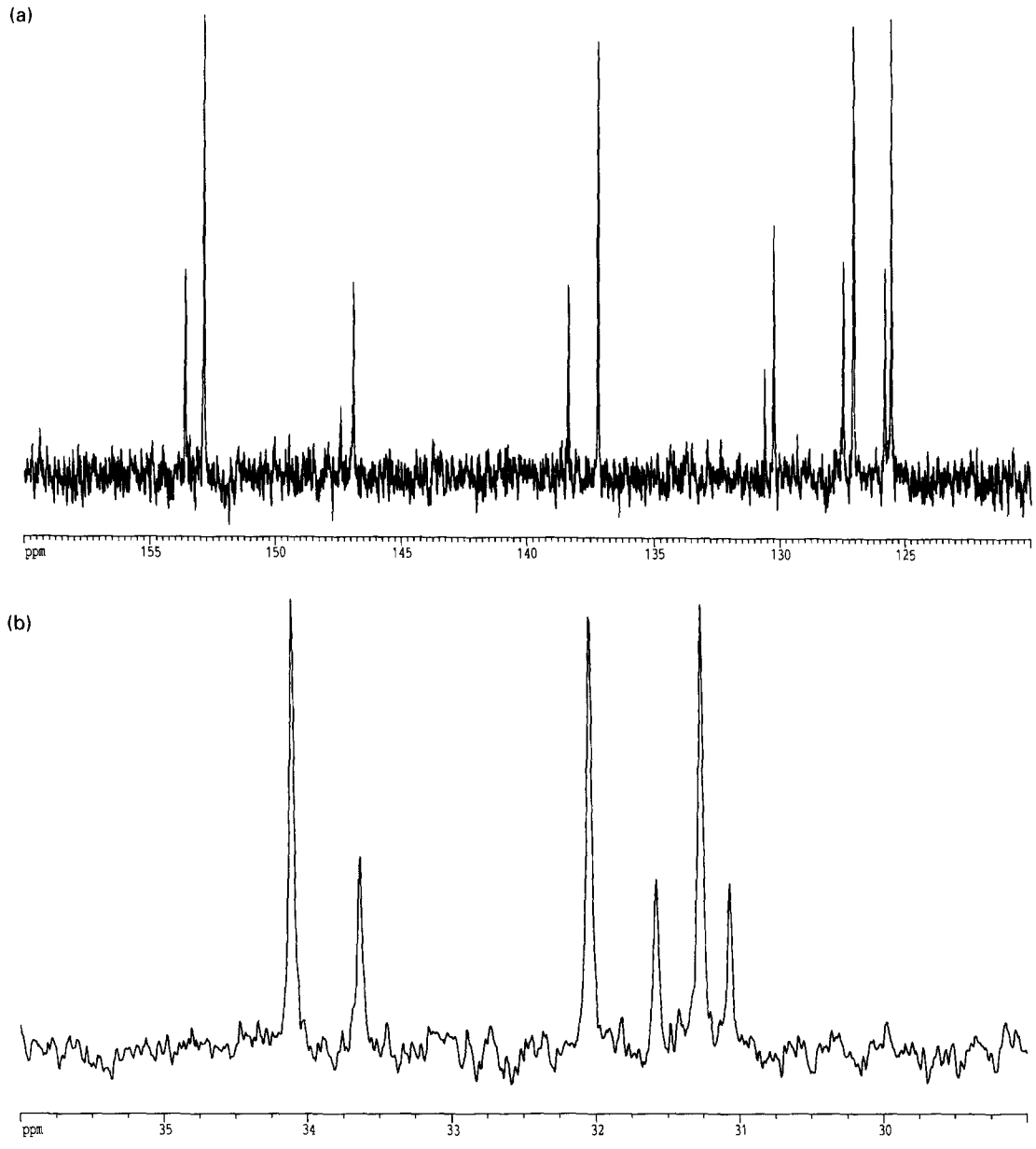


Fig. 2. (a) The aromatic region of the ^{13}C spectrum in D_2O at 303 K of complex **1**. (b) The aliphatic region of the ^{13}C spectrum of complex **1**.

the Ru—S bond lengths. The average bond lengths Ru—N 2.089(2) **1** and 2.106(2) **2** are similar to those observed for the octahedral complex $[Ru(NCMe)_3([9]aneS_3)]^{2+}$ 2.065(5) Å [18].

The angles in the equatorial plane involving the nitrogen atoms and metal centre differ from ideal octahedral values due to the small bite-angles of phen and bpy (78.8(2) and 78.0(2)° respectively). These values are similar to those seen for the octahedral complexes $[Ru([12]aneS_4)(phen)]^{2+}$ 79.5(4) and $[Ru([12]aneS_4)(bpy)]^{2+}$ 77.7(4) [19]. The remaining angles around the ruthenium atom in both cation complexes are very close to ideal octahedral values.

The conformation of any macrocyclic ligand can be described by a set of endocyclic torsion angles using an extended Dale nomenclature [20]. For example, the $[9]aneS_3$ macrocycle in complex cations **1** and **2** have values of the S—C—C—S, C—S—C—C and C—C—S—C torsion angles (listed in Table 1) which lead to a [333] conformation in the Dale nomenclature. This conformation has been found for many transition metal complexes characterised by X-ray diffraction where the $[9]aneS_3$ ligand adopts a facial arrangement [21]. The free $[9]aneS_3$ ligand also adopts, in the solid state, this conformation [22]. A molecular dynamics and mechanics study, in the gas

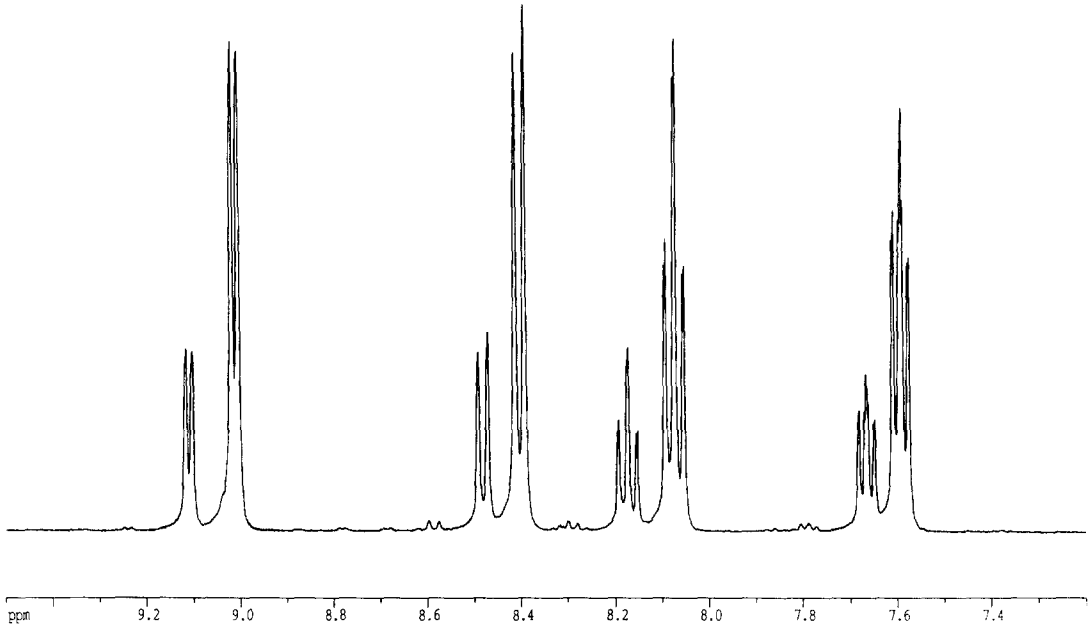


Fig. 3. The aromatic region of the ^1H spectrum of complex **2** in D_2O at 303 K.

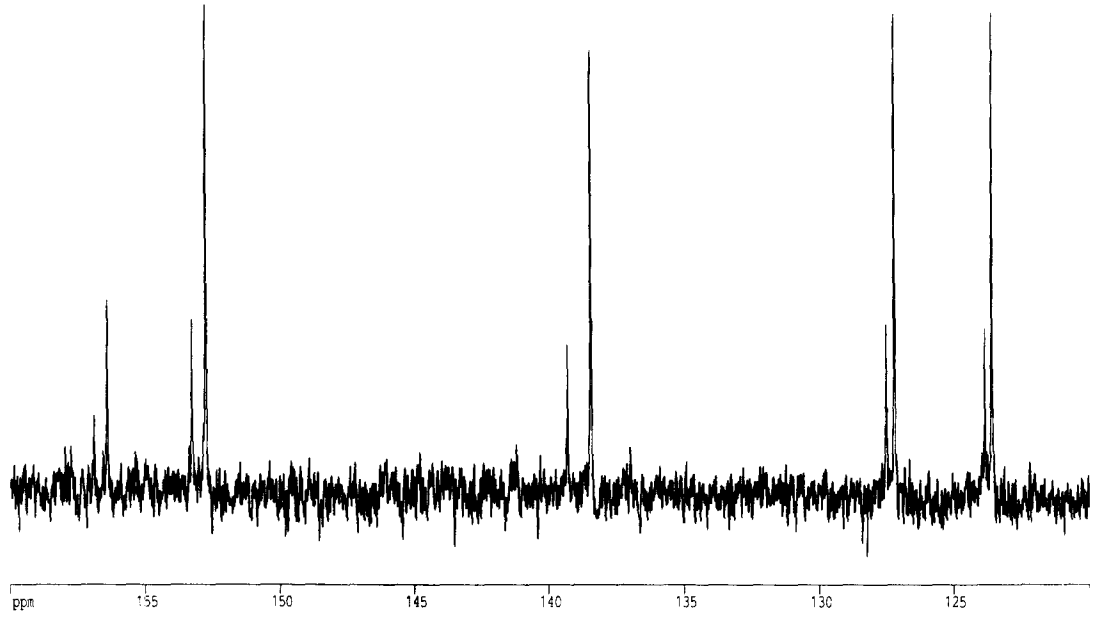


Fig. 4. The ^{13}C spectrum, of the aromatic region of complex **2**.

phase [23], gave 13 conformations with energies ranging from 4.5 to 8.3 kcal/mol, the lowest energy conformation again having a [333] arrangement.

Selected intermolecular contacts are given in Table 2. In crystals of both complexes, the backbone hydrogens of the macrocyclic ligand are involved in interactions with waters of crystallization (C—H $\cdots$ O) and chlorine anions (C—H $\cdots$ Cl). The distances of these interactions are close to the sum of van der Waals radii for H,Cl and H,O and could be considered as weak hydrogen bonds.

The results from the X-ray study are consistent with the NMR spectroscopic data for the complexes $[Ru([9]aneS_3)(phen)Cl]^+$ in solution, in that octahedral coordination with one thioether and one polypyridyl ligand is observed. However, the fact that the complexes **1** and **2** exist as two forms in solution and only one form is seen in the solid state suggests that

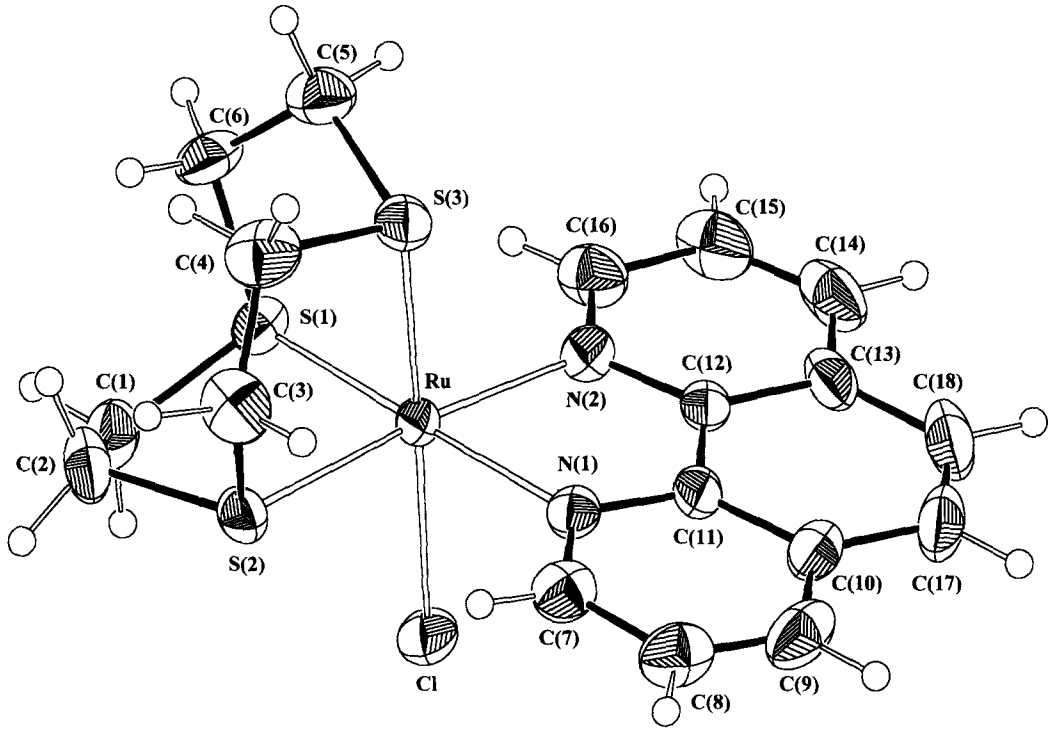


Fig. 5. Molecular structure of the $[Ru([9]aneS_3)(phen)Cl]^+$ complex cation showing the atomic labelling scheme. Thermal ellipsoids are drawn at the 30% probability level and the hydrogen atoms are represented with a U_{iso} of 0.01 Å^2.

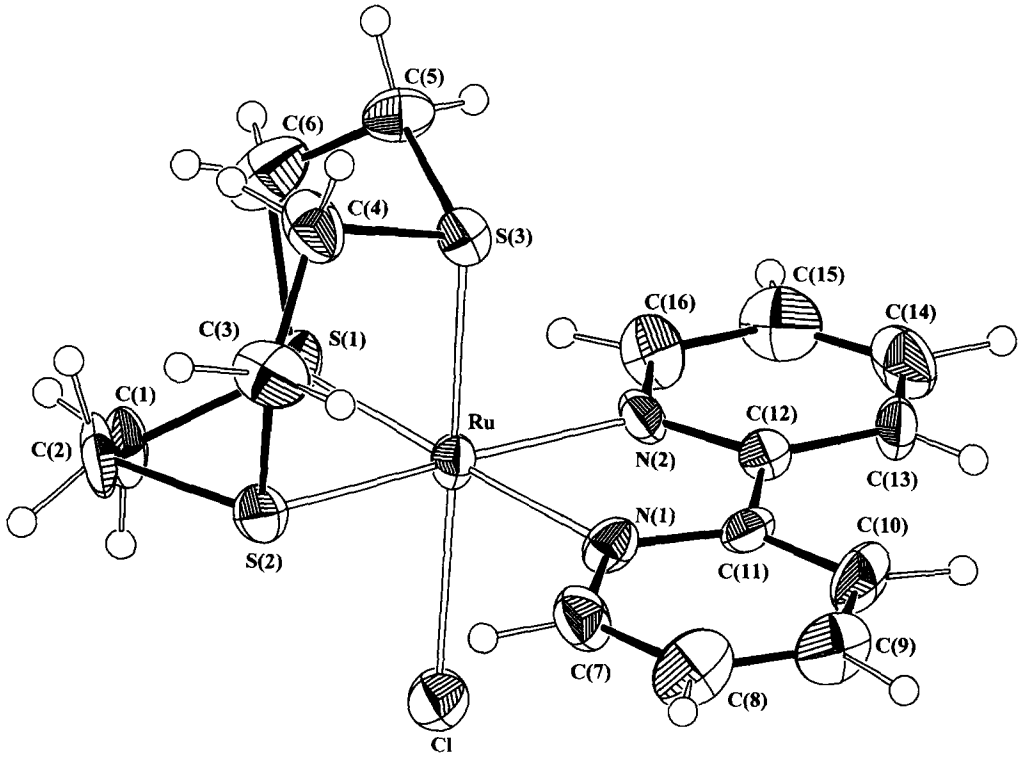


Fig. 6. Molecular structure of the $[Ru([9]aneS_3)(bpy)Cl]^+$ complex cation showing the atomic labelling scheme. Details are as in Fig. 5.

crystal packing forces, namely the hydrogen bonds C—H···O and C—H···Cl stabilize the conformation adopted by the macrocycle in the solid state. These forces are absent in solution allowing the [9]aneS$_3$ ligand to adopt two different conformations (both with C_S symmetry).

EXPERIMENTAL

The ligands [9]aneS$_3$, phen, bpy, dbp, and dip were purchased from the Aldrich Chemical Company and used without further purification.

Syntheses

[Ru(dmso)$_4$Cl$_2$]. The synthesis of [Ru(dmso)$_4$Cl$_2$] was carried out according to the method of Evans *et al.* [24] NMR: ^{1}H D_2O: 3.49, 3.48, 3.46, 3.43, 3.42, 3.37, 3.33 (dmso); ^{13}C, 46.73, 46.50, 45.70, 45.11, 44.67, 44.31 (all ppm). UV/Vis: λ_{max} nm($\varepsilon \times 10^{-3}$ M^{-1} cm^{-1}); 352(0.43), 312(0.33), 220(11.1), 202(26.9).

[Ru([9]aneS$_3$)(dmso)Cl$_2$]. [Ru(dmso)$_4$Cl$_2$] (0.5g, 1 mmol) was added to 0.186 g of [9]aneS$_3$ (1 mmol) in ethanol (*ca* 30 ml). The resulting suspension was refluxed for 90 min at 80 C. A colour change from pale to bright yellow indicated reaction. The solution was concentrated and a bright yellow solid obtained. The product was washed with ethanol and dried (0.39 g, 88%). [Note: care must be taken not to use excess [9]aneS$_3$ otherwise [Ru([9]aneS$_3$)$_2$]$^{2+}$ results.] NMR: ^{1}H D_2O; 3.38s(1.5 H), 3.35s(2.4 H), 3.26s(1.5 H), (dmso): 3.00–2.60m(12 H, [9]aneS$_3$); ^{13}C; 43.54, 43.50, 42.12, 35.02, 34.53, 34.39, 33.50, 33.29, 31.64, 31.01, 29.21, (all ppm). UV/Vis: λ_{max} nm($\varepsilon \times 10^{-3}$ M^{-1} cm^{-1}); 425(0.26), 352(0.40), 210(24.7).

[Ru([9]aneS$_3$)(1,10-phenanthroline)Cl]Cl (**1**). 1,10-phenanthroline (0.48 g, 2.42 mmol, 5% excess) was added to a solution of [Ru([9]aneS$_3$)(dmso)Cl$_2$] (0.1 g, 0.23 mmol) in ethanol. The yellow solution was refluxed for 15 min at 80 C or until a colour change to orange indicated reaction had taken place. The solution was concentrated until a yellow/orange needle or "glass wool"-like solid was obtained. On standing, large orange crystals developed. These were washed with water and dried (0.12 g, 95%). NMR: ^{1}H D_2O; {9.34d, 9.19d} 2H, {8.58d, 8.30d} 2H, {7.99s, 7.62s} 2H, {7.72q, 7.86q} 2H (phen), 3.1–2.3m (12H, [9]aneS$_3$); ^{13}C, 153.6, 152.8, 147.7, 146.9, 138.3, 137.2, 130.6, 130.2, 127.5, 127.1, 125.8, 125.5 (phen), 34.11, 33.64, 32.05, 31.58, 31.27, 31.07 ([9]aneS$_3$). UV/Vis: λ_{max} nm ($\varepsilon \times_3$)10^{-3} M^{-1} cm^{-1}); 411(3.0), 356(3.1), 297(9.6)sh, 260(22.2), 224(24.4), 200(36.0).

[Ru([9]aneS$_3$)(2,2′-bipyridyl)Cl]Cl (**2**). A 2% excess of 2,2′-bipyridyl (0.13g, 0.858 mmol) was added to 0.250 g of [Ru([9]aneS$_3$)(dmso)Cl$_2$] (0.36 g, 0.836 mmol) in ethanol. The yellow solution was refluxed for 20 min at 80 C and an orange/red solution obtained. The solution was concentrated to dryness and redissolved in EtOH/H_2O. On standing, orange/red crystals were obtained (0.42 g, 98%). NMR: ^{1}H D_2O; {9.11d, 9.01d} 2H, {8.47d, 8.38d} 2H, {8.17t, 8.06t} 2H, {7.66t, 7.56t} 2H (bpy); 2.96–2.21m 12H ([9]aneS$_3$): ^{13}C, 156.9, 156.4, 153.3, 152.8, 139.3, 138.4, 127.5, 127.2, 123.6 (phen), 34.27, 33.80, 32.09, 31.65, 31.34, 31.10 ([9]aneS$_3$). UV/Vis; λ_{max} nm($\varepsilon \times_3$)10^{-3} M^{-1} cm^{-1}); 413(3.0), 315(4.6), 283(15.7), 241(24.1), 203(24.1).

[Ru([9]aneS$_3$)(4,4′-diphenyl-2,2′-bipyridyl)Cl]Cl (**3**). The ligand 4,4′-diphenyl-2,2′-bipyridyl (0.062 g, 0.201 mmol) was added to a solution of [Ru([9]aneS$_3$)(dmso)Cl$_2$] (0.085 g, 0.197 mmol) in ethanol. Reflux for 2 h at 80 C gave an orange/brown solution. After concentration the brick-coloured precipitate was collected and dried (0.11 g, 84%). NMR: ^{1}H D_2O; 9.07d 2H, 9.00s 2H, 8.03d 4H, 7.90d 2H, 7.60m 6H (dbp), 3.20–2.60m 12H ([9]aneS$_3$). UV/Vis: λ_{max} nm($\varepsilon \times 10^{-3}$ M^{-1} cm^{-1}); 422(5.4), 295(26.9), 250(21.0), 202(36.5).

[Ru([9]aneS$_3$)(4,7′ - diphenyl - 1,10-phenanthroline)Cl]Cl (**4**). To the complex [Ru([9]aneS$_3$)(dmso)Cl$_2$] (0.2 g, 0.464 mmol) in ethanol was added 0.157 g (0.472 mmol) of 4,7′-diphenyl-1,10-phenanthroline. After refluxing for 2 h at 80 C a yel-

Table 2. Selected intermolecular contacts for crystal structures of the complexes **1** and **2**

Distances (Å)		Angles (°)	
Complex **1**			
H(12)···OW(1) [−1.0+*x*, *y*, *z*]	2.519	C(1)—H(12)···OW(1)[−1.0+*x*, *y*, *x*]	145.0
H(52)···OW(3)[*x*, 1.0+*y*, *z*]	2.485	C(5)—H(52)···OW(3)[*x*, 1.0+*y*, *z*]	164.5
H(42)···Cl(1)[*x*, 1.0+*y*, *z*]	2.903	C(4)—H(42)···Cl(1)[*x*, 1.0+*y*, *x*]	162.7
Complex **2**			
H(51)···OW(2)[−0.5−*x*, *y*, 0.5+*z*]	2.708	C(5)—H(51)···OW(2)[−0.5−*x*, *y*, 0.5+*z*]	150.2
H(41)···Cl(1)[−0.5−*x*, *y*, 0.5+*z*]	3.153	C(4)—H(41)···Cl(1)[−0.5−*x*, *y*, 0.5+*z*]	142.9
H(42)···Cl(1)[−*x*, 0.5−*y*, 0.5+*z*]	2.815	C(4)—H(41)···Cl(1)[−*x*, 0.5−*y*, 0.5+*z*]	150.9
H(22)···Cl(1)[−*x*, 0.5−*y*, 0.5+*z*]	2.838	C(2)—H(22)···Cl(1)[−*x*, 0.5−*y*, 0.5+*z*]	171.9
H(32)···Cl(1)[*x*, *y*, *z*]	2.933	C(32)—H(32)···Cl(1)[*x*, *y*, *z*]	160.1
H(11)···Cl(1)[0.5−*x*, *y*, 0.5+*z*]	2.848	C(32)—H(32)···Cl(1)[0.5−*x*, *y*, 0.5+*z*]	134.8

low/orange solution was obtained. Concentration of the solution yielded an orange solid (0.29 g, 91%). NMR: ^{1}H D_2O; 9.46d 2H, 8.12s 2H, 7.88d 2H, 7.87–7.59m 10H (dip), 3.29–2.64m 12H ([9]aneS_3). UV/Vis: λ_{max} nm($\varepsilon \times 10^{-3}$ M^{-1} cm^{-1}); 386(5.2), 276(28.5), 223(24.3), 205(38.6).

NMR spectroscopy

All spectra were recorded in either a Bruker AMX spectrometer operating at 300 MHz or a Bruker ARX spectrometer operating at 400 MHz. The ^{1}H spectra were obtained using 16k data points and a sweep width of 14.04 ppm. Deuterated methanol of D_2O were used as solvents with chemical shifts being referenced to HOD (4.75 ppm) or CD_2HOD (3.35 ppm). ^{13}C spectra were recorded using a sweep width of 250 ppm with 32k data points. Full proton decoupling was used. External dioxan (66.5 ppm) was used as a chemical shift reference. The 2D NOESY [25] spectrum (800 ms mixing time) was recorded at 400 MHz. A sweep width of 14.04 ppm and a recycle delay of 10 s was used. The number of t_1 increments was 512 with 8 scans being co-added for each increment. The number of data points used was 2048. The final matrix size was 2K × 2K with a qsine window applied in both dimensions.

Crystallographic measurements and processing

The pertinent crystal data and refinement details for complexes **1** and **2** are given in Table 3. Single crystal data for complex **1** were collected with an Enraf-Nonius CAD-4 diffractometer, using a graphite-monochromated Mo-K_α radiation ($\lambda = 0.71069$ Å). The unit cell parameters were calculated by least-squares refinement of 25 well centred reflections within the range $10 < \theta < 15°$. The intensity data were collected by ω-2θscan mode. Three strong reflections were measured every 3600 s and their intensities did not show appreciable decay. The data were corrected for absorption and polarization effects with CAD-4 software.

Data for complex **2** were collected with a MAR-research image plate system, using a graphite-monochromated Mo-K_α radiation ($\lambda = 0.71069$ Å). Single crystal was positioned at 75 mm from the plate. An exposure time of 2 min was used per 2° frame collected. Data analysis was carried out with XDS program [26]. Intensities were not corrected for absorption effects.

Structure analysis and refinement

The positions of the ruthenium atoms were obtained from three-dimensional Patterson maps and

Table 3. Crystal data and details of refinement of complexes **1** and **2**

	1	2
Formula	$C_{18}H_{26}Cl_2N_2O_3RuS_3$	$C_{16}H_{22}Cl_2N_2O_3RuS_3$
M	586.6	558.5
Crystal system	Monoclinic	Orthorhombic
Space group	$P2_1/n$	$Pbca$
a (Å)	11.753(2)	10.354(7)
b (Å)	8.047(6)	33.062(22)
c (Å)	23.952(4)	13.125(7)
β (°)	101.83(8)	(90)
V (Å^3)	2217.2(6)	4493.0
Z	4	8
D_c (g cm^{-3})	1.758	1.651
μ (Mo-K_α) (cm^{-1})	1.255	1.233
F(000)	1192	2256
Instrument	CAD-4 Four Circle Diffractometer	MAR-research Image Plate System
$2\theta_{max}$ (°)	50	50
Index ranges	$0 \leqslant h \leqslant 13$, $-2 \leqslant k \leqslant 9$, $-28 \leqslant l \leqslant 27$	$0 \leqslant h \leqslant 8$, $-38 \leqslant k \leqslant 38$, $-9 \leqslant l \leqslant 12$
Measured reflections	5657	5425
Unique reflections (R_{int})	3893 (0.0399)	2134 (0.0533)
Data-to-parameters ratio	3885/268	2134/272
Goodness-of-fit on F^2	0.914	0.869
Final R_1 and wR_2 values [$I > 2\sigma(I)$]	0.0412; 0.1031	0.0439, 0.1235
(all data)	0.0620, 0.1391	0.0564, 0.1361
Parameters a, b in weighting scheme[a]	0.0709, 11.69	0.1005, 31.74
Largest difference peak and hole (e Å^{-3})	0.978, −0.558	0.645, −0.839

[a] $w = 1/[\sigma^2(F_o^2) + (aP)^2 + bP]$, $P = [\mathrm{Max}(F_o^2) + 2F_o^2]/3$.

the remaining non-hydrogen atom positions by successive difference Fourier synthesis. The methylenic hydrogens were included in the refinement in calculated positions for idealized tetrahedral geometry while the aromatic hydrogens were found from difference Fourier maps. The hydrogen atoms of water molecules in both complexes were not found in final Fourier maps and were not included in the refinement. The hydrogens were refined with global isotropic thermal parameters. Anisotropic temperature factors were used for all non-hydrogen atoms. The structures were refined by least squares methods until convergence was achieved. The final refinements were made on F^2 using a weighting system, with the form $w = 1/[\sigma^2(F_o^2) + (aP)^2 + bP]$, $P = [\mathrm{Max}(F_o^2) + 2F_o^2]/3$ (see Table 3).

All calculations required to solve and refine the structures were carried out with SHELXS86 [27] and SHELX93 [28]. The atomic scattering factors were taken from [29]. The molecular diagrams were drawn with ORTEP II [30].

Additional material is available from the Cambridge Crystallographic Data Centre and comprises atomic coordinates, thermal parameters and the remaining bond lengths and angles.

Acknowledgements—We thank the E.P.S.R.C and the University of Reading for the image plate system and Insituto Superior Técnico for the CAD-4 diffractometer. We also thank Mr A. W. Johans for his technical assistance with crystallographic investigations. V. F. acknowledges the Junta Nacional de Investigação and British Council for a travel grant.

REFERENCES

1. J. K. Barton and E. Lolis, *J. Am. Chem. Soc.* 1985, **107,** 708.
2. C. V. Kumar, J. K. Barton and N. J. Turro, *J. Am. Chem. Soc.* 1985, **107,** 5518.
3. J. K. Barton, *Science* 1986, **233,** 727.
4. J. K. Barton, J. M. Goldberg, C. V. Kumar and N. J. Turro, *J. Am. Chem. Soc.* 1986, **108,** 2081.
5. A. M. Pyle, J. P. Rehmann, C. V. Kumar, N. J. Turro and J. K. Barton, *J. Am. Chem. Soc.* 1989, **111,** 3051.
6. A. M. Pyle and J. K. Barton, *Prog. Inorg. Chem: Bioinorg. Chem.* 1990, **38,** 413.
7. C. Hiort, B. Norden and A. Rodger, *J. Am. Chem. Soc.* 1990, **122,** 1971.
8. J. P. Rehmann and J. K. Barton, *Biochem.* 1990, **29,** 1710.
9. M. Eriksson, M. Leijon, C. Hiort, B. Nordem and A. Graslund, *J. Am. Chem. Soc.* 1992, **114,** 4933.
10. S. S. David and J. K. Barton, *J. Am. Chem. Soc.* 1993, **115,** 2984.
11. S. A. Tysoe, R. J. Morgan, A. D. Baker and T. C. Strekas, *J. Phys. Chem.* 1993, **97,** 1707.
12. K. Naing, M. Takahashi, M. Taniguchi and A. Yamagishi, *Inorg. Chem.* 1995, **34,** 350.
13. B. Rosenberg, L. VanCamp, J. E. Trosko and V. Mansour, *Nature* 1969, **222,** 385.
14. E. Alessio, G. Mestroni, G. Nardin, W. M. Attia, M. Calligaris, G., Sava and S. Zoret, *Inorg. Chem.* 1988, **27,** 4099.
15. B. K. Keppler, M. Henn, U. M. Juhl, M. R. Berger, R. Niebl and F. E. Wagner, *Prog. Clinical Biochem.* 1989, **10,** 41.
16. S. R. Cooper, S. C. Rawle, R. Yagbasan and D. J. Watkin, *J. Am. Chem. Soc.* 1991, **113,** 1600.
17. A. H. Krotz, L. Y. Kuo and J. K. Barton, *Inorg. Chem.* 1993, **32,** 5963.
18. C. Landgrafe and W. S. Sheldrick, *J. Chem. Soc., Dalton Trans.* 1994, 1885.
19. B. J. Goodfellow, S. M. D. Pacheco, J. Pedrosa de Jesus, M. G. B. Drew and Vitor Félix (unpublished results).
20. J.C. A. Boeyens and S. M. Dobson, *Stereochemical and Stereophysical Behavior of Macrocycles* (Edited by I. Bernal) Vol. 2. 1. Elsevier, Amsterdam (1987).
21. Cambridge Crystallographic Data Base, update (1996).
22. R. S. Glass, G. S. Wilson and W. N. Setzer, *J. Am. Chem. Soc.* 1980, **102,** 1068.
23. J. Beech, P. J. Cragg and M. G. B. Drew, *J. Chem. Soc., Dalton Trans.* 1994, 719.
24. I. P. Evans, A. Spencer and G. Wilkinson, *J. Chem. Soc., Dalton Trans.* 1973, 204.
25. S. Macura and R. R. Ernst, *Mol. Phys.* 1980, **41,** 95.
26. W. Kabsch, *J. Appl. Crystallogr.* 1988, **21,** 916.
27. G. M. Sheldrick, *SHELXS*-86, in *Crystallographic Computing* 3, (Edited by G. M. Sheldrick, C. Krüger and R. Goddard). Oxford University Press (1985).
28. G. M. Sheldrick, *SHELX*-93, *Program for Crystal Structure Refinement*, University of Göttingen (1994).
29. *International Tables for X-Ray Crystallography, Vol.* 4, Kynoch Press, Birmingham (1974).
30. C. K. Johnson, ORTEP II, A Fortran Thermal-ellipsoid, Plot Program, for Crystal Structure Illustrations. Report ORNL-5138, Oak Ridge National Laboratory, Oak Ridge, TN (1976).

Pergamon

PII: S0277-5387(96)00307-5

Polyhedron Vol. 16, No. 3, pp. 403–408, 1997
Copyright © 1996 Elsevier Science Ltd
Printed in Great Britain. All rights reserved
0277-5387/97 $17.00+0.00

Synthesis and characterization of the linear M—Hg—M trimetallic complexes $[\eta^5\text{-}Bz_5C_5(CO)_3M]_2Hg$ and $[\eta^5\text{-}HO_2CC_5H_4(CO)_3M]_2Hg$ (M = Cr, Mo, W). The X-ray crystal structure of $[\eta^5\text{-}Bz_5C_5(CO)_3W]_2Hg$

Li-Cheng Song,[a]* Lu-Yan Zhang,[a] Zhi-Fu Tao,[a] Qing-Mei Hu[a] and Xiao-Ying Huang[b]

[a]Department of Chemistry, Nankai University, Tianjin 300071, P.R. China

[b]State Key Laboratory of Structural Chemistry, Fuzhou 350002, P.R. China

(Received 15 May 1996; accepted 18 June 1996)

Abstract—The η^5-Bz_5C_5 ligand-containing trimetallic complexes $[\eta^5\text{-}Bz_5C_5(CO)_3M]_2Hg$ (M = Cr, Mo, W) were synthesized from the *in situ* reaction of phenylmercuric chloride with corresponding transition metal lithium salts $[\eta^5\text{-}Bz_5C_5(CO)_3M]$ Li in THF, whereas the η^5-$HO_2CC_5H_4$ ligand-containing trimetallic complexes $[\eta^5\text{-}HO_2CC_5H_4(CO)_3M]_2Hg$ were synthesized through hydrolysis of their corresponding esters in the presence of $KOH/EtOH/H_2O$, followed by acidification. These compounds were characterized by elemental analysis, IR, ^1H NMR and MS spectroscopy, while the structure of $[\eta^5\text{-}Bz_5C_5(CO)_3W]_2Hg$ was determined by an X-ray diffraction analysis. Copyright © 1996 Elsevier Science Ltd

Keywords: η^5-pentabenzylcyclopentadienyl; η^5-carboxycyclopentadienyl; group 6 metals; mercury; crystal structure.

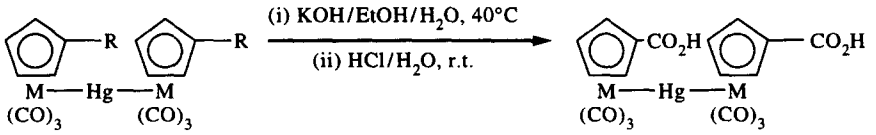
In view of the theoretical and practical importance of metal–metal bonded compounds [1], the organometallic complexes containing M—Hg—M (M = Cr, Mo, W) structural moieties have so far received considerable attention [2–4]. However, although the trimetallic M—Hg—M complexes containing mono-substituted cyclopentadienyl ligand have been known for several years [2–4], the study concerning their chemical reactions and synthesis regarding the M—Hg—M complexes containing poly-substituted cyclopentadienyl ligand has not been reported as yet. In order to further understanding of the properties of this kind of complex containing mono-substituted cyclopentadienyl ligand and to prepare the novel M—Hg—M complexes carrying η^5-pentabenzylcyclopentadienyl ligand η^5-Bz_5C_5, we initiated this study. Herein we report the synthesis and characterization of the new complexes $[\eta^5\text{-}HO_2CC_5H_4(CO)_3M]_2Hg$ and $[\eta^5\text{-}Bz_5C_5(CO)_3M]_2Hg$ (M = Cr, Mo, W) including the single-crystal structure of $[\eta^5\text{-}Bz_5C_5(CO)_3W]_2Hg$ determined by X-ray diffraction analysis.

* Author to whom correspondence should be addressed.

RESULTS AND DISCUSSION

Synthesis and characterization of $[\eta^5\text{-}HO_2CC_5H_4(CO)_3M]_2Hg$ (**2a–2c**)

On the basis of our work for synthesizing $[\eta^5\text{-}RC_5H_4(CO)_3M]_2Hg$ (M = Cr, Mo, W; R = CO_2Me, CO_2Et) (**1**) [3], an effort has been made to study further the preparation of their hydrolysis derivatives **2**. Fortunately, it was found that the M—Hg—M structural unit in the starting complexes **1** is quite stable towards both acidic and alkaline conditions; the starting complexes **1**, after the action of $NaOH/EtOH/H_2O$ and followed by acidification of the intermediate potassium salt with HCl/H_2O, gave rise to the cor-



1 **2**

R = CO_2Me, CO_2Et **2a** : M = Cr; **2b** : M = Mo; **2c** ; M = W

Scheme 1.

responding derivatives **2** in moderate yields, as shown in Scheme 1.

Products **2a–2c** are air-stable yellow solids and soluble in THF, DMSO and acetone but not in CH_2Cl_2 and other non-polar solvents. All of them were fully characterized by elemental analysis, IR, ^1H NMR and mass spectroscopies. In the IR spectra of **2a–2c,** there are three strong to very strong absorption bands in the range of 1884–1967 cm^{-1}, characteristic of their terminal carbonyls, one strong absorption band at about 1680 cm^{-1} and one broad band at about 3430 cm^{-1} characteristic of their carbonyl and hydroxyl group in the carboxylic substituent, respectively. Their ^1H NMR spectra have a pair of apparent triplets, in which the downfield triplet has been assigned to the H(2, 5) protons of the substituted cyclopentadienyl ring, while the upfield triplet is assigned to the H(3, 4) protons. Additionally, the triplet assigned to H(2, 5) or H(3, 4) is located in the lowest field in the case of the tungsten compound **2c,** the intermediate field for the molybdenum compound **2b** and in the highest field for the chromium compound **2a** and there are larger differences in chemical shifts between the corresponding triplets of **2a** and **2b** than between those of **2b** and **2c**. It follows that the ^1H NMR behaviour of the functionally substituted cyclopentadienyl ring of **2a–2c** are similar to that of starting complexes and other electron-withdrawing functional analogs [2, 3, 5]. It is worth pointing out that the ^1H NMR spectrum of the carboxylic functionality was not observed in the field as low as $\delta = 15$ ppm, perhaps due to the D/H exchange between **2** and the solvent DMSO.

Synthesis and characterization of $[\eta^5\text{-}Bz_5C_5(CO)_3M]_2$ Hg **(4a–4c)**

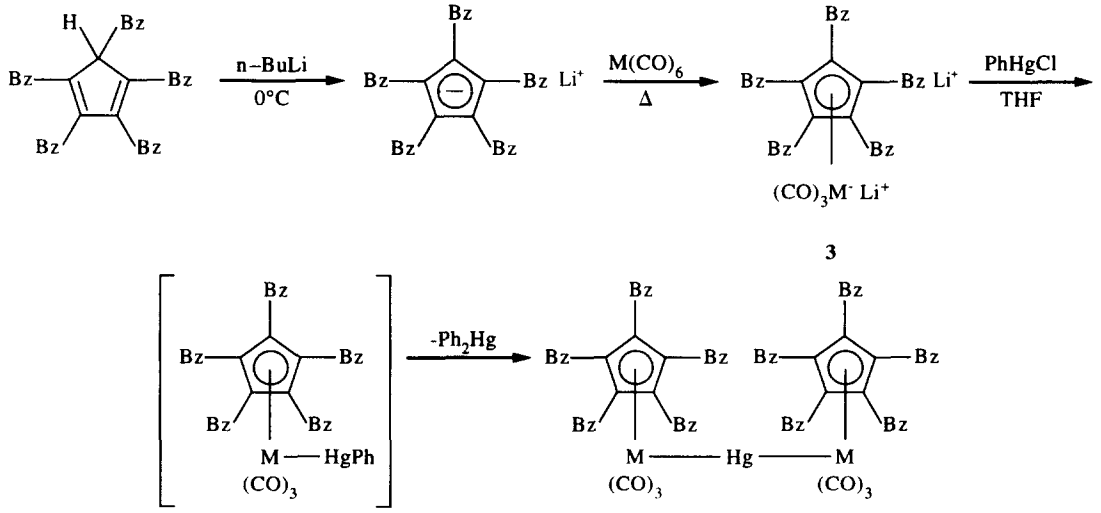
Similar to the lithium or sodium salts of monosubstituted cyclopentadienyltricarbonyl group 6 metal anions [2–4], the pentabenzylcyclopentadienyl analogs $\eta^5\text{-}Bz_5C_5(CO)_3MLi$ (**3**) derived from sequential reactions of pentabenzylcyclopentadiene, *n*-BuLi and group 6 metal carbonyls $M(CO)_6$, reacted with phenylmercuric chloride in THF to give the expected trimetallic compounds **4a–4c**. According to the related mechanistic study [3], the compounds **4a–4c** were most likely produced by a symmetrization process of the active bimetallic intermediate $\eta^5\text{-}Bz_5C_5M(CO)_3$-HgPh formed by a condensation reaction of **3** with PhHgCl, as shown in Scheme 2.

Compounds **4a–4c** are air-stable yellow crystalline solids, whose melting points increase in the order of **4a** < **4b** < **4c**. The yields of **4a–4c** are much lower than those of the analogs containing $\eta^5\text{-}C_P$ or $\eta^5\text{-}RC_5H_4$ ligand [2–4], the reason for which could be attributed to the special electronic and steric effects of $\eta^5\text{-}Bz_5C_5$ ligand [6–10] relative to those of $\eta^5\text{-}C_P$ and η^5-mono-substituted cyclopentadienyl ligand. For **4a–4c** all the characterizing data of the elemental analysis, IR and ^1H NMR spectroscopy are in good agreement with the structures shown in Scheme 2. However, it is worth noting that compounds **4a–4c** contain not only terminal carbonyls, but also bridging carbonyls. This is because in each of their IR spectra there is one strong absorption band at about 1860 cm^{-1} besides two absorption bands at the region of 1884–1959 cm^{-1}.

X-ray crystallography

In order to determine the structure of compounds **4a–4c** and establish the type of carbonyls in these compounds, an X-ray diffraction analysis for **4c** was undertaken. To the best of our knowledge, this is the first single-crystal molecular structure determination of an M—Hg—M trinuclear organometallic containing $\eta^5\text{-}Bz_5C_5$ ligand, although those of $\eta^5\text{-}Bz_5C_5$-containing mononuclear [8–10] and dinuclear [11] organometallics and $\eta^5\text{-}C_P$ [2, 12] or $\eta^5\text{-}RC_5H_4$ [3,4] containing M—Hg—M organometallics are known. Table 1 lists the crystallographic data. Table 2 and Table 3 list the selected bond lengths and bond angles, respectively. Figure 1 shows its molecular structure.

As seen from Fig. 1 complex **4c** consists of one mercury atom and two identical organometallic structural units $\eta^5\text{-}Bz_5C_5(CO)_3W$. The central Hg atom is located on a crystallographic inversion center so that the W—Hg—W skeleton is exactly linear ($\angle$W—Hg—W = 180°) and two substituted cyclopentadienyl rings are parallel and lie in a *trans* position with respect to the linear W—Hg—W axis. This is also the case for the ethoxycarbonylcyclopentadienyl molybdenum analog [3] but different from its parent compound, which is non-centrosymmetric and has a *cis* configuration of cyclopentadienyl ligands with respect to the W—Hg—W axis [2]. The bond angles



4a : M = Cr; **4b** : M = Mo; **4c** : M = W

Scheme 2.

Table 1. Crystal data and intensity collection details for **4c**

Empirical formula	$C_{86}H_{70}HgO_6W_2$
Formula weight	1767.79
Crystal system	monoclinic
Space group	$P2_1/n$(#14)
Lattice parameters	
a (Å)	12.536(1)
b (Å)	15.180(4)
c (Å)	18.322(4)
β (°)	94.04(1)
V (Å^3)	3478(1)
Z	2
D_{calc} (g cm^{-3})	1.69
F(000)	1724
μ (Mo-K_α) (cm^{-1})	56.25
Radiation	Mo-K_α, λ = 0.71069 Å graphite-monochromated
Temperature (°C)	23
$2\theta_{max}$(°)	49.9
No. of observation ($I \geqslant 3\sigma(I)$)	4202
No. of variables	430
Residuals R and Rw	0.042, 0.047
Goodness of fit indicator	1.07
Maximum shift in final cycle	0.00
Largest peak in final diff. map (eÅ^{-3})	0.80

Table 2. Selected bond lengths (Å) for **4c**

W—Hg	2.7532(7)	C(2)—C(3)	1.44(1)
W—C(03)	1.93(1)	C(2)—C(20)	1.52(1)
W—C(01)	1.94(1)	C(3)—C(4)	1.45(1)
W—C(02)	1.98(1)	C(3)—C(30)	1.48(1)
W—C(5)	2.310(9)	C(4)—C(5)	1.43(1)
W—C(1)	2.325(9)	C(4)—C(40)	1.51(1)
W—C(4)	2.336(8)	C(5)—C(50)	1.52(1)
W—C(2)	2.362(9)	C(10)—C(11)	1.51(1)
W—C(3)	2.376(8)	C(11)—C(16)	1.35(1)
O(1)—C(01)	1.16(1)	C(11)—C(12)	1.40(2)
O(2)—C(02)	1.16(1)	C(12)—C(13)	1.35(2)
O(3)—C(03)	1.17(1)	C(13)—C(14)	1.36(2)
C(1)—C(2)	1.42(1)	C(14)—C(15)	1.33(2)
C(1)—C(5)	1.44(1)	C(15)—C(16)	1.36(2)
C(1)—C(10)	1.52(1)	Hg—C(01)	2.843(9)

W—C(01)—O(1) and W—C(02)—O(2) [174(1) and 177(1)°, respectively] and Hg—W—C(01) and Hg—W—C(02) [72.2(3) and 69.9(3)°, respectively] indicate that the C(01)—O(1) and C(02)—O(2) carbonyl ligands are linear semi-bridging. Since the W—C(01) and Hg···C(01) distances D_1 and D_2 are 1.94(1) and 2.84(3) Å, for C(01)—O(1) the bridge asymmetry parameter $\alpha = 0.47$; since W—C(02) and Hg···C(02) distances D_1 and D_2 are 1.98(1) and 2.78(6) Å, for C(02)—O(2) $\alpha = 0.41$ ($\alpha = D_2 - D_1/D_1$) [13–14]. Apparently, the second W atom also has attached two corresponding carbonyls since **4c** is centrosymmetric. So, the fact that the semi-bridging cabonyls exist in **4c** is in good agreement with its IR spectroscopic data.

It is worth pointing out that for each of the two η^5-Bz_5C_5 ligands in complex **4c** four phenyl groups bonded to C(10), C(30), C(40) and C(50) of the benzyl substituents are situated on the opposite side of the tungsten atom with respect to substituted cyclopentadienyl ring, while the phenyl group attached to C(20) of the benzyl substituent approaches the tungsten atom. Similar to the mononuclear analogs of cobalt [6], manganese [7] and molybdenum [10], this

Table 3. Selected bond angles (°) for **4c**

W*—Hg—W	180.00	C(3)—C(4)—W	73.6(5)
C(01)—W—C(02)	102.7(4)	C(40)—C(4)—W	122.2(6)
C(01)—W—C(5)	101.1(4)	C(4)—C(5)—C(1)	107.2(8)
C(01)—W—C(1)	135.9(4)	C(4)—C(5)—C(50)	124(1)
C(01)—W—C(4)	92.5(4)	C(4)—C(5)—W	73.1(5)
C(01)—W—C(2)	151.2(4)	C(1)—C(5)—C(50)	128(1)
C(01)—W—C(3)	117.8(4)	C(1)—C(5)—W	72.5(5)
C(1)—W—Hg	137.6(2)	C(50)—C(5)—W	122.2(6)
C(4)—W—Hg	95.6(2)	C(03)—W—Hg	130.3(3)
C(2)—W—Hg	103.4(2)	C(01)—W—Hg	72.2(43)
C(3)—W—Hg	80.5(2)	C(02)—W—Hg	69.9(3)
W*—Hg—C(01)	139.4(3)	W*—Hg—C(02)	138.1(3)

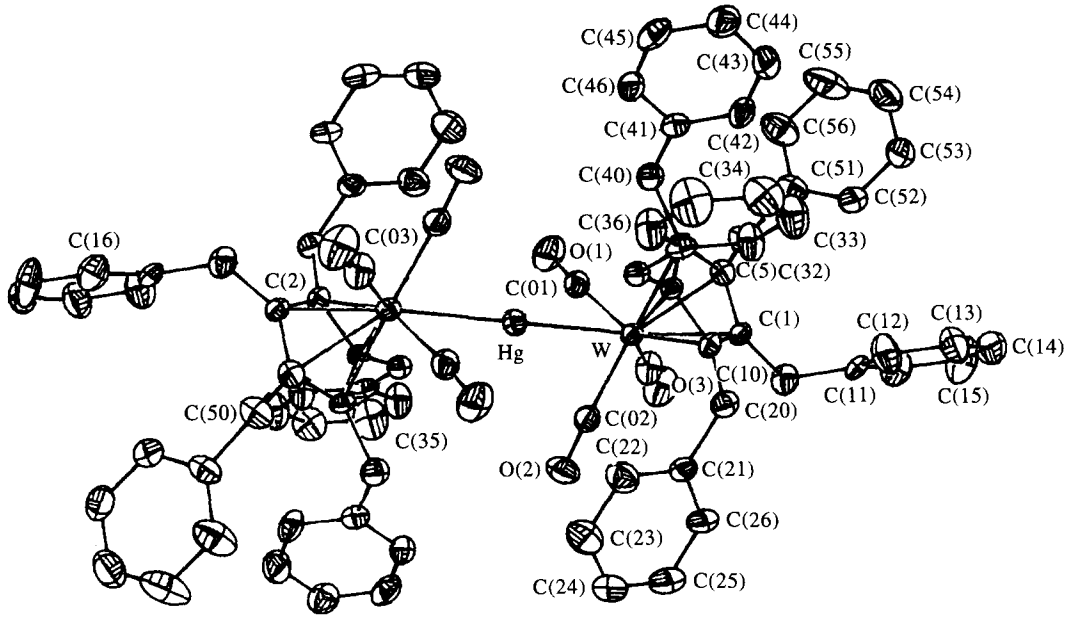


Fig. 1. Molecular structure of **4c**.

could be possibly caused by the smallest gap between the two phenyl groups bound to C(10) and C(30). However, this is not the case because the non-bonding distance of C(11)···C(31) (6.235 Å) lies midway between those of C(11)···C(41) (6.508 Å) and C(31)···C(51) (6.203 Å). So, besides the intramolecular non-bonding interactions, the intermolecular interactions could also be one of the reasons for this geometric arrangement of the five phenyl groups in complex **4c**. However, the real reasons remain unclear and further study is needed.

EXPERIMENTAL

The reactions were carried out under highly prepurified tank nitrogen. Diglyme and THF were rigorously dried and deoxygenated by distillation from Na/benzophenone ketyl. Bz_5C_5H [10], *n*-BuLi [15] and $[\eta^5\text{-}RO_2CC_5H_4(CO)_3M]_2Hg$ (M = Cr, Mo, W; R = CO_2Me, CO_2Et) [3] were prepared according to the literature. $M(CO)_6$(M = Cr, Mo, W) was purchased from Strem Chemicals Inc. and PhHgCl from Alfa Ventron. Silica gel for column chromatography was of about 300–400 mesh. Silica gel for TLC was GF-254 (10–40 μm). IR spectra were recorded on a Nicolet FT-IR 5DX spectrophotometer, ^1H NMR spectra on a Jeol FX 90Q spectrometer. Elemental analysis and MS determinations were performed by a 240 C analyzer and HP 5988A spectrometer, respectively. Melting points were determined on a Yanaco MP-500 apparatus.

Synthesis of $[\eta^5\text{-}HO_2CC_5H_4(CO)_3Cr]_2Hg$ (**2a**)

A 100 cm^3 two-necked flask equipped with a magnetic stir-bar, a serum cap and a reflux condenser, was charged with 0.697 g (0.96 mmol) of $[\eta^5\text{-}EtO_2$

$CC_5H_4(CO)_3Cr]_2Hg$, 20 cm^3 of C_2H_5OH and a solution prepared from 0.291 g (5.19 mmol) KOH and 10 cm^3 of distilled water. The reaction mixture was stirred for 8–10 h at about 40°C until TLC showed no starting complex left. After cooling to room temperature, the reaction mixture was filtered and to the filtrate was added about 50 cm^3 of distilled water followed by treatment with concentrated HCl until the yellow solid precipitated completely. The solid was filtered out and washed first with distilled water until the filtrate reached to the neutral and then washed with CH_2Cl_2 several times. Drying of the washed solid *in vacuo* gave 0.311 g (48%) of **2a** as a yellow solid, m.p. 158°C (dec.). Found: C, 31.6; H, 1.6. Calc. for $C_{18}H_{10}Cr_2HgO_{10}$: C, 31.3; H, 1.5%. IR (KBr, disc): νOH, 3435 (br.), $\nu_{C\equiv O}$, 1959(vs), 1915(s), 1893(vs), $\nu_{C=O}$, 1688(s) cm^{-1}. ^1H NMR (DMSO, δ, ppm): 5.29 [t, 4H, 2(H^3, H^4)], 5.67 [t, 4H, 2(H^2, H^5)]. MS(EI, Cr^{52}), *m/z* (relative intensity): 245 [$HO_2CC_5H_4Cr(CO)_3^+$, 7.3], 217[$HO_2CC_5H_4Cr(CO)_2^+$, 15.7], 202(Hg^+, 62.5), 189[$HO_2CC_5H_4Cr(CO)^+$, 17.2], 161($HO_2CC_5H_4Cr^+$, 56.8), 109($HO_2CC_5H_4^+$, 0.4), 65($C_5H_5^+$, 12.6), 52(Cr^+, 60.7), 45(CO_2H^+, 2.9).

Synthesis of [η^5-$HO_2CC_5H_4(CO)_3Mo]_2Hg$ (**2b**)

The same procedure for **2a** was followed, but the reagents were changed as follows: 0.597 g (0.74 mmol) of [η^5-$MeO_2CC_5H_4(CO)_3Mo]_2Hg$ and 0.201 g (3.59 mmol) of KOH; or 0.75 g (0.90 mmol) of [η^5-EtO_2C-$C_5H_4(CO)_3Mo]_2Hg$ and 0.219 g (3.91 mmol) of KOH. The former reaction gave 0.449 g (78%) of **2b,** while the latter reaction gave 0.589 g (84%) of **2b,** as a yellow solid, m.p. 195°C (dec.). Found: C, 27.7; H, 1.3. Calc. for $C_{18}H_{10}HgMo_2O_{10}$: C, 27.8; H, 1.3%. IR (KBr, disc): ν_{OH}, 3443 (br.), $\nu_{C\equiv O}$, 1967(vs), 1922(s), 1893(vs), $\nu_{C=O}$, 1680(s) cm^{-1}. ^1H NMR (DMSO, δ, ppm): 5.76[t, 4H, 2(H^3, H^4)], 6.14 [t, 4H, 2(H^2, H^5)]. MS(EI, MO^{98}), *m/z* (relative intensity): 291[HO_2C-$C_5H_4Mo(CO)_3^+$, 4.0], 263[$HO_2CC_5H_4Mo(CO)_2^+$, 2.9], 247[$C_5H_5Mo(CO)_3^+$, 1.2], 235[$HO_2CC_5H_4Mo(CO)^+$, 2.8], 207($HO_2CC_5H_4Mo^+$, 3.2), 202(Hg^+, 26.2), 66($C_5H_6^+$, 31.4), 45(CO_2H^+, 7.1).

Synthesis of [(η^5-$HO_2CC_5H_4(CO)_3W]_2Hg$ (**2c**)

The same procedure for **2a** was followed, but the reagents were changed as follows: 0.272 g (0.277 mmol) of [η^5-$MeO_2CC_5H_4(CO)_3W]_2Hg$ and 0.069 g (1.23 mmol) of KOH. 0.205 g (78%) of **2c** was given as a yellow solid, m.p. 224°C (dec.). Found: C, 22.7; H, 1.0; Calc. for $C_{18}H_{10}HgO_{10}W$: C, 22.7; H, 1.1%. IR (KBr, disc): ν_{OH}, 3418 (br.), $\nu_{C\equiv O}$, 1967(vs), 1909(s), 1885(vs), $\nu_{C=O}$, 1688(s) cm^{-1}. ^1H NMR (DMSO, δ, ppm): 5.84 [t, 4H, 2(H^3, H^4)], 6.20 [t, 4H, 2(H^2, H^5)]. MS(EI, W^{185}), *m/z* (relative intensity): 202(Hg^+, 40.3), 185(W^+, 18.5), 109($HO_2CC_5H_4^+$, 28.9), 64($C_5H_4^+$, 14.0), 45(CO_2H^+, 38.5).

Synthesis of [η^5-$Bz_5C_5(CO)_3Cr]_2Hg$ (**4a**)

A 100 cm^3 two-necked flask equipped with a magnetic stir-bar, a serum cap and a reflux condenser, was charged with 1.24 g (2.4 mmol) of η^5-Bz_5C_5H and 20 cm^3 of diglyme. To this mixture was added an equimolar aliquot of *n*-BuLi/hexane at 0°C and the solution turned to deep purple. After continuous stirring for 15 min, 0.538 g (2.4 mmol) of $Cr(CO)_6$ was added and the reaction mixture heated at about 130°C overnight. Solvent was removed at reduced pressure and 20 cm^3 of THF was added to give a THF solution of the salt η^5-$Bz_5C_5(CO)_3CrLi$. To this salt, 0.70 g (2.4 mmol) of PhHgCl was added at about 0°C and the solution turned to bright-yellow rapidly. After stirring for an additional 1 h, solvent was removed at reduced pressure to give a residue, which was extracted with CH_2Cl_2. The extracts were subjected to column chromatography and TLC separation with 50% CH_2Cl_2/petroleum ether as eluent, followed by recystallization from 50% CH_2Cl_2/petroleum ether to give 0.045 g (3%) of **4a** as a yellow solid, m.p. 140–142°C. Found: C, 68.2; H, 4.7. Calc. for $C_{86}H_{70}Cr_2HgO_6$: C, 68.7; H, 4.7%. IR (KBr, disc): $\nu_{C\equiv O}$, 1942(vs), 1885(s), 1860(vs) cm^{-1}. ^1H NMR ($CDCl_3$, δ, ppm): 3.90(s, 20H, $10CH_2$), 6.40–7.32(m, 50H, $10C_6H_5$).

Synthesis of [η^5-$Bz_5C_5(CO)_3Mo]_2Hg$ (**4b**)

A 100 cm^3 two-necked flask equipped with a magnetic stir-bar, a serum cap and a reflux condenser, was charged with 1.24 g (2.4 mmol) of η^5-Bz_5C_5H and 20 cm^3 of THF. The mixture was stirred and cooled to 0°C. To this mixture was added an equimolar aliquot of *n*-BuLi/hexane at 0°C. After stirring for 15 min, 0.62 g (2.4 mmol) of $Mo(CO)_6$ was added and the reaction mixture refluxed for about 24 h to give the salt η^5-$Bz_5C_5(CO)_3MoLi$. To this salt was added 0.70 g (2.4 mmol) of PhHgCl at about 0°C and the reaction mixture stirred for an additional 1 h. After the same work-up as that in the preparation of **4a,** 0.085 g (5%) of **4b** was given as a yellow solid, m.p. 188–189°C. Found: C, 64.8; H, 4.4. Calc. for $C_{86}H_{70}HgMo_2O_6$: C, 64.9; H, 4.4%. IR (KBr, disc): $\nu_{C\equiv O}$, 1959(vs), 1909(s), 1868(vs) cm^{-1}. ^1H NMR ($CDCl_3$, δ, ppm): 3.97(s, 20H, $10CH_2$), 6.70–7.27(m, 50H, $10C_6H_5$).

Synthesis of [η^5-$Bz_5C_5(CO)_3W]_2Hg$ (**4c**)

The same procedure for **4a** was followed, but use of 0.84 g (2.4 mmol) of $W(CO)_6$ instead of $Cr(CO)_6$ to give 0.121 g (6%) of **4c** as a yellow solid, m.p. 200–202°C. Found: C, 58.4; H, 3.8. Calc. for $C_{86}H_{70}HgO_6W_2$: C, 58.4; H, 4.0%. IR (KBr, disc): $\nu_{C\equiv O}$, 1950(vs), 1893(s), 1860(vs) cm^{-1}. ^1H NMR ($CDCl_3$, δ, ppm): 4.00(s, 20H, $10CH_2$), 6.63–7.25(m, 50H, $10C_6H_5$).

Single-crystal structure determination of [η^5-Bz_5C_5 $(CO)_3W]_2Hg$ (**4c**)

A yellow crystal measuring $0.16 \times 0.20 \times 0.50$ mm^3 obtained by recrystallization from CH_2Cl_2/hexane in a refrigerator, was mounted on a glass fiber and placed on an Enraf-Nonius CAD4 diffractometer equipped with a graphite monochromator. A total of 6386 independent reflections were collected at room temperature with Mo-K_α ($\lambda = 0.71069$ Å) radiation by ω-2θ scan mode, of which 4202 independent reflections with $I \geqslant 3\sigma(I)$ were considered to be observed and used in the subsequent refinement. Data were corrected for Lp factors.

The positions of tungsten and mercury atoms were found in an E-map by direct methods and the remaining non-hydrogen atoms found in the succeeding difference Fourier syntheses. The final refinement by full-matrix least-squares method used anisotropic thermal parameters for non-hydrogen atoms. All calculations were performed on a MICRO-VAX I computer using TEXSAN program system.

Acknowledgements—We are grateful to National Natural Science Foundation of China, Laboratory of Organometallic Chemistry at Shanghai Institute of Organic Chemistry, and State Key Laboratory of Elemento-Organic Chemistry for financial support of this work.

REFERENCES

1. G. Wilkinson, F. G. A. Stone and E. W. Abel, (Eds.) *Comprehensive Organometallic Chemistry*, Vol. 6, Ch. 40, p. 763 and Ch. 42, p. 983. Pergamon Press, Oxford (1982).
2. L.-C. Song, H. Yang, Q. Dong and Q.-M. Hu, *J. Organomet. Chem.* 1991, **414,** 137.
3. L.-C. Song, Q. Dong and Q.-M. Hu, *Acta Chim. Sin.* 1992, **50,** 193.
4. L.-C. Song, Z.-F. Tao, Q.-M. Hu, R.-J. Wang and H.-G. Wang, *Polyhedron* 1994, **13,** 2179.
5. D. W. Macomber and M. D. Rausch, *J. Organomet. Chem.* 1983, **258,** 331.
6. J. W. Chambers, A. J. Baskar, S. G. Bott, J. L. Atwood and M. D. Rausch, *Organometallics* 1986, **5,** 1635.
7. M. D. Rausch, W.-M. Tsai, J. W. Chambers, R. D. Rogers and H. G. Alt, *Organometallics* 1989, **8,** 816.
8. H. Schumann, C. Janiak, R. D. Cöhn, J. Loebel and A. Dietrich, *J. Organomet. Chem.* 1989, **365,** 137.
9. H. Schumann, *Pure and Appl. Chem.* 1991, **63,** 813.
10. L.-C. Song, L.-Y. Zhang, Q.-M. Hu and X.-Y. Huang, *Inorg. Chim. Acta* 1995, **230,** 127.
11. L.-C. Song, J.-Q. Wang, L.-Y. Zhang, Q.-M. Hu and X.-Y. Huang, *Youji Huaxue* 1995, **15,** 202.
12. M. M. Mickiewicz, C. L. Baston, A. H. White and S. B. Wild, *Australian J. Chem.* 1977, **30,** 1685.
13. M. D. Curtis and W. M. Butler, *J. Organomet. Chem.* 1978, **155,** 131.
14. R. J. Klinger, W. M. Butler and M. D. Curtis, *J. Am. Chem. Soc.* 1978, **100,** 5034.
15. (a) H. Gilman, W. Langham and F. W. Moore, *J. Am. Chem. Soc.* 1940, **62,** 2327; (b) W. G. Kofron and M. Baclawski, *J. Org. Chem.* 1976, **41,** 1879.

Pergamon

PII: S0277-5387(96)00311-7

Polyhedron Vol. 16, No. 3, pp. 409–415, 1997
Copyright © 1996 Elsevier Science Ltd
Printed in Great Britain. All rights reserved
0277-5387/97 $17.00+0.00

Preparation of molybdenum(II) η^2-vinyl complexes *via* sequential C—Cl activation and alkyne insertion

Jaqueline L. Kiplinger and Thomas G. Richmond*

Department of Chemistry, University of Utah, Salt Lake City, UT 84112, U.S.A

(Received 2 May 1996; accepted 18 June 1996)

Abstract—Reaction of the Schiff base ligand **1**, prepared by the condensation of 2-chlorobenzaldehyde and *N*,*N*-dimethylethylenediamine with $(\eta^6\text{-}C_6H_5CH_3)Mo(CO)_3$ **2** resulted in the formation of the seven-coordinate molybdenum(II) metallacycle, **3**, by oxidative addition of the strong aromatic C—Cl bond at molybdenum(0). The metallacycle **3** undergoes migratory insertion with electron-deficient internal acetylenes to afford novel η^2-vinyl complexes **4**, resulting in net replacement of a C—Cl bond by a C—C bond. Copyright © 1996 Elsevier Science Ltd

Keywords: oxidative addition; molybdenum; alkyne; insertion; bond activation; metallacycle.

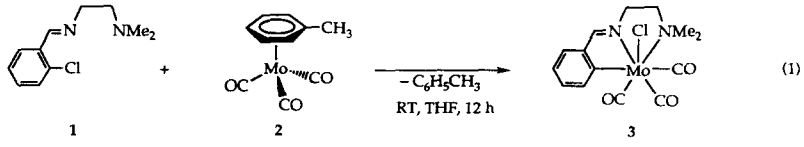
Organometallic η^2-vinyl complexes are of interest because of a variety of catalytic chemical transformations postulate the crucial participation of vinyl intermediates stabilized by a metal centre [1]. Most synthetic approaches to η^2-vinyl complexes have involved the external attack of nucleophiles (hydrides [2], thiols and thiolates [3], nitrogen [4] and phosphorus [5] reagents) on coordinated alkyne ligands. If the metal is electronically saturated, only an η^1-vinyl complex is formed [6].

Recently, we demonstrated that a rare migration reaction of a highly fluorinated ligand takes place at a tungsten(II) metal centre to afford robust η^2-vinyl compounds [7]. Importantly, it was shown that known oxidative addition chemistry, in conjunction with migratory insertion of unsaturated organic compounds, can be employed for the activation [8] and chemical modification [9] of C—F bonds.

We now report that this chemistry can be extended to chlorinated aromatic compounds and exploited for the construction of novel molybdenum(II) η^2-vinyl complexes. The key features of this work is that net replacement of an aromatic carbon–chlorine bond by a carbon–carbon linkage occurs under mild conditions *via* sequential oxidative addition and alkyne insertion at a molybdenum carbonyl complex.

RESULTS AND DISCUSSION

The Schiff base ligand **1** was prepared by condensation of 2-chlorobenzaldehyde and *N*,*N*-dimethylethylenediamine in ethanol and purified as a yellow oil by vacuum distillation [10]. As depicted in Eq. (1), treatment of a tetrahydrofuran solution of



1 2 3 (1)

* Author to whom correspondence should be addressed.

(η^6-$C_6H_5CH_3$)$Mo(CO)_3$ **2** [1], which generates the complex $Mo(CO)_3(thf)_3$ (thf = tetrahydrofuran) *in situ*, with **1** at room temperature for 12 h, affords a dark green solution from which **3** crystallizes as a dark green solid in 66% isolated yield.

Compound **3** exhibits several spectroscopic features that are virtually identical to structurally characterized tungsten(II) and platinum(IV) metallacycles [10,12]. Thus, **3** was formulated as a seven-coordinate molybdenum(II) metallacycle which was produced by chelate-assisted oxidative addition of the aromatic C—Cl bond in **1** to molybdenum(0). Loss of the C_{3v} symmetry of $Mo(CO)_3(thf)_3$ (ν_{CO} = 1920, 1790 cm^{-1}) was noted by the presence of three distinct carbonyl stretches at 2017, 1944 and 1903 cm^{-1} for **3** in thf solution.

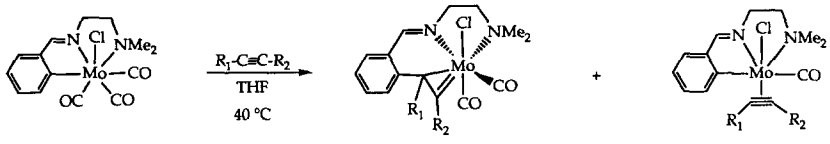
As shown in Fig. 1, the ^1H NMR spectra for **3** displays four distinct and highly coupled multiplet resonances (δ 4.55, 4.34, 3.90 and 2.41) for the methylene protons on the ethylene backbone; each integrate to one proton. This non-equivalence illustrates not only the chirality of the seven-coordinate molybdenum(II) metal centre but also the retained coordination of the ligand in solution. As evidenced by the presence of three uncoupled singlet resonances (δ 230.1, 224.1 and 223.8) for the carbonyl ligands at low field in the ^{13}C $\{^1H\}$ NMR spectrum, **3** is static on the NMR time-scale. In fact, the presence of three carbonyl resonances for complex **3** must reflect the rigid nature of the η^3-[C,N,N'] imine chelate ligand, as seven-coordinate complexes typically undergo non-rigid processes at the metal centre [13]. In contrast, related seven-coordinate tungsten(II) carbonyl systems containing a saturated monoanionic η^3-[C,N,N'] ligand exhibit dynamic behaviour at room temperature [14]. A carbon APT spectrum of **3** allowed for the facile identification of the iminic carbon and the metal-bound carbon as singlets at δ 178.4 and 169.6, respectively. The remaining aryl, methylene and methyl carbons afford eight additional resonances which are consistent with a capped octahedral structure for these compounds, with the aryl carbon as the capping group as noted for crystallographically characterized tungsten analogues [10,12,15].

The ability of this system to engage in facile C—Cl cleavage is attributed to several factors associated with ligand design. The nitrogen donor ligand supports a very basic metal centre which is required for oxidative addition. The chelating nature of the ligand is crucial since it reduces the entropic barrier to reaction by placing the C—Cl bond in close proximity to the Mo^0 metal centre. No evidence of bimolecular C—Cl activation of 2-chlorobenzaldehyde or chlorobenzene with **2** has been observed. Finally, the restricted conformation as well as the extended conjugation imparted by the imine moiety in the resulting metallacycle **3** are also important for promoting C—Cl activation in this system.

That cleavage of the carbon–chlorine bond (94 kcal/mol) [16] takes place in the presence of a C—H bond (110 kcal/mol) [16] is not surprising; however, that the facile cleavage of the robust C—Cl bond occurs under such mild conditions is noteworthy if one considers that carbon–chlorine bond activation is a fundamental step in the development of metal-based catalysts for the functionalization of chlorocarbons.

Reactivity studies

Further elaboration of the system was achieved by reaction of the molybdenum(II) chloride metallacycle **3** with internal acetylenes. As illustrated in Eq. (2),



(2)

3
υ_{CO} = 2017, 1944, 1903 cm^{-1}

4a: $R_1 = R_2$ = Ph
υ_{CO} = 1976, 1822 cm^{-1}
4b: R_1 = Ph; R_2 = CH_3
υ_{CO} = 1971, 1873 cm^{-1}

5a: $R_1 = R_2$ = Ph
υ_{CO} = 1921 cm^{-1}
5b: R_1 = Ph; R_2 = CH_3
υ_{CO} = 1925 cm^{-1}

treatment of **3** with either diphenyl acetylene or 1-phenyl-1-propyne in thf under reduced pressure at 40°C affords a dark green solution composed of two complexes, **4** and **5**, in a 3 : 1 ratio as quantified by ^1H NMR spectroscopy *via* integration of the imine resonance for each compound. The product ratio remained constant throughout the course of the reaction, which suggests that the resulting complexes are not interconvertible under the reaction conditions, and neither compound is an intermediate in the formation of the other. The minor product was identified as the unstable four-electron donor complex **5**. The major product in both systems was recognized as the η^2-vinyl complexes **4**, which were isolated in 50–55% yield as moderately air-stable, green crystalline solids.

Only the η^2-vinyl complexes were isolable from the reaction mixture. The existence of the four-electron donor complexes **5** was established through careful *in situ* IR monitoring of the strong IR band due to the single carbonyl ligand, and by comparison of spectral

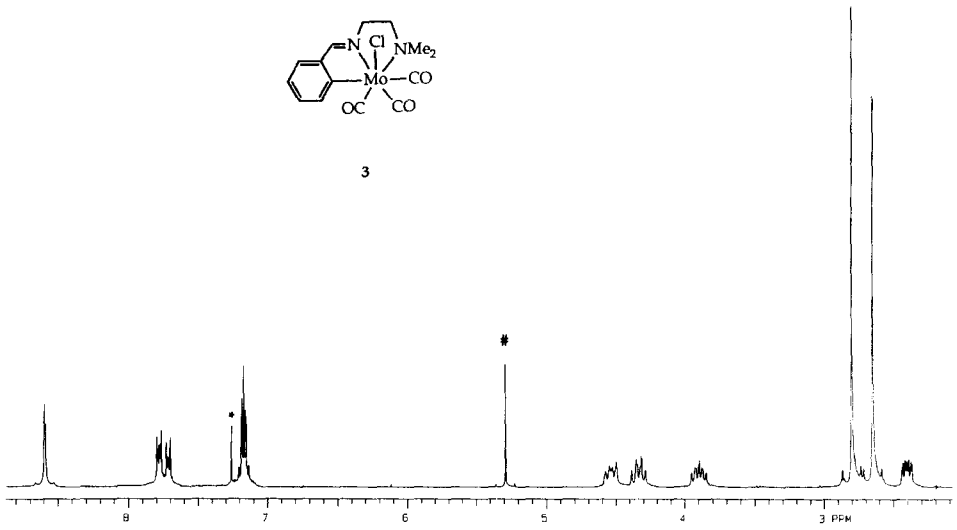


Fig. 1. ^{1}H NMR spectrum for **3**. * Denotes solvent peaks and # denotes the resonance due to methylene chloride of crystallization.

features to related, structurally characterized tungsten(II) fluoride systems in which four-electron donor complex formation is favoured by the electron-rich alkynes [7a].

Diagnostic resonances in the ^{13}C $\{^1$H$\}$ NMR spectra of **4a** and **4b** illustrate the salient features [17] of the η^2-vinyl systems. As shown in Fig. 2 for **4a,** the carbenoid character of C_α is reflected by a large downfield chemical shift at δ 258.2, whereas the four-coordinate carbon, C_β, has a significant upfield shift and resonates at δ 46.1 [18, 19]. Similarly, **4b** displays C_α at δ 264.2 and C_β at δ 41.2. Importantly, compounds **4** possess spectroscopic parameters compatible with other monomeric d^4 η^2-vinyl complexes as presented in Table 1 [2, 20].

Consistent with the low symmetry of the molecules, the pseudo six-coordinate η^2-vinyl complexes evince two carbonyl resonances that are located at δ 226.1 and 220.0 for **4a** and at δ 227.2 and 222.3 for **4b**. Interestingly, these η^2-vinyl complexes do not manifest any dynamic behaviour on the NMR time-scale. This contrasts the η^2-vinyl systems reported by Green and co-worker [2e], Templeton and co-workers [20], and Davidson and co-workers [3a,3c,5c,5d] that undergo a surfeit of fluxional processes that are attributed to a windshield wiper-type motion (less than 90 rotation)

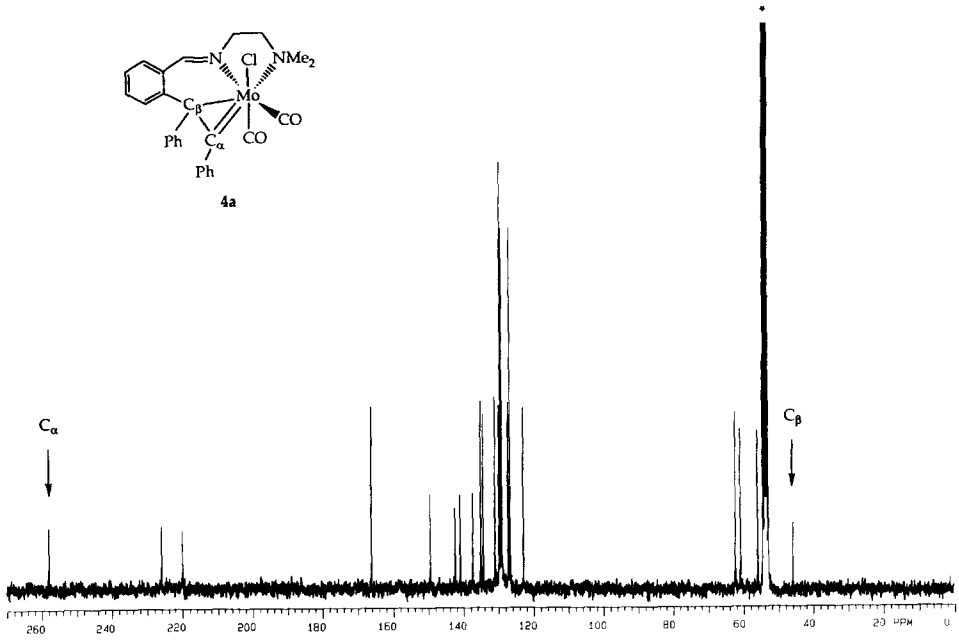


Fig. 2. ^{13}C$\{^1$H$\}$ NMR spectrum for **4a**. * Denotes solvent peaks.

Table 1. Relevant spectroscopic parameters for molybdenum(II) η^2-vinyl complexes

Complex	δ C_α (ppm)	δ C_β (ppm)	Ref.
$CpMo[P(OMe)_3]_2(\eta^2$-CPhCHPh)	255.5	26.8	2c,e
$CpMo[P(OMe)_3]_2(\eta^2$-CBu^{t}CHPh)	286.5	29.9	2e
$CpMo[P(OMe)_3]_2(\eta^2$-CMeCPh$_2$)	237.4	35.7	2e
$(\eta^5$-$C_9H_7)Mo[P(OMe)_3]_2(\eta^2$-CSiMe$_3CH_2$)	276.5	23.9	2d,e
[(Tp′)(CO)$_2$Mo(η^2-CPh=CH—CH=N(Me)(Bu^t)][BF$_4$]	242.6	40.7	20
4a	258.1	46.1	This work
4b	264.2	41.2	This work

of the η^2-vinyl fragment. Presumably, the steric constraint imposed by the rigid tridentate η^3-[C,N,N′] chelate ligand prevents this classical windshield wiper motion from occurring (rotation of the η^2-vinyl ligand). Any dynamic process would require a disconnection/reconnection between C_β and the aromatic carbon, which is highly unlikely.

The ^{1}H NMR spectra for **4a** and **4b** are essentially identical to that of **3,** the only difference being the resonances of the η^2-vinyl substituents. The 1-phenyl-1-propyne insertion product, **4b,** displays CO stretching frequencies somewhat lower than those of the diphenylacetylene insertion product, **4a,** which is probably an indication that the methyl group provides more electron density to the metal centre than the phenyl group, as would be expected. The assessment of the regiochemistry for the insertion of 1-phenyl-1-propyne was based upon the similarity of the spectral features of **4b** to those of a structurally characterized tungsten(II) fluoride 1-phenyl-1-propyne η^2-vinyl complex [21].

Consistent with the generally faster rates of CO dissociation for second row metals [22], the overall rate of η^2-vinyl formation is greater for the molybdenum(II) chloride than the tungsten(II) fluoride system. No information is available on the relative rates of migratory insertion since this reaction is fast at room temperature, as noted in the tungsten(II) fluoride system [7].

The η^2-vinyl complexes are chemically robust towards multiple insertions into the Mo—C_{aryl} bond. Although decomplexation of the metal as $Mo(CO)_6$ could be promoted by heating the η^2-vinyl complexes in the presence of 3 atm. CO(g), the resulting organic fragment could not be identified. This contrasts with other related later transition metal complexes, which readily undergo multiple insertion reaction with activated acetylenes to form large metallacycle complexes as well as heterocyclic ring systems upon metal extrusion [23].

Several groups have reported the preparation of η^2-vinyl complexes by external nucleophilic addition to four-electron donor alkyne ligands [2–5,17]. This work provides rare examples of η^2-vinyl formation involving intramolecular nucleophilic attack by the pendant aryl group [7]. A two-electron donor alkyne complex may be a common intermediate in these transformations which could either participate in the migratory insertion reaction or lose CO to afford the four-electron donor alkyne complex. It is interesting to note that the four-electron donor alkyne complex and the η^2-vinyl complexes are not interconvertible moieties, even in the presence of CO.

We have demonstrated that under mild conditions chelate-assisted oxidative addition of strong aromatic carbon–chlorine bonds in suitably designed ligands occurs at molybdenum(0) to afford seven-coordinate molybdenum(II) metallacycles. Further elaboration of the C—Cl bond is effected upon reaction of the molybdenum(II) metallacycle with electron-deficient acetylenes to produce molybdenum(II) η^2-vinyl complexes in which net replacement of a C—Cl bond with a C—C bond has ensued. Although these ligand-based systems are limited with respect to catalytic chemistry, they clearly serve as model compounds for the systematic study of structure and reactivity directed towards catalytic activation and functionalization of carbon–chlorine bonds.

EXPERIMENTAL

General procedures

All manipulations involving air-sensitive reagents were performed under purified nitrogen using standard Schlenk techniques or a Vacuum Atmosphere glovebox [25]. Tetrahydrofuran (thf) was dried with CaH_2 and distilled under nitrogen from sodium benzophenone ketyl radical. Diethyl ether and hexanes were dried with 4 Å molecular sieves and distilled under nitrogen from sodium benzophenone ketyl radical. Methylene chloride was dried and distilled under nitrogen from P_2O_5. Toluene was distilled under nitrogen from sodium metal. Literature methods were employed in the synthesis of $(\eta^6$-$C_6H_5CH_3)Mo(CO)_3$ [11]. All other chemicals were obtained from commercial sources and were used without further purification.

^{1}H- and ^{13}C-{^{1}H} NMR spectra were obtained on Varian XL-300 spectrometers at 300 and 75 MHz, respectively. All chemical shifts are reported in δ

(ppm) units with the following abbreviations: d = doublet, m = multiplet, q = quartet, s = singlet, and t = triplet. Deuterated methylene chloride ^1H NMR spectra were assigned to δ 5.32 and $^{13}C\{^1H\}$ NMR spectra were assigned to δ 53.8. For ^1H and $^{13}C\{^1H\}$ NMR spectra taken in $CDCl_3$, tetramethylsilane was used as an internal reference at δ 0.00. IR spectra were recorded using a Mattson model Galaxy Series 3000 FTIR spectrometer operating with 4.0 cm^{-1} resolution or a BioRad model FTS-40 FTIR spectrometer operating with a resolution of 2.0 cm^{-1}. Solution spectra were obtained in 0.1 mm CaF_2 cells. Solid-state spectra were obtained as KBr pellets for spectral acquisition. Melting points were obtained in open capillary tubes and reported in °C. Elemental analyses were performed by Atlantic Microlab, Norcross, GA.

Preparation of the compounds

Compound **1**. 2-Chlorobenzaldehyde (10.5 g, 0.119 mol) was dissolved in 100 cm^3 of a 75% ethanol/25% benzene solution. One equivalent of *N,N*-dimethylethylenediamine (16.7 g, 0.119 mol) was then added. The resulting solution was heated to boiling until the volume was reduced to approximately one-third. The remaining solvent was then removed by rotary evaporation to yield a yellow oil which was purified by short path vacuum distillation (b.p. 85–88°C, 0.15 mmHg) to yield **1** (20.4 g, 0.0968 mol), 81%. ^1H NMR ($CDCl_3$): δ 8.72 (s, 1H, N=CH); 8.02 (m, 1H, Ar-*H*); 7.28 (m, 3H, Ar-*H*); 3.76 (t, 2H, C=NCH_2); 2.63 (t, 2H, NCH_2); 2.29 (s, 6H, NCH_3). $^{13}C\{^1H\}$ NMR ($CDCl_3$): δ 157.9 (s, N=CH); 134.6 (s, Ar-C_{quat}); 132.8 (s, Ar-C_{quat}); 130.9 (s, Ar-*C*H); 129.2 (s, Ar-*C*H); 128.0 (s, Ar-*C*H); 59.64 (s, NCH_2); 45.43 (s, NCH_3).

Compound **3**. A 100-cm^3 Schlenk flask equipped with a stir bar was charged with (η^6-$C_6H_5CH_3$)$Mo(CO)_3$ **2** (3.02 g, 11.1 mmol) and flushed with nitrogen. Freshly distilled thf (30 cm^3) was added by syringe, and the resulting green-yellow $Mo(thf)_3(CO)_3$ solution was degassed and placed under nitrogen. The ligand **1** (2.43 g, 11.5 mmol) was placed in another Schlenk flask with freshly distilled thf (15 cm^3). The ligand solution was degassed and transferred by syringe to the $Mo(thf)_3(CO)_3$ solution resulting in a colour change to red within 5 min. Over the course of 12 h the solution slowly turned green, and IR spectroscopy confirmed the reaction was complete (ν_{CO} = 2017, 1944, 1903 cm^{-1}). The solvent was removed and the crude product redissolved in a minimal amount of CH_2Cl_2 and filtered through a pad of Celite to remove insoluble particulate matter. The volume was reduced and the product **3** was recrystallized by cooling a 1:5 CH_2Cl_2/Et_2O solution to −10 C for 24 h. Isolation by vacuum filtration gave 2.87 g (7.34 mmol, 66% yield) of **3** as a green crystalline solid. M.p. 116–118 C (dec.); IR ν_{CO} (KBr): 2010, 1938(sh), 1927, 1890 cm^{-1}. Found: C, 41.6; 3.8; N, 6.7. Calc. for $C_{14}H_{15}ClMoN_2O_3 \cdot 1/3\ CH_2Cl_2$ (418.98 g/mol): C, 41.1; H, 3.8; N, 6.7%. Note: CH_2Cl_2 was observed in the NMR spectra. ^1H NMR ($CDCl_3$): δ, 8.59 (s, 1H, N=CH); 7.78 (m, 1H, Ar-*H*); 7.72 (m, 1H, Ar-*H*); 7.17 (m, 2H, Ar-*H*); 4.55 (m, 1H, C=NCH_2); 4.34 (m, 1H, C=NCH_2); 3.90 (m, 1H, NCH_2); 2.80 (s, 3H, NCH_3); 2.65 (s, 3H, NCH_3); 2.41 (m, 1H, NCH_2). $^{13}C\{^1H\}$ NMR ($CDCl_3$): δ 230.1 (s, CO); 224.1 (s, CO); 223.8 (s, CO); 178.4 (s, N=CH); 169.6 (s, Mo-C); 145.5 (s, Ar-C_{quat}); 144.1 (s, Ar-*C*H); 131.8 (s, Ar-*C*H); 129.4 (s, Ar-*C*H); 123.6 (s, Ar-*C*H); 59.92 (s, NCH_2); 54.03 (s, NCH_2); 53.39 (s, NCH_3); 51.82 (s, NCH_3).

Compound **4a**. Under a nitrogen atmosphere, a 100-cm^3 Schlenk flask equipped with a magnetic stir bar was charged with **3** (0.22 g, 0.58 mmol) and diphenylacetylene (0.27 g, 1.5 mmol). Freshly distilled thf (25 cm^3) was added by syringe and the green slurry was degassed and heated to 40°C under reduced pressure to yield a maroon-coloured solution within 1 h. IR monitoring confirmed the reaction was complete in 4 h (ν_{CO} = 1976, 1882 cm^{-1}). Precipitation was achieved by the addition of hexanes and cooling to −10°C for 20 h. Isolation by filtration followed by hexane (2 × 20 cm^3) and Et_2O (5 × 50 cm^3) washings gave 0.17 g (0.31 mmol, 55% yield) of a red–brown powder, **4a**. M.p. 150–152 C (dec.); IR ν_{CO} (KBr): 1973, 1883 cm^{-1}. Found: C, 59.5; H, 4.8; N, 5.1. Calc. for $C_{27}H_{25}ClMoN_2O_2$ (540.90 g/mole): C, 60.0; H, 4.7; N, 5.2%. ^1H NMR (CD_2Cl_2): δ 8.52 (s, 1H, N=CH); 7.91 (m, 1H, Ar-*H*); 7.68 (m, 1H, Ar-*H*); 7.51 (m, 4H, Ar-*H*); 7.39 (m, 2H, Ar-*H*); 6.97 (m, 2H, Ar-*H*); 6.81 (m, 2H, Ar-*H*); 6.44 (m, 2H, Ar-*H*); 4.87 (m, 1H, C=NCH_2); 3.79 (m, 1H, C=NCH_2); 4.34 (m, 1H, C=NCH_2); 3.02 (m, 3H, NCH_3); 2.95 (m, 1H, NCH_2); 2.95 (s, 3H, NCH_3); 2.46 (m, 1H, NCH_2). $^{13}C\{^1H\}$ NMR (CD_2Cl_2): δ 258.1 (s, W=C_αPh); 226.1 (s, CO); 220.0 (s, CO); 166.31 (s, N=CH); 149.5 (s, Mo-C); 142.4 (s, Ar-C_{quat}); 140.0 (s, Ar-C_{quat}); 137.4 (s, Ar-C_{quat}); 135.1 (s, 2C, Ar-*C*H); 134.4 (s, 2C, Ar-*C*H); 130.9 (s, 2C, Ar-*C*H); 129.9 (s, Ar-*C*H); 129.5 (s, 2C, Ar-*C*H); 129.4 (s, Ar-*C*H); 129.0 (s, Ar-*C*H); 127.3 (s, Ar-*C*H); 126.8 (s, Ar-*C*H); 122.9 (s, Ar-*C*H); 62.51 (s, NCH_2); 61.01 (s, NCH_2); 56.06 (s, NCH_3); 53.78 (s, NCH_3); 46.1 (s, W-C_βPh).

Compound **4b**. Under a nitrogen atmosphere, a 100-cm^3 Schlenk flask equipped with a magnetic stir bar was charged with **3** (0.28 g, 0.72 mmol) and 1-phenyl-1-propyne (0.21 g, 1.8 mmol). Freshly distilled thf (30 cm^3) was added by syringe and the green slurry was degassed and heated to 40°C under reduced pressure to yield a red-green coloured solution within 1 h. IR monitoring confirmed the reaction was complete in 3 h (ν_{CO} = 1971, 1873 cm^{-1}). Precipitation was achieved by the addition of hexanes and cooling to −10°C for 20 h. Isolation by filtration followed by hexane (2 × 20 cm^3) and Et_2O (5 × 50 cm^3) washings gave 0.17 g (0.36 mmoles, 50% yield) of green-brown powder, **4b**. M.p.

85–87°C (dec.); IR ν_{CO} (KBr): 1954, 1863 cm^{-1}. Found: C, 55.2; H, 5.0; N, 5.6. Calc. for $C_{22}H_{23}ClMoN_2O_2$ (478.83 g/mole): C, 55.2; H, 4.8; N, 5.9%. ^1H NMR (CD_2Cl_2): δ 8.51 (s, 1H, N=CH); 7.82 (m, 2H, Ar-*H*); 7.51 (m, 5H, Ar—*H*); 7.23 (m, 2H, Ar-*H*); 4.92 (m, 1H, C=NCH_2); 3.84 (m, 1H, C=NCH_2); 3.04 (s, 3H, NCH_3); 2.94 (m, 1H, NCH_2); 2.90 (s, 3H, NCH_3); 2.42 (m, 1H, NCH_2); 2.11 (s, 3H, C_β-CH_3). $^{13}C\{^1H\}$ NMR (CD_2Cl_2): δ 264.2 (s, W=C_αPh); 227.2 (s, CO); 222.3 (s, CO); 166.33 (s, N=CH); 147.3 (s, Mo-C); 143.1 (s, Ar-C_{quat}); 135.6 (s, Ar-C_{quat}); 134.9 (s, Ar-*C*H); 134.1 (s, Ar-*C*H); 129.8 (s, Ar-*C*H); 129.1 (s, 2C, Ar—*C*H); 128.6 (s, Ar-*C*H); 127.8 (s, 2C, Ar-*C*H); 126.6 (s, Ar-*C*H); 62.14 (s, NCH_2); 61.34 (s, NCH_2); 55.87 (s, NCH_3); 52.76 (s, NCH_3); 41.2 (s, W-$C_\beta CH_3$).

Acknowledgements—The authors gratefully acknowledge support in the form of an AAUW American Fellowship (to J.L.K.) (1995–1996) and partial support from the National Science Foundation.

REFERENCES

1. B. C. Gates, J. R. Katzer and G. C. A. Schuit, *Chemistry of Catalytic Processes*. McGraw-Hill, New York (1979); L. Carlton, J. L. Davidson, P. Ewing, L. Manojlovic-Muir and K. W. Muir, *J. Chem. Soc., Chem. Commun.* 1985, 1474.
2. (a) S. G. Feng and J. L. Templeton, *Organometallics* 1992, **11,** 2168; (b) S. G. Feng, P. S. White and J. L. Templeton, *J. Am. Chem. Soc.* 1992, **114,** 2951; (c) M. Green, N. C. Norman and A. G. Orpen, *J. Am. Chem. Soc.* 1981, **103,** 1267; (d) S. R. Allen, M. Green, A. G. Orpen and I. D. Williams, *J. Chem. Soc., Chem. Commun.* 1982, 826; (e) S. R. Allen, R. G. Beevor, M. Green, N. C. Norman, A. G. Orpen and I. D. Williams, *J. Chem. Soc., Dalton Trans.* 1985, 435; (f) R. G. Beevor, M. Green, A. G. Orpen and I. D. Williams, *J. Chem. Soc., Chem. Commun.* 1983, 673.
3. (a) L. Carlton and J. L. Davidson, *J. Chem. Soc., Dalton Trans.* 1987, 895; (b) J. L. Davidson, *J. Organomet. Chem.* 1980, **186,** C19; (c) L. Carlton, J. L. Davidson, J. C. Miller and K. W. Muir, *J. Chem. Soc., Chem. Commun.* 1984, 11.
4. J. L. Davidson, I. E. P. Murray, P. N. Preston and M. V. Russo, *J. Chem. Soc., Chem. Commun.* 1981, 1059; J. L. Davidson, I. E. P. Murray and P. N. Preston and M. V. Russo, *J. Chem. Soc., Dalton Trans.* 1983, 1783.
5. (a) J. R. Morrow, T. L. Tonker and J. L. Templeton, *J. Am. Chem. Soc.* 1985, **107,** 6956; (b) S. G. Feng and J. L. Templeton, *Organometallics* 1992, **11,** 2168; (c) J. L. Davidson, W. F. Wilson, L. Manojlovic-Muir and K. W. Muir, *J. Organomet. Chem.* 1983, **254,** C6; (d) N. M. Agh-Atabay, L. J. Canoira, L. Carlton and J. L. Davidson, *J. Chem. Soc., Dalton Trans.* 1991, 1175; (e) J. L. Davidson, G. Vasapollo, L. Manojlovic-Muir and K. W. Muir, *J. Chem. Soc., Chem. Commun.* 1982, 1025.
6. D. L. Reger, K. A. Belmore, E. Mintz and P. J. McElligot, *Organometallics* 1984, **3,** 134; D. L. Reger and P. J. McElligot, *J. Am. Chem. Soc.* 1990, **102,** 5923; D. L. Reger, *Acc. Chem. Res.* 1988, **21,** 229.
7. (a) J. L. Kiplinger, M. A. King, A. M. Arif and T. G. Richmond, *Organometallics* 1993, **12,** 3382; (b) J. L. Kiplinger, T. G. Richmond, A. M. Arif, C. Dücker-Benfer and R. van Eldik, *Organometallics* 1996, **15,** 1545.
8. R. G. Harrison and T. G. Richmond, *J. Am. Chem. Soc.* 1993, **115,** 5303; B. K. Bennett, R. G. Harrison and T. G. Richmond, *J. Am. Chem. Soc.* 1994, **116,** 11165; J. L. Kiplinger, A. M. Arif and T. G. Richmond, *Inorg. Chem.* 1995, **34,** 399; J. L. Kiplinger and T. G. Richmond, *J. Am. Chem. Soc.* 1996, **118,** 1805; J. L. Kiplinger and T. G. Richmond, *Chem. Commun.* 1996, 1115.
9. For a comprehensive review of C—F activation by metal reagents, see J. L. Kiplinger, T. G. Richmond and C. E. Osterberg, *Chem. Rev.* 1994, **94,** 373.
10. For related ligand systems employed for chemistry at tungsten(0), see T. G. Richmond, M. A. King, E. P. Kelson and A. M. Arif, *Organometallics* 1987, **6,** 1995; B. P. Buffin and T. G. Richmond, *Polyhedron* 1990, **9,** 2887. For related ligand systems employed for chemistry at platinum(II), see C. M. Anderson, M. Crespo, M. C. Jennings, A. J. Lough, G. Ferguson and R. J. Puddephatt, *Organometallics* 1991, **10,** 2671; C. M. Anderson, M. Crespo, G. Ferguson, A. J. Lough and R. J. Puddephatt, *Organometallics* 1992, **11,** 1177; M. Crespo, M. Martinez and J. Sales, *Organometallics* 1993, **12,** 4297.
11. W. Strohmeier, *Chem. Ber.* 1961, **94,** 3337; F. A. Cotton and R. Poli, *J. Am. Chem. Soc.* 1988, **110,** 830.
12. C. E. Osterberg, M. A. King, A. M. Arif and T. G. Richmond, *Angew. Chem., Int. Ed. Engl.* 1990, **29,** 888; T. G. Richmond, *Coord. Chem. Rev.* 1990, **105,** 221.
13. R. G. Wilkins, *Kinetics and Mechanism of Reactions of Transition Metal Complexes*, 2nd edn. VCH Publishers, New York (1991).
14. B. P. Buffin, A. M. Arif and T. G. Richmond, *J. Chem. Soc., Chem. Commun.* 1993, 1432; B. P. Buffin, M. J. Poss, A. M. Arif and T. G. Richmond, *Inorg. Chem.* 1993, **32,** 3805.
15. For examples of chelate-stabilized aryl halide complexes at a Mo^{II} centre, see R. Harrison, A. M. Arif, G. Wulfsberg, R. Lang, T. Ju, G. Kiss, C. D. Hoff and T. G. Richmond, *J. Chem. Soc., Chem. Commun.* 1992, 1374.
16. B. E. Smart, in *The Chemistry of Functional Groups, Supplement D* (Edited by S. Patai and Z. Rappoport), Chapter 14. Wiley, New York (1983).
17. J. L. Templeton, *Adv. Organomet. Chem.* 1989, **29,** 1.
18. W. A. Nugent and J. M. Mayer, *Metal–Ligand Multiple Bonds*. Wiley, New York (1988).
19. B. E. Mann and B. F. Taylor, *^{13}C NMR Data for Organometallic Compounds*. Academic Press, New York (1981).

20. A. S. Gamble, P. S. White and J. L. Templeton, *Organometallics* 1991, **10,** 693.
21. J. L. Kiplinger, M. A. King, A. Fechtenkötter, A. M. Arif and T. G. Richmond, *Organometallics*, in press.
22. D. J. Darensbourg, *Adv. Organomet. Chem.* 1982, **21,** 113.
23. G. Wu, A. L. Rheingold and R. F. Heck, *Organometallics* 1986, **5,** 1922; F. Maassarani, M. Pfeffer and G. Le Borgne, *Organometallics* 1987, **6,** 2029.
24. D. F. Shriver and M. A. Drezdon, *Manipulation of Air Sensitive Compounds*, 2nd edn. Wiley, New York (1986).

Pergamon

PII: S0277-5387(96)00312-9

Polyhedron Vol. 16, No. 3, pp. 417–422, 1997
Copyright © 1996 Elsevier Science Ltd
Printed in Great Britain. All rights reserved
0277-5387/97 $17.00+0.00

Cadmium(II) halide complexes of pyrazine

Rosa D. Bailey and William T. Pennington*

Department of Chemistry, Clemson University, Clemson, SC 29634-1905, U.S.A.

(Received 22 September 1995; accepted 18 June 1996)

Abstract—Pyrazine forms 1 : 1 complexes with cadmium(II) halides, CdX_2 · pyrazine (X = Cl, Br, I). The structures of all three members of this series have been determined by single-crystal X-ray diffraction. All of the complexes crystallize as infinite CdX_2 chains in which cadmium atoms are doubly bridged by pairs of halide atoms; pyrazine ligands complete the pseudo-octahedral coordination of the cadmium atoms and link the CdX_2 chains to form extended two-dimensional layers. While this type of coordination is fairly common for chloro and bromo derivatives, the iodo compound represents, to the best of our knowledge, the first example of an iodo derivative with this coordination. In each case the layers stack along the crystallographic *a*-axis to complete the structure. In the bromo and iodo complexes, which are isomorphous, the pyrazine ring planes are perpendicular to the plane of the layer. The chloro derivative has a very similar structure; however, the pyrazine rings are rotated by 19.3° away from perpendicular, bringing the *ortho*-C—H groups into close proximity [2.89 (2) Å] to a chloride atom. Copyright © 1996 Elsevier Science Ltd

Keywords: cadmium halides; extended solids; C—H · · · Cl hydrogen-bonding.

In the search for molecular-based materials with interesting properties, much attention has been given to one-, two- and three-dimensional extended solids involving cadmium [1–5]. Cadmium is well suited for this, as its d^{10} configuration permits a wide variety of geometries and coordination numbers (four, five and six are common [6] and seven [3] and eight [7] are known). This structural diversity is particularly evident in cadmium(II) halide complexes. Complexes of the type CdX_2L_2 (X = Cl or Br; L = pyridine or similar small, monodentate ligand) typically form halogen-bridged chain compounds with six-coordinate, pseudo-octahedral cadmium [8]. However, in a number of studies, systematic structural variations over the halide series have been observed [9,10]. These variations have been attributed to factors such as crystal packing, hydrogen-bonding forces and halide dimensions [6], ease of disruption of the cadmium halide framework and relative Cd—X bond strength [9], and the increasing softness of the heavier halides [10]. Additional structural variation can be incorporated by replacing the monodentate ligands with a bidentate ligand (L′) to form complexes of the type CdX_2L'. A series of complexes, CdX_2(pyrazine) for X = Cl, Br and I (compounds **I–III**, respectively), which we have prepared and structurally characterized, are here discussed as an example of the structural variation that can occur in this class of compounds.

EXPERIMENTAL

Preparations

Pyrazine and all cadmium halides were obtained from Aldrich Chemical Company and were used as received; solvents were obtained from commercial houses and were dried and purified by standard techniques and stored over activated sieves. The compounds were prepared by combining ethanol (95%) solutions of the reactants in stoichiometric ratio. If dilute solutions were used, X-ray quality crystals could be grown by simply allowing the ethanol to evaporate slowly. At greater concentrations an immediate precipitate formed. The precipitate was redissolved for each compound by slight acidification of the solution; slow evaporation of the solvent from this acidic solution yielded data quality crystals, as well. The crystals were isolated by rinsing with cold ethanol and hexane, and dried under nitrogen. Powder diffraction spectra, used to identify solid phases in bulk, were measured on a Scintag XDS/2000 *θ–θ*

* Author to whom correspondence should be addressed.

diffractometer with Cu-$K_{\alpha 1}$ radiation (λ = 1.54060 Å) and an intrinsic germanium solid-state detection system (results can be found in the supplementary material). Far IR (500–100 cm^{-1}) and IR (4000–500 cm^{-1}) spectra were obtained as KBr pellets or as Nujol mulls in sealed polyethylene bags on Nicolet 20F and 510 spectrometers, respectively. Carbon, hydrogen, nitrogen analyses were performed by Atlantic Microlabs, Norcross, GA.

$CdCl_2(C_4H_4N_2)$ (**I**). Pyrazine (0.101 g, 1.24 mmol) was dissolved in ethanol (100 cm^3) and added to a solution of $CdCl_2$ (0.229 g, 1.25 mmol) in ethanol (100 cm^3). Slow evaporation yielded 0.206 g (62.6%) of prismatic crystals; m.p. >500°C. IR (cm^{-1}): 3104, 3049, 2919, 2858, 1601, 1474, 1425, 1388, 1172, 1129, 1055, 808, 746, 622, 446, 222, 178, 121. Elemental analyses: Found (Calc.): C, 18.5 (18.2); H, 1.6 (1.5); N, 10.7% (10.6%).

$CdBr_2(C_4H_4N_2)$ (**II**). Pyrazine (0.104 g, 1.30 mmol) was dissolved in ethanol (100 cm^3) and added to a solution of $CdBr_2 \cdot 4H_2O$ (0.426 g, 1.24 mmol) in ethanol (100 cm^3). Slow evaporation yielded 0.365 g (83.7%) of parallelepiped crystals; m.p. 447–449°C. IR (cm^{-1}): 3099, 3037, 2932, 1653, 1487, 1413, 1160, 1129, 1042, 789, 447, 280, 202, 180, 120. Elemental analyses: Found (Calc.): C, 13.8 (13.6); H, 1.1 (1.1); N, 7.9% (8.0%).

$CdI_2(C_4H_4N_2)$ (**III**). Pyrazine (0.102 g, 1.27 mmol) was dissolved in ethanol (100 cm^3) and added to a solution of CdI_2 (0.457 g, 1.25 mmol) in ethanol (100 cm^3). Slow evaporation yielded 0.470 g (84.4%) of light yellow, prismatic crystals; m.p. 409–412°C. IR (cm^{-1}): 3098, 3018, 1659, 1418, 1387, 1270, 1166, 1128, 1048, 795, 448, 172, 104. Elemental analyses: Found (Calc.): C, 11.0 (10.8); H, 0.9 (0.9); N, 6.1% (6.3%).

X-ray crystallography

All measurements were made at 22±1°C with graphite-monochromated Mo-K_α radiation (λ = 0.71073 Å) on either a Rigaku AFC7R (compounds **I** and **II**) or a Siemens R3m/V (compound **III**) diffractometer. Unit-cell dimensions and an orientation matrix were determined from the setting angles of several high-order reflections. Intensities were measured using an $\omega/2\theta$ scan technique at a speed of 4–32°/min for compounds **I** and **II** and 2°/min for **III**. The intensities of three reflections remeasured periodically throughout data collection fluctuated by less than ±1%, indicating crystal and electronic stability. The data were corrected for absorption (empirical, based on ψ-scans) and for Lorentz and polarization effects. The structures were solved by direct methods and refined on F by full-matrix least-squares techniques. Non-hydrogen atoms were refined with anisotropic thermal parameters and hydrogen atoms were refined isotropically. The weighting scheme was based on counting statistics and included a factor (0.0005) to downweight intense reflections. The final difference Fourier map for each of the structures was featureless. Scattering factors were taken from Table 2.2B and the real and anomalous dispersion corrections from Table 2.3.1 of ref. [11]. Relevant crystallographic data is given in Table 1. All calculations were performed using a combination of SHELXTL-Plus [12] and TEXSAN [13]. Atomic coordinates have been

Table 1. Crystallographic data for CdX_2(pyrazine) complexes

X (compound)	Cl (**I**)	Br (**II**)	I (**III**)
Formula	$C_4H_4N_2CdCl_2$	$C_4H_4N_2CdBr_2$	$C_4H_4N_2CdI_2$
Formula weight	263.39	352.31	446.29
Space group	*C2/m*	*Cmmm*	*Cmmm*
Cell reflections;			
2θ range (°)	25, 48.7–50.1	25, 43.6–48.6	42, 14.5–38.2
a (Å)	11.856(2)	12.571(2)	13.236(2)
b (Å)	7.549(2)	7.567(2)	7.627(2)
c (Å)	3.743(2)	3.889(2)	4.1537(7)
β (°)	93.15(3)		
V (Å^3)	334.5(2)	369.9(2)	419.3(1)
Z	2	2	2
D_{calc} (g cm^{-3})	2.62	3.16	3.54
μ (mm^{-1})	3.96	13.66	9.89
Transmission factors	0.72–1.00	0.84–1.00	0.79–1.00
2θ range (°)	5.0–50.0	5.0–55.0	3.5–50.0
Reflections collected	337	1684	1490
Reflections unique (R_{int})	321 (0.033)	270 (0.020)	241 (0.014)
Reflections observed [$I > 3\sigma(I)$]	318	237	226
Goodness-of-fit	1.38	1.10	0.71
R	0.0174	0.0135	0.0081
R_w	0.0221	0.0177	0.0125

deposited with the Cambridge Crystallographic Data Centre.

RESULTS AND DISCUSSION

General description of structures

A general view of CdX_2(pyrazine) showing the atomic numbering scheme is shown in Fig. 1. Selected bond distances and angles for the three compounds are given in Table 2.

All of the complexes crystallize as infinite CdX_2 chains in which cadmium atoms are doubly bridged by pairs of halide atoms; pyrazine ligands bonded in *trans*-positions complete the pseudo-octahedral coordination of the cadmium atoms and link the CdX_2 chains to form extended two-dimensional layers. The layers stack along the crystallographic *a*-axis, with adjacent layers related by C-centring, to complete the structure (Fig. 2; in Figs 2–4, the cadmium atoms are represented as boundary ellipsoids, the halide atoms as hatched ellipsoids, the nitrogen atoms as solid spheres, the carbon atoms as partially shaded circles and the hydrogen atoms as open circles). This layered structure is similar to that observed in CuX_2(pyrazine) (X = Br, Cl) [14]; the only major difference being the asymmetric nature of the halide bridges [Cu—Br distances of 2.427(2) and 3.034(2) Å] in the Cu^{II} complex, which is due to the pseudo-Jahn Teller distortion of the d^9 metal centre.

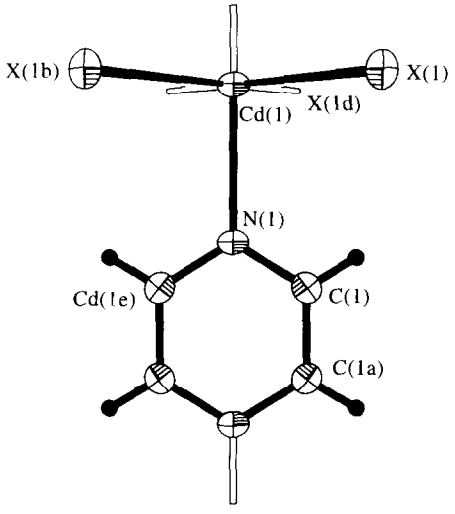


Fig. 1. A general view (50% probability ellipsoids) of CdX_2(pyrazine) showing the atom-numbering scheme used. Atom labels containing a lower case character were generated by the corresponding symmetry operation listed in Table 2.

Table 2. Bond distances (Å) and angles (°) for CdX_2(pyrazine) complexes

	X = Cl (I)	X = Br (II)	X = I (III)
Cd(1)—X(1)	2.612(2)	2.752(1)	2.947(1)
Cd(1)—N(1)	2.386(4)	2.397(3)	2.423(3)
N(1)—C(1)	1.335(3)	1.326(3)	1.328(3)
C(1)—C(1a)	1.377(6)	1.388(6)	1.386(6)
C(1)—H(1)	0.88(4)	0.89(3)	0.89(4)
X(1)—Cd(1)—X(1b)	88.5(1)	90.1(1)	90.4(1)
X(1b)—Cd(1)—X(1c)	91.5(1)	89.9(1)	89.6(1)
Cd(1)—X(1)—Cd(1d)	91.5(1)	90.1(1)	89.6(1)
Cd(1)—N(1)—C(1)	121.6(2)	121.5(2)	121.7(2)
C(1)—N(1)—C(1e)	116.7(3)	117.1(3)	116.6(3)
N(1)—C(1)—C(1a)	121.6(2)	121.5(2)	121.7(2)
N(1)—C(1)—H(1)	116(2)	121(2)	118(3)
C(1a)—C(1)—H(1)	123(2)	117(2)	120(3)

Symmetry operations: a: $x, 1-y, z$; b: $-x, -y, 1-z$; c: $-x, -y, -z$; d: $x, y, 1+z$; e: $-x, y, -z$.

The bonding distances and angles within the pyrazine ring for each of the complexes are typical of those observed in other compounds in which pyrazine bridges two metal centres [15].

Crystal structure of **I**

The cadmium atom lies on a crystallographic $2/m$ site at the origin; the twofold axis is coincident with the Cd—N bonds and the chloride ions lie on the mirror plane. The pyrazine ring also possesses $2/m$ symmetry, as it is situated about a site at $(0\,1/2\,0)$; a third $2/m$ site lies at the mid-point between the two bridging chloride ions at $(0\,0\,1/2)$. Adjacent cadmium atoms in the chloride-bridged chain are related by translation along the *c*-axis; adjacent chains in a layer are related by translation along the *b*-axis.

The Cd—N bond length of 2.386(4) Å is within the range of similar $Cd—N_{aromatic}$ bonding distances [2.36(6) $Å_{mean}$; 2.248(2)–2.448(6) $Å_{range}$] [16]. The Cd—Cl bond length of 2.612(2) Å is also within the range of typical values [2.62(4) $Å_{mean}$; 2.576(7)–2.731(2) $Å_{range}$] [17].

Crystal structure of **II**

The cadmium atom lies on a crystallographic *mmm* site at the origin. The pyrazine ring lies on the mirror plane perpendicular to the *c*-axis and the bridging halides lie on the mirror plane perpendicular to the *b*-axis. The layer is bisected by the mirror plane perpendicular to the *a*-axis. As in **I**, adjacent cadmium atoms in the bromide-bridged chain are related by translation along the *c*-axis, and adjacent chains in a layer are related by translation along the *b*-axis.

The Cd—N bond length of 2.397(3) Å observed in **II**, is slightly longer (2.75 σs) than that in **I**, but is still within the range of typical $Cd—N_{aromatic}$ bonding distances [16]. The Cd—Br bond length of 2.752(1) Å is experimentally equivalent to the value of 2.73(1) Å observed in $CdBr_2$(dioxane) [18], which has a similar layered structure. It has been observed that the length of Cd—Br distances in related compounds is depen-

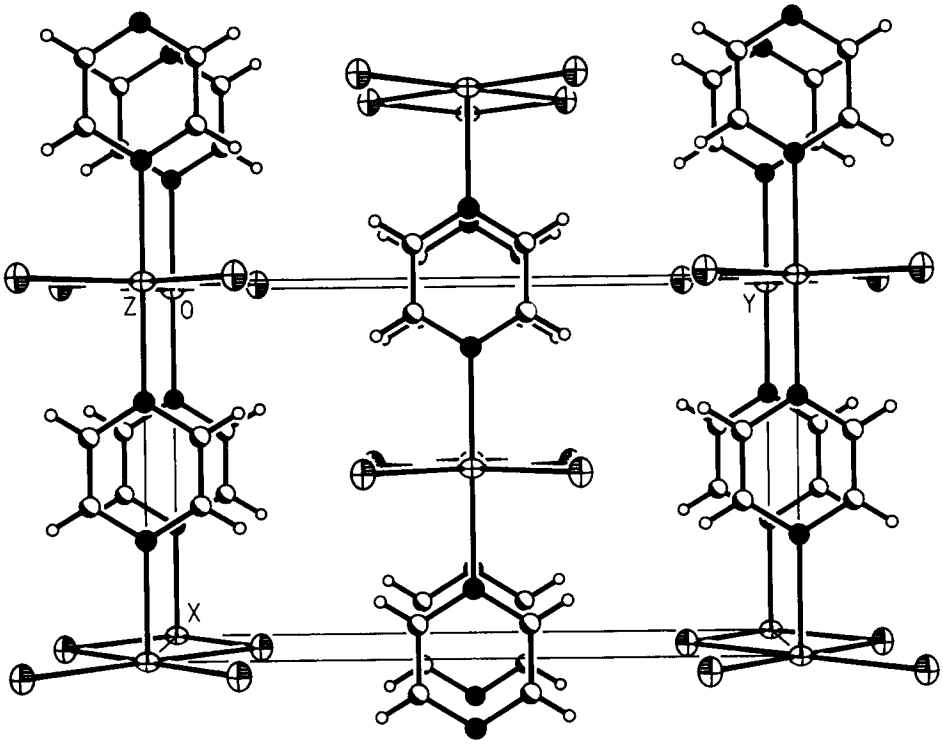


Fig. 2. Stacked layers of CdX_2(pyrazine) viewed down the *c*-axis, parallel to the CdX_2 chains.

dent on the nature of the atom bonded in a *trans* position [17e]. We have been unable to locate any compounds, other than $CdBr_2$(dioxane), in which bromine atoms are bonded in mutually *trans* positions of an octahedral cadmium coordination sphere. However, the value observed in **II** is within the range of values observed for a variety of $CdBr_2$ complexes [2.74(4) $Å_{mean}$; 2.691(1)–2.819(2) $Å_{range}$] [19].

Crystal structure of **III**

Compound **III** is isomorphous with **II**, the primary difference in the two structures being those expected as a result of the larger size of the iodine atoms.

The Cd—N bond length of 2.423(3) Å is somewhat longer than that observed in **I** (9.2 σs) and **II** (8.7 σs) and approaches the upper limit of observed Cd–$N_{aromatic}$ values [16]. To the best of our knowledge, this compound represents the first example of a complex with an octahedral CdI_4N_2 coordination sphere with bridging iodine atoms in *trans* positions. The Cd—I bond length of 2.947(1) Å is within the range of values for compounds in which cadmium atoms are bridged by iodine atoms [2.9(1) $Å_{mean}$; 2.741(1)–3.109(1) $Å_{range}$] [20].

Comparison of structures

In compounds **II** and **III** the pyrazine ring planes are perpendicular to the layers, while in **I** the rings are rotated by 19.3° away from the perpendicular to the layer (Fig. 3). This rotation lowers the symmetry of the layer from *mmm* to 2/*m*, resulting in the observed difference in crystal system and space group for **I** relative to **II** and **III**. This rotation appears to be owing to intra-layer C—H···Cl hydrogen bonding (Fig. 4). The H···Cl distance of 2.89(2) Å and the C—H···Cl angle of 129(1)° are both within the range of values attributed to this type of interaction (H···Cl = 2.569–2.944 Å; C—H···Cl = 119.3–169.2°) [21]. Packing differences for chloro versus bromo and iodo derivatives have recently been attributed to the presence of this type of interaction in a series of $Zn_2X_2L_2$ complexes (X = Cl, Br, I; L = oxo ligands) [22].

The increased Cd—N distance down the halide series might be a result of steric interactions between the pyrazine ring and the halide atoms within a CdX_2(pyrazine) layer. However, compression of the Cd—N distance in **II**, from the observed value of 2.397(3) Å to 2.386(4) Å, the value observed for **I**, would result in intra-layer contacts of 3.642 Å for N···Br, 3.731 Å for C···Br and 3.304 Å for H···Br, all of which are well outside the sum of van der Waal's radii for the atoms involved (H 1.20 Å [22], C 1.70 Å, N 1.55 Å, Br 1.85 Å, I 1.98 Å) [23]. Compression of the Cd—N distance in **III**, from the observed value of 2.423(3) Å to the value found in **I**, would also result in contacts much longer than their van der Waal's sums (N···I 3.792 Å, C···I 3.840 Å and H···I 3.360 Å). A more likely explanation for this trend is that

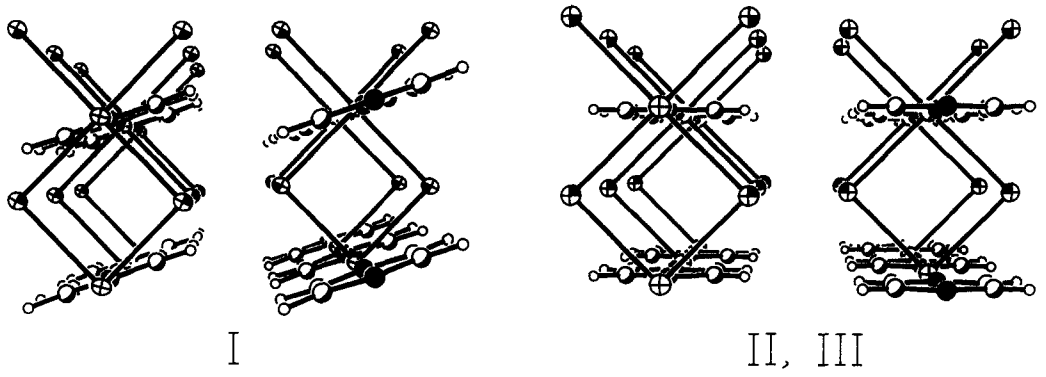


Fig. 3. Comparison of CdX_2(pyrazine) layers.

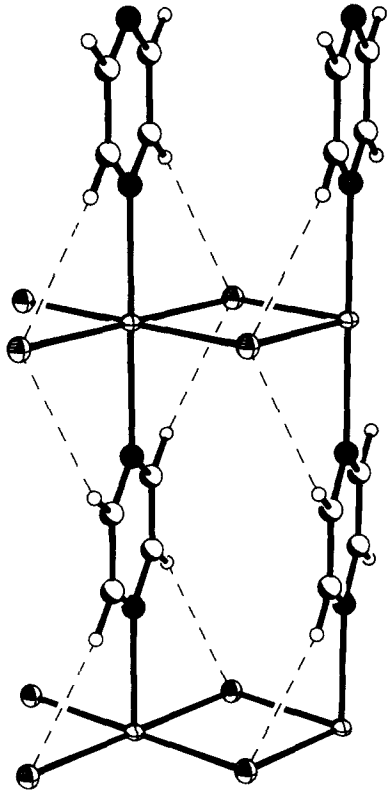


Fig. 4. Intra-layer C—H · · · Cl hydrogen bonding in **I**.

there is increased electron density at the cadmium with the heavier, softer halogens. This has been suggested as the reason for similar systematic structural changes observed in a series of cadmium halide complexes with chelating nitrogen macrocyclic ligands [10].

CONCLUSIONS

Systematic structural changes in the CdX_2(pyrazine) complexes can be attributed to steric factors associated with the increasing size of the bridging halides, down the series, and to electronic factors associated with the increasing softness of the heavier halogens. The symmetry breaking which occurs for the chloride derivative is associated with the presence of C—H · · · Cl hydrogen bonding which is not present for the bromo and iodo complexes. It is interesting to note that in a crystallographic study of a number of MX_2(pyridine)$_2$ complexes, the symmetries of the chloro derivatives have been found to be different to those of the heavier halo complexes [24]. Our continuing investigation of these types of complexes will examine the structural influence of C—H · · · Cl interactions.

Acknowledgements—We thank the National Science Foundation for funds to purchase the Rigaku and Scintag diffractometers used in this work. We are grateful to Sigma Xi for a Grant in Aid (to R.D.B.).

REFERENCES

1. B. F. Abrahams, M. J. Hardie, B. F. Hoskins, R. Robson and E. E. Sutherland, *J. Chem. Soc., Chem. Commun.* 1994, 1049.
2. T. Soma, H. Yuge and T. Iwamoto, *Angew. Chem., Int. Ed. Engl.* 1994, **33,** 1665.
3. M. Fujita, Y. J. Kwon, M. Miyazawa and K. Ogura, *J. Chem. Soc., Chem. Commun.* 1994, 1977.
4. H. Yuge and T. Iwamoto, *Acta Cryst.* 1995, **C51,** 374.
5. M. Hashimoto and T. Iwamoto, *Acta Cryst.* 1994, **C50,** 496.
6. D. G. Tuck, *Rev. Inorg. Chem.* 1979, **1,** 209.
7. C. K. Schauer and O. P. Anderson, *J. Am. Chem. Soc.* 1987, **109,** 3646.
8. V. H. Paulus, *Z. Anorg. Allg. Chem.* 1969, **369,** 38.
9. M. Neiuwenhuyzen, W. T. Robinson and C. J. Wilkins, *Polyhedron* 1991, **10,** 2111.
10. H. Strasdeit, W. Saak, S. Pohl, W. L. Driessen and J. Reedijk, *Inorg. Chem.* 1988, **27,** 1557.
11. *International Tables for X-ray Crystallography*, Vol. IV. Kynoch Press, Birmingham (1974).
12. G. M. Sheldrick, *SHELXTL-Plus*, Version 4.2.1. Structure Determination Software Programs. Sie-

mens Analytical X-ray Instruments Inc., Madison, Wisconsin, USA (1990).
13. P. N. Swepston, *TEXSAN*; *structure analysis software*. Molecular Structure Corporation, The Woodlands, Texas, USA (1993).
14. Th. Fetzer, A. Lentz and T. Debaerdemaeker, *Z. Naturforsch.* 1989, **44b,** 553.
15. See, for example: $Cu(pyrazine)_2(ClO_4)_2$: J. Darriet, M. S. Hadad, E. N. Duesler and D. N. Hendrickson, *Inorg. Chem.* 1979, **18,** 2679; $Co(pyrazine)_2Cl_2$: P. W. Carrick, M. Goldstein, E. M. McPartlin and W. D. Unsworth, *J. Chem. Soc., Chem. Commun.* 1971, 1634; $Cu(hfac)_2$ (pyrazine) and $(Cu(hfac)_2)_2$(pyrazine): R. C. E. Belton, D. E. Fenton and M. R. Truter, *J. Chem. Soc., Dalton Trans.* 1974, 17; $[(NH_3)_5Ru(pyrazine)Ru(NH_3)_5]^{5+}$: J. K. Beattie, N. S. Hush, P. R. Taylor, C. L. Raston and A. H. White, *J. Chem. Soc., Dalton Trans.* 1977, 1121; $Cu(NO_3)_2$(pyrazine): A. Santoro, A. D. Mighell and C. W. Reimann, *Acta Cryst.* 1970, **B26,** 979; $Cu(pyrazine)_2(CF_3SO_3)$: T. Otieno, S. J. Rettig, R. C. Thompson and J. Trotter, *Can. J. Chem.* 1989, **67,** 1964; $Cu(pyrazine)_2(CF_3SO_3)_2$: J. S. Haynes, S. J. Rettig, J. R. Sans, R. C. Thompson and J. Trotter, *Can. J. Chem.* 1987, **65,** 420.
16. Based on Cd—N bond lengths involving aromatic nitrogen heterocycles. (a) $CdCl_2$(benzotriazole): I. Sotofte and K. Nielsen, *Acta Chem. Scand.* 1984, **A38,** 257; (b) $CdCl_2(pyridine)_2$: H. Paulus, *Z. Anorg. Allg. Chem.* 1969, **369,** 38; (c) $CdCl_2(imidazole)_2$: R. J. Flook, H. C. Freeman, F. Huq and J. M. Rosalky, *Acta Cryst.* 1973, **B29,** 903; (d) $CdI_2(pyridine)_4$: M. Ito, T. Shibata and Y. Saito, *Acta Cryst.* 1984, **C40,** 2041; (e) $[Cd_2(1,2\text{-bis}(4\text{-pyridyl})ethane)_3](NO_3)_4$: ref. [3]; (f) [Cd(2,2′-bipyridine)][Ni(CN)$_4$]: ref. [5]; $Cd(CN)_2$(pyrazine): ref. [1].
17. Based on 20 Cd—Cl bond lengths involving octrahedral cadmium atoms doubly bridged by chlorine atoms. (a) $CdCl_2(benzotriazole)_2$: ref. [16a]; (b) $CdCl_2(pyridine)_2$: ref. [16b]; (c) $CdCl_2(imidazole)_2$: ref. [16c]; (d) $CdCl_2$(alaninato): K. I. Schaffers and D. A. Keszler, *Acta Cryst.* 1993, **C49,** 1156; (e) $CdCl_2$(MeOH)(dmso): M. Nieuwenhuyzen, W. T. Robinson and C. J. Wilkins, *Acta Cryst.* 1993, **C49,** 1173; (f) $CdCl_2 \cdot 4H_2O$: H. Leligny and J. C. Monier, *Acta Cryst.* 1979, **B35,** 569.
18. J. C. Barnes, L. J. Sesay and B. H. Nichols, *Inorg. Nucl. Chem. Lett.* 1977, **13,** 153.
19. Based on nine Cd—Br bond lengths involving bromine atoms bridging cadmium atoms. $CdBr_2$(dioxane): ref. [18]; (b) $CdBr_2$(MeOH)(dmso): ref. [17e]; (c) $CdBr_2$(pyridine-*N*-oxide): ref. [9].
20. Based on 10 Cd—I bond lengths involving iodine atoms bridging cadmium atoms. $CdI_2(PEt_3)$: N. A. Bell, T. D. Dee, M. Goldstein and I. W. Nowell, *Inorg. Chim. Acta* 1982, **65,** L87; CdI_2(propane-1,3-diamine)$_3$: G. Ciani, M. Moret, A. Sironi, S. Bruni, F. Cariati, A. Pozzi, T. Manfredini, L. Menabue and G. C. Pellacani, *Inorg. Chim. Acta* 1989, **158,** 9; $Cd_2I(S_2COi\text{-}Pr)_3$: B. F. Abrahams, B. F. Hoskins and G. Winter, *Acta Cryst.* 1990, **C46,** 391; $CdI(S_2CNEt_2)$: A. Duhme, S. Pohl and H. Strasdeit, *Inorg. Chim. Acta* 1990, **175,** 5; CdI_2(pyridine-*N*-oxide): G. Sawitzi and H.-G. von Schnering, *Chem. Ber.* 1974, **107,** 3266.
21. R. Taylor and O. Kennard, *J. Am. Chem. Soc.* 1982, **104,** 5063.
22. R. A. Edwards, O. P. Gladkikh, W. T. Robinson and C. J. Wilkins, *Abstracts of Papers*, Annual Meeting of the American Crystallographic Association, Montreal, Quebec, 1995; Abstract M178.
23. A. Bondi, *J. Phys. Chem.* 1964, **68,** 441.
24. A. A. McConnell and R. H. Nuttall, *J. Mol. Struct.* 1978, **49,** 207.

Pergamon

PII: S0277-5387(96)00298-7

Polyhedron Vol. 16, No. 3, pp. 423–425, 1997
Copyright © 1996 Elsevier Science Ltd
Printed in Great Britain. All rights reserved
0277-5387/97 $17.00+0.00

Selective reactions (hydrolysis or debenzotriazolation) of bis(benzotriazol-1-yl) methylimine by metal(II) salts

S. Thambidurai and S. K. Ramalingam*

School of Chemistry, Madurai Kamaraj University, Madurai 625 021, India

(Received 24 May 1996; accepted 17 June 1996)

Abstract—The reactions of bis(benzotriazol-1-yl)methylimine (BBTMI) with acetates and chlorides of Cu^{II}, Ni^{II}, Co^{II}, Zn^{II}, Cd^{II} and Mn^{II} were studied in ethanol. While the metal acetates induced debenzotriazolation to form 1-cyanobenzotriazole and benzotriazole, the chlorides induced hydrolysis of BBTMI to form 1,1′bis(benzotriazol-1-yl)carbonyl. These intermediates subsequently formed the mixed ligand complexes [1-cyanobenzotriazolediacetato M(II)] and [benzotriazolatochloro M(II)] respectively. The chemo-selectivity of the reactions could be attributed to a facile cleavage of one of the M—O bonds of the bidentately bound acetates and to the acidic nature in the case of the chloride solution. Copyright © 1996 Elsevier Science Ltd

Keywords: bis(benzotriazol-1-yl)methylimine; chemoselectivity; hydrolysis; debenzotriazolation; facile metal-oxygen bond cleavage; metal salts.

The reactions of N-unsubstituted imines are rarely reported in the literature since in many cases either the isolation of the imines themselves is difficult or even when formed many of them decompose or cyclise. Nevertheless, Tsutsumi *et al.*, and Smith *et al.*, studied the conversion of some aldimines to nitriles [1,2]. Katritzky *et al.*, reported the debenzotriazolation of N-unsubstituted imines which yielded cyanamide [3]. In a study of metal mediated organic reactions we have earlier reported that the imine BBTMI underwent debenzotriazolation upon using labile metal diketones in non-aqueous medium to bring about ultimately γ-cyanation on β-diketone ring [4]. The same substrate, however, was found to be without action on analogous but inert chelates. This was attributed to a facile breaking of one of the M—O bonds, accumulating a negative charge on the coordinated ligand which was responsible for further reaction. In this context it is of interest to test the influence of two different simple metal salts, one fully ionizing (chlorides) and the other partly ionizing (acetates), to test whether different end products could be obtained. The present paper reports the chemoselective reactions, *viz.* debenzotriazolation and hydrolysis of BBTMI brought about by the metal(II) acetates and chlorides respectively.

EXPERIMENTAL

Metal salts used were of reagent grade. Bis(benzotriazol-1-yl)methylimine was prepared by a method described in an earlier reported paper [4]. IR spectra were recorded on a Perkin-Elmer 577 spectrometer, and ^{1}H NMR spectra on a R 32 Bruker Instrument.

Reaction of BBTMI with acetates of Cu^{II}, Ni^{II}, Co^{II}, Zn^{II}, Cd^{II} and Mn^{II}

A mixture of equimolar amounts (0.002 mole) of the metal(II) acetate and the imine in 40 cm^3 of ethanol was kept stirred for 30 min. 1-Cyanobenzotriazolediacetatometal(II) complex which precipitated as a solid from the clear reaction mixture was filtered and washed with methanol and water.

Reaction of BBTMI chlorides of Cu^{II}, Ni^{II}, Co^{II}, Zn^{II} and Cd^{II}

An ethanolic solution containing 0.002 mole each of metal(II) chloride and BBTMI was kept stirred for

*Author to whom all correspondence should be addressed.

Table 1. Physical characteristics and elemental analysis of the complexes

Complex	Yield %	Elemental Analysis Expt. (Calc.) % C	N	H	M	μ_{eff} B.M.
$[Cu(OAc)_2(CNBTA)(H_2O)_2]$	75	36.1 (36.5)	15.7 (15.5)	3.7 (3.9)	17.9 (17.6)	1.35
$[Ni(OAc)_2(CNBTA)(H_2O)_2]$	65	37.3 (37.0)	15.5 (15.7)	3.8 (4.0)	16.1 (16.5)	3.10
$[Co(OAc)_2(CNBTA)(H_2O)_2]$	70	36.9 (37.0)	15.4 (15.7)	4.2 (4.0)	16.8 (16.5)	5.00
$[Zn(OAc)_2(CNBTA)]$	90	40.1 (40.3)	17.4 (17.1)	3.3 (3.1)	19.7 (20.0)	—
$[Cd(OAc)_2(CNBTA)]$	60	35.7 (35.3)	14.7 (15.50)	2.9 (2.7)	30.2 (30.0)	—
$[Mn(OAc)_2(CNBTA)(H_2O)_2]$	50	37.2 (37.4)	16.2 (15.9)	4.1 (4.0)	15.2 (15.6)	5.99

2 h. The solid benzotriazolatochlorometal(II) complex formed was filtered and washed with methanol.

RESULTS AND DISCUSSION

The reaction of acetates and chlorides of metal(II) ions with BBTMI yielded new dimeric 1-cyanobenzotriazolediacetatometal(II) and the known benzotriazolatochlorometal(II) complexes whose elemental analysis and physical characteristics are given in Table 1. The reaction products reveal that the metal(II) acetates induce debenzotriazolation to form 1-cyanobenzotriazole and benzotriazole and chlorides bring about hydrolysis to form 1,1′bis(benzotriazol-1-yl)carbonyl *in situ*. The chemo-selectivity of the BBTMI in undergoing a specific reaction with either the metal(II) acetates or chlorides and to bring about a specific reaction either debenzotriazolation or hydrolysis can be explained as follows:

1. In metal(II) acetates, the acetate group is bidentately bound to the metal ion. The cleavage of one of the facile M—O bonds places a negative charge on the oxygen atom of the acetate group rendering it a nucleophilic centre to bring about debenzotriazolation. The schematic steps are given below. We have earlier described the debenzotriazolation of BBTMI brought about by labile β-diketonates which involved the M—O bond cleavage as a key factor. This observation lends support for the above scheme.

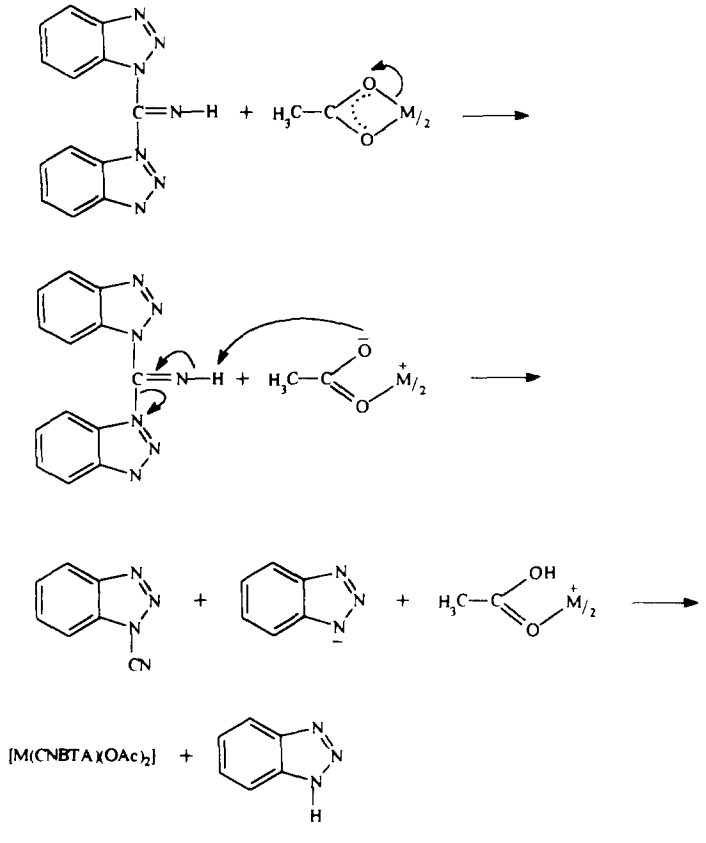
2. On the other hand metal chlorides seem to play a different role. They being a salt of weak base and strong acid, are necessarily acidic in ethanolic medium too. Such chlorides then bring about acid catalysed hydrolysis of BBTMI. The steps involved are: the formation of the ultimate product, *viz.* the benzotriazolatochloro complex, is obtained *via* decarbonylation of the intermediate 1,1′bis(benzotriazol-1-yl)carbonyl. This is possible due to the latter being a carbonylating agent [5]. The filtrate of the reaction product does not show the presence of any 1-substituted benzotriazoles, testifying the hydrolysis and the subsequent decarbonylation. However, the products in the filtrate could not be fully identified.

Identification

(*i*) *Benzotriazole chloro metal*(II). Elemental analysis shows that copper and cadmium complexes have the composition Cu(Cl)(BTA) and $Cd(BTAH)Cl_2$ respectively while other metal complexes have the composition $M(BTAH)_2Cl_2$. The identity of the complexes was confirmed by comparison with the spectra of authentic samples, prepared by the reported method [6].

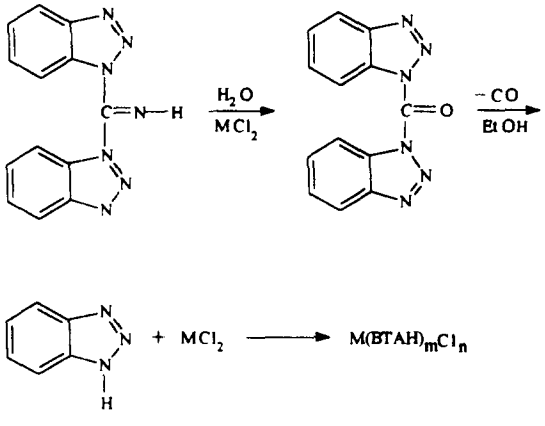
(*ii*) 1-*Cyanobenzotriazolediacetato metal*(II). The IR spectrum shows a strong absorption at 2180 cm^{-1} due to νCN which reveals the presence of a cyano group. The spectrum also shows bands attributable to benzotriazole, *viz.* at 745, 790, 1190, 1210 and 1270 cm^{-1}. The presence of an absorption band in the region 1630–1615 cm^{-1} is assignable to carbonyl stretching of the unidentately coordinated acetate groups [7]. The NMR spectrum of the zinc complex clearly indicates the presence of 1-cyanobenzotriazole and acetate groups through the appearance of the following peaks at 2.5 δ (s, 6H), 7.56 δ (s, 2H) and 8.1–8.3 δ (AA′BB′, 2H).

The identity of 1-cyanobenzotriazole is also confirmed by comparison of the demetallated ligand part with 1-cyanobenzotriazole prepared by the reported method [3].



M = Cu (II), Ni (II), Co (II), Zn (II), Mn (II) and Cd (II)

Scheme 1.



M = Ni(II), Co(II) and Zn(II) m=n=2

M = Cd (II) m=1 n=2

M = Cu (II) Cu(BTA)Cl

Scheme 2.

Acknowledgement—S. T. thanks the U.G.C. for award of a Fellowship.

REFERENCES

1. I. Rhee, M. Ryand and S. Tsutsumi, *Tetrahed. Letts* 1970, **39**, 3419.
2. W. Brackman and P. J. Smith, *Rec. Trav. Chim.* 1963, **82**, 757.
3. A. R. Katritzky, J. Z. Brzezinski and J. N. Lam, *Rev. Roum Chim.* 1991, **36**, 573.
4. S. Thambidurai, K. Jeyasubramanian, and S. K. Ramalingam, *Polyhedron* 1996, **15**, 4011.
5. W. S. Hancock, *J. Chromatography* 1981, **219**, 353.
6. J. Reedijk, A. R. Siedle, R. A. Velapoldi and J. A. M. Vankest, *Inorg. chim Acta.* 1983, **74**, 109.
7. K. Nakamoto (Ed.) *Infrared and Raman Spectra of Inorganic and Coordination Compounds*, John Wiley & Sons, New York (1977).

Pergamon

PII: S0277-5387(96)00297-5

Polyhedron Vol. 16, No. 3, pp. 427–431, 1997
Copyright © 1996 Elsevier Science Ltd
Printed in Great Britain. All rights reserved
0277-5387/97 $17.00+0.00

XPS and chiroptical studies on ternary lanthanide complexes of D-camphor-β-sulfonic acid and 1,10-phenanthroline

Dong Hengshan, Ma Hongzhu, Wang Bo and Yang Shiyan*

State Key Laboratory of Oxo Synthesis and Selective Oxidation, Lanzhou Institute of Chemical Physics, Chinese Academy of Sciences, Lanzhou 730000, P.R. China

(Received 1 April 1996; accepted 17 June 1996)

Abstract—Nine new chiral complexes of the type $Ln(Phen)_2L_2Cl$ (Ln = La^{III}, Pr^{III}, Nd^{III}, Ce^{III}, Sm^{III}, Eu^{III}, Tb^{III} and Ho^{III}, Phen = 1,10-phenanthroline, L = D-camphor-β-sulfonate ion) have been synthesized and characterized on the basis of elemental analysis, molar conductance, electronic, IR, XPS, circular dichroism (CD) and fluorescence spectra. A seven coordinated model has been proposed for these complexes. Copyright © 1996 Elsevier Science Ltd

Keywords: XP spectra; ternary lanthanide complexes; D-camphor-β-sulfonic acid; 1,10-phenanthroline; circular dichroism; fluorescence spectra.

In our earlier communications [1,2] we reported the preparation and properties of the lanthanide(III) complexes of D-camphor-β-sulfonic acid. As no chiroptical study on ternary lanthanide(III) complexes of D-camphor-β-sulfonic acid and 1,10-phenanthroline have been reported so far, in continuation of our systematic investigation of chiroptical lanthanide(III) chemistry we report here the synthesis and discussion of some of these complexes.

EXPERIMENTAL

Methods and materials

The reagents and solvents used were of AR grade and were used without further purification. Lanthanide(III) chlorides were made from the oxide and hydrochloric acid. Sodium D-camphor-β-sulfonate was made from sodium hydroxide and the acid.

Preparation of the complexes

The same method for the synthesis of all of these complexes was adopted. In a typical reaction to a sodium of 1,10-phenathroline (2 mmol) in anhydrous EtOH (30 cm^3), lanthanide(III) chloride (1 mmol) in EtOH (10 cm^3) was added, and the mixture was refluxed for 1 h. The white solids were separated and filtered, washed with EtOH and dried *in vacuo* (80 mm Hg) at 80°C for 1 h. The $Ln(Phen)_2Cl_3$ were obtained in the yield of 80–90%.

The solid, $Ln(Phen)_2Cl_3$ (1 mmol) was dissolved in absolute MeOH (30 cm^3), sodium D-camphor-β-sulphonate (3 mmol) in MeOH (20 cm^3) was added dropwise and the mixture was refluxed for 1 h. The white products were separated and filtered, washed with MeOH followed by Et_2O and dried *in vacuo* (80 mm Hg) at 80°C for 2 h.

Chemical and physical analyses

The lanthanide(III) contents in these complexes were determined by titration with EDTA in the presence of a buffer solution using xylenol orange as the indicator. C, H, N, S and Cl contents of the compounds were determined by standard procedures.

Molar conductance at room temperature was measured in 10^{-3} mol l^{-1} DMF solution using a DDS-IIA molar conductometer. IR spectra were taken on a NIC-5DX spectrophotometer (CsI pellets) in the range of 200–4000 cm^{-1}. Electronic spectra of the

* Author to whom correspondence should be addressed.

complexes in 10^4 mol l^{-1} DMF solution were recorded on a DJ-240 UV–vis spectrophotometer. The X-ray photoelectron spectra were measured on a PH1-550 spectrometer using Mg-K_α radiation (hν = 1253.6 eV). The peak areas and peak positions for the analyses were determined using a linear background. The accuracy of the measured BE values is $\pm$0.1 eV. All XP spectra were referenced to an assumed C 1*s* binding energy of 284.6 eV. Circular dichroism (CD) spectra were obtained at 20°C with a Cary Mode 60 spectropolarimeter with a CD model 6001 accessory in the 200–700 nm region. The molecular ellipticity (θ1) values are adjusted to an enantiometric excess (ee) of 100%. Fluorescence spectra of the complexes in 10^{-5} mol l^{-1} DMF were recorded on a 3070E spectrometer.

RESULTS AND DISCUSSION

Physical and analytical data on the new complexes are given in Table 1. Analytical results conform to the formula $Ln(Phen)_2L_2Cl$. The complexes are air stable and insoluble in ether, EtOH, acetone, THF and moderately soluble in MeOH and soluble in DMF and DMSO. The Λ_M values in DMF solution (Table 1) suggested that they are non-electrolytes [3]. The thermal analysis revealed that all the complexes are anhydrous.

IR spectra

The important bands observed in the IR spectra of the ligands as well as in their metal complexes are given in Table 2 along with their assignments.

The absorption bands of ν(C=O) at 1740 cm^{-1} in the ligand (NaL) and its metal complexes remains almost unchanged, indicative of the carbonyl oxygen being uncoordinated. Two stretching vibrations of —SO_3, $\nu_{as}(SO_3)$ and $\nu_s(SO_3)$ in the spectra of the complexes are observed at *ca* 1200 and 1047 cm^{-1} with the $\Delta\nu(SO_3)$ = 153 cm^{-1}. Comparing with the ligand, the two bands at 1190 and 1043 cm^{-1} with the difference $\Delta\nu(SO_3)$ = 147 cm^{-1} suggest that the —SO_3 group is coordinated with the metal ion in unidentate form. The band at 1620 cm^{-1} in the free ligand (Phen) attributed to the ν(C=N) stretching vibration shifts to lower frequencies at 1600 cm^{-1}, and the phen ring stretching vibration shifts from 1355 to 1346 cm^{-1} after complexation indicating that the nitrogen atoms are coordinated to the metal ion. Furthermore, three new bands are observed at *ca* 510, 320 and 270 cm^{-1} in the complexes assigned to ν(Ln—O), ν(Ln—N), and ν(Ln—Cl), respectively, confirms the participation of the ligands in the complexation [4, 5].

Electronic spectra

The electronic spectra of the complexes are similar, but are different from these of the ligands (Table 1).

Table 1. Elemental analysis and physical properties of the compounds

Compound	Found (Calc.) %						Λ_M	UV
	Ln	C	H	N	Cl	S	(S cm^2 mol^{-1})	(λ nm)
phen · H_2O								291, 325
NaL								285
$Eu(Phen)_2Cl_3$	24.1	46.9	2.6	8.3	17.0			300, 320
	(24.6)	(46.6)	(2.6)	(9.0)	(17.2)			
$Tb(Phen)_2Cl_3$	25.9	45.8	2.3	8.7	17.1			295
	(25.4)	(46.1)	(2.6)	(8.9)	(17.0)			320
$La(Phen)_2L_2Cl$	14.0	53.8	5.7	5.3	3.5	6.4	6	275, 295
	(14.3)	(54.5)	(5.2)	(5.8)	(3.7)	(6.6)		320
$Ce(Phen)_2L_2Cl$	14.0	54.1	5.5	6.0	3.6	6.3	5	276, 290
	(14.4)	(54.4)	(5.2)	(5.8)	(3.7)	(6.6)		320
$Pr(Phen)_2L_2Cl$	14.2	53.9	4.8	5.4	3.8	6.2	8	276, 290
	(14.5)	(54.4)	(5.2)	(5.8)	(3.7)	(6.6)		315
$Nd(Phen)_2L_2Cl$	14.3	54.0	5.1	5.0	3.4	6.7	8	275, 295
	(14.8)	(54.2)	(5.2)	(5.8)	(3.6)	(6.6)		318
$Sm(Phen)_2L_2Cl$	15.0	53.2	5.0	5.2	3.3	6.4	7	276, 296
	(15.3)	(53.9)	(5.1)	(5.7)	(3.6)	(6.5)		320
$Eu(Phen)_2L_2Cl$	15.1	53.3	4.7	5.4	3.7	6.2	6	278, 295
	(15.5)	(53.8)	(5.1)	(5.7)	(3.6)	(6.5)		320
$Tb(Phen)_2L_2Cl$	15.7	53.0	4.5	5.2	3.6	6.7	8	278, 297
	(16.1)	(53.2)	(5.1)	(5.7)	(3.6)	(6.5)		320
$Py(Phen)_2L_2Cl$	16.0	53.3	4.9	5.5	3.5	6.7	7	275, 295
	(16.4)	(53.2)	(5.1)	(5.6)	(3.6)	(6.5)		316
$Ho(Phen)_2L_2Cl$	16.1	53.3	5.0	5.4	3.3	6.4	6	275, 295
	(16.6)	(53.1)	(5.1)	(5.6)	(3.6)	(6.4)		318

Table 2. Significant IR bands of the ligands and the complexes (cm^{-1})

Compound	ν(C=O)	ν(C=N)	ν_{as}(—SO_3)	ν_s(—SO_3)	$\Delta\nu$(—SO_3)	ν(Ln—O)	ν(Ln—N)	ν(Ln—Cl)
phenH_2O		1620						
NaL	1740		1190	1050	140			
La(Phen)$_2L_2Cl$	1740	1600	1205	1045	160	512	320	270
Pr(Phen)$_2L_2Cl$	1741	1590	1204	1049	155	510	322	270
Ce(Phen)$_2L_2Cl$	1741	1585	1200	1048	152	513	325	272
Sm(Phen)$_2L_2Cl$	1740	1585	1200	1046	154	512	318	268
Eu(Phen)$_2L_2Cl$	1741	1685	1201	1046	155	514	320	270
Tb(Phen)$_2L_2Cl$	1741	1585	1203	1047	156	514	318	267
Nd(Phen)$_2L_2Cl$	1741	1585	1201	1045	156	513	316	270
Ho(Phen)$_2L_2Cl$	1740	1580	1200	1043	157	512	318	270
Dy(Phen)$_2L_2Cl$	1740	1584	1204	1045	159	512	320	271

Table 3. XP spectra data of the complexes and the ligands (BE eV)

Compound	N_{1s}	S_{2p}	O_{1s}	Cl_{2p}	Ln_{3d}	Ac%(Ln/C/N/O/S)[a]
Phen	401.2					
NaL		165.8	531.7, 533.1			
La(Phen)$_2L_2Cl$	399.5	165.6	531.5, 532.7	198.4	835.8	1.1:44:4.0:6.2:2.0:1
Pr(Phen)$_2L_2Cl$	399.4	165.4	531.4, 532.3	198.3	933.2	1.0:44.2:4.0:6.1:2.1:1
Nd(Phen)$_2L_2Cl$	399.5	165.6	531.2, 532.4	198.2	984.3	1.1:44.5:3.9:6.2:2.0:1
Ce(Phen)$_2L_2Cl$	399.6	165.6	531.3, 532.2	198.2	881.1	0.9:44.6:3.9:6.2:2.0:1
Sm(Phen)$_2L_2Cl$	399.5	165.5	531.3, 532.2	198.2	1084.1	1.0:44.5:4.1:6.0:1.9:1
Eu(Phen)$_2L_2Cl$	399.4	165.6	531.3, 532.2	198.2	1135.8	1.1:44.4:4.0:5.8:1.9:1
Ho(Phen)$_2L_2Cl$	399.4	165.5	531.4, 532.1	198.2	1190.6	1.0:44.6:4.2:5.9:2.1:1
Tb(Phen)$_2L_2Cl$	399.4	155.5	531.3, 532.1	198.1	1246.2	0.9:43.8:4.1:6.1:2.1:1
Dy(Phen)$_2L_2Cl$	399.4	165.5	531.3, 532.3	198.1	1217.5	0.9:44.0:4.1:6.0:2.1:1

[a]Atomic molar percent.

Table 4. CD spectra data of the complexes and the ligands

Compound	Conc. (c, DMF)	λ_{max} (nm)	α	$[\alpha]_D^{20}$ (°)
NaL	3.0	286	+0.0702	+23.4
La(Phen)$_2L_2Cl$	3.4	276, 300, 324	+0.2666	+86
Pr(Phen)$_2L_2Cl$	2.8	284, 300, 320	+0.3026	+89
Eu(Phen)$_2L_2Cl$	2.5	280, 302, 325	+0.3100	+124
Tb(Phen)$_2L_2Cl$	2.6	281, 305, 330	+0.3094	+119
Ce(Phen)$_2L_2Cl$	2.4	281, 304, 332	+0.3010	+125.4
Nd(Phen)$_2L_2Cl$	2.5	281, 304, 335	+0.2840	+113.6
Sm(Phen)$_2L_2Cl$	2.3	281, 305, 334	+0.2906	+126.3
Dy(Phen)$_2L_2Cl$	2.5	281, 305, 335	+0.2880	+1135.2
Ho(Phen)$_2L_2Cl$	2.4	281, 305, 334	+0.3100	+129.2

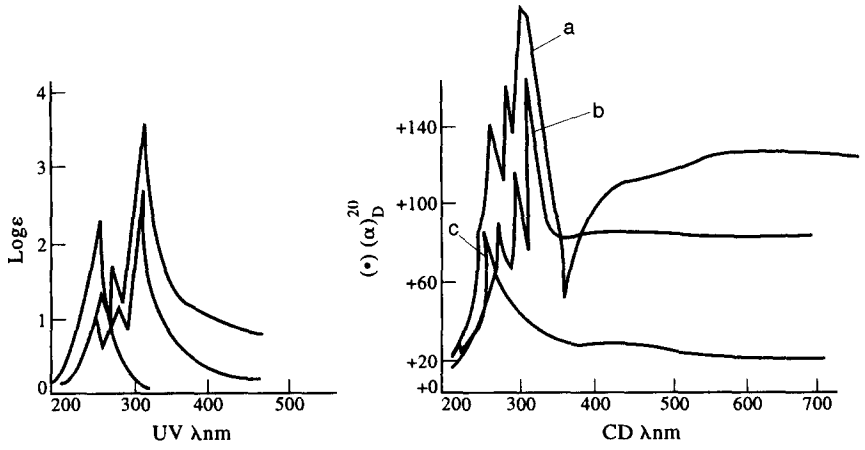


Fig. 1. CD(···) and electronic spectra of the complexes. (a) $Eu(Phen)_2L_2Cl$; (b) $La(Phen)_2L_2Cl$ and (c) NaL.

The bands are observed at *ca* 295 and 320 nm of the complexes due to the phen purple-shifted 4–8 nm relative to the free ligand, indicating the coordination of the nitrogen atom to the metal. The band at *ca* 280 nm and purple-shifted 5–10 nm in the complexes is attributed to the ν(C=O) absorption of L [4,5], indicating complexation.

Fluorescence spectra

A strong red-fluorescence of the solid complexes $Eu(Phen)_2L_2Cl$ and $Tb(Phen)_2L_2Cl$ was observed under a ultraviolet lamp (λ = 254 nm) but the solution fluorescence (1×10^{-5} mol l^{-1} DMF) of the complexes is very weak and a broad band at 404 nm of Eem are observed at Eex 345 nm for Eu^{III} complexes and Eex 364 nm for Tb^{III} complexes, respectively, indicating that the fluorescence is due to the interaction of phen with L. The result was confirmed by the determination of the solution (1×10^{-5} mol l^{-1} DMF) of the gel prepared from phen and HL in the mol ratio 1:1.

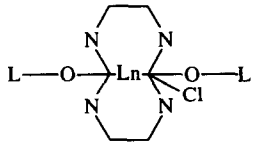
XP spectra

To obtain further insight concerning the nature of bonding, XP spectra of the complexes and ligands were recorded in the powder form at room temperature (25°C), and it was found that the data of atomic molar percent determined is very close to the elemental result. The electron BEs of the metal and the values of N 1*s*, O 1*s*, S 2*p* and Cl 2*p* are given in Table 3. The values for Ln 3*d* or 4*d* electron BE in the complexes are approximately the same and support the oxidation number of three.

The N 1*s* and S 2*p* electron spectra of the complexes are symmetric and their deconvolution revealed that related to the free ligands, the N 1*s* and S 2*p* BEs are both shifted lower, this can be explained as due to the increase of the electron density coordinated to the ligands and it is consistent with the electronic spectra date. The O 1*s* electron spectra of the complexes are asymmetric and deconvolution yields two components with an intensity ratio 1:3. The weaker component with a higher BE value at *ca* 532.7 eV remain almost unchanged and belongs to oxygen of the carbonyl, the more intense component with a lower BE value belongs to the oxygen of SO_3 group. The values are slightly lower than that of the NaL ligand [6].

CD spectra

The distinct positive Cotton effect of the spectra of the complex and the ligand (NaL) are observed (Table 4, Fig. 1), the positive value at *ca* 280 nm of the complexes is diagnostic of the preferred conformer with (s)-absolute configuration is dominant for dichroic absorption similar to a positive effect in the ligand [7].



On the basis of the above discussions a seven coordinated number bonding model is proposed for the complexes.

Acknowledgements—This project is supported by Union Laboratory of Asymmetric Synthesis (Chengdu Institute of

Organic Chemistry, Academia Sinica, Hong Kong Polytechnic, and Kuo Ching Chemical Co, Ltd.).

REFERENCES

1. Liu Jinxia, Wang Bo, Xie Wenjuan, Yang Shiyan and Jin Daosen, *Polyhedron* 1994, **13,** 2059.
2. Feng Dianzhong and Wang Bo, *Bull. Chem. Soc. Belg.* 1992, **101,** 167.
3. W. J. Geary, *Coord. Rev* 1971, **7,** 81.
4. Kazuo Nakamoto, *Infrared and Raman Spectra of Inorganic and Coordination Compounds*, 3rd Edn. Wiley-Interscience, New York (1978).
5. R. M. Silverstein, G. C. Bassier and T. C. Morril, *Spectrometric Identification of Organic Compounds*. Wiley, New York (1981).
6. H. Vaclav and P. Pavel, *Inorg. Chim. Acta* 1991, **179,** 267.
7. R. Rita, C. S. Manik and S. R. Parag, *Trans. Met. Chem.* 1990, **15,** 51.

Pergamon

PII: S0277-5387(96)00296-3

Polyhedron Vol. 16, No. 3, pp. 433–439 1997
Copyright © 1996 Elsevier Science Ltd
Printed in Great Britain. All rights reserved
0277-5387/97 $17.00+0.00

Preparation and characterization of iron(+2) and ruthenium(+2) diiminodiphosphine complexes. X-ray crystal structures of $[(\eta^5\text{-}C_5H_5)Fe(immpho)][BF_4]\cdot 0.5CH_2Cl_2$ and $\{[(\eta^5\text{-}C_5Me_5)Ru(CH_3CN)]_2[immpho]\}\{ZnCl_4\}\cdot 2CH_3CN\cdot 2H_2O$

Wai-Kwok Wong,[a]* Yang Chen[a] and Wing-Tak Wong[b]*

[a]Department of Chemistry, Hong Kong Baptist University, 224 Waterloo Road, Kowloon, Hong Kong

[b]Department of Chemistry, The University of Hong Kong, Pokfulam Road, Hong Kong

(Received 23 February 1996; accepted 17 June 1996)

Abstract—The interaction of *N,N'-bis*[*o*-(diphenylphosphino)benzylidene]ethylenediamine (immpho) with one and two equivalents of $[(\eta^5\text{-}C_5Me_5)Ru(CH_3CN)_3]^+$ (generated *in situ* from the reaction of $[(\eta^5\text{-}C_5Me_5)RuCl_2]_n$ with excess Zn granular in CH_3CN) in CH_3CN at room temperature gave $[(\eta^5\text{-}C_5Me_5)Ru(immpho)]_2[ZnCl_4]$ (**I**) and $\{[(\eta^5\text{-}C_5Me_5)Ru(CH_3CN)]_2[immpho]\}\{ZnCl_4\}$ (**II**) in 80% and 71% yield, respectively. Upon UV irradiation, immpho reacted with equal molar of $[(\eta^5C_5H_5)Fe(\eta^6\text{-mesitylene})][BF_4]$ in CH_3CN at room temperature to give $[(\eta^5\text{-}C_5H_5)Fe(immpho)][BF_4]$ (**III**) in 41% yield. Compounds **I**–**III** have been fully characterized by analytical and spectroscopic methods. The structures of **II** and **III** have been established by X-ray diffraction. Copyright © 1996 Elsevier Science Ltd

Keywords: ruthenium(+2); iron(+2); ruthenium(+2) dimer; diiminodiphosphine; cyclopentadienyl; pentamethylcyclopentadienyl.

We have been interested in the chemistry of diiminodiphosphines as these are polydentate ligands containing both phosphorus and nitrogen donor atoms which could behave as soft and hard bases, respectively, and act as bridging ligands for the preparation of heterometallic complexes with hard and soft metal centres. We have shown that these ligands exhibit a very rich coordination chemistry and can behave as bridging, *bi-*, *tri-* and *tetra*-dentate ligands depending on the reaction conditions [1–6]. As a tridentate ligand, the diiminodiphosphine ligand exhibits different modes of coordination toward different metal centres. The diiminodiphosphine ligands coordinate to the Group 6 metals (Cr, Mo) *via* the two imino groups and one of the phosphino groups with one of the phosphino groups remaining uncoordinated [2,6]; and coordinate to the Group 11 metals (Cu, Ag) *via* the two phosphino groups and one of the two imino groups only with one of the imino groups remaining uncoordinated [4,6]. In this paper, we report the coordination mode of *N,N'-bis*[*o*-(diphenylphosphino)benzylidene]ethylenediamine (immpho), a diiminodiphosphine ligand, toward Group 8 metals, Fe and Ru.

RESULTS AND DISCUSSION

Preparation of $[(\eta^5\text{-}C_5Me_5)Ru(immpho)]_2[ZnCl_4]$ (I)

An acetonitrile solution of $[(\eta^5\text{-}C_5Me_5)Ru(CH_3CN)_3]^+$, generated *in situ* from the reaction of $[(\eta^5\text{-}C_5Me_5)RuCl_2]_n$ with excess Zn granular in CH_3CN, was slowly added to a solution of CH_2Cl_2 containing one equivalent of immpho at room tem-

* Authors to whom correspondence should be addressed.

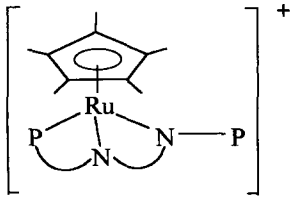
perature; after stirring the solution for an additional 12 h, work up gave dark-red crystals of stoichiometry $[(C_5Me_5)Ru(immpho)]_2[ZnCl_4]\cdot 2H_2O$, **I**$\cdot 2H_2O$, in good yield (80%) after recrystrallization from a CH_3CN/Et_2O mixture. The IR spectrum of **I** exhibits a $\nu_{C=N}$ stretch at 1626 cm^{-1} for the imino groups. The $^{31}P\text{-}\{^1H\}$ NMR spectrum of **I** exhibits two singlets of relative intensity 1 : 1 at δ 43.6 and -15.6 ppm which correspond to a coordinated and an uncoordinated phosphorus, respectively. This suggests that the immpho ligand behaves as a tridentate ligand with one of its phosphino groups remaining uncoordinated. This is further supported by the ^1H NMR spectrum of **I** which exhibits two broad multiplets of relative intensity of 1 : 1 at δ 9.80 and 8.18 ppm which corresponds to the —C*H*=N— proton of the uncoordinated and the coordinated benzylidene, respectively. Other than the phenyl protons, the ^1H NMR spectrum of **I** also exhibits a singlet at δ 1.09 ppm for the —C*H*$_3$ protons of the pentamethylcyclopentadienyl ring indicating that the pentamethylcyclo pentadienyl ring is bonded to the ruthenium metal in an η^5 fashion. Based on the above spectroscopic data, the following structure can be assigned to **I**.

This is confirmed by an X-ray diffraction study [7] which shows that the diiminodiphosphine ligand acts as a tridentate ligand with one of the two phosphino groups and the two imino groups coordinated to the ruthenium metal and an uncoordinated phosphino group.

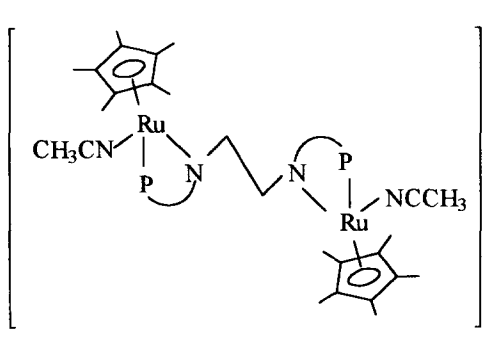
However, when the above reaction was carried out in the reverse order, that is by adding a CH_2Cl_2 solution of immpho into an equal molar solution of $[(\eta^5\text{-}C_5Me_5)Ru(CH_3CN)_3]^+$, generated *in situ* from the reaction of $[(\eta^5\text{-}C_5Me_5)RuCl_2]_n$ with excess Zn granular in CH_3CN, the $^{31}P\text{-}\{^1H\}$ NMR spectrum of the reaction mixture showed that a mixture of **I** and **II** (*via infra*) were obtained. Dark-red crystals of stoichiometry $\{[(\eta^5\text{-}C_5Me_5)Ru(CH_3CN)]_2[immpho]\}\{ZnCl_4\}$, **II**, were obtained in good yield (71%) after recrystallization from a CH_3CN/Et_2O mixture. The IR spectrum of **II** exhibits a $\nu_{C=N}$ stretch at 1637 cm^{-1} for the imino groups. The $^{31}P\text{-}\{^1H\}$ NMR spectrum of **II** exhibits only a singlet at δ 43.2 ppm. This suggests that the two phosphino groups of the immpho ligand were coordinated and equivalent. Other than the phenyl protons, the ^1H NMR spectrum of **II** also exhibits a broad multiplet of relative intensity of 2 at δ 8.30 ppm for the —C*H*=N— protons of the coordinated benzylidenes; two broad singlets of relative intensity 2 : 2 at δ 4.55 and 4.40 ppm for the —NCH_2CH_2N— protons; and a singlet of relative intensity of 30 at δ 1.40 ppm for the —C*H*$_3$ protons of the pentamethylcyclopentadienyl rings, indicating that the two pentamethylcyclopentadienyl rings are equivalent and bonded to the ruthenium metals in an η^5 fashion. Based on the above spectroscopic data the following structure can be assigned to **II**.

The structure of **II** was confirmed by an X-ray diffraction study. Crystals of stoichiometry $\{[(\eta^5\text{-}C_5Me_5)Ru(CH_3CN)]_2[immpho]\}\{ZnCl_4\}\cdot 2CH_3CN\cdot 2H_2O$ suitable for X-ray diffraction study were grown by slow diffusion of diethyl ether into a concentrated solution of **II** in CH_3CN. A perspective drawing of **II** is shown in Fig. 1. Selected bond lengths and bond angles are given in Table 1. The solid state structure is consistent with the spectroscopic data. The dimeric species is centro-symmetric with the pentamethylcyclopentadienyl rings bonded to the ruthenium metals in η^5-fashion having the Ru—C bond lengths ranging from 2.17(2) to 2.21(2) Å and the immpho ligand acted as a bidentate ligand having an imino group and a phosphino group coordinated to each of the two $[(\eta^5\text{-}C_5Me_5)Ru(CH_3CN)]^+$ moieties. Similar bonding behaviour has been reported for the immpho ligand [1]. Within the diiminodiphosphine ligand, the N(1)—C(11) bond length of 1.47(2) Å and the N(1)—C(12) bond length of 1.34(2) Å are in agreement with the C—N and C=N bond distances, respectively.

When a CH_3CN solution of equal molar of $[(\eta^5C_5H_5)Fe(\eta^6\text{-mesitylene})][BF_4]$ and immpho was irradiated at ambient temperature for 12 h, work up gave dark-red crystal of stoichiometry $[(\eta^5C_5H_5)Fe(immpho)][BF_4]\cdot CH_2Cl_2$, **III**$\cdot CH_2Cl_2$, in moderate yield (42%) after recrystallization from a CH_2Cl_2/Et_2O mixture. The IR spectrum of **III** exhibits a $\nu_{C=N}$ stretch at 1632 cm^{-1} for the imino groups. The $^{31}P\text{-}\{^1H\}$ NMR spectrum of **III** exhibits two singlets of relative intensity 1 : 1 at δ 67.8 and -12.6 ppm which correspond to a coordinated and an uncoordinated phosphorus, respectively. This suggests that the immpho ligand behaves as a tridentate ligand with one of its phosphino groups remaining unco-



Scheme 1.



Scheme 2.

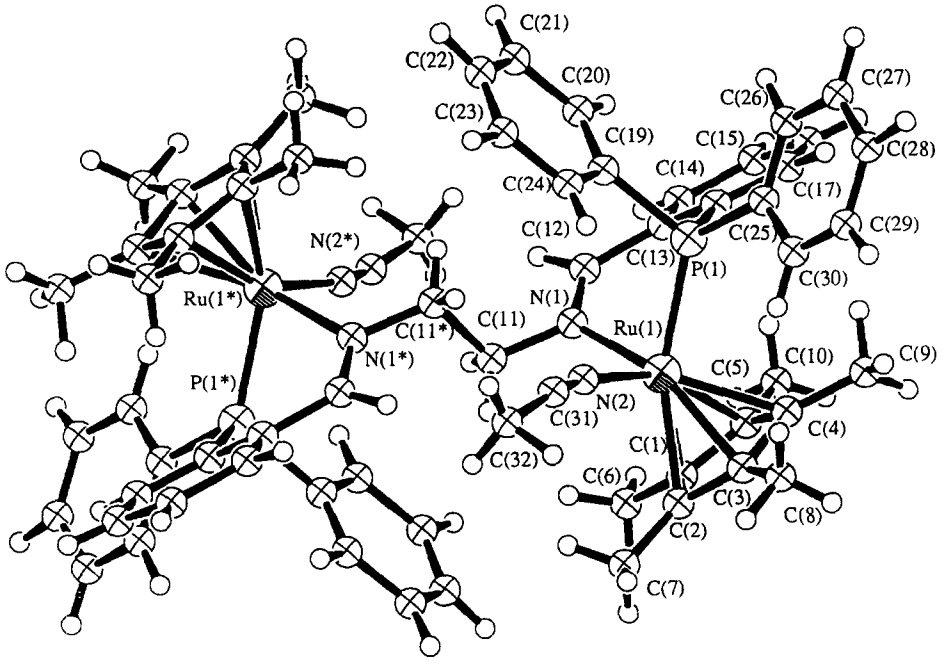


Fig. 1. A perspective drawing of the cation of **II**.

Table 1. Selected bond lengths (Å) and bond angles (°) for **II**

Ru(1)—P(1)	2.300(5)	Ru(1)—N(1)	2.11(1)
Ru(1)—N(2)	2.01(2)	Ru(1)—C(1)	2.21(2)
Ru(1)—C(2)	2.20(2)	Ru(1)—C(3)	2.17(2)
Ru(1)—C(4)	2.19(2)	Ru(1)—C(5)	2.20(2)
N(1)—C(11)	1.47(2)	N(1)—C(12)	1.34(2)
N(2)—C(31)	1.04(3)		

P(1)—Ru(1)—N(1)	80.8(4)	P(1)—Ru(1)—N(2)	93.5(5)
N(1)—Ru(1)—N(2)	91.7(6)	C(11)—N(1)—C(12)	113(1)
N(1)—C(12)—C(13)	122(1)	N(2)—C(31)—C(32)	172(2)
Ru(1)—N(2)—C(31)	166(2)		

ordinated. The resonances of the ^{1}H NMR spectrum of **III** are rather broad, indicating that the complex may be weakly paramagnetic. Other than the phenyl protons, the ^{1}H NMR spectrum of **III** exhibits two broad multiplets of relative intensity 1 : 1 at δ 9.45 and 8.76 ppm for the —C*H*=N— protons of the uncoordinated and coordinated benzylidene, respectively; two broad multiplets of relative intensity 2 : 2 at δ 4.70 and 3.75 ppm for the —NCH_2CH_2N— protons; and a broad singlet of relative intensity of 5 at δ 2.45 ppm for the protons of the cyclopentadienyl rings, indicating that the cyclopentadienyl ring is bonded to the iron metal in an η^5 fashion. The unusual high field shift of the cyclopentadienyl protons may probably be due to the weak paramagnetism of the complex. The above spectroscopic data suggest that the structure of **III** is similar to that of **I**.

This is confirmed by an X-ray diffraction study. Crystals of stoichiometry [(η^5-C_5H_5)Fe(immpho)][BF_4]·0.5CH_2Cl_2 suitable for X-ray diffraction study were grown by slow diffusion of diethyl ether into a concentrated solution of **III** in CH_2Cl_2. A perspective drawing of **III** is shown in Fig. 2. Selected bond lengths and bond angles are given in Table 2. The solid state structure is consistent with the spectroscopic data. The structure shows that the cyclopentadienyl ring is bonded to the iron metal in η^5 fashion with the Fe—C bond lengths ranging from 2.05(1) to 2.10(1) Å; and the immpho ligand acts as a tridentate ligand with one of the two phosphino groups and the two imino groups coordinated to the iron metal and an uncoordinated phosphino group. Within the diiminodiphosphine ligand, the N(1)—C(8) and the N(2)—C(27) bond lengths are 1.27(1) and 1.28(1) Å, respectively, and are in agreement with the C=N bond distance.

The present study shows that the mode of coordination of the diiminodiphosphine as a tridentate

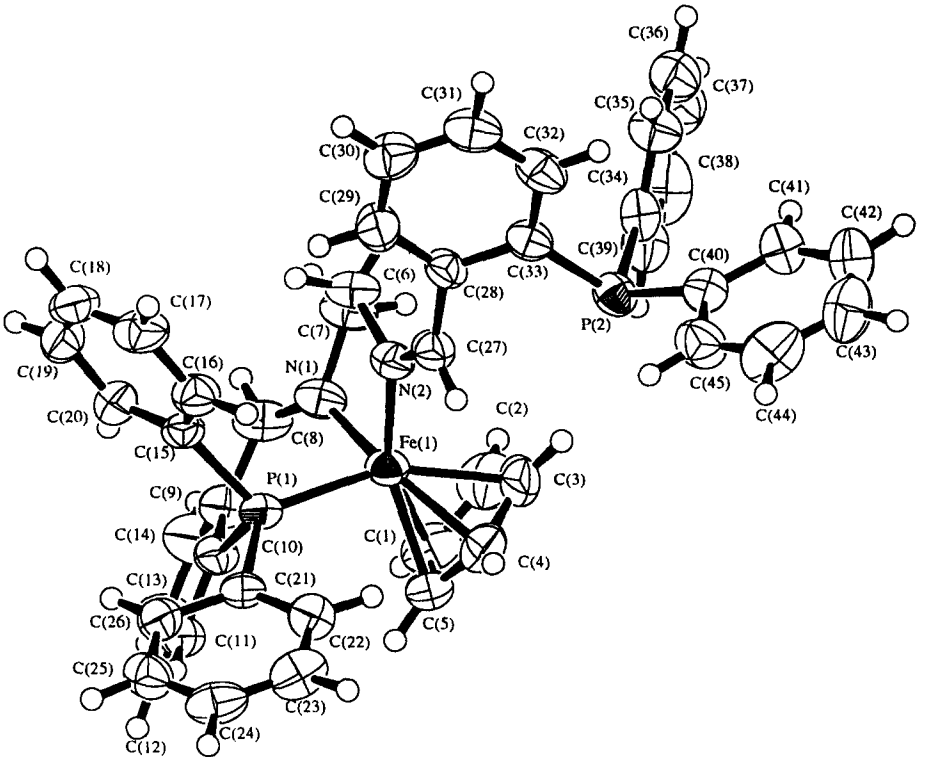


Fig. 2. A perspective drawing of the cation of **III**.

Table 2. Selected bond lengths (Å) and bond angles (°) for **III**

Fe(1)—P(1)	2.187(3)	Fe(1)—N(1)	1.937(9)
Fe(1)—N(2)	1.979(8)	Fe(1)—C(1)	2.05(1)
Fe(1)—C(2)	2.09(1)	Fe(1)—C(3)	2.09(1)
Fe(1)—C(4)	2.10(1)	Fe(1)—C(5)	2.06(1)
N(1)—C(8)	1.27(1)	N(1)—C(7)	1.46(1)
N(2)—C(6)	1.47(1)	N(2)—C(27)	1.28(1)
P(1)—Fe(1)—N(1)	83.5(3)	P(1)—Fe(1)—N(2)	98.5(2)
N(1)—Fe(1)—N(2)	82.6(3)	C(7)—N(1)—C(8)	120.1(9)
N(1)—C(8)—C(9)	122.4(9)	N(1)—C(7)—C(6)	106.1(8)
C(6)—N(2)—C(27)	120.7(8)	N(2)—C(27)—C(28)	127.2(10)
N(2)—C(6)—C(7)	108.0(8)		

ligand toward Group 8 metals (Fe and Ru) is similar to that of Group 6 metals; that is having one of the two phosphino groups and the two imino groups coordinated to the metal and the other phosphino group remaining uncoordinated. This may be a general trend for the diiminodiphosphine, acting as a tridentate ligand, coordinating to Group 8 metals.

EXPERIMENTAL

Microanalyses were performed by the Shanghai Institute of Organic Chemistry, Chinese Academy of Sciences, China. IR spectra (KBr pellets) were recorded on a Nicolet Nagna-IR 550 spectrometer; data are given in cm^{-1}. NMR spectra were recorded on a JEOL EX270 spectrometer. Chemical shifts of $^{31}P\{^1H\}$ NMR spectra were referenced to external 85% H_3PO_4. Chemical shifts of ^1H NMR spectra were referenced to internal deuterated solvents and then recalculated to TMS = δ 0.00 ppm. Low resolution mass spectra (LRMS) were obtained on a Finnigan MAT SSQ-710 spectrometer in FAB (positive) operation mode and are reported as m/z.

All operations were carried out under nitrogen or *in vacuo*. All chemicals used were of reagent grade. Solvents were dried by standard procedures. Distilled and deaerated prior to use. Melting points were taken in sealed capillaries and are uncorrected. Photochemical reactions were conducted at room temperature with a 450-W Conrad-Hanovia 7825

medium-pressure mercury lamp. $RuCl_3 \cdot 3H_2O$ was purchased from Aldrich and used without further purification. Immpho [6], $[(\eta^5C_5Me_5)RuCl_2]_n$ [8] and $[(\eta^5C_5H_5)Fe(\eta^6\text{-mesitylene})][BF_4]$ [9] were prepared according to literature methods.

Preparation of $[(\eta^5\text{-}C_5Me_5)Ru(immpho)]_2[ZnCl_4]$ (**I**)

A solution of $[(\eta^5\text{-}C_5Me_5)RuCl_2]_n$ (0.30 g, 1.0 mmol) and granular Zn (1.2 g, 18.5 mmol) in methanol (10 cm^3) was refluxed for 10 min. Then CH_3CN (10 cm^3) was added to the methanol solution and the resultant solution was maintained refluxing for another 5 h. The colour of the reaction mixture changed to orange. Upon cooling to room temperature, the solution was filtered. The filtrate was then added dropwise to a stirring solution of immpho (0.61 g, 1.0 mmol) in CH_2Cl_2 (10 cm^3). The reaction mixture was allowed to stir at room temperature for another 12 h to give a dark-red solution. The solvents were removed *in vacuo* to give a dark-red residue. The residue was redissolved in a minimum amount of CH_3CN and chromatographed on a silica gel column (2 × 15 cm) using CH_3CN as an eluant. The dark-red band obtained was concentrated to *ca* 5 cm^3 and then diethyl ether was added until the solution just turned cloudy. The CH_3CN/diethyl ether mixture was then cooled to −20 °C to give dark-red crystals, which were filtered and dried *in vacuo*. Yield: 0.83 g, 79%; m.p. 220–223 C. Found: C, 62.2; H, 5.1; N, 2.8. Calc. for $(C_{100}H_{98}N_4P_4Cl_4ZnRu_2)\cdot 2H_2O$: C, 62.4; H, 5.3; N, 2.9%. IR (cm^{-1}, in KBr): 3440 br, s, 3052 m, 2902 m, 1626 m, 1584 w, 1476 m, 1432 s, 1384 w, 1294 w, 1268 w, 1218 w, 1090 m, 1070 w, 1022 m, 920 w, 746 s, 694 vs, 508 s, 490 m. $^{31}P\text{-}\{^1H\}$ NMR ($CDCl_3$): uncoordinated PPh_2 group, δ −15.6(s) ppm; coordinated PPh_2 group, δ 43.6(s) ppm. ^1H NMR ($CDCl_3$): —C*H*=N— proton of uncoordinated benzylidene, δ 9.80 (1H, m) ppm; —C*H*=N— proton of coordinated benzylidene, δ 8.18 (1H, m) ppm; phenyl protons, δ 6.80–7.80 (28H, br, m) ppm; —NCH_2CH_2N— protons, δ 3.90–4.20 (4H, br, m) ppm; H_2O protons, δ 2.01 (2H, s) ppm; CH_3 protons, δ 1.09 (15H, s) ppm.

Preparation of $\{[(\eta^5\text{-}C_5Me_5)Ru(CH_3CN)]_2[immpho]\}\{ZnCl_4\}$ (**II**)

A solution of $[(\eta^5\text{-}C_5Me_5)RuCl_2]_n$ (0.30 g, 1.0 mmol) and granular Zn (1.2 g, 18.5 mmol) in methanol (10 cm^3) was refluxed for 10 min. Then CH_3CN (10 cm^3) was added to the methanol solution and the resultant solution was maintained refluxing for another 5 h. The colour of the reaction mixture changed to orange. Upon cooling to room temperature, the solution was filtered and stirred. Then a solution of immpho (0.30 g, 0.5 mmol) in CH_2Cl_2 (10 cm^3) was then added dropwise to the orange filtrate. The reaction mixture was allowed to stir at room temperature for another 12 h to give a dark-red solution. The solvents were removed *in vacuo* to give a dark-red residue. The residue was redissolved in a minimum amount of CH_3CN and chromatographed on a silica gel column (2 × 15 cm) using CH_3CN as an eluant to give a dark-red band. The solvent of the dark-red band was removed *in vacuo* to give a dark-red residue which was redissolved in a minimum amount of CH_2Cl_2. Then diethyl ether was added to the CH_2Cl_2 solution until it just turned cloudy. The CH_2Cl_2/diethyl ether mixture was then cooled to −20 °C to give dark-red crystals, which were filtered and dried *in vacuo*. Yield: 0.47 g, 71%; m.p. 231–232 °C. Found: C, 56.0; H, 5.2; N, 4.2. Calc. for $(C_{64}H_{70}N_4P_2Cl_4ZnRu_2)\cdot 0.5H_2O$: C, 55.9; H, 5.2; N, 4.1%. IR (cm^{-1}, in KBr): 3433 br, s, 3051 w, 2920 s, 2853 m, 1701 w, 1637 m, 1560 w, 1477 m, 1435 s, 1374 w, 1298 w, 1261 mw, 1188 w, 1089 s, 1068 m, 1026 s, 912 w, 800 m, 746 s, 730 m, 699 vs, 528 vs, 486 m. $^{31}P\text{-}\{^1H\}$ NMR ($CDCl_3$): coordinated PPh_2 group, δ 43.2(s) ppm. ^1H NMR ($CDCl_3$): —C*H*=N— protons, δ 8.34 (2H, br, m) ppm; phenyl protons, δ 6.68–7.80 (28H, br, m) ppm; —NCH_2CH_2N— protons, δ 4.55 (2H, br, s) and 4.40 (2H, br, s) ppm; —CH_3 protons of CH_3CN, δ 1.52–1.63 (6H, m) ppm; —CH_3 protons of C_5Me_5, δ 1.40 (30H, br, s) ppm.

Preparation of $[(\eta^5\text{-}C_5H_5)Fe(immpho)][BF_4]$ (**III**)

A solution of $[(\eta^5\text{-}C_5H_5)Fe(\eta^6\text{-mesitylene})][BF_4]$ (0.33 g, 1.0 mmol) and immpho (0.60 g, 1.0 mmol) in CH_3CN (30 cm^3) was irradiated at room temperature for 12 h. The colour of the solution changed from yellow to red–brown. The solvent of the resultant solution was removed *in vacuo* to give dark-red residue. The residue was redissolved in a minimum amount of CH_3CN and chromatographed on a silica gel volume (2 × 15 cm) using CH_3CN as an eluant to give a dark-red band. The solvent of the dark-red band was removed *in vacuo* to give a dark-red residue which was redissolved in a minimum amount of CH_2Cl_2. Then diethyl ether was added to the CH_2Cl_2 solution until it just turned cloudy. The CH_2Cl_2/diethyl ether mixture was then cooled to −20 °C to give dark-red crystals, which were filtered and dried *in vacuo*. Yield: 0.34 g, 42%; m.p. 182–184 °C. Found: C, 61.9; H, 4.5; N, 3.0. Calc. for $(C_{45}H_{39}N_2P_2BF_4Fe)\cdot CH_2Cl_2$: C, 61.6; H, 4.6; N, 3.1%. IR (cm^{-1}, in KBr): 3053 w, 2956 w, 2923 m, 2854 w, 1623 m, 1582 w, 1480 w, 1435 s, 1387 w, 1262 w, 1268 w, 1084 vs, 1055 vs, 1037 vs, 840 w, 815 w, 751 s, 698 s, 532 m, 519 s, 466 m. $^{31}P\text{-}\{^1H\}$ NMR (CD_2Cl_2): uncoordinated PPh_2 group, δ −12.6(s) ppm; coordinated PPh_2 group, δ 67.8(s) ppm. ^1H NMR (CD_2Cl_2): —C*H*=N— proton of uncoordinated benzylidene, δ 9.45 (1H, br, s) ppm; —C*H*=N— proton of coordinated benzylidene, δ 8.76 (1H, br, s) ppm; phenyl protons, δ 6.80–7.80 (26H, br, m) and 6.00 (2H, br, s) ppm; —NCH_2 CH_2N— protons, δ 4.60–4.83 (2H, br, m) and 3.52–4.00 (2H, br, m) ppm; C_5H_5 protons, δ 2.45 (5H, br, s) ppm. LRMS (FAB: +ve) m/z: 725.

X-ray diffraction studies

The general procedures for the X-ray diffraction studies are described as below. Crystals were mounted on glass fibres with epoxy resin. Intensity data were collected on a Rigaku AFC7R diffractometer with graphite monochromated Mo-K_α radiation ($\lambda = 0.71073$ Å) using ω-2θ scans ($2\theta_{max} \leqslant 45°$) at room temperature. The data were corrected for Lorentz, polarization effects and absorption correction using ψ-scan method [10]. Crystal data, data collection parameters, and results of the analysis are given in Table 3. The structures were solved by Direct Methods (SIR88) [11] and refined by full matrix least-squares technique. For compound **II,** an acetonitrile and a water molecule are found in the asymmetric unit. They were refined to give relatively high thermal displacement parameters. For compound **III,** a partially occupied solvate of dichloromethane is revealed in the asymmetric unit and their atomic positional and thermal parameters were refined with occupancy 0.5. With this model, the refinement converged to give the best R and Rw factors and more reasonable thermal parameters for this solvate. The hydrogen atoms were generated in their idealized positions (C—H bond fixed at 0.95 Å) and included in structure factor calculations but not refined. All calculations were performed on a Silicon-Graphics computer using the program package Texsan [12] from MSC.

(a) *Compound* **II.** Crystals of **II** suitable for X-ray diffraction study were grown from CH_3CN/diethyl ether as a solvate of stoichiometry $\mathbf{II} \cdot 2CH_3CN \cdot 2H_2O$. A red plate of dimensions of $0.24 \times 0.28 \times 0.34$ mm^3 was mounted on a glass fibre

Table 3. Data collection and processing parameters for **II** and **III**

	II	**III**
Empirical formula	$C_{68}H_{80}O_2N_6P_2Cl_4ZnRu_2$	$C_{45.5}H_{40}N_2P_2BF_4FeCl$
Colour and habit	Red plate	Red plate
Crystal size (mm)	$0.24 \times 0.28 \times 0.34$	$0.30 \times 0.38 \times 0.40$
Crystal system	Triclinic	Triclinic
Space group	$P\bar{1}$ (No. 2)	$P\bar{1}$ (No. 2)
Unit cell dimensions	$a = 13.391(1)$ (Å)	$a = 13.782(6)$ (Å)
	$b = 15.011(2)$ (Å)	$b = 15.935(3)$ (Å)
	$c = 12.225(2)$ (Å)	$c = 11.232(3)$ (Å)
	$\alpha = 91.08(1)$ (°)	$\alpha = 110.02(2)$ (°)
	$\beta = 103.93(1)$ (°)	$\beta = 100.47(3)$ (°)
	$\gamma = 113.28(1)$ (°)	$\gamma = 102.66(3)$ (°)
	$V = 2172.8(5)$ (Å^3)	$V = 2170(1)$ (Å^3)
	$Z = 1$	$Z = 2$
Formula weight	1484.70	854.88
Density (calc.)	1.135 (g cm^{-3})	1.308 (g cm^{-3})
Absorption coefficient	8.14 (cm^{-1})	5.33 (cm^{-1})
$F(000)$	762	882
Diffractometer	Rigaku AFC7R	Rigaku AFC7R
Radiation	Mo-K_α ($\lambda = 0.71073$ Å)	Mo-K_α ($\lambda = 0.71073$ Å)
Temperature (K)	298	301
Scan type	ω-2θ	ω-2θ
Scan speed	16.0 (° min (in ω)) (up to 4 scans)	16.0 (° min (in ω)) (up to 6 scans)
$2\theta_{max}$	45.0°	45.0°
Scan range (ω)	$(0.94 + 0.34 \tan\theta)°$	$(0.79 + 0.34 \tan\theta)°$
Reflections collected	5964	7236
Independent reflections	5673 ($R_{int} = 3.3\%$)	6821 ($R_{int} = 3.0\%$)
Observed reflections	3164 [$I > 3.0\sigma(I)$]	4617 [$I > 3.0\sigma(I)$]
Absorption correction	ψ-scan	ψ-scan
Transmission factors	0.8790–1.0000	0.9334–1.0000
Structure solution	Direct Methods (SIR88)	Direct Methods (SIR88)
Refinement method	Full-matrix least-squares	Full-matrix least-squares
Function minimized	$\Sigma w(\|F_o\| - \|F_c\|)^2$	$\Sigma w(\|F_o\| - \|F_c\|)^2$
Weighting scheme	$w = [\sigma_c^2(F_o) + (p/2)^2F_o^2]^{-1}$	$w = [\sigma_c^2(F_o) + (p/2)^2F_o^2]^{-1}$
p-factor	0.005	0.006
R indices (obs. data)	$R = 0.089$; $wR = 0.092$	$R = 0.081$; $wR = 0.091$
Goodness-of-fit	2.08	4.08
Largest Δ/σ	0.01	0.02
Number of parameters	270	509
Residual extrema (e Å^{-3})	1.04 to −1.09	1.22 to −0.88

with epoxy resin. A total of 5673 unique reflections ($2\theta \leqslant 45°$) were measured; 3164 of these had $I \geqslant 3\sigma(I)$ and were considered to be observed.

(b) *Compound* **III**. Crystals of **III** suitable for X-ray diffraction study were grown from CH_2Cl_2/diethyl ether as a solvate of stoichiometry **III** · $0.5CH_2Cl_2$. A red plate of dimensions of $0.30 \times 0.38 \times 0.40$ mm^3 was mounted on a glass fibre with epoxy resin. A total of 6821 unique reflections ($2\theta \leqslant 45°$) were measured; 4617 of these had $I \geqslant 3\sigma(I)$ and were considered to be observed.

Acknowledgements—W.-K.W. thanks the Hong Kong Baptist University and the Hong Kong Research Grants Council for financial support. W.-T.W. thanks the Hong Kong Research Grants Council and the University of Kong Hong for financial support.

REFERENCES

1. W. K. Wong, J.-X. Gao, Z.-Y. Zhou and T. C. W. Mak, *Polyhedron* 1992, **11,** 2965.
2. W. K. Wong, J.-X. Gao and W. T. Wong, *Polyhedron* 1993, **12,** 1647.
3. W. K. Wong, J.-X. Gao and Z.-Y. Zhou and T. C. W. Mak, *Polyhedron* 1993, **12,** 1415.
4. W. K. Wong, J.-X. Gao, W. T. Wong, W. C. Cheng and C. M. Che, *J. Organomet. Chem.* 1994, **471,** 277.
5. J.-X. Gao, H.-L. Wan, W. K. Wong, M. C. Tse and W. T. Wong, *Polyhedron* 1996, **15,** 1241.
6. J. C. Jeffrey, T. B. Rauchfuss and P. A. Tucker, *Inorg. Chem.* 1980, **19,** 3306.
7. W. K. Wong, Y. Chen and W. T. Wong, *Polyhedron* 1996, **15,** 1575.
8. P. J. Fagan, M. D. Ward, J. V. Caspar, J. C. Calabrese and P. J. Krusic, *J. Amer. Chem. Soc.* 1988, **110,** 2981.
9. A. M. McNair, J. L. Schrenk and K. R. Mann, *Inorg. Chem.* 1984, **23,** 2633.
10. A. C. T. North, D. C. Phillips and F. S. Mathews, *Acta Cryst. Sect A.* 1968, **24,** 351.
11. M. C. Burla, R. Camalli, G. Cascarano, C. Giacovazzo, G. Polidori, R. Spagna and D. Viterbo, *J. Appl. Cryst.* 1989, **22,** 389.
12. *Texsan: Crystal Structure Analysis Package.* Molecular Structure Corporation (1985, 1992).

Pergamon

PII: S0277-5387(96)00299-9

Polyhedron Vol. 16, No. 3, pp. 441–445, 1997
Copyright © 1996 Published by Elsevier Science Ltd
Printed in Great Britain. All rights reserved
0277-5387/97 $17.00+0.00

Synthesis and thermal behaviour of $(NH_4)_2Be(IO_3)_4 \cdot 2H_2O$

M. Georgiev and M. Maneva*

Department of Inorganic Chemistry, University of Chemical Technology and Metallurgy, 8 Kl.Ohridski Str., 1756 Sofia, Bulgaria

(Received 13 February 1995; accepted 17 June 1996)

Abstract—A new binary salt $(NH_4)_2Be(IO_3)_4 \cdot 2H_2O$ has been synthesised, and identified by elemental analysis, X-ray powder diffraction, IR spectra, DTA and DSC. The IR spectra show two absorption bands at 860 cm^{-1} and 460 cm^{-1}. The new compound showed thermal stability up to 160°C. A diagram of the thermal decomposition was offered by identifying the intermediate product. The kinetic parameters (E^* and A) were investigated on the basis of the TG data, and the kinetic equations were determined. It was proved that the process takes place in the kinetic region. Copyright © 1996 Published by Elsevier Science Ltd

Keywords: binary iodates; thermal decomposition; IR spectra; DSC; X-ray; kinetic parameters.

A number of publications [1–7] contain results from our investigations of beryllium iodates that have not been sufficiently studied. However, there are no data about binary beryllium iodates and this suggested to us to synthesize such iodates since they, much like the iodates, can be expected to possess valuable electrical properties.

The aim was to study the conditions of synthesis of a binary salt between NH_4IO_3 and $Be(IO_3)_2 \cdot 4H_2O$, the compound obtained being identified and described by the methods of quantitative analysis, DTA, DSC, TG, IR and X-ray.

EXPERIMENTAL

The initial products used in the synthesis of the newly obtained binary iodates were NH_4IO_3 and $Be(IO_3)_2 \cdot 4H_2O$. Solid $Be(IO_3)_2 \cdot 4H_2O$ was added to 0.2 M solution of $Be(IO_3)_2 \cdot 4H_2O$ heated to 70°C in quantities corresponding to the stoichiometric ratio $NH_4IO_3 : Be(IO_3)_2 \cdot 4H_2O = 2:1$. The solution obtained was filtered through a fibreglass filter and left to crystallise in a desiccator over H_2SO_4 or in the open at room temperature. The crystals were filtered off and dried.

The compound was analysed quantitatively: Be was determined by heating the substance to BeO at 900°C, I_2 was determined iodometrically [8] and NH_4^+ was determined with sodium tetrafluoroborate [9].

The data from the quantitative analysis of the newly synthesised compound agreed fairly well with those calculated for $(NH_4)_2Be(IO_3)_4 \cdot 2H_2O$, namely:

Table 1. Quantitative analysis data

	Be	NH_4^+	I
Theoretical, %	1.1	4.6	65.0
Experimental, %	1.1±0.1	5.1±0.1	65.1±0.5

The thermal investigations were carried out with MOM-OD-102 Paulic-Erday in the 20–1000°C temperature interval at a heating rate of 10°C min^{-1} and 200 mg sample. The DSC curves were taken on a Perkin-Elmer 4 at the rate of 10°C min^{-1} and 5 mg sample in the 30–400°C temperature interval. The IR spectra were taken in the 4000–2800 cm^{-1} interval in a hexachloroburadiene suspension and in the 3800–200 cm^{-1} interval in KBr tablets on a Philips PU 9712 spectrophotometer.

The X-ray data were obtained on DRON VM-1 powder diffractometer using Cu K_α radiation ($\lambda = 1.5418$ Å). They were processed using the computer programme ITO and LSUCR [16].

* Author to whom correspondence should be addressed.

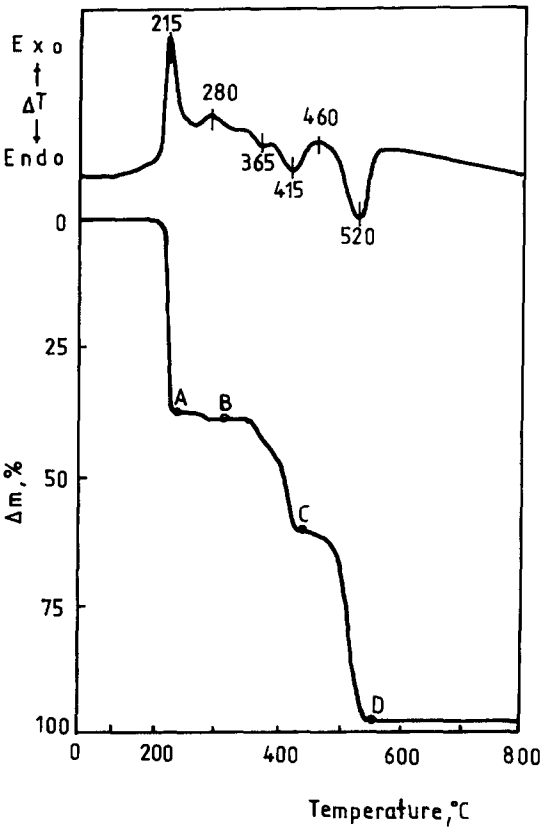


Fig. 1. DTA and TG curves of $(NH_4)_2Be(IO_3)_4 \cdot 2H_2O$.

RESULTS AND DISCUSSION

The DTA and TG curves of $(NH_4)_2Be(IO_3)_4 \cdot 2H_2O$ are shown in Fig. 1, while the DSC curves are shown in Fig. 2. The IR spectra are shown in Fig. 3, while Fig. 4 shows also the spectra of the products obtained from the thermal decomposition of the initial compound at 220°C and 320°C.

The compound crystallises in the triclinic crystallographic system with the following lattice parameters: $a = 7.514$ (1), $b = 9.824$ (2), $c = 6.689$ (2) Å, $\alpha = 103.29$ (2), $\beta = 106.14$ (2) and $\gamma = 107.17$ (1)°, $V = 443.0$ (1) Å^3; 2θ range (°) 9.869–82.868; reflections collected 543; pyknometrical density, 2.947 g cm^{-3}; $Z = 1$.

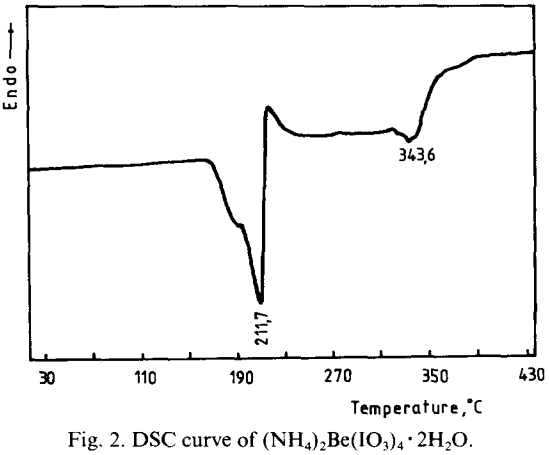


Fig. 2. DSC curve of $(NH_4)_2Be(IO_3)_4 \cdot 2H_2O$.

The course of the TG and DSC curves on Figs 1 and 2 showed that the compound is stable until 160°C, while the initial NH_4IO_3 undergoes decomposition at around 200°C with an exothermal effect [10], $Be(IO_3)_2 \cdot 4H_2O$ melts at $T_{max} = 70$°C and is dehydrated at $T_{max} = 95$°C [1]. These data are not recorded in the DTA of the newly obtained compound either (Fig. 1). This is yet another proof that what we have is a new compound with its IR spectra (Fig. 3). Its absorption curve in the 3200–3000 cm^{-1} region due to the stretching oscillations of the N—H bond from NH_4^+ differs in its character and position from those of NH_4IO_3. It is comparatively broader and is shifted toward the higher frequencies by about 40 cm^{-1}.

The stretching oscillations of the OH— groups from the hydrate water lie partially in this region, hence it is difficult to obtain a more accurate identification of the maximums observed in the absorption band. An analogous shift is to be observed also in the antisymmetric bending vibration (ν_4) of NH_4^+ (Fig. 3a) lying at 1410 cm^{-1}, compared to 1390 cm^{-1} in NH_4IO_3 [14]. Also noteworthy is the character of the stretching vibrations of the I—O bond from IO_3^- (ν_1 and ν_3) lying in the 850–650 cm^{-1} region. They appear as an absorption band broader than in NH_4IO_3 and $Be(IO_3)_2 \cdot 4H_2O$ (Fig. 3) and this character is probably due to structurally different iodate groups in the compound. The weak though distinct absorption band at 860 cm^{-1} may be attributed to Be—O. It appears as a shoulder in the $Be(IO_3)_2$ and $Be(IO_3)_2 \cdot 4H_2O$ spectra [5,6]. According to [12] the vibration at 460 cm^{-1} may refer to the Me—O—IO_2 groups or to the Be—O—IO_2 groups, respectively. This is to be expected, having in mind that the coordination saturation of Be^{2+} in the examined compound can be realised only by the incorporation also of the OIO_2— group in its polyhedron, due to shortage of hydrate water. This is confirmed by the fact that this particular absorption band is not found in the spectrum of $Be(IO_3)_2 \cdot 4H_2O$ containing $[Be(H_2O)_4]^{2+}$ but is found in $Be(IO_3)_2$. The coordination of Be^{2+} in the latter can be effected likewise solely by the oxygen of IO_3^-. The poor absorption band at 315 cm^{-1} is attributed to the Be—O bond from the BeO_4— group, this vibration being observed also in the spectrum of $Be(IO_3)_2 \cdot 4H_2O$ [4,5] (Fig. 3c).

Information about the thermal behaviour of the newly obtained compound is furnished by the DTA, DSC and TG curves in the investigated temperature range. For instance, corresponding to the exoeffect with $T_{max} = 215$°C (after DTA) is a sharp decrease of the mass of the sample $\Delta m = 38.3\%$. These changes can be attributed to the simultaneous dehydration and decomposition of $(NH_4)_2Be(IO_3)_4 \cdot 2H_2O$ to the obtaining of a solid product from HIO_3 and $Be(IO_3)_2$ according to the following equation:

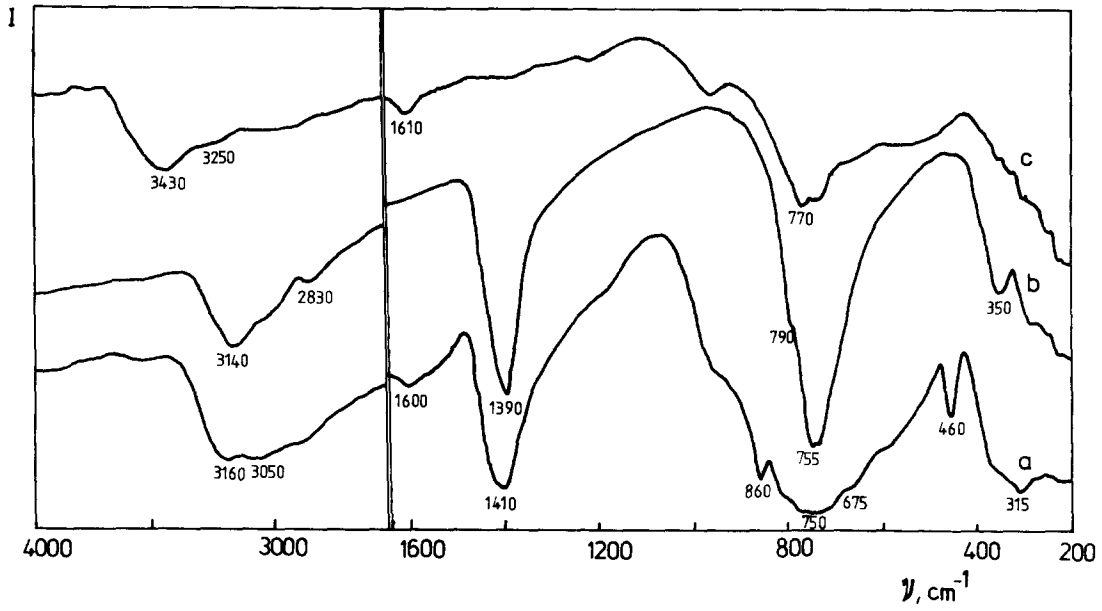


Fig. 3. IR spectra of (a) $(NH_4)_2Be(IO_3)_4 \cdot 2H_2O$; (b) NH_4IO_3; and (c) $Be(IO_3)_2 \cdot 4H_2$.

$$4.5[(NH_4)_2Be(IO_3)_4 \cdot 2H_2O] \rightarrow 3HIO_3 + 4.5Be(IO_3)_2 + \text{gaseous products} \quad (1)$$

The mass of the solid product calculated from equation (1) is $\Delta m = 61\%$. This value is in very good agreement with the experimental data from TG curves (Fig. 1). The product isolated from point A (Fig. 1) at $T = 220°C$ has been identified with its IR spectrum (Fig. 4). It shows both the characteristic absorption bands of the free HIO_3, most typical of which is that at 640 cm^{-1} related to the I—O—(H) bond, and those characteristic of $Be(IO_3)_2$.

The exoeffect observed is the result of a complex multi-stage process which includes both endo- and exo-processes. The latter are related mainly to the oxidation of NH_3 to different terminal products such as N_2O, NO, N_2 and H_2O [12]. The course of the respective TG-curve shows a sharp change up to $T = 220°C$. Indicative of the complex nature of this process is also the type of the respective peak observed

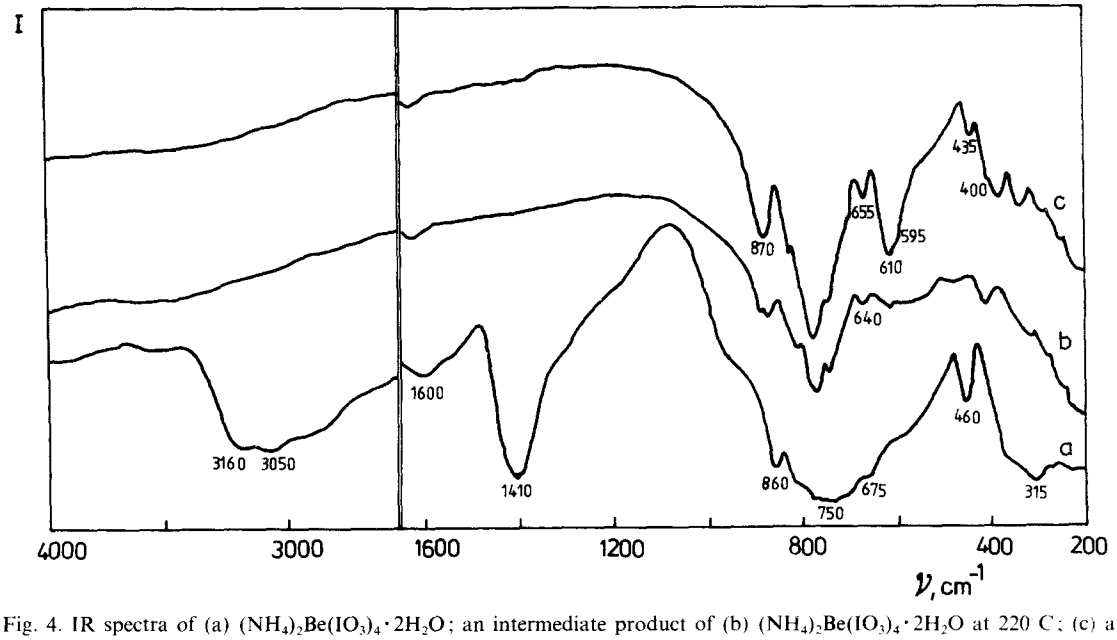


Fig. 4. IR spectra of (a) $(NH_4)_2Be(IO_3)_4 \cdot 2H_2O$; an intermediate product of (b) $(NH_4)_2Be(IO_3)_4 \cdot 2H_2O$ at 220 C; (c) at 320°C.

in DSC (Fig. 2) whose $T_{max} = 211.7°C$ and $\Delta H_{ph.tr.} = -147.5$ kJ mol^{-1}. It clearly distinguishes between two different exothermal effects which overlap partially. The TG-curve changes slowly in the 220–340°C temperature interval, the decrease in the mass for this interval alone being 0.5%; in other words it decreases by 39.5% from the beginning to this point. Corresponding to this part of the TG is an endoeffect in DTA which may be due to polymerisation and dehydration of HIO_3 according to the diagram.

$$3HIO_3 \rightarrow HI_3O_8 + H_2O$$

and crystallisation of the HI_3O_8 obtained (the exoeffect at 280°C is not related to changes in the mass—Fig. 1). This assumption is proved experimentally by the identification of a sample isolated in this interval (point B from TG on Fig. 1). Its IR spectra is presented in Fig. 4c and it shows the absorption bands characteristic of HI_3O_8 and of $Be(IO_3)_2$. The first one is identified by the stretching vibration of the I—O—I— group (characteristic for this acid) at 435, 400, 610 and 595 cm^{-1} [13–15]. The remaining absorption bands are of $Be(IO_3)_2$, according to [4, 6].

The endoeffect at $T_{max} = 365°C$ is attributed to the decomposition of HI_3O_8 following the diagram

$$2HI_3O_8 \rightarrow H_2O + 3I_2O_5$$

whereas that at $T_{max} = 415°C$ is attributed to the decomposition of I_2O_5 to O_2 and I_2. The release of I_2 can be visually ascertained as well. These two processes are not divided in the TG curve and show a common change in the mass $\Delta m = 60\%$, the theoretical one being $\Delta m = 54\%$. The 6% difference between the experimental and theoretical values can be explained by the partial decomposition within this interval of the $Be(IO_3)_2$ which is in the system. This assumption is corroborated by the change in Δm connected with the further decomposition of the pure $Be(IO_3)_2$ obtained at point C. Its presence is indicated by the course of the DTA and DTA and TG curves and by the nature of the residual product.

The exoeffect at $T_{max} = 468°C$ is related to the decomposition of $Be(IO_3)_2$, while the endoeffect at $T_{max} = 520°C$ is related to the decomposition of I_2O_5. The terminal product from $(NH_4)_2Be(IO_3)_4 \cdot 2H_2O$ is BeO. The overall theoretical change of the mass of the initial sample to BeO is 97.0%, recorded from the TG curve, while the theoretically calculated one is 96.8%. The BeO residue has been proved by X-ray powder diffraction and by the methods of IR spectroscopy. The data obtained fully coincided with those presented in [1–3].

The kinetic analysis used a computer program written in BASIC and based on a manual procedure for determining E^*_{deh} and A under non-isothermal conditions [17–20]. The general differential method was applied and the basic equation of non-isothermal kinetics was used in a logarithmic form [19].

$$\ln\left[\frac{d\alpha/dT}{F(\alpha)}\right] = \ln\frac{A}{b} - \frac{E^*}{R}\frac{1}{T}$$

where $\alpha = (m_0 - m_T)/(m_0/m_{end})$ is the conversion degree, m_0 and m_{end} are the initial and final mass of the hydrate in g, and m_T is the mass (in g) for a given T; b is the rate of heating in K s^{-1} ($b = dT/d\tau$), A is the pre-exponential factor in s^{-1}, $R = 8.314$ J K^{-1} mol^{-1}, and $F(\alpha)$ is the kinetics model (in a differential form).

The 25 kinetic equations taken from the relevant literature [17–19] describe a process of the type:

$$A(\text{solid}) \rightarrow B(\text{solid}) + C(\text{gas})$$

Numerical differentiation of the experimental $\alpha - T$ data is made after their approximation with a cubic parametric B-spline, as described in [18], which reflects most accurately the nature of the non-isothermal data processed.

The kinetic analysis involves determining the kinetic equations $F(\alpha)$, from those introduced into the program (25 in all), for which the dependence of ln $[(d\alpha/dT)/F(\alpha)]$ on $1/T$ is linear. The criteria for selecting $F(\alpha)$ are the values of the calculated correlation coefficients R and standard deviation σ. In cases where the dehydration process takes place in several stages, the kinetic analysis was carried out for each state separately.

The values obtained for the kinetic parameters of the principal stages of the process are shown in Table 2.

It follows from an analysis of the kinetic data (Table 2) determined under non-isothermal conditions that

Table 2. Kinetic data about the process of thermal decomposition of $(NH_4)_2Be(IO_3 \cdot 2H_2O)$ from the TG-curve

Temperature interval, °C	E^* kJ mol^{-1}	ln A, s^{-1}	Kinetic equation	R^*	σ^{**}
180–220	130	1.47	$F = (1-\alpha)^{2/3}$	0.9276	0.0803
360–400	42	14.92	$F = [(1-\alpha)^{-1/2} - 1]^{-1}$	0.9857	0.0086
400–420	120	52.56	$F = 1$	0.9999	0.0005
450–520	373	29.31	$F = \alpha(1-\alpha)$	0.9818	0.0141

R^* Correlation coefficient, σ^{**} Mean quadratic deviation, E^* Activation energy.

the principal stages of the process take place in the kinetic region. For the 360–400°C temperature interval the kinetic equation is of the diffusion type.

REFERENCES

1. M. Maneva and M. Georgiev, *Thermochim. Acta* 1985, **92,** 627.
2. M. Maneva and M. Georgiev, *Polyhedron* 1989, **8,** 357.
3. M. Maneva and M. Georgiev, *J. Therm. Anal.* 1989, **35,** 867.
4. M. Maneva and M. Georgiev, *Spectrosc. Letts* 1990, **23,** 831.
5. H. D. Lutz, N. Lange, M. Maneva and M. Georgiev, *Z. anorg. allg. Chem.* 1991, **594,** 77.
6. M. Maneva, M. Georgiev, H.D. Lutz and N. Lange, *Z. Naturforsch.* 1991, **46b,** 795.
7. J. Macicek, M. Maneva and M. Georgiev, *Z. Kristallogr.* 1992, **199,** 177.
8. I. M. Kolthof, W. A. Stenger and D. Mgasuyomo, *Obemnij Analiz.*, III, p. 571. Khimia Moskva (1961).
9. G. G. Russsakova, *Zh, Anal. Khim.* 1963, **18,** 154.
10. F. Solymosi and K. Jaky, *J. inorg. nucl. Chem.* 1971, **33,** 2829.
11. V. V. Boldyrev, T. Banchagi, O. P. Korobeinichev, Y. P. Savincev, T. V. Mulina, and Y. Ia. Karpenko, *Kinetika i kataliz* 1972, **13,** 80.
12. B. Emin-Ivanov, V. I. Pibina and B. E. Zaicev, *Koord. Khim.* 1979, **5,** 515.
13. P. M. A. Sherwood and J. J. Turner, *Spectrochim. Acta* 1970, **26a,** 1975.
14. T. Balicheva and G. Petrova, *Problemi Sovremennoi Khimii Koordinazionich Soedinenia*, **4,** p. 266. Leningr. Gos. Univ., Leningrad (1975).
15. M. B. Vassallo and I. L. Botto, *J. Therm. Anal.* 1992, **38,** 2593.
16. J. W. Visser, *J. Appl. Cryst.* 1969, **2,** 89.
17. M. Brown, D. Dollimore and A. Galveg, *Reakcii tverdih tel*, pp. 102, 104, 122. Mir, Moscow (1985).
18. Dzh. Foli and A. Van Dan, *Osnov interaktivniy grafiki.* Nauka, Moscow (1985).
19. J. Sestak, *Thermophysical Properties of Solids*, pp. 240, 430. Akademia, Prague (1984).
20. A. Bhatti and D. Dollimore, *Thermochim. Acta* 1984, **78,** 55.

Pergamon

PII: S0277-5387(96)00293-8

Polyhedron Vol. 16, No. 3, pp. 447–451, 1997
Copyright © 1996 Elsevier Science Ltd
Printed in Great Britain. All rights reserved
0277-5387/97 $17.00+0.00

Binuclear oxomolybdenum(V) complexes with mercaptocarboxylic acids: synthesis, characterization and electrochemistry

Subhasis Mitra, Hiranmay Biswas and Pinaki Bandyopadhyay*

Department of Chemistry, University of North Bengal, Darjeeling, PIN 734 430, India

(Received 17 April 1996; accepted 13 June 1996)

Abstract—A number of stable bis(μ-oxo) and μ-oxo-μ-sulfido binuclear oxomolybdenum(V) complexes of the type $R_2[Mo_2O_4L_2]\cdot 5H_2O$ (**1**) and $R_2[Mo_2O_3SL_2]\cdot 5H_2O$ (**2**) with different mercaptocarboxylic acids (H_2L) have been synthesized (where H_2L = 2-mercaptobenzoic acid, 2-mercaptoproprionic and 3-mercaptopropionic acid, and $R = Ph_4P^+$). The complexes have been characterized by elemental analysis, conductivity measurement and spectral (IR, UV-VIS and ^{1}H-NMR) data. The electrochemical behaviour of the complexes in DMF have also been examined by cyclic voltammetry at a glassy carbon electrode. Copyright © 1996 Elsevier Science Ltd

Keywords: binuclear oxomolybdenum complexes; bis(μ-oxo) bridge; μ-oxo-μ-sulfido bridge; mercaptocarboxylic acids; cyclic voltammetry.

Relevance of the molybdenum–sulfur bond to bioinorganic chemistry is well known [1–7] because of its presence in different molybdoenzymes. Some attention [8–12] has been given to oxomolybdenum(V) complexes of different mercaptocarboxylic acids. In continuation of our interest in this area [12], we now report the synthesis, spectroscopic characterization and electrochemical behaviour of binuclear oxomolybdenum complexes of mercaptocarboxylic acids with bis(μ-oxo) bridge and μ-oxo-μ-sulfido bridge. The mercaptocarboxylic acids used were 2-mercaptobenzoic acid (H_2L^1), 2-mercaptopropionic acid (H_2L^2) and 3-mercaptopropionic acid (H_2L^3).

EXPERIMENTAL

Materials

Sodium dithionite (E. Merck, India), hydrazine dihydrochloride and 3-mercaptopropionic acid (Merck, Germany), tetraphenylphosphonium chloride and 2-mercaptopropionic acid (Fluka AG, Switzerland) were used as received. 2-Mercaptobenzoic acid (Fluka AG, Switzerland) was purified by sublimation at reduced pressure as reported elsewhere [13].

Synthesis of complexes

$[(PPh_4)]_2[Mo_2O_4(L^1)_2]\cdot 5H_2O$ (**1a**). A solution of 2-mercaptobenzoic acid (0.3 g, 1.94 mmol) in methanol (15 cm^3) was added to a solution of sodium molybdate dihydrate (0.48 g, 1.98 mmol) in water (15 cm^3). A solution of sodium dithionite (0.175 g) in water (10 cm^3) was added to the above mixture and the pH of the solution was adjusted to *ca* 5.5. A solution of tetraphenylphosphonium chloride (0.75 g, 2.0 mmol) in water (10 cm^3) was added to the above mixture dropwise with stirring. Yellow precipitate appeared and it was collected by filtration, washed with water and dried *in vacuo*. Yield: 0.450 g, (*ca* 17%). Found: C, 55.5; H, 3.7; Mo, 13.9; S, 4.6. Calc. for $C_{62}H_{58}Mo_2O_{13}P_2S_3$: C, 56.0; H, 4.4; Mo, 14.5; S, 4.8%. Δ_M (in DMF) = 136 Ω^{-1} cm^2 mol^{-1}.

$[(PPh_4)]_2[Mo_2O_4(L^2)_2]\cdot 5H_2O$ (**1b**) was prepared using a similar method as described above. Yield: *ca* 25%. Found: C, 52.1; H, 4.4; Mo, 15.3, S, 5.0. Calc. for $C_{54}H_{58}Mo_2O_{13}P_2S_2$: C, 52.6; H, 4.7; Mo, 15.6; S, 5.2%. Δ_M (in DMF) = 137 Ω^{-1} cm^2 mol^{-1}.

* Author to whom correspondence should be addressed.

$[(PPh_4)]_2[Mo_2O_3S(L^1)_2]\cdot 5H_2O$ (**2a**). To a solution of sodium molybdate dihydrate (0.96 g, 3.96 mmol) in water (15 cm^3), hydrochloric acid (5 cm^3) was added followed by the addition of solid hydrazine dihydrochloride (1.0 g, 10 mmol). Then the mixture was heated over a water bath for 2 h and the hot solution was taken in a polythylene bottle containing $Na_2S\cdot 2H_2O$ (0.455 g, 4.0 mmol). The mixture was stirred till its temperature reached 298 K. A solution of 2-mercaptobenzoic acid (0.615 g, 4.0 mmol) in methanol (15 cm^3) was added to the above mixture with stirring and filtered the black precipitate off. The pH of the filtrate, cooled in an ice-bath, was raised to *ca* 12 with 13 M NaOH and the solution was kept at 278 K overnight. A yellow precipitate appeared which was washed with methanol and dissolved in water (15 cm^3). A solution of tetraphenylphosphonium chloride (0.5 g, 1.3 mmol) dissolved in water (10 cm^3) was added to it. A yellow precipitate was separated off, filtered, washed with water and dried *in vacuo*. Yield: 0.25 g (*ca* 47%). Found: C, 54.9; H, 3.9; Mo, 14.1, S, 6.9. Calc. for $C_{62}H_{58}Mo_2O_{12}P_2S_3$: C, 55.4; H, 4.3; Mo, 14.3; S, 7.1%. Δ_M (in DMF) = 134 Ω^{-1} cm^2 mol^{-1}.

$[(PPh_4)]_2[Mo_2O_3S(L^2)_2]\cdot 5H_2O$ (**2b**) and $[(PPh_4)]_2[Mo_2O_3S(L^3)_2]\cdot 5H_2O$ (**2c**). These complexes were prepared following the procedure for (**2a**), except that the pH was raised to *ca* 8 after the addition of mercaptocarboxylic acids. Yield: *ca* 12 (**2b**) and 18% (**2c**). Found (**2b**): C, 51.8; H, 4.2; Mo, 14.9; S, 7.4. Calc. for $C_{54}H_{58}Mo_2O_{12}P_2S_3$: C, 51.9; H, 4.6; Mo, 15.4; S, 7.7%. Δ_M (in DMF) = 136 Ω^{-1} cm^2 mol^{-1}. Found (**2c**): C, 51.5; H, 4.0; Mo, 15.1; S, 7.5. Calc. for $C_{54}H_{58}Mo_2O_{12}P_2S_3$: C, 51.9; H, 4.6; Mo, 15.4; S, 7.7%. Δ_M (in DMF) = 132 Ω^{-1} cm^2 mol^{-1}.

Physical measurements

The elemental analyses data, electrical conductance data, IR and electronic spectra were obtained as previously described [12]. The ^1H NMR spectra were recorded using a GE NMR QE 300 MHz, JEOL GSX400 or Varian EM-390 CW NMR spectrometer. Cyclic voltammetric measurements were done under dry nitrogen using a PAR model 370-4 electrochemistry system as reported earlier [12]. The potentials reported are uncorrected for junction potentials.

RESULTS AND DISCUSSION

The synthetic approach employed for the preparation of the complexes (**1**) involves the reaction of different mercaptocarboxylic acids with $Na_2MoO_4\cdot 2H_2O$ in the presence of sodium dithionite [14] as the reducing agent at pH 5.5. The pH of the reaction mixture plays an important role in the formation of complexes (**1**) and dithiodicarboxylic acid becomes the major product below pH 4.5. The existence of bis(μ-oxo) Mo^V complex with 3-mercaptopropionic acid (H_2L^3) in solution has been reported elsewhere [9]. Complexes (**2**) were synthesized by the preparation of the $[Mo_2O_3S]^{2+}$ core [15] followed by the addition of mercaptocarboxylic acids. In this synthetic route, precipitation of μ-oxo μ-sulfido complexes occurred in the higher range 8–12 depending upon the individual ligand.

The elemental analyses data of the complexes correspond to the above formulations. All the complexes are stable in air at room temperature and soluble in coordinating organic solvents. The molar conductance data indicate that all the complexes behave as 2 : 1 electrolytes [16].

The infrared spectra of all the complexes (Table 1) exhibit a very strong band in the range of 950–965 cm^{-1}, characteristic of the symmetric stretching vibration mode of the terminal Mo=O bond [17–20]. Although only the intense symmetric stretching mode is observed, this would agree with the prediction of a *cis*-disposition of the terminal Mo=O groups in the molybdenum(V) binuclears [21–23]. All the compounds exhibit the antisymmetric and symmetric stretching bands of Mo—O bridge bond [24,25] in the region 746–757 cm^{-1} and 453–470 cm^{-1} respectively. In the μ-oxo μ-sulfido complexes two prominent bands in the region 678–681 cm^{-1} and 415–422 cm^{-1} belong to the antisymmetric and symmetric stretching modes, respectively of the Mo—S bridge [21,22]. The intense antisymmetric ν_{COO} stretch of the metal bound carboxylate group [24,25] appear in the region 1590–1666 cm^{-1} (Table 1). The involvement of deprotonated thiol group in metal binding [26,27] is evident from the absence of ν_{SH} band in the region of 2400–2600 cm^{-1}. The strong and very broad absorption band between 3340–3495 cm^{-1} indicates the presence of water molecules in all the complexes [25].

The diamagnetic behaviour of all the complexes (**1**) and (**2**) at room temperature originates from strong coupling of the spins of the molybdenum(V) centres *via* dioxo or oxo-sulfido bridges. The ^1H NMR of all complexes (Table 1) show complete absence of the signal for sulfhydryl and carboxylic protons of free mercaptocarboxylic acids. This confirms the participation of different mercaptocarboxylic acids in coordination to molybdenum(V) through carboxylate anion and deprotonated sulfhydryl group. This is also supported by the remarkable shift of methylene proton signals to lower field in ^1H NMR spectra of complexes (**1b**), (**2b**) and (**2c**) containing mercaptopropionic acids [27]. ^1H NMR spectra of all complexes studied exhibit H_2O peak in the region 1.95–3.55 ppm (Table 1) depending upon the nature of the solvents. The H_2O peak shifts to higher field on shaking with D_2O.

The electronic spectral data of the complexes are given in Table 1. The strong absorptions around 290 nm and 430 nm are assigned [23] to intra-ligand and LMCT band, respectively.

Table 1.

Complexes	IR data[a]					^{1}H NMR[b]			Electronic spectra[c] $\lambda(\varepsilon)$	Electrochemical data[d]
	$\nu_{Mo=O}$[e]	ν_{Mo-O_b}	ν_{Mo-S_b}	ν_{COO}	ν_{H_2O}[f]	δ_{CH_3}	δ_{CH_2}[g]	δ_{H_2O}[h]		
(1a)	965	747[i]	—	1594[i]	3380	–	–	3.55[j]	292(29700), 370(8300), 445(sh)	−1.800
		463[k]		1432[k]						
(1b)	955	757[i]	—	1666[i]	3495	1.70[m]	4.16–4.23	1.95	290(sh), 360(5775), 435(1990)	−1.655
		470		1436				(1.75)		
(2a)	957	746	681	1590	3400	—	—	2.10[n]	290(36500), 325(sh), 435(1600)	−1.808
		468	415	1430				(1.95)		
(2b)	950	752	681	1616	3400	1.75[m]	4.03–4.10	2.10	295(14400), 430(1080)	−1.818
		453	420	1434				(1.90)		
(2c)	953	748	678	1613	3340	—	3.05–3.15[o]	2.56	315(6900), 360(3080), 450(770)	−1.780
		455	422	1434						

[a] As KBr disks in cm^{-1}.
[b] Values are in ppm from $SiMe_4$.
[c] λ = Absorption maxima in nm and ε = molar extinction coefficient ($dm^3\ mole^{-1}\ cm^{-1}$) in DMF.
[d] In DMF at 298 K; supporting electrolyte $[NBu_4^n]ClO_4$ (0.1 M); all potentials are referenced to SCE; E_{pc} is cathodic peak potential.
[e] Strong and sharp.
[f] Broad band.
[g] Appeared as multiplet.
[h] Data after shaking with D_2O given within parenthesis.
[i] ν_a.
[j] In DMF-d_7.
[k] ν_s.
[l] Shoulder.
[m] In $CDCl_3$.
[n] In CD_2Cl_2.
[o] In DMSO-d_6.

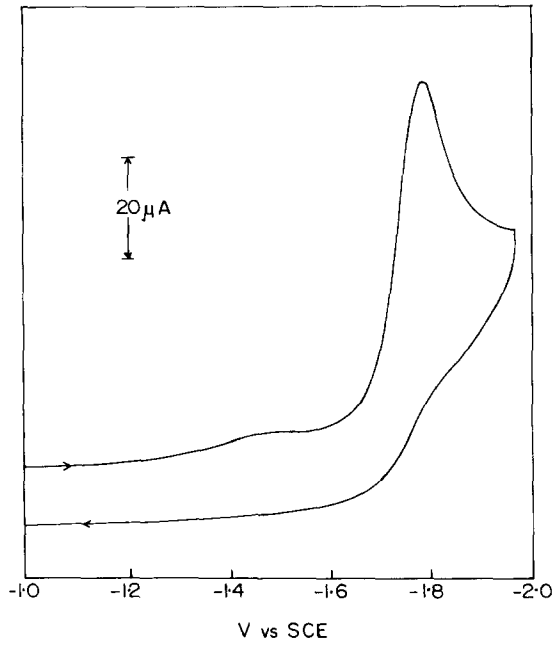


Fig. 1. Cyclic voltammogram of complex (**2c**) ($\sim 0.7 \times 10^{-3}$ M) in DMF (0.1 M in TBAP, 298 K) at glassy carbon electrode; scan rate 50 mV s^{-1}.

The electron transfer behaviour of complexes (**1**) and (**2**) have been examined voltammetrically in DMF (0.1 M in tetrabutylammonium perchlorate) at a glassy carbon electrode. All potentials (Table 1) are measured at 298 K and are referenced to saturated calomel electrode (SCE). All complexes undergo a reduction near -1.8 V and on scan reversal the anodic peak is virtually unobservable (Fig. 1). On comparison with the cathodic peak current of authentic two-electron reactions [28], the observed cathodic responses of complexes (**1**) and (**2**) show that the processes are of two-electron nature. Careful examination of the cathodic peak potentials reveals that the reduction potentials remain almost unaffected on variation of the different mercaptocarboxylates. This observation suggests that the electron transfer process is primarily localised on the metal centres. The single-step two-electron transfer implies that both the molybdenum(V) centers in complexes are reduced to molybdenum(V) simultaneously. The non-observance of anodic peak suggests that the reduced species, i.e. molybdenum(IV) binuclear complexes, undergo transformation to redox inactive products at a faster rate than the voltammetric time scale. In contrast to the prevalent two-step one-electron reduction of binuclear molybdenum(V) complexes having μ-oxo μ-sulfido bridge [20,28–30] in non-aqueous media, the one-step two-electron response of complexes (**1**) and (**2**) occurs rarely.

Acknowledgements—The financial support provided by University Grants Commission and Council of Scientific and Industrial Research, New Dehli, India is acknowledged. We also thank Dr. D. Bandyopadhyay and Professor R. N. Mukherjee for NMR spectra and electrochemical measurements respectively.

REFERENCES

1. S. P. Kramer, J. L. Johnson, A. A. Riberiro, D. S. Millington and K. V. Rajagopalon, *J. Biol. Chem.* 1987, **262,** 16357.
2. T. G. Spiro (Ed.) *Molybdenum Enzymes.* Wiley, New York (1985).
3. A. G. Sykes (Ed.) *Advances in Inorganic and Bioinorganic Mechanisms.* Academic Press, New York (1983).
4. S. P. Cramer, *Adv. Inorg. Bioinorg. Mech.* 1983, **2,** 259.
5. M. P. Coughlan (Ed.) *Molybdenum and Molybdenum Containing Enzymes.* Pergamon, New York (1983).
6. E. I. Stiefel, *Prog. Inorg. Chem.* 1977, **22,** 1.
7. R. C. Bray, *The Enzymes* (Edited by P. D. Boyer) 3rd Edn. Academic Press, New York (1975).
8. V. Sanz, T. Picher, P. Palanca, P. Gomez-Romero, E. Llopis, J. A. Ramirez, D. Beltran and A. Cervilla. *Inorg. Chem.* 1991., **30,** 3113.
9. G. P. Haight Jr, R. L. Belford and H. Chapman, *Third International Conference on* The Chemistry and Uses of Molybdenum, p. 245. Climax, Michigan (1979).
10. W. E. Newtion, G. J. J. Chen and J. W. McDonald, *J. Am. Chem. Soc.* 1976, **98,** 5387.
11. J. T. Spence, *Coord. Chem. Rev.* 1969, **4,** 475.
12. S. Mitra and P. Bandyopadhyay, *Indian. J. Chem.* 1995, **34A,** 493.
13. M. E. Bodini and M. A. Del Valle, *Polyhedron* 1990, **9,** 1181.
14. A. Kay and P. C. H. Mitchell, *J. Chem. Soc.* 1970, 2421.
15. T. Shibahara, H. Akashi, S. Nagahata, H. Hattori and H. Kuroya, *Inorg. Chem.* 1989, **28,** 362.
16. W. J. Geary, *Coord. Chem. Rev.* 1971, **7,** 81.
17. V. Lakshmanan, K. S. Nagaraja and M. R. Udupa, *Indian. J. Chem.* 1992, **31A,** 806.
18. A. L. Doadrio, M. T. Calabuig, C. V. Ragel and A. Doadrio, *Synth. React. Metal-Org. Chem.* 1989, **19,** 881.
19. C. Pickett, S. Kumar, P. A. Vella and J. Zubieta, *Inorg. Chem.* 1982, **21,** 908.
20. V. R. Ott, D. S. Swieter and F. A. Schultz, *Inorg. Chem.* 1977, **16,** 2538.
21. A. L. Doadrio-Villarejo, M. T. Calbuig, C. V. Ragel and A. Doadrio-Lopez, *Trans. Met. Chem.* 1991, **16,** 508.
22. R. Lozano, J. Roman, F. deJesus and E. Alarcon, *Trans. Met. Chem.* 1990, **15,** 141.
23. F. A. Cotton, D. L. Hunter, L. Richard and R. Weiss, *J. Coord. Chem.* 1974, **3,** 259.
24. A. Samotus, A. Kanas, M. Dudek, R. Grybos and E. Hodorowicz, *Trans. Met. Chem.* 1991, **16,** 495.
25. K. Nakamoto, *Infrared Spectra Of Inorganic and Coordination Compounds.* Wiley, New York (1963).

26. S. Purohit, A. P. Koley and S. Ghosh, *Polyhedron* 1990, **9,** 881.
27. A. Nakamura and N. Ueyama, *Molybdenum Chemistry of Biological Significance* (Edited by W. E. Newton and S. Otsuka), p. 369, Plenum Press, New York (1980).
28. F. A. Schultz, V. R. Ott, D. S. Rolison, D. C. Bravard, J. W. McDonald and W. E. Newtion, *Inorg. Chem.* 1978, **17,** 1758.
29. M. R. DuBois, *Inorg. Chem.* 1978, **17,** 2405.
30. H. C. Faulkner, *J. Electrochem. Soc.* 1978, **125,** 2870.

Pergamon

PII: S0277-5387(96)00291-4

Polyhedron Vol. 16, No. 3, pp. 453–461, 1997
Copyright © 1996 Elsevier Science Ltd
Printed in Great Britain. All rights reserved
0277-5387/97 $17.00+0.00

Synthesis and NMR studies of silver complexes with octaaza Schiff-base cryptands and the structure of a polymeric silver cryptate

Shu-Yan Yu,[a]* Qin-Hui Luo,[b] Biao Wu,[c] Xiao-Ying Huang,[c] Tian-Lu Sheng,[c] Xin-Tao Wu[c] and Da-Xu Wu[c]

[a] Fujian Institute of Research on the Structure of Matter, Chinese Academy of Sciences, Fuzhou 350002, P.R. China

[b] State Key Laboratory of Coordination Chemistry, Nanjing University, Nanjing 210093, P.R. China

[c] State Key Laboratory of Structural Chemistry, Chinese Academy of Sciences, Fuzhou 350002, P.R. China

(Received 23 February 1996; accepted 13 June 1996)

Abstract—Four binuclear and one polymeric silver complex of octaaza Schiff-base cryptands were synthesized by [2+3] condensation of tris(3-aminopropyl)amine (trpn) or tris(2-aminoethyl)amine (tren) with 5-R-2-methoxy-1,3-benzenedicarboxaldehyde (R = OCH_3, CH_3, Br or Ph) in the presence of excess of Ag^I ion. The polynucleating and extended coordination nature of the trpn-derived cryptand L^1 (R = OCH_3) was established by X-ray structure of $[\{Ag(Ag_2L^1)\}n][(ClO_4)_3 \cdot 2CH_3CN \cdot CH_3OH \cdot 2H_2O]_n$. The polymeric cation $[\{Ag(Ag_2L^1)\}_n]$ can be described as the bridge-twisted binuclear (Ag_2L^1) units linked together by silver atoms *via* a linear N—Ag—N bridging bonding mode in alternate (inward, outward) conformations relative to the benzene rings, resulting in an infinite single helical chain. The benzene rings in the helix chain are almost parallel to each other, with a π—π stacking distance of 3.84 Å. The coordination behaviour of cryptands have also been studied by NMR spectroscopy in solution. Copyright © 1996 Elsevier Science Ltd

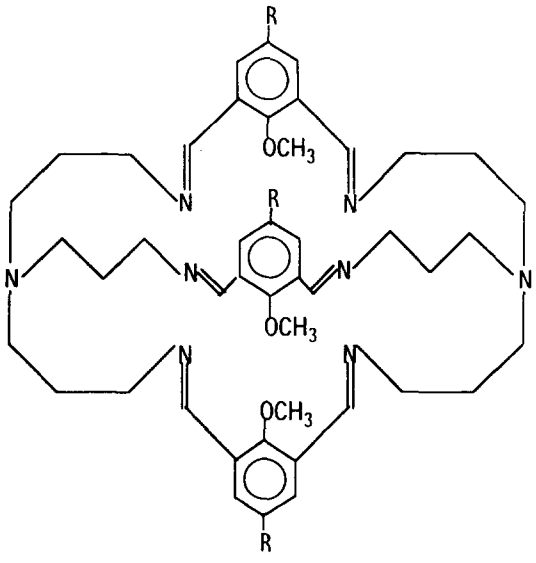
Keywords: cryptands; silver; cryptates; polymer; helix; structure.

Cryptands with large cavities and multiple recognizing functions have recently received a great deal of attention as hosts for metal ions which form cryptates from mono- to poly-nuclear [1,2]. The metal complexes are potentially important in the emerging fields of biomimetric chemistry [3], molecular electronics and supramolecular devices [4,5].

Polyaza Schiff-base cryptands and their metal complexes have been developed since Lehn [6] and Nelson [7] and their co-workers reported an efficient and facile synthetic method, based on [2+3] Schiff-base condensation of tris(2-aminoethyl)amine (tren) with rigid aromatic dialdehydes without template. This method opens a wide variety of new tren-derived polyaza Schiff-base and resulting amine cryptands and their mono- [8–10] bi- [11–15] and poly- [16–19] nuclear, cascade [20–22] and compartment [23–25] cryptates, which have been devoted to the studies of metal–metal bonding, magnetic coupling, electrochemical and photochemical processes, and modeling the active site of metalloproteins and metalloenzymes (especially, Cu, Zn-superoxide dismutase) [22]. However, only a few analogues derived from tris(3-aminopropyl) amine(trpn) with corresponding compounds have been reported to date [12,26–29]. This tardiness may in part be attributed to the labour involved in synthesis and characterization. It was anticipated that trpn, due to its longer chains than those of tren, would form cryptands and their metal complexes with novel conformations and host–guest properties. Recently, we reported a range of new binuclear polyaza cryptands by template condensation of trpn with 5-R-2-methoxy-1,3-benzenedicarboxaldehyde (R = OCH_3, CH_3, or Br). It is interesting that there are three variants of silver(I) cryptate with L^1 (R = OCH_3), two of which were described as a basket [27] and a bridge-twisted [28] shape. Here we present the third variant

* Author to whom correspondence should be addressed.

which possesses an infinite structure with single helix chain. Very few silver(I) polymeric helicates of all-nitrogen cryptands have been reported, although several silver(I) polymeric cryptates of poly-oxygen donor cryptates were structurally characterized earlier [30, 31]. Additionally, in order to elucidate the coordination nature of this type of ligands, we studied a series of silver(I) cryptates with trpn- and tren-derived Schiff-base octaaza-cryptands by NMR spectroscopy in solution (Fig. 1).



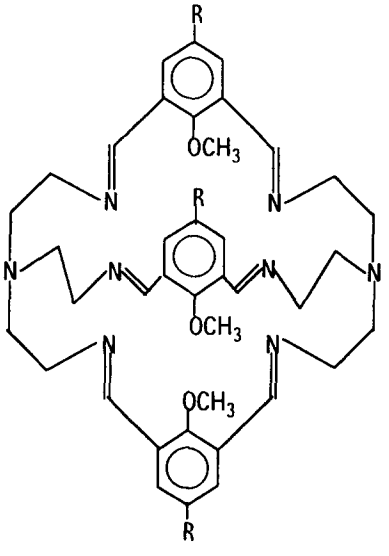


Fig. 1. Octaaza-cryptands derived from trpn and tren.

EXPERIMENTAL

Materials and physical measurements

In our earlier publications [27,28], we reported the physical measurements and synthesis of trpn, dialdehydes, and binuclear cryptates of L^1 ($R = OCH_3$), L^2 ($R = CH_3$) and L^3 ($R = Br$). 5-Ph-2-methoxy-1,3-benzenedicarboxaldehyde and tren were prepared with methods by Hu [32], and Kimura [33], respectively.

$[\{Ag(Ag_2L^1)\}_n][(ClO_4)_3 \cdot 2CH_3CN \cdot CH_3OH \cdot 2H_2O]_n$ (1)

To a stirred solution of $AgNO_3$ (0.425 g, 2.5 mmol) and 2,5-dimethoxy-1,3-benzenedicarboxaldehyde (0.582 g, 3.0 mmol) in anhydrous ethanol (100 cm^3) was added dropwise a solution of trpn (0.376 g, 2.0 mmol) in anhydrous ethanol (50 cm^3). After stirring for 3–4 h at 45°C, the mixture was filtered. Then an excess of $NaClO_4 \cdot H_2O$ (1.2, 10 mmol) in ethanol (20 cm^3) was added to the filtrate, yellowish microcrystals were isolated. This is a mixture of binuclear and polymeric complexes, characterized as $(Ag_{2.5}L^1)(ClO_4)_{2.5} \cdot 2H_2O$. Found: C, 41.1; H, 4.9; N, 8.0; Ag, 19.4. Calc. for $C_{48}H_{70}N_8O_{16}Ag_{2.5}Cl_{2.5}$: C, 41.0; H, 5.0; N, 8.2; Ag, 19.2%. The yellow block crystals of **1** suitable for X-ray analysis were obtained by slow diffusion of ether into 1 : 1 $CH_3CN \cdot CH_3OH$ solution, yield 58%. Found: C, 39.0; H, 5.0; N, 8.7; Ag, 19.8. Calc. for $C_{53}H_{80}N_{10}O_{21}Ag_3Cl_3$: C, 39.2; H, 4.9; N, 8.6; Ag, 19.9%. ^1H NMR(CD_3CN, TMS): δ 8.61, 8.59(d, 4H, HC=N); 8.52(s(br), 2H, HC=N); 7.10 (m, 4H, Ph-H); 6.52(s(br), 2H, Ph-H); 4.11–3.98 (m, 12H, CH_2—N(imino)); 3.78(s, 9H, 2-OCH_3); 3.40(s, 9H, 5-OCH_3); 3.00 ~ 2.78(m, 12H, CH_2—N-(bridgehead)); 1.96 ~ 1.92(m, 12H, CH_2). ^{13}C NMR (CD_3CN, TMS): δ 162(C=N); 155 ~ 152, 130, 114 (Ph-C); 65 ~ 64(CH_2—N(imino)), 57 ~ 55(CH_2—N (bridgehead)), 29(CH_2). Λ_{mol} (CH_3CN, 295 K): 378 S cm^2 mol^{-1}. IR(cm^{-1}): 3535w (νOH(H_2O)), 1637s(νC=N).

A similar procedure was adopted to synthesize the following complexes.

$[Ag_2L^4](ClO_4)_2$ (2)

Yellowish needle crystals of **2** (yield 83%). Found: C, 54.2; H, 4.9; N, 7.9; Ag, 15.5. Calc. for $C_{63}H_{72}N_8O_{11}Ag_2Cl_2$: C, 53.9; H, 5.2; N, 8.0; Ag, 15.4%. ^1H NMR(CD_3CN, TMS): δ 8.64(s(br), 2H, HC=N); 8.11, 7.95(d(br), 4H, HC=N); 7.66 (s(br), 2H, Ph(1)-H); 7.40(s(br), 2H, Ph(1)-H); 7.37 ~ 7.26(m, 15H, Ph(2)-H); 6.73(s(br), 2H, Ph(1)-H);

4.25, 4.17, 4.01(m, 12H, CH_2—N(imino)); 3.41, 3.39, 3.38(m, 9H, OCH_3); 3.16, 2.92, 2.72(m, 12H, CH_2—N(bridgehead)); 2.12, 1.99, 1.80(m, 12H, CH_2). Λ_{mol} (CH_3CN, 295 K): 331 S cm^2 mol^{-1}. IR(cm^{-1}): 1655 s(νC=N). UV–Vis spectrum (CH_3CN, 295 K): 280(ε_{mol} 23130), 316 nm (5820).

$[Ag_2L^5](ClO_4)_2 \cdot 4H_2O$ (**3**)

Yellowish microcrystals (yield 96%). Found: C, 40.0; H, 4.8; N, 9.2; Ag, 17.4. Calc. for $C_{42}H_{62}N_8O_{18}Ag_2Cl_2$: C, 40.2; H, 5.0; N, 8.9; Ag, 17.2%. ^1H NMR (CD_3CN, TMS): δ 8.85 (s, 4H, HC=N); 8.50(d, 2H, HC=N); 7.80(s, 2H, Ph-H); 7.45(s, 4H, Ph-H); 4.0 ~ 3.5(m, 30H, $OCH_3 + CH_2$—N (imino)); 2.95(m, 12H, CH_2—N-(bridgehead)). Λ_{mol} (CH_3CN, 295 K): 344 S cm^2 mol^{-1}. IR (cm^{-1}): 3472w (νOH(H_2O)); 2918, 2840(νCH), 1635s(νC=N). UV–vis (CH_3CN, 295 K): 340 (ε_{mol} 16000); 280 nm(10200).

$[Ag_2L^6](ClO_4)_2 \cdot 4H_2O$ (**4**)

White microcrystals (yield 83%). Found: C, 41.8; H, 4.8; N, 9.5; Ag, 18.0. Calc. for $C_{42}H_{62}N_8O_{15}Ag_2Cl_2$: C, 41.9; H, 5.1; N, 9.3; Ag, 17.9%. ^1H NMR(CD_3CN, TMS): δ 8.79; 8.52 (d, 6H, HC=N); 8.02, (s(br), 2H, Ph-H); 7.83(br, 4H, Ph-H); 3.85 ~ 3.54(m, 30H, CH_2—N (imino) + CH_3 + OCH_3); 3.00(m, 12H, CH_2—N (bridgehead). Λ_{mol} (CH_3CN, 295 K): 335 S cm^2 mol^{-1}. IR(cm^{-1}): 3481w (νOH(H_2O)); 2919, 2838(νCH); 1637s(νC=N). UV–vis spectrum (CH_3CN, 295 K): 320(ε_{mol} 14600), 280 nm(9800).

$[Ag_2L^7](ClO_4)_2 \cdot 2H_2O$ (**5**)

Yellow microcrystals (yield 80%). Found: C, 32.8; H, 4.0; N, 7.9; Ag, 15.0. Calc. for $C_{39}H_{55}N_8O_{16}Ag_2Br_3Cl_2$: C, 33.0; H, 3.9; N, 7.9; Ag, 15.2%. ^1H NMR (CD_3CN, TMS): δ 8.78(br, 4H, HC=N); 8.55(s(br), 2H, HC=N); 8.06(m, 6H, Ph-H); 3.98–3.85(m, 21H, $OCH_3 + CH_2$—N (imino)); 2.99 (m, 12H, CH_2—N(bridgehead)). Λ_{mol}(CH_3CN, 295 K): 311 S cm^2 mol^{-1}. IR(cm^{-1}): 3473w (νOH(H_2O)); 2912, 2844(νCH), 1637s(νC=N). UV–vis spectrum (CH_3 CN): 315(ε_{mol} 12500), 285 nm(7500).

X-ray crystal structure determination of $[\{Ag(Ag_2L^1)\}_n][(ClO_4)_3 \cdot 2CH_3CN \cdot CH_3OH \cdot 2H_2O]_n$ (**1**)

Crystal data. Formula $C_{53}H_{80}N_{10}O_{21}Ag_3Cl_3$, M = 1623.23, crystallizes from 1 : 1 acetonitrile–methanol with diffusion of ether as yellow blocks of photosensitive crystals, monoclinic space group $P2_1/c$, a = 13.308(3), b = 22.256(9), c = 23.066(9) Å, β = 102.18(2)°, V = 6678(4) Å^3, Z = 4, D_{calc} = 1.61 g cm^{-3}, $F(000)$ = 3312, graphite-monochromated Mo-K_α radiation (λ = 0.71069 Å), T = 296 K, μ (Mo-K_α) = 10.58 cm^{-1}. Enraf-Nonius CAD 4 diffractometer.

Data collection and processing. A single crystal encapsulated with gel, possessing approximate size 0.40 × 0.40 × 0.40 mm was mounted on a glass fibre and used for structure determination. The unit cell parameters were determined from least-squares refinement of the setting angles ($13.98 < \theta < 14.40$°) for 25 reflections. Using ω scan technique (scan speed < 5.49 min^{-1} scan width = $0.80 + 0.35 \tan\theta$, $0 \leqslant h \leqslant 15$, $-26 \leqslant k \leqslant 0$, $-27 \leqslant l \leqslant 27$), 12,423 unique reflections were collected to a maximum 2θ value of 50°. 4450 reflections with $I \geqslant 2\sigma(I)$ were used in the structural refinement. There was a linear decay during data collection, according to the intensities of three standard reflections (5, −12, 3; 6, −11, 2; −6, 11, −2) which were measured every 300 reflections (the final decay to 86.8%). Corrections for Lorentz-polarization, decay and absorption were applied, the latter using the DIFABS procedure [34]. The data were averaged (R_{int} = 0.82%).

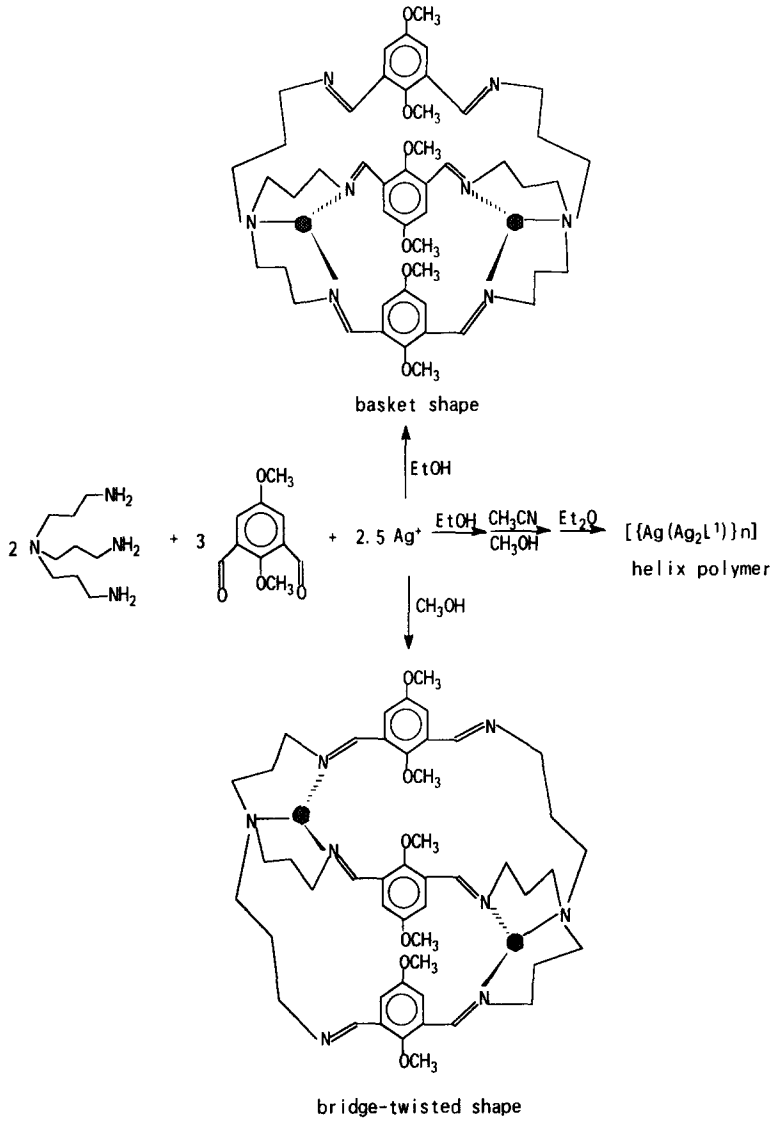
Structure analysis and refinement. The locations of silver atoms were determined by direct methods. The remaining non-hydrogen atoms were located through successive least-squares refinements on difference Fourier map using the TEXSAN(V2.1) structure solution package [35]. All of the non-hydrogen atoms were refined anisotropically, and the hydrogen atoms were included in calculated positions. The final least-squares cycle R = 0.097 and Rw = 0.091. The weighting scheme was $w^{-1} = \sigma^2(F)$. The polymeric silver cryptate is very sensitive to light, resulting in the poor quality of the data. Several atoms in the flexible ligand and solvents had high thermal motion and possibly disordered, although we were unable to refine a satisfactory model. The largest peak in final difference map is 1.33 e Å^{-3}. All calculations were performed on a Micro-VAX 3100 computer.

RESULTS AND DISCUSSION

Synthesis of cryptates

Using the same template technique, we synthesized the cryptates of trpn-derived cryptands $L^1 \sim L^4$ and tren-derived cryptands $L^5 \sim L^7$ in high yields (Fig. 1). Due to the steric hindrance, the cryptand derived from tren and 5-phenyl-2-methoxy-1,3-benzenedicarboxaldehyde was not obtained.

These cryptates were characterized as binuclear complexes, with the exception of the cryptates of L^1 (R = OCH_3). The cryptates of L^1 were obtained as three variants in different solvents. As shown in Scheme 1, the solvent plays an important role in isomerization and polymerization of the cryptates of L^1. From the highly polar solvents (methanol or acetonitrile), the product crystallizes with bridge-twisted



Scheme 1.

binuclear cryptate or depolymerizes in solution. From lower polarity solvents (ethanol or mixing with ether), the product crystallizes as basket-shaped binuclear cryptate or polymerizes in solution.

In addition, the appropriate excess of template material is also necessary in the synthesis of the polymeric cryptate of L^1, but does not effect the formation of the other cryptates.

NMR studies of coordinate conformations

All cryptates have similar IR and electronic spectroscopic features, consistent with our previous results [27,28]. All binuclear cryptates are easy to dissolve in acetonitrile and exhibit 1 : 2 electrolytic behaviour, while the polymeric cryptate **1** is difficult to dissolve in acetonitrile but easy to dissolve in DMSO or DMF and behaves as a 1 : 2 or 1 : 3 electrolyte. This is a significant difference between the polymeric cryptate and the binuclear cryptates.

The three variants of L^1 gave the same ^1H NMR or electronic spectra in CH_3CN solution, showing that the polymeric complex is not maintained and is depolymerized into binuclear cryptates.

Both the conformations of the binuclear cryptates (basket or bridge-twisted shapes as shown in their crystal structure [27,28]) are not distinguishable in

solution. Their proton chemical shifts give broad peaks, perhaps caused by the rapid exchange between the two conformations. To further elucidate the substituent and cavity size effects in coordinate conformation of the cryptands, we estimated supplementally the contribution of non-equivalent coordination to the proton chemical shifts of benzene rings in the cryptands based on our published results [27]. Their values are given in Table 1.

Since there are two conformations (basket and bridge-twisted shapes) for the cryptates, δ_c, δ_f, S_c and S_f need to be redefined. Here δ_c and δ_f denote the proton chemical shifts resulting from the coordinated and from the non-coordinated imino groups respectively. S_c and S_f denote the total contributions of the coordinated and of the non-coordinated, respectively. $|\delta_c-\delta_f|$ represents the non-equivalency in the cryptand ligand.

It can be seen from Table 1 that all of the complexes

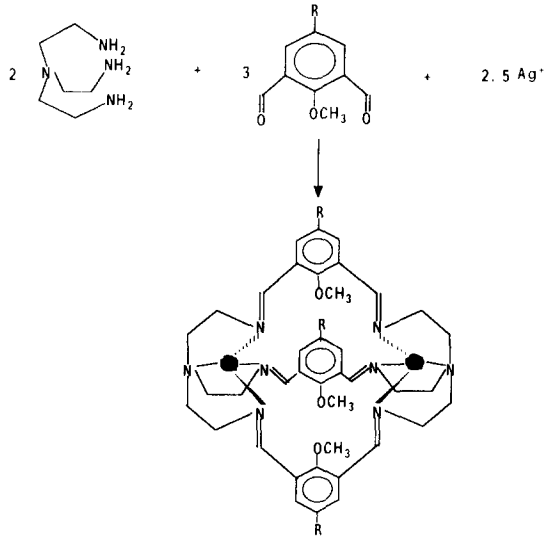


Table 1. The contribution of non-equivalent coordination to the proton chemical shifts of benzene rings in cryptates (ppm)

Cryptand	5-R	δ_c	δ_f	S_c	S_f	$\delta_c-\delta_f$
L^1	OCH_3	7.10	6.51	+0.41	−0.18	+0.59
L^2	CH_3	7.35	6.75	+0.38	−0.22	+0.60
L^3	Br	7.66	7.00	+0.31	−0.35	+0.66
L^4	Ph	7.66	6.73	+0.34	−0.59	+0.93
L^5	OCH_3	7.45	7.80	+0.76	+1.11	−0.35
L^6	CH_3	7.85	8.02	+0.86	+1.05	−0.09
L^7	Br	8.06	8.06	+0.71	+0.71	0

Values of L^2 and L^3 are quoted from [27]. $S_c = \delta_c - 7.26 - \Sigma$ s, $S_f = \delta_f - 7.26 - \Sigma$ s.

of trpn-derived cryptands ($L^1 \sim L^4$) have positive values of S_c and negative values of S_f. This indicates that all trpn-derived cryptates possess similar coordinate conformation. The S_c with positive value shows that the coordination of the equivalent four imino groups causes a deshielding effect, resulting in downfield shifts of the proton of benzene rings; meanwhile, the S_f with negative value shows the other two non-coordinated imino groups cause a shielding effect, resulting in upfield shifts of the proton of the benzene rings. Thus, all of the complexes of trpn-derived cryptands possess similar three-coordinate environment about each silver atom in solution, consistent with the crystal structures [27,28] of cation $[Ag_2L^1]^{2+}$. However, both S_c and S_f values of the complexes of tren-derived cryptands are positive, showing that all imino nitrogen donors are coordinated to silver atoms, resulting in deshielding effects. Thus, all of the complexes of tren-derived cryptands have approximately equivalent coordination for each imino N donor.

The values of $|\delta_c-\delta_f|$ have two sequences as follows:

Sequence I:

$$L^4(R = Ph) > L^3(R = Br) > L^2(R = CH_3) \approx L^1(R = OCH_3);$$

Sequence II:

$$L^5(R = OCH_3) > L^6(R = CH_3) > L^7(R = Br).$$

Comparison of sequence I with sequence II shows that the trpn-derived cryptands possess much larger non-equivalency than tren-derived cryptands. This may be due principally to the non-equivalent coordination of imino N donors of trpn-derived cryptands. The $L^4(R = Ph)$ possesses the highest value of $|\delta_c-\delta_f|$, attributed not only to the non-equivalent coordination but also to the steric effect of the substituents.

The crystal structures [27,28] reveal that internuclear distances of the two binuclear cryptates of L^1 are 7.468 (basket) and 8.266 Å (bridge-twisted), respectively. This shows that trpn-derived cryptand possesses a wide range of variable cavity size to satisfy the three coordination requirement of silver(I), resulting in large coordination non-equivalency for imino nitrogen donors.

The X-ray structure analysis and NMR studies [7, 11] show that the binuclear Ag^I complexes of cryptand derived from tren and phenyldialdehyde without substituent (i.e. isophthalaldehyde and terephthalaldehyde) possess equivalent four-nitrogen coordination about each silver atom. When we introduced a 2,5-substituent to benzene rings, the steric hindrance results in a little non-equivalency but does not change the four-coordination nature of the tren-derived cryptands, due to the rigidity of bridging chains and little variable cavity size.

Description of the helix structure of the polymeric cryptate **1**

The crystal structure of the polymeric cation complex $[\{Ag(Ag_2L^1)\}_n]$ is shown in Fig. 2. It consists of binuclear (Ag_2L^1) units linked together by silver atoms *via* a linear N—Ag—N bridging bonding mode. Selected interatomic distances and bond angles for **1** and a comparison with its precursor are given in Table 2. The fragment structure of the polymeric cryptate is shown in Fig. 3.

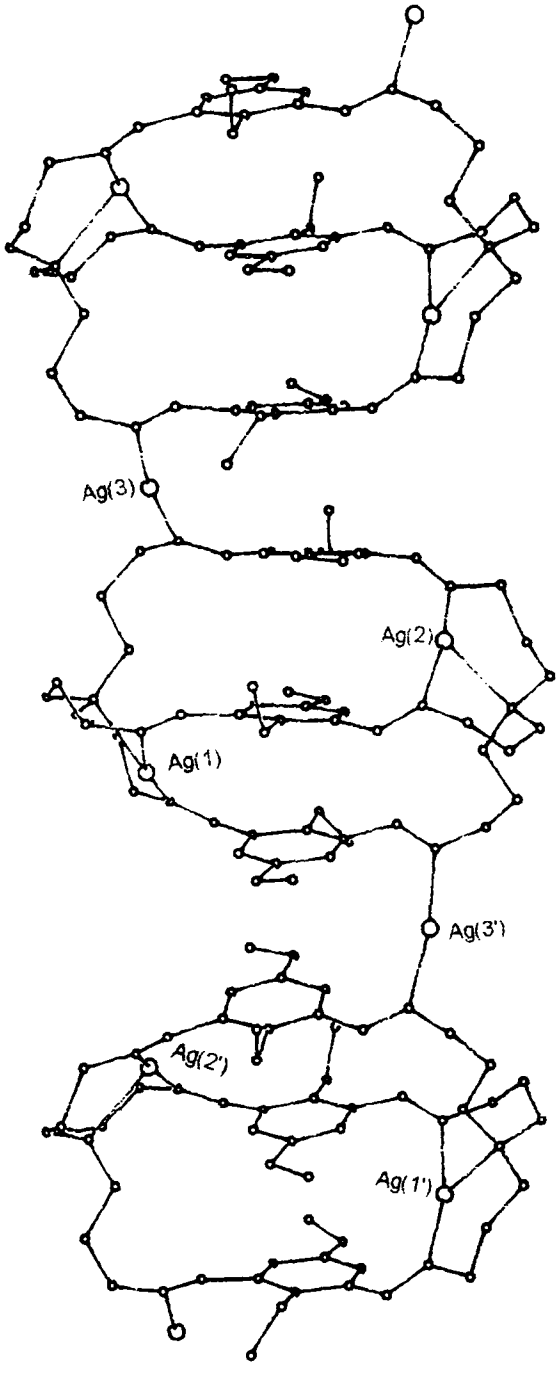
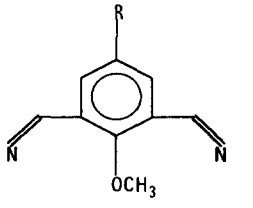
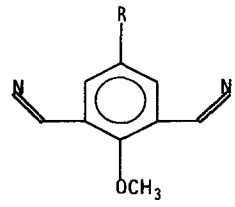


Fig. 2. A perspective view of the polymeric cation helix chain. $[\{Ag(Ag_2L^1)\}_n]$.

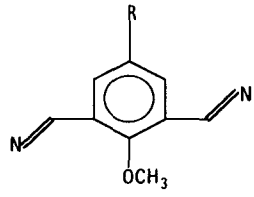
The fragment of the polymeric cryptate consists of Ag(3) and binuclear cryptate (Ag(1) Ag(2)L^1). Ag(3) is the bridging atom of inter-cavity. Both Ag(1) and Ag(2) are the bridging atoms of intra-cavity. In the cavity of (Ag_2L^1), Ag(1) and Ag(2) are situated in the different regions separated by the twisted bis (iminobenzene) bridging link consisting of N(5), N(6) and connected benzene ring. Each silver atom coordinates to three nitrogen atoms, two imino nitrogens and a bridgehead nitrogen, which has a slightly distorted trigonal environment. There are three possible arrangements of the C=N bonds relative to benzene rings illustrated as follows:



(in-, in-)



(out-, out-)



(in-, out-)

In the cavity, the twisted chain array composed of coordinate atoms and metal atoms N(3) → N(2) → Ag(1) → N(6) → N(5) → Ag(2) → N(8) → N(7) can be described as alternate (in-, out-) conformation. This coordinate chain possesses (out-, in-, Ag, in-, out-, Ag, out-, in-) conformation to form an S shape. The above-mentioned structural features are just equivalent to those of the bridge-twisted binuclear cryptate with the same cryptand [28], apparently being distinct from the basket shape out-, out-, Ag, out-, out-, Ag, out-, out-) [27]. Consequently, we consider that the bridge-twisted variant acts as a precursor unit to assemble the polymeric cryptate. By comparison of their bond lengths and angles (Table 2), we can further understand the relationship between them.

The average bond length of Ag—N (imino) of the polymeric cryptate is close to that of the precursor (2.18 Å). The average Ag—N (bridgehead) distance

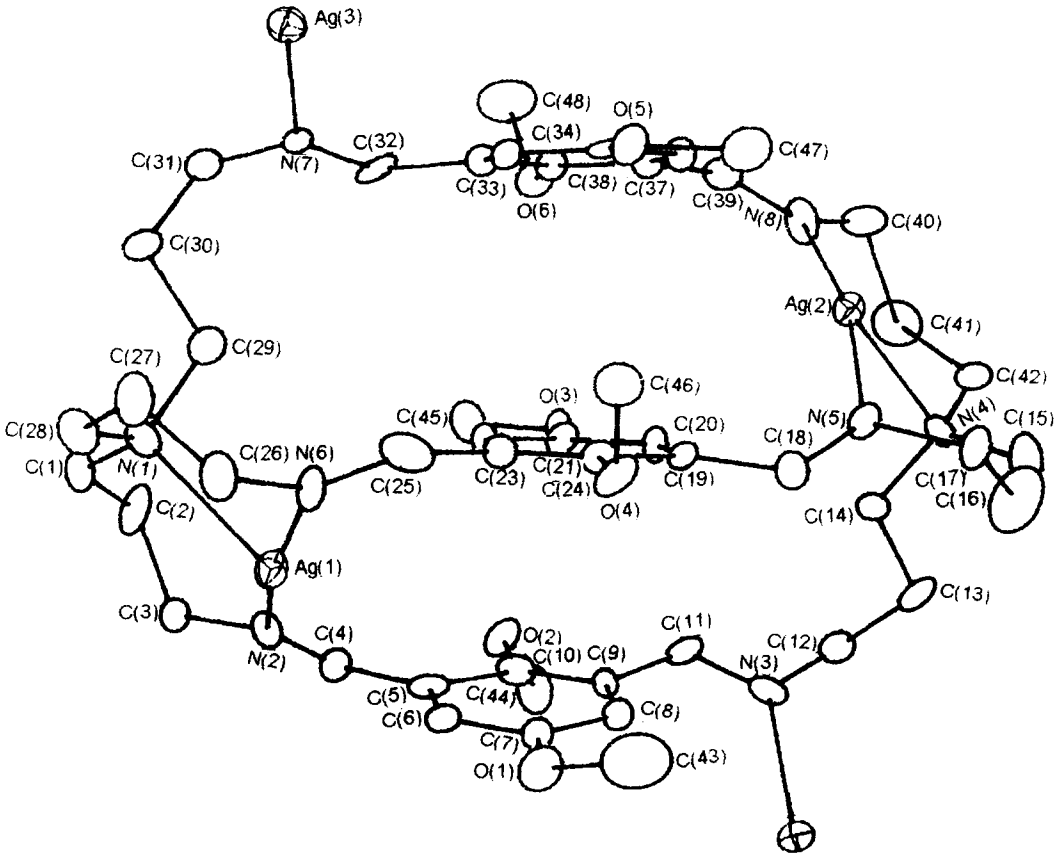


Fig. 3. Structure of the fragment $\{Ag(Ag_2L^1)\}$.

Table 2. Selected interatomic distances (Å) and bond angles ( ) for comparison of the polymeric cryptate **1** with its precursor

	Polymeric (p)	Binuclear (b)	p − b
Ag(1)—N(6)	2.20(2)	2.12(2)	+0.08
Ag(1)—N(2)	2.21(2)	2.22(2)	−0.01
Ag(1)—N(1)	2.46(2)	2.45(2)	+0.01
Ag(2)—N(8)	2.11(2)	2.17(2)	−0.06
Ag(2)—N(5)	2.17(2)	2.20(2)	−0.03
Ag(2)—N(4)	2.47(2)	2.43(2)	+0.04
Ag(3)—N(3)	2.19(2)	—	—
Ag(3)—N(7)	2.19(2)	—	—
Ag(1) ··· N(7)	5.783	4.860	+0.923
Ag(2) ··· N(3)	5.845	4.933	+0.912
Ag(1) ··· Ag(2)	8.367	8.266	+0.101
N(6)—Ag(1)—N(2)	166.1(7)	174.4(8)	−8.3(1)
N(6)—Ag(1)—N(1)	85.0(6)	91.1(8)	−6.1(2)
N(2)—Ag(1)—N(1)	96.2(7)	94.4(7)	+1.8(0)
N(8)—Ag(2)—N(5)	166.9(7)	172.9(8)	−6.0(1)
N(8)—Ag(2)—N(4)	98.7(9)	97.8(8)	+0.9(1)
N(5)—Ag(2)—N(4)	83.7(7)	89.1(7)	−5.4(0)
N(3)—Ag(3)—N(7)	169.7(7)	—	—

Data of binuclear cryptate (b) are quoted from [28].

Table 3. benzene ring planes in cryptate **1**

Plane	Orthonormal equation (e.s.d.)	Atoms
1	$0.0453x+0.9984y-0.0352z-3.3161=0$ (0.0097) (0.0006) (0.0093) (0.0762)	C(5) ~ C(10)
2	$0.1058x-0.9943y-0.0120z+6.4197=0$ (0.0093) (0.0010) (0.0092) (0.0782)	C(19) ~ C(24)
3	$0.1445x-0.9842y-0.1025z+10.3989=0$ (0.0093) (0.0017) (0.0095) (0.0734)	C(33) ~ C(38)

Dihedral: 1 ∧ 2 = 170.92(59); 1 ∧ 3 = 166.51(61); 2 ∧ 3 = 5.67(1.57)°.

of the former is 2.47 Å, being 0.03 Å longer than that of the latter. This indicates that the coordination between Ag and N (imino) in the former is slightly stronger than that in the latter, while the coordination between Ag and N (bridgehead) in the former is weaker than that in the latter.

It is noted that the corresponding bond angles and non-bond distances of the polymeric complex are quite different from the precursor. For example, the distance Ag(1)···N(7) or Ag(2)···N(3) is 0.9 Å, and Ag(1)···Ag(2) is 0.1 Å longer than that of the precursor. Moreover, in the cavity, the coordinate bond angle about the silver atom (N(6)—Ag(1)—N(2), N(6)—Ag(1)—N(1), N(8)—Ag(2)—N(5), or N(5)—Ag(2)—N(4)) is reduced by 5 ~ 8°, compared with the corresponding angle of the precursor. These changes were caused by the formation of the infinite chain *via* N(3)—Ag(3)—N(7) inter-cavity bridging bond.

The bond angle of inter-cavity bridge N(3)—Ag(3)—N(7) is 169.7(7)°, being 2.8 ~ 3.6° larger than that of the intra-cavity bridge N(6)—Ag(1)—N(2) or N(8)—Ag(2)—N(5). Both the inter-cavity bridge and intra-cavity bridge satisfy the distorted linear configuration of silver(I). The difference between the polymeric cryptate and its precursor reflects the steric requirement of the assembly process from the bridge-twisted shape to infinite chain. If we only take the linear N—Ag—N bonding coordination mode into consideration, the polymeric cation $[\{Ag(Ag_2L^1)\}_n]$ can be described as the conjugate bis(iminobenzene) moieties linked together *via* linear N—Ag—N bridges (inter- and intra-cavity) in alternate (in-, out-) conformations, resulting in the formation of an infinite single-helix chain. The helical array runs parallel to the crystallographic *b* axis.

As shown in Table 3, all benzene rings in the single helix chain are approximately parallel to each other, with a π–π stacking distance of 3.84 Å. Additionally, its isostructural analogous copper(I) and gold(I) polymeric cryptates were also synthesized in further studies.

Acknowledgements—We thank the state key laboratories of Structural Chemistry and Coordination Chemistry of China for support.

REFERENCES

1. J.-M. Lehn, *Angew. Chem., Int. Ed. Engl.* 1988, **27,** 89; *ibid* 1990, **29,** 1304; *Science* 1985, **227,** 849.
2. C. Seel and F. Vogtle, *Angew. Chem., Int. Ed. Engl.* 1992, **31,** 528.
3. J.-M. Lehn, in *Biomimetic Chemistry* (Edited by Z. I. Yoshida and N. Ise), p. 163. Elsevier, Amsterdam (1983).
4. J.-P. Launy (ed.), Molecular Electronics, *New J. Chem.* (special issue) 1991, **15,** 95.
5. N. Sabbatini, M. Guardigli, I. Manet, R. Ungaro, A. Casnati, R. Ziessel, G. Ulrich, Z. Asfari and J.-M. Lehn, *Pure Appl. Chem.* 1995, **67,** 135.
6. J. Zagwinski, J.-M. Lehn, R. Meric and J. P. Vigneron, *Tetrahedron Lett.* 1987, **28,** 3489.
7. D. McDowell and J. Nelson, *Tetrahedron Lett.* 1988, **29,** 385.
8. J. Hunter, C. Harding, M. McCann, V. McKee and J. Nelson, *J. Chem. Soc., Chem. Commun.* 1990, 1148.
9. T. Tsubomura, T. Sato, K. Yasaku, K. Sakat, K. Kobayashi and M. Morita, *Chem. Lett.* 1992, 731.
10. N. Martin, V. McKee and J. Nelson, *Inorg. Chim. Acta* 1994, **218,** 5.
11. C. J. Harding, Q. Lu, J. F. Malone, D. J. Marrs, N. Martin, V. McKee and J. Nelson, *J. Chem. Soc., Dalton Trans.* 1995, 1739 and references cited therein.
12. J. A. Farrar, V. McKee, A. H. R. Al-Obaidi, J. J. McGarvey, J. Nelson and A. J. Thomson, *Inorg. Chem.* 1995, **34,** 1302, and references cited therein.
13. J.-M. Lehn, J.-P. Vigneron, I. Bkouche-Waksman, J. Guilhem and C. Pascard, *Helv. Chim. Acta* 1992, **75,** 1069.
14. K. G. Ragunathan and P. K. Bharadwaj, *J. Chem. Soc., Dalton Trans.* 1992, 1653.
15. H. Adams, N. A. Bailey, D. E. Fenton, C. Fukuhara and M. Kanesato, *Supramol. Chem.* 1993, **2,** 325.
16. O. Kocian, R. J. Mortimer and P. D. Beer, *Tetrahedron Lett.* 1990, **31,** 5069; P. D. Beer, O. Kocian, R. J. Mortimer and P. Spencer, *J. Chem. Soc., Chem. Commun.* 1992, 602.
17. J. de Mendoza, E. Mesa, J.-C. Rodriguez-Ubis, P. Vazquez, F. Vögtle, P.-M. Windscheif, K. Rissanen, J.-M. Lehn, D. Lilienbaum and R. Ziessel, *Angew. Chem. Int. Ed. Engl.* 1991, **30,** 1331.
18. M. T. Youinou, J. Suffert and R. Ziessel, *Angew. Chem. Int. Ed. Engl.* 1992, **31,** 775.

19. M. Kumar, V. J. Aran and P. Navarro, *Tetrahedron Lett.* 1995, **36,** 2161.
20. Q. Lu, J.-M. Latour, C. J. Harding, N. Martin, D. J. Marrs, V. McKee and J. Nelson, *J. Chem. Soc., Dalton Trans.* 1994, 1471 and references cited therein.
21. D. Chen, R. J. Motekaitis, I. Murase and A. E. Martell, *Tetrahedron* 1995, **51,** 77 and references cited therein.
22. J.-L. Pierre, P. Chautemps, S. Refaif, C. Beguin, A. El-Marzouki, G. Serratrice, E. Saint-Aman and P. Rey, *J. Am. Chem. Soc.* 1995, **117,** 1965 and a reference therein.
23. M. G. B. Drew, C. J. Harding, V. McKee, G. G. Morgan and J. Nelson, *J. Chem. Soc., Chem. Commun.* 1995, 1035 and references therein.
24. M. D. Timken, W. A. Marritt, D. N. Hendrickson, R. A. Gagne and E. Sinn, *Inorg. Chem.* 1985, **24,** 4202.
25. P. Chakraborty and S. K. Chandra, *Polyhedron* 1994, **13,** 683.
26. M. P. Negwenya, A. E. Martell and J. Reibenspies, *J. Chem. Soc., Chem. Commun.* 1990, 1207.
27. S.-Y. Yu, Q.-H. Luo, M. C. Shen, X.-Y. Huang, W.-H. Yang and Z. Zhang, *Inorg. Chim. Acta* 1994, **223,** 181.
28. S.-Y. Yu, Q.-H. Luo, M.-C. Shen, Z. Zhang, X.-Y. Hang and Q.-J. Wu, *Polyhedron* 1994, **13,** 2467.
29. G. Morgan, V. McKee and J. Nelson, *Inorg. Chem.* 1994, **33,** 4427.
30. R. Wiest and R. Weiss, *J. Chem. Soc., Chem. Commun.* 1973, 678.
31. J. S. Bradshaw, C. W. McDaniel, B. D. Skidmore, R. B. Nielsen, B. E. Wilson, N. K. Dalley and R. M. Izatt, *J. Heterocycl. Chem.* 1987, **24,** 1085.
32. Y. Hu and H. Hu, *Chem. J. Chin. Univ.* 1986, **7,** 132.
33. E. Kimura, S. Young and J. P. Collman, *Inorg. Chem.* 1970, **9,** 1183.
34. N. Walker and D. Stuart, *Acta Cryst., Sect A* 1983, **39,** 158.
35. Molecular Structure Corporation, *TEXSAN, TEXRAY structure analysis package* (*version* 2.1). The Woodlands, TX (1989).

Pergamon

PII: S0277-5387(96)00290-2

Polyhedron Vol. 16, No. 3, pp. 463–471, 1997
Copyright © 1996 Elsevier Science Ltd
Printed in Great Britain. All rights reserved
0277-5387/97 $17.00+0.00

Structural characterization of nitrosodicyanomethanide and dicyanamide complexes of copper(II), nickel(II) and cobalt(II) with imidazole and 1-methylimidazole. X-ray crystallographic evidence of unusual nitrosodicyanomethanide O-bonding in $Cu\{ONC(CN)_2\}_2(1\text{-methylimidazole})_4$

Mária Hvastijová,[a]* Jozef Kožíšek,[a] Jiří Kohout,[a] Jerzy Mroziński,[b] Lothar Jäger[c] and Ingrid Svoboda[d]

[a]Department of Inorganic Chemistry, Slovak Technical University, 812 37 Bratislava, Slovakia

[b]Faculty of Chemistry, Wrocław University, Wrocław 30383, Poland

[c]Fachbereich Chemie, Martin-Luther University, Halle-Wittenberg, 0-4050 Halle-Saale, Germany

[d]Fachbereich Materialwissenschaft, Technische Hochschule Darmstadt, Petersenstrasse 20, D-642 87 Darmstadt, Germany

(Received 21 August 1995; accepted 13 June 1996)

Abstract—Pseudohalide complexes of the type $M\{ONC(CN)_2\}_2L_2$, with M = Cu, L = imidazole (iz), 1-methylimidazole (meiz); M = Ni, Co, L = meiz, $Cu\{ONC(CN)_2\}_2(meiz)_4$ $M\{ONC(CN)_2\}_2(iz)_4$, with M = Ni, Co, and $M\{N(CN)_2\}_2L_2$, with M = Cu, Co, L = meiz; M = Ni, L = iz, meiz have been prepared and characterized by spectroscopic and magnetic techniques. The crystal structure of $Cu\{ONC(CN)_2\}_2(meiz)_4$ has been determined by the X-ray diffraction method. The Cu^{II} environment is elongated pseudooctahedral, composed of four tertiary meiz nitrogens and two nitrosodicyanomethanide oxygens in longer axial distances. According to spectroscopic results, the remaining compounds show octahedral (Ni, Co) or pseudooctahedral (Cu) structures, realized in the M : L = 1 : 2 and probably also in the 1 : 4 compounds by bridging pseudohalide function. Such bridging is evidenced by magnetic properties of $Cu\{ONC(CN)_2\}_2(meiz)_2$, being affected by exchange coupling between the paramagnetic metal ions. Copyright © 1996 Elsevier Science Ltd

Keywords: nitrosodicyanomethanide; dicyanamide; X-ray structure; IR spectra; electronic spectra; magnetism.

The nitrosodicyanomethanide anion, $ONC(CN)_2^-$, contains as a ligand various donor atoms, but is preferentially coordinated through the nitroso–nitrogen or oxygen atom [1–6], depending on the character of the central atom. No well-documented case of oxygen coordinated nitrosodicyanomethanide in a transition *d*-metal complex is known until now. Further the $ONC(CN)_2^-$ anion can also act as a bidentate bridging ligand using its cyano nitrogen for additional binding [2,7,8].

Another pseudohalide used as a ligand in this work, the dicyanamide anion $N(CN)_2^-$, although potentially bidentate, much prefers forming coordination bonds *via* the cyano nitrogen [9]. This ligand shows more pronounced tendency to bridging function than

* Author to whom correspondence should be addressed.

nitrosodicyanomethanide [7], ligating either through both cyano or through amide and cyano nitrogens [9]. Even two isomers of $Cu\{N(CN)_2\}_2(imidazole)_2$ were isolated differing just by the mode of dicyanamide bridging [10].

In earlier papers the preparative and physical investigations of nitrosodicyanomethanide complexes of Cu^{II}, Co^{II}, Ni^{II} with ligands of pyrazole type [7,8], as well as of dicyanamide complexes of Cu^{II} and Co^{II} with imidazole and its methylderivatives [10,11] were performed. In further work, we have carried out a research of nitrosodicyanomethanide and dicyanamide complexes of Cu^{II}, Ni^{II}, Co^{II} with imidazole (iz) and 1-methylimidazole (meiz), including the X-ray crystallographic study of $Cu\{ONC(CN)_2\}_2(meiz)_4$.

EXPERIMENTAL

Preparation of the compounds

$Cu\{ONC(CN)_2\}_2(iz)_2$. Solutions of 2.5 mmol of $Cu(NO_3)_2 \cdot 3H_2O$ in 5 cm^3 of water and of 5.0 mmol of $NaONC(CN)_2$ in 5 cm^3 of water were mixed. The system obtained was alkalized with 2 cm^3 of 25% NH_3 and poured into a solution of 5.0 mmol of iz in 20 cm^3 of methanol. Under continuous stirring a suspension was formed which was filtered off and washed with diethylether. Yield 84%.

$Cu\{ONC(CN)_2\}_2(meiz)_4$. A solution of 5.0 mmol of $Cu(NO_3)_2 \cdot 3H_2O$ in 15 cm^3 of water and 20 mmol of meiz were poured into a solution of 11 mmol of $NaONC(CN)_2$ in 20 cm^3 of water. A green solution was formed from which a crystalline product was separated and washed with diethylether. Yield 81%.

$Cu\{ONC(CN)_2\}_2(meiz)_2$. A solution of 5.0 mmol of $Cu(NO_3)_2 \cdot 3H_2O$ in 3 cm^3 of water and 10 mmol of meiz were poured into a solution of 11 mmol of $KONC(CN)_2$ in 4 cm^3 of water. Under continuous stirring an oily suspension was formed from which a solid was isolated and washed with diethylether. Yield 79%.

$M\{ONC(CN)_2\}_2(iz)_4$ and $M\{ONC(CN)_2\}_2(meiz)_2$ (M = Ni, Co). Solution of 5.0 mmol of $M(NO_3)_2 \cdot 6H_2O$ in 6 cm^3 of water and of 11 mmol of iz or meiz in 8 cm^3 of water were poured into a solution of 11 mmol of $KONC(CN)_2$ in 5 cm^3 of water. Under continuous stirring the products in the form of microcrystalline powders were isolated and washed with methanol or diethylether. Yields 78–91%.

$M\{N(CN)_2\}_2L_2$ (M = Cu, Ni, Co; L = iz, meiz). Solutions of 4.0 mmol of $Cu(NO_3)_2 \cdot 3H_2O$ or $M(NO_3)_2 \cdot 6H_2O$ (M = Ni, Co) in 5 cm^3 of water and a solution of 8.5 mmol of $KN(CN)_2$ in 8 cm^3 of water were mixed with a solution of 9.0 mmol of L in 8 cm^3 of methanol. Under continuous stirring the respective compounds were precipitated and washed with 1 : 1 mixture of water and methanol. Yields 80–92%.

Analyses

Metal was determined chelatometrically after decomposition of the compounds by H_2SO_4 and $K_2S_2O_8$. The elemental analyses were carried out using a Carlo-Erba C,H,N-analyser. The analytical data are listed in Table 1.

X-ray structure analysis and refinement

A single crystal of dimension $0.15 \times 0.30 \times 0.45$ mm was used for data collection. The data were collected at 293(2) K on a Stoe-Siemens AED diffractometer using the ω-2θ scan technique with Mo-K_α filtered radiation ($\lambda = 0.71069$ Å). Lattice parameters were obtained by least-squares refinement of 48 reflections at $35.5 \leqslant 2\theta \leqslant 48.7°$. A total of 4374 reflections were collected ($2.2 \leqslant \theta \leqslant 25.0°$, $-10 \leqslant h \leqslant 10$, $-10 \leqslant k \leqslant 7$, $-12 \leqslant l \leqslant 12$), 2420 unique, of which 2327 with $F_o > 4\sigma(F_o)$ were considered as observed; $R_{int} = 0.0152$ and $R(\sigma) = 0.0179$. The intensities of three standard reflections were monitored every 3 h; no significant systematic fluctuation was found. Pro-

Table 1. Colour and analytical data for the compounds

Compound	Colour	C(%)(calc)	H(%)(calc)	N(%)(calc)	M(%)(calc)
$Cu\{ONC(CN)_2\}_2(iz)_2$	violet	36.8 (37.2)	2.0 (2.1)	35.9 (36.1)	16.3 (16.4)
$Cu\{ONC(CN)_2\}_2(meiz)_4$	green	45.6 (45.6)	3.9 (4.2)	33.9 (33.8)	11.0 (11.0)
$Cu\{ONC(CN)_2\}_2(meiz)_2$	dark green	40.0 (40.4)	3.1 (2.9)	33.1 (33.7)	15.0 (15.3)
$Ni\{ONC(CN)_2\}_2(iz)_4$	brown	41.1 (41.7)	3.0 (3.1)	37.3 (37.8)	11.0 (11.1)
$Ni\{ONC(CN)_2\}_2(meiz)_2$	dark brown	40.9 (40.9)	2.9 (2.9)	33.8 (34.1)	14.0 (14.3)
$Co\{ONC(CN)_2\}_2(iz)_4$	red brown	41.0 (41.6)	3.0 (3.1)	37.4 (37.8)	11.0 (11.4)
$Co\{ONC(CN)_2\}_2(meiz)_2$	orange	40.6 (40.9)	3.0 (2.9)	34.0 (34.1)	14.2 (14.3)
$Cu\{N(CN)_2\}_2(meiz)_2$	light blue	39.9 (40.1)	3.3 (3.4)	38.5 (38.9)	17.4 (17.7)
$Ni\{N(CN)_2\}_2(iz)_2$	rose	42.2 (42.8)	2.5 (2.5)	36.5 (36.7)	18.0 (18.0)
$Ni\{N(CN)_2\}_2(meiz)_2$	light blue	39.7 (40.6)	3.3 (3.4)	39.6 (39.5)	16.2 (16.5)
$Co\{N(CN)_2\}_2(meiz)_2$	rose	40.0 (40.6)	3.3 (3.4)	38.7 (39.4)	16.9 (16.6)

Table 2. Crystal and structure refinement data for $Cu\{ONC(CN)_2\}_2(meiz)_4$

Formula	$CuC_{22}H_{24}N_{14}O_2$
M_r	580.10
Crystallographic system	triclinic
a (Å)	8.776(2)
b (Å)	8.789(2)
c (Å)	10.225(2)
α (°)	65.176(10)
β (°)	86.228(8)
γ (°)	75.012(8)
V (Å^3)	690.6(2)
$F(000)$	299
Space group	$P\bar{1}$
Z	1
D_c (g cm^{-3})	1.395
μ(Mo-K_α) (mm^{-1})	0.838
No. of indep. refl.	2419
No. of indep. refl. $F_o > 4\sigma(F_o)$	2327
Goodness-of-fit on F^2	1.047
Final R [$I > 2\sigma(I)$]	0.0295
Final wR^a	0.0748
$\Delta\rho_{min}$ (e Å^{-3})	−0.23
$\Delta\rho_{max}$ (e Å^{-3})	0.26

[a] $w = 1/[s^2(F_o^2) + (0.0354P)^2 + 0.254P]$, where $P = (F_o^2 + 2F_c^2)/3$.

gram DIFABS [12] ($\mu = 0.838$ mm^{-1}) was used for absorption correction.

The structure was solved by Patterson methods using SHELXS86 [13] and refined on F^2 by SHELXL93 [14]. A difference map of the anisotropically refined structure gave the positions of all hydrogen atoms which were constrained: C—H = 0.93 or 0.96 Å for C—H and CH_3, respectively, with U(H) = 1.2 U_{eq} (C). In the final cycle of full-matrix least-squares refinement $R = 0.0295$ and $wR = 0.0748$. Geometrical analysis was performed using the program PARST [15].

Details about the data collection, the structure analysis and refinement are given in Table 2. Bond lengths and angles, atomic coordinates, displacement parameters and lists of structure factors for $Cu\{ONC(CN)_2\}_2(meiz)_4$ are deposited [16].

Physical measurements

The IR spectra were recorded using Philips Analytical PU9800 FTIR spectrometer in KBr disks (4000–400 cm^{-1}) and in Nujol mulls (500–200 cm^{-1}). The electronic spectra (0.4–2.8 μm^{-1}) were obtained on samples diluted by MgO with a Beckman UV 5240 spectrophotometer. Magnetic susceptibilities in the temperature range 4.2–*ca* 300 K were measured as described in detail previously [17].

RESULTS AND DISCUSSION

Description of the structure of $Cu\{ONC(CN)_2\}_2(meiz)_4$

The molecular entity $Cu\{ONC(CN)_2\}_2(meiz)_4$, with the detailed labeling of the atoms, is shown in Fig. 1. Significant bond lengths and angles are given in Table 3.

The central Cu^{II} atom, occurring in a special crystallographic position, is surrounded by four nitrogens of meiz molecules, forming the square basis of a distorted octahedron; the respective Cu—N bond lengths are 2.020(2) and 2.002(1) Å. The apical sites of the octahedron are occupied by two oxygens from nitrosodicyanomethanide anions at distances of 2.537(1) Å. The coordination geometry is therefore an elongated octahedron, the axial distances being considerably longer than the equatorial ones. There is an intricate system of hydrogen bonds as well as van der Waals contacts, as can be seen in Table 3.

It should be mentioned that in all the known nitrosodicyanomethanide complexes of *d*-elements the $ONC(CN)_2^-$ anions are coordinated through the nitroso nitrogen [1–4]. Thus, the structure solved here is the first example of the nitrosodicyanomethanide O-coordination in a *d*-metal complex.

Infrared spectra

The infrared spectra (Table 4) of the compounds under study contain in the middle region some bands characteristic for the ligation mode of the pseudohalide present [1–6,9]. The M^{II}: L = 1:2 nitrosodicyanomethanide complexes show the ν_{as}(CNO) and ν_s(CNO) frequencies in comparison with those in free $ONC(CN)_2^-$ ion [1,2,4] shifted by *ca* 93 cm^{-1} to

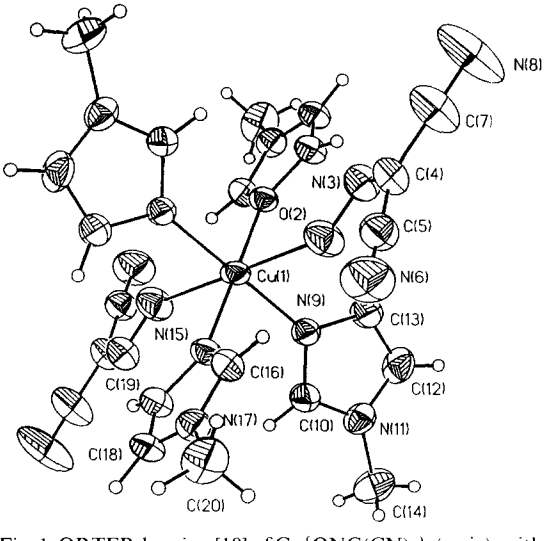


Fig. 1. ORTEP drawing [18] of $Cu\{ONC(CN)_2\}_2(meiz)_4$ with 50% probability thermal ellipsoids.

Table 3. Selected bond lengths (Å) and bond angles (°) in $Cu\{ONC(CN)_2\}_2(meiz)_4$

Cu(1)—N(9)	2.020(2)	N(9)—Cu(1)—N(15)	90.5(1)
Cu(1)—N(15)	2.002(1)	N(9)—Cu(1)—O(2)	89.9(1)
Cu(1)—O(2)	2.537(1)	N(15)—Cu(1)—O(2)	86.5(1)
O(2)—N(3)	1.259(2)	Cu(1)—O(2)—N(3)	136.3(1)
N(3)—C(4)	1.340(4)	Cu(1)—N(9)—C(10)	127.7(1)
C(4)—C(5)	1.412(3)	Cu(1)—N(9)—C(13)	127.1(1)
C(5)—N(6)	1.140(4)	Cu(1)—N(15)—C(16)	126.1(1)
C(7)—N(8)	1.132(4)	Cu(1)—N(15)—C(19)	128.2(1)
N(9)—C(10)	1.314(2)	O(2)—N(3)—C(4)	115.8(2)
N(9)—C(13)	1.367(2)		
N(15)—C(16)	1.314(3)		
N(15)—C(19)	1.375(2)		

D—H···A	D—H	H···A	D···A	D—H···A
C(10)—H(10A)···N(15)	0.930(2)	2.752(2)	3.091(3)	102.6(2)
C(16)—H(16A)···O(2)	0.930(2)	2.391(9)	3.008(2)	123.7(2)
C(13)—H(13A)···N(15)	0.930(2)	2.776(3)	3.085(3)	100.6(2)
C(19)—H(19A)···N(3)′	0.930(2)	2.502(3)	3.300(4)	144.0(2)
C(18)—H(18A)···N(8)″	0.930(2)	2.444(4)	3.370(4)	173.8(3)

Symmetry code: (I) $-x, -y, -z$; (II) $+x-1, +y+1, +z-1$.

higher values. These shifts are regarded as a strong indication of metal–ligand bonding through nitroso nitrogen: M—N(O)C(CN)$_2$ [1–3].

In the case of $Cu\{ONC(CN)_2\}_2(meiz)_4$ the oxygen ligation of $ONC(CN)_2^-$ should be distinctly manifested by the frequency change of the ν(C—N) and ν(N=O) vibrations. Köhler *et al.* [1,4] pointed out that O-bonded $ONC(CN)_2^-$ should have shifted the ν(C—N) mode to higher frequencies but the ν(N=O) mode to lower ones. The compound $Cu\{ONC(CN)_2\}_2(meiz)_4$ has bands at 1305 and 1285 cm^{-1} which can be assigned to the ν(C—N) and ν(N=O) vibrations, respectively. Since for the free $ONC(CN)_2^-$ ion the ν(CNO) modes occur in the regions of 1325 and 1275 cm^{-1} [1,2,4], both observed frequencies are only little changed in comparison with the respective free ion frequencies. In all likelihood this fact is caused by weak axial Cu—ONC(CN)$_2$ bonding, changing only insignificantly the bond electron density in the system C—N—O.

The Ni^{II}— and Co^{II}—ONC(CN)$_2$ complex of iz represent a further interesting case, since they exhibit an unusually great number of bands assignable to the ν(CNO) modes [1–5]. These bands should suggest the presence of two bonding non-equivalent ONC(CN)$_2$ groups, *viz.* coordinated and non-coordinated ones; the presence of the latter groups is supported especially by the bands around 1260 cm^{-1}.

For all nitrosodicyanomethanide complexes the (C≡N) modes are split by ≈25–10 cm^{-1}. Since in KONC(CN)$_2$ and AgONC(CN)$_2$ this mode is split nearly to the same extent [1,4] (asymmetric and symmetric C≡N stretches), no structural importance may be ascribed to this phenomenon.

From the dicyanamide complexes, the Ni^{II} and Co^{II} derivatives exhibit three bands belonging to the ν(C≡N) stretches, whose positions are mostly in good agreement with the bidentate N(CN)$_2$ groups [9]. On the other hand, $Cu\{N(CN)_2\}_2(miz)_2$ has both ν(C≡N) values well in the ranges for monodentate N(CN)$_2$ groups, although with respect to its polymeric structure (see next section) all N(CN)$_2$ groups must be bridging bidentate; similar inconsistencies were already observed in a number of other cases [11,17,19].

In the far-IR region the bands belonging to the M—N stretching vibrations were tentatively assigned (Table 4). In $Cu\{ONC(CN)_2\}_2(meiz)_4$ the symmetry of the CuN_4O_2 skeleton is nearly D_{2h} and 15 skeletal modes can be expected, nine of which are infrared active ($3B_{1u}+3B_{2u}+3B_{3u}$). Two of these modes appearing between ≈280–260 cm^{-1} can be assigned to the Cu—N stretches in the equatorial plane (B_{2u}, B_{3u}). It is clear that the Cu—O stretch (B_{1u}) cannot be observed in the far-IR region investigated here, since modes involving atoms at such long distances are usually revealed about 100 cm^{-1} and lower [20].

The remaining nitrosodicyanomethanide complexes show two to four absorptions between ≈335–≈240 cm^{-1} which can be attributed to the M—N stretching vibrations. These absorptions naturally comprise Cu—N stretches involving nitrogens from both ligand kinds; for bridged Ni^{II} and Co^{II} systems not only M—NO but also the M—NC stretches should contribute. On the analogy of nitrosodicyanomethanide complexes of Cu^{II} and Co^{II} with methylpyrazoles [7], it might be expected that the ν(M—N) frequencies are lowered approximately in the order of M—NO > M—NC > M—N(L) but a more detailed appreciation cannot be made at this stage.

The dicyanamide complexes exhibit a similar num-

Table 4. Characteristic IR data (cm^{-1}) for the MX_2L_4, MX_2L_2 and MY_2L_2 complexes[a]

$CuX_2(iz)_2$	$CuX_2(meiz)_4$	$CuX_2(meiz)_2$	$NiX_2(iz)_4$	$NiX_2(meiz)_2$	$CoX_2(iz)_4$	$CoX_2(meiz)_2$	$CuY_2(meiz)_2$	$NiY_2(iz)_2$	$NiY_2(meiz)_2$	$CoY_2(meiz)_2$	Assignment
							2297s	2278mw	2283s	2280s	$\nu_s+\nu_{as}$(C—N)
2219vs	2212vs	2240m	2218vs	2218s	2220s	2240s	2230s	2237s	2250s	2236ms	ν(C≡N)
2205vs	2200vs	2224s	2205s	2208sh	2205m	2214s	2164vs	2203s	2190vs	2185vs	
		2220s						2195vs	2168vs	2176vs	
		2199m									
1420s	1305s[b]	1420w[d]	1412mw	1418w	1410w	1420mw[d]					ν_{as}(CNO)
	1285vs[c,d]	1408m									
1371ms		1366s	1360sh	1367s	1363ms	1366ms					ν_s(CNO)
			1350s	1350s	1346m	1336s					
			1266s[e]		1265ms[e]						
			1256sh[e]		1260m[e]						
							1346m	[g]	1345m	1348mw[d]	ν_{as}(C—N)
1233s	1243s[c]	1198vs	1236vs	1219s	1233m	1233sh					ν(C—C)
1172w	1235s[c]	1187s	1212s		1209m	1215vs					
		1169vs(?)									
							953mw	[g]	945m	942m	ν_s(C—N)
							521ms	524s	517mw	525ms	δ(NCN)
							503mw	502m	507m	507m	
289ms	282m	302s	291s	305w	334w,br[d,f]	315m	295s	284ms	286s	260s[h]	ν(M—N)
264m	260mw	292s	267s	285m	255w	291ms	280ms[f]	264sh[h]	257sh[h]	250s[h]	
		287sh	255s[f]	262m		280m		246s[h]	246s[h]	235s[h]	
		258m		242m[f]		262ms[f]				244s[h]	

[a] X = $ONC(CN)_2$, Y = $N(CN)_2$.
[b] ν(C—N).
[c] ν(N=O).
[d] Cannot be distinguished unambiguously from the ligand L band.
[e] One of these bands may belong to the ligand L.
[f] Week splitting appears and the mean frequency is given.
[g] Obscured by the ligand L band.
[h] One of the bands in the respective region may belong to the $N(CN)_2$ group.

ber of absorptions between 290–≈230 cm^{-1} assignable to the M—N stretches as the previous complex group, however, some of these absorptions may also belong to the present ligands. Since none of the ν(M—N) frequencies occur above *ca* 300 cm^{-1}, the $N(CN)_2$ groups are very likely bridging through both cyano nitrogens [9,21].

Solid state electronic spectra

The electronic spectra (Table 5) of the copper(II) complexes with the Cu^{II} : L ratio of 1 : 2 exhibit broad visible bands resolved on the side of lower wavenumbers into one or two shoulders. The *d–d* spectral characteristics indicate the elongated pseudo-octahedral environment of the Cu^{II} central atom [22–25] in a polymeric structure. The equatorial positions are occupied by two tertiary nitrogens from the imidazole ligands and two nitroso or cyano nitrogens from the pseudohalides. In the axial sites are very likely located two cyano nitrogens from the pseudohalides of adjacent moieties [3,7,9,19].

From the relative positions of the *d–d* band maxima as well as the low-energy shoulders it is clear, that the tetragonal distortion [23,25] increase in the order of $Cu\{N(CN)_2\}_2(meiz)_2 < Cu\{ONC(CN)_2\}_2(meiz)_2 < Cu\{ONC(CN)_2\}_2(iz)_2$. If we tentatively assign the observed *d–d* absorptions to the pertinent transitions in D_{4h} symmetry according to Fig. 2, the ligand field parameter *Dq* can be calculated using the relation [24] $10\,Dq = \delta_3 - (1/2)\,\delta_1 - (1/3)(\delta_3 - \delta_2)$. The *Dq* values fluctuate around 870 cm^{-1}, inconsistently with the positions of both pseudohalides in the spectrochemical series [2], but in agreement with the relative basicity of iz and meiz [26].

The compound $Cu\{ONC(CN)_2\}_2(meiz)_4$ shows one broad unresolved band, which comprises all four *d–d* transitions in a low symmetry ligand field, thus, the *Dq* parameter cannot be calculated.

All nickel(II) complexes have electronic spectra with three spin-allowed *d–d* absorptions, being characteristic of octahedral surrounding of the Ni^{II} central atom [27]. The Ni^{II} : L = 1 : 2 compounds apparently adapt polymeric structures, similarly built as in the copper(II) compounds of the same type, but practically without tetragonal distortion. The compound $Ni\{ONC(CN)_2\}_2(iz)_4$ might have a molecular structure with monodentate $ONC(CN)_2$, but also a polymeric structure in which one half of $ONC(CN)_2$ groups bridges square-planar fragments $Ni(iz)_2$; the remaining $ONC(CN)_2$ groups should be anionic. A structure of this kind was recently established by X-ray crystallography for $Cu\{C(CN)_3\}_2(pyrazole)_4$ [28].

The spin-allowed absorptions in the increasing energy order are assigned to the transitions $^3T_{2g} \leftarrow {}^3A_{2g}$, $^3T_{1g}(F) \leftarrow {}^3A_{2g}$, and $^3T_{1g}(P) \leftarrow {}^3A_{2g}$; in the $ONC(CN)_2$ complexes the latter one is resolved only as a shoulder on the strong UV absorption. The *Dq* values are somewhat higher than for the copper(II) complexes and no explicit trend is perceptible. The β values, indicating the degree of covalency, are higher in the case of the $N(CN)_2$ complexes.

The cobalt(II) complexes have in their electronic spectra two spin-allowed *d–d* absorptions, whose positions give evidence for octahedral coordination geometry of the Co^{II} atom [29]. In substance structures of the same type can be postulated as for the corresponding nickel(II) complexes. The low and high energy absorptions are assigned to the transitions $^4T_{2g} \leftarrow {}^4T_{1g}(F)$ and $^4T_{1g}(P) \leftarrow {}^4T_{1g}(F)$ (in the $N(CN)_2$ complexes as a broad shoulder). The *Dq* values are very similar to those of the nickel(II) complexes and even so, the β values of the $N(CN)_2$ complexes (adding $Co\{N(CN)_2\}_2(iz)_2$ [11]) are obviously higher. Moreover, the β values in comparison with those of the corresponding nickel(II) complexes are—except for one case— practically invariably lower.

In the case of all nitrosodicyanomethanide complexes, between *ca* 1.9–2.9 μm^{-1} one or two absorptions occur, which belong to the transition in the $ONC(CN)_2$ group [2,4,30] or to some low-lying charge-transfer transition.

Table 5. Electronic spectral data for the compounds

Compound	ν_{max} (μm^{-1})[a]					*Dq* (cm^{-1})	*B* (cm^{-1})	β
$Cu\{ONC(CN)_2\}_2(iz)_2$	(1.66)	1.90	(2.05)	(2.65)		870		
$Cu\{ONC(CN)_2\}_2(meiz)_4$	1.74	2.25				[b]		
$Cu\{ONC(CN)_2\}_2(meiz)_2$	(1.34)[b]	1.67	(2.22)	(2.70)		890		
$Ni\{ONC(CN)_2\}_2(iz)_4$	1.00	(1.69)	2.07	(2.58)	(2.68)	1000	783	0.76
$Ni\{ONC(CN)_2\}_2(meiz)_2$	1.05	(1.58)	(1.92)	(2.60)	(2.86)	1050	712	0.69
$Co\{ONC(CN)_2\}_2(iz)_4$	0.94	(1.67)	(2.01)[b]	2.46		1060	792	0.82
$Co\{ONC(CN)_2\}_2(meiz)_2$	0.93	(1.91)[b]	(2.47)			1040	728	0.75
$Cu\{N(CN)_2\}_2(meiz)_2$	(1.21)	(1.31)	1.54			928		
$Ni\{N(CN)_2\}_2(iz)_2$	1.07	(1.33)	1.74	2.82		1070	860	0.86
$Ni\{N(CN)_2\}_2(meiz)_2$	1.02	1.70	2.74			1020	968	0.94
$Co\{N(CN)_2\}_2(meiz)_2$	0.91	(1.87)	2.12			1035	889	0.92

[a] The data in parentheses are related to shoulders, whose positions are only approximately determined.
[b] Not calculated; see text.

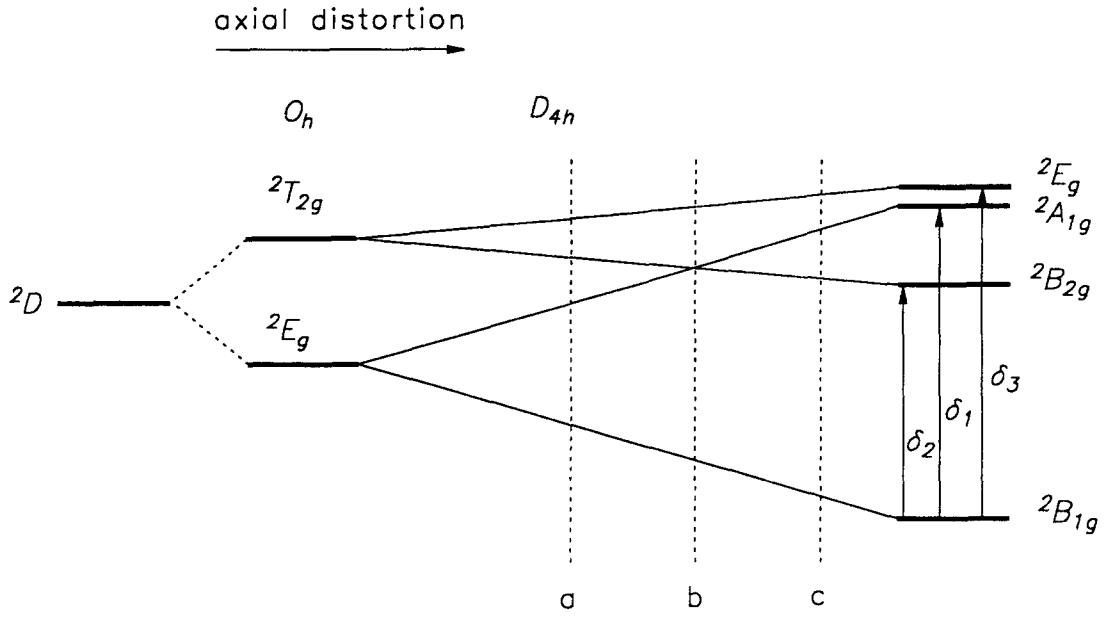


Fig. 2. Approximate regions of *d–d* transitions for (a) $Cu\{N(CN)_2\}_2(meiz)_2$, (b) $Cu\{ONC(CN)_2\}_2(meiz)_2$ and (c) $Cu\{ONC(CN)_2\}_2(iz)$.

Magnetism

The compound $Cu\{ONC(CN)_2\}_2(meiz)_2$ shows a sub-spin value of room temperature magnetic moment, ≈ 1.60 B.M., therefore temperature dependence of its magnetic susceptibility was measured (Fig. 3). The results obtained were fitted to the Curie–Weiss law in the higher-temperature region (Table 6). In the lowest temperature region some departures from the Curie–Weiss law behavior occur. The μ_{eff} values, though lower than the spin-only value, are only slightly temperature dependent (Fig. 3). One possibility for this behavior is some Cu^I species, but from the preparative point of view this is very unlikely, as no apparent reducing agent is present in the reaction system. Samples from different preparations were measured at room temperature and their magnetic moments were in the range of 1.59 ± 0.02 B.M. Furthermore, in the presence of Cu^I we should observe a non-linear course of the function $(\chi_{Cu})^{-1} = f(T)$.

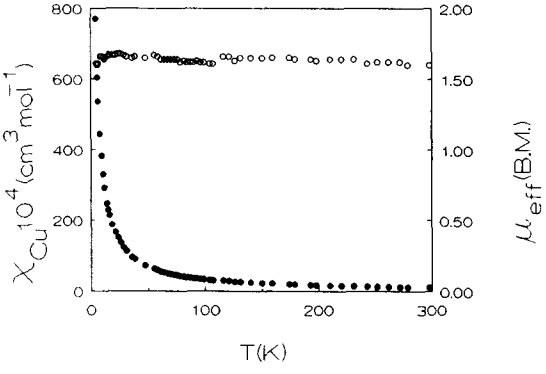


Fig. 3. Temperature dependence of molar susceptibility and effective magnetic moment for $Cu\{ONC(CN)_2\}_2(meiz)_2$.

The sub-spin copper μ_{eff} value may suggest that magnetism of the compound is influenced by both antiferromagnetic and ferromagnetic coupling between the magnetic Cu^{II} centers, which are bridged through the $ONC(CN)_2$ groups under formation of a polymeric system. In this system, two kinds of pathway for superexchange process are available, which can realize both ferromagnetic and antiferromagnetic exchange interaction. The orthogonal σ-orbitals of nitrosodicyanomethanide can mediate a ferromagnetic coupling, but the delocalized π-orbitals of this ligand can propagate an antiferromagnetic coupling. The latter coupling outweighs the former one to

Table 6. Parameters of the Curie-Weiss law for $Cu\{ONC(CN)_2\}_2(meiz)_2$ and $Co\{ONC(CN)_2\}_2(iz)_4$

Compound	Temperature range (K)	C (cm^3 K mol^{-1})	θ (K)	R^a
$Cu\{ONC(CN)_2\}_2(meiz)_2$	20–298	0.325	+2.5	2.52×10^{-2}
$Co\{ONC(CN)_2\}_2(iz)_4$	20–297	2.99	−18.4	7.05×10^{-2}

[a] The value $R = \sum_{i=1}^{n} [\chi_M(calc)_i - \chi_M(expt)_i]^2$ is the criterion determining the best fit.

cause an observed sub-spin lowering of μ_{eff}, but in their influence upon temperature behavior of μ_{eff} both kinds of magnetic exchange practically cancel out. The mutual ratio of greatness of these two kinds of magnetic interactions depends on the bridge geometric factors, mode of the polymeric system arrangement, its dimensionality, etc.

In this complex situation and in the absence of X-ray crystallographic data it seems that further attempts to rationalize the established magnetic properties are not justifiable. But it is important to note that complexes $Cu\{C(CN)_3\}_2$(3,4,5-trimethylpyrazole)$_2$ [31] and $Ni\{C(CN)_3\}_2$(2-methylbenzimidazole)$_2$ [17] were ascertained to show very similar magnetic behavior, but its fitting to the two-dimensional model in the first case did not lead to satisfying results.

For $Co\{ONC(CN)_2\}_2(iz)_4$ the temperature dependence of magnetic susceptibility was also measured (Fig. 4) and Curie–Weiss law parameters in the higher temperature region were calculated (Table 6). The experimental μ_{eff} values (4.73 B.M. at 297 K) with temperature decrease (Fig. 4) are very moderately lowered up to *ca* 100 K (4.60 B.M. at 99 K) and afterwards they fall continually more expressively as far as 2.52 B.M. at 4.2 K. In the low-temperature region the Curie–Weiss law is not obeyed by the susceptibility data.

The temperature behavior of μ_{eff} can be rationalized by the presumption of spin-orbit coupling in the octahedral $^4T_{1g}$ term [32]. Thus, the magnetic results cannot clear up the matter of the binding function of the $ONC(CN)_2$ group, because it is rather difficult to discover the potential presence of some magnetic exchange in combination with the spin-orbit effects. Similar magnetic behavior as that of $Co\{ONC(CN)_2\}_2(iz)_4$, only with somewhat less steep low temperature falling of the μ_{eff} values, but showing an anomalously low μ_{eff} value even at room temperature, was discovered for $Co\{N(CN)_2\}_2$(2-methylbenzimidazole)$_2$ having, according to the spectral results, polymeric octahedral structure with bridging $N(CN)_2$ groups [17]. The X-ray crystallography would be very desirable, but we were not able to obtain single crystals of $Co\{ONC(CN)_2\}_2(iz)_4$, nor of its Ni^{II} analogue.

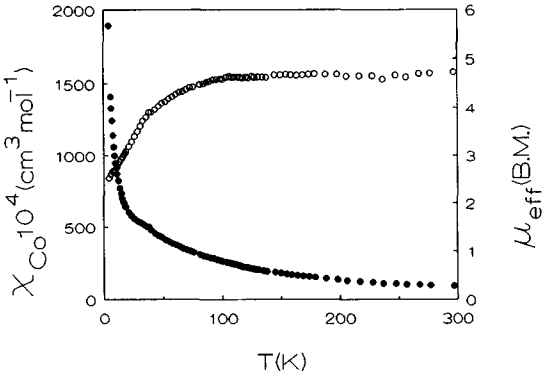


Fig. 4. Temperature dependence of molar susceptibility and effective magnetic moment for $Co\{ONC(CN)_2\}_2(iz)_4$.

REFERENCES

1. A. Kolbe and H. Köhler, *Z. Anorg. Allg. Chem.* 1970, **373,** 230.
2. H. Köhler and B. Seifert, *Z. Anorg. Allg. Chem.* 1970, **379,** 1.
3. H. Köhler and B. Seifert, *Z. Anorg. Allg. Chem.* 1968, **360,** 137.
4. V. V. Skopenko, Yu. L. Zub, V. F. Bolelij and H. Köhler, *Koord. Khim.* (Moscow) 1984, **10,** 1317.
5. E. Fritsch, K. Polborn, K. Sünkel, H. Köhler, L. Jäger and W. Beck, *Z. Anorg. Allg. Chem.* 1992, **617,** 110.
6. C. Tretner, L. Jäger, J. Kožíšek, M. Hvastijová and K. Sünkel, *Current Trends in Coordination Chemistry* (Edited by G. Ondrejovič and A. Sirota), p. 347. Slovak Technical University Press, Bratislava (1995).
7. M. Hvastijová, J. Kohout, D. Kováčová and R. Skirl, *Collect. Czech. Chem. Commun.* 1994, **59,** 2611.
8. M. Hvastijová, J. Kožíšek, J. Kohout and L. Jäger, *J. Coord. Chem.* 1995, **36,** 195.
9. H. Köhler, *Chemistry of Pseudohalides* (Edited by A. M. Golub, H. Köhler and V. V. Skopenko), p. 434. Elsevier, Amsterdam (1986).
10. J. Mroziński, M. Hvastijová and J. Kohout, *Polyhedron* 1992, **11,** 2867.
11. M. Hvastijová, J. Kožíšek, J. Kohout, L. Jäger and H. Fuess, *Trans. Met. Chem.* 1995, **20,** 276.
12. N. Walker and D. Stuart, *Acta Cryst.* 1983, **A39,** 158.
13. G. M. Sheldrick, *Acta Cryst.* 1990, **A46,** 467.
14. G. M. Sheldrick, *SHELXL93. Program for the Refinement of Crystal Structures.* University of Göttingen, Germany (1993).
15. M. Nardelli, *Comput. Chem.* 1983, **7,** 95.
16. Supplementary material, Tables 1–6.
17. M. Hvastijová, J. Kohout, J. Mroziński and L. Jäger, *Polish J. Chem.* 1995, **69,** 952.
18. C. K. Johnson, "ORTEPII", Report ORNL-3794, Oak Ridge National Laboratory, Tennessee (1971).
19. M. Hvastijová, J. Kohout, M. Okruhlica, J. Mroziński and L. Jäger, *Trans. Met. Chem.* 1993, **18,** 579.
20. J. Kohout, M. Hvastijová and J. Mroziński, *J. Mol. Struct.* 1984, **116,** 211.
21. H. Köhler, A. Kolbe and G. Lux, *Z. Anorg. Allg. Chem.* 1977, **428,** 103.
22. J. Reedijk, *Trans. Met. Chem.* 1981, **6,** 195.
23. B. J. Hathaway and D. E. Billing, *Coord. Chem. Rev.* 1970, **5,** 143.
24. D. E. Billing and A. E. Underhill, *J. Inorg. Nucl. Chem.* 1968, **30,** 2147.
25. B. J. Hathaway, *J. Chem. Soc., Dalton Trans.* 1972, 1196.
26. M. R. Grimmet, *Comprehensive Heterocyclic Chemistry*, Vol. 5, p. 383. Pergamon Press, Oxford (1984).

27. A. B. P. Lever, *Inorganic Electronic Spectroscopy*, 2nd ed., p. 507. Elsevier, Amsterdam (1984).
28. J. Kožíšek, M. Hvastijová, J. Kohout, J. Mroziński and H. Köhler, *J. Chem. Soc., Dalton Trans.* 1991, 1773.
29. See Reference 27, p. 480.
30. H. Köhler and G. Lux, *Inorg. Nucl. Chem. Lett.* 1968, **4,** 133.
31. J. Mroziński, J. Kohout and M. Hvastijová, *Polyhedron* 1989, **8,** 157.
32. B. N. Figgis, M. Gerloch, J. Lewis, F. E. Mabbs and G. A. Webb, *J. Chem. Soc. A.* 1968, 2086.

Pergamon

PII: S0277-5387(96)00287-2

Polyhedron Vol. 16, No. 3, pp. 473–479, 1997
Copyright © 1996 Elsevier Science Ltd
Printed in Great Britain. All rights reserved
0277-5387/97 $17.00+0.00

Chiral quadruple-bonded dimolybdenum complexes containing chelating diphosphine ligands; structural and chiroptical properties of α-Mo_2Cl_4[(R,R)-Me-DuPHOS]$_2$ and α-Mo_2Cl_4[(S,S)-Me-DuPHOS]$_2$, where Me-DuPHOS is 1,2-bis(2,5-dimethylphospholano)benzene

Chang-Tai Lee,[a] Jhy-Der Chen,[a]* Yui Whei Chen-Yang,[a] Lin-Shu Liou[b] and Ju-Chun Wang[b]

[a]Department of Chemistry, Chung-Yuan Christian University, Chung-Li, Taiwan, R.O.C.

[b]Department of Chemistry, Soochow University, Taipei, Taiwan, R.O.C.

(Received 25 April 1996; accepted 5 June 1996)

Abstract—The complexes α-Mo_2Cl_4[(R,R)-Me-DuPHOS]$_2$, **1**, and α-Mo_2Cl_4[(S,S)-Me-DuPHOS]$_2$, **2**, were prepared by reactions of $(NH_4)_5Mo_2Cl_9$ with (R,R)-Me-DuPHOS and (S,S)-Me-DuPHOS, respectively, in methanol. Their UV–vis and circular dichroism spectra have been recorded and the X-ray crystal structure of **1** has been determined. The chiral disphosphine ligands are chelated to the metal centers with an average twist angle of 5.2° about the metal–metal bond in the clockwise direction. The absorption spectra are typical for compounds with a Mo—Mo quadruple bond. The lowest energy bands at 690 nm for both **1** and **2** can be assigned to $\delta_{xy} \rightarrow \delta_{xy}^*$ transitions. The CD spectra of both ccomplexes **1** and **2** show two prominent bands at 695 and 520 nm and form mirror images of each other. Copyright © 1996 Elsevier Science Ltd

Keywords: quadruple bond; chelating diphosphine; circular dichroism; twist angle; chirality; CD sign rule.

Dimetallic complexes of the type $Mo_2X_4(PP)_2$, where PP is a disphosphine ligand and X is Cl, Br or I, have been extensively studied during recent years [1]. All the molecules of this type have d^4–d^4, Mo_2^{4+} moieties with two phosphorus atoms and two halogen atoms ligating to each of the molybdenum atoms. This type of complex can exist in two isomeric forms, i.e., α (chelating) and β (bridging), as shown in Fig. 1. In the α isomer the two phosphorus atoms of the same disphosphine ligands are coordinated to the same molybdenum metal centers, the chelate rings are *trans* to each other and the ligators are eclipsed. In the β isomer the similar atoms are disposed *trans* to each other and the two *trans* MoX_2P_2 units are rotated about the Mo—Mo quadruple bond such that the Mo—P (or the Mo—X) bond in one unit may or may not eclipse the Mo—P (or the Mo—X) bond in the other. Thus

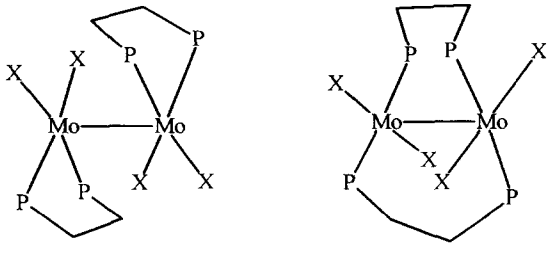


Fig. 1. Schematic drawing of the α (left) and β (right) isomer of an $Mo_2X_4(PP)_2$ compound.

*Author to whom correspondence should be addressed.

the torsional angle (P—Mo—Mo—P) may have any value $\geqslant 0°$.

Two types of chiral complexes of the form $Mo_2X_4(PP)_2$ have been structurally characterized. The first type has "class I" chromophores [2], that is, inherently chiral chromophores, and their CD spectra can be explained by the CD sign rule (Fig. 2) [3], which has been verified with the syntheses and structural characterization of the complexes, β-Mo_2X_4[(S,S)-dppb]$_2$ (X = Cl or Br) [4], β-Mo_2Cl_4[(S,S)-diop]$_2$ and β-Mo_2Cl_4[(R,R)-diop]$_2$ [5]. The other type of chiral complex has "class II" chromophores, [2] that is, an intrinsically achiral chromophore that displays chiroptical effects through perturbation by chiral surroundings. The chiral complex β-Mo_2Cl_4[(S,S)-dppm]$_2$ [6], which has an approximately 0° torsional angle, appears to belong to this category. The one-electron static coupling mechanism was invoked to explain the CD spectrum for this complex.

Here we report the first structurally characterized complexes that contain chiral, chelating disphosphine ligands and quadruply bonded chromophores. The preparation, structure, and optical activity of these chiral complexes form the subject of this report.

EXPERIMENTAL

General procedures

All manipulations were carried out under dry, oxygen-free nitrogen by using Schlenk techniques, unless otherwise noted. Solvents were dried and deoxygenated by refluxing over the appropriate reagents before use. Methanol was purified by distillation from magnesium, *n*-hexane from sodium/benzophenone, and dichloromethane from P_2O_5. The Visible absorption spectra were recorded on a Hitachi U-2000 spectrophotometer. The Circular Dichroism (CD) spectra were recorded on an Aviv 62A DS spectrometer. The NMR spectrum was recorded on a Bruker 200 MHz NMR spectrometer.

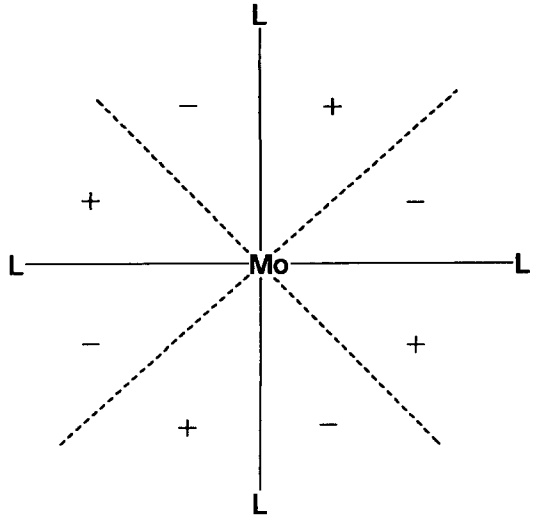


Fig. 2. Sector diagram for the $\delta_{xy} \rightarrow \delta^*_{xy}$ transition of a chiral $Mo_2L_nL'_{8-n}$ complex (CD sign rule).

Starting material

The complex $(NH_4)_5Mo_2Cl_9$ was prepared according to a previously reported procedure [7]. The reagents 1,2-bis[(2R,5R)-2,5-dimethylphospholano] benzene, (R,R)-Me-DuPHOS, and 1,2-bis[(2S,5S)-2,5-dimethylphospholano]benzene, (S,S)-Me-Du PHOS, were purchased from Strem Chemical Co.

Preparation of α-Mo_2Cl_4[(R,R)-Me-DuPHOS]$_2$ *and* α-Mo_2Cl_4[(S,S)-Me-DuPHOS]$_2$.

$(NH_4)_5Mo_2Cl_9$ (0.10 g, 0.16 mmol) and (R,R)-Me-DuPHOS or (S,S)-Me-DuPHOS (0.10 g, 0.33 mmol) were placed in a flask containing 15 cm^3 CH_3OH. The mixture was then stirred at room temperature for 3 h to yield a yellow–green solid and a yellow–green solution. The yellow–green product was filtered, washed by CH_3OH and ether and then dried under reduced pressure. Yield: 0.035 g (34.40%) for **1** and 0.051 g (50.20%) for **2**. Uv–vis: 675 nm in CH_2Cl_2 and 690 nm in THF. $^{31}P\{^1H\}$-NMR ($CDCl_3$): 63.65 (d, $J_{P\text{-}P}$ = 10.74 Hz, 63.49 (d, $J_{P\text{-}P}$ = 10.74 Hz) ppm.

X-ray crystallography

The diffraction data of α-Mo_2Cl_4[(R,R)-Me-DuPHOS]$_2$ were collected on a Siemens P4 diffractometer at 25°C, which was equipped with graphite-monochromated Mo—K_α (λ_α = 0.71037 Å) radiation. Data reduction was carried out by standard methods with use of well-established computational procedures [8]. Basic information pertaining to crystal parameters and structure refinement is summerized in Table 1. Table 2 lists selected bond distances and angles.

A yellow–green crystal of α-Mo_2Cl_4[(R,R)-Me-DuPHOS]$_2$ was mounted on the top of a glass fiber with epoxy cement. The unit cell constants were determined from 25 reflections with 2θ in the range from 24 to 27°. These were consistent with the monoclinic crystal system, and the space group was subsequently determined to be $P2_1$ from the systematic absences.

Routine $\theta-2\theta$ data collection was used to scan a possible 8516 data points in the range $4 < 2\theta < 50°$. The structure factors were obtained after Lorentz and polarization correlations. Empirical absorption based on azimuthal (ψ) scans of reflections of Eulerian angle χ near 90° were applied to the data. The positions of heavy atoms, including two molybdenum atoms, were located by direct methods. The remaining atoms were found in a series of alternating difference Fourier maps and least-square refinements. Anisotropic thermal parameters were used for all the atoms except the

Table 1. Crystal data for α-Mo_2Cl_4[(R,R)-Me-DuPHOS]$_2$ ·CH_2Cl_2

Formula	$Mo_2Cl_6P_4C_{37}H_{58}$
fw	1031.3
Space group	$P2_1$
a (Å)	10.675(1)
b (Å)	19.630(2)
c (Å)	10.952(1)
β ( )	104.790(0)
V (Å^3)	2219.0(4)
Z	2
d_{calc} (g cm^{-3})	1.544
Cryst size (mm)	0.4 × 0.4 × 0.5
μ (Mo-K_α) (mm^{-1})	1.097
Radiation monochromated in incident beam (*λ*Mo-K_α) (Å)	0.71073
Orientation reflections no.; range (2*θ*) ( )	25; 24 < 2*θ* < 27
Scan method	*θ*–2*θ*
Data Collection range (2*θ*) ( )	4 < 2*θ* < 50
No. of unique data	7815
No. of observed data	6884
Criterion for observed	$F > 4.0\sigma(F)$
No. of parameters refined	443
R^a	0.0340
R_w^b	0.0375
Quality-of-fit indicator^c	1.05
Largest shift/esd, final cycle	0.001
Largest peak (e Å^3)	1.03

$^aR = \Sigma \| F_o \| - \| F_c \| / \Sigma |F_o|$.
$^bR_w = [\Sigma w(|F_o| - |F_c|)^2 / \Sigma w|F_o|^2]^{1/2}$. $w = 1/[\sigma^2(F_o) + gF_o^2]$.
^{c}Quality-of-fit $= [\Sigma w(|F_o| - |F_c|)^2 / N_{observed} - N_{parameters})]^{1/2}$.

hydrogen atoms. The positions of the hydrogen atoms were fixed as riding models during the least-square refinements. The final residuals of the first refinement were $R = 0.0340$, $Rw = 0.0375$ and $S = 1.05$ with a (R,R) configuration for the ligands. An inversion of coordinates was made and the structure was refined to convergence with $R = 0.035$, $Rw = 0.039$ and $S = 1.09$. The results clearly confirmed that the (R,R) isomer was indeed correct. The reported *R* values for the structure [(COD)Rh((S,S)-Me-DuPHOS)]SbF_6 were $R = 0.046$ and $Rw = 0.035$ while its (R,R)-enantiomorph refined to $R = 0.049$ and $Rw = 0.039$ [9].

RESULTS AND DISCUSSION

Syntheses and structures

The yellow-green title complexes α-Mo_2Cl_4[(R,R)-Me-DuPHOS]$_2$, **1**, and α-Mo_2Cl_4[(S,S)-Me-DuPHOS]$_2$, **2**, were prepared by reactions of $(NH_4)_5Mo_2Cl_9$ with (R,R)-Me-DuPHOS and (S,S)-Me-DuPHOS, respectively in methanol. Crystals suitable for X-ray diffraction measurement were obtained by hexane-induced crystallization from a dichloromethane solution. The crystal of **1** conforms to the space group $P2_1$ with two molecules in the unit cell. Figure 3 shows the ORTEP diagram for **1**. It is seen from Fig. 1 that each molybdenum atom is coordinated with two chlorine atoms and two phosphorus atoms. The two phosphine ligands are chelated to the Mo centers to form five-membered rings. The achiral phosphorus atom of the free phosphine ligands become chiral upon coordination to the molybdenum atoms. The 1,2-phenylene unit remains essentially planar upon coordination of the phospholane moieties. However, in contrast to the slight (5.95) dihedral twist out of the P—Rh—P plane in the complex [(COD)Rh((S,S)-Me-DuPHOS)]SbF_6 [9], a large (average 25.8) dihedral twist out of the P—Mo—P plane is observed for **1**. The Mo—Mo bond distance of 2.147(1) Å for **1** is similar to those observed in α-Mo_2Cl_4(dppe)$_2$ (2.140(2) Å) [10], *anti*-α-Mo_2Cl_4(dpdt)$_2$ (2.147(1) Å) [11], and *anti*-α-Mo_2Cl_4(dpdbp)$_2$ (2.149(1) Å) [12]. Table 3 lists the important bond distances and angles for some structurally characterized quadruply-bonded complexes with chelating disphosphine ligands. It is noted that the average Mo—P bond distance is shorter for complex **1**, which indicate that Duphos ligands chelate the molybdenum atoms better than the other disphosphine ligands which possess two aryl substituents on phosphorus atoms. Complex **1** is the first structurally characterized compound of the type $Mo_2X_4(PP)_2$ in which the P in the free ligand is a cyclophosphine.

Figure 4 shows a view of the inner part of **1** looking down the Mo—Mo bond. It is seen that the twist includes the low Cl(1)—Mo(1)—Mo(2)—P(3) and P(1)—Mo(1)—Mo(2)—Cl(3), 3.3 and 5.6 , respectively, in counterclockwise direction and the high Cl(2)—Mo(1)—Mo(2)—P(2) and P(2)—Mo(1)—Mo(2)—Cl(4), 17.7 and 12.0 , respectively, in clockwise direction. The average value (χav) is taken as $\chi_{av} = 1/4(\chi_1 + \chi_2 + \chi_3 + \chi_4)$, where χ_1–χ_4 are the four smallest angles looking down the Mo—Mo bond, and is found to be 5.2 in the clockwise direction.

Absorption spectra

The absorption spectra (Fig. 5) are typical for compounds with a Mo—Mo quadruple bond. The lowest energy bands at 690 nm in THF solvent (675 nm in CH_2Cl_2) can be assigned to $\delta_{xy} \rightarrow \delta^*_{xy}$ transitions. The second lowest energy bands appear at 503 nm and can most probably be assigned to the forbidden transition $\delta_{xy} \rightarrow \delta_{x^2-y^2}$. The absorption energy of the lowest energy band is similar to those of the structurally characterized chelating complexes, i.e., 677 nm for α-Mo_2Cl_4(dppe)$_2$ [10], 675 nm for *anti*-α-Mo_2Cl_4(dpdt)$_2$ [11], and 669 nm for *anti*-α-Mo_2Cl_4(dpdbp)$_2$ [12].

CD spectrum

Figure 6 shows the CD spectra for **1** and **2** in THF solvent. It is seen that the phases of the CD bands

Table 2. Selected bond distances (Å) and angles (°) for α-Mo_2Cl_4[(R,R)-Me-DuPHOS]$_2$ ·CH_2Cl_2

Mo(1)—Mo(2)	2.147(1)	Mo(1)—Cl(1)	2.421(2)
Mo(1)—Cl(2)	2.408(2)	Mo(1)—P(1)	2.513(1)
Mo(1)—P(2)	2.519(2)	Mo(2)—Cl(3)	2.422(1)
Mo(2)—Cl(4)	2.422(2)	Mo(2)—P(3)	2.547(2)
Mo(2)—P(4)	2.529(1)	P(1)—C(2)	1.857(7)
P(1)—C(5)	1.868(7)	P(1)—C(7)	1.825(6)
P(2)—C(12)	1.823(5)	P(2)—C(14)	1.898(7)
P(2)—C(17)	1.866(7)	P(3)—C(20)	1.871(6)
P(3)—C(23)	1.891(7)	P(3)—C(25)	1.817(5)
P(4)—C(30)	1.828(6)	P(4)—C(32)	1.870(7)
P(4)—C(35)	1.863(7)		

Mo(2)—Mo(1)—Cl(1)	108.5(1)	Mo(2)—Mo(1)—Cl(2)	116.0(1)
Cl(1)—Mo(1) —Cl(2)	89.6(1)	Mo(2)—Mo(1)—P(1)	104.6(1)
Cl(1)—Mo(1)—P(1)	86.5(1)	Cl(2)—Mo(1)—P(1)	138.1(1)
Mo(2)—Mo(1)—P(2)	98.2(1)	Cl(1)—Mo(1)—P(2)	151.0(1)
Cl(2)—Mo(1)—P(2)	88.6(1)	P(1)—Mo(1)—P(2)	75.9(1)
Mo(1)—Mo(2)—Cl(3)	108.7(1)	Mo(1)—Mo(2)—Cl(4)	114.8(1)
Cl(3)—Mo(2)—Cl(4)	86.7(1)	Mo(1)—Mo(2)—P(3)	102.4(1)
Cl(3)—Mo(2)—P(3)	85.0(1)	Cl(4)—Mo(2)—P(3)	142.6(1)
Mo(1)—Mo(2)—P(4)	100.5(1)	Cl(3)—Mo(2)—P(4)	148.0(1)
Cl(4)—Mo(2)—P(4)	92.8(1)	P(3)—Mo(2)—P(4)	76.0(1)
Mo(1)—P(1)—C(2)	123.5(2)	Mo(1)—P(1)—C(5)	112.2(2)
C(2)—P(1)—C(5)	93.0(3)	Mo(1)—P(1)—C(7)	108.9(2)
C(2)—P(1)—C(7)	112.7(3)	C(5)—P(1)—C(7)	104.0(3)
Mo(1)—P(2)—C(12)	108.1(2)	Mo(1)—P(2)—C(14)	112.1(3)
C(12)—P(2)—C(14)	103.5(3)	Mo(1)—P(2)—C(17)	127.7(2)
C(12)—P(2)—C(17)	107.9(3)	C(14)—P(2)—C(17)	94.7(3)
Mo(2)—P(3)—C(20)	117.5(2)	Mo(2)—P(3)—C(23)	118.5(3)
C(20)—P(3)—C(23)	93.8(3)	Mo(2)—P(3)—C(25)	108.8(2)
C(20)—P(3)—C(25)	114.5(3)	C(23)—P(3)—C(25)	102.6(3)
Mo(2)—P(4)—C(30)	108.4(2)	Mo(2)—P(4)—C(32)	103.8(2)
C(30)—P(4)—C(32)	107.1(3)	Mo(2)—P(4)—C(35)	137.5(2)
C(30)—P(4)—C(35)	106.2(3)	C(32)—P(4)—C(35)	88.7(3)

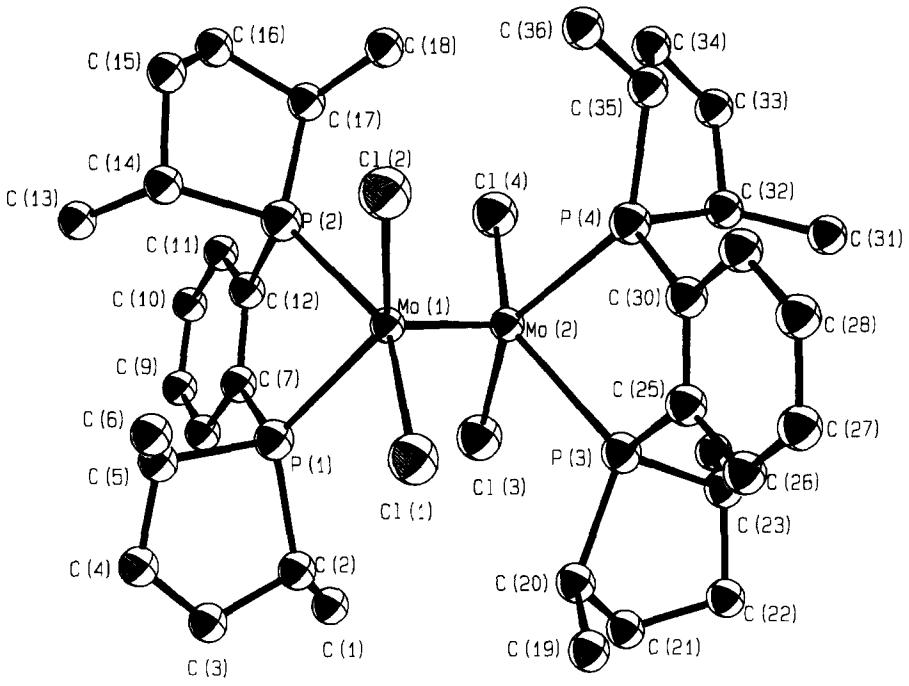


Fig. 3. ORTEP drawing of α-Mo_2Cl_4[(R,R)-Me-DuPHOS]$_2$ in its entirety.

under the $\delta_{xy} \rightarrow \delta^*_{xy}$ transition (695 nm) and $\delta_{xy} \rightarrow \delta_{x^2-y^2}$ transition (520 nm) of one complex are opposite to each other. It is also clearly seen that there is a mirror-image relationship between the spectra of the enantiomeric molecules **1** and **2**. This is expected since the ligands of the enantiomeric pair have opposite conformational preference that they produce isomers with opposite chiralities.

The previous discussion about the relationship between the absolute chirality of a twisted $Mo_2L_nL'_{8-n}$ molecule and the sign of the CD band for the $\delta_{xy} \rightarrow \delta^*_{xy}$ transitions can be summarized in a sector diagram as shown in Fig. 2. The CD sign rule predicts that the sign of the CD band under the $\delta_{xy} \rightarrow \delta^*_{xy}$ transitions of the conformer with $0 < \theta < 45°$ are opposite to those with $45 < \theta < 90°$ and the signs of the $\delta_{xy} \rightarrow \delta^*_{xy}$ transitions are opposite to those of $\delta_{xy} \rightarrow \delta_{x^2-y^2}$ transitions. According to the CD sign rule, complex **1** should show a positive sign for the $\delta_{xy} \rightarrow \delta^*_{xy}$ transitions. However, both the solution sample

Table 3. Some important bond distances and angles for **1**, anti-α-$Mo_2Cl_4(dpdt)_2$, **3**, α-$Mo_2Cl_4(dppe)_2$, **4** and anti-α-$Mo_2Cl_4(dpdbt)_2$, **5**

Complex	Mo—P	P—Mo—P	Mo—Mo—P	Cl—Mo—P
1	2.513 (1)	75.9 (1)	98.2 (1)	86.5 (1), 88.6 (1)
	2.519 (2)	76.1 (1)	100.5 (1)	85.0 (1), 92.8 (1)
	2.529 (1)		104.6 (1)	138.1 (1), 151.0 (1)
	2.547 (2)		102.4 (1)	142.6 (1), 148.0 (1)
3	2.547 (3)	74.82 (9)	98.53 (6)	92.45 (9), 146.69 (8)
	2.534 (3)		101.50 (6)	140.01 (8), 87.7 (9)
4	2.544 (4)	74.8 (2)	101.0 (1)	147.5 (2), 90.4 (2)
	2.553 (5)		100.0 (1)	88.4 (1), 147.4 (1)
5	2.550 (3)	74.74 (9)	99.85 (8)	92.45 (9), 146.69 (8)
	2.551 (3)		101.72 (7)	140.01 (8), 87.7 (9)

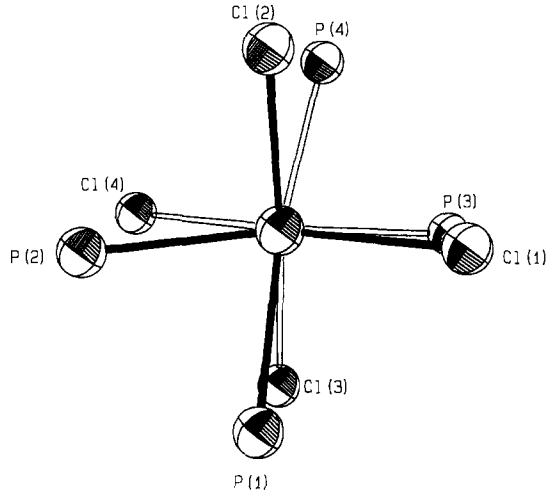


Fig. 4. View looking down the Mo—Mo bond for α-Mo_2Cl_4[(R,R)-Me-DuPHOS]$_2$.

prepared by dissolving the powders of complex **1** or **2** in THF solvents and the solid sample obtained by mulling powders as KBr disks displayed negative CD signs for the $\delta_{xy} \rightarrow \delta^*_{xy}$ transition, as shown in Fig. 6 for the solution spectra. It is noted that the average twist angle of about 5.2° in the clockwise direction is derived by taking the average of the four smallest angles looking down the Mo—Mo bond. Among the four angles there are two in the clockwise direction and the other two in the counterclockwise direction, which were observed in the crystal. Since the α-form complexes have no ligand constraints that limit the rotation of the Mo—Mo metal bond as β-form complexes, it is possible that the configuration and magnitude of the average twist angles in solution and in solid are not the same as that obtained in the crystal. The CD spectra of the crystals were not measured since a large amount of crystal was not available. It is safe to say that the twist angles of complexes **1** and **2** are still small (less than about 5°) in the solution. This can be verified by the fact that the g values ($g = 2R/D$ or $\Delta\varepsilon/\varepsilon$), which can be related to the twist angle by the equation $g = g_{max} \tan 2\theta$ [3], for the corresponding $\delta_{xy} \rightarrow \delta^*_{xy}$ transitions are about 2.4×10^{-4} and 9.2×10^{-4} for **1** and **2**, respectively in THF solvent. These are the smallest g values measured for quadruply-bonded complexes in the solution state. For example the g value for the complex [4] Mo_2Cl_4[(S,S)-dppb]$_2$ which has a twist angle of 22° is 5.8×10^{-3}. It is also noted that the g values for $\delta_{xy} \rightarrow \delta_{x^2-y^2}$ transition (4.9×10^{-3} and 9.1×10^{-3} for complexes **1** and **2**, respectively) are approximately an order of magnitude larger than those for the corresponding $\delta_{xy} \rightarrow \delta^*_{xy}$ transitions. The chelated complexes α-Mo_2Cl_4(S-chairphos)$_2$ and α-Mo_2Cl_4(R-dppp)$_2$ were reported to show no measurable CD spectra under either the $\delta_{xy} \rightarrow \delta^*_{xy}$ or $\delta_{xy} \rightarrow \delta_{x^2-y^2}$ transitions [3].

Supplementary material available

Atomic coordinates, bond distances, bond angles, anisotropic thermal parameters, H-atoms coordinates; torsion angles and a computer listing showing cell dimensions and symmetry operations. (8 pages); a listing of observed and calculated structural factors (18 pages).

Acknowledgement—The researchers wish to thank the National Science Council of the Republic of China for support.

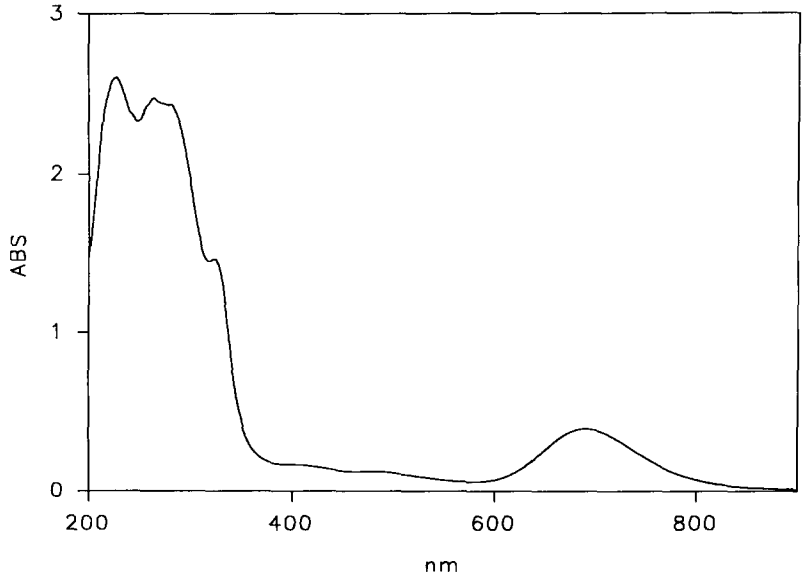


Fig. 5. UV-vis spectra of α-Mo_2Cl_4[(R,R)-Me-DuPHOS]$_2$ in THF.

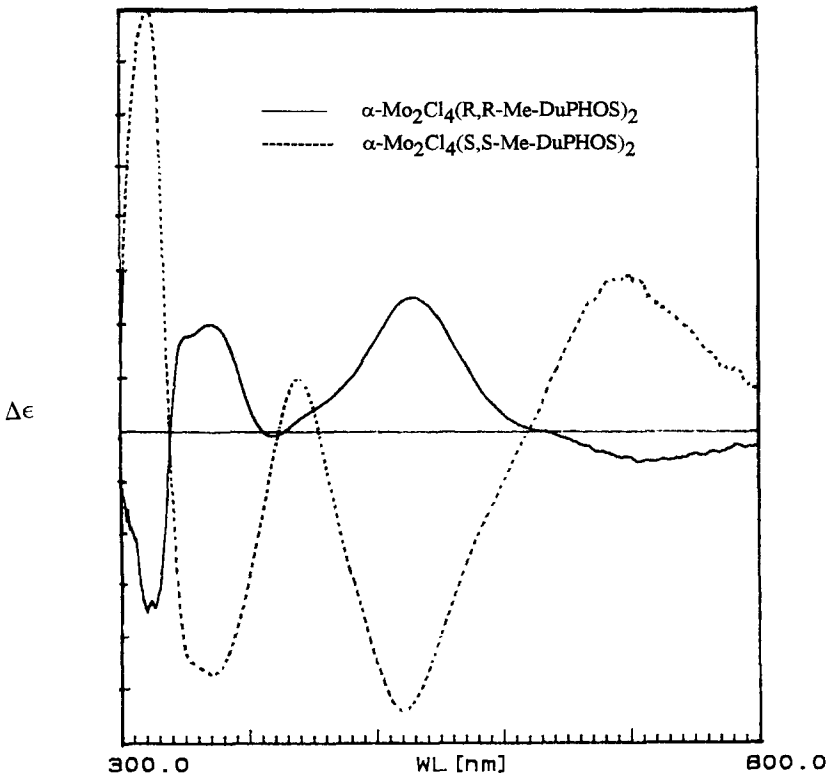


Fig. 6. CD spectra of α-Mo_2Cl_4[(R,R)-Me-DuPHOS]$_2$ and α-Mo_2Cl_4[(S,S)-Me-DuPHOS]$_2$ in THF.

REFERENCES

1. F. A. Cotton and R. A. Walton, *Multiple Bonds Between Metal Atoms*, 2nd ed. Oxford University Press, London (1993).
2. A. Moscowitz, *Tetrahedron* 1961, **13,** 48.
3. R. D. Peacock, *Polyhedron* 1987, **6,** 715.
4. P. A. Agaskar, F. A. Cotton, I. F. Fraser, M. M. Ljubica, K. W. Muir and R. D. Peacock, *Inorg. Chem.* 1986, **25,** 2511.
5. J.-D. Chen, F. A. Cotton and R. L. Falvello, *J. Am. Chem. Soc.* 1990, **112,** 1076.
6. J.-D. Chen and F. A. Cotton, *Inorg. Chem.* 1990, **29,** 1797.
7. J. V. Breneic and F. A. Cotton, *Inorg. Chem.* 1970, **9,** 351.
8. G. M. Sheldrick, *SHELXTL PLUS, Release* 4.1. Siemens Analytical X-ray Instruments Inc., Karlsruhe, Germany (1991).
9. M. J. Burk, M. J. E. Feaster, W. A. Nugent and R. L. Harlow, *J. Am. Chem. Soc.* 1993, **115,** 10125.
10. P. A. Agaskar and F. A. Cotton, *Inorg. Chem.* 1986, **25,** 15.
11. F. A. Cotton and S. Kitagawa, *Inorg. Chem.* 1987, **26,** 3463.
12. F. A. Cotton and S. Kitagawa, *Polyhedron* 1988, **7,** 463.

Pergamon

PII: S0277-5387(96)00285-9

Polyhedron Vol. 16, No. 3, pp. 481–487, 1997
Copyright © 1996 Elsevier Science Ltd
Printed in Great Britain. All rights reserved
0277-5387/97 $17.00+0.00

Synthesis and characterization of sulfur/iron/molybdenum (tungsten) cluster compounds containing functionally substituted cyclopentadienyl ligand. Single crystal structure of $[(\eta^5\text{-}MeO_2CC_5H_4)_2(\mu_3\text{-}CO)_2Mo_2Fe_2(\mu_3\text{-}S)_2(CO)_6]$

Li-Cheng Song,* Ji-Quan Wang, Qing-Mei Hu, Wen-Qi Gao and Bing-Song Han

Department of Chemistry, Nankai University, Tianjin 300071, P. R. China

(Received 27 March 1996; accepted 5 June 1996)

Abstract—Reaction of μ-$S_2Fe_2(CO)_6$ with Mo≡Mo triply bonded dimers $[\eta^5\text{-}RC_5H_4(CO)_2Mo]_2$ in CH_2Cl_2 at room temperature gave clusters $[(\eta^5\text{-}RC_5H_4)_2(\mu_3\text{-}CO)_2Mo_2Fe_2(\mu_3\text{-}S)_2(CO)_6]$ (**1a**, R = MeCO; **1b**, R = MeO_2C; **1c**, R = EtO_2C), whereas μ-$S_2Fe_2(CO)_6$ reacted with W≡W triply bonded dimers $[\eta^5\text{-}RC_5H_4(CO)_2W]_2$ to afford the clusters $[(\eta^5\text{-}RC_5H_4)_2(\mu_3\text{-}CO)_2W_2Fe_2(\mu_3\text{-}S)_2(CO)_6]$ (**2a**, R = MeO_2C; **2b**, R = EtO_2C) and $[[\eta^5\text{-}RC_5H_4(CO)_2]_2W_2Fe(\mu_3\text{-}S)(CO)_3]$ (**3a**, R = MeO_2C; **3b**, R = EtO_2C). While clusters **1a–1c** could also be produced by reaction of μ-$S_2Fe_2(CO)_6$ with Mo—Mo singly bonded dimers $[\eta^5\text{-}RC_5H_4(CO)_3Mo]_2$ in refluxing toluene, the reaction with W—W singly bonded dimers $[\eta^5\text{-}RC_5H_4(CO)_3W]_2$ failed to give the corresponding dimers **2a–2b** and **3a–3b**. In addition, cluster **1a** reacted with $NaBH_4$ in MeOH at room temperature to give the bis-hydroxyl derivative $[[\eta^5\text{-}MeCH(OH)C_5H_4]_2(\mu_3\text{-}CO)_2Mo_2Fe_2(\mu_3\text{-}S)_2(CO)_6]$ (**4**), whereas it afforded mono- and bis-hydrazone derivatives $[(\eta^5\text{-}MeCOC_5H_4)\ [\eta^5\text{-}2,4\text{-}(NO_2)_2C_6H_3NHNC(Me)C_5H_4](\mu_3\text{-}CO)_2Mo_2Fe_2(\mu_3\text{-}S)_2(CO)_6]$ (**5**) and $[[\eta^5\text{-}2,4\text{-}(NO_2)_2C_6H_3NHNC(Me)C_5H_4]_2(\mu_3\text{-}CO)_2Mo_2Fe_2(\mu_3\text{-}S)_2(CO)_6]$ (**6**) when reacted with 2,4-dinitrophenylhydrazine in EtOH at room temperature. All the new clusters were characterized by elemental analysis and spectroscopic methods, as well as for **1b** by X-ray diffraction techniques. Copyright © 1996 Elsevier Science Ltd

Keywords: group 6 metal–metal bonds; μ-$S_2Fe_2(CO)_6$; reactions; Fe/S/Mo (W) clusters; crystal structure.

In recent years there has been growing interest in group 6 metal/iron/sulfur clusters. This is most likely due to (i) the fact that some important biological systems contain such cluster cores, e.g. a Mo/Fe/S core in nitrogenase [1]; (ii) the potential applications of these clusters in hetero- and homogenous catalytic processes [2] and (iii) the novelty and diversity of the structures generated by means of various coordination modes of the sulfur atoms in the clusters [3]. So far, it has been reported that reactions of μ-$S_2Fe_2(CO)_6$ with group 6 metal–metal triply bonded dimers $[\eta^5\text{-}RC_5H_4(CO)_2M]_2$ (M = Mo, W; R = H, Me, M = Mo, R = MeO_2C) give a series of M/Fe/S cluster complexes [4–8], among which the clusters containing electron-withdrawing substituents on the cyclopentadienyl ring are little known. In order to prepare such interesting clusters, we carried out the reaction of μ-$S_2Fe_2(CO)_6$ with triply bonded dimers $[\eta^5\text{-}RC_5H_4(CO)_2M]_2$ or with singly bonded dimers $[\eta^5\text{-}RC_5H_4(CO)_3M]_2$ (M = Mo, W; R = electron-withdrawing functionality) and transformation reactions of functional substituents on cyclopentadienyl rings of some products. A preliminary account of the synthesis and structure of **1b** has been given [8]. Herein we further describe the detailed reaction procedures, the proper-

* Author to whom correspondence should be addressed.

ties and structural characterization of all the M/Fe/S clusters **1a–c, 2a–b** and **3a–b** obtained through this study.

RESULTS AND DISCUSSION

Synthesis and characterization of **1a–c, 2a–b** *and* **3a–b**

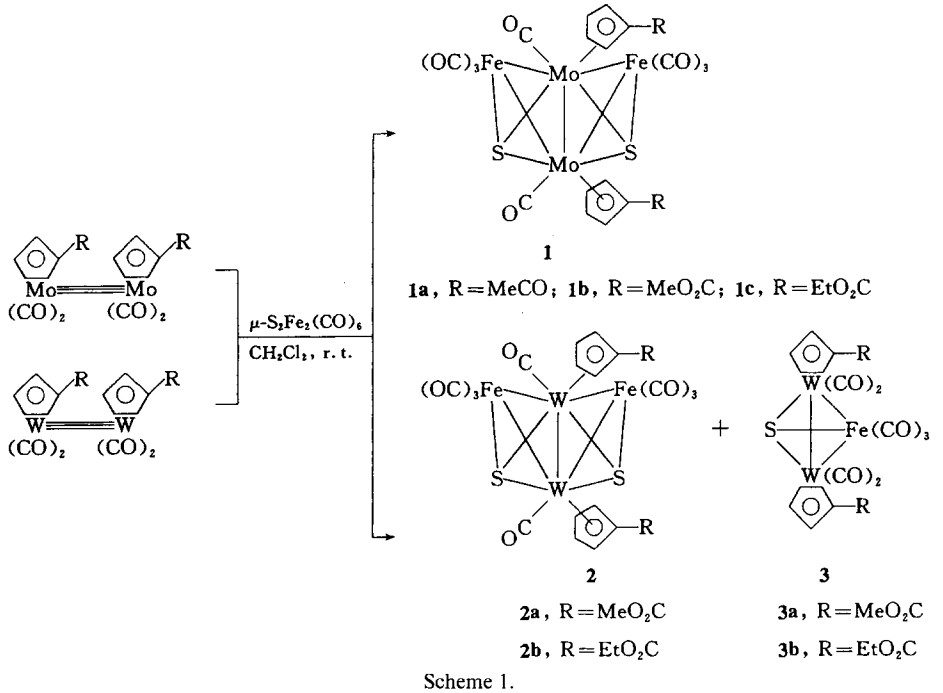
An equimolar amount of $[\eta^5\text{-}RC_5H_4(CO)_2Mo]_2$ reacted with $\mu\text{-}S_2Fe_2(CO)_6$ in CH_2Cl_2 at room temperature to give $Mo_2Fe_2S_2$ clusters $[(\eta_5\text{-}RC_5H_4)_2(\mu_3\text{-}CO)_2Mo_2Fe_2(\mu_3\text{-}S)_2(CO)_6]$ (**1a–c**), while the reaction of $[\eta^5\text{-}RC_5H_4(CO)_2W]_2$ gave $W_2Fe_2S_2$ clusters $[(\eta^5\text{-}RC_5H_4)_2(\mu_3\text{-}CO)_2W_2Fe_2(\mu_3\text{-}S)_2(CO)_6]$ (**2a–b**) and W_2Fe clusters $[[\eta^5\text{-}RC_5H_4(CO)_2]_2W_2Fe(\mu_3\text{-}S)(CO)_3]$ (**3a–b**) (Scheme 1).

Among these cluster compounds while **3a** was previously reported [9], **1a–c, 2a–b** and **3b** are new. Their formulation has been characterized by elemental analysis (for **2a** the satisfactory C/H analysis could not be obtained but FD mass spectroscopy gave its parent ion peak at *m/z* 1014) and by spectroscopic methods. Their IR spectra displayed three kinds of carbonyl absorption bands, one $\nu_{(CO)}$ band in the range of 1680–1721 cm^{-1} attributed to the carbonyls of the organic substituents, another $\nu_{(CO)}$ band between 1803–1844 cm^{-1} due to the semibridging carbonyls bonded to Mo or W atoms, and the third $\nu_{(CO)}$ consisting of three to four absorption bands in the range of 1893–2057 cm^{-1} attributed to the terminal carbonyls attached to iron atoms. The ^1H NMR spectra of **1a–c** and **2b** showed two apparent triplets at δ 5.07–6.16 ppm, while that of **2a** exhibited two broad singlets centered at δ 5.50 and δ 5.80 ppm. The downfield triplet or singlet was assigned to H^2 and H^5 close to the substituent of cyclopentadienyl ring and the upfield one to H^3 and H^4 remote from the substituent, since the substituents in cyclopentadienyl rings are electron-withdrawing [10]. Similar to **3a** [9], the four protons H^2—H^5 of **3b** showed two broad singlets upfield attributed to H^3 and H^4, and one multiplet downfield to H^2 and H^5.

As we know, the triply bonded dimers $[\eta^5\text{-}RC_5H_4(CO)_3M]_2$(M = Mo, W) were prepared by thermolysis of the corresponding singly bonded dimers $[\eta^5\text{-}RC_5H_4(CO)_3M]_2$. In order to make the synthetic procedures for those M/Fe/S clusters more convenient, we carried out the reactions of $\mu\text{-}S_2Fe_2(CO)_6$with the singly bonded dimers directly. As a result, the reaction of Mo—Mo singly bonded dimers $[\eta^5\text{-}RC_5H_4(CO)_3Mo]_2$ (R = MeCO, MeO_2C, EtO_2C) with $\mu\text{-}S_2Fe_2(CO)_6$ in toluene at reflux produced **1a–c** in 18%, 11% and 6% yield, respectively, whereas that of W—W singly bonded dimers $[\eta^5\text{-}RC_5H_4(CO)_3W]_2$ (R = MeO_2C, EtO_2C) did not give any isolable corresponding W/Fe/S cluster complexes.

Synthesis and characterization of **4–6**

On the basis of synthesis of the above functionally substituted cyclopentadienyl compounds, an effort has been made to prepare their derivatives through transformation reactions of their functional substituents on cyclopentadienyl rings. It was found that **1a** reacted with $NaBH_4$ in MeOH at room temperature for 3 h to afford the hydroxyl derivative $[\eta^5$-



Scheme 1.

$MeCH(OH)C_5H_4]_2(\mu_3\text{-}CO)_2Mo_2Fe_2(\mu_3\text{-}S)_2(CO)_6$ (**4**) in 78% yield, whereas its reaction with 2,4-dinitro phenylhydrazine at room temperature gave rise to corresponding mono- and bis-hydrazone derivatives $[(\eta^5\text{-}MeCOC_5H_4)$ $[\eta^5\text{-}2,4\text{-}(NO_2)_2C_6H_3NHNC(Me)C_5H_4](\mu_3\text{-}CO)_2Mo_2Fe_2(\mu_3\text{-}S)_2(CO)_6]$ (**5**) and $[[\eta^5\text{-}2,4\text{-}(NO_2)_2C_6H_3NHNC(Me)C_5H_4]_2(\mu_3\text{-}CO)_2Mo_2Fe_2(\mu_3\text{-}S)_2(CO)_6]$ (**6**), as shown in Scheme 2.

Derivatives **4**–**6** are deep brown colored, air-stable solids. The combustion analyses for **4**–**6** coincide with their compositions. The IR spectrum of **4** exhibited a broad $\nu_{(OH)}$ band centred at 3400 cm^{-1}, a bridging $\nu_{(CO)}$ at 1803 cm^{-1} and four terminal $\nu_{(CO)}$ bands in the range of 1950–2041 cm^{-1}. The IR spectrum of **5** showed a $\nu_{(CO)}$ band of acyl group at 1671 cm^{-1}, a $\nu_{(C=N)}$ band at 1614 cm^{-1}, a bridging $\nu_{(CO)}$ band at 1794 cm^{-1} and five terminal $\nu_{(CO)}$ bands at 1816–2057 cm^{-1}, whereas that of **6** displayed a $\nu_{(C=N)}$ band at 1614 cm^{-1}, a bridging $\nu_{(CO)}$ band at 1844 cm^{-1} and three terminal $\nu_{(CO)}$ bands at 1893–2041 cm^{-1}. The ^1H NMR spectrum of **4** indicated the presence of the functionally substituted cyclopentadienyl ligand η^5-$MeCH(OH)C_5H_4$. However, the ^1H NMR pattern of H^2—H^5 of the cyclopentadienyl rings is quite complicated and overlaps with the α-protons of the functional substituents. This might be attributed to the influences of the chiral substituent CH(OH)Me generated through reduction of the acyl group. In the ^1H NMR spectrum of **5** there was a multiplet at δ 1.96–2.36 ppm attributed to methyl groups attached to C=O and C=N double bonds, whereas in that of **6** there was one singlet at δ 2.16 ppm assigned to the methyl group on the C=N double bond. For the ^1H NMR spectrum of the substituted cyclopentadienyls **5** showed one singlet downfield assigned to the protons close to two different substituents and one doublet upfield to those remote from two different substituents, whereas **6** exhibited two multiplets attributed to the protons close to and remote from two same substituents respectively. In addition, the ^1H NMR spectra of **5** and **6** all indicated the presence of other hydrogen atoms in the functionally substituted cyclopentadienyl ligand η^5-$2,4\text{-}(NO_2)_2C_6H_3NHNC(Me)C_5H_4$.

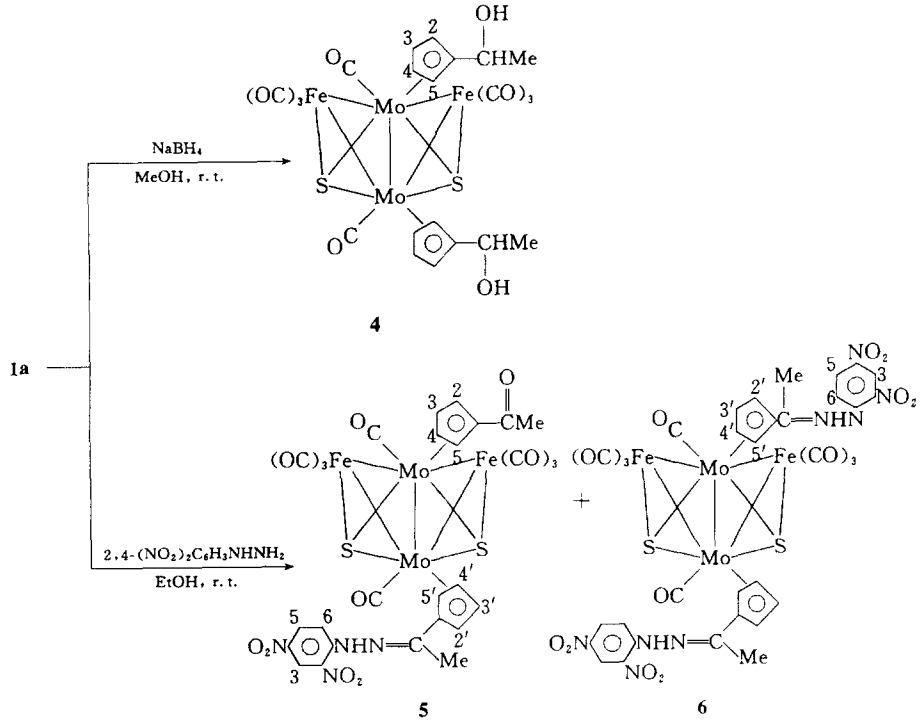
X-ray diffraction analysis for **1b**

Dark-brown crystals of **1b** were grown by slow evaporation of its THF solution at room temperature, and an X-ray diffraction analysis was undertaken. Selected bond distances and angles are listed in Tables 1 and 2, respectively. The molecular structure is shown

Table 1. Selected bond distances (Å)[a]

Mo(1)—Fe(2)	2.814(12)	Fe(2)—Mo(1a)	2.809(12)
Mo(1)—S(3)	2.339(8)	S(3)—Mo(1a)	2.348(8)
Mo(1)—C(4)	1.992(25)	Mo(1)—Mo(1a)	2.861(1)
Mo(1)—S(3a)	2.348(8)	Fe(2)—C(1)	1.782(9)
Fe(2)—S(3)	2.813(24)	Fe(2)—C(2)	1.767(8)
Fe(2)—C(3)	1.780(26)		

[a] Symmetry code a = $-x, -y, z$.



Scheme 2.

Table 2. Selected bond angles (°)[a]

Fe(2)—Mo(1)—S(3)	49.1(5)	Mo(1)—S(3)—Fe(2)	76.9(6)
Fe(2)—Mo(1)—C(4)	63.9(5)	Mo(1)—S(3)—Mo(1a)	75.2(3)
S(3)—Mo(1)—C(4)	112.9(7)	Mo(1)—C(4)—O(4)	158.9(10)
S(3)—Mo(1)—Mo(1a)	52.5(2)	Fe(2)—Mo(1)—Mo(1a)	59.3(1)
Fe(2)—Mo(1)—Fe(2a)	88.7(5)	C(4)—Mo(1)—Mo(1a)	97.8(3)
Mo(1a)—Mo(1)—Fe(2a)	59.5(1)	S(3)—Mo(1)—Fe(2a)	111.1(2)
Fe(2)—Mo(1)—S(3a)	110.7(2)	C(4)—Mo(1)—Fe(2a)	65.4(5)
S(3)—Mo(1)—S(3a)	92.7(4)	Fe(2a)—Mo(1)—S(3a)	49.1(5)
Mo(1a)—Mo(1)—S(3a)	52.2(2)	S(3)—Fe(2)—Mo(1a)	54.4(4)
Mo(1)—Fe(2)—S(3)	54.1(4)	C(1)—Fe(2)—Mo(1a)	91.2(5)
Mo(1)—Fe(2)—C(1)	145.4(10)	C(2)—Fe(2)—Mo(1a)	148.6(10)
Mo(1)—Fe(2)—C(2)	97.2(5)	C(3)—Fe(2)—Mo(1a)	115.2(5)
Mo(1)—Fe(2)—C(3)	114.1(5)	Fe(2)—S(3)—Mo(1a)	76.5(6)
Mo(1)—Fe(2)—Mo(1a)	61.2(3)		

[a] Symmetry code a = $-x, -y, z$.

in Fig. 1. The molecule consists of a butterfly metal cluster core Mo_2Fe_2 with molybdenum atoms in the hinge positions. Each wing face Mo_2Fe is capped by a μ_3-S atom *trans* to two iron atoms with respect to the Mo—Mo bond. Each molybdenum atom is coordinated by a η^5-$MeO_2CC_5H_4$ ligand and a semibridging carbonyl ligand, whereas each iron atom is bonded to three terminal carbonyls. Overall, the structure is very similar to that of its parent cluster [(η^5-$C_5H_5)_2(\mu_3$-$CO)_2Mo_2Fe_2(\mu_3$-$S)_2(CO)_6$] [6]. The butterfly angle and the Fe(2)—Fe(2a) non-bonding distance in **1b** are 108.57° and 3.930 Å, respectively. These values are slightly larger than those of its parent cluster (104.1° and 3.833(5) Å, respectively) [6]. Thus the two Mo_2Fe wings of **1b** are more open. Since the distances of C(4)—Fe(2), C(4)—Fe(2a) and C(4)—Mo(1) are 2.637, 2.683 and 1.992(25) Å, respectively, the asymmetric parameters [11] of the semibridging carbonyl C(4)O(4) are 0.32 and 0.35. These parameters are smaller than those of its parent cluster [6]. Based on the symmetry, the other carbonyl C(4a)O(4a) is also semibridging and μ_3-coordinated to one Mo atom and two Fe atoms. The X-ray diffraction analysis confirmed both semibridging carbonyls

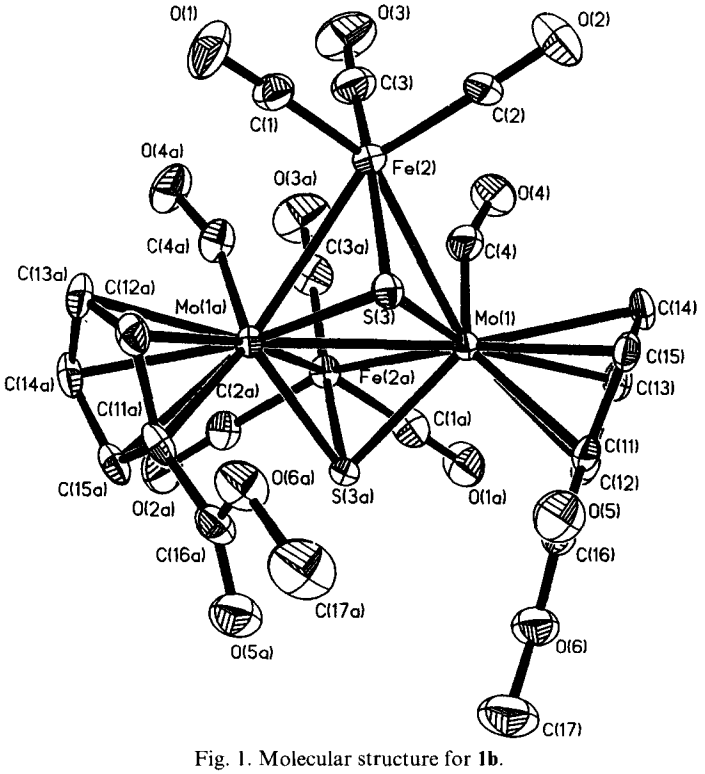


Fig. 1. Molecular structure for **1b**.

and terminal carbonyls present in the molecule of **1b**, which is in good agreement with its IR data as discussed above.

EXPERIMENTAL

All reactions were performed under purified tank nitrogen using vacuum line techniques. Toluene was distilled from Na/benzophenone ketyl under nitrogen. Dichloromethane, methanol and ethanol were deoxygenated by bubbling N_2 for about 15 min prior to use. $NaBH_4$ and 2,4-dinitrophenylhydrazine were used as purchased from commercial origin. μ-$S_2Fe_2(CO)_6$ [12], $[\eta^5$-$RC_5H_4(CO)_3M]_2$ (R = MeCO, MeO_2C, EtO_2C; M = Mo, W) [13] and $[\eta^5$-$RC_5H_4(CO)_2M]_2$ (R = MeCO, MeO_2C, EtO_2C; M = Mo, W) [14–15] were prepared according to literature methods. Preparative TLC was carried out on glass plates (26 × 19 cm) coated with silica gel G (10–40 μm). IR spectra were recorded on Nicolet FT-5DX and Nicolet Magna FT-750 infrared spectrophotometer. ^{1}H NMR spectra were recorded on Joel FX 90Q and Bruker AC-P200 spectrometers. C/H analyses and MS determinations were performed by a Perkin-Elmer 240C analyzer, and an HP 5988A and M-80 LC/MS spectrometers, respectively. Melting points were determined on a Yanaco MP-500 apparatus.

Preparation of **1a**

A two-necked flask (100 cm^3) fitted with a magnetic stir-bar, a rubber septum, and a nitrogen inlet tube was charged with 0.500 g (0.965 mmol) of $[\eta^5$-$MeCOC_5H_4(CO)_2Mo]_2$, 0.324 g (0.965 mmol) of μ-$S_2Fe_2(CO)_6$ and 40 cm^3 of CH_2Cl_2. The mixture was stirred at room temperature for 10 h. Solvent was removed under reduced pressure and the residue was dissolved in 5 cm^3 of acetone. The solution was subjected to TLC separation using 6 : 1 benzene : ether as eluent to give three bands. The upper two purple and red bands were known compounds $S_2Fe_3(CO)_9$ and $[\eta^5$-$MeCOC_5H_4(CO)_3Mo]_2$ [13]. The third dark-brown band was **1a** (0.179 g, 23%), m.p. 300°C(dec.). Found: C, 32.9; H, 1.7. Calc. for $C_{22}H_{14}Fe_2Mo_2O_{10}S_2$: C, 32.8; H, 1.7%. IR(KBr, disk): $\nu_{C\equiv O}$, 1803 s, 1967 vs, 2008 s, 2032 vs, 2057 vs; $\nu_{C=O}$, 1680 s cm^{-1}. ^{1}H NMR ($CDCl_3$, δ, ppm): 2.44(s, 6H, $2CH_3$), 5.07[t, 4H, 2(H^3, H^4)], 6.16[t, 4H, 2(H^2, H^5)]. MS(EI), *m/z* (^{56}Fe, ^{98}Mo, rel. int.); 754[(M-2CO)$^+$, 1.5%], 336[$Mo_2Fe(CO)_3^+$, 0.7], 252 (Mo_2Fe^+, 0.7), 196(Mo_2^+, 1.4), 140[$Fe(CO)_3^+$, 0.5], 112[$Fe(CO)_2^+$, 3.0], 107($MeCOC_5H_4^+$, 1.7), 98(Mo^+, 2.2), 88(SFe^+, 1.2), 84[$Fe(CO)^+$, 14.2], 64($C_5H_4^+$, 2.5), 56(Fe^+, 11.4).

Preparation of **1b**

The 100 cm^3 flask was charged with 0.500 g (0.909 mmol) of $[\eta^5$-$MeO_2CC_5H_4(CO)_2Mo]_2$, 0.305 g (0.909 mmol) of μ-$S_2Fe_2(CO)_6$ and 40 cm^3 of CH_2Cl_2. Similar work-up as above was followed using CH_2Cl_2 as eluent to give three bands. The upper two were known compounds $S_2Fe_3(CO)_9$ and $[\eta^5$-$MeO_2CC_5H_4(CO)_3Mo]_2$ [13].The third dark-brown band was **1b** (0.170 g, 22%), m.p. 260°C(dec.). Found: C, 31.6; H, 1.6. Calc. for $C_{22}H_{14}Fe_2Mo_2O_{12}S_2$: C, 31.5; H, 1.7%. IR(KBr, disk): $\nu_{C\equiv O}$, 1819 s, 1959 vs, 1983 s, 2032 vs, 2049 s; $\nu_{C=O}$, 1712 s cm^{-1}. ^{1}H NMR ($CDCl_3$, δ, ppm): 3.92(s, 6H, $2CH_3$), 5.08[t, 4H, 2(H^3, H^4)], 6.04[t, 4H, 2(H^2, H^5)]. MS(EI), *m/z*(^{56}Fe, ^{98}Mo, rel. int.): 400[$S_2Fe_2Mo_2(CO)^+$, 0.9%], 182[MoFe(CO)$^+$, 5.3], 154($MoFe^+$, 5.1), 144[$SFe(CO)_2^+$, 0.5], 140[$Fe(CO)_3^+$, 1.8], 130(SMo^+, 0.8), 126[$Mo(CO)^+$, 0.7], 123($MeO_2CC_5H_4^+$, 0.6], 116[$SFe(CO)^+$, 2.3], 92[$C_5H_4(CO)^+$, 1.4], 88(SFe^+, 1.2), 84[$Fe(CO)^+$, 0.6], 64($C_5H_4^+$, 3.7).

Preparation of **1c**

The 100 cm^3 flask was charged with 0.500 g (0.865 mmol) of $[\eta^5$-$EtO_2CC_5H_4(CO)_2Mo]_2$, 0.300 g (0.872 mmol) of μ-$S_2Fe_2(CO)_6$ and 40 cm^3 of CH_2Cl_2. Similar work-up as above was followed using CH_2Cl_2 as eluent to give three bands. The upper two were known compounds $S_2Fe_3(CO)_9$ and $[\eta^5$-$EtO_2CC_5H_4(CO)_3Mo]_2$ [13]. The third dark-brown band was **1c** (0.157 g, 21%), m.p. 203°C(dec.). Found: C, 33.1; H, 1.9. Calc. for $C_{24}H_{18}Fe_2Mo_2O_{12}S_2$: C, 33.3; H, 2.1%. IR(KBr, disk): $\nu_{C\equiv O}$, 1827 s, 1959 s, 1983 s, 2024 vs, 2049 s; $\nu_{C=O}$, 1712 s cm^{-1}. ^{1}H NMR ($CDCl_3$, δ, ppm): 1.42(t, 6H, $2CH_3$, J = 7.2 Hz), 4.38(q, 4H, $2CH_2$, J = 7.2 Hz), 5.16[t, 4H, 2(H^3, H^4)], 6.00[t, 4H, 2(H^2, H^5)].

Preparation of **2a** *and* **3a**

The 100 cm^3 flask was charged with 0.500 g (0.689 mmol) of $[\eta^5$-$MeO_2CC_5H_4(CO)_2W]_2$, 0.237 g (0.689 mmol) of μ-$S_2Fe_2(CO)_6$ and 30 cm^3 of CH_2Cl_2. Similar work-up as above was followed using 4 : 1 CH_2Cl_2 : petroleum ether as eluent to give four bands. The upper three were $S_2Fe_3(CO)_9$, $[\eta^5$-$MeO_2CC_5H_4(CO)_3W]_2$ [13] and **3a** [9] (0.036 g, 6%). The fourth dark-brown band was **2a** (0.017 g, 2%), m.p. 76–77°C. IR(KBr, disk): $\nu_{C\equiv O}$, 1844 m, 1893 s, 1950 vs, 1983 vs, 2049 vs; $\nu_{C=O}$, 1721 s cm^{-1}. ^{1}H NMR ($CDCl_3$, δ, ppm): 3.92(s, 6H, $2CH_3$), 5.50[br. s, 4H, 2(H^3, H^4)], 5.80[br. s. 4H, 2(H^2, H^5)]. MS(FD), *m/z*(^{56}Fe, ^{184}W, rel. int.): 1014(M^+, 4.9%).

Preparation of **2b** *and* **3b**

The 100 cm^3 flask was charged with 0.500 g (0.675 mmol) of $[\eta^5$-$EtO_2CC_5H_4(CO)_2W]_2$, 0.238 g (0.692 mmol) of μ-$S_2Fe_2(CO)_6$ and 30 cm^3 of CH_2Cl_2. Similar work-up was followed using 3 : 1 CH_2Cl_2 : petroleum ether as eluent to give four bands. The upper two were

$S_2Fe_3(CO)_9$ and $[\eta^5\text{-}EtO_2CC_5H_4(CO)_3W]_2$ [13]. The third brown band was **3b** (0.078 g, 12%) and the fourth dark-brown band was **2b** (0.050 g, 7%). **3b**: m.p. 98–99°C. Found: C, 29.9; H, 2.1. Calc. for $C_{23}H_{18}FeO_{11}SW_2$: C, 29.8; H, 2.0%. IR(KBr, disk): $\nu_{C\equiv O}$, 1844 s, 1893 s, 1983 vs, 2041 vs; $\nu_{C=O}$, 1712 s cm^{-1}. ^1H NMR ($CDCl_3$, δ, ppm): 1.28[t, 6H, $2CH_3$, $J = 7.2$ Hz), 4.28(q, 4H, $2CH_2$, $J = 7.2$ Hz), 5.24, 5.44[br. s, br. s, 4H, 2(H^3, H^4)], 5.64–6.04[m, 4H, 2(H^2, H^5)]. **2b**: m.p. 63–64°C. Found: C, 27.7; H, 1.8. Calc. for $C_{24}H_{18}Fe_2O_{12}S_2W_2$: C, 27.7; H, 1.7%. IR(KBr, disk): $C_{C\equiv O}$, 1835 s, 1893 s, 1950 vs, 1983 vs, 2049 vs; $\nu_{C=O}$, 1712 s cm^{-1}. ^1H NMR ($CDCl_3$. δ, ppm): 1.42(t, 6H, $2CH_3$, $J = 7.2$ Hz), 4.38(q, 4H, $2CH_2$, $J = 7.2$ Hz), 5.32[t, 4H, 2(H^3, H^4)], 6.12[t, 4H, 2(H^2, H^5)]. MS(FD), m/z(^{56}Fe, $^{182}W/^{183}W$, rel. int.): 1039(M^+, 100%).

Reaction of $[\eta^5\text{-}MeCOC_5H_4(CO)_3Mo]_2$ *with* $\mu\text{-}S_2Fe_2(CO)_6$

A two-necked flask (100 cm^3) fitted with a magnetic stir-bar, a rubber septum, and a reflux condenser topped with a nitrogen inlet tube was charged with 0.582 g (1.014 mmol) of $[\eta^5\text{-}MeCOC_5H_4(CO)_3Mo]_2$, 0.352 g (1.023 mmol) of $\mu\text{-}S_2Fe_2(CO)_6$ and 25 cm^3 of toluene. The mixture was refluxed for 5 h. Solvent was removed under reduced pressure and the residue was subjected to column chromatography using 1 : 5 ether : CH_2Cl_2 as eluent to give dark-brown solid **1a** (0.150 g, 18%).

Reaction of $[\eta^5\text{-}MeO_2CC_5H_4(CO)_3Mo]_2$ *with* $\mu\text{-}S_2Fe_2(CO)_6$

The 100 cm^3 flask was charged with 0.600 g (0.990 mmol) of $[\eta^5\text{-}MeO_2CC_5H_4(CO)_3Mo]_2$, 0.570 g (1.657 mmol) of $\mu\text{-}S_2Fe_2(CO)_6$ and 30 cm^3 of toluene. Similar work-up was followed to give dark-brown solid **1b** (0.072 g, 11%).

Reaction of $[\eta^5\text{-}EtO_2CC_5H_4(CO)_3Mo]_2$ *with* $\mu\text{-}S_2Fe_2(CO)_6$

The 100 cm^3 flask was charged with 0.600 g (0.946 mmol) of $[\eta^5\text{-}EtO_2CC_5H_4(CO)_3Mo]_2$, 0.488 g (1.419 mmol) of $\mu\text{-}S_2Fe_2(CO)_6$ and 30 cm^3 of toluene. Similar work-up was followed to give dark-brown solid **1c** (0.050 g, 6%).

Reaction of $[\eta^5\text{-}MeO_2CC_5H_4(CO)_3W]_2$ *with* $\mu\text{-}S_2Fe_2(CO)_6$

The 100 cm^3 flask was charged with 0.600 g (0.767 mmol) of $[\eta^5\text{-}MeO_2CC_5H_4(CO)_3W]_2$, 0.396 g (1.153 mmol) of $\mu\text{-}S_2Fe_2(CO)_6$ and 30 cm^3 of toluene. Similar work-up was followed. Apart from $S_2Fe_3(CO)_9$ and unreacted $[\eta^5\text{-}MeO_2CC_5H_4(CO)_3W]_2$, no other compounds were isolated.

Reaction of $[\eta^5\text{-}EtO_2CC_5H_4(CO)_3W]_2$ *with* $\mu\text{-}S_2Fe_2(CO)_6$

The 100 cm^3 flask was charged with 0.282 g (0.231 mmol) of $[\eta^5\text{-}EtO_2CC_5H_4(CO)_3W]_2$, 0.174 g (0.507 mmol) of $\mu\text{-}S_2Fe_2(CO)_6$ and 390 cm^3 of toluene. Similar work-up was followed. Apart from $S_2Fe_3(CO)_9$ and unreacted $[\eta^5\text{-}EtO_2CC_5H_4(CO)_3W]_2$, no other compounds were isolated.

Preparation of **4**

The 100 cm^3 was charged with 0.100 g (0.124 mmol) of **1a** and 10 cm^3 of methanol. During stirring 0.044 g (1.16 mmol) of $NaBH_4$ was added. The mixture was stirred at room temperature for 3 h. Solvent was removed under reduced pressure and the residue was dissolved in 5 cm^3 of acetone. The solution was subjected to TLC separation using 1 : 2 acetone : petroleum ether as eluent to give dark-brown solid **4** (0.078 g, 78%), m.p. 223°C(dec.). Found: C, 32.8; H, 2.2. Calc. for $C_{22}H_{18}Fe_2Mo_2O_{10}S_2$: C, 32.6; H, 2.2%. IR(KBr, disk): $\nu_{C\equiv O}$, 1803 s, 1950 vs, 1983 s, 2016 vs, 2041 s; ν_{O-H}, 3400 cm^{-1}. ^1H NMR ($CDCl_3$, δ, ppm); 1.52(d, 6H, $2CH_3$), 2.64(br. s, 2H, 2OH), 4.72–5.92[m, 10H, 2CH, 2(H^2—H^5)].

Preparation of **5** and **6**

The 100 cm^3 flask was charged with a solution of 0.065 g (0.081 mmol) of **1a** in 5 cm^3 of THF and 10 cm^3 of absolute ethanol. To this solution was added 2 cm^3 of 2,4-dinitrophenylhydrazine solution which was prepared by dissolving 1.0 g of 2,4-dinitrophenylhydrazine in 5 cm^3 of 98% concentrated sulfuric acid, 10 cm^3 of water and 35 cm^3 of 95% ethanol. The mixture was stirred at room temperature for 30 min to give a precipitate. The precipitate was filtered out, washed successively with water, ethanol and petroleum ether and subjected to TLC separation using CH_2Cl_2 as eluent to give brown solid **6** (0.011 g, 12%) and dark-brown solid **5** (0.035 g, 44%). **5**: m.p. 300°C(dec.). Found: C, 33.9; H, 1.7; N, 5.0. Calc. for $C_{28}H_{18}Fe_2Mo_2N_4O_{13}S_2$: C, 34.1; H, 1.8; N, 5.7%. IR(KBr, disk): $\nu_{C\equiv O}$, 1794 s, 1816 m, 1967 vs, 1988 vs, 2024 vs, 2057 vs; $C_{C=O}$, 1671 s; $\nu_{C=N}$, 1614 s, cm^{-1}. ^1H NMR ($CDCl_3$, δ, ppm): 1.96–2.36 [m, 6H, $C(O)CH_3$, $C(N)CH_3$], 5.08[d, 4H, (H^3, $H^{3'}$, H^4, $H^{4'}$, of substituted Cp rings)], 6.03[s, 4H, (H^2, $H^{2'}$, H^5, $H^{5'}$, of substituted Cp rings)], 7.87–8.12(m, 1H, H^6 of substituted benzene ring), 8.27–8.52(m, 1H, H^5 of substituted benzene ring), 9.15(s, 1H, H^3 of substituted benzene ring), 11.25(s, 1H, NH). **6**: m.p. 300°C(dec.). Found: C, 35.5; H, 2.1; N, 9.5. Calc. for $C_{34}H_{22}Fe_2Mo_2N_8O_{16}S_2$: C, 35.0; H, 1.9; N, 9.6%.

IR(KBr, disk): $C_{C\equiv O}$, 1844 m, 1893 m, 1983 vs, 2041 vs; $C_{C=N}$, 1614 vs, cm^{-1}. ^1H NMR ($CDCl_3$, δ, ppm): 2.16[s, 6H, $2C(N)CH_3$], 4.96–5.44[m, 4H, $2(H^3, H^4$ of substituted Cp rings)], 5.60–6.16[m, 4H, $2(H^2, H^5$ of substituted Cp rings)], 7.68–8.00(m, 2H, $2H^6$ of substituted benzene rings], 8.08–8.40(m, 2H, $2H^5$ of substituted benzene rings), 9.01(s, 2H, $2H^3$ of substituted benzene rings), 11.11(s, 2H, 2NH).

Crystal structure determination of **1b**

Suitable crystals of **1b** for X-ray diffraction study were obtained by slow evaporation of its THF solution at room temperature. Details of crystal parameters, data collections and structure refinements are given in Table 3. A brown crystal measuring $0.2\times0.3\times0.2$ mm was mounted on a glass fibre and placed on an Enraf-Nonius CAD4 diffractometer equipped with a graphite monochromator. A total of 1657 independent reflections was collected at room temperature, with Mo-K_α radiation ($\lambda = 0.71073$ Å) by the ω-2θ scan mode. Of the total reflections, 1565 reflections were considered to be observed with $I \geqslant 3\sigma(I)$ and used in structure solution and refinement. Data were corrected by Lorentz and polarization effects and empirical absorption. The structure was solved by the direct method. Mo, Fe and most of other non-hydrogen atoms were located by the E-map. Remaining non-hydrogen atoms were found in succeeding difference Fourier syntheses. The final refinement by full matrix least-squares method with anisotropic thermal parameters for non-hydrogen atoms converged to unweighted and weighted agreement factors of 0.029 and 0.038. The highest peak on the final difference Fourier map had a height of 0.56 e/Å^3. All calculations were performed on a PDP 11/44 and an IBM 486 computer using the SDP-PLUS and SHELXS program packages.

Table 3. Details of crystal parameters, data collections and structure refinements

Formula	$C_{22}H_{14}Fe_2Mo_2O_{12}S_2$
Molecular weight	838.05
Color and habit	brown plate
Crystal size (mm)	$0.2\times0.3\times0.2$
Crystal system	orthorhombic
Space group	*Fdd*2
a (Å)	15.735(3)
b (Å)	28.482(6)
c (Å)	12.014(2)
V (Å^3)	5384(3)
Z	8
Dx (g cm^{-3})	2.07
μ (cm^{-1})	21.56
$F(000)$	3280
Temperature (K)	299 ± 1
Scan type	ω-2θ
θ_{max} (°)	23
Unique reflections	1657
Observed reflections [$I \geqslant 3\sigma(I)$]	1565
R	0.029
Rw	0.038
Largest peak in final diff. map (e Å^{-3})	0.56

Acknowledgements—We are grateful to the National Natural Science Foundation of China and Special Foundation of State Education Committee of China for financial support of this work.

REFERENCES

1. (a) S. D. Conradson, B. K. Burgess, W. E. Newton, K. O. Hodgson, J. W. McDonald, J. F. Robinson, S. F. Ghellar, L. E. Mortensen, M. W. W. Adams, P. K. Mascharak, W. A. Armstrong and R. H. Holm, *J. Am. Chem. Soc.* 1985, **107**, 7935; (b) D. Coucouvanis, *Acc. Chem. Res.* 1991, **24**, 1.
2. (a) M. R. DuBois, M. C. VanDerveer, D. L. DuBois, R. C. Haltiwanger and W. K. Miller, *J. Am. Chem. Soc.* 1980, **102**, 7456; (b) M. R. DuBois, *Chem. Rev.* 1989, **89**, 1; (c) N. Y. Topsoe and H. Topsoe, *J. Catal.* 1983, **84**, 386; (d) M. D. Curtis, J. E. Penner-Hahn, J. Schwank, O. Baralt, D. J. McCabe, L. Thompson and G. Waldo, *Polyhedron* 1988, **7**, 2411.
3. P. Li and M. D. Curtis, *Inorg. Chem.* 1990, **29**, 1242 and the cited references therein.
4. M. D. Curtis, P. D. Williams and W. M. Butler, *Inorg. Chem.* 1988, **27**, 2853.
5. P. D. Williams and M. D. Curtis, *J. Organomet. Chem.* 1988, **352**, 169.
6. P. Braunstein, J.-M. Jud, A. Tiripicchio, M. Tiripicchio-Camellini and E. Sappa, *Angew. Chem. Int. Ed. Engl.* 1982, **21**, 307.
7. P. D. Williams, M. D. Curtis, D. N. Duffy and W. M. Butler, *Organometallics* 1983, **2**, 165.
8. L.-C. Song, J.-Q. Wang and Q.-M. Hu, *Polyhedron* 1995, **14**, 1101.
9. L.-C. Song, J.-Y. Shen, Q.-M. Hu and X.-D. Qin, *Polyhedron* 1995, **14**, 2079.
10. (a) D. W. Macomber and M. D. Rausch, *J. Organomet. Chem.* 1983, **258**, 331; (b) W. P. Hart and M. D. Rausch, *J. Organomet. Chem.* 1988, **355**, 455; (c) L.-C. Song, J.-Y. Shen, Q.-M. Hu, R.-J. Wang and H.-G. Wang, *Organometallics* 1993, **12**, 408; (d) L.-C. Song, J.-Y. Shen, Q.-M. Hu and X.-Y. Huang, *Organometallics* 1995, **14**, 98.
11. M. D. Curtis, K. R. Han and W. M. Butler, *Inorg. Chem.* 1980, **19**, 2096.
12. L. E. Bogan, Jr. D. A. Lesch and T. B. Rauchfuss, *J. Organomet. Chem.* 1983, **250**, 429.
13. L.-C. Song, J.-Y. Shen, *Chem. J. Chin. Univ.* 1992, **13**, 1227.
14. L.-C. Song and J.-Y. Shen, J.-Q. Wang, Q.-M. Hu, R.-J. Wang and H.-G. Wang, *Polyhedron* 1994, **13**, 3235.
15. L.-C. Song, J.-Q. Wang, W.-J. Zhao, Q.-M. Hu, Y.-Q. Fang, S.-J. Zhang, R.-J. Wang and H.-G. Wang, *J. Organomet. Chem.* 1993, **453**, 105.

Pergamon

PII: S0277-5387(96)00277-X

Polyhedron Vol. 16, No. 3, pp. 489–494, 1997
Copyright © 1996 Elsevier Science Ltd
Printed in Great Britain. All rights reserved
0277-5387/97 $17.00+0.00

Study of Cu^{II} binuclear complexes of binucleating hexadentate ligands

C. A. Sureshan and P. K. Bhattacharya*

Department of Chemistry, Faculty of Science, M.S. University of Baroda, Baroda 390 002, India

(Received 8 December 1995; accepted 3 June 1996)

Abstract—Three types of tridentate binucleating Schiff base ligands have been synthesised by condensation of 5,5′-methylenebis-salicylaldehyde with aminoalcohols, aminoacids or aminoethylpyridine. These ligands have two sets of tridentate phenolate O^-, azomethine N and O^-, COO^- or pyridyl nitrogen coordination sites. The binuclear Cu^{II} complexes of these ligands have been prepared and their spectral, magnetic and electrochemical properties have been studied. On the basis of these experimental results long range spin exchange interaction between two copper centres has been indicated. Copyright © 1996 Elsevier Science Ltd

Keywords: copper(II) complexes; binuclear complexes; hexadentate ligands; Schiff base; binucleating ligands; magnetic interactions.

In recent years the study of binuclear copper(II) complexes has been a subject of considerable interest because of their structural, magnetic, ESR and electrochemical properties.

In our laboratory Cu^{II} complexes of binucleating ligands with two bidentate sites separated by aromatic rings have been studied earlier [1–3]. In such complexes with π delocalised bridges, the spin exchange has been suggested to be through σ bonds [4,5]. Spin exchange interaction between Cu^{II} centres separated by σ bonding aliphatic chain has also been studied [6–9]. In the present study, binucleating ligands with two tridentate coordination sites have been synthesised. They are of three types. The first type of ligand was obtained by the condensation of 5,5′-methylenebis-salicylaldehyde (MBS) and aminoalcohols. These ligands have phenolate O^-, azomethine N and alkoxide O^- coordination sites. The second type of ligands was prepared by the condensation of above mentioned dialdehyde (MBS) and aminoacids and have phenolate O^-, azomethine N and carboxylate COO^- coordination sites. The third type of ligands was prepared by the condensation of MBS with aminoethylpyridine and have phenolate O^-, azomethine N and pyridyl N coordination sites. Binuclear complexes of these ligands with Cu^{2+} ions have been prepared and characterized by spectral, magnetic and electrochemical studies.

* Author to whom correspondence should be addressed.

EXPERIMENTAL

Chemicals

5′5-Methylenebis-salicylaldehyde (MBS) was prepared by the method reported earlier [10]. Glycine (gly), α-alanine (α ala), phenylalanine (pha), valine (val), ethanolamine (ea), propanolamine (pa), 2-aminobutanol (L_2ab), aminoethylpyridine, methanol, dimethylformamide, tetrabutylammonium tetrafluoroborate and $CuCl_2 \cdot 2H_2O$ used were of A.R. grade.

Preparation of binucleating ligands using MBS and aminoalcohols (I)

5′5-Methylenebis-salicylaldehyde (5 mmol) was dissolved in 50 cm^3 of benzene and to this 10 mmoles of aminoalcohol (ea, pa, L_2ab) solution in 20 cm^3 of benzene was added dropwise. The solution was refluxed for 3 h and the azeotrope was separated. Excess benzene was distilled out and the solid obtained was washed thoroughly with benzene and recrystallized from benzene. Yield: compound I_A 1.1 gm (62%); compound I_B 1.2 gm (65%); compound I_C 1.2 gm (63%).

Preparation of binucleating ligand using MBS and aminoacids (II) *or aminoethylpyridine* (III)

MBS (5 mmol) was suspended in 150 cm^3 of methanol. To this 10 mmoles of aminoacid (gly, ala, val or

pha) or aminoethylpyridine were added. The solutions were stirred for about five hours. The volumes of methanol were reduced to ~20 cm^3. The yellow crystalline products separated were washed with benzene and recrystallized from methanol. Yield: compound II_A 1.1 gm (62%); compound II_B 1.2 gm (60%); compound II_C 1.5 gm (66%); compound II_D 1.9 gm (70%); compound III_A 1.2 gm (53%).

Method I

Synthesis of binuclear complexes of ligand I *and* II

(a) To 2 mmol of binucleating ligand I or II in 50 cm^3 methanol, were added 8 mmoles of lithium methoxide, to raise the pH. This solution was added to 4 mmoles of $CuCl_2 \cdot 2H_2O$ in 10 cm^3 methanol. The resulting product was stirred for 1 h, filtered, washed thoroughly with methanol and dried *in vacuo*.

(b) To 2 mmol of MBS and 4 mmol of aminoalcohol (ea, pa, L_2ab) or aminoacid (gly, ala, pha, val) in 50 cm^3 of methanol, 8 mmol of lithium methoxide were added to raise the pH. The solutions were stirred for 2 h, 4 mmol of $CuCl_2 \cdot 2H_2O$ in 20 cm^3 of methanol were added. The reaction mixture was further stirred for one hour, the complex formed was filtered, washed with methanol and dried *in vacuo*.

Method II

(*a*) *Synthesis of binuclear complex of ligand* III *with* ClO_4^- *counter ion*

2 mmol of ligand III were dissolved in 25 cm^3 of methanol and to this were added 4 mmol of $Cu(ClO_4)_2 \cdot 6H_2O$ in 15 cm^3 methanol. The solution was stirred for 1 h. The solid obtained was filtered and washed with methanol and dried *in vacuo*.

(*b*) *Synthesis of binuclear complex of ligand* III *with* Cl^- *counter ion*

2 mmol ligand III were dissolved in 25 cm^3 methanol and to this were added 4 mmol of $CuCl_2 \cdot 2H_2O$ in 15 cm^3 methanol. The solution was stirred for ~10 h. The solid obtained was filtered and washed with methanol and dried *in vacuo*.

Physical measurements

C and H analyses were performed on Coleman analyzer model-33 and nitrogen was estimated by Dumas' method. Copper was estimated gravimetrically as copper oxide. Magnetic measurements were carried out using a Gouy balance at room temperature. The analytical data have been presented in Table 1. IR spectra (as KBr pellets) were recorded on a Shimadzu IR 408 spectrophotometer. The electronic spectra were recorded on a Shimadzu UV–vis spectrophotometer UV-240. Their diffuse reflectance spectra were recorded on the same instrument, equipped with spherical reflectance assembly, using $BaSO_4$ as a reference material. Thermogravimetric studies were carried out by using as thermal analyser, a Shimadzu D.T. 30 instrument. The ESR spectra were recorded by using a Varian E-15 spectrometer and TCNE was used as the marker.

The electrochemical unit consisted of model 174A polarographic analyzer, universal programmer, *x-y* recorder, platinum working electrode and Pt wire auxiliary electrode. $Ag/AgNO_3$ was used as the reference electrode.

RESULTS AND DISCUSSION

The analyses of the complexes correspond to the following binuclear formula (Fig. 1).

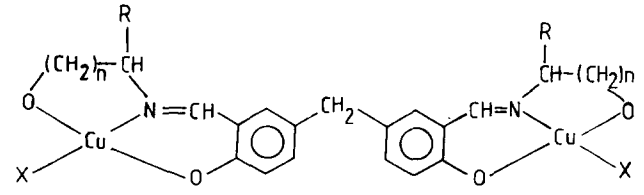
Electronic spectra

The electronic spectra of complexes II_B, II_C, II_D and III_A in DMF solution exhibit a broad band in the region 630–690 nm and four bands at 500, 380, 270 and 240 nm. Similar bands are observed in reflectance spectra of the complex also. The band in the 630–690 nm region corresponds to *d–d* transitions and is

Table 1. Preparative yields, analytical, magnetic and TGA data for the binuclear complexes[a]

Compound no.	Yield	C	H	N	Cu	μ_B	% Weight loss	Temperature range
I_A	0.68 g 68%	45.2 (45.5)	4.6 (4.4)	5.5 (5.5)	24.9 (25.3)	1.3	7	180–200
I_B	0.66 g 63%	47.5 (47.6)	4.7 (4.9)	5.1 (5.3)	23.7 (24.0)	1.1	7	170–190
I_C	0.73 g 65%	49.1 (49.2)	5.9 (6.1)	4.9 (5.0)	22.4 (22.6)	1.1	6	180–210
II_A	0.70 g 66%	42.9 (43.1)	3.5 (3.5)	5.1 (5.3)	23.8 (24.0)	1.3	—	—
II_B	0.70 g 63%	45.2 (45.1)	3.9 (3.9)	4.9 (5.0)	23.2 (22.7)	1.3	7	190–220
II_C	0.76 g 62%	51.4 (51.6)	5.3 (5.2)	4.8 (4.8)	21.4 (21.8)	1.2	—	—
II_D	0.85 g 60%	55.6 (55.8)	4.4 (4.2)	3.9 (3.9)	17.6 (17.9)	1.3	5	190–210
III_A	0.91 g 55%	42.5 (42.2)	3.9 (3.6)	6.7 (6.8)	15.1 (15.4)	1.2	—	—
III_B	0.61 g 46%	53.0 (52.7)	4.2 (3.9)	8.3 (8.5)	19.0 (19.2)	1.2	1	100–110

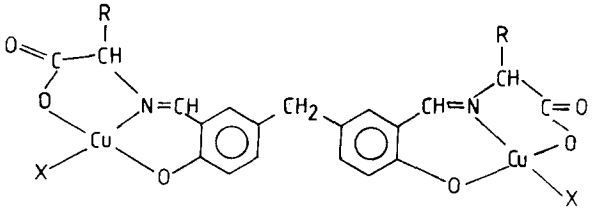
[a]Calculated values are in parentheses.



I_A n = 1 R = H X = H_2O

I_B n = 2 R = H X = H_2O

I_C n = 1 R = $-C_2H_5$ X = H_2O

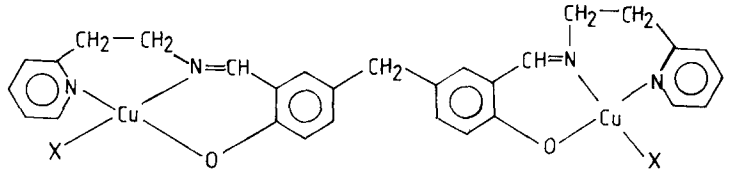


II_A R = H X = H_2O

II_B R = $-CH_3$ X = H_2O

II_C R = $-CH(CH_3)_2$ X = H_2O

II_D R = $-CH_2C_6H_5$ X = H_2O



III_A X = H_2O ClO_4^- as counter ion

III_B X = Cl

Fig. 1.

indicative of square planar geometry around the metal ion. The ligand occupies three positions with one water molecule completing the fourth coordination position [11,12]. The band at around 500 nm is a charge transfer band from phenolate oxygen to Cu^{II}. The bands 380, 270, 245 nm have previously been assigned to ligand related $\pi_1^* \leftarrow \pi$ and $\pi_2^* \leftarrow \pi$ transition [13,14] and appear in all spectra. They are consistent with dianionic form of Schiff base formed by salicylaldehyde and amino acids and their complexes previously reported [15–17]. This confirms the presence of the salicylaldimine group. The complexes I_A, I_B, I_C and II_A are insoluble and hence only reflectance spectra could be recorded. The bands appearing at 630–690 nm, 500, 380, 270 and 245 nm are similar to the spectra for the complexes II_B, II_C and II_D. The reflectance spectrum of complex III_B shows *d–d* band in the region 830–860 nm. Compared to the perchlorate containing complex III_A and neutral complexes I and II the bands in the complex III_B occurs at lower energy. Further, the spectra of II_B, II_C and II_D in DMF and III_A in DMF or dioxan/water solution do not show significant change from the reflectance spectra, whereas III_B on dissolution in water/dioxan exhibits spectra different from that in solid phase. A broad *d–d* band is observed in the range 630–690 nm similar to all other complexes in solution. This shows that there may be chloride bridges in the III_B complexes resulting in tetranuclear complexes. The chloride bridges break on dissolution in water with consequent change in the spectrum. The fact that the neutral complexes I and II and perchlorate complex III_B show no significant change on dissolution, indicates the absence of inter-dinuclear complex interaction in these complexes.

IR spectra

The IR spectra obtained for these complexes are in agreement with proposed structures. For the IR spectrum of the complex III_A perchlorate band is observed at 1100 cm^{-1}. The band at ~900 cm^{-1} is absent and there is no splitting of the 1100 cm^{-1} band indicating that perchlorate is tetrahedral and is outside the coordination sphere.

Magnetic and ESR data

Room temperature magnetic measurements showed μ_B 1.1–1.3 for binuclear complexes. These lower magnetic moments indicate antiferromagnetic interaction between the two metal centers at room temperature. The ESR spectra of samples I_C, II_A, II_B and II_D were carried out at room temperature in powder form and for III_A the spectra were recorded at room temperature in powder form as well as frozen solution spectra in DMF. The g values are shown in Table 2 and one spectrum is shown in Fig. 2. Observation of $g_\parallel$ and $g_\perp$ indicates tetragonal distortion and supports square planar structure. Even though the antiferromagnetic interaction is there the $\Delta ms = 2$ i.e., half field signals are not observed, probably due to large zero field splitting [6,18].

As the two metal atoms are far apart and the molecule is not flexible, the interaction can be through σ and π orbitals over the bridging atom. The p_x orbitals of the two phenoxo O^- combine with two Cu^{II} $d_{x^2-y^2}$ orbitals with unpaired electron. This results in the formation of two bonding and two antibonding molecular orbitals. The ligand atom orbitals which have less energy are comparable with the bonding molecular orbitals and ligand electrons occupy the bonding molecular orbitals. The two metal atom electrons occupy the antibonding molecular orbitals. They may be singly occupied in the two antibonding molecular orbitals, resulting in triplet state. If there is significant separation between the two antibonding orbitals there is pairing of electrons in the lower energy antibonding molecular orbital, resulting in antiferromagnetic spin coupling and a singlet state. The extent of spin exchange depends on the separation between the energies of singlet and triplet state (^2J). There is a temperature-dependent mixture of the singlet and triplet states and consequent lowering in the magnetic moment at room temperature. Long range spin exchange in bridges with delocalised π orbitals

Table 2. Electrochemical data and ESR parameters of some complexes

Compound no.	Cathodic peak potentials[a] E^1_{PC}	E^2_{PC}	$g_\parallel$	$g_\perp$
I_C	—	—	2.042	2.18
II_A	—	—	2.045	2.19
II_B	−0.97	−1.40	2.043	2.19
II_C	−0.98	−1.42	—	—
II_D	−0.98	−1.43	2.014	2.191
III_A	−0.92	−1.24	2.038	2.189

[a]Potentials are given in volts.

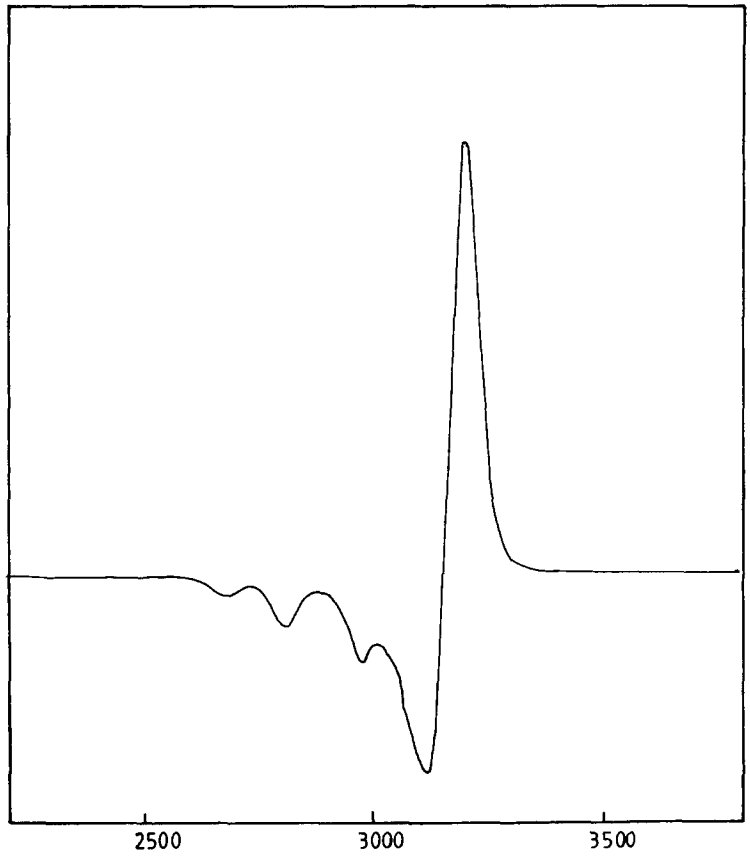


Fig. 2. The ESR spectra of a complex III_A in DMF at LNT.

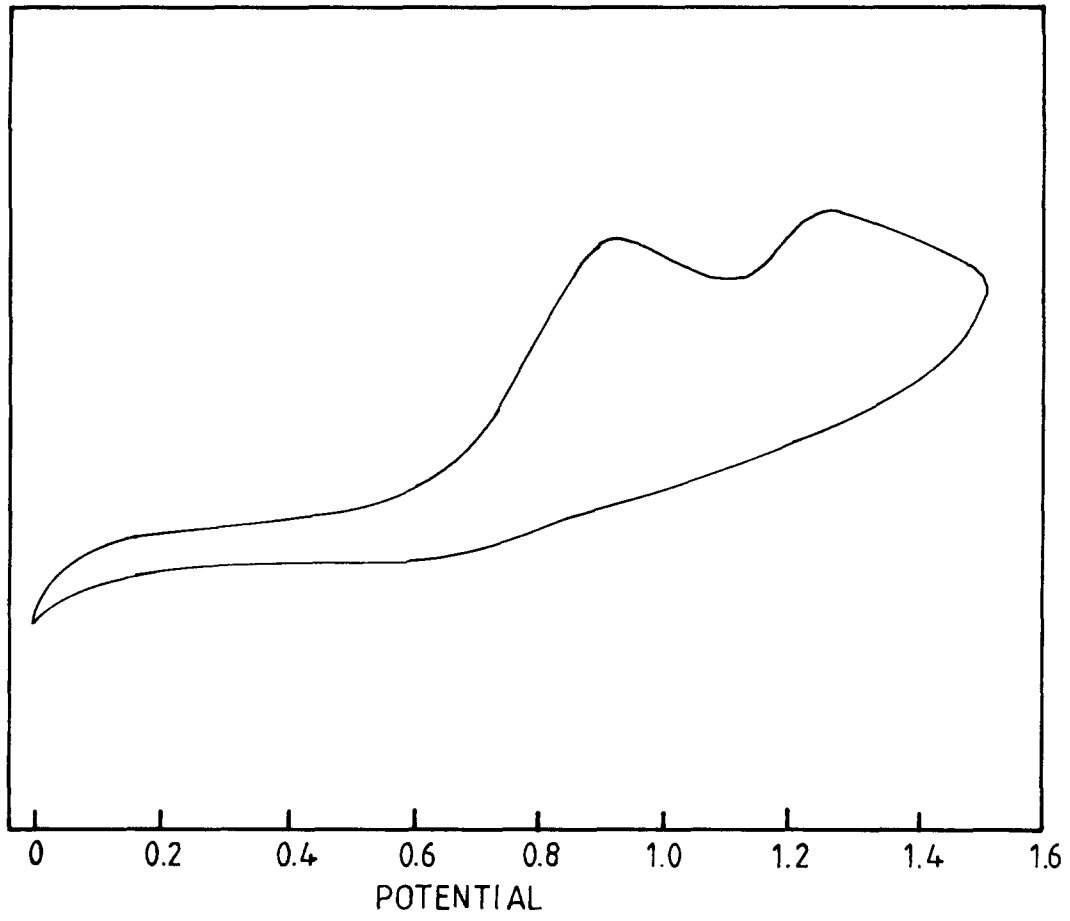


Fig. 3. Cyclic voltammogram of a complex III_A at 0.1 M. Electrolyte (tetrabutyl ammonium tetrafluoroborate) concentration in DMF.

have been extensively studied and in these cases also the exchange interaction is considered to be through σ orbitals [4,5]. In binuclear complexes with aliphatic bridges also spin exchange has been observed and X-ray crystal structure study shows that there is no interdinuclear complex interaction in such complexes [8,9], and hence antiferromagnetic interaction has been attributed to spin polarization of σ electrons. However, in the absence of X-ray and variable temperature magnetic data, attributing such a low magnetic moment, in the present study, to interaction through —CH_2— bridge is tentative and formation of tetranuclear structure, involving interdinculear interaction [19,20] cannot be ruled out.

Electrochemical studies

Cyclic voltammetric data of the complexes were recorded in DMF medium. The Schiff base ligands do not exhibit any redox peaks in the potential range investigated 0—1.7 V. The C.V. of mononuclear complex Cu (sal, ala) H_2O shows one quasireversible peak at $\sim -0.92/0.64$ corresponding to Cu^{II}/Cu^{I} couple. The electrochemical properties of four binuclear complexes II_B, II_C, II_D and III_A were studied. The electrochemical data are given in Table 2. A representative cyclic voltammogram is shown in Fig. 3. All these complexes exhibit completely irreversible behaviour. The binuclear complexes exhibit two reduction peaks which correspond to the stepwise reduction of two Cu^{II} centers to Cu^{I}:

$$Cu^{II}Cu^{II} \xrightarrow{+1e} Cu^{I}Cu^{II} \xrightarrow{+1e} Cu^{I}Cu^{I}.$$

The possibility that these two peaks correspond to simultaneous reduction of the two copper centres to Cu^{I} and finally to Cu^{0} is ruled out, since the mononuclear complex Cu (sal, ala) H_2O shows only one step reduction $Cu^{II} \rightarrow Cu^{I}$. The two-step reduction in the binuclear complexes indicates interaction between the two paramagnetic Cu^{II} centers [21]. This is in agreement with the magnetic data showing antiferromagnetic interaction.

The comparison of the reduction potentials of complexes II_B, II_C and II_D with that of complex III_A shows that the reduction of $Cu^{II} \rightarrow Cu^{I}$ in complex III_A occurs at less negative potential than that of complex II_B, II_C and II_D. This can be explained by σ and π

bonding nature of the ligands. In complexes II_B, II_C and II_D there is one phenolate O^-, one carboxylate COO^- and one imine coordination, where as in complex III_A there is one O^- coordination, one imine and one pyridyl N coordination. As there are two σ bonding in the first case the Cu^{II} gets reduced to Cu^{I} at more negative potential. In the second case III_A due to π bonding pyridyl nitrogen the $Cu^{II} \rightarrow Cu^{I}$ reduction occurs at less negative potential.

Thermogravimetric data

The thermogravimetric analysis (TGA) indicates loss of one water molecule per metal atom in the range of 180–200°C for the complexes. Loss of water at such high temperatures indicates that the H_2O molecules are coordinated and not lattice held. This is in agreement with C, H, N analysis presented in Table 1.

Acknowledgements—We thank the Department of Science and Technology (New Delhi) for the financial support for this work and Regional Sophisticated Instrumentation Centre, Indian Institute of Technology, Bombay for EPR measurements. Our thanks are due to Professor A. C. Shah, Head, Department of Chemistry, M.S. University of Baroda for providing laboratory facilities.

REFERENCES

1. N. D. Kulkarni and P. K. Bhattacharya, *Trans. Met. Chem.* 1989, **14,** 303.
2. N. D. Kulkarni, M. Jacob, K. V. Patel and P. K. Bhattacharya. *Synth. and React. Inorg. Met. Org. Chem.* 1992, **20,** 300.
3. B. Trivedi, V. Manjula and P. K. Bhattacharya. *J. Chem. Research (S)* 1994, 472.
4. T. R. Felthouse and D. N. Hendrickson. *Inorg. Chem.* 1978, **17,** 2636.
5. P. Chaudhuri, K. Oder, K. Wieghardt, S. Ghering, W. Haase, B. Nuber and J. Weiss. *J. Am. Chem. Soc.* 1988, **110,** 3657.
6. J. A. Real, M. Mollar, R. Ruiz, J. Faus, F. Lloret, M. Julve and M. P. Levisalles, *J. Chem. Soc. Dalton Trans.* 1993, 1483.
7. S. L. Stefan, M. E. Behairy, S. M. E. Khalil and H. F. A. E. Halim, *J. Chem. Res. (S)* 1994, 454.
8. R. Calvo, C. A. Steren, O. E. Piro, T. Rojo, F. J. Zuniga and E. E. Castellano. *Inorg. Chem.* 1993, **32,** 6016.
9. J. Glerup, P. A. Goodson, D. J. Hodgson and K. Michelsen. *Inorg. Chem.* 1995, **34,** 6255.
10. C. S. Marvel and N. Tarkoy, *J. Am. Chem. Soc.* 1957, **79,** 6000.
11. N. Arulsamy and P. S. Zacharias, *Trans. Met. Chem.* 1991, **16,** 255.
12. M. R. Wagner and F. A. Walker, *Inorg. Chem.* 1983, **22,** 3021.
13. D. L. Leussing and K. S. Bai, *Anal. Chem.* 1968, **40,** 575.
14. D. Heinert and A. E. Martell, *J. Am. Chem. Soc.* 1963, **85,** 188.
15. L. A. Zyzyck, H. Frummer and J. F. Villa, *J. Inorg. Nucl. Chem.* 1975, **37,** 1653.
16. S. T. Chow, D. M. Johns, C. A. McAuliffe and D. J. Machin, *Inorg. Chim. Acta* 1977, **22,** 1.
17. L. Casella, M. Gullotti and G. Pacchioni, *J. Am. Chem. Soc.* 1982, **104,** 2386.
18. Z. N. Chen, S. X. Liu, J. Qui, Z. M. Wang, J. L. Huang and W. X. Tang, *J. Chem. Soc., Dalton Trans.* 1994, 2989.
19. M. Julve, M. Verdaguer, J. Faus, F. Tinti, J. Moratal, A. Monge and E. Guiterrez-Puebla. *Inorg. Chem.* 1987, **26,** 3520.
20. J. P. Costes, F. Dahan and J. P. Laurent, *Inorg. Chim. Acta* 1995, **230,** 199.
21. E. L. Hasty, L. J. Wilson and D. N. Hendrickson, *Inorg. Chem.* 1978, **17,** 1834.

Pergamon

PII: S0277-5387(96)00273-2

Polyhedron Vol. 16, No. 3, pp. 495–505, 1997
Copyright © 1996 Elsevier Science Ltd
Printed in Great Britain. All rights reserved
0277-5387/97 $17.00+0.00

Synthesis, crystal structures and vibrational spectra of zinc hypophosphites

Peter A. Tanner,[a]* Liu Yu-Long[a] and Thomas C. W. Mak[b]

[a]Department of Biology and Chemistry, City University of Hong Kong, Tat Chee Avenue, Kowloon, Hong Kong

[b]Department of Chemistry, The Chinese University of Hong Kong, Shatin, New Territories, Hong Kong

(Received 7 April 1996; accepted 28 May 1996)

Abstract—The preparation, crystal structure, infrared and Raman spectra are reported for zinc hypophosphites, $Zn(hyp)_2$ and zinc hypophosphite monohydrate, $Zn(hyp)_2 \cdot H_2O$ (hyp = H_2PO_2). Both structures are polymeric, and the coordination geometry of zinc is octahedral. In $Zn(hyp)_2$ the coordination is to six oxygen atoms of the hypophosphite groups, and in $Zn(hyp)_2 \cdot H_2O$, *via* one oxygen atom of a water molecule, and five hypophosphite oxygen atoms. The hypophosphite vibrational modes give rise to multiple structures in the infrared and Raman spectra, and these bands are interpreted under unit cell group selection rules in a consistent manner with the crystallographic data. The infrared spectral region between 1940–2350 cm^{-1} comprises numerous combination bands, whose intensities are enhanced through Fermi resonance with the P—H stretching modes. The breadth and wavenumbers of water modes observed in the vibrational spectra of $Zn(hyp)_2 \cdot H_2O$ indicate the presence of medium-strong hydrogen bonding to hypophosphito-oxygen atoms. The X-ray data show a slight lengthening of the mean P—O bond distance, and shortening of the mean P—H distance for the hydrated compound. Whereas the changes in PH_2 stretching, and PH_2 and PO_2 bending wavenumbers between the two compounds are as expected from this, the PO_2 stretching modes show that change of the unit cell group symmetry must also be considered. The mean Zn—O bond distance is similar (near 2.1 Å) in both $Zn(hyp)_2$ and $Zn(hyp)_2 \cdot H_2O$, and the infrared active Zn—O antisymmetric stretching modes are observed near 328 and 300 cm^{-1}, respectively. Structural factors, in addition to the cation ionic radii, determine the trends in M^{II}-(O-hypophosphito) antisymmetric stretching modes for other divalent cations. Copyright © 1996 Elsevier Science Ltd

Keywords: infrared; Raman; hypophosphite complex; metal–ligand stretching vibration.

We have previously reported crystallographic and spectroscopic data for uranium(IV) hypophosphite compounds, $U(H_2PO_2)_4$ [1] and $UCl(H_2PO_2) \cdot 2H_2O$ [2] and $UBr(H_2PO_2)_3 \cdot 2H_2O$ [3]. In all of these compounds, the coordination geometry of the cation is square antiprismic. All structures were found to be polymeric, with the hypophosphito group acting as a bridging ligand between tetravalent cationic centres. The present study extends the investigations of the structural and spectral characteristics of hypophosphite compounds to those of the divalent cation zinc, for which the usual coordination number is four or six. Far infrared spectra and power diffraction data have previously been reported for $Zn(hyp)_2$ [4] (hyp = H_2PO_2). Brun *et al.* [5] have also reported infrared spectra and power diffraction data for other anhydrous divalent metal hypophosphites. Mayants and Matrosov [6] have reported infrared data for a compound identified as $Zn(hyp)_2 \cdot 0.5H_2O$ only on the basis of phosphorus elemental analysis.

EXPERIMENTAL

Syntheses of $Zn(hyp)_2$ *and* $Zn(hyp)_2 \cdot H_2O$

Both compounds were prepared from the reaction of 2 g of ZnO, or $ZnSO_4 \cdot 7H_2O$ (RG, Reidel-de-Haën) with 20 cm^3 of hypophosphorous acid (50% aqueous, RG, Reidel-de-Haën). The anhydrous compound was prepared at temperatures between 40–60°C, and the

* Author to whom correspondence should be addressed

hydrate between 4–25°C. Crystals were filtered from the liquor, quickly washed with water and air-dried. The crystals of the monohydrate were well-formed, stable in air, and up to 1 cm in length. Small needles were obtained, in several preparations, for the anhydrous compound, and thin plates formed on the surface of the solution in others.

Analytical results

A survey analysis of a single crystal of $Zn(hyp)_2 \cdot H_2O$ by a Jeol T300 scanning electron microscope, using electron microprobe analysis, showed only the presence of the elements Zn and P, with a mass ratio 0.98 (s.d. = 0.06). The calculated mass ratio Zn/P for $Zn(hyp)_2 \cdot H_2O$ is 1.055. Calc. (found) % by mass for $Zn(hyp)_2 \cdot H_2O$: Zn 30.6 (30.8 ± 0.13 by AAS); P 29.0 (29.8 by ICP-AES); H 2.8 (2.7 ± 0.23 by CHN analyser); H_2O 8.4 % (9.7% by loss in mass at 105°C). The Raman spectrum of the product obtained by heating the monohydrate at 105°C is identical with the spectrum of freshly prepared crystals at 40–60°C, sealed immediately in a capillary tube. Some bands in the infrared spectra of the dehydration product, at 105°C, of the monohydrate showed different relative intensities from those in the spectra of freshly-prepared samples, however. This change in composition must have occurred during the mulling process, since the Raman spectra show that these two initial products are identical. Very weak, sharp bands at 1661, 3324, 3449 and 3531 cm^{-1} were observed in the infrared spectra of $Zn(hyp)_2$, attributed to $\delta(H_2O)$, $2\delta(H_2O)$, ν_s, ν_{as} (H_2O) of weakly bound water. Calc. (found) % by mass for $Zn(hyp)_2$: Zn 33.5 (33.3 ± 0.10); P 31.7 (28.0); H 2.1% (2.0 ± 0.27).

Spectroscopic measurements

Raman spectra were recorded at room temperature using < 20 mW of 476.5 nm or 514.5 nm argon ion laser radiation. The resolution of the Spex 1403DM system was set at 2 cm^{-1}. Infrared Nujol mull spectra (4000–400 cm^{-1}) were recorded using Bomen MB120 and Perkin Elmer PE1600 spectrometers.

X-ray analyses

The details of the crystal parameters, data collection and structure refinement are given in Table 1. Raw intensities collected on a Nicolet R3m/V four-circle diffractometer at 294 K were processed with the profile fitting procedure of Diamond [7], and corrected for absorption using ψ-scan data. [8]. The zinc atom was located by the Patterson method, and the coordinates of the other non-hydrogen atoms and the hydrogens of the aqua ligands were obtained from successive difference Fourier synthesis. The hydrogen atoms of independent hypophosphite groups were generated geometrically. All non-hydrogen atoms were subjected to anisotropic refinement, and the hydrogen atoms were fixed and assigned the same isotropic temperature factor in structure factor calculations. Computations were performed using the SHELXTL–PLUS programme package [9] on a 486 PC. Analytic expressions of scattering factors for neutral atoms were employed, and anomalous dispersion corrections were incorporated [10]. The residual extrema in the last difference map all lie in the neighbourhood of the zinc atom.

RESULTS

Crystal structures of $Zn(hyp)_2$ *and* $Zn(hyp)_2 \cdot H_2O$

The atomic coordinates and thermal parameters are listed as supplementary data. Bond lengths and bond angles are given in Table 2.

$Zn(hyp)_2$. Figure 1(a) shows that the coordination sphere about the zinc atom comprises four symmetry-related oxygens derived from O(1), and two more distant oxygens from O(2), in a slightly distorted octahedral geometry. The two independent phosphorus atoms in the unit cell, P(1) and P(2), are each situated at a C_{2v} symmetry site. The bond distance P(1)—O(1) is about 1% longer than the distance P(2)—O(2). Both hypophosphito ligands exhibit a bridging complexation mode to generate a polymeric layer-type structure, but the oxygens of type O(1) are equidistant from two zinc atoms, whereas those of type O(2) coordinate with one zinc atom only. A stereoview of the crystal structure is shown in Fig. 2(a); note that the coordination layers match the (001) family of planes.

$Zn(hyp)_2 \cdot H_2O$. The eight phosphorus atoms in the unit cell form two distinct sets, 4P(1) and 4P(2), each with C_1 site symmetry. The phosphorus–oxygen bond distances in each of the hypophosphite anions are slightly (< 1%) different. For P(1), the bonds are labelled P(1)—O(1) and P(1)—O(2) and for P(2), the hypophosphito oxygens are O(3) and O(4). As shown in Fig. 1(b), the 6-coordination geometry of zinc involves one oxygen, O(1W), of a water molecule, three oxygens of P(2), and two oxygens of P(1). The Zn—O bond distances are shortest for the coordination with the oxygens of P(1). The longer Zn—O(1W) distance is similar to that of Zn—O(4c), with the Zn—O(4b) distance being longest. The O(4) atoms are linked to two zinc atoms, whereas all other oxygens link to only one zinc atom. The hypophosphito groups therefore bridge two or three zinc centres, generating a three-dimensional polymeric network. The hydrogen bonds between the water molecule and the oxygen of P(1), O(1W)...O(1g), are nearly linear, and comparable in length to those in ice. Weaker, bent hydrogen bonds, O(1W)...O(1h), also involve the water molecules. A stereoview of the crystal structure is shown in Fig. 2(b).

Table 1. Data collection and processing parameters

Molecular formula	$Zn(H_2PO_2)_2$	$Zn(H_2PO_2)_2 \cdot H_2O$
Relative molecular mass	195.3	213.36
Colour and habit	colourless flat prism	colourless prism
Crystal size (mm^3)	$0.12 \times 0.20 \times 0.40$	$0.40 \times 0.40 \times 0.50$
Crystal system	orthorhombic	monoclinic
Space group	*Pmma* (No. 51)	$P2_1/c$ (No. 14)
a (Å)	6.479(1)	7.685(3)
b (Å)	5.365(1)	7.376(1)
c (Å)	7.408(1)	10.468(2)
β ( )	—	104.16(2)
V ($Å^3$)	257.48(6)	575.4(2)
Z	2	4
$F(000)$	192	424
Density (calcd)(g cm^{-3})	2.520	2.463
Radiation	graphite-monochromatized	MoK_α, $\lambda = 0.71073$ Å
Standard reflections	(1, 2, 2); (3, 2, 1)	(−1, 2, 1); (3, 2, 4)
Intensity variation	±0.5%	±0.9%
R_{int} (from merging of equiv. reflections)	0.0288	0.0069
Absorption coefficient (mm^{-1})	5.29	4.76
Mean μr	0.40	0.70
Transmission factors	0.284 to 0.451	0.170 to 0.269
Scan type and rate (deg min^{-1})	ω-scan; 2.02-19.53	ω-scan; 3.50-29.30
Scan range	0.80° below K_{α_1} to 0.80° above K_{α_2}	0.70° below K_{α_1} to 0.70° above K_{α_2}
Background counting	stationary counts for one-fifth of scan time at each end of scan range	
Collection range	$0 \leqslant h \leqslant 11$; $-13 \leqslant k \leqslant 13$; $-16 \leqslant l \leqslant 16$; $2\theta_{max} = 100$	$0 \leqslant h \leqslant 16$; $0 \leqslant k \leqslant 15$; $-22 \leqslant l \leqslant 21$; $2\theta_{max} = 100$
Unique data measured	1525	5966
Obs. data with $\lvert F_o \rvert \leqslant 4\sigma \lvert F_o \rvert$, n	1145	4468
No. of variables, p	35	93
Extinction correction	$\chi = 0.0085(8)$ where $F^* = F[1 + 0.002\chi F^2/\sin(2\theta)]^{-1/4}$	$\chi = 0.0013(2)$
Weighting scheme	$w = [\sigma^2 \lvert F_o \rvert + 0.0003 \lvert F_o \rvert^2]^{-1}$	
R_F	0.027	0.036
wR	0.030	0.047
S	1.13	1.62
Largest and mean Δ/σ	0.000, 0.000	0.127, 0.011
Residual extrema in final difference map (e $Å^{-3}$)	+1.19 to −1.19	+1.59 to −0.93

$R_F = \Sigma \lVert F_o \rvert - \lvert F_c \rVert / \Sigma \lvert F_o \rvert$; $wR = [\Sigma w^2(\lvert F_o \rvert - \lvert F_c \rvert)^2 / \Sigma w^2 \lvert F_o \rvert^2]^{1/2}$; $S = [\Sigma w(\lvert F_o \rvert - \lvert F_c \rvert)^2/(n-p)]^{1/2}$.

Vibrational spectra of $Zn(hyp)_2$ *and* $Zn(hyp)_2 \cdot H_2O$

The free C_{2v} hypophosphite anion has nine non-degenerate modes of vibration:

$$\Gamma(\text{vib}, C_{2v}) \in \{4a_1; a_2; 2b_1; 2b_2\} \quad (1)$$

of which all are potentially Raman and infrared active, except for the a_2 mode which is infrared inactive. Normal coordinate calculations, deuteration studies, and the use of polarized radiation (cited in [2]), have enabled the assignments of specific vibrational motions from infrared and Raman data. The present study aimed to point out the distinctions between the spectra of $Zn(hyp)_2$ and $Zn(hyp)_2 \cdot H_2O$, and to investigate the spectral consequences resulting from the polymeric, rather than discrete molecular ion structures.

The Raman spectra of $Zn(hyp)_2$ and $Zn(hyp)_2 \cdot H_2O$ are shown in Fig. 3, and the wavenumbers are tabulated together with infrared data in Table 3. In many cases, multiple structure is observed in the spectra, and this correlates with one of the hypophosphite normal modes of vibration through the unit cell group analysis.

Spectra of $Zn(hyp)_2$

For $Zn(hyp)_2$, each molecular anion normal mode associated with each type of phosphorus atom transforms unchanged at the respective $H_2PO_2^-$ C_{2v} site, and gives rise to two unit cell group (C_{2h}) modes. For a_1 or a_2 molecular ion modes, these unit cell group modes are $a_g + a_u$, whereas for b_1 or b_2 modes, the

Table 2. Bond lengths (Å) and bond angles (°)

$Zn(hyp)_2$			
Zn(1)—O(1)	2.160(1)	Zn(1)—O(2)	2.003(1)
P(1)—O(1)	1.513(1)	P(1)—H(1)	1.35(2)
P(2)—O(2)	1.498(1)	P(2)—H(2)	1.35(3)
O(1)—Zn(1)—O(2)	89.8(1)	O(1)—Zn(1)—O(1b)	81.1(1)
Zn(1)—O(1)—Zn(1b)	97.2(1)	O(1)—P(1)—H(1)	108.1(5)
H(1)—P(1)—H(1a)	109(2)	O(1)—P(1)—O(1a)	115.2(1)
Zn(1)—O(1)—P(1)	127.9(1)	O(2)—P(2)—H(2)	110.0(5)
H(2)—P(2)—H(2b)	95.(1)	O(2)—P(2)—O(2b)	119.1(1)
Zn(1)—O(2)—P(2)	129.9(1)		
Symmetry transformations:	(a) $(0.5-x, -y, z)$; (b) $(0.5-x, 1-y, z)$; (c) $(-x, 1-y, -z)$; (d) $(-0.5+x, y, -z)$.		
$Zn(hyp)_2 \cdot H_2O$			
Zn(1)—O(1)	2.069(1)	Zn(1)—O(3)	2.090(1)
Zn(1)—O(1W)	2.118(2)	Zn(1)—O(2a)	2.048(1)
Zn(1)—O(4b)	2.147(1)	Zn(1)—O(4c)	2.113(1)
P(1)—O(1)	1.514(1)	P(1)—O(2)	1.501(1)
P(1)—H(1)	1.234(3)	P(1)—H(2)	1.222(3)
P(2)—O(3)	1.504(1)	P(2)—O(4)	1.517(1)
P(2)—H(3)	1.214(2)	P(2)—H(4)	1.230(2)
O(1W)—H(1WA)	0.860(3)	O(1W)—H(1WB)	0.860(3)
O(1)—Zn(1)—O(3)	96.2(1)	O(1)—Zn(1)—O(1W)	91.7(1)
O(3)—Zn(1)—O(1W)	171.2(1)	O(1)—Zn(1)—O(2a)	92.5(1)
O(3)—Zn(1)—O(2a)	94.4(1)	O(1W)—Zn(1)—O(2a)	89.1(1)
O(1)—Zn(1)—O(4b)	172.4(1)	O(3)—Zn(1)—O(4b)	89.6(1)
O(1W)—Zn(1)—O(4b)	82.2(1)	O(2a)—Zn(1)—O(4b)	92.0(1)
O(1)—Zn(1)—O(4c)	95.4(1)	O(3)—Zn(1)—O(4c)	89.6(1)
O(1W)—Zn(1)—O(4c)	85.9(1)	O(2a)—Zn(1)—O(4c)	170.7(1)
O(4b)—Zn(1)—O(4c)	79.7(1)	O(1)—P(1)—O(2)	114.6(1)
O(1)—P(1)—H(1)	98.5(1)	O(2)—P(1)—H(1)	112.5(1)
O(1)—P(1)—H(2)	112.4(1)	O(2)—P(1)—H(2)	114.8(1)
H(1)—P(1)—H(2)	102.1(2)	Zn(1)—O(1)—P(1)	129.5(1)
P(1)—O(2)—Zn(1d)	125.8(1)	O(3)—P(2)—O(4)	116.6(1)
O(3)—P(2)—H(3)	103.7(2)	O(4)—P(2)—H(3)	113.5(1)
O(3)—P(2)—H(4)	111.5(2)	O(4)—P(2)—H(4)	110.8(1)
H(3)—P(2)—H(4)	99.2(2)	Zn(1)—O(3)—P(2)	128.4(1)
P(2)—O(4)—Zn(1e)	126.6(1)	P(2)—O(4)—Zn(1f)	132.5(1)
Zn(1e)—O(4)—Zn(1f)	100.3(1)	Zn(1)—O(1W)—H(1WA)	134.2(2)
Zn(1)—O(1W)—H(1WB)	123.3(2)	H(1WA)—O(1W)—H(1WB)	93.0(3)
Hydrogen bonds:			
O(1W)···O(1g)	2.796	O(1W)···O(3h)	2.962
O(1W)—H(1WA)···O(1g)	171.4	O(1W)—H(1WB)···O(1h)	140.4
Symmetry transformations:	(a) $(1-x, -0.5+y, 0.5-z)$; (b) $(-x, -0.5+y, 0.5-z)$; (c) $(x, 0.5-y, -0.5-y, -0.5-z)$; (d) $(1-x, 0.5+y, 0.5-z)$; (e) $(-x, 0.5+y, 0.5-z)$; (f) $(x, 0.5-y, 0.5+z)$; (g) $(1-x, -y, -z)$; (h) $(-x, -y, -z)$.		

unit cell group modes are $b_g + b_u$. The gerade unit cell group modes are Raman active, and the ungerade modes are infrared active. To summarize, each molecular hypophosphite mode is expected to give rise to two infrared bands and two Raman bands. The difference between the infrared (or the Raman) wavenumbers of the molecular anion mode reflects the different environments of the two hypophosphite sites. The difference between the infrared and the Raman wavenumbers for a vibration at a particular site reflects the strength of the unit cell group vibrational coupling. The observed spectra are too complex for a simple interpretation, but are consistent with the above selection rules in that no more than two infrared and two Raman bands are observed for each moiety mode and that the mutual exclusion rule is obeyed (Table 3).

Spectra of $Zn(hyp)_2 \cdot H_2O$

In this case, the hypophosphite site group for each of the two sites is C_1 and the unit cell group is C_{2h}.

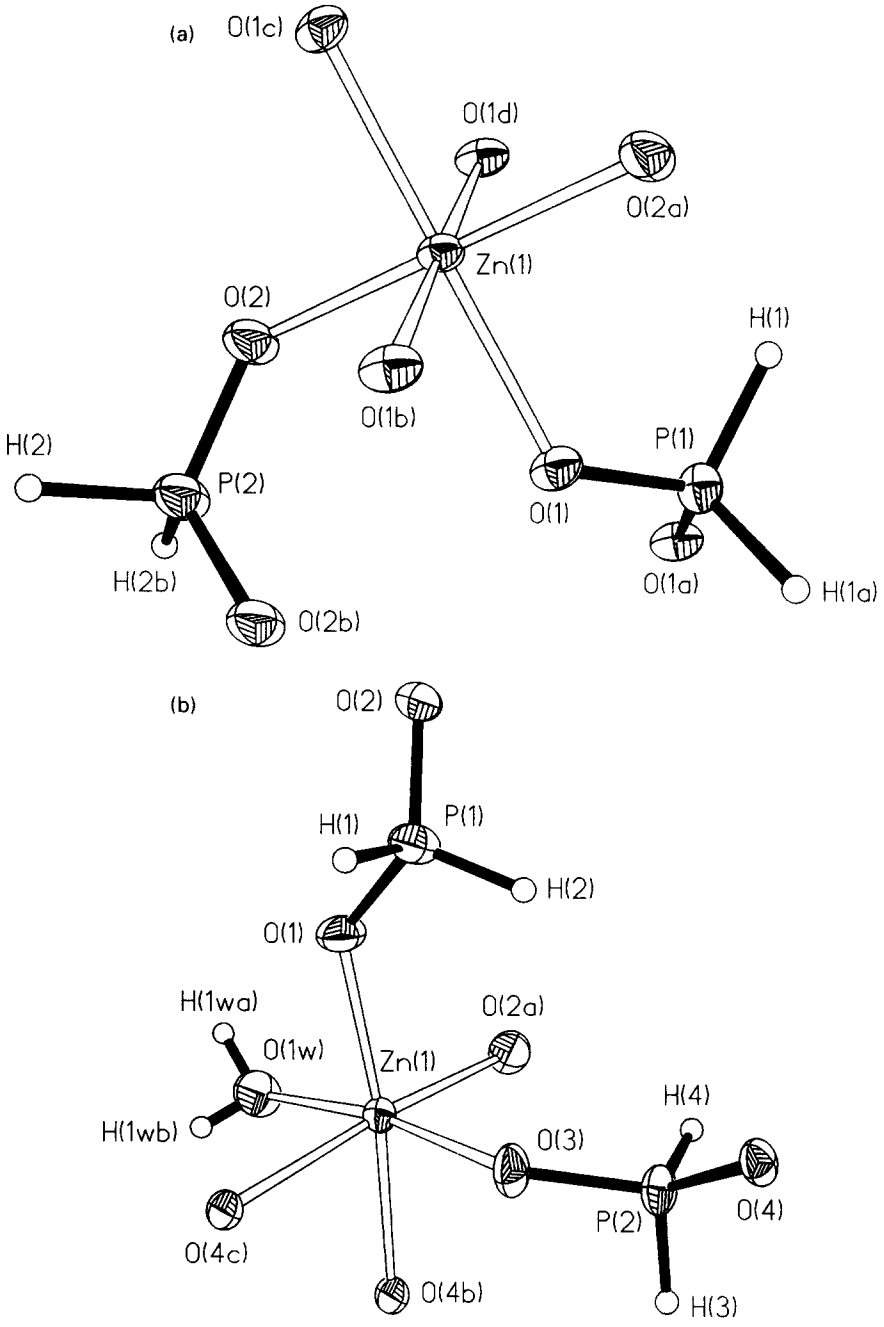


Fig. 1. Perspective views showing the atom numbering schemes and the coordination geometries about the zinc atoms in (a) $Zn(hyp)_2$ and (b) $Zn(hyp)_2 \cdot H_2O$. Symmetry codes are as given in Table 2.

The selection rules indicate that at each hypophosphite site, each parent anion mode gives rise to two potentially active infrared bands and two Raman bands in each case: i.e. to 4 IR and 4 Raman bands, with mutual exclusion. It is clear that not all of these are resolved in the room temperature unpolarized spectra, but more features are observed than in the spectra of $Zn(hyp)_2$. Other differences between the infrared spectra of the two compounds arise from the consequences of the presence of water in $Zn(hyp)_2 \cdot H_2O$. The water modes of vibration in this crystal are assigned in Table 3. Medium-strong hydrogen-bonding is indicated from the broad, medium-energy OH_2 stretching bands. The PO_2 scissor mode is at higher energy in $Zn(hyp)_2 \cdot H_2O$ than the anhydrous compound, since the longer mean P—O bond distance (1.509 Å, compared with 1.506 Å in $Zn(hyp)_2$) accompanies the closure of the (mean) OPO angle by 1.6°. A longer (mean) P—O bond distance in $Zn(hyp)_2 \cdot H_2O$ would enable contraction of the P—H bond length and an opening of the HPH angle and this is reflected by the PH_2 stretching and scissoring modes

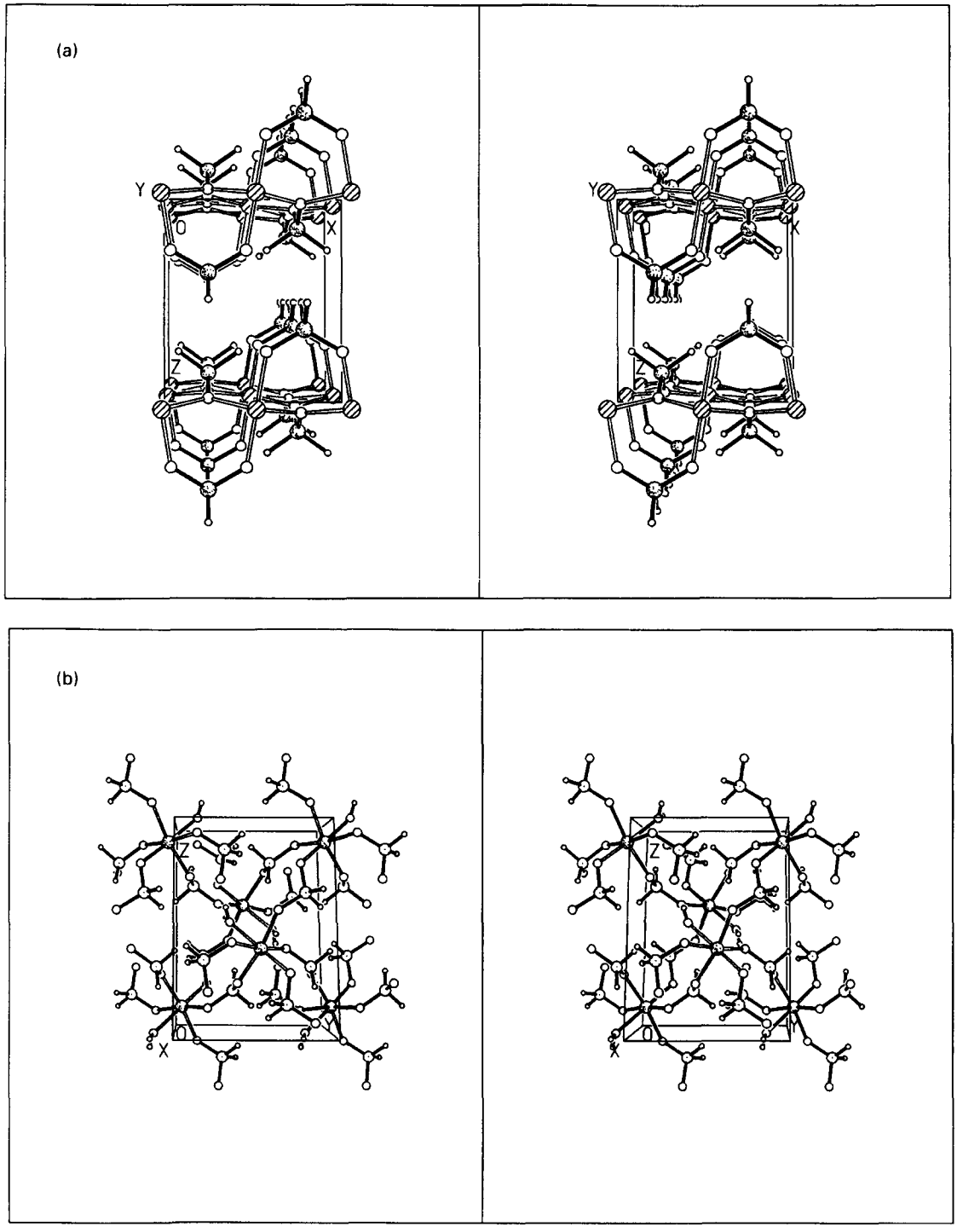


Fig. 2. Stereoview of the crystal structures of (a) $Zn(hyp)_2$ (the origin of the unit cell lies at the upper left corner, with x pointing from left to right, y toward the reader, and z downward) and (b) $Zn(hyp)_2 \cdot H_2O$ (the origin of the unit cell lies at the lower left corner with x toward the reader, y from left to right and z upward).

of the two compounds. The wavenumber of the P—O antisymmetric stretch normally shifts to lower energy upon hydrogen bonding [11,12]. However, in the present case, the changes in spectral selection rules from one crystal to another may complicate these simple arguments and a new, high energy feature is observed at 1180 cm^{-1} in the hydrated compound.

The low energy profiles of the PH_2 stretching bands in the infrared and Raman spectra of $Zn(hyp)_2$ and $Zn(hyp)_2 \cdot H_2O$ are broadened, and numerous features

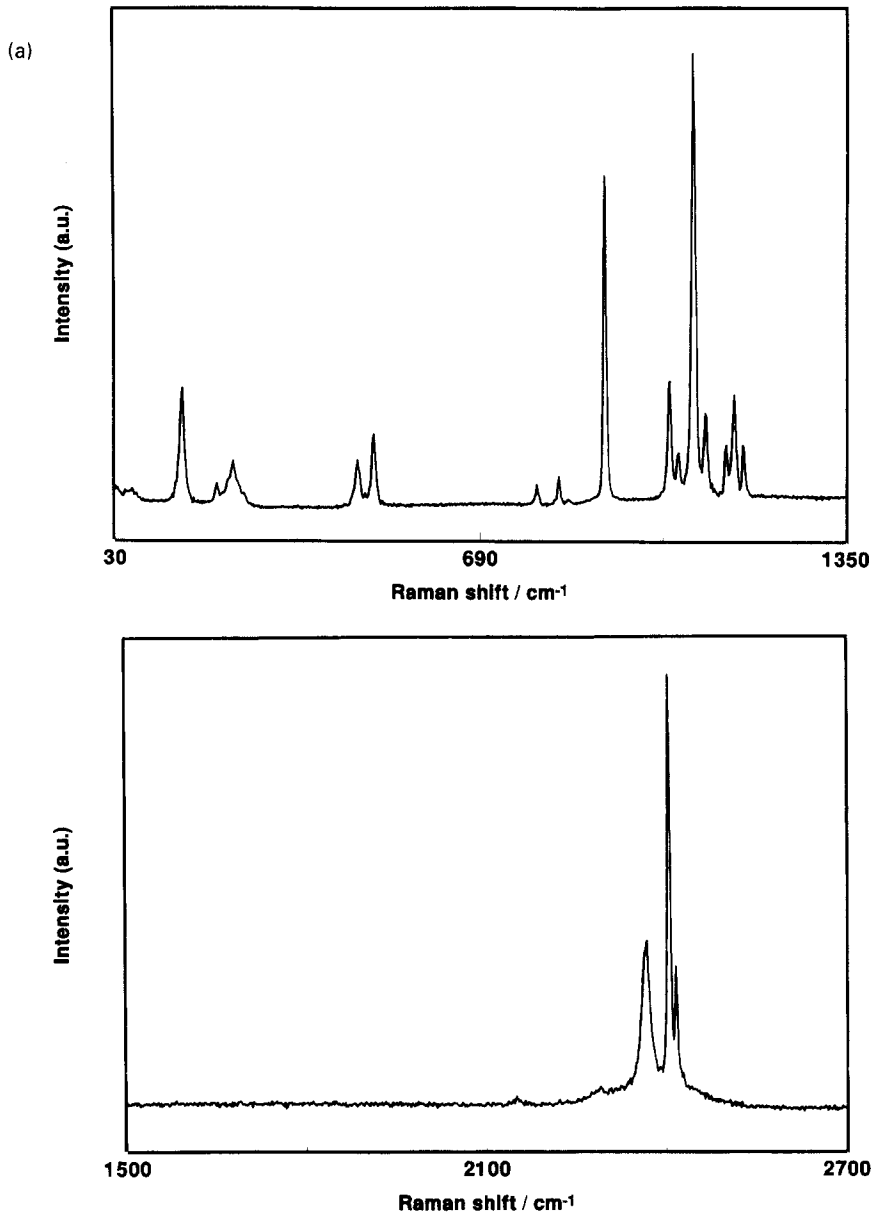


Fig. 3. 300 K Roman spectra of (a) $Zn(hyp)_2$ and (b) $Zn(hyp)_2 \cdot H_2O$ between 30 and 2700 cm^{-1}.

are superimposed. These infrared combination bands are assigned, in the case of $Zn(hyp)_2 \cdot H_2O$, in Table 4, and part of their intensities may be attributed to Fermi resonance with the PH_2 stretching modes. The assignments follow zero wavevector unit cell group selection rules, so that each combination band comprises one infrared active and one Raman active mode. To high energy of the PH_2 stretching bands, weak combination bands are observed which may involve one quantum of the OH_2 bending mode together with one quantum of the PH_2 rock, and/or combinations of P—H stretching modes with lattice modes (Table 4). Very weak bands are observed in the Raman spectrum near 1858 cm^{-1} and between 1940–1962 cm^{-1}, which are assigned to combination modes involving the PO_2 symmetric stretch with the PH_2 rock and PH_2 twist respectively.

Zinc–oxygen modes of vibration

Abenoza *et al.* [13] have assigned Mg—O vibrational modes in $Mg(hyp)_2 \cdot 6H_2O$, using a model of O_h site symmetry for the $Mg(OH_2)_6^{2+}$ moiety. The infrared active Mg—O antisymmetric stretch and the Raman active symmetric stretch were assigned at 430 cm^{-1} and 363 cm^{-1}, respectively. The Mg—O bond distances in $Mg(hyp)_2 \cdot 6H_2O$ (to O in H_2O, near

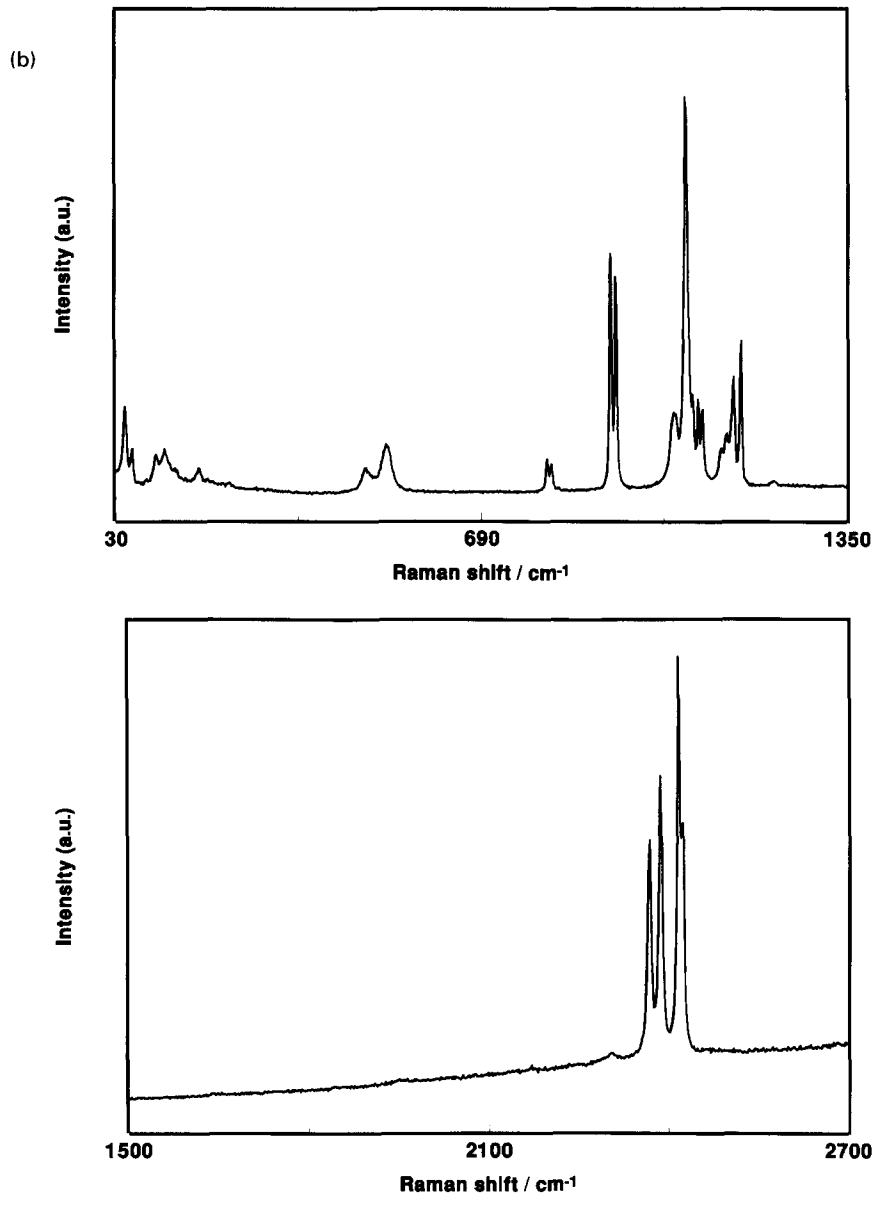


Fig. 3 – *continued.*

2.055 ± 0.011 Å [14]), are shorter than the mean Zn—O bond distances in $Zn(hyp)_2$ (to O in $H_2PO_2^-$, 2.108 Å) and $Zn(hyp)_2 \cdot H_2O$ (2.098 Å). The far infrared spectrum of $Zn(hyp)_2$ has been reported by Brun and Dumail [4]. A medium intensity band at 323 cm^{-1} and a weaker feature at 355 cm^{-1} were assigned to Zn—O antisymmetric stretching. The wavenumber of the stronger band is in agreement with the present study, and the bands could be attributed to ε_u and α_{2u} (D_{4h}) molecular point group components, associated with stretching of the long and short Zn—O bonds. This interpretation would neglect the coupling between different metal centres. The Raman data from the present study may indicate a symmetric stretching mode of Zn—O character at lower energy, near 245 and 234 cm^{-1} in $Zn(hyp)_2$ and $Zn(hyp)_2 \cdot H_2O$, respectively. Numerous Raman bands are observed below 230 cm^{-1} for $Zn(hyp)_2$ and $Zn(hyp)_2 \cdot H_2O$, so that specific assignments are tentative (Table 3) and are based upon the study of Abénoza and Martin [15].

A survey of the data for infrared-active M^{II}—O(hypophosphito) stretching mode wavenumbers in other complexes is collected in Table 5. $Cu(hyp)_2$ readily decomposes but has been shown to be isomorphous with $Zn(hyp)_2$ and $Co(hyp)_2$ [4]. Our infrared spectrum of $Cu(hyp)_2$ shows a resemblance to that of $Zn(hyp)_2$, but the wavenumber of ν(Cu—O) is different from that previously reported [19]. The G matrix element of this mode ν_{as} (M—O) in O_h symmetry is $(m_M)^{-1} + 2(m_O)^{-1}$, being virtually independent of the mass of the cation M. Although the wavenumbers show some relation to the cation ionic radii, it is clear

Table 3. Wavenumbers of bands in the room temperature Raman and infrared spectra of $Zn(hyp)_2$ and $Zn(hyp)_2 \cdot H_2O$

$Zn(hyp)_2$		$Zn(hyp)_2 \cdot H_2O$		Assignment[a]
Raman	Infrared	Raman	Infrared	
Wavenumber (cm^{-1})		Wavenumber (cm^{-1})		
48 mw		48 m		rot. or
60 mw		60 mw		transl.
		70 vw		ZnO_6
		86 vw		rot. H_2PO_2
		102 mw		rot. or trans. ZnO_6
116 w		118 mw		rot. H_2PO_2
		136 w		rot. H_2PO_2
152 m		180 mw		$\delta(ZnO_6)$
		196 w		$\delta(ZnO_6)$
228 mw		222 vw		$\delta(ZnO_6)$
245 m		234 vw		$\nu_s(ZnO_6)$
	328 ± 2 w		300 m	$\nu_{as}(ZnO_6)$
			323 w	$\nu_{as}(ZnO_6)$
			357 sh	$\nu_{as}(ZnO_6)$
434 vw				
469 m	471 mw	480 mw	475 m	PO_2 scissor, a_1
497 m	500 ms	518 m	515 ms	
792 w	798 ms	808 m	808 w	PH_2 rock, b_1
834 w	821 ms	816 m	817 s	
915 s	915 w	922 s	924 vw	PH_2 twist, a_2
	919 sh	932 s	932 vw	
1032 m		1036 bm	1024 s	PO_2 sym. str., a_1
1048 mw	1050 s	1058 vs	1043 ms	
1074 s	1071 ms	1070 m	1071 ms	PH_2 wag, b_2
	1081 ms	1080 m		
1097 m	(1094)	1088 m	1085 m	
	1123 s	1122 mw	1126 s	
1133 mw	1141 s	1132 mw	1138 s	PH_2 scissor, a_1
1148 m	1150 ms	1144 m	1146 s	
1165 mw	1160 s	1158 ms	1154 s	PO_2 antisym. str., b_2
1214 vw		1218 w	1180 s	
2300 wb	2291 w	2306 w	2302 w	combination
	2346 w		2344 m	bands, see Table 4
2367 s	2364 s	2368 ms	2362 s	$\nu_s(PH_2)$
			2385 ms	
2405 vs	2406 m	2416 s	2411 ms	and
2416 s	2414 m	2424 m	2421 m	$\nu_{as}(PH_2)$
			583 ms	water libration
		*ca*1650 vw	1631 s	$\delta(H_2O)$
			3230 m	$2\delta(H_2O)$
			3360 ms	$\nu_s(H_2O)$ and $\nu_{as}(H_2O)$
			3432 m	

[a]The internal $H_2PO_2^-$ modes are labelled according to the parent C_{2v} vibrations. Extensive mixing of the vibrational modes occurs, especially in the region 1000–1200 cm^{-1}, so that the assignment of a band to a specific vibrational coordinate is not implied.

that other factors such as the different crystal structures play a role in their magnitudes.

DISCUSSION

The compounds $Zn(hyp)_2$ and $Zn(hyp)_2 \cdot H_2O$ exhibit two- and three-dimensional polymeric structures respectively, with the hypophosphite anions acting as bridging ligands between metal centres. The zinc coordination is octahedral, but some hypophosphite oxygen atoms coordinate to one zinc atom only whereas others coordinate to two. The essential difference in the zinc coordination sphere for the two compounds is that one of the six oxygen atoms corresponds to a water molecule in the case of $Zn(hyp)_2 \cdot H_2O$. It is not surprising that the vibrational spectra of these polymeric compounds are also complex, but the multiple structure observed for internal anion modes in

Table 4. Combination bands observed in the infrared spectrum of $Zn(hyp)_2 \cdot H_2O$ between 1940–2485 cm^{-1}

Wavenumber(cm^{-1})	Assignment[a]
1944 vw	R808+IR1138 = 1946; R1132+IR808 = 1940
1960 vw	R808+IR1154 = 1962; R1158+IR808 = 1966
	R816+IR1146 = 1962; R1144+IR817 = 1961
1969 vw	R816+IR1154 = 1970; R1158+IR817 = 1975
1988 vw	R808+IR1180 = 1988
1994 vw	R817+IR1180 = 1997; R922+IR1071 = 1993
2011 vw	R1080+IR932 = 2012; R922, 932+IR1085 = 2012±5
2064 vw	R924+IR1138 = 2062; R1036+IR1024 = 2060
2076 vw	R932+IR1146 = 2078; R1144+IR932 = 2076; R1036+IR1043 = 2079
2143 sh	R1122+IR1024 = 2146
2158 vw	R1132+IR1024 = 2156; R1036+IR1126 = 2162
2166 w	R1122+IR1043 = 2165
2216 vw	R1144+IR1073 = 2217; R1070+IR1146 = 2216
2242 sh, b	R1158+IR1085 = 2243
2276 sh, b	R1144, 1158+IR1126 = 2277±7
2303 w	R1158+IR1146 = 2304; R1144+IR1154 = 2298
2345 w	R1158+IR1180 = 2338; R1218+IR1126 = 2344
2449 vw	R816+IR1631 = 2447; R86+IR2362 = 2448
2462 w	R102+IR2362 = 2464
2482 w	R118+IR2362 = 2480

[a]R = Raman; IR = infrared.

Table 5. Antisymmetric metal[II]–oxygen stretching wavenumbers in some hypophosphito complexes

Complex $M(hyp)_2$	Ionic radius of M^{2+} (Å)[a]	Crystal space group of $M(hyp)_2$	Wavenumber(cm^{-1}) of $\nu_{as}(M^{II}—O)$
Zn	0.88	Pmma (Z = 2)[b]	355 w, 323 m[c]
Co	0.88	Pmma (Z = 2)[b,c]	345 w, 303 m[c]
Cu	0.91	Pmma (Z = 2)[b,c]	394[b]
Cd	1.09	$P2_1/c$ (Z = 4)[d]	312, (255)[d]
Ca	1.14	C2/c (Z = 4)[d]	330, (280)[d]
Sr	1.32	Ccca (Z = 4)[d]	313[d]
Pd	0.79	Ccca (Z = 4)[d]	275[d]
Ba	1.49	Ccca (Z = 4)[d]	249[d]

[a]Reference 18, coordination number = 6.
[b]This study.
[c]Reference 4.
[d]Reference 5.

the infrared and Raman spectra is consistent with the predictions of unit cell group selection rules. It is emphasized that the vibrational spectra are not amenable to interpretation under "free molecule" selection rules, as has been attempted elsewhere [16,17] where structural data have not been available. Anhydrous zinc hypophosphite is apparently not isostructural with other divalent metal hypophosphites, where M = Ca, Cd, Sr, Pb, Ba [5], but appears to be isostructural with M = Cu, Co [4].

Supplementary data

Atomic coordinates and anisotropic thermal parameters.

Acknowledgements—This work is supported by the Hong Kong Research Grants Council Earmarked Grants No. 9040098 (to P.A.T.) and CUHK 311/94P (to T. C. W. M.). Jason Krishnan, Ng Chi Bun, Chan Ying Tai and Lau Ho Man are thanked for help in syntheses and analyses.

REFERENCES

1. P. A. Tanner, T.-H. Sze, T. C. W. Mak and W.-H. Yip, *J. Cryst. Spectr. Res.* 1992, **22,** 25.
2. P. A. Tanner, T.-H. Sze, T. C. W. Mak and R.-J. Wang, *Polyhedron* 1992, **11,** 817.
3. P. A. Tanner, J.-P. F. Silvestre and N. Q. Dao, *New J. Chem.* 1993, **17,** 263.

4. G. Brun and M. Dumail, *C. R. Acad. Sci. Paris* 1971, **272,** 1866.
5. G. Brun, A. Norbert and M. Caucanas-Dumail, *Rev. Chim. Minerale* 1972, **9,** 581.
6. L. S. Mayants and E. I. Matrosov, *Inorg. Mat.* 1965, **1,** 499.
7. R. Diamond, *Acta Cryst.* 1969, **A25,** 43.
8. G. Kopfmann and R. Hubber, *Acta Cryst.* 1968, **A24,** 348.
9. G. M. Sheldrick, in *Crystallographic Computing 3: Data Collection, Structure Determination, Proteins and Databases* (edited by G. M. Sheldrick, C. Krüger and R. Goddard), pp. 175–189. Oxford University Press, New York.
10. *International Tables for X-ray Crystallography*, Vol. IV, pp. 59, 99, 149. Kynoch Press, Birmingham, (1974). (Now distributed by Kluwer Academic Publishers, Dordrecht).
11. L. George, K. Sankaran, K. S. Viswanathan and C. K. Mathews, *Applied Spectrosc.* 1994, **48,** 801.
12. M. Tsuboi, *J. Am. Chem. Soc.* 1957, **79,** 1351.
13. M. Abénoza, P. Hilaire and R. Lafont, *C. R. Acad. Sc. Paris* 1971, **273,** 297.
14. J. L. Galigné and Y. Dumas, *Acta Cryst.* 1973, **B29,** 1115.
15. M. Abénoza and L. Martin, *J. Raman Spectrosc.* 1975, **4,** 185.
16. R. I. Bickley, H. G. M. Edwards, R. E. Gustar and J. K. F. Tait, *J. Mol. Struct.* 1992, **273,** 61.
17. E. J. Baran, S. B. Etcheverry and E. Diemann, *Polyhedron* 1985, **4,** 1711.
18. G. E. Rodgers, *Introduction to Coordination, Solid-State and Descriptive Inorganic Chemistry*, pp. 170–171. McGraw-Hill, New York (1994).
19. J. I. Michailow, O. I. Lomowski, A. B. Brosalin and W. W. Boldyrew, *Z. anorg. allg. Chem.* 1980, **463,** 199.

Pergamon

PII: S0277-5387(96)00264-1

Polyhedron Vol. 16, No. 3, pp. 507–514, 1997
Copyright © 1996 Elsevier Science Ltd
Printed in Great Britain. All rights reserved
0277-5387/97 $17.00+0.00

Amino acid–lanthanide interactions—2. The X-ray crystal structures of lanthanide and calcium complexes of 1-amino cyclohexane-1-carboxylic acid (Acc^6), $[Nd_2(Acc^6)_6(H_2O)_6](ClO_4)_6 \cdot (H_2O)_6$ (1), $[Er_2(Acc^6)_4(H_2O)_8](ClO_4)_6 \cdot (H_2O)_{11}$ (2) and $[Ca_5(Acc^6)_{12}(H_2O)_6](ClO_4)_{10} \cdot (H_2O)_4$ (3)

K. Aparna,[a] S. S. Krishnamurthy,[a]* M. Nethaji[a] and P. Balaram[b]

[a]Department of Inorganic and Physical Chemistry, Indian Institute of Science, Bangalore 560 012, India

[b]Molecular Biophysics Unit, Indian Institute of Science, Bangalore 560 012, India

(Received 10 April 1996; accepted 20 May 1996)

Abstract—The structures of $[Nd_2(Acc^6)_6(H_2O)_6](ClO_4)_6 \cdot (H_2O)_6$ (**1**) $[Er_2(Acc^6)_4(H_2O)_8](ClO_4)_6 \cdot (H_2O)_{11}$ (**2**) and $[Ca_5(Acc^6)_{12}(H_2O)_6](ClO_4)_{10} \cdot (H_2O)_4$ (**3**) (Acc^6 = 1-aminocyclohexane-1-carboxylic acid) have been determined by X-ray crystallography. The lanthanide complexes **1** and **2** are dimeric in which two lanthanide cations are bridged by four carboxylato groups of Acc^6 molecules. In addition, the neodymium complex (**1**) features the unidentate coordination of the carboxyl group of an Acc^6 molecule in place of a water molecule in the erbium complex (**2**). The coordination number in both **1** and **2** is eight. The calcium Acc^6 complex (**3**) is polymeric; three different calcium environments are observed in the asymmetric unit. Two calcium ions are hexa-coordinated and one is hepta-coordinated. Considerable differences are observed between the solid state structures of Ln^{III} and Ca^{II} complexes of Acc^6. Copyright © 1996 Elsevier Science Ltd

Keywords: lanthanide–amino acid complexes; crystal structures; 1-aminocyclohexane-1-carboxylic acid.

Lanthanide ions are often used as probes of Ca^{II} binding sites in biological systems. The ability of lanthanides to mimic Ca^{II} in diverse situations arises from the similarity in the sizes of the ions and their strong affinity to form complexes with oxygen donor ligands [1,2]. In continuation of our studies on amino acid [3] and peptide [4] complexes of lanthanides, we report here the structures of the lanthanide and calcium complexes of 1-aminocyclohexane-1-carboxylic acid (Acc^6).

The use of non-protein amino acid residues in the synthesis of peptides with restricted conformational flexibility has acquired increasing importance in the design of specifically folded analogues of biologically active peptides [5]. α,α-Dialkylated residues [—NH—CR^1R^2—CO—) have proved valuable in the construction of conformationally constrained peptide backbones [6–8]. The studies on Acc^6 residues of the N-blocked amino acids and peptides showed that the amino function is almost always found in the axial position [9–11]. The zwitterionic amino acid (Acc^6) is the only case where the amino function is equatorial [9]. In this context, it would be interesting to study the metal complexes of zwitterionic Acc^6 to assess the conformational preference of the amino group.

EXPERIMENTAL

Lanthanide perchlorates were prepared from the respective lanthanide oxides. 1-Aminocyclohexane 1-

* Author to whom correspondence should be addressed.

carboxylic acid (Acc^6) was prepared according to the literature procedure [12, 13].

Synthesis of $[Nd_2(Acc^6)_6(H_2O)_6](ClO_4)_6 \cdot (H_2O)_6$ **(1)** *and* $[Er_2(Acc^6)_4(H_2O)_8](ClO_4)_6 \cdot (H_2O)_{11}$ **(2)**

Lanthanide perchlorate hexahydrate (3.64×10^{-4} mol) and Acc^6 (0.05 g, 3.64×10^{-4} mol) were dissolved in 5 cm^3 of distilled water. On slow evaporation of the solution at room temperature, crystals of lanthanide-Acc^6 complexes were obtained. Yield: $\approx 75\%$.

Synthesis of $[Ca_5(Acc^6)_{12}(H_2O)_6](ClO_4)_{10} \cdot (H_2O)_4$ **(3)**

Calcium perchlorate (0.09 g, 2.80×10^{-4} mol) and Acc^6 (0.04 g, 2.80×10^{-4} mol) were dissolved in 5 cm^3 of distilled water. On slow evaporation of the solution at room temperature crystals of calcium perchlorate-Acc^6 complex were isolated. Yield: 70%.

Satisfactory C, H, N analysis could not be obtained for the complexes because of their hygroscopic nature. Lanthanide metal contents were determined by titration with EDTA using xylenol orange as the indicator and correspond to the empirical formulae noted above.

X-ray crystal structure analysis of **1–3**

A suitable crystal of each compound was mounted in a Lindemann capillary and sealed to protect it from moisture. The data were collected on an Enraf-Nonius CAD-4 diffractometer using graphite monochromated Mo-K_α radiation. The structures were solved by Patterson and Fourier techniques and refined by full matrix least squares procedures [14, 15]. All the non-hydrogen atoms were refined anisotropically. The methylene hydrogen atoms of the cyclohexane ring were fixed at geometrically calculated positions (C—H = 0.9 Å) and included in the structure factor calculations. The water and NH_3^+ hydrogen atoms were not located. This may be the reason for the high R-factor observed for complex **3**, which contains the relatively lighter calcium atoms compared to the other heavy atom structures **1** and **2**. The details pertaining to the data collection and refinement are given in Table 1.

RESULTS AND DISCUSSION

Spectroscopic data for the complexes

The Acc^6 complexes of neodymium (**1**), erbium (**2**) and calcium (**3**) perchlorates are prepared by dissolving stoichiometric amounts of Acc^6 and the respective metal salt in water. Slow evaporation of the resultant solution gave crystalline complexes in high yield. These complexes possess the characteristic color of the lanthanide ion.

The infrared spectra of the complexes show a broad and strong absorption in the 3300–2300 cm^{-1} region which can be assigned to the O—H and NH_3^+ stretching vibrations superimposed on each other. The strong band in the region 1600–1500 cm^{-1} arises from the asymmetric stretching vibration of the carboxylato group. The strong absorptions in the region of 1170–1050 and 620–630 cm^{-1} are assigned to ν_3 and ν_4 vibrations of the perchlorate ion.

The structure of the lanthanide-Acc^6 complexes in solution has been investigated by ^{13}C NMR spectroscopy. For this purpose, the ^{13}C resonances of Acc^6 are monitored upon successive addition of praseodymium perchlorate solution. The praseodymium complexes are expected to have a similar structure to that of the neodymium complex [16]. The advantage of using Pr^{3+} for NMR measurements is that it induces large chemical shifts, without causing appreciable line broadening compared to the Nd^{3+} ion [16]. Upon successive addition of praseodymium perchlorate solution, the resonances of carboxyl carbon (δ value in free Acc^6: 177.6 ppm, $\Delta\delta$: 1 ppm) and the carbon which is directly bonded to the carboxyl group (δ value in free Acc^6: 61.6 ppm, $\Delta\delta$: 6 ppm) show maximum chemical shift variations compared to the other resonances. Irrespective of the concentration of the praseodymium salt, only a single resonance is observed for the carboxyl carbon. This observation suggests that there is a dynamic equilibrium between differently coordinated carboxyl groups of the Acc^6 in solution. The X-ray crystal structure of the neodymium-Acc^6 complex shows two different types of coordination of the carboxyl group of Acc^6 (see below).

X-ray crystal structures

X-ray crystal structure analysis of neodymium-Acc^6 **(1)** *and erbium-Acc^6* **(2)** *complexes.* The structures of neodymium and erbium complexes were determined by X-ray crystallography. Perspective views of the molecules are shown in Figs 1 and 2. The selected bond distances and angles are listed in Table 2.

In both neodymium and erbium complexes, the two lanthanide ions are bridged by the carboxylato groups of four Acc^6 molecules. In the neodymium complex, in addition, each neodymium ion is also coordinated to a unidentate carboxyl group of an Acc^6 molecule. Such a unidentate coordination of the carboxyl group of an amino acid to lanthanides is observed for the first time. However, this type of unidentate carboxylato group is present in the solid state structures of the trifluoroacetato and *meta*-hydroxybenzoato complexes, $[Pr(O_2CCF_3)_3 \cdot 3H_2O]$ [17] and $[Ln_2(O_2C C_6H_4OH\text{-}3)_6(H_2O)_6] \cdot 2H_2O$ (Ln = Sm or Er) [18].

The metal to ligand ratio is 1 : 3 in the neodymium-Acc^6 complex but in the erbium-Acc^6 complex, it is decreased to 1 : 2 and the unidentate Acc^6 molecule is replaced by a water molecule. This difference is a

Table 1. Crystal data, details of intensity data collection, structure solution and refinement for **1**, **2** and **3**

	1	**2**	**3**
Molecular formula	$C_{42}H_{98}Cl_6Nd_2N_6O_{48}$	$C_{28}H_{90}Cl_6Er_2N_4O_{51}$	$C_{84}H_{176}Ca_5Cl_{10}N_{12}O_{74}$
Molecular weight	1956.5	1846.3	3093.3
Crystal system	Triclinic	Orthorhombic	Triclinic
a (Å)	11.429(1)	11.356(4)	14.952(5)
b (Å)	12.900(2)	22.707(7)	15.408(3)
c (Å)	14.653(2)	27.008(4)	16.109(4)
α ( )	71.87(1)	—	65.43(2)
β ( )	85.47(1)	—	83.73(2)
γ ( )	68.68(1)	—	82.23(2)
V (Å^3)	1911(13)	6964(3)	3338(10)
Space group	$P\bar{1}$	$Pcnn$	$P\bar{1}$
Z	1	4	1
D_c (g cm^{-3})	1.70	1.76	1.54
$F(000)$	992	3808	1622
Temperature (C)	20	20	20
Radiation (graphite monochromator)	Mo-K_α(0.7107 Å)	Mo-K_α(0.7107 Å)	Mo-K_α(0.7107 Å)
Scan technique	$\omega/2\theta$	ω	$\omega/2\theta$
Octants (collected)	$+h, \pm k, \pm l$	$+h, +k, +l$	$+h, \pm k, \pm l$
2θ range ( )	2–50	2–50	2–50
Decay	<1%	<1%	<1%
Color	Rose	Pale pink	Colorless
Size (mm)	0.20 × 0.50 × 0.40	0.18 × 0.88 × 0.25	0.40 × 0.40 × 0.40
Linear abs. coeff. (μ cm^{-1})	16.11	27.70	4.82
Total number of reflections	7246	6999	12019
Unique reflections	6244	6128	10115
Observed reflections	6235 $\{F_o > 5\sigma(F_o)\}$	3833 $\{F_o > 5\sigma(F_o)\}$	8017 $\{F_o > 5\sigma(F_o)\}$
No. of parameters	469	456	870
R^a	0.033	0.051	0.086
$R_w^{b,c}$	0.038	0.052	0.092
Residual peak in final diff. map (e/Å^3)	1.0	1.9	1.0
Shifts/e.s.d.(max)	0.1	0.1	0.1

[a] $R = \Sigma(||F_o|-|F_c||)/\Sigma|F_o|$.
[b] $R_w(\Sigma w(|F_o|-|F_c|)^2/\Sigma w|F_o|^2)^{1/2}$.
[c] w for **1** = $2.3568/(\sigma^2(F)+0.000441F^2)$; **2** = $2.7828/(\sigma^2(F)+0.000000F^2)$; **3** = $4.7977/(\sigma^2(F)+0.001727F^2)$.

consequence of the decreased ionic radius of the Er^{3+} ion compared to the Nd^{3+} ion as a result of "lanthanide contraction". In both **1** and **2**, the coordination number of the lanthanide ion is eight and the geometry around the metal is that of a square antiprism. The amino acids exist in the zwitterionic form and the perchlorate ions are outside the coordination sphere. In the neodymium complex **1**, the distance between the unidentate carboxylato oxygen [O(5)] and the neodymium ion is (2.485(3) Å) which is longer than the average distance of the bridging carboxylato oxygens to the neodymium ion (Table 2). The latter distances fall into two ranges [the mean of Nd(1)—O(2) and Nd(1)—O(3) is 2.447(3) Å; the mean of Nd(1)—O(1)′ and Nd(1)—O(4)′ is 2.375(4) Å]. The non-bonding distance between O(6) and Nd(1) ion is 3.912(4) Å. In both neodymium and erbium complexes, the average distance between the carboxylato oxygens and metal ion is shorter than the distance of the coordinated water oxygen to the metal.

X-ray crystal structure analysis of calcium-Acc^6 (**3**) *complex*. The structure of the calcium-Acc^6 complex (**3**) is shown in Fig. 3. The Acc^6 molecules are in their zwitterionic form and the perchlorate groups are outside the coordination sphere. The unit cell consists of five calcium atoms with one of them (Ca(3)) lying at the centre of inversion so that the asymmetric unit corresponds to the formula $[Ca_{2.5}(Acc^6)_6(H_2O)_3](ClO_4)_5 \cdot (H_2O)_2$. Unlike the lanthanide complexes of Acc^6, the calcium complex is polymeric with carboxylato bridges. Three different calcium environments are observed in the asymmetric unit, two calcium ions are hexa-coordinated with an octahedral geometry and one calcium ion is hepta-coordinated with pentagonal bipyramidal geometry. The Ca(1) and Ca(2) are bridged by three carboxylato groups of Acc^6 and Ca(2) and Ca(3) are bridged by two carboxylato groups. Each of the two centrosymmetrically related calcium ions Ca(1) and Ca(1)′ bears a chelated carboxylato group which also bridges

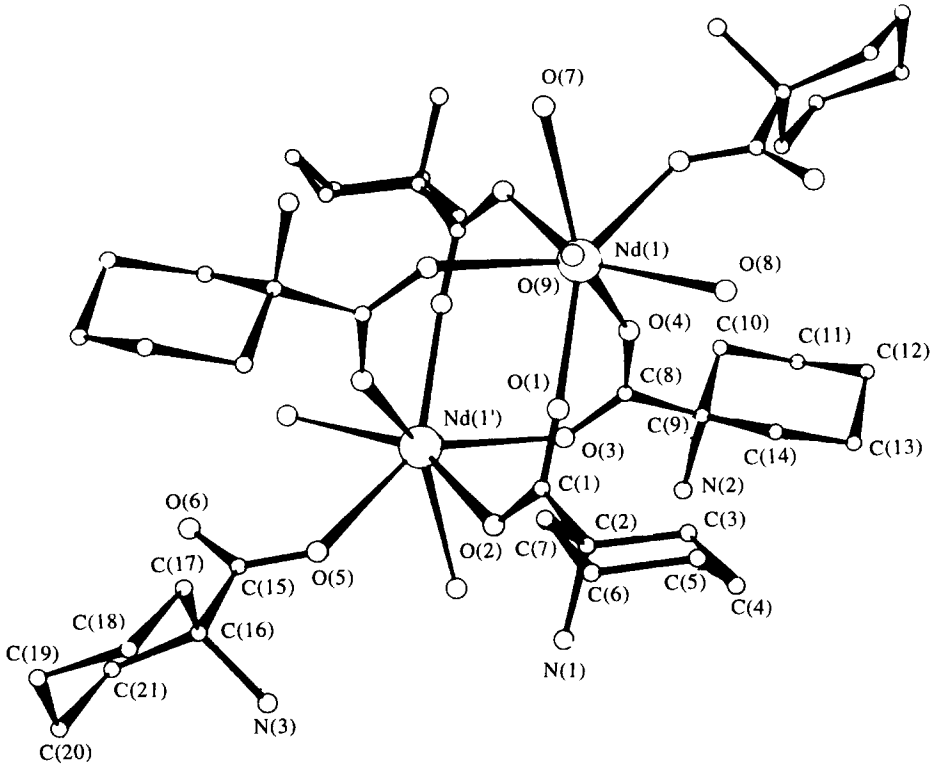


Fig. 1. The molecular structure of $[Nd_2(Acc^6)_6(H_2O)_6](ClO_4)_6 \cdot (H_2O)_6$ (**1**) omitting the perchlorate groups and lattice water molecules.

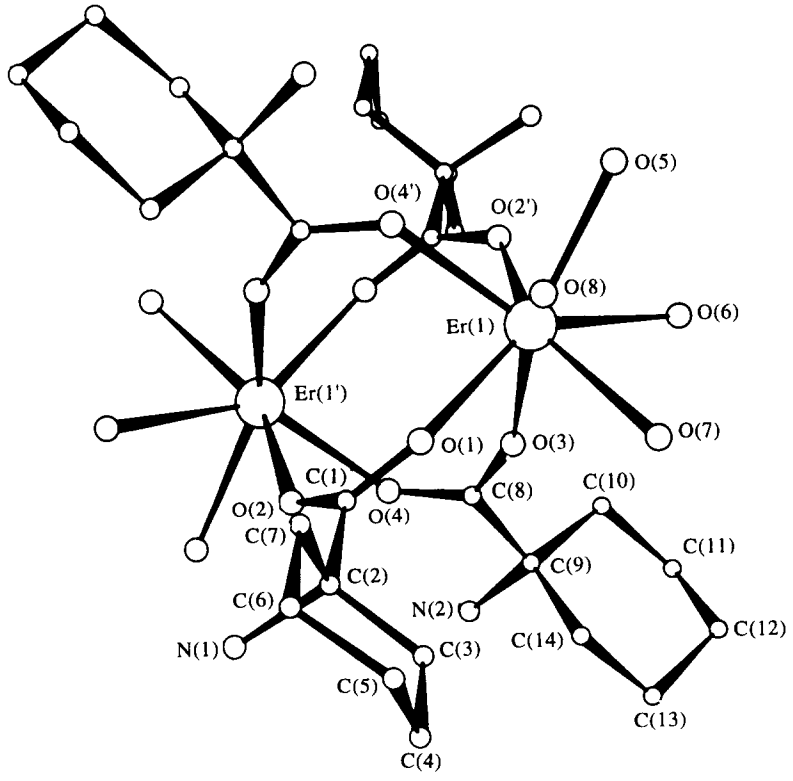


Fig. 2. The molecular structure of $[Er_2(Acc^6)_4(H_2O)_8](ClO_4)_6 \cdot (H_2O)_{11}$ (**2**) omitting the perchlorate groups and lattice water molecules.

Table 2. Selected bond distances (Å) and angles (°) in $[Nd_2(Acc^6)_6(H_2O)_6](ClO_4)_6 \cdot (H_2O)_6$ (**1**) and $[Er_2(Acc^6)_4(H_2O)_8](ClO_4)_6 \cdot (H_2O)_{11}$ (**2**)

Complex (**1**)	
Nd(1)—O(1) = 2.377(3)	O(1)—Nd(1)—O(4) = 73.7(1)
Nd(1)′—O(2) = 2.447(2)	O(4)—Nd(1)—O(8) = 84.8(1)
Nd(1)′—O(3) = 2.447(3)	Nd(1)—O(1)—C(1) = 173.1(3)
Nd(1)—O(4) = 2.372(4)	Nd(1)—O(4)—C(8) = 145.1(3)
Nd(1)—O(5) = 2.485(3)	Nd(1)—O(5)—C(15) = 138.8(4)
Nd(1)—O(7) = 2.544(3)	O(3)—C(8)—O(4) = 127.3(4)
Nd(1)—O(8) = 2.442(3)	O(5)—C(15)—O(6) = 125.5(4)
Nd(1)—O(9) = 2.508(3)	
Nd(1)···O(6) = 3.912(4)	
O(3)—C(8) = 1.245(6)	
O(4)—C(8) = 1.254(7)	
O(5)—C(15) = 1.256(5)	
O(6)—C(15) = 1.248(5)	
Complex (**2**)	
Er(1)—O(1) = 2.256(8)	O(1)—Er(1)—O(2)′ = 76.9(3)
Er(1)′—O(2) = 2.315(8)	O(3)—Er(1)—O(4)′ = 77.5(3)
Er(1)′—O(3) = 2.268(7)	Er(1)′—O(2)—C(1) = 136.9(6)
Er(1)′—O(4) = 2.300(7)	Er(1)′—O(4)—C(8) = 135.2(6)
Er(1)—O(5) = 2.393(7)	O(1)—C(1)—O(2) = 128.5(9)
Er(1)—O(6) = 2.431(8)	O(3)—C(8)—O(4) = 126.0(9)
Er(1)—O(7) = 2.359(8)	
Er(1)—O(8) = 2.408(6)	
O(1)—C(1) = 1.266(13)	
O(2)—C(1) = 1.243(13)	
O(3)—C(8) = 1.244(12)	
O(4)—C(8) = 1.262(12)	

the other calcium ion. Thus the carboxylato groups between Ca(1) and Ca(1)′ act as tridentate ligands.

The selected bond distances and angles are listed in Table 3. The distance between Ca(1)···Ca(1)′ (4.046(3) Å) is shorter than the distance between Ca(1)···Ca(2) (4.382(3) Å) or Ca(2)···Ca(3) (4.487 (2) Å). The Ca(1)—O(2) distance (2.365(6) Å) is shorter than the Ca(1)′—O(2) distance (2.737(4) Å).

Cyclohexyl ring conformation

The endocyclic cyclohexane ring angles in **1, 2** and **3** are close to an almost perfect chair conformation for the cyclohexane ring. The mean value is $\pm 54(1)^\circ$ as found for several Acc^6 containing compounds [9–12].

The amino functional group in the complexes **1**-**3** occupies an axial position with respect to the Acc^6 moiety. This feature is also observed in other Acc^6 containing compounds [10–12] except in the free zwitterionic Acc^6 where the amino functional group is in an equatorial position [9].

Comparison of the structures of lanthanide–amino acid complexes

Prior to this study, the structures of the lanthanide complexes of glycine [19], L-alanine [20] and α-amino isobutyric acid (Aib) [3] have been reported. In all these complexes, the amino acids exist in their zwitterionic form and the perchlorate or chloride ions reside outside the coordination sphere of the metal.

The glycine complex $[Nd_2(Gly)_6(ClO_4)_6 \cdot 9H_2O]$ [19] is polymeric with carboxylato bridges between two neodymium ions. The asymmetric unit consists of dimers in which neodymium ions are bridged by four glycine molecules; two of them act as bidentate ligands while the other two act as tridentate ligands chelating to one metal and bridging to the other metal. Each of the neodymium ion dimers, is linked to another such dimer by two carboxylato bridges. The L-Ala [20] and Aib [3] complexes of lanthanides are dimeric with four bridging carboxylato groups. The same feature is also observed in the lanthanide complexes of Acc^6 reported here. In addition, in the Nd-Acc^6 complex, a unidentate Acc^6 is present.

Comparison of the structures of calcium–amino acid complexes

The calcium-Acc^6 complex (**3**) shows considerable differences from the Ca-glycine complex. In the Ca-Acc^6 complex, bidentate and tridentate mode of bonding of the carboxylato groups are observed whereas in the calcium-glycine complex bidentate and unidentate bonding of the aminoacid are observed. In the calcium

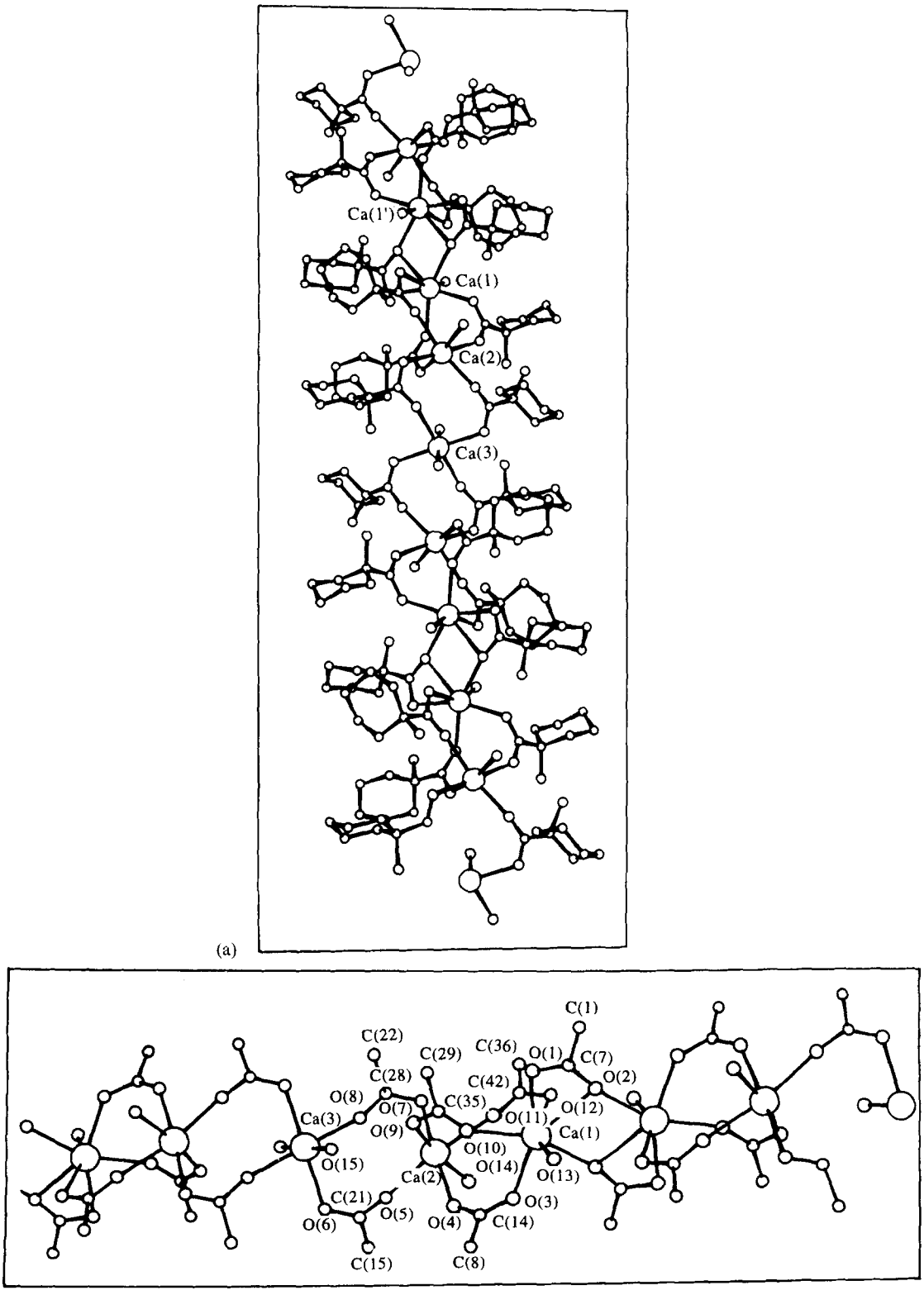


Fig. 3. (a) The molecular structure of $[Ca_5(Acc^6)_{12}(H_2O)_6](ClO_4)_{10}\cdot(H_2O)_4$ (**3**) omitting the perchlorate groups and lattice water molecules. (b) The molecular structure of $[Ca_5(Acc^6)_{12}(H_2O)_6](ClO_4)_{10}\cdot(H_2O)_4$ (**3**) omitting the perchlorate groups, lattice water molecules and ring carbon atoms.

Table 3. Selected bond distances (Å) and angles ( ) in $[Ca_5(Acc^6)_{12}(H_2O)_6](ClO_4)_{10}\cdot(H_2O)_4$ (3)

Ca(1)—O(1) = 2.426(5)	Ca(1)—O(1)—C7 = 100.4(4)
Ca(1)—O(2) = 2.365(6)	Ca(1)—O(2)—C7 = 169.0(4)
Ca(1)—O(3) = 2.363(6)	Ca(1)—O(3)—C14 = 131.9(5)
Ca(1)—O(10) = 2.359(6)	Ca(1)—O(10)—C35 = 143.0(4)
Ca(1)—O(12) = 2.395(4)	Ca(1)—O(12)—C42 = 108.6(4)
Ca(1)—O(13) = 2.374(5)	O(1)—C(7)—O(2) = 123.1(6)
Ca(2)—O(4) = 2.321(4)	O(5)—C(21)—O(6) = 122.9(6)
Ca(2)—O(5) = 2.304(5)	O(7)—C(28)—O(8) = 122.6(6)
Ca(2)—O(7) = 2.370(4)	O(9)—C(35)—O(10) = 125.9(7)
Ca(2)—O(9) = 2.326(7)	O(11)—C(42)—O(12) = 122.3(6)
Ca(2)—O(11) = 2.365(4)	
Ca(2)—O(14) = 2.356(9)	
Ca(3)—O(6) = 2.301(5)	
Ca(3)—O(8) = 2.312(4)	
Ca(3)—O(15) = 2.380(5)	
Ca(1)′—O(2) = 2.737(4)	

glycine complex [21], the coordination number for calcium is seven but in the calcium-Acc^6 complex, both six and seven coordinated calcium ions are observed.

Comparison of the structures of lanthanide and calcium amino acid complexes

Lanthanide complexes of Acc^6 show considerable structural differences from the calcium complex of Acc^6. The neodymium and erbium complexes of Acc^6 are dimeric whereas the Ca–Acc^6 complex is polymeric. In the Ca–Acc^6 complex both bi- and tridentate carboxylato bridges are present; in contrast, only bidentate carboxylato groups are present in the erbium-Acc^6 complex and bidentate and unidentate carboxylato groups are present in the neodymium–Acc^6 complex. Pronounced differences are also observed between the modes of binding of glycine to lanthanides and calcium as revealed by the structures of $[Nd_2(Gly)_6(ClO_4)_6\cdot 9H_2O]$ [19] and $[CaI_2(Gly)_3H_2O]$ [21]. In the calcium–glycine complex, only one glycine carboxylato group bridges two calcium ions while the other two glycine molecules are coordinated to a calcium ion in a unidentate fashion. On the other hand, the neodymium–glycine complex contains both bidentate and tridentate carboxyl groups (see above).

CONCLUSION

The results reported here reinforce our earlier conclusion [3,4] that there can be considerable variation in the modes of binding of amino acids to lanthanides as compared to calcium ions. The difference in the precise binding geometries suggests that structural alterations may accompany the interaction of lanthanides with calcium ion binding sites in biological systems.

Acknowledgements—One of the authors (KA) thanks CSIR, New Delhi, for a fellowship.

REFERENCES

1. J.-C. G. Bunzli and G. R. Choppin, *Lanthanide Probes in Life, Chemical and Earth Sciences*. Elsevier, Amsterdam (1989).
2. H. G. Brittain, F. S. Richardson and R. B. Martin, *J. Am. Chem. Soc.* 1976, **98,** 8255.
3. K. Aparna, S. S. Krishnamurthy, M. Nethaji and P. Balaram, *Polyhedron* 1994, **13,** 2993.
4. K. Aparna, P. Balaram, S. S. Krishnamurthy and M. Nethaji, *Int. J. Peptide Protein Res.* 1994, **43,** 19.
5. A. F. Spatola, *Chemistry and Biochemistry of Amino Acids, Peptides and Proteins*, (Edited by B. Weinstein) **7,** 267. Dekker, New York (1983).
6. G. R. Marshall, H. E. Bosshard, N. C. E. Kendrick, J. Turk, T. M. Balasubramanian, S. M. H. Cobb, M. Moore, L. Leduc and P. Needleman, *Peptide* (Edited by A. Loffet) p. 361. Editions de l'Universite de Bruxelles, Bruxelles (1976).
7. B. V. V. Prasad and P. Balaram, *CRC Crit. Rev. Biochem.* 1984, **16,** 307.
8. P. Balaram, *Curr. Opinion. Struct. Biol.* 1992, **2,** 840.
9. G. V. M. Crisma, C. Toniolo, N. Sen, M. Sukumar and P. Balaram, *J. Chem. Soc., Perkin Trans. II* 1988, 393.
10. R. Bardi, A. M. Piazzesi, C. Toniolo, M. Sukumar, P. A. Raj and P. Balaram, *Int. J. Peptide. Protein. Res.* 1985, **25,** 628.
11. P. K. C. Paul, M. Sukumar, R. Bardi, A. M. Piazzesi, G. Valle, C. Toniolo and P. Balaram, *J. Am. Chem. Soc.* 1986, **108,** 6363.
12. G. W. Kenner, J. Preston and R. C. Sheppard, *J. Chem. Soc.* 1965, 6239.
13. P. Tailleur and L. Berlinguet, *Can. J. Chem.* 1961, **39,** 1309.
14. G. M. Sheldrick *SHELXS* 86, *Program for Crys-*

tal Structure Solution. University of Göttingen, Germany (1986).
15. G. M. Sheldrick, *SHELX*76, *Program for Crystal Structure Determination.* University of Cambridge, U.K. (1976).
16. Ref. 1 Chapter 4, 93.
17. S. P. Bone, D. B. Sowerby and R. D. Verma, *J. Chem. Soc., Dalton Trans.* 1978, 1544.
18. Y. Koizumi, H. Sawase, Y. Suzuki, T. Takeuchi, M. Shimoi and A. Ouchi, *Bull. Chem. Soc. Jpn* 1984, **57,** 1809.
19. J. Legendziewicz, E. Huskowska, A. Waskowska and Gy. Argay, *Inorg. Chim. Acta.* 1984, **92,** 151.
20. D. C. Ngoan, T. Glowiak, E. Huskowska and J. Legendziewicz, *J. Less-common Met.* 1988, **136,** 339.
21. S. Natarajan and J. K. Mohan Rao, *J. Inorg. Nucl. Chem.* 1981, **43,** 1693.

Pergamon

PII: S0277-5387(96)00248-3

Polyhedron Vol. 16, No. 3, pp. 515–520, 1997
Copyright © 1996 Elsevier Science Ltd
Printed in Great Britain. All rights reserved
0277-5387/97 $17.00+0.00

Synthesis, spectroscopic and electrochemical properties of substituted bis(phthalocyaninato)lanthanide(III) complexes

Jianzhuang Jiang, Roger C. W. Liu, Thomas C. W. Mak, T. W. Dominic Chan* and Dennis K. P. Ng*

Department of Chemistry, The Chinese University of Hong Kong, Shatin, New Territories, Hong Kong

(Received 17 April 1996; accepted 13 May 1996)

Abstract—The sandwich-like bis(phthalocyaninato)lanthanide(III) complexes $Ln[Pc'(R)_8]_2$ (Ln = Eu, Gd; Pc′ = 2,3,9,10,16,17,23,24-octasubstituted phthalocyaninate; R = H, n-C_7H_{15}, OC_5H_{11}) have been prepared by treating $Ln(acac)_3 \cdot nH_2O$ (Ln = Eu, Gd; acac = acetylacetonate) with dilithium phthalocyaninate or with the corresponding disubstituted phthalonitriles in the presence of 1,8-diazabicyclo[5.4.0]undec-7-ene (DBU). The spectroscopic and electrochemical properties of the substituted sandwich complexes have been investigated and compared with those of the unsubstituted analogues. The matrix-assisted laser desorption/ionisation time-of-flight mass spectrometry (MALDI-TOF-MS) and electrospray ionisation mass spectrometry (ESI-MS) have also been employed to unambiguously characterise this novel class of compounds for the first time. Copyright © 1996 Elsevier Science Ltd

Since the discovery of electrochemically generated multicolour response in a solid film of bis(phthalocyaninato)lutetium(III) in 1970 [1], there has been a growing interest in the sandwich-like bis(phthalocyaninato) metal complexes. Apart from the electrochromic behaviour [2], this class of compounds also exhibits unusual electrical [3], magnetic [4], and mesogenic [5] properties. Most of the studies have so far focused in the unsubstituted bis(phthalocyaninato) complexes, in particular, of lutetium. It can be envisaged that by introducing substituents on the periphery of the phthalocyanine macrocycles rationally, the intrinsic properties of the molecule can be altered which may eventually tailor the bulk characteristics of the material. Substitution may also increase the solubility of complexes which facilitates the fabrication process. However, substituted bis(phthalocyaninato) metal complexes have been relatively little studied [5–9]. This paper describes the synthesis, spectroscopic characterisation and electrochemistry of the europium(III) and gadolinium(III) sandwich complexes of octasubstituted phthalocyanines.

* Authors to whom correspondence should be addressed.

EXPERIMENTAL

Hexanes and amyl alcohol were distilled from anhydrous $CaCl_2$ and sodium, respectively. 1,2,4-Trichlorobenzene (TCB) was dried over 4 Å molecular sieves and distilled under reduced pressure. All other reagents and solvents were used as received. The lanthanide acetylacetonates [10], 4,5-bis(pentyloxy) phthalonitrile [11], 4,5-diheptylphthalonitrile [12], and dilithium phthalocyaninate [$Li_2(Pc)$] [13] were prepared according to the literature prescriptions.

The ^1H NMR spectra were recorded on a Bruker WM 250 spectrometer (250 MHz). Spectra were referenced internally using residual solvent resonances relative to tetramethylsilane ($\delta = 0$). The UV–vis and near-IR absorption spectra were obtained on a Hitachi U-3300 and a Hitachi U-3100 spectrophotometers, respectively. IR spectra were recorded on a Nicolet 205 FT-IR spectrometer as KBr pellets. MALDI-TOF spectra were recorded on a Bruker bench TOF mass spectrometer equipped with a standard UV-laser desorption source. ESI mass spectra were measured on a Bruker APEX 47e ultra-high resolution Fourier transform ion cyclotron resonance (FTICR) mass spectrometer. Cyclic vol-

tammetry measurements were performed with a Princeton Applied Research (Model 273A) potentiostat. The cell used comprised a vacuum-tight chamber fitted with inlets for a glassy carbon working electrode, a platinum wire auxiliary electrode and a Ag–$AgNO_3$ reference electrode. Typically, experiments were carried out using *ca* 10 cm^3 of 0.1 mol dm^{-3} tetrabutylammonium hexafluorophosphate in dichloromethane containing *ca* 2 mg of sample under nitrogen at ambient temperature.

Preparation of bis(phthalocyaninato)lanthanide(III) *complexes* $Ln(Pc)_2$[Ln = Eu (**1**), Gd (**2**)]

A mixture of $Li_2(Pc)$ (53 mg, 0.1 mmol) and $Ln(acac)_3 \cdot nH_2O$ (Ln = Eu, Gd) (150 mg, 0.3 mmol) in TCB (10 cm^3) was refluxed for 10 h under nitrogen. The resulting dark blue solution was cooled and evaporated under reduced pressure to give a residue which was chromatographed on a silica gel column with $CHCl_3$ as eluent. A pale blue band containing a trace amount of the metal-free phthalocyanine $(Pc)H_2$ was developed followed by a greenish-blue band which was collected and concentrated. The crude product was purified by recrystallisation from a mixture of $CHCl_3$ and MeOH. Yield for Ln = Eu (19 mg, 32%). Yield for Ln = Gd (15 mg, 25%).

Preparation of bis[2,3,9,10,16,17,23,24-*octakis*(*pentyloxy*)*phthalocyaninato*]*lanthanide*(III)*complexes* $Ln[Pc'(OC_5H_{11})_8]_2$[Ln = Eu (**5**), Gd (**6**)]

Under a slow stream of nitrogen, a mixture of 4,5-bis(pentyloxy)phthalonitrile (**3**) (300 mg, 1.00 mmol), DBU (78 mg, 0.51 mmol) and $Ln(acac)_3 \cdot nH_2O$ (Ln = Eu, Gd) (30 mg, 0.06 mmol) was heated in amyl alcohol (4 cm^3) under reflux for 8 h to give a dark greenish-blue solution. The volatiles were removed *in vacuo*, then the residue was chromatographed with $CHCl_3$/hexanes (2 : 3) as eluent. Firstly, a green band was developed which contained a small amount of the metal-free phthalocyanine $[Pc'(OC_5H_{11})_8]H_2$ as determined by UV–vis spectrometry. Then a dark greenish-blue band containing the sandwich compound was developed which was collected and evaporated under reduced pressure. The crude product obtained was further purified by the same chromatographic procedure. Yield for Ln = Eu (121 mg, 79%). ^1H NMR [$(CD_3)_2SO + CDCl_3$ + hydrazine hydrate]: δ 10.64 (br s, 16 H, Pc′-H), 4.16 (br s, 32 H, OCH_2), 2.70–2.86 (m, 32 H, OCH_2CH_2), 2.32 (quintet, J = 7.3 Hz, 32 H, $OCH_2CH_2CH_2$), 2.02 (sextet, J = 7.3 Hz, 32 H, CH_2CH_3), 1.42 (t, J = 7.3 Hz, 48 H, CH_3). IR (KBr): 2965m, 2922m, 2856m, 1589w, 1500w, 1456m, 1372m, 1315m, 1272m, 1194m, 1094w, 1044w, 856w, 762w cm^{-1}. Yield for Ln = Gd (115 mg, 75%). IR (KBr): 2956m, 2926m, 2856m, 1606m, 1500m, 1456s, 1372m, 1317m, 1276s, 1194m, 1094w, 1044w, 863w, 762w cm^{-1}.

Preparation of bis(2,3,9,10,16,17,23,24-*octaheptylphthalocyaninato*)*lanthanide*(III)*complexes* $Ln[Pc'(C_7H_{15})_8]_2$[Ln = Eu (**7**), Gd (**8**)]

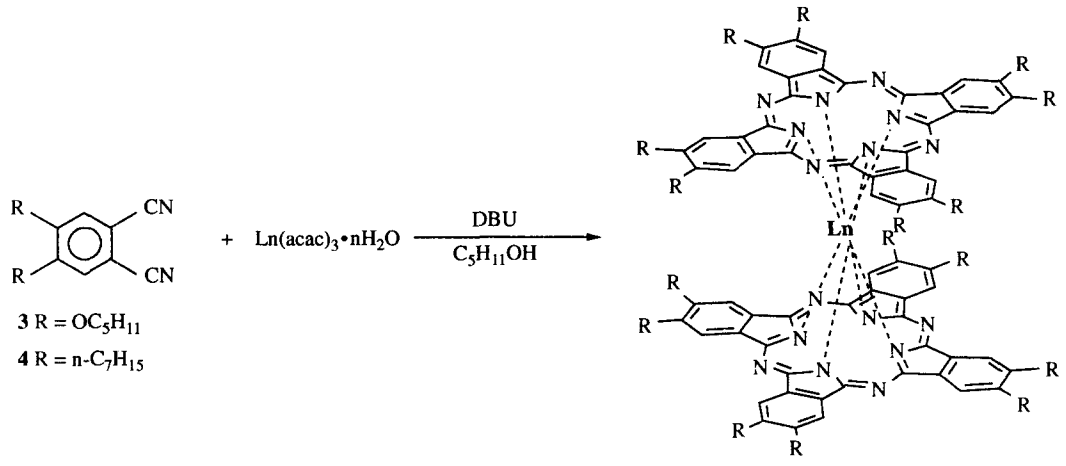
A mixture of 4,5-diheptylphthalonitrile (**4**) (150 mg, 0.46 mmol), DBU (39 mg, 0.26 mmol) and $Ln(acac)_3 \cdot nH_2O$ (Ln = Eu, Gd) (23 mg, 0.05 mmol) in amyl alcohol (2 cm^3) was refluxed for 13 h under a slow stream of nitrogen. The mixture was cooled to room temperature then filtered to remove most of the metal-free phthalocyanine $[Pc'(C_7H_{15})_8]H_2$, which was washed with amyl alcohol (2 cm^3). The combined filtrates were concentrated under reduced pressure then chromatographed with $CHCl_3$/hexanes (2 : 3) as eluent. After eluting out the residual $[Pc'(C_7H_{15})_8]H_2$, a dark blue solution containing the sandwich compound was collected and rotary-evaporated. The crude product was further purified by recrystallisation from a mixture of $CHCl_3$ and MeOH. Yield for Ln = Eu (92 mg, 72%). ^1H NMR [$(CD_3)_2SO$ + $CDCl_3$ + hydrazine hydrate]: δ 11.06 (br s, 16 H, Pc′-H), 4.31 (br s, 32 H, Pc′-CH_2), 3.13 (br s, 32 H, CH_2), 2.50 (br s, 32 H, CH_2), 2.21 (br s, 32 H, CH_2), 1.77–1.93 (m, 64 H, CH_2), 1.23 (t, J = 7.0 Hz, 48 H, CH_3). IR (KBr): 2965m, 2923s, 2856s, 1456m, 1371w, 1320s, 1106m, 756m, 722m cm^{-1}. Yield for Ln = Gd (87 mg, 68%). IR (KBr): 2964m, 2924s, 2848s, 1456s, 1369w, 1320s, 1102m, 757m, 724m cm^{-1}.

RESULTS AND DISCUSSION

Treatment of $Ln(acac)_3 \cdot nH_2O$ (Ln = Eu, Gd) with $Li_2(Pc)$ in TCB produced the sandwich complexes $Ln(Pc)_2$[Ln = Eu (**1**), Gd (**2**)] in moderate yields. The UV–vis spectra of the crude products obtained after chromatographic purification showed two broad bands at *ca* 640 nm and 670 nm in the Q band absorption region of phthalocyanines. The former band assignable to the species $LnH(Pc)_2$ or $[Ln(Pc)_2]^-$ diminished [2,8c] while the latter band assignable to the neutral $Ln(Pc)_2$ increased in intensity during further purification [14]. It suggested that the species $LnH(Pc)_2$ or $[Ln(Pc)_2]^-$ might be the primary products which converted slowly to the corresponding $Ln(Pc)_2$ in air.

In attempts to synthesise the substituted analogues of $Ln(Pc)_2$, we prepared the dilithium salt of 2, 3, 9, 10, 16, 17, 23, 24-octakis(pentyloxy)phthalocyanine $Li_2[Pc'(OC_5H_{11})_8]$ by treating 4,5-bis(pentyloxy) phthalonitrile (**3**) with lithium in amyl alcohol [6b]. The electronic absorption spectrum of the resulting green solution showed characteristic bands of metal phthalocyaninates [λ_{max} in $CHCl_3$: 355 nm (B band), 675 nm (Q band)]. The dilithium salt generated *in situ* was then treated with $Eu(acac)_3 \cdot nH_2O$ in refluxing TCB. The reaction gave a significant amount of the metal-free phthalocyanine $[Pc'(OC_5H_{11})_8]H_2$ with no indication of formation of the sandwich complex.

The substituted bis(phthalocyaninato)lanthanide



Scheme. 1.

(III) complexes $Ln[Pc'(R)_8]_2$ (Ln = Eu, Gd; R = OC_5H_{11}, n-C_7H_{15}) can however be prepared in good yields by treating the corresponding phthalonitriles with $Ln(acac)_3 \cdot nH_2O$ and DBU in amyl alcohol (Scheme 1). The reactions gave small amounts of metal-free phthalocyanines as the side products which were separated readily from the sandwich complexes by column chromatography and were characterised with UV–vis spectrometry {λ_{max}(nm) in $CHCl_3$: 348, 602, 636, 664 and 702 for $[Pc'(OC_5H_{11})_8]H_2$; 344, 610, 644, 672 and 708 for $[Pc'(C_7H_{15})_8]H_2$}. Satisfactory elemental analyses of these sandwich complexes could not be obtained even after repeated column chromatography and recrystallisation. As pointed out earlier [6c,15], this is quite usual for this class of compounds. Nevertheless, the new sandwich compounds were unambiguously characterised with a wide range of spectroscopic methods including ^{1}H NMR, UV–vis, near-IR, MALDI-TOF-MS and ESI-MS.

It is well documented that the sandwich complexes $Ln(Pc)_2$ can be formulated as $Ln^{3+}(Pc^{2-})(Pc^{\bullet -})$ or more precisely as $Ln^{3+}(Pc_2)^{3-}$ in which the unpaired electron delocalises in both of the Pc rings [16]. Because of the paramagnetic nature of these species, they are usually NMR silent. Recently, L'Her and coworkers have shown that by adding hydrazine hydrate (1% v/v) to solutions of lutetium sandwiches in deuterated dimethylformamide or dimethylsulfoxide, satisfactory NMR data can be obtained because the paramagnetic neutral species are reduced to the corresponding anions in which both of the macrocycles are diamagnetic dianions [6b,c]. By using a similar strategy, we could obtain ^{1}H NMR spectra of the europium complexes **5** and **7**. As these complexes are only sparingly soluble in $(CD_3)_2SO$, the spectra were measured in $CDCl_3$ and $(CD_3)_2SO$ (v/v 1 : 1) in the presence of *ca* 5% (v/v) hydrazine hydrate. Both spectra showed a broad downfield band at δ 10.64 (for **5**) or 11.06 (for **7**) due to the ring protons together with signals assignable to the protons in the side chains. ^{1}H NMR spectra of the gadolinium complexes **6** and **8** could not be obtained due to the strong paramagnetic nature of the metal centre.

The electronic absorption spectra of **5–8** were similar to those of other bis(phthalocyaninato)lanthanide(III) complexes and could be assigned similarly [6b, 7, 17]. Fig. 1 gives the UV–vis and near-IR spectra of compound **8**, which show two B bands at 329 and 355 nm, a Q band at 686 nm and two π-radical anion bands at 492 and 925 nm. Interestingly, the splitting of the B bands has rarely been observed previously [5c]. A broad near-IR absorption peaking at 1633 nm was also observed which could be attributed to an intramolecular ring-to-ring charge transfer, from dianion to radical anion [17].

The electronic spectral data for compounds **5–8** are

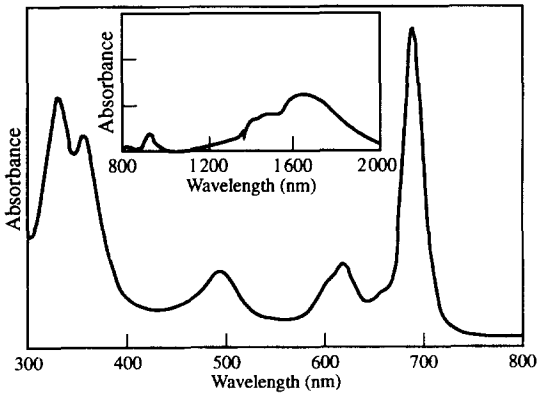


Fig. 1. UV–vis and near-IR spectra of $Gd[Pc'(C_7H_{15})_8]_2$ (**8**) in $CHCl_3$.

Table 1. The UV–vis and near-IR data for bis(phthalocyaninato)lanthanide(III) complexes in $CHCl_3$

Compound	λ_{max}/nm (log ε)
$EuPc_2$ (**1**)	322, 461, 605, 671, 906, 1406, 1607
$GdPc_2$ (**2**)	323, 459, 605, 670, 910, 1410, 1573
$Eu[Pc'(OC_5H_{11})_8]_2$ (**5**)	337 (4.89), 371 (4.96), 492 (4.51), 613 (4.43), 679 (5.01), 906 br, 1693 br
$Gd[Pc'(OC_5H_{11})_8]_2$ (**6**)	337 (4.95), 371 (5.02), 490 (4.54), 612 (4.47), 677 (5.09), 911 br, 1674 br
$Eu[Pc'(C_7H_{15})_8]_2$ (**7**)	331 (5.03), 357 (4.94), 497 (4.47), 618 (4.54), 690 (5.09), 922 br, 1677 br
$Gd[Pc'(C_7H_{15})_8]_2$ (**8**)	329 (4.99), 355 (4.92), 492 (4.47), 616 (4.49), 686 (5.09), 925 br, 1633 br

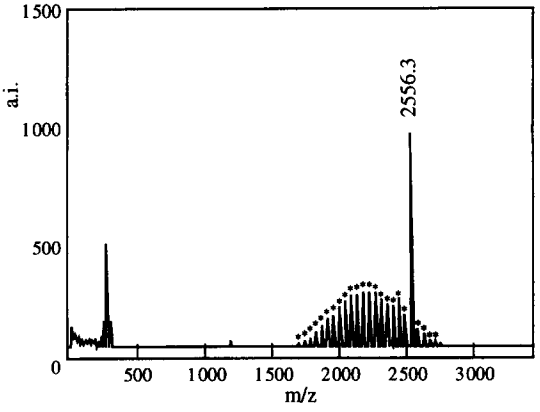


Fig. 2. MALDI-TOF mass spectrum of $Eu[Pc'(OC_5H_{11})_8]_2$ (**5**). * indicates the internal calibrant poly(ethylene glycol).

summarised in Table 1. The data for unsubstituted **1** and **2** are also included for comparison. It can be seen that all of the absorptions are red-shifted when substituents are introduced onto the macrocycles. For example, the Q band is red-shifted by 7–8 nm in compounds **5** and **6** or 16–19 nm in compounds **7** and **8**. It is also worth noting that the lower-energy near-IR band of the europium complexes appears at longer wavelength than that of the corresponding gadolinium complexes. The compounds **1** and **2** also give a lower energy charge transfer band compared with the Dy (1536 nm), Tm, Yb and Lu (1530 nm) analogues [17]. These are consistent with the results reported recently showing that for $Ln(Por)_2$ [18] and Ln(Pc)(Por) [19] (Por = general porphyrinato dianion), when the ionic radius of the central metal ion increases, the absorption maximum of the lower-energy near-IR band is shifted to longer wavelength.

Compounds **5–8** were also mass-measured using two newly developed desorption/ionisation techniques, namely matrix-assisted laser desorption/ ionisation (MALDI) and electrospray ionisation (ESI). Fig. 2 shows a typical positive-ion MALDI time-of-flight mass spectrum of compound **5** using pretreated all-*trans*-retinoic acid as matrix. Poly(ethylene glycol) was used as internal calibrant. Apart from the envelop of peaks originating from the poly(ethylene glycol), an intense ion signal corresponding to the intact singly-charged molecular ion was observed. Ion signals with mass-to-charge ratio less than 500 were commonly attributed to the ions derived from the matrix materials. In all cases, the molecular ion was either the most abundant high mass ion or the only high mass ion present in the mass spectrum. Because of the low resolution of the time-of-flight mass spectra, only average molecular masses can be assigned which are tabulated in Table 2.

The ESI mass spectra of compounds **5–8** were measured using a FTICR mass spectrometer with chloroform as solvent. The molecular ions were essentially the only ions present in the mass spectra. Fig. 3 displays the molecular-ion region in the spectrum of **5** in which distinct isotopic distribution can be observed. The relative abundance of the isotopic cluster is in good agreement with the simulated spectrum of $\{Eu[Pc'(OC_5H_{11})_8]_2\}^+$ as shown in the top-insert. It is therefore concluded that the observed molecular ions were monocations rather than protonated species. The mass spectral results are summarised in Table 2.

Cyclic voltammetric studies revealed that compounds **5–8** undergo one reversible oxidation and one reversible reduction. The data are listed in Table 3, which also includes the half-wave potentials ($E_{1/2}$) of related sandwich compounds for comparison. The potentials were referenced to the ferrocenium–ferrocene couple at +0.355 V relative to the saturated calomel electrode (SCE), and the reversibility was judged by comparison of the separation between the anodic and cathodic potentials at various scan rates

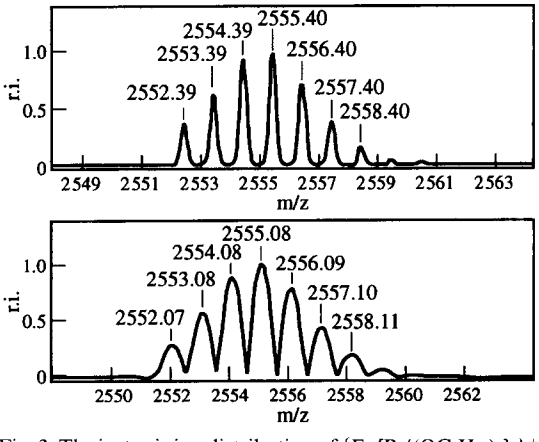


Fig. 3. The isotopic ion distribution of $\{Eu[Pc'(OC_5H_{11})_8]_2\}^+$ ($\mathbf{5}^+$) observed in the ESI mass spectrum of **5**. The top spectrum shows the corresponding simulated pattern.

Table 2. The mass spectral data for bis(phthalocyaninato)lanthanide(III) complexes

Compound	Mass (m/z) ESI-FTICR Calculated[a] value	Measured value	Error (Dalton)	MALDI-TOF Calculated[b] value	Measured value	Error (Dalton)
$Eu[Pc'(OC_5H_{11})_8]_2$ (**5**)	2555.40	2555.08	0.32	2555.09	2556.31	1.22
$Gd[Pc'(OC_5H_{11})_8]_2$ (**6**)	2559.39	2559.10	0.29	2560.32	2561.30	0.98
$Eu[Pc'(C_7H_{15})_8]_2$ (**7**)	2747.98	2747.65	0.33	2747.97	2749.50	1.53
$Gd[Pc'(C_7H_{15})_8]_2$ (**8**)	2752.99	2752.62	0.37	2753.21	2755.00	1.79

[a] Mass corresponding to the most abundant isotopic peak of the molecular ion.
[b] Mass corresponding to the average molecular weight of the compound.

Table 3. Electrochemical potentials of selected lanthanide(III) sandwich complexes of phthalocyanines vs SCE

Compound	$E_{1/2}$(red.)/V	$E_{1/2}$(ox.)/V	Reference
$Eu[Pc'(OC_5H_{11})_8]_2$ (**5**)	−0.21[a]	+0.19[a]	This work
$Gd[Pc'(OC_5H_{11})_8]_2$ (**6**)	−0.20[a]	+0.20[a]	This work
$Eu[Pc'(C_7H_{15})_8]_2$ (**7**)	−0.22[a]	+0.17[a]	This work
$Gd[Pc'(C_7H_{15})_8]_2$ (**8**)	−0.22[a]	+0.18[a]	This work
$Yb[Pc'(OC_4H_9)_8]_2$	−0.15	+0.26	7
$Lu[Pc'(OC_4H_9)_8]_2$	−0.19	+0.25	7
$Lu[Pc'H_4(tert\text{-}C_4H_9)_4]_2$	−0.17	+0.25	6a
$Lu[Pc'H_4(tert\text{-}C_4H_9)_4](Pc)$	−0.13	+0.29	6a
$LuPc_2$	−0.07	+0.34	6a

[a] Recorded with NBu_4PF_6 as electrolyte in CH_2Cl_2 (0.1 mol dm^{-3}) at ambient temperature. Scan rate = 100 mV s^{-1}.

with that of the ferrocenium–ferrocene internal standard [20].

It is generally believed that all of the redox processes in this class of compounds occur on the conjugated macrocyclic ligands; the oxidation state of the central metal ion does not change [6c,7,21]. Thus by incorporating electron donating groups onto the macrocycles, the compound should become more reducing and less oxidising. This is well demonstrated by the $E_{1/2}$ values of **5**–**8** obtained (Table 3). The eight pentyloxy and n-heptyl groups greatly increase the electron density in the macrocycle to roughly the same extent. It is worth mentioning that the difference between the oxidation and reduction potentials, which is a good estimate of the thermal activation energy for the conduction process in these sandwich complexes [22], remains relatively constant (*ca* 0.40 V) in this series of compounds.

Acknowledgements—We thank Rebecca L. C. Lau and Y.-M. Keung for recording the mass spectra, Drs. W.-H. Leung and L. L. Yeung for assistance in cyclic volammetric measurements. This work was supported by the Hong Kong Research Grants Council (Earmarked Grant CUHK 311/94P) and The Chinese University of Hong Kong (Incentive Fund 94/95).

REFERENCES

1. P. N. Moskalev and I. S Kirin, *Opt. Spektrosk.* 1970, **29,** 414; *Russ. J. Phys. Chem. (Engl. Transl.)* 1972, **46,** 1019.
2. M. M. Nicholson, in *Phthalocyanines: Properties and Applications*, Eds. C. C. Leznoff and A. B. P. Lever, Vol. 3, pp. 71–117. VCH, New York (1993).
3. J.-J. André, K. Holczer, P. Petit, M.-T. Riou, C. Clarisse, R. Even, M. Fourmigue and J. Simon, *Chem. Phys. Lett.* 1985, **115,** 463; P. Turek, P. Petit, J.-J. André, J. Simon, R. Even, B. Boudjema, G. Guillaud and M. Maitrot, *J. Am. Chem. Soc.* 1987, **109,** 5119; M. Maitrot, G. Guillaud, B. Boudjema, J.-J. André, H. Strzelecka, J. Simon and R. Even, *Chem. Phys. Lett.* 1987, **133,** 59; J. Padilla and W. E. Hatfield, *Synth. Metals* 1989, **29,** F45; M. Bouvet and J. Simon, *Chem. Phys. Lett.* 1990, **172,** 299; K. R. Rickwood, D. R. Lovett, B. Lukas and J. Silver, *J. Mater. Chem.* 1995, **5,** 725.
4. K. L. Trojan, W. E. Hatfield, K. D. Kepler and M. L. Kirk, *J. Appl. Phys.* 1991, **69,** 6007; J. L. Paillaud, M. Drillon, A. De Cian, J. Fischer, R. Weiss and G. Villeneuve, *Phys. Rev. Lett.* 1991, **67,** 244; K. L. Trojan, J. L. Kendall, K. D. Kepler and W. E. Hatfield, *Inorg. Chim. Acta* 1992,

198–200, 795; P. Petit, *Synth. Metals* 1992, **46,** 147.
5. (a) C. Piechocki, J. Simon, J.-J. André, D. Guillon, P. Petit, A. Skoulios and P. Weber, *Chem. Phys. Lett.* 1985, **122,** 124; (b) Z. Belarbi, M. Maitrot, K. Ohta, J. Simon, J.-J. André and P. Petit, *Chem. Phys. Lett.* 1988, **143,** 400; (c) Z. Belarbi, C. Sirlin, J. Simon and J.-J. André, *J. Phys. Chem.* 1989, **93,** 8105.
6. (a) A. Pondaven, Y. Cozien and M. L'Her, *New J. Chem.* 1991, **15,** 515; (b) *New J. Chem.* 1992, **16,** 711; (c) F. Guyon, A. Pondaven, P. Guenot and M. L'Her, *Inorg. Chem.* 1994, **33,** 4787.
7. K. Takahashi, Y. Tomita, Y. Hada, K. Tsubota, M. Handa, K. Kasuga, K. Sogabe and T. Tokii, *Chem. Lett.* 1992, 759.
8. (a) Y. Liu, K. Shigehara, M. Hara and A. Yamada, *J. Am. Chem. Soc.* 1991, **113,** 440; (b) M. L. Rodriguez-Mendez, R. Aroca and J. A. DeSaja, *Chem. Mater.* 1992, **4,** 1017; (c) D. Battisti, L. Tomilova and R. Aroca, *Chem. Mater.* 1992, **4,** 1323.
9. L. G. Tomilova, E. V. Chernykh, T. T. Ioffe and E. A Luk'yanets, *J. Gen. Chem. USSR* (*Engl. Transl.*) 1983, **53,** 2339; N. B. Subbotin, L. G. Tomilova, E. V. Chernykh, N. A. Kostromina and E. A. Luk'yanets, *J. Gen. Chem. USSR* (*Engl. Transl.*) 1986, **56,** 208.
10. J. G. Stites, C. N. McCarty and L. L. Quill, *J. Am. Chem. Soc.* 1948, **70,** 3142.
11. M. Hanack, A. Gül, A. Hirsch, B. K. Mandal, L. R. Subramanian and E. Witke, *Mol. Cryst. Liq. Cryst.* 1990, **187,** 365.
12. H. Nishi, N. Azuma and K. Kitahara, *J. Heterocycl. Chem.* 1992, **29,** 475; M. Hanack, P. Haisch, H. Lehmann and L. R. Subramanian, *Synthesis* 1993, 387.
13. P. A Barrett, D. A. Frye and R. P. Linstead, *J. Chem. Soc.* 1938, 1157.
14. C. Clarisse and M. T. Riou, *Inorg. Chim. Acta* 1987, **130,** 139; M. M'Sadak, J. Roncali and F. Garnier, *J. Chim. Phys.* 1986, **83,** 211.
15. W. T. Ford, L. Sumner, W. Zhu, Y. H. Chang, P.-J. Um, K. H. Choi, P. A. Heiney and N. C. Maliszewskyj, *New J. Chem.* 1994, **18,** 495.
16. A. T. Chang and J.-C. Marchon, *Inorg. Chim. Acta* 1981, **53,** L241; E. Orti, J. L. Brédas and C. Clarisse, *J. Chem. Phys.* 1990, **92,** 1228; N. Ishikawa, O. Ohno and Y. Kaizu, *Chem. Phys. Lett.* 1991, **180,** 51.
17. D. Markovitsi, T.-H. Tran-Thi, R. Even and J. Simon, *Chem. Phys. Lett.* 1987, **137,** 107.
18. J. W. Buchler, K. Elsässer, M. Kihn-Botulinski, B. Scharbert and S. Tansil, *ACS Symp. Ser.* 1986, **321,** 94; J. W. Buchler, P. Hammerschmitt, I. Kaufeld and J. Löffler, *Chem. Ber.* 1991, **124,** 2151.
19. D. Chabach, M. Tahiri, A. De Cian, J. Fischer, R. Weiss and M. El Malouli Bibout, *J. Am. Chem. Soc.* 1995, **117,** 8548.
20. H. M. Koepp, H. Wendt and H. Stehlow, *Z. Electrochem.* 1960, **64,** 483.
21. H. Konami, M. Hatano, N. Kobayashi and T. Osa, *Chem. Phys. Lett.* 1990, **165,** 397.
22. J. Simon and J. J. Andre, *Molecular Semi-conductors.* Springer Verlag, Berlin (1985); M. Bouvet and J. Simon, *Chem. Phys. Lett.* 1990, **172,** 299.

Pergamon

PII: S0277-5387(96)00247-1

Polyhedron Vol. 16, No. 3, pp. 521–524, 1997
Copyright © 1996 Elsevier Science Ltd
Printed in Great Britain. All rights reserved
0277-5387/97 $17.00+0.00

The $Cr_2O_7^{2-}$–CrO_4^{2-}–$HCrO_4^-$ system revisited

V. G. Poulopoulou,[a] E. Vrachnou,[a] S. Koinis[b] and D. Katakis[b]*

[a]N.C.R.S. "Demokritos", P.O.B. 60228, 153 10 Aghia Paraskevi Attiki, Greece

[b]Inorganic Chemistry Laboratory, Department of Chemistry, University of Athens, Panepistimiopolis, 157 01 Athens, Greece

(Received 1 April 1996; accepted 13 May 1996)

Abstract—The electronic spectra of aqueous Cr^{VI} solutions in the pH range 3–11 have four isosbestic points, located at 246, 293, 338 and 441 nm. These positions are independent of the total concentration of Cr^{VI}. The existence of the isosbestic points indicates that only two species are present, namely CrO_4^{2-} and $Cr_2O_7^{2-}$, and that $HCrO_4^-$ is spectrophotometrically undetectable. This conclusion is further supported by factor analysis, which gives the number of linearly independent species in solution to be two, and also by the method of spectral displacement. At the isosbestic points absorbance is linear in total Cr^{VI} concentration. In this sense Beer's law is valid, and the results can be used for analytical purposes. Copyright © 1996 Elsevier Science Ltd

Current interest in protonated oxochromium(VI) species originates in the role these species play in the corresponding mechanisms of substitution or redox reactions. It is well known [1] that replacement of an oxide ion by a hydroxide, results in a dramatic increase of both self-lability and of the lability of the other ligands. In oxidations by tetraoxoanions *via* a bridged pathway, fast protonation is a prerequisite. For oxidations by CrO_4^{2-} and/or $Cr_2O_7^{2-}$ in particular, it is important to know whether $HCrO_4^-$ is present in significant amounts or not. This is more so in biological systems, in order to understand the mutagenic action of Cr^{VI} compounds, which depends on their ability to cross the cell membrane, and to react with the components of the cell [2].

In the early literature it was believed that aqueous solutions of chromium(VI), at pH 3 to 11, in addition to CrO_4^{2-} and $Cr_2O_7^{2-}$, also contain $HCrO_4^-$. The methods used to study these systems include freezing point and conductivity measurements [3], potentiometry [4], spectrophotometry [5,4d–f], vapour pressure measurements [6], and calorimetry [7]. Reference 4f contains the bibliography up to 1960.

In none of these papers is the existence of $HCrO_4^-$ questioned, and this confidence was transferred to the textbooks and comprehensive works dealing with the subject [8]. Yet the early results do *not prove* the existence of $HCrO_4^-$; they are merely consistent with it, but they can be interpreted without assuming its existence. Furthermore Michel and Machiroux [9] failed to find direct Raman evidence for the existence of $HCrO_4^-$, and came to the conclusion that in aqueous Cr^{VI} solutions, at pH 3–11, there is no $HCrO_4^-$, that only two species are present in detectable amounts, namely $Cr_2O_7^{2-}$ and CrO_4^{2-}, related to each other through the equilibrium:

$$2CrO_4^{2-} + 2H^+ \rightleftharpoons Cr_2O_7^{2-} + H_2O \quad \log K_1 = 14.85 \tag{1}$$

the value of K_1 being given at zero ionic strength and 25°C.

On the basis of these data estimates [10] of the percentages of various species, which include $HCrO_4^-$, were questioned. Moreover, Michel and Cahay [11] extended their investigation to more acidic solutions, up to 12 M HNO_3 and again, they found no evidence for protonated species.

Hence the matter of the existence of $HCrO_4^-$, in considerable equilibrium amounts, cannot be considered settled, and this is what the present paper deals with. We tried to detect $HCrO_4^-$ using an assortment of sensitive UV–vis spectrophotometric techniques, and it was found, that its concentration, instead of being as high as 99.6% (pH 4, $[Cr^{VI}]_{total} = 10^{-6}$ M)or

* Author to whom correspondence should be addressed.

91.05% (pH 4, $[Cr^{VI}]_{total} = 10^{-3}$ M) as estimated [10], it is within experimental error zero. The affinity of CrO_4^{2-} and $Cr_2O_7^{2-}$ for protons, and for that matter of the protonated forms as well for a second proton, is extremely small.

EXPERIMENTAL

The solutions were prepared using proanalysis $Na_2Cr_2O_7$ (Mallinckrodt) and doubly distilled water. Air was excluded by purging with argon, passed through a NaOH solution in order to avoid formation of carbonates, which interfere with the spectrum at short wavelengths [4]. The pH was adjusted with NaOH or $HClO_4$ and measured with an E520 Metrohm–Herisau pH-meter. Electronic spectra were obtained with a Hitachi U-2000, in quarts cell.

RESULTS AND DISCUSSION

Among the concentrations of CrO_4^{2-}, $HCrO_4^-$ and $Cr_2O_7^{2-}$, at different pH values, there is no linear relation of the form:

$$\alpha[CrO_4^{2-}] + \beta[HCrO_4^-] + \gamma[Cr_2O_7^{2-}] = 0$$

α, β, γ being pH-independent constants, not all zero [12]. Hence, if all three species were contributing to light absorbance at different wavelengths, the corresponding matrix would have rank three [13]. However, factor analysis [14] shows that there are only two significant elements in the diagonalized matrix, i.e., that the rank is two. Since CrO_4^{2-} and $Cr_2O_7^{2-}$ are known to exist at high and low pH values, respectively, we must conclude that these are the only species present; $HCrO_4^-$ is not present in measurable amounts, even at the pH values where it was believed to dominate [10].

The spectra at different pH values and different total Cr^{VI} concentrations exhibit four well-defined isosbestic points at 246, 293, 338, and 441 nm (Fig. 1). The spectra in this figure were obtained at constant ionic strength (1 M $NaClO_4$). If in addition to the total concentration and the pH, a third variable is changed, namely ionic strength, slightly different spectra are obtained, but the change in the environment does not seem to affect the electronic transitions themselves, nor the positions of the isosbestic points.

It is seen in Fig. 1 that the position of the isosbestic points does not depend on the total concentration of Cr^{VI} or pH.

The absorbance at the isosbestic points at various totals Cr^{VI} concentrations are given in Table 1. The corresponding average absorptivities per chromium equivalent are $\varepsilon_{441} = (2.45 \pm 0.05) \times 10^2$, $\varepsilon_{338} = (1.59 \pm 0.1) \times 10^3$, $\varepsilon_{293} = (1.34 \pm 0.08) \times 10^3$, $\varepsilon_{246} = (2.19 \pm 0.1) \times 10^3$. For at least three orders of magnitude in the concentration, at the isosbestic points, Beer's law is valid, as indicated by the constant values of the ratio

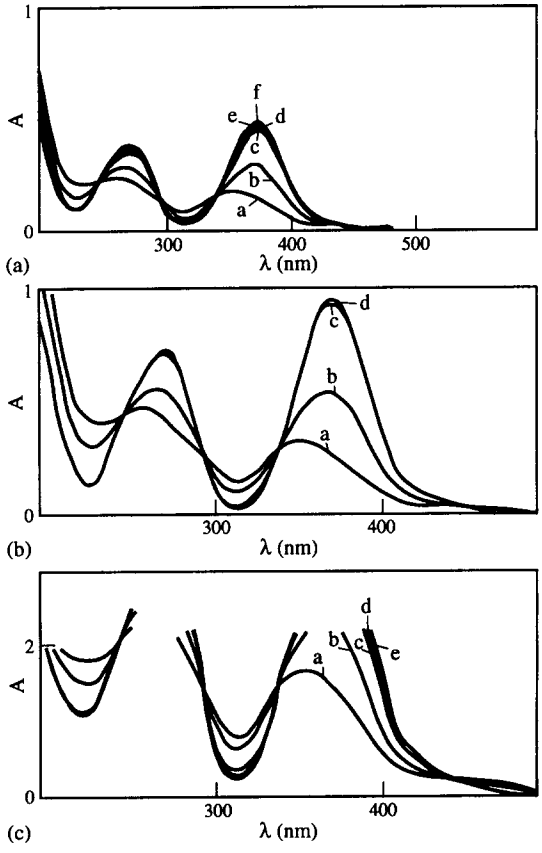


Fig. 1. Spectra (Absorbance) of Cr^{VI} solutions at various total Cr^{VI} concentrations and pH values, at constant ionic strength 1 M $NaClO_4$, 28°C. (a) $[Cr^{VI}]_{total} = 1.0 \times 10^{-4}$ M, pH, a:4, b:5, c:6, d:7, e:8, f:9; 1 cm cell. (b) $[Cr^{VI}]_{total} = 1.0 \times 10^{-3}$ M, pH, a:3, b:5, c:7 8, d:9; 0.2 cm cell. (c) $[Cr^{VI}]_{total} = 1.0 \times 10^{-2}$ M, pH, a:3, b:5, c:7, d:8, e:9; 0.1 cm cell.

$A_{isosb}/[Cr^{VI}]_{total}$, and this can obviously be used analytically; knowledge of the distribution among species is not necessary.

The behaviour at the isosbestic points should be contrasted with that at the rest of the spectrum, where Beer's law is not valid.

For a long time, the appearance of isosbestic points was considered to be proof for the existence of only two absorbing species in a system [15]. Later, this assumption was questioned, but our system is not among the special cases examined [16]. The appearance of the four isosbestic points, combined with the factor analysis results, must be taken as strong evidence for the existence of only two species indeed.

However, for further support we applied the method of spectral displacement, developed by T. Nowicka-Jankowska [17]. According to this method, if we take the linear combinations of absorbances at two wavelengths, differing by a constant $\Delta\lambda$:

$$\xi_{1,2} = \alpha A_1 + \beta A_2$$

Table 1. Absorbances[a] at the four isosbestic points of Cr^{VI} solutions in the pH range 3–11. In parenthesis Abs/$[Cr^{VI}]_{total}$

Total Cr^{VI} (M)	A_{441}	A_{338}	A_{293}	A_{246}
1.6×10^{-5}	0.004 (250)	0.025 (1562)	0.022 (1375)	0.034 (2125)
6.6×10^{-5}	0.016 (242)	0.013 (1712)	0.087 (1318)	0.140 (2121)
1.0×10^{-4}[b]	0.024 (240)	0.154 (1540)	0.125 (1250)	0.220 (2200)
6.0×10^{-4}	0.150 (250)	1.025 (1708)	0.825 (1375)	1.450 (2416)
1.0×10^{-3}[b]	0.24 (240)	1.53 (1520)	1.25 (1250)	2.17 (2170)
1.0×10^{-2}[b]	2.5 (250)	15.0 (1500)	14.6 (1460)	21.2 (2120)

[a] All measurements but the last were made with 1 cm quartz cells at 28°C. The concentrated solutions (10^{-2} M) were measured in 0.1 and 0.2 cm cells, respectively and the values were multiplied by 10 and 5 to be comparable with the others.

[b] Ionic strength 1 M ($NaClO_4$).

the new curve should also have isosbestic points. What this means in practical terms is that if we displace the spectra by a given $\Delta\lambda$ (positive or negative) and then take the sum or difference or any linear combination of the original spectra with the displaced ones, if there is a hidden peak or shoulder, this combination *will not* have isosbestic points. Generally, the linear combination of the displaced spectra with the original one may:

(1) Still have isosbestic points, which is strong evidence that the original isosbestic points were real, and that only two species exist;

(2) The new curves cross each other but not at common points, which indicates that the original isosbestic points were coincidental;

(3) The curves do not cross each other. In this case there is no new information.

In our case we varied three experimental variables (pH, total Cr^{VI}, ionic strength) and scanned the entire spectrum, which was recorded in digital form, every 2 nm, applying the method with different $\Delta\lambda$'s, and coefficients α and β. In fact, we used 60 values of $\Delta\lambda$, from -30 to $+30$ nm and a random choice of α and β; this essentially means an infinite number of combinations. In all cases the isosbestic points either persisted or there was no crossing of the curves.

The Cambridge Structural Database (1989) contains no $HCrO_4^-$ entry, and Gmelin gives only one relevant compound, $KHCrO_4^-$, assumed to be present in mixed crystals with $KMnO_4$. This, combined with the Raman evidence and the evidence presented here, lead to the conclusion that hydrogen chromate is a strong acid, and by analogy with the H_2SO_4/HSO_4^- couple, H_2CrO_4 is expected to be even stronger; this is probably the reason why these species were not detected.

The fact then that $HCrO_4^-$ was not observed directly by modern Raman techniques and in the present investigation indicate the presence, in equilibrium mixtures, of CrO_4^{2-} and $Cr_2O_7^{2-}$ only, unless, in the case of the spectroscopic data, it is accepted that $Cr_2O_7^{2-}$ and $HCrO_4^-$ have exactly the same spectrum, which is very unlikely [18]. The hypothetical O_3CrOH has C_{3v} symmetry, the same as the O_3CrO chromophore of dichoromate, and resemblance is expected, but not the identity required to explain the accuracy and the persistence of the position of the isosbestic points.

On a more general, and perhaps more important basis, it is noted that the rate laws of many substitution and redox reactions with oxoanions [1], including those of Cr^{VI}, allow no doubt for the existence of protonated species, not however necessarily in quantities detectable by Raman and or UV–vis spectroscopic techniques. Yet, even with a small quantity of protonated species (equilibrium or steady state) the corresponding reaction is greatly accelerated, and the proton catalyzed term becomes comparable with the non-catalyzed one. The increase in lability due to the protonation must be orders of magnitude greater than that estimated on the basis of the hitherto accepted equilibrium quantities of $HCrO_4^-$.

Saito and Sasaki point out [19] that if the rate constants for substitution reactions for Cr^{VI} on one hand, and Mo^{VI}, W^{VI} on the other, are compared on the basis of the rate laws [20].

$$\text{Rate} = k[HCrO_4^-][X][H^+] \quad (2)$$

$$\text{Rate} = k'[MO_4^{2-}][X][H^+] \quad M = Mo, W \quad (3)$$

the conclusion is reached that $HCrO_4^-$ is much less reactive than MoO_4^{2-} or WO_4^{2-}. However, k in (2) is actually $k''K[H^+]$, where K the equilibrium constant for the formation of $HCrO_4^-$. The small reactivity of $HCrO_4^-$ may be due to the small value of K; this is essentially our claim. A common mechanism for the Cr, Mo, and W oxoanions [20] (possibly concerted) then becomes possible.

Similar remarks can probably be made for oxygen exchange, and oxidation reaction as well.

Acknowledgements—The authors wish to thank Mr N. Liadakis who prepared the P.C. software for the application of the spectral displacement method.

REFERENCES

1. (a) H. Taube and G. Gordon, *Inorg. Chem.* 1962, **1,** 69; (b) H. Gamjager and R. K. Murmann, *Adv. Inorg. Bioinorg. Mechanisms* 1983, **2,** 317; (c) D. Katakis and G. Gordon, *Mechanisms of Inorganic Reactions*, pp. 188, 241, Wiley, New York (1987).
2. (a) T. Norseth, *Environ. Health Perspect.* 1981, **40,** 121; (b) M. A. Sirover, *Environ. Health Perspect.* 1981, **40,** 163; (c) R. A. Zakour, T. A. Kunkel and L. A. Loeb, *Environ. Health Perspect.* 1981, **40,** 197; (d) K. W. Jennette, *Environ. Health Perspect.* 1981, **40,** 233; (e) K. W. Jennette, *Biol. Trace Elements Res.* 1979, **1,** 55; (f) P. H. Connett and K. E. Wetterhahn, *Structure and Bonding* 1983, **54,** 93.
3. (a) P. Walden, *Z. Physik, Chem.* 1888, **2,** 49; (b) W. Ostwald, *Z. Physik. Chem.* 1888, **2,** 78; (c) M. S. Sherrill, *J. Am. Chem. Soc.* 1907, **29,** 1641; (d) E. Spitalski, *Z. Anorg. Chem.* 1907, **54,** 265.
4. (a) K. Beck and P. Stegmuler, *Arb. Kaiserl Gesundh* 1910, **34,** 446; (b) J. D. Neuss and W. J. Reiman, *J. Am. Chem. Soc.* 1934, **56,** 2238; (c) G. Schwarzenbach and J. Meier, *J. Inorg. & Nuclear Chem.* 1958, **8,** 302; (d) J. R. Howard, V. S. K. Nair and G. H. Nancollas, *Trans. Faraday Soc.* 1958, **54,** 1034; (e) N. Bailey, A. Carrington, K. A. K. Lott and M. C. R. Symons, *J. Chem. Soc.* 1960, 290; (f) Y. Sasaki, *Acta Chem. Scand.* 1962, **16,** 719; (g) H. Linge and A. L. Jones, *Aust. Chem.* 1968, **21,** 2189.
5. (a) Job, *Compt. rend.* 1928, **186,** 1546; (b) W. G. Davies and J. E. Prue, *Trans. Faraday Soc.* 1955, **51,** 1045; (c) J. Y. Tong and E. L. King, *J. Am. Chem. Soc.* 1953, **75,** 6180; (d) G. P. Haight Jr, D. C. Richardson and H. Coburn, *Inorg. Chem.* 1964, **3,** 1777; (e) J. Y. Tong, *Inorg. Chem.* 1964, **3,** 1805; (f) G. Linge and A. L. Jones, *Aust. Chem.* 1968, **21,** 1445.
6. R. H. Stokes, J. M. Wilson and R. A. Robinson, *Trans. Faraday Soc.* 1941, **37,** 566.
7. L. G. Hepler, *J. Am. Chem. Soc.* 1958, **80,** 6181.
8. See for example: (a) J. K. Beattie and G. P. Haight Jr, *Progr. Inorg. Chem.* 1972, **17,** 93; (b) F. A. Cotton and G. Wilkinson, *Advanced Inorganic Chemistry*. Wiley, New York, (1988); (c) L. F. Larkworthy, K. B. Nolan and P. O'Brien, *Chromium Comprehensive Coord. Chem.* eds G. Wilkinson, R. D. Gillard and J. A. McCleverty, Vol. 3, p. 699, Pergamon, Oxford (1987).
9. G. Michel and R. Machiroux, *J. Raman Spect.* 1983, **14,** 22.
10. R. K. Tandon, P. T. Crisp, J. Ellis and R. S. Baker, *Talanta* 1984, **31,** 227.
11. G. Michel and R. Cahay, *J. Raman Spect.* 1986, **17,** 79.
12. S. P. Koinis, A. T. Tsatsas and D. F. Katakis, *J. Chemometrics* 1991, 21.
13. D. Katakis, *Anal. Chem.* 1965, **37,** 876.
14. D. T. Harvey and A. Bowman, *J. Chem. Educ.* 1990, **67,** 470.
15. (a) G. Scheibe, *Z. Angew. Chem.* 1937, **50,** 212; (b) R. S. Drago, *Physical Methods of Chemistry*, p. 92, W. B. Saunders Company, Philadelphia, (1977).
16. (a) M. D. Cohen and E. Fischer, *J. Chem. Soc.* 1968, 3044; (b) J. R. Morey, *J. Phys. Chem.* 1962, **66,** 2169; (c) J. R. Morey, *J. Phys. Chem.* 1963, **67,** 1569; (d) F. Kwjatkowski, *Roczniki Chem.* 1966, **40,** 177.
17. Teresa Nowicka-Jankowska, *J. Inorg. Nucl. Chem.* 1971, **33,** 2043.
18. V. Miskowski, N. B. Gray and C. J. Ballhausen, *Mol. Phys.* 1974, **28,** 729.
19. K. Saito and Y. Sasaki, *Inorg. Bioinorg. Mech.* 1982, 179.
20. (a) A. Haim, *Inorg. Chem.* 1972, **11,** 3147; (b) S. Fanahashi, Y. Kato, M. Nakayama and M. Tanaka, *Inorg. Chem.* 1981, **20,** 1752.

Pergamon

PII: S0277-5387(96)00245-8

Polyhedron Vol. 16, No. 3, pp. 525–529, 1997
Copyright © 1996 Elsevier Science Ltd
Printed in Great Britain. All rights reserved
0277-5387/97 $17.00+0.00

Synthesis, spectroscopy and crystal structure of $Ag(TLA) \cdot NO_3$ [TLA = tris(6-methyl-2-pyridylmethyl)amine]

Zhi Hui Zhang,* Zhi Ang Zhu, Xian He Bu, Yu Liu and Yun Ti Chen

Department of Chemistry, Nankai University, Tianjin 300071, P.R. China

(Received 8 February 1996; accepted 13 May 1996)

Abstract—The title complex has been synthesized and characterized by X-ray diffraction. The Ag^I atom is in a distorted square pyramidal geometry with two pyridyl nitrogen atoms, one alkylamine nitrogen atom from TLA and two oxygen atoms from the nitrate group which is coordinated as a bidentate ligand. There are two different independent configurations in the same unit cell, and the internuclear distance Ag(1) ··· Ag(2) is 9.246 Å. The solution behaviors of $Ag(TLA)NO_3$ have been further studied with ^1H NMR. The two β-protons on each pyridine are resolved from each other and are assigned to the two peaks at 7.50 and 7.08 ppm. The methene protons and methyl protons are shifted slightly upfield compared with those of free TLA due to the formation of coordinate bonds of $N_{pyridyl}$ with Ag^I atom. Copyright © 1996 Elsevier Science Ltd

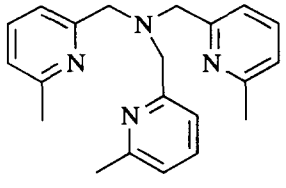
Keywords: silver(I) complex; synthesis; crystal structure; tris(6-methyl-2-pyridylmethyl)amine; ^1H NMR; spectroscopic study.

Studies of mononuclear and polynuclear complexes have attracted much interest in recent years. The main reason is probably that many metalloproteins and enzymes have multi-metal sites which are essential for their biological and catalytic functions. Thus, the syntheses, and crystal structures of new complexes are of significance for understanding the biological phenomena and exploiting artificial models. The tripodal tetradentate ligands including nitrogen atoms are versatile and useful for assembly new molecules, because they can be coordinated to many transition metal ions to form new compounds as biomimetic systems. For instance, the complexes of iron with tris(2-pyridylmethyl)amine (TPA) have been studied as the models of methyl monooxydase (MMO) [1,2], copper complexes with the same ligands, as the models of copper protein [3,4], and nickel complexes, as the models of carbon monoxide dehydrogenase (CODH) [5,6]. It is reported that some Ag^I complexes show excellent antimicrobial activities against some bacteria [7]. More recently, we have synthesized some new complexes by using tripodal ligands [8,9]. In order to extend our knowledge in this field, we now report the synthesis, spectroscopic properties and X-ray crystal structure of the complex of $AgNO_3$ with [tris(6-methyl-2-pyridylmethyl)]amine (TLA), which is a potential tripodal tetradentate ligand.

EXPERIMENTAL

Materials and general methods

All of the starting materials and solvents for synthesis were of analytical grade as purchased commercially and used without further purification. IR absorption spectra were recorded on a 170SX (Nicolet) FT-IR spectrophotometer using KBr discs. Elemental analysis was taken on a Perkin–Elmer ana-



Structure 1. TLA ligand.

*Author to whom correspondence should be addressed.

lyzer model 240. ^{1}H NMR was recorded on a Bruker AC-P200 spectrometer (200 MHz, 25°C) in CD_3OD. Chemical shifts (in ppm) are referenced to the residual protonic solvant peaks.

Synthesis

The TLA ligand was prepared by using the published procedure [10]. A solution of $AgNO_3$ (0.170g, 1 mmol) in 50 cm^3 absolute methanol was added to a stirred solution of TLA (0.40g, 1.2 mmol) in 60 cm^3 absolute methanol. After stirring for 1–1.5 h, the mixture was filtered and then covered with a piece of black material (to avoid light). By slow evaporation of the filtrate at room temperature, colourless crystals of $Ag(TLA)NO_3$(1) suitable for X-ray structure determination were obtained. Found: C, 50.0; H, 5.0; N, 14.0. Calc. for $C_{21}H_{24}N_5O_3Ag$: C, 50.2; H, 4.8; N, 13.9%.

Crystallographic studies

The crystal and intensity data were obtained from a crystal mounted on a glass fibre and using an Enraf–Nonius CAD-4 diffractionmeter equipped with a graphite monochromator. The determination of unit cell parameters and the data collection were performed with Mo–k_α radiation ($\lambda = 0.71073$ Å). Unit cell dimensions were obtained by least-square refinements of setting angles of 25° reflections. The structure was solved by direct methods (MULTAN 82) [11]. The metal atoms were located from an E-map. The location of the other non-hydrogen atoms was achieved by successive difference Fourier syntheses. Final refinement by full matrix least-square methods was carried out with anisotropic thermal parameters for non-hydrogen atoms. All the calculations were performed on a PDP 11/44 computer using the SDP-PLUS program systems [12]. The crystallographic data and data collection parameters for the complex 1 are summarized in Table 1.

Table 1. Crystallographic data and details of refinement for $Ag(TLA)NO_3$

Formula	$C_{21}H_{24}AgN_5O_3$
Formula weight	502.33
Crystal system	monoclinic
Space group	PZ_1/a
Unit cell dimensions	
a (Å)	17.183 (3)
b (Å)	14.134 (2)
c (Å)	19.980 (4)
β (°)	115.23 (1)
V (Å^3)	4390 (2)
Z	8
μ (MoK_α) mm^{-1}	0.938
Dc (Mg·M^{-3})	1.52
Linear absorption coefficient	1.133–0.831
F(000)	2048
Crystal size (mm)	$0.3 \times 0.3 \times 0.25$
Scan mode	$\omega/2\theta$
λ (Å)	0.71073
max. 2θ (°)	46
Scan speed (°/min)	0.92–5.49
Index range h, k, l	−18 to 18, 0 to 15, 0 to 22
No. of indep. reflcns.	5106 ($R_{int} = 0.028$)
No. of uniq. reflcns.	2389 [$I > 3\sigma(I)$]
Absorption correction	empirical (DIFABS) [15]
No. of parameters refined	541
R	0.047
R_w	0.054
Goodness of fit	0.82
Maximum Δ/σ	0.761
Residual extrema in difference map	0.51, −0.39
Weighting scheme	$w = 1/(\sigma^2(F) + 0.0001F^2)$

RESULTS AND DISCUSSION

Crystal structure of $Ag(TLA)NO_3$

A perspective view of 1 and a packing diagram are shown in Figs 1 and 2, respectively. Selected bond lengths and bond angles are given in Table 2.

It can be seen from Fig. 1 that in the same unit cell there are two independent metal configurations which are somewhat different. Each Ag^I atom lies in the distorted square pyramidal environment composed of one amine nitrogen atom [N(1) or N(5)], two pyridyl nitrogen atoms [N(2) and N(3) or N(6) and N(7)] and two oxygen atoms [O(11) and O(12) or O(21) and O(22)] from the nitrate. The nitrogen atoms of two pyridyl groups from TLA [one includes N(2) and N(6), the other includes N(3) and N(7)] coordinate to the silver(I) atoms. One of the 2-pyridylmethyl arms in the potentially tetradentate TLA ligand remains uncoordinated to the metal centre. The distances Ag(1)–N(1) and Ag(2)–N(5) are 2.462(11) and 2.482(10) Å, respectively, and they are longer than normal ones. This indicates a weaker interaction between silver(I) and the tertiary nitrogen [13]. The distances between Ag(1)–N(3) (2.466 Å) or Ag(2)–N(7) (2.504 Å) are longer than Ag(1)–N(2) (2.346 Å) or Ag(2)–N(6) (2.331 Å), respectively. This may be due to the steric effect of the coordinated nitrate ligand which pushes away the coordinated pyridyl group [N(3), C(21), C(22), C(23), C(24), C(25)] or [N(7), C(51), C(52), C(53), C(54), C(55)] from the nitrate group [N(11), O(11), O(12), O(13)] or [N(12), O(21), O(22), O(23)], respectively. The nitrate group which lies in the *trans*-position to the coordinated pyridyl groups is coordinated to the Ag^I atom as a bidentate ligand with Ag(1)–O(11) = 2.483(13) Å, Ag(1)–O(12) = 2.605(12) Å or Ag(2)–O(21) = 2.411(9) Å, Ag(2)–O(23) = 2.686(10) Å, and these are normal coordinated bonds. However, there are no chemical bonds formed between the Ag(1) or Ag(2) and the pyridyl nitrogen of the other pyridyl group which

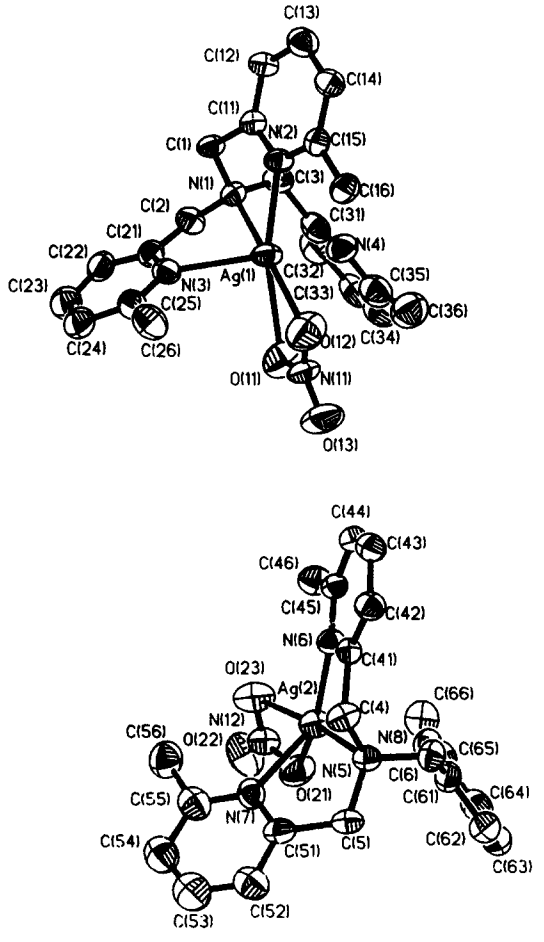


Fig. 1. ORTEP view and labeling scheme for $Ag(TLA)\cdot NO_3$.

includes N(4) or N(8), and the distances of Ag(1)···N(4) and Ag(2)···N(8) are 2.699 Å and 2.686 Å, respectively. The distance of O(13)···C(44) is 3.253 Å, and there is no interaction between the two atoms and the distance of Ag(1)···Ag(2) is 9.246 Å. Apparently there are two kinds of different independent molecular structures in the same unit cell. The Ag^{I} atoms are situated out of the coordinated pyridyl planes 1 [C(11), C(12), C(13), C(14), C(15), N(2)] and plane 2 [C(21), C(22), C(23), C(24), C(25), N(3)] or 4 [C(41), C(42), C(43), C(44), C(45), N(6)] and 5 [C(51), C(52), C(53), C(54), C(55), N(7)] by 0.43 Å or 0.33 Å. The dihedral angles between planes 1 and 2 or planes 4 and 5 are 50.03 or 54.36 , respectively. The dihedral angles between planes 2 and 3 [C(31), C(32), C(33), C(34), C(35) N(4)] or planes 5 and 6 [C(61), C(62), C(63), C(64), C(65), N(8)] are 81.46 or 79.90 , respectively.

Spectroscopic studies

In the IR spectra of $Ag(TLA)NO_3$, the broad bands appearing at about 3434 cm^{-1} imply the existence of water, but no water molecule is coordinated to Ag^{I} in the crystal structure. The strong peaks at 1596, 1575, 1462 cm^{-1} are attributed to the vibration of pyridyl rings. There are two new stronger absorption bands of 1 at 1384 and 1309 cm^{-1} which are assigned to the nitrate group [14]. ^{1}H NMR data and spectra are shown in Table 3 and Fig. 3, respectively. From the ^{1}H NMR data of complex 1, it can be seen that the chemical shift appearing at 7.65 ppm implies the py-γ-H. The two β-protons on each pyridyl ring are

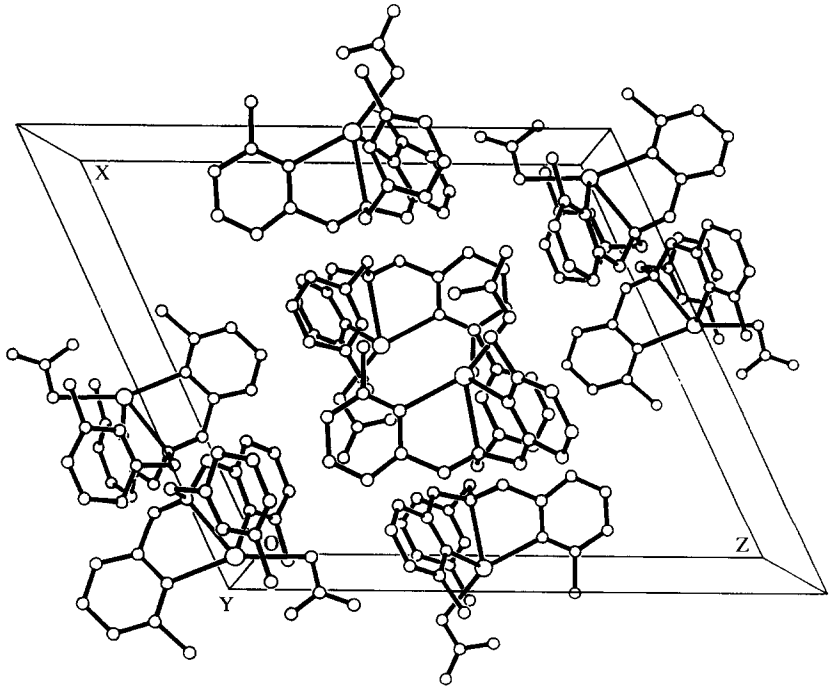


Fig. 2. Perspective view of molecular stacking in unit cell of $Ag(TLA)\cdot NO_3$.

Table 2. Selected bond length (Å) and bond angle (°) for $Ag(TLA) \cdot NO_3$ with estimated standard deviations in parentheses

Ag(1)–O(11)	2.483(13)	Ag(1)–O(12)	2.605(12)
Ag(1)–N(1)	2.462(11)	Ag(1)–N(2)	2.346(9)
Ag(1)–N(3)	2.466(10)	Ag(2)–O(21)	2.411(9)
Ag(2)–O(23)	2.686(10)	Ag(2)–N(5)	2.482(10)
Ag(2)–N(6)	2.331(9)	Ag(2)–N(7)	2.504(12)

N(1)–Ag(1)–N(2)	72.7(3)	N(1)–Ag(1)–N(3)	68.6(4)
N(2)–Ag(1)–N(3)	109.5(4)	N(5)–Ag(2)–N(6)	72.5(3)
N(5)–Ag(2)–N(7)	69.0(3)	N(6)–Ag(2)–N(7)	107.4(3)
O(11)–Ag(1)–N(3)	88.6(4)	O(12)–Ag(1)–N(1)	174.6(4)
O(21)–Ag(2)–N(5)	130.9(4)	O(21)–Ag(2)–N(6)	154.6(4)
O(23)–Ag(2)–N(5)	173.3(3)	O(21)–Ag(2)–N(7)	92.5(3)
O(23)–Ag(2)–N(6)	110.8(3)	O(12)–Ag(1)–N(2)	112.0(4)
O(12)–Ag(1)–N(3)	111.2(4)	Ag(1)–O(11)–N(11)	103.1(8)

Table 3. The ^1H NMR data of complex 1 and assignment

Chemical shift (ppm)	py–β–H	py–γ–H	$-CH_2-$	$-CH_3-$
TLA	7.22, 7.18	7.64	3.97	2.57
$Ag(TLA) \cdot NO_3$	7.50, 7.08	7.65	3.80	2.47

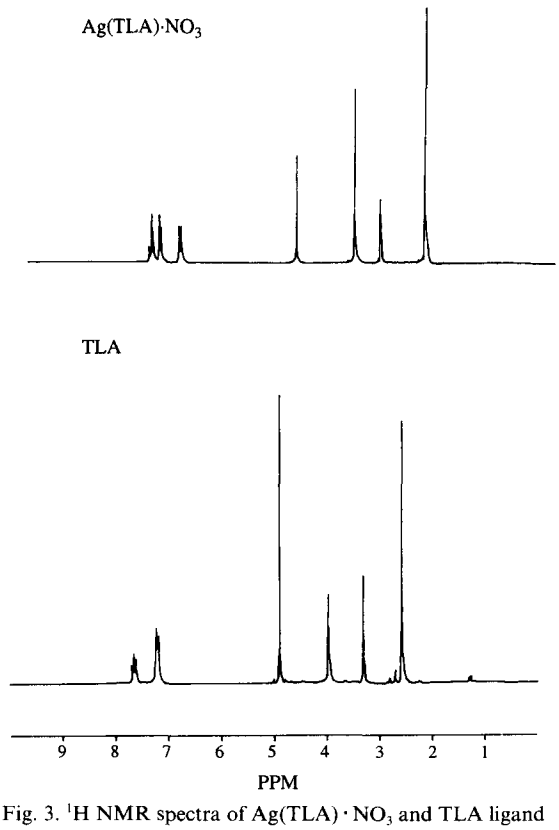


Fig. 3. ^1H NMR spectra of $Ag(TLA) \cdot NO_3$ and TLA ligand in CD_3OD.

resolved from each other and are assigned to the two peaks at 7.50 and 7.08 ppm. The proton number ratio of the three pyridyl-H peaks at 7.65, 7.50 and 7.08 ppm is 1 : 1 : 1. The chemical shift of the methylene potons is at δ 3.80 ppm and that of methyl protons is at δ2.47 ppm, and the proton number ratio of the two peaks is 2 : 3, and they are shifted slightly upfield compared with those of TLA because of the formation of coordination bonds of $N_{pyridyl}$ with Ag^I atom.

Supplementary material—Full details of the crystal data and data collections, thermal parameters, bond distances and angles, mean plane and dihedral angles between the planes, listings of observed and calculated structural factors for complex 1 are available from the authors on request.

Acknowledgements—The project was financially supported by the Elementary Organic Chemistry Institute Key laboratory and the National Natural Science Foundation of China.

REFERENCES

1. Y. Dong, H. Fujii, M. P. Hendrich, R. A. Leising, G. Pan, C. R. Randall, E. C. Wilkinson, Y. Zang, L. Que Jr., B. G. Fox, K. Kauffmann and E. Münck, *J Am. Chem. Soc.* 1995, **117,** 2778.
2. Y.-M. Chiou and L. Que, *J. Am. Chem. Soc.* 1992, **114,** 7567.
3. N. Wei, N. N. Murthy and K. D. Karlin, *Inorg. Chem.* 1994, **33,** 6093.
4. S. Chen, J. F. Richardson, R. M. Buchanan, *Inorg. Chem.* 1994, **33,** 2376.
5. S. W. Ragsdale, *Crit. Rev. Biochem. Mol. Biol.* 1991, **26,** 261.
6. C.-P. Wang, R. Franco, J. J. G. Moura, I. Moura and E. P. Day, *J. Biochem.* 1992, **11,** 7378.
7. K. Nomiya, K.-I. Onoue, Y. Kondoh and N. C. Kasuga, *Polyhedron* 1995, **10,** 1359.
8. Z. H. Zhang, X. H. Bu, Z. A. Zhu and Z. H.

Jiang, Y. T. Chen, *Trans. Met. Chem.* 1996, **21,** 235.
9. Z. H. Zhang, X. H. Bu, Z. A. Zhu and Y. T. Chen, *Polyhedron* 1996, **16,** 2787.
10. M. M. De Mota, J. Rodgers and S. M. Nelson, *J. Chem. Soc. A.* 1969, 2036.
11. Main, P. Fiske, S. J. Hull, S. E. Lessinger, G. Germain, J. P. De Clereq and M. M. Woolfson, *MULTAN*82. *A system of computer programs for the automatic solution of crystal structures from X-ray diffraction data*, Universities of York and Louvain (1982).
12. *SDP Structure Determination Package*, Enraf-Nonius, Delft (1985).
13. S.-Y. Yu, Q.-H. Luo, M.-C. Shen, X.-Y. Huang, W.-H. Yang and Z. Zhang, *Inorg. Chim. Acta* 1994, **223,** 181.
14. Kazuo Nakamoto, *Infrared and Raman Spectra of Inorganic and Coordination Compounds*, Third Ed., Chap. 3, John Wiley (1978); (in Chinese), translated by D. R. Huang and R. Q. Wang, The Publishing House of the Chinese Chemical Industry, Beijing (1986).
15. N. Walker and D. Stuart, *Acta Cryst.* 1983, **A39,** 158.

Pergamon

PII: S0277-5387(96)00244-6

Polyhedron Vol. 16, No. 3, pp. 531–534, 1997
Copyright © 1996 Elsevier Science Ltd
Printed in Great Britain. All rights reserved
0277-5387/97 $17.00+0.00

Synthesis, structure and magnetic properties of oxalate-bridged complex $[Cu_2(bpy)_2(C_2O_4)(H_2O)_2][Cu(bpy)(C_2O_4)](NO_3)_2$

Juan Shi, Guang-Ming Yang, Peng Cheng, Dai-Zheng Liao,* Zong-Hui Jiang and Geng-Lin Wang

Department of Chemistry, Nankai University, Tianjin, P.R. China

(Received 9 January 1996; accepted 13 May 1996)

Abstract—The complex $[Cu_2(bpy)_2(C_2O_4)(H_2O)_2][Cu(bpy)(C_2O_4)](NO_3)_2$ has been synthesized by electrophilic attack of $[Cu(bpy)(H_2O)_2]^{2+}$ on $K_3[Cr(C_2O_4)_3]$ (where bpy stands for 2,2′-bipyridyl). The crystal structure of the complex consists of a binuclear species $[Cu_2(bpy)_2(C_2O_4)(H_2O)_2]^{2+}$ and a mononuclear species $[Cu(bpy)(H_2O)(C_2O_4)]$. The temperature dependences of the magnetic susceptibilities of the complex have been studied in the 4.2–300 K range, giving the exchange integral $J = -340\ cm^{-1}$, indicating rather strong antiferromagnetic interaction between the copper(II) ions within the binuclear unit. Copyright © 1996 Elsevier Science Ltd

Keywords: trinuclear copper complex; crystal structure; magnetic properties.

Polymetallic complexes with extended bridged structures are of current interest due to spin-exchange and charge transfer between metal ions and the domain of metalloenzymes and novel magnetic materials [1,2].

The oxalate has been proved to be an appropriate bridging unit to design magnetic centers and many oxalato-bridged complexes have been reported [1,3–7]. However, to our knowledge, only a few crystal structures showing this binding feature of oxalates have been determined by X-ray diffraction methods. In this paper, we report the synthesis, characterization and structural and magnetic study of a new trinuclear copper complex of formula $[Cu_2(bpy)_2(C_2O_4)(H_2O)_2][Cu(bpy)(C_2O_4)](NO_3)_2$, where bpy refers to 2,2′-bipyridyl. Furthermore, we have attempted to verify the reaction mechanism of electrophilic attack of the $[Cu(bpy)(H_2O)_2]^{2+}$ ion on the coordinated oxalate ligands in tris(oxalato)chromate(III) ion which emerged mainly from the work of Goswami *et al.* [7, 8] and Basok *et al.* [9].

EXPERIMENTAL

Materials

$K_3[Cr(C_2O_4)_3]$ and $Cu(bpy)(NO_3)_2 \cdot 3H_2O$ were prepared by the literature methods [10,11]. 2,2′-bipyridine(bpy) was of analytical grade.

Synthesis of $[Cu_2(bpy)_2(C_2O_4)(H_2O)_2][Cu(bpy)(C_2O_4)](NO_3)_2$

To 420 mg (1 mmol) of $Cu(bpy)(NO_3)_2 \cdot 3H_2O$ stirred in 10 cm^3 of H_2O was added a solution of 163 mg (0.33 mmol) of $K_3[Cr(C_2O_4)_3]$ in 10 cm^3 of H_2O. Sky-blue single crystals suitable for X-ray investigations were obtained by slow evaporation at room temperature of the mixed aqueous solutions over 2 weeks. (Found: C, 40.6; H, 2.5; N, 11.4; Cu, 19.0. Calc. for $[C_{34}H_{28}N_8O_{16}Cu_3]$: C, 41.0; H, 2.8; N, 11.3; Cu, 19.1%.)

Measurements

Elemental analyses for carbon, hydrogen and nitrogen were carried out on Perkin–Elmer elemental analyser model 240. Metal contents were determined by EDTA titration. Variable temperature magnetic susceptibilities were measured on a vibrating sample magnetometer Model CF. Diamagnetic corrections were made with Pascal's constants for all the constituent atoms, and the magnetic moments were calculated by the equation $\mu_{eff} = 2.828\ (\chi_M T)^{1/2}$.

* Author to whom correspondence should be addressed.

X-ray structure determination

A blue single crystal of $[Cu_2(bpy)_2(C_2O_4)(H_2O)_2][Cu(bpy)(C_2O_4)](NO_3)_2$, having the approximate dimensions $0.2 \times 0.3 \times 0.3$ mm, was mounted on a glass fibre. Determination of the unit cell and data collection were performed with MoK_α radiation ($\lambda = 0.71074$ Å) on a CAD4 diffractometer equipped with a graphite monochromator. A total of 4205 independent reflections was collected by the $\omega - 2\theta$ scan technique in the range $2^\circ \leqslant \theta \leqslant 23$, from which 2498 reflections [$I \geqslant 3\sigma(I)$] were corrected for Lorentz and Polarization factors.

The complex crystallizes in the monoclinic space group C2/c with $a = 21.700(4)$, $b = 10.446(3)$, $c = 16.005(2)$ Å and $\beta = 95.63(1)^\circ$, $V = 3610(2)$ Å^3, $Mr = 995.27$, $Z = 4$, $Dx = 1.839$ cm^{-2}, F(000) = 2012.

The structure was solved by direct methods (MULTAN 82). The copper atom positions were located from an E-map. The other non-hydrogen atoms were determined with successive difference-Fourier syntheses. The final refinement by the full-matrix least-squares method with anisotropic thermal parameters for the non-hydrogen atoms converged with the unweighted and weighted agreement factors 0.050 and 0.053, respectively. The highest peak in the final difference Fourier map had a height of 0.96 eÅ^{-3}. All calculations were performed on a PDP 11/44 computer using the SDP-PLUS program system. The related bond lengths and angles for the complex are given in Table 1.

RESULTS AND DISCUSSION

The crystal structure of the complex

The crystal structure consists of a binuclear species $[Cu_2(bpy)_2(C_2O_4)(H_2O)_2](NO_3)_2$ and a mononuclear species $[Cu(bpy)(C_2O_4)]$. A sketch of the unit cell is shown in Fig. 1. A perspective view of $[Cu_2(bpy)_2(C_2O_4)(H_2O)_2]^{2+}$ is shown in Fig. 2. The $[Cu_2(bpy)_2(C_2O_4)(H_2O)_2]^{2+}$ ion is centrosymmetric, with the symmetry centre at the mid-point of the C(1)—C(1)′

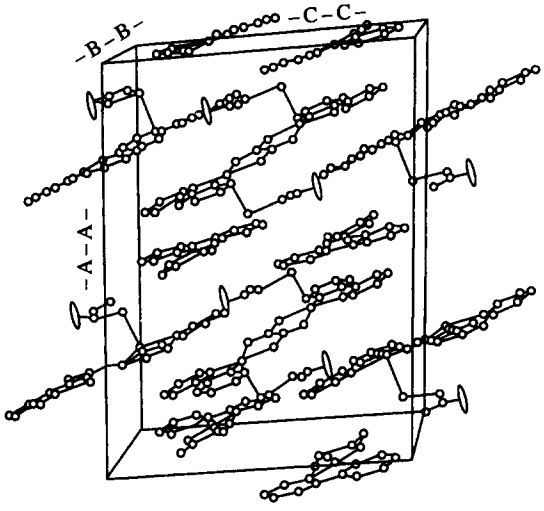


Fig. 1. A sketch of the unit cell of complex.

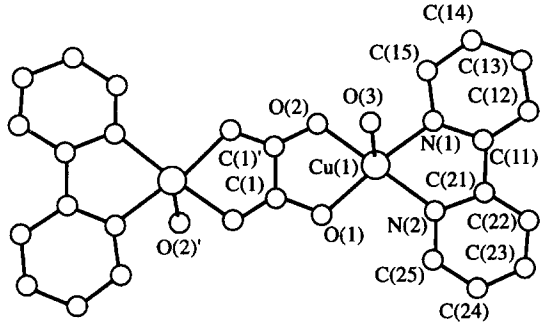


Fig. 2. A perspective view of $[Cu_2(bpy)_2(C_2O_4)(H_2O)_2]^{2+}$.

Table 1. Related bond lengths (Å) and angles (°)

Cu(1)–O(1)	1.971(1)	O(1)–Cu(1)–O(2)	84.64(3)
Cu(1)–O(2)	1.974(1)	O(1)–Cu(1)–O(3)	92.37(4)
Cu(1)–O(3)	2.247(1)	O(1)–Cu(1)–N(1)	173.58(5)
Cu(1)–N(1)	1.977(1)	O(1)–Cu(1)–N(2)	95.50(4)
Cu(1)–N(2)	1.970(1)	O(2)–Cu(1)–O(3)	94.01(4)
Cu(2)–O(4)	1.908(1)	O(2)–Cu(1)–N(1)	96.31(4)
Cu(2)–N(3)	1.948(2)	O(2)–Cu(1)–N(2)	168.17(4)
		O(3)–Cu(1)–N(1)	93.91(4)
		O(3)–Cu(1)–N(2)	97.79(4)
		N(1)–Cu(1)–N(2)	82.28(5)
		O(4)–Cu(2)–O(4)	85.67(5)
		O(4)–Cu(2)–N(3)	95.82(5)
		O(4)–Cu(2)–N(3)	175.60(5)
		N(3)–Cu(2)–N(3)	83.00(6)

bond. The coordination polyhedron of Cu(1) is formed by two oxygen atoms O(1), O(2) of $C_2O_4^{2-}$, two nitrogen atoms N(1), N(2) of bpy and O(3) of H_2O. The Cu(1) is five coordinate and lies only 0.138 Å away from the least-squares plane through the atoms N(1), N(2), O(1), O(2). The in-plane Cu—O bond distances average 1.97(8) Å and Cu—N bond distances are 1.98(9) Å and 1.97(1) Å, respectively, which are in the normal range. The Cu(1)—O(3) bond distance is 2.247 Å. Thus, the coordination geometry around the copper(1) ion can be described as a distorted tetragonal pyramid.

A perspective view of the mononuclear species is shown in Fig. 3. In $[Cu(bpy)(C_2O_4)]$, copper(2) is four coordinate with a square planar environment: from two oxygen atoms O(4), O′(4) from $C_2O_4^{2-}$ and two nitrogen atoms(s) N(3), N′(3) from bpy. Copper(2) lies on a 2-fold axis and on the least-squares plane though the N(1), N(2), O(1), O(2). The in-plane Cu—O and Cu—N bond distances average to 1.91(8) Å and 1.95(2) Å which are the normal values. The complex $[Cu_2(bpy)_2(C_2O_4)(H_2O)_2][Cu(bpy)(C_2O_4)](NO_3)_2$ was synthesized by electrophilic attack of $[Cu(bpy)(H_2O)_2]^{2+}$ on the coordinated oxalate ligands of the tris(oxalato)chromate(III) ion. Mechanistic studies of this type have been reported [7–9]. In line with these studies, the reaction scheme shown below can be envisaged for the formation of the title compound.

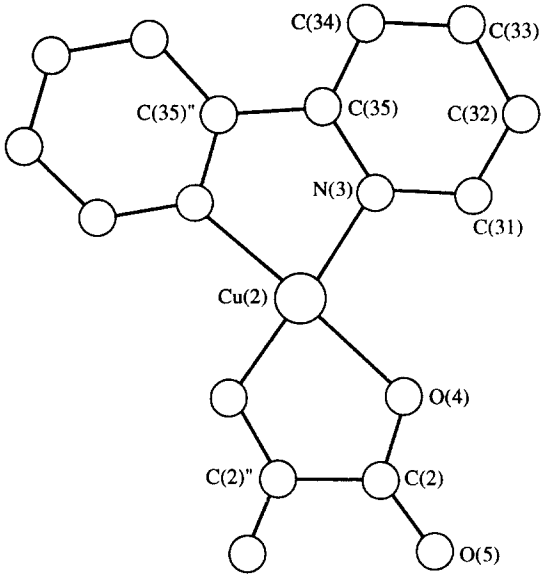
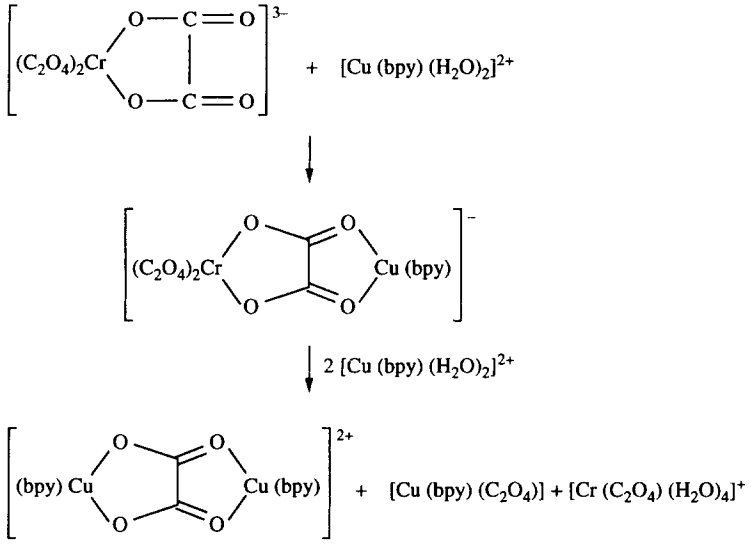


Fig. 3. A perspective view of $[Cu(bpy)(C_2O_4)]$.



Magnetic properties

Variable-temperature susceptibility data in the range 4.2–300 K were collected for the title complex. The X-ray structure analysis has shown that binuclear $[Cu_2(bpy)_2(C_2O_4)(H_2O)_2]^{2+}$ is present in the title complex, in which the two copper ions are bridged by oxalate. The other copper ions in $[Cu(bpy)(C_2O_4)]$ appear to be essentially isolated. Therefore we tried to fit the magnetic data to a theoretical expression (Eq. (1)) based a model which takes into account exchange interaction within the $[Cu_2(bpy)_2(C_2O_4)(H_2O)_2]^{2+}$ unit and neglects interactions involving the remaining copper ion:

$$\chi_M = \frac{2Ng^2\beta^2}{KT}\left[3+\exp\left(\frac{-2J}{KT}\right)\right]^{-1} + \frac{N\beta^2g^2}{4KT}. \quad (1)$$

χ_M denotes the susceptibility per trinuclear complex, the second term denotes the contribution of

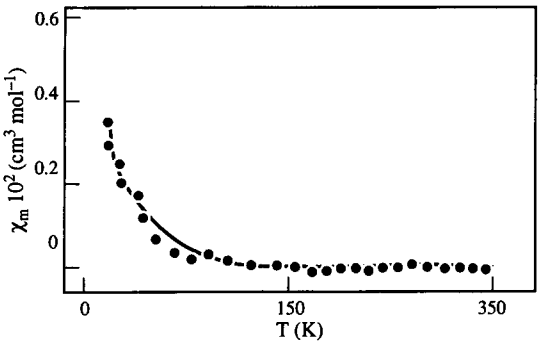


Fig. 4. Temperature variation of the magnetic susceptibility of complex. This curve was calculated using Eq. (1).

the copper ion in mononuclear species [Cu(bpy)$(H_2O)(C_2O_4)$] and the remaining symbols have their usual meanings. As shown in Fig. 3, good fits to experimental data were obtained for $J = -340$ cm^{-1}, $g = 2.12$. The agreement factor F defined here as $F = \Sigma[(\chi_M)_{obs} - (\chi_M)_{calc}]^2/(\chi_M)_{obs}$ is then equal to 1.1×10^{-4}.

For the binuclear species $[Cu_2(bpy)_2(C_2O_4)(H_2O)_2]^{2+}$ the coordination geometry around each copper(II) ion is approximated to square pyramidal. The Cu—oxalato—Cu core is almost planar. In this 4+1 environment, the Cu^{II} unpaired electron is described by a d_{xy} type orbital pointing from the metal toward the four nearest neighbours in an antibonding fashion [12, 13]. This coordination geometry is the most favourable to achieve a strong antiferromagnetic interaction through the oxalato bridge since the magnitude of the antiferromagnetic contribution, related to the square of the overlap between the magnetic orbitals centered on each Cu^{II} ion, is essentially governed by their delocalization onto the oxygen atoms of the oxalato bridge [13].

Acknowledgement—This project was supported by the national Natural Science Foundation of China.

REFERENCES

1. R. D. Willett, D. Gatteschi and O. Kahn (Eds.), *Magneto-Structural Correlation in Exchange-Coupled Systems*. NATO ASI Series, Reidel, Dordrecht, Holland (1985).
2. J. S. Miller and A. Epstein, *Angew. Chem. Int. Ed. Engl.* 1994, **33,** 385.
3. T. R. Felthouse, E. J. Laskowski and D. N. Hendrickson, *Inorg. Chem.* 1977, **16,** 1077.
4. M. Julve, J. Faus, M. Verdaguer and A. Gleizes, *J. Am. Chem. Soc.* 1984, **106,** 8306.
5. M. Julve, M. Verdaguer, O. Kahn, A. Gleizes and M. Philoche-Levisalles, *Inorg. Chem.* 1983, **22,** 258; *Inorg. Chem.* 1984, **23,** 3808.
6. A. Bencini, C. Benelli, D. Gatteschi, C. Zanchini and A. C. Fabretti, *Inorg. Chim. Acta* 1984, **86,** 169.
7. P. Chaudhuri and K. Oder, *J. Chem. Soc. Dalton Trans.* 1990, 1597.
8. L. Goswami, S. Sarker and D. Banerjea, *Z. Anorg. Allg. Chem.* 1977, **435,** 301.
9. A. K. Basak and C. Chatterjee, *Bull. Chem. Soc. Jpn* 1983, **56,** 318.
10. E. Bushra and C. H. Johnson, *J. Chem. Soc.* 1939, 1937.
11. F. M. Jaeger and J. A. Dijk, *Z. Anorg. Chem.* 1936, **227,** 273.
12. O. Kahn, *Angew. Chem. Int. Ed. Engl.* 1985, **24,** 834.
13. M. Julve, M. Verdaguer, O. Kahn, A. Gleizes and M. Philoche-Levisalles, *Inorg. Chem.* 1983, **22,** 368.

Pergamon

PII: S0277-5387(96)00226-4

Polyhedron Vol. 16, No. 3, pp. 535–539, 1997
Copyright © 1996 Elsevier Science Ltd
Printed in Great Britain. All rights reserved
0277–5387/97 $17.00+0.00

Chiroptical lanthanide(III) Schiff base complexes derived from D-camphor-β-sulfonic acid

Ma Hongzhu,[a] Wang Bo,[a]* Xu Xingzhong[a] and Feng Wu[b]

[a]Research Institute of Qilu Petrochem. Corp., Zibo, Shandong 255400, P.R. China

[b]Teaching and Research Section of Chemistry, Agriculture School, Lanzhou 730000, P.R. China

(Received 8 December 1995; accepted 15 April 1996)

Abstract—Ten new chiral complexes of optical Schiff base ligand (NaHL) derived from D-camphor-β-sulfonic acid and *o*-aminophenol with La^{III}, Pr^{III}, Nd^{III}; Sm^{III}, Eu^{III}, Gd^{III}, Tb^{III}, Dy^{III}, Ho^{III} and Er^{III} have been synthesized and characterized by elemental analysis, molar conductance, XPS, fluorescence, IR, electronic spectra and magnetic susceptibility measurements and thermal (TG,DTA,DTG) methods. Their dominant conformers were determined from CD spectra and supported by ^{1}H NMR data. Copyright © 1996 Elsevier Science Ltd

Keywords: lanthanide; complexes; chiroptical; Schiff base; D-camphor-β-sulfonic acid; preparation.

In our earlier paper,[1] we have reported the preparation and properties of several chiral lanthanide(III) complexes of D-camphor-β-sulfonic acid. The paper continues in that direction and as part of our studies on the coordination chemistry of chiral lanthanide(III) complexes we describe here the synthesis and discussion of some of these complexes derived from D-camphor-β-sulfonic acid.

EXPERIMENTAL

Methods and materials

The chemical reagents used were of AR grade and employed without further purification. Lanthanide(III) perchlorate were made from the oxide and perchloric acid.

Preparation of the ligand (NaHL)

The ligand (NaHL) were isolated as the sodium salt by boiling a mixture of D-camphor-β-sulfonic acid, *o*-amoinophenol and NaOH under reflux (1 : 1 : 1 molar ratio) in dry MeOH. The product gave satisfactory elemental analysis, IR and ^{1}H NMR spectra.

Preparation of the complexes

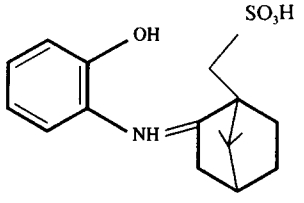
The same synthesis method for the complexes was adopted. In a typical reaction, an EtOH solution of the lanthanide(III) perchlorate and the Schiff base ligand in 1 : 2 molar ratio was stirred for 2 h followed by concentration to small volume and cooled, whereupon the product precipitated. It was filtered off, washed with cooled EtOH followed by Et_2O and dried *in vacuo*.

Characterization of the complexes

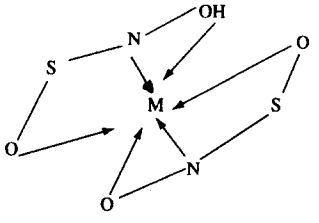
Lanthanide, C, H, N and S contents of the ligand and complexes were estimated by standard procedures. Molar conductance values at room temperature were measured in 10^{-3} M MeOH solution using a DDS-IIA molar conductor. Room-temperature magnetic susceptibility measurements were made on solid samples by the Guoy method using $Hg[Co(CNS)_4]$ as calibrant. IR spectra were recorded

* Author to whom correspondence should be addressed.

in CsI pellets using an NIC-5DX spectrophotometer in the region 200–4000 cm^{-1}. Electronic spectra were recorded on a DJ-240 UV–vis spectrophotometer with 10^{-3} M solutions of the complexes in MeOH. Fluorescence spectra of the complexes in MeOH solution were obtained using an X-ray 3070E fluorescence spectrophotometer. The X-ray photoelectron spectra were measured on a PHI-550 spectrometer using Mg-K_α radiation. The samples were finely pulverized and set on a gold holder as thin disks. The X-ray gun operated at 15 KV and 20 mA taking C1s binding energy (284.8 eV) as a standard. The background pressure during the measurements was lower than 10^{-6} Pa. All spectra were recorded using the same spectrometer parameters of 20 eV pass energy and 6 mm slit width. The peak areas and peak positions for the measured BE value is ± 0.05 eV. The ^1H NMR spectra were measured on a Bruker AC 80 spectrometer using DMSO-d_6 solvent. CD spectra were obtained at 20°C with a Cary model 60 spectroplarimeter with a CD model 6001 accessory. Thermal analysis were made under nitrogen between room temperature and 800°C using a thermoflex Q-1500D meter.



ligand



bonding model

RESULTS AND DISCUSSION

Physical and analytical data for the trivalent lanthanide(III) complexes are given in Table 1. The complexes have the general formulae [La(HL)L], where Ln = La, Pr, Nd, Sm, Eu, Gd, Tb, Dy, Ho and Er. The complexes are insoluble in ether, petroleum and benzene, moderately soluble in chloroform, dichloromethane and THF and soluble in methanol, ethanol, acetone, DMSO and water. The complexes are air stable and can exist in alkazid solution even in strong basic aqueous solution such as 6 M NaOH to form a clear yellow solution and in acidic solution such as concentrated hydrochloride acid to form a clear red solution. Λ_M values in methanol solution (concentration range $0.8–1.0 \times 10^{-3}$ M, Table 1) indicate that the complexes behave as non-electrolytes.[2]

IR spectra

The main IR bands with their tentative assignments are listed in Table 2. For the complexes several additional bands are present, indicative of an unneutralized coordinated phenolic OH group. The bands at 3370 cm^{-1} in the ligand due to phenolic ν(OH) group has shifted up to *ca* 3400 cm^{-1} in the complexes. The ν(C—O) mode coupled with the δ(OH) mode of the phenolic OH group are observed at 1400 cm^{-1}, which is some broadened possibly due to coordination. While the ν(C=N) band at 1639 cm^{-1} has shifted down to 1600 cm^{-1} in the complexes, indicating participation of the azomethine nitrogen[3,4] in the complexation. Two stretching vibrations of —SO_3—, $\nu_{as}(SO_3)$ and $\nu_s(SO_3)$, in the spectra of the complexes are observed at *ca* 1205 and 1143 cm^{-1}, a higher frequency by *ca* 10 cm^{-1} and lower by 30 cm^{-1}, respectively, compared with the bands at 1215 and 1170 cm^{-1}, which assigned are to $\nu(SO_3)$ of the ligand, NaHL. Bands assignable to ν(Ln—O) and ν(Ln—N) are observed at *ca* 510 and 340 cm^{-1}, respectively.[5]

Electronic spectra and magnetic properties

The electronic spectra (Table 3) of the complexes reveal the presence of most of the ligand bands. A strong peak observed at 293 nm and a weak one at 262 nm are attributed to the $\pi \rightarrow \pi^*$ transition of the —C=N group and phenyl, respectively. Comparing with the ligand, a red shift at *ca* 10–15 and 2–3 nm is observed respectively, which indicates bonding between the lanthanide(III) ion and the ligand.[6,7] Additionally, new bands are observed in the 410–450 nm region and a high-intensity structureless continum is observed almost up to 500 nm. These characteristics may be related to electronic transitions based mainly on the ligand moieties and ligand-to-metal charge-transfer bands may be present.

The paramagnetic behaviour of the lanthanide(III) ion is consistent with the presence of unpaired electrons. The room-temperature magnetic moments of all the complexes show very little deviation from the Van Vleck values,[8] indicating little participation of 4*f*-electrons in bond formation.

CD spectra

The CD spectra data in the range 200–600 nm of the lanthanide complexes and the ligand NaHL are

Table 1. Physical properties and analytical data of the ligand and complexes prepared

Compound	Colour	μ_{eff} (B.M.)	Found (Calc.)‰ Ln	C	H	N	S	Decomposition temperature (°C)	Λ_M (S cm^2 mol^{-1})
NaHL	Pale yellow			55.2	5.1	4.1	9.3		
				(55.4)	(5.2)	(4.0)	(9.2)	217	
La(HL)L	Yellow	dia.	18.0	49.0	4.4	3.6	8.1		
			(17.9)	(49.4)	(4.5)	(3.6)	(8.2)	196–546	41.6
Pr(HL)L	Green	2.71	18.0	49.2	4.4	3.6	8.2		
			(18.1)	(49.2)	(4.5)	(3.6)	(8.2)	172–530	25.2
Nd(HL)L	Grey	3.64	18.3	48.9	4.4	3.4	8.1		
			(18.4)	(49.0)	(4.5)	(3.6)	(8.2)	206–550	36.4
Sm(HL)L	Pale yellow	1.79	19.0	48.7	4.4	3.6	8.0		
			(19.1)	(48.6)	(4.4)	(3.5)	(8.1)	184–542	35.1
Eu(HL)L	Grey–white	3.51	19.0	48.6	4.3	3.5	8.1		
			(19.2)	(48.5)	(4.4)	(3.5)	(8.1)	209–523	40.8
Gd(HL)L	Yellow–green		19.7	48.0	4.3	3.5	8.0		
			(19.7)	(48.2)	(4.4)	(3.5)	(8.0)	164–558	24.3
Tb(HL)L	Blackish	8.99	19.9	48.2	4.4	3.6	8.4		
			(19.9)	(48.1)	(4.4)	(3.5)	(8.0)	176–523	30.6
Dy(HL)L	Pink	9.82	20.2	48.4	4.2	3.5	8.0		
			(20.3)	(47.9)	(4.4)	(3.5)	(8.0)	162–541	25.8
Ho(HL)L	Pale yellow	9.98	20.4	47.6	4.0	3.4	8.1		
			(20.5)	(47.8)	(4.4)	(3.5)	(8.0)	160–540	39.2
Er(HL)L	Greyish	10.06	20.5	47.5	4.3	3.5	7.8		
			(20.7)	(47.6)	(4.3)	(3.5)	(7.9)	158–560	31.6

Table 2. Significant IR bands of NaHL and its complexes (cm^{-1})

Compound	ν(OH) (phenolic)	ν(C—O)	ν(C=N)	$\nu_{as}(SO_3)$	$\nu_s(SO_3)$	ν(Ln—O)	ν(Ln—N)
Na(HL)	3370	1226	1639	1215	1170		
La(HL)L	3400	1200	1608	1205	1143	510	342
Pr(HL)L	3392	1400	1615	1206	1148	511	340
Nd(HL)L	3390	1402	1614	1205	1143	510	341
Sm(HL)L	3395	1400	1615	1204	1146	511	340
Eu(HL)L	3386	1401	1609	1208	1144	512	340
Gd(HL)L	3400	1401	1601	1207	1146	511	341
Tb(HL)L	3405	1403	1615	1207	1147	510	342
Dy(HL)L	3400	1400	1605	1200	1152	514	344
Ho(HL)L	3395	1402	1608	1205	1160	518	346
Er(HL)L	3390	1400	1609	1200	1148	520	341

given in Table 3. The complexes and ligand show the positive cotton effect, the positive value at *ca* 310 nm is diagnostic of the preferred conformation (refer to the salicylidienamino chirality rule) and the conformer is dominant for dichroic absorption which next to the chiral centre.[9] The positive cotton effect at *ca* 450 nm in all these complexes may be attributed to a charge-transfer transition from a ligand $p\ \pi$ orbital to a $5d$ or $4f$ orbital of the lanthanide(III) ion and related to the distortion of the chelate ring system.[10] It is likely that other conformers [by rotation about the (N—C α) band] are absent as the observed CD curves and for the lanthanide(III) complexes prepared the overall electronic situation is much the same, as indicated by the almost identical electronic spectra.

Fluorescence spectra

To obtain the detailed nature of the ligand-lanthanide(III) environment. The fluorescence spectra of

Table 3. Electronic and CD spectra data

Compound	Electronic		CD		
	λ_{max} (nm)	log ε	λ_{max} (nm)	$[\alpha]^{20}_{max}$ (°)	$[\alpha]^{20}_{589}$ (°)
NaHL	292	4.2	300	+124.8	+64.2
	260	4.8	270	+248.6	
	228	4.0	230br	+118.6	
	213sh	3.63			
La(HL)L	429	2.1	450sh	+68.6	+66.3
	300	4.7	309	+236.4	
	272	4.5	270	+222.7	
	226	4.4	220br	+90.5	
	215sh	3.0			
Pr(HL)L	434	1.8	438sh	+68.0	+67.2
	306	4.9	310	+243.5	
	270	4.1	274	+116.4	
	226	3.2	228br	+90.5	
	231sh	3.0			
Nd(HL)L	429	3.0	436	+94.6	+58.5
	295	4.6	301	+250.4	
	274sh	4.5	280	+213.6	
	225	3.6	220br	+160.0	
	213	2.8			
Sm(HL)L	428	3.9	440	+104.7	+66.1
	301	4.6	312	+214.2	
	275	4.9	281	+310.5	
	226	4.2	230	+201.0	
			218sh	350.8	
Eu(HL)L	430	4.0	445	+84.1	+67.1
	305	4.6	310	+106.2	
	275	4.8	284	+206.4	
	228	3.4	230br	+244.3	
	215	3.1			
Gd(HL)L	435	2.6	451	+80.8	+63.2
	305	4.6	310	+121.3	
	270	4.0	278	+209.4	
	224br	3.6	230br	+316.9	
Tb(HL)L	434	2.9	441	+90.1	+64.6
	301	3.4	312	+132.5	
	270	2.8	275	+146.9	
	226	2.4	225	+188.6	
	213sh	1.8	215sh	+209.4	
Dy(HL)L	430	4.0	435	+82.6	+64.6
	300	4.6	308	+133.4	
	275	4.5	289	+167.2	
	226	3.0	231br	+208.9	
	213	2.8			
Ho(HL)L	431	1.8	446	+76.3	+68.9
	300	5.9	308br	+114.9	
	274	4.6	275sh	+201.6	
	226	3.8	230br	+314.1	
	213sh	3.0			
Er(HL)L	440	2.0	445	+81.2	+66.5
	302	4.6	310	+104.0	
	275	4.2	285	+150.9	
	226	3.6	228	+212.7	
	213sh	2.8	215sh	269.3	

Eu^{III} and Tb^{III} complexes have been recorded under the excitation. $\lambda = 333.7$ nm, with high resolution. The room-temperature emission show some structuring in each of the transition regions, for Eu(HL)L, with $^5Do \rightarrow {}^7F_1$ and $^7F_2$ at 591 and 624 nm, respectively, which suggest a strong magnetic dipole character of the Eu—L bonding, for Tb(HL)L, with $^5D_4 \rightarrow {}^7F_6$, $^7F_5$, $^7F_4$ and $^7F_3$ at 490, 542, 587 and 614 nm, respectively, which can be attributed to ligand-field-induced changes in the inherent transition probabilities of the respective $^5D_4 \rightarrow {}^7F_4$ transition processes compared with the related hydrated ions.

^{1}H *NMR spectra*

The ^{1}H NMR data of the lanthanide(III) complexes indicate that only one set of signals is observed for the phenolic (—OH) hydrogen at 5.1 ppm (1 H,s) compared with the ligand at 5.3 ppm (1H,s) and other functional groups, indicating that the two residues in these complexes (Ln : L ratio 1 : 2) are in identical chemical environments on the ^{1}H NMR spectra.

XPS spectra

To investigate the nature of bonding, XPS spectra of the complexes and ligand were recorded. The results of the XPS semi-quantitative analyses of the surface layers are in agreement with the sample composition and the ratio of La : C : O : S : N is *ca* 1 : 33 : 8 : 2 : 2, which is consistent with the elemental analysis data. Only one symmetric sulfur 2*p* peak for all the complexes was observed, but the BE value is a little higher than that of the ligand, while the nitrogen 1*s* peak of the C=N group appeared at 400.5 eV and shows an identical chemical environment. The O1*s* peaks of the complexes are complicated. However, attempts have been made to identify some important information regarding the mode of bonding. Compared with the ligand, their deconvolution yields three components with an intensity ratio 1 : 1 : 3. The more intense component with BE value at 530.6 eV belongs to the oxygen of the $-SO_3$ group. The weaker components of the O1*s* peaks at 531.6 and 533.0 eV are assigned to the deprotoned and protoned phenolic oxygen, respectively. It may be reasonably inferred from the above discussion that an overall coordination number of six is achieved in all these complexes and a plausible octahedral structure proposed.

Thermal analysis

Thermal data (*ca* 5 C min^{-1}) indicate that the complexes sustain weight loss in the 160–540 °C region and are less thermally stable than the ligand and that the complexes are anhydrous. The main features of the complex follow this pattern. The complexes decompose exothermally in four main steps: the first corresponding to a loss of the C=N group and phenolic group in range 160–204 C; the second probably corresponding to a decarbonization process and the sulforite compound may be formed between 231–308 C; the third contacted with the loss of sulfur dioxide under 340–470 °C; the fourth linking to the pyrolysis of the organic matter existing in these complexes and together with the crystallization at 450–540 C. The final product of the decomposition is the lanthanide(III) oxide, as confirmed by X-ray diffraction detection and IR spectroscopy, as well as from the experimental and expected weight losses.

REFERENCES

1. J. X. Liu, B. Wang, W. J. Xie, S. Y. Yang and D. S. Jin, *Polyhedron* 1994, **13**, 3095.
2. W. J. Geary, *Coord. Chem. Rev.* 1971, **7**, 81.
3. R. M. Silverstein and G. C. Bassler, *Spectrophotometric Identification of Organic Compounds*. Wiley, New York (1967).
4. K. Nakamoto, *Infrared and Raman Spectra of Inorganic and Coordination Compounds*, 3rd edn. Wiley-Interscience, New York (1978).
5. J. R. Ferroro, *Low Frequency Vibration of Inorganic Coordination Compounds*. Plenum Press, New York (1976).
6. A. B. D. Lever, *Inorganic Electronic Spectroscopy*. Elsevier, Amsterdam (1968).
7. B. N. Figgs, *Introduction to Ligand Fields*. Wiley Easter Ltd, New York (1976).
8. J. H. Vleck and A. Frand, *J. Chem. Phys.* 1990, **29A**, 494.
9. H. E. Smith, *Chem. Rev.* 1988, **83**, 359.
10. R. M. Silver, G. C. Bassler and T. C. Morril, *Spectrometric Identification of Organic Compounds*. Wiley, New York (1981).

Pergamon

PII: S0277-5387(96)00221-5

Polyhedron Vol. 16, No. 3, pp. 541–550, 1997
Copyright © 1996 Elsevier Science Ltd
Printed in Great Britain. All rights reserved
0277–5387/97 $17.00+0.00

Structural studies of formamidine compounds: from neutral to anionic and cationic species

F. Albert Cotton,[a]* Steven C. Haefner,[a] John H. Matonic,[a] Xiaoping Wang[a] and Carlos A. Murillo[b]*

[a]Department of Chemistry and Laboratory for Molecular Structure and Bonding, Texas A&M University, College Station, TX 77843, U.S.A.

[b]Department of Chemistry and Laboratory for Molecular Structure and Bonding, Texas A&M University, College Station, TX 77843, U.S.A. and Department of Chemistry, University of Costa Rica, Ciudad Universitaria, Costa Rica

(Received 19 February 1996; accepted 10 April 1996)

Abstract—N,N′-Di(*p*-tolylformamidine), HDTolF, reacts with an ether solution of methyl lithium to give $Li_2(\mu\text{-DTolF})_2(Et_2O)_2$ (**I**), while N,N′-diphenylformamidine, HDPhF, reacts with a THF solution of MeMgCl to give the bioctahedral molecule $(DPhF)(THF)Mg(\mu\text{-THF})(\mu\text{-Cl})_2Mg(THF)(DPhF)$ (**II**), in which one of the THF molecules is bonded to both Mg atoms. Crystal structures of **I**, **II**, as well as the neutral molecule HDTolF (**III**) and the salt $[H_2DTolF][BF_4]$ (**IV**) are presented. The neutral molecule shows distinct amine and imine C—N distances, while the ionic species show identical C—N distances. Copyright © 1996 Elsevier Science Ltd

Amidinato ligands of the type $[RNC(R')NR]^-$ have been especially useful for the preparation of classic lantern-type dinuclear species with the general formula $[M_2(amidinato)_4]^{0,1,2+}$.[1] At present, this type of ligand forms dinuclear compounds with a greater variety of metal atoms than any other ligand, including the well-known carboxylates. Frequently, new compounds show interesting characteristics such as very short interatomic distances between metal atoms which lead to high magnetic anisotropies, such as in the case of $V_2(DTolF)_4$ [DTolF = di(*p*-tolylformamidinate)]. Other fascinating properties are displayed by the new type of dinuclear compounds of the type $M_2(amidinato)_3$, M = Fe, Co,[2] which show a very large number of unpaired electrons [seven in the case of $Fe_2(DPhF)_3$].

In general, when the amidinato groups bridge two metal atoms in a symmetrical way their C—N distances are similar, as expected from the delocalization of π-electrons. The same is true when they chelate, as in $M(amidinato)_3$ compounds.[3]

However, many other bonding modes are possible,[4] in which inequalities of the C—N distances are found. Some differences are clearly present when the parent amidine coordinates to the metal atom in compounds such as in $MCl_2(amidine)_2$, M = Fe, Co, Pt and Mn,[5] where short and long imide and amine distances are well-defined. Such differences are also observed in some,[6] but not all,[7] neutral amidines structurally characterized.

In our studies we have also found that in acidic conditions amidines are capable of forming cations, as in $[H_2DTolF][CoCl_3(HDTolF)]$.[5a] Even though this type of cation is easily formed there are very few crystallographically well-characterized compounds where such cations are present. One of the few examples is that of $[H_2DPhAc][C_2O_4]$ (DPhAc = diphenylacetamidinate).[8]

We present detailed crystallographic work on cationic, neutral and anionic amidine ligands in this paper. The latter were obtained by reaction of butyl lithium (or methyl lithium) and the Grignard reagent MeMgCl, which are some of the most frequently employed reagents to form the anionic species used in the preparation of many transition metal complexes.

* Authors to whom correspondence should be addressed.

We also show some of the structural characteristics which differentiate anions from cations and neutral amidines.

EXPERIMENTAL

Materials and methods

Manipulations were performed under nitrogen using standard Schlenk techniques, except for the syntheses of HDTolF and $[H_2DTolF][BF_4]$. Solvents were purified by conventional methods and were freshly distilled under nitrogen prior to use. All other reagents were purchased from Aldrich and were used as received. IR spectra were recorded on a Perkin–Elmer 16PC FT-IR spectrophotometer as Nujol mulls between KBr plates. ^{1}H NMR spectral measurements were performed on a JEOL-JNM GX-200 spectrometer.

$[Li_2(\mu\text{-DTolF})_2(Et_2O)_2]$ (I)

An ether solution of 1.4 M methyl lithium (1.5 cm^3, 2.1 mmol) was slowly added to a cold (−30°C) solution of HDTolF (0.45 g, 2.0 mmol) in Et_2O (40 cm^3). The resulting pale yellow solution was allowed to warm to room temperature with stirring. Partial evaporation of the solvent (30 cm^3) under reduced pressure gave **I** as a white precipitate. The product was collected by filtration and washed with hexanes (2 × 5 cm^3). Yield 0.58 g, 95%. Crystals suitable for X-ray analysis were obtained from an Et_2O solution at −20°C. IR (cm^{-1}): 2980–2832(br, s), 1664(m), 1608(w), 1587(w), 1522(sh, w), 1507(m), 1468(s), 1449(s), 1377(s), 1312(m), 1303(sh, w), 1202(m), 987(w), 936(w), 827(sh, w), 818(w), 807(m), 721(m), 583(w), 515(w), 696(w). ^{1}H NMR (C_6D_6, δ, ppm): 8.20 (CH), 6.97, 6.93, 6.88, 6.83 (arom.), 2.14 (*p*-CH_3), 3.28 (CH_2) and 1.13 (CH_3).

[(DPhF)(THF)Mg(μ-THF)(μ-Cl)$_2$Mg(THF)(DPhF)] (II)

To HDPhF (2.00 g, 10.2 mmol) suspended in toluene (20 cm^3) at −70°C was added a 3.0 M THF solution of MeMgCl (3.4 cm^3, 10.2 mmol). The mixture was slowly allowed to return to room temperature. As bubbling occurred, a thick suspension was formed. Most of the solid dissolved upon addition of toluene (40 cm^3) at 35°C. The solvent was removed *in vacuo*. The greyish solid was extracted with toluene (30 cm^3) at 40°C and was filtered. The remaining solid was discarded. To the pale yellow solution was added a layer of hexanes (20 cm^3). After 2 days at room temperature large colourless crystals were filtered and washed with hexanes (2 × 10 cm^3). After drying over a stream of dry nitrogen the yield was 1.58 g (43%). IR (cm^{-1}): 1682(vs), 1651(s), 1587(s), 1376(m), 1310(s, br), 1209(s), 1171(w), 1153(w), 1076(w), 1029(w), 986(w), 899(w), 806(w), 754(s), 695(s), 593(w), 519(w). ^{1}H NMR (C_6D_6, δ, ppm): 7.81 (CH), 7.25, 7.20, 7.10, 7.04, 7.00, 6.93, 6.65 (arom.), 3.87 (THF), 1.78 (THF).

HDTolF (III)

N,N′-Di(*p*-tolyl)formamidine was prepared by a slightly modified published procedure.[9] The product was washed repeatedly with warm hexanes. Single crystals of **III** were obtained from toluene/hexanes at −15°C. IR (cm^{-1}): 3200–2831(br, s), 1658(m), 1606(w), 1586(m), 1505(sh, w), 1459(s), 1377(s), 1311(m), 1301(m), 1200(w), 852(sh, w), 828(w), 817(sh, w), 808(m), 720(m), 582(w), 570(w), 514(w), 496(w). ^{1}H NMR (C_6D_6, δ, ppm): 12.28 (NH), 8.01 (CH), 6.99, 6.94, 6.93, 6.88 (arom.) and 2.14 (CH_3).

$[H_2DTolF][BF_4]$ (IV)

To a solution of HDTolF (0.20 g, 0.88 mmol) in diethyl ether (20 cm^3) was added dropwise a solution of $HBF_4 \cdot Et_2O$ (85%, 0.25 cm^3) in diethyl ether (10 cm^3). The resulting precipitate was filtered and washed with diethyl ether (3 × 15 cm^3). After drying *in vacuo*, the yield was 0.26 g (92%). Single crystals of **IV** suitable for X-ray diffraction studies were obtained by slow diffusion of a layer diethyl ether into a methylene chloride solution of **IV**. IR (cm^{-1}): 3275(m), 3225(m), 3165(m), 3113(m), 3065(m), 1695(s), 1613(m), 1595(m), 1560(w), 1516(s), 1347(s), 1314(m), 1290(w), 1217(m), 1145(m), 1129(m), 1105(s), 1060(s), 1018(s), 965(m), 911(w), 835(m), 819(s), 801(m), 766(m), 642(w), 524(m), 509(s), 446(m), 431(w). ^{1}H NMR (d$_6$-acetone, δ, ppm): 9.16 (CH), 7.49, 7.45, 7.34, 7.29 (arom.), 2.35 (CH_3).

Structure determinations

Geometric and intensity data for **I** and **II** were measured on an Enraf–Nonius FAST area-detector system utilizing the program MADNES.[10] Data were collected at room temperature on a Rigaku AFC5R diffractometer equipped with a rotating Cu anode for **III** and **IV**. Detailed procedures have been described previously.[11,12]

Reflections for cell indexing were found by an automated search routine (Rigaku) or using 50 reflections taken from three 10° ω rotations in the range $0 \leqslant \omega \leqslant 110°$ (FAST). In each case, the cell dimensions and correct Laue group were confirmed by axial images. For **I** and **II**, the refined cell used 250 reflections in the range $20 \leqslant 2\theta \leqslant 32°$, and data collection was performed with the detector set at a distance of 40 mm and a swing angle of 22.5°. All data were corrected for Lorentz and polarization effects. An empirical absorption correction based on a series of

Table 1. Crystal data for $Li_2(\mu\text{-DTolF})_2(Et_2O)_2$ (**I**), (THF)(DPhF)Mg(μ-THF)(μ-Cl)$_2$Mg(THF)(DPhF) (**II**), HDTolF (**III**) and $[H_2DTolF][BF_4]$ (**IV**)

	I	II	III	IV
Formula	$C_{38}H_{50}Li_2N_4O_2$	$C_{38}H_{46}C_{12}Mg_2N_4O_3$	$C_{15}H_{16}N_2$	$C_{15}H_{17}BF_4N_2$
Formula weight	608.70	726.31	224.30	312.12
Space group	$P\bar{1}$	$P2_1/a$	$P\bar{1}$	$C2/c$
a (Å)	8.279(3)	11.355(2)	10.121(1)	16.670(2)
b (Å)	10.390(3)	28.229(6)	10.530(2)	8.241(1)
c (Å)	12.156(4)	11.728(2)	6.101(1)	11.755(1)
α (°)	69.57(2)	90	99.17(1)	90
β (°)	79.47(3)	96.29(3)	96.38(1)	90.284(9)
γ (°)	70.12(2)	90	86.79(1)	90
V (Å^3)	919.0(5)	3736(1)	637.3(2)	1614.8(3)
Z	1	4	2	4
d_{calc} (g cm^{-3})	1.100	1.291	1.169	1.284
Crystal size (mm^3)	$0.42\times0.38\times0.34$	$0.32\times0.35\times0.40$	$0.45\times0.41\times0.37$	$0.50\times0.30\times0.10$
Absorption coefficient (mm^{-1})	0.067	0.249	0.535	0.926
Data collection instrument	FAST		Rigaku AFC5R	
Radiation (monochromated in incident beam)	Mo-K_α(λ_α = 0.71073 Å)		Cu-K_α(λ_α = 1.54184 Å)	
Temperature (K)	213(2)	293(2)	293(2)	293(2)
Data collection range, θ (°)	2.19–22.49	1.44–22.41	4.26–60.11	5.3–59.96
Number of unique data, total with $F_o^2 > 2\sigma(F_o^2)$	2293	3767	1902	1205
Number of parameters refined	208	452	197	128
Transmission factors, min., max.	—	—	0.964, 1.000	0.9578, 1.0000
R^a	0.088	0.085	0.041	0.048
wR_2^b	0.178	0.176	0.124	0.130
Quality-of-fit indicator^c	1.070	1.051	1.119	1.105

$^a R = [\Sigma(F_o - F_c)/\Sigma F_o]$.

$^b wR_2 = [\Sigma w(F_o^2 - F_c^2)^2/\Sigma w(F_o^2)^2]^{1/2}$, $w = 1/[\sigma^2(F_o^2) + (ap)^2 + bp]$, $p = [\max(F_o^2 \text{ or } 0) + 2(F_c^2)]/3$. $a = 0.0483$ and $b = 1.72$ for **I**. $a = 0.0814$ and $b = 0.00$ for **II**, $a = 0.0693$ and $b = 0.09$ for **III**, $a = 0.0624$ and $b = 0.8591$ for **IV**.

psi-scans was applied to the data for compounds **III** and **IV**. A correction for extinction was applied to the data for **IV** [refined extinction parameter $x = 0.0017(4)$].[13]

The structures for **I**, **II** and **III** were solved by direct methods and refined using the SHELXTL[14] structure refinement package, structure **IV** was refined using SHELXL-93.[15] For **I** and **II** the structure factors were calculated with hydrogen atoms placed at the expected positions. Except for the methyl protons, all other hydrogen atoms were refined isotropically for **III**. For **IV** the positions of the hydrogen atoms were determined from the difference-Fourier map, and were refined using a common isotropic displacement parameter.

The bridging THF molecule in **II** was found to be conformationally disordered, attempts to model the disorder failed. This disorder is shown by the large displacement parameters of the constituent carbon atoms. Pertinent information regarding data collection and refinement is given in Table 1. Selected bond distances and angles are given in Tables 2, 3, 4 and 5 for compounds **I**, **II**, **III** and **IV**, respectively. Supplementary data for **I**, **II**, **III** and **IV** have been deposited with the Cambridge Crystallographic Data Centre.*

RESULTS AND DISCUSSION

$[Li_2(\mu\text{-DTolF})_2(Et_2O)_2]$

The reaction of butyllithium or methyllithium with HDTolF in the presence of Et_2O affords crystals of a dilithium compound. As far as we know this is the first time that a crystal structure has been determined on a lithium amidinato compound in spite of the fact that these compounds are so widely used in the preparation of transition-metal amidinato complexes. The reason for the lack of crystal structure determinations is probably the facility which the crystals lose ether.

The crystal structure of **I** reveals a centrosymmetric

* Supplementary material available: Tables of positional parameters for **I**, **II**, **III** and **IV**, full tables of displacement parameters and molecular dimensions (41 pages).

Table 2. Selected bond lengths (Å) and angles (°) for $Li_2(\mu_2\text{-DTolF})_2(Et_2O)_2$ (**I**)

Li···Li′	2.61(2)	Li—N(2)	2.231(9)
Li—N(1)	2.045(8)	Li—N(2′)	2.078(8)
Li—O	1.914(9)	N(1)—C	1.307(5)
C—N(2)	1.337(5)	N(1)—C(11)	1.403(5)
N(2)—C(21)	1.413(5)	C(1)—O	1.455(8)
O—C(3)	1.413(8)	C(2)—C(1)	1.39(1)
N(1)—Li—N(2)	64.6(3)	N(1)—Li—N(2′)	116.9(4)
N(2)—Li—N(2′)	105.7(3)	O—Li—N(1)	121.6(4)
O—Li—N(2)	123.4(5)	O—Li—N(2′)	114.6(4)
C—N(1)—Li	89.5(3)	C—N(2)—Li	81.2(3)
Li—N(2)—Li′	74.3(3)	N(1)—C—N(2)	120.0(4)
C—N(1)—C(11)	118.0(4)	C—N(2)—C(21)	117.6(4)
C(1)—O—Li	117.0(4)	C(3)—O—Li	131.4(6)
C(3)—O—C(1)	110.6(6)	C(4)—C(3)—O	113.5(7)

Primed atoms are symmetry generated.

Table 3. Selected bond distances (Å) and angles (°) for (THF)(DPhF)Mg(μ-THF)(μ-$Cl)_2$Mg(THF)(DPhF) (**II**)

Mg(1)···Mg(2)	3.141(4)	Mg(1)—Cl(1)	2.398(4)
Mg(2)—Cl(1)	2.462(4)	Mg(1)—Cl(2)	2.452(4)
Mg(2)—Cl(2)	2.400(4)	Mg(1)—O(3)	2.357(6)
Mg(2)—O(3)	2.322(6)	Mg(1)—N(1)	2.131(8)
Mg(1)—N(2)	2.135(8)	N(1)—C(1)	1.27(1)
N(2)—C(1)	1.30(1)	N(3)—C(2)	1.26(1)
N(4)—C(2)	1.33(1)	N(1)—C(11)	1.37(1)
Mg(1)—Cl(1)—Mg(2)	80.5(1)	N(1)—C(1)—N(2)	118.4(9)
N(3)—C(2)—N(4)	116.0(9)	C(1)—N(1)—C(11)	121.4(8)
C(2)—N(3)—C(31)	120.3(8)	C(1)—N(2)—C(21)	122.1(8)
C(2)—N(4)—C(41)	122.4(8)	Mg(1)—O(3)—Mg(2)	84.3(2)
Mg(1)—Cl(2)—Mg(2)	80.6(1)	O(2)—Mg(1)—N(1)	95.6(3)

Table 4. Selected bond lengths (Å) and angles (°) for HDTolF (**III**)

N(1)—C(1)	1.340(2)	N(2)—C(1)	1.277(2)
N(1)—C(2)	1.414(2)	N(2)—C(9)	1.415(2)
N(1)—H(1)	0.88(2)	H(1)—N(2′)	2.20(2)
N(1)—N(2′)	3.074(2)		
H(1)—N(1)—C(1)	118(1)	H(1)—N(1)—C(2)	117(1)
C(1)—N(1)—C(2)	124.3(1)	N(2)—C(1)—N(1)	123.6(1)
C(1)—N(2)—C(9)	116.8(1)	C(14)—C(9)—N(2)	119.6(1)
C(3)—C(2)—N(1)	118.9(1)	C(10)—C(9)—N(2)	122.3(1)
C(7)—C(2)—N(1)	122.4(1)	N(1)—H(1)—N(2′)	175(1)

Primed atoms are symmetry generated.

Table 5. Selected bond and non-bonded distances (Å) and angles (°) for $[H_2DTolF][BF_4]$ (**IV**)

C(1)—N(1)	1.305(2)	C(1)—H(1)	0.96(5)
N(1)—C(2)	1.422(3)	N(1)—H(10)	0.92(4)
		C(3)—H(3)	0.93(3)
C(1)···F(2)	3.387(4)	H(1)···F(2)	2.50(5)
C(3)···F(2)	3.404(4)	H(3)···F(2)	2.49(4)
C(3)···F(2′)	3.527(3)	H(3)···F(2)′	2.77(3)
N(1)···F(1)	2.792(3)	H(10)···F(1)	1.88(5)
N(1)—C(1)—N(1)′	122.3(3)	N(1)—C(1)—H(1)	118.8(2)
C(1)—N(1)—C(2)	127.4(2)	C(1)—N(1)—H(10)	119(2)
C(3)—C(2)—N(1)	123.0(2)	C(2)—N(1)—H(10)	114(2)
C(1)—H(1)—F(2)	154(2)	N(1)—H(10)···F(1)	175(2)
C(3)—H(3)···F(2)	170(2)		

Primed atoms are symmetry generated.

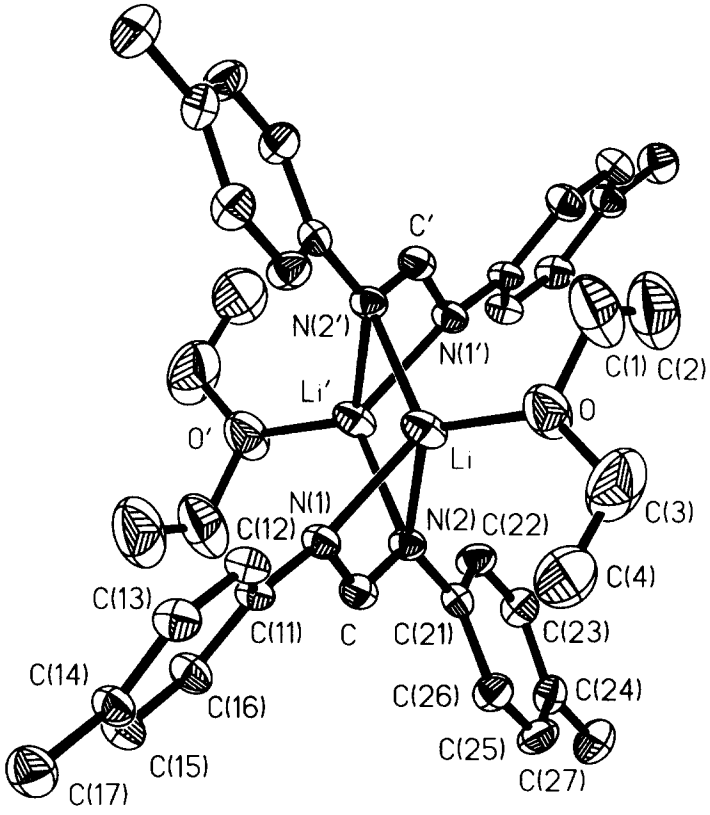


Fig. 1. A drawing of the molecular structure of $Li_2(\mu\text{-DTolF})_2(Et_2O)_2$. Non-hydrogen atoms are represented by their 30% probability ellipsoids.

dinuclear molecule. The ligand bonding mode is unusual in that each DTolF group has one nitrogen atom bonded exclusively to a lithium atom but the second nitrogen atom is bonded to each of the two lithium atoms. The fourth coordination site of each pseudo-tetrahedral lithium atom is occupied by an oxygen atom of a diethylether molecule as seen in Fig. 1.

The three-way bonding mode has been observed only once before in a triazenide compound of rhodium.[16] Perhaps we will see this type of bonding mode more frequently in the future.

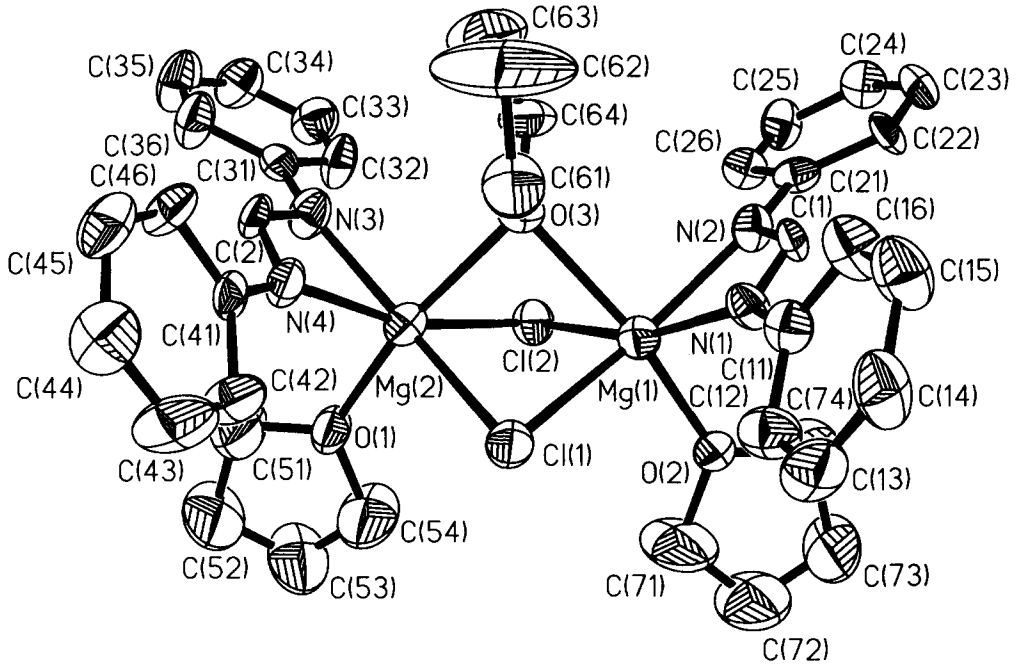


Fig. 2. Perspective view of the dinuclear (THF)(DPhF)Mg(μ-Cl)$_2$(μ-THF)Mg(DPhF)(THF) molecule showing the atom labelling scheme. Non-hydrogen atoms are represented by their 40% probability ellipsoids.

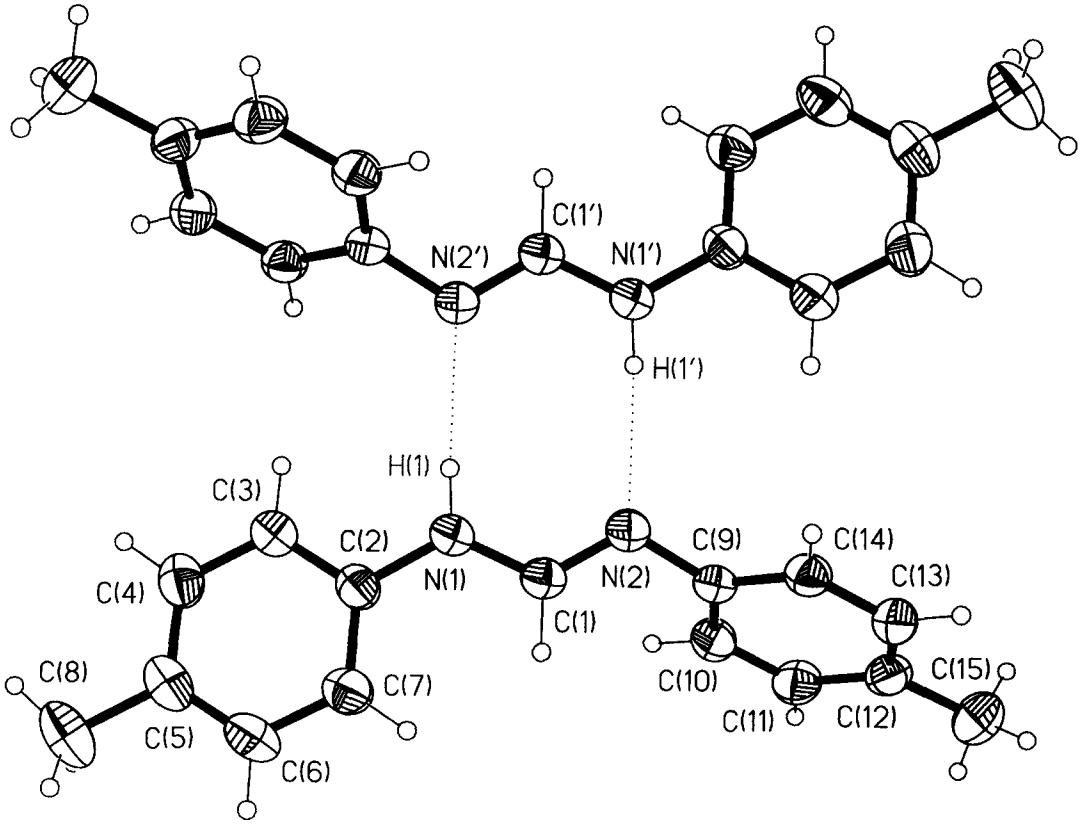


Fig. 3. A plot of a pair of HDTolF molecules showing the hydrogen bonding interactions. Non-hydrogen atoms are represented by their 40% probability ellipsoids. Hydrogen atoms are drawn as arbitrarily sized circles.

As expected, the shortest Li—N bond is the unshared bond [2.045(8) Å]. The second nitrogen atom has two different bonds to the lithium atoms [2.078(8) and 2.231(9) Å]. The shorter Li—N bond lengths are in good agreement with those of typical lithium to pyridine-like ligands and lithium amides.[17] The Li—O distance is also very similar to those found in other compounds such as $[LiBr \cdot Et_2O]_4$.[18]

(THF)(DPhF)Mg(μ-Cl)$_2$(μ-THF)Mg(DPhF)(THF)]

When the deprotonation of HDPhF is carried out using a Grignard reagent, MeMgCl, in the presence of THF it affords crystals of **II**. It is a dinuclear compound consisting of a face-sharing bioctahedron.

Each DPhF group is chelated to a Mg atom. The coordination sphere is completed by a THF molecule, two bridging chloride ions and a bridging THF molecule which is essentially *trans* to the singly coordinated THF, as seen in Fig. 2. This is only the second time that such μ-type coordination has been observed in a THF molecule. The first one was in $[(C_5H_4Me)TiF_3]_2$ (μ-THF).[19] However, this point was not emphasized in that report. The bridge is somewhat similar to that formed by tetrahydrothiophene, THT, in $[MCl_6(\mu\text{-THT})_3]^{2-}$, M = Nb, Ta.[20] In **II** both terminal Mg—O bonds are *ca* 0.3 Å shorter than the bridging ones. The Mg—O—Mg bridge is nearly symmetrical with distances of 2.322(6) and 2.357(6) Å.

HDTolF

The molecular structure of **III** is shown in Fig. 3. The compound forms dimers in which the molecules are associated by a pair of hydrogen bonds. The two molecules are related by a crystallographic inversion centre. The hydrogen atom bonded to the nitrogen atom was located on a Fourier map and was refined without constraints to give a N—H distance of 0.88(2) Å. The N—C—N skeleton shows well-defined C—N amine bonds [1.340(2) Å] and imine bonds [1.277(2) Å]. The difference of 0.06 Å in these bonds compares reasonably well with those in other amidine compounds as shown in Table 6. An exception might appear to be that of N,N′-di(*p*-chlorophenyl) formamidine (HDClPhF), which is reported to form dimers that contain identical skeletal C—N bond lengths as well as H atoms located at the midpoint between the pairs of nitrogen atoms. Our results as well as the others shown in Table 6 support the probable existence of the disorder in the structure of HDClPhF as hinted in the publication.

Another important feature shown in the structure of **III** is the marked difference found in the C—N—C bond angles. The one at the amine nitrogen is 7.5° greater than that at the imine nitrogen. A similar pattern is observed in other amidines including those

Table 6. Comparison of N—C bond distances (Å) of imine and amine type linkages in neutral amidine compounds

Amidine species	R	R′	M	d(C—N(1)) (amine)		d(C—N(2)) (imine)		C—N—C at N(1)		C—N—C at N(2)		Reference
$HNCHNH_2$	H	H		1.344(1)		1.298(1)		—		—		6a
(tol)NCPhN(tol)H	*p*-tolyl	Ph		1.359(11)		1.299(12)		128.4(7)		116.5(7)		6b
(tol)NCMeN(tol)H	*p*-tolyl	Me		1.368(4)		1.283(4)		127.6(3)		119.6(3)		6c
(Ph)NCHN(Ph)H	H	Ph		1.351(7)	1.310(8)	1.295(6)	131.2(5)		130.6(5)	119.2(5)	119.2(4)	6d
(*p*-ClC$_6$H$_4$)$_2$N$_2$HCH	H			1.309(3)	—	—	122.9(3)		121.6(3)	—	—	7a
(Ph)NCHN(Ph)H	H			1.314(3)	1.311(3)	1.305(3)	120.3(2)		120.5(2)	120.1(2)	119.8(2)	7b
(tol)NCHN(tol)H	*p*-tolyl	H		1.339(2)	—	—	124.3(1)		116.8(1)		—	This work
$FeCl_2$(HDPhF)$_2$	Ph	H	Fe	1.305(2)	1.318(3)	1.322(2)	128.1(2)		124.3(2)	116.6(2)	115.1(2)	5b
$FeCl_2$(HDTolF)$_2$	*p*-tolyl	H	Fe	1.339(5)	1.301(4)	1.315(4)	126.1(4)		123.9(3)	117.0(3)	115.2(3)	5a
$CoCl_2$(HDTolF)$_2$	*p*-tolyl	H	Co	1.349(6)	1.308(5)	1.291(5)	125.4(4)		125.6(4)	116.2(3)	116.5(4)	5a
PtCl(HDTolF)$_3$	*p*-tolyl	H	Pt	1.33(2)	1.32(2)	1.30(2)	122(2)	123(1)	126(1)	116(1)	117(1)	119(1)	5a
PtCl(DTolF)(HDTolF)$_2$	*p*-tolyl	H	Pt	1.349(9)	1.32(1)	1.31(1)	1.319(9)	123.1(4)	123.9(7)	116.7(6)	117.3(7)	5a
$[MnCl_2(HDPhF)_2]_2$	Ph	H	Mn	1.349(6)	1.298(5)	1.298(5)	1.297(5)	123.9(4)	125.6(4)	114.8(3)	114.6(4)	5c
$CoCl_2$(HDTolF)$^{-}$	*p*-tolyl	H	Co	1.32(2)		1.34(2)		125(1)		118(1)		5a
[H_2DTolF][BF_4]	*p*-tolyl	H		1.305(2)		—		127.4(2)				This work
[HDPhAc][C_2O_4]	Ph	Me		1.320(3)		1.305(3)		122.8(2)		125.8(2)		8

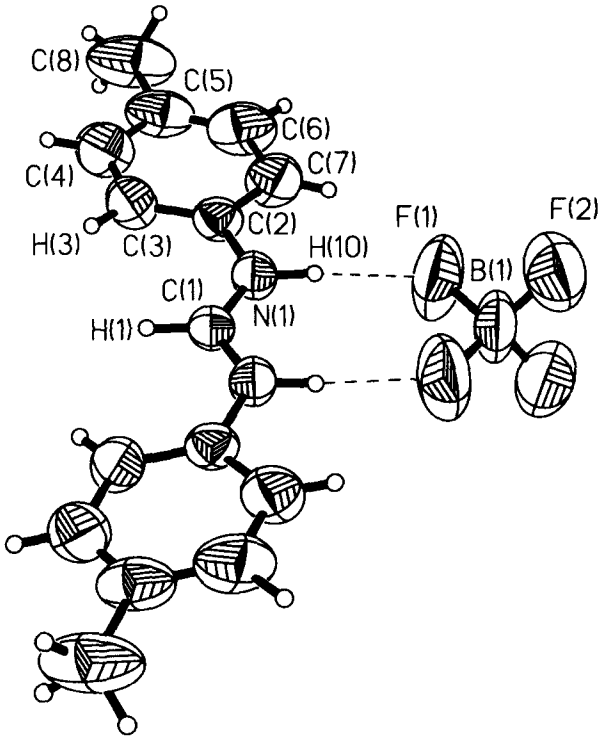


Fig. 4. A drawing of a cation and an anion in $[H_2DTolF][BF_4]$. Non-hydrogen atoms are represented by their 50% probability ellipsoids.

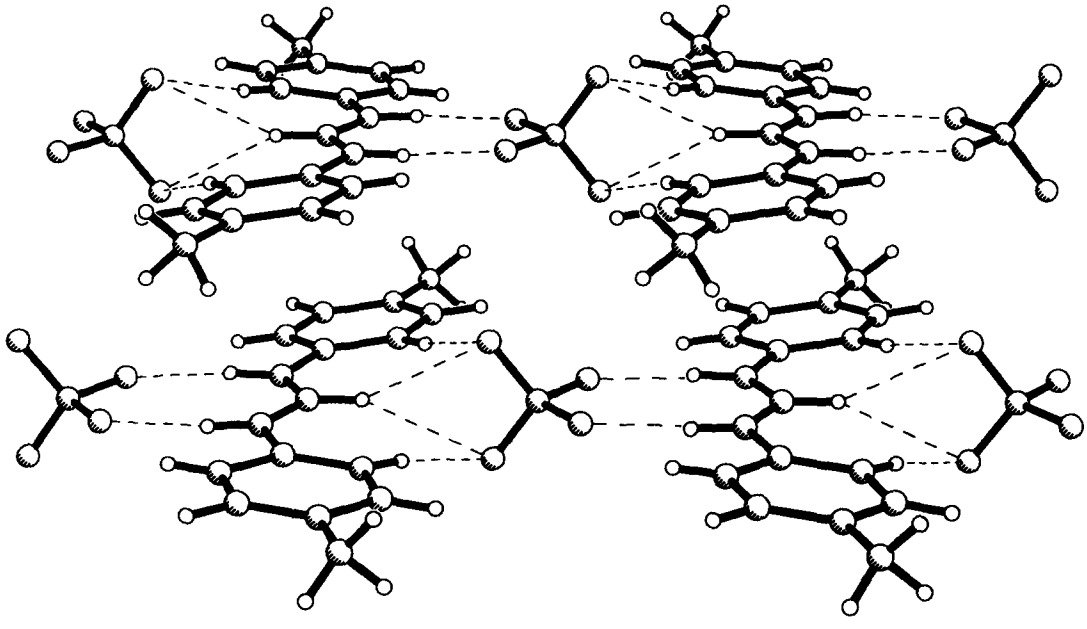


Fig. 5. A drawing that shows two layers of the stacking in the crystal.

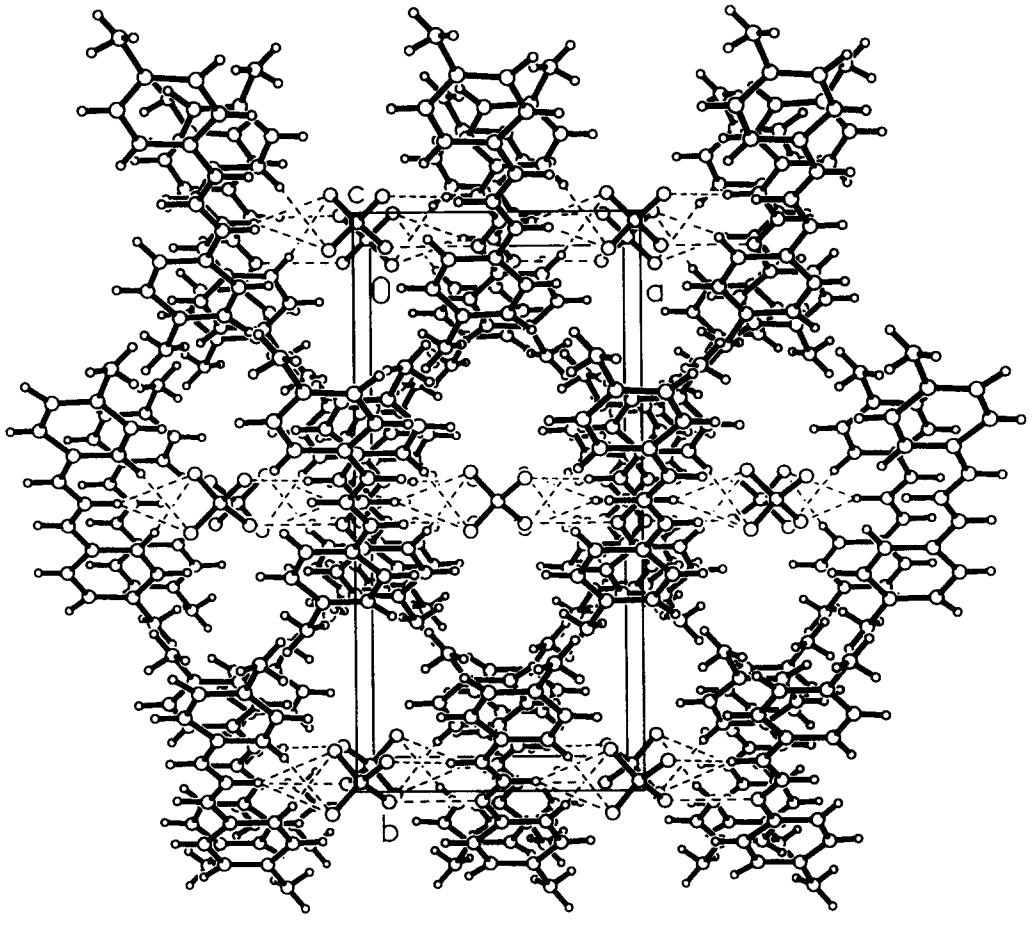


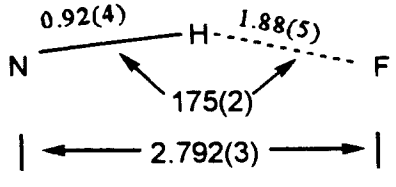
Fig. 6. A drawing of a portion of the extended structure of $[H_2DTolF][BF_4]$ showing the hydrogen bonding pattern viewed down the *c* axis.

where the amidine is coordinated to a metal atom as shown in Table 6.

$[H_2DTolF][BF_4]$

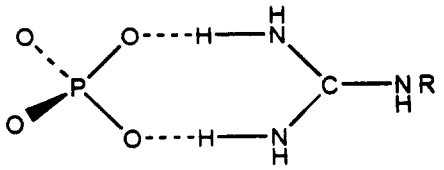
A drawing of the salt is shown in Fig. 4. There is a crystallographic two-fold axis along the methyne C—H bond that requires the C—N bonds of the N—C—N skeleton to be identical, contrary to the case with the neutral molecule, compound **III**. Equality of the N—C bond lengths is also observed in another structurally characterized cationic amidinium salt,[8] as well as in most symmetrically bonded amidinato complexes. As in the neutral parent species, the C—N—C bond angles for **IV** are greater than 120°. The two N—H groups are directed towards the $[BF_4]^-$ anion and participate in hydrogen bonding with the F atoms of the anion H · · · F = 1.88(5) Å; consequently, the tolyl groups are swept back to the other side of the cation. In contrast to the acetamidinium ion in the structure of $[H_2DPhA][C_2O_4]$, the entire H_2DTolF cation is nearly planar, exhibiting only a small dihedral angle [7.4(9)°] between the plane described by N(1), C(1), N(1) and the plane of the tolyl rings.

A partial packing diagram for compound **IV** is shown in Fig. 5 and a more extended one in Fig. 6. In addition to generalized electrostatic attractions that occur in all ionic crystals, these crystals are also stabilized by hydrogen bonds from the two N—H groups of each cation to two of the fluorine atoms of a BF_4^- ion. These crystallographically equivalent hydrogen bonds have the dimensions:



This nice fit of the cations to the BF_4^- anion is reminiscent of the way in which the cationic guanidyl groups of arginine residues nicely fit onto phosphate

ions by the formation of pairs of hydrogen bonds (**I**),[21] in certain phosphatases.



Closer examination of Figs 5 and 6 shows that there may be still another set of localized interactions that are necessary for the stabilization of the beautiful structure shown. It would appear that certain C—H bonds are attracted to the other two fluorine atoms of each BF_4^- ion. Thus C(1) lies at 3.387(4) Å of F(2) and F(2)′. The C(1)—H(1)···F(2) angles are 154(2)° and the C(1)—H(1) and H(1)···F(2) distances are 0.96(5) and 2.50(5) Å, respectively. In addition, there are two equivalent C(3)—H(3)···F(2) interactions that are also practically linear, 170(2)°, with a C(3)—F(2) distance of 3.404(4) Å and C(3)—H(3) and H(3)···F(2) distances of 0.93(3) and 2.49(4) Å, respectively. When compared with C—H···O-type hydrogen bonds,[22] these C—H···F interactions seem to merit serious consideration as C—H···F hydrogen bonds.[23]

*Acknowledgements*We are grateful to the Vicerrectoría de Investigación U. C. R. (Project 115-87-516) and the Department of Chemistry for support of work at the University of Costa Rica and to the National Science Foundation for support of work at Texas A&M University.

REFERENCES

1. F. A. Cotton, L. M. Daniels and C. A. Murillo, *Inorg. Chem.* 1993, **32**, 2881, and refs therein.
2. (a) F. A. Cotton, L. M. Daniels, L. R. Falvello and C. A. Murillo, *Inorg. Chim. Acta* 1994, **219**, 7; (b) F. A. Cotton, L. M. Daniels, D. J. Maloney and C. A. Murillo, *Inorg. Chim. Acta* 1996, **249**, 9.
3. F. A. Cotton, L. M. Daniels, D. J. Maloney and C. A. Murillo, *Inorg. Chim. Acta* 1996, **242–243**, 1, and refs therein.
4. See for example J. Barker and M. Kilner, *Coord. Chem. Rev.* 1994, **133**, 219.
5. (a) F. A. Cotton, L. M. Daniels, D. J. Maloney, J. H. Matonic and C. A. Murillo, *Polyhedron* 1994, **13**, 815; (b) F. A. Cotton, L. M. Daniels and C. A. Murillo, *Inorg. Chim. Acta* 1994, **224**, 5; (c) D. I. Arnold, F. A. Cotton, D. J. Maloney, J. H. Matonic and C. A. Murillo, *Polyhedron* 1996, **16**, 133.
6. (a) R. Norrestam, S. Mertz and I. Crossland, *Acta Cryst.* 1983, **C39**, 1554; (b) N. W. Alcock, N. C. Blacker, W. Errington, M. G. H. Wallbridge and J. Barker, *Acta Cryst.* 1994, **C50**, 456; (c) E. Ciszak, M. Gdaniec, M. Jaskólski and Z. Kosturkiewicz, *Acta Cryst.* 1988, **C44**, 2144; (d) N. W. Alcock, J. Barker and M. Kilner, *Acta Cryst.* 1988, **C44**, 712.
7. (a) R. Anulewicz, T. M. Krygowski and B. Pniewska, *Acta Cryst.* 1990, **C46**, 2121; (b) R. Anulewicz, T. M. Krygowski and N. Pniewska, *J. Crystallogr. Spectr. Res.* 1987, **17**, 661.
8. B. Kratochvíl, J. Novotný, S. Smrčková and J. Krechl, *Collect. Czech. Chem. Commun.* 1990, **55**, 479.
9. R. M. Roberts, *J. Org. Chem.* 1949, **14**, 277.
10. J. Pflugrath and A. Messerschmitt, MADNES, Munich Area Detector (New EEC) System, Version EEC 11/1/89, with enhancements by Enraf-Nonius Corp., Delft, The Netherlands. A descriptive of MADNES appears in: A. Messerschmitt and J. Pflugrath, *J. Appl. Cryst.* 1987, **20**, 30.
11. (a) J. C. Bryan, F. A. Cotton, L. M. Daniels, S. C. Haefner and A. P. Sattelberger, *Inorg. Chem.* 1995, **34**, 1875; (b) W. R. Scheidt and I. Turowska-Turk, *Inorg. Chem.* 1994, **33**, 1314.
12. (a) A. Bino, F. A. Cotton and P. E. Fanwick, *Inorg. Chem.* 1979, **18**, 3558; (b) F. A. Cotton, B. A. Frenz, G. Deganello and A. Shriver, *J. Organomet. Chem.* 1973, **50**, 227.
13. The extinction parameter x as refined by least-squares, where F_c is multiplied by $k[1 = 0.001(x)(F_c^2)(\lambda)^3/\sin(2\theta)]^{1/4}$, k = overall scale factor.
14. SHELXTL, Version 5.03. Siemens Industrial Automation, Inc., Madison, Wisconsin (1990).
15. G. M. Sheldrick, SHELXL-93. *A Program for Crystal Structure Refinement*. University of Göttingen, Germany (1993).
16. N. G. Connelly, P. M. Hopkins, A. G. Orpen, G. M. Rosair and F. Viguri, *J. Chem. Soc., Dalton Trans.* 1992, 2907.
17. (a) W.-P. Leung, L.-H. Weng, R.-J. Wang and T. C. W. Mak, *Organometallics* 1995, **14**, 4832; (b) K. Gregory and P. v. R. Schleyer, *Adv. Organomet. Chem.* 1991, **37**, 67.
18. F. Neumann, F. Hampel and P. v. R. Schleyer, *Inorg. Chem.* 1995, **34**, 6553.
19. A. Herzog, F.-Q. Liu, H. W. Roesky, A. Demsar, K. Keller, M. Noltemeyer and F. Pauer, *Organometallics* 1994, **13**, 1251.
20. F. A. Cotton and M. P. Diebold and W. J. Roth, *J. Am. Chem. Soc.* 1987, **109**, 5506.
21. F. A. Cotton, V. W. Day, E. E. Hazen, Jr., S. Larsen and S. T. K. Wong, *J. Am. Chem. Soc.* 1974, **96**, 4471.
22. T. Steiner and W. Saenger, *J. Am. Chem. Soc.* 1992, **114**, 10146.
23. A study of the dimensions of other possible examples is in hand and results will be published soon.

Pergamon

Polyhedron Vol. 16, No. 4, pp. 551–566, 1997
Copyright © 1996 Published by Elsevier Science Ltd
Printed in Great Britain. All rights reserved
PII: S0277-5387(96)00243-4
0277-5387/97 $17.00+0.00

POLYHEDRON REPORT NUMBER 64

Some recent coordination chemistry of lead(II)

Jonathan Parr

Department of Chemistry, Loughborough University, Loughborough, Leics LE11 3TU, U.K.

CONTENTS

1. INTRODUCTION 551
2. CONVENTIONAL LIGANDS 551
2.1. Group 14: donor ligands 551
2.2. Group 15: nitrogen ligands 552
2.3. Group 15: phosphorous ligands 555
2.4. Group 16: oxygen ligands 556
2.5. Group 16: sulfur and selenium ligands 557
2.6. Miscellaneous 559
3. MACROCYCLIC LIGANDS 559
3.1. Nitrogen donor macrocyclic ligands 559
3.2. Nitrogen/oxygen mixed donor macrocyclic ligands 560
3.3. Nitrogen/sulfur mixed donor macrocyclic ligands 564
3.4. Oxygen donor macrocyclic ligands 564
4. CONCLUSION 564

1. INTRODUCTION

There has been a resurgence of interest in the coordination chemistry of heavy p-block elements in recent years, and this review is concerned with reports of new coordination chemistry of lead(II) that have been published during this renaissance. Since it is a rather large area of chemistry, this report is not comprehensive, but even limiting it to only the most interesting examples has allowed the inclusion of many varied compounds. The expansive literature dealing with macrocyclic ligands is treated in a separate section as it merits being considered as a "special case" of coordination chemistry.

Of all p-block elements, lead(II) has a particular fascination for coordination chemists, as it can adopt many different geometries in its complexes, allowing a degree of tolerance for ligand configurations which is not seen in, for example, *d*-block elements. Coupled with the ability to bind well to both hard and soft donor atoms, these properties make lead(II) an interesting metal to study, forming as it often does complexes which are different from those which might be conventionally expected.

The toxic nature of lead and its widespread occurrence in the environment, subsequent to its many applications in technology, adds a focus to the search for powerful and selective lead binding materials and ligand systems. For example, there is no oral chelator available for therapeutic uses in the treatment of lead poisoning that has been specifically designed for lead. Certainly much remains to be discovered in the field of lead coordination chemistry, despite the large body of work already published, of which this review covers only a part.

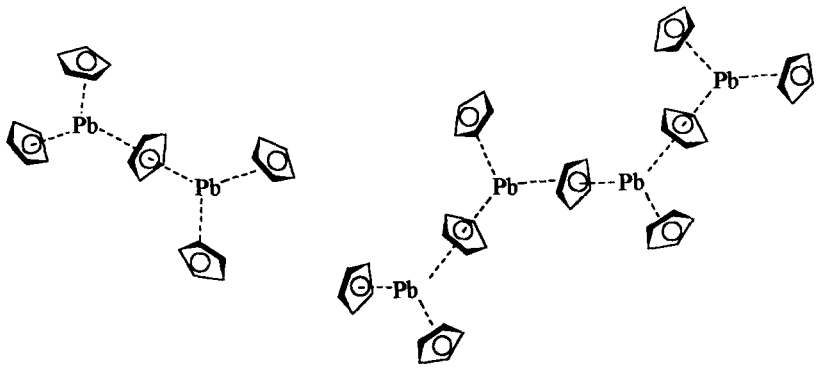
2. CONVENTIONAL LIGANDS

2.1. *Group* 14: *donor ligands*

The family of substituted plumbocenes has been expanded to include examples where 1,2,3,4,1′,2′,3′,4′ = Ph, 5,5′ = 4-(*t*-Bu)Ph [1], and where 1,2,3,4,5,1′,2′,3′,4′,5′ = Ph [2] or Me [3]. The half sandwich complexes [Cp*PbX] (where X = Cl^-, $[BF_4]^-$ or $CF_3SO_3^-$) were also prepared [8] and their exchange reactions with 2,2′ bipyridyl (bipy) and 1,10 phenanthroline (1,10 phen) explored.

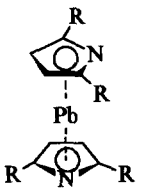
The reaction of plumbocene with an excess of [LiCp] yields the fascinating compound $[Li(12\text{-}C\text{-}4)]_2$

$[(C_5H_5)_9Pb_4][(C_5H_5)_5Pb_2]$, **1**, crystallised on addition of a crown of ether to the reaction mixture. The structure comprises both triple and quintuple decker sandwich moieties [4].



The two anions present in 1.

Heteroatom analogues of $(Cp)^-$ have been used to prepare the plumbocene like complex **2** where R = (*t*-Bu). The crystal structure of **2** reveals a tilt angle of 142.7° indicating that as with other plumbocene type compounds, the remaining lone pair on the lead is stereochemically active [5].



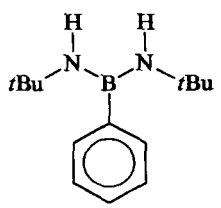
2

2.2. *Group* 15 : *nitrogen ligands*

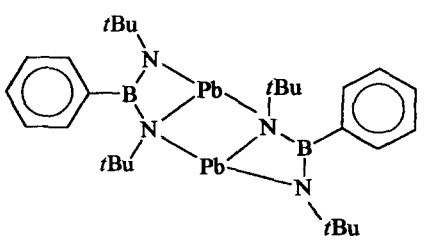
Aminoborane ligands have widespread utility in the coordination chemistry of most metals and lead(II) is no exception. The interaction of polypyrazolylborates with simple lead(II) salts yields a variety of products, depending upon the substitution of the Tp ligands and the reaction stoichiometry (Scheme 1).

Compounds **3, 4,** and **5** were analysed by X-ray crystallography to reveal a distorted trigonal bipyramidal (TB) geometry for **3,** and irregular octahedral geometries for both **4** and **5** [6].

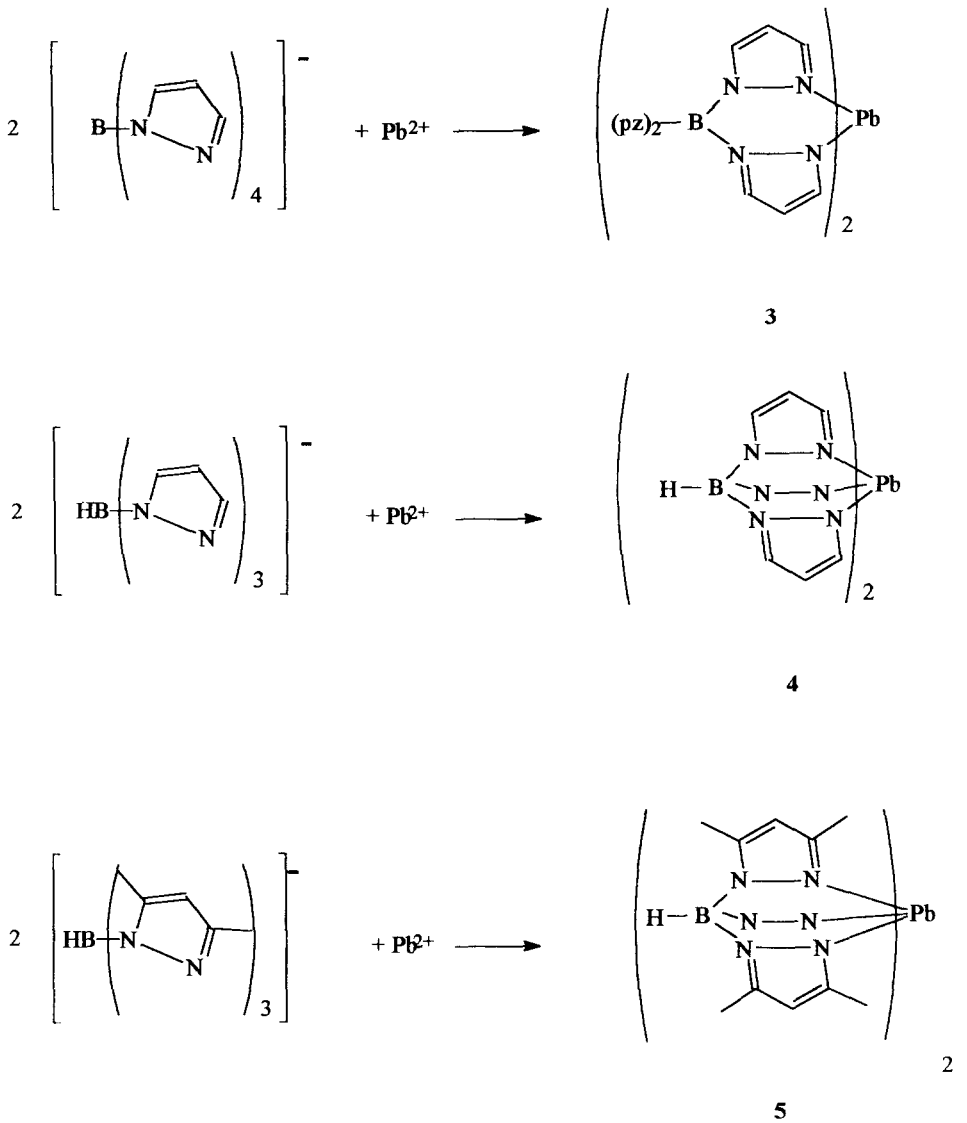
The dilithium salt of the aminoborane **6** reacts with lead(II) chloride to give the dimeric compound **6a** where in each of the lead(II) centres is tricoordinate, exhibiting two kite shaped [PbNBN] rings linked together through two further Pb–N bonds [7]. A related structural motif is seen in $[Pb(NR_2)]_4$ [8].



6



6a

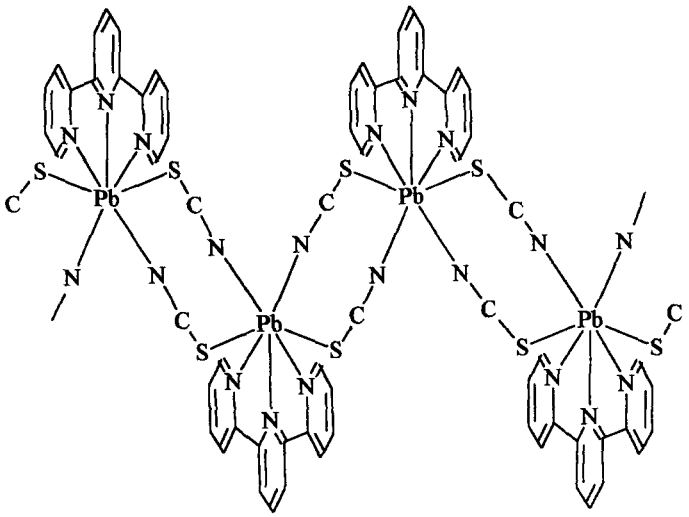


Scheme. 1.

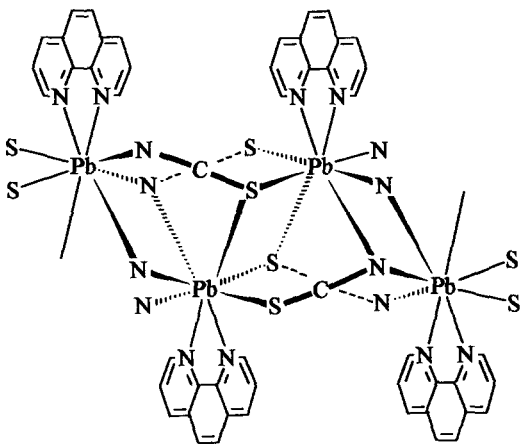
The synthesis of $[(t\text{-Bu})(Ph)C{=}N]_8Pb \cdot Li(THF)$ from the reaction of benzonitrile and *t*-butylithium with lead(II) chloride was reported, a further example of tricoordination of lead(II) as well as being the first reported imino complex of lead(II) [9]. The product exists in the solid state as a regular tetrahedron, with the lead(II) in the apical position and the three imino nitrogens defining the basal triangle. The lithium bridges the three nitrogens on the opposite face of the triangle to the lead and coordinates a molecule of THF.

The versatile ligand triazacyclononane forms 1 : 1 complexes with lead(II) nitrate and with lead(II) perchlorate. In the solid state these both form irregular hexacoordinate complexes with intermolecular bridging through the oxygen atoms of the nitrate or perchlorate counterions to form arrays in the solid state that show considerable similarity despite the apparent steric differences between nitrate and perchlorate ions [10]. The stability of the 1 : 1 complex in aqueous solution has been measured at $\log K = 10.35$ [10].

Complexes formed between lead(II) thiocyanate and (1,10 phen) and 2,2′ : 6′2″ terpyridine (terpy) have been investigated [11,12]. Despite the seeming simplicity of the system a variety of compounds can be prepared by subtle adaption of the reaction stoichiometry, including **7** and **8**.



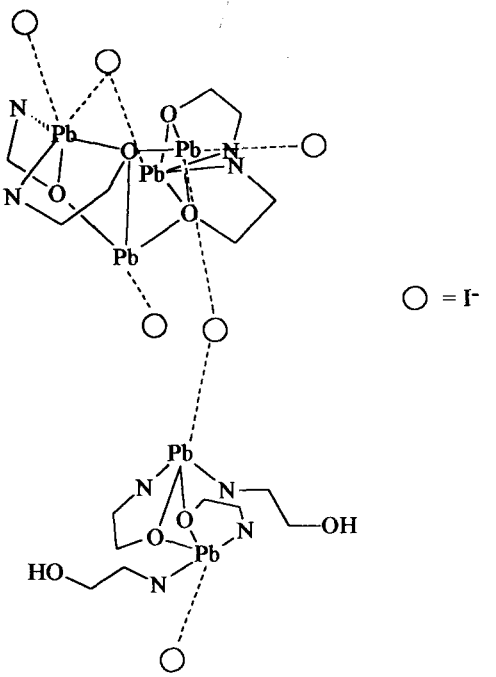
7



8

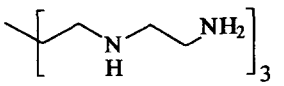
The linear polymer **7** comprises $[Pb(terpy)]^{2+}$ units lined by four bridging thiocyanates to two further $[Pb(terpy)]^{2+}$ units. Compound **8** is again a linear polymer with an octacoordinate lead(II) binding to one (1,10 phen) and six bridging thiocyanates, connecting each lead(II) to four neighbouring lead(II) centres [12].

The neutral bidentate ligand tetramethylethylenediamine (tmeda) reacts with lead monoxide in the presence of ammonium iodide to yield the simple chelated complex $[Pb(tmeda)_2I_2]$ [13] which has a linear polymer array of $[Pb(tmeda)]^{2+}$ units linked by bridging iodides to give an overall irregular octahedral geometry to the plead(II) centre. By the same authors, the analogous reaction with ethanolamine replacing tmeda was explored [14] resulting in the slightly more unusual compound $[Pb_6(Ea)_6(HEa)_2I_6]$ **9**.



9

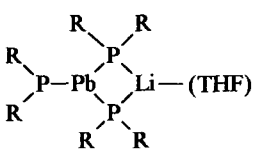
Nitrilotriacetamide (NTA) has been used to prepare a 1 : 1 complex $[(NTA)Pb(NO_3)](NO_3)$ [15]. This decacoordinate structure represents the highest coordination number routinely observed for lead(II), exhibiting in the solid state a configuration which suggests that the remaining lone pair is steroechemically inactive in this compound. Stability constants are reported for the formation of complexes of 5-(4′-amino-2′-azabutane)-5-methyl-3,7-diazanonane-1,9-diamine, **10,** with lead(II) in water ($\log K = 9.2$) [16]. This tripodal ligand is related to macrocyclic ligands such as cryptands, ($\log K$ for (2,2,2-crypt) with lead(II) in MeOH = 12.5) [17].



10

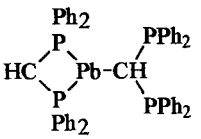
2.3. *Group* 15 : *phosphorus ligands*

The first report of a simple compound of empirical formula $[Pb(PR_2)_2]$ was from Cowley *et al* [18]. These dimeric neutral complexes form from the reaction of lead(II) chloride with lithium di-*t*-butylphosphide in stoichiometry 1 : 2, the nature of the product was confirmed by X-ray crystallography [18]. The same reaction in 1 : 3 stoichiometry gives the trisubstituted anionic lead compound **11** [19].



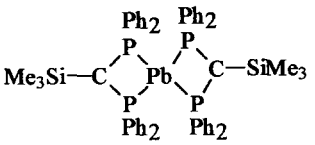
11

An excellent and thoroughgoing study of complexes of the phosphorus analogue of the well-known *bis*-(trimethylsilyl)amide was reported by Buhro *et al.* [20]. Perhaps unsurprisingly, the complex of empirical formula $[Pb(P(SiMe_3)_2)]$ is not monomeric, but dimeric. The structural characterisation of this complex shows a puckered (Pb_2P_2) ring, with a terminal phosphide on each lead(II) centre, the whole crystallising with a *cis*-configuration [20].



12

A further example of tricoordinate lead(II) is given by Balch and Oran. The lithium salt of deprotonated *bis*-(diphenylphosphino)methane (dppm) reacts with lead(II) chloride to give **12**, and the trimethylsilyl substituted analogue of dppm forms a tetracoordinate species **13** [21]. NMR studies reveal that at ambient temperatures both molecules are fluxional, **12** exchanging between a tri- and a tetracoordinate species, (between η^1 C- bound and η^2 $(P)_2$- bound), **13** exchanging between different tetracoordinate geometries [21].

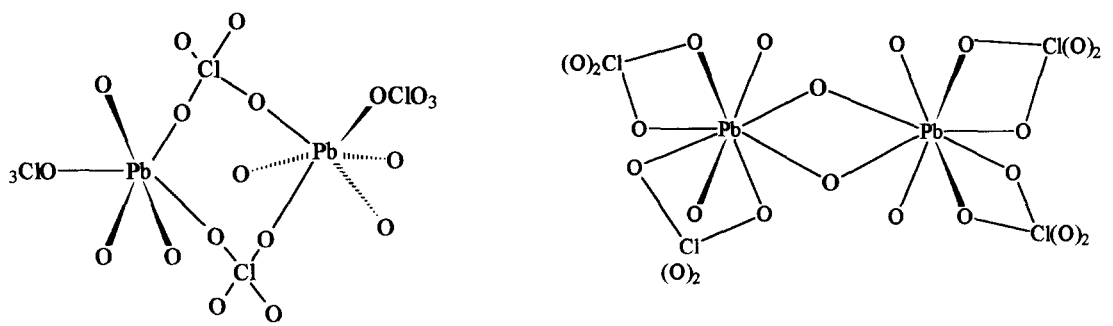


13

2.4. *Group* 16 : *oxygen ligands*

Tetrameric $[Pb_4(OH)_4](N)_3)_4$ was isolated from a basic aqueous solution of lead(II) nitrate, and the X-ray structure reported [22]. The compound exists in the solid state as a cubane type arrangement of four lead(II) atoms occupying four opposite corners of a cube with four hydroxyl ions completing the array. This remarkable ion is an important addition to the understanding of the speciation of lead(II) ions in aqueous solution, and is unusual of its kind.

A number of compounds have been isolated from the system $Pb(ClO_4)_2$/DMSO, and crystal structures were reported for $Pb(DMSO)_x(ClO_4)_2$, where $x = 3$ or 5 [23]. Two isomers were isolated for the case $x = 3$ (**14**) where the bridging oxygen is either from a perchlorate or a DMSO moiety. The report also contains a useful discussion on the potential difficulties of relating the composition of species in solution to the nature of the species which crystallise therefrom.

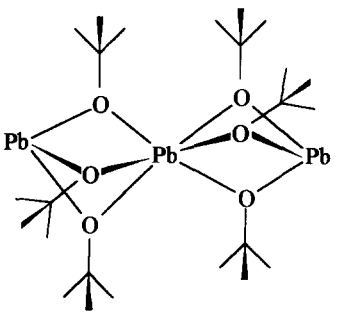


O = DMSO Oxygen

Perchlorato and DMSO bridged isomers of 14

Lead(II) alkoxides have received much attention particularly due to their potential application as precursors to metal films. In another extensive study by Buhro *et al.* [24] the alcoholysis of $Pb[N(Si(Me)_3)]_2$ with various

alcohols was shown to lead to a series of alkoxides with varying structural features. Sterically undemanding alcohols (isopropanol, 2-methoxyethanol) give linear polymeric compounds $[Pb(OR)_2]_n$ where the lead exhibits a distorted trigonal bipyramidal structure, bound to four μ^2 alkoxide oxygens. More encumbered alcohols (*t*-butanol, neopentyl alcohol) form tri-metallic compounds $[Pb_3(OR)_6]$ (**15**) [24]. Using an excess of alcohol, or by direct reactions of lead(II) chloride with an excess of sodium alkoxides, products of the type $[Pb_4(OR)_6]$ can be formed [25].



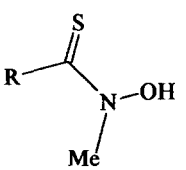
15

A similar polymeric motif is seen in the product of the reaction of lead monoxide with triethanolamine $[N(CH_2CH_2OH)_3]$ and ammonium iodide [26] which comprises a repeating $[Pb_4I_4N(CH_2CH_2)_3(EtOH)_2(EtOH)]$ unit, where triethanolamine is a tetradentate ligand, doubly deprotonated. A structurally related compound is reported by Veith *et al.* [27].

Aminosquaric acid reacts with lead(II) nitrate in methanol solution to give $[Pb(C_4O_3CH_2)\cdot 2H_2O]_n$ where each octacoordinate lead(II) is bound once to each of four aminosquarate residues and to the oxygens of four μ^2 bridging water molecules [28]. Another seemingly simple system, lead(II) acetate and phthalic acid, has been shown by crystallography to give a series of interesting products [29]. The mixed compound lead(II) acetophthalate comprises three distinct lead(II) centres, each of which exhibit a different coordination geometry.

2.5. *Group* 16: *sulfur and selenium ligands*

Thiohydroxamates (**16**) have been show to form simple 2:1 complexes with lead where R = Ph, Me. Both complexes exhibit a distorted trigonal bipyramidal geometry in the solid state [30]. Dithiocarbamate complexes have been investigated by vibrational spectroscopy [31], mass spectroscopy, ^{207}Pb NMR and electrochemical techniques [32]. Whilst it is proposed that $[RNCS_2]^-$ is always present as a bidentate ligand, these ligands are shown in some cases to be labile in experiments measuring the rate of scrambling of ligands in mixtures of the type $\{[Pb(S_2CNR)_2]+[Pb(S_2CNR')_2]\}$ [32].

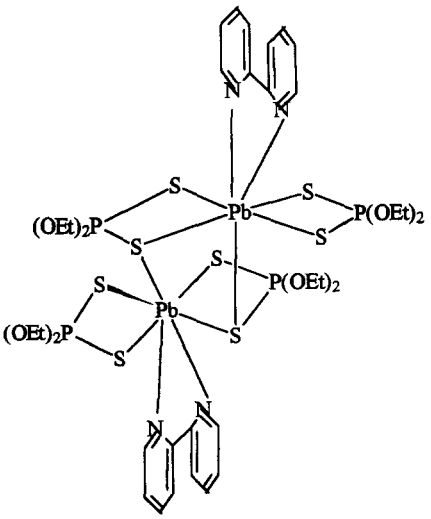


16

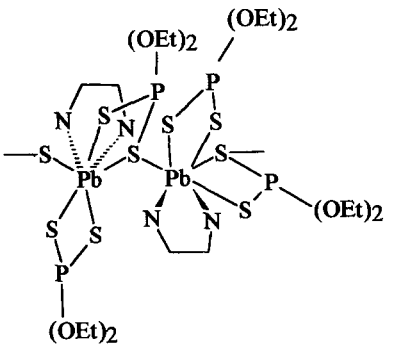
The dipotassium salt *bis*-(2,2-dicyanoethylene-1,1-dithiolato)plumbate was isolated as a hydrate from the reaction of lead(II) acetate with the potassium dithiolate. The anion exhibits a pyramidal geometry in the solid state by X-ray crystallography, a disposition found by calculation to be favoured over a planar arrangement by 25 kJ mol^{-1} [33].

An elegant investigation of the simple yet significant diothiolate complex [Pb(ethane-1,2,-dithiolate)] reveals that the compound exists in the solid state as an extended array, with intermolecular Pb–S interactions giving an overall hexacoordinate configuration to the oligometric lead centres [34]. Less tractable was the $[Pb(C_4S_4)]_n$ tetrathiosquarate complex of lead(II), a high melting insoluble violet polymer [35].

Thiophosphates of various kinds have been shown to form complexes with lead(II) [36–38]. The mixed complexes $[Pb(S_2P(OEt)_2(bipy)]_2$ and $[(Pb(S_2P(OEt)_2)_2(en)]_n$ shown in **17** have been prepared and their isolation has been used to infer a mechanism for the reaction of simple amines with [lead(II)*bis*-(O,O) dialkyldithiophosphates] [36].



The dimeric $[Pb(bipy)(S_2P(OEt)_2)_2]_2$

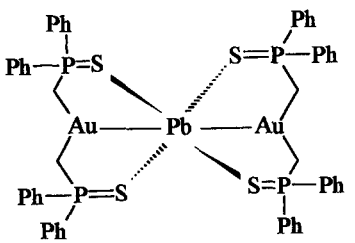


The repeating unit of $[(Pb(S_2P(OEt)_2)_2(en)]_n$

17

Inorganic chelate rings have enjoyed much popularity recently and lead(II) has been complexed by tetraphenyldithiomidophosphinate, which forms a simple neutral 2 : 1 complex with a trigonal bipyramidal geometry in the solid state [37], giving a complex which comprises two [PbSPNPS] rings.

A slightly more sophisticated system reported by Fackler *et al.* [38] uses an organogold dithiophosphinate **18** to prepare 2 : 1 complex of octahedral geometry exhibiting two Au–Pb interactions of 2.896 and 2.963 Å.



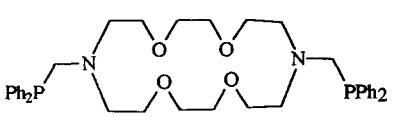
18

The dianion *bis*-(2,2-dicyanoethylene-1,1-diselenato)plumbate was prepared from the reaction of lead(II) acetate and the potassium salt of the diselenodicyanoethylene, and isolated as the tetraphenyl arsonium salt.

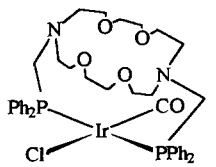
The solid state structure of this by X-ray methods is found to be intermediate between square pyramidal and trigonal bipyramidal [40].

2.6. *Miscellaneous*

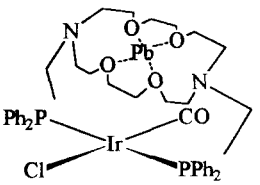
The diphosphine **19** which has a crown ether backbone has been coordinated to an [Ir(Cl)(CO)] fragment to yield **19a** which can further bind [Pb^{2+}] in the crown ether function to give the dication **19b**. The Pb–Ir distance in the crystal structure is 3.117 Å [41]. The related complex **20** is reported by the same authors [42] which exhibits shorter Pb–Ir interactions (2.855 and 2.831 Å), and is an example of tricoordinate lead(II). This tricoordination is also observed in a complex reported by Lappert and Power [43] where the sterically encumbered species $Pb[N(Si(Me)_3)_2]$ acts as a two electron donor ligand complexing to [η3(allyl)PdCl]. Although this seems an isolated example for lead(II), both tin(II) and germanium(II) form a range of complexes of this type [43].



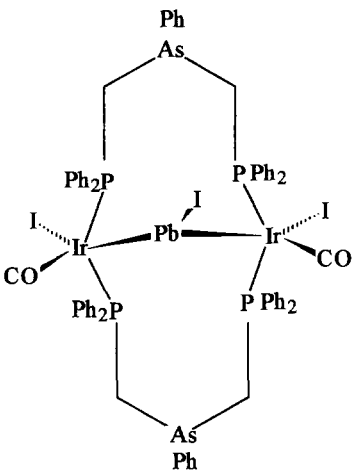
19



19a



19b

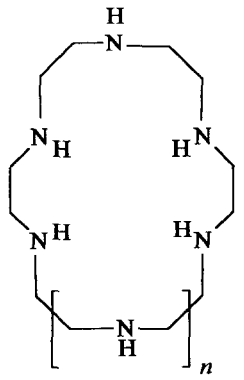


20

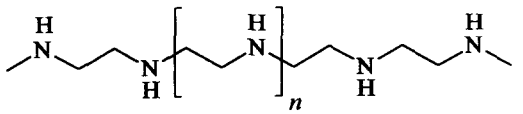
3. MACROCYCLIC LIGANDS

3.1. *Nitrogen donor macrocyclic ligands*

Lead(II) is a popular metal amongst macrocyclic chemists in part because it exhibits a wide degree of flexibility in the geometry and coordination number of its complexes. A comparative study of complexes of lead(II) with linear and cyclic polyamines reveals an enhancement in stability in smaller cyclic amines over their straight chain analogues, an enhancement which decreases as the size of the polyamine increases [44]. In addition, the larger cyclic polyamines form bi- and tri-nuclear complexes of good stability, and the crystal structure of $[30]aneN_{10}Pb_2(ClO_4)_4$ is also reported. The values for log K for mononuclear complexes do not vary greatly for **22–24**, with **21** exhibiting a significantly higher stability. Values for the analogous linear amines **26** and **27** are very close to those seen for **22** and **23**, with the log K for **28** greater than log K for **24**.

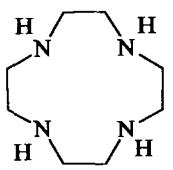


$n = 1$, **21**, $\log K = 14.13$
$n = 2$, **22**, $\log K = 10.02$
$n = 3$, **23**, $\log K = 10.83$
$n = 4$, **24**, $\log K = 9.77$

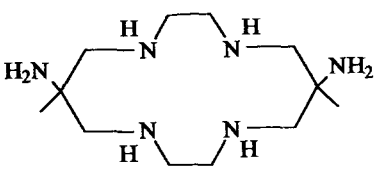


$n = 2$, **25**, $\log K = 9.97$
$n = 3$, **26**, $\log K = 9.86$
$n = 4$, **27**, $\log K = 10.37$
$n = 5$, **28**, $\log K = 11.32$

In a related study, a series of tetraazacycles and oxatriazacycles with various spacing groups were prepared and their stabilities with lead(II) and other metals were investigated, with the highest value of log K reported for the 1 : 1 complex with lead(II) of the smallest tetraazacycle ligand, **29**, ($\log K = 15.9$) [45]. Tetraazacycle **30**, incorporating two pendant amine functions allowing a potentially hexadentate ligand was prepared and its 1 : 1 complex with lead(II) examined by X-ray crystallography [46]. The compound has in the solid state all six amine groups bound to the lead centre and the nonacoordinate geometry is completed by one molecule of water and two oxygens form a perchlorate anion. The log K of this species is reported as 11.8.



29



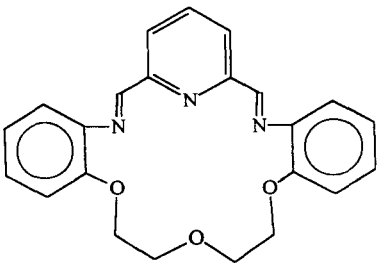
30

An unusual result arising from the interaction of lead(II) nitrate and 24(pyridinium)-C-6 is reported by Cramer *et al.* [47] where the product which is formulated as[Pb(24(pyridinium)-C-6)]$(NO_3)_6$ is revealed by crystallography to contain a $[Pb(NO_3)_6]^{4-}$ ion and [24(pyridinium)-C-6]$^{4+}$ with an empty cavity.

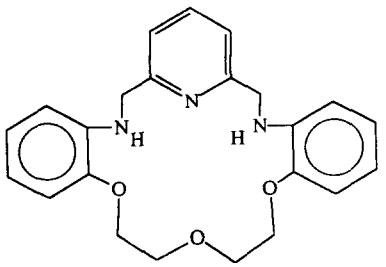
3.2. *Nitrogen/oxygen mixed donor macrocyclic ligands*

A wide variety of N,O donor macrocycles have been reported in coordination studies with lead(II). Ligands of this class derived from Schiff base condensations on pyridine-2,6-dicarboxaldehyde (**31**–**36**) have been widely

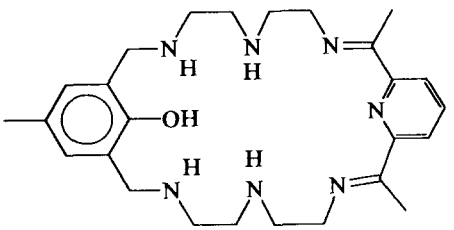
studied. A 1 : 1 complex of lead(II) with ligand **31** was reported with bidentate nitrates lending an overall decacoordination for the metal [48]. The reduced form of the ligand is also reported with a concomittant change of conformation of its lead(II) complex associated with the increased flexibility of the ligand. The macrocycle **33** contains phenolic and pyridine donor sites, and forms a complex with lead(II), $[Pb_2(L)]$ which is a linear polymer in the solid state [49]. The potentially octadentate macrocycle **34,** which comprises alcohol and pyridine donor groups, forms 1 : 1 complexes with lead(II) [50] despite a similar configuration to **35,** which forms both mono- and bi-nuclear complexes [51].



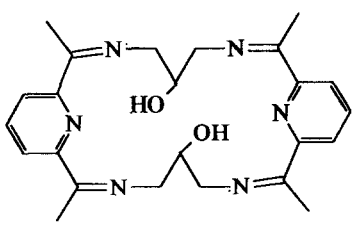
31



32



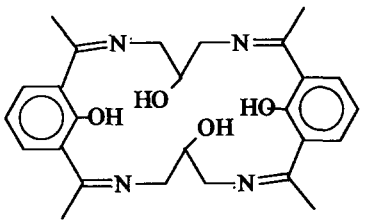
33



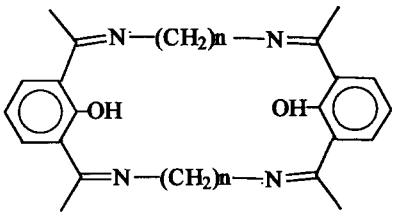
34

36 and **37** are two- and three-dimensional analogues of the same ligand type. **37** forms a 1 : 1 complex with a heptacoordinate configuration [52] whereas **36** is reported to form an intriguing dimetallic complex, $[Pb(Cu\mathbf{36})_2](ClO_4)_2$ [53].

An elegant ^{13}C NMR study on the fluxional processes seen for the lead(II) complex of **38** [54,55] reveals that a hexacoordinate structure is favoured in solution with exchange between the four pendant groups, the macrocyclic donor atoms being bound throughout the exchange process.

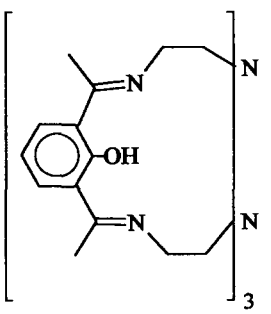


35

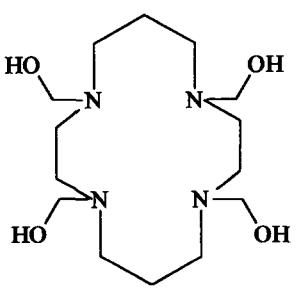


n = 2 or 3

36

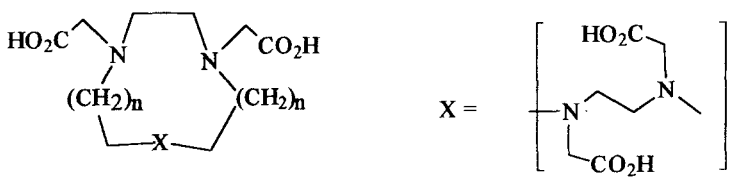


37

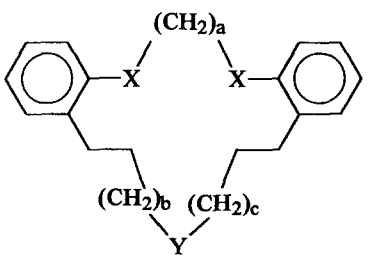


38

A series of ligands based upon **39** were prepared and their relative binding efficiency with lead(II) was investigated to elucidate preference for binding site type, with 1,4,7,10-tetraazacyclododecane-*N*,*N*′,*N*″,*N*‴-tetraacetic acid forming the most stable complex of this family of ligands [56]. An expansive series of ligands of general formula **40** were reported and their complexation behaviour with lead(II) investigated [57, 58]. The crystal structure of the complex formed between lead(II) and **40** where X = S, Y = NH was reported. The highest log *K* value for this set of ligands is observed for the case where all donor atoms are nitrogens (log *K* = 9.5), decreasing to a minimum when all X,Y donor sites are thioethers (log *K* ~ 3). This comprehensive study illuminates the preferences of lead(II) for donor atom type, maintaining as it does a fixed structure and configuration to the ligands, changing only donor atom type.

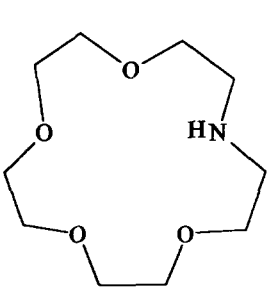


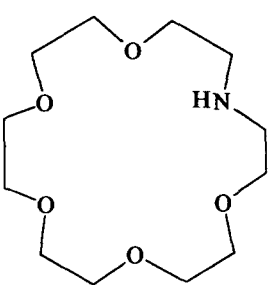
39



where a = 1-4, b = c = 2
X = (NH), O, S
Y = (NH), O, S

40



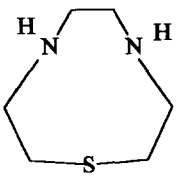


41 **42**

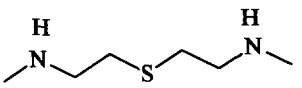
The azacrown ethers 1,4,7,10-tetraoxa-13-azacyclopentadecane (**41**) and 1,4,7,10,13-pentaoxa-16-aza-cyclooctadecane (**42**) have been show to form more stable complexes with lead(II) than their oxygen analogues 15-C-5 and 18-C-6, (*vide infra*) with log *K* $[Pb(\mathbf{41})]^{2+}$ = 6.0 (*cf* 3.92) [59] $[Pb(\mathbf{42})]^{2+}$ = 8.4 (*cf* 6.99) [60]. Structural characterisation of $[Pb(\mathbf{41})(NO_3)_2]$ shows an asymmetric structure with the pentadentate macrocycle bound on one side of the lead(II) with two bidentate nitrate groups bound on the other face, giving a significantly distorted coordination sphere, whereas $[Pb(\mathbf{42})(NO_3)_2]$ has a planar equatorial disposition of the hexadentate macrocycle, with the two bidentate nitrate functions disposed on opposite sides, giving an altogether more symmetrical decacoordinate structure [61].

3.3. *Nitrogen/sulfur mixed donor macrocyclic ligands*

A comparison of ring and chain configurations of the ligands [9]aneN$_2$S and atam (**43**) and their complexes with lead(II) was given by Herman *et al.* [62]. The relatively low values for log K (6.9 and 5.3, respectively) compare well with the result reported by McPartlin *et al.* [57, 58] where inclusion of thioether functions reduced ligand efficiency relative to the nitrogen analogue. The neutral mixed S,N donor ligands. **44a, 44b** and their complexes with lead(II) were reported by Murphy *et al.* [63]. The crystal structure of the complex [Pb(**44a**)(MeOH)(H$_2$O)](ClO$_4$)$_2$ was also given.

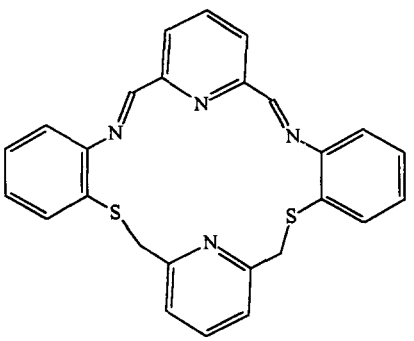


[9]aneN$_2$S

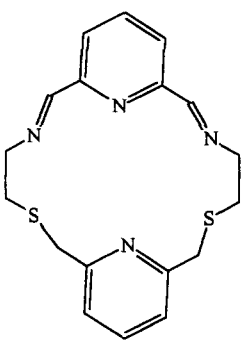


atam

43



44a



44b

3.4. *Oxygen donor macrocyclic ligands*

The structure of the complex [Pb(15-C-5)(SCN)$_2$] has been shown in the crystal structure to comprise two distinct types of coordinated lead(II). In one, the lead is octacoordinate binding five oxygens from the crown ether and three thiocyanato N atoms, the second being similarly bound to the crown ether and one thiocyanato N and two thiocyanato S atoms [64]. IR studies of the prepared complex in the solid state show bands consistent with this change in going from S- to N- bound thiocyanates [64]. Single crystal X-ray structures of the complexes [Pb18-C-6(SCN)$_2$], and [Pb(*cis-anti-cis*dicyclohexyl 18-C-6(SCN)$_2$] were reported along with spectroscopically characterised [Pb(*cis-syn-cis*dicyclohexyl 18-C-6(NCS)$_2$] [65]. In both structures the lead(II) exists in a hexagonal bipyramidal array, with the macrocycle describing the median plane. For [Pb(*cis-anti-cis*dicyclohexyl 18-C-6(SCN)$_2$] both thiocyanate groups are monodentate S bound, whereas in [Pb18-C-6(SCN)$_2$] one is monodentate S bound, the other monodentate N bound [65].

The complex formed from lead(II) acetate and 18-C-6 has also been investigated in the solid state, revealing a somewhat different configuration [66]. The decacoordinate [Pb18-C-6(CH$_3$CO$_2$)$_2$] has both bidentate acetate groups disposed *cis* on one side of the lead(II) and the hexacoordinate crown ether on the opposite face (cf [Pb(**42**)(NO$_3$)$_2$] (*vide supra*).

Sulfur donor macrocycles based upon trithiacycladecane have been shown to complex lead(II) with moderate stability, although no critical stability data has been reported [67].

4. CONCLUSION

The conclusion that is drawn from the foregoing collection of reported research is that there is a wealth of lead(II) coordination chemistry. It is not bounded by the constraints of a requirement for a particular ligand

conformation, nor by a requirement for a specific donor atom type, forming complexes with coordination number ranging from three to ten, with many donor atom types. The significance that lead has as an environmental contaminant and as a poison to humans ensures its future as a metal of interest to coordination chemists.

REFERENCES

1. H. Schumann, C. Janiak and J. Zuckerman, *Chem. Ber.* 1988, **121,** 207.
2. C. Janiak, H. Schumann, C. Stader, B. Wrackmeyer and J. J. Zuckerman, *Chem. Ber.* 1988, **121,** 175.
3. P. Jutzi, R. Dickbreder and H. Nöth, *Chem. Ber.* 1989, **122,** 865.
4. M. J. Duer, N. A. Page, M. A. Paver, P. R. Raithby, M.-A. Rennie, C. A. Russell, C. Stourton, A. Steiner and D. S. Wright, *J. Chem. Soc., Chem. Comm.* 1995, 1141.
5. N. Kuhn, G. Henkel and S. Stubenrauch, *Angew. Chem. Int. Ed. Engl.* 1992, **31,** 778.
6. D. L. Reger, M. F. Hudd, A. L. Rheingold, and B.S. Haggerty, *J.Am. Chem. Soc.* 1992, **144,** 579.
7. A. Heine, D. Fest, D. Stalke, C. D. Habben, A. Meller and G. M. Sheldrick, *J. Chem. Soc., Chem. Comm.* 1990, 742.
8. H. Chen, R. A. Bartlett, H. V. Rasika Dias, M. O. Olmstead, and P. P. Power, *Inorg. Chem.* 1991, **30,** 3390.
9. A. J. Edwards, M. A. Paver, P. R. Raithby, C. A. Russell and D. S. Wright, *J. Chem. Soc., Chem. Comm.* 1993, 1086.
10. K. Wieghardt, M. Kleine-Boymann, B. Nuber, J. Weiss, L. Zsolnai and G. Huttner, *Inorg. Chem.* 1986, **25,** 1647.
11. L. M. Englehardt, B. M. Furphy, J. McB. Harrowfield, J. M. Patrick, B. W. Skelton and A. H. White, *J. Chem. Soc. Dalton Trans.* 1989, 595.
12. L. M. Englehardt, B. M. Furphy, J. McB. Harrowfield, J. M. Patrick and A. H. White, *Inorg. Chem.* 1989, **28,** 1410.
13. V. N. Kokozay and A. V. Sienkiewicz, *Polyhedron* 1995, **14,** 1547.
14. V. V. Skopenko, V. N. Kokozay, V. R. Polyakov and A. V. Sienkiewicz, *Polyhedron* 1994, **13,** 15.
15. D. A. Smith, S. Sucheck and A. A. Pinkerton, *J. Chem. Soc., Chem. Comm.* 1992, 367.
16. G. K. Hollingshed, G. A. Lawrance, M. Maeder and M. Rossignoli, *Polyhedron* 1991, **10,** 409.
17. H.-J.Buschmann, *Chem. Ber.* 1985, **118,** 3408.
18. A. H. Cowley, D. M. Giolando, R. A. Jones, C. M. Nunn and J. M. Power, *Polyhedron* 1988, **7,** 1909.
19. A. M. Arif, A. H. Cowely, R. A. Jones and J. M. Power, *J. Chem. Soc., Chem. Comm.* 1986, 1446.
20. S. C. Goel, M. Y. Chiang, D.J. Rauscher and W. E. Buhro, *J. Am. Chem. Soc.* 1993, **115,** 160.
21. A. L. Balch and D. E. Oram, *Inorg. Chem.* 1987, **26,** 1906.
22. S. M. Grimes, S. R. Johnston and I. Abrahams, *J. Chem. Soc. Dalton Trans.* 1995, 2081.
23. J. M. Harrowfield, B. W. Skelton and A. H. White, *J. Chem. Soc. Dalton Trans.* 1993, 2011.
24. S. C. Goel, M. Y. Chiang and W. E. Buhro, *Inorg. Chem.* 1990, **29,** 4640.
25. R. Papierink, L. G. Hubert-Pfalzgraf and M. C. Massiani, *Polyhedron* 1991, **10,** 1657.
26. V. Kokozay and A. V. Sienkiewicz, *Polyhedron* 1993, **12,** 2421.
27. M. Veith and J. Hans, *Angew. Chem. Int. Ed. Engl.* 1991, **30,** 878.
28. D. Narinesingh, M. Ramcharitar, L. A. Hall and D. J. Williams, *Polyhedron* 1994, **13,** 45.
29. D. J. Williams, S. J. Maginn and R. J. Davey, *Polyhedron* 1994, **13,** 1683.
30. K. Abu-Dari, F. E. Hahn and K. N. Raymond, *J. Am. Chem. Soc.* 1990, **112,** 1519.
31. A. C. Fabretti, A. Giusti, C. Preti, G. Tosi and P. Zannini, *Polyhedron* 1986, **5,** 871.
32. A. M. Bond, R. Colton and A. F. Hollenkamp, *Inorg. Chem.* 1990, **29,** 1991.
33. H.-U. Hummel and H. Meske, *J. Am. Chem. Soc., Dalton Trans.* 1989, 627.
34. P. A. W. Dean, J. J. Vittal and N. C. Payne, *Inorg. Chem.* 1985, **24,** 3594.
35. R. Grenz, F. Götzfried, U. Nagel and W. Beck, *Chem. Ber.* 1986, **119,** 1217.
36. P. G. Harrison, M. G. Begley, T. Kikabhai, A. T. Steel and M. I. Khalil, *J. Chem. Soc., Dalton Trans.* 1989, 2443.
37. J. S. Casas, A. Castiñeiras, I. Haiduc, A. Sánchez, J. Sordo and E. M. Vásquez-López, *Polyhedron* 1994, **13,** 2873.
38. S. Wang, G. Garzón, C. King, J.-C. Wang and J. P. Fackler, *Inorg. Chem.* 1989, **28,** 4623.
39. P. Bhattacharyya and J. D. Woollins, *Polyhedron* 1995, **14,** 3367.
40. H. U. Hummel, E. Fischer, T. Fischer, D. Gruß, A. Franke and W. Dietzsche, *Chem. Ber.* 1992, **125,** 1565.
41. A. L. Balch, F. Neve and M. O. Olmstead, *Inorg. Chem.* 1991, **30,** 3395.
42. A. L. Balch, V. J. Catalano, M. A. Chatfield, J. K. Nagle, M. O. Olmstead and P. E. Reedy, Jr, *J. Am. Chem. Soc.* 1991, **113,** 1252.
43. M. F. Lappert and P. P. Power, *J. Chem. Soc., Dalton Trans.* 1985, 51.
44. A. Andrés, A. Bencini, A. Carachalios, A. Bianchi, P. Dapporto, E. García-España, P. Paoletti and P. Paoli, *J. Chem. Soc., Dalton Trans.* 1993, 3507.
45. M. T. S. Amorim, S. Chaves, R. Delgado and J. J. R. Fraústo da Silva, *J. Chem. Soc., Dalton Trans.* 1991, 3065.

46. P. G. Lye, G. A. Lawrence, M. Maeder, B. W. Skelton, H. Wen and A. H. White, *J. Chem. Soc., Dalton Trans.* 1994, 793.
47. R. E. Cramer, K. A. Mitchell, A. Y. Hirazumi and S. L. Smith, *J. Chem. Soc., Dalton Trans.* 1994, 563.
48. A. Bashall, M. McPartlin, B. P. Murphy, D. E. Fenton, S. J. Kitchen and P. A. Tasker, *J. Chem. Soc., Dalton Trans.* 1990, 505.
49. S. Brooker and P. D. Croucher. *J. Chem. Soc., Chem. Comm.* 1993, 1278.
50. H. Adams, N. A. Bailey, D. E. Fenton, R. J. Good, R. Moody and C. O. Rodriguez de Barbarin, *J. Chem. Soc., Dalton Trans.* 1987, 207.
51. S. S. Tandon and V. McKee, *J. Chem. Soc., Dalton Trans.* 1989, 19.
52. M. G. B. Drew, O. W. Howarth, G. G. Morgan and J. Nelson, *J. Chem. Soc., Dalton Trans.* 1994, 3149.
53. M. Tadoroko, H. Okawa, N. Matsumoto, M. Koikawa and S. Kida, *J. Chem. Soc., Dalton Trans.* 1991 1657.
54. P. Clarke, S. F. Lincoln and K. P. Wainwright, *Inorg. Chem.* 1991, **30,** 134.
55. P.-A. Pittet, G. S. Laurence, S. F. Lincoln, M. L. Turonek and K. P. Wainwright, *J. Chem. Soc., Chem. Comm.* 1991, 1205.
56. K. Kumar, M. Magerstädt and O. A. Gansow, *J. Chem. Soc., Chem. Comm.* 1989, 145.
57. K. R. Adams, D. S. Baldwin, P. A. Duckworth, l. F. Lindoy, M. McPartlin, A. Bashall, H. R. Powell and P. A. Tasker, *J. Chem. Soc., Dalton Trans.* 1995, 1127.
58. K. R. Adams, D. S. Baldwin, A. Bashall, L. F. Lindoy, M. McPartlin and H. R. Powell, *J. Chem. Soc., Dalton Trans.* 1994, 238.
59. H.-J. Buschmann, in *Stereochemistry of Organometallic and Inorganic Compounds* (Edited by I. Bernal), **2,** 103, Elsevier, Amsterdam (1987).
60. H.-J. Buschmann, *Thermochim. Acta* 1986, **107,** 219.
61. K. Byriel, K. R. Dunster, L. R. Gahan, C. H. L. Kennard, J. L. Latten, I. L. Swann and P. A. Duckworth, *Polyhedron* 1992, **11,** 1205.
62. D. M. Wambeke, W. Lippens, G. G. Herman, A. M. Goeminne and G. P. Van der Kelen, *Polyhedron* 1992, **11,** 2989.
63. A. Bashall, M. McPartlin, B. P. Murphy, H. R. Powell and S. Waikar, *J. Chem. Soc., Dalton Trans.* 1994, 1383.
64. H. J. Brügge, R. Fäsing, A. Knöchel and W. Dreißig, *Polyhedron* 1985 **4,** 1493.
65. A. Y. Nazarenko and E. B. Rusanov, *Polyhedron* 1994, **13,** 2549.
66. Y.-G. Shin, M. J. Hampden-Smith, T. T. Kodas and E. N. Deusler, *Polyhedron* 1993, **12,** 1453.
67. W. N. Setzer, E. l. Cacioppo, Q. Guo, G. J. Grant, D. D. Kim, J. L. Hubbard and D. G. VanDerveer, *Inorg. Chem.* 1990, **29,** 2672.

Pergamon

PII: S0277-5387(96)00333-6

Polyhedron Vol. 16, No. 4, pp. 567–572, 1997
Copyright © 1996 Elsevier Science Ltd
Printed in Great Britain. All rights reserved
0277-5387/97 $17.00+0.00

Complexes of lead(II) and lanthanide(III) ions with a macrocyclic ligand containing a furan head unit. Crystal structure of a methanol inclusion compound of a novel macrocycle

Harry Adams,[a] Rufina Bastida,[b]* Andres de Blas,[c] Marina Carnota,[c] David E. Fenton,[a] Alejandro Macías,[b] Adolfo Rodriguez[b] and Teresa Rodriguez-Blas[c]

[a]Department of Chemistry, The University, Sheffield S3 7HF, U.K.

[b]Departamento de Química Inorgánica, Universidad de Santiago de Compostela, Avda. de las Ciencias s/n, 15706 Santiago de Compostela, Spain

[c]Departamento de Química Fundamental e Industrial, Universidad de La Coruña, Campus de la Zapateira s/n, 15071 La Coruña, Spain

(Received 14 June 1996; accepted 2 July 1996)

Abstract—A Schiff-base polyoxaazamacrocycle derived from 2,5-diformylfuran and 1,5-bis(2-aminophenoxy)-3-oxapentane was obtained by a template procedure as mononuclear lanthanide(III) and lead(II) complexes. In the absence of the metal salt the macrocycle was not formed. The complexes were characterized by elemental analysis, molar conductivity, mass spectrometry and IR, ^{1}H NMR and ^{13}C NMR spectroscopy. The reduction of the Pb^{II} complex with sodium borohydride yielded a novel polyoxaazamacrocycle containing a furan head and aromatic lateral units; the X-ray crystal structure of its methanol inclusion compound is reported.
Copyright © 1996 Elsevier Science Ltd

Keywords: template synthesis; lanthanide(III) complexes; polyoxaazamacrocycle; Schiff base; inclusion compound; X-ray crystal structure.

The coordination chemistry of macrocyclic ligands is a fascinating area which has attracted the attention of inorganic chemists. Macrocyclic ligands form stable complexes with lanthanides and they serve as a springboard to explore the coordination chemistry of these metal ions. The ability of lanthanide(III) metal ions to promote the Schiff-base condensation of the appropriate diamine and dicarbonyl precursors, resulting in the formation of metal complexes of otherwise inaccessible macrocyclic ligands, is well established [1,2].

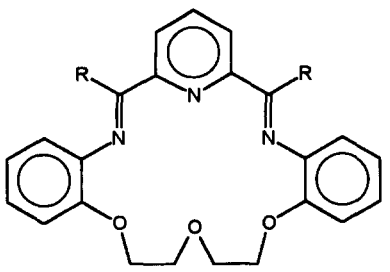
In previous papers [3,4] we have reported the template synthesis of lanthanide(III) complexes of polyoxaaza Schiff-base macrocycles containing aromatic, head and lateral units (L^1, L^2). Herein, we describe an extention of the investigation of the Ln^{III}-promoted synthesis to the macrocycle L^3, which contains a furan head unit, instead of pyridine. In addition, using lead as the templating agent, we have prepared the corresponding complex of L^3 which can be reduced in order to obtain the novel polyoxaazamacrocycle, L^4.

* Author to whom correspondence should be addressed.

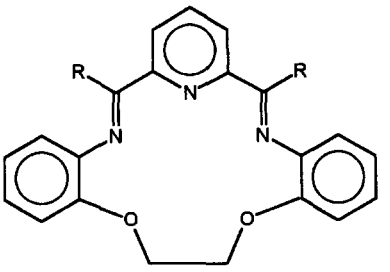
EXPERIMENTAL

Measurements

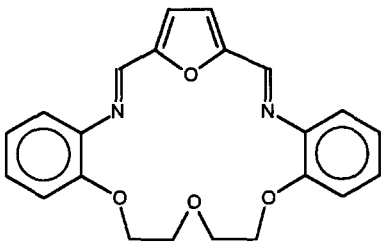
Elemental analyses, ^{1}H and ^{13}C NMR and mass spectra were carried out by Servicios Generales de Apoyo a la Investigación de la Universidad de La Coruña: elemental analyses were carried out on a Carlo Erba EA 1108 elemental analyser; ^{1}H and ^{13}C NMR spectra were recorded using a Bruker AC 200 F spectrometer and FAB-mass spectra using a Fisons



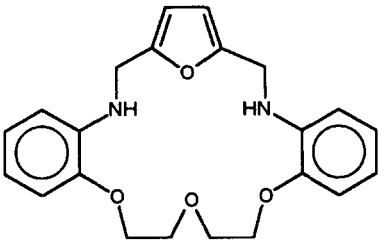
L1 a) R = H b) R = Me



L2 a) R = H b) R = Me



L3



L4

Quattro mass spectrometer with 3-nitrobenzyl alcohol as the matrix. The IR spectra were recorded, as KBr discs, using a Perkin–Elmer 1330 spectrophotometer.

Conductivity measurements were carried out in 10^{-3} mol.dm^{-3} dimethylformamide solutions at 20°C using a Crison Micro CM 2201 conductivimeter.

Chemicals and starting materials

2,5-Diformylfuran was prepared according to the literature method [5], and 1,5-bis(2-aminophenoxy)-3-oxapentane was prepared by reduction of the corresponding dinitro precursor [3]. Metal salts were commercial reagents from Aldrich and Alfa Laboratories, used without further purification. Solvents were of reagent grade purified by the usual methods.

Condensation between 2,5-diformylfurane and 1,5-bis(2-aminophenoxy)-3-oxapentane in the absence of metal ions

A methanolic solution of 1,5-bis(2-aminophenoxy)-3-oxapentane (1 mol in 20 cm^3) was added dropwise to methanolic solution of 2,5-diformylfuran (1 mmol in 25 cm^3) with stirring and heating. The solution was gently refluxed with magnetic stirring for *ca* 18 h. The solid was filtered off and washed with diethyl ether and air dried. No identifiable product could be isolated.

Reaction of 2,5-diformylfurane and 1,5-bis(2-aminophenoxy)-3-oxpentane in the presence of lanthanide(III) ions

To a refluxing solution of 2,5-diformylfuran (1 mmol) in methanol (50 cm^3) was added a solution of hydrated lanthanide nitrate (1 mmol) in methanol (25 cm^3). The solution was stirred vigorously and heated while a methanolic solution of 1,5-bis(2-aminophenoxy)-3-oxapentane (1 mmol in 50 cm^3) was slowly added. After the addition was complete, the resulting solution was refluxed for *ca* 24 h. The brown powder precipitated was filtered off, washed with diethyl either and dried *in vacuo* (Ln = La, Ce). The complexes of Nd, Eu, Ho, Pr, Sm and Gd were recovered from the resulting solution after evaporation and addition of diethyl ether.

All products appear to be air stable and are soluble in dimethylformamide.

Reaction of 2,5-diformylfurane and 1,5-bis(2-aminophenoxy)-3-oxapentane in the presence of lead(II) perchlorate

To a refluxing solution of 2,5-diformylfuran (1 mmol) in methanol (50 cm^3) was added a solution of hydrated lead(II) perchlorate (1 mmol) in methanol (50 cm^3). The solution was stirred vigorously and heated while a methanolic solution of 1,5-bis(2-aminophenoxy)-3-oxapentane (1 mmol in 50 cm^3) was slowly added. Reflux was maintained for *ca* 24 h. After filtration, the lead complex was recovered from the solution. M.p.: 245–250°C. (decomp.) Found: C, 32.0; H, 2.5; N, 3.8%. Calc. for $[PbL^3](ClO_4)_2 \cdot H_2O$: C, 33.0; H, 2.7; N, 3.5%.

Preparation of the reduced Schiff base macrocycle L^4

To a refluxing solution of 2,5-diformylfuran (2 mmol) and hydrated lead nitrate (2 mmol) in meth-

anol (125 cm^3) was slowly added a methanolic solution of 1,5-bis(2-aminophenoxy)-3-oxapentane (2 mmol in 50 cm^3). After the addition was complete, the resulting solution was refluxed for *ca* 24 h. The lead–Schiff base complex thus formed was reduced *in situ* with $NaBH_4$. The solid formed was filtered off and extracted with dichloromethane. The filtrate was rotary-evaporated to dryness, dissolved in water, filtered and extracted with dichloromethane.

The product recovered from the CH_2Cl_2 solution was recrystallized from acetonitrile/methanol (5 : 1) to give a methanol inclusion compound of L^4 as pale yellow crystals suitable for X ray diffraction. Yield: 40%. M.p.: 206–207 C. Found: C, 66.9; H, 6.65; N, 6.9. Calc. for $L^4 \cdot CH_3OH$: C, 67.0; H, 6.8; N, 6.8%. ^{13}C NMR [$(CD_3)SO$]: 66.70, 69.05, 108.24, 109.75, 109.85, 116.54, 120.90, 136.93, 145.43, 151.20.

Structure determination of $L^4 \cdot CH_3OH$

Suitable pale yellow single crystals of the methanol inclusion compound of L^4 were obtained by cooling an acetonitrile/methanol (5 : 1) solution.

Crystal data. $C_{23}H_{28}N_2O_5$; M = 412.47. Crystallizes as pale yellow oblongs; crystal dimensions $0.48 \times 0.23 \times 0.23$ mm^3. Orthorhombic, $a = 20.808(6)$, $b = 15.212(4)$, $c = 6.641(2)$ Å, $U = 2102.1(10)$ $Å^3$, $Z = 4$, $D_c = 1.303$ g cm^{-3}, space group *Pnma* (D_h^{16}, No. 62), Mo-K_α radiation ($\lambda = 0.71073$ Å), μ(Mo-K_α) = 0.092 mm^{-1}, $F(000) = 880$.

Data collection and processing. Three-dimensional, room temperature X-ray data were collected in the range $3.5 < 2\theta < 45$ on a Nicolet R3 diffractometer by the ω scan method. Of the 1997 reflections measured, all of which were corrected for Lorentz and polarization effects (but not for absorption), 1092 independent reflections exceeded the significance level $|F|/\sigma(|F|) > 4.0$. The structure was solved by direct methods and refined by full-matrix least-squares methods on F^2. Hydrogen atoms were included in calculated positions and refined in riding mode. Refinement converged at a final $R = 0.0488$ ($wR_2 = 0.1366$, for all unique 1438 data, 142 parameters, mean maximum δ/σ 0.000, 0.000), with allowance for thermal anisotropy of all non-hydrogen atoms. Minimum and maximum final electron density: 0.237 and 0.299 e $Å^{-3}$. A weighting scheme $w = 1/[\sigma^2(F_o^2) + (0.0768*P)^2 + 0.2855*P]$ where $P = (F_o^2 + 2*F_c^2)/3$ was used in the latter stages of refinement. Complex scattering factors were taken from the program package SHELXL93 [6] as implemented on the Viglen 486dx computer. Bond lengths and angles, with estimated standard deviations, are listed in Table 1.

Anisotropic thermal vibrational parameters with e.s.d.s., atom position parameters and observed structure amplitudes and calculated structure factors have been deposited at the Cambridge Crystallographic Data Centre.

RESULTS AND DISCUSSION

Complexes of lanthanides with L^3

The reaction between furan-2,5-dicarbaldehyde and 1,5-bis(2-aminophenoxy)-3-oxapentane in a 1 : 1 molar ratio in methanol yields a garnet coloured solid which appears to be a mixture of monomeric and possible polymeric products. We have previously found that lanthanide(III) ions can act as effective templates in the formation of oxaaza Schiff base macrocycles derived from 1,5-bis(2-aminophenoxy)-3-oxapentane and 2,6-diformyl- and 2,6-diacetylpyridine [3,4] and Fenton and co-workers have studied the complexation of L^3 with alkaline earth metals, proving that the higher alkaline earth ions (Ca^{2+}, Sr^{2+} and Ba^{2+}) can act as effective templates in the formation of this macrocycle [7,8]. Owing to the similar radii of lanthanide and alkaline earth metal cations it was therefore of interest to investigate the potential application of lanthanide ions as templating ions for the formation of L^3.

When a 1+1 condensation between equimolar amounts of 2,5-diformylfuran and 1,5-bis(2-aminophenoxy)-3-oxapentane was carried out in the presence of hydrated lanthanide(III) nitrates in refluxing methanol for *ca* 24 h, complexes of L^3 with La^{3+}, Ce^{3+}, Nd^{3+}, Eu^{3+} and Ho^{3+} in 1 : 1 ratio were formed in good yields (Table 2).

The complexes were characterized by elemental analysis (C, H, N), molar conductance, mass spectrometry and IR spectroscopy. The analytical and conductivity data are presented in Table 2. The former are consistent with the general formula $[LnL^3][NO_3]_3 \cdot xH_2O \cdot yEt_2O$. The conductivity data in dimethylformamide (dmf) are in the range reported [9] for 2 : 1 electrolytes in this solvent for lanthanum and cerium compounds, and in the range reported [9] for 1 : 1 electrolytes for the europium and holmium complexes. The sparing solubility of the neodymium complex in different solvents restricted the conductivity measurements.

All the complexes have similar IR spectra (Table 3), indicating that they have similar structures. The absence of carbonyl and amine bands, together with the appearance of an imine band at *ca* 1615 cm^{-1}, indicates that condensation and cyclization has occurred [10]. Information about the bonding mode of the nitrate ions may also be obtained from the IR spectra. The free nitrate ion has relatively high symmetry (D_{3h}). When a nitrate ion becomes coordinated in monodentate, bidentate or bridged fashion its effective symmetry is reduced to only C_{2v} or C_s. This causes the degeneracies to split and all modes to be infrared active. Hence, it is possible to distinguish between ionic and coordinated nitrate groups [11]. The presence of a band at 1384 cm^{-1} is characteristic of ionic nitrate present in the outer coordination sphere [12]. The absorption bands occurring in the regions 1466–1452, 1294–1288 and 1040–1030 cm^{-1}

Table 1. Bond lengths (Å) and angles (°) for $L \cdot CH_3OH$

N(1)—C(6)	1.379(3)	N(1)—C(7)	1.454(3)
O(1)—C(8)	1.375(3)	O(2)—C(1)	1.387(3)
O(2)—C(9)	1.424(3)	O(3)—C(10)	1.431(3)
C(1)—C(2)	1.370(4)	C(1)—C(6)	1.414(4)
C(2)—C(3)	1.399(4)	C(3)—C(4)	1.361(4)
C(4)—C(5)	1.385(4)	C(5)—C(6)	1.397(4)
C(7)—C(8)	1.486(4)	C(8)—C(11)	1.339(4)
C(9)—C(10)	1.501(4)	C(11)—C(11a)	1.426(6)
O(1S)—C(1S)	1.399(5)		
C(6)—N(1)—C(7)	120.4(2)	C(1)—O(2)—C(9)	117.3(2)
C(2)—C(1)—O(2)	124.5(2)	C(2)—C(1)—C(6)	121.0(3)
O(2)—C(1)—C(6)	114.5(2)	C(1)—C(2)—C(3)	120.4(3)
C(4)—C(3)—C(2)	119.5(3)	C(3)—C(4)—C(5)	120.7(3)
C(4)—C(5)—C(6)	121.2(3)	N(1)—C(6)—C(5)	123.5(3)
N(1)—C(6)—C(1)	119.3(2)	C(5)—C(6)—C(1)	117.2(3)
N(1)—C(7)—C(8)	111.5(2)	C(11)—C(8)—O(1)	109.3(2)
C(11)—C(8)—C(7)	134.2(3)	O(1)—C(8)—C(7)	116.4(2)
O(2)—C(9)—C(10)	109.2(2)	O(3)—C(10)—C(9)	110.1(2)
C(8)—O(1)—C(8a)	107.2(3)	C(10)—O(3)—C(10a)	112.8(3)
C(8)—C(11)—C(11a)	107.1(2)		

Symmetry transformations used to generate equivalent atoms: a; x, $-y+\frac{3}{2}z$.

Table 2. Analytical, yield and molar conductance (in dmf) data for the complexes $[LnL^3][NO_3]_3 \cdot xH_2O \cdot yEt_2O$

			Analysis (%)[a]				
Ln	x	y	C	H	N	Yield (%)	$\Lambda_M/\Omega^{-1}\,cm^2\,mol^{-1}$
La	2	—	35.8 (35.8)	2.7 (3.2)	8.9 (9.5)	64	149.7
Ce	—	—	38.3 (37.6)	2.9 (2.9)	9.9 (9.9)	93	160.8
Nd	—	1.5	41.8 (41.1)	3.7 (4.3)	8.8 (8.6)	17	—
Eu	—	2	42.4 (41.8)	3.9 (4.6)	8.2 (8.1)	13	95.6
Ho	—	2	40.8 (41.1)	3.9 (4.6)	7.9 (8.0)	25	110.8

[a] Required values are given in parentheses.

Table 3. Infrared spectral data (cm^{-1}) for the complexes $[LnL^3][NO_3]_3 \cdot xH_2O \cdot yEt_2O$

Ln	ν (C=N)$_{imine}$	ν (NO_3^-)
La	1612	1462; 1384; 1294; 1032
Ce	1614	1466; 1384; 1294; 1032
Nd	1622	1456; 1384; 1288; 1045
Eu	1616	1454; 1384; 1290; 1051
Ho	1612	1452; 1384; 1290; 1030

are assignable to the ν(N=O), $\nu_a(NO_2)$ and $\nu_s(NO_2)$ vibrations [13] and clearly identify these species as containing coordinated nitrate groups. The two highest frequency bands are separated by *ca* 160 cm^{-1}. This magnitude indicates a strong interaction between oxygen atoms from the nitrate with the lanthanide ions and it is typical of bidentate coordination [14,15].

The FAB-mass spectra of the complexes show the peak corresponding to the free macrocycle L^3 at m/z 377, which confirms the monomeric [1 + 1] nature of the ligand. The mass spectrum of the holmium complex shows a peak corresponding to $[HoL^3(NO_3)_2]^+$ at m/z 666.

Even though the presence of the lighter lanthanide(III) ions is essential for the formation of the diimine macrocycle L^3, the corresponding complexes seems to lose the metal very easily. When the complexes are dissolved in dimethyl sulfoxide, a precipitate is observed in a few minutes and the ^1H and ^{13}C NMR spectra of all resultant solutions are identical and correspond to the free macrocycle L^3: δ_H 3.89 (t, 4 H, —CH_2—O), 4.22 (t, 4 H, —CH_2—O), 6.96–7.38 (m, 10 H, furan H and aryl H), 8.60 (s, 2 H, CH=N) and δ_C 68.96, 70.20, 115.19, 117.38, 118.09, 121.52, 128.19, 138.88, 144.00, 153.44, 153.75.

Condensation between equimolar amounts of 2,5-diformylfuran and 1,5-bis(2-aminophenoxy)-3-oxapentane in the presence of praseodymium, samarium and gadolinium nitrates yielded products whose

elemental analyses (Table 4) agreed with the general formula $[Ln(L^3)_2](NO_3)_3 \cdot xH_2O \cdot yEt_2O$. The IR spectra show bands corresponding to imine and nitrates in the same range as was found for the La, Ce, Nd, Eu and Ho complexes. The FAB-mass spectra show the peak corresponding to the free macrocycle L^3 at *m/z* 377. The behaviour in dimethyl sulfoxide is similar to that found for the complexes of La, Ce, Nd, Eu and Ho, and the NMR spectra correspond to the free macrocycle L^3 (no signals of dialdehyde and amine are observed). From this, it seems that Pr, Sm and Gd also act as templates in the formation of L^3.

Complex of lead with L^3

Condensation between equimolar amounts of 2,5-diformylfuran and 1,5-bis(2-aminophenoxy)-3-oxapentane in the presence of lead(II) perchlorate in refluxing methanol for *ca* 24 h yielded a complex with formula $[PbL^3](ClO_4)_2 \cdot H_2O$. The presence of the imine band at 1620 cm^{-1}, together with the absence of carbonyl and amine bands in the IR spectrum indicated that condensation and cyclization had occurred. Bands attributable to perchlorate appear at 1120 and 630 cm^{-1}.

Table 4. Analytical data (%)[a] for the complexes $[Ln(L^3)_2][NO_3]_3 \cdot xH_2O \cdot yEt_2O$

Ln	*x*	*y*	C	H	N
Pr		1	50.2 (50.0)	4.6 (4.3)	8.9 (8.5)
Sm	1	—	47.7 (47.7)	4.2 (3.8)	8.3 (8.8)
Gd	—	2	53.0 (52.1)	4.5 (4.8)	8.3 (7.9)

[a] Required values are given in parentheses.

The FAB-mass spectrum of the complex exhibits a peak corresponding to the free macrocycle, as well as a peak at *m/z* 683 which corresponds to $[PbL^3(ClO_4)]^+$.

Unlike the lanthanide complexes, the lead compound does not undergo demetallation in dimethyl sulfoxide and the ^1H NMR spectrum shows signals at δ 3.93 (4 H, $-CH_2-O$), 4.28 (t, 4H, $-CH_2-O$), 7.03–7.45 (m, 10 H, furan H and aryl H), 8.87 (s, 2 H, CH=N). When this spectrum is compared with the one for the free macrocycle, some changes in the chemical shifts are observed: the most important one occurs for the imine proton signal which is shifted downfield by *ca* 0.27 ppm. The ^{13}C NMR spectrum exhibits signals at δ 67.34, 69.92, 113.76, 118.60, 119.44, 121.62, 129.03, 145.61, 153.17, 153.41.

Reduction of the lead(II) complex $[PbL^3]^{2+}$ with sodium borohydride yielded a novel polyoxaazamacrocycle, L^4, whose IR spectrum did not show the band attributable to the imine bond but displayed bands attributable to >NH groups.

Crystal structure of $L^4 \cdot CH_3OH$

Single crystals of this macrocycle, as a methanol inclusion compound, suitable for X-ray analysis were obtained on cooling an acetonitrile/methanol (5:1) solution. The crystal structure is shown in Figs 1 and

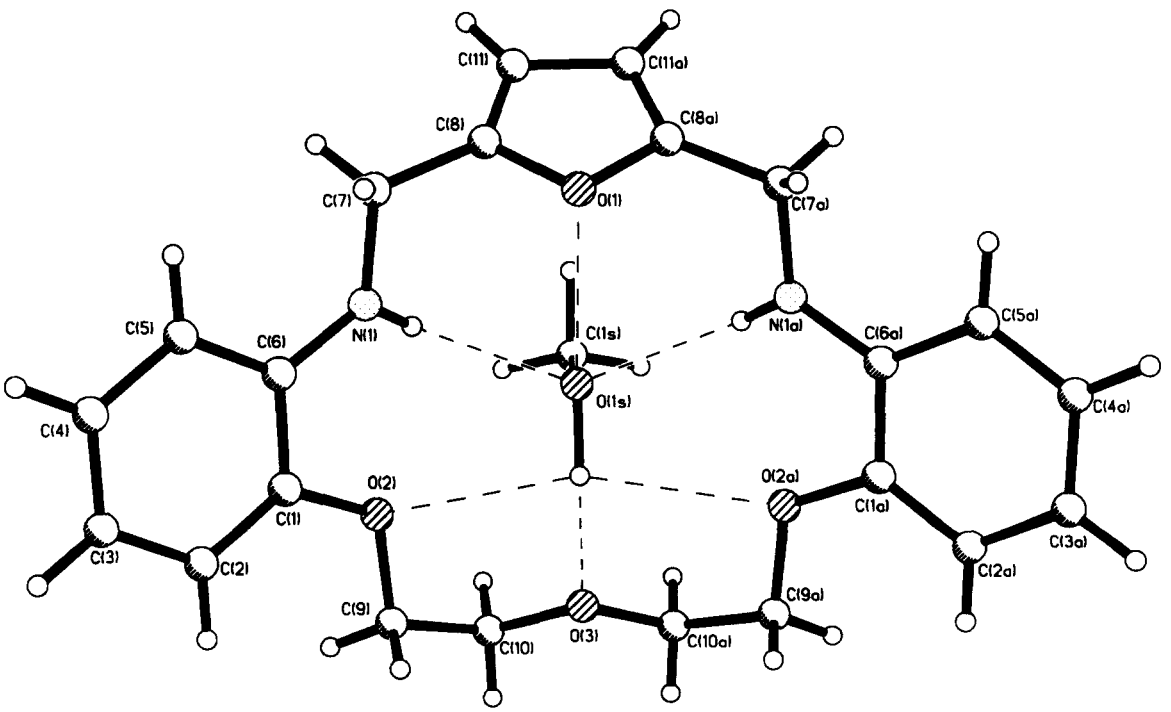


Fig. 1. Top view of the molecular structure of the methanol inclusion.

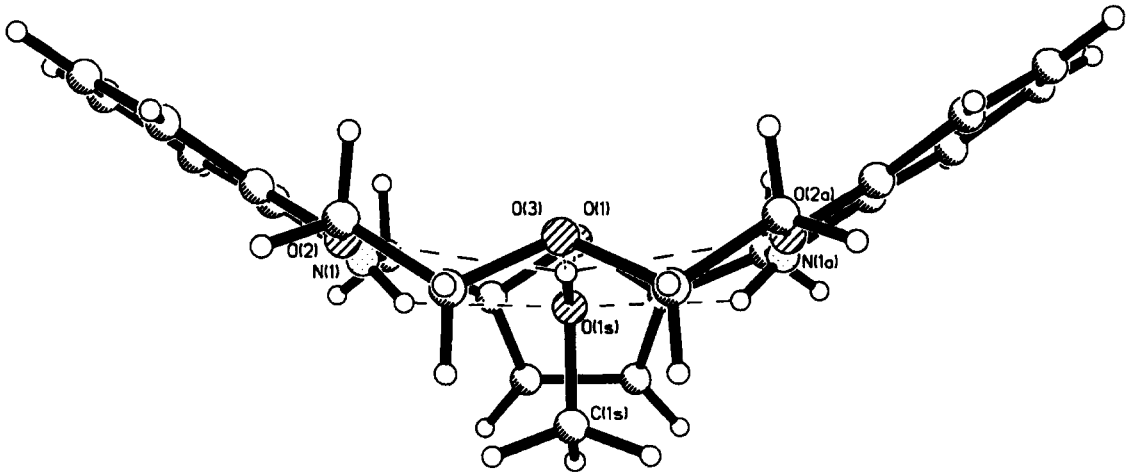


Fig. 2. Side view of the host–guest unit.

2. The molecular geometry is characterized by a crystallographic mirror plane running through O(3) and dividing the furan ring. Heteroatoms are coplanar and the furan ring and both of the benzene nuclei are bent towards opposite sides of the assumed plane, probably to avoid steric overcrowding. The guest methanol is involved in a strong, almost linear, hydrogen bonding interaction between the central oxygen of the polyether chain and the guest hydroxyl [O(1s)···O(3) 2.796, HO(1s)···O(3) 1.667, O(1s)···HO(1s)···O(3) 172.2°] and seems to be involved with both NH groups of the host and the guest oxygen [O(1s)···N(1) 2.956, O(1s)···HN(1) 2.200 Å, O(1s)···HN(1)···N(1) 141°].

The perfect accommodation of the guest methanol by the host molecule is also obvious from steric reasons; that is, the "endo" orientation of the lipophilic methyl group with respect to the host cavity.

The ^{1}H NMR spectrum of a dimethyl sulfoxide solution, derived from the crystals from which the X-ray sample was selected, show peaks corresponding to the macrocycle at δ 3.80 (d, 4 H, —CH_2—N), 4.10 (t, 4 H, —CH_2—O), 4.21 (t, 4 H, —CH_2—O), 4.62 (t, 2 H, —NH), 6.34 (s, 2 H, furan H), 6.60 (m, 4 H, aryl H), 6.80 (m, 4 H, aryl H), together with a doublet centred at δ 3.158 due to the methyl group of the methanol.

Any attempt to prepare complexes of this macrocycle with lanthanide(III) nitrates by direct reaction of the lanthanide salt with L^4 in acetonitrile or methanol were unsuccessful.

Acknowledgements—We thank La Xunta de Galicia (XUGA 20903B94) and Universidad de La Coruña for financial support.

REFERENCES

1. D. E. Fenton and P. A. Vigato, *Chem. Soc. Rev.* 1988, **17,** 69.
2. L. M. Villarino, *J. Less-Common. Met.* 1989, **149,** 21.
3. R. Bandín, R. Bastida, A. de Blas, P. Castro, D. E. Fenton, A. Macías, A. Rodriguez and T. Rodriguez, *J. Chem. Soc., Dalton Trans.* 1994, 1185.
4. R. Bastida, A. de Blas, P. Castro, D. E. Fenton, A. Macías, R. Rial, A. Rodriguez and T. Rodríguez-Blas, *J. Chem. Soc., Dalton Trans.* 1996, 1493.
5. A. F. Oleinik and Yu, Novitskii, *J. Org. Chem. USSR* 1970, **6,** 2643.
6. G. M. Scheldrick, *SHELXL*93, *An integrated system for solving and refining crystal structures from diffraction data* (*Revision* 5.1), University of Gottingen, Germany (1993).
7. D. E. Fenton, D. H. Cook, I. W. Nowell and P. E. Walker, *J. Chem. Soc., Chem. Commun.* 1977, 623.
8. D. H. Cook and D. E. Fenton, *J. Chem. Soc., Dalton Trans.* 1979, 810.
9. W. J. Geary, *Coord. Chem. Rev.* 1971, **7,** 81.
10. S. C. Cummings and D. H. Busch, *J. Am. Chem. Soc.* 1970, **92,** 1924.
11. W. T. Carnall, S. Siegel, J. R. Ferrano, B. Tani and E. Gebert, *Inorg. Chem.* 1973, **12,** 560.
12. D. S. Kumar and V. Alexander, *Inorg. Chim. Acta* 1995, **238,** 63.
13. K. Nakamoto, *Infrared and Raman Spectra of Inorganic and Coordination Compounds*, 3rd edn. Wiley-Interscience, New York (1977).
14. P. Guerriero, U. Casellato, S. Tamburini, P. A. Vigato and R. Graziani, *Inorg. Chim. Acta* 1987, **129,** 127.
15. J. H. Forsberg and T. Moeller, *Gmelin Handbook. Anorg. Chem.*, Part D1. Springer-Verlag, Berlin (1980).

Pergamon

PII: S0277-5387(96)00334-8

Polyhedron Vol. 16, No. 4, pp. 573–576, 1997
Copyright © 1996 Elsevier Science Ltd
Printed in Great Britain. All rights reserved
0277-5387/97 $17.00+0.00

Molecular adducts of diorganotin dichloride with *N*-(2-oxidoarylideneaminoacidato) diorganotin(IV) complexes. Crystal structure of $[Ph_2Sn(2\text{-}OC_{10}H_6CH{=}NCH_2COO)]SnPh_2Cl_2$

Lian Ee Khoo,[a]* Yan Xu,[a] Ngoh Khang Goh,[a] Lian Sai Chia[a] and Lip Lin Koh[b]

[a]National Institute of Education, Nanyang Technological University, 469 Bukit Timah Road, 259756 Singapore, Singapore

[b]Chemistry Department, National University of Singapore, Lower Kent Ridge Road, 119260 Singapore, Singapore

(Received 14 June 1996; accepted 2 July 1996)

Abstract—Three new dinuclear tin complexes, $[Me_2Sn(2\text{-}OC_6H_4CH{=}NCH\{Pr^i\}COO)]SnMe_2Cl_2$ (**1**), $[Me_2Sn(2\text{-}OC_{10}H_6CH{=}NCH_2COO)]SnMe_2Cl_2$ (**2**) and $[Ph_2Sn(2\text{-}OC_{10}H_6CH{=}NCH_2COO)]SnPh_2Cl_2$ (**3**), were prepared and characterized by spectroscopic studies and elemental analyses as a 1 : 1 adduct between diorganotin dichloride (acceptor) and bicycloazastannoxide (donor). A full X-ray crystal structure analysis was performed on **3** and the results confirmed that the donor and the acceptor moieties of **3** are bonded with an Sn—O bond distance of 2.307 Å. Copyright © 1996 Elsevier Science Ltd

Keywords: X-ray structure; diorganotin(IV) complexes; spectroscopic studies.

The chemotherapeutic properties, especially the anti-tumour activities of diorganotins, continue to be the focus of many reports [1,2]. Recent studies have shown that many diorganotin(IV) compounds exhibit anti-tumour activity against human tumour cell lines: in particular the symmetric diorganotin diesters [3] derived from iminodiacetic acid and 2,6-pyridinedicarboxylic acid, as well as the bicyclic diorganotin monocarboxylates [4] like dialkyltin derivatives of dipeptides.

In addition to this biological activity, diorganotin carboxylates are of interest for structural reasons [5]. Dimethyltin iminodiacetate monohydrate [6] and bis[aquadi-n-butyl(2,6-pyridine-dicarboxylato)tin (IV)] [7], both analogues of bicyclic diorganotin dicarboxylates, were reported to crystallize as dimers, with a seven-coordinate distorted pentagonal bipyramidal structure around the tin atom. In contrast, the bicyclic diorganotin monocarboxylates, like dialkyltin diglycylglycinates [4,8] and diorgano(*N*-arylidene-α-aminoacidato)tin(IV) complexes [9–11], were reported to be monomeric, with the tin atom in a distorted trigonal bipyramidal geometry and the carboxylate moiety in the tridentate ligand in unidentate mode. In line with these studies on the chemistry of bicycloazastannoxides [9–11] we now report the donating property of the carbonyl oxygen in bicyclic diorganotin monocarboxylates *via* the synthesis and characterization of the molecular adduct between diorganotin dichloride and *N*-(2-oxidoarylideneaminoacidato)diorganotin(IV). The results of a full X-ray structural analysis of $[Ph_2Sn(2\text{-}OC_{10}H_6CH{=}NCH_2COO)]SnPh_2Cl_2$, a new dinuclear tin adduct, are also presented.

EXPERIMENTAL

Carbon, hydrogen and nitrogen analyses were performed in the Schwarzkopf Microanalytical Labora-

* Author to whom correspondence should be addressed.

tory, Woodside, New York, U.S.A. The ^1H and ^{13}C NMR spectra of the samples dissolved in $CDCl_3$ were recorded on a Jeol FX90 MHz spectrometer with TMS as internal standard. IR spectral data of the compounds were recorded using a Perkin–Elmer model 1725 FT-IR spectrometer in the frequency range 4000–450 cm^{-1}. About 5 mg of sample were used for the preparation of KBr disks and 2–10 scans were accumulated for an FT-IR spectrum.

Diphenyltin dichloride was recrystallized in hexanes, and dimethyltin dichloride from Aldrich Chemical Co. was used without purification. Diorgano(*N*-arylidene-α-aminoacidato)tin(IV) were prepared according to published procedures [9–11].

Preparation of the 1 : 1 *adduct of diorgano*(N-*arylidene-α-aminoacidato*)*tin*(IV) *and diorganotin dichloride*

(*a*) $[Me_2Sn(2\text{-}OC_6H_4CH{=}NCH\{Pr^i\}COO)]SnMe_2Cl_2$ (**1**). To $Me_2Sn(2\text{-}OC_6H_4CH{=}NCH\{Pr^i\}COO)$ (0.43 g, 1.1 mmol) in benzene (7 cm^3) was added dimethyltin dichloride (0.26 g, 1.1 mmol) in cm^3 benzene (3 cm^3). The mixture was heated to boiling (2 min). On cooling, petroleum ether (b.p. 60–80°C) was added dropwise until the solution turned turbid (10 cm^3). In the freezer, a yellow solid (0.6 g, 86% yield) was deposited which was recrystallized from benzene/hexanes to give the 1 : 1 adduct, $[Me_2Sn(2\text{-}OC_6H_4CH{=}NCH\{Pr^i\}COO]SnMe_2Cl_2$, m.p. 135–135°C. Found: C, 32.6; H, 4.13; N, 2.5. Calc. for $C_{16}H_{25}Cl_2NO_3Sn_2$: C, 32.7; H, 4.3; N, 2.4%. IR (cm^{-1}): 1622 $\nu(OCO_{asym})$. ^{13}C NMR: δ 173.06 (COO); 173.55 (CH=N); 73.91 (=NCH—); 2.00, 0.16 ($SnMe_2$); 15.68, 19.02, 18.45 (Pr^i); 168.91, 137.84, 135.97, 122.65, 117.76, 117.40 (aromatic carbons). ^1H NMR: δ 8.41 (CH=N); 3.96 (NCH-$\{Pr^i\}$CO); 2.3–2.5, 1.14, 1.06 ($CHMe_2$); 1.17, 0.83 ($SnMe_2$); 7.9–7.2 (ArH).

(*b*) $[Me_2Sn(2\text{-}OC_{10}H_6CH{=}NCH_2COO)]SnMe_2Cl_2$ (**2**). To a stirred solution of $Me_2Sn(2\text{-}OC_{10}H_6CH{=}NCH_2COO)$ (0.78 g, 2 mmol) in toluene (60 cm^3) was added dimethyltin dichloride (0.50 g, 0.2 mmol) in toluene (30 cm^3). The mixture was heated to boiling and the solvent was removed (*ca* 40 cm^3) by evaporation *in vacuo*. On cooling to 4°C, the yellow adduct, $Me_2Sn(2\text{-}OC_{10}H_6CH{=}NCH_2COO)Me_2SnCl_2$ (1.1 g, 83% yield), m.p. 178–180°C was obtained. Found: C, 34.5; H, 3.8; N, 2.9. Calc. for $C_{17}H_{21}Cl_2NO_3Sn_2$: C, 34.3; H, 3.6; N, 2.4%. IR (cm^{-1}): 1620 $\nu(OCO_{asym})$. ^{13}C NMR: δ 171.68 (COO); 167.20 (CH=N); 57.54 (=NCH_2—); 15.63, 1.18 ($SnMe_2$); 171.43, 139.30, 133.83, 129.33, 128.76, 126.93, 124.46, 123.71, 118.86, 108.32 (aromatic carbons). ^1H NMR: δ 9.23 (CH=N); 4.47 (NCH_2CO); 1.17, 0.83 ($SnMe_2$); 7.9–7.2(ArH).

(*c*) $[Ph_2Sn(2\text{-}OC_{10}H_6CH{=}NCH_2COO)]SnPh_2Cl_2$ (**3**). Preparation of compound **3** was accomplished according to the procedure used for **2**. Diphenyltin dichloride (0.70 g, 2 mmol) and $Ph_2Sn(2\text{-}OC_{10}H_6CH{=}NCH_2COO)$ (1.0 g, 2 mmol) were refluxed in benzene (80 cm^3). The product (1 g, 58% yield) was recrystallized from benzene at room temperature to give crystals of $[Ph_2Sn(2\text{-}OC_{10}H_6CH{=}NCH_2COO)]SnPh_2Cl_2$, m.p. 188–190°C. Found: C, 54.0; H, 3.6; N, 1.9. Calc. for $C_{37}H_{29}Cl_2NO_3Sn_2$: C, 52.7; H, 3.5; N, 1.7%. IR (cm^{-1}): 1618 $\nu(OCO_{asym})$. ^{13}C NMR: δ 172.78 (COO); 166.63 (CH=N); 57.82 (=NCH_2—); 171.52, 140.45, 137.60, 137.23, 136.37, 135.15, 133.69, 131.61, 130.92, 129.61, 129.09, 127.29, 124.57, 124.16, 118.42, 108.48 (aromatic carbons). ^1H NMR: δ 9.18 (CH=N); 4.44 (NCH_2CO); 7.9–7.2 (ArH).

X-ray crystallography of $[Ph_2Sn(2\text{-}OC_{10}H_6CH{=}NCH_2COO)]Ph_2SnCl_2$

Crystal data. $C_{37}H_{29}Cl_2NO_3Sn_2$, F.W. = 843.9, monoclinic, $C2/c$; $a = 27.055(7)$, $b = 16.221(4)$, $c = 17.445(4)$ Å; $\beta = 115.44(4)°$; $D_{calc} = 1.622$ Mg m^{-3}; $F(000) = 3328$; $V = 6914(3)$ $Å^3$; $\mu = 1.64$ mm^{-1} for $Z = 8$. A total of 6296 reflections were collected from a selected single crystal of dimensions $0.30 \times 0.30 \times 0.20$ mm^3 using a Siemens R3M/V2000 diffractometer with Mo-K_α radiation by ω scan (2.50 to 30.00° min^{-1} between $3.0 < 2\theta < 50.0°$). These intensity data were reduced and corrected for Lorentz and polarization factors resulting in a total of 6137 independent reflections. The structure was solved by direct methods [12] and refined by full-matrix least squares on F [the total of observed reflections: 4251 ($F > 4\sigma(F)$)] using SHELXTL PLUS. The tin, carbon, nitrogen, oxygen and chlorine atoms were refined with anisotropic thermal parameters. Hydrogen atoms were placed at calculated positions with assigned isotropic thermal parameters. The final refinement gave $R = 0.042$ and $R_w = 0.050$ (data-to-parameter ratio: 10.4 : 1). Selected bond angles and interatomic distances are listed in Table 1.

Supplementary material, including non-hydrogen and hydrogen atomic coordinates and thermal parameters have been deposited at the Cambridge Crystallographic Data Centre, and observed and calculated structural factors are available upon request from the corresponding author.

RESULTS AND DISCUSSION

The crystal structure of $[Ph_2Sn(2\text{-}OC_{10}H_6CH{=}NCH_2COO)SnPh_2Cl_2$ reveals a monomeric 1 : 1 donor–acceptor dinuclear tin complex (Fig. 1). Each of the two tin atoms, Sn(1) and Sn(2), has a five-coordination geometry in a distorted trigonal bipyramidal arrangement.

The Sn(1) atom lies in the ligand plane and forms a five-membered and a six-membered chelate ring with the ligand. Thus, the two phenyl groups and the imino nitrogen take up the equatorial positions, while the oxygen atoms, O(2) and O(14A), take up the axial

Table 1. Selected bond lengths (Å) and bond angles (°) for $[Ph_2Sn(2\text{-}OC_{10}H_6CH{=}NCH_2COO)]SnPh_2Cl_2$

Sn(1)—N	2.136(5)	N—Sn(1)—O(2)	83.8(2)
Sn(1)—O(2)	2.068(4)	N—Sn(1)—O(14A)	75.8(2)
Sn(1)—O(14A)	2.188(3)	O(2)—Sn(1)—O(14A)	159.5(2)
Sn(1)—C(21)	2.108(8)	N—Sn(1)—C(21)	114.6(2)
Sn(1)—C(31)	2.127(8)	O(2)—Sn(1)—C(21)	95.5(2)
Sn(2)—Cl(1)	2.333(2)	O(14A)—Sn(1)—C(21)	95.2(2)
Sn(2)—Cl(2)	2.477(2)	N—Sn(1)—C(31)	125.8(3)
Sn(2)—O(14)	2.307(4)	O(2)—Sn(1)—C(31)	95.4(2)
Sn(2)—C(41)	2.122(7)	O(14A)—Sn(1)—C(31)	94.5(2)
Sn(2)—C(51)	2.113(8)	C(21)—Sn(1)—C(31)	119.4(3)
N—C(11)	1.295(7)	Cl(1)—Sn(2)—Cl(2)	94.5(1)
N—C(13)	1.458(7)	Cl(1)—Sn(2)—O(14)	83.1(1)
O(2)—C(2)	1.323(8)	Cl(2)—Sn(2)—O(14)	176.6(1)
O(14)—C(14)	1.250(6)	Cl(1)—Sn(2)—C(41)	110.9(2)
O(14A)—C(14)	1.258(7)	Cl(2)—Sn(2)—C(41)	93.8(2)
C(1)—C(2)	1.406(8)	O(14)—Sn(2)—C(41)	89.2(2)
C(1)—C(11)	1.407(7)	Cl(1)—Sn(2)—C(51)	112.3(2)

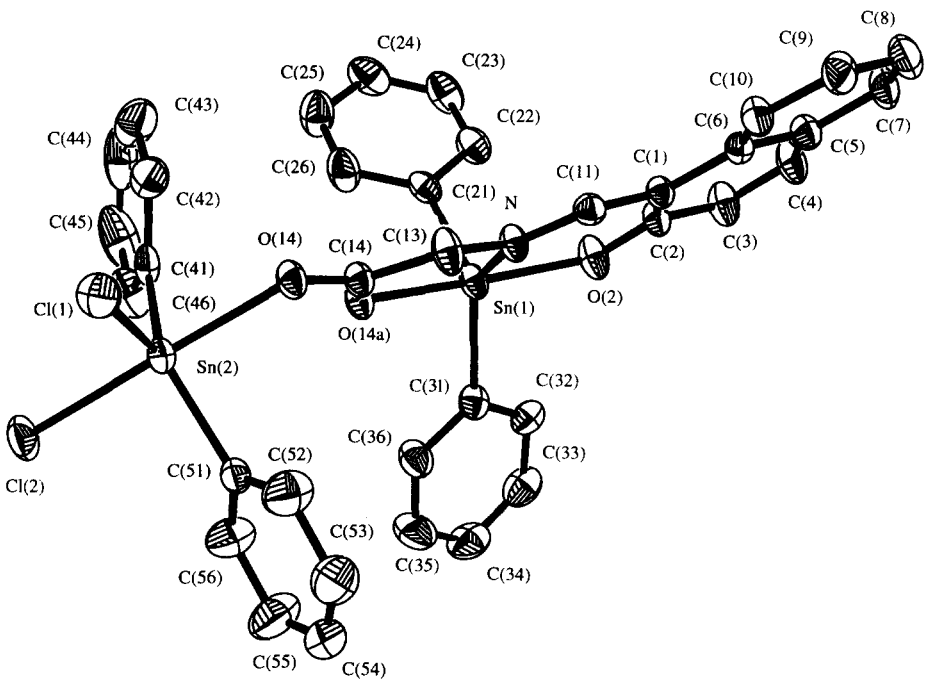


Fig. 1. Molecular structure and crystallographic numbering scheme employed for $[Ph_2Sn(2\text{-}OC_{10}H_6CH{=}NCH_2COO)]SnPh_2Cl_2$.

sites around the Sn(1) atom. The bond lengths and bond angles (Table 1) around the Sn(1) atom, including Sn(1)—N (2.136 Å), Sn(1)—O(2) (2.068 Å); O(2)—Sn(1)—O(14A) (159.5°) and N—Sn(1)—O(14A) (75.8°), remain practically unchanged compared with the donor, $Ph_2Sn(2\text{-}OC_{10}H_6CH{=}NCH_2COO)$ [11].

The Sn(2) atom, which forms the acceptor fragment of the title compound **3**, is bonded to the carbonyl oxygen, O(14), with an Sn(2)—O(14) bond distance of 2.307 Å. Thus, the Sn(2) atom is surrounded by O(14) and Cl(2) along the axial direction while the second chlorine atom, Cl(1), and the *ipso* carbons, C(41) and C(51), of the two phenyl groups form the equatorial plane. The trigonal bipyramidal geometry of Sn(2) is distorted as indicated by bonding angles of 135.6(2), 112.3(2), 110.9(2) and 176.6(1)° for C(41)—Sn(2)—C(51), C(51)—Sn(2)—Cl(1), Cl(1)—Sn(2)—C(41) and Cl(2)—Sn(2)—O(14), respectively.

All the phenyl rings in **3** are nearly planar, with very small deviations of 0.0050(4) for C(21)–C(26),

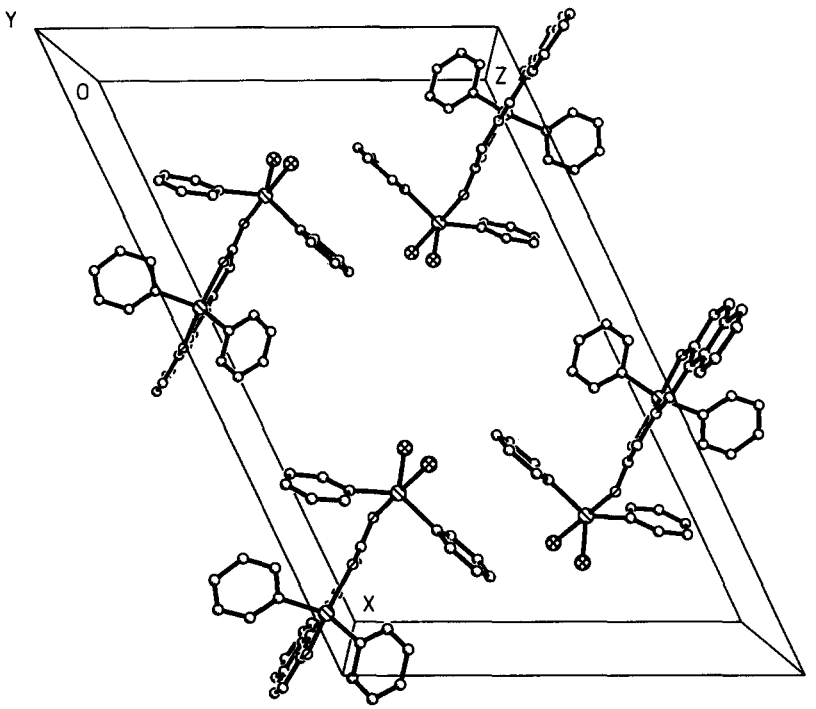


Fig. 2. The packing view of the unit cell of $[Ph_2Sn(2\text{-}OC_{10}H_6CH{=}NCH_2COO)]SnPh_2Cl_2$.

0.0079(5) for C(31)–C(36), 0.0109(6) for C(41)–C(46) and 0.0027(6) for C(51)–C(56). The naphthyl ring formed by C(1)–C(10) is close to coplanar with the O(2), Sn(1), O(14A), C(14), C(13), N and C(11) atoms, with a deviation of 0.0778(4) Å [Sn(1) plane] (Fig. 2). The crystal structure of **3** (Fig. 2) adopts a "butterfly-shape" headed by Sn(2) with the four phenyl rings as the "wings" and the Sn(1) plane as the "body". The dihedral angles between the "body" and the "wings" are 112.7(4) [C(21)–C(26)], −136.2(5) [C(31)–C(36)], 104.1(6) [C(41)–C(46)] and −101.7(6)° [C(51)–C(56)].

The IR carbonyl stretching frequency appears as a strong broad band at 1680 cm^{-1} for $Ph_2Sn(2\text{-}OC_{10}H_6CH{=}NCH_2COO)$ [11] and shifts by 62 cm^{-1} for **3**, confirming the interaction between the Sn and the carbonyl oxygen atoms. Similar shifts were observed for the adducts **1** and **2**. The proton and ^{13}C NMR spectra for **1**, **2**, and **3** are very similar. Compared with their respective donors, a shift in the carbonyl ^{13}C absorption (*ca* 0.3–0.5 ppm) was observed. The marked similarities in the spectra of the three adducts, which have the same stoichiometry and are prepared in like manner, provide strong evidence that they are isostructural with each other.

Acknowledgement—We thank Nanyang Technological University (RP9/92) for financial support.

REFERENCES

1. M. Gielen, *Metal-Based Drugs* 1994, **1**, 213.
2. A. J. Crowe, *Drugs of the Future* 1987, **12**, 40.
3. M. Gielen, M. Bouâlam, A. Meriem, B. Mahieu, M. Biesemans and R. Willem, *Heteroatom Chem.* 1992, **3**, 449.
4. F. Huber, M. Vornefeld, H. Preut, E. von Angerer and G. Ruisi, *Appl. Organomet. Chem.* 1992, **6**, 597.
5. E. R. T. Tiekink, *Appl. Organomet. Chem.* 1991, **5**, 1.
6. F. L. Lee, E. J. Gabe, L. E. Khoo, W. H. Leong, G. Eng and F. E. Smith, *Inorg. Chim. Acta* 1989, **166**, 257.
7. F. Huber, H. Preut, E. Hoffmann and M. Gielen, *Acta Cryst.* 1989, **C45**, 51.
8. F. Huber, H. J. Haupt, H. Preut, R. Barbieri and M. T. Z. Lo Giudice, *Anorg. Allg. Chem.* 1977, **432**, 51.
9. F. E. Smith, R. C. Hynes, T. T. Ang, L. E. Khoo and G. Eng, *Can. J. Chem.* 1992, **70**, 1114.
10. J. T. Wang, Y. W. Zhang, Y. M. Xu and Z. W. Wang. *Heteroatom Chem.* 1992, **3**, 599.
11. F. E. Smith, L. E. Khoo, N. K. Goh, R. C. Hynes and G. Eng, *Can. J. Chem.* in press.
12. G. M. Sheldrick, *SHELXTL PC™ Release* 4.1. Siemens Crystallographic Research Systems, Madison, WI (1990).

Pergamon

PII: S0277-5387(96)00331-2

Polyhedron Vol. 16, No. 4, pp. 577–580, 1997
Copyright © 1996 Elsevier Science Ltd
Printed in Great Britain. All rights reserved
0277-5387/97 $17.00+0.00

Reaction of $[Ru_3(CO)_{12}]$ with 2-(chloromethyl)pyridine, syntheses of pyrid-2-ylacetyl ruthenium(II) complexes and crystal structure of $[RuCl(C_5H_4N\text{-}2\text{-}CH_2CO)(CO)(PPh_3)_2]$

Mayumi Shimizu, Yukio Nakamura* and Makoto Tadokoro

Department of Chemistry, Faculty of Science, Osaka City University, Sugimoto-3, Sumiyoshi-ku, Osaka 558, Japan

(Received 6 June 1996; accepted 1 July 1996)

Abstract—The cycloruthenated pyrid-2-ylacetyl complex $[\{RuCl(C_5H_4N\text{-}2\text{-}CH_2CO)(CO)_2\}_2]$ (**1**) was obtained by reaction of $[Ru_3(CO)_{12}]$ with an excess of 2-(chloromethyl)pyridine in refluxing toluene. Subsequent reaction of **1** with two equivalents of triphenylphosphine in refluxing benzene afforded the bis(phosphine) derivative $[RuCl(C_5H_4N\text{-}2\text{-}CH_2CO)(CO)(PPh_3)_2]$ (**2**). X-ray analysis of **2** shows that the complex is monomeric with the ruthenium atom coordinated by ring nitrogen and acyl carbon atoms from the cycloruthenated pyrid-2-ylacetyl group, *cis* chlorine and carbonyl carbon atoms, and *trans* phosphorus atoms, to form a distorted octahedral geometry. Copyright © 1996 Elsevier Science Ltd

Keywords: ruthemium(II) complex; triruthenium dodecacarbonyl; oxidative addition; nitrogen heterocycle; X-ray structure; 2-(chloromethyl)pyridine.

We have previously studied the reactions of 2-(chloromethyl)- and 2,6-bis(chloromethyl)-pyridine (abbreviated as 2-cmpy and 2,6-cmpy, respectively) with low-valent palladium and rhodium complexes. For example, 2-cmpy reacted with $[Pd(PPh_3)_4]$ to give a C,N-bridged dinuclear complex $[\{PdCl(\mu\text{-}C_5H_4N\text{-}2\text{-}CH_2)PPh_3\}_2]$, [1] while 2,6-cmpy gave a tandem tetranuclear complex $[\{Pd_2Cl(\mu\text{-}Cl)[\mu\text{-}C_5H_3N\text{-}2,6\text{-}(CH_2)_2](PPh_3)_2\}_2]$ in addition to a dinuclear complex analogous to that mentioned above [2]. In the reaction with $[RhCl(PPh_3)_3]$, 2-cmpy afforded C,N-chelated mononuclear complexes *cis* (PP)- and *trans* (PP)-$[RhCl_2(C_5H_4N\text{-}2\text{-}CH_2)(PPh_3)_2]$, whereas 2,6-cmpy gave the corresponding *cis* (PP) and *trans* (PP) complexes or a novel dinuclear complex $[Rh_2Cl_4\{C_5H_3N\text{-}2,6\text{-}(CH_2)_2\}(PPh_3)_2]$ according to the reactant's mole ratio, in which the 2,6-dimethylpyridine-α,α'-diyl ligand is C,N-chelated to one rhodium atom and bound to the second one in an η^3-pseudo-1-aza-allylic fashion [3].

Recently, much attention has been devoted to the reactivities of dodecacarbonyltriruthenium towards N-donor ligands, especially those containing N heterocycles [4]. The reaction of the carbonyl cluster with pyridine gave a cycloruthenated complex $[Ru_3(\mu\text{-}H)(\mu\text{-}C_5H_4N)(CO)_{10}]$ [5]. Similar μ-hydrido-triruthenium cluster complexes have been obtained with 2-aminopyridine [6] and pyridine-2-thiol [7]. Although the reactions with other substituted pyridines, like 2-pyridinecarbinol [8], 2-pyridone [6] and 2-(diphenylphosphino)pyridine [9], have been investigated too, no reactions with halo- and halomethyl-substituted pyridines have been described to our knowledge. Here, we report on the products obtained from reaction of $[Ru_3(CO)_{12}]$ with 2-cmpy, followed by reaction with triphenylphosphine.

EXPERIMENTAL

All the reactions were performed under nitrogen, using solvents that were redistilled under argon. The reagent 2-cmpy was freed from its hydrogen chloride

* Author to whom correspondence should be addressed.

adduct by the action of NEt_3. The carbonyl cluster $[Ru_3(CO)_{12}]$ was purchased from Aldrich Chemical Company Inc. and used without further purification. IR spectra were obtained as Nujol mulls with a JASCO A-702 spectrophotometer. ^1H and ^{13}C NMR spectra were recorded on Jeol JNM GX-400 instrument at 400 and 100 MHz, respectively. ^{31}P NMR spectra were measured using a Jeol α-400 instrument at 24.2 MHz. Internal TMS (^1H, ^{13}C) and external H_3PO_4 (^{31}P) were used as references. FAB-mass spectra were obtained with a Jeol JMS AX-500 spectrometer in the positive-ion mode using 3-NBA as a matrix, dichloromethane as a solvent and xenon as a bombardment gas.

Reaction of $[Ru_3(CO)_{12}]$ *with* 2-cmpy. *Synthesis of* $[\{RuCl(C_5H_4N\text{-}2\text{-}CH_2CO)(CO)_2\}_2]$ (**1**)

To a suspension of $[Ru_3(CO)_{12}]$ (0.31 g, 0.48 mmol) in toluene (10 cm^3) was added 2-cmpy (7.1 mmol), and the mixture was heated at 110°C for 2 h. A wine-red solution was obtained at 90°C and then a precipitate separated out gradually, which was collected, washed with ether and dried *in vacuo*. Yield 0.40 g (89%). Yellow ochre. IR (cm^{-1}): ν(CO) 2020, 1975, 1952, 1930(sh), 1665. ^1H NMR (CD_3CN): δ 4.14, 3.80 (2H, ABq, J = 20.5 Hz, CH_2); Py-ring 7.48 (1H, t, J = 6.7 Hz, H^5), 7.56 (1H, d, J = 7.9 Hz, H^3), 7.97 (1H, t, J = 7.3 Hz, H^4), 8.81 (0.8H, br s, H^6), 9.51 (0.2H, br s. $H^{6'}$). ^{13}C NMR (CD_3CN): δ 63.3 (CH_2); Py-ring 123.7, 124.0 (C^3, C^5), 140.3 (C^4), 150.3 (C^6), 162.6 (C^2). Found: C, 34.3; H, 1.9; N, 4.5: Calc for $C_9H_6ClNO_3Ru$: C, 34.6; H, 1.9; N, 4.5%.

Reaction of **1** *with* PPh_3. *Synthesis of the bis(phosphine) derivative* $[RuCl(C_5H_4N\text{-}2\text{-}CH_2CO)(CO)(PPh_3)_2]$ (**2**)

A suspension of **1** (0.06 g, 0.20 mmol) in benzene (8 cm^3) containing PPh_3 (0.13 g, 0.55 mmol) was heated at 80°C for 2 h. In a few minutes the suspension turned pink. The crude product was filtered, washed with diethyl ether and dried *in vacuo*. Recrystallization from $CHCl_3/Et_2O$ gave **2** (pink). After drying, the residue was redissolved in dichloromethane and diethyl ether was added to reprecipitate **2** (white). Total yield 97%. The pink and white products were the same based on their NMR data. IR (cm^{-1}): ν(CO) 1928, 1605. ^1H NMR ($CDCl_3$): δ 2.96 (2H, s, CH_2); Py-ring 6.37 (1H, triple d, J = 7.3, *ca* 2 Hz, H^5), 6.93 (1H, d, J = 7.3 Hz, H^3), 7.36 (1H, triple d, J = 7.3, *ca* 2 Hz, H^4), 8.21 (1H, d, J = 7.3 Hz, H^6); PPh_3 7.1–7.5. ^{13}C NMR($CDCl_3$): δ 62.1 (CH_2), 120.0 (C^5), 122.7 (C^3), 135.9 (C^4), 152.1 (C^6), 161.2 (C^2); PPh_3 127–135. ^{31}P NMR ($CDCl_3$): δ 32.9. FAB-MS *m/z*: 809 (M^+), 774 ($M-Cl^+$), 746 ($M-Cl-CO^+$), 717 ($M-Cl-2CO^+$). Found: C, 65.2; H, 4.4; N. 1.8. Calc. for $C_{44}H_{36}ClNO_2P_2Ru$: C, 65.3; H, 4.5; N, 1.7%.

X-ray crystallography

Pale yellow crystals of **2**·Et_2O were obtained by slow evaporation from a chloroform/diethyl ether solution. A crystal of appropriate dimensions, $0.40 \times 0.22 \times 0.15$ mm^3, mounted in a glass capillary was used for data collection at a temperature of 23°C on a Rigaku AFC5R diffractometer with graphite-monochromated Cu-K_α (λ = 1.54178 Å) radiation and the ω–2θ scan technique. Accurate cell dimensions and crystal orientation matrices were determined by least-squares refinement of 25 reflections ($57.9 < 2\theta < 59.8°$) for complex **2**·Et_2O. A total of 7041 reflections were collected to a maximum 2θ value of 120.2°; 6710 of them were unique, and of these 4933 were assumed as observed [$I > 3.0\ \sigma\ (I)$], and were used for refinement (506 parameters), converging to R = 0.037 and R_w = 0.048. For all these structures the data were corrected for Lorenz, polarization, and absorption effects. A decay correction was also applied.

The structure of **2**·Et_2O was solved by the heavy-atom Patterson methods (DIRDIF92 PATTY) [10] and expanded using Fourier techniques. All non-hydrogen atoms were refined anisotropically. Hydrogen atoms were located on a ΔF map and refined isotropically. The maximum and minimum peaks on the final difference Fourier map, and goodness-of-fit corresponded to 0.41 and -0.42 $eÅ^{-3}$, and 1.67, respectively. All calculations were performed using the teXsan [11] crystallographic software package.

Crystal data for **2**·Et_2O. Formula = $[C_{44}H_{36}ClNO_2P_2Ru][C_4H_{10}O]$, F.W. = 883.37, monoclinic, space group $P2_1/c$ (No. 14), a = 13.015(4), b = 15.611(3), c = 21.257(3) Å, β = 93.15(2)°, V = 4312(1) $Å^3$, Z = 4, $D_{calc.}$ = 1.360 g cm^{-3}.

RESULTS AND DISCUSSION

Reactions of $[Ru_3(CO)_{12}]$ with an excess of 2-cmpy in refluxing toluene afforded the cycloruthenated dinuclear complex $[\{RuCl(C_5H_4N\text{-}2\text{-}CH_2CO)(CO)_2\}_2]$ (**1**). Complex **1** is insoluble in non-coordinating solvents, but readily dissolves in CH_3CN, from which the complex could not be recovered as a pure solid. Bridge-splitting reaction and subsequent substitution of the one carbonyl group of **1** with triphenylphosphine in a benzene suspension at 80°C gave the monomeric, organic-soluble bis(phosphine) derivative $[RuCl(C_5H_4N\text{-}2\text{-}CH_2CO)(CO)(PPh_3)_2]$ (**2**). Such a substitution of the carbonyl group with triphenylphosphine has been observed in the complexes $[\{RuCl(phpy)(CO)_2\}_2]$ and $[\{RuCl(bzqn)(CO)_2\}_2]$ (Hphpy = 2-phenylpyridine; Hbzqn = benzo[*h*]quinoline) and is explained by the skeletal conjugation of the cyclometalated organic groups [12]. The ^{31}P NMR spectrum of **2** in $CDCl_3$ shows a sharp singlet, and hence the *trans*-bis(phos-

Table 1. Selected bond lengths (Å), bond angles (°) and torsion angles (°)

Ru(1)—Cl(1)	2.549(1)	Ru(1)—P(1)	2.381(1)
Ru(1)—P(2)	2.400(1)	Ru(1)—N(1)	2.163(3)
Ru(1)—C(7)	2.000(4)	Ru(1)—C(8)	1.847(4)
Cl(1)—Ru(1)—P(1)	87.08(4)	Cl(1)—Ru(1)—P(2)	86.40(4)
Cl(1)—Ru(1)—N(1)	88.82(10)	Cl(1)—Ru(1)—C(8)	101.6(1)
P(1)—Ru(1)—N(1)	91.0(1)	P(1)—Ru(1)—C(7)	94.6(1)
P(1)—Ru(1)—C(8)	89.7(1)	P(2)—Ru(1)—N(1)	89.6(1)
P(2)—Ru(1)—C(7)	92.0(1)	P(2)—Ru(1)—C(8)	90.9(1)
N(1)—Ru(1)—C(7)	81.0(2)	C(7)—Ru(1)—C(8)	88.5(2)
Ru(1)—C(7)—C(6)—C(5)	9.4(5)	O(1)—C(7)—Ru(1)—N(1)	176.8(5)
O(1)—C(7)—C(6)—C(5)	−174.3(4)	C(1)—N(1)—Ru(1)—C(7)	−176.5(4)
C(4)—C(5)—C(6)—C(7)	176.3(5)		

phine) structure can be assigned for **2**. The ^{1}H NMR spectrum of **2** in $CDCl_3$ exhibits a sharp singlet assignable to the CH_2 group, indicating that complex **2** has a symmetrical plane including the pyridyl and cycloruthenated rings. Two geometrical isomers of *trans* (N, CO) and *trans* (N, Cl) are possible for **2**. The IR spectrum of this complex exhibits a comparatively low frequency ν(CO) band. This low stretching frequency of the carbonyl group is known to reflect the structure possessing the carbonyl group *trans* to a nitrogen donor ligand [13,14]. X-ray analysis finally established the exact structure of **2** (Fig. 1). Selected bond lengths, bond angles and torsion angles are listed in Table 1.

The structure is monomeric and has a distorted octahedral geometry. The ruthenium atom is coordinated by the N, C (acyl), C (carbonyl) and Cl atoms in an equatorial plane and the two axially situated phosphorus atoms. The pyrid-2-ylacetyl group is cycloruthenated and constitutes a five-membered ring with the ruthenium atom. The pyridyl and cycloruthenated rings are almost coplanar to one another.

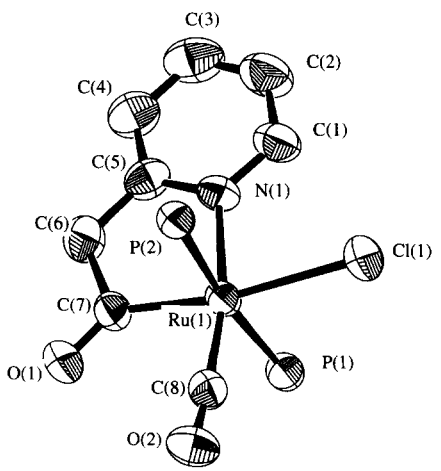
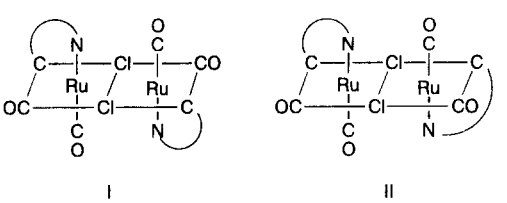


Fig. 1. The crystal structure of **2** with hydrogen and phenyl carbon atoms omitted for clarity. The solvent of crystallization is also omitted.

As is to be expected from the above discussion, the carbonyl group is situated in the position *trans* to the ring nitrogen atom. The bite angle (N(1)—Ru(1)—C(7)) is relatively small and as a result the angle Cl(1)—Ru(1)—C(8) is spread out. Other bond lengths and angles are generally normal. Complex **2** (pink) is photosensitive and turns white gradually when irradiated with the sunlight. It cannot be ruled out that the *trans* (N, CO) to *trans* (N, Cl) isomerization is responsible for this colour change.

The IR spectrum of **1** shows two strong bands in the terminal carbonyl region suggesting a *cis* arrangement of the two carbonyl groups coordinated to each ruthenium atom in the dinuclear complex [12]. The spectrum also shows an additional ν(CO) band at 1665 cm^{-1} indicating the presence of a CH_2CO group formed by cycloruthenation of the pyrid-2-ylmethyl group followed by CO insertion. The presence of the cycloruthenated pyrid-2-ylacetyl group is also shown by the ^{1}H and ^{13}C NMR spectra of **1** in CD_3CN. In addition to these facts and the consideration mentioned above for the structure of complex **2**, the appearance of the two separate signals (approximately 1 : 4 in intensity) which can be assigned to the H^6 pyridyl ring proton, suggests the coexistence of the two kinds of isomers (**I** and **II**) coming from different



arrangements of the other ligands around the metal. Only a few examples of the cyclometalated pyrid-2-ylacetyl complexes have been described to our knowledge: $[PdCl(C_5H_4N\text{-}2\text{-}CH_2CO)(PPh_3)]$ [1a], $[Mn(C_5H_4N\text{-}2\text{-}CH_2CO)(CO)_4]$ [15] and $[Mo(C_5H_4N\text{-}2\text{-}CH_2CO)(\eta^5\text{—}C_5H_5)(CO)_2]$ [15]. All these complexes, as well as **2**, have a symmetrical plane

including the cycloruthenated ring, and hence the methylene protons appeared as a singlet, while those of complex **1** appear as an AB quartet, indicating that the structure of **1** is unsymmetrical about the cycloruthenated ring. The tendency for metal carbonyl anions to form a cyclic derivation on reaction with 2-cmpy is directly related to the tendency for the derivatives formed from the same metal carbonyl anions and acyl halides to undergo decarbonylation on heating or irradiation [15]. Both of these tendencies are thought to be directly related to the strength of the M—CO bond in these compounds [16].

REFERENCES

1. (a) K. Isobe, Y. Nakamura and S. Kawaguchi, *Bull. Chem. Soc. Jpn* 1989, **62,** 1802; (b) K. Nakatsu, K. Kafuku, H. Yamaoka, K. Isobe, Y. Nakamura and S. Kawaguchi, *Inorg. Chim, Acta* 1981, **54,** L69. For other independent work, see, M. Onishi, K. Hiraki, K. Maeda and T. Itoh, *J. Organomet. Chem.* 1980, **188,** 245.
2. K. Higashimura and Y. Nakamura, *J. Chem. Soc., Dalton Trans.* 1993, 3075.
3. N. Shinkawa, A. Sato, J. Shinya, Y. Nakamura and S. Okeya, *Bull. Chem. Soc. Jpn* 1995, **68,** 183; Y. Nakamura and N. Shinkawa, *Rhodium Ex.* 1994, **6,** 14.
4. For recent reviews, see, E. Sappa, in *Comprehensive Organometallic Chemistry* (Edited by E. W. Abel, F. G. A. Stone and G. Wilkinson), Vol. 7, p. 803. Pergamon, Oxford (1995); M. I. Bruce, M. P. Cifuentes and M. G. Humphrey, *Polyhedron* 1991, **10,** 277.
5. M. I. Bruce, M. G. Humphrey, M. R. Snow, E. R. T. Tiekink and R. C. Wallis, *J. Organomet. Chem.* 1986, **314,** 311.
6. P. L. Andreu, J. A. Cabeza, V. Riera, Y. Jeannin and D. Miguel, *J. Chem. Soc., Dalton Trans.* 1990, 2201.
7. A. J. Deeming, K. I. Hardcastle and M. Karim, *Inorg. Chem.* 1992, **31,** 4792.
8. D. J. Darensbourg, B. Fontal, S. S. Chojnacki, K. K. Klausmeyer and J. H. Reibenspies, *Inorg. Chem.* 1994, **33,** 3526.
9. A. Maisonnat, J. P. Farr, M. M. Olmstead, C. T. Hunt and A. L. Balch, *Inorg. Chem.* 1982, **21,** 3961.
10. P. T. Beurskens, G. Admiraal, G. Beurskens, W. P. Bosman, S. Garcia-Granda, R. O. Gould and J. M. M. Smykalla, *C. PATTY*, 1992. *Structure Analysis Programs with Intelligent Control*, Rigaku Corp., Tokyo (1991).
11. *teXsan. Crystal Structure Analysis Package*, Molecular Structure Corp., The Woodlands, TX (1985, 1992).
12. K. Hiraki, Y. Obayashi and Y. Oki, *Bull. Chem. Soc. Jpn* 1972, **52,** 1372.
13. S. D. Robinson and G. Wilkinson, *J. Chem. Soc. A* 1966, 300.
14. M. I. Bruce, M. Z. Iqbal and F. G. A. Stone, *J. Chem. Soc. A* 1971, 2820.
15. R. B. King and M. B. Bisnette, *Inorg. Chem.* 1966, **5,** 293.
16. R. B. King and M. B. Bisnette, *J. Organomet. Chem.* 1964, **2,** 15.

Pergamon

PII: S0277-5387(96)00330-0

Polyhedron Vol. 16, No. 4, pp. 581–585, 1997
Copyright © 1996 Elsevier Science Ltd
Printed in Great Britain. All rights reserved
0277–5387/97 $17.00+0.00

Metal alkoxides with polymerizable ligands: synthesis and molecular structure of $[Nb_4(\mu\text{-}O)_4(\mu,\eta^2\text{-}O_2CMe{=}CH_2)_4(OPr^i)_8]$

Liliane G. Hubert-Pfalzgraf,[a]* Valerie Abada,[a] Sabine Halut[b] and Jacques Roziere[c]

[a]Laboratoire de Chimie Moléculaire, URA-CNRS, Université de Nice Sophia-Antipolis, Parc Valrose, 06108 Nice Cedex 2, France

[b]Laboratoire de Chimie des Métaux de Transition, URA-CNRS, 4 Place Jussieu, 75230 Paris Cedex 05, France

[c]Laboratoire des acides minéraux, URA-CNRS, 34065 Montepellier Cedex, France

(Received 24 May 1996; accepted 1 July 1996)

Abstract—The reaction between $[Nb(OPr^i)_5]_2$ and methacrylic acid $[CH_2C(CH_3)CO_2H{=}McOH]$, and subsequent controlled microhydrolysis, gave $[Nb_4(\mu\text{-}O)_4(\mu,\eta^2\text{-}Mc)_4(OPr^i)_8]$ which was characterized by X-ray diffraction. The compound is based on a planar Nb_4O_4 core with terminal isopropoxide ligands, while the functional carboxylates act as bridging chelating ligands. The Nb—O bond lengths vary from 1.840(3) to 2.203(4) Å and follow the order Nb—OR ~ Nb—O < Nb—O(Mc). The Nb—O—Nb angles are bent with values of 146.2(2) and 150.2(2)°, respectively. The polymerization behaviour is discussed. Copyright © 1996 Elsevier Science Ltd

Keywords: niobium; oxoalkoxide; sol–gel; carboxylates; polymerizable ligands.

Hybrid organic–inorganic materials have gained increasing interest over the last few years [1]. The versatility and mild experimental conditions of the sol–gel process allow the incorporation of a large variety of organic functional compounds and thus opens up a large palette of technological applications. The use of heteroleptic alkoxides $M(OR)n-xG_x$ is one of the strategies employed to avoid phase separation between the organic and inorganic components in the final oxide materials. Indeed, such precursors can give access to an inorganic network in which the organic groups G are chemically bonded as a result of differential hydrolysis between the ligands of type OR and G. The organic groups G can be polymerizable, thermo- or photolabile, or mono- or polyfunctionalized. The synthesis of transition metal oxo clusters capped with polymerizable ligands, which can be used to extend the network to form hybrid organic–inorganic polymers, has recently been reported [2].

We have recently shown the limits of the use of 2-hydroxyethylmethacrylate as a ligand for oxophilic metals [3]. Acids were anticipated to provide more stable derivatives [4]. We report here the reaction of $[Nb(OPr^i)_5]_2$ with methacrylic acid followed by subsequent microhydrolysis. The cluster $[Nb(\mu\text{-}O)_4(\mu,\eta^2\text{-}Mc)_4(OPr^i)_8]$ ($Mc = O_2CCMeCH_2$) was thus obtained. Its characterization has been achieved by X-ray diffraction, FT-IR and NMR. Its reactivity was also investigated.

EXPERIMENTAL

All reactions were achieved under inert atmosphere using Schlenk tube techniques. Solvents were dried and purified by distillation. $[Nb(OPr^i)_5]_2$ was obtained according to the literature [5,6]. Methacrylic acid (Aldrich) was stored over molecular sieves, ^1H, ^{13}C NMR and IR spectra were recorded on Bruker AC-200 and IR-FTS 45 spectrometers, respectively. IR spectra were obtained as Nujol mulls between KBr

* Author to whom correspondence should be addressed.

plates. Analyses were obtained from the Centre de Microanalyses du CNRS.

Synthesis of $[Nb_4(\mu\text{-}O)_4(\mu,\eta^2\text{-}Mc)_4(OPr^i)_8]$

Methacrylic acid (0.225 ml, 2.65 mmol) in toluene (10 cm^3) was slowly added to a solution of $[Nb(OPr^i)_5]_2$ (1.03 g, 1.32 mmol) in toluene (20 cm^3). The reaction medium was stirred at room temperature for 5 h and evaporated. The resulting oil was dissolved in isopropanol (5 cm^3) and a solution of water in isopropanol (0.53 cm^3, 1 M) was added ($h = 0.2$). Crystallization led to 0.52 g (63%) of white, air-sensitive crystals of **1,** soluble in toluene, cyclohexane, THF and diethyl ether, but insoluble in hexane and alcohols. Found: C: 38.8; H: 6.3. Calc. for $C_{40}OH_{76}O_{20}Nb_4C$: 38.5; H: 6.1%. IR (cm^{-1}): 1647m ν(C=C); 1578vs $\nu_{as}(CO_2)$; 1462s, 1416s, $\nu_s(CO_2)$; 1377s, 1130m, 1244m; 1152vs, 1126vs ν(C—O); 1003sh; 998vs ν(Nb—O—Nb); 935m, 854m, 831w, 763sh; 733vs ν(Nb—O—Nb); 605sh, 590vs, 469m, 430m, 401m ν(Nb—OR). ^{1}H NMR (C_6D_6, ppm): δ 6.5, 6.3 (t, 4H (1 : 1), CH, $J = 2.2$ Hz), 5.4, 5.3 (t, 4H (1 : 1), CH, $J = 2.2$ Hz), 5.1 (sept, 4H, OCH, $J = 6.6$ Hz), 4.9 (sept, 4H, OCH, $J = 6.6$ Hz), 2.17s, 1.97 (s, 12H (1 : 1), CH_3), 1.47–1.28 (overlapping of doublets, 48H, CH_3, $J = 6.6$ Hz). ^{13}C NMR (C_6D_6, ppm): δ 174.8, 174.6 (CO_2); 140.6 140.3 ($C{=}CH_2$); 125.5, 125.4 ($CH_2{=}C$); 79.2, 73.9 (CH); 25.6 25.4, 25.2, 25.1 (CH_3, Pr^i); 19.8, 19.3 (CH_3, Mc).

The same product was obtained by reacting $[Nb(OPr^i)_5]_2$ and methacrylic acid directly in isopropanol and hydrolysis ($h = 0.3$), but the yield was lower (20%) owing to some esterification of the methacrylic acid.

Table 1. Crystallographic data for $[Nb_4(\mu\text{-}O)_4(\mu,\eta^2\text{-}O_2CMe{=}CH_2)_4(OPr^i)_8]$

Formula	$C_{40}H_{76}O_{20}Nb_4$
F.w.	1248.64
System	Triclinic
Space group	$P\bar{1}$
a, Å	10.811(2)
b, Å	11.731(3)
c, Å	12.576(2)
α, °	103.58(2)
β, °	104.76(1)
γ, °	102.24(2)
V, Å^3	1435(16)
Z	1
μ(Mo-K_α), cm^{-1}	8.05
$d_{calc.}$, g cm^{-3}	1.44
2θ range, °	$2 < 2\theta < 50$
Scan type	$\omega/2\theta$
Scan width, °	$0.8 + 0{,}34 \tan\theta$
Scan speed, °min^{-1}	$1.6 <$ sp. < 16.5
Diffractometer	CAD4F
No. of reflections collected	5366
No. of unique reflections	5028
Merging R factor	0.02
No. of reflections with $I > 3\sigma I$	3390
Abs. coeff. corr.	$0.89 <$ coeff < 1.11
R	0.033
R_w	0.034
Weighting scheme	unity
No. of variables	292

Crystallography of $[Nb_4(\mu\text{-}O)_4(\mu,\eta^2\text{-}Mc)_4(Opr^i)_8]$

A selected crystal (obtained directly from the reaction medium) was mounted in a Lindemann glass capillary and set up on an automatic diffractometer. Unit-cell dimensions with estimated standard deviations were obtained from least-squares refinements of the setting angles of 25 well-centred reflections. Two standard reflections were monitored periodically; they showed no change during data collection. Crystallographic data and other pertinent information are summarized in Table 1. Corrections were made for Lorentz and polarization effects. Empirical absorption corrections (Difabs) [7] were applied.

Computations were performed by using CRYSTALS adapted on a MicroVax II [8]. Atomic structure factors for neutral C, O, Nb and H were taken from ref. [9]. Anomalous dispersion was taken into account. The structure was solved by the Patterson method and subsequent Fourier maps. Almost all hydrogen atoms were found on difference maps, the others were geometrically located. Their positions were not refined and they were given an overall isotropic thermal parameter. Non-hydrogen atoms were anisotropically refined. Least-squares refinements with approximation in three blocks to the normal matrix were carried out by minimizing the function $\Sigma w(|F_0| - |F_c|)_2$, where F_0 and F_c are the observed and calculated structure factors. Unit weight was used. Models reached convergence with $R = \Sigma(||F_0| - |F_c||)/\Sigma|F_0|$ and $R_w = [\Sigma w(|F_0| - |F_c|)^2/[\Sigma w(F_0)^2]]^{1/2}$ having the values listed in Table 1. Criteria for a satisfactory complete analysis were the ratios of rms shift to standard deviations being less than 0.1 and no significant features in the final difference map.

Tables of atomic coordinates anisotropic temperature factors, and observed and calculated structure factors have been deposited at the Cambridge Crystallographic Data Centre.

RESULTS AND DISCUSSION

The reaction between $[Nb(OPr^i)_5]_2$ and methacrylic acid (1 : 2 stoichiometry) in toluene at room temperature yields an oily product. FT-IR shows the presence of uncoordinated acid (1690 cm^{-1}). Subsequent controlled microhydrolysis (hydrolysis ratio $h = [H_2O]/[Nb(OR)_5]$ of 0.2) in Pr^iOH allowed the isolation of a white crystalline material, **1,** in 63% yield. The same compound was obtained if the reaction and subsequent microhydrolysis were carried out

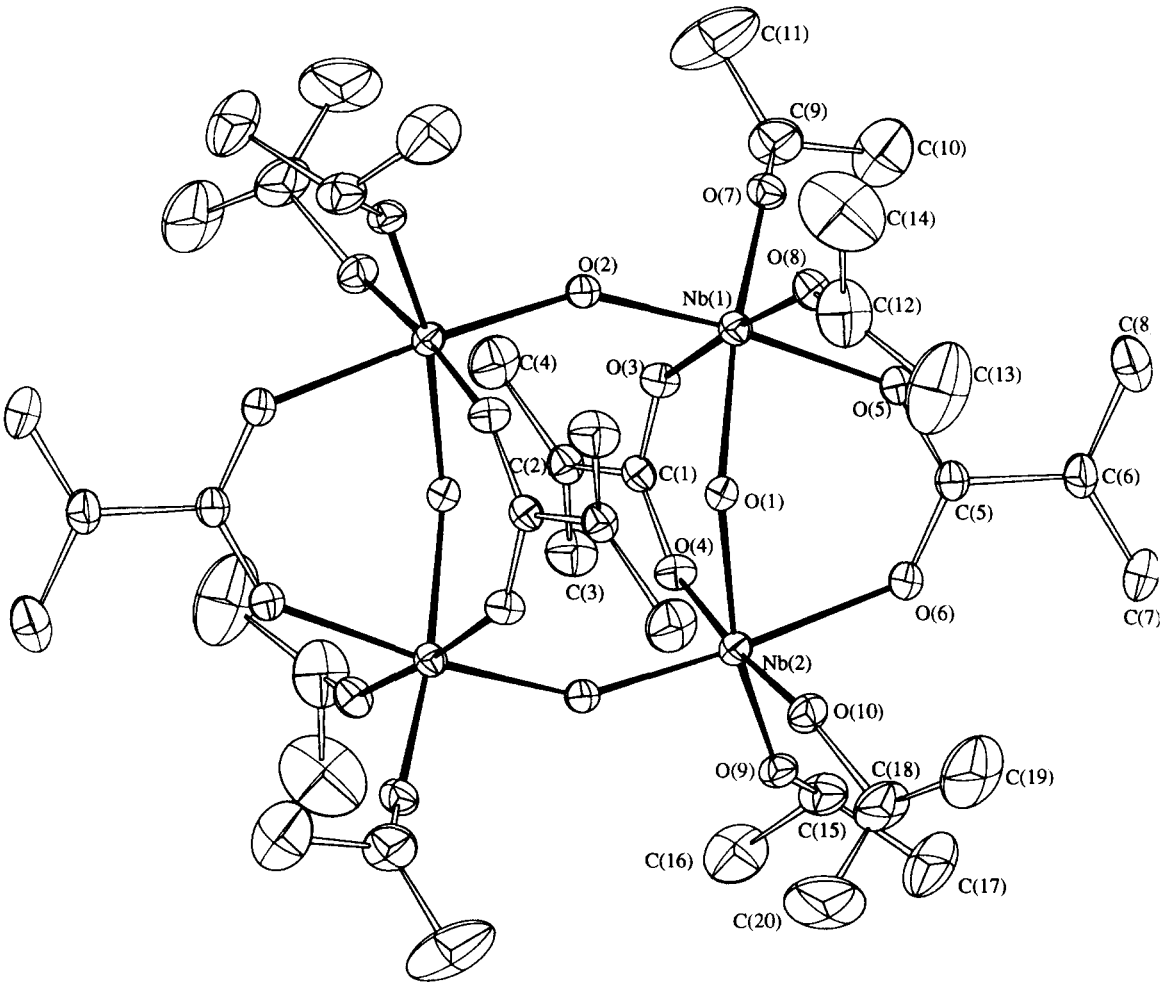


Fig. 1. Molecular structure of $[Nb_4(\mu\text{-}O)_4(\mu,\eta^2\text{-}Mc)_4(OPr^i)_8]$ using the program CAMERON[11] (thermal ellipsoids at 20% probability).

directly in isopropanol, but the yield was lower owing to esterification (as evidenced by the νCO_2 absorption band of the ester at 1721 cm^{-1}), and, thus, simultaneous uncontrolled microhydrolysis. The same compound was also obtained when larger amounts of acid (up to four equivalents) were used. The infrared spectrum of **1** showed the absorption bands characteristic of the CO_2 asymmetric stretching vibration at 1578 cm^{-1} and $\nu_s CO_2$ at 1462 and 1416 cm^{-1}. The difference $\Delta_\nu = \nu_{as}CO_2 - \nu_s CO_2$ for the methacrylate groups suggests chelating or bridging coordination modes [10]. A band at 1647 cm^{-1}, assigned to ν(C=C) vibrations shows the presence of uncoordinated double bonds (1637 cm^{-1} in free methacrylic acid). Strong and sharp absorption bands at 998 and 733 cm^{-1} can be tentatively assigned to Nb—O—Nb vibrations [11]. The ^1H NMR spectra indicate the presence of OPr^i and OMc ligands in a 1 : 2 integration ratio. The presence of two types of signals in a 1 : 1 integration ratio for each ligand furthermore suggests the formation of a species having magnetic non-equivalent surroundings for the isopropoxo and methacrylate ligands.

The identity of compound **1** was established by X-ray diffraction [12]. Its molecular structure consists of a centrosymmetric $Nb_4(\mu\text{-}O)_4(\mu,\eta^2\text{-}Mc)_4(OPr^i)_8]$ species as shown in Fig. 1. Relevant interatomic distances and angles are collected in Table 2. The metal atoms are linked together by bridging methacrylate and μ_2-oxo ligands and they are six-coordinated. The Nb—O bond lengths are in the range 1.840(3)–2.203(4) Å, with the gradation Nb-OPr^i ~ Nb—O < Nb —O(Mc). These data are in agreement with the literature [11]. The structure is built around a nearly planar Nb_4O_4 core with a Nb(1) · · · Nb(2) distance of 3.668(2) Å The niobium–oxo bond lengths vary from 1.889(3) to 1.936(3) Å, thus resulting in a slightly assymmetrical Nb_4O_4 ring. The short Nb—O bond distances indicate some π bonding. The angles at the bridging oxo ligands, O(1) and O(2), are 146.2(2) and 150.2(2)°, respectively [13]. The stereochemistry around the niobium centres is severely distorted

Table 2. Selected bond lengths (Å) and angles (°) for $[Nb_4(\mu\text{-}O)_4(\mu,\eta^2\text{-}O_2CMe{=}CH_2)_4(OPr^i)_8]$

Nb(1)—O(1)	1.936(3)	Nb(1)—O(2)	1.897(3)
Nb(1)—O(3)	2.153(3)	Nb(1)—O(5)	2.156(4)
Nb(1)—O(7)	1.876(3)	Nb(1)—O(8)	1.840(3)
Nb(2)—O(1)	1.897(3)	Nb(2)—O(2)	1.889(3)
Nb(2)—O(4)	2.173(3)	Nb(2)—O(6)	2.203(4)
Nb(2)—O(9)	1.883(3)	Nb(2)—O(10)	1.860(3)
Nb(1)···Nb(2)	3.668(2)	Nb(1)···Nb(2′)	3.658(2)
O(2)—Nb(1)—O(1)	94.0(1)	O(3)—Nb(1)—O(1)	82.6(1)
O(3)—Nb(1)—O(2)	86.7(1)	O(5)—Nb(1)—O(1)	81.5(1)
O(5)—Nb(1)—O(2)	171.5(1)	O(5)—Nb(1)—O(3)	85.6(1)
O(7)—Nb(1)—O(1)	158.6(1)	O(7)—Nb(1)—O(2)	98.8(1)
O(7)—Nb(1)—O(3)	81.1(1)	O(7)—Nb(1)—O(5)	83.5(1)
O(8)—Nb(1)—O(1)	95.8(1)	O(8)—Nb(1)—O(2)	98.1(2)
O(8)—Nb(1)—O(3)	175.1(2)	O(8)—Nb(1)—O(5)	89.6(2)
O(8)—Nb(1)—O(7)	99.3(2)	O(2)—Nb(2)—O(1)	96.8(1)
O(4)—Nb(2)—O(1)	84.5(1)	O(4)—Nb(2)—O(2)	88.5(1)
O(6)—Nb(2)—O(1)	81.8(1)	O(6)—Nb(2)—O(2)	172.5(1)
O(6)—Nb(2)—O(4)	84.0(1)	O(9)—Nb(2)—O(1)	158.2(1)
O(9)—Nb(2)—O(2)	98.5(1)	O(9)—Nb(2)—O(4)	80.5(1)
O(9)—Nb(2)—O(6)	81.0(1)	O(10)—Nb(2)—O(1)	97.3(1)
O(10)—Nb(2)—O(2)	98.8(2)	O(10)—Nb(2)—O(4)	172.2(1)
O(10)—Nb(2)—O(6)	88.7(2)	O(10)—Nb(2)—O(9)	95.5(2)
Nb(2)—O(1)—Nb(1)	146.2(2)	Nb(2)—O(2)—Nb(1)	150.2(2)
C(1)—O(3)—Nb(1)	137.1(3)	C(1)—O(4)—Nb(2)	133.9(3)
C(5)—O(5)—Nb(1)	135.8(3)	C(5)—O(6)—Nb(2)	133.3(3)
C(9)—O(7)—Nb(1)	146.1(4)	C(12)—O(8)—Nb(1)	151.8(5)
C(15)—O(9)—Nb(2)	143.7(4)	C(18)—O(10)—Nb(2)	140.6(5)

toward a trigonal prism. The ^1H and ^{13}C NMR provide support for the retention of the solid state structure in solution.

Compound **1** can be considered as resulting from the assembly of two $Nb_2O(Mc)_2(OR)_4$ units *via* bridging oxo ligands. The dinuclear unit is structurally analogous to that of $[NbCl_3(O_2CPh)]_2O$ (obtained in low yield by reacting $NbCl_5$ and benzoic acid in 2 : 3 stoichiometry) [14], but two terminal OR ligands have been used here for the hydrolysis condensation reaction. The overall tetranuclear structure of **1** is similar to that of $[Ta_4O_4Cl_8(O_2CC_6H_4Me\text{-}p)_4]$ obtained when the reaction between $TaCl_5$ and the acid is conducted in a 1 : 2 stoichiometry and in refluxing toluene [15]. The special stability of the tetranuclear unit for group 5 carboxylate derivatives is also illustrated by the formation of $Nb_4O_4(OAc)_4(OPr^i)_8$ obtained by reacting $Nb(OPr^i)_5$ and $La(OAc)_3 \cdot 2AcOH$ [16]. The number of oxo ligands in compound **1**, larger than expected on the basis of the hydrolysis ratio, indicates that they are, in part, derived from the carboxylic acid. It can be noted that the carboxylato alkoxide aggregates obtained so far for group 5 metals are of smaller nuclearity than for titanium or zirconium [4].

Compound **1** is soluble in a variety of solvents and its potential as precursor to materials—accessibility of the double bonds of the methacrylate ligands for organic homo- and copolymerization reactions, hydrolytic behaviour— was considered. No evolution of **1** is observed in refluxing THF in the presence of ABN after 2 h ; the unsaturated organic functionalities are probably inaccessible for steric reasons as shown by space-filling models. Compound **1** is, however, a potential candidate for organic microcellular doped solids [17]. Hydrolysis–polycondensation reactions of **1** in isopropanol offer turbid sols.

REFERENCES

1. U. Schubert, N. Hùsing and A. Lorenz, *Chem. Mater.* 1995, **7**, 2010.
2. C. Sanchez, M. In. P. Toledano and P. Griesmar, *Better Ceramics through Chemistry VI, Mater. Res. Soc. Symp. Proc.* 1992, **271**, 669.
3. N. Pajot, R. Papiernik, L. G. Hubert-Pfalzgraf and J. Vaissermann, *J. Chem. Soc., Chem. Commun.* 1995, 1817.
4. U. Schubert, E. Arpac, W. Glaubitt, A. Helmerich and C. Chau, *Chem. Mater.* 1992, **3**, 291 and references therein.
5. D. C. Bradley, W. Wardlaw and A. Whitley, *J. Chem. Soc.* 1955, 726.
6. D. C. Bradley, B. N. Chakravarti and W. Wardlaw, *J. Chem. Soc.* 1956, 2381.

7. N. Walker and D. Stuart, *Acta Cryst.* 1983, **39,** 158.
8. D. J. Watkin, J. R. Carruthers and P. W. Betteridge, *CRYSTALS, An Advanced Crystallographic Program System*, Chemical Crystallography Laboratory, University of Oxford, Oxford (1988).
9. *International Tables for X-ray Crystallography*, Vol IV. Kynoch Press, Birmingham (1974).
10. G. B. Deacon and R. J. Philips, *Coord. Chem. Rev.* 1980, **33,** 227.
11. L. G. Hubert-Pfalzgraf, M. Postel and J. G. Riess, *Comprehensive Coordination Chemistry*, Vol. 3, Chap. 34. Pergamon Press, London (1987); L. G. Hubert-Pfalzgraf, *Encyclopedia of Inorganic Chemistry*, Vol 5, p. 2444. Dekker, London (1995); W. A. Nugent and R. L. Harlow, *J. Am. Chem. Soc.* 1994, **116,** 6142.
12. L. J. Pearce and D. J. Watkin, *CAMERON*, Chemical Crystallography Laboratory, University of Oxford, Oxford (1992).
13. C. Lecomte, J. Protas, R. Guilard, B. Fliniaux and P. Fournari, *J. Chem. Soc., Chem. Commun.* 1976, 434.
14. D. A. Brown, M. G. H. Wallbridge and N. W. Alcock, *J. Chem. Soc., Dalton Trans.* 1993, 2037.
15. D. A. Brown, W. Errington and M. G. H. Wallbridge, *J. Chem. Soc., Dalton Trans.* 1993, 1163.
16. S. Boulmaaz, L. G. Hubert-Pfalzgraf and J. Vaissermann, unpublished work.
17. L. G. Hubert-Pfalzgraf, N. Pajot, R. Papiernik and S. Parraud, *Better Ceramics through Chemistry VII, Mater. Res. Soc. Symp. Proc.* (1996), in press.

Pergamon

PII: S0277-5387(96)00327-0

Polyhedron Vol. 16, No. 4, pp. 587–592, 1997
Copyright © 1996 Elsevier Science Ltd
Printed in Great Britain. All rights reserved
0277–5387/97 $17.00+0.00

Synthesis and structural study of a tetranuclear magnesium alkoxide: $[Mg_4(\mu_3, \eta^2\text{-}OR)_2(\mu_2, \eta^2\text{-}OR)_4(OR)_2]$ with $OR{=}OCH(CH_3)CH_2OCH_3$

Laure Albaric,[a] Nadine Hovnanian,[a]* Anne Julbe,[a] Christian Guizard,[a] Angel Alvarez-Larena[b] and Joan F. Piniella[b]

[a]Laboratoire des Matériaux et Procédés Membranaires, UMR CNRS 9987, ENSCM, 8 rue de l'école normale, 34053 Montpellier Cedex 1, France

[b]Departament de Geología, Unidad de Cristalographía y de Mineralogía, Universidad Autónoma de Barcelona, 08193 Bellaterra, Spain

(Received 10 April 1996; accepted 1 July 1996)

Abstract—Direct reaction between magnesium and 1-methoxy-2-propanol yielded the title complex which has been characterized by X-ray crystallography. The molecular structure consists of a centrosymmetric tetrameric unit in which the Mg atoms are five- or six-coordinated by terminal, triple- and double-bridging chelating alkoxo ligands. Copyright © 1996 Elsevier Science Ltd

Keywords: magnesium; alkoxide; X-ray crystallography; sol–gel; molecular precursor of oxide material.

The increasing application of molecular chemistry in the elaboration of high-technology materials by sol-gel or chemical vapour deposition techniques provides a better understanding of the influence of the organic part on the properties of the precursor (solubility, thermodynamic stability, volatility, etc.) and a better control of the performance of the material. In this context, metal alkoxides have drawn increasing scrutiny as sources of oxide materials [1].

In order to elaborate catalytic V–Mg multicomponent oxide membranes by the sol–gel process, we have investigated the properties of metal alkoxides derived from 1-methoxy-2-propanol [2]. The advantages of the functional alcohols have already been exploited for the sol–gel process [3]. They ensure homogeneous media yielding soluble complexes and slow down the hydrolysis rates [4]. They can also allow the formation of heterobimetallic structures, since they are chelating ligands.

Little structural information about homometallic magnesium alkoxides is known. Dimers with four-membered Mg_2O_2 rings are found in which each magnesium atom is three [5] or four coordinated [6]. A monomeric structure with the sterically hindered 2,4,6-tris(trifluoromethyl)phenoxo group [7] is known. A heterocubane structure forming tetrameric complexes is observed in $[CpMgOEt]_4$ [8] and $Mg(OCH_3)_2 \cdot 2CH_3OH$ [9]. This latter compound, recently characterized by X-ray diffraction, presents an extensive structural disorder which prevents good structure refinement. This feature is frequently observed for alkoxide compounds and makes the structural determination difficult. Structural analyses on heterobinuclear complexes including the Mg atom are more numerous [10]. In particular, the heterometallic aluminium magnesium alkoxides have been investigated with different OR groups since these compounds are sol-gel precursors for $MgAl_2O_4$ [11]. Here, we report the synthesis, the X-ray characterization and the hydrolysis reactions of a novel tetranuclear magnesium alkoxide derived from 1-methoxy-2-propanol.

EXPERIMENTAL

All the manipulations were routinely performed under high purity argon using Schlenk tubes and vac-

* Author to whom correspondence should be addressed.

uum line techniques with solvents purified by standard methods. Before use, magnesium turnings (Prolabo, 99.8% purity) were washed with ether, dried at 110°C in air and purged with argon. Analytical data were obtained from the Centre de Microanalyses du CNRS de Vernaison. IR spectra were obtained as Nujol mulls between KBr plates on an IR-FT Nicolet 5ZDX spectrometer. ^{1}H NMR spectra were recorded on a Bruker AC-200 spectrometer in CD_2Cl_2. Mass spectra were recorded on a 300DX JEOL spectrometer by electronic impact. Thermogravimetric analysis was made under argon and the heating rate was 5°C min^{-1}. Specific area B.E.T. measurements from N_2 adsorption–desorption were performed from ASAP 2000 Micromeritics.

Synthesis of $[Mg(OCH(CH_3)CH_2OCH_3)_2]_4$

Magnesium alkoxide was synthesized from the reaction of magnesium turnings (8 g, 0.329 mol) with 1-methoxy-2-propanol (120 cm^3, 1.228 mol) in toluene (120 cm^3). The mixture was stirred vigorously and heated at reflux temperature until all the metal was consumed (10 h). The resulting grey, fine suspension of particles was filtered off and the colourless filtrate was evaporated to dryness. The white powder obtained was purified by recrystallization. Magnesium alkoxide (5 g) was stirred with 20 cm^3 of n-heptane at 50°C. The addition of 30 cm^3 of toluene changes the initial suspension into a slightly turbid solution. When the temperature reached 60°C a clear solution formed from which colourless crystals sensitive to moist air were formed by a slow decrease of temperature to ambient temperature. Yield based on magnesium: 99%. Found: C, 46.1; H, 8.8; Mg, 12.2. Calc. for $C_8H_{18}MgO_4$: C, 47.4; H, 8.6; Mg, 12.0%. FT-IR (cm^{-1}): 1328sh, 1313w, 1258w, 1205m, 1174sh, 1156sh, 1086s, 987s, 927w, 916w, 869m, 795w, 681w, 585m, 568sh, 520m, 493w. ^{1}H NMR (CD_2Cl_2, ppm): δ 0.98–1.23 (m, CH_3, 3 H), 3.13–3.58 (m, OCH_2 and OCH_3, 5 H), 3.93–4.05 (m, OCH, 1 H). MS (*m/z*, EI$^+$), OR = OCH(Me)CH_2OMe: OMe (100%), $CH_2OCH_3/MgOCH_3$ (65%), $OMeCH_2CH(CH_3)$ (28%), OR (22%), MgO(OR) (3%), Mg(OR)OCH_3 (12%), Mg(OR)($MeOCH_2CH_3$) (1.8%), $Mg(OR)_2$ (1.5%).

Crystallographic study

A suitable crystal of $[Mg(OCH(CH_3)CH_2OCH_3)_2]_4$ was mounted in a Lindemann capillary with a diameter of 0.3 mm on to an Enraf Nonius CAD4 diffractometer with graphite-monochromated Mo-K_α radiation. Unit-cell parameters were obtained from a least-squares fit to automatically centred settings for 25 reflections. The crystal parameters and data collection and structure refinement details are summarized in Table 1. Three standard reflections were monitored every hour and no decay was observed during the data collection. The data were corrected for Lorentz and polarization effects. No correction for absorption was made. The structure was solved by direct methods using the SHELXS-86 program [12]. The structure refinement was carried out using the SHELXL-93 program [13]. Anisotropic temperature factors were used for all non-hydrogen atoms. Hydrogen atoms were placed in calculated positions. The isotropic temperature factors were fixed at 1.5 (for the methylic H) or 1.2 (for the rest of H) times U_{eq} of the corresponding C atoms. The geometric calculations were performed with PLATON [14]. Positional and thermal parameters are available as supplementary material, deposited at the Cambridge Crystallographic Data Centre.

RESULTS AND DISCUSSION

We have investigated the synthesis of the 1-methoxy-2-propoxide of magnesium and its reactivity towards water. 1-Methoxy-2-propanol reacted directly with the electropositive magnesium following the exothermic reaction:

$$4Mg + 8HOCH(CH_3)CH_2OCH_3 \xrightarrow{\text{Toluene}} [Mg(OCH(CH_3)CH_2OCH_3)_2]_4 + 4H_2.$$

The IR spectrum of the resulting compound $[Mg(OCH(CH_3)CH_2OCH_3)_2]_4$ (**1**) exhibits bands at 585, 568, 520 and 493 cm^{-1} which belong to ν(Mg—O) stretching frequencies with the characteristic ν(C—O) bands lying at 1258, 1205, 1174 and 1156 cm^{-1}.

The ^{1}H NMR spectrum shows complex signals (multiplets) corresponding to the $OCH(CH_3)CH_2OCH_3$ alkoxide groups which obscure structural conclusions. Thus, the NMR study is complicated by intra- and/or intermolecular exchange phenomema occurring in solution owing to the lability of the alkoxide groups. This common feature of alkoxide chemistry generally requires an X-ray diffraction study for an unambiguous structural characterization.

Mass spectrometry is sometimes used in order to ascertain the degree of condensation, with respect to disproportionation reactions in the vapour phase. Here, the ion of the highest molecular mass can be assigned to $[Mg(OR)_2]^+$. Thus, the mass spectrum does not show the tetrameric nature of the compound as proved by the X-ray diffraction analysis. The ionization method used for mass spectral analysis is that of electronic impact, which causes a strong fragmentation into ions of low molecular mass.

The molecular structure of $[Mg(OCH(CH_3)CH_2OCH_3)_2]_4$ is shown in Fig. 1. Relevant bond lengths and angles are collected in Table 2. The complex consists of a centrosymmetric tetramer in which the four Mg atoms form a nearly perfect rhomb (Table 2). The asymmetric unit is only half of the

Table 1. Crystal data and structure refinement for $[Mg(OCH(CH_3)CH_2OCH_3)_2]_4$

Empirical formula	$C_{32}H_{72}Mg_4O_{16}$
Formula weight	810.14
Temperature (K)	293(2)
Wavelength, λ (Å)	0.71069
Crystal system	Monoclinic
Space group	$P2_1/n$ (no. 14)
Unit-cell dimensions	$a = 11.399(2)$ Å
	$b = 10.787(5)$ Å
	$c = 18.157(3)$ Å
	$\beta = 90.42(2)$
Volume (Å^3)	2232(1)
Density (calculated) (g cm^{-3})	1.205
Z	2
Absorption coefficient (cm^{-1})	1.43
$F(000)$	880
Crystal size (mm)	$0.36 \times 0.25 \times 0.14$
θ Range for the data collection (°)	2.10–24.99
Index ranges	$-13 \leqslant h \leqslant 13, 0 \leqslant k \leqslant 12, 0 \leqslant l \leqslant 21$
Independent reflections	3917
Refinement method	Full-matrix least squares on F^2 (all reflections)
Data/restraints/parameters	3917/24/235
Goodness-of-fit on F^2	0.735
Final R indices [1198 refl. with $I > 2\sigma(I)$][a]	$R(F) = 0.0642$, $R_w(F^2) = 0.1218$
R indices (all data)	$R(F) = 0.2298$, $R_w(F^2) = 0.1452$
Largest diffraction peak and hole (e Å^{-3})	0.299 and −0.233
Scan type	ω–2θ
Scan width	$0.8 + 0.35 \tan\theta$
Reference reflections	3 every 400
(Δ/σ) max[b]	0.04

[a] The quantity minimized in the least-squares procedure is: $R_w(F^2) = [\Sigma w(F_o^2 - F_c^2)^2/\Sigma(F_o)^2]^{1/2}$, $w = 1/[\sigma^2(F_o^2) + (0.0626P)^2]$ where $P = [\max(F_o^2, 0) + 2F_c^2]/3$.

[b] Maximum ratio of the r.m.s. shift to standard deviation observed for the last cycle of refinement.

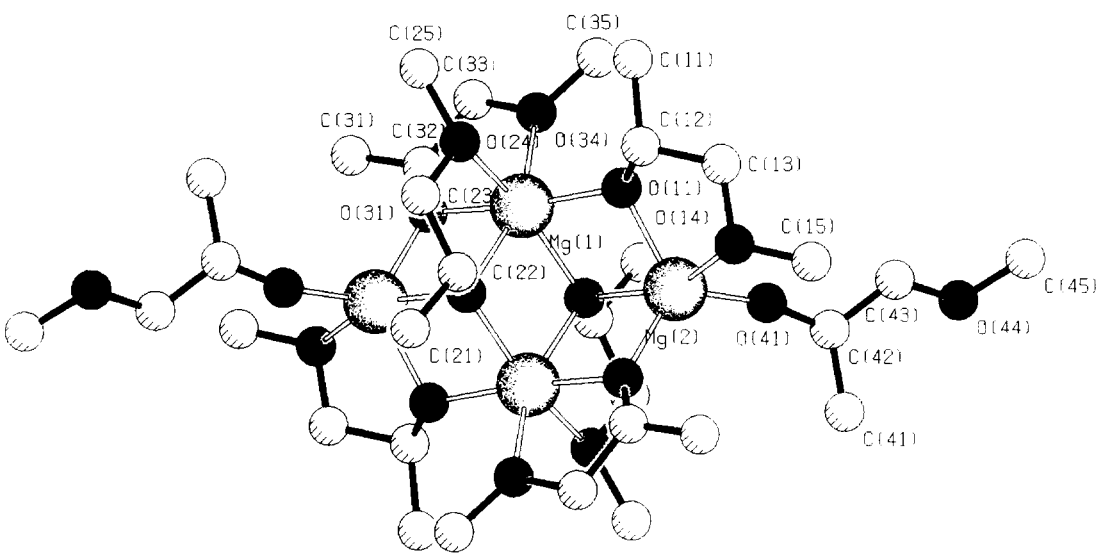


Fig. 1. View of the $[Mg(OCH(CH_3)CH_2OCH_3)_2]_4$ molecule showing the atom-numbering scheme.

tetramer. The Mg(1)···Mg(1a) $[-x, -y, -z]$ distance is close to that of Mg(1)···Mg(2) and, therefore, these three atoms define an almost equilateral triangle [the same disposition is obviously observed for Mg(1), Mg(1a) and Mg(2a)]. Every two neighbouring magnesium atoms are joined by two oxygen atoms. So two O-centred hexagons defined by alternating Mg and O atoms (three of each) can be

Table 2. Selected metal···metal distances (Å), bond lengths (Å) and angles (°) for $[Mg_4(\mu_3, \eta^2\text{-}OR)_2(\mu_2, \eta^2\text{-}OR)_4(OR)_2]$ with OR = $OCH(CH_3)CH_2OCH_3$ (standard deviations in parentheses) (a = $-x, -y, -z$)

Mg(1a)···Mg(1)	3.114(3)				
Mg(2)···Mg(1)	3.098(3)				
Mg(2a)···Mg(1)	3.075(3)				
Mg(2a)···Mg(2)	5.330(3)				
Mg(1a)···Mg(2)	3.075(3)				
Mg(1)—O(11)	η^2, μ_2	2.000(4)	Mg(2)—O(11)	η^2, μ_2	2.010(3)
Mg(1)—O(21)	η^2, μ_3	2.090(4)	Mg(2)—O(14)	η^2, μ_2	2.272(4)
Mg(1)—O(24)	η^2, μ_3	2.211(4)	Mg(2)—O(31a)	η^2, μ_2	1.965(4)
Mg(1)—O(21a)	η^2, μ_3	2.082(4)	Mg(2)—O(41)	terminal	1.848(4)
Mg(1)—O(31)	η^2, μ_2	2.018(4)	Mg(2)—O(21a)	η^2, μ_3	2.133(3)
Mg(1)—O(34)	η^2, μ_2	2.128(4)			
O(11)—Mg(1)—O(21)		106.18(15)	O(11)—Mg(2)—O(14)		77.65(14)
O(11)—Mg(1)—O(24)		90.54(14)	O(11)—Mg(2)—O(31a)		114.00(15)
O(11)—Mg(1)—O(21a)		81.16(13)	O(11)—Mg(2)—O(41)		126.04(18)
O(11)—Mg(1)—O(31)		171.45(16)	O(11)—Mg(2)—O(21a)		79.70(14)
O(11)—Mg(1)—O(34)		94.75(15)	O(14)—Mg(2)—O(31a)		98.38(15)
O(21)—Mg(1)—O(24)		76.20(15)	O(14)—Mg(2)—O(41)		92.67(16)
O(21)—Mg(1)—O(21a)		83.45(14)	O(14)—Mg(2)—O(21a)		155.53(15)
O(21)—Mg(1)—O(31)		82.35(14)	O(31a)—Mg(2)—O(41)		119.93(18)
O(21)—Mg(1)—O(34)		158.32(16)	O(31a)—Mg(2)—O(21a)		82.50(14)
O(24)—Mg(1)—O(21a)		154.95(17)	O(41)—Mg(2)—O(21a)		108.18(17)
O(24)—Mg(1)—O(31)		92.10(15)	Mg(1)—O(11)—Mg(2)		101.14(17)
O(24)—Mg(1)—O(34)		98.43(16)	Mg(1a)—O(21)—Mg(2a)		94.58(15)
O(21a)—Mg(1)—O(31)		99.59(15)	Mg(2)—O(31a)—Mg(1a)		101.08(16)
O(21a)—Mg(1)—O(34)		105.75(15)	Mg(1)—O(21)—Mg(1a)		96.55(14)
O(31)—Mg(1)—O(34)		76.81(15)	Mg(1)—O(21)—Mg(2a)		93.45(14)

observed (Fig. 2). Two coordination geometries around the magnesium atoms are observed. In the first one, Mg(1) is coordinated to six oxygens in a very distorted octahedral disposition: the Mg—O bond lengths are in the range 2.000(4)–2.211(4) Å, and some angles deviate greatly from the ideal values [e.g. 158.3(2)° and 154.9(2)°]. The second coordination geometry, around Mg(2), can be described as a very

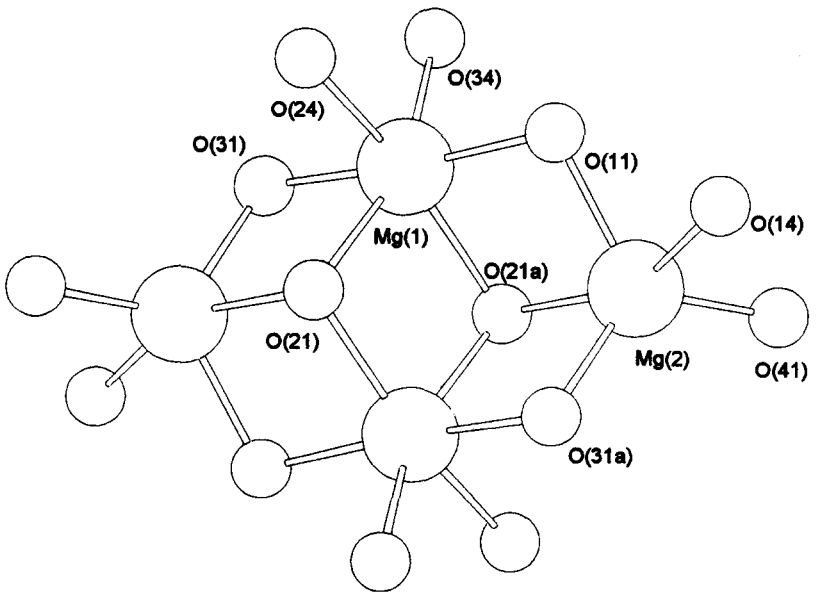


Fig. 2. View of the coordination geometries around the Mg atoms.

distorted trigonal bipyramid. The basal plane is defined by O(11), O(41) and O(31a) $[-x, -y, -z]$ and shows the shortest Mg—O bond lengths: 1.848(4)–2.010(4) Å. The two Mg—O apical bond lengths are greater: 2.133(3) and 2.272(4) Å. Magnesium coordinated by five oxygens occurs infrequently [7,11a,15]. The functional alkoxides can adopt different types of coordination around the metal atoms (Table 3). In the title compound, three of them have been found: terminal; μ_2, η^2; and μ_3, η^2. The oxygen coordination polyhedron around each five-coordinate magnesium atom results from one terminal monodentate alkoxo group, one μ_2, η^2- and one μ_3, η^2-OR ligands whereas each six-coordinate metal atom is bonded to two μ_2, η^2- and one μ_3, η^2-alkoxide ligands. The μ_3-oxygen, O(21), joins two six-coordinate magnesiums to one five-coordinate magnesium. It is clearly pyramidal (the sum of the Mg—O—Mg angles is 284.59° average). The triple- and double-bridging chelating coordination modes of the alkoxide ligands have been already found in $\{VOCl[OCH(CH_3)CH_2OCH_3]\}_2$, [2a] $[Y_3(OCH_2CH_2OMe)_5(acac)_4]$, [16] $Cd_9(OC_2H_4OMe)_{18}$ [17], $[Y(OC_2H_4OMe)]_{10}$ [18], $[Ca_9(OC_2H_4OMe)_{18}(HOC_2H_4OMe)_2]$ [19] and the cation $[Mg(OCH_2CH_2OMe)_6(DME)_2]^+$ [20]. This latter has been obtained by the reaction of Mg metal with $Hg(SiMe_2Ph)_2$ in DME with the cleavage of the carbon–oxygen bond of 1,2-dimethoxyethane. In this structure, the Mg atoms are joined together in the same way as in **1**.

The Mg—O(μ_3, η^2) bond lengths [2.13(4) Å av] and the μ_2, η^2 ones [2.06(4) Å av] are longer than those observed for terminal $[OCH(CH_3)CH_2OCH_3]$ groups [1.848(4) Å]. The same pattern has been already observed for other compounds derived from $HOCH_2CH_2OCH_3$ [17–20]. The Mg—μ_3-O, the Mg—μ_2-O and the Mg—O terminal bond lengths encountered in other magnesium alkoxides are comparable to those observed in **1** [5–8,20].

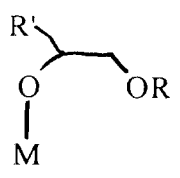
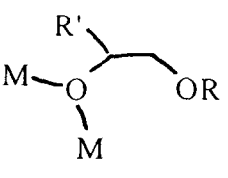
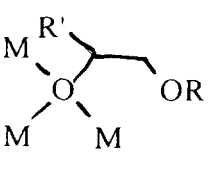
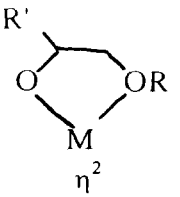
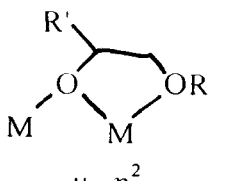
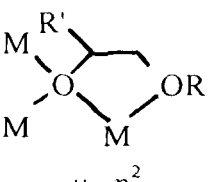
These results show that functional and versatile ligands such as $[OCH(CH_3)CH_2OCH_3]$ allow the magnesium atoms to attain high coordination numbers in clusters.

Compound **1** has good solubility in polar organic solvents such as the parent alcohol, tetrahydrofuran or chlorinated solvents ($CHCl_3$, CH_2Cl_2). It is slightly soluble in toluene and insoluble in aliphatic solvents such as n-heptane. Its solubility has been applied to the sol-gel process. The 1-methoxy-2-propanol solution of **1** was hydrolysed. It gave immediate gelification when $h \geqslant 2$ (h = degree of hydrolysis = $[H_2O]/[M(OR)_n]$) or a sol when $h = 1$, which gelled in a few hours.

The thermogravimetric analysis of **1** shows a four-step process with weight losses at 100, 200, 335 and 380°C. The successive percentages of weight losses are approximately 10, 11, 29 and 23.3%. The successive removal of the organic groups of the molecule shows that compound **1** is not volatile.

The calcination in air at 600°C of the resulting gel provided magnesium oxide which had a specific surface area (130 $m^2 g^{-1}$) higher than that obtained when MgO was synthesized at the same temperature from ionic precursors such as magnesium chloride or nitrate (30 and 85 $m^2 g^{-1}$, respectively). This makes com-

Table 3. Different modes of coordination of alkoxyalcohols on metal M

 terminal	 μ_2, η^1	 μ_3, η^1
 η^2	 μ_2, η^2	 μ_3, η^2

pound **1** an interesting precursor for catalytic applications. Further work on the elaboration of V–Mg multicomponent oxide membranes from this alkoxide compound, as well as their catalytic properties, are in progress.

Acknowledgement—The authors would like to thank M. Prof. Mihai Dimonie from Fac. Chemie Industriatà of Bucaresti in Romania for helpful discussions of this work.

REFERENCES

1. L. G. Hubert-Pfalzgraf, *New J. Chem.* 1987, **11,** 663.
2. (a) G. Foulon, J.-D. Foulon and N. Hovnanian, *Polyhedron* 1993, **12,** 2507; (b) N. Hovnanian, G. Foulon and L. Cot, *J. Sol-gel Sci. Tech.* 1994, **2,** 57.
3. P. Ravindranathan, S. Komarneni, A. Bhalla, R. Roy and L. E. Cross, *J. Mater. Res.* 1988, **3,** 810.
4. D. J. Eichorst and D. A. Payne, *Better Ceramics Through Chemistry III, Material Research Society Symp. Proc.* 1988, **121,** 773; J. T. J. Davies, H. C. Winterton and N. N. Hughes, *Better Ceramics Through Chemistry II*, 1986, **73,** 111.
5. J. Calabrese, M. A. Cushing, Jr and S. D. Ittel, *Inorg. Chem.* 1988, **27,** 867.
6. N. A. Bell, P. T. Moseley and H. M. M. Shearer, *Acta Cryst.* 1984, **C40,** 602.
7. H. W. Roesky, M. Scholz and M. Noltemeyer, *Chem. Ber.* 1990, **123,** 2303.
8. H. Lehmkuhl, K. Mehler, R. Benn, A. Rufinska and C. Krüger, *Chem. Ber.* 1986, **119,** 1054.
9. H. Thoms, M. Epple, H. Viebrock and A. Reller, *J. Mater. Chem.* 1995, **5,** 589.
10. U. Bemn, K. Lashgari, R. Norrestam, M. Nygren and G. Westin, *J. Solid State Chem.* 1993, **103,** 366; M. Antapin, Y. Struchkov, A. Shilov and A. Shilova, *Gazz. Chim. Ital.* 1993, **123,** 265; M. Veith, D. Käfer, J. Koch, P. May, L. Stahl and V. Huch, *Chem. Ber.* 1992, **125,** 1033; M. Yu. Antipin, L. P. Didenko, L. M. Kachapina, A. E. Shilov, A. K. Shilova and Y. T. Struchkov, *J. Chem. Soc., Chem. Commun.* 1989, 1467; L. Malpezzi, U. Zucchini and T. Dall'Occo, *Inorg. Chim. Acta* 1991, **180,** 245; M. Veith, J. Hans, L. Stahl, P. May, V. Huch and A. Sebald, *Z. Naturforsch.* 1991, **46b,** 403.
11. (a) J. A. Meese-Markscheffel, R. Fukuchi, M. Kido, G. Tachibana, C. M. Jensen and J. W. Gilje, *Chem. Mater.* 1993, **5,** 755; (b) J. A. Meese-Marktscheffel, R. E. Cramer and J. W. Gilje, *Polyhedron* 1994, **13,** 1045; (c) J. Sabmannshausen, R. Riedel, K. B. Pfanz and H. Chmiel, *Z. Naturforsch* 1993, **48b,** 7; (d) C.-C. Chang, W.-H. Lee, T.-Y. Her, G.-H. Lee, S.-M. Peng and Y. Wang, *J. Chem. Soc., Dalton Trans.* 1994, 315; (e) C.-C. Chang, T.-Y. Her, M.-D. Li, R. Williamson, G.-H. Lee, S.-M. Peng and Y. Wang, *Inorg. Chem.* 1995, **34,** 4296.
12. G. M. Sheldrick, *SHELXS-86*, Crystallographic computing (Edited by G. M. Sheldrick, C. Krüger and R. Goddard), Vol. 3, p. 175. Oxford University Press, Oxford (1985).
13. G. M. Sheldrick, *SHELX93, program for the refinement of crystal structure*. University of Göttingen, Germany (1993).
14. A. L. Spek, *PLATON 94*, *Acta Cryst.* 1990, **A46,** C34.
15. Y. S. Ng, G. A. Rodley and W. T. Robinson, *Inorg. Chem.* 1976, **15,** 303.
16. O. Poncelet, L. G. Hubert-Pfalzgraf and J.-C. Daran, *Inorg. Chem.* 1990, **29,** 2883.
17. S. Boulmaaz, R. Papiernik and L. G. Hubert-Pfalzgraf, *Polyhedron* 1992, **11,** 1331.
18. O. Poncelet, L. G. Hubert-Pfalzgraf, J.-C. Daran and R. Astier, *J. Chem. Soc., Chem. Commun.* 1989, 1846.
19. S. C. Goel, M. A. Matchett, M. Y. Chiang and W. E. Buhro, *J. Am. Chem. Soc.* 1991, **113,** 1844.
20. E. A. Sadurski, W. H. Ilsley, R. D. Thomas, M. D. Glick and J. P. Oliver, *J. Am. Chem. Soc.* 1978, **100,** 7761.

Pergamon

PII: S0277-5387(96)00325-7

Polyhedron Vol. 16, No. 4, pp. 593–597, 1997
Copyright © 1996 Elsevier Science Ltd
Printed in Great Britain. All rights reserved
0277-5387/97 $17.00+0.00

Synthesis and structural characterization of the pentaruthenium cluster $[(\mu\text{-H})_2Ru_5\{\mu_4\text{-}CC(CH_3)COOC_2H_5\}(CO)_{14}]$

Xue-Wen Dong,[a] Yu-Zhong Lun[a]* and Kai-Bai Yu[b]

[a]National Engineering Research Center for Fine-Petrochemical Intermediates, Lanzhou Institute of Chemical Physics, Chinese Academy of Sciences, Lanzhou 730000, P.R. China

[b]Chengdu Center of Analysis and Measurement, Chinese Academy of Sciences, Chengdu 610041, P.R. China

(Received 16 February 1996; accepted 1 July 1996)

Abstract—The reaction between $Ru_3(CO)_{12}$ with ethyl methacrylate in octane followed by separation by TLC has given the new pentaruthenium cluster $[(\mu\text{-H})_2Ru_5\{\mu_4\text{-}CC(CH_3)COOC_2H_5\}(CO)_{14}]$. The product was characterized by elemental analyses, IR, and NMR and the X-ray was determined by diffraction analysis.
Copyright © 1996 Elsevier Science Ltd

Keywords: cluster; synthesis; pentaruthenium; characterization; ethyl methacrylate; dodecacarbonyl triruthenium.

The investigation of pentaruthenium clusters in recent years has been focused mainly on two aspects; one is the reactivity of the cluster $[(Ru_5(CO)_{15}(\mu_5\text{-}C_2PPh_2)(\mu\text{-}PPh_2)]$ which has been reviewed and reported in several papers [1–7]; the other concerns benzene derivatives of the square pyramidal carbido cluster $Ru_5C(CO)_{15}$ which has been reviewed recently [8, 9].

In the present study, a new pentaruthenium cluster $[(\mu\text{-H})_2Ru_5\{\mu_4\text{-}CC(CH_3)COOC_2H_5\}(CO)_{14}]$ has been synthesized by the direct reaction of $Ru_3(CO)_{12}$ with ethyl methacrylate. The synthesis and characterization of the title cluster is reported herein as well as an X-ray crystal structure determination.

RESULTS AND DISCUSSION

Synthesis and characterization of $[(\mu\text{-H})_2Ru_5\{\mu_4\text{-}CC(CH_3)COOC_2H_5\}(CO)_{14}]$

Treatment of $Ru_3(CO)_{12}$ with ethyl methacrylate in octane gave the new title cluster (Fig. 1). The elemental analysis corresponded to the given formula. The presence of the terminal carbonyl ligands was confirmed by the IR absorptions in the range 1977–2098 cm^{-1}. In the ^1H NMR spectra, characteristic resonances were observed consistent with the structure of the title cluster. In the group of ^{13}C NMR signals δ 64.7 and 28.9 for OC_2H_5, δ 14.3 for CH_3, the small signal at δ 61.5 is due to C(18) (Fig. 2). The seven resonances in the ^{13}C NMR spectrum at δ 184.5, 189.8, 192.3, 192.6, 194.4, 196.1 and 197.4 correspond to the carbonyl ligands coordinated to five ruthenium atoms.

Crystal structure of $[(\mu\text{-H})_2Ru_5\{\mu_4\text{-}CC(CH_3)COOC_2H_5\}(CO)_{14}]$

Suitable crystals of $[(\mu\text{-H})_2Ru_5\{\mu_4\text{-}CC(CH_3)COOC_2H_5\}(CO)_{14}]$ were obtained by slowly lowering the temperature of its $CHCl_3$ solution. The molecular structure and crystal cell is illustrated in Figs 1 and 2. Bond lengths and angles with estimated standard deviations are collected in Tables 1 and 2.

The metal core adopts the shape of a distorted pyramid. One edge is bridged by C(18) and O(15) of the ligands [with Ru(1)—C(18) 2.194(6) and Ru(2)—O(15) 2.122 Å]; C(20) is bonded to four Ru

* Author to whom correspondence should be addressed.

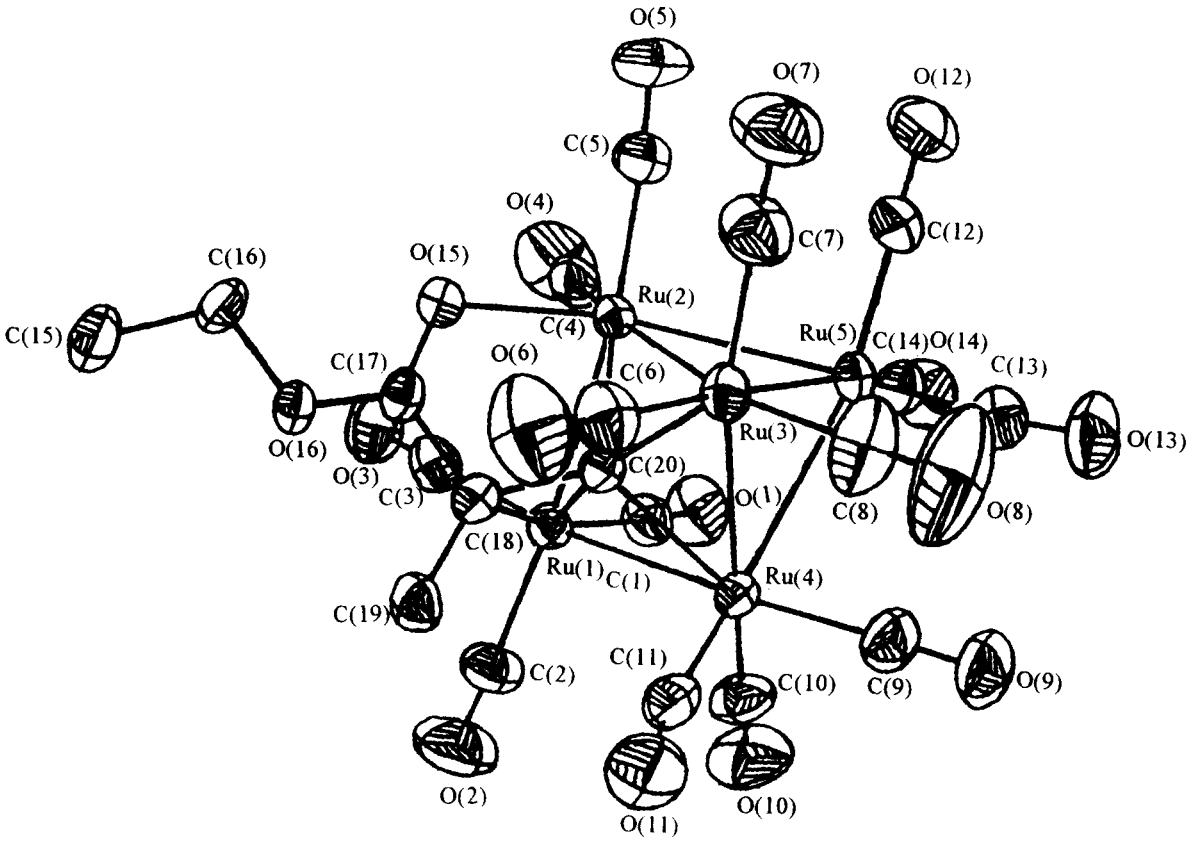


Fig. 1. ORTEP drawing of $[(\mu\text{-H})_2Ru_5\{\mu_4\text{-CC}(CH_3)COOC_2H_5\}(CO)_{14}]$.

atoms. The 14 remaining CO ligands are terminal. The double bond in the ligand has been opened, C(20) is coordinated to four different ruthenium atoms Ru(1), Ru(2), Ru(3), Ru(4) and C(18) is coordinated to Ru(1). The oxygen atom O(15) in the ligand is coordinated to Ru(2). The five ruthenium atoms give a square-pyramidal structure. The location of two bridging H atoms in the complex was conjectured to be between Ru(2)—Ru(5) and Ru(1)—Ru(4), respectively. The Ru—Ru distances in

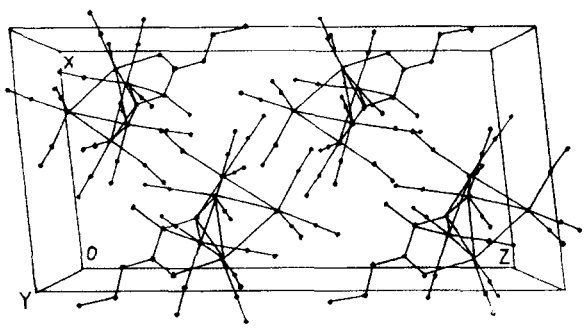


Fig. 2. Unit Cell of $[(\mu\text{-H})_2Ru_5\{\mu_4\text{-CC}(CH_3)COOC_2H_5\}(CO)_{14}]$.

Table 1. Bond lengths (Å) for the title compound

Ru(1)—Ru(2)	2.811(1)	Ru(1)—Ru(4)	2.896(1)
Ru(1)—C(1)	1.932(6)	Ru(1)—C(2)	1.928(7)
Ru(1)—C(18)	2.194(6)	Ru(1)—C(3)	1.901(7)
Ru(1)—C(20)	2.118(6)	Ru(2)—Ru(3)	2.856(1)
Ru(2)—Ru(5)	2.950(1)	Ru(2)—O(15)	2.122(4)
Ru(2)—C(4)	1.877(7)	Ru(2)—C(5)	1.909(8)
Ru(2)—C(20)	2.121(6)	Ru(3)—Ru(4)	2.803(1)
Ru(3)—Ru(5)	2.787(1)	Ru(3)—C(6)	1.908(7)
Ru(3)—C(7)	1.887(9)	Ru(3)—C(8)	1.898(8)
Ru(3)—C(20)	2.115(6)	Ru(4)—Ru(5)	3.036(1)
Ru(4)—C(9)	1.913(7)	Ru(4)—C(10)	1.906(8)
Ru(4)—C(20)	2.185(5)	Ru(5)—C(12)	1.904(7)
Ru(5)—C(13)	1.906(7)	Ru(5)—C(14)	1.927(7)
O(1)—C(1)	1.141(8)	O(2)—C(2)	1.119(10)
O(3)—C(3)	1.126(8)	O(4)—C(4)	1.145(10)
O(5)—C(5)	1.136(10)	O(6)—C(6)	1.137(9)
O(7)—C(7)	1.140(10)	O(8)—C(8)	1.143(11)
O(9)—C(9)	1.129(8)	O(10)—C(10)	1.138(10)
O(11)—C(11)	1.137(9)	O(12)—C(12)	1.137(9)
O(13)—C(13)	1.121(9)	O(14)—C(14)	1.138(9)
O(15)—C(17)	1.248(7)	O(16)—C(16)	1.464(7)
O(16)—C(17)	1.312(6)	C(15)—C(16)	1.486(9)
C(17)—C(18)	1.464(8)	C(18)—C(19)	1.522(9)
C(18)—C(20)	1.466(8)		

Table 2. Bond angles (°) for the title compound

Ru(2)—Ru(1)—Ru(4)	81.4(1)	Ru(2)—Ru(1)—C(1)	92.6(2)
Ru(4)—Ru(1)—C(1)	89.8(2)	Ru(2)—Ru(1)—C(2)	169.1(2)
Ru(4)—Ru(1)—C(2)	96.0(2)	C(1)—Ru(1)—C(2)	98.0(3)
Ru(2)—Ru(1)—C(3)	89.7(2)	Ru(4)—Ru(1)—C(3)	170.8(2)
C(1)—Ru(1)—C(3)	92.8(3)	C(2)—Ru(1)—C(3)	92.3(3)
Ru(2)—Ru(1)—C(18)	70.6(2)	Ru(4)—Ru(1)—C(18)	77.6(1)
C(1)—Ru(1)—C(18)	160.1(3)	C(2)—Ru(1)—C(18)	98.5(3)
C(3)—Ru(1)—C(18)	97.5(2)	Ru(2)—Ru(1)—C(20)	48.5(2)
Ru(4)—Ru(1)—C(20)	48.7(1)	C(1)—Ru(1)—C(20)	120.8(2)
C(2)—Ru(1)—C(20)	122.4(3)	C(3)—Ru(1)—C(20)	123.0(3)
C(18)—Ru(1)—C(20)	39.7(2)	Ru(1)—Ru(2)—Ru(3)	93.3(1)
Ru(1)—Ru(2)—Ru(5)	92.9(1)	Ru(3)—Ru(2)—Ru(5)	57.3(1)
Ru(1)—Ru(2)—O(15)	84.2(1)	Ru(3)—Ru(2)—O(15)	97.4(1)
Ru(5)—Ru(2)—O(15)	154.5(1)	Ru(1)—Ru(2)—C(4)	84.5(2)
Ru(3)—Ru(2)—C(4)	168.1(2)	Ru(5)—Ru(2)—C(4)	111.0(2)
O(15)—Ru(2)—C(4)	93.9(2)	Ru(1)—Ru(2)—C(5)	172.4(2)
Ru(3)—Ru(2)—C(5)	93.1(2)	Ru(5)—Ru(2)—C(5)	93.8(2)
O(15)—Ru(2)—C(5)	91.1(2)	C(4)—Ru(2)—C(5)	90.0(3)
Ru(1)—Ru(2)—C(20)	48.4(2)	Ru(3)—Ru(2)—C(20)	47.5(2)
Ru(5)—Ru(2)—C(20)	80.4(1)	O(15)—Ru(2)—C(20)	78.8(2)
C(4)—Ru(2)—C(20)	132.6(3)	C(5)—Ru(2)—C(20)	136.4(3)
Ru(2)—Ru(3)—Ru(4)	82.2(1)	Ru(2)—Ru(3)—Ru(5)	63.0(1)
Ru(4)—Ru(3)—Ru(5)	65.8(1)	Ru(2)—Ru(3)—C(6)	109.7(2)
Ru(4)—Ru(3)—C(6)	107.6(2)	Ru(5)—Ru(3)—C(6)	170.1(2)
Ru(2)—Ru(3)—C(7)	89.2(3)	Ru(4)—Ru(3)—C(7)	159.2(2)
Ru(5)—Ru(3)—C(7)	93.4(2)	C(6)—Ru(3)—C(7)	93.2(3)
Ru(2)—Ru(3)—C(8)	156.3(2)	Ru(4)—Ru(3)—C(8)	90.4(3)
Ru(5)—Ru(3)—C(8)	93.4(2)	C(6)—Ru(3)—C(8)	94.0(3)
C(7)—Ru(3)—C(8)	90.0(4)	Ru(2)—Ru(3)—C(20)	47.7(2)
Ru(4)—Ru(3)—C(20)	50.4(1)	Ru(5)—Ru(3)—C(20)	84.5(1)
C(6)—Ru(3)—C(20)	85.6(3)	C(7)—Ru(3)—C(20)	132.2(3)
C(8)—Ru(3)—C(20)	137.7(3)	Ru(1)—Ru(4)—Ru(3)	92.6(1)
Ru(1)—Ru(4)—Ru(5)	89.5(1)	Ru(3)—Ru(4)—Ru(5)	56.8(1)
Ru(1)—Ru(4)—C(9)	165.9(2)	Ru(3)—Ru(4)—C(9)	93.6(3)
Ru(5)—Ru(4)—C(9)	83.4(2)	Ru(1)—Ru(4)—C(10)	79.4(2)
Ru(3)—Ru(4)—C(10)	168.3(2)	Ru(5)—Ru(4)—C(10)	114.1(2)
C(9)—Ru(4)—C(10)	92.4(4)	Ru(1)—Ru(4)—C(11)	104.0(2)
Ru(3)—Ru(4)—C(11)	96.2(2)	Ru(5)—Ru(4)—C(11)	150.8(2)
C(9)—Ru(4)—C(11)	87.8(3)	C(10)—Ru(4)—C(11)	94.0(3)
Ru(1)—Ru(4)—C(20)	46.7(2)	Ru(3)—Ru(4)—C(20)	48.2(1)
Ru(5)—Ru(4)—C(20)	77.5(1)	C(9)—Ru(4)—C(20)	141.7(3)
C(10)—Ru(4)—C(20)	125.6(3)	C(11)—Ru(4)—C(20)	93.0(2)
Ru(2)—Ru(5)—Ru(3)	59.6(1)	Ru(2)—Ru(5)—(4)	76.8(1)
Ru(3)—Ru(5)—Ru(4)	57.4(1)	Ru(2)—Ru(5)—C(12)	90.1(2)
Ru(3)—Ru(5)—C(12)	93.3(2)	Ru(4)—Ru(5)—C(12)	150.7(2)
Ru(2)—Ru(5)—C(13)	155.4(2)	Ru(3)—Ru(5)—C(13)	96.0(2)
Ru(4)—Ru(5)—C(13)	93.6(2)	C(12)—Ru(5)—C(13)	87.5(3)
Ru(2)—Ru(5)—C(14)	109.7(2)	Ru(3)—Ru(5)—C(14)	164.8(2)
Ru(4)—Ru(5)—C(14)	111.3(2)	C(12)—Ru(5)—C(14)	97.7(3)
C(13)—Ru(5)—C(14)	94.9(3)	Ru(2)—O(15)—C(17)	112.5(3)
C(16)—O(16)—C(17)	116.4(5)	Ru(1)—C(1)—O(1)	176.0(6)
Ru(1)—C(2)—O(2)	177.8(7)	Ru(1)—C(3)—O(3)	178.3(7)
Ru(2)—C(4)—O(4)	178.6(6)	Ru(2)—C(5)—O(5)	174.0(6)
Ru(3)—C(6)—O(6)	176.9(7)	Ru(3)—C(7)—O(7)	175.9(8)
Ru(3)—C(8)—O(8)	178.2(8)	Ru(4)—C(9)—O(9)	177.0(9)
Ru(4)—C(10)—O(10)	176.2(6)	Ru(4)—C(11)—O(11)	171.1(6)
Ru(5)—C(12)—O(12)	177.9(6)	Ru(5)—C(13)—O(13)	173.9(7)
Ru(5)—C(14)—O(14)	178.8(6)	O(16)—C(16)—C(15)	108.0(5)
O(15)—C(17)—O(16)	120.4(5)	O(15)—C(17)—C(18)	122.1(5)
O(16)—C(17)—C(18)	117.5(5)	Ru(1)—C(18)—C(17)	108.5(4)
Ru(1)—C(18)—C(19)	117.8(4)	C(17)—C(18)—C(19)	114.7(5)

Table 2.—*continued*

Ru(1)—C(18)—C(20)	67.4(3)	C(17)—C(18)—C(20)	111.4(5)
C(19)—C(18)—C(20)	127.2(5)	Ru(1)—C(20)—Ru(2)	83.1(2)
Ru(1)—C(20)—Ru(3)	153.8(3)	Ru(2)—C(20)—Ru(3)	84.8(2)
Ru(1)—C(20)—Ru(4)	84.6(2)	Ru(2)—C(20)—Ru(4)	119.6(2)
Ru(3)—C(20)—Ru(4)	81.4(2)	Ru(1)—C(20)—C(18)	72.9(3)
Ru(2)—C(20)—C(18)	108.4(4)	Ru(3)—C(20)—C(18)	133.1(4)
Ru(4)—C(20)—C(18)	123.5(4)		

the cluster average 2.877 Å which compares well with the average Ru—Ru distance of 2.85 Å in $Ru_3(CO)_{12}$ [10].

There are several interesting features of the structure. The seven Ru—Ru separations range between 2.78 and 3.04 Å but fall into three groups. (i) The Ru(1)—Ru(2) bond is bridged by C(18), O(15), C(20) [2.811(1) Å]. (ii) The Ru(2)—Ru(3), Ru(3)—Ru(4), Ru(1)—Ru(4) bonds are bridged by C(20) [2.856(1), 2.803(1) and 2.896(1) Å]. (iii) The three non-bridged basal Ru—Ru bonds, the longest Ru(4)—Ru(5), the shortest Ru(3)—Ru(5) and Ru(2)—Ru(5) bonds [3.036(1), 2.787(1) and 2.950(1) Å].

The electron count requires the ligand chain to donate six electrons to the cluster, these come formally from C(18) (one), C(20) (three), O(15) (two) and two come from the two hydrogens. Together with the 14 CO groups (28), the cluster has a 76-cluster valence electron (c.v.e.) configuration.

EXPERIMENTAL

General procedure

All operations were carried out under nitrogen on a standard Schlenk line. Solvents were purified by conventional methods and distilled under nitrogen prior to use. NMR spectra were obtained with a Bruker AM 400 NMR spectrometer. The peak positions are reported downfield of TMS. The IR spectrum was recorded on a Nicolet 10 DX FT-IR spectrometer. The C and H analyses were carried out with a Carlo–Erba 1106 microanalyser. $Ru_3(CO)_{12}$ was prepared as described in the literature [11]. Ethyl methacrylate was obtained commercially and used as received.

Preparation of $[(\mu\text{-H})_2Ru_5\{\mu_4\text{-CC}(CH_3)COOC_2H_5\}(CO)_{14}]$

A solution of $Ru_3(CO)_{12}$ (200 mg, 0.3 mmol) and ethyl methacrylate (100 mg, 0.9 mmol) in octane (50 cm^3) was heated for 22 h at 110°C. After cooling to room temperature the solvent was removed under reduced pressure and the residue was purified by preparative TLC. Eluting with petroleum ether (30–60°C), gave a fraction from which the red cluster $[(\mu\text{-H})_2Ru_5\{\mu_4\text{-CC}(CH_3)COOC_2H_5\}(CO)_{14}]$ (20 mg, 10%) was obtained. Found: C, 23.7; H, 1.0. Calc. for $C_{20}H_{10}O_{16}Ru_5$: C, 23.7; H, 1.0%; IR (KBr pellet) cm^{-1}: 2099 w, 2074 s, 2045 vs, 2025 s, 1993 s, 1977 w. ^1H NMR ($CDCl_3$): δ 1.84 (s, CH_3), 1.25 (t, CH_3), 4.12 (q, CH_2), −21.17, −28.56 (2 × s, Ru—H—Ru). ^{13}C NMR ($CDCl_3$): δ 184.5, 189.8, 192.3, 192.6, 194.4, 196.1, 297.4 (7 × s, CO), 61.52 (d, C(18)), 64.7 (s, CH_2), 29.0 (s, CH_3), 14.3 (s, CH_3).

Single-crystal X-ray diffraction analysis

A red crystal of the title cluster having approximate dimensions of 0.20 × 0.22 × 0.40 mm was mounted on a R3M/E four-circle diffractometer. Graphite monochromated Mo K_α radiation (λ = 0.71073 Å) and a θ–2θ scan type were used to measure the intensity data in the range $2 \leqslant 2\theta \leqslant 45°$. The unit cell was determined and refined with 25 reflections in the 2θ range 9.64–23.74°. Crystal data for $[(\mu\text{-H})_2Ru_5\{\mu_4\text{-CC}(CH_3)COOC_2H_5\}(CO)_{14}]$: $C_{20}H_{10}O_{16}Ru_5$, monoclinic space group $P2_1/c$, a = 10.541(2), b = 13.275(2), c = 20.300(3) Å, $\alpha = \gamma = 90.00(0)$, β = 95.97(1)°, V = 2825.1(9) Å^3, Z = 4, D_c = 2.38 g cm^{-3}, μ(Mo K_α) = 26.2 cm^{-1}, $F(000)$ = 1920. The 3140 independent reflections with $I \geqslant 1.5\,\sigma(I)$ of 4243 measured were corrected for Lorentz and polarization effects.

The structure was solved by the heavy-atom technique and refined by full-matrix least-squares methods. Refinement converged at a final R of 0.0305 (Rw = 0.0250, largest shift/esd −0.039), with allowance for the thermal anisotropy of all non-hydrogen atoms. Complex scattering factors were taken from the program package SHELXTL [12], as implemented on an Eclipse S140 computer, which was used for structure solution and refinement. A weighting scheme $\omega = \{1-\exp\}[-5(\sin\theta/\lambda)^2)/[\sigma^2(F)+0.0001F^2]$ was used in the later stages of refinement. Pertinent results are given in Figs 1 and 2 and Tables 1 and 2. Tables of coordinates, structure amplitudes, thermal and full non-hydrogen parameters have been deposited at the Cambridge Crystallographic Data Centre.

Acknowledgement—We acknowledge financial support of this work from the State Key Laboratory for Oxo Synthesis and Selective Oxidation, Lanzhou Institute of Chemical Physics, Chinese Academy.

REFERENCES

1. M. I. Bruce, *J. Organomet. Chem.* 1990, **394,** 365.
2. M. I. Bruce and M. J. Liddell, *J. Organomet. Chem.* 1991, **410,** 211.
3. C. J. Adams, M. I. Bruce and B. W. Skelton, *J. Organomet. Chem.* 1991, **420,** 87.
4. C. J. Adams, M. I. Bruce and M. J. Liddell, *J. Organomet. Chem.* 1991, **420,** 105.
5. M. I. Bruce, M. J. Liddell and B. W. Skelton, *Organometallics* 1991, **10,** 3282.
6. C. J. Adams and M. I. Bruce, *J. Organomet. Chem.* 1992, **430,** 181.
7. C. J. Adams, M. I. Bruce, B. W. Skelton and A. H. White, *J. Chem. Soc., Chem. Commun.* 1992, 26.
8. B. F. G. Johnson, *J. Organomet. Chem.* 1994, **475,** 31.
9. D. Braga, P. J. Dyson, Fabrizia Grepioni and B. F. G. Johnson, *Chem. Rev.* 1994, **94,** 1585.
10. S.-H. Han, S. T. Nguyen and G. L. Geoffroy, *Organometallics*, 1988, **7,** 2034.
11. C. R. Eady and D. E. Jackson, *J. Chem. Soc., Dalton Trans.* 1980, 383.
12. G. M. Sheldrick, SHELXTL, *An integrated system for solving, refining and displaying crystal structures from diffraction data* (Revision 5.1). University of Gottingen, Germany (1985).

Pergamon

PII: S0277-5387(96)00319-1

Polyhedron Vol. 16, No. 4, pp. 599–602, 1997
Copyright © 1996 Elsevier Science Ltd
Printed in Great Britain. All rights reserved
0277-5387/97 $17.00+0.00

Comparative formation constants for metal ions with macrocycles based on 1,4,8,11-tetraazacyclotetradecane and carrying diamine, dicarboxylate or amine-carboxylate pendants

Yakup Baran,[a] Geoffrey A. Lawrance[b]* and Eric N. Wilkes[b]

[a]Department of Chemistry, Art and Science Faculty, The University of Karaelmas, 67100 Zonguldak, Turkey

[b]Department of Chemistry, The University of Newcastle, Callaghan 2308, Australia

(Received 14 June 1996; accepted 27 June 1996)

Abstract—Acid dissociation constants for the newly isolated dihydrogen *anti*-1,4,8,11-tetraazacyclotetradecane-6,13-dicarboxylate (diacmac), as well as for hydrogen *anti*-6-methyl-1,4,8,11-tetraazacyclotetradecane-6-amine-13-carboxylate (acammac) and *anti*-6,13-dimethyl-1,4,8,11-tetraazacyclotetradecane-6,13-diamine (diammac) are reported. The ligands differ somewhat in their selection of metal ions, which is reflected in the formation constants for complexation (log K_{ML}, 25°C) which have been determined for the d^{10} metal ions Zn^{2+} (diammac, 14.9; acammac, 14.7; diacmac, 26.3), Cd^{2+} (diammac, 10.6; acammac, 16.7; diacmac, 15.9), Hg^{2+} (diammac, 10.5; acammac, 17.3; diacmac, 21.8) and Pb^{2+} (diammac, 10.8; acammac, 10.7; diacmac, 19.0) and the d^5 Mn^{2+} ion (diammac, 6.2; acammac, 12.0; diacmac, 18.3). Differences arise in part from the increasing availability of potential O donors versus N donors in stepping from diammac to diacmac, and imply a clear role for the pendants in binding metal ions. Copyright © 1996 Elsevier Science Ltd

Keywords: macrocycles; metal complexes; formation constants.

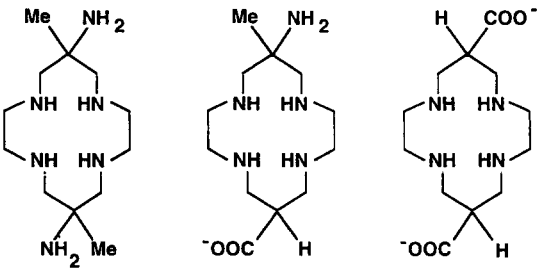
Pendant arm analogues of the 14-membered parent macrocycle 1,4,8,11-tetraazacyclotetradecane (cyclam) with groups pendant to the ring at both carbons in the centre of the opposite propyl chains have been described previously [1,2]. Macrocycles with two primary amine groups, one primary amine group and one carboxylate group, or two carboxylate groups attached to these carbons as potential donor groups have been prepared *via* copper(II)-directed condensation of ethane-1,2-diamine complexes with formaldehyde and nitroethane and/or diethyl malonate [3–5]. Subsequent reduction and/or decarboxylation and hydrolysis reactions lead to the three potentially sexidendate macrocycles diammac (**1**) [3], acammac (**2**) 4 and diacmac (**3**). Analogues based on related 1,2-diamines are also known [6]. All these macrocycles can, in principle, exist in two geometric forms, with the potential pendant donor groups in *syn* or *anti* dispositions relative to the macrocyclic ring [1]. Separation and isolation of the two geometric forms of **1** was only established relatively recently [7], as were the differing stability constants for the complexation of metal ions [8]. Both **2** and **3** exist only, or at least predominantly, as the *anti* isomer, arising from control of stereochemistry during their formation reactions [4]. The isolation of **3** as a free ligand salt is described here. Furthermore, a comparison of the variation in selective complexation by this series of ligands has been carried out and is described in this paper.

* Author to whom correspondence should be addressed.

EXPERIMENTAL

Syntheses

Syntheses of both hydrogen *anti*-6-methyl-1,4,8,11-tetraazacyclotetradecane-6-amine-13-carboxylate (acammac) and *anti*-6,13-dimethyl-1,4,8,11-tetraaza-



1 2 3

cyclotetradecane-6,13-diamine (diammac) and their isolation as hydrochloride salts have been reported previously [4, 7].

Dihydrogen anti-1,4,8,11-*tetraazacyclotetradecane*-6,13-*dicarboxylate hydrochloride*, (H_2*diacmac*·4HCl). Bis(ethane-1,2-diamine)copper(II) perchlorate (16.3 g) was dissolved in methanol (300 cm^3) and heated to 50°C. To this solution were added diethyl malonate (12.5 cm^3), formaldehyde solution (12 cm^3, 38% aq.) and triethylamine (10.5 cm^3), and the solution was refluxed for 3 h. Additional diethylmalonate (2 cm^3) and formaldehyde (2 cm^3) were added, and the solution stirred and allowed to cool slowly to room temperature. Following refrigeration, a pink precipitate was collected, dissolved in water (2 dm^3) and sorbed on to a column of SP-Sephadex C-25 resin (20 cm × 5 cm). Only one major band was recovered upon elution with 1 mol dm^{-3} NaCl. As the volume of the solution was reduced by rotary evaporation, a pink solid precipitated, and was collected washed with ethanol and air dried (1.4 g, 5%). The synthesis was repeated to obtain more of the intermediate tetraethyl 1,4,8,11-tetraazacyclotetradecane-6,6,13,13-tetracarboxylate complex [5]. This complex (2.8 g) was dissolved in methanol (200 cm^3) containing 4 cm^3 of water by heating to 60°C, the pH was raised to > 10 by addition of triethylamine, and the solution stirred for 20 h. After dilution to 2 dm^3 with water, the solution was sorbed on to a column of SP-Sephadex C-25 resin (20 cm × 5 cm) and eluted with 0.2 mol dm^{-3} $NaClO_4$ solution. One major acid-stable band and two minor bands, which were not acid stable and not macrocyclic compounds, were collected. The major band and a solution of 3M HCl (30 cm^3) were placed in separate dropping funnels and added dropwise with stirring to powdered zinc (6 g). The reducing solution was stirred at 60°C after addition for a further 30 min, then filtered to remove reduced copper and unreacted zinc metal. After dilution to 2 dm^3, the solution was sorbed on to a column of Dowex 50Wx2 resin (4 cm × 15 cm), washed with 0.2 dm^3 water and 0.5 mol dm^{-3} HCl, then eluted with 3 mol dm^{-3} HCl, the product being detected by testing small aliquots regularly with copper ions and base addition. The product was taken to dryness on a rotary evaporator, collected, washed with ethanol and diethyl ether, and dried thoroughly (0.9 g). (Found: C, 32.7; H, 6.9; N, 12.8. Calc. for $C_{12}H_{24}N_4O_4 \cdot 4HCl \cdot 0.5H_2O$: C, 32.5; H, 6.6; N, 12.7%; acid content confirmed by potentiometric titration). NMR (D_2O): $^1H\delta$ 3.4–3.9 (q × 3, overlapping); $^{13}C\delta$ 41.0, 45.4, 48.2 174.6.

Physical methods

NMR spectra (in D_2O) were recorded using a Bruker Avance DPX300 spectrometer, with sodium TSP as reference. Elemental analyses were performed by the Australian National University Microanalysis Service. Potentiometric titrations were carried out essentially as described previously [9] using a Metrohm 665 automated burette and an IBM clone computer fitted with a Fylde Scientific pH card connected to a Metrohm combined glass electrode. All measurements were fully automated under control of the IBM clone computer. Titrations were performed at 25.0 ± 0.1°C in constant ionic strength (I = 0.5 mol dm^{-3}, KCl) aqueous solutions under nitrogen. Solutions of ligand (6×10^{-4} mol dm^{-3}), alone and in the presence of 0.9 or 0.5 equivalents of metal ion, were titrated with 83 increments (of 4×10^{-6} dm^3) of 0.4 mol dm^{-3} NaOH. Equilibrium constants were calculated from potentiometric data with a TURBO BASIC version of the program TITFIT [10]. For each system, each titration was repeated at least three times, with good reproducibility (*ca* ± 0.1 log units) in the determined constants.

RESULTS AND DISCUSSION

The macrocycles examined contain four secondary amines and either two pendant primary amines (**1**), one pendant primary amine and one pendant carboxylic acid group (**2**), or two pendant carboxylic acid groups (**3**), all capable of coordination to metal ions. They adopt similar *anti* geometry in terms of location of the pendants relative to the macrocycle plane. The basic fourteen-membered macrocyclic ring in all three, ignoring the pendants, is that of the classical macrocycle cyclam (1,4,8,11-tetraazacyclotetradecane, **4**) in all cases. Although **1** and **2** have been described as free ligands obtained in good yield previously, [4, 7] **3** is accessible by only low-yield routes and the isolation of **3** in an acceptable, though modest yield has not

been detailed earlier. Whereas **1** exists as both *syn* and *anti* isomers [3], both **2** and **3** form only one isomer (*anti*) dominantly or exclusively, which is presumably associated with a relatively strong axial interaction of a pendant carboxylate group during synthesis directing the stereochemistry with high stereospecificity, a process which cannot occur with the poor nitro group pendants that are involved in the synthetic route that eventually yields **1**, All three ligands can act as sexidentate ligands, as has been described in detail for **1** and **2**, and to a limited extent for **3**. The pendant groups enforce boat geometries on the chelate rings to which they are attached when they coordinate to a metal ion, with strain and associated distortions greater in the case of the amine pendant than the carboxylate pendant [4].

The transition from two primary amine pendant donors to two carboxylate pendant donors *via* the species with one of each donor presents an opportunity to examine the influence of different pendants on the metal ion-binding capabilities in a series where the pentants are attached directly to the macrocycle ring. Given the common framework linking **1–4** it is not unreasonable to find that the protonation constants of all ligands are somewhat similar (Table 1) [8,11,12]. In the data presented in Table 1, L is the neutral hexamine (**1**), or else the deprotonated amino acid (**2** and **3**), and hence six protonation steps can be expected for each ligand. The first and second protonations occur with log K_a values near 11 and 10 in all ligands, and are associated with proton addition to the secondary amines in the macrocycle ring, with the protons shared between adjacent pairs of amines within the ring [11,12]. The next two steps in **1** (and the next step in **2**), which are absent in the unsubstituted cyclam, are assigned to protonation of the pendant primary amines. Introduction of the last two protons into the ring only occurs with difficulty, and only one of the two can be observed (log K_a *ca* 2), the final protonation being inaccessible in dilute aqueous acid. Protonation of the two carboxylate groups in **3** and the single group in **2** occur with pK_a values near 4, as anticipated for such groups. Where two acid groups are present, the pK_a values are lower. In both **2** and **3** the protonation assigned to the final amines occurs more readily, presumably as a result of electronic influences of the carboxylate groups, or else as a result of zwitterionic behaviour.

Binding of the d^{10} metal ions shows a significant difference in formation constants for **1** compared with **3**, employing a common model for analysis of titration data, and imply that the pendant groups play a role in metal ion binding. Of the metal ions examined, only zinc(II) has been shown to be capable of (although not necessarily having a preference for) sexidentate coordination to **1** [1], and presumably this will be the case with **2** and **3** also. The significant difference for log K_{ML} from **1** to **3** with zinc ion probably reflects formation of a highly preferred, neutral sexidentate complex with **3**, whereas **1** and **2** may not participate in sexidentate coordination at all under the conditions employed. The other metal ions are too large to be incorporated into the macrocycle ring, and thus differences between ligands are subsequently not generally so marked. However, with **3**, even where metal ions bind in a five-coordinate mode as a square-based pyramid, at least one of the carboxylate pendant groups must be coordinated, whereas **2** has a choice of amine or carboxylate axial donors and **1** only axial amine donors, accounting for differences between **1** and **3** with all metal ions and less substantial differences between **1** and **2**. Both protonated species, MLH and MLH_2, modelled exhibit significantly lower stabilities than ML species, consistent with proton incorporation into the macrocycle which makes binding involving the ring unfavourable, without any obvious trends; these species may involve only simple chelation involving a pendant and one ring secondary amine exo to the ring. A MLH_{-1} species can be modelled reasonably consistently, presumably associated with a deprotonated coordinated water and reduced

Table 1. The logarithms of the protonation and formation constants for **1**, **2** and **3** with various metal ions; some comparative values for cyclam (**4**) are included (charges are omitted for clarity)[a]

M	Complex	1	2	3	4
H^+	$H+L \rightleftharpoons HL$	11.0	10.5	10.6	11.6
	$HL+H \rightleftharpoons H_2L$	10.0	9.9	9.9	10.6
	$H_2L+H \rightleftharpoons H_3L$	6.2	6.4	4.0	
	$H_3+H \rightleftharpoons H_4L$	5.5	5.5	3.2	
	$H_4L+H \rightleftharpoons H_5L$	1.5[b]	3.2[c]	3.1[c]	1.6[d]
Zn^{2+}	$M+L \rightleftharpoons ML$	14.9	14.7	26.3	15.5
	$ML+H \rightleftharpoons MLH$	6.8	6.6	5.4	
	$MLH+H \rightleftharpoons MLH_2$	6.0	5.0	4.8	
	$ML \rightleftharpoons MLH_{-1}+H$	10.5	10.8	10.5	
Cd^{2+}	$M+L \rightleftharpoons ML$	10.6	16.7	15.9	11.3
	$ML+H \rightleftharpoons MLH$	7.5	6.8	7.1	
	$MLH+H \rightleftharpoons MLH_2$	5.7	6.0	3.4	
	$ML \rightleftharpoons MLH_{-1}+H$		7.1	7.2	
Hg^{2+}	$M+L \rightleftharpoons ML$	10.5	17.3	21.8	23.0
	$ML+H \rightleftharpoons M$	7.5	6.8	8.2	
	$MLH+H \rightleftharpoons MLH_2$	5.7	6.0	5.9	
	$ML \rightleftharpoons MLH_{-1}+H$		7.8	13.4	
Pb^{2+}	$M+L \rightleftharpoons ML$	10.8	10.7	19.0	10.8
	$ML+H \rightleftharpoons MLH$	7.5	6.1	7.3	
	$MLH+H \rightleftharpoons MLH_2$	4.1	3.0	4.2	
	$ML \rightleftharpoons MLH_{-1}+H$			8.0	
Mn^{2+}	$M+L \rightleftharpoons ML$	6.2	12.0	18.3	
	$ML+H \rightleftharpoons MLH$	8.2	8.6	8.9	
	$MLH+H \rightleftharpoons MLH_2$		5.9	3.7	
	$ML \rightleftharpoons MLH_{-1}+H$	4.6	8.7	9.3	

[a] 25 C, I = 0.5 mol dm^{-3} KCl, standard errors are ±0.1 units.

[b] Approximate only; sixth protonation not determined (< 1.5).

[c] Sixth protonation not determined (< 2).

[d] Third protonation; fourth protonation not determined (< 1.5).

coordination by the multidentate ligand. Formation constants with both **2** and **3** appear higher for this species than is the case with **1** for larger metal ions, presumably reflecting an enhanced stability of neutral or anionic species possible only with these ligands and not with **1**.

Whereas zinc can be considered a special case because it alone can accommodate six coordination, with all metal ions there will nevertheless be an interplay between O anion donor versus N donor preference in determining the size of the formation constant. With mercury(II), there is a trend in increasing formation constants for both ML and MLH_{-1} species with increasing number of available O donors, in line with the expected behaviour for O anion donor preference (Hg > Pb > Zn > Cd) [11, 12], but opposed to the expected behaviour for N donor preference (Hg > Cd > Zn > Pb) [11,12]. Lead typically shows a relatively strong O versus N preference, consistent with the step in formation constant from **1** to **3**, whereas, by contrast, Cd typically shows a relatively strong N versus O preference, again consistent with no major change from **1** to **3**. The trend for **3**, whereby log K_{ML} for Zn is significantly higher than that for Cd and Pb, inferring a strong selectivity towards zinc, is similar to that observed with the cyclic polyaminoacid 1,4,7-triazacyclononane-1,4,7-triacetate (log K_{ML} 26.6, Zn; 16.8, Cd; 16.6, Pb) [13]. The trend with the d^5 manganese(II) ion is consistent with an expected preference for O anion donors. Overall, the polyaminoacid diacmac is both a stronger binder of the d^{10} and d^5 metal ions examined compared with diammac, but at the same time more selective, as a result of the mixed donor set offered, including the sterically more efficient carboxylate donors.

Acknowledgement—Financial assistance from the Australian Research Council is gratefully acknowledged.

REFERENCES

1. P. V. Bernhardt and G. A. Lawrance, *Coord. Chem. Rev.* 1990, **104,** 297.
2. G. A. Lawrance, M. Maeder and E. N. Wilkes, *Rev. Inorg. Chem.* 1993, **13,** 199.
3. P. Comba, N. F. Curtis, G. A. Lawrance, A. M. Sargeson, B. W. Skelton and A. H. White, *Inorg. Chem.* 1986, **25,** 4260.
4. G. A. Lawrance, M. Maeder, T. W. Hambley and E. N. Wilkes, *J. Chem. Soc., Dalton Trans.* 1992, 1283.
5. N. F. Curtis, L. Xin and D. C. Weatherburn, *Trans. Met. Chem.* 1992, **17,** 147; *Inorg. Chem.* 1993, **32,** 5838.
6. P. V. Bernhardt, P. Comba, B. Elliott, G. A. Lawrance, M. Maeder, M. A. O'Leary, G. Wei and E. N. Wilkes, *Aust. J. Chem.* 1994, **47,** 1171.
7. P. V. Bernhardt, P. Comba, T. W. Hambley, G. A. Lawrance and K. Varnagy, *J. Chem. Soc., Dalton Trans.* 1992, 355.
8. P. G. Lye, G. A. Lawrance, M. Maeder, B. W. Skelton, H. Wen and A. H. White, *J. Chem. Soc., Dalton Trans.* 1994, 793.
9. G. K. Hollingshed, G. A. Lawrance, M. Maeder and M. Rossignoli, *Polyhedron* 1991, **10,** 409.
10. A. Zuberbühler and T. Kaden, *Talanta* 1982, **29,** 201.
11. A. Bianchi, M. Micheloni and P. Paoletti, *Coord. Chem. Rev.* 1991, **116,** 17.
12. R. D. Hancock and A. E. Martell, *Chem. Rev.* 1989, **89,** 1875.
13. P. Chaudhuri and K. Wieghardt, *Prog. Inorg. Chem.* 1986, **35,** 329.

Pergamon

PII: S0277-5387(96)00320-8

Polyhedron Vol. 16, No. 4, pp. 603–606, 1997
Copyright © 1996 Elsevier Science Ltd
Printed in Great Britain. All rights reserved
0277-5387/97 $17.00+0.00

T symmetrical gaseous tetra-tert-butyltetraboratetrahedrane: an electron diffraction study

Drahomír Hnyk*

Institute of Inorganic Chemistry, Academy of Sciences of the Czech Republic, CZ-250 68 Řež near Prague, Czech Republic

(Received 14 June 1996; accepted 26 June 1996)

Abstract—The structure of tetra-tert-butyltetraboratetrahedrane in the gas phase has been studied by electron diffraction. Analysis of the experimental data obtained by electron scattering from the tetra-tert-butyltetraboratetrahedrane vapour confirmed that the molecule consisted of a B_4 tetrahedron with a B—B edge distance of 170.4(4) pm. The B—C distances, which coincided with the C_3 axes of the tetrahedron, were determined to be 158.0(6) pm. There is an overall agreement between the solid state and gaseous structures of the B_4C_4 core. The approximately staggered conformations around the C—C and B—C bonds in the gas phase resulted in an overall symmetry of *T*. Copyright © 1996 Elsevier Science Ltd

Keywords: tetraboratetrahedrane; electron diffraction; gas phase; geometry; *T* symmetry; conformations.

The molecules B_4X_4 (X = Cl, R) are of considerable interest because of their four-orbital bonding scheme for the B_4 framework which does not comply with the rule indicating that $n+1$ electron pairs are optimal for *n*-deltahedral framework bonding [1]. According to tensor surface harmonics theory [2] the four electron pairs occupy one radial $S^{\sigma}(a_1)$ orbital and three surface $P^{\pi}(t_2)$ orbitals, the latter being three-fold degenerate. In the electron-precise P_4 molecule two non-bonded surface orbitals possessing e symmetry are also occupied.

The B atoms in the molecule $B_4(Bu^t)_4$ (**1**, Fig. 1) are extremely deshielded [$\delta(^{11}B)$ = 135.4 ppm] [3]; this is also true, but to a lesser extent, for B_4Cl_4 [$\delta(^{11}B)$ = 85.5 ppm] [4]. These high frequency shifts may be satisfactorily reproduced computationally only by taking into account correlated wave functions in the calculations of magnetic properties (*cf.* 139 and 81.4 ppm, respectively, at the GIAO-MP2/TZP′ level of *ab initio* theory) [3].

Although the X-ray diffraction analysis (XRD) of tetra-tert-butyltetraboratetrahedrane, $B_4(Bu^t)_4$ [5], revealed a slight distortion of the B_4C_4 framework from the ideal T_d symmetry (point group in the crystal: C_2), there are no grounds for believing that the gaseous molecule **1** departs from this symmetry at all.

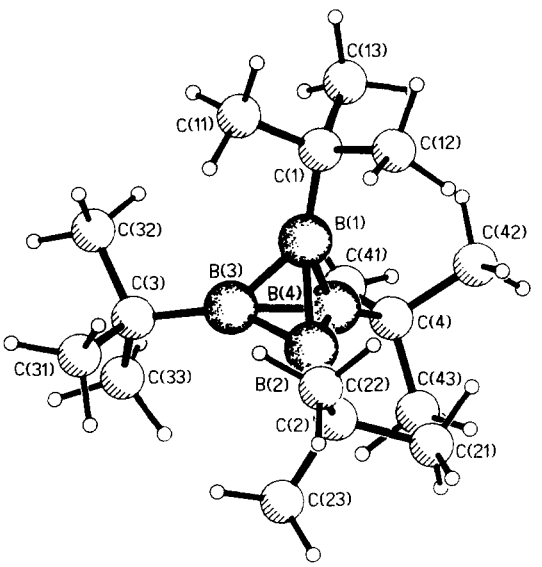


Fig. 1. A view of the $B_4(Bu^t)_4$ molecule in the optimum refinement of the electron diffraction data.

*Present address: Department of Chemistry, The University of Edinburgh, West Mains Road, Edinburgh EH9 3JJ, U.K.

Table 1. Results of the refinements for B_4 $(Bu^t)_4$

(a) Interatomic distances (r_a, pm)[a] and mean amplitudes of vibration (u, pm)

	Atomic pair	r_a^b	u_a^b	Key to the coupling scheme
$p_1 = d_1$	B—B	170.4(4)	5.5[c]	
$p_2 = d_2$	B—C	158.0(6)	4.7(1)	i
$p_3 = d_3$	C—C	155.0(2)[d]	4.2	i
$p_4 = d_4$	C—H	110.1(1)	6.2(2)	ii
d_5	B(2)···C(1)	313.0(4)	8.5(4)	iii
d_6	C(11)···B(1)	259.0(3)	8.1(3)	iv
d_7	C(1)···C(2)	428.4(8)	13.6(4)	v
d_8	C(11)···C(12)	249.5(3)	6.7	iv
d_9	B(1)···C(21)	395.0(4)[e]	16.1	v
d_{10}	B(1)···C(22)	362.5(4)[e]	12.3(7)	vi
d_{11}	B(1)···C(23)	424.9(4)[e]	16.1	v
d_{12}	C(1)···C(21)	497.6(6)[e]	20.0[e]	
d_{13}	C(1)···C(22)	431.1(6)[e]	16.1	v
d_{14}	C(1)···C(23)	556.1(6)[e]	32.1(17)	vii
d_{15}	C(11)···C(21)	596.1(9)[e]	38.2	vii
d_{16}	C(11)···C(22)	466.8(9)[e]	16.0[e]	
d_{17}	C(11)···C(23)	606.8(6)[e]	38.2	vii
d_{18}	C(12)···C(23)	578.4(7)[e]	38.2	vii
d_{19}	C(12)···C(22)	404.3(12)[e]	20.6	v
d_{20}	C(13)···C(23)	681.3(6)[e]	30.0[e]	
d_{21}	C(1)···H[C(12)]	218.3(4)	9.4(3)	viii
(b) Angular parameters (°)[b]				
p_5	∠BCC	111.7(2)		
p_6	∠CCH	109.7(4)		
p_7	τ_1(Me)	42.4(8)		
p_8	τ_2(Bu^t)	30.0(3)		

[a] The B···H, all other C···H and H···H nonbonded distances were included in the refinement, but they are not listed here. Their fixed vibrational amplitudes, were within the range 10.8–35.0 pm.

[b] Least-squares standard deviations in the last digit are given in parentheses.

[c] Fixed.

[d] The correlation coefficients with p_1 and p_2 are 0.71 and −0.92, respectively; all other elements of the correlation matrix have absolute values of less than 0.70.

[e] Dependent on the Bu^t twist angle (τ_2).

In addition, high quality *ab initio* optimization of the structure of B_4Me_4, which turned out to be a suitable model for **1**, support this assumption unambiguously [3]. In order to verify this assumption the electron-scattering pattern of **1** was analysed and its molecular structure determined.

EXPERIMENTAL

The sample of tetra-tert-butyltetraboratetrahedrane, provided by Professor P. Paetzold, was prepared according to the literature [5]. The purity was established by ^{11}B NMR spectra.

Electron-diffraction patterns were recorded in Kodak electron image plates using the Balzers Eldigraph KDG-2 instrument at the University of Oslo [6,7]. The nozzle was held at 346 K during the experiment. The electron beam was accelerated by a voltage of 42 kV and the electron wavelength and nozzle-to-plate distance were calibrated using the scattering pattern of benzene as a reference. The normal method of data treatment of the Norwegian group was employed [8]. Six plates from the long (498.79 mm), and five from the short (248.90 mm), nozzle-to-plate distances were selected for the analysis. Data from the long and short camera distances used in the refinements were within the ranges $20.0 \leqslant s \leqslant 143.75$ nm^{-1} and $42.5 \leqslant s \leqslant 282.5$ nm^{-1}, respectively [$s = (4\pi/\lambda)\sin(\theta/2)$, where λ, the electron wavelength, was 5.863 pm for both camera distances and θ is the scattering angle]. The least-squares method was applied to molecular intensities modified by s^4. The least-squares refinements were performed with a modified PC version of the program by Seip and co-workers [8]. Atomic scattering factors were taken from ref. [9].

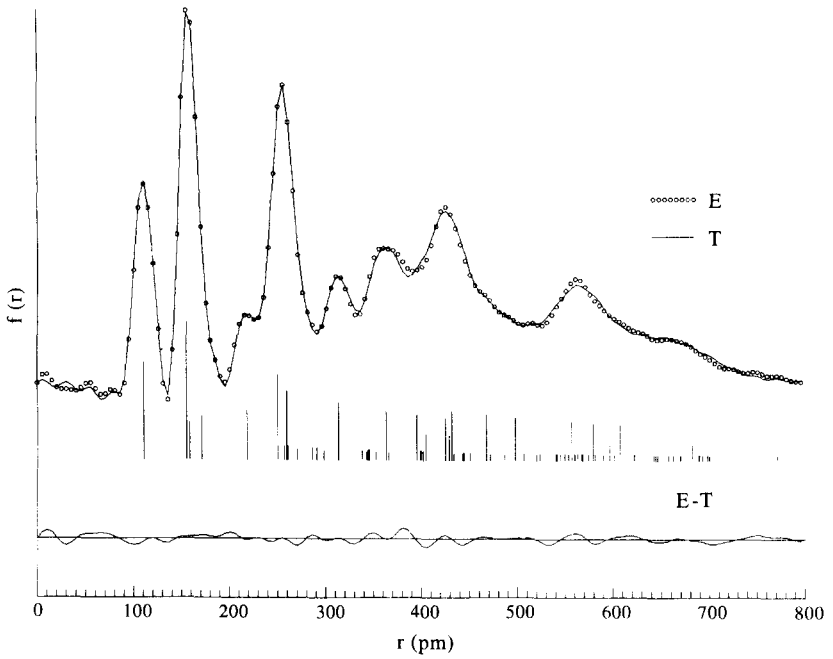


Fig. 2. Radial distribution curves (E, experimental; T, theoretical) calculated with an artificial damping factor exp(−0.000 $02s^2$). Theoretical values are used in the region $0.0 \leqslant s \leqslant 25.0$ nm^{-1}. The positions of the distances excluding H···H are marked with the vertical bars of height proportional to the weight of the distance. The positions of the most important distances can be deduced from Table 1. The difference curve is given below.

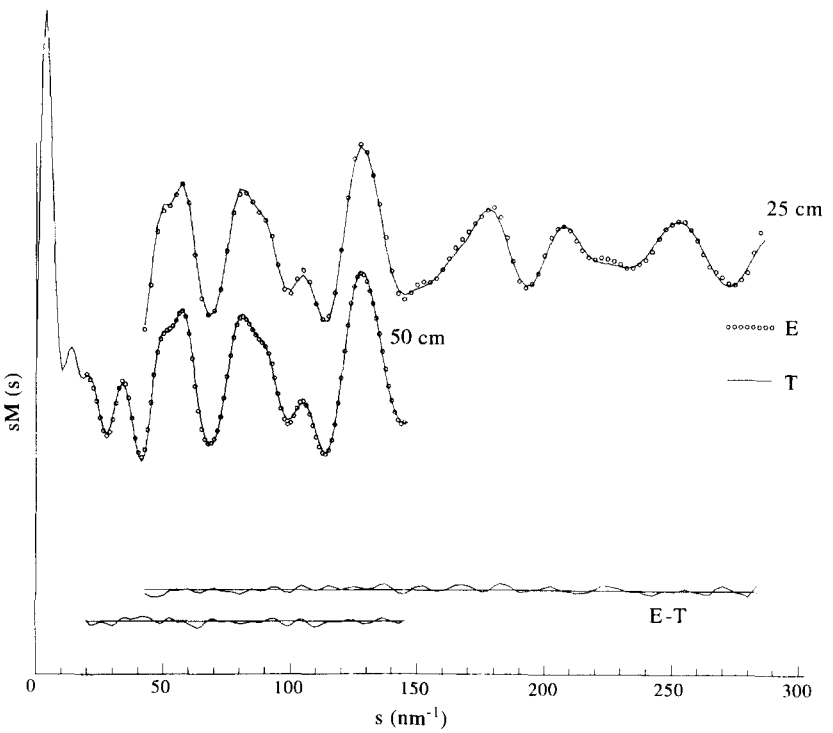


Fig. 3. Molecular intensity curves for the two camera distances (E, experimental; T, theoretical). The difference curves (experimental–theoretical) are also shown.

MOLECULAR MODEL

The molecular model of the boron atom skeleton, used in analysis of electron diffraction data, was based on a tetrahedron, the centre of which coincided with the origin of the coordinate system. C_2 and C_3 symmetry operations (the B—C bonds lay on the C_3 axes) were used to generate the appropriate geometry, including the positions of the four tert-butyl groups attached to the boron atoms of the B_4 core. The structure was then defined by four bonded distances [p_1–p_4; r(B—B), r(B—C), r(C—C), and r(C—H)], and by four angular parameters (p_5–p_8), see Table 1. The latter include the BCC and CCH bond angles as well as the twist angles (τ) of the methyl and tert-butyl groups around the C—C and B—C bonds, respectively. The twist angles τ_1 and τ_2 were defined to be zero when the B(1)—C(1)—C(11)—H (τ_1) and B(2)—B(1)—C(1)—C(12) (τ_2) (and other combinations of atoms according to symmetry) chains of atoms were coplanar and eclipsed. The B(2)—B(1)—C(1)—C(11) twist is consequently $-120°$. Values of τ_1 and $\tau_2 > 0$ indicate clockwise rotation around the C(1)—C(11) and B(1)—C(1) bonds, viewed from C(1) to C(11) and from B(1) to C(1), respectively. Overall the molecule had T symmetry.

RESULTS AND DISCUSSION

The refinement of the geometric parameters proceeded smoothly. It was possible to refine all the parameters, including both the torsion angles. The refinement of the latter led to approximately staggered conformations around the C—C and B—C bonds. The vibrational amplitude of the B—B distance could not be refined, but proved to have little influence on the final geometry. Its fixed value is optimal in terms of the lowest R factor. The success of the determination of conformational interactions between the tert-butyl groups may be judged by reference to the conformationally dependent area in the radial distribution curve; no problems were encountered when fitting the peaks in the range 360–680 pm (Fig. 2). Figure 3 shows the experimental and calculated molecular intensity. The structural details and vibrational amplitudes of the optimum refinement, for which the R factor was 0.065, are listed in Table 1.

There is excellent agreement between the B—B bond lengths established in the two phases [XRD: 170.7(6) pm; the largest standard deviation from those associated with the four different B—B bonds reported in ref. [5] is cited]. Moreover, this nearest-neighbour separation in **1** also agrees quite well with that determined for B_4Cl_4 [GED: 170.3(11) pm [10]; MP2/6–31G*: 169.0 pm [3]]. The B—B bond length is much closer to that for a two-centre, two-electron B—B bond than to that usually found for a n-deltahedral cluster obeying the $n+1$ bonding scheme [11]. The values of the other two distances related to the B_4C_{16} body, the B—C and C—C bond lengths, are in good accord with those of the corresponding average solid state parameters, 157.3(4) and 153.5(4) pm, respectively. For comparison, the B—B and B—C bond lengths in B_4Me_4, as computed at the MP2/6–31G* level of theory, are 168.8 and 156.2 pm, respectively [3].

Acknowledgements—I thank Professor P. Paetzold for providing the sample and his continuous interest during the course of this work, Mr Hans V. Volden for recording the experimental data and Mrs Snefrid Gundersen for technical assistance. I acknowledge the Grant Agency of the Academy of Sciences of the Czech Republic (Grant No. A4032502) for financial support. I am also grateful to Professor David W. H. Rankin for helpful comments.

REFERENCES

1. See, for example K. Wade, *Adv. Inorg. Chem. Radiochem.* 1976, **18,** 1.
2. See, for example A. J. Stone, *Inorg. Chem.* 1981, **20,** 563.
3. M. Bühl, J. Gauss, M. Hofmann and P. v. R. Schleyer, *J. Am. Chem. Soc.* 1993, **115,** 12385 and references therein.
4. L. Ahmed, J. Castilla and J. A. Morrison, *Inorg. Chem.* 1992, **31,** 1858.
5. T. Mennekes, P. Paetzold, R. Boese and D. Bläser, *Angew. Chem. Int. Ed. Engl.* 1991, **30,** 173.
6. W. Zeil, J. Haase and L. Wegmann, *Z. Instrumentenkd.* 1966, **74,** 84.
7. O. Bastiansen, R. Graber and L. Wegmann, *Balzers High Vak. Rep.* 1966, **25,** 1.
8. B. Andersen, H. M. Seip, T. G. Strand and R. Stølevik, *Acta Chem. Scand.* 1969, **23,** 3224.
9. A. W. Ross, M. Fink and R. Hilderbrandt, *International Tables for Crystallography* (Edited by A. J. C. Wilson), vol C, p. 245. Kluwer Academic Publishers, Dordecht (1992).
10. P. T. Brain, A. J. Downs, M. Fanfarillo, M. J. Goode, A. G. Massey, D. W. H. Rankin and H. E. Robertson, *J. Mol. Struct.* 1989, **192,** 163.
11. P. T. Brain, D. W. H. Rankin, H. E. Roberston, I. A. Alberts, A. J. Downs., T. M. Greene, M. Hofmann and P. v. R. Schleyer, *J. Chem. Soc., Dalton Trans.* 1995, 2193 and references therein.

Pergamon

PII: S0277-5387(96)00318-X

Polyhedron Vol. 16, No. 4, pp. 607–612, 1997
Copyright © 1996 Elsevier Science Ltd
Printed in Great Britain. All rights reserved
0277-5387/97 $17.00+0.00

A new three-dimensional, hydrogen-bonded metal–pteridine complex: synthesis, characterization and crystal structure of diaqua bis(1,3-dimethylpteridine-2,4(1*H*,3*H*)-dione-O^4,N^5) copper(II) nitrate dihydrate

Francisco Hueso-Ureña,[a] Sonia B. Jiménez-Pulido,[a] Miguel N. Moreno-Carretero,[a]* Miguel Quirós-Olozábal and Juan M. Salas-Peregrín

[a]Departamento de Química Inorgánica y Orgánica, Universidad de Jaén, 23071 Jaén, Spain

[b]Departamento de Química Inorgánica, Universidad de Granada, 18071 Granada, Spain

(Received 6 June 1996; accepted 26 June 1996)

Abstract—In absolute methanol, copper(II) nitrate reacted with 1,3-dimethyl-(1*H*,3*H*)-pteridin-2,4-dione (1,3-dimethyllumazine, DMLM) giving a complex with formula $[Cu(DMLM)_2(H_2O)_2](NO_3)_2 \cdot 2H_2O$. This compound has been characterized by means of analytical techniques (elemental analysis and TG), spectral methods (IR, UV–vis–NIR, EPR), magnetic measurements (77–290 K) and single-crystal X-ray diffraction. The copper(II) ion occupies an inversion centre and exhibits an elongated octahedral coordination. The equatorial plane consists of two N(5) atoms of the pteridine ligands and two oxygen atoms from water molecules, and the two axial sites are occupied by two O(4) atoms of the ligands. The non-coordinated water molecules and nitrate anions, as well as the pteridine ligands are involved in a two-dimensional H-bond network, the metal–pteridine moieties being linked to the non-coordinated water molecules and nitrate anions of neighbouring molecules through the O(2) atom of the pteridine ligands. The molecules are packed in planes parallel to the *b*-axis, these planes being stacked at a mean distance of 3.297 Å to each other. A three-dimensional arrangement is defined by the involvement of the coordinated water molecules in a hydrogen bond with one oxygen atom from the uncoordinated water and another oxygen from the nitrate group of the adjacent layers. Copyright © 1996 Elsevier Science Ltd

Keywords: complexes; crystal structure; pteridine; lumazine.

Pteridines, as well as their structurally related flavins and pterins, are biochemically important molecules owing to their capability of undergoing either one- or two-electron transfer reactions through their potentially metal-chelating α-carbonylpyrazine moiety [1, 2]. For this reason, they have attracted great attention from several points of view. These ligands have recently been used as models to determine the reactivity of metal sites in several enzymes [3–13]. Nevertheless, there are only a few X-ray-determined structures [14–22]. Lumazine [pteridine-2,4(1*H*,3*H*)-dione] derivatives were also used as flavin analogues in order to determine the effect of solvent polarity on coordination patterns [23,24].

From another point of view, and in order to explain the control of the cooperative interaction between electron transfer and proton transfer in hydrogen-bonded charge-transfer (HBCT) systems, pteridines have been used as a basic skeleton to construct models in which the establishment of metallosupramolecular H-bonded systems takes place. This interaction could be related to the redox properties of the metal atoms and the stacking interaction between the ligands. This would be a new way to regulate electronic properties in the solid state [25–27].

* Author to whom all correspondence should be addressed.

As a part of a programme aimed at the structural characterization of metal complexes with lumazine methylated derivatives, we now report a complete study, including the crystal structure, of a copper(II) complex with 1,3-dimethyllumazine (hereafter, denoted as DMLM) having a three-dimensional H-bond network, $[Cu(DMLM)_2(H_2O)_2]$ $(NO_3)_2 \cdot 2H_2O$.

EXPERIMENTAL

Synthesis

The pteridine-derived ligand was prepared from water solution with acid pH by adding dropwise a glyoxal solution (*ca* 40%) to a boiling solution of the 5,6-diamino-1,3-dimethyluracil. The resulting solution was stirred for *ca* 6 h and then the 1,3-dimethyllumazine (DMLM) was isolated as a yellow solid.

Synthesis of the title complex was carried out as follows: DMLM (0.192 g, 1 mmol) dissolved in hot MeOH (*ca* 30 ml) was added slowly, with stirring, to $Cu(NO_3)_2 \cdot 3H_2O$ (0.241 g, 1 mmol) dissolved in the minimum amount of methanol. The resulting solution was allowed to stand at room temperature. Following evaporation over several days green crystals were isolated. These were filtered off and air dried. Found: C, 29.7; H, 3.6; N, 21.4; Cu, 7.3. Calc. for $[Cu(DMLM)_2(H_2O)_2]$ $(NO_3)_2 \cdot 2H_2O$: C, 29.8; H, 3.7; N, 21.7; Cu, 7.0%.

Crystallographic study

A prismatic green crystal with dimensions $0.45 \times 0.30 \times 0.25$ mm^3 was mounted in a Stoe–Siemens AED-2 diffractometer ($T = 292$ K) with Mo-K_α radiation ($\lambda = 0.71073$ Å) monochromatized with a highly oriented graphite crystal. The unit cell was determined from 25 random reflections. The intensities were collected using the ω–2θ scan mode, in the range $3.8 < 2\theta < 55°$. A total of 4569 reflections were measured with $-2 \leqslant h \leqslant 11$, $-2 \leqslant k \leqslant 18$, $-13 \leqslant l \leqslant 13$. They were averaged to 2892 independent reflections ($R_{int} = 0.020$), 2075 with $F > 4\sigma(F)$ being retained for structure solution and refinement. Data were corrected for Lorentz and polarization effects but not for absorption. Three standard reflections were monitored every ninety minutes and showed no significant decay in intensity.

Crystal data. $C_{16}H_{24}N_{10}O_{14}Cu$, Formula weight = 644.0, monoclinic, space group, $P2_1/n$ unit-cell dimensions: $a = 8.7460(8)$, $b = 13.874(1)$, $c = 10.678(1)$ Å, $\beta = 92.64(1)°$, $V = 1294.4(4)$ Å^3, $Z = 2$, density (calc.) = 1.652 Mg m^{-3}, absorption coefficient 0.932 mm^{-1}, $F(000) = 662$.

The metal atom was placed in an inversion centre (the only possibility for $Z = 2$), and the remaining atoms were located in successive ΔF maps. Non-H atoms were refined anisotropically by full-matrix least squares and hydrogen atoms from the ligand were idealized whereas those of the water molecules were refined with fixed O—H (0.86 Å) and H—H (1.40 Å) distances. A common isotropic displacement coefficient was refined for all H atoms. A weighting scheme, $w^{-1} = \sigma^2(F) + 0.032\,F^2$, was used and 206 parameters refined.

Final R indices for observed data were $R = 0.047$ and $wR = 0.088$, goodness-of-fit = 0.48. Δ/σ in the last cycle was below 0.015 for non-H atoms, data-to-parameter ratio 10.1:1, ΔF values in the final difference map were -0.43 and 0.39 e Å^{-3}.

All calculations and drawings have been performed on a Microvax II computer (Technical Services of University of Granada) using the Siemens SHELXTL PLUS system.

Apparatus

Microanalyses (C, H, N) were performed by Technical Services of the University of Granada (STUGRA); the metal and water contents of the complex were determined from the TG plot. Conductivity measurements have been carried out using freshly prepared dimethylformamide and dimethylsulfoxide solutions on a Hanna HI8820 instrument. Thermogravimetric studies were carried out under pure air on a Mettler TG-50 thermobalance, using 4.22 mg of sample and a 10°C min^{-1} heating rate. Infrared spectra were obtained on a Perkin–Elmer FT-IR 1760X (KBr pellets, 4000–400 cm^{-1}) and Perkin–Elmer 983G spectrophotometer (polyethylene pellets, 600–180 cm^{-1}). The electron paramagnetic resonance spectrum was obtained in the X-band at room temperature on a Bruker ESP 300E apparatus, with a microwave frequency of 9.79 GHz and a modulation frequency of 100 kHz. Magnetic measurements were carried out on a Manics DSM-8 system between 77 and 290 K. Diffuse reflectance spectra (240–1500 nm) were recorded on a Perkin–Elmer UV–vis–NIR Lambda-19 machine using a $BaSO_4$ pellet as reference.

RESULTS AND DISCUSSION

A view of the molecular unit is shown in Fig. 1 and bond lengths and angles in the coordination sphere and the pteridine ligand are given in Table 1. In the crystal structure, the complex possesses an inversion centre. The metal ion exhibits an elongated octahedral coordination (tetragonality factor $T = 0.85$). The equatorial plane consists of two N(5) atoms [Cu—N(5), 2.026(3) Å] from the pteridine ligands and two water molecules [Cu—O(1w), 1.957(3) Å]; the two axial sites are occupied by two O(4) atoms from the DMLM ligands [Cu—O(4), 2.353(3) Å]. The ratio between the apical metal–ligand bond lengths and the basal ones, R(A/B) $\approx$ 1.18, is lower than that needed ($\leqslant$1.4) to force a square-planar complex [28]. This tetragonal elongation is consistent with the align-

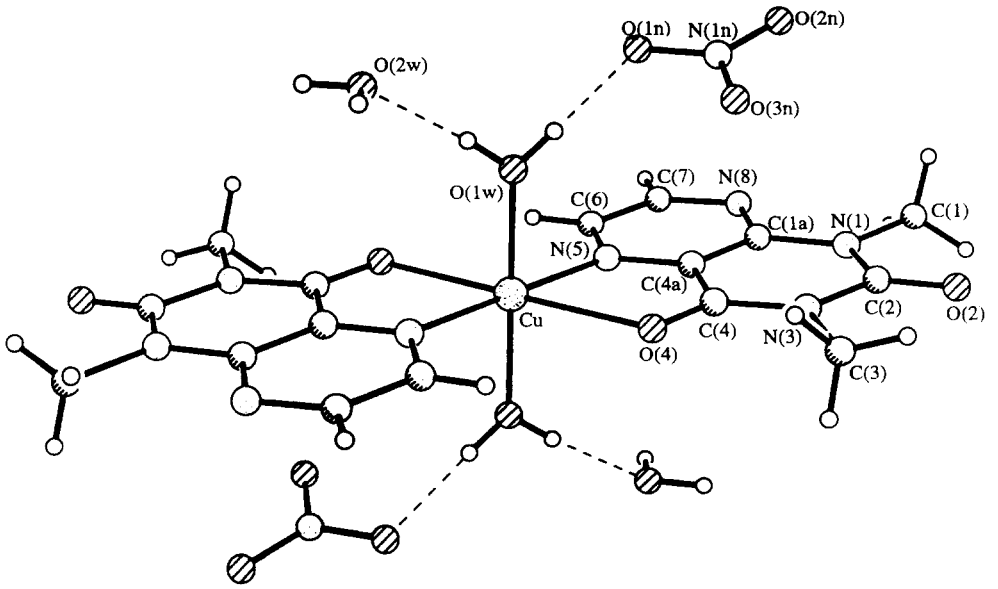


Fig. 1. Molecular drawing and numbering scheme for the monomeric unit.

ment of both O(4) donor atoms in the z-axis, the Cu^{II} ion ground state being $d_{x^2-y^2}$.

The DMLM ligand is practically planar, the greatest deviations being 0.029 Å [O(4)] for the exocyclic atoms and 0.017 Å [C(1a)] for the endocyclic ones. However, the pteridine ligands are not coplanar because the least-squares plane of the DMLM and the coordination plane around the copper atom [Cu, N(5), O(4), N(5′) and O(4′)] deviate slightly from coplanarity and define an acute angle of 4.0°. Owing to the centrosymmetric character of the molecular unit, the distance of the metal ion to the pteridine plane is 0.121 Å, both pteridine planes being parallel but displaced by 0.242 Å from each other. As

Table 1. Bond lengths (Å) and angles (°) around the metal ion and in the pteridine ligand

Metal ion			
		O(4)—Cu—N(5)	77.1(1)
Cu—O(4)	2.353(3)	O(4)—Cu—O(1w)	89.7(1)
Cu—N(5)	2.026(3)	N(5)—Cu—O(1w)	88.8(1)
Cu—O(1w)	1.957(3)	Cu—O(4)—C(4)	107.3(2)
		Cu—N(5)—C(4a)	115.6(2)
		Cu—N(5)—C(6)	125.9(2)
Pteridine ligand			
N(1)—C(1)	1.479(6)	N(3)—C(4)	1.363(5)
N(1)—C(1a)	1.382(5)	C(4)—O(4)	1.223(5)
N(1)—C(2)	1.376(6)	C(4)—C(4a)	1.467(5)
C(1a)—C(4a)	1.389(5)	C(4a)—N(5)	1.332(4)
C(1a)—N(8)	1.346(5)	N(5)—C(6)	1.338(5)
C(2)—O(2)	1.195(6)	C(6)—C(7)	1.388(6)
C(2)—N(3)	1.389(6)	C(7)—N(8)	1.316(6)
N(3)—C(3)	1.485(6)	C(3)—N(3)—C(4)	117.8(4)
C(1)—N(1)—C(1a)	120.0(4)	N(3)—C(4)—O(4)	123.3(3)
C(1)—N(1)—C(2)	117.3(4)	N(3)—C(4)—C(4a)	115.3(3)
C(1a)—N(1)—C(2)	122.6(3)	O(4)—C(4)—C(4a)	121.4(3)
N(1)—C(1a)—C(4a)	119.2(3)	C(1a)—C(4a)—C(4)	120.4(3)
N(1)—C(1a)—N(8)	119.2(3)	C(1a)—C(4a)—N(5)	121.1(3)
C(4a)—C(1a)—N(8)	121.6(3)	C(4)—C(4a)—N(5)	118.5(3)
N(1)—C(2)—O(2)	122.2(5)	C(4a)—N(5)—C(6)	118.3(3)
N(1)—C(2)—N(3)	117.1(4)	N(5)—C(6)—C(7)	119.0(4)
O(2)—C(2)—N(3)	120.8(4)	C(6)—C(7)—N(8)	124.5(4)
C(2)—N(3)—C(3)	116.8(3)	C(1a)—N(8)—C(7)	115.6(4)
C(2)—N(3)—C(4)	125.4(3)		

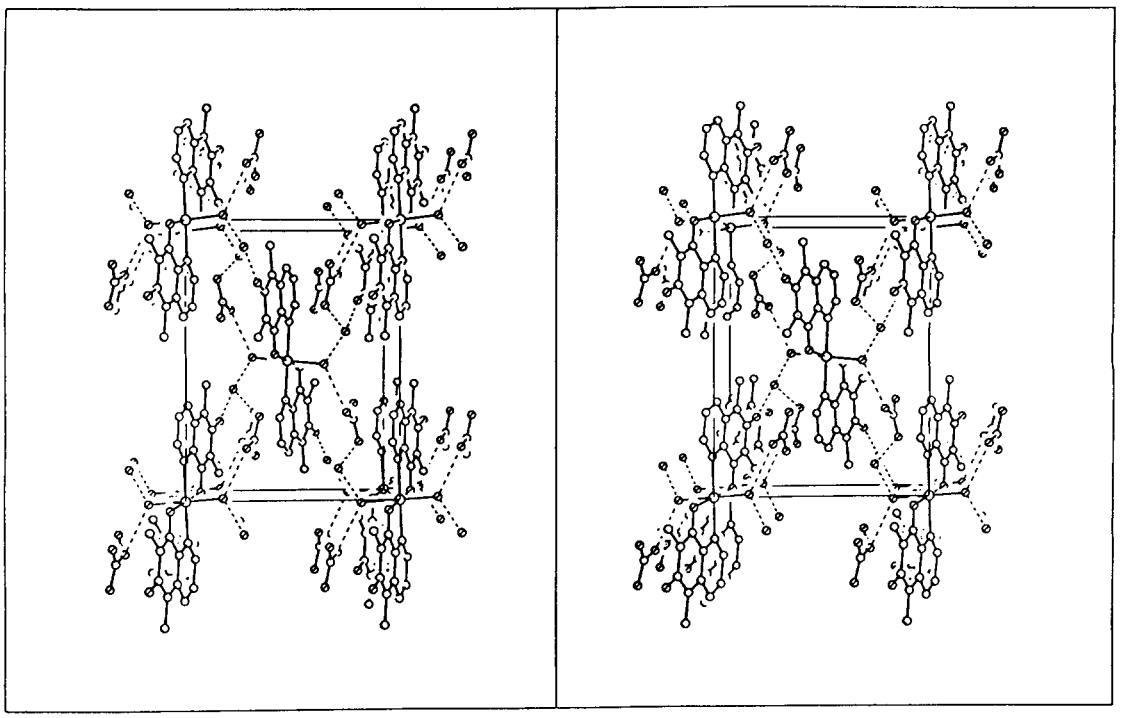


Fig. 2. A view of the hydrogen-bond network and the packing scheme.

expected, all geometric data in the organic ligand indicate significant electronic delocalization; the C(2)—O(2) distance [1.195(6) Å] is a little shorter than that of C(4)—O(4) [1.223(5) Å] as a consequence of the involvement of the O(4) atom in the coordination sphere. This structure is very similar to that by Mitsumi *et al.* [25] for the analogous copper(II) complex with monodeprotonated lumazine; the only difference being the presence of nitrate counteranions because of the inability of DMLM to undergo deprotonation.

Hydrogen bonding plays a very important role in the packing scheme of this compound. The hydrogen-bonding network is shown in Fig. 2 and geometrical data are listed in Table 2. The molecular units are linked in two-dimensional networks perpendicular to the [1 0 3] direction, in which each non-coordinated water molecule establishes two hydrogen bonds, one with the O(2) atom of a pteridine ligand [O(2w)—H(21)···O(2)] and another with the O(2n) of the nitrate group [O(2w)—H(22)···O(2n)]. The coordinated water molecules are hydrogen bonded with a nitrate group [O(1w)—H···O(1n)] and a non-coordinated water molecule [O(1w)—H···O(2w)] of the adjacent layer, thus defining a three-dimensional H-bond network in which the planes containing the metal–pteridine moieties are stacked at a mean distance of 3.297 Å.

Table 2. Hydrogen bonding (A—H···B) in the title complex

A	B	d(A···B) (Å)	d(H···B) (Å)	∠(A—H···B) (°)
O(1w)	O(2w)	2.584(5)	1.73(5)	172(5)
O(1w)	O(1n)	2.727(4)	1.88(3)	174(5)
O(2w)	O(2)[a]	2.794(5)	1.97(5)	158(4)
O(2w)	O(2n)[b]	2.909(6)	2.04(5)	170(5)

[a] $\frac{3}{2}-x, \frac{1}{2}+y, \frac{1}{2}-z$.
[b] $\frac{1}{2}-x, \frac{1}{2}+y, \frac{1}{2}-z$.

Conductivity values obtained in both DMF (110 mho cm^{-1} mol^{-1}) and DMSO (76 mho cm^{-1} mol^{-1}) solutions lie at the lower limit indicated for a 2:1 electrolyte [29]. The thermal decomposition of this compound in air has been studied using TG and DSC plots. These indicate that four water molecules are lost in only one clearly defined step between 77 and 121°C (exp. weight loss 11.7%, calc. 11.2%). The corresponding endothermic peak appears at 103°C (ΔH = 48.3 kJ mol^{-1} H_2O). The desolvated compound is stable at temperatures up to 220°C. At this point, an abrupt weight loss occurs as a consequence of the combustion of the organic matter. The pyrolysis finishes at 400°C, leaving a final residue of copper oxide, as corroborated from the corresponding infrared spectrum.

The infrared spectrum shows bands at 3450 cm^{-1} assignable to ν(O—H) from water. The AM1 semi-empirical method, implemented in the HYPERCHEM 4.0 program, was used to make assignments of the vibrational modes of the IR spectrum. The bands at 1672 and 1737 cm^{-1} may be assigned to a combination of the stretching vibrations of both

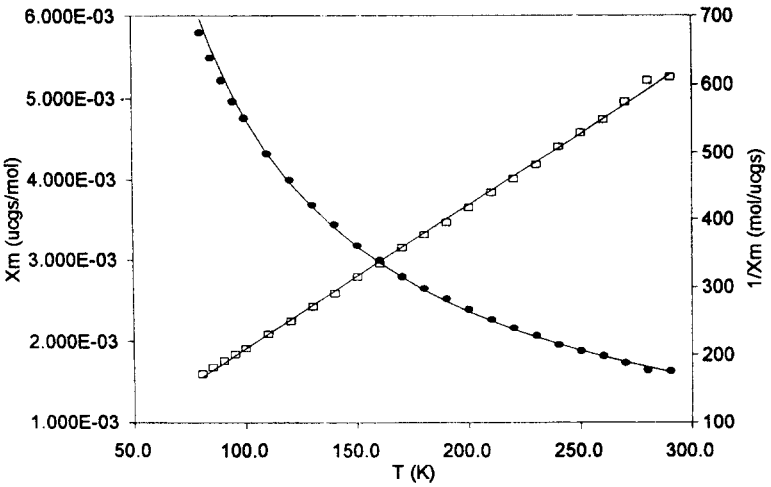


Fig. 3. Molar susceptibility values of the title compound at different temperatures (circles, χ_M; squares, $1/\chi_M$).

exocyclic carbonyl groups, the first being mainly owing to ν(C(4)=O) whereas in the second the greater component seems to be ν(C(2)=O). Other vibration modes related to potential donor atoms may be assigned as follows: ν(C=N) (1602 cm^{-1}), ν(C=C)+ν(C—N) (1483 and 1304 cm^{-1}). These bands appear shifted to higher wavelength by *ca* 10 cm^{-1} with respect to their position in the IR spectrum of the free ligand, the only exception being the band mainly assignable to ν(C(4)=O), which is in accord with the involvement of O(4) and N(5) atoms in the M—L bond [30]. The strong band corresponding to ν(N—O) of the free nitrate group appears at 1385 cm^{-1}. The far-infrared spectrum clearly shows a new band at 245 cm^{-1}, which may be assigned to the ν(Cu—N) vibration [31].

The complex displays an axial EPR powder spectrum with $g_\perp = 2.03$ and $g_\parallel = 2.39$ and may be interpreted, according to refs [32] and [33], by the existence of rhombic symmetry with the tetragonal axes parallel, but where the rhombic component is so small that it is not resolved by the powder technique.

As shown in Fig. 3, molar susceptibility values at different temperatures have been fitted to the Curie law ($\theta = 2.2 \pm 0.7$ K, $C = 0.484 \pm 0.003$ cgsu K mol^{-1}, $r^2 = 0.9996$). The value of θ reveals that only a small antiferromagnetic interaction exists between the metallic centres owing to their tetragonal axes being quasi-parallel but not aligned. The effective magnetic moment for the Cu^{II} atom, once diamagnetic corrections have been made, was 2.04 ± 0.04 B.M. in accord with the existence of magnetically dilute monomeric units [34].

The vis–NIR diffuse reflectance spectrum (25,000–9000 cm^{-1}) shows a broad, asymmetric band at 13,000–20,000 cm^{-1}, with maximum absorbance at 15,100 cm^{-1}. This band is typical for 4+2 tetragonal ("square-plane") copper(II) complexes with the chromophore group CuN_2O_2 [35] and may be deconvoluted into four components (17,000, 15,400, 14,300, 11,800 cm^{-1}) corresponding to the expected transitions in six-coordinated D_{2h} Cu^{II} ion with a $d_{x^2-y^2}$ ground state.

Supplementary material.—A list of structure factors and tables with (i) atomic coordinates and isotropic thermal parameters for non-H atoms, (ii) bond lengths and angles, (iii) anisotropic temperature factors for non-H atoms, (iv) hydrogen atom coordinates and (v) equations of planes and dihedral angles have been deposited at the Cambridge Crystallographic Data Centre.

REFERENCES

1. C. Bessenbacher, C. Vogler and W. Kaim, *Inorg. Chem.* 1989, **28**, 4645.
2. C. Bessenbacher and W. Kaim, *Z. Anorg. Allg. Chem.* 1989, **577**, 39.
3. S. J. N. Burgmayer, A. Baruch, K. Kerr and K. Yoon, *J. Am. Chem. Soc.* 1989, **111**, 4982.
4. M. J. Clarke, M. G. Dowling, A. R. Garafalo and T. F. Brennan, *J. Am. Chem. Soc.* 1979, **101**, 223.
5. M. J. Clarke, M. G. Dowling, A. R. Garafalo and T. F. Brennan, *J. Biol. Chem.* 1980, **255**, 3472.
6. M. W. Yu and C. J. Fritchie, Jr, *J. Biol. Chem.* 1975, **250**, 946.
7. R. H. Benno and C. J. Fritchie, Jr, *Acta Cryst.* 1973, **B29**, 2493.
8. W. T. Garland, Jr and C. J. Fritchie, Jr, *J. Biol. Chem.* 1974, **249**, 2228.
9. P. Kierkegaard, M. Leijonmarck and P. E. Werner, *Acta Chem. Scand.* 1972, **26**, 2980.
10. B. Fischer, H. Schmalle, E. Dubler, A. Schafer and M. Viscontini, *Inorg. Chem.* 1995, **34**, 5726.
11. F. M. Hornung and W. Kaim, *J. Chem. Soc., Faraday Trans.* 1994, **90**, 2909.
12. B. Schwederski and W. Kaim, *Inorg. Chim. Acta* 1992, **195**, 123.

13. B. Fischer, J. Strahle and M. Viscontini, *Helv. Chim. Acta* 1991, **74,** 1544.
14. J. N. Burgmayer and E. I. Stiefel, *J. Am. Chem. Soc.* 1986, **108,** 8310.
15. J. N. Burgmayer and E. I. Stiefel, *Inorg. Chem.* 1988, **27,** 4059.
16. J. Perkinson, S. Brodie, Y. Keum, K. Mosny, P. J. Carroll, T. V. Morgan and S. J. N. Burgmayer, *Inorg. Chem.* 1991, **30,** 719.
17. A. Odani, H. Masuda, K. Inukai and O. Yamauchi, *J. Am. Chem. Soc.* 1992, **114,** 6294.
18. T. Kohzuma, H. Masuda and O. Yamauchi, *J. Am. Chem. Soc.* 1989, **111,** 3431.
19. O. Heilmann, H. D. Hausen and W. Kaim, *Z. Naturforsch.* 1994, **49B,** 1554.
20. M. S. Nasir, K. D. Karlin, Q. Chen and J. Zubieta, *J. Am. Chem. Soc.* 1992, **114,** 2264.
21. A. Abelleira, R. D. Galang and M. J. Clarke, *Inorg. Chem.* 1990, **29,** 633.
22. K. J. Black, H. Huang, S. High, L. Starks, M. Olson and M. E. Mcguire, *Inorg. Chem.* 1993, **32,** 5591.
23. M. Goodgame and M. A. Schmidt, *Inorg. Chim. Acta* 1979, **36,** 151.
24. T. Kohzuma, A. Odani, Y. Morita, M. Takani and O. Yamauchi, *Inorg. Chem.* 1988, **27,** 3854.
25. M. Mitsumi, J. Toyoda and K. Nakasuji, *Inorg. Chem.* 1995, **34,** 3367.
26. K. Nakasuji, K. Sugiura, T. Kitagawa, J. Toyoda, H. Okamoto, K. Okamura, H. Yamamoto, I. Murara, A. Kawamoto and J. Tanaka, *J. Am. Chem. Soc.* 1991, **113,** 1862.
27. T. Mirani, G. Saito and H. Uruyama, *Phys. Rev. Lett.* 1988, **60,** 2299.
28. D. L. Kepert, *Inorganic Stereochemistry.* Springer-Verlag, Berlin (1982).
29. W. J. Geary, *Coord. Chem. Rev.* 1971, **7,** 81.
30. K. Nakamoto, *Infrared and Raman Spectra of Inorganic and Coordination Compounds*, 4th edn. Wiley & Sons, New York, (1986).
31. J. R. Ferraro, *Low-Frequency Vibrations of Inorganic and Coordination Compounds.* Plenum Press, New York (1971).
32. J. R. Pilbrow, *Transition Ion Electron Paramagnetic Resonance.* Clarendon Press, Oxford (1990).
33. B. J. Hathaway and D. E. Billing, *Coord. Chem. Rev.* 1970, **5,** 143.
34. R. L. Carlin, *Magnetochemistry.* Springer-Verlag, Berlin (1986).
35. A. B. P. Lever, *Inorganic Electronic Spectroscopy*, 2nd edn. Elsevier, Amsterdam (1984).

Pergamon

PII: S0277-5387(96)00317-8

Polyhedron Vol. 16, No. 4, pp. 613–621, 1997
Copyright © 1996 Elsevier Science Ltd
Printed in Great Britain. All rights reserved
0277-5387/97 $17.00+0.00

Metallation of 2-sulfanilamidopyrimidine (sulfadiazine). X-ray diffraction structure and solution behaviour of bis(sulfadiazinato) mercury(II) bis(dimethylsulfoxide)

Angel García-Raso,[a]* Juan J. Fiol,[a] G. Martorell,[a] Adela López-Zafra[a] and Miguel Quirós[b]

[a]Department de Química, Universitat de les Illes Balears, 07071 Palma de Mallorca, Spain

[b]Departamento de Química Inorgánica, Facultad de Ciencias, Universidad de Granada, 18071 Granada, Spain

(Received 28 May 1996; accepted 26 June 1996)

Abstract—The X-ray crystal structure of $Hg(Sulfa)_2 \cdot 2DMSO$ (**1**) was determined. Compound **1** was obtained from the reaction of sulfadiazine (2-sulfanilamidopyrimidine (Sulfa-H)) with mercury(II) acetate in methanol and crystallization in DMSO/methanol. The coordination geometry about the mercury atom is approximately linear [N—Hg: 2.087(4) Å; N—Hg—N: 175.0(2)°]. Two secondary DMSO molecules are loosely bound to the mercury atom, [Hg—O(DMSO): 2.769(7) Å]. No π-aryl stacking interaction was observed in either the solid or solution state. The IR, electronic and ^1H and ^{13}C NMR spectral data for **1** suggest binding of mercury to the sulfonamide nitrogen, in agreement with the crystal structure determination. Copyright © 1996 Elsevier Science Ltd

Keywords: mercury(II) complex; sulfadiazine; X-ray structure; NMR structural elucidation.

Many sulfanilamide derivatives possess antibacterial activity, and sulfadiazine also has a strong antibacterial property. Thus, sulfadiazine compounds are widely used for their bactericidal action and X-ray structures of many of them have been solved [1]. On the other hand, some metal complexes of these ligands promote rapid healing of skin disorders [e.g. the Ag^I complex [2,3]—commercially named "Flammazine" (marketed in Spain by Duphar) or "Silvederma" (marketed in Spain by Aldo Union) is used for human burn treatment and the Zn^{II} complex [4,5] in preventing bacterial infection in burned animals]. The effectiveness of these burn treatment compounds does not appear to depend solely on the presence of a metal ion (slow release of the Ag^I or Zn^{II}) but depends strongly on the nature of the material to which the metal ion is bound [4].

A few Hg^{II} complexes [6] are still used in topical medicine as antiseptics, although it is known that interactions of heavy metal ions with biomolecules can yield potentially toxic effects. In this context we report the synthesis, spectroscopic characterization and X-ray structure determination of $Hg(Sulfadiazinato)_2 \cdot 2DMSO$.

* Author to whom correspondence should be addressed.

EXPERIMENTAL

Analyses and physical measurements

Analytical measurements were carried out using a Carlo–Erba model 1106 microanalyser. The infrared spectra were registered in the solid state (KBr pellets) on a PE 683 with an infrared data station PE 1600, and the electronic spectra were registered on a PE 552 spectrophotometer. Thermogravimetic data in the temperature range 30–700°C were recorded in a flowing nitrogen atmosphere (heating rate 10°C min^{-1}) on a PE TGA-2 thermobalance. 1D and 2D ^1H and ^{13}C NMR spectra were carried out on a Bruker AMX 300 spectrometer. Proton and carbon chemical shifts in

DMSO-d_6 were referenced to DMSO-d_6 (^{1}H NMR, δ(DMSO) = 2.60 ppm; ^{13}C NMR, δ(DMSO) = 43.5 ppm). The 2D NMR experiments were performed at 20°C without sample spinning.

^{1}H *Detected heteronuclear multiple quantum coherence spectroscopy* (*HMQC*) [7]. The one-bond ^{1}H–^{13}C shift correlation spectra resulted from a 502 × 2048 data matrix with 48 scans (preceded by 16 dummy scans) per t_1 value. Pre-delay was 1.0 s and a 10.3 μs 90° ^{13}C pulse width was used. A sine-bell squared filter was used prior to Fourier transformation in the t_2 and t_1 dimensions.

^{1}H *Detected multiple-bond heteronuclear multiple quantum coherence spectroscopy* (*HMBC*) [8]. The multiple-bond ^{1}H–^{13}C shift correlation spectra resulted from a 479 × 2048 data matrix with 160 scans (preceded by 16 dummy scans) per t_1 value. Pre-delay was 1.0 s and a 10.3 μs 90° ^{13}C pulse width was used. The delay between the first and the second 90° ^{13}C pulses was 75 ms. A sine-bell squared filter was used prior to Fourier transformation in the t_2 and t_1 dimensions.

Rotating frame Overhauser effect spectroscopy (*ROESY*) [9]. The ^{1}H–^{1}H shift correlation spectra resulted from a 237 × 2048 data matrix with 64 scans (preceded by 16 dummy scans) per t_1 value. Pre-delay was 2.0 s and a 5.1 μs 90° ^{1}H pulse width and 2.0 kHz (23 dB) of ^{1}H r.f. power and 22 μs 90° ^{1}H pulse width were used. Mixing time = 500 ms. A sine-bell squared filter was used prior to Fourier transformation in the t_2 and t_1 dimensions. The 2D spectra were processed by using commercial Bruker software.

Sulfadiazine (Roig-Farma) and mercury(II) acetate (Merck) were used without further purification.

Crystallographic studies

Crystallographic studies were performed on a Siemens Nicolet P4 diffractometer with graphite-monochromated Mo-$K\alpha$ radiation (λ = 0.71073 Å). The unit cell and orientation matrix were obtained from 25 randomly oriented reflections. 4653 reflections (4267 independent) were collected using ω–2θ scans in the range ($0 \leqslant h \leqslant 28$, $0 \leqslant k \leqslant 12$, $-26 \leqslant l \leqslant 25$, $2\theta < 60°$), and corrected for Lorentz and polarization effects and empirically (ψ scans) for absorption (transmission range: 0.360–0.702). 3551 reflections with $F_0 > 4\sigma(F_0)$ were retained for solving and refining the structure. The structure was solved by the heavy-atom method and refined by full-matrix least squares on F using anisotropic temperature factors for non-H atoms. Hydrogen atoms were idealized. The final indices were R = 0.042, R_w = 0.043, S = 1.04. Shift/esd in the final cycle was below 0.001. Residues in the final delta (F) map were between −2.26 and 1.09 eÅ^{-3}. All calculations performed with the SHELXTL-Plus program package [10].

Crystal data and structure solution parameters are summarized in Table 1. Tables of crystal data, final atomic coordinates, anisotropic thermal parameters, final hydrogen coordinates and a listing of observed and calculated structure factors are included in the supplementary material, deposited at the Cambridge Crystallographic Data Centre.

Table 1. Selected crystallographic data for bis(sulfadiazinato)mercury(II) bis(dimethylsulfoxide) (**1**)

Crystal data	
Empirical formula	$C_{24}H_{30}HgN_8O_6S_4$
Colour habit	White laminae
Crystal size (mm)	0.25 × 0.35 × 0.08
Crystal system	Monoclinic
Space group	$C2/c$
Unit-cell dimensions (Å, °)	a = 20.537(7)
	b = 8.653(3)
	c = 18.846(6)
	β = 106.68(2)
Volume (Å^3)	3207(3)
Z	4
Formula weight	855.4
Density (calc.) (Mg m^{-3})	1.772
Absorption coefficient (mm^{-1})	5.111
F(000)	1688
Data collection	
Diffractometer used	Siemens Nicolet P4
Radiation	Mo-K_α (λ = 0.71073 Å)
Temperature (K)	291
2θ Range (°)	2.0–60.0
Standard reflections	3 measured every 90 min
Index ranges	$0 \leqslant h \leqslant 28$, $0 \leqslant k \leqslant 12$, $-26 \leqslant l \leqslant 25$
Reflections collected	4653
Independent reflections	4267 (R_{int} = 39.41%)
Observed reflections	3551 [$F > 4.0\sigma(F)$]
Absorption correction	Empirical (lamina)
Transmission Range	0.360–0.702
Solution and refinement	
Solution	Heavy atom
Refinement method	Full-matrix least squares
Quantity minimized	$\Sigma w(F_o - F_c)^2$
Hydrogen atoms	Riding model, refined common isotropic U
Weighting scheme	$w^{-1} = \sigma^2(F) + 0.0012\,F^2$
Number of parameters refined	196
Final R indices (obs. data)	R = 4.18%,
	wR = 5.12%,
	R_w = 4.32%
R indices (all data)	R = 5.27%,
	wR = 5.42%
Goodness-of-fit	1.04
Largest and mean Δ/σ	0.001, 0.000
Data-to-parameter ratio	18.1:1
Largest difference peak (eÅ^{-3})	1.09
Largest difference hole (eÅ^{-3})	−2.26

$R = \Sigma(|F_o| - |F_c|)/(\Sigma|F_o|)$.
$R_w = [\Sigma w(|F_o| - |F_c|)^2/\Sigma w|F_o|^2]^{1/2}$.

Table 2. Bond distances (Å) and angles (°) for **1**

Mercury coordination sphere			
Hg—N(2a)	2.087(4)		
Contact Hg—DMSO			
Hg—O(1d)	2.769(7)	Hg—S(1d)	3.733(3)
Ligand			
N(1a)—C(2a)	1.360(7)	N(1a)—C(6a)	1.342(8)
C(2a)—N(2a)	1.399(6)	C(2a)—N(3a)	1.357(6)
N(2a)—S(1b)	1.654(4)	N(3a)—C(4a)	1.363(7)
C(4a)—C(5a)	1.379(9)	C(5a)—C(6a)	1.414(9)
S(1b)—O(1b)	1.463(4)	S(1b)—O(2b)	1.453(5)
S(1b)—C(1b)	1.775(7)	C(1b)—C(2b)	1.393(10)
C(1b)—C(6b)	1.413(9)	C(2b)—C(3b)	1.395(12)
C(3b)—C(4b)	1.394(13)	C(4b)—N(4b)	1.383(14)
C(4b)—C(5b)	1.387(16)	C(5b)—C(6b)	1.420(13)
S(1d)—O(1d)	1.515(6)	S(1d)—C(1d)	1.801(11)
S(1d)—C(2d)	1.788(10)		
N(2a)—Hg—N(2a′)	175.0(2)	C(2a)—N(1a)—C(6a)	115.3(5)
N(1a)—C(2a)—N(2a)	113.3(4)	N(1a)—C(2a)—N(3a)	127.0(7)
N(1a)—C(2a)—N(2a)	119.6(4)	Hg—N(2a)—C(2a)	116.9(3)
Hg—N(2a)—S(1b)	117.9(2)	C(2a)—N(2a)—S(1b)	123.6(3)
C(2a)—N(3a)—C(4a)	115.4(5)	N(3a)—C(4a)—C(5a)	122.7(5)
C(4a)—C(5a)—C(6a)	116.7(5)	N(1a)—C(6a)—C(5a)	122.8(6)
N(2a)—S(1b)—O(1b)	104.0(2)	N(2a)—S(1b)—O(2b)	111.9(3)
O(1b)—S(1b)—O(2b)	116.9(3)	N(2a)—S(1b)—C(1b)	106.6(3)
O(1b)—S(1b)—C(1b)	109.1(3)	O(2b)—S(1b)—C(1b)	107.9(3)
S(1b)—C(1b)—C(2b)	122.1(4)	S(1b)—C(1b)—C(6b)	118.0(4)
C(2b)—C(1b)—C(6b)	119.8(6)	C(1b)—C(2b)—C(3b)	120.2(7)
C(2b)—C(3b)—C(4b)	121.4(9)	C(3b)—C(4b)—N(4b)	122.8(10)
C(3b)—C(4b)—C(5b)	118.5(9)	N(4b)—C(4b)—C(5b)	118.7(9)
C(4b)—C(5b)—C(6b)	121.5(8)	C(1b)—C(6b)—C(5b)	118.5(7)
O(1d)—S(1d)—C(1d)	106.0(5)	O(1d)—S(1d)—C(2d)	107.2(4)
C(1d)—S(1d)—C(2d)	97.6(5)		

Preparation of $Hg(sulfadiazinato)_2 \cdot 2DMSO$), **1**

A mixture of a methanol solution of sulfadiazine (Sulfa-H) and a methanol solution of mercury(II) acetate (2:1) afforded a white precipitate, which was filtered and washed with methanol. The resulting solid was crystallized in DMSO/MeOH (1:25) yielding white prisms (3–5 days) of **1** suitable for X-ray diffraction. The complex obtained exhibited a weight loss between 120 and *ca* 175°C, corresponding to the loss of two DMSO molecules per formula unit (mass loss calc., 18.3%; mass loss found, 18.1%). Found: C, 33.6; H, 3.7; N, 13.6; S, 15.0. Calc. for $C_{24}H_{30}N_8O_6S_4Hg$: C, 33.7; H, 3.5; N, 13.1; S, 15.0%. IR(cm^{-1}): 294vw, 351vw, 389w, 532w, 564m, 588s, 639w, 666w, 685m, 718w, 801m, br, 834m, 980m, 1018m, 1081s, 1091s, 1130s, 1184w, 1228m, 1265m, 1301m, 1360m, 1421s, br, 1449s, br, 1504m, 1548m, 1588s, 1598s, 1627m, 3230m, br, 3355m, br. UV(DMSO): 272nm (3.3×10^5), Λ_M (Ω^{-1} cm^2 mol^{-1}) of 10^{-3} M in DMSO, 20°C = 5. ^1H NMR (DMSO-d_6): δ 8.59 d [2H, H(4a)/H(6a), J = 4.8 Hz], 7.87 bd [2H, H(2b)/H(6b), J = 8.5 Hz], 7.08t [1H, H(5a), J = 4.8 Hz], 6.67d [2H, H(3b)/H(5b), J = 8.7 Hz], 6.01bs (2H, NH_2), 2.64s (12H, 2DMSO). ^{13}C NMR (DMSO-d_6): δ 163.7 [C(2a)], 162.4 [C(4a)/C(6a)], 156.6 [C(4b)], 134.3 [C(2b)/C(6b)], 129.8 [C(1b)], 118.4 [C(5a)], 116.0 [C(3b)/C(5b)], 39.2 (DMSO).

RESULTS AND DISCUSSION

Description of the structure

The molecular structure of $Hg(Sulfadiazinato)_2 \cdot 2DMSO$ (**1**) and the atom-numbering scheme are shown in Fig. 1. The two deprotonated sulfadiazinato ligands are related by a binary axis through the metal atom and bound to the mercury via the heterocyclic nitrogen in a nearly linear arrangement [N(2a)—Hg—N(2a′) = 175.0(2)°] Table 2). The Hg—N bond distance [Hg—N(2a) = 2.087(4) Å] is similar to previously reported distances in other Hg—N systems [11]. Figure 2a shows the angles corresponding to the trigonal arrangement of the imido nitrogen in the different metal [Ag^I [2,3], Zn^{II} [4,5], Cu^{II} [12] and Hg^{II}]–sulfadiazinato complexes. As can be observed, a more or less distorted trigonal arrangement appears in all of them but the values corresponding most closely to a trigonal arrangement are found in the Hg complex.

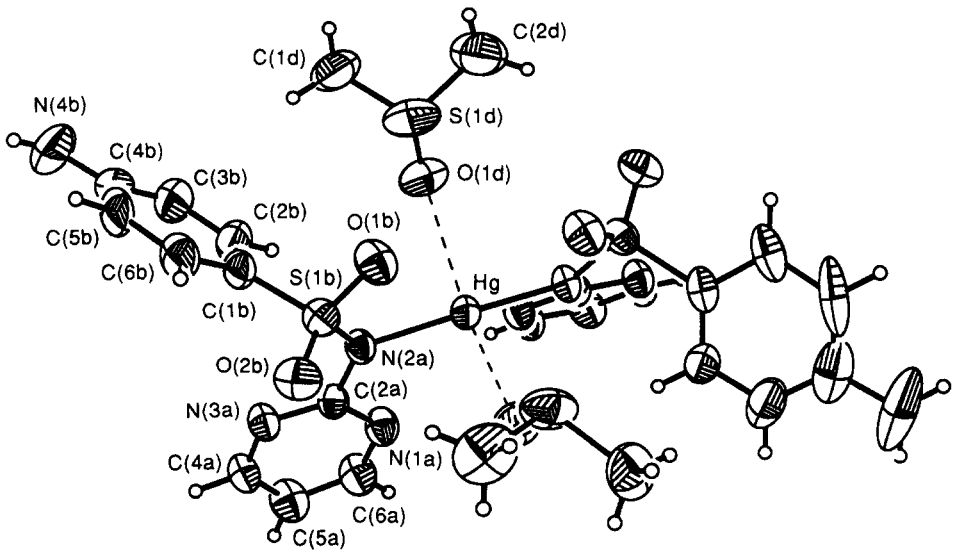


Fig. 1. Molecular structure of the complex showing the atom-numbering scheme.

The C(4b)—N(4b) distance of 1.383(14) Å, is in good agreement with the corresponding bond in sulfadiazine [1.43(3) [1a] or 1.41(2) Å [1b] and other metal–sulfadiazinato complexes [Ag^{I} 1.393(9) Å [2], Zn^{II} 1.377(9) and 1.382(14) Å [5] and Cu^{II} 1.372(17) and 1.373(27) Å [12]], and appreciably shorter than the 1.470(5) Å proposed by Camerman for the length of a C(sp^2)—N(sp^2) single bond [13], suggests considerable double bond character in that bond. There does not appear to be any extension of the phenyl ring electron delocalization to include S(1b), as the S(1b)—C(1b) distance of 1.775(7) Å is a normal single bond. This value is similar to other metal–sulfadiazinato complexes [2–5,12,14]. Analogously, the S(1b)—N(2a) distance [1.654(4) Å] is also nearly a single bond showing no π bond character. The interatomic distance is equivalent to the free ligand [1.65(1) [1a] or 1.66(2) Å [1b]] and Cu^{II} complex [1.657(17) and 1.680(12) Å [12]], but higher than in Ag^{I} [1.600(6) [2,3]] and Zn^{II} [1.568(4) Å and 1.609(4) Å [4,5]] complexes. The S(1b)—O(1b) and S(1b)—O(2b) bonds are very similar but are not completely equal [1.463(4) and 1.453(5) Å, respectively] and are equivalent to the other metal–sulfadiazinato complexes, but higher than in free sulfadiazine [1.41(2) and 1.42(2) Å [1a] or 1.41(1) Å [1b]]. The bond lengths and angles in pyrimidine (mean C—C: 1.397 Å; mean C—N: 1.356 Å, mean angle: 118.8°) and phenyl rings (mean C—C = 1.400 Å; mean C—C—C = 120.0°) are in good agreement with the values observed for such rings in free sulfadiazine and metal–sulfadiazinato complexes studied. The bonding around the sulfur atom is distorted from the ideal tetrahedral geometry. The maximum and minimum values of angles around the sulfur atom are 116.9(3)° [O(1b)—S(1b)—O(2b)] and 106.6(3)° [N(2a)—S(1b)—C(1b)]. A general tetrahedral behaviour is present in all the metal complexes with the same maximum angle (O—S—O), but the minimum varies with each molecule [N—S—C for Ag^{I} and Hg^{II} complexes and O—S—N for Cu^{II} and Zn^{II} complexes and for sulfadiazine).

The molecule maintains a *gauche* conformation (Fig. 2b) about the S(1b)—N(2a) bond with a torsion angle [C(1b)—S(1b)—N(1a)—C(2a)] of −73.3°, similar to the Zn^{II} [−75.4 and −74.0°] and Cu^{II} [−74.6°] complexes, but it is higher than in the ionic sodium 3,5-dimethylsulfadiazinato (−60.6°) [14] and Ag^{I} (−53.9°) complex. On the other hand, although the *gauche* structure between the two rings is very similar in Zn^{II}, Cu^{II} and Hg^{II}, the relative disposition of the metal is clearly different as can be observed by the torsion angles [O(1b)—S(1b)—N(1a)—metal] with values of −36.8, −28.4 and 5.79°.

The crystal packing is depicted in Fig. 3a. The packing of the complex units is governed by long chains formed by weak hydrogen bonds between the NH_2 of the aromatic ring of one complex unit and the N of the two pyrimidines of the next complex unit [N(4b)—H···N(1a) (other complex unit) = 2.44 and N(4b)—H···N(1a)(other complex unit) = 2.90 Å]. On the other hand, no stacking interactions are present in the crystal structure because the aromatic rings are practically perpendicular (Fig. 3b).

Infrared data

The IR spectrum of the complex was recorded down to the far-IR region of 200 cm^{-1} and compared with that of sulfadiazine. Tentative band assignments (cm^{-1}) of some characteristic bands of sulfadiazine were made by analogy with other related systems [15, 16]. The bands at 3355 and 3230 cm^{-1} assigned to ν_a and ν_s (N—H) vibrations of the NH_2 group are significantly shifted with respect to those of the free

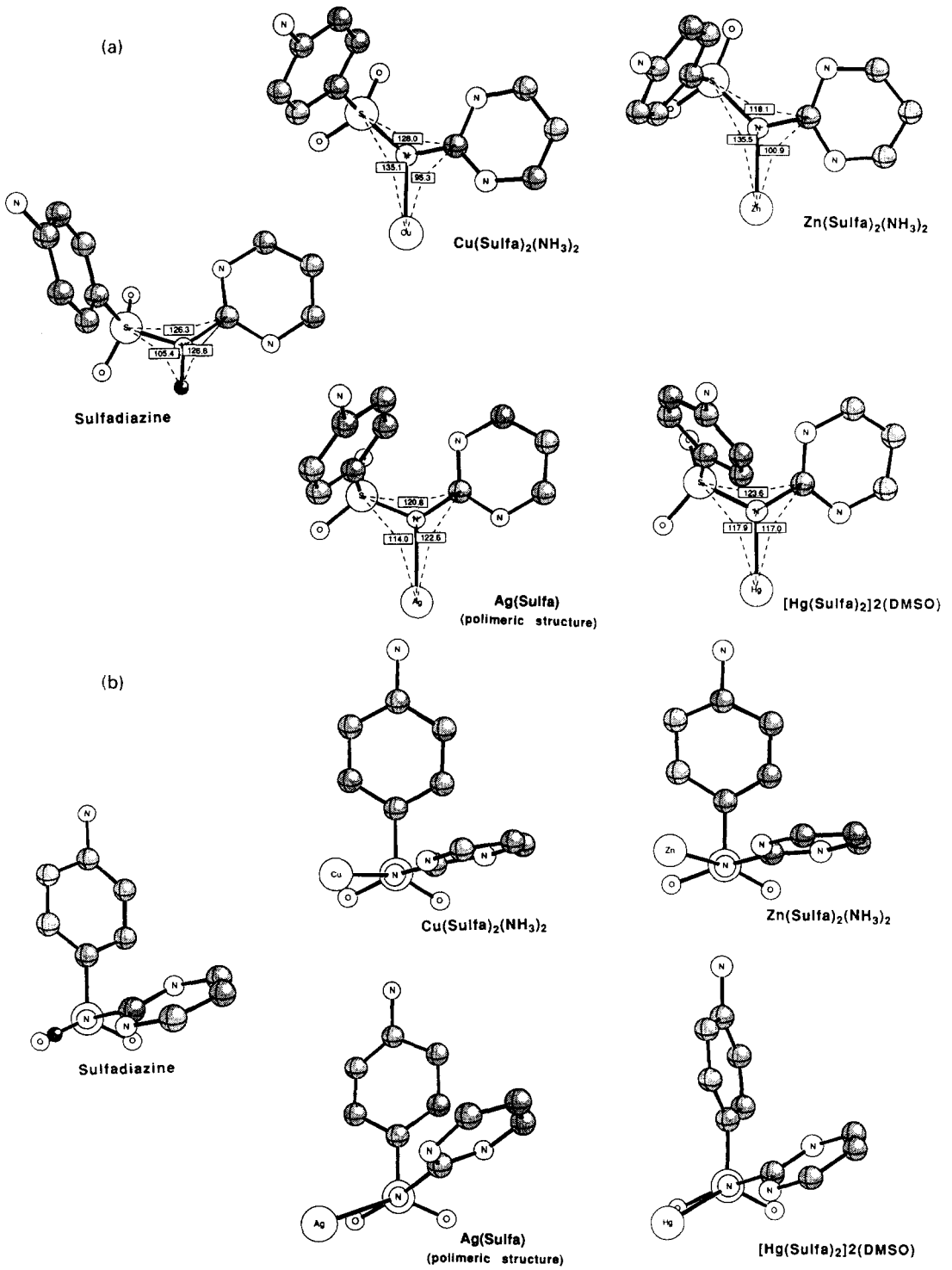


Fig. 2. (a) Trigonal arrangement of imido nitrogen in different metal–sulfadiazine complexes; (b) *gauche* disposition of two aromatic rings of Sulfa in different metal–sulfadiazine complexes. (Data obtained from refs [1a,1b,2–6].)

ligand (3425 and 3360 cm^{-1}) as a consequence of the change in their hydrogen bonding scheme. The strong bands related to ν_a and ν_s of the (SO_2—N) moiety at 1325 and 1155 in the sulfadiazine show important changes upon complexation. The first splits into two peaks at 1360 and 1301 cm^{-1} and the second appears at 1130 cm^{-1}. The band at 945 cm^{-1} corresponding to ν (S—N) is shifted to higher frequencies (980 cm^{-1}) upon complexation [15]. All these changes suggest binding of the mercury atom to the sulfonamide nitro-

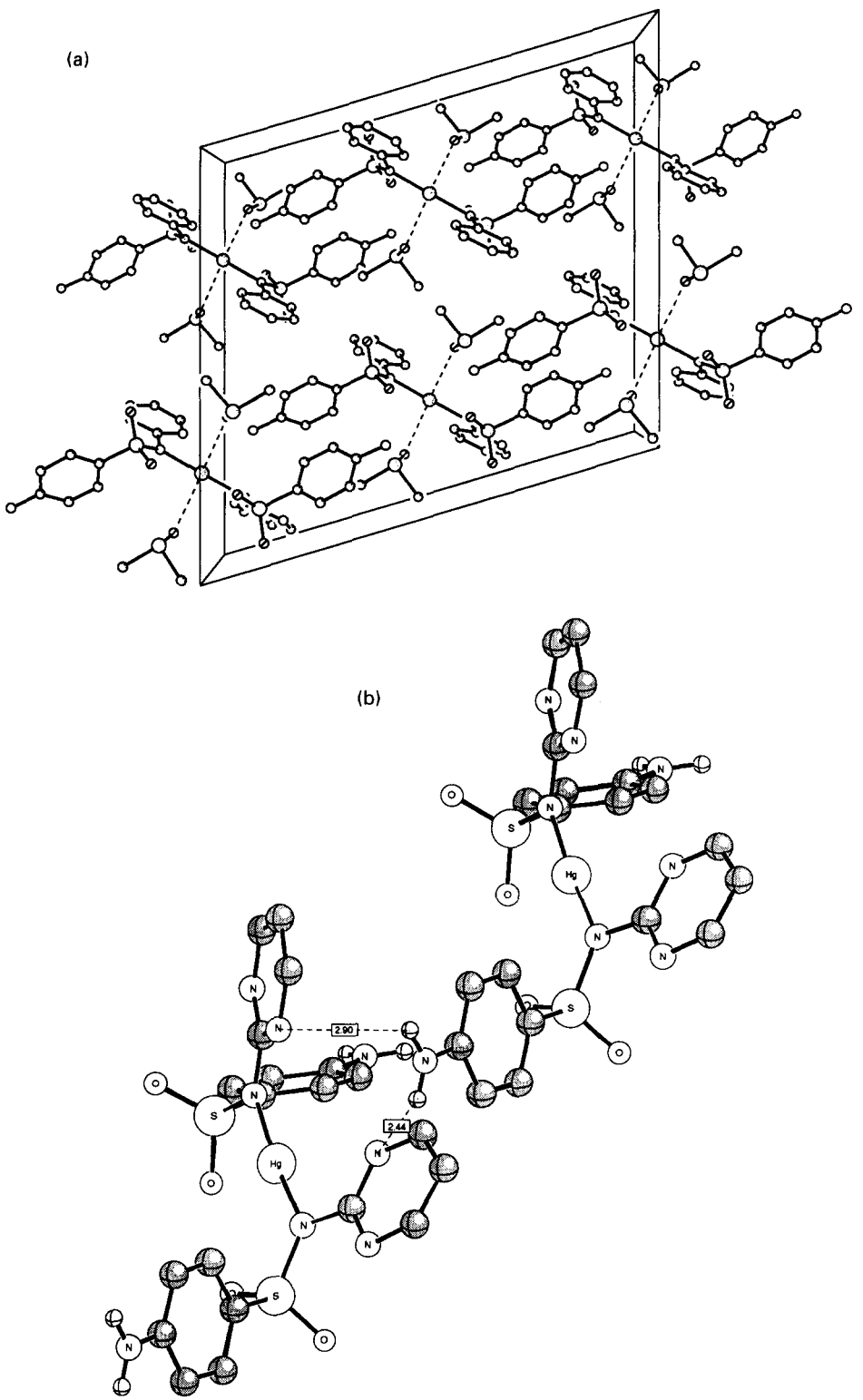


Fig. 3. (a) View of the unit cell down the *b*-axis. (Hydrogen atoms have been omitted for clarity.) (b) Packing of two complex units showing hydrogen bonds between them and the relative disposition of the different aromatic rings. (DMSO and hydrogen atoms have been omitted for clarity.)

gen. The assignment of the band at 1018 cm^{-1} [ν (S=O)DMSO] [17] in the IR spectrum of the mercury complex suggests that the two DMSO molecules of crystallization are loosely bound to the Hg through the oxygen atom.

Electronic spectra

The electronic spectrum in DMSO of sulfadiazine shows two bands at 273 ($\varepsilon = 3.94 \times 10^6$) and 366 nm ($\varepsilon = 2.9 \times 10^5$), assignable to aromatic ring transitions. No frequency changes were observed in the spectrum of the complex. The intensity of the band near 272 nm decreases sharply upon complexation (3.3×10^5), the second one appearing as a shoulder.

^{1}H and ^{13}C NMR spectra

^{1}H NMR spectra can be easily assigned by $J_{H\,H}$ couplings and ROESY (supplementary material). HMQC (Fig. 4a) and HMBC (Fig. 4b) were used to assign the ^{1}H and ^{13}C NMR spectra of the mercury complex. The ^{1}H and ^{13}C assignments of sulfadiazine and Hg(Sulfadiazinato)$_2$·2DMSO (**1**) are shown in Table 3. The non-protonated carbon resonance of 1 were recognized from the HMQC spectrum and

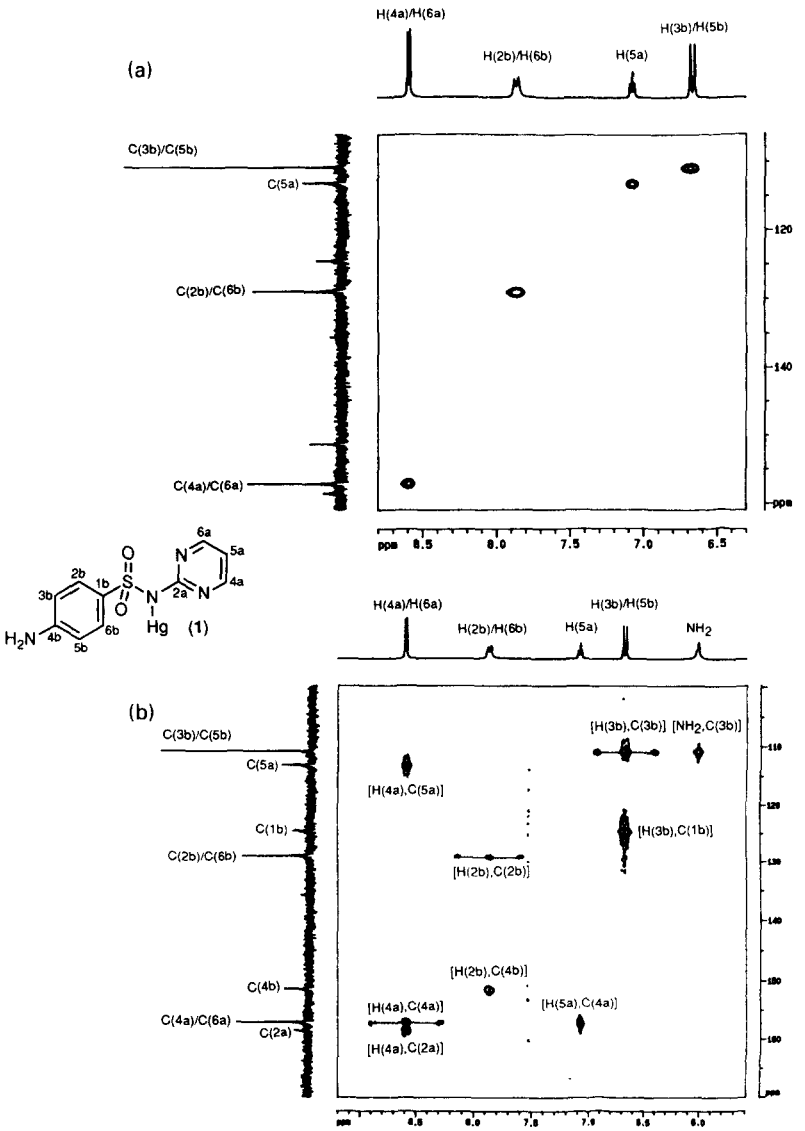
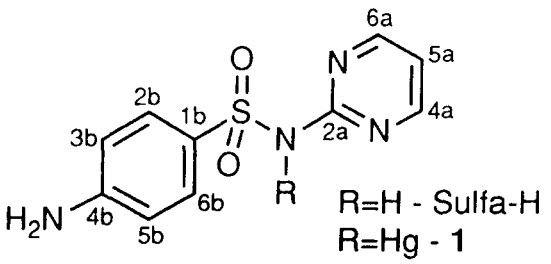


Fig. 4. (a) ^{1}H-detected ^{1}H–^{13}C multiple quantum shift correlation (HMQC) spectrum of [Hg(Sulfa)$_2$]·2DMSO in DMSO-d_6. (b) ^{1}H-detected ^{1}H–^{13}C multiple-bond shift correlation (HMBC) spectrum of [Hg(Sulfa)$_2$]·2DMSO in DMSO-d_6. (Incompletely suppressed "satellite" peaks from C(4a), C(2b) and C(3b) are also present.)

Table 3. ^1H and ^{13}C NMR shift assignments for sulfadiazine (Sulfa-H) and $[Hg(Sulfa)_2]\cdot 2DMSO$ (1) in DMSO-d_6[a]



Assignment	^1H (1)	^1H (Sulfa-H)	$\Delta\delta$ (^1H)[b]	^{13}C (1)	^{13}C (Sulfa-H)	$\Delta\delta$ (^{13}C)[b]
N(2a)—H	—	11.35	—	—	—	—
C(2a)	—	—	—	163.7	161.2	+2.5
C(4a)—H/C(6a)—H	8.59	8.57	+0.02	162.4	162.2	+0.2
C(5a)—H	7.08	7.11	−0.03	118.4	119.5	−1.1
C(1b)	—	—	—	129.8	128.8	+1.0
C(2b)—H/C(6b)—H	7.87	7.70	+0.17	134.3	133.8	+0.5
C(3b)—H/C(5b)—H	6.67	6.65	+0.02	116.0	116.1	+0.1
C(4b)	—	—	—	156.6	157.0	−0.4

[a] Relative to TMS with DMSO-d_6 peak as reference (^1H: 2.60 and ^{13}C: 43.5 ppm).
[b] $\Delta\delta = \delta_{(1)} - \delta_{(Sulfa\text{-}H)}$.

assigned from the HMBC spectrum. Thus C(1b), C(4b) and C(2a) were assigned as the resonances at 129.8, 156.6 and 163.7 from the HMBC correlations to H(3b), H(2b) and H(4a)/H(6a), respectively.

Upon complexation a downfield shift was observed for the C(2a) resonance of Sulfa-H. In addition, the Sulfa-H imino ^1H signal disappeared (Table 3). These changes are consistent with binding of mercury to sulfadiazine through N(2a), as suggested by the X-ray structure. The downfield shift for the C(2a) and H(2b)/H(6b) resonances of Sulfa-H could be related to the proximity of the Hg^{II} atom. No significant changes in ^1H and ^{13}C chemical shifts were observed for other atoms upon complexation, suggesting that, in solution, the aromatic rings are not involved in stacking interactions.

On the other hand, the existence of a nOe between H(2b)/H(6b) and H(4a) indicates, if aggregates do not exist in solution, that the phenyl and the pyrimidyl aromatic rings are, probably, nearer in solution than in the solid structure, because in the crystal the distances are very large [H(2b)···H(4a) = 5.72 and H(6b)···H(4a′) = 6.10 Å for a structural unit $Hg(Sulfadiazinato)_2\cdot 2DMSO$].

Acknowledgement—We are grateful to DGICYT Ref. PB94-0922-C02-02 for financial support.

REFERENCES

1. See, for example, 2-Sulfanilamido-pyrimidine (Sulfadiazine): (a) H. S. Shin, G. S. Ihn, H.-S. Kim and C. H. Koo, *J. Korean Chem. Soc.* 1974, **18,** 329; (b) V. V. Joshi, R. K. Tiwari, T. C. Patel and T. P. Singh, *Indian J. Phys.* 1983, **A57,** 79; 2-Sulfanilamido-5-methoxypyrimidine: (c) A. Guiseppetti, C. Tadini, G. P. Bettinetti and F. Giordano, *Cryst. Struct. Commun.* 1977, **6,** 263; 2-Sulfanilamido-4-methylpyrimidine (Sulphamerazine): (d) N. Deo, R. K. Tiwari and T. P. Singh, *J. Sci. Res. Bhopal, India* 1980, **2,** 137; (e) K. R. Acharya, K. N. Kuchela and G. Kartha, *J. Cryst. Spectrosc.* 1982, **12,** 369; (f) M. R. Caira and R. Mohamed, *Acta Cryst.* 1992, **B48,** 492; 2-Sulfanilamido-4,6-dimethylpyrimidine (Sulfamethazine or Sulfadimidine): (g) L. Maury, J. Rambaud, B. Pauvert, Y. Lasserre, G. Berge and M. Audran, *J. Pharm. Sci.* 1985, **74,** 422; (h) R. K. Tiwari, M. Haridas and T. P. Singh, *Acta Cryst.* 1984, **C40,** 655; (i) M. R. Caira, *J. Cryst. Spectrosc.* 1991, **21,** 641.
2. N. C. Baezinger and A. W. Struss, *Inorg. Chem.* 1976, **15,** 1807.
3. D. S. Cook and M. F. Turner, *J. Chem. Soc., Perkin Trans* 2 1975, 1021.
4. N. C. Baezinger, S. L. Modak and C. L. Fox, Jr, *Acta Cryst.* 1983, **C39,** 1620.
5. C. J. Brown, D. S. Cook and L. Sengier, *Acta Cryst.* 1985, **C41,** 718.
6. P. J. Sadler, *Adv. Inorg. Chem.* 1991, **36,** 1.
7. A. Bax and S. Subramanian, *J. Magn. Reson.* 1986, **67,** 565.
8. A. Bax and M. F. Summers, *J. Am. Chem. Soc.* 1986, **108,** 2093.
9. A. Bax and D. G. Davis, *J. Magn. Reson.* 1985, **63,** 207.
10. Release 3.4 for Nicolet R3m/v crystallographic system, Nicolet Instrument Corporation, Madison, Wisconsin, USA.

11. See, for example, L. D. Kosturko, C. Folzer and R. F. Stewart, *Biochemistry* 1974, **13,** 949; D. M. L. Goodgame, A. M. Khaled, C. A. O'Mahoney and D. J. Williams, *J. Chem. Soc., Chem. Commun.* 1990, 1765; D. M. L. Goodgame, S. P. W. Hill and D. J. Williams, *Polyhedron* 1992, **11,** 1507; A. García-Raso, J. J. Fiol, E. Molins, A. M. Calafat, P. A. Marzilli and L. G. Marzilli, *Metal-Based Drugs* 1995, **2,** 81.
12. C. J. Brown, D. S. Cook and L. Sengier, *Acta Cryst.* 1987, **C43,** 2332.
13. A. Camerman, *Can. J. Chem.* 1970, **48,** 179.
14. S. S. Hanan and A. N. Talukdar, *Acta Cryst.* 1992, **C48,** 2021.
15. F. Blasco, R. Ortiz, L. Perelló, J. Borrás, J. Amigó and T. Debaerdemaeker, *J. Inorg. Biochem.* 1994, **53,** 117.
16. J. Casanova, G. Alzuet, J. Borrás, J. Timoneda, S. García-Granda and I. Cándano-González, *J. Inorg. Biochem.* 1994, **56,** 65.
17. E. Alessio, G. Balducci, A. Lutman, G. Mestroni, M. Calligaris and W. M. Attia, *Inorg. Chim. Acta* 1993, **203,** 205; V. Yu Kukushin, V. K. Belsky, V. E. Konovalov, G. A. Kirakosyan, L. V. Konovalov, A. I. Moiseev and V. M. Tkachuk, *Inorg. Chim. Acta* 1991, **185,** 143; K. Nakamoto, *Infrared and Raman Spectra of Inorganic and Coordination Compounds*, 4th edn. John Wiley & Sons, New York.

Pergamon

PII: S0277-5387(96)00315-4

Polyhedron Vol. 16, No. 4, pp. 623–627, 1997
Copyright © 1996 Elsevier Science Ltd
Printed in Great Britain. All rights reserved
0277-5387/97 $17.00+0.00

Identification of the dysprosium(III) chloride solvate $DyCl_3(THF)_{3.5}$: crystal structure of the ion pair [*trans*-$DyCl_2(THF)_5$][*trans*-$DyCl_4(THF)_2$]

Gerald R. Willey,[a]* Paul R. Meehan,[a] Timothy J. Woodman[a] and Michael G. B. Drew[b]

[a]Department of Chemistry, University of Warwick, Coventry CV4 7AL, U.K.

[b]Department of Chemistry, University of Reading, Whiteknights, Reading, RG6 2AD, U.K.

(Received 24 May 1996; accepted 26 June 1996)

Abstract—Treatment of $DyCl_3(H_2O)_6$ with thionyl chloride in the presence of tetrahydrofuran provided colourless crystals of $DyCl_3(THF)_{3.5}$, subsequently identified as the ionic salt [*trans*-$DyCl_2(THF)_5$][*trans*-$DyCl_4(THF)_2$] by an X-ray diffraction study. The dysprosium atom in the monocation is seven coordinate with the *trans*-$DyCl_2$ unit [Dy—Cl, 2.624(5) Å] surrounded by five tetrahydrofuran molecules (Dy—O, mean 2.41(2) Å) in a regular pentagonal bipyramidal geometry. For the anion the dysprosium atom is six coordinate with an octahedral geometry comprising four equatorial chlorine atoms (Dy—Cl, mean 2.642(5) Å) and two axial tetrahydrofuran molecules (Dy—O, 2.41(2) Å). Copyright © 1996 Elsevier Science Ltd

Keywords: structure; auto-ionisation; dysprosium(III); tetrahydrofuran; adduct.

Lanthanide halide solvates $MX_3(S)_n$, particularly those involving X = Cl and S = THF, are convenient and useful precursors to organometallic lanthanide species such as alkoxides, hydrides, etc., which, in addition to their intrinsic coordination chemistry, attract considerable commercial interest, e.g. catalytic activity for alkene polymerization [1]. Given that there are no dramatic or wholesale size differences across the lanthanide series M^{III} (Ce → Lu) but rather more subtle variations [2], it might be expected that a common solvation species would dominate. To some extent this is true with the emergence of the structurally characterized seven coordinate pentagonal bipyramidal species $MCl_3(S)_4$, and the related $MCl_3(B)_2$ (B = bidentate ligand). Examples here include: M = Gd, B = dimethoxyethane (DME) [3]; M = Sm, S = THF [4]; M = Sm, 2S (THF) and B = DME [5]; M = Eu, S = pyridine [6]. However, a cursory glance at the literature reveals that the level of solvation is by no means regular, or even predictable, and examples of solvate stoichiometry range from $n = 1.5$ to $n = 4$: typical representatives include $LaCl_3(THF)_{1.5}$ [7]; $CeCl_3(THF)_2$ [7]; $GdCl_3(THF)_3$ [8]; $ErCl_3(THF)_{3.5}$ [8] and $EuCl_3(THF)_4$ [9]. Even for one and the same metal there is often an interesting gradation, e.g. for $NdCl_3(THF)_n$ there are exemplars for $n = 1.5$ [10], 2 [8] and 4 [11].

Specifically, for dysprosium(III), $DyCl_3(THF)_{3.5}$ is the sole representative, but although there are several reports giving synthetic details [7] the structure has not been clarified. Herein we describe the isolation of this particular solvate from the reaction system $DyCl_3(H_2O)_6/SOCl_2/THF$ and its structural identity (X-ray diffraction) as the ion pair [*trans*-$DyCl_2(THF)_5$][*trans*-$DyCl_4(THF)_2$].

EXPERIMENTAL

Manipulations of materials were carried out using Schlenk techniques, in conjunction with a conventional dinitrogen atmosphere glovebox. Solvents were dried over CaH_2, and subsequently over P_4O_{10}, and were distilled over Na/benzophenone in an inert atmosphere prior to use. $DyCl_3(H_2O)_6$ was purchased

* Author to whom correspondence should be addressed.

from Aldrich Chemical Co. and used without further purification. IR spectra were obtained as Nujol mulls between CsI plates using a Perkin–Elmer 580B instrument, and elemental analyses were carried out using a Leeman Labs Inc., PS 1000 sequential inductively coupled plasma (ICP) spectrometer and a CE 440 elemental (C, H, N) analyser.

Preparation of $DyCl_3(THF)_{3.5}$

$SOCl_2$ (25 cm^3, 343 mmol) was added dropwise to a cooled (0°C), stirred solution of $DyCl_3(H_2O)_6$ (6.02 g, 15.97 mmol) in tetrahydrofuran (75 cm^3) and the mixture was heated at reflux for 75 h. Removal of solvent *in vacuo* from the resulting solution afforded an off-white solid which was washed with ether (3×20 cm^3) and hexane (3×20 cm^3) and pumped *in vacuo* at room temperature for several hours. Subsequent recrystallization from THF in the presence of activated charcoal gave the title compound as cubic crystals. Yield 7.24 g, 87.2%. Found: C, 30.8; H, 5.3; Cl, 20.1; Dy, 30.9. Calc. for $C_{28}H_{56}O_7Dy_2Cl_6$: C, 32.3; H, 5.4; Cl, 20.4; Dy, 31.2%. IR $\bar{\nu}_{max}/cm^{-1}$ (Nujol): 1306m, 1170s, 1075m, 1010s, ν_{as}(COC); 919m, 858s, ν_s(COC); 771w, 722s, 668w, 565vw, 497vw (ligand), 276vs br, 240 br sh ν(DyCl).

X-ray crystallography

Crystal data are given in Table 1, together with refinement details. Data were collected with Mo-K_α radiation using the MARresearch Image Plate System. The crystal was positioned at 75 mm from the image plate. A total of 95 frames were measured at 2° intervals with a counting time of 2 minutes. Data analysis was carried out with the XDS program [12]. The structure was solved using direct methods with the SHELX86 program [13]. The non-hydrogen atoms were refined with anisotropic thermal parameters. The hydrogen atoms were included in geometric positions and given thermal parameters equivalent to 1.2 times those of the atom to which they were attached. An empirical absorption correction was applied [14]. The structure was then refined on F^2 using SHELXL [15]. The light atoms have high thermal motion. All calculations were carried out on a Silicon Graphics R4000 workstation at the University of Reading. Additional material available from the Cambridge Crystallographic Data Centre comprises hydrogen atom coordinates, thermal parameters, a complete set of bond distances and angles and observed and calculated structure factors.

Table 1. Crystal data and structure refinement for [*trans*-$DyCl_2(THF)_5$][*trans*-$DyCl_4(THF)_2$]

Empirical formula	$C_{28}H_{56}Cl_6Dy_2O_7$
Formula weight	1042.43
Temperature (K)	293(2)
Wavelength (Å)	0.7107
Crystal system	monoclinic
Space group	$C2/c$
Unit-cell dimensions (Å, °)	$a = 12.758(7)$
	$b = 11.736(7)$
	$c = 27.695(13)$
	$\beta = 91.49(1)$
Volume (Å^3)	4145(4)
z	4
Density (calculated) (mg/m^3)	1.670
Absorption coefficient (mm^{-1})	4.000
$F(000)$	2056
Crystal size (mm)	$0.25 \times 0.25 \times 0.20$
θ range for data collection (°)	2.46–25.12
Index ranges	$0 \leqslant h \leqslant 13$,
	$-7 \leqslant k \leqslant 11$,
	$-32 \leqslant l \leqslant 32$
Reflections collected	3445
Independent reflections	2463
	[R(int) = 0.0446]
Weighting scheme $(a, b)^a$	0.84, 27.34
Data/restraints/parameters	2461/0/199
Goodness-of-fit on F^2	0.431
Final R indices [$I > 2\sigma(I)$]	$R_1 = 0.0838$,
	$wR_2 = 0.2750$
R indices (all data)	$R_1 = 0.1072$,
	$wR_2 = 0.3757$
Largest diff. peak and hole (e Å^{-3})	2.244, −1.364

[a] Weighting scheme $w = 1/(\sigma^2(F_o^2) + (aP)^2 + bP)$, where $P = (F_o^2 + 2F_c^2)/3$.

RESULTS AND DISCUSSION

Dehydration of $DyCl_3(H_2O)_6$ using thionyl chloride in an excess of tetrahydrofuran provided colourless cubic crystals of the anhydrous solvate $DyCl_3(THF)_{3.5}$. The infrared spectrum contains characteristic bands at 1010 cm^{-1} ν_{as}(C—O—C), 858 cm^{-1} ν_s(C—O—C) and 276, 240 (sh) cm^{-1} ν(Dy—Cl) with no sign of the presence of water molecules. The true nature of the product was obtained by an X-ray diffraction study which revealed the 1:1 ionic salt [*trans*-$DyCl_2(THF)_5$][*trans*-$DyCl_4(THF)_2$]. The structures of the individual ions are presented in Fig. 1 with the atom numbering scheme used. Selected bond distances and angles for each ion are listed in Table 2. It is interesting that auto-ionization of dysprosium(III) chloride in the strongly polar THF has produced an ion pair comprising seven coordinate $DyCl_2^+$ (solvated) cations and six coordinate $DyCl_4^-$ (solvated) anions. The coordination number seven is commonplace for lanthanide(III) halide complexes, but even under the umbrella of pentagonal bipyramidal geometry perhaps some clear distinction should be made between *neutral* monomeric compounds $MCl_3(S)_4$/$MCl_3(B)_2$ [Type X] and *cationic* species based on solvated MCl_2^+ where auto-ionisation in a polar donor solvent has occurred, i.e. [Type Y]

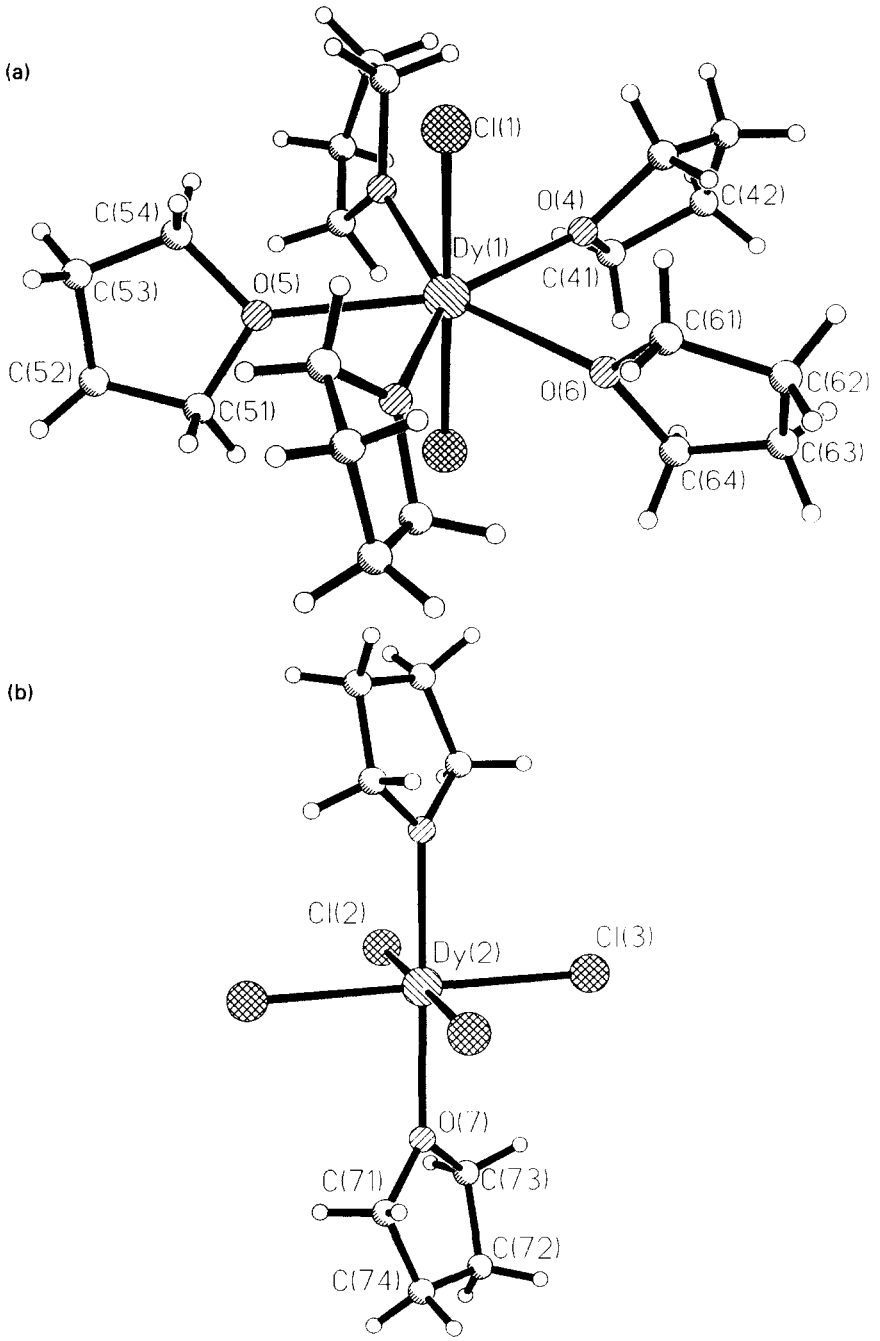


Fig. 1. Perspective views of the structures of (a) the [*trans*-$DyCl_2(THF)_5$]$^+$ cation and (b) the [*trans*-$DyCl_4(THF)_2$]$^-$ anion.

$$2MCl_3(S)_{3.5} \xrightarrow{S} [MCl_2(S)_5]^+ + [MCl_4(S)_2]^-.$$

Examples of each type include: [Type X] M = Gd, B = DME [3]; M = Eu, S = THF [9]; M = Nd, S = THF [11]; M = Sm, 2S(THF) and B(DME) [5]; M = Eu, S = pyridine [6]; M = Sm, S = THF [4]; M = Sm, S = isopropanol [16]; M = Lu, S = THF [17]; M = Y, B = DME [18]. For [Type Y] M = Tb, S = THF [19] and M = Y, S = THF [20] and S = NIM [21] where NIM = *N*-methylimidazole ($C_4H_6N_2$). However, it should be noted that an alternative to [Type Y] exists which features solvated MX_2^+ cations, but not as derived from auto-ionisation, namely, $[SmI_2(THF)_5][Co(CO)_4]$ [22]; $[SmI_2(Ph_2MeP{=}O)_5]I$ [23]; $[YCl(OCMe_3)(THF)_5][PBh_4]$ [24].

In the present structure, the *trans*-$DyCl_2$ unit of the cation is linear with identical Dy—Cl bond distances 2.624(5) Å and Cl—Dy—Cl 179.3(3)°. By way of comparison, the seven coordinate pentagonal bipyramidal (some distortion noted) $DyCl_3$(triethyleneglycol)·18-crown-6 adduct [25] shows an

Table 2. Bond lengths (Å) and angles (°) for the coordination spheres of [*trans*-$DyCl_2(THF)_5$][*trans*-$DyCl_4(THF)_2$]

Dy(1)—O(4)	2.37(2)
Dy(1)—O(6)	2.379(12)
Dy(1)—O(5)	2.453(11)
Dy(1)—Cl(1)	2.624(5)
O(4)—Dy(1)—O(6)	72.2(4)
O(6)#1—Dy(1)—O(6)	144.5(8)
O(6)—Dy(1)—O(5)#1	72.4(5)
O(4)—Dy(1)—O(5)	143.6(3)
O(6)—Dy(1)—O(5)	142.6(5)
O(5)#1—Dy(1)—O(5)	72.7(6)
O(4)—Dy(1)—Cl(1)	90.36(13)
O(6)#1—Dy(1)—Cl(1)	84.7(4)
O(6)—Dy(1)—Cl(1)	95.5(4)
O(5)#1—Dy(1)—Cl(1)	84.9(3)
O(5)—Dy(1)—Cl(1)	94.6(3)
Cl(1)#1—Dy(1)—Cl(1)	179.3(3)
Dy(2)—O(7)	2.41(2)
Dy(2)—Cl(3)	2.641(5)
Dy(2)—Cl(2)	2.644(5)
O(7)—Dy(2)—Cl(3)	90.4(6)
O(7)—Dy(2)—Cl(2)	90.5(5)
Cl(3)—Dy(2)—Cl(2)	88.1(2)
O(7)#2—Dy(2)—O(7)	179.998(1)

Symmetry transformations used to generate equivalent atoms; #1 $-x, y, -z+1/2$; #2 $-x+1/2, -y+1/2, -z$.

essentially linear $DyCl_2$ fragment with Cl—Dy—Cl 163.96(8)° and Dy—Cl mean 2.626(2) Å. In a subsequent determination of a more ordered form of this particular molecule [26] the dimensions showed some minor changes, namely Dy—Cl mean 2.607(1); Cl—Dy—Cl 162.65(7)°. Some measure of how close the present structure approaches the ideal is seen by the fact that Cl—Dy—O (ten of these) lie in the range 84.7(4)–95.5(4)° and O—Dy—O (five of these) fall within the very narrow range 72.2(4)–72.7(6)°. The equatorial DyO_5 segment is coplanar; a least-squares plane carried through these six atoms shows deviations of ±0.25 Å. With regard to the bound solvent molecules there is a steric alignment about the Dy←O linkages leaving the individual five-membered rings in a steam-paddle arrangement; the three independent Cl(1)—Dy(1)—O_{ring}—C_{ring} torsion angles are 21.0, 25.1 and 12.2°, indicative that the ring planes are much more axially than equatorially aligned. For the centrosymmetric $[DyCl_4(THF)_2]^-$ anion the coordinated THF molecules are mutually *trans* in axial locations with Dy—O 2.41(2) Å and O—Dy—O, 179.998(1)°. The equatorial $DyCl_4$ unit is perforce planar with Dy—Cl bond distances in the range 2.641(5)–2.644(5), mean 2.642(5) Å and *cis*-Cl—Dy—Cl angles lying between 88.1(2) and 91.9(2)°. There is precious little difference between the anion and cation dimensions; the Dy—Cl bond distances are marginally longer in the anion, but the Dy—O bonds are identical for both. For a direct comparison the neutral six-coordinate $DyCl_3(HMPA)_3$ [27] shows Dy—Cl 2.626(4), 2.637(2) and 2.634(3) Å, mean 2.632(4) Å.

In summary, we note that although solvated lanthanide MCl_2^+ cations with a *trans* pentagonal bipyramidal metal geometry are fairly commonplace, only three previous examples originate strictly from autoionisation. As listed above these are M = Y (Group 3) (two examples) and Tb and all three feature a steam-paddle arrangement of the five equatorial solvent molecules associated with the MCl_2^+ cation. The present structural study confirms a fourth (and still rare) representative with M = Dy, and it is tempting to associate all such "3.5 complexes", both present and future, with this ionic formulation. The question of why the more orthodox mononuclear adduct $DyCl_3(THF)_4$ (Type X) was not obtained, and, indeed, whether it can be obtained, is under evaluation. One point that emerges from the brief survey above is that even with a specific donor solvent (S) such as tetrahydrofuran there is no one singular structural type that encompasses MCl_3–THF complexation. Some of the factors that appear relevant to the observed structural diversity of such complexes have been admirably set out and discussed by Evans *et al* [19].

Acknowledgements—We thank the University of Warwick for postgraduate scholarship awards (to P.R.M. and T.J.W.). Financial support by the EPSRC and the University of Reading for the image plate system is gratefully acknowledged and we thank Mr A. W. Johans for technical assistance with the X-ray crystallographic studies.

REFERENCES

1. H. Schumann and W. Genthe, in *Handbook on the Physics and Chemistry of Rare Earth Elements*, Edited by K. A. Gschneidner and L. Eyring, Vol. 7, Ch. 53. Elsevier, Amsterdam (1984); F. A. Hart, in *Comprehensive Co-ordination Chemistry* (Edited by G. Wilkinson, R. D. Gillard and J. A. McCleverty), Vol. 3, Ch. 39. Pergamon Press, Oxford (1987); R. M. Mehrotra, A. Singh and U. M. Tripathi, *Chem. Rev.* 1991, **91,** 1287.
2. A. F. Wells, *Structural Inorganic Chemistry*, 5th Edn. Clarendon Press, Oxford (1986).
3. G. Wei, H. Gao, Z. Jin and Q. Shen, *J. Struct. Chem.* (*Jiegou Huaxue*) 1989, **8,** 61.
4. G.-Y. Lin, G.-C. Wei, Z.-S. Jin and W.-Q. Chen, *J. Struct. Chem.* (*Jiegou Huaxue*) 1992, **11,** 200.
5. Z. Jin, G. Nie, N. Hu and W. Chen, *Chin. J. Appl. Chem.* (*Yingyong Huaxue*) 1989, **6,** 69.
6. N.-H. Hu, Y.-H. Lin, Q. Shen, Y. Xing and E.-D. Shi, *Acta Chim. Sin.* (*Huaxue Xuebao*) 1986, **44,** 388.
7. J. H. Freeman and M. L. Smith, *J. Inorg. Nucl. Chem.* 1958, **7,** 224; M. D. Taylor, *Chem. Rev.* 1962, **62,** 503; S.-H. Wu, Z.-B. Ding and X.-J. Li, *Polyhedron* 1994, **13,** 2679.

8. G. B. Deacon, T. Feng, S. Nickel, B. W. Skelton and A. H. White, *J. Chem. Soc., Chem. Commun.* 1993, 1328.
9. S.-H. Lin, Z.-C. Dong, J.-S. Huang, Q.-F. Zhang and J.-X. Lu, *Acta Cryst.* 1991, **C47,** 426.
10. G. B. Deacon, T. D. Tuong and D. L. Wilkinson, *Inorg. Synth.* 1990, **28,** 286.
11. W. Chen, Z. Jin, Y. Xing, Y. Fan and G. Yang, *Inorg. Chim. Acta* 1987, **130,** 125.
12. W. Kabsch, *J. Appl. Crystallogr.* 1988, **21,** 916.
13. G. M. Sheldrick, SHELX86, *Acta Cryst.* 1990, **A46,** 467.
14. N. Walker and D. Stuart, *Acta Cryst.* 1983, **A39,** 158.
15. G. M. Sheldrick, *SHELXL, Program for crystal structure refinement.* University of Gottingen, Germany (1993).
16. L. E. Depero, M. T. Arienti, M. Zocchi and M. C. Gallazzi, *Struct. Chem.* 1991, **2,** 595.
17. G. K.-I. Magomedov, A. Z. Voskoboinikov, N. I. Kirillova, A. I. Gusev, I. N. Parshina and I. P. Bele, *Metalloorg. Khim.* (*Organometallic Chem. in USSR*), 1992, **5,** 679.
18. W. J. Evans, T. J. Boyle and J. Ziller, *J. Am. Chem. Soc.* 1993, **115,** 5084.
19. W. J. Evans, J. L. Shreeve, J. W. Ziller and R. J. Doedens, *Inorg. Chem.* 1995, **34,** 576.
20. Z.-W. Xie, C.-T. Qian, J. Sun and X.-L. Jin, *J. Struct. Chem* (*Jiegou Huaxue*) 1993, **12,** 107; P. Sobota, J. Utko and S. Szafert, *Inorg. Chem.* 1994, **33,** 5203.
21. W. J. Evans, J. L. Shreeve, T. J. Boyle and J. W. Ziller, *J. Coord. Chem.* 1995, **34,** 229.
22. W. J. Evans, I. Bloom, J. W. Grate, L. A. Hughes, W. E. Hunter and J. L. Atwood, *Inorg. Chem.* 1985, **24,** 4620.
23. A. Sen, V. Chebolu and E. M. Holt, *Inorg. Chim. Acta* 1986, **118,** 87.
24. W. J. Evans, J. M. Olotson and J. W. Ziller, *J. Am. Chem. Soc.* 1990, **112,** 2308.
25. R. D. Rogers, E. J. Voss and R. D. Etzenhouser, *Inorg. Chem.* 1988, **27,** 533.
26. R. D. Rogers and R. D. Etzenhouser, *Acta Cryst.* 1988, **C44,** 1533.
27. X.-W. Zhang, X.-F. Li, F. Benetollo and G. Bombieri, *Inorg. Chim. Acta* 1987, **139,** 103.

Pergamon

PII: S0277-5387(96)00316-6

Polyhedron Vol. 16, No. 4, pp. 629–634, 1997
Copyright © 1996 Elsevier Science Ltd
Printed in Great Britain. All rights reserved
0277-5387/97 $17.00+0.00

Synthesis and structure of $[(CH_3)_4N]_4[H_2MoV_9O_{28}]Cl\cdot 6H_2O$

Neven Strukan, Marina Cindrić and Boris Kamenar*

Laboratory of General and Inorganic Chemistry, Faculty of Science, University of Zagreb, POB 153, 10000 Zagreb, Croatia

(Received 24 May 1996; accepted 26 June 1996)

Abstract—$[(CH_3)_4N]_4[H_2MoV_9O_{28}]Cl\cdot 6H_2O$ has been synthesized from ammonium vanadate and molybdenum(VI) oxide in acidic aqueous solution by adding tetramethylammonium chloride, and its structure determined by single-crystal X-ray analysis. The polyoxomolybdovanadate anion has the structure of the decavanadate anion with the molybdenum atom substituted at one "capping" vanadium site. Owing to the $2/m$ symmetry of the anion, this molybdenum atom is randomly distributed over four "capping" metal atom positions. Two hydrogen atoms are bonded to triply bridging oxygen atoms. Copyright © 1996 Elsevier Science Ltd

Keywords: molybdovanadates; crystal structure determination; protonation site.

Molybdovanadates have been studied in aqueous solution by NMR spectroscopy and potentiometry, and a number of polyoxoanion species observed and identified [1–3]. Although the crystal structures of a few molybdovanadate anions have been reported, such as α-$[Mo_6V_2O_{26}]^{6-}$ [4], β-$[Mo_6V_2O_{26}]^{6-}$ [5], $[Mo_8V_5O_{40}]^{7-}$ [6], $[Mo_4V_8O_{36}]^{8-}$ [7] and $[(V^{IV}V^{V}Mo_{10})VO_{40}]^{6-}$ [8,9], none of these structures correlates with any of the major species observed in solution. It seems that crystals appear because of their insolubility rather than the relative stability of the solution species [3]. However, our recent paper revealed the structure of the $[Mo_4V_5O_{27}]^{5-}$ anion as the first example of a structurally characterized molybdovanadate that is dominant in aqueous solution [10].

In general, while the molybdenum-rich region of the molybdovanadates is structurally complex, the vanadium-rich region essentially retains the decavanadate structure characterized by three species containing either one or two (positioned *cis* or *trans*) "capping" vanadium sites substituted by molybdenum atoms [2]. The synthesis and crystal structure determination of $[(CH_3)_4N]_4[H_2MoV_9O_{28}]Cl\cdot 6H_2O$, described here, confirms the results found in solution [1].

* Author to whom correspondence should be addressed.

EXPERIMENTAL

Reagents and apparatus

All chemicals were of reagent grade and used as purchased from commercial sources. The IR spectrum was recorded in KBr with an FTIR 1600 spectrophotometer in the 4500–450 cm^{-1} region.

Preparation and elemental analyses

The title complex was prepared by mixing a 2M ammonium solution (25 cm^3) of MoO_3 (1.80 g) and a hot water solution (25 cm^3) of NH_4VO_3 (2.9 g). When 2M HCl (13 cm^3) was added to the resulting solution its colour turned to orange. Undissolved NH_4VO_3 was filtered off and solid $(CH_3)_4NCl$ (5.49 g) was added. After standing for 10 days at room temperature orange crystalline product (0.15 g, 0.83%) was filtered off and recrystallized from water solution. Found: C, 12.8; H, 3.5; N, 4.0; Mo, 6.3; V, 30.9; Cl, 2.0. Calc. for $C_{16}H_{62}N_4O_{34}MoV_9Cl$: C, 13.3; H, 4.3; N, 3.9; Mo, 6.6; V, 31.7; Cl, 2.5%. IR (cm^{-1}): 3501m, 3144m, 3034m, 1485s, 1461m, 1448m, 962s, 848s, 751s, 543s.

Crystal structure determination

Crystal data. $C_{16}H_{62}N_4O_{34}MoV_9Cl$, monoclinic, space group $I2/m$, $M = 1444.54$, $a = 10.600(2)$,

$b = 20.117(4)$, $c = 11.129(8)$ Å, $\beta = 92.39(3)^\circ$, $V = 2371(3)$ Å^3, $Z = 2$, $D_X = 2.02$ g cm^{-3}, $F(000) = 1448$, $\mu(\text{Mo-}K_\alpha) = 20.40$ cm^{-1}. A single crystal of dimensions $0.12 \times 0.26 \times 0.38$ mm^3 was used for the data collection on a STOE modified Philips PW1100 diffractometer with graphite-monochromatized Mo-K_α radiation ($\lambda = 0.7107$ Å). Four standard reflections measured every 80 min showed a drop of intensity of 16%. The 3974 reflections (3519 unique) were collected ($2 \leqslant \theta \leqslant 30^\circ$, $-14 \leqslant h \leqslant 14$, $0 \leqslant k \leqslant 28$, $0 \leqslant l \leqslant 15$) by ω scans at room temperature. Data were corrected for decay, Lorentz and polarization effects, and also for absorption (by integration from crystal shape using the ACXR [11] program).

The structure was solved by a heavy-atom method and successive Fourier syntheses. While the Patterson map revealed the positions of three metal atoms in the asymmetric unit, subsequent Fourier maps showed the positions of all other non-hydrogen atoms. Inspection of the difference maps revealed the existence of residual electron density around metal atom M(2) (~ 6 e Å^{-3}) indicating a partial molybdenum substitution at the "capping" vanadium sites. Refinement of site occupancy factors gave a V:Mo ratio of 0.78:0.22. Owing to the overall symmetry of the molybdovanadate anion ($2/m$) the ratio V:Mo was fixed as 0.75:0.25 and, as such, included in the further refinement. The refinement was performed by full-matrix least-squares calculations with anisotropic thermal parameters for all non-hydrogen atoms, V(2) and Mo(2) were refined with the same coordinates and anisotropic thermal parameters. Following the absorption correction all hydrogen atoms were located in a difference Fourier map, and included in structure factor calculations. Since water oxygen O(w1) and hydrogen H(11) are positioned in a mirror plane, the other hydrogen atom H(12), located in a general position, is distributed over two symmetrically related equivalent positions. The calculations converged at $R = 0.030$ over 1948 reflections with $I\xi \geqslant 3\sigma(I)$ and 157 refined parameters, $wR = 0.045$, $w = 0.8011/[\sigma^2(F) + 0.0008F^2]$ and $S = 0.987$. Two low refections (110 and 011) were omitted owing to secondary extinction. The largest remaining difference peak was 0.37 e Å^{-3}. All calculations were performed on an IBM PC/AT compatible microcomputer (processor 80486/66MHz) using the SHELXS86 [12] and SHELX76 [13] programs. The distances and angles were calculated using the CSU program [14], the molecular and crystal structure using ORTEP [15] and PLUTON [16] programs.

RESULTS AND DISCUSSION

The structure of the molybdovanadate anion is shown in Fig. 1 and the packing of anions with surrounding tetramethylammonium cations, chlorine ions and water molecules is shown in Fig. 2. Interatomic distances are listed in Table 1 and hydrogen bonding parameters in Table 2, while the relative

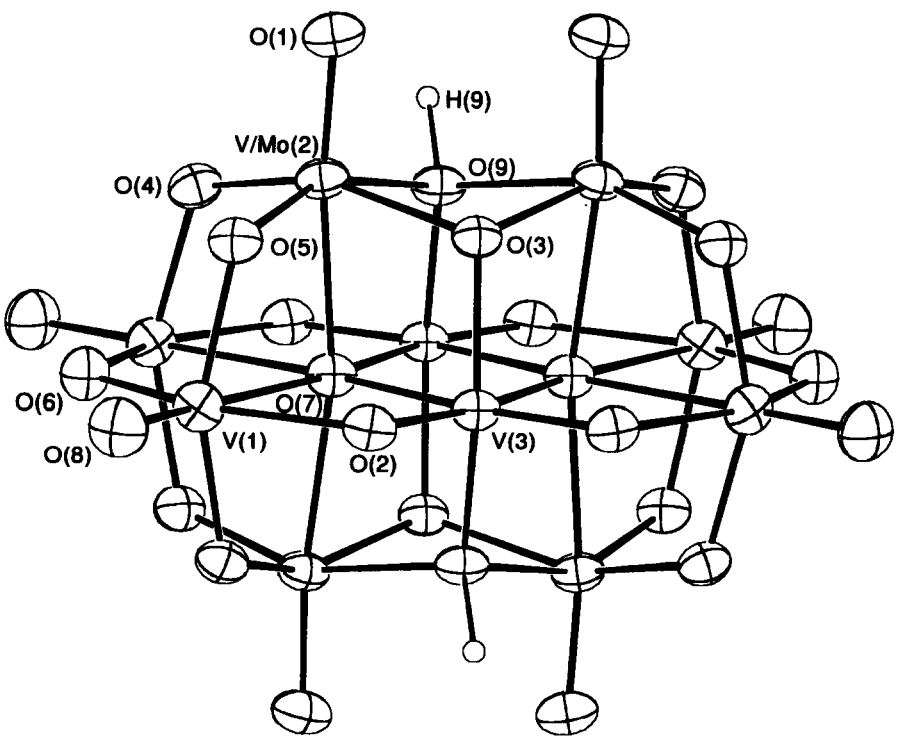


Fig. 1. View of the $[H_2MoV_9O_{28}]^{3-}$ anion with the atomic numbering scheme.

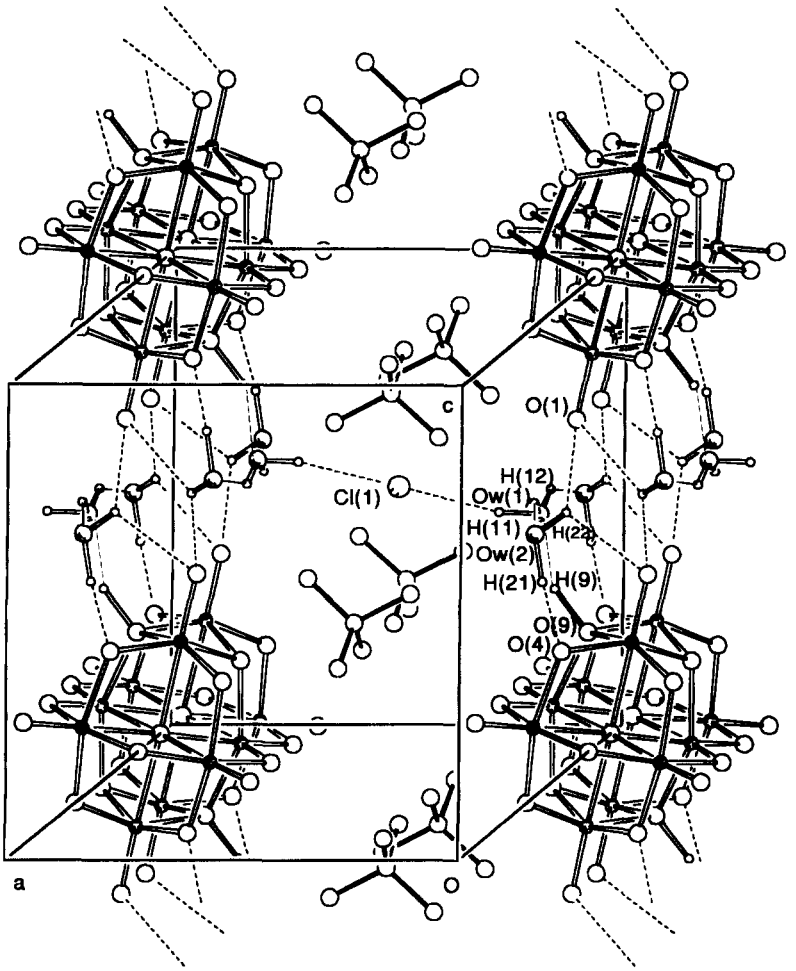


Fig. 2. Part of the unit cell ($0.75 \leqslant y \leqslant 1.25$) of $[N(CH_3)_4]_4[H_2MoV_9O_{28}]Cl \cdot 6H_2O$. Hydrogen bonds are shown by broken lines. Tetramethylammonium hydrogens are omitted for clarity.

values of the M—O bond strengths are given in Table 3. The final atomic coordinates, thermal parameters, and list of observed and calculated structure factors have been deposited as supplementary material at the Cambridge Crystallographic Data Centre.

The monomolybdovanadate anion has a well-known decavanadate structure, built up of 10 edge-sharing MO_6 octahedra. However, since the polyanion has a crystallographically imposed $2/m$ symmetry one molybdenum atom should be distributed over four "capping" metal atom positions. All metal-to-metal distances vary from 3.065 to 3.207 Å and are comparable with those found in the structures of other decavanadate salts [17–22]. The V—O distances within VO_6 octahedra [V(1) and V(3)] are also similar to those already observed and depend upon the type of oxo ligand: bond length to the terminal oxo oxygen $V{=}O_t$ is 1.609 Å, $V—O_b$ bond lengths to the oxygen bonded to two V atoms vary from 1.688 to 2.052 Å, $V—O_{3b}$ bond lengths to the oxygen bonded to three V atoms are 1.921 and 1.929 Å and, finally, $V—O_{6b}$ bond lengths to the oxygen shared between six V atoms are 2.139 and 2.321 Å. The VO_6 octahedra are significantly distorted, with the bond angles at the V atoms ranging from 74.7 to 108.1°. In the "capping" octahedron, with a random distribution of molybdenum and vanadium atoms, the metal-to-oxygen distances are between the values found for Mo—O and V—O bond lengths and vary as follows: to one terminal oxo oxygen atom 1.621 Å, to two doubly bridging oxygens 1.819 and 1.841 Å, to two triply bridging oxygens 2.006 and 2.034 Å, and to one oxygen bridging six metal atoms 2.261 Å. The bond angles at the metal atom range from 75.3 to 105.1°.

The location of proton H(9), bonded to O(9), was of particular interest since it was suggested that the basic oxygen site has an important role regarding the reactivity of such polyanions. The distance between the water oxygen O(w1) and the polyoxo oxygen atom O(9) of 2.968 Å is indicative of a moderately strong hydrogen bond. However, since both protons belonging to water molecule w1 are engaged in the hydrogen bonding with the water oxygen O(w2) and chlorine atom Cl(1), it is reasonable to suppose that the above-

Table 1. Interatomic distances (Å) and angles (°)

V(1)···V(1)^{ii}	3.065(1)	Mo/V(2)···Mo/V(2)^{ii}	4.502(3)
V(1)···Mo/V(2)	3.126(1)	Mo/V(2)···Mo/V(2)^{i}	3.083(1)
V(1)···Mo/V(2)^{ii}	3.129(2)	Mo/V(2)···V(3)	3.207(1)
V(1)···V(3)	3.082(1)	Mo/V(2)···V(3)^{ii}	3.192(2)
V(1)···V(3)^{ii}	4.443(1)	V(3)···V(3)^{ii}	3.341(1)
V(1)—O(2)	2.052(2)	V(3)—O(2)	1.688(2)
V(1)—O(4)	1.875(3)	V(3)—O(2)^{i}	1.688(2)
V(1)—O(5)^{ii}	1.891(3)	V(3)—O(3)^{ii}	1.921(4)
V(1)—O(6)	1.826(2)	V(3)—O(7)	2.139(3)
V(1)—O(7)	2.321(3)	V(3)—O(7)^{iii}	2.139(3)
V(1)—O(8)	1.609(2)	V(3)—O(9)	1.929(4)
Mo/V(2)—O(1)	1.621(3)	N(1)—C(1)	1.509(5)
Mo/V(2)—O(3)	2.006(2)	N(1)—C(2)	1.497(5)
Mo/V(2)—O(4)	1.841(2)	N(1)—C(3)	1.486(5)
Mo/V(2)—O(5)	1.819(2)	NN(1)—C(4)	1.486(5)
Mo/V(2)—O(7)	2.261(2)		
Mo/V(2)—O(9)	2.034(2)	O(9)—H(9)	1.256
O(2)—V(1)—O(4)	83.9(1)	O(2)—V(3)—O(2)^{i}	108.1(1)
O(2)—V(1)—O(5)^{ii}	83.5(1)	O(2)—V(3)—O(3)^{ii}	97.3(1)
O(2)—V(1)—O(6)	156.3(1)	O(2)—V(3)—O(7)	87.3(1)
O(2)—V(1)—O(7)	74.7(1)	O(2)—V(3)—O(7)^{i}	164.6(1)
O(2)—V(1)—O(8)	99.6(1)	O(2)—V(3)—O(9)	97.4(1)
O(4)—V(1)—O(5)^{ii}	154.6(1)	O(3)^{ii}—V(3)—O(7)	79.9(1)
O(4)—V(1)—O(6)	92.1(1)	O(3)^{ii}—V(3)—O(9)	154.8(1)
O(4)—V(1)—O(7)	78.0(1)	O(7)—V(3)—O(7)^{iii}	77.3(1)
O(4)—V(1)—O(8)	102.6(1)	O(7)—V(3)—O(9)	80.4(1)
O(5)^{ii}—V(1)—O(6)	90.7(1)		
O(5)^{ii}—V(1)—O(7)	77.5(1)	V(1)—O(2)—V(3)	110.6(1)
O(5)^{ii}—V(1)—O(8)	101.2(1)	Mo/V(2)—O(3)—Mo/V(2)^{i}	100.5(1)
O(6)—V(1)—O(7)	81.6(1)	Mo/V(2)—O(3)—V(3)^{ii}	108.7(1)
O(6)—V(1)—O(8)	104.1(1)	V(1)—O(4)—Mo/V(2)	114.5(1)
O(7)—V(1)—O(8)	174.2(1)	V(1)^{ii}—O(5)—Mo/V(2)	115.0(1)
		V(1)—O(6)—V(1)^{ii}	114.1(1)
O(1)—Mo/V(2)—O(3)	99.9(1)	V(1)—O(7)—V(1)^{ii}	82.6(1)
O(1)—Mo/V(2)—O(4)	103.5(1)	V(1)—O(7)—Mo/V(2)	86.0(1)
O(1)—Mo/V(2)—O(5)	105.1(1)	V(1)—O(7)—Mo/V(2)^{ii}	86.1(1)
O(1)—Mo/V(2)—O(7)	172.8(1)	V(1)—O(7)—V(3)	87.3(1)
O(1)—Mo/V(2)—O(9)	98.5(1)	C(1)—O(7)—V(3)^{ii}	170.0(1)
O(3)—Mo/V(2)—O(4)	153.7(1)	Mo/V(2)—O(7)—Mo/V(2)^{ii}	169.6(1)
O(3)—Mo/V(2)—O(5)	90.4(1)	Mo/V(2)—O(7)—V(3)	93.6(1)
O(3)—Mo/V(2)—O(7)	75.3(1)	Mo/V(2)—O(7)—V(3)^{ii}	93.0(1)
O(3)—Mo/V(2)—O(9)	76.5(1)	V(3)—O(7)—V(3)^{ii}	102.7(1)
O(4)—Mo/V(2)—O(5)	94.8(1)	Mo/V(2)—O(9)—Mo/V(2)^{i}	98.6(1)
O(4)—Mo/V(2)—O(7)	80.2(1)	Mo/V(2)—O(9)—V(3)	108.0(1)
O(4)—Mo/V(2)—O(9)	88.3(1)		
O(5)—Mo/V(2)—O(7)	80.5(1)	C(1)—N(1)—C(2)	109.3(3)
O(5)—Mo/V(2)—O(9)	154.8(1)	C(1)—N(1)—C(3)	109.1(3)
O(7)—Mo/V(2)—O(9)	75.4(1)	C(1)—N(1)—C(4)	109.9(3)
		C(2)—N(1)—C(3)	109.3(3)
Mo/V(2)—O(9)—H(9)	112.4(2)	C(2)—N(1)—C(4)	109.1(3)
V(3)—O(9)—H(9)	116.1(2)	C(3)—N(1)—C(4)	110.2(3)

Symmetry code: (i) $x, -y, -z$; (ii) $-x, y, -z$; (iii) $-x, -y, -z$.

Table 2. Hydrogen bonding parameters[a]

D	H	A	D—H	H···A	D···A	∠D—H···A
O(9)	H(9)	O(w1)	1.256	1.795	2.968(6)	152.7
O(w1)	H(11)	Cl(1)	0.957	2.419	3.362(4)	168.4
O(w1)	H(12)	O(w2)	1.097	2.094	3.061(4)	145.4
O(w2)	H(21)	O(4)	1.138	1.727	2.856(4)	170.3
O(w2)	H(22)	O(1)	0.949	2.503	3.013(4)	113.7
O(w2)	H(22)	O(1)^{i}	0.949	2.261	2.994(4)	133.3

[a] D = donor, A = acceptor. Symmetry code: (*i*) $-x, y, 1-z$.

Table 3. Bond strength calculations for $[H_2MoV_9O_{28}]^{3-}$[a]

	V(1)	Mo/V(2)	V(3)	Σs	s(O···H)	Σs[b]
O(1)		1.86		1.86	0.10, 0.12	2.08
O(2)	0.50		1.35	1.85		
O(3)		0.59	0.71	1.88		
O(4)	0.79	0.94		1.73	0.22	1.95
O(5)	0.76	1.00		1.76		
O(6)	0.91			1.82		
O(7)	0.27	0.31	0.40	1.96		
O(8)	1.73			1.73		
O(9)		0.55	0.68	1.78	0.44	2.22
Σs	4.96	5.25	4.88			

[a] s(V—O) = $[d(V—O)/1.791]^{-5.1}$, s(Mo—O) = $[d(Mo—O)/1.882]^{-6}$, s(O···H) = $[d(O···H)/0.86]^{-2.17}$, s(Mo/V—O) = $\frac{1}{4}s$(Mo—O) + $\frac{3}{4}s$(V—O).
[b] Including s(O···H).

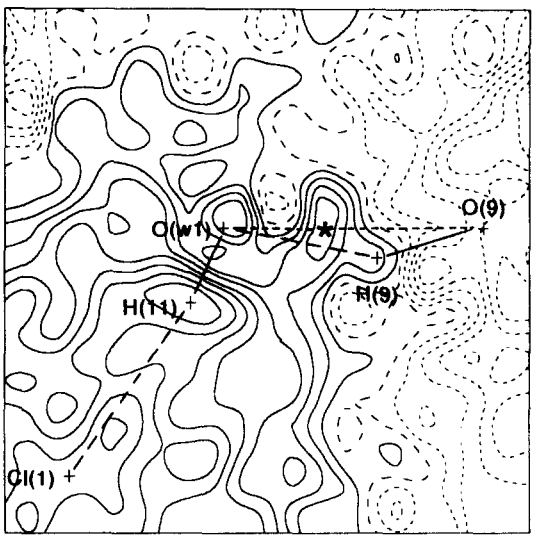


Fig. 3. Contour electron density map in the region around water oxygen O(w1) and polyoxoanion oxygen O(9). Residual peak (0.34 e Å^{-3}), marked by asterisk, indicates a possible dynamic disorder of H(9) between the water molecule and the molybdovanadate anion.

mentioned hydrogen bond O(9)···O(w1) is realized through the hydrogen atom attached to O(9). In this way an endless column is formed along the *c*-axis between the $[H_2MoV_9O_{28}]^{3-}$ anions and water molecules. The columns are mutually interconnected by the lateral O(w1)···Cl(1) hydrogen bond of 3.362 Å.

However, whereas the same location of a hydrogen atom at the triply bonded oxygen atom was also proposed in the paper describing the structure of tetrakis(n-hexylammonium) dihydrogendecavanadate [23], in the structure of tetrakis-adenosinium dihydrogendecavanadate undecahydrate such protonation was assigned to the doubly-bridging oxygen atoms [18]. Our finding is in agreement with the results of ^{17}O NMR spectroscopy and with the suggestion that triply bridging oxygen atoms are favoured protonation sites, whereas the doubly bridging oxygens are a second choice and are protonated to a lesser extent [24]. These results agree well with an analysis of the distribution of the electrostatic potential determined by *ab initio* methods, as well as of the Laplacian charge density calculated for the $[V_{10}O_{28}]^{6-}$ anion [25].

In fact, an additional residual peak close to the water oxygen atom O(w1) found in a final difference electron density map (1.22 Å, 0.34 e Å^{-3}, Fig. 3), is probably indicative of dynamic disorder of H(9) between O(w1) and the polyoxo oxygen atom, O(9).

The protonation of the oxygen atom O(9) is also supported by the bond strength calculation using the relation s(V—O) = $[d(V—O)/1.791]^{-5.1}$ for all non-substituted VO_6 octahedra [26], and s(Mo/V—O) = $\frac{1}{4}s$(Mo—O) + $\frac{3}{4}s$(V—O) for a "capping" Mo/VO_6 octahedron (Table 3). Whereas the bond numbers for oxygens O(1) and O(4), engaged in hydrogen bonding, are close to 2, and correspond to the theoretical value for oxygen atoms, a relatively high value for O(9) of 2.22 is also indicative of a possible disorder of H(9). The M—O bond number within the $(Mo/V)O_6$ octahedron amounts to 5.25, exactly the same value required for the metal site to be occupied by vanadium and molybdenum in the ratio 3 : 1.

Acknowledgement—This research was supported by the Ministry of Science and Technology of the Republic of Croatia.

REFERENCES

1. R. I. Maksimovskaya and N. N. Chumachenko, *Polyhedron* 1987, **6,** 1813.
2. O. W. Howarth, L. Petterson and I. Andersson, *J. Chem. Soc., Dalton Trans.* 1989, 1915.
3. O. W. Howarth, L. Petterson and I. Andersson, *J. Chem. Soc., Dalton Trans.* 1991, 1799.
4. A. Björnberg, *Acta Cryst.* 1979, **B35,** 1995.
5. A. M. Nenner, *Acta Cryst.* 1985, **C41,** 1703.
6. A. Björnberg, *Acta Cryst.* 1980, **B36,** 1530.
7. A. Björnberg, *Acta Cryst.* 1979, **B35,** 1989.
8. A. Björnberg and B. Hedman, *Acta Cryst.* 1980, **B36,** 1018.
9. M. Cindrić, B. Kamenar, N. Strukan and Z. Veksli, *Polyhedron* 1995, **14,** 1045.
10. B. Kamenar, M. Cindrić and N. Strukan, *Polyhedron* 1994, **13,** 2271.
11. S. Harkema, *ACXR. Program for absorption correction.* Department of Chemical Technology, University of Twente, Enschede, The Netherlands (1979).
12. G. M. Sheldrick, *SHELXS*86. *Program for the solution of crystal structures.* University of Göttingen, Germany (1986).
13. G. M. Sheldrick, *SHELX*76. *Program for crystal structure determination.* University of Cambridge, England (1976).
14. I. Vicković, *J. Appl. Cryst.* 1988, **21,** 987.
15. C. K. Johnson, *ORTEP II, Report ORNL*-3794, *revised.* Oak Ridge National Laboratory, Tennessee, U.S.A. (1971).
16. A. L. Spek, *The EUCLID Package.* In *Computational Crystallography* (Edited by D. Sayre), p. 528. Clarendon Press, Oxford (1982).
17. H. T. Evans, Jr., *Inorg. Chem.* 1966, **5,** 967.
18. M. V. Capparelli, D. M. Goodgame, P. B. Hayman and A. C. Skapski, *J. Chem. Soc., Chem. Commun.* 1986, 776.
19. V. W. Day, W. G. Klemperer and D. J. Maltbie, *J. Am. Chem. Soc.* 1987, **109,** 2991.
20. J. M. Arrieta, A. R. Arnaiz, C. Santiago, L. Lorente, F. J. Zuñiga, G. Madariaga and G. Germain, M. Vlassi, *Acta Cryst.* 1993, **C49,** 1417.
21. J. M. Nieto, P. Salagre, F. Medina, J. E. Sueiras and X. Solans, *Acta Cryst.* 1993, **C49,** 1879.
22. M.-T. Averbuch-Pouchot and A. Durif, *Eur. J. Solid State Inorg. Chem.* 1994, **31,** 351.
23. P. Roman, A. Aranzabe, A. Luque, J. M. Gutierrez-Zorrilla and M. Martinez-Ripoll, *J. Chem. Soc., Dalton Trans.* 1995, 2225.
24. W. G. Klemperer and W. Schum, *J. Am. Chem. Soc.* 1977, **99,** 3544.
25. J.-Y. Kempf, M.-M. Rohmer, J. M. Poblet, C. Bo and M. Benard, *J. Am. Chem. Soc.* 1992, **114,** 1136.
26. I. D. Brown, *Structure and Bonding in Crystals,* (Edited by M. O'Keefe and A. Navrotsky), Vol. II, pp. 1–30. Academic Press, New York (1981).

Pergamon

PII: S0277-5387(96)00324-5

Polyhedron Vol. 16, No. 4, pp. 635–641, 1997
Copyright © 1996 Elsevier Science Ltd
Printed in Great Britain. All rights reserved
0277–5387/97 $17.00+0.00

Synthesis of tris(dicyclohexylamido) titanium and zirconium chloride and the structure of $(c\text{-Hex}_2\text{N})_3\text{TiCl}$

Zhibang Duan,* Leonard M. Thomas and John G. Verkade†

Department of Chemistry, Iowa State University, Ames, IA 50011, U.S.A.

(Received 24 April 1996; accepted 26 June 1996)

Abstract—Reaction of $MCl_4(THF)_2$ (M = Ti and Zr) with excess $LiNCy_2$ in pentane affords crystalline $(c\text{-Hex}_2\text{N})_3\text{MCl}$ in greater than 70% yields. The products were characterized by ^1H, ^{13}C, ^1H and ^{13}C HETCOR NMR, and MS techniques. Crystalline $(c\text{-Hex}_2\text{N})_3\text{TiCl}$ was also characterized by a single-crystal X-ray structure. Trends in the structural dimensions of $(R_2N)_3\text{TiCl}$ are noted. Copyright © 1996 Elsevier Science Ltd

Keywords: titanium; zirconium; amides; NMR.

Titanium and zirconium nitrides find uses as wear-resistant coatings on machine tools [1], gold substitutes for decorative coatings [2], reflectance and hardness coatings for microelectronic devices [3], diffusion barriers in various semiconductor metallization schemes [4] and as ceramics with high thermal impact resistance [5]. Tris(dialkylamido) halides of these metals, $(R_2N)_3MX$, are of interest because of their potential as single-source MOCVD precursors to their corresponding nitride and carbonitride films, and also for their applications in important synthetic transformations. Thus, $[(Me_3Si)_2N]_3\text{TiF}$ was recently studied for its ability to deposit TiN and TiCN films on silicon and steel substrates under N_2, H_2 and He [6]. Its analogue $(Et_2N)_3\text{TiCl}$ is efficacious as a reagent in titanating allylmetal compounds [7,8], enolates [9], cyanomethyl lithium [10], benzylmagnesium bromide [10] and lithiated hydrazones [11] for use in chemo- and stereoselective additions to carbonyl substrates [10]. Conversion of $(Et_2N)_3\text{TiCl}$ to $(Et_2N)_3\text{TiMe}$ allows the latter to be used for aminomethylation of aromatic aldehydes [10,12]. To our knowledge, however, no reports concerning the ring-substituted analogues $(c\text{-Hex}_2\text{N})_3\text{MCl}$ (M = Ti and Zr) have been reported. In connection with our interest in tricyclic azatranes of group 4 [13] as precursors for MOCVD, we report here the first synthesis and characterization of $(c\text{-Hex}_2\text{N})_3\text{TiCl}$ (**1**) and $(c\text{-Hex}_2\text{N})_3\text{ZrCl}$ (**2**), as well as the molecular and crystal structure of **1**. Trends in the angles around titanium in $(R_2N)_3\text{TiCl}$ derivatives are observed and discussed.

EXPERIMENTAL

General procedures

All reactions were carried out under argon with strict exclusion of moisture using standard Schlenk or dry-box techniques [14]. Solvents were dried over, and distilled from, Na/benzophenone and stored prior to use over 4 Å molecules sieves under argon. Lithium dicyclohexylamide (97%) was purchased from Aldrich and was used as received. $TiCl_4(THF)_2$ and $ZrCl_4(THF)_2$ were synthesized according to literature procedures [15].

NMR spectra were recorded at 20°C on a Nicolet NT300 (^1H) or a Varian VXR300 spectrometer in C_6D_6 using the protio impurity of the solvent as an internal reference for ^1H spectra and the ^{13}C resonance of C_6D_6 as a reference for the ^{13}C NMR spectra. Two-dimensional COSY 90 and HETCOR spectra were recorded on a Bruker DRX 400 spectrometer. Mass spectra were obtained on a Finnigan TSQ 700 instrument or a Kratos MS-50 spectrometer. Melting points (uncorrected) were determined with a Thomas–

* Current address: YTC America Inc., 550 Via Alondra, Camarillo, CA 93012, U.S.A.

† Author to whom correspondence should be addressed.

Hoover capillary apparatus. Elemental analyses were performed by Desert Analytics.

Tris(dicyclohexylamido)titanium chloride, **1**

$TiCl_4(THF)_2$ (1.10 g, 3.28 mmol) was added to a suspension of $LiNCy_2$ (2.95 g, 97%, 15.3 mmol) in pentane (90 cm^3) at −78°C. The reaction mixture was warmed to room temperature, stirred for 17 h and then filtered through Celite. The residue was washed copiously with pentane. The filtrate and the washings were combined and concentrated to about 20 cm^3. The solution was kept in a freezer to allow crystals to grow. The crystals were filtered off, washed with cold pentane (4 × 3 cm^3) and dried *in vacuo* to give 1.47 g of product in 72% yield. M.p.: >148°C (dec.). Found: C, 69.2; H, 10.7; N, 6.6. Calc. for $C_{36}H_{66}ClN_3Ti$: C, 69.3; H, 10.7; N, 6.7%. ^1H NMR (400 MHz): δ 4.06 [tt, 6 H, $^3J_{H_aH_a}$ = 11.3 Hz, $^3J_{H_aH_e}$ = 2.9 Hz, $H(1_a)$], 2.10 [apparent d, 12 H, $^2J_{H_aH_e}+{}^3J_{H_aH_e}+{}^3J_{H_eH_e}$ = 11.7 Hz, $H(2_e)$], 1.82 [apparent d, 12 H, $^2J_{H_aH_e}+{}^3J_{H_aH_e}+{}^3J_{H_eH_e}$ = 12.7 Hz, $H(3_e)$], 1.66 [apparent qd, 12 H, $^2J_{H_aH_e}+{}^3J_{H(1_a)H(2_a)}+{}^3J_{H(2_a)H(3_a)}$ = 12.3 Hz, $^3J_{H(2_a)H(3_e)}$ = 3.0 Hz, $H(2_a)$], 1.60 [apparent d, 6 H, $^2J_{a}H_e+{}^3J_{H_aH_e}+{}^3J_{H_eH_e}$ = 13.5 Hz, $H(4_e)$], 1.38 [apparent qt, 12 H, $^2J_{H_aH_e}+{}^3J_{H(2_a)H(3_a)}+3J_{H(3_a)H(4_a)}$ = 13.0 Hz, $^3J_{H(2_e)H(3_a)}+{}^3J_{H(3_a)H(4_e)}$ = 3.1 Hz, $H(3_a)$], 1.15 [apparent qt, 6 H, $2J_{H_aH_e}+{}^3J_{H(3_a)H(4_a)}$ = 13.0 Hz, $^3J_{H(3_e)H(4_a)}$ = 3.8 Hz, $H(4_a)$]. $^{13}C\{^1H\}$ NMR (75.43 MHz, C_6D_6): δ 62.28 (C(1)), 36.60 (C(2)), 27.46 (C(3)), 26.28 (C(4)). For proton and carbon subscript labels for **1** (and **2**) see Fig. 1 in Results and Discussion. MS(EI) *m/z* [ion (M represents the most intense peak in a group of peaks due to the isotope distribution), relative intensity]: 623 (M^+, 7.7), 586 ($M-Cl-2H^+$, 98), 541 ($M-C_6H_{10}^+$, 4.2), 442 [$M-HN(c\text{-Hex})_2^+$, 100], 357 [$M-HN(c\text{-Hex})_2-HCy-H^+$, 17.2], 181 [$HN(c\text{-Hex})_2^+$, 11.7]. CIMS ($NH_3$) *m/z* (ion, relative intensity): 624 ($M+H^+$, 3.2), 182 [$HN(c\text{-Hex})_2+H^+$, 100], 138 (35.9).

Tris(dicyclohexylamido)zirconium chloride, **2**

The synthetic procedure for **2** was the same as that for **1** except that $ZrCl_4(THF)_2$ was used instead of $TiCl_4(THF)_2$. Yield: 73%. Found: C, 65.2; H, 10.4; N, 6.7. Calc. for $C_{36}H_{66}ClN_3Zr$: C, 64.8; H, 10.0; N, 6.3%. ^1H NMR (400 MHz): δ 3.32 [tt, 6 H, $^3J_{H_aH_a}$ = 11.3 Hz, $^3J_{H_aH_e}$ = 3.2 Hz, $H(1_a)$], 2.03 [apparent d, 12 H, $^2J_{H_aH_e}+{}^3J_{H_aH_e}+{}^3J_{H_eH_e}$ = 11.7 Hz, $H(2_e)$], 1.81 [apparent d, 12 H, $^2J_{H_aH_e}+{}^3J_{H_aH_e}+{}^3J_{H_eH_e}$ = 13.0 Hz, $H(3_e)$], 1.66 [apparent qd, 12 H, $^2J_{H_aH_e}+{}^3J_{H(1_a)H(2_a)}+{}^3J_{H(2_a)H(3_a)}$ = 12.3 Hz, $^3J_{H(2_a)H(3_e)}$ = 3.0 Hz, $H(2_a)$], 1.59 [apparent d, 6 H, $^2J_{H_aH_e}+{}^3J_{H_aH_e}+{}^3J_{H_eH_e}$ = 13.5 Hz, $H(4_e)$] 1.38 [apparent qt, 12 H, $^2J_{H_aH_e}+{}^3J_{H(2_a)H(3_a)}+{}^3J_{H(3_a)H(4_a)}$ = 13.0 Hz, $^3J_{H(2_e)H(3_a)}+{}^3J_{H(3_a)H(4_e)}$ = 3.1 Hz, $H(3_a)$], 1.13 [apparent qt, 6 H, $^2J_{H_aH_e}+{}^3J_{H_aH_a}$ = 13.0 Hz, $^3J_{H_aH_e}$ = 3.8 Hz, $H(4_a)$]. $^{13}C\{^1H\}$ NMR (75.43 MHz, C_6D_6): δ 57.21 (C(1)), 37.42 (C(2)), 27.16 (C(3)), 26.06 (C(4)). MS (EI) *m/z* [ion (M represents the most intense peak in a group of peaks due to the isotope distribution), relative intensity]: 665 (M^+, 7.5), 582 ($M-C_6H_{11}^+$, 12.0), 484 [$M-HN(c\text{-Hex})_2^+$, 44.9], 401 [$M-HN(c\text{-Hex})_2-C_6H_{11}^+$, 14.9], 317 [$M-HN(c\text{-Hex})_2-C_6H_{11}-C_6H_{12}^+$, 10.1], 181 [$HN(c\text{-Hex})_2$, 16.2], 138 (51.0), 83 ($C_6H_{11}^+$, 100).

Crystal structure determination of **1**

A yellow crystal of **1** with dimensions of 0.2 × 0.1 × 0.05 mm^3 was mounted on a Siemens P4RA diffractometer for data collection at 213(2) ± 1 K. The unit-cell constants were determined from reflections found from a rotation photograph. Twenty-five reflections in the θ range 15–25° were used to determine precise cell constants. Lorentz and polarization corrections were applied to the data, as were nonlinear corrections based on the decay in the standard reflections. A semi-empirical absorption correction based on azimuthal scans was applied.

The space group *P*1 was chosen based on systematic absences and intensity statistics. This assumption proved to be correct as determined by a successful direct-methods solution [16] and subsequent refinement. All non-hydrogen atoms were placed directly from the *E* map. All non-hydrogen atoms were refined with anisotropic displacement parameters. All hydrogens were treated as riding atoms with individual isotropic displacement parameters. Crystal data and refinement parameters are summarized in Table 1. Selected bond distances and angles are listed in Table 2. There was a significant amount of disorder in the final structure. Some of the atoms associated with the cyclohexyl rings exhibit a high degree of thermal motion. Atoms C(26) and C(29) were refined with a split occupancy of about 51–49% for each site. Refinement calculations were performed on a Digital Equipment Micro VAX 3100 computer using SHELXTL-Plus [16] and SHELXL-93 [17,18].

RESULTS AND DISCUSSION

The reaction of $MCl_4(THF)_2$ (M = Ti and Zr) with $LiNCy_2$ in pentane led to the formation of the title compounds in yields over 70%:

$$MCl_4(THF)_2 + 3LiN(c\text{-Hex})_2 \xrightarrow{\text{pentane}} (c\text{-Hex}_2N)_3MCl + 3LiCl + 2THF. \quad (1)$$

Similar reactions were utilized to prepare $(R_2N)_3MCl$ (R = Me [19], Et [19], and $SiMe_3$ [20] using MCl_4 instead of $MCl_4(THF)_2$.

The molecular structure of $(c\text{-Hex}_2N)_3TiCl$ shown in Fig. 1 displays a distorted tetrahedral titanium

Table 1. Crystallographic data for **1**

Formula	$C_{36}H_{66}N_3ClTi$
Formula weight	624.27
Colour	Yellow
Crystal size (mm)	$0.2 \times 0.1 \times 0.05$
Crystal system	Triclinic
Space group	$P\bar{1}$
a (Å)	9.606(5)
b (Å)	10.292(6)
c (Å)	20.258(11)
α ( )	98.76(5)
β ( )	90.27(4)
γ ( )	113.13(4)
V (Å^3)	1815.7(17)
Z	2
d_{calc} (g cm^{-3})	1.142
μ (mm^{-1})	2.857
λ (Cu-K_α) (Å)	1.54178
Weighting scheme, w^{-1}	$\sigma(F_0^2)+(0.0800P)^2$ where $P=(F_0^2+2F_c^2)/3$
Final R indices [$I \geqslant 2\sigma(I)$]	$R_1{}^a = 0.0828$, $wR_2{}^b = 0.1949$
R indices (all data)	$R_1{}^a = 0.1666$, $wR_2{}^b = 0.2273$
GoF,[c] observed and all data	1.134, 0.831

[a] $R_1 = \Sigma\|F_0|-|F_c\|/\Sigma|F_0|$.
[b] $wR_2 = [\Sigma[w(F_0^2-F_c^2)^2]/\Sigma[w(F_0^2)^2]]^{0.5}$ where $w = 1/[\sigma^2(F_0^2)+(aP)^2+bP+d+e\sin\theta]$.
[c] GoF $= [\Sigma[w(F_0^2-F_c^2)^2]/(n-p)]^{0.5}$.

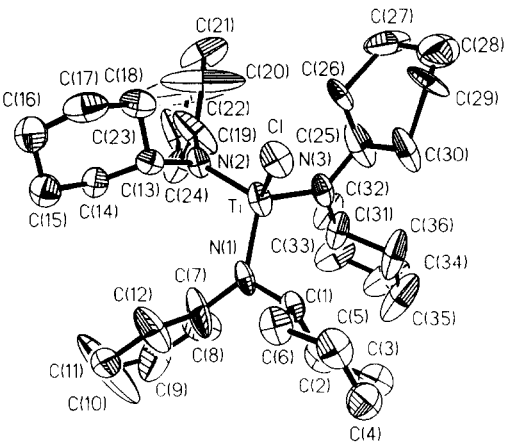


Fig. 1. Drawing of **1** with the atom-labelling scheme. Ellipsoids are drawn at the 50% probability level.

geometry with a propeller-like arrangement of the *c*-Hex_2N groups. There are two independent molecules in the unit cell. The geometries around each of the nitrogens is trigonal planar with average angle sums of 359.7(6)°. However, each of the angles around any given nitrogen is quite different (Table 2) implying a certain amount of flexibility which allows the rings to pack efficiently into the structure. Thus, the angles involving the carbon proximal to the chlorine are 107.5(4), 108.5(4) and 122.8(7)° for C(1)N(1)Ti, C(13)N(2)Ti and C(25)N(3)Ti, respectively, while those containing the carbon distal to the chlorine are 123.5(5), 131.0(6) and 133.6(6)° for C(31)N(3)Ti, C(19)N(2)Ti and C(7)N(1)Ti, respectively. Interestingly, the C—C—C angle sums of the three Cy rings proximal to the chlorine (665–668°) and one of the distal Cy rings [C(31)—C(36) 665°] are not far from the value expected for an unstrained cyclohexane ring (654.0°). However, the other two distal C_6H_{11} rings have angle sums (719°) close to that expected for a planar C_6 ring. Indeed the C(7)–C(12) and the C(19)–C(24) rings are each planar within 0.031 and 0.024 Å, respectively. This structural feature suggests that the distal rings experience substantial steric compression.

Although the overall geometries of $(R_2N)_3TiCl$ for R = Me [19], Et [19], *c*-Hex and $SiMe_3$ [20] are similar, there are significant differences in the dimensions. Table 3 summarizes some of the structural parameters for these complexes. For compound **1**, the average ClTiN and NTiN angles are almost the same. However, it can be seen that the average of the ClTiN angles decreases in the order R = Me > Et > *c*-Hex > $SiMe_3$, with a concomitant increase of the average NTiN angles (Fig. 2). Since the bulk of the R

Table 2. Selected bond lengths (Å) and angles ( ) for **1**

Ti—N(1)	1.879(6)	N(2)—C(13)	1.472(8)
Ti—N(3)	1.878(6)	N(2)—C(19)	1.485(9)
Ti—N(2)	1.890(6)	N(3)—C(25)	1.436(10)
N(1)—C(7)	1.458(9)	N(3)—C(31)	1.485(9)
N(1)—C(1)	1.489(9)		

N(1)—Ti—N(3)	107.9(3)	C(1)—N(1)—Ti	107.5(4)
N(1)—Ti—N(2)	110.1(3)	C(13)—N(2)—C(19)	120.0(7)
N(3)—Ti—N(2)	110.1(3)	C(13)—N(2)—Ti	108.5(4)
N(1)—Ti—Cl	110.0(2)	C(19)—N(2)—Ti	131.0(6)
N(3)—Ti—Cl	110.9(2)	C(25)—N(3)—C(31)	113.5(8)
N(2)—Ti—Cl	107.8(2)	C(25)—N(3)—Ti	122.8(7)
C(7)—N(1)—C(1)	118.8(7)	C(31)—N(3)—Ti	123.5(5)
C(7)—N(1)—Ti	133.6(6)		

Table 3. Selected structural parameters for $(R_2N)_3TiCl$

R	ClTiN[a] (°)	NTiN[a] (°)	XNTi(proximal)	XNTi(distal)	Cl—Ti (Å)	Ti—N (Å)[a]	Ref.
Me	113.3(2)	105.4(2)	114.7(4)[b]	131.1(3)[b]	2.300(3)	1.866(4)	[19]
Et	111.4(1)	107.5(2)	112.6(3)[a,b]	132.7(4)[a,b]	2.300(2)	1.861(4)	[19]
c-Hex (**1**)	109.6(2)	109.4(2)	112.9(5)[a,b]	129.4(6)[a,b]	2.309(3)	1.882(6)	This work
$SiMe_3$	104.1(3)	114.3(3)	116.0(5)[c]	127.2(6)[c]	2.259(6)	1.940(10)	[20]

[a]Average value.
[b]X = C.
[c]X = Si.

groups increases in the order Me < Et < *c*-Hex < $SiMe_3$, it is reasonable to assume that increasingly bulky R groups enlarge the NTiN angles and concomitantly shrink the ClTiN angles. Thus, the trends displayed in Fig. 2 seem to be dominated by steric rather than electronic effects of the R groups.

The average C(or Si)NTi angles proximal to Cl are smaller than those distal to Cl (Table 3). Although steric compression among the distal $SiMe_3$ groups in $[(Me_3Si)_2N]_3TiCl$ would give rise to the largest average NTiN angles compared with the corresponding angles in the remaining $(R_2N)_3TiCl$ compounds, the distal SiNTi angle in $[(Me_3Si)_2N]_3TiCl$ is smaller than the distal CNTi angles for the $(R_2N)_3TiCl$ complexes. This suggests that by opening the NTiN angle sufficiently, the distal carbons (or silicon) move radially outwards to locations that permit the distal C (or Si)NTi angle to decrease. The Cl—Ti bond lengths are comparable for complexes with R = Me, Et and *c*-Hex and the same is true for Ti—N bond distances. However, the Cl—Ti bond length [2.259(6) Å] in $[(Me_3Si)_2N]_3TiCl$ is smaller than those in the $(R_2N)_3TiCl$ complexes, while the average TiN distance in the former is longer than in the latter species. Although the more sterically demanding $SiMe_3$ groups may be expected to favour a longer TiN bond, it is not clear on steric grounds why the Cl—Ti bond in $[(Me_3Si)_2N]_3TiCl$ should be shorter, since the average ClTiN angle (which is the smallest among these complexes) is expected sterically to elongate the ClTi bond in $[(Me_3Si)_2N]_3TiCl$. If however, N → Si π bonding is sufficiently strong, the Ti—N bonds are expected to lengthen and the Ti—Cl bond could be expected to shorten *via* a compensatory Cl → Ti π interaction.

Compounds **1** and **2** exhibited a group of peaks at *m/z* 623 and 665, respectively, in their EI mass spectra, which exactly matched the theoretical isotopic pattern for the parent compound, confirming the volatility of this type of compound. Several groups of peaks corresponding to the removal of cyclohexyl, dicyclohexylamine and a combination of both cyclohexyl and dicyclohexylamine from the parent species were

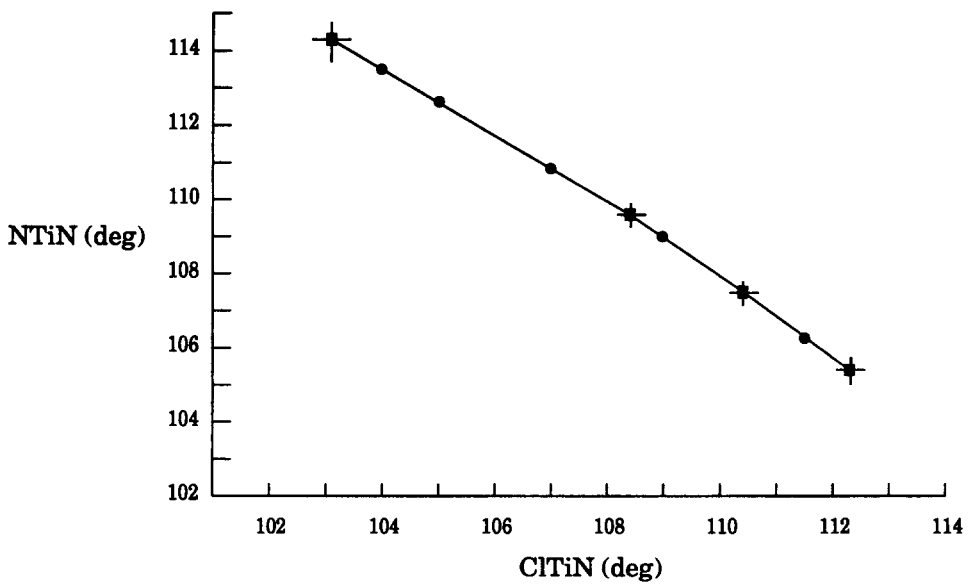


Fig. 2. Plot of average NTiN angle against ClTiN angle in $(R_2N)_3TiCl$. The dots represent values based on the geometrical relationship for a trigonal pyramid $\cos\alpha = -0.500\sin^2\beta + \cos^2\beta$ where α and β are the NTiN and ClTiN angles, respectively. The squares in ascending order of average ClTiN angle and descending average NTiN angle represent R = $SiMe_3$, *c*-Hex, Et, Me in $(R_2N)_3TiCl$. The crosses on the squares are error bars.

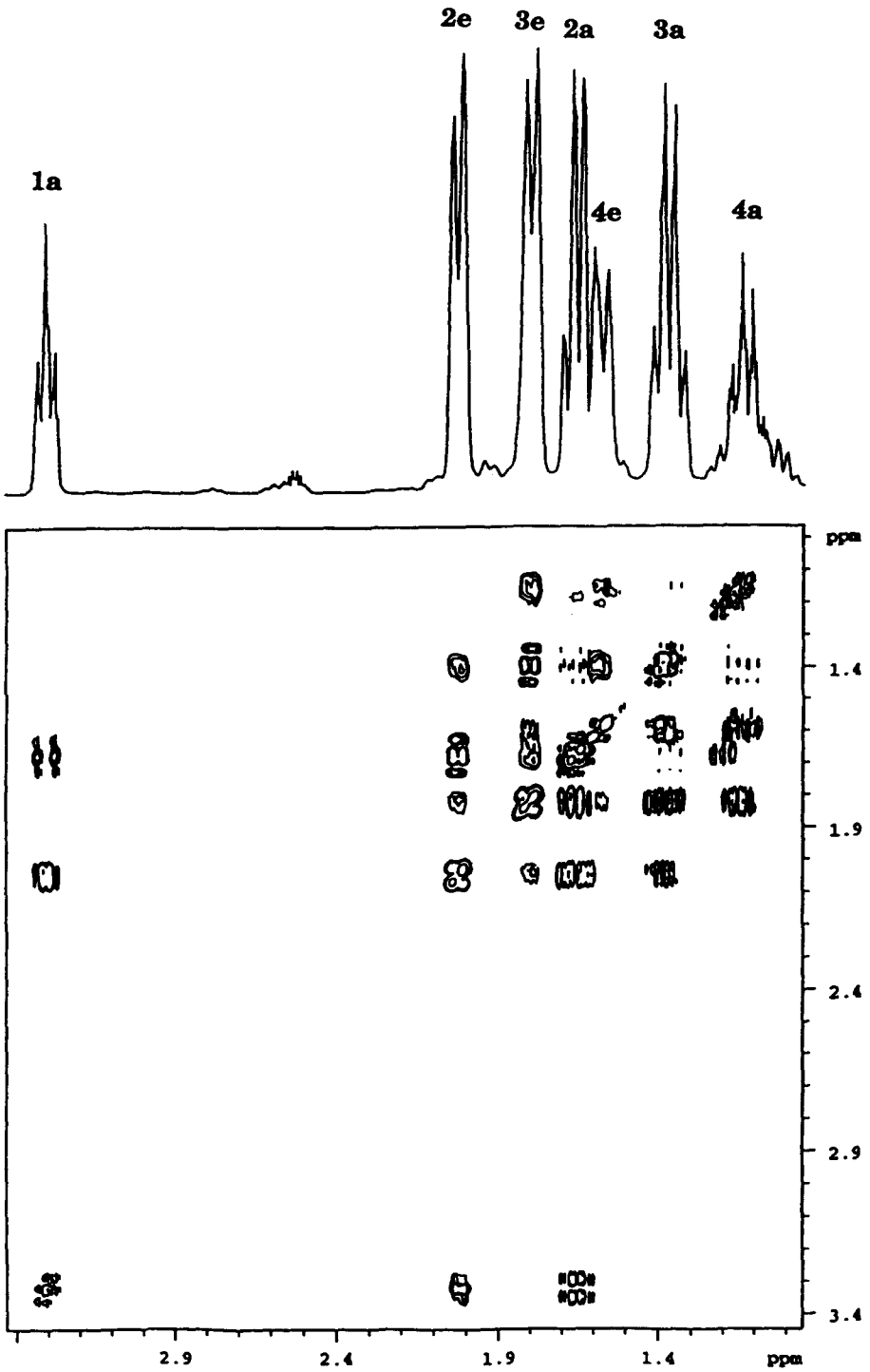


Fig. 3. ^{1}H NMR spectrum of **2** in C_6D_6 and its ^{1}H^{1}H COSY 90 2D NMR spectrum. For labels see Results and Discussion.

also observed. From the NH_3/CI mass spectrum of the titanium complex, however, only a group of peaks at m/z 624 with low intensity for $(M+H^+)$ and a base peak at m/z 182 for $[HN(c\text{-Hex})_2+H^+]$ were found, probably owing to reactions of the complex with NH_3.

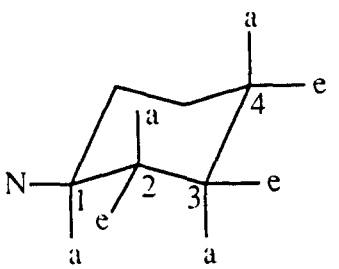
The ^{1}H NMR spectra of **1** and **2** displayed similar patterns, as did the $^{13}C\{^1H\}$ NMR spectra, indicating the isostructural nature of these complexes. Although the ^{1}H NMR spectra in benzene-d_6 exhibited seven signals with different multiplicities (Fig. 3), the $^{13}C\{^1H\}$ spectra showed only four singlets with relative intensities of approximately 1 : 2 : 2 : 1, indicative of the relative numbers of carbon atoms for each cyclohexyl ring. Since the single crystal structure of **1**

Table 4. Correlation of ^1H and ^{13}C NMR chemical shifts for **1** and **2**

1		2	
$\delta(^1H)$ (ppm), assgnt[a]	$\delta(^{13}C)$ (ppm), assgnt[a]	$\delta(^1H)$ (ppm), assgnt[a]	$\delta(^{13}C)$ (ppm), assgnt[a]
4.06, $H(1_a)$	62.28, C(1)	3.32, $H(1_a)$	57.21, C(1)
2.10, $H(2_e)$; 1.66, $H(2_a)$	36.60, C(2)	2.03, $H(2_e)$; 1.66, $H(2_a)$	37.42, C(2)
1.82, $H(3_e)$; 1.38, $H(3_a)$	27.46, C(3)	1.81, $H(3_e)$; 1.38, $H(3_a)$	27.16, C(3)
1.60, $H(4_e)$; 1.15, $H(4_a)$	26.28, C(4)	1.59, $H(4_e)$; 1.13, $H(4_a)$	26.06, C(4)

[a] For atom-labelling scheme, see Fig. 1.

revealed a tetrahedral coordination environment about the metal centre, it is reasonable to suggest that both **1** and **2** have virtual C_{3v} symmetry in solution, as was the case for $(Me_2N)_3TiCl$ [19], $(Et_2N)_3TiCl$ [19] and $[(Me_3Si)_2N)_3TiCl]$ [20]. This symmetry accounts for the four carbon resonances observed for **1** and **2** assuming rapid rotation on the NMR time-scale of the six-membered rings around the M—N and N—Cl bonds. The ^{13}C chemical shifts obtained at lower field (75.4 MHz) for **1** and **2** are identical to those obtained at higher field (100.6 MHz). Similar phenomena were observed in their ^1H NMR spectra, except that those obtained at lower field (300 MHz) exhibited much lower resolution than at high field (400 MHz). A depiction for the assignment of the ^{13}C and ^1H NMR spectra is shown below with a indicating the axial protons and e representing the equatorial protons. The assignments of the signals in the ^1H and $^{13}C\{^1H\}$



NMR spectra of **1** and **2** are based on NMR integrations, couplings in the ^1H NMR spectra and on ^1H–^{13}C hetero correlated NMR spectra. The cross-peaks in the ^1H–^{13}C HETCOR 2D NMR spectra of **1** and **2** give the connectivities between the proton and the carbon signals (Table 4). Each of the three carbon resonances at higher field corresponds to two (axial and equatorial) proton signals, while the one at lower field is seen to exhibit one proton resonance which can be assigned to the axial proton in the methine group. This assignment was further confirmed by its coupling pattern of a triplet of triplets, consistent with couplings to the neighbouring two axial and two equatorial methylene protons, respectively. Because axial–axial coupling constants are larger than the axial–equatorial and the equatorial–equatorial couplings in general [21], the 11.3 Hz coupling was assigned to the $H(1_a)H(2_a)$ interaction while the 2.9 and 3.0 Hz couplings were assigned to the $H(1_a)H(2_e)$ couplings for the Ti and Zr complex, respectively. From the ^1H–^1H 2D COSY 90 NMR spectrum (Fig. 3) it can be seen that the $H(1_a)$ proton couples to only two proton signals, which are likely to be $H(2_a)$ and $H(2_e)$. Each of the $H(2_a)$ and $H(2_e)$ signals should be a doublet of doublets of doublets of doublets, owing to the geminal and neighbouring proton couplings. However, simpler coupling patterns with an apparent doublet and an apparent doublet of quartets for these protons were observed, probably owing to accidental overlap. Based on the above discussion, the peaks located at δ 1.66 were assigned to the $H(2_a)$ resonance, for which relatively large axial–axial couplings are expected, while those at δ 2.10 and 2.03 were assigned to the $H(2_e)$ peaks for **1** and **2**, respectively. From the coupling relationship to $H(2_a)$ and $H(2_e)$ in the COSY 90 NMR spectrum (Fig. 3) the H(3) protons were easily recognized. For reasons analogous to the foregoing, the peaks at δ 1.38 were attributed to the $H(3_a)$ resonances which exhibit an apparent doublet of quartets pattern, while those at δ 1.81 were assigned to the $H(3_e)$ resonances, which display an apparent doublet. The signals for $H(4_a)$ and $H(4_e)$ were similarly assigned.

It is noteworthy that the chemical shifts in the titanium compound are more downfield in general than the zirconium derivative for both the ^1H and ^{13}C NMR peaks, except for the $H(2_a)$, $H(3_a)$ and C(2) resonances (Table 4). This may be associated with the differences in metal electronegativities [22]. The same trend was observed for azametallatrane analogues containing these metals [13b].

Acknowledgement—The authors thank the National Science Foundation for grant support of this research.

REFERENCES

1. W. Schintlmeister, O. Pacher and K. Pfaffinger, *J. Electrochem Soc.* 1976, **123,** 924; G. R. Fenske, N. Kaufherr, R. H. Lee, B. M. Kramer, R. F. Bunshah and W. D. Sproul, *Surf. Coat. Technol.* 1988, **36,** 791; B. O. Johansson, J.-E. Sundren, U. Helmersson and M. K. Hibbs, *Appl. Phys. Lett.* 1984, **44,** 670; W. D. Münz, D. Hofman and K. Hartig, *Thin Solid Films* 1982, **96,** 79; J. M.

Molarius, A. S. Korhonen and E. O. Ristolainen, *J. Vac. Sci. Technol A* 1985, **3,** 2419; P. C. Johnson and H. Randhawa, *Surf. Coat. Technol.* 1987, **33,** 53.
2. M. Hirose, T. Yasui, Y. Ochi and M. Nakagawa, U.S. Patent 4,420,498; R. Buhl, H. K. Pulker and E. Moll, *Thin Solid Films* 1981, **80,** 265.
3. K. Suzuki, M. Tada, T. Oyama and S. Suzuki, Jpn Kokai Tokyo Koho JP 01 308 848 [89,308,848], *Chem. Abstr.* **113,** 83675z; M. Ogita and K. Yokoyama, Jpn Kokai Tokyo Koho JP 02 68926 [9068,926], *Chem. Abstr.* **113,** 124683w.
4. C. Y. Ting, *J. Vac. Sci. Technol.* 1982, **21,** 14; M. Wittmer, *Appl. Phys. Lett.* 1980, **37,** 540; H. von Seefeld, N. W. Cheung, M. Maenpaa and M.-A. Nicolet, *IEEE Trans. Electron Devices* 1980, **27,** 873; N. W. Cheung, H. von Seefeld, M.-A. Nicolet, F. Ho and P. Iles, *J. Appl. Phys.* 1981, **52,** 4297.
5. Y. Fujinaka, Jpn Kokai Tokyo Koho JP 03,152,892 [91,152,892], *Chem. Abstr.* **115,** 268398m.
6. F. Laurent, O. Cyr-Athis, J.-P. Legros, R. Choukroun and L. Valade, *New J. Chem.* 1994, **18,** 575.
7. M. T. Reetz, R. Steinbach, B. Wenderoth and J. Westermann, *Chem. Ind. (London)* 1981, 541; M. T. Reetz and B. Wenderoth, *Tetrahedron Lett.* 1982, **23,** 5259.
8. R. Hanko and D. Hoppe, *Angew. Chem.* 1982, **94,** 378; *Angew. Chem. Int. Ed. Engl.* 1982, **21,** 372.
9. M. T. Reetz and R. Peter, *Tetrahedron Lett.* 1981, **22,** 4691.
10. M. T. Reetz, *Top. Curr. Chem.* 1982, **106,** 1.
11. M. T. Reetz, R. Steinbach and K. Kebeler, *Angew. Chem.* 1982, **94,** 872; *Angew. Chem. Int. Ed. Engl.* 1982, **21,** 864; *Angew. Chem. Suppl.* 1982, 1899.
12. D. Seebach and M. Schiess, *Helv. Chim. Acta* 1982, **65,** 2598; *Angew. Chem. Int. Ed. Engl.* 1983, **22,** 31.
13. (a) A. A. Naiini, W. M. P. B. Menge and J. G. Verkade, *Inorg. Chem.* 1991, **30,** 5009; (b) Z. Duan, A. A. Naiini, J.-H. Lee and J. G. Verkade, *Inorg. Chem.* 1995, **34,** 5477; (c) Z. Duan and J. G. Verkade, *Inorg. Chem.* 1995, **34,** 4311; (d) Z. Duan and J. G. Verkade, *Inorg. Chem.*, in press.
14. D. F. Shriver and M. A. Drezdon, *The Manipulation of Air Sensitive Compounds*. John Wiley & Sons, New York (1986).
15. L. E. Manzer, *Inorg. Synth.* 1982, **21,** 135.
16. SHELXTL-PLUS, Siemens Analytical X-ray, Inc., Madison, WI, U.S.A. (1990).
17. SHELXL-93, G. M. Sheldrick, *J. Appl. Cryst.* in preparation.
18. All X-ray scattering factors and anomalous dispersion terms were obtained from *International Tables for Crystallography*, Vol. C, pp. 4.2.6.8 and 6.1.1.4. Kluwer, Dordrecht (1992).
19. D. G. Dick, R. Rousseau and D. W. Stephan, *Can. J. Chem.* 1991, **69,** 357.
20. C. Airoldi, D. C. Bradley, H. Chudzynska, M. B. Hursthouse, K. M. A. Malik and P. R. Raithby, *J. Chem. Soc., Dalton Trans.* 1980, 2010.
21. R. M. Silverstein, G. C. Bassler and T. C. Morill, *Spectrometric Identification of Organic Compounds*, 5th edn. John Wiley & Sons, Inc., New York, (1991); H. Friebolin, *Basic One- and Two-Dimensional NMR spectroscopy*, 2nd edn (Transl. by J. K. Becconsall). VCH Publishers, New York (1993).
22. J. E. Huheey, *Inorganic Chemistry: Principles of Structure and Reactivity*, 3rd edn. Harper & Row Publishers, New York (1983).

Pergamon

PII: S0277-5387(96)00304-X

Polyhedron Vol. 16, No. 4, pp. 643–651, 1997
Copyright © 1996 Elsevier Science Ltd
Printed in Great Britain. All rights reserved
0277-5387/97 $17.00+0.00

Synthesis and characterization of vanadyl(IV) complexes of Schiff bases derived from anthranilic acid and salicylaldehyde (or its derivatives) or acetylacetone. Single crystal X-ray structures of the oxidized products

Gebray Asgedom,[a] Alavattam Sreedhara,[a] Jussi Kivikoski[b] and Chebrolu P. Rao[a]*

[a]Bioinorganic Laboratory, Department of Chemistry, Indian Institute of Technology, Powai, Bombay 400 076, India

[b]Department of Chemistry, University of Jyvaskyla, Fin 40351, Jyvaskyla, Finland

(Received 24 May 1996; accepted 24 June 1996)

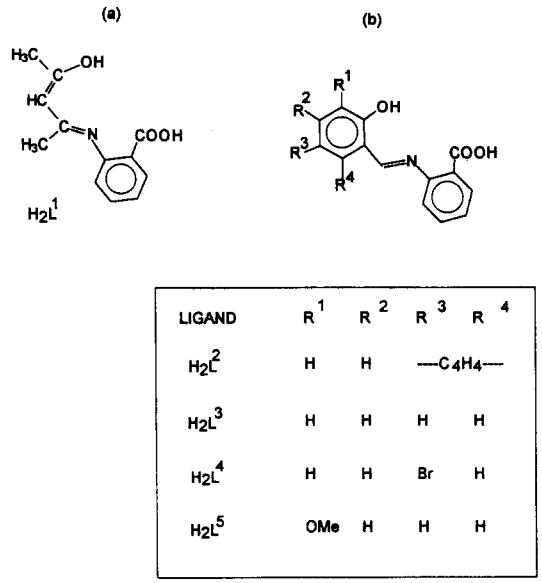
Abstract—Anhydrous, dimeric vanadyl(IV) complexes of Schiff bases derived from [1 + 1] condensation of salicylaldehyde (or its derivatives) and anthranilic acid, have been synthesized from CH_3CN and were characterized by elemental analysis, FTIR, EPR, absorption, TGA, cyclic voltammetry and room temperature magnetic susceptibility measurements. These complexes were found to be oxidized by air in polar solvents like MeOH and DMF to V^V products. The $E_{1/2}$ values were found to be around 660 mV indicating that the carboxylate group favours vanadyl(IV) binding when compared to the alkoxo-bound vanadium complexes. Oxidative instability of these complexes are dependent on the substituent on the salicylaldehyde ring and follow an order, 5,6-benzo > H ⩾ 3-OMe in MeOH and DMF. Attempted recrystallization of the dimeric vanadyl(IV) complex from pyridine led to products of oxidation, polymerization and loss of Schiff base ligand. Single crystal X-ray diffraction showed the oxidation product to be a decavanadate with the pyridinium counter cation, $[C_5NH_6]_6\ V_{10}O_{28} \cdot 2H_2O$. When the dinuclear vanadyl(IV) complex was recrystallized from MeOH, it gave a product of mononuclear carboxylate bound octahedral VO^{3+} moiety along with the presence of both MeOH and OMe units in the coordination sphere with a formula, VO(L)(OMe)(MeOH), where L = 1 + 1 Schiff base derived from 5,6-benzosalicylaldehyde and anthranilic acid, as studied through single crystal X-ray diffraction. Copyright © 1996 Elsevier Science Ltd

Keywords: dimeric vanadyl(IV); oxidative instability; decavanadate; mononuclear octahedral VO^{3+}; single crystal X-ray; Schiff bases.

Important structural moieties in the coordination chemistry of vanadium are VO^{2+} and VO_2^+ and relatively few well characterized complexes containing mononuclear VO^{3+} are known [1]. The isolation and characterization of a novel haloperoxidase [2], requiring vanadium in its +5 oxidation state has motivated many [1, 3–6], including us [7–9] to synthesize, characterize and study various ligand systems coordinated to V^V in its LVO_2^{n-} ($n = 0, 1$) or VO^{3+} forms. The binding of the monooxovanadium(V) moiety (VO^{3+}) to the carboxylate oxygen atom is of current interest not only because this has been proposed to be the structural unit in haloperoxidases [10], but also for the fact that very few have been structurally characterized.

As reported in the literature, reaction of Schiff bases formed between salicylaldehyde and amino acids like glycine, alanine and leucine with $VOSO_4$ in alcoholic-aqueous solution resulted in mononuclear water bound vanadyl(IV) complexes [11,12]. Attempts to dehydrate these by heating to 160°C and to study the properties of the anhydrous complexes were unsuc-

* Author to whom correspondence should be addressed.



LIGAND	R^1	R^2	R^3	R^4
H_2L^2	H	H	—C_4H_4—	
H_2L^3	H	H	H	H
H_2L^4	H	H	Br	H
H_2L^5	OMe	H	H	H

Fig. 1. (a) Structure of H_2L^1; (b) structures of H_2L^2–H_2L^5.

cessful [13]. This paper deals with the synthesis of dinuclear vanadyl(IV) complexes of Schiff bases derived from anthranilic acid and salicylaldehyde (and its derivatives) or acetylacetone in poorly coordinating solvents such as CH_3CN, their stability and conversion to V^V products in coordinating solvents like MeOH and DMF. The structure of the ligands is given in Fig. 1. Attempts to crystallize the vanadyl(IV) dimeric complexes from MeOH or pyridine led to oxidized products of different chemical nature and structure and were structurally characterized by single crystal X-ray methods.

EXPERIMENTAL

Materials and methods

All the methods of analysis (i.e. elemental, ICPAES, EPR, UV-vis, ^{51}V NMR, magnetic and X-ray diffractometer) and synthesis of 2-hydroxy-1-naphthaldehyde (5,6-benzosal), 5-bromosalicylaldehyde (5-brsal) and $VO(acac)_2$ are described in our earlier papers [7–9]. Salicylaldehyde (sal) and acetylacetone (Hacac) (SD Fine, India) were distilled before use, other chemicals were used as received from commercial sources. CH_3CN was distilled over CaH_2 and stored over molecular sieves prior to use.

Preparation of Schiff bases

To an ice cooled 3.5 cm^3 (35 mmol) of Hacac in 10 cm^3 EtOH was added 4.1 g (30 mmol) of anthranilic acid dissolved in 20 cm^3 ice cooled EtOH and the mixture was stirred for 10 min while cold. The solution was brought to room temperature and left for 36 h to result in the precipitation of white crystalline material of the Schiff base (H_2L^1) in 36% yield.

The Schiff bases between anthranilic acid and salicylaldehyde or its derivatives were prepared by the addition of methanolic solution of anthranilic acid to methanolic solution of respective aldehydes in a 1 : 1 ratio followed by stirring for 3 h. The Schiff bases H_2L^2 and H_2L^3 precipitated out; H_2L^4 gave an orange precipitate and H_2L^5 an oil on vacuum drying. Yield of the products obtained was in the range 67–70%.

Synthesis of oxovanadium complexes

Complex **1**. To H_2L^1 (0.430 g, 2 mmol) in 30 cm^3 CH_3CN was added $VO(acac)_2$ (0.530 g, 2 mmol) in 50 cm^3 CH_3CN to result in the formation of an immediate green precipitate. This was refluxed for 3 h, cooled and filtered. The green compound was purified by stirring in hot CH_3CN for 2 h, followed by filtration, washing with ether and drying *in vacuo* to give a product with yield of 66% based on vanadium content. IR(cm^{-1}): 1620 ($\nu_{C=N}$), 1550 (ν_{asym} of COO^-), 1400 and 1390 ($\delta_{CH_3} + \nu_{COO^-}$), 990 ($\nu_{V=O}$).

Complex **1a**. Complex **1** was dissolved in pyridine, to result in a brownish-green solution, which after 2 weeks gave orange crystals of **1a** in 23% yield. These crystals lose their crystallinity and change to yellow powder when removed from solvent. IR (cm^{-1}): 3517 (ν_{OH}, free), 3408 (ν_{OH}, H-bonded), 2133 and 2018 (ν_{asym} and ν_{sym} of $C{=}NH^+$), 975 ($\nu_{V=O}$), 835–470 (ν_{asym} and ν_{sym} of V—O—V).

Complex **2**. To H_2L^2 (0.582 g, 2 mmol) suspended in 50 cm^3 hot CH_3CN was added $VO(acac)_2$ (0.530 g, 2 mmol) in 50 cm^3 CH_3CN. This resulted in a red solution followed by the formation of a brown precipitate. The mixture was refluxed for 12 h, cooled and filtered. The brown product was washed by stirring in hot CH_3CN for 3 h followed by filtration. The same purification procedure was employed for a second time. The filtered product **2** was washed with ether and dried *in vacuo* to give a pure product in 66% yield. IR (cm^{-1}): 1620 ($\nu_{C=N}$), 1550 and 1390 (ν_{asym} and ν_{sym} of COO^-), 995 ($\nu_{V=O}$).

Complex **2a**. Complex **2** (0.661 g) was stirred under reflux in 30 cm^3 MeOH for 6 h. The solution was filtered and the filtrate was kept at room temperature to give compound **2a** as dark red crystals suitable for X-ray analysis in 64% yield. IR (cm^{-1}): 3228 (ν_{OH}), 1626 ($\nu_{C=N}$), 1534 and 1389 (ν_{asym} and ν_{sym} of COO^-), 955 ($\nu_{V=O}$).

Complex **3**. $VO(acac)_2$ (0.795 g, 3 mmol) in 50 cm^3 CH_3CN was added to a hot solution of H_2L^3 (0.723 g, 3 mmol) in 50 cm^3 CH_3CN to result in a red solution that immediately gives a minute golden precipitate. The mixture was refluxed for 4 h, cooled to room temperature and filtered. The precipitate was washed by stirring in hot CH_3CN for 2 h, filtered, and then washed with ether and dried *in vacuo*. Yield of pure product is 49%. IR (cm^{-1}): 1620 ($\nu_{C=N}$), 1555 and 1389 (ν_{asym} and ν_{sym} of COO^-), 997 ($\nu_{V=O}$).

Complex **4**. To H_2L^4 (0.638 g, 2 mmol) in 30 cm^3 hot CH_3CN was added $VO(acac)_2$ (0.530 g, 2 mmol) in 40 cm^3 CH_3CN to result in greenish-brown suspension upon addition. The mixture was refluxed for 5 h, cooled and filtered to give a dark yellow precipitate. Purification of this compound was done as described for complex **3** to give a yield of 42%. IR (cm^{-1}): 1622 ($\nu_{C=N}$), 1560 and 1390 (ν_{asym} and ν_{sym} of COO^-), 997 ($\nu_{V=O}$).

Complex **5**. The Schiff base H_2L^5 (6 mmol) was dissolved in 20 cm^3 CH_3CN and to this was added $VO(acac)_2$ (1.590 g, 6 mmol) in 100 cm^3 CH_3CN to result in a dark brown solution followed by immediate precipitation. The mixture was refluxed for 5 h, cooled and filtered to give yellow precipitate. This complex was purified as described for complex **3** to give a pure product in 46% yield. IR (cm^{-1}): 1620 ($\nu_{C=N}$), 1570 and 1390 (ν_{asym} and ν_{sym} of COO^-), 990 ($\nu_{V=O}$). Elemental analysis of all the products is given in Table 1.

Table 1. Elemental analysis of complexes **1–5**

Compound	Formula	% C	% H	% N	% V
1	$C_{24}H_{22}N_2O_8V_2$	c50.7	3.9	4.9	17.9
		o50.2	3.9	5.2	17.5
1a	$C_{30}H_{38}N_6O_{30}V_{10}$	c24.5	2.6	5.7	34.6
		o24.0	2.8	6.0	35.0
2	$C_{36}H_{22}N_2O_8V_2$	c60.7	3.1	3.9	14.3
		o60.2	3.0	4.2	14.0
2a	$C_{20}H_{18}NO_6V$	c57.3	4.3	3.3	12.2
		o57.5	4.4	3.2	11.7
3	$C_{28}H_{18}N_2O_8V_2$	c54.9	2.9	4.6	16.7
		o54.3	2.8	4.5	16.1
4	$C_{28}H_{16}N_2O_8V_2Br_2$	c43.6	2.1	3.6	13.2
		o43.2	2.5	3.5	13.6
5	$C_{30}H_{22}N_2O_{10}V_2$	c53.5	3.3	4.2	15.2
		o53.1	3.2	4.1	14.8

X-ray crystallography of **1a**

Single crystal X-ray diffraction data were collected on an Enraf-Nonius CAD4 diffractometer using Mo-K_α radiation. The crystal of **1a** was mounted using a drop of perfluoropolyether and data collection was done at −90°C. Two standard reflections were measured every hour, 3% loss in intensity was detected and was accordingly corrected. The structure was solved using SHELXS86 [14], refined with CRYSTALS [15] and the diagrams were generated using ORTEP [16]. Details of the data collection and refinement parameters are given in Table 2.

The hydrogen atoms bonded to C were placed geometrically (C—H distance 1.00 Å). The hydrogen atoms bonded to N(21), N(31) and O(100) were located from a difference Fourier map and their coordinates and isotropic temperature factors were refined. The hydrogen atoms bonded to C atoms were treated as riding atoms with fixed temperature factor [U(iso) = 0.08]. Full matrix least squares refinement with anisotropic temperature factors for all non-hydrogen atoms was used. Empirical (ψ scan) absorption correction was applied using five reflections.

Table 2. Summary of crystallographic data and parameters of compounds **1a** and **2a**

Compound	**1a**	**2a**
Formula	$C_{30}H_{38}N_6O_{30}V_{10}$	$C_{20}H_{18}NO_6V$
Formula weight	1472.07	419.31
Crystal system	Monoclinic	Monoclinic
Space group	$P2_1/c$	$P2_1/c$
a (Å)	9.357(4)	11.901(6)
b (Å)	18.121(5)	8.058(1)
c (Å)	14.000(5)	18.996(2)
β (°)	93.46(3)	101.46(2)
V (Å^3)	2369(1)	1785.4(9)
Z	2	4
D_c (g cm^{-3})	2.06	1.56
Temperature (K)	183(2)	295(1)
Collected data	4099	3747
Unique data	3693	3481
Observed data [$I > 2\sigma(I)$]	2065	2840
Parameters	359	243
Final R	0.045	0.034
R_w[a]	0.043	0.037

[a] $R_w = [\Sigma w(|F_o| - |F_c|)^2/\Sigma w|F_o|^2]^{1/2}$, where a Chebychev weighting scheme was employed.

X-ray crystallography of **2a**

Single crystal X-ray diffraction data were collected on an Enraf-Nonius CAD4 diffractometer using Mo-K_α radiation. Two standard reflections were measured every hour, no systematic variations were observed. The structure was solved using SHELXS86 [14] refined with CRYSTALS [15] and the diagrams were generated using ORTEP [16]. Details of the data collection and refinement parameters are given in Table 2.

In solving the crystal structure of **2a** the hydrogen atoms bonded to C (except to C(41)) were placed geometrically (C—H distance 1.00 Å) whereas Fourier difference syntheses were used to place the hydrogen atom associated with the O(41) and C(41) atoms. Full-matrix least squares refinement with anisotropic temperature factors for all non-hydrogen atoms was used. All hydrogen atoms were treated as riding atoms with fixed temperature factor [U(sio) = 0.08]. Empirical (ψ-scan) absorption correction was applied using three reflections in this structure.

Coordinates and isotropic temperature factors of all non-hydrogen atoms of **1a** and **2a** are given in supplementary data. The bond angles of **1a** are also given in supplementary data

RESULTS AND DISCUSSION

Description of the structure of **1a**

Attempts to crystallize the complexes of **1** and **2** from pyridine resulted in the decomposition along with oxidation of V^{IV} and formation of decavanadate [V^{V}]. Both the complexes gave the same decavanadate crystal with the loss of the Schiff base ligand. The crystals when taken out of the solution lose their crystallinity and change to yellow powder. Many decavanadate salts such as $Na_6V_{10}O_{28}$ [17], $[NH_4]_2Na_2H_2V_{10}O_{28}$ [18], $[(C_5H_5NH)_4][H_2V_{10}O_{28}]$ [19], $[(C_6H_5)_4P]_3H_3V_{10}O_{28}$ [20] and $[(C_6H_{13})NH_3]_4$ $(H_2V_{10}O_{28})$ [21] have been structurally characterized. The new decavanadate with pyridinium counter cation, $[C_5H_6N]_6V_{10}O_{28}\cdot 2H_2O$, in the present case is EPR inactive confirming the oxidation of the vanadium(IV) to (V) in pyridine. The molecular ORTEP of the decavanadate ion at 50% probability is shown in Fig. 2. The crystal packing diagram is shown in Fig. 3. There are five hydrogen bonds in the molecule. Three of these are from pyridinium cations and the other two are from water molecules and all these act as hydrogen donors. N(11), N(21) and N(31) of pyridinium ions form hydrogen bonds with O(7), O(1) and O(3) of the decavanadate anionic unit respectively. The water molecule forms a H-bond with O(13), and also with O(6) of a neighbouring decavanadate unit. Thus, four of the hydrogen bonds are between the decavanadate anions and the corresponding counter cations, whereas in the fifth the water molecule forms hydrogen bonds between two different decavanadate units. Some important bond lengths are given in Table 3. The V—V distances (3.054–3.300 Å) and V—O distances in the decavanadate are similar to the other decavanadates reported. The loss of crystallinity when removed from solvent is presumably due to the partial loss of water or pyridine or both that stabilise the crystal through hydrogen bonding.

In the decavanadate there are three types of vanadium ions present in the ratio of 2 : 2 : 1 based on the nearest oxygen coordination as shown in Fig. 2. These three types are designated as type *a* (V1), type *b* (V2 and V3) and type *c* (V4 and V5). The ^{51}V NMR of **1a** in pyridine showed peaks at −472 and −507 ppm in the intensity ratio 1 : 1 and these are attributable to (type *b*) and (type *c*) vanadium ions respectively. Similar ^{51}V NMR has been reported in the literature [20] for V(*b*-type) and V(*c*-type). However, it was not possible to locate V(*a*-type) possibly due to small intensity and larger line width. Other workers have detected a broad peak around −420 ppm, but

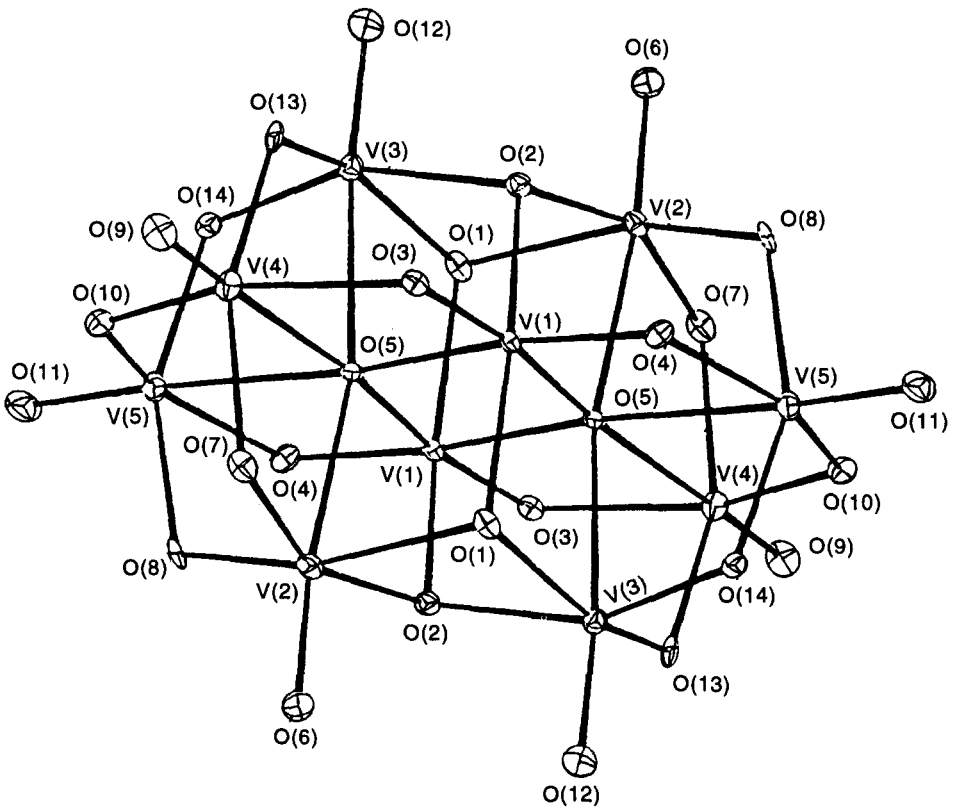


Fig. 2. ORTEP diagram of decavanadate anion **1a** with thermal ellipsoids at 50% probability.

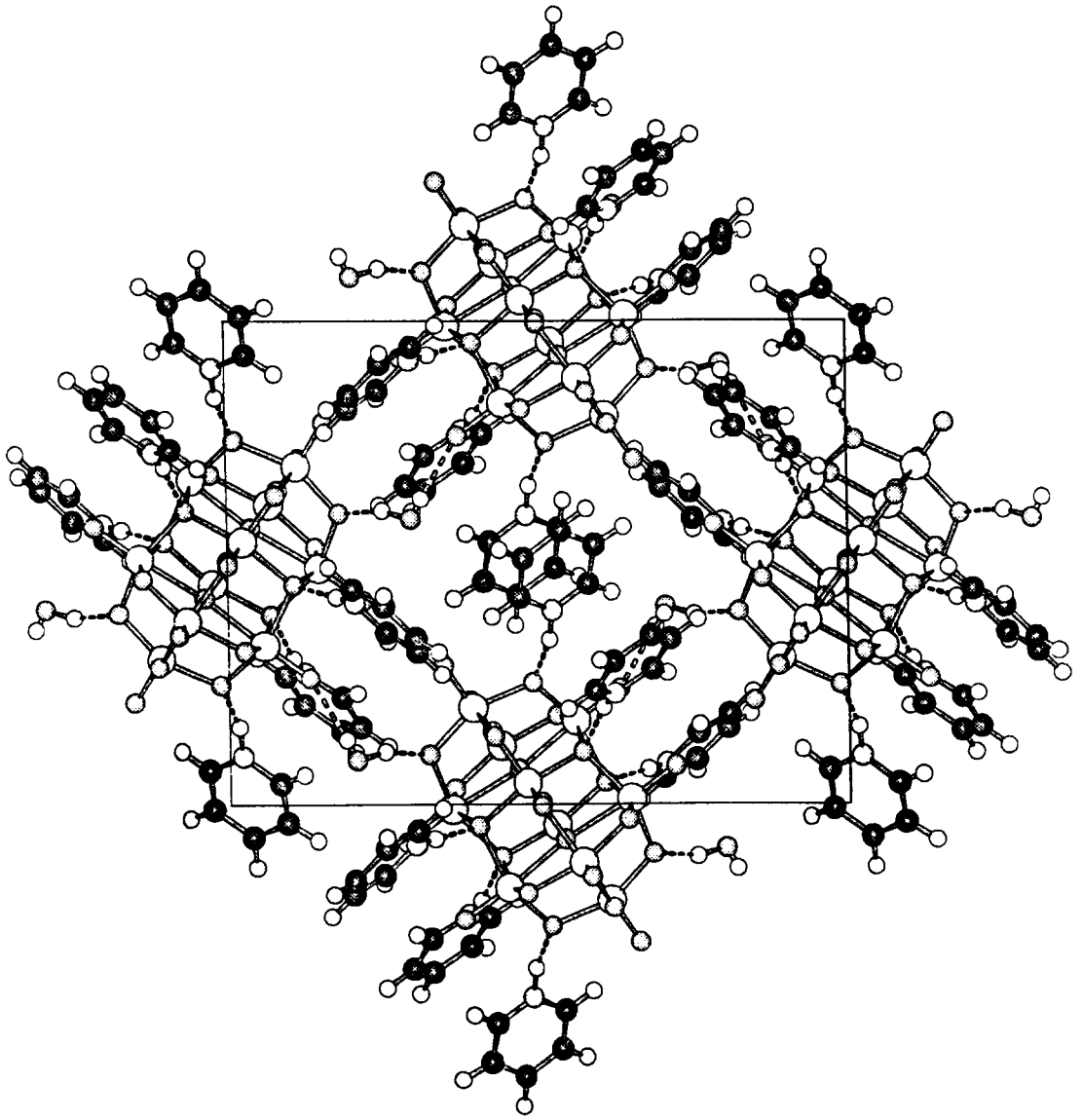


Fig. 3. Unit cell packing diagram of **1a** showing H-bonding as broken lines, viewed along the "b" axis.

Table 3. V—O bond lengths for **1a** in (Å)

V(1)—O(1)	1.940(5)	V(1)—O(4)	1.678(5)
V(1)—O(2)	1.945(5)	V(1)—O(5)	2.086(5)
V(1)—O(3)	1.671(5)	V(1)—O(5)	2.159(5)
V(2)—O(1)	2.060(5)	V(2)—O(6)	1.612(5)
V(2)—O(2)	1.984(5)	V(2)—O(7)	1.867(5)
V(2)—O(5)	2.217(5)	V(2)—O(8)	1.751(5)
V(3)—O(1)	1.992(5)	V(3)—O(12)	1.605(5)
V(3)—O(5)	2.279(5)[a]	V(3)—O(13)	1.833(5)
V(3)—O(5)	2.279(5)[a]	V(3)—O(14)	1.802(5)
V(4)—O(3)	2.072(5)	V(4)—O(9)	1.592(5)
V(4)—O(5)	2.284(5)	V(4)—O(10)	1.824(5)
V(4)—O(7)	1.928(5)	V(4)—O(13)	1.843(5)[a]
V(5)—O(4)	2.028(5)[a]	V(5)—O(10)	1.833(5)
V(5)—O(5)	2.347(5)	V(5)—O(11)	1.597(5)
V(5)—O(8)	1.930(5)	V(5)—O(14)	1.858(5)

[a] From symmetry related ones.

this peak was dependent on the amount of water added during measurement of spectra [20].

The description of structure **2a**

The important bond lengths and angles are given in Table 4. This complex has a distorted octahedral VO^{3+} species in which the terminal oxo and the methanol occupy the apical positions with a *trans* angle of 174.79(4). The tridentate Schiff base and the methoxide together form the basal plane of the molecule. The ORTEP diagram of **2a** is given in Fig. 4. The V—O(1) and the V—O(3) bond distances, 1.890(1) and 1.940(1) Å, are in the range observed for many vanadium Schiff base complexes [1,3–6]. The V atom is displaced towards the terminal oxygen by 0.242 Å

Table 4. Selected bond lengths (Å) and bond angles (°) for **2a**

V(1)—O(1)	1.890(1)	O(3)—V(1)—O(1)	161.75(6)
V(1)—O(3)	1.940(1)	O(31)—V(1)—O(1)	99.31(6)
V(1)—O(31)	1.781(1)	O(31)—V(1)—O(3)	91.40(7)
V(1)—O(41)	2.236(1)	O(41)—V(1)—O(1)	82.62(6)
V(1)—O(50)	1.591(1)	O(41)—V(1)—O(3)	84.00(6)
V(1)—N(1)	2.135(1)	O(41)—V(1)—O(31)	83.39(6)
		O(50)—V(1)—O(1)	96.33(7)
		O(50)—V(1)—O(3)	95.87(7)
		O(50)—V(1)—O(31)	101.82(7)
		O(50)—V(1)—O(41)	174.79(7)
		N(1)—V(1)—O(1)	82.47(6)
		N(1)—V(1)—O(3)	83.19(6)
		N(1)—V(1)—O(31)	163.75(6)
		N(1)—V(1)—O(41)	80.82(6)
		N(1)—V(1)—O(50)	93.99(7)

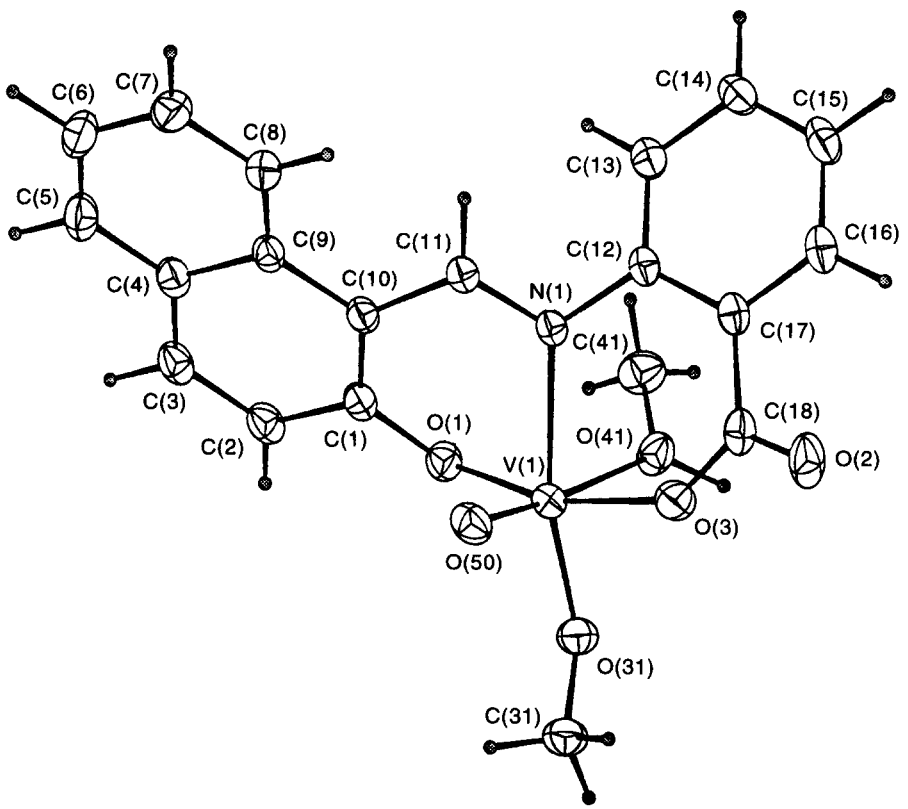


Fig. 4. ORTEP diagram of complex **2a** with thermal ellipsoids at 50% probability.

from the least square plane defined by O(1), O(31), O(3) and N(1). The V=O(50) distance, 1.591(1) Å is close to that observed for six coordinate complexes [22]. There is an intermolecular hydrogen bond between the C=O of the carboxylate and the OH of the methanol group of the neighbouring molecule with O(2)···O(41) distance of 2.668(2) Å. A similar complex LVO(OEt)(HOEt) (H_2L = N-(2-carboxyphenyl)salicyldeneamine) prepared from $VO(OEt)_3$ has been characterized by X-ray diffraction [4], but the present compound is a result of the synthesis through a different route.

Electronic absorption spectra

Complexes **1**–**5** are soluble in donor organic solvents but are insoluble in non-polar solvents. The absorption spectra were measured in the solid state, and in DMF and pyridine solution. The absorption

spectral data is given in Table 5. The reflectance spectra of each of the complexes **1–4** showed three bands in the range 560–585 nm, 740–780 nm and 450–470 nm. Based on the Ballhausen and Gray model [23] the bands are assigned as $^2B_2(d_{xy}) \rightarrow {}^2B_1(d_x2-d_y2)$, $^2B_2 \rightarrow {}^2E(d_{xz}, d_{yz})$ and $^2B_2 \rightarrow {}^2A_1(d_z2)$ transitions, respectively. These values are in agreement with values observed for dimeric five coordinate vanadyl(IV) complexes [24]. However, the third transition (450–475 nm) may also arise from LMCT transition. Three *d–d* bands were observed in solution for **2, 3** and **4** and these were centered around 770 (broad), 550 and 520 nm (sh). The spectra are similar both in DMF and in pyridine solutions. The diffuse reflectance spectrum of complex **5** showed four bands at 780, 655, 562 and 461 nm, however, in solution the bands are observed at 780, 557 and 408 nm.

Stability of complexes **2, 3** and **5** were monitored in DMF solutions, in air, as a function of time using UV-visible absorption spectral studies. While complex **2** showed complete conversion to the V^V form in 2 h, oxidation for **3** and **5** took at least 48 h.

The UV–vis spectrum of complex **1a** showed a doublet centered at 255 and 250 nm and another band at 198 nm. The bands at 255 and 250 nm are assignable to pyridinium cation. The band at 198 nm is due to $O \rightarrow V^V$ charge transfer band. Complex **2a** in DMF showed a band around 550 nm due to LMCT transition.

EPR and magnetic studies

The oxovanadium(IV) complexes are paramagnetic and gave typical axial EPR spectra for frozen samples (77 K) in DMSO. The samples **1–5** showed two sets of overlapping eight line spectra (^{51}V, $I = 7/2$). While the $g_\parallel$ (1.947–1.949) and $g_\perp$ (1.981–1.983) values of the present complexes are similar to those observed for N-salicylideneamino acid complexes, their $A_\parallel$ (183.21–184.29) and $A_\perp$ (66.29–66.86) values deviate considerably [25]. However, the values obtained for complexes **1–5** are close to those reported for the mixed ligand complex of a Schiff base N-(2-carboxyphenyl)salicylideneamine and 8-hydroxyquinoline, and 2,2′-dihydroxyazobenzene and 8-hydroxyquinoline [26]. The large hyperfine coupling constants observed in the present case are due to the weak interaction of carboxylate in delocalization of the unpaired electron density away from the metal center.

The room temperature values of effective magnetic moment per vanadium are in the range 1.70–1.94 B.M. for complexes **1** and **5** corresponding to the d^1 configuration, and showing marginal or negligible electron exchange interactions in these complexes due to carboxylate bridging. Phenolate bridged dimeric complexes have shown weak antiferromagnetic interactions and a magnetic moment of 1.55 B.M. has been reported for the complex bis[oxovanadium(IV)2-(2′-hydroxyphenyl)iminomethylphenato] [27]. Magnetic moment values for alkoxy bridged complexes $[VO(acac)OMe]_2$ was found to be 1.80 B.M. and exhibits only a weak interaction between the vanadium ions [28].

Table 5. Electronic absorption data of **1–5**

Compound	λ, nm, (ε, mol dm^{-3} cm^{-1})
1	DMF: 776(56), 560(112), 460(sh, 205), 349(9400)
	Py: 740(70), 547(304), 467(378)
	Reflectance: 780, 575, 476, 395
1a	H_2O: 255, 250, 198
2	DMF: 755(71), 585(323), 418 (24000)
	Py: 750(92), 582(310), 530(281)
	Reflectance: 740, 585, 460
2a	DMF: 560(1714), 429(23700), 327(22738)
3	DMF: 780(46), 560(192), 510(241), 391(15512), 299(26787)
	Py: 780(49), 533(256), 507(275)
	Reflectance: 780, 560, 452
4	DMF: 780(66), 565(226), 525(246)
	Py: 780(32), 560(159)
	Reflectance: 770, 560, 450
5	DMF: 780(36), 557(155), 408(8989)
	Py: 770(49), 550(229)
	Reflectance: 780, 655, 562, 461

Electrochemical studies

The electrochemical behavior of complexes **1, 3** and **5** were studied by cyclic voltammetry in the range +1.00 to −2.00 V in DMF at Pt working electrode and Ag/AgCl reference electrode using NEt_4Cl or NEt_4Br as supporting electrolyte. Complex **1** showed an irreversible anodic peak at +0.65V and complexes **3** and **5** gave a quasi-reversible cyclic voltammetric response due to VO^{3+}/VO^{2+} couple at $E_{1/2} = +0.66$ (Fig. 5). Complexes with NO_5 core of alkoxo binding showed reduction at more negative potential (−0.41V) [7]. On the other hand, the mixed ligand complexes [1] of N_3O_3 core showed VO^{3+}/VO^{2+} redox behavior in the range +0.61 to +0.80 V where the potentials are similar to those observed for **1, 3** and **5**. While the alkoxy rich dinuclear V^V complexes showed $E_{1/2}$ around −0.42 V, those with carboxylate bound vanadium complexes showed around 0.66 V. The potentials seem to indicate the nature and influence of the bound ligands (alkoxy or carboxylate) on the redox behaviour of vanadium. The potentials also indicate that the alkoxy-bound V^V centers are favoured by about 104 kJ mol^{-1} over the carboxylate bound counterparts. Thus this study strongly suggests the stabilization of V^{IV} center by carboxylate ligands. It is understood from the literature that phenolate and alkoxide donors generally favour VO^{3+} and VO_2^+ centers.

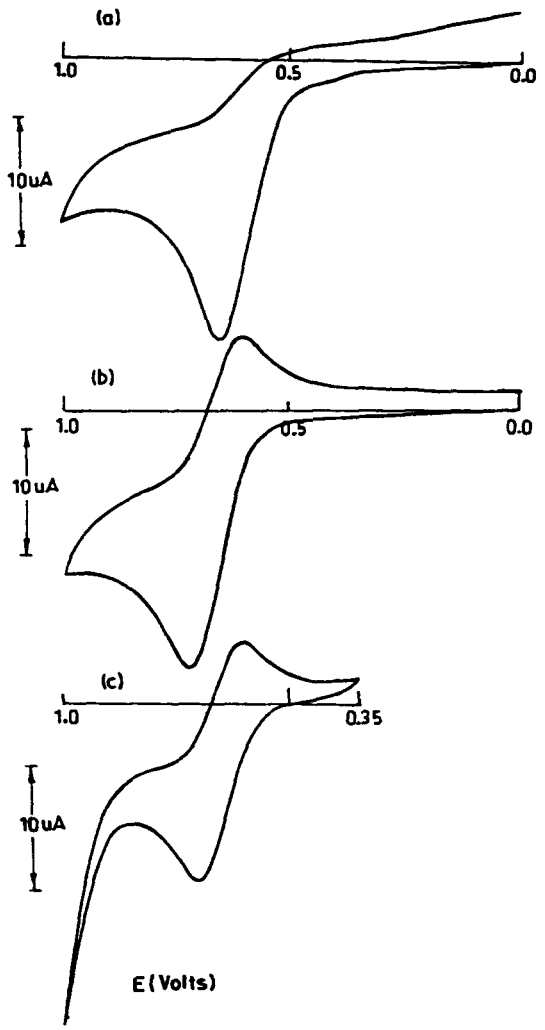


Fig. 5. Cyclic voltammograms of complexes (a), **1**; (b) **3**; (c) **5**, in DMF at a Pt working electrode and Ag/AgCl reference electrode using NEt_4Cl or NEt_4Br supporting electrolyte.

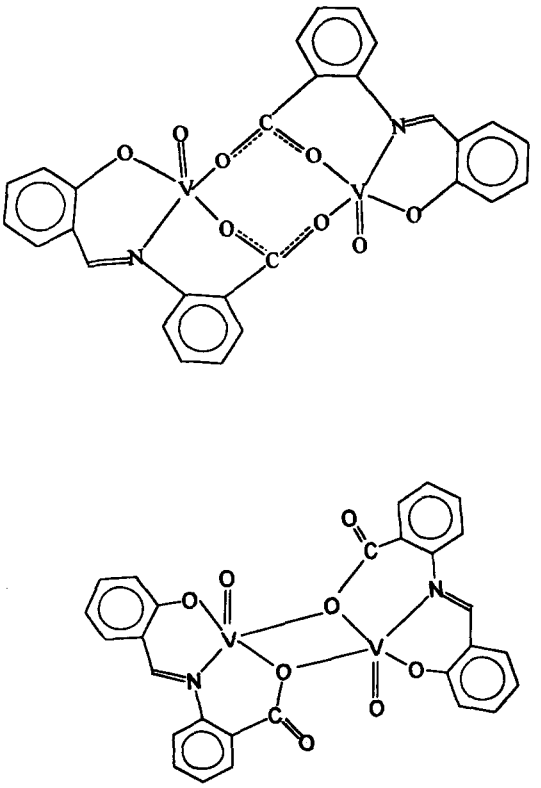


Fig. 6. Schematic representation of the proposed structures of complex **3**.

Thermogravimetric and differential thermal analysis

The thermogravimetric and differential thermal analysis curves for **1** showed that there is no weight loss up to 250°C. However, three weight losses were observed with starting temperatures of 270, 400 and 470°C. The loss of 270°C for complex **1**, which is absent in the other complexes, is attributable to the decomposition of the acetylacetonate and those at higher temperatures are due to the decomposition of the benzene ring. The weight of the final residue at 700°C matches with the V_2O_5 which is 32% of the molecular weight of the compound. Complexes **2**, **3**, **4** and **5** start to lose weight at 400°C and this loss is assigned to the decomposition of the benzene ring. Complex **2a** showed weight loss at 180°C that accounts for 15% of the molecular weight and is attributable to the loss of methanol and a methoxide. The other weight loss is observed at 400°C.

Based on the mono and bidentate nature of the carboxylate group, two possible structures are proposed for **3** as shown in Fig. 6.

Acknowledgements—G.A. thanks the Indian Council of Cultural Relations for a research fellowship and the Govt. of Ethiopia for grant of leave; A.S. thanks the Department of Atomic Energy, India, for the award of a Dr K.S. Krishnan research fellowship; C.P.R. is grateful to DST for funding the project; J.K. thanks the Academy of Finland for support. We thank Dr E. Kolehmainen, University of Jyvaskyla, Finland for recording the ^{51}V NMR of complex **1a**. Regional Sophisticated Instrumentation Centre, IIT-Bombay is gratefully acknowledged for help in recording EPR, TGA-DTA and for ICPAES analysis.

REFERENCES

1. J. Chakravarty, S. Dutta, S. K. Chandra, P. Basu and A. Chakravorty, *Inorg. Chem.* 1993, **32**, 4249; S. Mondal, S. Dutta and A. Chakravorty, *J. Chem. Soc., Dalton Trans.* 1995, 1115.
2. H. Vilter, *Phytochemistry* 1984, **23**, 1387; R. Wever, E. de Boer, H. Plat and B. E. Krenn, *FEBS Lett.* 1987, **216**, 1.
3. V. Vergopoulos, W. Priebsch, M. Fritsche and D. Rehder, *Inorg. Chem.* 1993, **32**, 1844.

4. M. J. Clague, N. L. Keder and A. Butler, *Inorg. Chem.* 1993, **32,** 4754.
5. G. I. Colpas, B. J. Hamstra, J. W. Kampf and V. L. Pecoraro, *Inorg. Chem.* 1994, **33,** 4669.
6. C. J. Carrano, M. Mohan, S. M. Holmes, R. de la Rosa, A. Butler, J. M. Charnock and C. D. Garner, *Inorg. Chem.* 1993, **32,** 646.
7. G. Asgedom, A. Sreedhara and C. P. Rao, *Polyhedron* 1995, **14,** 1873; G. Asgedom, A. Sreedhara, J. Kivikoski, J. Valkonen, E. Kolehmainen and C. P. Rao, *Inorg. Chem.* 1996, **35,** 5674.
8. G. Asgedom, A. Sreedhara, J. Kivikoski, J. Valkonen and C. P. Rao, *J. Chem. Soc., Dalton Trans.* 1995, 2459; G. Asgedom, A. Sreedhara, J. Kivikoski, E. Kolehmainen and C. P. Rao, *J. Chem. Soc., Dalton Trans.* 1996, 93.
9. G. Asgedom, A. Sreedhara, E. Kolehmainen and C. P. Rao, *Polyhedron* 1996, **16,** 3731.
10. D. Rehder, C. Weidemann, A. Duch and W. Priebsch, *Inorg. Chem.* 1988, **27,** 584.
11. K. Nakajima, M. Kojima, K. Toriumi, K. Saito and J. Fujita, *Bull. Chem. Soc. Jpn.* 1989, **62,** 760.
12. L. J. Theriot, G. O. Carlisle and H. J. Hu, *J. Inorg. Nucl. Chem.* 1969, **31,** 2841.
13. R. H. Holm, G. W. Everett, Jr and A. Chakravorty, *Prog. Inorg. Chem.* 1996, **7,** 119.
14. G. M. Sheldrick, *SHELXS* 86, *Program for the Solution of Crystal Structures.* University of Gottingen (1986).
15. D. J. Watkin, J. R. Carruthers and P. W. Betteridge, *CRYSTALS.* Chemical Crystallography Laboratory, University of Oxford (1990).
16. C. K. Johnson, ORTEP, Report ORNL-5138. Oak Ridge National Laboratory, Oak Ridge, TN (1976).
17. P. A. Durif, M. T. Averbuch-Pouchot and J. C. Guitel, *Acta Cryst.* 1980, **B36,** 680.
18. I. Cavaco, J. C. Pessoa, S. M. Luz, M. T. Duarte, P. M. Matias, R. Henriques and R. D. Gillard, *Polyhedron* 1995, **14,** 429.
19. J. M. Arrieta, *Polyhedron* 1992, **11,** 3045.
20. V. W. Day, W. G. Klemperer and D. J. Maltbie, *J. Am. Chem. Soc.* 1987, **109,** 2991.
21. P. Roman, A. Aranzabe, A. Luque, J. M. Guitierrez-Zorilla and M. Martinez-Ripoll, *J. Chem. Soc., Dalton Trans.* 1995, 2225.
22. J. A. Bonadies, W. M. Butler, V. L. Pecoraro and C. J. Carrano, *Inorg. Chem.* 1987, **26,** 1218.
23. C. J. Ballhausen and H. B. Gray, *Inorg. Chem.* 1962, **1,** 111.
24. A. Syamal and K. S. Kale, *Inorg. Chem.* 1979, **18,** 992.
25. L. Casella, M. Gullotti, A. Pintar, S. Colonna and A. Manfredi, *Inorg. Chim. Acta* 1988, **144,** 89.
26. J. J. R. Frausto da Silva, R. Wootton and R. D. Gillard, *J. Chem. Soc. (A),* 1970, 3369; I. Cavaco, J. C. Pessoa, D. Costa, M. T. Duarte, R. D. Gillard and P. Matias, *J. Chem. Soc., Dalton Trans.* 1995, 149.
27. P. A. Vigato, R. Graziani, M. Vidali, F. Milani and M. M. Musiani, *Inorg. Chim. Acta* 1982, **61,** 121.
28. M. M. Musiani, F. Milani, R. Graziani, M. Vidali, U. Caellato and P. A. Vigato, *Inorg. Chim. Acta* 1982, **61,** 115.

Pergamon

PII: S0277-5387(96)00306-3

Polyhedron Vol. 16, No. 4, pp. 653–661, 1997
Copyright © 1996 Elsevier Science Ltd
Printed in Great Britain. All rights reserved
0277-5387/97 $17.00+0.00

Possible binding modes for dinitrogen activation by the FeMo-cofactor in nitrogenase

Shi-Jun Zhong[a]* and Chun-Wan Liu[b]*

[a] Center of Computer Network, Xiamen University, Xiamen, Fujian 361005, P.R. China

[b] State Key Laboratory of Structural Chemistry, Fujian Institute of Research on the Structure of Matter, Chinese Academy of Sciences, Fuzhou, Fujian 350002, P.R. China

(Received 12 April, 1996; accepted 19 June 1996)

Abstract—Dinitrogen activation at the FeMo-cofactor site of nitrogenase was studied based upon the quantum chemical CNDO calculations performed on possible processes of dinitrogen approaching and binding to the FeMo-cofactor. The best dinitrogen binding mode suggested in this article is the dinitrogen-inserting end-on mode, in which one nitrogen atom is located at the geometrical center of the FeMo-cofactor, and another nitrogen atom keeps out of the Fe_4 surface of the Fe_6 prism of the FeMo-cofactor. The mechanism of protonation of dinitrogen at the FeMo-cofactor site is discussed based upon the suggested binding mode.
Copyright © 1996 Elsevier Science Ltd

Keywords: binding mode; calculation; CNDO; dinitrogen; FeMo-cofactor; protonation mechanism.

The structural model proposed by Kim–Rees [1–3] and Bolin [4] for the iron–molybdenum cofactor (FeMoco) of the nitrogenase molybdenum–iron protein, which provides a structural basis for interpreting biological dinitrogen reduction, can be represented by two joined incomplete cubane clusters of composition 4Fe : 3S and 1Mo : Fe : 3S, with three iron atoms from each cluster bridged by what are apparently sulfur atoms. The structure contains six coordinately unsaturated FeS_3 sites with their central Fe atoms located in a trigonal prismatic arrangement. The remaining Mo and Fe atoms, capping the trigonal faces of the Fe_6 (or 6Fe) prism, serve as cluster anchor points. The six-coordinated Mo atom, being bound to three sulfur atoms within the cluster, is ligated by the imidazole group of the His-442 residue, as well as a bidentate homocitrate (HC) through hydroxyl and carboxyl oxygen atoms. It should be pointed out that the nitrogen atom of the imidazole provides two electrons for bonding to Mo. The anchor Fe atom is coordinated by the sulfur atom of the Cys-275 residue. Table 1 lists some interatomic distances selected from the reported structural data based on the X-ray crystallographic analyses [1,3,4] (at 2.7 Å and 2.2 Å resolution), the iron EXAFS [5] and the molybdenum EXAFS [6]. In fact, many structural details about the FeMoco already were derived from earlier EXAFS spectroscopy [7–10].

The FeMoco is regarded as the likely site of substrate binding and reduction [11–13]. In order to reveal some insights into N_2 binding mode, many theoretical calculations including earlier researches [14] of simple metal center models and recent researches [15–20] of the Kim–Rees model, have been performed on some individual structures proposed for the complex of N_2 with the FeMoco. Based on extended Huckel (EHMO) calculations, Deng and Hoffmann [15] suggested that the best N_2 coordinated mode is that one in which N_2 occupies the site of a bridging sulfur and binding in the side-on fashion to two Fe atoms of the FeMoco. However, other researchers [16–19] favor dinitrogen binding modes on the Fe_4 face of the FeMoco. Plass [16] employed the EHMO method to discuss the similarities and differences between the FeMo-, FeV- and FeFe-cofactors as dinitrogen is in the end-on fashion to bind to the Fe_4 face. Shestakov's EHMO calculations [17] also suggested the end-on mode on the Fe_4 face. Dance [18] supposed that dinitrogen is in the side-on fashion to bind the Fe_4 face, and studied various configurations related to the Fe_4 face site using density

* Authors to whom correspondence should be addressed.

Table 1. Some selected interatomic distances for the FeMoco

Fe—Fe	Fe—Mo	Fe—S	Mo—S	Mo—O	Mo—N	Year	Method	Reference
2.7–2.8	—	—	—	—	—	1992	X-ray (2.7 Å)	1
2.4–2.6	—	—	—	—	—	1993	X-ray (2.2 Å)	3
2.64	2.73	2.32	2.4	2.2	2.2	1993	Fe-EXAFS[a]	5
2.66	2.70	2.29	2.4	2.2	2.2	1993	Fe-EXAFS[b]	5
—	2.72	—	2.37	2.19	2.19	1994	Mo-EXAFS[c]	6
—	2.70	—	2.37	2.22	2.22	1994	Mo-EXAFS[d]	6

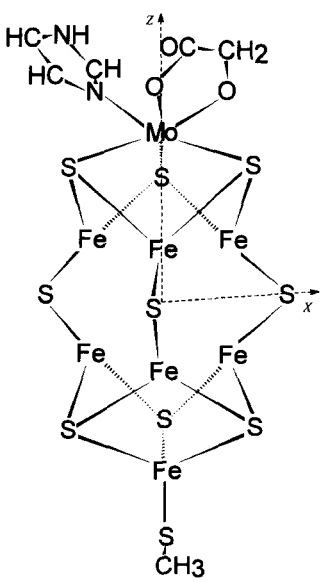
[a] For the dithionite-reduced *Azotobacter vinelandii* nitrogenase Mo–Fe protein.
[b] For the thionine-oxidized Mo–Fe protein.
[c] For the isolated FeMoco.
[d] For the Mo–Fe protein.

functional theory. The calculations by Dance were performed on an FeFe-model other than the FeMoco. Machado and Davidson [19] investigated *ab initio* results of dinitrogen side-on and end-on coordination to one, two and four iron centers of some iron–sulfur cofactor models. Although the above calculations have provided valuable ideas about this complex problem of dinitrogen binding, there are some details which need to be investigated in much more comprehensive ways. First, models used in calculations must well characterize the FeMoco. The replacement of the residues on the Mo atom and the anchor Fe atom by simple groups such as H atoms would have a large effect on results, as pointed out by Stavrev and Zerner [20] based on the INDO calculations of oxidized rubredoxin. Secondly, dinitrogen binding would be considered as a moving process of dinitrogen approaching to the FeMoco while some geometrical changes may occur, such as the fluctuation of the skeleton of the FeMoco and the flapping of the bridging sulfur atoms. During the process, many intermediates of the complex of dinitrogen with the FeMoco can be generated as the possible dinitrogen binding mode. A rational binding model must be selected from these intermediates by comparison of some factors such as the net charge on dinitrogen, the N—N bond order and the barrier for forming the complex of dinitrogen with the FeMoco. In addition, the geometric space maintained for the entry of protons and the exit of ammonia also is an important factor.

In this paper, quantum chemical calculations are performed on the processes of dinitrogen approaching in several manners to the FeMoco. The results will suggest an alternative dinitrogen binding mode. The mechanism for the protonation of dinitrogen also is discussed based upon the selected binding mode.

GEOMETRICAL CONSIDERATION AND CALCULATIONAL DETAILS

The model for the FeMoco used in our calculations is chosen as **1** of stoichiometry $[MoFe_7S_9(:N(CH)_2NHCH)(—OCH_2COO—)(—SCH_3)]$, which involves all ligand groups directly ligating to the metal atoms. These terminal ligand groups are coordinately saturated by hydrogen atoms, after removing the outer residues. The terminal ligands on the Mo atom are chosen by replacement of homocitrate with a simple group (—OCH_2COO—) and by replacement of the imidazole of His-442 with a simple imidazole (:$N(CH)_2NHCH$), the later providing two electrons to bond to Mo. The ligand on the anchor Fe atom is SCH_3. This calculation model guarantees that the metal–ligand bonding of the FeMoco keeps unchanged. In addition, the 193 valence electrons of this model, may fit in with the $S = 3/2$ spin state [21, 22] of the isolated FeMoco in its semireduced (or the "native") state. The interatomic distances are chosen according to Table 1 to be: 2.65 Å (Fe—Fe), 2.70 Å (Fe—Mo), 2.30 Å (Fe—S), 2.40 Å (Mo—S), 2.20 Å (Mo—O), and 2.20 Å (Mo—N). For dinitrogen, the N—N bond length is chosen to be 1.1 Å. Besides, the Fe—N distances thought to present direct interaction between Fe and N are chosen to be 1.9 Å to 2.0 Å, values being close to the sum of the valence radii of Fe and N.



1

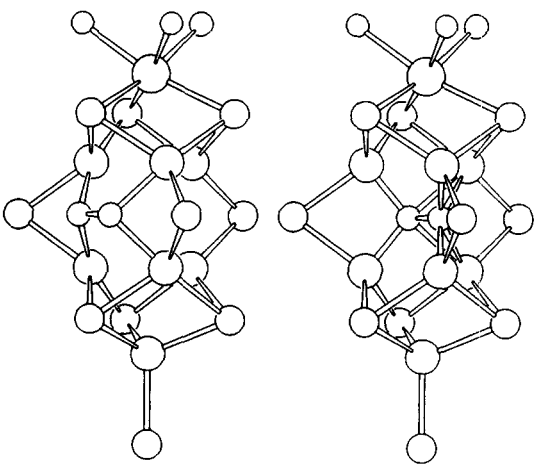
Up to now, there is no direct experimental evidence to indicate where the active sites are. If molybdenum is at the active site, the structure for the FeMoco does not yet help us define its function [23]. In addition, mono-atom site hardly provides effective activation according to our preliminary calculations as well as the reported calculated results [15]. On the other hand, the suggestion of the iron sites [24] was reformulated based upon firmer chemical evidence [25,26]. The multicentric binding fashion provided by the Fe_6 prism can transfer more charge to dinitrogen and effectively activate it. Therefore, it focus our attention on the Fe_6 prism which center (or the cavity), three Fe_4 surfaces (or the windows), and one Fe_2 gap caused by release of one bridging sulfur atom, can serve as active sites. The possible binding modes contain three types: the center-site modes (**3, 5, 7, 8, 9, 10, 11, 12, 14** and **16**), the face-site modes (**2, 4,** and **6**) and the bridge-site modes (**13** and **14**).

Dinitrogen can utilize the end-on or/and side-on fashions to bind to these active sites. It is certainly possible that a variety of different binding modes are utilized by the intermediates generated during dinitrogen moving toward the FeMoco. To describe the moving of dinitrogen, we define a coordinate frame (see **1**, the dotted lines) with the origin located at the geometrical center of the FeMoco, the z axis pointing to the Mo atom and the x axis pointing to one of the three bridging sulfur atoms. Six schemes expressing the moving of dinitrogen are considered below.

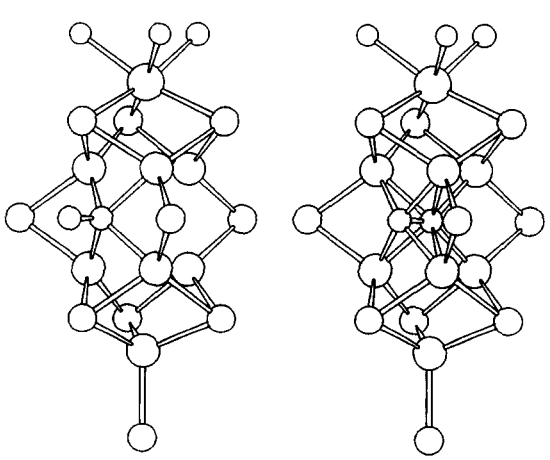
Scheme **I** (**2** → **3**): Along the negative x axis, dinitrogen moves toward the FeMoco. If dinitrogen is in the end-on fashion (or dinitrogen being vertical to the Fe_4 square surface), the first nitrogen atom begins to interact with the four atoms while the second nitrogen atom does not direct interaction with the FeMoco. This results in mode **2**. The 3.8 Å distance between two diagonal Fe atoms of the Fe_4 window is large enough to allow the inserting of dinitrogen in the end-on fashion. When the first nitrogen enters the cavity and goes near the geometrical center, the second nitrogen atom still stays out of the Fe_4 surface. We have mode **3**, where four Fe—N distances correlative to the outer nitrogen atom are about 1.9 Å and the six ones correlative to the centric nitrogen atom are about 2.0 Å.

Scheme **II** (**4** → **5**): Along the negative x axis, dinitrogen moves in a horizontal side-on fashion (or the bond axis of dinitrogen being parallel to the Fe_4 face but orthogonal with the z axis). As each nitrogen atom begins to interact with two of the four iron atoms, we obtain mode **4**. If dinitrogen can penetrate through the Fe_4 window which is considerably small to the dinitrogen in the side-on fashion, and enter the Fe_6 cavity, we arrive at mode **5**.

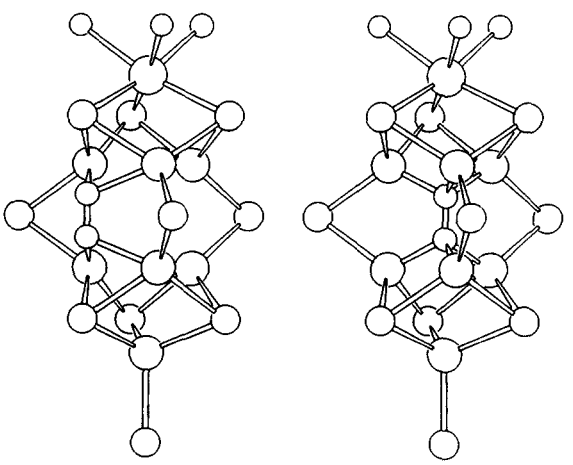
Scheme **III** (**6** → **7**): It is similar to Scheme **II**, but dinitrogen being in a vertical side-on fashion (or the bond axis of dinitrogen being parallel to both the Fe_4 face and the z axis). We have mode **6** and mode **7**.



Scheme II



Scheme I



Scheme III

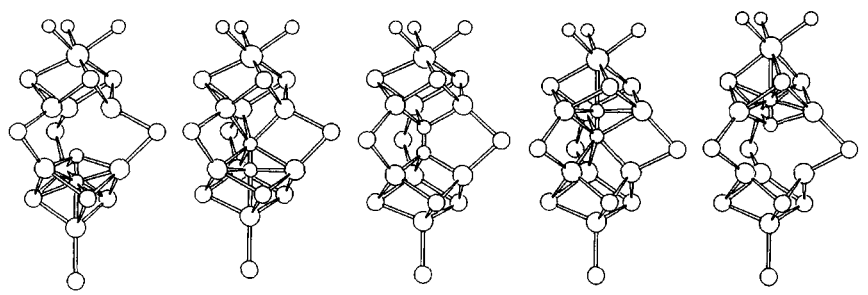
The latter is just the mode proposed by Chan, Kim, and Rees [3]. However, the Fe_6 cavity is too small for dinitrogen binding in mode **7**. The Fe_6 prism must increase its Fe—Fe edges up to 3.0 Å.

Scheme **IV** (**10** ← **9** ← **8** → **11** → **12**): Mode **8** is like mode **7**, but has a larger Fe_6 cavity of 3.0 Å Fe—Fe edges which can satisfy the demand of 2.0 Å Fe—N distances [3,15]. When dinitrogen drops down to and into the Fe_4S_3 cluster, we have two binding modes. One is mode **9** in which the first nitrogen atom is on the Fe_3 trigonal face of the Fe_4S_3 cluster, while the Fe—Fe distances are expanded to 3.4 Å. Another one is mode **10** in which dinitrogen inserts its half in the Fe_4S_3 bag while the Fe—Fe distances recover a little to 3.3 Å. Similarly, we have modes **11** and **12** as dinitrogen jumps up to and into the $MoFe_3S_3$ cluster. At each step, other atoms will change their sites according to the interatomic distances described previously.

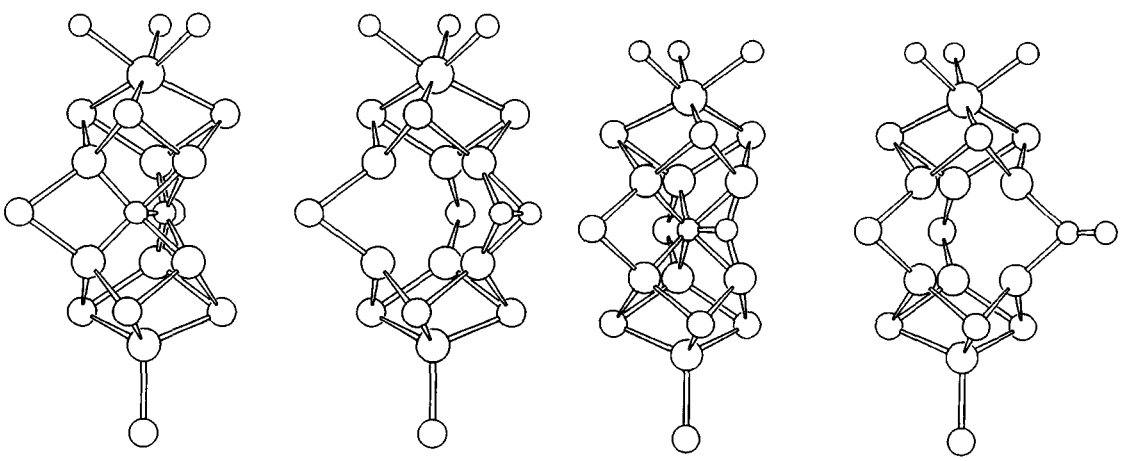
Scheme **V** (**14** ← **13**): Dinitrogen approaches the FeMoco in a horizontal side-on fashion along the positive x axis (contrary to Scheme **II**), while the bridging sulfur atom has been released to generate a Fe_2 gap which can grasp dinitrogen. When each nitrogen atom has interaction with the two Fe atoms, we have mode **13**, which is just Orme-Johnson's first mode [27] and supported by the EHMO calculations by Deng and Hoffmann [15]. If the Fe_2 gap enlarges enough to swallow dinitrogen, we have mode **14** in which dinitrogen lays in the center of the Fe_6 cavity like in mode **5**.

Scheme **VI** (**16** ← **15**): Along the positive x axis, dinitrogen moves in the end-on fashion to approach the Fe_2 gap. When the first nitrogen atom begins to interact with the two Fe atoms of the Fe_2 gap, we have mode **15**. As dinitrogen enters the cavity, we have mode **16** in which dinitrogen also lays in the center of the cavity.

About 50 configuration points are calculated during each process of dinitrogen moving toward the FeMoco. The calculations are divided into two steps. First, for comparing the possible binding modes involved in the above six schemes, the geometry of the FeMoco keeps unchanged for six schemes. Secondly, for further analysis of binding process, the fluctuation of the FeMoco skeleton and the lengthening of N—N bond are taken into account. Although DFT calculation [17] and *ab initio* calculation [18] have been



Scheme IV



Scheme V

Scheme VI

performed on some individual structures to model the complex of dinitrogen with FeMoco, such a laborious problem as the above described process of dinitrogen moving toward the FeMoco is not easy to calculate at a high level. Therefore we employ the semi-empirical CNDO method [28], by which calculations of a series of continuous geometrical configurations are believable because the energy differences computed from the values in CNDO calculations may be compared directly with the results computed from jobs using other methods [29].

POSSIBLE DINITROGEN BINDING MODES

A rational binding mode should be consistent with the following criteria: (1) a lower barrier of the total energy for forming the complex of dinitrogen with the FeMoco; (2) a negative net charge on dinitrogen; (3) A significant weakening of the triple bond of dinitrogen; (4) enough spacious sites for the entry of the protons and for the exit of the product ammonia.

For each scheme described above for expressing dinitrogen binding, we examine the variations of three important quantities: (1) the N—N bond order, (2) the net charge on dinitrogen, and (3) the relative values of the total energy (in atomic unit, au) of the system consisting of dinitrogen and the FeMoco. The three quantities for each scheme are expressed by three curves in order from the top to the bottom of the left vertical axis in each sub-figure of Fig. 1, where the FeMoco keeps its original electron number and the $S = 3/2$ spin state [23,24]. In Fig. 1, the horizontal axis for sub-figures (a), (b), (c), (e), and (f) is the x axis, but the z axis for sub-figure (d). The vertical dotted lines in each sub-figure indicate where exist explicit Fe—N interaction of about 1.9–2.0 Å Fe—N distance, and correspond to possible binding modes which numbers (Nos.) are also marked on the tops of the dotted lines.

Figure 1(a) expresses Scheme **I**. When dinitrogen stays far away (the left of Fig. 1(a)) from the FeMoco, it almost has no interaction with the FeMoco, and keeps the triple bond (the Wiberg bond order is 3.0) and the zero net charge. When it approaches the Fe Moco and begins to bind to the Fe_4 surface, mode **2** is formed around the point of $x = -1.2$ in the horizontal axis, where dinitrogen has the negative net charge of -0.6 and the N—N bond order of 1.7. When dinitrogen inserts its half in the Fe_6 prism to form mode **3** which is indicated by a dotted line at the point $x = 0$ of the horizontal axis, the negative net charge accumulates to about -1.4 and the N—N bond order further decreases to 1.0. In mode **3**, it is obvious that much charge has been transferred to dinitrogen from the metal centers of the FeMoco, and dinitrogen has already been activated greatly. There is no explicit barrier in the smooth energy curve which shows the possibility of dinitrogen inserting. Orme-Johnson's second dinitrogen binding mode [30] is somewhat like mode **3**. The complete entry of dinitrogen into the cavity in Orme-Johnson's second mode requires a light expansion of the Fe_6 frame. Our calculation on this expansion, shows that it is possible with respect to the total energy. However, this entry does not bring further weakening of the bond order of dinitrogen, and is not helpful to the subsequent process of dinitrogen reduction which is associated to the entry of protons and the exit of ammonia. In mode **3**, one nitrogen atom keeps out of the Fe_4 surface, thus granting large space for the addition of protons. The further calculation of local geometry optimization shows that the N—N bond length in mode **3** can be elongated to near 1.5 Å, it just being the length of N—N single bond.

Figure 1(b) expresses Scheme **II**, by which dinitrogen attaches to the Fe_4 surface in the horizontal side-on fashion. Mode **4** is indicated by the dotted line at about $x = -1.9$ in the horizontal axis, where the correlative N—N bond order is 1.7 and the net charge on dinitrogen is -0.7. When going near the Fe_4 face, dinitrogen will be much activated. Mode **4** is the binding mode suggested by Dance [17]. A higher barrier for the entry of dinitrogen in the side-on fashion, shows the difficulty of the formation of mode **5** in this scheme. In view of the different path, mode **5** may be regarded as a derivative of mode **3** when dinitrogen rotates an angle of 30 and the nitrogen atom in the cavity moves out of another Fe_4 surface. Our further calculation shows that this rotation is not difficult in energy, as long as the N—N bond length is stretched gradually during the rotation.

Figure 1(c) expresses Scheme **III** by which dinitrogen attaches to the Fe_4 surface in the vertical side-on fashion. Mode **6** is indicated by the dotted line at the point $x = -1.9$ of the horizontal axis, in which the net charge on N_2 is -0.7 and the N—N bond order is 1.5. Both mode **6** and mode **4** which are similar, have not made dinitrogen sufficiently activated. Mode **7** is just the binding mode proposed by Chan, Kim and Rees [3], which requires the entry of dinitrogen. However this entry is inhibited by a higher barrier which arises from the restriction of the smaller Fe_4 window to the entry of the dinitrogen in side-on fashion. This binding mode **7** can be expressed better as mode **8** below, which has an enlarged Fe_6 cavity with Fe—Fe distances of 3.0 Å, geometrically allowing the standing of dinitrogen in the center.

Figure 1(d) expresses Scheme **IV** by which dinitrogen in the cavity of the prism is artificially moved down to the Fe_4S_3 cluster to form modes **9** and **10** (the left of Fig. 1(d)), and up to the $MoFe_3S_3$ cluster to form modes **11** and **12** (the right of Fig. 1(d)). Mode **8** (the center of Fig. 1(d)) is preferable to other correlative modes **9**, **10**, **11** and **12**, for it has the smaller N—N bond order of 1.1, larger negative net charge of -1.5, and the lower energy. Here, it must be pointed out that the five modes are generated after the entry of dinitrogen in the vertical side-on fashion into the Fe_6 cavity, which is inhibited by a barrier shown

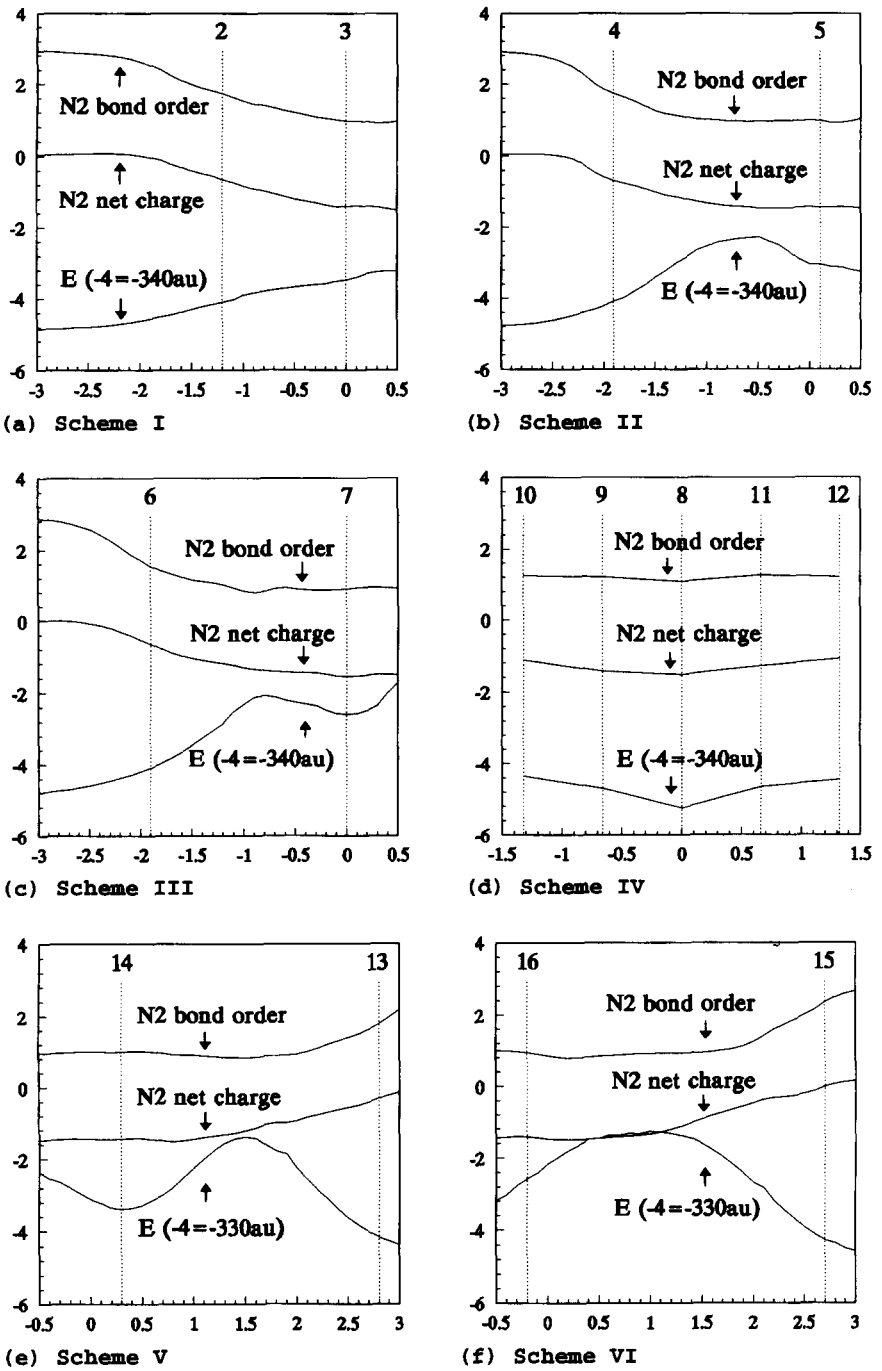


Fig. 1. Variation of the N—N bond order, the net charge on dinitrogen, and the relative value of the total energy (in au), during the process of dinitrogen approaching and binding to the FeMoco according to the six schemes. The dotted lines indicate the positions of possible binding modes.

in Fig. 1(c). In addition, there are not enough spaces in the five modes for the protonation. Therefore, we think that the five modes are not good binding modes.

The fixation of dinitrogen perhaps relates to the release of a bridging sulfur atom. One reason for this suggestion is that the release of the bridging sulfur provides a Fe_2 gap to grasp dinitrogen. Figure 1(e) shows the process (i.e., Scheme V) that dinitrogen in side-on fashion approaches to the gap and enters the cavity. The dotted line at the point $x = 2.8$ of the horizontal axis, expresses mode **13** where the N—N bond order is about 1.8 and the net charge is -0.3. Figure 1(f) expresses a similar process (i.e., Scheme **VI**), in which dinitrogen is in the end-on fashion. The dotted line indicates mode **15,** where the N—N bond order is about 2.4 and the net charge is almost zero.

Both Scheme V and **VI** encounter a high barrier which inhibits the entry of dinitrogen into the cavity. The two central modes **14** and **16** indeed may be regarded the derivatives of modes **5** and **3**, respectively, when losing a bridging sulfur.

In both modes **13** and **15**, the interactions between metal atoms and dinitrogen are not strong. Therefore, the dinitrogen in both mode **13** and mode **15** will be easily replaced by a stronger substrate such as C_2H_4. However, C_2H_4 cannot affect the dinitrogen reduction at the FeMoco site [31]. This evidence suggests that dinitrogen binding prefers a stronger binding mode such as the dinitrogen-inserting mode **3** or the central modes. Therefore, modes **13** and **15** are not good binding modes. Certainly, there are some other possible binding modes, such as that one of dinitrogen bridging over the Fe_2 gap in the vertical side-on fashion. These binding modes including one-metal-center modes, however, cannot sufficiently activate dinitrogen, and are disregarded here.

Table 2 lists the calculated results of typical binding modes. It can be seen that the N—N bond orders in mode **3** and the center-site modes **5, 8, 14** and **16,** are smaller than those in face-site modes **4** and **6,** and also smaller than those in bridging-site modes **13** and **15**. However, the barrier for forming each central binding mode is high, but smooth for mode **3**. This means that dinitrogen can insert in or/and enters into the cavity only through the Fe_4 window and only in the end-on fashion. Therefore, we suggest that mode **3** could best express dinitrogen binding. Other central modes such as **5, 14,** and **16** may be regarded as derivatives of mode **3**.

The six schemes expressed in Fig. 1 correlate to the $S = 3/2$ spin state of the semi-reduced FeMoco. However, the characteristic $S = 3/2$ EPR signal will be lost when one electron transferred from the Fe-protein to the MoFe-protein ends up on the FeMoco [24,32]. There are two distinct viewpoints [23] about which state dinitrogen should bind to. One is that N_2 and possibly other substrates can only bind after the MoFe protein has been reduced by more than one electron. The other is that substrates should bind to the $S = 3/2$ state of isolated FeMoco. To check if mode **3** is or not still the preferable binding mode in each state of the FeMoco, we have calculated eight sets of figures each involving six schemes. The eight cases correlate to four redox states, i.e. the original semi-reduced state and its three reduced states by one, two and three electrons, respectively, while each redox state may have two spin states. We make laborious calculations in order to remedy the defect of the CNDO method when treating systems with significant spin problems. There are some differences between the results of calculations of the eight cases. For example, the total energy decreases with the reduction of the FeMoco. However, comprehensive analysis of the four criteria described above for a rational binding mode, still suggests that mode **3** is the best candidate. Furthermore, to investigate the effect of the variation of interatomic distances, we have also performed the same calculation jobs on larger FeMoco skeletons with larger interatomic distances. Although some significant changes are encountered with the total energy, the net charge and the N—N bond order for individual binding mode, mode **3** still is preferable to other modes.

In conclusion, mode **3** is the best dinitrogen binding mode. As a derivative of mode **3,** mode **5** is a possible mode, in which the lengthened N—N bond allows two nitrogen atoms located at sites just out of the centers of two Fe_4 faces respectively. This arrangement of nitrogen atoms retains larger space for protonation. In addition, mode **4** is also possible because the two nitrogen atoms can easily grasp protons transferred by bridging sulfur atoms, as pointed out by Dance [18]. Certainly, the activation of dinitrogen in mode **4** is not sufficient as in modes **3** and **5**.

Table 2. The net charge and the Wiberg bond order of dinitrogen binding to the FeMoco in typical binding modes

Mode	Net charge on N_2	N—N bond order
2	−0.6	1.7
3	−1.4	1.0
4	−0.7	1.6
5	−1.4	1.0
6	−0.7	1.5
8	−1.5	1.1
9	−1.4	1.2
10	−1.1	1.3
11	−1.3	1.3
12	−1.1	1.2
13	−0.3	1.8
14	−1.4	1.0
15	0.0	2.4
16	−1.4	1.0

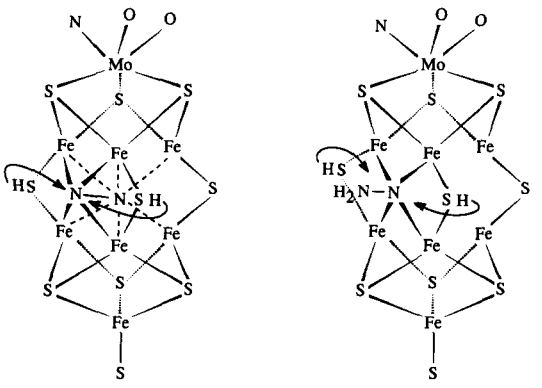
MECHANISM FOR THE PROTONATION OF DINITROGEN

Dinitrogen reduction at the FeMoco site mainly consists of two processes. One is the binding of dinitrogen and the transfer of electrons. The other is the transfer of protons and the release of product NH_3. Certainly, the two processes could be fulfilled in a parallel manner. This suggests that electrons could be transferred both before the transfer of protons and during the protonation of dinitrogen. In the first process, dinitrogen approaches and binds to the FeMoco, meanwhile charge is transferred from the metal centers of the FeMoco to dinitrogen, and dinitrogen is activated with the significant weakening of the N—N bond. Based on the calculations provided in the previous sections, we have determined the best dinitrogen binding mode, i.e., mode **3**. To check the transfer of electrons, let us cut the FeMoco model into

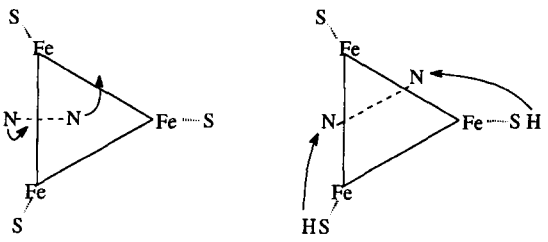
three parts, i.e., the $MoFe_3S_3$ cluster including ligands on Mo atom, three bridging sulfur atoms, and the Fe_4S_3 cluster including the ligand on the anchor Fe atom. The distribution of the charge in mode **3** is, -1.4 on dinitrogen, 1.6 on the $MoFe_3S_3$ cluster, -1.2 on three bridging S atoms and 1.0 on the Fe_4S_3 cluster. This result makes clear the transfer of charge from the metal centers of the FeMoco to dinitrogen. In the second process, protons are transferred from surrounding proteins to dinitrogen, possibly through the bridging sulfur atoms which have hydrogen-bond interaction with surrounding residues. Dance [18] has analyzed the details of proton transfer *via* the wing sulfurs, and proposed a mechanism for the protonation of dinitrogen binding to the Fe_4 face as in mode **4**. Here, we propose two alternative mechanisms for the protonation of dinitrogen at the FeMoco site, based upon the just selected dinitrogen binding mode **3**.

One mechanism for the protonation of dinitrogen is shown in Scheme **VII** which contains two steps. The first step (see **17**) is the transfer of protons from the bridging sulfur atoms to the nitrogen atom exposed out of the Fe_4 surface. Then the nitrogen atom which has caught two protons, will try to go away from the Fe_4 face both for weakening of N—Fe interactions by formation of N—H bonds and for the tension of the bent hydrogen bond N—H···S. Sequentially, the moving of the outer nitrogen atom could bring the inner nitrogen atom to exit the 4Fe window, because there still exists a weak interaction between two nitrogen atoms although the adding of two protons has further decreased the N—N bond order (but the N—N bond order still keeps a smaller value near 0.7). Thus, this process reaches an intermediate state (see mode **18**), in which H_2N—N is in the end-on fashion to binding the Fe_4 face. The bridging sulfur atoms which have just passed two protons to the outer nitrogen atom, will flap toward the surrounding residue (e.g. Arg-96 according to Ree's structure [1–3,18] to grasp other protons, and continuously transfer them to nitrogen atoms. The second step of the protonation of dinitrogen, is the adding of other protons to H_2N—N, probably in two ways. One way is from [H_2N—N : (Fe_4 face)] to [H_3N+HN : (Fe_4 face)] and finally to [$2NH_3$ + FeMoco]. Another way is from [H_2N—N : (Fe_4 face)] to [H_2N—H_2N···(Fe_4 face)] and finally to [$2NH_3$ + FeMoco]. It can be noted that in the second way the intermediate H_2NNH_2 could release. However, H_2NNH_2 has not been experimentally observed in nitrogenase yet. Therefore, the first way seems more plausible.

Another possible mechanism for the protonation of dinitrogen is shown in Scheme **VIII**. As previously discussed, mode **5** can be derived from mode **3** when dinitrogen rotates an angle of about 30°. This transformation is shown as **19** which is the bird's-eye view of the FeMoco in mode **3**, but only keeping the top Fe_3 triangle and three bridging sulfurs for the sake of clarity. This rotation is feasible in energy when the



Scheme VII



Scheme VIII

N—N bond length slightly increases. After this rotation, each nitrogen atom is located almost at the center of a Fe_4 face, see **20**. Then the bridging sulfurs repeatedly transfer protons to dinitrogen until two NH_3 form and release.

Acknowledgements—This work was supported by the CP-NKPFR of China. S.-J.Z. would like to thank Mr Chun-Xi Zhang of Fujian Institute of Research on the Structures of Matter and Dr Jing-Wei Huang of Xiamen University, for helpful discussions and suggestions.

REFERENCES

1. J. Kim and D. C. Rees, *Science* 1992, **257,** 1677; *Nature* 1992, **369,** 553.
2. J. Kim, D. Woo and D. C. Rees, *Biochemistry* 1993, **32,** 7104.
3. M. K. Chan, J. Kim and D. C. Rees, *Science* 1993, **260,** 792.
4. (a) J. T. Bolin, A. E. Ronce, T. V. Morgan, L. E. Mortenson and N. H. Xuong, *Proc. Natl Acad. Sci. U.S.A.* 1993, **90,** 1078; (b) J. T. Bolin, N. Campobasso, S. W. Muchmore, W. Minor, T. V. Morgan and L. E. Mortenson, in *New Horizons in Nitrogen Fixation* (Edited by R. Palacios, J. Mora and W. Newton) pp. 89–94. Kluwer Academic Publishers (1993).

5. J. Chen, J. Christiansen, R. C. Tittsworth, B. J. Hales, S. J. George, D. Coucouvanis and S. P. Cramer, *J. Am. Chem. Soc.* 1993, **115,** 5509.
6. H. I. Liu, A. Filipponi, N. Gavini, B. K. Burgess, B. Hedman, A. De Cicco, C. R. Natoli and K. O. Hodgson, *J. Am. Chem. Soc.* 1994, **116,** 2418.
7. M. R. Antonio, B. K. Teo, W. H. Orme-Johnson, M. J. Nelson, S. E. Groh, P. A. Lindahl, S. M. Kawzlarich and B. A. Averill, *J. Am. Chem. Soc.* 1982, **104,** 4703.
8. S. D. Conradson, B. K. Burgess, W. E. Newton, L. E. Mortenson and K. O. Hodgson, *J. Am. Chem. Soc.* 1987, **109,** 7507.
9. J. M. Arber, A. C. Flood, C. D. Garner, C. A. Gormal, S. S. Hasnain and B. E. Smith, *Biochem. J.* 1988, **252,** 421.
10. S. P. Cramer, Biochemical Applications of X-ray Absorption Spectroscopy in *Extended X-ray Absorption Fine Structure* (Edited by D. Konigsberger and R. Prins) pp. 257–320. Plenum, New York (1988).
11. V. K. Shsh and W. J. Brill, *Proc. Natl Acad. Sci. U.S.A.* 1977, **74,** 3249.
12. T. R. Hawkes, P. A. McLean and B. E. Smith, *Biochem. J.* 1984, **217,** 317.
13. D. J. Scott, H. D. May, W. E. Newton, K. E. Brigle and D. R. Dean, *Nature* 1990, **343,** 188.
14. P. Peliken and R. Boca, *Coord. Chem. Rev.* 1984, **55,** 55.
15. H. Deng and R. Hoffmann, *Angew. Chem. Int. Ed. Engl.* 1993, **32,** 1062.
16. W. Plass, *J. Mol. Struct. (THEOCHEM)* 1994, **315,** 53.
17. A. F. Shestakov, *10th International Congress on Nitrogen Fixation*, Saint-Petersburg, Russia, 28 May–3 June, 1995, p. 6.
18. I. G. Dance, *Aust. J. Chem.* 1994, **47,** 979.
19. F. B. C. Machado and E. R. Davidson, *Theor. Chim. Acta* 1995, **92,** 315.
20. K. Stavrev and M. Zerner, *Int. J. Quant. Chem., Quant. Biol. Symp.* 1995, **22,** 155.
21. B. K. Burgess, *Chem. Rev.* 1990, **90,** 1377.
22. L. Ma, N. Gavini, H. I. Liu, B. Hedman, K. O. Hodgson and B. K. Burgess, *J. Biol. Chem.* 1994, **269,** 18007.
23. D. Sellman, *Angew. Chem. Int. Ed. Engl.* 1993, **32,** 64.
24. M. E. Winfield, *Rev. Pure Appl. Chem. (Australia)* 1964, **156,** 1102.
25. M. Jimeniz-Tenorio and G. J. Leigh, *J. Am. Chem. Soc.* 1991, **113,** 5662.
26. G. J. Leigh, *New J. Chem.* 1994, **18,** 157.
27. W. H. Orme-Johnson, *Science* 1992, **257,** 1639.
28. (a) G. Segal and J. A. Pople, *J. Chem. Phys.* 1966, **46,** 3289; (b) J. A. Pople and D. L. Beveridge, *Approximate Molecular Orbital Theory*. McGraw-Hill (1970).
29. M. J. Frisch, A. E. Frisch and J. B. Foresman, *Gaussian 94 User's Reference*, pp. 51–52. Gaussian, Inc., Pittsburgh (1995).
30. W. H. Orme-Johnson, in *Molybdenum Enzymes, Cofactors and Models* (Edited by E. I. Stiefel, D. Coucouvanis and W. E. Newton) pp. 257–270. American Chemistry Society, Washington D.C. (1993).
31. J.-W. Huang, H.-T. Zhang, R. Yang, M.-Y. Zhou, H.-L. Wan and Q.-R. Cai, *Gaodeng Xuexiao Huaxue Xuebao (Chem. J. Chinese Univ.)*, 1995, **16,** 920.
32. R. N. F. Thorneley, G. A Ashby, K. Fisher and D. J. Lowe, in *Molybdenum Enzymes, Cofactors and Models* (Edited by E. I. Stiefel, D. Coucouvanis and W. E. Newton) pp. 290–302. American Chemistry Society, Washington D.C. (1993).

Pergamon

PII: S0277-5387(96)00305-1

Polyhedron Vol. 16, No. 4, pp. 663–670, 1997
Copyright © 1996 Elsevier Science Ltd
Printed in Great Britain. All rights reserved
0277-5387/97 $17.00+0.00

Bimetallic alkoxides of aluminium-hafnium and aluminium-zirconium. X-ray structure of $Al_2Hf(OPr^i)_{10}$

E. P. Turevskaya,[a] D. V. Berdyev,[a] N. Ya. Turova,[a]* Z. A. Starikova,[b] A. I. Yanovsky,[b] Yu. T. Struchkov† and A. I. Belokon[b]

[a]M. V. Lomonosov Moscow State University, Department of Chemistry, 119899 Moscow, Russia

[b]A. N. Nesmeyanov Institute of Organoelement Compounds, Russian Academy of Science, 117813 Moscow, Russia

(Received 20 March 1996; accepted 18 June 1996)

Abstract—The solubility studies in the $Al(OR)_3$-$M(OR)_4 \cdot ROH$-ROH (R = Pr^i) systems at 20°C revealed the existence of the only complex, $Al_2M(OR)_{10}$, [M = Hf(**I**), Zr(**II**)]. The literature data on the existence of the $AlM(OR)_7$ species were disproved. According to the results of the single crystal X-ray diffraction study of **I**, its molecule has a two-fold symmetry axis and involves two peripheral tetrahedrally coordinated Al atoms, each of their coordination tetrahedra sharing one common edge with the coordination octahedron of the central Hf atom, $[(RO)_2Al(\mu\text{-}OR)_2]_2Hf(OR)_2$. The mean planes of almost planar $[AlO_2Hf]$ cycles form the dihedral angle of 82° with each other. Mass-spectra of **I** and **II** show two fragmentation pathways, *viz.*: (1) the elimination of the ether molecule accompanied by the formation of oxo groups, and (2) the $Al(OR)_3$ molecule abstraction producing the $AlM(OR)_6^+$ ions. According to the X-ray powder diffraction data crystals of **I** and **II** are isostructural. The influence of the oligomeric Zr and Hf oxoalkoxides, formed as a result of partial thermolysis of $M(OR)_4 \cdot ROH$, on the processes of formation of complexes with $Al(OR)_3$ has been elucidated. The non-crystalline solid $Al_2Hf(OEt)_{10}$ was isolated from ethanol solution, its mass-spectral fragmentation being analogous to that of **I** and **II**. Copyright © 1996 Elsevier Science Ltd

Keywords: aluminium alkoxozirconates; -hafnates; single-crystal X-ray diffraction; mass-spectral study; physico-chemical analysis.

The alkoxy-derived Al_2O_3 and MO_2 (M = Zr, Hf) based materials find extensive applications in the production of optical, refractory materials and solid electrolytes. The existence of aluminium alkoxozirconates and alkoxohafnates of two compositions, $Al_2M(OR)_{10}$ and $[AlM(OR)_7]_2$ ‡ has been reported in the earlier literature [1–4]. Later on the physico-chemical analysis of the $Al(OR)_3$-$Zr(OR)_4 \cdot ROH$-ROH system led to the conclusion, that in this system only one complex, *viz.*, $AlZr(OR)_7$, actually exists [5].

The present paper reports the results of the studies of composition of aluminium alkoxohafnates and alkoxozirconates by means of physico-chemical analysis, single crystal X-ray diffraction, and mass spectrometry.

EXPERIMENTAL

Drying of ROH (R = Pr^i, Et) was carried out by the prolonged refluxing over crystalline $Al(OPr^i)_3$ or $Ca(OEt)_2$ respectively and subsequent distillation. $Al(OR)_3$ (R = Pr^i, Et) was prepared by reaction of the metal with absolute ROH, complexes $M(OR)_4 \cdot ROH$ (M = Zr, Hf; R = Pr^i) and $Hf(OEt)_4$ were synthesized by anodic oxidation of the metal in the alcohol in the presence of LiCl [6].

Zr and Hf in the presence of Al were determined by complexonometric titration in acidic medium (pH = 1–2) using xylenol orange for indication (the solution colour changed from pink to yellow). The

* Author to whom correspondence should be addressed.
† Deceased, 16 August 1995.
‡ In this case and further on in the text R = Pr^i.

Al content was calculated from the difference after determination of the sum of all oxides, obtained after calcination of the solutions or solid phases at 800°C.

Synthesis of aluminium alkoxohafnate and -zirconate

Reactions were carried out by 1–2 h refluxing of the mixture of the solutions of crystalline $Al(OR)_3$ and $Hf(OR)_4 \cdot ROH$ in ROH taken in the ratio of 2:1. The concentration of the initial solutions after complete dissolution of the components amounted to 8–10% with respect to the sum of both alkoxides. It is noteworthy that simple cooling of the hot initial solutions containing both alkoxides without the refluxing resulted in the crystallization of the starting material $Hf(OR)_4 \cdot ROH$ solvate. The precipitation of a fine crystalline sample of $Al_2Hf(OR)_{10}$ (**I**) from reaction solutions obtained after partial removal of the solvent (up to the concentration of 40–50%) begins after about 3 days. After complete evaporation of the solvent the yellowish liquids are formed which become solid after standing for about a month. The recrystallization of the fine powder of **I** from the alcohol produced the single crystals suitable for X-ray diffraction study (yield ~50%). Found: Al 6.5; Hf 21.1; C 43.3; H 8.5. Calc. for $Al_2Hf(OR)_{10}$: Al 6.6; Hf 21.7; C 43.8; H 8.5%.

It should be also mentioned that large crystals of **I** were isolated along with the fine crystalline powder of $Hf(OR)_4 \cdot ROH$ (according to the X-ray powder diffraction data) from the reaction mixture in those cases, where the starting solutions were taken in Al:Hf = 1:1 ratio. Crystals of **I** melt at 57–62°C.

When carrying out the synthesis of alkoxozirconate of the 2:1 composition under the conditions described above for the synthesis of **I**, the crystallization of the fine crystalline powder from the 40–50% solutions was observed only after 7–10 days (yield ~30%). Found: Al 7.5; Zr 12.5; C 48.4; H 9.5. Calc. for $Al_2Zr(OR)_{10}$: Al 7.3; Zr 12.4; C 48.9; H 9.5%.

Attempts to use the solutions with higher concentrations has led to the solidification of the entire reaction mixture and no crystalline phase could be isolated. Further efforts to obtain the bimetallic complex by recrystallization of the solidified mass yielded only the well-formed crystalline product, which, according to the X-ray powder diffraction data, represented $Al(OR)_3$.

In order to determine the composition of zirconium and hafnium isopropoxides after their refluxing in isopropanol, the special experiments were carried out. Thus, after refluxing of the 6% solution of $Zr(OR)_4 \cdot ROH$ in ROH for 1 h the crystallization of monosolvate was observed, and the concentration of the mother liquor proved to be significantly higher than the equilibrium values for 20°C (3.3% $Zr(OR)_4$ rather than 1.7% [6]). The refluxing of 3–4% solution is accompanied by even more profound destruction, so that the concentration of the mother liquor over the 1:1 sample turns out to be as high as 10% (after evaporation of the solvent *in vacuo*). The melting of these samples occurs in a rather wide temperature range of 100–128°C (according to [6] m.p. of $Zr(OR)_4 \cdot ROH$ is equal to 138–141°C). The results are analogous to those observed for the desolvation of Zr and Hf isopropoxides, which occurs at higher temperatures and results in the formation of $M_3O(OR)_{10}$ and $Zr_4O(OR)_{14}$ oxoisopropoxides [6].

The reaction of "$Hf(OEt)_4$" with $Al(OEt)_3$ was carried out under the same conditions as the synthesis of complexes **I** and **II**. A few crystals of hafnium ethoxoaluminate (**III**) were in some cases precipitated from the viscous solution obtained by evaporation of the solvent from reaction mixture *in vacuo*. Found: Al 7.3; Hf 25.9; C 35.7; H 7.6. Calc. for $Al_2Hf(OEt)_{10}$: Al 7.9; Hf 26.1; C 35.2; H 7.3%.

Study of the solubility diagrams

The solubility in the $Al(OR)_3$-$M(OR)_4 \cdot ROH$-ROH systems were studied by the analytical method at 20°C. Solubilities of **I** and **II** were determined by saturation of alcohol with the corresponding crystalline complexes. The euthonics were obtained after agitation of alcohol with two solid phases: $Al(OPr^i)_3$ and **I** (or **II**) and $M(OPr^i)_4 \cdot Pr^iOH$ with **I** (or **II**), respectively.

In each of the binary systems, $M(OR)_4 \cdot ROH$-ROH (M = Hf, Zr), there exists the only solid phase, *viz.* monosolvate, which shows rather low solubility (1.9% and 1.5% for M = Hf and Zr, respectively) [6]. The solubility of $Al(OR)_3$ (with m.p. of 140°C) in the alcohol is equal to 4.3% at 20°C [7]. Figure 1 shows that **I** and **II** are congruently soluble and may be crystallized from a sufficiently broad region on both sides of the 2:1 section. It has already been mentioned that **I** also precipitates from the solutions with 1:1 component ratio. It should be particularly emphasized that in many cases in these systems supersaturated solutions are formed, which have concentrations significantly higher than those corresponding to the equilibrium values and yet do not yield the crystalline phase even after standing for several days.

The crystallization region of **II** is sufficiently large. The solubility values are substantially higher than those reported in [5] (Tables 1 and 2).

X-ray diffraction study

$C_{30}H_{70}Al_2HfO_{10}$, M = 823.31, monoclinic, space group $C2/c$, at 293° $a = 23.311(5)$, $b = 11.176(2)$, $c = 17.372(4)$ Å, $\beta = 104.94(3)°$, $V = 4373(2)$ Å^3, $Z = 4$, $D_c = 1.251$ g cm^{-3}, $D_{exp} = 1.249$ g cm^{-3}. X-ray diffraction experiment was carried out with a Siemens P3/PC diffractometer ($T = 293$ K, graphite-monochromated Mo-$K\alpha$ radiation, $\lambda = 0.71073$ Å $\theta/2\theta$ scan technique, no absorption correction was applied, μ(Mo-Kα) = 24.67 cm^{-1}, $\theta = 2$–29°). The structure

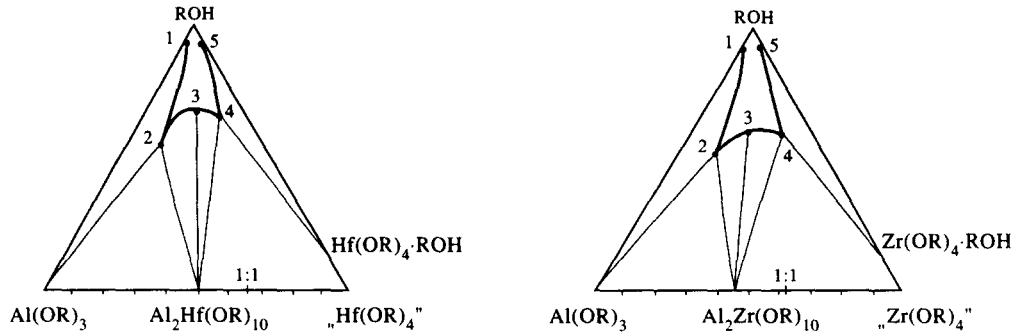


Fig. 1. Solubility in the $Al(OR)_3$-$M(OR)_4 \cdot ROH$-ROH systems at 20°C (mass. %).

was solved by direct methods and refined by the full-matrix least-squares technique in the anisotropic approximation. All H atoms were placed in geometrically calculated positions and included in the refinement using the riding model approximation with the $U_{iso}(H) = 1.2U_{eq}(C)$ for the methyne and $U_{iso}(H) = 1.5U_{eq}(C)$ for methyl groups, where the $U_{eq}(C)$ is the equivalent isotropic temperature factor of the carbon atom bonded to the corresponding H atom. Final discrepancy factors are: $R1 = 0.0500$ (on F for 4057 reflections with $I > 2\sigma(I)$), $wR2 = 0.1458$ (on F^2 for all 5810 reflections used in the refinement of 195 parameters). All calculations were carried out on IBM PC with the help of SHELXTL PLUS 5 (gamma version) program. Atomic coordinates are available from the Cambridge Crystallographic Data Centre, 12 Union Road, Cambridge CB2 1EZ, U.K.

Mass-spectra were measured using an AEI MS-30 mass-spectrometer, the temperature of the injected sample was 150°C, ionization potential was 70 eV, the masses of the ions involving the ^{180}Hf, ^{90}Zr and ^{12}C isotopes are listed.

RESULTS AND DISCUSSION

It is noteworthy that the mere simultaneous presence of two alkoxides in the solution does not provide sufficient condition for their chemical interaction. Complex formation actually occurs only in the course of the prolonged refluxing of the solutions. It was established that this process, as well as the desolvation of $[M(OR)_4(ROH)]_2$ in the absence of the solvent [6], is accompanied by the partial thermolysis of the components.

One may suggest that it is actually the presence of the oxo group in Zr and Hf alkoxides, which makes possible the formation of bimetallic isopropoxide complexes. We have already come across the similar phenomena earlier, when studying the chemistry of

Table 1. Solubility in the $Al(OR)_3$-$Hf(OR)_4 \cdot ROH$-ROH system at 20°C

Number of the point	The composition of solution (mass %) $Al(OR)_3$	$Hf(OR)_4$	Solid phase
1	4.3	—	$Al(OR)_3$
2	36.2	11.5	$Al(OR)_3 + Al_2Hf(OR)_{10}$
3	15.5	15.8	$Al_2Hf(OR)_{10}$
4	8.9	24.8	$Al_2Hf(OR)_{10} + Hf(OR)_4 \cdot ROH$
5	—	1.9	$Hf(OR)_4 \cdot ROH$

Table 2. Solubility in the system $Al(OR)_3$-$Zr(OR)_4 \cdot ROH$-ROH at 20°C

Number of the point	The composition of solution (mass %) $Al(OR)_3$	$Zr(OR)_4$	Solid phase
1	4.3	—	$Al(OR)_3$
2	34.6	12.5	$Al(OR)_3 + Al_2Zr(OR)_{10}$
3	21.1	16.9	$Al_2Zr(OR)_{10}$
4	8.6	31.1	$Al_2Zr(OR)_{10} + Zr(OR)_4 \cdot ROH$
5	—	1.5	$Zr(OR)_4 \cdot ROH$

polymeric $M(OR)_2$ (M = Co, Ni, Cr, Fe). These alkoxides react with Al, Nb and other alkoxide species only in the presence of traces of water, i.e. only after oxo groups are introduced into the coordination sphere of metal atom [8,9]. Another process, which is known to be a source of oxo groups in alkoxide molecules, thus promoting the formation of complexes, is the oxidation by traces of oxygen, occurring, for instance, for alkaline and alkaline-earth alkoxides. Such oxidation process is especially well documented in case of the reaction between Ba and Ti alkoxides [10].

The present work provides additional evidence for the role of the presence of the traces of oxo groups in the process of complex formation. It does not exclude, however, the possibility of crystallization of bimetallic alkoxides, without oxo groups from such solutions. Along with the complexes **I** and **II** we have observed the crystallization of such complexes in the course of the synthesis of $LaNb_2(OR)_{13}\cdot 2ROH$ [8] and $Ba_2Zr(OR)_8\cdot 5ROH$ [11]. The yields in all cases were far from being quantitative, as the mother liquors in both cases were known to contain oxo groups, either within the $La_5O(OR)_{13}$ component (in case of the lanthanum–niobium system) or as a result of $Ba(OR)_2$ oxidation (in case of barium–zirconium complex). The composition of the bimetallic complexes, which are formed eventually, *viz.*, the presence or absence of the oxo groups in such complexes, is determined in each particular case by the energy of crystal lattice. Therefore, on carrying out the synthesis of bimetallic alkoxides, one should pay special attention to the possibly full separation of the crystalline phase from the mother liquors, as the oxo complexes are frequently accumulated in one of the phases. Otherwise, it may well happen that it would be impossible to have definite data on the individual character and composition of bimetallic complexes. Thus, the difficulties with crystallization of complexes **II** and its incomplete separation from the liquid phase resulted in incorrect determination of its composition as 1:1 [5].

The single-crystal X-ray diffraction study has shown that the crystal of **I** is built of trinuclear molecules (Fig. 2, Table 3) which have the structure, first suggested by Mehrotra [3]. The molecule occupies a special position on the two-fold axis, which passes through the Hf atom and involves the central coordination octahedron $[Hf(OR)_6]$ sharing common edges with each of the two peripheral coordination tetrahedra $[Al(OR)_4]$. The metal–oxygen core of the complex **I** is analogous to that of the trinuclear aluminium isopropoxochloride derivative, $Al_3Cl_5(OPr^i)_4$ [12] (the latter is believed to be structurally related to trimeric aluminium isopropoxide, $[Al(OPr^i)_3]_3$), the only difference being the higher coordination number of the central atom in case of six-coordinated Hf rather than five-coordinated aluminium. Molecule **I** also shows some structural similarity with tetranuclear alkoxides $[Al(OPr^i)_3]_4$ [13, 14] and

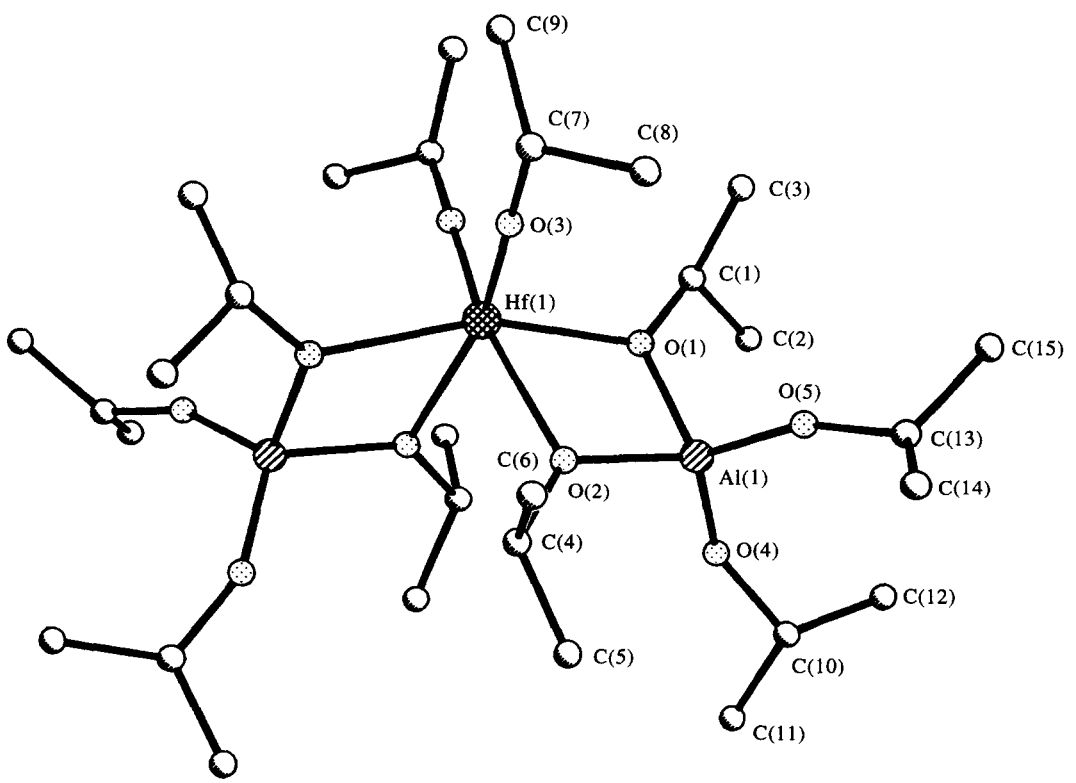


Fig. 2. Molecular structure of $Al_2Hf(OPr^i)_{10}$ (**I**).

Table 3. Bond lengths (Å) and angles (°) in **I**

Hf(1)—O(3)	1.913(4)	O(5)—C(13)	1.288(12)
Hf(1)—O(1)	2.140(4)	C(1)—C(2)	1.40(2)
Hf(1)—O(2)	2.213(3)	C(1)—C(3)	1.425(14)
Hf(1)—Al(1)	3.125(2)	C(4)—C(5)	1.434(12)
Al(1)—O(5)	1.667(6)	C(4)—C(6)	1.491(12)
Al(1)—O(4)	1.689(5)	C(7)—C(9)	1.37(2)
Al(1)—O(2)	1.787(4)	C(7)—C(8)	1.43(2)
Al(1)—O(1)	1.803(5)	C(10)—C(11)	1.47(2)
O(1)—C(1)	1.454(8)	C(10)—C(12)	1.481(14)
O(2)—C(4)	1.450(6)	C(13)—C(15)	1.40(2)
O(3)—C(7)	1.377(9)	C(13)—C(14)	1.45(2)
O(4)—C(10)	1.379(9)		

O(3)—Hf(1)—O(3A)	100.8(3)	Al(1)—O(2)—Hf(1)	102.2(2)
O(3)—Hf(1)—O(1)	100.7(2)	C(7)—O(3)—Hf(1)	177.4(7)
O(3A)—Hf(1)—O(1)	92.4(2)	C(10)—O(4)—Al(1)	138.5(6)
O(1)—Hf(1)—O(1A)	159.4(2)	C(13)—O(5)—Al(1)	160.9(12)
O(3)—Hf(1)—O(2)	92.1(2)	C(2)—C(1)—C(3)	120.0(12)
O(3A)—Hf(1)—O(2)	158.3(2)	C(2)—C(1)—O(1)	112.2(8)
O(1)—Hf(1)—O(2)	67.9(2)	C(3)—C(1)—O(1)	111.0(8)
O(1A)—Hf(1)—O(2)	96.1(2)	C(5)—C(4)—O(2)	111.3(6)
O(2)—Hf(1)—O(2A)	81.5(2)	C(5)—C(4)—C(6)	113.8(9)
O(5)—Al(1)—O(4)	118.7(4)	O(2)—C(4)—C(6)	108.5(6)
O(5)—Al(1)—O(2)	112.2(3)	C(9)—C(7)—O(3)	115.0(12)
O(4)—Al(1)—O(2)	114.3(2)	C(9)—C(7)—C(8)	117.0(12)
O(5)—Al(1)—O(1)	112.4(4)	O(3)—C(7)—C(8)	113.5(10)
O(4)—Al(1)—O(1)	109.1(2)	O(4)—C(10)—C(11)	112.7(9)
O(2)—Al(1)—O(1)	85.3(2)	O(4)—C(10)—C(12)	113.3(9)
C(1)—O(1)—Al(1)	128.7(5)	C(11)—C(10)—C(12)	114.2(11)
C(1)—O(1)—Hf(1)	126.3(5)	O(5)—C(13)—C(15)	120(2)
Al(1)—O(1)—Hf(1)	104.5(2)	O(5)—C(13)—C(14)	119.5(12)
C(4)—O(2)—Al(1)	129.8(4)	C(15)—C(13)—C(14)	115.9(12)
C(4)—O(2)—Hf(1)	127.9(4)		

Atoms labelled by letter A are generated from the reference atoms by the $-x, y, -z+1/2$ symmetry transformation.

$Er[Al(OR)_4]_3$ [15], which, in contrast to **I**, involve three, rather than two, peripheral $[Al(OR)_4]$ groups. Although compound **I** has two *cis*-terminal OR groups at the central Hf atom instead of the third four-membered cycle, two $[HfO_2Al]$ cycles, which are present in the structure are geometrically close to those observed in the tetranuclear complexes. In particular the mean planes of two almost planar $[HfO_2Al]$ cycles in **I** form the dihedral angle of 82° with each other, which is quite close to values of the corresponding dihedral angles in the structure of $[Al(OR)_3]_4$.

The angular distortions of the Hf coordination octahedron and the Al tetrahedra are naturally due to the formation of the four-membered rings and are manifested in the significant decrease of the endocyclic bond angles [O(1)—Hf(1)—O(2), 67.9(2)° and O(1)—Al(1)—O(2), 83.5(2)°] and the simultaneous increase of most of those bond angles which are not involved in any cycles [O(1)—Hf(1)—O(3), 100.7(2); O(1)—Hf(1)—O(3A), 92.4(2); O(3)—Hf(1)—O(3A), 100.8(3)° and O(1)—Al(1)—O(4), 109.1(2); O(1)—Al(1)—O(5), 112.4(4); O(2)—Al(1)—O(4), 114.3(2); O(2)—Al(1)—O(5), 112.2(3), O(4)—Al(1)—O(5), 118.7(4)°]. The bridging as well as the terminal Hf—O bond lengths in **I** [Hf(1)—O(1) 2.140(4), Hf(1)—O(2) 2.213(3) Å and Hf(1)—O(3) 1.913(4) Å] do not differ from the distances observed for the corresponding Zr(Hf)—OR bonds in the $[M(OR)_4(ROH)]_2$ solvates [16]. The increased bond order of the terminal Hf—O bonds is reflected in the widening of the corresponding HfOC bond angles, which is even more pronounced in complex **I** [Hf(1)—O(3)—C(7) 177.4(7)°] than in the $Hf(OR)_4 \cdot ROH$ structure, wherein the relevant HfOC angles span the range of 167.3–177.6°. The regular increase of the O—C bond lengths and simultaneous decrease of the HfÔC bond angles are observed in molecule **I** on going from terminal [O(3)—C(7) 1.377(9) Å] to bridging OR groups [O(1)—C(1) 1.454(8), O(2)—C(4) 1.450(6) Å, Hf(1)—Ô(1)—C(1) 126.3(5), Hf(1)—Ô(2)—C(4) 127.9(4)°].

Analogous geometrical differences are found in the coordination environment of the Al atoms. The Al—O and C—O bond lengths both terminal [Al(1)—O(4) 1.689(5), O(4)—C(10) 1.379(9) Å and

Table 4. The results of the indexing of X-ray powder diffraction patterns for **I** and **II** (DRON-3M, Co-$K\alpha$) using the cell parameters determined in the single crystal X-ray study of **I**

$Al_2Hf(OR)_{10}$ (I)				$Al_2Zr(OR)_{10}$ (II)	
I	d_{exp}	d_{calc}	hkl	I	d_{exp}
5	10.1	10.01	110	32	10.7
5	9.25	9.07	$\bar{1}10$	20	9.64
100	8.74	8.39	002	100	8.86
40	7.96	8.19	111	85	8.12
				60	7.97
50	7.79	7.76	$\bar{2}02$	30	7.56
10	6.25	6.23	310	15	6.15
14	6.09	6.10	112	10	6.07
15	5.45	5.47	311	—	—
15	5.39	5.36	$\bar{4}02$	—	—
10	5.01	5.00	220	12	5.10
10	4.97	4.95	$\bar{2}21$	—	—
15	4.56	4.56	312	10	4.58
5	4.21	4.20	402	20	4.13
5	4.08	4.10	222	5	3.97
8	3.88	3.88	$\bar{4}04$	30	3.81
20	3.79	3.81	$\bar{5}13$	10	3.76
10	3.55	3.56	131	—	—
5	3.36	3.36	422	—	—
13	3.30	3.30	$\bar{1}15$	10	3.31
5	3.26	3.20	331	7	3.26
10	3.14	3.13	$\bar{1}33$	12	3.13

Al(1)—O(5) 1.667(6), O(5)—C(13) 1.288(12) Å*] and bridging [Al(1)—O(1) 1.803(5) and Al(1)—O(2) 1.787(4) Å], as well as the terminal and bridging AlOC bond angles [Al(1)—Ô(4)—C(10) 138.5(6), Al(1)—Ô(5)—C(13) 160.19(12)° and Al(1)—Ô(1)—C(1) 128.7(5), Al(1)—Ô(2)—C(4) 129.8(4)° respectively] are quite close to those observed earlier in the structures of $[Al(OR)_3]_4$ [13] and $Al_3(OR)_4Cl_5$ [12]. The sums of the bond angles at the bridging oxygen atoms are approximately equal to 360°, which indicates that these atoms are evidently sp^2-hybridized.

The results of the indexing of the powder diffraction pattern of **I** and **II** using the unit cell parameters, found in the single-crystal X-ray study of **I** (*vide infra*), are listed in Table 4.

Solubility studies of the $Al(OR)_3$-$M(OR)_4 \cdot ROH$-ROH (M = Hf, Zr) systems at 20°C (Fig. 1, Tables 1 and 2) lead to the conclusion that in each case there exists the only one complex, *viz.* complex $Al_2M(O\text{-}Pr^i)_{10}$ (M = Hf(**I**), Zr(**II**)) with the 2:1 composition. Both complexes are sufficiently stable and crystallize in a broad range of concentrations on both sides of the 2:1 section. According to the mass-spectroscopic data, these complexes are also present in the vapour phase (Fig. 3, Table 5). Mass-spectroscopic study of **I** and **II** shows that the complexes exhibit two main fragmentation pathways on electron impact, *viz.*, (1) the consecutive elimination of OR, R_2O and CH_2 groups; and (2) the abstraction of $Al(OR)_3$ with the formation of $AlM(OR)_7$ and subsequent fragmentation of the latter, proceeding similarly to the decomposition of molecule **I** to **II**.

Table 5. Mass spectra of $Al_2M(OR)_{10}$, M = Hf (**I**) and Zr (**II**)[a]

I		II[5]		
m/Z	I	m/Z	I	Interpretation
765	100	675	100	$Al_2M(OR)_9^+$
664	32	574	87	$Al_2MO(OR)_7^+$
650	10	560	25	$Al_2MO(OR)_6(OEt)^+$
620	7	530	12	$AlM(OR)_7^+$
621	7	531	12	$Al_2MO_2(OR)_6^+$
605	7	515	25	$Al_2MO(OR)_6^+$
561	11	471	100	$AlM(OR)_6^+$
				$Al_2MO_2(OR)_5^+$
547	—	457	—	$AlM(OR)_5(OEt)^+$
518	4.7	428	18	$AlMO(OR)_5^+$
503	4.7	413	18	$Al_2MO_2(OR)_4^+$
502	10	412	18	$AlM(OR)_5^+$
475	5	—	—	$Al_2MO_2(OR)_3(OMe)^+$
459	3.5	369	—	$AlMO(OR)_4^+$
401	2	311	37	$Al_2MO_3(OR)_2^+$

[a]Along with the listed ions in both mass-spectra the ions corresponding to the products of the $[Al(OR)_3]_n$ (n = 3, 4) fragmentation are present: 757 $[Al_4(OR)_{11}^+]$, 553 $[Al_3(OR)_8^+]$, 349 $[Al_2(OR)_5^+]$.

In the X-ray powder diffraction pattern for the samples of "$AlZr(OR)_7$" only those diffraction lines which may be attributed to complex **II** were present; the same is, by the way, true for the hafnium derivatives. It may be, therefore, assumed that the excess of the zirconium alkoxide is found in the sample in the form of amorphous thermolysis product $Zr(OR)_4 \cdot ROH$ [6] (this fact may account for the variations of the solubility values of the samples having the 1:1 composition).

The mass-spectrum of the "$AlZr(OR)_7$" samples, reported earlier [5] may find more natural interpretation in the assumption of the presence of both complex **II** and the $Zr(OR)_4 \cdot ROH$ solvate in these samples. It may, therefore, be concluded that alkoxozirconates and -hafnates of the 1:1 composition do not exist.

The study of the interaction of Al and Hf ethoxides is of particular interest, taking into account, that in this case both components contain oxo groups. Thus, according to the preliminary results of the X-ray diffraction study the $Hf(OEt)_4$ samples contain the $[Hf_3O(OEt)_{10}(EtOH)]_2$ species [18]. The reaction of complex formation with polymer aluminium ethoxide

*The Al—O bond lengths in the almost regular tetrahedron in the structure of $[C_6H_{11}NH_3]^+[Al(OR)_4]^-$ are equal to 1.73–1.76 Å [17].

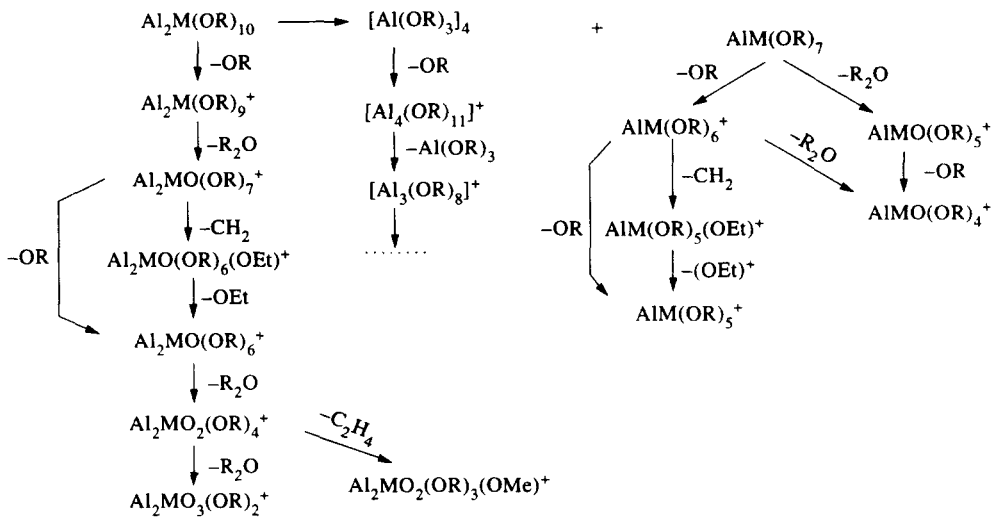


Fig. 3. Fragmentation scheme for complexes $Al_2M(OR)_{10}$ (M = Zr, Hf).

Table 6. Mass spectrum of $Al_2Hf(OEt)_{10}$[a]

m/Z	I	Interpretation
686	17	$Al_2Hf(OEt)_{10}^+$
670	19	$Al_2Hf(OEt)_9(OCH_3)^+$
643	100	$Al_2Hf(OEt)_9^+$
569	20	$Al_2HfO(OEt)_7^+$
521	7	$AlHf(OEt)_7^+$
499	4	$Al_2HfO_2(OEt)_5^+$
477	5	$AlHf(OEt)_6^+$
419	10	$Al_2HfO_3(OEt)_3^+$
403	5	$AlHfO(OEt)_4^+$
345	10	$Al_2HfO_4(OEt)^+$

[a]The ions corresponding to the fragmentation of $[Al(OEt)_3]_n$ (973 $[Al_6(OEt)_{18}^+]$, 779 $[Al_5(OEt)_{14}CH_2^+]$, 691 $[Al_5(OEt)_{12}O^+]$, 529 $[Al_4(OEt)_9O^+]$, 442 $[Al_3(OEt)_8^+]$, 323 $[Al_2(OEt)_6^+]$) and "hafnium ethoxide" ions (956 $[Hf_3O(OEt)_9^+]$, 817 $[Hf_3O_3(OEt)_5^+]$) are also present.

proceeds only after prolonged refluxing with the solution of "$Hf(OEt)_4$" in ethanol, which probably increases the concentration of oxo ligands. Nevertheless, it is possible to isolate from the concentrated solutions (in rather low yields) the crystals of $Al_2Hf(OEt)_{10}$ (**III**). Mass-spectrum of **III**, and that of the foam-like sample, formed after evaporation of the solvent from the 2 : 1 aluminium and hafnium ethoxide solution *in vacuo*, turned out to be identical and their fragmentation scheme (Table 6) was similar to that of **I** and **II**. It means, therefore, that molecules of **III** exist also in the vapour phase, and the ions of the $Al_2HfO_n(OR)_{9-n}^+$ type (n = 1–4) are formed only in the process of the elimination of ether from **III**.

Acknowledgements—The authors are indebted to the Russian Foundation for Basic Research (Project No 94-03-08338) and INTAS (Grant 94-771) for financial support.

REFERENCES

1. R. C. Mehrotra and A. Mehrotra, *Inorg. Chim. Acta Rev.* 1971, 127.
2. D. C. Bradley, R. C. Mehrotra and D. P. Gaur, *Metal Alkoxides*, Academic Press, London (1978).
3. R. C. Mehrotra and J. Singh, *J. Indian Chem. Soc.* 1977, **54**, 109.
4. R. C. Mehrotra and A. Mehrotra, *J. Chem. Soc.* 1972, 1203.
5. N. Ya. Turova, S. I. Kucheiko and N. I. Kozlova, *Soviet J. Coord. Chem.* 1983, **9**, 513 (English).
6. E. P. Turevskaya, N. I. Kozlova, N. Ya. Turova, A. I. Belokon', D. V. Berdyev, V. G. Kessler and Yu. K. Grishin, *Russ. Chem. Bull.* 1995, 734 (English).
7. V. A. Kozunov and N. Ya. Turova, *Russ. J. Inorg. Chem.* 1978, **23**, 680 (English).
8. E. P. Turevskaya, N. Ya. Turova, A. V. Korolev, A. I. Yanovsky and Yu. T. Struchkov, *Polyhedron* 1995, **14**, 1531.
9. T. V. Rogova, N. Ya. Turova and N. I. Kozlova, *Soviet J. Coord. Chem.* 1986, **12**, 440 (English).
10. E. P. Turevskaya, M. I. Yanovskaya, V. K. Limar and N. Ya. Turova, *Russ. J. Inorg. Chem.* 1993, **38**, 563 (English).
11. E. P. Turevskaya, D. V. Berdyev, N. Ya. Turova and I. M. Yanovskaya, *Russ. J. Inorg. Chem.* 1995, **40**, 1527 (English).
12. A. I. Yanovsky, V. A. Kozunov, N. Ya. Turova, N. G. Furmanova and Yu. T. Struchkov, *Doklady Chem. Proc. Acad. Sci. USSR* 1979, **244**, 26 (English).
13. N. Ya. Turova, V. A. Kozunov, A. I. Yanovsky, N. G. Bokiy, Yu. T. Stuchkov and V. L. Tarnopolsky, *J. Inorg. Nucl. Chem.* 1979, **41**, 5.
14. K. Folting, W. E. Streib, K. G. Cauton, O. Poncelet and L. G. Hubert-Pfalzgraf, *Polyhedron* 1991, **10**, 1639.
15. M. Wijk, R. Norrestam, M. Nygren and G. Westin, *Inorg. Chem.* 1996, **35**, 1077.
16. B. A. Vaartstra, J. C. Huffman, P. S. Gradeff, J. C.

Daran, S. Parraud, K. Yunlu and K. G. Caulton, *Inorg. Chem.* 1990, **29,** 3126.
17. B. Beagley, K. Jones, P. Parkes and R. G. Pritchard, *Synth. React. Inorg. Met. Org. Chem.* 1988, **18,** 465.
18. Z. A. Starikova, A. I. Yanovsky, E. P. Turevskaya, N. Ya. Turova and D. V. Berdyev (unpublished results).

Pergamon

PII: S0277-5387(96)00294-X

Polyhedron Vol. 16, No. 4, pp. 671–680, 1997
Copyright © 1996 Elsevier Science Ltd
Printed in Great Britain. All rights reserved
0277-5387/97 $17.00+0.00

First-row transition and group 12 element bis{poly[4-methyl-1*H*-pyrazol-1-yl)borate]} derivatives. X-ray crystal structure of $Zn[HB(4\text{-}Mepz)_3]_2 \cdot CHCl_3$

Giancarlo Gioia Lobbia,[a]* Bruna Bovio,[b] Carlo Santini,[a] Claudio Pettinari[a] and Fabio Marchetti[a]

[a]Dipartimento di Scienze Chimiche, Università di Camerino, via S. Agostino 1, I-62032 Camerino, Italy

[b]Dipartimento di Chimica Generale, Università di Pavia, viale Taramelli 12, I-27100 Pavia, Italy

(Received 15 May 1996; accepted 13 June 1996)

Abstract—A series of new metal complexes of general formula $M[Tp^{\#}]_2$ (where $Tp^{\#}$ = hydridotris(4-methyl-1*H*-pyrazol-1-yl)borate (Tp^{4Me}) or tetrakis(4-methyl-1*H*-pyrazol-1-yl)borate ($pzTp^{4Me}$) and M = Mn, Fe, Co, Ni, Cu, Zn, Cd) were synthesized from the appropriate metal chloride and $KTp^{\#}$ in aqueous solution. These compounds are air-stable solids, sparingly soluble in most organic solvents; they have been characterized by elemental analysis, conductivity and molecular weight measurements, IR, UV, visible spectra and, in the case of diamagnetic compounds, also with ^1H and ^{13}C NMR spectra. The X-ray crystal structure of bis[hydridotris(4-methyl-1*H*-pyrazol-1-yl)borate]zinc(II) · $CHCl_3$ has been determined. The metal is six-coordinate in a distorted octahedral geometry. The N—Zn—N intraligand bond angles range from 84.3(1) to 86.3(1)°. The Zn—N distances vary from 2.114(3) to 2.205(4) Å. The geometry around the B atoms is tetrahedral. The angles N—B—N range from 106.8(3) to 111.0(3)°, the B—N bond distances vary from 1.528(6) to 1.564(5) Å. Comparison is made with some related compounds. Copyright © 1996 Elsevier Science Ltd

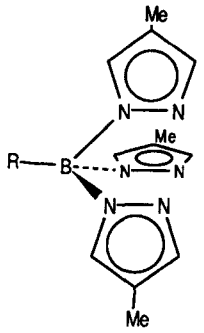
Keywords: polypyrazolylborates; X-ray; UV–visible; IR; metal(II) derivatives; NMR.

The poly(1*H*-pyrazolyl)borate donors $[H_nB(pz)_{4-n}]$ $[Tp^{\#}]$ ($n \leqslant 2$) constitute an important and versatile family of ligands. It is possible to change easily their electronic and steric features and prepare coordination compounds characterized by different stoichiometries and geometries [1]. The donors $[H_nB(pz)_{4-n}]^-$ can generally act as bidentate ($n = 0$ or 2) or tridentate ligands ($n = 0$ or 1). In the latter coordination mode they are particularly interesting: for example it is possible to synthesize simple models for active sites of bio-organic macromolecules such as enzymes [2–4]. Moreover, this class of compounds is useful in this study of the electronic spin-state transitions induced by pressure [5] or temperature [6]. Most of the research into the coordination chemistry of tris- and tetrakis(pyrazolyl)borates has been focused on the first-row transition metals [1, 7, 8]. The data obtained from spectroscopic techniques [8] and from the X-ray crystal structures of $M(Tp^{\#})_2$ with Tp [9], Tp* [10], or Tp^{3Me} [11], have conveyed direct information on structural parameters of the slightly distorted octahedral complexes.†

Here we report the synthesis of the anionic polydentate chelating ligands, hydridotris(4-methyl-1*H*-pyrazol-1-yl)borate (Tp^{4Me}) and tetrakis(4-methyl-1*H*-pyrazol-1-yl)borate ($pzTp^{4Me}$) (Fig. 1), obtained by heating KBH_4 in the corresponding molten pyrazole. Through careful temperature control it was possible to stop at the tri-substitution stage or to continue until tetra-substitution of the hydrogens with pyrazole moieties. The potassium salts are water soluble and their hydrolytic stability increases with increasing substitution of B-bonded hydrides by pyrazolate groups. These monoanionic N-donors have been chosen in

* Author to whom correspondence should be addressed.

† The ligand abbreviations are according to Trofimenko (refs [1,8]) and the symbol $Tp^{\#}$ stands for any pyrazolylborate.



R = H or 4-Methypyrazole

Fig. 1. Ligands used in this work.

view of the fact that, differently from the 3- or 3,5-substituted parent ligands, they offer the 3-position free from steric hindrance. The presence of a methyl group in the 4-position increases the donating ability of the donors.

The coordination chemistry of these ligands towards transition metal M^{2+} ions (M = Mn, Fe, Co, Ni, Cu, Zn, Cd), is described and the tridentate chelating character of tris(pyrazolyl)borates in the solid state is conclusively demonstrated from the X-ray crystal structure determination of $Zn[Tp^{4Me}]_2 \cdot CHCl_3$.

RESULTS AND DISCUSSION

Coordination compounds derived from the anionic $[Tp^{4Me}]$ or $[pzTp^{4Me}]$, and divalent first-row transition or group 12 metal ions can be readily prepared by metathesis reaction:

$$MX_2 + 2KTp^{\#} \xrightarrow{H_2O} M[Tp^{\#}]_2 + 2KX$$
1–14

M = Mn, Co, Ni, Zn or Cd, X = Cl;
M = Fe or Cu, $X_2 = SO_4$;
$Tp^{\#} = Tp^{4Me}$ or $pzTp^{4Me}$.

The analytical data of derivates **1–14** are given in Table 1. Most of the $M[Tp^{\#}]_2$ derivatives gradually decompose on heating, without melting: this behavior

Table 1. Analytical data of compounds **1–14**

Compound[a]	No.	Colour	Yield %	M.p. °C	Elemental analysis[b] C	H	N	Conductivity[c] conc.	Λ
$Mn(Tp^{4Me})_2$	**1**	colourless	88	300 dec	50.7	5.8	29.5	0.8	0.14
$C_{24}H_{32}B_2N_{12}Mn$					(51.0)	(5.7)	(29.7)		
$Fe(Tp^{4Me})_2$	**2**	red-violet	91	265 dec	50.7	5.7	29.4	1.0	0.82
$C_{24}H_{32}B_2N_{12}Fe$					(50.9)	(5.7)	(29.7)		
$Co(Tp^{4Me})_2$	**3**	pink yellow	89	>350 dec	50.3	5.5	29.3	0.8	0.56
$C_{24}H_{32}B_2N_{12}Co$					(50.6)	(5.7)	(29.5)		
$Ni(Tp^{4Me})_2$	**4**	pale lilac	90	340 dec	50.3	5.8	29.2	0.9	0.10
$C_{24}H_{32}B_2N_{12}Ni$					(50.7)	(5.7)	(29.5)		
$Cu(Tp^{4Me})_2$	**5**	blue-sky	92	282–286	49.9	5.7	29.2	0.6	0.18
$C_{24}H_{32}B_2N_{12}Cu$					(50.2)	(5.6)	(29.3)		
$Zn(Tp^{4Me})_2$	**6**	colourless	87	335 dec	50.5	5.4	29.4	0.8	0.07
$C_{24}H_{32}B_2N_{12}Zn$					(50.1)	(5.6)	(29.2)		
$Cd(Tp^{4Me})_2$	**7**	colourless	88	312–314	46.4	5.2	26.9	0.8	0.09
$C_{24}H_{32}B_2N_{12}Cd$					(46.3)	(5.2)	(27.0)		
$Mn(pzTp^{4Me})_2$	**8**	colourless	85	300 dec	52.6	5.5	30.6	0.9	0.11
$C_{32}H_{40}B_2N_{16}Mn$					(53.0)	(5.6)	(30.9)		
$Fe(pzTp^{4Me})_2$	**9**	red-brown	94	>340 dec	52.6	5.6	30.7	0.9	0.32
$C_{32}H_{40}B_2N_{16}Fe$					(52.9)	(5.5)	(30.9)		
$Co(pzTp^{4Me})_2$	**10**	pink yellow	93	>350 dec	52.9	5.5	30.5	0.8	2.02
$C_{32}H_{40}B_2N_{16}Co$					(52.7)	(5.5)	(30.7)		
$Ni(pzTp^{4Me})_2$	**11**	pale lilac	86	340 dec	52.4	5.3	30.3	0.9	0.10
$C_{32}H_{40}B_2N_{16}Ni$					(52.7)	(5.5)	(30.7)		
$Cu(pzTp^{4Me})_2$	**12**	blue-sky	95	263–270	52.1	5.6	30.3	1.0	0.12
$C_{32}H_{40}B_2N_{16}Cu$					(52.4)	(5.5)	(30.5)		
$Zn(pzTp^{4Me})_2$	**13**	colourless	95	300 dec	52.0	5.6	30.4	1.3	0.07
$C_{32}H_{40}B_2N_{16}Zn$					(52.2)	(5.5)	(30.5)		
$Cd(pzTp^{4Me})_2$	**14**	colourless	92	300 dec	49.2	5.2	28.5	0.8	0.10
$C_{32}H_{40}B_2N_{16}Cd$					(49.1)	(5.1)	(28.6)		

[a] Tp^{4Me} is hydridotris(4-methyl-1*H*-pyrazol-1-yl)borate, $C_{12}H_{16}BN_6$, and $pzTp^{4Me}$ is tetrakis(4-methyl-1*H*-pyrazol-1-yl)borate, $C_{16}H_{20}BN_8$.

[b] Calculated values in parentheses.

[c] Molar conductivity in CH_2Cl_2 solution ($ohm^{-1}\ cm^2\ mol^{-1}$) at room temperature, the molar concentration $\times 10^{-3}$.

has been previously observed also in other poly(pyrazolyl)borato derivatives [12].

Compounds **1–14** are sparingly soluble in polar solvents such as acetone or methanol, and soluble in DMSO and chlorinated solvents, from which they may be suitably recrystallized. The solubility of compounds **8–14** is generally lower than that of compounds **1–7**. The $M[pzTp^{4Me}]_2$ have the same colours as their $M[Tp^{4Me}]_2$ counterparts, except in the case of the iron derivatives $Fe[Tp^{4Me}]_2$ and $Fe[pzTp^{4Me}]_2$, which are violet and red, respectively. Conductivity measurements carried out in dichloromethane solution indicate that all the derivates are non-electrolytes in this solvent. Molecular weight determinations have shown also that compounds **1–14** are not dissociated in chloroform: for example the ratio between the vaporimetric and the calculated molecular weight is 0.90 (=441/491) for **6** and 0.92 (=577/624) for **13**.

IR data

Selected infrared data of $M[Tp^{4Me}]_2$ and $M[pzTp^{4Me}]_2$ derivatives are reported in Table 2. In the spectra of $M[Tp^{4Me}]_2$ we have observed a ν(B—H) absorption in the region 2400–2500 cm^{-1}: it is found at higher frequencies shifted with respect to the potassium ligand salt (a similar behaviour likely due to solid state effects, has been previously found in other poly(pyrazolyl)borato derivatives [13]) and it is generally split into two components.

Over 3000 cm^{-1} we have found weak absorptions, assigned to heterocyclic ν(C—H) vibrations. The spectra of **1–14** exhibit in the 1500–1600 cm^{-1} region strong or medium bands due to the "breathing" of the pyrazole rings. Finally, the medium intensity absorption at *ca* 1410 cm^{-1} in $M[Tp^{4Me}]_2$ and at *ca* 1420 cm^{-1} in $M[pzTp^{4Me}]_2$ derivatives can be tentatively assigned to ν(B—N) stretch [14]. It has not been possible to assign with certainty the metal–ligand absorptions in the far-IR region because of the presence of several overlapped ligand bands.

NMR data

The ^1H and ^{13}C NMR spectra have been performed in the case of zinc and cadmium derivatives (Table 3). The NMR spectra of **6** and **7** suggest that the three pyrazolyl rings are equivalent over the temperature range of 220–300 K, in accordance with the presence of tridentate ligands. However we cannot exclude the possibility of lower coordination numbers in solution, due to a fluxional behaviour similar to those previously observed in related Tp and Tp* complexes [15, 16]. The pyrazole ring exchange may be very rapid, as observed for MeHg(Tp) [17], which doesn't allow the direct observation of signal splitting even at −90°C.

Consequently the determination of the coordination mode of the donor in solution is not possible.

The ^{13}C NMR spectrum of $Cd[Tp^{4Me}]_2$ exhibits an interesting feature: we observed at room temperature the coupling constant (21 Hz) between $^{111,113}Cd$ and C(3). This coupling is of the same order of magnitude of that previously observed (14 Hz) in the spectrum of $Cd[Tp^*]_2$ at 263 K [18]. In the spectra of cadmium derivatives a slightly deshielding of the H(3) and C(3) nuclei with respect to those of zinc derivatives is detected, thus indicating a likely stronger donation of the ligand in the former compounds.

In the spectra of derivatives **13** and **14** we observed at room temperature only one set of signals. Cooling the samples to −50°C an initial splitting of the signals appeared, whereas at −80°C the splitting was complete, two different sets of signals, in 3 : 1 intensity ratio, being detected. This suggests that in the frame of an octahedral structure, one pyrazole ring is different from the other three, but also that at room temperature a fluxional behavior, which makes all pyrazoles indistinguishable, is operating in solution. As previously indicated for derivatives of (pzTp), the exchange rate of pyrazoles is fast compared with the NMR time scale, at room temperature.

UV–visible data

The UV-visible spectra of derivatives **1–14** have been carried out in chloroform solutions. The position of absorption maxima and the extinction coefficients are given in Table 4.

All the complexes exhibit a very intense band at *ca* 240 nm, which corresponds to pyrazolic intraligand transition. Moreover at the limit of the UV part of the spectra (at *ca* 290 nm) and in the visible region (at *ca* 340 nm) some absorptions of medium intensity are often detected, which should be attributed to "metal to ligand charge transfer" (MLCT) [9a]: the relatively high extinction coefficient may be a conclusive proof for this attribution.

In the spectrum of nickel(II) derivative **4** we observed a weak absorption at 354 nm, (ε = 35), typical of *d–d* transitions.

In the spectra of iron(II) derivatives **2** and **9** we observed three absorptions between 290 and 490 nm, due to MLCT transitions. Moreover an additional absorption at *ca* 580 nm was found, which could be tentatively assigned to $^1T_{1g}(^1I) \leftarrow {}^1A_{1g}$ transition, on the basis of previous reports on low and high spin iron d^6 six-coordinated complexes [9b].

In the spectra of copper(II) derivatives **5** and **12** a weak broad band at 592 nm was detected, which may be assigned to $^2T_{2g} \leftarrow {}^1E_g$ transition in skewed octahedral $Cu(N\text{-donor})_6$ complexes [19]. The broadening and the splitting of the absorption is caused by the trigonal component of the field, spin-orbital coupling and Jahn-Teller distortion, in accordance with that previously indicated for distorted octahedral $Cu(Tp^{\#})_2$ complexes, structurally investigated [9f,h]. The apparent octahedral splitting parameter Δ, neglecting Jahn–Teller effects, is ~16,000 cm^{-1}, thus indicating

Table 2. IR and far-IR data (Nujol mull) of compounds **1–14**

Compound	No	ν(C—H)	ν(B—H)	1500–1600	ν(B—N)	<650
$K(Tp^{4Me})$		3115w	2407s	1568s 1562m		636vs, 624vs, 552br, 460w, 393m, 367m, 354m, 256m, 233mbr, 203w
$Mn(Tp^{4Me})_2$	**1**	3087w	2489m 2434s	1567s	1411m	633vs, 380s, 340m, 279s, 229s
$Fe(Tp^{4Me})_2$	**2**	3127w 3089w	2483s 2459s	1565m 1560m	1426m 1400s	631vs, 426m, 384s, 350m, 286m, 253s, 236s, 210m
$Co(Tp^{4Me})_2$	**3**	3119w 3088w	2481m 2452s	1566s	1410m	632vs, 419w, 387s, 373m, 286s, 278s, 262s, 253s, 207s
$Ni(Tp^{4Me})_2$	**4**	3122w 3089w	2481s 2459	1566s	1419m	631vs, 390s, 374m, 289s, 269s, 255vs
$Cu(Tp^{4Me})_2$	**5**	3123w 3093w	2485m 2447	1567s	1418m	633vs, 394m, 386m, 300m, 279m, 226vs, 206m
$Zn(Tp^{4Me})_2$	**6**	3118w 3087w	2480m 2456s	1567s	1417m	633vs, 383s, 303m, 282s, 256s, 247s, 228s, 215s, 208s
$Cd(Tp^{4Me})_2$	**7**	3090w	2484m 2456s	1568s 1560sh	1408m 1390sh	633vs, 377s, 280s, 255m, 247m, 224m, 203m
$K(pzTp^{4Me})$				1573m	1434m	624vs, 398s, 385sh, 364m, 352m, 303m, 279s, 252m, 247s, 225s
$Mn(pzTp^{4Me})_2$	**8**	3151w 3129w 3087w		1570m 1559w	1424m 1419m	648s, 618vs, 552br, 419w, 392m, 385sh, 376w, 352m, 325m, 302m, 290m, 280vs, 276m, 255m, 247m, 215s
$Fe(pzTp^{4Me})_2$	**9**	3161w 3086w		1569m 1560w	1420m	631w, 618vs, 484br, 448m, 383m, 354s, 326w, 302m, 289w, 279s, 266w, 246m, 211m, 202m
$Co(pzTp^{4Me})_2$	**10**	3150w 3088w		1570m	1418m	625w, 618vs, 398vs, 373w, 352m, 303m, 281s, 253m, 249m, 229s, 210s
$Ni(pzTp^{4Me})_2$	**11**	3150w 3124w 3092		1576m 1570m	1411m 1419m	649m, 619s, 552br, 417w, 401s, 385w, 376m, 352m, 326w, 303m, 289s, 280s, 266w, 255sh, 257m, 225vs, 203m
$Cu(pzTp^{4Me})_2$	**12**	3151w 3129w 3082w		1570m 1560w	1412m	648m, 618s, 552m, 418m, 398w, 386w, 378w, 352m, 326m, 303s, 290m, 280s, 266w, 255sh, 247s, 230s, 224s
$Zn(pzTp^{4Me})_2$	**13**	3151w 3087w		1570m 1560m	1412m	649s, 618vs, 405sh, 393s, 370w, 304m, 285m, 279s, 228m, 200s
$Cd(pzTp^{4Me})_2$	**14**	3150w 3126w		1570m	1410sh	645s, 632w, 618vs, 402sh, 389vs, 325m, 279m, 266m, 247m, 227m, 208m

a relatively strong ligand field, similar to those caused by the donors (Tp) and (pzTp) [9a]. As indicated by Jesson [9a] the extinction coefficient (ε) increases *ca* 60 cm^{-1} with the substitution of the hydrido group with a pyrazole molecule. A similar trend is found in the spectra of iron derivatives **2** and **9** for the MLCT absorption (342 nm), where ε increase from 6900 in $Fe[Tp^{4Me}]_2$ to 11400 cm^{-1} in $Fe[pzTp^{4Me}]_2$.

X-ray crystal structure of $Zn[Tp^{4Me}]_2 \cdot CHCl_3$

The molecular structures of the two independent molecules of $Zn[Tp^{4Me}]_2 \cdot CHCl_3$ is shown in Fig. 2 together with its numbering scheme [20]. The molecules exhibit crystallographic symmetry -1 because the Zn atoms occupy special positions *a* (0, 0, 0) and *h* (1/2, 1/2, 1/2).

Since the differences among chemically equivalent interatomic distances and angles in the molecules have only relative meaning, their average values are given in Table 5, whereas the individual values in the coordination sphere are listed in Table 6. The individual distances and angles in the ligands are available as Supplementary Material.

The packing of the complex molecules in the crystal leaves space for the chloroform molecules. The

Table 3. ^1H and ^{13}C NMR data ($CDCl_3$) of the ligands KTp^{4Me} and $KpzTp^{4Me}$ and of compounds **6, 7, 13** and **14**

Compound	No	Solvent	^1H			^{13}C			
			3- or 5-H		4-Me	C(3) or C(5)		C(4)	4-Me
KTp^{4Me}		$CDCl_3$	7.22s	6.82s	2.00s	142.1	134.7	115.6	9.3
		$(CD_3)_2CO$	7.32s	7.18s	1.98s	140.5	134.4	113.6	9.4
		D_2O	7.37s	7.03s	1.94s				
$Zn(Tp^{4Me})_2$	**6**	$CDCl_3$	7.33s	6.92s	1.99s	139.6	133.5	114.0	9.2
$Cd(Tp^{4Me})_2$	**7**	$CDCl_3$	7.50s	7.18s	2.00s	141.1[a]	135.9	115.4	9.0
$KpzTp^{4Me}$		$CDCl_3$	7.22s	6.83s	1.99s	140.3	133.4	113.2	8.2
			7.24s	6.94s	1.97s				
$Zn(pzTp^{4Me})_2$	**13**	$CDCl_3$	7.14s	7.08s	2.00s	142.1	134.8	115.9	9.2
$Cd(pzTp^{4Me})_2$	**14**	$CDCl_3$	7.48s	7.31s	2.06s	141.9	134.8	115.6	9.3

[a] $J_{(Cd-C)} = 21$ Hz.

Table 4. UV–visible data of compounds **1–14**

Compound	No.	Λ^a	ε^b	C^c	Assignment[d]
$Mn(Tp^{4Me})_2$	**1**	240	9100	1.3×10^{-4}	intraligand
		356	330	1.3×10^{-4}	MLCT
$Fe(Tp^{4Me})_2$	**2**	240	10200	1.7×10^{-4}	intraligand
		296 shoulder	4600	1.7×10^{-4}	MLCT
		342	6900	1.7×10^{-4}	MLCT
		476	1600	1.7×10^{-4}	MLCT
		572	500	1.1×10^{-3}	*d–d*
$Co(Tp^{4Me})_2$	**3**	240	11400	1.2×10^{-4}	intraligand
$Ni(Tp^{4Me})_2$	**4**	240	8600	1.7×10^{-4}	intraligand
		354	35	1.7×10^{-4}	*d–d*
$Cu(Tp^{4Me})_2$	**5**	240	7400	0.9×10^{-4}	intraligand
		338	400	0.9×10^{-4}	MLCT
		582	70	1.3×10^{-3}	*d–d*
$Zn(Tp^{4Me})_2$	**6**	240	5200	0.6×10^{-4}	intraligand
		354	230	0.6×10^{-4}	MLCT
$Cd(Tp^{4Me})_2$	**7**	240	6300	0.8×10^{-4}	intraligand
$Mn(pzTp^{4Me})_2$	**8**	244	9100	4.8×10^{-4}	intraligand
$Fe(pzTp^{4Me})_2$	**9**	240	13100	0.8×10^{-4}	intraligand
		296 shoulder	5600	0.8×10^{-4}	MLCT
		344	11400	0.8×10^{-4}	MLCT
		490	1200	1.1×10^{-3}	MLCT
		590	450	1.1×10^{-3}	*d–d*
$Co(pzTp^{4Me})_2$	**10**	240	17300	1.0×10^{-4}	intraligand
		310	1000	1.0×10^{-4}	MLCT
$Ni(pzTp^{4Me})_2$	**11**	244	7000	6.3×10^{-4}	intraligand
$Cu(pzTp^{4Me})_2$	**12**	244	6600	7.4×10^{-4}	intraligand
		314 shoulder	1300	7.4×10^{-4}	MLCT
		592 very broad	130	7.4×10^{-4}	*d–d*
$Zn(pzTp^{4Me})_2$	**13**	240	11300	0.9×10^{-4}	intraligand
$Cd(pzTp^{4Me})_2$	**14**	240	10400	1.0×10^{-4}	intraligand

[a] Λ in nm.
[b] ε in (mol l^{-1} cm^{-1}.
[c] C in mol l^{-1}.
[d] MLCT stands for metal to ligand charge transfer.

crystal cohesion is ensured by intermolecular short approaches: C(5B)···C(6E) 3.546(6) Å, N(1B)···C(6E) 3.550(7) Å, C(4A)···C(1) 3.577(7) Å, C(5A)···C(1) 3.381(8) Å, C(5A)···Cl(3) 3.542(5) Å, C(5C)···Cl(3) $(1-x, 1-y, 2-z)$ 3.534(5) Å and Cl(1)···Cl(1) $(-x, 1-y, 1-z)$ 3.582(3) Å.

The Zn—N distances vary from 2.114(3) to 2.205(4) Å with a weighted average of 2.13(1) Å. The

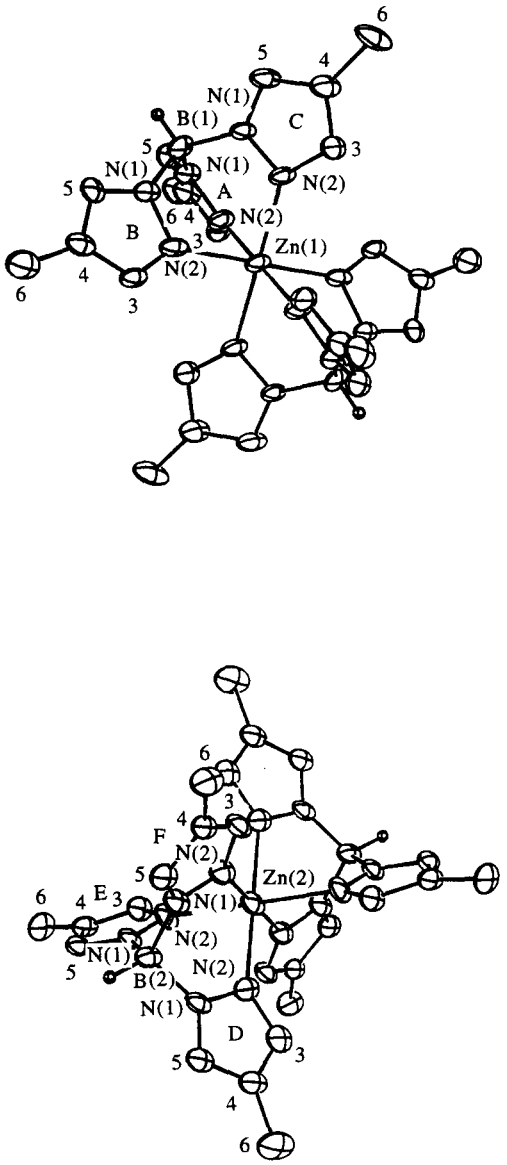


Fig. 2. ORTEP plot and numbering scheme of atoms of two crystallographically independent molecules of [HB(4-Mepz)$_3$]$_2$Zn. Thermal ellipsoids enclose 25% of the electron density. Carbon atoms are indicated only by numbers. Hydrogen atoms are omitted for clarity, except those bonded to B atoms.

Table 5. Average bond distances (Å) and angles (°) with their standard errors[a] of Zn[Tp^{4Mc}]$_2$·CHCl$_3$

Zn—N	6	2.135	0.015	0.001
B—N	6	1.547	0.006	0.002
N(1)—N(2)	6	1.360	0.010	0.002
N(2)—C(3)	6	1.346	0.010	0.002
C(3)—C(4)	6	1.387	0.007	0.003
C(4)—C(5)	6	1.376	0.006	0.002
C(4)—C(6)	6	1.529	0.002	0.003
C(5)—N(1)	6	1.348	0.009	0.002
N(2)—Zn—N(2)	6	85.16	0.31	0.05
N(2)—Zn—N(2′)	6	94.84	0.31	0.05
Zn—N(2)—N(1)	6	119.1	0.4	0.1
Zn—N(2)—C(3)	6	135.6	0.9	0.1
N(2)—N(1)—C(5)	6	110.7	0.4	0.1
N(2)—N(1)—B	6	119.5	0.8	0.1
C(5)—N(1)—B	6	129.7	0.8	0.1
N(1)—N(2)—C(3)	6	105.1	0.9	0.1
N(2)—C(3)—C(4)	6	111.3	0.9	0.2
C(3)—C(4)—C(5)	6	104.9	0.5	0.2
C(3)—C(4)—C(6)	6	127.7	0.3	0.2
C(5)—C(4)—C(6)	6	127.4	0.4	0.2
C(4)—C(5)—N(1)	6	107.9	0.5	0.1
N(1)—B—N(1)	6	108.7	0.7	0.1

[a] All values calculated according to A. Domenicano, A. Vaciago and C. A. Coulson, *Acta Crystal.*, **B3**, 1975, 221.

octahedral N—Zn—N intraligand bond angles range from 84.3(1) to 86.3(1)° [weighted average 85.2(3)°], whereas the interligand corresponding angles range from 93.7(1) to 95.7(1)° [weighted average 94.8(3)°]. These values are comparable with those found in the bis[hydridotris(1-pyrazolyl-N^2)borato]zinc(II) [21].

In the pyrazole rings without a free lone pair, the following pattern for the angles is observed: Zn—N(2)—C(3) > Zn—N(2)—N(1) [weighted average 135.6(9) > 119.1(4)°], N(2)—N(1)—C(5) > N(1)—N(2)—C(3) [weighted average 110.7(4) > 105.1(9)°] and N(2)—C(3)—C(4) > C(4)—C(5)—N(1) [weighted average 111.3(9) > 107.9(5)°], consistent with the empirical rules concerning the bond angles in pyrazoles [22]. A similar trend was observed in [HB—(μ-pz)$_3$—Cu(PPh$_3$)] [23].

The weighted average N···N intraligand distance of 2.902(3) Å is shorter than the average interligand N···N distance of 3.15(2) Å. The least-squares planes of the pyrazole rings suggest the following probability that the rings are non-planar: $P > 99\%$ for N(1A)—C(5A), N(1C)—C(5C), N(1D)—C(5D), and N(1E)—C(5E), $P = 81.5\%$ for N(1B)—C(5B), $P = 53.9\%$ for N(1F)—C(5F); maximum out-of-plane displacements (Å): C(5A) −0.019(4), C(5C) −0.010(5), C(3D) 0.020(5) and C(3E) −0.012(4).

The steric demands of ligands were recognized as important in determining the stability of complexes, in ligand competition and exchange [24]. It is of value to calculate effective cone angles of ligands from the crystallographic structural data. The effective cone angles of the ligand HB(4-Mepz)$_3$ were calculated assuming the midpoint of three Zn—N vectors as the cone axes and the Zn atoms as the cone vertexes. The angle between the cone axes and the vector which touches the van der Waals radii of the hydrogen atoms closest to Zn (r = 1.17 Å for H) for each end of the tridentate ligand is: 102.4° for H(3A), 103.8° for H(3B) and 105.8° for H(3C) and 102.4° for H(3D), 111.6 for H(3E) and 104.1° for H(3F). These angles correspond to a total average value θ: 208.0° for Zn(1) ligand and 212.0° for Zn(2) ligand. These values are consistent with the value 212.2° found in the parent ligand [HB-(μ-pz)$_3$] [23].

Table 6. Selected interatomic distances (Å) and bond angles (°) with e.s.d.s in parentheses of $Zn[Tp^{4Me}]_2 \cdot CHCl_3$

Zn(1)—N(2A)	2.185(4)	Zn(2)—N(2D)	2.205(4)
Zn(1)—N(2B)	2.117(3)	Zn(2)—N(2E)	2.114(3)
Zn(1)—N(2C)	2.119(3)	Zn(2)—N(2F)	2.116(4)
N(2A)—Zn(1)—N(2B)	85.5(1)	N(2D)—Zn(2)—N(2E)	84.3(1)
N(2A)—Zn(1)—N(2C)	84.8(1)	N(2D)—Zn(2)—N(2F)	84.4(1)
N(2B)—Zn(1)—N(2C)	86.3(1)	N(2E)—Zn(2)—N(2F)	85.2(1)
N(2A)—Zn(1)—N(2B′)	94.5(1)	N(2D)—Zn(2)—N(2E′)	95.7(1)
N(2A)—Zn(1)—N(2C′)	95.2(1)	N(2D)—Zn(2)—N(2F′)	95.6(1)
N(2B)—Zn(1)—N(2C′)	93.7(1)	N(2E)—Zn(2)—N(2F′)	94.8(1)

The geometry around the B atom is tetrahedral. The B–N bond distances vary from 1.528(6) to 1.564(5) Å, with weighted average 1.547(6) Å. The angles N—B—N range from 106.8(3) to 111.0(3)° with weighted average 108.7(7)°.

The B(1)···Zn(1) and B(2)···Zn(2) distances are 3.183(5) and 3.237(6) (weighted average 3.20(3) Å) comparable with the values found in $Zn[HB(pz)_3]_2$ [21].

Bond distances and angles within the solvent molecule $CHCl_3$ and: C(1)—Cl(1) 1.728(7), C(1)—Cl(2) 1.771(7) and C(1)—Cl(3) 1.769(5) Å; Cl(1)—C(1)—Cl(2) 109.2(4), Cl(1)—C(1)—Cl(3) 110.9(3) and Cl(2)—C(1)—Cl(3) 106.9(3)° respectively.

In Table 7, selected bond distances and angles of $Zn[Tp^{4Me}]_2$ are compared with the values reported for other six-coordinate octahedral $M[Tp^{\#}]_2$-type compounds [9, 16, 21, 25–33]. Several general patterns emerge; for example for M—N bond distance is nearly equal to the sum of Shannon's ionic radii [34] and increases when alkyl groups are in the 3-position of the heterocyclic rings of the ligand, near to coordination sites. We also observed the mean M—N value increases on going from the metals of the (n) to those of ($n+1$) period.

According to Shannon and Prewitt [35], two very different Fe—N distances are found in the case of low ($Fe[Tp]_2$) and high-spin ($Fe[Tp^*]_2$) derivatives respectively. Between all the derivatives the shortest M—N distance is found in $Fe[Tp]_2$ whereas the longest is found in the $Pb[Tp^{\#}]_2$ derivatives, where, if the lone pair is also stereochemically inactive, the structure is a trigonally distorted octahedron due to strong interligand steric effects.

Only in the $Cu[Tp^{\#}]_2$ derivatives did we observe three different sets of Cu—N distances. The structure can be described as an elongated rhombic octahedron. The marked distortion could be ascribed to the Jahn–Teller effect.

The average N—M—N bite angles range from 73.2 in $Pb[Tp]_2$ to 91.2 in $Fe[Tp^{3Me}]_2$. It is worth noting that N—M—N values decrease with increasing of the M—N distances, i.e. the mean N—M–N value decreases on going from the metal of the (n) to those of ($n+1$) period.

In the case of Mg, Ca, Co, Ni, Cu, Zn, Cd and Pb derivatives we observed that the presence of an alkyl group in the 3-, 4- and 5-position of the heterocyclic ring doesn't seem to produce relevant effects on the molecular parameters reported in Table 8. Only in the case of the iron derivatives the steric hindrance exerted by a Me group in 3 position is the decisive factor to determine the stability of high-spin states and consequently the lengthening of the Fe—N bonds and the opening of the N—Fe—N bites.

EXPERIMENTAL

General laboratory equipment

Concentration was always carried out under reduced pressure (water aspirator). The samples were dried *in vacuo* till constant weight (20°C, *ca* 0.1 Torr). Carbon, hydrogen, and nitrogen analyses were carried out with a Fisons Instruments 1108 CHNS-O Elemental analyzer. Molecular weight determinations were performed with a Knauer membrane osmometer. Infrared spectra were recorded from 4000 to 200 cm^{-1} on a Perkin–Elmer 2000 System Series FTIR instrument. ^1H- and ^{13}C-NMR spectra were recorded on a Varian VXR-300 spectrometer operating at room temperature (300 MHz for ^1H, 75 MHz for ^{13}C). The conductances of solutions were measured with a Crison CDTM 522 conductimeter at room temperature.

Synthesis of the donors

Potassium[hydridotris(4-methyl-1H-pyrazol-1-yl) borate]. Potassium borohydride (2.7 g, 0.05 mol) and 4-methyl-pyrazole (16.4 g, 0.20 mol) were gradually heated under stirring in a 1-litre flask at temperature not exceeding 190°C. Potassium borohydride dissolved slowly with evolution of hydrogen. After 60 h the melt was poured dropwise into 300 cm^3 of stirred hot xylene. Upon cooling, a solid precipitated and, after repeated washings in *n*-heptane/diethy ether (2 : 1

Table 7. Comparison of relevant structural data for distorted octahedral M[Tp#]$_2$-type compounds

Complex	M—N	M—N$_{av}$	N—M—N (bite)	N—M—N$_{av}$ (bite)	Reference
Mg(Tp)$_2$	2.149(4), 2.190(4), 2.214(4)	2.18	85.8(1), 81.7(1), 86.0(1)	84.5	[25]
Mg(Tp)$'_2$	2.149(3), 2.199(4), 2.206(4)	2.18	85.9(1), 81.9(1), 86.6(1)	84.8	[25]
Mg(pzTp)$_2$	2.202(3), 2.158(3), 2.108(3)	2.16	84.8(1), 83.0(1), 86.2(1)	84.7	[25]
Mg(pzTp)$'_2$	2.172(3), 2.143(3), 2.167(3)	2.16	85.5(1), 83.7(1), 85.1(1)	84.8	[25]
Ca(Tp)$_2$	2.407(4), 2.449(4), 2.447(4)	2.43	76.5(1), 80.6(1), 80.7(1)	79.3	[25]
Ca(Tp)$'_2$	2.460(4), 2.458(4), 2.425(4)	2.45	76.0(1), 80.6(1), 80.7(1)	79.1	[25]
Fe(Tp)$_2$	1.973(3), 1.980(3), 1.972(3)	1.97	88.3(2), 88.1(2), 88.3(2)	88.2	[9c]
Fe(Tp)$'_2$	1.979(3), 1.960(3), 1.971(4)	1.97	88.0(2), 88.5(2), 88.5(2)	88.3	[9c]
Fe(Tp*)$_2$	2.190(4), 2.179(4), 2.147(4)	2.17	87.1(1), 86.3(1), 86.3(1)	86.6	[9c]
Fe(Tp^{3Me})$_2$	2.197(4), 2.200(4), 2.201(5)	2.20	86.6(2), 93.7(2), 93.4(2)	91.2	[26]
Fe(Tp^{3Me})$'_2$	2.215(5), 2.201(4), 2.208(5)	2.21	86.4(2), 93.7(2), 93.6(3)	91.2	[26]
Co(Tp)$_2$	2.123(7), 2.120(7), 2.130(7), 2.133(8), 2.128(8), 2.140(7)	2.13	85.9(3), 85.8(3), 85.3(3), 84.6(3), 85.3(3), 86.2(3)	85.5	[9d]
Co(Tp^A)$_2$[a]	2.170(2), 2.164(2), 2.012(2)	2.14	84.45(6), 88.77(6), 88.58(6)	87.3	[27]
Co(Tp^B)$_2$[b]	2.151(3), 2.207(3), 2.086(3)	2.15	84.8(1), 87.3(1), 89.6(1)	87.2	[27]
Co(Tp^C)$_2$(CHCl$_3$)[c]	2.154(3), 2.154(3), 2.157(3)	2.15	89.7(1), 89.6(1), 90.3(1)	89.9	[28]
Co(Tp^C)$_2$(C$_6$H$_6$)[c]	2.182(2), 2.190(2), 2.139(2)	2.17	88.44(7), 88.62(7), 90.52(7)	89.2	[28]
Ni(Tp)(Tp$^{3\text{-}iPr}$)	2.124(4), 2.177(6), 2.061(4), 2.076(6)	2.11	88.3(2), 88.4(2), 87.0(2)	87.9	[29]
Ni(Tp^{3Me})$_2$	2.101(6), 2.134(4), 2.106(5)	2.11	87.8(2), 92.1(2), 92.4(2)	90.8	[11]
Cu(Tp)$_2$	2.018(3), 1.991(2), 2.528(4)	2.00[d]	88.7(1), 80.3(1), 86.2(1)	85.1	[9f]
	2.082(2), 2.356(4), 1.998(2)	2.04[d]	81.9(1), 86.6(1), 87.9(1)	85.5	[9f]
Cu(Tp*)$_2$	2.142(3), 2.020(2), 2.284(3)	2.08[d]	87.6(2), 85.7(2), 87.1(2), 88.6(3), 86.4(2), 86.1(2)	86.9	[30]
Zn(Tp)$_2$	2.148(2), 2.150(2), 2.162(2), 2.152(2), 2.175(2), 2.143(2)	2.15	85.93(8), 85.13(7), 85.69(8), 85.96(8), 85.15(8), 85.67(8)	85.6	[21]
Zn(Tp*)$_2$	2.187(3), 2.146(2), 2.183(2)	2.17	87.2(1), 86.1(1), 85.9(1)	86.4	[31]
Zn(Tp^{4Me})$_2$	2.185(4), 2.117(3), 2.119(3), 2.205(4), 2.114(3), 2.116(4)	2.14	85.5(1), 84.8(1), 86.3(1)	85.5	This work
		2.14	84.3(1), 84.4(1), 85.2(1)	84.6	
Cd(Tp)$_2$	2.341(6), 2.282(5), 2.357(6), 2.355(6), 2.293(6), 2.371(6)	2.33	83.4(2), 78.9(2), 83.8(3), 83.5(2), 78.2(2), 83.2(2)	81.8	[32]
Cd(Tp^{3Ph})$_2$	2.389(6), 2.415(6), 2.351(6)	2.38	84.23(2), 85.57(2), 85.76(2)	85.2	[32]
Cd(pzTp)(Tp^{3Ph})	2.380(11), 2.411(10), 2.392(11), 2.313(11), 2.397(11), 2.369(10)	2.38	81.5(4), 81.5(4), 84.3(4), 80.6(4), 81.1(4), 79.6(4)	81.4	[32]
Cd(Tp*)$_2$	2.348(5)	2.35	82.7(1)	82.7	[33]
Cd(pzTp^{3Me})$_2$	2.362(8), 2.308(8), 2.365(8)	2.34	81.0(3), 82.3(3), 82.3(3)	81.9	[33]
Cd(pzTp)$_2$	2.314(3), 2.387(3), 2.284(3)	2.33	78.7(1), 84.4(1), 79.1(1)	80.9	[33]
Pb(Tp)$_2$	2.462(13), 2.623(16), 2.477(13), 2.750(14), 2.806(13), 2.523(14)	2.61	73.5(4), 73.2(4), 72.5(4), 78.6(5), 71.6(4), 69.4(4)	73.2	[16]
Pb(Tp*)$_2$	2.610(5)	2.61	75.2(1)	75.2	[16]

[a] Tp^A is HB(3-iPrpz)$_2$(5-iPrpz).
[b] Tp^B is HB(3-iPr, 4-Brpz)$_2$(5-iPr,4-Brpz).
[c] Tp^C is HB(3-thienyl)pz$_3$.
[d] Average of the two short bands.

v/v) the mixture was filtered, yielding 12.2 g of a white solid (83%) with m.p. 258–260°C; Found: C, 48.9; H, 5.5; N, 28.4; Calc. for $C_{12}H_{16}BN_6K$: C, 49.0; H, 5.5; N, 28.6%.

The ligand potassium[tetrakis(4-methyl-1H-pyrazol-1-yl)borate] was prepared similarly, heating at 220°C. Yield: 72%; m.p. 247–249°C. Found: C, 51.1; H, 5.5; N, 29.7; Calc. for $C_{16}H_{20}BN_8K$: C, 51.3; H, 5.4; N, 29.9%.

Synthesis of the complexes

Zinc(II) *bis*[*hydridotris*(4-*methyl*-1H-*pyrazol*-1-*yl*) *borate*]. $ZnCl_2$ (0.14 g, 1 mmol) was dissolved in distilled water (*ca* 50 cm^3) and added under stirring with an aqueous solution (*ca* 50 cm^3) of potassium hydridotris(4-methyl-1*H*-pyrazol-1-yl)borate (0.59 g, 2 mmol). A colorless precipitate was immediately obtained, which was filtered, washed with water–

Table 8. Crystal data, data collection and refinement of the structure of $Zn[Tp^{4Me}]_2 \cdot CHCl_3$

Formula	$C_{25}H_{33}B_2N_{12}Cl_3Zn$
Formula weight	694.98
Space group	$P\bar{1}$
Color	colourless
a (Å)	11.971(2)
b (Å)	13.499(2)
c (Å)	11.469(3)
α (°)	100.47(2)
β (°)	111.87(2)
γ (°)	96.84(1)
V_c (Å^3)	1655.5(6)
Z	2
D_{calcd} (g cm^{-3})	1.39
Crystal size (mm)	$1.05 \times 0.21 \times 0.17$
μ (Cu-K_α) (cm^{-1})	35.87
Data collection instrument	Enraf-Nonius CAD4
Radiation (monochromated)	Cu-K_α (λ = 1.5418 Å)
Temperature of data collection (K)	293
Scan mode	$\omega/2\theta$
Data collection range	$4° < 2\theta < 70°$
Stds (measured every 300 min)	−2 2 2, 1 −2 1, 0 3 −1
No. of unique reflections measured	6013 ($h, \pm k, \pm l$)
No. of data with $F_o^2 > 3\sigma(F_o^2)$	4499
No. of parameter refined	391
R^a	0.045
R_w^b	0.050

[a] $R = (\Sigma \| F_o| - k|F_c\|)/\Sigma|F_o|$.
[b] $R_w = \{\Sigma_w(|F_o| - k|F_c|)^2/\Sigma_w|F_o|^2\}^{1/2}$.

methanol (10 cm^3, 1 : 1 v/v) and dried under reduced pressure. The crude product was recrystallized with $CHCl_3$ and shown to be compound **6**. Compounds **1–5** and **7–14** were prepared similarly.

X-ray analysis

A needle-shaped colourless crystal of $Zn[Tp^{4Me}]_2$, **6**, with dimension $1.05 \times 0.21 \times 0.17$ mm was selected for the X-ray analysis and mounted on the Enraf-Nonius CAD4 diffractometer with graphite-monochromated Cu-K_α radiation of the Centro Grandi Strumenti dell'Università, Pavia, Italy.

The SEARCH program was used to obtain 25 reflections, from which approximate cell dimensions were derived by the INDEX program. Accurate lattice parameters were obtained by least-squares refinement of these reflections.

The triclinic cell quoted was confirmed by the TRACER program [36]. The $\omega/2\theta$ scan technique was used to collect the intensities. Three standard reflections were measured every 300 min and showed small random deviations within the limits of statistical fluctuation. The intensities were corrected for Lorentz and polarization factors; an empirical absorption correction [37] with minimum and maximum absorption factors of 0.5589 and 0.9942 was applied. The structure factors were put on an absolute scale [38] and an overall isotropic thermal factor of 5.651 Å^2 was obtained thereby.

Table 8 lists crystal data, data-collection parameters and details of structure refinement.

4499 reflections having $I > 3\sigma(I)$ were considered observed and used in the structure analysis.

Structure determination and refinement

The structure was obtained by Patterson and Fourier methods. A difference Fourier synthesis phased on the two Zn atoms revealed the positions of all the non-hydrogen atoms of the complex molecules. Residual electronic density, observed on successive difference-Fourier syntheses is due to the crystallization solvent $CHCl_3$. The positions of the hydrogen atoms were calculated from the geometry of the compound and checked in a final difference-Fourier map. The final least-squares anisotropic refinement included the hydrogen atoms in fixed positions with the equivalent isotropic thermal parameters of their bonded atoms. In the early refinement stages the observed reflections were given unit weight. The maximum ratio of the parameter shift to the e.s.d. in the final refinement cycle was 0.01. The largest residual peaks on the final difference-Fourer map were 0.432 and −0.303 e Å^{-3} both close to the Zn(2) atom. No extinction correction was applied.

All calculations were carried out with the Enraf-Nonius SDP crystallographic computing package [39] and with local programs.

Supplementary material available

Tables of atomic positional parameters of all atoms, anisotropic thermal parameters, bond distances and bond angles involving non-hydrogen atoms and hydrogen atoms, planarity of molecular regions and a listing of observed and calculated structure factors (total of 45 pages).

Acknowledgements—We gratefully acknowledge the CNR and Universities of Camerino and Pavia for financial support.

REFERENCES

1. (a) S. Trofimenko, *J. Am. Chem. Soc.* 1967, **89,** 3170; (b) S. Trofimenko, *J. Am. Chem. Soc.* 1967, **89,** 6288.
2. D. Qiu, L. T. Kilpatrick, N. Kitajima and T. G. Spiro, *J. Am. Chem. Soc.* 1994, **116,** 2585.
3. R. Alsfasser, A. K. Powell and H. Vahrenkamp, *Angew. Chem.* 1990, **29,** 898.

4. J. C. Calabrese, S. Trofimenko and J. S. Thompson, *J. Chem. Soc., Chem. Commun.* 1986, 1122.
5. C. Hannay, R. Thissen, V. Briois, M. J. Hubin-Franskin, F. Grandejean, G. J. Long and S. Trofimenko, *Inorg. Chem.* 1994, **33,** 5983; G. J. Long and B. B. Hutchinson, *Inorg. Chem.* 1987, **26,** 608; E. Köning, *Prog. Inorg. Chem.* 1987, **35,** 527.
6. F. Grandejean, G. J. Long, B. B. Hutchinson, L. Ohlhausen, P. Neill, J. D. Holcomb, *Inorg. Chem.* 1989, **28,** 4406.
7. S. Trofimenko, *Prog. Inorg. Chem.*, 1986, **34,** 115.
8. S. Trofimenko, *Chem. Rev.* 1993, **93,** 943.
9. (a) J. P. Jesson, S. Trofimenko and D. R. Eaton, *J. Am. Chem. Soc.* 1967, **89,** 3148; (b) J. P. Jesson, S. Trofimenko and D. R. Eaton, *J. Am. Chem. Soc.* 1967, **89,** 3158; (c) J. D. Oliver, D. F. Mullica, B. B. Hutchinson and W. O. Milligan, *Inorg. Chem.* 1980, **19,** 165; (d) M. R. Churchill, K. Gold and C. E. Maw Jr, *Inorg. Chem.* 1970, **9,** 1597; (e) G. Bandoli, D. A. Clemente, G. Paolucci and L. Doretti, *Cryst. Struct. Commun.* 1979, **8,** 965; (f) A. Murphy and B. J. Hathaway, *J. Chem. Soc., Dalton Trans.* 1979, 1646; (g) O. J. Curnow and B. K. Nicholson, *J. Organomet. Chem.* 1984, **267,** 257; (h) R. E. Marsh, *Acta Cryst. C: Cryst. Struct. Commun.* 1989, **45,** 1269.
10. S. H. Cho, D. Whang and K. Kim, *Bull. Korean Chem. Soc.* 1991, **12,** 107; (*CA* 115: 63312s); M. K. Chan and W. H. Armstrong, *Inorg. Chem.* 1989, **28,** 3777; S. H. Cho, D. Whang, K.-N. Han and K. Kim, *Inorg. Chem.* 1992, **31,** 519.
11. P. Cecchi, G. Gioia Lobbia, F. Marchetti, G. Valle and S. Calogero, *Polyhedron* 1994, **13,** 2173.
12. U. B. Ceipidor, M. Tomassetti, F. Bonati, R. Curini and G. D'Ascenzo, *Therm. Acta* 1983, **63,** 59.
13. F. G. Lalor, S. Miller and N. Garvey, *J. Organomet. Chem.* 1988, **356,** C57.
14. S. A. A. Zaidi, T. A. Khan, S. R. Zaidi and Z. A. Siddiqi, *Polyhedron* 1985, **4,** 1163.
15. D. L. Reger and M. E. Tarquini, *Inorg. Chem.* 1983, **22,** 1064.
16. D. L. Reger, M. F. Huff, A. L. Reingold and B. S. Haggerty, *J. Am. Chem. Soc.* 1992, **114,** 579.
17. A. J. Canty, N. J. Minchin, J. M. Patrick and A. M. White, *Aust. J. Chem.* 1983, **36,** 1107.
18. W. R. McWhinnie, Z. M. Mirzai, M. C. Perry, N. Shaikh and T. A. Hamor, *Polyhedron* 1993, **12,** 1193.
19. R. J. Dudley and B. J. Hathaway, *J. Chem. Soc. (A)* 1970, 2794.
20. C. K. Johnson, ORTEP. Report ORNL-3793. Oak Ridge National Laboratory, Tennessee, U.S.A. (1965).
21. K. Nakata, S. Kawabata and K. Ichikawa, *Acta Cryst.* 1995, **C51,** 1092.
22. F. Bonati and B. Bovio, *J. Crystallogr. Spectrosc. Res.* 1990, **20,** 233; F. Bonati, *Gazz. Chim. Ital.* 1989, **120,** 341.
23. G. Gioia Lobbia, C. Pettinari, F. Marchetti, B. Bovio and P. Cecchi, *Polyhedron* 1996, **15,** 881.
24. C. A. Tolman, *Chem. Rev.* 1977, **77,** 313.
25. Y. Sohrin, H. Kokusen, S. Kihara, M. Matsui, Y. Kushi and M. Shiro, *J. Am. Chem. Soc.* 1993, **115,** 4128.
26. S. Calogero, G. Gioia Lobbia, P. Cecchi, G. Valle and J. Friedl, *Polyhedron* 1994, **13,** 87.
27. S. Trofimenko, J. C. Calabrese, P. J. Domaille and J. S. Thompson, *Inorg. Chem.* 1989, **28,** 1091.
28. J. C. Calabrese, P. J. Domaille, S. Trofimenko and G. J. Long, *Inorg. Chem.* 1991, **30,** 2795.
29. J. C. Calabrese, P. J. Domaille, J. S. Thompson and S. Trofimenko, *Inorg. Chem.* 1990, **29,** 4429.
30. R. E. Marsh, *Acta Cryst.* 1989, **C45,** 1269.
31. A. Looney, R. Han, I. B. Gorrell, M. Cornebise, K. Yoon, G. Parkin and A. L. Rheingold, *Organometallics* 1995, **14,** 274.
32. D. L. Reger, S. M. Myers, S. S. Mason, D. J. Darensbourg, M. W. Holtcamp, J. H. Reibenspies, A. S. Lipton and P. D. Ellis, *J. Am. Chem. Soc.* 1995, **117,** 10998.
33. D. L. Reger, S. S. Mason, A. L. Rheingold and R. L. Ostrander, *Inorg. Chem.* 1993, **32,** 5217.
34. R. D. Shannon, *Acta Cryst.* 1976, **32A,** 751.
35. R. D. Shannon and C. T. Prewitt, *Acta Cryst.* 1970, **B26,** 1076.
36. S. L. Lawton and R. A. Jacobson, *TRACER, a cell reduction program.* Ames Laboratory, Iowa State University of Science and Technology, Ames, IA, U.S.A. (1965).
37. A. C. North, D. C. Phillips and F. C. Mathews, *Acta Cryst.* 1968, **A24,** 351.
38. A. J. C. Wilson, *Nature* 1942, **150,** 152.
39. B. A. Frenz and Associates Inc., College Station, TX 77840 and Enraf-Nonius, Delft, The Netherlands (1985).

Pergamon

PII: S0277-5387(96)00288-4

Polyhedron Vol. 16, No. 4, pp. 681–688, 1997
Copyright © 1996 Elsevier Science Ltd
Printed in Great Britain. All rights reserved
0277-5387/97 $17.00+0.00

Molecular structure of acetato *meso*-tetra (4-methoxyphenylporphyrinato)thallium(III), Tl(tmpp)(OAc), and ^{13}C NMR investigation of its homolog cyano *meso*-tetra (4-methoxyphenylporphyrinato)thallium(III), Tl(tmpp)(CN)

Yeong-Horng Sheu,[a] Tay-Ning Hong,[a] Chu-Chieh Lin,[a] Jyh-Horung Chen[a]* and Shin-Shin Wang[b]

[a]Department of Chemistry, National Chung-Hsing University, Taichung 40227, Taiwan, R.O.C.

[b]Union Chemical Laboratories, Hsin-Chu 30043, Taiwan, R.O.C.

(Received 25 April 1996; accepted 5 June 1996)

Abstract—The new compound acetato *meso*-tetra(4-methoxyphenylporphyrinato)thallium(III), Tl(tmpp)(OAc), has been synthesized and its molecular structure determined by X-ray analysis. The displacement of the thallium atom from the porphyrin mean plane was 0.808 Å. The geometry around the thallium centre of the Tl(tmpp)(OAc) molecule has Tl—O(1) = 2.29(1) and Tl—O(2) = 2.48(1) and average Tl—Np = 2.211(8)Å. An asymmetric-bidentate acetato group is coordinated to the thallium(III) atom. The free energy of activation $\Delta G^{\ddagger}_{224}$ for the acetato group of Tl(tmpp)(OAc) in CD_2Cl_2 solvent undergoing intramolecular exchange has been derived to be 48.4 kJ mol^{-1} through ^1H NMR temperature-dependent measurements. In the intermediate exchange region, neither the carbonyl nor methyl signals of the acetate ligand for Tl(tmpp)(OAc) in CD_2Cl_2 solvent in ^{13}C NMR spectra was found at 20°C. In the slow exchange region, the methyl and carbonyl carbons of the acetato group are separately located at 17.7 ppm [with ^3J(Tl—^{13}C) coupling constant 275 Hz] and 173.9 ppm [with ^2J(Tl—^{13}C) coupling constant 230 Hz], respectively, for the Tl(tmpp)(OAc) in CD_2Cl_2 at −90°C. The ^{13}C resonance of the axial cyano ligand in the title compound cyano *meso*-tetra(4-methoxyphenylporphyrinato)thallium(III), Tl(tmpp)(CN), was observed at 139.9 ppm (20°C) [with ^1J(^{205}Tl—^{13}C) coupling constant 5287.3 Hz and ^1J(^{203}Tl—^{13}C) coupling constant 5238.0 Hz]. This indicates that the cyano group is, as cyanide type, axially coordinated to the Tl atom in Tl(tmpp)(CN).
Copyright © 1996 Elsevier Science Ltd

Keywords: crystal structure; thallium porphyrins; NMR analysis; asymmetric-bidentate ligand; intra- and intermolecular exchange; acetate.

The molecular structure and dynamical NMR studies of acetato *meso*-tetraphenylporphyrinatothallium (III), Tl(tpp)(OAc) [1–3], and acetato *meso*-tetra(4-pyridyl)porphyrinatothallium(III), Tl(tpyp)(OAc) [4, 5], have been reported by ourselves and others. It turned out that the acetato ligand exchange for Tl(tpyp)(OAc) in CD_2Cl_2 solvent was intermolecular [4, 5], whereas the exchange for Tl(tpp)(OAc) in the same solvent was intramolecular [1, 2]. The driving force for the intermolecular exchange might be due to hydrogen bonding between Tl(tpyp)(OAc) and HOAc. When the tpp or tpyp was replaced by tmpp, the new complex, acetato *meso*-tetra(4-methoxyphenyl) porphyrinatothallium(III), Tl(tmpp)(OAc) was obtained. The acetato exchange of Tl(tpyp)(OAc) and

* Author to whom correspondence should be addressed.

Tl(tpp)(OAc) in CD_2Cl_2 encouraged us to investigate similar exchange of Tl(tmpp)(OAc) in the same solvent by a dynamical NMR method.

Previously, Senge *et al.* [6] reported the X-ray crystallographic characterization of cyano *meso*-tetra(4 - methoxypheyl)porphyrinatothallium(III), Tl(tmpp)(CN) and Coutsolelos *et al.* [7] reported the crystal structure of isocyano *meso*-tetraphenylporphyrinatothallium(III), Tl(tpp)(NC). However, they were not able unambiguously to solve the dichotomy of isocyanide versus cyanide binding to the thallium centre on the basis of the crystalographic data for Tl(tmpp)(CN) [6] and Tl(tpp)(NC) [7]. As described in our previous papers, with a pulse delay of 3.5 s (i.e. longer than 3.0 s), the ^{13}C signal of CN instead of bonding to Tl(tpp)(NC) [7] but bonding to cyano *meso*-tetraphenylporphyrinatothallium(III), Tl(tpp)(CN) [8], [or cyano *meso*-tetra(4-pyridyl)porphyrinatothallium(III), Tl(tpyp)(CN), [9] appears as two pairs of doublets at 139.2 ppm with $^1J(^{205}Tl—C) = 5394$ Hz and $^1J(^{203}Tl—C) = 5344$ Hz [or at 137.7 ppm with $^1J(^{205}Tl—C) = 5852$ Hz and $^1J(^{203}Tl—C) = 5795$ Hz].

In this paper, the synthesis, its NMR spectroscopic studies, and the molecular structure of the crystalline Tl(tmpp)(OAc) by X-ray analysis are reported. The long pulse delay technique was used to observe the ^{13}C resonance of the cyano ligand of Tl(tmpp)(CN) and resolve the ambiguous binding for both types.

Table 1. Crystal data for Tl(tmpp)(OAc)·$1CH_2Cl_2$ (or $C_{51}H_{41}Cl_2N_4O_6Tl$)

Formula	$C_{51}H_{41}Cl_2N_4O_6Tl$
Formula weight	1081.1
a (Å)	12.943(2)
b (Å)	14.741(2)
c (Å)	24.034(3)
β (°)	102.76(1)
V (Å^3)	4472(1)
Z	4
Dc (g cm^{-3})	1.606
Space group	$P2_1/n$
$F(000)$	2152
μ (cm^{-1})	37.87
R^a (%)	5.00
R_w^b (%)	6.50
GOF	1.43
A^b	1
B^b	10^{-3}
Largest feature final Diff. map (e Å^{-3})	1.22
Crystal size (mm^3)	$0.3 \times 0.5 \times 0.5$
Data collected	7631
$2\theta_{max}$ (°)	48
Temperature (K)	293
Data used	5140
Discrimination	$F > 4.0\sigma(F)$

$^aR = [\Sigma \| F_o \| - \| F_c \| / \| F_o \|]$.

$^bR_w = [(\Sigma w(\| F_o \| - \| F_c \|^2 / \Sigma w \| F_o \|^2)^{1/2}]$; $w = A/(\sigma^2 F_o + BF_o^2)$.

EXPERIMENTAL

Crystallography

Crystal Data and other information for Tl(tmpp)(OAc)·$1CH_2Cl_2$ (or $C_{51}H_{41}Cl_2N_4O_6Tl$) are given in Table 1. Measurements were made on a Siemens R3m/V diffractometer using monochromatized Mo-K_α radiation ($\lambda = 0.71073$ Å) *via* the $\theta-2\theta$ scan technique. Semi-empirical absorption corrections were applied. The range of transmission factors was 0.416–1.000. The structure was solved by direct methods (SHELXTL PLUS) and refined by full-matrix least-squares. All non-hydrogen atoms were refined with anisotropic thermal parameters, whereas all hydrogen atoms were calculated using a riding model and included in the structure factor calculations. Selected bond distances and angles are given in Table 2.

NMR spectra

Proton and ^{13}C NMR spectra were recorded at 400.13 and 100.61 MHz, respectively, on a Bruker AM-400 spectrometer in CD_2Cl_2 (or $CDCl_3$) locked on solvent deuterium, and referenced to the solvent peak. The temperature of the spectrometer probe was calibrated by the shift difference of methanol resonance in the ^1H NMR spectrum. Solid-state ^{13}C CP/MAS NMR spectra were recorded at 20°C at 50.33 MHz on a Bruker MSL-200 solid-state NMR spectrometer. Dry nitrogen gas was used to drive MAS rates of 3.6 Hz.

Preparation of Tl(tmpp)(OAc)

Free base (tmpp); 146.1 mg, 0.19 mmoles, from Aldrich) and $Tl(OAc)_3$ (236.4 mg, 0.62 mmoles) were refluxed for 5 h in 20 cm^3 of acetic acid containing sodium acetate 70.9 mg. After cooling, water (150 cm^3) was added, and the solid collected and dried by suction. The filter cake was dissolved with CH_2Cl_2 and collected by vacuum filtration. Recrystallization from CH_2Cl_2–hexane gave violet crystals (181 mg, 91.4%). The crystals were grown by diffusion of ether vapour into a $CHCl_3$ solution. It was dissolved in CD_2Cl_2 for ^1H and ^{13}C NMR measurement (shown in Tables 3 and 4).

Preparation of Tl(tmpp)Cl

Tl(tmpp)(OAc) (101.1 mg, 0.101 mmoles) was passed down an alumina column (10 g, neutral, activity I). The major purple band eluting with chloro-

Table 2. Selected bond distances (Å) and angles (°)

Tl—O(1)	2.29(1)	Tl—N(1)	2.215(7)
Tl—O(2)	2.48(1)	Tl—N(2)	2.178(8)
O(1)—C(21)	1.19(2)	Tl—N(3)	2.222(8)
O(2)—C(21)	1.21(2)	Tl—N(4)	2.230(8)
C(21)—C(22)	1.49(2)		
O(1)—Tl—O(2)	51.2(4)	N(1)—Tl—N(2)	84.9(3)
O(2)—C(21)—O(1)	119(1)	N(1)—Tl—N(3)	141.6(3)
O(2)—C(21)—C(22)	120(1)	N(1)—Tl—N(4)	84.0(3)
O(1)—C(21)—C(22)	121(2)	N(2)—Tl—N(3)	83.2(3)
O(1)—Tl—N(1)	121.4(3)	N(2)—Tl—N(4)	140.0(3)
O(1)—Tl—N(2)	125.8(3)	N(3)—Tl—N(4)	82.1(3)
O(1)—Tl—N(3)	94.9(4)	O(2)—Tl—N(1)	90.8(3)
O(1)—Tl—N(4)	92.4(4)	O(2)—Tl—N(2)	85.9(4)
Tl—O(2)—C(21)	89.7(8)	O(2)—Tl—N(3)	124.4(4)
Tl—O(1)—C(21)	100(1)	O(2)—Tl—N(4)	132.5(4)

Table 3. Proton chemical shifts (δ) and thallium–proton coupling constants (J in Hz) for the Tl(tmpp)(OAc), Tl(tmpp)Cl, Tl(tmpp)(CN) complexes in $CDCl_3$ (or CD_2Cl_2) in the absence of the axial ligand[a]

Compound	Temp(°C)	H_β(β-pyrrole)	$H_{2,6}$		$H_{3,5}$		p-O-CH_3
Tl(tmpp)(OAc) in CD_2Cl_2	20	9.06	8.22	8.05	7.33	7.28	4.07
		(63)[b]	(8)[c]	(8)	(8)	(8)	
	−90	9.04	8.13	7.92	7.27	7.13	3.95
		(64)	(8)	(8)	(8)	(8)	
Tl(tmpp)Cl in CD_2Cl_2	20	9.14	8.28	8.01	7.34	7.22	4.03
		(64)	(8)	(8)	(8)	(8)	
	Room temp[d]	9.09	8.15(m)[e]		7.32(m)		4.13
		(65)					
Tl(tmpp)(CN) in $CDCl_3$	20	9.10	8.31	8.02	7.4	7.3	4.10
		(59)	(8)	(8)	(8)	(7)	
	Room temp[d]	9.08	8.15(m)		7.41-7.27(m)		4.12
		(62)					

[a]Chemical shifts in ppm relative to CD_2Cl_2 at 5.3 ppm and to $CDCl_3$ at 7.24 ppm, respectively.
[b]Value in parentheses beneath are ^4J(Tl—H) coupling constants in Hz.
[c]Value in parentheses beneath are ^3J(H—H) coupling constants in Hz.
[d]From [6].
[e]m = multiplet.

form was collected and concentrated. The crystalline product obtained was purple (91.5 mg, 94.7%). It was dissolved in CD_2Cl_2 for NMR measurement at 20°C (shown in Tables 3 and 4).

Preparation of Tl(tmpp)(CN)

The compound Tl(tmpp)Cl (370 mg, 0.387 mmoles) was dissolved in $CHCl_3$ (20 cm^3). After the addition of a solution of NaCN (189.67 mg) in dry methanol (15 cm^3), the mixture was stirred for 3 days at room temperature [9], then extracted with distilled water thrice (50 × 3 cm^3). The purple crystals, Tl(tmpp)(CN), (333 mg, 90.8%) were collected by vacuum filtration and dried. It was dissolved in $CDCl_3$ for ^1H (Table 3) and ^{13}C (Table 4) NMR measurement at 20°C.

RESULTS AND DISCUSSION

Molecular structure of Tl(tmpp)(OAc)

The skeletal framework of the Tl(tmpp)(OAc) molecule is illustrated in Fig. 1. It reveals the six-coordination of the thallium atom with the four nitrogen atoms (N_p) of the porphyrinato group and the asymmetric-bidentate OAc^- ligand, the bond distances are: Tl—O(1) = 2.29(1), Tl—O(2) = 2.48(1), O(1)—C(21) = 1.19(2), O(2)—C(21) = 1.21(2), C(21)—C(22) = 1.49(2) Å and the mean Tl—N_p = 2.211(8) Å. The thallium atom lies 0.741

Table 4. ^{13}C chemical shifts (δ) and thallium–carbon coupling constants (J in Hz) of Tl(tmpp)(OAc), Tl(tmpp)Cl, Tl(tmpp)(CN) complexes in CD_2Cl_2 (or $CDCl_3$)[a]

Compound	Temp (°C)	C_4	C_α	$C_{2,6}$ ($C_{2,2'}$)	C_1	C_β	C_m	$C_{3,5}$ ($C_{3,3'}$)	*p*-OCH_3	COC^*H_3	C^*OCH_3	CN
Tl(tmpp)(OAc) in CD_2Cl_2	20	160.0	150.5	135.7	136.3	134.5	132.8	122.2	112.6	55.8	—	—	—
			(20)	(23)	(23)	(28)	(120)	(150)	112.5				
	−85	158.4	149.1	135.3	135.7	133.0	132.1	121.3	111.5	54.7	17.7	173.9	—
			(18)	(22)	(22)	(28)	(119)	(148)	111.3		(275)	(230)	
Tl(tmpp)(OAc), ^{13}C CP/MAS (solid)	20	158.9	150.6		132.9			122.4	109.9	55.8	16.9	173.9	—
								(144)			(268)	(240)	
Tl(tmpp)Cl in CD_2Cl_2	20	160.1	150.4	135.7	136.4	134.2	132.2	122.3	112.7	55.8	—	—	—
			(13)	(18)	(19)	(25)	(120)	(142)	122.6				
Tl(tmpp)(CN)inCDCL$_3$	20	159.7	150.1	136.3	135.3	134.1	132.6	121.8	112.5	55.6	—	—	$^1J(^{205}Tl—CN) = 5287.3$
						(17)	(102)	(117)	112.3				$^1J(^{203}Tl—CN) = 5238.0$

[a]Chemical shifts in ppm relative to the centre line of CD_2Cl_2 at 53.2 ppm or to the centre line of $CDCl_3$ at 77.0 ppm. Values in parentheses beneath are $J(Tl—^{13}C)$ coupling constants in Hz.

and 0.808 Å from the four porphyrin nitrogens (N_p) and the 24-atom porphyrin plane ($C_{20}N_4$), respectively, and the O(1)—Tl—O(2) bond angle is 51.2(4)°. The dihedral angles between the mean plane of the porphyrin skeleton and the mean planes of four phenyl groups are 59.6° [C(31)], 96.8° [C(41)], 59.5° [C(51)], and 110.4° [C(61)].

Hoard and co-workers [10] have calculated that the radial strain in the core of a metalloporphyrin is minimized for a "radius of the central hole" of about 2.01 Å. The radius of core size (i.e. C_t—N, the distance from the geometrical centre of the mean plane of the 24-atom core to the porphyrinato-core N atoms) of Tl(tmpp)(OAc) is 2.084 Å, which is larger than 2.01 Å. The Tl^{III} atom is bonded in a highly expanded porphyrinato core ($C_{20}N_4$) in Tl(tmpp)(OAc) and the porphyrin ($C_{20}N_4$ and Tl) can be viewed as dome shaped. Figure 2 shows the displacement (in Å) of each atom of the porphyrin ($C_{20}N_4$ and Tl) from the porphyrin mean plane ($C_{20}N_4$). The average out-of-plane displacements of the thallium, nitrogen (N_p), C_α, C_{meso}, and C_β atom are 0.81, 0.07, 0.02, 0.02, and −0.06 Å, respectively (shown in Fig. 2). This structure shows marked "doming" with atoms approximately in descending planes thallium, N_p, Cα, C_{meso}, C_β. The difference between the displacement of the metal centre from the mean plane of the four pyrrole nitrogens ($4N_p$) and the mean plane of the $C_{20}N_4$ porphyrin skeleton has been used to describe the degree of doming. The net doming is ~ 0.07 Å (≈ 0.808–0.741).

Dynamical NMR of Tl(tmpp)(OAc) *in* CD_2Cl_2

When a 0.02 M solution of Tl(tmpp)(OAc) in CD_2Cl_2 (Fig. 3) was cooled, the methyl proton signal, a single peak at 20°C (δ = 0.01 ppm) first broadened (temperature of coalescence, T_c = −49°C) and then split into two peaks with a separation of 14.2 Hz. The process is completely reversible, and the results measured at 400 MHz confirm the separation as a coupling $^4J(Tl—H)$ rather than a chemical-shift difference. This process is treated as a two-site intramolecular exchange [11], a comparison of observed and computed spectra yields $\Delta G^*_{224} = 48.4$ kJ/mol. ^{13}C NMR data for Tl(tmpp)(OAc) at 20 and −85°C is shown in Table 4. At −85°C, the rate of intramolecular exchange of OAc^- for Tl(tmpp)(OAc) in CD_2Cl_2 is 5.8 Hz. This exchange rate is slow comparable with the coupling frequency $Tl—^{13}C$, i.e. 253 ± 23 Hz. The methyl and carbonyl carbons of the acetato group are observed at 17.7 ppm [with $^3J(Tl—^{13}C) = 275$ Hz] and 173.9 ppm [with $^2J(Tl—^{13}C) = 230$ Hz], respectively. At 20°C, the intramolecular exchange rate of the acetato ligand is comparable with the coupling frequency of $Tl—^{13}C$. In this intermediate exchange region, the signals are broadened beyond detection. Hence, no signal of the axial ^{13}C has been found at 20°C.

Tl(tmpp)(OAc) does not hydrolyze in CD_2Cl_2.

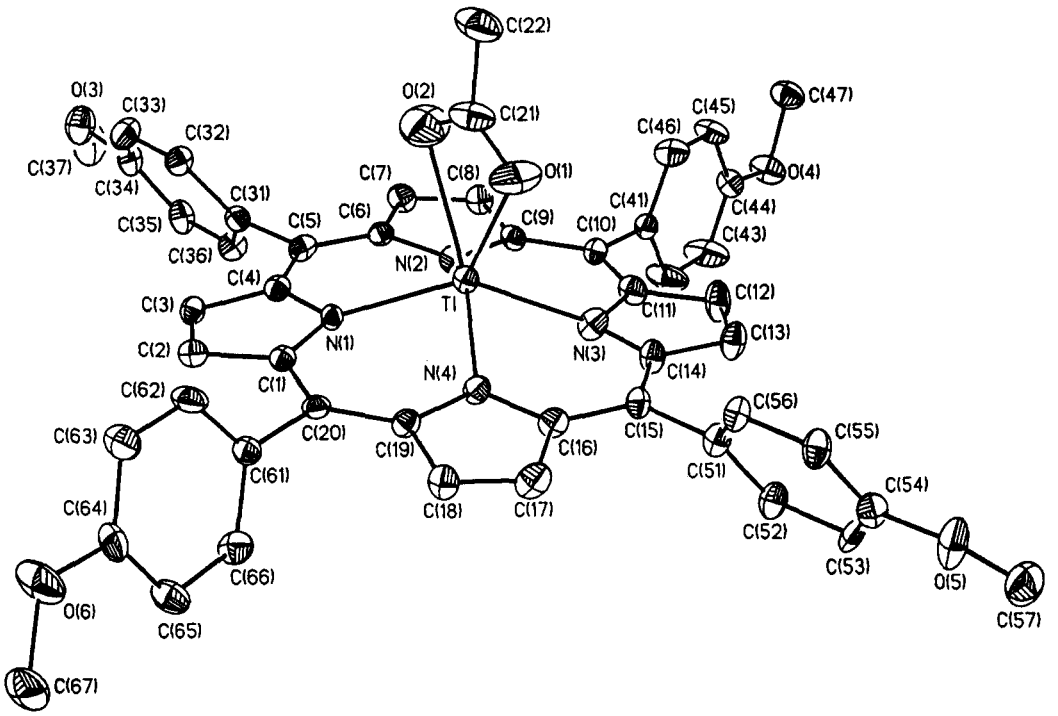
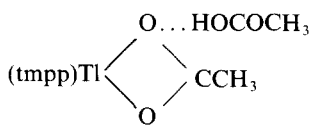


Fig. 1. Molecular configuration and atoms labelling scheme for Tl(tmpp)(OAc)·$1CH_2Cl_2$. Hydrogen atoms and solvent [C(71)H_2Cl(1)Cl(2)] are omitted for clarity.

Hence, the exchange of OAc^- for Tl(tmpp)(OAc) in CD_2Cl_2 solvent is intramolecular. If ~ 0.05 cm^3 of acetic acid (HOAc) is intentionally added to the solution of Tl(tmpp)(OAc) in CD_2Cl_2, the OAc^- exchange switches from intramolecular to intermolecular. At −90°C, the singlet peak with population 99% at 2.03 ppm corresponds to added HOAc and the other singlet peak with population 1% at −0.09 ppm is due to Tl(tmpp)(OAc). These two sets of peaks arise from the slow exchange of OAc^- between Tl(tmpp)(OAc) and HOAc. The slow exchange limit should be at temperature below −90°C. At 20°C, the sharp singlet at 1.99 ppm is due to the fast exchange of OAc^- between two compounds. This result indicates that two stages occur. The first stage is possibly a hydrogen bonding between Tl(tmpp)(OAc) and HOAc:



The other stage is a reversible intermolecular OAc^- exchange between Tl(tmpp)(OAc) and HOAc. The key step for the occurrence of intermolecular OAc^- exchange is the existence of HOAc externally added.

Solid-state ^{13}C *NMR data for* Tl(tmpp)(OAc)

Solid-state ^{13}C CP/MAS data of crystalline Tl(tmpp)(OAc) at 20°C are shown in Table 4. Eight major resonances with the methyl carbon at δ = 16.9, carbonyl carbon at δ = 173.9, *p*-O-CH_3 at δ = 55.8. *meta* carbon ($C_{3,5}$) at δ = 109.9, *meso* carbon (C_m) at δ = 122.4, $C_{1,2,6,\beta}$ at δ = 132.9, α carbon (C_α) at δ = 150.6, and *para* carbon (C_4) at δ = 158.9 ppm were observed. Both the ^{13}C chemical shift and thallium–carbon coupling constant data for the crystalline are consistent with the low-temperature solution data of Tl(tmpp)(OAc) in CD_2Cl_2 at −90°C. This provides evidence that the acetate is asymmetric-bidentate chelating to the thallium atom in CD_2Cl_2 at −90°C. As the temperature increases from −90 to 20°C, it becomes dynamical symmetric bidentate (or symmetrically pseudo-chelating) [2,12], and the acetate exchange is fast on the ^1H NMR time-scale at this temperature. This explains how the methyl protons of the apical acetate ligand were observed at 20°C as a sharp singlet at δ = 0.01 ppm, with no evidence of coupling of the thallium nuclei with the acetate group.

The intermolecular exchange of the OAc^- group is rapid for Tl(tmpp)(OAc) in CD_2Cl_2 at 20°C, whereas the rotation of the anisole group along C_1—C_{meso} bond is slow at the same temperature on the NMR time-scale. It is supported either by the assignment of 135.7, 136.3 ppm to $C_{2,6}$ carbons and 112.6, 112.5 ppm due to the $C_{3,5}$ carbons (shown in Table 4) or by the assignment of 8.22, 8.05 ppm to $H_{2,6}$ protons and 7.33, 7.28 ppm due to the $H_{3,5}$ protons (shown in Table 3) for Tl(tmpp)(OAc) at 20°C. Likewise, inequivalent *o*-H and *m*-H protons at 20°C are observed for

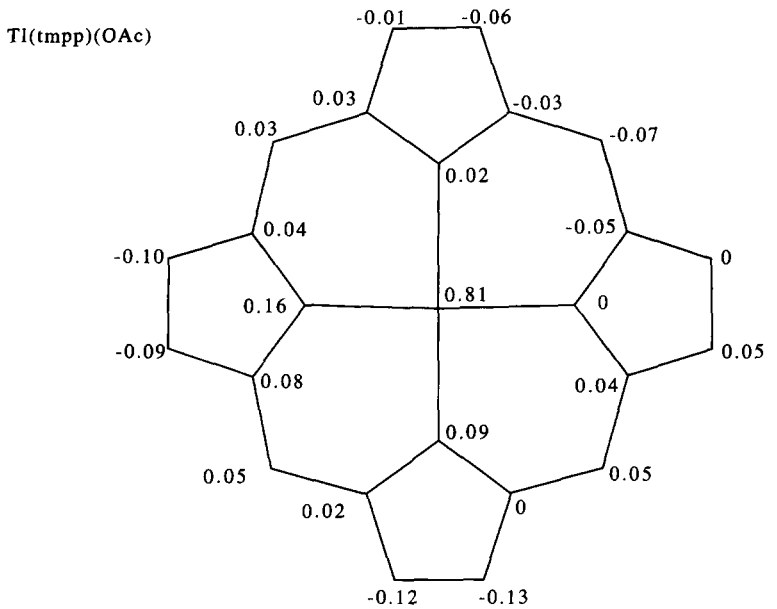


Fig. 2. Formal diagram for the porphyrin core ($C_{20}N_4$ and Tl) of Tl(tmpp)(OAc) in which each atom symbol is replaced by a number showing the displacement (in unit of Å) of that atom from the mean plane of the porphyrin ($C_{20}N_4$).

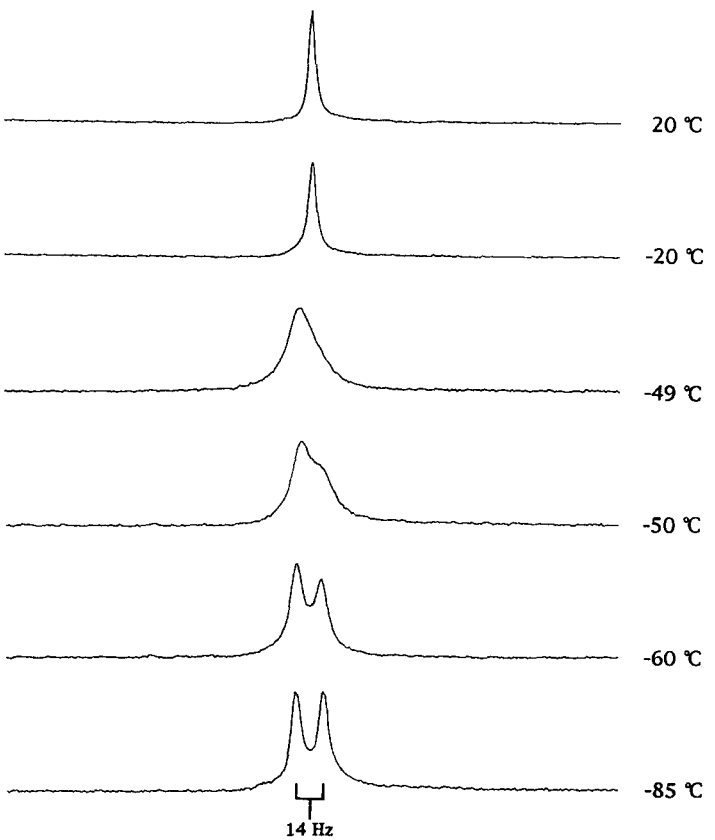


Fig. 3. 400.13 MHz ^{1}H NMR spectra for the axial acetato protons of Tl(tmpp)(OAc) in CH_2Cl_2 at various temperatures.

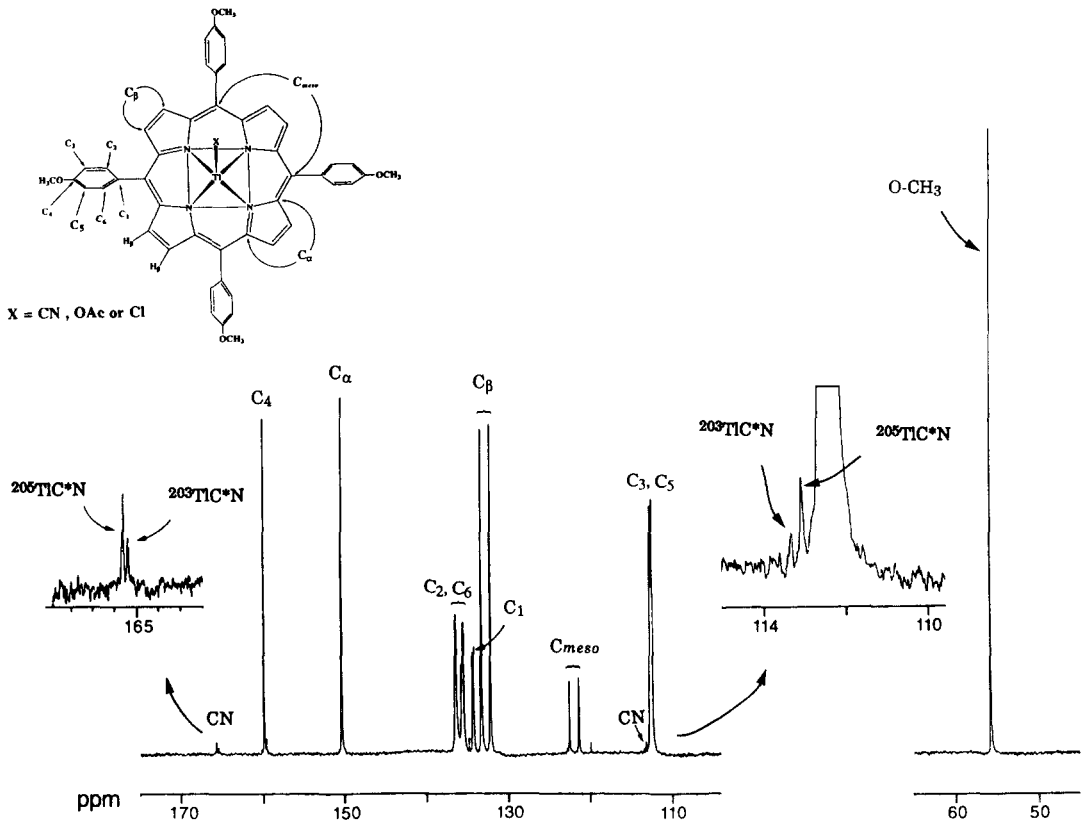


Fig. 4. 100.61 MHz ^{13}C Broad band NMR spectrum of Tl(tmpp)(CN) in $CDCl_3$ at 20°C with a pulse delay of 3.5 s.

Tl(tmpp)(OAc), Tl(tmpp)Cl and Tl(tmpp)(CN) (shown in Table 3) while the literature data appear to show average values at room temperature [6].

^{13}C *NMR for* Tl(tmpp)(CN) in solution

Figure 4 shows the representative broad band ^{13}C spectrum of Tl(tmpp)(CN) in $CDCl_3$ solvent at 20°C with a pulse delay of 3.5 s. The ^{13}C signal of CN bonded to Tl(tmpp)(CN) appears as two pairs of doublets at 165.57 and 113.02 ppm and 165.33 and 113.27 ppm for the outer and inner pairs, respectively. The outer pair arises from $^{205}Tl—^{13}C$ coupling (5287.3 Hz) and the inner one from $^1J(^{203}Tl—^{13}C)$ (5238.0 Hz). This is confirmed by noting that $^1J(^{205}Tl—^{13}C)/^1J(^{203}Tl—^{13}C) = 1.0094$, which is quite close to the theoretical value calculated from $\gamma(^{205}Tl)/\gamma(^{203}Tl) = 1.0098$. The ^{13}C chemical shifts of axial CN are upfield shift about 29.2 ppm from 168.5 ppm (obtained on saturated aqueous solution of the KCN salts) [13] to 139.3 ppm. The value of $^1J(^{203,205}Tl—^{13}C)$ obtained from Tl(tmpp)(CN) are agreeable to those obtained {5852[$^1J(^{205}Tl—^{13}C)$], 5795 [$^1J(^{203}Tl—^{13}C)$]} from Tl(tpyp)(CN) [9] and {5394[$^1J(^{205}Tl—^{13}C)$], 5344 [$^1J(^{203}Tl—^{13}C)$]} from Tl(tpp)(CN) [8].

Acknowledgements—Financial support of the National Research Councils of the R.O.C. under Grant NSC 85-2113-M-005-019 is gratefully acknowledged. J. H. Chen wishes to thank Miss Suh-Yung Fang (Hsinchu Major Instrument Centre) for help in measuring the solid state ^{13}C CP/MAS spectrum with a Bruker MSL-200 solid state NMR spectrometer.

REFERENCES

1. J. C. Chen, H. S. Jang, J. H. Chen and L. P. Hwang, *Polyhedron* 1991, **10,** 2069.
2. S. C. Suen, W. B. Lee, F. E. Hong, T. T. Jong, J. H. Chen and L. P. Hwang, *Polyhedron* 1992, **11,** 3025.
3. R. J. Abraham, G. E. Barnett and K. M. Smith, *J. Chem. Soc., Perkin Trans. I* 1973, 2142.
4. J. J. Fuh, S. S. Tang, Y. H. Lin, J. H. Chen, T. S. Liu, S. S. Wang and J. C. Lin, *Polyhedron* 1994, **13,** 3031.
5. S. S. Tang, Y. H. Lin, M. T. Sheu, C. C. Lin, J. H. Chen and S. S. Wang, *Polyhedron* 1995, **14,** 1241.

6. M. O. Senge, K. R. Senge, K. J. Reli and K. M. Smith, *J. Chem. Soc., Dalton Trans.* 1993, 3519.
7. A. G. Coutsolelos, A. Tsapara, D. Daphnomili and D. L. Ward, *J. Chem. Soc., Dalton Trans.* 1991, 3413.
8. W. B. Lee, S. C. Suen, T. T. Jong, F. E. Hong, J. H. Chen, H. J. Lin and L. P. Hwang, *J. Organomet. Chem.* 1993, **450,** 63.
9. T. W. Cheng, Y. J. Chen, F. E. Hong, J. H. Chen, S. L. Wang and L. P. Hwang, *Polyhedron* 1994, **13,** 403.
10. D. M. Collins and J. L. Hoard, *J. Am. Chem. Soc.* 1970, **92,** 3761.
11. I. O. Sutherland, *Annual Reports on Nuclear Magnetic Resonance Spectroscopy*, (Edited by E. F. Mooney) Vol. 4, p. 71. Academic Press, London and New York (1971).
12. N. W. Alcock and V. M. Tracy, *J. Chem. Soc., Dalton Trans.* 1976, 2243.
13. G. E. Maciel and D. A. Beatty, *J. Phys. Chem.* 1965, **69,** 3920.

Pergamon

PII: S0277-5387(96)00286-0

Polyhedron Vol. 16, No. 4, pp. 689–694, 1997
Copyright © 1996 Elsevier Science Ltd
Printed in Great Britain. All rights reserved
0277-5387/97 $17.00+0.00

Preparation, crystal structure, magnetic and EPR properties of a heptacoordinated manganese(II) chain of $[Mn(bipy)(H_2O)(TBD)]_n$ (H_2TBD = *trans*-2-butene diacid, bipy = 2,2′-bipyridine)

Xiang Shi Tan,[a] Dao Feng Xiang,[a] Wen Xia Tang[a]* and Jie Sun[b]

[a]State Key Laboratory of the Coordination Chemistry, Coordination Chemistry Institute, Nanjing University, Nanjing 210093, P.R. China

[b]Laboratory of Organometallic Chemistry, Shanghai Institute of Organic Chemistry, Chinese Academy of Sciences, Shanghai 200032, P.R. China

(Received 10 April 1996; accepted 5 June 1996)

Abstract—An infinite zigzag chain manganese(II) complex $[Mn(bipy)(H_2O)TBD)]_n$ (bipy = 2,2′-bipyridine; H_2TBD = trans-2-butene diacid) has been prepared and characterized by single-crystal X-ray diffraction, and magnetic measurements. The structure was solved by direct methods and refined by least-squares methods to $R(Rw)$ values of 0.031 (0.042). Each TBD is bound to two manganese(II) ions through carboxylate oxygens, affording the manganese(II) ions bridged by TBD group to yield a infinite chain running along the a axis. The intrachain Mn···Mn separation is 9.05 Å, while the shortest interchain Mn···Mn distance is 5.86 Å. The manganese(II) ion displays a distorted pentagonal bipyramid coordination by virtue of a bidentate bipyridine, two carboxylate groups of two TBD and a H_2O molecule. The variable temperature magnetic susceptibility of the title complex in the temperature range 3.3–302 K has been interpreted in terms of Heisenberg chain model with a molecular field, the values obtained for J, g and zJ' being: 0.58 cm^{-1}, 2.01, and −0.09 cm^{-1}, respectively, indicating weakly antiferromagnetic intra- and interchain exchange interactions. The x-band EPR spectrum of the complex exhibits a six-line manganese hyperfine pattern centered at $g = 2.001$, $A = 94.5$ G, together with five "forbidden" hyperfine doublets. Copyright © 1996 Elsevier Science Ltd

Keywords: manganese complexes; chain complexes; crystal structures; magnetism; trans-2-butene diacid; z,z′-bipyridine.

The study of magnetic exchange interaction through extended bridging ligands has been of major interest in the field of molecular magnetism in the past few years [1]. In consideration of this reason, a number of homo- and(or) heteronuclear one-dimensional chain manganese(II) complex polymers [2–7] has been designed and synthesized, and magnetic exchange interactions of these complexes have been revealed by single crystal X-ray and magnetic analyses. However, to our knowledge, no polymeric manganese(II) complexes bridged by TBD (dianion of *trans*-2-butene diacid) ligands has been reported up to now. In the present paper we describe the preparation, crystal structure and magnetic and EPR properties of an infinite chain manganese(II) complex with bridging TBD ligand, $[Mn(bipy)(H_2O)(TBD)]_n$. This complex is also the first example of a heptacoordinated manganese(II) compound in an infinite zigzag chain.

* Author to whom correspondence should be addressed.

EXPERIMENTAL

Preparations

All reagents were reagent grade and used as received. The piperidinium salt of *trans*-2-butene

diacid was prepared in the similar method to piperidinium salt of terephthalic acid [8].

$[Mn(bipy)H_2O)\ (TBD)]_n$. A methanolic solution (30 cm^3) of 2,2′-bipyridine (2.0 mmol) and piperidinium salt of *trans*-2-butene diacid (2.0 mmol) was slowly added to the solution (30 cm^3) of manganese(II) perchlorate hexahydrate (2.0 mmol) in the same solvent with continuous stirring. The light yellow powder separated during the addition was obtained by filtration. Yellow rhombohedra of the title complex suitable for X-ray analysis were obtained in a 65% yield after 2 weeks by slow evaporation of the mother-liquor at room temperature. Found: C, 49.4; H, 3.6; N, 8.2; Mn, 16.4. Calc. for $C_{14}H_{12}N_2O_5Mn$: C, 48.9; H, 3.5; N, 8.2; Mn, 16.0%.

Physical measurements

Magnetic measurements on powder samples were carried out with a CF-1 type extracting sample magnetometer in the temperature range 3.3–302 K, and corrections for the diamagnetism of the title complex was estimated from Pascal's constants to be -175.0×10^{-6} cm^3/mol. The X-band EPR spectrum was recorded with a Bruker ER 200D-SRC spectrometer in MeOH/DMF solution at 110 K, employing X-band radiation and cylindrical cavity with 100 KHz magnetic field modulation. Calibrations of the microwave frequency were performed with an EIP 845A microwave frequency counter.

X-ray crystallography

Diffraction data were collected at 293(1) K on a Rigaku AFC7R four-circle diffractometer with graphite monochromated Mo-K_α radiation (λ = 0.71069 Å) and a 12 kW rotating anode generator. Details of the crystallographic data collection and structure refinement are listed in Table 1. The cell parameters were determined from least-squares refinement of the setting angles of 22 reflections in the range $23.45 < 2\theta < 26.67°$. A total of 2769 reflections were collected using the ω-2θ scan technique to a maximum 2θ value of 50.0°. The intensities of three representative reflections were measured after every 200 reflections. Over the course of data collection, the standards decreased by −0.5%. A linear correction factor was applied to the data to account for this phenomenon. The linear absorption coefficient, μ, for Mo-K_α radiation is 9.4 cm^{-1}. An empirical absorption correction based on azimuthal scans of several reflections was applied which results in transmission factors ranging from 0.67 to 1.00. The data was corrected for Lorentz and polarization effects. The structure was solved by direct methods and expanded using Fourier techniques. The non-hydrogen atoms were refined anisotropically, while hydrogen atoms were refined isotropically. The final cycle of full-matrix least-squares refinement was based on 1874 observed reflections ($I > 3.00\sigma(I)$) and 248 variable parameters and converged with unweighted and weighted agreement factor of $R = \Sigma||F_o| - |F_c||/\Sigma|F_o| = 0.031$, $Rw = [\Sigma w(|F_o| - |F_c|)^2/\Sigma F_o^2]^{1/2} = 0.043$. The standard deviation of an observation of unit weight was 1.46. The maximum and minimum peaks on the final difference Fourier map corresponded to 0.28 and −0.32 $eÅ^{-3}$, respectively. All calculations were performed using the TEXSAN crystallographic software package of Molecular Structure Corporation.

Table 1. Summary of crystal data, data collection and structure refinement for the title complex

Formula	$C_{14}H_{12}N_2O_5Mn$
M	343.20
Crystal size (mm)	$0.2\times0.2\times0.3$
Crystal system	orthorhombic
Space group	P_{bca}
a (Å)	15.997(2)
b (Å)	19.718(4)
c (Å)	9.102(2)
V (Å^3)	2871.0(9)
Z	8
D_c (g cm^{-1})	1.588
μ(Mo-K_α) (cm^{-1})	9.44
F(000)	1400
λ(Mo-K_α) (Å)	0.71069
Scan type	ω-2θ
2θ range (°)	0–50
No. of total reflections	2769
No. of observed reflections $[I > 3\sigma(I)]$	1874
R^a	0.031
Rw^b	0.043
GOF	1.46

[a] $R = \Sigma||F_o| - |F_c||/\Sigma|F_o|$.
[b] $Rw = [\Sigma w(|F_o| - |F_c|)^2/\Sigma F_o^2]^{1/2}$.

RESULT AND DISCUSSION

Structure description

Selected bond lengths and angles are listed in Table 2. The structure of the title complex consists of infinite zigzag chains of $[Mn(bipy)\ (H_2O)\ (TBD)]_n$ (Figs 1 and 2). One of the independent structure units is shown in Fig. 1 together with the atom-numbering scheme. The TBD (dianion of *trans*-2-butene diacid) group acts as a tetrakis (monodentate) ligand which is bound on each side to one manganese(II) ion through the carboxylate oxygens in a *syn* configuration yielding a chain which runs parallel to the *a* axis of the orthorhombic cell, as shown in Fig. 2. The intrachain Mn···Mn separation is 9.05 Å, while the shortest interchain Mn···Mn distance is 5.86 Å. These infinite zig-zig chains are cross-linked by O—H···O hydrogen bonds, involving water O(5) with symmetry related O(2*) and O(3*) (* denotes the symmetry

Table 2. Selected bond lengths (Å) and bond angles (°) for the title complex

Mn—O(1)	2.385(2)	Mn—O(2)	2.245(2)
Mn—O(3)	2.302(2)	Mn—O(4)	2.328(2)
Mn—O(5)	2.167(2)	Mn—N(1)	2.281(2)
Mn—N(2)	2.263(2)		
O(1)—Mn—O(2)	55.66(7)	O(1)—Mn—O(3)	135.74(7)
O(1)—Mn—O(4)	159.58(8)	O(1)—Mn—O(5)	79.98(8)
O(1)—Mn—N(1)	107.73(8)	O(1)—Mn—N(2)	82.56(7)
O(2)—Mn—O(3)	83.36(7)	O(2)—Mn—O(4)	139.85(7)
O(2)—Mn—O(5)	104.72(9)	O(2)—Mn—N(1)	92.54(9)
O(2)—Mn—N(2)	128.80(8)	O(3)—Mn—O(4)	56.49(6)
O(3)—Mn—O(5)	97.19(8)	O(3)—Mn—N(1)	88.18(8)
O(3)—Mn—N(2)	141.38(7)	O(4)—Mn—O(5)	82.14(8)
O(4)—Mn—N(1)	86.97(8)	O(4)—Mn—N(2)	89.01(7)
O(5)—Mn—N(1)	162.38(9)	O(5)—Mn—N(2)	94.21(8)
N(1)—Mn—N(2)	71.70(8)		

Hydrogen bonding parameters

D	H	A	D—H (Å)	H···A (Å)	D···A (Å)	D—H···A (°)
O(5)	H(11)	O(3*)	0.893	1.868	2.705	155.4
O(5)	H(12)	O(2*)	0.821	1.932	2.726	162.7
O(5′)	H(12′)	O(2)	0.821	1.932	2.726	162.7
O(5′)	H(11′)	O(3)	0.893	1.868	2.705	155.4

Symmetry codes: * x, $1/2-y$, $z+1/2$; ′ x, $1/2-y$, $z-1/2$.

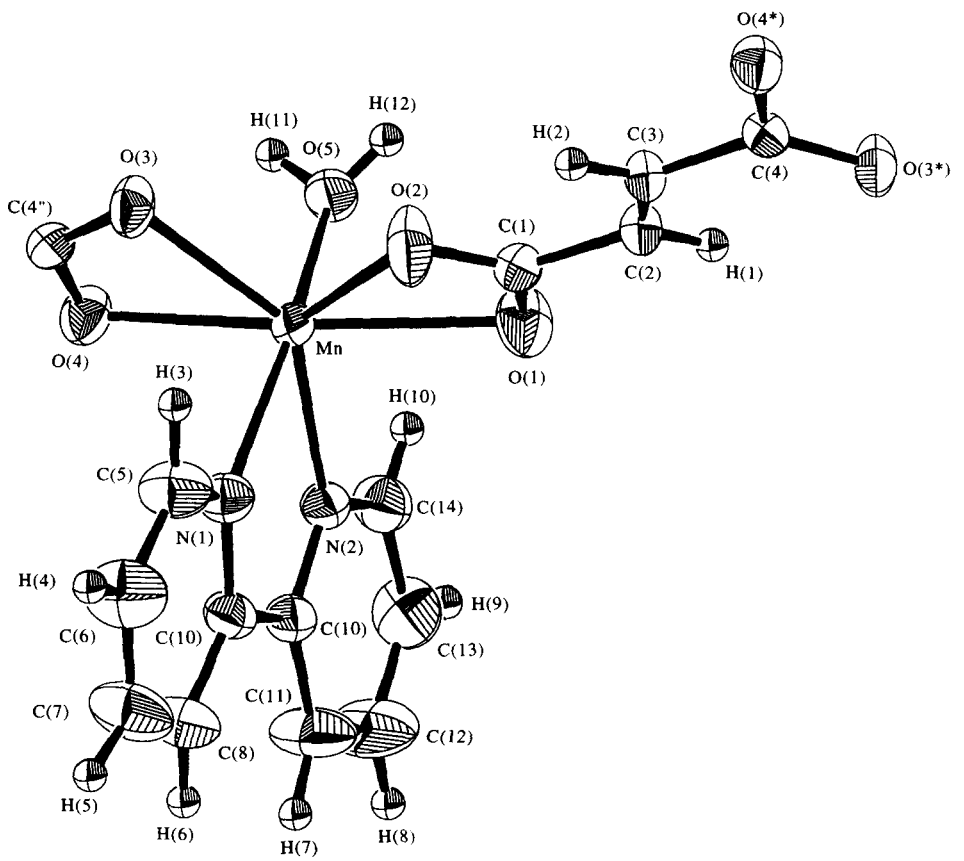


Fig. 1. Molecular structure of [Mn(TBD)(bipy)(H_2O)] with thermal ellipsoids (50% probability level).

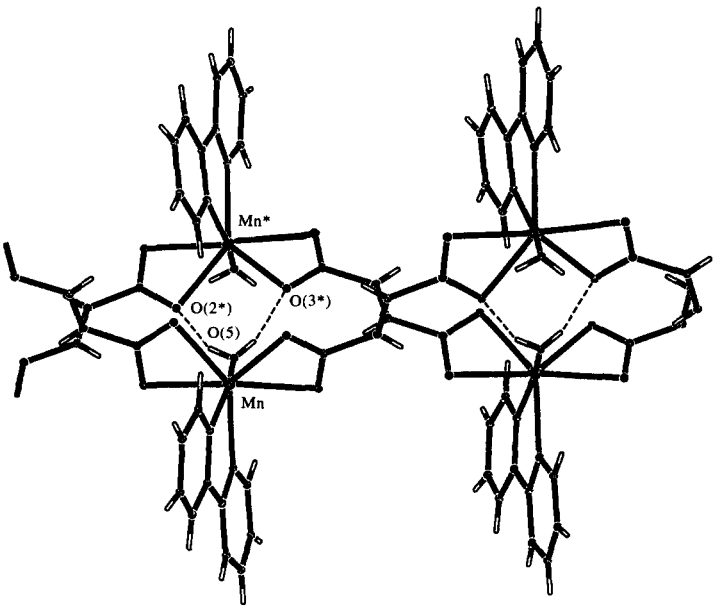


Fig. 2. Part of the chain structure of $[Mn(TBD)(bipy)(H_2O)]_n$ indicating the chain character.

operation x, $1/2-y$, $z+1/2$), as shown in Fig. 2. The hydrogen-bonding parameters are listed in Table 2.

Every Mn^{II} ion is heptacoordinate and possesses an N_2O_5 ligand environment by virtue of four oxygen atoms of two TBD ligands, two nitrogen atoms of one bipyridine and one oxygen atom of a coordinated water molecule. The manganese(II) ion displays a distorted pentagonal bipyramid with the approximate equatorial plane defined by O(1), O(2), O(3), O(4) and N(2) atoms and the Mn(II) ion is 0.046 Å out of this plane. The Mn—O average length is 2.285 Å, which is slightly longer than those of hexacoordinate Mn^{II} complex, and the Mn—N average distance (2.275 Å) is similar to those in reported manganese(II) complexes [9,10]. The bond angles of O(1)—Mn—O(2) [55.66(7)°] and O(3)—Mn—O(4) [56.49(6)°] in the equatorial plane deviate from 72°, which are restricted by the four-membered chelate rings. Similarly the large deviation from the idealized orthogonal geometry is found at the Mn atom in the five-membered Mn—N(1)—C(9)—C(10)—N(2) chelate ring [71.70(8)°] as expected due to the small bite distance of the bipyridine ligand [6,11]. The all carbon and nitrogen atoms of the bipy ligand are coplanar with deviations from the mean plane not greater than ±0.06 Å.

Magnetic and EPR properties

The temperature dependence of the molar magnetic susceptibility and magnetic moment per 1 Mn ion unit of the title complex in the form of χ_M *vs* T (μ_{eff} *vs* T) is shown in Fig. 3(a, b). the effective magnetic moment at 302.51 K is 5.95 B.M. which is in accord with the spin-only moment (5.92 B.M.) in the absence of any exchange interaction for Mn^{II} ions. Upon cooling, the value of μ_{eff} remains unchanged down to about 52 K (5.93 B.M.), then it decreases very slowly from 5.91 B.M. at 47 K to 5.74 B.M. at 15.45 K, below 15 K it decreases rapidly to 3.59 B.M. at 3.32 K, thus showing the presence of a very weakly intrachain antiferromagnetic exchange interaction. The decrease of the μ_{eff} below 15 K may be attributed to an interchain antiferromagnetic interaction and/or a zero-field splitting of the Mn^{II} ion.

Owing to the large spin of Mn^{II}, the data in the low-dimensional regime may be fitted with the expression calculated by Fisher for a classical-spin Heisenberg chain [12,13], scaled to a real spin $S = 1/2$:

$$\chi_M = [2Ng^2\mu_{B2}S(S+1)/3kT] \times (1-U)/(1+U) \quad (1)$$

where $U = -\coth K + 1/K$, $K = J(S+1)/kT$, and the exchange Hamiltonian is written as $H = -JS_iS_j$.

A molecular field correction [14,15] was added to account for the actual nature of the compound. Thus the expression for the magnetic susceptibility of the title complex becomes:

$$\chi_M = \chi_M/[1-2zJ'\chi_M/Ng^2\mu_B^2]. \quad (2)$$

Using eq. (2), a very close agreement with experiment is obtained with $J = -0.58$ cm^{-1}, $g = 2.01$, $zJ' = -0.09$ cm^{-1} and $R = 1.35 \times 10^{-3}$ [$R = \Sigma(\chi_{calc} - \chi_{obs})^2/\Sigma(\chi_{obs})^2$]. The magnetic susceptibility calculated by using the fit parameters is shown as the solid line in Fig. 3(a).

The weakly magnetic exchange interaction through bridging TBD ligands with a large intramolecular Mn···Mn separation (*ca* 9.05 Å) is consistent with those of other Mn^{II} and Co^{II} complexes bridged by terephthalate or isophthalate ligands ($J = -1.04 \rightarrow$

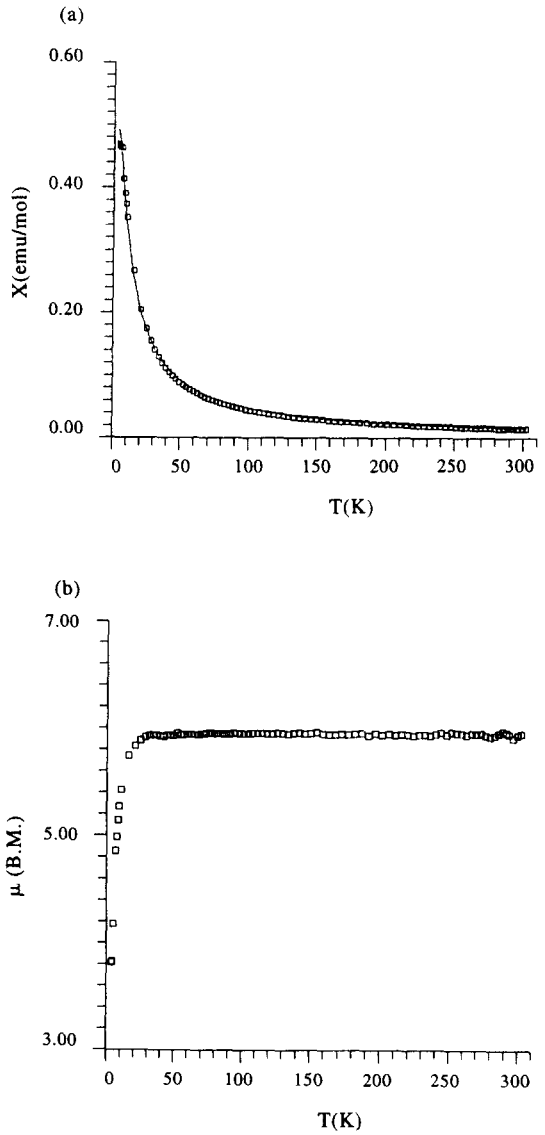


Fig. 3. (a) The Plot of $X-T$ for the title complex. The solid line represents best fit of data according to eq. (2). (b) Plot of μ_{eff} *vs* T for the title complex.

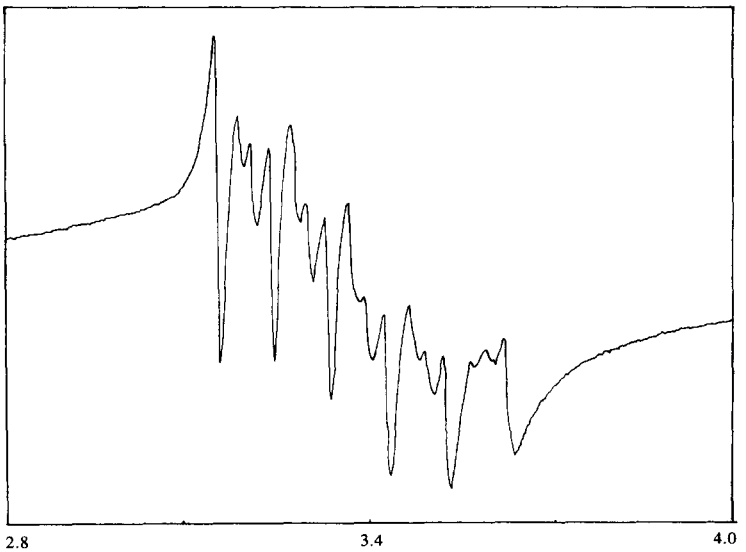


Fig. 4. X-band EPR spectrum for the title complex.

0.53 cm^{-1}) [16–19]. Despite the weakness of the exchange interaction, the fact that the magnetic data can be described without considering other factors as single-ion zero-field splitting and/or the local anisotropy or Mn^{II} ion, suggests that their effects are negligible as can be seen in other case [11].

The X-band EPR spectrum was measured in dilute frozen MeOH/DMF solution at 110 K. The spectrum (Fig. 4) exhibits a six-line manganese hyperfine pattern centered at $g = 2.001$, $A = 94.5$ G, which is that expected of an odd unpaired electron system ($S = 5/2$), $m_s = \pm 5/2, \pm 3/2, \pm 1/2$; and $I = 5/2$, $m_I = \pm 5/2, \pm 3/2, \pm 1/2$) with the g, A tensors isotropic, resulting from "allowed" transitions ($\Delta m_s = \pm 1$, $\Delta_I = 0$) [11,20]. Besides, between every adjacent pair of the "allowed" six hyperfine lines of the $g \sim 2$ resonance there is a pair of relatively weak "forbidden" ($\Delta m_s = \pm 1$, $\Delta m_I = \pm 1$) transitions [21, 22]. The average separation of the "forbidden" hyperfine doublets in the spectrum is 23.25 G.

REFERENCES

1. *Magneto-Structure Correlations in Exchange Coupled System* (Edited by R. D. Willett, D. Catteschi and O. Kahn). NATP ASI, Reidel, Dordrecht (1985).
2. M. Cavaluzzo, Q. Chen, and J. Zubieta, *J. Chem. Soc., Chem. Commun.* 1991, 1657.
3. J. J. Borras-Almenar, R. Burriel, E. Coronado, D. Gatteschi, C. J. Gomez-Garcia and C. Zanchini, *Inorg. Chem.* 1991, **30,** 947.
4. Y. Pei, M. Verdaguer, O. Kahn, J. Sletten and J.-P. Renard, *Inorg. Chem.* 1987, **26,** 138.
5. Y. Pei, O. Kahn, J. Sletten, J.-P. Renard, R. Georges, J.-C. Gianduzzo, J. Curely and Q. Xu, *Inorg. Chem.* 1988, **27,** 47.
6. J. Cano, G. D. Munno, J. Sanz, R. Ruiz, F. Lioret, J. Faus, and M. Julve, *J. Chem. Soc., Dalton Trans.* 1994, 3465.
7. J. J. Borras-Almenar, R. Burriel, E. Corondo, D. Gatteschi, C. J. Gomez-Garcia and C. Zanchini, *Inorg. Chem.* 1991, **30,** 947.
8. M. Verdaguer, J. Gouterson, S. Jeannin, Y. Jeannin, and O. Kahn, *Inorg. Chem.* 1984, **23,** 4291.
9. P. A. Marioni, W. Marty, S. Stoeckli-Evans, and C. Whitaker, *Inorg. Chimi. Acta* 1994, **219,** 161.
10. M. Devereux, M. McCann, M. T. Casey, M. Curran, G. Ferguson, C. Candin, M. Converg and V. Quillet, *J. Chem. Soc., Dalton Trans.* 1995, 771.
11. (a) X. T. Tan, J. Chen, P. J. Zheng and W. X. Tang, *Inorg. Chim. Acta* 1995, **234,** 27; (b) X. S. Tan, J. Chen, P. J. Zheng and W. X. Tang, *Acta Cryst.* 1995, **C51,** 1268.
12. M. Drillon, E. Coronado, D. Beltran, R. Georges, *J. Chem. Phys.* 1983, **79,** 449.
13. M. E. Fisher, *Am. J. Phys.* 1964, **32,** 343.
14. R. L. Carlin, *Magnetochemistry.* Springer, Berlin, Heidelberg, (1986).
15. B. J. Kennedy, K. S. Murray, *Inorg. Chem.* 1985, **24,** 1552.
16. X. S. Tan, J. Sun and W. X. Tang, *Inorg. Chim. Acta* 1995, in press.
17. J. Cano, G. D. Munno, J. Sanz, R. Ruiz, F. Lloret, J. Faus and M. Julve, *J. Chem. Soc., Dalton Trans.* 1994, 3465.
18. Z.-H. Jiang, S.-L. Ma, D.-Z. Liao, S.-P. Yan and G.-L. Wang, *Science in China (series B)* 1993, **23,** 1009.
19. S.-L. Ma, D.-Z. Liao, Z.-H. Jiang, S.-P. Yan, F.-C. Xue and G.-L. Wang, *Syn. React. Inorg. Met.-Org. Chem.* 1994, **24,** 137.
20. K. Chen, *J. of Zhejiang University (nature science)* 1993, **27,** 69.
21. H. W. Dewijn, and R. F. Van Balderen, *J. Chem. Phys.* 1972, **46,** 1381.
22. S. K. Chandra, and A. Chakravorty, *Inorg. Chem.* 1992, **31,** 760.

Pergamon

PII: S0277-5387(96)00283-5

Polyhedron Vol. 16, No. 4, pp. 695–699, 1997
Published by Elsevier Science Ltd
Printed in Great Britain. All rights reserved
0277-5387/97 $17.00+0.00

Transition metal complexes with the thiosemicarbazide-based ligands.—XXIX. Crystal and molecular structure of β-bis(S-methylisothiosemicarbazide)nickel(II) bromide and the energies of electronic states of Ni^{II} in similar structures

D. Ž. Obadović,[a]* V. Divjaković[a] and V. M. Leovac[b]

[a] Institute of Physics, Faculty of Sciences, Trg D. Obradovića 4, 21000 Novi Sad, Yugoslavia

[b] Institute of Chemistry, Faculty of Science, Trg D. Obradovića 3, 21000 Novi Sad, Yugoslavia

(Received 23 February 1996; accepted 5 June 1996)

Abstract—The crystal structure of the β-$(NiL_2)Br_2$ (L = S-methylisothiosemicarbazide, $C_2H_7N_3S$) complex was solved on the basis of X-ray diffraction data. It was established that the central Ni^{II} atom has a square-planar coordination, with the four nitrogen atoms of two chelate ligands. In the case of $[NiL_2]X_2$ (X = Br, I) the crystallographic data for the Ni—N bond length, together with the experimentally obtained values for frequencies of electronic *d–d* transitions represented the basis for the calculation of the ionization potentials H_{dd}, constants of partial population of *s* and *p*, as well as the charge *q* of the Ni^{II} ion in these complexes. In addition, the energies of the electronic *d* levels of Ni^{II} were calculated and the most probable MO scheme has been constructed. Published by Elsevier Science Ltd

Keywords: transition metal complexes; square-planar Ni^{II}; crystal structure; electronic spectra; orbital energy; MO scheme.

This work represents a continuation of our experimental and theoretical studies of Ni^{II} complexes with different ligands [1,2]. The synthesis of the investigated complexes of the formula $[NiL_2]X_2$ (L = S-methylisothiosemicarbazide, X = Br, I) has been reported earlier [3], as well as the structure of the $[NiL_2]I_2$ complex [4]. In the case of the $[NiL_2]Br_2$ complexes two crystal modifications: triclinic (α) and orthorhombic (β) were established. The crystal and molecular structure of α-$[NiL_2]Br_2$ has been reported elsewhere [5], whereas the structure of β-$[NiL_2]Br_2$ complex is the subject of the present work. Also, the calculation of the energies of the Ni^{II} electronic states and the most probable MO scheme are presented.

* Author to whom correspondence should be addressed.

EXPERIMENTAL

Physical measurements

The crystal structure was solved from three-dimensional intensity data collected on an Enraf-Nonius CAD-4 diffractometer using Mo-K_α radiation (λ = 0.071069 nm), monochromatized with a graphite crystal and the ω-2θ scan mode. Of the 956 unique reflections recorded in the range $3 \leqslant 2\theta \leqslant 50°$, 730 reflections with $F_o \geqslant 4\sigma$ (F_o) were included in the crystal structure analysis ($0 \leqslant h \leqslant 4, 0 \leqslant k \leqslant 23$, $0 \leqslant l \leqslant 14$) and refinement (9 atoms, 73 parameters), $w = 1.5799/\sigma^2(F_o)$. No absorption correction was applied. All calculations were carried out using SHELX-76 program [6].

The crystal data are: orthorhombic, *P*bnm,

Table 1. Bond distances (nm) and angles (°)

	β-[NiL$_2$]Br$_2$	α-[NiL$_2$]Br$_2$	[NiL$_2$]I$_2$
Ni—N(1)	0.1851(11)	0.1883(11)	0.1873(11)
Ni—N(3)	0.1928(10)	0.1931(10)	0.1923(10)
S—C(1)	0.1727(18)	0.1735(12)	0.1761(12)
S—C(2)	0.1825(17)	0.1836(13)	0.1802(13)
C(1)—N(1)	0.1322(19)	0.1344(12)	0.1284(12)
C(1)—N(2)	0.1345(19)	0.1313(12)	0.1315(12)
N(2)—N(3)	0.1433(18)	0.1452(12)	0.1429(12)
N(3)—Ni—N(1)	84.6(3)	86.0(6)	84.1(6)
Ni—(3)—N(2)	108.7(4)	107.3(9)	108.5(9)
C(1)—N(1)—Ni	115.1(3)	111.7(10)	113.5(11)
N(3)—N(2)—C(1)	115.1(5)	116.1(12)	114.3(13)
C(2)—S—C(1)	102.3(8)	103.2(9)	102.6(8)
N(2)—C(1)—N(1)	116.5(4)	118.7(14)	119.3(14)
S—C(1)—N(1)	128.7(6)	125.2(13)	126.8(12)
S—C(1)—N(2)	114.8(5)	116.0(12)	113.9(11)

$a = 0.4399(3)$, $b = 1.9663(4)$, $c = 1.5293(4)$ nm, $V = 1.3228(2)$ nm^3, $Z = 4$, $D_0 = 2.21$ g cm^{-3}, $D_c = 2.25$ g cm^{-3}.

The positions of Br and Ni atoms were determined from the three-dimensional Patterson function; the coordinates of the other atoms were found from electron density maps. Both Ni and Br atoms occupy special positions of the *P*bnm space group, the remaining atoms are located in general position. The structure was refined anisotropically by the least-squares routine to an R value of 0.059 (R_w was 0.052). Hydrogen atoms have not been located. Bond distances and angles are given in Table 1.

Reflectance spectra were measured in the 10,000–45,000 cm^{-1} range at room temperature using a monochromator SPM-2 (Veb Zeiss, Jena) with a R-45/0 type reflection cell. MgO was used as "white" standard.

CALCULATION OF THE ENERGIES OF Ni^{II} ELECTRONIC STATES

Spectral investigations [7] have afforded experimental values of the electronic *d–d*, intraligand (IL) and charge-transfer (CT) transitions (Table 2). These values represented the basis for calculation of the energies of molecular orbitals of the investigated complexes.

The energies of electronic states b_{1g}, a_{1g}, b_{2g} and e_g of the d level of square-planar Ni^{II} complexes were calculated by solving the secular equation [8]:

$$|H_{ij} - WG_{ij}| = 0$$

where G_{ij} represents the group overlap integral, and H_{ij} is the exchange integral which can be expressed in terms of Coulomb integral H_{jj} and group overlap integral G_{ij} as:

$$H_{ij} = F\left(\frac{H_{ii} + H_{jj}}{2}\right)G_{ij}.$$

The group overlap integrals can be calculated on the basis of the two-atom overlap integral, S, taken from the tables [9], and they represent a function of the parameters p and τ:

$$p = \frac{1}{2}(\mu_A + \mu_B)\frac{R}{R_0}, \quad \tau = \frac{\mu_A - \mu_B}{\mu_A + \mu_B}$$

where R_0 represents the first Bohr radius, and μ_A and μ_B (the index A stands for the N atoms of the surroundings, and B is referred to the Ni^{II} atom) are the exponents of the radial part of the Slater wave functions [10]. On the basis of the solved crystal structures, the parameter p was calculated taking an average value for the Ni—N bond distance $\bar{R}_{Ni-N} = 1.898$, 1.907 and 1.889 Å for [NiL$_2$]I$_2$, α-[NiL$_2$]Br$_2$ and β-[NiL$_2$]Br$_2$, respectively. The values of parameters p and τ thus obtained, as well as the two-atom overlap integrals, are presented in Table 3.

The group overlap integrals, calculated on the basis of the two-atom overlap integrals are presented in

Table 3. Parameters p, τ and the two-atom overlap integrals, S for square planar Ni^{II} complexes

Compound	p	τ	$S(2p_\pi, 3d_\pi)$	$S(2p_\sigma, 3d_\sigma)$
[NiL$_2$]I$_2$	6.817	0.0253	0.155	0.216
α-[NiL$_2$]Br$_2$	6.849	0.0253	0.145	0.200
β-[NiL$_2$]Br$_2$	6.777	0.0253	0.160	0.215

Table 2. Electronic spectral data of Ni^{II} complexes

	Transition (10^3 cm^{-1})					
		d–d		CT		IL
Compound	$b_{2g} \rightarrow b_{1g}$	$a_{1g} \rightarrow b_{1g}$	$e_g \rightarrow b_{1g}$	$a_{1g} \rightarrow a_{2u}$	$e_g \rightarrow a_{2u}$	$a_{2u}(\pi^*) \rightarrow a_{2u}(\pi^b)$
[NiL$_2$]I$_2$	11.1	20.0	23.3	30.8	34.0	41.2
[NiL$_2$]Br$_2$	11.0	20.1	23.3	30.8	34.0	41.2

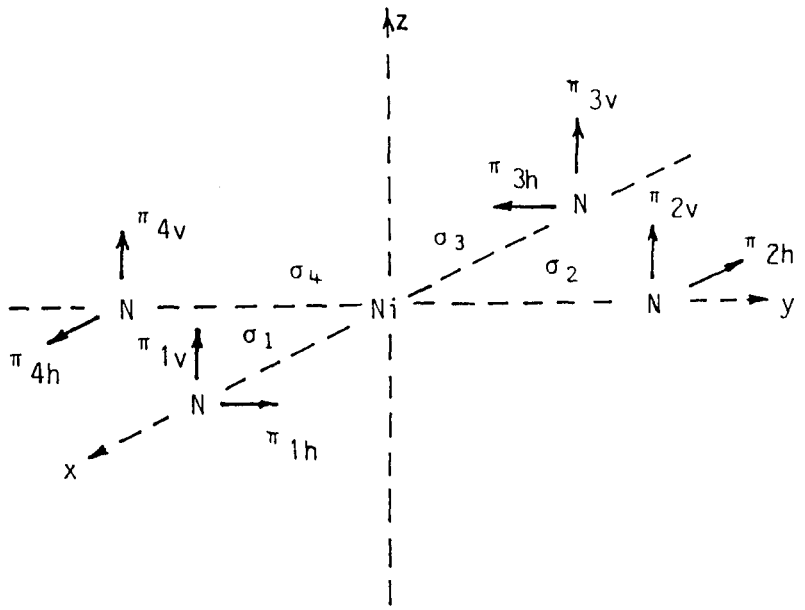


Fig. 1. Coordinate system for σ- and π-molecular orbitals for square planar Ni^{II} complexes.

Table 4, whereas in Fig. 1 is presented the coordinate system of square-planar Ni^{II} complexes.

The Coulomb integral H_{jj} was approximated by the ionization potential of the N atoms of the Ni^{II} surroundings, and $H_{ii} = H_{dd}$ was calculated on the basis of the relation:

$$H_{dd} = \mathrm{d(VSIE)} = (1-s-p)(\mathrm{dVSIE}: d^n) + s(\mathrm{dVSIE}: d^{n-1}s) + p(\mathrm{dVSIE}: d^{n-1}p)$$

where VSIE stands for the valence state ionization energies [10]. On the basis of this procedure we calculated the matrix elements $H_{ij}(b_{1g})$, $H_{ij}(b_{2g})$, $H_{ij}(a_{1g})$ and $H_{ij}(e_g)$, as well as the energies of the corresponding d-levels of Ni^{II} presented in Table 5. The experimental values of the frequencies of d–d transitions (Table 2) enabled the calculation of the constants of partial population of s and p, as well as of q for Ni^{II} in the investigated complexes. By a reverse iterative calculation, the more exact values of ionization energies H_{dd}, i.e. of the electronic energies of the d levels, were calculated. The process was repeated until the calculated values agreed with the experimental ones within the limits of experimental errors.

DISCUSSION

Crystal structure of β-[NiL$_2$]Br$_2$ complex

The crystal structure consists of the centrosymmetric complex cation of the type $[NiL_2]^{2+}$ and

Table 4. Basic functions and group overlap integrals for square-planar Ni^{II} complexes

Irreducible representation in D_{4h}	Metal function	Ligand function	G_{ij}	G_{ij} (calc.) [NiL$_2$]I$_2$	α-[NiL$_2$]Br$_2$	β-[NiL$_2$]Br$_2$
a_{1g}	$3d_{z^2}$	$\frac{1}{2}(\sigma_1+\sigma_2+\sigma_3+\sigma_4)$	$S(d,\sigma)$	0.216	0.200	0.215
b_{1g}	$3d_{x^2-y^2}$	$\frac{1}{2}(\sigma_1-\sigma_2+\sigma_3-\sigma_4)$	$\sqrt{3}S(d,\sigma)$	0.374	0.346	0.367
b_{2g}	$3d_{xy}$	$\frac{1}{2}(\pi_{1h}-\pi_{2h}+\pi_{3h}-\pi_{4h})$	$2S(d,\pi)$	0.309	0.290	0.320
e_g	$3d_{yz}$	$\frac{1}{\sqrt{2}}(\pi_{2v}-\pi_{4v})$	$\sqrt{2}S(d,\pi)$	0.218	0.204	0.225
	$3d_{zx}$	$\frac{1}{\sqrt{2}}(\pi_{1v}-\pi_{3v})$				

Table 5. Calculated orbital energy ($\times 10^3$ cm^{-1}) of Ni^{II} complexes

MO	$[NiL_2]I_2$ calc.	$[NiL_2]I_2$ exp.	α-$[NiL_2]Br_2$ calc.	α-$[NiL_2]Br_2$ exp.	β-$[NiL_2]Br_2$ calc.	β-$[NiL_2]Br_2$ exp.[a]
$a_{2u}(\pi^*)$		−64.8		−64.8		
$b_{1g}(\sigma^*)$	−75.5	−75.6	−75.3	−76.8	−75.8	
$b_{2g}(\pi^*)$	−87.2	−86.7	−86.5	−86.5	−86.9	
$a_{1g}(\sigma^*)$	−97.5	−95.6	−95.6	−95.6	−96.8	
$e_g(\pi^*)$	−99.7	−98.8	−98.1	−98.8	−98.3	
$a_{2u}(\pi^b)$		−106		−106		
Ni charge	0.19		0.19		0.19	
Ni configuration		$d^{8.58}s^{0.73}p^{0.5}$		$d^{8.94}s^{0.37}p^{0.5}$		$d^{8.83}s^{0.73}p^{0.25}$

[a] Experimental values for α-$[NiL_2]Br_2$ and β-$[NiL_2]Br_2$ are identical, as the spectra were recorded for the sample containing both crystal modifications.

bromine anions, where L is S-methylisothiosemicarbazide bonded to the Ni ion as a chelate *via* two N atoms, from both the amine and hydrazine groups. The complex cation is formed by two S-methylisothiosemicarbazide moieties in a *trans* position, planarly coordinated to the Ni atom (Fig. 2). This can also be inferred from the diamagnetic behaviour of the complex [7]. The *imido* form of the S-methylthiosemicarbazide ligand, which is a characteristic for the majority of the S-alkyl derivatives of thiosemicarbazides and thiosemicarbazones [11], has also been confirmed. The electronic charge density is well localised along the N(1)—C(1)—N(2) fragment as indicated by the values of the bond distances C(1)—N(1) and C(1)—N(2). The similar bond distances in the same fragment were also found in related structures of bis(S-methylthiosemicarbazide) nickel(II)iodide [4]. Bond distances and angles of the β-$[NiL_2]Br_2$ are given in Table 1 and compared with corresponding values of similar compounds α-$[NiL_2]Br_2$ and $[NiL_2]I_2$ [4,5]. The Ni–N bond distances are similar to those found in the similar planar complexes with the same ligand [4,5]. No Ni—Ni bonding interactions were observed and the Ni atom did not exhibit the tendency of assuming an octahedral surrounding. The complex cations are also well separated from the bromine anions, and none of the distances are shorter than 0.365 nm.

The energies of Ni^{II} *electronic states*

The orbitals of the metal atom participating in the formation of σ-bonding MO in the square-planar Ni^{II} complexes are $3d_{z^2}$, $3d_{x^2-y^2}$, $4s$, $4p_x$ and $4p_y$. As the contribution of the atomic orbitals to the formation of molecular orbitals is proportional to the atomic orbital overlap, which is expressed by the value of the group overlap integral, it is evident from Table 4 that the contribution of the $3d_{x^2-y^2}$ orbital to σ molecular orbitals is much greater than that of the d_{z^2} orbital.

The a_{2u} π molecular orbital is formed by overlapping of the Ni^{II} orbital with four π_v ligand orbitals of the N-surroundings, (Fig. 1) giving the so-called "ring" π^b orbital, which stabilizes the square-planar coordination of the metal ion in these complexes. The ionization potential of the N atoms of the ligand is $\simeq 13.2$ eV (106×10^3 cm^{-1}), and the energies $e_g(\pi^*)$, $a_{1g}(\sigma^*)$ of the d levels of Ni^{II} are $\simeq 12.4$ eV and 12.2 eV, respectively. Since the $a_{2u}(\pi^*)$ level is stabilized by the empty $4p_z$ metal orbital, and if $3d_{xy}$, $3d_{yz}$, $3d_{yz}$ and $3d_{z^2}$ are weakly antibonding, the bands at 30.8×10^3 and 34.0×10^3 cm^{-1} can be ascribed to charge-transfer transitions of the metal-ligand type, between the d-orbital of the Ni^{II} and the π^* orbital of the N atom. The experimentally obtained energy difference of 41.2×10^3 cm^{-1} corresponds to the transition between the ligand $a_{2u}(\pi^b)$ and $a_{2u}(\pi^*)$ levels, which is in agreement with the results of our calculations. The results obtained by calculating the energies of the molecular orbitals (Table 5) show that the distance between the $b_{1g}(\sigma^*)$ and $b_{2g}(\pi^*)$ levels is greater than the difference between the $b_{2g}(\pi^*)$ and $a_{1g}(\sigma^*)$ levels, and much greater than the distance of the $a_{1g}(\sigma^*)$ and $e_g(\pi^*)$ levels. This indicates that $d_{x^2-y^2}$ orbital, which has the highest energy with respect to all other d-orbitals, takes part in formation of four dsp^2 hybrid orbitals, which are then involved in bonding with ligand N-atoms [12].

The values obtained for the energies of the corresponding MO's are in agreement with the square-planar coordination of the four N atoms of the first coordination sphere, as well as with the crystallographic data about the Ni—Cl and Ni—Br bond length, which exclude the possibility of formation of a distorted octrahedron. The calculated MO energies are fully consistent with the experimental data obtained from electronic spectra, giving the exact difference between the one-electron molecular orbital levels, and resulting in the most probably MO scheme presented in Figure 3.

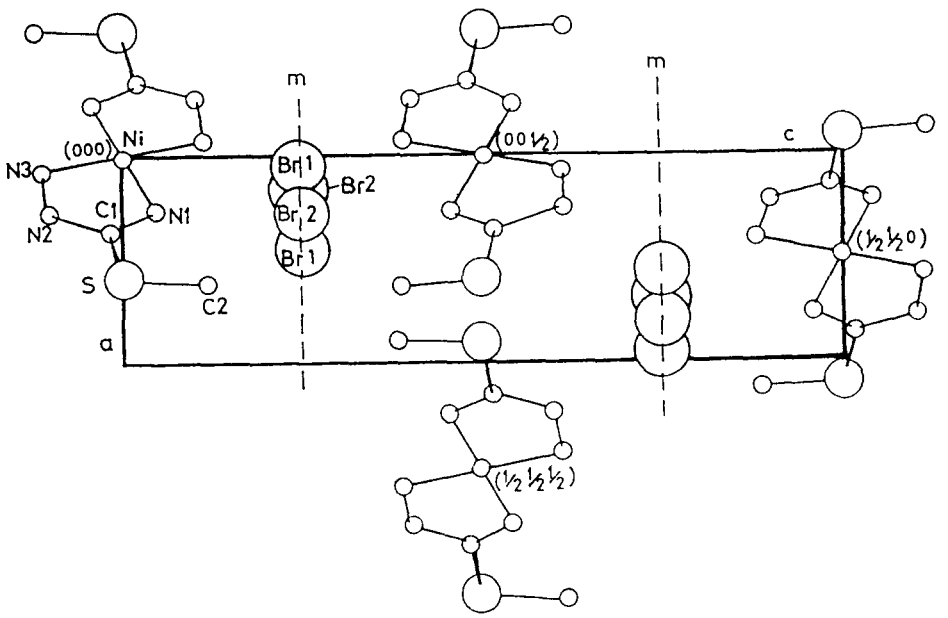


Fig. 2. The crystal structure of β-$[NiL_2]Br_2$ complex.

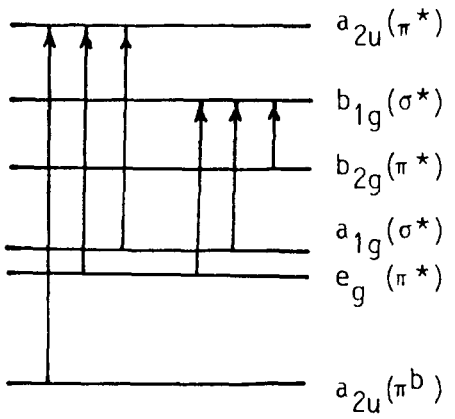


Fig. 3. Most probable MO scheme of the investigated square-planar Ni^{II} complexes.

REFERENCES

1. D. Ž. Obadović, A. F. Petrović, V. M. Leovac and S. Yu. Chundak, *J. Phys. Chem.* 1990, **42,** 3611.
2. V. M. Leovac, D. Ž. Obadović, S. Yu. Chundak and F. Skuban, *Thermochim. Acta* 1992, **4214**, 193.
3. V. M. Leovac, M. Babin, V. Canić and N. V. Gerbeleu, *Z. Anorg. Allg. Chem.* 1980, **471,** 227.
4. V. Divjaković and V. M. Leovac, Associazione Italiana di Cristalografia, *III Congresso Italo-Yugoslavo, Parma*, p. 68. (1979). Instituti di Chimica Generale, University Parma.
5. V. Divjaković, V. M. Leovac and B. Ribar, *Rev. Research, Physics Series*, Faculty of Sciences, Novi Sad, 1983, **413,** 25.
6. G. M. Sheldrick, SHELX76. *Program for crystal structure determination.* Univ. of Cambridge, England (1976).
7. D. Obadović, A. F. Petrović and S. Lukić, *Rev. Research, Physics Series*, Faculty of Sciences, Novi Sad, 1981, **411,** 1.
8. C. J. Ballhausen and H. B. Gray, *Inorg. Chem.* 1961, **41,** 111.
9. H. H. Jaffe, *J. Chem. Phys.* 1953, **21,** 258.
10. J. C. Slater, *Phys. Rev.* 1930, **436,** 57.
11. V. Divjaković, V. M. Leovac, B. Ribar and N. V. Gerbeleu, *Zeit. Krist.* 1989, 154.
12. H. B. Gray and C. J. Ballhausen, *J. Am. Chem. Soc.* 1963, **85,** 260.

Pergamon

PII: S0277-5387(96)00282-3

Polyhedron Vol. 16, No. 4, pp. 701–706, 1997
Copyright © 1996 Elsevier Science Ltd
Printed in Great Britain. All rights reserved
0277-5387/97 $17.00+0.00

Degradative oxidation of D-ribono-1,4-lactone by Cr^{VI} in perchloric acid

S. Signorella, S. Garcia and L. F. Sala*

Area Inorgánica, Facultad de Ciencias Bioquímicas y Farmacéuticas (UNR), Suipacha 531, 2000 Rosario, Argentina

(Received 16 January 1996; accepted 5 June 1996)

Abstract—The oxidation of D-ribono-1,4-lactone by Cr^{VI} yielded D-erythronic acid, erythrose, carbon dioxide and Cr^{III} as final products when a 15-fold or higher excess of sugar over Cr^{VI} was used. The kinetics of the redox processes involving the Cr^{VI}/Cr^{III} couple were determined and a mechanism is proposed. The complete rate law for the Cr^{VI} oxidation reaction is expressed by: $-d[Cr^{VI}]/dt = \{a[S]+b[S][H^+]+c[H^+]^3\}\ [Cr^{VI}]_T$, where $a = 3.09\times10^{-3}\ M^{-1}\ s^{-1}$, $b = 4.98\times10^{-2}\ M^{-2}\ s^{-1}$, $c = 1.07\times10^{-3}\ M^{-3}\ s^{-1}$ and S refers to the total reductant concentration, at 60°C. Cr^{V} is formed in a fast step by reaction of the CO_2^- radical and Cr^{VI}, and Cr^{V} reacts with the organic substrate faster than Cr^{VI} does. The EPR spectra show that the intermediate Cr^{V} complex (g = 1.978) is formed and decays by a first-order process. Copyright © 1996 Elsevier Science Ltd

Keywords: ribonolactone; chromium; oxidation; kinetics; mechanism; Cr^{V}; Cr^{VI}.

Hexavalent chromium, in many different compounds, is a well established carcinogen and mutagen [1–4]. There is, therefore, appreciable interest in determining the mode of action of chromium species derived from initial uptake of Cr^{VI} compounds [5]. Ligands that possess two oxygen atoms able to form five-membered rings about the metal atom, such as 1,2-diols and α-hydroxyacids are reported to stabilize Cr^{V} intermediates after further interaction with biological reductants [6–10]. For this reason, some sugars, or their derivatives, may play an important role in the chemistry of Cr^{VI}. Aldonic acids (or their lactones) have been found as metabolic intermediates in animals, plants and microorganisms, as products of the action of microorganisms on carbohydrates and as constituents of acidic polysaccharides [11].

As part of a general project dealing with the interaction of carbohydrates and transition metal ions, we have studied the reaction of Cr^{VI} with low molecular weight model reductants [12–20].

Chromic oxidation of α-hydroxyacids has been extensively studied [12,21–26]. These oxidations may yield products coming from either C—C [12, 23–26] or C—H, [22,26] depending on the particular molecular characteristics, through mechanisms involving either two-electron or three-electron initial oxidation of substrate by Cr^{VI}. Polyhydroxyacids offer additional binding sites to form the chromic ester precursor of the slow electron-transfer steps and might help to elucidate stereoelectronic effects affecting the reaction course [26]. In this paper we report the results obtained in our investigation of the chromic oxidation of D-ribono-1,4-lactone (RL) (Scheme I) in perchloric acid.

EXPERIMENTAL

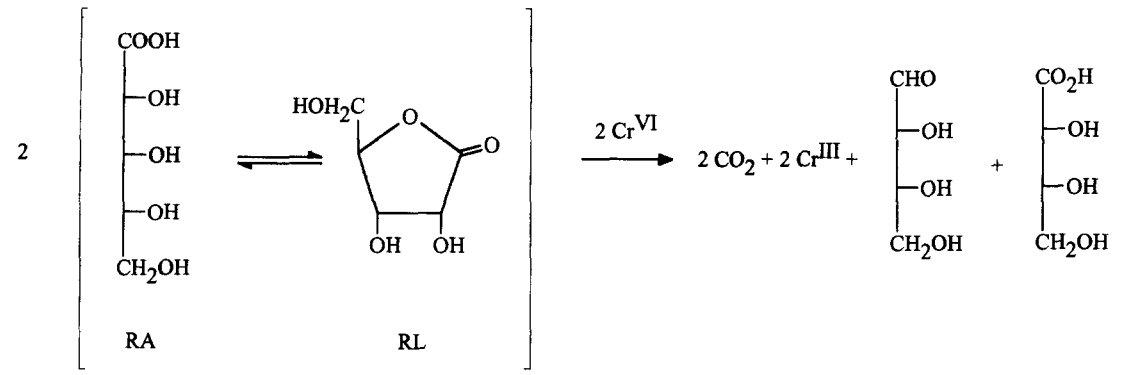
Materials

D-Ribono-1,4-lactone (sigma grade), potassium dichromate (Cicarelli c.a), perchloric acid (P.A. Merck), acrylonitrile (Aldrich grade) and sodium perchlorate (Sigma grade) were used without further purification.

Spectrophotometric measurements

Kinetic measurements were made at 350 nm by monitoring the absorbance changes on a Guilford Response II spectrophotometer with fully thermostated cell compartments. Pseudo-first-order rate constants, determined from the slope of ln(Abs) *vs*

* Author to whom correspondence should be addressed.



Scheme I.

time, were deduced from multiple determinations and were within ±5% of each other. In most experiments the concentration of Cr^{VI} was kept constant at 7.75 10^{-4} M while the RL was varied from 0.0116 to 0.062 M. Mixtures of sodium perchlorate and perchloric acid were used to maintain a constant ionic strength of 1.0 M.

Disappearance of Cr^{VI} was followed until at least 80% conversion. Reactant solutions were previously thermostated and transferred into a cell of 1 cm path length immediately after mixing. Experiments were performed at 60°C unless otherwise mentioned.

The acid : lactone proportion of the reductant in the starting solution was calculated by optical rotation measurements at given hydrogen ion concentrations [27]. Table 1 shows the composition of the substrate solution at different perchloric acid concentrations. Ribonic acid (RA) is the major form in solution over the whole acid concentration range (0.2–1.0 M $HClO_4$), and as expected, the lactone proportion increases with increasing [$HClO_4$]. In order to confirm that no cooxidation process occurs at the primary hydroxy group, RL was methylated at C-5OH to yield the 5-O-methyl-D-ribono-1,4-lactone (MRL) [29]. The chromic oxidation of MRL and RL affords the same k_{obs} values, under the same reaction conditions.

Product analysis

Under conditions employed in the kinetic measurements (ratios of RL over Cr^{VI} from 15/1 to 80/1) qualitative identification of D-erythronic acid (EA) and erythrose as the reaction products was carried out by paper chromatography. EA and erythrose were identified against authentic samples using *n*-butanol/acetic acid/water (4 : 1 : 5) as eluent. Paper chromatograms were visualized by two kinds of development reagents: a three-stage dip of silver nitrate, sodium hydroxide and sodium thiosulfate [30] and *p*-anisidine reagent [31]. Under these conditions, carbon dioxide was detected and the quantitative determination of this gas afforded 1 mole of CO_2 per mole of Cr^{VI}.

Test for free radicals

A solution of potassium dichromate (1.16×10^{-3} M) in 1 cm^3 of 0.5 M $HClO_4$ was added to a mixture of 1.16×10^{-3} M RL in 0.5 M $HClO_4$ (2 cm^3) and acrylonitrile (0.5 cm^3) at 20°C. After 20 min a white precipitate of a polymer slowly appeared. Blank experiments in the absence of organic substrate or

Table 1. Concentration of ribonolactone and ribonic acid in the starting solution[a]

[$HClO_4$]/M	C_T[b]/M	R[c]	10^2[RL]/M	10[RA]/M	10^5[R^-]/M
0.2–0.3	0.1623	+0.200	0.476	1.575	7.75
0.4–0.5	0.1360	+0.189	1.710	1.190	2.00
0.6	0.1317	+0.200	2.68	1.049	2.10
0.75	0.1370	−0.222	3.640	1.006	1.74
0.9–1	0.14	+0.234	4.16	0.984	1.34

[a] Values used in calculations: molar rotations: +5.65 (RL), +2.37 (RA), +0.95 (R^-); K [28] = $[H^+][R^-]/([RL]+[RA]) = 9.55 \times 10^{-5}$.
[b] $C_T = [RA]+[RL]+[R^-]$, where R^- refers to ribonate.
[c] Optical rotation.

oxidant agent did not show formation of any such precipitate.

EPR measurements

EPR spectra were recorded with a Bruker spectrometer model ER-200. Spectra were acquired at a frequency of *ca* 9.8 GHz with a center field of 3500 G, a swept width of 100–1000 G and variable modulation amplitude. The cavity and sample tube were kept at 25°C. Initial Cr^{VI} concentration in all the EPR measurements was 7.75×10^{-4} M.

RESULTS AND DISCUSSION

Over the whole range of perchloric acid concentrations used in the kinetic measurements, spectrophotometric studies showed that the reaction of RL and Cr^{VI} resulted in an absorbance band at 350 nm and a shoulder at 420–500 nm characteristic of the $Cr_2O_7^{2-}$ ion. It is known that Cr^V species, usually formed in these oxidation reactions, absorb at 350 nm and may superimpose Cr^{VI} absorbance yielding the wrong interpretation of spectrophotometric absorbance decay values [22]. However, if Cr^V reacts faster than Cr^{VI} and exists in solution in a sufficiently small concentration, changes in absorbance at 350 nm essentially reflect changes in Cr^{VI} concentration. We observed deviations from first-order decay over very short time periods and we calculated pseudo-first-order rate constants from the slopes of the linear part of the ln(Abs) *vs* time curves; a good criterion only if Cr^V decays faster than Cr^{VI}. The relative values of the Cr^{VI} *vs* Cr^V oxidation rates constants obtained from the Cr^V EPR signal intensities during the reaction course (discussed below) demonstrate this is the case for the present reaction.

Unlike that observed for the chromic oxidation of gluconic acid [16], in the present case, Cr^V was not detected spectrophotometrically at 750 nm under conditions used in the kinetic experiments. Fortunately, it could be easily detected by EPR measurements. The reaction of Cr^{VI} with excess RL generates an EPR spectrum dominated by a single detectable sharp signal at $g_{iso} = 1.978$ (Fig. 1 inset (a)), typical of five-coordinate oxochromate(V) complexes [32,33]. The Cr^V signal grows and decays with time to yield the broad Cr^{III} signal ($g_{iso} = 1.981$) as the ultimate fate of chromium in this reaction (Fig. 1 inset (b)). Figure 1 shows a curve for peak-to-peak heights of Cr^V EPR signal *vs* time obtained on a reacting solution. Values of the rates of disappearance of Cr^{VI} (k_6) and Cr^V (k_5), respectively, may be calculated by eq. (1) [12,16], which fits well the experimentally observed Cr^V intermediate growth and decay curve in Fig. 1.

$$h = Ak_6\{\exp(-k_5t) - \exp(-2k_6t)\}/(2k_6 - k_5). \quad (1)$$

It has been shown that any rate profiles dealing with the build up and decay of an intermediate by first order processes can be described by a pair of solutions having the same numerical values for the rate constants, but with the order of the assignment reversed [34]. For conditions stated in Fig. 1, $k_6 = 8.35 \times 10^{-5}\ s^{-1}$ and $k_5 = 0.00768\ s^{-1}$ and the time of maximum Cr^V concentration, $T_{max} \approx 8.5$ min. We have chosen this assignment for the rate constant values and not the reverse one, for several reasons. In the EPR measurements, the temperature is lower than that used in the spectrophotometric experiments. Since the redox rates increase when the temperature rises, k_6 obtained from EPR data (at 25°C) should be lower than values obtained from the spectrophotometric measurements at 60°C (a value of 0.00768 exceeds all the k_{obs} values in Table 3). Besides, we have evaluated $k_{obs}(2k_6)$ spectrophotometrically at 25°C under conditions used in the EPR experiments, and we have reproduced the $k_{obs}(2k_6)$ value (the value obtained by this technique, for conditions in Fig. 1, is: $1.84 \times 10^{-4}\ s^{-1}$). Thus, the fact that k_5 is 91 times higher than k_6 justifies our initial assumption that changes in absorbance at 350 nm essentially reflect changes in Cr^{VI} concentration.

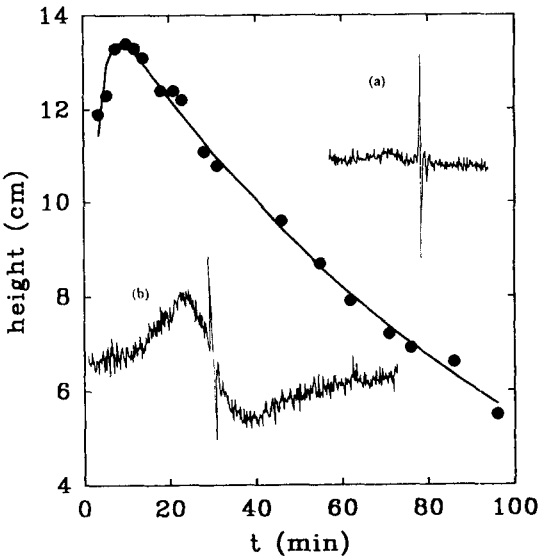


Fig. 1. Peak-to-peak heights of Cr^V EPR signals *vs* time [*S*] = 0.039 M; $[Cr^{VI}]_0 = 7.75 \times 10^{-4}$ M; $[HClO_4] = 1$ M; $T = 25$°C. Inset: (a) Cr^V EPR signal recorded at $t = 5$ min; (b) superimposition of Cr^V and Cr^{III} EPR signals as Cr^{III} builds up during the run ($t = 35$ min).

In order to verify the dependence of rate upon Cr^{VI}, pseudo-first order rate constants were calculated at various $[Cr^{VI}]_0$ ($4–26 \times 10^{-4}$ M) but at constant temperature, [RL], $[H^+]$ and ionic strength (Table 2). The rate constant was found to increase with increasing $[Cr^{VI}]_0$. However, values of $k_{obs}[Cr^{VI}]_0/[Cr_2O_7^{2-}]$ at various $[Cr^{VI}]_0$ were found to be constant, meaning that the dimeric species, *viz.* $Cr_2O_7^{2-}$, is the effective oxidant. The equilibrium $HCrO_4^-/Cr_2O_7^{2-}$ ($K = 76$) [35] was used to calculate $[Cr_2O_7^{2-}]$, neglecting the

Table 2. Effect of oxidant on the oxidation of ribonolactone. [RL] = 0.08 M; $[HClO_4]$ = 1 M; T = 35°C

$10^4[Cr^{VI}]_0$/M	$10^3 k_{obs}[Cr^{VI}]_0/[Cr_2O_7^{2-}]$
4	14.7
8	13.0
14	12.9
20	14.1
26	13.7

subsidiary equilibrium $HCrO_4^-/CrO_4^{2-}$ because of the high $[HClO_4]$ employed.

Table 3 summarizes values of k_{obs} for various concentrations of RL at fixed concentrations of perchloric acid. Plots of k_{obs} *vs* [RL+RA] ([*S*]) (Fig. 2) gave straight lines with a positive intercept from which values of k_1 and k_2 were determined (Table 4). Dependence of k_1 and k_2 with $[HClO_4]$ is shown in Fig. 3 and may be expressed by:

$$k_1 = a + b[H^+], \quad (2)$$

$$k_2 = c[H^+]^3, \quad (3)$$

where $a = 3.09 \times 10^{-3}$ M^{-1} s^{-1}, $b = 4.98 \times 10^{-2}$ M^{-2} s^{-1}, $c = 1.07 \times 10^{-3}$ M^{-3} s^{-1}.

The complete rate law is then given by:

$$-d[Cr^{VI}]/dt = k_{obs}[Cr^{VI}]_T = (k_1[S] + k_2)[Cr^{VI}]_T =$$

$$\{(a + b[H^+])[S] + c[H^+]^3\}[Cr^{VI}]_T, \quad (4)$$

where [*S*] refers to the total organic substrate concentration: RL+RA.

Table 3. Observed pseudo-first-order rate constants (k_{obs}) for different concentrations of $HClO_4$ and organic substrate. T = 60°C; $[Cr^{VI}]_0 = 7.75 \times 10^{-4}$ M; I = 1 M

	$[HClO_4]$/M $[10^4 k_{obs}(s^{-1})]$					
[*S*]/M	0.2	0.4	0.5	0.6	0.75	0.9
0.0116		3.47	4.85	6.90	9.51	12.7
0.0155			5.77	8.41	9.99	13.6
0.019		4.54	7.16		14.2	17.0
0.023		5.70	7.78			18.2
0.027		6.63		12.8	16.3	
0.031	4.10	7.77	10.2	13.9	17.0	
0.035		8.23	11.8		19.3	
0.039	4.80	9.57	13.2	16.4	20.1	25.2
0.043	5.24					
0.047	5.95					
0.054	6.94					
0.062	7.38					

Table 4. Values of k_1 and k_2 for different $[HClO_4]$

$[HClO_4]$/M	0.2	0.4	0.5	0.6	0.75	0.9
$10^2 k_1/M^{-1} s^{-1}$	1.14	2.25	3.03	3.49	3.97	4.65
$10^5 k_2/s^{-1}$	4.9	5.80	11.6	30.0	50.9	72.8

According to all experimental kinetic data, oxidation of the substrate by Cr^{VI} should occur through three parallel slow steps leading to the redox products. A mechanism considering this fact and fitting the

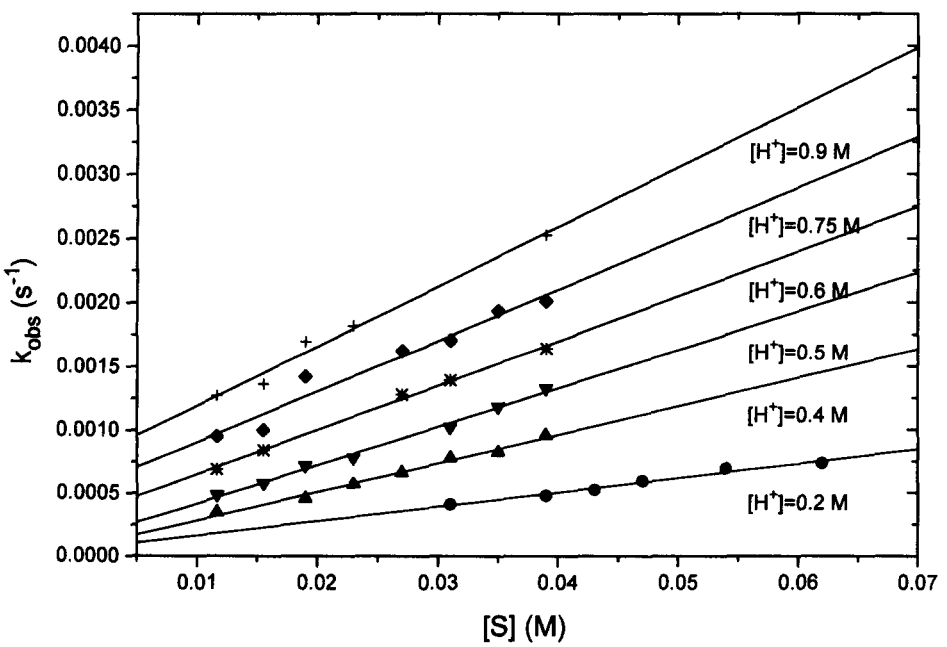


Fig. 2. k_{obs} as a function of the total reductant concentration at different acidities.

$$RL + H_2O \overset{K_h}{\rightleftharpoons} RA$$

$$RA + Cr_2O_7^{=} \overset{K_1}{\rightleftharpoons} A^{=} \overset{K_2,H^+}{\rightleftharpoons} AH^- \overset{K_3,H^+}{\rightleftharpoons} AH_2$$

$$k_1\,|\,RA \qquad k_2\,\downarrow\,RA \qquad k_3\,|\,H^+$$

$$\rightarrow P \leftarrow$$

where $P = {}^{0}CO_2^- + CH_2OH(CHOH)_2CHO^+ + Cr^{III}$

$$H_2O \;|\; \rightarrow CH_2OH(CHOH)CO_2H$$

Scheme II.

experimental kinetic law well, is proposed in Scheme II.

In this mechanism we have assumed that the open carboxylic acid is the reactive form of the organic substrate. This assumption is based on previous findings showing the enhanced ability of hydroxyacids to bind Cr^{VI} and Cr^{V} [21–26]. In any case, a possible mechanism involving the lactone may not be discarded. However, if the lactone was the reactive form of the organic reductant, coordination of Cr^{VI} should be favored at the pair of *syn* hydroxyl groups of the molecule, C(2)—OH and C(3)—OH [36]. The intermediate complex formed in this way might be present in the equilibrium mixture but should not be a direct precursor of the slow redox steps. Opening of the lactone ring and rearrangement should be required for the slow electron-transfer steps to take place within a complex with the carboxylate bound to Cr^{VI}.

Thus, the first step of the proposed mechanism may be interpreted as the formation of a monochelate with RA acting as a bidendate ligand bound to Cr^{VI} at C(1)—O and C(2)—O to yield the anionic species $[(RA)(O)_2(OH_2)CrOCrO_3]^{2-}$ (A^{2-}). This intermediate, or its monoprotonated form (AH^-), may decompose to the products in the presence of a second RA molecule, whereas the diprotonated form (AH_2) yields the products through an acid catalyzed step. We propose here that redox paths involving either the anionic or neutral complexes, are three-electron steps, just as observed for the chromic oxidation of mandelic acid [23], and Cr^{III} is formed with the oxidation products.

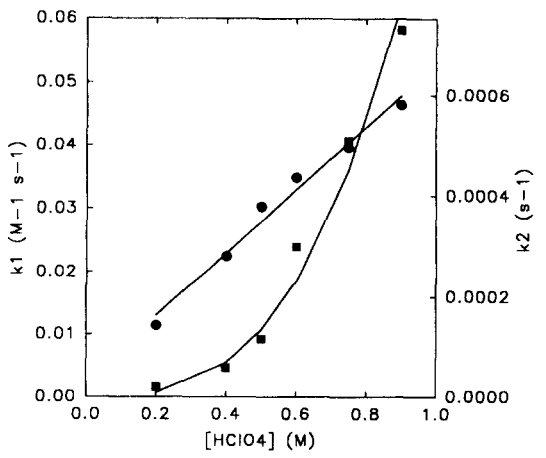


Fig. 3. Effect of acidity on k_1 and k_2.

If A^{2-}, AH^- and AH_2 are formed in rapid equilibria, the rate law corresponding to this mechanism may be expressed as:

$$v = -d[Cr^{VI}]/dt$$
$$= \{k_1K_1[RA]^2 + k_2K_2K_1[RA]^2[H^+] + k_3K_3K_2K_1[H^+]^3[RA]\}[Cr_2O_7^{2-}]. \quad (5)$$

Since

$$[Cr^{VI}]_T = [Cr_2O_7^{2-}]\{1 + 1/K_d + K_1[RA] + K_1K_2[RA][H^+] + K_1K_2K_3[H^+]^2[RA]\}. \quad (6)$$

Replacing $[Cr_2O_7^{2-}]$ in eq. (6)

$$v = \{k_1K_1[RA]^2 + k_2K_2K_1[RA]^2[H^+] + k_3K_3K_2K_1[H^+]^3[RA][Cr^{VI}]_T\} \times \{1 + 1/K_d + K_1[RA] + K_1K_2[RA][H^+] + K_1K_2K_3[H^+]^2[RA]\}^{-1}. \quad (7)$$

If $K_1[RA]$ is the largest term in the denominator (a reasonable assumption since K_1 corresponds to a complex formation constant while K_2 and K_3 are protonation ones), eq. (7) will be simplified to the experimentally observed form:

$$v = \{k_1[RA] + k_2K_2[RA][H^+] + k_3K_3K_2[H^+]^3\}[Cr^{VI}]_T. \quad (8)$$

Equation (8) may be expressed as a function of the total organic substrate concentration:

$$v = \{(k_1[S] + k_2K_2[S][H^+])K_h/(1 + K_h) + k_3K_3K_2[H^+]^3\}[Cr^{VI}]_T. \quad (9)$$

Polymerization after addition of acrylonitrile supports the formation of $^{\cdot}CO_2^-$ radicals. These radicals formed in the slow steps may react with Cr^{VI} to yield Cr^{V} and carbon dioxide:

$$^{\cdot}CO_2^- + Cr^{VI} \overset{fast}{\rightarrow} CO_2 + Cr^{V}. \quad (10)$$

Finally, Cr^{V} may react with excess substrate to yield erythrose, carbon dioxide and Cr^{III} in a two-electron step:

$$Cr^{V} + RA \overset{fast}{\rightarrow} CH_2OH(CHOH)_2CHO + CO_2 + Cr^{III}. \quad (11)$$

CONCLUSIONS

The present results indicate that the oxidation of RA occurs by a Cr^{VI}/Cr^{III} three-electron path yielding erythronic acid and the $^{\cdot}CO_2^-$ radical; followed by a $Cr^{VI}/Cr^{V}/Cr^{III}$ one-electron/two-electron path, leading to erythrose and carbon dioxide. This mechanistic proposal fits the experimental kinetics well and explains the products detected after the reaction completion, when an excess of sugar acid over Cr^{VI} is used. The present results are consistent with those obtained for a number of reported α-hydroxy acids chromic oxidations [12,23–26]. However, a reactant structure/cleaved bond type relation may not be easily rationalized upon comparison with other polyhydroxy acids. In the case of gluconic acid, C2—H break occurs through a two-electron transfer process [16] and the α-keto-acid is the only reaction product. On the other hand, galactonic acid yields lyxonic acid and carbon dioxide as products [37]. It seems reasonable to suggest that the relative C2, C3, C4 configuration influences the reaction course. Thus, the C2, C3, C4 *ribo* configuration behaves as the *arbino* (in galactonic acid) but different from the *xylo* (in gluconic acid). Even when any conclusive explanation may not be given at present, we think that after studying the chromic oxidation of a number of sugar acids of the same carbon-chain length it will be possible to find correlations between the structure of the reactants and the type of bond cleavage.

Acknowledgements—We thank the National Research Council of Argentina (CONICET), the International Science Foundation (IFS), the Third World Academy of Science (TWAS) and the National University of Rosario, Argentina, for financial support.

REFERENCES

1. P. O'Brien and G. Wang, *Polyhedron* 1993, **12,** 1409.
2. V. Ramana and K. Sastry, *J. Inorg. Biochem.* 1994, **56,** 87.
3. J. Alexander and J. Aaseth, *Analyst* 1995, **120,** 931.
4. S. Katz and H. Salem, *The Biological and Environmental Chemistry of Chromium.* VCH Publishers, Inc., New York (1994).
5. A. Fan and L. Harden-Barlow, *Adv. Mod. Environ. Toxicol.* 1987, **11,** 87.
6. K. Wetterhahn, *J. Am. Chem. Soc.* 1982, **104,** 874.
7. S. Rossi, N. Grorman and K. Wetterhahn, *Chem. Res. Toxicol.* 1988, **1,** 101.
8. S. Brauer and K. Wetterhahn, *J. Am. Chem. Soc.* 1991, **113,** 3001.
9. D. Goodgame, P. Hayman and D. Hathway, *Polyhedron* 1992, **1,** 497.
10. D. Goodgame and M. Joy, *J. Inorg. Biochem.* 1986, **26,** 219.
11. W. Pigman and D. Horton, *The Carbohydrates. Chemistry and Biochemistry,* Vol. 1B, p. 1014. Academic Press, Inc., New York (1980).
12. S. Signorella, S. García and L. Sala, *Polyhedron* 1992, **11,** 1391.
13. L. Sala, S. Signorella, M. Rizzotto, M. Frascaroli and F. Gandolfo, *Can. J. Chem.* 1992, **70,** 2046.
14. L. Sala, C. Palopoli, V. Alba and S. Signorella, *Polyhedron* 1993, **12,** 2227.
15. S. García, S. Signorella, S. Acebal, E. Piagio and L. Sala, *Oxidation Commun.* 1993, **16,** 313.
16. S. Signorella, M. Santoro, M. Mulero and L. Sala, *Can. J. Chem.* 1994, **72,** 398.
17. M. Rizzotto, S. Signorella, M. Frascaroli, V. Daier and L. Sala, *J. Carbohyd. Chem.* 1995, **14,** 45.
18. S. Signorella, C. Palopoli and L. Sala, *Polyhedron* 1995, **14,** 1725.
19. M. Rizzotto, M. Frascaroli, S. Signorella and L. Sala, *Polyhedron* 1996, **15,** 1517.
20. S. Signorella, M. Rizzotto, A. Bousseckson, C. Palopoli and L. Sala, *J. Chem. Soc., Dalton Trans.* 1996, 1607.
21. M. Mitewa and P. Bontchev, *Coord. Chem. Rev.* 1985, **61,** 241.
22. G. Haight, G. Jwisich, M. Kelso and P. Merril, *Inorg. Chem.* 1985, **24,** 2740.
23. D. Ip and J. Rocek, *J. Am. Chem. Soc.* 1979, **101,** 6311.
24. M. Krumpolk and J. Rocek, *J. Am. Chem. Soc.* 1977, **99,** 137.
25. S. Ramesh, S. Mahapatro, J. Lui and J. Rocek, *J. Am. Chem. Soc.* 1981, **103,** 5772.
26. K. Srinivasan and J. Rocek, *J. Am. Chem. Soc.* 1978, **100,** 2789.
27. D. Sawyer and J. Bagger, *J. Am. Chem. Soc.* 1959, **81,** 5302.
28. G. Escandar, Ph.D. Thesis, National University of Rosario (1992).
29. L. Hough, J. Jones and D. Mitchell, *Can. J. Chem.* 1958, **36,** 1720.
30. W. Travelyan, D. Proctor and J. Harrison, *Nature* 1950, **166,** 44.
31. L. Haugh, J. Jones and N. Wadman, *J. Chem. Soc.* 1950, 1702.
32. R. Bramley, J. Ji, R. Rudd and P. Lay, *Inorg. Chem.* 1990, **29,** 3089.
33. G. Barr-David, M. Charara, R. Codd, R. Farrell, J. Irwin, R. Bramley, S. Brumby, J. Ji, G. Hanson and P. Lay, *J. Chem. Soc., Faraday Trans.* 1995, **91,** 1207.
34. J. Moore and R. Pearson, *Kinetics and Mechanism,* p. 295, 3rd. edn. Wiley, New York (1981).
35. H. Spenson and R. Kinney, *Inorg. Chem.* 1971, **10,** 1376.
36. M. Branca, A. Dessi, H. Kozlowski, G. Micera and J. Swiatek, *J. Inorg. Biochem.* 1990, **39,** 217.
37. S. Signorella, M. Santoro and L. Sala, unpublished work.

Pergamon

PII: S0277-5387(96)00267-7

Polyhedron Vol. 16, No. 4, pp. 707–712, 1997
Copyright © 1996 Elsevier Science Ltd
Printed in Great Britain. All rights reserved
0277-5387/97 $17.00+0.00

Metal substitution reaction in the cluster $(\mu\text{-H})_2Fe_3(\mu_3\text{-Se})(CO)_9$—II.* Crystal and molecular structure of $[FeW_2(\mu_3\text{-Se})(CO)_7Cp_2]$ and $[FeMoW(\mu_3\text{-Se})(CO)_7Cp_2]$ ($Cp = \eta^5\text{-}C_5H_5$)

Sergei N. Konchenko,† Alexander V. Virovets, Sergei V. Tkachev and Nina V. Podberezskaya

Institute of Inorganic Chemistry, Siberian Division of RAS, Acad. Lavrentyev str. 3, Novosibirsk 630090, Russia

(Received 7 May 1996; accepted 22 May 1996)

Abstract—The sequential substitution of two $Fe(CO)_3$ groups in $[(\mu\text{-H})_2Fe_3(\mu_3\text{-Se})(CO)_9]$ with isolobal fragments $CpW(CO)_2$ (the first stage) and $CpMo(CO)_2$ (the second stage) has been shown to result in the title heterotrimetal cluster $[FeMoW(\mu_3\text{-Se})(CO)_7Cp_2]$. Its structure and the structure of its $[FeW_2(\mu_3\text{-Se})(CO)_7Cp_2]$ analog obtained previously have been determined by X-ray analysis. Copyright © 1996 Elsevier Science Ltd

Keywords: iron; molybdenum; selenium; tungsten; heterometallic clusters; synthesis; crystal and molcular structure.

The directed synthesis of heterometal clusters containing three or more different transition metals is one of the most interesting and important, but complicated problems of modern cluster chemistry [2]. One approach to this problem is the sequential metal substitution in homometal clusters and their heteronuclear derivatives. For example, in the last two decades many heterotrimetal complexes were obtained when the compounds $[(\mu\text{-H})_2Fe_3(\mu_3\text{-S})(CO)_9]$ and $[FeCo_2(\mu_3\text{-S})(CO)_9]$ were used as the starting reagents [2–4]. In this work an analogous approach has been shown to be useful for the parent selenide iron cluster $[(\mu\text{-H})_2Fe_3(\mu_3\text{-Se})(CO)_9]$ (**I**).

EXPERIMENTAL

The reaction of $[(\mu\text{-H})Fe_2W(\mu_3\text{-Se})(CO)_8Cp]$ (**II**) with $[CpMo(CO)_3]_2$ was carried out under argon; the other manipulations were performed in the air. All solvents were distilled from appropriate drying agents. The IR spectra were recorded on the Bruker IFS85 spectrometer. The NMR spectra were recorded on Bruker SXP-4-100 (^1H at 90 MHz) and CXP-300 (^{77}Se at 57.3 MHz) spectrometers. The chemical shift of ^{77}Se (positive downfield) was referenced to the saturated water solution of H_2SeO_3 as an external standard and counted relative to dimethylselenide [1]. Complexes **II** and $[FeW_2(\mu_3\text{-Se})(CO)_7Cp_2]$ (**III**) were obtained by a slight modification of the method recently described [1].

Synthesis of 1,1,2,2,3,3,3-heptacarbonyl-1,2-bis-(η^5-cyclopentadienyl)-(1,2,3,μ_3-selenido)-triangulo-tungsten-molybdenum-iron

Compound **I** (0.12 g, 0.18 mmol) and $[CpMo(CO)_3]_2$ (0.17 g, 0.35 mmol) in *m*-xylene (5 cm^3) were refluxed for 8 h and the volatiles then removed *in vacuo*. The solid residue was extracted with several portions of $CHCl_3$ and concentrated *in vacuo*. The mixture of soluble products thus obtained was separated by TLC on "Silufol" plates (hexane–benzene in a 3:2 ratio). Four major fractions were collected:

* See Ref. 1 for Part I.

† Author to whom correspondence should be addressed.

(1) The pale red fraction: small amounts of unreacted $[CpMo(CO)_3]_2$.

(2) The red-brown fraction: trace amounts of $[FeMo_2(\mu_3\text{-Se})(CO)_7Cp_2]$ (**IV**) [5].

(3) The red-violet fraction: $[FeMoW(\mu_3\text{-Se})(CO)_7Cp_2]$ (**V**), the black crystals (from toluene–pentane), yield 0.053 g (40%). Found: C, 27.9; H, 1.4. Calc. for $C_{17}H_{10}FeO_7MoSeW$: C, 27.5; H, 1.35%. IR ($CHCl_3$, ν_{CO}, cm^{-1}): 2038 s; 2024 s; 1985 vs; 1954 vs; 1941 sh; 1886 m, br; 1845 m, br. ^1H NMR ($CDCl_3$, TMS, δ, ppm): 5.28 (s, MoC_5H_5); 5.32 (s, WC_5H_5).

(4) The dark red fraction: trace amounts of **III**.

X-ray structure determination

The structures of **III** and **V** were determined by X-Ray analysis. Single crystals were prepared by the slow diffusion of pentane into toluene solutions of these compounds (Table 1). Absorption corrections were applied using the integration method on crystal shape. The structures were solved by direct methods ("SHELXS-86") [6] and refined by the full-matrix least squares method on F^2 using all independent reflections ("SHELXL-93") [7]. Hydrogen atoms were refined in the rigid body approximation (C—H distance is 0.96 Å). It has been found that in the structure of **V**, Mo and W positions were not located and both M(1) and M(2) contain a Mo/W mixture. After a final refinement M(1) and M(2) was found to be 34.3(5)% W+65.7(5)% Mo and 65.7(5)% W+34.3(5)% Mo, respectively. Atomic coordinates and thermal parameters are deposited in the Cambridge Crystallographic Database. Molecules of **III** and **V** are shown in Figs 1 and 2 with selected bond distances in the captions. Crystal packing is shown in Fig. 3.

RESULTS AND DISCUSSION

Synthesis and spectroscopy

Cluster **I** was recently shown to react with the dineric complexes $[CpM(CO)_3]_2$ (M = Mo, W) in *m*-xylene at the boiling point of the solvent resulting in metal substituted derivatives formation. [1,5] Now we have found that the first-step tungsten substituted produce **II** can be used to obtain the heterotrimetal cluster **V** in an analogous manner (Scheme 1).

III, **V** and **IV** can be considered as a series of clusters obtained by the sequential substitution of the group $CpW(CO)_2$ with $CpMo(CO)_2$. Their IR spectra ($CHCl_3$ solution) are very similar, but there are some differences in the peak locations and the intensity ratio.

The ^{77}Se NMR spectra of those complexes show signals for μ_3-Se. It is interesting that their chemical

Table 1. Crystallographic data for **III** and **V**

	III	**V**
Formula	$C_{17}H_{10}FeO_7SeW_2$	$C_{17}H_{10}FeMoO_7SeW$
fw	828.76	740.85
Crystal system	monoclinic	monoclinic
a (Å)	30.682(8)	30.712(5)
b (Å)	8.544(3)	8.565(1)
c (Å)	15.085(6)	15.099(2)
β (°)	102.95(3)	102.88(1)
V (Å^3)	3854(2)	3871.8(9)
Space group, *Z*	*C*2/*c* (No.15), 8	*C*2/*c* (No. 15), 8
D_x (g cm^{-3})	2.857	2.542
μ (cm^{-1})	300.5	243.9
Crystal shape	±(100), 0.060,	±(100), 0.050,
[faces, distances	±(21$\bar{2}$), 0.314,	±(001), 0.286,
between them (mm)]	±(2$\bar{1}\bar{2}$), 0.300	±(01$\bar{1}$), 0.258,
		±(011), 0.228
Diffractometer	Syntex $P2_1$	Syntex $P2_1$
Radiation	Cu-K_α (λ = 1.5418 Å)	Cu-K_α (λ = 1.5418 Å)
$2\theta_{max}$ (°)	85	90
$N_{total/independ.}$[a]	1577/1358	1606/1567
R_{int}	0.0433	0.0231
Transmission	0.02326–0.19734	0.03445–0.29806
R(*F*)	0.0457 for 1143 $F > 4\sigma$	0.0442 for 1253 $F > 4\sigma$
	0.0538 for all	0.0573 for all
wR (F^2)	0.1236 for 1143 $F > 4\sigma$	0.0973 for 1253 $F > 4\sigma$
	0.1292 for all	0.1040 for all

[a] Reflections with $h+k = 2n$ were measured alone.

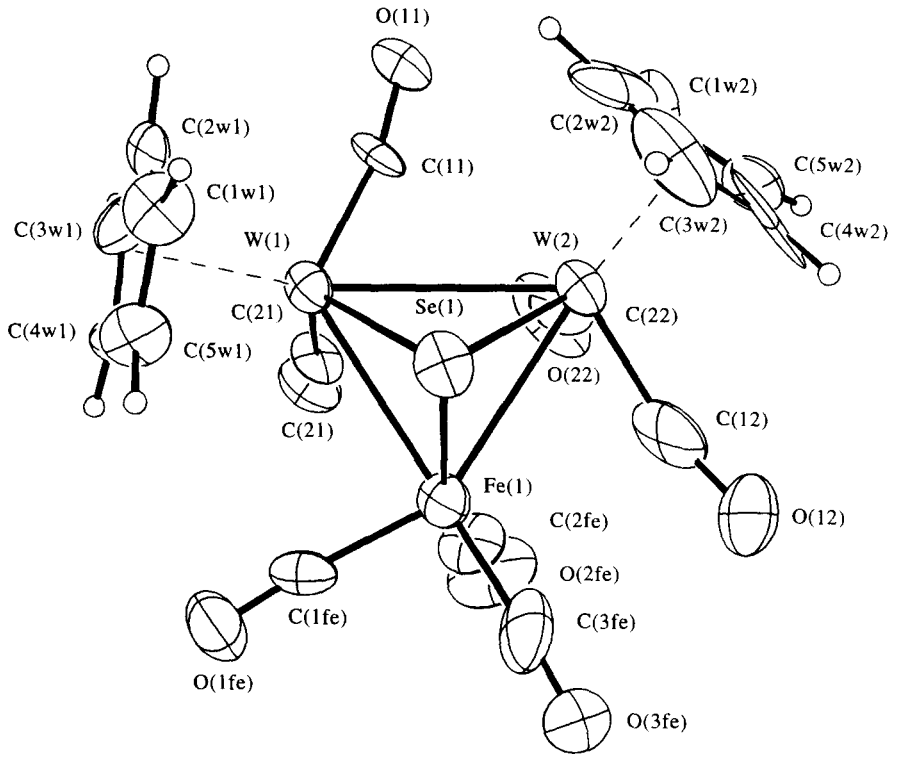


Fig. 1. The molecule of $[FeW_2(\mu_3\text{-Se})(CO)_7Cp_2]$ (**III**) (thermal ellipsoids on 50% probability level). Selected bond distances (Å): W(1)—W(2), 3.071(2), W(1)—Fe(1), 2.819(4), W(2)—Fe(1), 2.835(4), W(1)—Se(1), 2.495(3), W(2)—Se(1), 2.510(3), Fe(1)—Se(1), 2.334(4), W—C(CO), 1.90(2)–1.96(3), W—C(Cp), 2.28(3)–2.37(2), Fe—C(CO), 1.77(3)–1.85(4).

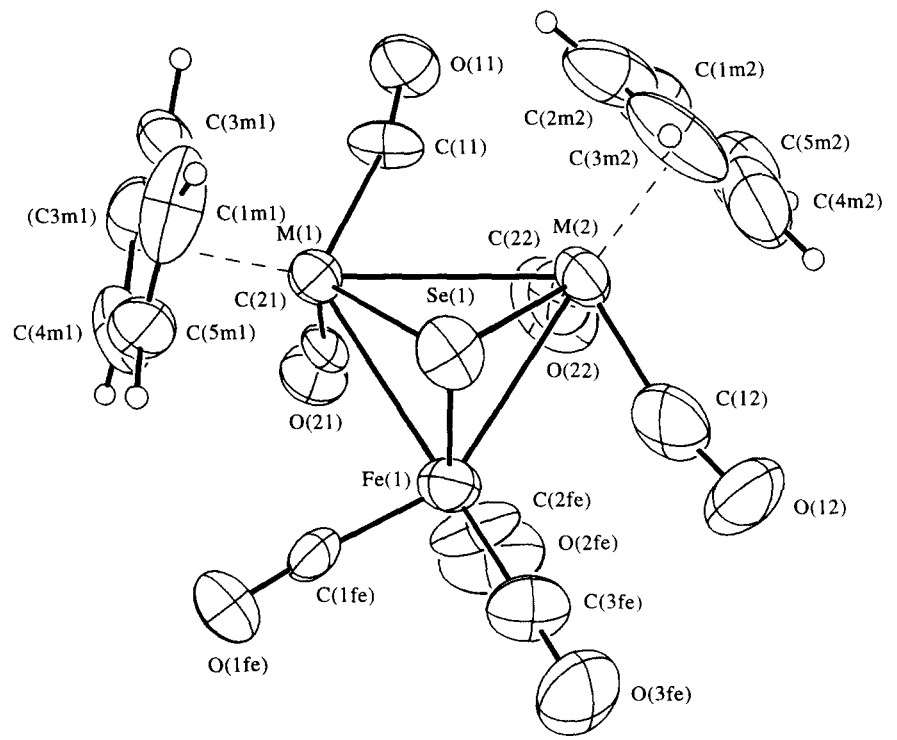


Fig. 2. The molecule of $[FeMoW(\mu_3\text{-Se})(CO)_7Cp_2]$ (**V**) (thermal ellipsoids on 50% probability level). Selected bond distances (Å): M(1)—M(2), 3.079(2), M(1)—Fe(1), 2.820(3), M(2)—Fe(1), 2.836(3), M(1)—Se(1), 2.499(2), M(2)—Se(1), 2.497(2), Fe(1)—Se(1), 2.322(4), MGC(CO), 1.93(2)–2.01(2), M—C(Cp), 2.25(3)–2.37(2), Fe—C(CO), 1.74(2)–1.77(2).

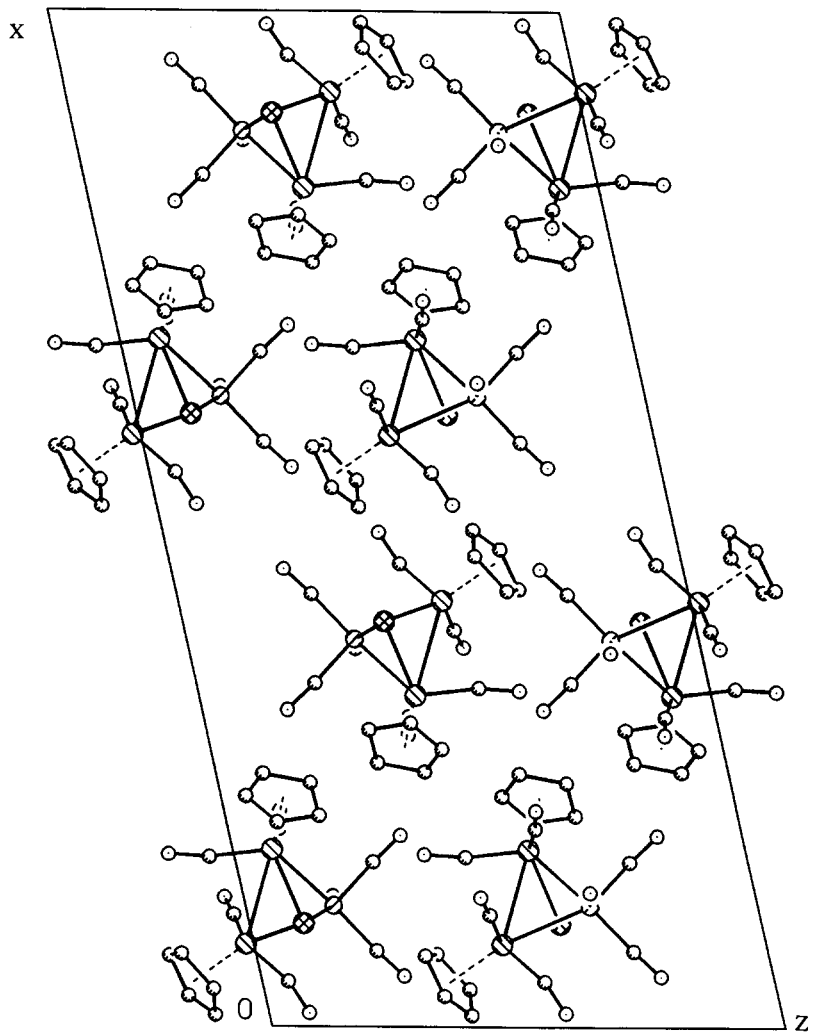
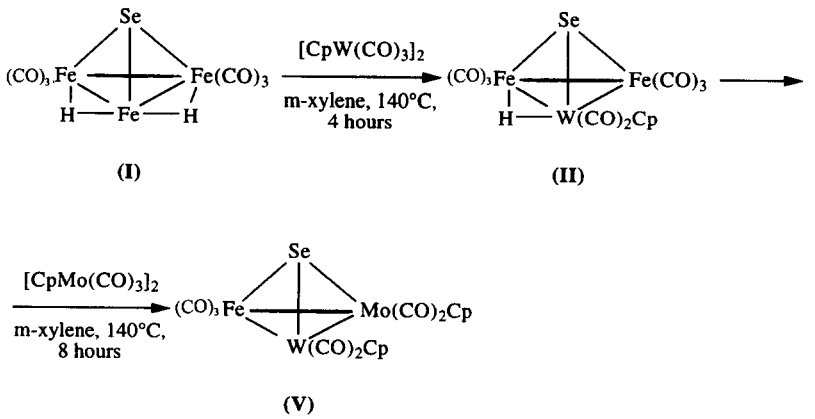


Fig. 3. Crystal packing of **III** and **V** (view along *y* axis).



(I) **(II)** **(V)**

Scheme 1.

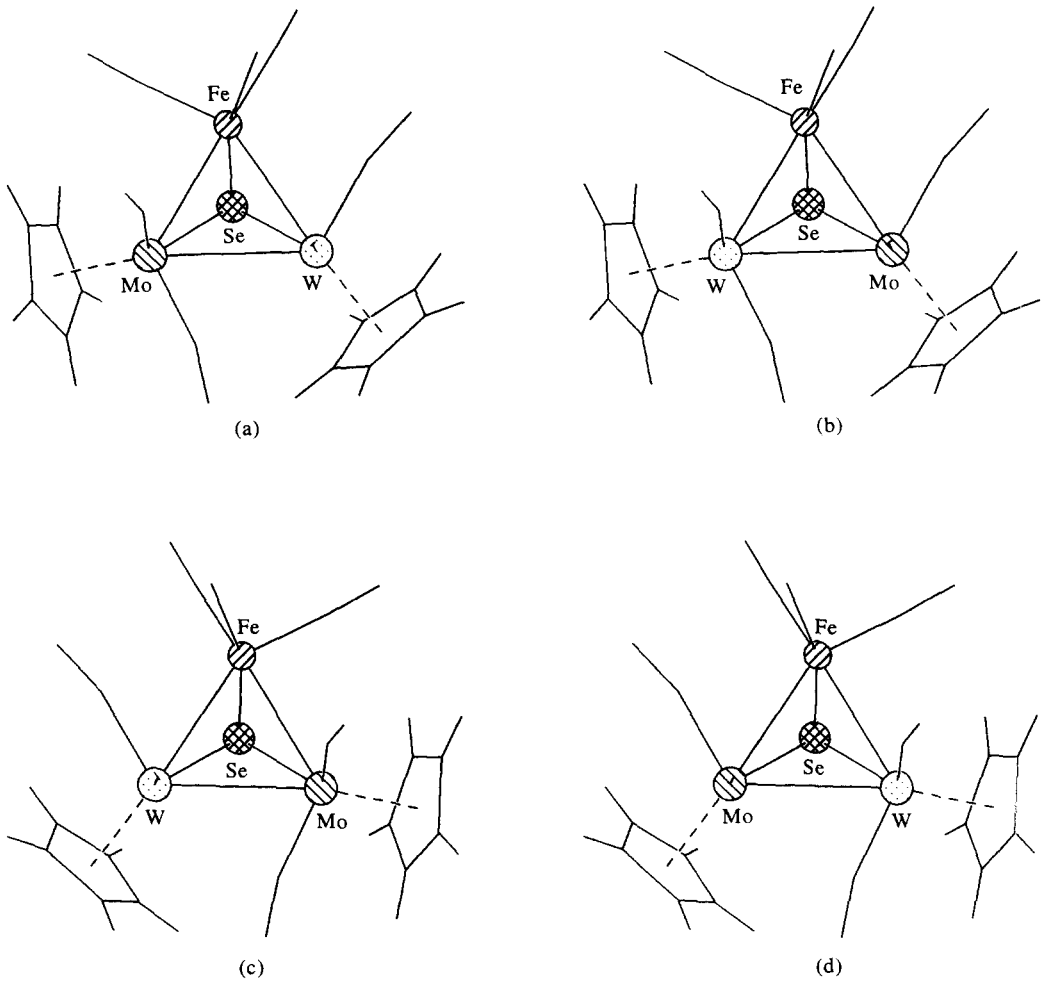


Fig. 4. Four isomers of cluster **V** occurring in the crystalline state shown in a common orientation: μ_3-Se atom is situated over the FeM(1)M(2) plane. Isomers **a** and **b** (as well as **c** and **d**) occupy a common crystallographic position giving a Mo/W disorder.

shifts are additively increased in the row: **III** ($\delta = -51$ ppm) [1], **V** ($\delta = 183$ ppm) and **IV** ($\delta = 421$ ppm)* [5]. In each step the $\Delta\delta$ values are nearly equal: 234 and 238 ppm, respectively.

The ^{1}H NMR spectrum of **V** contains two singlet signals for protons of two Cp ligands bonded to W and Mo. Their chemical shifts (see Experimental Section) are approximately the same as those in the cases of **III** [5.31 ppm] [1] and **IV** [5.28 ppm] [5].

Crystal and molecular structures of **III** *and* **V**

X-Ray structural analysis has shown **III** and **V** to be isostructural. They are also isostructural to one of the two known polymorphous modifications of [$FeMo_2$ (μ_3-Se) $(CO)_7Cp_2$] (**IV**) [8], but differ in the crystal packing from the other one [5]. Also the structures of two analogous sulfide clusters [FeW_2 (μ_3-S) $(CO)_7Cp_2$] (**VI**) [9] and [$FeMo_2$ (μ_3-S) $(CO)_7$ (η^5-$CH_3C_5H_4)_2$] (**VII**) [10] are known.

From our point of view the most interesting feature of **III, IV, VI** and **VII** is an unexpected chirality of their molecules in the crystalline state resulting from the ligands disposition asymmetry: these clusters have pseudo mirror symmetry within the tetrahedral FeM_2 (μ_3-X) core and at the same time have no symmetry in the ligand arrangement (Fig. 1). The latter fact causes the formation of two optical isomers related by crystallographic symmetry operations: the inversion and glide reflection (Fig. 4).

In the case of **V** the situation is more interesting: in addition to a ligand disposition asymmetry the tetrahedral FeMoW(μ_3-X) core has no symmetry elements. Therefore, in theory, **V** would exist in the crystalline state as a mixture of four isomers resulting from the combination of these two chirality types (Fig. 4). Molybdenum and tungsten atoms have been determined to be statistically distributed in the M(1) and (2) positions (Fig. 2). Based on the ^{77}Se NMR and IR spectra

* All ^{77}Se NMR spectra were recorded for CH_2Cl_2 solutions of clusters.

of **V** and the result of chromatography separation results (see previous sections), we can conclude that **V** is an individual compound but not a mixture of **III** and **IV**. Therefore, X-ray data can be interpreted in the following manner: all four isomers of **V** occur in a crystal as the statistically distributed blocks of enantiomer pairs **V(a,c)** and **V(b,d)** (see Figs 3 and 4) in a 34.3 : 65.7 ratio. This occurs because Mo and W are closely related in size. The bond distances in **III** and **V** are very close. The M(1)—M(2) bond in **V** is slightly longer than W(1)—W(2) that in **III** due to the presence of the Mo atoms in M positions. In **III** as well as in **V**, the M—Se distances are virtually equal for M(1) and M(2).

CONCLUSION

The method which we have used to obtain clusters **II**–**V** is based on the cooperative degradation of both reaction partners at a high temperature resulting in a new cluster core formation. It is not predictable *a priori* and requires an experimental testing for each new object. In this work this approach has been shown to have some success in the case of the selenide iron carbonyl clusters as well as in the case of a number of parent compounds containing other μ_3-coordinated non-transition elements [2,3].

REFERENCES

1. S. N. Konchenko, A. V. Virovets, S. V. Tkachev, V. I. Alekseev and N. V. Podberezskaya, *Polyhedron* 1996, **15,** 1221.
2. S. P. Gubin, *Koord. Khim.* 1994, **20,** 403 (in Russian).
3. K. H. Whitmire, *J. Coord. Chem.* 1988, **17,** 95.
4. K. Fisher, W. Deck, M. Schwarz and H. Vahrenkamp, *Chem. Ber.* 1985, **118,** 4946.
5. S. N. Konchenko, A. V. Virovets, V. A. Varnek, S. V. Tkachev, N. V. Podberezskaya and V. A. Maksakov, *Zh. Strukt. Khum.* 1996, **37,** 337 (in Russian).
6. G. M. Sheldrick, *Acta Cryst.* 1990, **A46,** 467.
7. G. M. Sheldrick, *Acta Cryst.* 1993, **A49** (Suppl.), C53.
8. P. Mathur, M. M. Hossain and A. L. Rheingold, *Organometallics* 1994, **13,** 3909.
9. P. D. Williams and M. D. Curtis, *J. Organomet. Chem.* 1988, **352,** 169.
10. Wen-Hua Sun, Shi-Yan Yang, Han-Qing Wang, Quan-Fu Zhou and Kai-Bei Yu, *J. Organomet. Chem.* 1994, **465,** 263.

Pergamon

PII: S0277-5387(96)00250-1

Polyhedron Vol. 16, No. 4, pp. 713–719, 1997
Copyright © 1996 Elsevier Science Ltd
Printed in Great Britain. All rights reserved
0277-5387/97 $17.00+0.00

Preparation, characterization and X-ray crystal structure of a charge transfer salt $(DMNP)_4[SiW_{12}O_{40}] \cdot 2DMF$

Xiao-Min Zhang,[a] Bao-Zhen Shan,[a] Xiao-Zeng You,[a]* Zhou Zhong-Yuan[b] and Zhou Xiang-Ge[b]

[a]Coordination Chemistry Institute, The State Key Laboratory of Coordination Chemistry, Nanjing University; The Center for Advanced Studies in Science and Technology of Microstructure, Nanjing 210093, P.R. China

[b]Chengdu Institute of Organic Chemistry, The Chinese Academy of Science, Chengdu, P.R. China

(Received 8 February 1996; accepted 22 May 1996)

Abstract—The title compound, $[(DMNP)_4SiW_{12}O_{40} \cdot 2DMF]$ (DMNP = 4-dimethylamino-1-methylpyridylammonium; DMF = N,N-dimethyl formamide) has been synthesized from $(TBA)_4SiW_{12}O_{40}$ (TBA- = tetrabutylammonium) and DMNP iodide in acetonitrile. The compound crystallized in $P2_1/n$ space group from DMF solution, and was characterized by elemental analysis, XPS study, IR, ESR and electronic spectra. X-ray structure analysis confirmed the presence of the Keggin structure of $SiW_{12}O_{40}^{4-}$. The sites of four oxygen atoms bonded to Si atom are disordered over 8 possible locations in each anion in the crystal, which increases the symmetry of the polyanion. The bond distances of Si—O and W=O are 1.636(5)–1.655(5) and 1.632–1.726 Å, respectively. Copyright © 1996 Elsevier Science Ltd

Keywords: X-ray structure; charge-transfer; Keggin structure; DMNP; donor; acceptor.

The design and synthesis of new magnetic molecular materials based on charge-transfer (CT) compounds has been developed rapidly in recent years [1–3]. These materials are made up of organic donors such as tetrathiafulvalene (TTF) and its derivatives and inorganic acceptors derived from the polyoxometalates whose structures are made by association of MO_6 (M = Mo, W) octahedra [4,5]. These polyanions present a field of interest because of their reversible high electron-acceptor capabilities such as the Keggin structure $[(XM_{12}O_{40})^{n-}$, M = W, Mo; X = P, Si, Ge ...] and Dawson structure $[(X_2M_{18}O_{62})^{n-}$, M = W, Mo; X = P, Si, As ...], which also keep their gross structures [6]. We focus our investigations on polyanions having the Keggin structure. This paper deals with the preparation and characterization of a CT compound obtained from the reaction with DMNP and the tetrabutyl ammonium salt of $SiW_{12}O_{40}^{4-}$.

* Author to whom correspondence to be addressed.

EXPERIMENTAL

Materials

All chemicals were procured commercially and used without subsequent purification. The polyoxometalate $(TBA)_4SiW_{12}O_{40}$ was synthesized according to the procedure described earlier [7]. The DMNP iodide was prepared by the literature method.

Synthesis of $(DMNP)_4SiW_{12}O_{40} \cdot 2DMF$

In 50 cm^3 acetonitrile solution, $(TBA)_4SiW_{12}O_{40}$ (0.3 mmol, 1.15 g) and the DMNP iodide (1.2 mmol, 0.422 g) were mixed and refluxed for 2 h. After cooling to room temperature, the yellow precipitates were filtered by suction and washed several times by acetonitrile. Yield: 0.98 g, 95%. The yellow crystals of the title complex were obtained by recrystallization in

DMF. Found: C, 12.5; H, 1.6; N, 3.8. Calc. for $C_{38}H_{66}N_{10}O_{42}SiW_{12}$: C, 12.8; H, 1.8; N, 3.9%.

Measurements

Elemental analysis was performed on a Perkin-Elmer 240C analytical Instrument. The IR spectrum was recorded on a Nicolet FT-IR 170SX spectrophotometer with KBr pellet. The XPS was performed on a VG ESCALAB MK-II. The low temperature powder ESR spectrum was obtained on a Bruker 2000D-SRC spectrometer.

Crystallography

Data collection. A prismatic crystal of size $0.22 \times 0.28 \times 0.30$ mm was used for data collection on Siemens P4/PC diffractometer with graphite monochromated Mo—K_α ($\lambda = 0.71073$ Å) radiation using ω scan type with variable scan speed of 4.0–29.30° min^{-1}. Three standard reflections were measured every 100 reflections. No absorption correction was made. From a total of 12,767 reflections measured for $4.0 \leqslant 2\theta \leqslant 50.0°$ ($-16 \leqslant h \leqslant 16$, $-24 \leqslant k \leqslant 24$, $-18 \leqslant l \leqslant 0$), 7144 were independent and 3638 reflections were considered observed using the criteria $F > 6.0\sigma(F)$.

Structure solution and refinement. The structure was solved by direct methods using Siemens SHELXTL P4/PC and refined by full-matrix least-squares. All non-hydrogen atoms were refined anisotropically. All the hydrogen atoms were refined using the riding model with fixed isotropic thermal parameter U. The final reliability factors were $R = 0.072$, $R_w = 0.0962$. The weighting scheme is $w = 1/[\sigma^2(F) + 0.0055F^2]$. All computations were performed on an IBM compatible 486/DX2 personal computer. The high R value is due to the poor crystal and disorder of the anion. The crystal data are summarized in Table 1. The final atomic coordinates and thermal parameters, together with observed and calculated structure factors, have been deposited as supplementary material with the Editor, from whom copies are available on request.

Table 1. Crystallographic data for $(DMNP)_4SiW_{12}O_{40} \cdot 2DMF$

Molecular formula	$C_{38}H_{66}N_{10}O_{42}SiW_{12}$
Molecular weight	3569.3
Colour and habit	Yellow prism
Crystal system	Monoclinic
Space group	$P2_1/n$
Unit cell dimensions	
a (Å)	13.109(3)
b (Å)	19.283(4)
c (Å)	14.364(3)
β (°)	90.10(4)
Z	2
D_{calc} (g/cm^{-1})	3.265
$F(000)$	3204
Absorption coefficient (mm^{-1})	19.034
R_{int}	0.0905
Parameters refined	474
F_{Gof}	1.93
Largest and mean Δ/σ	0.031, 0.003
Data-to-parameter ratio	7.7:1
$\Delta\rho_{max}$ (eÅ^{-3})	1.46
$\Delta\rho_{min}$ (eÅ^{-3})	−1.13

RESULTS AND DISCUSSION

IR spectrum

The IR data of the title compound and $(TBA)_4SiW_{12}O_{40}$ are shown in Table 2. It can be seen that the related vibration bands of the polyoxometalate remain almost unchanged in the title complex, ν(W—Od) from 967.6 to 969 cm^{-1}, ν(Si—Oa) 919 cm^{-1} [unchanged], ν(W—Ob—W) 884 to 883 cm^{-1}, and ν(W—Oc—W) 792 to 791 cm^{-1} [7]. This suggests that the interaction between organic donor and polyoxoanion is very weak, which can be verified by UV spectra in DMF solution that has only one strong absorption near 290 nm and no charge-transfer band appears.

UV spectra

Figure 1 compares the UV spectra of the title compound and $(TBA)_4SiW_{12}O_{40}$ in DMF solution. The only one strong absorption band appeared at 290 nm which is a characterization band of $SiW_{12}O_{40}^{4-}$ polyanion [4]. The spectra indicates that the organic cation is a weak donor, and the $SiW_{12}O_{40}^{4-}$ is a weak acceptor. The interactions between the polyoxometalate and DMNP are very weak, and the title complex is almost entirely dissociated in solution [6]. This result agrees with the IR spectra.

ESR spectra

The low temperature ESR spectra of the title compound irradiated by Hg lamp for 1 h is displayed in Fig. 2. The appearance of the Mo^V signal is because small amounts of molybdenum (from the raw materials, about 0.005%) are always contained in the polytungstate. They behave as selective electron traps under reducing conditions. The signal of $g_\parallel = 1.912$, $g_\perp = 1.933$, is ascribed to Mo^V [4]. The ESR signal of polytungstosilicate was not observed in the spectra, which may be due to the fact that the signal from the 12-tungstate blues rapidly decreased in intensity without broadening significantly and were unobservable as the temperature was raised [8].

Table 2. IR data of the title complex and $(TBA)_4SiW_{12}O_{40}$

	$\nu(W—O^d)$	$\nu(Si—O^a)$	$\nu(W—O^b—W)$	$\nu(W—O^c—W)$
$(TBA)_4SiW_{12}O_{40}$	967.6	919	884	792
$(DMNP)_4SiW_{12}O_{40}\cdot 2DMF$	969	919	883	791

[a] Tetrahedral.
[b] Corner sharing.
[c] Edge sharing.
[d] Terminal.

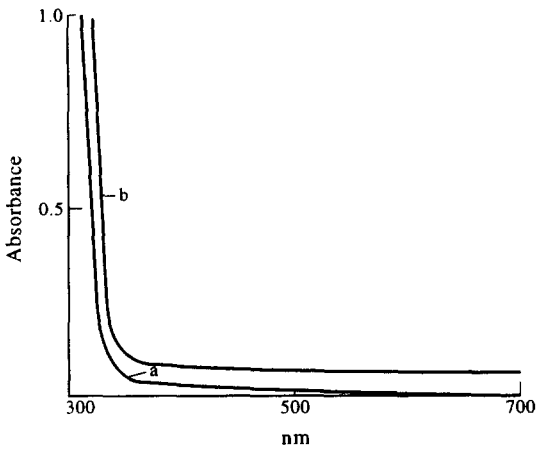


Fig. 1. Comparison of the electronic spectra of $(TBA)_4SiW_{12}O_{40}$ and the title compound in DMF solution. (a) $(TBA)_4SiW_{12}O_{40}$, (b) the title compound. All spectra were obtained on 2×10^{-3} M solution in 1 cm cell at 18°C.

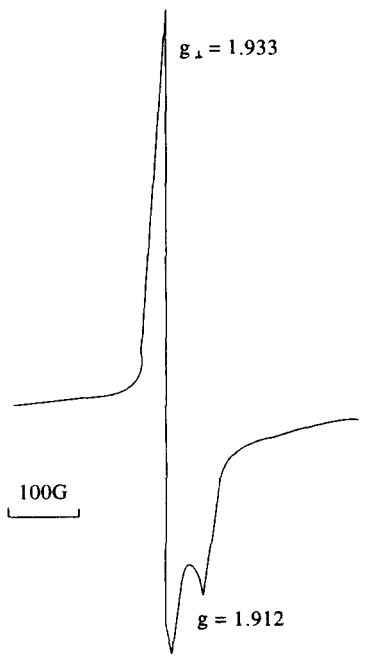


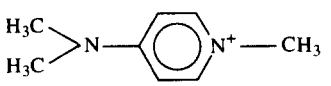
Fig. 2. X-Band ESR spectrum of the title compound at low temperature (100 K). The powder sample was irradiated for 1 h by a 500 W Hg lamp.

XPS study

The XPS data of related compounds for W_{4f}, Si_{2p}, and O_{1s} are shown in Table 3. The yellow title compound turned into grey-blue in the course of being irradiated under the 500 W Hg lamp. From Table 3, it can be seen that the XPS data of W_{4f}, Si_{2p} and O_{1s} in the title compound are 35.6, 101.9 and 530.7 eV, respectively. The core electron binding energies are higher, 0.3, 0.4 and 0.3 eV respectively than those in $(TBA)_4SiW_{12}O_{40}$. The related binding energies of irradiated compound are higher at 0.6, 0.2 and 0.5 eV than those in the unirradiated title compound. The above results are not consistent with the earlier reports [9,10], but similar to the compounds of TTF and its derivatives [11]. Further work is being carried out on this case.

Structural studies

Selected bond distances and bond angles are listed in Tables 4 and 5, respectively. The diagram rep-



Scheme 1.

resentation of the cation DMNP is given in Scheme 1. The view of the molecule and polyoxoanion structure of the title compound and its atomic numbering are shown in Fig. 3. A stereoview of the packing diagram viewed down the *Y* axis is given in Fig. 4. The X-ray

Table 3. XPS data of the title compound and $(TBA)_4SiW_{12}O_{40}$ (eV)

	W_{4f}	Si_{2p}	O_{1s}
$(TBA)_4SiW_{12}O_{40}$	35.3	101.5	530.4
[a] $(DMNP)_4SiW_{12}O_{40}\cdot 2DMF$	35.6	101.9	530.7
[b] $(DMNP)_4SiW_{12}O_{40}\cdot 2DMF$	36.2	102.1	531.2

[a] Before irradiated.
[b] After irradiated.

Table 4. Selected bond distances (Å)

Si(1)—O(7)	1.655(5)	Si(1)—O(7′)	1.644(6)
Si(1)—O(8)	1.636(5)	Si(1)—O(8′)	1.649(5)
Si(1)—O(7A)	1.655(5)	Si(1)—O(7′A)	1.644(6)
Si(1)—O(8A)	1.636(5)	Si(1)—O(8′A)	1.649(5)
W(1)—O(1)	1.632(6)	W(1)—O(7)	2.361(5)
W(1)—O(8)	2.441(5)	W(1)—O(9)	2.082(5)
W(1)—O(19)	1.903(6)	W(1)—O(10A)	1.907(5)
W(1)—O(15A)	1.833(5)	W(2)—O(2)	1.709(5)
W(2)—O(8)	2.289(5)	W(2)—O(9)	1.726(5)
W(2)—O(11)	1.925(5)	W(2)—O(20)	1.999(6)
W(2)—O(12A)	1.949(5)	W(3)—O(3)	1.731(4)
W(3)—O(11)	1.863(5)	W(3)—O(13)	1.937(6)
W(3)—O(15)	1.859(5)	W(3)—O(7A)	2.378(5)
W(3)—O(14A)	1.870(6)	W(4)—O(4)	1.701(5)
W(4)—O(12)	1.864(5)	W(4)—O(14)	1.983(6)
W(4)—O(16)	1.866(5)	W(4)—O(17)	1.874(5)
W(5)—O(5)	1.695(5)	W(5)—O(8)	2.482(6)
W(5)—O(16)	1.939(5)	W(5)—O(18)	1.797(6)
W(5)—O(19)	1.957(6)	W(5)—O(20)	2.007(5)
W(6)—O(6)	1.658(6)	W(6)—O(10)	1.842(5)
W(6)—O(13)	1.922(5)	W(6)—O(17)	1.917(5)
W(6)—O(18)	1.924(5)	W(6)—O(7A)	2.418(6)
O(7)—W(3A)	2.378(5)	O(7)—W(6A)	2.418(6)
O(10)—W(1A)	1.907(5)	O(12)—W(2A)	1.949(5)
O(14)—W(3A)	1.870(6)	O(15)—W(1A)	1.833(5)

analysis of the complex indicates the presence of the Keggin structure for the polyoxometalate. The silicon atom is in the centre of the polyanion and the four oxygen atoms of the SiO_4 tetrahedron are disordered. Every oxygen atom has two equal sites, O(7) and O(7A), O(8) and O(8A), O(7′) and O(7′A), O(8′) and O(8′A). The relevant Si—O bond lengths are 1.655(5), 1.635(5), 1.644(6) and 1.649(5) Å, respectively. The bond distances of the polyoxometalate are in the range of 1.632(6)–1.731(4) Å for the terminal oxygen, 1.726(3)–2.082(5) Å for the bridging oxygens, and 2.289(5)–2.482(6) Å for the oxygens of the SiO_4 group. The shortest bond distances of W—O in the anion is W(1)—O(1) 1.632(6) Å, and the longest W—O bond length W(5)—O(8) is 2.482(6) Å, which indicate the severe distortion of the WO_6 octahedra in the polyanion. The bond lengths and angles relating to the organic cation are normal and are not discussed further. In the crystal structure, the large spherical polyoxometalate anions and DMNP cations form an interval layer arrangement along the [010] direction. The DMNP cations act as interstitial species at specific sites. The part of positive charge in the organic donor is closer to the polyoxoanion. The organic cation has two kinds of arrangement in the unit cell. One type has a compact parallel alignment in the form of head-to-head and tail-to-tail. The other four cations located on both sides of the polyoxoanion formed an overlapping head-to-head arrangement, respectively. Planes of the two kinds of cations have certain dihedral angles. The shortest contact distances between the cation and polyoxoanion are O(6)—C(6) 3.11 Å and O(2)—C(6) 3.37 Å, which suggest that the interaction may occur in the organic donor and inorganic acceptor.

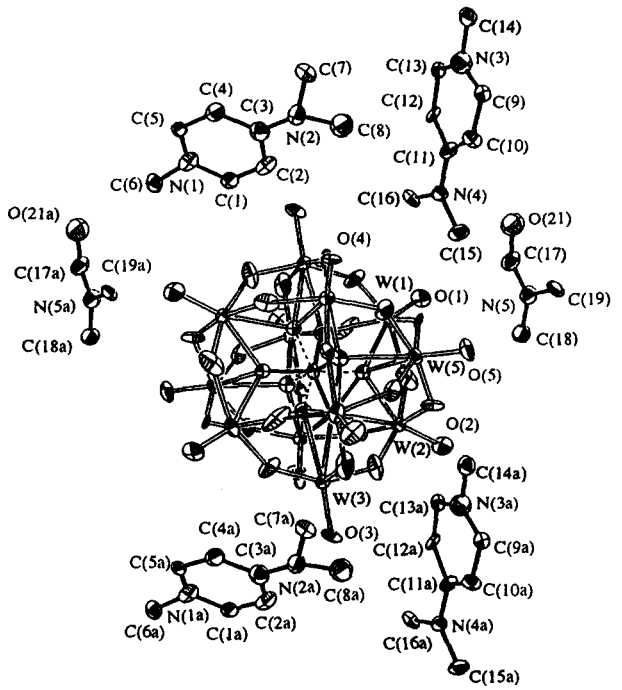
Acknowledgements—The authors would like to thank the State Science and Technology Commission and the National Nature Science Foundation of China for a major key research project.

REFERENCES

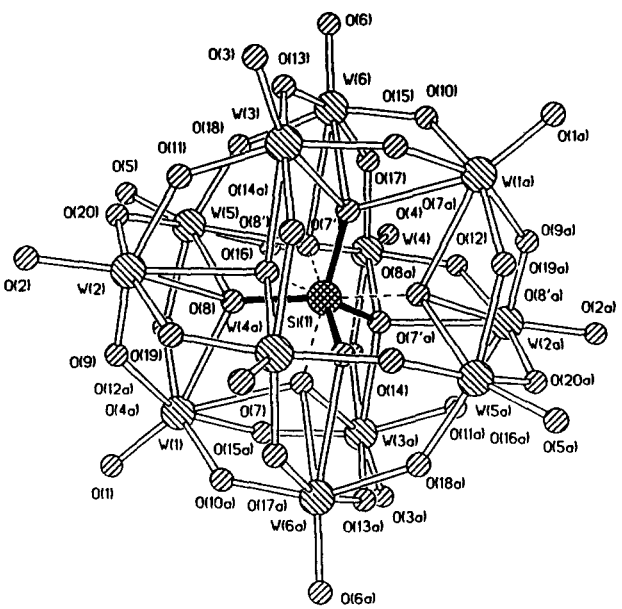
1. C. J. Gomez-Garcia, C. Gimenez-Saiz, S. Triki,

Table 5. Selected bond angles (°)

O(7)—Si(1)—O(8′)	109.4(3)	O(8)—Si(1)—O(7A)	108.8(2)
O(7)—Si(1)—O(8A)	108.8(2)	O(7A)—Si(1)—O(8′A)	109.4(3)
O(1)—W(1)—O(7)	156.7(2)	O(1)—W(1)—O(8)	154.9(2)
O(1)—W(1)—O(9)	97.5(2)	O(7)—W(1)—O(9)	97.3(2)
O(1)—W(1)—O(19)	102.4(3)	O(7)—W(1)—O(19)	96.7(2)
O(1)—W(1)—O(10A)	99.6(3)	O(8)—W(1)—O(10A)	91.4(2)
O(19)—W(1)—O(10A)	157.8(2)	O(1)—W(1)—O(15A)	109.0(2)
O(8)—W(1)—O(15A)	94.2(2)	O(9)—W(1)—O(15A)	153.4(2)
O(19)—W(1)—O(15A)	90.2(2)	O(2)—W(2)—O(8)	153.3(2)
O(2)—W(2)—O(9)	94.0(2)	O(2)—W(2)—O(11)	105.4(2)
O(8)—W(2)—O(11)	93.0(2)	O(9)—W(2)—O(11)	160.3(2)
O(2)—W(2)—O(20)	88.0(2)	O(9)—W(2)—O(20)	89.3(2)
O(11)—W(2)—O(20)	87.6(2)	O(2)—W(2)—O(12A)	106.8(2)
O(8)—W(2)—O(12A)	92.2(2)	O(9)—W(2)—O(12A)	88.2(2)
O(11)—W(2)—O(12A)	89.8(2)	O(20)—W(2)—O(12A)	165.0(2)
O(3)—W(3)—O(11)	97.9(2)	O(3)—W(3)—O(13)	95.4(2)
O(3)—W(3)—O(15)	109.3(2)	O(11)—W(3)—O(15)	152.4(2)
O(13)—W(3)—O(15)	86.4(2)	O(3)—W(3)—O(7A)	156.9(3)
O(11)—W(3)—O(7A)	95.9(2)	O(3)—W(3)—O(14A)	102.5(2)
O(11)—W(3)—O(14A)	91.0(2)	O(13)—W(3)—O(14A)	162.0(2)
O(15)—W(3)—O(14A)	88.4(2)	O(7A)—W(3)—O(14A)	95.6(2)
O(4)—W(4)—O(12)	97.9(2)	O(4)—W(4)—O(14)	100.0(2)
O(12)—W(4)—O(14)	90.8(2)	O(4)—W(4)—O(16)	104.2(2)
O(12)—W(4)—O(16)	157.9(2)	O(14)—W(4)—O(16)	85.4(2)
O(4)—W(4)—O(17)	101.2(3)	O(12)—W(4)—O(17)	88.6(2)
O(14)—W(4)—O(17)	158.7(2)	O(16)—W(4)—O(17)	87.1(2)
O(5)—W(5)—O(8)	154.1(3)	O(5)—W(5)—O(16)	103.9(2)
O(8)—W(5)—O(16)	96.9(2)	O(5)—W(5)—O(18)	101.5(3)
O(8)—W(5)—O(18)	95.4(2)	O(16)—W(5)—O(18)	85.1(2)
O(5)—W(5)—O(19)	99.5(2)	O(16)—W(5)—O(19)	87.7(2)
O(18)—W(5)—O(19)	158.9(2)	O(5)—W(5)—O(20)	90.7(2)
O(16)—W(5)—O(20)	165.4(2)	O(18)—W(5)—O(20)	92.5(2)
O(19)—W(5)—O(20)	89.4(2)	O(6)—W(6)—O(10)	106.8(3)
O(6)—W(6)—O(13)	97.4(2)	O(10)—W(6)—O(13)	92.7(2)
O(6)—W(6)—O(17)	100.9(2)	O(10)—W(6)—O(17)	86.9(2)
O(13)—W(6)—O(17)	161.0(3)	O(6)—W(6)—O(18)	98.8(2)
O(10)—W(6)—O(18)	153.8(3)	O(13)—W(6)—O(18)	89.3(2)
O(17)—W(6)—O(18)	82.9(2)	O(6)—W(6)—O(7A)	158.6(2)
O(17)—W(6)—O(7A)	96.8(2)	O(18)—W(6)—O(7A)	95.2(2)
Si(1)—O(7)—W(1)	122.6(2)	Si(1)—O(7)—W(3A)	121.7(3)
W(1)—O(7)—W(3A)	97.2(2)	Si(1)—O(7)—W(6A)	119.6(2)
W(1)—O(7)—W(6A)	94.8(2)	W(3A)—O(7)—W(6A)	94.4(2)
Si(1)—O(8)—W(1)	119.1(2)	Si(1)—O(8)—W(2)	129.2(2)
W(1)—O(8)—W(2)	96.6(2)	Si(1)—O(8)—W(5)	116.3(5)
W(1)—O(8)—W(5)	92.6(2)	W(2)—O(8)—W(5)	94.9(2)
W(1)—O(9)—W(2)	136.0(3)	W(6)—O(10)—W(1A)	139.5(3)
W(2)—O(11)—W(3)	138.8(3)	W(4)—O(12)—W(2A)	136.8(3)
W(3)—O(13)—W(6)	131.5(3)	W(4)—O(14)—W(3A)	135.0(2)
W(3)—O(15)—W(1A)	148.6(3)	W(4)—O(16)—W(5)	138.4(3)
W(4)—O(17)—W(6)	138.0(4)	W(5)—O(18)—W(6)	142.9(3)
W(1)—O(19)—W(5)	134.4(2)	W(2)—O(20)—W(5)	122.8(2)



ORTEP of the polyoxometalate $(DMNP)_4SiW_{12}O_{40}\cdot 2DMF$



Structure of the polyanion $SiW_{12}O_{40}^{4-}$

Fig. 3. Crystal structure of the title compound and its polyoxoanion, showing 50% thermal ellipsoids and atom numbering.

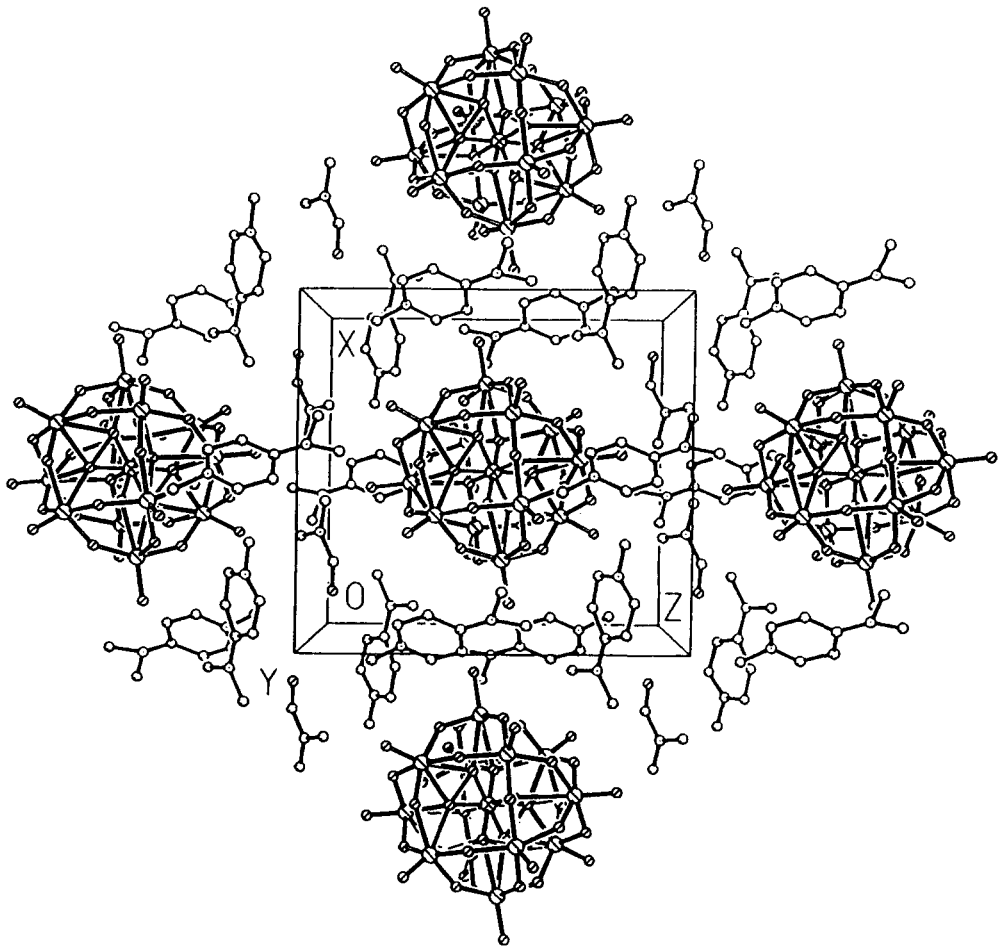


Fig. 4. Crystal packing of the title compound viewed along the *Y*-axis.

E. Coronado, P. Le Magueres, L. Ouahab, L. Ducasse, C. Sourisseau and P. Delhaes, *Inorg. Chem.* 1995, **34**, 4139.
2. P. Le Magueres, L. Ouahab, S. Golhen, D. Grandjean, O. Pena, J. C. Jegaden, C. J. Gomez-Garcia and P. Delhaes, *Inorg. Chem.* 1994, **33**, 5180.
3. E. Coronado and C. J. Gomez-Garcia, *Comments Inorg. Chem.* 1995, **17**, 255 and references therein.
4. M. T. Pope, *Heteropoly and Isopoly Oxometalates*. Springer-Verlag, New York (1983).
5. C. Rocchiccioli-Deltcheff, M. Fournier, R. Franck and R. Thouvenot, *Inorg. Chem.* 1983, **22**, 207.
6. N. Jing-Ying, Y. Xiao-Zeng, D. Cun-Ying, F. Hoong-Kun and Z. Zhong-Yuan, *Inorg. Chem.*, 1996, accepted.
7. M. Filowitz, R. K. C. Ho, W. G. Klemperer, and W. Shum, *Inorg. Chem.* 1979, **1**, 93.
8. G. M. Varga, E. Papaconstantinou and M. T. Pope, *Inorg. Chem.* 1970, **3**, 662.
9. W. Jun, W. Zhi-Yuan, Z. Heng-Bin, Z. Zhong-Qing, W. Xiao-Ren and W. Wuan, *Chem. J. Chin. Univ.* 1992, **11**, 1428.
10. Z. Bao-Jian, Q. Lun-Yu, L. Jing-Fu, and Z. Shi-Liang, *Acta Chim. Sin.* 1987, **45**, 232.
11. D. Attanasio, C. Bellitto, M. Bonamico, G. Righint and G. Staulo, *Mat. Res. Soc. Symp. Proc.* 1992, **247**, 545.

Pergamon

PII: S0277-5387(96)00269-0

Polyhedron Vol. 16, No. 4, pp. 721–731, 1997
Copyright © 1996 Elsevier Science Ltd
Printed in Great Britain. All rights reserved
0277-5387/97 $17.00+0.00

Organometallic tantalum complexes with phosphine, phosphanido and phosphinidene ligands. Syntheses and crystal structures of $[Cp'TaCl_4\{PH_2(2,4,6\text{-}Pr^i_3C_6H_2)\}]$, $[Cp'Ta(\mu\text{-}PPh_2)(PPh_2)]_2 \cdot C_7H_8$ and $[Cp'TaCl\{\mu\text{-}P(2,4,6\text{-}Pr^i_3C_6H_2)\}]_2 \cdot C_7H_8$ ($Cp' = C_5H_4Me$)†

Ghasan A. Abdul Hadi, Katharina Fromm,‡ Steffen Blaurock, Svea Jelonek and Evamarie Hey-Hawkins§

Institut für Anorganische Chemie der Universität, Talstr. 35, D-04103 Leipzig, Germany

(Received 7 May 1996; accepted 20 May 1996)

Abstract—The reaction of $[Cp'TaCl_4]$ ($Cp' = C_5H_4Me$) with $KPPh_2(dioxane)_2$ (1 : 1) in diethyl ether at room temperature gave the phosphanido-bridged tantalum(III) complex $[Cp'Ta(\mu\text{-}PPh_2)(PPh_2)]_2$ (**1**)$\cdot C_7H_8$ as black crystals. $[Cp'TaCl_4]$ reacted with 2,4,6-triisopropylphenylphosphine with formation of the adduct $[Cp'TaCl_4\{PH_2(2,4,6\text{-}Pr^i_3C_6H_2)\}]$ (**2**). Attempts to eliminate HCl from **2** with DBU (DBU = 1,8-diazabicyclo-[5,4,0]-undec-7-ene) gave the phosphinidene-bridged tantalum(IV) complex $[Cp'TaCl\{\mu\text{-}P(2,4,6\text{-}Pr^i_3C_6H_2)\}]_2$ (**3**)$\cdot C_7H_8$. It was shown independently that DBU acts as a base and as a reducing agent. **1**–**3** were characterized spectroscopically (IR, MS, NMR) as well as by crystal structure determinations. Copyright © 1996 Elsevier Science Ltd

Keywords: methylcyclopentadienyl tantalum complexes; phosphide ligand; phosphanido ligand; phosphinidene ligand.

Organometallic dialkyl- and diarylphosphanido complexes of early transition metals have been studied intensively, while complexes derived from functionalised phosphines which exhibit a reactive phosphorus-ligand bond have been largely neglected [1]. It was recently shown that Zr [2] and Mo [3] complexes react with primary phosphines or alkali metal phosphanides to yield a wide variety of products, whose formation depends on the nature of the organic substituents on phosphorus and the transition metal. The zirconocene derivatives with functionalised phosphorus-based ligands exhibit remarkable reactivity; thus, substitution of the P-based ligand by polar or protic reagents, and insertion of multiply-bonded inorganic or organic systems into the metal–phosphorus bond are observed [2]. The latter yields novel functionalised phosphorus ligands in the coordination sphere of the transition metal that are not available by other routes.

We have now extended our work on zirconocene [2] and molybdenum [3] chemistry to cyclopentadienyl tantalum complexes to investigate the influence of the nature of the transition metal on the reactivity observed in reactions with primary phosphines and alkali metal phosphanides. While the P—Si or P—H bond in zirconium complexes is generally less reactive

† Dedicated to Professor Hans Georg von Schnering, on the occasion of his 65th birthday.

‡ Present address: Institut für Anorganische Chemie der Universität, Auf der Morgenstelle 18, D-72076 Tübingen, Germany.

§ Author to whom correspondence should be addressed.

[2], we expect this bond to be more reactive when the P ligand is coordinated to a group 5 or 6 metal; thus, modification of the ligand should be possible.

To date, only a few phosphanido derivatives of organometallic [4] and inorganic [5,6] tantalum compounds and two stable terminal phosphinidene complexes [6,7] have been described in the literature, although potential starting materials such as cyclopentadienyl-substituted tantalum halides, alkyls, hydrides or carbonyls [8] are accessible, as are inorganic tantalum halides [9].

We now report the synthesis of a tantalum phosphanido complex $[Cp'Ta(\mu\text{-}PPh_2)(PPh_2)]_2$ (**1**) ($Cp' = C_5H_4Me$), as well as the preparation of the first organometallic tantalum complex with a *primary* phosphine ligand $[Cp'TaCl_4\{PH_2(2,4,6\text{-}Pr^i_3C_6H_2)\}]$ (**2**). The latter can be utilised as starting material for the synthesis of the tantalum phosphinidene complex $[Cp'TaCl\{\mu\text{-}P(2,4,6\text{-}Pr^i_3C_6H_2)\}]_2$ (**3**).

RESULTS AND DISCUSSION

Synthesis and properties of $[Cp'Ta(\mu\text{-}PPh_2)(PPh_2)]_2$ (**1**)$\cdot C_7H_8$

Phosphanido complexes of tantalum are rare. Thus, $[Cp_2TaH_2(PPh_2)]$ was mentioned as an intermediate in the formation of the diphosphene complex $[Cp_2TaH(\eta^2\text{-}P_2Ph_2)]$ in 1989 [4a], but it was only in 1995 that its synthesis and spectroscopic details were reported [4c]. Another monophosphanido complex, $[Cp^*TaMe(\eta^2\text{-}C_2H_4)(PPh_2)]$ ($Cp^* = C_5Me_5$), which is accessible from $[Cp^*TaMe_2(\eta^2\text{-}C_2H_4)]$ and $PHPh_2$, was reported in 1993 [4b]. Hydrogenation of this complex in the presence of $PHPh_2$ gives the tris-phosphanido complex $[Cp^*TaH(PPh_2)_3]$. Both complexes exhibit fluxional behaviour at room temperature [4b].

Our attempts to utilise the salt elimination reaction as a synthetic approach to tantalum(V) phosphanido complexes were thwarted due to the high reducing potential of alkali metal phosphanides. Thus, the reaction of $[Cp'TaCl_4]$ with $KPPh_2(dioxane)_2$ (1 : 1) in ether afforded after work up black, rhombic crystals of $[Cp'Ta(\mu\text{-}PPh_2)(PPh_2)]_2$ (**1**)$\cdot C_7H_8$, which could be handled in air for a short time without decomposition. Similar to the reaction of cyclopentadienyl-substituted molybdenum(V) complexes with $KPPh_2(dioxane)_2$ [10], both reduction of the Ta^V starting material to Ta^{III} (formally $[Cp'TaCl_2]$; comparable Ta^{III} complexes $[Cp^RTaCl_2]$ with $Cp^R = C_5H_5$, C_5Me_5, C_5Me_4Et have been obtained by controlled reduction of $[Cp^RTaCl_4]$) [11] and substitution of the chloro ligands by PPh_2 are observed. Surprisingly, $[Cp^*NbCl_4]$ reacted with $LiPPh_2$ at low temperature to give only the substitution product $[Cp^*NbCl_3(PPh_2)]$, which was characterised by IR and ^1H NMR spectroscopy [12]. However, when a fourfold excess of lithium phosphanide was employed, only reduction products were observed [12].

In the mass spectrum of **1**, a signal for toluene is observed at *ca* 140°C, and at *ca* 290°C the molecular ion peak is observed at $m/z = 1260$, as well as signals for fragments arising from loss of Cp′ ligands and phenyl groups.

No signals due to **1** are observed in the ^1H and ^{31}P NMR spectrum, suggesting the presence of a paramagnetic species.

Synthesis and properties of $[Cp'TaCl_4\{PH_2(2,4,6\text{-}Pr^i_3C_6H_2)\}]$ (**2**) *and* $[Cp'TaCl\{\mu\text{-}P(2,4,6\text{-}Pr^i_3C_6H_2)\}]_2$ (**3**)

When equimolar amounts of $PH_2(2,4,6\text{-}Pr^i_3C_6H_2)$ are added to a toluene solution of $[Cp'TaCl_4]$, a colour change from yellow to orange indicates the formation of the adduct $[Cp'TaCl_4\{PH_2(2,4,6\text{-}Pr^i_3C_6H_2)\}]$ (**2**), which can be isolated as yellow crystals.

The Lewis acidity of tantalum(V) and niobium(V) complexes has been extensively studied and a large number of adducts of $[Cp^RMCl_4]$ with ethers, amines, nitriles, and isonitriles has been reported [13]. Up to now, only a few phosphine complexes of cyclopentadienyl tantalum (or niobium) tetrachloride are known, all of which possess *tertiary* phosphine ligands. While $[CpMCl_4(PMe_3)]$ (M = Nb, Ta) [13d, 14] and $[CpNbCl_4(PEt_3)]$ [14] were earlier reported to be unstable, it was shown only recently that stable adducts can be obtained provided there is *no excess* of phosphine present. Thus, the complexes $[Cp^*NbCl_4(L)]$ ($L = PMe_3$, PMe_2Ph, $PMePh_2$), $[Cp^*NbCl_3(Me)(PMe_2Ph)]$ and $[\{Cp^*NbCl_4\}_2(\mu\text{-dmpe})]$ (dmpe = $Me_2PCH_2CH_2PMe_2$) are accessible in high yield [12], as are the phosphine adducts $[CpNbCl_4(L)]$ ($L = PMe_3$, PMe_2Ph, $PMePh_2$) [15]. With excess phosphine, these complexes are readily reduced to niobium(IV) compounds, with PMe_3 being the best reducing agent (formation of $PMe_3H^+Cl^-$) [12, 15]. With **2**, no reaction is observed with excess phosphine.

In the NMR spectra, $[Cp'TaCl_4\{PH_2(2,4,6\text{-}Pr^i_3C_6H_2)\}]$ (**2**) exhibits dynamic behaviour which we attribute to rotation about the Ta—P bond. Thus, at room temperature only broad signals are observed for the PH_2 group in the ^1H and ^{31}P NMR spectra. Below 290 K a triplet is observed in the proton-coupled ^{31}P NMR spectrum [$\Delta G^‡$ (288 K) = 67 ± 2 kJ mol^{-1} [16]. Similarly, the dynamic behaviour of $[Cp^*TaMe(\eta^2\text{-}C_2H_4)(PPh_2)]$ was attributed to restricted rotation about the Ta—P bond [$\Delta G^‡ = 48 \pm 1.3$ kJ mol^{-1}] [4b]. Inversion barriers of terminal phosphanido groups lie in the same range (e.g., 48–60 kJ mol^{-1} for Nb, Re, Fe, and W complexes [17].

As expected on coordination to a transition metal, the signal of the phosphine ligand is shifted to low field compared to the free phosphine (−158.2 ppm, J(PH) 203 Hz) [18b, 18c] by 122.5 ppm, and the P—H coupling constant increases by 158 Hz. Accordingly,

a low-field shift of the P—H signal by 2.80 ppm is observed in the proton NMR spectrum. Similarly, low-field shifts are observed for the resonances of the *ortho*-Pr^i groups of the aromatic ligand (free phosphine: 1.19 CH*Me*$_2$, 3.41 C*H*Me$_2$ [18], coordinated: 1.29 and 3.90, respectively), while the differences in the chemical shifts of the *para*-Pr^i ligand and the *meta*-H atoms of the phenyl ligand are less pronounced. Comparable effects are observed in the ^{31}P NMR spectra of LiPH(2,4,6-Pr$^i_3$C$_6$H$_2$) (−165 ppm, *J*(PH) 166 Hz) [19] and the corresponding phosphanido complex [Cp$'_2$Zr(Cl){PH(2,4,6-Pr$^i_3$C$_6$H$_2$)}] (−4.6 ppm, *J*(PH) 230 Hz) [19]. For most tantalum and niobium complexes with tertiary phosphine ligands, no ^{31}P NMR data have been reported. However, for those complexes for which data are available, e.g. [Cp*NbCl$_3$(X)(PMe$_2$Ph)] (X = Cl: 2 ppm, X = Me: −1.9 ppm) [12], [CpNbCl$_4$(L)] (L = PMe$_3$: 5 ppm, L = PMe$_2$Ph: 12 ppm, L = PMePh$_2$: 17 ppm) [15] and the cationic complex [Cp$_2$TaH$_2$(PHPh$_2$)]$^+$ (0.2 ppm, *J*(PH) 389 Hz) [4c], broad signals and a low-field shift compared to the free phosphines (PMe$_3$: −62 ppm, PMe$_2$Ph: −46 ppm, PMePh$_2$: −26 ppm, PHPh$_2$: −41.1 ppm, ^{1}*J*(PH) 214.3 Hz) [20] are also observed; however, here the difference is less pronounced.

In the ^{1}H NMR spectrum of **2** and **3**, the signals of the Cp′ ligand are shifted to high field by up to 1 ppm compared to [Cp′TaCl$_4$] [21]. In **2**, the *ipso*-C atom of the triisopropylphenyl ligand (152.2 ppm, *J*(PC) 28 Hz) exhibits the expected chemical shift [18c], however, the PC coupling constant is smaller than in the free phosphine (*J*(PC) 57.2 Hz) [18c] and in [Cp*TaMe(η^2-C$_2$H$_4$)(PPh$_2$)] (145.9 ppm, *J*(PC) 41 Hz) [4b].

No molecular ion peak is observed in the mass spectrum of **2**. Only signals for [Cp′TaCl$_4$] and PH$_2$(2,4,6-Pr$^i_3$C$_6$H$_2$) as well as fragmentation products thereof are observed.

The phosphinidene-bridged tantalum(IV) complex [Cp′TaCl{μ-P(2,4,6-Pr$^i_3$C$_6$H$_2$)}]$_2$ (**3**) is obtained on reacting **2** with DBU (1:2 or 1:3) in *ca* 55% yield. Also, when [Cp′TaCl$_4$] is reacted *in situ* with PH$_2$(2,4,6-Pr$^i_3$C$_6$H$_2$) and DBU (1:1:1), only **3** can be isolated, in low yield (*ca* 10–15%). The formation of an intermediate phosphanido complex was not observed. While no reaction of **2** was observed with excess phosphine, we were able to show that [Cp′TaCl$_4$] is reduced by equimolar amounts of DBU to give a paramagnetic Ta^{IV} species (Experimental Section). Thus, in the reaction between [Cp′TaCl$_4$], PH$_2$(2,4,6-Pr$^i_3$C$_6$H$_2$) and DBU, the amine is the reducing agent even in the absence of primary phosphine. Similarly, [MCl$_5$] (M = Nb, Ta) have been reported to be reduced to M^{IV} by aliphatic [22] and aromatic [23] amines. Surprisingly, in the reaction of [Cp*TaCl$_4$] with aniline the adduct [Cp*TaCl$_4$(NH$_2$Ph)] is formed [24]. This adduct also reacts with base (LiNEt$_2$) undergoing elimination of HCl (without reduction) and formation of the Ta^V imido complex [Cp*TaCl$_2$(NPh)] [24].

Stable terminal phosphinidene complexes of inorganic tantalum derivatives, [(SiMe$_3$NCH$_2$CH$_2$)$_3$NTa=PR] (R = Ph, Cy, Bu^t) [7] (yellow) and [(Bu$^t_3$SiO)$_3$Ta=PPh] [6] (red), have been reported, in addition to those known for Mo [25], W [26] and Zr [27]. [(SiMe$_3$NCH$_2$CH$_2$)$_3$NTa=PR] [175.1 (R = Cy) and 227.3 ppm (R = Bu^t)] [7] and [(Bu$^t_3$SiO)$_3$Ta=PPh] [6] (334.6 ppm) have ^{31}P chemical shifts which indicate the presence of a linear MPR unit (bent MPR unit: 660 to 800 ppm [25]), for **3**, a ^{31}P chemical shift of 391.5 ppm is observed. Also, the deshielding effect on coordination to a transition metal is even more pronounced in **3**. Thus, all resonances of the triisopropylphenyl ligand are shifted to low field by 0.1 to 0.5 ppm in the ^{1}H NMR spectrum.

In the mass spectrum, the molecular ion peak of **3** (*m/z* 1060) as well as a signal for the monomeric compound (*m/z* 530) and fragmentation products of the Cp′TaCl and P(2,4,6-Pr$^i_3$C$_6$H$_2$) fragment are observed.

Molecular structures of [Cp′Ta(μ-PPh$_2$)(PPh$_2$)]$_2$(**1**)·C$_7$H$_8$, [Cp′TaCl$_4$\{PH$_2$(2,4,6-Pr$^i_3$C$_6$H$_2$)\}] (**2**) *and* [Cp′TaCl{μ-P(2,4,6-Pr$^i_3$C$_6$H$_2$)}]$_2$ (**3**)·C$_7$H$_8$

Single crystals of **1** were obtained by covering a saturated toluene solution with a layer of n-heptane. The compound crystallises in the triclinic space group $P\bar{1}$ and has one formula unit per unit cell (Table 1, Table 4). The unit cell also contains a disordered toluene molecule without bonding interactions. Single crystals of **2** are obtained as yellow needles on cooling a saturated pentane solution to 5 C. **2** crystallises in the triclinic space group $P\bar{1}$ and has two formula units per unit cell (Table 2, Table 4). **3** is obtained as dark red cubes on cooling a saturated toluene/pentane solution to −20 C. The compound crystallises in the monoclinic space group $P2_1/n$ with two formula units per unit cell (Table 3, Table 4). The unit cell also contains two disordered toluene molecules without bonding interactions.

The pronounced tendency of low-valent Ta^{III} and Ta^{IV} complexes to form binuclear complexes is also exhibited in the molecular structures of **1** and **3**. Both consist of centrosymmetric dimeric molecules in which Ta atoms are bound by two bridging phosphanido (PPh$_2$, **1**) or phosphinidene [P(2,4,6-Pr$^i_3$C$_6$H$_2$), **3**] groups. In **1** each Ta atom also bears a terminal PPh$_2$ ligand (Fig. 1), in **3** there are terminal chloro ligands (Fig. 2). In both complexes, a Cp′ group completes the coordination of the Ta atom. The centrum of the Ta$_2$P$_2$ rings in **1** and **3** coincides with a crystallographic inversion centre [**1**: 0, 1/2, 0 (c), **3**: 0, 0, 1/2 (b)].

The four-membered metallacycles Ta(1)—P(2)—Ta(1)′—P(2)′ (**1**) and Ta—P—Ta′—P′ (**3**) are planar. The bond lengths and angles of the central Ta$_2$P$_2$ ring in **1** [Ta(1)—P(2)$_{br}$ 2.458(2), 2.486(2) Å;

Table 1. Selected bond lengths [Å] and bond angles [°] for **1** · C_7H_8

Ta(1)—P(1)	2.390(2)	Ta(1)—P(2)	2.486(2)
Ta(1)—P(2)′	2.458(2)	Ta(1)—Ta(1)′	3.024(2)
P(1)—C101	1.822(5)	P(1)—C(201)	1.821(6)
P(2)—C(301)	1.851(5)	P(2)—C(401)	1.849(5)
C(101)—C(102)	1.372(9)	C(101)—C(106)	1.412(8)
C(102)—C(103)	1.401(10)	C(103)—C(104)	1.40(2)
C(104)—C(105)	1.38(2)	C(105)—C(106)	1.394(11)
C(201)—C(206)	1.386(9)	C(210)—C(202)	1.398(9)
C(202)—C(203)	1.393(10)	C(203)—C(204)	1.36(2)
C(204)—C(205)	1.39(2)	C(205)—C(206)	1.389(10)
C(301)—C(306)	1.397(8)	C(301)—C(302)	1.382(9)
C(302)—C(303)	1.395(10)	C(303)—C(304)	1.391(14)
C(304)—C(305)	1.363(13)	C(305)—C(306)	1.402(8)
C(401)—C(406)	1.387(8)	C(401)—C(402)	1.392(8)
C(402)—C(403)	1.381(11)	C(403)—C(404)	1.36(2)
C(404)—C(405)	1.372(13)	C(405)—C(406)	1.389(8)
C(1)—C(5)	1.426(8)	C(1)—C(2)	1.432(8)
C(1)—C(6)	1.492(8)	C(2)—C(3)	1.433(9)
C(3)—C(4)	1.408(8)	C(4)—C(5)	1.408(8)
Ta—C(Cp) 2.379(5) to 2.471(5)			
Ta(1)—P(2)—Ta(1)′	75.43(5)	P(2)—Ta(1)—P(2)′	104.58(5)
P(1)—Ta(1)—P(2)	104.15(6)	P(1)—Ta(1)—P(2)′	99.97(6)
C(201)—P(1)—C(101)	100.3(3)	C(201)—P(1)—Ta(1)	126.4(2)
C(101)—P(1)—Ta(1)	133.1(2)	C(102)—C(101)—C(106)	118.2(6)
C(102)—C(101)—P(1)	120.4(4)	C(106)—C(101)—P(1)	121.4(5)
C(101)—C(102)—C(103)	122.4(7)	C(104)—C(103)—C(102)	118.4(9)
C(105)—C(104)—C(103)	120.3(7)	C(104)—C(105)—C(106)	120.3(9)
C(105)—C(106)—C(101)	120.3(8)	C(202)—C(201)—C(206)	118.6(6)
C(202)—C(201)—P(1)	119.6(5)	C(206)—C(201)—P(1)	121.6(5)
C(201)—C(202)—C(203)	119.4(8)	C(204)—C(203)—C(202)	121.7(8)
C(205)—C(204)—C(203)	119.4(7)	C(204)—C(205)—C(206)	119.9(8)
C(205)—C(206)—C(201)	120.9(8)	C(401)—P(2)—C(301)	98.1(2)
C(401)—P(2)—Ta(1)′	117.6(2)	C(301)—P(2)—Ta(1)′	121.0(2)
C(401)—P(2)—Ta(1)	122.4(2)	C(301)—P(2)—Ta(1)	123.7(2)
Ta(1)′—P(2)—Ta(1)	75.43(5)	C(302)—C(301)—C(306)	118.3(5)
C(302)—C(301)—P(2)	120.1(5)	C(306)—C(301)—P(2)	121.6(4)
C(301)—C(302)—C(303)	121.3(7)	C(304)—C(303)—C(302)	119.8(8)
C(305)—C(304)—C(303)	119.7(6)	C(304)—C(305)—C(306)	120.7(7)
C(305)—C(306)—C(301)	120.3(6)	C(402)—C(401)—C(406)	117.7(5)
C(402)—C(401)—P(2)	121.3(5)	C(406)—C(401)—P(2)	120.7(4)
C(401)—C(402)—C(403)	120.4(7)	C(404)—C(403)—C(402)	120.5(8)
C(405)—C(404)—C(403)	121.2(8)	C(404)—C(405)—C(406)	118.5(7)
C(405)—C(406)—C(401)	121.8(6)	C(5)—C(1)—C(2)	107.0(5)
C(5)—C(1)—C(6)	126.7(5)	C(2)—C(1)—C(6)	126.1(6)
C(3)—C(2)—C(1)	107.3(5)	C(4)—C(3)—C(2)	108.6(5)
C(3)—C(4)—C(5)	107.8(5)	C(4)—C(5)—C(1)	109.1(5)

Ta(1)—P(2)—Ta(1)′ 75.43(5)°; P(2)—Ta(1)—P(2)′ 104.58(5)°] are comparable to those of the central Ta_2Cl_2 rings in inorganic binuclear complexes of type $[TaCl_2L_2(\mu\text{-}Cl)]_2$ (L = SMe_2 [28], PMe_3 [29], $Me_2PCH_2CH_2PMe_2$ [30]), while the central Ta_2P_2 ring in **3** is nearly square [Ta—P 2.317(6), Ta—P′ 2.338(2) Å, P—Ta—P′ 96.49(8), Ta—P—Ta′ 83.51(8)°] indicating substantial p_π-d_π back bonding of the phosphorus lone pair.

Even though the 18-electron rule predicts the presence of a Ta=Ta double bond in **1** and a Ta—Ta single bond in **3**, the Ta—Ta distance of 3.024(2) Å in **1** is longer than the Ta=Ta double bond lengths reported in the literature (2.55–2.85 Å in inorganic octahedral ditantalum(III) complexes) [31]. Although the Ta—Ta bond length is strongly dependent on the number and type of ligands (e.g., hydrido-bridged complexes generally have shorter Ta—Ta bonds than comparable halogen-bridged complexes) [31], and in the Ta^{IV} complex $[TaCl_2(PMe_3)_2(\mu\text{-}Cl)_2]_2$ [32] a value of 2.83 Å is given for a Ta—Ta single bond, the long Ta—Ta distance in **1** and the paramagnetic behaviour indicate the absence of a Ta=Ta double bond. The lengthening of the Ta—Ta bond in **1** can also be

Table 2. Selected bond lengths [Å] and bond angles [°] for **2**

Ta(1)—Cl(1)	2.402(2)	Ta(1)—Cl(2)	2.417(2)
Ta(1)—Cl(3)	2.416(2)	Ta(1)—Cl(4)	2.386(2)
Ta(1)—C(Cp′)	2.423(8) to 2.496(8)		
Ta—Cp(Centre)	2.145		
P(1)—H(1A)	1.42	P(1)—H(1B)	1.42
Ta(1)—P(1)	2.710(2)	P(1)—C(7)	1.841(8)
C(1)—C(5)	1.413(13)	C(1)—C(2)	1.426(13)
C(1)—C(6)	1.506(13)	C(2)—C(3)	1.392(13)
C(3)—C(4)	1.401(14)	C(4)—C(5)	1.40(2)
C(7)—C(8)	1.407(12)	C(7)—C(12)	1.404(12)
C(8)—C(9)	1.385(12)	C(8)—C(13)	1.535(12)
C(9)—C(10)	1.405(13)	C(10)—C(11)	1.391(13)
C(10)—C(16)	1.521(12)	C(11)—C(12)	1.395(13)
C(12)—C(19)	1.524(12)	C(13)—C(14)	1.50(2)
C(13)—C(15)	1.537(14)	C(16)—C(18)	1.50(2)
C(16)—C(17)	1.53(2)	C(19)—C(21)	1.50(2)
C(19)—C(20)	1.531(14)		
Cl(4)—Ta(1)—Cl(1)	88.07(10)	Cl(4)—Ta(1)—Cl(3)	86.50(8)
Cl(1)—Ta(1)—Cl(3)	153.37(7)	Cl(4)—Ta(1)—Cl(2)	150.88(7)
Cl(1)—Ta(1)—Cl(2)	86.07(9)	Cl(3)—Ta(1)—Cl(2)	86.10(7)
Cl(4)—Ta(1)—P(1)	78.56(8)	Cl(1)—Ta(1)—P(1)	77.12(7)
Cl(3)—Ta(1)—P(1)	76.25(7)	Cl(2)—Ta(1)—P(1)	72.33(7)
C(7)—P(1)—H(1A)	105.9(3)	Ta(1)—P(1)—H(1A)	105.9(5)
C(7)—P(1)—H(1B)	105.9(3)	Ta(1)—P(1)—H(1B)	105.91(5)
H(1A)—P(1)—H(1B)	106.2	Cl(1)—Ta(1)—Cp(Centre)	103.8
Cl(2)—Ta(1)—Cp(Centre)	104.0	Cl(3)—Ta(1)—Cp(Centre)	102.8
Cl(4)—Ta(1)—Cp(Centre)	105.1	P(1)—Ta(1)—Cp(Centre)	176.3
C(7)—P(1)—Ta(1)	125.7(3)	C(5)—C(1)—C(2)	105.7(8)
C(5)—C(1)—C(6)	127.7(9)	C(2)—C(1)—C(6)	126.5(8)
C(3)—C(2)—C(1)	109.5(8)	C(2)—C(3)—C(4)	107.4(8)
C(5)—C(4)—C(3)	108.6(8)	C(4)—C(5)—C(1)	108.8(9)
C(8)—C(7)—C(12)	120.4(8)	C(8)—C(7)—P(1)	119.7(6)
C(12)—C(7)—P(1)	119.9(6)	C(9)—C(8)—C(7)	118.6(8)
C(9)—C(8)—C(13)	117.5(7)	C(7)—C(8)—C(13)	123.9(8)
C(8)—C(9)—C(10)	122.8(8)	C(11)—C(10)—C(9)	117.0(8)
C(11)—C(10)—C(16)	122.7(8)	C(9)—C(10)—C(16)	120.3(7)
C(10)—C(11)—C(12)	122.6(8)	C(11)—C(12)—C(7)	118.7(8)
C(11)—C(12)—C(19)	116.4(8)	C(7)—C(12)—C(19)	124.8(8)
C(14)—C(13)—C(8)	112.0(8)	C(14)—C(13)—C(15)	111.6(9)
C(8)—C(13)—C(15)	109.8(8)	C(18)—C(16)—C(10)	112.6(8)
C(18)—C(16)—C(17)	110.2(9)	C(10)—C(16)—C(17)	110.2(8)
C(21)—C(19)—C(12)	112.2(8)	C(21)—C(19)—C(20)	111.3(9)
C(12)—C(19)—C(20)	110.1(8)		

attributed to the high steric demand of the bridging PPh_2 ligands. In **3**, The Ta—Ta bond length of 3.100(3) Å is comparable to that observed in **1**. As **3** exhibits diamagnetic behaviour, the presence of a Ta—Ta single bond must be assumed. A comparable value of 3.165 Å is observed for a Ta—Ta bond in $[TaCl_3(SMe_2)(\mu\text{-SPh})]_2$ [33].

The Ta(1)—P(1) bond length of the terminal phosphanido ligand in **1** of 2.390(2) Å is only slightly shorter than that in $[TaH(PPh_2)_2(dmpe)]$ [Ta—P 2.430(6) and 2.404(6) Å] [5]. In both compounds, the P atom of the terminal phosphanido group is trigonal-planar (sum of bond angles *ca* 360°), indicating that the PPh_2 group is acting as a three-electron donor. In contrast, an increase in the Ta—P bond length and a pyramidal geometry of the P atom are observed when the phosphanido ligand acts as a one-electron donor (e.g., $[Cp_2TaH_2(PPh_2)]$, Ta—P 2.595(3) Å) [4c].

In **3**, the Ta—P bond lengths of the bridging phosphinidene ligand are comparable to that observed for the terminal phosphanido group in **1**. The dependence of the Ta—P bond length on the substituents and geometrical arrangement at phosphorus is demonstrated in the following complexes: Thus, the Ta—P double bond in $[(SiMe_3NCH_2CH_2)_3NTa{=}PCy]$ [7] of 2.145(7) Å (TaPC is linear) is much shorter than that observed for $[(Bu^t_3SiO)_3Ta{=}PPh]$ [6] (2.317(4) Å, Ta—P—C 110.2(4)°, bent TaPC). However, all these distances are shorter than the sum of the covalent radii of Ta and P (2.44 Å) [34].

The Ta—Cl bond length in **3** [2.350(2) Å] is shorter

Table 3. Selected bond lengths [Å] and bond angles [°] for $3 \cdot C_7H_8$

Ta—P	2.317(6)	Ta—P′	2.338(2)
Ta—Cl(1)	2.350(2)	Ta—Ta′	3.100(3)
P—C(7)	1.824(8)	P—Ta′	2.338(2)
Ta—Cp(Centre)	2.071	Ta—C(Cp)	2.349(10) to 2.451(9)
C(1)—C(5)	1.40(2)	C(1)—C(2)	1.43(2)
C(2)—C(3)	1.41(2)	C(3)—C(4)	1.39(2)
C(4)—C(5)	1.416(14)	C(5)—C(6)	1.50(2)
C(7)—C(12)	1.385(11)	C(7)—C(8)	1.419(11)
C(8)—C(9)	1.388(11)	C(8)—C(13)	1.508(12)
C(9)—C(10)	1.376(12)	C(10)—C(11)	1.384(11)
C(10)—C(16)	1.517(11)	C(11)—C(12)	1.406(11)
C(12)—C(19)	1.513(11)	C(13)—C(15)	1.52(2)
C(13)—C(14)	1.53(2)	C(16)—C(17)	1.500(14)
C(16)—C(18)	1.527(13)	C(19)—C(21)	1.52(2)
C(19)—C(20)	1.54(2)		
P—Ta—P′	96.49(8)	P—Ta—Cl(1)	105.02(12)
P′—Ta—Cl(1)	105.57(8)	P—Ta—Ta′	48.54(8)
P′—Ta—Ta′	47.95(11)	Cl(1)—Ta—Ta′	113.34(8)
C(7)—P—Ta	139.9(3)	C(7)—P—Ta′	136.6(3)
Ta—P—Ta′	83.51(8)	Cl(1)—Ta—Cp(Centre)	112.8
P—Ta—Cp(Centre)	118.3	P′—Ta—Cp(Centre)	116.7
C(5)—C(1)—C(2)	108.3(10)	C(3)—C(2)—C(1)	106.4(10)
C(4)—C(3)—C(2)	109.6(10)	C(1)—C(5)—C(4)	108.2(10)
C(3)—C(4)—C(5)	107.5(10)	C(4)—C(5)—C(6)	124.9(12)
C(1)—C(5)—C(6)	126.9(12)	C(12)—C(7)—P	119.9(6)
C(8)—C(7)—P	119.2(6)	C(9)—C(8)—C(7)	117.3(8)
C(12)—C(7)—C(8)	120.8(7)	C(7)—C(8)—C(13)	122.8(7)
C(9)—C(8)—C(13)	119.9(7)	C(9)—C(10)—C(11)	118.2(8)
C(10)—C(9)—C(8)	123.4(8)	C(11)—C(10)—C(16)	118.7(8)
C(9)—C(10)—C(16)	123.1(7)	C(7)—C(12)—C(11)	118.9(7)
C(10)—C(11)—C(12)	121.4(8)	C(11)—C(12)—C(19)	117.4(7)
C(7)—C(12)—C(19)	123.6(7)	C(8)—C(13)—C(14)	113.2(9)
C(8)—C(13)—C(15)	110.7(9)	C(17)—C(16)—C(10)	109.9(8)
C(15)—C(13)—C(14)	112.4(11)	C(10)—C(16)—C(18)	113.1(7)
C(17)—C(16)—C(18)	112.7(9)	C(12)—C(19)—C(20)	109.7(8)
C(12)—C(19)—C(21)	113.1(8)	C(21)—C(19)—C(20)	111.9(11)

than those in octahedral Ta derivatives (e.g., $[TaCl_2(\mu\text{-}Cl)(\mu\text{-dmpm})]_2$, dmpm = $Me_2PCH_2PMe_2$, Ta—Cl (terminal) 2.435(7), 2.457(6) Å [35], *trans*-$[CpTaCl_2(CO)(PMe_2Ph)_2]$, Ta—Cl 2.518(4), 2.539(4) Å [13d], $[Cp^*TaCl_3(PMe_3)]$, Ta—Cl 2.395(3) to 2.416(3) Å [11b], *cis*-$[Cp^*TaCl_2(CO)_2(PMe_3)]$, Ta—Cl 2.504(2), 2.512(2) Å [11b]), indicating a less pronounced *trans* effect of the bridging phosphorus ligand.

$[Cp'TaCl_4\{PH_2(2,4,6\text{-}Pr^i_3C_6H_2)\}]$ (**2**) (Figs 3 and 4) is the first phosphine adduct of $[Cp'TaCl_4]$ to be crystallographically characterised. A niobium complex, $[CpNbCl_4(PMePh_2)]$ [15], an amine complex, $[Cp^*TaCl_4(NH_2Ph)]$ [24], and an isocyanide complex $[Cp^*TaCl_4(CN\text{-}2,6\text{-}Me_2C_6H_3)]$ [24] which are structurally related, have been reported.

In **2**, the Ta atom has a pseudo-octahedral geometry, with the phosphine ligand located *trans* to the Cp′ ligand and the four chlorine ligands bent away from the Cp′ ligand [Cl(4)—Ta(1)—Cl(1) 88.07(10), Cl(4)—Ta(1)—Cl(3) 86.50(8), Cl(1)—Ta(1)—Cl(2) 86.07(9), Cl(3)—Ta(1)—Cl(2) 86.10(7)]. The Ta atom is shifted towards the Cp′ ligands and lies 0.58 Å above the plane defined by the four chlorine ligands, which is parallel to the plane defined by the Cp′ ring.

The Ta—Cl bond lengths [Ta(1)—Cl(1) 2.402(2), Ta(1)—Cl(2) 2.417(2), Ta(1)—Cl(3) 2.416(2), Ta(1)—Cl(4) 2.386(2)] are comparable to those observed in related compounds [e.g. $Cp^*TaCl_3(PMe_3)$], Ta—Cl 2.395(3) to 2.416(3) Å] [11b], while an increase in bond length is observed due to a strong *trans* effect in *cis*-$[Cp^*TaCl_2(CO)_2(PMe_3)]$ [Ta—Cl 2.504(2), 2.512(2) Å] [11b].

While the Ta—P bond lengths of phosphine adducts are in the range 2.59–2.67 Å [11b,13,14, 35–38], **2** exhibits a rather long Ta(1)—P(1) bond length of 2.710(2) Å, which is possibly due to the steric influence of the chlorine ligands or the *trans* effect of the Cp′ ligand. In the structurally related complexes $[CpNbCl_4(PMePh_2)]$ [Nb—P 2.7844(9) Å] [15] and

Table 4. Crystal data and structure refinement for $[Cp'Ta(\mu\text{-}PPh_2)(PPh_2)]_2$ (**1**)·C_7H_8, $[Cp'TaCl_4\{PH_2(2,4,6\text{-}Pr^i_3C_6H_2)\}]$ (**2**), and $[Cp'TaCl\{\mu\text{-}P(2,4,6\text{-}Pr^i_3C_6H_2)\}]_2$ (**3**)·C_7H_8

	1·C_7H_8	**2**	**3**·C_7H_8
Formula	$C_{67}H_{62}P_4Ta_2$	$C_{21}H_{32}Cl_4PTa$	$C_{49}H_{68}Cl_2P_2Ta_2$
Molecular weight	1353.03	638.19	1151.78
Temperature (K)	213(2)	200(2)	200(2)
Crystal system	triclinic	triclinic	monoclinic
Space group	$P\bar{1}$ (no. 2)	$P\bar{1}$ (no. 2)	$P2_1/n$ (no. 14)
a (Å)	10.083(5)	6.6244(13)	10.5457(12)
b (Å)	11.212(6)	10.159(2)	16.39(5)
c (Å)	13.191(7)	18.944(4)	14.021(2)
α (°)	102.62(4)	86.90(3)	90
β (°)	97.99(4)	81.93(3)	94.957(11)
γ (°)	101.03(4)	76.45(3)	90
V (Å^3)	1403(1)	1226.8(4)	2415(7)
Z	1	2	2
d_{calc} (g cm^{-3})	1.601	1.728	1.584
2Θ range (°)	3–60	4–47	4–50
h (min., max.)	0/14	−6/7	−12/12
k (min., max.)	−15/15	−11/9	0/19
l (min., max.)	−18/18	−21/15	−16/16
Total reflections	8040	4804	4389
Independent reflections	7609 [R(int.) 0.0439]	3441 [R(int.) 0.0904]	4298 [R(int.) 0.0186]
Parameters	345	273	382
Absorption coefficient (μ cm^{-1})	38.73	49.86	47.36
Largest diff. peak/hole (e Å^{-3})	4.3/−3.7[a]	1.7/−2.2	2.0/−1.1
Final R indices [$I > 2\sigma(I)$]	$R1$ = 0.0520, $wR2$ = 0.1450	$R1$ = 0.0407, wR = 0.1110	$R1$ = 0.0355, wR = 0.0806
R indices (all data)	$R1$ = 0.0522, $wR2$ = 0.1454	$R1$ = 0.0495, $wR2$ = 0.1147	$R1$ = 0.0840, wR = 0.0933
Goodness-of-fit (F^2)	1.078	1.106	0.997

[a] Located on the Ta—Ta vector.

$[Cp^*TaCl_2(CO)_2(PMe_3)]$ [Ta—P 2.707(2) Å] [11b], in which the phosphine ligand is in a position *trans* to the cyclopentadienyl ligand, lengthening of the metal–P bond was also observed.

EXPERIMENTAL

All experiments were carried out under purified dry nitrogen (for **1**) or argon (for **2** and **3**). Solvents were dried and freshly distilled under nitrogen or argon. For **1**: the IR spectrum was recorded on a Perkin-Elmer 883 in the range 200–4000 cm^{-1}; MS: Varian MAT 711 (EI, 70 eV, source temperature 180°C). For **2** and **3**, the IR spectra were recorded on a FT spectrometer System 2000 (Perkin-Elmer) in the range 200–4000 cm^{-1}; NMR spectra with an AVANCE DRX 400 spectrometer (Bruker), ^{1}H NMR: internal standard solvent (e.g., benzene, toluene), ^{31}P NMR: external standard 85% H_3PO_4; MS: with a Sektorfeldgerät AMD 402 (AMD Intectra GmbH) (EI, 70 EV). The EPR spectrum was recorded with a Bruker ESP 300E. The melting points were determined in sealed capillaries under nitrogen or argon and are uncorrected. $[Cp'TaCl_4]$ [13b], $KPPh_2(dioxane)_2$ [39], and $PH_2(2,4,6\text{-}Pr^i_3C_6H_2)$ [18] were prepared by literature procedures.

Synthesis of $[Cp'Ta(\mu\text{-}PPh_2)(PPh_2)]_2$ (**1**)·C_7H_8

$[Cp'TaCl_4]$ (0.50 g, 1.24 mmol) and $KPPh_2(dioxane)_2$ (0.49 g, 1.24 mmol) were placed in a Schlenk tube. 20 cm^3 of ether was added at room temperature. A brown solution was obtained. The solvent was removed to dryness and the residue extracted with toluene. After filtering, the solution was covered with a layer of n-heptane. After several days at room temperature black rhombic crystals of **1** were obtained: *ca* 40 mg (20% based on $KPPh_2(dioxane)_2$), m.p. 167°C. EI-MS (70 eV), m/z (%): 1260 (28.4) [$M^+ = [Cp'Ta(\mu\text{-}PPh_2)(PPh_2)]_2^+$], 1181 (12.0) [(M-Cp′)$^+$], 1104 (19.4) [(M-2Cp′)$^+ = [Ta(\mu\text{-}PPh_2)(PPh_2)]_2^+$], 1026(5.7) [(M-Ph-2Cp′)$^+$], 998 (5.8) [(M-2Ph-2Cp′)$^+$], 920 (4.3) [(M-3Ph-2Cp′)$^+$], 552 (3.9) [$(Ta(PPh_2)_2)^+$], and fragmentation products thereof. IR (KBr, cm^{-1}): $\tilde{\nu}$ = 3056 m, 2957 w, 2920 w, 2850 w, 2350 w, 2322 vw, 1954 vw, 1879 vw, 1804 vw, 1750 vw, 1610 vw, 1578 m, 1474 m, 1429 m, 1379 m, 1300 m, 1266 m, 1177 m, 1154 w, 1127 w, 1081 w, 1063 w, 1026 m, 997 w, 890 vw, 865 w, 843 w, 800 m, 737 s, 696 vs, 560 vw, 512 s, 484 m, 452 m, 425 m, 308 w.

Synthesis of $[Cp'TaCl_4\{PH_2(2,4,6\text{-}Pr^i_3C_6H_2)\}]$ (**2**)

$[Cp'TaCl_4]$ (1.95 g, 4.88 mmol) was suspended in 30 cm^3 toluene and with stirring $PH_2(2,4,6$-

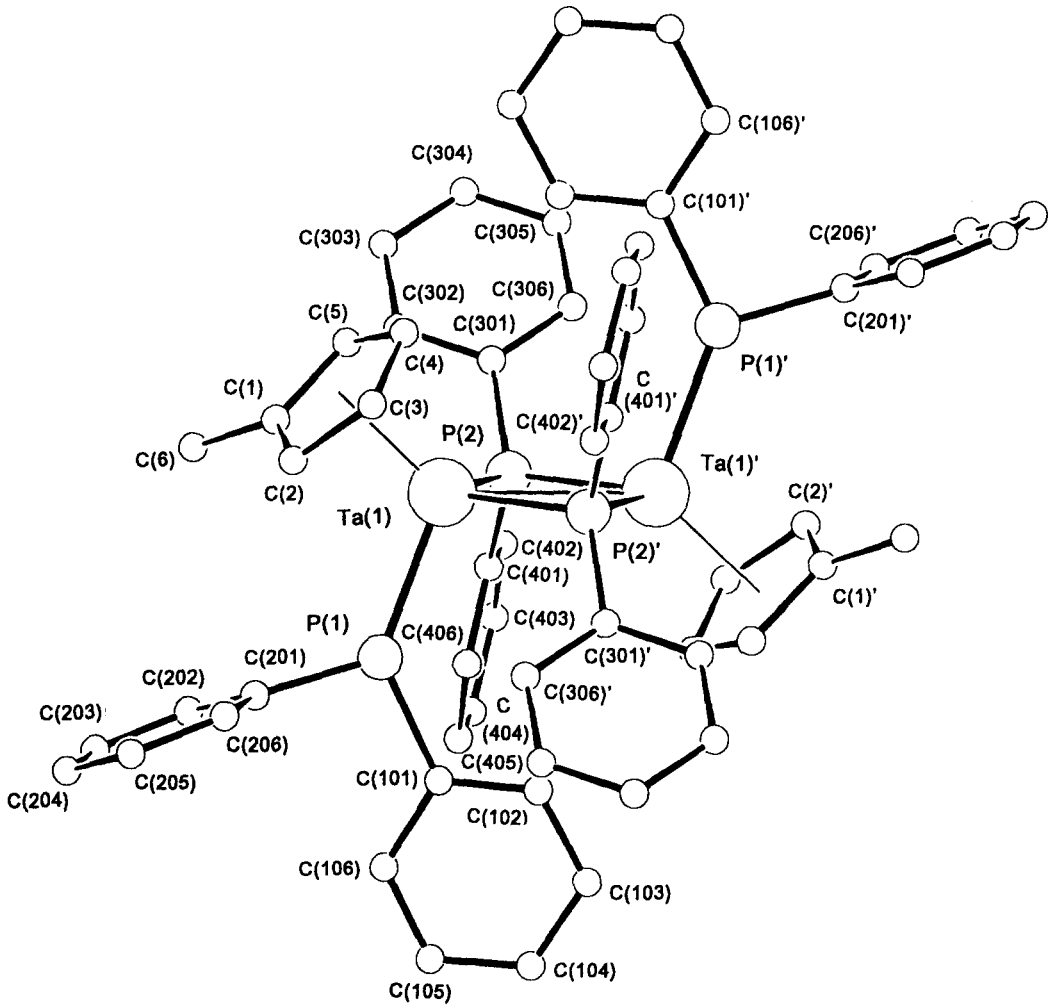


Fig. 1. Molecular structure of $[Cp'Ta(\mu\text{-}PPh_2)(PPh_2)]_2$ (**1**) showing the atom numbering scheme employed (SCHAKAL plot) [43]. Hydrogen atoms are omitted for clarity.

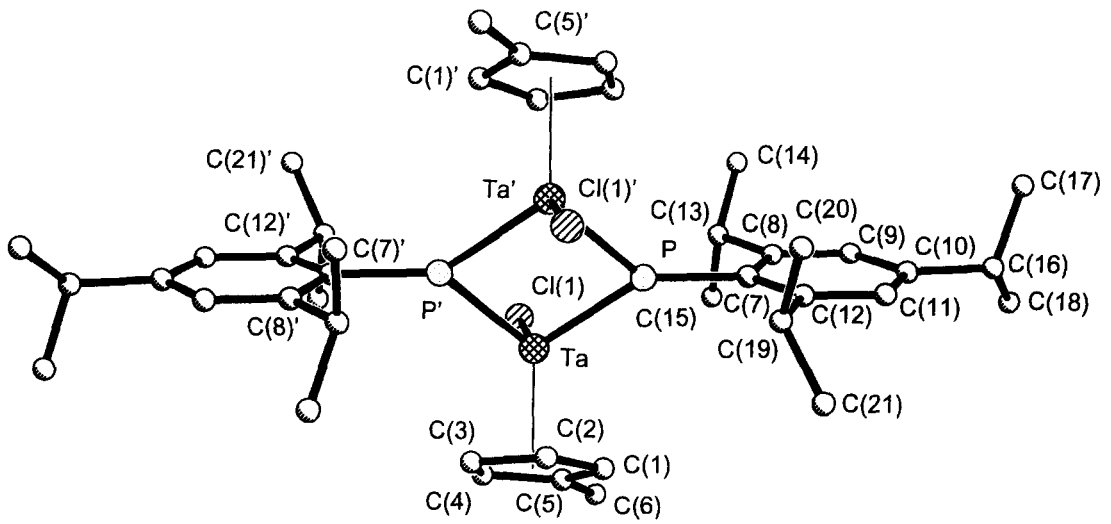


Fig. 2. Molecular structure of $[Cp'TaCl\{\mu\text{-}P(2,4,6\text{-}Pr^i_3C_6H_2)\}]_2$ (**3**) showing the atom numbering scheme employed (SHELXTL PLUS; XP) [41]. Hydrogen atoms are omitted for clarity.

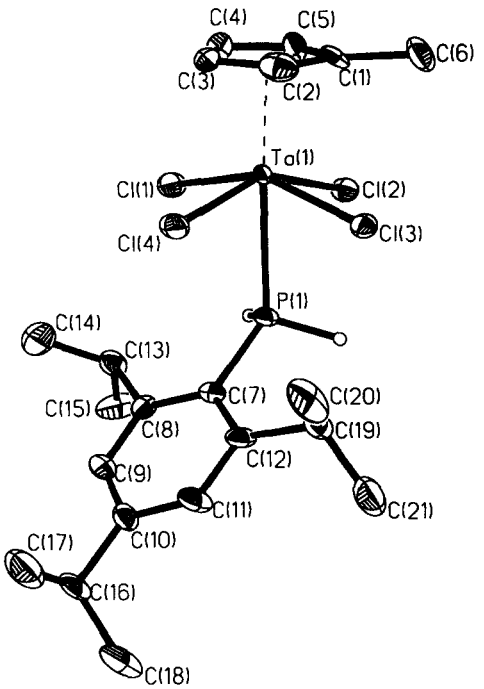


Fig. 3. Molecular structure of [Cp′TaCl$_4${PH$_2$(2,4,6-Pr$^i_3$C$_6$H$_2$)}] (**2**) showing the atom numbering scheme employed (ORTEP plot, 50% probability, SHELXTL PLUS; XP) [41]. Hydrogen atoms (other than P—H) are omitted for clarity.

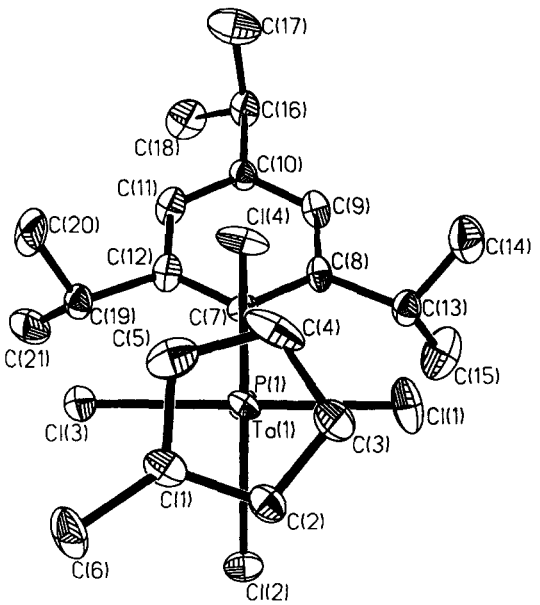


Fig. 4. View along the Ta—P bond axis of [Cp′TaCl$_4${PH$_2$(2,4,6-Pr$^i_3$C$_6$H$_2$)}] (**2**) (ORTEP plot, 50% probability, SHELXTL PLUS; XP) [41]. Hydrogen atoms are omitted for clarity.

Pr$^i_3$C$_6$H$_2$) (1.15 g, 4.88 mmol) was added with a syringe. The reaction is exothermic and a clear orange solution is obtained. The solution was stirred overnight. Then the solvent was removed to dryness and the residue extracted with pentane. Cooling to 5°C afforded yellow needles of **2**: 2.8 g (90%). The product is only slightly air sensitive but is hydrolysed rapidly. **2** is soluble in CH_2Cl_2 and $CHCl_3$ without decomposition. M.p. 147°C.

^{1}H NMR (400 MHz; C_7D_8; 298 K, ppm): 1.12 [d, ^3J(HH) 6.8 Hz, 6 H, 4-(*Me*$_2$CH)C$_6$H$_2$], 1.29 [d, ^3J(HH) 6.5 Hz, 12 H, 2,6-(*Me*$_2$CH)$_2$C$_6$H$_2$], 2.09 (s, br, 3H, C$_5$H$_4$*Me*), 2.68 [sept, ^3J(HH) 6.8 Hz, 1 H, 4-(Me$_2$C*H*)C$_6$H$_2$], 3.90 [broad with fine structure, 2 H, 2,6-(Me$_2$C*H*)$_2$C$_6$H$_2$], 5.69 (s, br 2 H, C$_5$*H*$_4$Me), *ca* 5.8 [br, 1 H, P*H*$_2${2,4,6-(Me$_2$CH)$_3$C$_6$H$_2$}], 6.23 (s, 2H, C$_5$*H*$_4$Me), *ca* 6.7 [br, 1 H, P*H*$_2${2,4,6-(Me$_2$CH)$_3$C$_6$H$_2$}], 7.12 [s, 2 H, 2,4,6-(Me$_2$CH)$_3$C$_6$*H*$_2$]. ^{1}H NMR (400 MHz; toluene-d_8; 263 K, ppm): all signals broaden apart from the broad signals at *ca* 5.8 and 6.7 ppm; the broad P—H resonances are observed as sharp singlets at 6.10 and 6.99 ppm [J(PH) 357 Hz] at low temperature. ^{31}P NMR (C_7D_8, ppm): (a) 300 K, *ca* −36, broad, $\nu_{1/2}$ *ca* 800 Hz, (b) T < 290 K, −35.7 t [^1J(PH) 360.9 Hz]. ^{13}C NMR (C_7D_8 298 K, ppm): 16.1 (C$_5$H$_4$*Me*); 24.4, 24.9 [2,4,6-(*Me*$_2$CH)$_3$C$_6$H$_2$]; 34.3, 35.1 [2,4,6-(Me$_2$*C*H)$_3$C$_6$H$_2$]; 121.1, 122.5, 135.1 (*C*$_5$H$_4$Me); 152.2 (d, J(PC) 28 Hz, C$_{ipso}$-PH$_2$), other signals for 2,4,6-(Me$_2$CH)$_3$*C*$_6$H$_2$ are obscured by those of toluene. EI-MS (70 eV): no molecular ion peak is observed. Only signals for [Cp′TaCl$_4$] and PH$_2$(2,4,6-Pr$^i_3$C$_6$H$_2$) as well as fragmentation products thereof are observed, *m/z* (%): 402 (100) ([Cp′TaCl$_4$]$^+$), 236 (35) [PH$_2$(2,4,6-Pr$^i_3$C$_6$H$_2$)$^+$], 204 (90) [(2,4,6-Pr$^i_3$C$_6$H$_2$)$^+$], 79 (25) [(Cp′)$^+$], 43 (30) [(Pr^i)$^+$]. IR (KBr, cm^{-1}): $\tilde{\nu}$ = 3113 s, 2926 m, 2866 m, 1600 m, 1561 sh, 1498 m, 1459 m, 1424 m, 1382 m, 1361 m, 1170 sh, 1105 m, 1080 m, 1048 m, 938 s, 869 m, 746 m, 414 sh. Found: C 39.1; H 5.3; Cl 22.4. Calc. for $C_{21}H_{32}Cl_4PTa$ (638.2): C 39.5; H 5.1; Cl 22.2%.

Synthesis of [Cp′TaCl{μ-P(2,4,6-Pr$^i_3$C$_6$H$_2$)}]$_2$ (**3**)·C$_7$H$_8$

With stirring, DBU (0.96 g, 6.29 mmol, 1 cm^3) was added with a syringe to a yellow solution of [Cp′TaCl$_4${PH$_2$(2,4,6-Pr$^i_3$C$_6$H$_2$)}] (**2**) (2.0 g, 3.14 mmol) in 30 cm^3 toluene. A colour change to red-brown was observed. The solution was stirred at r.t. for 2 h. Then the solvent was removed to dryness and the residue dissolved in 20 cm^3 pentane/2 cm^3 toluene giving a red-brown solution. Cooling to −20 C yielded dark red cubic crystals of **3**·C$_7$H$_8$. **3** is soluble in CH_2Cl_2 and $CHCl_3$ without decomposition. The product is only slightly air sensitive but hydrolysed rapidly. The crystals were ground and the resulting powder dried *in vacuo* to remove the included toluene. Yield: 0.91 g (55%). M.p. 268°C. ^{1}H NMR (400 MHz, C_6D_6, 298 K, ppm): 1.28 [d, ^3J(HH) 5.6 Hz, 24 H, 2,6-(*Me*$_2$CH)$_2$C$_6$H$_2$], 1.51 [d, ^3J(HH) 6.6 Hz, 12 H, 4-(*Me*$_2$CH)C$_6$H$_2$], 1.96 (s, 6 H, C$_5$H$_4$*Me*), 3.27 [sept, ^3J(HH) 6.6 Hz, 2 H, 4-(Me$_2$C*H*)C$_6$H$_2$], 3.93 [broad

with fine structure, 4 H, 2,6-$(Me_2CH)_2C_6H_2$], 5.24 (s, br, 4 H, C_5H_4Me), 5.91 (s, br, 4 H, C_5H_4Me), 7.36 [s, 4 H, 2,4,6-$(Me_2CH)_3C_6H_2$]. ^{31}P NMR (C_6D_6, ppm): 391.5, s. EI-MS (70 eV, *m/z* (%)): 1060 (100) [M^+ = [Cp′TaCl{μ-P(2,4,6-$Pr^i_3C_6H_2$)}]$_2^+$], 530 (1.0) [Cp′TaCl{μ-P(2,4,6-$Pr^i_3C_6H_2$)}$^+$], 204 (60) [(2,4,6-$Pr^i_3C_6H_2$)$^+$], 79 (20) [(Cp′)$^+$], 43 (40) [(Pr^i)$^+$], as well as fragmentation products thereof. IR (KBr, cm^{-1}): $\tilde{\nu}$ = 2958 s, 2924 m, 2865 m, 1596 m, 1490 sh, 1459 m, 1419 m, 1379 m, 1359 m, 1313 m, 1262 m, 1099 m, 1031 m, 936 sh, 876 m, 805 s, 753 sh, 506 sh. Found: C, 47.1; H, 5.8. Calc. for $C_{42}H_{60}Cl_2P_2Ta_2$ (1059.7): C, 47.6, H, 5.7%.

Reaction of [Cp′$TaCl_4$] *with DBU*

DBU (0.8 g, 5.0 mmol) was added with a syringe to a stirred yellow suspension of [Cp′$TaCl_4$] (2.0 g, 5.0 mmol) in 30 cm^3 toluene. A colour change to red-brown was observed. The solution was stirred at r.t. for 5 h. Then the solvent was removed to dryness and the residue was washed with 20 cm^3 pentane and dissolved in 30 cm^3 CH_2Cl_2. An EPR spectrum of the CH_2Cl_2 solution showed the 8-line spectrum expected for a paramagnetic tantalum compound (Ta: $I = 7/2$).

Data collection and structure refinement for [Cp′Ta(μ-PPh_2)(PPh_2)]$_2$ (**1**)·C_7H_8, [Cp′$TaCl_4$ {PH_2(2,4,6-$Pr^i_3C_6H_2$)}] (**2**), *and* [Cp′TaCl{μ-P(2,4,6-$Pr^i_3C_6H_2$)}]$_2$ (**3**)·C_7H_8

Data (Mo-K_α = 0.71069 Å) were collected with a Stoe STADI 4 diffractometer (for **1** and **3**) and with a Siemens CCD (SMART) (for **2**). 25 reflections (2Θ range: 2–25°) (**1**) or 80 reflections (2θ range: 28–40°) (**3**) were used for determination of the unit cell parameters; for **2**, 1930 reflections (2θ range: 12–25°) were used for refinement of the unit cell parameters. Absorption correction: psi-scans. The structures were solved by direct methods (**1**, **3**: SHELXS-86 [40], **2**: SHELXTL PLUS [41]) and subsequent difference Fourier syntheses and refined by full-matrix least-squares on F^2 (**1**, **3**: SHELXL-93 [42], **2**: SHELXTL PLUS [41]). Restrictions for **1**: Ta, P and C atoms anisotropic, H atoms isotropic in calculated positions. One molecule of toluene (disordered, only C atoms located and refined isotropically) per formula unit of **1** is present in the unit cell. Restrictions for **2**: Ta, P, Cl and C atoms anisotropic, H atoms isotropic in calculated positions. Restrictions for **3**: Ta, P, Cl and C atoms anisotropic, H atoms isotropic in calculated positions. One molecule of toluene (disordered, only C atoms located and refined isotropically) per formula unit of **3** is present in the unit cell. A summary of data collection parameters is given in Table 4. Anisotropic atomic parameters and full lists of bond lengths and angles have been deposited as supplementary material with the Cambridge Crystallographic Data Centre.

Acknowledgements—We gratefully acknowledge support of this work by the Landesgraduiertenförderung (Baden-Württemberg) (scholarship for K. Fromm), the Fonds der Chemischen Industrie and the Deutsche Forschungsgemeinschaft. We thank the company Chemetall for a generous donation of lithium alkyls, H. C. Starck GmbH & Co. KG for a generous donation of $TaCl_5$ and Hoechst AG for a generous donation of chemicals.

REFERENCES

1. *Comprehensive Organometallic Chemistry II* (Edited by E. W. Abel, F. G. A. Stone, G. Wilkinson) Volumes 4 and 5. Pergamon Press, Oxford (1995).
2. (a) E. Hey-Hawkins, *Chem. Rev.* 1994, **94,** 1661; (b) J. Ho, R. Rousseau and D. W. Stephan, *Organomet.* 1994, **13,** 1918 and references therein.
3. E. Hey-Hawkins and K. Fromm, *Polyhedron* 1995, **14,** 2825.
4. (a) J. C. Leblanc and C. Moise, *J. Organomet. Chem.* 1989, **364,** C3; (b) R. T. Baker, J. C. Calabrese, R. L. Harlow and I. D. Williams, *Organometallics* 1993, **12,** 830; (c) G. I. Nikonov, L. G. Kuzmina, P. Mountford and D. A. Lemenovskii, *Organometallics* 1995, **14,** 3588; (d) G. Bonnet, O. Lavastre, J. C. Leblanc and C. Moise, *New. J. Chem.* 1988, **12,** 551.
5. P. J. Domaille, B. M. Foxmann, T. J. McNeese and S. S. Wreford, *J. Am. Chem. Soc.* 1980, **102,** 4114.
6. J. B. Bonanno, P. T. Wolczanski and E. B. Lobkovsky, *J. Am. Chem. Soc.* 1994, **116,** 11159.
7. C. C. Cummins, R. R. Schrock and W. M. Davis, *Angew. Chem.* 1993, **105,** 758.
8. J. A. Labinger in *Comprehensive Organometallic Chemistry* (Edited by G. Wilkinson) Vol. 3, Chapter 25, p. 705 ff. Pergamon Press, Oxford (1982).
9. N. N. Greenwood and A. Earnshaw, *Die Chemie der Elemente.* VCH Verlagsgesellschaft, Weinheim (1988).
10. (a) K. Fromm and E. Hey-Hawkins, *Z. Anorg. Allg. Chem.* 1993, **619,** 261; (b) E. Hey-Hawkins and K. Fromm, *Polyhedron* 1995, **14,** 2027.
11. (a) C. Ting, N. C. Baenziger and L. Messerle, *J. Chem. Soc., Chem. Commun.* 1988, 1133; (b) V. C. Gibson, T. P. Kee and W. Clegg, *J. Chem. Soc., Dalton Trans.* 1990, 3199.
12. M. I. Alcalde, J. de la Mata, M. Gomez, R. Royo and F. Sanchez, *J. Organomet. Chem.* 1995, **492,** 151.
13. (a) M. J. Bunker, A. de Cian and M. L. H. Green, *J. Chem. Soc., Chem. Commun.* 1977, 59; (b) M. J. Bunker, A. de Cian, M. L. H. Green and N. Siganporia, *J. Chem. Soc., Dalton Trans.* 1980, 2155; (c) W. A. Herrmann, W. Kalcher, H. Biersack, I. Bernal and M. Creswick, *Chem. Ber.* 1981, **114,** 3558; (d) R. J. Burt, G. Leigh and D. L. Hughes, *J. Chem. Soc., Dalton Trans.* 1981, 793; (e) A. Nakamura, T. Okamoto and H. Yasuda, *Organomet. Synth.* 1988, **4,** 20 and references therein.
14. R. J. Burt and G. J. Leigh, *J. Organomet. Chem.* 1978, **148,** C19.

15. J. C. Fettinger, D. W. Keogh and R. Poli, *Inorg. Chem.* 1995, **34,** 2343.
16. M. Hesse, H. Meier and B. Zech, *Spektroskopische Methoden in der Organischen Chemie*, 4. Ed. Georg-Thieme-Verlag, Stuttgart-New York (1991).
17. G. Bonnet, M. M. Kubicki, C. Moise, R. Lazzaroni, P. Salvadori and G. Vitulli, *Organometallics* 1992, **11,** 964 and references therein.
18. (a) H. Ranaivonjatovo, J. Escudié, C. Couret and J. Stagé, *J. Organomet. Chem.* 1991, **415,** 327; (b) Y. van den Winkel, H. M. M. Bastiaans and F. Bickelhaupt, *J. Organomet. Chem.* 1991, **405,** 183; (c) P. Kölle, G. Linti, H. Nöth, G. L. Wood, C. K. Narula and R. T. Paine, *Chem. Ber.* 1988, **121,** 871.
19. E. Hey-Hawkins, S. Kurz and G. Baum, *Z. Naturforsch.* 1995, **50B,** 239.
20. V. Mark, C. H. Dungan, M. M. Crutchfield and J. R. Van Wazer, *Compilation of* ^{31}P-NMR *Data*, in: *Topics Phosphorus Chem.* Vol. 5, pp. 169–226. (1968).
21. ^{1}H and ^{13}C NMR data for [Cp′TaCl$_4$]: ^{1}H NMR (400 MHz, $CDCl_3$, 298 K, ppm): 2.93 (s, 3H, C_5H_4*Me*); 6.66 (t, 2H, ^{3}J(HH) 2.6 Hz; C_5*H*$_4$Me) 7.05 (t, 2H, ^{3}J(HH) 2.7 Hz, C_5*H*$_4$Me). ^{13}C NMR ($CDCl_3$, 298 K, ppm): 18.1 (C_5H_4*Me*); 121.3, 121.6, 137.0 (C_5H_4Me).
22. F. A. Cotton and G. Wilkinson, Advanced Inorganic Chemistry, 4. Ed. Verlag Chemie; Interscience Publishers, John Wiley & Sons; New York (1990).
23. (a) R. E. McCarley and B. A. Torp, *Inorg. Chem.* 1963, **2,** 540; (b) R. E. McCarley and J. C. Boatman, *Inorg. Chem.* 1963, **2,** 547.
24. M. Gomez, P. Gomez-Sal, M. Pilar Nicolas and P. Royo, *J. Organomet. Chem.* 1995, **491,** 121.
25. P. B. Hitchcock, M. F. Lappert and W. P. Leung, *J. Chem. Soc., Chem. Commun.* 1987, 1282.
26. A. H. Cowley and B. Pellerin, *J. Am. Chem. Soc.* 1990, **112,** 6743.
27. Z. Hou, T. L. Breen and D. W. Stephan, *Organomet.* 1993, **12,** 3158.
28. J. M. Canich and F. A. Cotton, *Inorg. Chem.* 1987, **26,** 3473.
29. A. P. Sattelberger, R. B. Wilson and J. C. Huffmann, *Inorg. Chem.* 1982, **21,** 2392.
30. F. A. Cotton, L. R. Falvello and R. C. Najjar, *Inorg. Chem.* 1983, **22,** 375.
31. L. Messerle, *Chem. Rev.* 1988, **88,** 1229.
32. (a) P. D. W. Boyd and C. E. F. Rickard, *J. Chem. Soc., Dalton Trans.* 1987, 307; (b) F. A. Cotton, M. P. Diebold and W. J. Roth, *Polyhedron* 1985, **4,** 1103.
33. G. C. Campbell, J. A. M. Canich, F. A. Cotton, S. A. Duraj and J. F. Haw, *Inorg. Chem.* 1986, **25,** 287.
34. L. Pauling, *Die Natur der chemischen Bindung.* Verlag Chemie, Weinheim (1962).
35. A. R. Chakravarty, F. A. Cotton, M. P. Diebold, D. B. Lewis and W. J. Roth, *J. Am. Chem. Soc.* 1986, **108,** 971.
36. M. L. Leutkens Jr, W. L. Elcesser, J. C. Huffmann and A. P. Sattelberger, *J. Chem. Soc., Chem. Commun.* 1983, 1072.
37. F. A. Cotton, S. A. Duraj and W. J. Roth, *Inorg. Chem.* 1984, **23,** 4046.
38. Q. Jiang, P. J. Carrol and D. H. Berry, *Organometallics* 1991, **10,** 3648.
39. K. Issleib and A. Tzschach, *Chem. Ber.* 1959, **92,** 1118.
40. G. M. Sheldrick, *SHELXS*-86, *Program for Crystal Structure Solution*, University of Göttingen, Germany (1986).
41. SHELXTL PLUS, *XS*: *Program for Crystal Structure Solution*; *XL*: *Program for Crystal Structure Determination*; *XP*: *Interactive Molecular Graphics*. Siemens Analyt. X-ray Inst. Inc., (1990).
42. G. M. Sheldrick, *SHELXL*-93, *Program for Crystal Structure Determination*. University of Göttingen, Germany (1993).
43. E. Keller, *SCHAKAL* 88, *A Fortran Program for the Graphic Representation of Molecular and Crystallographic Models*. Freiburg (1988).

Pergamon

PII: S0277-5387(96)00214-8

Polyhedron Vol. 16, No. 4, pp. 733–740, 1997
Copyright © 1996 Elsevier Science Ltd
Printed in Great Britain. All rights reserved
0277-5387/97 $17.00+0.00

Synthesis and characterization of copper–ibuprofenate complexes with 2,2′-bipyridine and 1,10-phenanthrolines and their hydrolytic activities in phosphate diester cleavage

A. Latif Abuhijleh

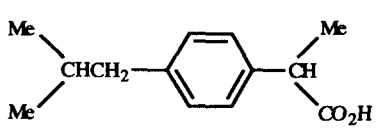
Department of Chemistry, Birzeit University, P.O. Box 14, West Bank—via Israel

(Received 6 February 1996; accepted 29 April 1996)

Abstract—A synthetic investigation of copper(II) ibuprofenate (Ibup) addition compounds with 2,2′-bipyridine (bpy), 1,10-phenanthroline (phen) and 2,9-dimethyl-1,10-phenanthroline (dmph) has led to the isolation of dinuclear adducts of the forms $[Cu(Ibup)_2(bpy)]_2 \cdot 4H_2O$ (**1**) and $[Cu(Ibup)_2(phen)]_2$ (**2**) and a mononuclear adduct $Cu(Ibup)_2(dmph)$ (**3**). Spectroscopic data for adducts **1** and **2** are consistent with a dinuclear structure with two CuN_2O_2+O chromophors. Each copper is coordinated with two ibuprofenate bridges, a terminal diimine molecule and a monodentate ibuprofenate group complete five-coordination at each metal atom. Spectroscopic data for adduct **3** are consistent with a mononuclear structure having a very distorted square-pyramidal CuN_2O_2+O chromophore. The Cu^{II} atom is coordinated to two nitrogen atoms from a chelating dmph ligand, two carboxylic oxygens of a bidentate ibuprofenate ion and an oxygen atom of a monodentate carboxylic group of a second ibuprofenate ion. The reduction of adduct (**3**) by ascorbic acid produced stable red copper(I) complex of the form $[Cu(dmph)_2]$ (Ibup) (**4**). Spectral data of this adduct indicated that the cation has distorted tetrahedral geometry about the copper atom. The effect of **1** and **2** on the rate of hydrolysis of bis(*p*-nitrophenyl) phosphate (BNPP) have been examined in aqueous methanol solution at 70°C and pH 7.4. Copyright © 1996 Elsevier Science Ltd

Keywords: copper complexes; ibuprofen; diimines; hydrolysis; phosphate.

It has been suggested that copper(II) complexes of anti-inflammatory drugs are often more active and desirable drugs than the parent ligands themselves [1]. Ibuprofen [2-(4-isobutylphenyl)propionic acid], [Scheme 1] is a non-steroidal anti-inflammatory drug and has been used for many years in the treatment of inflammatory diseases. Physical studies of copper(II) ibuprofenate [2] have shown that it contains dinuclear units with bridging carboxylates, similar to the familiar copper acetate and many other copper(II) carboxylates [3]. It is well known that many copper(II) carboxylates form dinuclear adducts with basic ligands [3,4]; however, with certain bases many copper(II) carboxylates also form mononuclear adducts [3b,4–8]. Several studies from our laboratories and others have been designed to investigate the factors which influence the adoption of either dinuclear or mononuclear complexes for copper(II) carboxylate adducts [3a,4–10]. In general, it has been found that by increasing the acidity of the alkyl (or aryl) carboxylate ligands, such as through halogenation of alkyl groups and/or by increasing the basicity of the other ligands, the tendency towards formation of mononuclear complexes increases [2b,4–10].



Scheme 1.

Our interest in copper(II) carboxylate complexes with nitrogen-donor ligands evolves from their biological implications [1,4,7,11]. As an example, the imidazole and carboxylate groups are the ligating moieties found in proteins and in many naturally occurring mixed-ligand complexes [12]. In addition, mononuclear and dinuclear copper(II) carboxylates and their nitrogen-donor adducts have been found

to have a variety of pharmacological effects, such as antitumour [1,13], superoxide dismutase [14], catecholase [4,7], cytotoxicity and antiviral activities [11]. Chelators such as 2,2′-bipyridine and 1,10-phenanthroline have potential antitumour activity and their activity may be increased through their chelation to the copper ion [15]. A complex between the chelating agent 1,10-phenanthroline and copper(II) is able to induce the degradation of DNA in the presence of reducing agents[16] and 2,2′-bipyridine complexes of copper(II) have been used as non-enzymatic catalysts for the hydrolytic cleavage of phosphodiester backbone of DNA and RNA [17,18]. There has been interest in developing metal complexes which can promote hydrolysis of phosphate esters as model systems for metallo-phosphatase enzymes and as catalysts for the detoxification of man-made phosphorus(V) toxins of some pesticides and chemical weapons [17,18]. In addition, the development of new artificial photosynthetic assemblies capable of harvesting solar energy is of great interest in inorganic photochemistry [19]. Cuprous diimine chromophores have received considerable attention since these chromophores display metal-to-ligand charge transfer (MLCT) bands in the visible region [20]. Recently, light excitation into these bands leads to room-temperature emission in argon dichloromethane solution and the photo-driven energy transfer from cuprous phenanthroline derivatives has been demonstrated [21]. As part of an ongoing investigation into the biological and photochemical activities of copper compounds, this article reports the synthesis and spectroscopic characterization of ternary complexes of copper(II) ibuprofenate with 2,2′-bipyridine, 1,10-phenanthroline and 2,9-dimethyl-1,10-phenanthroline and examines the activities of the first two complexes for the hydrolysis of bis(*p*-nitrophenyl)phosphate. In addition, the reduction of copper(II) ibuprofenate adduct of 2,9-dimethyl-1,10-phenanthroline to bis(2,9-dimethyl-1,10-phenanthroline) copper(I) ibuprofenate is also reported.

EXPERIMENTAL

Materials

2,2′-Bipyridine (bpy), 1,10-phenanthroline(phen) and 2,9-dimethyl-1,10-phenanthroline (dmph) were purchased from Aldrich; sodium bis(*p*-nitrophenyl)phosphate (BNPP) and biological buffer HEPES [N-(2-hydroxyethyl) piperazine-N′-ethanesulfonic acid] were from Sigma and used without further purification. Tetrakis(μ-ibuprofenato) dicopper(II), $[Cu_2(Ibup)_4]$ (Ibup = ibuprofenate ion), was prepared as described previously [2b] and recrystallized from anhydrous diethylether: dichloromethane (1 : 1).

Preparation of complexes

$[Cu(Ibup)_2(bpy)]_2 \cdot 4H_2O$ (**1**). A solution of 2,2′-biypridine (0.164 g, 1.05 mmol) in methanol (50 cm^3) was added to Cu_2 $(Ibup)_4$ (0.496, 0.524 mmol). The mixture was stirred at room temperature for 2 h. The blue solution was filtered and left in the hood to evaporate. The bluish-green precipitate that formed was recrystallized from chloroform and air dried. Yield 0.58 g (83%). Found: C 65.0; H, 7.0; N, 4.1. Calc. for $C_{72}H_{92}N_4O_{12}Cu_2$: C, 64.9; H, 6.9; N, 4.2%.

$[Cu(Ibup)_2(phen)]_2$ (**2**). A solution of 1,10-phenanthroline (0.133 g, 0.68 mmol) in methanol (50 cm^3) was added to $Cu_2(Ibup)_2$ (0.319 g, 0.337 mmol). The mixture was stirred at room temperature for 2 h. The bluish-green solution was filtered and left in the hood to evaporate. The sky-blue precipitate that formed was recrystallized from chloroform and air dried. Yield 0.38 g (86%). Found: C 70.0; H, 6.6; N, 4.2. Calc. for $C_{76}H_{84}N_4O_8Cu_2$: C, 69.8; H, 6.4; N, 4.3%.

$Cu(Ibup)_2(dmph)$ (**3**). A solution of 2,9-dimethyl-1,10-phenanthroline (0.176 g, 0.845 mmol) in methanol (50 cm^3) was added to $Cu_2(Ibup)_4$ (0.398 g, 0.420 mmol). The solution was protected from the light and stirred at room temperature for 3 h. The green solution was filtered and left in the hood to evaporate. The green precipitate that formed was recrystallized from chloroform and air dried. Yield 0.37 g (65%). Found: C, 70.1; H, 6.9; N, 4.0. Calc. for $C_{40}H_{46}N_2O_4Cu$: C, 70.4; H, 6.8; N, 4.1%.

$[Cu(dmph)_2]Ibup$ (**4**). Solid ascorbic acid (0.053 g, 0.30 mmol) was added to the green solution of **3** (0.2 g, 0.29 mmol) in acetonitrile (15 cm^3). The red solution which formed was stirred for 15 min, filtered and left in the hood to evaporate. The red oily product was dissolved in dichloromethane (20 cm^3) and filtered. The red filtrate was concentrated by slow evaporation to *ca* 2 cm^3 then anhydrous diethylether was added to the solution with stirring until the red precipitate formed. The complex was filtered under reduced pressure, washed several times with anhydrous diethyether and dried *in vacuo*. Yield 0.045 g (45%). Found: C, 71.2; H, 6.1; N, 8.4. Calc. for $C_{41}H_{41}N_4O_2Cu$: C, 71.9; H, 6.0; N, 8.2%.

Physical measurements

Elemental analyses for C, H and N were performed by Galbraith Laboratories, Knoxville, Tennessee, U.S.A. Room-temperature (298 K) magnetic susceptibility measurements of powdered and solution samples were determined as described previously [4,6]. Electronic data of dichloromethane solutions were obtained with a Bausch and Lomb Spectronic 2000. IR spectra of Nujol or hexachlorobutadiene mulls sealed between polyethylene sheets were obtained in the 4000–200 cm^{-1} region with a Perkin–Elmer model 843 IR spectrophotometer. X-band ESR spectra of polycrystalline material and of methanol/toluene solu-

tions were obtained at room temperature and 77 K with an ESPIT-330 Vol. 501 spectrometer. Diphenylpicrylhydrazide (DPPH, $g = 2.0036$) was used as the calibrating field marker. A Varian 360A-60MHz spectrometer was used to obtain NMR spectra and chemical shifts were referenced to $SiMe_4$.

Kinetics

All kinetic studies were performed at 70°C and pH 7.4 with temperature compensation probe. The Sigma biological buffer HEPES (5 mmol dm^{-3}) was used to maintain a constant pH at 7.4. The pH of the buffer solutions was adjusted with NaOH or HNO_3 and checked at 70°C. Kinetic measurements were performed with the use of Bausch and Lomb 2000 UV–vis spectrophotometer equipped with a thermostated cell compartment.

The hydrolysis of sodium bis(*p*-nitrophenyl) phosphate (BNPP) by copper(II) complexes was monitored spectrophotometrically by following the production of *p*-nitrophenolate at 400 nm ($\varepsilon = 14\,000$ M^{-1} cm^{-1}, pH = 7.4) [17a]. The reactions were carried out under pseudo-first-order conditions with an excess copper(II) complex over BNPP concentrations. In a typical kinetic experiment, 1.5 cm^3 (2×10^{-3} M) of copper(II) complex dissolved in methanol and 1.5 cm^3 (1×10^{-4} M) of BNPP dissolved in HEPES buffer (pH 7.4) were combined in a 1 cm quartz cell and the absorbance changes at 400 nm were recorded at 70°C against the reference cell under identical conditions, except copper(II) complex was omitted. The final concentrations in the cell were (1×10^{-3} M) copper(II) complex and (5×10^{-5} M) BNPP.

First-order rate constants, k_{obs} (s^{-1}), were calculated from the slope of the linear plots of absorbance against time by converting to concentration units and dividing by the initial BNPP concentration. All experiments were run in triplicate and the first-order rate constants represent the average of these experiments.

RESULTS AND DISCUSSION

Magnetic and spectroscopic characterization

The ESR parameters, g and A, for frozen solutions and solid-state spectra of complexes studied are given in Table 1. The room-temperature ESR spectra of solid state samples of **1, 2** and **3** are anisotropic and contain $g_\parallel$ and $g_\perp$ components. Two of the four copper(II) hyperfine components in the $g_\parallel$ region for complex **3** are partially resolved. These spectra are of axial type ($g_\parallel > g_\perp > 2.040$), suggesting for all compounds $d_{x^2-y^2}$ (or d_{xy}) ground state, characteristic of a square-planar, square-based pyramidal or octahedral stereochemistry [22].

Frozen-solution ESR spectra of complexes **1** and **2** in 3.0 kG region exhibit a resolved structure with $g_\parallel > g_\perp$ (Table 1) and a representative frozen solution spectrum is that of **1** shown in Fig. 1. In addition to the hyperfine structure of copper(II) in the $g_\parallel$ region, the $g_\perp$ regions of these spectra exhibit ^{14}N-super-hyperfine structure consisting of five lines. This structure is attributed to the presence of two nitrogen atoms in the plane of the copper(II) ion. The spectral parameters for the complexes are comparable to those previously reported complexes that have square-based CuN_2O_2 of tetragonally elongated CuN_2O_2+O or $CuN_2O_2+O_2$ chromophore, including those reported for copper(II) carboxylates with α,α'-diimine [4–7, 23]. In these complexes the copper(II) ion is bonded to two unidentate nitrogen donors (e.g. imidazoles) or one bidentate chelate α,α'-diimine ligand and one oxygen atom from each of the two carboxylate anions. The second oxygen atom of each carboxylate ligand is in a weakly pseudo-axial position [5,7,9,11,24].

In addition to the above signals expected for $\Delta M_s = 1$ allowed transition of magnetic dilute copper(II) complexes $S = \frac{1}{2}$, the ESR spectra for complexes **1** and **2** in the full ESR region show another three weak signals at about 1200, 2230 and 3830 G and a representative spectrum is that of **2** shown in Fig. 2(a). These signals are attributed to the spin-

Table 1. ESR data for copper(II) ibuprofenates

Compound	State (temperature)	g_0^a	$g_\parallel$	$g_\perp$	$A_\parallel Cu$ ($\times 10^4$ cm^{-1})	$A_\perp N$ ($\times 10^4$ cm^{-1})
1	Solid (room)	2.128	2.255	2.064	—	—
	Frozen (77 K)	2.134	2.277	2.063	221	14
2	Solid (room)	2.122	2.243	2.061	—	—
	Frozen (77 K)	2.141	2.286	2.069	222	14
3	Solid (room)	2.172	2.362	2.082	—	—
	Frozen (77 K)	2.169	2.337	$g_x = 2.035$ $g_y = 2.134$	167	—

[a] g_0 values are calculated from the equation $g_0 = \frac{1}{3}(g_\parallel + 2g_\perp)$.

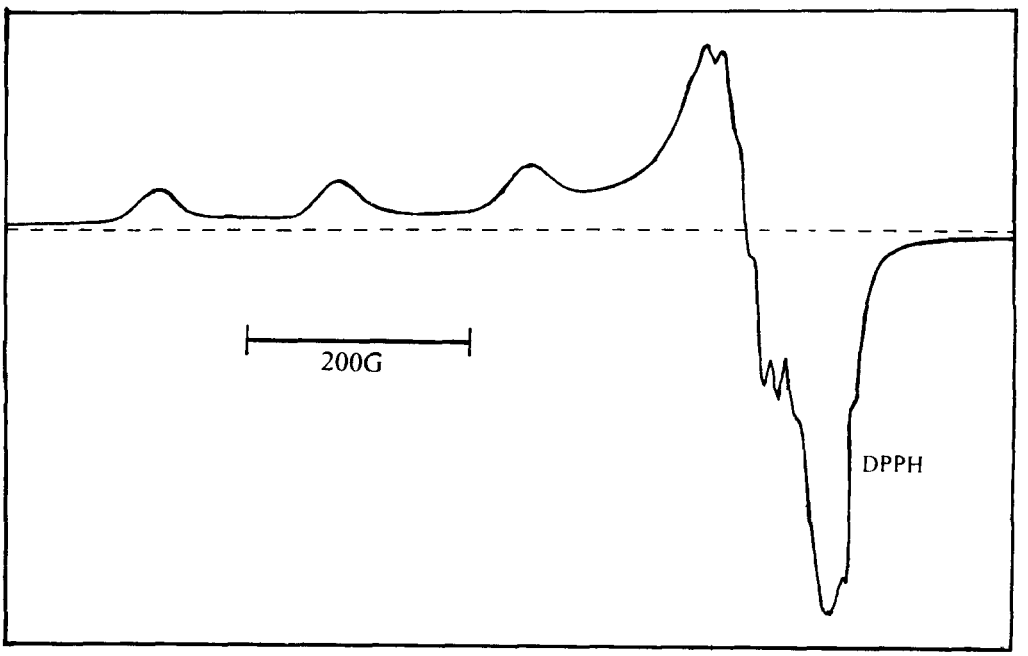


Fig. 1. Frozen-solution ESR spectrum of compound **1**.

triplet state with $S = 1$. The signals at 2230 and 3830 G are devoid of any hyperfine structure, they are assigned to the $\Delta M_s = 1$ transitions Hxy_1 and Hxy_2 [24a]. The weak signal at 1200 G showed a resolved seven-line hyperfine structure ($A = 100 \times 10^{-4}$ cm^{-1}) and is attributed to the half-field $\Delta M_s = 2$ forbidden transition in dinuclear copper(II) complexes [25]. The positions and the assignment of these signals are comparable with those found for dicopper(II) complexes having an acetate ion-bridged ligand [25] and with those reported recently for ternary dinuclear copper(II) complexes of 4-aminobenzoic acid with 4,7-disubstituted phenanthrolines [26]. In these complexes each copper atom is coordinated with two 4-aminobenzoate bridges, a terminal diimine molecule and the fifth coordination position is occupied by a water molecule. In addition, the hyperfine coupling constant observed, 100×10^{-4} cm^{-1}, is about one half of that of mononuclear copper(II) units of axial symmetry (Table 1) and is comparable to those of the spin-triplet states of magnetically coupled dicopper(II,II) complexes [25,27]. Based on these ESR spectral properties along with other spectral data, dinuclear structure are proposed for these complexes of the type $[Cu(Ibup)_2(diimine)]_2$ (diimine = bpy or phen) in the solid state and the dinuclearity of these complexes is, at least partially, preserved in methanolic solutions with the monomeric units being bridged by two ibuprofenato ligands. In addition, spectral parameters for complexes **1** and **2** are comparable to those of previously reported for other dinuclear copper(II) carboxylates with diimines [26,28], such as $[Cu(4\text{-aminobenzoate})_2(H_2O)(phen)]_2(NO_3)_2$ [26] and $[Cu(acetate)_2(OClO_3)(bpy)]_2$ [28]. X-ray analysis of these complexes showed that the geometry at each copper(II) atom is distorted square-pyramidal. The basal coordination sites are occupied by the nitrogen atoms of a chelating diimine and two oxygen atoms of bridging carboxylates and the apical position is occupied by an oxygen atom of a monodentate ligand (water or perchlorato group). The dinuclear structure is stabilized by diimine–diimine stacking interactions. The structure of complex **1** or **2** (Scheme 2) can be described in the same manner, except ibuprofenato groups replaced both the bridging 4-aminobenzoato or acetato groups and the terminal monodentate ligands (water or perchlorato group).

The frozen-solution ESR spectrum of complex **3** [Fig. 2(b)] is clearly of rhombic type (Table 1), suggesting a distortion from square symmetry in solution. No signals due to a triplet state were observed in the spectrum of this compound, which is consistent with its mononuclear structure. The lowest g value (2.035) lies between the values obtainable in rhombic spectra for distorted square-based pyramidal or for distorted trigonal-bipyramidal geometry [22]. The structure deviation from square symmetry is attributed to the presence of methyl groups in the 2 and 9 positions on the phenanthroline moiety, close to the coordinated nitrogens to copper(II). In addition, the absence of the ^{14}N superhyperfine splitting may be attributed to the deviation from square symmetry. The ESR and other spectral parameters for complex **3** (Scheme 3) are comparable to those of ternary mononuclear copper(II) complexes of 2,5-dimethoxycinnamic acid or 3,5-disubstituted salicylates and 2,9-dimethyl-1,10-phennthroline [11, 23]. The crystal structure of the ternary complex of 2,5-dimethoxycinnamic acid have

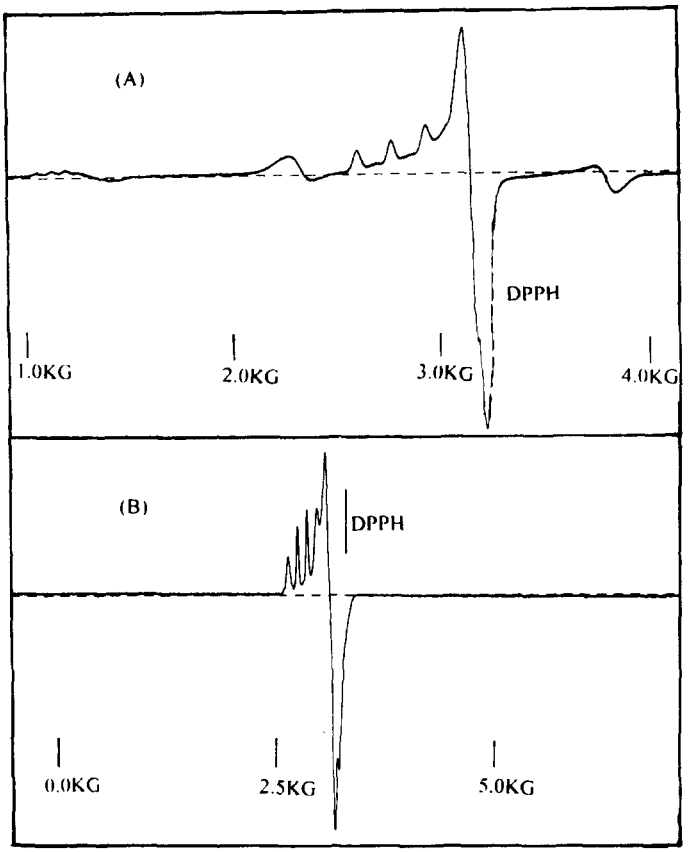
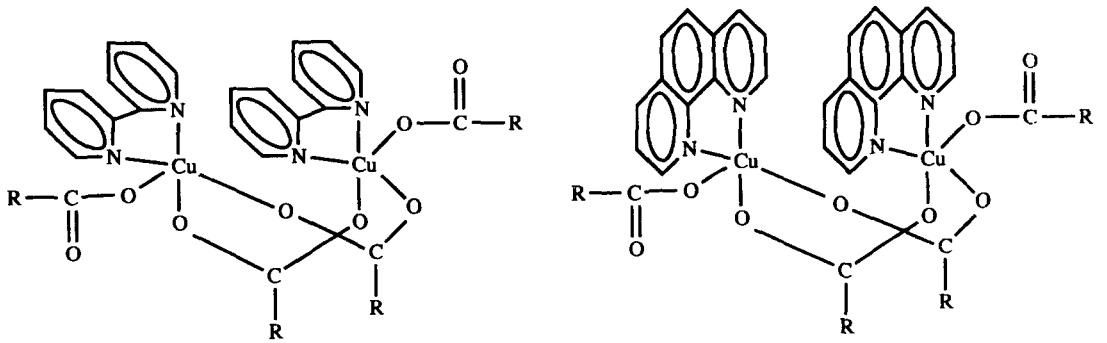
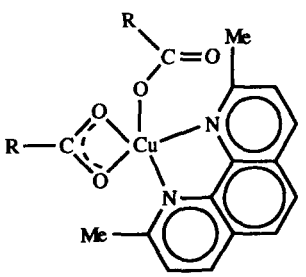


Fig. 2. Frozen-solution ESR spectra of compound (a) **2** and (b) **3**.



RCOO = ibuprofenate anion

Scheme 2.



RCOO = ibuprofenate anion

Scheme 3.

been determined [23]. The copper(II) ion in this complex is five-coordinated and complexes by two nitrogen atoms from 2,9-dimethyl-1,10-phenanthroline, two carboxylic oxygens of a bidentate cinnamic acid and one oxygen atom of a monodentate carboxyl group of a second cinnamic acid molecule. The geometry of the complex has been described as a very distorted square pyramid or trigonal bipyramid.

Inspection of the ESR parameters (Table 1) shows that $A_{\perp}$ values for complexes **1** and **2** are greater than $A_{\parallel}$ for complex **3**, while $g_{\parallel}$ values in the former complexes are smaller. These results are consistent with the presence of a stronger equatorial ligand-field in complexes **1** and **2** with an in-plane CuN_2O_2 chro-

mophore, compared with complex **3** with a very distorted an in-plane CuN_2O_2 chromophore.

The magnetic moments and electronic and IR spectral data are summarized in Table 2. Complexes **1** and **2** exhibit magnetic moments values at room temperature a little lower than normally found in magnetically dilute copper(II) ion complexes, as found in complex **3**. This is attributed to the presence of weak antiferromagnetic coupling in complexes **1** and **2**, which are proposed to have dinuclear structure as shown from spectral data. Facilities to carry out detailed magnetic properties with temperature variation were not available to us. However, it is worth noting that dinuclear copper(II) complexes with doubly bridged carboxylate groups, including those of 2,2′-bipyridine as a secondary ligand, are known to be weakly antiferromagnetically coupled [26–30]. Their $-2J$ values are much less than those found in the familiar tetracarboxylato-ligand complexes of the type $Cu_2(O_2CR)_4L_2$. This decrease has been attributed [30] to the decrease in the number of bridging carboxylato groups by which the superexchange interaction is mediated [26–30].

The electronic spectra for complexes **1** and **2** obtained in CH_2Cl_2 solutions exhibit one very broad absorption band near 675 nm and shoulder near 400 nm (Table 2). The broad band is assigned to the copper(II) *d–d* transitions. The position of this band fall within the range expected for a distorted-tetragonal copper(II) environment with an in-plane CuN_2O_2 chromophore [4–7], including those reported for copper(II) carboxylates with α,α^--diimine [11, 23, 27, 28]. The shoulder near 400 nm is assigned to the charge-transfer band, as expected when π–π interactions between aromatic system are present [36].

The electronic spectrum of complex **3** in CH_2Cl_2 solution exhibits a very broad *d–d* band at 820 nm, similar to that seen for mononuclear copper(II) carboxylates with 2,9-dimethyl-1,10-phenanthroline [11, 23]. The copper(II) ion is five-coordinated, contains the CuN_2O_2+O chromophore and complexes by a chelating 2,9-dimethyl-1,10-phanenthroline, one bidentate and one monodentate carboxylate groups. The low energy of the *d–d* electronic transitions is due to the presence of a pronounced distortion from planar symmetry in this complex and it is consistent with the ESR spectral data.

In the solid-state IR spectra, complexes **1** and **2** possess similar spectra for the ν_{as}(COO) and ν_s(COO) bands (Table 2), supporting similar structures. Two ν_{as}(COO) and two ν_s(COO) are observed, indicating the presence of two types of ibuprofenate groups. The bands at 1610 and 1395–1380 cm^{-1} with large separation, $\Delta\nu$ [ν_{as}(COO) − ν_s(COO)] value of 230–215 cm^{-1}, are assigned to the stretching modes of the monodentate carboxyl group. The positions and separation between them are comparable to those associated with a monodentate coordination of carboxylate group [31]. The bands at 1595 and *ca* 1420–1415 cm^{-1} with $\Delta\nu$ value of 175–180 cm^{-1} are assigned to the "bridging" bidentate carboxylate ligand. The positions and separation between these frequencies are similar to those associated with classical carboxylate bridges (Cu—O—C—O—Cu), including those of $Cu_2(Ibup)_4$ [2, 8, 31]. These IR spectral results are consistent with the proposed structures of these complexes in which two ibuprofenate are bridging two copper atoms and one ibuprofenate is coordinated as a monodentate ligand to each copper atom. In addition to bands of carboxyl groups in complex **1**, bands due to water molecules were observed at 3530–3460 cm^{-1}. When this complex was heated at 110°C for *ca* 10–15 min these bands only disappeared from the IR spectra, while the rest of the spectrum retained its features. This observation indicated that water molecules in this complex are not coordinated, but are present as lattice molecules which were lost on heating.

Solid-state IR spectra for complex **3** exhibit two ν_{as}(COO) and two ν_s(COO) stretching bands (Table 2), indicating the presence of two types of ibuprofenate ligands. The 1610 and 1380 cm^{-1} ($\Delta\nu$ = 230 cm^{-1}) pair observed in the solid-state are assigned to the carboxylate group that acts as a monodentate ligand and the 1600 and 1410 cm^{-1} ($\Delta\nu$ = 190 cm^{-1}) pair are assigned to the other carboxylate that acts as

Table 2. Magnetic moments and electronic and IR spectral data for copper-ibuprofenate complexes

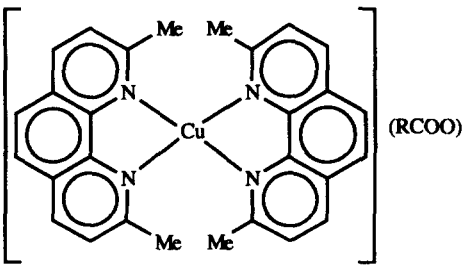
Compound	μ_{eff} (BM) (298 K) Solution	Solid	λ_{max} (nm) (ε = $dm^3\ mol^{-1}\ cm^{-1}$)[a]	ν_{asym} (CO_2) (cm^{-1})	ν_{sym} (CO_2) (cm^{-1})	$\Delta\nu$ (cm^{-1})
1	1.85	1.80	675(180)	1595	1420	175
			sh. 390(170)[b]	1610	1395	215
2	1.84	1.80	680(170)	1595	1415	180
			sh. 400(155)[b]	1610	1380	230
3	1.90	1.87	820(120)	1600	1410	190
				1610	1380	230
4	Diamagnetic		456(6400)	1585	1380	205

[a] ε is per dimer unit for complex **1** and **2**.
[b] sh. is shoulder.

asymmetric bidentate ligand [31]. These results are consistent with the proposed mononuclear structure containing CuN_2O_2+O chromophore, as discussed in the above spectral properties.

In conclusion, all physical measurements carried out in this study suggest that complexes **1** and **2** have essentially identical dinuclear structures of the type $[Cu(Ibup)_2(diimine)]_2$, in which a dinuclear structure results from the bridging of two ibuprofenate molecules by bidentate carboxylic groups (Scheme 2). In these adducts intermolecular stacking which is usually connected with π–π interactions between the diimine ligands (bpy or phen) may be important in determining the dinuclear structure. The steric hindrance caused by the presence of methyl groups in the 2 and 9 positions on the diimine (dmph) aromatic rings close to the coordination sites, which resulted in a pronounced distortion in the sphere of coordination, complex **3**, precludes the possibility of obtaining an intermolecular stack between diimine ligands and then obtaining the dinuclear structure; instead only mononuclear complex of the type $Cu(Ibup)_2(dmph)$ was obtained (Scheme 3).

Complex **4**, bis(2,9-dimethyl-1,10-phenanthroline) copper(I) ibuprofenate, which was obtained by the reduction of complex **3** was identified by UV–vis, IR and NMR spectral data, in addition to its elemental analyses. Its electronic spectrum obtained in CH_2Cl_2 solution exhibited the metal-to-ligand charge-transfer (MLCT) at 456 nm ($\varepsilon = 6400\ M^{-1}\ cm^{-1}$). The position of this band and its molar absorptivity are comparable with those previously reported for the $Cu(dmph)_2^+$ cation [20, 32]. Examination of the ^1H NMR spectrum, especially the methyl groups of the ligand (dmph), showed an upfield change in the chemical shift of the six proton at *ca* 2.4 ppm compared with those of the free ligand at *ca* 2.8 ppm. This shift was ascribed to an aromatic ring current effect [32] exhibited by cations of the type $[(2,9\text{-dialkyl-1,10-phenanthroline})_2Cu]^+$. The structure of these cations are known to have the distorted tetrahedral geometry about the copper atom [20,32]. The other protons of dmph ligand were not resolved, but relatively broad signals were observed between 7 and 9 ppm. An IR spectrum of the complex revealed peaks of coordinated dmph ligands at 1635, 1505, 1362, 855, 730 and 550 cm^{-1} and peaks of the carboxyl group of ibuprofenate ion at 1585 and 1380 cm^{-1}. The positions of these peaks are comparable with those recently reported for $CuCl(dmph)_2$ [32a] and $(dmph)_2$ Cu(butyrate) [32b]. Collectively, these spectral data suggest that complex **4** has structure of the type $[(dmph)_2Cu](Ibup)$ (Scheme 4).



RCOO = ibuprofenate anion

Scheme 4.

Hydrolysis of BNPP

Since the hydrolysed product *p*-nitrophenolate anion shows a characteristic band at 400 nm ($\varepsilon = 14\,000\ M^{-1}\ cm^{-1}$, at pH 7.4) [17a], the hydrolysis of BNPP [bis(*p*-nitrophenyl)phosphate] by copper(II) complexes **1** and **2** can be easily followed spectrophotometrically. The change in absorbance at 400 nm versus time of the reaction with complexes **1** and **2** was obtained and the pseudo-first-order rate constants, k_{obs}, for the two complexes were found to be $1.0\times10^{-5}\ s^{-1}$ and $0.7\times10^{-5}\ s^{-1}$, respectively. These values showed rate enhancement of *ca* 3.6×10^3 and 2.6×10^3 in the presence of 1 mM of complex **1** or **2**, respectively, compared with the rate constant of the uncatalysed reaction (k_{unc}) of *ca* $2.75\times10^{-9}\ s^{-1}$ at 70°C and pH 7.4 [17d]. It was not possible to obtain kinetic data for complex **3** due to its reduction to copper(I) diimine adduct at 70°C in aqueous methanol solution. This was judged by the disappearance of the copper(II) *d*–*d* transition band at 820 nm and the appearance of an intense metal-to-ligand charge-transfer band at 456 nm characteristic of the copper(I) diimine adduct, **4**.

BNPP has been used as a model for hydrolytic cleavage of the phosphodiester backbone of DNA and RNA [18a,b]. Several possible mechanisms for the hydrolysis of phosphate diesters, including BNPP, by transition-metal complexes have been proposed [17, 18]. In these mechanisms the metal ions supply electrophilic acceptor sites for the phosphodiester's P—O^- followed by an external nucleophilic (H_2O or OH^-) attack or an intramolecular metal hydroxide attack at P=O, which then facilitates the hydrolysis of *p*-nitrophenolate groups. In addition, cooperation between metal ions and carboxyl groups of the ibuprofenate ions which may make a nucleophilic attack at phosphodiester cannot be ruled out in the hydrolysis of BNPP in the presence of complex **1** or **2**. Detailed kinetic studies and the potential application of these new complexes in the hydrolysis of biological phosphoric ester is being investigated.

Acknowledgements—I am grateful to Professor Jan Reedijk and to Mr G. A. Van Albada of Leiden University, The Netherlands, for obtaining the ESR spectra and to Birzeit University for the support of this research under Grant No. 235/17/15/9.

REFERENCES

1. J. R. J. Sorenson, *Prog. Med. Chem.* 1989, **26**, 437, and refs therein.

2. (a) C. D. Samara, D. P. Kessissoglou, G. E. Manoussakis, D. Mentzafos and A. Terzis, *J. Chem. Soc., Dalton Trans.* 1990, 959; (b) D. R. Fraiser, S. K. Lynch and G. O. Garlisle, *J. Inorg. Nucl. Chem.* 1981, **43,** 2747.
3. (a) J. Catterick and P. Thornton, *Adv. Inorg. Chem. Radiochem.* 1977, **20,** 291; (b) M. Melnik, *Coord. Chem. Rev.* 1981, **36,** 1; (c) M. Kato and Y. Muto, *Coord. Chem. Rev.* 1988, **92,** 45.
4. A. L. Aubhijleh, *J. Inorg. Biochem.* 1994, **55,** 255, and refs therein.
5. A. L. Abuhijleh, *Polyhedron* 1989, **8,** 2777.
6. A. L. Abuhijleh and C. Woods, *J. Chem. Soc., Dalton Trans.* 1992, 1249.
7. A. L. Abuhijleh, J. Pollitte and C. Woods, *Inorg. Chim. Acta* 1994 **215,** 131, and refs therein.
8. C. D. Samara, P. D. Jannakoudakis, D. P. Kessissoglou, G. E. Manoussakis, D. Mentzafor and A. Terzis, *J. Chem. Soc., Dalton Trans.* 1992, 3259.
9. F. T. Greenaway, A. Pezesh, A. W. Cordes, M. C. Nobel and J. R. J. Sorenson, *Inorg. Chim. Acta* 1984, **93,** 67.
10. I. Y. Ahmed and A. L. Abuhijleh, *Inorg. Chim. Acta* 1982, **61,** 241.
11. J. D. Ranford, P. J. Sadler and D. A. Tocher, *J. Chem. Soc., Dalton Trans.* 1993, 3393.
12. H. Beinert, *Coord. Chem. Rev.* 1980, **33,** 55.
13. H. Tamura, H. Imai, J. Kuwahara and Y. Suguira, *J. Am. Chem. Soc.* 1987, **109,** 6870.
14. R. G. Bhjirud and T. S. Srivastava, *Inorg. Chim. Acta* 1990, **173,** 121.
15. N. Farrell, *Transition Metal Complexes as Drugs and Chemotherapeutic Agents.* Kluwer Academic Publishers, Dordecht (1989).
16. (a) D. S. Sigman, *Accts Chem. Res.* 1986, **19,** 180; (b) D. S. Sigma, A. Mazunder and D. M. Perrin, *Chem. Rev.* 1993, **93,** 2295.
17. (a) B. Anderson, R. M. Milburn, J. M. Harrowfield, G. B. Robertson and A. M. Sargeson, *J. Am. Chem. Soc.* 1977, **99,** 2652; (b) J. R. Morrow and W. C. Trogler, *Inorg. Chem.* 1989, **28,** 2330; (c) J. N. Burstyn and K. A. Deal, *Inorg. Chem.* 1993, **32,** 3585; (d) J. Chin, M. Banaszuk, V. Jubain and X. Zou, *J. Am. Chem. Soc.* 1989, **111,** 186.
18. (a) J. Chin, *Accts Chem. Res.* 1991, **24,** 145: (b) P. Hendry and A. M. Sargeson, *Prog. Inorg. Chem.* 1990, **38,** 201; (c) B. C. Barras, *Chem. Br.* 1988, 677.
19. M. A. Fox and M. Chanon, *Photoinduced Electron Transfer.* Elsevier, Amsterdam (1988).
20. D. R. McMillin, J. R. Kirchhoff and K. V. Goodwin, *Coord. Chem. Rev.* 1985, **64,** 83, and refs therein.
21. F. N. Castellano, M. Ruthkosky and G. J. Meyer, *Inorg. Chem.* 1995, **34,** 3, and refs therein.
22. B. J. Hathaway and A. A. G. Tomlinson, *Coord. Chem. Rev.* 1970, **5,** 1.
23. L. P. Battaglia, A. B. Corradi, M. A. Zoroddu, G. Manca, R. Basosi and C. Solina, *J. Chem. Soc., Dalton Trans.* 1991, 2109.
24. (a) G. Lusuardi, L. Menabue and M. Saladini, *Inorg. Chim. Acta* 1994, **218,** 53; (b) L. Forti, M. Saldini and M. Sola, *Inorg. Chim. Acta* 1991, **187,** 197.
25. T. Kamiuski, H. Okawa, E. Kituara, M. Koikawa, N. Matsumoto, S. Kida and H. Oshio, *J. Chem. Soc., Dalton Trans.* 1989, 2077.
26. (a) M. A. Zoroddu, R. Dallocchio and S. Mosca, *Polyhedron* 1996, **15,** 277, and refs therein; (b) L. B. Battaglia, A. C. Bonamartini, S. Ianelli, M. A. Zoroddu and G. Sanna, *J. Chem. Soc., Faraday Trans.* 1991, **87,** 3863.
27. J. P. Maher, P. H. Rieger, P. Thornton and M. D. Ward, *J. Chem. Soc., Dalton Trans.* 1992, 3353.
28. (a) S. P. Perlepes, J. C. Huffman and G. Christou, *Polyhedron* 1992, **11,** 1471; (b) S. Meenakumari and A. Chakravarty, *Polyhedron* 1993, **12,** 374.
29. S. P. Perlepes, J. C. Huffman and G. Christou, *Polyhedron* 1991, **10,** 2301, and refs therein.
30. T. Tokii, N. Watanbe, M. Nakashima, Y. Muto, M. Morooka, S. Ohba and Y. Saito, *Bull. Chem. Soc.* 1990, **63,** 364.
31. G. B. Deacon and R. J. Phillips, *Coord. Chem. Rev.* 1980, **33,** 227.
32. (a) A. J. Pallenberg, K. S. Koenig and D. M. Barnhart, *Inorg. Chem.* 1995, **34,** 2833; (b) D. J. Darensbourg, M. W. Holtcamp, B. Khandelwal, K. K. Klausmeyer and J. H. Reibenspies, *Inorg. Chem.* 1995, **34,** 2389.

Pergamon

PII: S0277-5387(96)00217-3

Polyhedron Vol. 16, No. 4, pp. 741–747, 1997
Copyright © 1996 Elsevier Science Ltd
Printed in Great Britain. All rights reserved
0277-5387/97 $17.00+0.00

Studies on the formation and decomposition of copper(III) and nickel(III) complexes with macrocyclic ligands containing amide groups

Fuping Kou, Shourong Zhu,* Huakuan Lin, Keqin Ma and Yunti Chen

Department of Chemistry, Nankai University, Tianjin 300071, P. R. China

(Received 23 February 1996; accepted 26 April 1996)

Abstract—The spectral characteristics of 13- and 14-membered C-functionalized macrocyclic dioxotetraamine and the corresponding saturated polyamine copper(II), copper(III) and nickel(III) complexes have been studied. It was shown that C-functionalized substituents, although not coordinating to the metal ion, have significant effects on the spectral properties of their M^{III} complexes. As for copper(II) complexes, substituents increase the in-plane ligand field and decrease the wavelength of the *d–d* absorption of their complexes. Substituents increase the π-CT wavelength and decrease the absorption coefficients. Rate constants and activation parameters for the oxidation of Cu^{II} complexes by peroxodisulfate and decomposition reactions of copper(III) complexes in aqueous solution were also measured. Activation parameters were shown to be dependent on ligand structure. Copyright © 1996 Elsevier Science Ltd

Keywords: macrocyclic dioxotetraamine; copper(III) complex; nickel(III) complex; formation; decomposition; kinetics.

Square-planar saturated and unsaturated N_4 ligands have been well demonstrated to stabilize various oxidation states of enclosed iron [1], cobalt [2,3] or nickel [4,5] in aprotic solvents. The redox properties are determined by various structural parameters: a large ring, the presence of alkyl side chains to interfere with axial solvation or unsaturation of N donors for the lower valence states, while the absence of these factors or the presence of negative charge on N donors stabilizes higher oxidation states. Another efficient ligand factor facilitating higher oxidation states of metal ions in aqueous solutions was discovered in oligopeptide complexes of Cu^{II} [6] and Ni^{II} [7], where anionic imide N donors reduce the electrode potentials for M^{III}/M^{II} couples. Highly deprotonated peptide complexes have extremely low potentials [8]. It is postulated that oxidative cleavage of peptides by air in the presence of Cu^{II} or Ni^{II} involves M^{III}-peptide complexes as intermediates. The stabilization of high-oxidation states of 3*d* transition metal ions, in particular Cu^{III}, is of great current interest. This is due to the fact that such compounds can serve as models for some enzymes such as galactose oxidase [9] and may be used as effective oxidants and redox catalysts [10]. However, it is necessary to bear in mind that thermodynamic stabilization of the high oxidation state (i.e. lowering $M^{III}L/M^{II}L$ couple potential) prevents its use as an effective oxidant. More attractive in this sense would be compounds possessing high redox potentials along with high kinetic stability.

Among copper(II) stabilizing ligands, macroscopic tri- and tetrapeptides have been most widely studied [10]. The data obtained show that an increase in the number of deprotonated amide groups in the macrocycles cause a thermodynamic stabilization of copper(III). On the other hand, saturated tetraaza macrocycles containing only secondary amine donors do not stabilize copper(III), but are good nickel(III)-stabilizing ligands [11]. From this point of view, macrocyclic ligands containing both secondary amines and amide groups are of interest. Recently, we have developed a simple and versatile method for the synthesis of C-functionalized macrocyclic dioxotetraamine [12] that produce appropriate ligand fields and steric environments so as to reproduce certain essential redox functions that occur in natural metal-containing enzymes. On the basis of our pre-

* Author to whom correspondence should be addressed.

vious studies [13–17], copper and nickel complexes with macrocyclic dioxotetraamine ligand I_1–I_4 were chosen to investigate the effects of ligand structure on their spectral properties, formation and decomposition kinetics of Cu^{III} and Ni^{III} complex (Fig. 1).

EXPERIMENTAL

Reagents

All chemicals and solvents used in the synthesis and determination were of reagent grade and were used without further purification.

Synthesis

All reagents used were of analytical grade. L_1–L_4 were prepared according to the new method recently developed by us [12]. The corresponding saturated polyamine macrocycles were prepared by B_2H_6 reduction of dioxotetraamine [16].

Apparatus and instruments

Cyclic voltammetry was used to determine the electrode potentials E of a series of the present M^{II}-macrocycle complexes in a similar fashion as before [12]. A PARC model 273 electrochemical apparatus was used. The working electrode used was glassy carbon. Platinum was used as an auxiliary electrode. Saturated calomel was used as reference electrode. Voltammograms were obtained in 0.5 mol dm^{-3} Na_2SO_4 solution at 25°C and a scan rate of 100 mV s^{-1} for metal complexes (3×10^{-3} mol dm^{-3}). Complex solutions were prepared by mixing equimolar quantities of the ligand and copper(II)/nickel(II) sulfate. The E values (V versus SCE) were obtained from an average of three independent solution measurements and have a reproducibility of 5 mV. As a supporting electrolyte, we have consistently used 0.5 mol dm^{-3} sodium sulfate. The separation of the anodic and cathodic peaks was 70–110 mV and the peak current ratios were near unity. These features are indicative of quasi-reversible electrochemical behaviour and, therefore, the midpoint between the oxidation peak and the reduction peak was taken as the electrode potential E for M^{III}/M^{II} couples. All of the E values thus obtained were summarized in Table 1.

Kinetic measurements

Kinetic measurements were carried out spectrophotometrically in a thermostatted (±0.1°C) quartz cell (1 cm) using a Shimadzu UV–Vis 160A spectrophotometry. Extinction coefficient ε were determined by oxidation of the complex (5×10^{-4} mol dm^{-3}) in $K_2S_2O_8$ (0.1 mol dm^{-3}). Solutions of reagents were thermostatted before measurement for *ca* 15 min. Solutions of $K_2S_2O_8$ were prepared immediately before use. The formation of copper(III) and nickel(III) complexes and their disappearance was followed at their absorption maximum (−410 nm), where absorption of the initial copper(II) complexes is negligible. All measurements unless otherwise stated were carried out at ionic strength $I = 0.1$ M $NaClO_4$. The $K_2S_2O_8$ concentration was 2.0×10^{-3} mol dm^{-3}. The complex concentration was 3×10^{-3}–1.0×10^{-4} mol dm^{-3}. pH values were adjusted to 6–7 with NaOH. All solutions were prepared with twice distilled water.

RESULTS AND DISCUSSION

Reaction of dioxotetraamine macrocycles with transition metal ions proceeds according to the following equations to yield positively charged and neutral complexes [12b]:

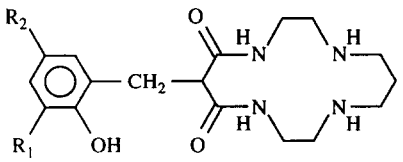
$$M^{2+} + L = MH_{-1}L^{+} + H^{+} \quad (1)$$

$$M^{2+} + L = MH_{-2}L + 2H^{+}. \quad (2)$$

The mechanism of this reaction includes coordination of the metal ion to secondary amine nitrogen atoms and a subsequent deprotonation of amide groups. It must be noted that, unlike in previous reports, two amido groups are different, that is, when coordinated to the metal ion, especially copper(II), the amido hydrogen does not dissociate simultaneously [13]. As shown in the reaction equation, the equilibrium strongly depends on pH; at pH 4.8, the positively charged $[CuH_{-1}L]^{+}$ has a maximum value about 15%, when pH rise to 5.5 or higher, all metal ions existed in the form of $MH_{-2}L$ (Fig. 2). In the present kinetic study, the initial pH of the complex is 6–7, in which range $MH_{-1}L$ does not exist. Since phenolic oxygen does not coordinate to copper(II), substituents have little effect on properties of their M^{II} complexes. However, there are some differences between the complex with and without substituents. Table 1 summarizes some spectral data and Cu^{II}/Cu^{III} half-wave potentials.

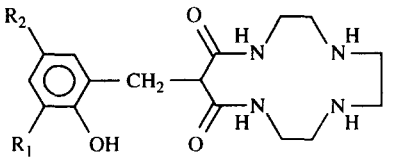
The position of the *d–d* absorption band in the electronic spectra is typical of square-planar complexes. The data presented show that the absorption maxima shifted to short wavelength with the introduction of a substituent. The greater *d–d* transition energy of complexes with substituents indicate the evidence that they have greater in-plane ligand field strength. To our knowledge, these complexes have the greatest in-plane ligand field strength.

It is well known that the most suitable macrocycles for Cu^{II} ions are 14-membered ligands. Apparently, in complexes with 13-membered ligands, the coordination polyhedron of the metal ion has some distortion from planarity and this distortion decreases the in-plane ligand field strength, thus the wavelength of the copper(II) complexes are larger than corresponding 14-membered ligands. Due to this distor-



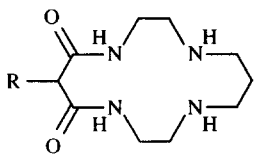
L_1 R_1=R_2=H; L_2 R1=OCH_3, R_2=H

L_3 R_1=H, R_2=Br; L_4 R_1=R_2=Br

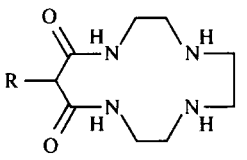


L_5 R_1=R_2=H; L_6 R1=OCH_3, R_2=H

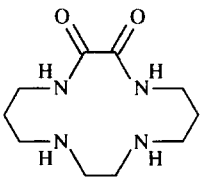
L_7 R_1=H, R_2=Br; L_8 R_1=R_2=Br



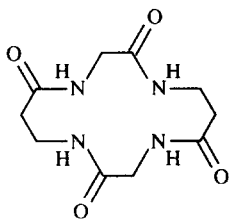
L_9 R=H; L_{10} R=$ArCH_2$



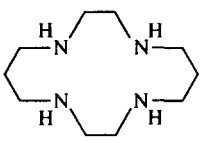
L_{11} R=H; L_{12} R=$ArCH_2$



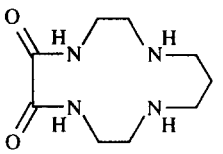
L_{13}



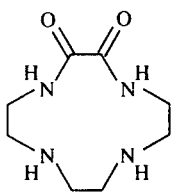
L_{14}



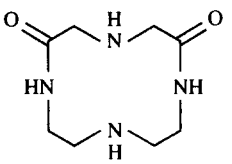
L_{15}



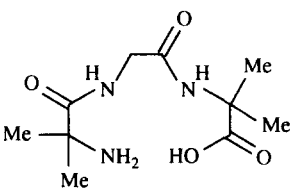
L_{16}



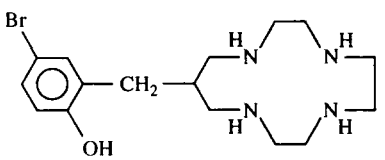
L_{17}



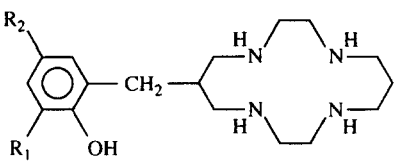
L_{18}



L_{19}



L_{20}



L_{21} R_1=R_2=H; L_{22} R1=H, R_2=Br

L_{23} R_1=OCH_3, R_2=H

Fig. 1. The structure of the tetraaza ligands containing the amide groups used in the study.

Table 1. Spectral characteristic and Cu^{II}/Cu^{III} half-wave potential (V versus S.C.E.) of the copper(II) complex

Ligand	L_1	L_2	L_3	L_4	L_5	L_9	L_{11}	L_{15}	L_{20}	L_{21}	L_{22}	L_{23}
λ_{max} (nm)	500	505	495	490	510	515	520	505				
Extinction coefficient	80	77	75	73	90	90	100					
Cu^{III}/Cu^{II}	0.64	0.62	0.66	0.68	0.58	0.64	0.56		1.00	1.00		
Ni^{III}/Ni^{II}	0.72	0.72	0.73	0.73	0.81				0.64	0.46	0.46	0.45

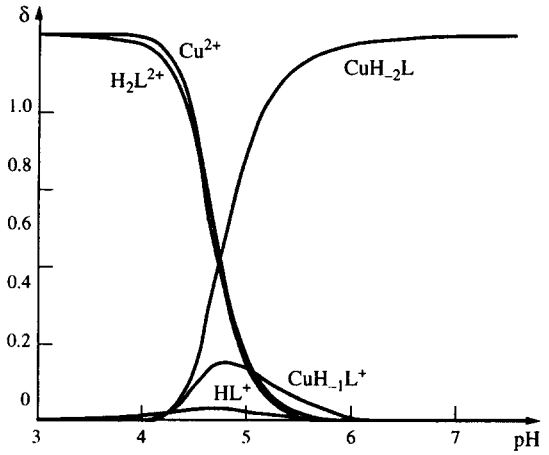


Fig. 2. Distribution diagram of Cu^{II}-L_1 complexes.

tion, the absorption coefficient increased. All oxidation processes of the complexes in aqueous solution are quasi-reversible. Substituents increase the Cu^{II}/Cu^{III} potential of the complex. Lower $E_{1/2}$ values for complexes with 13-membered ligands compared with 14-membered ones are due to a better fit of the 13-membered ring to the copper(III) ion. However, substituents decrease the Ni^{II}/Ni^{III} potential. This is quite different from that in copper(II) complexes and indicates that there must be some interaction between substituents and Ni^{II} or Ni^{III} ions because d^7-Ni^{III} tends to form a distorted octrahedral complex; the phenol substitute interacts and stabilizes the Ni^{III} complex, thus decreasing the Ni^{III}/Ni^{II} potentials. For 13-membered macrocyclic dioxotetraamine, it is the strong ligand field that stabilizes copper(III) efficiently. However, macrocyclic polyamine, especially 14-membered macrocyclic polyamine, stabilizes nickel(III) effectively. Substituents in macrocyclic polyamines can further stabilize the Ni^{III} state.

Due to the low Cu^{II}/Cu^{III} potential, one expects that macrocyclic dioxotetraamine copper(II) can easily by oxidized. When the macrocyclic dioxotetraamine copper(II) complex was oxidized chemically or electrochemically, brown copper(III) complexes were formed. Their charge-transfer absorption bands have been reported. In our study, potassium peroxodisulfate was used as an oxidant, since both potassium peroxodisulfate and its reduction products do not absorb in the visible and the near-UV region and its reactions with copper(II) complexes are slow enough to study them by conventional spectrophotometric techniques.

After addition of oxidant to a solution of the copper(II) complexes, an intense new absorption band appears in the near UV and visible spectral region (Fig. 3).

Both in ligands and complexes there are no absorptions in the 380–440 nm region in our experimental conditions. When free ligands were oxidized by potassium peroxodisulfate, no absorption in this region was observed even in a longer time interval (1 h). Hay [18] attributed this band to be a *d–d* transition, while Lampeka [19] reported it to be a CT band. We assign the 380–440 nm absorption to be an L–M CT band of the copper(III) complex, because of its large absorption coefficient. This M^{III} CT band does not change in 0.1 mol dm^{-3} $HClO_4$. Absorption maxima and extinction coefficients were summarized in Table 2.

We can see from Table 2 that, as in copper(II) complexes, the absorption maximum varies with the substituents. Compared with L_9 complexes, the presence of substituents leads to a substantial intensity decrease and wavelength increase. This indicates that a significant π-interaction of the phenol substituent

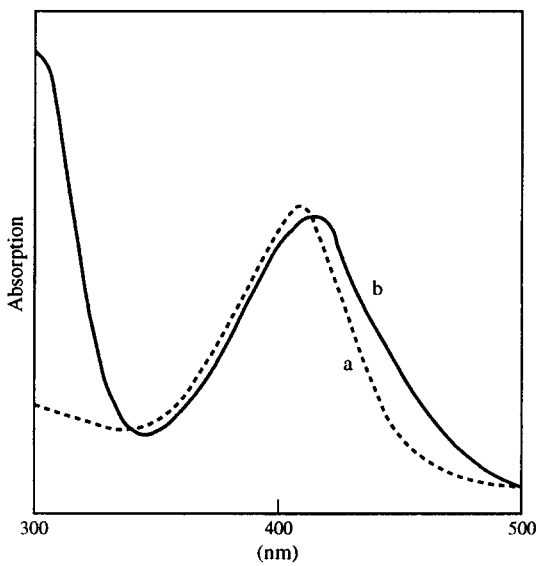


Fig. 3. The π-CT spectra of M^{III}-L_1 complexes (a) Cu^{III} and (b) Ni^{III} complexes.

Table 2. Parameters of CT band spectra of M^{III} complexes at 25 °C

Cu^{III} complex	λ_{max}	Extinction coefficient	Ni^{III} complex	λ_{max}	Extinction coefficient
L_1	410	1700	L_1	410	3050
L_3	400	1170	L_2	440	5300
L_5	410	1500	L_3	400	2110
L_6	440	3190	L_4	390	2370
L_7	400	1150	L_5	410	1800
L_8	390	2230	L_9	300	8170
L_9	300	15000	L_{21}	410	5690

with the central M^{III} ion may exist, in agreement with Lampeka [19]. However, some different structure macrocyclic dioxotetraamine copper(III) complexes have a similar absorption maximum [20] (350 nm), such as L_{11} (300 nm), L_{10} and L_{12} (300 nm) [19], L_{14} (365 nm) [21], L_{15} (Ni^{III} complex, 370 nm) [22], L_{13}, L_{16} and L_{17} (350 nm) [18], L_{18} (355 nm) [20], and L_{19} (395 nm) [21]. Both λ_{max} and the absorption coefficient of the present C-functionalized copper(III) complexes are similar to the tripeptide copper(III) and nickel(III) complexes [23]. Unlike in acid solution, all the M^{III} complexes decomposed quickly in strong alkaline solution. This further supports the view that the absorption at 350–450 nm is caused by M^{III} complexes [22,23].

Oxidation kinetics

Despite the availability of a large number of papers concerning the properties of copper(III) and nickel(III) complexes, kinetic investigations of copper(II) or nickel(II) on corresponding M^{III} states are few. Only the oxidation of some peptide complexes by $IrCl_8^{2-}$ and several cross reactions between peptide complexes appear to have been studied [24,25]. Figure 4 shows spectral changes occurring during oxidation of a C-functionalized macrocyclic dioxotetraamine copper(II) complex by peroxodisulfate. From Fig. 4 we can see that the reaction processes are characteristic of consecutive reaction. In fact, the absorption increase at 410 nm is contributed to the copper(III) complex formation. While the decrease indicates the decomposition of the copper(II) complex.

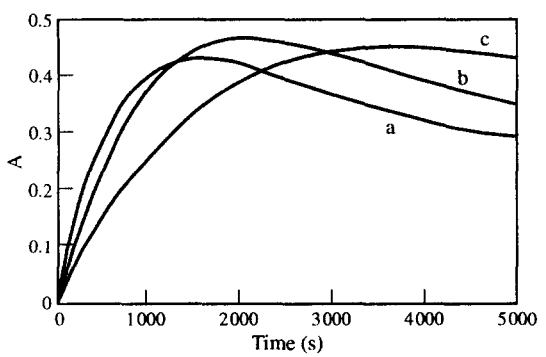


Fig. 4. Spectroscopic changes at 410 mm during oxidation of $Cu^{II}L$.

Rate constants for the oxidation were calculated from the initially linear regions of kinetic curves using the calculated ε values for the copper(III) and nickel(III) complexes. The M^{III} complexes formation rate was found to be first-order in both reagents. That is:

$$d[Cu^{III}L]/dt = k_{obs}[Cu^{II}L][S_2O_8^{2-}].$$

The observed second-order rate constants of Cu^{II} and Ni^{II} complexes are summarized in Tables 3 and 4.

Comparison of k_{obs} and $E_{1/2}$ values shows that complexes of 13-membered ligands having lower redox potentials will oxidize more slowly. Substituents

Table 3. Observed second-order rate constants k_{obs} ($M^{-1}s^{-1}$) of the oxidation process of copper(II) complexes with $K_2S_2O_8$ (I = 0.1 M $NaClO_4$)

	5 °C	15 °C	25 °C	35 °C	45 °C
L_1	0.418	0.668	1.01	1.67	
L_3		0.247	0.365	0.567	0.960
L_5	0.087	0.149	0.259	0.489	
L_6		0.190	0.310	0.514	0.953
L_7		0.125	0.194	0.357	0.650
L_8		0.102	0.178	0.320	0.577

Table 4. Observed second-order rate constants k_{obs} ($M^{-1}s^{-1}$) of the oxidation process of nickel(II) complexes with $K_2S_2O_8$ (I = 0.1 M $NaClO_4$)

	15 °C	25 °C	35 °C	45 °C
L_1	0.363	0.607	1.09	1.97
L_2	0.475	0.750	1.29	2.28
L_3	0.263	0.501	0.738	1.55
L_4	0.193	0.377	0.667	1.12
L_5	0.610	1.00	1.55	2.69
L_9	6.65	8.11	9.71	11.3
L_{21}	2.67	4.19	7.86	13.7

decrease the redox rate considerably, which may be due to the fact that the steric hindrance of the substituents decreased the stability of the intermediate complexes because the phenol substituent covered the metal ions [13].

In accordance with the literature results [11, 19], the following scheme can be used to describe the oxidation mechanism:

$$M^{II}L + S_2O_8^{2-} \overset{K}{\rightleftharpoons} [M^{II}L \cdot S_2O_8]^{2-}$$

$$[M^{II}L \cdot S_2O_8]^{2-} \overset{k}{\rightarrow} M^{III}L^{+} + SO_4^{2-} + SO_4^{-}$$

$$M^{II}L + SO_4^{-} \overset{\text{fast}}{\rightarrow} M^{III}L^{+} + SO_4^{2-}.$$

The first step is a fast pre-equilibrium process; an outer-sphere intermediate complex was formed between oxidant and reductant. The second step is the activation and electron-transfer step, which is the rate-determining step. The free radical is active and is quickly reduced as shown in step 3. After oxidation, $BaCl_2$ solution was added to the mixture and a white precipitate formed, which indicated that $S_2O_8^{2-}$ was reduced to SO_4^{2-}.

According to the mechanism, we have:

$$d[M^{III}L^{+}]/dt = kK[M^{II}L][S_2O_8]^{2-},$$

therefore, $k_{obs} = kK$.

In the formation of the outer-sphere intermediate complex, there is no bonding formation, i.e. the enthalpy is small in the formation of the intermediate complex.

Using Eyring's formula, the activation parameters of the rate-determining step were obtained (Table 5).

From Tables 5 and 6 we can see that, for complexes with 13-membered ligands, the values of $\Delta H_m^{\ddagger}$ are considerably higher than those for complexes with 14-membered analogues, while the difference of $\Delta S_m^{\ddagger}$ values are small. This reflects different stereochemistry in both types of complexes.

The data presented may lead us to ascertain the effect of the substituents on activation parameters. It is the large $\Delta H_m^{\ddagger}$ value of complexes with substituents that greatly reduced their oxidation rates. On comparison with 13-membered copper(II) complexes, k_{obs} of 14-membered copper(II) complexes are larger because of their small $\Delta H_m^{\ddagger}$ value. In our opinion, the reason is that 14-membered macrocycles are best fitted to the copper(II) ion, the strong coordinative interactions exerted by the 14-membered macrocyclic dioxotetraamine ligand raising the energy of the antibonding level (essentially metallic in character) from which the electron is abstracted, thus decreases the $\Delta H_m^{\ddagger}$ values. While 13-membered macrocyclics most readily fit the nickel(II) ion [26], therefore, their oxidation rates are larger than 14-membered analogues. Electron-giving substituents increase the level of the highest occupying orbitals of the metal ions, thus k_{obs} values were increased compared with the electron-withdrawing substituent.

Table 5. Activation parameters of the oxidation of Cu^{II} complexes with potassium peroxosulfate

Ligand	$\Delta H_m^{\ddagger}$ (kJ mol^{-1})	$\Delta S_m^{\ddagger}$ (J mol^{-1} K^{-1})
L_1	30.1	−144
L_3	31.8	−146
L_5	38.4	−127
L_6	38.1	−127
L_7	39.7	−125
L_8	41.5	−120

Table 6. Activation parameters of the oxidation of Ni^{II} complexes with potassium peroxosulfate

Ligand	$\Delta H_m^{\ddagger}$ (kJ mol^{-1})	$\Delta S_m^{\ddagger}$ (J mol^{-1} K^{-1})
L_1	40.5	−113
L_2	36.8	−124
L_3	42.9	−107
L_4	42.0	−112
L_5	34.7	−129
L_9	11.10	−191
L_{21}	39.6	−99.5

Decomposition of copper(III) *and nickel*(III) *complexes*

Copper(III) and nickel(III) complexes formed in the oxidation reactions are not stable enough and decompose via intramolecular redox reaction. Our experiments have shown that the decompositions are first-order in copper(III) or nickel(III) complexes:

$$-d[M^{III}L^{+}]/dt = k_d[M^{III}L^{+}].$$

Since the decomposition reactions are slow, rate constants for the oxidation were calculated from the initially linear regions of kinetic curves. The starting point was chosen 5–10 min. after the absorption maximum to ensure all the copper(II) complexes were oxidized. Rate constants and activation parameters for the decomposition of M^{III} complexes are summarized in Table 7.

Analysis of the data presented in Table 7 shows little effect of ring size on decomposition rate constants and activation parameters of copper(III) complexes, but the effect of the substituents is more pronounced. Electron-withdrawing substituents not only decrease the oxidation rate of copper(II) complexes, but also decrease the decomposition rate of copper(III) complexes. The introduction of substituents greatly increased the kinetic stability of copper(III) complexes. The half-lives of Cu^{III} complexes of macrocyclic-dioxotetraamine at 25°C are 2.5 to 5 h, while Ni^{III} complexes have half-lives of 4–18 h.

Nickel(III) complexes of macrocyclic dioxotetraamines are thermodynamically unstable,

Table 7. Rate constants and activation parameters for decomposition of M^{III} complexes

Complex	k_d ($s^{-1} \times 10^5$) 15°C	25°C	35°C	$\Delta H_m^{\ddagger}$ (kJ mol^{-1})	$\Delta S_m^{\ddagger}$ (J mol^{-1} K^{-1})
$Cu^{III}L_1$	7.00	11.7	16.8	28.3	−226
$Cu^{III}L_5$	6.34	10.1	13.5	25.5	−236
$Cu^{III}L_7$	4.79	7.04	11.7	32.6	−218
$Cu^{III}L_8$	3.51	5.41	8.06	30.2	−229
$Cu^{III}L_9$		21		61	−111
$Ni^{III}L_1$	1.93	2.94	4.95	30.2	−230
$Ni^{III}L_3$	1.51	2.22	3.40	27.5	−242
$Ni^{III}L_4$	1.13	1.57	1.99	18.5	−122
$Ni^{III}L_5$	2.95	6.81	14.7	56.8	−134
$Ni^{III}L_9$	7.21	14.5	27.5	47.0	−161

however, they do have considerable kinetic stability. As in the case of copper(III) complexes, substituents, especially electron-withdrawing substituents, increase the kinetic stability of Ni^{III} complexes. Substituted polyamine Ni^{III} complexes even have no noticeable spectral change over 1 week.

Decomposition of the M^{III} complex was very slow compared with the oxidation process: in 0.1 mol dm^3 $K_2S_2O_8$ solution the decomposition rate was even less than 1% of the oxidation rate, according to formula $28\ \beta = K^{K/(1-K)}$, where β is the mole ratio of the M^{III} complex and K is the ratio of decomposition and formation rate of the M^{III} complex, 95% or higher M^{III} complex existed in the absorption maxima, therefore, we can easily determine the absorption coefficient by the oxidation of M^{II} complex in 0.1 mol dm^{-3} $K_2S_2O_8$ solution.

In conclusion, our study shows that though phenols do not coordinate to M^{II}, they do affect the spectral characteristics and M^{II}/M^{III} potentials. Substituents increasing the in-plane ligand field can increase redox potentials, but decrease the oxidation rate of their M^{II} complexes and decomposition rates of their M^{III} complexes.

REFERENCES

1. N. Herron and D. H. Busch, *J. Am. Chem. Soc.* 1981, **103,** 1236.
2. A. M. Tait, F. V. Lovecchio and D. H. Busch, *Inorg. Chem.* 1977, **16,** 2006.
3. Y. Hung, L. Y. Martin, S. C. Jackels, A. M. Tait and D. H. Busch, *J. Am. Chem. Soc.* 1977, **99,** 4029.
4. D. G. Pillsbury and D. H. Busch, *J. Am. Chem. Soc.* 1976, **98,** 7836.
5. D. H. Busch, *Accts. Chem. Res.* 1978, **11,** 392.
6. F. P. Bossu, K. L. Chellappa and D. W. Margerum, *J. Am. Chem. Soc.* 1977, **99,** 2195.
7. F. P. Bossu and D. W. Margerum, *Inorg. Chem.* 1977, **16,** 1210.
8. A. G. Lappin, C. K. Murry and D. W. Margerum, *Inorg. Chem.* 1978, **17,** 1630; E. Kimura, *J. Coord. Chem.* 1986, **15,** 1.
9. B. J. Hathaway, *Comprehensive Coordination Chemistry* (Edited by G. Wilkinson), Vol. 5, p. 533. Pergamon Press, Oxford (1987).
10. D. W. Margerum and G. D. Owens, *Metal Ions in Biological Systems* (Edited by H. Sigel), Vol. 12, p. 75. Marcel Dekker Inc., New York (1981).
11. S. V. Rosokha and Y. D. Lampeka, *Tero. Eksp. Khim. (Russ. Ed)* 1988, **24,** 577.
12. (a) S. R. Zhu, H. K. Lin, C. C. Lin, F. P. Kon and Y. T. Chen, *Inorg. Chim. Acta* 1995, **228,** 225; (b) S. R. Zhu, F. P. Kou, H. K. Lin and Y. T. Chen, *Inorg. Chem.* 1996, **35,** in press.
13. F. P. Kou, S. R. Zhu, H. K. Lin, Y. T. Chen, H. G. Wang and X. K. Yao, *J. Chem. Soc., Chem. Commun.* 1996, 59.
14. Q. H. Luo, S. R. Zhu, M. C. Shen, A. R. Dai, A. D. Liu, H. C. Gu, F. M. Li and S. J. Di, *Kexue Tongbao* 1992, 1288.
15. Q. H. Luo, S. R. Zhu, M. C. Shen, S. Y. Yu, Z. Zhang, X. Y. Huang and Q. J. Wu, *J. Chem. Soc., Dalton Trans.* 1994, 1873.
16. H. K. Lin, S. R. Zhu, Z. X. Gu and Y. T. Chen, *J. Chem. Soc., Dalton Trans.* 1995, 1879.
17. Q. H. Luo, S. R. Zhu and M. C. Shen, *Huaxue Xuebao* 1994, **52,** 699.
18. R. W. Hay, R. Rembi and W. Sommerville, *Inorg. Chim. Acta* 1982, **59,** 147.
19. Y. D. Lampeka and S. P. Gavrish, *J. Coord. Chem.* 1990, **21,** 351.
20. L. Fabbrizzi, *Inorg. Chem.* 1986, **25,** 321; L. Fabbrizzi and A. Poggi, *J. Chem. Soc., Chem. Commun.* 1980, 646.
21. J. S. Rybka and D. W. Margerum, *Inorg. Chem.* 1981, **20,** 1453.
22. E. Zeigerson, *J. Chem. Soc., Chem. Commun.* 1974, 241.
23. S. T. Kirksey Jr, T. A. Neubecker and D. W. Margerum, *J. Am. Chem. Soc.* 1979, **101,** 1631.
24. J. M. Anast, A. W. Hamburg and D. W. Margerum, *Inorg. Chem.* 1983, **22,** 2139.
25. G. D. Owens and D. W. Margerum, *Inorg. Chem.* 1981, **20,** 1446.
26. L. L. Diaddario, W. R. Robinson and D. W. Margerum, *Inorg. Chem.* 1983, **22,** 1021.
27. J. W. Moore and R. G. Pearson, *Kinetics and Mechanism—A study of Homogeneous Chemical Reactions* 3rd edn, p. 336. John Wiley, New York (1981), Chinese translation.

Pergamon

PII: S0277-5387(96)00347-6

Polyhedron Vol. 16, No. 5, pp. 749–763, 1997
Copyright © 1996 Elsevier Science Ltd
Printed in Great Britain. All rights reserved
0277-5387/97 $17.00 + 0.00

Lanthanide coordination polymers with dicarboxylate-like ligands: crystal structures of polymeric neodymium(III) and erbium(III) complexes with flexible double betaines

Ping-Rong Wei,* De-Dong Wu, Zhong-Yuan Zhou, Song-Lin Li and Thomas C. W. Mak†

Department of Chemistry, The Chinese University of Hong Kong, Shatin, New Territories, Hong Kong

(Received 28 June 1996; accepted 17 July 1996)

Abstract—Four novel two-dimensional lanthanide(III) coordination polymers of two flexible double betaines with different numbers of methylene groups bridging two quaternary nitrogen atoms, namely $[\{Nd(L^2)_2(H_2O)_2\}_n][ClO_4]_{3n}$ (**1**), $[\{Nd(L^2)_2(H_2O)_2\}_n][ClO_4]_{3n}\cdot nH_2O$ (**2**), $[\{Er(L^1)_2(H_2O)_2\}_n][ClO_4]_{3n}\cdot nH_2O$ (**3**) and $[\{Er(L^2)_2(H_2O)\}_n][ClO_4]_{3n}\cdot nH_2O$ (**4**) [L^1 = *N,N′*-dicarboxymethyl-*N,N,N′,N′*-tetramethyl-1,3-propanediammonium: $^-O_2CCH_2N^+Me_2—(CH_2)_3—N^+Me_2CH_2CO_2^-$; L^2 = *N,N′*-dicarboxymethyl-*N,N,N′,N′*-tetramethyl-1,4-butanediammonium: $^-O_2CCH_2N^+Me_2—(CH_2)_4—N^+Me_2CH_2CO_2^-$], have been prepared and characterized by X-ray crystallography. Each complex contains a centrosymmetric paddle-wheel-like dimeric subunit in which each pair of adjacent metal atoms is bridged by four *syn–syn* μ-carboxylato-*O,O′* groups that are oriented nearly perpendicular to each other about the metal–metal axis. The dimeric subunits are extended into a polymeric chain through the linkage of each metal centre to carboxylato groups of an adjacent dimer. Such infinite chains are extended into a plane wave-like layer structure by cross-linkage of the molecular skeletons of double betaine ligands. The neodymium(III) atom is (**1**) is surrounded, in a distorted monocapped square-antiprismatic geometry, by seven carboxylato oxygen atoms and two aqua ligands, and the carboxylato groups are involved in three different coordination modes: the common bidentate bridging, unidentate and unusual tridentate bridging. In (**2**), (**3**) and (**4**), the lanthanide(III) atom exhibits eight coordination in a distorted square antiprism, and the carboxylato groups in the dimeric subunits adopt the common unidentate and bidentate bridging modes. In addition, the uncommon bidentate chelate mode of carboxylato groups also occurs in (**4**). Copyright © 1996 Elsevier Science Ltd

Keywords: betaine; carboxylate; neodymium; erbium; lanthanide; coordination polymer.

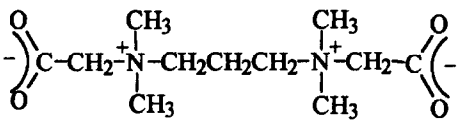
There has been considerable interest in the coordination chemistry of lanthanide complexes with carboxylato ligands owing to their potential application as luminescent probes in systems of biological relevance [1], particularly as resonance contrasting agents [2,3]. Of the numerous lanthanide complexes that have been widely studied [4–7], most have been found to possess a variety of dimeric or infinite chain structures in which the carboxylate groups act as bridges between metal atoms, and the number of bridging carboxylato groups varies in different complexes. In the case of the acetate ligand, the cerium(III) complex adopts a linear polymeric structure with respective pairs of metal atoms bridged by three acetato groups [8], whereas the holmium(III) complex takes a dimeric form in which the lanthanide atoms are bridged by only two carboxylate groups [9]. The neodymium(III) (methylthio)acetate complex has nine-coordinate lanthanide atoms that are bridged in pairs by two or four carboxylato ligands into a linear polymeric chain [10]. In ytterium(III) (methylthio)acetate, which takes a linear polymeric form, adjacent metal atoms are linked by only one carboxylato group [11]. In contrast, lanthanide carboxylates with a two-dimensional polymeric network

* On sabbatical leave from the Department of Chemistry, Zhengzhou University, Zhengzhou 450052, P. R. China.

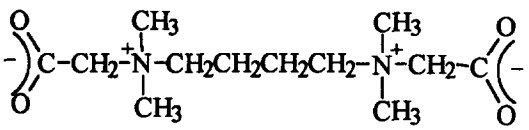
† Author to whom correspondence should be addressed.

are rare, although the formate has been found to exhibit a layered structure [12].

Our recent studies have demonstrated that betaine ($Me_3N^+CH_2CO_2^-$; IUPAC name, trimethylammoniumacetate) and its derivatives, considered as structural analogues of the corresponding carboxylate anions, are useful in the preparation of carboxylate complexes of transition metals [13–17]. Furthermore, by virtue of their overall charge neutrality, betaine compounds have been used to prepare metal complexes with new structural features compared with the common metal carboxylates [18–22]. In previous studies we have obtained two-dimensional crystalline mercury(II) chloride adducts, as well as silver and sodium coordination polymers with layer-type or three-dimensional networks by using a series of flexible double betaines with an adipic acid skeleton, or different polymethylene bridges between the quaternary nitrogen atoms [23–27]. Lanthanide complexes of betaine and its derivatives are much less well known, although several examples have been reported recently [28]. In this paper, we describe the preparation and characterization of four new neodymium(III) and erbium(III) complexes containing two-dimensional frameworks constructed from two flexible dicarboxylate-like double betaines with different numbers of methylene groups linking two quaternary nitrogen atoms, namely $[\{Nd(L^1)_2(H_2O)_2\}_n][ClO_4]_{3n}$ (**1**), $[\{Nd(L^2)_2(H_2O)_2\}_n][ClO_4]_{3n} \cdot nH_2O$ (**2**), $[\{Er(L^1)_2(H_2O)_2\}_n][ClO_4]_{3n} \cdot nH_2O$ (**3**) and $[\{Er(L^2)_2(H_2O)\}_n][ClO_4]_{3n} \cdot nH_2O$ (**4**) [L^1 = *N*,*N*′-dicarboxymethyl-*N*,*N*,*N*′,*N*′-tetramethyl-1,3-propanediammonium: $^-O_2CCH_2N^+Me_2$—$(CH_2)_3$—$N^+Me_2CH_2CO_2^-$; L^2 = *N*,*N*′-dicarboxylmethyl-*N*,*N*,*N*′,*N*′-tetramethyl-1,4-butanediammonium: $^-O_2CCH_2N^+Me_2$—$(CH_2)_4$—$N^+Me_2CH_2CO_2^-$].



L^1



L^2

Structural formulas of L^1 and L^2

EXPERIMENTAL

The flexible double betaines L^1 and L^2 were synthesized as described previously [27]. The C, H and N microanalyses were carried out on a Perkin–Elmer 240 elemental analyser. Infrared spectra were recorded from KBr pellets in the range of 4000–400 cm^{-1} on a Perkin–Elmer 1600 FT-IR spectrometer.

Synthesis of $[\{Nd(L^1)_2(H_2O)_2\}_n][ClO_4]_{3n}$ (**1**)

Perchloric acid (2 N) was added slowly to an aqueous suspension (10 cm^3) of neodymium oxide (Nd_2O_3; 0.084 g, 0.25 mmol) with stirring at *ca* 60°C. The resulting clear solution of neodymium(III) perchlorate (0.5 mmol) was mixed with an aqueous solution (5 cm^3) of L^1 (0.26 g, 1.0 mmol). After stirring at *ca* 60°C for a few minutes, a clear solution was obtained by filtration. Storage of the solution in a desiccator charged with drierite for a few days yielded pink prismatic crystals. Found: C, 27.1; H, 5.1; N, 5.6. Calc. for $C_{22}H_{48}N_4O_{22}Cl_3Nd$: C, 27.2; H, 4.9; N, 5.8%. IR: 3433s, 3011w, 2978w, 2078w, 1661m, 1622vs, 1478m, 1406s, 1328m, 1272w, 1144s, 1117s, 983w, 939w, 906m, 717m, 628m and 546w cm^{-1}.

Synthesis of $[\{Nd(L^2)_2(H_2O)_2\}_n][ClO_4]_{3n} \cdot nH_2O$ (**2**)

To an aqueous solution (10 cm^3 of neodymium(III) perchlorate (0.5 mmol) was added a solution of L^2 (0.274 g, 1.0 mmol) in water (5 cm^3) with stirring at *ca* 60°C for a few minutes. After filtration, pink block-like crystals were obtained by diffusing ethanol into the aqueous solution. Found: C, 28.6; H, 5.2; N, 5.5. Calc. for $C_{24}H_{54}N_4O_{23}Cl_3Nd$: C, 28.3; H, 5.3; N, 5.5%. IR: 3435s, 3065w, 2967w, 2075w, 1613vs, 1488m, 1405m, 1341m, 1145s, 1118s, 1080s, 1009w, 938w, 894m, 715m, 628m and 552w cm^{-1}.

Synthesis of $[\{Er(L^1)_2(H_2O)_2\}_n][ClO_4]_{3n} \cdot nH_2O$ (**3**)

The aqueous solution (10 cm^3) of erbium(III) perchlorate (0.5 mmol) prepared in a similar manner to that above was mixed with a solution of L^1 (260 mg, 1.0 mmol) in water (5 cm^3) with stirring at *ca* 60°C for a few minutes. The solution was filtered, and ethanol was diffused into the resulting solution for a week to yield pink crystals. Found: C, 26.5; H, 5.1; N, 5.4. Calc. for $C_{22}H_{48}N_4O_{22}Cl_3Er$: C, 26.1; H, 4.9; N, 5.5%. IR: 3424s, 3011w, 2978w, 2020w, 1635s, 1613s, 1482m, 1406s, 1355m, 1275w, 1145s, 1118s, 1080s, 982w, 938w, 900m, 709w, 628w and 541w cm^{-1}.

Synthesis of $[\{Er(L^2)_2(H_2O)\}_n][ClO_4]_{3n} \cdot nH_2O$ (**4**)

To an aqueous solution (10 cm^3) of erbium(III) perchlorate (0.5 mmol) was added L^2 (274 mg, 1.0 mmol) in water (5 cm^3) with stirring under heating.

After filtration pink prismatic crystals were obtained by diffusing ethanol into the aqueous solution. Found: C, 28.3; H, 5.1; N, 5.5. Calc. for $C_{24}H_{52}H_4O_{22}Cl_3Er$: C, 28.2; H, 5.1; N, 5.5%. IR: 3446s, 3065w, 2967w, 2031w, 1607s, 1482m, 1411s, 1346m, 1139s, 1118s, 932w, 894m, 726m, 622m and 562w cm^{-1}.

CAUTION. Metal perchlorate salts containing organic ligands are potentially explosive and should be handled with great care.

Crystal structure determinations

Information concerning crystallographic data and structure refinement of the four complexes is summarized in Table 1. Raw intensities of complexes **1, 3** and **4** were collected at 293 K on a MSC/Rigaku RAXIS-IIC imaging plate system with a rotating anode Mo-K_α X-ray source ($\lambda = 0.71073$ Å, 50 kV, 150 mA) [29], and corrected for absorption using the ABSCOR program [30]. Raw intensities of complex **2** were collected on a Siemens R3m/V diffractometer in the variable ω-scan mode [31] using Mo-K_α radiation ($\lambda = 0.71073$ Å) at 293 K. Unit-cell parameters were calculated from least-squares fitting of 2θ angles for 25 reflections. Crystal stability was monitored by recording three check reflections at intervals of 150 data measurements, and no significant variation was detected. The raw data were processed with a learnt-profile procedure [32], and empirical absorption corrections based on ψ-scan data were also applied.

All calculations were performed on a PC 486 computer with the SHELXTL-PC program package [33]. Each crystal structure was solved with the Patterson superposition method. The non-hydrogen atoms were refined anisotropically, except for the oxygen atoms of the slightly disordered perchlorate groups in complexes **1–4,** which were subjected to interatomic distance constraints of Cl—O 1.42 ± 0.01 Å and O···O 2.31 ± 0.02 Å and refined isotropically. All the hydrogen atoms were generated geometrically (C—H = 0.96 Å), assigned fixed isotropic thermal parameters and included in the structure factor calculations. Analytical expressions of neutral-atom scattering factors were employed, and anomalous dispersion corrections were incorporated [34]. Selected bond lengths and angles are given in Table 2.

Additional material deposited at the Cambridge Crystallographic Data Centre comprises atom coordinates, thermal parameters and remaining bond lengths and angles.

Table 1. Data collection and processing parameters for complexes **1–4**

Complex	**1**	**2**	**3**	**4**
Formula	$C_{22}H_{48}NdCl_3N_4O_{22}$	$C_{24}H_{54}NdCl_3N_4O_{23}$	$C_{22}H_{50}ErCl_3N_4O_{23}$	$C_{24}H_{52}ErCl_3N_4O_{22}$
M	971.2	1017.3	1012.3	1022.3
Colour, habit	Pink prism	Pink block	Pale pink prism	Pale pink prism
Crystal size/mm	$0.06 \times 0.10 \times 0.22$	$0.10 \times 0.18 \times 0.20$	$0.06 \times 0.18 \times 0.38$	$0.16 \times 0.18 \times 0.34$
Crystal system	Monoclinic	Triclinic	Monoclinic	Triclinic
Space group	$P2_1/c$ (No. 14)	$P\bar{1}$ (No. 2)	$P2_1/c$ (No. 14)	$P\bar{1}$ (No. 2)
a/Å	12.567(1)	12.002(6)	13.752(1)	11.975(2)
b/Å	26.352(1)	13.596(5)	25.617(1)	12.873(3)
c/Å	11.834(1)	14.911(6)	12.171(1)	13.395(3)
α/°	90	114.64(3)	90	78.36(3)
β/°	92.97(2)	106.34(4)	112.42(2)	75.30(3)
γ/°	90	96.29(4)	90	81.79(3)
U/Å^3	3914(2)	2049.3(16)	3964(2)	1947.1(10)
Z	4	2	4	2
$F(000)$	1980	1042	2052	1038
D(calcd)/g cm^{-3}	1.648	1.649	1.696	1.744
μ/mm^{-1}	1.62	1.55	2.41	2.45
Collection range; $2\theta_{max}$	$\pm h, \pm k, l$; 45°	$h, \pm k, \pm l$; 46°	$\pm h, \pm k, l$; 45°	$\pm h, -k, \pm l$; 45°
Unique data measured	7335	5691	8089	7525
Observed data, n	6714 [$F \geqslant 6\sigma(F)$]	4324 [$F \geqslant 4\sigma(F)$]	6301 [$F \geqslant 6\sigma(F)$]	6956 [$F \geqslant 6\sigma(F)$]
No. of variables, p	505	492	515	524
R	0.047	0.051	0.056	0.040
R'	0.079	0.050	0.072	0.060
S (goodness-of-fit)	1.91	1.41	1.95	1.64
Residual extremes in final difference map/e Å^{-3}	+0.83, −1.19 +0.89, −1.07	+1.91, −1.46	+1.62, −0.89	

$R = \Sigma\Delta/\Sigma|F_o|$, $R' = [\Sigma\omega\Delta^2/\Sigma\omega|F_o|^2]^{1/2}$ and $S = [\Sigma\omega\Delta^2/(n-p)]^{1/2}$ where $\omega = [\sigma^2(F_o) + K|F_o|^2]^{-1}\Delta = ||F_o| - |F_c||$, $10^4 K = 10$, 2, 4 and 8 for complexes **1, 2, 3** and **4,** respectively.

Table 2. Selected interatomic distances (Å) and angles (°) for complexes **1**–**4**

$[\{Nd(L^1)_2(H_2O)_2\}_n][ClO_4]_{3n}$ **1**			
Nd(1)—O(1)	2.459(3)	Nd(1)—O(5)	2.772(3)
Nd(1)—O(6)	2.554(3)	Nd(1)—O(1W)	2.541(3)
Nd(1)—O(2W)	2.527(4)	Nd(1)—O(2a)	2.453(3)
Nd(1)—O(3c)	2.407(3)	Nd(1)—O(5a)	2.424(3)
Nd(1)—O(7b)	2.435(4)	O(1)—C(1)	1.246(5)
O(2)—C(1)	1.248(5)	C(1)—C(2)	1.531(6)
C(2)—N(1)	1.517(5)	N(1)—C(3)	1.506(5)
C(11)—O(3)	1.225(6)	C(11)—O(4)	1.231(6)
O(5)—C(12)	1.262(5)	O(6)—C(12)	1.226(5)
C(12)—C(12)	1.527(6)	C(13)—N(3)	1.511(6)
N(3)—C(15)	1.496(6)	N(3)—C(16)	1.512(6)
C(22)—O(7)	1.266(6)	C(22)—O(8)	1.231(6)
Nd(1)···Nd(1a)	4.243(3)		
O(1)—Nd(1)—O(5)	66.4(1)	O(1)—Nd(1)—O(6)	83.6(1)
O(1)—Nd(1)—O(5a)	74.1(1)	O(2a)—Nd(1)—O(5a)	73.7(1)
O(5)—Nd(1)—O(6)	48.2(1)	O(5)—Nd(1)—O(2a)	67.5(1)
O(6)—Nd(1)—O(2a)	79.7(1)	O(1W)—Nd(1)—O(3c)	72.0(1)
O(2W)—Nd(1)—O(3c)	73.3(1)	O(5)—Nd(1)—O(5a)	70.7(1)
O(1W)—Nd(1)—O(7b)	73.0(1)	O(2W)—Nd(1)—O(7b)	66.9(1)
Nd(1)—O(1)—C(1)	139.4(3)	C(1)—O(2)—Nd(1a)	137.6(3)
O(1)—C(1)—O(2)	128.1(4)	O(1)—C(1)—C(2)	111.8(3)
O(2)—C(1)—C(2)	120.0(4)	C(1)—C(2)—N(1)	118.2(3)
C(2)—N(1)—C(3)	110.9(3)	C(2)—N(1)—C(4)	111.1(3)
C(3)—N(1)—C(4)	110.0(3)	C(2)—N(1)—C(5)	107.6(3)
C(3)—N(1)—C(5)	109.9(3)	C(4)—N(1)—C(5)	107.2(3)
N(1)—C(5)—C(6)	113.6(3)	C(5)—C(6)—C(7)	106.8(3)
C(6)—C(7)—N(2)	113.6(3)	C(7)—N(2)—C(8)	109.3(3)
C(7)—N(2)—C(9)	105.7(3)	C(8)—N(2)—C(9)	111.6(4)
C(7)—N(2)—C(10)	110.3(3)	C(8)—N(2)—C(10)	110.1(3)
C(9)—N(2)—C(10)	109.7(4)	N(2)—C(10)—C(11)	116.7(3)
C(10)—C(11)—O(3)	120.1(4)	C(10)—C(11)—O(4)	113.2(4)
O(3)—C(11)—O(4)	126.7(5)	C(11c)—O(3c)—Nd(1)	145.7(3)
Nd(1)—O(5)—C(12)	88.5(2)	Nd(1)—O(5)—Nd(1a)	109.3(1)
C(12)—O(5)—Nd(1a)	160.4(3)	Nd(1)—O(6)—C(12)	99.8(3)
O(5)—C(12)—O(6)	122.7(4)	O(5)—C(12)—C(13)	114.1(4)
O(6)—C(12)—C(13)	123.1(4)	C(12)—C(13)—N(3)	117.1(4)
C(13)—N(3)—C(14)	105.9(4)	C(13)—N(3)—C(15)	110.5(4)
C(14)—N(3)—C(15)	111.1(4)	C(13)—N(3)—C(16)	108.2(4)
C(14)—N(3)—C(16)	109.2(4)	C(15)—N(3)—C(16)	111.7(4)
N(3)—C(16)—C(17)	114.8(4)	C(16)—C(17)—C(18)	111.8(5)
C(17)—C(18)—N(4)	114.2(5)	C(18)—N(4)—C(19)	111.3(5)
C(18)—N(4)—C(20)	109.4(4)	C(19)—N(4)—C(20)	108.2(5)
C(18)—N(4)—C(21)	110.8(4)	C(19)—N(4)—C(21)	106.8(4)
C(20)—N(4)—C(21)	110.3(4)	N(4)—C(21)—C(22)	118.8(4)
C(21)—C(22)—O(7)	111.6(4)	C(21)—C(22)—O(8)	120.6(5)
O(7)—C(22)—O(8)	127.7(5)	C(22b)—O(7b)—Nd(1)	142.4(3)

Table 2.—*Continued.*

Hydrogen bonding:			
O(2w)···O(9)	2.875(7)	O(2w)···O(11)	2.783(7)
$[\{Nd(L^2)(H_2O)_2\}_n][ClO_4]_{3n}\cdot nH_2O$ **2**			
Nd(1)—O(1)	2.390(5)	Nd(1)—O(5)	2.448(4)
Nd(1)—O(7)	2.435(3)	Nd(1)—O(1W)	2.492(4)
Nd(1)—O(2W)	2.583(4)	Nd(1)—O(2a)	2.497(5)
Nd(1)—O(3b)	2.425(5)	Nd(1)—O(8a)	2.445(3)
O(1)—C(1)	1.247(7)	O(2)—C(1)	1.239(6)
O(3)—C(12)	1.252(8)	O(4)—C(12)	1.233(5)
C(11)—C(12)	1.540(6)	O(5)—C(13)	1.265(8)
O(6)—C(13)	1.251(5)	N(3)—C(14)	1.502(5)
C(17)—C(18)	1.511(5)	C(18)—C(18e)	1.548(11)
O(7)—C(19)	1.253(6)	O(8)—C(19)	1.252(6)
C(24)—C(24d)	1.521(7)	Nd(1)···Nd(1a)	4.376(3)
O(1)—Nd(1)—O(7)	74.7(1)	O(5)—Nd(1)—O(1W)	72.9(2)
O(5)—Nd(1)—O(2W)	69.6(1)	O(7)—Nd(1)—O(2a)	81.8(1)
O(1W)—Nd(1)—O(3b)	70.4(1)	O(2W)—Nd(1)—O(3b)	71.4(2)
O(1)—Nd(1)—O(8a)	73.2(1)	O(2a)—Nd(1)—O(8a)	77.7(1)
Nd(1)—O(1)—C(1)	166.9(3)	C(1)—O(2)—Nd(1a)	107.9(4)
C(12c)—O(3c)—Nd(1a)	142.4(3)	C(2)—N(1)—C(3)	106.6(4)
C(2)—N(1)—C(4)	109.5(3)	C(3)—N(1)—C(4)	109.6(4)
C(2)—N(1)—C(5)	109.5(4)	C(3)—N(1)—C(5)	108.3(3)
C(4)—N(1)—C(5)	113.2(4)	C(8)—N(2)—C(9)	110.3(4)
C(8)—N(2)—C(10)	107.4(4)	C(9)—N(2)—C(10)	107.8(4)
C(8)—N(2)—C(11)	112.9(4)	C(9)—N(2)—C(11)	107.3(3)
C(10)—N(2)—C(11)	111.0(4)	O(1)—C(1)—O(2)	123.6(5)
O(1)—C(1)—C(2)	114.7(4)	O(2)—C(1)—C(2)	121.6(5)
N(1)—C(2)—C(1)	117.4(4)	N(1)—C(5)—C(6)	115.1(5)
C(5)—C(6)—C(7)	114.5(4)	C(6)—C(7)—C(8)	110.3(4)
N(2)—C(8)—C(7)	115.9(4)	N(2)—C(11)—C(12)	116.8(3)
O(3)—C(12)—O(4)	127.5(4)	O(3)—C(12)—C(11)	109.9(3)
O(4)—C(12)—C(11)	122.6(5)	Nd(1)—O(5)—C(13)	140.4(3)
C(14)—N(3)—C(15)	110.6(3)	C(14)—N(3)—C(16)	105.6(4)
C(15)—N(3)—C(16)	107.9(4)	C(14)—N(3)—C(17)	110.6(4)
C(15)—N(3)—C(17)	111.6(4)	C(16)—N(3)—C(17)	110.3(3)
O(5)—C(13)—O(6)	125.9(4)	O(5)—C(13)—C(14)	120.3(3)
O(6)—C(13)—C(14)	113.9(5)	N(3)—C(14)—C(13)	118.7(5)
N(3)—C(17)—C(18)	115.5(4)	C(17)—C(18)—C(18e)	110.5(4)
Nd(1)—O(7)—C(19)	138.9(3)	C(19)—O(8)—Nd(1a)	141.6(3)
C(20)—N(4)—C(21)	110.3(4)	C(20)—N(4)—C(22)	110.6(4)
C(21)—N(4)—C(22)	109.2(4)	C(20)—N(4)—C(23)	109.2(4)
C(21)—N(4)—C(23)	108.0(4)	C(22)—N(4)—C(23)	109.5(4)
O(7)—C(19)—O(8)	128.3(3)	O(7)—C(19)—C(20)	112.2(4)
O(8)—C(19)—C(20)	119.5(4)	N(4)—C(20)—C(19)	118.1(4)
N(4)—C(23)—C(24)	115.1(4)	C(23)—C(24)—C(24d)	110.2(5)

Table 2.—*Continued.*

Hydrogen bonding:			
O(3w)···O(2w)	2.815(7)	O(1w)···O(14)	2.880(7)
$[\{Er(L^1)(H_2O)_2\}_n][ClO_4]_{3n}\cdot nH_2O$ **3**			
Er(1)—O(1)	2.289(4)	Er(1)—O(5)	2.291(4)
Er(1)—O(1W)	2.409(3)	Er(1)—O(2W)	2.470(3)
Er(1)—O(3b)	2.347(3)	Er(1)—O(4c)	2.338(3)
Er(1)—O(7d)	2.343(3)	Er(1)—O(8e)	2.264(4)
O(1)—C(1)	1.256(5)	O(2)—C(1)	1.230(5)
C(1)—C(2)	1.521(7)	C(2)—N(1)	1.516(5)
C(11)—O(3)	1.260(5)	C(11)—O(4)	1.245(4)
O(5)—C(12)	1.184(5)	O(6)—C(12)	1.314(5)
C(22)—O(7)	1.253(3)	C(22)—O(8)	1.236(5)
Er(1)···Er(1a)	4.423(4)		
O(1)—Er(1)—O(1W)	72.8(1)	O(5)—Er(1)—O(1W)	69.3(1)
O(1)—Er(1)—O(2W)	71.9(1)	O(5)—Er(1)—O(2W)	73.0(1)
O(3b)—Er(1)—O(7d)	76.6(1)	O(4c)—Er(1)—O(7d)	76.3(1)
O(3b)—Er(1)—O(8e)	74.2(1)	O(4c)—Er(1)—O(8e)	75.9(1)
Er(1)—O(1)—C(1)	147.1(3)	O(1)—C(1)—O(2)	125.1(5)
O(1)—C(1)—C(2)	120.9(3)	O(2)—C(1)—C(2)	114.0(4)
C(1)—C(2)—N(1)	117.6(3)	C(2)—N(1)—C(3)	111.5(3)
C(2)—N(1)—C(4)	111.5(3)	C(3)—N(1)—C(4)	108.2(3)
C(2)—N(1)—C(5)	108.7(3)	C(3)—N(1)—C(5)	106.9(3)
C(4)—N(1)—C(5)	110.0(3)	N(1)—C(5)—C(6)	114.6(3)
C(5)—C(6)—C(7)	109.2(3)	C(6)—C(7)—N(2)	113.6(3)
C(7)—N(2)—C(8)	109.0(3)	C(7)—N(2)—C(9)	107.4(3)
C(8)—N(2)—C(9)	110.5(3)	C(7)—N(2)—C(10)	107.9(3)
C(8)—N(2)—C(10)	112.0(3)	C(9)—N(2)—C(10)	109.9(3)
N(2)—C(10)—C(11)	118.5(3)	C(10)—C(11)—O(3)	120.3(3)
C(10)—C(11)—O(4)	111.8(3)	O(3)—C(11)—O(4)	127.8(4)
C(11c)—O(3c)—Er(1a)	139.3(3)	C(11c)—O(4c)—Er(1)	143.9(3)
Er(1)—O(5)—C(12)	158.2(4)	O(5)—C(12)—O(6)	115.9(4)
O(5)—C(12)—C(13)	120.2(4)	O(6)—C(12)—C(13)	119.1(4)
C(12)—C(13)—N(3)	127.7(3)	C(13)—N(3)—C(14)	116.1(3)
C(13)—N(3)—C(15)	100.0(2)	C(14)—N(3)—C(15)	95.7(4)
C(13)—N(3)—C(16)	116.4(4)	C(14)—N(3)—C(16)	119.6(3)
C(15)—N(3)—C(16)	102.6(3)	N(3)—C(16)—C(17)	117.8(4)
C(16)—C(17)—C(18)	109.0(4)	C(17)—C(18)—N(4)	115.3(4)
C(18)—N(4)—C(19)	112.5(2)	C(18)—N(4)—C(20)	108.1(3)
C(19)—N(4)—C(20)	108.8(4)	C(18)—N(4)—C(21)	109.2(4)
C(19)—N(4)—C(21)	110.9(3)	C(20)—N(4)—C(21)	107.2(2)
N(4)—C(21)—C(22)	116.8(2)	C(21)—C(22)—O(7)	121.1(4)
C(21)—C(22)—O(8)	113.6(2)	O(7)—C(22)—O(8)	125.3(3)
C(22d)—O(7d)—Er(1)	119.3(3)	C(22d)—O(8d)—Er(1a)	168.6(3)

Table 2.—*Continued.*

Hydrogen bonding:			
O(2W)···O(2)	2.719(7)	O(2W)···O(6)	2.909(7)
$[\{Er(L^2)_2(H_2O)_2\}_n][ClO_4]_{3n}\cdot nH_2O$ **4**			
Er(1)—O(1)	2.488(4)	Er(1)—O(2)	2.418(4)
Er(1)—O(5)	2.329(3)	Er(1)—O(1W)	2.360(4)
Er(1)—O(3c)	2.321(3)	Er(1)—O(4d)	2.323(4)
Er(1)—O(6a)	2.266(4)	Er(1),O(7b)	2.289(3)
O(1)—C(1)	1.252(6)	O(2)—C(1)	1.252(6)
O(3)—C(12)	1.241(6)	O(4)—C(12)	1.257(7)
O(5)—C(13)	1.239(6)	O(6)—C(13)	1.256(7)
O(7)—C(24)	1.265(7)	O(8)—C(24)	1.231(8)
N(1)—C(2)	1.507(7)	C(23)—C(24)	1.518(6)
Er(1)···Er(1a)	4.492(3)		
O(1)—Er(1)—O(2)	53.2(1)	O(2)—Er(1)—O(1W)	73.7(1)
O(5)—Er(1)—O(3c)	73.8(1)	O(5)—Er(1)—O(4d)	75.8(1)
O(3c)—Er(1)—O(6a)	77.6(1)	O(4d)—Er(1)—O(6a)	76.2(1)
O(1)—Er(1)—O(7b)	72.5(1)	O(1W)—Er(1)—O(7b)	79.0(1)
Er(1)—O(1)—C(1)	90.1(3)	Er(1)—O(2)—C(1)	93.3(3)
C(12c)—O(3c)—Er(1)	148.4(3)	C(12c)—O(4c)—Er(1a)	135.3(3)
Er(1)—O(5)—C(13)	134.4(4)	C(13)—O(6)—Er(1a)	152.7(3)
C(24b)—O(7b)—Er(1)	128.8(3)	C(2)—N(1)—C(3)	109.5(4)
C(2)—N(1)—C(4)	107.6(4)	C(3)—N(1)—C(4)	107.7(4)
C(2)—N(1)—C(5)	114.3(4)	C(3)—N(1)—C(5)	107.9(4)
C(4)—N(1)—C(5)	109.7(4)	C(8)—N(2)—C(9)	106.4(4)
C(8)—N(2)—C(10)	109.4(4)	C(9)—N(2)—C(10)	109.0(4)
C(8)—N(2)—C(11)	109.1(4)	C(9)—N(2)—C(11)	110.8(4)
C(10)—N(2)—C(11)	112.0(4)	C(14)—N(3)—C(15)	111.6(4)
C(14)—N(3)—C(16)	110.3(4)	C(15)—N(3)—C(16)	109.6(4)
C(14)—N(3)—C(17)	105.7(4)	C(15)—N(3)—C(17)	109.8(4)
C(16)—N(3)—C(17)	109.8(4)	C(20)—N(4)—C(21)	109.8(4)
C(20)—N(4)—C(22)	108.3(4)	C(21)—N(4)—C(22)	108.0(4)
C(20)—N(4)—C(23)	112.1(4)	C(21)—N(4)—C(23)	107.4(4)
C(22)—N(4)—C(23)	111.1(4)	O(1)—C(1)—O(2)	122.7(5)
O(1)—C(1)—C(2)	115.2(4)	O(2)—C(1)—C(2)	122.2(4)
N(1)—C(2)—C(1)	118.1(4)	N(1)—C(5)—C(6)	115.9(4)
C(5)—C(6)—C(7)	108.2(4)	C(6)—C(7)—C(8)	112.4(4)
N(2)—C(8)—C(7)	113.4(4)	N(2)—C(11)—C(12)	118.3(4)
O(3)—C(12)—O(4)	127.7(4)	O(3)—C(12)—C(11)	120.3(5)
O(4)—C(12)—C(11)	112.1(4)	O(5)—C(13)—O(6)	127.4(4)
O(5)—C(13)—C(14)	121.0(5)	O(6)—C(13)—C(14)	111.6(4)
N(3)—C(14)—C(13)	117.5(4)	N(3)—C(17)—C(18)	116.2(4)
C(17)—C(18)—C(19)	109.2(5)	C(18)—C(19)—C(20)	109.3(5)
N(4)—C(20)—C(19)	115.3(5)	N(4)—C(23)—C(24)	117.5(4)
O(7)—C(24)—O(8)	125.1(4)	O(7)—C(24)—C(23)	119.8(5)
O(8)—C(24)—C(23)	115.0(5)		
Hydrogen bonding:			
O(2W)···O(11′)	2.912(7)	O(1W)···O(8)	2.726(7)

Symmetry codes.

for **1**: (a) $-1-x, -y, -2-z$; (b) $-1-x, -y, -1-z$; (c) $x, 0.5-y, 0.5+z$; (d) $x, y, -1+z$; (e) $-1-x, -0.5+y, -2.5-z$.

For **2**: (a) $1-x, 1-y, 1-z$; (b) $1+x, y, z$; (c) $-x, 1-y, 1-z$; (d) $1-x, -y, -z$; (e) $-x, -y, -z$.

For **3**: (a) $-x, -y, -z$; (b) $-x, -0.5+y, -z$; (c) $x, 0.5-y, -0.5+z$; (d) $-x, -y, 1-z$; (e) $x, y, -1+z$.

For **4**: (a) $-x, 1-y, -z$; (b) $-x, 2-y, -z$; (c) $-x, 1-y, 1-z$; (d) $x, y, -1+z$; (e) $x, 1+y, z$.

RESULTS AND DISCUSSION

Crystal structure of $[\{Nd(L^1)_2(H_2O)_2\}_n][ClO_4]_{3n}$ (**1**)

Complex **1** comprises discrete perchlorate anions and a two-dimensional cationic polymeric layer containing tetrakis(carboxylato-*O*,*O*′)-bridged centrosymmetric dimeric subunits. As illustrated in Fig. 1a, four carboxylato groups from respective L^1 ligands link a pair of neodymium(III) atoms in the *O*,*O*′-bridging mode to generate a paddle-wheel-like centrosymmetric [Nd_2(carboxylato-*O*,*O*′)$_4$] dimer. The Nd···Nd separation [4.243(3) Å] is significantly shorter than that [4.315 Å] in $[\{Nd(ClCH_2CO_2)_3\}_3(H_2O)_5]_n$ [7]. Each neodymium atom is coordinated by seven carboxylato oxygen atoms from L^1 ligands and two aqua ligands in a nine-coordinate environment. The carboxylato groups are involved in three different coordination modes: a common bidentate bridging mode in the *syn–syn* configuration [C(1)—O(1)—Nd(1), 139.4(3) and C(1)—O(2)—Nd(1a) 137.6(3)°], a unidentate mode [C(11c)—O(3c)—Nd(1), 145.7(3) and C(22b)—O(7b)—Nd(1), 142.4(3)°], as well as an unusual tridentate bridging coordination mode [C(12)—O(6)—Nd(1), 99.8(3), C(12)—O(5)—Nd(1), 88.5(2) and C(12)—O(5)—Nd(1a), 160.4(3)°] in which the Nd(1)—O(5) distance [2.772(3) Å] is much longer than those of Nd(1)—O(6) [2.554(3) Å] and Nd(1a)—O(5) [2.424(3) Å] bonds. This latter coordination mode involves both *syn–syn* and *syn–anti* bridging and is rarely encountered in betaine lanthanide complexes with two- and three-dimensional polymeric networks, although the bridging tridentate carboxylato group is known in chloroacetate lanthanide complexes, which adopt infinite chain structures [7]. The coordination geometry about the neodymium atom may be described as a distorted NdO_9 monocapped, square antiprism as shown in Fig. 2a. One square face comprises four carboxylato oxygen atoms [O(1), O(5a), O(2a) and O(6)] with large mean deviation (0.117 Å) from the least-squares plane, whereas the other face as defined by two carboxylato oxygen atoms [O(3b) and O(7c)] and two aqua oxygen atoms [O(1w) and O(2w)] having a mean deviation of 0.041 Å from the least-squares plane. The dihedral angle between the square faces is *ca* 6.7°. The Nd—O distances vary from 2.407(3) to 2.772(3) Å, among which the shortest one is associated with the unidentate bridging carboxylato oxygen atom, and the longest one with the tridentate bridging carboxylato oxygen atom.

The molecular backbone of each of the two independent, flexible, double betaine ligands is extended to achieve a longer separation between its two quaternary nitrogen atoms. The conformation of the double betaine is similar to that in its hydrated form [27], but different from that in its mercury adduct, in which the symmetry of the molecular backbone of L^1 has a C_2-axis at the middle methylene carbon atom [24]. A perspective view of complex **1** is shown in Fig. 1b, where the dimeric subunits are extended into a polymeric chain running along the *c*-direction. Such chains are further cross-linked by the molecular skeleton of the double betaine ligand, thereby extending the structure into a plane wave-like layer corresponding to the plane [200]. The crystal structure is built up by a packing of these layers such that the perchlorate groups (one of which exhibits orientational disorder and forms an acceptor hydrogen bond [O(2w)···O(9) 2.875(7) Å] with one coordinated aqua oxygen atom [O(2w)]) are accommodated in the interlayer regions.

Crystal structure of $[\{Nd(L^2)_2(H_2O)_2\}_n][ClO_4]_{3n} \cdot nH_2O$ (**2**)

There are one complete and two half molecules of L^2 in the asymmetric unit of complex **2**. The resulting dimeric moiety is similar to that in complex **1**, being also a paddle-wheel-like structure based on tetrakis(carboxylato-*O*,*O*′) bridging (Fig. 3a). However, the neodymium(III) atom is coordinated by six carboxylato oxygen atoms from L^2 ligands and two aqua ligands in an eight-coordinate environment, being different from that of complex **1**. As shown in Fig. 2b, the coordination geometry about the neodymium atom in complex **2** may be described as a square antiprism with Nd—O distances in the range of 2.390(5) to 2.583(4) Å. The upper square face consists of two carboxylato oxygen atoms [O(3b) and O(5)] and two aqua oxygen atoms [O(1w) and O(2w)] with negligible mean deviation (0.005 Å) from the least-squares plane. The lower face is defined by oxygen atoms [O(1), O(7), O(2a) and O(8a)] from four carboxylato groups of L^2 ligands with a mean deviation of 0.078 Å from the least-squares plane. The dihedral angle between the square face is *ca* 3.4°.

Unlike complex **1**, in which the carboxylato groups exhibit three different coordination modes (unidentate, bidentate bridging and tridentate bridging), the carboxylato groups in complex **2** functions only in the unidentate [C(12c)—O(3c)—Nd(1a), 142.4(3) and C(13)—O(5)—Nd(1), 140.4(3)°] and bidentate bridging modes [C(1)—O(1)—Nd(1), 166.9(3), C(1)—O(2)—Nd(1a), 107.9(4), C(19)—O(7)—Nd(1), 138.9(3) and C(19)—O(8)—Nd(1a), 141.6(3)°]. Coexistence of uni- and bidentate modes has been found in some dimeric lanthanide carboxylates [28]. The Nd···Nd separation [4.376(3) Å] is comparable to that in $[\{Nd(ClCH_2CO_2)_3\}_3(H_2O)_5]_n$ [7] but is significantly longer than that in complex **1**. It is noteworthy that the conformations of the independent double betaine ligands are different: two ligands each have an inversion centre located between the two middle methylene carbons, being similar to that in its hydrated form [27] but different from that in its mercury adduct, in which the molecular backbone of L^2 has a C_2-axis [24], but the other ligand has no crystallographically imposed symmetry. A perspective view of complex **2** (Fig. 3b) shows that col-

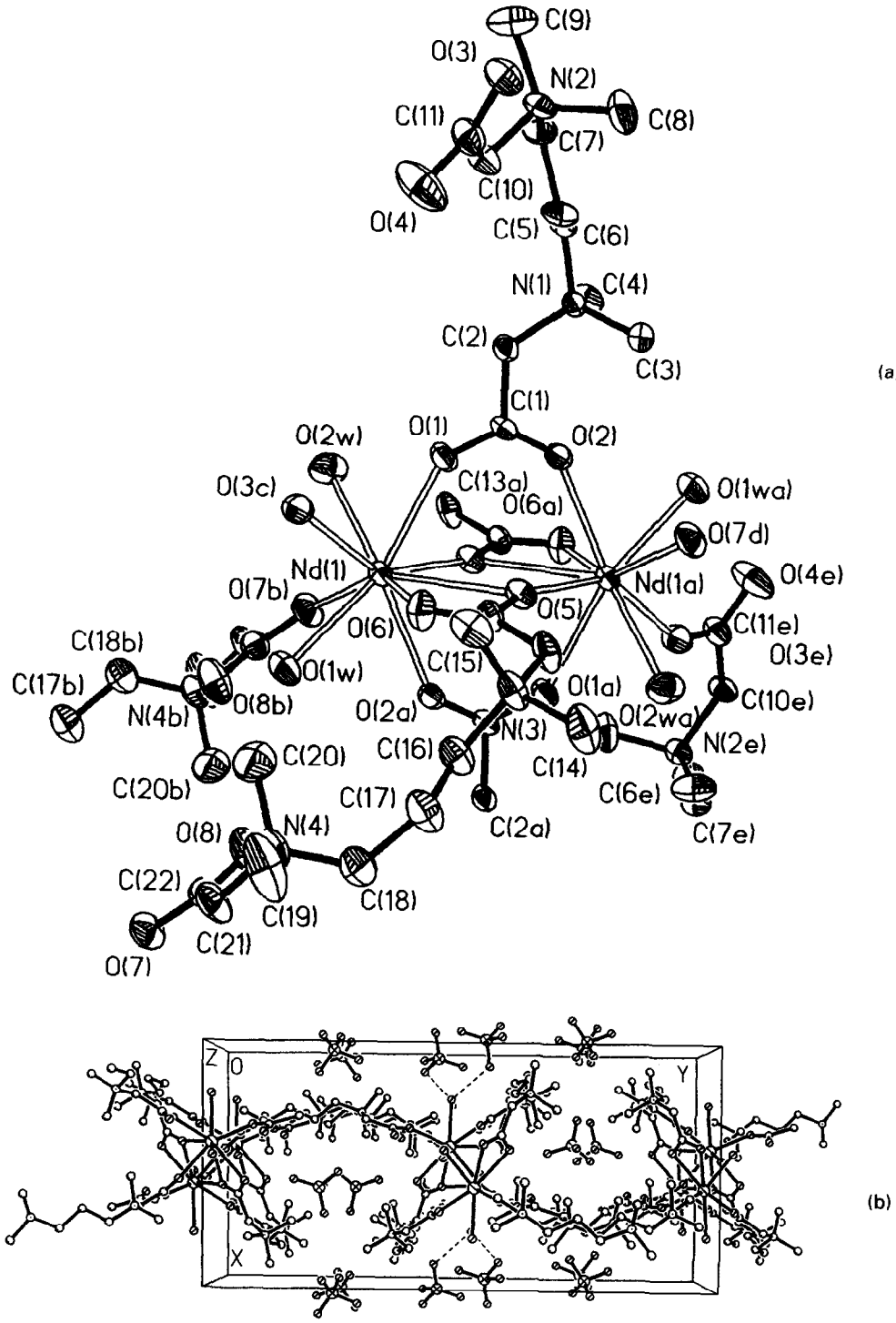


Fig. 1. (a) Structural skeleton of the asymmetric unit (35% thermal ellipsoid) of $[\{Nd(L^1)_2(H_2O)_2\}_n][ClO_4]_{3n}$ (**1**) with atom labelling. (b) Packing drawing showing the plane wave-like layer structure corresponding to [200] in the crystal structure of **1**.

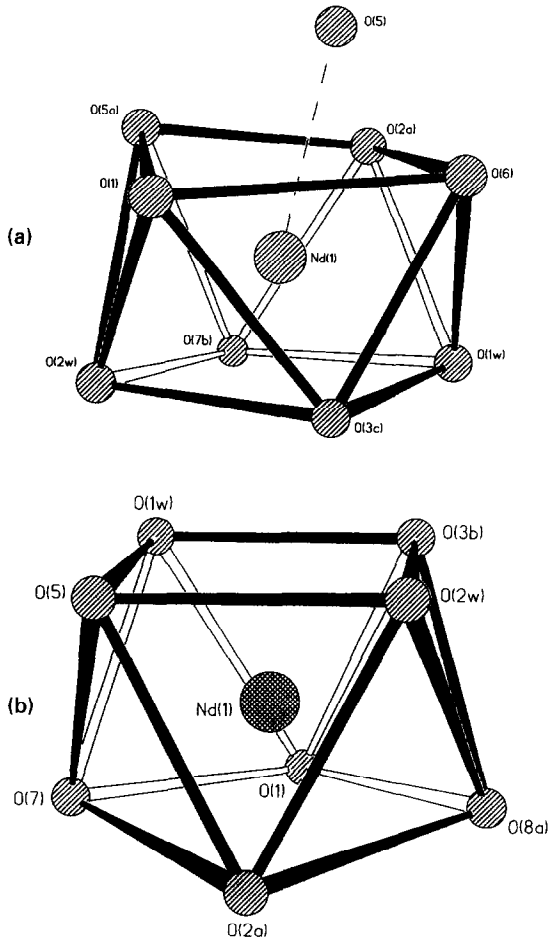


Fig. 2. Perspective view showing the coordination polyhedron about (a) the neodymium(III) atom in **1** and (b) the neodymium(III) and erbium(III) atoms in **2**, **3** and **4**.

umns of paddle-wheel-like dimeric subunits [Nd_2(carboxylato-*O*,*O*′)$_4$] stacked parallel to the *a* direction are cross linked by the double betaine skeletons to generate a two-dimensional polymeric network corresponding to the [01$\bar{1}$] plane. The perchlorate groups, one of which forms an acceptor hydrogen bond [O(1w)···O(14), 2.880(7) Å] with an aqua ligand oxygen atom [O(1w)], occupy the interlayer regions. The lattice water molecule [O(3w)] forms a hydrogen bond [O(3w)···O(2w), 2.815 Å] with the other aqua oxygen atom [O(2w)].

Crystal structure of [{Er(L^1)$_2$(H$_2$O)$_2$}$_n$][ClO$_4$]$_{3n}$·nH$_2$O (**3**)

Complex **3** comprises discrete perchlorate anions and a two-dimensional cationic polymeric layer containing tetrakis (*μ*-carboxylato-*O*,*O*′)-bridged centrosymmetric dimeric subunits (Fig. 4a). In the dimeric subunit, four carboxylato groups from respective L^1 ligands oriented nearly perpendicular to each other about the Er···Er direction bridge the metal centers in a *syn–syn* manner to yield a paddle-wheel-like [Er_2(carboxylato-*O*,*O*′)$_4$] dimer. The Er(1)···Er(1a) separation is 4.423(4) Å, and the erbium(III) atom in the present complex is coordinated by eight oxygen atoms from four bidentate L^1, two monodentate L^1 and two aqua ligands in a square-antiprismatic environment. One square face consists of two carboxylato oxygen atoms [O(1) and O(5)] and two aqua oxygen atoms [O(1w) and O(2w)] with a mean deviation 0.0704 Å from the least-squares plane. The other face is defined by oxygen atoms [O(3b), O(4c), O(7d) and O(8e)] from four carboxylato groups of L^1 ligands with a mean deviation 0.0249 Å from the least-squares plane. The dihedral angle between the square faces is *ca* 2.5°.

The Er—O distances lie between 2.264(4) and 2.470(3) Å, which are comparable to those found for other related erbium(III) complexes [6,35]. The carboxylato ligands around the erbium atom not only act in the bidentate bridging mode [C(11c)—O(3c)—Er(1a), 139.3(3), C(11c)—O(4c)—Er(1), 143.9(3), C(22d)—O(7d)—Er(1), 119.3(3) and C(22d)—O(8d)—Er(1a), 168.6(3)°], but also in the unidentate mode [C(1)—O(1)—Er(1), 147.1(3) and C(12)—O(5)—Er(1), 158.2(4)°], being similar to that in complex **2**. The extended conformation of the flexible double betaine skeleton is similar to that in complex **1**. Intramolecular hydrogen bonds [O(2)···O(2w) 2.719(7) and O(6)···O(2w) 2.909(7) Å] between the uncoordinated oxygen atoms [O(2) and O(6)] of the two unidentate carboxylato groups and one of the aqua ligands [O(2w)] are formed (Fig. 4a). A perspective view of complex **3** is given in Fig. 4b, showing a wavy polymeric layer network corresponding to the plane [100]. The crystal structure is built up by a packing of these infinite layers such that the interlayer interactions are mainly of the van der Waal's type. The perchlorate groups, having no contact with the metal ions, are packed between the layers.

Crystal structure of [{Er(L^2)$_2$(H$_2$O)}$_n$][ClO$_4$]$_{3n}$·nH$_2$O (**4**)

Complex **4** is a coordination polymer featuring a centrosymmetric tetrakis(carboxylato-*O*,*O*′)-bridged dimer similar to those of **1**–**3**. The Er···Er separation [4.492(3) Å] in the dimer is comparable to that in complex **3**. As shown in Fig. 5a, the erbium atom is coordinated by seven carboxylato oxygen atoms from L^2 ligands and one aqua oxygen atom in a square-antiprismatic geometry similar to that in complexes **2** and **3**, with Er—O bond distances lying in the range of 2.266(4) to 2.488(4) Å. The mean deviations of the sets of oxygen atoms [O(3c), O(4d), O(5), O(6a) and O(1), O(2), O(7b), O(1w)] from their least-squares planes are 0.001 and 0.099 Å, respectively. The dihedral angle between the least-squares planes is *ca* 4.5°.

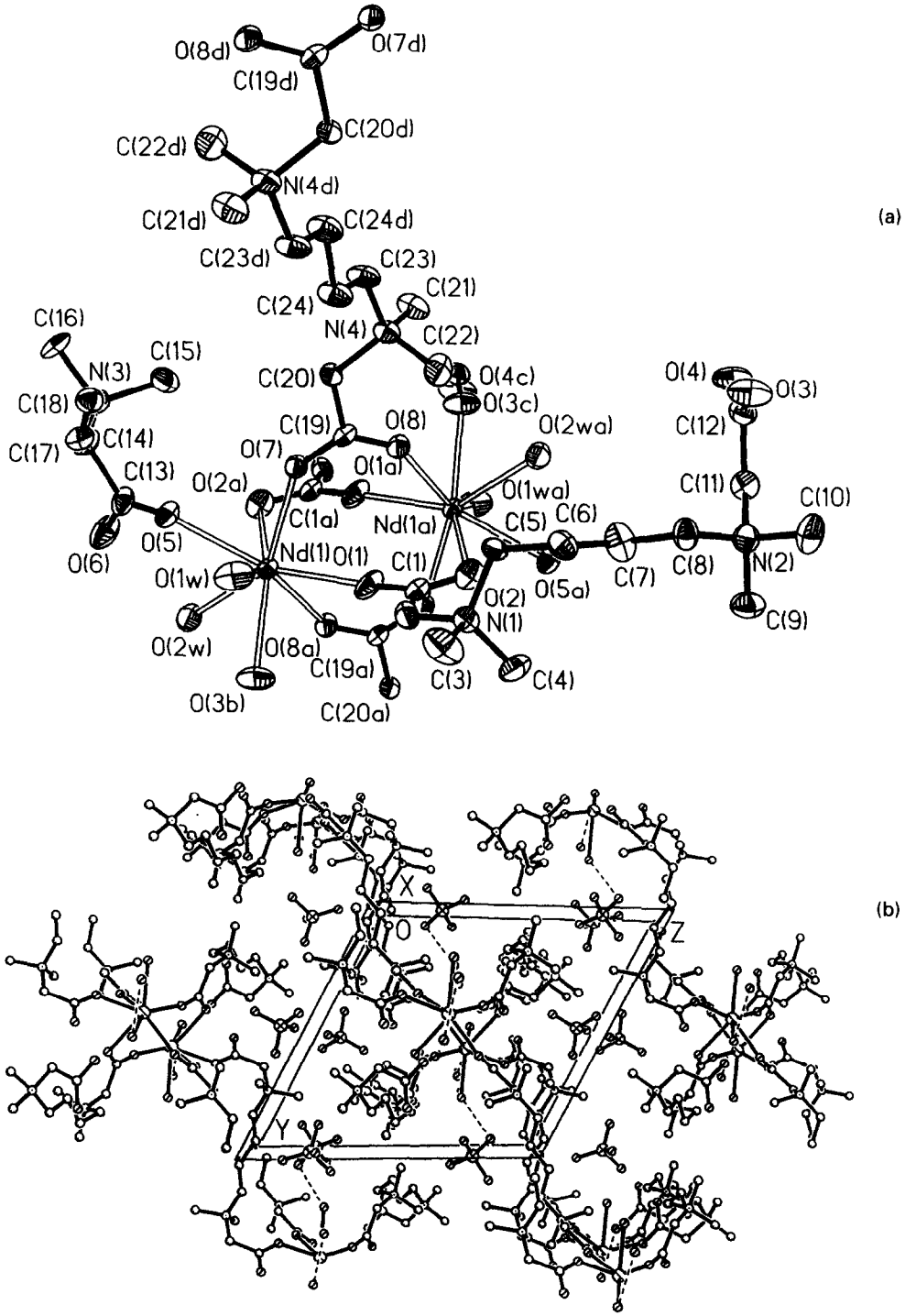


Fig. 3. (a) Structural skeleton of the asymmetric unit (35% thermal ellipsoid) of $[\{Nd(L^2)_2(H_2O)_2\}_n][ClO_4]_{3n} \cdot nH_2O$ (**2**) with atom labelling. (b) Packing drawing showing the plane wave-like layer structure corresponding to [01$\bar{1}$] in the crystal structure of **2**.

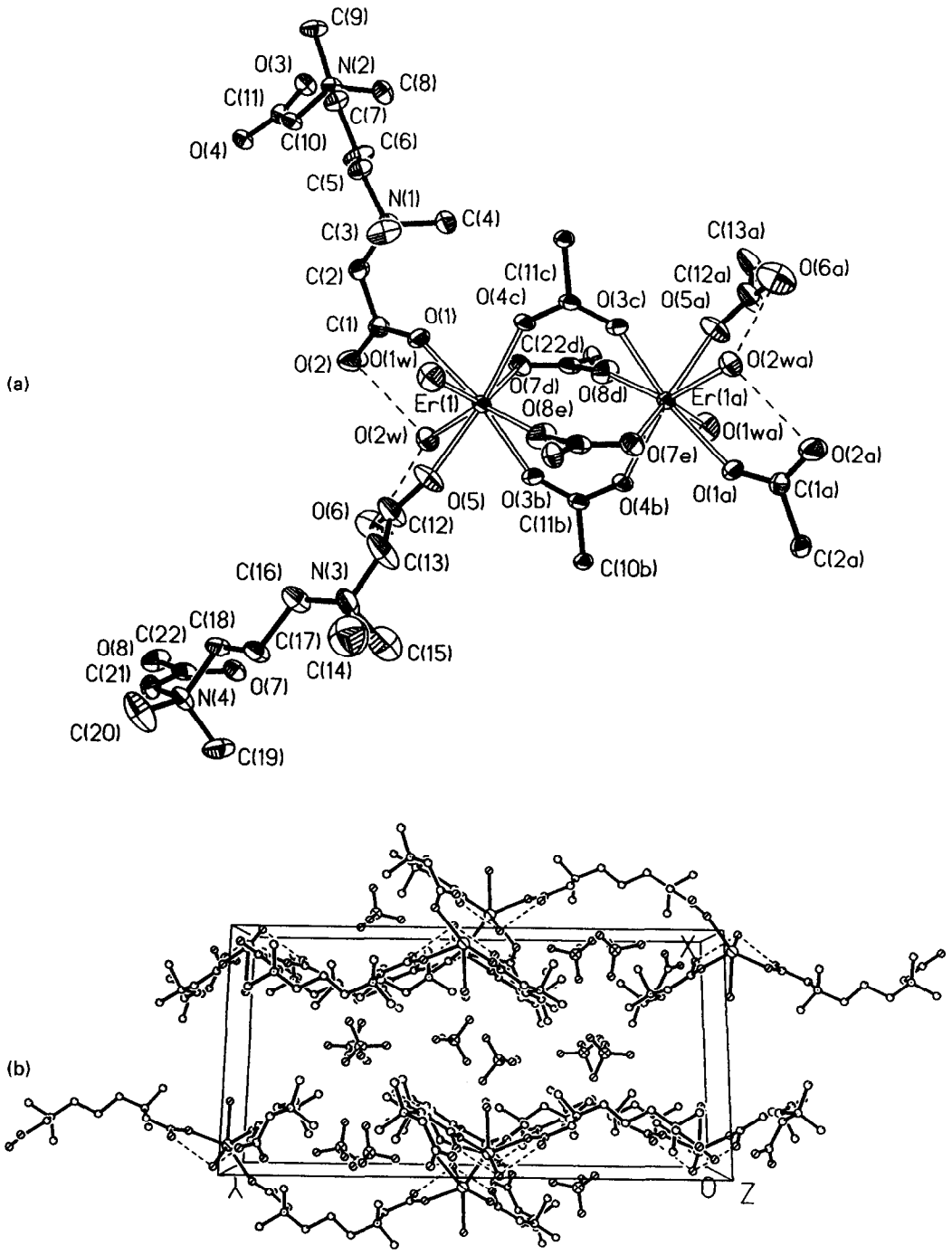


Fig. 4. (a) Structural skeleton of the asymmetric unit (35% thermal ellipsoid) of $[\{Er(L^1)_2(H_2O)_2\}_n][ClO_4]_{3n}\cdot nH_2O$ (**3**) with atom labelling. (b) Packing drawing showing the plane wave-like layer structure corresponding to [200] in the crystal structure of **3**.

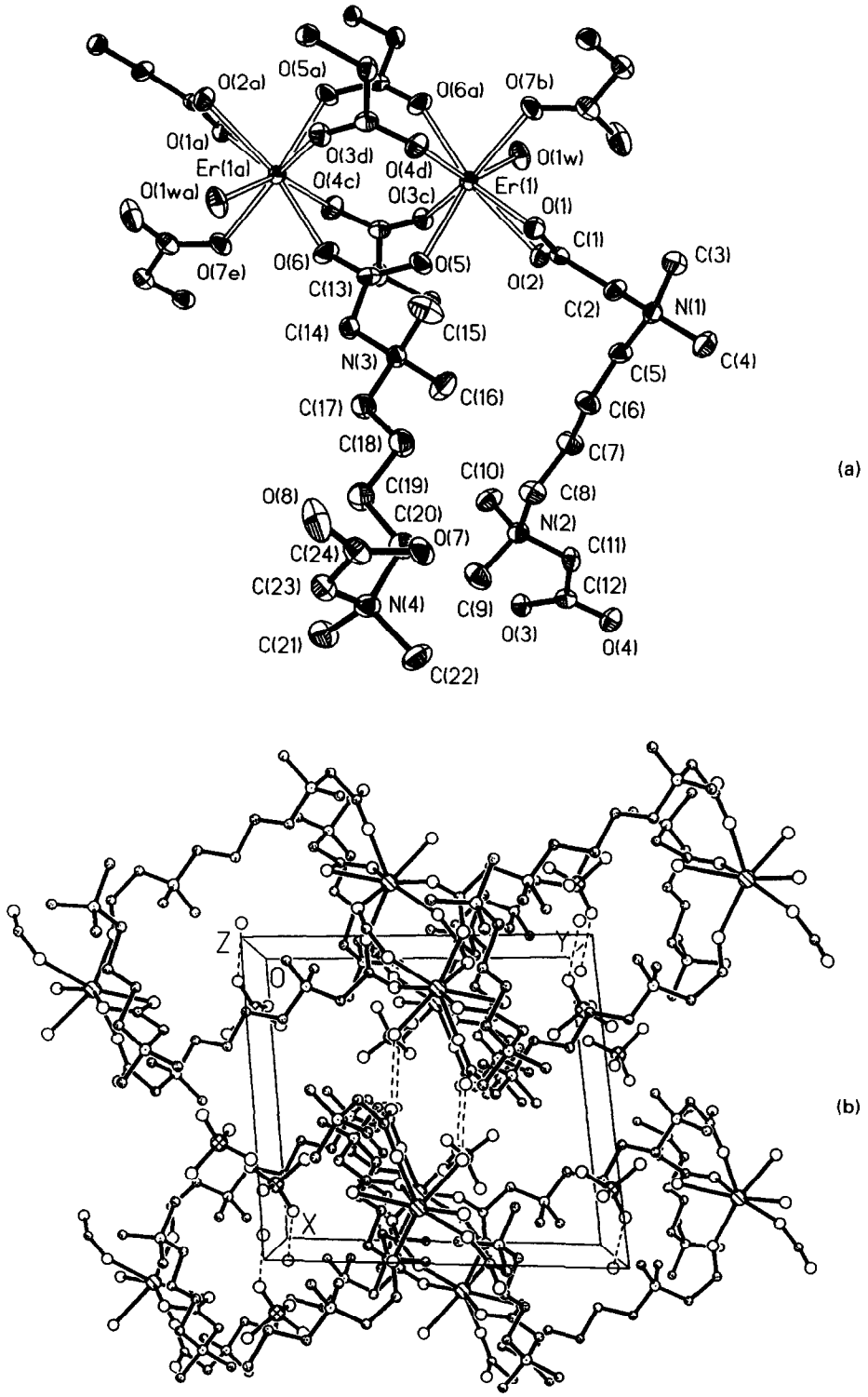


Fig. 5. (a) Structural skeleton of the asymmetric unit (35% thermal ellipsoid) of $[\{Er(L^2)_2(H_2O)\}_n][ClO_4]_{3n} \cdot nH_2O$ (**4**) with atom labelling. (b) Packing drawing showing the plane wave-like layer structure corresponding to [100] in the crystal structure of **4**.

Unlike complex **3**, in which the carboxylato groups act only in the unidentate and bridging bidentate coordination modes, the carboxylato groups of L^2 in complex **4** show three coordination modes: the common bridging bidentate [C(12c)—O(3c)—Er(1), 148.4(3); C(12c)—O(4c)—Er(1a), 135.3(3); C(13)—O(5)—Er(1), 134.4(4) and C(13)—O(6)—Er(1a), 152.7(3)°], unidentate [C(24b)—O(7b)—Er(1), 128.8(3)°], as well as bidentate chelate modes [C(1)—O(1)—Er(1) 90.1(3) and C(1)—O(2)—Er(1) 93.3(3)°]. The bidentate chelate mode is uncommon in polymeric lanthanide carboxylates, although some monomeric lanthanide carboxylate complexes are known to exhibit this type of ligand coordination [36,37]. The coexistence of the above types of coordination modes of carboxylato groups in complex **4** is rare among lanthanide carboxylates. The conformation of each of the two independent double betaines L^2 is different from that in complex **2**, and also different from that in its hydrated form and mercury adduct, in which the symmetry of the molecular backbone of L^2 has an inversion centre [24,27] at the midpoint between the two middle methylene carbons (Fig. 6). As shown in Fig. 5b, the wave-like, two-dimensional polymeric network in the crystal structure of complex **4** corresponds to the [100] plane. The aqua ligand [O(1w)] about the erbium atom in one layer forms an intermolecular hydrogen bond [O(1w)···O(8), 2.726(7) Å] with one of the uncoordinated unidentate carboxylato oxygen atoms from an adjacent layer, and *vice versa*, so that each neighbouring pair of layers are linked by such hydrogen bonds. An anionic perchlorate group, which exhibits orientational disorder and forms an acceptor hydrogen bond [O(2w)···O(11′), 2.912(7) Å] with the aqua ligand O(2w), is stacked inside the resulting partially open channels. The remaining perchlorate groups occupy the interlayer regions.

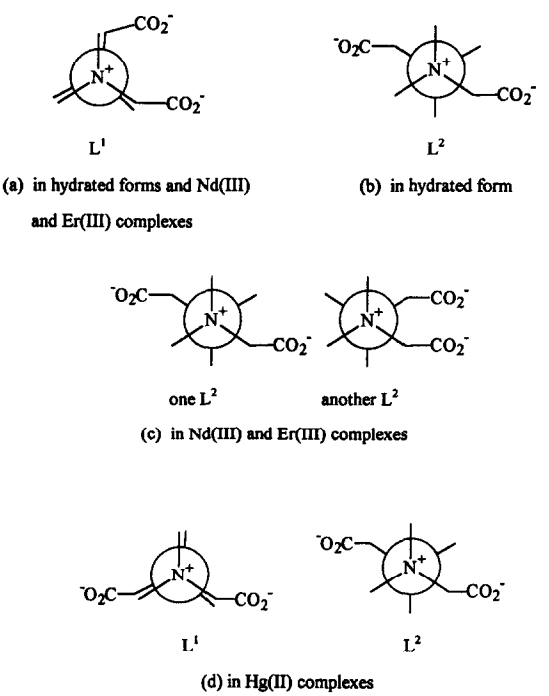


Fig. 6. Conformations of the flexible double betaines L^1 and L^2 in their hydrated forms and metal complexes.

CONCLUSIONS

The present study has demonstrated that two-dimensional coordination polymeric networks can be generated from neodymium(III) and erbium(III) perchlorates with flexible double betaines. The resulting four complexes in the present study are all based on the cross-linkage of tetrakis(carboxylato)-bridged dimers with a paddle-wheel-like structure by the double betaine molecular backbones. Variation of the number of methylene units linking the two positively charged quaternary nitrogen atoms in the double betaine skeleton, the particular lanthanide(III) species employed, as well as the presence or absence of lattice water molecules, results in different skeletal configurations and carboxylate coordination modes of the flexible betaine ligands, and consequently the coordination geometries adopted by the lanthanide(III) atoms.

Acknowledgement—This work is supported by a Hong Kong Research Grants Council Earmarked Grants (Ref. No. CUHK 89/93E).

REFERENCES

1. Choppin, G. R. and Bunzli, J.-C. G., *Lanthanide Probes in Life, Chemical and Earth Science*. Elsevier, Amsterdam, 1989.
2. Lauffer, R. B., *Chem. Rev.*, 1987, **87,** 901.
3. Hart, F. A., in *Comprehensive Coordination Chemistry*, eds Wilkinson, G., Gillard, R. D. and McCleverty, J. A., Vol. 3. Pergamon Press, Oxford, 1987, p. 1059.
4. Ouchi, A., Suzuki, Y., Ohki, Y. and Koizumi, Y., *Coord. Chem. Rev.*, 1988, **92,** 29.
5. Sawase, H., Koizumi, Y., Suzuki, Y., Shimoi, M. and Ouchi, A., *Bull. Chem. Soc. Jpn*, 1984, **57,** 2730.
6. Wei, P.-R., Jin, T.-Z., Yang, Q.-C. and Xu, G.-X., *J. Rare Earths*, 1992, **10,** 166.
7. Sugita, Y. and Ouchi, A., *Bull. Chem. Soc. Jpn*, 1987, **60,** 171; Imai, T., Shimoi, M. and Ouchi, A., *Bull. Chem. Soc. Jpn*, 1987, **60,** 159.
8. Sadikov, G. G., Kukina, G. A. and Porai-Koshits, M. A., *Zh. Strukt. Khim*, 1967, **8,** 551.
9. Bats, J. W., Kalus, R. and Fuess, H., *Acta Cryst.*, 1979, **B35,** 1225.
10. Kondo, S., Shimoi, M., Ouchi, A. and Takeuchi, T., *Bull. Chem. Soc. Jpn*, 1982, **55,** 2840.
11. Ouchi, A., Shimoi, M. and Kondo, S., *Bull. Chem. Soc. Jpn*, 1985, **58,** 1053.
12. Antsyshkina, A. S., Porai-Koshits, M. A., Arkhangel'ski, I. V. and Butman, L. A., *Koord. Khim.*, 1976, **2,** 565.

13. Chen, X.-M. and Mak, T. C. W., *J. Crystal Spectros. Res.*, 1001, **27,** 471.
14. Chen, X.-M. and Mak, T. C. W., *Acta. Cryst.*, 1993, **C48,** 1211.
15. Chen, X.-M. and Mak, T. C. W., *Inorg. Chim. Acta.*, 1991, **182,** 139.
16. Chen, X.-M. and Mak, T. C. W., *J. Crystal Spectros. Res.*, 1991, **21,** 27.
17. Chen, X.-M. and Mak, T. C. W., *Aust. J. Chem.*, 1991, **44,** 639.
18. Chen, X.-M., Mak, T. C. W., Huang, W.-Y. and Lu, L., *Acta Cryst.*; 1992, **C11,** 2567.
19. Chen, X.-M. and Mak, T. C. W., *Struct. Chem.*, 1992, **3,** 369; *ibid.*, 1993, **4,** 247.
20. Chen, X.-M. and Mak, T. C. W., *Inorg. Chim. Acta*, 1991, **189,** 3.
21. Chen, X.-M. and Mak, T. C. W., *J. Chem. Soc., Dalton Trans.*, 1991, 1585, 1219, 3253.
22. Chen, X.-M. and Mak, T. C. W., *Inorg. Chem. Acta.*, 1993, **203,** 97.
23. Wu, D.-D. and Mak, T. C. W., *Inorg. Chim. Acta*, 1995, **237,** 163.
24. Wu, D.-D. and Mak, T. C. W., *J. Chem. Soc., Dalton Trans.*, 1995, 139.
25. Wu, D.-D. and Mak, T. C. W., *J. Chem. Soc., Dalton Trans.*, 1995, 2671.
26. Wu, D.-D. and Mak, T. C. W., *Struct. Chem.*, 1996, **7,** 91.
27. Wu, D.-D. and Mak, T. C. W., *J. Mol. Struc.* 1994, **326,** 193.
28. Chen, X.-M. and Mak, T. C. W., *Inorg. Chem.*, 1994, **33,** 2444; Chen, X.-M. and Mak, T. C. W., *Polyhedron*, 1994, **13,** 1087; Chen, X.-M., Aubin, S. M. J., Wu, Y.-L., Yang, Y.-S., Mak, T. C. W. and Hendrickson, D. N., *J. Am. Chem. Soc.*, 1995, **117,** 9600; Chen, X.-M., Wu, Y.-L., Wang, R.-J. and Mak, T. C. W., *Polyhedron*, 1995, **15,** 739.
29. Sato, M., Yamamoto, M., Imada, K., Katsube, Y., Tanaka, N. and Higashi, T., *J. Appl. Cryst.*, 1992, **25,** 348; Tanner, J. and Krause, K. L., *The Rigaku Journal*, 1992, **11,** 4.
30. *ABSCOR—An Empirical Absorption Correction Based on Fourier Coefficient Fitting*, T. Higashi, Rigaku Corporation, Tokyo, 1995.
31. Sparks, R. A., In *Crystallographic Computing Techniques*, ed. Ahmed, F. R., Munksgaard, Copenhagen 1976, p. 452.
32. Kopfmann, G. and Huber, R., *Acta Cryst.*, 1968, **A24,** 348.
33. Sheldrick, G. M., in *Computational Crystallography*, ed. Sayre, D. Oxford University Press, New York, 1982 p. 506; Sheldrick, G. M., in *Crystallographic Computing* 3 : *Data Collection, Structure Determination, Proteins and Databases*, eds Sheldrick, G. M., Kruger, C. and Goddard, R. Oxford University Press, New York, 1985, p. 175.
34. *International Tables for X-ray Crystallography*, ed. Ibers, J. A. and Hamilton, W. C., Kynock Press, Birmingham (now distributed by Kluwer Academic Press, Dordrecht), 1974, Vol. 4. pp. 55, 99, 149.
35. Imai, T. and Ouchi, A., *Bull. Chem. Soc. Jpn*, 1987, **60,** 408.
36. Zeng, H.-D. and Pan, K.-Z., *Jiegou Huaxue*, 1992, **11,** 388.
37. Koziol, A. E., Klimek, B., Stepniak, K., Rzacynska, Z., Brzyska, W., Bodak, O. I., Akselrud, L. G., Pavlyuk, V. V. and Tafeenko, V. A., *Z. Kristallogr*, 1992, **200,** 25.

Pergamon

PII: S0277-5387(96)00348-8

Polyhedron Vol. 16, No. 5, pp. 765–776, 1997
Copyright © 1996 Elsevier Science Ltd
Printed in Great Britain. All rights reserved
0277 5387/97 $17.00+0.00

Synthesis and characterization of platinum(0) alkene complexes; X-ray crystal structure determinations on [Pt(*trans*-PhCH=CHCHO)(PPh_3)$_2$] and [Pt(*trans*-PhCH=CHCOMe)(PPh_3)$_2$]

Penny A. Chaloner,* Sîan E. Davies and Peter B. Hitchcock

School of Chemistry and Molecular Sciences, University of Sussex, Falmer, Brighton, BN1 9QJ, U.K.

(Received 28 June 1996; accepted 17 July 1996)

Abstract—Reaction of [Pt(C_2H_4)(PPh_3)$_2$] with a range of alkenes gave the complexes [Pt(alkene)(PPh_3)$_2$]. Complexes of alkenes bearing electron-withdrawing ligands were, predictably, more stable than those of electron-rich alkenes. The complexes were characterized by multinuclear (^{1}H, ^{13}C, ^{31}P and ^{195}Pt) NMR spectroscopy and the structures of the derivatives of *trans*-PhCH=CHCHO and *trans*-PhCH=CHCOMe were established by X-ray diffraction studies. The complexes reacted with PCy_3 to give [Pt(alkene)(PCy_3)(PPh_3)], usually as a mixture of regioisomers. Copyright © 1996 Elsevier Science Ltd

Keywords: platinum(0); alkene complexes; NMR spectroscopy; X-ray crystallography.

We have been interested for some time in the substitution chemistry of platinum(0), and have shown that the reaction of [Pt(C_2H_4)(PPh_3)$_2$] with bulky phosphines at low temperature results in substitution of the phosphine rather than the ethene [1]. A number of platinum alkene complexes have been prepared by displacement of ethene by another alkene. The reactions are clean, as the only by-product is gaseous ethene which is easily removed [2]. Alkene complexes isolated by this method include derivatives of ketenes [3], cumulenes [4], allenes [5], $C_2H_{4-n}X_n$ (X = CN or COOMe, n = 0–4 [6], styrene [7], strained cycloalkenes [8], Dewar benzenes [9], cyclooctene [10] and others [11]. The reaction of [Pt(C_2H_4)(DIOP)] with chiral alkenes has been used to indicate the enantiometric purity of the alkene [12], and alkynes have also been shown to displace ethene [13]. We have recently reported the preparation and characterization of a range of complexes in which the added alkene is a propenoate or a 2-methylpropenoate ester [14], and we now extend this to more varied alkenes.

RESULTS AND DISCUSSION

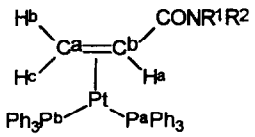
Reaction of alkenes with [Pt(C_2H_4)(PPh_3)$_2$]

Addition of a wide range of alkenes [15] to a toluene solution of [Pt(C_2H_4)(PPh_3)$_2$] resulted in clean conversion to the complexes **1–7**, which were generally isolated by reduction of the volume of toluene and precipitation with light petroleum (b.p. 30–40°C) to give white or cream powders. Analytically pure material was obtained in this way in several cases. However, the complexes decomposed when attempts were made to recrystallize them. The yields were generally good, except for **2a**, which was rather unstable and decomposed completely in solution at room temperature in less than 1 h. Since bonding in these complexes is dominated by metal to ligand back-bonding, we would expect that complexes of electron-rich alkenes would be less stable than those of alkenes bearing electron-withdrawing groups.

^{31}P *NMR spectra* (Table 1)

It proved possible (*vide infra*) to establish which phosphorus atom was which, and the structures show

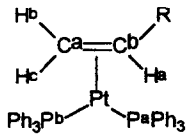
* Author to whom correspondence should be addressed.



1a R1, R2 = H

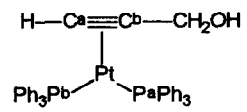
1b R1 = H, R2 = CMe_2CH_2COMe

1c R1 = Me, R2 = Ph

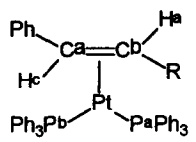


2a R = OCOMe

2b R = CH_2OH



3



4a R = H

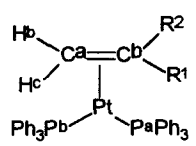
4b R = Ph

5a R = COPh

5b R = COMe

5c R = CHO

5d R = COCH=CHPh



6a R1 = H, R2 = CHO

6b R1 = Me, R2 = CHO

7a R1 = H, R2 = CN

7b R1 = Me, R2 = CN

the labelling convention used. The presence of electron-withdrawing substituents on the alkenes causes a decrease in the coupling constant $^1J(Pt–P_a)$ and an increase in $^1J(Pt–P_b)$ relative to $[Pt(C_2H_4)(PPh_3)_2]$. This follows the trend previously established for the propenoates, and may be attributed to the *trans* influence of the electron-withdrawing group. The substitution of an α-methyl group on the double bond (compare complexes **6a**, and **6b**, and **7a** and **7b**) causes an increase in $^1J(Pt–P_a)$ and a decrease in $^1J(Pt–P_b)$. The methyl group is an inductive donor, and might be expected to weaken the Pt–P bond *trans* to it; hence $^1J(Pt–P_b)$ is decreased.

For complexes **1a–c**, $^1J(Pt–P_a)$ increases with substitution at nitrogen, but the effect is small. This parallels the results with propenoate ester complexes; we can postulate that as the alkene becomes more hindered, bonding to it is weakened and there is a concomitant increase in the strength of the platinum–phosphorus bonds [16].

Complexes of alkenes bearing electron-donating groups, **2**, show a decrease in both phosphorus–platinum coupling constants relative to $[Pt(C_2H_4)(PPh_3)_2]$, whilst $^2J(PP)$ increases to 50–52 Hz. The complex of *trans*-PhCH=CHPh gave data comparable with the ethene complex. In the less symmetrical styrene derivative, however, the α-phenyl substitution decreases the value of $^1J(Pt–P_b)$ by approximately 40 Hz; the phenyl might appear to be acting as a donor of electron density into the platinum–phosphorus bond *trans* to it. However, it is more likely that the phenyl substituent has an effect on the position of the

Table 1. ^{31}P NMR spectra of platinum(0) alkene complexes **1–7**

Complex	$\delta(P_a)$ (ppm)	$^1J(Pt–P_a)$ (Hz)	$\delta(P_b)$ (ppm)	$^1J(Pt–P_b)$ (Hz)	$^2J(P_a–P_b)$ (Hz)
1a	32.3	3626	32.5	4012	45
1b	32.8	3673	32.1	3939	46
1c	33.4	3686	30.4	3989	46
2a	32.0	3349	34.8	3717	50
2b	34.8	3572	33.9	3562	52
3	30.4	3578	33.7	3642	35
4a	31.8	3749	33.7	3790	56
4b	35.6	3731	—	—	—
5a	27.9	3650	28.9	4245	38
5b	29.2	3659	28.0	4173	40
5c	28.5	3648	29.5	4249	40
5d	27.4	3674	29.8	4234	37
6a	32.1	3624	31.7	4169	40
6b	33.2	3748	30.0	3959	44
7a	30.5	3496	31.3	3947	34
7b	29.4	3600	30.4	3685	40

$\{Pt(PPh_3)_2\}$ moiety relative to the carbon–carbon double bond. The steric bulk of the phenyl group could cause slippage of the platinum towards the less hindered terminus, which would have the same effect on the observed coupling constant.

^{195}Pt *NMR spectra* (Table 2)

In platinum NMR spectroscopy chemical shifts are relatively insensitive to small changes in molecular structure, but they are indicative of the oxidation state of platinum [17]. The chemical shifts of compounds **1–7** confirm that they are platinum(0) complexes. The appearance of each spectrum is a doublet of doublets, since coupling to the two phosphorus atoms is distinct in each case (Fig. 1).

Table 2. ^{195}Pt NMR spectra of platinum(0) alkene complexes **1–7**

Compound	$\delta(Pt)$ (ppm)	$^1J(Pt–P_a)$ (Hz)	$^1J(Pt–P_b)$ (Hz)
1a	−5094	3609	4006
1b	−5090	3665	3957
1c	−5131	3692	3988
2a	−5030	3354	3718
2b	−5085	3590	3723
3	−4694	3562	3610
4a	−5023	3749	3788
4b	−5050	3742	3742
5a	−5087	3650	4246
5b	−5100	3656	4177
5c	−5039	3634	4261
5d	−5076	3667	4239
6a	−5098	3621	4167
6b	−5123	3750	3957
7a	−5042	3496	3950
7b	−5053	3604	3681

^{13}C *NMR spectra* (Table 3)

The alkene carbons in the complexes resonate at higher fields than in the free alkenes (upfield shift *ca* 80 ppm), as is common in metal alkene complexes [18]. A typical spectrum is shown in Fig. 2. The notation for the labelling of the carbon atoms is shown in structures **1–7**.

The effect of a methyl substituent on the double bond is to change the chemical shift of the carbon atom to which it is bonded, C_b. Thus, in the free alkene the shift moves downfield; δ for C_b in $CH_2{=}CHCHO$ is 138.6, whereas for $CH_2{=}C(Me)CHO$ it is 145.6. In the complexes this effect is accentuated. An α-phenyl substituent causes a downfield shift of the resonance of the carbon atom to which it is bonded by 20 ppm relative to a proton. For example, in **6a** $\delta(C_a) = 39.8$ whereas for **5c** $\delta(C_a) = 60.7$.

Each carbon atom has one large (*ca* 24–30 Hz) and one small (*ca* 3–7 Hz) coupling constant associated with the two phosphorus atoms. The large coupling constant is assumed to be that associated with the pseudo *trans* phosphorus atom. These are significantly smaller than those reported for highly strained and pyramidalized alkenes, but are comparable with that in $[Pt(C_2H_4)(PPh_3)_2]$ [9]. As the signals were relatively weak, ^{195}Pt satellites could be identified only in one complex, that of PhCH=CHCOPh, **5a**, *viz.* $^1J(Pt—C_b) = 149$ Hz. This is smaller than the coupling found in $[Pt(C_2H_4)(PPh_3)_2]$ [$^1J(PtC) = 194$ Hz]. This may suggest that the steric hindrance in **5a** results in a longer Pt—C distance, and hence a smaller coupling constant, but more examples would be needed for a definitive answer. An α-methyl or an α-phenyl group

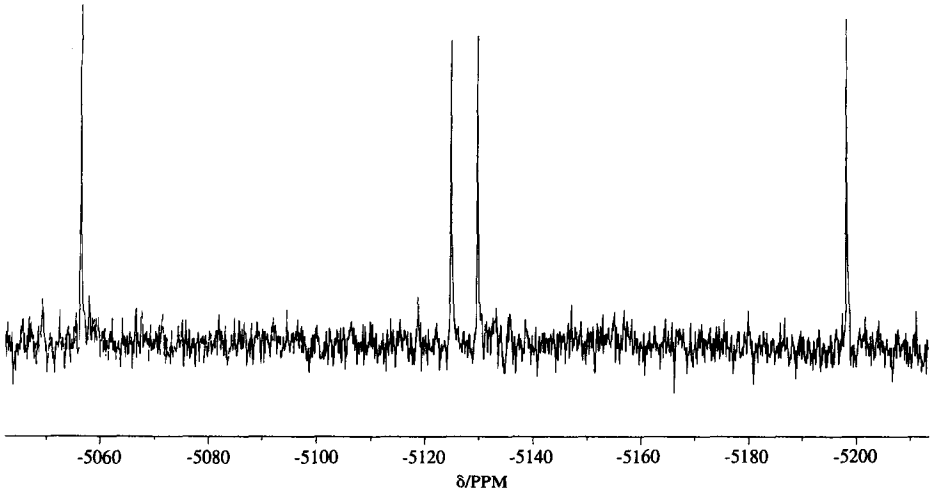


Fig. 1. ^{195}Pt NMR spectrum of [Pt(*trans*-PhCH=CHCHO)(PPh_3)$_2$] **5c**.

Table 3. ^{13}C NMR spectroscopic data for complexes **1–7**

Compound	$\delta(C_a)^a$ (ppm)	$\delta(C_b)^a$ (ppm)	$\delta(C_a)$ (ppm)	$\delta(C_b)$ (ppm)	$^2J(C_a–P_a)$ (Hz)	$^2J(C_a–P_b)$ (Hz)	$^2J(C_b–P_b)$ (Hz)	$^2J(C_b–P_a)$ (Hz)
1b	132.8	137.6	53.0	40.8	25.7	2.9	32.4	2.9
1c	137.8	144.3	49.0	42.1	30.3	6.4	33.2	5.7
2b	137.9	114.6	58.5	40.9	29.1	4.3	28.6	3.8
4a	137.3	137.8	59.1	39.8	29.0	5.3	26.7	4.7
4b	137.3	137.3	59.3	52.0	20.5	5.3	26.7	4.7
5a	138.8	144.3	57.7	61.2	24.7	5.6	29.3	3.3
5b	137.6	142.4	60.2	63.0	32.0	3.3	24.8	5.7
5c	134.4	152.4	60.7	64.5	32.4	1.9	22.8	4.3
5d	137.5	142.7	60.1	64.9	32.4	3.8	23.8	5.7
6a	138.0	138.6	39.6	62.4	28.6	1.0	16.2	1.9
6b	137.1	145.6	46.5	72.0	nd	nd	22.9	5.7
7a	137.7	117.5	39.8	23.8	29.2	3.0	38.6	4.5
7b	137.7	130.6	44.5	33.5	38.0	5.5	35.6	4.9

[a] Data for the uncomplexed alkenes.
nd: not determined; the signal was broad.

increases $^2J(C_aP_a)$ and decreases $^2J(C_bP_b)$. No significant effect was found on $^2J(C_aP_b)$ or $^2J(C_bP_a)$. We suggest that this is a result of the fact that the α substituent causes some slippage of the platinum towards the less hindered end of the double bond.

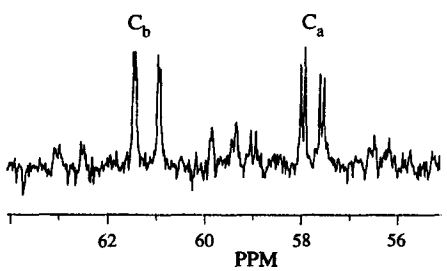


Fig. 2. Alkene region of the ^{13}C NMR spectrum of [Pt(*trans*-PhCH=CHCOPh)(PPh_3)$_2$], **5a**.

^{1}H *NMR spectra* (Tables 4 and 5)

The chemical shift of the protons attached to the carbon–carbon double bond is moved upfield by 3–4 ppm up on coordination, as is typical for this type of complex [20]. An expansion of the alkene region of the spectrum of **6a** is shown in Fig. 3; this illustrates the complexity of the assignments. The coupling constants were determined by ^{1}H {^{31}P} decoupling experiments followed by simulation using PANIC [21], but even this did not allow complete assignment in every case (the spectra of **1a, 1b, 2a, 2b, 6a** and **7a** were not assigned).

The interproton coupling is very different from that in the free alkenes. Both *trans* and *cis* couplings are reduced and the geminal coupling is increased. These data are all consistent with the lowering of the carbon–carbon bond order in the complex. For each proton

Table 4. ^{1}H NMR spectroscopic data for complexes **1–7**

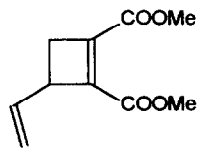
Complex	$\delta(H_a)^a$ (ppm)	$\delta(H_b)^a$ (ppm)	$\delta(H_c)^a$ (ppm)	$\delta(H_a)$ (ppm)	$\delta(H_b)$ (ppm)	$\delta(H_c)$ (ppm)	$^3J(H_aH_b)^a$ (Hz)	$^3J(H_aH_c)^a$ (Hz)	$^2J(H_bH_c)^a$ (Hz)	$^3J(H_aH_b)$ (Hz)	$^3J(H_aH_c)$ (Hz)	$^2J(H_bH_c)$ (Hz)
1c	5.9	5.1	6.4	3.51	2.13	3.05	10.1	16.9	2.0	8.61	10.40	3.16
3			4.42			4.41						
4a	6.5	5.1	5.5	2.74	2.90	3.86	10.9	17.6	1.0	8.48	10.52	4.92
4b			7.18			4.10						
5a	7.25		7.8	4.79		4.66		15.7			8.75	
5b	6.4		7.2	4.33		4.08		16.3			9.30	
5c	6.5		7.1	4.14		4.00		15.9			8.71	
5d	6.7		7.6	4.61		4.30		15.9			9.17	
6b		5.85	6.15		2.36	2.41			0.97			4.0
7b		5.2	5.0		1.99	2.46			0.8			4.51

[a] Data for the uncomplexed alkenes.

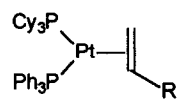
there is a large coupling to one phosphorous atom, and a smaller one to the other. The ^3J(PH) couplings are similar to those in related complexes. For example, in [Pt{MeOCH=C(CN)$_2$}(PPh$_3$)$_2$] $^3J(HP_a)$ = 6.9 Hz and $^3J(HP_b)$ = 3.6 Hz [22]. As it is known which phosphorus has the larger coupling to each proton (from the decoupling experiments) and we know which phosphorus was decoupled, we can tell which phosphorus was which. The significance of the coupling of the alkene protons to ^{195}Pt was not analysed in detail, but varied between 38 and 66 Hz. $^2J(Pt–H_a)$ is typically 60–66 Hz.

Structure of [Pt(*trans*-PhCH=CHCHO)(PPh$_3$)$_2$], **5c**

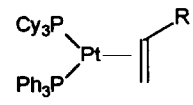
A number of platinum(0) complexes of the type [Pt(alkene)(PPh$_3$)$_2$] have been characterized crystallographically including those for which the alkene was *trans*-4-$O_2NC_6H_4CH$=CHC_6H_4-4-NO_2 [23], *trans*-Ph(CN)C=C(CN)Ph [24], $(NC)_2C$=$C(CN)_2$ [25], $(MeO_2C)_2C$=$CHCO_2Me$ [26], Cl_2C=CCl_2 [27], *trans*-NCCH=CHCN [28] and **8** [29]. The geometry of these complexes is characterized by a trigonal planar arrangement of the ligands with the alkene in the plane of the triangle. There is a non-zero angle between the PtP_2 and PtC_2 planes.



8



9a



9b

Crystals of **5c** were grown by slow evaporation of a perdeuterotoluene solution. The molecular structure is shown in Fig. 4, and selected bond lengths and angles are given in Table 6. The Pt—P bond lengths [2.252(3), 2.272(4) Å] are slightly shorter than those in [Pt{$(MeO_2C)_2C$=$CHCO_2Me$}(PPh$_3$)$_2$] [26] [2.283(4), 2.286(3) Å], reflecting lower steric hindrance, but the carbon–carbon bond length of the bound alkene [1.43(1) Å versus 1.44(2) Å] is essentially identical. The P—Pt—P bond angle [113.5(1)°] is larger than is usually found in this type of complex. For example P—Pt—P is 100.6(2)° in [Pt(Cl_2C=CCl_2)(PPh$_3$)$_2$] [27], 104.4(2)° in [Pt(*trans*-NCCH=CHCN)(PPh$_3$)$_2$] [30] and 103.90(3)° in [Pt{*trans*-Ph(CN)C=C(CN)Ph}(PPh$_3$)$_2$] [24]. The reason for this unusually high value is not immediately apparent, except that

Table 5. ^{1}H–^{31}P coupling constants for **1**–**7**

Complex	$^{3}J(H_aP_a)$ (Hz)	$^{3}J(H_aP_b)$ (Hz)	$^{3}J(H_bP_a)$ (Hz)	$^{3}J(H_bP_b)$ (Hz)	$^{3}J(H_cP_a)$ (Hz)	$^{3}J(H_cP_b)$ (Hz)	$^{3}J(H_aPt)$ (Hz)	$^{3}J(H_bPt)$ (Hz)	$^{3}J(H_cPt)$ (Hz)
1c	8.80	4.18	8.31	4.68	8.52	5.68	66	48	48
3						nd			60
4a	7.60	4.89	8.53	4.35	9.51	8.90	64	58	nd
4b						nd			60
5a	8.77	3.23			8.78	5.00	60		50
5b	9.10	3.40			8.78	5.33	60		52
5c	8.26	3.77			8.69	5.37	56		52
5d	9.38	3.46			9.03	5.63	62		58
6b			8.10	4.7	10.4	7.4		nd	50
7b			7.53	4.36	7.43	5.24		46	56

nd : not determined.

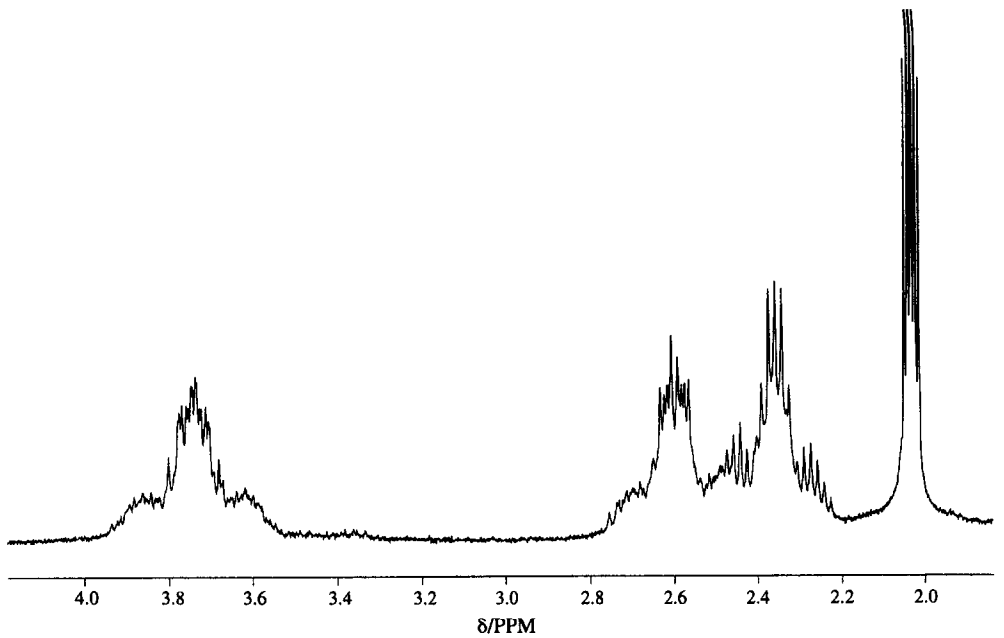


Fig. 3. Alkene region of the ^{1}H NMR spectrum of $[Pt(CH_2{=}CHCHO)(PPh_3)_2]$, **5c**.

the Pt—P bond lengths are short in comparison with related complexes, so that the bond angle is opened to minimize steric repulsions. The angle between the PtC_2 and PtP_2 planes is 5(3)°, in the expected range.

Structure of $[Pt(trans\text{-}PhCH{=}CHCOMe)(PPh_3)_2]$, **5b**

Crystals of **5b** were grown by evaporation of a per-deuterotoluene solution. The structure is shown in Fig. 5, and selected bond lengths and angles are given in Table 7. The structure is quite similar to that of **5c**. The Pt—P bond lengths are a little longer, as are the Pt—C bond distances, and the P—Pt—P angle has been closed to 109.87(3)°. These changes all reflect the increased steric demand of the alkene. Strain is also alleviated by twisting the PtC_2 and PtP_2 planes relative to each other; the dihedral angle in this case is 12.2(4)°.

In the complex of PhCH=CHCHO there is little or no slippage [31] of the platinum away from the midpoint of the carbon–carbon double bond. However, in **5b** the platinum has slipped towards the less hindered end of the bond [Pt—C_a = 2.124(3) Å, Pt—C_b = 2.139(4) Å]. The reason is unclear, since study of a model reveals no severe interactions on moving the platinum to the midpoint of the double bond.

Reactions of the complexes with PCy_3

It was known that reaction of $[Pt(C_2H_4)(PPh_3)_2]$ with bulky phosphines at low temperature gave $[Pt(C_2H_4)(PPh_3(PR_3)]$, and that, of these complexes,

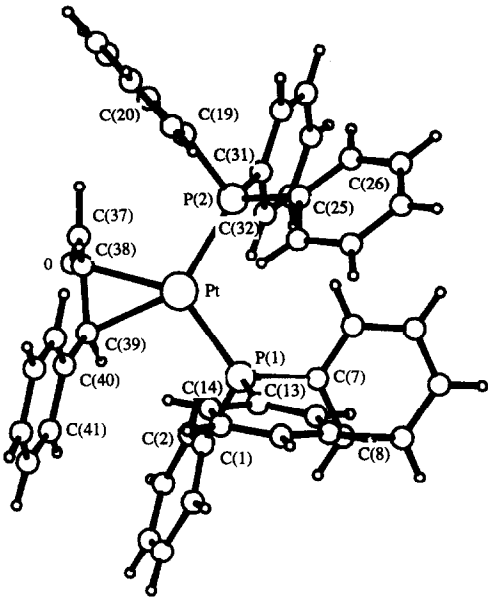


Fig. 4. Structure of [Pt(*trans*-PhCH=CHCHO)(PPh_3)$_2$], **5c**.

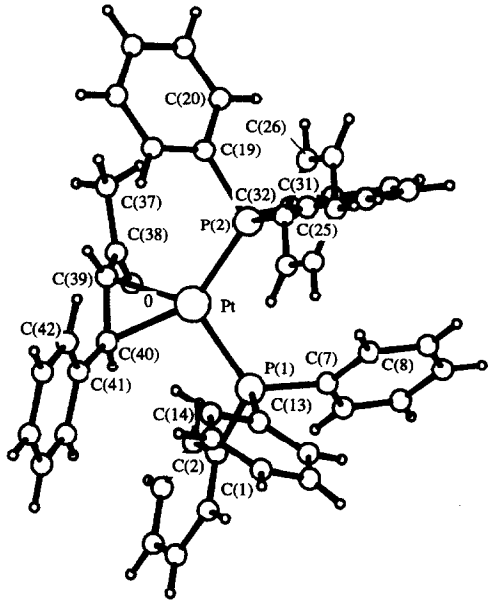


Fig. 5. Structure of [Pt(*trans*-PhCH=CHCOMe)(PPh_3)$_2$], **5b**.

the one with PCy_3 was the most stable. PCy_3 has a large cone angle [32], and since it is appreciably more basic than PPh_3, the chemical shift is sufficiently different from that for PPh_3 that the ^{31}P NMR spectra should be readily interpreted. PCy_3 was therefore added to complexes **1**–**7** at −50°C. The ^{31}P NMR spectra of the products show one or more AB quartets, and the reaction appears to go to completion in most cases, although some of the products were very insoluble. The same reaction products were obtained by addition of the relevant alkene to [Pt(C_2H_4)(PCy_3)(PPh_3)], formed *in situ*. In each case there are two possible regioisomers, which are shown as **9a** and **9b** for a monosubstituted alkene complex. The reaction mixture was stored at −20°C for 1–2 weeks and any equilibration monitored by ^{31}P NMR spectroscopy.

Details of the complexes formed and the ratios between the regioisomers are given in Table 8. In some cases (**1a, 4b, 5c,** minor isomers from **5d, 6b**) complete data were not obtained owing to the low solubility of the complexes. The reaction of **2a** was unsuccessful because of decomposition; this was not surprising as this was much the least stable of the complexes prepared. Complex **7b** did not appear to react. The complexes of CH_2=CHCONH$_2$, *trans*-PhCH=CHCHO, HC≡CCH$_2$OH and CH_2=CHCHO gave a single regioisomer on reaction with PCy_3, and the complex of PhCH=CHPh gave a single product because of its symmetry. It seems that the selective production of a single regioisomer is confined to complexes of ligands with low steric demand. This suggests that only in these complexes is there no barrier to PCy_3, the bulkier and more basic ligand, taking up the electronically favourable site.

Equilibration studies on alkene complexes

In order to gain some insight into the relative stabilities of the complexes, the displacement of one alkene by another was followed by ^{31}P NMR spectroscopy. One molar equivalent of a second alkene was added at −50°C to [Pt(alkene)(PPh_3)$_2$] prepared *in situ*. The resulting solution was warmed slowly in the NMR probe, and the ^{31}P NMR spectrum recorded. The solu-

Table 6. Selected bond lengths (Å) and angles (°) for [Pt(*trans*-PhCH=CHCHO)(PPh_3)$_2$], **5c**

Pt—M(1)	2.037	Pt—P(1)	2.252(3)
Pt—P(2)	2.272(4)	Pt—C(38)	2.159(14)
Pt—C(39)	2.158(14)	C(37)—C(38)	1.44(2)
C(38)—C(39)	1.43(2)	O—C(37)	1.21(2)
M(1)—Pt—P(1)	121.2	M(1)—Pt—P(2)	125.3
P(1)—Pt—P(2)	113.5(1)	O—C(37)—C(38)	126(1)
C(37)—C(38)—C(39)	122(1)	C(38)—C(39)—C(40)	121(1)

M(1) is the midpoint of the C(38)–C(39) bond.

Table 7. Selected bond lengths (Å) and angles (°) for [Pt(*trans*-PhCH=CHCOMe)(PPh_3)$_2$], **5b**

Pt—M(1)	2.008	Pt—P(1)	2.270(1)
Pt—P(2)	2.275(1)	Pt—C(39)	2.139(4)
Pt—C(40)	2.124(3)	O—C(38)	1.228(4)
C(37)—C(38)	1.508(5)	C(38)—C(39)	1.472(5)
C(39)—C(40)	1.437(5)		
M(1)—Pt—P(1)	121.7	M(1)—Pt—P(2)	128.3
P(1)—Pt—P(2)	109.87(3)	O—C(38)—C(37)	120.2(3)
O—C(38)—C(39)	123.3(3)	C(37)—C(38)—C(39)	116.5(3)
C(38)—C(39)—C(40)	118.9(2)	C(39)—C(40)—C(41)	122.6(3)

M(1) is the midpoint of the C39–C40 bond.

Table 8. ^{31}P NMR spectroscopic data for the products of the reactions of **1–7** with PCy_3

Starting complex	$\delta(PPh_3)$ (ppm)	^1J(Pt–PPh_3) (Hz)	$\delta(PCy_3)$ (ppm)	^1J(Pt–Pcy_3) (Hz)	^2J(PP) (Hz)	Ratio[a]
1a	30.8	[b]	41.6	[b]	46	100:0
1b	25.2	3551	35.1	3855	48	57:43
	25.1	3806	34.9	3855	46	
1c	27.5	3662	34.2	3894	49	57:43
	25.5	4014	28.5	3666	47	
2b	34.3	3476	42.1	4267	57	67:33
	33.2	3364	39.4	3993	53	
3	30.6	4462	38.7	3488	37	100:0
4a	32.3	3724	41.2	3651	57	63:27
	29.8	3592	40.4	3694	55	
4b	29.9	[b]	36.9	[b]	40	
5a	21.5	3354	32.7	3989	35	67:33
	26.8	4179	33.9	3534	35	
5b	31.8	4229	39.1	3961	37	58:42
	30.5	3652	38.6	3517	42	
5c	29.9	[b]	36.9	[b]	40	100:0
5d	25.5	3749	38.6	4045	34	71:29
	37.1	[b]	44.7	[b]	38	
6a	30.5	4213	35.4	3461	40	100:0
6b	28.6	3939	36.6	3647	43	74:26
	30.3	[b]	38.0	[b]	46	
7a	29.6	3929	38.7	3433	34	60:40
	28.7	3435	39.7	3821	37	

[a] The date for the major complex is given first in each case.
[b] Not determined owing to low solubility.

tion was then kept at 25°C and the ^{31}P NMR spectrum recorded at intervals until no further change was observed. It was shown that it did not matter in which order the reaction was carried out; the same ratio of final products was obtained. The spectra for a typical experiment involving the reaction of [Pt(*trans*-PhCH=CHCOMe)(PPh_3)$_2$] with CH_2=$CHCO_2$Me are shown in Fig. 6. Some of the data obtained are shown in Table 9. This allowed us to construct a stability series for the platinum(0) alkene complexes as follows:

CH_2=CHCN ~ CH_2=CHCHO > CH_2=$CHCO_2$

CH_2Ph > CH_2=$CHCO_2$Me > CH_2=$CHCO_2$Bu^t >

HC≡CCH_2OH ~ CH_2=C(Me)CN ~

CH_2=C(Me)CHO > *trans*-PhCH=CHCHO >

trans-PhCH=CHCOCH=CHPh >

CH_2=$CHCONH_2$ > CH_2=CHCONMePh >

trans-PhCH=CHCOMe > *trans*-PhCH=CHCOPh :

CH_2=C(Me)COOR > CH_2=$CHCH_2OH$ >

CH_2=CHPh > *trans*-PhCH=CHPh >

CH_2=CHOCOMe

It can be clearly seen that two factors are important.

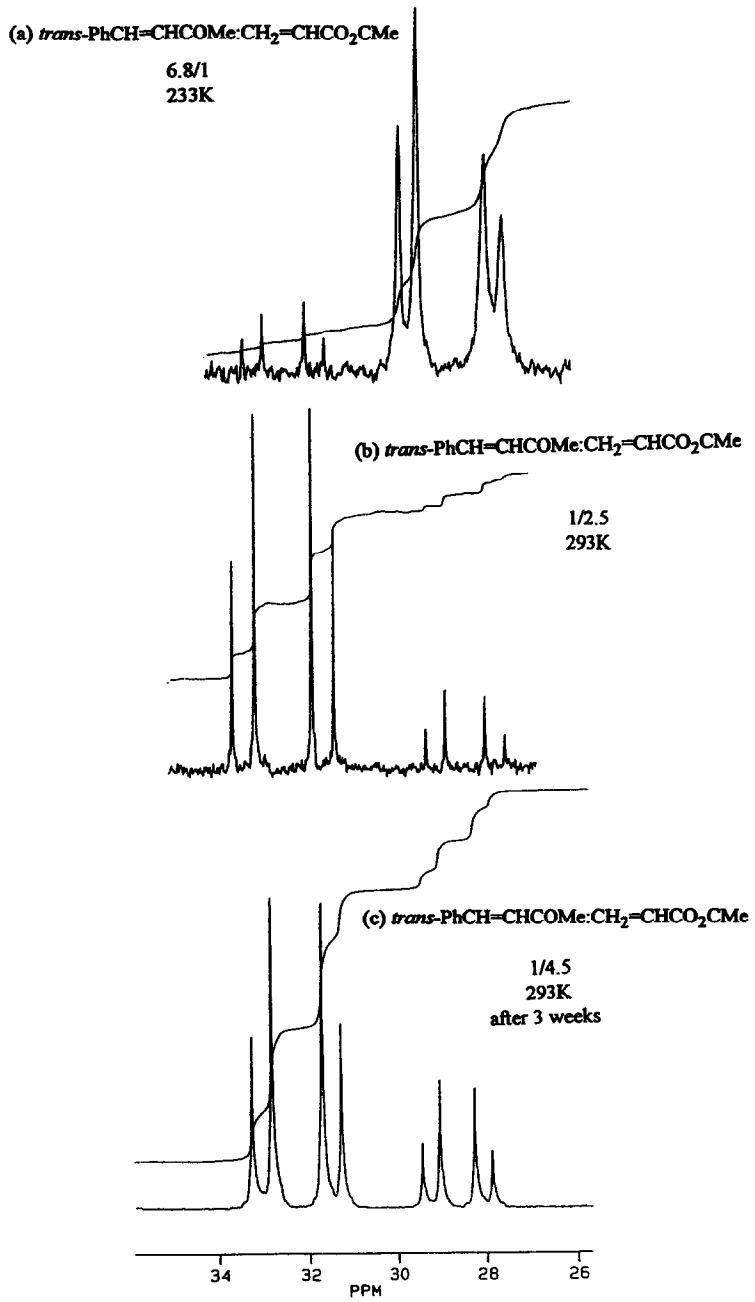


Fig. 6. ^{31}P NMR spectra of the products of the reactions between [Pt(*trans*-PhCH=CHCOMe)(PPh_3)$_2$] **5b**, and CH_2=$CHCO_2Me$.

The most stable complexes are those bearing alkenes with the most electron-withdrawing groups; thus CH_2=CHCHO > CH_2=$CHCO_2Me$ > CH_2=$CHCONH_2$ > CH_2=$CHCH_2OH$. However, steric factors are also important. The substitution of an α-methyl group contributes to both effects, and the phenyl group is even bulkier. Bulky groups tend to cause twisting of the alkene, which decreases orbital overlap. The results described here have parallels in the work of Tolman [33]. He determined the equilibrium constants for the reaction of [Ni(alkene){$P(OC_6H_4$-2-Me)$_3$}$_2$] with 38 alkenes. He concluded that the most important contribution to bonding was back-bonding from the metal into the π^* orbital of the alkene, and that steric effects were less significant than electronic ones.

CONCLUSIONS

Spectroscopic parameters for complexes **1**–**7** may be rationalized in terms of steric and electronic effects. The bonding to the metal is strongest, and the com-

Table 9. Equilibration studies on platinum(0) alkene complexes

Alkene 1	Alkene 2	Final ratio of alkene 1 : alkene 2
CH_2=CHCN	CH_2=CHCHO	56 : 44
CH_2=CHCN	CH_2=CHCOOMe	75 : 25
CH_2=CHCN	CH_2=C(Me)CN	100 : 0
CH_2=CHCHO	CH_2=CHCOOMe	62 : 38
CH_2=CHCHO	HC≡CCH_2OH	50 : 50
CH_2=CHCHO	CH_2=C(Me)CHO	100 : 0
CH_2=CHCOOMe	HC≡CCH_2OH	50 : 50
CH_2=CHCOOMe	*trans*-PhCH=CHCHO	79 : 21
CH_2=CHCOOMe	CH_2=$CHCONH_2$	80 : 20
CH_2=CHCOOMe	CH_2=$CHCONHCMe_2CH_2COCH_3$	67 : 33
CH_2=CHCOOMe	*trans*-PhCH=CHCOPh	75 : 25
CH_2=CHCOOMe	*trans*-PhCH=CHCOMe	71 : 29
CH_2=$CHCOOBu^t$	*trans*-PhCH=CHCOPh	83 : 17
CH_2=$CHCOOBu^t$	*trans*-PhCH=CHCOMe	80 : 20
CH_2=C(Me)CN	*trans,trans*-PhCH=CHCOCH=CHPh	83 : 17
CH_2=C(Me)CN	CH_2=CHPh	100 : 0
HC≡CCH_2OH	CH_2=CHPh	100 : 0
CH_2=C(Me)CHO	*trans,trans*-PhCH=CHCOCH=CHPh	83 : 17
CH_2=C(Me)CHO	CH_2=$CCONHCMe_2CH_2COCH_3$	50 : 50
CH_2=C(Me)CHO	*trans*-PhCH=CHCOMe	100 : 0
trans-PhCH=CHCHO	*trans,trans*-PhCH=CHCOCH=CHPh	72 : 28
trans-PhCH=CHCHO	CH_2=$CHCONH_2$	67 : 33
trans-PhCH=CHCHO	CH_2=CHCON(Me)Ph	64 : 36
trans-PhCH=CHCHO	*trans*-PhCH=CHCOMe	67 : 33
trans,trans-PhCH=CHCOCH=CHPh	*trans*-PhCH=CHCOPh	60 : 40
trans,trans-PhCH=CHCOCH=CHPh	*trans*-PhCH=CHCOMe	67 : 33
trans,trans-PhCH=CHCOCH=CHPh	CH_2=C(Me)COOEt	86 : 14
trans,trans-PhCH=CHCOCH=CHPh	CH_2=CHPh	83 : 17
CH_2=$CHCONH_2$	*trans*-PhCH=CHCOMe	78 : 22
trans-PhCH=CHCOPh	*trans*-PhCH=CHCOMe	50 : 50
trans-PhCH=CHCOPh	CH_2=CHPh	50 : 50

plexes are most stable, when the alkene bears electron-withdrawing groups, and has a low steric demand; the major component of the bonding is back-donation from platinum(0) to the π^* orbital of the alkene. When PCy_3 is reacted with **1–7** two regioisomers are generally formed, but a few complexes, usually of unhindered alkenes, gave a single regioisomer.

EXPERIMENTAL

All preparations were carried out under nitrogen using standard Schlenk line techniques. Solvents were dried, distilled and degassed prior to use. NMR spectra were recorded using a Bruker ACP250 FT spectrometer operating at 250 (^{1}H), 62.82 (^{13}C), 101.20 (^{31}P) or 53.78 MHz (^{195}Pt). Chemical shifts are reported relative to external TMS (^{1}H, ^{13}C), 85% H_3PO_4 (^{31}P) or $Na_2[PtCl_6]$ (^{195}Pt). Microanalyses were performed using a Perkin–Elmer 400 CHN analyser. Melting points were determined using a Stuart melting point apparatus and are uncorrected.

Synthesis of cis-$[Pt(PPh_3)_2Cl_2]$

The synthesis was carried out as described by Gillard and Pilbrow with 87% yield [34].

Synthesis of $[Pt(C_2H_4)(PPh_3)_2]$

The synthesis was carried out as described by Nagel with 90% yield [35].

Synthesis of complexes of the type $[Pt(alkene)(PPh_3)_2]$

In a typical synthesis $[Pt(C_2H_4)(PPh_3)_2]$ (0.1483 g, 19.8 mmol) was placed in a Schlenk line and dissolved in dry degassed toluene (3 cm^3). The alkene (1 : 1 molar ratio with platinum) was added to the solution, which was then stirred for 2 h. After cooling to 0°C, light petroleum (b.p. 30–40°C, 10 cm^3) was added and the complex was precipitated. The precipitate was collected by filtration under nitrogen, washed (light petroleum, b.p. 30–40°C, 10 cm^3) and dried *in vacuo*.

In many cases analytically pure material was obtained in this way. However, recrystallization proved difficult as all the complexes deteriorated slowly in solution. Details of the preparations and the microanalytical data (where available) are given in Table 10.

Structure of [Pt(*trans*-PhCH=CHCHO)(PPh_3)$_2$], **5c**

Data were collected using a crystal grown by slow evaporation from perdeuterotoluene, *ca* $0.15 \times 0.15 \times 0.10$ mm^3 on an Enraf–Nonius CAD4 diffractometer operating in the θ–2θ mode with $\Delta\theta = (0.8 + 0.35 \tan\theta)$ and a maximum scan time of 1 min, monochromated Mo-K_α radiation, $\lambda = 0.71069$ Å, $\mu = 39.9$ cm^{-1}. Unit-cell parameters were obtained from a least-square fit of 25 reflections, $7.3 < \theta < 10.4°$. A total of 3635 independent reflections were measured for $2 < \theta < 25°$ and h 0–39, k 0–15, l 0–13. 2236 observed reflections with $|F^2| > 3\sigma(F^2)$, $\sigma(F^2) = \{\sigma^2(I) + (0.04I)^2\}^{1/2}/Lp$ were used in the refinement. Two reference reflections were remeasured every 60 min and showed a maximum deviation of 0.2%. Lorentz and polarization corrections and absorption correction by DIFABS [36] (max. 1.12, min. 0.92) were applied. The structure was solved by routine heavy-atom methods and non-hydrogen atoms refined anisotropically by full-matrix least squares. The phenyl hydrogen atoms were fixed at calculated positions ($B_{iso} = 1.4B_{eq}$ for parent atom) and the other hydrogen atoms were freely refined. The absolute structure was determined by refinement of a $\Delta F''$ multiplier. The weighting scheme was $w = 1/\sigma^2(F)$, $\Sigma w(|F_o|-|F_c|)^2$ minimized, and the final residuals were $R = 0.031$, $wR = 0.037$. $C_{45}H_{38}OP_2Pt$, $M_w = 851.8$, orthorhombic, $Pna2_1$ (No. 33), $a = 24.513(3)$, $b = 13.292(2)$, $c = 11.227(4)$ Å, $V = 3657.8$ Å^3, $Z = 4$, $D_x = 1.55$ g cm^{-3}, $F(000) = 1696$, 453 variables, $S = 1.24$, $\Delta/\sigma_{max}0.05$, $\Delta\rho_{max,min} = +0.81, -0.83$ eÅ^3.

Structure of [Pt(*trans*-PhCH=CHCOMe)(PPh_3)$_2$], **5b**

Data were collected using a crystal grown by slow evaporation from perdeuterotoluene, *ca* $0.35 \times 0.25 \times 0.20$ mm^3 on an Enraf–Nonius CAD4 diffractometer operating in the θ–2θ mode with $\Delta\theta = (0.8 + 0.35 \tan\theta)$ and a maximum scan time of 1 min, monochromated Mo-K_α radiation, $\lambda = 0.71069$ Å, $\mu = 38.8$ cm^{-1}. Unit-cell parameters were obtained from least squares fit of 25 reflections, $7.3 < \theta < 10.3°$. A total of 6616 independent reflections were measured for $2 < \theta < 25°$ and h 0–11, k −15 to 15, l −19 to 19. 5926 observed reflections with $|F^2| > 3\sigma(F^2)$, $\sigma(F^2) = \{\sigma^2(I) + (0.04I)^2\}^{1/2}/Lp$ were used in the refinement. Two reference reflections were remeasured every 60 min and showed a maximum deviation of 0.7%. Lorentz and polarization corrections and absorption correction by DIFABS [36] (max 1.19, min 0.89) were applied. The structure was solved by routine heavy-atom methods and non-

Table 10. Yield, melting point and analyses for complexes **1**–**7**

Complex	Yield (%)	M.p. (°C)[a]	Found (Calc.) (%) C	H	N
1a	84	188–194			
1b	85	136–140	60.7 (60.8)	5.3 (5.1)	1.5 (1.6)
1c	24	138–146			
2a	10	118–130			
2b	78	94–102			
3	82	120–124	60.5 (60.7)	4.6 (4.4)	
4a	70	105–108			
4b	83	118–124			
5a	92	190–196	65.1 (66.0)	4.7 (4.6)	
5b	60	178–182	63.0 (63.8)	4.6 (4.7)	
5c	92	182–188	64.2 (63.5)	4.7 (4.5)	
5d	94	172–184			
6a	96	139–143			
6b	81	126–134	60.3 (60.8)	4.7 (4.6)	
7a	96	150–160			
7b	63	124–128			

[a] All the complexes decompose on melting, hence the long melting ranges.

hydrogen atoms refined anisotropically by full-matrix least squares. The phenyl hydrogen atoms were fixed at calculated positions ($B_{iso} = 1.3B_{eq}$ for parent atom) and the other hydrogen atoms were freely refined. The weighting scheme was $w = 1/\sigma^2(F)$, $\Sigma w|F_o|-|F_c|)^2$ minimized, and the final residuals were $R = 0.019$, $wR = 0.026$. $C_{46}H_{40}OP_2Pt$, $M_w = 865.9$, triclinic, $P\bar{1}$, $a = 9.667(1)$, $b = 12.859(2)$, $c = 16.571(3)$ Å, $\alpha = 76.62(1)$, $\beta = 84.13(1)°$, $\gamma = 70.04(1)°$, $V = 1883.0$ Å^3, $Z = 2$, $D_x = 1.53$ g cm^{-3}, $F(000) = 864$, Δ/σ_{max} 0.4, $\Delta\rho_{max,min} = +0.85, -0.83$ eÅ^3.

Reactions of complexes **1–7** *with* PCy_3

The complexes **1–7** were formed *in situ* by addition of the relevant alkene (1 : 1 molar ratio) to a dry, degassed solution of $[Pt(C_2H_4)(PPh_3)_2]$ in $C_6D_5CD_3$ (0.5 cm^3) in an NMR tube. The tube was then cooled to −70°C and a solution of PCy_3 (1 : 1 molar ratio with platinum) in $C_6D_5CD_3$ (0.5 cm^3) was added. The NMR tube was shaken carefully and the ^{31}P NMR spectrum recorded at −70 and −50°C, and then allowed to equilibrate at 5°C over 2–3 weeks.

Acknowledgements—We thank the EPSRC and Johnson Matthey plc for a CASE grant (to S.E.D.) and Johnson Matthey plc for a generous loan of platinum salts.

REFERENCES

1. Chaloner, P. A. and Broadwood-Strong, G. T. L., *J. Organomet. Chem.*, 1989, **362,** C21.
2. Chicote, M. T., Green, M., Spencer, J. L., Stone F. G. A. and Vicente, J., *J. Organomet. Chem.*, 1977, **137,** C8.
3. Schorpp, K. and Beck, W., *Z. Naturforsch.*, 1973, **28B,** 738.
4. White, M. R. and Stang, P. J., *Organometallics*, 1983, **2,** 1654; Sharp, T. R., White, M. R., Davis, J. F. and Stang, P. J., *Org. Mass Spectrom.*, 1984, **19,** 107.
5. Osborn, J. A., *J. Chem. Soc., Chem. Commun.*, 1968, 1231.
6. Pellizer, G., Graziani, M., Lenarda, M. and Heaton, B. T., *Polyhedron*, 1983, **2,** 657; Cenini, S., Ugo, R. and La Monica, G., *J. Chem. Soc., A*, 1971, 409; Cenini, R., Ugo, R., Bonati, F. and La Monica, G., *Inorg. Nucl. Chem. Lett.* 1967, **3,** 191.
7. Chatt, J., Shaw, B. L. and Williams, A. A., *J. Chem. Soc.*, 1962, 3269.
8. Visser, J. P., Schipperijn, A. J. and Lukas, J., *J. Organomet. Chem.*, 1973, **47,** 433.
9. Cook, D. J., Green, M., Mayne N. and Stone, F. G. A., *J. Chem. Soc., A*, 1968, 1771; Booth, B. L., Haszeldine R. N. and Tucker, N. I., *J. Organomet. Chem.*, 1968, **11,** P5.
10. Gilchrist, T. L., Graveling F. J. and Rees, C. W., *J. Chem. Soc., Chem. Commun.*, 1968, 821; Sanders, W. D., Laird, B. B. and Davies, R. E., *J. Am. Chem. Soc.*, 1981, **103,** 970.
11. Gassman, P. G. and Cesa, I. G. *Organometallics*, 1984, **3,** 119; Godleski, S. A., Gundlach K. B. and Valpey, R. S., *Organometallics*, 1985, **4,** 296.
12. Parker D. and Taylor, R. J., *J. Chem. Soc., Chem. Commun.*, 1987, 1781; *Tetrahedron*, 1988, **44,** 2241.
13. Halpern, J. and Weil, T. A., *J. Chem. Soc., Chem. Commun.*, 1973, 631; Nelson, J. H., Jonassen, H. B. and Roundhill, D. M., *Inorg. Chem.*, 1969, **8,** 2591; Tripathy, P. B. and Roundhill, D. M., *J. Organomet. Chem.*, 1970, **24,** 247; Newkome, G. R. and McClure, G. L., *J. Am. Chem. Soc.*, 1974, **96,** 617; Bennett, M. A. and Yoshida, T. *J. Am. Chem. Soc.*, 1978, **100,** 1750; Smart, L. E., Browning, J., Green, M., Laguna, A., Spencer, J. L. and Stone, F. G. A., *J. Chem. Soc., Dalton Trans.*, 1977, 1777.
14. Chaloner, P. A., Davies, S. E. and Hitchcock, P. B., *J. Organomet. Chem.*, in press.
15. We thank Chris DeArmitt for a sample of CH_2=CHCONMcPh.
16. Mason R. and Meek, D. W., *Angew. Chem., Int. Ed. Engl.*, 1978, **17,** 183.
17. Pregosin, P. S., *Ann. Rep. NMR Spec.*, 1986, **17,** 285.
18. Pellizer, G., Lenarda, M., Ganzerla, R. and Graziani, M., *Gazz. Chim. Ital.*, 1986, **116,** 155.
19. Nicolaides, A., Smith, J. M., Kumar, A., Barnhart D. M. and Borden, W. T., *Organometallics*, 1995, **14,** 3475.
20. Hall, P. W., Puddephatt, R. J. and Tipper, C. F. H., *J. Organomet. Chem.*, 1974, **71,** 145.
21. Castellano, S. and Bothney-By, A. A., *J. Chem. Phys.* 1964, **41,** 3863.
22. Lenarda, M., Ganzerla, R., Lisini, A., Graziani, M. and Boschi, T., *Trans. Met. Chem.*, 1981, **6,** 199.
23. Barbaran, J. M. and McGinnety, J. A., *Inorg. Chem.*, 1974, **13,** 2864.
24. Osborne, R. B., Lewis, H. C. and Ibers, J. A., *J. Organomet. Chem.*, 1981, **208,** 125.
25. Cheng, P.-T. and Nyberg, S. C., *Can. J. Chem.*, 1972, **50,** 912.
26. Caruso, F., Camalli, M., Pellizer, G., Asaro, F. and Lenarda, M., *Inorg. Chim. Acta*, 1991, **181,** 167.
27. Francis, J. N., McAdam, A. and Ibers, J. A. *J. Organomet. Chem.*, 1971, **29,** 131.
28. Pannattoni, C., Graziani, R., Bandoli, G., Clements, D. A. and Belluco, U., *J. Chem. Soc., B*, 1970, 371.
29. Choi, H., Hershberger, J. W., Pinhas, A. R. and Ho, D. M., *Organometallics*, 1991, **10,** 2930.
30. Jason, M. E. and McGinnety, J. A., *Inorg. Chem.*, 1975, **14,** 3025.
31. Albright, T. A., Hoffmann, R., Thibeault, J. C. and Thorn, D. L., *J. Am. Chem. Soc.*, 1979, **101,** 3801.
32. Tolman, C. A., *Chem. Rev.* 1977, **77,** 313.
33. Tolman, C. A., *J. Am. Chem. Soc.*, 1974, **96,** 2780.
34. Gillard, R. D. and Pilbrow, M. F., *J. Chem. Soc., Dalton Trans.*, 1974, 2320.
35. Nagel, U., *Chem. Ber.*, 1982, **115,** 1998.
36. Walker, N. and Stuart, D., *Acta Cryst.* 1983, **A39,** 158.

Pergamon

PII: S0277-5387(96)00353-1

Polyhedron Vol. 16, No. 5, pp. 777–780, 1997
Copyright © 1996 Elsevier Science Ltd
Printed in Great Britain. All rights reserved
0277-5387/97 $17.00 + 0.00

Crystal and molecular structure of cyclo-tetrakis[μ-oxo-bis(2,2,6,6-tetramethylheptan-3,5-dionate)titanium(IV)] pentane adduct

Sergei I. Troyanov* and Oleg Yu. Gorbenko

Moscow State University, Chemistry Department, Vorobjevy Gory, 119899 Moscow, Russia

(Received 1 April 1996; accepted 17 July 1996)

Abstract—The X-ray crystal structure of titanium(IV) oxo-bis-2,2,6,6-tetramethylheptan-3,5-dionate, pentane (1 : 1) adduct has been determined. The tetrameric molecule of $[TiO(thd)_2]_4$ contains a nearly planar $(Ti—O)_4$ ring with two Ti atoms on a twofold axis. Compared with the dimeric titanium oxo-bis-(acetylacetonate), another type of TiO_6 octahedral connection takes place, namely through vertices instead of edges. Copyright © 1996 Elsevier Science Ltd

Keywords: β-diketonates; titanium; crystal structure.

Various volatile titanium compounds, firstly alkoxides, have been used as precursors for CVD of ferroelectrics like $(Ba,Sr)TiO_3$ and $PbZr_{1-x}Ti_xO_3$. Besides high volatility, important characteristics of the precursors are their thermal and hydrolytic stability, decomposition mechanism and by-products. It has been shown that $(Ba,Sr)TiO_3$ thin films, prepared by liquid source CVD using $TiO(thd)_2$ (thd = 2,2,6,6-tetramethylheptan-3,5-dionate) instead of the more volatile $Ti(OPr^i)_4$ and $Ti(OPr^i)_2(thd)_2$, demonstrated better step coverage and improved electrical properties [1,2]. The thermal properties of $TiO(thd)_2$ have been reported [3,4].

The molecular structure of $TiO(thd)_2$, which could be useful for understanding its properties, has not been reported so far. The analogous acetylacetonate (=acac) derivative, $TiO(acac)_2$, is known to be dimeric [5].

EXPERIMENTAL

Synthesis

Titanium oxo-β-diketonates can be prepared by the hydrolysis of bis(alkoxy)bis(β-diketonate)titanium(IV) [6] or dihalobis(β-diketonate)titanium(IV) [7] and by oxidation of tris(β-diketonate) titanium(III) [3,8]. With excess β-diketone some titanium(IV) alkoxides convert to titanium oxo-β-diketonates [9].

Preliminary study had shown that $Ti(OPr^i)_2(thd)_2$ is rather stable to hydrolysis, in accordance with the considerations in ref. [10]: no mass change was observed for a 1 g sample held in air for 6 h. Under the same conditions $Ti(OPr^i)_2(acac)_2$ was completely converted to $TiO(acac)_2$ in 2 h. More severe conditions should be used to hydrolyse $Ti(OPr^i)_2(thd)_2$. To our knowledge the compound is not inclined to ether elimination, at least up to 150°C. Thus, we believe that the procedure described below resulted from hydrolysis rather than from an elimination reaction.

About 1 g of $Ti(OPr^i)_2(thd)_2$ was dissolved in the minimal quantity of acetone containing traces of water at room temperature. The solution was heated to boiling point for a few minutes. After slow cooling fine, plate-like crystals were formed, which were separated by decantation and recrystallized from pentane.

Crystal structure determination

The selected crystal with approximate dimensions $0.2 \times 0.2 \times 0.3$ mm^3 was sealed in a Lindemann glass capillary. The data were collected at room temperature on an Enraf–Nonius CAD-4 diffractometer

* Author to whom correspondence should be addressed.

(Mo-K_α radiation, graphite monochromator, θ–2θ scan method, $\theta_{max} = 24°$). The crystallographic calculations were performed using the SHELXS-86 and SHELXL-93 program packages [1]. The structure was solved using a combination of direct and Fourier methods and refined by the full-matrix least-squares technique with anistropic thermal parameters for all non-hydrogen atoms.

The tert-butyl groups have been found to be strongly disordered between two positions around their pseudo-threefold axes. After refinement the occupancies of the more abundant configurations have been found to be in the range 0.56–0.83. The positions of the hydrogen atoms were calculated using a riding model and included in the structure factor calculation. Crystal data and structure refinement parameters for $[TiO(thd)_2]_4 \cdot C_5H_{12}$ are given in Table 1. Selected bond lengths are summarized in Table 2 and selected angles in Table 3. Atomic coordinates, bond lengths and distances and thermal parameters have been deposited at the Cambridge Crystallographic Data Centre.

Powder diffraction measurement (θ–2θ scan) was performed with a DRON-3M diffractometer using Co-K_α radiation in the 2θ range 6–50°. The experimental and calculated diffraction patterns (see Supplementary data) agree satisfactorily, indicating a formation of only one solid phase.

RESULTS AND DISCUSSION

The tetrameric molecule of $[TiO(thd)_2]_4$ with two Ti atoms [Ti(2) and Ti(3)] lying on a crystallographic two-fold axis is shown in Fig. 1. The pentane molecules, strongly disordered in the $[TiO(thd)_2]_4 \cdot C_5H_{12}$ structure, are trapped in the holes between tetrameric molecules near the centre of inversion at coordinates (0.25, 0.25, 0). No chemical bonding to $[TiO(thd)_2]_4$ takes place.

Four Ti atoms lie in a plane forming a square. Two independent Ti—Ti distances are equal 3.598 Å. The μ-oxo atoms are nearly in the same plane, but they are shifted out from the square sides. Similar tetranuclear $(Ti—O)_4$ rings have been found in $[Cp'TiX(\mu\text{-}O)]_4$ derivatives, where $Cp' = C_5H_{5-n}Me_n$; $n = 0, 1, 4, 5$; X = Cl, Br [12–14]. In the Br complex [12], there is a planar (but not square) Ti—O arrangement with Ti—O 1.80–1.82 Å, and the O—Ti—O angle of 103–106. In most other structures, the Ti—O distances are 1.78–1.82 Å with O—Ti—O angles in the range 103–105°.

In the $[TiO(thd)_2]_4$ molecule each titanium atom has a distorted octahedral coordination. Three pairs of Ti—O bonds are present: the short Ti—O bonds

Table 1. Crystal data and structure refinements for $[TiO(thd)_2]_4 \cdot C_5H_{12}$

Formula	$Ti_4O_{20}C_{88}H_{152} \cdot C_5H_{12}$
Formula weight	1793.83
Crystal system	Monoclinic
Space group	*C*2/*c*
a (Å)	25.016(5)
b (Å)	18.267(4)
c (Å)	26.492(5)
β (°)	116.77(3)
V (Å^3)	10809(4)
Z	4
D_c (g cm^{-3})	1.103
μ (cm^{-1})	3.43
Radiation (Å)	Mo-K_α, 0.71073
Reflections measured	7133
Unique reflections	6749 [*R*(int) = 0.1080]
Data/restraints/parameters	6500/116/792
Goodness-of-fit on F^2	0.939
wR_2(on F^2)	0.1236
R_1 [$I > 2\sigma(I)$]	0.0525
Largest diff. peak and hole (eÅ^{-3})	0.293 and −0.239

Table 2. Selected bond lengths for $[TiO(thd)_2]_4$

Ti(1)—O(2)	1.804(3)	Ti(1)—O(1)	1.818(3)
Ti(1)—O(7)	1.965(3)	Ti(1)—O(10)	1.969(3)
Ti(1)—O(8)	2.116(3)	Ti(1)—O(9)	2.117(4)
Ti(2)—O(2)	1.810(3)	Ti(2)—O(5)	1.969(3)
Ti(2)—O(6)	2.120(3)	Ti(3)—O(1)	1.793(3)
Ti(3)—O(3)	1.968(3)	Ti(3)—O(4)	2.132(4)
O(3)—C(3)	1.283(6)	O(4)—C(5)	1.234(6)
O(5)—C(14)	1.286(6)	O(6)—C(16)	1.263(6)
O(7)—C(25)	1.280(6)	O(8)—C(27)	1.241(6)
O(9)—C(36)	1.282(6)	O(10)—C(38)	1.279(5)
C(3)—C(4)	1.345(7)	C(4)—C(5)	1.425(7)
C(14)—C(15)	1.364(7)	C(15)—C(16)	1.397(7)
C(25)—C(26)	1.376(7)	C(26)—C(27)	1.421(7)
C(36)—C(37)	1.391(7)	C(37)—C(38)	1.375(7)

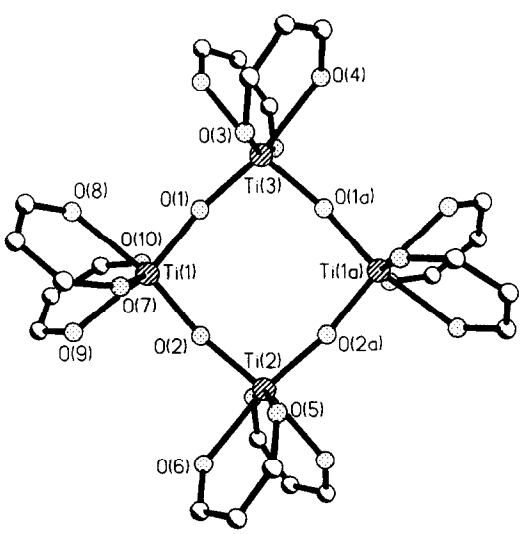


Fig. 1.

Table 3. Selected bond angles for $[TiO(thd)_2]_4$

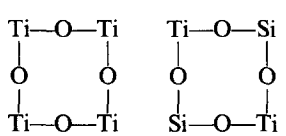
O(2)—Ti(1)—O(1)	100.47(13)	O(2)—Ti(1)—O(7)	90.31(14)
O(1)—Ti(1)—O(7)	102.88(14)	O(2)—Ti(1)—O(10)	102.47(14)
O(1)—Ti(1)—O(10)	90.12(14)	O(7)—Ti(1)—O(10)	159.91(14)
O(2)—Ti(1)—O(8)	168.37(14)	O(1)—Ti(1)—O(8)	88.62(14)
O(7)—Ti(1)—O(8)	80.52(14)	O(10)—Ti(1)—O(8)	84.60(14)
O(2)—Ti(1)—O(9)	92.0(2)	O(1)—Ti(1)—O(9)	165.57(14)
O(7)—Ti(1)—O(9)	84.09(14)	O(10)—Ti(1)—O(9)	80.07(13)
O(8)—Ti(1)—O(9)	80.00(14)	O(2)—Ti(2)—O(2)′	100.3(2)
O(2)—Ti(2)—O(5)	103.14(14)	O(2)′—Ti(2)—O(5)	89.93(13)
O(2)′—Ti(2)—O(5)′	103.14(14)	O(5)—Ti(2)—O(5)′	159.7(2)
O(2)—Ti(2)—O(6)′	166.95(14)	O(5)—Ti(2)—O(6)′	84.02(13)
O(2)—Ti(2)—O(6)	90.52(14)	O(5)—Ti(2)—O(6)	80.42(13)
O(6)′—Ti(2)—O(6)	79.8(2)	O(1)′—Ti(3)—O(1)	99.4(2)
O(1)—Ti(3)—O(3)′	101.99(14)	O(1)—Ti(3)—O(3)	90.03(14)
O(3)′—Ti(3)—O(3)	161.5(2)	O(1)—Ti(3)—O(4)′	91.38(14)
O(3)—Ti(3)—O(4)′	85.27(14)	O(1)—Ti(3)—O(4)	166.94(14)
O(3)—Ti(3)—O(4)	80.45(14)	O(4)′—Ti(3)—O(4)	79.0(2)
Ti(3)—O(1)—Ti(1)	170.3(2)	Ti(1)—O(2)—Ti(2)	169.3(2)
C(3)—O(3)—Ti(3)	133.4(4)	C(5)—O(4)—Ti(3)	130.7(4)
C(14)—O(5)—Ti(2)	133.2(3)	C(16)—O(6)—Ti(2)	130.6(4)
C(25)—O(7)—Ti(1)	133.3(3)	C(27)—O(8)—Ti(1)	131.7(4)
C(36)—O(9)—Ti(1)	131.0(4)	C(38)—O(10)—Ti(1)	133.9(3)
O(3)—C(3)—C(4)	124.2(5)	O(3)—C(3)—C(2)	113.1(5)
C(4)—C(3)—C(2)	122.7(5)	O(4)—C(5)—C(4)	122.7(5)
C(3)—C(4)—C(5)	122.8(5)	O(5)—C(14)—C(15)	123.4(5)
O(4)—C(5)—C(6)	118.1(5)	O(6)—C(16)—C(15)	123.0(5)
O(5)—C(14)—C(13)	113.9(5)	O(7)—C(25)—C(26)	123.5(5)
C(14)—C(15)—C(16)	122.8(5)	C(25)—C(26)—C(27)	122.0(5)
O(6)—C(16)—C(17)	116.0(5)	O(8)—C(27)—C(28)	118.2(5)
O(7)—C(25)—C(24)	114.3(5)	O(9)—C(36)—C(35)	116.3(5)
O(8)—C(27)—C(26)	122.8(5)	O(10)—C(38)—C(37)	122.1(5)
O(9)—C(36)—C(37)	120.9(5)	O(10)—C(38)—C(39)	114.5(5)
C(38)—C(37)—C(36)	124.8(5)		

Symmetry transformation code (′): $-x, y, \frac{1}{2}-z$.

in nearly linear Ti—O—Ti bridges (*ca* 1.81 Å), the long Ti—O bonds with oxygen, *trans* to μ-O (*ca* 2.12 Å) and the Ti—O bonds of the intermediate length with O, *cis* to μ-O (*ca* 1.96 Å). This last value is close to the Ti—O distances in rutile (1.944 and 1.988 Å) [15]. Variations in O—Ti—O angles in the TiO_6 octahedra follow the change of bond lengths (Table 3): the angle between short Ti—O bonds is *ca* 100°, that between long bonds is *ca* 80°, deviations from 90°C being equal in magnitude. Thus, the strong *trans* influence is clearly observed in the plane of the $(Ti—O)_4$ ring. Similar pairs of bonds were found in $[TiO(acac)_2]_2$, with bond lengths 1.83, 1.97 and 2.06 Å, respectively.

Owing to the rigidity of the β-diketonate ligand only one coordination mode is possible: with one oxygen atom in the *cis* position to μ-O and another one in the *trans* position. The latter is out of the $(Ti—O)_4$ ring plane by more than 0.25 Å. The Ti—O(*cis*) bond is nearly orthogonal to the Ti—O bond with μ-O, which is in the *trans* position to another oxygen of the same β-diketonate ligand; for example, O(1)—Ti(1)—O(10) $\approx$ O(2)—Ti(1)—O(7) $\approx 90°$. Corresponding angles in dimeric $[TiO(acac)_2]_2$ are more distorted (*ca* 93°). This is probably owing to the difference in the oxygen bridges: Ti—O—Ti angle *ca* 170° in $[TiO(thd)_2]_4$ and *ca* 97° in $[TiO(acac)_2]_2$. The TiO_6 octahedra are connected by edges in the latter compound and by vertices in the former. Such behaviour is not surprising taking into account that *tert*-butyl groups occupy more space than methyl groups, thus some steric hindrance would occur in the case of edge connection.

Recently, the structure of $[TiO(acac)_2]_2[SiO(OBu^t)_2]_2$ has been reported [16]. It is very similar to that of $[TiO(thd)_2]_4$. The bond lengths and angles in the TiO_6 octahedra are close: for instance the Ti—O distance in the bridge is 1.80 Å, and the O—Ti—O angles in the chelate rings are *ca* 83°. The eight-membered titanosiloxane cycle is also nearly planar:



One could expect that such a molecular structure could be a template for special oxide phases formed

by decomposition of the precursors. For instance, the $(Ti—O)_4$ ring can easily support the formation of the (TiO_2) plane of the perovskite structure of $(Ba,Sr)TiO_3$.

Acknowledgement—This work was partly supported by Volkswagen Foundation grant NI/69341.

REFERENCES

1. Kawahara, T., Yamamuka, M., Makita, T., Naka, J., Yuuki, A., Mikami, N. and Ono, K., *Jpn J. Appl. Phys.*, 1994, **33,** 5129, 5897.
2. Kawahara, T., Yamamuka, M., Makita, T., Yuuki, A., Mikami, N. and Ono, K., *Mat. Res. Soc. Proc.*, 1995, **361,** 361.
3. Kandybin, M. V., Durasov, V. B. and Igumenov, I. K., *Sib. Khim. Zh.*, 1993, 19.
4. Kandybin, M. V., Igumenov, I. K. and Yushina, I. V., *Zh. Neorg. Khim.*, 1994, **39,** 773.
5. Smith, G. D., Caughlan, C. N. and Campbell, J. A., *Inorg. Chem.*, 1972, **11,** 2989.
6. Yamamoto, A. and Kambara, S., *J. Am. Chem. Soc.*, 1957, **79,** 4344.
7. Serpone, N. and Fay, R. C., *Inorg. Chem.*, 1967, **6,** 1835.
8. Collis, R. E., *J. Chem. Soc. (A)*, 1969, 1895.
9. Puri, C. M., Pande, K. C. and Mehrotra, R. C., *J. Less-Common Met.*, 1962, **4,** 393.
10. Rubtzov, E. M., *Koord. Khim.*, 1989, **15,** 579.
11. Sheldrick, G. M., SHELXL-93, Program for crystal structure refinement, University of Göttingen, Göttingen, 1986; Sheldrick, G. M., *Acta Cryst.*, 1990, **A46,** 467.
12. Troyanov, S. I., Varga, V. and Mach, K., *J. Organomet. Chem.*, 1991, **201,** 402.
13. Petersen, J. L., *Inorg. Chem.*, 1980, **19,** 181.
14. Skapsky, A. C. and Troughton, P. G. H., *Acta Cryst.*, 1970, **B26,** 716.
15. Baier, W H., *Acta Cryst.*, 1956, **9,** 515.
16. Gunji, T., Kasahara, Fuji, A., Abe, Y. and Kawano, M., *Bull. Chem. Soc. Jpn*, 1995, **68,** 2975.

Pergamon

PII: S0277-5387(96)00344-0

Polyhedron Vol. 16, No. 5, pp. 781–787, 1997
Copyright © 1996 Elsevier Science Ltd
Printed in Great Britain. All rights reserved
0277-5387/97 $17.00+0.00

Supramolecular self-organization in methyl(diphenylphosphinothioato)mercury(II), [HgMe{S(O)PPh$_2$}], a polymer containing $Hg_2O_2P_2S_2$ eight-membered rings interconnected through secondary Hg···O bonds

José S. Casas,* Alfonso Castiñeiras, Ionel Haiduc,*† Agustín Sánchez, José Sordo and Ezequiel M. Vázquez-López

Departamento de Química Inorgánica, Facultade de Farmacia, Universidade de Santiago de Compostela, E-15706 Santiago de Compostela, Galicia, Spain

(Received 19 January 1995; accepted 17 July 1996)

Abstract—Methyl- and phenylmercury(II) diphenylphosphinothioates [HgR{S(O)PPh$_2$}] (R = Me and Ph) were synthesized. In [HgMe{S(O)PPh$_2$}] the mercury atom is coordinated to the methyl carbon atom and to the ligand sulfur atom. Intermolecular Hg···O interactions form a supramolecular ribbon structure along the *b*-axis. The IR and NMR (^{1}H, ^{13}C, ^{31}P and ^{199}Hg) spectra of the two compounds are discussed. Copyright © 1996 Elsevier Science Ltd

Keywords: supramolecular chemistry; methylmercury(II); phenylmercury(II); phosphinothioates; X-ray structure; multinuclear NMR.

Organometallic derivatives of oxo and thio phosphorus acids are frequently supramolecular compounds, in which the molecular units are associated through secondary and/or dative bonds. This association is due to the tendency of the metal in the organometallic coordination centre to increase its coordination number, and to the ability of the oxo and thio organophosphorus moieties to act as bridging ligands. From supramolecular chemistry being defined as "the chemistry of molecular assemblies and of intermolecular bond", dealing with "organized entities that result from the association of two or more chemical species held together by intermolecular forces" [1], it follows that the structures of the type reported here can be described as "supramolecular".

Among the organophosphorus anions which serve as ligands, the phosphinothioates (monothiophosphinates), R_2POS^-, are particularly interesting, due to their ambident character and to the simultaneous presence in the molecule of soft donor (sulfur) and hard donor (oxygen) sites. This may have interesting structural consequences. It has been shown previously that organometallic derivatives of these anionic ligands are associated into supramolecular, polymeric structures. Examples include [SbPh$_2${O(S)PPh$_2$}]$_n$ [2], [SnMe$_3${O(S)PMe$_2$}]$_n$ [3], [SnMe$_2${O(S)PPh$_2$}$_2$]$_n$ [4] and [TlMe$_2${O(S)PPh$_2$}]$_n$ [5]. Supramolecular structures are also found in phosphorodithioates (dithiophosphates), phosphinodithioates (dithiophosphinates), dithioarseniates and other functional organometallic derivatives [6].

The formation of supramolecular structures involves a process of self-organization, which goes beyond the simple packing of molecules in the crystal lattice. In addition to the primary bonds which connect the ligand to the organometallic coordination centre, such structures may contain intramolecular and intermolecular secondary bonds, that are defined by interatomic distances intermediate between the sum of covalent radii and the sum of van der Waals radii [7]. The former usually lead to cyclizations and

* Authors to whom correspondence should be addressed.
† European Community Visiting Scientist from Facultatea de Chimie, Universitatea "Babes-Bolyai", RO-3400 Cluj-Napoca, Romania.

the latter connect the building units into supramolecular structures.

We now report the supramolecular structure of methyl(diphenylphosphinothioato)mercury(II), $[HgMe\{S(O)PPh_2\}]_n$, as determined by X-ray diffraction. The probably isostructural phenylmercury derivative, $[HgPh\{S(O)PPh_2\}]$, was also prepared.

EXPERIMENTAL

Diphenylphosphinothioic acid, $Ph_2P(S)OH$, was prepared according to a literature method [8]. Methylmercury(II) hydroxide and phenylmercury(II) acetate (Ventron) were used as received. The instruments used for spectroscopic characterization were as described earlier [9–11].

Preparation of $[HgMe\{S(O)PPh_2\}]_n$

Diphenylphosphinothioic acid (0.234 g, 1 mmol), dissolved in 20 cm^3 ethanol, was mixed with a solution of 0.233 g (1 mmol) methylmercury(II) hydroxide in water at room temperature, and stirred for 2 h. A white crystalline substance deposited after concentrating the solution. The solid was filtered, washed with heptane and dried. Yield: 0.331 g (73.8%), m.p. 137–138°C (with decomposition). Found: C, 34.3; H, 3.0; S, 7.8. $C_{13}H_{13}OPSHg$ requires: C, 34.8; H, 2.9; S, 7.1%. IR spectrum (cm^{-1}, KBr pellets): $\nu(P\cdots O)$ = 1163 vs, $\nu(P—S)$ = 696s.

Preparation of $[HgPh\{S(O)PPh_2\}]$

A solution containing 0.674 g (2 mmol) phenylmercury(II) acetate in 30 cm^3 ethanol was mixed with a solution containing 0.468 g (2 mmol) of diphenylphosphinothioic acid in 25 cm^3 ethanol, and allowed to stand without stirring. After *ca* 10 min, a white crystalline precipitate (long needles) deposited. That was filtered, washed with heptane and dried. Yield: 0.733 g (75.7%), m.p. 181–183°C (with decomposition). Found: C, 42.9; H, 3.0; S, 6.7. $C_{18}H_{15}OPSHg$ requires: C, 42.3; H, 3.0; S, 6.3%. IR spectrum (cm^{-1}, KBr pellets): $\nu(P\cdots O)$ = 1169vs, $\nu(P—S)$ = 698s.

Crystal structure determination of $[HgMe\{S(O)PPh_2\}]$

Collection and reduction of X-ray data. A colourless prismatic crystal of approximate dimensions $0.02 \times 0.2 \times 0.4$ mm^3 was analysed in a CAD4 Enraf–Nonius diffractometer, at room temperature (293 K), using Mo-K_α ($\lambda = 0.71073$ Å) graphite monochromated radiation.

Crystal data. $C_{13}H_{13}OPSHg$, $M = 448.88$, monoclinic, space group $C2/c$ (no. 15), $a = 26.339(2)$, $b = 6.177(1)$, $c = 17.702(5)$ Å, $\beta = 96.118(1)°$ and $V = 2863.7(9)$ $Å^3$, $Z = 8$, $D_{calc} = 2.082$ g cm^{-3}, $F(000) = 1680$, $\mu = 10.988$ mm^{-1}.

The ω–2θ scan technique was used in the range 3–30°. Cell parameters were refined by a least-square procedure on the setting angles of 25 reflections ($6.5 \leqslant \theta \leqslant 13.6°$). Corrections were applied for Lorentz and polarization effects and for absorption [12]. A total of 4275 reflections were collected, of which 4144 were unique ($R_{int} = 0.0254$) and of these 3227 with $I > 2\sigma(I)$ were used for refinement.

The structure was solved by direct methods [13] and refined by a full-matrix least square procedure based on F^2 [14]. Non-hydrogen atoms were refined with anisotropic displacement parameters. Hydrogen atoms were included in the model at geometrically calculated positions [14]. The final R (on F) was 0.0356, R_w (on F^2) 0.0895 and goodness of fit was 1.078 for all observed reflections.

Further details of the crystal structure determination have been deposited with the Editor and the Cambridge Crystallographic Data Centre.

RESULTS AND DISCUSSION

The structure of methyl(diphenylphosphinothioato)mercury(II) consists of dimers, connected into an infinite ribbon running along the *b*-axis of the crystal. An ORTEP [15] drawing of the dimer, with the atom numbering scheme, is shown in Fig. 1 and that of the polymeric ribbon in Fig. 2. Selected interatomic distances and bond angles are given in Table 1.

The structure of the dimeric unit

In the monomeric $[HgMe\{S(O)PPh_2\}]$ moiety, the mercury atom forms the primary bonds with the methyl group [Hg—C(1) = 2.073(6) Å], and with the sulfur atom of the thiophosphorus ligand [Hg—S = 2.391(2) Å]. The phosphorus–oxygen bonds seem to retain a certain degree of double bond character [P—O = 1.489(4) Å] [5]. The phosphorus–sulfur bond is a single bond [P—S = 2.047(2) Å] [5]. The two primary bonds are basically co-linear [S—Hg—C = 177.3(2)°].

Monomeric units are joined in pairs through mercury–oxygen secondary interactions [$Hg\cdots O^{ii}$ = 2.897(4) Å, ii = $-x$, $-y+1$, $-z+2$, thereby forming an eight-membered ring of chair conformation (see Fig. 1)].

The transannular $Hg\cdots O$ distances are longer than the sum of the Van der Waals radii (3.23 Å) [16] and they suggest no secondary interaction.

The conformation of the eight-membered ring is clearly described by the bond angles S—P—O = 115.7(2)° (angle at phosphorus larger than tetrahedral) and Hg—S—P = 100.24(7)°. Other significant angles are $S—Hg\cdots O^{ii}$ = 91.96(9)°. Torsion angles are listed in Table 2.

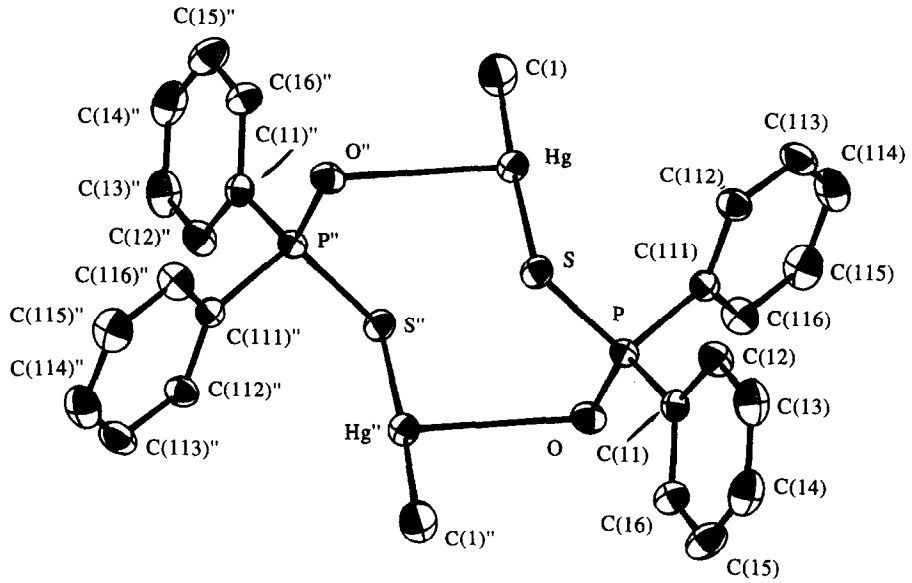


Fig. 1. ORTEP drawing showing asymmetric unit and the atom numbering scheme used.

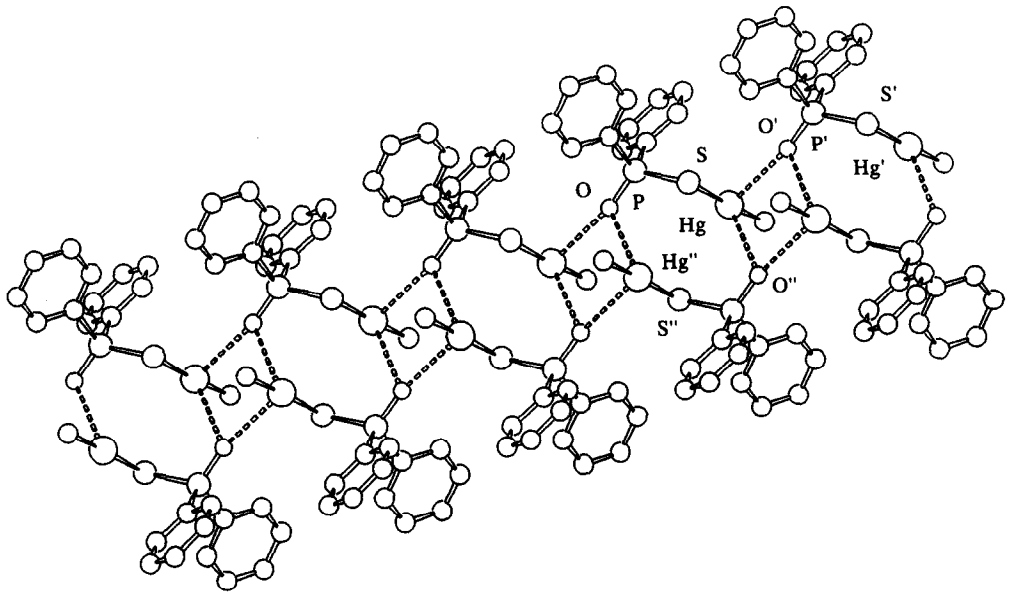


Fig. 2. View of polymeric ribbon along the *b*-axis (hydrogen atoms have been omitted).

Table 1. Selected interatomic distances (Å) and angles (°)[a]

Hg—C(1)	2.073(6)	P—S	2.047(2)
Hg—S	2.391(2)	P—O	1.489(4)
Hg—O^{i}	2.831(4)	P—C(11)	1.810(5)
Hg—O^{ii}	2.897(4)	P—C(111)	1.810(5)
Hg—S^{ii}	3.516(2)		
C(1)—Hg—S	177.3(2)	O^{i}—Hg—S^{ii}	149.24(8)
C(1)—Hg—O^{i}	94.8(2)	O^{ii}—Hg—S^{ii}	54.94(7)
S—Hg—O^{i}	84.49(9)	O—P—C(111)	110.6(2)
C(1)—Hg—O^{ii}	90.7(2)	O—P—C(11)	111.3(2)
S—Hg—O^{ii}	91.96(9)	C(111)—P—C(11)	107.0(2)
O^{i}—Hg—O^{ii}	95.61(9)	O—P—S	115.7(2)
C(1)—Hg—S^{ii}	94.2(2)	C(111)—P—S	108.9(2)
S—Hg—S^{ii}	87.65(4)	C(11)—P—S	102.7(2)
P—S—Hg	100.24(7)		

[a] Symmetry code: i = $x, -1+y, z$; ii = $-x, -y+1, -z$.

Table 2. Torsion angles (°)

Atom 1	Atom 2	Atom 3	Atom 4	Angle
C(1)	Hg	S	P	55.90(4.64)
Hg	S	P	O	79.74(0.19)
Hg	O^{i}	P^{i}	S^{i}	−13.30(0.23)
Hg	O^{ii}	P^{ii}	S^{ii}	−162.15(0.84)

Supramolecular association

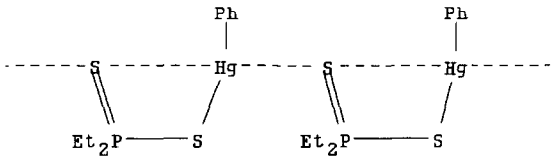
The dimers are further connected into a supramolecular ribbon structure (SCHAKAL [17] drawing is shown in Fig. 2) through additional Hg···O secondary interactions [Hg···O^{i} = 2.831(3) Å, i = $x, y-1, z$] slightly shorter than the Hg···O secondary bonds leading to the formation of the dimeric units. In the ribbon, eight-membered $Hg_2O_2P_2S_2$ rings alternate with four-membered Hg_2O_2 rings; the latter consist only of Hg···O secondary bonds. Figure 3 shows the Hg_2O_2 units as planar, and with the P—S bond (part of the eight-membered ring). Only the *ipso* carbons of the phenyl groups are shown, for clarity. When viewed along the *b*-axis, the mercury atoms are delineated in two parallel rows and the building units are in the eclipsed arrangement (Fig. 4). It can be seen that, within the ribbon, which is enveloped on the outside of the phenyl and methyl groups, there are channels delimited by the mercury, oxygen sulfur and phosphorus atoms.

If the secondary bonds are considered, the coordination geometry around the metal atom can be described as ψ-trigonal bipyramidal (distorted), with the sulfur atom and methyl group in axial positions and two Hg···O secondary interactions in equatorial positions; the distortion comes mostly from the O···Hg···O angles [O^{i}···Hg···O^{ii} = 95.61(9)°].

Comparison with other structures

In organoantimony [2] and organotin [3,4] phosphinothioate(monothiophosphinate) compounds, the metal–ligand primary bond is to oxygen (Sb—O, Sn—O), whereas in the organothallium compound [$TlMe_2\{S(O)PPh_2\}$] [5] the primary bond is through sulfur although, in this case, there are also a strong dative intermolecular O → Tl bond. According with the "softer" character of the mercury atom, in the compound discussed here the primary bond is Hg—S.

An interesting comparison can be made with other organomercury derivatives of dithiophosphorus ligands (phosphorodithioates and phosphinodithioates). Thus, both [$HgMe(S_2PPh_2)$] [9] and [$HgPh\{S_2P(OEt)_2\}$] [10] are discrete cyclic dimers, in which an eight-membered $Hg_2S_4P_2$ ring is formed through Hg···S intermolecular secondary interactions (*cf.* Hg—S = 2.379 Å and Hg···S = 3.152 Å in the phenyl derivative, and Hg—S = 2.383 Å and Hg···S = 3.323 Å in the ethoxy derivative). Unlike these, the compound [$HgPh(S_2PEt_2)$] [11] is a polymer (**1**) formed through Hg···S secondary bonds (3.183 Å) between four-membered chelate rings, which contain both primary (Hg—S = 2.375 Å) and secondary intermolecular (Hg···S = 3.182 Å) bonds.



1

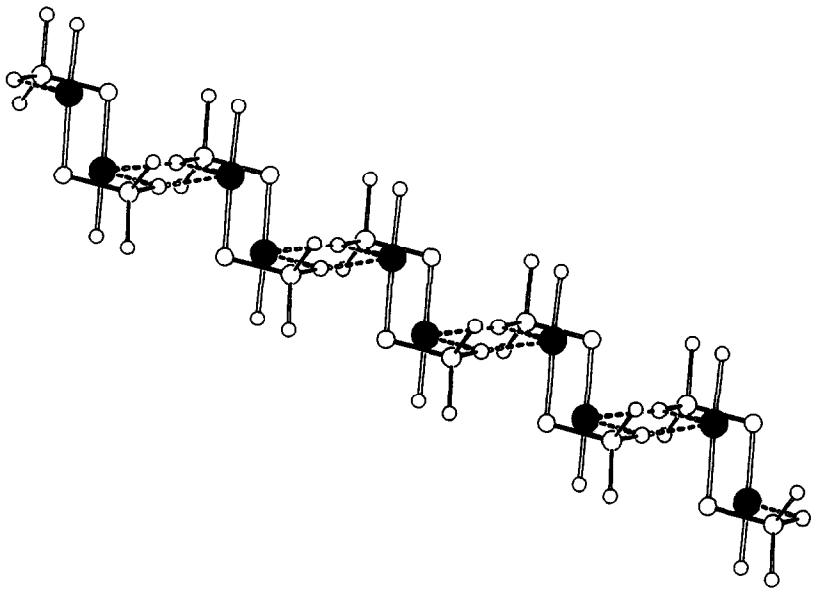


Fig. 3. View showing the ladder chain along the *b*-axis. For clarity hydrogen and carbon atoms, except those which are directly bonded to phosphorus and mercury atoms, are omitted.

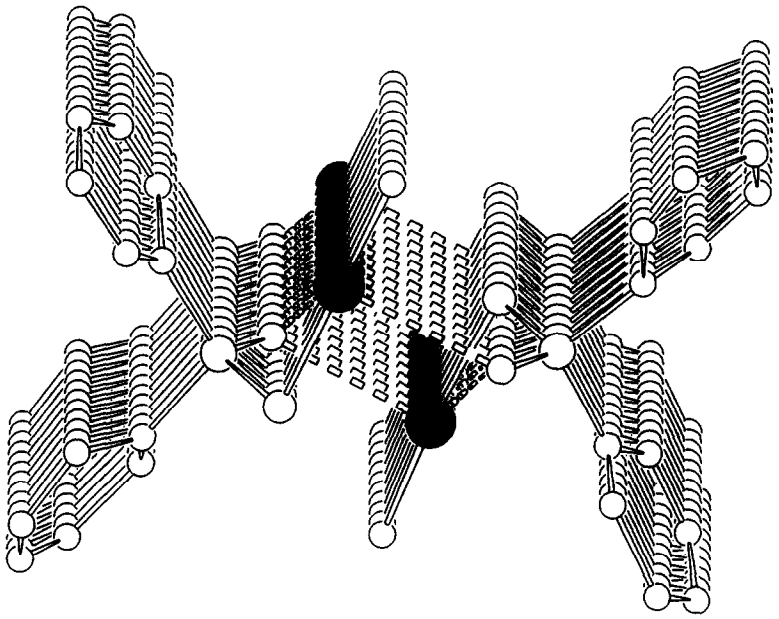


Fig. 4. View showing the eclipsed arrangement of the dimers (hydrogen atoms have been omitted).

Table 3. Significant NMR parameters[a]

Compound	$\delta(^1H(R—Hg))$	$^2J(^1H—^{199}Hg)$	$\delta(^{13}C(R—Hg))$	$^nJ(^{13}C—^{199}Hg)$	$\delta(^{31}P)$	$^2J(^{31}P—^{199}Hg)$	$\delta(^{199}Hg)$
$[HgMe\{S(O)PPh_2\}]$	0.95	183.6	12.57	1303	48.5s	106	−629s
$[HgPh\{S(O)PPh_2\}]$	$H_o = 7.28$[b]	177.4	$C_i = 157.95$	2099	48.2s	105	−967s
			$C_o = 135.99$	113			
			$C_m = 128.99$	179			
			$C_p = 128.40$	—			

[a] δ in ppm and J in Hz; s = singlet.
[b] Other signals are obscured by those of the ligand.

The compound described here are cyclic dimers connected by secondary Hg···O bonds (Fig. 2).

It is also worth mentioning that the structural diversity of inorganic mercury(II) [18] and organomercury(II) compounds of mono- and dithiophosphorus ligands, derived from a change in the peripheral organic groups, either at the metal or at phosphorus. This suggests that structural investigations of related derivatives is worthwhile and further work along these lines is in progress in our laboratory.

Spectroscopic studies

The similar values of the IR ν(P—S) and ν(P═O) bands (see Experimental section) suggest a similar coordination mode of the ligand in the two organomercury complexes.

Table 3 lists the relevant NMR data obtained in $CDCl_3$ for both compounds. The phosphorus is more shielded than in the dimethylthallium derivative [5] in accordance with the different behaviour of the ligand. It is interesting to note the presence of $^{31}P—^{199}Hg$ coupling satellites with a $^2J(^{31}P—^{199}Hg)$ value similar to that described for $[Hg(SCN)_2(SPBu_3)_2]$ [19]. This coupling is usually not observed in monoorganomercury(II) dithiophosphinates and dithiophosphates [9–11], suggesting a lower lability for the monothiophosphinato ligands [20]. The $\delta(^{13}C(R—Hg))$ and $^nJ(^{13}C—^{199}Hg)$ values are similar and in the phenylmercury derivative the $\delta(^{199}Hg)$ value is intermediate between those found in organomercuric dithiophosphinates and dithiophosphates [9–11].

Acknowledgements—We gratefully acknowledge partial financial support of this work and a visiting fellowship grant to I.H. from the Commission of the European Communities, Directorate for Science, Research and Development (Contract No. ERD-CIPA-CT-92-2108) under the Action "Cooperation in Science and Technology with Central and East European Countries". One of us (I.H.) also wishes to thank his colleagues at the University of Santiago de Compostela for their hospitality and spirit of cooperation during his stay in Spain (September–October 1993).

REFERENCES

1 (a) Lehn, J. M., in *Perspectives in Coordination Chemistry*, ed. Williams, A. F., Floriani, C. and Merbach, A. E. Verlag Helvetica Chimica Acta, Basel and VCH, Weinheim, 1992, p. 447; (b) Lehn, J. M., *Pure Appl. Chem.*, 1978, **50,** 871; (c) Lehn, J. M., *Angew. Chem.* 1988, **100,** 91; *Angew, Chem., Int. Edn Engl.* 1988, **27,** 89.
2. Begley, M. J., Sowerby, D. B., Wesolek, D. M., Silvestru, C. and Haiduc, I., *J. Organomet. Chem.*, 1986, **316,** 281.
3. Shihada, A. F., Jasim, I. A. A. and Weller, F., *J. Organomet. Chem.*, 1984, **268,** 125.
4. Silvestru, C., Haiduc, I., Caruso, F., Rossi, M., Mahieu, B. and Gielen, M., *J. Organomet. Chem.*, 1993, **448,** 75.
5. Casas, J. S., Castiñeiras, A., Haiduc, I., Sánchez, A., Sordo, J. and Vázquez-López, E. M., *Polyhedron*, 1994, **13,** 1805.
6. Haiduc, I., *Supramolecular Associations in Main Group Organometallic Chemistry*. Lecture given at the 12th Colloquio de la Academia Mexicana de Química Inorganica, "Química de los Elementos Representativos", UNAM, Mexico, DF, 5–6 August 1993 (to be published).
7. Alcock, N. W., *Adv. Inorg. Chem. Radiochem.*, 1972, **15,** 1.
8. Higgins, W. A., Vogel, P. W. and Graig, W. G., *J. Am. Chem. Soc.*, 1955, **77,** 1864.
9. Zukerman-Schpector, J., Vázquez-López, E. M., Sánchez, A., Casas, J. S. and Sordo, J., *J. Organomet. Chem.*, 1991, **405,** 67.
10. Vázquez-López, E. M., Castiñeiras, A., Sánchez, A., Casas, J. S. and Sordo, J., *J. Cryst. Spectrosc. Res.*, 1992, **22,** 403.
11. Casas, J. S., Castiñeiras, A., Sánchez, A., Sordo, J. and Vázquez-López, E. M., *J. Organomet. Chem.*, 1994, **468,** 1.
12. Walker, N. and Stuart, D., *Acta Cryst.*, 1983, **A39,** 158.
13. Sheldrick, G. M., SHELXS86, A Program for the Solution of Crystal Structure from X-ray Diffraction Data. University of Göttigen, Germany, 1986.
14. Sheldrick, G. M., SHELXL93, A Program for the Refinement of Crystal Structures from X-ray Diffraction Data. University of Göttingen, Germany, 1993.
15. Johnson, C. R., ORTEP. Report ORNL-3794.

Oak Ridge National Laboratory, TN, U.S.A., 1965.
16. Bondi, A., *J. Phys. Chem.*, 1964, **68,** 441; Canty, A. J. and Deacon, G. B., *Inorg. Chim. Acta*, 1980, **45,** 225.
17. Keller, E., SCHAKAL, A Program for Plotting Molecular and Crystal Structures. University of Freiburg, Germany, 1988.
18. Haiduc, I., *Rev. Inorg. Chem.* 1981, **3,** 353.
19. Colquhoun, I. J. and McFarlane, W., *J. Chem. Soc., Dalton Trans.*, 1981, 658.
20. Bond, A. M., Colton, R., Dakternieks, D., Dillon, M. L., Hauenstain, J. and Moir, J. E., *Aust. J. Chem.*, 1981, **34,** 1393.

Pergamon

PII: S0277-5387(96)00343-9

Polyhedron Vol. 16, No. 5, pp. 789–794, 1997
Copyright © 1996 Elsevier Science Ltd
Printed in Great Britain. All rights reserved
0277-5387/97 $17.00+0.00

Synthesis and characterization of 3-hydroxy-4-pyridinone-oxovanadium(IV) complexes

John Burgess,[a] Baltazar De Castro,[b] Celeste Oliveira,[c] Maria Rangel[c]* and Walkiria Schlindwein[d]

[a]Department of Chemistry, University of Leicester, Leicester LE1 7RH, U.K.

[b]Departamento de Química, Faculdade de Ciências do Porto, 4050 Porto, Portugal

[c]Instituto de Ciências Biomédicas de Abel Salazar, 4050 Porto, Portugal

[d]Chemistry Department, De Montfort University, Leicester LE1 9BH, U.K.

(Received 28 June 1996; accepted 12 July 1996)

Abstract—The synthesis and characterization of several new bis-ligand-oxo-vanadium(IV) complexes containing 1,2-substituted-3-hydroxy-4-pyridinonates or ethylmaltolate (3-hydroxy-2-ethyl-pyranonate) are reported. Structures are proposed based on EXAFS data. Copyright © 1996 Elsevier Science Ltd

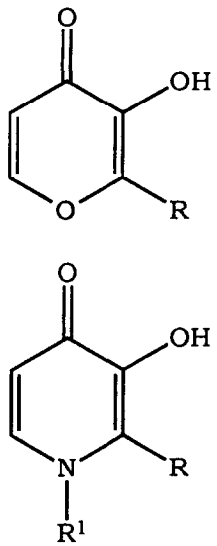
Keywords: vanadium(IV) complexes; pyranonate and pyridinonate complexes; EXAFS; UV–vis spectra.

Since the seventies, vanadium has been associated with insulin and its role in the body [1]. Control of glucose levels in plasma has been achieved, *in vitro* and *in vivo*, by means of vanadium administration in the form of inorganic salts [2]. However, as these compounds are poorly absorbed, the required high doses have been associated with undesirable side effects. In order to achieve better absorption and so reduce the doses of the element, it seemed appropriate to administer it in the form of an organic matrix. The synthesis of a potential insulin substitute, bis(maltolato)oxovanadium(IV) [$VO(ma)_2$, BMOV], was reported in 1992 by Orvig and co-workers [3]; its structure and properties have since been fully documented [4]. This compound was administered to diabetic rats and the studies demonstrated that BMOV is effective, at a lower dose than inorganic vanadium salts, in regulating glucose levels in the plasma [5]. It lowered cholesterol and triglyceride levels and ameliorated the cardiac disfunction normally observed in diabetic patients [6]. It exhibited no significant toxic effects on hepatic and kidney functions [7].

Maltol (3-hydroxy-2-methyl-4-pyranone) (**1a**) is a permitted food additive, used in the baking industry. It, or ethyl maltol (**1b**), reacts with primary amines to yield 3-hydroxy-2-methyl(ethyl)-4-pyridinones (**2a–h**). This class of ligands has recognized pharmaceutical importance, in iron and aluminium oral chelation therapy [8] and in the administration of gallium and indium isotopes in radiodiagnosis and radiotherapy [9]. Pyridinone ligands are not only good chelators of M^{III} and M^{II} metal ions, but also permit modulation of the hydrophilic/lipophilic balance (HLB), of ligands and of complexes, by changing the substituent on the ring nitrogen atom. Such a possibility of tailoring the HLB is of paramount importance for substances to be used *in vivo*, as this parameter is crucial for the transport properties of ligands and complexes across biological membranes.

We now report the synthesis and characterization of oxovanadium(IV) (vanadyl) complexes VOL_2, in which the ligands L are anions of the 3-hydroxy-4-pyranone (**1b**) and of the 3-hydroxy-4-pyridinones (**2a–h**) (Fig. 1); the synthesis and solution chemistry of the analogous complex of **1a** have been described earlier [4]. The new complexes have been characterized by elemental analysis and mass spectrometry, and structurally by vibrational, electronic

* Author to whom correspondence should be addressed.



PYRONES

	R	
1a	Me	Hma
1b	Et	Hetma

PYRIDINONES

	R	R^1	
2a	Me	H	Hmpp
2b	Me	Me	Hdmpp
2c	Et	Me	Hempp
2d	Me	C_6H_5	Hppp
2e	Et	C_6H_5	Hepp
2f	Me	4-MeC_6H_4	Hptp
2g	Me	4-(n-C_4H_9)C_6H_4	Hpbp
2h	Me	4-(n-C_6H_{13})C_6H_4	Hphp

Fig. 1. Formulae of, and abbreviations for, the pyranone and pyridinone ligands used in this investigation.

and electron spin resonance (ESR) spectroscopy, and by EXAFS.

EXPERIMENTAL

The oxovanadium(IV) complexes were synthesized by adding the stoichiometric amounts of vanadyl sulfate and the pyranone or pyridinone ligand in water, adjusting the pH to 5, and refluxing the mixture for about 1 h. The blue–grey solids that formed were filtered while the solution was still warm, washed with cold water or, for complexes of the more hydrophobic ligands, with methanol–water, and dried over phosphorus pentoxide. Elemental analyses were performed at the Microanalytical Laboratory of the University of Manchester; thermogravimetric analysis was carried out on a TA3000 instrument; mass spectra were obtained on a Kratos Concept instrument (fast atom bombardment and electron impact modes).

Vibrational spectra were obtained in potassium bromide discs on a Mattson 5000 FTIR spectrometer. Reflectance electronic spectra were recorded in the range 300–1200 nm at room temperature on a Shimadzu UV-3101PC spectrometer, using barium sulfate as reference material. X-band ESR spectra were recorded in solution at room temperature and at 77 K on a Bruker ESP300E spectrometer using diphenylpicrylhydrazyl as reference. The solutions for ESR were prepared under anaerobic conditions in 1 : 1 chloroform–toluene mixtures.

EXAFS experiments were performed in the region of the vanadium K-edge using station 7.1 at the Synchrotron Radiation Source, Daresbury, U.K. The beam energy was 2 GeV and a typical average stored ring current was 150 mA in multibunch mode and brilliance configuration. Data were acquired in the EXAFS transmission mode with argon-filled ion chambers using an Si(111) monochromator with 50% harmonic rejection. The data analysis was performed using the Daresbury EXAFS suite of programs.

RESULTS AND DISCUSSION

In exploratory experiments, the compounds were prepared either by adjusting the pH of the solution to 9, as described for the bis(maltolato) oxovanadium(IV) complex [3], or by adjusting the pH of the solution to 5, as described for other oxovanadium(IV) complexes with bidentate oxygen ligands [10]. The latter conditions were chosen, as the resulting products gave better elemental analyses.

Mass spectra show the expected peaks for the complexes VOL_2 and for fragments VOL and L. The results relating to the most intense peak, together with the results of elemental analyses (CHN), are shown in Table 1 for the 10 compounds prepared. It is clear that all compounds must contain five-coordinate vanadium except for complex **2a**, in which a water molecule appears to be bound in the sixth coordination position (also see below, in the EXAFS section). Thermogravimetric analyses are consistent with **2a** being a monohydrate; the remaining complexes are anhydrous.

The IR spectra exhibit in the range 1600–1440 cm^{-1} a set of four bands characteristic of pyranones or pyridinones [11]. Upon coordination, the band characteristic of the O—H stretching vibration is lost, as expected, but the band characteristic of the V=O vibration remains well defined and appears, for all the compounds, within the range 965–993 cm^{-1} (Table

Table 1. Data for elemental analysis, mass spectra, vibrational and electronic spectra

Compound[a]		%C	%H	%N	MS (MH^+)	ν(V=O) (cm^{-1})	λ_{vis} (nm)	
$VO(ma)_2$	**1a**	45.6 (45.5)	3.2 (3.2)	—	318	993	410; 534; 609; 703
$VO(etma)_2$	**1b**	48.8 (48.7)	4.1 (4.1)	—	346	993	399; 544; 621; 710
$VO(mpp)_2 \cdot H_2O$	**2a**	43.5 (43.3)	4.2 (4.2)	8.3 (8.4)	316	983	393; 532; 622; 660
$VO(dmpp)_2$	**2b**	49.1 (49.0)	4.7 (4.7)	8.2 (8.2)	344	965	415; 528; 651; 784
$VO(empp)_2$	**2c**	51.2 (51.7)	5.3 (5.4)	7.5 (7.5)	372	967	417; 529; 643; 773
$VO(ppp)_2$	**2d**	62.2 (61.7)	4.3 (4.3)	5.8 (6.0)	468	986	412; 542; 624; 683
$VO(eppp)_2$	**2e**	62.5 (63.0)	4.9 (4.9)	5.7 (5.7)	496	969	397; 537; 627; 725
$VO(ptpp)_2$	**2f**	64.1 (63.0)	4.9 (4.9)	5.7 (5.7)	496	979	406; 549; 634; 714
$VO(pbpp)_2$	**2g**	66.3 (66.3)	6.2 (6.3)	4.9 (4.8)	580	976	405; 547; 641; 716
$VO(phpp)_2$	**2h**	68.4 (68.0)	7.0 (7.0)	4.3 (4.4)	636	977	406; 550; 634; 716

[a] See Fig. 1 for definitions of abbreviations used for ligands.

1), thus confirming the stability of the +4 oxidation state in the solid state.

Comparison of solution and reflectance electronic spectra of several of our complexes persuaded us to concentrate on the latter. Figure 2 shows some typical reflectance spectra. The solution spectra suffered from the disadvantage that it often proved difficult or impossible to locate the weakest band in the visible region, and from the complication of the introduction of solvation effects at too early a stage in the investigation. Reflectance electronic spectra exhibit for all compounds four bands in the visible region, which appear in the following ranges: 393–417, 528–549, 609–651 and 700–784 nm. Spectra of **1a**, **2c** and **2f** are shown in Fig. 2; the data for all compounds are summarized in Table 1. The optical spectra of vanadyl complexes are normally interpreted in terms of the energy level scheme derived originally by Ballhausen and Gray from a molecular orbital study for a square-pyramidal structure of C_{4v} symmetry [12], with the z-axis taken as the vanadium–oxygen double bond and the x- and y-axes along the equatorial bonds. In this scheme b_2 $(d_{xy}) < e(d_{xz}, d_{yz}) < b_1(d_{x^2-y^2}) < a_1$ (d_{z^2}), and three electronic transitions are predicted, and indeed normally observed, for vanadyl complexes. However, some complexes exhibit four bands, and it is then assumed that the $^2E(xy, yz)$ state is split in low symmetry. The three- or four-band patterns observed in optical spectra of vanadyl complexes and the assignment of the electronic transitions have been discussed and interpreted not only in terms of symmetry but also of stereochemistry and size of chelate ring [10, 13–17]. Furthermore, for vanadyl complexes for which *cis–trans* isomerism is possible, and for which the chelate rings are five-membered, the four-band pattern has been associated with the *trans* isomer, the three-band pattern with the *cis*. Using α-hydroxycarboxylates as examples, the *cis*-tartrate exhibits three bands, the *trans*-tartrate four, with the same pattern for lactate, glycolate and diphenylglycolate complexes [10,18].

The bis(pyranonato) and bis(pyridinonato) oxovanadium(IV) complexes described here have electronic spectra with four bands, and as the transition energies are very similar to those reported for the α-hydroxycarboxylato complexes, the assignment developed for these latter complexes will be used: $\Delta E_{xy} < \Delta E_{xz} < \Delta E_{x^2-y^2} < \Delta E_{z^2}$ (or CT) [16]. This analogy can be extended further to postulate that our solid products consist of the *trans* isomer in each case. This is consistent with the recently reported crystal structure of $VO(ma)_2$, which shows the vanadium to be five-coordinate with distorted square-pyramidal geometry (the vanadium atom lies 0.07 Å above the equatorial plane defined by the donor oxygen atoms) and the two maltolate ligands *trans* to each other [4]. Also, for $VO(ma)_2$ the three low-energy bands appear at 534, 609 and 703 nm, in reasonable accordance with those reported in chloroform (where the authors implied four bands but quoted only three λ_{max} values, 549, 602 and 752 nm) [10]. These λ_{max} values are very different from those in strongly coordinating solvents such as pyridine (476, 610, 769 and 847 nm) [10] or water (three bands only reported, at 441, 625 and 860 nm) [4].

For series of closely related ligands, as here, it is to be expected that differences in donor strength should arise from σ donating power, and so the stretching

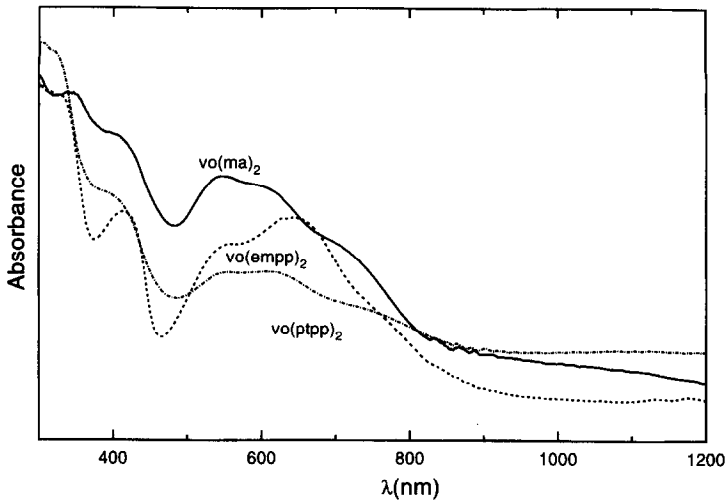


Fig. 2. Diffuse reflectance spectra of the complexes $VO(ma)_2$, $VO(empp)_2$ and $VO(ptpp)_2$.

frequency of the V=O bond can be a measure of its strength. A decrease in stretching frequency has been interpreted as resulting from an increase in electron donation to vanadium, thereby making it less able to accept charge from the oxygen, thus reducing the bond order. For the five-coordinate complexes [i.e. excluding results for the hydrated complex, $VO(mpp)_2H_2O$] values of ν(V=O) correlate with expected stabilities, with the lowest value for the most strongly bonding ligand (**2b**) and the highest for the least strongly bonding (**1a**). Furthermore, a reasonable linear correlation is observed between the energy (E cm^{-1}) of the $(xy) \rightarrow (z^2)$ or $(xy) \rightarrow (x^2-y^2)$ transitions and ν(V=O) for the five-coordinate bis(pyridinonato)oxovanadium(IV) complexes.

ESR spectra were obtained, in chloroform–toluene solutions, at room temperature and at 77 K. At both temperatures they are well resolved and typical of a d^1 electron configuration ($S = 1/2$). At ambient temperature the isotropic spectra exhibit eight well-defined lines resulting from the hyperfine interaction of the unpaired electron with the vanadium nucleus (^{51}V, $I = 7/2$). The frozen solution spectra are similar for all the compounds, exhibiting strong anisotropy. It is possible to distinguish in the low-field and high-field regions lines representative of the parallel splitting due to the hyperfine interaction of the unpaired electron with the vandium nucleus (^{51}V, $I = 7/2$) and a central region where different sets of lines corresponding to the x and y components of the hyperfine interaction are superimposed. According to the optical spectra, and bearing in mind the low symmetry of our compounds, rhombic spectra are to be expected. Table 2 summarizes the values of g_{iso} and A_{iso}, obtained directly from the spectra at ambient temperature by averaging the separation of the $-mI$ to $+mI$ transitions, as well as $g_\parallel$ and $A_\parallel$, obtained directly from frozen solution spectra. The ESR parameters are practically invariant for all the compounds and are indicative of similar metal–ligand covalency.

In order to gain insight into the local structure of the synthesized complexes, EXAFS experiments were carried out, since it proved impossible to grow crystals of sufficient quality for single-crystal X-ray diffractometry.* The vanadium–oxygen bond distances obtained are given in Table 3, which also includes data for $VO(ma)_2$ determined by X-ray diffraction for comparison. Both EXAFS and X-ray diffraction show two oxygen atoms at 3.7 Å from each vanadium, which are the nearest neighbours in adjacent layers. A detailed report and analysis of our EXAFS results will be published elsewhere [19]. The results confirm

Table 2. ESR parameters for the complexes in chloroform–toluene solution at room temperature and at 77 K

Compound[a]	Ligand	g_{iso}	A_{iso}	$g_\parallel$	$A_\parallel$
$VO(ma)_2$	**1a**	1.98	92	1.94	171
$VO(etma)_2$	**1b**	1.98	92	1.94	171
$VO(dmpp)_2$	**2b**	1.99	89	1.94	171
$VO(empp)_2$	**2c**	1.99	89	1.94	171
$VO(ppp)_2$	**2d**	1.97	89	1.95	169
$VO(eppp)_2$	**2e**	1.99	89	1.95	169
$VO(ptpp)_2$	**2f**	1.99	89	1.98	169
$VO(pbpp)_2$	**2g**	1.98	91	1.96	169
$VO(phpp)_2$	**2h**	1.99	89	1.94	167

[a] See Fig. 1 for definitions of abbreviations used for ligands.

* It may be noted that it took the authors of Ref. [4] several years and some good fortune to obtain an X-ray diffraction quality crystal of $VO(ma)_2$.

Table 3. EXAFS results for the compounds studied

Complex[a]	Ligand	Nearest neighbour atom	Number of neighbour atoms	Distance from vanadium (Å)
$VO(ma)_2$[b]	**1a**	O	1	1.60
		O	4	1.95
$VO(mpp)_2 \cdot H_2O$	**2a**	O	1	1.60
		O	4	1.95
		O	1	2.32
$VO(dmpp)_2$	**2b**	O	1	1.60
		O	4	1.94
$VO(ppp)_2$	**2d**	O	1	1.59
		O	4	1.94
$VO(ptpp)_2$	**2f**	O	1	1.61
		O	4	1.94
$VO(pbpp)_2$	**2g**	O	1	1.60
		O	4	1.94
$VO(phpp)_2$	**2h**	O	1	1.61
		O	4	1.94

[a] See Fig. 1 for definitions of abbreviations used for ligands.
[b] X-ray diffraction data: V=O = 1.596 Å; VO = 1.971, 1.998, 1.958, 2.204 Å.

that all the compounds are five-coordinate, with the exception of **2a**, for which a bound water molecule was detected at 2.3 Å from the vanadium in the sixth coordination position. The other bond lengths are similar for all the compounds and are indicative of the presence of five oxygen atoms coordinated to the vanadium: the vanadyl-oxygen at 1.59–1.16 Å, the four other oxygens at 1.94–1.95 Å. These results are as expected, both in relation to the structure of $VO(ma)_2$ and to the corresponding distances in $VO(acac)_2$ and $VO(bzac)_2$, which, from single-crystal X-ray diffraction, are between 1.56 and 1.61 Å and between 1.95 and 1.99 Å, respectively [20].

The EXAFS results we have obtained for $VO(ma)_2$ are in very good agreement with the X-ray diffraction data. We believe that the information obtained from the absorption technique is of great importance, as it permits the accurate establishment of structure in the vicinity of the metal in circumstances where single-crystal X-ray diffraction is not possible. In the present context, this means that we can obtain structural information on related complexes containing long hydrocarbon chain substituents in the pyridinone ligands, and on these complexes in solution; in other words, we shall be able to probe solvation of this group of complexes in a range of solvent media.

Table 3 indicates that the vanadium–oxygen bond lengths do not vary significantly between the various pyridinone complexes, thus showing that the local structure around the metal centre is not appreciably modified by changing the substituents on the ring nitrogen atom. This indicates that the HLB of these complexes can be tuned without altering the structure around the metal centre. Indeed, all our structural and spectroscopic data suggest that inclusion of substituents on the ring nitrogen does not significantly affect such properties of these complexes.

Acknowledgements—We are grateful to the JNICT and to the British Council for their support, and to Dr John Fawcett for structural calculations.

REFERENCES

1. Shechter, Y. and Karlish, S. D. J., *Nature*, 1980, **284**, 556.
2. (a) Shechter, Y. and Karlish, S. D. J., *Biochemistry*, 1981, **20**, 5795; (b) Shechter, Y. and Meyerovitch, J., *J. Biol. Chem.*, 1987, **262**, 6658; (c) Underwood, E. J., *Trace Elements in Human and Animal Nutrition*. Academic Press, New York, 1977; (d) Heylieger, C. E., Tahiliani, A. G. and McNeill, J. H., *Science*, 1985, **227**, 1474.
3. McNeill, J. H., Yuen, V. G., Hoveyda, H. R. and Orvig, C., *J. Med. Chem.*, 1992, **35**, 1489.
4. Caravan, P., Gelmini, L., Glover, N., Herring, F. G., Li, Huali, McNeill, J. H., Rettig, S. J., Setyawati, I. A., Shuter, E., Sun, Yan, Tracey, A. S., Yuen, V. G. and Orvig, C., *J. Am. Chem. Soc.*, 1995, **117**, 12759.
5. Yuen, V. G., Orvig, C. and McNeill, J. H., *Can. J. Physiol. Pharmacol.*, 1993, **71**, 263.
6. Yuen, V. G., Orvig, C., Thompson, K. H. and McNeill, J. H., *Can J. Physiol. Pharmacol.*, 1993, **71**, 270.
7. Dai, S., Yuen, V. G., Orvig, C. and McNeill, J. H., *Pharmacol. Commun.*, 1993, **3**, 311.
8. Kontoghiorghes, G. J., *Analyst*, 1995, **120**, 845.
9. Hider, R. C. and Hall, A. D., *Prog. Med. Chem.*, 1991, **28**, 41.

10. Stewart, C. P. and Porte, A. L., *J. Chem. Soc., Dalton Trans.*, 1972, 1661.
11. (a) Katritzky, A. R. and Jones, R. A., *J. Chem. Soc.*, 1960, 2947; (b) Katritzky, A. R. and Jones, R. A., *Spectrochim. Acta*, 1961, **17,** 64; (c) Batts, B. D. and Spinner, E., *Aust. J. Chem.*, 1976, **22,** 2581; (d) Finnegan, M. M., Lutz, T. G., Nelson, W. O., Smith, A. and Orvig, C., *Inorg. Chem.*, 1987, **26,** 2171.
12. (a) Ballhausen, C. J. and Gray, J. B., *Inorg. Chem.*, 1962, **1,** 111; (b) Guzy, C. M., Raynor, J. B. and Symons, M. C. R., *J. Chem. Soc. (A)*, 1969, 2791.
13. Forrest, J. G. and Prout, C. K., *J. Chem. Soc. (A)*, 1967, 1312.
14. Selbin, J. and Morpugo, L., *J. Inorg. Nucl. Chem.*, 1965, **27,** 673.
15. Chasteen, N. D., Belford, R. L. and Paul, I. C., *Inorg. Chem.*, 1969, **8,** 408.
16. Holyk, N. M., M. S. Thesis, University of New Hampshire, 1979.
17. Valek, M. H., Yeranos, W. A., Basu, G., Hon, P.-K. and Belford, R. L., *J. Molec. Spectrosc.*, 1971, **37,** 228.
18. Hon, P.-K., Belford, R. L. and Pfluger, C. E., *J. Chem. Phys.*, 1965, **43,** 1323.
19. Burgess, J., Rangel, M., Schlindwein, W. and Waltham, E., submitted for publication.
20. (a) Dodge, R. P., Templeton, D. H. and Zalkin, A., *J. Chem. Phys.*, 1961, **35,** 55; (b) Hon, P.-K., Belford, R. L. and Pfluger, C. E., *J. Chem. Phys.*, 1965, **43,** 3111; (c) Shuter, E., Rettig, S. J. and Orvig, C., *Acta Cryst.* 1995, **51C,** 12.

Pergamon

PII: S0277-5387(96)00341-5

Polyhedron Vol. 16, No. 5, pp. 795–800, 1997
Copyright © 1996 Elsevier Science Ltd
Printed in Great Britain. All rights reserved
0277-5387/97 $17.00+0.00

The crystal structure and hydrolysis equilibrium of triphenyl(2-mercapto-1-methylimidazolato)tin(IV)

José S. Casas, Alfonso Castiñeiras, Emilia García Martínez, Angeles Sánchez González, Agustín Sánchez and José Sordo*

Departamento de Quíimica Inorgánica, Universidade de Santiago de Compostela, 15706 Santiago de Compostela, Galicia, Spain

(Received 25 June 1996; accepted 12 July 1996)

Abstract—The title compound was prepared from 1-methyl-2(3H)-imidazolinethione and triphenyltin(IV) hydroxide, and its crystal structure was determined by X-ray diffraction. The crystal consists of discrete molecules with the tin atom coordinated to one carbon atom of each of the three phenyl groups and to the sulfur atom of the deprotonated ligand. An Sn—N interaction [2.920(3) Å] slightly distorts the tin coordination geometry from that of a perfect tetrahedron. NMR spectroscopy was used to study the hydrolysis of this compound in $CDCl_3$. Copyright © 1996 Elsevier Science Ltd

Keywords: tin; X-ray structure; NMR; triphenyltin complex.

Increasing industrial use of organotin compounds containing an Sn—S bond, especially as stabilizers of polyvinyl chlorides [1], and recognition of the importance of this bond for the biological properties of organotin compounds [2], have together spurred on the study of thiolates of tin. An interesting class of such compounds comprises those of general formula $SnR_3(SR')$, where R′ contains a donor atom (D) capable of forming a secondary bond with the tin atom. The coordination polyhedra of these compounds are thus intermediate between tetrahedra and trigonal bipyramids, the degree of distortion of the former towards the latter depending on the strength of the Sn—D bond.

In a previous paper [3] we reported the preparation and structural characterization of triphenyl(5-mercapto-1-phenyl-1,2,3,4-tetrazolato)tin(IV), [$SnPh_3$(MPT)], which has both an Sn—S bond of normal length and an Sn—N bond length of 3.275(3) Å (shorter than the sum of the van der Waals radii of tin and nitrogen, but too long to substantially distort the tetrahedral tin environment). We now describe the synthesis and structure of [$SnPh_3$(mimt)] (Hmimt = 1-methyl-2(3H)-imidazolinethione), another compound in which the presence of a nitrogen atom contiguous to a C—S bond leads to the possible formation of a four membered Sn—S—C—N ring. In [$SnPh_3$(mimt)], the Sn—N bond [2.920(3) Å] is shorter than in [$SnPh_3$(MPT)], with the result that this bond affects the coordination polyhedron of the tin atom. The temperature dependence of a hydrolytic equilibrium detected in the NMR spectra of solutions of this compound in $CDCl_3$ is also described.

EXPERIMENTAL

1-Methyl-2(3H)-imidazolinethione (Aldrich) and triphenyltin(IV) hydroxide (Aldrich) were used as supplied.

Preparation of [$SnPh_3$(mimt)]

Triphenyltin(IV) hydroxide (0.288 g, 0.79 mmol) and 1-methyl-2(3H)-imidazolinethione (0.100 g, 0.88 mmol) were suspended in 60 cm^3 of benzene (**caution**) in a 100 cm^3 round-bottomed flask fitted with a condenser and a Dean-Stark moisture trap. The reaction mixture was refluxed for 22 h, filtered and the clear filtrate concentrated to dryness, yielding an oil which afforded a crystalline solid, isolated and identified as

* Author to whom correspondence should be addressed.

[$SnPh_3$(mimt)], m.p. 94°C. Found: C, 56.7; H, 4.2; N, 6.2; S, 6.4. Calc. for $C_{22}H_{20}N_2SSn$: C, 56.9; H, 4.3; N 6.0; S, 6.9%. When the clear filtrate of the synthesis was slowly concentrated without reaching dryness, it afforded initially a crystalline solid, which was identified as the ligand (Hmimt).

Physico-chemical measurements

Analytical data were obtained with a Carlo-Erba 1108 apparatus. Melting points were determined in a Büchi apparatus. NMR spectra of samples as 0.1 M solutions in $CDCl_3$ were recorded in a Bruker AMX 500 spectrometer operating at 500.14 MHz (^1H; 5 mm o.d. NMR tube) or 125.76 MHz (^{13}C; 5 mm o.d. NMR tube) and at 186.50 MHz (^{119}Sn; 5 mm o.d. sealed tubes); the internal lock and reference to tetramethylsilane was provided by $CDCl_3$ for the ^1H (7.26 ppm) and ^{13}C (77.0 ppm) spectra, and by tetramethyltin for the ^{119}Sn spectra.

Crystal structure determination of [$SnPh_3$(mimt)]

Crystals suitable for X-ray diffraction studies were selected from the first batch of the synthesis. No further purification was necessary.

Crystal data. $C_{22}H_{20}N_2SSn$, $M = 463.17$, monoclinic, space group $P2_1/c$, $a = 11.362(1)$, $b = 9.808(1)$, $c = 19.111(2)$ Å, $\beta = 105.44(1)°$, $V = 2052.9(6)$ Å^3, $Z = 4$, $D_x = 1.449$ g cm^{-3}, $F(000) = 928$.

Intensity data for a colourless prismatic crystal ($0.35 \times 0.35 \times 0.40$ mm^3) were obtained at room temperature (293 K) in an Enraf–Nonius CAD4 diffractometer using graphite-monochromated Mo-K_α radiation ($\lambda = 0.71073$ Å). The ω–2θ scan technique was used to measure the intensities of 6552 reflections up to a maximum Bragg angle of 30°. Cell parameters were obtained by a least-squares procedure from the setting angles of 25 reflections ($8.3 \leqslant \theta \leqslant 11.9°$) [4]. No decomposition of the crystal occurred during data collection. Corrections were applied for Lorentz and polarization effects and for absorption ($\mu = 1.35$ mm^{-1}) [5]. Of the 6552 reflections collected, 5988 were unique ($R_{int} = 0.035$); of these, 3905 satisfied the $I \geqslant 3.0\ \sigma(I)$ criterion of observability and were used in the subsequent analysis.

The structure was solved by Patterson and Fourier methods [6] and was refined on F by a full-matrix least-squares procedure [4] using anisotropic displacement parameters for non-hydrogen atoms. Hydrogen atoms were located from difference Fourier syntheses and refined with isotropic B_{eq} values fixed at 4.0 Å^2. The weighting scheme $w = 1/\sigma^2(F)$ was used. Refinement proceeded smoothly to convergence with a maximum of Δ/σ 0.02 ($R = 0.035$, $R_w = 0.034$) and goodness-of-fit = 1.38 for 296 variables. A correction for extinction was made in the last cycle of refinement [7]. The secondary extinction coefficient refined to $g = 1.587 \times 10^{-8}$ $\{F_c = F_c/[1 + g(F_c)^2 Lp]\}$. Analysis of variance showed no special features, and the maximum and minimum residual electron density peaks in the final difference map were +0.89 and −0.77 e Å^{-3}, respectively.

Atomic scattering factors and anomalous dispersion corrections for all atoms were taken from *International Tables for X-ray Crystallography* [8].

RESULTS AND DISCUSSION

Description of the structure of [$SnPh_3$(mimt)]

In Fig. 1, an ORTEP drawing [9] shows the structure of [$SnPh_3$(mimt)] and the atomic numbering scheme used. Table 1 lists interatomic distances and angles.

The crystal consists of discrete molecules in which the tin atom is coordinated to the sulfur atom of the mimt ligand and to the one carbon atom of each of the three phenyl groups. The Sn—S bond length lies towards the lower end of the range recently reported for triphenyltin thiolates (2.405–2.481 Å) [10–12], close to the sum of the covalent radii of tin and sulfur (2.42 Å) [13]. The Sn—C bond distances are within the range 2.12–2.18 Å reported for triphenyltin compounds [10]. The Sn—S distance and the orientation of the mimt ligand [the torsion angle Sn—S—C(2)—N(1) is 163.4(3)°] places N(3) at 2.920(3) Å from the tin atom. This distance, longer than the sum of the covalent radii of tin and nitrogen (2.15 Å), but shorter than the sum of the van der Waals radii (3.75 Å) [13], lies towards the upper end of the range (2.601–3.057 Å) reported for [$SnPh_3$(L)] complexes, in which L coordinates to the tin *via* sulfur and nitrogen atoms [10–12] and is also longish compared with intramolecular Sn—N distances in other tin compounds [14].

Around the tin atom, the angles C(21)—Sn—C(31) and S—Sn—C(31) are wider and S—Sn—C(11) and C(11)—Sn—C(21) are narrower than the ideal tetrahedral angle. By contrast, in [$SnPh_3$(SPh)] [15] there is only minimal distortion of the tetrahedral environment (C—Sn—C = 112.1°). Since mimt and SPh would be expected to exert similar steric effects, this difference may be attributed to the Sn—N(3) interaction in [$SnPh_3$(mimt)]. Although this might suggest description of the tin environment in [$SnPh_3$(mimt)] as a *cis*-trigonal bipyramid with N(3) and C(11) in the apical positions and sulfur, C(21) and C(31) in the equatorial positions, this bipyramid is extremely distorted: the tin atom lies 0.539 Å out of the S—C(21)—C(31) equatorial plane, the sum of the equatorial angles is only 342.8° and the axial Sn—C bond length is close to the equatorial ones. In contrast, pentacoordinate tin complexes containing a five-membered Sn—S—C—C—N ring have only very slightly distorted trigonal bipyramids [10,11]. Thus, the environment of tin in [$SnPh_3$(mimt)] is best described as a distorted tetrahedron. Similarly distorted tin

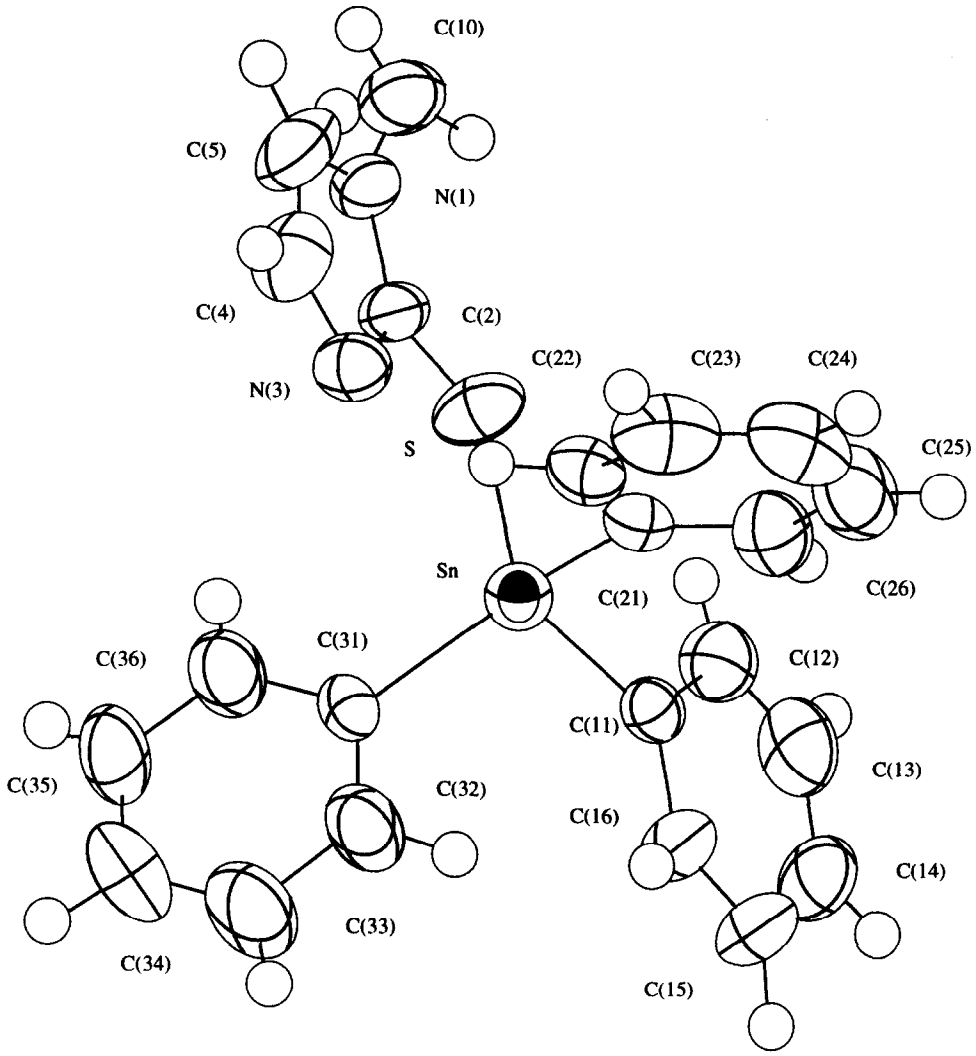


Fig. 1. Perspective view of $[SnPh_3(mimt)]$ showing the atom numbering scheme and the coordination geometry about the tin atom.

coordination polyhedra have been described for triphenyltin *o*-quinolinylthiolate [Sn—S, 2.42(1) Å; Sn—N, 2.836(3) Å] [11] and for triphenyltin pyrimidine-2-thionate [Sn—S, 2.442(3) Å; Sn—N, 2.88(5) Å] [12], which also contain a four-membered Sn—S—C—N ring.

The bond lengths of mimt in $[SnPh_3(mimt)]$ are very similar to those found previously in complexes in which this ligand is S, N-bridged ($[\{Cu(mimt)\}_4]$ [16] and $[GaMe_2(mimt)]_2$ [17]). The angle S—C(2)—N(3) is narrower in the tin complex, and N(3)—C(2)—N(1) is wider; however, and as expected, the greatest difference concerns the M—S—C angle, which is much wider in the complexes of copper [106.8(2)°] and gallium [100.97(9)°] than in $[SnPh_3(mimt)]$ [91.8(1)°], probably due to the disposition of mimt in copper and gallium complexes to form tetramers and dimers, respectively. The M—S—C angle in $[SnPh_3(mimt)]$ is also narrower than the 95.5(7)° found in [HgMe(mimt)] [18] (in which mimt is S-monodentate), possibly due to the Sn—N(3) interaction in the tin complex. High e.s.d. values preclude comparison of bond distances in both compounds.

NMR spectra

Table 2 lists ^1H and ^{13}C chemical shifts for the free ligand Hmimt and the complex $[SnPh_3(mimt)]$. The ^1H NMR spectrum of the complex contains two broad signals at 7.39 and 7.68 ppm attributable to the $SnPh_3$ moiety and the signals of the mimt ligand, slightly shielded with respect to Hmimt. The presence of a

Table 1. Selected bond distances (Å) and angles (°) in $[SnPh_3(mimt)]$

Sn—S	2.437(1)	C(14)—C(15)	1.357(9)
Sn—N(3)	2.920(3)	C(15)—C(16)	1.382(7)
Sn—C(11)	2.134(3)	C(21)—C(22)	1.378(6)
Sn—C(21)	2.129(4)	C(21)—C(26)	1.370(6)
Sn—C(31)	2.121(5)	C(22)—C(23)	1.389(8)
S—C(2)	1.746(4)	C(23)—C(24)	1.370(8)
N(1)—C(2)	1.350(5)	C(24)—C(25)	1.345(8)
N(1)—C(5)	1.384(7)	C(25)—C(26)	1.407(8)
N(1)—C(10)	1.459(7)	C(31)—C(32)	1.378(6)
N(3)—C(2)	1.310(6)	C(31)—C(36)	1.358(7)
N(3)—C(4)	1.376(5)	C(32)—C(33)	1.391(8)
C(4)—C(5)	1.321(9)	C(33)—C(34)	1.341(8)
C(11)—C(12)	1.388(7)	C(34)—C(35)	1.336(8)
C(11)—C(16)	1.382(6)	C(35)—C(36)	1.407(8)
C(12)—C(13)	1.392(6)	C(13)—C(14)	1.350(7)

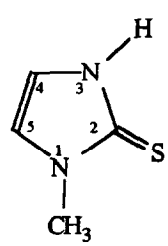
S—Sn—N(3)	59.9(1)	C(11)—C(12)—C(13)	121.4(5)
S—Sn—C(11)	99.3(1)	C(12)—C(13)—C(14)	120.6(6)
S—Sn—C(21)	111.6(2)	C(13)—C(14)—C(15)	119.6(4)
S—Sn—C(31)	112.3(2)	C(14)—C(15)—C(16)	120.0(5)
C(11)—Sn—C(21)	105.4(1)	C(11)—C(16)—C(15)	122.6(5)
C(11)—Sn—C(31)	107.1(1)	C(22)—C(21)—C(26)	118.0(4)
C(21)—Sn—C(31)	118.9(2)	C(21)—C(22)—C(23)	121.0(4)
C(2)—N(1)—C(5)	105.6(5)	C(22)—C(23)—C(24)	120.3(5)
C(2)—N(1)—C(10)	126.8(4)	C(23)—C(24)—C(25)	119.5(5)
C(5)—N(1)—C(10)	127.6(5)	C(24)—C(25)—C(26)	120.8(5)
C(2)—N(3)—C(4)	104.6(5)	C(21)—C(26)—C(25)	120.5(5)
S—C(2)—N(1)	123.7(4)	C(32)—C(31)—C(36)	118.8(4)
S—C(2)—N(3)	124.0(3)	C(31)—C(32)—C(33)	119.7(5)
N(1)—C(2)—N(3)	112.3(4)	C(32)—C(33)—C(34)	120.8(6)
N(3)—C(4)—C(5)	111.1(6)	C(33)—C(34)—C(35)	120.2(5)
N(1)—C(5)—C(4)	106.6(4)	C(34)—C(35)—C(36)	120.3(5)
C(12)—C(11)—C(16)	115.7(4)	C(31)—C(36)—C(35)	120.0(4)

Table 2. ^1H and ^{13}C NMR data in $CDCl_3$ solution[a]

^1H	N—CH_3	H(4)	H(5)	N(H)	Ph—Sn (*o*)	Ph—Sn (*m-p*)
Hmimt	3.61(s)	6.67(d)	6.71(d)	11.36(s,b)		
$[SnPh_3(mimt)]$	3.56(s)	6.63(s)	6.66(d)	—[b]	7.39(m)	7.68(m)

^{13}C	N—CH_3	C(4)	C(5)	C(2)	C_i (^1J)	C_o (^2J)	C_m (^3J)	C_p (^4J)
Hmimt	34.0	114.0	118.7	160.2				
$[SnPh_3(mimt)]$	34.4	119.9(vb)	119.9(vb)	138.7(vb)	137.1 (—)[c]	136.6 (44.7)	128.6 (59.4)	129.6 (—)[c]

[a] b = broad, d = doublet, m = multiplet, s = singlet, vb = very broad. δ in ppm. J in Hz.
[b] Very weak, broad singlet at $\approx$ 11 ppm.
[c] Not observed.
Numbering scheme:



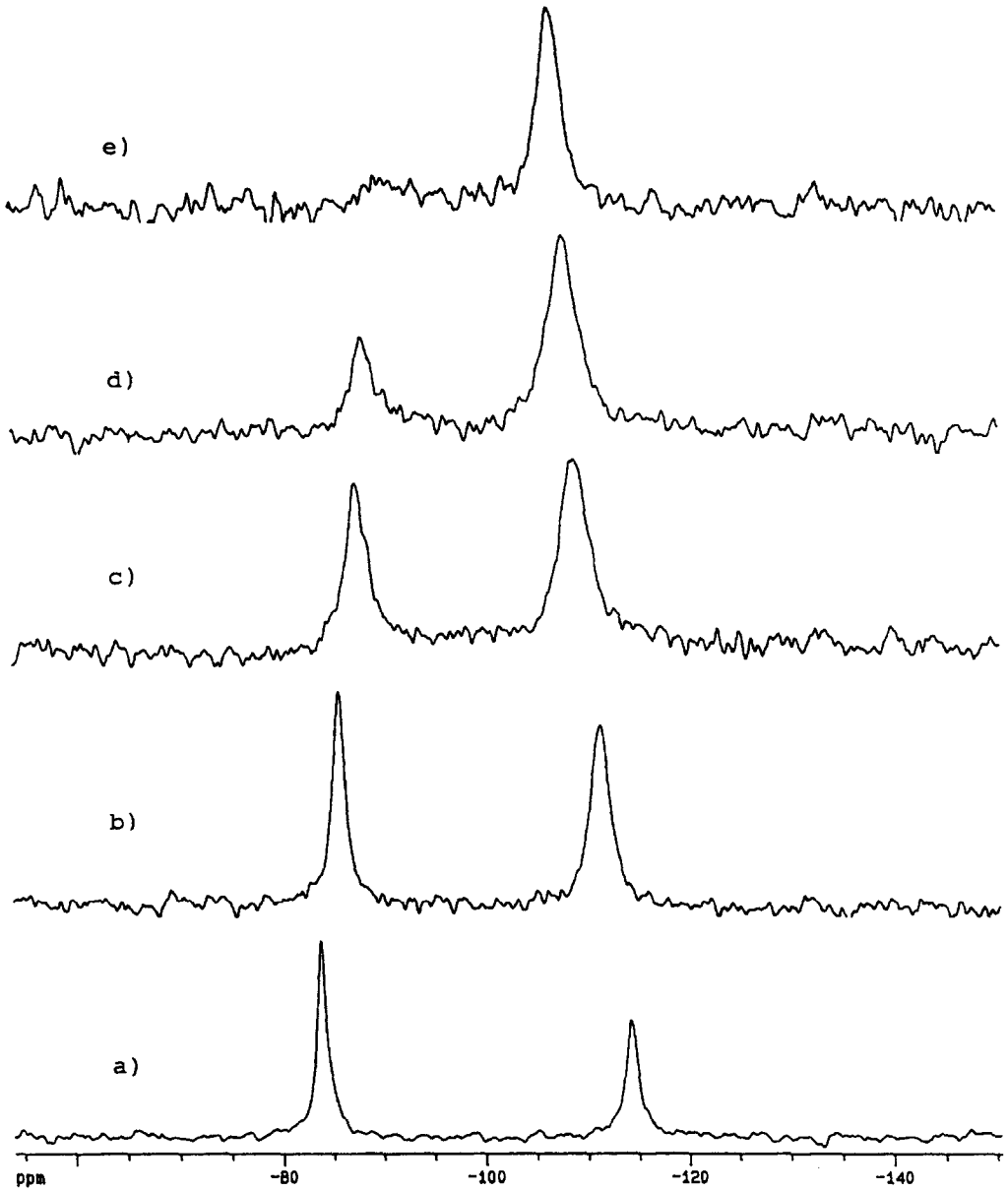


Fig. 2. ^{119}Sn NMR spectra of [$SnPh_3$(mimt)] at 280 K (a), 300 K (b), 320 K (c), 330 K (d) and 340 K (e).

very weak, broad singlet at $\approx$ 11 ppm attributable to N(3)H, together with the liberation of free Hmimt ligand in the synthesis if water is present in the reaction (see Experimental section), suggested the occurrence of a hydrolytic equilibrium:

$$[SnPh_3(mimt)] + H_2O = SnPh_3OH + Hmimt \quad (1)$$

Since no other signals due to the individual or complexed species were observed in the ^{1}H or ^{13}C spectra of the complex {the main feature in the latter spectrum is the shift of the signal of C(2) to higher field upon complexation, as expected for a process involving deprotonation of N(3) and a partial evolution of the thione form at C(2) into a thiolate form [3]}, equilibrium (1) must be fast at room temperature on the ^{1}H and ^{13}C NMR timescales. In the ^{119}Sn spectrum, however, signals due to both $SnPh_3OH$ (−85.8 ppm) and [$SnPh_3$(mimt)] (−111.2 ppm) were detected. Furthermore, addition of a few drops of water to the NMR sample increased the intensity of the $SnPh_3OH$ signal without changing its position, thus confirming the existence of equilibrium (1) by showing it to have been displaced to the right.

The influence of temperature on the above equilibrium was investigated using ^{119}Sn NMR spectroscopy in the range 280–340 K (Fig. 2). At 280 K, $SnPh_3OH$ and [$SnPh_3$(mimt)] gave signals at −83.8 and −114.3 ppm, respectively. Increasing the tem-

perature caused the $SnPh_3OH$ signal to move upfield and to decrease in intensity, while the [$SnPh_3$(mimt)] signal moved downfield and increased in intensity. At 340 K, a single signal attributed to [$SnPh_3$(mimt)] was observed at −106.5 ppm, the equilibrium (1) at this temperature being displaced towards complex formation even when H_2O is present. Note that upon varying the temperature, the position of the ^{119}Sn NMR signal of the complex remained in the narrow range −114.6 to −106.5 ppm, which is towards the upper end of the usual range for a tetracoordinate tin atom in a triphenyltin compound in $CDCl_3$ [19].

Acknowledgement—We thank the Xunta de Galicia, Spain, for financial support under Project XUGA 20314B91.

REFERENCES

1. (a) Evans, C. J. and Karpel, S, *Organotin Compounds in Modern Technology*. Elsevier, Amsterdam, 1985, p. 23; (b) Evans, C., *Spec. Chem.* 1991, **11,** 152.
2. Barbieri, R., Silvestri, A., Lo Giudice, M., Ruisi, G. and Musmeci, M. T., *J. Chem. Soc., Dalton Trans.* 1989, 519.
3. Bravo, J., Cordero, M. B., Casas, J. S., Sánchez, A., Sordo, J., Castellano E. E. and Zukerman-Schpector, J., *J. Organomet. Chem.* 1994, **482,** 147.
4. Franz, B. A., The Enraf–Nonius CAD4 SDP—A real-time system for concurrent X-ray data collection and crystal structure solution, in *Computing in Crystallography*, Vol. 2.2, ed. Schenk, H., Olthof-Hazekamp, R., van Koningsveld, H. and Bassi, G. C. Delft University Press, The Netherlands 1985, p. 64.
5. Walker, N. and Stuart, D., *Acta Cryst.* 1983, **A39,** 158.
6. Sheldrick, M., SHELX 86: Program for the Solution of Crystal Structures. University of Göttingen, Germany, 1986.
7. Zachariasen, W. H., *Acta Cryst.* 1963, **16,** 1139.
8. *International Tables for X-ray Crystallography*, Vol. IV. Kynoch Press, Birmingham, 1974. (Present distributor: Kluwer Academic, Dordrecht.)
9. Johnson, C. K., ORTEP II. Report ORNL-5138, Oak Ridge National Laboratory, Tennessee, U.S.A., 1976.
10. James, B. D., Magee, R. J., Patalighug, W. C., Skelton, B. W. and White, A. H., *J. Organomet. Chem.* 1994, **467,** 51.
11. Rau, D. N, Ph.D. thesis, University of Massachusetts, U.S.A., 1988. University Microfilm International, Ann Arbor, MI, 1990.
12. Petrilli, L., Caruso, F. and Rivarola, E., *Main Group Met. Chem.* 1994, **17,** 439.
13. Huheey, J. E., *Inorganic Chemistry, Principles of Structure and Reactivity*, 3rd edn. Harper International, 1983, p. 258.
14. Cea-Olivares, R., Jimenez Sandoval, O., Espinosa Pérez, G. and Silvestru, D., *Polyhedron* 1994, **13,** 2809 and references therein.
15. Speziali, N. L., Guimaraes, B. G., Silva, R. M., Duarte, P. H. and Aguiar, S. R., *Acta Cryst.* 1994, **C50,** 1059.
16. Raper, E. S., Creighton, J. R. and Clegg, W., *Inorg. Chim. Acta* 1991, **183,** 179.
17. Copper, D. A., Rettig, S. J., Storr, A. and Trotter, J., *Can. J.Chem.*, 1986, **64,** 1643.
18. Norris, A. R., Taylor, S. E., Buncel, E., Bélanger-Gariépy, F. and Béauchamp, A. L., *Can. J. Chem.* 1983, **63,** 1536.
19. Holecek, J., Nádvorník, M., Handlír, K. and Lycka, A., *J. Organomet. Chem.* 1983, **241,** 177.

Pergamon

PII: S0277-5387(96)00340-3

Polyhedron Vol. 16, No. 5, pp. 801–804, 1997
Copyright © 1996 Elsevier Science Ltd
Printed in Great Britain. All rights reserved
0277-5387/97 $17.00 + 0.00

Synthesis of two heterobimetallic complexes (dppe)$PdMS_4$ (M = W, Mo), and X-ray structure of the tungsten complex

Biao Wu, Wenjian Zhang, Xiaoying Huang, Xintao Wu* and Shuyan Yu

State Key Laboratory of Structural Chemistry, Fujian Institute of Research on Structure of Matter, Chinese Academy of Sciences, Fuzhou, Fujian 350002, P.R. China

(Received 25 June 1996; accepted 12 July 1996)

Abstract—The heterobimetallic complexes (dppe)$PdMS_4$ [dppe = $(CH_2PPh_2)_2$, M = W, Mo] have been synthesized by the reaction of (dppe)$PdCl_2$ and $(NH_4)_2MS_4$ in CH_2Cl_2–CH_3CN solvent, and characterized by elemental analysis, UV–vis and IR spectroscopies. The structure of (dppe)$PdWS_4$ has been determined by single-crystal X-ray analysis. The Pd—W distance is 2.89 Å, the average distance of the W—S bridge is 2.23 Å, and that of terminal W—S is 2.14 Å. Copyright © 1996 Elsevier Science Ltd

Keywords: heterobimetallic; palladium; tetrathiometallate; synthesis; structure.

Transition metal sulfido complexes have stimulated profound research interest due to their solid-state properties, applications in catalysis and structural similarity to the cluster core of metal–sulfur metalloenzymes [1]. The tetrathiometallate anions, WS_4^{2-} and MoS_4^{2-}, which are useful and versatile reagents, play a key role in some biological processes [2, 3]. Many types of compound which are interesting from the standpoint of structural chemistry are formed with the aid of doubly, triply and quasi-quadruply bridging tetrathiometallate ligands. The MoS_4^{2-} anion has been claimed to be the most effective antagonist of copper metabolism [4]. There has been extensive research on WS_4^{2-}/$Cu(Ag^I)$ and MoS_4^{2-}/$Cu(Ag^I)$ complexes [5], which has shown a rich structural variation.

Recently, a series of heterometallic sulfido complexes with $\{MWS_4M'\}$ and $\{MMoS_4M'\}$ cores (M = Ag, Cu; M′ = Cu, Fe) were synthesized by the unit construction method in our laboratory [6]. However, heterometallic sulfido complexes derived from MS_4^{2-} (M = W, Mo) with palladium metal are rare [7]. Herein, we report the syntheses of two heterometallic sulfido complexes [(dppe)$PdWS_4$] (**I**) and [(dppe)$PdMoS_4$) (**II**) and the structure of **I**.

* Author to whom correspondence should be addressed.

EXPERIMENTAL

All solvents were A.R. grade. $(NH_4)_2WS_4$, $(NH_4)_2MoS_4$ [8] and (dppe)$PdCl_2$ [9] were synthesized according to the literature methods. Elemental analyses were carried out by the Elemental Analysis laboratories of our institute. UV–vis spectra were obtained on a Schimadzu UV-3000 spectrophotometer. IR spectra were recorded on a Perkin–Elmer 750 spectrometer as KBr discs.

Syntheses

Preparation of [(dppe)$PdWS_4$] (**I**). (dppe)$PdCl_2$ (0.40 g, 0.70 mmol) and $(NH_4)_2WS_4$ (0.35 g, 1.00 mmol) were added to 20 cm^3 of a mixed solution of CH_2Cl_2 and CH_3CN (1 : 1 v/v), and the mixture was stirred for 1 day at ambient temperature. After filtering, the product was washed with CH_2Cl_2, distilled H_2O, EtOH and Et_2O, respectively. The yellow product was dried in air (yield: 88%). Single yellow crystals were obtained by diffusing ethyl ether into DMF solution. Found: C, 38.4; H, 2.7. Calc. for $C_{26}H_{24}P_2PdWS_4$: C, 38.2; H, 3.0%. IR (KBr): 1583, 1483(m), 1435(s), 717(s), 530(s), 497(s), 482(s), 441(m) cm^{-1}.

Preparation of [(dppe)$PdMoS_4$] (**II**). The method was similar to that for **I**; (dppe)$PdCl_2$ (0.40 g, 0.70

Table 1. Crystallographic data and refinement parameters for I

Chemical formula	$C_{26}H_{24}PdP_2S_4W$
Formula weight	816.94
$F(000)$	788
Crystal colour	yellow
Crystal system	triclinic
Space group	$P\bar{1}$
Unit cell parameters	
a	9.213(4) Å
b	10.410(4) Å
c	15.478(7) Å
α	82.19(4)°
β	103.00(4)°
γ	100.63(3)°
U	1414.7 Å^3
Z	2
$D_{calc.}$	1.92 g cm^{-3}
μ	51.9 cm^{-1}
Range of *hkl*	0–10, −12 to 12, −18 to 18
Scan rate	3–5° min^{-1} (in ω)
Scan width (°)	$1.3+0.350\tan\theta$
$2\theta_{max}$	50.0°
No. of reflections measured	4962 unique
Parameters refined	307
Residuals: R/R_w[a]	0.072/0.085
Goodness of fit: S[b]	4.668
E.s.d. of observed unit weight	1.06
High/low peak in final diff. map	3.75 (1 Å to *W*)/ −0.32 eÅ^{-3}

[a] $R = \Sigma\|F_o\|-|F_c\|/\Sigma|F_o|$, $R_w = [\Sigma(|F_o|-|F_c|)^2/\Sigma wF_o^2]^{1/2}$.
[b] $S = [\Sigma w(|F_o|-|F_c|)^2/(N_{obs}-N_{var})]^{1/2}$, $w = 1.000/[\sigma(F_o)^2+(0.030F_o)^2+1.000$.

mmol) and $(NH_4)_2MoS_4$ (0.26 g, 1.00 mmol) were added to 20 cm^3 of a mixed solution of CH_2Cl_2 and CH_3CN (1:1 v/v), and an orange-red powder was obtained (yield: 81%). Found: C, 42.1; H, 3.1. Calc. for $C_{26}H_{24}P_2PdMoS_4$: C, 42.8; H, 3.3%. IR (KBr): 1583, 1483(m), 1435(s), 717(s), 530(s), 503(s), 482(m), 436(m) cm^{-1}.

X-ray structure determination of [(dppe)PdWS$_4$] (I)

A crystal of *ca* $0.50\times0.14\times0.08$ mm^3 was used for the structure determination. Some experimental conditions are reported in Table 1. Data were collected on an Enraf–Noniuns CAD4 diffractometer using Mo-K_α radiation ($\lambda = 0.71073$ Å) *via* the ω–2θ scan technique at *ca* 296 K. A total of 5301 reflections for I were collected, of which 4962 were unique. The data were corrected for Lorentz and polarization factors and for absorption using empirical scan data and DIFABS [10]. The maximum and minimum absorption corrections were 1.0829 and 0.8757, respectively, with an average value of 0.9780.

The structure was solved by using the Patterson heavy atom method, which revealed the heavy atoms. The remaining atoms were located in successive difference Fourier syntheses. The structure was refined using a full-matrix least-squares technique. All non-hydrogen atoms were refined with anisotropic thermal parameters, whereas all hydrogen atoms were calculated using a riding model and included in the structure factor calculation. The 2730 reflections with $I \geqslant 3\sigma(I)$ were considered to be observed and used in the refinement. All calculations were performed on a Compaq computer using. MolEN/PC [11].

RESULTS AND DISCUSSION

Because the chloride ligands are good leaving groups in the palladium complex (dppe)PdCl$_2$, they are easily displaced by a strong nucleophilic group, especially a bidentate ligand, like MS_4^{2-} (M = W, Mo). The resulting products were obtained according to the following equation:

$$(dppe)PdCl_2 + (NH_4)_2MS_4 \longrightarrow (dppe)PdMS_4 + 2NH_4Cl \quad (M = W, Mo).$$

The products have poor solubility in common solvents, and slight solubility in DMF, DMSO and CH_3NO_2.

The band maxima and their intensities in the UV–vis spectra of I and II are summarized in Table 2; the recorded spectra of I and II are given in Fig. 1. λ_1 and λ_2 of these spectra belong to the π–π^* transition of the dppe ligand. The λ_3 values of I and II, assigned to the charge transition of S_t—M, are similar to those of MS_4^{2-} (M = W, Mo) [12].

The crystal of compound I is a neutral compound consisting of a distorted tetrahedral WS_4 unit with a palladium atom and two sulfur atom bridges (Fig. 2).

Table 2. Band maxima λ_{max} (in nm), extinction coefficients ε_{mol} (dm^3 cm^{-1} mol^{-1}) in UV–vis spectra of I and II (in DMF)

Complex	λ_1 (ε_{mol})	λ_2 (ε_{mol})	λ_3 (ε_{mol})
I	278 (33,495)	306 (28,594)	391 (11,233)
$(NH_4)_2WS_4$			392 (1.5×10^4) [12]
II	272 (20,413)	312 (34,786)	462 (5624)
$(NH_4)_2MoS_4$			467 (1.5×10^4) [12]

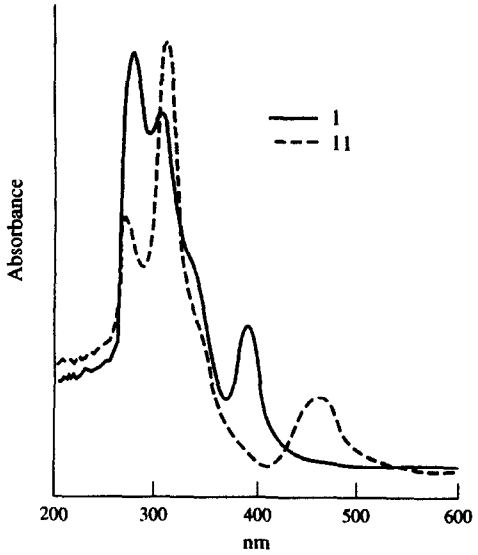


Fig. 1. The UV–vis spectra of I and II in DMF.

Table 3. Selected bond lengths (Å) for I

W—Pd	2.887(2)	Pd—P(2)	2.264(5)
W—S(1)	2.236(5)	P(1)—C(1)	1.87(2)
W—S(2)	2.228(6)	P(1)—C(111)	1.82(2)
W—S(3)	2.147(8)	P(1)—C(121)	1.82(2)
W—S(4)	2.135(7)	P(2)—C(2)	1.84(3)
Pd—S(1)	2.354(5)	P(2)—C(211)	1.79(2)
Pd—S(2)	2.351(6)	P(2)—(221)	1.82(2)
Pd—P(1)	2.275(5)	C(1)—C(2)	1.49(3)

The important bond lengths and bond angles are given in Tables 3 and 4. The palladium atom has a *cis*-quasi-square coordination geometry, with two phosphorus donors of dppe and two sulfur donors of WS_4^{2-}. The Pd—S distances (2.35 Å average) are slight longer than in $[[(allyl)Pd]_2WS_4]$ (2.34 Å average) [13]. The Pd—P distances (2.27 Å average) are in the region of

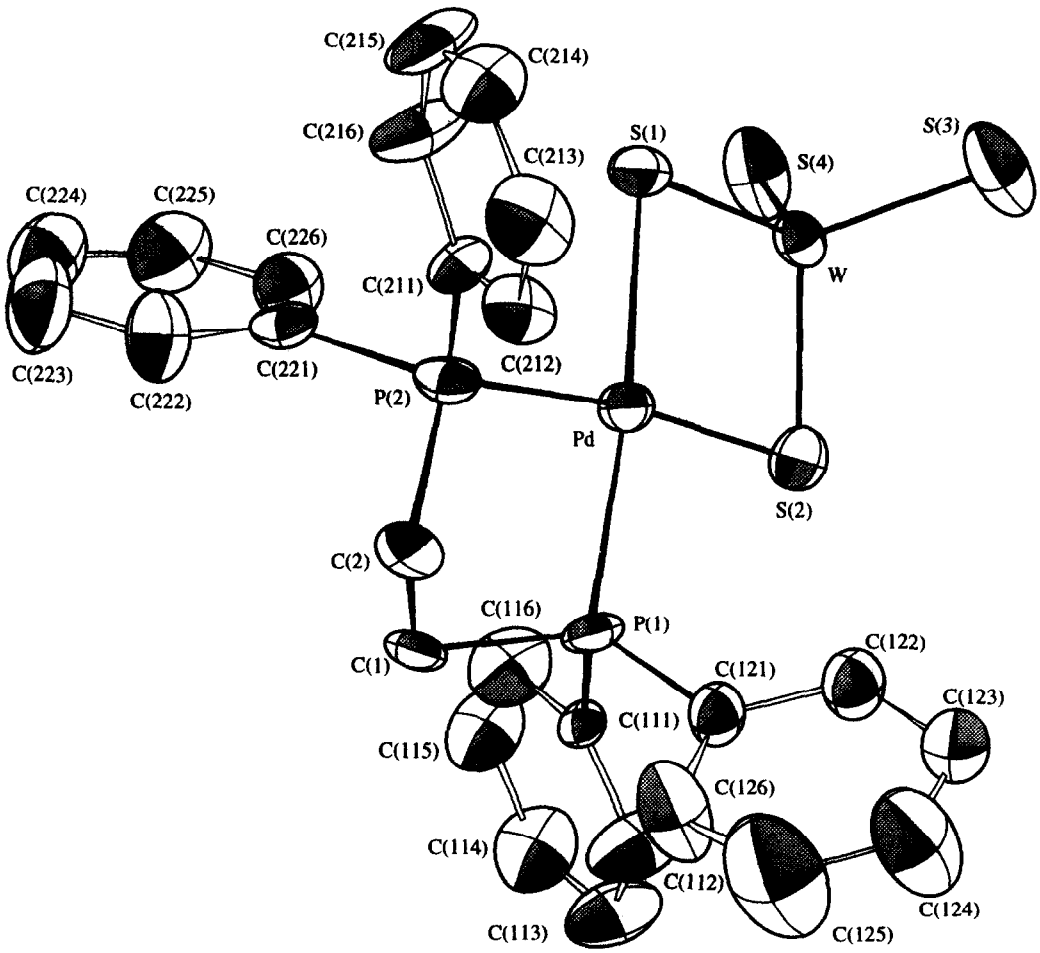


Fig. 2. The ORTEP drawing of I with 50% probability level.

Table 4. Selected bond angles (°) for **I**

Pd—W—S(1)	52.9(1)	S(2)—Pd—P(2)	173.7(2)
Pd—W—S(2)	52.8(2)	P(1)—Pd—P(2)	86.1(2)
Pd—W—S(3)	125.1(2)	W—S(1)—Pd	77.9(2)
Pd—W—S(4)	125.0(2)	W—S(2)—Pd	78.1(2)
S(1)—W—S(2)	105.7(3)	Pd—P(1)—C(1)	104.8(6)
S(1)—W—S(3)	110.2(2)	Pd—P(1)—C(111)	116.6(7)
S(1)—W—S(4)	110.4(2)	Pd—P(1)—C(121)	112.8(8)
S(1)—W—S(3)	110.5(3)	C(1)—P(1)—C(111)	105(1)
S(2)—W—S(4)	110.0(2)	C(1)—P(1)—C(121)	108(1)
S(3)—W—S(4)	109.9(3)	C(111)—P(1)—C(121)	108.8(9)
W—Pd—S(1)	49.2(1)	Pd—P(2)—C(2)	106.3(7)
W—Pd—S(2)	49.0(2)	Pd—P(2)—C(211)	120.2(8)
W—Pd—P(1)	136.9(1)	Pd—P(2)—C(221)	113.5(7)
W—Pd—P(2)	136.9(1)	C(2)—P(2)—C(211)	105(1)
S(1)—Pd—S(2)	98.3(3)	C(2)—P(2)—C(221)	105(1)
S(1)—Pd—P(1)	173.8(3)	C(211)—P(2)—C(221)	104.8(9)
S(1)—Pd—P(2)	87.7(2)	P(1)—C(1)—C(2)	107(2)
S(2)—Pd—P(1)	87.9(3)	P(2)—C(2)—C(1)	108(1)

those for (dppe)$PdCl_2$ [14]. The W—S—Pd angles (78.0° average) are 2.0° larger and the W—Pd distance (2.89 Å) is 0.08 Å longer than those in [[(allyl)$Pd]_2WS_4$] (76.0° and 2.81 Å average, respectively). The terminal W—S distances (2.14 Å average) are shorter than in $(NH_4)_2WS_4$ (2.17 Å) [15], but the W—S bridge distances (2.23 Å average) are slightly longer than those in [[(allyl)$Pd]_2WS_4$] (2.21 Å) [13].

Acknowledgements—This research was supported by grants from the State Key Laboratory of Structural Chemistry and National Science Foundation of China and the Science Foundation of Province.

REFERENCES

1. (a) Gates, B. C., *Catalytic Chemistry*. Wiley, New York, 1991; (b) *Metalloproteins, Chemical Properties & Biological Effects*, ed. Otsuka, S. and Yamanaka, T. Elsevier, New York, 1988.
2. Croughan, M. P., *Molybdenum and Molybdenum-containing Enzymes*. Pergamon Press, Oxford, 1980.
3. Muller, A., Diemann, E., Jostes, R. and Bogge, H., *Angew. Chem., Int. Edn Engl.* 1981, **20,** 934.
4. Mills, C. F., *Chem. Ber.*, 1979, **15,** 512.
5. Wu, X.-T., Chen, P.-C., Du, S.-W., Zhu, N.-Y. and Lu, J.-X., *J. Clust. Sci.*, 1994, **5,** 265 and references therein.
6. (a) Zhu, N.-Y., Du, S.-W., Chen, P.-C., Wu, X.-T. and Lu, J.-X., *J. Coord. Chem.*, 1992, **26,** 35; (b) Du, S.-W., Zhu, N.-Y., Chen, P.-C. Wu, X.-T. and Lu, J.-X., *J. Chem. Soc., Dalton Trans.*, 1992, 339; (c) Du, S.-W., Zhu, N.-Y., Chen, P.-C., Wu X.-T. and Lu, J.-X., *Polyhedron*, 1992, **11,** 109; (d) Sheng, T.-L., Du, S.-W. and Wu, X-T., *J. Clust. Sci.*, 1994, **5,** 303.
7. (a) Muller, A., Diemann, E., Jostes, R. and Bogge, H., *Angew. Chem., Int. Edn Engl.*, 1981, **20,** 957; (b) Adams, R. D., *Polyhedron*, 1985, **4,** 2003; (c) DuBois, M. R., *Chem. Rev.*, 1989, **89,** 1; (d) Dobbs, D. A. and Bengman, R. G., *J. Am. Chem. Soc.*, 1992, **114,** 6908.
8. McDonald, J. W., Friesen, G. D., Rosenhien, L. D. and Newton, W. F., *Inorg. Chim. Acta*, 1987, **72,** 205.
9. Steffen W. L. and Palenik, G. J., *Inorg. Chem.*, 1976, **15,** 2432.
10. Walker, N. and Stuart, D., *Acta Cryst.*, 1983, **A39,** 159.
11. MolEN, An Interactive Structure Solution Procedure. Enraf–Nonius, Delft, The Netherlands, 1990
12. Muller, A., Diemann, E., *Chem. Phys. Lett.*, 1971, **9,** 369.
13. Howard, K. E., Rauchfuss, T. B. and Wilson, S. R., *Inorg. Chem.*, 1988, **27,** 3561.
14. Singh, S., Jha, N. K., Narula, P. and Singh, T. P., *Acta Cryst.*, 1995, **C51,** 593.
15. Sasvari, K., *Acta Cryst.*, 1963, **36,** 3090.

Pergamon

PII: S0277-5387(96)00338-5

Polyhedron Vol. 16, No. 5, pp. 805–813, 1997
Copyright © 1996 Elsevier Science Ltd
Printed in Great Britain. All rights reserved
0277-5387/97 $17.00+0.00

Copper(II)–diethylenetriamine complexes with monodentate N-donor ligands: crystal and molecular structure of diethylenetriamine 2-cyanoguanidine copper(II) nitrate

Michael J. Begley, Peter Hubberstey* and Jo Stroud

Department of Chemistry, Nottingham University, Nottingham NG7 2RD, U.K.

(Received 18 June 1996; accepted 8 July 1996)

Abstract—Mixed ligand copper(II) complexes, $[Cu(dien)(cnge)X_2 \cdot nH_2O]$ ($X = NO_3^-$, NO_2^- or $0.5SO_4^{2-}$), containing diethylenetriamine (dien) and cyanoguanidine (cnge), have been prepared and characterized. Similar complexes, $[Cu(dien)(ImH)X_2 \cdot nH_2O]$ ($X = Cl^-$, NO_3^-, NO_2^- or $0.5SO_4^{2-}$), containing diethylenetriamine (dien) and imidazole (ImH), were prepared for comparison. Under identical reaction conditions, the corresponding pyridine complexes could not be isolated, the copper(II)–dien complexes, $[Cu(dien)X_2 \cdot nH_2O]$ ($X = Br^-$, Cl^-, NO_3^-, NO_2^- or $0.5SO_4^{2-}$) being formed. The structure of $[Cu(dien)(cnge)(ONO_2)_2]$ (**5**) has been determined by single-crystal X-ray diffraction methods. It comprises discrete molecular units based on a tetragonally elongated octahedral copper(II) coordination sphere with equatorially bound dien (average Cu---N = 2.004 Å) and cnge (Cu---N = 1.945 Å) and axially bound nitrate (Cu---O = 2.517, 2.567 Å). Marked shifts ($\sim 25\ cm^{-1}$) to higher frequency in the ν_{as}(NCN) band of cnge on coordination to copper(II) in **5** and related complexes are shown to be consistent with strongly bound cnge, as evidenced by short Cu—N distances and near linear CuNC bond angles. FAB-MS studies gave comparable patterns for all complexes, inferring structural types similar to that for $[Cu(dien)(cnge)(ONO_2)_2]$. Copyright © 1996 Elsevier Science Ltd

Keywords: copper(II); diethylenetriamine; 2-cyanoguanidine.

2-Cyanoguanidine (cnge) readily coordinates later transition metals [1–8], complexes with copper(I) [1], copper(II) [2–6] and cadmium(II) [7] having been structurally characterized. In the absence of multidentate ligands, copper(II) normally binds two *trans*-located cnge ligands [2,3]; in the presence of bidentate chelating 2,2′-bipyridine (bipy), it coordinates two *cis*-located cnge ligands [4]. In the presence of tridentate chelating 1-(2-aminoethyl)biguanide (aebg), copper(II) binds a single cnge ligand [5]. In all cases, the cnge molecules occupy equatorial positions of the tetragonally elongated copper(II) (d^9) coordination sphere; the only example of axially located cnge occurs in the unique tetrakis(acetato) bridged dinuclear copper(II) complex [6]. We now describe the coordination of cnge to copper(II) in a complex containing the tridentate chelating ligand, diethylenetriamine [bis(2-aminoethyl)amine, 3-azapentane-1,5-diamine, dien].

Although mixed ligand complexes of copper(II) containing dien have been known for many years [9–11], structural data are limited. Of those which have been structurally characterized, very few contain dien and a monodentate ligand [10]; the majority contain dien and a bidentate ligand [11]. The latter adopt five-coordinate distorted square pyramidal geometries, with dien located equatorially and the bidentate ligand occupying one equatorial and one axial position; anions are not coordinated [11]. The former adopt six-coordinate tetragonally elongated octahedral geometries, with both ligands located equatorially and anions weakly bound axially [10]. Surprisingly, analogous pentamethyldiethylenetriamine (Me_5dien) complexes all adopt five-coordinate square pyramidal geometries [12,13]. Those with Me_5dien and a bidentate ligand are structurally analogous to the corresponding dien complexes [12]; those with Me_5dien and a monodentate ligand bind a

* Author to whom correspondence should be addressed.

third ligand (either solvent or anion) in the axial position [13].

RESULTS AND DISCUSSION

Mixed ligand copper(II) complexes, containing dien and either imidazole (ImH), 2-cyanoguanidine (cnge) or pyridine (py), were targeted. Anions varied from bromide through chloride, nitrate and nitrite to sulfate. The general synthetic route comprised treatment of an aqueous solution of the copper(II) salt with an aqueous solution containing dien and the appropriate monodentate N-donor ligand. Of the 15 possible mixed ligand products only seven formed; they are listed in Table 1. Imidazole was the most effective monodentate ligand, forming complexes **1–4** with all anions except bromide; cnge formed complexes **5–7** with the oxoanions, but not the halides, and pyridine did not form any complexes. The products of the other eight systems were the simple copper(II)–dien complexes (**8–12**), which were also produced in the absence of the monodentate ligand. Of the 12 products, only eight (**1, 2, 4, 5, 7–10**) could be satisfactorily characterized by analytical and spectroscopic methods; the other four (**3, 6, 11, 12**) were so deliquescent that quantitative analysis was not attempted. Vibrational spectroscopy was used, however, to confirm the presence of dien, monodentate ligand and anion, as appropriate. Analytical and spectroscopic data are collated in Table 1. UV–vis spectra of all products were similar, comprising a single broad band with λ_{max} close to 660 nm. They had magnetic moments close to 1.7 B.M., typical of mononuclear copper(II) d^9 systems. Fast atomic bombardment mass spectroscopy (FAB-MS) studies of all 12 products, plus $Cu(Me_5dien)(cnge)(NO_3)_2$ (**13**), were undertaken. Although the parent ions were not observed, the fragmentation and combination patterns were consistent with the proposed product identities.

X-ray crystal structure of $[Cu(dien)(cnge)(ONO_2)_2]$ (**5**)

After recrystallization, $[Cu(dien)(ImH)Cl_2 \cdot 2H_2O]$ (**1**), $[Cu(dien)(ImH)(NO_3)_2 \cdot H_2O]$ (**2**) and $[Cu(dien)(cnge)(NO_3)_2]$ (**5**) gave good quality crystals. However, structural analysis was only pursued for **5**, the structure of the imidazole (ImH) and 1-ethylimidazole (EtImH) complexes, $[Cu(dien)(L)(OClO_3)_2]$ [L = ImH (**14**) or EtImH (**15**)] having been determined previously [10]. The molecular structure of **5** is shown in Fig. 1; selected interatomic distances and angles are given in Table 2. It comprises discrete molecular units based on a tetragonally elongated octahedral copper(II) coordination sphere, typical of Jahn–Teller distorted d^9 $[(d_{z^2})^2 (d_{x^2-y^2})^1]$ systems, with strongly bonded N-donor ligands in the equatorial sites and weakly bonded

Table 1. Analytical and spectroscopic data for copper–dien complexes

Complex		Analytical data				IR spectroscopic data (cm^{-1})[a]		
		C	H	N	Cu	dien	ligand	anion
$Cu(dien)(ImH)Cl_2 \cdot 2H_2O$	**1**	24.4 (24.6)	6.4 (6.2)	20.4 (20.5)	17.2 (18.6)	2917s, 1597m	1733m, 1024m	
$Cu(dien)(ImH)(NO_3)_2 \cdot H_2O$	**2**	22.0 (22.3)	4.8 (5.1)	26.5 (26.0)	16.8 (16.9)	2920s	1734m, 1024m	1383s
$Cu(dien)(ImH)(NO_2)_2 \cdot nH_2O$[b]	**3**					2885s, 1597m, 1459m	1729m, 1024m	1265s
$Cu(dien)(ImH)(SO_4) \cdot 2H_2O$	**4**	24.9 (25.4)	6.3 (5.2)	20.9 (21.2)	18.6 (19.4)	2927s, 1597m	1730s, 1020s	1118s
$Cu(dien)(cnge)(NO_3)_2$	**5**	19.1 (19.3)	4.8 (4.6)	34.0 (33.7)	16.6 (17.0)	2922s	2235s, 2191s	1380s
$Cu(dien)(cnge)(NO_2)_2 \cdot nH_2O$[b]	**6**					2919s, —, 1445m	2191s, 2148s	1269s
$Cu(dien)(cnge)(SO_4) \cdot 3H_2O$	**7**	17.6 (18.0)	6.1 (5.8)	24.8 (24.5)	15.7 (15.9)	2929s, 1600m	2240s, 2189s	1112s
$Cu(dien)Br_2$	**8**	14.6 (14.7)	4.1 (4.0)	12.9 (12.9)	19.2 (19.5)	2939s, 1576m, 1470m		
$Cu(dien)Cl_2$	**9**	20.6 (20.2)	5.9 (5.5)	18.0 (17.7)	25.5 (26.8)	2923s, 1610m, 1541m		
$Cu(dien)(NO_3)_2$	**10**	16.7 (16.6)	4.5 (4.5)	24.0 (24.1)	20.8 (21.9)	2920s, 1599m, 1458m		1385s
$Cu(dien)(NO_2)_2 \cdot nH_2O$[b]	**11**					2925s, 1594m, 1480m		1260s
$Cu(dien)(SO_4) \cdot nH_2O$[b]	**12**					2927s, 1599m, 1460m		1115s

[a] IR data for the free ligands and anions. dien: 2930s, 1598m, 1458m cm^{-1}; ImH: 1735s, 1025s cm^{-1}; cnge: 2209s, 2165s cm^{-1}; $\nu_3(NO_3)$ 1390 cm^{-1}, $\nu_3(NO_2)$ 1244s, cm^{-1}, $\nu_3(SO_4)$ 1105 cm^{-1}.

[b] Analytical data are not available for these complexes due to their deliquescent nature.

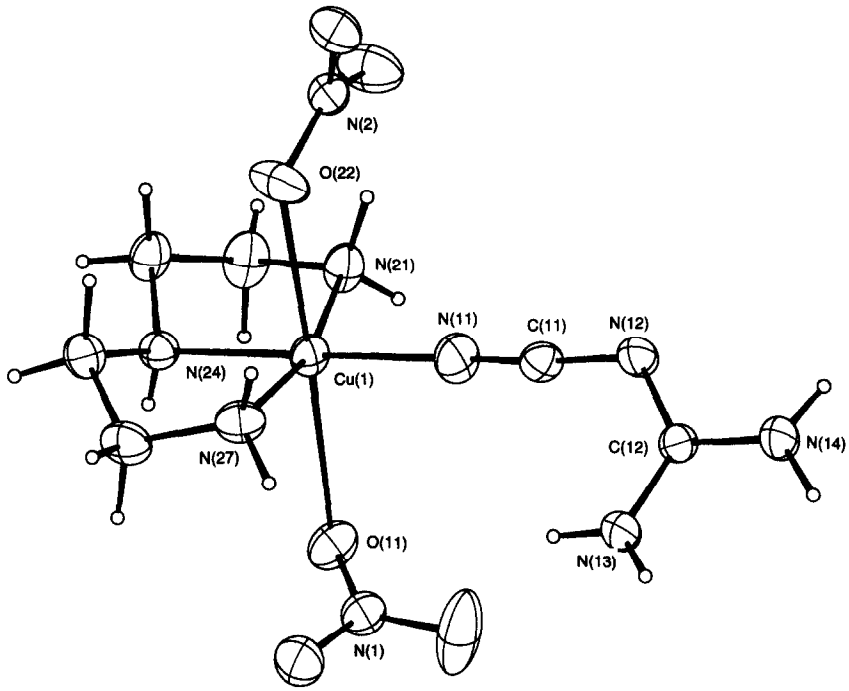


Fig. 1. Molecular structure of $[Cu(dien)(cnge)(ONO_2)_2]$.

Table 2. Interatomic distances (Å) and angles (°) in $[Cu(dien)(cnge)(ONO_2)_2]$

Copper coordination sphere			
Cu(1)—N(11)	1.945(4)	N(11)—Cu(1)—N(21)	95.2(2)
Cu(1)—N(21)	2.006(4)	N(21)—Cu(1)—N(24)	84.3(2)
Cu(1)—N(24)	1.988(4)	N(24)—Cu(1)—N(27)	84.0(2)
Cu(1)—N(27)	2.019(4)	N(11)—Cu(1)—N(27)	96.6(2)
Cu(1)—O(11)	2.567(3)	N(11)—Cu(1)—N(24)	179.4(2)
Cu(1)—O(22)	2.517(3)	N(21)—Cu(1)—N(27)	165.5(2)
		N(11)—Cu(1)—O(11)	91.0(2)
		N(21)—Cu(1)—O(11)	97.2(2)
		N(24)—Cu(1)—O(11)	89.4(2)
		N(27)—Cu(1)—O(11)	91.2(2)
		N(11)—Cu(1)—O(22)	88.7(2)
		N(21)—Cu(1)—O(22)	89.8(2)
		N(24)—Cu(1)—O(22)	91.0(2)
		N(27)—Cu(1)—O(22)	81.9(2)
		Cu(1)—O(11)—N(1)	110.9(3)
		Cu(1)—O(22)—N(2)	127.6(3)
Cyanoguanidine			
N(11)—C(11)	1.146(5)	N(11)—C(11)—N(12)	174.6(5)
C(11)—N(12)	1.287(5)	C(11)—N(12)—C(12)	119.2(4)
N(12)—C(12)	1.345(5)	N(12)—C(12)—N(13)	123.2(4)
C(12)—N(13)	1.313(5)	N(12)—C(12)—N(14)	117.6(4)
C(12)—N(14)	1.309(5)	N(13)—C(12)—N(14)	119.2(4)
		Cu(1)—N(11)—C(11)	176.4(4)

nitrates in the axial sites. The analogous ImH and EtImH complexes are very similar, with equatorially located dien and imidazole molecules and axially located perchlorate anions. Pertinent structural data for the copper(II) coordination spheres of all three complexes are compared in Table 3. The most significant difference lies in the copper to anion distances, those to perchlorate being somewhat longer than those to nitrate. It is also interesting to note that the Cu—N distances increase in the sequence, cnge (1.945

Table 3. Structural parameters [distances (Å) and angles (°)] in the copper(II) coordination spheres of [Cu(dien)(cnge)$(ONO_2)_2$] (**5**), [Cu(dien)(ImH)$(OClO_3)_2$] (**14**) and [Cu(dien)(EtImH)$(OClO_3)_2$] (**15**)

	5	**14**[a]	**15**[a]
Cu---N(dien)	1.988–2.019 (2.004)[b]	2.006–2.012 (2.008)[b]	2.009–2.016 (2.012)[b]
Cu---N(L)[c]	1.945	1.970	1.971
Cu---O (anion)	2.517, 2.567	2.571, 2.763	2.570, 2.686
O---Cu---N	81.9–97.2[d]	80.6–101.8[d]	80.6–95.8[d]
N(dien)—Cu—N(dien)	84.0, 84.3	84.1	83.2, 83.6
N(dien)—Cu—N(L)[c]	95.2, 96.6	96.3	96.1, 96.9

[a] Reference [10].
[b] Range (average).
[c] L = cnge, ImH or EtImH.
[d] Range.

Å) < ImH (1.970 Å) ~ EtImH (1.971 Å) < dien (1.988–2.019 Å), owing to the change from *sp* through sp^2 to sp^3 hybridization.

The cnge molecule bonds to the copper(II) ion in an equatorial position. As for other examples of cnge coordinated to copper(II) [2–6], its geometry (Table 2) does not differ significantly from that for free cnge [14]. Although effectively planar [maximum deviation from the least squares mean plane = 0.047 Å, C(12)], the cnge molecule is twisted out of the plane formed by the four ligating nitrogen atoms (dihedral angle = 36.1°). The latter is slightly distorted, the *trans*-located terminal dien nitrogens lying above the mean plane [N(21), 0.073 Å; N(27), 0.072 Å] and the pivotal dien nitrogen and cnge nitrile nitrogen lying below the mean plane [N(24), −0.079 Å; N(11), −0.066 Å]. The copper atom lies 0.077 Å below the mean plane, between the pivotal dien and cnge nitrogens [N(11)—Cu—N(24) 179.4(2)]. The nitrate anions are planar and subtend dihedral angles of 20.0° [$N(1)O_3^-$] and 67.4° [$N(2)O_3^-$] with the N_4 plane.

The monodentate coordination of the nitrate anions in **5** differs from that of the nitrate anions in [Cu(dien)(NO_3)](NO_3) (**16**) [15] and [Cu(dien)$_2$]$(NO_3)_2$ (**17**) [16]. In **16**, one nitrate acts as a bidentate bridging ligand and the other is non-coordinated, as are both nitrates in **17**. The distorted trigonal bipyramidal copper(II) coordination sphere in **16** is completed by a single tridentate chelating dien molecule [15]. The copper(II) in **17** is surrounded by two tridentate chelating dien ligands, its six-coordinate geometry, the relatively rare, compressed tetragonally distorted octahedron, the alternative Jahn–Teller distorted d^9 [$(d_{x^2-y^2})^2 (d_{z^2})^1$] system, being dictated by the steric requirements of the dien ligand [16]. The differing strength of nitrate binding in **5** and **17** can be traced to the copper(II) coordination geometry. Whereas the nitrate anions bind weakly in the axial positions of the tetragonally elongated octahedron in **5** (Cu···O = 2.52, 2.57 Å), it is much more strongly coordinated in the bridging equatorial positions of the distorted trigonal bipyramid in **16** (Cu···O = 2.12, 2.29 Å). Nitrate binding in **16** is enhanced by secondary interactions, giving a pseudo-bidentate chelating coordination for both copper–nitrate contacts (Cu···O = 2.58, 2.89 Å) and hence a pseudo-seven-fold coordination geometry.

The molecules of **5** are held in place in the crystal predominantly by hydrogen bonding interactions between the cnge amino moieties and the nitrate anions. Hydrogen bond contacts also occur between terminal dien amino groups and the nitrate anions. These interactions are shown in Fig. 2 and structural details for all possible hydrogen bond contacts are collected in Table 4.

A marked increase in the frequency of the doublet assigned to ν_{as}(NCN) [17] is observed on coordination of cnge in [Cu(dien)(cnge)$(ONO_2)_2$] (Table 1). This change is typical of coordinated cnge, as shown by comparison with data for the five previously structurally characterized copper(II)–cnge complexes (Table 5). Only one complex, [$(\mu$-OAc$)_4${Cu(cnge)}$_2$], does not exhibit such a change in ν_{as}(NCN). Although the marked shifts in ν_{as}(NCN) cannot be related to trends in the geometry of the ligating nitrile moiety of the cnge molecule, they do appear to be sensitive to the cnge coordination geometry and the strength of the Cu---N coordinate bond. Marked increases in ν_{as}(NCN) are consistent with short Cu···N distances and near linear Cu—N—C bond angles, presumed indicative of strongly bound cnge. Virtually no change in ν_{as}(NCN) occurs for [$(\mu$-OAc$)_4${Cu(cnge)}$_2$], which has the longest Cu---N distance and smallest Cu—N—C angle (Table 5). Thus despite the increasing database on copper(II)–cnge complexes, ν_{as}(NCN) can only be used as a crude indicator of the strength of cnge bonding.

Although coordination of cnge in Cu(dien)(cnge)$(SO_4)\cdot 3H_2O$ (**7**) results in an increase in ν_{as}(NCN) similar to that observed in **5**, a decrease in ν_{as}(NCN) is observed for Cu(dien)(cnge)$(NO_2)_2\cdot nH_2O$ (**6**) (Table 1). Hence, similar coordination geometries may be inferred for **5** and **7**, but not **6**. As **6** is the first copper(II)–cnge complex for which a decrease has been observed and we have not been able to obtain a pure crystalline sample, an assessment of its structural chemistry is not possible.

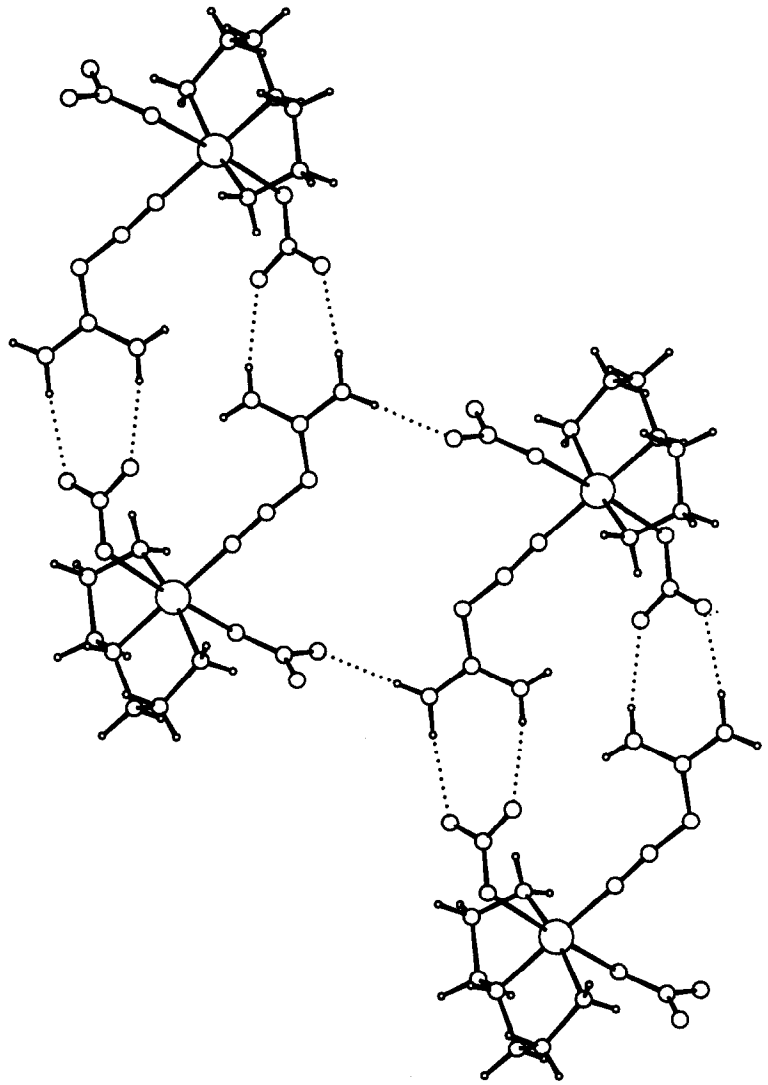


Fig. 2. Hydrogen bonding interactions between centrosymmetrically related $[Cu(dien)(cnge)(ONO_2)_2]$ molecules.

Table 4. Hydrogen bonding interactions in $[Cu(dien)(cnge)(ONO_2)_2]$ (5)

Interaction N—H···X	Symmetry of X	N—H (Å)	N—X (Å)	H···X (Å)	NHX (°)
N(13)—H(131)···O(21)	$(1-x, 1-y, -z)$	0.85(7)	3.109(5)	2.36(7)	147(6)
N(13)—H(132)···O(13)	$(1-x, 2-y, -z)$	0.78(7)	2.899(5)	2.14(8)	166(7)
N(14)—H(141)···O(12)	$(1-x, 2-y, -z)$	0.91(7)	3.037(5)	2.13(7)	174(6)
N(14)—H(142)···O(21)	$(2-x, 1-y, -z)$	0.87(6)	3.003(5)	2.13(8)	178(6)
N(21)—H(211)[a]		0.88(6)			
N(21)—H(212)···O(23)	(x, y, z)	0.95(7)	2.996(6)	2.14(7)	150(6)
N(24)—H(241)[a]		0.79(4)			
N(27)—H(271)···O(21)	$(1-x, 1-y, -z)$	0.88(6)	3.144(5)	2.35(6)	151(5)
N(27)—H(272)[a]		0.78(6)			

[a] H···X contacts < 2.40 Å do not occur with these amino hydrogen atoms.

Table 5. Molecular geometries and IR spectroscopic data for structurally characterized copper–cnge complexes

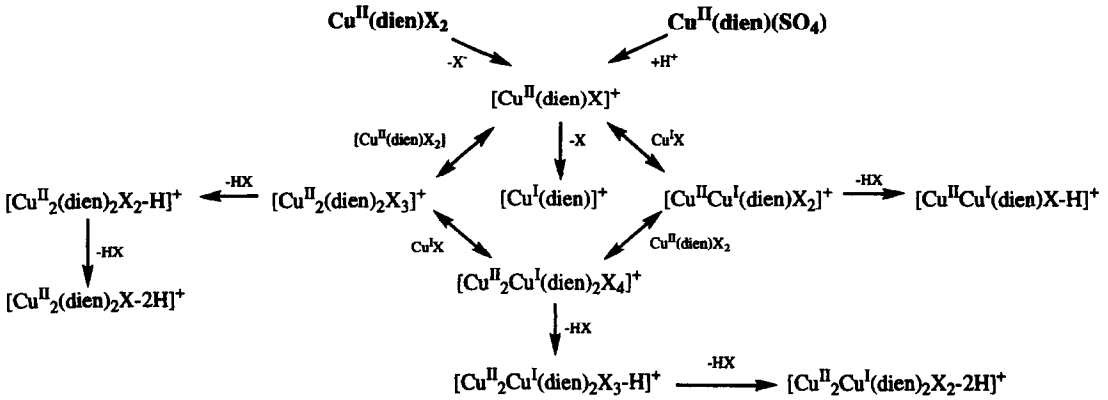
Complex	Geometrical data					IR spectroscopic data
	Cu—N(1) (Å)	N(1)—C(1) (Å)	C(1)—N(2) (Å)	Cu—N(1)—C(1) (°)	N(1)—C(1)—N(2) (°)	ν_{as} (NCN) (cm^{-1})
Free cnge[a]	—	1.169	1.305	—	175.1	2209/2165
$[Cu(dien)(cnge)(ONO_2)_2]$[b]	1.945(4)	1.146(5)	1.287(5)	176.4(4)	174.6(5)	2235/2191
$[Cu(bipy)(cnge)_2(FBF_3)_2]$[c]	1.931	1.159	1.309	151.0	174.7	2232/2209
$[Cu_2(O_2CMe)_4(cnge)_2]$[d]	2.136	1.146	1.300	135.9	175.1	2209/2168
$[Cu(cnge)_2(H_2O)_2](NO_3)_2 \cdot 2H_2O$[e]	1.92	1.16	1.29	168.8	173.2	2240/2200
$[Cu(cnge)_2Cl_2(H_2O)_2]$[f]	1.92	1.16	1.29	164.9	170.6	2250/2200
$[Cu(cnge)(aebg)]SO_4 \cdot H_2O$[g]	1.96	1.17	1.28	[h]	172.6	[h]

[a] Reference [14].
[b] This work.
[c] Reference [4].
[d] Reference [6].
[e] Reference [2].
[f] Reference [3].
[g] Reference [5].
[h] Not quoted.

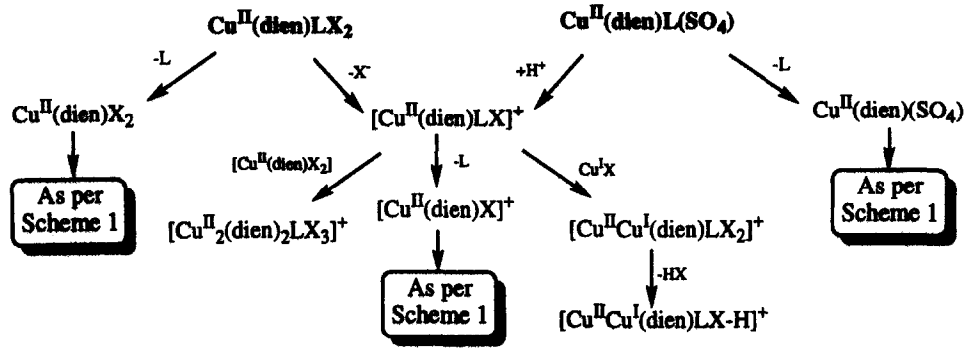
Mass spectrometric studies of copper(II)–dien complexes

FAB-MS studies of copper(II)–dien complexes have been particularly valuable, the spectra following a consistent pattern. The fragmentation and combination patterns for $Cu(dien)X_2$ and $Cu(dien)LX_2$ (L = ImH or cnge; X = Br, Cl, NO_3 or NO_2) complexes are summarized in Schemes 1 and 2, respectively. The ions (minimum *m/z* values) observed for individual complexes are collated in Table 6. In neither case is the parent ion observed. In the absence of a mondentate N-donor ligand (Scheme 1), however, loss of X^- gives the observed $[Cu^{II}(dien)X]^+$ cation, which either loses X to form $[Cu^{I}(dien)]^+$ or combines with $[Cu^{II}(dien)X_2]$ or $[Cu^{I}X]$ moieties to form species which consecutively lose up to two HX fragments. For complexes containing a monodentate N-donor ligand (Scheme 2), a similar behaviour pattern emerges, loss of X^- giving $[Cu^{II}(dien)LX]^+$, which either loses L to form $[Cu^{I}(dien)X]^+$ or combines with $[Cu^{II}(dien)X_2]$ or $[Cu^{I}X]$ moieties to form species which exhibit HX loss. The formation of $[Cu^{I}(dien)X]^+$, which could also arise from $Cu(dien)LX_2$ *via* $Cu(dien)X_2$ by sequential loss of L and X^-, leads to those ions observed in the spectra of $Cu(dien)X_2$ (Scheme 1).

The spectra for the sulfates (Schemes 1 and 2; Table 6) are analogous to those for the complexes containing singly charged ions, the only significant difference involving the formation of the pivotal ions, addition of H^+ giving $[Cu^{II}(dien)(SO_4H)]^+$ (Scheme 1) and



Scheme 1.



Scheme 2.

$[Cu^{II}(dien)L(SO_4H)]^+$ (Scheme 2), which behave as $[Cu^{II}(dien)X]^+$ and $[Cu^{II}(dien)LX]^+$, HSO_4^- being the singly charged X^- anion.

EXPERIMENTAL

Elemental analysis, mass spectrometry, IR and UV–vis spectroscopy and magnetic measurements were used to characterize all products, except for the highly deliquescent nitrites and sulfates, which were studied using spectroscopic methods only; pertinent data are collated in Table 1. Carbon, nitrogen and hydrogen analyses (microanalysis) and copper analyses (atomic absorption spectroscopy) and mass spectral data acquisition were carried out in the University of Nottingham Chemistry Department by Mr T. J. Spencer, Mr M. Guyler and Mr T. Hollingworth, respectively. IR spectra were obtained as KBr pressed pellets on either a Perkin–Elmer PE983G or PE 1600 series FTIR spectrophotometer and UV–vis spectra on either a Perkin–Elmer Lambda 5 or Unicam UV2-100 spectrometer.

Copper(II) nitrite was prepared *in situ* by treatment of $CuSO_4 \cdot 5H_2O$ with $Ba(NO_2)_2$. The other copper(II) salts [$CuBr_2$, $CuCl_2 \cdot 2H_2O$, $Cu(NO_3)_2 \cdot 3H_2O$, $CuSO_4 \cdot 5H_2O$] were obtained from Aldrich Chemical Company Ltd and recrystallized from deionized water prior to use. The N-donor ligands, dien, ImH, cnge and py, were obtained from Aldrich Chemical Company Ltd and used without further purification.

Preparation of bromide salts

An aqueous solution (50 cm^3) of $CuBr_2$ (4.00 g, 17.9 mmol) was added to an aqueous solution (50 cm^3) containing either dien (1.93 g, 18.0 mmol) alone or dien (1.39 g, 18.0 mmol) with either ImH (1.24 g, 18.2 mmol), cnge (1.50 g, 17.8 mmol) or py (1.43 g, 18.1 mmol). The resulting blue solution was heated to 90°C

Table 6. Ions (minimum m/z values) observed in the FAB mass spectra of Cu(dien)Br_2 (**8**), Cu(dien)Cl_2 (**9**), Cu(dien)(ImH)$Cl_2 \cdot 2H_2O$ (**1**), Cu(dien)$(NO_3)_2$ (**10**), Cu(dien)(ImH)$(NO_3)_2 \cdot H_2O$ (**2**), Cu(dien)(cnge)$(NO_3)_2$ (**5**), Cu(dien)$(NO_2)_2 \cdot nH_2O$ (**7**), Cu(dien)(cnge)$(NO_2)_2 \cdot nH_2O$ (**6**), Cu(dien)$(SO_4) \cdot nH_2O$ (**12**), Cu(dien)(ImH)$(SO_4) \cdot 2H_2O$ (**4**), Cu(dien)(cnge)$(SO_4) \cdot 3H_2O$ (**7**) and Cu(Me_5deta)(cnge)$(NO_3)_2$ (**13**)

Ion	Anion: / Complex:	Br^-	Cl^-		NO_3^-			NO_2^-		SO_4^{2-}			
		8	**9**	**1**	**10**	**2**	**5**	**11**	**6**	**12**	**4**	**7**	**13**[a]
$[Cu^{II}(dien)X]^+$		245	201	201	228	228	228	212	212	263	263	263	298
$[Cu^{II}_2(dien)_2X_3]^+$		—	437	437	—	518	518	—	—	—	—	—	—
$[Cu^{II}_2(dien)_2X_2-H]^+$		—	401	401	—	455	455	—	—	525	525	525	—
$[Cu^{II}_2(dien)_2X-2H]^+$		—	—	—	—	392	392	—	—	428	428	428	—
$[Cu^{II}_2Cu^{I}(dien)_2X_4]^+$		—	535	535	—	—	—	—	—	—	—	—	—
$[Cu^{II}_2Cu^{I}(dien)_2X_3-H]^+$		—	499	499	—	580	—	—	—	—	—	—	—
$[Cu^{II}_2Cu^{I}(dien)_2X_2-2H]^+$		—	—	—	—	517	—	—	—	587	587	587	—
$[Cu^{II}Cu^{I}(dien)X_2]^+$		—	299	299	353	—	—	321	—	423	423	423	—
$[Cu^{II}Cu^{I}(dien)X-H]^+$		307	263	263	290	—	—	—	—	325	325	325	—
$[Cu^{I}(dien)]^+$		166	166	166	166	166	166	166	166	166	166	166	236
$[Cu^{II}(dien)LX]^+$		—	—	269	—	296	312	—	—	—	331	347	382
$[Cu^{II}Cu^{I}(dien)LX_2]^+$		—	—	367	—	421	437	—	—	—	490	506	507
$[Cu^{II}Cu^{I}(dien)LX-H]^+$		—	—	331	—	358	374	—	—	—	393	409	444
$[Cu^{II}_2(dien)_2LX_3]^+$		—	—	—	—	586	—	—	—	—	—	—	—

[a] For these ions read Me_5dien for dien.

for 30 min, before the solvent volume was reduced to yield a blue gum. For all four experiments, washing with ethanol gave a dark blue solid, which after recrystallization from aqueous ethanol was found to be $Cu(dien)Br_2$ (4.95 g, 15.2 mmol, 85%).

Preparation of chloride salts

An aqueous solution (60 cm^3) of $CuCl_2 \cdot 2H_2O$ (5.00 g, 29.3 mmol) was added to an aqueous solution (60 cm^3) containing either dien (3.10 g, 28.9 mmol) alone or dien (3.10 g, 28.9 mmol) with either ImH (1.95 g, 28.6 mmol), cnge (2.45 g, 29.1 mmol) or py (2.30 g, 29.1 mmol). The resulting blue solution was heated to 90°C for 30 min, solvent volume was reduced and ethanol added to yield a blue solid. Recrystallization from aqueous ethanol gave $Cu(dien)Cl_2$ (4.90 g, 20.6 mmol, 71%) or $Cu(dien)(ImH)Cl_2 \cdot 2H_2O$ (5.05 g, 14.8 mmol, 52%).

Preparation of nitrate salts

An aqueous solution (60 cm^3) of $Cu(NO_3)_2 \cdot 3H_2O$ (5.00 g, 20.7 mmol) was added to an aqueous solution (60 cm^3) containing either dien (2.22 g, 20.7 mmol) alone or dien (2.22 g, 20.7 mmol) with either ImH (1.40 g, 20.6 mmol), cnge (1.75 g, 20.8 mmol) or py (1.65 g, 20.9 mmol). The resulting blue solution was heated to 90°C for 30 min, solvent volume reduced, ethanol added and the mixture left at 5°C for 16 h. All four experiments gave blue solids, which after recrystallization from aqueous ethanol analysed for $Cu(dien)(NO_3)_2$ (4.20 g, 14.5 mmol, 70%), $Cu(dien)(ImH)(NO_3)_2 \cdot H_2O$ (6.25 g, 16.6 mmol, 80%), $Cu(dien)(cnge)(NO_3)_2$ (5.95 g, 15.8 mmol, 77%) and $Cu(dien)(NO_3)_2 \cdot H_2O$ (3.65 g, 11.8 mmol, 57%), respectively.

Preparation of nitrite salts

An aqueous solution (30 cm^3) of $CuSO_4 \cdot 5H_2O$ (3.26 g, 13.1 mmol) was added to an aqueous solution (30 cm^3) of $Ba(NO_2)_2$ (3.00 g, 13.1 mmol). A white precipitate of $BaSO_4$, which formed immediately, was filtered off to leave a lime green solution, which was then added to an aqueous solution (40 cm^3) containing dien (1.35 g, 12.6 mmol) alone or dien (1.35 g, 12.6 mmol) with either ImH (0.86 g, 12.6 mmol), cnge (1.05 g, 12.5 mmol) or py (1.00 g, 12.6 mmol). The resulting blue solution was heated to 90°C for 30 min, solvent volume reduced, ethanol added and the mixture left at 5°C for 16 h. In none of the experiments did precipitation occur. Other diverse solvent combinations (H_2O–Pr^iOH, MeCN–Et_2O, MeCN–toluene) were tried but without success. A solid product could only be obtained by removal of all solvent *in vacuo*.

Preparation of sulfate salts

An aqueous solution (60 cm^3) of $CuSO_4 \cdot 5H_2O$ (8.00 g, 32.0 mmol) was added to an aqueous solution (60 cm^3) containing either dien (3.45 g, 32.2 mmol) alone or dien (3.45 g, 32.2 mmol) with either ImH (2.15 g, 31.6 mmol), cnge (2.69 g, 32.0 mmol) or py (2.55 g, 32.2 mmol). The resulting blue solution was heated to 90°C for 30 min, solvent volume reduced, ethanol added and the mixture left at 5°C for 16 h. In the presence of ImH or cnge, highly deliquescent blue solids analysing for $Cu(dien)(ImH)(SO_4) \cdot 2H_2O$ (6.10 g, 16.6 mmol, 53%) and $Cu(dien)(cnge)(SO_4) \cdot 3H_2O$ (6.45 g, 16.1 mmol, 50%) were recovered. In the presence of py or with dien alone, precipitation did not occur. As for the nitrites, various solvent combinations (H_2O–Pr^iOH, MeCN–Et_2O, MeCN–toluene) were tried but without success. A solid product could only be obtained by removal of all solvent *in vacuo*.

X-ray crystallography

Oscillation and Weissenberg photographs revealed preliminary cell parameters for selected crystals of **5** (triclinic) mounted in Lindemann tubes under dry nitrogen. X-ray diffraction data for the refinement of cell parameters and structure determination were collected using a Hilger and Watts Y290 four-circle diffractometer.

Crystal data. $C_6H_{17}CuN_9O_6$, M = 374.80, triclinic, space group $P\bar{1}$, $a = 7.949(3)$, $b = 10.217(4)$, $c = 10.351(4)$ Å, $\alpha = 66.08(5)°$, $\beta = 75.39(5)°$, $\gamma = 85.45(5)°$, $U = 743.36$ Å^3, $Z = 2$, $F(000) = 386$, D_m (bromoform/hexane) = 1.68 g cm^{-3}, $D_c = 1.67$ g cm^{-3}, Mo-K_α radiation, $\lambda = 0.71073$ Å, $\mu_{calc} = 15.15$ cm^{-1}, crystal dimensions $0.08 \times 0.20 \times 0.25$ mm^3.

One unique set of data (2199 reflections; index ranges $-9 < h < 9$, $-10 < k < 12$, $0 < l < 12$) was collected at 298 K in the range $1 < \theta < 25°$ (scan mode: ω–2θ) using graphite monochromated Mo-K_α radiation. Standard reflections were constant throughout the course of the data collection, indicating that the crystals were stable. Data were corrected for Lorentz and polarization effects; absorption corrections were not applied.

The positions of the copper atoms were determined by identifying the copper–copper $2x$, $2y$, $2z$ vector in the Patterson map (CRYSTALS [18]). The positions of the remaining atoms were obtained by Fourier difference syntheses. All atoms were refined with anisotropic displacement parameters with the exception of the hydrogen atoms, which were refined isotropically. Full least squares matrix refinement (CRYSTALS [18]) against F values [2199 data with $I > 3\sigma(I)$] with unit weights converged to $R = 0.040$ and $R_w = 0.042$ for 257 parameters in space group $P\bar{1}$; residual $\Delta\rho_{min} = -0.513$, $\Delta\rho_{max} = 0.619$, $(\Delta/\sigma)_{max} = 0.065$.

Atomic coordinates, thermal parameters, a complete list of interatomic distances and angles, and observed and calculated structure factors have been deposited with the Editor as supplementary material.

Acknowledgement—We thank the EPSRC for a maintenance grant (to J.S.).

REFERENCES

1. Begley, M. J., Hubberstey, P. and Walton, P. H., *J. Chem. Soc., Chem. Commun.*, 1989, 502; Begley, M. J., Eisenstein, O., Hubberstey, P., Jackson, S., Russell, C. E. and Walton, P. H., *J. Chem. Soc., Dalton Trans.*, 1994, 1935; Begley, M. J., Hubberstey, P., Russell, C. E. and Walton, P. H., *J. Chem. Soc., Dalton Trans.*, 1994, 2483; Begley, M. J., Hubberstey, P. and Walton, P. H., *J. Chem. Soc., Dalton Trans.*, 1995, 957; Hubberstey, P. and Russell, C. E., *J. Chem. Soc., Chem. Commun.*, 1995, 959.
2. Begley, M. J., Hubberstey, P. and Moore, C. H. M., *J. Chem. Res. (S)*, 1985, 378.
3. Chiesi-Villa, A., Coghi, L., Mangia, A., Nardelli, M. and Pelizzi, G., *Acta Cryst.* 1971, **B27,** 192.
4. Batsanov, A. S., Hubberstey, P. and Russell, C. E., *J. Chem. Soc., Dalton Trans.*, 1994, 3189.
5. Coghi, L., Mangia, A., Nardelli, M., Pelizzi, G. and Sozzi, L., *J. Chem. Soc., Chem. Commun.*, 1968, 1475.
6. Begley, M. J., Hubberstey, P., Spittle, P. H. and Walton, P. H., *Acta Cryst.* 1993, **C49,** 1047.
7. Chiesi-Villa, A., Coghi, L., Mangia, A., Nardelli, M. and Pelizzi, G., *J. Cryst. Molec. Struct.*, 1971, **1,** 291; Chiesi-Villa, A., Coghi, L., Gaetani-Manfredotti, A. and Guastini, C., *Cryst. Struct. Commun.*, 1974, **3,** 739; Hubberstey, P. and Falshaw, C. P., *J. Chem. Res. (S)*, 1982, 176.
8. Avakyan, S. N. and Eminyan, R. S. *Izv. Akad. Nauk. Arm. SSR, Khim.*, 1963, **16,** 13; Balahura, R. J. and Jordan, R. B., *J. Am. Chem. Soc.*, 1971, **93,** 625; Shafranskii, V. N. and Drankin, I. V., *Russ. J. Inorg. Chem.*, 1977, **22,** 712.
9. Bew, M. J., Hathaway, B. J. and Fereday, R. J., *J. Chem. Soc. (A)*, 1972, 1229; Gampp, H., Sigel, H. and Zuberbühler, A. D., *Inorg. Chem.*, 1982, **21,** 1190; Mori, W., Sakurai, T., Nakahara, A. and Nakao, Y., *Inorg. Chim. Acta.*, 1987, **132,** 247; Jiang, F., McCracken, J. and Peisach, J., *J. Am. Chem. Soc.*, 1990, **112,** 9035; Gerfen G. J. and Singel, D. J., *J. Chem. Phys.*, 1994, **100,** 4127.
10. Miki, K., Kaida, S., Saeda, M., Yamatoya, K., Kasai, N., Sato, M. and Nakaya, J.-I., *Acta Cryst.*, 1986, **C42,** 1004.
11. Ray, N. J. and Hathaway, B. J., *Acta Cryst.*, 1978, **B34,** 3224; Druhan, G. and Hathaway, B. J., *Acta, Cryst.* 1979, **B35,** 344; Ray, N. J., Hulett, L., Sheahan, R. and Hathaway, B. J., *J. Chem. Soc., Dalton Trans.*, 1981, 1463; Bray, K. L. and Drickamer, H. G., *J. Phys. Chem.*, 1989, **93,** 7604.
12. Shintani, N., Nukui, E., Miyamae, H., Fukuda, Y. and Sone, K., *Bull. Chem. Soc. Japan*, 1994, **67,** 1828.
13. van Koningsbruggen, P. J., van Hal, J. W., Müller, E., de Graaf, R. A. G., Haasnoot, J. G. and Reedijk, J., *J. Chem. Soc., Dalton Trans.*, 1993, 1371; Scott, M. J., Lee, S. C. and Holm, R. H., *Inorg. Chem.*, 1994, **33,** 4651; Scott, M. J. and Holm, R. H., *J. Am. Chem. Soc.*, 1994, **116,** 11357.
14. Hirschfeld, F. L. and Hope, R., *Acta Cryst.* 1980, **B36,** 406.
15. Allmann, R., Krestl, M., Bolos, C., Manoussakis, G. and Nikolov, G. St., *Inorg. Chim. Acta* 1990, **175,** 255.
16. Stephens, F. S., *J. Chem. Soc. (A)*, 1969, 883.
17. Jones, W. J. and Orville-Thomas, W. J., *Trans. Faraday Soc.*, 1959, **55,** 193.
18. Watkin, D. J., Carruthers, J. R. and Betheridge, P. W., *Crystals Users Guide.* Chemical Crystallography Laboratory, Oxford University, Oxford, 1985.

Pergamon

PII: S0277-5387(96)00337-3

Polyhedron Vol. 16, No. 5, pp. 815–823, 1997
Copyright © 1996 Elsevier Science Ltd
Printed in Great Britain. All rights reserved
0277–5387/97 $17.00 + 0.00

Chloride anion recognition by neutral platinum(II) and palladium(II) 5,5′-bis-amide substituted bipyridyl receptor molecules

Paul D. Beer,[a]* Nicholas C. Fletcher,[a] Michael G. B. Drew[b] and Trevor J. Wear[c]

[a]Inorganic Chemistry Laboratory, University of Oxford, South Parks Road, Oxford OX1 3QR, U.K.

[b]Department of Chemistry, University of Reading, PO Box 224, Reading RG2 6AD, U.K.

[c]Kodak Ltd, Headstone Drive, Harrow, Middlesex HA1 4TY, U.K.

(Received 24 May 1996; accepted 8 July 1996)

Abstract—A series of new acyclic platinum(II) and palladium(II) 5,5′-bis-amide substituted 2,2′-bipyridyl receptors have been synthesized and single-crystal structural investigations of two receptors are described. Proton NMR anion binding studies reveal that these neutral receptors recognize chloride anions in dimethyl sulfoxide solution. Copyright © 1996 Elsevier Science Ltd

Keywords: anion; recognition; platinum; palladium; bipyridyl; chloride.

The molecular recognition [1] and sensing [2] of anionic species is a rapidly expanding area of host–guest chemistry. A variety of positively charged and neutral electron-deficient abiotic receptor molecules have been synthesized and shown in some cases to selectively recognize anions [3, 4]. As part of a research programme aimed at designing new optical and electrochemical sensory reagents for anions [2], we have recently reported new classes of anion receptor that contain positively charged organometallic and coordination transition metal Lewis acidic binding sites in combination with amide N—H groups [5,6]. For example, spectral and electrochemical recognition of anions has been demonstrated by ruthenium(II) 4,4′- and 5,5′-bis-disubstituted bipyridyl derivatives [7,8]. In an effort to investigate the effect of charge of the Lewis acidic centre upon the anion recognition process, we describe here the preparation and anion complexation ability of new neutral platinum(II) and palladium(II) bipyridyl receptors.

RESULTS AND DISCUSSION

Anion receptor syntheses

The preparation of the 5,5′-bis-amide substituted 2,2′-bipyridyl ligands has been described previously (Fig. 1) [8]. Attempts were made to coordinate the ligands L^1, L^2, L^3 and L^4 to platinum(II) using $K_2[PtCl_4]$ (Scheme 1). The literature procedures for the preparation of such complexes are usually made in water [9]. However, all the ligands demonstrated an extreme hydrophobicity. Consequently, ligand L^1 was dissolved in methanol (using the preparation of $Pt(phen)Cl_2$ as a precedent [10]), to which was added the platinum precursor $K_2[PtCl_4]$ in aqueous acetonitrile, with stirring for several hours. The product $Pt(L^1)Cl_2$ was isolated following removal of the solvent and recrystallized from methanol as a yellow solid in 70% yield. Ligands L^{2-4} proved insoluble in methanol, so warm DMSO was used as the reaction solvent. After several hours of heating with $K_2[PtCl_4]$ the solvent was removed by vacuum distillation, and the products $Pt(L^{2-4})Cl_2$ were obtained as yellow solids.

The analogous palladium complexes $Pd(L^{1,3,4})Cl_2$ were prepared similarly using $K_2[PdCl_4]$ in good yields as yellow–brown solids. Unfortunately, extreme insolubility problems with the palladium complex product of L^2 prevented its characterization.

It is noteworthy that with the platinum complexes the addition of water caused a dramatic colour change from yellow to bright red. This colour change has also been observed under extreme conditions with Pt(bipy)Cl_2, and typically is derived from refluxing [Pt(bi-

* Author to whom correspondence should be addressed.

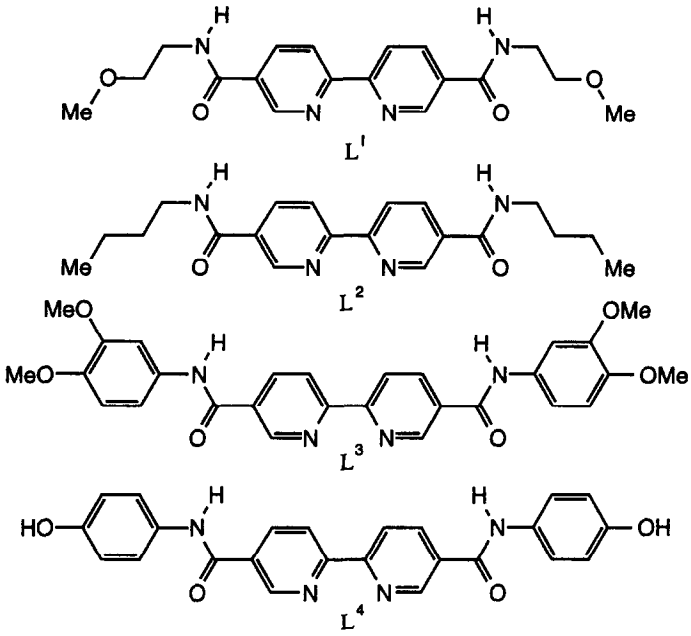
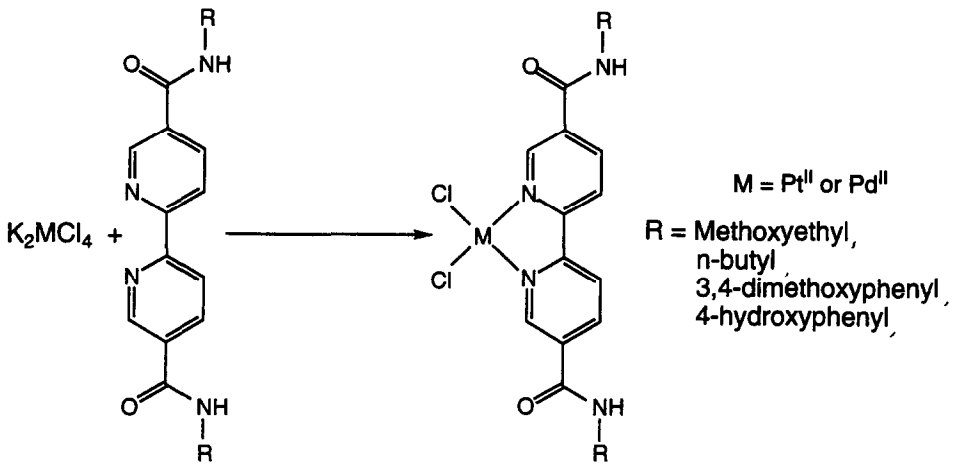


Fig. 1. 5,5'-Bis-amide-substituted bipyridyl ligands.



Scheme 1.

$py)(NH_3)_2]^{2+}$ in hydrochloric acid to give the red form [11,12]. There is substantial evidence that the yellow and red complexes are monomeric structures and so it has been postulated that the colour change is due to differing spatial arrangements in the crystal structure. Since the amide functionalized complexes readily change colour on the addition of water, this could be attributed to hydrogen bonding to water by the complexes, forcing the crystal structure to rearrange in some manner. Unfortunately, the poor solubility of the complexes prevented a solution investigation into this phenomenon using electronic spectroscopy.

Structural studies

$Pt(L^2)Cl_2$. Crystals of complex $Pt(L^2)Cl_2$ suitable for X-ray structural analysis were obtained as yellow needles by dissolving in warm DMSO and subsequent slow evaporation over 9 months. The structure is shown in Fig. 2, together with the atomic numbering scheme. The platinum complex has crystallographic C_2 symmetry and there is a DMSO solvent molecule per complex, with a hydrogen bond between the amide nitrogen atom N(12) and the oxygen atom in the solvent DMSO [N(12)···O(1S) $(-x,-y,1-z)$ 2.838

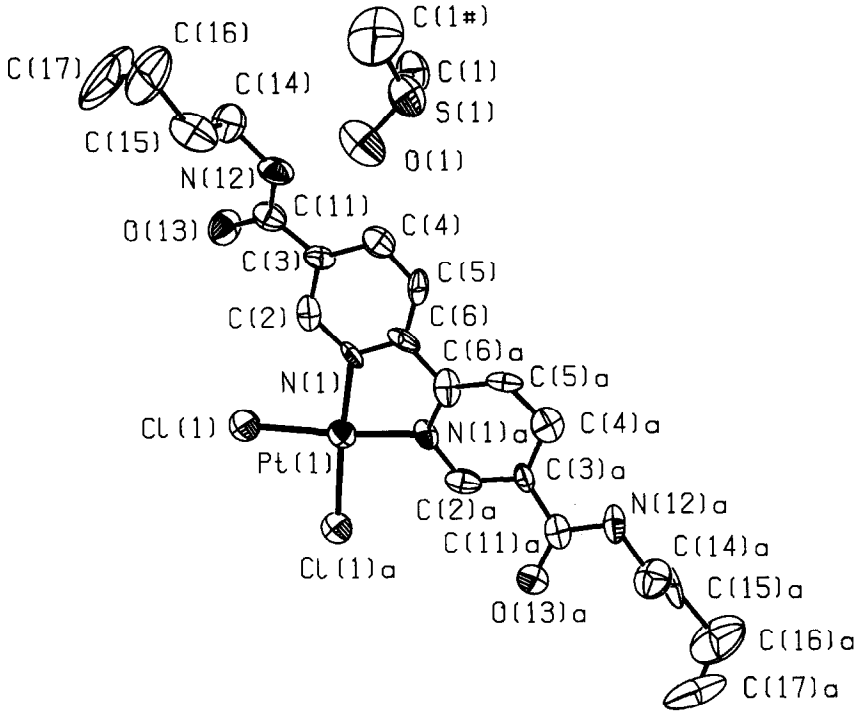


Fig. 2. Thermal motion ellipsoid plot of $Pt(L^2)Cl_2$, with ellipsoids drawn at the 30% probability level.

Å]. The bond lengths and angles for the bipyridyl platinum fragments are in good agreement with those for $Pt(bipy)Cl_2$ (both the red and yellow forms) [12] (Table 1). It was observed that the bond distances between the platinum centre and the ligated atoms were slightly smaller than with $Pt(bipy)Cl_2$ [12]. This is probably due to the electron-withdrawing effect of the new amide functionalized ligand, causing better d–π^* back bonding, and consequently shorter bond lengths are observed and the reduced electron density on the platinum centre facilitates stronger bonding to the chloride ligands.

The molecules are planar and stack in a staggered array of overlapping units, as shown in Fig. 3a and b. The structure does not, however, demonstrate the configuration of either the yellow or the red isomorph of $Pt(bipy)Cl_2$, with the Pt—Pt distance being comparatively much larger (6.695 Å) [12]. The individual units lie in line with each other as in the red form, but the two platinum atoms do not sit directly over each other. It is presumed that on the addition of water, a rearrangement can occur which brings the two platinum centres closer together, by virtue of a change in the hydrogen bonding arrangement, giving the distinct colour change observed.

$Pd(L^1)Cl_2$. Crystals of complex $Pd(L^1)Cl_2$ suitable for X-ray structure analysis were obtained as yellow needles by dissolving in warm DMSO and subsequent

Table 1. Dimensions (Å) and angles (°) in the metal coordination spheres for $Pt(L^2)Cl_2$, yellow and red forms of $Pt(bipy)Cl_2$ [12]

Parameter	$Pt(L^2)Cl_2$	Yellow forms of $Pt(bipy)Cl_2$	Red forms of $Pt(bipy)Cl_2$
Pt(1)—N(1)	1.94(2)	2.006(10) 2.011(10)	2.001(6)
Pt(1)—Cl(1)	2.248(7)	2.281(4) 2.300(3)	—
N(1)—Pt(1)—N(1)#1	79.3(9)	—	80(1)
N(1)—Pt(1)—Cl(1)	96.1(5)	94.3(3)	96(1)
N(1)—Pt(1)—Cl(1)#1	175.1(5)	175.9(3) 174.7(3)	184[a]
Cl(1)—Pt(1)—Cl(1)#1	88.6(4)	89.1(1)	88(1)
Inter Pt—Pt	6.965	4.435	3.45

[a] Calculated value.

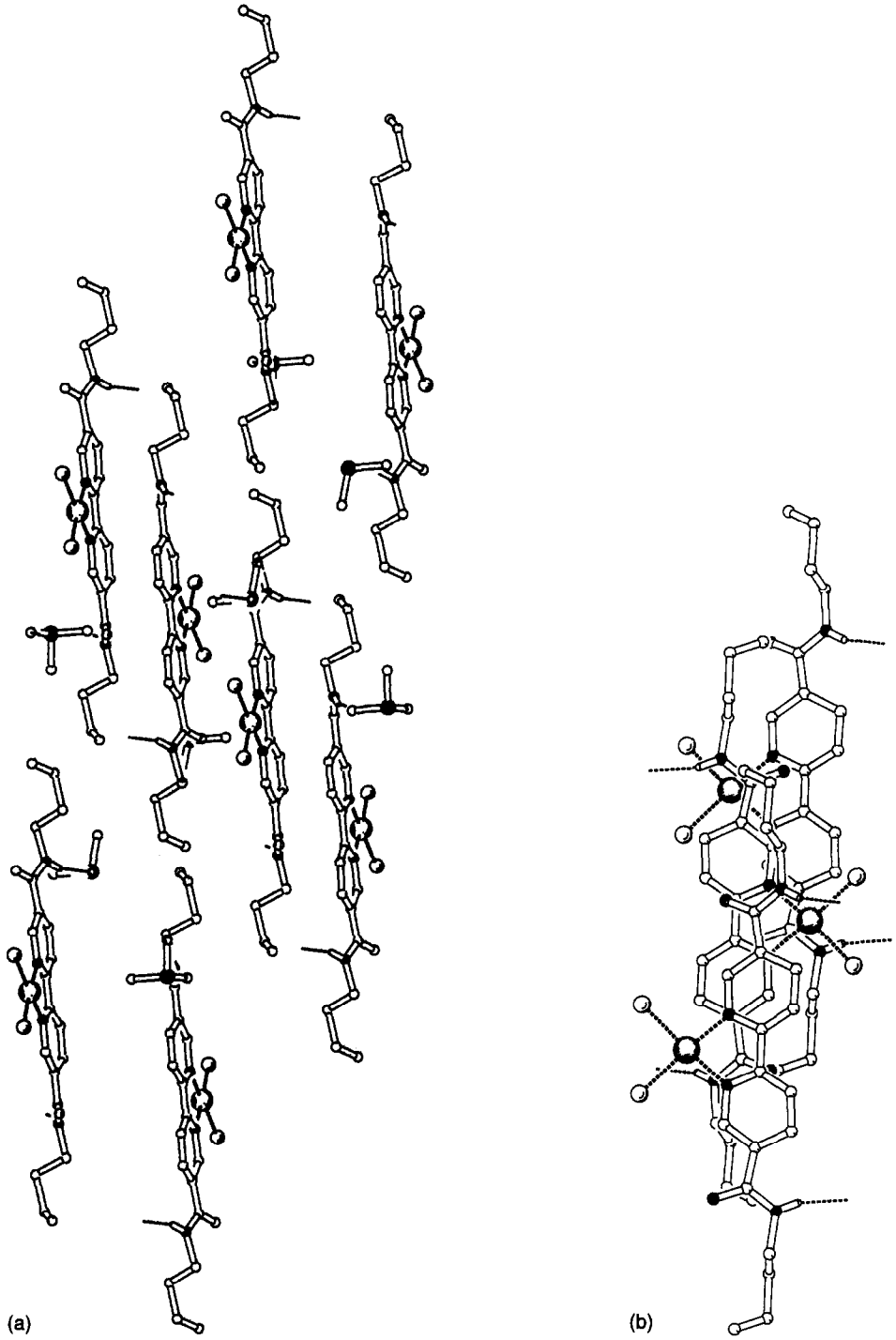


Fig. 3. PLUTON straw plots of the structure of $Pt(L^2)Cl_2$, illustrating the linear array of the complexes.

slow evaporation over 6 months. The structure is shown in Fig. 4, together with the atomic numbering scheme. The units themselves indicate that the bond lengths and distances are similar to those of Pd(bipy)Cl_2 [13], with changes in the metal-to-ligand bond distances again associated with the additional electron-withdrawing nature of the amide groups (Table 2).

These planar molecules also pack closely in a linear stack (Fig. 5a, b); however, in this case the packing is more similar to the literature (compare the Pd—Pd distances in Table 2) [13], where the packing is isomorphic with the yellow form of Pt(bipy)Cl_2. There is no solvent in this structure and two types of hydrogen bond link the individual units together in a two-dimensional lattice. One is formed between an amide

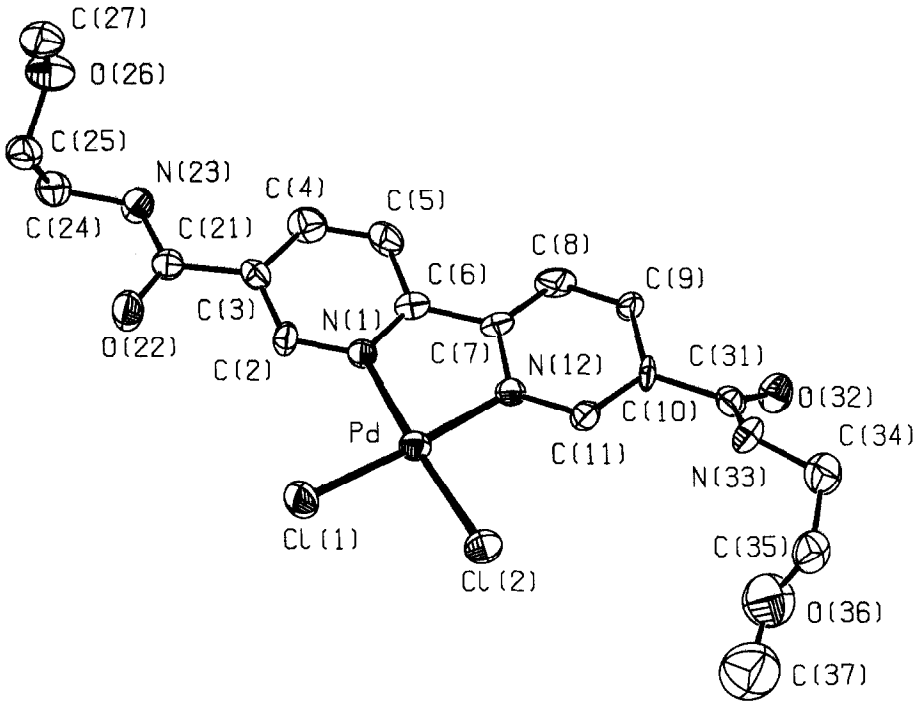


Fig. 4. Thermal motion ellipsoid plot of $Pd(L^1)Cl_2$, with ellipsoids drawn at the 50% probability level.

Table 2. Dimensions (Å) and angles (°) in the metal coordination spheres for $Pd(L^1)Cl_2$, yellow and red forms of $Pd(bipy)Cl_2$ [13]

Parameter	$Pd(L^1)Cl_2$	$Pd(bipy)Cl_2$
Pd(1)—N(12)	2.002(12)	2.03(1)
Pd(1)—N(1)	2.028(10)	2.03(1)
Pd(1)—Cl(1)	2.261(4)	2.317(3)
Pd(1)—Cl(2)	2.271(4)	2.277(3)
N(12)—Pd(1)—N(1)	81.2(4)	80.5(4)
N(12)—Pd(1)—Cl(1)	175.6(3)	175.0(3)
N(1)—Pd(1)—Cl(1)	94.4(3)	95.3(3)
N(12)—Pd(1)—Cl(2)	94.6(3)	94.4(4)
N(1)—Pd(1)—Cl(2)	175.8(3)	174.5(3)
Cl(1)—Pd(1)—Cl(2)	89.8(2)	89.9(1)
Closest inter Pd—Pd	4.9148	4.587

nitrogen [N(23)] atom and an adjacent chloride [Cl(2)] ligand lying in the plane [N(23)—Cl(2) $(0.5-x,-y,0.5+z)$ 3.321 Å]. The other is formed from the amide nitrogen [N(33)] atom and an amide oxygen [O(22)] atom in the molecule directly above the stack [N(33)—O(32) $(0.5+x,y,0.5-z)$ 2.907 Å]. In order to achieve this hydrogen bond, there are two differences in the conformation of the ligand in the palladium complex relative to the platinum complex, where both carbonyl groups are positioned on the same side as each other and on the same side as the metal atom. By contrast, in the palladium complex, while one carbonyl group is on the metal side, the other is rotated around to point away from the metal so that it can participate in hydrogen bonding. In addition, this atom is severely twisted out of the plane of the pyridine ring to which it is attached, thus the C(11)—C(10)—C(31)—N(33) torsion angle is 37.1° compared to the more expected angle for C(2)—C(3)—C(21)—N(23) of −2.1° (Table 3).

Proton NMR anion coordination studies

The addition of tetrabutylammonium chloride to DMSO-d_6 solutions of the neutral platinum and palladium(II) bipyridyl receptors resulted in significant downfield perturbations of the 4,4′-bipyridyl and especially the amide protons (Table 4). Typically, an amide proton shift of $\Delta\delta = 0.1$ ppm was observed after the addition of two equivalents of the chloride salt. As noted previously, these results suggest that favourable amide CONH---Cl^- hydrogen bonding is a crucial contributing factor to the overall anion complexation process. Disappointingly, precipitation problems with the $ML^{2,3}$ Cl_2 (M = Pt, Pd) receptors precluded complete titration curves being obtained. However, stability constants for 1:1 receptor:chloride anion stoichiometry were determined from the titration data of the other receptors using the least squares curve fitting program EQNMR [14], and the results are summarized in Table 4. Within experimental error all four neutral platinum(II) and palladium(II) receptors complex the chloride anion with similar magnitudes of stability constant, suggesting neither the nature of the metal nor the alkyl or aryl

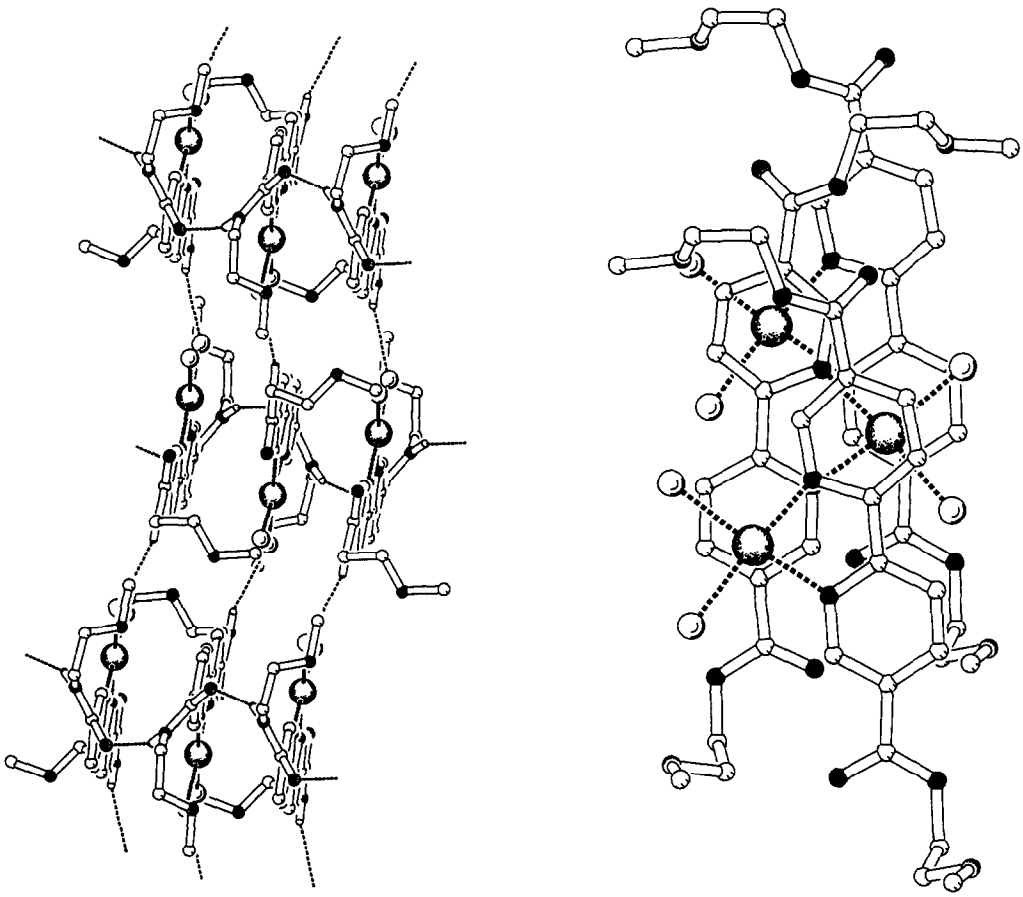


Fig. 5. PLUTON straw plot of the structure of $Pd(L^1)Cl_2$, illustrating the two-dimensional array of the molecules, held together by intermolecular hydrogen bonding.

substituent greatly influences the strength of halide anion binding. Interestingly, charged ruthenium(II) 5,5′-bis-amide-substituted 2,2′-bipyridyl receptor analogues [8] exhibited only slightly larger magnitudes of stability constant with chloride in DMSO, of typical value 45 $dm^3\ mol^{-1}$, implying that the charged or neutral character of the transition metal bipyridyl coordinated Lewis acid centre is not critical to the inclusive thermodynamic stability of anion binding in these systems.

Table 3. Selected torsion angles (°) in $Pt(L^2)Cl_2$ and $Pd(bipy)Cl_2$ [13]

$Pt(L^2)Cl_2$	
C(2)—C(3)—C(11)—N(12)	163.3
C(3)—C(11)—N(12)—C(14)	171.7
C(11)—N(12)—C(14)—C(15)	104.1
N(12)—C(14)—C(15)—C(16)	173.9
C(14)—C(15)—C(16)—C(17)	72.4
$Pd(bipy)Cl_2$	
C(2)—C(3)—C(21)—N(23)	−2.1
C(3)—C(21)—N(23)—C(24)	177.0
C(21)—N(23)—C(24)—C(25)	−75.9
N(23)—C(24)—C(25)—C(26)	−70.6
C(24)—C(25)—C(26)—C(27)	164.4
C(11)—C(10)—C(31)—N(33)	37.1
C(10)—C(31)—N(33)—C(34)	−172.9
C(31)—N(33)—C(34)—C(35)	134.4
N(33)—C(34)—C(35)—C(36)	−60.5
C(34)—C(35)—C(36)—C(37)	172.8

CONCLUSIONS

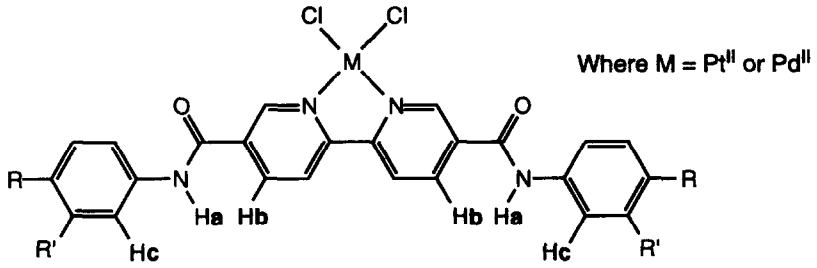
New acyclic neutral platinum(II) and palladium(II) 5,5′-bis-amide-substituted 2,2′-bipyridyl receptors have been prepared and the single-crystal structures of two receptors determined. Proton NMR chloride anion binding studies in deuteriated DMSO solution reveal that these neutral receptors complex the halide anion *via* favourable amide CO—NH---Cl^- hydrogen bonding interactions. Stability constant evaluations suggest the strength of halide anion binding is largely independent of the nature of the d^8 metal or the alkyl/aryl amide-linked substituent.

EXPERIMENTAL

Instrumentation

NMR spectra were recorded on a Bruker AM300 instrument using the solvent deuterium signal as an

Table 4. Magnitudes of shift ($\Delta\delta$, ppm) in peak position of various protons in the ^{1}H NMR spectrum of receptors $M(L^{1,4})Cl_2$ (M = Pt,Pd) after the addition of two equivalents of chloride anion in DMSO-d_6 and stability constant evaluations



Compound	Proton a $\Delta\delta$ (ppm)	Proton b $\Delta\delta$ (ppm)	Proton c $\Delta\delta$ (ppm)	K_{stab}[a] (dm^3 mol^{-1})
$Pt(L^1)Cl_2$	0.10	0.07	—	32
$Pt(L^4)Cl_2$	0.10	0.07	0.03	32
$Pd(L^1)Cl_2$	0.09	0.05	—	36
$Pd(L^4)Cl_2$	0.11	0.09	0.12	34

[a] Errors estimated to be $\leqslant 10\%$.

internal reference. Mass spectrometry was performed by the analytical services at Kodak Ltd, Harrow. Elemental analyses were performed at the Inorganic Chemistry Laboratory, University of Oxford. Unless stated to the contrary, commercial grade chemicals were used without further purification.

The preparation of the ligands have been described previously [8].

Synthesis

Platinum(II) (5,5′-*bis*(*methoxyethylamido*)-2,2′-*bipyridine*) *dichloride* (PtL^1Cl_2). Ligand L^1 (36 mg, 0.101 mmol) was dissolved in methanol (20 cm^3) with gentle heating, to which was added $K_2[PtCl_4]$ (47 mg, 0.114 mmol) in 50% aqueous acetonitrile (20 cm^3). The reaction mixture was stirred for 4.5 h and filtered. The solvent was removed from the filtrate giving a yellow residue, and the product was isolated after recrystallization from methanol. Yield 44 mg, 70%. ^{1}H NMR (DMSO): δ 3.29 (4H, m, $NHCH_2CH_2$), 3.32 (6H, s, OCH_3), 3.50 (4H, m, CH_2CH_2O), 8.75 (2H, d, $J = 8.4$ Hz, bipyC*H*^{4}), 8.79 (2H, d, $J = 8.5$ Hz, bipyC*H*^{3}), 9.15 (2H, bt, N*H*), 9.88 (2H, s, bipy C*H*^{6}). Found: C, 34.9; H, 3.7; N, 7.7. Calc. for $C_{18}H_{22}N_4O_4Cl_2Pt$: C, 34.6; H, 3.6; N, 8.0%. FAB-MS: $[MH]^+$ 625, $[M-Cl]^+$ 589.

Platinum(II) (5,5′-*bis*(*butylamido*)-2,2′-*bipyridine*) *dichloride* (PtL^2Cl_2). Ligand L^2 (46 mg, 0.130 mmol) and $K_2[PtCl_4]$ (85 mg, 0.205 mmol) were mixed in DMSO (20 cm^3) and heated at 60°C for 1 h. Following additional stirring for 22 h at room temperature, the solvent was removed at reduced pressure at approx. 60°C to give a yellow solid. The residue was ground up, stirred in water (50 cm^3) for 2 h, filtered and dried *in vacuo*, giving a red solid which went yellow on drying. Yield 51 mg, 63%. ^{1}H NMR (DMSO): δ 0.91 (6H, t, $J = 7.2$ Hz, CH_2CH_3), 1.33 (4H, m, $CH_2CH_2CH_3$), 1.54 (4H, m, $CH_2CH_2CH_2$), 2.37 (4H, m, $NHCH_2CH_2$), 8.75 (4H, s, bipyC*H*^{3} and bipyC*H*^{4}), 9.01 (2H, t, $J = 5.3$ Hz, N*H*), 9.87 (2H, d, $J = 2.0$ Hz, bipyC*H*^{6}). Found: C, 37.8; H, 4.1; N, 8.3. Calc. for $C_{20}H_{26}N_4O_2Cl_2Pt \cdot 2H_2O$: C, 38.7; H, 4.2; N, 9.0%. FAB-MS: $[MH]^+$ 620, $[M-Cl]^+$ 579.

Platinum(II) (5,5′-*bis*(3,4-*dimethoxyphenylamido*)-2,2′-*bipyridine*) *dichloride* (PtL^3Cl_2). Using ligand L^3, an analogous synthetic procedure was used as in the preparation of $Pt(L^2)Cl_2$. Yield 78%. ^{1}H NMR (DMSO): δ 3.76 (6H, s, OCH_3), 3.78 (6H, s, OCH_3), 6.98 (2H, d, $J = 9.3$ Hz, ArC*H*^{5}), 7.33 (2H, d, $J = 8.2$ Hz, ArC*H*^{6}), 7.45 (2H, s, ArC*H*^{2}), 8.84 (2H, d, $J = 9.8$ Hz, bipyC*H*^{4}), 8.94 (2H, d, $J = 7.8$ Hz, bipyC*H*^{3}), 9.96 (2H, s, bipyC*H*^{6}), 10.68 (2H, s, N*H*). Found: C, 42.2; H, 3.1; N, 6.8. Calc. for $C_{28}H_{26}N_4O_6Cl_2Pt$: C, 43.1; H, 3.4; N, 7.2%. FAB-MS: $[MH]^+$ 780, $[M-Cl]^+$ 744.

Platinum(II) (5,5′-*bis*(4-*hydroxyphenylamido*)-2,2′-*bipyridine*) *dichloride* (PdL^4Cl_2). Using ligand L^4, an analogous synthetic procedure was used as in the preparation of $Pt(L^1)Cl_2$. Yield 68%. ^{1}H NMR (DMSO): δ 6.78 (4H, d, $J = 8.3$ Hz, PhC*H*^{2}), 7.55 (4H, d, $J = 8.2$ Hz, PhC*H*^{3}), 8.82 (2H, d, $J = 8.2$ Hz, bipyC*H*^{4}), 8.92 (2H, d, $J = 8.0$ Hz, bipyC*H*^{3}), 9.41 (2H, s, bipyC*H*^{6}), 9.92 (2H, s, O*H*), 10.59 (2H, s, N*H*). Found: C, 39.5; H, 2.8; N, 6.9. Calc. for $C_{24}H_{18}N_4O_4Cl_2Pt \cdot 2H_2O$: C, 39.6; H, 3.0; N, 7.7%.

Palladium(II) (5,5′-*bis*(*methoxyethylamido*)-2,2′-*bipyridine*) *dichloride* (PdL^1Cl_2). Using ligand L^1, an analogous synthetic procedure was used as in the preparation of $Pt(L^1)Cl_2$. Yield 89%. ^{1}H NMR (DMSO):

δ 3.28 (4H, m, $NHCH_2CH_2$), 3.34 (6H, s, OCH_3), 3.49 (4H, m, CH_2CH_2O), 8.74 (2H, d, $J = 8.4$ Hz, bipyCH^4), 8.76 (2H, d, $J = 8.4$ Hz, bipyCH^3), 9.12 (2H, bt, NH), 9.50 (2H, s, bipyCH^6). Found: C, 40.2; H, 3.8; N, 10.5. Calc. for $C_{18}H_{22}N_4O_4Cl_2Pd$: C, 40.4; H, 4.1; N, 10.5%. FAB-MS: $[MH]^+$ 535, $[M-Cl]^+$ 501, $[MH-2Cl]^+$ 460.

Palladium(II) (5,5′-*bis*(3,4-*dimethoxyphenylamido*)-2,2′-*bipyridine*) *dichloride* (PdL^2Cl_2). Using ligand L^3, an analogous synthetic procedure was used as in the preparation of $Pt(L^2)Cl_2$, giving a brown solid. Yield 68%. ^{1}H NMR (DMSO): δ 3.77 (6H, s, OCH_3), 3.79 (6H, s, OCH_3), 7.00 (2H, bd, ArCH^5), 7.35 (2H, bd, Hz, ArCH^6), 7.47 (2H, s, ArCH^2), 8.8–8.9 (4H, m, bipyCH^4 and bipyCH^3), 9.62 (2H, s, bipyCH^6), 10.68 (2H, s, NH). Found: C, 44.7; H, 3.4; N, 7.1. Calc. for $C_{28}H_{26}N_4O_6Cl_2Pd$: C, 48.6; H, 3.8; N, 8.1%.

Palladium(II) (5,5′-*bis*(4-*hydroxyphenylamido*)-2,2′-*bipyridine*) *dichloride* (PdL^4Cl_2). Using ligand L^4, an analogous synthetic procedure was used as in the preparation of $Pt(L^2)Cl_2$. Yield 67%. ^{1}H NMR (DMSO): δ 6.78 (4H, d, $J = 8.4$ Hz, PhCH^2), 7.54 (4H, d, $J = 8.4$ Hz, PhCH^3), 8.82 (2H, d, $J = 8.2$ Hz, bipyCH^4), 8.87 (2H, d, $J = 8.1$ Hz, bipyCH^3), 9.41 (2H, s, bipyCH^6), 9.53 (2H, s, OH), 10.57 (2H, s, NH). Found: C, 46.0; H, 3.0; N, 8.7. Calc. for $C_{24}H_{18}N_4O_4Cl_2Pd \cdot H_2O$: C, 46.4; H, 3.2; N, 9.0%.

Crystal structure analysis

Crystal data are given in Table 5, together with refinement details. Data for both crystals were collected with Mo-K_α radiation using the MARresearch Image Plate System. The crystals were positioned at 75 mm from the Image Plate. Ninety-five frames were measured at 2° intervals with a counting time of 2 min. Data analysis was carried out with the XDS program [15]. Both structures were solved using heavy atom methods with the SHELX86 program [16]. In both structures the non-hydrogen atoms were refined with anisotropic thermal parameters. The hydrogen

Table 5. Crystal data and structure refinement for $Pt(L^2)Cl_2$ and $Pd(L^1)Cl_2$

Compound	$Pt(L^2)Cl_2$	$Pd(L^1)Cl_2$
Empirical formula	$C_{24}H_{38}Cl_2N_4O_4PtS_2$	$C_{18}H_{22}Cl_2N_4O_4Pd$
Formula weight	1553.38	1071.39
Temperature (K)	293(2)	293(2)
Wavelength (Å)	0.71072	0.71072
Crystal system	monoclinic	orthorhombic
Space group	*C*2/*c*	*Pbca*
Unit cell dimensions		
a (Å)	28.64(2)	8.147(8)
b (Å)	9.066(9)	27.319(17)
c (Å)	11.907(11)	17.769(12)
β (°)	103.31(1)	(90)
Volume (Å^3)	3008(5)	3955(3)
Z	4	8
Density (calculated) (Mg m^{-3})	1.715	1.799
Absorption coefficient (mm^{-1})	5.017	1.243
F(000)	1544	2160
Crystal size (mm^3)	0.2 × 0.3 × 0.2	0.15 × 0.25 × 0.25
θ range for data collection	2.84–24.88	2.29–24.94
Index ranges	$0 \leqslant h \leqslant 33$	$0 \leqslant h \leqslant 9$
	$-9 \leqslant k \leqslant 9$	$-32 \leqslant k \leqslant 32$
	$-13 \leqslant l \leqslant 13$	$-20 \leqslant l \leqslant 20$
Reflections collected	2604	11,508
Independent reflections	1723	3245
R(int)	0.0581	0.0738
Data/parameters	1723/170	3205/268
Weighting scheme (*a*, *b*)[a]	0.21, 20.56	0.06, 111.28
Goodness-of-fit on F^2	1.202	1.179
Final *R* indices [$I > 2\sigma(I)$]		
R_1	0.0872	0.0772
R_{w2}	0.2724	0.1426
R indices (all data)		
R_1	0.0996	0.1120
R_{w2}	0.2959	0.1871
Largest diff. peak and hole (e Å^{-3})	1.664, −1.555	1.102, −0.706

[a] Weighting scheme: $w = 1/(\sigma^2(F_o^2) + (aP)^2 + bP)$, where $P = (F_o^2 + 2F_c^2)/3$.

atoms were included in geometric positions and were given thermal parameters equivalent to 1.2 times that of the atom to which they were bonded. Both structures were refined using SHELXL [17]. All calculations were carried out on a Silicon Graphics R4000 Workstation at the University of Reading. Unfortunately, in the structure refinement of $Pt(L2)Cl_2$, C(4) and C(5) could not be refined with positive definite thermal parameters, presumably because of some slight disorder, and were given isotropic thermal parameters. Diagrams were prepared using PLATON [18] and PLUTON [19].

Acknowledgements—We thank the EPSRC for a CASE studentship (N.C.F.) and Kodak Ltd for additional financial support. Additionally, we thank the EPSRC and the University of Reading for funds for the Image Plate System.

REFERENCES

1. Dietrich, B., *Pure Appl. Chem.*, 1993, **65,** 1457; Pierre, J. L. and Baret, P., *Bull. Soc. Chim. Fr.*, 1983, 367; Dietrich, B., in *Inclusion Compounds*, Vol. 2, ed Atwood, J. L., Davies, J. E. D. and MacNicol, D. D., Academic Press, New York, 1984, p. 337; F. P. Schmidtchen, *Nachr. Chem. Tech. Lab.*, 1988, **36,** 8.
2. Beer, P. D., *Chem. Commun.*, 1996, 689.
3. Hosseini, M. W., Blacker, A. J. and Lehn, J.-M., *J. Am. Chem. Soc.*, 1900, **112,** 3896 and refs therein; Schmidtchen, F. P., *J. Org. Chem.*, 1986, **51,** 5161; Beer, P. D., Wheeler, J. W., Greive, A., Moore, C. and Wear, T., *J. Chem. Soc., Chem. Commun.*, 1992, 1225; Furuta, H., Cyr, M. and Sessler, J. L., *J. Am. Chem. Soc.*, 1991, **113,** 6677.
4. Katz, H. E., *Organometallics*, 1987, **6,** 1134; Wuerst, J. D. and Zacharie, B., *J. Am. Chem. Soc.*, 1987, **109,** 4714; Blandon, M. T., Horner, J. N. and Newcombe, M., *J. Org. Chem.* 1989, **54,** 4626; Reetz, M. T., Niemeyer, C. M. and Harms, K., *Angew. Chem., Int. Edn Engl.*, 1991, **30,** 1472; Rudkevich, D. M., Stauthamer, W. P. R. V., Verboom, W., Engbersen, J. F. J., Harkema, S. and Reinhoudt, D. N., *J. Am. Chem. Soc.*, 1992, **114,** 9671.
5. Beer, P. D., Hazlewood, C., Hesek, D., Hodacova, J. and Stokes, S. E., *J. Chem. Soc., Dalton Trans.*, 1993, 1327; Beer P. D., Chen, Z., Goulden, A. J., Graydon, A. R., Stokes, S. E. and Wear, T., *J. Chem. Soc., Chem. Commun.* 1993, 1834; Beer, P. D., Drew, M. G. B., Graydon, A. R., Smith, D. K. and Stokes, S. E., *J. Chem. Soc., Dalton Trans.*, 1995, 403.
6. Beer, P. D., Dickson, C. A. P., Fletcher, N. C., Goulden, A. J., Grieve, A., Hodacova, J. and Wear, T. *J. Chem. Soc., Chem. Commun.*, 1993, 828.
7. Beer, P. D., Chen, Z., Goulden, A. J., Grieve, A., Hesek, D., Szemes, F. and Wear, T., *J. Chem. Soc., Chem. Commun.*, 1994, 1269; Szemes, F. and Beer, P. D., *J. Chem. Soc., Chem. Commun.*, 1995, 2245.
8. Beer, P. D., Fletcher, N. C. and Wear, T., *Polyhedron*, 1996, **15,** 1339.
9. Morgan, G. T. and Burstall, F. H., *J. Chem. Soc.*, 1934, 965.
10. Palocsay, F. A. and Rund, J. V., *Inorg. Chem.*, 1969, **8,** 524.
11. Textor, Von M. and Oswald, H. R., *Z. Anorg. Allg. Chem.*, 1974, **407,** 244; Bielli, E., Gidney P. M., Gillard, R. D. and Heaton, B. T., *J. Chem. Soc., Dalton Trans.*, 1974, 2133.
12. Osborn, R. S. and Rodgers, D., *J. Chem. Soc., Dalton Trans.*, 1974, 102; Herber, R. H., Croft, M., Coyer, M. J., Bilash, B. and Sahiner, A., *Inorg. Chem.*, 1994, **33,** 2422.
13. Canty, A. J., Minchin, N. J., Skelton, B. W. and White, A. H., *Aust. J. Chem.*, 1992, **45,** 423.
14. Hynes, M. J., *J. Chem. Soc., Dalton Trans.*, 1993, 311.
15. Kabsch, W., *J. Appl. Cryst.* 1988, **21,** 916.
16. Sheldrick, G. M., *Acta Cryst.* 1990, **A46,** 467.
17. Sheldrick, G. M., SHELXL: Program for Crystal Structure Refinement. University of Gottingen, 1993.
18. Spek, A. L., *Acta Cryst.* 1990, **A46,** C34.
19. PLUTON: Molecular Graphics Program, Utrecht University, Utrecht, The Netherlands, 1996.

Pergamon

PII: S0277-5387(96)00335-X

Polyhedron Vol. 16, No. 5, pp. 825–831, 1997
Copyright © 1996 Elsevier Science Ltd
Printed in Great Britain. All rights reserved
0277-5387/97 $17.00+0.00

A copper(II) azide compound of pyrazinic acid containing a new dinuclear complex anion $[Cu_2(N_3)_6]^{2-}$. Synthesis, spectral and structural study of KCu_2(pyrazinato)$(N_3)_4$

Mohamed A. S. Goher,[a]* Najeeb A. Al-Salem,[a] Franz A. Mautner,[b]* and Kurt O. Klepp[c]

[a]Department of Chemistry, Faculty of Science, Kuwait University, P.O. Box 5969 Safat, 13060 Kuwait

[b]Institut für Physikalische und Theoretische Chemie, Technische Universität Graz, A-8010 Graz, Austria

[c]Abteilung für Allgemeine und Anorganische Chemie, Johannes Kepler Universität Linz, A-4040 Linz, Austria

(Received 18 June 1996; accepted 4 July 1996)

Abstract—A new complex of copper(II) azide with pyrazinic acid, of general formula KCu_2(pyrazinato)$(N_3)_4$ has been synthesized and characterized by spectroscopic and crystallographic methods. The structure of the complex consists of a new dinuclear complex anion $[Cu_2(N_3)_6]^{2-}$, potassium cations and neutral polymeric complex [Cu(pyrazinato)(N_3)]. Each distorted square-planar copper centre [Cu(1)] in the complex anion is coordinated to four nitrogen atoms from two terminal and two μ-(1,1) bridging azido ligands [Cu—N distances 1.940(6)–2.011(5) Å]. In the polymeric complex, each copper atom, Cu(2), is coordinated to N(41) of a terminal azido group and N(61), N(62) and O(31) from pyrazinato anions to form infinite, "neutral" chains of polyhedra with orientations along [010]. The potassium cations are located in broad channels which are a consequence of stacking of the copper complexes. The IR spectrum confirms the presence of different asymmetric azido ligands. The absorption frequencies of diagnostic values are given and discussed. The electronic spectrum displays three absorption bands associated with N_3^-—Cu^{II} charge transfer transitions. The EPR spectrum of the solid complex suggests an axial structure with non-coupled copper(II) atoms. Copyright © 1996 Elsevier Science Ltd

Keywords: copper(II) azide; pyrazinic acid; complex; spectra; structure.

It has long been accepted [1–4] that picolinic acid, also known as 2-pyridinecarboxylic acid, chelates divalent metal ions to form a five-membered ring through the ligation of the picolinate anion, which serves as a *N,O*-bidentate ligand. The picolinate anion also acts as a *N,O,O'*-tridentate chelating bridging ligand as found in the structure of [Cu(picolinato)$_2$]·2(H_2O) [5]. Recently we established that the picolinate anion can act as a *N,O,O*,-tridentate ligand as in [Mn(picolinato)$(N_3)(H_2O)]_n$ [6], and as a *N,O,O,O'*-tetradentate ligand as found in the structure of $[Cu(picolinato)Cl]_n$ [7] or $[Cd(picolinato)X]_n$ (X = N_3 or NCS) [8]. Both coordinative interactions to transition metal centres and ionic interaction to alkali metals, have been observed in the crystal structures of $[NaCu(picolinato)_2(N_3)(H_2O)_2]_n$ [9] and $[MCu(picolinato)(N_3)_2]_n$ (M = Na or K) [10]. Thus, the picolinato anion is a versatile ligand that can bind metal ions in a variety of bonding modes.

Pyrazine and pyrazine-2-carboxylic acid, also called pyrazinic acid (hereafter abbreviated as H-pyz) combine the coordinating properties of the pyridine-2-carboxylic acid with the fact that the pyrazine moiety may act as a bridge and thus aid the formation of polymeric derivatives [11]. Pyrazinic acid is, therefore, expected to be at least as versatile as the azide ion, a ligand which can bind metal ions in a different matter [12–18]. Combination of these two versatile ligands with copper(II) ion was anticipated to yield interesting

* Authors to whom correspondence should be addressed.

results. The present work constitutes part of our continuing study of metal pseudo-halides containing substituted pyridine ligands [19,20].

EXPERIMENTAL

Pyrazinic acid was obtained from Aldrich and other chemicals were of analytical grade quality.

Preparation of KCu_2(pyrazinato)$(N_3)_4$ *complex*

Copper(II) nitrate trihydrate (0.48 g, *ca* 2 mmol) dissolved in ethanol (10 cm^3) and pyrazinic acid (0.26 g, *ca* 2 mmol) in water/ethanol (30 cm^3) were mixed together. To this mixture an aqueous solution (5 cm^3) of KN_3 (0.34 g, *ca* 4 mmol) was added dropwise until a deep green solution was obtained. If a green precipitate formed after several minutes, the mixture was filtered off. In order to obtain suitable crystals, two drops of the azide solution were added to the green filtrate and the solution was left undisturbed for several weeks. Olive-green crystals of the complex were deposited along with an unidentified blue crystalline material. Found: C, 13.3; H, 0.8; N, 43.2; Cu, 28.0; K, 8.0. Calc. for KCu_2(pyrazinato)$(N_3)_4$: C, 13.1; H, 0.7; N, 42.9; Cu, 27.8; K, 8.6%.

X-ray crystallography

For the X-ray structure determination a prism-shaped single crystal was used (Enraf–Nonius, CAD4, graphite-monochromatized Mo-K_α radiation). Data were collected at 295 K (ω–θ scans, variable scan width and scan time) and processed in the usual way. Crystallographic data and processing parameters are given in Table 1.

The Mo1EN program package was used for structure solution and subsequent refinement [21]. Anisotropic displacement parameters were applied only to the non-hydrogen atoms in full-matrix least-squares refinements. The occupation factors of the three split positions of the disordered potassium atoms were adjusted by taking into account the corresponding electron density maxima obtained from Fourier maps. Selected bond distances and bond angles are given in Table 2. Positional parameters, anisotropic displacement parameters, hydrogen atom coordinates, a full list of bond lengths and angles have been deposited at the Cambridge Crystallographic Data Centre.

Physical measurements

The procedures and instruments used for other measurements were as described previously [22].

Table 1. Crystallographic data and processing parameters

Compound	**1**
Molecular formula	$C_5H_3Cu_2KN_{14}O_2$
Molecular weight	457.36
Crystal system	Orthorhombic
a (Å)	17.297(8)
b (Å)	13.410(6)
c (Å)	6.341(2)
V (Å^3)	1471(1)
Space group	*Pba*2 (No. 32)
Z	4
$F(000)$	896
μ(Mo-K_α) (mm^{-1})	3.22
D_{calc}/D_{obs} (Mg m^{-3})	2.065/2.05(3)
Approx. crystal size (mm)	$0.08 \times 0.08 \times 0.25$
Data collection limits	$h,k,\pm l$; $2\theta < 54°$
Unique reflections	3183
Observed data	2792
Cut-off	$3.50\sigma(F_0)^2$
Least-squares parameters	235
$R = \Sigma\|F_0\| - \|F_0\|/\Sigma\|F_0\|$	0.042
$R_w = [\Sigma w\|F_0\| - \|F_c\|^2/\Sigma w\|F_0\|^2]^{1/2}$	0.051
$w = [\sigma(F_0^2)^2 + (0.005F_0^2)^2]^{-1/2}$	
Residual electron density in final difference map (eÅ^{-3})	3.11

RESULTS AND DISCUSSION

The interaction of copper(II) ion and pyrazinic acid in the presence of potassium azide afforded an olive green-complex of empirical formula KCu_2(pyrazinato)$(N_3)_4$, along with an unidentified blue crystalline compound.

The structure of the title complex, **1**, consists of a packing of $[Cu_2(N_3)_6]^{2-}$ anions, potassium cations and a polymeric neutral complex [Cu(pyrazinato)$(N_3)]_n$ (Figs 1 and 2). Each copper centre, Cu(1), in the dinuclear complex anion is coordinated by four nitrogen atoms; two nitrogens from two terminal azido groups at Cu—N distances of 1.940(6) and 1.979(5) Å and two nitrogen atoms from two μ-(1,1) bridging azido ligands [Cu—N = 1.997(6) and 2.011(5) Å]. The coordination environment about each copper atom may be described as distorted square planar. This complex anion is the first to have been isolated and structurally characterized in the case of copper(II) azido complexes. The Cu—Cu separation within the dinuclear complex anion is 3.126(2) Å. The Cu—Cu distances in copper(II) azido complexes fall in the range 3.78 in $CuL'(N_3)_3$ [L = (2-aminoethyl)pyridine] [23] to 3.08 Å in $[Cu(N_3)_2]_n$ [24], which has infinite chains of planar $Cu(N_3)_2$ units. The terminal azido ligands are asymmetric [N(11)—N(12) = 1.216(8), N(12)—N(13) = 1.141(9) and N(21)—N(22) = 1.213(9) and N(22)—N(23) = 1.141(11) Å] with $\Delta d = 0.075$ and 0.072 Å, respectively [Δd is the difference between the two N—N distances within an azide group]. The μ-(1,1) azido ligands, on the other hand, are less asym-

Table 2. Selected bond distances (Å) and angles (°)

K(11)···K(12)	0.835(6)	K(11)···K(13)	2.67(1)
Complex anion $[Cu_2(N_3)_6]^{2-}$			
Cu(1)···Cu(1c)	3.126(2)	Cu(1)—N(21)	1.940(6)
Cu(1)—N(31)	2.011(5)	Cu(1)—N(11)	1.979(5)
Cu(1)—N(31c)	1.997(6)	N(11)—N(12)	1.216(8)
N(12)—N(13)	1.141(9)	N(21)—N(22)	1.213(9)
N(22)—N(23)	1.141(11)	N(31)—N(32)	1.194(8)
N(32)—N(33)	1.152(10)		
N(11)—Cu(1)—N(21)	96.3(3)	N(11)—Cu(1)—N(31)	161.0(2)
N(11)—Cu(1)—N(31c)	96.5(3)	N(21)—Cu(1)—N(31)	92.2(2)
N(21)—Cu(1)—N(31c)	166.6(2)	N(31)—Cu(1)—N(31c)	76.8(2)
Cu(1)—N(11)—N(12)	117.5(5)	N(11)—N(12)—N(13)	179.4(8)
Cu(1)—N(21)—N(22)	118.8(5)	N(21)—N(22)—N(23)	176.8(9)
Cu(1)—N(31)—N(32)	123.3(4)	Cu(1)—N(31)—Cu(1c)	102.5(2)
Cu(1c)—N(31)—N(32)	126.2(4)	N(31)—N(32)—N(33)	178.6(6)
Polymeric neutral complex $[Cu(pyrazinato)(N_3)]_n$			
Cu(2)—O(31)	1.954(5)	Cu(2)—N(41)	1.943(5)
Cu(2)—N(61)	2.022(4)	Cu(2)—N(62a)	2.010(4)
O(31)—C(30a)	1.260(8)	O(32)—C(30)	1.237(8)
N(41)—N(42)	1.186(8)	N(42)—N(43)	1.136(10)
N(61)—C(13)	1.347(8)	N(61)—C(14)	1.330(8)
N(62)—C(11)	1.341(7)	N(62)—C(12)	1.325(8)
C(11)—C(14)	1.381(8)	C(11)—C(30)	1.502(8)
C(12)—C(13)	1.404(9)		
O(31)—Cu(2)—N(41)	173.4(2)	O(31)—Cu(2)—N(61)	87.6(2)
O(31)—Cu(2)—N(62a)	81.9(2)	N(41)—Cu(2)—N(61)	95.2(3)
N(41)—Cu(2)—N(62a)	94.4(3)	N(61)—Cu(2)—N(62a)	166.3(2)
Cu(2)—O(31)—C(30a)	116.2(4)	Cu(2)—N(41)—N(42)	121.9(5)
N(41)—N(42)—N(43)	177.0(8)	Cu(2)—N(61)—C(13)	119.4(4)
Cu(2)—N(61)—C(14)	122.1(4)	C(13)—N(61)—C(14)	118.5(5)
C(11)—N(62)—C(12)	117.5(5)	C(11)—N(62)—Cu(2b)	112.1(4)
C(12)—N(62)—Cu(2b)	130.4(4)	N(62)—C(11)—C(14)	123.0(5)
N(62)—C(11)—C(30)	114.1(5)	C(14)—C(11)—C(30)	122.9(5)
N(62)—C(12)—C(13)	120.4(6)	N(61)—C(13)—C(12)	120.9(6)
N(61)—C(14)—C(11)	119.6(6)	O(32)—C(30)—O(31b)	124.9(6)
O(32)—C(30)—C(11)	119.4(6)	C(11)—C(30)—O(31b)	115.7(6)

Symmetry code: (a) $\frac{3}{2}-x, -\frac{1}{2}+y, z$; (b) $\frac{3}{2}-x, \frac{1}{2}+y, z$; (c) $1-x, 1-y, z$.

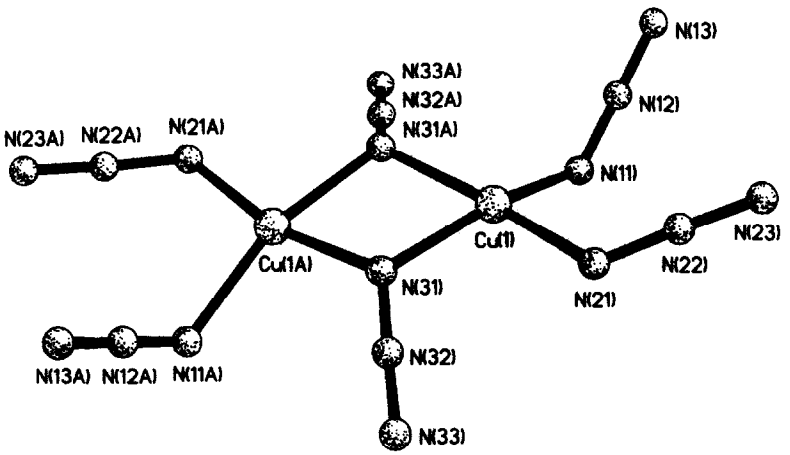


Fig. 1. The molecular geometry and atom-numbering scheme of the binuclear $[Cu_2(N_3)_6]^{2-}$ anion.

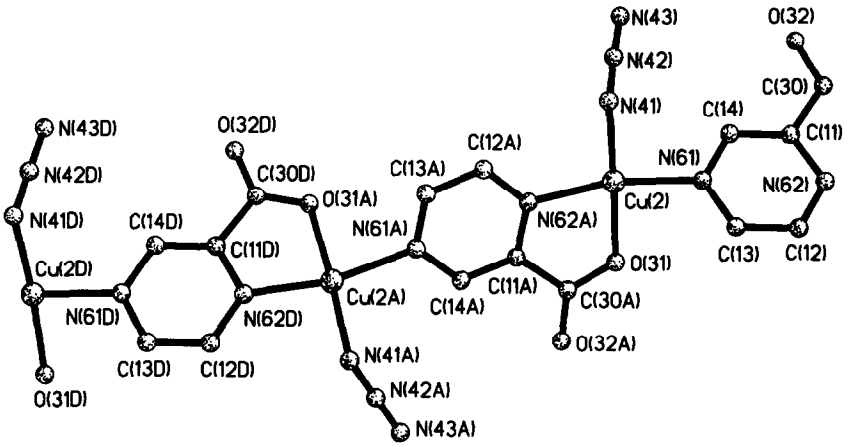


Fig. 2. the molecular geometry and atom-numbering scheme of the polymeric complex [Cu(pyrazinato)(N_3)]$_n$. The chains of polyhedra are oriented along [010].

metric than the terminal azido ligands [N(31)—N(32) = 1.194(8) and N(32)—N(33) = 1.152(10) Å; Δd = 0.042 Å]. In both cases, however, the long N—N distance is that between the central nitrogen atom and the nitrogen atom bonded to the copper atom, as found in the structures of other copper(II) azido complexes [25]. Both types of azido ligand are linear within experimental error (Table 2).

A dinuclear azido complex anion of the type $[M_2(N_3)_6]^{2-}$ has previously been reported only for M = Pd [26]. In the palladium anion, the azido ligands of both types are significantly asymmetric and the M—N—N angles are larger than the corresponding values in the present anion; reported values are: N_α—N_β = 1.239(14), N_β—N_γ = 1.142(17) Å, Δd = 0.097 Å (terminal); N_α—N_β = 1.205(18), N_β—N_γ = 1.139(16) Å, Δd = 0.066 Å; (μ-1,1); Pd—N—N = 127.6(13) and 120.6(14)°.

In the neutral complex, each copper atom [Cu(2)] is also four-coordinated to N(41) of a terminal azido ligand at a Cu—N distance of 1.943(5) Å, N(61) and N(62) of two pyrazinato anions [Cu—N = 2.022(4) and 2.010(4) Å], and an oxygen atom O(31) at Cu—O bond length of 1.954(5) Å. The pyrazinato anion, therefore, acts as an *N,N',O*-tridentate ligand bridging two metal centres [angle N(61)—Cu—N(62a) = 166.3(2)°] *via* both nitrogen atoms to form infinite, "neutral" chains of polyhedra (Figs 2 and 3). The five-membered chelate ring deviates 0.019 Å from planarity. The Cu—N(pyz) distances are comparable with corresponding values found in the structures of [MCu(picolinato)$(N_3)_2$]$_n$ [Cu—N(pic) = 2.012(5) Å for M = Na, 2, and 2.003(3) Å for M = K, **3**] [10], but significantly longer than Cu—N(pic) = 1.961(3) Å found in the structure of [NaCu(picolinato)$_2(N_3)(H_2O)_2]_n$, **4** [9]. The Cu—O(pyz) bond length, on the other hand, is significantly shorter than corresponding values [Cu—O(pic) = 1.997(5) and 1.990(3) Å] in **2** and **3**, respectively, but agrees very well those [1.951(3) and 1.944(3) Å] found in the structure of **4**. The terminal azide group is linear and asymmetric, as found in the above anion.

Both anionic and neutral copper complexes are arranged in sheets of polyhedra with orientation normal to [001] (Fig. 3). The potassium cations are located in broad channels. These channels are a consequence of stacking of the copper polyhedra. The location of the potassium ion is split into three different positions; i.e. K(11), K(12) and K(13) with occupation factors of 0.45, 0.40 and 0.15, respectively. K(11) and K(12) are arranged within 1.5 Å in the same height as the sheets of $[Cu_2(N_3)_6]^{2-}$ whereas K(13) is almost within the height of the chains of Cu(2) polyhedra.

The structure of the present complex differs from that of the polymeric [NaMn(pyrazinato)$(N_3)_2(H_2O)_2]_n$, complex **5**, which also contains two azido groups and a single pyrazinato anion [27]. Complex **5** crystallizes with two aqua ligands and the pyrazinato anion functions only as a chelating *N,O*-bidentate ligand, as compared with the tridentate anion in the present structure. Complex **5** features octahedrally coordinated manganese and sodium atoms, μ-1,1,3 bridging azido ligands, bridging and terminally bonded aqua molecules and heterodinuclear units, Na—$\mu(N_3)\mu(OH_2)$—Mn.

The IR spectrum of free pyrazinic acid exhibits the following absorption bands: (cm^{-1}, v = very, w = weak, m = medium, s = strong, br = broad); 1725vs, br [ν(C=O)], 1316vs [ν(C—O)], 1020s, 825m, 789s, 705m, 410m (pyrazine vibrations) [28]. The spectrum of the complex, on the other hand, shows a substantial shift to lower wavenumber of the ν_{as}(CO_2^-) which appears at 1684 cm^{-1}, and increase of the $\nu_s(CO_2^-)$ to 1384 cm^{-1}. This large separation between the two ν(C—O) indicates a monodentate coordination to the metal atoms as found for many metal complexes of carboxylic acids [29–32]. Vibrations related to the pyrazine moiety are shifted to higher wavenumbers and appear at 1050m, 855m,

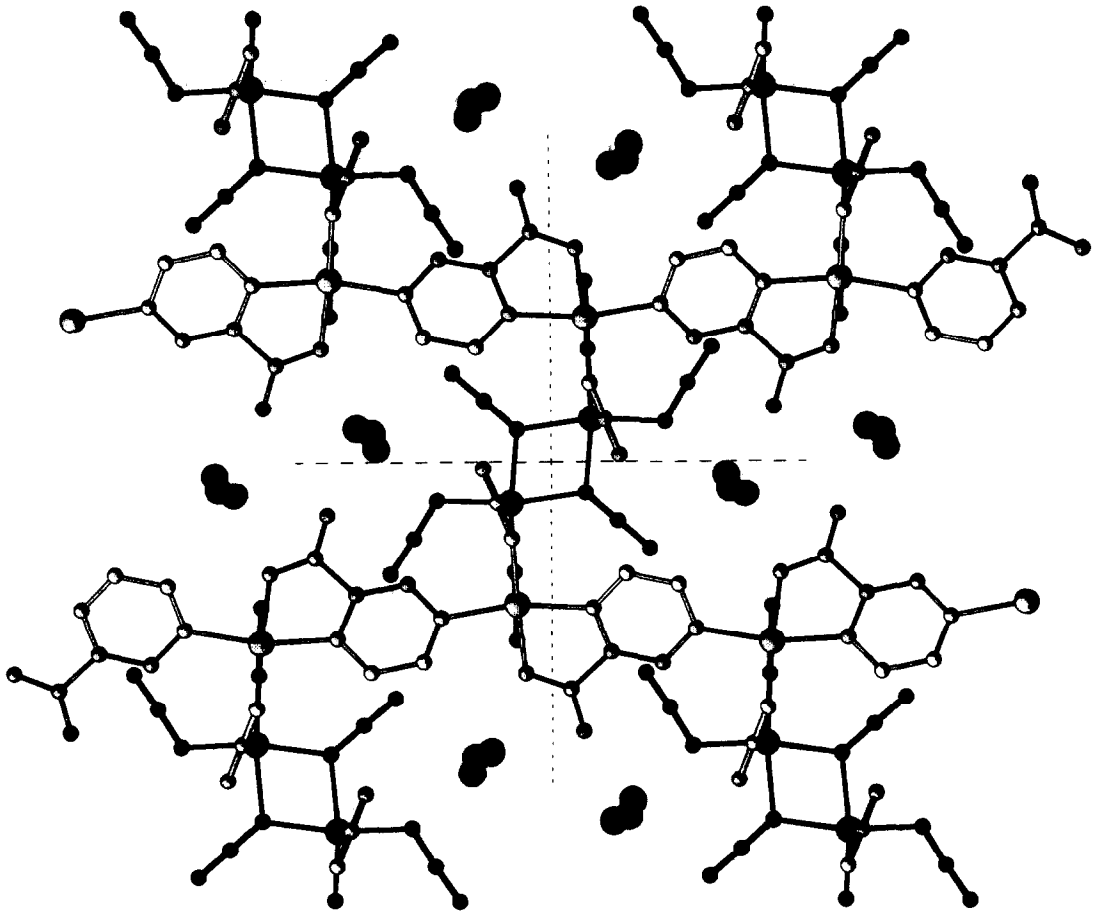


Fig. 3. Packing of KCu_2(pyrazinato)$(N_3)_4$ viewed along the *c*-axis of the unit cell. The binuclear $[Cu_2(N_3)_6]^{2-}$ anions (dark) and linear chains of polymeric $[Cu(pyrazinato)(N_3)]_n$ molecules (light) form alternating sheets normal to [001]. Disordered potassium ions (isolated spheres) are located in broad channels oriented along [001].

815m, 725m and 430w. While these results are indicative of the coordination of the pyrazine moiety it could not be distinguish whether one or both nitrogen atoms are coordinated.

The IR spectrum of the present complex also shows at least three bands of different intensities at 2128vs, 2055s and 2010m, associated with the $\nu_{as}(N_3)$ mode. The crystal structure determination reveals that the complex contains four independent azido groups with different Δd values, and hence four absorption bands are expected owing to the asymmetric stretching vibrations of these azides. In fact, the Δd values for two pairs of these azides are very close; 0.075 and 0.072 Å for N(11)—N(12)—N(13) and N(21)—N(22)—N(23) and 0.042 and 0.050 Å for N(31)—N(32)—N(33) and N(41)—N(42)—N(43). These values suggest the possibility that the corresponding four vibrations may appear as two superimposed bands. However, according to the relationship between Δd and $\nu_{as}(N_3)$ given by Agrell [33], the observed Δd values suggest the higher and lower frequency bands should appear near 2080 and 2040 cm^{-1}, respectively. In contrast, the higher and lower frequency bands appear in the spectrum at 2128 and 2010 cm^{-1}, respectively. It is possible that the coincidence of the vibrations related to the two azides with Δds of 0.075 and 0.072 Å leads to some kind of resonance or configuration interaction, which in turn leads to the appearance of two bands at 2128 and 2055 cm^{-1}, instead of just one band at approx. 2080 cm^{-1}. The same may be true for the other two ν_{as} vibrations leading to two bands at 2055 and 2010 cm^{-1} rather than one at *ca* 2045 cm^{-1}. In the region 1350–1250 cm^{-1}, where the symmetric stretch mode of the azide usually appears, we could not locate any related band owing to the strong absorption of the ligand itself.

The electronic spectrum of the solid complex (Fig. 4) exhibits its *d–d* transition as a very broad band centred around 14,400 cm^{-1} as found for four- and six-coordinated copper(II) complexes [34,35]. The spectrum also exhibits two very strong broad bands centred around 27,500 and 22,440 cm^{-1}. These bands are a result of $N_3^- \rightarrow Cu^{II}$ charge transfer transitions. For terminal copper(II) azide monomers one feature is reported, Π_σ^{nb}-to-copper(II) charge transfer, whereas two bands are observed for μ-1,3 or μ-1,1

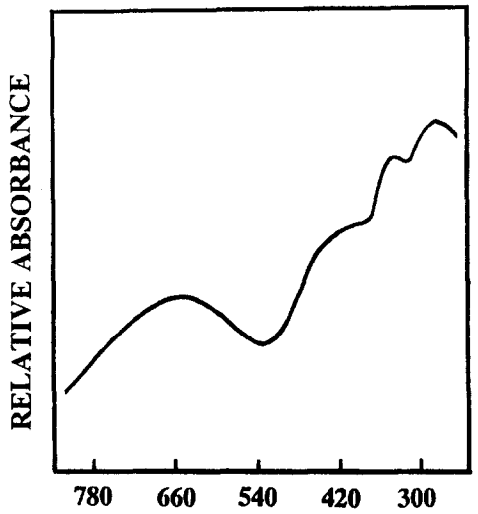


Fig. 4. Reflectance spectrum of solid KCu_2(pyrazinato)$(N_3)_4$.

dimers [36]. The present complex contains both types of azide ligands, hence three CT bands are expected. In fact, the lower energy CT band is so broad that it covers the range 27,000–19,500 cm^{-1}.

The powder EPR spectrum of the title solid complex measured at room temperature is of the axial type, with $g_{\|} = 2.233$ and $g_{\perp} = 2.061$. The G value of 3.82 calculated as the ratio of $(g_{\|}-2)/(g_{\perp}-2)$, is a little lower than 4, suggesting some exchange coupling between bridged copper atoms in this complex. The spectrum, however, displays no absorption in the lower field region.

Acknowledgement—Financial support by the Kuwait University Research Administration Project (no. SC 077) is gratefully acknowledged.

REFERENCES

1. A. Anagnostopoulos, R. A. Matthews and R. A. Walton, *Can. J. Chem.* 1972, **50,** 1307.
2. G. W. A. Fowles, R. A. Matthews and R. A. Walton, *J. Chem. Soc. (A)* 1968, 1108.
3. A. Kleinstein and G. A. Webb, *J. Inorg. Nucl. Chem.* 1971, **33,** 405.
4. S. C. Chang, J. K. H. Ma, J. S. Wang and N. C. Li, *J. Coord. Chem.* 1972, **2,** 31.
5. A. Takenaka, N. Utsumi, T. Yamamoto and I. Nita, *Nippon Kagaku Zsashi* 1970, **91,** 928.
6. M. A. S. Goher, M. A. M. Abu-Youssef, F. A. Mautner and A. Popitsch, *Polyhedron* 1992, **11,** 2137.
7. M. A. S. Goher, A. K. Hafez, M. A. M. Abu-Youssef, A. Popitsch, H. P. Fritzer and F. A. Mautner, *Monatsh. Chem.* 1994, **125,** 833.
8. F. A. Mautner, M. A. M. Abu-Youssef and M. A. S. Goher, *Polyhedron* 1997, **16,** 235.
9. M. A. S. Goher and F. A. Mautner, *Polyhedron* 1994, **13,** 2149.
10. M. A. S. Goher and F. A. Mautner, *Polyhedron* 1995, **14,** 1439.
11. R. W. Matthews and R. A. Walton, *Inorg. Chem.* 1971, **7,** 1433.
12. K. D. Karlin, J. C. Hayes, J. P. Hutchinson and J. Zubieta, *J. Chem. Soc., Chem. Commun.* 1983, 376; K. D. Karlin, A. Farooq, J. C. Hayes, B. L. Cohen, T. M. Rowe, E. Sinn and J. Zubieta, *Inorg. Chem.* 1987, **27,** 1271.
13. O. Kahn, S. Sikorav, J. Gouterson, S. Jeannin and Y. Jeannin. *Inorg. Chem.* 1983, **22,** 2877; P. Pickardt, *Z. Naturforsch.* 1982, **37b,** 110; J. Comarmand, P. Plumiere, J.-M. Lehn, Y. Agnus, R. Louis, D. Weiss, O. Kahn and L. Morgenstern-Badarau, *J. Am. Chem. Soc.* 1982, **104,** 6330.
14. M. G. B. Drew, J. Nelson, F. Esho, V. McKee and S. M. Nelson, *J. Chem. Soc., Dalton Trans.* 1982, 1837; S. Sikorav, I. Bkouche-Waksman and O. Kahn, *Inorg. Chem.* 1984, **23,** 490.
15. M. A. S. Goher and T. C. W. Mak, *Inorg. Chim. Acta* 1984, **89,** 119; V. McKee, J. V. Dagdigian, R. Bau and C. A. Reed, *J. Am. Chem. Soc.* 1981, **103,** 7000.
16. V. McKee, M. Zvagulis, J. V. Dagdigian, M. G. Patch and C. A. Reed, *J. Am. Chem. Soc.* 1984, **106,** 4765; T. N. Sorrell, C. J. O'Connor, J. P. Hutchinson and J. Zubieta, *J. Am. Chem. Soc.* 1985, **107,** 4199.
17. M. A. S. Goher and T. C. W. Mak, *Inorg. Chim. Acta* 1985, **99,** 223; I. Agrell, *Acta Chem. Scand.* 1967, **21,** 2647; I. Agrell and S. Lamnevik, *Acta Chem. Scand.* 1968, **22,** 450; R. Soderquist, *Acta Cryst.* 1968, **24B,** 2038.
18. M. A. S. Goher, R.-J. Wang and T. C. W. Mak, *J. Mol. Struct.* 1991, **243,** 179; C. S. Choi and H. P. Boutin, *Acta Cryst.* 1969, **25B,** 982.
19. M. A. S. Goher and F. A. Mautner, *Polyhedron* 1996, **15,** 5.
20. F. A. Mautner and M. A. S. Goher, *Struct. Chem.* 1994, **5,** 171.
21. *MolEN: An Interactive Structure Solution Procedure.* Enraf–Nonius, Delft, The Netherlands (1990).
22. M. A. S. Goher, M. A. M. Abu-Youssef and F. A. Mautner, *Polyhedron* 1996, **15,** 453.
23. N. A. Baily, D. E. Fenton and C. H. McLean, *Inorg. Chim. Acta* 1991, **179,** 1.
24. R. Soderquist, *Acta Cryst.* 1968, **24B,** 450.
25. M. A. S. Goher and T. C. W. Mak, *Inorg. Chim. Acta* 1984, **85,** 117; T. C. W. Mak and M. A. S. Goher, *Inorg. Chim. Acta* 1986, **115,** 17; M. A. S. Goher and F. A. Mautner, *Z. Naturforsch.* 1991, **46b,** 687.
26. W. P. Fehlhammer and L. F. Dahl, *J. Am. Chem. Soc.* 1972, **94,** 3377.
27. M. A. S. Goher and F. A. Mautner, *Polyhedron* 1993, **12,** 2557.
28. J. Bus, Th.J. Liefkens and W. Schwaiger, *Recl. Trav. Chim. Phys. Pays-Bas* 1973, **92,** 123.
29. A. L. Magri, A. D. Magri, F. Balestrieri, E. Cardarelli, G. D'Ascenzo and E. Chiacchierini, *Thermochim. Acta* 1980, **38,** 225.
30. J. R. Allan, A. D. Paton, K. Turvey, H. J. Bowley

and D. L. Garrad, *Inorg. Chim. Acta* 1987, **132,** 41.
31. C. L. Klein, L. M. Trefonas, J. C. O'Connor and R. J. Majeste, *Cryst. Struct. Commun.* 1981, **10,** 891.
32. J. C. O'Connor and E. K. K. Sinn, *Inorg. Chem.* 1981, **20,** 545.
33. I. Agrell, *Acta Chem. Scand.* 1971, **25,** 2965.
34. R. C. Aggarwal, N. K. Singh and R. P. Singh, *Inorg. Chim. Acta* 1979, **32,** L87.
35. W. E. Estes, D. P. Gavel, W. E. Hatfield and D. J. Hodgson, *Inorg. Chem.* 1978, **17,** 1415.
36. J. E. Pate, P. K. Ross, T. J. Thamann, C. A. Reed, K. D. Karlin, T. N. Sorrell and E. J. Solomon, *J. Am. Chem. Soc.* 1989, **111,** 5198.

Pergamon

PII: S0277-5387(96)00328-2

Polyhedron Vol. 16, No. 5, pp. 833–838, 1997
Copyright © 1996 Elsevier Science Ltd
Printed in Great Britain. All rights reserved
0277-5387/97 $17.00+0.00

A series of novel one-dimensional polymeric clusters $[W_4Ag_5S_{16}]_n \cdot n[Ln(DMF)_8]$ (Ln = Nd, Pr and La) derived from the assembly system of tetrathiotungstate and silver nitrate. X-ray crystal structure of $[W_4Ag_5S_{16}]_n \cdot n[Nd(DMF)_8]$

Qun Huang, Xintao Wu* and Jiaxi Lu

State Key Laboratory of Structural Chemistry, Fujian Institute of Research on Structure of Matter, Chinese Academy of Sciences, Fuzhou, Fujian 350002, P.R. China

(Received 17 April 1996; accepted 2 July 1996)

Abstract—The title complexes have been obtained from reaction of ammonium tetrathiotungstate and silver nitrate in the presence of lanthanide nitrate in DMF and CH_3CN. The one-dimensional polymeric cluster anionic structure can be viewed as square-type $[W_4Ag_4S_{16}]^{4-}$ fragments bridged by Ag^+ cations. The valence and dimensions of the lanthanide-coordinated cations play significant roles in the assembly reaction of ammonium tetrathiotungstate and silver nitrate. In addition, the IR and Raman spectra are discussed. Copyright © 1996 Elsevier Science Ltd

Keywords: chalcogenide; clusters; tungsten–silver compounds; polymeric tungsten–silver–sulfur compounds; structure; lanthanide compounds.

Thiometalates and their related multi-metal sulfides have been extensively researched. Many reports have shown the considerable variety of structures of such complexes and their role in the chemistry of life processes [1]. In addition, polymeric transition metal chalcogenides have attracted much attention owing to their useful properties derived directly from their structural peculiarities [2].

In the M/Ag/S system (M = Mo, W), many discrete, and a few polymeric, M—Ag—S cluster complexes have been obtained, such as: $[(PPh_3)_2AgS_2MS_2Ag(PPh_3)\cdot 0.8CH_2Cl_2]$ (linear) [3], $[Et_4N][(PPh_3)_2AgS_3MOCu(CN)]$ (butterfly-type) [4], $[Ag_6S_6M_2(SCMe_3)_2(O)_2(PPh_3)_4]$ (double-cubane-like) [5], $[(PPh_3)_4Ag_4W_2S_8]$ (cage) [6], $[AgWS_4\cdot HNEt_3\cdot DMF]_n$ [7] and $[AgMS_4\cdot 4\text{-}MePyH]_n$ [8] (M = Mo, W). Recently, the assembly reaction system of tetrathiotungstate and silver nitrate has been explored in our laboratory, and the polymeric complex $[WS_4Ag\cdot NH_3C(CH_2OH)_3\cdot H_2O]_n$ (double-chain) [9] with a novel polymeric cluster configuration has been isolated. Herein, the detailed synthesis, characterization and structure of the title complexes $[W_4Ag_5S_{16}\cdot Ln(DMF)_8]_n$ [10], which are also derived from the assembly system of tetrathiotungstate and silver nitrate, are reported.

EXPERIMENTAL

All operations were performed at room temperature in air. $(NH_4)_2WS_4$ was synthesized according to the literature [11]. Other chemicals were used as purchased. Elemental analyses were performed by the Elemental Analysis Laboratories of our institute. IR and Raman spectra were recorded on a Nicolet Magna 750 FT-IR spectrometer and a Nicolet 910 FT-Raman laser spectrometer, respectively.

Preparation of $[W_4Ag_5S_{16}]_n\cdot n[Ln(DMF)_8]$

To a solution of $(NH_4)_2WS_4$ (0.70 g, 2 mmol) in DMF (5 cm^3) was added a solution of $AgNO_3$ (0.68

* Author to whom correspondence should be addressed.

g, 4 mmol), $Ln(NO_3)_3 \cdot 6H_2O$ (1 mmol) and *p*-nitroaniline (0.28 g, 2 mmol) in CH_3CN (15 cm^3). The dark precipitate was filtered off, and 0.30 g of red crystals were obtained from allowing the red filtrate to stand in air for one day.

Found: C, 11.9; H, 2.2; N, 4.7. Calc. for $[W_4Ag_5S_{16}][Nd(DMF)_8]$: C, 11.5; H, 2.2; N, 4.5%. IR (KBr pellet, cm^{-1}): 1647, 677, 496, 472, 461, 455, 442, 426 and 413. Raman (diluted with KBr, cm^{-1}): W—S, 498, 472, 466, 445 and 430; Ag—S, 259 and $\delta(WS_4)$, 191 and 171.

Found: C, 11.3; H, 2.3; N, 4.6. Calc. for $[W_4Ag_5S_{16}][Pr(DMF)_8]$: C, 11.5; H, 2.3; N, 4.5%. IR (KBr pellet, cm^{-1}): 1647, 677, 496, 472, 461, 455, 442, 426 and 413.

Found: C, 11.8; H, 2.2; N, 4.6. Calc. for $[W_4Ag_5S_{16}][La(DMF)_8]$: C, 11.5, H, 2.3; N, 4.5%. IR (KBr pellet, cm^{-1}): 1647, 675, 496, 472, 461, 455, 442, 426 and 413.

Table 1. Crystal data and experimental details

Compound	$[W_4Ag_5S_{16}]_n \cdot n[Nd(DMF)_8]$
Formula	$C_{24}H_{56}N_8O_8NdS_{16}Ag_5W_4$
M_r	2516.78
Crystal dimension (mm)	$0.35 \times 0.20 \times 0.17$
Crystal appearance	Red, rhombic
Crystal system	Triclinic
Space group	*P*-1
a (Å)	16.104(9)
b (Å)	16.328(4)
c (Å)	12.608 (2)
α (°)	94.23(2)
β (°)	94.47(3)
γ (°)	100.19(3)
V (Å^3)	3240(2)
Z	2
D_c (g cm^{-3})	2.58
μ(Mo-K_α) (cm^{-1})	100.1
F(000)	2334
Scan type	2θ–ω
Scan rate (° min^{-1})	8
Scan width	$1.0+0.350\tan(\theta)$
2θ(max) (°)	50
h, *k*, *l* ranges	0–19, −19 to 19, −15 to 15
R_{int}	0.044
Measured reflections	11841
Unique reflections	11396
Obs. reflections [$I > 3\sigma(I)$]	4106
Minimum, maximum transmission coefficients	0.75, 1.03
No. of parameters	395
R^a	0.056
R'^b	0.063
Goodness-of-fit	1.13
Maximum Δ/σ	0.07
Maximum, minimum $\Delta\rho$ (e Å^{-3})	1.56, −0.31

$^aR = \Sigma(|F_o| - |F_c|)/\Sigma|F_o|$.
$^bR' = [\Sigma w(|F_o| - |F_c|)^2/\Sigma w|F_o|^2]^{1/2}$;
$w = [\sigma^2(|F_o|^2) + (0.020 \times |F_o|)^2 + 1.00]^{-1} - F_o$.

Crystal structure determination

Crystals of $[W_4Ag_5S_{16}]_n \cdot n[Nd(DMF)_8]$ were selected and mounted on glass fibres for the single-crystal X-ray diffraction experiment. The crystallographic and experimental data are given in Table 1. Diffraction data were collected on a Rigaku AFC-5R diffractometer using Mo-K_α radiation ($\lambda = 0.71069$ Å) at room temperature. Cell constants and orientation matrices were obtained from least squares by using the setting angles of 20 reflections in the range $12 < 2\theta < 50°$. Intensities were corrected for polarization and Lorentz factors and for absorption by using empirical ψ-scan data and the method of Walker and Stuart (DIFABS) [12].

The structures were solved by direct methods using MULTAN, and the positions of two heavy atoms were obtained from the *E*-map. The remaining non-hydrogen atoms were located from a difference Fourier map. No attempt was made to locate hydrogen atoms. Metal and sulfur atoms were refined anisotropically. The refinement of the structure was performed by full-matrix least-squares techniques using the MolEN program package [13]. All calculations were carried out on a Compaq Prolinea 4/50 computer. Atomic scattering factors were taken from ref. [14].

The cell dimensions for $[W_4Ag_5S_{16}]_n \cdot n[La(DMF)_8]$ were also determined and the values are $a = 16.162(7)$, $b = 16.354(9)$, $c = 12.621(5)$ Å, $\alpha = 94.24(4)$, $\beta = 94.57(4)$, $\gamma = 100.37(4)°$ and $V = 3258(3)$ Å^3.

RESULTS AND DISCUSSION

Synthesis of $[W_4Ag_5S_{16}]_n \cdot n[Ln(DMF)_8]$

Equation (1) shows the reaction of WS_4^{2-} anions and Ag^+ cations in the presence of Ln^{3+} cations.

$$WS_4^{2-} + Ag^+ \xrightarrow{Ln^{3+}} [(W_4Ag_5S_{16})^{3-}]_n. \quad (1)$$

In the syntheses of the title complexes, the trivalent Ln^{3+} cations were added in the reaction solution. These cations are oxygen and nitrogen philic and do not react with WS_4^{2-} moieties. However, through charge- and other interactions they can influence the assembly of WS_4^{2-} and Ag^+, and induce the formation of $[(W_4Ag_5S_{16})^{3-}]_n$ with the trinegative $(W_4Ag_5S_{16})^{3-}$ cluster anion fragments as cyclic units. In addition, Ln^{3+} cations are readily coordinated by oxygen atoms of DMF groups, and form large tripositive ions $[Ln(DMF)_8]^{3+}$. These mononuclear metal-coordinated ions $[Ln(DMF)_8]^{3+}$ occupy the interstices between the polymeric cluster anions $[(W_4Ag_5S_{16})^{3-}]_n$ in the crystalline product.

Description of the structure

Selected bond lengths and angles are listed in Tables 2 and 3, respectively. The structure of a portion of the

Table 2. Selected bond lengths (Å) in $[W_4Ag_5S_{16}]_n \cdot n[Nd(DMF)_8]$

W(1)—Ag(1)	2.971(3)	Ag(1)—S(13)	2.556(9)
W(1)—Ag(2)	2.989(3)	Ag(1)—S(41)	2.530(10)
W(1)—Ag(5a)	2.966(3)	Ag(1)—S(44)	2.552(12)
W(1)—S(11)	2.243(8)	Ag(2)—S(11)	2.557(9)
W(1)—S(12)	2.179(9)	Ag(2)—S(12)	2.566(9)
W(1)—S(13)	2.243(9)	Ag(2)—S(21)	2.559(9)
W(1)—S(14)	2.181(8)	Ag(2)—S(23)	2.508(10)
W(2)—Ag(2)	2.967(3)	Ag(3)—S(21)	2.518(9)
W(2)—Ag(3)	2.966(3)	Ag(3)—S(22)	2.577(9)
W(2)—S(21)	2.255(9)	Ag(3)—S(31)	2.552(9)
W(2)—S(22)	2.204(8)	Ag(3)—S(33)	2.564(9)
W(2)—S(23)	2.211(9)	Ag(4)—S(31)	2.533(11)
W(2)—S(24)	2.134(11)	Ag(4)—S(34)	2.567(10)
W(3)—Ag(3)	2.999(3)	Ag(4)—S(41)	2.513(10)
W(3)—Ag(4)	2.960(3)	Ag(4)—S(42)	2.498(11)
W(3)—Ag(5)	2.951(3)	Ag(5)—S(13b)	2.523(9)
W(3)—S(31)	2.239(9)	Ag(5)—S(14b)	2.572(10)
W(3)—S(32)	2.179(9)	Ag(5)—S(32)	2.536(10)
W(3)—S(33)	2.237(9)	Ag(5)—S(33)	2.528(9)
W(3)—S(34)	2.159(10)	Nd—O(1)	2.48(2)
W(4)—Ag(1)	2.935(3)	Nd—O(2)	2.43(2)
W(4)—Ag(4)	2.933(3)	Nd—O(3)	2.39(2)
W(4)—S(41)	2.268(11)	Nd—O(4)	2.52(3)
W(4)—S(42)	2.197(10)	Nd—O(5)	2.39(3)
W(4)—S(43)	2.123(12)	Nd—O(6)	2.41(3)
W(4)—S(44)	2.206(11)	Nd—O(7)	2.42(3)
Ag(1)—S(11)	2.527(10)	Nd—O(8)	2.43(3)

a: $(x, y, 1+z)$; b: $(x, y, z-1)$.

anion is shown in Fig. 1. This linear polymeric anion can be viewed as octanuclear cyclic cluster fragments, $[W_4Ag_4S_{16}]^{4-}$, bridged by Ag^+ cations. In the $[W_4Ag_4S_{16}]^{4-}$ fragment, the W atoms are arrayed in an approximate square; and the Ag atoms lie nearly along the edges of the square, between the W atoms. A similar square-type configuration has been shown in the reported cluster complex $[Et_4N]_4[W_4Cu_4S_{12}O_4]$ [15].

In the anion, the tungsten atoms retain their tetrahedral coordination geometry as in isolated WS_4^{2-} ions, but in two slightly different coordination environments; namely, one coordinated by one terminal sulfur atom, two μ_2-S atoms and one μ_3-S atom, and the other by two μ_2-S and two μ_3-S atoms. Compared with that of tungsten atoms, the coordination geometry of the silver atoms with two μ_2-S and two μ_3-S atoms is largely distorted from tetrahedral; the S—Ag—S angles range from 91.2 to 127.7°, similar to those reported in $[AgWS_4 \cdot 4\text{-MePyH}]_n$ (93.5–133.1°) [8] $[WS_4Ag \cdot NH_3C(CH_2OH)_3 \cdot H_2O]_n$ (92.1–126.7°) [9].

With three kinds of sulfur atoms in the anion, namely, terminal sulfur atoms, μ_2-S atoms and μ_3-S atoms, the W—S bond lengths range from 2.123 to 2.268 Å. The mean W—S_t, W—(μ_2-S) and W—(μ_3-S) bond lengths are 2.128, 2.190 and 2.248 Å, respectively. In comparison, the W—S_t bond length is 2.177 Å in isolated WS_4^{2-} ions [1a], and the W—S_t, W—(μ_2-S) and W—(μ_3-S) bond lengths are 2.144(3), 2.217(2) and 2.242(3) Å, respectively, in $[WS_4Ag_3(PPh_3)_3(S_2P(OCH_2CH_3)_2)]$ [16]. The average Ag—S bond length is 2.542 Å, which is comparable with those in other polymeric complexes (see Table 4). The average W—Ag distance of 2.964 Å is shorter than the values observed in $[(PPh_3)_3Ag_2WS_4 \cdot 0.8CH_2Cl_2]$ (2.971 Å) [3], $[WS_4Ag \cdot NH_3C(CH_2OH)_3 \cdot H_2O]_n$ (2.980 Å) [9], $[AgWS_4 \cdot HNEt_3 \cdot DMF]_n$ (2.983 Å) [7] and in $[WS_4Ag_3(PPh_3)_3(S_2P(OCH_2CH_3)_2)]$ (3.080 Å) [16], but longer than those in polymeric linear-chain complexes $[AgWS_4 \cdot 4\text{-MePyH}]_n$ (2.949 Å) [8] and $[WS_4Ag \cdot NH_3C(CH_2OH)_3 \cdot 2DMF]_n$ (2.931 Å) [9]. Comparison of the main bond lengths and angles of some polymeric W—Ag—S complexes is shown in Table 4.

In general, Ln atoms tend to attain high coordination numbers. Figure 2 shows that the Nd atoms is surrounded by eight DMF molecules. The average Nd—O bond length is 2.43 Å and the O—Nd—O coordination angles range from 70.4 to 144.8°.

The packing diagram of the unit cell viewed down the c-axis is shown in Fig. 3. The linear anionic $[(W_4Ag_5S_{16})^{3-}]_n$ cluster chains run parallel to the crys-

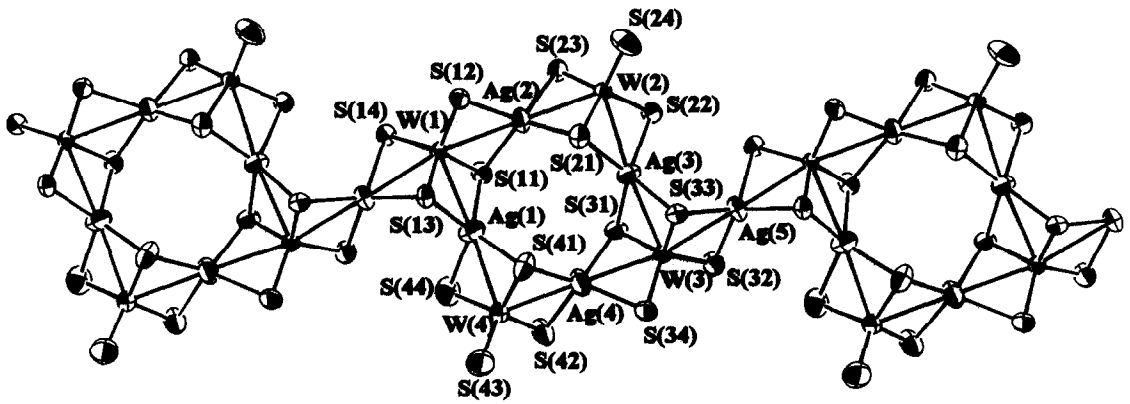


Fig. 1. Structure of a portion of the anion of $[W_4Ag_5S_{16}]_n \cdot n[Nd(DMF)_8]$.

Table 3. Selected bond lengths (Å) in $[W_4Ag_5S_{16}]_n \cdot n[Nd(DMF)_8]$

Ag(1)—W(1)—Ag(2)	88.12(9)	S(13b)—Ag(5)—S(14b)	91.8(3)
Ag(1)—W(1)—Ag(5a)	80.0(1)	S(13b)—Ag(5)—S(32)	124.3(4)
Ag(2)—W(1)—Ag(5a)	168.0(1)	S(13b)—Ag(5)—S(33)	113.2(3)
S(11)—W(1)—S(12)	112.5(3)	S(14b)—Ag(5)—S(32)	115.7(4)
S(11)—W(1)—S(13)	112.4(4)	S(14b)—Ag(5)—S(33)	121.8(3)
S(11)—W(1)—S(14)	107.0(4)	S(32)—Ag(5)—S(33)	92.8(4)
S(12)—W(1)—S(13)	106.8(3)	W(1)—S(11)—Ag(1)	76.8(3)
S(12)—W(1)—S(14)	106.5(3)	W(1)—S(11)—Ag(2)	76.7(3)
S(13)—W(1)—S(14)	111.6(3)	Ag(1)—S(11)—Ag(2)	109.2(4)
Ag(2)—W(2)—Ag(3)	87.39(9)	W(1)—S(12)—Ag(2)	77.6(3)
S(21)—W(2)—S(22)	113.0(3)	W(1)—S(13)—Ag(1)	76.2(3)
S(21)—W(2)—S(23)	112.2(3)	W(1)—S(13)—Ag(5a)	76.7(2)
S(21)—W(2)—S(24)	108.7(4)	Ag(1)—S(13)—Ag(5a)	97.5(3)
S(22)—W(2)—S(23)	107.5(3)	W(1)—S(14)—Ag(5a)	76.8(2)
S(22)—W(2)—S(24)	106.4(4)	W(2)—S(21)—Ag(2)	75.8(2)
S(23)—W(2)—S(24)	108.7(4)	W(2)—S(21)—Ag(3)	76.6(3)
Ag(3)—W(3)—Ag(4)	86.59(9)	Ag(2)—S(21)—Ag(3)	107.7(3)
Ag(3)—W(3)—Ag(5)	80.53(9)	W(2)—S(22)—Ag(3)	76.2(3)
Ag(4)—W(3)—Ag(5)	166.7(2)	W(2)—S(23)—Ag(2)	77.6(3)
S(31)—W(3)—S(32)	106.7(3)	W(3)—S(31)—Ag(3)	77.2(3)
S(31)—W(3)—S(33)	112.0(3)	W(3)—S(31)—Ag(4)	76.4(2)
S(31)—W(3)—S(34)	111.9(3)	Ag(3)—S(31)—Ag(4)	107.0(4)
S(32)—W(3)—S(33)	112.3(3)	W(3)—S(32)—Ag(5)	77.1(3)
S(32)—W(3)—S(34)	107.2(4)	W(3)—S(33)—Ag(3)	77.0(2)
S(33)—W(3)—S(34)	106.6(4)	W(3)—S(33)—Ag(5)	76.2(3)
Ag(1)—W(4)—Ag(4)	88.6(1)	Ag(3)—S(33)—Ag(5)	98.1(3)
S(41)—W(4)—S(42)	112.2(4)	W(3)—S(34)—Ag(4)	77.0(3)
S(41)—W(4)—S(43)	108.0(5)	W(4)—S(41)—Ag(1)	75.2(3)
S(41)—W(4)—S(44)	113.6(5)	W(4)—S(41)—Ag(4)	75.5(3)
S(42)—W(4)—S(43)	107.9(5)	Ag(1)—S(41)—Ag(4)	108.8(4)
S(42)—W(4)—S(44)	107.7(4)	W(4)—S(42)—Ag(4)	77.0(4)
S(43)—W(4)—S(44)	107.3(4)	W(4)—S(44)—Ag(1)	75.8(3)
W(1)—Ag(1)—W(4)	176.6(1)	O(1)—Nd—O(2)	70.4(7)
S(11)—Ag(1)—S(13)	94.4(3)	O(1)—Nd—O(3)	76.4(7)
S(11)—Ag(1)—S(41)	126.5(3)	O(1)—Nd—O(4)	119.0(7)
S(11)—Ag(1)—S(44)	115.1(3)	O(1)—Nd—O(5)	143.8(7)
S(13)—Ag(1)—S(41)	107.8(3)	O(1)—Nd—O(6)	74.6(8)
S(13)—Ag(1)—S(44)	120.2(3)	O(1)—Nd—O(7)	140.4(8)
S(41)—Ag(1)—S(44)	94.9(4)	O(1)—Nd—O(8)	74.9(8)
W(1)—Ag(2)—W(2)	170.9(1)	O(2)—Nd—O(3)	85.1(8)
S(11)—Ag(2)—S(12)	91.7(3)	O(2)—Nd—O(4)	71.2(8)
S(11)—Ag(2)—S(21)	123.8(4)	O(2)—Nd—O(5)	144.3(8)
S(11)—Ag(2)—S(23)	121.0(3)	O(2)—Nd—O(6)	103.5(8)
S(12)—Ag(2)—S(21)	111.0(3)	O(2)—Nd—O(7)	81.5(8)
S(12)—Ag(2)—S(23)	116.8(4)	O(2)—Nd—O(8)	143.3(9)
S(21)—Ag(2)—S(23)	94.1(3)	O(3)—Nd—O(4)	142.9(7)
W(2)—Ag(3)—W(3)	173.1(1)	O(3)—Nd—O(5)	109.0(8)
S(21)—Ag(3)—S(22)	93.7(3)	O(3)—Nd—O(6)	144.8(9)
S(21)—Ag(3)—S(31)	127.7(3)	O(3)—Nd—O(7)	73.8(9)
S(21)—Ag(3)—S(33)	111.1(3)	O(3)—Nd—O(8)	75.2(8)
S(22)—Ag(3)—S(31)	111.8(4)	O(4)—Nd—O(5)	78.9(8)
S(22)—Ag(3)—S(33)	122.4(3)	O(4)—Nd—O(6)	70.6(8)
S(31)—Ag(3)—S(33)	93.0(3)	O(4)—Nd—O(7)	74.7(8)
W(3)—Ag(4)—W(4)	174.7(1)	O(4)—Nd—O(8)	139.3(8)
S(31)—Ag(4)—S(34)	91.2(4)	O(5)—Nd—O(6)	84.0(8)
S(31)—Ag(4)—S(41)	122.3(3)	O(5)—Nd—O(7)	71.9(8)
S(31)—Ag(4)—S(42)	117.9(3)	O(5)—Nd—O(8)	72.3(9)
S(34)—Ag(4)—S(41)	119.4(3)	O(6)—Nd—O(7)	140.8(9)
S(34)—Ag(4)—S(42)	112.3(3)	O(6)—Nd—O(8)	78.2(8)
S(41)—Ag(4)—S(42)	95.3(4)	O(7)—Nd—O(8)	120.7(9)
W(1b)—Ag(5)—S(3)	170.4(1)		

a: $(x, y, 1+z)$; b: $(x, y, z-1)$.

Table 4. Comparison of main bond lengths (Å) and angles (°) of some polymeric W—Ag—S cluster complexes

Complex	I	II	III	IV	V
W—Ag	2.964(3)	2.931(6)	2.949(1)	2.983(6)	2.980(2)
W—S_t	2.128(11)	—	—	—	—
W—μ_2-S	2.190(9)	2.22(2)	2.206(4)	2.203(9)	2.204(6)
W—μ_2-S	2.248(9)	—	—	—	—
Ag—μ_2-S	2.547(10)	2.52(2)	2.533(4)	2.547(11)	2.565(7)
Ag—μ_2-S	2.538(9)	—	—	—	—
W—Ag—W	173.1(1)	176.4(5)	180.0(1)	177.1(2)	—
Ag—W—Ag	167.4(2)	176.4(3)	180.0(1)	177.1(2)	—
Ag—W—Ag	85.21(9)	—	—	—	—
S—W—S	106.4(4)–113.6(5)	106.7(9)–114.5(4)	107.3(1)–113.5(2)	106.6(4)–113.0(3)	106.3(2)–113.2(3)
S—Ag—S	91.2(4)–127.7(3)	94.1(4)–119.1(9)	93.5(2)–133.1(1)	91.5(4)–123.0(4)	92.1(2)–126.7(2)

I: $[W_4Ag_5S_{16}]_n \cdot n[Nd(DMF)_8]$; II: $[WS_4Ag \cdot NH_3C(CH_2OH)_3 \cdot 2DMF]_n$ [9]; III: $[AgMS_4 \cdot 4\text{-MePyH}]_n$ [8]; IV: $[AgWS_4 \cdot HNEt_3 \cdot DMF]_n$ [7]; V: $[WS_4Ag \cdot NH_3C(CH_2OH)_3 \cdot H_2O]_n$ [9].

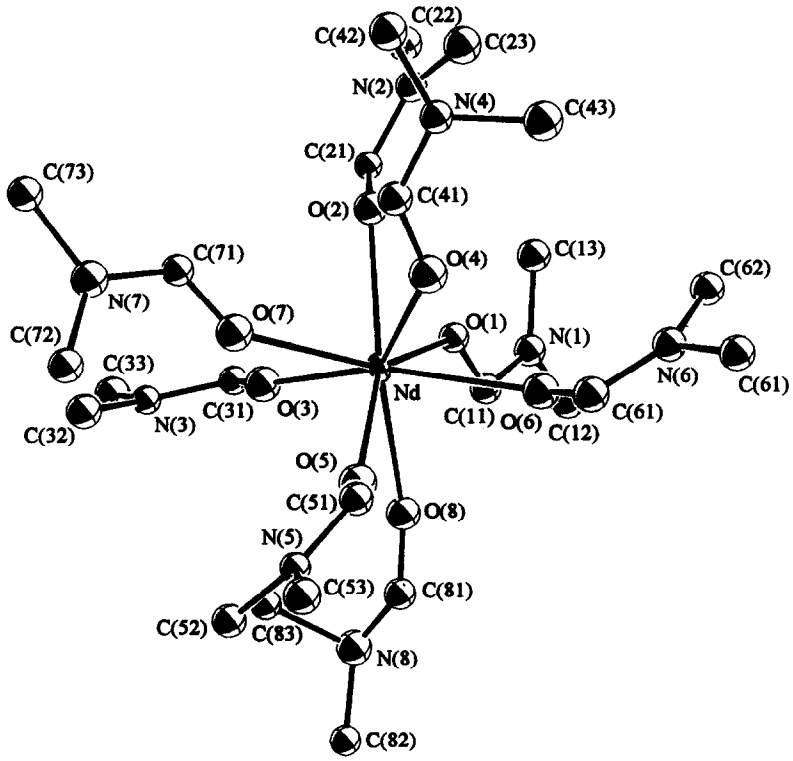


Fig. 2. Configuration of the cation $[Nd(DMF)_8]^{3+}$.

tallographic *c*-axis, and the $[Nd(DMF)_8]^{3+}$ cations are located along these chains with the distance between two neighbouring Nd atoms being 12.608 Å.

IR and Raman spectra

IR spectra of the title complexes are very similar. The strongest absorption band at 1647 cm^{-1} in each IR spectrum can be undoubtedly attributed to the C=O stretching vibration. In principle, W—S characteristic vibration absorption bands appear in the 400–500 cm^{-1} area. The complicated absorption peaks in this area of each spectrum suggest that there are many kinds of sulfur atoms in the complex. This is consistent with the results of the X-ray single-crystal diffraction. The crystal structure determination shows that three kinds of sulfur atoms exist in these complexes (terminal atoms, μ_2-S atoms and μ_3-S atoms).

Only the polymeric complex $[W_4Ag_5S_{16}]_n \cdot n[Nd(DMF)_8]$ was characterized by Raman spectroscopy. Compared with the IR spectrum, the Raman spectrum is simpler. The strongest absorption band at 1647 cm^{-1} in the IR spectrum disappears in the Raman spectrum because of prohib-

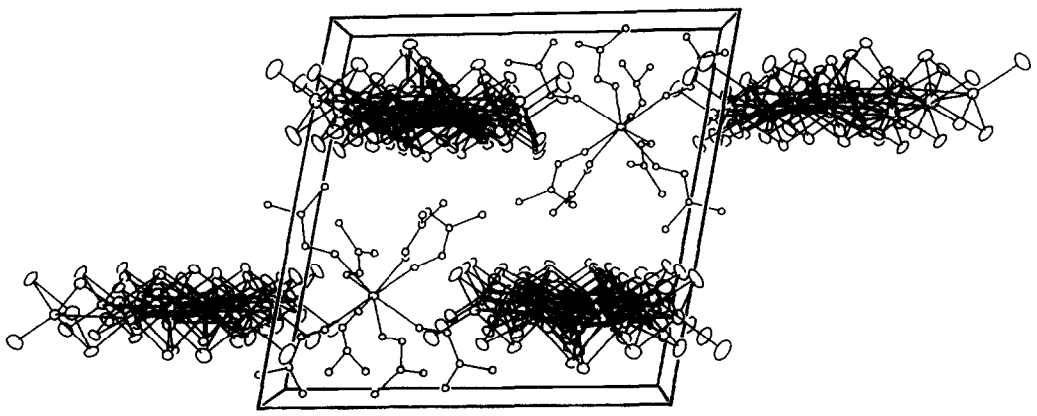


Fig. 3. Packing diagram of the unit cell viewed down the *c*-axis.

ition of the transition. In the 400–500 cm^{-1} area, the Raman spectrum also displays complicated bands of W—S vibration similar to those in the IR spectrum. The bands at 259 and 191 (and 171 cm^{-1}) can be assigned to ν_s(Ag—S) and $\delta(WS_4)$, respectively [17].

Acknowledgements—This research was supported by grants from the State Key Laboratory of Structural Chemistry, Fujian Institute of Research on Structure of Matter, Chinese Academy of Sciences, the National Science Foundations of China, and the Provincial Science Foundations of Fujian.

REFERENCES

1. (a) A. Müller, E. Diemann, R. Jostes and H. Bögge, *Angew. Chem. Int. Ed. Engl.* 1981, **20,** 934; (b) C. F. Mills, *Chem. Ber.* 1979, **15,** 512; (c) C. E. Holloway and M. Melnik, *Rev. Inorg. Chem.* 1993, **13,** 233; (d) B. Krebs and G. Henkel, *Angew. Chem. Int. Ed. Engl.* 1991, **30,** 769; (e) X. T. Wu, P. C. Chen, S. W. Du, N. Y. Zhu and J. X. Lu, *J. Clust. Sci.* 1994, **5,** 265.
2. D. W. Murphy and P. A. Christian, *Science* 1979, **205,** 651; M. S. Whittingham, *Prog. Solid State Chem.* 1978, **12,** 41; R. R. Chianelli, T. A. Pecoraro, T. R. Halbert, H. W. Pan and E. I. Stiefel, *J. Catal.* 1984, **86,** 226.
3. A. Müller, H. Bögge and E. Koniger-Ahlborn, *Z. Naturforsch.* 1979, **34b,** 1698.
4. N. Y. Zhu, S. W. Du, P. C. Chen, X. T. Wu and J. X. Lu, *J. Coord. Chem.* 1992, **26,** 35; S. W. Du, N. Y. Zhu, P. C. Chen, X. T. Wu and J. X. Lu, *J. Chem. Soc., Dalton Trans.* 1992, 339.
5. S. W. Du and X. T. Wu, *J. Coord. Chem.* 1993, **30,** 183.
6. A. Müller, H. Bögge and E. Koniger-Ahlborn, *J. Chem. Soc., Chem. Common.* 1978, 739.
7. Q. Huang, X. T. Wu, T. L. Sheng and Q. M. Wang, *Acta Cryst.* 1996, **C52,** 795.
8. J. P. Lang, J. G. Li, S. Bao and X. Q. Xin, *Polyhedron* 1993, **12,** 801.
9. Q. Huang, X. T. Wu, T. L. Sheng and Q. M. Wang, *Inorg. Chem.* 1995, **34,** 4931.
10. Q. Huang, X. T. Wu, Q. M. Wang, T. L. Sheng and J. X. Lu, *Angew. Chem. Int. Ed. Engl.* 1996, **35,** 868.
11. J. W. McDonald, G. D. Friesen, L. D. Rosenhein and W. E. Newton, *Inorg. Chim. Acta* 1983, **72,** 205.
12. N. Walker and D. Stuart, *Acta Cryst.* 1983, **A39,** 158.
13. MolEN, *An Interactive Structure Solution Procedure.* Enraf–Nonius, Delft, The Netherlands (1990).
14. D. T. Cromer and J. T. Waber, *International Tables for X-ray Crystallography*, Vol. 4, Tables 2.2a, 2.3.1. Kynoch Press, Birmingham (1974).
15. Q. Huang, X. T. Wu, Q. M. Wang, T. L. Sheng and J. X. Lu, *Inorg. Chem.* 1996, **35,** 893.
16. S. W. Du, N. Y. Zhu, P. C. Chen and X. T. Wu, *J. Mol. Struct.* 1993, **291,** 167.
17. A. Müller and W. Hellmann, *Spectrochim. Acta* 1985, **41A,** 359.

Pergamon

PII: S0277-5387(96)00332-4

Polyhedron Vol. 16, No. 5, pp. 839–847, 1997
Copyright © 1996 Elsevier Science Ltd
Printed in Great Britain. All rights reserved
0277-5387/97 $17.00+0.00

Further studies of the reactions involving ethyne and $M_2(OBu^t)_6$, where M = Mo and W. Polyacetylene formation versus formation of ethyne adducts and C—C coupled products

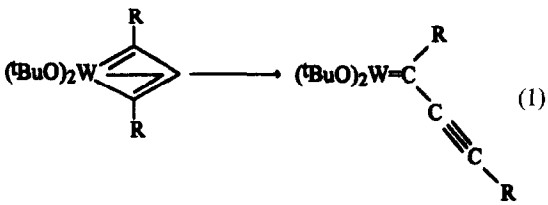
Malcolm H. Chisholm,* David M. Hoffman, Jill McCandless Northius and John C. Huffman

Department of Chemistry and Molecular Structure Center, Indiana University, Bloomington, IN 47405, U.S.A.

(Received 6 June 1996; accepted 1 July 1996)

Abstract—$M_2(OBu^t)_6$ compounds in hydrocarbon solvents react with ethyne to give a mixture of *cis*- and *trans*-polyacetylene and ethyne- and μ-C_4H_4 adducts of $M_2(OBu^t)_6$ by competing pathways. The degree of ethyne polymerization is shown to *decrease* with increasing concentration of $M_2(OBu^t)_6$, to increase with increasing volumes of solvent for constant concentration and to be greater for M = Mo than for M = W. The kinetically labile complex $Mo_2(OBu^t)_6(\mu\text{-}C_2H_2)$, originally reported by Strutz and Schrock [*Organometallics* 1984, **4**, 1600], has been trapped by the addition of pyridine and 4-methylpyridine at −20°C and the structure of the latter compound determined by a single crystal X-ray study. There is a pseudo-tetrahedral Mo_2C_2 core, Mo—Mo = 2.645(1) Å, C—C = 1.39(1) Å and Mo—C = 2.092(7) Å (ave.), supported by a single OR bridge. Each metal atom has a pseudo-trigonal bipyramidal geometry. In the presence of an excess of ethyne, $Mo_2(OBu^t)_6$ yields a mixture of compounds, two of which are proposed to be isomers of formula $Mo_2(OBu^t)_6(\mu\text{-}C_4H_4)$. Addition of CO to a hydrocarbon solution of the latter gives $Mo_2(OBu^t)_6(\mu\text{-}C_4H_4)(CO)$ which is shown to be structurally related to its tungsten analogue by a single crystal X-ray determination. [ν(CO) = 1908 (M = Mo) and 1883 cm^{-1} (M = W).] The isolated compounds show no activity towards ethyne polymerization which is proposed to occur by way of a carbene/alkylidene mechanism. Consistent with this proposal is the finding that $Mo_2(OBu^t)_6$, which is unreactive towards norbornene, can be activated towards norbornene polymerization by the addition of ethyne (5 equiv.). Copyright © 1996 Elsevier Science Ltd

The polymerization of acetylenes by metal carbene complexes was first proposed and demonstrated by Katz and Lee [1]. Subsequently Schrock and co-workers [2] reported alkyne polymerization in alkyne metathesis systems and studied this process by well-defined alkylidene complexes. Alkynes are known to react with $W_2(OBu^t)_6$ to give $(Bu^tO)_3W{\equiv}CR$ complexes, which are alkyne metathesis catalysts [3], and, in related reactions involving $W_2(OR)_6$ compounds, alkyne polymerization has been observed [4]. Terminal acetylenes are also known to react to give deprotiometallacycles [5] and in the reaction between $W_2(OBu^t)_6$ and $Bu^tC{\equiv}CH$, the deprotiometallacyclic complex $W(OBu^t)_2(C_3Bu^t_2)$ was found to initiate the fast polymerization of alkynes [6]. In the latter reaction ring opening according to Eq. (1) may account for generation of the alkylidene ligand responsible for the initiation of alkyne polymerization.



(1)

$Mo_2(OBu^t)_6$ has been shown to react with alkynes to give alkylidynes in only a few instances [7] whereas $Mo_2(OR)_6$ compounds, where R = Pr^i and CH_2Bu^t, have been shown to effect cyclotrimerization to benzene [8]. Knox *et al.* [9] have also documented oligomerization of alkynes at a dinuclear centre [9] but

* Author to whom correspondence should be addressed.

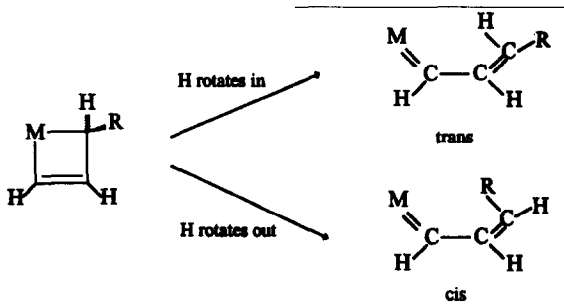
to our knowledge no example of catalytic polymerization by a dinuclear centre has been documented. We return here to a study of the reactions between $M_2(OBu^t)_6$ compounds and ethyne, which are known to give polyacetylene and the kinetically labile complexes $Mo_2(OBu^t)_6(\mu\text{-}C_2H_2)$ [7] and $W_2(OBu^t)_6(\mu\text{-}C_2H_2)$, the latter having been trapped as a pyridine adduct and shown to exist in equilibrium with a methylidyne complex, as given by Eq. (2) [10]. In the presence of excess ethyne

$$W_2(OBu^t)_6(\mu\text{-}C_2H_2)(py) \rightleftharpoons 2[(Bu^tO)_3W{\equiv}CH]^+py \quad (2)$$

$W_2(OBu^t)_6(\mu\text{-}C_4H_4)$ was also detected and spectroscopically characterized [11]. We address the question of what role, if any, do dinuclear species derived from ethyne play in the polymerization of ethyne, and we characterize the previously elusive $\mu\text{-}C_2H_2$ and $\mu\text{-}C_4H_4$ adducts of $Mo_2(OBu^t)_6$ by trapping with pyridine and carbon monoxide, respectively.

RESULTS AND DISCUSSION

Black, shiny metallic looking polyacetylene formed upon exposure of C_2H_2 to hydrocarbon solutions of $M_2(OBu^t)_6$ compounds (M = Mo and W). These films were collected by filtration and dried *in vacuo*. In all instances we observed IR bands at 802 and 1013 cm^{-1} indicative of a mixture of *cis*- and *trans*-polyacetylene [12]. Polymerization of ethyne by a metal–carbene/alkylidene intermediate would be expected to proceed through a metallacyclobutene [13] which could open to give both *cis* and *trans* stereochemistry about the C—C double bond as shown in Eq. 3.



(3)

However, the observed stereochemistry does not rule out alternative mechanisms of polymerization such as Ziegler–Natta polymerization by way of a *cis*-migratory insertion involving a metal–vinyl (alkenyl), because the activation energy for *cis* to *trans* isomerization could be provided by the preparation of a Nujol mull or KBr pellet owing to local heating effects. [The *cis*-to-*trans* isomerization has a relatively low activation barrier, *ca* 17 kcal mol^{-1}] [14].

In an attempt to distinguish between a possible carbene/alkylidene mechanism and Ziegler–Natta type polymerization we investigated the reaction between $Mo_2(OBu^t)_6$ and norbornene. No reaction occurred between this strained olefin and $Mo_2(OBu^t)_6$ in hydrocarbon solvents at room temperature. However, addition of norbornene to hydrocarbon solutions of $Mo_2(OBu^t)_6$ followed by 5 equiv. of ethyne produced a rapid polymerization of norbornene. It is well known that metal–carbene/alkylidene complexes can affect the ring opening polymerization methathesis (ROMP) of norbornene [15] and, in our case, work-up of the polymer derived in the above reaction revealed the same ^1H and $^{13}C\{^1H\}$ NMR data as that reported by the polymer when formed from an authentic alkylidene catalyst precursor [16].

An estimation of the catalytic activity of the system with respect to ethyne polymerization was undertaken as follows.

(a) Polymerization of ethyne by $Mo_2(OBu^t)_6$ was first conducted in hexane as solvent with varying concentrations of catalysts and solution volumes: 1.59×10^{-4} M (40 mg/5 cm^3); 1.59×10^{-3} M (40 mg/50 cm^3) and 0.79×10^{-3} M (40 mg/100 cm^3), yielding consumption of 50, 71 and 117 monomer equivalents, respectively. From this result it is apparent that the system is not very catalytically active. Because PA (PA = polyacetylene) is virtually insoluble in hexane it is reasonable to speculate that the catalyst died as the metal catalyst was incorporated with the PA. Thus, in this interpretation, the increase in volume of the solution allowed for a greater degree of polymerization before all the molybdenum-containing catalyst was precipitated from solution.

(b) The catalyst concentration was changed by keeping the solvent volume constant (along with all other factors) and changing the amount of solute. For $Mo_2(OBu^t)_6$ concentrations of 1.27×10^{-5}, 2.43×10^{-3} and 4.44×10^{-3} M in 15 cm^3 of hexane the monomer equivalents of ethyne consumed were 157, 91 and 39, respectively.

From (a) and (b) we conclude that active catalyst is *not* $Mo_2(OBu^t)_6$, but rather some species derived from its decomposition.

Similar experiments were carried out in toluene as solvent and similar results were obtained, although the monomer equivalents of ethyne consumed were

somewhat larger (by *ca* 40%), presumably because PA is slightly more soluble in toluene than hexane.

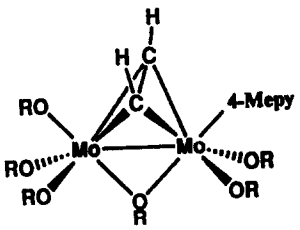
Polymerization of propyne was also carried out in hexane employing $Mo_2(OBu^t)_6$ as catalyst precursor; in this case, 5.29×10^{-3} M (50 mg/15 cm^3), 2.66×10^{-3} M (50 mg/30 cm^3) and 1.98×10^{-3} M (50 mg/40 cm^3) solutions consumed, respectively, 68, 167 and 300 equivalents of propyne.

The catalytic activity of $Mo_2(OBu^t)_6$ and $W_2(OBu^t)_6$ were also compared under otherwise identical conditions and $Mo_2(OBu^t)_6$ solutions were found to be more active by a factor of two. This is an interesting observation since ethyne and $W_2(OBu^t)_6$ are known to produce the methylidyne species $(Bu^tO)_3W{\equiv}CH$ and alkylidynes are readily converted to alkylidenes with relatively mild protio sources such as those present on silica surfaces [17]. In addition, Freudenberger and Schrock [18] have shown that $(Bu^tO)_3W{\equiv}CBu^t$ reacts with various Brønstead acids, HX, to give $X_2(Bu^tO)_2W{=}CH(Bu^t)$ compounds, where X = PhO, Cl and RCOO.

Detection and characterization of organometallic compounds formed upon the addition of ethyne to hydrocarbon solutions of $Mo_2(OBu^t)_6$

Addition of $^{13}C_2H_2$ to $Mo_2(OBu^t)_6$ in toluene-d_8 was studied by ^{13}C and ^1H NMR spectroscopy. At -80 to -60°C only free $^{13}C_2H_2$ and $Mo_2(OBu^t)_6$ were detected by NMR spectroscopy, but the formation of PA was seen as a fine black film on the walls of the NMR tube at these temperatures. At -40 to -20°C, $Mo_2(OBu^t)_6(\mu\text{-}^{13}C_2H_2)$ was observed [$\delta(^{13}C)$ 127.2] in addition to free acetylene and $Mo_2(OBu^t)_6$. As the temperature was raised two other sets of ^{13}C signals were observed which are assignable to the metallacyclic species $Mo_2(OBu^t)_6(\mu\text{-}C_4H_4)$ (see later). The fact that the latter did not form until 0°C and that the ethyne adduct formed between -40 and -20°C led us to believe that the ethyne adduct could be independently synthesized and indeed this was achieved.

The addition of an excess of ethyne to a hydrocarbon solution of $Mo_2(OBu^t)_6$ in the presence of pyridine leads to the formation of $Mo_2(OBu^t)_6(py)(\mu\text{-}C_2H_2)$, which is isolated as a dark green crystalline solid. This compound is spectroscopically analogous to the tungsten congener, giving rise to four OBu^t signals in the low-temperature ^1H NMR spectrum in the integral ratio 1 : 1 : 2 : 2. The compound is thermally unstable in solution above 0°C, where $Mo_2(OBu^t)_6$ is formed along with free pyridine and some PA. Solutions containing $[Mo_2(OBu^t)_6(py)(\mu\text{-}^{13}C_2H_2)]$ and $[Mo_2(OBu^t)_6(py)(\mu\text{-}C_2D_2)]$ provided no evidence for the formation of a $Mo_2(\mu\text{-}H^{13}CCD)$-containing species [10]. Thus, in contrast to the tungsten analogue, there is no evidence that $Mo_2(OBu^t)_6(\mu\text{-}C_2H_2)$ is in equilibrium with the methylidyne complex $(Bu^tO)_3Mo{\equiv}CH$. From reactions between $Mo_2(OBu^t)_6$ and ethyne in the presence of 4-methylpyridine (4-Mepy) a green crystalline compound $[Mo_2(OBu^t)_6(4\text{-Mepy})(\mu\text{-}C_2H_2)]$ was isolated. The 4-Mepy adduct has been characterized crystallography (see later); the structure is shown schematically in **I**. It is akin to the previously reported tungsten compound $W_2(OBu^t)_6(py)(\mu\text{-}C_2H_2)$ [10].



I

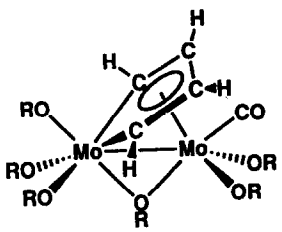
The addition of ethyne-$^{13}C_2H_2$ (in excess) to a toluene-d_8 solution of $Mo_2(OBu^t)_6$ at room temperature leads to a mixture of products, including PA as a dark precipitate, $Mo_2(OBu^t)_6(\mu\text{-}C_2H_2)$[$\delta(^{13}C)$ 127.2, $^1J_{C-H}$=190 Hz] and ^1H-coupled ^{13}C resonances at δ 209.8 and 115.3 and at δ 179.8 and 124.6. Each of the signals is a multiplet that is one-half of an AA′XX′ spin system.

It should be emphasized that there are resonances owing to two AA′XX′ spin systems corresponding to a, roughly, 60 : 40 product mixture. It seems likely that one is akin to that of the μ-C_4H_4 groups previously seen in $[Mo_2(OCH_2Bu^t)_6(\mu\text{-}C_4H_4)(py)]$ and $[W_2(OPr^i)_6(\mu\text{-}C_4H_4)(\eta^2\text{-}C_2H_2)]$ and proposed for $W_2(OBu^t)_6(\mu\text{-}C_4H_4)$ [11]. The nature of the other μ-C_4H_4 group remains a mystery. It could be only σ bonded to one metal, or it could bridge the two metal atoms in a symmetrical perpendicular manner akin to that reported by Green and Mountford [19] for $Cp'_2W_2Cl_4(C_4Me_4)$.

Upon addition of carbon monoxide to the $Mo_2(OBu^t)_4(C_4H_4)$ compounds a red-orange solution of $Mo_2(OBu^t)_6(\mu\text{-}C_4H_4)(CO)]$ is formed. This compound is also accessible (and best prepared) from the reaction between $Mo_2(OBu^t)_6(\mu\text{-}C_2H_2)(py)]$ and an excess of ethyne followed by addition of carbon monoxide. Similarly addition of carbon monoxide to $W_2(O^tBu)_6(\mu\text{-}C_4H_4)$ formed *in situ* from the reaction between $Mo_2(OBu^t)_6(\mu\text{-}C_2H_2)(py)$ and an excess of ethyne, followed by addition of carbon monoxide. Similarly, addition of carbon monoxide to $W_2(OBu^t)_6(\mu\text{-}C_4H_4)$ formed *in situ* from the reaction between $W_2(OBu^t)_6$ and an excess of ethyne in hydrocarbon solutions, yielded $W_2(OBu^t)_6(\mu\text{-}C_4H_4)(CO)$. The compounds adopt a common structure, depicted by **II** and described in more detail below. The value of ν(CO) is 1908 for M = Mo and 1883 cm^{-1} for M = W, indicating greater M d_π to CO π^* back-bonding for the 3rd row element, W compared with the 2nd row Mo.

Table 1. Summary of crystal data

	I	II	III
Empirical formula	$C_{32}H_{63}Mo_2N_1O_6$	$C_{29}H_{58}Mo_2O_7$	$C_{29}H_{58}O_7W_2$
Molecular weight	749.73	710.65	886.47
Colour	Dark brown	Black	Black
Crystal dimensions (mm)	$0.20 \times 0.30 \times 0.30$	$0.04 \times 0.28 \times 0.32$	$0.08 \times 0.08 \times 0.10$
Space group	$P2_1/n$	*Pbca*	*Pcab*
Cell dimensions			
Temperature (°C)	−175	−170	−160
a (Å)	11.377(2)	15.817(4)	41.906(23)
b (Å)	22.909(3)	41.778(10)	10.395(4)
c (Å)	14.392(2)	10.420(3)	10.395(4)
β (°)	91.04(1)		
Z	4	8	8
V (Å^3)	3750.43	6885.26	6893.35
D_{calc} (g cm^{-3})	1.328	1.371	1.708
Wavelength (Å)	0.71069	0.71069	0.71069
Linear absorption coefficient	6.887	7.476	68.505
Detector to sample distance	22.5	22.5	22.5
Sample to source distance	23.5	23.5	23.5
Average ω scan width at half height	0.25	0.25	0.25
Scan speed (° min^{-1})	6.0	6.0	4.0
Scan width (° + dispersion)	2.0	1.2	0.8
Individual background (s)	6	6	4
Aperture size (mm)	3.0×4.0	3.0×4.0	3.0×4.0
2θ range (°)	6–45	6–45	6–45
Total number of reflections collected	5520	6160	6113
Number of unique intensities	4891	4513	4529
Number with $F > 0.0$	5465	3928	
Number with $F > 3\sigma(F)$	3390	3235	3659
$R(F)$	0.0463	0.0765	0.0332
$Rw(F)$	0.0480	0.0714	0.0353
Goodness-of-fit for the last cycle	0.976	1.223	0.756
Maximum Δ/σ for last cycle	0.01	0.12	0.05



II

Solid-state and molecular structure of [$Mo_2(OBu^t)_6$(4-Mepy)(μ-C_2H_2)]

A summary of the crystal data is given in Table 1. Selected bond distances and bond angles are given in Tables 2 and 3, respectively. An ORTEP drawing of the molecule is shown in Fig. 1, along with the central $Mo_2O_6C_2N$ core giving the atom-numbering scheme used in the tables. If the μ-C_2 moiety is considered to occupy a single coordination site then the geometry may be described as a fusing of two trigonal bipyramids along a common equatorial (μ-C_2) and axial (μ-OR) edge. The Mo—Mo distance of 2.645(1) Å is consistent with a M—M single bond and the C—C distance of 1.39(1) Å is longer than that in ethylene,

Table 2. Selected bond distances (Å) for $Mo_2(OBu^t)_6$(4-Mepy)(μ-C_2H_2)

Mo(1)—Mo(2)	2.645(1)
Mo(1)—O(3)	1.914(5)
Mo(1)—O(4)	1.915(5)
Mo(1)—O(8)	1.980(5)
Mo(1)—N(9)	2.284(6)
Mo(1)—C(10)	2.080(7)
Mo(1)—C(11)	2.091(7)
Mo(2)—O(5)	1.931(5)
Mo(2)—O(6)	1.927(5)
Mo(2)—O(7)	1.968(5)
Mo(2)—O(8)	2.078(5)
Mo(2)—C(10)	2.089(7)
Mo(2)—C(11)	2.108(8)
C(10)—C(11)	1.39(1)

Table 3. Selected bond angles (°) for $Mo_2(OBu^t)_6$(4-Mepy)(μ-C_2H_4)

O(3)—Mo(1)—O(4)	118.56(21)
O(3)—Mo(1)—O(8)	95.56(20)
O(3)—Mo(1)—N(9)	82.14(21)
O(4)—Mo(1)—N(9)	82.78(20)
C(10)—Mo(1)—C(11)	39.0(3)
O(5)—Mo(2)—O(6)	127.69(21)
O(5)—Mo(2)—O(7)	88.29(21)
O(5)—Mo(2)—O(8)	87.10(20)
O(6)—Mo(2)—O(7)	88.99(20)
C(10)—Mo(2)—C(11)	38.7(3)
Mo(1)—O(8)—Mo(2)	81.34(18)
Mo(1)—C(10)—Mo(2)	78.77(25)
Mo(1)—C(11)—Mo(2)	78.10(25)

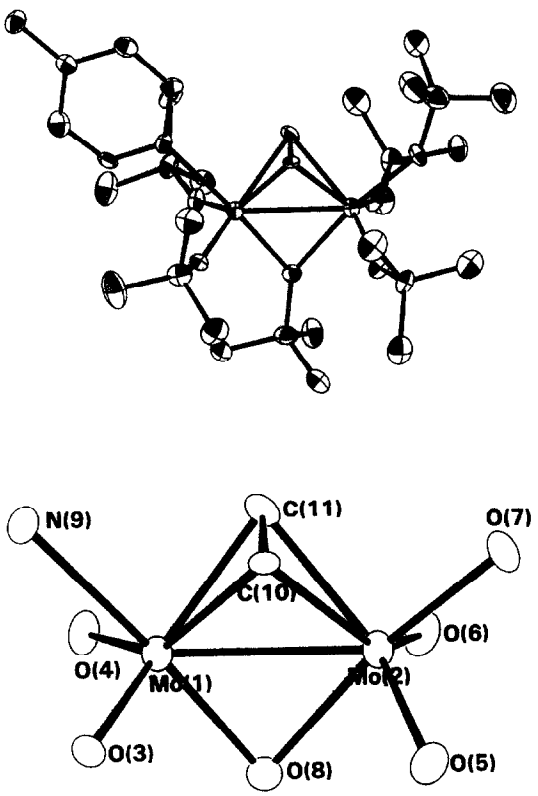


Fig. 1. An ORTEP drawing of the $Mo_2(OBu^t)_6$(4-Mepy)(μ-C_2H_2) molecule and the numbering scheme of its $Mo_2O_6NC_2$ core.

1.34 Å, and acetylene, 1.21 Å, collectively indicating that the central moiety can be viewed as a dimetallatetrahedrane [10]. The metric parameters differ little from those for the tungsten analogue: W—W = 2.665(1), W—C = 2.11(2) (ave) and C—C = 1.441(14) Å [10].

$M_2(OBu^t)_6(\mu\text{-}C_4H_4)(CO)$. A summary of the crystal data is given in Table 1 for the two compounds (M=Mo and W) and a comparison of bond distances and bond angles is given in Tables 4 and 5. An ORTEP drawing of the molybdenum compound is given in Fig. 2, together with a ball-and-stick diagram showing the central $Mo_2(O)_6C_4(CO)$ core.

The two molecules are remarkably similar. In each, one metal atom has a pseudo-octahedral geometry, forming four bonds to oxygen and two to carbon. The M—O(7) distances are asymmetric, with M(1)—O(7) being notably shorter. In a formal sense M(1) could be viewed as M(6+) and M(2) as a d^4 M(2+) centre being bonded datively to μ-OR, two terminal alkoxides, a terminal carbonyl and a butadiene ligand

Table 4. A comparison of selected bond distances (Å) for the central core of $Mo_2(OBu^t)_6(\mu\text{-}C_4H_4)(CO)$, where M = Mo or W

	M = Mo	M = W
M(1)—M(2)	2.8886(17)	2.901(1)
M(1)—O(7)	2.025(8)	2.000(6)
M(1)—O(12)	1.919(8)	1.921(6)
M(1)—O(17)	1.911(8)	1.918(6)
M(1)—O(22)	1.856(8)	1.863(7)
M(1)—C(3)	2.073(12)	2.101(9)
M(1)—C(6)	2.114(12)	2.150(11)
M(2)—O(7)	2.196(8)	2.224(6)
M(2)—O(32)	1.909(8)	1.905(6)
M(2)—O(27)	1.919(8)	1.911(6)
M(2)—C(3)	2.359(12)	2.376(9)
M(2)—C(4)	2.295(13)	2.300(10)
M(2)—C(5)	2.313(13)	2.277(11)
M(2)—C(37)	1.979(14)	1.966(9)
M(2)—C(6)	2.302(12)	2.323(9)
O(38)—C(37)	1.160(15)	1.168(11)
C(3)—C(4)	1.369(18)	1.393(14)
C(4)—C(5)	1.434(20)	1.438(16)
C(5)—C(6)	1.407(17)	1.425(15)

Table 5. A comparison of selected bond angles (°) for $M_2(OBu^t)_6(\mu\text{-}C_4H_4)(CO)$, where M = Mo or W

	M = Mo	M = W
O(7)—M(1)—O(12)	170.3(3)	170.29(25)
O(7)—M(1)—O(17)	85.8(3)	85.20(25)
O(7)—M(1)—O(22)	92.0(3)	89.67(26)
O(12)—M(1)—O(17)	84.6(4)	85.17(27)
O(12)—M(1)—O(22)	92.9(3)	92.59(27)
O(17)—M(1)—O(22)	113.0(3)	110.47(27)
O(7)—M(2)—O(32)	84.7(3)	79.06(24)
O(7)—M(2)—O(27)	78.9(3)	84.12(24)
O(7)—M(2)—C(37)	173.4(4)	173.9(3)
O(32)—M(2)—O(27)	107.1(3)	106.19(26)
O(32)—M(2)—C(37)	92.3(4)	96.2(3)
O(27)—M(2)—C(37)	96.6(4)	93.7(3)
M(1)—O(7)—M(2)	86.27(27)	86.71(22)
M(1)—C(3)—M(2)	81.1(4)	80.6(3)
M(2)—C(37)—O(38)	178.6(12)	179.3(8)
M(1)—C(6)—M(2)	81.6(4)	80.9(3)

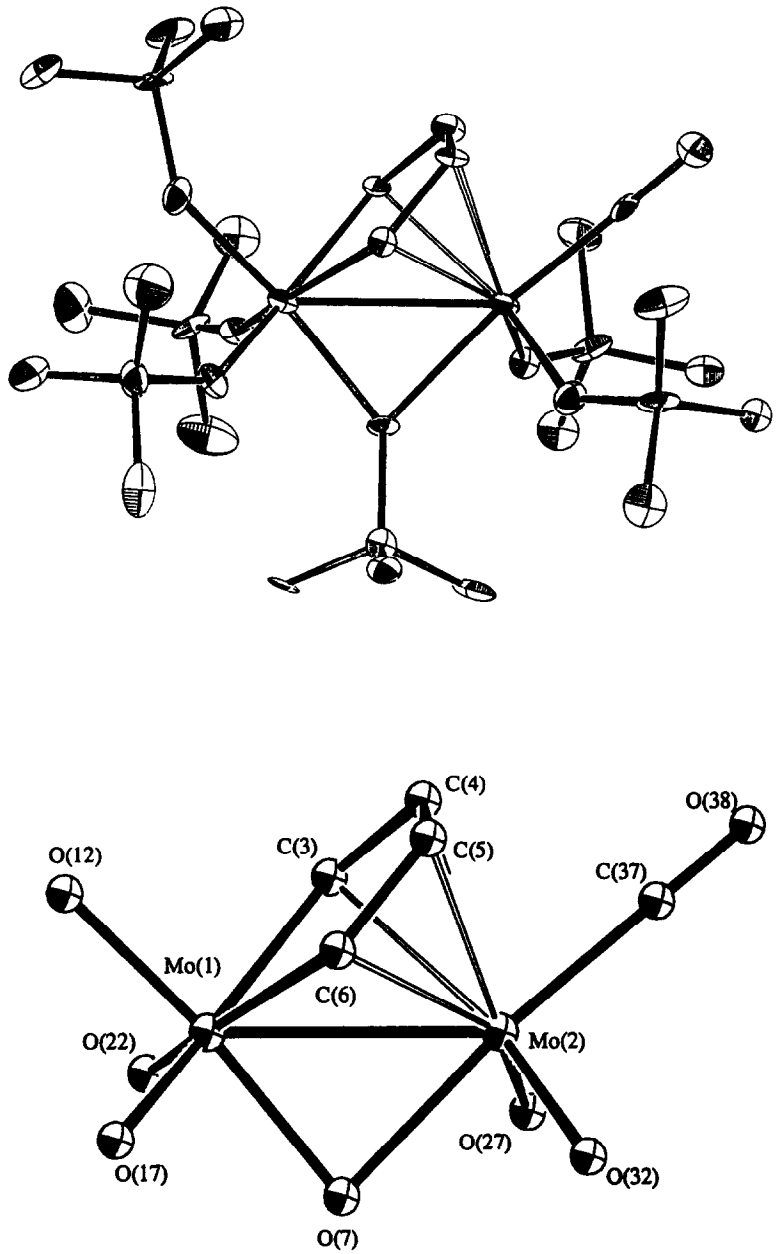


Fig. 2. An ORTEP drawing of the $Mo_2(OBu^t)_6(\mu\text{-}C_4H_4)(CO)$ molecule giving the atom-numbering scheme used for the central skeleton.

[C(3)—C(4)—C(5)—C(6)]. Since M(1) is contained in the C(3)—C(4)—C(5)—C(6) plane, one can also view the bridge as a metallacyclopentadiene. The structure is closely related to that of $Mo_2(OCH_2Bu^t)_6(py)(\mu\text{-}C_4H_4)$ [20], but with a CO ligand in place of pyridine.

Investigation of the role of $Mo_2(OBu^t)_6(\mu\text{-}C_2H_2)$ *and* $Mo_2(OBu^t)_6(\mu\text{-}C_4H_4)$ *in ethyne polymerization*

$Mo_2(OBu^t)_6(\mu\text{-}C_2H_2)$ and $Mo_2(OBu^t)_6(\mu\text{-}C_4H_4)$ are not thermally stable at room temperature. The dimolybdenum ethyne complex liberated ethyne, which was polymerized to PA, and reformed $Mo_2(OBu^t)_6$. At low temperatures, below $-20°C$, polymerization of added ethyne proceeded without the detectable involvement of the complexes. At these low temperatures, when labelled ethyne was added no labels were incorporated into the Mo_2-containing complexes. Previously, we showed that $Mo_2(OPr^i)_6(py)_2(\mu\text{-}C_2H_2)$ and $Mo_2(OCH_2Bu^t)_6(py)(\mu\text{-}C_4H_4)$ were not involved in alkyne polymerization but only in alkyne cyclotrimerization to given benzene [8]. In the present case we find no evidence for the formation of benzene and no evidence for participation in ethyne polymerization.

CONCLUSIONS

Careful synthetic studies have allowed us to prepare and characterize the previously elusive $Mo_2(\mu\text{-}C_2H_2)$- and $Mo_2(\mu\text{-}C_4H_4)$-containing compounds supported by six tert-butoxide ligands. Although ethyne is polymerized by solutions containing $Mo_2(OBu^t)_6$, the aforementioned compounds are not involved in the catalytic cycle. It seems likely that only a small impurity in solutions of $Mo_2(OBu^t)_6$ is responsible for ethyne polymerization and that this process may well involve the metal–carbene polymerization mechanism. The evidence in favour of a metal-mediated carbene mechanism is based on the observation that, whereas hydrocarbon solutions of $Mo_2(OBu^t)_6$ and norbornene do not react, the addition of ethyne produces a catalytically active system for polymerization of norbornene, and the NMR spectra for the polymer are identical to those for polymer produced by a well-defined metal–carbene catalyst precursor [16].

EXPERIMENTAL

All reactions were carried out under dry, oxygen-free N_2 employing standard Schlenk and glove-box techniques. Solvents were dried and freed from oxygen by distillation under N_2 over either sodium benzophenone ketal (hexane, toluene, benzene) or from CaH_2 (CH_2Cl_2). Freshly distilled solvents were stored under nitrogen over 3 Å molecular sieves. Reagent grade methanol was stored over molecular sieves and degassed to remove oxygen. The preparations of $Mo_2(OBu^t)_6$ [20] and $W_2(OBu^t)_6$ [21] have been described previously. Ethyne was purified by passing the gas through a cold trap at −78°C.

^1H, $^{13}C\{^1H\}$, proton-coupled ^{13}C and variable temperature NMR spectra were obtained on a Varian XL300 spectrometer. The ^1H spectra are referenced to protio impurities in commercial benzene-d_6, toluene-d_8 and dichloromethane-d_2. Infrared spectra were recorded as KBr pellets. Elemental analyses were performed by Oneida Research Services, Inc.

Preparation of $Mo_2(OBu^t)_6(py)(\mu\text{-}C_2H_2)$

$Mo_2(OBu^t)_6$ (1.365 g, 2.174 mmol) was taken up in hexane/pyridine (50 cm^3/5 cm^3). The resulting orange solution was then cooled to −196°C by immersion in a liquid nitrogen bath. With the use of a calibrated gas manifold, acetylene was added (2.826 mmol, 2.3 equiv.). The mixture was warmed to −20°C. The solution colour changed from yellow to dark green after stirring for 4 h at −20°C. The resulting green solution was concentrated to approximately one-half its original volume. The concentrated solution, when placed in the freezer overnight, yielded a dark green crystalline solid. The solution was removed *via* cannula and the resulting solid dried *in vacuo* (890 mg, 1.196 mmol) (55% yield). Elemental analyses were not obtained owing to the thermal instability of the compound. ^1H NMR (C_6D_6, 25°C), δ 8.56 (br m, 2H, py), 6.94 (br m, 1H, py), 6.65 (br m, 2H, py), 6.00 (s, 2H, C_2H_2), 1.46 (s, 54H, $OC(CH_3)_3$). ^1H NMR ($C_6D_5CD_3$, −60°C): δ 8.85 (br, py), 8.58 (br, py), 8.28 (br, py), 6.54 (br, py), 6.30 (br, 2H, C_2H_2), 6.18 (br, py), 2.18 (s, 9H, $OC(CH_3)_3$), 1.89 (s, 9H, $OC(CH_3)_3$), 1.71 (s, 18H, $OC(CH_3)_3$), 1.14 (s, 18H, $OC(CH_3)_3$). ^{13}C NMR (C_6D_6, 25°C): δ 127.2 (s, J_{C-H} = 190 Hz, C_2H_2), 82.0 (s, $OC(CH_3)_3$), 32.3 (q, J_{CH} = 130 Hz, $OC(CH_3)_3$).

Synthesis of $Mo_2(OBu^t)_6(\mu\text{-}C_4H_4)(CO)$

$Mo_2(OBu^t)_6(\mu\text{-}C_2H_2)(py)$, synthesized as above (151 mg, 0.205 mmol) was dissolved in hexane (30 cm^3). The resulting brown solution was frozen with the use of liquid nitrogen, and the flask evacuated. By using standard gas line techniques the flask was exposed to acetylene (0.247 mmol, 1.2 equiv.). Warming of this solution to room temperature for 1 h gave no noticeable colour change. The solution was again frozen in liquid nitrogen and the flask evacuated. Carbon monoxide (0.342 mmol, 1.7 equiv.) was added to the system with the use of a calibrated gas syringe. Again, the solution was warmed to room temperature. While warming, the solution changed from an emerald green to an orange-red colour. The colour change took place approximately 15 min after the solution was at, or near, room temperature. A noticeable precipitate (polyacetylene by analysis), also formed. To remove the polyacetylene, the solution was filtered with a medium filter frit giving a clear orange-red solution. Reducing the volume of the solution by one-half afforded red crystals after several days at −20°C. ^1H NMR (C_6D_6, 25°C): δ 7.53 (m, 2H, C_4H_4), 5.85 (m, 2H, C_4H_4), 1.99 (s, 9H, $OC(CH_3)_3$), 1.53 (s, 18H, $OC(CH_3)_3$), 1.44 (s, 9H, $OC(CH_3)_3$), 1.27 (s, 18H, $OC(CH_3)_3$). ^{13}C NMR (C_6D_6, 25°C): δ 243.2 (s, CO), 182.8 (s, C_α-sigma bound), 106.9 (s, C_β-π bound). IR (KBr, cm^{-1}): 2971m, 1908m (CO), 135m, 1171s, 949s.

Preparation of $W_2(OBu^t)_6(\mu\text{-}C_4H_4)(CO)$

This was prepared by the addition of an excess of acetylene to a hydrocarbon solution of $W_2(OBu^t)_6$, followed by the addition of CO. Crystals for the X-ray study were obtained by crystallization from a concentrated solution of hexane after removing PA by filtering through a fine frit.

Single-crystal X-ray studies

The general operating procedures used have been described previously [22].

Preparation and structure of $Mo_2(OBu^t)_6(4\text{-Mepy})(\mu\text{-}C_2H_2)$

The sample was prepared in an analogous manner to that described for $Mo_2(OBu^t)_6(py)(\mu\text{-}C_2H_2)$ but

employing 4-methylpyridine in place of pyridine. The crystals were grown slowly at −20°C from a 4:1 hexane/4-methylpyridine mixture. A brown crystal of dimensions $0.20 \times 0.30 \times 0.30$ mm^3 was mounted in a nitrogen-filled glove-bag by using silicone grease and was transferred to a goniostat. The sample was cooled to −175°C for characterization and data collection.

The structure was solved by the usual combination of direct methods (MULTAN78) and Fourier techniques. The Mo atom positions were obtained from an initial *E*-map and the remainder of the non-hydrogen atoms were found in subsequent iterations of least-squares refinement and difference Fourier calculations. After partial refinement of the non-hydrogen atoms, a difference Fourier revealed many, but not all, hydrogen atoms. All hydrogen atom positions were therefore calculated by using idealized geometries [d(C—H) = 0.95 Å].

Structure of $Mo_2(OBu^t)_6(\mu\text{-}C_4H_4)(CO)$

A suitable sample was transferred to the goniostat and cooled to −170°C for data collection.

The structure was solved by the usual combination of direct methods (MULTAN78) and Fourier techniques. The positions of the Mo atoms were determined from an E-map. The remaining non-hydrogen atoms were obtained from subsequent iterations of least-squares refinement and difference Fourier calculations. In the final cycles of refinement, four atoms with poorly behaved anisotropic thermal parameters were refined isotropically and all other non-hydrogen atoms were refined with anisotropic thermal parameters.

Structure of $W_2(OBu^t)_6(\mu\text{-}C_4H_4)(CO)$

A large, well-formed crystal was cleaved to obtain a nearly equidimensional cube and transferred to the goniostat using standard inert atmosphere handling techniques. The crystal was then cooled to −160°C for characterization and data collection.

Owing to a rather long b axis (*ca* 42 Å!), a short scan width was required. Experimentation revealed that a scan width of 0.8° resolved the peaks with little difficulty; fortunately, the crystal diffracted nearly perfectly, allowing the narrow scan width.

The two tungsten atoms were located by direct methods (MULTAN78) and all other non-hydrogen atoms were present in a difference Fourier phased on the two metal atoms. Hydrogen atoms were clearly visible in a difference Fourier phased on the refined non-hydrogen atoms, and were included in the final cycles of refinement (anisotropic thermal parameters for W, O and C; isotropic for H). A final difference Fourier map was featureless, with the largest peaks (1.2 and 1.1 e Å^3) lying adjacent to the two tungsten atoms. Ψ scans of several reflections were flat, so no absorption correction was deemed necessary.

Representative polymerization reactions

$Mo_2(OBu^t)_6$+HCCH. By using standard gas line techniques a hexane solution (40 cm^3) of $Mo_2(OBu^t)_6$ (50 mg, 0.79 mmol) at room temperature was exposed to 1 atm. of ethyne. The initial pale orange solution darkened and a dark precipitate formed. After 10–15 min the uptake of acetylene ceased (4.02 mmol, 50.3 equiv.). The solution was stirred for an additional hour before filtering through a medium porosity frit. The resulting precipitate was insoluble in all common solvents. The filtrate, analysed by NMR spectroscopy, appeared to contain three products.

Precipitate-polyacetylene: IR (KBr, cm^{-1}): 3030w, 2980s, 1645m, 1401m, 1262m, 1102m, 1013s (*trans*), 803m (*cis*).

Filtrate (when $^{13}C_2H_2$ was used): ^{1}H NMR (C_6H_6, 25°C): δ 6.32 (m), 5.64 (m), 4.21 (br, s), 3.18 (s), 2.67 (br, s), 1.88 (s), 1.73 (s), 1.57 (s), 1.52 (s), 1.47 (s), 1.40 (s), 1.04 (s). $^{13}C\{^1H\}$ NMR (C_6D_6, 25°C): δ 209.8 (m, AA′XX′), 179.3 (m, AA′XX′), 127.2 (s), 124.6 (m, AA′XX′), 115.2 (m, AA′XX′).

$Mo_2(OBu^t)_6$+CH_3CCH. Either hexane or toluene solutions (40 cm^3) of $Mo_2(OBu^t)_6$ (50 mg, 0.080 mmol) were exposed to 1 atm. propyne (CH_3CCH) by using a calibrated gas line. The orange solution darkened and after 10–15 min a dark precipitate formed. Continual exposure (90 minutes total) to approximately 1 atm. propyne resulted in a total propyne uptake of 24.2 mmol, 303 equiv. of hexane and 28.1 mmol, 351.3 equiv. of toluene. The solution was stirred for an additional 1 h before the volatile components were removed *in vacuo* leaving an oily red solid. A Katz and Lee procedure for work-up was followed [1]. The solid was extracted with CH_2Cl_2 (30 cm^3) giving a deep cherry red solution which was passed through a frit before precipitating the red polypropyne with MeOH (30 cm^3). [If worked-up in the presence of air the polymer is yellow.] ^{1}H NMR (CD_2Cl_2, 25°C): δ 6.8 (br s, 1H, CH), 1.8 (br s, 3H, CH_3). ^{13}C NMR (CD_2Cl_2, 25°C): δ 132.0 (br s), 22.6 (br s). IR (KBr, cm^{-1}): 2967s, 1717m, 1684m, 1652m, 1632m, 1443s, 1377s, 1252m, 1159m, 1066s, 1024s (*trans*), 874m (*cis*), 808m.

Synthesis of poly(norbornene). By using standard gas line techniques a toluene solution (15 cm^3) of $Mo_2(OBu^t)_6$ (42 mg, 0.067 mmol) was exposed to C_2H_2 (0.34 mmol, 5.1 equiv.). After 0.5 h this solution was black and polyacetylene had precipitated. A toluene solution (10 cm^3) of norbornene (598 mg, 6.36 mmol, 95 equiv.) was transferred *via* cannula to the black solution. The resulting mixture was stirred at room temperature for 24 h during which time a colour change from black to purple occurred. ^{1}H NMR (C_6D_6, 25°C): δ 5.50 (s), 5.36 (s), 2.91 (br s), 2.50 (br s), 2.04 (br s), 1.83 (br s), 1.47 (br s), 1.23 (br m). ^{13}C-$\{^1H\}$ NMR (C_6D_6, 25°C): δ 134.3 (s), 134.2 (s), 133.7 (2), 133.5 (s), 133.3 (s), 43.9 (s), 43.6 (s), 39.1 (s), 38.8 (s), 33.3 (s), 32.8 (s), 32.6 (s).

$Mo_2(OBu^t)_6$+$^{13}C_2H_2$. A hexane solution (10 cm^3)

of $Mo_2(OBu^t)_6$ (84 mg, 0.133 mmol) was exposed, using standard gas line techniques, to $^{13}C_2H_2$ (0.266 mmol, 2.0 equiv.). Warming the solution to room temperature gave a dark solution. Half of this solution was transferred to another flask where the volatile components were removed. The ^{13}C-$\{^1H\}$ NMR spectrum of the dark oil was obtained and the data are listed below as Sample A. To the other half of the solution was added, by using gas line techniques, ^{13}CO (0.133 mmol, > 1 equiv.). While warming this solution to room temperature a colour change through emerald green to red-black occurred. The volatile components were removed and the resulting oil was characterized by ^{13}C-$\{^1H\}$ spectroscopy; listed as Sample B. ^{13}C-$\{^1H\}$ NMR (C_6D_6, 25°C): Sample A: δ (C_4H_4) 209.8 (m, AA′XX′), 179.5 (m, AA′XX′), 124.7 (m, AA′XX′), 115.2 (m, AA′XX′), 127.2 (s, μ-C_2H_2); Sample B: δ (CO) 243.4 (s), (C_4H_4) 208.9 (m, AA′XX′), 182.7 (m, AA′XX′), 115.2 (m, AA′XX′), 106.9 (m, AA′XX′), 127.1 (s, μ-C_2H_2).

$Mo_2(OBu^t)_6 + {}^{13}C_2H_2$ *followed by addition of* $^{13}C_2H_2$. A hexane solution (10 cm^3) of $Mo_2(OBu^t)_6$ (60 mg, 0.095 mmol) was exposed to $^{13}C_2H_2$ (0.190 mmol, 2.0 equiv.). The solution was stirred at room temperature for 0.5 h. The solution was then exposed to $^{12}C_2H_2$ (uptake 13.6 equiv. based on Mo). The dark solution was filtered with a medium filter frit to remove the polyacteylene that had formed. The ^{13}C-$\{^1H\}$ NMR spectrum of the filtrate shows that the ^{13}C label remains with the ethyne adduct and the metallacyclic species. ^{13}C-$\{^1H\}$ NMR (C_6D_6, 25°): δ 209.8 (m, AA′XX), 179.6 (m, AA′XX′), 127.4 (m, AA′XX′), 115.2 (m, AA′XX′), 127.2 (s).

Acknowledgement—We thank the National Science Foundation for support.

REFERENCES

1. T. J. Katz and S. J. Lee, *J. Am. Chem. Soc.* 1980, **102,** 422.
2. (a) L. G. McCullough and R. R. Schrock, *J. Am. Chem. Soc.* 1984, **106,** 4067; (b) R. Schlund, R. R. Schrock and W. E. Crowe, *J. Am. Chem. Soc.* 1989, **111,** 8004.
3. R. R. Schrock, M. L. Listemann and L. G. Sturgeoff, *J. Am. Chem. Soc.* 1982, **104,** 4291; M. L. Listemann and R. R. Schrock, *Organometallics* 1985, **4,** 74.
4. J. H. Freudenberger, S. F. Pedersen and R. R. Schrock, *Bull. Soc. Chim. Fr.* 1985, 349.
5. R. R. Schrock, *Acc. Chem. Res.* 1986, **19,** 342; J. S. Murdzek and R. R. Schrock, in *Carbyne Complexes.* VCH Publishers, New York (1988).
6. A. Bray, A. Mortreaux, F. Petit, and Szymanska-Buz, *J. Chem. Soc., Chem. Commun.* 1993, 197.
7. H. Strutz and R. R. Schrock, *Organometallics* 1984, **4,** 1600.
8. M. H. Chisholm, K. Folting, J. C. Huffman and I. P. Rothwell, *J. Am. Chem. Soc.* 1982, **104,** 4389.
9. S. A. R. Knox, A. F. Dyke, S. R. Finnimore, R. J. Naish, A. G. Orpen, G. H. Riding and G. E. Taylor, *ACS Symp. Ser.* 1981, **155,** 259.
10. M. H. Chisholm, K. Folting, D. M. Hoffman and J. C. Huffman, *J. Am. Chem. Soc.* 1984, **106,** 6794.
11. M. H. Chisholm, D. M. Hoffman and J. C. Huffman, *J. Am. Chem. Soc.* 1984, **106,** 6806.
12. J. C. W. Chien, *Polyacetylene: Chemistry, Physics and Material Science*, p. 85. Academic Press, New York (1985).
13. R. R. Schrock, R. T. DePue, J. Feldman, C. J. Schavarien, J. C. Devan and A. H. Liu, *J. Am. Chem. Soc.* 1988, **110,** 1423 and ref. [2b].
14. T. Ito, H. Shirakawa and S. Ikeda, *J. Polym. Sci. Polym. Chem. Ed.* 1975, **13,** 1943.
15. J. Kress, J. A. Osborn, R. M. E. Greene, K. J. Ivin and J. J. Rooney, *J. Chem. Soc., Chem. Commun.* 1985, 874; R. R. Schrock, J. Feldman, L. F. Cannizo and R. H. Grubbs, *Macromolecules* 1987, **20,** 1169; K. C. Wallace and R. R. Schrock, *Macromolecules* 1987, **20,** 448.
16. L. R. Gillion and R. H. Grubbs, *J. Am. Chem. Soc.* 1986, **108,** 733.
17. K. Weiss and G. Lössel, *Angew. Chem. Int. Ed. Engl.* 1989, **28,** 63.
18. J. H. Freudenberger and R. R. Schrock, *Organometallics* 1985, **4,** 1937.
19. M. L. H. Green and P. Mountford, *Organometallics* 1990, **9,** 886; M. L. H. Green and P. Mountford, *J. Chem. Soc. Rev.* 1992, 27.
20. M. H. Chisholm, F. A. Cotton, C. A. Murillo and W. W. Reichert, *Inorg. Chem.* 1977, **16,** 1801.
21. M. Akiyama, D. Little, M. H. Chisholm, F. A. Cotton, M. W. Extine, D. A. Haitko and P. E. Fanwick, *Inorg. Chem.* 1979, **18,** 2266.
22. M. H. Chisholm, K. Folting, C. C. Kirkpatrick and J. C. Huffman, *Inorg. Chem.* 1984, **23,** 1021.

Pergamon

PII: S0277-5387(96)00326-9

Polyhedron Vol. 16, No. 5, pp. 849–854, 1997
Copyright © 1996 Elsevier Science Ltd
Printed in Great Britain. All rights reserved
0277–5387/97 $17.00 + 0.00

Kinetics and equilibria of the ternary complex formation of nitrilotriacetatoferrate(III) with 2,2′-bipyridyl in aqueous solutions

Sanjoy Kumar Bhattacharyya and Rupendranath Banerjee*

Department of Chemistry, Jadavpur University, Calcutta-700032, India

(Received 3 April 1996; accepted 1 July 1996)

Abstract—In the pH range 2.7–3.7, $[Fe(nta)(H_2O)_2]$ (**1**) reacted with $Hbipy^+$ and bipy to form the ternary complex, [Fe(nta)(bipy)] (**2**), which was also formed in the reaction between $[Fe(nta)(H_2O)(OH)]^-$ and $Hbipy^+$. The equilibrium constant determined spectrophotometrically agreed well with the kinetically determined value. Rate constants and corresponding activation parameters have been evaluated for different pathways leading to compound **2** and its dissociation. Bond dissociation appears to be important in the transition state. The greater thermodynamic stability of [Fe(nta)(benzohydroxamate)]$^-$ (**3**) than **2** is a consequence of a much greater rate of dissociation of compound **2** than of compound **3**; formation rate constants for compounds **2** and **3** are similar. Copyright © 1996 Elsevier Science Ltd

Keywords: kinetics; equilibrium; ternary complex; nitrilotriacetate; iron(III); 2,2′-bipyridyl.

Ternary complexes of $[Fe(nta)(H_2O)_2]$ (**1**, H_3nta = nitrilotriacetic acid) have a proven role in iron binding to transferrin [1,2] and in strongly enhancing the antimicrobial action of ciprofloxacin [3]. Thus, several ternary complexes with **1** have been prepared and their biological activity described [4]. The binary complex **1** is itself an analogue for the active centre in pyrocatechase [5], but **1** induces tissue damage in rats in the presence of H_2O_2 [6].

The kinetics and equilibria of formation and dissociation of ternary complexes formed with **1** are therefore interesting subjects for investigation. To our knowledge, only one such kinetic study has been reported [7] and no equilibrium study has appeared so far on the complexation of N donor ligands to **1**. This is somewhat surprising because substitution at $Fe^{3+}(aq)$ and $Fe(OH)^{2+}(aq)$ centres has been the subject of much kinetic investigation [8], which has been valuable in the emergence of general mechanistic patterns for substitution at these two aqua ions.

* Author to whom correspondence should be addressed.

EXPERIMENTAL

Materials

All reagents used were of analytical grade and all solutions were in distilled water, redistilled from alkaline permanganate in an all-glass apparatus. The iron(III) nitrate solutions (*ca* 0.02 mol dm^{-3}) were prepared by dissolving $Fe(NO_3)_3 \cdot 9H_2O$ (Merck) in dilute HNO_3 (*ca* 0.05 mol dm^{-3}). Higher concentrations of Fe^{III} were avoided to eliminate dimeric Fe^{III} species. Iron(III) was first precipitated as $Fe_2O_3 \cdot xH_2O$ with dilute NH_3, thoroughly washed and then dissolved with 1 : 1 HCl. For standardization, the Fe^{III} solution thus produced was reduced with tin(II) chloride followed by oxidation with $K_2Cr_2O_7$ as usual [9]. Iron(III) was also quantified by complexometric titration with EDTA solution using variamine B as indicator [9]. The two results agreed within $\pm 1\%$.

Aqueous solutions of **1** were prepared from a mixture of equal volumes (100 dm^3) of equimolar (0.02 mol dm^{-3}) solutions of Fe^{III} and H_3nta; the pH being adjusted to 3.0 with dilute KOH. Under these conditions **1** is formed quantitatively and it is reasonably

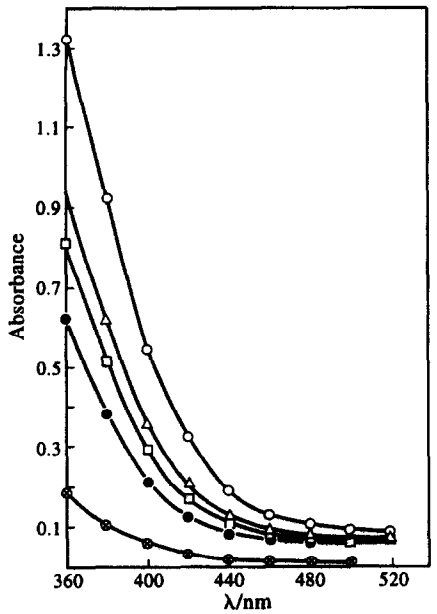


Fig. 1. UV–vis spectra of 1.0 m mol dm^{-3} $[Fe(nta)(H_2O)_2]$ at pH, 2.7 (⊗). Complex+0.01 mol dm^{-3} bipy at pH, 2.33 (●); 2.77 (□); 2.97 (△); 3.64 (○).

stable against thermal and photochemical decompositions [10–13].

Solutions of KNO_3 (BDH) were standardized with a cation exchange resin in H^+-form. Melting points of the supplied ligands 2,2′-bipyridyl (Merck) and H_3nta (Koch-light, England) agreed within ±1°C with the literature values, and were used as received.

Physical measurements and kinetics

Rate measurements were performed on a Hi-Tech SF-5A stopped-flow spectrophotometer coupled to a data acquisition system [7]. The mixing chamber of the instrument was thermostatted. Rate constants were measured under pseudo first-order conditions and the corresponding $\ln(A_e - A)$ *vs* time (t) plots were linear for at least 90% attainment of the equilibrium. The reported rate constants (k_0) were calculated with a standard least-squares program and are mean values from at least five kinetic runs.

UV–vis spectra were recorded on a Carl–Zeiss Jena (VSU-2P) spectrophotometer. This, and the stopped-flow machine, were used to measure the equilibrium optical density, A_e.

The uncertainties of the reported kinetic and equilibrium parameters are the standard deviations obtained from the scattering of the points on the least-squares lines. All pH values were measured on a Systronics (335) instrument having combined electrodes calibrated with standard solutions as described earlier [14].

Perchlorate media were avoided because $[Hbipy]^+[ClO_4^-]$ has very limited solubility in such a media below pH 4.5.

RESULTS AND DISCUSSION

Solutions of **1** give, upon addition of bipy, a sufficient increase in absorption at 400 nm (Fig. 1), the lower limit of wavelengths sensed by our stopped-flow apparatus. At this wavelength absorbances of equilibrated reaction mixtures showed the presence of complex formation equilibrium (1):

$$[Fe(nta)(H_2O)_2] + Hbipy^+ \overset{K_1}{\rightleftharpoons} [Fe(nta)(bipy)] + H^+ \quad (1)$$

(1) **(2)**

At 400 nm only **1** and **2** absorb. Equation (2) can, therefore, be obtained:

$$\frac{C_{Fe}[H^+](K_h + [H^+])^{-1}}{(A_e - A_0)} = \frac{1 + K_H[H^+]}{K_1 K_H C_{bipy} \Delta\varepsilon} + \frac{1}{\Delta\varepsilon} \quad (2)$$

where A is the absorbance, K_H is the protonation constant of bipy, K_h is the first hydrolysis equilibrium constant of **1** [see Eq. (3)], $\Delta\varepsilon$ is the difference in the

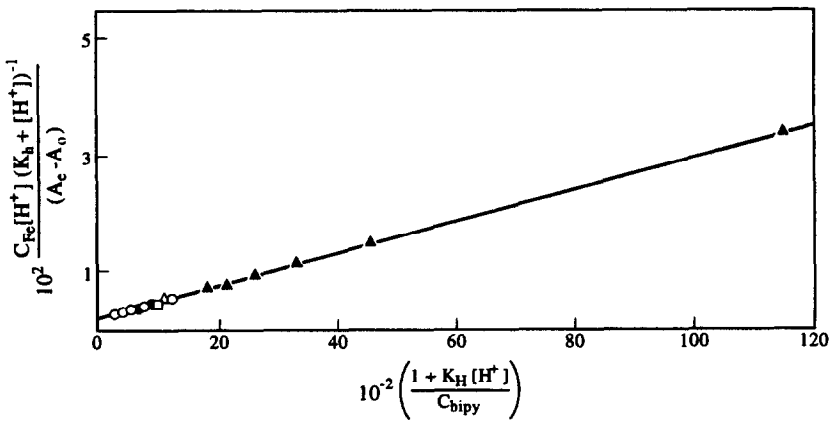


Fig. 2. Evaluation of equilibrium constant for the formation of [Fe(nta)(bipy)] according to Eq. (2), at 25°C, I = 0.1 mol dm^{-3}. Data at pH, 2.7 (□); 2.9 (▲); 3.2 (△); 3.35 (■); 3.5 (●); and 3.75 (○).

$$[Fe(nta)(H_2O)_2] \overset{k_h}{\rightleftharpoons} [Fe(nta)(H_2O)(OH)]^- + H^+ \quad (3)$$

$$Hbipy^+ \overset{K_a}{\rightleftharpoons} bipy + H^+ \quad (4)$$

$$[Fe(nta)(H_2O)_2] + Hbipy^+ \underset{k_{-1}}{\overset{k_1}{\rightleftharpoons}} [Fe(nta)(bipy)] + H^+ \quad (1a)$$

$$[Fe(nta)(H_2O)(OH)]^- + Hbipy^+ \underset{k_{-2}}{\overset{k_2}{\rightleftharpoons}} [Fe(nta)(bipy)] + 2H_2O \quad (5)$$

$$[Fe(nta)(H_2O)_2] + bipy \underset{k_{-3}}{\overset{k_3}{\rightleftharpoons}} [Fe(nta)(bipy)] + 2H_2O \quad (6)$$

$$[Fe(nta)(H_2O)(OH)]^- + bipy \underset{k_{-4}}{\overset{k_4}{\rightleftharpoons}} [Fe(nta)(bipy)] + OH^- \quad (7)$$

Scheme 1.

molar absorptivity between **2** and **1** and C_{Fe} and C_{bipy} are the total metal and total ligand concentrations. The linearity of plots of the left-hand side of Eq. (2) as a function of $(1+K_H[H^+])/C_{bipy}$ (Fig. 2) confirms the validity of the stoichiometry reported in Eq. (1). Therefore, no protonated and/or hydrolysed complexes are formed under the present conditions. This was further verified from an ion-exchange experiment. A mixture of **1** and bipy equilibrated under kinetic conditions was eluted consecutively through a Dowex 50 W × 8 cation exchanger bed in K^+-form and an Amberlite IRA 400 anion exchanger bed in NO_3^--form. The total amount of iron initially charged passed out unabsorbed, indicating the absence of any ionic species of iron at analytically significant concentrations.

The K_1 and ε values for the ternary complex, **2**, obtained from Fig. 2 are 0.025 and 554 mol^{-1} dm^3 cm^{-1} at 25°C and $I = 0.1$ mol dm^{-3} (KNO_3).

Table 1 reports the k_0 data. The nature of the dependence of k_0 on different reaction conditions (see later) suggests the kinetics shown in Scheme 1.

For the present experimental conditions, Eq. (8) can be obtained from Scheme 1.

$$k_0 = k_f C_{bipy} + k_r \quad (8)$$

where

$$k_f = \left(k_1[H^+] + k_2 K_h + k_3 K_a + \frac{k_4 K_h K_a}{[H^+]} \right) (K_a + [H^+])^{-1} \quad (9)$$

and

$$k_r = k_{-1}[H^+] + k_{-2} + k_{-3} + \frac{k_{-4} K_w}{[H^+]}. \quad (10)$$

Plots of k_0 against C_{bipy} at different fixed acidities were linear with significant intercept k_r and slope k_f. Figure 3 shows the excellent linear dependence of k_f $(K_a + [H^+])$ on $[H^+]$. The k_r *vs* $[H^+]$ plot (Fig. 3) is also excellent straight line with significant intercepts. Linearity such as that shown in Fig. 3 suggests that

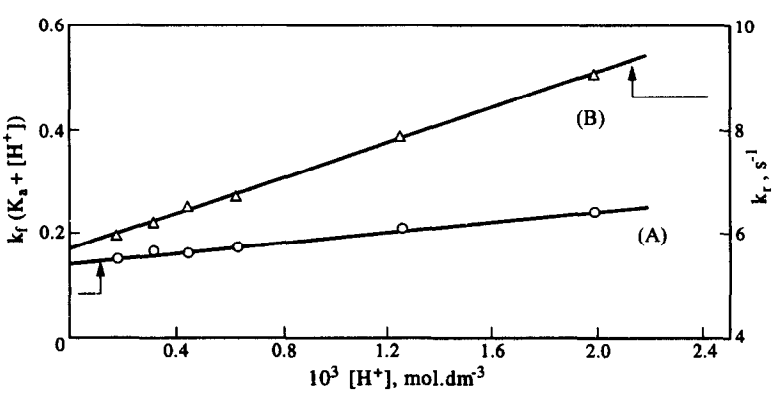


Fig. 3. Evaluation of rate constants. Temperature 25°C; I, 0.1 mol dm^{-3}.

Table 1. Rate data for the complexation of $[Fe(nta)(H_2O)_2]$ (0.5 mmol dm^{-3}) with 2,2′-bipyridyl, $I = 0.1$ mol dm^{-3}

pH	C_{bipy} (mmol dm^{-3})	k_0 (s^{-1})	pH	C_{bipy} (mmol dm^{-3})	k_0 (s^{-1})
		20.0°C			
2.7	5.0	5.50	3.55	5.0	5.55
	8.0	5.75		8.0	6.45
	11.0	6.10		11.0	7.40
	14.0	6.40		14.0	8.45
	17.0	6.65		17.0	9.35
	20.0	7.00		20.0	10.45
		$10^{-2}k_f = 1.0 \pm 0.01^a$			$10^{-2}k_f = 3.26 \pm 0.03^a$
		$k_r = 4.98 \pm 0.02^b$			$k_r = 3.86 \pm 0.04^b$
3.1	5.0	5.10	3.85	5.0	6.35
	8.0	5.40		8.0	8.15
	11.0	5.95		11.0	9.75
	14.0	6.30		14.0	11.3
	17.0	6.80		17.0	13.15
	20.0	7.30		20.0	14.65
		$10^{-2}k_f = 1.48 \pm 0.03^a$			$10^{-2}k_f = 5.53 \pm 0.05^a$
		$k_r = 4.29 \pm 0.05^b$			$k_r = 3.65 \pm 0.06^b$
					25.0°C
3.35	5.0	5.25			
	8.0	5.90	2.7	5.0	9.4
	11.0	6.50		8.0	9.95
	14.0	7.35		11.0	10.2
	17.0	8.00		14.0	10.6
	20.0	8.65		17.0	10.8
				20.0	11.2
		$10^{-2}k_f = 2.30 \pm 0.03^a$			$10^{-2}k_f = 1.13 \pm 0.04^a$
		$k_r = 4.07 \pm 0.04^b$			$k_r = 8.93 \pm 0.06^b$
2.9	5.0	8.65	3.75	5.0	9.50
	8.0	9.00		8.0	11.50
	11.0	9.40		11.0	13.40
	14.0	9.95		14.0	15.60
	17.0	10.35		17.0	17.75
	20.0	10.95		20.0	19.90
		$10^{-2}k_f = 1.53 \pm 0.04^a$			$10^{-2}k_f = 6.95 \pm 0.06^a$
		$k_r = 7.8 \pm 0.06^b$			$k_r = 5.92 \pm 0.08^b$
35.0°C					
3.2	5.0	8.00			
	8.0	8.55	2.85	5.0	22.5
	11.0	9.50		8.0	23.6
	14.0	10.20		11.0	24.7
	17.0	11.00		14.0	25.4
	20.0	11.70		17.0	26.8
				20.0	27.5
		$10^{-2}k_f = 2.52 \pm 0.04^a$			$10^{-2}k_f = 3.31 \pm 0.1^a$
		$k_r = 6.66 \pm 0.06^b$			$k_r = 20.9 \pm 0.13^b$
3.35	5.0	8.20			
	8.0	9.10			
	11.0	10.10	3.1	5.0	21.4
	14.0	11.25		8.0	22.6
	17.0	12.00		11.0	24.3
	20.0	13.15		14.0	26.0
				17.0	27.2
				20.0	29.1
		$10^{-2}k_f = 3.29 \pm 0.05^a$			$10^{-2}k_f = 5.08 \pm 0.06^a$
		$k_r = 6.51 \pm 0.07^b$			$k_r = 18.41 \pm 0.08^b$

Table 1—Continued.

pH	C_{bipy} (mmol dm^{-3})	k_0 (s^{-1})	pH	C_{bipy} (mmol dm^{-3})	k_0 (s^{-1})
3.5	5.0	8.55			
	8.0	9.90	3.3	5.0	21.5
	11.0	11.40		8.0	23.5
	14.0	12.55		11.0	26.0
	17.0	14.30		14.0	28.2
	20.0	15.55		17.0	29.3
				20.0	33.1
		$10^{-2}k_f = 4.70\pm0.06^a$			$10^{-2}k_f = 7.46\pm0.08^a$
		$k_r = 6.17\pm0.09^b$			$k_r = 17.3\pm0.11^b$
3.5	5.0	22.1	3.7	5.0	23.9
	8.0	25.2		8.0	27.9
	11.0	28.5		11.0	32.8
	14.0	31.8		14.0	37.0
	17.0	34.7		17.0	42.2
	20.0	38.1		20.0	46.7
		$10^{-2}k_f = 10.64\pm0.07^a$			$10^{-2}k_f = 15.36\pm0.20^a$
		$k_r = 16.55\pm0.10^b$			$k_r = 16.01\pm0.27^b$

[a] mol^{-1} dm^3 s^{-1}.
[b] s^{-1}.

the active path could be as given in Eqs (1a), (5) and (6) and that path (7) is kinetically insignificant, probably owing to the small value for the quotient $K_aK_h[H^+]^{-1}$ under the experimental conditions used. k_1 and $(k_2K_h+k_3K_a)$ were evaluated from the slopes and intercepts, respectively, of Fig. 3A. Similarly, Fig. 3B gave k_{-1} as its slope and $(k_{-2}+k_{-3})$ as its intercept. These kinetic parameters are collected in Table 2 along with the activation parameters corresponding to k_1 and k_{-1}.

The equilibrium quotient K_1 for equilibrium 1 is equal to $k_1/k_{-1} = 0.027$ at 25°C, $I = 0.1$ mol dm^{-3} (KNO_3). This kinetically evaluated K_1 agrees with our equilibrium measurements ($K_1 = 0.025$) and lends support to the proposed mechanism. Once K_1 is known, the equilibrium constants for reaction (5) ($K_2 = K_1/K_h = 2700$ mol^{-1} dm^3) and for reaction (6) ($K_3 = K_1/K_a = 765$ mol^{-1} dm^3) may also be evaluated.

Das *et al.* [7] have studied the reaction of **1** with benzohydroxamic acid (Hbha) and found

$$[Fe(nta)(H_2O)_2] + Hbha \underset{k'_{-1}}{\overset{k'_1}{\rightleftharpoons}} [Fe(nta)(bha)]^- + H^+ \quad (11)$$

$k'_1 = 18.3$ mol^{-1} dm^3 s^{-1} ($\Delta H^{\neq} = 42.3$ kJ mol^{-1}, $\Delta S^{\neq} = -80$ J K^{-1} mol^{-1}) and $k'_{-1} = 168$ mol^{-1} dm^3 s^{-1} ($\Delta H^{\neq} = 41.3$ kJ mol^{-1}, $\Delta S^{\neq} = -65$ J K^{-1} mol^{-1}) at 25°C. The equilibrium constant K'_1 for reaction (11) is 0.108.

Within the range of experimental error the activation parameters for the k'_1 path [Eq. (11)] are the same as those for the k_1 path (Table 2). The value for k'_1 is also quite close to k_1, inspite of the wide difference in the nature of the entering ligands, *viz.* bha and bipy. This proximity in kinetic parameters for two widely different entering ligands strongly suggests an interchange mechanism, where Fe^{III}—OH_2 bond dissociation is more important than bond formation.

The presence of strong donors in the coordination

Table 2. Kinetic parameters for the formation and dissociation of [Fe(nta)(bipy)]

Temp. (°C)	k_1 (mol^{-1} dm^3 s^{-1})	$10^{-3}k_{-1}$ (mol^{-1} dm^3 s^{-1})	$10^2(k_2k_h+k_3k_a)$ (s^{-1})	$(k_{-2}+k_{-3})$ (s^{-1})
20	38±0.9	1.00±0.04	9.1±0.1	3.55±0.03
25	44±2.1	1.65±0.03	14.3±0.2	5.67±0.03
35	89.7±4.3	4.00±0.03	36.0±0.3	15.25±0.02
$\Delta H^{\neq}$, kJ mol^{-1}	42.8±4.4	67±5		
$\Delta S^{\neq}$, J K^{-1} mol^{-1}	−70±15	40.8±7		

sphere of Fe^{III} induces dissociative activation. A well-known case in point is the observation that the reaction of $Fe(H_2O)_6^{3+}$ mostly follows an I_a pathway, while that of $Fe(H_2O)_5(OH)^{2+}$ prefers I_d. Such effects of donor ligands are also manifested in the replacement of H_2O from $[Fe(edta)(H_2O)]^-$ by S^{IV} [15]; the reaction proceeding through an I_d pathway. Similar situations were also found [16–18] in the formation of different ternary complexes with $[M(nta)(H_2O)_2]^-$ [$M = Ni^{II}$, Co^{II}, Mn^{II}].

Attachment of the strong σ-donor ligand nta to the Fe^{III} centre in **1** definitely weakens the remaining Fe^{III}—OH_2 bonds and thus favours a dissociative mechanism. Such bond weakening is probably reflected in the low $\Delta H^{\neq}$ value for the k_1 and k'_1 paths compared with $\Delta H^{\neq}$ (64 kJ mol^{-1}) for water exchange in Fe^{3+} [8b]. Unfortunately, no information is available on the water exchange rate for **1** and so its comparison with k_1 is not possible. Rate constant and activation parameters for the reverse pathways k_{-1} and k'_{-1} are widely different, indicating their dependence on the nature of the replaceable ligand and thus suggesting that bond dissociation is primarily important in the reverse reactions as well.

Dissociation of bipy from **2** is almost 10 times faster than the dissociation of bha from **3**. This is most likely a manifestation of stronger Fe^{III}—O bonds than Fe^{III}—N bonds [19,20], and the well-known affinity of Fe^{III} for hydroxamic acids. The lower stability of the bipyridyl complex **2** ($K_1 = 0.025$) compared with the bha complex **3** is therefore a consequence of the much higher rate of dissociation for **2**; the formation rate constant for **2** is close to that for **3**.

Acknowledgement—R.B. gratefully acknowledges financial assistance from D.S.T. (New Delhi).

REFERENCES

1. P. K. Bali, W. R. Harris and D. N. Nesset-Tollefson, *Inorg. Chem.* 1991, **30,** 502.
2. J. M. El Hage Chahine and D. Fain, *J. Chem. Soc., Dalton Trans.* 1993, 3137.
3. S. C. Wallis, L. R. Gahan, B. G. Charles and T. W. Hambley, *Polyhedron* 1995, **14,** 2835.
4. L. S. White, P. V. Nilsson, L. H. Pignolet and L. Que, *J. Am. Chem. Soc.* 1984, **106,** 8312.
5. M. G. Weller and U. Weser, *J. Am. Chem. Soc.* 1982, **104,** 3752.
6. Y. Nishida and I. T. Sayo, *Polyhedron* 1995, **14,** 2301.
7. P. K. Das, S. G. Bhattacharya, R. Banerjee and D. Banerjee, *J. Coord. Chem.* 1989, **19,** 311.
8. (a) C. P. Brink and A. L. Crumbliss, *Inorg. Chem.* 1984, **23,** 4708; (b) M. Grant and R. B. Jordan, *Inorg. Chem.* 1981, **20,** 55.
9. *Vogel's Text book of Quantitative Chemical Analysis* (revised by G. H. Jeffery, J. Bassett, J. Mendham and R. C. Denney), 5th edn., p. 326, 725. ELBS with Longman, London (1989).
10. R. L. Gustafson and A. E. Martell, *J. Phys. Chem.* 1963, **67,** 576.
11. G. Schwarzenbach and J. Heller, *Helv. Chim. Acta* 1951, **34,** 1889.
12. V. V. Vekshin, V. I. Kornev, I. P. Doinikova and A. V. Elenskii, *Russ. J. Inorg. Chem.* 1983, **28,** 1448.
13. S. L. Heath, A. K. Powell, H. L. Utting and M. Helliwell, *J. Chem. Soc., Dalton Trans.* 1992, 305.
14. S. Mukhopadhyay and R. Banerjee, *J. Chem. Soc., Dalton Trans.* 1994, 1349.
15. M. D. Rutter and R. van Eldik, *J. Chem. Soc., Dalton Trans.* 1992, 1037.
16. D. W. Margerum and H. M. Rosen, *J. Am. Chem. Soc.* 1967, **89,** 1088.
17. M. A. Cobb and D. N. Hague, *Trans. Farad. Soc.* 1971, **67,** 3069.
18. D. N. Hague and M. S. Zetter, *Trans. Farad. Soc.* 1970, **66,** 1176.
19. F. A. Cotton and G. Wilkinson, *Advanced Inorganic Chemistry*, 5th edn, p. 718. John Wiley & Sons, Chichester (1988).
20. K. H. Weiler, M. Ghisletta, L. Hansherr-Primo, T. Kredolfer, H. W. Schmalle and V. Gramlich, *Inorg. Chem.* 1995, **34,** 1950.

Pergamon

PII: S0277-5387(96)00323-3

Polyhedron Vol. 16, No. 5, pp. 855–862, 1997
Copyright © 1996 Elsevier Science Ltd
Printed in Great Britain. All rights reserved
0277-5387/97 $17.00+0.00

Synthetic and spectroscopic investigations of N(4)-substituted isatin thiosemicarbazones and their copper(II) complexes

Gordon A. Bain,[a] Douglas X. West,[a]* Jacqueline Krejci,[a] Jesús Valdés-Martínez,[b] Simón Hernández-Ortega,[b] and Rubén A. Toscano[b]

[a]Department of Chemistry, Illinois State University, Normal, IL 61790-4160, U.S.A.

[b]Instituto de Química, Universidad Nacional Autónoma de México, Circuito Exterior, Ciudad Universitaria, Coyoacán, México D.F.

(Received 20 April 1996; accepted 28 June 1996)

Abstract—A series of N(4)-substituted thiosemicarbazones of isatin were synthesized and their copper(II) complexes prepared from copper(II) chloride. X-ray crystal structures of two of the thiosemicarbazones, isatin 3-(hexamethylenimylthiosemicarbazone) and isatin 3-(N(4)-ethylthiosemicarbazone), have been solved and are compared with a previously published structure of isatin 3-(N(4)-*p*-tolythiosemicarbazone). The coordination chemistry of the copper(II) complexes of these and other isatin thiosemicarbazones is reported and discussed.
Copyright © 1996 Elsevier Science Ltd

Keywords: isatin; thiosemicarbazone; copper(II).

The 3-thiosemicarbazones of isatin have been of interest since 1-methylisatin-3-thiosemicarbazone (Marboran™) was found to be active in the treatment of smallpox 40 years ago [1–3]. Although substitution at the N(4) position (Fig. 1) of the thiosemicarbazone moiety was found to reduce anti-smallpox activity, substitution of two butyl groups at the N(4) position yields a compound with demonstrated activity against ectromelia (a vaccina virus unaffected by Marboran™) and also against type 2 polio, which is an enterovirus and quite unrelated to the vaccina family [4].

It has been suggested that thiosemicarbazone drugs may act to inhibit viruses by binding to copper ions, which are constituents of the virus [4]. Others have prepared and partially characterized metal complexes of N(4)-2-pyridyl ITSC [5], N(4)-phenyl ITSC [6], N(4)-ethyl ITSC [7] and N(4)-dimethyl ITSC [8]. These previously prepared complexes were of different stoichiometry to those described here, a result of the different preparative conditions.

Here, we present spectroscopic data on the ITSCs substituted at the N(4) position with one and two methyl, ethyl or propyl groups and with cyclic hydrocarbon groups which result in piperidine or hexamethylenimine rings, and their complexes prepared from copper chloride. We also include crystal structures of the isatin 3-(hexamethyleniminylthiosemicarbazone) (H_2Ishexim) and isatin 3-(N(4)-ethylthiosemicarbazone) (H_2Is4E).

EXPERIMENTAL

The thiosemicarbazones were prepared by reaction of equimolar amounts of the appropriate N(4)-substituted thiosemicarbazide, either purchased from Aldrich [N(4)-methyl- and N(4)-ethylthiosemicarbazide] or synthesized following the procedure developed by Holmberg and Psilanderhielm [9] and modified by Scovill [10], with isatin (Aldrich, 98%) at room temperature in absolute ethanol with a catalytic amount of conc. H_2SO_4. The products precipitated as yellow powders in 15 min to an hour, and were collected by suction filtration and washed with cold absolute ethanol.

Complexes were prepared by dissolving equimolar amounts of anhydrous copper(II) chloride and the

* Author to whom correspondence should be addressed.

desired ITSC in warm absolute ethanol. The resulting mixture was then refluxed for 1 h. Solids were collected by suction filtration and rinsed with EtOH and Et_2O to apparent dryness.

The NMR spectra were recorded in DMSO-d_6 with a Varian Gemini 2000 300 MHz spectrometer. Infrared and electronic spectra were recorded with Perkin–Elmer 783 and 330 spectrophotometers, respectively, and EPR spectra were recorded in the solid state and in DMSO solution in an insert Dewar with a Varian E104 spectrometer. The EPR spectra were calibrated with DPPH.

The X-ray crystal structures of H_2Ishexim and H_2Is4E were solved at room temperature using a Siemens P4 diffractometer. Yellow crystals of both compounds were grown by slow evaporation at 35°C of a DMSO/EtOH solution, and a pure DMSO solution, respectively. Complete crystallographic experimental parameters are given in Table 1. Lattice parameters were obtained from 25 reflections with $7.25 \leqslant 2\theta \leqslant 25.98°$ (H_2Ishexim) and $8.61 \leqslant 2\theta \leqslant 28.98°$ (H_2Is4E). Crystal stability was monitored using three standard reflections every 97 reflections, for both crystals. Intensity data corrections were made for background, Lorentz and polarization effects. The structures were solved by direct methods, and refined by full-matrix least-squares techniques using the Siemens SHELEXTL-Plus (PC version) [11] program. The absolute conformation of H_2Is4E was established by the method of Rogers ($\eta = 1.0(1)$) [12]. Anisotropic temperature factors were used for all non-H atoms. Hydrogen atoms attached to carbon were included using a riding model, except for the atoms N(1)—H and N(3)—H, which were located on a difference Fourier map at an advanced stage of refinement and then had their coordinates further refined. All H atoms were constrained and assigned fixed isotropic temperature factors; $U = 0.06$ Å^2, $\Sigma\omega(F_o - F_c)^2$ minimized, $\omega = [\sigma^2(F_o) + g(F_o)^2]^{-1}$, with final $g = 0.0005$ (where g is a "fudge factor" refined each cycle to prevent unrealistic weight). Residual electron density was between -0.34 and $+0.55$ eÅ^{-3} (H_2Ishexim) and -0.35 and $+0.29$ eÅ^{-3} (H_2Is4E). Scattering factors were taken from ref. [13].

Table 1. Crystallographic data for isatin 3-(hexamethyleniminylthiosemicarbazone), H_2Ishexim and isatin 3-(N(4)-ethylthiosemicarbazone), H_2Is4E

Symbol	H_2Ishexim	H_2Is4E
Empirical formula	$C_{15}H_{18}N_4OS$	$C_{11}H_{22}N_4OS$
Formula weight	298.4	248.3
Crystal colour; habit	Yellow; laminar	Light yellow, prism
Crystal dimensions (mm)	$0.40 \times 0.30 \times 0.04$	$0.38 \times 0.16 \times 0.16$
Crystal system	Orthorhombic	Orthorhombic
Space group	$Pna2_1$ No. 33	$P2_12_12_1$ No. 19
a (Å)	11.871(2)	4.6400(10)
b (Å)	24.443(5)	11.620(2)
c (Å)	5.266(1)	22.049(4)
V (Å^3)	1527.8(8)	1188.7(6)
Z	4	4
F(000)	624	520
Radiation (λ, Å)	Cu-K_α (1.54178)	Cu-K_α (1.54178)
Temperature (K)	293	293
Absorption coefficient (mm^{-1})	1.917	2.343
ρ_{calc} (g cm^{-3})	1.297	1.387
2θ range (°)	3.0–110.0	3.0–105.0
Scan type	θ–2θ	ω
Scan speed (° min^{-1})	Variable; 4.00–29.30	Variable; 3.00–29.30
Scan range (°)	$2.00 + \Delta[k_{\alpha1}k_{\alpha2}]$	1.00 (plus k_α separation)
Index ranges	$-12 \leqslant h \leqslant 12$	$-4 \leqslant h \leqslant 4$
	$-25 \leqslant k \leqslant 25$	$-11 \leqslant k \leqslant 11$
	$-5 \leqslant l \leqslant 5$	$-22 \leqslant l \leqslant 22$
Reflections collected	2364	1672
Independent reflections	1925 ($R_{int} = 3.10\%$)	1672 ($R_{int} = 3.39\%$)
Observed reflections	1853 [$F > 3.0\sigma(F)$]	1549 [$F > 4.0\sigma(F)$]
Absorption correction	Face-indexed numerical	Face-indexed numerical
Min./max. transmission	0.8770/0.9327	0.4967/0.8242
No. of parameters refined	214	165
Data/parameter ratio	8.7	9.4
$R = \Sigma(\|F_o\| - \|F_c\|)/\Sigma\|F_o\|$	5.77	4.83
$R_w = [\Sigma(\|F_o\| - \|F_c\|)^2/\omega\|F_o\|^2]^{1/2}$	8.20	8.04
Goodness-of-fit	1.36	1.43

RESULTS AND DISCUSSION

Perspective views of H_2Ishexim and H_2Is4E are presented in Fig. 1. Table 1 shows a summary of crystal data and X-ray analysis information for both compounds, and relevant bond distances and angles are listed in Table 2. A complete listing of bond distances and angles is included in the supplementary material. Despite repeated and varied efforts we have been unable to obtain a diffraction-quality single crystal of a copper(II) complex of any of the isatin thiosemicarbazones discussed.

Carbon atoms C(13) and C(14) of H_2Ishexim were found to be disordered with occupancy factors of 0.5586 and 0.4414 for C(13) and C(13a); 0.5698 and 0.4302 for C(14) and C(14a), respectively.

The six- and five-membered rings of the isatin moiety are very nearly planar. The dihedral angles between the mean planes of both rings are only 2.1 and 0.5° in H_2Ishexim and H_2Is4E, respectively, but the angle between the best least-squares plane describing the entire isatin moiety and that for the thiosemicarbazone (TSC) moiety [N(2)—N(3)—C(10)—S(1)—N(4)] is 18.1°(H_2Ishexim) and 10.77°(H_2Is4E), a significant deviation from planarity.

In H_2Ishexim, this deviation might be expected to be owing to a solid-state effect, but examination of the packing diagram revealed no significant intermolecular interaction. It therefore appears to be intrinsic and may be caused by overlap of lone pairs of electrons on S and N(2) that would occur if these moieties were coplanar. The hexamethylenimine ring (hexim) lies partly within the thiosemicarbazone plane, atoms N(4) and C(11) being in the plane; the remainder of the carbon atoms in the ring are angled out of the plane, similar to other TSCs with this functional group [14]. Interestingly, the oxygen atom lies above the plane of the isatin moiety of H_2Ishexim by 0.018(4) Å. This deviation is a consequence of being involved in hydrogen bonding with the N(3)—H atom which is attached to the TSC moiety and therefore lies above the plane of the isatin function.

In contrast, the packing diagram for H_2Is4E shows a possible interaction between sulfur and the N(4)—H

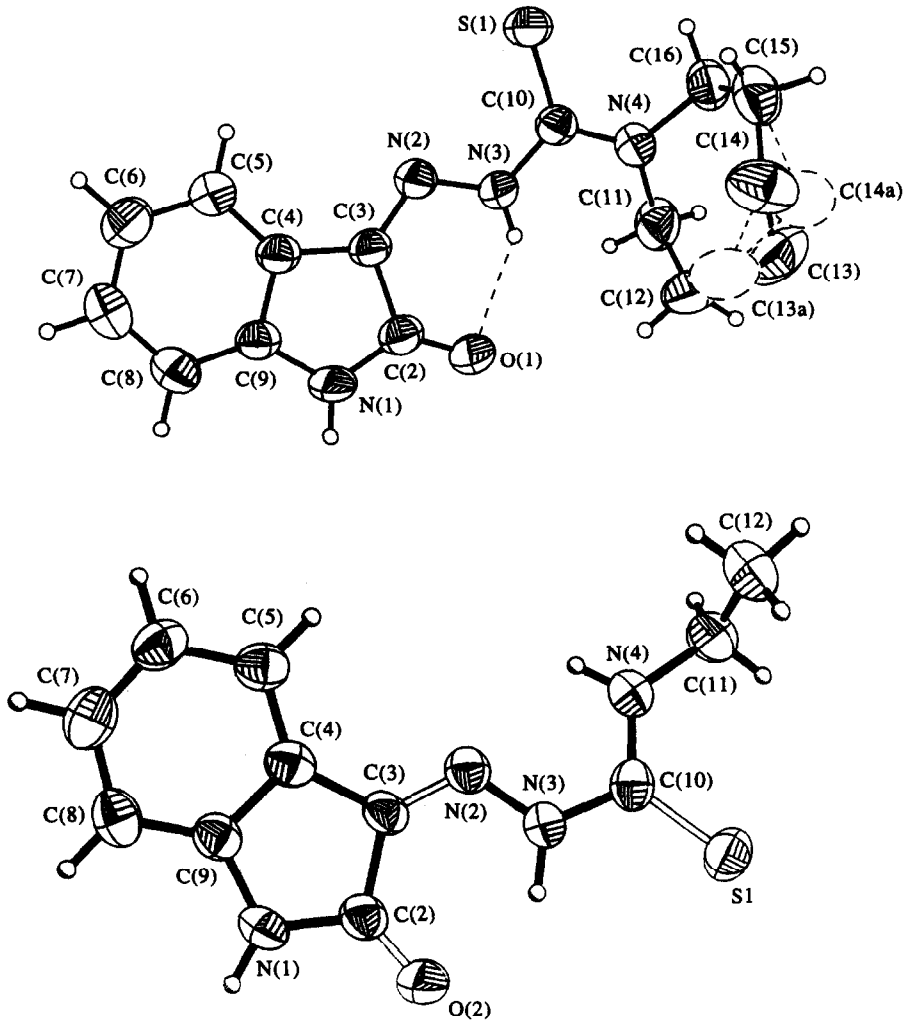


Fig. 1. Ortep diagrams of H_2Ishexim and H_2Is4E from X-ray data.

of a neighbouring molecule. This distance is 2.81(6) Å, which is comparable to the 2.77 Å distance observed in the related (to the point of crystallizing in the same space group) thiosemicarbazone HFo4M [14]. This indicates considerable interaction between the molecules and may therefore account for the deviation of the sulfur from the mean plane of the molecule.

In both structures, the thiosemicarbazone moiety is *Z* about the C(3)=N(2) double bond as a consequence of hydrogen bonding between N(3)—H and O(2). H_2Ishexim is also *Z* about the N(3)—C(10) bond. This latter *Z* conformation is thought to be owing to the lesser overlap of the lone pair of electrons on N(2) with an eclipsing sulfur atom than would be the case with an eclipsing hexim ring. The configuration about the N(3)—C(10) bond in H_2Is4E is *E*, the same as that found in the previously published isatin 3-(N(4)-paratoluylthiosemicarbazone) (H_2Is4pT) [15]. This conformation is brought about by a five-membered ring formed by H-bonding between N(4)—H and N(2). Although five-membered H-bonding rings are generally less favourable than the six-membered rings, the presence of such a hydrogen bond is supported by the inversion of configuration relative to H_2Ishexim, which lacks an N(4)—H atom. The reported structure of H_2Is4pT did not include refined coordinates for N(4)—H which might have helped substantiate the presence of hydrogen bonding. A comparison of bond distances and angles (Table 2) across the TSC and isatin moieties shows the only significant difference between the three molecules to lie in the extent to which the sulfur atom is deflected away from N(2). In H_2Ishexim, the *Z* configuration about the N(3)—C(10) bond places the sulfur in a position where its lone pairs overlap the lone pair on N(2). This results in a greater N(3)—C(10)—S(1) angle than is seen in H_2Is4E and H_2Is4pT, where the *E* configuration about this bond prevents interaction between sulfur and N(2).

Table 2. Comparison of relevant bond distances and angles in H_2Ishexim, H_2Is4E and H_2Is4pT

	H_2Ishexim	H_2Is4E	H_2Is4pT
N(1)—C(2)	1.340(6)	1.347(6)	1.350(5)
C(2)—O(2)	1.236(7)	1.236(6)	1.232(5)
C(2)—C(3)	1.502(6)	1.488(6)	1.504(5)
C(3)—C(4)	1.447(6)	1.456(6)	1.451(5)
C(3)—N(2)	1.305(5)	1.285(5)	1.288(4)
N(2)—N(3)	1.362(6)	1.348(5)	1.346(4)
N(3)—C(10)	1.375(5)	1.383(5)	1.383(4)
C(10)—S(1)	1.672(4)	1.676(5)	1.662(4)
C(10)—N(4)	1.339(6)	1.321(6)	1.333(5)
N(3)—H(3′)	0.90(3)	0.98(5)	
H(3′)···O(2)	1.97(4)	1.99(5)	2.05
N(4)—H(4′)		0.86(6)	
N(2)···H(4′)		2.21(6)	2.12
C(9)—N(1)—C(2)	111.8(4)	111.4(3)	111.4(3)
N(1)—C(2)—O(2)	127.7(4)	126.6(4)	127.0(3)
O(2)—C(2)—C(3)	126.3(4)	126.7(4)	126.8(3)
N(1)—C(2)—C(3)	106.0(4)	106.7(4)	106.1(3)
C(2)—C(3)—N(2)	127.2(4)	128.3(4)	127.6(3)
C(3)—N(2)—N(3)	115.4(4)	117.2(4)	117.7(3)
N(2)—N(3)–C(10)	119.8(4)	119.8(3)	120.4(3)
N(3)—C(10)—S(1)	121.5(4)	118.1(3)	116.8(3)
S(1)—C(10)—N(4)	123.9(3)	126.7(3)	130.2(3)
N(3)—C(10)—N(4)	114.6(4)	115.3(4)	112.8(3)
C(10)—N(4)—C(11)	124.2(4)	127.4(4)	
C(10)—N(4)—C(16)	120.6(4)		
N(3)—H(3′)—O(2)	139(3)	134(3)	137
N(2)—H(4′)—N(4)		109(4)	113

H_2Ishexim, H_2Is4E and the other ITSCs of this study were identified by their ^{1}H and ^{13}C NMR spectra (Table 3). In the ^{1}H spectra, we assign the signal at δ 11.0–11.2 to N(1)—H based on the position of this peak in the spectrum of the parent isatin molecule. This assignment differs from earlier work [7] on the N(4)-ethyl compound in which this peak was ascribed to the N(3)-H; however, our assignment of the peak at δ 12.5–13.5 as the N(3)-H is supported both by its location at lower field (indicative of an intramolecularly hydrogen-bonded proton) and by the greater dependency of its position on the nature of the N(4) substituent. Further support for our assignment of the δ 13.12 peak as intramolecularly hydrogen bonded N(3)-H is found in a comparison of spectra of H_2Ispip recorded in DMSO-d_6 and $CDCl_3$.

A 0.8–1.0 ppm difference in the chemical shift of the N(3)-H (hydrogen bonded to the isatin oxygen) was observed with the N(4) dialkyl- and cycloalkyl-substituted compounds having the lower field chemical shift. It is likely that this difference in chemical shift lies in the configuration about the N(3)—C(10) bond. In the presence of bulky dialkyl or azacyclo functions at N(4), overlap of these groups and the lone pair at N(2) would be minimized by adoption of a *Z* configuration about the N(3)—C(10) bond (lone pair and S on the same side). For the N(4)-monoalkyl TSC this interaction would be minimized, and the formation of N(4)—H···N(2) intramolecular hydrogen bonds facilitated, by adoption of an *E* configuration.

No previous reports of ^{13}C spectra for these TSCs exist; however, a report of both ^{1}H and ^{13}C spectra of isatin [16] gives the amide C(2) at δ 159.4 and the ketonic C(3) at δ 184.4, respectively. Upon formation of the TSC, the ketonic (now azomethine) carbon signal is at significantly higher field (i.e. δ 131.5–134.8), the exact position being dependent on the nature of the N(4) substituent. A difference in the spectra of mono- and di-/cycloalkyl TSCs is also seen in the chemical shift of C(3) where the former appears 2–3 ppm further upfield (*ca* 134.5) than the latter (*ca* 131.5). The amide carbon {C(2)} resonance changes only slightly, moving upfield by *ca* 3 ppm.

Partial elemental analyses of the copper(II) complexes showed all to be of acceptable purity (Table 4). Magnetic moments for all complexes were close to the spin-only value of μ_{eff} = 1.7 B.M.

Table 3. ^{1}H and ^{13}C NMR data for isatin thiosemicarbazones

Compound	N(1)-*H*	N(3)-*H*	N(4)-*H*	*C*(2)	*C*(3)	*C*(9)	*C*(10)
Isatin	11.01			159.42	184.45	150.77	
H_2IsDH	11.17	12.46	9.01, 8.63	162.68	132.15	142.38	178.73
H_2Is4M	11.193	12.595	9.24	162.61	131.55	142.21	177.67
H_2IsDM	11.275 85%	13.411 85%		162.86	134.74	141.68	182.12
2nd Isomer	10.936 15%	13.115 15%		162.66			178.99
H_2Is4E	11.183[a]	12.547[b]	9.258[c]	162.62	131.62	142.23	176.70
H_2IsDE	11.215 85%	13.432 85%		162.73	134.34	141.64	177.80
2nd isomer	10.94 15%	13.12 15%					
H_2Is4P	11.19	12.56	9.26	162.85	131.80	142.43	177.29
H_2IsDP	11.24	13.56		162.91	134.83	141.65	177.99
H_2Ispip[d]	11.269	13.121		162.69	133.57	141.80	178.64
H_2Ishexim	11.258	13.504		162.85	134.81	141.70	178.47

[a] N(1)-H appears to hydrogen bond to the DMSO as suggested by the shifts for H_2Ispip in *d*.

[b] This assignment is based on the discussion in *d* and is contrary to the assignment in ref. [8].

[c] Based on the spectrum of H_2IsDH and the assignment in ref. [8], the N(4)-H hydrogen of H_2Is4E is intramolecularly hydrogen bonded to N(2), in agreement with the solid-state result. Similar behaviour is suggested for H_2Is4M and H_2Is4P.

[d] When H_2Ispip was recorded in $CDCl_3$, the signal at δ 11.269 was found at δ 8.154, but the signal at δ 13.12 did not change. This suggests that the δ 13 signal is N(3)-H and is intramolecularly hydrogen bonded, whereas the signal at δ 11.2 (DMSO) and δ 8.15 ppm is N(1)-H and hydrogen bonds in DMSO solution.

The vibrational spectra of the isatin TSCs (Table 5) show little difference between the members of the series. Upon formation of the copper(II) complexes, the anticipated changes in frequency of those vibrations involved in donation to the metal, and the difference between the neutral and monoanionic ligands, are plainly visible. The frequency of the ν(C=O) vibration shifts to lower energy by *ca* 30 cm^{-1} upon complexation as the anionic ligand. This is in keeping with a transfer of charge from the oxygen to the copper(II) centre and the corresponding decrease of the bond order in the carbonyl bond. In contrast, the frequency of ν(C=O) for the complexes of the neutral ligand, $[Cu(H_2Is4E)Cl_2]$ and $[Cu(H_2Is4P)Cl_2]$, remains relatively unchanged, suggesting little or no charge donation from oxygen to copper in these complexes. This observation is mirrored in the ν(C—S) vibration (i.e. thioamide IV), which also decreases in frequency by *ca* 70 cm^{-1} upon formation of the anionic ligand and is reduced only slightly in the neutral ligand. The apparent non-coordination of oxygen in the neutral complexes suggests that the TSC moiety coordinates in a bidentate fashion through N and S. There is no significant difference in the vibrational frequencies of the copper–ligand bonds throughout the series. In keeping with the stoichiometry of the compounds, two peaks (presumably symmetric and antisymmetric stretches) are found for ν(Cu—Cl) in $[Cu(H_2Is4E)Cl_2]$ and $[Cu(H_2Is4P)Cl_2]$. For the remainder of the complexes, the changes in frequency of the carbonyl, imine and thiocarbonyl bonds and the appearance of bands assignable to ν(Cu—O), ν(Cu—N), ν(Cu—S) and ν(Cu–Cl) in the spectra of the complexes strongly support the proposed structure of an anionic, tridentate chelating thiosemicarbazone with one chloride ligand completing the coordination sphere around copper.

Solid-state UV–vis spectra of the ligands and com-

Table 4. Colours, partial elemental analyses and magnetic susceptibilities of the copper(II) complexes of isatin N(4)-substituted thiosemicarbazones

Compound	Colour	Found(Calc.) (%) C	H	N	μ(B.M.)
[Cu(HIs4M)Cl]	Dark brown	36.5(36.2)	2.9(2.7)	16.1(16.9)	1.7
$[Cu(H_2Is4E)_2Cl_2]$	Tan	35.3(34.5)	3.2(3.2)	14.2(14.6)	1.7
$[Cu(H_2Is4P)_2Cl_2]$	Brown	37.2(36.3)	3.4(3.6)	14.8(14.1)	1.7
[Cu(HIs4DM)Cl]	Green	38.4(38.2)	2.9(3.2)	16.2(16.2)	1.6
[Cu(HIs4DE)Cl]	Dark grey	42.1(41.7)	4.0(4.0)		1.7
[Cu(HIs4DP)Cl]	Black	45.0(44.8)	4.6(4.8)	13.5(13.9)	1.8
[Cu(HIspip)Cl]	Brown	43.9(43.5)	3.9(3.9)	13.8(14.5)	1.7
[Cu(HIshexim)Cl]	Brown	45.2(45.0)	4.1(4.3)	13.5(14.0)	1.9

Table 5. Infrared spectroscopic assignments for isatin thiosemicarbazones and their copper(II) complexes

Compounds	ν(N{1}H)	ν(C=O)	ν(C=N)	ν(CS)	ν(CuN)	ν(CuO)	ν(CuS)	ν(CuCl)
H_2Is4M	3232m	1683s	1591w	810w				
H_2IsDM	3180m	1684s	1588w	802m				
H_2Is4E	3257m	1677s	1590m	817m				
H_2IsDE	3180m	1682s	1588w	802m				
H_2Is4P	3150w	1679s	1588w	815w				
H_2IsDP	3218m	1693s	1596s	802m				
H_2Ispip	3200s	1688s	1584m	799m				
H_2Ishexim	3185m	1678s	1588w	800m				
[Cu(HIs4M)Cl]	[a]	1669vs	1557w	795m	450m	418m	382m	315m
[Cu(HIsDM)Cl]	3150	1655s	1580w	780w	450w	430m	381m	310m
								337m
[Cu(H_2Is4E)Cl_2]	3180m	1695s	1584m	808w	448w		372w	317m
[Cu(HIsDE)Cl]	3200w	1650s	1578w	811m	450w	425w	383w	326w
								323m
								315m
[Cu(H_2Is4P)Cl_2]	3160w	1682s	1571s	808w	450w		372w	299m
[Cu(HIsDP)Cl]	3279m[b]	1651s	1592m	811m	473w	417vw	372w	326m
[Cu(HIspip)Cl]	3285[b]	1647s	1593s	798m	441w	418w	370sh	313m
[Cu(HIshexim)Cl]	3262m[b]	1639s	1583s	808m	405vw	412w	379w	328m

[a] Obscured by N(4)-H.

[b] The spectra for [Cu(HIsDP)Cl], [Cu(HIspip)Cl], and [Cu(HIshexim)Cl] have a peak at *ca* 3275 cm^{-1} which seems unlikely to be ν{N(1)H}. This peak might be more reasonably assigned as ν{N(3)H} suggesting that the bulkier TSCs lose N(1)H, whereas the lighter TSCs lose N(3)H upon complexation with the copper. However, C=O and C=S IR bands and other spectral data do not show significant differences between complexes with bulky and less bulky substituents at N(4) to support this suggestion.

plexes (Table 6) show a strong π–π^* band in the ligand at *ca* 36,000 cm^{-1} (not shown in Table 6) which is obscured in the spectra of the complexes. The TSC moiety n—π^* band at 27,500–29,500 cm^{-1} is generally lower in energy in the anionic ligand complexes than in the uncomplexed TSCs, whereas the energy of the band increases slightly in the coordinated neutral ligand. This is consistent with the loss of N(3)H and the resultant formation of the conjugated TSC moiety for the anionic ligand. The low energy of the *d–d* transition in the neutral complexes suggests either coordination of an additional molecule in an axial position or tetrahedral distortion of the coordination sphere. This band in the complex [Cu(HIs4M)Cl] is found at higher than expected energy (15,150 cm^{-1}). The remaining complexes in the series have *d–d* bands around 14,000 cm^{-1}, suggesting a more distorted environment around copper owing to their bulkier N(4) substituents.

Table 6. Solid-state UV–visible spectroscopic data for isatin thiosemicarbazones and their copper(II) complexes

Compound	$n \rightarrow \pi^*$ and charge transfer	$d \rightarrow d$
H_2Is4M	27,930 24,750	
H_2IsDM	27,780 25,250 22,730	
H_2Is4E	28,410 25,450	
H_2IsDE	28,570 25,640 21,880	
H_2Is4P	29,010 25,910 23,530	
H_2Is4DP	29,410 27,170 24,390	
H_2Ispip	30,580 28,760 22,570	
H_2Ishexim	29,590 27,930 23,810	
[Cu(HIs4M)Cl]	27,030 24,690	15,150
[Cu(HIsDM)Cl]	28,330 26,530 20,830	18,120 14,710
[Cu(H_nIs4E)Cl_n]	29,410 26,600 22,220	12,630
[Cu(HIsDE)Cl]	28,570 24,150 20,410	18,180 14,270
[Cu(H_2Is4P)Cl_2]	30,300 26,880 22,220	13,160
[Cu(HIsDP)Cl]	28,570 23,090 21,980	17,540 14,290
[Cu(HIspip)Cl]	28,410 23,260 20,830	19,690 14,310
[Cu(HIshexim)Cl]	27,030 24,270 21,410	18,380 14,710

The solid-state EPR spectra (Table 7) also provide information about the coordination environment around copper(II) in these complexes. A previous EPR study [17] involving the 4-methylpiperidine N(1) Mannich base of isatin thiosemicarbazone (no substitution at the N(4) position) coordinated to copper(II) showed an isotropic powder spectrum. In contrast, only one of the present compounds has an isotropic spectrum [Cu(HIsDE)Cl], while all others gave approximately axial spectra. The spectrum for [Cu(HIsDE)Cl] is two orders of magnitude weaker than the spectra for the other complexes in this study, suggesting considerable internuclear interaction (i.e. binuclear or polynuclear).

EPR data for the neutral ligand complexes have higher values for both $g_\parallel$ and $g_\perp$ resulting in higher

Table 7. Solid-state EPR data for copper(II) complexes of isatin TSCs

Complex		Temp.	$g_{\parallel}$ or g_1	g_2	g_3 or $g_{\perp}$	g_{av} or g_{iso}
[Cu(HIs4M)Cl]	Solid	RT	2.149	2.081	2.047	2.092
		77 K	2.154	2.082	2.044	2.093
[Cu(HIsDM)Cl]	Solid	RT	2.199	2.057	2.035	2.097
		77 K	2.198	2.055	2.035	2.096
[Cu(H_2Is4E)Cl_2]	Solid	RT	2.243		2.058	2.119
		77 K	2.242		2.056	2.111
[Cu(HIsDE)Cl]	Solid	RT				2.080
		77 K				2.083
[Cu(H_2Is4P)Cl_2]	Solid	RT	2.232		2.058	2.116
		77 K	2.232	2.066	2.053	2.117
[Cu(HIsDP)Cl]	Solid	RT	2.192	2.056	2.032	2.093
		77 K	2.196		2.040	2.092
[Cu(HIspip)Cl]	Solid	RT	2.169		2.046	2.087
		77 K	2.186		2.045	2.092
[Cu(HIshexim)Cl]	Solid	RT				2.082
		77 K	2.164	2.082	2.043	2.096

values of g_{av}. The largest shift occurs for $g_{\parallel}$ which is *ca* 2.23 at both room and liquid nitrogen temperatures. This suggests a 4+1 or 4+2 coordination geometry for both [Cu(H_2Is4E)Cl_2] and [Cu(H_2Is 4P)Cl_2] in which the two chloro ligands of the complex are coordinated in the plane and chlorine(s) or sulfur(s) from the equatorial sphere of a neighbouring molecule occupy an axial position, resulting in either a paired or chain structure in the solid state. The complexes with anionic tridentate ligands are all thought to be planar with no significant axial interaction resulting in low values of $g_{\parallel}$ (and $g_{\perp}$). Some spectral variation occurs within this series of complexes, some having high $g_{\parallel}$ values ([Cu(HIs DM)Cl]) and some low $g_{\parallel}$ values ([Cu(HIs4M)Cl]), and most display some rhombic distortion. Higher values of $g_{\parallel}$ in these complexes are related to increased axial interaction(s).

Application of a combination of UV–vis adsorption and EPR spectral data permits the calculation of covalency parameters, $k_{\parallel}$ and $k_{\perp}$, for two of the complexes [18]. A value for either of 0.73 indicates minimal π-bond contribution, while smaller values indicate greater π-bonding. The values of $k_{\parallel}$ and $k_{\perp}$ for [Cu(HIs4M)Cl] are 0.66 and 0.69, and for [Cu(HIspip) Cl] they are 0.60 and 0.72, respectively. The low values of $k_{\parallel}$ suggest a marked amount of π bonding in the square-planar environment of each of these complexes, whereas the π contribution to axial bonding is much smaller. This is expected given that copper has filled π-bonding orbitals, but sulfur and chlorine (empty *d*) and nitrogen (π^*) have a limited π-acceptor capacity.

Supplementary material—Atomic coordinates, packing diagrams, complete listings of bond distances and angles and structure factors have been deposited at the Cambridge Crystallographic Data Centre.

Acknowledgements—Acknowledgement is made to the donors of the Petroleum Research Fund, administered by the American Chemical Society, and the Camille and Henry Dreyfus Foundation for partial support of this research. J.V.-M. thanks Universidad Nacional Autónoma de México PAPIIT Program (IN1038393) and Consejo Nacional de Ciencia y Tecnología (3920-E).

REFERENCES

1. R. L. Thompson, S. A. Milton, J. E. Officer and G. H. Hitchings, *J. Immunol.* 1953, **70,** 229.
2. D. J. Bauer, *Brit. J. Exp. Path.* 1956, **36,** 105.
3. D. J. Bauer and P. W. Sadler, *Brit. J. Pharmacol.* 1960, **15,** 101.
4. C. L. Hoagland, S. M. Ward, L. E. Smadel and T. M. Rivers, *J. Exptl. Med.* 1941, **74,** 69.
5. G. M. Abu El Reash, M. A. Khattab and U. I. El-Ayaan, *Synth. React. Inorg. Met.-Org. Chem.* 1992, **22,** 1417.
6. K. M. Ibrahim, A. A. El-Asmy, M. M. Bekheit and M. M. Mostafa, *Synth. React. Inorg. Met.-Org. Chem.* 1985, **15,** 1247.
7. K. M. Ibrahim, *Synth. React. Inorg. Met.-Org. Chem.* 1993, **23,** 1351.
8. R. N. Pathak and L. K. Mishra, *J. Indian Chem. Soc.* 1988, **65,** 119.
9. B. Holmberg and B. Psilanderhielm, *J. Prakt. Chem.* 1910, **82,** 440.
10. J. P. Scovill, *Phosphorus, Sulfur Silicon* 1991, **60,** 15.
11. Siemens Analytical X-ray Inst., Inc., XS-Crystal Structure Solution Program, version 4.0/360 for MS-DOS (1990).
12. R. D. Rogers, *Acta Cryst.* 1981, **A37,** 734.
13. *International Tables for X-ray Crystallography*, Vol. IV. Kynoch Press, Birmingham (1974).
14. D. X. West, G. A. Bain, R. J. Butcher, J. P. Jasinski, R. Y. Pozdniakiv, J. Valdés-Martínez,

R. A. Toscano and S. Hernández-Ortega, *Polyhedron* 1996, **15,** 665.
15. M. D. Revenko, V. Kh. Kravstov and Y. A. Siminov, *Krystallographia* 1994, **39,** 50.
16. M. S. Morales-Rios and P. Joseph-Nathan, *Magn. Res. Chem.* 1991, **29,** 893.
17. Y. K. Bhoon, *Indian J. Chem.* 1983, **22A,** 430.
18. R. K. Ray, *Polyhedron* 1989, **8,** 7.

Pergamon

PII: S0277-5387(96)00322-1

Polyhedron Vol. 16, No. 5, pp. 863–868, 1997
Copyright © 1996 Elsevier Science Ltd
Printed in Great Britain. All rights reserved
0277-5387/97 $17.00+0.00

Crystal and molecular structure of [ammonia–silver(I)-2-(4-chlorobenzoyl)benzoate]: $[(NH_3)\cdot Ag(C_{14}H_8ClO_3)]$, a silver complex containing both linear and three-coordinate silvers

David R. Whitcomb[a]* and Robin D. Rogers[b]

[a]Dry Media Systems Laboratory, Imation Corporation, St. Paul, MN 55144-1000, U.S.A.

[b]Department of Chemistry, University of Alabama, Tuscaloosa, AL 35487, U.S.A.

(Received 11 March 1996; accepted 26 June 1996)

Abstract—The crystal and molecular structure of [ammonia–silver(I)-2-(4-chlorobenzoyl)benzoate], $[(NH_3)\cdot Ag(C_{14}H_8ClO_3)]$, has been solved by X-ray diffraction techniques. The carboxylate is bound to the silver in two modes, a linear two-coordinate silver (68%) and an asymmetrically chelated three-coordinate silver (32%). An unusually short Ag—N bond, 2.098(2) Å, is observed for the two-coordinate silver. Based on the structure of the $[(NH_3)\cdot Ag(C_{14}H_8ClO_3)]$ complex, and the similarities in the IR and thermal properties, the ammine free $[Ag(C_{14}H_8ClO_3)]$ complex starting material is proposed to have the normal eight-membered silver carboxylate structure. Copyright © 1996 Elsevier Science Ltd

Keywords: silver; carboxylate; ammine.

In our continuing effort to develop further understanding of silver carboxylate chemistry [1] the silver complex of 2-(4-chlorobenzoyl)benzoic acid, (CBBA) was investigated. The marginal solubility of the AgCBBA complex, however, prohibited preparation of X-ray quality crystals.

Silver carboxylates are known to be poorly soluble in common organic solvents [2], the main exception to this rule seems to be the halogenated hydrocarbon derivatives [3]. Pyridine has been reported as a co-solvent (with ethanol) for the recrystallization of silver carboxylates having long alkyl chains [4]. While this observation has been confirmed the crystals obtained by this technique have been found to be poorly formed on a molecular level [1e]. The poor quality of the crystals can be attributed to the slow diffusion of equilibrium-released pyridine; thus, alternative routes to the preparation of high quality crystals would have great utility. Silver carboxylates have been successfully recrystallized from aqueous ammonia without incorporation of the ammine into the complex [5] although ammine has since been found to be incorporated into the silver coordination sphere in some structures [6]. In recrystallizing AgCBBA from ammonia we have found that the ammine is incorporated into the silver's coordination sphere. This report summarizes the properties of two silver CBBA complexes, $[(NH_3)\cdot AgCBBA]$, including characterization of its molecular structure and the ammine-free [AgCBBA] complex. Based on the structure of the $[(NH_3)\cdot AgCBBA]$ complex, the ammine-free complex is proposed to have a silver coordination sphere analogous to known silver carboxylate structures [7].

EXPERIMENTAL

Instrumentation

Differential scanning calorimetry, (DSC) and thermal gravimetric analysis, (TGA) were carried out on a TA Instruments 2100 thermal analyser with a dual

* Author to whom correspondence should be addressed.

sample DSC (model 910) and a TGA (model 951). The heating rate for the DSC and TGA was 5°C min^{-1}, under a nitrogen purge of approximately 50 cm^3 min^{-1}. FTIR spectra were obtained on a BOMEM-MB 102 FTIR spectrometer as a Nujol paste between KBr plates (some samples run in KBr without Nujol appeared to form free carboxylic acid, owing to halide exchange).

X-ray data collection, structure determination and refinement

The space group of the transparent single crystal of the title compound was determined to be the centric $P2_1/c$. Two positions were readily apparent for the silver atom: they were refined to occupancy factors of 68% (Ag) and 32% (Ag′) in alternate least-squares cycles. The geometrically constrained hydrogen atoms were placed in calculated positions and allowed to ride on the bonded atom with $B = 1.2 \times U_{eqv}(C)$. The ammine hydrogen atoms were included as a rigid group with rotational freedom at the bonded nitrogen atom [$B = 1.2 \times U_{eqv}(N)$]. Two sets of these hydrogen atoms were included, one with 68% occupancy and one with 32% occupancy corresponding to the silver disorder. Refinement of non-hydrogen atoms was carried out with anisotropic temperature factors. Crystal data and structure refinement data and selected bond distances and angles are given in Tables 1 and 2.

Preparation of compounds

[AgCBBA]. 2-(4-Chlorobenzoyl)benzoic acid (2.80 g, 11.0 mmol, Aldrich Chemical Co.) and sodium hydroxide (0.40 g, 10 mmol) were dissolved in water (100 cm^3). A slight solid was removed by filtration and silver nitrate, (1.70 g, 10.0 mmol) in water (10 cm^3) was added. After 15 min of stirring the white solid was filtered, dispersed in an equal volume of water, filtered and allowed to dry in the dark. Found: C, 45.5; H, 2.1. Calc. for $C_{14}H_8ClO_3Ag$: C, 45.8; H, 2.2%.

[$(H_3N)\cdot$AgCBBA]. Silver-2-(4-chlorobenzoyl)benzoate (0.30 g, 0.81 mmol) was dispersed in ethanol (10 cm^3) and sufficient 30% aqueous NH_3 added to obtain a clear solution. The vessel was closed with a septum and vented, to allow slow NH_3 loss, with a #16 gauge needle. Standing in the dark for one week resulted in the formation of large, colourless cubic crystals. The solution was decanted and the air- and light-stable crystals allowed to dry. Found: C, 43.3; H, 2.9; N, 3.7. Calc. for $C_{14}H_{11}NClO_3Ag$: C, 43.7; H, 2.9; N, 3.6%.

RESULTS AND DISCUSSION

While silver carboxylates are well known to exhibit eight-membered ring structures [7], the *o*-benzoyl car-

Table 1. Crystal data and structure refinement for [$(NH_3)\cdot$AgCBBA]

Temperature (K)	293(2)
Crystal system	Monoclinic
Space group	$P2_1/c$
Unit cell dimensions (Å,°) (4061 reflections in full θ range)	$a = 11.6107(10)$ $b = 7.7178(6)$ $c = 15.5340(13)$ $\beta = 90.8860(10)$
Volume (Å^3)	1391.8(2)
Z	4
Density (calculated) (g cm^{-3})	1.835
Absorption coefficient (mm^{-1})	1.645
Diffractometer/scan	Siemens SMART/CCD area detector
Radiation/wavelength (Å)	Mo-K_α (graphite-monochrom.)/0.71073 Å
$F(000)$	760
Crystal size (mm)	$0.10 \times 0.10 \times 0.20$
θ range for data collection (°)	1.75–23.28
Index ranges	$-6 \leqslant h \leqslant 12$, $-8 \leqslant k \leqslant 8$, $-17 \leqslant l \leqslant 17$
Reflections collected	5410
Independent/observed refls.	2006($R_{int} = 0.0325$)/ 1853([$I > 2\sigma(I)$])
Absorption correction	Semi-empirical from ψ-scans
Range of relat. transm. factors	0.9606 and 0.6886
Refinement method	Full-matrix-block least-squares on F^2
Computing	SHELXTL, V.5[a]
Data/restraints/parameters	1996/0/191
Goodness-of-fit on F^2	1.086
SHELXTL, V.5 weight parameters	0.0379, 0.5763
Final R indices [$I > 2\sigma(I)$]	$R_1 = 0.0275$, $wR_2 = 0.0719$
R indices (all data)	$R_1 = 0.0312$, $wR_2 = 0.0793$
Largest diff. peak and hole (eÅ^{-3})	0.200 and −0.364

[a] SHELXTL, V.5., Siemens Industrial Automation, Inc., Analytical Instrumentation Business Unit, 1994, Madison, WI, U.S.A.

Table 2. Selected bond lengths (Å) and angles (°) for [$(NH_3)\cdot$AgCBBA]

Ag—N	2.098(2)	N—Ag′—O(1)	133.53(8)
Ag—O(1)	2.180(2)	O(2)—Ag′—O(1)	54.81(7)
Ag′—N	2.169(2)	C(1)—O(1)—Ag	103.9(2)
Ag′—O(2)	2.309(2)	C(1)—O(1)—Ag′	86.9(2)
Ag′—O(1)	2.468(2)	C(1)—O(2)—Ag′	94.5(2)
Cl—C(12)	1.747(3)	O(2)—C(1)—O(1)	123.4(3)
O(1)—C(1)	1.256(3)	O(2)—C(1)—C(2)	118.6(2)
O(2)—C(1)	1.246(3)	O(1)—C(1)—C(2)	117.9(2)
O(3)—C(8)	1.220(3)	O(2)—C(1)—Ag′	58.23(14)
N—Ag—O(1)	170.55(8)	O(1)—C(1)—Ag′	65.5(2)
N—Ag′—O(2)	171.39(8)	C(2)—C(1)—Ag′	171.8(2)

bonyl of the CBBA ligand is in a position to coordinate with the silver in the eight-membered ring. The $[(NH_3)\cdot AgCBBA]$ complex resulting from recrystallization of AgCBBA from ammonia could form three quite different structures.

1. Axially coordinated NH_3 in which the eight-membered silver carboxylate ring is maintained, analogous to $[Ag_2(C_9H_8NO_3)_2(H_2O)_2]\cdot 2H_2O$ [5c].
2. Monomeric silver which is chelated by one carboxylate, analogous to the known $[AgSt(PPh_3)_2]$ complex [1b].
3. Polymeric silver carboxylate in which the silver is coordinated by an imine (resulting from NH_3 reaction with the *o*-benzoyl carbonyl) from an adjacent ligand.

All three structures would give the same elemental analysis and would be difficult to characterize by normal techniques such as IR and MS. We have determined the actual structure, by X-ray diffraction techniques, of the $[(NH_3)\cdot AgCBBA]$ complex to be a form of 2 : the two unique structures are shown in Fig. 1. The solid-state packing diagram is shown in Fig. 2.

Description of the $[(NH_3)\cdot AgCBBA]$ *structure*

Two different silver environments appear in the $[(NH_3)\cdot AgCBBA]$ complex; two-coordinate silver at 68% occupancy and three-coordinate silver at 32% occupancy. The carboxylate and the ammine are positionally unchanged in either configuration in the structure.

The two different types of silver coordination are clearly illustrated by the fact that one silver is approximately linearly coordinated by the carboxylate and the other is chelated. The two-coordinate silver exhibits a Ag—O bond [2.180(2) Å] that is slightly short compared to known silver carboxylates, which are normally 2.2–2.4 Å [7]. This distance is consistent, however, with the silver's low coordination number. The three-coordinate silver is asymmetrically chelated by the carboxylate, the Ag′—O bonds are 2.309(2) [O(2)] and 2.468(2) Å [O(1)]. The shorter bond length is quite normal for a stable Ag—O bond, and the longer bond is not unusual [7].

The two-coordinate silver in the $[(NH_3)\cdot AgCBBA]$ complex exhibits an unusually short Ag—N bond, [2.098(2) Å] which is substantially shorter than other silver complexes containing nitrogen ligands [1,5c,8]. The second Ag—N bond [2.169(2) Å], associated with the three-coordinate silver, is in the expected range for normal Ag—N bonds. The only $Ag—N_{ammine}$ bond distances reported in a carboxylate complex are 2.158(5) and 2.154(5) Å [6]. Simple $[Ag(NH_3)_2]^+$ complexes, on the other hand, exhibit shorter $Ag—N_{ammine}$ bond lengths of 2.11–2.18 Å [9].

As far as other potential bonding interactions within the $[(NH_3)\cdot AgCBBA]$ complex are concerned, such as those from the *o*-benzoyl oxygen which is in a position to coordinate with the silver, the *o*-benzoyl oxygen can be seen clearly to be uninvolved in silver complexation. The closest $Ag\cdots O_{benzoyl}$ contact distance is found to be 3.8 Å. In addition, the silver–chlorine separations, 3.516 (Ag···Cl) and 3.605 Å (Ag′···Cl), between adjacent ligands in the solid state, are not within the van der Waal's radii of the two atoms (3.5 Å). Bond distances for $Ag—Cl_{organic}$ systems fall in the range 2.626(3)–3.000(3) Å [10], although significant interactions have been reported for Ag···Cl as long as 3.160 Å [11].

IR spectra of $[(NH_3)\cdot AgCBBA]$ *and* [AgCBBA]

The IR spectrum (Table 3) suggests that the ammine is present as the NH_3 ligand and not the imine. The IR spectrum is not definitive, however, since imines exhibit NH stretches in this same region, although the number of imine stretches are usually fewer [12] than the four observed for the

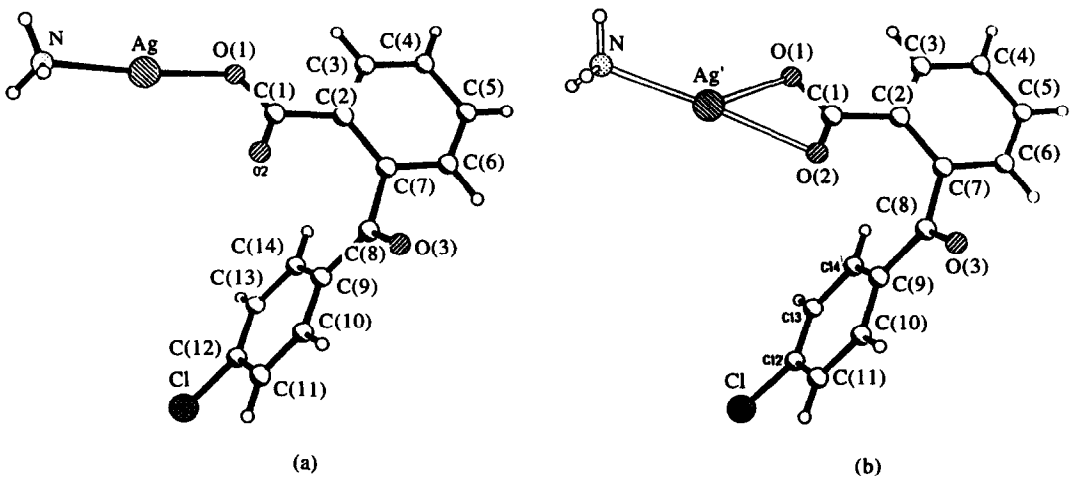


Fig. 1. Molecular structure of $[(NH_3)\cdot AgCBBA]$: (a) 68% occupancy; (b) 32% occupancy.

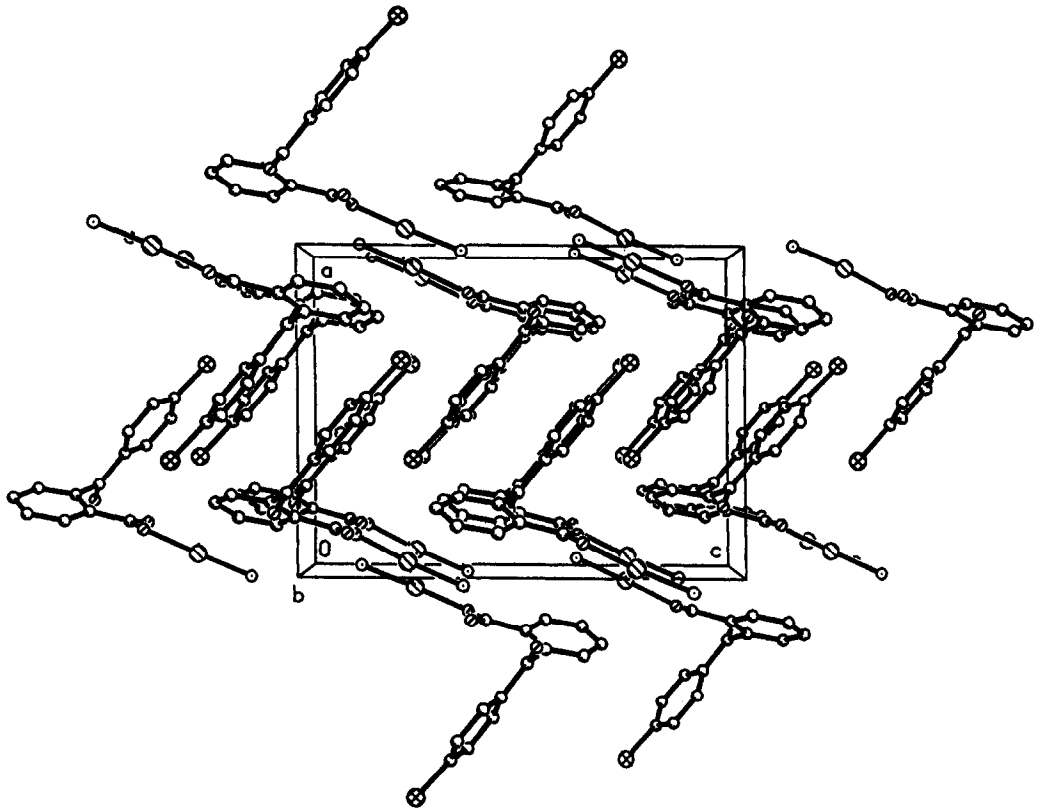


Fig. 2. Solid-state packing diagram of [(NH_3) · AgCBBA].

Table 3. Selected IR stretches (cm^{-1}) for [(NH_3) · AgCBBA] and [AgCBBA]

Complex	$\nu(NH_3)$	$\nu(C{=}O_{benzoyl})$	$\nu_{asym}(CO_2^-)$	$\nu_{sym}(CO_2^-)$
CBBA	—	1677	1682	—
[(NH_3) · AgCBBA]	3331, 3241, 3238, 3182	1661	1581, 1556	1377
[AgCBBA]	—	1657	1576, 1547	1382
$[Ag(NH_3)_2]_2SO_4$ [13]	3320, 3230, 3150	—	—	—

[$(NH_3$)AgCBBA] complex. On the other hand, the NH_3 stretches are quite similar to those reported for $[Ag(NH_3)_2]SO_4$ [13]. In addition, the weak absorptions seen in the spectrum of the [(NH_3) · AgCBBA] complex, but not in that of the ammine-free [AgCBBA] complex, in the 1600–1650 cm^{-1} region are most likely the δ (HNH) bands of NH_3. In addition, the NH_3 bands in the 3180–3330 cm^{-1} region are lost upon heating (see TGA results).

The *o*-benzoyl carbonyl stretch is in the same position for both [(NH_3) · AgCBBA] and [AgCBBA] complexes. Since the benzoyl carbonyl is not coordinated in the [(NH_3) · AgCBBA] complex, it may be concluded that this group is uncoordinated in the [AgCBBA] complex as well. The carboxylate carbonyl stretches in both complexes are very similar but not identical.

Thermal analysis of [(NH_3) · AgCBBA] *and* [AgCBBA] *complexes*

The thermal phase changes in the DSC of the [(NH_3) · AgCBBA] and [AgCBBA] complexes are the same, with the exception of the additional endothermic decomposition observed in the [(NH_3) · AgCBBA] complex centred at 186°C. Decomposition is confirmed in the TGA, (Fig. 3) by the observation of a weight loss at this temperature which is equivalent to one mole of NH_3 (6.1% = 23

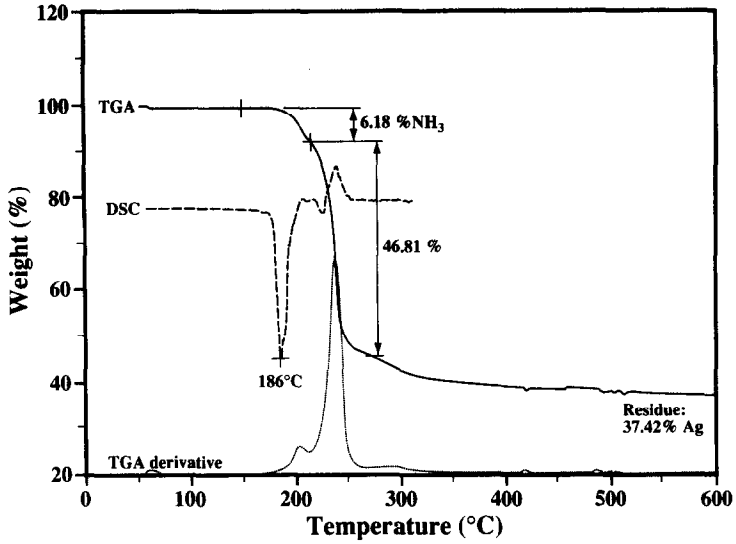


Fig. 3. DSC and TGA of [(NH_3) · AgCBBA].

amu), taking into account some convoluting of the NH_3 with subsequent weight losses. In addition, the IR spectrum of the [(NH_3) · AgCBBA] complex taken after cooling from heating past the first thermal transition (cooled from 200°C) clearly shows the loss of *ca* 100% of the ammine.

The TGAs of both complexes above 200°C are virtually superimposable, including the main decomposition in both cases (centred at *ca* 240°C) which is equivalent to *ca* 185 amu, and suggest a very similar species. Unfortunately, this latter mass does not readily correlate to identifiable fragments. Convoluted decomposition is not surprising in the case of [(NH_3) · AgCBBA] since the sample is still black at 600°C and the theoretical weight for residual Ag° is 28.3% (compared with the observed 37.4%), but the silvery residue in the ammine-free [AgCBBA] case should be 29.5%, which is quite close to the observed 30.3%.

Acknowledgements—We are grateful to R. Gould and C. Spicer (3M Analytical & Properties Research Laboratory) who obtained the IR spectra.

REFERENCES

1. (a) D. R. Whitcomb and R. D. Rogers, *J. Chem. Crystallogr.* 1995, **25,** 137; (b) D. R. Whitcomb and R. D. Rogers, *J. Chem. Crystallogr.* 1996, **26,** 99; (c) D. R. Whitcomb and R. D. Rogers, *Inorg. Chim. Acta* in press; (d) J. Blair, R. Patel, R. D. Rogers and D. R. Whitcomb, *J. Imag. Sci. Tech.* 1996, **40,** 117; (e) B. P. Tolochko, S. V. Chernov, S. G. Nikitenko and D. R. Whitcomb, *Nuclear Instruments and Methods in Physics Research A*, accepted.
2. W. U. Malik, A. K. Jain and O. P. Jhamb, *J. Chem. Soc.* (*A*) 1971, 1514; N. A. Izmailov and V. S. Chernyi, *Russ. J. Phys. Chem.* 1960, **34,** 149; P. N. Cheremisinoff, *J. Am. Oil Chem. Soc.* 1951, 278; C. A. Jacobson and A. Holmes, *J. Biol. Chem.* 1916, **25,** 29; H. Stephen and T. Stephen (Eds), *Solubilities of Inorganic and Organic Compounds*. Pergamon Press, Oxford (1963).
3. E. Szlyk, I. Lakomska and A. Grodzicki, *Thermochim. Acta* 1993, **223,** 207; D. Shanefield, *J. Inorg. Nucl. Chem.* 1962, **24,** 1014.
4. M. Ikeda and Y. Iwata, *Photogr. Sci. Eng.* 1980, **24,** 273.
5. (a) T. C. W. Mak, W.-H. Yip, C. H. L. Kennard, G. Smith and E. J. O'Reilly, *Aust. J. Chem.* 1986, **39,** 541; (b) G. Smith, D. S. Sagatys, C. Dahlgren, D. E. Lynch, R. C. Bott, K. A. Byriel and C. H. L. Kennard, *Z. Kristallogr.* 1995, **210,** 44; (c) G. Smith, A. N. Reddy, K. A. Byriel and C. H. L. Kennard, *Polyhedron* 1994, **13,** 2425; (d) G. Smith, A. N. Reddy, K. A. Byriel and C. H. L. Kennard, *J. Chem. Soc., Dalton Trans.* 1995, 3665.
6. F. Jaber, F. Charbonnier and F. Faure, *Eur. J. Solid State Inorg. Chem.* 1995, **32,** 25; F. Jaber, F. Charbonnier and R. Faure, *J. Chem. Crystallogr.* 1994, **24,** 681.
7. R. C. Mehrotra and R. Bohra, *Metal Carboxylates*. Academic Press, New York (1983); X.-M. Chen and T. C. W. Mak, *J. Chem. Soc., Dalton Trans.* 1991, 1219; (c) X.-M. Chen and T. C. W. Mak, *Polyhedron* 1991, **10,** 1723; D.-X. Chen and T. C. W. Mak, *J. Chem. Soc., Dalton Trans.* 1991, 1219; B. T. Usbaliev, M. Movsumov, I. R. Amiraslanov, A. I. Akhmedov, A. A. Musaev and Kh. S. Mamedov, *Zhur. Struk. Khim.* 1981, **22,** 98.
8. v-M. Hedrich and H. Hartl, *Acta Cryst.* 1983, **C39,** 533; v-M. Hedrich and H. Hartl. *Acta Cryst.* 1983, **C39,** 1649.
9. U. Zachwieja, and H. Jacobs, *Z. Anorg. Allg. Chem.* 1989, **571,** 37; U. Zachwieja and H. Jacobs, *Z. Krist.* 1992, **201,** 207.
10. D. M. Van Seggen, O. P. Anderson and S. H. Strauss, *Inorg. Chem.* 1992, **31,** 2987; M. R. Col-

sman, T. D. Newbound, L. J. Marshall, M. D. Noirot, M. M. Miller, G. P. Wulfsberg, J. S. Frye, O. P. Anderson and S. H. Strauss, *J. Am. Chem. Soc.* 1990, **112,** 2349; M. R. Colsman, M. M. Miller, G. P. Wulfsberg, O. P. Anderson and S. H. Strauss, *J. Am. Chem. Soc.* 1989, **111,** 3762; D. M. Van Seggen, O. P. Anderson and S. H. Strauss, *Inorg. Chem.* 1992, **31,** 2987.

11. G. Wulfsberg, D. Jackson, W. Ilsey, S. Dou, A. Weiss and J. Gagliardi, *Z. Naturforsch.* 1992, **47a,** 75.
12. L. J. Bellamy, *The Infrared Spectra of Complex Molecules*, 2nd edn. J. Wiley & Sons, New York (1958).
13. K. Nakamoto, *Infrared and Raman Spectra of Inorganic and Coordination Compounds*, 3rd edn, p. 202, J. Wiley & Sons, New York (1978).

Pergamon

PII: S0277-5387(96)00295-1

Polyhedron Vol. 16, No. 5, pp. 869–875, 1997
Copyright © 1996 Elsevier Science Ltd
Printed in Great Britain. All rights reserved
0277-5387/97 $17.00 + 0.00

Reactivity studies on some η^1-alkenyl complexes of iron

Leoné Hermans and Selwyn F. Mapolie*

Department of Chemistry, University of the Western Cape, Bellville, 7535, South Africa

(Received 17 May 1996; accepted 13 June 1996)

Abstract—The η^1-alkenyl complexes $[\eta^5\text{-}C_5H_5(CO)_2Fe(CH_2)_nCH{=}CH_2]$ (n = 2 and 3) have been prepared by the reaction of $Na[\eta^5\text{-}C_5H_5(CO)_2Fe]$ with 4-bromo-1-butene and 5-bromo-1-pentene respectively. The reactivity of the σ-olefin complexes in hydrogenation, hydroboration and hydroformylation reactions are reported as are reactions with Lewis acids such as $TiCl_4$ and the electrophile HCl. Copyright © 1996 Elsevier Science Ltd

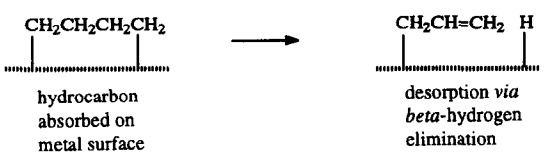
Keywords: iron-alkenyl; σ-olefins; iron-butenyl; iron-pentenyl; reactivity; functionalised-alkyls.

η^1-Alkenyl complexes are compounds in which an alkene ligand is bonded to a metal centre *via* a M—C σ bond. This class of compounds has the general formula shown below:

$L_nM{-}(CH_2)_y$ ⟋⟍

(L_nM = metal and its associated ligands)

With the exception of the allyl complexes [1,2] i.e. compounds where $y = 1$ in the above structure, not many examples of these complexes have been reported in the literature. This is quite surprising since these η^1-alkenyl complexes have often been implicated as potential model compounds for intermediates in a number of catalytic cycles involving transition metals as catalysts. Thus, for example, they could be models for hydrocarbons absorbed onto a catalytic metal surface in a process such as the Fischer–Tropsch reaction. In particular, they could represent hydrocarbon fragments at the stage at which desorption of these organic fragments from the catalyst surface occurs *via* β-hydrogen elimination.



Again with the exception of the allyl complexes, there is a great paucity of information with regard to the reactivity of these compounds. Very little indeed has been reported on the reactivity of the longer-chain alkenyl compounds of iron in particular. We have encountered only two reports [3,4] in which the iron–butenyl compound is briefly mentioned. It is in light of this that we embarked on our investigation of the reactivity of some iron complexes of the type $Cp(CO)_2Fe(CH_2)_nCH{=}CH_2$ ($Cp = \eta^5\text{-}C_5H_5$). We now report on some of these results.

EXPERIMENTAL

All reactions were performed under dry nitrogen using standard Schlenk tube techniques to manipulate air-sensitive compounds. $[CpFe(CO)_2]_2$, purchased from Strem Chemicals and the n-bromo-1-alkenes, purchased from Aldrich, were used without further purification. $HRh(CO)(PPh_3)_3$ [5] and $ClRh(PPh_3)_3$ [6] were prepared *via* literature methods. Tetrahydrofuran and hexane were distilled from sodium/benzophenone ketyl under nitrogen. Dichloromethane was dried by refluxing over P_2O_5 and distilling under nitrogen.

Infrared spectra were recorded on a Perkin–Elmer, Paragon 1000 FT-IR spectrophotometer and NMR spectra on a Varian EM 390 or a Varian VXR 200 spectrometer operating at 90 MHz and 200 MHz respectively. Tetramethylsilane was used as an internal standard (δ 0.00 ppm) for ^1H spectra while ^{13}C signals were measured relative to $CHCl_3$. Mass

* Author to whom correspondence should be addressed.

spectra were recorded on a V.G. Micromass 16F spectrometer operating at 70 eV and using an accelerating voltage of 4 kV. Microanalyses were performed by the microanalytical laboratory at the University of Cape Town.

Preparation of $Cp(CO)_2Fe(CH_2)_nCH{=}CH_2$, $n = 2$ *and* 3, *i.e. compounds* **1** *and* **2**

A solution of $[CpFe(CO)_2]_2$ (1 g, 2.83 mmol) in tetrahydrofuran (20 cm^3) was stirred over a sodium amalgam (0.2 g Na in 3 cm^3 Hg) for 2 h at room temperature. The resulting solution of $Na[CpFe(CO)_2]$ (5.68 mmol) was transferred using a syringe to a Schlenk tube, and the *n*-bromo-1-alkene, $CH_2{=}CH(CH_2)_nBr$, ($n = 2$ or 3) (5.86 mmol) was added dropwise with stirring. The resulting green-brown reaction mixture was stirred for 2 h at room temperature. The solvent was removed to give a green residue which was extracted with CH_2Cl_2 (2×30 cm^3) and filtered. The filtrate was evaporated on a rotary evaporator resulting in a yellow-brown oily residue. This was dissolved in a minimum of hexane and the solution chromatographed on an alumina column (10×2.5 cm). A yellow band was eluted with hexane and removal of the solvent gave the η^1-alkenyl compound as a yellow oil. The crude oil was purified by low temperature (-78°C) recrystallisation from hexane. Thus the crude oil was dissolved in a minimum of hexane in a Schlenk tube under nitrogen and the resulting yellow solution cooled to -78°C. This result in the formation of a yellow solid. The supernatant liquid was removed using a syringe and the yellow solid washed with ice-cold hexane (2×10 cm^3). The washings were also syringed off. On allowing the solid to warm up to room temperature, it melted giving a yellow-brown oil. This was then dried under reduced pressure. Yields and characterization data are given in Table 1.

Hydrogenation of $Cp(CO)_2Fe(CH_2)_nCH{=}CH_2$, $n = 2$ *and* 3

$ClRh(PPh_3)_3$ (0.02 g, 0.022 mmol) was dissolved in dichloromethane (2 cm^3). Hydrogen gas was bubbled through the solution for 30 min in order to activate the catalyst. A solution of the iron–alkene complex (0.64 mmol) dissolved in dichloromethane (5 cm^3), was added to the catalyst solution. The resulting mixture was allowed to stir under hydrogen for 2 h at room temperature after which the solvent was removed under reduced pressure. This resulted in the formation of a yellow-brown oil. The residue was dissolved in a minimum of hexane and then chromatographed on an alumina column (5×2.5 cm). A pale yellow band was eluted with pure hexane and gave a yellow-orange oil on removal of the solvent. Recrystallisation from hexane at -78°C gave a bright yellow solid which melts to a yellow-brown oil on warming to room temperature. The product was identified as the corresponding iron alkyl compound **3** or **4**, yields 60% and 54% respectively.

Oxidative hydroboration of the iron–alkenyl complexes

The oxidative hydroboration of the iron–butenyl compound **1**, is described to illustrate the procedure used for the iron alkenyl compounds in general. **1** (0.22 g, 0.90 mmol) was dissolved in THF (3 cm^3) in a Schlenk tube under nitrogen. The solution was cooled to 0°C and BH_3 (0.9 cm^3 of 1 M solution in THF) was added dropwise. The solution changes colour from yellow to dark greenish-yellow. The mixture was allowed to warm up to room temperature and then stirred for a further 1.5 h at this temperature. Water (2 drops) was added followed by 3 M NaOH (0.60 cm^3). The dark green-brown solution was treated dropwise with 30% H_2O_2 (0.20 cm^3). This results in the reaction mixture changing colour to light yellow. The resulting mixture was then refluxed for 1 h after which it was allowed to cool to room temperature. Any undissolved salts were filtered off. The filtrate was dried over $MgSO_4$. The mixture was filtered and the solvent removed, leaving a yellow-brown oil. The residue was redissolved in a minimum of CH_2Cl_2 and the solution chromatographed on an alumina column (2.5×2 cm). Elution with CH_2Cl_2 results in a two yellow bands *viz.* a pale yellow band moving with the solvent front and a second, more intense yellow band moving much slower. The first band was identified as the starting material, while the second band was found to be the hydroboration-oxidation product **5**, in 70% yield.

The hydroboration of **2** was carried out in a similar manner yielding compound **6** as product in 64% yield.

Hydroformylation of compounds **1** *and* **2**

The method for the hydroformylation of the iron–pentenyl compound **2** is described here but the procedure has also been applied with equal success to the iron–butenyl compound **1**.

The hydroformylation catalyst, $HRh(CO)(PPh_3)_3$ (0.063 g, 0.04 mmol) was dissolved in THF (5 cm^3) in a Schlenk tube. Synthesis gas ($CO : H_2$; 1 : 1) was bubbled through the solution for 10 min. A solution of **2** (0.33 g, 1.30 mmol) in THF (4 cm^3) was added to the catalyst solution and the mixture refluxed for 3.5 h under an atmosphere of syngas. The yellow reaction mixture turns dark brown during this period. After cooling to room temperature, the solvent was removed on a rotary evaporator leaving a brown oil. This was dissolved in a minimum of hexane and the solution chromatographed on an alumina column (2.5×5 cm), made up in hexane. Three components were observed, the first of which was eluted with pure hexane. Removal of the solvent results in a pale yellow oil which was identified as unreacted starting material

(32%). The second dark yellow band was eluted using a 1 : 1 hexane–dichloromethane mixture. On removing the solvent, a yellow-brown oil was obtained. This was identified as the aldehyde compound **8** (42% yield). The last yellow fraction was eluted with pure dichloromethane. Removal of the solvent resulted in a pale yellow oil which was found to be the ω-hydroxyhexyl species **9** (18% yield).

The corresponding iron–butenyl compound **1**, undergoes a similar reaction to yield **6** and **7** as the major products in 22 and 48% yields, respectively.

Reaction of **1** *with* $TiCl_4$

Compound **1** (0.2 g, 0.86 mmol) was dissolved in hexane (5 cm^3). To this was added dropwise a solution of $TiCl_4$ (0.15 cm^3, 1.37 mmol) in hexane (5 cm^3). The solution changes colour from bright yellow to dark brown almost immediately. The mixture was allowed to stir at room temperature for 1.5 h. During this time, the reaction mixture goes darker with a black precipitate forming. Methanol (2 cm^3) was added to the reaction mixture with rapid stirring which was continued for a further 15 min at room temperature. The solvent was removed from the reaction mixture leaving a dark brown oily residue. The oil was dissolved in a small amount of dichloromethane and the resulting solution chromatographed on an alumina column (2.5 × 5 cm) made up with dichloromethane. Elution with dichloromethane gave an orange-yellow band which on removal of the solvent from the eluent, yielded an orange-yellow solid. This was identified as the metallocycle **10** (60%, yield). A second yellow band yielded a small amount of a pale yellow solid which showed no ν(CO) bands in its IR spectrum. A third faint yellow band could not be eluted from the column.

Reaction of iron–alkenyl compounds with HCl

The reaction of **1** with HCl is outlined below; but again this procedure can be extended to compound **2**.

1 (0.15 g, 0.65 mmol) was dissolved in dry hexane (5 cm^3) at −20°C. Anhydrous HCl gas was bubbled through the solution for 1 h at this temperature. During this time the solution goes orange-red with an oily substance being deposited on the walls of the reaction flask. The solvent together with the excess HCl was removed *in vacuo*, resulting in an orange-red sticky residue. This was dissolved in a minimum of dichloromethane and the solution filtered by gravity. Hexane was carefully layered onto the filtrate until the mixture went cloudy. Cooling the mixture to −5°C resulted in the formation of a brick-red precipitate which was filtered off and identified as $CpFe(CO)_2Cl$ (90% yield).

A similar reaction using compound **2** as starting material resulted in the same product in 84% yield.

RESULTS AND DISCUSSION

The iron–butenyl compound **1** and the iron–pentenyl species **2** were isolated as yellow-brown oils from the reaction of $Na[CpFe(CO)_2]$ with 4-bromo-1-butene and 5-bromo-1-pentene, respectively.

$$Na[CpFe(CO)_2] + CH_2{=}CH(CH_2)_nCH_2Br \rightarrow Cp(CO)_2FeCH_2(CH_2)_nCH{=}CH_2 \quad (1)$$

1 $n = 1$
2 $n = 2$

Compounds **1** and **2** are both air and light sensitive. The decomposition of the compounds is further accelerated in solution, especially in the presence of air. They can however be stored for several weeks if kept at −20°C and in the absence of air and light. Both compounds were characterized by IR, ^1H and ^{13}C NMR spectroscopy as well as by elemental analysis. The characterization data are given in full in Table 1.

The IR spectra of the compounds in the ν(CO) region resemble those of the corresponding alkyl compounds with the general formula, $CpFe(CO)_2R$ (R = alkyl), showing two sharp bands at 1999 and 1949 cm^{-1}. The examination of the ^1H NMR spectra of both compounds clearly show the characteristic olefinic protons being present around δ 4.90 and δ 5.80 ppm.

Reactivity of the iron–alkenyl complexes

Most of the reactions described below were carried out on both the butenyl and the pentenyl compounds.

(*a*) *Catalytic hydrogenation of* **1** *and* **2**. It is well known that unsaturated hydrocarbons such as alkenes and alkynes undergo facile hydrogenation in the presence of Wilkinson's catalyst [6,7]. We thus considered it feasible that the iron–alkenyl compounds would also undergo a similar reaction. Under the relatively mild conditions employed one would expect that the Fe—C bond to remain intact and not to be susceptible to reductive elimination in the presence of hydrogen. We find that this is indeed the case. We observe that even refluxing the reaction mixture at temperatures between 40 and 50°C, results only in the hydrogenation of the pendant alkene functional group. The Fe—C bond is not affected under these conditions. The hydrogenation process results in the complete conversion of the iron–alkenyl compounds to the corresponding alkyl compounds, **3** and **4**. The latter were characterized by comparing their characterization data with those of authentic samples prepared using methods reported in the literature [8,9].

$$Cp(CO)_2FeCH_2(CH_2)_nCH{=}CH_2 \xrightarrow{H_2} Cp(CO)_2Fe(CH_2)_nCH_2CH_3 \quad (2)$$

1 $n = 1$
2 $n = 2$

3 $n = 1$
4 $n = 2$

Table 1. Yields and characterization data for new compounds

Compound number	Yield (%)	Microanalysis[a] (%)	IR ν(CO)[b] (cm^{-1})	^{1}H NMR[c] (δ ppm)	^{13}C NMR[c] (δ ppm)
1	74	C 56.8 (56.9) H 5.0 (5.3)	1942(s) 2002(s)[d]	1.48(br t, 2H) $FeCH_2CH_2CH{=}CH_2$ 2.17 (br m, 2H) $FeCH_2CH_2CH{=}CH_2$ 4.75 (s, 5H) C_5H_5 4.88 (br m, 2H) $FeCH_2CH_2CH{=}CH_2$ 5.86 (br m, 1H) $FeCH_2CH_2CH{=}CH_2$	2.13 $FeCH_2$ 41.83 $FeCH_2CH_2{=}CH_2$ 85.31 C_5H_5 112.27 $Fe(CH_2)_2CH{=}CH_2$ 142.53 $Fe(CH_2)_2CH{=}CH_2$ 217.508 CO
2	66	C 58.3 (58.6) H 5.9 (5.7)	1943(s) 2001(s)[d]	1.48 (br s, 4H) $Fe(CH_2)_2CH_2CH{=}CH_2$ 2.07 (br m, 2H) $Fe(CH_2)_2CH_2CH{=}CH_2$ 4.73 (s,5H) C_5H_5 4.94 (br m, 2H) $Fe(CH_2)_3CH{=}CH_2$ 5.80 (br m, 1H) $Fe(CH_2)_3CH{=}CH_2$	3.05 $FeCH_2$ 37.65, 38.98 $FeCH_2CH_2CH_2CH{=}CH_2$ 85.7 C_5H_5 113.94 $Fe(CH_2)_3CH{=}CH_2$ 139.15 $Fe(CH_2)_3CH{=}CH_2$ 217.60 CO
5[d]	70	C 52.6 (52.8) H 5.6 (5.6)	1943(s) 2000(s)	1.45–152 (br s, 7H) $Fe(CH_2)_3CH_2OH$ 3.62 (br s, 2H) $Fe(CH_2)_3CH_2OH$ 4.63 (s, 5H) C_5H_5	3.12 $FeCH_2(CH_2)_2CH_2OH$ 34.70, 38.45 $FeCH_2(CH_2)_2CH_2OH$ 62.48 $Fe(CH_2)_3CH_2OH$ 85.40 C_5H_5 217.60 CO
6[e]	64	C 54.4 (54.6) H 6.2 (6.1)	1942(s) 2001(s)	1.31–1.58 (br s, 9H) $Fe(CH_2)_4CH_2OH$ 3.63 (br s, 2H) $Fe(CH_2)_4CH_2OH$ 4.67 (s, 5H) C_5H_5	3.25 $FeCH_2(CH_2)_3CH_2OH$ 30.71, 32.47, 37.92 $FeCH_2(CH_2)_3CH_2OH$ 63.16 $Fe(CH_2)_4CH_2OH$ 85.30 C_5H_5 217.64 CO
7	48	C 54.8 (55.0) H 5.2 (5.4)	1945(s) 2001(s)	0.89–1.90 (m, 6H) $Fe(CH_2)_3CH_2CHO$ 2.30 (br t, 2H) $Fe(CH_2)_3CH_2CHO$ 4.67 (s, 5H) C_5H_5 9.72 (s, 1H) $Fe(CH_2)_3CH_2CHO$	*
8	42	C 56.7 (56.5) H 5.6 (5.8)	1721(m), 1934(s) 1995(s)	0.92–1.80 (br m, 8H) $Fe(CH_2)_4CH_2CHO$ 2.34 (br t, 2H) $Fe(CH_2)_4CH_2CHO$ 4.62 (s, 5H) C_5H_5 9.70 (s, 5H) $Fe(CH_2)_4CH_2CHO$	*
9[f]	18	C 56.3 (56.1) H 6.4 (6.5)	1995 1934(s)	1.36–1.52 (br s, 11H) $Fe(CH_2)_5CH_2OH$ 3.66 (br s, 2H) 4.76 (s, 5H) C_5H_5	3.20 $FeCH_2(CH_2)_4CH_2OH$ 31.46, 32.60 $FeCH_2(CH_2)_2CH_2CH_2CH_2OH$ 34.70, 38.45 $FeCH_2$ $CH_2CH_2CH_{22}CH_2OH$ 62.62 $Fe(CH_{25}CH_2OH)$ 85.60 C_5H_5 217.66 CO

[a] Calculated values in parentheses; [b] Neat film between NaCl plates; [c] $CDCl_3$ as solvent unless otherwise stated; [d] Prepared by the hydroboration of the Fp-butenyl compound (Fp = C_5 $H_5Fe(CO)_2$); [e] Prepared by the hydroboration of the Fp-pentenyl compound; [f] Prepared *via* hydroformylation of the Fp-pentenyl compound; *Data not obtained.

As stated earlier, under the reaction conditions employed no iron–carbon bond cleavage occurs. This is confirmed by the fact that the expected cleavage product, $CpFe(CO)_2H$ is not detected during the reaction. There is also no sign of the dimer, $[CpFe(CO)_2]_2$ which would be an indication of the presence of the hydride since the latter has the tendency to decompose to the dimer in the presence of air.

(*b*) *Hydroboration-oxidation reactions.* Olefinic hydrocarbons readily undergo hydroboration to produce organoborane species which can be oxidized to 1° alcohols. Both the iron–butenyl and iron–pentenyl compounds undergo facile hydroboration followed by *in situ* oxidation to produce a ω-hydroxyalkyl compound of this type, $Cp(CO)_2Fe(CH_2)_yCH_2OH$ where $y = 3$ and 4.

$$\begin{array}{l} Cp(CO)_2FeCH_2(CH_2)_nCH{=}CH_2 \xrightarrow{\text{(i)}} \\ \quad \mathbf{1}\ \ n = 1 \\ \quad \mathbf{2}\ \ n = 2 \end{array}$$

$$\xrightarrow[\text{(iii)}]{\text{(ii)}} Cp(CO)_2Fe(CH_2)_yCH_2OH$$

$$\begin{array}{l} \mathbf{5}\ \ y = 3 \\ \mathbf{6}\ \ y = 4 \end{array}$$

(i) $BH_3 \cdot THF$ (ii) H_2O_2 (iii) NaOH (3)

The intermediate borane compounds were not isolated but were oxidized *in situ*. There are thus no characterization details available for these compounds. The ω-hydroxyalkyls were however fully characterized and these details are outlined in Table 1. The IR spectra of both compounds show two strong bands in the ν(CO) region and are at positions similar to those of the starting iron–alkenyl compounds. This is an indication that the metal environment remains unaffected during the reaction. The full range IR spectra (4000–600 cm^{-1}) of both **5** and **6**, show a strong band around 3350 cm^{-1} which can be assigned to the O—H stretching frequency of the hydroxy functionalised alkyl species. The spectra also show the absence of any C=C stretching frequency around 1630 cm^{-1} which is present in the parent alkenyl species. This clearly indicates that unsaturation is no longer present in the hydrocarbon chain of the products.

Only the mass spectrum of compound **6** shows a molecular ion, whereas that of **5** shows the highest mass peak representing the species M^+—CO. In both cases there appear to be two fragmentation patterns. The one involves initially the sequential loss of the terminal carbonyl groups from the parent ion followed by the loss of the hydroxy group of the alcohol functionality. This is then followed by the elimination of the hydrocarbon chain. The second fragmentation route again involves the initial loss of the terminal CO groups. However, in this case the hydroxy group is only eliminated after the loss of the aliphatic chain.

Table 2. Mass spectral data for the compounds $Cp(CO)_2Fe—(CH_2)_yCH_2OH$, **5** and **6**

Ion[a]	Relative peak intensities 5[b]	6[c]
M	—	2
M—CO	06	7
M—2CO	30	25
M—2CO—OH	08	04
M—2CO—H_2O	16	26
M—2CO—OH—$C_{1/2n}H_n$	14	—
M—2CO—OH—C_nH_{2n}	61	100
M—2CO—OH—C_nH_{2n}—Cp	42	15
M—2CO—C_nH_{2n}	100	96
M—2CO—Cp	22	33
M—2CO—Cp—OH	03	05
M—2CO—Cp—H_2O	51	23
M—2CO—Cp—H_2	02	05
M—2CO—Cp—$C_{1/2n}H_n$	03	—
M—2CO—Cp—C_nH_{2n}	02	05

[a] M = $Cp(CO)_2Fe(CH_2)_yCH_2OH$, Cp = η^5-C_5H_5; all ions have a single positive charge, ion refers to suggested assignment.

[b] Peak intensities relative to $m/z = 138$.

[c] Peak intensities relative to $m/z = 121$.

The full assignment of the various peaks in the mass spectra is given in Table 2.

(*c*) *Hydroformylation of compounds* **1** *and* **2.** The compound $HRh(CO)(PPh_3)_3$ is a well known hydroformylation catalyst and has been used to promote the hydroformylation of normal alkenes at room temperature and ambient pressure [10, 11]. It is for this reason that we employed this compound in the attempted hydroformylation of the metal–alkenyl compounds. The iron–alkenyl compounds were subjected to hydroformylation at atmospheric pressure at both 25°C and at 70°C. Both **1** and **2** undergo hydroformylation to some extent in each case a mixture of the hydroxy functionalised and aldehydic functionalised iron alkyl compounds were isolated together with some unreacted starting material.

$$\begin{array}{l} CpFe(CO)_2FeCH_2(CH_2)_nCH{=}CH_2 \\ \quad \mathbf{1}\ \ n = 1 \\ \quad \mathbf{2}\ \ n = 2 \end{array}$$

$$\xrightarrow[\text{THF}]{H_2/CO} Cp(CO)_2FeCH_2(CH_2)_{n+1}CH_2CHO$$

$$\begin{array}{l} \mathbf{7}\ \ n = 1 \\ \mathbf{8}\ \ n = 2 \end{array} \qquad (4)$$

$$+$$

$$\begin{array}{l} Cp(CO)_2FeCH_2(CH_2)_{n+1}CH_2CH_2OH \\ \mathbf{6}\ \ n = 1 \\ \mathbf{9}\ \ n = 2 \end{array}$$

Both the aldehyde and the alcohol are obtained

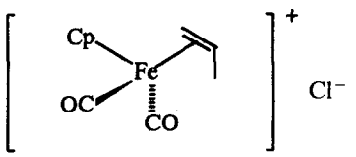
irrespective of the temperature at which the reaction is performed at room temperature or at 70°C. However, the selectivity to the alcohol is increased when the reaction is allowed to proceed at the higher temperature. This is in line with what normally occurs in the case of the hydroformylation of conventional alkenes. We also detect small amounts of the hydrogenation product i.e. the iron–alkyl species but this is less than 10% in both cases. The products obtained in these reactions are all new and the characterization details are given in Table 1. The alcohol obtained using compound **1** as starting material is the same as the compound obtained when **2** is subjected to oxidative hydroboration. The stability of alcohol **8** appears to be lower than the homologous compound **6,** decomposing rapidly when in solution and in the absence of nitrogen. Both the alcohols and the aldehydes were isolated as yellow-brown oils.

The aldehydes obtained in these reactions are also not very stable in solution. It can be stored for only short periods (a couple of days), even at −20°C and in the absence of air.

Reaction of compounds **1** *and* **2** *with* HCl

Green and Nagy [1], have shown that the iron–alkyl compound, $Cp(CO)_2Fe—CH_2CH=CH_2$, undergoes a facile reaction with mineral acids such as HCl to produce a cationic complex in which the allyl group undergoes rearrangement to be bonded in a η^2 fashion as shown below.

$$Cp(CO)_2Fe—CH_2CH=CH_2 \xrightarrow{HCl}$$



(5)

We attempted similar reactions with the homologous iron–butenyl and iron–pentenyl complexes to investigate whether related cationic species as above would be obtained. In our hands, we found that the longer chain alkenyl compounds to not yield the η^2 cationic species, but rather undergo iron–carbon bond cleavage to produce $CpFe(CO)_2Cl$ and the chloroalkene.

$$Cp(CO)_2FeCH_2(CH_2)_nCH=CH_2 \xrightarrow[20°C]{HCl}$$

1 $n = 1$
2 $n = 2$

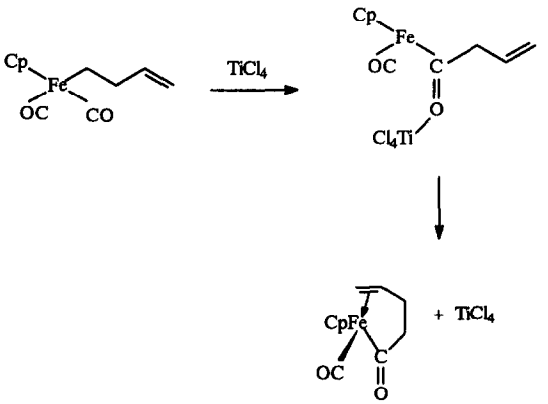
$$CpFe(CO)_2Cl + ClCH_2(CH_2)_nCH=CH_2 \qquad (6)$$

The above cleavage reactions occur even under mild conditions such as low temperatures of −20°C. The organometallic product of the reaction was identified by comparing its IR and ^1H NMR spectra with that of an authentic sample [12]. The organic products were identified by GC analysis of the reaction mixture.

In both reactions we observed no evidence for electrophilic interactions between HCl and the double bond of the pendant alkene ligand.

Reaction of **1** *with* $TiCl_4$

The reactivity of the iron–butenyl compound with a Lewis acid such as $TiCl_4$ was investigated. The rationale behind this reaction was to attempt the coordination of the pendant alkene to the titanium centre. This unfortunately did not occur; instead the $TiCl_4$ acted as a Lewis acid promoter of alkyl migration leading to a coordinatively unsaturated iron centre (see below). This unsaturated species undergoes intramolecular cyclization in which the pendant alkene moiety coordinates to the iron centre in a η^2 fashion. The species isolated from this reaction has previously been isolated and characterized by Green and Smith [3] as a decomposition product of the iron–butenyl compound.



We observe a similar reaction if $AlCl_3$ is employed instead of $TiCl_4$ supporting our contention that the conversion to the cyclic acyl species is promoted by a Lewis acid. In the case of the pentenyl compound, we do not observe the formation of an analogous cyclic compound, instead the only product isolated is $CpFe(CO)_2Cl$.

CONCLUSION

The iron–alkenyl compounds have proved to be valuable starting materials to new functionalised alkyl complexes of iron. They have thus successfully been employed to produce iron–borane compounds as well as new hydroxy and aldehydic functionalised complexes. We are at present investigating the reactivity as well as the thermal properties of these new functionalised iron alkyls.

REFERENCES

1. Green, M. L. H. and Nagy, P. L., *J. Chem. Soc.*, 1963, 189.

2. Kurosa, H., *J. Organomet. Chem.* 1987, **334,** 234.
3. Green, M. L. H. and Smith, M. J., *J. Chem. Soc.*, 1971, 3220.
4. Bodnar T. and Cutler, A. R., *Organometallics*, 1985, **4,** 1558.
5. Bath, S. S. and Vaska, L., *J. Am. Chem. Soc.* 1963, **85,** 3500.
6. Osborn, J. A., Jardine, F. H. and Wilkinson, G., *J. Chem. Soc. A*, 1966, 1711.
7. Halpern, J., Okamoto, T. and Zakhariev, A., *J. Mol. Catal.* 1976, **2,** 65.
8. King, R. B., Ed., *Organometallic Synthesis*, vol. 1. Academic Press New York, 1965, p. 151.
9. Kasluaskas R. J. and Wrighton, M., *Organometallics*, 1982, **1,** 602.
10. Yagupsky, G., Brown, C. K. and Wilkinson, G., *J. Chem. Soc. A*, 1970, 1392.
11. Brown, C. K. and Wilkinson, G., *J. Chem. Soc. A*, 1970, 2753.
12. Piper, T. S., Cotton, F. A. and Wilkinson, G., *Inorg. Nucl. Chem.*, 1955, **1,** 167.

Pergamon

PII: S0277-5387(96)00358-0

Polyhedron Vol. 16, No. 5, pp. 877–879, 1997
Copyright © 1996 Elsevier Science Ltd
Printed in Great Britain. All rights reserved
0277-5387/97 $17.00+0.00

COMMUNICATION

Esterolytic activity of metal complexes of 2,6-diacetylpyridine dioxime

Paola Gómez Tagle and Anatoly K. Yatsimirsky*

Facultad de Química, Universidad Nacional Autónoma de México (UNAM), México D.F., 04510 México

(Received 10 May 1996; accepted 17 July 1996)

Abstract—The rate constants of the cleavage of 4-nitrophenyl acetate ($4\text{-}O_2NC_6H_4O_2CCH_3$) by the complexes of 2,6-diacetylpyridine dioxime with Ni^{II}, Hg^{II}, Zn^{II}, Pb^{II}, Mn^{II} and Cd^{II} range from 2 to *ca* 6000 times higher than that of the free ligand under the same conditions. Complexation of the oxime ligand with Co^{II} and Cu^{II} does not affect the reaction rate. The complex with Cd^{II} operates in a catalytic regime with respect to the oxime ligand. The activities of the complexes with different metals, excluding Co^{II}, correlate with those of metallocarboxypeptidases towards an ester substrate. Copyright © 1996 Elsevier Science Ltd

Keywords: ester hydrolysis; oxime; metal complexes; catalysis.

Catalytic properties of metal-substituted hydrolytic metalloenzymes were studied with the aim of clarifying the role of the metal centre in substrate activation [1]. The interpretation of such results is not straightforward, however, and a similar study with a model system would help to find a reasonable approach. In this communication we report the esterolytic activity of a series of metal complexes of 2,6-diacetylpyridine dioxime (H_2dapd). We chose this ligand for three reasons. Firstly, because earlier, the esterolysis by the zinc(II) [2,3] and palladium(II) [4] coordinated oxime group was studied as a mimic of acyl transfer enzyme mechanism. Secondly, because it usually forms tridentate complexes with the fourth position occupied by a solvent molecule or a counter ion [5], thus repeating a coordination motif typical of many zinc enzymes [6]. Finally, because it should form more stable metal complexes than the previously employed bidentate 2-pyridinealdoxime [2], allowing study of a wide series of metal cations in neutral and weakly basic aqueous solutions without concomitant cation hydrolysis and/or precipitation of hydroxides.

* Author to whom correspondence should be addressed

H_2dapd was synthesized from 2,6-diacetylpyridine (Aldrich) and hydroxylamine *via* a modified procedure of ref. [5c]. 4-Nitrophenyl acetate (NPA, Aldrich) was purified by recrystallization from acetic acid–ethyl acetate. The reaction course was monitored by the appearance of 4-nitrophenolate anion using a Hewlett–Packard 8452A diode array spectrophotometer equipped with a thermostatted cell holder. Owing to the low solubility of H_2dapd all solutions contained 24% (v/v) ethanol. Stock solutions of NPA were prepared in dry acetonitrile. Kinetic measurements normally used 4×10^{-5} mol dm^{-3} NPA and varied concentrations of metal salts and H_2dapd in 0.01 mol dm^{-3} BisTris or borate buffer solutions (used at appropriate pH intervals) with ionic strength 0.1 mol dm^{-3} (NaCl) at 25°C. The pseudo-first-order rate constants (k_{obs}) were calculated by the integral method, or, for slow reactions, from initial rates.

Kinetics of the cleavage of NPA by free H_2dapd was first order in both NPA and H_2dapd, the second-order rate constant being directly proportional to the OH^- concentration in pH range 7.92–9.94. Spectrophotometric titration of H_2dapd revealed the values $pK_{a1}^{LH} = 11.15$ and $pK_{a2}^{LH} = 11.74$ (no statistical

Pergamon

PII: S0277-5387(96)00376-2

Polyhedron Vol. 16, No. 6, pp. 881–888, 1997
Copyright © 1996 Elsevier Science Ltd
Printed in Great Britain. All rights reserved
0277–5387/97 $17.00+0.00

Crystal structures of $[(IMe_2SnOSnMe_2OEt)_2]$ and $[\{(PrCO_2)Me_2SnOSnMe_2(O_2CPr)_2\}_2]$

Julian A. Blair,[a] R. Alan Howie,[a] James L. Wardell[a]* and Philip J. Cox[b]

[a]Department of Chemistry, University of Aberdeen, Meston Walk, Old Aberdeen AB9 2UE, U.K.

[b]School of Pharmacy, The Robert Gordon University, Schoolhill, Aberdeen AB9 1FR, U.K.

(Received 14 June 1996; accepted 31 July 1996)

Abstract—Centrosymmetric $[(\mu\text{-}Me_2Sn)_2(\mu\text{-}IMe_2Sn)_2(\mu\text{-}OEt)_2(\mu_3\text{-}O_2)]$ (**3**), obtained from 1,2:5,6-di-*O*-isopropylidene-3-*C*-iododimethylstannyl-α-D-allofuranoside on solvolysis in aqueous EtOH, has a ladder structure, made up of three fused Sn_2O_2 rings. There are two pairs of distinct five-coordinate tin centres in **3**. The ethoxide ligands bridge the two distinct Sn centres essentially symmetrically [Sn(1)—O(2) and Sn(2)—O(2) = 2.171(6) and 2.178(6) Å]. In centrosymmetric, solid $[(\mu\text{-}Me_2Sn)_2\{\mu\text{-}(PrCO_2)Me_2Sn\}_2(\mu\text{-}PrCO_2)_2(\mu_3\text{-}O)_2]$ (**4**) obtained from Me_2SnCl_2 and $CH_3CH_2CH_2CO_2H$ in H_2O, there are also two distinct tin sites. The Sn(1) atoms are bonded to 2 C and 4 O atoms, with tin–oxygen bond lengths between 2.027(6) and 2.712(8) Å. The immediate coordination sphere of Sn(2) consists of 2 C and 3 O [Sn(2)—O bond lengths between 2.020(5) and 2.216(11) Å]; there are also intramolecular, Sn(2)—O(5) [2.990(12)], and intermolecular, Sn(2)—O(5^{ii}) [3.109(11) Å] contacts. The core of the structure of **4** is a five rung ladder, made up of Sn_2O_2 rings, with additionally two side rings, composed of Sn_2O_3C units. Copyright © 1996 Elsevier Science Ltd

Keywords: organotin; crystal structure; carboxylate; organotin oxycarboxylate.

The Sn_2O_2 planar ring is a commonly found structural feature in organotin oxides and related compounds. In a search through the Cambridge Crystallographic Data Base (in Spring, 1996) over 130 compounds had been listed having this fragment. About 40 of these compounds were of the dimeric tetraorganodistannoxane type, $[(\mu\text{-}R_2Sn)_2(\mu\text{-}XR_2Sn)_2(\mu\text{-}Y)_2(\mu_3\text{-}O)_2]$ (**1**; X and Y = univalent anions).[1,2] For compounds (**1**, X = OH, Cl or NCS; Y = OH or Cl), the solid-state structure is the ladder structure [1b,1f, 3], illustrated in Fig. 1. For compounds in which X and Y are chelating anions, e.g. as in (**1**, X = Y = carboxylate), the structures are modified as a consequence of the bidentate nature of these ligands [1a, c]; for (**1**, X = Y = O_2CR) different structural motifs have been identified [2], one frequently found is that shown in Fig. 2.

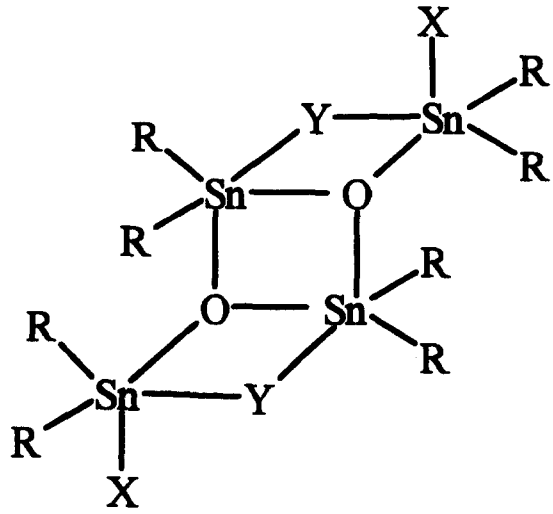


Fig. 1.

The oxyhalides are generally obtained by partial hydrolysis of diorganotin dihalides [4]. We have found that the stannylated carbohydrate 3-(iododimethylstannyl)-1,2:5,6-di-*O*-isopropylidene-α-D-glucofuranose (**2**) undergoes solvolysis in 95% ethanol to provide $[(\mu\text{-}Me_2Sn)_2(\mu\text{-}IMe_2Sn)_2\ (\mu\text{-}OEt)_2(\mu_3\text{-}O)_2]$ (**3**). Compound **3** is the first reported compound of type **1** to contain iodide and ethoxide groups. We now report the structure (and stability) of **3**. The

* Author to whom correspondence should be addressed.

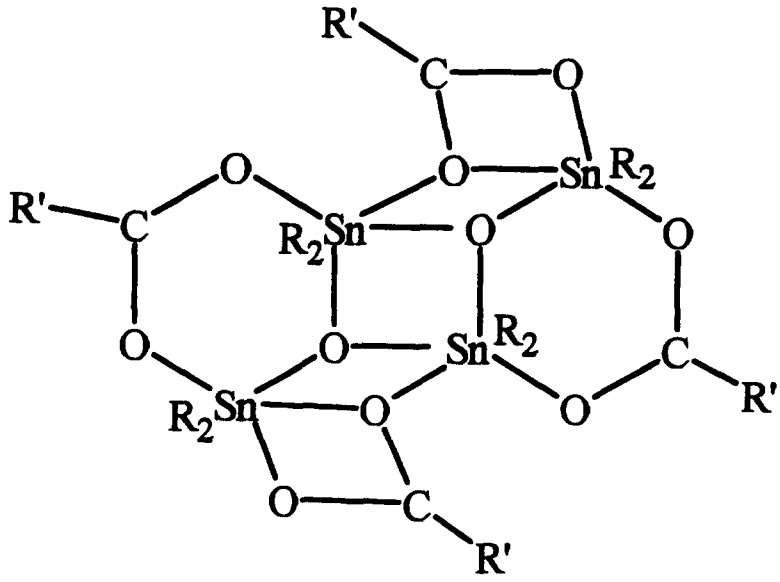


Fig. 2.

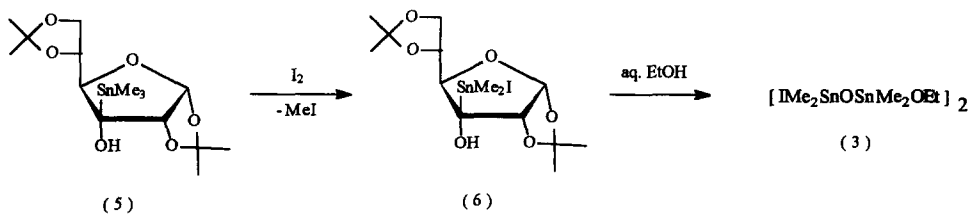
crystal structure of $[(\mu\text{-}Me_2Sn)_2\{\mu\text{-}(PrCO_2)Me_2Sn\}_2(\mu\text{-}PrCO_2)_2(\mu_3\text{-}O)_2]$ (**4**) has also been determined: **4** was obtained from the reaction of Me_2SnCl_2 and butanoic acid in water.

RESULTS AND DISCUSSION

Compound 3

Reaction of the stannylated carbohydrate **5** with equimolar I_2 in CCl_4 had been previously reported to produce **6** as the major tin-containing product; Me_3SnI was also obtained as a minor product [5]. Characterization of **6** was simply achieved from the NMR spectra data. Attempts to obtain a pure crystalline sample of **6** failed. Removal of all volatiles from the reaction mixture from **5** and I_2 and subsequent crystallisation of the resulting solid residue from 95% ethanol led to the isolation of crystalline **3**; the structure of solid **3**, a formal dimer of $[IMe_2Sn OSnMe_2OEt]$, was confirmed by X-ray diffraction (see later). Compound **3** is only sparingly soluble in $CDCl_3$ solution and only poorly resolved NMR spectra, e.g. without Sn—C coupling constants, were obtained. However, it was possible to detect from the ^1H and ^{13}C NMR spectra that two species (probably either different aggregates or stereoisomers) were present in $CDCl_3$ solution. For the OCH_2CH_3 units, there were two sets of δ^1H values [1.10 and 3.58 ppm (major compound) and 1.24 and 3.72 ppm (minor compound)], and two sets of $\delta^{13}C$ values [12.3 and 57.4 (major species) and 14.0 and 58.4 (minor species)]. In the ^1H NMR spectrum, three signals assignable to Me_2Sn groups were detected: these were at 0.96, 0.98 and 1.15 ppm, in the approximate ratio 6 : 1 : 5. It was possible to resolve these δ^1H values to give 0.96 and 1.15 ppm for the distinct Me_2Sn units of a major species and values of 0.98 and 1.15 ppm for those of a minor species. The ^{13}C NMR spectrum showed considerable complexity in the region 8–20 ppm, with $\delta^{13}C$ values of 8.1, 8.4, 9.4, 9.8, 18.1 and 19.7 ppm values. No compound of type **1**, having alkoxy groups, has been previously reported; aryloxy-containing compounds, $[(\mu\text{-}R_2Sn)_2(\mu\text{-}ArOR_2Sn)_2(\mu\text{-}OAr)_2(\mu_3\text{-}O)_2]$, however, have been prepared [3a] from $[R_2SnO]_n$ and ArOH. The $\delta^1H(Me_2Sn)$ values for $[(\mu\text{-}Me_2Sn)_2(\mu\text{-}ArOMe_2Sn)_2(\mu\text{-}Me_2Sn)_2(\mu\text{-}OAr)_2(\mu_3\text{-}O)_2]$ were 1.02 and 0.84 ppm (Ar = Ph) and 0.89 and 0.77 ppm (Ar = C_6H_4OMe-*p*); $\delta^{13}C(Me_2Sn)$ values were 2.4 and 4.5 ppm (Ar = Ph) and 5.2 and 7.2 ppm (Ar = C_6H_4OMe-*o*).

Compound **3** is considered to result from solvolytic cleavage of the tin–carbohydrate bond of **6**, on attempted recrystallization. The identification of the



(5) (6) (3)

resulting sugar species was not attempted. Compound **3** itself is also unstable to hydrolysis. As shown by NMR spectra, **6** on storage in air or on further crystallizations from 95% EtOH loses ethoxide units with the formation of $[(\mu\text{-}Me_2Sn)_2(\mu\text{-}IMe_2Sn)_2(\mu\text{-}OH)_2(\mu_3\text{-}O)_2]$ [$\delta^1H(Me_2Sn)$ = 0.99 and 1.15 ppm].

A number of halodialkylstannyl-saccharide derivatives has also been found to be unstable on storage in moist air or on attempted recrystallization from protic solvents. Compound **3**, the first such "decomposition" product to be characterized, may well be representative of these hydrolysis products. Earlier we had reported [6] that the trimethylstannyl-saccharide 1,2:5,6-di-*O*-isopropylidene-3-*O*-[(trimethylstannyl)-methyl]-α-D-glucofuranose (**7**) on storage in air underwent decomposition to Me_3SnO_2CH, Eq. (1). The type of dealkylation and other transformations of the triorganostannyl-carbohydrates in aqueous/aerial environments are of significance when considering their biological activities.

Crystal structure of **3**. As a consequence of the complex solution NMR spectra of **3**, it was decided to undertaken an X-ray diffraction study. The crystal of **3** used in the X-ray diffraction study was obtained directly from the crystallization of the total solid residue isolated on evaporation of the reaction mixture from **5** and I_2 in $CHCl_3$ solution. The atom arrangements for **3** are shown in Figure 3; bond lengths and angles are listed in Table 1. The ethoxide groups, but not the iodides, act as bridging units. The ladder structure of centrosymmetric **3** possesses two distinct Sn sites: each Sn centre is five-coordinate. Sn(1) is bonded to two C, I and to two O and has a distorted trigonal bipyramidal geometry and EtO and I ligands in the axial sites: I—Sn(1)—O = 160.88(14)°. The sum of the equatorial angles about Sn(1) is 359.9(12)°. The Sn(1)—I(1) bond is appreciably longer [2.9458(14) Å] than the single Sn—I bond lengths found in tetrahedral organotin iodides (2.69–2.729 Å)[7]. The Sn(1)—O bond lengths are 2.014(5) and 2.171(6) Å.

A greater distortion from a trigonal bipyramidal geometry is found for Sn(2), which is bonded to two C and to three O atoms. The angles at tin range from 72.8(2) to 147.0(2)°, the largest angle [O(1')—Sn(2)—O(2), symmetry operation; (i) $1-x$, $-y$, $2-z$], being the quasi-axial angle. The sum of the equatorial angles about Sn(2) is 362.8(11)°. The Sn(2)—O bond lengths are in the range 2.051(5)–2.178(6) Å. The central $Sn(2)_2O_2$ ring has O—Sn—O and Sn—O—Sn bond angles of 74.2(2) and 105.8(2)°, respectively. The very near planar arrangement of the tin, iodide and oxygen atoms in **3** can be seen in Fig. 4, the carbon atoms being the only major atoms significantly out of the plane.

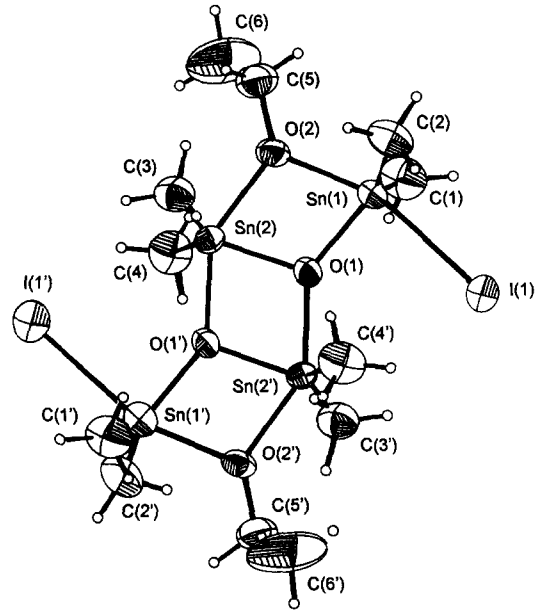
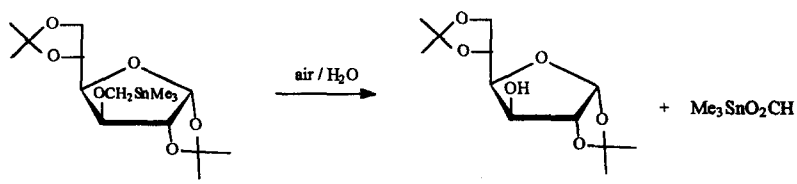


Fig. 3. Atom arrangements for **3**; ellipsoids are drawn at 40%.

The structure of the compound, $[(\mu\text{-}Bu_2Sn)_2[\mu\text{-}(o\text{-}MeOC_6H_4OBu_2Sn)\}_2$ $(\mu\text{-}o\text{-}MeOC_6H_4O)_2(\mu_3\text{-}O)_2]$ has also been reported [3a], this compound, which contains both bridging and nonbridging aroxy ligands, has a similar structure to that of **3**, with the nonbridging aroxy groups replacing the iodide units in **3**.

Compound **4**

Compound **4** was required for a study on the encapsulation and release of organotin species from controlled-release systems, based on metal carboxylate glasses [8]. It was prepared from Me_2SnCl_2 and butanoic acid in H_2O. Compound **4** is a further example of a compound with the general formula $[(R_2Sn)_4(R'CO_2)_4(O)_2]$. The NMR spectra of **4** in $CDCl_3$ solution indicated only a single species, with two different Me_2Sn sites. Figure 5 shows the atom arrangements for **4** in the solid state for a crystal



(7)

Table 1. Bond lengths (Å) and angles (°) for compound **3**

I(1)—Sn(1)	2.9458(14)	Sn(2)—O(1^{i})	2.131(6)
Sn(1)—O(1)	2.014(5)	Sn(2)—C(3)	2.133(10)
Sn(1)—C(2)	2.124(9)	Sn(2)—O(2)	2.178(6)
Sn(1)—C(1)	2.126(10)	O(1)—Sn(2^{i})	2.131(6)
Sn(1)—O(2)	2.171(6)	O(2)—C(5)	1.420(11)
Sn(2)—O(1)	2.051(5)	C(5)—C(6)	1.49(2)
Sn(2)—C(4)	2.104(9)		
O(1)—Sn(1)—C(2)	111.2(4)	C(4)—Sn(2)—C(3)	135.3(4)
O(1)—Sn(1)—C(1)	115.4(4)	O(1′)—Sn(2)—C(3)	96.7(3)
C(2)—Sn(1)—C(1)	133.3(4)	O(1)—Sn(2)—O(2)	72.8(2)
O(1)—Sn(1)—O(2)	73.7(2)	C(4)—Sn(2)—O(2)	95.2(4)
C(2)—Sn(1)—O(2)	95.5(4)	O(1^{i})—Sn(2)—O(2)	147.0(2)
C(1)—Sn(1)—O(2)	93.6(3)	C(3)—Sn(2)—O(2)	94.3(3)
O(1)—Sn(1)—I(1)	87.4(2)	Sn(1)—O(1)—Sn(2)	111.7(3)
C(2)—Sn(1)—I(1)	93.9(3)	Sn(1)—O(1)—Sn(2^{i})	141.8(3)
C(1)—Sn(1)—I(1)	92.0(3)	Sn(2)—O(1)—Sn(2^{i})	105.8(2)
O(2)—Sn(1)—I(1)	160.88(14)	C(5)—O(2)—Sn(1)	125.8(6)
O(1)—Sn(2)—C(4)	111.4(4)	C(5)—O(2)—Sn(2)	129.0(6)
O(1)—Sn(2)—O(1^{i})	74.2(2)	Sn(1)—O(2)—Sn(2)	101.3(2)
C(4)—Sn(2)—O(1^{i})	98.6(4)	O(2)—C(5)—C(6)	111.9(10)
O(1)—Sn(2)—C(3)	113.1(3)		

Symmetry operations: (i) $1-x, -y, 2-z$.

grown from MeOH solution; it has the general type of structure shown in Fig. 2. Selected bond lengths and angles are listed in Table 2.

Many of the previously reported [2] $[(R_2Sn)_4(R'CO_2)_4(O)_2]$ compounds, as the one here, have triclinic unit cells. The tetra-tin molecule **4** is centrosymmetric and contains two distinct tin atoms. The Sn(1) atom is bonded to two carbon and to four oxygen atoms, the longest Sn—O bond is that to O(4^{i}) [Sn(1)—O(4^{i}) = 2.712(8) Å, symmetry operation, (i) $1-x, 1-y, 1-z$], while the others are between 2.027(6) and 2.296(10) Å. The immediate coordination sphere of Sn(2) consists of two C and three O atoms, with Sn(2)—O bond lengths of 2.020(5) to 2.216(11) Å. There are, in addition, an intra-dimer contact, Sn(2)—O(5) [2.990(12) Å], and an inter-dimer contact, Sn(2)—O(5^{ii}) [3.109(11) Å, symmetry operation (ii), $1-x, 1-y, -z$]. Although these are clearly much weaker interactions, these are considered to be significant. There are two pairs of carboxylate groups: one is bidentate and bridges Sn(1) and Sn(2), while the other is chelated to Sn(2) atom and is bonded to Sn(1), within the molecule, and also is linked to a Sn(2) centre of an adjacent molecule. There are reports of other $[(Me_2Sn)_4(RCO_2)_4(O)_2]$ (e.g. R = CF_3 and CH_2Cl) having weak molecule–molecule

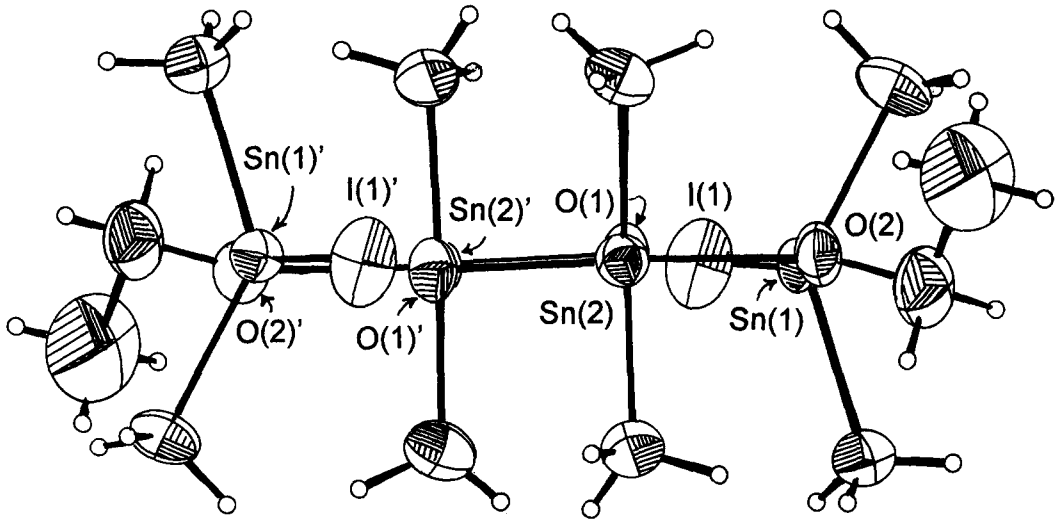


Fig. 4. View of the near planar arrangement of Sn, I and O atoms in **3**.

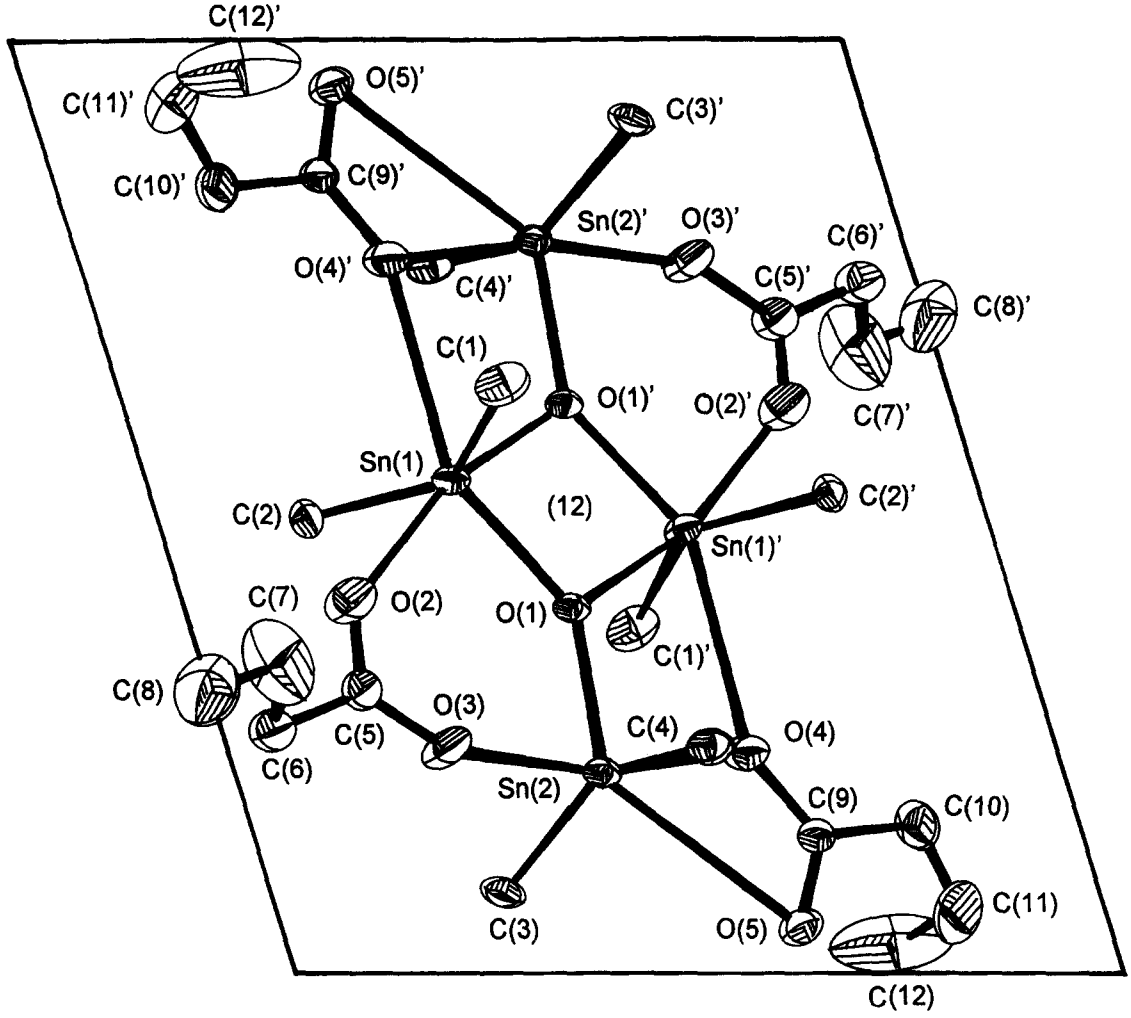


Fig. 5. The cell of **4** showing atom labels and 40% probability ellipsoids. The direction of view is along *b* (down into the page) and *x* and *z* as shown are the projections of *b* and *c*. H atoms have been omitted for clarity.

links with Sn—O connections between 3.0 and 3.2 Å [9]. Such interactions connect the tetra-nuclear molecules into chains running parallel to *c*. A stronger inter-molecule Sn—O interaction [2.56(1) Å] was reported [10] for the less symmetric $[(Me_2Sn)_4(AcO)_4(O)_2]$. The angles in the central Sn_2O_2 ring in **4** are 76.8(3) and 103.2(3)°.

The geometry of the molecule as a whole can be discussed in terms of displacements from the plane defined by the four tin atoms. The Sn/O nucleus of the molecule is remarkedly planar with out-of-plane distances for O(1), O(2), O(3), O(4) and O(5) of 0.003(6), 0.089(16), −0.104(15), 0.028(9) and 0.027(12) Å, respectively. For the tin–methyl carbon atoms, C(1), C(2), C(3) and C(4), the corresponding distances are −1.981(19), 1.989(14), 1.986(14) and −2.015(14) Å. A feature of **4** is the very high thermal parameters exhibited at room temperature; this is especially pronounced for the terminal carbons of the carboxylate units.

EXPERIMENTAL

Solution NMR spectra were obtained on a Bruker 250 MHz instrument and IR spectra on Philips Analytical PU 9800 FTIR and Nicolet 205 FTIR instruments. The X-ray diffraction data for 3 were collected by the EPSRC service, based at the University of Wales, Cardiff and that for **4** on a Nicolet P3 diffractometer.

Preparation of **3**

To a solution of 1,2 : 5,6-di-*O*-isopropylidene-3-*C*-trimethylstannyl-α-D-allofuranose [5] (0.588 g, 13.9×10^{-4} mol) in $CHCl_3$ (10 cm^3) was added I_2 (0.305 g, 13.9×10^{-4} mol). The reaction mixture was maintained at room temperature until the solution was decolourized (36 h). All volatiles were removed *in vacuo* and the solid residue was recrystallized from

Table 2. Bond lengths (Å) and angles (°) for compound **4**

C(1)—Sn(1)	2.067(17)	C(2)—Sn(1)	2.104(12)
O(1)—Sn(1)	2.027(6)	O(2)—Sn(1)	2.296(10)
O(1^{i})—Sn(1)	2.137(7)	O(4^{i})—Sn(1)	2.712(8)
Sn(1)—Sn(1)	3.264(2)	C(3)—Sn(2)	2.093(11)
C(4)—Sn(2)	2.098(12)	O(1)—Sn(2)	2.020(5)
O(3)—Sn(2)	2.216(11)	O(4)—Sn(2)	2.193(8)
O(5)—Sn(2)	2.990(12)	O(5^{ii})—Sn(2)	3.109(11)
C(5)—O(2)	1.145(15)	C(5)—O(3)	1.191(16)
C(9)—O(5)	1.211(14)	C(9)—O(4)	1.222(14)
C(2)—Sn(1)—C(1)	144.3(7)	O(1)—Sn(1)—C(1)	106.0(5)
O(1)—Sn(1)—C(2)	108.4(4)	O(2)—Sn(1)—C(1)	87.3(7)
O(2)—Sn(1)—C(2)	83.5(6)	O(2)—Sn(1)—O(1)	89.8(3)
C(1)—Sn(1)—Sn(1^{i})	105.4(5)	C(1)—Sn(1)—O(1^{i})	98.3(6)
C(1)—Sn(1)—O(4^{i})	80.1(6)	C(2)—Sn(1)—Sn(1^{i})	107.1(4)
C(2)—Sn(1)—O(1^{i})	98.6(4)	C(2)—Sn(1)—O(4^{i})	78.9(4)
O(1)—Sn(1)—Sn(1^{i})	39.6(2)	O(1)—Sn(1)—O(1^{i})	76.8(3)
O(1)—Sn(1)—O(4^{i})	141.9(3)	O(2)—Sn(1)—Sn(1^{i})	129.4(4)
O(2)—Sn(1)—O(1^{i})	166.4(4)	O(2)—Sn(1)—O(4^{i})	128.3(4)
Sn(1^{i})—Sn(1)—O(1^{i})	37.2(2)	Sn(1^{i})—Sn(1)—O(4^{i})	102.3(2)
O(1^{i})—Sn(1)—O(4^{i})	65.1(3)	C(3)—Sn(2)—O(5)	83.6(5)
C(3)—Sn(2)—O(5^{ii})	71.4(5)	C(4)—Sn(2)—O(5)	81.2(5)
C(4)—Sn(2)—C(3)	145.9(5)	O(1)—Sn(2)—C(3)	107.7(4)
C(4)—Sn(2)—O(5^{ii})	74.5(4)	O(1)—Sn(2)—O(5)	123.7(3)
O(1)—Sn(2)—O(5^{ii})	172.5(3)	O(3)—Sn(2)—O(5)	146.6(5)
O(1)—Sn(2)—C(4)	106.2(4)	O(3)—Sn(2)—C(3)	88.1(6)
O(3)—Sn(2)—C(4)	88.0(6)	O(3)—Sn(2)—O(1)	89.7(3)
O(3)—Sn(2)—O(5^{ii})	82.8(4)	O(4)—Sn(2)—O(5)	45.6(3)
O(4)—Sn(2)—C(3)	97.4(5)	O(4)—Sn(2)—C(4)	93.5(5)
O(4)—Sn(2)—O(1)	78.0(3)	O(4)—Sn(2)—O(3)	167.5(4)
O(4)—Sn(2)—O(5^{ii})	109.5(3)	O(5)—Sn(2)—O(5^{ii})	63.9(3)
Sn(1)—O(1)—Sn(1^{i})	103.2(3)	Sn(2)—O(1)—Sn(1^{i})	121.9(3)
Sn(2)—O(1)—Sn(1)	134.9(3)	C(5)—O(2)—Sn(1)	141.8(11)
C(5)—O(3)—Sn(2)	144.4(10)	O(3)—C(5)—O(2)	177.9(13)
C(9)—O(4)—Sn(2)	116.0(8)	O(5)—C(9)—O(4)	122.4(13)

Symmetry operations: (i) $1-x, 1-y, 1-z$; (ii) $1-x, 1-y, -z$.

ethanol. Colourless crystals of **3** (0.10 g) were obtained; compound **3** decomposed on heating. Found: C, 15.2; H, 3.8. Calc. For $C_{12}H_{34}I_2O_4Sn_4$: C, 14.8; H, 3.5%.

^{1}H NMR (250 MHz, $CDCl_3$): *major species* δ: 0.96 [s, 6H, $J(^{119,117}Sn—^1H)$ = *ca* 80 Hz, Me_2Sn], 1.10 [t, 6H, J = 7.3 Hz, CH_2CH_3], 1.15 [s, 6H, $J(^{119,117}Sn—^1H)$ = *ca* 80 Hz, Me_2Sn], 3.58[q, 4H, J = 7.3 Hz, CH_2CH_3].

minor species δ: 0.98 [s, 6H, $J(^{119,117}Sn—^1H)$ = *ca* 80 Hz, Me_2Sn], 1.15 [s, 6H, $J(^{119,117}Sn—^1H)$ = *ca* 80 Hz, Me_2Sn], 1.24 [t, 6H, J = 7.3 Hz, CH_2CH_3], 3.72 [br, 4H, CH_2CH_3].

^{13}C NMR (62.9 MHz, $CDCl_3$) δ: 8.0, 8.4, 9.5, 9.8, 12.3, 14.0, 18.3, 19.7, 57.7, 58.4.

Preparation of **4**

Dimethyltin dichloride (3.27 g, 0.0149 mol) in CH_2Cl_2 (100 cm^3) was shaken with sodium butanoate (3.28 g, 0.030 mol) in H_2O (50 cm^3) at room temperature for 12 h. The organic fraction was collected, washed with water and dried over $MgSO_4$. The solvent was removed under reduced pressure to leave an oil, which slowly crystallized. The product was recrystallized from MeOH; m.p. 161–162°C. Found: C, 29.9; H, 5.3. Calc.: C, 29.6; H, 5.3%.

^{1}H NMR ($CDCl_3$, 250 MHz); δ 0.77 [s, 6H, $J(^{119,117}Sn—H)$ = 84 Hz, Me_2Sn], 0.79 [s, 6H, $J(^{119,117}Sn—H)$ = 84 Hz, Me_2Sn], 0.93 (t, 3H, J = 7.3 Hz, $MeCH_2$), 1.61 (quintet, 2H, J = 7.3 Hz, $MeCH_2CH_2$), 2.16 (t, 2H, J = 7.3 Hz, CH_2CO).

^{13}C NMR ($CDCl_3$, 62.9 MHz): δ 6.3 [$J(^{119}Sn—^{13}C)$ = 755 Hz, $J(^{117}Sn—^{13}C)$ = 721 Hz, Me_2Sn], 8.6 [$J(^{119}Sn—^{13}C)$ 796 Hz, $J(^{117}Sn—^{13}C)$ = 761 Hz, Me_2Sn], 13.8 [$MeCH_2$ CH_2CO_2], 19.0 [$MeCH_2CH_2CO_2$], 38.1 [$MeCH_2$ CH_2CO_2], 180.1 [CO].

^{119}Sn NMR ($CDCl_3$, 93.3 MHz) δ: −175.5, 187.5.

Crystal structure determination of **3**

A colourless crystal was obtained from 95% ethanol solution. The unit cell and intensity data were col-

Table 3. Crystal data and structure refinement

	Compound **3**	Compound **4**
Formula	$C_{12}H_{34}I_2O_4Sn_4$	$C_{24}H_{52}O_{10}Sn_4$
Formula weight	970.96	975.44
Temperature (K)	150 (2)	298
Wavelength (Å)	0.71069	0.71069
Crystal system	Monoclinic	Triclinic
Space group	$P2_1/n$	PT
Unit-cell dimensions		
a (Å)	7.459(9)	9.578(6)
b (Å)	11.995(8)	9.535(4)
c (Å)	15.615(5)	11.466(6)
α (°)	90	106.63 (4)
β (°)	94.82(4)	103.37(4)
γ (°)	90	98.99(4)
Volume (Å^3)	1392(2)	947.9(9)
Z	2	1
Density (calc) (Mg m^{-1})	2.316	1.709
Absorption coefficient (mm^{-1})	5.774	2.66
F(000)	888	476
Crystal size (mm)	$0.22 \times 0.22 \times 0.11$	$0.54 \times 0.52 \times 0.50$
Range (°)	2.14 to 25.03	max: 25
Index range	$-8 \leqslant h \leqslant 8$	$-10 \leqslant h \leqslant 10$
	$-14 \leqslant k \leqslant 12$	$-11 \leqslant k \leqslant 10$
	$-18 \leqslant l \leqslant 17$	$0 \leqslant l \leqslant 13$
Reflections collected	5793	3346
Independent reflections	2139 [R(INT) = 0.1101]	2975 [R(INT) = 0.007]
Observed reflections	1889 (I > 2σ (I))	2221 (F > 4σ (F))
Refinement method	Full-matrix least-squares on F^2	Full-matrix least-squares on F
No. of parameters refined	105	193
Goodness-of-fit on F^2 (s)	1.041	—
Final R indices	$R1 = 0.0504$; $wR2 = 0.1229$ [$I > 2\sigma(I)$]	$R = 0.052$; $wR = 0.065$
R indices (all data)	$R1 = 0.0563$; $wR2 = 0.1257$	—
Final weighting scheme	$w = 1\ [\sigma^2(F_o^2 0 + (0.0686P)^2$ where $P = (F_o^2 + 2F_c^2)/3$	$w = 1\ [\sigma^2(F) + 0.001F^2]$
Residual diffraction (e Å^{-3})	2.433 (at Sn1 site) −1.117	1.05 (*ca* 1.0 Å from Sn1) −0.44

lected on a Delft Instruments FAST diffractometer using the routines ENDEX, REFINE and MADONL in the MADNES software [11] and processed using ABSMAD [12], detailed procedures have been described [13]. The structure was elucidated [14] with SIR92 and refined [15] with SHELXL93. A correction for absorption was made [16] with DIFABS. The non-H atoms were refined with anisotropic temperature factors and H atoms were refined to ride on their attached carbon atoms with isotropic temperatures 1.2° greater than their hosts. The molecular plot was obtained [17] using ZORTEP. Crystal data and structure refinement details are listed in Table 3.

Crystal structure determination of **4**

A colourless crystal was grown from MeOH solution. Data were collected on a Nicolet P3 diffractometer with Mo-K_α radiation; data collection used ω scan rates of 1.0 ($Ip < 150$) to 29.3 ($Ip > 2500$)° min^{-1}, where Ip was the prescan intensity. Scan width was 0.6° ω. Background counts were taken at $\pm 1.0°$ in ω from the Bragg angle of each reflection. Cell refinement was carried out using P3 diffractometer software [18]. Data reduction employed the program RDNIC [19]. Absorption correction utilised an empirical method based on psi scans [20]. The structure was solved by the heavy atom method, followed by successive Fourier and difference syntheses and refined by full-matrix least-squares. All non-H were refined anisotropically. The H-atoms were placed in calculated positions with C—H = 0.95 Å and refined upon the C to which they were attached with common group $U_{iso's}$ for each of Sn—methyl—H, alkyl methylene—H and alkyl methyl—H [refined values 0.23(2), 0.29(4) and 0.32(5), respectively]. All of the atoms in this structure display remarkedly high thermal vibration amplitudes. This is particularly so for the terminal atoms of the carboxylate anions which are clearly suffering from considerable disorder. All computations were performed on the SUN

SPARCserver (UNIX operating system) of the Computing Centre of the University of Aberdeen. Structure solution and refinement involved [21] SHELXS86 and SHELX76 [22], respectively. Molecular graphics utilized the ORTEX program [23] and the software used [24] for publication was XPUB. Crystal data and structure refinement details are listed in Table 3.

Acknowledgement—The use of the EPSRC X-ray crystallographic service at the University of Wales, Cardiff is gratefully acknowledged.

REFERENCES

1. For recent references, see (a) Ng, S. W. and Kumar Das, V. G., *Acta Cryst.* 1995, **C51,** 1774; (b) Kresinski, R. A., Staples, R. J. and Fackler, J. P., *Acta Cryst.* 1994, **C50,** 401; (c) Gielen, M., Bouhdid, A., Willem, R., Bregadze, V. I., Ermanson, L. V. and Tiekink, E. R. T., *J. Organomet. Chem.* 1995, **501,** 277; (d) Tiekink, E. R. T., Gielen, M., Bouhdid, A., Biesermans, M. and Willems, R., *J. Organomet. Chem* 1995, **494,** 247; (e) Mokal, V. B., Jain, V. K. and Tiekink, E. R. T., *J. Organomet. Chem.* 1994, **471,** 53; (f) Cox, M. J. and Tiekink, E. R. T., *Z. Krist.* 1994, **209,** 622.
2. For reviews of carboxylato–tin complexes, see Tiekink, E. R. T., *Appl. Organomet. Chem.* 1991, **5,** 1.
3. For example, see (a) Vatsa, C., Jain, V. K., Das, T. K. and Tiekink, E. R. T., *J. Organomet. Chem.* 1991, **418,** 329; (b) Puff, H., Friedrichs, E. and Visel, F., *Z. Anorg. Allg. Chem.* 1981, **477,** 50.
4. Harrison, P. G., in *The Chemistry of Tin.* Blackie, Glasgow, 1989.
5. Burnett, L. A., Doidge-Harrison, S. M. S. V., Garden, S. J., Howie, R. A., Taylor, O. J. and Wardell, J. L., *J. Chem. Soc., Perkin Trans.* 1; 1993, 1621.
6. Taylor, O. J. and Wardell, J. L., *J. Chem. Res. (S),* 1989, 98; *J. Chem. Res. (M),* 1989, 852.
7. Alcock, N. W. and Sawyer, J. F., *J. Chem. Soc., Dalton Trans.* 1977, 1090; Cody, V. and Cory, E. R., *J. Organomet. Chem.* 1969, **19,** 359; Zakharov, L. H., Betrov, B. I., Lobedev, V. A., Kuzmin, E. A. and Belov, N. V., *Kristallografiya,* 1978, **23,** 1049.
8. Duffy, J. A., Harston, P., Wardell, J. L. and Smith, P. J., *Appl. Organomet. Chem.* 1990, **4,** 69–71; Blair, J. A., Duffy, J. A. and Wardell, J. L., *Phys. Chem. Glasses,* 1992, **33,** 191; Blair, J. A., Mordue, A. J., Duffy, J. A. and Wardell, J. L., *J. Controlled Release,* 1994, **31,** 145; Blair, J. A., Ph.D. Thesis, University of Aberdeen, 1992.
9. Faggiani, R., Johnson, J. P., Brown, I. D. and Birchall, T., *Acta Cryst.* 1978, **B34,** 3743; Vialle, G., Peruzzo, V., Tagliavini, G. and Ganis, P., *J. Organomet. Chem.* 1984, **276,** 325.
10. Lockhart, T. P., Manders, W. F. and Holt, E. M., *J. Am. Chem. Soc.* 1986, **108,** 6611.
11. Pflugrath, J. W. and Messerschmidt, A., MADNES. Version 11, September. Distributed by Delft Instruments, Delft, The Netherlands, 1989.
12. Karaulov, A. I., *ABSMAD. Program for FAST Data Processing.* University of Wales, Cardiff, 1992.
13. Darr, J. A., Drake, S. R., Hursthouse, M. B. and Malik, K. M. A., *Inorg. Chem.* 1993, **32,** 5704.
14. Altomare, A., Burla, M. C., Camalli, M., Gascarino, G., Giacovazzo, C., Guagliardi, A. and Polidori, G., *J. Appl. Chem.* 1994, **27,** 435.
15. Sheldrick, G. M., *SHELXL93. Program for the Refinement of Crystal Structures.* University of Gottingen, Germany, 1994.
16. Walker, N. and Stuart, D., *Acta Cryst.* 1983, **A39,** 158.
17. Zsolnai, L., *ZORTEP. An Interactive ORTEP Program.* University of Heidelberg, Germany, 1995.
18. *Nicolet P3/R3 Data Collection Operator's Manual.* Nicolet XRD Corporation, 10061 Bubb Road, Cupertino, CA 95014, U.S.A., 1980.
19. Howie, R. A., *RDNIC. Data Reduction Program for Nicolet P3 Diffractometer.* University of Aberdeen, U.K., 1980.
20. North, A. C. T., Phillips, D. C. and Mathews, F. S., *Acta Cryst.* 1968, **A24,** 351.
21. Sheldrick, G. M., *Acta Cryst.* 1990, **A46,** 467.
22. Sheldrick, G. M., *SHELX76. Program for Crystal Structure Determination.* University of Cambridge, U.K., 1977.
23. McArdle, P., *J. Appl. Cryst.* 1994, **27,** 438.
24. Low, J. N., *XPUB. Program for the Preparation of Tabular Crystallographic Data.* University of Dundee, U.K., 1980.

Pergamon

PII: S0277-5387(96)00371-3

Polyhedron Vol. 16, No. 6, pp. 889–895, 1997
Copyright © 1996 Elsevier Science Ltd
Printed in Great Britain. All rights reserved
0277-5387/97 $17.00+0.00

A polymeric complex of copper(II) bridged simultaneously by tridentate glycinato and μ(N,S)-thiocyanato anions. Synthesis, spectral, structural and thermal properties of the complex $[Cu(Glycinato)(NCS)(H_2O)]_n$

Mohamed A. S. Goher,[a]* Laila A. Al-Shatti[a] and Franz A. Mautner[b]

[a] Department of Chemistry, Faculty of Science, Kuwait University, P.O. Box 5969 Safat, 13060 Kuwait

[b] Institut für Physikalische und Theoretische Chemie, Technische Universität Graz, A-8010 Graz, Austria

(Received 24 May 1996; accepted 31 July 1996)

Abstract—The copper(II)–glycine–thiocyanate ion system, which has been studied, afforded a new 1:1:1 complex which crystallized with an additional water molecule. The IR spectrum of the solid complex suggests an aquo ligand, a bridging thiocyanato ligand and a *N,O*-bidentate chelating glycinato ligand. Room-temperature magnetic moment, electronic spectra and ESR spectra suggested a tetragonally distorted octahedral structure for the complex $[Cu(glycinato)(NCS)(H_2O)]_n$, which was confirmed by X-ray crystallography. The complex contains $\mu(N,S)$-thiocyanato ligands and an aqua molecule. The glycinato anion chelates a copper atom *via* its N and O atoms. The second O atom of the glycinato group links another Cu atom at a long distance of 2.908(5) Å, giving rise to *N,O,O*-tridentate chelating bridging glycinato ligand. The structure of the complex is further consolidated by hydrogen bonds of the type O—H···O between aqua molecules and carboxylate O atoms. The thermal decomposition of the complex was investigated under nitrogen. Copyright © 1996 Elsevier Science Ltd

Keywords: glycinato; thiocyanato; copper(II) complex; crystal structure.

Binding of small ligand molecules to copper proteins has been widely employed as a method to obtain structural or mechanistic information on the metal sites [1]. For instance, the azide ion has been used in binding studies on amine oxidases [2], superoxide dismutase [3], galactose oxidase [4], laccase [5] and ascorbate oxidase [6]. Casella *et al.* have initiated a systematic investigation of the binding of azide and thiocyanate ions to a series of copper(II) complexes with ligands containing nitrogen and oxygen donor atoms which can be considered as mimics of the potential ligands of type 2 and 3 copper centers in the proteins [7,8]. In such cases binding of anions such as azide, thiocyanate and bromide to copper(II) is generally accompanied by the appearance of LMCT transitions in the visible or near-UV region and produce changes in the EPR spectra that may be potentially very useful for empirical correlations between spectra and structure.

X-ray analysis indicates that in $[M(gly)_2]\cdot nH_2O$, where M = Ni, Zn or Cd, n = 2 or 1 and gly = glycino anion, the two glycino anions coordinate *via* their N and O atoms to the metal by forming a *trans*-square planar structure [9,10]. Furthermore, it has been shown that the oxygens of the carbonyl groups that are not coordinated to the metal are hydrogen bonded either to the amino group of the neighboring molecule or to water of crystallization, or they are bounded weakly to the metal of the neighboring complex.

Recently we established that a substitution of one of the two picolinate anions in the parent [M(picolinato)$_2$] complex by other anion, such as Cl^-, NCS^- or N_3^-, leads to new mode of bonding of the picolinato anion [11–13]. As binding of pseudohalide ions to copper(II)–amino acid systems have not yet been

* Author to whom correspondence should be addressed.

investigated, we studied the binding of the thiocyanate anion to copper(II)–glycine complex in order to appraise the influence of these anions on the mode of bonding of each other. This system afforded a new polymeric 1 : 1 : 1 thiocyanato–copper(II)–glycinato complex which crystallizes with one water molecule. The synthesis and structural properties of this complex as elucidated by spectroscopic and X-ray crystallographic methods are reported here

EXPERIMENTAL

Glycine was obtained from Aldrich and the other chemicals were of analytical grade quality.

Preparation of the complexes

Cu(glycinato)$_2 \cdot H_2O$. This complex was prepared [14, 15] by mixing a solution of copper(II) nitrate trihydrate dissolved in acetone with an aqueous solution of glycine in 1 : 2 molar ratio. The mixture was stirred, heated for several minutes and allowed to stand until blue crystals were isolated. Found: C, 20.6; H, 4.5; N, 12.6; Cu, 27.9. Calc.: C, 20.9; H, 4.4; N, 12.2; Cu, 27.7%.

[Cu(glycinato)(NCS)$(H_2O)]_n$ (**1**). $Cu(NO_3)_2 \cdot 3H_2O$ (1.2 g, 5 mmol) dissolved in distilled water (20 cm^3) was mixed with glycine (0.75 g, 10 mmol) dissolved in water (20 cm^3). To this mixture, NaNCS (0.24 g, 3 mmol) dissolved in water (3 cm^3) was added dropwise. The final mixture should be filtered if some white precipitate is formed and the filtrate allowed to stand over several days until blue (green tinted) colored crystals are produced. Found: C, 16.7; H, 3.0; N, 13.2; S, 15.6; Cu, 29.5. Calc.: C, 16.9; H, 2.8; N, 13.1; S, 15.0; Cu, 29.7%.

Physical measurements

Procedures and instruments used for other physical measurements are as described previously [16].

X-ray crystallography

A modified STOE four-circle diffractometer was used for single-crystal X-ray measurements. Orientation matrix and lattice parameters were obtained by least-squares refinement of the diffraction data from 45 reflections in the 2θ range 10–29°. Data were collected at 298(1) K using graphite crystal-monochromatized Mo-K_α radiation ($\lambda = 0.71069$ Å) and the ω-scan technique. The intensities were corrected for Lorentz and polarisation effects and for absorption [17]. Crystallographic data are given in Table 1.

The structure was solved by Patterson superposition methods and subsequent Fourier analyses. Anisotropic displacement parameters were applied to the non-hydrogen atoms in full-matrix least-squares refinements. Hydrogen-atom positions were obtained from ΔF maps and included in the final refinement cycles by use of geometrical constraints. The programs DIFABS [17], SHELX-76 [18], SHELXS-86 [19], PLATON [29] and THE XRAY SYSTEM [21] were used for computations. Analytical expressions of neutral-atom scattering factors were employed and anomalous dispersion corrections were incorporated [22]. Selected bond distances and bond angles are given in Table 2. Positional parameters, anisotropic displacement parameters, hydrogen-atom coordinates, a full list of bond lengths and angles and observed and calculated structure factors have been deposited with the Editor as supplementary material.

RESULTS AND DISCUSSION

When thiocyanate was added to an aqueous solution of bis(thiocyanato)copper(II) complex no change of the blue color occurred whatever the amount of added thiocyanate. This is in contrast to what we have observed [23] in the case of the addition of the azide ion to the same system. In the latter case a new absorption band occurred at 354 nm. Addition of thiocyanate to an aqueous solution of a mixture of copper(II) ions and glycine in 1 : 2 molar ratio, however, was accompanied by a new absorption band at 339 nm. The electronic absorption spectrum of Cu(gly-

Table 1. Crystallographic data and processing parameters

Molecular formula	$C_3H_6CuSN_2O_3$
Molecular weight	213.70
Crystal system	Monoclinic
a (Å)	5.161(2)
b (Å)	7.461(3)
c (Å)	8.357(4)
β (°)	94.72(3)
V (Å^3)	320.7(2)
Space group	$P2_1$ (no. 4)
Z	2
$F(000)$	214
μ(Mo-K_α) (mm^{-1})	0.37
D_{calc}/D_{obs} (mg m^{-3})	2.213/2.19(3)
Approximate crystal size (mm)	0.50 × 0.20 × 0.15
Data collection limits	$\pm h, \pm k, l$; $2\theta < 60°$
Scan mode	ω-scan, $\Delta\omega = 1.50°$
$F_o > 3\sigma(F_o)$	1373
Least-squares parameters	105
R	0.048
R_w	0.048
Weighting scheme	$5.880\sigma^{-2}(F_o)$
Residual extrema in final difference map (e Å^{-3})	+1.16/−0.98

Table 2. Selected bond distances (Å) and bond angles (°)

Cu(1)—S(1)	2.894(2)	Cu(1)—O(2c)	2.908(5)
Cu(1)—O(1)	1.954(5)	Cu(1)—O(3)	1.945(6)
Cu(1)—N(2)	2.015(5)	Cu(1)—N(1d)	1.905(7)
S(1)—C(1)	1.628(6)	O(1)—C(2)	1.270(7)
O(2)—C(2)	1.239(7)	N(1)—C(1)	1.165(9)
N(2)—C(3)	1.480(8)	C(2)—C(3)	1.500(8)
S(1)—Cu(1)—O(1)	91.1(2)	S(1)—Cu(1)—O(3)	100.1(2)
S(1)—Cu(1)—N(2)	91.7(2)	S(1)—Cu(1)—O(2c)	170.5(1)
O(1)—Cu(1)—O(3)	84.0(2)	O(1)—Cu(1)—N(2)	83.1(2)
O(1)—Cu(1)—O(2c)	90.3(2)	O(3)—Cu(1)—N(2)	162.6(2)
O(3)—Cu(1)—O(2c)	89.3(2)	N(2)—Cu(1)—O(2c)	79.2(2)
Cu(1)—S(1)—C(1)	101.2(2)	Cu(1)—O(1)—C(2)	116.6(4)
C(2)—O(2)—Cu(1a)	99.6(4)	C(1)—N(1)—Cu(1b)	176.2(6)
Cu(1)—N(2)—C(3)	109.3(4)	S(1)—C(1)—N(1)	178.4(6)
O(1)—C(2)—O(2)	123.5(6)	O(1)—C(2)—C(3)	117.4(5)
O(2)—C(2)—C(3)	119.1(5)	N(2)—C(3)—C(2)	110.4(5)
Hydrogen bonds			
O(3)—H(5)	0.90(2)	O(3)—H(6)	0.80(10)
H(5)···O(2)	1.94(4)	H(6)···O(2)	1.91(10)
O(3)—H(5)···O(2)	162(10)	O(3)—H(6)···O(2)	158(9)
O(3)···O(2)	2.812(7)	O(3)···O(2)	2.766(8)

Symmetry codes: (a) $-x, -1/2+y, -z$; (b) $-x, -1/2+y, 1-z$; (c) $-x, 1/2+y, -z$; (d) $-x, 1/2+y, 1-z$.

cinato)$_2 \cdot H_2O$ complex in water exhibited a single absorption band at 637.5 nm, whereas that of a mixture of copper(II) ions and glycine (1 : 2 molar ratio) showed the corresponding band at 732 nm. Thus, the complexes that exist in both cases are different. This result was confirmed by measuring the EPR spectra of both solutions. These spectra differ in number and positions of the EPR lines. Thus, while the thiocyanate does not bind the bis(glycinato) complex of copper(II), it interacts with the complex formed by mixing copper(II) ions and glycine.

Mixing of copper(II) ions, glycine and thiocyanate anions in a molar ratio of 1 : 2 : 1 in aqueous solution, however, afforded a green-colored solution from which a blue copper(II) complex of the empirical formula Cu(glycinato)(NCS)(H_2O) deposited. This complex is insoluble in water, alcohol, chloroform, carbon tetrachloride and acetone, but soluble in DMF and DMSO giving rise to nonconducting solutions. This result is an indication of the polymeric nature of the complex.

The principal structural features of the [Cu(glycinato)(NCS)(H_2O)] complex are illustrated in Fig. 1. The stereochemistry about each six-coordinated copper center is best described as a tetragonal bipyramid (4+2). The glycinato anion chelates a copper atom, Cu(1), *via* its amino nitrogen atom, N(2) [Cu—N = 2.015(5) Å], and a carboxylate oxygen atom, O(1) [Cu—O = 1.954(5) Å], to form a five-membered ring. The Cu(1) atom is further coordinated by a second oxygen atom, O(2c), of the carboxylate group of another glycinato anion at a Cu—O distance of 2.908(5) Å. Thus, the glycinato anion behaves as a *N,O,O*-tridentate chelating bridging ligand in the present complex. Each metal atom is further linked by an oxygen atom of an aquo molecule

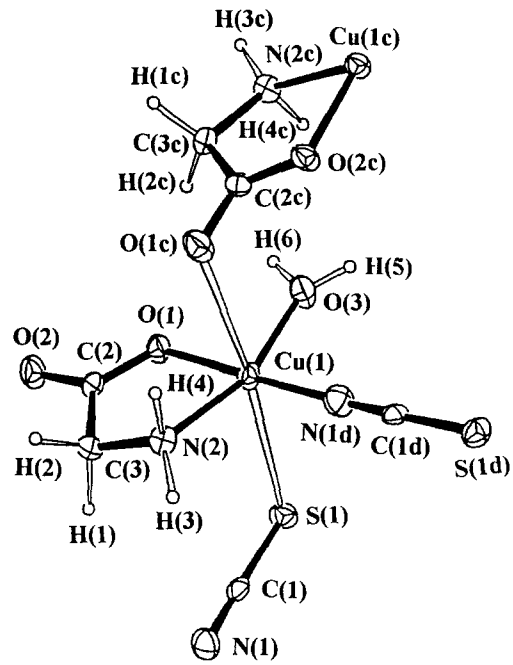


Fig. 1. Molecular geometry and atom labeling scheme of $Cu(C_2H_4O_2N)(NCS)(H_2O)$. Symmetry code according to Table 2.

[Cu—O = 1.945(6) Å]. The thiocyanato groups are functioning in the $\mu(N,S)$ fashion to bridge each copper atom with its nearest copper neighbor [Cu—NCS and Cu—SCN distances are 1.905(7) Å and 2.894(2) Å, respectively], forming a three-dimensional network structure. The C—S bond length of 1.628(6) Å found in the present complex is very close, whereas the N—C distance of 1.165(9) Å is larger than corresponding values [1.646(4) Å for C—S and 1.148(6) Å for N—C] found in [Cd(picolinato)(NCS)]$_n$-containing $\mu(N,S)$ thiocyanato ligands [13]. The N—C bond length is much larger than the corresponding value [1.140(11) Å] found in the [Mn(H-quin)(quin)(NCS)$(H_2O)_2$] complex (H-quin is quinaldic acid) with terminal nitrogen-bonded thiocyanato ligands [24]. The thiocyanato ligand in the present structure is linear [$\angle$NCS = 178.5(6)°]. Intermolecular hydrogen bonds of the type O—H $\cdots$ O between the aquo molecules and the oxygen atoms of the carboxylate groups (Fig. 2, and Table 2) consolidate the structure of the present complex.

The structure of the title complex may be compared with that of [Cd(picolinato)(NCS)]$_n$ [13], which also exhibits $\mu(N,S)$-thiocyanato ligands and six-coordinated metal centers. In the cadmium complex the picolinato anion is coordinated *via* N(1) and O(1) to Cd(1), forming a chelating five-membered ring. O(1) and O(2) are further coordinated to another cadmium center, Cd(1c) (see Fig. 3, ref. [13]), forming an additional chelating four-membered ring. As a consequence the cadmium atoms and O(1) atoms of the picolinate anions form the backbone of a zigzag chain structure oriented along the short *b* axis of the monoclinic unit cell. The picolinato anion in the cadmium complex functions as a *N,O,O,O'*-tetradentate chelating bridging ligand.

The IR spectrum of the solid complex (**1**) shows a very broad band in the range 3500–2200 cm^{-1}, due to νO—H $\cdots$ O [25], between aqua molecules and COO$^-$ groups of glycinato ligands. The absorption vibrations due to the bonded NH_2 group appear as strong bands at 3300 and 3260 cm^{-1}, similar to those for

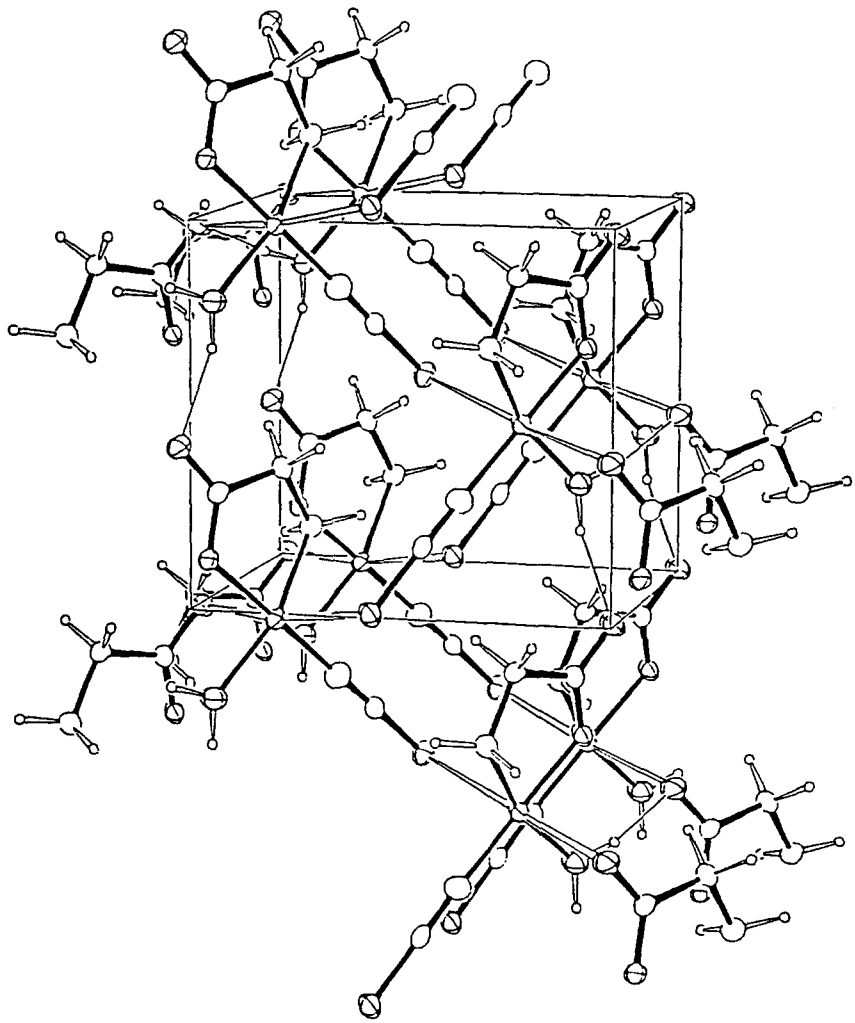


Fig. 2. Unit-cell plot (stereo) of Cu($C_2H_4O_2N$)(NCS)(H_2O), viewed along the *a* axis of the unit cell. Hydrogen bonds are indicated by thin lines.

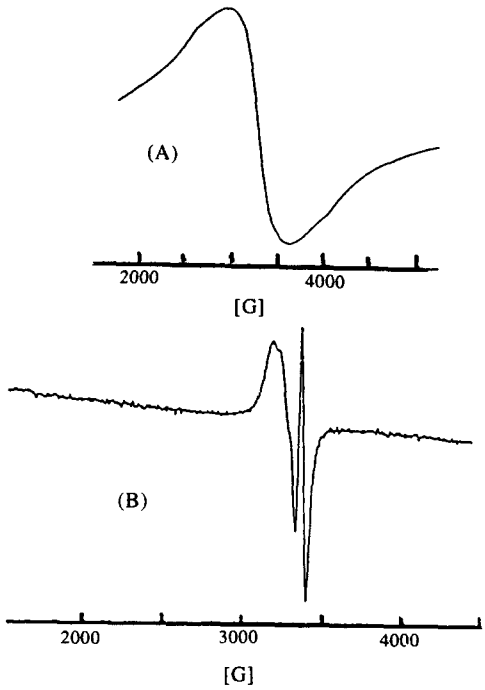


Fig. 3. ESR spectra of $Cu(C_2H_4O_2N)(NCS)(H_2O)$ complex: (a) polycrystalline powder and (b) DMSO saturated solution.

$Cu(gly)_2 \cdot H_2O$. The carbonyl stretching absorption band [ν(C=O)] appears at 1653 cm^{-1}, whereas ν(C—O) appears at 1401 cm^{-1} compared with the corresponding bands (1593 and 1392 cm^{-1}, respectively) in the spectrum of $[Cu(gly)_2]$ [26]. We tentatively assigned the following frequencies [27]: the band at 532 cm^{-1} due to [$\rho_w(H_2O)$], at 462 cm^{-1} to [δNCS + ν(Cu—OH_2)] and at 422 cm^{-1} to [ν(Cu—N(gly))].

The IR spectrum of complex **1** shows a very strong band at 2100 cm^{-1} due to the ν(C—N) mode, in addition to two medium bands at 809 and 770 cm^{-1} related to ν(C—S). Bridging *N,S*-thiocyanato groups are expected to exhibit two ν(C—N) bands above and below 2100 cm^{-1} as well as two ν(C—S) bands [28–32]. While the appearance of two ν(C—S) bands is consistent with the X-ray structural results of the complex, the band at 2100 cm^{-1} is on the borderline between N- and S-bonded thiocyanato ligands. The appearance of a single ν(C—N) absorption band in the IR spectrum, however, is not unusual and has been observed for many μ(*N,S*)-thiocyanato complexes [13, 33,34].

The room-temperature magnetic moment of 1.82 B.M. found for complex **1** is consistent with magnetically dilute tetragonal copper(II) systems, show-

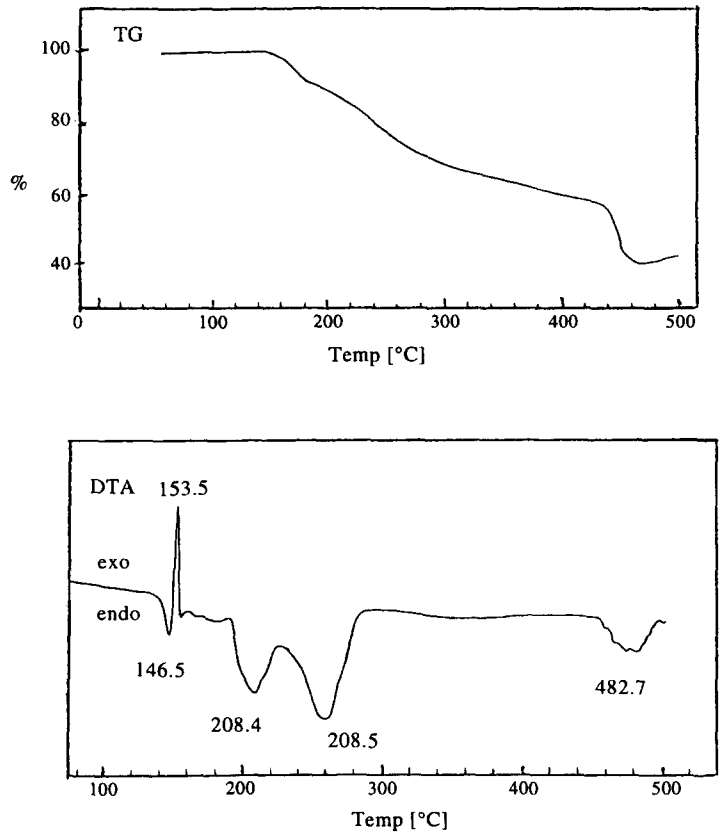


Fig. 4. Thermal decomposition of $[Cu(C_2H_4O_2N)(NCS)(H_2O)]$.

ing an orbitally nondegenerate groundstate [35]. The electronic absorption spectrum of the title complex as a solid mulled in Nujol displays a broad *d–d* band centered around 641 nm, which is consistent with a tetragonal, octahedral geometry around copper(II) [36]. The spectrum of a saturated DMSO solution of complex **1** shows the *d–d* band at 754 nm; a position which is suggestive of five-coordination geometry of copper(II) [37,38]. Thus, complex **1** does not maintain its solid-state structure in DMSO solution. This may be achieved by breaking the long Cu—O bond of 2.908 Å value in DMSO solvent.

The ESR spectrum of a polycrystalline powder of the title complex at room temperature is of one *g*-value type with a *g* value of 2.146 (Fig. 3). As reported for other complexes of Cu^{II} [39], a grossly misaligned set of tetragonal axes seems to be a more plausible explanation. As a result of the poor dissolution of this complex, its ESR spectrum in DMSO displays a poor resolution of the four hyperfine lines of uncoupled copper(II) as can be seen from Fig. 3.

The thermal decomposition of [Cu(glycenato)(NCS)$(H_2O)]_n$ is represented in Fig. 4. The first step of the thermal decomposition consists of a dehydration at 146°C [loss of weight (%); experimental 8.5 and theoretical 8.4]. The DTA curve [Fig. 4(b)] starts this step with a narrow endotherm (melting endotherm), immediately followed by an exotherm. This may be interpreted as a rearrangement of the amorphous system in the crystalline phase. The following, well-separated step 2 for the dehydrated compound does not reflect a simple one-stage process and the DTA curve shows two endotherms. The experimental loss of weight of 34.65%, however, indicates that $C_2H_4NO_2$ is released (theoretical 34.66%) in the second step. A reductive [Cu^{II}–Cu^{I}] degradation is completed at *ca* 440°C in dynamic nitrogen atmosphere. A polymer residue of the empirical formula $[Cu(SCN)]_n$ is indicated by the calculated weight loss of the complex. The weight loss of 16.84% in the temperature range 440–500°C (T_{max} = 482.6°C, Fig. 4) may indicate the release of sulfur (calc. 15.0%) with the formation of another polymer residue $[Cu(CN)]_n$. This suggestion was borne in mind because of the fact that the thermal decomposition of $K[Cu_2(CN)_3] \cdot H_2O$ and $[(CH_3)_2(C_6H_5)S][Cu_2(CN)_3]$ [40] ended with the formation of CuCN at 420 and 470°C, respectively.

Acknowledgments—Financial support by the College of Graduate Studies, Kuwait University, is gratefully acknowledged. The authors thank Professor Ch. Kratky for the use of the STOE diffractometer.

REFERENCES

1. Dooley, D. M., *Life Chem. Rep.* 1987, **5,** 91.
2. Dooley, D. M. and Cote, C. E., *Inorg. Chem.* 1985, **24,** 3996.
3. Dooley, D. M. and McGuirl, M. A., *Inorg. Chem.* 1986, **25,** 1261.
4. Bereman, R. D., Ettinger, M. J., Kosman, D. J. and Kurland, R. J., *Adv. Chem. Ser.* 1977, **162,** 263.
5. Spira-Solomon, D. J. and Solomon, E. I., *J. Am. Chem. Soc.* 1987, **109,** 6421.
6. Casella, L., Gullotti, M., Pallenza, G., Pintar, A. and Marchesini, A., *Biochem. J.* 1988, **251,** 441.
7. Casella, L., Gullotti, M., Pallanza, G. and Buga, M., *Biol. Metals* 1990, **3,** 137.
8. Casella, L., Gullotti, M., Pallenza, G. and Buga, M., *Inorg. Chem.* 1991, **30,** 221.
9. Stosick, A. J., *J. Am. Chem. Soc.* 1945, **67,** 365.
10. Low, B. M., Hershfeld, F. H. and Richards, F. M., *J. Am. Chem. Soc.* 1959, **81,** 4412.
11. Goher, M. A. S., Abu-Youssef, M. A. M., Mautner, F. A. and Popitsch, A., *Polyhedron*, 1992, **11,** 2137.
12. Goher, M. A. S., Hafez, A. K., Abu-Youssef, M. A. M., Popitsch, A., Fritzer, H. P. and Mautner, F. A., *Monatsh. Chem.* 1994, **125,** 833.
13. Mautner, F. A., Abu-Youssef, M. A. M. and Goher, M. A. S., *Polyhedron*, 1997, **16,** 235.
14. Low, B. W., Hirshfeld, F. L. and Richards, F. M., *J. Am. Chem. Soc.* 1959, **18,** 4412.
15. Hitchman, M. A. and Kwan, L., *J. Chem. Soc., Dalton Trans.* 1987, 457.
16. Goher, M. A. S., Abu-Youssef, M. A. M., Mautner, F. A. and Popitsch, A., *Polyhedron*, 1993, **12,** 1751.
17. Walker, N. and Stuart, D., *Acta Cryst.* 1983, **A39,** 158.
18. Sheldrick, G. M., *SHELX-76, A Program for Crystal Structure Determination.* University Chemical Laboratory, Cambridge, 1976.
19. Sheldrick, G. M., *SHELXS-86.* Universitat Gottingen, Germany, 1986.
20. Spek, A. L., in *Computational Crystallography*, ed. D. Sayre, Clarendon Press, Oxford, 1982, p. 528.
21. Stewart, J. M., *The X-RAY SYSTEM*, version of 1976, Technical Report TR-466. University of Maryland, College Park, 1976.
22. *International Tables for X-Ray Crystallography*, Vol. IV. Kynoch Press, Birmingham. 1974, pp. 99 and 149.
23. Goher, M. A. S., Al-Salem, N. A. and Mautner, F. A., to be published.
24. Goher, M. A. S. and Mautner, F. A., *Polyhedron*, 1993, **12,** 1863.
25. Gelfand, L. S., Pytlewski, L. L., Speca, A. N., Mikulski, C. M. and Karayannics, N. M., *J. Inorg. Nucl. Chem.* 1980, **42,** 209.
26. Lane, T. J., Dukin, J. A. and Hooper, R. J., *Spectrochim. Acta*, 1964, **20,** 1013; Tomita, K., *Bull. Chem. Soc. Jpn.* 1961, **34,** 280, 286; Condrate, R. A. and Nakamoto, K., *J. Chem. Phys.* 1965, **42,** 2590.
27. Nakamoto, K., *Infrared Spectra of Inorganic and Coordination Compounds*, 2nd edn. John Wiley, New York, 1970.
28. Mitchell, P. C. H., and Williams, R. J. P., *J. Chem. Soc.* 1960, 1912; Tramer, A., *J. Chim. Phys.* 1962, **59,** 232.

29. Lewis, J., Nyholm, R. S. and Smith, P. N., *J. Chem. Soc.* 1961, 4590.
30. Sabatini, A. and Bertini, I., *Inorg. Chem.* 1965, **4,** 959.
31. Clark, R. J. H. and Williams, C. S., *Spectrochim. Acta*, 1966, **22,** 1081; Aslam, M. and Assai, W. H. S., *Inorg. Nucl. Chem. Lett.* 1971, **7,** 96.
32. Goher, M. A. S., *Coll. Czech. Chem. Commun.* 1977, **42,** 1478.
33. Chatt, J. and Duncanson, L. A., *Nature*, 1956, **178,** 997; Chatt, J., Duncanson, L. A., Hart, F. A. and Owston, P. G., *Nature*, 1958, **181,** 43.
34. Owston, P. G. and Rowe, J. M., *Acta Cryst.* 1960, **13,** 253.
35. Figgis, B. N. and Lewis, J., *Prog. Inorg. Chem.* 1964, **6,** 37.
36. Kohout, J., Quastlerova-Hvastijova, M., Kohoutova, M. and Gazo, J., *Monatsch.* 1971, **102,** 350; *ibid.* 1973, **104,** 779.
37. Bew, M. J., Dudley, R. J., Fereday, R. J. and Hathaway, B. J., *J. Chem. Soc. A*, 1971, 1437.
38. Bamfield, P., Price, R. and Miller, R. G. J., *J. Chem. Soc. A*, 1966, 1447.
39. Hathaway, B. J. and Billing, D. E., *Coord. Chem. Rev.* 1970, **5,** 143.
40. Cernak, J., Gooryova, K., and Sabolova, S., *Inorg. Chim. Acta*, 1991, **185,** 119.

Pergamon

PII: S0277-5387(96)00365-8

Polyhedron Vol. 16, No. 6, pp. 897–902, 1997
Copyright © 1996 Elsevier Science Ltd
Printed in Great Britain. All rights reserved
0277-5387/97 $17.00+0.00

A dinuclear manganese(II) complex doubly bridged by *skew–skew* μ-carboxylato groups: synthesis and X-ray structure of $[\{Mn(bpy)_2(p\text{-}Me_2N^+C_5H_4NCH_2CO_2^-)\}_2](ClO_4)_4$

Ping-Rong Wei,* Qi Li, Wing-Por Leung and Thomas C. W. Mak†

Department of Chemistry, The Chinese University of Hong Kong, Shatin, New Territories, Hong Kong

(Received 5 July 1996; accepted 24 July 1996)

Abstract—In the novel centrosymmetric dinuclear manganese(II) complex $[\{Mn(bpy)_2(p\text{-}Me_2N^+C_5H_4NCH_2CO_2^-)\}_2](ClO_4)_4$, the bridging betaine ligand functions in an abnormal non-planar *skew–skew* mode, with both Mn^{II} atoms lying on the same side of the mean plane of each bridging carboxylato group. The intramolecular metal–metal separation in the dinuclear cation agrees well with those in the range 4.64–4.79 Å found for known doubly carboxylato-bridged manganese(II) complexes. Copyright © 1996 Elsevier Science Ltd

Keywords: dinuclear manganese(II) complex; betaine; 4-dimethylaminopyridinioacetate; carboxylate; bridging ligand.

There has been considerable interest in the coordination chemistry of manganese complexes with carboxylato ligands, owing to the fact that there is an increased recognition of the role of this metal in biological systems [1–3]. Dinuclear manganese(II) complexes are of special interest, since such systems are known to exist at the active centres of some manganese-containing enzymes [4]. Recently, dinuclear units with one to three carboxylato bridges were suggested to be plausible structures of the dinuclear sites in Mn catalases [5,6].

Our recent studies have demonstrated that betaine ($Me_3N^+CH_2CO_2^-$; IUPAC name: trimethylammonioacetate) and its derivatives, considered as structural analogues of the corresponding carboxylate anions, are useful in the preparation of soluble carboxylate-like complexes of transition metals [7–11]. The crystal structures of manganese(II) carboxylates have been widely studied, and polymeric structures generally predominate [12,13]. Several dinuclear manganese(II) carboxylates containing one to three carboxylate bridges that are stabilized by the incorporation of bidentate terminal ligands such as 2,2′-bipyridine have been reported [14–19]. Among these, the bridging carboxylato group exhibits the common bidentate coplanar *syn–syn* mode in $[Mn_2(bpy)_4(ta)](ClO_4)_2$ (ta = terephthalate dianion) [14] and the coplanar *syn–anti* bridging mode in $[\{Mn(bpy)_2(H_2O)\}_2(Me_3N^+CH_2CO_2^-)](ClO_4)_4\cdot 2H_2O$ [15]. The non-planar *skew–skew* bridging mode of the carboxylato group was previously found in the manganese(II) complexes $[\{Mn(Me_3N^+CH_2CO_2^-)_3\}_n]\cdot(MnCl_4)_n$ [20], $[Mn(tpa)(\mu\text{-}OAc)]_2(TCNQ)_2\cdot 2CH_3CN$ and $[Mn(tpa)(TCNQ)(CH_3OH)](TCNQ)_2\cdot CH_3CN$ (tpa = tris(2-pyridylmethyl)amine, TCNQ = tetracyanoquinodimethane) [21], $[Mn_2(L)_2(\mu\text{-}OAc)_2](ClO_4)_2$ [L = *N*,*N*′-dimethyl-*N*,*N*′-bis(2-pyridylmethyl)ethane-1,2-diamine] [22], as well as the iron(II) complex $[Fe_2(tpa)(\mu\text{-}OAc)_2](BPh_4)_2$, in which the coordination geometry of the iron atom is similar to that of the corresponding manganese ion [23]. In these complexes two metal centres lie on different sides of the mean plane of each bridging carboxylate. We now report the synthesis and single-crystal X-ray analysis of a novel dinuclear manganese(II) complex with 4-dimethylaminopyridinioacetate and 2,2′-bipyridine (bpy), namely $[\{Mn(bpy)_2(p\text{-}Me_2N^+C_5H_4NCH_2CO_2^-)\}_2](ClO_4)_4$ (**1**), in which the two metal ions are bridged by a pair of *skew–skew* car-

* On sabbatical leave from the Department of Chemistry, Zhengzhou University, Zhengzhou 450052, P. R. China.

† Author to whom correspondence should be addressed.

boxylato groups but lie on the same side of the mean plane of each bridging ligand.

EXPERIMENTAL

4-Dimethylaminopyridinioacetate was synthesized by the reaction of 4-dimethylaminopyridine with ethylchloroacetate as described previously [24]. C, H, N microanalyses were carried out on a Perkin–Elmer 240 elemental analyser. Infrared spectra were recorded from KBr pellets in the range of 4000–400 cm^{-1} on a Perkin–Elmer 600 FT-IR spectrometer.

Synthesis

To an aqueous solution (10 cm^3) of 4-dimethylaminopyridinioacetate (180 mg, 1.0 mmol) was added $MnCl_2 \cdot 4H_2O$ (98 mg, 0.5 mmol) with stirring for 10 min at 60°C. Then bpy (78 mg, 0.5 mmol) and $NaClO_4 \cdot H_2O$ (144 mg, 1.0 mmol) were added and the mixture was stirred for 20 min. After filtration the resulting solution was allowed to stand in air for a few days, from which yellow block crystals deposited. The yield was 86 mg (*ca* 46% based on Mn) of **1**. Found: C, 46.3; H, 3.4; N, 11.2. Calc. for $C_{29}H_{28}N_6O_{10}Cl_2Mn$: C, 46.7; H, 3.8; N, 11.3%. IR data (cm^{-1}): 3423s, 3092m, 3060m, 1654vs, 1622m, 1595s, 1568s, 1472m, 1435s, 1381s, 1306m, 1211m, 1178m, 1141vs, 1111vs, 1082vs, 1013m, 943w, 906w, 821w, 772s, 730m, 687w, 623s, 548w.

CAUTION! Perchlorate salts of metal complexes with organic ligands are potentially explosive. Only a small amount of compound should be prepared, and it must be handled with caution.

X-ray data collection and structure refinement

A selected single crystal of **1** was used to collect X-ray data at 292 K on a MSC/Rigaku RAXIS-IIC imaging plate system with a rotating anode X-ray generator (Mo-K_α, $\lambda = 0.71073$ Å, 50 kV, 150 mA) [25] and corrected for absorption using the REQAB program [26]. Crystallographic data are summarized in Table 1.

All computations were performed on a PC-486 computer with the SHELXTL-PLUS program package [27]. The direct method yielded the positions of all non-hydrogen atoms, and the hydrogen atoms of the betaine ligands were generated geometrically (C—H = 0.96 Å) and allowed to ride on their respective parent carbon atoms. The final refinement cycles were performed by full-matrix least squares with anisotropic thermal parameters for all non-hydrogen atoms and assigned isotropic thermal parameters for hydrogen atoms. Analytic expressions of neutral-atom scattering factors were employed, and anomalous dispersion corrections were incorporated [28].

Table 1. Crystallographic data for **1**

Formula	$C_{29}H_{28}N_6O_{10}Cl_2Mn$
Formula weight	746.4
Colour; habit	yellow; block
Crystal size, mm^3	$0.20 \times 0.26 \times 0.32$
a, Å	14.490(1)
b, Å	14.233(1)
c, Å	16.546(1)
β, °	105.73(1)
V, $Å^3$	3282(2)
Z	4
Space group	$P2_1/n$ (No. 14)
$F(000)$	1532
ρ_{calc}, g cm^{-3}	1.510
μ, mm^{-1}	0.630
Transm. coeff.	0.776/1.035
Collection range, $2\theta_{max}$, °	18, 16, ±21; 50
Unique data measured	6024
Observed data [$F > 4\sigma(F)$], n	3114
No. of variables, p	433
R_F[a]	0.048
R_w[b]	0.064
S(GOF)	1.59

[a] $R_F = \Sigma\Delta/\Sigma|F_0|$.

[b] $R_g = [\Sigma w\Delta^2/\Sigma w|F_0|^2]^{1/2}$ and $S = [\Sigma w\Delta^2/(n-p)]^{1/2}$ where $w = [\sigma^2(F_0)^2 + 0.0004|F_0|^2]^{-1}$, $\Delta = \|F_0| - |F_c\|$.

Selected bond lengths and angles are given in Table 2 and lists of the remaining bond lengths and angles, hydrogen atom coordinates and anisotropic thermal parameters have been deposited at the Cambridge Crystallographic Data Centre.

RESULTS AND DISCUSSION

The crystal structure of complex **1** consists of a packing of discrete dinuclear cations and perchlorate anions. As illustrated in Fig. 1, a pair of symmetry-related manganese(II) atoms, separated by a non-bonding distance of 4.874(2) Å, are bridged by two carboxylato groups into a centrosymmetric eight-membered metallacyclic ring. Each manganese(II) atom in the resulting dinuclear cation has a distorted octahedral coordination geometry comprising two carboxylato oxygen atoms [O(1) and O(2a)] from two betaine ligands which occupy *cis* positions, and four nitrogen atoms [N(3), N(4), N(5) and N(6)] from a pair of chelate bpy groups; the most distorted angles of the octahedron are the bite angles of the chelate bpy ligands [72.8(1)–73.4(1)°]. The Mn—N(bpy) bond lengths lie in the range 2.229(1)–2.266(1) Å and are significantly longer than those of Mn—O(carboxylate) (average 2.108 Å). These bond distances are in agreement with literature values for both bpy- and carboxylato-containing manganese(II) complexes [14, 15, 29]. The best equatorial plane is defined by atoms O(1), N(3), N(5) and N(6) [the largest deviation from the mean plane is 0.040 Å for N(6)] and

Table 2. Selected bond lengths (Å) and angles (°)

Mn(1)—O(1)	2.107(1)	Mn(1)—N(3)	2.232(1)
Mn(1)—N(4)	2.265(2)	Mn(1)—N(5)	2.266(1)
Mn(1)—N(6)	2.229(1)	Mn(1)—O(2a)	2.109(2)
O(1)—C(1)	1.257(2)	O(2)—C(1)	1.249(2)
C(1)—C(2)	1.508(2)	C(2)—N(1)	1.466(2)
N(1)—C(3)	1.334(2)	N(1)—C(7)	1.345(2)
C(3)—C(4)	1.354(2)	C(4)—C(5)	1.421(2)
C(5)—C(6)	1.398(2)	C(5)—N(2)	1.342(2)
C(6)—C(7)	1.361(2)	N(2)—C(8)	1.452(2)
N(2)—C(9)	1.446(2)	C(10)—C(11)	1.381(2)
C(10)—N(3)	1.333(2)	C(11)—C(12)	1.338(2)
C(12)—C(13)	1.396(2)	C(13)—C(14)	1.367(2)
C(14)—C(15)	1.474(2)	C(14)—N(3)	1.359(2)
C(15)—C(16)	1.372(2)	C(15)—N(4)	1.337(2)
C(16)—C(17)	1.340(2)	C(17)—C(18)	1.317(2)
C(18)—C(19)	1.373(2)	C(19)—N(4)	1.331(2)
C(20)—C(21)	1.381(2)	C(20)—N(5)	1.337(2)
C(21)—C(22)	1.363(2)	C(22)—C(23)	1.368(2)
C(23)—C(24)	1.378(2)	C(24)—C(25)	1.485(2)
C(24)—N(5)	1.351(2)	C(25)—C(26)	1.389(2)
C(25)—N(6)	1.338(2)	C(26)—C(27)	1.348(2)
C(27)—C(28)	1.354(2)	C(28)—C(29)	1.367(2)
C(29)—N(6)	1.346(2)		

O(1)—Mn(1)—N(3)	100.3(1)	O(1)—Mn(1)—N(4)	91.1(1)
N(3)—Mn(1)—N(4)	73.4(1)	O(1)—Mn(1)—N(5)	164.3(1)
N(3)—Mn(1)—N(5)	95.1(1)	N(4)—Mn(1)—N(5)	90.5(1)
O(1)—Mn(1)—N(6)	91.6(1)	N(3)—Mn(1)—N(6)	166.6(1)
N(4)—Mn(1)—N(6)	100.6(1)	N(5)—Mn(1)—N(6)	72.8(1)
O(1)—Mn(1)—O(2a)	94.8(1)	N(3)—Mn(1)—O(2a)	92.8(1)
N(4)—Mn(1)—O(2a)	165.8(1)	N(5)—Mn(1)—O(2a)	87.3(1)
N(6)—Mn(1)—O(2a)	92.2(1)	Mn(1)—O(1)—C(1)	141.6(1)
C(1)—O(2)—Mn(1a)	134.6(1)	O(1)—C(1)—O(2)	125.3(2)
O(1)—C(1)—C(2)	117.4(1)	O(2)—C(1)—C(2)	117.3(1)
C(1)—C(2)—N(1)	111.9(1)	C(2)—N(1)—C(3)	121.4(1)
C(2)—N(1)—C(7)	120.4(1)	C(3)—N(1)—C(7)	117.8(1)
N(1)—C(3)—C(4)	123.8(1)	C(3)—C(4)—C(5)	119.2(1)
C(4)—C(5)—C(6)	116.3(1)	C(4)—C(5)—N(2)	121.7(1)
C(6)—C(5)—N(2)	121.9(1)	C(5)—C(6)—C(7)	120.2(1)
N(1)—C(7)—C(6)	122.7(1)	C(5)—N(2)—C(8)	122.2(1)
C(5)—N(2)—C(9)	121.3(1)	C(8)—N(2)—C(9)	116.4(1)
C(11)—C(10)—N(3)	122.0(2)	C(10)—C(11)—C(12)	118.1(1)
C(11)—C(12)—C(13)	121.5(1)	C(12)—C(13)—C(14)	117.9(2)
C(13)—C(14)—C(15)	122.4(1)	C(13)—C(14)—N(3)	120.7(1)
C(15)—C(14)—N(3)	116.7(1)	C(14)—C(15)—C(16)	123.8(1)
C(14)—C(15)—N(4)	115.8(1)	C(16)—C(15)—N(4)	120.4(1)
C(15)—C(16)—C(17)	119.6(1)	C(16)—C(17)—C(18)	120.8(2)
C(17)—C(18)—C(19)	118.5(1)	C(18)—C(19)—N(4)	122.3(1)
Mn(1)—N(3)—C(10)	123.7(1)	Mn(1)—N(3)—C(14)	116.0(1)
C(10)—N(3)—C(14)	119.5(1)	Mn(1)—N(4)—C(15)	116.1(1)
Mn(1)—N(4)—C(19)	125.0(1)	C(15)—N(4)—C(19)	118.1(1)
C(21)—C(20)—N(5)	123.0(1)	C(20)—C(21)—C(22)	117.5(1)
C(21)—C(22)—C(23)	120.8(1)	C(22)—C(23)—C(24)	119.0(1)
C(23)—C(24)—C(25)	123.3(1)	C(23)—C(24)—N(5)	121.2(1)
C(25)—C(24)—N(5)	115.5(1)	C(24)—C(25)—C(26)	122.9(1)
C(24)—C(25)—N(6)	116.6(1)	C(26)—C(25)—N(6)	120.5(1)
C(25)—C(26)—C(27)	120.5(1)	C(26)—C(27)—C(28)	119.1(1)
C(27)—C(28)—C(29)	119.3(1)	C(28)—C(29)—N(6)	122.4(1)
Mn(1)—N(5)—C(20)	124.8(1)	Mn(1)—N(5)—C(24)	116.6(1)
C(20)—N(5)—C(24)	118.5(1)	Mn(1)—N(6)—C(25)	117.6(1)
Mn(1)—N(6)—C(29)	123.4(1)	C(25)—N(6)—C(29)	118.2(1)

Symmetry codes: (a) $2-x, -y, 1-z$.

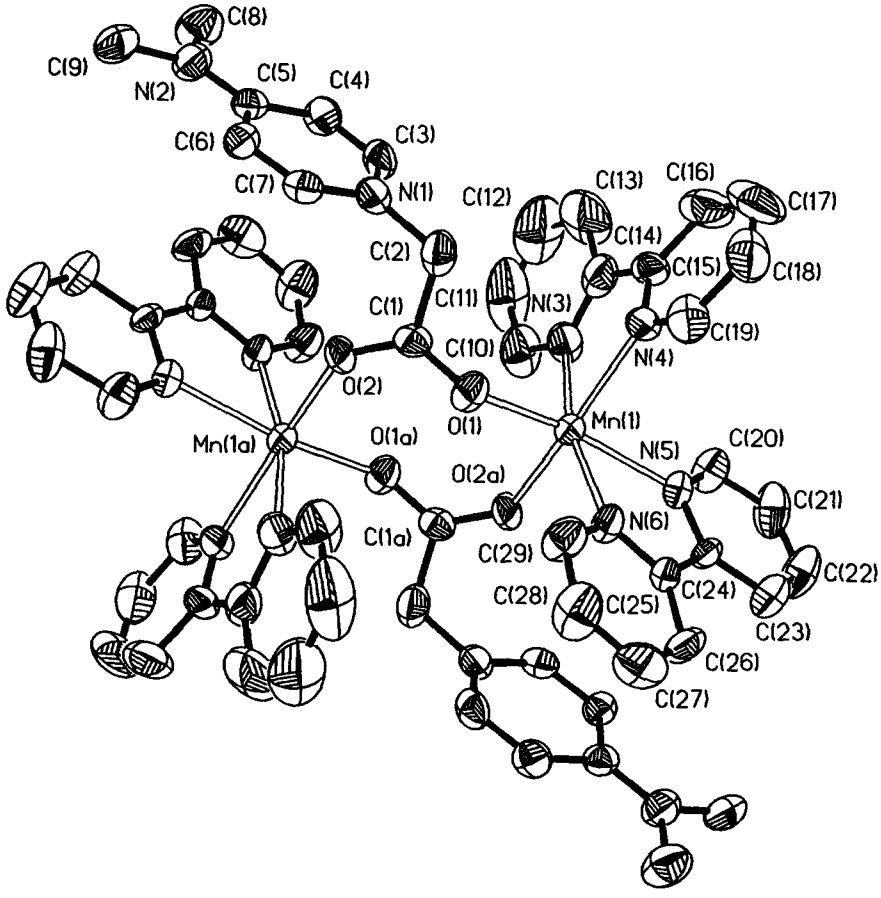


Fig. 1. ORTEP drawing (35% thermal ellipsoids) of the dinuclear $[\{Mn(bpy)_2(p\text{-}Me_2NC_5H_4NCH_2CO_2)\}_2]^{2+}$ cation in **1**. Symmetry code is given in Table 1.

the manganese atom is displaced 0.061 Å out of this plane towards atom O(2a).

The most interesting structural feature in complex **1** is that the carboxylato group of the betaine ligand bridges the Mn^{II} atoms in an abnormal non-planar *skew–skew* (e) mode, which differs from the coplanar *syn–syn* (a), *syn–anti* (b) and *anti–anti* (c) bridging modes commonly occurring in metal carboxylates [13], as well as the unusual non-planar *syn–skew* (d) mode found in $[Cd_3(C_5H_4N^+CH_2CO_2^-)_4Cl_6]$ [30] (see Fig. 2). The O(2) atom coordinates Mn(1a) in an out-of-plane fashion with a torsion angle Mn(1a)—O(2)—C(1)—C(2) = 152.3(2)°, and the Mn(1)—O(1) bond is rotated out of the plane of the carboxylato group by an even greater extent [torsion angle Mn(1)—O(1)—C(1)—C(2) = −72.5(2)°]. The Mn(1) and Mn(1a) atoms thus lie on the same side of the mean plane containing the carboxylato group of the bridging betaine ligand. This non-planar *skew–skew* coordination mode (e) is therefore different from mode (f) as found in the above-mentioned Mn^{II} and Fe^{II} complexes [20–23]. The intramolecular metal–metal separation in the present dinuclear cation agrees well with those in the range 4.64–4.79 Å found for known doubly carboxylato-bridged manganese(II) complexes [14, 29c, 31]. In contrast, the metal–metal distance is considerably longer than those [4.03–4.44 Å] reported for triply μ-carboxylato-bridged manganese(II) complexes [18, 32, 33] and much shorter than those [5.60–5.67 Å] found for singly carboxylato-bridged manganese(II) complexes [15,34], implying that the metal–metal separation in the $(\mu$-carboxylato$)_n$ bridged systems may be controlled by varying the number of such bridges, as well as their coordination modes.

The carboxylato group in the molecular skeleton of the betaine ligand deviates from being perpendicular to the dimethylaminopyridinium moity, the dihedral angle between the plane containing atoms O(1), O(2), C(1), C(2) (mean deviation 0.007 Å) and the plane containing atoms N(1), C(3), C(4), C(5), N(2), C(6), C(7), C(8), C(9) (mean deviation 0.025 Å) being 74.2°. The conformation of the betaine ligand is thus similar to that in its hydrochloride form (dihedral angle 60.7°), but different from that in its hydrate form (dihedral angle 96.3°), in which the molecular skeleton of the betaine ligand possesses approximate C_s symmetry [24].

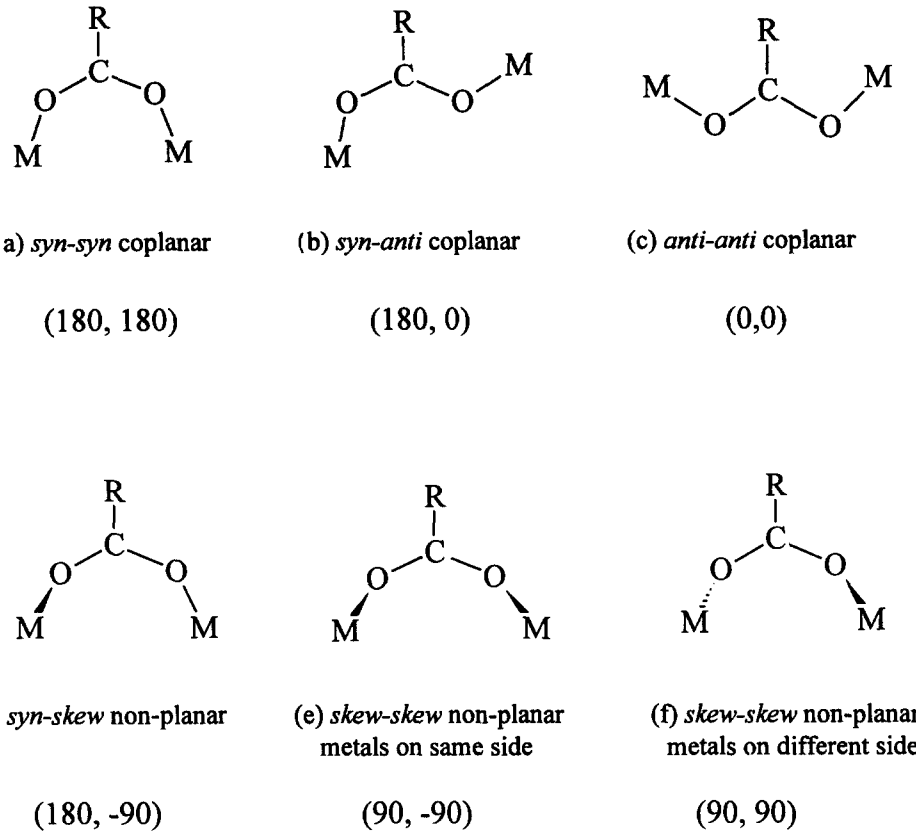


Fig. 2. Six idealized bridging modes of carboxylate and betaine ligands in their metal complexes. Enclosed in parentheses are the representative numerical values of the pair of R—C—O—M torsion angles (°) for each type of geometry.

Acknowledgement—This work was supported by the Hong Kong Research Grants Council, Earmarked Grant CUHK 89/93E.

REFERENCES

1. Pecoraro, V. L., *Manganese Redox Enzymes*. VCH, New York, 1992.
2. Christou, V., *Acc. Chem. Res.*, 1989, **22,** 328.
3. Wieghardt, K., *Angew. Chem., Int. Ed. Engl.*, 1989, **28,** 1153; Que, L. and True, A. E., *Prog. Inorg. Chem.*, 1990, **38,** 97.
4. Sheats, J. E., Czermuszewicz, R. S., Dismukes, G. C., Rheingold, A. L., Petrouleus, V., Stubbe, J., Armstrong, W. H., Beer, R. H. and Lippard, S. J., *J. Am. Chem. Soc.*, 1987, **109,** 1435; Wieghardt, K., Bossek, U., Ventur, D. and Weiss, J., *J. Chem. Soc., Chem. Commun.*, 1985, 347.
5. Fono, Y. and Fridovich, I., *J. Biol. Chem.*, 1983, **258,** 6015; Beyer, W. F., Jr, and Fridovich, I., *Biochemistry*, 1985, **24,** 6460; Algood, G. S. and Perry, J. J., *J. Bacteriol.*, 1986, **168,** 563.
6. Waldo, G. S., Yu, S. and Penner-Hahn, J. E., *J. Am. Chem. Soc.*, 1992, **114,** 5869; Fronko, R. M., Penner-Hahn, J. E. and Bender, C. J., *J. Am. Chem. Soc.*, 1988, **110,** 7554.
7. Chen, X.-M., Mak, T. C. W., Huang, W.-Y. and Lü, L., *Acta Cryst.*, 1992, **C11,** 2567.
8. Chen, X.-M. and Mak, T. C. W., *Struct. Chem.*, 1992, **3,** 369; *ibid.*, 1993, **4,** 247.
9. Chen, X.-M. and Mak, T. C. W., *Inorg. Chim. Acta.*, 1991, **189,** 3.
10. Chen, X.-M. and Mak, T. C. W., *J. Chem. Soc., Dalton Trans.*, 1991, 1585, 1219, 3253.
11. Wu, D.-D. and Mak, T. C. W., *J. Chem. Soc., Dalton Trans.*, 1995, 139.
12. Chishwell, B., McKenzie, E. D. and Lindoy, L. F., *Comprehensive Coordination Chemistry*, Vol. 5. Pergamon, Oxford 1987, p. 43.
13. Mehrotra, C. and Bohra, R., *Metal Carboxylates*. Academic Press, New York, 1983.
14. Cano, J., Munno, G. D., Sanz, J., Ruiz, R., Lloret, F., Faus, J. and Julve, M., *J. Chem. Soc., Dalton Trans.*, 1994, 3465.
15. Chen, X.-M., Tong, Y.-X., Xu, Z.-T. and Mak, T. C. W., *J. Chem. Soc., Dalton Trans.*, 1995, 4001.
16. Menage, S., Girerd, J.-J. and Gleizes, A., *J. Chem. Soc., Chem. Commun.*, 1988, 431.
17. Wieghardt, K., Bossek, U., Ventur, D. and Weiss, J., *J. Chem. Soc., Chem. Commun.*, 1985, 347.
18. Wieghardt, K., Bossek, U., Weiss, J., Bonvoisin, J., Corbella, M., Vitols, S. E. and Girerd, J.-J., *J. Am. Chem. Soc.*, 1988, **110,** 7398.
19. Sheats, J. E., Czernuszewicz, R. S., Dismukes, G. C., Rheingold, A., Petrouleas, V., Stubbe, J., Armstrong, W. H., Beer, R. H. and Lippard, S. J., *J. Am. Chem. Soc.*, 1987, **109,** 1435.

20. Chen, X.-M. and Mak, T. C. W., *Inorg. Chim. Acta.*, 1991, **189,** 3.
21. Oshio, H., Ino, E., Mogi, I. and Ito, T., *Inorg. Chim.*, 1993, **32,** 5697.
22. Che, C.-M., Tang, W.-T., Wong, K.-Y., Wong, W.-T. and Lai, T.-F., *J. Chem. Res.*, 1991, **30,** 401.
23. Ménage, S., Zhang, Y., Hendrich, M. P. and Que, L., Jr, *J. Am. Chem. Soc.*, 1992, **114,** 7786.
24. Wei, P.-R., Li, Q. and Mak, T. C. W., *J. Chem. Crystallogr.*, 1996, **26,** 133.
25. Krause, K. L. and Phillips, G. N., *J. Appl. Crystallogr.*, 1992, **25,** 146; Sato, M., Yamamoto, M., Imada, K., Katsube, Y., Tanaka, N. and Higashi, T., *ibid.*, 1992, **25,** 348; Tanner, J. and Krause, K. L., *Rigaku Journal*, 1994, **11,** 4.
26. Miller, L. L. and Jacobson, R. A., *Computers Chem.*, 1989, **13,** 1.
27. Sheldrick, G. M., *SHELXTL-PC, Program Package for X-ray Crystal Structure Determination.* Siemens Analytical Instruments Inc., Karlsruhe, 1990; Sheldrick, G. M., in *Computational Crystallography*, ed. D. Sayre. Oxford University Press, New York, 1982, p. 506; Sheldrick, G. M., in *Crystallographic Computing* 3: *Data Collection, Structure Determination, Proteins, and Databases*; ed. G. M. Sheldrick, C. Krüger, and R. Goddard. Oxford University Press, New York, 1985, p. 175.
28. *International Tables for X-ray Crystallography*, Vol. 4. Kynoch Press, Birmingham, 1974. (Now distributed by Kluwer Academic Publishers, Dordrecht) pp. 55, 99, 149.
29. (a) Deguenon, D., Bernardelli, G., Tuchagues, J. P. and Castan, P., *Inorg. Chem.*, 1990, **29,** 3031; (b) Jiang, Z.-H., Ma, S.-L., Liao, D.-Z., Yan, S.-P., Wang, G.-L., Yao, X.-K. and Wang, R.-J., *J. Chem. Soc., Chem. Commun.*, 1993, 745; (c) Andrah, M., Roesky, H. W., Noltemeyer, M. and Schmidt, H. G., *Polyhedron*, 1993, **12,** 2901; (d) Oshio, H., Ino, E., Mogi, I. and Ito, T., *Inorg. Chem.*, 1993, **32,** 5697.
30. Mak, T. C. W. and Chen, X.-M., *J. Aust. Chem.*, 1991, **44,** 639.
31. Rardin, R. L., Tolman, W. B. and Lippard, S. J., *New J. Chem.*, 1991, **15,** 417.
32. Menage, S., Vitols, S. E., Bergerat, P., Codjovi, E., Kahn, O., Girerd, J.-J., Guillot, M., Solans, X. and Calvet, T., *Inorg. Chem.*, 1991, **30,** 2666.
33. Hübner, K., Roesky, H. W., Noltemeyer, M. and Bohra, R., *Chem. Ber.*, 1991, **124,** 515.
34. Aurangzeb, N., Hulme, C. E., McAuliffe, C. A., Pritchard, R. G., Watkinson, M., Bermejo, M. R. and Sousa, A., *J. Chem. Soc., Chem. Commun.*, 1994, 2193.

Pergamon

PII: S0277-5387(96)00370-1

Polyhedron Vol. 16, No. 6, pp. 903–908, 1997
Copyright © 1996 Elsevier Science Ltd
Printed in Great Britain. All rights reserved
0277-5387/97 $17.00+0.00

Effect of hydrogenation on electronic and distant magnetic properties in copper(II) complexes with derivatives of tetrahydrosalen and salen. X-ray crystal structure of [Cu{Bu,Me(saltmen)}] complex

M. Valko,[a]* R. Boča,[a] R. Klement,[a] J. Kožíšek,[a] M. Mazúr,[a] P. Pelikan,[a] H. Morris,[b] H. Elias[c] and L. Müller[c]

[a] Faculty of Chemical Technology, Slovak Technical University, Radlinskeho 9, SK-812 37 Bratislava, Slovak Republic

[b] School of Pharmacy and Chemistry, Liverpool John Moores University, Byrom Street, Liverpool L3 3AF, U.K.

[c] Institut für Anorganische Chemie, Technische Hochschule Darmstadt, D-64287 Darmstadt, Germany

(Received 15 May 1996; accepted 30 July 1996)

Abstract—The salen complex CuL and the corresponding tetrahydrosalen complex Cu[H_4]L were investigated by ESR spectroscopy and molecular orbital calculations [H_2L = *N*,*N*′-bis(3-*tert*-butyl-5-methylsalicylidene)-2,3-diamino-2,3-dimethylbutane; H_2[H_4]L = *N*,*N*′-bis(2-hydroxy-3-*tert*-butyl-5-methylbenzyl)-2,3-diamino-2,3-dimethylbutane]. X-ray structure determination of CuL confirmed a slightly distorted planar geometry of the CuN_2O_2 coordination core. The ESR spectra of CuL at both 77 K and room temperature revealed that very well resolved lines cannot be attributed to the interaction with copper nuclear spin and ^{14}N donor nuclei alone. Computer simulation showed that in addition to copper hyperfine (g_{iso} = 2.094, $|A^{Cu}(iso)|$ = 270 MHz, room temperature) and nitrogen superhyperfine structure [$|A^{N}(iso)|$ = 46 MHz] a distant interaction with two equivalent protons is also present [$|A^{H}(iso)|$ = 23 MHz]. These protons are attached to the carbon atoms adjacent to ^{14}N nuclei. In contrast the number of lines in the spectrum of the hydrogenated analogue Cu[H_4]L is greatly reduced. At room temperature only a quintet with considerable smaller nitrogen shf constant [$|A^{N}(iso)|$] = 25 MHz is observed. Thus, both factors planarity and conjugation, are essential for the observation of distant hydrogen shf splitting in CuL. The ESR findings are in good agreement with calculated spin densities by QR-INDO/1 method. Copyright © 1996 Elsevier Science Ltd

Keywords: copper salen complexes; effect of hydrogenation; crystal structure; superhyperfine splitting; EPR; MO calculations.

In order to emulate the biological activity of proteins [1], various model metal complexes containing Schiff base ligands have been prepared and in some cases dioxygen activation and its relevance in oxidative catalysis investigated [2]. These studies on model systems indicate that the key attributes for a metalloprotein to carry out a specific biological function are the environment around the metal center and conformational flexibility. For example, the flexibility of the ethylene diamine backbone in salen [3] plays a crucial role in the dioxygen activation. Most of the studies were carried out with the tetradentate Schiff base ligand salen, while tetrahydrosalens have rarely been studied with the exception of the hydrogenation product of nonsubstituted salen. The coordination chemistry of this ligand with nickel [4,5], zinc [4,5], cobalt [5,6], molybdenum [7,8], copper [5,9], and iron

* Author to whom correspondence should be addressed. E-mail: mvalko@cvt.stuba.sk. The Royal Society visiting scientist 1994–1995.

[10] has been reported as well as dinuclear complexes [6, 10a, 11]. More recently a trinuclear cobalt [12] complex was prepared and characterized.

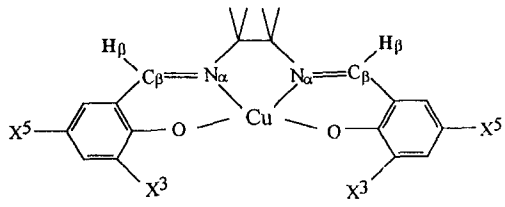
We have recently reported on metal-catalysed oxidative dehydrogenation of the C—N bond in coordinated tetrahydrosalens [13, 14]. Comparing the ligand properties of salen and tetrahydrosalen, one expects both an increased *N*-basicity and greater conformational flexibility as a consequence of C=N bond hydrogenation. The loss of conjugation in coordinated tetrahydrosalens might generate interesting electronic and magnetic properties of such complexes, reflected in absence of weak *distant* magnetic interactions. The aim of this short contribution is to present a comparative study of electronic and *distant* magnetic interactions on the substituted salen and tetrahydrosalen copper(II) complexes depicted in Fig. 1.

RESULTS AND DISCUSSION

From the crystal structure analysis for the molecule **1** the chromophore is of the *cis*-$\{CuN_2O_2\}$ type with distances Cu—N = 1.932(3) and Cu—O = 1.890(2) Å, respectively (Fig. 2). The planar arrangement of the chromophore is somewhat distorted, which follows from the O—Cu—O, O—Cu—N and N—Cu—N angles deviating from 90 and 180°, slightly (Tables 1 and 2).

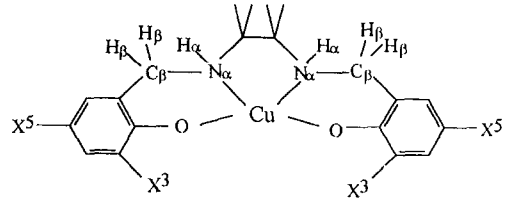
The ESR spectrum of **1** in frozen toluene solution is shown in Fig. 3. It corresponds to an axially symmetric species with $g_{\parallel} = 2.191$ and $g_{\perp} = 2.040$ and detailed analysis shows that the very well resolved high-field perpendicular band of the spectrum cannot be attributed to the interaction with the copper nuclear spin ($I^{Cu} = 3/2$) and ^{14}N ($I^N = 1$) donor nuclei alone. Computer simulation [15, 16] showed that, in addition to copper hyperfine and nitrogen shf structure, a *distant* interaction with two equivalent protons is also present. These protons are attached to the carbon atoms adjacent to ^{14}N nuclei (depicted in Fig. 1). In addition, an "overshoot line" resulting from the angular spectral dependence of the copper hyperfine lines in perpendicular region is observed. In order to obtain exact values for both the hydrogen as well as nitrogen shf constants, room-temperature spectra were taken (Fig. 4). The isotropic spectrum, $g_{iso} = 2.094$, $|A^{Cu}(iso)| = 270$ MHz, shows m_I-dependent linewidth with clearly defined superhyperfine structure on the high-field line. Two equivalent nitrogen nuclei should give five lines which are further split into triplets by the interaction with two equivalent protons giving a 15 line spectrum. This interpretation gives a good match between the theoretical and the second derivative experimental spectrum, for which $|A^N(iso)| = 46$ MHz and $|A^H(iso)| = 23$ MHz were found. These values and those for the solid-state spectrum are in a good agreement with the monocrystal study of Maki and McGarvey [17a] as well as with ENDOR [17b] study on copper(II) bis-salicylaldehyde-imine 1 : 200 diluted in the corresponding nickel chelate.

In contrast the number of lines in the spectrum of the hydrogenated analog **2** is greatly reduced. Again the solution spectrum shows m_I-dependent linewidth with discernable hyperfine structure on the high-field line, however, in this case only a quintet with a considerable smaller nitrogen shf constant $|A^N(iso)| = 25$ MHz is observed, which is also confirmed in the low-temperature study (spectrum not shown). All spectral parameters are summarized in Table 3.



CuL

1



$Cu[H_4]L$

2

ligand	X3	X5
H_2L	t-Bu	Me
$H_2[H_4]L$	t-Bu	Me

Fig. 1. Structural formulas of the complexes. Abbreviations: H_2L = *N*,*N*′-bis(3-*tert*-butyl-5-methylsalicylidene)-2,3-diamino-2,3-dimethylbutane; $H_2[H_4]L$ = *N*,*N*′-bis(2-hydroxy-3-*tert*-butyl-5-methyl-benzyl)-2,3-diamino-2,3-dimethylbutane.

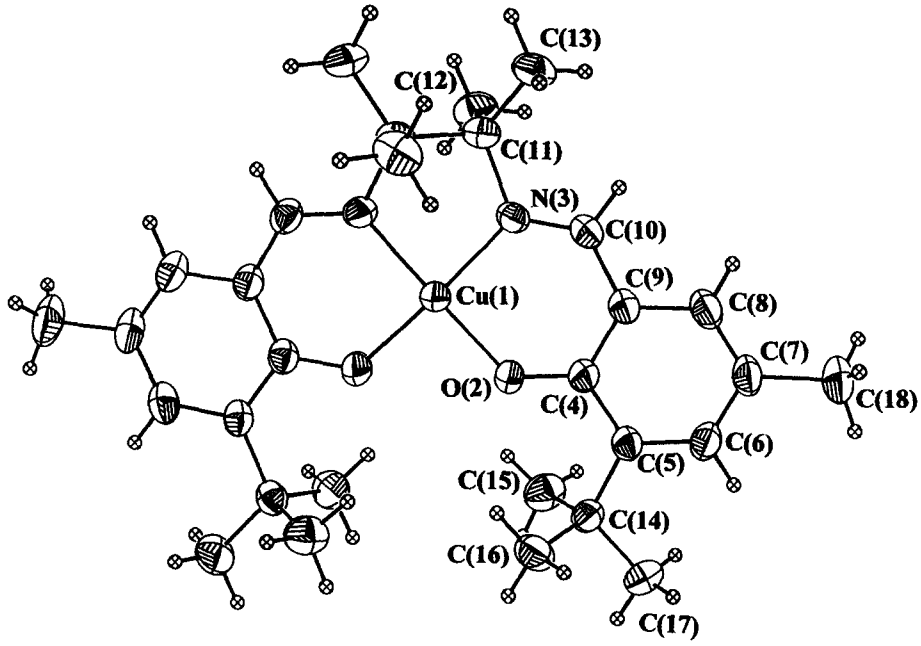


Fig. 2. View of the coordination geometry in the complex **1**.

Table 1. Crystallographic data for complex CuL (**1**)

Formula	$C_{30}H_{42}N_2O_2Cu$
Formula weight	526.2
Space group	$C222_1$ (no. 20)
a (Å)	10.211(5)
b (Å)	23.979(11)
c (Å)	11.715(4)
V (Å^3)	2868.4(11)
Z	4
d_{calc} (g cm^{-3})	1.219
μ(Mo-K_α) (cm^{-1})	7.40
Temperature (°C)	25(2)
$R(F_o)^a$	0.0394
$R_w(F_o)^{b,c}$	0.1101
S (Goodness-of-fit)^d	1.128^d

[a] $R(F_o) = \Sigma(|F_o - F_c|)/\Sigma|F_c|$.

[b] $R_w(F_o) = \Sigma w^{1/2}|F_o - F_c|/\Sigma w^{1/2}|F_c|$.

[c] $w = 1[\sigma^2(F_0^2) + (0.0468P)^2 + 2.11P]$, where $P = (F_0^2 + 2F_c^2)/3$ with $\sigma(F_0^2)$ from computing statistics.

[d] $S = \{\Sigma[w(F_o - F_c)^2]/(n-p)\}^{1/2}$, where n is the number of observed reflections and p is the number of parameters refined.

An increase in $g_\parallel$ value and decrease in $|A_\parallel|$ for **2** can be attributed to an increased positive charge on a donor set as concluded by Peisach and Blumberg (P-B diagram) [18]. This is further reflected by a significant reduction in the nitrogen shf splitting constant 25 MHz, compared with 46 MHz for the non-hydrogenated complex. The decrease in nitrogen shf splitting for the hydrogenated analog is what may be expected for isotropic coupling of Cu^{II} to a sp^3 nitrogen versus a sp^2 nitrogen (i.e. less s-character). The shift to smaller $g_\parallel$ values in **1** indicates increased delocalization of the unpaired spin density away from the copper nucleus and may also be interpreted in terms of increased covalency of the metal–ligand bond.

The ratio of $g_\parallel/|A_\parallel|$ is a good measure of degree of tetrahedral distortion [19]. The value of this ratio for **1** is 105 cm, which correlates well with the square-planar arrangement around the copper center, the corresponding value of 112 cm for **2** reveals a slight tetrahedral distortion. Thus, the results of low-temperature frozen solution study are in good agreement with X-ray analysis, indicating that inert toluene does not affect the planarity of copper surroundings. Since the X-ray data for **2** are not available at present, the Ni counterpart data recently reported can be used [20]. The X-ray analysis revealed that the NiO_2N_2 plane does in fact show a slight tetrahedral distortion and that the two benzene rings are bent slightly upwards and downwards, respectively. Also Ni—O (1.866 and 1.850 Å) and Ni—N (1.930 and 1.890 Å) distances differ a little more. Assuming similar X-ray data for **2**, a good match between the X-ray and ESR conclusions may be derived.

In spite of the fact that we are aware of relative validity of calculated spin densities and their comparison against shf constants, particularly for a set of two compounds, we have carried out MO calculations within the INDO method (Table 4). They show that for both **1** and **2** the spin density is delocalized within the molecular plane over the chromophore: the donor nitrogen and oxygen atoms bear 0.047 and 0.050 spin density, respectively. This finding is quite typical for planar Cu^{II} complexes with Schiff-base type ligands. What is rather atypical is the nonvanishing spin density on the hydrogen atoms H_β approaching a value of 0.006. Such a value is manifestated in the ESR

Table 2. Selected bond lengths (Å) and bond angles (°) for $C_{30}H_{42}N_2O_2Cu$ (**1**)

Cu(1)—O(2)	1.890(2)	O(2)—C(4)	1.315(4)
Cu(1)—N(3)	1.932(3)	N(3)—C(10)	1.293(4)
N(3)—C(11)	1.497(4)	C(9)—C(10)	1.430(5)
C(4)—C(9)	1.423(5)	C(11)—C(12)	1.527(5)
O(2)′—Cu(1)—O(2)	88.7(2)	O(2)′—Cu(1)—N(3)′	93.75(10)
O(2)′—Cu(1)—N(3)	176.72(11)	C(4)—O(2)—Cu(1)	128.9(2)
O(2)—Cu(1)—N(3)	93.74(10)	C(10)—N(3)—C(11)	121.2(3)
O(2)—Cu(1)—N(3)′	176.72(12)	C(10)—N(3)—Cu(1)	124.5(2)
N(3)—Cu(1)—N(3)′	83.9(2)	C(11)—N(3)—Cu(1)	114.3(2)
N(3)—C(10)—C(9)	126.4(3)	C(4)—C(9)—C(10)	123.6(3)

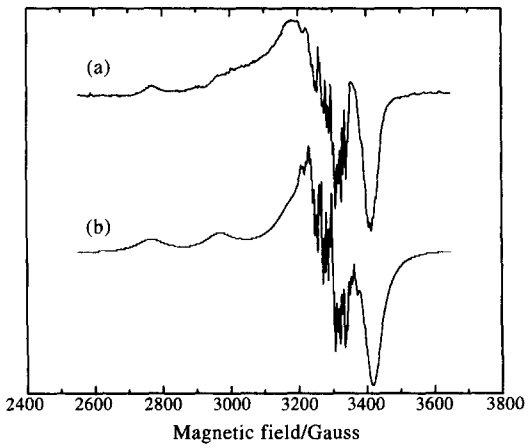


Fig. 3. First-derivative ESR spectrum of a frozen toluene solution at 100 K due to **1** (1 mmol): (a) experimental spectrum; (b) computer simulation using the spin Hamiltonian parameters in Table 3.

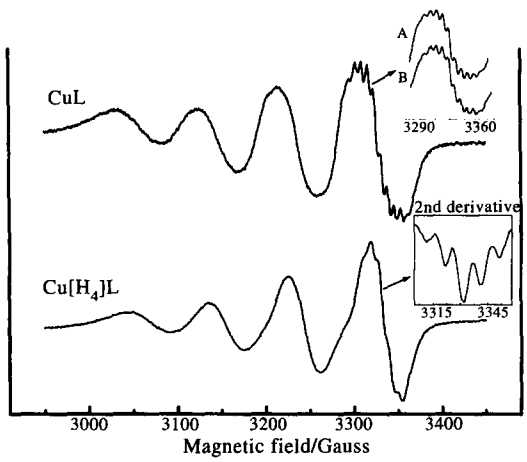


Fig. 4. First-derivative ESR spectrum of a toluene solution at room temperature due to **1** (1 mmol) and **2** (1 mmol). Upper inset: high field copper band of **1**. (A) Simulation using the spin Hamiltonian parameters in Table 3; (B) experiment. Lower inset: 2nd derivative high field copper band of **2**.

spectra: the superhyperfine splitting can be observed even from a rather *distant* hydrogen atom. Comparison of the QR-INDO/1 and INDO/2 (not presented) values show that both sets of data lead to the same conclusion. It should be noted that the donor oxygen atoms and C_β atoms also bear some spin density. Since these atoms have zero nuclear spin, the effect of these spin densities is not seen in shf splitting of the ESR spectra. Thus, the only ESR active spin densities are those on the Cu, N and H atoms. The relatively high spin density on the H_α and H_β in the case of **1** is a consequence of the practically planar rearrangement of the respective hydrogen atoms. In the case of the hydrogenated analog **2** the spin density at the H_α and H_β atom is so low (these hydrogens are situated out of the planar rearrangement) that additional superhyperfine splitting in the ESR spectra is not observed.

EXPERIMENTAL

Preparation

The synthesis of the ligands H_2L and $H_2[H_4]L$ and preparation of the complexes CuL (**1**) and $Cu[H_4]L$ (**2**) was described earlier [13].

ESR spectroscopy

The ESR spectra were recorded on a Bruker SRC-200 D spectrometer operating at X-band. Spectral simulations were performed using computer programs described elsewhere [15,16].

X-ray structure determination

For X-ray diffraction a suitable specimen of **1** of dimensions $0.22 \times 0.22 \times 0.62$ mm (0.030 mm^3) was mounted on a STOE-STADI4 diffractometer with graphite-monochromatized Mo-K_α radiation. The final lattice constants (Table 1) were determined from the 2θ values of 56 reflections in the range 45–55°. The intensities of 2730 reflections ($-14 < h < 14$,

Table 3. ESR data for the toluene solutions of CuL (**1**) and Cu[H_4]L (**2**)[a]

100 K toluene solution	$g_\perp$	$g_\parallel$	$\lvert A_\perp^{Cu}\rvert$	$\lvert A_\parallel^{Cu}\rvert$	$\lvert A_\perp^{N}\rvert$	$\lvert A_\parallel^{N}\rvert$	$\lvert A_\perp^{H}\rvert$
1	2.040	2.191	80	627	41		17
2	2.042	2.213	32	590	32		
Room temperature	g_{iso}		$\lvert A_{iso}^{Cu}\rvert$		$\lvert A_{iso}^{N}\rvert$		$\lvert A_{iso}^{H}\rvert$
1	2.094		270		46		23
2	2.100		253		25		

[a] Hyperfine and shf splitting constants in MHz.

Table 4. Calculated spin densities by QR-INDO/1 method

Atom	Complex **1**	Complex **2**			
Cu	0.7912	0.7636			
O	0.0498	0.0611	0.0700		
N_α	0.0466	0.0464	0.0410		
H_α		−0.0003	−0.0010		
C_β	−0.0040	−0.0015	−0.0021		
H_β	0.0061	−0.0004	0.0029	−0.0003	0.0054

$-33 < k < 33$, $-16 < l < 16$) were measured in the interval $1.70 < \theta < 30°$. Independent reflections: 2581 ($R_{int} = 0.0121$). Reflections used with $F > 4.0\sigma(F)$: 2087. An empirical absorption correction was carried out. The structure was solved by the Patterson method and refined by full-matrix weighted least-squares techniques [21,22]. The *U*s for all the hydrogen atoms were fixed and isotropic. The final difference map was featureless with the highest peak of 0.48 and −0.36 e $Å^{-3}$, respectively.

Molecular orbital calculations

The MO calculations were performed within the approximate INDO (Intermediate Neglect of Differential Overlap) method. Two variants of the method have been applied; (i) standard INDO/2 extended to transition metals [23–26]. (ii) the nonempirical quasi-relativistic INDO/1 [27–29]. All 77 atoms in **1** were considered and the basis set consisted of 187 valence orbitals. The hydrogenated counterpart **2** was taken in geometry determined for a nickel analog [20]. UHF spin densities have been projected in order to eliminate the higher spin multiplicity components.

Supplementary material available. Atomic coordinates, thermal parameters and complete bond length and angles for complex **1** have been deposited with the Editor as supplementary data. Atomic coordinates have also been deposited with the Cambridge Crystallographic Data Centre.

Acknowledgements—Sponsorship of this work by the Deutsche Forschungsgemeinschaft, Verband der Chemischen Industrie e.V., Otto-Röhm-Stiftung (to H.E.), Ministry of Education of the Slovak Republic [grants No. 1/999437/93 (to R.B.) and 1/990945/93 (to P.P.)] and The Royal Society (to M.V.) is gratefully acknowledged. The cooperation between Bratislava and Liverpool supported by the British Council, Bratislava, is gratefully acknowledged.

REFERENCES

1. (a) Solomon, E. I., in *Copper Coordination Chemistry: Biochemical & Inorganic Perspectives*, ed. K. D. Karlin and J. Zubieta. Adenine Press, New York, 1982; p. 1. (b) Gray, H. B. and Solomon, E. I., in *Copper Proteins*, ed. T. G. Spiro. Wiley, New York, 1981; (c) Shadle, S. E., Penner-Hahn, J. E., Schugar, H. J., Hedman, B., Hodgson, K. O. and Solomon, E. I., *J. Am. Chem. Soc.* 1993, **115,** 767; (d) Zubieta, J., Karlin, K. D. and Hayes, J. C., in *Copper Coordination Chemistry: Biochemical & Inorganic Perspectives*, ed. K. D. Karlin and J. Zubieta. Adenine Press, New York, 1982, p. 97.
2. (a) Holm, R. H., *Chem. Rev.* 1987, **87,** 1401; (b) Dixit, P. S. and Srinivasan, K., *Inorg. Chem.* 1988, **27,** 4507; (c) Srinivasan, K., Michaud, P. and Kochi, J. K., *J. Am. Chem. Soc.* 1986, **108,** 2309; (d) Groves, J. T., Haushalter, R. C., Nakamura, M., Nemo, T. E. and Evans, B. J., *J. Am. Chem. Soc.* 1981, **103,** 2884; (e) Groves, J. T., Nemo, T. E. and Meyers, R. S., *J. Am. Chem. Soc.* 1979, **101,** 1032.
3. (a) Kessel, S. L., Emberson, R. M., Debrunner, P. G. and Hendrickson, D. N., *Inorg. Chem.* 1980, **19,** 1170; (b) Lauffer, R. B., Heistand II, R. H. and Que Jr, L., *Inorg. Chem.* 1983, **22,** 50; (c) Lloret, F., Julve, M., Mollar, M., Castro, I., Lattore, J., Faus, J., Solans, X. and Morgenstern-

Badaran, I., *J. Chem. Soc., Dalton Trans.* 1989, 729.
4. Connor, M. J. and West, B. O., *Aust. J. Chem.* 1967, **20,** 2077.
5. Gruenwedel, D. W., *Inorg. Chem.* 1968, **7,** 495.
6. Macke, H. and Fallab, S. *Chimia* 1972, **26,** 422.
7. Mitchell, P. C. H. and Parker, D. A., *J. Chem. Soc., Dalton Trans.* 1972, 1828.
8. (a) Subramanian, P., Spence, J. T., Ortega, R. and Enemark, J. H., *Inorg. Chem.* 1984, **23,** 2546; (b) Hinshaw, C. J., Peng, G., Singh, R., Spence, J. T., Enemark, J. H., Bruck, J. M., Kristofzski, J., Merbs, S. L., Ortega, R. B. and Wexler, P. A., *Inorg. Chem.* 1989, **28,** 4483.
9. Amundsen, A. R., Whelan, J. and Bosnich, B., *J. Am. Chem. Soc.* 1977, **99,** 6730.
10. (a) Borer, L., Thalken, L., Ceccarelli, C., Glick, M., Hua Zhang, J., and Reiff, W. M., *Inorg. Chem.* 1983, **22,** 1719; (b) Borer, L., Thalken, L., Hua Zhang, J., and Reiff, W. M., *Inorg. Chem.* 1983, **22,** 3174.
11. Patel, K. V. and Bhattacharya, P. K., *Indian J. Chem.* 1984, **23A,** 527.
12. Solari, E., Floriani, C., Cunningham, D., Higgins, T. and McArdle, P. *J. Chem. Soc., Dalton Trans.* 1991, 3139.
13. Böttcher, A., Elias, H., Jäger, E.-G., Langfelderova, H., Mazur, M., Müller, L., Paulus, H., Pelikan, P., Rudolph, M. and Valko, M., *Inorg. Chem.* 1993, **32,** 4131.
14. Valko, M., Klement, R., Pelikan, P., Boca, R., Dlhan, L., Bottcher, A., Elias, H. and Muller, L., *J. Phys. Chem.* 1995, **99,** 137.
15. (a) Nigels, M. J., Ph.D. thesis, University of Illinois, Urbana, IL, 1979; (b) Belford, R. L. and Nigels, M. J., Presented at the International Electron Paramagnetic Resonance Symposium, 21st Rocky Mountain Conference, Denver, CO, 1979; (c) Maurice, A. M., Ph.D. thesis, University of Illinois, Urbana, IL, 1981.
16. Rieger, P. H., in *Special Periodical Report* 13*B* ed. M. C. R. Symons. The Royal Society of Chemistry, Thomas Graham House, Cambridge, 1993, pp. 178–199.
17. (a) Maki, A. H. and McGarvey, B. R., *J. Chem. Phys.* 1958, **29,** 35; (b) Kita, S., Hashimoto M., and Iwaizumi, M., *Inorg. Chem.* 1979, **18,** 3432.
18. Peisach, J. and Blumberg, W. E., *Arch. Biochem. Biophys.* 1974, **165,** 691.
19. (a) Sakaguchi, V. and Addison, A. W., *J. Chem. Soc., Dalton Trans.* 1979, 600; (b) Mabbs, F. and Collison, D., *Electron Paramagnetic Resonance of d-Transition Metals Ions.* Elsevier, Amsterdam, 1992; (c) Symons, M. C. R., West, D. X. and Wilkinson, J. G., *J. Chem. Soc., Dalton Trans.* 1975, 1696; (d) Symons, M. C. R., *Chemical and Biochemical Aspects of Electron Spin Resonance Spectroscopy.* Van Nostrand-Reinhold, New York, 1978; (e) Goodman, B. A. and Raynor, J. B., in *Advanced Inorganic Radiochemistry*, Vol. 13, ed. H. J. Emelens and A. G. Sharpe. Academic Press, New York, 1970, p. 135.
20. Böttcher, A., Elias, H., Müller, L. and Paulus, H., *Angew. Chem., Int. Ed. Engl.* 1992, **31,** 623.
21. Sheldrick, G. M., *SHELX*-86. *Program for Crystal Structure Determination.* University of Cambridge, Cambridge, England, 1986.
22. Sheldrick, G. M., *SHELX*-93 *Fortran*-77 *Program for the Refinement of Crystal Structures from Diffraction Data.* University of Göttingen, Germany 1993.
23. Pople, J. A. and Beveridge, D. L., *Approximate Molecular Orbital Theory.* McGraw-Hill, New York, 1970.
24. Clack, D. W., *Mol. Phys.* 1974, **27,** 1513.
25. Boca, R. and Pelikan, P., *Coord. Chem. Rev.* 1992, **118,** 270.
26. Zerner, M. and Gouterman, M., *Theor. Chim. Acta.* 1966, **4,** 44.
27. Boca, R., *Int. J. Quantum Chem.* 1988, **34,** 385.
28. Pyykkö, P. and Lohr Jr., J. J., *Inorg. Chem.* 1981, **20,** 1950.
29. Boca, R., *Program MOSEM*8. Slovak Technical University, Bratislava, 1993.

Pergamon

PII: S0277-5387(96)00363-4

Polyhedron Vol. 16, No. 6, pp. 909–914, 1997
Copyright © 1996 Elsevier Science Ltd
Printed in Great Britain. All rights reserved
0277-5387/97 $17.00+0.00

Crystal structure characterization of a polynuclear complex between copper(II), tris(2-aminoethyl)amine and ferrocyanide

Zhong-Lin Lu,[a] Chun-Ying Duan,[a]* Yu-Peng Tian,[a] Zhen-Wei Wu,[a]† Jing-Jing You,[a]† Zhong-Yuan Zhou[b] and Thomas C. W. Mak[b]

[a] The State Key Laboratory of Coordination Chemistry, Nanjing University, Nanjing 210093, P.R. China

[b] Department of Chemistry, The Chinese University of Hong Kong, Shatin, New Territories, Hong Kong

(Received 25 April 1996; accepted 24 July 1996)

Abstract—The addition of $[Fe(CN)_6]^{4-}$ to $[Cu(tren)]^{2+}$ [tren = tris(2-aminoethyl)amine] gives a polynuclear complex of formula $[(tren)Cu(NC)Fe(CN)_4(CN)Cu(tren)]\cdot 12H_2O$, which has been characterized by spectroscopic techniques and single crystal X-ray analysis. The asymmetric unit comprises half a molecule and the iron atom is at the centre of symmetry. The $[Cu(tren)]^{2+}$ and $[Fe(CN)_6]^{4-}$ ions are linked together through cyanide bridges. Of the six CN^- groups around the iron atom, four are not bonded to copper atoms, but only interact through hydrogen bonds with the water molecules present in the lattice, the remaining two coordinate to copper atoms of adjacent $[Cu(tren)]^{2+}$ moieties, leading to a non-linear Fe—C≡N—Cu chain. The presence of six water molecules per asymmetric unit of the complex gives rise to an extensive hydrogen-bonded system. Infrared and electronic spectral results are discussed and related to the crystal structure. Copyright © 1996 Elsevier Science Ltd

Keywords: crystal structure; polynuclear complex; ferrocyanide; tris(2-aminoethyl)amine; copper(II) complex; characterization.

Interaction of ferrocyanide with copper proteins may lead to electron transfer between the two metals, the copper ion(s) being reduced. It is believed that outer-sphere charge-transfer (CT) complexes are formed during the process, and the binding in such complexes is suggested to occur *via* electrostatic interactions and hydrogen bonding. However, direct information on this process is not available [1]. In some cases, such as ferrocyanide with bovine superoxide dismutase and copper-substituted carbon anhydes [2,3], formation of CT complexes without electron exchange takes place. In the hope of throwing some light on the actual binding model of ferrocyanide, both with the copper enzymes and with copper complexes, we chose to study the copper(II) complex with tris(2-aminoethyl)amine, which commonly serves as a model for copper proteins and enzymes [4,5], to form the polynuclear complex $Cu^{(II)}$–$Fe^{(II)}$–$Cu^{(II)}$ and we report the single crystal structure.

EXPERIMENTAL

Materials

All chemicals were reagent grade and used without further purification. $[Cu(tren)][ClO_4]_2$ was synthesized according to the procedure described earlier [6].

CAUTION! Although no problems were encountered in this work, perchlorate salts containing

* Author to whom correspondence should be addressed.

† *Present address*: Institute of Food and Fermentation of Jiang Su, Nanjing, P.R. China.

organic ligands are potentially explosive. They should be prepared in small quantities and handled with care.

Preparation of the complex

A mixture of $[Cu(tren)][ClO_4]_2$ (0.82 g, 2 mmol) and $K_4[Fe(CN)_6]\cdot 3H_2O$ (1 mmol, 0.37 g) in water (10 cm^3) was stirred for 1 h. Dark green precipitates were formed after filtering off and slowly evaporating the water solution in air. Found: C, 25.2; H, 5.6; N, 22.6. Calc. for $C_{18}H_{36}N_{14}Cu_2Fe\cdot 12H_2O$: C, 25.5; H, 5.9; N, 23.1%.

Physical measurement

Elemental analyses were performed on a Perkin–Elmer 240C analytical instrument. IR spectra were recorded on a Nicolet 170SX FT spectrophotometer with KBr pellets in the range from 4000–500 cm^{-1}. The far-IR spectra (500–100 cm^{-1}) were recorded as Nujol mulls between polyethylene sheets. Electronic reflectance and solution (water) spectra were recorded on a Shimadzu 240 and 3100 spectrophotometers, respectively. Powder ESR spectra were measured at 100 K using a Bruker 200-D SRC spectrometer.

Crystallographic data collection and structure determination

The relevant crystal data and structural parameters are summarized in Table 1. The intensities were collected at 294 K on a Riguka RAXIS IIC imaging-plate diffractometer using Mo-K_α radiation ($\lambda = 0.71073$ Å) from a rotating-anode generator operating at 50 kV and 90 mA ($2\theta_{max} = 55.2°$); 60 oscillation frames in the range of 0 ~ 180°, exposure 8 min per frame for the complex [7].

Table 1. Crystal data for the complex

Formula	$[Cu(Cu_6H_{18}N_4)]_2$ $[Fe(CN)_6]\cdot 12H_2O$
Formula weight	956.8
Colour habit	Dark blue prism
Size (mm)	$0.20\times 0.14\times 0.36$
Crystal system	Monoclinic
Space group	$P2_1/c$
a/Å	13.582(1)
b/Å	10.112(1)
c/Å	13.940(1)
α/°	90
β/°	95.33(1)
γ/°	90
V/Å^3	1906.3(10)
Z	2
d_{cal}/g cm^{-3}	1.477
μ	1.548
$F(000)$	892
Reflections collected	6891
Reflections unique	3933 ($R_{int} = 0.017$)
Reflections observed ($I > 3\sigma(I)$)	2443
R, R_w	0.027, 0.041
w^{-1}	$\sigma^2(F)+0.002F^2$
GOF	1.10
$\Delta(\rho)$ max, min/e Å^{-3}	0.25, −0.40

The structure was solved by direct methods. All non-hydrogen atoms were refined anisotropically by full-matrix least squares. Hydrogen atoms of the ligand and the solvent molecules were placed in their calculated positions with C—H 0.96 Å, assigned fixed isotropic thermal parameters and allowed to ride on their respective parent atoms. The contributions of these hydrogen atoms were included in the structure factor calculations.

All computations were carried out on a PC-486 using the SHELXTL-PLUS program package [8]. Analytical expressions of neutral-atom scattering factors were employed, and anomalous dispersion corrections were incorporated [9]. Bond distances and angles are listed in Table 2.

Additional material deposited at the Cambridge Crystallographic Data Centre comprises atom coordinates and thermal parameters.

RESULTS AND DISCUSSION

IR spectrum

The principal IR-active bands of the title complex fall in the regions 3100–3500 and 2000–2100 cm^{-1}, the first being characteristic of ν(O—H) and ν(N—H), the second of ν (C≡N). In the first interval, the band at 3450 cm^{-1} and a shoulder at 3500 cm^{-1} are assigned to the stretching vibrations of water molecules. The bands at 3338, 3277 and 3146 cm^{-1} are some of the expected NH_2 stretching vibrations of the tren ligand [10]. For the ν(C≡N) mode of $[Fe(CN)_6]^{4-}$ two main bond systems of comparable intensity are observed: one at 2058 cm^{-1} is assigned to the intermetallic C—N stretching [11], and another at 2041 cm^{-1} is assigned to terminal stretching modes. The two bands are derived from the T_{1u} species of ferrocyanide in the O_h point group by lowering of the symmetry [12]. The Cu—N (NH_2 of tren) stretching modes are at 422 and 472 cm^{-1}. The weak but sharp band at 534 cm^{-1} can be assigned to the Cu—N stretching mode of the imino nitrogen [13], while the band at 273 cm^{-1} might be assigned to the Cu—N stretching relative to CN^- group, and bands at 421 and 442 cm^{-1} might be due to the Fe—C stretching mode [14]. All of these indicate that the complex not only contains the ferrocyanide moiety, but also the copper(II) moiety with the CN^- group coordinated to it, as well as water molecules.

Electronic spectra and ESR spectrum

The solid reflectance electronic spectrum (Fig. 1) shows a band at 18,400 cm^{-1} and a shoulder at *ca*

Table 2. Selected bond lengths (Å) and angles (°) and intermolecular contacts

Fe(1)—C(1)	1.924(2)	O(1w)···O(2w)	2.692(5)
Fe(1)—C(2)	1.935(2)	O(1w)···O(3w)	2.813(5)
Fe(1)—C(3)	1.894(2)	O(1w)···O(4w)	2.782(5)
Cu(1)—N(3)	1.958(2)	O(1w)···O(5w)	2.805(5)
Cu(1)—N(4)	2.049(2)	O(2w)···O(6wb)	2.791(5)
Cu(1)—N(5)	2.046(2)	O(2w)···O(4wc)	2.847(5)
Cu(1)—N(6)	2.167(2)	O(4w)···O(5wb)	2.792(5)
Cu(1)—N(7)	2.050(2)	O(4w)···O(6w)	2.836(5)
C(1)—N(1)	1.155(3)	N(1)···O(6wa)	2.906(5)
C(2)—N(2)	1.146(3)	N(2)···O(3wa)	2.864(5)
C(3)—N(3)	1.156(3)	N(5)···O(3wd)	3.090(5)
N(4)—C(4)	1.465(4)	O(3wa)···N(1e)	3.061(5)
N(5)—C(6)	1.468(3)		
N(6)—C(8)	1.463(4)		
N(7)—C(5)	1.485(3)		
N(7)—C(7)	1.491(3)		
N(7)—C(9)	1.474(3)		

C(1)—Fe(1)—C(2)	89.4(1)	N(3)—Cu(1)—N(4)	93.1(1)
C(1)—Fe(1)—C(3)	94.1(1)	N(3)—Cu(1)—N(5)	91.7(1)
C(2)—Fe(1)—C(3)	87.6(1)	N(4)—Cu(1)—N(5)	140.7(1)
C(1)—Fe(1)—C(1a)	180.0(1)	N(3)—Cu(1)—N(6)	107.4(1)
C(2)—Fe(1)—C(1a)	90.6(1)	N(4)—Cu(1)—N(6)	104.0(1)
C(3)—Fe(1)—C(1a)	85.9(1)	N(5)—Cu(1)—N(6)	111.7(1)
C(1)—Fe(1)—C(2a)	90.6(1)	N(3)—Cu(1)—N(7)	169.4(1)
C(2)—Fe(1)—C(2a)	180.0(1)	N(4)—Cu(1)—N(7)	84.2(1)
C(3)—Fe(1)—C(2a)	92.4(1)	N(5)—Cu(1)—N(7)	84.0(1)
C(1)—Fe(1)—C(3a)	85.9(1)	N(6)—Cu(1)—N(7)	83.2(1)
C(2)—Fe(1)—C(3a)	92.4(1)	Fe(1)—C(3)—N(3)	173.7(2)
C(3)—Fe(1)—C3a)	180.0(1)	Cu(1)—N(3)—C(3)	144.1(2)

Symmetry code: a $(1-x, 1-y, 1-z)$; b $(-x, 1-y, 1-z)$; c $(-x, 0.5+y, 1.5-z)$; d $(1-x, -0.5+y, 1.5-z)$; e $(1-x, 0.5+y, 1.5z)$.

14,600 cm^{-1}, the former can be assigned to the metal to metal charge transfer transition (MMCT) (15), and the latter to a *d–d* transition of the Cu^{II} moiety. However, the broadness and overlapping characteristics of the spectrum prevented us from obtaining further information about the coordination geometry

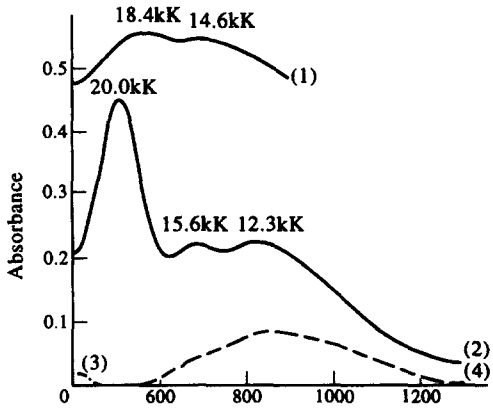


Fig. 1. The electronic reflectance (1) and absorption in water (2) of the title complex (——), comparing with the absorption in water for $K_4Fe(CN)_6 \cdot 3H_2O$(3) (-·--·-) and [Cu (tren)][ClO$_4$]$_2$ (4) (- - -).

of the copper(II) atoms. The solution electronic spectrum (Fig. 1) of the complex exhibits three well-separated bands at 20,000 (980), 15,600 (700) and 12,300 cm^{-1} (710 dm^{-3} mol^{-1} cm^{-1}). The band at 20,000 cm^{-1} is ascribed to a MMCT transition, the other two bands are assigned to *d–d* transitions of the copper(II) moiety, the equal intensity of the two bands indicated that the coordination geometry of Cu^{II} might be a *cis* octahedron or a geometry intermediate between the square pyramidal and trigonal bipyramidal topolgies [16,17]. However, discarding the tail of the MMCT band, it might be expected that the intensity of the band at *ca* 15,600 cm^{-1} will be lowered, and thus we can suggest that the coordination geometry of the copper(II) is square pyramidal with considerable trigonal bipyramidal distortion. This suggestion is also supported by the solid-state ESR spectrum at 100 K which has the $g_{\parallel} = 2.107$, $A_{\parallel} = 3.2 \times 10^{-3}$, $g_{\perp} = 2.077$ and $A_{\perp} = 5.7 \times 10^{-3}$.

Description of the structure of the complex

The stereochemistry of the complex is shown in Fig. 2. The structure consists of a neutral [(tren) Cu(NC)Fe(CN)$_4$(CN)Cu(tren)] unit as a separate

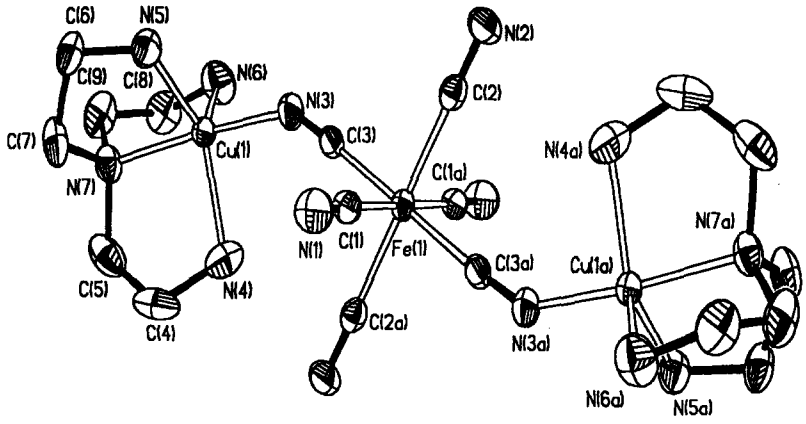


Fig. 2. Molecular structure and atom numbering of the complex.

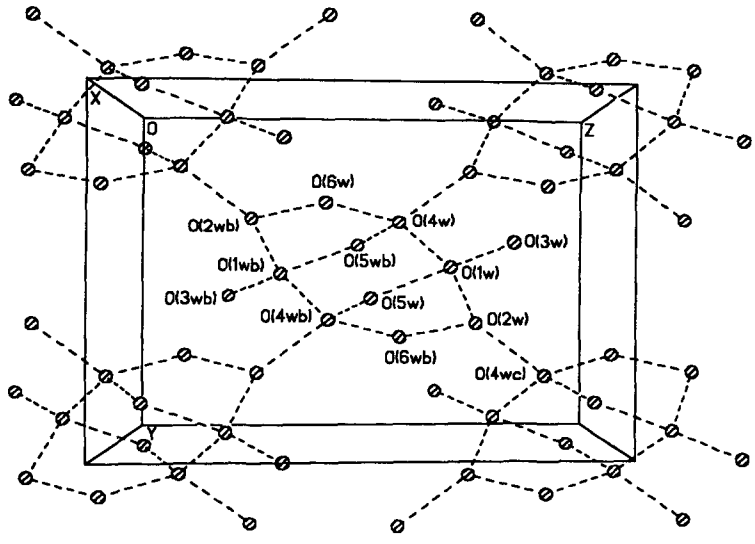


Fig. 3. Hydrogen bonding scheme for the water molecules in the molecular packing.

trinuclear complex. Within the polynuclear complex, the iron atom of the hexacyanoferrate ion occupies the centre of symmetry, and four of the six CN^- groups, namely C(1)≡N(1) and C(2)≡N(2), as well as the centrosymmetrically related ones, are bonded to iron and to water molecules. The other two cyanide ligands around iron reveal their amibdentate and bridging nature, forming bonds with the copper atoms of the nearest $[Cu(tren)]^{2+}$ ions and giving rise to non-linear Fe—C≡N—Cu sequences, with the Cu—N≡C bond angle of *ca* 144.1°. An intermediate geometry between regular, square-based pyramidal and trigonal bipyramidal around each copper atom is thus present, as suggested by the spectroscopy, and the geometrical parameter [18] $\tau = 0.48$ also indicates that there is some shift towards square pyramidal, as expected. This structure is quite different from the general mononuclear [17,19,20] and binuclear [21, 22] copper(II) complexes with the tren as ligand, which always give an almost regular trigonal bipyramidal arrangement around the copper(II), with τ close to 1.0, owing to the rigid C_{3v} structure of the tren ligand. In the basal plane the copper atom is coordinated by two primary amine nitrogen atoms, N(4), N(5), and the tertiary amine nitrogen atom, N(7), of the tren, and the nitrogen atom, N(2), belonging to the cyanide group, whereas, the other primary amine nitrogen atom of tren, N(6), is in an apical position of the square pyramid. The bond lengths and angles within each $[Fe(CN)_6]^{4-}$ and $[Cu(tren)]^{2+}$ unit do not differ significantly from values reported previously [6,20,23,24]

A two-dimensional network (Fig. 3) of the water molecules, connected by hydrogen bonds and in groups of six for each asymmetric unit of the polynuclear complex, is present in the lattice. Four of the

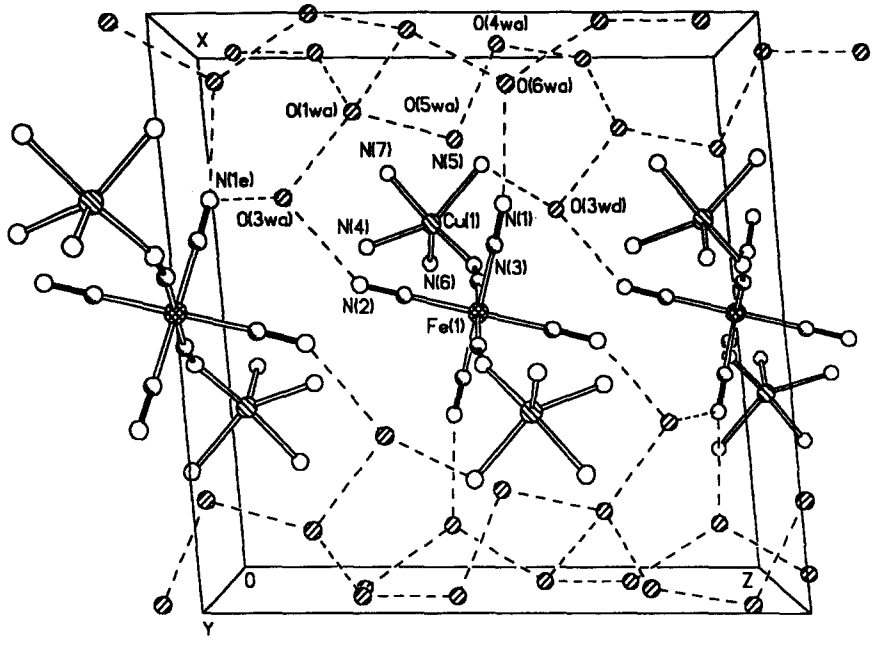


Fig. 4. Hydrogen bonding scheme in the molecular packing. Carbon atoms of the $[Cu(tren)]^{2+}$ moiety were omitted for clarity.

six water molecules, O(1w), O(2w), O(4w), O(6w), are connected together to form a main chain, the remaining two, O(5w) and O(3w), are connected to the chain through hydrogen bonds to water molecule O(1w). The main chain, together with the centrosymmetrically related ones, connect together to form the eight-membered ring. The rings are connected *via* hydrogen bonds $O(2w)\cdots O(4wc)$ $(-x, 0.5+y, 1.5-z)$ to form a two-dimensional network. This develops along the *a*-axis of the cell, and is associated with each of the separate polynuclear units through an extensive hydrogen-bond system involving some of the nitrogens of the hexacyanoferrate moiety, to form the three-dimensional networks shown in Fig. 4. Of the six water molecules, only two of them, O(3w) and O(6w), form hydrogen bonds to the nitrogen of the terminal CN^- group. Of the three primary amine nitrogen atoms, only one, N(5), forms a hydrogen bond to the water molecule. The intermolecular contacts of those water molecules and nitrogen atoms are listed in Table 2. No other intermolecular contacts are less than 3.15 Å.

Acknowledgements—This work was supported by a major research project grant from the State Science and Technology Commission and the National Science Foundation of China.

REFERENCES

1. Goldberg, M. and Pecht, I., *Biochemistry*, 1976, **15,** 4197.
2. Morpurgo, L., Mavelli, I., Carabreses, L., Finazzi, A. and Rotilio, G., *Biochem. Biophys. Res. Comm.*, 1976, **70,** 607.
3. Morpurgo, G. O., Mosini, V. and Porte, P., *J. Chem. Soc., Dalton Trans.*, 1980, 1272.
4. Malachowski, R., Huynh, H. B., Tomlinson, L. J., Kelly, R. S. and Furbee, J. W. Jr, *J. Chem. Soc., Dalton Trans.*, 1995, 31.
5. Mcllachlan, G. A., Fallon, G. D., Martin, R. J. and Spiccia, L., *Inorg. Chem.*, 1995, **34,** 254.
6. Lu, Z. L., Duan, C. Y., Tian, Y. P., You, X. Z., Fun, H. K. and Yip, B. C., *Polyhedron*, 1996, **15,** 1769.
7. Tanner, J. and Krause, K., *Riguka Journal*, 1994, **11,** 4; *ibid.*, 1990, **7,** 28; Kraus, K. L. and Phillips, G. N., *J. Appl. Crystallogr.*, 1992, **25,** 146.
8. Sheldrick, G. M., in *Computational Crystallography*, ed. D. Sayre. Oxford University Press, New York, 1982, pp. 506–514.
9. *International Tables for X-ray Crystallography*, Vol. 4. Kynoch Press, Birmingham (now distributed by Kluwer Academic Press, Dordrecht), 1974, pp. 55, 99, 14.
10. Schmidtke, H. H. and Garthoff, G., *Inorg. Chim. Acta*, 1968, **2,** 357.
11. Does, D. A., Haim, A. and Wilmarth, W. K., *J. Inorg. Nuclear Chem.*, 1961, **21,** 33.
12. Shriver, D. F., Shriver, S. H. and Anderson, S. E., *Inorg. Chem.*, 1965, **4,** 725.
13. Hathaway, B. J. and Tomlinson, A. A. G., *Coord. Chem. Rev.*, 1970, **5,** 1.
14. Cauzzi, D. A., Mari, G., Predieri, G., Tiripicchio, A. and Cavatorta, F., *Inorg. Chem. Acta*, 1993, **204,** 181.
15. Suzuki, M. and Uehara, A., *Bull. Chem. Soc. Jpn*, 1984, **57,** 3134.
16. Duggan, M., Ray, N., Hathaway, B. J., Tomlin-

son, G., Brint, P. and Pelin, K., *J. Chem. Soc., Dalton Trans.*, 1980, 1342.
17. Chan-Cheng, S., Wen-Shuh, L., Tsy-Yan, H., Tsung-Yi, C., Sue-Lein, W. and Fen-Lin, L., *Polyhedron*, 1993, **12,** 2249.
18. Addison, A. W., Rao, T. W., Reedijk, J., Van Rijn, J. and Verscher, G. C., *J. Chem. Soc., Dalton Trans.*, 1984, 1349.
19. Jain, P. C. and Lingafelter, E. C., *J. Am. Chem. Soc.*, 1967, **89,** 6131.
20. Fun, H. K., Yip, B. C., Lu, Z. L., Duan, C. Y., Tian, Y. P. and You, X. Z., *Trans. Met. Chem.*, 1996, **15,** 1769.
21. Duggan, D. M. and Hendrickson, D. N., *Inorg. Chem.*, 1974, **13,** 1911.
22. Lasowski, E. J., Duggan, D. M. and Hendrickson, D. N., *Inorg. Chem.*, 1975, **14,** 2249.
23. Ludi, A. and Gudel, H. U., *Structure and Bonding*, 1973, **14,** 1.
24. Gentil, L. A., Olasle, J. A. and Riggutie, G. E., *Inorg. Chim. Acta*, 1991, **179,** 89.

Pergamon

PII: S0277-5387(96)00361-0

Polyhedron Vol. 16, No. 6, pp. 915–919, 1997
Copyright © 1996 Published by Elsevier Science Ltd
Printed in Great Britain. All rights reserved
0277-5387/97 $17.00+0.00

Synthesis and crystal structure of a new μ_2-phenoxy oxygen bridged macrocyclic binuclear cadmium(II) complex with pendant arms

Xin-You Xu,[a] Qin-Hui Luo,[a]* Meng-Chang Shen,[a] Xiao-Yun Huang,[b] and Qiang-Jin Wu[b]

[a] Coordination Chemistry State Key Laboratory, Nanjing University, Nanjing 210008, P.R. China

[b] Fuzhou State Key Laboratory of Structure Chemistry, Fuzhou 350002, P.R. China

(Received 20 March 1996; accepted 24 July 1996)

Abstract—A new binuclear cadmium(II) macrocyclic complex has been synthesized by [2+2] Schiff-base condensation of tris(3-aminopropyl)amine with sodium 2,6-diformyl-4-methoxylphenolate in the presence of $Cd(ClO_4)_2 \cdot 6H_2O$. The crystal structure, spectral characterization and molar conductivity show that two cadmium(II) ions were bridged by two μ_2-phenoxy oxygen atoms. Each cadmium(II) is located in a trigonal prismatic coordination environment (N_4O_2). Copyright © 1996 Published by Elsevier Science Ltd

Keywords: cadmium(II); binuclear complex; macrocycle; oxygen bridge; crystal structure; trigonal prism.

Pilkington and Robson [1] obtained a new kind of macrocyclic ligand for the first time by the template condensation of 2,6-diformyl-4-methylphenol with diamines. The ligands contain strong donors, namely, phenoxy oxygen atoms as well as amine nitrogen atoms, therefore they are excellent for catalysis and biological simulation [2,3] because of their special coordination ability with transition metal ions. The polyaza macrocyclic ligands also have these properties and have attracted much attention [4–6]. Cadmium is an environmental pollutant which inhibits RNA polymerase activity *in vivo* [7,8] and reacts readily with proteins and other biological molecules, and so the macrocyclic chemistry of cadmium has been developed recently [9]. Although many studies have been made on cadmium(II) macrocyclic complexes [10–12], only a few crystal structures have been reported, and most were found to be mononuclear complexes [13–17]. In this paper we report the synthesis, characterization and X-ray crystal structure of a new η-oxo-bridged binuclear cadmium(II) complex of a 28-membered macrocyclic complex with pendant arms (Fig. 1). To our knowledge, only a few of these kinds of structures have hitherto been reported.

* Author to whom correspondence should be addressed.

EXPERIMENTAL

Materials

2,6-Diformyl-4-methoxylphenol (dmop) was prepared using the method described in the literature [18]. Sodium 2,6-diformyl-4-methoxylphenolate (sdmop) was obtained by mixing equimolar amounts of dmop and NaOH in ethanol. Tris(3-aminopropyl)amine was prepared by a modified literature method [19] with a purity of over 99%. All starting materials were of chemical purity.

Physical measurements

Solution electrical conductivity was measured by a BDS-A numerical conductometer (Jiangsu, China) with solution concentrations of *ca* 10^{-4} mol dm^{-3} in acetonitrile. IR spectra were measured as KBr discs

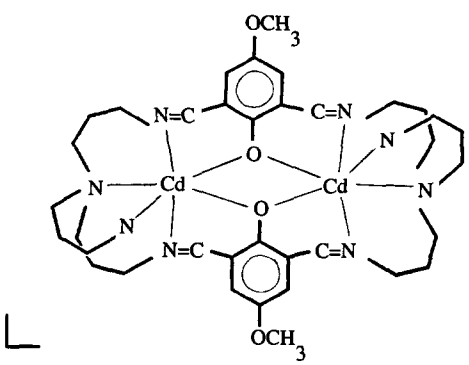


Fig. 1. The structure of the binuclear complex cation $[Cd_2(H_{-2}L)]^{2+}$.

using a Nicolet 5DX FT-IR spectrophotometer. Electronic spectra were recorded on Shimadazu UV-240 spectrophotometer.

Preparation of the complex $[Cd_2(H_{-2}L)](ClO_4)_2 \cdot 0.5CH_3OH$

To a stirred solution of sodium 2,6-diformyl-4-methoxyphenolate (0.101 g, 0.5 mmol) and $Cd(ClO_4)_2 \cdot 6H_2O$ (0.261 g, 0.625 mmol) in absolute methanol (30 cm^3) was added dropwise a solution of tris(3-aminopropyl)amine (0.094 g, 0.5 mmol) in absolute methanol (15 cm^3) at 0°C. After stirring for 2 h at 35°C, yellowish microcrystals were precipitated and filtered off, washed with methanol and dried *in vacuo* (yield 45%). Found: C, 40.2; H, 5.5; N, 10.5; Cd, 19.9. Calc. for $C_{36.5}H_{56}N_8O_{12.5}Cd_2Cl_2$; C, 39.8; H, 5.1; N, 10.2; Cd, 20.4%. IR (KBr, cm^{-1}): 3400 br, ν(OH)(CH_3OH); 3354s, $\nu_{as}(NH_2)$; 3300s, $\nu_s(NH_2)$; 1641s, ν(C=N); 1544s, ν(Ar—O); 1102 (ClO_4^-). UV–vis (λ_{max} nm, CH_3CN); 270 (9763 mol^{-1} dm^3 cm^{-1}); 430 (10078). Λ_M (CH_3CN, 279 K): 236 S cm^2 mol^{-1}. The yellowish crystals of $[Cd_2(H_{-2}L)](ClO_4)_2 \cdot 5CH_3OH$ suitable for X-ray structure determination were obtained by slow evaporation of the mother liquor at ambient temperature.

CAUTION. Perchlorate salts of metal complexes with organic ligands are potentially explosive. Only small amounts of material should be prepared, and these should be handled with caution. The complex described in this report has, so far, been found to be safe when used in small quantities.

X-ray crystal structure determination of $[Cd_2(H_{-2}L)](ClO_4)_2 \cdot 5CH_3OH$

Crystal data. $C_{36.5}H_{56}N_8O_{12.5}Cd_2Cl_2$, $M = 1102.65$, yellowish crystal, dimensions $0.9 \times 0.9 \times 0.45$ mm^3, triclinic, space group P_{-1}(#2), $a = 10.455(6)$, $b = 11.451(4)$, $c = 20.130(6)$ Å, $\alpha = 105.75(3)$, $\beta = 82.84(3)$, $\gamma = 97.21(3)°$, $V = 2291(2)$ $Å^3$, $F(000) = 1122$, $Z = 2$, $D_c = 1.60$ g cm^{-3}, $T = 296$ K, $\mu = 11.06$ cm^{-1}.

Data collection and refinement. A single crystal was mounted on a glass fibre. The crystal data were collected on an Enraf–Nonius CAD4 four-circle diffractometer with graphite-monochromated Mo-K_α radiation ($\lambda = 0.71069$ Å) using an ω–2θ scan mode with ω scan width $0.95 + 0.350 \tan\theta$, scan rate 5.49° min^{-1}. A total of 8067 independent reflections were collected in the range $2 < 2\theta < 50°$, of which 6421 reflections with $I > 3\sigma(I)$ were used in the structure determination and refinement, after L_p corrections. The structure was solved by the MITHRIL direct method. The remaining non-hydrogen atoms were located from a difference Fourier map. Hydrogen atoms were introduced in calculated positions but not refined. The final least-squares cycle gave $R = 0.052$, $R_w = 0.064 (w = 1/\sigma^2(F_0))$. The maximum and minimum residuals had values of 0.63 and −0.89 $eÅ^{-3}$, respectively. All calculations were performed on a MICRO VAX-3100 computer using the programs contained in the TEXSAN [20].

RESULTS AND DISCUSSION

Characterization of the complex

In the infrared spectrum a strong peak appears at 1641 cm^{-1} corresponding to the stretching vibration of imino C=N bonds. The symmetric and asymmetric stretching frequencies (3300 and 3354 cm^{-1}) for NH_2 groups are also present, but no strong peaks at 1650–1700 cm^{-1} for the carbonyl groups. This means that two NH_2 groups and carbonyl groups have been condensed into C=N bonds, whilst another NH_2 group is unchanged. A broad band at *ca* 3400 cm^{-1}, characteristic of the OH group of CH_3OH, showed that CH_3OH molecules exist in the crystalline complex, in agreement with the elemental analysis. The strong peak at 1102 cm^{-1} without splitting showed that ClO_4^- did not take part in coordination with Cd^{II} ions. This is also confirmed by the molar conductivity of the complex ($\Lambda_M = 236$ S cm^2 mol^{-1}) which is attributable to a 2:1 electrolyte. Two intense absorptions in the electronic spectrum of the complex are designated to π–π^* transitions of the K band of the benzene rings and of C=N groups.

Description of the structure of $[Cd_2(H_{-2}L)](ClO_4)_2 \cdot 0.5CH_3OH$

A perspective view of the cation $[Cd_2(H_{-2}L)]^{2+}$ and a packing diagram are displayed in Figs 2 and 3, respectively. Selected bond distances and bond angles are given in Tables 1 and 2, respectively.

Figure 3 shows that each unit cell contains two complex associations, each consisting of one molecule of the macrocyclic complex cation $[Cd_2(H_{-2}L)]^{2+}$, two perchlorate anions and half of a methanol solvent

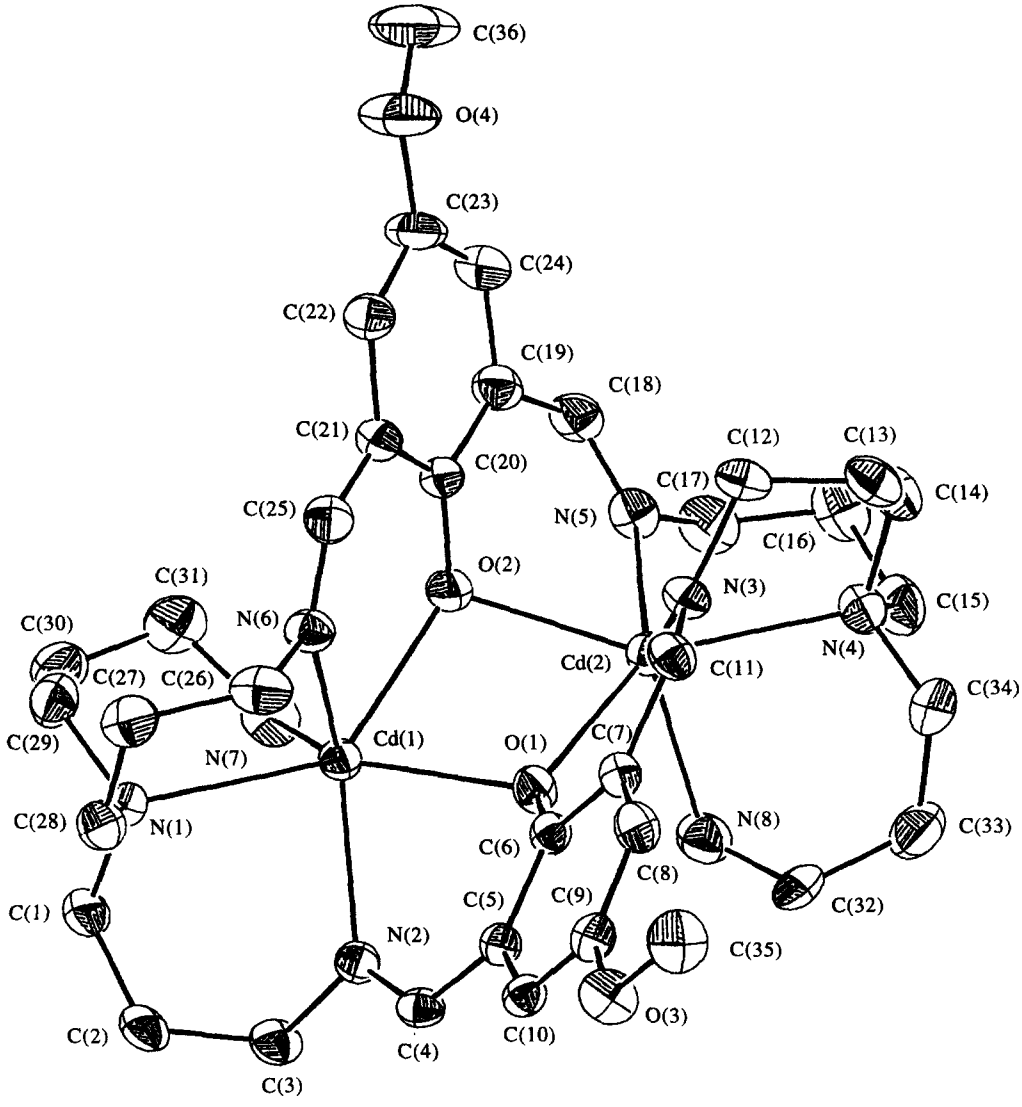


Fig. 2. A perspective view of the cation $[Cd(H_{-2}L)]^{2+}$.

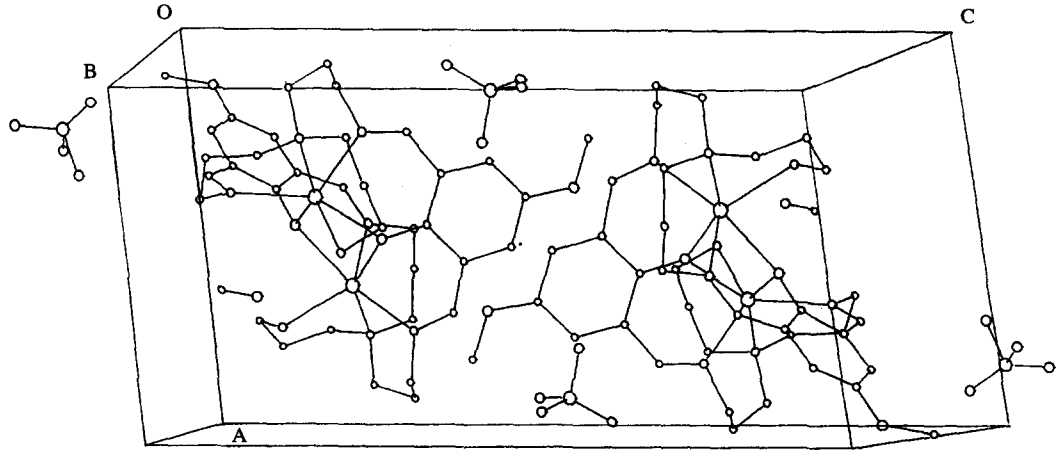


Fig. 3. A packing diagram of the complex $[Cd_2(H_{-2}L)](ClO_4)_2 \cdot 0.5CH_3OH$.

Table 1. Selected bond distances (Å)

Cd(1)—N(7)	2.294(6)	Cd(2)—N(3)	2.295(5)
Cd(1)—N(6)	2.300(5)	Cd(2)—N(8)	2.302(6)
Cd(1)—N(2)	2.311(5)	Cd(2)—N(5)	2.305(5)
Cd(1)—O(1)	2.282(4)	Cd(2)—O(1)	2.318(4)
Cd(1)—O(2)	2.350(4)	Cd(2)—O(2)	2.328(4)
Cd(1)—N(1)	2.455(5)	Cd(2)—N(4)	2.483(5)
O(1)—C(6)	1.303(6)	O(2)—C(20)	1.315(7)
O(3)—C(9)	1.374(7)	O(4)—C(23)	1.369(8)
O(3)—C(35)	1.397(9)	O(4)—C(36)	1.40(1)
Cd(1)—Cd(2)	3.689(2)	Cd(2)—N(1)	6.133(5)
Cd(1)—N(4)	6.158(5)	N(1)—N(4)	8.608(8)

molecule. The methanol and perchlorate anions are disordered over two interpenetrating sites. It can be seen from Fig. 2 that in the cation of the complex each Cd^{II} ion is enclosed within the polyaza macrocycle and coordinated by one bridgehead nitrogen atom, two imino nitrogen atoms, one amine nitrogen atom of the pendant arms and two oxygen atoms of phenoxy groups. Each Cd^{II} is located in a trigonal prismatic N_4O_2 coordination environment with coordination number of six. For the Cd(1) centre, the phenoxy oxygens O(1), O(2) and the amino nitrogen N(6) forms one trigonal face, the Cd(1) deviates downwards by 1.5181 Å from the face. The amino nitrogen atoms N(2), N(7) and the bridgehead nitrogen N(1) form another trigonal face, the Cd(1) deviates upwards by 1.2522 Å from the face. The dihedral angle between the two faces is 11.13°. For the Cd(2) centre, the phenoxy oxygens O(1), O(2) and amino nitrogen N(3) form one trigonal face and the Cd(2) deviates upwards by 1.4849 Å from the face. The amino nitrogens N(4), N(5) and the bridgehead nitrogen N(8) form another trigonal face and the Cd(2) deviates downwards by 1.2423 Å from the face. The dihedral angle between the two faces is 12.74°C. The dihedral angle between the plane consisting of Cd(1), O(1), Cd(2) and the plane consisting of Cd(1), O(2), Cd(2) is 151.00°. The phenoxy oxygens O(1) and O(2) bridge the two Cd^{II} ions. The bond distances of Cd(1)—N(imino) and Cd(2)—N(imino) are approximately equal, being in the range 2.294–2.311 Å. These Cd—N bond distances are shorter than the standard bond distance of 233 ± 0.005 Å [20]. This means that these imino groups have strong coordination ability towards Cd^{II}. Conversely, the two bond distances Cd(1)—N(1), Cd(2)—N(4) are 2.455 and 2.483 Å, respectively, implying weak interaction between the Cd^{II} ions and the bridgehead nitrogen atoms.

Table 2. Selected bond angles (°)

O(1)—Cd(1)—N(7)	126.1(2)	N(3)—Cd(2)—N(8)	121.8(2)
O(1)—Cd(1)—N(6)	91.9(2)	N(3)—Cd(2)—N(5)	120.4(2)
O(1)—Cd(1)—N(2)	75.1(1)	N(3)—Cd(2)—O(1)	77.9(2)
O(1)—Cd(1)—O(2)	72.0(1)	N(3)—Cd(2)—O(2)	95.5(2)
O(1)—Cd(1)—N(1)	148.0(2)	N(3)—Cd(2)—N(4)	81.9(2)
N(7)—Cd(1)—N(6)	121.7(2)	N(8)—Cd(2)—N(5)	111.9(2)
N(7)—Cd(1)—N(2)	110.9(2)	N(8)—Cd(2)—O(1)	75.5(2)
N(7)—Cd(1)—O(2)	76.1(2)	N(8)—Cd(2)—O(2)	122.7(2)
N(7)—Cd(1)—N(1)	82.5(2)	N(8)—Cd(2)—N(4)	82.7(2)
N(6)—Cd(1)—N(2)	121.6(2)	N(5)—Cd(2)—O(1)	142.8(2)
N(6)—Cd(1)—O(2)	77.0(2)	N(5)—Cd(2)—O(2)	74.2(2)
N(6)—Cd(1)—N(1)	82.1(2)	N(5)—Cd(2)—N(4)	81.0(2)
N(2)—Cd(1)—O(2)	142.7(1)	O(1)—Cd(2)—O(2)	71.8(1)
N(2)—Cd(1)—N(1)	81.5(2)	O(1)—Cd(2)—N(4)	135.9(2)
O(2)—Cd(1)—N(1)	135.5(1)	O(2)—Cd(2)—N(4)	149.6(2)
C(20)—O(2)—Cd(1)	132.3(4)	C(6)—O(1)—Cd(1)	115.0(3)
C(20)—O(2)—Cd(2)	111.0(3)	C(6)—O(1)—Cd(2)	130.8(3)
Cd(2)—O(2)—Cd(1)	104.1(1)	Cd(1)—O(1)—Cd(2)	106.6(2)
C(9)—O(3)—C(35)	117.3(5)	C(23)—O(4)—C(36)	117.9(8)
C(28)—N(1)—C(29)	108.4(5)	C(15)—N(4)—C(14)	108.9(5)
C(28)—N(1)—C(1)	108.3(5)	C(15)—N(4)—C(34)	107.3(5)
C(28)—N(1)—Cd(1)	112.2(4)	C(15)—N(4)—Cd(2)	112.5(4)
C(32)—N(8)—Cd(2)	108.6(4)	C(14)—N(4)—C(34)	108.7(5)
C(29)—N(1)—C(1)	108.1(5)	C(14)—N(4)—Cd(2)	111.6(4)
C(29)—N(1)—Cd(1)	108.2(4)	C(34)—N(4)—Cd(2)	107.7(4)
C(1)—N(1)—Cd(1)	111.4(3)	C(18)—N(5)—C(17)	116.4(5)
C(4)—N(2)—C(3)	117.2(5)	C(18)—N(5)—Cd(2)	123.1(4)
C(4)—N(2)—Cd(1)	122.7(4)	C(17)—N(5)—Cd(2)	119.9(4)
C(3)—N(2)—Cd(1)	119.2(4)	C(25)—N(6)—C(26)	116.5(5)
C(11)—N(3)—C(12)	117.1(5)	C(25)—N(6)—Cd(1)	130.3(4)
C(11)—N(3)—Cd(2)	128.6(4)	C(26)—N(6)—Cd(1)	113.2(3)
C(12)—N(3)—Cd(2)	114.2(4)	C(31)—N(7)—Cd(1)	110.3(4)

However, in the cadmium cryptate synthesized by condensation of tris(2-aminoethyl)amine with 2,6-diformyl-4-methylphenol [21], the corresponding bond distance of Cd—N(bridgehead) 2.787 Å, was larger than that reported in this paper. The long Cd(1)···Cd(2) distance (3.689 Å) indicates that there is no interaction between the two metal atoms. The bond distances Cd(1)—O(1), Cd(2)—O(2), Cd(2)—O(1) and Cd(2)—I(2) are 2.282, 2.350, 2.318 and 2.328 Å, respectively, being close to those reported by Drew *et al.* [21], also implying that Cd(1) is similar to Cd(2) in coordination environment but slightly different to Cd(2) in degree of distortion. An analogous complex $[Cu_2L'(OH)](ClO_4)_3$ which was synthesized by [2+2] Schiff-base condensation of tris(2-aminoethyl)amine with isophthalic aldehyde in the presence of $Cu(ClO_4)_2 \cdot 6H_2O$ is unstable [22]. In our complex, however, the flexibility of the carbon chain strengthened the coordination ability of the bridgehead nitrogen atoms, and the phenoxy oxygen atoms bridging the two Cd^{II} atoms enhanced the stability of the complex as well as forming the six-membered chelate rings and so stabilizing the structure of the complex.

Acknowledgements—This project was supported by the Natural Science Foundation of China and Fuzhou State Key Laboratory of Structure Chemistry.

REFERENCES

1. Pilkington, N. H. and Robson, R., *Aust. J. Chem.*, 1970, **23,** 2225.
2. Zanello, P., Tamburini, S., Vigato, P. A. and Mazzochim, G. A., *Coord. Chem. Rev.*, 1987, **77,** 165.
3. Vigato, P. A., Tamburini, S. and Fenton, D. E., *Coord. Chem. Rev.*, 1990, **106,** 105.
4. Bailey, N. A., Rodriguez de Barbarin, C. O., Fenton, D. E., Hellier, P. C., Hempstead, P. D., Kanesato. M. and Leeson, P. B., *J. Chem. Soc., Dalton Trans.*, 1995, 765.
5. Ngwenya, M. P., Chen, D., Martell, A. E. and Reibenspies, J., *Inorg. Chem.*, 1991, **30,** 2732.
6. Fenton, D. E., *Pure Appl. Chem.*, 1986, **58,** 1437.
7. Jacobson, K. B. and Turner, J. E., *Toxicology*, 1980, **60,** 1.
8. Hidalgo, H. A., Koppa, V. and Bryan, E. S, *FEBS Lett.*, 1976, **64,** 159.
9. Dakternieks, D., *Coord. Chem. Rev.*, 1990, **98,** 288.
10. Marchetti, P. S., Bank, S., Bell, T. W., Kennedy, M. A. and Ellis, P. D., *J. Am. Chem. Soc.*, 1989, **111,** 2063.
11. Thom, V. J., Hosken, G. D. and Hancock, R. D., *Inorg. Chem.*, 1985, **24,** 3378.
12. Richens, D. T., in *Annual Reports on the Progress of Chemistry*, 86 (sect. A), The Royal Society of Chemistry, Cambridge, 1989, p. 66.
13. Adam, K. R., Dancey, K. P., Leong, A. J., Lindoy, L. F., McCool, B. J., McPartlin, M. and Tasker, P. A., *J. Am. Chem. Soc.*, 1988, **110,** 8471.
14. Drew, M. G. B., Mcfall, S. G. and Nelson, S. M., *J. Chem. Soc., Dalton Trans.*, 1979, 575.
15. Adam, K. R., Arshad, S. P. H., Baldwin, D. S., Duckworth, P. A., Leong, A. J., McCool, B. J., McPartlin, M., Tailor, B. A. and Tasker, P. A., *Inorg. Chem.*, 1994, **33,** 1194.
16. Drew, M. G. B., Howarth, O. W., Morgan, G. G. and Nelson, J., *J. Chem. Soc., Dalton Trans.*, 1994, 3149.
17. Bencini, A., Bianch, A., Castello, M., Varia, M. D., Garcia-Espana, E., Micheloni, M. and Paoletti, P., *Inorg. Chem.*, 1989, **28,** 347.
18. Taniguchi, S., *Bull. Chem. Soc. Jpn*, 1984, **57,** 268.
19. Chin, J., Banaszczyk, M., Jubian, V. and Zou, X., *J. Am. Chem. Soc.*, 1989, **111,** 186.
20. *TEXSAN, TEXRAY Structure Analysis Package*, Molecular Structure Corporation, The Woodlands, TX, U.S.A. 1989.
21. Drew, M. G. B., Howarth, O. W., Morgan, G. G. and Nelson, J., *J. Chem. Soc. Dalton Trans.*, 1994, 3149.
22. Harding, C. J., Lu, Q., Malone, J. M., Marrs, D. J., Martin, N., McKee, V. and Nelson, J., *J. Chem. Soc., Dalton Trans.*, 1995, 1739.

Pergamon

PII: S0277-5387(96)00360-9

Polyhedron Vol. 16, No. 6, pp. 921–925, 1997
Copyright © 1996 Elsevier Science Ltd
Printed in Great Britain. All rights reserved
0277-5387/97 $17.00+0.00

Structure of [2-(aminomethyl)pyridine]silver(I) nitrate and EPR studies of its oxidation product*

G. Swarnabala and M. V. Rajasekharan†

School of Chemistry, University of Hyderabad, Hyderabad 500 046, India

(Received 8 January 1996; accepted 24 July 1996)

Abstract—Reaction of $AgNO_3$ with excess 2-(aminomethyl)pyridine (amp) in water led to the crystallization of Ag(amp)NO_3 (**1**). Nearly linear coordination of silver(I) by pyridine-N and amino-N from two different amp molecules results in a polymeric chain structure of **1**. The packing is stabilized by ring–ring stacking interactions between two inversion-related polymer chains. Oxidation of **1** with $(NH_4)_2S_2O_8$ resulted in an orange solution from which a magnetically dilute Ag^{II} complex was crystallized by the addition of NH_4PF_6. It gave a well-resolved EPR spectrum and is formulated as silver(II) picolinate co-crystallized with NH_4PF_6.
Copyright © 1996 Elsevier Science Ltd

Keywords: polymeric coordination compound; silver(I); silver(II); EPR.

2-(Aminomethyl)pyridine (amp), being a flexible ligand, can either form chelates or act as a bridging ligand. While several examples are known for tris-chelates with this ligand [1–4], there is only one example [5] for the bridging mode, namely, the polymeric $[Rh_2(OAc)_4(amp)]_n$ complex. Solution studies [6,7] indicated the formation of several Ag^I-containing species such as $[AgHL]^+$, $[AgL]^+$, $[Ag_2L_2]^{2+}$, $[AgL_2]^+$ and $[Ag_2L]^{2+}$ where L = amp. As part of our continuing interest in the complexes of Ag with N-heterocyclic ligands [8,9], we have now investigated Ag(amp)NO_3 (**1**) which has a polymeric structure analogous to that of Ag(pz)NO_3 [10] (where pz = pyrazine). Reaction of **1** with $(NH_4)_2S_2O_8$ resulted in the oxidation of Ag^I to Ag^{II}, as well as the conversion of the $—CH_2NH_2$ group to carboxylate. The EPR of the oxidation product is also presented.

EXPERIMENTAL

All chemicals were of reagent grade. Amp and 2-picolinic acid (picH) were purchased from Fluka. IR (KBr disks) and UV–vis spectra were recorded on Perkin–Elmer 1310 and Lambda-3B spectrometers, respectively. C, H, N analyses were performed using a Perkin–Elmer 240C analyser. Silver was estimated gravimetrically [11]. EPR spectra were measured using a Jeol-FE-3X spectrometer.

Synthesis

Ag(amp)NO_3. To a solution of $AgNO_3$ (0.169 g, 1.00 mmol) in water (2 cm^3), amp (0.20 cm^3, 1.9 mmol) was added. The resulting clear solution was allowed to evaporate slowly in a desiccator. Colourless rod-shaped, thick crystals of Ag(amp)NO_3 (**1**) deposited after two days which were washed with water and methanol and dried. Yield: 0.185 g (0.665 mmol) 66.5%, based on $AgNO_3$. Found: C, 26.3; H, 3.1; N, 15.0; Ag, 37.4. Calc. for $C_6H_8N_3O_3Ag$: C, 25.9; H, 2.9; N, 15.1; Ag, 38.8%. IR data (KBr): 3267b, 1763s, 1595s, 1388b, 1151s, 997s, 825s, 760s, 611m cm^{-1}.

X-ray crystallography

Single-crystal data were collected on an Enraf–Nonius CAD-4 diffractometer using graphite-monochromated Mo-K_α radiation. Unit-cell parameters are based on 25 accurately centred reflections. An empirical absorption correction based on ψ-plot [12] was applied to the intensity data. There was no significant crystal decay. Crystallographic data are given in Table 1. The structure was solved by a combination of heavy

* Dedicated to Professor P. T. Manoharan on the occasion of his 60th birthday.

† Author to whom correspondence should be addressed.

Table 1. Crystallographic data for Ag(amp)NO_3

Formula	$C_6H_8AgN_3O_3$
Formula weight	278.02
a (Å)	11.850(3)
b (Å)	6.402(1)
c (Å)	11.038(4)
V (Å^3)	837.4(4)
Z	4
Space group	*Pnma*
T (K)	293(2)
λ (Å)	0.71073
$\rho_{calc.}$ (g cm^{-3})	2.205
μ (mm^{-1})	2.384
θ range (°)	2–24.97
Data/restraints/parameters	808/4/85
$R_1{}^a/wR_2{}^b$ [$I > 2\sigma(I)$]	0.0320/0.0973

$^a R_1 = \Sigma \| F_o| - |F_c \| / \Sigma |F_o|$.
$^b wR_2 = [\Sigma\{w(F_o^2 - F_c^2)^2\}/\Sigma(wF_o^4)]^{1/2}$.
$w^{-1} = [\sigma^2(F_o^2) + (0.0773\,P)^2]$, $P = (\text{Max.}\,(F_o^2, 0) + 2\,F_c^2)/3$.
$S = [\Sigma\{w(F_o^2 - F_c^2)^2\}/(n-p)]^{1/2}$.

atom and direct methods using SHELXS-86 [13] and refined over F^2 using SHELXL-93 [14]. The non-hydrogen atoms were refined anisotropically. The hydrogen atoms were located by geometrical considerations. The ring H atoms and CH_2 H atoms were allowed to ride upon the C atoms to which they were attached. The positional parameters of amine H atoms were refined, but restrained with respect to the adjacent CH_2 and Ag. The three common H atom thermal parameters (for ring, amine and CH_2) were refined isotropically. Refinement* converged with $wR_2 = 0.0973$, $R_1 = 0.0320$ [$I > 2\sigma(I)$] for 742 reflections; the goodness-of-fit (S) was = 1.208. The final difference map showed a residual electron density of 0.771 eÅ^{-3}. Molecular diagrams were obtained using the ORTEP program [18].

RESULTS AND DISCUSSION

Synthesis

Two types of crystals were obtained when amp was added to an aqueous solution of $AgNO_3$, in 1 : 1 and 2 : 1 proportions. The crystals reported here were obtained from the latter solution. It has been observed that the polymeric material is being formed only in the presence of excess ligand. The yield quoted is based on the first crop of pure crystals. The polymer has been synthesized several times by this method and checked by IR, and C, H, N analyses. The C, H, N analyses and the IR of the flake-like crystals formed in the former synthesis, using a 1 : 1 ratio, do not agree with that of the polymer. These crystals are being investigated further.

Structure

The structure is made up of a one-dimensional polymeric chain. Figure 1 shows the molecular structure of the repeating unit of the polymer while Fig. 2 shows the packing of the polymer chains in the unit cell. The coordination around the Ag atom is approximately linear [N(1)—Ag—N(2) = 164.9(2)°], and the Ag atom is bound by N atoms of pyridine and amine from two different ligands. The two oxygens of the nitrate ion are weakly bonded to Ag at a distance of 2.72(3) Å[Ag—O(1)]. These distances are outside the range of 2.3–2.6 Å usually expected for a weak Ag—O interaction. Nevertheless, the presence of these oxygens seems to be partly responsible for the deviation of the coordination from linearity. The structure is analogous to that of Ag(pz)NO_3 [10] where the silver atom is perturbed by distant nitrate oxygens [Ag—O = 2.72(2)–2.94(2) Å] leading to even greater deviation from linearity [N—Ag—N = 159.3(9)°]. The Ag—N(pyridine) and Ag—N(amine) distances are comparable to those observed in other Ag^I complexes with these types of ligands [9,10,19]. The two inversion-related polymeric chains lie nearly along the a-axis. The packing is stabilized by ring–ring stacking interactions (Fig. 2). The nitrogen atoms of the two pyridine rings are *anti* to each other. The shortest interplanar distance is 3.213(1) Å [C(5)···N(1)].

Oxidation of Ag(amp)NO_3 (1)

When $(NH_4)_2S_2O_8$ was added to a saturated solution of **1** at 4°C, the colour of the solution slowly changed to pink, from which pink, needle-shaped crystals (**2**) separated in a few hours. When NH_4PF_6

*Since systematic absences do not distinguish between $Pna2_1$ and its centrosymmetric counterpart, *Pnma*, structure solution and refinements were performed in both space groups. Both refinements converged readily (maximum shift/e.s.d. less than 0.01 for both), provided the starting coordinates are obtained from Fourier maps calculated in the respective space groups. (However, singularities result if refinement is attempted in *Pnma* with parameters refined in $Pna2_1$ or vice versa.) The residuals (R_1) are 0.030 for $Pna2_1$ and 0.032 for *Pnma*. One disadvantage of refining in $Pna2_1$ was that the z-coordinates were found to show significantly higher (about four times) standard deviations ($\sigma(z)$) compared to $\sigma(x, y)$. A survey of the recent literature [15] showed that such a discrepancy is often seen for nearly planar molecules in the $Pna2_1$ space group, and it probably has to do with correlations in the refinement process owing to the presence of pseudo symmetry (mirror plane). In the present case, even though intensity statistics and the Hamilton test [16] are in favour of the non-centrosymmetric space group, as pointed out by Marsh [17] as well as by a referee such tests are not definitive, especially for structures with heavy atoms. Since the geometrical parameters are identical in both space groups within one standard deviation, and there is no disorder in either refinement, the data in the more symmetric space group (*Pnma*) are presented here, while the $Pna2_1$ data are available from the corresponding author on request.

Table 2. Selected bond lengths (Å) and angles (°) for $Ag(amp)NO_3$

Ag—N(1)	2.180(4)	Ag—N(2#1)	2.197(4)
N(1)—Ag—N(2#1)	164.9(2)	C(5)—N(1)—Ag	117.3(4)
C(1)—N(1)—Ag	125.1(3)	C(6)—N(2)—Ag(#2)	118.8(3)

Symmetry transformations used to generate equivalent atoms: #1 $x+1/2$, y, $-z+1/2$; #2 $x-1/2$, y, $-z+1/2$.

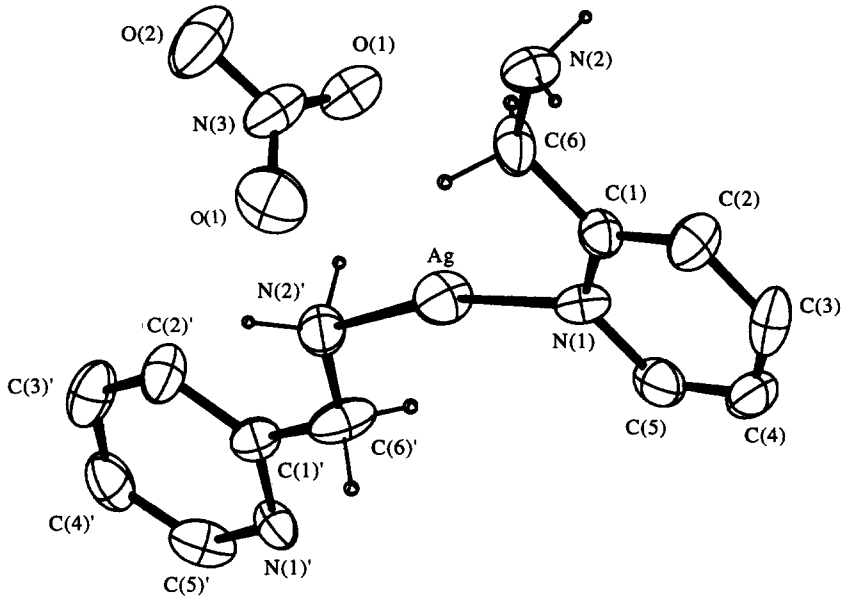


Fig. 1. The molecular structure of the repeating unit. Symmetry transformations: $' = 0.5+x, y, 0.5-z$ and $'' = x, 0.5-y, z$. Atoms are represented by displacement ellipsoids at 50% probability level.

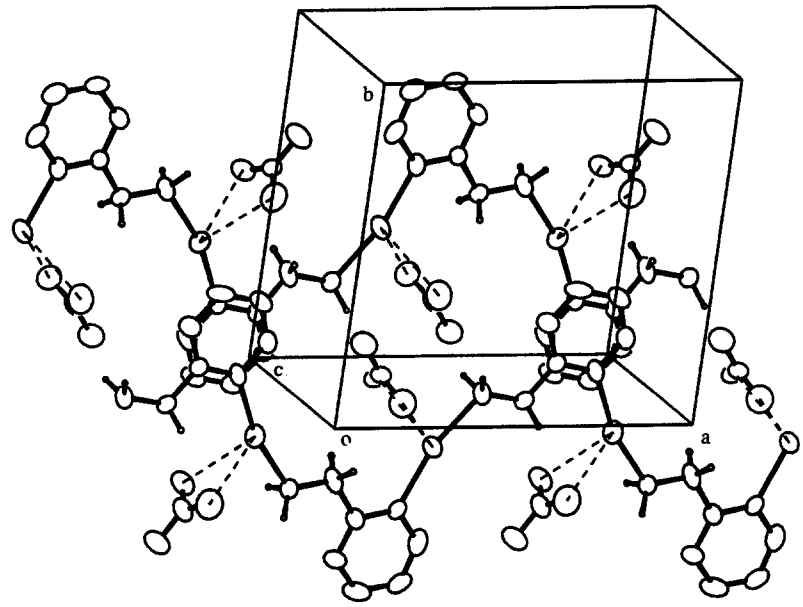


Fig. 2. The packing of polymer chains in the crystal illustrating the stacking of the pyridine rings of the ligand. The weak interactions of the nitrate oxygens with the silver ion are indicated by broken lines.

was added to the mother liquor a light pink precipitate (**3**) was formed. The rest of the solution, when kept in the refrigerator (4°C) for several days, deposited some pink crystals (**4**).

Owing to the instability of **3** and **4** when removed from mother liquor, definitive analytical data could not be obtained. The pink solution has electronic absorption bands at 19.6 and 27.8 kK. These may be assigned to *d–d* and LMCT transitions, respectively, of an Ag^{II} species [8,20]. The IR spectrum of **2**, as well as of **3**, shows a strong peak at 1690 cm^{-1} (typical for COO—) which is absent in **1**. Closer examination revealed that the IR spectrum of **2** matches that of the previously reported [20] $Ag(pic)_2$. These observations imply that our experimental conditions lead to the conversion of the aminomethyl side chain to carboxylate, as well as oxidation of Ag^{I} to Ag^{II}. Silver(I)-catalysed oxidation in the presence of persulfate, of amine to aldehyde, and aldehyde to carboxylate have been noted before [21]. It was further observed that the treatment of $Ag(pic)\cdot H_2O$, prepared using a reported procedure [22], with $(NH_4)_2S_2O_8$ followed by NH_4PF_6 leads to the precipitation of an unstable pink crystalline product identical in properties to **3**. All these observations lead to the conclusion that the Ag^{II} species resulting from the $S_2O_8^{2-}$ oxidation of $Ag(amp)NO_3$ is $Ag(pic)_2$.

The unique feature of **3** is that it gives a well-resolved EPR spectrum showing hyperfine splitting from $^{107,108}Ag$ ($I = 1/2$) and superhyperfine from two ^{14}N ($I = 1$) nuclei (Fig. 3b). However, a typical magnetically concentrated spectrum with $g_\parallel = 2.191$ and $g_\perp = 2.059$, was obtained for **2** (Fig. 3a). The computer simulation of the spectrum of **3** (Fig. 3c), using a previously described program [8], led to the following parameters: $g_\parallel = 2.184$, $g_\perp = 2.054$, $A_\parallel(Ag) = 45.8 \times 10^{-4}$ cm^{-1}, $A_\perp(Ag) = 18.0 \times 10^{-4}$ cm^{-1}, $A(N) = 25.7 \times 10^{-4}$ cm^{-1}, $B(N) = 15.3 \times 10^{-4}$ cm^{-1}. The nitrogen superhyperfine interaction was modelled assuming the tensors to be equivalent and axial with the Ag—N bond direction as the symmetry axis. For a square-planar coordination, $A_\parallel(Ag)$ is in the (x,y)-planes of the nitrogen tensors. The components of the ligand tensors along the principal direction of the Ag tensor, namely $A_\parallel(N)$ and $A_\perp(N)$ are then equal to $B(N)$ and $(1/\sqrt{2})\,(A^2+B^2)^{1/2}$, respectively. The observation of eight lines in the parallel region and six lines in the perpendicular region implies the following relation between the Ag and N hyperfine components: $A_\parallel(Ag) \cong 3A_\parallel(N)$ and $A_\perp(Ag) \cong A_\perp(N)$. The EPR spectrum showing coupling with only two N atoms, conforms with formulation of the paramagnetic species as $Ag(pic)_2$.

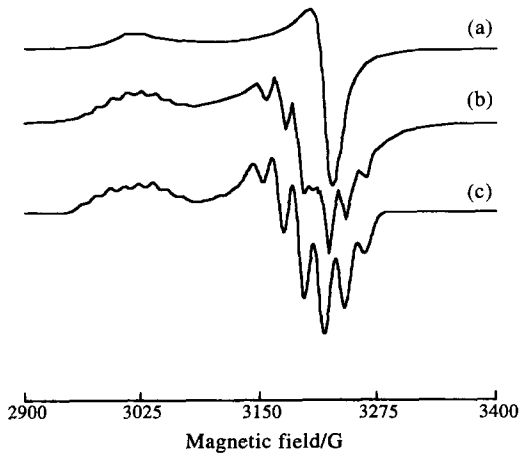


Fig. 3. EPR spectra (X-band, 300 K) of polycrystalline samples: (a) **2**, (b) **3** and (c) computer simulation of (b).

Well-resolved EPR spectra having similar parameters were observed previously [8] for Ag (dmbp) NO_3^+ and $Ag(dmp)NO_3^+$, where dmbp = 6,6′-dimethyl-2,2′-bipyridine and dmp = 2,9-dimethyl-1,10-phenanthroline, when the Ag^{II} species were precipitated by the addition of NH_4PF_6. Comparing with these two systems and other previously reported [23] Ag^{II} species, the EPR parameters of **3** also imply 35–50% delocalization of the odd electron. Detailed characterization of these magnetically dilute materials is hampered by the difficulty in obtaining stable crystals. However, IR spectra reveal the presence of NH_4^+ and PF_6^- ions, as well as strong features from the organic ligand. Since the observation of resolved EPR spectra require magnetic dilution at the molecular level, the compounds may be double salts or clathrate hydrates.

Unlike dmbp [9a] and dmp [9b], which form monochelates with $AgNO_3$, having a 3+1 (nearly) planar coordination at Ag, amp forms a polymeric complex having linear coordination with practically no involvement of the NO_3^- in the coordination sphere. The flexibility of the aminomethyl side chain and the stabilization of the crystal structure by stacking interactions between adjacent polymeric chains are responsible for this difference. Stacking interaction between aromatic rings makes an important contribution to the packing of dmbp and dmp complexes as well [9].

All three complexes, $Ag(L)NO_3$ (L = dmbp, dmp, amp), when treated with $S_2O_8^{2-}$ followed by NH_4PF_6 yielded magnetically dilute Ag^{II} species. This is puzzling because, based on EPR and IR, as well as confirmation by independent preparation, $Ag(amp)NO_3$ produces the neutral $Ag(pic)_2$ species, while $Ag(L)NO_3$ (L = dmbp, dmp) gave [8] $Ag(L)NO_3^+$. While the formation of double salts with NH_4PF_6 is plausible for the latter (as implied by analytical data), a host–guest complex between $Ag(pic)_2$ and NH_4PF_6*

*NH_4PF_6 has an NaCl-type lattice [24]. Size considerations preclude both substitutional and interstitial doping of the Ag^{II} species in NH_4PF_6. Formation of a clathrate phase upon crystallization from aqueous medium containing Ag^{II} species having appropriate size and shape may possibly account for the magnetically dilute EPR spectra. While the structures of hydrates of NH_4PF_6 are not available, $HPF_6\cdot 6H_2O$ does have a clathrate structure [24c].

is more likely for the former. It is noteworthy that $Ag(bpy)_2^{2+}$ (bpy = 2,2′-bipyridine) and $Ag(py)_4^{2+}$ (py = pyridine) do not yield magnetically dilute EPR spectra when crystallized with NH_4PF_6. Further studies using different paramagnetic species and other PF_6^- salts are in progress.

Supplementary material available

Tables of (i) complete crystal data, (ii) atomic coordinates and equivalent isotropic displacement parameters, (iii) complete bond lengths and angles, (iv) and anisotropic thermal parameters, (v) hydrogen coordinates and observed and calculated structure factors have been deposited at the Cambridge Crystallographic Data Centre.

Acknowledgements—We thank Dr Babu Varghese for collecting the X-ray data at R.S.I.C, I.I.T, Madras. G.S. thanks C.S.I.R., New Delhi for the award of a Research Associateship.

REFERENCES

1. Michelsen, K., *Acta Chem. Scand.*, 1970, **24,** 2003.
2. Hodgson, D. J., Michelsen, K. and Pedersen, E., *Acta Chem. Scand.*, 1990, **44,** 1002.
3. Katz, B. A. and Strouse, C. E., *Inorg. Chem.*, 1980, **19,** 658 and references therein.
4. Mikami-Kido, M. and Saito, Y., *Acta Cryst.*, 1982, **B38,** 452.
5. Crawford, C. A., Day, E. F., Streib, W. E., Huffman, J. C. and Christou, G., *Polyhedron*, 1994, **13,** 2933.
6. Gmelin Handbuch der Anorganische Chemie, Main Series, 8th Edn, Vol. B6, Springer-Verlag, Berlin, 1975, p. 96.
7. Goeminne, A. M. and Eeckhaut, Z., *J. Inorg. Nucl. Chem.*, 1974, **36,** 357.
8. Swarnabala, G. and Rajasekharan, M. V., *Inorg. Chem.*, 1989, **28,** 662.
9. (a) Venkatalakshmi, N., Rajasekharan, M. V. and Mathews, I. I., *Trans. Met. Chem.*, 1992, **17,** 455; (b) Swarnabala, G. and Rajasekharan, M. V., *Polyhedron*, 1996, **15,** 3197.
10. Vranka, G. and Amma, E. L., *Inorg. Chem.*, 1966, **5,** 1020.
11. Bassett, J., Denney, R. C., Jeffery, G. H. and Mendham, J., *Vogel's Text Book of Quantitative Analysis*. ELBS, London, 1978.
12. North, A. C. T., Phillips, D. C. and Mathews, F. S., *Acta Cryst.*, 1968, **A24,** 351.
13. Sheldrick, G. M., SHELXS-86, *Acta Cryst.*, 1990, **A46,** 467.
14. Sheldrick, G. M., SHELXL-93, *J. Appl. Cryst.*, under preparation.
15. Hamzaouii, F. and Baert, F., *Acta Cryst.*, 1994, **C50,** 757; Lis, T., *Acta Cryst.*, 1994, **C50,** 484; Pavlyuk, V. V., Yanson, T. I. and Bodak, O. I., *Acta Cryst.*, 1995, **C51,** 792; Blake, A. J. and Parsons, S., *Acta Cryst.*, 1995, **C51,** 571.
16. Hamilton, W. C., *Acta Cryst.*, 1965, **18,** 502.
17. Marsh, R. E., *Acta. Cryst.*, 1986, **B42,** 193.
18. Johnson, C. K., ORTEP, *Report ORNL* 3794, Oak Ridge National Laboratory, Oakridge, U.S.A., 1965.
19. Yamaguchi, T. and Lindquist, O., *Acta Chem. Scand.*, 1983, **37,** 685.
20. Fowles, G. W. A., Mathews, R. W. and Walton, R. A., *J. Chem. Soc.* (*A*), 1968, 1108.
21. Fieser, L. F. and Fieser, M., *Reagents for Organic Synthesis*. John Wiley, New York, 1967.
22. Deloume, J.-P. and Faure, R., *Acta Cryst.*, 1977, **B33,** 2709.
23. Buch, T., *J. Chem. Phys.*, 1965, **43,** 761; Manoharan, P. T. and Rogers, M. T., in *Electron Spin Resonance of Metal Complexes*, Ed. T. F. Yen, Plenum Press, New York, 1968, p. 143; Halpern, T., McKoskey, S. M. and McMillan, J. A., *J. Chem. Phys.*, 1970, **52,** 3526; Rajasekharan, M. V., Sethulakshmi, C. N., Manoharan, P. T. and Güdel, H., *Inorg. Chem.*, 1976, **15,** 2657; Evans, J. C., Gillard, R. D., Lancashire, R. J. and Morgan, P. H., *J. Chem. Soc., Dalton Trans.*, 1980, 1277; Brown, T. G. and Hoffman, B. M., *Mol. Phys.*, 1980, **39,** 1073; Sontum, S. F. and Case, D. A., *J. Phys. Chem.*, 1982, **86,** 1596.
24. (a) Seifert, H., *Z. Krist.*, 1931, **76,** 455; (b) Bode, H. and Clausen, H., *Z. Anorg. Allg. Chem.*, 1951, **265,** 229; (c) Bode, V. H. and Teufer, G., *Acta Cryst.*, 1955, **8,** 611.

Pergamon

PII: S0277-5387(96)00350-6

Polyhedron Vol. 16, No. 6, pp. 927–931, 1997
Copyright © 1996 Elsevier Science Ltd
Printed in Great Britain. All rights reserved
0277-5387/97 $17.00+0.00

Nitrosyl ruthenium complexes with general formula $[RuCl_3(NO)(P–P)]$ ($P–P = \{PPh_2(CH_2)_nPPh_2\}$, $n = 1–3$ and $\{PPh_2\text{-}CH = CH\text{-}PPh_2\}$). X-ray structure of $[RuCl_3(NO)\{PPh_2(CH_2)_3PPh_2\}]$

Alzir A. Batista,[a]* Cid Pereira,[a] Salete L. Queiroz,[b] Luiz A. A. de Oliveira,[b] Regina H. de A. Santos[c] and Maria Teresa do P. Gambardella[c]

[a] Departamento de Química/UFSCAR-CP, 676-CEP, 13565-905 São Carlos (SP), Brazil

[b] Instituto de Química/UNESP-CP, 355-CEP, 14800-900 Araraquara (SP), Brazil

[c] Instituto de Química de São Carlos/USP-CP, 780-CEP, 13560-970 São Carlos (SP), Brazil

(Received 15 May 1996; accepted 22 July 1996)

Abstract—Ruthenium(II) complexes with general formula $[RuCl_3(NO)(P–P)]$ were obtained in the solid state, where $P–P = PPh_2(CH_2)_nPPh_2$ ($n = 1–3$) and $PPh_2\text{-}CH = CH\text{-}PPh_2$. The ^{31}P NMR spectra of these compounds measured in CH_2Cl_2 showed only singlets, consistent with a *fac* configuration containing two equivalent phosphorus atoms. However the X-ray diffraction data show that the $[RuCl_3(NO)\{PPh_2(CH_2)_3PPh_2\}]$ complex crystallizes in a *mer* configuration, where one of the phosphorus atoms is *trans* to the NO group, in a slightly distorted octahedral geometry. Copyright © 1996 Elsevier Science Ltd

Keywords: ruthenium; nitrosyl; complexes; biphosphines; X-ray structure; isomerism.

The nitrosyl ligand has been shown to exist in both linear and bent forms corresponding to three-electron and one-electron donors, respectively. Crystallographic and spectroscopic studies have been used to distinguish between these two geometries in mononuclear nitrosyl complexes [1–6]. There is some evidence that bulky ligands present in ruthenium nitrosyl complexes govern the intramolecular geometry of these species [7–9]. Thus, bulky ligands in the ruthenium complexes bend away from the nitrosyl group towards less sterically crowded sites in order to relieve the strain caused by these coordinating molecules. In the complex $[OsCl_3(NH_3)(PPh_3)_2]$ [8], which contains an ammine ligand, less bulky than the nitrosyl, the phosphines bend towards the NH_3 by a small amount (0.3°) compared with $[RuCl_3(NO)(P\text{-}Ph_2Me)]$, where the phosphine bends away from the NO by a greater amount (4.1°) [9]. In this paper we report the preparation and characterization of ruthenium(II) complexes with general formula $[RuCl_3(NO)(P–P)]$, where P–P is one of the following diphosphine ligands: bis(diphenylphosphino)methane (dppm), 1,2-bis(diphenylphosphino)ethane (dppe), 1,3-bis(diphenylphosphino)propane (dppp), 1,2-bis (diphenylphosphino)ethylene (dppen), and the X-ray structure of the complex $[RuCl_3(NO)(dppp)]$. Our aim was mainly to provide information about the structure of this complex in solution and in the solid state, and to investigate the ability of coordinated NO^+ to cause a *trans* strengthening effect in $\{Ru^{II}–NO^+\}$-type complexes containing strong π acceptor ligands.

* Author to whom correspondence should be addressed.

EXPERIMENTAL

Measurements

The infrared spectra of the complexes were measured from powder samples diluted in CsI on an FT-IR Bomem-Michelson 102 spectrometer in the 4000–200 cm^{-1} region. The ^{31}P $\{^1H\}$ spectra were recorded in CH_2Cl_2 on a Bruker 400 MHz spectrometer, with H_3PO_4 (85%) as the internal reference.

Synthesis

The $[RuCl_3(NO)\{PPh_2(CH_2)_nPPh_2\}]$ complexes were synthesized from $[RuCl_3(NO)]$, which was prepared by passing a stream of NO through a solution of commercial ruthenium chloride (Degussa S.A.) in dichloromethane until the solution became red, followed by evaporation to dryness. The dried solid obtained was kept in a vacuum desiccator for at least 3 days before use. The NO was generated by reaction of dilute nitric acid (*ca* 33%) over copper metal. The NO gas was dried by passing it through a column containing anhydrous $CaCl_2$. A typical synthesis of the $[RuCl_3(NO)\{PPh_2(CH_2)_nPPh_2\}]$ complexes was done by refluxing for about 4 h the deoxygenated methanolic solution (5 cm^3) of $[RuCl_3NO]$ (0.1 g, 0.42 mmol) and the corresponding diphosphine (0.42 mmol). In all cases solids were precipitated, which were filtered off and well washed with diethyl ether (yield: *ca* 80%).

$[RuCl_3(NO)(dppm)]$ (**1**). Orange microcrystalline powder. Found: C, 48.7; H, 3.4; N, 2.5. Calc. for $C_{25}H_{22}Cl_3NOP_2Ru$: C, 48.3; H, 3.6; N, 2.2%. IR: ν(NO) 1867, ν(Ru—Cl) 330 and 288 cm^{-1}. ^{31}P-$\{^1H\}$ NMR: δ −16.5.

$[RuCl_3(NO)(dppe)]$ (**2**). Yellow microcrystalline powder. Found: C, 49.3; H, 4.0; N, 2.1. Calc. for $C_{26}H_{24}Cl_3NOP_2Ru$: C, 49.1; H, 3.8; N, 2.2%. IR: ν(NO) 1861, ν(Ru—Cl) 331 and 278 cm^{-1}. ^{31}P-$\{^1H\}$ NMR: δ 46.70.

$[RuCl_3(NO)(dppp)]$ (**3**). Yellow microcrystalline powder. Found: C, 49.4; H, 3.9; N, 2.2. Calc. for $C_{27}H_{26}Cl_3NOP_2Ru$: C, 49.9; H, 4.0; N, 2.2%. IR: ν(NO) 1875, ν(Ru—Cl) 325 and 291 cm^{-1}. ^{31}P-$\{^1H\}$ NMR: δ 14.17.

$[RuCl_3(NO)dppen]$ (**4**). Yellow microcrystalline powder. Found: C, 49.7; H, 3.6; N, 2.2. Calc. for $C_{26}H_{22}Cl_3NOP_2Ru$: C, 49.3; H, 3.5; N, 2.2%. IR: ν(NO) 1875, ν(Ru—Cl) 330 and 283 cm^{-1}. ^{31}P-$\{^1H\}$ NMR: δ 54.10.

Crystal structure of **3**

Suitable crystals of complex **3** were grown by slow evaporation of a dichloromethane/diethyl ether solution. A single crystal was used for data collection and cell parameter determination on an Enraf–Nonius CAD-4 diffractometer, with graphite-monochromated Mo-K_α radiation at room temperature (T = 298 K). Unit-cell parameters were obtained by least squares from the setting angles of 25 reflections. Intensity data were collected in the ω scan mode up to θ_{max} = 26.32°, with scan rates between 3.3 and 16.5° min^{-1}. The intensity of three standard reflections were essentially constant during the measurement. Data were corrected for Lorentz polarization and absorption effects using the empirical Psi Scan method [10]. The structure was solved using the SIR method [11] and difference Fourier techniques. In the final cycles of least-squares refinement, all non-hydrogen atoms were treated anisotropically. All hydrogen atoms were assumed in their calculated position by the geometry of the ligand atom and included in the least-squares calculation with a fixed isotropic temperature factor (6.0 $Å^2$). The function minimized was $\Sigma w(|F_0| - |F_c|)^2$, where $w^{-1} = \sigma^2(F_0)$. Scattering factors for non-hydrogen atoms were taken from Cromer and Mann [12] with corrections for anomalous dispersion from Cromer and Liberman [13], and for hydrogen atoms from Stewart *et al.* [14].

All the calculations were performed with the system Mo1EN [10]. The data collection and experimental details are summarized in Table 1. The relevant interatomic bond lengths and angles are listed in Table 2.

Table 1. Crystal data, data collection details and structure refinement results for $[RuCl_3(NO)\{PPh_2(CH_2)_3PPh\}]$

Molecular formula	$C_{27}Cl_3H_{26}NOP_2Ru$
Molecular weight	649.89
Crystal system	Monoclinic
Space group	$P2_1/c$
Z	4
D_c (g cm^{-3})	1.603
a (Å)	12.091(1)
b (Å)	13.973(1)
c (Å)	16.639(1)
β (°)	107.271(7)
V ($Å^3$)	2684.4(4)
$F(000)$	1312
Crystal size (mm)	0.23 × 0.25 × 0.15
λ (Mo-K_α) (Å)	0.71073
μ (cm^{-1})	10.1
Scan mode	ω–2θ
θ limits (°)	2.33–26.32
Range of hkl; min.	0, −17, −20
Range of hkl; max.	15, 0, 20
Unique reflections	5447
Reflections used [$I > 3\sigma(I)$]	3387
Number of variables	317
Goodness-of-fit	1.67
R, R_w, R_{all}	0.047, 0.056, 0.099
Max. shift/e.s.d.	0.01
Max., min. density in final difference map (e $Å^{-3}$)	1.43, −0.18
Minimized function	$\Sigma w(\|F_0\| - \|F_c\|)^2$
Max., min. absorption correction (%)	99.99, 94.39

Table 2. Selected bond lengths (Å) and angles (°) for $[RuCl_3(NO)\{PPh_2(CH_2)_3PPh_2\}]$, with esds in parentheses

Ru—Cl(1)	2.376(2)	P(1)—C(1b)	1.827(5)
Ru—Cl(2)	2.354(2)	P(1)—C(3)	1.832(6)
Ru—Cl(3)	2.366(2)	P(2)—C(1c)	1.833(6)
Ru—P(1)	2.460(1)	P(2)—C(1d)	1.813(6)
Ru—P(2)	2.436(2)	P(2)—C(1)	1.808(6)
Ru—N	1.880(4)	O—N	0.906(7)
P(1)—C(1a)	1.826(5)		

Cl(1)—Ru—Cl(2)	92.54(6)	Ru—P(1)—C(1a)	120.3(2)
Cl(1)—Ru—Cl(3)	176.64(5)	Ru—P(1)—C(1b)	113.1(2)
Cl(1)—Ru—P(1)	81.42(5)	Ru—P(1)—C(3)	107.8(2)
Cl(1)—Ru—P(2)	98.32(6)	C(1a)—P(1)—C(1b)	101.4(2)
Cl(1)—Ru—N	88.4(2)	C(1a)—P(1)—C(3)	107.5(3)
Cl(2)—Ru—Cl(3)	86.65(6)	C(1b)—P(1)—C(3)	105.7(3)
Cl(2)—Ru—P(1)	86.41(5)	Ru—P(2)—C(1c)	109.8(2)
Cl(2)—Ru—P(2)	167.31(6)	Ru—P(2)—C(1d)	125.0(2)
Cl(2)—Ru—N	93.0(2)	Ru—P(2)—C(1)	107.5(2)
Cl(3)—Ru—P(1)	95.27(5)	C(1c)—P(2)—C(1d)	99.8(2)
Cl(3)—Ru—P(2)	82.13(5)	C(1c)—P(2)—C(1)	108.1(3)
Cl(3)—Ru—N	94.9(2)	C(1d)—P(2)—C(1)	105.6(3)
P(1)—Ru—P(2)	88.72(5)	Ru—N—O	172.0(6)
P(1)—Ru—N	169.8(2)	P(2)—C(1)—C2	115.3(4)
P(2)—Ru—N	93.8(2)	P(1)—C(3)—C2	115.3(4)

Figure 1 shows the ORTEP [15] drawing of the molecule with the atom-numbering scheme.

RESULTS AND DISCUSSION

In all the diphosphine complexes studied in this work, the ν(NO) in the infrared spectra were close to 1870 cm^{-1}, indicating that they were indeed of the $\{Ru^{II}—NO^{+}\}$ type [1,2].

The $^{31}P-\{^{1}H\}$ NMR data mentioned in the experimental section show that these complexes present only a singlet, suggesting that in all cases the phosphorus atoms are *trans* to the chlorines. However, the crystal structure of the $[RuCl_3(NO)(dppp)]$ complex (Fig. 1) shows that the NO group is *trans* to a phosphorus atom, suggesting that this compound can be found as a *fac* isomer in solution and prefers, probably because of steric effects, to be crystallized as a *mer* isomer.

The ν(NO) in the IR spectrum obtained from crystals of the $[RuCl_3(NO)(dppp)]$ complex is at 1841 cm^{-1}, different from the 1875 cm^{-1} found for the sample prepared from powder of the same complex. Considering that the chlorine is a better donor than the phosphorus atom, in this case the back-bonding Ru → NO should be more intense for the structure where the NO is *trans* to the chlorine (*fac* isomer) and the ν(NO) should be expected to shift to a lower energy, which was not observed experimentally. In this case the shift of 34 cm^{-1} observed in the IR spectra

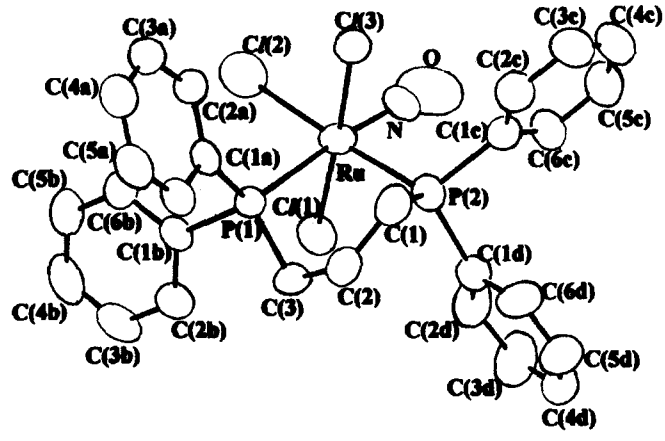


Fig. 1. Molecular structure and crystallographic numbering scheme for $[RuCl_3(NO)\{PPh_2(CH_2)_3PPh_2\}]$.

of the samples probably is not due to electronic effects, but is the consequence of steric effects. Thus, when the nitrosyl group is close to three chlorine atoms (*mer* isomer) for steric reasons it becames less linear, compared with the NO species which is only close to two chlorine atoms (*fac* isomer), and in this case the ν(NO) shifts to a lower energy [7]. For the crystal sample the IR spectra shows $\nu_{Ru\text{-}Cl}$ at 336 and 311 cm^{-1}.

It is interesting to point out that the isomerization process from the *mer* to the *fac* isomer was observed through $^{31}P\text{-}\{^1H\}$ experiments. In this case the $^{31}P\text{-}\{^1H\}$ spectra (A) of a fresh solution prepared with crystals of the $[RuCl_3(NO)(dppp)]$ in CH_2Cl_2 shows two doublets ($\delta = 10.13$ and $\delta = 0.27$, $J_{P\text{-}P} = 48.6$ Hz) as expected for the *mer* isomer. The intensity of these two doublets decreased with time and the singlet at $\delta = 14.17$, which belongs to the *fac* isomer, appeared (B) and at the end of this isomerization process only this isomer was present in the solution (C) (Fig. 2).

In the structure of the $[RuCl_3(NO)(dppp)]$ *mer* isomer (Fig. 1), three mutually perpendicular coordination planes are well defined and their angles are of a slightly distorted octahedron. Their angles are close to 90°. In this complex the Ru atom is displaced 0.099 Å towards the NO group, out of the best plane consisting of the three chlorines and the P(2) phosphorus atom. For the analogous series of *mer*-$[RuX_3(NO)(en)]$ complexes, where X = Cl, Br, I, these values were found to be 0.176(2), 0.1518(7) and 0.106(2) Å, respectively [16]. These distortions were attributed to the steric hindrance between the bulky Ru—NO bond orbital and the halogen. The distortion is decreased in the order Cl, Br, I because the bigger the halogen is the longer is the Ru—X length [average Ru—X lengths are 2.36, 2.50, 2.71 Å for X = Cl, Br and I, respectively]. This rationalization seems to be reasonable in order to explain the smaller value of the distortion (0.099 Å) found for the $[RuCl_3(NO)(dppp)]$ complex compared with those found for the halogen complexes $[RuX_3(NO)(en)]$, considering that the diphosphine is bulkier than the en ligand. This effect becomes evident when the average Ru—Cl distance in $[RuCl_3(NO)(en)]$ and $[RuCl_3(NO)(dppp)]$ are found to be essentially the same (*ca* 2.37 Å), but the Ru—N(2) and Ru—P(2), 2.092(9) [16] and 2.436(2) Å, respectively, are substantially different. In the case of $[RuCl_3(NO)(dppp)]$ the average interatomic distance between the nitrogen atom of the NO and the chlorine ligands is 3.07 Å, identical to that found in the *mer*-$[RuCl_3(NO)(en)]$ complex [16]. The identical distances found in these two complexes can be rationalized if we consider that, although the diphosphine ligand is bulkier than the en ligand, this effect is compensated for by the longer Ru—P(2) distance.

The observed Ru—N—O bond angle [172.0(6)°] is smaller than those found for $[RuX_3(NO)(en)]$ [16] [174.1(7), 176.9(5) and 179.4(2)° for X = Cl, Br and I, respectively]. This effect is attributed to the repulsion between the extensive molecular orbital of the NO ligand and the phenyl rings bonded to the P(2) atom of the diphosphine. The same effect is reflected in the angle P(1)—Ru—N, which is smaller than 180° [169.8(2)°], and in the angles Cl(3)—Ru—P(2) [82.13(5)°] and Cl(1)—Ru—P(2) [98.32(6)°]. The bulky NO molecular orbitals show influence even in the Cl(2)—Ru—P(1) and the Cl(2)—Ru—N angles. As can be seen in Table 2 these angles are equal to 86.41(5) and 93.0(2)°, respectively, which can be explained by considering that the NO molecular orbital pushes Cl(2) towards the P(1) atom. The Ru—P(1) and Ru—P(2) distances of 2.460(1) and 2.436(2) Å, respectively (see Table 2) are near to the expected values, which usually fall in the range 2.41–2.44 Å [17], and in this case the *trans* strengthening effect in the $[RuCl_3(NO)(dppp)]$ complex was not observed. It is likely that the essentially linear nitrosyl group does not achieve strong bonding (particularly through Ru—NO π back-bonding) when *trans* to phosphorus, which is not a very good donor atom [18]. Indeed, this crystal structure shows the oxygen atom of the NO group with a high thermal parameter, indicating some flexibility for the orientation of the nitrosyl with respect to the Ru—N bond. The distance Ru—N is longer [1.880(4) Å] when NO is *trans* to the phosphine, as in our complex, than when it is *trans* to bromine [1.787(9) Å] or *trans* to oxygen from the ethylsulfoxide [1.72(1) Å] as in $[RuBr_3(NO)(Pr^n_2S)_2]$ and $[RuBr_3(NO)(Et_2S)(Et_2SO)]$ complexes, respectively [19]. The Ru—N distance of 1.880(4) Å is a little larger than the expected metal–nitrogen double bond distance of 1.75(3) Å in ruthenium and osmium complexes that contain linear nitrosyl ligands [7]. The N—O distance [0.906(7) Å] is close to those found for the bis(dipropyl)sulfide [1.047(26) Å] and for the sulfide/sulfoxide [1.09(1) Å] complexes mentioned above [19].

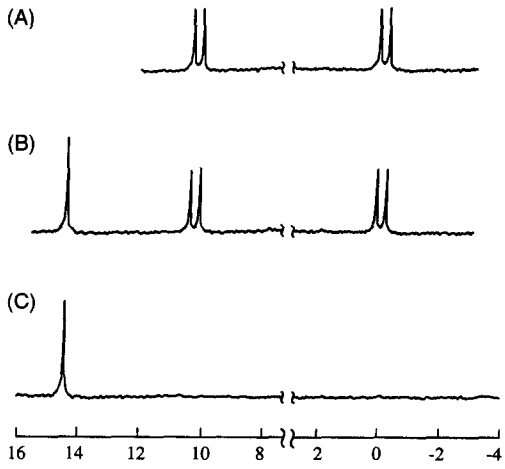


Fig. 2. (A) $^{31}P\text{-}\{^1H\}$ NMR spectrum of a fresh solution at room temperature of $[RuCl_3(NO)\{PPh_2(CH_2)_3PPh_2\}]$ (*mer* isomer) in CH_2Cl_2. (B) $^{31}P\text{-}\{^1H\}$ NMR spectrum of (A) after 3 h. (C) $^{31}P\text{-}\{^1H\}$ NMR spectrum of (A) after 12 h.

Supplementary material—Atomic coordinates, anisotropic thermal parameters and a complete list of the bond distances and angles have been deposited with the Cambridge Crystallographic Data Centre.

Acknowledgements—This work was supported by grants from the FAPESP, CNPq, CAPES and FINEP.

REFERENCES

1. Bottomley, F., *Coord. Chem. Rev.*, 1978, **26,** 7.
2. Enemark, J. H. and Feltham, R. D., *Coord. Chem. Rev.*, 1974, **13,** 339.
3. Pierpont, C. G. and Eisenberg, R., *Inorg. Chem.*, 1972, **11,** 1088.
4. Gaughan, A. P. Jr, Corden, B. J., Eisenberg, R. and Ibers, J. A., *Inorg. Chem.*, 1974, **13,** 786.
5. Pierpoint, C. G. and Eisenberg, R., *Inorg. Chem.*, 1973, **12,** 199.
6. Seddon, E. A. and Seddon, K. R., *The Chemistry of Ruthenium.* Elsevier, Amsterdam, 1984, pp. 1130–1138.
7. Haymore, B. L. and Ibers, J. A., *Inorg. Chem.*, 1975, **14,** 3060.
8. Bright, D. and Ibers, J. A., *Inorg. Chem.*, 1969, **8,** 1078.
9. Schultz, A. J., Henry, R. L., Reed, J. and Eisenberg, R., *Inorg. Chem.*, 1974, **13,** 732.
10. Fair, C. K., *MolEN: Structure Determination System.* Enraf–Nonius, Delft, The Netherlands, 1990.
11. Burla, M. C., Camalli, M., Cascarano, G., Ciacovazzo, C., Polidori, G., Spagna, R. and Viterbo, D., *J. Appl. Cryst.*, 1989, **22,** 389.
12. Cromer, D. T. and Mann, J. B., *Acta Cryst.*, 1968, **A24,** 321.
13. Cromer, D. T. and Liberman, D., *J. Chem. Phys.*, 1970, **53,** 1891.
14. Stewart, R. F., Davidson, E. R. and Simpson, W. T., *J. Chem. Phys.*, 1965, **42,** 3175.
15. Johnson, C. K., *ORTEP-II: A Fortran Thermal Ellipsoid Plot Program for Crystal. Illustration,* ORNL-5138. Oak Ridge National Laboratory, Oak Ridge, Tennessee, (1976).
16. Tomizawa, H., Harada, K., Miki, E., Mizumachi, K., Ishimori, T., Urushiyama, A. and Nakahara, M., *Bull. Chem. Soc. Jpn,* 1993, **66,** 1658.
17. Haymore, B. L. and Ibers, J. A., *J. Am. Chem. Soc.*, 1975, **97,** 5369.
18. Elschenbroich, Ch. and Salzer, A., *Organotransition Metal Chemistry—A Concise Introduction.* VCH, Weinheim, Germany, 1989, p. 229.
19. Coll, R. K., Fergusson, J. K., McKee, V., Page, C. T., Robinson, W. T. and Keong, T. S., *Inorg. Chem.*, 1987, **26,** 106.

Pergamon

PII: S0277-5387(96)00349-X

Polyhedron Vol. 16, No. 6, pp. 933–938, 1997
Copyright © 1996 Elsevier Science Ltd
Printed in Great Britain. All rights reserved
0277-5387/97 $17.00+0.00

Spectroscopic and electrochemical studies of Ni^{II}, Cu^{II}, Pd^{II} and VO^{II} complexes with naphthoquinonic ligands

Juan Camus,[a]* Aurelia Meghea[b] and J. R. Anacona[c]

[a] Facultad de Ciencias, Universidad de Playa Ancha, Casilla 34-V, Valparaiso, Chile

[b] National Institute of Chemistry, Department of Physical Chemistry, 1 Polizu Str, 78126, Bucharest, Romania

[c] Departamento de Química, Universidad de Oriente, Apartado postal 208, Cumaná, Venezuela

(Received 29 March 1996; accepted 19 July 1996)

Abstract—The electron transfer complexes of general type $[M(L^1)_2]$, $[M(L^2)_2]$ and $[M(L^3)_2]$ with M = Ni^{II}, Cu^{II}, Pd^{II} and VO^{II} ions have been investigated using 2-hydroxy-3-methylmercaptan-1,4-naphthoquinone (HL^1), 2-amino-3-methylmercaptan-1,4-naphthoquinone (HL^2) and 2, 3-diamino-1,4-naphthoquinone (HL^3) as ligands. Polarographic results confirmed that some the these neutral compounds underwent reversible or quasi-reversible one-electron reduction processes, and the reduction potentials for the $[M(L^1)_2]$ and $[M(L^3)_2]$ complexes were lower than those of the corresponding $[M(L^2)_2]$ complexes. EPR spectra of the prepared compounds, except the $[Pd(L^2)_2]$ complex, show that they are paramagnetic and some of them behave as free radicals stabilized through the cation. An attempt to correlate spectroscopic and redox parameters has been made. Copyright © 1996 Elsevier Science Ltd

Keywords: spectroscopy; electrochemical; napthoquinone; complexes.

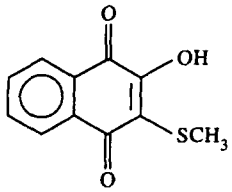
Transition metal charge transfer complexes have been the subject of a considerable amount of research over the past twenty years, and several reviews dealing with the unusual chemical and physical properties of these complexes have been published [1–5]. One of the most interesting properties of these compounds is their ability to undergo facile electron-transfer reactions, and the structural and spectroscopic changes that accompany these reactions have attracted much attention. As a result of these studies, it has been concluded that the accessibility of a range of oxidation states of the complex is the result of the accessibility of a number of formal oxidation states for the ligand, and that the electron density in the metal orbitals does not change significantly as the oxidation state is changed [3,5–6]. On the other hand, the observations indicate that it should be possible to stabilize new magnetic states in a planar geometry with appropriate extended π-system ligands containing *ortho* donor atoms in the nitrogen and oxygen families.

The easy isolation and characterization of the neutral naphthoquinonic complexes suggests reasonable stabilities associated with their electronic arrangements and raises the possibility that they can be reducible to mono- and/or dinegative anions. The data from this work referring to charge transfer complexes of the general types $[M—O_2S_2]$, $[M—N_2S_2]$ and $[M—N_4]$ used 1,4-naphthoquinonic derivatives as ligands. The following ligands were used: 2-hydroxy-3-mercaptomethyl-1,4-naphthoquinone (HL^1), 2-amino-3-mercaptomethyl-1,4-naphthoquinone (HL^2) and 2,3-diamino-1,4-naphthoquinone (HL^3). The ligands investigated have the structures shown.

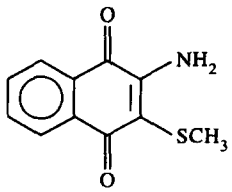
EXPERIMENTAL

All operations leading to the formation of the complexes and isolation of the final product were carried out using degassed solutions and solvents and under nitrogen that had been freed from oxygen. The general method to obtain the complexes consists of adding,

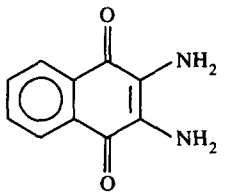
* Author to whom correspondence should be addressed



HL_1



HL_2



HL_3

under continuous stirring, to an ethanolic solution of metal(II) chloride salts or vanadyl sulfate, a ligand solution in a 40% aqueous solution of tetrabutylammonium hydroxide. The formation of the complex compound takes place immediately. Stirring was continued for 2 h, at room temperature, and then the fine crystallized precipitate was filtered and dried *in vacuo*. The ligands were prepared following published methods [7] and wherever possible reagents of analytical grade were used without further purification. All solvents were dried following published methods.

EPR measurements were carried out at room temperature by means of an X-band spectrometer employing 100 kHz modulation of the magnetic field and operating at 9060 Mhz and using a Mn^{II} standard ($g_3 = 2.03584$, $g_4 = 1.98040$, $H_3 = 3179.5$ and $H_4 = 3268.5$ G). The polarographic measurements were obtained with an Orion KTS device. The half-wave potentials were measured at room temperature using the calomel reference electrode and the dropping mercury measuring electrode. Solutions of the complexes (1×10^{-3} mol dm^{-3}) were used and the supporting electrolyte was a 0.1 M solution of tetra-n-butylammonium perchlorate. The electronic spectra were recorded with a Zeiss–Jena VSU-1 spectrophotometer using spectral grade solvents. The IR spectra were run on a Zeiss–Jena UR-10 spectrophotometer, using anhydrous KBr pellets.

RESULTS AND DISCUSSION

Analytical data and molar conductivities, which establish the formulaes $[M(L^1)_2]$, $[M(L^2)_2]$ and $[M(L^3)_2]$, are given in Table 1. The results show that the ligands coordinate to metal ions with a molar ratio of 2:1. In dimethylformamide, the conductivity of the complexes ranges between 11.4 and 55 cm^2 mol^{-1} ohm^{-1}, which is in good agreement with their non-electrolyte character [8]. The minimum value that would allow characterization as a 1:1 electrolyte is 65 cm^2 mol^{-1} ohm^{-1} in this solvent. All the compounds are stable in air.

IR spectra

The IR spectra of the ligands in the region 4000–400 cm^{-1} show significant bands at 1650–1670 and 1575–1590 cm^{-1} as expected for C=O and C=C stretching vibrational modes. They are also characterized by two medium bands at 835–865 and 755–785 cm^{-1}, which are assigned to the C—H out-of-plane deformations of the naphthoquinonic ring. The observed characteristic absorption frequencies at 3380 (HL^1), 680 (HL^1 and HL^2), 3240 and 3380 (HL^2 and HL^3) cm^{-1} were assigned respectively, to the O—H and S—CH_3 vibrations and the symmetric and antisymmetric N—H vibrations of the ammino group.

The IR spectra of the coordination compounds obviously changed compared with those of the corresponding ligands. Modification or disappearance of the absorption band owing to the vibration of the O—H bond in the spectra of the $[M(L^1)_2]$ complexes proves that the coordination takes place through the oxygen atoms. In the same way, the characteristic absorption bands produced by the amino groups in the spectra of the $[M(L^2)_2]$ and $[M(L^3)_2]$ complexes disappeared and a new characteristic absorption band owing to N—H vibrations of the imino group was observed in the 3280–3320 cm^{-1} region. These results show that the HL^1 and HL^2 ligands are deprotonated and coordinate with metal ions to form neutral coordination compounds through the negative oxygen and imino ions of the hydroxyl and amino groups, respectively. The HL^3 ligand would participate in the formation of complexes in mono- or dianion forms, but, considering the composition data, it is inferred that HL^3 behaves as a bidentate monoanion. Furthermore, these ligands have a delocalized π orbital system which permits their participation in redox processes and they are able to coordinate to the central metal ion under the semiquinonic or quinonic forms.

EPR spectra

The metal complexes synthesized with ligands HL^1–HL^3 gave unusually strong EPR spectra, some of them with a good hyperfine resolution (Table 2). The non-isotropic values of the tensors were determined in all cases on polycrystalline powder samples at room temperature. Some of the isotropic g values in solution have already been published [9].

The species, NiL_2, of whatever ligand type, are para-

Table 1. Elemental analyses[a] and molar conductivities

Compound	C (%)	H (%)	N (%)	M (%)	S (%)	Λ_M ($cm^2 M^{-1} ohm^{-1}$)
HL^1	59.4 (60.0)	3.4 (3.6)			22.1 (21.8)	
HL^2	60.5 (60.3)	4.0 (4.1)	6.0 (6.4)			
HL^3	63.7 (63.9)	4.8 (4.3)	14.9 (14.9)			
$[Ni(L^1)_2]$	52.9 (53.0)	3.4 (3.2)		11.6 (11.8)	11.4 (12.8)	23
$[Cu(L^1)_2]$	52.5 (52.4)	3.5 (3.2)		12.7 (12.6)	12.3 (12.7)	12.8
$[VO(L^1)_2]$	52.0 (52.0)	2.4 (3.2)		13.4 (13.2)		24
$[Ni(L^2)_2]$	50.9 (50.6)	2.8 (3.1)	4.9 (5.4)	11.1 (11.2)		55
$[Cu(L^2)_2]$	50.7 (50.2)	3.5 (3.0)	5.4 (5.3)	12.1 (12.1)		27
$[Pd(L^2)_2]$	50.0 (50.2)	3.2 (2.5)	11.6 (11.7)	22.4 (22.2)		11.4
$[Ni(L^3)_2]$	54.9 (55.7)	3.1 (2.8)	12.0 (13.0)	13.3 (13.6)		28.5
$[Cu(L^3)_2]$	54.9 (55.1)	2.7 (2.8)	12.9 (12.9)	14.5 (14.6)		12.7
$[Pd(L^3)_2]$	45.9 (46.4)	2.8 (2.8)	5.0 (4.9)	18.9 (18.7)		34
$[VO(L^3)_2]$	54.7 (54.7)	2.7 (3.0)		11.7 (11.6)		28

[a] Calculated values are given in parentheses.

Table 2. EPR parameters

Compound	$A_\parallel$	$A_\perp$	g_1 $g_\parallel$	g_2 $g_\perp$	g_3 A_T	A_T	g_{sv}
$[Cu(L^1)_2]$	158.93	29.30	2.25	2.07		619.82	2.130
$[Cu(L^2)_2]$	58.61	23.14	2.245	2.04		89.00	2.108
$[Cu(L^3)_2]$	86.16	28.95	2.24	2.02		86.88	2.093
$[Ni(L^1)_2]$			2.006	2.004		201.31	2.005
$[Ni(L^2)_2]$			2.06	2.02		97.90	2.032
$[Ni(L^3)_2]$			2.08	2.05	2.0025	169.52	2.044
$[Pd(L^3)_2]$					2.0009	18.26	2.001
$[VO(L^1)_2]$	63.49	20.88	1.98	1.99		458.35	1.987
$[VO(L^3)_2]$				1.96		1.07	1.966

magnetic, which is not consistent with the presence of a deprotonated ligand system containing planar nickel(II). The signals obtained, are, however, proof of the semiquinonic character of the ligands. The signals support the definition proposed by Holm and co-workers [10] for these complexes as free radicals stabilized through the cation in which the unpaired electron is delocalized over the ligands, and to some extent over the central ion.

The $[Ni(L^1)_2]$ complex presents a hyperfine structure that is split into five hyperfine components with the intensity ratio 1:4:6:4:1, probably owing to interaction with four equivalent protons of the ligand. The $[Ni(L^2)_2]$ compound has a spectrum consisting of three components. It is suggested that two components ($g_\parallel, g_\perp$) originate in the splitting of the unpaired electron in the axial symmetry field of the complex, while the third component is the result of the donor–acceptor interaction between the ligands and the central ion ($g_3 = 2.0025$). The $[Ni(L^3)_2]$ complex has a signal with pronounced asymmetry and third-order anisotropy, indicating a distortion from square-planar configuration.

Both parallel and perpendicular features of ^{63}Cu are clearly resolved in polycrystalline powder samples of Cu^{II} complexes at room temperature. The $g_\parallel$ and $g_\perp$ values deviate considerably from the free spin value, and the trend $g_\parallel > g_\perp > 2.0023$ observed in the copper(II) complexes shows that the unpaired electron is in the $d_{x^2-y^2}$ orbital of the copper(II) ion [11]. A lower value of the total width for $[Cu(L^2)_2]$ and $[Cu(L^3)_2]$ compared with that of the $[Cu(L^1)_2]$ complex is indicative of more covalency in the in-plane σ bonding character of the former complexes [9].

The EPR of the palladium complexes show that $[Pd(L^2)_2]$ is diamagnetic while $[Pd(L^3)_2]$ presents a highly intense, symmetric and sharp signal (Fig. 1) with a g value of 2.0009 and total width of 18.26 G, suggesting the presence of a free radical stabilized through the cation. However, the observed paramagnetism may also be due to the strong donor–acceptor interaction observed in charge transfer complexes.

At room temperature the EPR spectrum of $[VO(L^1)_2]$ shows eight hyperfine lines characteristic of the vanadium nucleus ($I = \frac{7}{2}$). The oxovanadium com-



Fig. 1. EPR spectrum (X-band) at room temperature of $[Pd(L^3)_2]$ powder.

plex is likely to possess a tetragonal pyramidal structure [12] which is the basic type of coordination known for many oxovanadium compounds with a local C_{2v} symmetry [13]. The single unpaired electron is expected to be located in A_1 orbital which mainly consists of the vanadium $3d_{x^2-y^2}$ orbital [14,15]. The narrowing of the spectrum in the case of the $[VO(L^3)_2]$ complex and its poorer resolution indicate an increase in the covalent character of the metal–ligand bond. In this case the EPR signal consists of a single, extremely narrow line, characteristic of the donor–acceptor interactions present in typical charge transfer complexes.

Electronic spectra

In order to clarify the mode of bonding, the electronic spectra of the free ligands and metal chelates were studied and assigned on the basis of a careful comparison of the latter with the free ligands. In the spectra of the naphthoquinonic ligands, the aromatic bands at 47,200–35,700 cm^{-1} are attributed to naphthoquinone $\pi \rightarrow \pi^*$ transitions. The bands at 33,300–29,000 cm^{-1} are assigned to $n \rightarrow \pi^*$ transitions together with single bands detected at 21,000, 20,400 and 18,200 cm^{-1} for HL^1, HL^2 and HL^3 ligands, respectively. The electronic spectra of the complexes are summarized in Table 3. The electronic spectral data for the nickel(II) complexes are characterized by single *d–d* bands at 24,500 cm^{-1} for $[Ni(L^1)_2]$ in acetonitrile, 12,500 cm^{-1} for $[Ni(L^2)_2]$ and 20,200 cm^{-1} for $[Ni(L^3)_2]$ in acetone, which could be due to $d_{xy} \rightarrow D_{x^2-y^2}$ transitions in square-planar complexes.

The electronic spectra of the copper(II) complexes, $[Cu(L^1)_2]$ and $[Cu(L^2)_2]$ in acetonitrile exhibited three bands appearing at 12,500–13,500, 14,100–15,100 and 15,300–16,400 cm^{-1}, the positions of which were similar to those reported for square-planar or distorted tetrahedral geometries [16–18]. Tetrahedral complexes of Cu^{II} are rare owing to the Jahn–Teller effect and hence a square-planar geometry for these Cu^{II} derivatives can be suggested. The bands may reasonably be assigned, considering C_{4v} symmetry, as $^2B_{1g} \rightarrow {}^2A_{1g}$, $^2B_{1g} \rightarrow {}^2B_{2g}$, and $^2B_{1g} \rightarrow {}^2E_g$ transitions, respectively, which may be a result of the splitting of the ^2D state of the free ion in the four-coordinate state. The electronic spectrum of the $[Cu(L^3)_2]$ complex in 1:1 MeOH-dichloromethane solution contains a single band at 14,200 cm^{-1} which falls in the borderline region for square planar and tetrahedral types, indicating distortion from tetrahedral towards square-planar symmetry [19].

The electronic spectra of the palladium complexes, $[Pd(L^2)_2]$, in acetonitrile, and $[Pd(L^3)_2]$ in acetone, are consistent with a D_{4h} square–planar geometry [20], the *d–d* absorption bands at 15,800–16,000 and 18,500–21,200 cm^{-1} have been assigned to $^1A_{1g} \rightarrow {}^1B_{1g}$ and $^1A_{1g} \rightarrow {}^1E_g$ transitions, respectively.

The electronic spectra of the oxovanadium(IV) complexes have been studied very intensively, since it is the easiest of the d^1 systems to use experimentally. Unfortunately, the interpretation of the spectra has been complicated by the deviation of the complexes from regular octahedral or square-pyramidal stereochemistries. Only a single band at 16,100 cm^{-1} was detected for the oxovanadium(IV) complex and a second band is probably obscured by the strong charge transfer band observed at 25,400 cm^{-1}. These spectral features are comparable with those of various oxovanadium(IV) complexes already reported [12, 21]. We propose a C_{4v} symmetry for our five-coordinated oxovanadium(IV) complex.

Polarographic results

Polarographic measurements in acetonitrile have revealed several waves corresponding to reversible or quasi-reversible reductions of the complex species, and most of these present easily measurable and reproducible polarograms. A summary of polarographic potentials for complexes of HL^1, HL^2 and HL^3 is given in Table 3. The polarographic results indicate evidence for the existence of monoanions and dianions in solutions, but pure samples of these reduction processes were not isolated. The polarographic reduction of the complexes proceeds in two or three monoelectronic steps, some of them being reversible or quasi-reversible. The first wave was assigned to the reduction of the neutral complex species to the monoanionic species. The second wave was assigned to the reduction of the monoanionic species to the dianionic species. The third wave appears from $E_{1/2} = -0.87$ to -1.43 V and was assigned to the reduction of the naphthoquinone ring. The stability of the dianion

Table 3. Electronic spectral (cm^{-1}) and half-wave reduction potential data (V)

Compound	*d–d* transitions	*v*(CT)	$[complex]^0 \rightarrow [complex]^-$	$[complex]^- \rightarrow [complex]^{2-}$	Ligand-based reduction
$[Ni(L^1)_2]$	24,500	27,400	−0.115	−0.48	−0.87
$[Ni(L^2)_2]$	12,500	26,200			
$[Ni(L^3)_2]$	20,200	27,200	+0.36	+0.20	−1.43
$[Cu(L^1)_2]$	12,500; 14,100; 15,300	25,800	−0.15		−1.18
$[Cu(L^2)_2]$	13,500; 15,100; 16,400	26,500	−0.55	−0.80	−1.05
$[Cu(L^3)_2]$	14,800	24,000	−0.26		−1.38
$[Pd(L^2)_2]$	16,000; 18,500	27,000	−0.61	−0.80	−1.22
$[Pd(L^3)_2]$	18,500; 21,200	26,000	+0.025	−0.22	−0.91
$[VO(L^1)_2]$	16,100	25,400	−0.30		−1.01

relative to the monoanion and the stability of the monoanion relative to neutral species is greater for the $[M(L^2)_2]$ complexes than for the corresponding $[M(L^1)_2]$ and $[M(L^3)_2]$ complexes. The most significant result that emerges from consideration of these potentials is their variation as the ligand is changed, for complexes of the same metal and charge type. For every metal investigated so far, the differences between the potentials for the $[M(L^3)_2]$ complexes and those for the $[M(L^2)_2]$ complexes are in the vicinity of 0.6 V. In contrast, the potentials for the monoanion of any one ligand with the entire series of metals cover a much smaller range. The conclusion appears to be that the ligand is assuming a commanding role in the ease of reduction and must participate somehow in the electron transfer process.

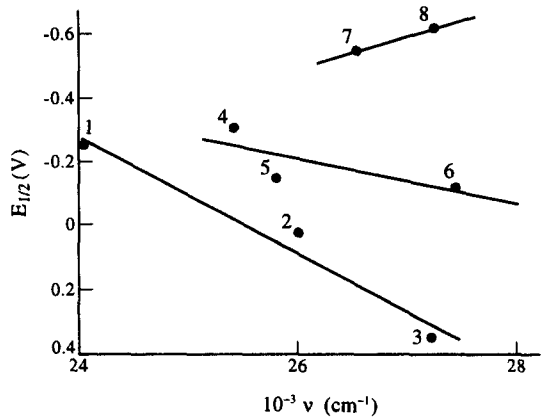


Fig. 2. Linear correlation between half-wave reduction potential and MLCT band energy. Numbers are as follows: 1, $[Cu(L^3)_2]$; 2, $[Pd(L^3)_2]$; 3, $[Ni(L^3)_2]$; 4, $[VO(L^1)_2]$; 5, $[Cu(L^1)_2]$; 6, $[Ni(L^1)_2]$; 7, $[Cu(L^2)_2]$; 8, $[Pd(L^2)_2]$.

Correlations between spectroscopic and electrochemical results

Square-planar complexes in which the ligands have a π electron system will have both π bonding and π^* antibonding ligand orbitals, and charge transfer (CT) bands of lowest energy are expected to involve transitions from the highest occupied metal orbitals (HOMOs) and the most stable (lowest) unoccupied ligand molecular orbital (LUMO). The detected charge transfer transitions can be seen in Table 3. A good approach to estimate the energies of the metal ligand charge transfer transitions from electrochemical data or *vice versa* [22] has been the correlation observed between the low energy electronic transition and the first potential reduction of the metal complex involved. The basis of such correlations lies in the fact that the same orbitals are involved in both the MLCT transition and in the electrochemical process. When the first reduction potential for the $[complex]^0/[complex]^{-1}$ couple and the lowest energy absorption band of the complexes were plotted a good relationship was obtained for each ligand with different metal ions (Fig. 2). The MLCT assignment of the lowest energy transitions in the metal complexes was thus established.

In Fig. 3 a range of A_T values, the total width of the EPR spectral band, are displayed as a function of the isotropic *g* factor for some of the charge transfer complexes. It can be appreciated that a smooth correlation was obtained since the extent of

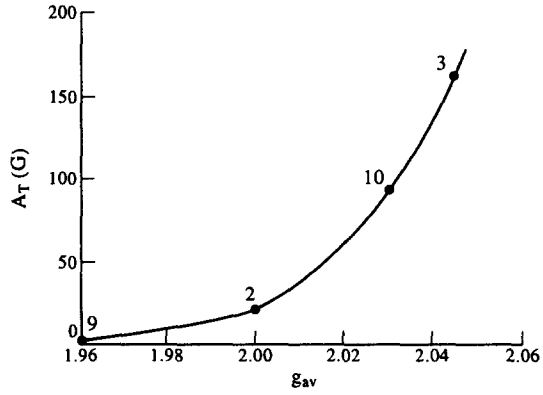


Fig. 3. Variation of the total width of the EPR spectrum with the g_{av} values. Numbers 2 and 3 as in Fig. 2; 9, $[VO(L^3)_2]$; 10, $[Ni(L^2)_2]$.

delocalization of the unpaired electron from the metal atom increases along the curve, moving towards $g = 2.0023$ as A_T falls. Deviations from the curve arise for the $[Cu(L^2)_2]$, $[Cu(L^3)_2]$ and $[Ni(L^1)_2]$ complexes and this is likely to be owing to the fact that they do not have full D_{4h} symmetry. These complexes might present distorted square-planar symmetry with third-order anisotropy.

On the other hand, the covalent character of the metal–ligand bonding would relate to the reduction potential of the metal ions having d^1 or d^9 electronic configurations. They present strong, well-resolved EPR spectra as a result of the interaction of the electron with the central metal ion. The higher the charge delocalization, the higher the covalent character of the metal–ligand bond and the ease of separation of an electron from the HOMO increases, so that the reduction potential increases. From Table 3 it can be appreciated that the total width, A_T, of the EPR spectra decreases along the series $[Cu(L^1)_2] > [VO(L^1)_2] > [Cu(L^2)_2]$, as the first reduction potential increases.

REFERENCES

1. McCleverty, J. A. *Prog. Inorg. Chem.*, 1968, **10,** 49.
2. Schrauzer, G. N. *Acc. Chem. Res.*, 1969, **2,** 72.
3. Eisenberg, R. *Prog. Inorg. Chem.*, 1970, **12,** 295.
4. Wicklund, P. A. and Brown, D. G. *Inorg. Chem.*, 1976, **2,** 396.
5. Burns, R. P. and McAuliffe, C. A. *Adv. Inorg. Chem. Radiochem.*, 1979, **22,** 303.
6. Holm, R. H. and O'Connor, M. J. *Prog. Inorg. Chem.*, 1971, **14,** 241.
7. Hoover, J. R. E. and Day, A. E. *J. Am. Chem. Soc.*, 1954, **76,** 148.
8. Geary, W. J. *Coord. Chem. Rev.*, 1971, **7,** 81.
9. Camus, J., Meghea, A. and Anacona, J. R. *Polyhedron*, 1996, **15,** 2953.
10. Balch, A. L., Dance, I. G. and Holm, R. H. *J. Am. Chem. Soc.*, 1968, **90,** 1139.
11. Goodman, B. A. and Raynar, J. B. *Adv. Inorg. Chem. Radiochem.*, 1970, **13,** 313.
12. Wasson, J. R. *Inorg. Chem.*, 1979, **10,** 1581.
13. Sato, M., Fujita, Y. and Kwan, T. *Bull. Chem. Soc. Jpn*, 1973, **46,** 3007.
14. Kivelson, D. and Lee, S. K. *J. Chem. Phys.*, 1964, **41,** 1896.
15. McGarvey, B. R. *Trans. Met. Chem.*, 1966, **3,** 89.
16. Lever, A. B. P. *Inorganic Electronic Spectroscopy.* Elsevier, Amsterdam, 1984.
17. El-Dissouky, A. *Indian J. Chem.*, 1983, **22A,** 427.
18. Patel, K. G. and Singh, R. P. *J. Inorg. Nucl. Chem.*, 1977, **39,** 1325.
19. Ray, P. and Sen, D. N. *J. Indian Chem. Soc.*, 1948, **25,** 473.
20. El-Sonbati, A. Z., El-Sayed., Mabrouk, M. and Megahed, H. E. *Trans. Met. Chem.*, 1991, **16,** 280.
21. Selbin, J. *Chem. Rev.*, 1965, **65,** 153.
22. Caspar, J. V., Sullivan, B. P. and Meyer, T. J. *Inorg. Chem.*, 1984, **23,** 2104.

Pergamon

PII: S0277-5387(96)00346-4

Polyhedron Vol. 16, No. 6, pp. 939–944, 1997
Copyright © 1996 Elsevier Science Ltd
Printed in Great Britain. All rights reserved
0277-5387/97 $17.00+0.00

X-ray crystal structure and electronic properties of chlorobis(mepirizole)copper(II) tetrafluoroborate (mepirizole = 4-methoxy-2-(5-methoxy-3-methyl-1*H*-pyrazol-1-yl)-6-methylpyrimidine)

Julia García-Lozano,[a]* Juan Server-Carrió,[a] Emilio Escrivà,[a] José-Vicente Folgado,[a] Carmen Molla[a] and Luis Lezama[b]

[a]Department de Química Inorgànica, Universitat de València, c/Vicent Andrés Estellés, s/n, 46100 Burjassot, València, Spain

[b]Departamento de Química Inorgánica, Universidad del País Vasco, Apdo. 644, 48080 Bilbao, Spain

(Received 24 May 1996; accepted 17 July 1996)

Abstract—The crystal structure of $[Cu(mep)_2Cl](BF_4)$ [mep = 4-methoxy-2-(5-methoxy-3-methyl-1*H*-pyrazol-1-yl)-6-methylpyrimidine] has been determined by X-ray diffraction. The crystal structure is built up of $[Cu(mep)_2Cl]^+$ cations and BF_4^- anions. The structure of the cation involves a five-coordinated CuN_4Cl chromophore, with a stereochemistry near to a compressed trigonal bypyramid (TBP) but with a significant degree of distortion towards the square pyramidal (SP) topology. The EPR spectrum is indicative of a mixed $d_{z^2}/d_{x^2-y^2}$ ground state for the copper(II) ions, in agreement with the structural data. Copyright © 1996 Elsevier Science Ltd

Keywords: copper(II) complexes; stereochemistry; five-coordination; distortion; EPR; bidentate ligand.

As a part of our studies on the coordination behaviour of the pyrazole, pyrimidine and related nitrogen-containing heterocyclic derivatives, we have previously reported [1–6] the preparation and characterization of several complexes of divalent 3*d* ions with mepirizole [4-methoxy-2-(5-methoxy-3-methyl-1*H*-pyrazol-1-yl)-6-methylpyrimidine; hereafter, mep] a biologically active pyrimidine–pyrazole derivative. All structural studies show that mepirizole behaves as a bidentate ligand through two nitrogen atoms, one from each ring, with significant steric hindrance in the formation of metal complexes. Here we report the crystal structure and electronic properties of a new five-coordinated mepirizole-containing copper(II) complex, $[Cu(mep)_2Cl](BF_4)$. The stereochemistry of this compound is compared with those reported for related $[Cu(N\sim N)_2Cl]$ entities (where N∼N represents a N-donor bidentate ligand), which have been the focus of crystallographic and spectroscopic studies [7–9].

* Author to whom all correspondence should be addressed.

EXPERIMENTAL

Preparation of the complex

A solution of $NaBF_4$ (1 mmol) in water (25 cm^3) was added with stirring to a mixture of an ethanolic solution of mepirizole (1 mmol in 25 cm^3) and an aqueous solution of copper(II) chloride (0.5 mmol in 20 cm^3). The resulting green solution was left at room temperature and within 72 h a fine crystalline solid formed. This was filtered off, washed with a water/ethanol mixture, dried and stored over silica gel. By slow evaporation of the mother liquor at room temperature prismatic green crystals appeared, which were separated by filtration, washed and dried. Found: C, 40.8; Cl 5.4; N 17.2; Cu 9.6. Calc. for

$C_{22}H_{28}BClCuF_4N_8O_4$: C, 40.4; Cl, 5.4; N 17.1; Cu 9.7%.

Physical measurements

The IR spectrum (KBr pellets) was recorded on a Pye Unicam SP 2000 spectrophotometer. The diffuse reflectance spectrum was obtained using a Perkin–Elmer Lambda 9 UV/VIS/IR spectrophotometer. Polycrystalline powder EPR spectra were recorded at room temperature on Bruker ER 200D (X-band) and ESP-300 (Q-band) spectrometers.

Crystal structure

A green prismatic crystal of the complex with approximate dimensions ($0.2 \times 0.3 \times 0.4$ mm^3) was mounted on an Enraf–Nonius CAD-4 diffractometer. Intensity data and the 25 reflections for the unit cell determination (least-squares fit with $7 < \theta < 15°$) were measured at room temperature using graphite-monochromated Mo K_α radiation. The $\omega/2\theta$ scan technique was used, with variable speed, width $(0.8 + 0.35 \tan\theta)°$ in ω, and θ limits $1 < \theta < 26°$. No intensity decay was detected. From the 5570 independent reflections 4021 with $I > 2\sigma(I)$ were considered observed. Empirical absorption correction was made using Ψ-scan (max. and min. transmission factors 1.00 and 0.89).

The structure was solved by direct methods using the program SIR92 [10]. All non-hydrogen atoms were refined anisotropically by least squares on F_o using the XRAY76 System [11]. The hydrogen atoms were included as isotropic fixed contributors (370 refined parameters). In the final stages an empirical weighting scheme was chosen as to give no trends in $\langle w\Delta^2 F\rangle$ *vs* $\langle F_o\rangle$ and *vs* $\langle \sin\theta/\lambda\rangle$ using the program PESOS [12]. The final ΔF map showed a maximum peak of 0.38 e Å^{-3}.

All calculations were done with a VAX6410 computer and the atomic scattering factors and anomalous dispersion corrections were taken from ref. [13]. Other relevant parameters for the crystal structure analysis are listed in Table 1.

Table 1. Crystal data for $[Cu(mep)_2Cl](BF_4)$

Formula	$C_{22}H_{28}BClCuF_4N_8O_4$
Symmetry	Triclinic, $P\bar{1}$
a, b, c (Å)	7.821(1), 13.652(2), 14.300(1)
α, β, γ(°)	103.54(1), 104.57(1), 94.34(1)
V(Å^3), Z	1421.9(2), 2
D_c(g cm^{-3}), M	1.53, 654.32
F(000), μ(cm^{-1})	670, 9.3
Max. final shift/error	0.0014 [y of F(3)]
Max. thermal value	0.144 [U_{33} of F(3)]
Final ΔF peak	0.38 e Å^{-3}
Extinction correction	None
S, unit weight standard deviation	1.09
Final R and R_w	0.065, 0.067

RESULTS AND DISCUSSION

Description of crystal structure

The crystal structure of the title compound is built up of $[Cu(mep)_2Cl]^+$ cations and BF_4^- anions. Figure 1 shows a perspective view of the $[Cu(mep)_2Cl]^+$ entity with the atomic-numbering scheme. Selected bond distances and angles are listed in Table 2.

The structure of the cation involves a five-coordinated CuN_4Cl chromophore, with no evidence for even semi-coordination of the BF_4 groups. In short, the stereochemistry of the coordination polyhedron can be viewed as near to a compressed trigonal bypiramid (TBP), similar to those reported [8,9] for several $[Cu(N\sim N)_2Cl]^+$ cations. Such a stereochemistry for five-coordinated copper(II) systems is slightly stabilized if significant steric hindrance is present [14]. There are two molecules per unit cell, but both copper(II) ions are in crystallographically equivalent sites with their trigonal axes parallel.

Two nitrogen atoms (one of each mepirizole molecule) and the chlorine atom define the equatorial plane, whereas the other two coordinated nitrogen atoms occupy the axial positions. The Cu—N_{ax} bond distances [mean value 2.001(5) Å] are not significantly different and are *ca* 0.13 Å shorter than the two equatorial ones [mean value of 2.135(4) Å]. On the other hand, the Cu—Cl bond length [2.264(2) Å] is longer than Cu—N distances consistent with the larger size of the chlorine atom. Furthermore, this copper–chlorine bond distance is significantly greater than that previously found [2] in $Cu(mep)Cl_2$ (2.19 Å), where distorted tetrahedral CuN_2Cl_2 chromophores are present.

The in-plane bond angles are far from the value of 120° corresponding to a regular TBP stereochemistry. In particular, the N_{eq}—Cu—N_{eq} angle [100.6(2)°] is appreciably lower than the ideal value, clearly indicating the distortion of the coordination polyhedron. We have quantified this distortion—from an ideal TBP geometry towards a square pyramidal (SP) one—by applying the method of Muetterties and Guggenberger [15] using the analytical formula proposed by Galy *et al.* [16]. The dihedral angles and the deviation (Δ) for both TBP and SP ideal geometries and the $[Cu(mep)_2Cl]^+$ cation are given in Table 3. The value of $\Delta = 0.22$ clearly indicates the predominance of the TBP form but with a significant degree of distortion towards the SP topology.

In addition, we have also used the τ parameter as defined by Addison *et al.* [17] to quantify the degree of distortion of the polyhedron. This is a simpler parameter but it affords similar qualitative results. So, for the title compound, $\tau = 0.67$ ($\tau = 1$ for a regular

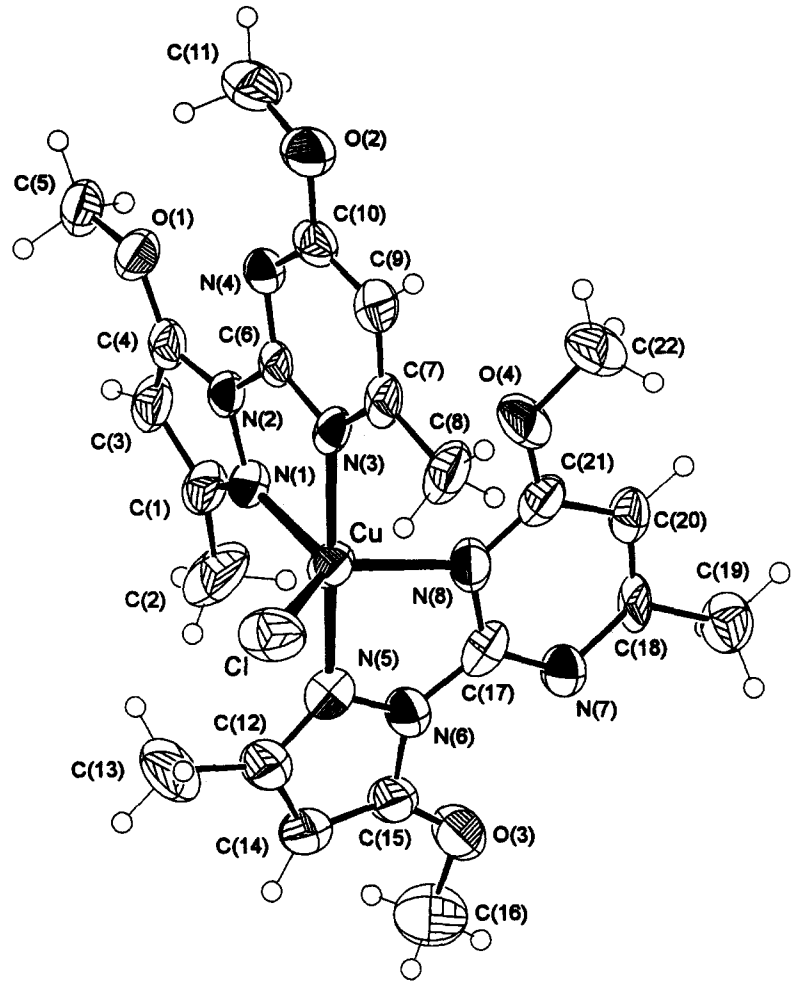


Fig. 1. Perspective view of the $[Cu(mep)_2Cl]^+$ cation showing the atom labelling.

TBP stereochemistry and $\tau = 0$ for a SP one), thus supporting the above conclusions.

Hathaway and co-workers [8] have studied the correlation between several molecular parameters for a series of five-coordinated $[Cu(bipy)_2Cl]^+$ cations that contain distorted trigonal bipyramidal CuN_4Cl chromophores. They pointed out that the in-plane bond lengths and angles vary systematically in the CuN_4Cl polyhedra. We have now reconsidered some of these correlations, including the title compound and others five-coordinated $[Cu(N\sim N)_2Cl]^+$ cations, using the τ parameter as a criterion for the degree of distortion. The graphic representation of the N_{eq}—Cu—N_{eq} angle versus τ is shown in Fig. 2a. If the compound $[Cu(bpy)_2Cl][CuCl_2]$ [18] (where the chlorine atom is involved in a bridging role to the copper atom in the anion $CuCl_2^-$) is omitted, a reasonable correlation is obtained, with the N_{eq}—Cu—N_{eq} angle increasing as τ increases.

With regard to the bond distances, it must be

Table 2. Bond lengths (Å) and angles (°) for the copper coordination sphere

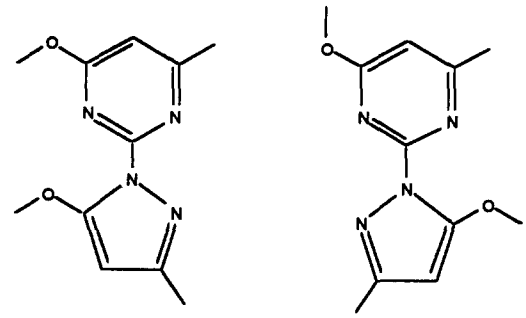
Cu—Cl	2.264(2)	Cu—N(5)	1.995(6)
Cu—N(1)	2.113(4)	Cu—N(8)	2.156(5)
Cu—N(3)	2.007(5)		
Cl—Cu—N(1)	125.1(2)	N(1)—Cu—N(5)	97.1(2)
Cl—Cu—N(8)	134.8(2)	N(1)—Cu—N(3)	78.3(2)
Cl—Cu—N(5)	92.6(2)	N(3)—Cu—N(8)	100.6(2)
Cl—Cu—N(3)	92.2(2)	N(3)—Cu—N(5)	174.7(2)
N(1)—Cu—N(8)	100.0(2)	N(5)—Cu—N(8)	77.6(2)

Table 3. Dihedral angles (°) and distortion (Δ) of the coordination polyhedron for $[Cu(mep)_2Cl]BF_4$ compared with the ideal trigonal bipyramid (TBP) and regular square pyramid (SP) geometries

Dihedral angle	TBP	$[Cu(mep)_2Cl]^+$	SP
δa_1	101.5	90.8	121.8
δa_3	101.5	98.1	121.8
δa_4	101.5	112.0	121.8
δa_6	101.5	103.1	121.8
δa_2	101.5	84.1	73.9
δa_5	101.5	111.1	73.9
δe_1	53.1	67.0	73.9
δe_2	53.1	53.2	73.9
δe_3	53.1	48.7	0
Δ	0	0.22	1

stressed that the Cu—N_{ax} lengths are practically insensitive to the degree of distortion, whereas the Cu—N_{eq} distances vary with τ, but no explicit correlation can be established. So, only the Cu—Cl bond distance exhibits a roughly regular correlation with τ. A plot of d(Cu—Cl) against τ is showed in Fig. 2b. Again, with the exception of $[Cu(bipy)_2Cl][CuCl_2]$, an agreeable correlation is obtained, with d(Cu—Cl) decreasing with the degree of distortion.

In relation to the mepirizole molecules, the more striking feature is that they exhibit different conformations (hereafter noted as **A** and **B** conformations). In fact, to date only in the tris complex $[Cu(mep)_3](PF_6)_2$ has the **B** conformation been observed [6]. The two conformations are essentially related through rotation around the central C—N bond between the pyrimidinic and pyrazolic nuclei.



A *B*

Conformational analysis according to the rigid approximation in the MMX program [19] affords an energy barrier for this rotation of *ca* 50 kJ mol^{-1}. Thus, if significant steric restrictions are present they can stabilize the two conformers.

In other respects, there are no unusual bond distances or angles in the mepirizole molecules. In both molecules **A** and **B** the individual pyrimidine and pyrazole rings are planar (deviation from planarity ranging from 0.01 to 0.03 Å), with dihedral angles between both nuclei of 12.0° for the **A** molecule and 5.6° for the **B** molecule, clearly indicating significant torsions.

Finally the bite parameter defined by $b = 2d_0/(d_1+d_2)$ (where d_0 is the non-bonding distance between the two donor atoms, and d_1 and d_2 are the distances of these atoms to the metal centre) is $b = 1.27$ for molecule **A** and $b = 1.25$ for molecule **B**. The former compares well with the mean value of 1.29(2) for bidentate mepirizole molecules with conformation **A**. On the other hand, the **B** molecule exhibits a lower b value as occurs in the tris complex $[Cu(mep)_3](PF_6)_2$ ($b = 1.20$).

The BF_4^- anions exhibit a near-regular tetrahedral structure, with a mean B—F distance of 1.37(1) Å and a mean F—B—F angle of 109.5(7)°. The shortest Cu—F distance is 5.82 Å, in agreement with non-coordination of the tetrafluoroborate groups.

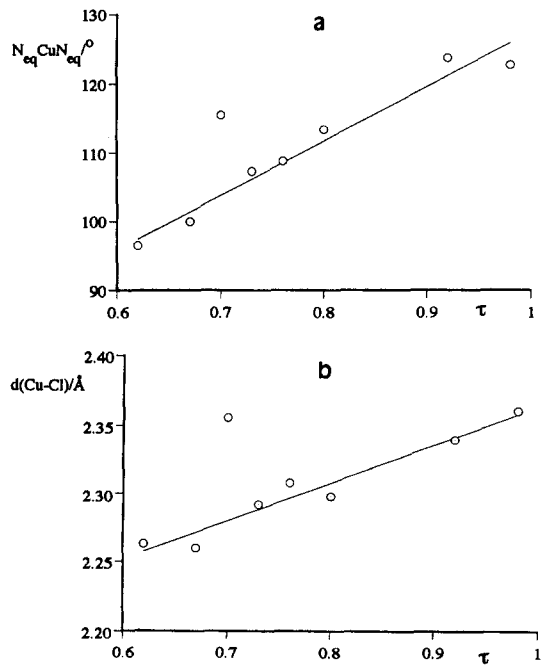


Fig. 2. (a) Correlation between the N_{eq}—Cu—N_{eq} angle and the τ parameter; (b) correlation between the Cu—Cl bond distance and the τ parameter (see text).

Vibrational and electronic spectra

The IR spectrum of the title compound shows a large number of absorption bands in the range 1700–1100 cm^{-1}, assigned to different vibrational modes of the mepirizole molecule. In addition, a strong band is observed at *ca* 1060 cm^{-1}, consistent with the presence of non-coordinated BF_4^- groups with T_d symmetry [20]. Finally, the absorption observed in the low

energy region at *ca* 390 cm^{-1} is assigned to Cu—Cl stretching vibrations [21].

The electronic reflectance spectrum of the compound studied exhibits a very broad structure in the visible region centred at 15,100 cm^{-1}. Taking into account the topology of the CuN_4Cl chromophores it may be assumed that the unresolved *d–d* band arises from overlap of the $(d_{xz}, d_{yz})\rightarrow d_{z^2}$ and $(d_{x^2-y^2}, d_{xy})\rightarrow d_{z^2}$ transitions in a point group symmetry close to C_{2v}. These observations compare well with those reported for similar CuN_4Cl chromophores [8].

EPR spectroscopy

The room-temperature X-band EPR powder spectrum of the title compound is clearly orthorhombic, although it was not fully resolved owing to the width of the signals, and leads to approximate *g* values of 2.03, 2.12 and 2.25. In the Q-band spectrum, the three lines are clearly defined giving more accurate *g* values of 2.017, 2.121 and 2.250 ($g_{average} = 2.129$). These values are very similar to those found in the complexes $Cu(terpy)X_2$ (X = Br, I, NCS) [22] which contain pentacoordinate CuN_3X_2 chromophores having a coordination geometry close to C_{2v}, and $[Cu(bipy)_2(NH_3)](BF_4)_2$ with CuN_5 chromophores intermediate between the ideal square pyramidal (C_{4v}) and trigonal bipyramidal (D_{3h}) [23]. In our compound, we can roughly consider that the local geometry of the CuN_4Cl entities is close to C_{2v} with the CuCl direction defining the twofold axis. Following the vibrational model proposed by Reinen and Atanasov [14], the ground-state wave function of a five-coordinated copper(II) complex can be expressed as follows:

$$\varphi_g = (1+c^2)^{-1/2}[d_{z^2} + c\, d_{x^2-y^2}].$$

The mixing coefficient *c* is zero for the trigonal bipyramid (d_{z^2} ground state) and is $1/\sqrt{3}$ for the square pyramid ($d_{z^2-y^2}$ ground state). The corresponding expressions for the *g* values are:

$$g_z = g_0 + 8[c^2/(1+c^2)]u_z$$

$$g_y = g_0 + 2[c^2/(1+c^2)][1-\sqrt{3}/c]^2 u_y$$

$$g_x = g_0 + 2[c^2/(1+c^2)][1+\sqrt{3}/c]^2 u_x$$

where u_i are the orbital contributions. Taking u_i as 0.032 ($g_{average} = g_0 + 4u_i$), the experimental *g* values can be reproduced nicely with *c* values of 0.33(3), very close to the value of 1/3 expected for a C_{2v} geometry, thus implying a ground state for the Cu(II) ions between d_{z^2} (TBP) and $d_{x^2-y^2}$ (SP). Hence, there is a full agreement between the structural and spectroscopic results.

Acknowledgements—Financial support from DGICYT (PB93-0688) is gratefully acknowledged. We also thank Dr M. Martínez-Ripoll and the U.E. de Cristalografía at the Instituto Rocasolano (CSIC, Madrid) for providing access to computing facilities in the crystal structure determination.

REFERENCES

1. Molla, M. C., García-Lozano, J., Borrás, J., Foces-Foces, C., Cano, F. H. and Martínez-Ripoll, M. *Transition Met. Chem.*, 1985, **10,** 460.
2. Soto, L., Legros, J.-P., Molla, M. C. and García-Lozano, J., *Acta Cryst.*, 1987, **C43,** 834.
3. Soto, L., García-Lozano, J., Escrivà, E., Legros, J.-P., Tuchagues, J.-P., Dahan, F. and Fuertes, A., *Inorg. Chem.*, 1989, **28,** 3378.
4. Benetó, M., Soto, L., García-Lozano, J., Escrivà, E., Legros, J.-P. and Dahan, F., *J. Chem. Soc., Dalton Trans.*, 1991, 1057.
5. Soto, L., García-Lozano, J., Escrivà, E., Benetó, M., Dahan, F., Tuchagues, J.-P. and Legros, J.-P., *J. Chem. Soc., Dalton Trans.*, 1991, 2619.
6. Soto, L., García-Lozano, J., Escrivà, E. and Legros, J.-P., *Polyhedron*, 1992, **6,** 647.
7. Harrison, W. D. and Hathaway, B. J., *Acta Cryst.*, 1980, **B36,** 1069.
8. Harrison, W. D., Kennedy, D. C., Power, M., Sheahan R. and Hathaway, B. J., *J. Chem. Soc., Dalton Trans.*, 1981, 1556.
9. Carugo, O. and Castellani, C. B., *J. Chem., Dalton Trans.*, 1990, 2895.
10. Altomare A., Burla M. C., Camalli, M., Cascarano, G., Giacovazzo, G., Guagliardi, A. and Polidori, G., *J. Appl. Cryst.*, 1994, **27,** 435.
11. Stewart, J. M., Machin, P. A., Dickinson, C. W., Ammon, H. L., Heck, H. and Flack, H., *The XRAY76 System*, Computer Science Center, University of Maryland, College Park, Maryland, 1976.
12. Martínez-Ripoll, M. and Cano, F. H., *PESOS: a computer program for the automatic treatment of weighting schemes*, Instituto Rocasolano, CSIC, Madrid, 1975.
13. *International Tables for X-Ray Crystallography*, Vol. 4. Kynoch Press, Birmingham, 1974, p. 72.
14. Reinen, D. and Atanasov, M., *Chem. Phys.*, 1989, **136,** 27.
15. Muetterties, E. L. and Guggenberger, L. J., *J. Am. Chem. Soc.*, 1974, **96,** 1748.
16. Galy, J., Bonnet, J. J. and Anderson, S., *Acta Chem. Scand.*, 1979, **A33,** 383.
17. Addison, A. W., Rao, T. N., Reedijk, J., van Rijn, J. and Verschoor, G. C., *J. Chem. Soc., Dalton Trans.*, 1984, 1349.
18. Kaiser, J., Brauer, G., Schröder, F. A., Taylor, F. and Rasmussen, S. E., *J. Chem. Soc., Dalton Trans.*, 1974, 1490.
19. The MMX program package from Serena Software Ltd., Bloomington N.Y. The MMX molecular-mechanics program was established from the MM2 and MMP1 programs (Allinger QCPE 395 and QCPE 318) by K. E. Gilbert and J. J. Gajeswki.
20. Quist, A. S., Bates, J. B. and Boyd, G. E., *J. Chem. Phys.*, 1971, **54,** 4896.
21. Ferraro, J. R., *Low Frequency Vibrations of Inor-*

ganic Coordination Compounds. Plenum Press, New York, 1971.
22. Arriourtua, M. I., Mesa, J. L., Rojo, T., Debaermaeker, T., Beltrán, D., Stratemeier, H. and Reinen, D., *Inorg. Chem.*, 1988, **27**, 2976; A. Kutoglu, R. Allmann, J. V. Folgado, M. Atanasov and D. Reinen, *Z. Naturforsch.*, 1991, **46b**, 1193.
23. Tyagi, S., Hathaway, B., Kremer, S., Stratemeier, H. and Reinen, D., *J. Chem. Soc., Dalton Trans.*, 1984, 2087.

Pergamon

PII: S0277-5387(96)00345-2

Polyhedron Vol. 16, No. 6, pp. 945–948, 1997
Copyright © 1996 Elsevier Science Ltd
Printed in Great Britain. All rights reserved
0277-5387/97 $17.00+0.00

Optical non-linearity of distorted cubic cage-shaped cluster compounds $\{MAg_3S_3[S_2P(OCH_2CH_3)_2]\}(S)(Ph_3P)_3$ (M = W, Mo)

Xintao Wu,[a]* Quanming Wang[a] and Shu Shi[b]

[a] State Key Laboratory of Structural Chemistry, Fujian Institute of Research on the Structure of Matter, Fuzhou, Fujian 350002, P.R. China

[b]Department of Chemical Engineering, National University of Singapore, Singapore 0511

(Received 24 May 1996; accepted 15 July 1996)

Abstract—The non-linear optical (NLO) properties of two distorted cage clusters $\{WAg_3S_3[S_2P(OCH_2CH_3)_2]\}(S)(Ph_3P)_3$ (**1**) and $\{MoAg_3S_3[S_2P(OCH_2CH_3)_2]\}(S)(Ph_3P)_3$ (**2**) were studied. Both NLO absorption and refraction were observed with **1** and **2**, third-order effects were detected with $\alpha_2 = 6 \times 10^{-10}$ mW^{-1} for **1** and $\alpha_2 = 8 \times 10^{-10}$ mW^{-1} for **2**. NLO refraction was also found on **1** and **2**, with $n_2 = 1 \times 10^{-16}$ m^2 W^{-1} for **2**. The non-linearity of these two clusters was compared with some related NLO materials. Copyright © 1996 Elsevier Science Ltd

Keywords: optical non-linearity; cluster compound; tungsten; molybdenum; silver; incomplete cubane-like.

Traditionally, non-linear optical (NLO) research has been largely focused on semiconductors, conjugated polymers and discrete organic molecules [1,2]. Recently, studies on these clusters have been expanded to include their non-linear optical (NLO) properties. A series of studies on structure and NLO properties of Mo(W)–S(O)–Cu(Ag) clusters has been undertaken in the search for better NLO materials [3–8]. The butterfly-shaped clusters $[MOS_3Cu_2(PPh_3)x]$ (M = Mo, W; x = 3, 4) exhibit strong NLO refractive effect (self-focusing) [7], but their nest-shaped derivatives, $(n\text{-}Bu_4N)_2[MoOS_3Cu_3BrCl_2]$ and $(n\text{-}Bu_4N)_2[MoOS_3Cu_3(NCS)_3]$, behave quite differently. The self-focusing effect observed in this family of butterfly-shaped clusters is replaced by a self-focusing effect in the family of the nest-shaped clusters [5,6]. Here, we report a study on two novel distorted cubic cage-shaped inorganic clusters $\{MAg_3S_3[S_2P(OCH_2CH_3)_2]\}(S)(Ph_3P)_3$ [M = W(**1**), Mo(**2**)]. From a structural point of view, these two clusters can be considered as closed derivatives of the nest-shaped clusters. We discuss their structures, electronic spectra and NLO absorptive and refractive properties.

EXPERIMENTAL

Synthesis

Clusters **1** and **2** were prepared and characterized using published methods [9,10].

Synthesis of cluster **1**. $\{WAg_2S_4\}(Ph_3P)_3$ (0.6 g, 0.46 mmol) and $AgS_2P(OCH_2CH_3)$ (0.134 g, 0.46 mmol) were reacted in CH_2Cl_2 (40 cm^3) for about 3 h and then filtered. The orange filtrate was mixed with Pr^{i}OH (20 cm^3) and Et_2O (20 cm^3). Orange crystals (0.35 g) were obtained by cooling the filtrate at 5–10°C for several days.

Synthesis of cluster **2**. The synthesis was similar to that of cluster **1**, using $\{MoAg_2S_4\}(Ph_3P)_3$ instead of $\{WAg_2S_4\}(Ph_3P)_3$.

Optical measurements

Acetonitrile solutions of 5.2×10^{-4} g cm^{-3} of **1** and 2.6×10^{-4} g cm^{-3} of **2** were placed in 1 mm quartz

* Author to whom correspondence should be addressed.

cuvettes for optical measurements. Their non-linear absorption and non-linear refraction were measured with a linearly polarized laser light ($\lambda = 532$ nm; pulse width = 7 ns) generated from a Q-switched and frequency-doubled Nd-YAG laser. The spatial profiles of the optical pulses were nearly Gaussian. The laser beam was focused with a 25 cm focal-length focusing mirror. The radius of the beam waist was measured to 40 ± 5 μm (half-width at $1/e^2$ maximum). The incident and transmitted pulse energy were measured simultaneously by two Laser Precision detectors (RjP-735 energy probes) which were linked to the computer by an IEEE interface. The non-linear optical properties of the samples were manifested by moving the samples along the axis of the incident beam (Z-direction) with respect to the focal points [11]. An aperture of radius 0.5 mm was placed in front of a detector that was positioned behind the sample to assist the measurement of the self-defocusing effect of the sample.

RESULTS AND DISCUSSION

Molecular structure

Clusters **1** and **2** have the same molecular configuration, as shown in Fig. 1. The core $\{WAg_3S_3\}$ of cluster **1** is an incomplete cubane-like one, which is completed by three Ag atoms, and the terdentate WS_4^{2-}. Three PPh_3 ligands are terminally attached to the three Ag atoms, respectively. One sulfur of the bridging $S_2P(OCH_2CH_3)_2^{2-}$ is linked to a Ag atom and the other bridges the other two Ag atoms. In cluster **2** the W atoms are replaced by Mo.

Linear and non-linear optical properties

The electronic spectra were measured and absorption maxima were observed at 405 and 250 mm for **1** and at 256 nm for **2**. Both NLO absorption and NLO refraction were observed with **1** and **2**.

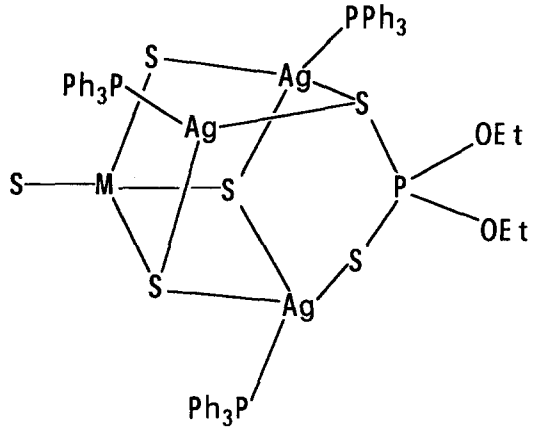


Fig. 1. The molecular configuration of **1** (M = W) and **2** (M = Mo).

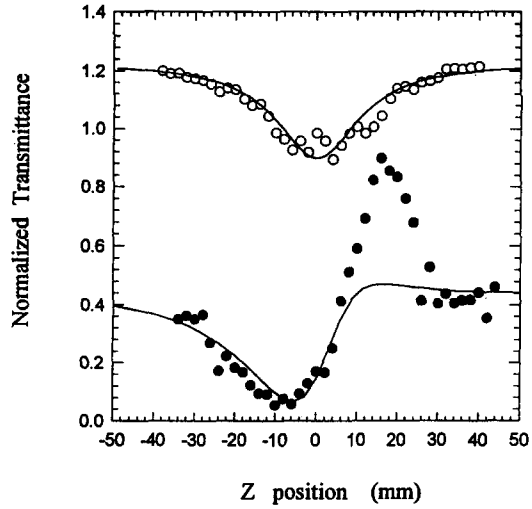


Fig. 2. Z-scan data for **1**. Observed under an open aperture configuration; upper solid curve: theoretical curve based on Eq. (1). Filled circles: Z-scan data observed under a closed aperture configuration divided by those obtained under the open aperture configuration to filter out the influence of NLO absorption. Lower solid curve: a theoretical curve obtained from Eq. (2). Cluster concentrations are 5.2×10^{-4} g cm^{-3} for **1** and 2.6×10^{-4} g cm^{-3} for **2**.

The NLO properties of **1** and **2** were revealed using a Z-scan technique [11]. Their non-linear absorptive properties are depicted by the open circles in Figs 2 and 3 while their non-linear refractive properties are

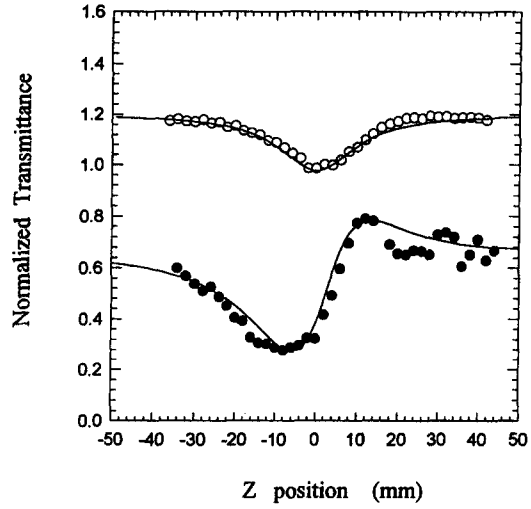


Fig. 3. Z-scan data for **2**. Observed under an open aperture configuration; upper solid curve: theoretical curve based on Eq. (1). Filled circles: Z-scan data observed under a closed aperture configuration divided by those obtained under the open aperture configuration to filter out the influence of NLO absorption. Lower solid curve: a theoretical curve obtained from Eq. (2). Cluster concentrations are 5.2×10^{-4} g cm^{-3} for **1** and 2.6×10^{-4} g cm^{-3} for **2**.

depicted by the filled circles in the figures. The solid curves in the figures are generated theoretically using Eqs (1) and (2):

$$T(z) = \frac{1}{\sqrt{\pi q(z)}} \int_{-\infty}^{+\infty} \ln[1+q(z)]e^{-\tau^2}\,d\tau \qquad (1)$$

$$T(z,s) = \frac{\int_{-\infty}^{+\infty} P_T(t)\,dt}{S\int_{-\infty}^{+\infty} P_i(t)\,dt} \qquad (2)$$

Equation (1) describes the typical and pure absorptive behaviour of a hypothetical third-order NLO process. The function $q(z)$ is defined by

$$q(r) = \int_0^{\infty}\int_0^{\infty} \alpha_2 I_i(r,t,z) L_{eff} r\,dr\,dt$$

where α_2 is the non-linear absorption coefficient of the cluster at 532 nm; $L_{eff} = [1-\exp(-\alpha_0 L)]/\alpha_0$, with α_0 being the linear absorption coefficient of the cluster and L being the sample thickness (1 mm in this study); $I_i(r,t,z) = \{I_0/[1+(z/z_0)^2]\}\exp[-2(r/\omega_0)^2-(t/t_0)^2]$ is the incident irradiance with $z_0 = \pi\omega_0^2/\lambda$ and $\omega^2 = \omega_0^2[1+(z/z_0)^2]$, where I_0 is the peak irradiance at focus, r is the radial coordinate, t is the time, t_0 is the pulse width, ω_0 is the spot radius of the laser beam at focus (40 μm in this study) and λ is the wavelength of the laser (532 nm). The peak irradiance used in the experiments are 85 MW cm^{-2} for **1** and 99 MW cm^{-2} for **2**.

It is obvious that the theoretical curves of the third-order NLO absorption reproduce well the general pattern of the observed experimental data (open circles). This suggests an effectively third-order characteristic for the experimentally detected NLO effects. The best fits of Eq. (1) to the open circles of Figs 2 and 3 give $\alpha_2 = 6\times10^{-10}$ m W^{-1} for **1** and $\alpha_2 = 8\times10^{-10}$ m W^{-1} for **2**.

Equation (2) describes the transmittance change detected behind a pinhole (0.5 mm radius) when both NLO absorptive and NLO refractive properties are considered.

$$P_i(t) = (1/2)I_0\pi\omega_0^2\exp[-(t/t_0)^2]$$

and

$$P_T(z,t) = \varepsilon_0 c n_0 \pi \int_0^{r_a} |E_a(r,t,z)|^2 r\,dr,$$

where ε_0 and c are the permittivity and speed of light in vacuum and n_0 is the linear refractive index of the sample. At the aperture, the electric component of the optical field is given by

$$E_a(r,t,z) = \{[2\pi/i\lambda(1-z)]\exp[i\pi r^2/\lambda(1-z)]\} \times \int_0^{\infty} \{r'E(r',t,z)J_0(2\pi r'r/\lambda(1-z)) \times \exp(i\pi r'^2/\lambda(1-z))\}dr'$$

in which 1 is the distance between the aperture and the focus,

$$E(r',t,z) = [2\sqrt{I(r',t,z)}/\varepsilon_0 c n_0] \times \exp\{(kn_2/\alpha_2)\ln[1+q(r',t,z)]\}$$

and $J_0(x)$ is the zeroth-order Bessel's function.

In the lower plots of Figs 2 and 3, the valley–peak pattern of the detected transmission behind the aperture indicates that the sign of the NLO refraction is positive, i.e. the materials have self-focusing capability. It is noted that the theoretical curves calculated from Eq. (2) can reproduce the qualitative trend of the experimental data represented by the filled circles in Figs 2 and 3, but significant deviation exists between the theoretical and experimental data for **1**. Since all of the even-order NLO effects are zero owing to the presence of a macroscopic inversion centre in the solutions, it seems plausible that higher odd-order NLO processes (such as fifth-order processes) are making significant contributions to the observed NLO refraction of **1**.

A control experiment shows that neither the photo damage of the quartz cells containing the solutions of **1** and **2**, nor the bubble formation in the solutions owing to local heating occurs to any detectable extent under the conditions used in this study. From the best

Table 1. Optical parameters of selected NLO chromophores

Compound	Conc. (M)	λ (nm)	α_2 (mW^{-1})	n_2 (m^2 W^{-1})	Ref.
GaInAs	Neat	1500		4.5×10^{-16}	12
AlGaAs	Neat	1560		2×10^{-17}	12
PTS	Neat	1600		1.5×10^{-16}	12
DAN	Neat	630		5×10^{-16}	12
$MoOS_3Cu_2(PPh_3)_3$	7.4×10^{-5}	532	2.6×10^{-10}	5×10^{-17}	7
$Mo_2S_8Ag_4(PPh_3)_4$	1.3×10^{-4}	532	1.3×10^{-9}	1.6×10^{-16}	13
$MoOS_3(CuNCS)_3^{2-}$	6.1×10^{-3}	532	1.1×10^{-10}	-2.3×10^{-16}	5
1	5.2×10^{-4} g cm^{-3}	532	6×10^{-10}		This work
2	2.6×10^{-4} g cm^{-3}	532	8×10^{-10}	1×10^{-16}	This work

fit of Eq. (2) to the filled circles of Fig. 3, one obtains a value of $n_2 = 1 \times 10^{-16}$ m^2 W^{-1} for **2**.

To put the optical non-linearities of the clusters **1** and **2** in a proper perspective with reference to other known third-order NLO materials, these effective α_2 and n_2 values are listed in Table 1 along with the reported α_2 and n_2 values of related inorganics clusters and a few best-performing semiconductors and organic polymers. Most of the well-performing third-order NLO materials reported in the literature are solid materials (e.g. semiconductors and conjugated polymers). These are neat materials. One notices from Table 1 that impressive optical non-linearity is achieved with much-diluted inorganic clusters. Since both α_2 and n_2 values are expected to be proportional to the concentration of the NLO chromophore, superior NLO performance can be expected if the solubilities of the inorganic clusters can be improved significantly. Currently, the upper limit of the concentration of these clusters, which are close to the concentrations quoted in Table 1, are set by their log solubility in common organic solvents.

REFERENCES

1. Chemla, D. S. and Zyss, J. (ed), *Nonlinear Optical Properties of Organic Molecules and Crystals.* Academic, Orlando, 1987.
2. Huang, H. (ed), *Optical Nonlinearities and Instabilities in Semiconductors.* Academic, Boston, 1988.
3. Shi, S., Ji, W., Tang, S. H., Lang, J. P. and Xin, X. Q., *J. Am. Chem. Soc.*, 1994, **116,** 3615.
4. Shi, S., Ji, W., Lang, J. P. and Xin, X. Q., *J. Phys. Chem.*, 1994, **98,** 3570.
5. Shi, S., Ji, W., Xie, W., Chong, T. C., Zeng, H. C., Lang, J. P. and Xin, X. Q., *Mater. Chem. Phys.*, 1995, **39,** 298.
6. How, H. W., Ye, X. R., Xin, X. Q., Liu, J., Chen, M. Q. and Shi, S., *Chem. Mater.*, 1995, **7,** 472.
7. Shi, S., Hou, H. W. and Xin, X. Q., *J. Phys. Chem.*, 1995, **99,** 4050.
8. Hou, H. W., Xin, X. Q., Liu, J., Chen, M. Q. and Shi, S., *J. Chem. Soc., Dalton Trans.*, 1994, 3211.
9. Du, S. W., Zhu, N. Y., Chen, P. C. and Wu, X. T., *J. Mol. Struct.*, 1993, **291,** 167.
10. Du, S. W. and Wu, X. T., *Acta Cryst.*, 1994, **C50,** 700.
11. Sheik-Bahae, M., Said, A. A., Wei, T. H., Hagan, D. J. and Van Stryland, E. W., *IEEE J. Quant. Electron*, 1990, **26,** 760.
12. Stegeman, G. I. and Torruellas, W., *Mat. Res. Soc. Symp. Proc.*, 1994, **328,** 397.
13. Ji, W., Shi, S., Du, H. J. and Xin, X. Q., *J. Phys. Chem.*, 1995, **99,** 894.

Pergamon

PII: S0277-5387(96)00354-3

Polyhedron Vol. 16, No. 6, pp. 949–961, 1997
Copyright © 1996 Elsevier Science Ltd
Printed in Great Britain. All rights reserved
0277-5387/97 $17.00+0.00

Metal–oxygen versus metal–sulfur bonding of the ambident monothiophosphinato ligand in some triphenylmetal(IV) derivatives, $Ph_3M[OSPR_2]$ (M = Ge, Sn, Pb). Crystal structures of $Ph_3Ge[O(S)PPh_2]$ and $[Ph_2Sn\{O(S)PPh_2\}(\mu\text{-}OH)]_2$

Anca Silvestru,[a] Cristian Silvestru,[a]* Ionel Haiduc,[a]* John E. Drake,[b]* Jincai Yang[b] and Francesco Caruso[c]

[a] Facultatea de Chimie, Universitatea Babes-Bolyai, R-3400 Cluj-Napoca, Romania

[b] Department of Chemistry and Biochemistry, University of Windsor, Windsor, Ontario, Canada, N9B 3P4

[c] Consiglio Nazionale delle Ricerche, Istituto di Strutturistica Chimica "G. Giacomello", I-00016 Monterotondo Stazione, Roma, Italy

(Received 7 May 1996; accepted 15 July 1996)

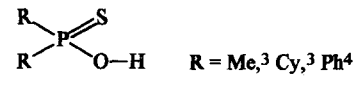
Abstract—Diorganomonothiophosphinato–triphenylmetal(IV) derivatives, $Ph_3M(OSPR_2)$ (M = Ge, Sn, Pb; R = Me, Et, Ph), were prepared and investigated. The IR and multinuclear (^1H, ^{13}C, ^{31}P) NMR spectra are discussed in relation to the M—O and/or M—S bonding of the ambident $OSPR_2^-$ ligand. The crystal and molecular structures of $Ph_3Ge[O(S)PPh_2]$ (**1**) and $[Ph_2Sn\{O(S)PPh_2\}(\mu\text{-}OH)]_2$ (**2**) were determined by X-ray diffractometry. The asymmetric unit for $Ph_3Ge[O(S)PPh_2]$ contains two independent molecules. The monothiophosphinato group is bonded to germanium only through oxygen (av. Ge—O 1.826, Ge···S 3.892 Å), leading to a tetrahedral coordination around the germanium atom. The crystal of $[Ph_2Sn\{O(S)PPh_2\}(\mu\text{-}OH)]_2$ consists of dimeric units built up through Sn—O—Sn bridges involving the oxygen atom of the hydroxy groups. The monothiophosphinato group is again monodentate [Sn(1)—O(1) 2.089(3), Sn(1)···S(1) (non-bonding) 4.164 Å] and the coordination geometry around tin is trigonal bipyramidal, with the O(1) atom of the phosphorous ligand and the O(2′) atom of a bridging hydroxy group in axial positions. Copyright © 1996 Elsevier Science Ltd

Keywords: monothiophosphinato ligand; organogermanium(IV); organotin(IV); organolead(IV) compounds.

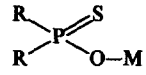
In contrast to the large amount of research work concerned with metal derivatives of dithiophosphorus ligands [1,2], there are comparatively few investigations of the related monothiophosphinates. In the free acids (**a**) the presence of O—H groups was established by X-ray diffractometry. The corresponding $[R_2PSO]^-$ anion is an ambident nucleophile and can exhibit primary coordination through either oxygen (**b**) or sulfur (**c**), depending on the "hard/soft" acid character of the metallic centre.

Thus, X-ray diffraction studies show that in $N(CH_2CH_2O)_3SiO(S)PPh_2$ [5] or $Me_3Sb[O(S)PPh_2]_2$ [6] the diphenylmonothiophosphinato ligand is attached to the metal only through oxygen, while in the gold complex $[(C_6F_5)_2Au\{S(O)PPh_2\}(CH_2PPh_2Me)$ [7] it is linked only through the sulfur atom. Moreover, this type of ligand not only could exhibit monometallic monoconnective (monodentate) coordination, but also could act in a monometallic biconnective (bidentate) fashion or in various bridging patterns (bi-

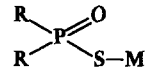
* Authors to whom correspondence should be addressed.



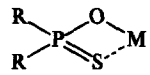
a



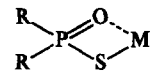
b



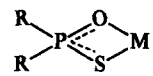
c



d



e



f

metallic biconnective or triconnective, trimetallic tetraconnective). Thus, anisobidentate coordination with primary bonds to oxygen (**d**) or to sulfur (**e**), or isobidentate coordination (**f**), is, in principle, possible. Secondary bonds [M···S in (**d**) and M···O in (**e**)] are longer than covalent bond lengths but shorter than van der Waals interatomic distances. Generally, with borderline Lewis acids, both oxygen and sulfur atoms of the $[R_2PSO]^-$ unit are involved in the coordination to the metallic centre (Table 1), as established by single-crystal X-ray diffraction studies. When such compounds are dissolved the crystal lattice is generally destroyed and the weak intra- or intermolecular chalcogen–metal interactions observed in the solid state are probably broken. In this case the magnitude of the ^{31}P NMR chemical shift is indicative of the coordination pattern of the $[R_2PSO]^-$ ligand, i.e. monodentate coordination with primary bonds through the oxygen or the sulfur atom, or a biconnective pattern involving both chalcogen atoms.

We now report the synthesis and spectroscopic characterization of triphenylmetal(IV) diorganomonothiophosphinates, $Ph_3M[OSPR_2]$ (M = Ge, Sn, Pb; R = Me, Et, Ph), and the crystal and molecular structures of $Ph_3Ge[O(S)PPh_2]$ and $[Ph_2Sn\{O(S)PPh_2\}(\mu\text{-}OH)]_2$.

EXPERIMENTAL

The starting materials were prepared according to literature methods: Ph_3GeCl [14], $Na[OSPMe_2]\cdot 1.5H_2O$, $Na[OSPEt_2]\cdot 3H_2O$[15], and $NH_4[OSPPh_2]$ [6,16]. Ph_3ECl (E = Sn, Pb) were commercial products. $Ph_3Sn[OSPEt_2]$ and $Ph_3Sn[OSPPh_2]$ were prepared as previously described [8,9]. Infrared spectra were run in the range 4000–400 cm^{-1} on a Perkin–Elmer 283B spectrometer, as KBr disks. ^1H, ^{13}C and ^{31}P NMR spectra were recorded on a Varian Gemini 300S instrument operating at 299.5, 75.4 and 121.4 MHz, respectively. The chemical shifts are reported in ppm relative to TMS and 85% H_3PO_4, respectively.

Preparation of the title compounds, $Ph_3M[OSPR_2]$ (Table 2)

A reaction mixture containing triphenylmetal chloride, Ph_3MCl, and the corresponding sodium or ammonium diorganomonothiophosphinate, $M^I[OSPR_2]\cdot nH_2O$ (excess was used for R = Me, Et) in 50 cm^3 organic solvent was stirred at room temperature for 8 h. The insoluble solid (the resulting M^ICl and the excess starting materials) was filtered off, the clear filtrate was dried over anhydrous Na_2SO_4 and then the solvent was evaporated to dryness in a rotary evaporator. The remaining solid product was recrystallized from organic solvents. When oily products were obtained (M = Ge, R = Me, Et), treatment with n-hexane led to the title compounds as white solids.

Crystal structure determinations

Colourless block crystals of $Ph_3Ge[O(S)PPh_2]$ (**1**) and $[Ph_2Sn\{O(S)PPh_2\}(\mu\text{-}OH)]_2$ (**2**) were mounted on glass fibres and sealed with epoxy glue. Data were collected on a Rigaku AFC6S diffractometer with graphite-monochromated Mo-K_α radiation, operating at 50 kV and 35 mA. Cell constants and an orientation matrix for data collection, obtained from 24 carefully centred reflections in the range $8.56 < 2\theta < 11.50°$ for **1** and $8.40 < 2\theta < 14.58°$ for **2** corresponded to a monoclinic and triclinic cell, respectively, whose dimensions are given in Table 3. The systematic absences ($h0l$, $l = 2n+1$; $0k0$, $k = 2n+1$) were observed for **1**. Based on statistical analyses of intensity distributions and the successful solution and refinement of the structure, the space group was determined to be $P-1$ for **2**.

The data were collected at a temperature of 23 ± 1°C using the ω–2θ scan technique to a maximum of 2θ value of 50.0°. The ω scans of several intense reflections, made prior to data collection, had an average width at half-height of 0.29° for compound **1** and 0.35° for **2**, with a take-off angle of 6.0°. Scans of $(1.37+0.30\tan\theta)°$ for **1** and $(1.68+0.30\tan\theta)°$ for **2**

Table 1. Single-crystal X-ray diffraction and ^{31}P NMR data (solution) for some metal monothiophosphinates

Compound	Single-crystal X-ray diffractometry data					$\delta(^{31}P)$ (ppm)	Ref.
	Molecular dimensions (Å)				Coordination pattern		
$N(CH_2CH_2O)_3SiO(S)PPh_2$	P—O	1.549(3)	Si—O	1.700(3)	monometallic	63.2[a]	[5]
	P—S	1.934(1)	Si···S	4.044[b,c]	monoconnective		
$Me_3Sb[O(S)PPh_2]_2$	P—O	1.55(1)[d]	Sb—O	2.111(5)[d]	monometallic	75.3[e]	[6]
	P—S	1.95(2)[d]	Sb···S	3.96(5)[c,d]	monoconnective		
$(C_6F_5)_2Au\{S(O)PPh_2\}(CH_2PPh_2Me)$	P—O	1.467(18)	Au···O	4.055[b,c]	monometallic	45.9[e]	[7]
	P—S	2.026(12)	Au—S	2.363(7)	monoconnective		
$Me_2Sn[O(S)PEt_2]_2$	P—O	1.57(4)[d]	Sn—O	2.06(8)[d]	monometallic		[8]
	P—S	1.98(1)[d]	Sn···S	3.29(17)[d,f]	biconnective		
$[Me_2Sn\{O(S)PPh_2\}_2]_n$	P(1)—O(1)	1.554(8)	Sn(1)—O(1)	2.041(8)	bimetallic		[9]
	P(1)—S(1)	1.984(4)	Sn(1)···S(1)	3.901(3)[f]	biconnective		
			Sn(1a)—S(1)	2.939(3)[g]			
	P(2)—O(2)	1.538(9)	Sn(1)—O(2)	2.081(8)	monometallic		
	P(2)—S(2)	1.957(5)	Sn(1)···S(2)	3.530(4)[f]	biconnective		
$[Me_3SnOSPMe_2]_n$	P—O(1)	1.505(7)	Sn(1)—O(1)	2.267(6)	bimetallic	76.6	[10]
	P—S(1)	1.997(3)	Sn(1)···S(1)	5.180[b,c]	biconnective		
			Sn(1a)—S(1)	2.737(3)			
$[Ph_2SbOSPPh_2]_n$	P—O(1)	1.504(3)	Sb—O(1)	2.299(3)	bimetallic	51.7[e,f]	[11]
	P—S(1)	2.010(3)	Sb···S(1)	4.524[b,c]	biconnective		
			Sb(1a)—S(1)	2.753(1)			
$[Me_2TlOSPPh_2]_n$	P—O(1)	1.487(7)	Tl(1)···O(1)	3.143(7)[g]	trimetallic	60.3[e]	[12]
	P—S(1)	1.994(3)	Tl(1)—S(1)	2.919(3)	tetraconnective		
			Tl(1a)—O(1)	2.509(7)[h]			
			Tl(1b)···S(1)	3.402(3)			

[a] In CD_3CN.
[b] Calculated from published atomic coordinates.
[c] Non-bonding distance.
[d] Averaged values; esds for average bond lengths are calculated from the equation $\sigma = \left\{\left[\sum_{i=1}^{i=N}(x_i-x)^2/(N-1)\right]\right\}^{1/2}$, where x_i is ith bond length and x is the mean of the n equivalent bond lengths [13].
[e] In $CDCl_3$.
[f] This work.
[g] Weak intramolecular metal–sulfur interaction.
[h] Intermolecular interaction.

were made at a speed of 32.0° min^{-1} (in ω). The weak reflections [$I < 10.0\sigma(I)$] were rescanned (maximum of four rescans) and the counts were accumulated to assure good counting statistics. Stationary background counts were recorded on each side of the reflection. The ratio of peak counting time to background counting time was 2:1. The diameter of the incident beam collimator was 1.0 mm, and the crystal to detector distance was 285.0 mm.

Of the 10,281 reflections for compound **1** and 4277 for **2** that were collected, 9971 and 4047, respectively, were unique (R_{int} = 0.153 and 0.061). The intensities of three representative reflections that were measured after every 150 reflections remained constant throughout data collection, indicating crystal and electronic stability (no decay correction was applied).

The linear absorption coefficient for Mo-K_α is 12.84 cm^{-1} for compound **1** and 12.88 cm^{-1} for **2**. An empirical absorption correction, based on azimuthal scans of several reflections was applied which resulted in transmission factors ranging from 0.76 to 1.00 for **1** and 0.64 to 1.00 for **2**. The data were corrected for Lorentz and polarization effects.

The structures were solved by direct methods [17]. The non-hydrogen atoms, other than carbon, were refined anisotropically. The hydrogen atom attached to oxygen in compound **2** was found from the Fourier map and its position then fixed. The hydrogen atoms attached to carbon were included in their idealized positions with C—H set at 0.95 Å. Their isotropic thermal parameters were set at 1.2 times that of the atom to which they were attached. The final cycle of full-matrix least-squares refinement [18] was based on 2677 observed reflections for **1** and 2967 for **2** [$I > 3.00\sigma(I)$] and 314 variable parameters for **1** and 262 for **2**.

The standard deviations of an observation of unit weight [19] were 1.97 and 1.53 for compounds **1** and

Table 2. Preparation of $Ph_3M[OSPR_2]$

Starting materials					
Ph_3MCl g (mmol)	$M^I[OSPR_2]\cdot nH_2O$ g (mmol)	Reaction solvent	Product [yield : g(%)]	M.p. (°C)	Recryst. solvent
Ph_3GeCl 1.13 (3.33)	$Na[OSPMe_2]\cdot 1.5H_2O$ 0.85 (5.35)	$CHCl_3$	$Ph_3Ge[OSPMe_2]$ 1.00 (75)	85–87	—
Ph_3GeCl 1.13 (3.33)	$Na[OSPEt_2]\cdot 3H_2O$ 1.14 (5.33)	$CHCl_3$	$Ph_3Ge[OSPEt_2]$ 1.00 (67)	55–57	$CHCl_3$
Ph_3GeCl 0.34(1.00)	$NH_4[OSPPh_2]$ 0.25 (1.00)	C_6H_6	$Ph_3Ge[OSPPh_2]$ 0.47 (87)	136–137	cyclohexane
Ph_3SnCl 0.84 (2.18)	$Na[OSPMe_2]\cdot 1.5H_2O$ 0.051 (3.27)	$CHCl_3$	$Ph_3Sn[OSPMe_2]$ 0.72 (72)	296	
Ph_3PbCl 0.95 (2.00)	$Na[OSPMe_2]\cdot 1.5H_2O$ 0.51 (3.20)	$CHCl_3$	$Ph_3Pb[OSPMe_2]$ 0.63 (57)	dec.	
Ph_3PbCl 0.95 (2.00)	$Na[OSPEt_2]\cdot 3H_2O$ 0.68 (3.18)	$CHCl_3$	$Ph_3Pb[OSPEt_2]$ 0.92 (80)	dec.	
Ph_3PbCl 0.48 (1.00)	$NH_4[OSPPh_2]$ 0.25 (1.00)	$CHCl_3$	$Ph_3Pb[OSPPh_2]$ 0.60 (89)	145–147	$CHCl_3$/hexane

Table 3. Crystal data and details of structure refinement for $Ph_3Ge[O(S)PPh_2]$ (**1**) and $[Ph_2Sn\{O(S)PPh_2\}(\mu\text{-}OH)]_2$ (**2**)

	1	**2**
Formula	$C_{30}H_{25}GeOPS$	$C_{48}H_{42}O_4P_2S_2Sn_2$
Crystal size (mm)	$0.42\times0.33\times0.24$	$0.31\times0.24\times0.23$
M	537.15	1046.30
Crystal system	Monoclinic	Triclinic
Space group	$P2_1/c$	$P\text{-}1$
a (Å)	19.515(8)	11.098(4)
b (Å)	14.990(7)	12.395(7)
c (Å)	20.889(7)	9.844(4)
α (°)		108.09(4)
β (°)	117.37(3)	92.49(4)
γ (°)		114.33(3)
V (Å^3)	5426(4)	1149(1)
Z	8	1
D_{calc} (g cm^{-3})	1.32	1.51
μ (Mo-K_α) (cm^{-1})	12.84	12.88
$F(000)$	2208.00	524.00
$R = \Sigma(\|F_o\|-\|F_c\|)/\Sigma\|F_o\|$	0.0549	0.032
$R' = [\Sigma w(\|F_o\|-\|F_c\|)^2/\Sigma wF_o^2]^{1/2}$	0.0347	0.0255
Goodness-of-fit, $S = [\Sigma(\|F_o\|-\|F_c\|)/\sigma]/(N_o\text{-}N_v)$	1.97	1.53

2, respectively. The weighting scheme was based on counting statistics and included a factor ($p = 0.004$ for **1** and 0.003 for **2**) to downweight the intense reflections. Plots of $\Sigma w(|F_o|-|F_c|)^2$ versus $|F_0|$, reflection order in data collection, $\sin\theta/\lambda$ and various classes of indices showed no unusual trends. The maximum and minimum peaks on the final difference Fourier map corresponded to 0.41 and -0.40 for **1** and 0.67 and -0.53 eÅ^{-3} for **2**.

Neutral-atom scattering factors were taken from Cromer and Waber [20]. Anomalous dispersion effects were included in F_c [21]; the values for Δf and $\Delta f'$ were those of Creagh and McAuley [22]. All calculations were performed using the TEXSAN [23] crystallographic software package.

Additional material available from the Cambridge Crystallographic Data Center comprises the final atomic coordinates of the non-hydrogen atoms, H-atom coordinates, thermal parameters and all of the bond lengths and angles. Structure factor tables are available from the authors.

RESULTS AND DISCUSSION

The title compounds were prepared as colourless, crystalline solids, by reacting the sodium or

ammonium salts of the diorganomonothiophosphinate with the appropriate triphenylmetal(IV) chloride, in chloroform or benzene, according to Eq. (1):

$$Ph_3MCl + M^I[OSPR_2]\cdot nH_2O \rightarrow Ph_3M[OSPR_2] + M^ICl + nH_2O$$

$$M = Ge, Sn, Pb; \quad M^I = Na; \quad R = Me, Et$$

$$M^I = NH_4; \quad R = Ph \qquad (1)$$

The triphenylgermanium(IV) and triphenyltin(IV) derivatives are stable compounds and can be stored in the solid state in the absence of air and moisture for months. An old sample of $Ph_3Sn[O(S)PPh_2]$ stored for years in a sealed flask showed no sign of decomposition as proved by NMR analysis. In contrast, the triphenyllead(IV) monothiophosphinates are quite unstable. Thus, for R = Me and Et, the solid compounds become grey in about 24 h.

In solution, however, the stability of the title tin and lead compounds is lower. Thus, a $CHCl_3$ solution of $Ph_3Pb[OSPPh_2]$ kept in the refrigerator turned orange and a red solid product deposited within days. Attempts to grow crystals of $Ph_3Sn[OSPR_2]$ for X-ray diffractometry investigations have failed, and only for R = Ph were some crystals separated that proved (NMR data, X-ray diffractometry) to be the unexpected hydroxo-bridged diphenyltin(IV) dimer, $[Ph_2Sn\{O(S)PPh_2\}(\mu\text{-}OH)]_2$. Indeed the magnitude of $^3J_{SnH}$ [^{1}H NMR ($CDCl_3$): δ 7.3 (m, P-C_6H_5, Sn-C_6H_5, *−meta+para*), 7.66 (dd, $^3J_{HH}$ 7.7, $^4J_{HH}$ 1.2, $^3J_{SnH}$ 85.9 Hz, Sn-C_6H_5, *−ortho*), 7.80 (ddd, $^3J_{HH}$ 7.6, $^4J_{HH}$ 1.4, $^3J_{PH}$ 13.5 Hz, P-C_6H_5, *−ortho*)] and of $^2J_{SnC}$ and $^3J_{SnC}$ [^{13}C NMR ($CDCl_3$): δ 127.96 (d, $^3J_{PC}$ 12.8 Hz, P-C_m), 128.79 (s, $^3J_{SnC}$ 94.9 Hz, Sn-C_m), 130.43 (s, P-C_p), 130.67 (s, Sn-C_p), 130.75 (d, $^2J_{PC}$ 11.0 Hz, P-C_0), 135.84 (s, $^2J_{SnC}$ 65.0 Hz, Sn-C_0). 138.48 (d, $^1J_{PC}$ 106.7 Hz, P-C_i)], 139.19 (s, Sn-C_i) are consistent with the presence of only two phenyl groups attached to tin (*cf.* ^{13}C NMR data for PH_2SnCl_2 ;$^2J_{SnC}$ 63, $^3J_{SnC}$ 90Hz, and for Ph_3SnCl: $^2J_{SnC}$ 49, $^3J_{SnC}$ 68 Hz) [24]. Moreover, the ^{31}P resonance of the hydroxo-bridged diphenyltin(IV) derivative was found to be surrounded by satellites due to phosphorous–tin coupling [^{31}P NMR ($CDCl_3$): δ 68.1 (s, $^2J_{PSn}$ 126.0 Hz)], a pattern that was not observed for the $Ph_3Sn[OSPR_2]$ compounds. The same hydroxobridged derivative was obtained upon attempted monocrystal growth of $Ph_2Sn[OSPPh_2]_2$, described previously [9]. This is in line with a previous report that bis(diorganomonothiophosphinato)diorganotin(IV) derivatives, $R_2Sn[OSP(OR')_2]_2$, are sensitive to atmospheric moisture and a monothiophosphinato group is readily hydrolysed to give $[R_2Sn\{O(S)P(OR')_2\}(\mu\text{-}OH)]_2$ or $[R_2Sn\{O(S)P(OR')_2\})_2O]_2$, depending on the nature of the R groups on the tin or phosphorous atoms [25, 26]. In our case the same compound was formed both by hydrolytic splitting of a phenyl group from $Ph_3Sn[OSPPh_2]$ or a monothiophosphinato group from $Ph_2Sn[OSPPh_2]_2$. Crystal samples of both origins were subjected to complete X-ray diffraction analysis in two different, independent laboratories (by J.E.D. and F.C.) and the results were practically identical. The data reported here are for the sample obtained from $Ph_3Sn[OSPPh_2]$ (J.E.D.'s laboratory).

The compounds were investigated by IR and multinuclear NMR spectroscopy and the crystal and molecular structure of $Ph_3Ge[O(S)PPh_2]$ and $[Ph_2Sn\{O(S)PPh_2\}(\mu\text{-}OH)]_2$ were determined by X-ray diffractometry.

Infrared spectra

The analysis of the infrared spectra was focused on the ν(PO) and ν(PS) stretching vibrations that proved to be a useful tool in establishing the coordination pattern of the monothiophosphinato ligand. The IR data for the present compounds are listed in Table 4, and compared with data for the corresponding O- and S-alkyl esters of the monothiophosphinic acids and their sodium or ammonium salts.

The infrared spectra of the O—R′ esters, $R_2P(S)OR'$, exhibit medium to very strong absorption bands in the regions of 1040–990 cm^{-1} and 590–580 cm^{-1} (R = Me, Et) or 630 cm^{-1} (R = Ph) which were assigned to single bond P—O(R) and double bond P=S stretching vibrations. For the S—R′ esters, $R_2P(O)SR'$, the absorption bands corresponding to the double bond P=O and single bond P—S(R) stretching vibrations are shifted, as expected, to higher (1200–1180 cm^{-1}) and lower [520–510 cm^{-1} (R = Me, Et) or 570 cm^{-1} (R = Ph)] wavenumbers, respectively. The infrared spectra of the sodium or ammonium salts exhibit absorption bands at intermediate values between those observed for the O—R′ and S—R′ esters, corresponding to a delocalization of the π electrons over the PSO fragment.

All triphenylgermanium(IV) derivatives exhibit medium to strong bonds at about 906 and 660–620 cm^{-1} which clearly indicate the coordination of the monothiophosphinato ligand only through the oxygen atom. Therefore, it is reasonable to propose a monomeric structure (**g**) for $Ph_3Ge[O(S)PR_2]$ in the solid state. In contrast, for triphenyltin(IV) and -lead(IV) analogues the positions of the bands assigned to the phosphorus–oxygen and phosphorous–sulfur stretching vibrations (Table 4) suggest bidentate behaviour of the monothiophosphinato ligand, i.e. coordination through both oxygen and sulfur atoms, thus leading to an increase of the coordination number of the central metal atom from four to five. As a result either monomeric **h** or polymeric **i** structures might be considered for $\{Ph_3M[OSPR_2]\}_n$ (M = Sn, Pb) in the solid state. In this case, on the basis of infrared data it is impossible to distinguish between isobidentate and anisobidentate coordination, and to assign a primary coordination of

Table 4. Infrared data for $Ph_3M[OSPR_2]$ derivatives and related compounds

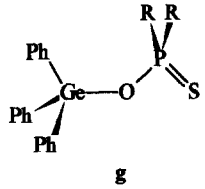
Compound	ν(P—O)	ν(P···O)	ν(P=O)	ν(P—S)	ν(P···S)	ν(P=S)	Ref
$Me_2P(S)OMe$	1038					581	[27]
$Me_2P(O)SMe$			1184	510			[27]
Me_2PSONa		1075vs			562s		[28]
$Ph_3GeOSPMe_2$	960vs					617vs	This work
$Ph_3SnOSPMe_2$		1080vs			545s		This work
$Ph_3PbOSPMe_2$		1110vs			535vs		This work
$Et_2P(S)OPr^n$	990s					580m	[29]
$Et_2P(O)SPr^n$			1180s	520m			[29]
Et_2PSONa		1084vs			553ms		[28]
$Ph_3GeOSPEt_2$	965s					622m	This work
$Ph_3SnOSPEt_2$		1100s			535m		This work
$Ph_3PbOSPEt_2$		1100vs			530m		This work
$Ph_2P(S)OMe$	1027vs					635s	[30]
$Ph_2P(O)SMe$			1200vs	568vs			[30]
Ph_2PSONH_4		1045s			628vs		[31]
		1051s					
$Ph_3GeOSPPh_2$	965vs					660m	This work
$Ph_3SnOSPPh_2$		1063s			595s		This work
$Ph_3PbOSPPh_2$		1055s			590s		This work

the monothiophosphinato ligand through oxygen or sulfur respectively. Single-crystal X-ray diffractometry investigations have confirmed a structure of type **g** for $Ph_3Ge[O(S)PPh_2]$(see below) and of type **i** for the $\{Me_3Sn[OSPMe_2]\}_n$ analogue [10].

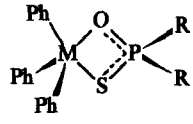
NMR spectra

All of the triphenylmetal(IV) derivatives were investigated in solution by multinuclear NMR spectroscopy. Their ^1H NMR spectra (Table 5) exhibit two sets of resonances corresponding to the organic groups attached to phosphorous and metal atoms, respectively. For the protons of the diorganomonothiophosphinato ligands only one resonance with the expected splitting pattern owing to the proton–proton and phosphorous–proton couplings was observed for the P-C*H*$_3$ (doublet), P-C*H*$_2$-C*H*$_3$ (doublet of triplets), P-C*H*$_2$-CH$_3$ (doublet of quartets), P-C_6H_5 (*ortho*-H, doublet of multiplets), respectively. This indicates the equivalence of the organic groups attached to the same phosphorous atom on the NMR time-scale. The phenyl groups attached to the metal atom exhibit two multiplet resonances for the *ortho* and *meta*+*para* protons. In the case of Ph_3Sn^{IV} and Ph_3Pb^{IV} derivatives the resonance of the *ortho* protons is surrounded by satellites caused by the tin–proton and lead–proton couplings, with the expected magnitude of the ^3J(SnH) (*ca*, 60 Hz) and $^3J(^{207}PbH)$ (*ca* 105 Hz) coupling constants.

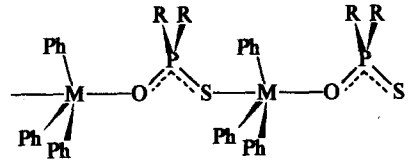
The ^{13}C NMR spectra (Table 6) show the expected downfield resonances for the carbon atoms of the phenyl groups attached to the metal. For the tin and lead derivatives the signals for the *ortho* and *meta* carbons are surrounded by satellites due to the metal–carbon couplings, with a magnitude of the ^2J(MC)



g



h



i

Table 5. ^1H NMR data for $Ph_3M[OSPR_2]$ derivatives

	Ph_3M			PEt		PPh	
Compound	*ortho*	*meta+para*	PMe	CH_2	CH_3	*ortho*	*meta+para*
$Ph_3GeOSPMe_2$	7.74dd $^3J_{HH}$ 7.6 $^4J_{HH}$ 2.0	7.48m	1.74d $^2J_{PH}$ 13.2				
$Ph_3SnOSPMe_2$	7.77dd $^3J_{HH}$ 6.4 $^4J_{HH}$ 2.8 $^3J_{SnH}$ 61.8	7.44s,br	1.67d $^2J_{PH}$ 13.2				
$Ph_3PbOSPMe_2$	7.82d $^3J_{HH}$ 7.1 $^3J_{PbH}$ 106.0	7.54dd (*meta*) $^3J_{HH}$ 7.5 7.41t (*para*) $^3J_{HH}$ 7.5	1.63d $^2J_{PH}$ 13.1				
$Ph_3GeOSPEt_2$	7.73dd $^3J_{HH}$ 7.7 $^4J_{HH}$ 1.8	7.46m		1.84dq $^2J_{PH}$ 12.5 $^3J_{HH}$ 7.4	1.09dt $^3J_{PH}$ 19.7 $^3J_{HH}$ 7.4		
$Ph_3SnOSPEt_2$	7.80d $^3J_{HH}$ 6.0 $^3J_{SnH}$ 57.8	7.45m		1.82dq $^2J_{PH}$ 12.0 $^3J_{HH}$ 7.7	1.07dt $^3J_{PH}$ 19.5 $^3J_{HH}$ 7.7		
$Ph_3PbOSPEt_2$	7.86d $^3J_{HH}$ 6.8 $^3J_{PbH}$ 104.9	7.51dd (*meta*) $^3J_{HH}$ 7.1 7.40t (*para*) $^3J_{HH}$ 7.1		1.79dq $^2J_{PH}$ 11.8 $^3J_{HH}$ 7.6	1.07dt $^3J_{PH}$ 19.3 $^3J_{HH}$ 7.6		
$Ph_3GeOSPPh_2$	7.66dd $^3J_{HH}$ 7.7 $^4J_{HH}$ 1.8	7.37m[a]				7.81ddd $^3J_{PH}$ 13.7 $^3J_{HH}$ 8.0 $^4J_{HH}$ 1.6	7.37m[a]
$Ph_3SnOSPPh_2$	7.65d $^3J_{HH}$ 6.7 $^3J_{SnH}$ 54.7	7.29m[a]				7.70dd $^3J_{PH}$ 13.4 $^3J_{HH}$ 7.4	7.29m[a]
$Ph_3PbOSPPh_2$	7.77d $^3J_{HH}$ 7.1 $^3J_{PbH}$ 105.6	7.38m[a]				7.72dd $^3J_{PH}$ 13.1 $^3J_{HH}$ 7.3	7.38m[a]–

[a] Resonances for M—Ph and P—Ph overlapped.

and $^3J(MC)$ corresponding to a triphenylmetal moiety. No resonances suggesting the presence of a Ph_2Sn derivative were observed in the spectrum of $Ph_3Sn[OSPPh_2]$. Regardless of the nature of the metal atom in the Ph_3M moiety, the ^{13}C NMR spectra show only one set of signals for each carbon atom of the $OSPR_2$ ligand, thus indicating the equivalence of the organic groups attached to the same phosphorous atom on the NMR time-scale. These resonances exhibit the expected doublet pattern caused by the phosphorous–carbon couplings.

For all (diorganomonothiophosphinato)triphenylmetal(IV) the ^{31}P NMR spectra are seen as singlets. The magnitude of ^{31}P chemical shift of diorganomonothiophosphinic acid derivatives can be used to distinguish between the $R_2P(=S)O$—, $R_2P(=O)S$— or $[R_2PSO]$ structure of the coordinated ligands. Thus, the resonance for the S ester is shifted about 40–60 ppm to higher field, as expected, compared with the signal observed for the free acid (which contains an O—H group) and its O—Me ester, for the same R group attached to phosphorous. The resonances for the corresponding sodium or ammonium salts have intermediate values between these two extremes. A comparison of the ^{31}P chemical shifts of the Ph_3M derivatives with those of the free acids, their O— and S—Me esters and their sodium or ammonium salts is given in Table 7 and reveals interesting results. Thus, for all Ph_3Ge^{IV} derivatives the ^{31}P chemical shift is of the same magnitude as observed for the corresponding free acid or its O—Me ester. This behaviour is consistent with monodentate coordination of the monothiophosphinato moiety only through its oxygen atom, structure **g** found in the solid state for $Ph_3Ge[O(S)PPh_2]$ and indicated by the IR spectra, being also preserved in solution.

For the Ph_3M^{IV} (M = Sn, Pb) derivatives, with one exception, the ^{31}P chemical shift has an intermediate magnitude between those observed for the O— and S—Me esters of the corresponding monothiophosphinic acid. Taking into account the presence of only one set of ^1H and ^{13}C resonances, respectively,

Table 6. ^{13}C NMR data for $Ph_3M[OSPR_2]$ derivatives

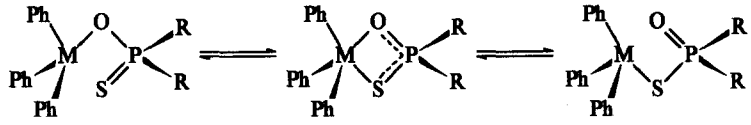
Compound	Ph_3M				PMe	PEt		PPh			
	C_i	C_o	C_m	C_p		CH_2	CH_3	C_i	C_o	C_m	C_p
$Ph_3GeOSPMe_2$	134.43s	134.76s	128.63s	130.74s	26.43d						
					$^1J_{PC}$ 74.2						
$Ph_3SnOSPMe_2$	139.05s	136.92s	130.02s	128.89s	25.43d						
		$^2J_{SnC}$ 47.8	$^3J_{SnC}$ 62.2		$^1J_{PC}$ 71.8						
$Ph_3PbOSPMe_2$	150.09s	137.10s	130.18s	129.53s	25.28d						
		$^2J_{PbC}$ 89.3	$^3J_{PbC}$ 103.0		$^1J_{PC}$ 71.2						
$Ph_3GeOSPEt_2$	134.44s	134.82s	128.54s	130.62s		28.93d	7.31d				
						$^1J_{PC}$ 71.5	$^2J_{PC}$ 4.3				
$Ph_3SnOSPEt_2$	139.05s	137.02s	128.83s	129.93s		28.36d	6.86d				
		$^2J_{SnC}$ 47.6	$^3J_{SnC}$ 62.5			$^1J_{PC}$ 68.4	$^2J_{PC}$ 4.6				
$Ph_3PbOSPEt_2$	155.57s	137.27s	129.96s	129.39s		28.36d	6.88d				
		$^2J_{PbC}$ 85.6	$^2J_{PbC}$ 101.0			$^1J_{PC}$ 67.5	$^2J_{PC}$ 4.6				
$Ph_3GeOSPPh_2$	128.64s	129.72s	123.40s	125.46s				132.98d	125.80d	123.02d	125.82d
								$^1J_{PC}$ 110.2	$^2J_{PC}$ 11.4	$^3J_{PC}$ 13.5	$^4J_{PC}$ 3.3
$Ph_3SnOSPPh_2$	137.92s	136.76s	128.79s	130.05s				137.96d	130.71d	127.98d	130.79s
		$^2J_{SnC}$ 48.7	$^3J_{SnC}$ 63.8					$^1J_{PC}$ 109.0	$^2J_{PC}$ 11.6	$^3J_{PC}$ 13.9	
$Ph_3PbOSPPh_2$	155.35s	137.13s	130.06s	129.49s				138.38d	130.77d	128.09d	130.85s
		$^2J_{PbC}$ 86.0	$^3J_{PbC}$ 101.5					$^1J_{PC}$ 112.6	$^2J_{PC}$ 10.8	$^3J_{PC}$ 12.9	

Table 7. ^{31}P NMR data for $Ph_3M[OSPR_2]$ derivatives and related compounds

Compound	δ[P(=S)O]	δ[PSO]	δ[P(=O)S]	Ref
$Me_2P(S)OH$	87.9[a]			[32]
$Me_2P(S)OMe$	94.3[a]			[32]
$Me_2P(O)SMe$			45.9	[33]
Me_2PSONa		63.9[b,c]		This work
$Ph_3GeO(S)PMe_2$	84.3[a]			This work
$Ph_3SnOSPMe_2$		68.1br[a]		This work
$Ph_3PbOSPMe_2$		55.6[a]		This work
$Et_2P(S)OH$	99.7[d]			[32]
$Et_2P(S)OMe$	108.8[a]			[34]
$Et_2P(O)SMe$			58.6	[33]
Et_2PSONa[b]		77.9[c,e]		This work
$Ph_3GeO(S)PEt_2$	98.4[a]			This work
$Ph_3SnOSPEt_2$		83.2[a]		This work
$Ph_3PbOSPEt_2$		71.2[a]		This work
$Ph_2P(S)OH$	76.0[a]			This work
$Ph_2P(S)OMe$	83.5			[33]
$Ph_2P(O)SMe$			42.8	[33]
Ph_2PSONH_4		58.1[b]		This work
$Ph_3GeO(S)PPh_2$	71.9[a]			This work
$Ph_3SnOSPPh_2$		64.9[a]		This work
$Ph_3PbS(O)PPh_2$			48.1[a]	This work

[a] In $CDCl_3$.
[b] In CD_3OD.
[c] $\delta = 62.4$ in CD_3OD [32].
[d] In CD_3COCD_3.
[e] $\delta = 67.7$ in CD_3COCD_3 [32].

for both organic groups attached to phosphorous, this suggests that the ligand coordinates to the metallic centre through both chalcogen atoms and has fluxional behaviour in solution according to the following scheme:



In contrast, for M = Pb, R = Ph the ^{31}P chemical shift displays a value of δ 48.1, which compares very well with that of the S—Me ester, $Ph_2P(=O)SMe$ (*cf.* δ 42.8). This indicates that the structural formulation of this compound in solution should be $Ph_3PbS(O)PPh_2$, with a monodentate ligand attached to lead only through the sulfur atom.

On the basis of the above data we conclude that ^{31}P NMR can distinguish not only between the monodentate and bidentate coordination pattern of the monothiophosphinato ligands, but also between the $R_2P(=S)O$— or $R_2P(=O)S$— nature in the former situation. In addition, these data confirm the versatility of the monothiophosphinato ligand, i.e. its capacity to coordinate through oxygen to a "hard" metallic centre, to involve both chalcogen atoms, or to coordinate only through the sulphur atoms to a "soft" metallic centre.

Crystal and molecular structure of $Ph_3Ge[O(S)PPh_2]$

The solid state structure of $Ph_3Ge[O(S)PPh_2]$ was determined by single-crystal X-ray diffractometry. The asymmetric unit contains two, very similar, independent monomeric molecules, which are separated by normal van der Waals distances. Selected bond distances and angles for both molecules **1a** and **1b** are listed in Table 8, but in the subsequent discussion we will refer only to molecule **1a** (Fig. 1) (the same considerations can be used to describe molecule **1b**).

The monothiophosphinato ligand is coordinated through the oxygen atom in a clearly monodentate pattern. The phosphorous–oxygen and phosphorous–sulphur bond distances are characteristic for single P—O [1.563(7) Å] and double P=S [1.931(5) Å] bonds [*cf.* 1.582(2) and 1.956(1) Å in the free $Ph_2P(S)OH$ acid, [35] or 1.60(2) and 1.936(6) Å in its O—Me ester, $Ph_2P(S)OMe$ [36]. The tetrahedral geometry around the phosphorous atoms in both ligands is distorted with an O(1)—P(1)—S(1) angle [116.7(3)°] of the same magnitude as in the free $Ph_2P(S)OH$ acid [O—P—S 115.4(1)°] [35].

Table 8. Relevant interatomic distances (Å) and bond angles (°) for $Ph_3Ge[O(S)PPh_2]$ (**1**)

	Molecule (**1a**)		Molecule (**1b**)	
Ge(1)—O(1)	1.825(7)	Ge(2)—O(2)	1.826(8)	
Ge(1)—C(1)	1.91(1)	Ge(2)—C(31)	1.90(1)	
Ge(1)—C(7)	1.93(1)	Ge(2)—C(37)	1.91(1)	
Ge(1)—C(13)	1.92(1)	Ge(2)—C(43)	1.93(1)	
Ge(1)···S(1)	3.843(4)	Ge(2)···S(2)	3.940(4)	
P(1)—O(1)	1.563(7)	P(2)—O(2)	1.562(8)	
P(1)—S(1)	1.931(5)	P(2)—S(2)	1.920(5)	
P(1)—C(19)	1.79(1)	P(2)—C(49)	1.80(1)	
P(1)—C(25)	1.79(1)	P(2)—C(55)	1.78(1)	
O(1)—Ge(1)—C(1)	112.4(4)	O(2)—Ge(2)—C(31)	112.4(4]	
O(1)—Ge(1)—C(7)	102.5(4)	O(2)—Ge(2)—C(37)	102.5(4)	
O(1)—Ge(1)—C(13)	103.6(4)	O(2)—Ge(2)—C(43)	101.7(4)	
C(1)—Ge(1)—C(7)	111.2(6)	C(31)—Ge(2)—C(37)	113.6(6)	
C(1)—Ge(1)—C(13)	114.8(5)	C(31)—Ge(2)—C(43)	113.4(5)	
C(7)—Ge(1)—C(13)	111.5(5)	C(37)—Ge(2)—C(43)	112.2(5)	
Ge(1)—O(1)—P(1)	132.2(5)	Ge(2)—O(2)—P(2)	132.6(5)	
O(1)—P(1)—S(1)	116.7(3)	O(2)—P(2)—S(2)	116.8(4)	
O(1)—P(1)—C(19)	104.6(5)	O(2)—P(2)—C(49)	102.7(5)	
O(1)—P(1)—C(25)	101.2(6)	O(2)—P(2)—C(55)	105.4(6)	
S(1)—P(1)—C(19)	114.2(5)	S(2)—P(2)—C(49)	113.5(5)	
S(1)—P(1)—C(25)	114.3(5)	S(2)—P(2)—C(55)	113.5(5)	
C(19)—P(1)—C(25)	104.2(6)	C(49)—P(2)—C(55)	103.5(6)	

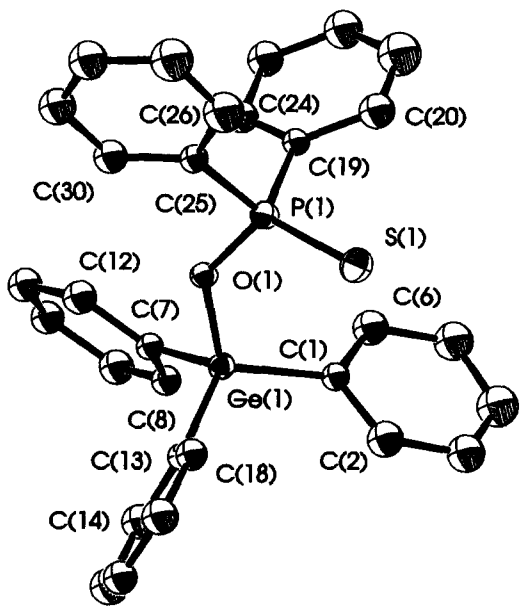


Fig. 1. ORTEP plot of the molecule $Ph_3Ge[O(S)PPh_2]$ (**1a**).

The Ge(1)—O(1) bond length is slightly longer [1.825(7) Å] than in $(Ph_3Ge)_2O$ [average 1.77(5) Å] [37], and close to the sum of the covalent radii of Ge and O, Σ_{cov}(Ge, O) = 1.95 [38]. The Ge(1)—O(1)—P(1) angle of 132.2(5)° is slightly less than the Ge—O—Ge angle of 135.7(7)° in $(Ph_3Ge)_2O$ [37]. The relative position of the sulfur atom double bonded to phosphorous with respect to the germanium atom is similar to that observed in the dithiophosphinato analogues, $Ph_3Ge[S(S)PR_2]$ (R = Me, Ph) [39], i.e. the monothiophosphorus ligand is twisted to bring the non-bonded sulfur atom much closer to the germanium atom, thus leading to a *syn* conformation of the Ge—O—P=S fragment. This situation contrasts to that observed in the dithiophosphinato derivative, $Ph_3GeS(S)P(OMe)_2$, for which the non-bonded sulfur atom is twisted as far as possible from the germanium atom (Ge···S 5.253 Å) [40]. The magnitude of the germanium-sulfur distances [Ge(1)···S(1) 3.843(4) and Ge(2)···S(2) 3.940(4) Å in molecules **1a** and **1b**, respectively] is in the range of van der Waals distances and too large to suggest any significant secondary interaction between these atoms.

The distortion from tetrahedral angles around Ge is not large but all C—Ge—C angles are greater than those for all tetrahedral angles (Table 8). In each independent molecule two O—Ge—C angles are well below all tetrahedral angles, while the third one is of the same value as the C—Ge—C angles. In comparison, the tetrahedral distortion is slightly less for the two germanium centres in $(Ph_3Ge)_2O$ [37], with the average C—Ge—C angle still larger than that for all tetrahedral angles at 111.4°, but only one O—Ge—C

angle in each half of the molecule significantly less, at 101.9(7) and 103.5(7)°. The above is essentially as expected from Bent's rule [41], which seems to operate well for germanium compounds; according to this rule "more electronegative substituents 'prefer' hybrid orbitals having less *s* character, and more electropositive substituents 'prefer' those having more *s* character". Alteratively, the distortion of the tetrahedral coordination polyhedron at germanium might be owing to the spatial requirements of the phenyl groups attached to germanium and of the non-bonded sulfur atom.

Crystal and molecular structure of $[Ph_2Sn\{O(S)PPh_2\}(\mu\text{-}OH)]_2$

The solid state structure of $[Ph_2Sn\{O(S)PPh_2\}(\mu\text{-}OH)]_2$ was also determined by single-crystal X-ray diffractometry. Selected bond distances and angles are listed in Table 9. Figure 2 shows the ORTEP view of the molecular structure, with the atom-numbering scheme.

The monothiophosphinato ligand is monodentate and linked to tin through the oxygen atom. The tin–sulfur interatomic distance is 4.164 Å, significantly longer than the sum of van der Waals radii of the corresponding atoms, $\Sigma_{vdW}(Sn, S) = 4.0$ Å [38]. As a result, each tin atom is five coordinated, in a distorted trigonal bipyramidal geometry (Fig. 3). The axial positions are occupied by the O(1) atom of the monothiophosphinato ligand and the O(2′) hydroxo oxygen

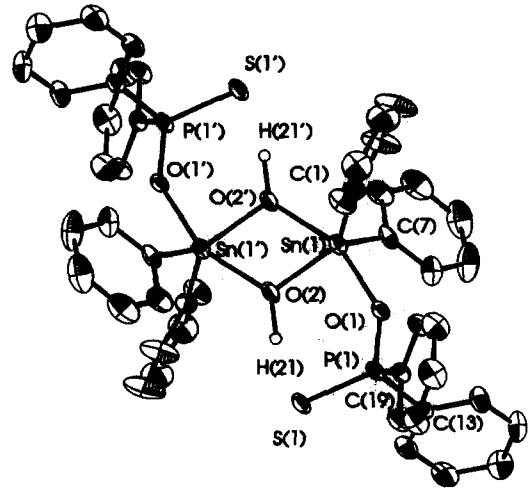


Fig. 2. ORTEP plot of the molecule $[Ph_2Sn\{O(S)PPh_2\}(\mu\text{-}OH)]_2$ (**2**) (the atoms are drawn with 30% probability ellipsoids and hydrogen atoms are omitted for clarity).

of the other molecular unit of the dimer, with an O(1)—Sn(1)—O(2′) angle of 156.76°, which reflects the distortion of the coordination polyhedron. The equatorial bond angles at tin range between 117.0 and 121.8°, and the O(2)Sn(1)C(1)C(7) system is basically planar [the deviations from the best equatorial plane are: Sn(1) −0.079, O(2) 0.028, C(1) 0.025, C(7) 0.026 Å]. The four-membered Sn_2O_2 ring is planar. The O(1)P(1)S(1) and O(1′)P(1′)S(1′) fragments are almost coplanar with the Sn_2O_2 system, being sym-

Table 9. Relevant interatomic distances (Å) and bond angles (°) for $[Ph_2Sn\{O(S)PPh_2\}(OH)]_2$ (**2**)[a]

Sn(1)—O(1)	2.089(3)	P(1)—O(1)	1.548(3)
Sn(1)—O(2)	2.024(3)	P(1)—S(1)	1.972(2)
Sn(1)—O(2′)	2.174(3)	P(1)—C(13)	1.807(4)
Sn(1)···S(1)[b]	4.164	P(1)—C(19)	1.799(4)
Sn(1)—C(1)	2.116(4)	O(1)···S(1)[b]	2.993
Sn(1)—C(7)	2.122(4)	O(2)—H(21)	1.15
		S(1)···H(21)	1.96
O(1)—Sn(1)—O(2)	86.8(1)	O(2′)—Sn(1)—O(2)	70.0(1)
O(1)—Sn(1)—C(1)	96.0(1)	O(2′)—Sn(1)—C(1)	97.1(2)
O(1)—Sn(1)—C(7)	96.0(2)	O(2′)—Sn(1)—C(7)	95.1(2)
O(1)—Sn(1)—O(2′)	156.76(9)	C(1)—Sn(1)—C(7)	117.0(2)
		O(2)—Sn(1)—C(1)	120.5(2)
		O(2)—Sn(1)—C(7)	121.8(1)
Sn(1)—O(1)—P(1)	145.0(2)	Sn(1)—O(2)—H(21)	118.6
Sn(1)—O(2)—Sn(1′)	110.0(1)	Sn(1′)—O(2)—H(21)	130.0
O(1)—P(1)—S(1)	116.0(1)	S(1)—P(1)—C(13)	111.4(1)
O(1)—P(1)—C(13)	106.4(2)	S(1)—P(1)—C(19)	110.4(1)
O(1)—P(1)—C(19)	106.0(2)	C(13)—P(1)—C(19)	106.1(2)
O(2)—H(21)···S(1)	157.3		

[a] Symmetry equivalent position $(1-x, 1-y, -z)$ is denoted by prime.
[b] Non-bonding distance.

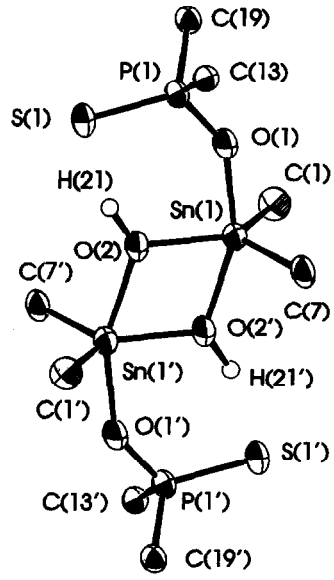


Fig. 3. ORTEP plot of the core of the molecule $[Ph_2Sn\{O(S)PPh_2\}(\mu\text{-}OH)]_2$ (**2**) showing the trigonal bipyramidal coordination around tin (the atoms are drawn with 50% probability ellipsoids and the phenyl rings, except for the carbon atoms attached to tin and phosphorous, are omitted for clarity).

metrically displaced on each side of the Sn_2O_2 plane [the deviations from the best Sn(1)O(2)Sn(1')O(2') plane are: O(1) −0.057, P(1) −0.028, S(1) −0.028 Å]. The equatorial planes at both tin atoms are almost perpendicular to the Sn_2O_2 ring ($OSnC_2/Sn_2O_2$ dihedral angle 88.6°).

The monodentate character of the ligand is supported by the phosphorus–chalcogen distances [P(1)—O(1) 1.548(3), P(1)—S(1) 1.972(2) Å; for comparison see the above discussion of the molecular structure of the germanium compound]. The hydrogen bond interactions between the sulfur and hydroxo oxygen atoms within each molecular unit might account for the slightly longer phosphorus–sulfur bond distance. A similar hydrogen bond interaction was observed for the monothiophosphinato analogue, $[Ph_2Sn\{O(S)OPh_2\}(\mu\text{-}OH)]_2$ [25], where the sulfur and hydroxo oxygen atoms within each molecular unit are brought together at 3.121 Å, compared with 3.050 Å in the present compound.

Acknowledgements—We are grateful to the companies Hoechst and Schering A.G. for gifts of triphenyltin chloride used as starting material. This work was partially supported by the National Council for Academic Research, Bucharest, under Grant Nos 4010-B16, B21/1995.

REFERENCES

1. Haiduc, I., Sowerby, D. B. and Lu, S.-F., *Polyhedron*, 1995, **14,** 3389.
2. Mehrotra, R. C., Srivastava, G. and Chauhan, B. P. S., *Coord. Chem. Rev*, 1984, **55,** 207.
3. Mattes, R., Mühlsiepen, K.-M. and Rühl, D., *Z. Anorg. Allg. Chem.*, 1983, **499,** 75.
4. Mattes, R. and Rühl, D., *Acta Cryst.*, 1984, **C40,** 106.
5. Uh, D. S., Do, Y., Lee, J.-H. and Suh, L.-H., *Main Group Metal Chem.*, 1993, **16,** 131.
6. Silvestru, C., Haiduc, I., Ebert, K. H., Breunig, H. J. and Sowerby, D. B., *J. Organomet. Chem.*, 1994, **468,** 113.
7. Uson, R., Laguna, A., Laguna, M., Lazaro, I., Jones, P. G. and Fittschen, C., *J. Chem. Soc., Dalton Trans.*, 1988, 2323.
8. Haiduc, I., Silvestru, C., Caruso, F., Rossi, M. and Gielen, M., *Rev. Roum. Chim. (Bucharest)*, 1994, **39,** 53.
9. Silvestru, C., Haiduc, I., Caruso, F., Rossi, M., Mahieu, B. and Gielen, M., *J. Organomet, Chem.*, 1993, **448,** 75.
10. Shihada, A. F., Jassim, A. A. and Weller, F., *J. Organomet. Chem.*, 1984, **268,** 125.
11. Begley, M. J., Sowerby, D. B., Wesolek, D. M., Silvestru, C. and Haiduc, I., *J. Organomet. Chem.*, 1986. **316,** 281.
12. Casas, J. L., Castineiras, A., Haiduc, I., Sanchez, A., Sordo, J. and Vasquez-Lopez, E. M., *Polyhedron*, 1994, **13,** 1805.
13. Churchill, M. J., Cooke, J., Wormald, J., Davison, A. and Switkes, E. S., *J. Am. Chem. Soc.*, 1969, **91,** 6518.
14. Kuhlein, K. and Neumann, W. P., *Liebigs Ann. Chem.*, 1967, **702,** 17.
15. Mastryukova, T. A., Shipov, A. E. and Kabachnick, M. I., *Zh. Obshch. Khim.*, 1962, **32,** 3579.
16. Higgins, W. A., Vogel, R. W. and Craig, W. G., *J. Am. Chem. Soc.*, 1955, **77,** 1864.
17. Sheldrick, G. M., *Crystallographic Computing* 3, ed. G. M. Sheldrick, C. Kruger and R. Goddard. Oxford University Press, Oxford, 1985, p. 175.
18. Least-squares: function minimized: $\Sigma w(|F_o|-|F_c|)^2$, where $w = 4F_0^2/\sigma^2(F_0^2)$, $\sigma^2(F_0^2) = [S^2(C+R^2B)+(pF_0^2)^2]/(Lp)^2$, S = scan rate, C = total integrated peak count, R = ratio of scan time to background counting time, Lp = Lorentz–polarization factor, and p = p factor).
19. Standard deviation of an observation weight unit: $\Sigma w(|F_o|-|F_c|)^2/(N_o-N_v)^{1/2}$, where N_0 = number of observations and N_v = number of variables.
20. Cromer, D. T. and Waber, J. T., *International Tables for X-ray Crystallography*, Vol. 4. Kynoch Press, Birmingham, 1974, Table 2.2A.
21. Ibers, J. A. and Hamilton, W. C., *Acta Cryst.*, 1964, **17,** 781.
22. Creagh, D. C. and McAuley, W. J., *International Tables for X-ray Crystallography*, Vol. C. Kluwer Academic Publishers, Boston, 1992, Table 4.2.6.8.
23. TEXSAN-TEXRAY, Structure Analysis Package (SHELX93), Molecular Structure Corporation, Woodlands, TX, 1985.
24. Mitchell, T. N., *J. Organomet. Chem.*, 1973, **59,** 189.
25. Naser, F. A. K., Hossain, M. B., van der Helm, D. and Zuckerman, J. J., *Inorg. Chem.*, 1983, **22,** 3107.
26. Mokal, V. B., Jain, V. K. and Tiekink, E. R. T., *J. Organomet. Chem.*, 1994, **471,** 53.
27. Kabachnik, M. I., Mastryukova, T. N., Matro-

sov, E. I. and Fisher, B., *Zh. Strukt. Khim.*, 1965, **6,** 691; *Chem. Abstr.*, 1966, **64,** 5945.
28. Lindner, E. and Ebinger, H. M., *Z. Naturforsch.*, 1973, **28b,** 113.
29. Mastryukova, T. A., Kalyanova, R. M., Ghenkina, G. K., Scherbina, T. M., Svoren, V. A. and Kabachnik, M. I., *Zh. Obshch. Khim.*, 1977,**47,** 2723.
30. Lindner, E. and Ebinger, H. M., *Chem. Ber.*, 1974, **107,** 135.
31. Begley, M. J., Sowerby, D. B., Wesolek, D. M., Silvestru, C. and Haiduc, I., *J. Organomet. Chem.*, 1986, **316,** 281.
32. Haegele, G., Kuchen, W. and Steinberger, H., *Z. Naturforsch.*, 1974, **29b,** 349.
33. Tebby, J. C. (Ed.), *CRC Handbook of Phosphorus-31 Nuclear Magnetic Resonance Data.*, CRC Press, Boca Raton, 1991, **13,** p. 364.
34. Keck, H., Kuchen, W. and Kuehlborn, S., *Phosphorus Sulfur*, 1985, **24,** 343.
35. Mattes, R. and Rühl, D., *Acta Cryst.*, 1984, **C40,** 106.
36. Lepicard, G., de Saint-Giniez-Liebig, D., Laurent, A. and Rerat, C., *Acta Cryst*, 1969, **B25,** 617.
37. Kuz'mina, L. G. and Struchkov, Yu. T., *Zh. Strukt. Khim.*, 1972, **13,** 946.
38. Huheey, J. E., *Inorganic Chemistry*. Walter de Gruyter, Berlin, 1988, p. 278.
39. Silvestru, C., Toscano, R. A., Cardenas, J., Cea-Olivares, R., Silvestru, A. and Haiduc, I., *Polyhedron*, 1995, **14,** 2231.
40. Chadha, R. K., Drake, J. E. and Sarkar, A. B. A., *Inorg. Chem.*, 1985, **24,** 3156.
41. Bent, H., *Chem. Rev.*, 1961, **61,** 275.

Pergamon

PII: S0277-5387(96)00352-X

Polyhedron Vol. 16, No. 6, pp. 963–966, 1997
Copyright © 1996 Elsevier Science Ltd
Printed in Great Britain. All rights reserved
0277–5387/97 $17.00+0.00

Synthesis and crystal structure of a novel lanthanide–copper mixed metal complex: $Gd_2Cu_3\{O(CH_2COO)_2\}_6 \cdot 9H_2O$

Jiang-Gao Mao, Ling Song, Xiao-Ying Huang and Jin-Shun Huang*

State Key Laboratory of Structure Chemistry, Fujian Institute of Research on the Structure of Matter, Chinese Academy of Sciences, Fuzhou 350002, P. R. China

(Received 8 February 1996; accepted 15 July 1996)

Abstract—The reaction of diglycolic acid $O(CH_2COOH)_2$ with $Cu(NO_3)_2 \cdot 2H_2O$ and hydrated gadolinium nitrate at pH 7 produced a novel Ln–Cu mixed metal complex: $[Gd_2Cu_3\{O(CH_2COO)_2\}_6 \cdot 9H_2O]$, which was characterized by elemental analysis, IR spectrum and X-ray crystallography. In the complex, the Gd^{3+} ions and the Cu^{2+} ions are connected by the carboxylate groups of the ligand molecules, thus resulting in the formation of the complicated network structure. Copyright © 1996 Elsevier Science Ltd

Keywords: synthesis; crystal structure; rare earth copper complex; carboxylate acid.

The synthesis of polynuclear mixed copper–lanthanide complexes is of interest for several reasons [1–4]. These complexes are important in understanding the nature of the magnetic exchange interactions between lanthanide and transition metal ions, and they can possibly be used as magnetic materials [2, 3], and high temperature superconductors [5]. The structural chemistry of these compounds has also attracted our attention, most Ln–Cu complexes with Schiff-bases are polynuclear, such as $LnCu_2$, $LnCu_3$, Ln_2Cu_2, Ln_2Cu_4 [2,3,6]. The Ln–Cu complexes with pyridinioacetate have the octadecanuclear Ln_6Cu_{12}, in which the lanthanide ions form an octahedron with twelve Cu^{2+} ions occupying the edges of the octahedron and one ClO_4^- anion encapsulated in the centre [7]. The complex with the highest nuclearity reported so far contains a core of $[La_8Cu_{12}(OH)_{24}]$. It was synthesized through a metallomacrocycle route [8]. The lanthanide complexes with Cu(pba) form the so-called "ladder" structure, which differs slightly along the "lanthanide contraction" [9]. We deemed that the multidentate polycarboxylate acids would be good ligands for the preparation of the Ln–Cu mixed metal complexes since the metal ions can be bridged by the bidentate carboxylate groups. We selected the diglycolic acid as the ligand and successfully prepared the novel Gd–Cu title complex, and here we report its preparation and crystal structure.

EXPERIMENTAL

Preparation

$Cu(NO_3)_2 \cdot 2H_2O$ (1.5 mmol) and hydrated lanthanide nitrate (1 mmol) were dissolved in water (10 cm^3) and mixed with stirring. Diglycolic acid (3 mmol) was dissolved in another 10 cm^3 water and the pH was adjusted to 7.0 with $NH_3 \cdot H_2O$. These two solutions were then mixed with vigorous stirring, the green precipitates formed were filtered off and the clear solution was allowed to evaporate at room temperature, where upon prismatic green–blue crystals were isolated after several days. Found: C, 20.1; H, 3.1; Cu, 13.3; Gd, 21.3. Calc. C, 19.7; H, 2.9; Cu, 13.1; Gd, 21.5%. IR studies indicated that ν_{COO} (1724, 1419 cm^{-1}) of the free ligand were shifted to 1604 and 1425 cm^{-1}, proving the bidentate complexation of the carboxylate groups. Upon complexation, ν_{COC} of 1149 cm^{-1} for the free ligand was shifted to 1114 cm^{-1}. These results

* Author to whom correspondence should be addressed.

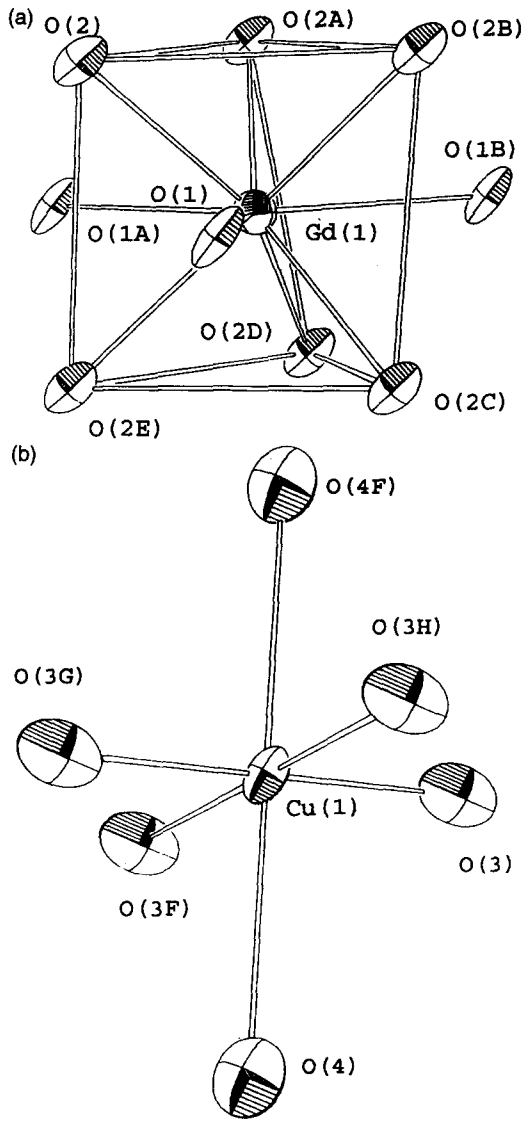


Fig. 1. (a) The coordination geometry of the Gd^{3+} ion; (b) the coordination polyhedron of the Cu^{2+} ion.

are in good agreement with the structure determined by X-ray diffraction.

Data collection, structural determination and refinement

Data collection was performed on an Enraf–Nonius CAD4 diffractometer with graphite-monochromated Mo-K_α radiation ($\lambda = 0.71069$ Å) operating at 298 K using ω–2θ scan methods. Data were corrected for Lorentz and polarization factors, and an empirical absorption correction applied based on the ψ scan technique.

From the systematic absences and statistical results, the space group was uniquely determined to be *P6/mcc* (#192). The structure was solved by direct methods, which revealed the coordinates of the Gd atom ($\frac{2}{3}, \frac{1}{3}, \frac{1}{4}$) and those of the Cu atom ($\frac{1}{2}, 0, \frac{1}{2}$). All remaining non-hydrogen atoms were located from subsequent difference Fourier syntheses. All non-hydrogen atoms except O(5) were refined by full-matrix least-squares procedures with anisotropic thermal parameters. The O(5) atom, with coordinates (0.195, 0.266, 0.500) and a peak height of 6.2 eÅ^3, which represents the free water molecule, was refined isotropically with its occupancy of $\frac{1}{4}$ according to the results from the occupancy refinement. All calculations were performed on a COMPAQ Prolinea 4/50 computer using the Molen program package [10] and published scattering factors [11].

A summary of data collection, structure determination and refinement is presented in Table 1.

RESULTS AND DISCUSSION

Selected bond lengths and angles for the complex are listed in Table 2. The coordination polyhedra for the Gd^{3+} and Cu^{2+} ions are shown in Fig. 1. The Gd^{3+} ion is nine coordinated by three ether oxygen atoms and six carboxylato oxygen atoms from three ligand molecules. The Gd—O(ether) and Gd—

Table 1. Experimental data for the X-ray diffraction studies of the Gu—Cu complex

Complex	Gd—Cu
Formula	$Gd_2Cu_3O_{39}C_{24}H_{42}$
Molecular weight	1459.70
Crystal system	Hexagonal
Space group	P6/mcc (#192)
a/Å	15.126(3)
c/Å	14.690(8)
V/Å^3	2911(2)
Z	2
Dc/gcm^{-3}	1.665
F(000)	1426
Crystal Description	greenish-blue, prism
Crystal size/mm	0.40 × 0.10 × 0.05
2θ range/°	3–50
μ(Mo-K_α)/cm^{-1}	34.3
Absorption correction	Yes
Maximum and Mini transition factor hkl ranges:	0.876–1.00
	h = 0–15
	k = 0–15
	l = −17–0
No. of unique data	1997
Reflections included ($I > 3\sigma(I)$)	1377
Solution	Direct methods
No. of Parameters refined	57
Hydrogen atoms	Not included
R	0.036
R_w	0.038
Weighting scheme · w^{-1} =	$\sigma^2(F)$
Goodness of fit	1.01
Maximum shift/σ ratio	0.05
Largest difference peak and hole/eÅ^{-3}	1.40, −0.15

Table 2. Important bond lengths (Å) and angles (deg.)

Gd(1)—O(1)[a,b]	2.552(2)(3x)	Gd(1)—O(2)	2.448(2)(6x)
Cu(1)—O(3)[f,g,h]	1.956(3)(4x)	Cu(1)—O(4)[f]	2.519(4)(2x)
O(1)—C(1)	1.409(4)	O(1)—C(1)[c]	1.409(5)
O(2)—C(2)[c]	1.234(6)	O(3)—C(2)	1.255(4)
C(1)—C(2)	1.519(6)		
O(1)—Cd(1)—O(1)[a]	119.99(5)	O(1)—Gd(1)—O(2)	61.81(7)
O(1)—Gd(1)—O(2)[a]	138.69(6)	O(1)—Gd(1)—O(2)[b]	73.82(7)
O(2)—Gd(1)—O(2)[a]	82.24(9)	O(2)—Gd(1)—O(2)[c]	123.62(9)
O(2)—Gd(1)—O(2)[d]	147.63(7)	O(2)—Gd(1)—O(2)[e]	82.60(8)
O(3)—Cu(1)—O(3)[f]	91.0(1)	O(3)—Cu(1)—O(3)[g]	180.0(2)
O(3)—Cu(1)—O(3)[h]	89.0(1)	C(1)—O(1)—C(1)[c]	113.1(3)
O(1)—C(1)—C(2)	107.8(4)	O(2)—C(2)—O(3)[c]	127.2(4)
O(2)—C(2)—C(1)[c]	118.6(3)	O(3)—C(2)—C(1)	114.9(4)

[a] $1-y, x-y, z$. [b] $1-x+y, 1-x, z$. [c] $1-y, 1-x, 1/2-z$. [d] $1-x+y, y, 1/2-z$.
[e] $x, x-y, 1/2-z$. [f] $1-x, 1-y, z$. [g] $1-x, 1-y, 1-z$. [h] $x, y\ 1-z$.

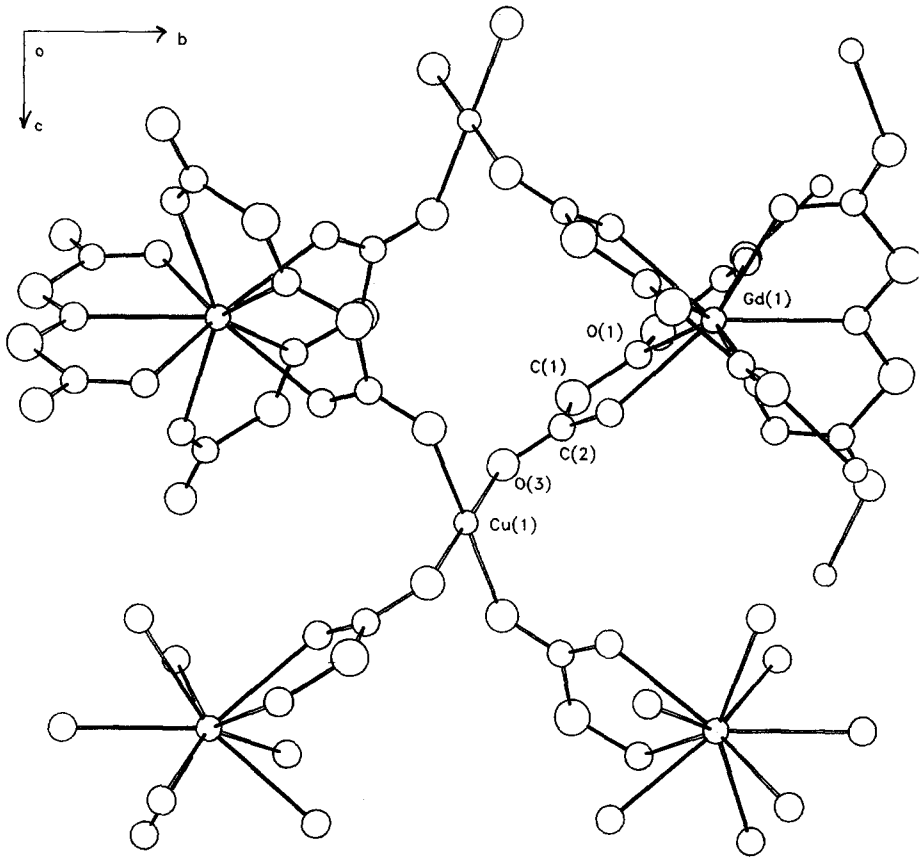


Fig. 2. Crystal structure of $Gd_2Cu_3(O(CH_2COO)_2)_6$ with atomic labelling along the (100) plane.

$O(COO^-)$ distances are 2.522(2) and 2.448(2) Å, respectively (Table 2). From these bond lengths we can see that the coordination ability of carboxylato group is much stronger than that of the ether oxygen atom. There coordination geometry of the gadolinium ion can be best described as a tricapped trigonal prism; the six carboxylato oxygen atoms form a trigonal prism with three ether oxygen atoms as capping atoms (Fig. 1a). The copper ion is four coordinated to four carboxylato oxygen atoms with a Cu—O bond length of 1.956(3) Å. There are also two weak Cu—$O(H_2O)$ bonds, with Cu—O separations of 2.519(4) Å. The O—Cu—O (oxygen atoms from the COO^- groups) bond angles are 180.0(2), 91.0(1) and 89.0(1)°, respectively. Thus, the Cu^{2+} ion has a slightly distorted square-planar coordination geometry. With

the two weak bonds, the geometry of the copper ion in the complex can best be described as distorted octahedral with the two axial bonds greatly elongated (Fig. 1b), resulting from the "Jahn–Teller effect".

The structure of the complex is shown in Fig. 2. The lanthanide ions and the copper ions are connected by the carboxylate groups. Each carboxylate group is bidentate, so every ligand molecule is pentadentate, being bonded to one lanthanide ion and two copper ions. This kind of connection results in the formation of a complicated three-dimensional network structure. The shortest Gd—Gd, Gd—Cu and Cu—Cu distances are 7.345(0), 5.706(0) and 7.345(0) Å, respectively.

Besides bonding weakly to the copper ions, the water molecules also form hydrogen bonds. The separations O(2)···O(4c), O(3)···O(4i) and O(5)···O(4j) (symmetry codes: c: $1-y, 1-x, \frac{1}{2}-z$; i: $1-x, -y, z$; j: $y, -x+y, z$) are 2.795(6), 3.007(7) and 2.78(3) Å, respectively, demonstrating the presence of hydrogen bonds.

REFERENCES

1. Blake, A. J., Cherepeno, Y. A., Duntop, A. A., Grant, C. M., Milne, P. E. Y., Rawson, J. M. and Winpenny, R. E. P., *J. Chem. Soc., Dalton Trans.*, 1994, 2719.
2. Andruk, M., Ramade, L., Codjovi, E., Guilliou, O., Kahn, O. and Trombe, J. C., *J. Am. Chem. Soc.*, 1993, **115,** 1822; Georges, R., Kahn, O. and Guilliou, O., *Phys. Rev. B*, 1994, **49,** 3235; Andruh, M., Bakalbassis, E., Kahn, O., Trombe, J. C. and Porcher, P., *Inorg. Chem.*, 1993, **32,** 1616.
3. Benelli, C., Caneschi, A., Gatteschi, D., Guilliou, O. and Pardi, L., *J. Magn. Magn. Mater.*, 1990, **83,** 522; Benelli, C., Caneschi, A., Gatteschi, D., Guilliou, O. and Pardi, L., *Inorg. Chem.*, 1990, **29,** 1750; Bencini, A., Benelli, C., Caneschi, A., Dei, A. and Gatteschi, D., *Inorg. Chem.*, 1986, **25,** 572; Bencini, A., Benelli, C., Caneschi, A., Carlin, R. L., Dei, A. and Gatteschi, D., *J. Am. Chem. Soc.*, 1985, **107,** 8128.
4. Keller, S. W., Carson, V. A., Sandford, D., Stenzel, F., Stacy, A. M., Kwei, G. H. and Alario-Franco, M., *J. Am. Chem. Soc.*, 1994, **116,** 8070.
5. Nelson, D. L., Willingham, M. S. and George, T. F. (ed.) *Chemistry of High-Temperature Superconductors*, ACS Symposium Series, 351. American Chemical Society, Washington D.C., 1987.
6. Bidell, W., Doring, J., William, H., Hans-Ulrich Hund, Bsch, Plappert, E. and Berke, H., *Inorg. Chem.*, 1993, **32,** 502; Blake, A. J., Milne, P. E. Y. and Winpenny, R. E. P., *J. Chem. Soc., Dalton Trans.*, 1993, 3727.
7. Chen Xiao-Ming, Aubin, S., M. J., Wu, Yu-Luan, Yang, Yan-Sheng, Mak, T. C. W. and Hendrickson, D. N., *J. Am. Chem. Soc.*, 1995, **117,** 9600.
8. Blake, A. J., Gould, R. O., Milne, P. E. Y. and Winpenny, R. E. P., *J. Chem. Soc., Chem. Commun.*, 1991, 1453.
9. Guilliou, O., Kahn, O., Oushoorn, R. L., Boubekear, K. and Batail, P., *Inorg. Chim. Acta*, 1992, **198–200**, 119; Guilliou, O., Bergerat, P., Kahn, O., Bakalbassis, E., Boubekaar, K., Batail, P. and Guillot, M., *Inorg. Chem.*, 1992, **31,** 110.
10. Fair, C. K., MolEN, *An Interactive Intelligent System for Crystal Structure Analysis*. Enraf–Nonius, Delft, The Netherlands, 1990.
11. Cromer, D. T. and Waber, J. T., *International Tables for X-ray Crystallography*, Vol. IV. Kynoch Press, Birmingham, 1974. (Present distributor Kluwer Academic Publisher, Dordrecht.)

Pergamon

PII: S0277-5387(96)00339-7

Polyhedron Vol. 16, No. 6, pp. 967–974, 1997
Copyright © 1996 Elsevier Science Ltd
Printed in Great Britain. All rights reserved
0277-5387/97 $17.00+0.00

The structure of the crystal solvate of magnesium methoxide with methanol, $Mg(OMe)_2 \cdot 3.5MeOH$

Z. A. Starikova,[a] A. I. Yanovsky,[a] E. P. Turevskaya[b] and N. Ya. Turova[b]*

[a]A. N. Nesmeyanov Institute of Organoelement Compounds, Russian Acad. Sci., 28 Vavilov St., Moscow 117813, Russia

[b]M. V. Lomonosov Moscow State University, Department of Chemistry, Vorobyovy Gory, Moscow 119899, Russia

(Received 25 June 1996; accepted 12 July 1996)

Abstract—The X-ray diffraction study of the crystals deposited from the solution obtained by the reaction of magnesium with methanol allowed the formulation of the product as $Mg(OMe)_2 \cdot 3.5MeOH$ (**I**). Its structure is built of the residues of four types, namely cubane $[Mg_4(\mu_3\text{-}OR)_4(OR)_4(ROH)_8]$ neutral molecules, $[Mg_4(\mu_3\text{-}OR)_4(OR)_2(ROH)_{10}]^{2+}$ cations, $[(RO)_2H]^-$ anions (R = Me) and eight crystallographically independent non-coordinated solvating methanol molecules. All residues are linked into a three-dimensional framework by means of a complicated hydrogen-bonding system. The crystal structure provides the basis for discussion of the possible mechanism of desolvation of **I**. Copyright © 1996 Elsevier Science Ltd

Keywords: magnesium methoxide; methanol solvate; structure; cubane.

Magnesium, as well as the alkaline-earth metal alkoxides, have been extensively studied due to the possibility of their application in the synthesis of inorganic materials, in particular the perovskite-type mixed oxide phases. Special attention has recently been paid to the II group metal alkoxides with bulky branched alkoxy groups, preventing the possible oligomerization and thus producing species which may potentially act as precursors in MOCVD processes. The studies of the structure and properties of the derivatives of the simplest alkoxy homologues, the so-called "ionic" alkoxides, soluble in polar solvents and employed as starting solutions for the sol–gel processes, are much less numerous. A few years ago we reported [1] the structure of the solvate formerly known as "$Ca(OEt)_2 \cdot 2EtOH$", prepared by the prolonged refluxing of ethanol solutions of calcium ethoxide. The solvate was proved to be the $Ca_6O_2(OEt)_8 \cdot 14EtOH$ oxocomplex, built of two $[Ca_4O_4]$ cubanes sharing a common $[Ca_2(oxo\text{-}O)_2]$ face.

Here we report the structure of magnesium methoxide solvate, which readily deposits on cooling from the freshly prepared solutions obtained by the reaction of magnesium with absolute MeOH. Two possible compositions of this solvate, namely $Mg(OR)_2 \cdot 3ROH$ [2] and $Mg(OR)_2 \cdot 4ROH$ [3] (R = Me) were suggested. The tensimetric study of the $Mg(OR)_2$ (solid)–ROH (vapour) system has led to the conclusion that the composition of the solvate is close to 1:4 [4]. Crystals of $Mg(OMe)_2 \cdot 3.5MeOH$ (**I**) easily lose the solvent in a dry atmosphere at 20°C; on heating above 39°C under mother liquor they decompose, yielding a powder whose composition is close to that of the monosolvate. The analogous product precipitates from the methanol solutions at temperatures higher than 40°C and again partially dissolves on cooling. On heating of the monosolvate *in vacuo* up to 50–70°C the non-solvated $Mg(OR)_2$ is formed [4].

EXPERIMENTAL

The reaction of magnesium with absolute MeOH occurs at room temperature. In order to avoid boiling of the alcohol, the metal is introduced into the solution in small portions. Otherwise, the solution quickly becomes opaque and immediately yields the monosolvate precipitate. On further cooling or evaporation

* Author to whom correspondence should be addressed.

of the solvent at 20°C, the transparent rhomboid or rectangular plates of $Mg(OR)_2 \cdot 3.5ROH$ (**I**) are deposited. Their composition, determined by X-ray diffraction, is in good agreement with the results of elemental analysis. Found: Mg, 12.2, 12.0. Calc.: Mg, 12.1%.

The crystallo-optical properties of the crystals are as follows. Crystals are biaxial, $\angle 2V \sim 90°$, the extinction is direct or slanting ($< 31°$); the elongation direction is positive and the optical sign is positive, $n'_g = 1.447$, $n'_p = 1.444$.

X-ray diffraction study

$C_{44}H_{160}Mg_8O_{44}$, $M = 1588.20$, orthorhombic, space group *Aba*2, at 188 K, $a = 23.60(1)$, $b = 24.331(8)$, $c = 31.954(9)$ Å, $V = 18{,}348(11)$ Å^{-3}, $Z = 8$, $D_c = 1.15$ g cm^{-3}. The X-ray diffraction experiment was carried out with a Syntex $P2_1$ diffractometer ($T = 188$ K, Mo-K_α radiation, θ–2θ scan technique, $\theta \leqslant 24°$, $\mu = 10.42$ cm^{-1}; no absorption correction was applied). The structure was solved by direct methods and refined by the full-matrix least-squares techniques in the anisotropic approximation. All methyl hydrogen atoms were placed in the geometrically calculated positions and included in the refinement using the riding model approximation with $U_{iso}(H) = 1.5U_{eq}(C)$, where $U_{eq}(C)$ is the equivalent isotropic temperature factor of the corresponding methyl carbon atom. The hydroxyl hydrogen atoms were not located. The determination of the absolute structure was impossible due to the lack of sufficiently strong anomalous scatterers. Final discrepancy factors are: $R_1 = 0.0885$ [on F for 3564 unique reflections with $I \geqslant 2\sigma(I)$], $R_{w2} = 0.2966$ (on F^2 for all 7253 reflections used in the refinement of 865 parameters). All calculations were carried out on an IBM PC with the help of the SHELXTL PLUS 5 program (gamma version). Bond lengths and angles are given in Tables 1 and 2. Atomic coordinates are available from the Cambridge Crystallographic Data Centre, 12 Union Road, Cambridge CB2 1EZ, U.K.

Table 1. Bond lengths (Å) in the structure of **I**[a]

Mg(1)—O(11)	2.040(12)	Mg(8)—O(83)	2.117(10)
Mg(1)—O(2)	2.067(10)	Mg(8)—O(81)	2.126(12)
Mg(1)—O(1)	2.081(10)	O(1)—C(1)	1.45(2)
Mg(1)—O(12)	2.094(11)	O(2)—C(2)	1.46(2)
Mg(1)—O(4)	2.101(12)	O(3)—C(3)	1.43(2)
Mg(1)—O(13)	2.117(11)	O(4)—C(4)	1.39(2)
Mg(2)—O(23)	2.055(11)	O(5)—C(5)	1.45(2)
Mg(2)—O(21)	2.083(12)	O(6)—C(6)	1.42(2)
Mg(2)—O(2)	2.094(11)	O(7)—C(7)	1.42(2)
Mg(2)—O(3)	2.096(11)	O(8)—C(8)	1.44(2)
Mg(2)—O(1)	2.121(10)	O(11)—C(11)	1.41(2)
Mg(2)—O(22)	2.130(10)	O(12)—C(12)	1.42(2)
Mg(3)—O(4)	2.064(10)	O(13)—C(13)	1.40(2)
Mg(3)—O(33)	2.090(13)	O(21)—C(21)	1.41(2)
Mg(3)—O(2)	2.109(12)	O(22)—C(22)	1.41(2)
Mg(3)—O(31)	2.109(11)	O(23)—C(23)	1.41(2)
Mg(3)—O(3)	2.116(9)	O(31)—C(31)	1.42(2)
Mg(3)—O(32)	2.123(10)	O(32)—C(32)	1.40(2)
Mg(4)—O(1)	2.050(11)	O(33)—C(33)	1.41(2)
Mg(4)—O(41)	2.061(10)	O(41)—C(41)	1.43(2)
Mg(4)—O(42)	2.091(11)	O(42)—C(42)	1.39(2)
Mg(4)—O(3)	2.102(10)	O(43)—C(43)	1.43(2)
Mg(4)—O(4)	2.107(10)	O(51)—C(51)	1.43(2)
Mg(4)—O(43)	2.130(10)	O(52)—C(52)	1.47(2)
Mg(5)—O(53)	2.031(12)	O(53)—C(53)	1.36(2)
Mg(5)—O(5)	2.048(13)	O(61)—C(61)	1.43(2)
Mg(5)—O(6A)	2.110(10)	O(62)—C(62)	1.52(2)
Mg(5)—O(52)	2.127(11)	O(63)—C(63)	1.41(2)
Mg(5)—O(51)	2.127(11)	O(71)—C(71)	1.40(2)
Mg(5)—O(6)	2.141(10)	O(72)—C(72)	1.38(2)
Mg(6)—O(61)	2.009(14)	O(73)—C(73)	1.46(2)
Mg(6)—O(6A)	2.085(12)	O(81)—C(81)	1.40(2)
Mg(6)—O(63)	2.104(11)	O(82)—C(82)	1.33(2)
Mg(6)—O(5A)	2.103(10)	O(83)—C(83)	1.39(2)
Mg(6)—O(5)	2.102(10)	O(1C)—C(1C)	1.37(3)
Mg(6)—O(62)	2.147(11)	O(2C)—C(2C)	1.46(2)
Mg(7)—O(71)	2.024(11)	O(3C)—C(3C)	1.24(2)
Mg(7)—O(7A)	2.083(10)	O(4C)—C(4C)	1.43(2)
Mg(7)—O(7)	2.096(9)	O(5C)—C(5C)	1.39(2)
Mg(7)—O(72)	2.111(10)	O(6C)—C(6C)	1.46(2)
Mg(7)—O(73)	2.123(11)	O(7C)—C(7C)	1.40(3)
Mg(7)—O(8)	2.138(11)	O(8C)—C(8C)	1.44(2)
Mg(8)—O(82)	2.037(10)	O(9C)—C(9C)	1.39(2)
Mg(8)—O(8A)	2.064(10)	O(10C)—C(10C)	1.38(2)
Mg(8)—O(7)	2.073(12)	O(11C)—C(11C)	1.44(3)
Mg(8)—O(8)	2.100(9)	O(12C)—C(12C)	1.49(3)

[a] For labelling of the symmetry-derived atoms, see the caption to Fig. 2.

RESULTS AND DISCUSSION

The crystal of the solvate of magnesium methoxide with methanol (**I**) is built of the residues belonging to four types, namely $[Mg_4(\mu_3\text{-}OMe)_4(OMe)_2(MeOH)_{10}]^{2+}$ cations (Ct), $[(MeO)_2H]^-$ anions, $[Mg_4(\mu_3\text{-}OMe)_4(OMe)_4(MeOH)_8]$ neutral molecules (NM) and non-coordinated solvating MeOH molecules linked together into an infinite three-dimensional hydrogen-bonding framework (Figs 1–3). Therefore, complex **I** should be formulated as $[Mg_4(OR)_6(ROH)_{10}]^{2+}[(RO)_2H]_2^- \cdot [Mg_4(OR)_8(ROH)_8] \cdot 8ROH$. Tetranuclear NM and Ct have the cubane $[Mg_4O_4]$ cage, with the magnesium and methoxide oxygen atoms occupying the alternating vertices. Each magnesium atom has a coordination octahedron formed by three μ_3-OR groups and three oxygen atoms of the terminal OR groups and solvating ROH molecules. The latter were identified taking into account the longer Mg—O(R)H as compared to Mg—OR distances, their participation in the intramolecular ROH···OR hydrogen bonds, and the general pattern of the hydrogen-bonding system in the structure. It turns out that two of the three terminal ligands at each magnesium atom belong to ROH, whereas the third terminal ligand corresponds to the OR group, the overall ROH : OR(terminal) ratio in

Table 2. Bond angles (°) in the structure of I[a]

O(11)—Mg(1)—O(2)	91.4(5)	O(71)—Mg(7)—O(73)	93.1(5)
O(11)—Mg(1)—O(1)	94.1(4)	O(7A)—Mg(7)—O(73)	96.8(4)
O(2)—Mg(1)—O(1)	83.3(4)	O(7)—Mg(7)—O(73)	93.4(4)
O(11)—Mg(1)—O(12)	89.2(5)	O(72)—Mg(7)—O(73)	86.8(4)
O(2)—Mg(1)—O(12)	95.8(4)	O(71)—Mg(7)—O(8)	91.3(5)
O(1)—Mg(1)—O(12)	176.6(5)	O(7A)—Mg(7)—O(8)	78.4(4)
O(11)—Mg(1)—O(4)	170.0(5)	O(7)—Mg(7)—O(8)	83.6(4)
O(2)—Mg(1)—O(4)	79.1(4)	O(72)—Mg(7)—O(8)	95.8(4)
O(1)—Mg(1)—O(4)	81.9(4)	O(73)—Mg(7)—O(8)	174.7(4)
O(12)—Mg(1)—O(4)	94.7(5)	O(82)—Mg(8)—O(8A)	167.8(5)
O(11)—Mg(1)—O(13)	102.0(5)	O(82)—Mg(8)—O(7)	90.0(5)
O(2)—Mg(1)—O(13)	163.3(5)	O(8A)—Mg(8)—O(7)	80.3(4)
O(1)—Mg(1)—O(13)	85.9(4)	O(82)—Mg(8)—O(8)	90.9(4)
O(12)—Mg(1)—O(13)	94.2(5)	O(8A)—Mg(8)—O(8)	80.9(4)
O(4)—Mg(1)—O(13)	86.9(5)	O(7)—Mg(8)—O(8)	85.1(4)
O(23)—Mg(2)—O(21)	102.0(5)	O(82)—Mg(8)—O(83)	95.4(4)
O(23)—Mg(2)—O(2)	93.1(4)	O(8A)—Mg(8)—O(83)	92.8(4)
O(21)—Mg(2)—O(2)	86.3(5)	O(7)—Mg(8)—O(83)	94.8(4)
O(23)—Mg(2)—O(3)	91.7(4)	O(8)—Mg(8)—O(83)	173.7(4)
O(21)—Mg(2)—O(3)	163.4(4)	O(82)—Mg(8)—O(81)	94.3(5)
O(2)—Mg(2)—O(3)	83.5(4)	O(8A)—Mg(8)—O(81)	95.6(5)
O(23)—Mg(2)—O(1)	168.9(5)	O(7)—Mg(8)—O(81)	175.3(5)
O(21)—Mg(2)—O(1)	87.5(4)	O(8)—Mg(8)—O(81)	96.6(5)
O(2)—Mg(2)—O(1)	81.7(4)	O(83)—Mg(8)—O(81)	83.0(5)
O(3)—Mg(2)—O(1)	78.1(4)	C(1)—O(1)—Mg(4)	118.5(8)
O(23)—Mg(2)—O(22)	92.9(4)	C(1)—O(1)—Mg(1)	121.7(8)
O(21)—Mg(2)—O(22)	92.4(5)	Mg(4)—O(1)—Mg(1)	98.0(4)
O(2)—Mg(2)—O(22)	174.0(5)	C(1)—O(1)—Mg(2)	117.0(8)
O(3)—Mg(2)—O(22)	96.3(4)	Mg(4)—O(1)—Mg(2)	101.6(4)
O(1)—Mg(2)—O(22)	92.4(4)	Mg(1)—O(1)—Mg(2)	95.6(4)
O(4)—Mg(3)—O(33)	92.0(5)	C(2)—O(2)—Mg(1)	119.8(8)
O(4)—Mg(3)—O(2)	79.0(4)	C(2)—O(2)—Mg(2)	117.1(9)
O(33)—Mg(3)—O(2)	170.5(5)	Mg(1)—O(2)—Mg(2)	96.9(4)
O(4)—Mg(3)—O(31)	98.4(4)	C(2)—O(2)—Mg(3)	121.2(8)
O(33)—Mg(3)—O(31)	92.4(5)	Mg(1)—O(2)—Mg(3)	100.7(5)
O(2)—Mg(3)—O(31)	91.8(5)	Mg(2)—O(2)—Mg(3)	96.0(4)
O(4)—Mg(3)—O(3)	83.6(4)	C(3)—O(3)—Mg(2)	119.3(8)
O(33)—Mg(3)—O(3)	93.5(4)	C(3)—O(3)—Mg(4)	119.8(8)
O(2)—Mg(3)—O(3)	82.7(4)	Mg(2)—O(3)—Mg(4)	100.7(4)
O(31)—Mg(3)—O(3)	173.7(6)	C(3)—O(3)—Mg(3)	121.0(8)
O(4)—Mg(3)—O(32)	162.3(5)	Mg(2)—O(3)—Mg(3)	95.7(4)
O(33)—Mg(3)—O(32)	101.9(5)	Mg(4)—O(3)—Mg(3)	95.0(4)
O(2)—Mg(3)—O(32)	86.5(5)	C(4)—O(4)—Mg(3)	118.8(9)
O(31)—Mg(3)—O(32)	92.0(4)	C(4)—O(4)—Mg(1)	117.4(9)
O(3)—Mg(3)—O(32)	84.6(4)	Mg(3)—O(4)—Mg(1)	101.1(5)
O(1)—Mg(4)—O(41)	93.2(4)	C(4)—O(4)—Mg(4)	122.7(9)
O(1)—Mg(4)—O(42)	163.3(4)	Mg(3)—O(4)—Mg(4)	96.4(4)
O(41)—Mg(4)—O(42)	99.2(5)	Mg(1)—O(4)—Mg(4)	95.6(4)
O(1)—Mg(4)—O(3)	79.5(4)	C(5)—O(5)—Mg(5)	120.4(9)
O(41)—Mg(4)—O(3)	172.4(5)	C(5)—O(5)—Mg(6A)	116.4(8)
O(42)—Mg(4)—O(3)	87.4(4)	Mg(5)—O(5)—Mg(6A)	101.4(5)
O(1)—Mg(4)—O(4)	82.5(4)	C(5)—O(5)—Mg(6)	119.6(9)
O(41)—Mg(4)—O(4)	93.8(4)	Mg(5)—O(5)—Mg(6)	99.9(5)
O(42)—Mg(4)—O(4)	85.6(5)	Mg(6A)—O(5)—Mg(6)	94.6(4)
O(3)—Mg(4)—O(4)	82.9(4)	C(6)—O(6)—Mg(6A)	121.9(10)
O(1)—Mg(4)—O(43)	98.2(4)	C(6)—O(6)—Mg(5A)	121.7(10)
O(41)—Mg(4)—O(43)	92.2(4)	Mg(6A)—O(6)—Mg(5A)	98.5(4)
O(42)—Mg(4)—O(43)	92.4(5)	C(6)—O(6)—Mg(5)	117.0(9)
O(3)—Mg(4)—O(43)	91.2(4)	Mg(6A)—O(6)—Mg(5)	99.0(5)
O(4)—Mg(4)—O(43)	173.9(4)	Mg(5A)—O(6)—Mg(5)	92.9(4)
O(53)—Mg(5)—O(5)	166.9(4)	C(7)—O(7)—Mg(8)	119.4(8)

Table 2.—*Continued.*

O(53)—Mg(5)—O(6A)	91.7(5)	C(7)—O(7)—Mg(7A)	119.6(8)
O(5)—Mg(5)—O(6A)	80.8(4)	Mg(8)—O(7)—Mg(7A)	101.4(5)
O(53)—Mg(5)—O(52)	92.3(5)	C(7)—O(7)—Mg(7)	119.2(9)
O(5)—Mg(5)—O(52)	95.3(5)	Mg(8)—O(7)—Mg(7)	94.9(4)
O(6A)—Mg(5)—O(52)	176.0(6)	Mg(7A)—O(7)—Mg(7)	97.5(4)
O(53)—Mg(5)—O(51)	93.4(5)	C(8)—O(8)—Mg(8A)	124.1(9)
O(5)—Mg(5)—O(51)	98.3(5)	C(8)—O(8)—Mg(8)	119.7(9)
O(6A)—Mg(5)—O(51)	98.9(4)	Mg(8A)—O(8)—Mg(8)	98.8(4)
O(52)—Mg(5)—O(51)	81.0(4)	C(8)—O(8)—Mg(7)	115.5(9)
O(53)—Mg(5)—O(6)	89.2(4)	Mg(8A)—O(8)—Mg(7)	99.8(5)
O(5)—Mg(5)—O(6)	79.6(4)	Mg(8)—O(8)—Mg(7)	92.9(4)
O(6A)—Mg(5)—O(6)	85.5(4)	C(11)—O(11)—Mg(1)	122.9(11)
O(52)—Mg(5)—O(6)	94.4(4)	C(12)—O(12)—Mg(1)	126.6(10)
O(51)—Mg(5)—O(6)	174.8(4)	C(13)—O(13)—Mg(1)	142.3(11)
O(61)—Mg(6)—O(6A)	166.9(5)	C(21)—O(21)—Mg(2)	146.7(12)
O(61)—Mg(6)—O(63)	94.9(5)	C(22)—O(22)—Mg(2)	126.4(11)
O(6A)—Mg(6)—O(63)	95.8(5)	C(23)—O(23)—Mg(2)	124.7(10)
O(61)—Mg(6)—O(5A)	91.8(5)	C(31)—O(31)—Mg(3)	124.9(10)
O(6A)—Mg(6)—O(5A)	79.7(4)	C(32)—O(32)—Mg(3)	141.5(10)
O(63)—Mg(6)—O(5A)	94.8(4)	C(33)—O(33)—Mg(3)	122.7(10)
O(61)—Mg(6)—O(5)	89.0(5)	C(41)—O(41)—Mg(4)	122.1(9)
O(6A)—Mg(6)—O(5)	80.2(4)	C(42)—O(42)—Mg(4)	137.0(11)
O(63)—Mg(6)—O(5)	175.8(6)	C(43)—O(43)—Mg(4)	123.9(10)
O(5A)—Mg(6)—O(5)	83.2(4)	C(51)—O(51)—Mg(5)	136.5(10)
O(61)—Mg(6)—O(62)	91.3(5)	C(52)—O(52)—Mg(5)	122.1(11)
O(6A)—Mg(6)—O(62)	97.2(5)	C(53)—O(53)—Mg(5)	136.7(11)
O(63)—Mg(6)—O(62)	85.2(5)	C(61)—O(61)—Mg(6)	140.4(13)
O(5A)—Mg(6)—O(62)	176.9(6)	C(62)—O(62)—Mg(6)	125.7(12)
O(5)—Mg(6)—O(62)	96.5(4)	C(63)—O(63)—Mg(6)	127.4(11)
O(71)—Mg(7)—O(7A)	167.0(5)	C(71)—O(71)—Mg(7)	133.6(10)
O(71)—Mg(7)—O(7)	89.4(4)	C(72)—O(72)—Mg(7)	126.8(10)
O(7A)—Mg(7)—O(7)	81.8(4)	C(73)—O(73)—Mg(7)	126.6(9)
O(71)—Mg(7)—O(72)	95.1(4)	C(81)—O(81)—Mg(8)	135.1(12)
O(7A)—Mg(7)—O(72)	93.7(4)	C(82)—O(82)—Mg(8)	143.4(13)
O(7)—Mg(7)—O(72)	175.5(5)	C(83)—O(83)—Mg(8)	126.0(11)

[a] For labelling of the symmetry-derived atoms, see the caption to Fig. 2.

NM thus becoming equal to 8:4. The number of coordinated ROH molecules in Ct is higher, as only two of their four magnesium atoms have terminal OR groups and the overall ROH : OR(terminal) ratio becomes equal to 10 : 2. The Mg—μ_3-OR and terminal Mg—O(R)H bond lengths are almost equal (2.05–2.14 and 2.08–2.15 Å, respectively), whereas the terminal bonds involving the OR groups are noticeably shorter (2.01–2.09 Å; see Table 1). The distortion of the cubane cages is similar in both cases and is clearly manifested in the decrease of the OMgO angle and corresponding increase of the MgOMg angle (78.4–85.5° and 92.9–101.4°, respectively).

It is noteworthy that $[Ba(OBu^t)_2(Bu^tOH)_2]_4$ has a quite similar structure, each barium atom bearing two terminal Bu^tOH molecules as well as one terminal OBu^t group [5]. However, the intramolecular hydrogen bonds in this barium complex are formed between those terminal ligands which are bonded to the same barium atom, in contrast to NM in **I**, wherein such hydrogen-bonds link the terminal ligands at different magnesium atoms, thus bridging four of the six $[Mg_2O_2]$ faces of the cubane $[Mg_4O_4]$ cage.

Both crystallographically independent cations Ct1 and Ct2 in structure **I** occupy special positions on the two-fold axis; Ct1 involves Mg(5) and Mg(6) as well as the symmetry related Mg(5A) and Mg(6A) atoms, whereas Ct2 involves the Mg(7), Mg(8) and Mg(7A) and Mg(8A) atoms. Two pairs of oxygen atoms in each cation participate in intracationic ROH ···OR bonds, which correspond to the short O(61)···O(61A) and O(53)···O(53A) in Ct1 and O(71)···O(82) and O(71A)···O(82A) contacts in Ct2. This is probably due to different functions of these hydrogen-bonds relative to the two-fold axis, which ultimately determine the crystallographic uniqueness of each of the two cations Ct1 and Ct2. It is noteworthy that the pairs of oxygen atoms involved in the intracationic hydrogen bonds do not take part in the interionic hydrogen-bonding. At the same time, in contrast with the oxygen atoms of the cations, four of these eight oxygen atoms of NM, which

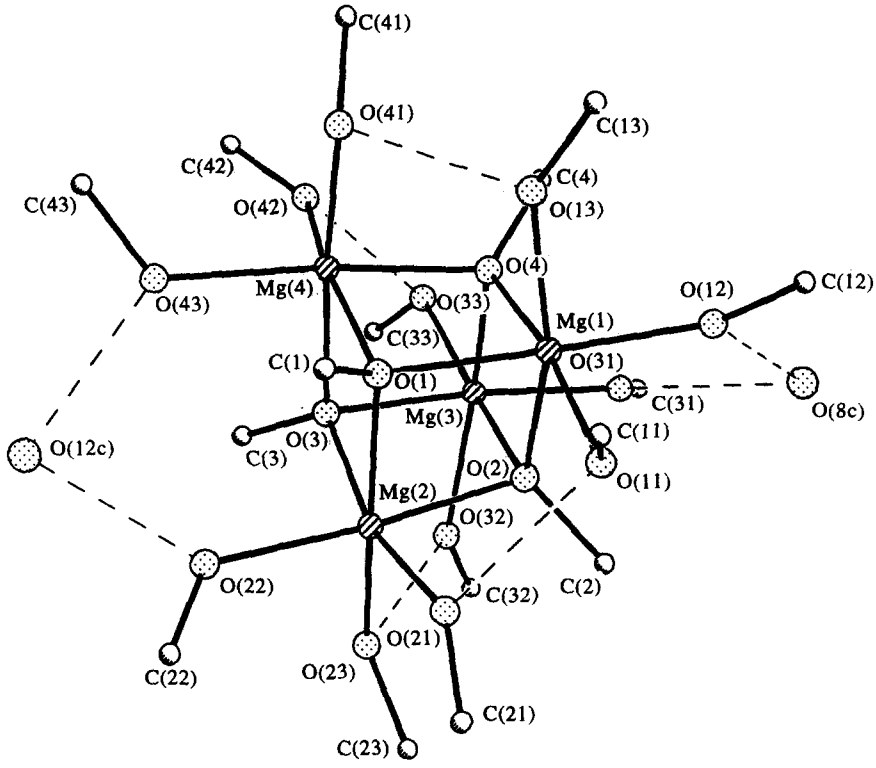


Fig. 1. Structure of the neutral molecule $[Mg_4(\mu_3\text{-}OMe)_4(OMe)_4(MeOH)_8]$ in the crystal of **I**. The O···O contacts corresponding to the intra- and intermolecular hydrogen bonds are shown as dashed lines.

form the intramolecular bonds O(11)···O(21), O(23)···O(32), O(33)···O(42) and O(41)···O(13), are involved in the intermolecular hydrogen bonds with the ROH molecules as well [O(11)···O(3c), O(23)···O(11c), O(33)···O(1c) and O(41)···O(9c)] (Fig. 3). One may therefore assume that this fact may lead to the weakening of the intramolecular hydrogen bonds in NM, which is reflected in the noticeably longer O···O distances in NM (2.49–2.59 Å) as compared to that in Ct1 [2.38(2) and 2.47(2) Å] and Ct2 [2.43(1) Å]. These values of the O···O distances allow us to assign the observed hydrogen bonds in **I** to the category of strong hydrogen bonds (O···O 2.4–2.7 Å) according to the classification suggested in Ref. [6].

All oxygen atoms in **I** participate in hydrogen-bonding, the OH groups acting both as donors and acceptors with the exception of those oxygen atoms and OH groups which are involved in the intracationic hydrogen bonds. NM, on one hand, and Ct1 and Ct2

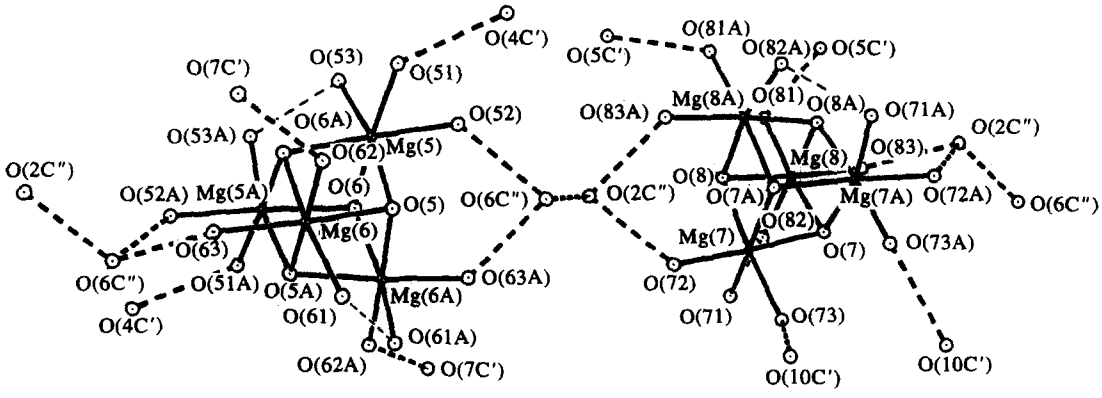


Fig. 2. The fragment of the ···Ct1···Ct2··· chain in the structure of **I**. The atoms related to the reference atoms of the Ct1 and Ct2 cations by the $x, -y, z$ and $1-x, y, z$ symmetry operations, respectively, are designated by the letter A in the atom label. The apostrophe and quotation marks indicate the participation of the oxygen atoms of the solvating molecules in the hydrogen bond links between and within the chains, respectively.

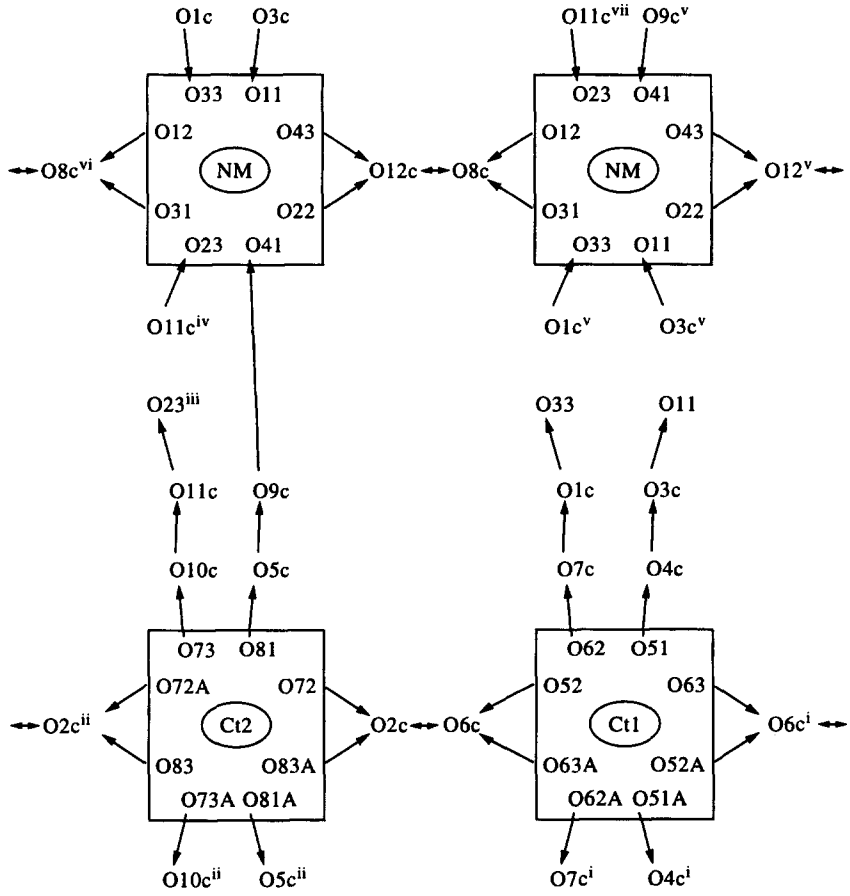


Fig. 3. The general scheme of hydrogen-bonding pattern in the structure of **I**. The arrows indicate the directions of the hydrogen bonds O—H → O. The superscripts are used for designating the oxygen atoms involved in various residues of the structure and derived from the reference atoms by means of the following symmetry operations: (i) $-x, -y, z$; (ii) $1-x, -y, z$; (iii) $1-x, 0.5-y, z-0.5$; (iv) $1-x, 0.5-y, 0.5+z$; (v) $x-0.5, 0.5-y, z$; (vi) $0.5+x, 0.5-y, z$; (vii) $0.5-x, y, 0.5+z$.

on the other, are engaged in two different infinite chains ···NM···NM··· and ···Ct1···Ct2···, both of which stretch along the *a*-axis (Fig. 2 shows a fragment of the cationic chain). The NM and Ct residues within both chains are linked *via* the $[(RO)_2H]^-$ anions each of which consists of one OR group and one solvating alcohol molecule, the O(8c)···O(12c) and O(2c)···O(6c) distances in the two crystallographically independent anions being equal to 2.423(15) and 2.419(15) Å, respectively. The ···NM···NM··· and ···Ct1···Ct2··· chains are connected with each other through the solvating ROH molecules. The general scheme of hydrogen-bonding in **I** is given in Fig. 3; the O···O distances corresponding to the hydrogen bonds are listed in Table 3. It may be seen in Fig. 3 that the solvating ROH molecules form tightly bound pairs which act as links between the ···NM···NM··· and ···Ct1···Ct2··· chains, thus producing the infinite three-dimensional hydrogen-bonding framework in the crystal of **I**.

The cubane $[M_4O_4]$ cage found in **I** presents one of the two main structural patterns known for tetranuclear mono- or bimetallic alkoxides or oxoalkoxides. Such a cage is formed by fusion of two four-membered $[M_2O_2]$ rings along all four Mg—O edges and involves the tetrahedral array of metal atoms, whereas the alternative structural pattern involves the planar array of the metal atoms. The cubane-shaped complexes are formed by the above mentioned calcium oxoethoxide [1], as well as by a number of molecular aggregates, namely $[MOBu^t]$, where M = K, Rb, Cs [7], $[NaO\text{-}CH(CF_3)_2]_4$ [8], $[MOSiMe_3]_4$ (M = Li to Cs) [7] and $[Ti(OR)_4]$, where R = Me or $SiPh_3$ [9, 10]. In all cases the cubane cage exhibits the same geometric distortions as those observed in the structure of **I**, i.e. the increase of the bond angles at the oxygen atoms and simultaneous decrease of the bond angles at the metal atoms. It is noteworthy that the minimal angular distortions of the cubane cage were observed for the derivatives of the alkaline metals. The cubane alkoxide molecules were proved to be much more stable than tetranuclear alkoxides with the alternative structure, e.g. titanium complexes $[Ti(OMe)_4]$ [11]; many cubanes were proved to exist in the vapour as well as

Table 3. Interatomic O···O distances (Å) corresponding to inter- and intramolecular hydrogen bonds in the structure of I[a]

O(11)···O(21)	2.539 (0.016)	O(12C)···O(8C)	2.423 (0.015)
O(23)···O(32)	2.491 (0.015)	O(33)···O(1C)	2.586 (0.016)
O(42)···O(33)	2.552 (0.015)	O(1C)···O(7C)	2.721 (0.018)
O(13)···O(41)	2.594 (0.014)	O(23)···O(11C)^{iv}	2.604 (0.016)
O(61)···O(61A)	2.383 (0.023)	O(11C)···O(10C)	2.666 (0.017)
O(53)···O(53A)	2.468 (0.020)	O(62)···O(7C)	2.654 (0.017)
O(71)···O(82)	2.434 (0.012)	O(63)···O(6C)^{i}	2.555 (0.016)
O(11)···O(3C)	2.585 (0.017)	O(6C)···O(2C)	2.419 (0.015)
O(3C)···O(4C)	2.586 (0.020)	O(51)···O(4C)	2.665 (0.016)
O(12)···O(8C)^{vi}	2.634 (0.015)	O(52)···O(6C)	2.657 (0.016)
O(31)···O(8C)^{vi}	2.620 (0.015)	O(72)···O(2C)	2.609 (0.015)
O(41)···O(9C)	2.582 (0.014)	O(83)···O(2C)^{ii}	2.610 (0.014)
O(9C)···O(5C)	2.627 (0.017)	O(81)···O(5C)	2.657 (0.016)
O(22)···O(12C)	2.617 (0.016)	O(73)···O(10C)	2.725 (0.016)
O(43)···O(12C)	2.653 (0.015)		

[a] For labelling of the symmetry-derived atoms, see the caption to Fig. 3.

in the solid phase [7, 8]. It is also remarkable that the $[Mg_4(OR)_6(ROH)_{10}]^{2+}$ cations found in the structure of I most probably exist in solution. This conclusion may be drawn from the fact that the crystals of methoxochlorides $[Mg_4(\mu_3\text{-}OR)_4(OR)_2(ROH)_{10}]Cl_2$ [12] with the same cation were isolated as one of the products of the reaction of I with $MgCl_2$ in ROH.

In conclusion we can try to use the information obtained from the crystal structure of I in order to gain some insight into the process of its desolvation. The isotherms of dissociation vapour pressure (Fig. 4) show that the equilibrium process takes place in the range of compositions from 1 : 3.5 up to approximately 1 : 1. At temperatures of 40–50°C the irreversible destruction of I starts for the compositions of 1 : 2 and 1 : 1.5, and is completed when the composition reaches 1 : 0.75. Further desolvation leads to the formation of the phases of variable composition and no longer represents the equilibrium process.

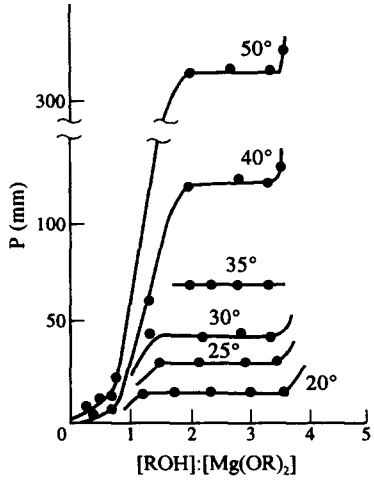


Fig. 4. The isotherms of the dissociation vapour pressure in the $Mg(OMe)_2$–MeOH system.

On degradation of I up to the composition of $Mg(OR)_2 \cdot 0.75ROH$, 2.75 M of ROH per 1 M of $Mg(OR)_2$ are lost. As was mentioned above, in the structures of the NM and Ct cubanes there exist ROH molecules which are bound more tightly than the others due to intramolecular hydrogen bonds; there are four such tightly bound molecules in NM and two such molecules in Ct. If we assume that these tightly bound molecules are the last to be eliminated in the desolvation process, we may suggest the existence of an intermediate with the composition $Mg(OR)_2 \cdot 0.75ROH$, which is in good agreement with the results of the tensimetry study. It is noteworthy that up to this composition the isolated cubane aggregates are retained in the intermediate complexes and, therefore, the desolvation process still remains reversible. The desolvation most probably begins with the elimination of eight solvating ROH molecules, thus producing the species of the overall composition $[Mg_8(OR)_{14}(ROH)_{18}]^{2+}[(RO)_2H]_2^-$, i.e. "$Mg(OR)_2 \cdot 2.5ROH$". Thereafter, the destruction of the anion occurs and the formation of the product consisting of the neutral cubanes, $Mg_4(OR)_8(ROH)_8$, i.e. "$Mg(OR)_2 \cdot 2ROH$", may be anticipated. Ultimately, the ROH molecules, which do not participate in hydrogen-bonding, are eliminated. Thus, after elimination of 22 ROH molecules from the starting $[Mg_4(OR)_6(ROH)_{10}]^{2+}[(RO)_2H]_2^-[Mg_4(OR)_8(ROH)_8] \cdot 8ROH$ compound, neutral molecules of $[Mg_4(OR)_8(ROH)_3]$ are formed. The magnesium atoms' coordination numbers in these molecules cannot attain the normal value of six and would remain equal to four or five, which provokes the aggregation of cubane cages, accompanied by the formation of stable polymeric structure and the increase of the coordination numbers of metal atoms. Indeed, the samples corresponding to the 1 : 1 to 1 : 0.75 compositions are amorphous and insoluble in alcohol. Their desolvation proceeds at temperatures $\geqslant$ 50°C and is

accompanied by partial thermolysis, which normally occurs at lower temperatures for methoxides than for their higher homologues. Therefore, the alkoxide with the "$Mg(OR)_2$" composition should contain oxo bridges, and the above-mentioned calcium ethoxide [1] may be considered as an example of such a species.

The X-ray powder diffraction pattern of $Mg(OR)_2$ shows diffuse reflections, which may be indexed on the basis of the hexagonal unit cell reported for the alkaline-earth methoxides, belonging to the CdI_2 structural type [4,13]. One can therefore suggest the formation of $[Mg(OR)_2]_\infty$ orthogonal to the six-fold symmetry axis. However, most of the $Mg(OR)_2$ sample consist of the amorphous phase, which is reflected, in particular, in the considerable difference (up to 40%) between the experimental and calculated density values [4]. It is noteworthy that the calcium, strontium and barium methoxides, which are also formed as a result of the destruction of the corresponding $M(OR)_2 \cdot 4ROH$ solvates, yield samples with significantly higher degrees of crystallinity, so that the corresponding experimental/calculated density ratio is in the range of 96–98% [4].

Note added in proof

After this manuscript was submitted for publication, we became acquainted with the paper by H. Thoms, M. Epple, H. Viebrock and A. Reller (*J. Mater. Chem.*, 1995, vol. 5, p. 589) wherein the crystal structure of the $Mg(OMe)_2 \cdot 2(MeOH)$ solvate is reported. The striking similarity of the unit cell dimensions and the closeness of the symmetries of both crystals make us believe that one and the same compound was in fact studied in both cases. The elemental analysis reported by H. Thoms *et al.* and the corresponding disolvate formulation would not have differed significantly for the 3.5-solvate and may have easily been affected by the instability of the product, which readily loses the solvating methanol molecules.

Acknowledgements—The authors gratefully acknowledge the financial support of INTAS (Grant No. 94-771) and Russian Foundation for Basic Research (Project Nos 94-08338 and 96-33553).

REFERENCES

1. Turova, N. Ya., Turevskaya, E. P., Kessler, V. G., Yanovsky, A. I. and Struchkov, Yu. T., *J. Chem. Soc., Chem. Commun.*, 1993, 21.
2. Szarwasy, E., *Chem. Ber.* 1897, **30,** 806, 1836.
3. Quinet, M., *Bull. Soc. Chim. Fr.*, 1935, **5**(2), 1201.
4. Turowa, N. Ya., Popowkin, B. A. and Nowoselowa, A. W., *Z. Anorg. Allg. Chem.*, 1969, **365,** 100.
5. Borup, B., Samuels, J. A., Streib, W. E. and Caulton, K. G., *Inorg. Chem.*, 1994, **33,** 994.
6. Brown, I. D., *Acta Cryst.*, 1976, **A32,** 24.
7. Weiss, E., Alsdorf, H. and Grützmacher, H.-F., *Ber.* 1968, **101,** 3777; 1970, **103,** 1190.
8. Samuels, J. A., Lobkovsky, E. B., Streib, W. E., Folting, K., Huffman, J. C., Zwanziger, J. W. and Caulton, K. G., *J. Am. Chem. Soc.*, 1993, **115,** 5093.
9. Dahl, L. F., Davis, G. L., Wampler, D. L. and West, R., *J. Inorg. Nucl. Chem.*, 1962, **24,** 357.
10. Harvey, S., Lappert, M. F., Raston, C. L., Skelton, B. W., Srivastava, G. and White, A. H., *J. Chem. Soc., Chem. Commun*, 1988, 1216.
11. Wright, D. A. and Williams, D. A., *Acta Cryst.*, 1968, **B24,** 1107.
12. Botchkova, R. I., Golovatchev, V. P., Turevskaya, E. P. and Belov, N. V., *Doklady AN SSSR*, 1969, **189,** 1246.
13. Stäglich, H. and Weiss, E., *Chem. Ber.*, 1978, **111,** 901.

Pergamon

PII: S0277-5387(96)00342-7

Polyhedron Vol. 16, No. 6, pp. 975–981, 1997
Copyright © 1996 Elsevier Science Ltd
Printed in Great Britain. All rights reserved
0277–5387/97 $17.00+0.00

Preparation and characterization of zinc(II) and palladium(II) complexes with 16-ethyl-5,6,7,8,9,14-hexahydrodibenzo[*b*,*i*][1,4,8,11]-tetraazacyclotetradecine

Mamoru Hashimoto and Kazunori Sakata*

Department of Chemistry, Faculty of Engineering, Kyushu Institute of Technology, Tobata-ku, Kitakyushu 804, Japan

(Received 25 June 1996; accepted 12 July 1996)

Abstract—The zinc(II) and palladium(II) complexes of 16-ethyl-5,6,7,8,9,14-hexahydrodibenzo [*b*,*i*][1,4,8,11]tetraazacyclotetradecine (HL^1) and 5,14-dihydro-7,16-diethyldibenzo[*b*,*i*][1,4,8,11]tetraazacyclotetradecine (H_2L^2) have been synthesized and their spectroscopic data determined. The absorption bands of ML^1X (M = Zn, Pd; X = Cl, NCS, ClO_4) observed in the 20,400–23,900 cm^{-1} region were attributable to $\pi \rightarrow \pi^*$ and charge transfer transitions. Those bands for the three palladium(II) complexes (PdL^1X) are similar to each other in various solvents, but the bands of ZnL^1X are slightly different from one another. The ^{13}C NMR signals for $NiL^1(ClO_4)$ and $PdL^1(ClO_4)$ are similar to each other, but the C(15) and C(17) carbon signals for $ZnL^1(ClO_4)$ exhibit downfield shifts upon metal coordination. Judging from the molar conductances for the complexes, $ZnL^1(ClO_4)$ and PdL^1X (X = Cl, NCS, ClO_4) are 1:1 electrolytes in acetonitrile and nitromethane, but ZnL^1Cl and ZnL^1 (NCS) are non-electrolytes. The treatment of PdL^1X (X = Cl, NCS, ClO_4) in methanol solution with an excess of base in air gave (7-ethyldibenzo [*b*,*i*][1,4,8,11]tetraazacyclotetradecinato)palladium(II) (PdL^3). Copyright © 1996 Elsevier Science Ltd

Keywords: dibenzotetraazaannulene; macrocycle; zinc complex; palladium complex; NMR spectrum; absorption spectrum.

Our recent research has been concerned with structural and spectroscopic properties of tetraazamacrocyclic complexes. Although much attention has been paid to the chemistry of transition-metal complexes with dibenzotetraaza[14]annulene macrocycles [1], there have been only a few studies of zinc and palladium complexes and/or a conjugated π-electron system [2]. Recently, we have synthesized (16-ethyl-5,6,7,8-tetrahydro-9*H*-dibenzo[*b*,*i*][1,4,8,11] tetraazacyclotetradecinato) nickel(II) complexes with eight types of counteranions [3]. Furthermore, we have reported the counteranion effect of their nickel(II) complexes.

In the present work, we have synthesized zinc(II) and palladium(II) complexes of 16-ethyl-5,6,7,8,9,14-hexahydrodibenzo[*b*,*i*][1,4,8,11]tetraazacyclotetradecine (HL^1) having three types of counteranions. The palladium(II) complexes of HL^1 in methanol are oxidized by the addition of excess base, and lead to (7-ethyldibenzo[*b*,*i*][1,4,8,11]tetraazacyclotetradecinato)-palladium(II) (PdL^3). We also prepared the zinc(II) and palladium(II) complexes of 5,14-dihydro-7,16-diethyldibenzo[*b*,*i*][1,4,8,11]tetraazacyclotetradecine (H_2L^2) following the procedure of NiL^2 [4]. We have characterized the spectral properties of ZiL^1X, PdL^1X, ZnL^2, PdL^2 and PdL^3 (X = Cl, NCS and ClO_4).

EXPERIMENTAL

Physical measurements

UV and visible spectra covering the 12,500–50,000 cm^{-1} region were recorded on a Shimadzu UV 200S

* Author to whom correspondence should be addressed.

double beam spectrophotometer at room temperature. IR spectra in the range of 400–4000 cm^{-1} were recorded on a Jeol JIR-5500 FT-IR spectrophotometer and a Hitachi 260-30 spectrophotometer at room temperature as Nujol mulls and using the potassium bromide disc method. ^1H and ^{13}C NMR measurements were recorded using a Jeol JNM-FX 60 spectrometer. The NMR spectra were obtained in $CDCl_3$, DMSO-d_6 and DMF-d_7. Chemical shifts are given in ppm relative to tetramethylsilane as an internal reference. Conductivity measurements were performed with acetonitrile and DMF solutions of the complexes kept at 25.0 ± 0.1°C using a Coolnics Thermo-Bath (model CTE-310). Conductivities were measured with a TOA Electronics Ltd CM-20E. FAB mass spectra (in a matrix of neat glycerin) for ZnL^1X and PdL^1X (X = Cl, NCS and ClO_4) and EI mass spectra (at 70 eV) for ZnL^2, PdL^2, NiL^3 and PdL^3 were obtained on a Jeol JMS-DX 300 gas chromatograph mass spectrometer. Argon was employed as the fast-atom beam. Melting points were determined with a Yanaco MP-S3 micro melting point apparatus (hot-plate type).

Preparation of macrocycles and their complexes

16-*Ethyl*-5,6,7,8,9,14-*hexahydrodibenzo*[*b*,*i*]-[1,4,8,11]*tetraazacyclotetradecine* (HL^1). The synthetic procedures for HL^1 and its nickel(II) complexes have been reported previously [3].

(16-*Ethyl*-5,6,7,8-*tetrahydro-9H-dibenzo*[*b*,*i*]-[1,4,8,11]*tetraazacyclotetradecinato*)*zinc*(II) *chloride* (ZnL^1Cl). A mixture of HL^1 (0.160 g, 0.50 mmol), zinc(II) chloride (0.082 g, 0.60 mmol) and methanol (30 cm^3) was heated at 50°C for 1 h with stirring. Water (30 cm^3) and ammonium chloride (1.0 g, 0.019 mol) were added to the reaction mixture. A precipitate was isolated by filtration and washed with water to give 154 mg (73%) of yellow needles, m.p. 140°C (dec.). IR KBr: 1609, 1461, 1310, 1283, 748 cm^{-1}. MS *m*/*z* (relative intensity): 383 (100), 384 (38.3), 385 (65.6), 386 (32.3), 387 (44.1). UV (acetonitrile): λ_{max} 472 (21,300), 271 (17,500), 246sh (18,700) nm.

(16-*Ethyl*-5,6,7,8-*tetrahydro-9H-dibenzo*[*b*,*i*]-[1,4,8,11]*tetraazacyclotetradecinato*)*zinc*(*II*) *isothiocyanate* (ZnL^1NCS). A mixture of HL^1 (0.160 g, 0.50 mmol), zinc(II) acetate dihydrate (0.132 g, 0.60 mmol) and methanol (30 cm^3) was heated at 50°C for 1 h with stirring. Water (60 cm^3) and ammonium thiocyanate (2.0 g, 0.026 mol) were added to the reaction mixture. A precipitate was separated by filtration and washed with water to give 215 mg (97%) of yellow needles, m.p. 155°C (dec.). IR (KBr): 3150 (N—H), 2074 (NCS), 1609, 1461, 1308, 1280, 751 cm^{-1}. MS *m*/*z* (relative intensity): 383 (100), 384 (39.4), 385 (63.1), 386 (33.1), 387 (42.1). UV (acetonitrile): λ_{max} 470 (23,200), 270 (17,500), 253 (17,200) nm.

(16-*Ethyl*-5,6,7,8-*tetrahydro-9H-dibenzo*[*b*,*i*]-[1,4,8,11]*tetraazacyclotetradecinato*)*zinc*(II) *perchlorate* (ZnL^1ClO_4). A mixture of HL^1 (0.160 g, 0.50 mmol), zinc(II) perchlorate (0.159 g, 0.60 mmol) and methanol (30 cm^3) was heated at 50°C for 1 h with stirring. Water (60 cm^3) and ammonium perchlorate (3.0 g, 0.026 mol) was added to the reaction mixture. A precipitate was recovered by filtration and washed with water to give 168 mg (69%) of yellow needles, m.p. 128°C (dec.). IR (KBr): 3252 (N—H), 1593, 1455, 1308, 1283, 1120–1040 (Cl—O), 748, 622 (Cl—O) cm^{-1}. MS *m*/*z* (relative intensity): 383 (100), 384 (37.4), 385 (64.3), 386 (30.4), 387 (42.0). UV (acetonitrile): λ_{max} 468 (21,300), 270 (17,400) nm.

(16-*Ethyl*-5,6,7,8-*tetrahydro-9H-dibenzo*[*b*,*i*]-[1,4,8,11]*tetraazacyclotetradecinato*)*palladium*(II) *chloride* (PdL^1Cl). A mixture of HL^1 (0.160 g, 0.50 mmol), palladium(II) acetate (0.150 g, 0.67 mmol) and methanol (60 cm^3) was treated at 20°C for 2 h with stirring while nitrogen was continuously bubbled through it. The reaction mixture was filtered and water (100 cm^3) and ammonium chloride (2.0 g, 0.037 mol) were added to the filtrate. A precipitate was separated by filtration and washed with water to give 219 mg (95%) of yellow needles, m.p. 247°C (dec.). IR (KBr): 1588, 1443, 1320, 1280, 1233, 742 cm^{-1}. MS *m*/*z* (relative intensity): 423 (41.3), 424 (79.9), 425 (100), 426 (32.9), 427 (83.3), 428 (27.3), 429 (38.7). UV (acetonitrile): λ_{max} 487 (21,900), 463 (16,000), 265 (16,500), 233 (18,500) nm.

(16-*Ethyl*-5,6,7,8-*tetrahydro-9H-dibenzo*[*b*,*i*]-[1,4,8,11]*tetraazacyclotetradecinato*)*palladium*(II) *isothiocyanate* (PdL^1NCS). This was prepared from HL^1 (0.160 g, 0.50 mmol), palladium(II) acetate (0.150 g, 0.67 mmol), methanol (60 cm^3), water (100 cm^3) and ammonium thiocyanate (2.0 g, 0.026 mol) following the above procedure, and was recovered by filtration to obtain 232 mg (96%) of brown–yellow plates, m.p. 257°C (dec.). IR (KBr): 3055 (N—H), 2050 (NCS), 1590, 1440, 1319, 1278, 1234, 745 cm^{-1}. MS *m*/*z* (relative intensity): 423 (37.7), 424 (80.4), 425 (100), 426 (33.6), 427 (82.9), 428 (24.3), 429 (37.9). UV (acetonitrile): λ_{max} 487 (22,000), 464sh (17,000), 266 (17,200), 234 (20,500) nm.

(16-*Ethyl*-5,6,7,8-*tetrahydro-9H-dibenzo*[*b*,*i*]-[1,4,8,11]*tetraazacyclotetradecinato*)*palladium*(II) *perchlorate* (PdL^1ClO_4). This complex was prepared from HL^1 (0.160 g, 0.50 mmol), palladium(II) acetate (0.150 g, 0.67 mmol), methanol (60 cm^3), water (100 cm^3) and ammonium perchlorate (3.0 g, 0.026 mol) following the above procedure, and was isolated by filtration to yield 242 mg (92%) of brown–yellow needles, m.p. 279°C (dec.). IR (KBr): 3210 (N—H), 1588, 1440, 1315, 1265, 1231, 1120–1040 (Cl—O), 740, 620 (Cl—O) cm^{-1}. MS *m*/*z* (relative intensity): 423 (41.2), 424 (80.6), 425 (100), 426 (34.0), 427 (77.9), 428 (25.5), 429 (45.3). UV (acetonitrile): λ_{max} 487 (20,300), 464 (16,100), 264 (12,100), 232 (15,100) nm.

5,14-*Dihydro*-7,16-*diethyldibenzo*[*b*,*i*][1,4,8,11]-*tetraazacyclotetradecine* (H_2L^2). The synthetic procedure for H_2L^2 and its nickel(II) complex have been described previously [4].

(7,16-*Diethyldibenzo*[*b*,*i*][1,4,8,11]*tetraazacyclotetradecinato*)*zinc*(II) (ZnL^2). A mixture of H_2L^2 (0.172 g, 0.50 mmol), zinc(II) acetate dihydrate (0.154 g, 0.70 mmol), sodium acetate trihydrate (0.150 g, 1.10 mmol) and ethanol (60 cm^3) was refluxed for 20 h with stirring while nitrogen was continuously bubbled through it. The product was collected and washed with ethanol to give 146 mg (72%) of brown needles, m.p. 243°C (dec.). IR (KBr): 1580, 1470, 1376, 1332, 1208, 734 cm^{-1}. MS *m*/*z* (relative intensity): 391 (100), 392 (27.9), 393 (60.8), 394 (22.7), 395 (36.3), 404 (17.3), 405 (8.5), 406 (71.5), 407 (22.0), 408 (43.2), 409 (16.9), 410 (25.9), 411 (6.4); UV (DMF): λ_{max} 504 (18,100), 486sh (17,200), 420 (69,000), 402sh (41,700), 291 (28,300) nm.

(7,16)-*Diethyldibenzo*[*b*,*i*][1,4,8,11]*tetraazacyclotetradecinato*)*palladium*(II) (PdL^2). A mixture of H_2L^2 (0.344 g, 1.00 mmol), palladium(II) sodium chloride trihydrate (0.350 g, 1.00 mmol) and DMF (25 cm^3) was refluxed for 1 h with stirring while nitrogen was continuously bubbled through it. Palladium(II) sodium chloride trihydrate (0.150 g, 0.43 mmol) was added to the reaction mixture, which was further refluxed for 1 h and filtered to remove the inorganic residue. Upon cooling the filtrate with an ice water bath, the product was separated and washed several times with methanol (10 cm^3) to give 186 mg (41%) of dark brown plates, m.p. 217°C (dec.). IR (KBr): 1595, 1470, 1443, 1338, 1228, 740 cm^{-1}. MS *m*/*z* (relative intensity): 431 (12.1), 432 (26.9), 433 (38.0), 434 (12.9), 435 (28.7), 436 (10.7), 437 (13.7), 446 (77.1), 448 (100), 449 (24.9), 450 (82.3), 451 (21.2), 452 (37.0), 453 (9.3). UV (DMF): λ_{max} 498 (16,700), 476 (14,800), 438 (29,900), 346 (5650), 274 (22,000) nm.

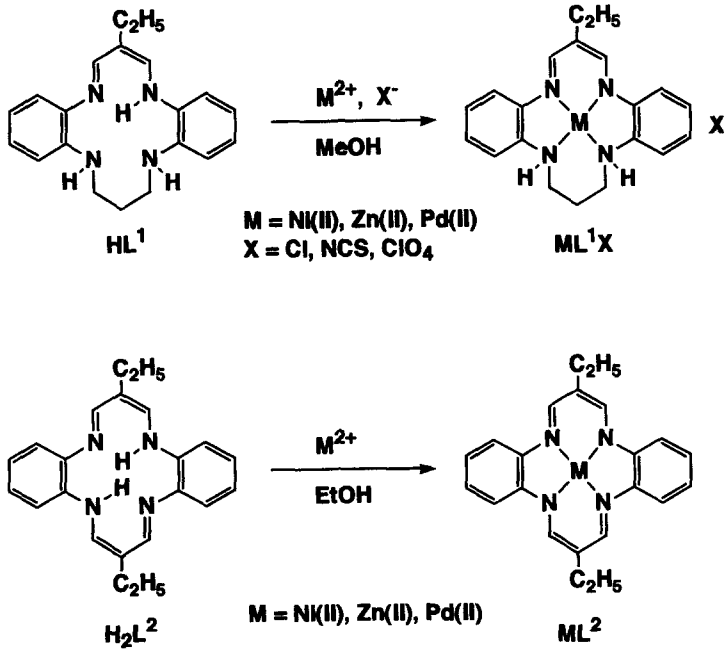
(16-*Ethyldibenzo*[*b*,*i*][1,4,8,11]*tetraazacyclotetradecinato*)*palladium*(II) (PdL^3). A mixture of PdL^2Cl (0.100 g, 0.22 mmol), sodium hydroxide (0.10 g, 2.5 mmol) and methanol (100 cm^3) was heated at 40°C for 6 h with stirring. Upon cooling the reaction mixture with an ice water bath, the crystalline solid was recovered by filtration and washed several times with methanol (10 cm^3) to give 50 mg (55%) of dark brown microcrystals, m.p. 262°C (dec.). IR (KBr): 1573, 1442, 1328, 732 cm^{-1}. MS *m*/*z* (relative intensity): 403 (36.0), 404 (79.1), 405 (100), 406 (24.9), 407 (84.6), 408 (21.7), 409 (39.1), 417 (20.3), 418 (47.1), 419 (60.8), 420 (82.1), 421 (23.9), 422 (66.3), 423 (16.6), 424 (25.4). UV (acetonitrile): λ_{max} 476 (13,300), 454 (12,400), 427 (32,500), 308 (4280), 268 (13,900) mm.

(16-*Ethyldibenzo*[*b*,*i*][1,4,8,11]*tetraazacyclotetradecinato*)*nickel*(II) (NiL^3). A mixture of methanol (100 cm^3), NiL^1Cl (0.100 g, 0.24 mmol) and sodium hydroxide (0.10 g, 2.5 mmol) was reacted as described above for 6 h to yield 73 mg (80%) of reddish violet needles, m.p. 244°C (dec.). IR (KBr): 1598, 1471, 1336, 1257, 739 cm^{-1}. MS *m*/*z* (relative intensity): 357 (100), 358 (23.8), 359 (41.2), 360 (11.1), 372 (81.0), 373 (21.3), 374 (32.1), 375 (9.0), 376 (6.1). UV (acetonitrile): λ_{max} 510 (7350), 470 (7370), 429 (59,400), 307 (15,700), 272 (19,900) nm.

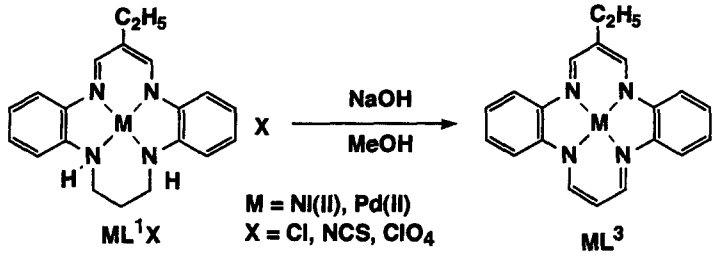
RESULTS AND DISCUSSION

Preparation and properties of the metal complexes

The reaction of macrocycle HL^1 and/or H_2L^2 with zinc(II) and/or palladium(II) salts gave the cor-



Scheme 1.



Scheme 2.

responding zinc(II) and/or palladium(II) complexes (ML^1X, ML^2: M = Zn, Pd, X = Cl, NCS, ClO_4) in good yield. PdL^1X and NiL^1X in methanol are oxidized by the addition of base and by molecular oxygen, and then PdL^3 and NiL^3 are obtained [3,5]. On the other hand, ZnL^1X are recovered unchanged in methanol solution following the above procedure. The analytical data of the zinc(II), palladium(II) and nickel(II) complexes are listed in Table 1. Elemental analyses of these crystalline samples were in fair agreement with the compositions of these compounds.

Electronic spectra

The electronic absorption spectra covering the 15,000–40,000 cm^{-1} range in acetonitrile are shown in Fig. 1 for HL^1, $PdL^1(ClO_4)$ and PdL^3. The intense absorption bands for $PdL^1(ClO_4)$ observed in the 20,500–21,600 cm^{-1} region are reasonably attributed to $\pi \rightarrow \pi^*$ transitions within a ligand molecule and charge transfer transitions from metal to ligand, since the molar extinction coefficients are much larger than those normally assigned to ligand-field transitions.

Table 1. Analytical data for the complexes

Complex	Empirical formula	Elemental analyses Calc./Found (%) C	H	N
ZnL^1Cl	$C_{20}H_{23}N_4ZnCl$	57.2	5.5	13.3
		56.9	5.7	13.3
$ZnL^1(NCS)$	$C_{21}H_{23}N_5ZnS$	57.0	5.2	15.8
		57.1	5.4	15.6
$ZnL^1(ClO_4)$	$C_{20}H_{23}N_4ZnClO_4$	49.6	4.8	11.6
		49.3	5.1	11.6
PdL^1Cl	$C_{20}H_{23}N_4PdCl$	52.1	5.0	12.2
		52.2	5.3	11.8
$PdL^1(NCS)$	$C_{21}H_{23}N_5PdS$	52.1	4.8	14.5
		51.9	4.8	14.1
$PdL^1(ClO_4)$	$C_{20}H_{23}N_4PdClO_4$	45.7	4.4	10.7
		46.0	4.4	10.5
NiL^3	$C_{20}H_{18}N_4Ni$	64.4	4.9	15.0
		64.1	5.2	14.8
PdL^3	$C_{20}H_{18}N_4Pd$	57.1	4.3	13.3
		56.9	4.4	13.3
ZnL^2	$C_{22}H_{22}N_4Zn$	64.8	5.4	13.7
		65.1	5.5	13.8
PdL^2	$C_{22}H_{22}N_4Pd$	58.9	4.9	12.5
		58.9	5.2	12.6

Those bands for the three palladium(II) complexes (PdL^1X; X = Cl, NCS, ClO_4) are similar to each other, and are not influenced by any anion [3]. The ligand-field bands were not assigned for the present complexes, because all the ligand-field bands were obscured by the $\pi \rightarrow \pi^*$ and charge transfer transition bands of high intensity. The spectral behaviour is consistent with the square-planar coordination and is similar to that observed for tetraaza[14]annulene metal(II) complexes [1g, 4].

The electronic absorption spectra for $ZnL^1(ClO_4)$ and ZnL^2 are shown in Fig. 2. The intense absorption bands for ZnL^1X (X = Cl, NCS, ClO_4) observed in the 21,100–21,400 cm^{-1} range slightly differ from one another. The difference of these bands is observed in various solvents, such as ethyl acetate, chloroform, acetonitrile, DMF, *etc.* Namely, the absorption bands are affected by the counteranion and the solvent. This fact may show that the coordination structures of the zinc(II) complexes assume distorted square-planar and/or pentacoordinated configurations because of their ability to take the tetrahedral coordination of zinc(II).

General features of the spectra for ML^2 and ML^3 (M = Zn, Pd and Ni) are similar to each other. A pair of weaker bands (ε = 7000–18,000) are observed in the 19,600–22,000 cm^{-1} region, and the extremely intense absorption bands (ε = 30,000–69,000) observed in the 22,800–23,800 cm^{-1} range are assigned to the so-called Soret-type transition, as estimated for metal porphyrins [6]. Since the nickel(II) and palladium(II) complexes do not indicate any significant absorption below *ca* 19,000 cm^{-1}, they may be square-planar coordinations.

Molar conductivity

The molar conductances for zinc(II) and palladium(II) complexes are listed in Table 2, together with those for nickel(II) complexes. $ZnL^1(ClO_4)$ and PdL^1X (X = Cl, NCS, ClO_4) are 1 : 1 electrolytes in acetonitrile and nitromethane, but ZnL^1Cl and $ZnL^1(NCS)$ are non-electrolytes [7]. $NiL^1(ClO_4)$ $ZnL^1(ClO_4)$ and $PdL^1(ClO_4)$ are 1 : 1 electrolytes and

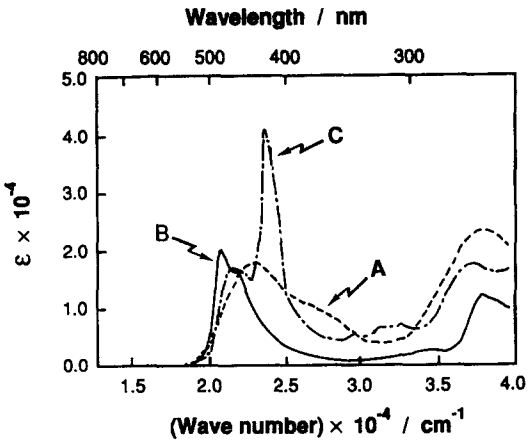


Fig. 1. Electronic absorption spectra for macrocycle and palladium(II) complexes in acetonitrile at room temperature. (A) HL^1; (B) $PdL^1(ClO_4)$; (C) PdL^3.

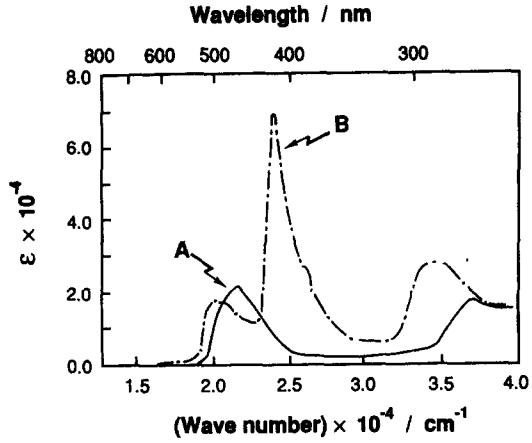


Fig. 2. Electronic absorption spectra for zinc(II) complexes in acetonitrile at room temperature. (A) $ZnL^1(ClO_4)$; (B) ZnL^2.

Table 2. Molar conductances for ML^1X complexes at 25°C[a]

Complex	Λ_M (Ω^{-1} cm^2 mol^{-1})		Type of Electrolyte[b]	Ref.
	Acetonitrile	Nitromethane		
ZnL^1Cl	5.0	4.3	0	
$ZnL^1(NCS)$	4.8	7.2	0	
$ZnL^1(ClO_4)$	131.2	48.6	2 (1 : 1)	
PdL^1Cl	94[c]	37[c]	2 (1 : 1)	
$PdL^1(NCS)$	103.4	55.0	2 (1 : 1)	
$PdL^1(ClO_4)$	124.6	74.8	2 (1 : 1)	
NiL^1Cl	24.2	16.1	0	3
$NiL^1(NCS)$	121.7	68.5	2 (1 : 1)	3
$NiL^1(ClO_4)$	139.7	86.6	2 (1 : 1)	3

[a] Measured in acetonitrile, for *ca* 10^{-3} mol dm^{-3} solutions.

[b] Assignment of the type of electrolyte presented in solutions was made on the basis of the conductance data compiled by Geary [7].

[c] For *ca* 10^{-4} mol dm^{-3} solutions.

are tetracoordinated complexes in acetonitrile and nitromethane solutions. Therefore, it is noted that the perchlorate anions of $ML^1(ClO_4)$ (M = Ni, Zn, Pd) ionize in these solvents. ZnL^1Cl, $ZnL^1(NCS)$ and NiL^1Cl become pentacoordinated complexes by taking up a chloride and/or an isothiocyanate anion in the axial state. On the other hand, the chloride and isothiocyanate anions of $NiL^1(NCS)$, PdL^1Cl and $PdL^1(NCS)$ ionize. These facts show that ML^1X (M = Ni, Zn, Pd; X = Cl, NCS) tend to increase coordination from four to five in the following order: Zn > Ni > Pd. This is ascribed to the characteristics of the metal(II) cations.

NMR spectra

The ^1H and ^{13}C NMR data of the zinc(II), palladium(II) and nickel(II) complexes are collected in Tables 3 and 4, respectively. The pattern of all ^1H NMR signals of ZnL^1X and PdL^1X (X = Cl, NCS and ClO_4) is similar to that of NiL^1X [3]. It is found

Table 3. ^{1}H NMR data for the metal complexes[a]

Compound	Arom.	H^a H^b	H^c	H^d	H^e	$-CH_2-$	$-CH_3$	Ref.
HL^1	6.6–7.2(m)	4.70(s) 12.37(t) (J = 5.1 Hz)	7.83(d) (J = 5.1 Hz)	3.43(t) (J = 5.1 Hz)	1.8–2.3(m)	2.36(q) (J = 7.3 Hz)	1.18(t) (J = 7.3 Hz)	3
ZnL^1Cl	6.7–7.2(m)	4.3(s)	8.16(s)	3.44(m)	2.1(m)	2.37(q) (J = 7.4 Hz)	1.19(t) (J = 7.4 Hz)	
$ZnL^1(NCS)$	6.7–7.4(m)		8.10(s)	3.42(m)	2.1(m)	2.34(q) (J = 7.3 Hz)	1.19(t) (J = 7.3 Hz)	
$ZnL^1(ClO_4)$	6.5–7.2(m)	3.4(s)	8.21(s)	3.42(m)	2.1(m)	2.48(q) (J = 7.3 Hz)	1.17(t) (J = 7.3 Hz)	
$PdL^1(NCS)$	6.9–7.4(m)	3.76(s)	7.78(s)	3.1(m)	2.2(m)	2.54(q) (J = 7.3 Hz)	1.23(t) (J = 7.3 Hz)	
$PdL^1(ClO_4)$	6.9–7.7(m)	3.77(s)	7.79(s)	3.04(m)	2.2(m)	2.52(q) (J = 7.3 Hz)	1.22(t) (J = 7.3 Hz)	
NiL^3	6.7–7.4(m)		7.59(s)	7.64(s) (J = 6.7 Hz)	5.32(t) (J = 6.7 Hz)	2.40(q) (J = 7.4 Hz)	1.18(t) (J = 7.4 Hz)	
PdL^3	6.6–7.3(m)		7.42(s)	7.46(d) (J = 5.6 Hz)	5.60(t) (J = 5.6 Hz)	2.32(q) (J = 7.2 Hz)	1.16(t) (J = 7.2 Hz)	

[a] Chemical shift in ppm from TMS. Multiplicity of a proton signal is given in parentheses: s = singlet, d = doublet, t = triplet, q = quartet, m = multiplet. Measured in $CDCl_3$.

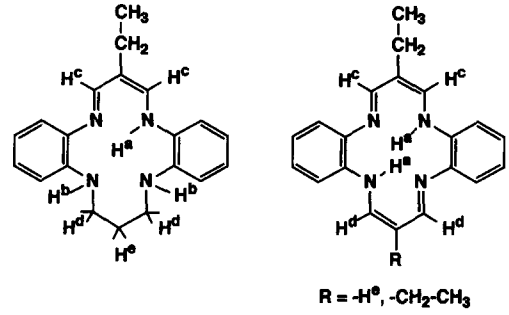
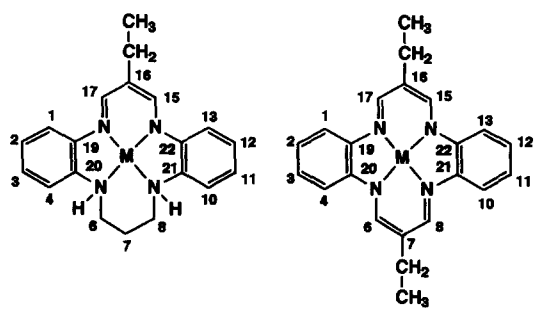


Table 4. ^{13}C NMR data for the macrocycle and its metal complexes[a]

Compound	C(1) C(4) C(10) C(13)	C(2) C(3) C(11) C(12)	C(19) C(22)	C(20) C(21)	C(15) C(17)	C(6) C(8)	C(16)	C(7)	$-CH_2-$	$-CH_3$
HL^1	123.7 118.3	113.3 112.5	140.0	134.3	145.5	45.0	109.6	25.6	27.4	17.3
$ZnL^1(ClO_4)$	127.6 125.9	122.8 113.9	143.8	137.2	153.7	55.2	107.3	26.9	28.9	18.9
$PdL^1(ClO_4)$	128.7 125.7	124.4 115.1	148.0	139.4	142.5	52.5	112.4	25.6	30.2	18.8
$NiL^1(ClO_4)$	128.6 124.9	124.0 114.8	148.0	138.5	145.1	52.4	112.8	24.4	28.1	18.1
H_2L^{2b}	124.8	114.4	138.2		147.7		111.3		26.4	17.2

[a] Measured in DMSO-d_6. Chemical shifts in ppm from internal TMS.
[b] Measured in DMF-d_7.



that the metal-free macrocycle (HL^1) releases an H^a-amine proton upon metal coordination and the metal ions are chelated by four nitrogens of the ligand in the nickel(II) complexes. The H^c-methine proton signals of PdL^1X are observed at higher field than those of HL^1, whereas those of ZnL^1X are observed at lower fields. This indicates that the coordination structures of PdL^1X and ZnL^1X are different. The ^{13}C NMR spectra were used to distinguish clearly NiL^1X, PdL^1X and ZnL^1X. That is to say the aromatic C(15) and C(17) signals for $NiL^1(ClO_4)$ and $PdL^1(ClO_4)$ are observed at slightly higher field (0.4, 3.0 ppm) than that for HL^1, but that of $ZnL^1(ClO_4)$ is observed at lower field (8.2 ppm). The C(19) and C(22) signals for the former are shifted to lower field than for the latter. In the nickel(II) and palladium(II) complexes with analogous ligands, 5,14-dihydro-7,16-diethyl-(*Z*)-dipyrido[*b*,*i*][1,4,8,11]tetraazacyclotetradecine [4c],5,14-dihydro-6,8,15,17-tetramethyldibenzo[*b*,*i*]-[1,4,8,11]tetraazacyclotetradecine [8] and 3,3′-(1,2-phenylenediimino)diacrolein [9], the C(15) and C(17) peaks exhibit upfield shifts (0–7 ppm) upon metal coordination, and the C(19) and C(22) peaks reveal downfield shifts (6–10 ppm). These facts show that the coordination structures of $NiL^1(ClO_4)$ and $PdL^1(ClO_4)$ are similar to each other and assume a square-planar configuration, while $ZnL^1(ClO_4)$ may have a distorted square-planar and/or a pentacoordinated structure. The bridged aliphatic ring C(6) and C(8) signals for $NiL^1(ClO_4)$, $ZnL^1(ClO_4)$ and $PdL^1(ClO_4)$ indicate lower field shifts on metal coordination. This is due to the electron-withdrawing effect of the metal cations.

Acknowledgement—Special thanks are due to the Center for Instrumental Analysis, Kyushu Institute of Technology for elemental analyses, mass spectra and NMR spectra.

REFERENCES

1. (a) Sakata, K., Hashimoto, M., Hamada, T. and Matsuno, S., *Polyhedron*, 1996, **15,** 967; (b) Davies, D. L. and Grist, A. J., *Inorg. Chim. Acta*, 1995, **236,** 89; (c) Davies, D. L. and Grist, A. J. *Inorg. Chim. Acta*, 1994, **216,** 217; (d) Giannini, L., Solari, E., Floriani, C., Chiesi-Villa, A. and Rizzoli, C., *Angew. Chem., Int. Edn. Engl.*, 1994, **33,** 2204; (e) Angelis, S. D., Solari, E., Gallo, E., Floriani, C., Chiesi-Villa, A. and Rizzoli, C., *Inorg. Chem.*, 1992, **31,** 2520; (f) Magull, J. and Simon, A., *Z. Anorg. Allg. Chem.*, 1992, **615,** 81; (g) Housmekerides, C. E., Ramage, D. L., Kretz, C. M., Shntz, J. T., Pilato, R. S., Geoffrey, G. L., Rheingold, A. L. and Haggerty, B. S., *Inorg. Chem.*, 1992, **31,** 4453; (h) Lelj, F., Morelli, G., Ricciardi, G. and Rosa, A., *Polyhedron*, 1991, **10,** 523; (i) Giraudon, J. M., Sala-Pala, J., Guerchais, J. E. and Toupet, L., *Inorg. Chem.*, 1991, **30,** 891; (j) Cotton, F. A. and Czuchajowska, J., *Polyhedron*, 1990, **9,** 2553; (k) Giraudon, J.-M., Mandon, D., Sala-Pala, J., Guerchais, J. E., Kerbaol, J.-M., Kerbaol, J.-M., Mest, Y. L. and L'Harison, P., *Inorg. Chem.*, 1990, **29,** 707; (l) Adams, F., Gompper, R. and Kujath, E., *Angew. Chem., Int. Edn. Engl.*, 1989, **28,** 1060; (m) Boiko, A. N. and Muzychenko, V. I., *Russ. J. Inorg. Chem.*, 1989, **34,** 393; (n) Sakata, K., Annoura, T. and Hashimoto, M., *Inorg. Chim. Acta*, 1988, **150,** 153; (o) Yang, C.-H., Ladd, J. A. and Goedken, V. L., *J. Coord. Chem.*, 1988, **19,** 235.
2. (a) Hochgesang, P. J. and Bereman, R. D., *Inorg. Chim. Acta*, 1988, **149,** 69; (b) Tsutsui, M., Bobsein, R. L., Cash, G. and Pettersen, R., *Inorg. Chem.*, 1979, **18,** 758; (c) Makin, S. M., Broido, P. I., Pomogaev, A. I. and Nikulina, S. A., *Chem. Heterocyclic Compounds*, 1989, 103.
3. Hashimoto, M. and Sakata, K., *J. Heterocyclic Chem.*, 1994, **31,** 489.
4. (a) Sakata, K., Hashimoto, M. and Naganawa, T., *Inorg. Chim. Acta*, 1985, **98,** L11; (b) Sakata, K., Hayashida, Y., Hashimoto, M., Terada, K. and Kato, Y., *Inorg. Chim. Acta*, 1985, **105,** L25; (c) Sakata, K., Hayashida, Y., Yanagida, S. and Hashimoto, M., *Inorg. Chim. Acta*, 1987, **134,** 269; (d) Lelj, F., Morelli, G., Ricciardi, G. and Rosa, A., *Polyhedron*, 1991, **10,** 523; (e) Snopok, B. A. and Lampeka, Y. D., *Opt. Spectrosk.*, 1992, **73,** 678.
5. (a) Hashimoto, M. and Sakata, K., *J. Heterocyclic Chem.*, 1992, **29,** 493; (b) Ansell, C. W. G., Chang, M. F. H. Y. J., McPartlin, M. and Tasker, P. A., *J. Chem. Soc., Dalton Trans.*, 1982, 2113.
6. (a) Smith, K. M., *Porphyrins and Metalloporphyrins*. Elsevier, Amsterdam, 1975; (b) Dolpin, D., *The Porphyrins*, Vols I–V. Academic Press, New York, 1978.
7. Geary, W. J., *Coord. Chem. Rev.*, 1971, **7,** 81.
8. Sakata, K., Yamamura, F. and Hashimoto, M., *Synth. React. Inorg. Met.-Org. Chem.*, 1990, **20,** 1043.
9. Sakata, K., Kaji, M., Kitagawa, K., Yusa, Y. and Hashimoto, M., *Inorg. Chim. Acta*, 1988, **146,** 65.

Pergamon

PII: S0277-5387(96)00336-1

Polyhedron Vol. 16, No. 6, pp. 983–988, 1997
Copyright © 1996 Elsevier Science Ltd
Printed in Great Britain. All rights reserved
0277-5387/97 $17.00+0.00

Studies on some mixed-ligand complexes of ruthenium(II) involving dithiocarboxylates, dithiocarbamates, triphenylphosphine and bipyridine

Sujoy Baitalik,[a]* Sasankasekhar Mohanta[a] and Bibhutosh Adhikary[b]*

[a]Department of Inorganic Chemistry, Indian Association for the Cultivation of Science, Calcutta 700 032, India

[b]Department of Chemistry, Bengal Engineering College (Deemed University), Shibpur, Howrah 711 103, India

(Received 30 April 1996; accepted 8 July 1996)

Abstract—Ruthenium(II) complexes $[Ru(R\text{-}acda)_2(PPh_3)_2]$ (**1a–e**), $[Ru(R\text{-}acda)(bpy)_2](ClO_4)$(**2a–d**), $[Ru(R\text{-}acda)(phen)_2](ClO_4)$(**2e–g**), $[Ru(R_2\text{-}dtc)(bpy)_2](ClO_4)$(**3a, b**) and $[Ru(R_2\text{-}dtc)(phen)_2](ClO_4)$(**3c, d**) (where R-acdaH = 2-alkylamino-1-cyclopentene-1-dithicarboxylic acid, R_2-dtcNa = sodium *N,N'*-dialkyl dithiocarbamate, bpy = 2,2′-bipyridine and phen = 1,10-phenanthroline) have been synthesized and characterized. The ^1H NMR spectra of the phosphine complexes (**1a–e**) show that, with the increase in the chain length of the alkyl group of R-acda$^-$, the N-alkylamino proton becomes more deshielded and is accompanied by a shift of the NH stretching frequency ν(NH) to lower energy. A linear relationship is obtained between the chemical shift δ(NH) and ν(NH). All the complexes exhibit absorption bands due to $d\pi \rightarrow \pi^*$ (bpy, phen or PPh_3), $d\pi \rightarrow \pi^*$ (R-acda$^-$ or R_2-dtc$^-$) charge transfer transitions and $\pi \rightarrow \pi^*$ intraligand transition. Complexes **1a–e** undergo two irreversible oxidations, $Ru^{II} \rightarrow Ru^{III}$ and $Ru^{III} \rightarrow Ru^{IV}$, while the other complexes (**2, 3**) exhibit one reversible (Ru^{II}/Ru^{III}) and one irreversible ($Ru^{III} \rightarrow Ru^{IV}$) oxidation process. Copyright © 1996 Elsevier Science Ltd

Keywords: Ru^{II} complexes; mixed-ligand Ru^{II} complexes; dithiocarboxylates of Ru^{II}; dithiocarbamates of Ru^{II}; thioacid ligands; electrochemistry of Ru^{II}.

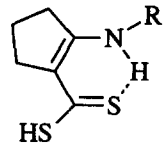
Mononuclear ruthenium(II) polypyridine complexes have been the focus of attention because of their unique chemical stability and interesting redox properties [1–5]. However, the chemistry of mixed-ligand mononuclear ruthenium(II) complexes containing polypyridine and dithiocarboxylates or dithiocarbamates has not been studied much. Herein, we report the synthesis, characterization and electrochemical behaviour of a series of monomeric mixed-ligand ruthenium(II) complexes (**1a–e, 2a–g, 3a–d**) derived from the (S, S$^-$) donor ligands HL [1–5], NaL [6, 7] and using PPh_3, 2,2′-bipyridine and 1,10-phenanthroline as co-ligands.

* Authors to whom correspondence should be addressed.

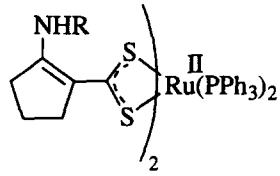
EXPERIMENTAL

Physical measurements

IR spectra were recorded on a Perkin–Elmer 783 spectrophotometer using KBr discs and electronic spectra on a Shimadzu UV-160 spectrophotometer. The electrochemical data were obtained with a BAS 100B electrochemistry system. A three-electrode assembly (BAS) comprising a platinum working electrode, a platinum auxilliary electrode and an Ag–AgCl reference electrode was used. The concentration of the supporting electrolyte tetraethylammonium perchlorate (TEAP) was maintained at 0.1 mol dm^{-3}. ^1H NMR spectra were obtained in $CDCl_3$ solutions on a 270 MHz Bruker WH 270 spectrometer using $Si(CH_3)_4$ ($\delta H = 0$) as the internal standard. Carbon,

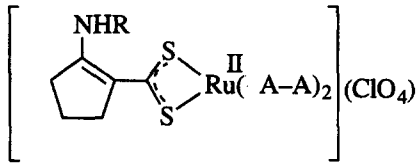


HL^{1-5}(R–acda H; R = H, Me, Et, Bu, C_6H_{11})



1a–1e

R = H(a), Me(b), Et(c), Bu(d), C_6H_{11}(e)



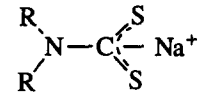
2a–2g

	R	(A–A)
2a:	H	bpy
2b:	Me	bpy
2c:	Et	bpy
2d:	Bu	bpy
2e:	H	phen
2f:	Me	phen
2g:	Et	phen

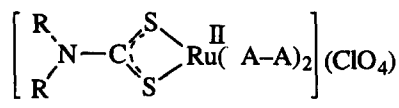
hydrogen and nitrogen analyses were carried out on a Perkin–Elmer 240C elemental analyser.

Materials

All reagents and solvents were purchased from chemical sources and used as received. 2-Alkylamino-1-cyclopentene-1-dithiocarboxylic acids were prepared by reported methods [6,7]. $Ru(bpy)_2Cl_2$, $Ru(phen)_2Cl_2$ and $Ru(PPh_3)_3Cl_2$ were prepared by the published methods [8,9]. Silver perchlorate was prepared from silver carbonate and perchloric acid, and recrystallized from benzene [10].



Na $L^{6,7}$(R_2dtc^-; R = Et, Pr)



3a–3d

	R	(A–A)
3a:	Et	bpy
3b:	Pr	bpy
3c:	Et	phen
3d:	Pr	phen

CAUTION! Silver perchlorate and the other perchlorate salts described below are potentially explosive. Although $AgClO_4$ was recrystallized in gram quantities without any difficulty, **extreme caution should be exercised in handling this material.**

Preparation of the complexes

All the reactions were carried out under nitrogen using dry solvents.

General procedure for the synthesis of the complexes $[Ru(R\text{-}acda)_2(PPh_3)_2]$ (**1a–e**). A typical procedure for the preparation of **1a** is given below.

$[Ru(H\text{-}acda)_2(PPh_3)_2]$(**1a**). To a stirred suspension of $Ru(PPh_3)_3Cl_2$(0.96 g, 1 mmol) in C_6H_6 (25 cm^3) was added a C_6H_6 solution (10 cm^3) of H-acdaH (0.32 g, 2.0 mmol). The mixture was stirred at room temperature for 5 h, during which time a clear solution was obtained. The solution was concentrated on a rotary evaporator to a small volume (*ca* 5 cm^3) and added dropwise to 50 cm^3 vigorously stirred petroleum ether (b.p. 40–60°C). The product precipitated was collected by filtration and purified by column chromatography using neutral alumina and C_6H_6 as the eluant; yield 0.75 g (80%).

General method for the preparation of $[Ru(A\text{-}A)_2(L^{1-4,6,7})](ClO_4)$ (A-A = bpy *or* phen) *complexes.* $[Ru(Me\text{-}acda)(bpy)_2](ClO_4)$ (**2b**). A stirred suspension of $[Ru(bpy)_2Cl_2]\cdot 2H_2O$ (0.26 g, 0.5 mmol) in EtOH (40 cm^3) was treated with $AgClO_4$ (0.21 g, 1 mmol) and filtered after 2 h to remove the AgCl precipitated. To the filtrate was added Me-acdaH (0.08 g, 0.5 mmol) dissolved in EtOH (10 cm^3). The solution was stirred at room temperature for 10 h, during which time the product deposited as microcrystals. These were collected by filtration and recrystallized from EtOH; yield 0.25 g (75%).

In the case of complexes **3a–d** the sodium salts of dialkyldithiocarbamates were used instead of Me-acdaH.

RESULTS AND DISCUSSION

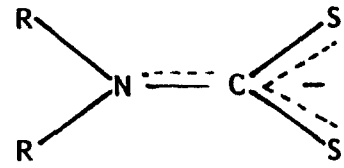
The synthetic routes involved in the formation of the phosphine complexes (**1a–e**) and polypyridine complexes (**2a–g, 3a–d**) are given by Eqs (1) and (2), respectively:

$$Ru(PPh_3)_3Cl_2 \xrightarrow[C_6H_6]{\text{R-acdaH}} [Ru(\text{R-acda})_2(PPh_3)_2]$$

$$[Ru(bpy)_2Cl_2/Ru(phen)_2Cl_2] \xrightarrow[\text{(ii) R-acdaH/Na[R}_2\text{dtc]}]{\text{(i) AgClO}_4\text{, EtOH}} \textbf{(1a–e)} \quad (1)$$

$$[Ru(\text{R-acda/R}_2\text{-dtc})\langle(bpy)_2/(phen)_2\rangle](ClO_4) \quad \textbf{(2a–g, 3a–d)} \quad (2)$$

All the complexes have been isolated in good yield and their microanalytical data (Table 1) confirm the composition given. The IR spectra of the phosphine complexes exhibit three NH stretching frequencies between 3400 and 3200 cm^{-1} for **1a**, while for complexes **1b–e** only a single ν(NH) vibration is observed. Significantly, the ν(NH) frequencies of these compounds, 3250 (**1b**), 3240 (**1c**), 3230 (**1d**) and 3220 (**1e**) cm^{-1}, are progressively shifted to lower energy with the increase in size of the alkyl group R of R-acda$^-$. Complexes **1a–e** show a characteristic sharp band at about 820 cm^{-1} which has previously been assigned to $\nu_{as}(CS_2^-)$ [6,11–13]. Three diagnostic IR bands for the dithiocarbamate complexes **3a–d** are observed due to ν(C---N), $\nu_{as}(CS_2^-)$ and $\nu_s(CS_2^-)$ vibrations of the delocalized ligand moiety at about



1500, 1280 and 780 cm^{-1}, respectively [10]. Although the ν(CN) frequency of these complexes at 1500 cm^{-1} is almost independent of the substituents, it is shifted to a higher energy relative to those of the free ligands (*ca* 1480 cm^{-1}) due to the increased double bond character upon coordination to the metal centre [14,15]. All the perchlorate complexes show a broad band at about 1100 cm^{-1} and a sharp band at 620 cm^{-1}, indicating the presence of free ClO_4^- anion.

The UV–vis spectra data of the complexes are given in Table 2. All the phosphine complexes (**1a–e**) have similar spectra, exhibiting three bands. The lowest energy band observed at 460 nm may be attributed to a $d\pi \rightarrow \pi^*$ (PPh_3) metal-to-ligand charge transfer (MLCT) transition. The next highest energy band, observed at about 380 nm, is also an MLCT $d\pi \rightarrow \pi^*$ (R-acda$^-$) transition [16,17]. The intra-ligand transition occurs at about 330 nm.

Complexes **2a–g** also exhibit two MLCT bands at 490 and 350 nm, and an intra-ligand transition at 330 nm, of which the 490 nm band is assignable to a $d\pi \rightarrow \pi^*$ (bpy or phen) transition and the band at 350 nm to a $d\pi \rightarrow \pi^*$ (R-acda$^-$) transition. It may be mentioned that the MLCT transition of $[Ru(bpy)_3](ClO_4)_2$ occurring at 452 nm [18] is displaced to lower energies on substituting bpy with one or two ligands [19]. In the case of complexes **3a–d** the two MLCT bands are shifted to relatively higher wavelengths, 515 and 460 nm.

The ^{1}H NMR spectral data of the phosphine–R-acdaH complexes (**1a–e**) are given in Table 3. The spectrum of complex **1b** shows two overlapping but discernible singlets at 2.85 and 2.87 ppm for the methyl

Table 1. Analytical data[a] for some selected complexes

Complex	Analysis (%)		
	C	H	N
1a	63.5 (63.6)	5.4 (5.1)	2.8 (2.7)
1b	62.5 (61.9)	5.5 (5.2)	2.9 (2.9)
1c	62.3 (62.5)	5.8 (5.4)	3.1 (2.8)
1d	64.8 (63.8)	6.7 (5.9)	2.9 (2.7)
1e	65.8 (65.1)	6.2 (6.0)	2.6 (2.5)
2a	46.0 (46.1)	3.9 (4.0)	9.2 (9.9)
2c	46.7 (46.9)	4.2 (4.2)	9.1 (9.7)
2d	45.5 (45.0)	4.6 (5.0)	7.9 (8.7)
3a	43.5 (44.1)	4.1 (4.1)	10.4 (10.3)
3b	46.8 (47.0)	4.3 (4.3)	9.9 (10.1)
3c	48.7 (49.3)	4.0 (4.2)	9.5 (9.3)

[a]Calculated values are given in parentheses.

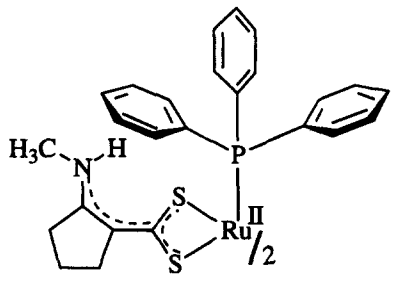
Table 2. UV–vis data for the complexes

Complex	λ_{max} (nm)/ε ($M^{-1}cm^{-1}$)		
1a	460 (16,400),	370 (14,800),	320 (18,000)
1b	460 (15,100),	380 (11,000),	330 (16,500)
1c	460 (13,300),	380 (10,000),	325 (16,000)
1d	460 (17,000),	380 (15,700),	300 (13,000)
1e	470 (18,000),	385 (22,000),	330 (15,000)
2a	490 (18,500),	350 (21,000),	300 (30,000)
2b	485 (18,200),	350 (20,800),	300 (28,000)
2c	485 (21,000),	350 (22,000),	300 (29,000)
2d	490 (21,500),	350 (20,500),	300 (32,000)
2e	490 (16,500),	400 (14,700),	345 (16,000)
2f	490 (20,000),	400 (16,500),	350 (22,700)
2g	490 (18,200),	400 (9500),	350 (15,000)
3a	520 (9600),	460 (6400),	350 (14,500)
3b	520 (9400),	475 (9600),	360 (12,400)
3c	510 (9800),	460 (10,000),	265 (35,000)
3d	515 (9700),	450 (9000),	265 (34,000)

Table 3. ^{1}H NMR ($CDCl_3$) spectral data for some complexes

Complex	δ(ppm)
1a	1.59–1.72 (m, 4H, 4-CH_2), 2.38–2.50 [m, 8H, (3, 5)-CH_2], 6.14 (s, 4H, NH_2), 7.02–7.08 (m, 12H, *m*-Ph), 7.14–7.19 (m, 6H, *p*-Ph), 7.29–7.38 (m, 12H, *o*-Ph)
1b	1.57–1.72 (m, 4H, 4-CH_2), 2.37–2.61 [m, 8H, (3, 5)-CH_2], 2.85, 2.87 (s, 6H, N-CH_3), 7.01–7.07 (m, 12H, *m*-Ph), 7.13–7.18 (m, 6H, *p*-Ph), 7.29–7.41 (m, 12H, *o*-Ph), 8.25–8.30 (t, 2H, NH)
1c	1.11–1.16 (t, 6H, 7-Ch_3), 1.56–1.76 (m, 4H, 4-CH_2), 2.32–2.61 [m, 8H, (3, 5)-CH_2], 3.13–3.22 (m, 4H, 6-CH_2), 7.01–7.06 (m, 12H, *m*-Ph), 7.12–7.23 (m, 6H, *p*-Ph), 7.28–7.42 (m, 12H, *o*-Ph), 8.37–8.39 (t, 2H, NH)
1d	0.77–0.96 (m, 6H, 9-CH_3), 1.25–1.36 (m, 4H, 8-CH_2), 1.40–1.52 (m, 4H, 7-CH_2), 1.57–1.70 (m, 4H, 4-CH_2), 2.43–2.57 [m, 8H, (3, 5)-CH_2], 3.09–3.16 (m, 4H, 6-CH_2], 7.00–7.05 (m, 12H, *m*-Ph), 7.12–7.17 (m, 6H, *p*-Ph), 7.28–7.39 (m, 12H, *o*-Ph), 8.46–8.50 (m, 2H, NH)
1e	1.17–1.52 [m, 10H, (7–11)-CH_2], 1.58–1.82 (m, 4H, 4-CH_2), 2.45–2.64 [m, 8H, (3, 5)-CH_2], 3.24–3.25 (m, 2H, 6-CH), 6.99–7.05 (m, 12H, *m*-Ph), 7.11–7.16 (m, 4H, *p*-Ph), 7.30–7.36 (m, 12H, *o*-Ph), 8.64 (br, 2H, NH)

group of Me-acda, indicating the presence of two structural isomers. The occurrence of the two isomers can be rationalized by taking into consideration the restricted rotation of the N-methyl group of Me-acda in the delocalized structure **1** [6]. From the almost identical heights of the two peaks it may be concluded that the two isomers are present in a 1 : 1 ratio. In the case of **1c**, a broad multiplet due to the —CH_2— group of the N-ethyl moiety of Et-acda is observed between 3.13 and 3.22 ppm. Although a quartet is expected for a single isomer, the broad multiplet again indicates the presence of two isomers.



I

Another interesting aspect of the NMR spectra is that, with the increase in chain length of the alkyl group (cyclohexyl derivative included) in complexes **1b–e**, the chemical shift due to the NH proton increases. In other words, the NH proton becomes more deshielded as the substituent R of R-acda$^-$ is changed in the order Me, Et, Bu and cyclohexyl. Furthermore, with the increase in chain length of the alkyl group of R-acda$^-$, the NH stretching frequency is also shifted to a lower energy. Indeed, a linear correlation is obtained in a ν(NH) *vs* δ(NH) plot (Fig. 1). This observation indicates that along the series **1b–e**, a gradual change of the N—H bond distance probably occurs. However, in the absence of crystallographic results, it is not possible to ascertain the cause of such variation. It is important to note that the observed effect contradicts the trend expected purely on the basis of inductive influence of the alkyl groups. We note that Cole-Hamilton and Stephenson have reported the stereochemical features of $[Ru(PR_3)_2(S_2CNMe_2)_2]$ complexes [20].

The redox properties of the complexes were studied by cyclic voltammetry and differential pulse voltammetry, and the results are given in Table 4. The cyclic voltammograms of the phosphine complexes (**1a–e**) are consistent with two stepwise irreversible metal-centred oxidations, as shown in Eqs (3) and (4).

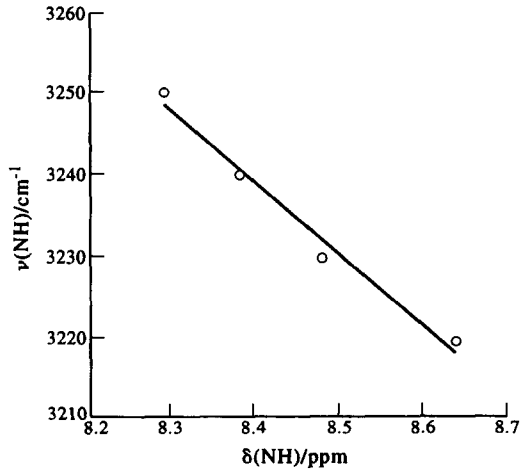


Fig. 1. Plot of chemical shift δ(NH) *vs* the stretching frequency ν(NH) of the phosphine complexes **1b–e**.

Table 4. Electrochemical data for the complexes

Complex	$E^1_{1/2}$(V)	ΔE_p (mV)	E^1_{pa}(V)	E^2_{pa}(V)
1a			0.26	0.72
1b			0.22	0.67
1c			0.24	0.67
1d			0.24	0.69
1e			0.23	0.69
2a	0.49	65		1.25
2b	0.45	64		1.15
2c	0.46	65		1.26
2d	0.45	63		1.26
2e	0.49	64		1.28
2f	0.45	64		1.20
2g	0.45	65		1.20
3a	0.56	60		1.60
3b	0.53	61		1.59
3c	0.55	63		1.57
3d	0.53	61		1.57

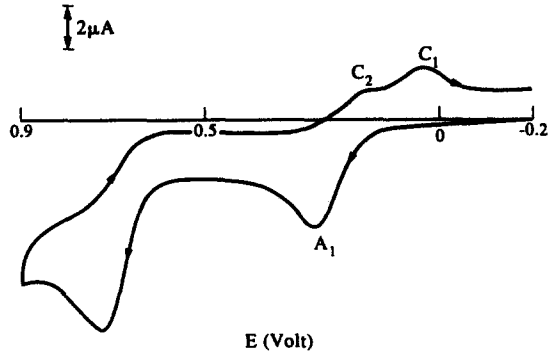


Fig. 2. Cyclic voltammogram of **1a** in CH_3CN with a platinum electrode at a scan rate of 100 mV s^{-1}. Concentration of the complex: 1.0×10^{-3} mol dm^{-3}; concentration of supporting electrolyte, $[Et_4N](ClO_4)$: 0.1 mol dm^{-3}.

$$[Ru^{II}(R\text{-acda})_2(PPh_3)_2]^0 \xrightarrow{E^1_{pa}} [Ru^{III}(R\text{-acda})_2(PPh_3)_2]^+ \quad (3)$$

$$[Ru^{III}(R\text{-acda})_2(PPh_3)_2]^+ \xrightarrow{E^2_{pa}} [Ru^{IV}(R\text{-acda})_2(PPh_3)_2]^{2+} \quad (4)$$

The E^1_{pa} and E^2_{pa} values of **1a** and **1b** are 0.26 and 0.72 V, and 0.21 and 0.67 V, respectively, indicating that the oxidation of **1a** is relatively somewhat more difficult than that of **1b**. This observation is in agreement with the greater electron-releasing ability of the methyl group in **1b** as compared to the hydrogen atom in **1a**. A similar trend is also observed for the oxidation of $R^{III} \rightarrow R^{IV}$ (E^2_{pa}). E^1_{pa} values for all substituted complexes (**1b–e**) lie in the narrow range of 0.21–0.24 V.

Recently, Chakravorty and co-workers have made extensive studies on the reactivities of ruthenium(II) complexes with S,S^- donor ligands containing phosphine and its derivatives, and have observed that the preferred geometries of these complexes are *cis* for ruthenium(II) and *trans* for ruthenium(III) [21–23]. They have demonstrated that at a lower temperature, *cis*-Ru^{II} oxidizes to *cis*-Ru^{III}, which, being unstable, isomerizes to stable *trans*-Ru^{III}. In the reverse scan, *trans*-Ru^{III} is reduced to *trans*-Ru^{II}, which is also unstable and isomerizes to *cis*-Ru^{II} [21–24].

The cyclic voltammogram of **1a** (Fig. 2) shows an indication of isomerism even at room temperature. As may be noted, the anodic peak $A_{(1)}$ has two components in the return sweep, $C_{(1)}$ and $C_{(2)}$, of which $C_{(1)}$ may be considered as due to *trans*-Ru^{II}, which then isomerizes to the more stable *cis*-Ru^{II}, which is indicated by $C_{(2)}$. Clearly, the isomerization rate is slow on the cyclic voltammetric time scale (100 mV s^{-1}).

Cyclic voltammograms of the mixed-ligand complexes (**2a–g**) exhibit reversible and irreversible metal-centred oxidation processes and two reversible reductions of bpy or phen. Thus, while the Ru^{II}/Ru^{III} couple is reversible, the conversion of $Ru^{III} \rightarrow Ru^{IV}$ takes place irreversibly. The criteria of reversibility were checked by observing the constancy of peak separation ($E_{pa} - E_{pa} = 60$–65 mV) and the ratio of peak heights ($i_{pa}/i_{pc} \approx 1$) with the variation of scan rates (50–500 mV s^{-1}). It may be noted that the $E^1_{1/2}$ value of **2a** (0.49 V) is again somewhat higher than the other alkyl derivatives **2b–d** (0.45 V); the latter compounds show practically no dependence on the substituents.

The reduction of bpy and phen in all the complexes occurs in two steps according to Eqs (5) and (6), typically at about −1.50 and −1.80 V:

$$[Ru(R\text{-acda})(bpy)_2]^+ + e \rightleftharpoons [Ru(R\text{-acda}(bpy)(bpy^{\cdot-})] \quad (5)$$

$$[Ru(R\text{-acda})(bpy)(bpy^{\cdot-})] + e \rightleftharpoons [Ru(R\text{-acda})(bpy^{\cdot-})_2] \quad (6)$$

Inasmuch as each bpy or phen can accept two electrons in this lowest unoccupied molecular orbital [25, 26], one should expect to observe four such reduction steps in the series **2a–g** and **3a–d**. The observation of only two couples up to −2.0 V was limited by the cut-off potential of the supporting electrolyte (TEAP) in acetonitrile.

Complexes **3a–d**, similar to **2a–g**, undergo reversible and irreversible meter-centred oxidation processes. The reduction behaviours of bpy or phen in these compounds are very similar to the preceding series. The $E^1_{1/2}$ values of **3a–d** (0.52–0.56 V) show a small substitutional effect.

A comparison of the electrochemical data for Ru^{II}/Ru^{III} in the three series of compounds (Table 4) reveals that the phosphine–R–acda$^-$ complexes (series **1**) are most easily oxidized relative to those of series **2** and **3**. The most important factor that contributes to the easier oxidation of the compounds of series **1** is

that they are uncharged, while those belonging to series **2** and **3** are monocationic. Another important difference lies in the number of (S,S^-) ligands attached, which is two for series **1** and one for series **2** and **3**. Between series **2** and **3,** the greater stability of ruthenium(II) in series **3** can be attributed to greater σ-donor capacity of the dithiocarbamate ligands relative to R-acda$^-$.

Acknowledgement—We thank Prof. K. Nag (Indian Association for the Cultivation of Science) for helpful suggestions and laboratory facilities.

REFERENCES

1. Juris, A., Balzani, V., Barigelletti, F., Campagna, S., Belser, P. and Von Zelewsky, A., *Coord. Chem. Rev.*, 1988, **84,** 85.
2. Meyer, T. J., *Pure Appl. Chem.*, 1986, **58,** 1193.
3. Meyer, T. J., *Accts. Chem. Res.*, 1989, **22,** 163.
4. Kalyanasauduram, K., *Coord. Chem. Rev.*, 1982, **46,** 159.
5. Seddon, E. A. and Seddon, K. R., *The Chemistry of Ruthenium.* Elsevier, Amsterdam, 1984.
6. Nag. K. and Joardar, D. S., *Inorg. Chim. Acta*, 1975, **14,** 133.
7. Bordas, B., Sohar, P., Matolcsy, G. and Berencsi, P., *J. Org. Chem.*, 1972, **37,** 1727.
8. Stephenson, T. A. and Wilkinson, G., *J. Inorg. Nucl. Chem.*, 1966, **28,** 945.
9. Sullivan, B. P., Salmon, D. J. and Meyer, T. J., *Inorg. Chem.*, 1978, **17,** 3334.
10. Chakladar, S., Paul, P. and Nag, K., *Polyhedron.*, 1991, **13,** 1513.
11. Dutta, S. K., Kumar, S. B., Bhattacharya, S. and Chaudhury, M., *J. Chem. Soc., Dalton Trans.*, 1994, 97.
12. Chaudhury, M., *Inorg. Chem.*, 1985, **24,** 3011.
13. Chaudhury, M., *J. Chem. Soc., Dalton Trans.*, 1984, 115.
14. Connor, C. O., Gilbert, J. D. and Wilkinson, G., *J. Chem. Soc. A.*, 1969, 84.
15. Chatt, J., Duncanson, L. A. and Venanzi, L. M., *Nature (London).*, 1966, **177,** 1042.
16. Rillema, D. P., Taghdiri, D. G., Jones, D. S., Keller, C. D., Worl, L. A., Meyer, T. J. and Levy, H. A., *Inorg. Chem.*, 1987, **26,** 578.
17. Allen, G. H., White, R. P., Rillema, D. P. and Mayer, T. J., *J. Am. Chem. Soc.*, 1984, **106,** 2613.
18. Curtis, J. C., Sullivan, B. P. and Meyer, T. J., *Inorg. Chem.*, 1983, **22,** 224.
19. Haga, M., Ano, T., Ishizaki, T., Kano, K., Nozaki, K. and Ohno, T., *J. Chem. Soc., Dalton Trans.*, 1994, 263.
20. Cole-Hamilton, D. J. and Stephenson, T. A., *J. Chem. Soc., Dalton Trans.*, 1974, 739.
21. Bag, N., Lahiri, G. K. and Chakravorty, A., *J. Chem. Soc., Dalton Trans.*, 1990, 1557.
22. Pramanik, A., Bag, N., Roy, D., Lahiri, G. K. and Chakravorty, A., *Inorg. Chem.*, 1991, **30,** 410.
23. Menon, M., Pramanik, A., Bag, N. and Chakravorty, A., *J. Chem. Soc., Dalton Trans.*, 1995, 1543.
24. Ballester, L., Esterbani, O., Gutierrez, A., Perpinary, M. F., Valero, C. R., Puebla, E. G. and Gonzalez, M. J., *Polyhedron.*, 1992, **11,** 3173.
25. Vlcek, A. A., *Coord. Chem. Rev.*, 1982, **43,** 39.
26. Kahl, J. L., Hanck, K. W. and DeArmond, K., *J. Phys. Chem.*, 1978, **82,** 540.

Pergamon

PII: S0277-5387(96)00356-7

Polyhedron Vol. 16, No. 6, pp. 989–991, 1997
Copyright © 1996 Elsevier Science Ltd
Printed in Great Britain. All rights reserved
0277-5387/97 $17.00+0.00

COMMUNICATION

The first observation of a Th^{3+} ion in aqueous solution

Thomas M. Klapötke* and Axel Schulz

Department of Chemistry, University of Glasgow, Glasgow G12 8QQ, U.K.

(Received 5 July 1996; accepted 12 July 1996)

Abstract—The reaction of $ThCl_4$ and HN_3 aqueous solution yielded the $Th^{3+}(aq)$ ion which was identified by its absorption (UV–vis, 200–1300 nm) and ESR spectra. In the high energy region of the electronic spectrum just below 650 nm, a significant and constant signal occurs until 420 nm (maximum at 460 nm), which sees the onset of a very intense, broad band with maxima at *ca* 332 (shoulder), 190 and below 185 nm. The ESR spectrum of a frozen solution revealed a very broad signal and a main g value of 2.19. Copyright © 1996 Elsevier Science Ltd

Keywords: thorium chemistry; hydrazoic acid; azides; ESR spectra; electronic spectra.

Recently the electronic structure of f^1 complexes of the early actinide elements (An = Pa, U, Np) has been studied experimentally and theoretically using non-relativistic and relativistic calculations of the optical transition energies of AnX_6^{q-} complexes [1,2]. Examples of actinide f^1 complexes include the tetrahedral borohydride compounds $[Pa(BH_4)_4]$ and $[Pa(BH_3CH_3)_4]$ [3], $[Pa(\eta^8\text{-}C_8H_8)_2]$ [4] and $[U(\eta^5\text{-}C_5H_5)_3NPh]$ [5], and the isoelectronic octahedral hexahalide complexes $[PaX_6]^{2-}$ (X = F, Cl, Br, I), $[UX_6]^-$ (X = F, Cl, Br) and NpF_6 [6, 7]. Thorium(III) complexes are very rare but intensely coloured organometallic systems such as blue $[\{Th(\eta^5\text{-}C_5H_3)(SiMe_3)_2\}_3]$ [8], violet $[Th(\eta^5\text{-}C_5H_5)_3]$ [9], green $[Th(\eta^5\text{-}C_5H_4Me)_3]$ [10] or brown $[Th(\eta^5\text{-}C_5H_5)_2Cl]$ [9] have been reported. In this communication we report the first observation and identification of a Th^{3+} ion in aqueous solution. As far as we are aware, there are no previous reports on a Th^{3+} ion and it is well-known textbook knowledge that: (i) "the oxidation state III is the only oxidation state which, with the possible exceptions of Th and Pa, is displayed by all actinides" [11a] and (ii) "Th^{3+} and Pa^{3+} do not exist in aqueous solution] [11b]. (N.B. For organometallic examples compare with refs [8–10].)

We have previously studied the chemistry and bonding of covalent azides and recently extended our studies to hydrazoic acid, HN_3 [12a–c]. The instability of Th^{3+} in aqueous solution can be attributed to the fact that it is rapidly oxidized by air and it reduces water with evolution of H_2 [11a]. The most recent value recommended for the system Th^{4+}/Th^{3+} is $E^0 = -3.0$ V [13a] (the earlier recommendation was -3.7 V) [13b]. On the other hand, the reduction potential of HN_3 is more negative than that of any other reducing agent in acidic aqueous solution [Eq. (1)] [11a]. The ΔE^0 value for a reaction according to Eq. (2) can be estimated to $\Delta E^0(2) = +0.54$ V and the reaction is therefore thermodynamically allowed [14]:

$$1.5N_2 + H^+(aq) + e^- \rightarrow HN_3(aq)$$

$$E^0 = -3.54 \text{ V (pH 3.5, 25°C) [15]} \quad (1)$$

$$Th^{4+} + HN_3 \rightarrow Th^{3+} + 1.5N_2 + H^+ \quad (2)$$

A solution of Th^{3+} was prepared from aqueous solutions of $ThCl_4$ and HN_3 [16a]. A solution of $ThCl_4$ (2.76 g, 7.38 mmol) in 10 cm^3 water ($c = 0.74$ mol l^{-1}) was added to 15 cm^3 of a fresh stirred, solution of HN_3 ($c = 2.0$ mol l^{-1}) under nitrogen. An amber solution of Th^{3+} was obtained immediately ($c = 0.3$ mol

* Author to whom correspondence should be addressed.

l^{-1} [16b]; pH *ca* 3.5 [*cf.* $pK_a(HN_3)$ 4.77] [11a]; characterization see below) with evolution of N_2. The aqueous Th^{3+} solution in hydrazoic acid is stable for more than 1 h before Th^{3+} is slowly oxidized by water to form an insoluble, white, gel-like precipitate of thorium oxide hydroxide [17,18].

Recently, it has been shown that for f^1 complexes most of the $f \rightarrow f$ transitions are orbitally forbidden (N.B. the labels "$f \rightarrow f$" and "$f \rightarrow d$" refer to the predominant atomic orbital (AO) character of the molecular orbitals (MOs) involved in the transition) and are therefore observed experimentally as very weak, or are nonexistent [2]. Other transitions are permitted in their own right, and consequently $f \rightarrow d$ and certain charge-transfer bands will have much greater oscillator strengths and will obscure the weaker $f \rightarrow f$ peaks should they occur in the same energy range [2]. Figure 1 shows the higher energy transitions (200–1300 nm) for Th^{3+} [19]. As expected, the spectrum is very similar to the spectrum reported for the f^1 system $[Et_4N]_2[PaBr_6]$ [1] (*cf.* also ref. [20a,b] and for NpF_6 ref. [20c]). There are no well-defined $f \rightarrow f$ transitions below 1300 nm. At just below 650 nm, a significant and constant signal occurs until 420 nm (maximum at 460 nm), which sees the onset of a very intense, broad band with maxima at *ca* 332 (shoulder), 190 and below 185 nm. Since $5f \rightarrow 6d$ and metal $\rightarrow$ ligand charge transfers are allowed transitions, which are usually rather broad and occur in the UV region, the broad band centred at 460 nm as well as the intense absorptions at 332, 190 and below 185 nm can be assigned to such transitions. A number of small shoulders on the main peak occur over the energy range 270–190 nm, but these cannot be justifiably ascribed to well-defined electronic absorptions. Although it is clearly possible that $f \rightarrow f$ transitions occur in this range, there is no means by which they can be assigned with confidence to features in the experimental spectrum (Fig. 1). It should be mentioned, however, that it cannot be completely ruled out that the single electron in Th^{3+}

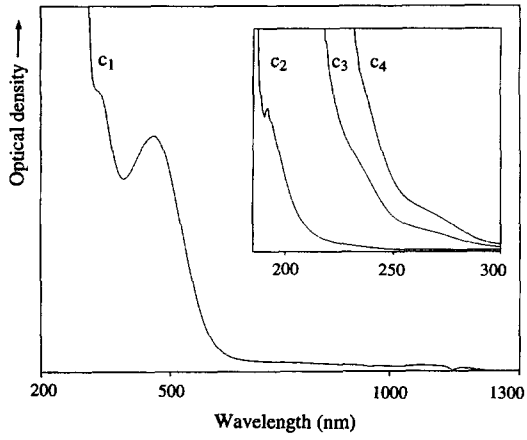


Fig. 1. Room temperature optical spectrum of Th^{3+} in HN_3 solution ($c_1 = 0.3$ mol l^{-1} [16b], $c_2 = 0.01$ mol l^{-1}, $c_3 = 5 \times 10^{-3}$ mol l^{-1}, $c_4 = 2 \times 10^{-4}$ mol l^{-1}) [21].

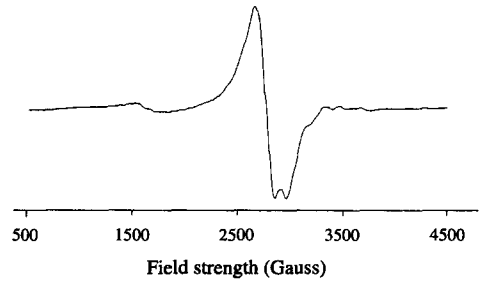


Fig. 2. ESR spectrum of a frozen solution of $[Th(H_2O)_x(N_3)_y(Cl)_z]^{(3+)-(y+z)}$ ($x+y+z=9$, *cf.* the CN of La^{3+} in aqueous solution is 9) [11a, 23].

(aq) is a $6d$ rather than a $5f$ electron. In Th^{3+} (g), the $6d$ level lies 9200 cm^{-1} above $5f$, but in the aqueous ion the d orbitals will be stabilized by the ligand field [13b,17]. In this interpretation, the band at 460 nm could be assigned to a d–d transition equal to the ligand field stabilization energy (*cf.* ref. [1]).

The ESR spectrum of a frozen solution (Fig. 2) shows a very broad signal, very similar in shape to that of the f^1 system $UCl_5 \cdot SOCl_2$ [22]. The observed main g value of 2.19 compares with those found for other f^1 systems [6]. The overall shape of the spectrum may well correspond to a system with axial symmetry. However, further experimental and especially theoretical studies have to be carried out to assign the different anisotropic g values with confidence.

Acknowledgements—We thank the University of Glasgow for financial support of this work. We are especially indebted to Dr K. J. Taylor for recording the ESR spectrum.

REFERENCES

1. Edelstein, N., Krupa, J. C., Naik, R. C., Rajnak, K., Whittaker, B. and Brown, D., *Inorg. Chem.*, 1988, **27**, 3186.
2. Kaltsoyannis, N. and Bursten, B. E., *Inorg. Chem.*, 1995, **34**, 2735.
3. Kot, W. K., Ph.D. thesis, University of California (1991).
4. Blake, P. C., Lappert, M. F., Atwood, J. L. and Zhang, J., *J. Chem. Soc. Chem. Commun.*, 1986, 1148.
5. Brennan, J. G. and Andersen, R. A., *J. Am. Chem. Soc.*, 1985, **107**, 514.
6. Selbin, J. and Ortego, J. D., *Chem. Rev.*, 1969, **69**, 657.
7. Reisfeld, M. J. and Crosby, G. A., *Inorg. Chem.*, 1965, **4**, 65.
8. Starks, D. F., Parsons, T. C., Streitweiser, A. and Edelstein, N. M., *Inorg. Chem.*, 1974, **13**, 1307.
9. Marks, T. J. and Ernst, R. D., in *Comprehensive Organometallic Chemistry*, Vol. 3, ed. Wilkinson, G., Stone, F. G. A. and Abel, E. W. Pergamon Press, Oxford, 1982, ch. 21.
10. Bruno, J. W., Kalina, D. G., Mintz, E. A. and Marks, T. J., *J. Am. Chem. Soc.*, 1982, **104**, 1860.
11. (a) Greenwood, N. N. and Earnshaw, A., *Chem-*

istry of the Elements. pp. 497, 500, 1476, 1483, Pergamon Press, Oxford, (1984); (b) Holleman, A. F., Wiberg, E. and Wiberg, N., *Lehrbuch der Anorganischen Chemie*, pp. 1286, 1289 and 1304. Walter de Gruyter, Berlin, New York, 1985.

12. (a) Tornieporth-Oetting, I. C. and Klapötke, T. M., *Angew. Chem. Int. Ed. Engl.*, 1995, **34,** 511; (b) Klapötke, T. M., *Acc. Chem. Res.*, submitted for publication; (c) Klapötke, T. M., White, P. S. and Tornieporth-Oetting, I. C., *Polyhedron*, 1996, **15,** 2579.
13. (a) Bratsch, S. G. and Lagowski, J. J., *J. Phys. Chem.*, 1986, **90,** 307; (b) Nugent, L. J., Baybarz, R. D. and Burnett, J. L., *J. Phys. Chem.*, 1973, **77,** 1528.
14. $\Delta E^0(2) = E^0(Th^{4+}/Th^{3+}) - E^0$ [Eq. (1)] = -3.0 V $+ 3.54$ V = $+0.54$ V.
15. US Department of Commerce, National Bureau of Standards, *Selected Values of Chemical Thermodynamic Properties*, United States Government Printing Office, Washington, D.C., 1982.
16. (a) **Safety Note:** Thorium is radioactive and hydrazoic acid is very toxic and, as pure material, explosive [12a]; (b) The quoted concentration of 0.3 mol l^{-1} for Th^{3+} (aq) is not the result of measurement, but is based on the assumption of a 100% yield.
17. *Gmelin Handbook of Inorganic Chemistry, Th Thorium*, Vol. C1, Vol. D1, 8th edn, Springer, Berlin, 1978 and 1988.
18. The chemical analysis of the gel formed gave: N, 1.94 and H, 1.89% roughly corresponding to an empirical formula of $[Th(OH)_2(N_3)_2(H_2O)_3]$ (Calc: N, 2.08 and H, 1.99%). IR (KBr, cm^{-1}): $\nu_{as}(N_3)$ 2095 [*cf.* $\nu_{as}(N_3, NaN_3)$ 2130]. We also tried to precipitate a Th^{III} azide from a fresh Th^{3+} solution in HN_3 by adding a large amount of acetone. However, only a white Th^{IV} oxide hydroxide was recovered after filtration.
19. The low energy $f \rightarrow f$ transitions (>1300 nm) could not be observed because of strong absorptions of water (solvent) in this region.
20. (a) Eisenstein, J. C. and Pryce, M. L. H., *Proc. R. Soc. London, Ser. A*, 1960, **255,** 181; (b) Steindler, M. J. and Gerding, T. J., *Spectrochim. Acta*, 1996, **22,** 1197; (c) Goodman, G. L. and Fred, M., *J. Chem. Phys.*, 1959, **30,** 850.
21. Absorption spectra: Shimadzu UV-3101 PC UV–vis-NIR spectrophotometer; spectra recorded at room temperature in 5-mm quartz cells.
22. Selbin, J., Ortego, J. D. and Gritzner, G., *Inorg. Chem.*, 1968, **7,** 976.
23. ESR spectra: Bruker ESR 200 D-SRC spectrometer; 9.48 GHz, 2 dB attenuation, sweeptime 50 s, modulation 25 G; sample temperature -140°C.

Pergamon

Polyhedron Vol. 16, No. 6, p. 993, 1997
Copyright © 1996 Published by Elsevier Science Ltd
Printed in Great Britain. All rights reserved
0277–5387/97 $17.00+0.00

BOOK REVIEWS

Metal Complexes in Aqueous Solutions, by A. E. Martell and R. D. Hancock, 253 pp., Plenum, New York, 1996, $59.50, ISBN 0-306-45248.

If you are one of those chemists who is suspicious of numerical data and trusts only in the formation of crystals, you will learn a lot from this book. The measurement of formation constants often baffles outsiders. Complicated equilibria are described, even more complicated computer programs are run, and some numbers emerge into the light of publication, there to slumber peacefully for evermore. This book shows it need not be like that. We now have this integrated account of the whole subject of the thermodynamics of metal complexes in aqueous solution. It reads coherently and rationalizes the subject in a way that will teach experts and novices alike more than most other books in this area.

The authors have essentially expanded and modernized their 1989 *Chemical Review* article. The first three substantial chapters present an orderly development of why some ligand–metal complexes are more stable than others. Steric effects, enthalpy and entropy contributions, ligand field effects, hardness and softness, chelate effects and inductive effects are introduced when appropriate, and data are summarized with numerous clear structural diagrams and graphs. Some complex structures have been redrawn by the authors from literature data, giving a homogeneous style to the diagrams' appearance and often improving on the pictures provided by the original crystallographers.

The rational argument as to what effect generates what result is presented most persuasively by a series of examples. Just when you think one trend is safely established, another set of complexes is produced that bucks that trend, but the new anomaly can then be explained by some other development. Sceptics may think this all sounds rather like special pleading. After all, every complex has its own peculiarities, and nobody expects simple rules to apply in complicated situations. There is little discussion of kinetics, or of ligand synthesis, and many of the examples come from the authors' own research, with some other active groups being less frequently cited. Nevertheless, the whole story is very effective, and readers will find here an excellent rationalization of why chemists should select particular ligands to react with particular metals, and not select other combinations.

The second half of the book uses the principles already developed to design appropriate complexes for medicinal and radiopharmaceutical applications of metal complexes and to rationalize selected aspects of metallobiochemistry. The layout of these chapters is that of a review ordered by metals rather than ligands, and it is noticeable that various biological constraints now enter the argument. There is a certain amount of jargon, so that you will need to know what a myocardial pervasion agent is, and there is a rather elementary discussion of general technetium chemistry which could have been taken for granted. However, the principles the authors developed earlier allow us to see why, for example, hydroxide ions are bound to zinc effectively in carbonic anhydrase when the binding is much weaker in ordinary aqueous solutions. There are also five effective pages on magnetic resonance imaging. This would be a good introduction to the field for novices, but this section in particular is bound to be obsolete soon, whereas the principles of ligand design will remain valuable for a very long time to come.

The last chapter is a clear account of how to measure stability constants. Expert readers will probably know this already, and the topic is covered for novices elsewhere, but this account is certainly very clear.

There are a few minor mistakes, like the representation of pyridine as C_6H_5N (p. 34), and the assertion on p. 1 that there is a glossary for technical terms in the Appendix (there is neither a Glossary nor an Appendix). The index is really terrible, even by the standards of chemistry books. For one thing it is too brief, and the selection of entries is perverse. Successive entries feature Desferriferrioxamine (that is what we used to call desferrioxamine), DFO (an abbreviation of the previous entry), ΔH^0, ΔS^0 and Dibenzo-30-crown-10. I wonder when chemistry publishers will realize that indexes are supposed to be helpful rather than entertaining.

PETER THORNTON
Queen Mary and Westfield College,
London E1 4NS, U.K.

Energetics of Organometallic Species, edited by J. A. Martinho Simões, NATO ASI Series: Series C: Mathematical and Physical Sciences, Vol. 367. xii+442 pp. Kluwer Academic Publishers, Dordrecht 1992. Price: not stated. ISBN 0-7923-1707-6.

The days are long gone when organometallic compounds of the transition metals were automatically regarded as "unstable", now we know a bit more about thermodynamic and kinetic stability. But how strong are the bonds? This volume, a collection of 20 papers by participants at a 1991 Study Institute, sets out to answer this.

It is a measure of the sophistication attained nowadays that a large majority of papers are not concerned with either classical combustion or solution methods, although one of these latter is an important study of f-block thermochemistry (T. J. Marks). Instead, use is made of equilibrium methods, kinetic methods; short-lived species are studied by voltammetry. Mass spectra and other methods are employed in the gas phase. How do gas phase and solution data relate? Two papers show us. Concepts such as bond enthalpy transferability are explored (J. A. Connor). Quantitative theoretical calculations are reported. The overall impression is that this is a diverse and increasingly sophisticated field. Much of this material has by now been published in the learned journals. The benefits of such a meeting are obviously to those who attend the Institute, but also subsequently to the non-specialists who read these proceedings and obtain an overall view under one cover, a state-of-the-art snapshot, not easily obtained by reading the literature.

SIMON COTTON
Uppingham School,
Uppingham,
Rutland LE15 9QE
U.K.

Pergamon

Polyhedron Vol. 16, No. 6, p. 993, 1997
Copyright © 1996 Published by Elsevier Science Ltd
Printed in Great Britain. All rights reserved
0277–5387/97 $17.00+0.00

BOOK REVIEWS

Metal Complexes in Aqueous Solutions, by A. E. Martell and R. D. Hancock, 253 pp., Plenum, New York, 1996, $59.50, ISBN 0-306-45248.

If you are one of those chemists who is suspicious of numerical data and trusts only in the formation of crystals, you will learn a lot from this book. The measurement of formation constants often baffles outsiders. Complicated equilibria are described, even more complicated computer programs are run, and some numbers emerge into the light of publication, there to slumber peacefully for evermore. This book shows it need not be like that. We now have this integrated account of the whole subject of the thermodynamics of metal complexes in aqueous solution. It reads coherently and rationalizes the subject in a way that will teach experts and novices alike more than most other books in this area.

The authors have essentially expanded and modernized their 1989 *Chemical Review* article. The first three substantial chapters present an orderly development of why some ligand–metal complexes are more stable than others. Steric effects, enthalpy and entropy contributions, ligand field effects, hardness and softness, chelate effects and inductive effects are introduced when appropriate, and data are summarized with numerous clear structural diagrams and graphs. Some complex structures have been redrawn by the authors from literature data, giving a homogeneous style to the diagrams' appearance and often improving on the pictures provided by the original crystallographers.

The rational argument as to what effect generates what result is presented most persuasively by a series of examples. Just when you think one trend is safely established, another set of complexes is produced that bucks that trend, but the new anomaly can then be explained by some other development. Sceptics may think this all sounds rather like special pleading. After all, every complex has its own peculiarities, and nobody expects simple rules to apply in complicated situations. There is little discussion of kinetics, or of ligand synthesis, and many of the examples come from the authors' own research, with some other active groups being less frequently cited. Nevertheless, the whole story is very effective, and readers will find here an excellent rationalization of why chemists should select particular ligands to react with particular metals, and not select other combinations.

The second half of the book uses the principles already developed to design appropriate complexes for medicinal and radiopharmaceutical applications of metal complexes and to rationalize selected aspects of metallobiochemistry. The layout of these chapters is that of a review ordered by metals rather than ligands, and it is noticeable that various biological constraints now enter the argument. There is a certain amount of jargon, so that you will need to know what a myocardial pervasion agent is, and there is a rather elementary discussion of general technetium chemistry which could have been taken for granted. However, the principles the authors developed earlier allow us to see why, for example, hydroxide ions are bound to zinc effectively in carbonic anhydrase when the binding is much weaker in ordinary aqueous solutions. There are also five effective pages on magnetic resonance imaging. This would be a good introduction to the field for novices, but this section in particular is bound to be obsolete soon, whereas the principles of ligand design will remain valuable for a very long time to come.

The last chapter is a clear account of how to measure stability constants. Expert readers will probably know this already, and the topic is covered for novices elsewhere, but this account is certainly very clear.

There are a few minor mistakes, like the representation of pyridine as C_6H_5N (p. 34), and the assertion on p. 1 that there is a glossary for technical terms in the Appendix (there is neither a Glossary nor an Appendix). The index is really terrible, even by the standards of chemistry books. For one thing it is too brief, and the selection of entries is perverse. Successive entries feature Desferriferrioxamine (that is what we used to call desferrioxamine), DFO (an abbreviation of the previous entry), ΔH^0, ΔS^0 and Dibenzo-30-crown-10. I wonder when chemistry publishers will realize that indexes are supposed to be helpful rather than entertaining.

PETER THORNTON
Queen Mary and Westfield College,
London E1 4NS, U.K.

Energetics of Organometallic Species, edited by J. A. Martinho Simões, NATO ASI Series: Series C: Mathematical and Physical Sciences, Vol. 367. xii+442 pp. Kluwer Academic Publishers, Dordrecht 1992. Price: not stated. ISBN 0-7923-1707-6.

The days are long gone when organometallic compounds of the transition metals were automatically regarded as "unstable", now we know a bit more about thermodynamic and kinetic stability. But how strong are the bonds? This volume, a collection of 20 papers by participants at a 1991 Study Institute, sets out to answer this.

It is a measure of the sophistication attained nowadays that a large majority of papers are not concerned with either classical combustion or solution methods, although one of these latter is an important study of f-block thermochemistry (T. J. Marks). Instead, use is made of equilibrium methods, kinetic methods; short-lived species are studied by voltammetry. Mass spectra and other methods are employed in the gas phase. How do gas phase and solution data relate? Two papers show us. Concepts such as bond enthalpy transferability are explored (J. A. Connor). Quantitative theoretical calculations are reported. The overall impression is that this is a diverse and increasingly sophisticated field. Much of this material has by now been published in the learned journals. The benefits of such a meeting are obviously to those who attend the Institute, but also subsequently to the non-specialists who read these proceedings and obtain an overall view under one cover, a state-of-the-art snapshot, not easily obtained by reading the literature.

SIMON COTTON
Uppingham School,
Uppingham,
Rutland LE15 9QE
U.K.

Pergamon

PII: S0277-5387(96)00419-6

Polyhedron Vol. 16, No. 7, pp. 995–998, 1997
Copyright © 1997 Elsevier Science Ltd
Printed in Great Britain. All rights reserved
0277-5387/97 $17.00+0.00

Synthesis and structure of $Nb_2(\mu_2\text{-}Se_2)_2(Te_2I_6)_2$

Vladimir P. Fedin,[a]* Vladimir E. Fedorov,[a] Hideo Imoto[b] and Taro Saito[b]

[a] Institute of Inorganic Chemistry of the Russian Academy of Sciences, pr. Lavrentjeva 3, 630090, Novosibirsk, Russia

[b] Department of Chemistry, School of Science, The University of Tokyo, Hongo, Bunkyo-ku, Tokyo 113, Japan

(Received 30 July 1996; accepted 16 August 1996)

Abstract—Compound $Nb_2(\mu_2\text{-}Se_2)_2(Te_2I_6)_2$ was obtained in high yield by high-temperature reaction (500 C) of the dinuclear cluster complex $Nb_2(\mu_2\text{-}Se_2)_2I_4$ with Te and I_2 in a 1:4:4 ratio. The structure of $Nb_2Se_4Te_4I_{12}$ has been determined by single-crystal X-ray diffraction. It is characterized by the presence of isolated molecules of $[Nb_2(\mu_2\text{-}Se_2)_2(Te_2I_6)_2]$. The inner skeleton is formed by a dinuclear $[Nb_2(\mu_2\text{-}Se_2)_2]^{4+}$ fragment with a Nb—Nb distance of 2.926(2) Å; the Se—Se distances are 2.310(2) and 2.311(2) Å. Each Nb atom is ligated (formally) by $Te_2I_6^{2-}$ ligands. The terminal Te—I distances in the $Te_2I_6^{2-}$ ligands range from 2.735(2) to 2.786(2) Å. The bridging Te—I distances are rather long, ranging from 3.175(1) to 3.261(2) Å. Copyright © 1997 Elsevier Science Ltd

Keywords: crystal structure; niobium complexes; selenium complexes; tellurium complexes.

The coordination chemistry of tellurium(II) halides and halotellurate(II) inorganic ligands is relatively undeveloped [1–3]. A limited number of complexes has been obtained recently and structurally characterized. The first example, a $Nb_2Te_8I_{12}$ complex, was described by Leist and Tremel in 1993 [4]. The structure of the compound was characterized by the presence of two $Te_2I_6^{2-}$ ligands coordinated to a $Nb_2(\mu_2\text{-}Te_2)_2^{4+}$ centre. TeI_3^- ligands coordinated to a triangular cluster fragment $[Mo_3(\mu_3\text{-}Te)(\mu_2\text{-}Te_2)_3]^{4+}$ were found for the first time in the structure of $Mo_3Te_{10}I_{10}$ [5]. In 1996 Strähle and co-workers described the tetrahedral $[Re_4(\mu_3\text{-}Te)_4(TeBr_2)_4Br_8]$ cluster complex [6]. This compound contains neutral $TeBr_2$ ligands. All of these compounds were obtained by direct combination of the elements. Hexanuclear Re_6 tellurohalide cluster complexes, $Re_6Te_6Cl_6(TeCl_2)_2$ and $[Re_6Te_8(TeBr_2)_6]Br_2$, have been obtained by reaction of rhenium halides with Te [7].

Our recent efforts have focused on the development of a high-temperature technique to synthesize tellurohalide cluster complexes by extrusion reactions from cluster chalcogenides or halochalcogenides of the transition elements. A new $[Re_6Te_8(TeI_2)_6]I_2$ complex has been prepared by the reaction of the octahedral cluster complex $[Re_6Te_8](Te_7)_{0.6}$ with I_2 [8].

Here we report the synthesis and crystal structure determination of $[Nb_2Se_4Te_4I_{12}]$ formally containing $Te_2I_6^{2-}$ ligands coordinated to niobium atoms of the $Nb_2(\mu_2\text{-}Se_2)_2^{4+}$ cluster fragment.

RESULTS AND DISCUSSION

The compound $[Nb_2Se_4Te_4I_{12}]$ was obtained in quantitative yield by the high-temperature reaction of the dinuclear cluster compound $Nb_2Se_4I_4$ with tellurium and iodine, according to Eq. (1).

$$Nb_2Se_4I_4 + 4Te + 4I_2 \rightarrow Nb_2Se_4Te_4I_{12} \qquad (1)$$

The initial compound, $[Nb_2(\mu_2\text{-}Se_2)_2]I_{8.2}$, has a polymeric layer structure [9,10]. High-temperature reaction with tellurium and iodine leads to the formation of isolated molecules of $[Nb_2(\mu_2\text{-}Se_2)_2(Te_2I_6)_2]$ (extrusion reaction [11]).

The structure of $[Nb_2Se_4Te_4I_{12}]$ has been determined by single-crystal X-ray diffraction. The complex has a central $Nb_2(\mu_2\text{-}Se_2)_2^{4+}$ core, in which the coordination of diselenium ligands resembles acetylene-type $\eta^2:\eta^2$:

* Author to whom correspondence should be addressed.

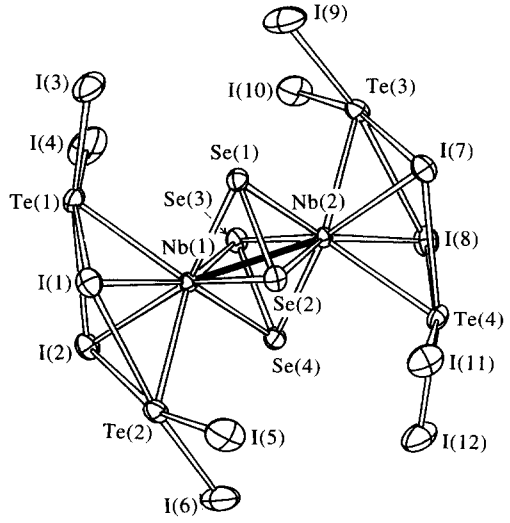


Fig. 1. ORTEP drawing of the $[Nb_2Se_4Te_4I_{12}]$ molecule. Thermal ellipsoids are drawn at the 50% probability level.

μ_2 coordination (Fig. 1). The Se_2 ligands coordinate almost symmetrically, with Nb—Se distances ranging from 2.602(2) to 2.614(2) Å. The Se—Se distances at 2.310(2) and 2.311(2) Å are similar to the corresponding values found in $Nb_2Se_4I_4$ [10]. The Nb—Nb distance of 2.926(2) Å is somewhat longer than the Nb—Nb distance in niobium metal (2.858 Å) and is comparable with the Nb—Nb distances in related Nb^{IV} compounds in which Nb—Nb single bonds are present [12].

The bond lengths and angles of the $Te_2I_6^{2-}$ ligands coordinated to the niobium atoms in $Nb_2(\mu_2\text{-}Se_2)_2(Te_2I_6)_2$ and $Nb_2(\mu_2\text{-}Te_2)_2(Te_2I_6)_2$ [4] are significantly different from those in the free $Te_2I_6^{2-}$ anion. In the planar anion, $Te_2I_6^{2-}$, the four-membered Te_2I_2 ring system is strongly asymmetric, with bridging Te—I bond lengths of 3.061 and 3.215 Å [3]. The corresponding distances for the compound $[Nb_2(\mu_2\text{-}Se_2)_2(Te_2I_6)_2]$ are appreciably longer and range from 3.212(2) to 3.257(2) Å and from 3.175(2) to 3.261(2) Å for $Te_2I_6^{2-}$ ligands coordinated to Nb(1) and Nb(2) atoms, respectively. (For the compound $Nb_2(\mu_2\text{-}Te_2)_2(Te_2I_6)_2$ the bridging Te—I distances are also rather long and span 3.167(1)–3.217(1) Å [4].) Moreover, the terminal Te—I bond lengths of the compound $Nb_2(\mu_2\text{-}Se_2)_2(Te_2I_6)_2$ are up to about 0.12 Å shorter than the corresponding value previously determined for the free $Te_2I_6^{2-}$ anion [3]. On the other hand the terminal Te—I distances (average 2.75 Å) are similar to the corresponding value, 2.76 Å, found in the octahedral cluster complex $[Re_6Te_8(TeI_2)_6]I_2$, with neutral TeI_2 ligands [8]. Therefore, we have some grounds to suppose that the structure of the compound $[Nb_2(\mu_2\text{-}Se_2)_2(Te_2I_6)_2]$ is half way between that of the $[(Nb^{4+})_2(\mu_2\text{-}Se_2^{2-})_2(Te_2I_6^{2-})_2]$ (complex with halochalcogenate ligands $Te_2I_6^{2-}$) and $[(Nb^{4+})_2(\mu_2\text{-}Se_2^{2-})_2(TeI_2)_4(I^-)_4]$ (complex with TeI_2 neutral ligands) extreme formulations.

The structure of $Nb_2Se_4Te_4I_{12}$ has two short intermolecular iodine–iodine distances, which are 3.552(2) Å for I(10)—I(10′) and 3.656(2) Å for I(5)—I(11′). These distances compare favourably with those found in polyiodide structures [13]. These interactions make a chain of molecules along the [212] direction as shown in Fig. 2. Other intermolecular distances are longer than 3.8 Å.

EXPERIMENTAL

Preparation of $Nb_2Se_4Te_4I_{12}$

The compound $Nb_2Se_4I_4$ was prepared by the literature method [10]. A mixture of $Nb_2Se_4I_4$ (2.0185 g,

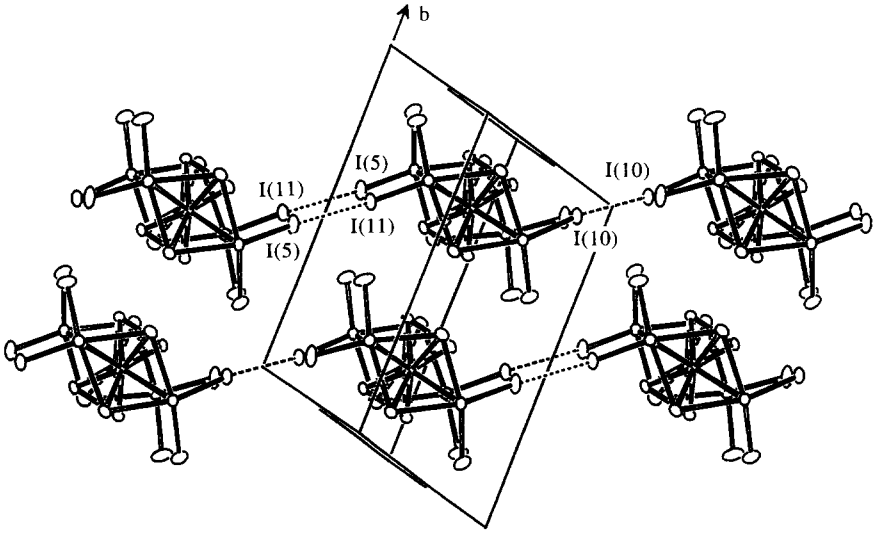


Fig. 2. ORTEP drawing of the crystal structure of $[Nb_2Se_4Te_4I_{12}]$ projected on a [101] plane showing intermolecular interactions. The horizontal direction is [212]. Thermal ellipsoids are drawn at the 50% probability level.

Table 1. Crystal data and refinement results for $Nb_2(Se_2)_2(Te_2I_6)_2$

Formula	$I_{12}Nb_2Se_4Te_4$	Formula weight	2534.9
a/Å	11.745(2)	Space group	$P\bar{1}$ (No.2)
b/Å	14.960(2)	Crystal size/mm^3	$0.08 \times 0.14 \times 0.22$
c/Å	10.831(2)	T/K	295
α/°	95.67(1)	λ/Å	0.7107
β/°	116.19(1)	ρ_{calcd}/(g cm^{-3})	4.69
γ/°	98.19(1)	μ/mm^{-1}	19.65
V/Å^3	1661.9(5)	R^a	0.036
Z	2	R_w^b	0.029

$^a R = \Sigma\|\|F_o\| - \|F_c\|\|/\Sigma|F_o|$ for 6175 reflections.
$^b R_w = [\Sigma w(|F_o| - |F_c|)^2/\Sigma w|F_o|^2]^{1/2}$ where $w = 1/\sigma^2(|F_o|)$.

Table 2. Selected bond distances (Å) and angles (°) for $Nb_2(Se_2)_2(Te_2I_6)_2$

Nb(1)—Nb(2)	2.926(2)	Te(1)—I(4)	2.744(2)
Nb(1)—Se(1)	2.614(2)	Te(2)—i(1)	3.238(2)
Nb(1)—Se(2)	2.612(2)	Te(2)—I(2)	3.221(2)
Nb(1)—Se(3)	2.614(2)	Te(2)—I(5)	2.755(2)
Nb(1)—Se(4)	2.613(2)	Te(2)—I(6)	2.739(2)
Nb(1)—Te(1)	2.912(2)	Te(3)—I(7)	3.177(1)
Nb(1)—Te(2)	2.911(2)	Te(3)—I(8)	3.255(2)
Nb(1)—I(1)	2.946(2)	Te(3)—I(9)	2.736(2)
Nb(1)—I(2)	2.951(2)	Te(3)—I(10)	2.786(2)
Nb(2)—Se(1)	2.602(2)	Te(4)—I(7)	3.261(2)
Nb(2)—Se(2)	2.609(2)	Te(4)—I(8)	3.175(1)
Nb(2)—Se(3)	2.613(2)	Te(4)—I(11)	2.779(2)
Nb(2)—Se(4)	2.608(2)	Te(4)—I(12)	2.735(2)
Nb(2)—Te(3)	2.907(2)	I(1)—Te(1)—I(2)	77.69(3)
Nb(2)—Te(4)	2.908(2)	I(3)—Te(1)—I(4)	96.05(5)
Nb(2)—I(7)	2.944(2)	I(1)—Te(2)—I(2)	77.84(3)
Nb(2)—I(8)	2.941(2)	I(5)—Te(2)—I(6)	96.95(5)
Se(1)—Se(2)	2.310(2)	I(7)—Te(3)—I(8)	77.02(3)
Se(3)—Se(4)	2.311(2)	I(9)—Te(3)—I(10)	95.04(5)
Te(1)—I(1)	3.212(2)	I(7)—Te(4)—I(8)	76.96(3)
Te(1)—I(2)	3.257(2)	I(11)—Te(4)—I(12)	94.35(5)
Te(1)—I(3)	2.746(2)		

2.00 mmol), Te (1.0208 g, 8.00 mmol) and I_2 (2.0431 g, 8.05 mmol) was heated (500°C, 72 h) in an evacuated, fused silica tube. The tube was cooled at 10°C h^{-1} to promote crystal growth. Excess of iodine was evaporated *in vacuo* at 60°C, allowing the isolation of well-formed crystals of $Nb_2Se_4Te_4I_{12}$. Yield: 5.06 g (99%). Found: Nb, 7.3. Calc. for $I_{12}Nb_2Se_4Te_4$: Nb, 7.3%.

In order to ensure product homogeneity, the X-ray powder diffraction pattern of the product was obtained and found to be identical with that calculated from the single-crystal data.

The electrical conductivity, σ, of $Nb_2Se_4Te_4I_{12}$ crystals at room temperature was measured by a four-point contact method: $\sigma = 1 \times 10^{-11}$ ohm^{-1} cm^{-1}.

Crystal structure determination of $Nb_2Se_4Te_4I_{12}$

X-ray data were measured at 295 K on a Rigaku AFC-7R diffractometer with graphite-monochromated Mo-K_α radiation ($\lambda = 0.7107$ Å) using the 2θ–ω scan mode and an empirical absorption correction was applied (relative transmission factor: 0.502–0.994). A slight decay (3.3% in intensity) was detected during the data collection and the data were linearly corrected for the decay. The structure was solved by direct methods (SHELXS86) [14] and all atoms were refined anisotropically using the full-matrix least-squares analysis (ANYBLK) [15]. An extinction correction was made following Zachariasen's method [16], and the extinction parameter τT was refined to be 1.54×10^{-7}.

Crystal data and refinement results for $Nb_2Se_4Te_4I_{12}$ are given in Table 1. Selected interatomic distances and angles are given in Table 2.

Acknowledgement—This work was supported by the Russian Foundation for Basic Research (research grant no. 96-03-33018).

REFERENCES

1. Beck, J., *Angew. Chem., Int. Ed. Engl.* 1994, **33,** 163.
2. Roof, L. C. and Kolis, J. W., *Chem. Rev.* 1993, **93,** 1037.
3. Krebs, B. and Ahlers, F.-P., *Adv. Inorg. Chem.* 1990, **35,** 235.
4. Leist, A. and Tremel, W., *Angew. Chem., Int. Ed. Engl.* 1993, **32,** 1751.
5. Fedin, V. P., Imoto, H. and Saito, T., *J. Chem. Soc., Chem. Commun.* 1995, 1559.
6. Lang, E. S., Abram, U. and Strähle, J., *Z. Anorg. Allg. Chem.* 1996, **622,** 251.
7. Mironov, Y. V., Pell, M. A. and Ibers, J. A., *Inorg. Chem.* 1996, **35,** 2709.
8. Fedin, V. P., Fedorov, V. E., Imoto, H. and Saito, T., *Polyhedron*, accepted for publication.
9. Schäfer H. and Beckmann, W., *Z. Anorg. Allg. Chem.* 1966, **347,** 225.
10. Rijnsdorp, J., de Lange, G. J. and Wiegers, G. A., *J. Solid State Chem.* 1979, **30,** 365.
11. Lee, S. C. and Holm, R. H., *Angew. Chem., Int. Ed. Engl.* 1990, **29,** 840.
12. Sokolov, M., Virovets, A., Nadolinnyi, V., Hegetschweiler, K., Fedin, V., Podberezskaya, N. and Fedorov, V., *Inorg. Chem.* 1994, **33,** 3503.
13. Herbstein, F. H., Reisner, G. M. and Schwotzer, W., *J. Inclusion Phenom.* 1985, **3,** 173.
14. Sheldrick, G. M., *Program for crystal structure determination*, University of Cambridge (1986).
15. Imoto, H., Hayakawa, S., Morita, N. and Saito, T., *Inorg. Chem.* 1990, **29,** 2007.
16. Zachariasen, W. H., *Acta Cryst.* 1967, **23,** 558.

Pergamon

PII: S0277-5387(96)00420-2

Polyhedron Vol. 16, No. 7, pp. 999–1002, 1997
Copyright © 1997 Elsevier Science Ltd
Printed in Great Britain. All rights reserved
0277-5387/97 $17.00+0.00

Sulfur–hydrogen bond activation of thiols by the fragment CpFe(dppe)$^+$: cyclopentadienyl iron(III) thiolate complexes

C. Díaz

Departamento de Química, Facultad de Ciencias, Universidad de Chile, Casilla 653—Santiago, Chile

(Received 29 July 1996; accepted 16 August 1996)

Abstract—Oxidative addition of thiols RSH, R = CH_3, $CH_2CH_2CH_3$, $CH_2C_6H_5$, $C(CH_3)_3$ and C_6H_4Br, by the complex [CpFe(dppe)I] afforded the oxidized thiolate complexes [CpFe(dppe)-SR]PF_6. The reaction of [CpFe(dppe)I] with $HSC_6H_4NH_2$ produces the diamagnetic [CpFe(dppe)$HSC_6H_4NH_2$]PF_6 instead of the expected thiolate product. The reaction of the dithiol $HS(CH_2)_4SH$ with the same iron fragment, gives the binuclear complex [CpFe(dppe)-$S(CH_2)_2$S-CpFe(dppe)][PF_6]$_2$. The formation of the thiol-containing complexes as intermediates in the activation of the S—H bonds is discussed. Copyright © 1997 Elsevier Science Ltd

Keywords: thiol activation; sulfur–hydrogen bond; thiolate complexes; non-sulfur complexes; non III-thiolate complexes.

The hydrodesulfurization process is an essential step in the effective utilization of crude oil and high sulfur coal [1]. The elimination of organosulfur compounds from these hydrocarbon feedstock mixtures are processes catalysed by a variety of metal and organometallic compounds [2]. A fundamental step in the interaction between a catalyst and sulfur-containing substrates, such as hydrogen sulfide or thiols, is the oxidative addition of S—H bonds to the metal centres [3]. Activation of the S—H bond generally occurs with organometallic fragments in low oxidation states [3, 4]. In the majority of cases the activation is promoted by some drastic conditions, i.e. temperature [5] or UV radiation [6].

Previously we have reported the activation of the S—S bond in dithioethers by the electron-rich fragment CpFe(dppe)$^-$, to give the iron–thiolate complexes [CpFe(dppe)-SR]PF_6 [7]. Now we report the mild oxidative addition of thiols to the fragment CpFe(dppe)$^+$, to give the paramagnetic complexes [CpFe(dppe)-SR]PF_6.

RESULTS AND DISCUSSION

CpFe(dppe)I reacted with the thiols RSH to give the blue paramagnetic [CpFe(dppe)-SR]PF_6 complexes according to Eq. (1)

$$\text{CpFe(dppe)I} + \text{RSH} \xrightarrow[\text{CH}_3\text{OH}]{\text{NH}_4\text{PF}_6} \text{[CpFe(dppe)-SR]PF}_6 \qquad (1)$$

where R = CH_3 (**1**), $CH_2CH_2CH_3$ (**2**), $CH_2C_6H_5$ (**3**), C_6H_5 (**4**), t-$C(CH_3)_3$ (**5**) or C_6H_4Br (**6**). The complexes **1–4** have been previously obtained by oxidative addition of the corresponding dithioethers RSSR to the fragment CpFedppe$^+$ [7]. The new complexes **5** and **6** were characterized by elemental analysis and IR and UV–vis spectroscroptic methods.

The IR spectra (see Table 1) of **5** and **6** exhibit the typical absorption bands of the CpFe(dppe)$^+$ moiety [8]. Absorption bands were observed at 3060, ν(C—H), 1435, ν(C—C) and 1098 cm^{-1} δ (C—H), characteristic of an η^5-bonded cyclopentadienyl group. An intense band around 700 cm^{-1} assigned to the δ (C—H) out-of-plane vibration of the phenyl group of dppe, was also observed. The $\nu(PF_6)$ vibration of complexes **5** and **6** was observed normally at 840 cm^{-1} [8, 9].

The characteristic blue colour exhibited by the complexes is associated with their paramagnetic nature [7]. The lowest absorption bands observed around 450 and 590 nm are assigned to a *d–d* transition [7]. The spectrum of **5** is shown in Fig. 1.

On the other hand the reaction of CpFe(dppe)I with

Table 1. Selected spectroscopic data for the thiolate and thiol complexes

Complex	IR (KBr) (cm^{-1})			Visible λ max (CH_2Cl_2) (nm)	
	C_5H_5[a]	dppe[b]	$\nu(PF_6)$		
5	1098	700	846	457	587
6	1095	698	841	456	590
7[c]	1094	696	842	420	
8	1097	699	847	429	593

[a] (C—H) bending, in-plane vibration.
[b] (C—H) bending, out-of-plane vibration.
[c] ^1H NMR: δ 7.7–7.5 (m, C_6H_5), 4.5 (s, C_5H_5), 2.76 (m, CH_2—CH_2—). ^{31}P NMR: δ 90 (s, dppe), −143 (s, PF_6).

$NH_2C_6H_4SH$ afforded the diamagnetic [CpFe(dppe)($HSC_6H_4NH_2$)]PF_6 (**7**) instead of the expected iron–thiolate oxidized complex. The compound was obtained as a yellow-green oil which

$$CpFe(dppe)I + HS\text{-}C_6H_4\text{-}NH_2 \xrightarrow[CH_3OH]{NH_4PF_6} [CpFe(dppe)(HS\text{-}C_6H_4NH_2)]PF_6 \quad (2)$$

was characterized by IR, ^1H, ^{31}P NMR and UV–vis spectroscopic methods. The IR spectrum showed the typical bands of the CpFe(dppe) moiety [8] (see Table 1).

The ν(S—H) and ν(NH) bands were observed at 2558 and 3461, 3376 cm^{-1}, respectively. Comparing the IR spectra of the free 4-aminothiophenol with the coordinated ligand, the major changes are observed for the ν(S—H) band which suggests an S-coordination to the metal. In the free ligand ν(S—H) appears as a broad band around 2500 (owing to the association) while in the complex a narrow band was observed. More detailed studies in solution are precluded because of the low intensity exhibited by the ν(SH) band in solution [6a].

The ^{31}P NMR spectrum of **7** exhibits the signal for dppe at δ 90, a value typical of cationic [CpFe[dppe)L]$^+$ complexes with L = sulfur donor atom [9,10]. The PF_6 septuplet was observed at δ −143. The ^1H NMR spectrum exhibited the multiplet of C_6H_5 protons of dppe in the range δ 7.0–7.5 and the signal for the CH_2 protons was observed at δ 2.76, also as a multiplet. The C_5H_5 proton signal appeared at δ 4.5. All these values are typical of [CpFe(dppe)L]PF_6 complexes [9,10].

The UV–vis spectrum showed the absorption maximum around 420 nm, characteristic of [CpFe(dppe)L]$^+$ complexes where L is a neutral donor ligand [9,11]. The position of this maximum suggests S coordination rather than N coordination; amine complexes CpFe(dppe)NR_3^+ absorb around 500 nm [12].

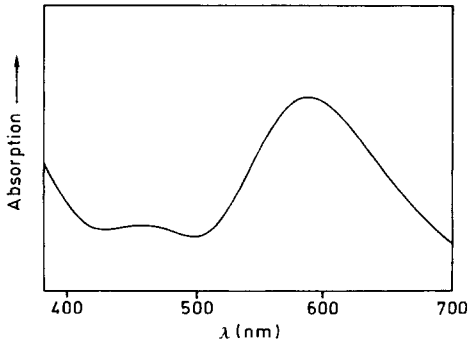


Fig. 1. UV–vis absorption spectrum of [CpFe(dppe)-S-Bu^t]PF_6 in CH_2Cl_2 solution at room temperature.

Reaction of $HS(CH_2)_2SH$ *with* CpFe(dppe)I

Reaction of $HS(CH_2)_2SH$ with CpFe(dppe)I afforded the binuclear product [CpFe(dppe)-S$(CH_2)_2$-S-CpFe(dppe)]$(PF_6)_2$ according to Eq. (3)

$$2CpFe(dppe)I + HS(CH_2)_2SH \xrightarrow[CH_3OH]{NH_4PF_6} [CpFe(dppe)\text{-}S\text{-}(CH_2)_2\text{-}S\text{-}CpFe(dppe)](PF_6)_2 \quad (3)$$

8

Complex **8** was characterized by elemental analysis as well as IR and UV–vis spectroscopic methods.

As observed for the monothiolate complexes, the IR spectrum of **8** exhibits the characteristic bands of the CpFe(dppe)$^+$ moiety [8]. As expected, the ν(S—H) band is absent. The $\nu(PF_6)$ band was observed in the normal range (see Table 1).

Compound **8** which was obtained as a blue solid, exhibited similar absorptions in the UV–vis spectrum to those of the monothiolate complexes **1**–**4**. Data are given in Table 1.

Coordination versus S—H *bond cleavage in thiols*

As suggested for the activation of dithioethers by the fragment CpFe(dppe)$^+$ [7], the activation of the S–H bond in thiols appears to occur through an intermediate involving the sulfur molecule coordinated to the metal fragment (see Fig. 2).

This assumption is supported by molecular orbital calculations [13] which indicate a favourable HOMO [CpFe(dppe)$^+$]–LUMO [RSH] back bonding interaction as shown in Fig. 3. The enhancement of the electron density of the LUMO of the thiol, which has a S—H, S—C antibonding character, produces a weak S—H bond. Thus the isolation of the complex [CpFe(dppe)$HSC_6H_4NH_2$]$^+$, probably coordinated to the metal *via* the sulfur atom, affords additional evidence for the activation mechanism.

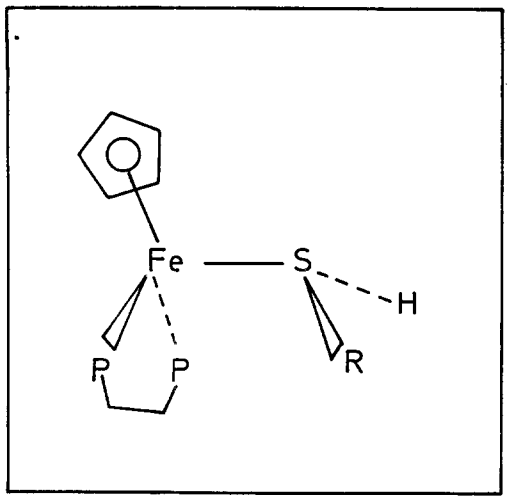


Fig. 2. Possible intermediate involved in the activation of thiols.

EXPERIMENTAL

Infrared spectra were recorded on a Perkin–Elmer FT-IR 2000 spectrophotometer. NMR spectra were recorded on a Bruker AMX 300 instrument. Chemical shifts are given relative to TMS (^{1}H) or 85% H_3PO_4 (^{31}P proton decoupled) with the shift reference being positive. Visible absorption spectra were measured on a Varian DMS-90 spectrophotometer in 1-cm curvettes. Elemental analyses were performed with a Perkin–Elmer 240 microanalyser.

All reactions were carried out under N_2 using standard Schlenk techniques. Solvents were purified using standard procedures. Thiols (Aldrich) were used without additional purification. CpFe(dppe)I was prepared using previously reported methods [10].

Reaction of thiols with CpFe(dppe)I

The complex CpFe(dppe)I (0.14 g, 0.2 mmol) was placed in a Schlenk vessel with the calculated amount

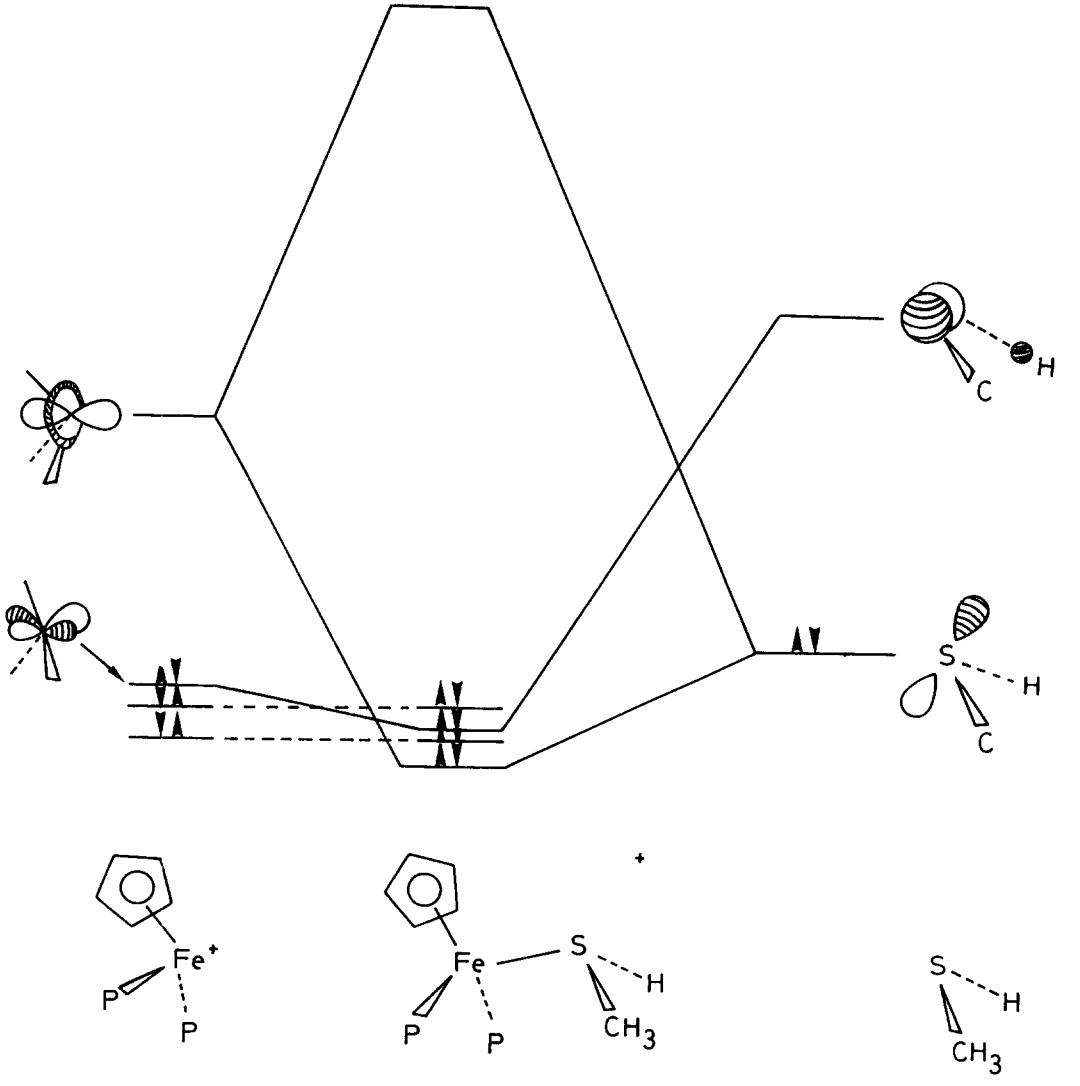


Fig. 3. Simplified molecular orbital diagram for [CpFe(dppe)HSR]$^+$. Possible geometries of the complexes adapted from refs [6a] and [14].

of thiol, RSH (R = CH_3, $CH_2CH_2CH_3$, $CH_2C_6H_5$ and C_6H_5) in the molar ratio 1 : 1 and in the presence of NH_4PF_6. A total of 20 cm^3 of CH_3OH was added and the reaction mixture was stirred for 12 h. After this, the solution, initially black, changed to blue. The solvent was removed *in vacuo* and the solid residue was extracted with CH_2Cl_2. The solutions were filtered through Celite and the solvent was partially evaporated *in vacuo*. Upon addition of a 1 : 10 mixture of n-hexane/diethyl ether the product, a dark blue powder, precipitated and was washed twice with the same solvent mixture. Identification of the products was by comparison of their IR and UV–vis spectra with those of an authentic sample [7].

For the reaction with methanethiol, the mercaptan was bubbled through the solution of [CpFe(dppe)I] in the presence of NH_4PF_6.

[CpFe(dppe)-S-Bu^t]PF_6 (**5**). The complex CpFe(dppe)I (0.14 g, 0.2 mmol) and $(CH_3)_3C$—SH (0.13 cm^3, 1.15 mmol) in the presence of NH_4PF_6 (0.21 g, 1.28 mmol) were stirred for 16 h in CH_3OH (20 cm^3). The solution changed from black to blue after 1 h. The solvent was removed *in vacuo* and the solid extracted with CH_2Cl_2, and then filtered through Celite. The solvent was partially evaporated at reduced pressure and a 1 : 10 mixture of n-hexane/diethyl ether was added. The blue–green powder precipitated was washed twice with the same solvent mixture and dried *in vacuo*. Yield 0.1 g (61%). Found: C, 55.6; H, 5.5. Calc. for $C_{35}H_{38}F_6SP_3Fe$: C, 55.8; H, 5.0%.

[CpFe(dppe)-S-C_6H_4Br]PF (**6**). CpFe(dppe)I (0.14 g, 0.2 mmol) and HSC_6H_4Br (0.061 g, 0.32 mmol) were stirred in the presence of NH_4PF_6 (0.24 g, 0.15 mmol) for 18 h at room temperature in CH_3OH. Separation and purification procedures similar to that for (**5**) afforded a black–blue powder. Yield 0.12 g, (65%). Found: C, 53.2; H, 3.4. Calc. for $C_{37}H_{33}F_6SP_3BrFe$: C, 52.1; H, 3.9%.

[CpFe(dppe)$HSC_6H_4NH_2$]PF_6 (**7**). CpFe(dppe)I (0.14 g, 0.2 mmol) and HS-C_6H_4-NH_2 (0.054 g, 0.43 mmol) in the presence of NH_4PF_6 (0.2 g, 0.6 mmol) and using CH_3OH as solvent were stirred for 20 h at room temperature. After this the solution changed from black to yellow–green. The solvent was removed *in vacuo* and the solid residue extracted with CH_2Cl_2 and filtered through Celite. Elimination of the solvent to dryness affords an oil which could not be converted to a solid in spite of various attempts with several solvents. The dark yellow product was identified spectroscopically: ^1H and ^{31}P NMR data are shown in Table 1. IR(film): 3461s, 3376vs, 3215m, 3055m, 3030m, 2924m, 2558w, 1889w, 1623vs, 1623vs, 1493vs, 1431m, 1289vs, 1177m, 1094s, 1007w, 842vs, 745m, 696s.

[CpFe(dppe)-S$(CH_2)_2$S-CpFe(dppe)]$PF_6)_2$ (**8**). CpFe(dppe)I (0.2 g, 0.31 mmol) and $HS(CH_2)_2SH$ (0.02 cm^3, 0.208 g, 1.7 mmol) were stirred in the presence of NH_4PF_6 (0.29 g, 1.7 mmol) using CH_3OH as solvent (30 cm^3) at room temperature. After 5 min the solution changed from black to blue. The solution was stirred additionally for a further 5 h, and the solvent removed *in vacuo*. The solid residue was extracted with CH_2Cl_2 and filtered through Celite. The solution was concentrated to *ca* 10 cm^3 and then a mixture of 1 : 10 ether/n-hexane was added. The black-blue solid precipitated was washed twice with the same mixture and dried *in vacuo*. Yield 0.18 g (81%). Found: C, 53.8; H, 4.6. Calc. for $C_{66}H_{66}F_{12}P_6S_2Fe_2$: C, 54.7; H, 4.5%.

Acknowledgements—This work was financially supported by FONDECYT (Grant 1950305) and DTI. U. de Chile (Grant Q 3280).

REFERENCES

1. Schuman, S. C. and Shalit, H., *Catal. Rev.* **4,** 245; Mitchell, P. C. H., *Catalysis (London)* 1981, **4,** 175.
2. Angelici, R. J., *Acc. Chem. Res.* 1988, **21,** 387; Angelici, R. J., *J. Coord. Chem. Rev.* 1990, **105,** 61; Friend, C. M. and Robert, J. T., *Acc. Chem. Res.* 1988, **21,** 394.
3. McDonald, R. and Cowie, M., *Inorg. Chem.* 1993, **32,** 1671 and refs therein.
4. Philipp, C. C., Young, C. G., White, P. S. and Templeton, J. L., *Inorg. Chem.* 1993, **32,** 5437.
5. Cooke, J., Green, M. and Stone, F. G. A., *J. Chem. Soc.(A)* 1968, 170; Singer H. and Wilkinson, G., *J. Chem. Soc.(A)* 1968, 2516.
6. (a) Darensbourg, M. Y., Longridge, E. M., Payne, V., Reibenspies, J., Riordan, Ch. G., Spring, J. J. and Calabrese, J. C., *Inorg. Chem.* 1990, **29,** 2721; (b) Winter, A., Scheidsteger, O. and Huthner O., *Z. Naturforsch.* 1983, **38B,** 1525.
7. Díaz, C., Leal, C. and Yutronic, N., *Bol. Soc. Chil. Quím.* 1996, **41,** 99; Díaz, C., Leal, C. and Yutronic, N., *J. Organomet. Chem.* 1996, **516,** 59.
8. Campos, M. M., Díaz, C., Figueroa, K., Padilla, L., Lara, N. and Díaz, G., *Vibrat. Spectrosc.* 1994, **7,** 61.
9. Díaz, C. and Arancibia, A., *Polyhedron* 1994, **13,** 117.
10. Díaz, C. and Latorre, R., *Bol. Soc. Chil. Quím.* 1992, **37,** 211.
11. Díaz, C. and Weiss, B., *Polyhedron* 1993, **12,** 1403.
12. Díaz, C. and Yutronic, N., *Polyhedron* 1996, **15,** 1001.
13. An approximate molecular orbital diagram for [CpFe(L_2)-HSR]+ can be established considering the following theoretical studies on similar systems: refs. 11 and 12; Kostic, N. M. and Fenske, R. F., *Organometallics* 1992, **1,** 979. For MO results on HSR see: Belen'Kii, L. I., *Chemistry of Organosulfur Compounds: General Problems.* Ellis Horwood, England, 1990, p. 363; Matsushita, T., Osamura, Y., Misawa, N., Nishimoto, K. and Tsuno, Y., *Bull. Chem. Soc. Jpn* 1979, **52,** 2521.
14. Schuman, H., Arif, A., Rheingold, A., Janiak, Ch., Hoffmann, R. and Kuhn, N., *Inorg. Chem.* 1991, **30,** 1618.

Pergamon

PII: S0277-5387(96)00385-3

Polyhedron Vol. 16, No. 7, pp. 1003–1011, 1997
Copyright © 1997 Elsevier Science Ltd
Printed in Great Britain. All rights reserved
0277-5387/97 $17.00+0.00

Platinum(II) and palladium(II) complexes of tetrakis(pyrazolyl)cyclotriphosphazenes

K. R. Justin Thomas,[a]*† V. Chandrasekhar,[a] Piero Zanello[b] and Franco Laschi[b]

[a]Department of Chemistry, Indian Institute of Technology, Kanpur-208 016, India

[b]Departimento di Chimica dell' Universitá di Siena, Pian dei Mantellini 44, 53100 Siena, Italy

(Received 28 June 1996; accepted 16 August 1996)

Abstract—Reactions of tetrakis(pyrazolyl)cyclotriphosphazene derivatives, *gem*-$N_3P_3Ph_2Pz_4$ (**2**) and *gem*-$N_3P_3Ph_2(dmpz)_4$ (**4**), with $PdCl_2(PhCN)_2$ or $PtCl_2(PhCN)_2$ afforded complexes of the type MCl_2L (L = **2** or **4**). The detailed spectroscopic (proton, ^{13}C and ^{31}P NMR) investigations revealed that in these complexes the phosphazenes act as bidentate N_2-donor ligands *via* the two geminal pyrazolyl pyridinic nitrogen atoms, thus forming six-membered chelate rings. The platinum derivative $N_3P_3Ph_2Pz_4 \cdot PtCl_2$ (**6**) reacted further with $CuCl_2$ to yield a new heterobimetallic derivative, $N_3P_3Ph_2Pz_4 \cdot PtCl_2 \cdot CuCl_2$ (**9**). The EPR spectra of **9** indicated a distorted five-coordinate geometry around copper. The electrochemistry of **9** is also reported. Copyright © 1997 Elsevier Science Ltd

Keywords: cyclotriphosphazene ligand; pyrazole; platinum(II); palladium(II); copper(II) complexes; NMR.

Interest in the donor groups attached to cyclophosphazenes and their transition metal complexes arises from the fact that such small molecules can function as structural and functional models for their linear high molecular weight polymer analogs, which should exhibit unusual physical and chemical properties [1]. Ever since the pyrazolylcyclotriphosphazenes were introduced by Paddock and coworkers [2] into coordination chemistry, several novel pyrazolyl-substituted cyclotriphosphazene derivatives have been examined as ligands for transition metals [3–8]. Depending on the nature of the substituents other than pyrazolyl groups and the metals, four different modes of interaction between the pyrazolylcyclotriphosphazene and transition metals are observed (Fig. 1). In general they coordinate to the metal through the exocyclic pyrazolyl and the phosphazene skeletal nitrogens. The hexakis- and tetrakis(pyrazolyl)cyclotriphosphazenes $N_3P_3(dmpz)_6$ and $N_3P_3Ph_2(dmpz)_4$ form five-coordinate complexes with copper(II) and nickel(II) halides [3–5], in which the metal is bound to the ligand *via* two nongeminal pyr-

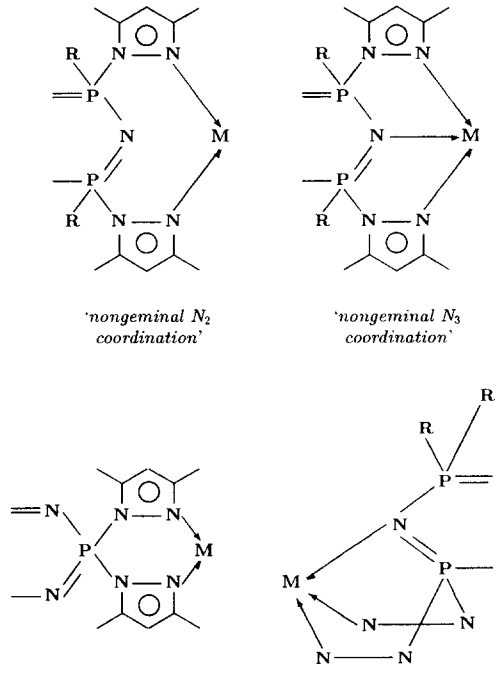


Fig. 1. Coordination modes of pyrazolylcyclotriphosphazenes.

* Author to whom correspondence should be addressed.

† Present address: Dr K. R. Justin Thomas, Regional Sophisticated Instrumentation Centre, Indian Institute of Technology, Madras 600 036, India.

azolyl and one cyclotriphosphazene ring nitrogen. However, with platinum(II) and palladium(II) chlorides they produced mainly four-coordinate complexes with the N_2 donor set derived from two geminal pyrazolyl nitrogens [2,8]. The nongeminal coordination leads to five-membered chelate rings, while in the geminal (N_2) mode the complexes possess six-membered chelates with the boat conformation. In the geminal pattern the ring phosphazene nitrogen involvement in coordination is scarce and is identified only with certain group VI metal carbonyl complexes [9].

The interaction of the cyclophosphazene skeletal nitrogen with the transition metal is of σ-type and is generally weak. It was believed that the basicity of the cyclotriphosphazene ligand and the coordination number of the metals are the important factors affecting the ligating response of a particular pyrazolylcyclotriphosphazene. The basicity of a cyclophosphazene ligand may be affected by changing substituents other than donor groups with electron-rich moieties and/or by modifying the substituents on the exocyclic donor groups. To unravel the basicity factor we have synthesized a new ligand $N_3P_3Ph_2Pz_4$ (**2**), which contains four simple pyrazolyl groups as donors. The difference between **2** and $N_3P_3Ph_2(dmpz)_4$ (**4**) is the presence or absence of methyl substituents at the pyrazole nucleus and the basicity of **2** would be comparatively low. Our aim here is to compare the electronic and steric effects in the spectral and electrochemical properties of the complexes. We describe here in particular the mononuclear Pt^{II} and Pd^{II} chloride complexes of **2** and a heterobimetallic compound with Pt and Cu metal centers and an attempt is also made to compare with the related systems known in the literature.

EXPERIMENTAL

Abbreviations

Hdpctp: hexakis(3,5-dimethyl-1-pyrazolyl)cyclotriphosphazene, tdpctp: 2,2-diphenyl-4,4,6,6-tetrakis (3,5-dimethyl-1-pyrazolyl)cyclotriphosphazene, tpctp: 2,2-diphenyl-4,4,6,6-tetrakis (1-pyrazolyl) cyclotriphosphazene, dmpzH: 3,5-dimethylpyrazole, PzH: pyrazole.

Materials

The platinum and palladium precursors used in this study were obtained by known literature methods [10]. $N_3P_3[NH(CH_2)_3NH]Cl_4$, $N_3P_3Ph_2Cl_4$ and $N_3P_3Ph_2(dmpz)_4$ synthesized by adopting the reported procedures [11, 12, 4]. Solvents dichloromethane, benzene, hexane and acetonitrile were distilled from P_2O_5 and stored over molecular sieves.

Synthesis of the ligand **2**

A solution of $N_3P_3Ph_2Cl_4$ (4.31 g, 10 mmol) dissolved in benzene (50 cm^3) was added to a stirred mixture of pyrazole (2.72 g, 40 mmol) and triethylamine (6.06 g, 60 mmol) at 25°C. The reaction mixture was heated under reflux for 2 days, cooled and the precipitated triethylamine hydrochloride salt was filtered off. From the filtrate the solvent was stripped off *in vacuo*, leaving a residue. The residue was thoroughly washed with water (3×20 cm^3) and ether (3×20 cm^3) and subsequently dried *in vacuo*. A colorless solid obtained was crystallized from a 1 : 1 mixture of hexane and dichloromethane (4.18 g, Yield: 75%). M.p.: 219°C. Found: C, 51.6; H, 3.9; N, 27.8. Calc. for $C_{24}H_{22}N_{11}P_3$: C, 51.7; 3.9; N, 27.6%. IR (cm^{-1}): 1470 m, ν(C=N); 1280 vs; 1220 vs, br; 1165 vs, br, ν(P=N).

Synthesis of **3**

The title compound was obtained in 60% yield by using a very similar procedure that of above except that $N_3P_3Ph_2Cl_2$ was substituted by $N_3P_3[NH(CH_2)_3NH]Cl_4$ M.p.: 216°C.

Synthesis of the complexes

The complexes **5–8** were essentially made by following a same procedure. A general description is as follows: The ligand (1 mmol) and the metal precursor (1 mmol) were taken in benzene (20 cm^3) and heated to reflux for 2–4 h. The palladium complexes **5** and **7** were isolated as insoluble residues from the reaction mixture, while the platinum complexes **6** and **8** required the evaporation of the solvent followed by precipitation from diethyl ether. The solids obtained were crystallized from dichloromethane/benzene or hexane mixtures. The physical and analytical data presented in Table 1.

Synthesis of **9**

To a stirred solution of **6** (0.1646 g) dissolved in dichloromethane (20 cm^3) was added anhydrous $CuCl_2$ (0.030 g). The turbid mixture was stirred for 6 h. The light green precipitate formed was separated by filtration and dried *in vacuo*. Yield: 0.182 g (95%).

Physical measurements

IR spectra were recorded on a Perkin–Elmer 1320 spectrophotometer. The samples were prepared as potassium bromide pellets and the wavenumber was calibrated using polystyrene as calibrant. ^1H and ^{13}C NMR spectra were obtained on a Bruker spectrometer operating at 400 MHz and chemical shifts are reported with reference to internal tetramethylsilane. ^{31}P NMR

Table 1. Physical data for the complexes[a]

Compound	Color	Melting point (°dec.)	Elemental Analyses Found (Calc.) C	H	N
5	Orange	140	39.2[38.7]	3.0[3.3]	21.0[20.8]
6[b]	Yellow	134	42.1[42.2]	3.3[3.4]	16.4[16.25]
7	Orange	238	45.4[45.1]	4.5[4.7]	18.2[17.9]
8	Light yellow	125	41.1[41.2]	4.1[3.85]	16.5[16.2]
9[c]	Light green	120	30.1[30.2]	2.3[2.5]	16.1[16.0]

[a] The formulae of the complexes **4**–**9** are $N_3P_3Ph_2Pz_4 \cdot PdCl_2$, $N_3P_3Ph_2Pz_4 \cdot PtCl_2$, $N_3P_3Ph_2(dmpz)_4 \cdot PdCl_2$, $N_3P_3Ph_2(dmpz)_4 \cdot PtCl_2$ and $N_3P_3Ph_2Pz_4 \cdot PtCl_2 \cdot CuCl_2$.

[b] Includes half a molecule of benzene.

[c] Cu: 6.6[6.45].

spectra were recorded on a Bruker spectrometer operating at 164.5 MHz. Phosphorus chemical shifts are reported with reference to external 85% H_3PO_4; upfield shifts are negative. Electrochemical measurements were performed with a BAS 100A electrochemical analyser [13]. The three-electrode cell consisted of a glassy-carbon working electrode, a platinum wire as a counter electrode and reference electrode saturated calomel electrode. All potential values are referred to the saturated calomel electrode. Under the present experimental conditions the one-electron oxidation of ferrocene occurs at +0.38 V.

RESULTS AND DISCUSSION

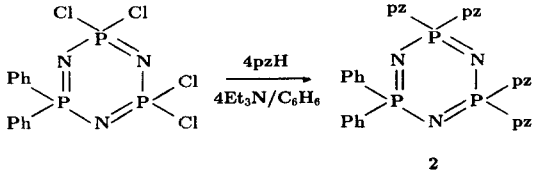
Synthesis

The geminal tetrakis(pyrazolyl)cyclotriphosphazene, $N_3P_3Ph_2pz_4$ (**2**), is obtained from the reaction of *gem*-$N_3P_3Ph_2Cl_4$ with pyrazole in the presence of triethylamine in refluxing benzene. Similarly, **3** is accessed by a facile nucleophilic substitution reaction of *spiro*-$N_3P_3[NH(CH_2)_3NH]Cl_4$ with pyrazole (Scheme 1). The phosphazenes **2** and **3** are obtained in relatively good yields. The pyrazolylcyclotriphosphazenes have been characterized by multinuclear NMR and IR spectroscopy and by C, H and N elemental analyses.

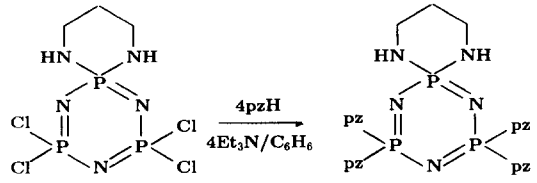
The reaction of **2** and $N_3P_3Ph_2(dmpz)_4$ (**4**) with $PdCl_2(NCPh)_2$ or $PtCl_2(NCPh)_2$ in benzene give the complexes of the general formula $[MCl_2 \cdot L]$, where L = **2**; M = Pd (**5**) or Pt (**6**) and L = **4**; M = Pd (**7**) or Pt (**8**), in good yields. The complexes are highly soluble in common halogenated solvents, such as dichloromethane, chloroform, etc. In these complexes the two geminal pyrazolyl pyridinic nitrogen atoms are involved in coordination. The coordinating ability of these "metallo-ligands" has been illustrated by the preparation of a heterobimetallic compound $2 \cdot PtCl_2 \cdot CuCl_2$ (**9**). All the complexes have been characterized by elemental analysis and multinuclear NMR spectroscopy. Electrochemical and ESR spectral studies have been performed on the heterobimetallic derivative **9**.

NMR spectroscopy

The ^1H NMR spectra of **2** and **3** show that the four pyrazolyl groups are equivalent. They exhibit three

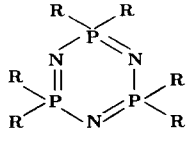


2

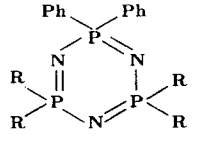


3

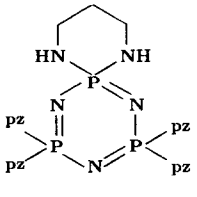
Scheme 1.



R = dmpz (1)



R = pz (2)
R = dmpz (4)



3

Scheme 2.

different signals due to the 4-C, 5-C and 3-C protons of pyrazole nucleus at *ca* 6.2, 7.7 and 7.9 ppm, respectively (Fig. 2). The unresolved multiplet at *ca* 6.2 ppm is assigned to the 4-C protons. Recent studies on the polypyrazolyl borates and their complexes indicate that the 3-C protons resonate at lower fields than that of 5-C [12,13]. Considering the criterion to be compatible with the case for these pyrazolylphosphazenes also, we attribute the doublet in the downfield region to the 3-C protons and the other doublet at *ca* 7.7 ppm to the 5-C protons. In addition, the pyrazolylcyclotriphosphazenes **2** and **3** show features due to the phenyl and 1,3-diaminopropane moieties, respectively. The proton NMR spectrum of **2** shows a cluster of signals in the region 7.21–7.81 ppm for the phenyl groups, while that of **3** exhibits a multiplet at 1.67, a triplet at 3.35 and a broad signal at 4.86 ppm due to the $—CH_2—$, $—NCH_2—$ and the —NH— protons, respectively, of the 1,3-diamino propane *spiro* loop. After coordination to palladium (in complexes **5** and **7**) all the four pyrazolyl groups become nonequivalent and give rise to approximately four sets of signals at room temperature (Figs 3 and 4, Table 2). This is surprising to compare with the results reported by other authors who observe that the palladium derivatives of polypyrazolyl borate [14]

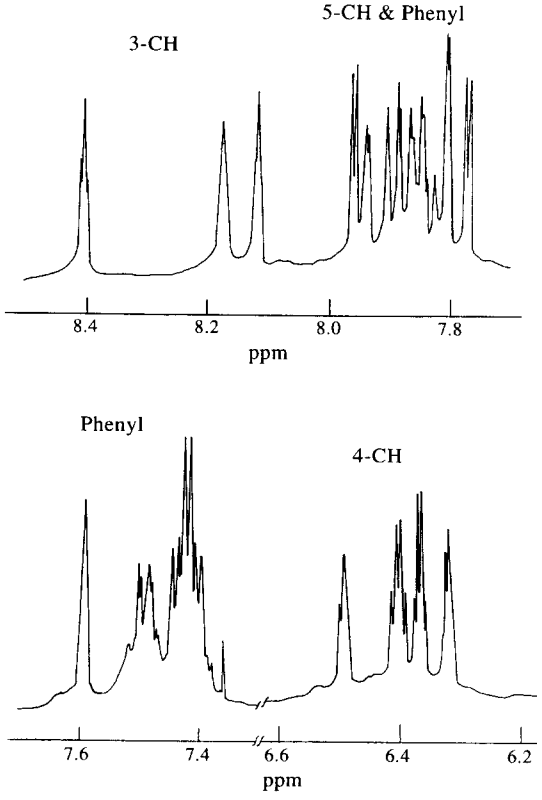


Fig. 3. ^1H NMR spectrum of the palladium complex **5** indicating the presence of four different pyrazole groups.

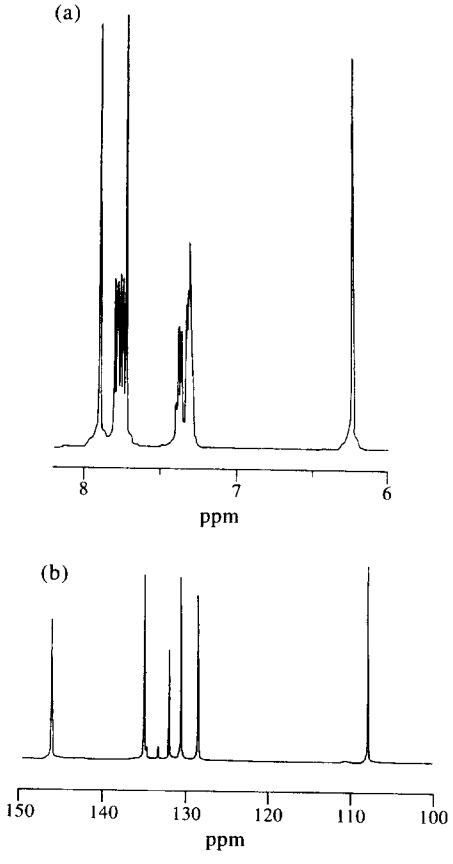


Fig. 2. (a) ^1H and (b) ^{13}C NMR spectra of **2**, showing only one type of pyrazole group.

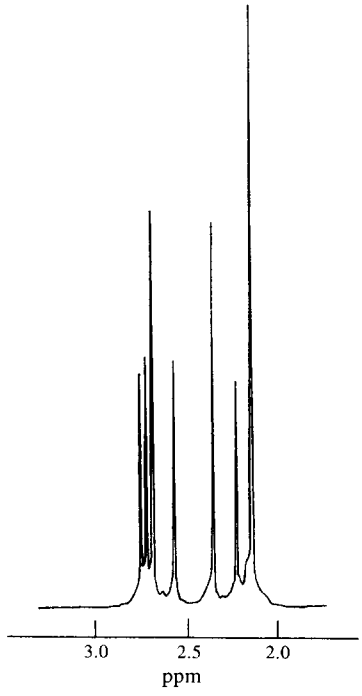


Fig. 4. ^1H NMR spectrum of the palladium complex **7** in the methyl region.

Table 2. Proton NMR data for the ligand and complexes[a]

No.	3-CH_3 (or) 3-CH	5-CH_3 (or) 5-CH	4-CH	Phenyl
2	7.90 (d, 4H)	7.73 (d, 4H)	6.23 (t, 4H)	7.29–7.81 (m, 10H)
5	7.60, 7.78	7.95, 8.16	6.32, 6.37	7.37–7.90 (m, 10H)
	7.81, 7.98 (d, 4H)	8.19, 8.41 (t, 4H)	6.41, 6.50 (q, 4H)	
6	7.98 (4H)	7.80 (4H)	6.35 (4H)	7.38–7.87 (m, 10H)
4	2.26 (s, 12H)	2.15 (s, 12H)	5.88 (s, 4H)	7.31–7.94 (m, 10H)
7	2.75, 2.72, 2.68, 2.57		5.79, 5.80	7.37–8.24 (m, 10H)
	2.35, 2.22, 2.14 (s, 24H)[b]		5.98, 6.00 (s, 4H)	
8	2.19 (s, 12H)	2.08 (s, 12H)	5.86 (br, 4H)	7.36–8.09 (m, 10H)
3	8.10 (d, 4H)	7.75 (d, 4H)	6.42 (t, 4H)	4.86 (br, NH, 2H)
				3.35 (t, NCH_2, 4H)
				1.63 (m, CH_2, 2H)

[a] Multiplicity given in parentheses.
[b] Intensity ratio $\alpha:\alpha:\beta:\alpha:\beta:\alpha:2\beta$.

or pyrazolylphosphazenes [8] are fluxional in nature at room temperature.

This observation stimulated us to reinvestigate the spectra of the palladium complex **7**, derived from tdpctp, which was earlier reported by Paddock and Gallicano [2]. They have observed only three signals for 3- and 5-methyl protons. Interestingly, the spectra recorded at 400 MHz shows seven signals in the ratio $\alpha:\alpha:\beta:\alpha:\beta:\alpha:2\beta$ (Fig. 4). The observation of nonequivalent pyrazolyl groups are well explained by considering the two possible isomers for these complexes (Fig. 5). In isomer **A** the uncoordinated pyrazolyl groups are away from the metal center and constitute a stereochemically equivalent set. However, in isomer **B** the uncoordinated pyrazolyl groups are stereochemically nonequivalent. These differences, due to the spatial arrangement of pyrazolyl groups lead to a multitude of signals. Similar and somewhat less pronounced effects have been noticed in the ^{13}C NMR spectra of the compounds also (Table 3).

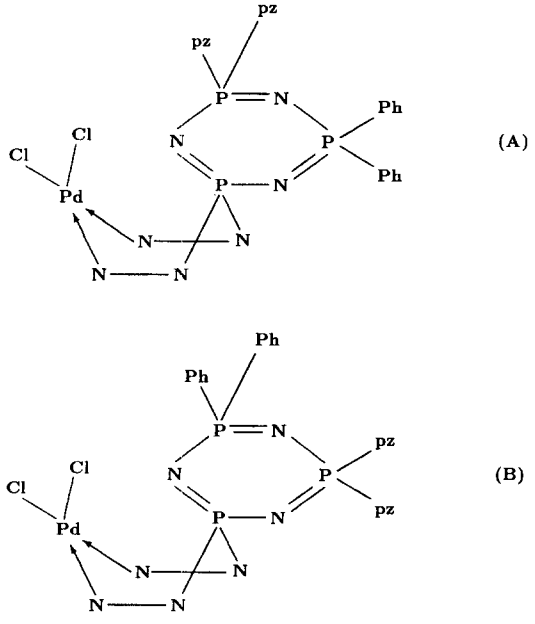


Fig. 5. Isomeric structures of the complexes with geminal N_2 coordination.

The ^{31}P NMR spectra of **2** and **3** display a AX_2 pattern with a doublet at −1.99 and 1.15 and a triplet at 24.10 and 14.58, respectively. The upfield doublet is readily assigned to the Ppz_2 groups by comparison with the value for $N_3P_3(dmpz)_4$ and **4**. The two bond coupling observed for Ppz_2 and PPh_2 or P_{spiro} centers in **2** and **3** are larger than that observed for PCl_2 and PPh_2 or P_{spiro} groups in their parent compounds $N_3P_3[NH(CH_2)_3NH]Cl_4$ [12] and $N_3P_3Ph_2Cl_4$ [15], respectively. The chemical shift of a particular phosphorus atom depends on several factors, such as the nature of the substituents (steric and electronegatively), extent of π-bonding with the substituents, bond angles at phosphorus, etc. The substituents on the adjacent phosphorus may also influence the chemical shift of the phosphorus nucleus under consideration [18]. It is clearly evident from Table 4 that the bulkiness of the pyrazolyl substituent is responsible for the drastic upfield shift when compared with the other aminocyclotriphosphazenes. A slight down-field shift for the Ppz_2 group in **3** may be attributed to the electronic effect exerted by the electron rich *spiro* loop.

The ^{31}P NMR spectra of palladium complexes **5** and **7** show an ABX pattern (see Table 4). The two ppz_2 phosphorus nuclei which are equivalent in **1** and **4** have become nonequivalent and the phosphorus bearing the coordinated pyrazole are shielded and phosphorus nucleus associated with the uncoordinated pyrazolyl groups are slightly deshielded. The PPh_2 phosphorus nuclei in the palladium complexes are also deshielded. The platinum complexes show only two broad signals at room temperature, suggestive of fluxional motions in solution. However, the nature of the dynamic processes are not clear at this stage.

Table 3. ^{13}C NMR data for the ligand and complexes

Compound	3-C	4-C	5-C	Methyl	Phenyl
2	145.9	107.8	134.8		134.5, 133.1, 131.8 130.5, 128.4
5	146.1 142.0	107.9 106.6	136.2 135.0		132.0, 130.7, 130.1 128.6, 128.5
6	146.1	107.9	135.3		135.0, 133.8, 132.0 130.7, 128.6
4	152.1	109.4	146.7	13.7, 12.8	135.7, 134.3, 131.6 131.4, 127.6
7	157.5, 157.4 153.7, 153.6	111.0, 110.9 110.7	149.2	15.4, 13.8 13.5, 12.5	131.6, 131.1, 130.9 128.6, 128.4
8	153.4	108.8	136.1	13.4, 12.1	134.5, 132.8, 130.3 128.6, 127.1
3	145.0	107.4	135.0		40.0 (NCH_2) 25.6 (CH_2)

Table 4. ^{31}P NMR data for the ligand and complexes

Compound	Pattern	$\delta P(Ph_2)$	$\delta P(pz_2)$	^3J(p-p) Hz
2	AX_2	24.10	−1.99	51.4
5	ABX	25.00	−0.41	71.5
			−3.52	33.4, 24.6
6	AX_2	24.08(br)	−1.95(br)	
4	AX_2	20.35	−5.41	58.8
7	ABX	21.05	−1.82	68.9
			−5.97	45.6, 22.3
8	AX_2	22.73(br)	−3.61(br)	
3	AX_2	14.58[a]	1.15	50.7
$N_3P_3[H(CH_2)_3NH]Cl_4$[b]	AX_2	12.3[a]	23.1[c]	43.7
$N_3P_3Ph_2Cl_4$[d]	AX_2	19.5	17.1[c]	12.0
$N_3P_3(NHBu^t)_2Cl_4$[e]	AX_2	2.3[c]	19.6[c]	44.7
$N_3P_3(Az)_2Cl_4$[f]	AX_2	34.2[f]	21.9[c]	30.0

[a] δP(spiro).
[b] From ref. [12].
[c] δP (Cl_2).
[d] From ref. [15].
[e] δP ($(NHBu^t)_2$), from ref. [16].
[f] δP (Az_2), from ref. [17].

EPR spectroscopy

The EPR spectrum of **9** recorded at room temperature as polycrystalline powder sample was isotropic and do not exhibit any metal or ligand splitting features. However, in solution it displayed informative spectra. Figure 6(b) shows the X-band EPR spectrum of tpctp·$PtCl_2$·$CuCl_2$ in acetonitrile solution recorded at 100 K. The well resolved lineshape is indicative of a $S = 1/2$ paramagnetic species in an axial symmetry ($g_\parallel > g_\perp$) with hyperfine resolution in the parallel region; a poorly but informative resolution of nine superhyperfine lines is also detectable in the perpendicular region. The overall lineshape is accounted for by magnetic coupling of the $S = 1/2$ unpaired electron with the copper nucleus ($I = 3/2$); the minor superhyperfine multiplet is attributable to the electron spin interaction with four nitrogen nuclei ($I = 1$; theoretical intensity of ratio = 1 : 5 : 10 : 14 : 19 : 14 : 10 : 5 : 1). The second derivative analysis affords a better resolution of the absorption pattern and gives the experimental values of the $A_\perp$(N) superhyperfine coupling constant. The poor resolution of the spectrum in the perpendicular region and corresponding linewidth are consistent with the non-equivalence of the four coordinating nitrogen nuclei, as confirmed by computer simulation. This further supports the proposed tetragonal arrangement [19] of the copper environment with the three nitrogens originating from two geminal pyrazolyl groups and one acetonitrile molecule lying in the equatorial plane (higher $A_\perp$(N)) and the fourth of the cyclo-

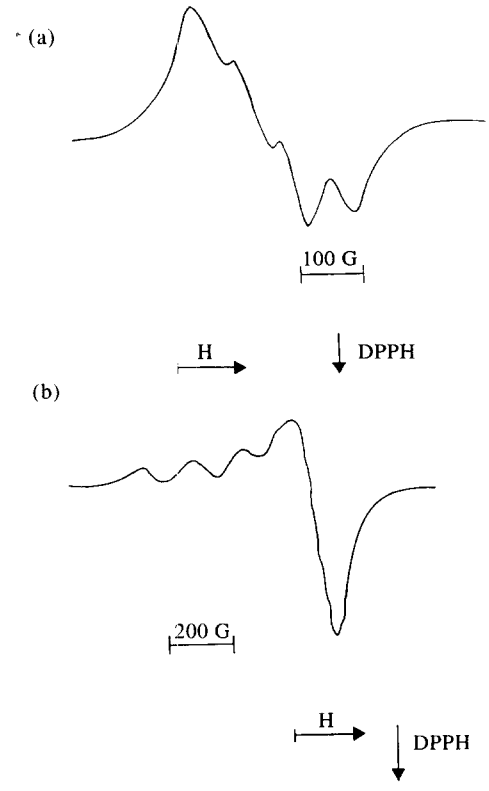


Fig. 6. EPR spectra of **9** (a) at room temperature (298 K) and (b) at 100 K in acetonitrile solution.

triphosphazene nitrogen occupying an apical position. The $A_{\parallel}$ values suggest that the equatorial plane is more tetrahedrally distorted [20]. The involvement of acetonitrile is further supported by the fact that when the spectrum was recorded in DMF the super hyperfine splitting collapsed. The parameters of the simulated spectrum are:

$g_{\parallel} = 2.270$	$g_{\perp} = 2.059$
$g_{av} = 1/3(g_{\parallel}+2g_{\perp}) = 2.130$	
$A_{\parallel} = 148.0$ G	$A_{\perp} = 10.0$ G
$A_{av} = 1/3(A_{\parallel}+2A_{\perp}) = 56.0$ G	
$A_{\parallel}(3N) = 4.0$ G	$A_{\perp}(3N) = 13.8$ G
$A_{\parallel}(N) = 3.7$ G	$A_{\perp}(N) = 12.7$ G.

Figure 6(a) shows the room-temperature X-band EPR spectrum of **9** in acetonitrile solution. Both the first and the second derivative spectra are poorly resolved and do not exhibit superhyperfine resolution. The relevant isotropic parameters ($g_{iso} = 2.132$; $A_{iso} = 58.3$ G) well fit the low temperature (100 K) ones. It must be noted that no absorption attributable to paramenetic platinum centered species have been detected neither in the original complex nor in solution from exhaustive electrolysis.

Electrochemistry

The unusual EPR spectral observations of the complex tpctp·$PtCl_2$·$CuCl_2$ prompted us to investigate the electrochemical behavior of it. The redox pattern exhibited by the heterodimetal complex is intriguing. As illustrated in Fig. 7, in acetonitrile solution it undergoes three subsequent cathodic steps at peaks A, B and C, respectively. Controlled potential coulometric tests served to elucidate overall reduction path. The catho-anodic peak system A/G ($E^{\circ} = +0.46$ V) proved to involve a chemically reversible electron transfer, in that controlled potential electrolysis ($E_w = 0.0$ V) consumes one electron per molecule. Concommitantly the initially EPR-active (see the previous section), yellow–green solution turns colorless and EPR silent. Such a final solution exhibits a cyclic voltammetric profile quite complementary to that illustrated in Fig. 7(c). Subsequent exhaustive one-electron reduction at the second cathodic step ($E_w = -1.0$ V) causes deposition of copper metal on the microelectrode surface. The resulting solution displays only the reduction process C, which we confidently assign to the reduction of the platinum(II) center, in analogy with the results on the platinum complexes of tpctp and tdpctp, which exhibit an irreversible Pt^{II}/Pt^{0} reduction at very negative potential values (in the range from -1.5 V to -1.6 V). Upon reoxidation of the electrodeposited copper metal

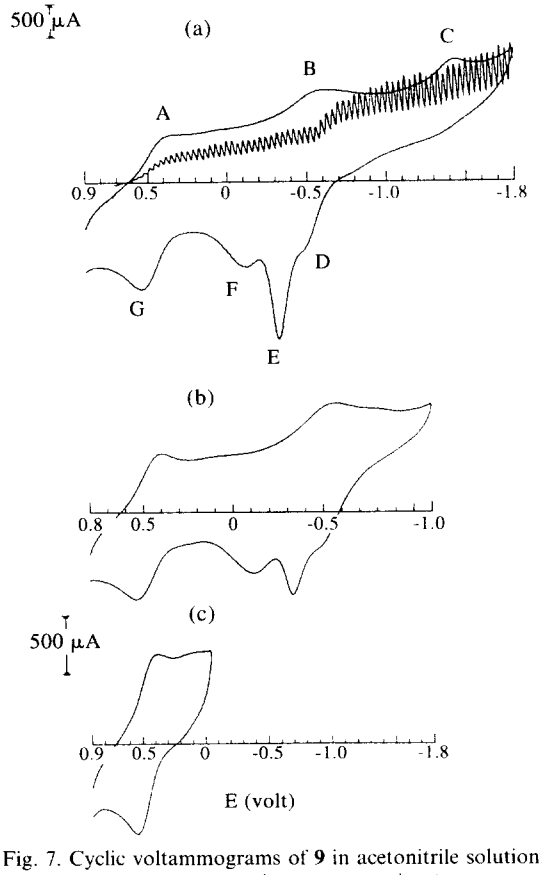


Fig. 7. Cyclic voltammograms of **9** in acetonitrile solution. Scan rates: (a), (c) 0.2 V s^{-1}; (b) 0.1 V s^{-1}. Direct current voltammetric scan rate: (a) 0.01 V s^{-1}.

($E_w = +0.6$ V), the solution restores the original voltammetric response shown in Fig. 7. In summary, the overall redox propensity of complex tpctp · $PtCl_2$ · $CuCl_2$ is so schematizable:

$$[LCu^{II}Pt^{II}] \underset{-e(G)}{\overset{+e(A)}{\rightleftharpoons}} [LCu^{I}Pt^{II}]^- \underset{-e(D)}{\overset{+e(B)}{\rightleftharpoons}} [LCu^{0}Pt^{II}]^{2-}$$

$$\downarrow$$

$$Cu^0 + [Pt^{II}L]^{2-}$$

$$-e\downarrow(E) \qquad (C)\downarrow +2e$$

$$Cu^I + [Pt^0L]^{4-}$$

$$-e\downarrow \qquad (F)\downarrow$$

$$Cu^{II} \qquad \text{degradation}$$

Finally a few further points deserve comment. (i) The thermodynamically easy access to the $Cu^IPt^{II}L$ (L = ligand) congener is quite rare [21], particularly when compared with the corresponding complex hdpctp · $CuCl_2$ · $PtCl_2$, which under the same experimental conditions undergoes the $[Cu^{II}Pt^{II}L]/[Cu^0Pt^{II}L]^{2-}$ reduction process through a single-stepped irreversible process ($E_p = -0.55$ V), without any stabilization of the intermediate mixed-valent species [22]. This is likely attributable to the electronic factors arising from the substitution of two pyrazolyl groups for two electron-withdrawing phenyl groups and removal of methyl groups from 3- and 5-positions of pyrazole ring, which makes easier the addition of electrons. (ii) The analysis of the peak system A/G with scan rates varying from 0.02 to 2 V s^{-1} shows that the peak-to-peak separation progressively increases from 140 to 315 mV. This high departure from the constant values of 59 mV expected for an electrochemically reversible one-electron transfer denotes that a considerable geometrical strain accompanies the $[Cu^{II}Pt^{II}L]/[Cu^0Pt^{II}L]^{2-}$ redox change [21].

CONCLUSION

The new pyrazolylcyclophazene ligand **1** reacts in a facile manner with the platinum and palladium salts to give the corresponding mononuclear complexes. The possibility of using these complexes as ligands for the assembly of heterobimetallic compounds has been demonstrated for the platinum complex **6**. It is also interesting to note that the absence of methyl groups in the pyrazolyl nucleus affects mainly the electrochemical property of the heterobimetallic derivative. However, the final conclusion on the role of substituents on pyrazolyl and cyclophosphazene moieties awaits more elaborate studies with more sensitive metals such as copper, cobalt, etc., and various suitably modified pyrazolylcyclotriphosphazenes. Work in this direction is in progress at our laboratories.

REFERENCES

1. Allcock, H. R., *Polymer*, 1980, **21,** 673; Potin, Ph. and De Jaeger, R., *Eur. Polym. J.* 1991, **27,** 341; Chandrasekhar, V. and Justin Thomas, K. R., *Appl. Organomet. Chem.* 1993, **7,** 1; Allcock, H. R., Desorcie, J. L. and Riding, G. H., *Polyhedron*, 1987, **6,** 119.
2. Gallicano, K. D., Paddock, N. L., Rettig, S. J. and Trotter, J., *Inorg. Nucl. Chem. Lett.* 1979, **15,** 417; Gallicano, K. D. and Paddock, N. L., *Can. J. Chem.* 1982, **60,** 521.
3. Justin Thomas, K. R., Chandrasekhar, V., Pal, P., Scott, S. R., Hallford, R. and Cordes, A. W., *Inorg. Chem.* 1993, **32,** 606; Justin Thomas, K. R., Chandrasekhar, V., Scott, S. R., Hallford, R. and Cordes, A. W., *J. Chem. Soc., Dalton Trans.* 1993, 2589.
4. Justin Thomas, K. R., Tharmaraj, P., Chandrasekhar, V. and Tiekink, E. R. T., *J. Chem. Soc., Dalton Trans.* 1994, 1301.
5. Justin Thomas, K. R., Tharmaraj, P., Chandrasekhar, V., Scott, S. R. and Cordes, A. W., *Polyhedron*, 1995, **14,** 977.
6. Justin Thomas, K. R., Tharmaraj, P., Chandrasekhar, V., Bryan, C. D. and Cordes, A. W., *Inorg. Chem.* 1994, **34,** 5382.
7. Chandrasekaran, A., Krishnamurthy, S. S. and Nethaji, M., *Curr. Sci.* 1991, **60,** 700.
8. Chandrasekaran, A., Krishnamurthy, S. S. and Nethaji, M., *Inorg. Chem.* 1993, **32,** 6102.
9. Chandrasekaran, A., Krishnamurthy, S. S. and Nethaji, M., *J. Chem. Soc., Dalton Trans.* 1994, 63.
10. Kharasch, M. S., Seyler, R. C. and Mayo, F. R., *J. Am. Chem. Soc.* 1938, **60,** 882.
11. McBee, E. T., Okuhara, K. and Morton, C. J., *Inorg. Chem.* 1965, **4,** 1672.
12. Chandrasekhar, V., Krishnamurthy, S. S., Manohar, H., Vasudevamurthy, A. R., Shaw, R. A. and Woods, M., *J. Chem. Soc., Dalton Trans.* 1984, 621.
13. Zanello, P., Opromolla, G., Casarin, M., Herberhold, M. and Xeitner, P., *J. Organomet. Chem.* 1993, **443,** 199.
14. Onishi, M. and Hirachi, K., *Inorg. Chim. Acta*, 1994, **224,** 131; Reger, D. L., Swift, C. A. and Leboida, L., *Inorg. Chem.* 1984, **23,** 249; Trofimenko, S., *Prog. Inorg. Chem.* 1986, **34,** 115; Cabildo, P., Claramont, R. M. and Elguero, J., *Org. Magn. Res.* 1984, **22,** 603.
15. Keat, R., Shaw, R. A. and Woods, M., *J. Chem. Soc., Dalton Trans.* 1976, 1582.
16. Allen, C. W., Brown, D. E., Cordes, A. W. and Craig, S. C., *J. Chem. Soc., Dalton Trans.* 1988, 1405.
17. Van der Huizen, A. A., Van de Grampel, J. C., Rusch, J. W., Witting, T., Bolhuis, E. and Meetsma, A., *J. Chem. Soc., Dalton Trans.* 1986, 1317.
18. Chandrasekhar, V. and Justin Thomas, K. R., *Struct. Bonding (Berlin)*, 1993, **81,** 43.
19. Hathaway, B. J. and Billing, D. E., *Coord. Chem. Rev.* 1970, **5,** 143.
20. Additon, A. W., Rao, T. N., Reedijk, J., van Rijn,

J. and Verschoor, G. C., *J. Chem. Soc., Dalton Trans.* 1984, 1349.
21. Zanello, P., *Stereochemistry of Organometallic and Inorganic Compounds*, Vol. 4, ed. I. Bernal. Elsevier, Amsterdam 1990, p. 181.
22. Justin Thomas, K. R., Zanello, P. and Chandrasekhar, V., Manuscript in preparation.

Pergamon

PII: S0277-5387(97)00417-2

Polyhedron Vol. 16, No. 7, pp. 1013–1021, 1997
Copyright © 1997 Elsevier Science Ltd
Printed in Great Britain. All rights reserved
0277-5387/97 $17.00+0.00

Syntheses and structural studies on copper(II) complexes derived from ethyl(2-benzothiazolyl)aminoformate

Xu Shen,[a]* Hui-Nan Guan,[a] Xiao-Ying Huang,[a] Qiu-Tian Liu,[a] Bei-Sheng Kang,[b]* Xiao-Lin Wu,[b] Lian-Quan Gu[b] and Jie Sun[c]

[a] State Key Laboratory of Structural Chemistry and Fujian Institute of Research on the Structure of Matter, Chinese Academy of Sciences, Fuzhou 350002, P.R. China

[b] Department of Chemistry, Zhongshan University, Guangzhou 510275, P.R. China

[c] Laboratory of Organometallic Chemistry and Shanghai Institute of Organic Chemistry, Chinese Academy of Sciences, Shanghai 200032, P.R. China

(Received 25 June 1996; accepted 16 August 1996)

Abstract—The reaction of copper(II) acetate with ethyl(2-benzothiazolyl)aminoformate (HL) gave red crystals of $[Cu_2L_4]_2$ (**1**). When complex **1** was treated with pyridine (Py) in chloroform/toluene, red crystals of $CuL_2(Py)_2$ (**2**), were deposited. Both complexes have been characterized by single-crystal X-ray diffraction methods, showing that the binuclear complex **1** has the copper atoms each located in a four-coordinate square-planar geometry of N_4, with two independent molecules in an asymmetric unit. The average bond distances of Cu—N(amine) and Cu—N(bta) (bta = benzothiazoyl) are 1.98 and 2.07 Å, respectively. Complex **2** is mononuclear with the Cu atom also in a square plane. The bond distances of Cu—N(py) and Cu—N(amine) are 2.011(4) and 1.997(4)Å, respectively. Copyright © 1997 Elsevier Science Ltd

Keywords: crystal structure; Cu^{II} complexes; syntheses; pyridine complex; amine complexes; ethyl(2-benzothiazolyl)aminoformate.

Amide-containing ligands have long invoked the interest of coordination chemists and biochemists, because of their biological significance [1]. It is believed that the coordination of amide to metal ions could provide simple models for more complex enzymes [2]. In recent years, the literature has reported many studies on the coordination behaviour of amide oxygen or deprotonated nitrogen to metal ions [3]. Amino acids are the basic units of proteins whose importance in living cells has been known for a long time. Amino acid esters can be hydrolysed directly into amino acids. In most cases, the biological activities associated with a given compound are often traceable to the coordination behaviour of the metals present in the biosystem. Thus, inspired by these facts, we have synthesized a new ligand, ethyl(2-benzothiazolyl)aminoformate (Fig. 1), and obtained two copper complexes **1** and **2**. In this paper, we report the characterization including the X-ray crystal structures, of **1** and **2**.

EXPERIMENTAL

Ethyl(2-benzothiazolyl)aminoformate (HL)

The ligand HL was prepared by the reaction of 2-aminobenzothiazole (1.50 g, 0.01 mol) with ethyl-

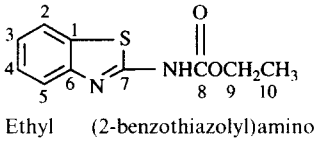


Fig. 1. Ethyl (2-benzothiazolyl)amino formate ($C_{10}H_{10}O_2N_2S$).

* Authors to whom correspondence should be addressed.

chloroformate (1.09 g, 0.01 mol) in boiling ethylacetate for 3–4 h by the method described in the literature [4]. Yield, 1.81 g (70%). M.p. 202–203°C. Found: C, 54.2; H, 4.4; N, 12.5; S, 14.6. Calc. for $C_{10}H_{10}O_2N_2S$: C, 54.1; H, 4.5; N, 12.6; S, 14.4%. ^{1}H NMR (DMSO-d_6): δ(NH) 12.03 (s, 1H, NH); δ(CH) 7.26–7.96 (m, 4H, aromatic ring); δ(CH) 4.23–4.27 (q, 2H, OCH_2); δ(CH) 1.26–1.30 (t, 3H, CH_3), ^{13}C NMR (DMSO-d_6) 159.93 $\delta(C_7)$, 154.26 (C_8), 149.50 (C_1), 131.82 (C_6), 120.45–126.21 (C_2–C_5), 62.14 (C_9), 14.56 (C_{10}).

Synthesis of complex **1** $[(Cu_2L_4)_2]$

To a boiling anhydrous ethanol solution (30 cm^3) containing HL (0.31 g, 1.40 mmol) was added $Cu(CH_3COO)_2 \cdot H_2O$ (0.14 g, 0.70 mmol). The mixture was refluxed for 2–3 h then cooled to room temperature, whereupon the solid precipitated was isolated by filtration, washed repeatedly with anhydrous ethanol and methanol and dried in a vacuum desiccator over anhydrous $CaCl_2$. Recrystallization from $CHCl_3/Et_2O$ gave red crystals of **1**. Yield, 0.36 g (79%). Found: C, 47.5; H, 3.8; N, 10.8; S, 12.4. Calc. for $C_{20}H_{18}O_4N_4S_2Cu$: C, 47.4; H, 3.6; N, 11.1; S, 12.6%.

Synthesis of complex **2** $[CuL_2(Py)_2]$

Complex **1** (0.2 g) was dissolved in a mixed chloroform/toluene/pyridine (2 : 2 : 1, v/v/v; 30 cm^3) solvent. After slow evaporation of this red solution at room temperature in air over a period of several days (the volume of the solution was reduced to about 5 cm^3), red crystals of **2** were obtained, which were filtered and dried in air. Yield, 0.08 g (40%). Found: C, 54.2; H, 4.3; N, 12.8; S, 9.5. Calc. for $C_{30}H_{28}O_4N_6S_2Cu$: C, 54.2; H, 4.2: N, 12.6; S, 9.6%.

Physical measurements

Elemental analyses (C, H, N) were performed on a Carlo–Erba 1106 elemental analyser. IR spectral data were recorded on a Magna 750 spectrometer. NMR (^{1}H and ^{13}C) spectra were collected on an AM 500 spectrometer in DMSO-d_6 solution.

X-ray diffraction analysis

A summary of data collection, crystallographic data and details of the structure refinement is listed in Table 1. For both complexes, the structures were solved by direct methods, refinements were carried out by full-matrix least-squares cycles and the hydrogen atoms were included in structural calculations but not refined. Some non-hydrogen atoms were refined anisotropically, while the rest were refined isotropically. All the calculations were performed using the TEXSAN crystallographic software package from the Molecular Structure Corporation.

RESULTS AND DISCUSSION

Complex **1** $[Cu_2L_4]_2$

Views of the molecular structures of the $Cu_{1,2}$ and $Cu_{3,4}$ units in complex **1** are shown in Fig. 2a, b, respectively, and the packing arrangement is given in Fig. 3. Selected atomic distances and bond angles are listed in Table 2.

The asymmetric unit contains two crystallographically independent molecules, each consisting of two four-coordinate copper(II) centres. The anionic L group acts as a bidentate ligand and coordinates to the central copper atoms with nitrogen atoms from the benzothiazoyl (bta) group and the amino group, respectively. Each of the copper atoms is in a distorted square plane composed of the N donor atoms from the four L groups, with two from the bta and two from the amino groups.

As shown in Table 2, the Cu—N(amino) distances range from 1.95(2) to 2.01(2) Å (mean 1.98 Å) and the Cu—N(bta) distances range from 1.98(2) to 2.07(2) Å (mean 2.01 Å) and are comparable with those found in related complexes [5–7]. It is noticed that the average Cu—Cu distance of 2.559 Å is shorter than the Cu—Cu van der Waals distance of 2.86 Å and much closer to that of 2.56 Å in metallic Cu [8], indicating the existence of a bonding interaction for Cu—Cu in complex **1**. This Cu—Cu distance is longer than that in $[Cu_2(NPhCPhNPh)_4]$ [9] which has a similar structure where the bridging NPhCPhNPh ligands result in an even shorter Cu—Cu distance of 2.45 Å.

The nitrogen atoms from the amino and bta groups coordinate to the Cu atoms in the *trans* form, with angles N_{bta}—Cu—N_{amino} of 89.7° (mean), N_{bta}—Cu—N_{bta} of 166.7° (mean) and N_{amino}—Cu—N_{amino} of 174.3° (mean). Inside the five-membered chelate rings [Cu—Cu—N_{amino}—C—N_{bta}], the Cu—N_{bta}—C angle ranges from 120(1) to 125(1)° (mean 123°), Cu—N(amino)—C ranges from 115(1) to 121(1)° (mean 118.5°), N_{bta}—Cu—Cu ranges from 82.5(5) to 85.1(5)° (mean 83.4°) and N_{amino}—Cu—Cu ranges from 84.9(5) to 88.8(5)° (mean 87.0°).

As shown in the structure, there are four chelate rings with each pair of Cu atoms in an independent molecule, and the average dihedral angle between each pair of *cis*-coordinated chelate rings is 87.7°, nearly perpendicular to each other. In addition, the average dihedral angle between each pair of *trans*-coordinated chelate rings is 1.08°, nearly parallel to each other.

Complex **2** $[CuL_2(Py)_2]$

The structure of complex *2* is illustrated in Fig. 4, and its packing arrangement is shown in Fig. 5. Selected bond distances and bond angles are also given in

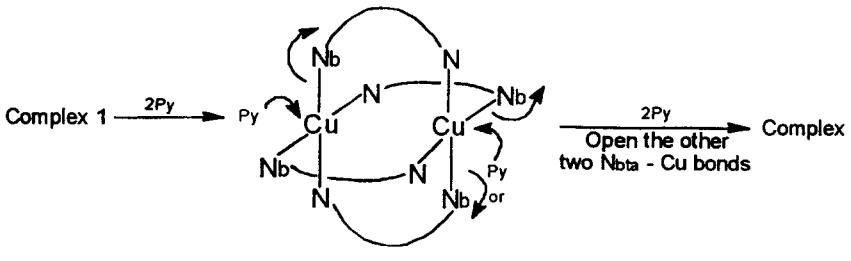
Table 1. Crystallographic and data collection parameters

Complex	**1**	**2**
Formula	$C_{80}H_{72}O_{16}S_8Cu_4$	$C_{30}H_{28}O_4N_6S_2Cu$
Formula weight	2024.22	664.26
Crystal colour, habit	red, prismatic	red, prismatic
Crystal dimensions mm	$0.20 \times 0.20 \times 0.40$	$0.20 \times 0.17 \times 0.14$
Crystal system	triclinic	orthorhombic
Space group	*P*-1 (No. 2)	*Pbca* (No. 61)
a/Å	17.816(8)	16.462(6)
b/Å	18.747(5)	16.568(5)
c/Å	13.952(5)	11.270(5)
α/°	90.49(3)	
β/°	108.43(3)	
γ/°	98.41(3)	
V/Å^3	4365(2)	3074(2).
Z	2	4
D_{calc}/cm^{-3}	1.540	1.44
$F(000)$	2072	1372
μ(Mo-K_α)/cm^{-1}	12.27	8.85
Diffractometer	Rigaku AFC7R	Enraf–Nonius CAD4
Temperature/°C	20.0	23.0
Scan type	ω-2θ	ω-2θ
Scan rate/min^{-1}	4.0 ~ 16.0	< 5.49
Scan width/°	$1.63+0.30\tan\theta$	$0.55+0.35\tan\theta$
2θmax/°	35.0	49.9
No. of reflections measured	5739	3080
No. of unique reflections	5469 (R_{int} = 0.039)	3080 (R_{int} = 0)
No. of reflections with $I > 3\sigma(I)$	3698	1714
No. of variables	718	196
R	0.073	0.045
R_w	0.085	0.055
GOF	2.82	1.33
Max. shift in final cycle	0.10	0.05
$\Delta\rho_{max, min}$/e Å^{-3}	0.60, −0.55	0.51, −0.27

Table 2. The copper(II) atom is in a four-coordinate square-planar geometry, in which either of the two L groups provides one nitrogen donor atom from the dehydrogenated amino group, and the other coordinated atoms are from the two nitrogen atoms contributed by two pyridine molecules. Unlike the structure of complex **1**, the benzothiazolyl nitrogen of the L group in **2** does not bind to the Cu^{II} ion. The Cu—N(1) bond distance is 2.011(4) Å, which agrees well with the bond distance for Cu—$N_{pyridine}$ elsewhere [10]. The bond Cu—N(2) of 1.997(4) Å is within the range of the corresponding bond found in complex **1**. The other bond distances in the ligand do not change much relative to those in complex **1**. This can be explained by the fact that the benzothiazolyl nitrogen atom coordinates to Cu^{II} only with its non-bonding electron pairs. The bond angle N(2)—Cu—N(1) of 90.4(1)° indicates that the square-planar geometry of Cu is quite exact. The angle C(6)—N(2)—Cu of 108.0(3)° is smaller than the corresponding one in complex **1** (average of 120°), where the angle is expanded for bridging.

The formation of the complexes can be depicted in Scheme 1 where the binuclear complex **1** dissociates into the mononuclear complex **2** in pyridine by dissociation of the N_{bta}—Cu bond.

This can be readily explained based on two facts. (i) The coordination ability of pyridine to copper is



Scheme 1.

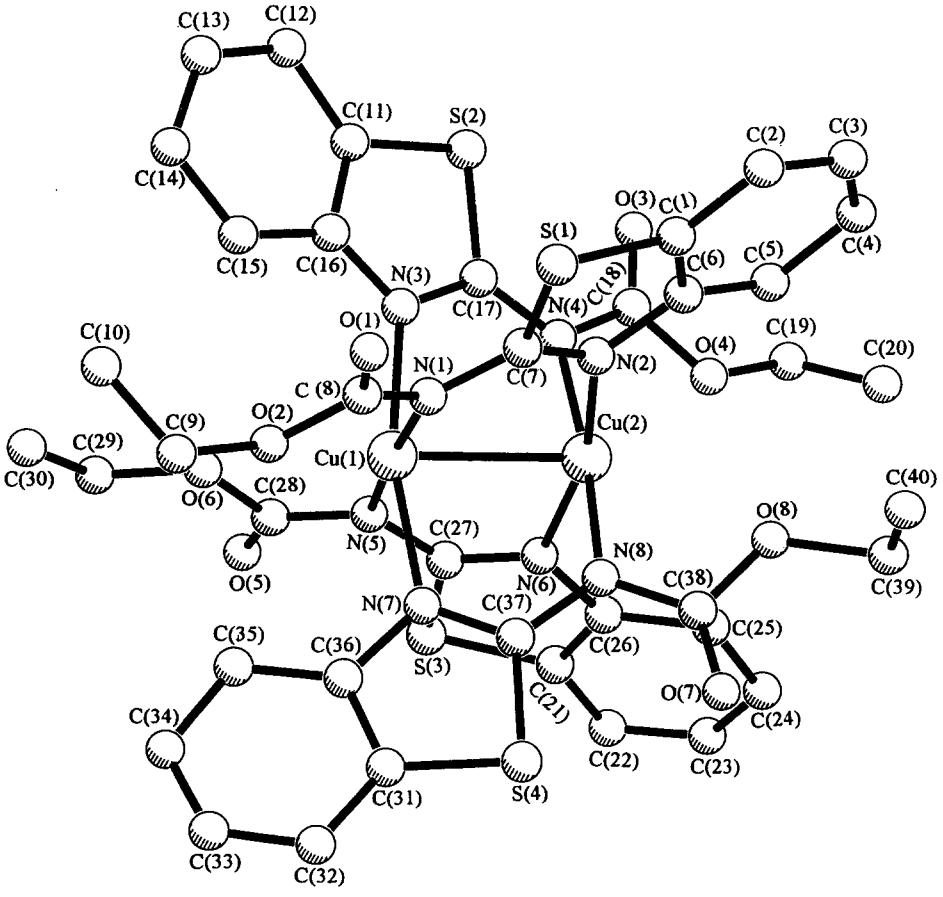


Fig. 2a. Molecular structures of $Cu_{1,2}$ and $Cu_{3,4}$ unit in complex **1**.

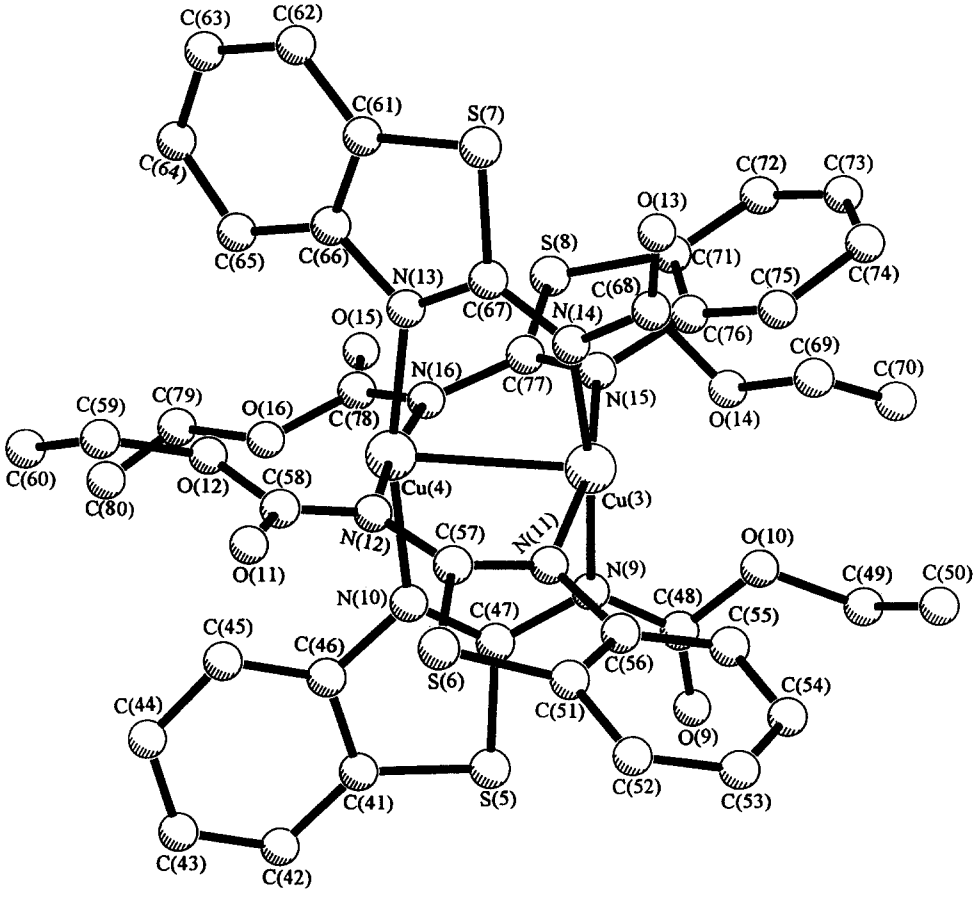


Fig. 2b. Molecular structure of $Cu_{3,4}$ unit in complex **1**.

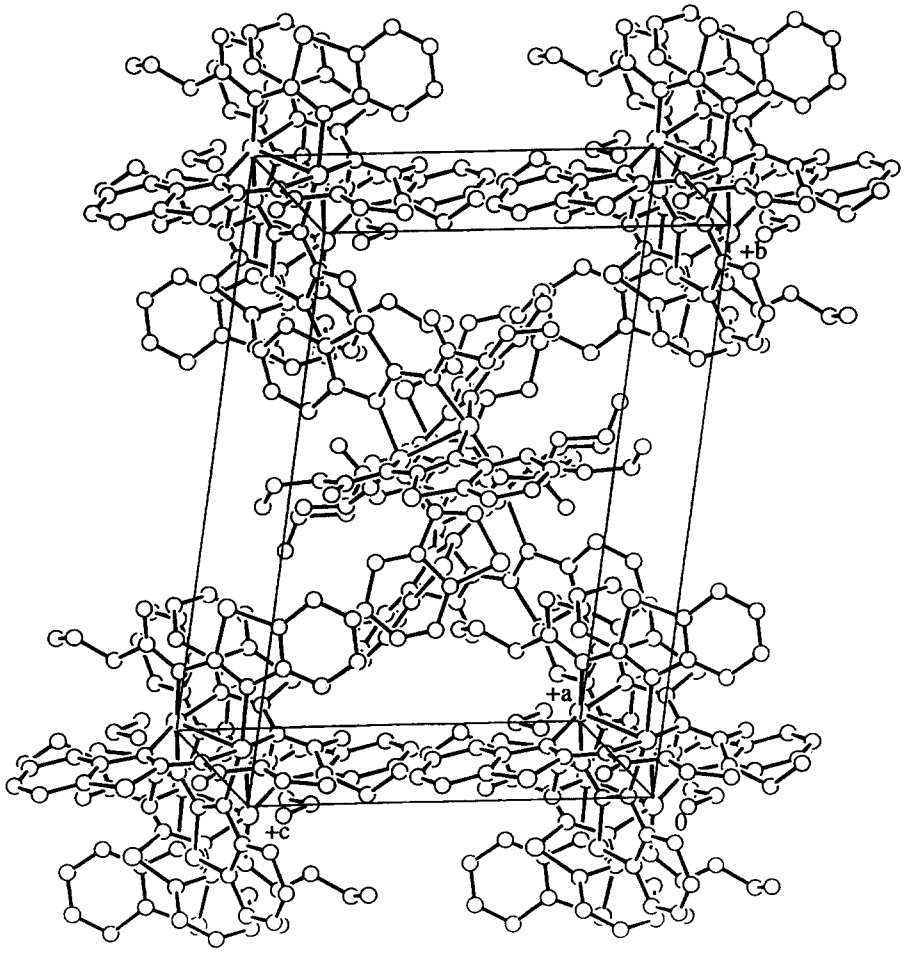


Fig. 3. Packing arrangement for complex **1**.

Table 2. Selected bond distances (Å) and angles ( ) for **1** and **2**

1

Cu(1)		Cu(2)		Cu(3)		Cu(4)	
Cu(1)—N(1)	1.99(2)	Cu(2)—N(2)	2.02(2)	Cu(3)—N(9)	1.99(2)	Cu(4)—N(10)	2.00(2)
Cu(1)—N(3)	2.04(2)	Cu(2)—N(4)	1.95(2)	Cu(3)—N(11)	2.00(2)	Cu(4)—N(12)	2.00(2)
Cu(1)—N(5)	1.99(2)	Cu(2)—N(6)	1.99(2)	Cu(3)—N(14)	1.95(2)	Cu(4)—N(13)	1.98(2)
Cu(1)—N(7)	2.07(2)	Cu(2)—N(8)	1.96(2)	Cu(3)—N(15)	1.99(2)	Cu(4)—N(16)	2.01(2)
Cu(1)—Cu(2)	2.562(3)			Cu(3)—Cu(4)	2.555(3)		
N(1)—Cu(1)—N(4)	88.0(6)	N(2)—Cu(2)—N(4)	87.5(6)	N(9)—Cu(3)—N(11)	88.7(6)	N(10)—Cu(4)—N(16)	91.4(6)
N(1)—Cu(1)—N(5)	175.3(6)	N(2)—Cu(2)—N(6)	165.6(7)	N(9)—Cu(3)—N(14)	127.8(7)	N(10)—Cu(4)—N(1)	87.4(6)
N(1)—Cu(1)—N(7)	90.4(6)	N(2)—Cu(2)—N(8)	91.5(6)	N(9)—Cu(3)—N(15)	91.1(7)	N(10)—Cu(4)—N(13)	168.0(6)
N(3)—Cu(1)—N(5)	91.7(6)	N(4)—Cu(2)—N(6)	91.7(6)	N(11)—Cu(3)—N(14)	90.5(6)	N(12)—Cu(4)—N(13)	91.2(6)
N(3)—Cu(1)—N(7)	166.2(6)	N(4)—Cu(2)—N(8)	174.3(7)	N(11)—Cu(3)—N(15)	167.5(6)	N(12)—Cu(4)—N(16)	173.6(7)
N(5)—Cu(1)—N(7)	88.8(6)	N(6)—Cu(2)—N(8)	87.9(6)	N(14)—Cu(3)—N(15)	88.1(7)	N(13)—Cu(4)—N(16)	88.7(6)
Cu(1)—N(1)—C(7)	117(1)	Cu(2)—N(2)—C(7)	123(1)	Cu(3)—N(9)—C(47)	116(1)	Cu(4)—N(10)—C(47)	124(1)
Cu(1)—N(3)—C(17)	120(1)	Cu(2)—N(4)—C(17)	121(1)	Cu(3)—N(11)—C(57)	122(1)	Cu(4)—N(12)—C(57)	119(1)
Cu(1)—N(5)—C(27)	120(1)	Cu(2)—N(6)—C(27)	123(1)	Cu(3)—N(14)—C(67)	121(1)	Cu(4)—N(13)—C(67)	121(1)
Cu(1)—N(7)—C(37)	122(1)	Cu(2)—N(8)—C(37)	119(1)	Cu(3)—N(15)—C(77)	125(1)	Cu(4)—N(16)—C(77)	115(1)
Cu(2)—Cu(1)—N(1)	88.8(5)	Cu(1)—Cu(2)—N(2)	82.5(5)	Cu(4)—Cu(3)—N(9)	87.9(5)	Cu(3)—Cu(4)—N(10)	82.9(5)
Cu(2)—Cu(1)—N(3)	83.4(4)	Cu(1)—Cu(2)—N(4)	86.5(5)	Cu(4)—Cu(3)—N(11)	84.4(4)	Cu(3)—Cu(4)—N(12)	86.1(5)
Cu(2)—Cu(1)—N(5)	86.5(5)	Cu(1)—Cu(2)—N(6)	83.1(5)	Cu(4)—Cu(3)—N(14)	84.9(5)	Cu(3)—Cu(4)—N(13)	85.1(5)
Cu(2)—Cu(1)—N(7)	82.9(5)	Cu(1)—Cu(2)—N(8)	87.8(5)	Cu(4)—Cu(3)—N(15)	83.2(5)	Cu(3)—Cu(4)—N(16)	87.6(5)

2

Cu—N(1)	2.011(4)	Cu—N(2)	1.997(4)	N(2)—Cu—N(1)	90.4(1)	C(6)—N(2)—Cu	108.0(3)

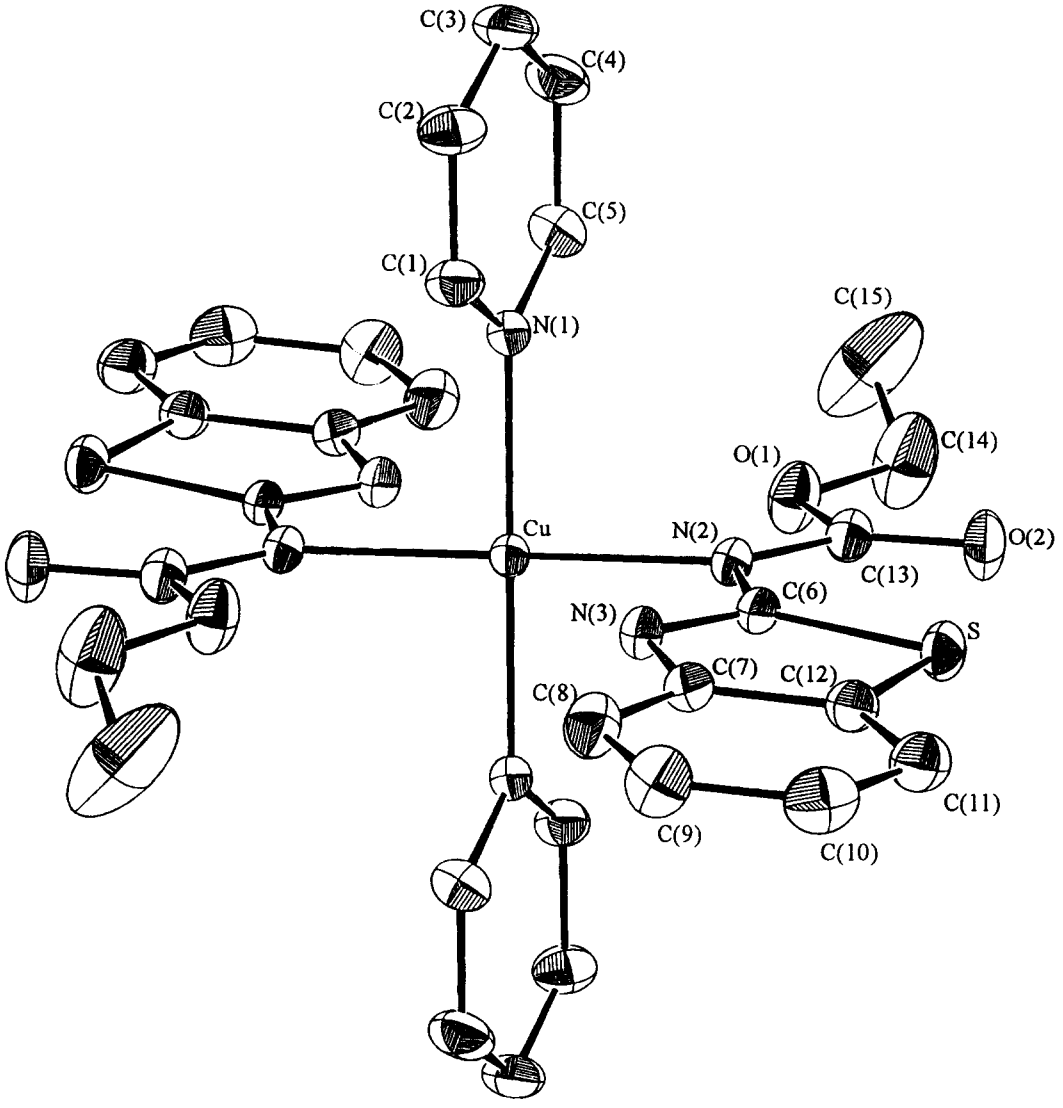


Fig. 4. Structure of complex **2**.

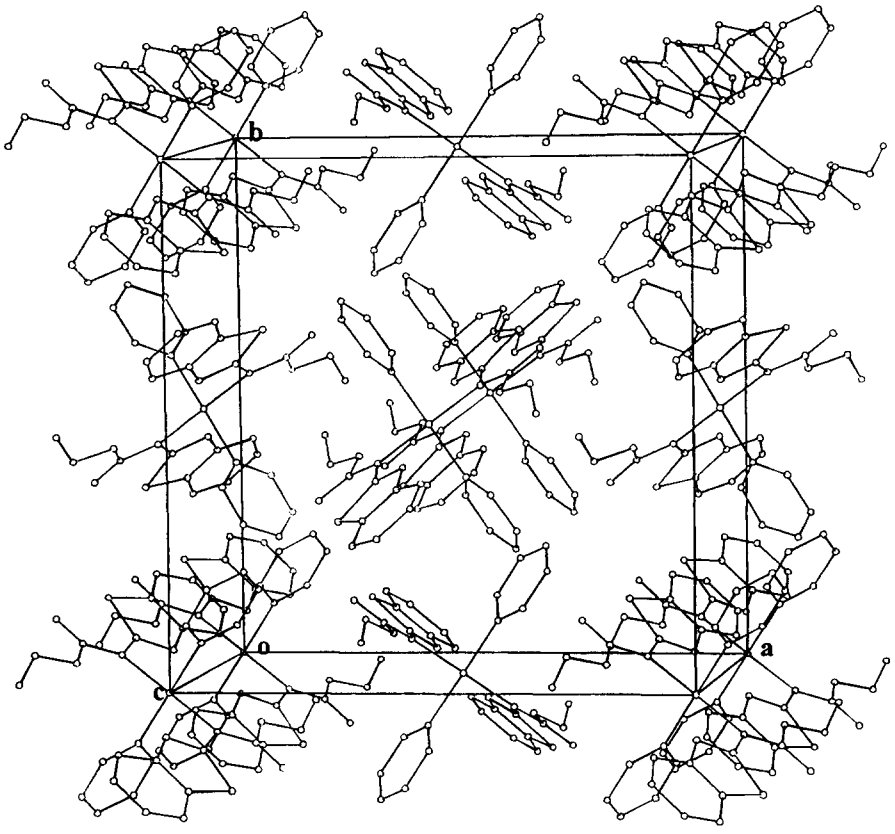


Fig. 5. Packing arrangement for complex **2**.

stronger than that of N_{bta}, which can be seen from the atomic distances for N_{bta}—Cu (average 2.01 Å) and N_{py}—Cu [1.997(4) Å]. (ii) The binuclear complex **1** is asymmetric and more sterically congested, while the mononuclear complex **2** is symmetric and more stable thermodynamically.

IR spectra

The IR spectra of complexes **1** and **2** are very similar to each other because of their similar bond distances. In the IR spectra, ν(NH) is found at *ca* 3178 and 3140 cm^{-1} for the free ligand HL, but is absent in the complexes, indicating that the amino group has coordinated to the Cu^{II} ion through release of the hydrogen atom. The ν(C—O) at *ca* 1722 cm^{-1} for the free ligand is found to shift to lower frequency at *ca* 1686 cm^{-1} in the complexes. The Amide-II absorption band for HL appears at 1564 cm^{-1}, which is shifted to a higher frequency, 1573 cm^{-1}, in the complexes. This fact could be interpreted by back donation involving electron transfer in the direction copper→amide [11]. In addition, the absorption bands at *ca* 405 and 389 cm^{-1} are ascribed to ν(Cu—N_{amino}), and 366 cm^{-1} to ν(Cu—N_{bta}) [11].

Acknowledgements—Financial support from the Natural Science Foundation of Guangdong Province and NNSF of China as well as the Postdoctoral Foundation of China (X.S.) are greatly appreciated.

REFERENCES

1. Sigel, H. and Martin, R. B., *Chem. Rev.* 1982, **82,** 385.
2. Hay, R. W. and Morris, P. J., *Metal Ions in Biological Systems*, Vol. 5, ed. H. Sigel. Marcel Dekker, New York, (1976).
3. Sekizaki, M. and Yamasaki, K., *Inorg. Chim. Acta* 1970, **4,** 296; Bault. J. and Brisdon, B. J., *Inorg. Chim. Acta* 1976, **19,** 159; Airoldi, C. and Goncalves, A. S., *J. Inorg. Nucl. Chem.* 1978, **40,** 1817; Garg, B. S., Kumar V. and Reddy, M. J., *Indian J. Chem.* 1993, **32A,** 726.
4. Jaiswal, K., Parmar, S. S. and Singh, S. P., *J. Heterocyc. Chem.* 1979, **16,** 561.
5. Li, M., Zou, J., Xu, Z., You, X. Z. and Huang, X. Y., *Polyhedron* 1995, **14,** 639.
6. Chen, Z. N., Wang, J. L., Qiu, J., Miao, F. M. and Tang, W. X., *Inorg. Chem.* 1995, **34,** 2255.
7. Ojima, H. and Nonoyama, K., *Coord. Chem. Rev.* 1988, **92,** 85.
8. Wasson, J. R., Shyr, C. I. and Trpp, C., *Inorg. Chem.* 1968, **7,** 469.
9. Harris, C. M., Hoskins, B. F. and Martin, R. L., *J. Chem. Soc.* 1959, 3728.
10. Li, S., Liu, D., Meny, F., Zhou, J. and Yang, Z., *Jiegou Huaxue.* 1995, **14,** 55.
11. Burger, K., *Coordination Chemistry: Experimental Methods*, (English transl. ed. I. T. Millar). Akademiai Kiado, Budapest, (1973), pp. 53–122.

Pergamon

PII: S0277-5387(96)00415-9

Polyhedron Vol. 16, No. 7, pp. 1023–1030, 1997
Copyright © 1997 Elsevier Science Ltd
Printed in Great Britain. All rights reserved
0277-5387/97 $17.00+0.00

Mixed valence complexes incorporating Ru^{III} and Fe^{II}: synthesis, characterization, kinetics and physico-chemical studies

Amitava Das* and H. C. Bajaj*

Central Salt and Marine Chemicals Research Institute, Bhavnagar 364002, India

(Received 14 June 1996; accepted 16 August 1996)

Abstract—A set of new mixed valence complexes of the type $Na_3[(edtaH)Ru^{III}LFe^{II}(CN)_5]$, where L = pyz, bp, dmbp, etybp or tmbp, has been synthesized and characterized by physico-chemical methods. The kinetics of formation of these binuclear complexes were studied using a stopped-flow spectrophotometer. Electrochemical studies for these complexes show only a weak metal–metal interaction in the ground state. All these complexes, except the one incorporating tmbp, gave an MMCT band in the region $900 < \lambda < 1000$ nm and belong to the Robin–Day class II type. Copyright © 1997 Elsevier Science Ltd

Keywords: synthesis; ruthenium; binuclear complexes; kinetics; mixed-valence.

The measurement of intramolecular rather than intermolecular electron transfer offers distinct advantages for investigating the detailed mechanism of electron transfer reactions [1]. In order to investigate the electron transfer in mixed valance systems, the study of binuclear metal complexes, in which the two redox active centres are linked by an unsaturated bridging ligand, have become increasingly popular [2]. The most widely studied mixed valence binuclear system is the Creutz–Taube ion, the theoretical study of which has contributed considerably to our understanding of electron transfer theory [3]. One of the most popular bridging ligands is 4,4′-bipyridyl and its derivatives [4]. A number of mixed valence homo- and heterobinuclear complexes has been synthesized using these bridging ligands to enable examination of metal–metal interactions and electron transfer processes across the molecular bridge, and also to determine the effects of length of the "molecular wire" on these [5].

The chemistry of polyaminopolycarboxylate complexes of ruthenium(III/II) is of continued interest owing to their biochemical importance [6] and catalytic ability [7] in oxidation and reduction reactions. $K[Ru^{III}(edtaH)Cl]$ is known to exist as Ru(edtaH)(H_2O) in aqueous solution [8,9] and to react with pyridine or substituted pyridine to form the corresponding pyridyl derivative through a facile aqua substitution path [8a,10]. To date, examples are scanty [10b] where the remarkable lability of the aqua ligand has been utilized for the design and synthesis of binuclear complexes. $Na_3[Fe(CN)_5(H_2O)]$ is known to react with N-heterocyclic ligands though a facile aqua substitution path [11]. We have taken advantage of these two aqua substitution reactions to synthesize a set of mixed valence heterobinuclear complexes of the type $Na_3[Ru(edtaH)LFe(CN)_5]$, where L = pyrazine (pyz), 4,4′bipyridyl (bp), 3,3-dimethyl-4,4′-bipyridyl (dmpb), *trans*-1,2-bis-4-pyridylethylene (etybp) and trimethyl bis-4-bipyridyl (tmbp) (Fig. 1). In this paper, we report the kinetics of the formation of the five mixed valence binuclear complexes **VI–X** using mononuclear complexes, **I–V** as ligands, their synthesis, characterization and physico-chemical studies. The mononuclear complex **I** was reported earlier by Matsubara and Creutz [8a] in aqueous solution. Synthesis and characterization of the mononuclear complex **I**, [Ru(edtaH)(Pyz)], along with complexes **II–V** are also included.

EXPERIMENTAL

Materials

$K[Ru(edtaH)Cl]\cdot 2H_2O$ and $Na_3[Fe(CN)_5(NH_3)]\cdot 3H_2O$ were prepared following the published

* Authors to whom correspondence should be addressed.

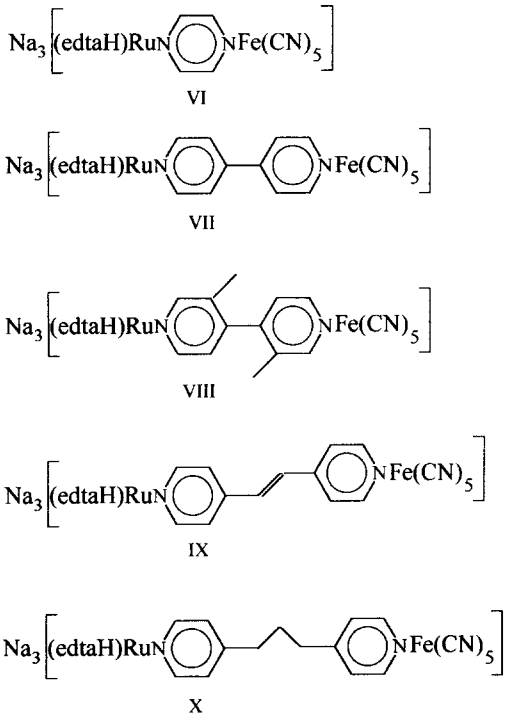


Fig. 1. Structures of binuclear complexes **VI–X**.

procedures [12,13]. Pyrazine (pyz), 4,4′-bipyridyl (bp), *trans*-1,2-bis(4-pyridyl)ethylene (etybp) and 1,3-bis(4-pyridyl)propane (tmbp) were used as received from Aldrich. 3,3′-Dimethyl-4,4′-bipyridyl (dmpb) was synthesized following a known method [14]. Solvents were purified and dried before use by standard methods and double distilled water was used. $[Bu_4N]ClO_4$ was used as background electrolyte for electrochemical studies.

Physical measurements

Microanalysis (C, H, N) were carried out with a Carlo–Erba elemental analyser. Absorption spectra were recorded on a Shimadzu UV 3101 PC spectrophotometer. IR spectra were recorded on a Carl–Zeiss specord M80 spectrometer as KBr pellets. EPR studies were carried out using a Bruker 300X spectrometer either at room temperature or at 77 K using a Dewar insert in the sample chamber. Electrochemical experiments were performed by using Princeton Applied Research (PAR 273A) electrochemical instruments. A conventional three electrode cell assembly was used. Saturated calomel electrode as reference and Pt as working electrode were used for this purpose. pH measurements were carried out with Digisun pH meter. For spectrophotometric and cyclic voltammetric studies of binuclear complexes, freshly prepared solutions were used throughout.

Kinetic studies

Kinetic studies were performed on a High-Tech SF51 stopped-flow spectrophotometer. The measurements were carried out by following the absorbance increase in the wavelength region 380–550 nm [the MLCT band for the $Fe(CN)_5$ unit upon coordination to the remote N atom of L in the Ru(edtaH)L unit] or at λ_{max} for the MMCT band for complexes **VI–IX**. In all instances pseudo first-order conditions were maintained {excess $[Ru(edta)L^-]$} and the corresponding first-order plots were linear for at least 2–3 half-lives of the reaction. Rate constant data are represented as an average of triplicate runs and are reproducible within $\pm 4\%$. pH for the kinetic solutions was maintained using acetic acid–acetate buffer and the ionic strength of the solution was maintained with KCl solution.

Synthesis

$Ru(edtaH)(L)\cdot 2H_2O$, *where* L = pyz, bp, dmbp, etybp *or* tmbp. $K[Ru(edtaH)Cl]\cdot 2H_2O$ (260 mg; 0.4 mM) was dissolved in warm water (5 cm^3), to which 4 mM of L (pyz, 320 mg; bp, 624 mg; dmbp, 736 mg; etybp, 728 mg; tmbp, 792 mg) dissolved in *ca* 5–10 cm^3 of ethanol was added and stirred at *ca* 50°C for 15 min. Then the volume was reduced to *ca* 5 cm^3, to which excess acetone was added and cooled to *ca* 5°C. The desired compound was precipitated, filtered off and washed thoroughly with methanol and acetone to remove excess L. Further purification involved recrystallization from water–methanol mixture and drying *in vacuo* (yield, 80–85%). Elemental analysis data (see Table 1) for these mononuclear complexes (**I–V**) agree well with the proposed formulation.

$Na_3[Ru(edtaH)LFe(CN)_5\cdot 3H_2O$, *where* L = pyz, bp, dmbp, etybp *or* tmbp. All binuclear complexes were synthesized by reaction of 0.4 mM Ru(edtaH)L with 0.4 mM (102 mg) of $Na_3[Fe(CN)_5(NH_3)]\cdot 3H_2O$ at room temperature in water (10 cm^3). The reaction mixture was stirred for 20 min and then concentrated at room temperature *in vacuo* to *ca* 3 cm^3. The desired binuclear complexes (**VI–X**) were precipitated on addition of cooled (5°C) and excess methanol and were allowed to stand for 1 h. Precipitate was filtered and washed with 8 : 2 (v/v) methanol/water mixture. Complexes **VI–X** were further purified by recrystallization from a water/methanol mixture (7 : 3; v/v) (yield 75–80%). Analytical data for complexes **VI–X** are given in Table 1 and are in good agreement with the proposed formulation.

RESULTS AND DISCUSSION

K[Ru(edtaH)Cl] hydrolysed [8,9] rapidly in aqueous solution to give $Ru(edtaH)(H_2O)$, which reacts with N-heterocyclic ligands through rapid aqua substitution pathway to yield mononuclear complexes (**I–**

Table 1. Elemental analysis and spectral data for complexes **I–X**

Complex	Analyses[a]			UV–vis/nm	IR (cm^{-1})
	C	*H*	*N*	($10^3 \times \varepsilon/M^{-1} cm^{-1}$)	
$[Ru(edtaH)pyz]\cdot 2H_2O$	33.0 (33.2)	4.2 (4.1)	10.9 (11.0)	260(6.3), 288(5.0), 350(1.5)	1735, 1650
$[Ru(edtaH)bp]\cdot 2H_2O$	41.1 (41.2)	4.3 (4.3)	9.5 (9.6)	280(2.4), 300(sh), 355(sh)	1740, 1645
$[Ru(edtaH)dmbp]\cdot 2H_2O$	43.1 (43.3)	4.8 (4.7)	9.1 (9.2)	270(2.5), 292(sh) 350(sh)	1740, 1640
$[Ru(edtaH)etybp]\cdot 2H_2O$	42.3 (43.4)	4.3 (4.4)	9.4 (9.2)	299(6.2), 352(1.8)	1745, 1645
$[Ru(edtaH)tmbp]\cdot 2H_2O$	44.0 (44.2)	4.9 (4.9)	8.8 (8.9)	253(2.4), 282(1.3), 360(sh)	1740, 1645
$Na_3[Ru(edtaH)pyzFe(CN)_5]\cdot 3H_2O$	29.2 (29.3)	3.0 (2.9)	16.2 (16.3)	290(sh), 475(1.9), 916(2.7)	2060, 1735, 1650
$Na_3[Ru(edtaH)bpFe(CN)_5]\cdot 3H_2O$	34.9 (35.1)	3.3 (3.2)	14.6 (14.7)	418(1.9), 933(2.5)	2065, 1730 1650
$Na_3[Ru(edtaH)dmbpFe(CN)_5]\cdot 3H_2O$	36.6 (36.7)	3.5 (3.5)	14.0 (14.2)	374(3.9), 983(2.4)	2060, 1730 1645
$Na_3[Ru(edtaH)etybpFe(CN)_5]\cdot 3H_2O$	36.9 (36.8)	3.4 (3.3)	14.1 (14.3)	453(3.4), 997(2.2)	2060, 1735 1645
$Na_3[Ru(edtaH)tmbpFe(CN)_5]\cdot 3H_2O$	37.3 (37.4)	3.8 (3.7)	13.9 (14.0)	260(sh), 306(sh), 384(1.4)	2060, 1740 1650

[a] Calculated values in parentheses.

V). For synthesis of these mononuclear complexes, a large excess of L (five-fold equimolar excess) was used to avoid the possibility of the formation of homobinuclear complexes [10b]. $[Fe(CN)_5(H_2O)]^{3-}$ is also known to react with N-donor heterocyclic ligands through substitution of the aqua molecule within the stopped-flow time-scale [11]. We have utilized these two specific reactions to synthesize the binuclear complexes **VI–X** (Fig. 1). IR spectra of all the complexes (Table 1) exhibit a sharp band at around 1735 cm^{-1} for the uncoordinated —COOH group, and a broad band at 1645 cm^{-1} for the coordinated $—COO^-$ group [10]. Bands at 1600 cm^{-1} and 1460 cm^{-1} appear owing to the stretching and bending of C=C and C=N, respectively, of the coordinated pyrazine or derivatives of the 4,4′-bipyridyl. The binuclear complexes (**VI–X**) also exhibit bands at around 2060 cm^{-1}, which are assigned to the —C≡N stretching of the $Fe(CN)_5^{3-}$ fragment [15]. All these complexes (**I–X**) exhibit a broad absorption band at around 3400 cm^{-1} owing to the H_2O molecule, present as water of crystallization.

The stability of the binuclear complexes (**VI–IX**) in aqueous solution at room temperature was monitored spectrophotometrically at the metal to metal charge transfer (MMCT) band (*vide infra*) and were found to be stable within the time-scale for EPR, electrochemical and spectrophotometric studies. However, decrease in the intensity at the MMCT band, i.e. decomposition of the mixed valence binuclear complex, was observed on prolonged storage of the aqueous solution.

Kinetic studies

Preliminary experiments showed that the aqueous solution of $Ru(edta)L^-$ (L = pyz, bp, dmbp, etybp or tmbp) and $Fe(CN)_5H_2O^{3-}$ on mixing, yielded binuclear complexes of the type $[(edta)Ru^{III}LFe^{II}(CN)_5]^{4-}$ within the stopped-flow time-scale. The kinetics of the formation of the binuclear complexes **VI–X** [Eq. (1)] were studied using mononuclear complexes, $Ru(edta)L^-$, as the incoming ligand under pseudo first-order conditions at pH = 5.0, where $Ru(edta)L^-$ and $Fe(CN)_5H_2O^{3-}$ are the only reactive species. The uncoordinated N atom on the remove side of L in $Ru(edta)L^-$ reacts with $Fe(CN)_5H_2O^{3-}$ through an aqua substitution path and a new MLCT band for Fe—L coordination develops in the visible region (*vide infra*). An additional, relatively intense, MMCT band appears at $900 < \lambda < 1000$ nm (*vide infra*) for complexes **VI–IX**. Reactions were studied at these two different wavelengths and k_{obs} were found to be same. A plot of k_{obs} *vs* $[Re(edta)L^-]$ gives a straight line with a small intercept, which signifies a reverse aquation reaction [Eq (2)]. Representative plots for reactions of $Fe(CN)_5H_2O^{3-}$ with $Ru(edta)(bp)^-$ and $Ru(edta)(etybp)^-$ are presented in Fig. 2. Rates for the formation (k_f) and aquation reactions (k_r) were obtained from the slope and intercept of the plot k_{obs} *vs* $[Ru(edta)L^-]$, respectively, and are summarized in Table 2 along with K ($=k_f/k_r$). These rate data are comparable with the related aqua substitution reaction [2b,9] in $Fe^{II}(CN)_5(H_2O)$ by N-heterocyclic ligands of the type $\{(NH_3)ML^{n+}\}$, where

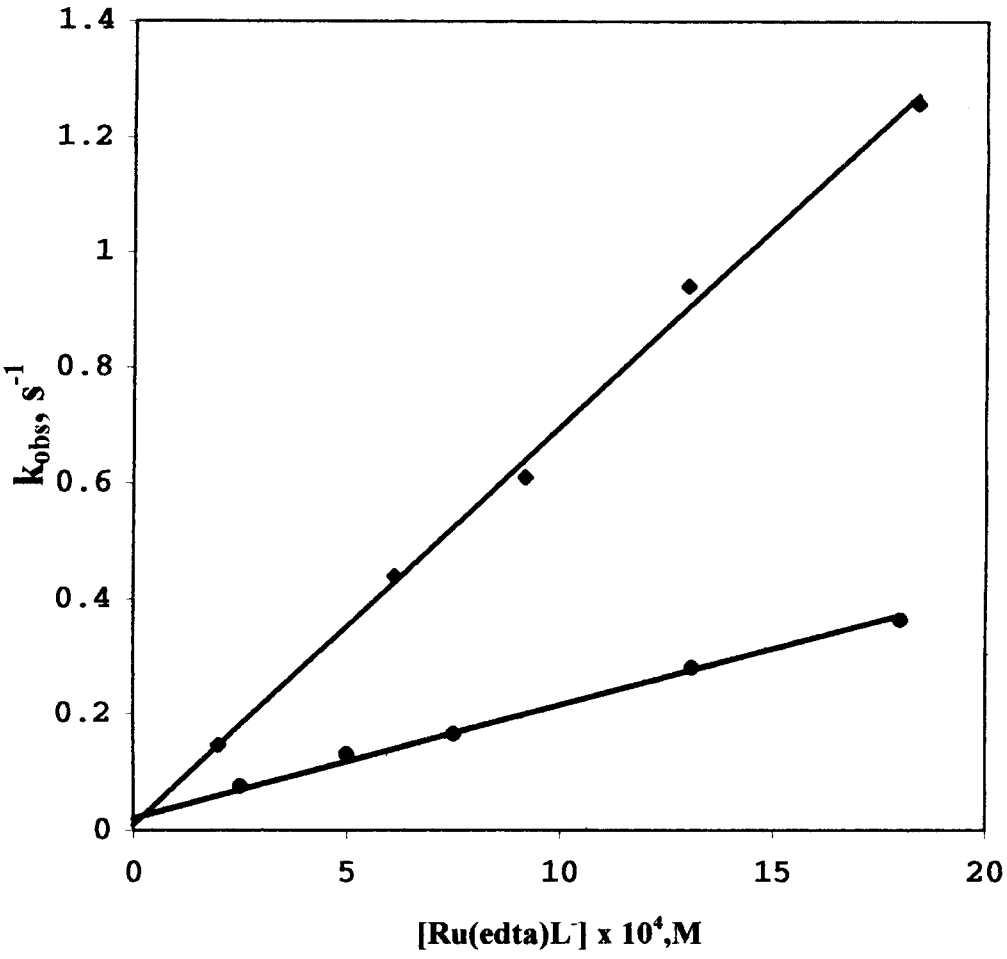


Fig. 2. Dependence of k_{obs} on [Ru(edta)L^-] for the reaction of $Fe(CN)_5H_2O^{3-}$ with Ru(edta)(bp)$^-$ (●) and Ru(edta)(etybp)$^-$ (◆): [$Fe(CN)_5H_2O^{3+}$] = 1.35×10^{-5} M; pH = 5.0 (acetic acid–acetate buffer, 0.2 M); ionic strength = 0.5 M (KCl); T = 25±0.1°C.

Table 2. Summary of rate parameters reaction (1)[a]

L	k_f ($M^{-1}s^{-1}$)	k_r (10^3) (s^{-1})	K (10^{-4}) (M^{-1})
pyz	150±10	2±0.6	7.5
bp	175±15	20±20	0.87
dmpb	146±10	35±10	0.42
etybp	684±35	9±5	7.6
tmbp	154±10	154±20	0.1

[a] At pH = 5.0, acetic acid–acetate buffer, T = 25.0±0.1°C; μ = 0.5 M (KCl).

M = Ru, Rh, Co. For tmbp, two pyridyl units are separated by a standard —CH_2—CH_2—CH_2— group and behaves more like 4-picoline, and is less effective as a π-acid ligand in stabilizing Fe^{II} owing to lower $\pi_M \rightarrow \pi_{py}$ back bonding which is reflected in higher value for k_r, compared with others (Table 2). Presumably, extended conjugation in etybp is responsible for more efficient $\pi_M \rightarrow \pi_{py}$ back bonding in complex **IX** and is reflected in higher k_f and relatively low k_r values. The steric constraint associated with the methyl groups in dmpb prevents the two pyridine ring from adopting the coplanar conformation necessary for good delocalization, hence the degree of conjugation is lower for dmbp and is reflected in slightly higher k_r value (Table 2). Thus it is interesting that the increasing stability of the binuclear complexes follows the order that would be expected on the basis of increasing back-bonding interaction. However, the important effect of ligand basicity has not been assessed.

$$Fe(CN)_5H_2O^{3-} + Ru(edta)L^- \underset{k_r}{\overset{k_f}{\rightleftharpoons}} [(edta)Ru^{III}LFe^{II}(CN)_5]^{4-} + H_2O \quad (1)$$

$$k_{obs} = k_f[Ru(edta)L^-] + k_r \quad (2)$$

EPR spectroscopy

All mononuclear and binuclear complexes (**I–X**) were found to be EPR active and exhibited broad

spectra at room temperature, while at 77 K [water/glycerol; 1:3 (v/v)] characteristic spectra were observed as reported for other complexes of Ru^{III} (edta) with π-acid ligands [10b,16]. Respective g_x, g_y and g_z values for the complexes are 2.61, 2.3 and 1.91. Comparison of the EPR spectra for mono- and binuclear complexes reveals that presence of a diamagnetic Fe^{II} centre does not have any influence on the nature of the EPR spectra for the Ru^{III} centre in the binuclear complexes **VI–X**.

Cyclic voltammetry

Cyclic voltammetric studies of complex **I–X** were carried out in water and the results are summarized in Table 3. The $E_{1/2}$ values for the $Ru^{II/III}$ couple for the mononuclear complex **I** (L = pyz) is comparable to that reported earlier [17]. Other mononuclear complexes, **II–V** have $E_{1/2}$ values comparable with that of the Ru^{III}(edta)Py^- complex [8a]. The ΔE ($E_{pa} - E_{pc}$) values for Ru^{II-III} couples are *ca* 140 mV, while those for the $Fe^{II/III}$ couple are *ca* 90 mV. Under identical experimental condition, the value of ΔE for the $Fe^{II/III}$ couple in $K_4Fe(CN)_6$ is 75 mV. The higher ΔE value for the $Ru^{II/III}$ couple signifies its quasi-reversible nature. Comparison of $E_{1/2}$ values for the mononuclear components [18] (Table 3) with those for the binuclear complexes **VI–X** (Table 3) reveals a little shift in the $E_{1/2}$ values of the individual component in binuclear complexes and thus there exists only a very weak electrochemical interaction between the two metal centres, linked by a hydrocarbon bridge, in the ground state.

UV-vis spectra

The ruthenium(III) centres in Ru(edta)pyridine-type complexes are known to be very weak σ donors and generally do not have any appreciable and characteristic absorption in the visible region [9,10], whereas the Fe^{II} centre in $[Fe(CN)_5Py]^{3-}$-type complexes, being a good π donor, is expected to have a strong MLCT band in the visible region. Thus, in the binuclear complexes, spectra in the visible region are dominated by the Fe^{II} to Py MLCT band (Table 1). The MLCT band for the Fe^{II} centre in complexes **VI–IX** appears almost in the same region as in the $[Fe(CN)_5Py]^{3-}$-type complexes. However, spectra in the UV region for complexes **VI–X** are dominated by the strong $n \rightarrow \pi^*$ transition of the coordinated edta group, which is intense enough to mask the expected $\pi \rightarrow \pi^*$ transition for the bipyridyl ligands, L. For complex **X**, the electronic spectrum is essentially the sum of the spectrum of the two monomeric units, [Ru(edtaH)tmbp] and $[Fe(CN)_5tmbp]^{3-}$. This is expected as the two π systems of the bridging ligand are separated by a saturated —CH_2—CH_2—CH_2— linkage and thus behave as a non-interacting chromophore. While all the other binuclear complexes (**VI–IX**) exhibit an additional relatively intense absorption band in the range $1000 > \lambda_{max} > 900$ nm, with $\varepsilon \sim 2.2\text{–}2.7 \times 10^3$ M^{-1} cm^{-1}, which disappear either on oxidation of the Fe^{II} by oxone or on reduction of the Ru^{III} centre by ascorbic acid in complexes **VI–IX**. Thus, the band in the near infrared region for complexes **VI–IX** is assigned as the metal to metal charge transfer absorption (MMCT) band [Eq. (3)]. ε Values observed for the MMCT band of the binuclear complexes **VI–IX** are comparable with those reported for similar mixed valence heterobinuclear complexes [10,15b] $[Ru^{III}(edtaH)NCFe^{II}(CN)_5]^{4-}$ and $[Ru^{III}(NH_3)_5CNFe^{II}(CN)_5]^-$. The MMCT band in mixed valence complexes provides information about the extent of electronic coupling between the metal centres and the rate of electron transfer from one metal centre to the other [1b,19–21].

$$[(edtaH)Ru^{III}\text{–}L\text{–}Fe^{II}(CN)_5]^{3-} \overset{E_{op}}{\underset{E_{th}}{\rightleftarrows}} [(edtaH)Ru^{II}\text{–}L\text{–}Fe^{II}(CN)_5]^{3-} \quad (3)$$

Experimentally obtained values for wave number

Table 3. Redox potentials[a] for the complexes **I–X**

Complex	$-E^{1}_{1/2}(Ru^{III-II})$/V	$E^{1}_{1/2}(Fe^{II-III})$/V
$[Ru(edtaH)pyz]\cdot 2H_2O$[b]	0.002	—
$[Ru(edtaH)bp]\cdot 2H_2O$	0.08	—
$[Ru(edtaH)dmbp]\cdot 2H_2O$	0.07	—
$[Ru(edtaH)etybp]\cdot 2H_2O$	0.08	—
$[Ru(edtaH)tmbp]\cdot 2H_2O$	0.09	—
$Na_3[Ru(edtaH)pyzFe(CN)_5]\cdot 3H_2O$	0.16	0.55
$Na_3[Ru(edtaH)bpFe(CN)_5]\cdot 3H_2O$	0.13	0.48
$Na_3[Ru(edtaH)dmbpFe(CN)_5]\cdot 3H_2O$	0.09	0.45
$Na_3[Ru(edtaH)etybpFe(CN)_5]\cdot 3H_2O$	0.09	0.44
$Na_3[Ru(edtaH)tmbpFe(CN)_5]\cdot 3H_2O$	0.11	0.42

[a] Redox potentials are reported *vs* SCE at 25 ± 0.1°C, $\mu = 0.2$ M ($[Bu^n_4N]ClO_4$).
[b] From ref. [17].

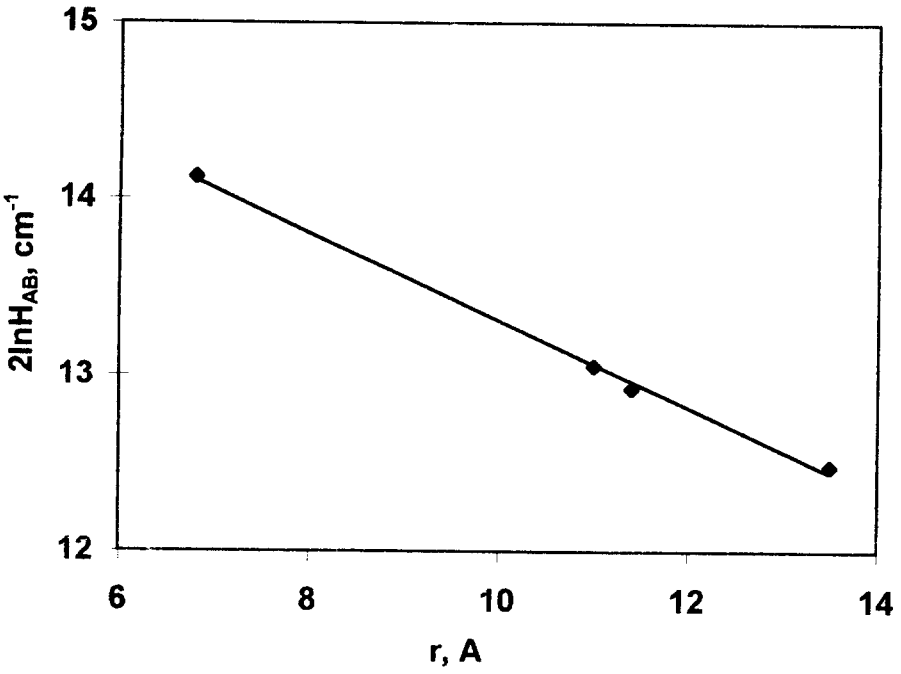


Fig. 3. Logarithmic plot of the square of the electronic coupling elements H_{AB} vs. metal to metal distance, r, in Na_3 [(edtaH)Ru^{III}–L–Fe^{II} $(CN)_5$] complexes; L : 1, pyz; 2, bp; 3, dmbp; 4, etybp.

(ν), molar absorbance at λ_{MMCT} (ε) and full width at the half maxima ($\Delta\nu_{1/2}$) for the intervalence charge transfer band (MMCT) for complexes **VI–IX** are presented in Table 4. Assuming a Gaussian band shape, a lower limit for the bandwidth ($\Delta\nu_{1/2}$) at room temperature can be calculated from Eq. (4) and the values are presented in Table 4.

$$\Delta\nu_{1/2} = (2310\nu_{max})^{1/2} \quad (4)$$

$\Delta\nu_{1/2}$ is related to the oscillator strength, f by Eq. (5) and f can also be expressed [1b,22] in terms of α (degree of mixing) and r (the metal–metal separation distance) (Eq. (6)].

$$f = 4.6 \times 10^{-9}\, \varepsilon_{max}\Delta\nu_{1/2} \quad (5)$$

$$f = 1.085 \times 10^{-5}\, \nu_{max}(\alpha r)^2 \quad (6)$$

Thus

Table 4. Mixed valence data for Na_3[(edtaH)Ru^{III}–L– Fe^{II} $(CN)_5$]

L Parameters	pyz	bp	dmbp	etybp
ν_{max} (cm^{-1})	10,917	10,718	10,163	10,030
$\Delta\nu_{1/2}$ (cm^{-1}) (calc.)	5020	4976	4845	4813
$\Delta\nu_{1/2}$ (cm^{-1})(expt)	5400	5200	5100	5000
α^2	0.01138	0.0041	0.004	0.0026
H_{AB} (cm^{-1})	1164	683	640	513

$$\alpha^2 = 4.24 \times 10^{-4}\varepsilon\Delta\nu_{1/2}/\nu_{max}r^2 \quad (7)$$

and

$$H_{AB} = \nu_{max}\alpha, \quad (8)$$

where α^2 is the measure of the ground state delocalization in the mixed valence complex and H_{AB} is the measure of electronic coupling. Values for α^2 and H_{AB}, calculated using Eqs. (4)–(8) are also summarized in Table 4. It is apparent that an increase in bridge length (metal–metal distances for pz, bp, dmbp and etybp are 6.8, 11, 11.4 and 13.5 Å, respectively) attenuates the communication between the metal centres. The delocalization parameter α^2 is in the order of 0.01 or less corresponding to an electron delocalization of only $< 1\%$. This is further consolidated by the lower, theoretically obtained, value for $\Delta\nu_{1/2}$ compared with the observed $\Delta\nu_{1/2}$ values [11b,23] for complexes **VI–IX**. Thus all these mixed valence complexes belongs to Robin–Day class II valence trapped system [1b,h,i,3a,24]. The plot of $2\ln H_{AB}$ *vs* r gives a straight line (Fig. 3) with $\beta = 0.25$ Å^{-1}, which reveals the measure of attenuation of the electronic overlap of donor and acceptor with the bridge [1e,23] and is close to that reported for polyene-bridged ruthenium amine complexes (0.22 Å^{-1}) [1e]. While for the complex **X**, there exists an interrupted π-system and thus no orbital pathway is available for metal–metal interaction. This is an example of a Robin–Day class I system [3a]. The decrease of electronic interaction with increase in the metal–metal distance has also been predicted theoretically [25]. As delocalization

from Fe^{II} to Ru^{III} is small [21,26] in complexes **VI–IX**, E_{th} can be given by Eq (9)

$$E_{th} = E_{op}/4 - H_{AB} \quad (9)$$

Thus, for reaction (1), assuming $T\Delta S \approx 0$ [26], the thermal electron transfer rate constant, k_{th}, can be expressed by

$$k_{th} = \nu_{et} \exp[-(\Delta G^*/RT)] \approx \nu_{et} \exp[-(E_{th}/RT)] \quad (10)$$

where ν_{et} is the electron hopping frequency and can be estimated [26] roughly ($\approx 10^{14}\ s^{-1}$ for **VI** and $\approx 10^{13}$ for complexes **VII–IX**) from the relation $\nu_{et} \approx 4H_{AB}/h$, [$h$ = Planck's constant] and this allows us to predict approximate values of k_{th} ($\approx 10^{10}$ for complex **VI** and $\approx 10^{9}\ s^{-1}$ for complexes **VII–IX**). Values obtained for k_{th} for complexes **VI–IX** are close to that reported for other related mixed valence binuclear complexes [21]. Moreover, the experimentally obtained value for k_{th} for the related mixed valence complex, $[(NH_3)_5Ru^{III}(NC)Fe^{II}(CN)_5]^-$ is $8 \times 10^{11}\ s^{-1}$ i.e. one/two orders of magnitude higher than that predicted for complexes **VI–IX**, which is a realistic one if the increased metal–metal distances are considered for these complexes.

Acknowledgements—The authors are grateful to DST, India for financial support and Prof. P. Natarajan, Director, Central Salt and Marine Chemicals Research Institute, Bhavnagar for his encouragement in this work.

REFERENCES

1. (a) Haim, A., *Prog. Inorg. Chem.* 1983, **30,** 273; (b) Creutz, C., *Prog. Inorg. Chem.* 1983, **30,** 1; (c) Hush, N. S., *Coord. Chem. Rev.* 1985, **64,** 135; (d) Newton, M. and Sutin, M., *Annu. Rev. Phys. Chem.* 1984, **35,** 437; (e) Woitellier, S., Launay, J. P. and Spangler, C. W., *Inorg. Chem.* 1989, **28,** 758; (f) Richardson, D. E. and Taube, H., *Coord. Chem. Rev.* 1984, **60,** 107; (g) Geselowitz, D. A., Kutner, W. and Meyer, T. J., *Inorg. Chem.* 1986, **25,** 2015; (h) Reimers, J. R. and Hush, N. S., *Inorg. Chem.* 1990, **29,** 4510; (i) Ribou, A. C., Launay, J. P., Takahashi, K., Nihira, T., Tarutani, S. and Spangler, C. W., *Inorg. Chem.* 1994, **33,** 1325.
2. (a) Sutton, J. E., Sutton, P. M. and Taube, H., *Inorg. Chem.* 1979, **18,** 1017; (b) Lee, G.-H., Ciana, L. D. and Haim, A., *J. Am. Chem. Soc.* 1989, **111,** 2535; (c) Hupp, J. T., *J. Am. Chem. Soc.* 1990, **112,** 1563; (d) Clark, R. J. H., Michael, D. J. and Yamashita, M., *J. Chem. Soc., Dalton Trans.* 1991, 3447; (e) Das, A., Jeffery, J. C., Maher, J. P., McCleverty, J. A., Schatz, E., Ward, M. D. and Wollermann, G., *Inorg. Chem.* 1993, **32,** 2145; *Angew. Chem., Int. Ed. Engl.* 1992, **31,** 1515; (f) Launay, J. P., Tourrel-Pagis, M., Lipskier, J. F., Marvaud, V. and Joachim, C., *Inorg. Chem.* 1991, **30,** 1033; (g) Thomas, J. A., Jones, C. J., McCleverty, J. A., Collison, D., Mabbs, F. E., Hoarding, C. J. and Hutchings, M. G., *J. Chem. Soc., Chem. Commun.* 1992, 1796.
3. (a) Robin, M. B. and Day, P., *Adv. Inorg. Chem. Radio Chem.* 1967, **10,** 247; (b) Meyer, T. J., *Acc. Chem. Res.* 1978, **11,** 94; (c) Cooper, B. J., Vess, T. M., Kalsbeck, W. A. and Wertz, D. W., *Inorg. Chem.* 1991, **30,** 2286; (d) Day, P. A., *J. Phys. Chem.* 1986, **90,** 878.
4. (a) Tom, G. M., Creutz, C. and Taube, H., *J. Am. Chem. Soc.* 1976, **96,** 7827; (b) Powers, M. J., Callahan, R. W., Salmon, D. J. and Meyer, T. J., *Inorg. Chem.* 1976, **15,** 894; (c) Blackbourn, R. L. and Hupp, J. T., *J. Phys. Chem.* 1988, **92,** 2817; (d) Constable, E. C. and Ward, M. D., *J. Chem. Soc., Dalton Trans.* 1990, 1405; (e) Downard, A. J., Honey, G. E., Phillips, L. F. and Steel, P. J., *Inorg. Chem.* 1991, **30,** 2259; (f) McWhinie, S. L. W., Jones, C. J., McCleverty, J. A., Collison, D., Mabbs, F. E., *J. Chem. Soc., Chem. Commun.* 1990, 940; (g) Amorose, A. J., Mehar, J. P., McCleverty, J. A. and Ward, M. D., *J. Chem. Soc., Chem. Commun.* 1994, 1273.
5. (a) Bhadbhade, M. M., Das, A., Jeffery, J. C., McCleverty, J. A., Badiola, J. A. N. and Ward, M. D., *J. Chem. Soc., Dalton Trans.* 1995, 2769; (b) Amorose, A. J., Thompson, A. M. C., Maher, J. P., McCleverty, J. A., and Ward, M. D., *Inorg. Chem.* 1995, **34,** 4828.
6. (a) Clarke, M. J., In *Metal Ions in Biological Systems*, Vol. 11. Wiley, New York, 1980, p. 231; (b) Zhang, S., Holl, L. A. and Shepherd, R. E., *Inorg. Chem.* 1990, **29,** 1012; (c) Shepherd, R. E., Zhang, S., Lin, F.-T. Kortes, R. A., *Inorg. Chem.* 1992, **31,** 1457; (d) Chatterjee, D., Bajaj, H. C. and Das, A., *J. Chem. Soc., Dalton Trans.* 1995, 2497.
7. (a) Taqui Khan, M. M., Siddiqui, M. R. H., Hussain, A. and Moiz, M. A., *Inorg. Chem.* 1986, **25,** 2765; (b) Taqui Khan, M. M., Shukla, R. S. and Rao, A. P., *Inorg. Chem.* 1989, **28,** 452; (c) Zhang, S. and Shepherd, R. E., *Inorg. Chim. Acta*, 1992, **217,** 1993.
8. (a) Matsubara, T. and Creutz, C., *Inorg. Chem.* 1979, **18,** 1956; (b) Toma, H. E., Santos, P. S., Mattioli, M. P. P. and Oliveira, L. A. A., *Polyhedron*, 1987, **6,** 603; (c) Bajaj, H. C. and Van Eldik, R., *Inorg. Chem.* 1988, **27,** 4052.
9. (a) Matsubara, T. and Creutz, C., *J. Am. Chem. Soc.* 1978, **100,** 6255; (b) Oliveira, L. A. A., Ciana, L. D. and Haim, A., *Inorg. Chim. Acta*, 1994, **225,** 129.
10. (a) Chatterjee, D., Bajaj, H. C. and Das, A., *Inorg. Chem.* 1993, **32,** 4049; (b) Das, A., Bajaj, H. C. and Chatterjee, D., *Polyhedron*, 1995, **14,** 3585; (c) Chatterjee, D., Bajaj, H. C., and Das, A., *Inorg. Chim. Acta* 1994, **224,** 189.
11. (a) Toma, H. E. and Malin, J. M., *Inorg. Chem.* 1973, **12,** 1039; (b) Felix, F. and Ludi, A., *Inorg. Chem.* 1978, **17,** 1782.
12. Diamantis, A. A. and Dubrawski, J. V., *Inorg. Chem.* 1981, **20,** 1142.
13. Jwo, J.-J. and Haim, A., *J. Am. Chem. Soc.* 1976, **98,** 1172.
14. Das, A., Maher, J. P., McCleverty, J. A., Navas Badiola, J. A. and Ward, M. D., *J. Chem. Soc., Dalton Trans.* 1993, 681.

15. (a) Dong, Y. and Hupp, J. T., *Inorg. Chem.* 1992, **31,** 3322; (b) Walker, C. C., Barbara, P., Doorn, S. K., Dong, Y. and Hupp, J. T., *J. Phys. Chem.* 1991, **95,** 5712.
16. (a)Wilkinson, G., Gillard, R. D. and McCleverty, J. A. (ed.), *Comprehensive Coordination Chemistry*, Vol 5. Pergamon Press, Oxford, 1987; (b) Bunker, B. C., Drago, R. S., Hendrickson, D. N., Richman, R. M. and Kesse, S. L., *J. Am. Chem. Soc.* 1978, **100,** 3805.
17. Creutz, C., Kroger, P., Matsubara, T., Netzet, T. L. and Sutin, N., *J. Am. Chem. Soc.* 1979, **101,** 5442.
18. Burewicz, A. and Haim, A., *Inorg. Chem.* 1988, **27,** 1611.
19. Callahan, R. W., Brown, G. M. and Meyer, T. J., *Inorg. Chem.* 1975, **14,** 1449.
20. Hush, N. H., *Prog. Inorg. Chem.* 1967, **8,** 391.
21. Callahan, R. W., Keene, A. R., Meyer, T. J. and Salmon, D. J., *J. Am. Chem. Soc.* 1977, **99,** 1064.
22. Yeh, A. and Haim, A., *J. Am. Chem. Soc.* 1985, **107,** 369.
23. Fagalde, F. and Katz, N. E., *Polyhedron*, 1995, **14,** 1213.
24. Dowling, N., Henry, P. M., Lewis, N. A. and Taube, H., *Inorg. Chem.* 1981, **20,** 2345.
25. (a) Larsson, S., *Chem. Phys. Lett.* 1982, **90,** 136; (b) Joachim, C., *Chem. Phys. Lett.* 1987, **116,** 339.
26. Reynolds, W. L. and Lumry, R. W., *Mechanisms of Electron Transfer*. Ronald Press, New York, 1966, pp. 128–129.

Pergamon

PII: S0277-5387(96)00411-1

Polyhedron Vol. 16, No. 7, pp. 1031–1045, 1997
Copyright © 1997 Elsevier Science Ltd
Printed in Great Britain. All rights reserved
0277-5387/97 $17.00+0.00

A survey of terminal chalcogenido complexes of the transition metals: trends in their distribution and the variation of their M=E bond lengths

Tina M. Trnka and Gerard Parkin*

Department of Chemistry, Columbia University, New York, NY 10027, USA

(Received 25 June 1996; accepted 12 August 1996)

Abstract—The distribution of structurally characterized terminal chalcogenido complexes as a function of both the chalcogen and transition metal has been surveyed with the aid of the Cambridge Structural Database. The majority of these complexes are concentrated along the vanadium–molybdenum–rhenium diagonal with oxo derivatives being the most prevalent. Terminal chalcogenido derivatives of the early and late transition metals, and terminal tellurido complexes of all the transition metals, are particularly rare. Trends in the variation of metal–chalcogenido bond lengths are also described. Copyright © 1997 Elsevier Science Ltd

Keywords: metal; chalcogen; oxo; sulfido; selenido; tellurido.

Transition metal complexes with metal–ligand multiple bonds have attracted considerable attention over recent years [1]. The majority of these complexes feature multiple bonds to carbon, nitrogen and oxygen, with relatively few examples involving multiple bonding to their heavier congeners. In this regard, the chalcogens (E = O, S, Se, Te, Po) [2] are distinct from other groups of elements, since they represent the first group of non-metals for which all of the non-radioactive members (i.e. with the exclusion of Po) are known to form multiple bonds to the transition metals [3]. For this reason, it is timely to survey transition metal terminal chalcogenido complexes, and in this article we describe current trends in their distribution and the variation of the M=E bond lengths. The present study covers all transition metal terminal chalcogenido complexes, and, as such, is intended to complement Mayer's 1988 review concerned exclusively with oxo derivatives [4].

RESULTS AND DISCUSSION

We have surveyed the distribution of terminal chalcogenido complexes as a function of both the transition metal and chalcogen by using the Cambridge Structural Database (Version 5.11, April 1996). At the outset, it must be recognized that a survey of this type necessarily excludes complexes that have not been structurally characterized. However, since X-ray diffraction is often required to authenticate the presence of a terminal [M=E] moiety for the heavier chalcogens (S, Se, Te) [5], it is reasonable to consider that the distribution of structurally characterized complexes reflects their actual distribution. In contrast, the identification of terminal oxo complexes does not rely so heavily upon X-ray diffraction; for example, the terminal oxo moiety is frequently recognized by characteristic IR absorptions in the range *ca* 750–1100 cm^{-1} [1,6]. Consequently, the actual number of terminal oxo complexes may be significantly underestimated by surveying a structural database, a fact that should be considered when evaluating trends in distribution.

Distribution of terminal chalcogenido complexes

The distribution of structurally characterized terminal chalcogenido complexes of the transition metals is summarized in Table 1 and described below as a function of both the chalcogen and the transition metal.

Distribution as a function of the chalcogen. The occurrence of terminal chalcogenido complexes as a

* Author to whom correspondence should be addressed.

function of the chalcogen is illustrated in Fig. 1 [7], from which it is evident that their occurrence diminishes rapidly in the sequence O ≫ S > Se > Te. Furthermore, since the total number of oxo complexes is considerably greater than the number of structurally characterized examples, the difference between the actual distributions of oxo complexes and their heavier counterparts is in reality much more pronounced than is illustrated. In fact, the terminal metal–oxo moiety is the most common class of transition metal–ligand multiple bond [1,4], and studies on these complexes dominate those of their sulfido, selenido and tellurido counterparts [5,8,9]. Such a trend is in accord with the commonly observed preference for the heavier main group elements to form single rather than multiple bonds [5,10], but it must be recognized that the distribution also reflects other factors. For example, the oxidising nature of the atmosphere must be a consideration when rationalizing the abundance of terminal oxo complexes, while the scarcity of terminal tellurido complexes may simple be attributed to less research effort into the chemistry of tellurium compared with its lighter congeners [7].

Distribution as a function of the transition metal. The distribution of terminal chalcogenido complexes as a function of the transition metal is illustrated in Figs

Table 1. Structurally characterized terminal chalcogenido complexes of the transition metals[a]

	O	S	Se	Te	Total
Sc	0	0	0	0	0
Ti[b]	13	0	0	0	13
	1.648[43]				
V	399	9	1	0	409
	1.608[71]	2.098[26]	2.196(3)		
Cr	50	0	0	0	50
	1.595[42]				
Mn	6	0	0	0	6
	1.511[71]				
Fe[c]	0	0	0	0	0
	1.60–1.67				
Co	0	0	0	0	0
Ni	0	0	0	0	0
Y	0	0	0	0	0
Zr[d]	1	2	1	2	6
	1.804(4)	2.326[12]	2.480(1)	2.690[56]	
Nb	36	17	0	0	53
	1.738[109]	2.205[66]			
Mo[e]	783	71	7	2	863
	1.706[79]	2.154[87]	2.301[58]	2.566[31]	
Tc	101	0	0	0	101
	1.676[43]				
Ru	17	0	0	0	17
	1.721[38]				
Rh	0	0	0	0	0
Pd	0	0	0	0	0
La	0	0	0	0	0
Hf[f]	1	1	1	2	5
	1.826(9)	2.311(3)	2.467(1)	2.677[40]	
Ta[g]	1	3	3	2	9
	1.720[30]	2.217[24]	2.341[26]	2.578[14]	
W	212	80	14	3	309
	1.716[68]	2.150[72]	2.306[51]	2.546[34]	
Re	286	8	0	0	294
	1.700[64]	2.099[16]			
Os	48	0	0	0	48
	1.713[32]				
Ir	1	0	0	0	1
	1.725(9)				
Pt	0	0	0	0	0
Total	1955	191	27	11	2184

2–8, from which it is apparent that their occurrence varies markedly with the location of the metal in the Periodic Table. The distribution as a function of Group is illustrated in Fig. 2, which indicates a rather peaked profile reaching a maximum with the Group 6 metals (Cr, Mo, W). The frequency of terminal chalcogenido complexes falls off quite dramatically on both sides of Group 6; indeed, there are no structurally characterized terminal chalcogenido complexes of either the Group 3 (Sc, Y, La) or Group 10 (Ni, Pd, Pt) transition metals. Moreover, there is only one such complex of the Group 9 metals, namely the iridium–oxo complex $(2,4,6\text{-}Me_3C_6H_2)_3IrO$ [11].

The lack of terminal oxo complexes for the late transition metals has already been noted by Mayer [12], who rationalized that their scarcity is a consequence of the necessarily high *d* electron count on late transition metal centers [13]. Specifically, π antibonding interactions resulting from the overlap of filled π orbitals on the oxo ligand with the filled d_π metal orbitals (so-called "filled–filled" repulsions [14]) destabilize a terminal metal–oxo interaction with respect to a bridged structure. Such an explanation, however, is clearly not applicable to the early transition metals (e.g. Sc, Y, La, Ti, Zr, Hf). For these elements, it is likely that the presence of a highly electrophilic metal center results in M=O moieties that are exceptionally reactive towards a variety of possible degradation reactions. For example, the zirconium–oxo complex, $Cp^*_2Zr(O)(NC_5H_5)$, reacts instantaneously with water to give the hydroxide derivative, $Cp^*_2Zr(OH)_2$ [6], whereas its tungsten counterpart, Cp^*_2WO, is stable with respect to $Cp^*_2W(OH)_2$ [15].

Concerning their distribution as a function of the transition series, the greatest number of structurally characterized terminal chalcogenido complexes are known for the second transition series, as illustrated in Fig. 3. However, rather than interpreting this as an indication of enhanced stability of their multiple bonds, it is more likely that the larger number of terminal chalcogenido complexes for the second versus third transition series is merely a consequence of more research effort being placed on the elements of the former series [16].

The distribution of terminal chalcogenido moieties

---

[a] The search of the Cambridge Structural Database (CSD) (Version 5.11, April 1996) was performed for the doubly bonded M=E moiety (where M = Groups 3–10 transition metals), restricting the coordination number of E to 1 and using the "insist-on-coordinates" and "insist-perfect-match" parameters in order to help eliminate inaccurate data. As a result of these constraints, not all complexes that have been structurally characterized may be retrieved in a particular search. For each transition metal, the number of terminal chalcogenido complexes is listed in the first line, with the mean M=E bond length (in Å) listed below. The number following the mean bond length in brackets indicates the sample standard deviation, while a number in parentheses indicates the esd for a single measurement.

[b] The titanium complex $[Et_4N][TiCl_4(S)]$ was excluded since the Ti—S interaction does not comprise a multiple bond. See: Müller, U. and Krug, V., *Angew. Chem., Int. Ed. Engl.* 1988, **27,** 293.

[c] Although no molecular terminal iron–oxo complexes were retrieved from the CSD search, the structure of the ferrate derivative K_2FeO_4, with a bond length of 1.67[1] Å, has been determined (see: Hoppe, M. L., Schlemper, E. O. and Murmann, R. K., *Acta. Cryst.* 1982, **B38,** 2237). Also, the X-ray structure of a complex proposed to be an iron(IV)–oxo–porphyrin complex has been cited in footnote 28 of Schappacher, M., Weiss, R., Montiel-Montoya, R. and Trautwein, A., *J. Am. Chem. Soc.* 1985, **107,** 3736. However, the sample was contaminated with an Fe^{III} bromide derivative, so that the derived Fe=O bond length [1.604(19) Å] should be regarded with caution (see: Parkin, G., *Chem. Rev.* 1993, **93,** 887). In addition to the above complexes that have been studied by X-ray diffraction, EXAFS studies on horseradish peroxidase and model compounds indicate Fe—O bond lengths in the range of 1.60–1.65 Å (see: Penner-Hahn, J. E., Eble, K. S., McMurry, T. J., Renner, M., Balch, A. L., Groves, J. T., Dawson, J. H. and Hodgson, K. O., *J. Am. Chem. Soc.* 1986, **108,** 7819 and Penner-Hahn, J. E., McMurry, T. J., Renner, M., Latos-Grazynsky, L., Eble, K. S., Davis, I. M., Balch, A. L., Groves, J. T., Dawson, J. H. and Hodgson, K. O., *J. Biol. Chem.* 1983, **258,** 12761.

[d] The CSD search did not retrieve the following anionic zirconium–oxo complexes which contain four-membered $[M_2O_2]$ rings (M = Li, K) owing to interaction of the oxo ligand with the counterion: $[\{\eta^5\text{-}\eta^1\text{-}\eta^5\text{-}\eta^1\text{-}Et_8C_4(C_4H_2N)_3(C_5H_3N)Zr=O\}_2(\mu\text{-}K)_2]$, with $d(Zr=O) = 1.813(2)$ Å, Jacoby, D., Floriani, C., Chiesi-Villa, A. and Rizzoli, C., *J. Am. Chem. Soc.* 1993, **115,** 7025; $[\{\eta^5\text{-}\eta^1\text{-}\eta^5\text{-}\eta^1\text{-}Et_8C_4(C_4H_2N)_3(3\text{-}EtC_5H_2N)Zr=O\}_2(\mu\text{-}K)_2]$, with $d(Zr=O) = 1.804(2)$ Å, Jacoby, D., Isoz, S., Floriani, C., Chiesi-Villa, A. and Rizzoli, C., *J. Am. Chem. Soc.* 1995, **117,** 2793; $[\{\eta^1\text{-}\eta^1\text{-}\eta^5\text{-}\eta^1\text{-}Et_7C_4(C_4H_2N)_3(CH_2CH_2C_5H_2N)Zr=O\}_2(\mu-Li)_2]$ with $d(Zr=O) = 1.838(7)$ Å, Jacoby, D., Isoz, S., Floriani, C., Chiesi-Villa, A. and Rizzoli, C., *J. Am. Chem. Soc.* 1995, **117,** 2805.

[e] The number of molybdenum–chalcogenido complexes and the Mo=E bond lengths include the complexes $Mo(PMe_3)_4(E)_2$ [S, 2.54(1) Å; Se, 2.381(1) Å; Te, 2.597(1) Å] (see: ref. [21]) and $[(3,5\text{-}Me_2C_6H_3)NBu^t]_3Mo=E$ [O, 1.706(2) Å; S, 2.168(1) Å; Se, 2.312(1) Å; Te, 2.535(1) Å] (C. C. Cummins, personal communication) which were not listed in Version 5.11 of the CSD.

[f] The number of hafnium–tellurido complexes and the mean Hf=Te bond length includes $[(Me_3Si)_3SiTe]_2Hf(Te)(dmpe)_2$ [2.637(2) Å] which was not listed in Version 5.11 of the CSD. See: Gerlach, C. P., Christou, V. and Arnold, J., *Inorg. Chem.* 1996, **35,** 2758.

[g] The value of 1.720[30] Å for Ta=O is different to that listed in the Cambridge Structural Database; it is the average value for two structure determinations of $Cp^*_2Ta(O)H$. See: Parkin, G., van Asselt, A., Leahy, D. J., Whinnery, L., Hua, N. G., Quan, R. W., Henling, L. M., Schaefer, W. P., Santarsiero, B. D. and Bercaw, J. E., *Inorg. Chem.* 1992, **31,** 82.

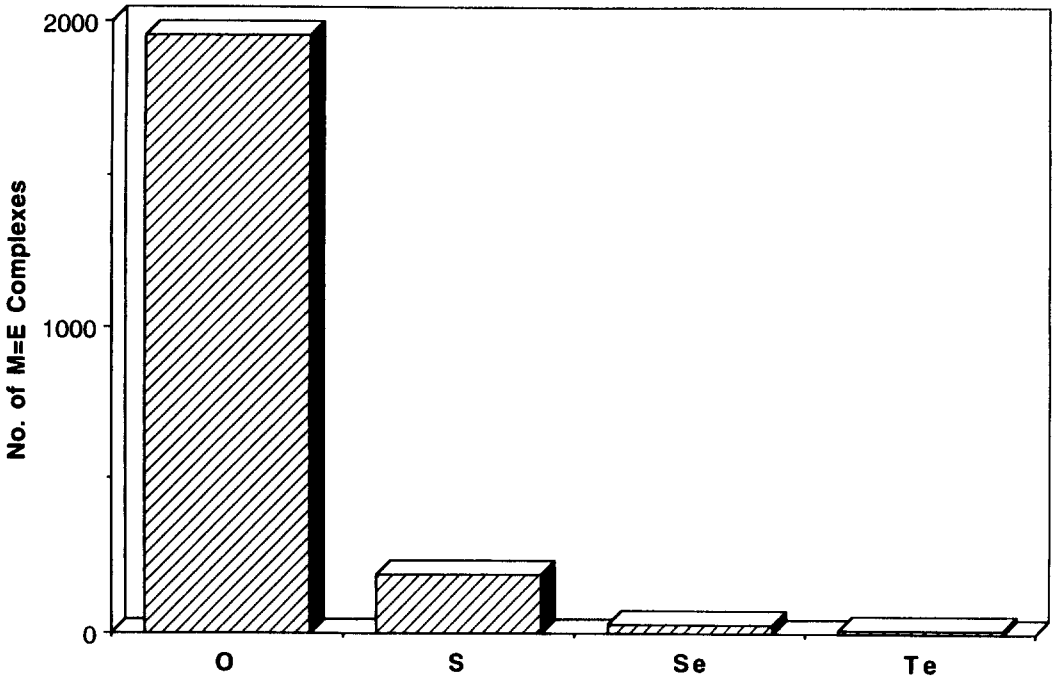


Fig. 1. Structurally characterized terminal chalcogenido complexes as a function of the chalcogen.

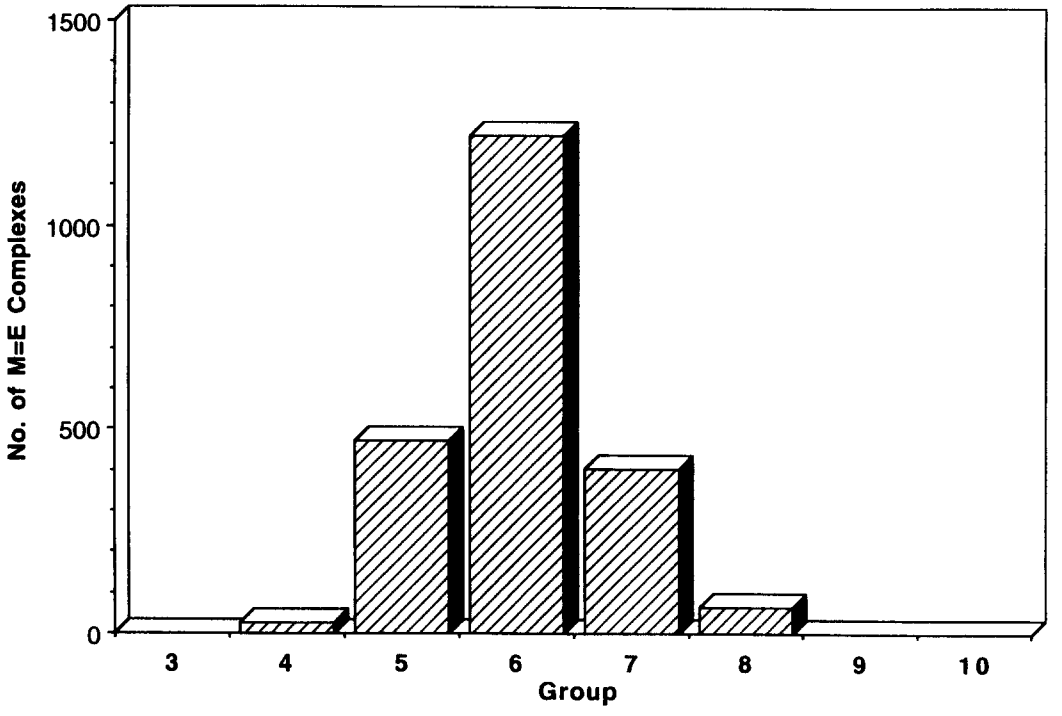


Fig. 2. Structurally characterized terminal chalcogenido complexes as a function of periodic group.

for each transition metal is illustrated in Fig. 4. Focusing attention on the Groups 5–7 metals, it is apparent that upon progressing from the first to the second to the third transition series, the peak in the distribution shifts from earlier to later transition metals. Thus, the element with the largest number of structurally characterized terminal chalcogenido complexes is vanadium (Group 5) in the first transition series, molybdenum (Group 6) in the second series, and rhenium (Group 7) in the third transition series. Not surprisingly, since metal–oxo complexes belong to the most common class of metal–ligand multiple bond, such a

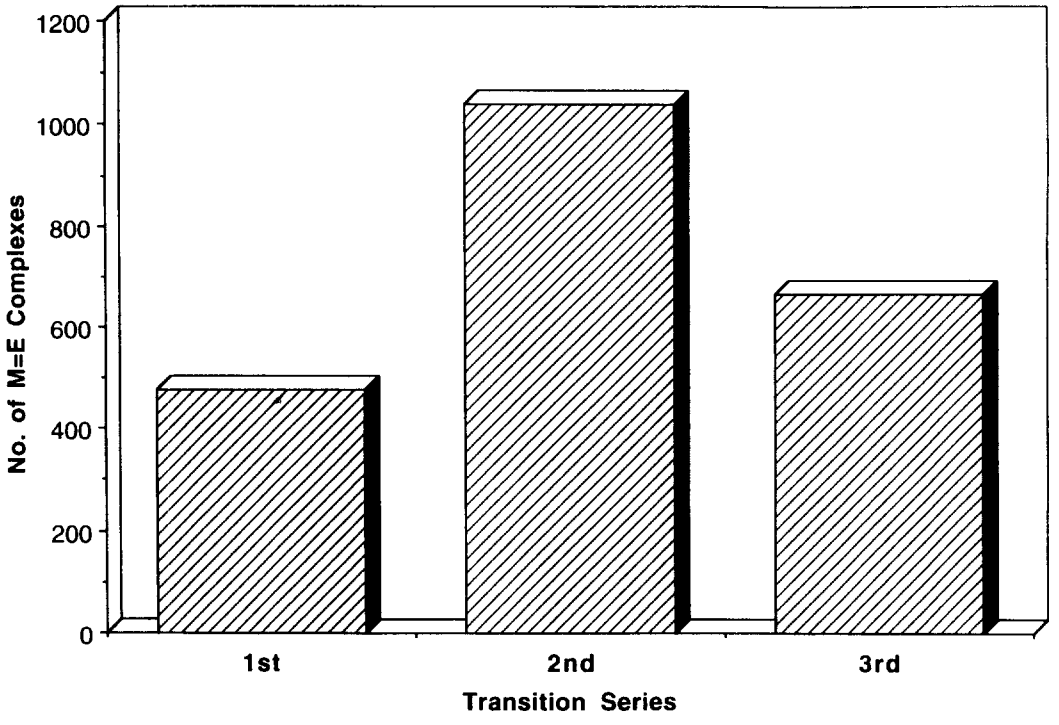


Fig. 3. Structurally characterized terminal chalcogenido complexes as a function of the transition series.

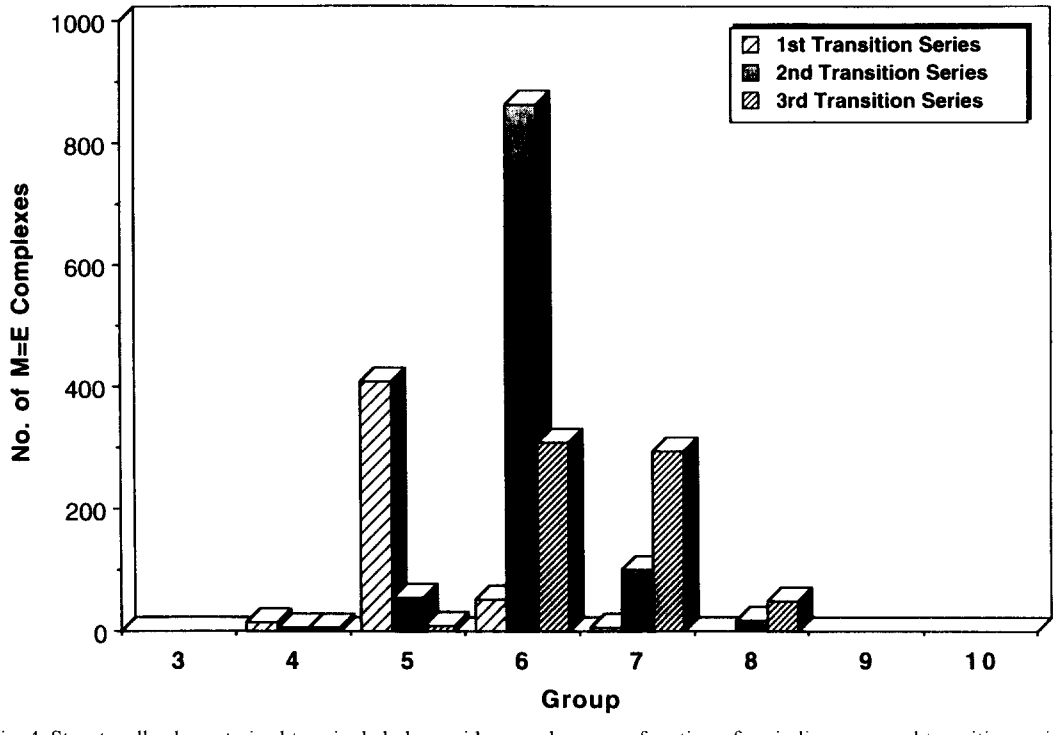


Fig. 4. Structurally characterized terminal chalcogenido complexes as a function of periodic group and transition series.

trend closely parallels that described for metal–ligand multiple bonds in general, for which the majority of complexes are concentrated on the vanadium–molybdenum–rhenium diagonal [1].

Finally, the distribution of terminal chalcogenido complexes for each individual transition metal as a function of the chalcogen is illustrated in Figs 5–8, with Fig. 8 emphasizing the distributions for com-

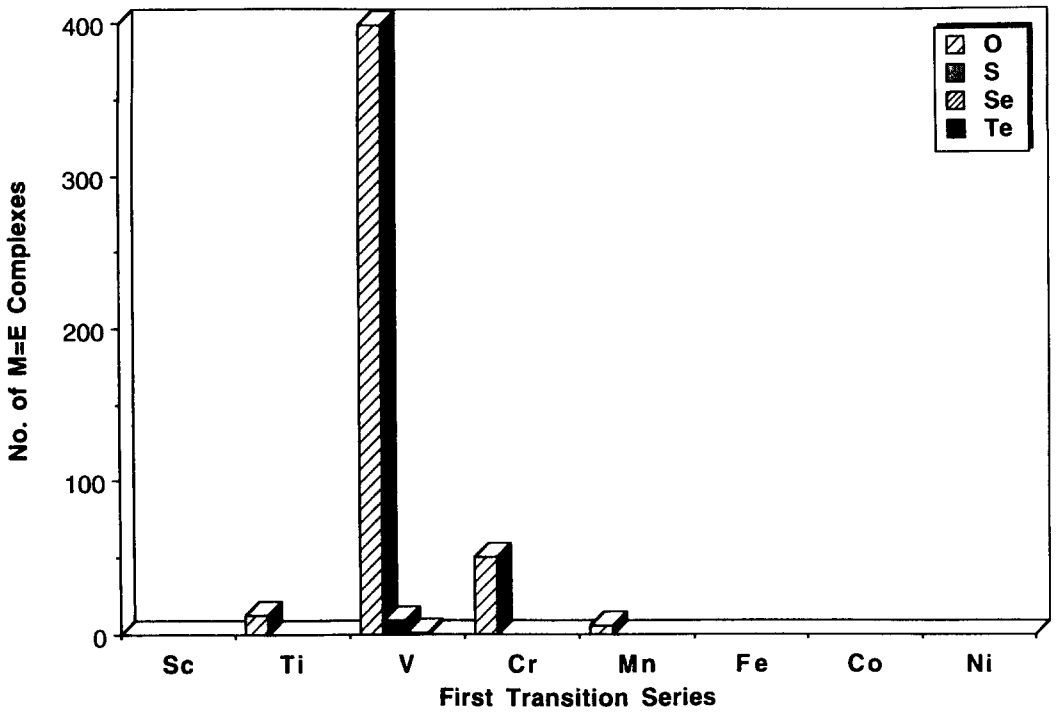


Fig. 5. Structurally characterized terminal chalcogenido complexes of the 1st transition series.

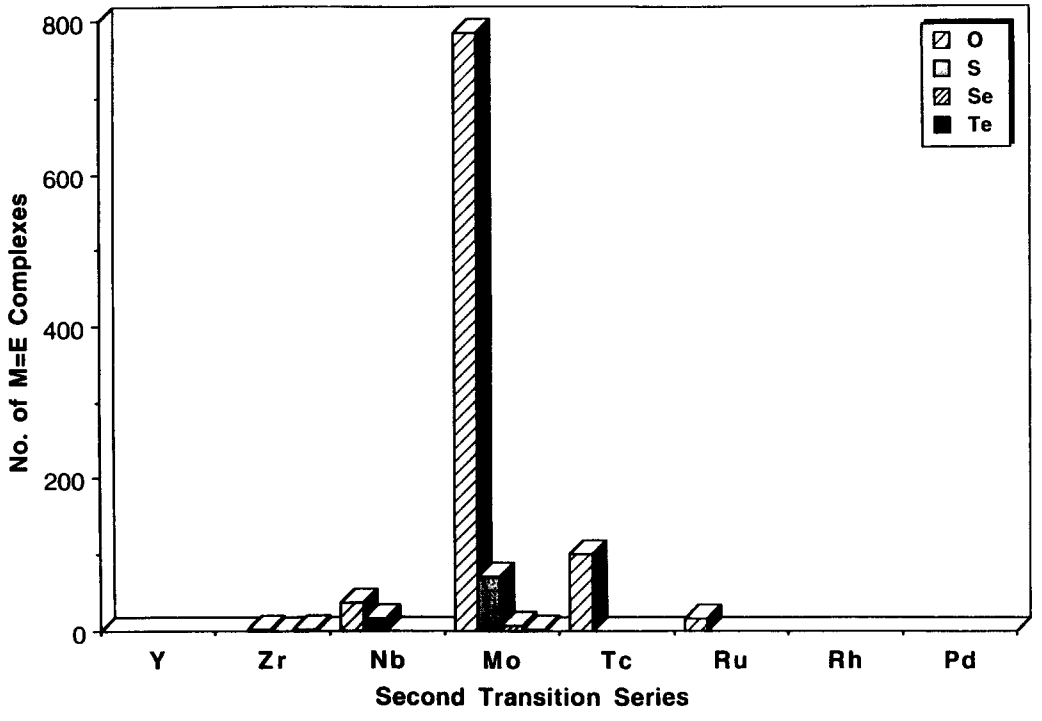


Fig. 6. Structurally characterized terminal chalcogenido complexes of the 2nd transition series.

plexes with low abundance. For each transition metal where a significant number (>20) of terminal chalcogenido complexes have been structurally characterized, the number of terminal oxo complexes outweighs that of the other derivatives, as would be expected from the trend shown in Fig. 1. Coupled with the fact that the occurrence of terminal chalcogenido complexes decreases rapidly with the early and late metals, it is no surprise that terminal selenido and tellurido complexes are particularly scarce for these

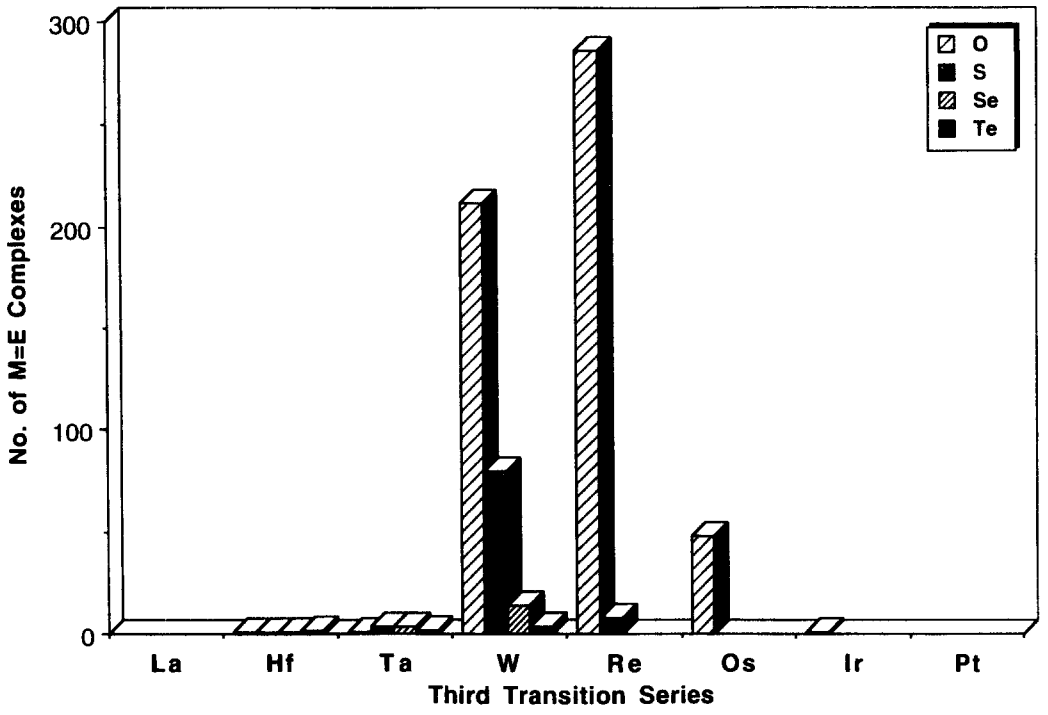


Fig. 7. Structurally characterized terminal chalcogenido complexes of the 3rd transition series.

elements. For example, we are not aware of any simple molecular terminal selenido or tellurido complexes of Cr, Mn, Tc, Re, Fe, Ru, Os and Ir, though each is known to form terminal oxo complexes. Consequently, the syntheses of terminal chalcogenido complexes at the extremes of these distributions represent a challenging goal for the synthetic chemist.

Variation of M=E bond lengths in terminal chalcogenido complexes

The distribution of M=E bond lengths for each of the transition metals has also been analyzed with the aid of the Cambridge Structural Database, and the mean d(M=E) bond lengths for all structurally characterized terminal chalcogenido complexes of the transition metals are summarized in Table 1 [17]. As an illustration, the bond length distributions for tungsten, one of the elements that forms terminal chalcogenido complexes with all of the chalcogens, are presented in Figs 9–11. Inspection of Figs 9 and 10 indicates that the distributions for W=O and W=S bond lengths are reasonably narrow, although there are clearly some outliers. For example, the average W=S bond length of 2.54(1) Å in $[W_4S_8(H_2NCH_2CH_2NH_2)_4]S$ [18] is approximately 0.4 Å longer than the mean (2.150 Å) of all terminal tungsten sulfido complexes (Fig. 10); furthermore, it is longer than the mean W—S single bond length (2.390 Å) of complexes listed in the Cambridge Structural Database [19]. In fact, the terminal sulfido bond length in $[W_4S_8(H_2NCH_2CH_2NH_2)_4]S$ is so long that it is comparable to the mean tungsten–tellurido bond length (2.546 Å). The anomalous W=S bond length in $[W_4S_8(H_2NCH_2CH_2NH_2)_4]S$ thus raises the issue of whether or not the complex actually contains a multiply bonded terminal sulfido ligand. Another example is provided by $Mo(dppe)_2(O)(S)$, with a Mo=S bond length of 2.415(7) Å [20], significantly longer than the mean value of 2.154 Å for all other terminal molybdenum–sulfido complexes. A possible explanation for the anomalous bond length was suggested [21] to be a consequence of the X-ray structure having been performed on a crystal of composition $(dppe)_2Mo(O)(S)\cdot SO_2\cdot H_2SO_4\cdot PhCH_3\cdot EtOH$ [20]; thus, in view of the proposed presence of H_2SO_4, it is possible that the sulfido ligand is actually protonated, i.e. $[(dppe)_2Mo(O)(SH)]^+$, so that the derived Mo—S bond length is that of a single bond, not that of a double bond [22]. Moreover, the anomalous Mo=O bond lengths for the *cis-mer*-$MoOCl_2(PR_3)_3$ complexes listed in Mayer's review [4,23], so-called "distortional" or "bond-stretch" isomers [24,25], are now recognized to be an artifact due to compositional disorder [26]. Thus, in the instances where a substantial body of data is available, it is prudent to scrutinize bond lengths that deviate significantly from the mean, for the true interpretation (e.g. correct atom/ligand assignment or problems with contamination) may not be so straightforward.

Mayer has previously noted that M=O bond lengths are generally insensitive to both coordination

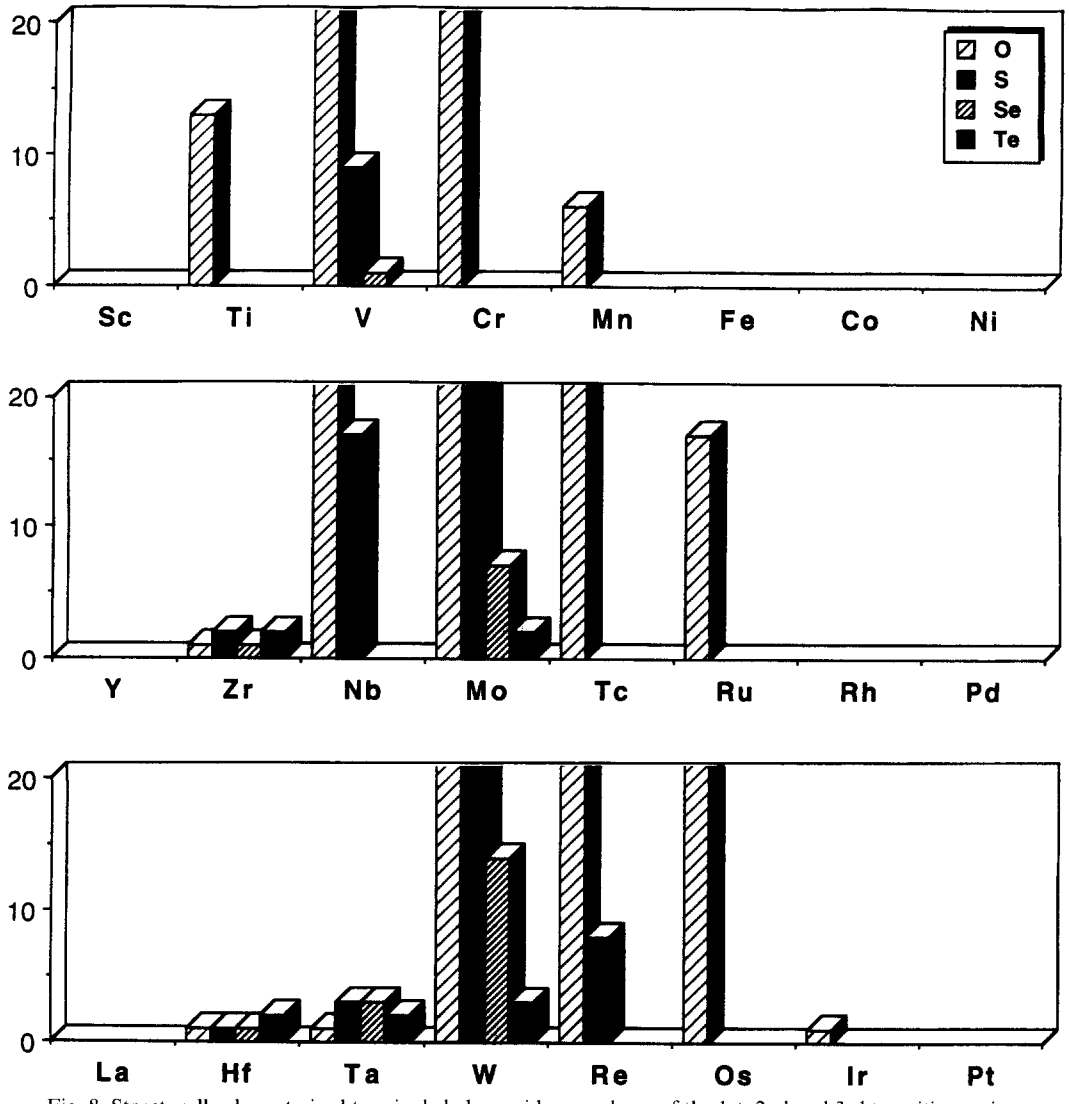


Fig. 8. Structurally characterized terminal chalcogenido complexes of the 1st, 2nd and 3rd transition series.

number and oxidation state of the metal [4,27]. Nevertheless, for a closely related series of complexes, the M=E bond length would be expected to correlate with bond order, which may vary between one and three, as illustrated by the resonance structures:

$$\overset{+}{M}\text{—}\overset{-}{E} \leftrightarrow M{=}E \leftrightarrow \overset{-}{M}{\equiv}\overset{+}{E}$$

Such a trend is aptly illustrated for the tungsten sulfido and selenido complexes listed in Table 2 [28]. Thus, a progressive decrease in bond length is observed as the formal bond order increases from 2 in the 18-electron complexes $W(PMe_3)_2(L)_2(E)_2$ and $W(PMe_4)_4(Se)H_2$, to 2.5 in the "16"-electron complexes $W(PMe_3)_2(E)_2(\eta^2\text{-OCHR})$, and to 3 in the "12"-electron complexes $W(E)X_4$ (E = S, Se; X = F, Cl, Br). Likewise, Mayer has rationalized that the long ruthenium–oxo bond lengths in d^4 octahedral ruthenium–oxo complexes is a consequence of reduced bond order [4]. Specifically, rather than possessing a $\overset{-}{Ru}{\equiv}\overset{+}{O}$ triple bond, the formal ruthenium–oxo bond order is restricted to 2 in 18-electron d^4 octahedral complexes of the type $[Ru(O)L_4X]^+$ [29], owing to the occupation of metal–oxygen π^* orbitals. Thus, such complexes exhibit ruthenium–oxo bond lengths at the long end of the distribution illustrated in Fig. 12. Further variations in M=E bond length are described in the following sections as a function of both the chalcogen and transition metal.

Variation in M=E bond length as a function of the chalcogen. Examination of Table 1 reveals that only five of the transition elements (Zr, Hf, Ta, Mo and W) are known to form terminal chalcogenido complexes with all of the non-radioactive chalcogens. The variation in mean M=E bond length for each of these transition metals is represented graphically in Fig. 13, which, for comparison, also includes the variation of the double bond covalent radii of the chalcogens. Thus, the change in M=E bond length as a function

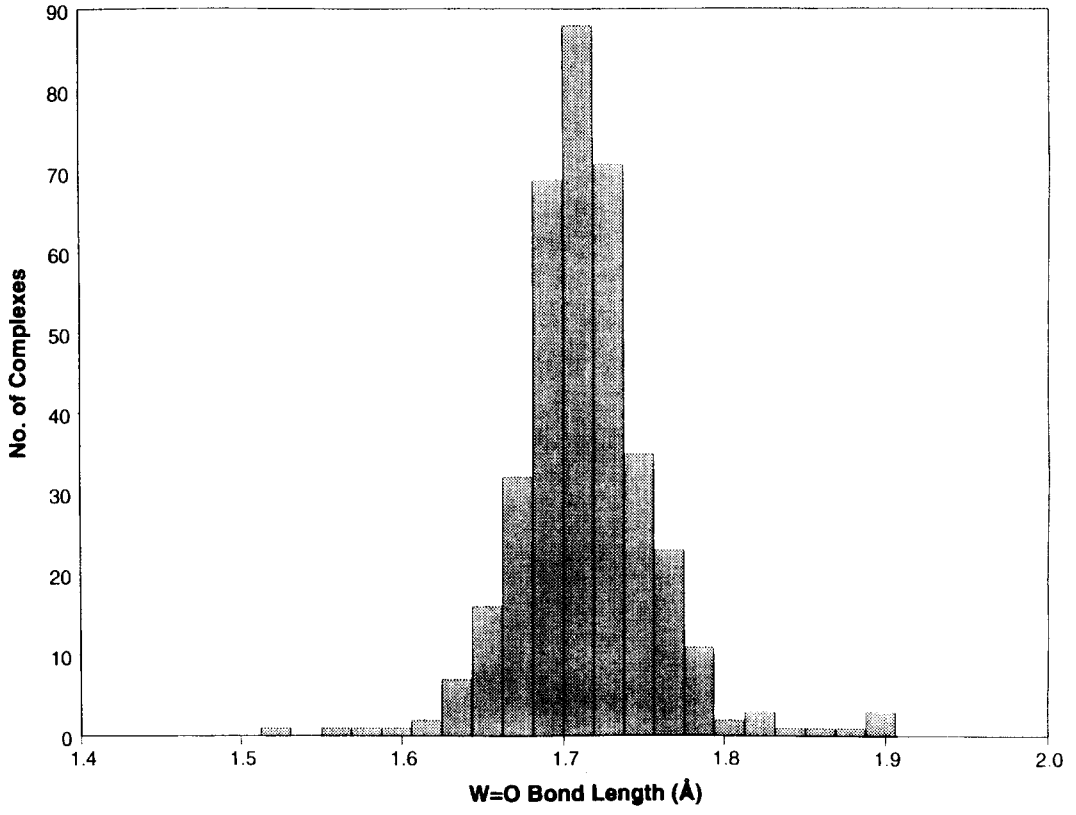


Fig. 9. Distribution of W=O bond lengths in tungsten–oxo complexes.

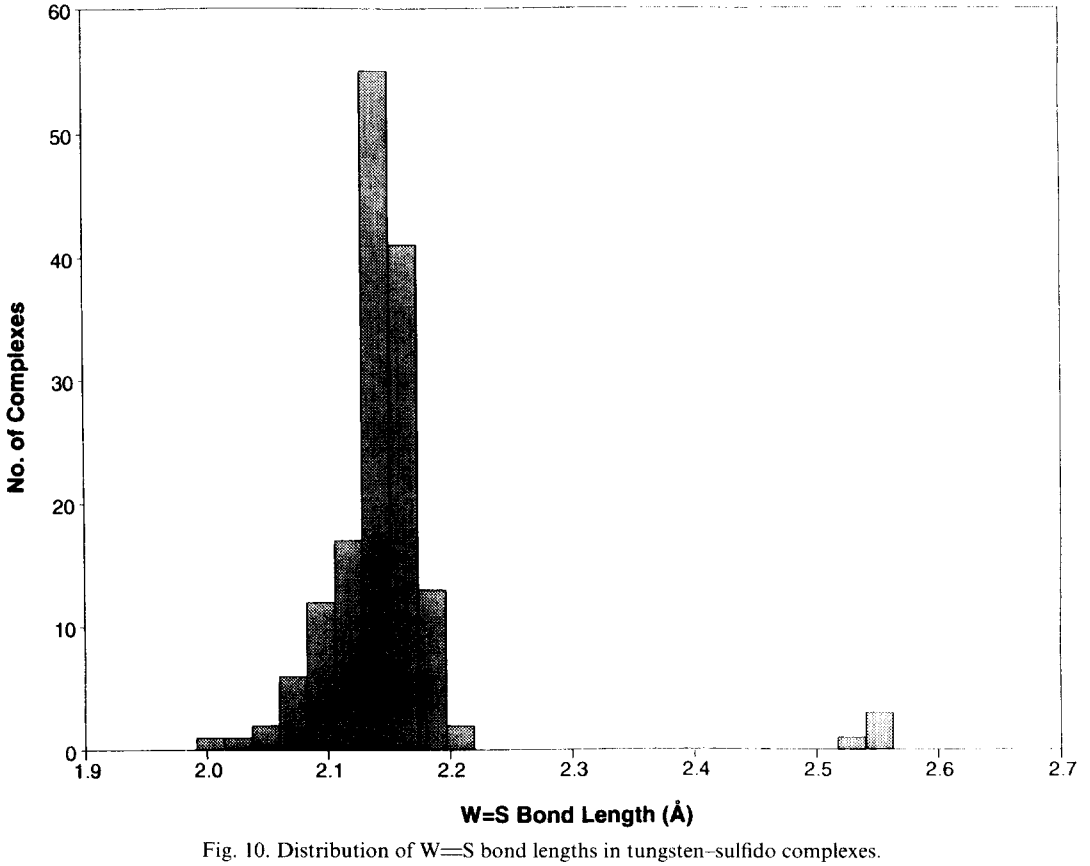


Fig. 10. Distribution of W=S bond lengths in tungsten–sulfido complexes.

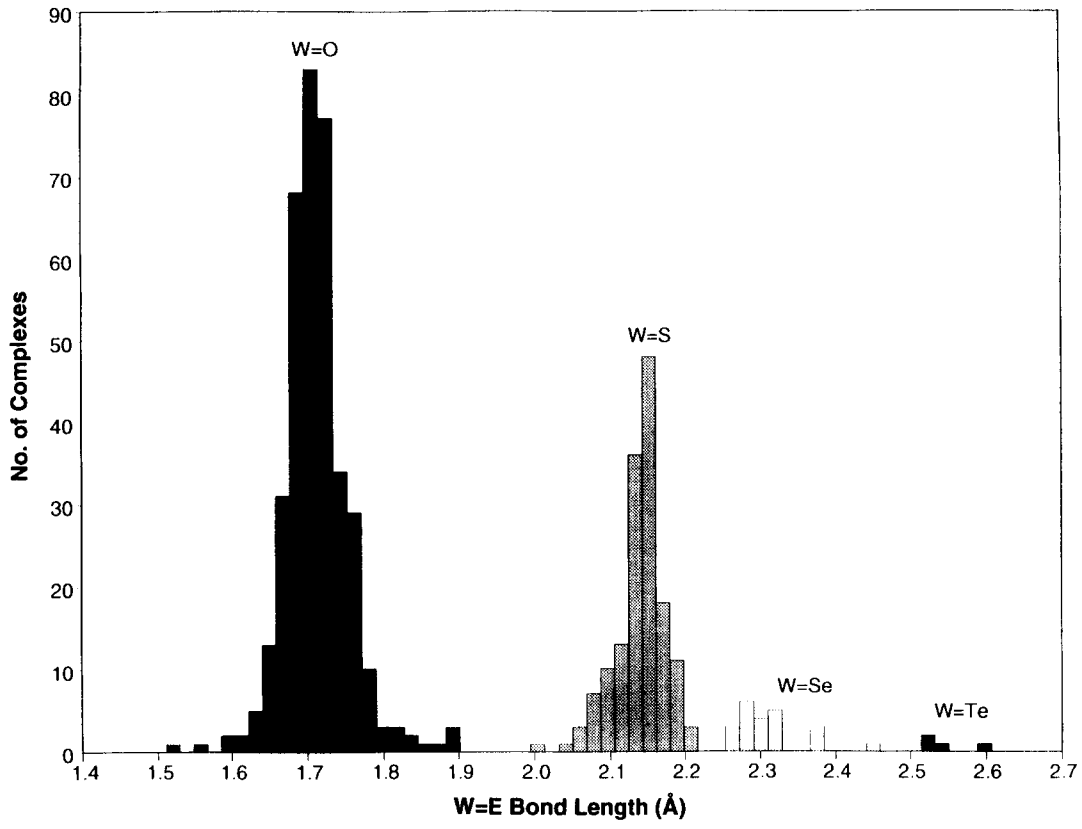


Fig. 11. Distribution of W=E bond lengths in tungsten–chalcogenido complexes (the W=S outliers of Fig. 10 are not included).

Table 2. Variation of W=E bond length with bond order

	Bond order	S	Se	Ref.
$W(PMe_3)_4(E)H_2$	2		2.445(2)	28
$W(PMe_3)_4(E)_2$	2	2.253[3]	2.380[1]	28
$W(PMe_3)_2(CNBu^t)_2(E)_2$	2	2.248(2)	2.375(2)	28
$W(PMe_3)_2(E)_2(\eta^2\text{-OCHPh})$	2.5	2.186[2]	2.317[4]	28
$W(E)F_4$	3	2.104(7)	2.226(7)	35
$W(E)Cl_4$	3	2.086(6)	2.203(4)	35
$W(E)Br_4$	3	2.109(11)	2.220(22)	35

of the chalcogen is similar for each of the transition metals and correlates reasonably well with the change in double bond covalent radii. However, upon closer inspection of the data summarized in Table 3 and Fig. 14, it is evident that the difference in M=O and M=Te bond lengths for a given transition metal (0.83–0.89 Å) is consistently greater than the difference in double bond covalent radii of oxygen and tellurium (0.72 Å). For the case of zirconium, the discrepancy has been attributed to the particularly large increase of 0.52 Å in bond length between the oxo and sulfido derivatives, compared with the difference of 0.39 Å in covalent radii of oxygen and sulfur [30]. In comparison, the increments in bond lengths between the sulfido, selenido and tellurido derivatives are close to those predicted by the differences in covalent radii of the chalcogens. Thus, the metal–oxo bond lengths are anomalously short, an observation that has been rationalized in terms of the resonance structure [Zr—O] for $(\eta^5\text{-}C_5Me_4Et)_2Zr(O)(NC_5H_5)$ [30], with bond shortening attributed to an ionic component [31]. Since the heavier chalcogens are both less electronegative and larger than oxygen, the corresponding zirconium–chalcogenido interactions would be subject to less ionic shortening,

Cundari has recently carried out computational

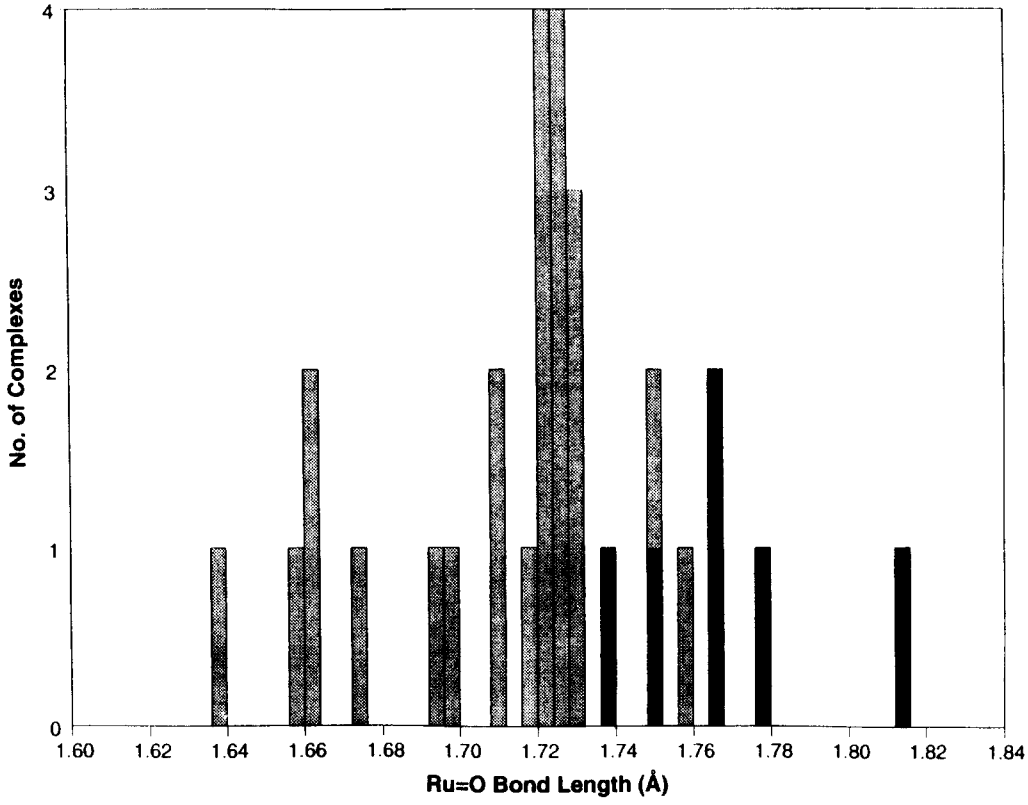


Fig. 12. Distribution of Ru=O bond lengths in ruthenium–oxo complexes, with the solid bars representing d^4 complexes.

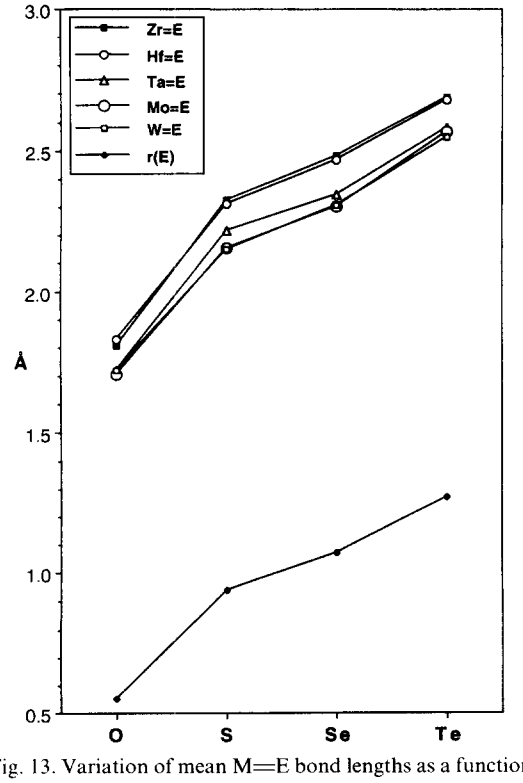


Fig. 13. Variation of mean M=E bond lengths as a function of the chalcogen.

studies on a comprehensive series of terminal chalcogenido complexes [32]. Significantly, the computational results are in excellent agreement with the experimental data. For example, computational studies on the hypothetical species $[Cp_2Zr{=}E]$ (E=O, S, Se, Te) demonstrated that, compared with the other derivatives, the oxo species shows a significant contribution from a singly bonded Zr—O structure, with the π bonds localized on the oxo ligand. Such a result is consistent with the proposed resonance structure $[\overset{+}{Z}r{-}\overset{-}{O}]$ for the zirconium–oxo complex $(\eta^5\text{-}C_5Me_4Et)_2Zr(O)(NC_5H_5)$ [30]. Furthermore, Cundari's calculations also predict the trend in which the difference in metal–oxo and metal–sulfido bond lengths decreases in going from the Group 4 to Group 6 transition metals (see Table 3 and Fig. 14). However, in view of the errors inherently associated with measuring the differences in mean bond lengths for limited datasets, further structural studies are warranted to establish the generality of these apparent trends.

Variation in M=E bond length as a function of the metal. In view of the paucity of heavier terminal chalcogenido complexes for all of the transition metals, it is only possible to illustrate the variation in M=E bond length as a function of the metal for the oxo derivatives. Thus, the variation of M=O bond lengths is shown in Fig. 15, which also includes the metallic radii of the transition metals [33] for purposes of comparison. Figure 15 also includes data for Zr, Hf and

Table 3. Comparison of M=E bond length increments with respect to the M=O derivative

	r_{db}(E)/Å[a]	$[r_{db}(E)-r_{db}(O)]$/Å	d(M=E) − d(M=O)/Å[b]				
			Zr	Hf	Ta	Mo	W
O	0.55	0	0	0	0	0	0
S	0.94	0.39	0.52	0.49	0.50	0.45	0.43
Se	1.07	0.52	0.67	0.64	0.62	0.60	0.59
Te	1.27	0.72	0.89	0.85	0.86	0.86	0.83

[a] r_{db}(E) is the double bond covalent radii of the chalcogens. Data taken from Pauling, L., *The Nature of the Chemical Bond*, 3rd edn. Cornell University Press, Ithaca, 1960, p. 224, with the exception of r_{db}(O) which was taken from Jolly, W. L., *Modern Inorganic Chemistry*, McGraw-Hill, New York, 1984, p. 53.

[b] See Table 1 for individual d(M=E) values.

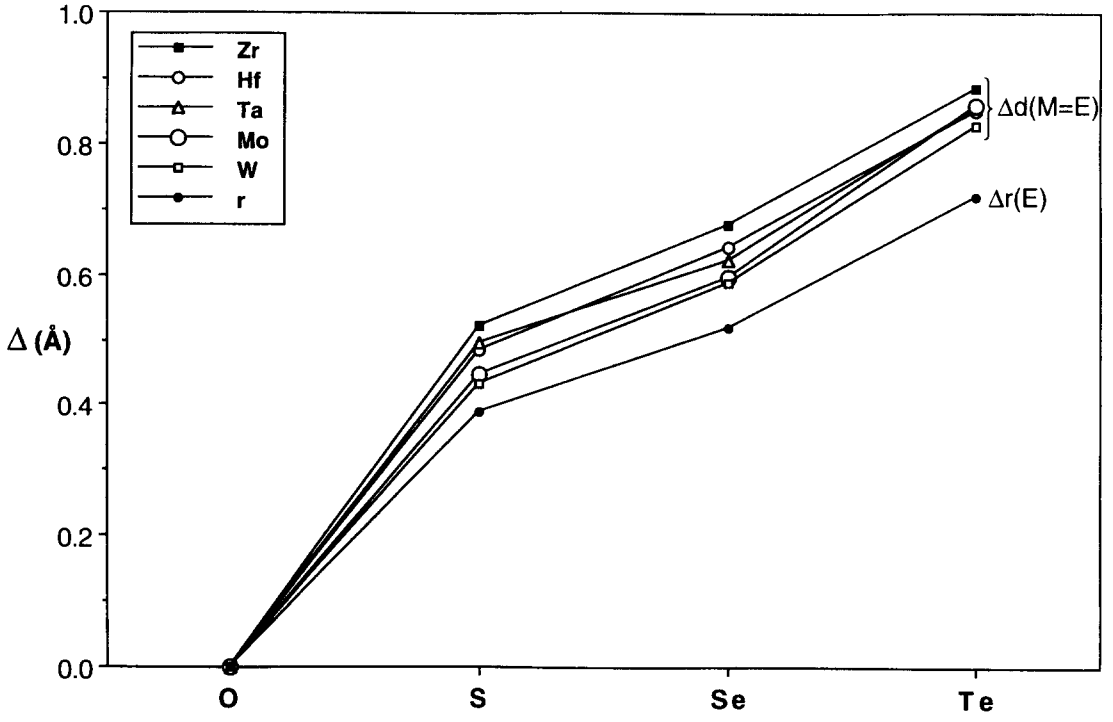


Fig. 14. Incremental changes relative to oxygen of (i) d(M=E) and (ii) r_{db}(E). Δd(M=E) = d(M=E) − d(M=O); Δr(E) = r_{db}(E) − r_{db}(O).

Ir which were not known to form terminal oxo complexes prior to 1988 when the last review on this topic was published [4]. Overall, there is a general decrease in mean M=O bond length upon crossing a period, with the largest incremental change for the earlier metals. With the exception of Mn and Fe (for which the available data is minimal), such a trend correlates reasonably well with the variation in covalent radii of the transition metals.

CONCLUDING REMARKS

The present paper has attempted to provide an account of the distribution of terminal chalcogenido complexes of the transition metals. Thus, at present, the majority of such complexes are oxo derivatives along the vanadium–molybdenum–rhenium diagonal. Particularly rare are terminal chalcogenido derivatives of the early and late transition metals, while terminal tellurido complexes are scarce for all the transition metals. While it would not be wise to correlate the distribution of terminal chalcogenido complexes with their stability in an absolute sense, it seems reasonable to consider that their distribution may indeed be a reflection of their intrinsic reactivity. For example, the zirconium–oxo complex $Cp^*_2Zr(O)(NC_5H_5)$ has been shown to be highly reactive, even with substrates such as H_2 [6]. Likewise, the terminal tellurido complex $W(PMe_3)_4(Te)_2$ exhibits a reductive coupling reaction with Bu^tNC to give the ditellurido complex

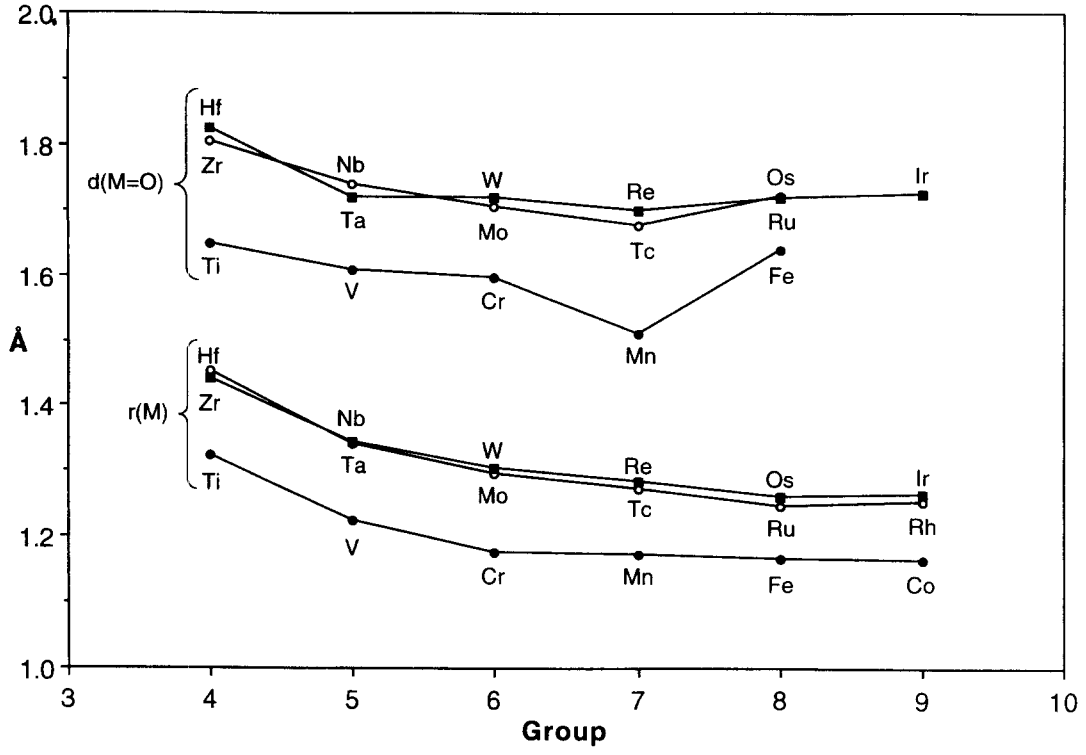


Fig. 15. Variation of mean M=O bond lengths as a function of the metal.

$W(PMe_3)(CNBu^t)_4(\eta^2\text{-}Te_2)$, a reaction that is unprecedented for the sulfido and selenido analogues [28]. Interestingly, both $Cp^*_2Zr(O)(NC_5H_5)$ and $W(PMe_3)_4(Te)_2$ represent classes of molecules (terminal zirconium–oxo and terminal–tellurido complexes) that were not known in 1988, when the classic text *Metal–Ligand Multiple Bonds* by Nugent and Mayer was published [1]. It is, therefore, likely that the most exciting future developments in the chemistry of terminal chalcogenido complexes will derive from the syntheses of presently unknown functionalities ranging from Sc=O to Ir=Te.

Acknowledgements—We thank the US Department of Energy, Office of Basic Energy Science (#DE-FG02-93ER14339) for support of this research. G. P. is the recipient of a Camille and Henry Dreyfus Teacher-Scholar Award (1991–1996) and a Presidential Faculty Fellowship Award (1992–1997). T. M. T. acknowledges the Camille and Henry Dreyfus Foundation for the Jean Dreyfus Boissevain Undergraduate Scholarship in Chemistry (1994–1995).

REFERENCES

1. Nugent, W. A. and Mayer, J. M., *Metal–Ligand Multiple Bonds*. Wiley-Interscience, New York, 1988.
2. There is some controversy as to whether or not oxygen should be considered a chalcogen. The term chalcogen appears to have developed directly from the words "chalkosphäre" and "chalkophile", coined in the earlier part of this century by Goldschmidt, a geochemist [2a,b]. Goldschmidt used "chalkosphäre" to describe a region of the earth that is rich in metal oxides and sulfides, i.e. ores, while "chalkophile" was used to describe elements found in this region (e.g. Fe, Cu, Zn). Since these names derived from the Greek word "chalkos" (χαλκοσ) meaning copper, a literal translation of chalcogen is "copper-former". However, Jensen has rationalized that since "chalkos" may also be interpreted as copper alloy or ore, and since copper is not the only element considered to be a "chalkophile", a more pertinent interpretation of the term chalcogen is "ore-former" [2c]. Consequently, oxygen is appropriately considered to be a chalcogen, a term that has, in fact, been approved by IUPAC as the collective name for the group 16 elements: O, S, Se, Te, Po [2d]. (a) Goldschmidt, V. M., *J. Chem. Soc. (London)*, 1937, 655; (b) Goldschmidt, V. M., *Die Naturwissenschaften*, 1930, **18,** 999; (c) Jensen, K. A., *Chemistry and Industry*, 1964, **49,** 2016; (d) *IUPAC Nomenclature of Inorganic Chemistry, Recommendations* 1990, ed. G. J. Leigh. Blackwell, London, 1990.
3. For example, only the first three members of the pnictogens are known to form isolable complexes with multiple bonds to transition metals, with $Bu^t_3SiO)_3Ta = EPh$ (E = N, P, As) being the first series of such complexes [3a]. The terminal stibido complexes, $[(CO)_4M{\equiv}Sb]^-$ (M = Cr, Mo, W) and $[(CO)_3Fe{\equiv}Sb]^-$, however, have been generated in the gas phase [3b]. (a) Bonanno, J. B., Wolczanski, P. T. and Lobkovsky, E. B., *J. Am. Chem. Soc.* 1994, **116,** 11159; (b) Arnold, F. P.

Jr, Ridge, D. P. and Rheingold, A. L., *J. Am. Chem. Soc.* 1995, **117,** 4427.
4. Mayer, J. M., *Inorg. Chem.* 1988, **27,** 3899.
5. For example, rather than forming terminal chalcogenido complexes, the heavier chalcogens are commonly found either (i) to bridge two or more metal centers [5a–e] or (ii) to form polychalcogenide ligands [5f–q]. (a) Herrmann, W. A., *Angew. Chem., Int. Ed. Engl.* 1986, **25,** 56; (b) Compton, N. A., Errington, R. J. and Norman, N. C., *Adv. Organomet. Chem.* 1990, **31,** 91; (c) Housecroft, C. E., in *Inorganometallic Chemistry*, ed. T. P. Fehlner. Plenum Press, New York, 1992, Ch 3, pp. 73–178; (d) Fenske, D., Ohmer, J., Hachgenei, J. and Merzweiler, K., *Angew. Chem., Int. Ed. Engl.* 1988, **27,** 1277; (e) Dance, I. and Fisher, K., *Prog. Inorg. Chem.* 1994, **41,** 637; (f) Müller, A. and Diemann, E., *Adv. Inorg. Chem.* 1987, **31,** 89; (g) Draganjac, M. and Rauchfuss, T. B., *Angew. Chem., Int. Ed. Eng.* 1985, **24,** 742; (h) Wachter, J., *Angew. Chem., Int. Ed. Engl.* 1989, **28,** 1613; (i) Beck, J., *Angew. Chem., Int. Ed. Engl.* 1994, **33,** 163; (j) Böttcher, P., *Angew. Chem., Int. Ed. Engl.* 1988, **27,** 759; (k) Kanatzidis, M. G., *Comm. Inorg. Chem.* 1990, **10,** 161; (m) Kolis, J. W., *Coord. Chem. Rev.* 1990, **105,** 195; (n) Roof, L. C. and Kolis, J. W., *Chem. Rev.* 1993, **93,** 1037; (o) Ansari, M. A. and Ibers, J. A., *Coord. Chem. Rev.* 1990, **100,** 223; (p) Kanatzidis, M. G. and Huang, S.-P., *Coord. Chem. Rev.* 1994, **130,** 509; (q) Ansari, M. A., McConnachie, J. M. and Ibers, J. A., *Acc. Chem. Res.* 1993, **26,** 574.
6. Howard, W. A., Waters, M. and Parkin, G., *J. Am. Chem. Soc.* 1993, **115,** 4917; Howard, W. A., Trnka, T. M., Waters, M. and Parkin, G., *J. Organomet. Chem.*, in press.
7. For a recent review describing the distribution of structurally-characterized alkoxide, thiolate, selenolate and tellurolate complexes, see: Arnold, J., *Prog. Inorg. Chem.* 1995, **43,** 353.
8. Rice, D. A., *Coord. Chem. Rev.* 1978, **227,** 199; Vahrenkamp, H., *Agnew. Chem., Int. Ed. Engl.* 1975, **14,** 322; Müller, A., Diemann, E., Jostes, R. and Bögge, H., *Angew. Chem., Int. Ed. Engl.* 1981, **20,** 934; Müller, A. and Diemann, E., in *Comprehensive Coordination Chemistry*, Vol. 2, ed. G. Wilkinson, R. D. Gillard and J. A. McCleverty. Pergamon Press, Oxford, 1987, Ch. 16.1, pp. 515–550; Müller, A., *Polyhedron*, 1986, **5,** 323–340.
9. Berry, F. J., in *Comprehensive Coordination Chemistry*, Vol. 2, ed. G. Wilkinson, R. D. Gillard and J. A. McCleverty. Pergamon Press: Oxford, 1987, Ch. 17, pp. 661–674.
10. For some leading articles on multiple bonding of the heavier main group elements, see: Kutzelnigg, W., *Angew. Chem., Int. Ed. Engl.* 1984, **23,** 272; Gusel'nikov, L. E. and Nametkin, N. S., *Chem. Rev.* 1979, **79,** 529; Jutzi, P., *Angew Chem., Int. Ed. Engl.* 1975, **14,** 232; Norman, N. C., *Polyhedron* 1993, **12,** 2431; Schmidt, M. W., Truong, P. N. and Gordon, M. S., *J. Am. Chem. Soc.* 1987, **109,** 5217; Jacobsen, H. and Ziegler, T., *J. Am. Chem. Soc.* 1994, **116,** 3667; Huheey, J. E., Keiter, E. A. and Keiter, R. L., *Inorganic Chemistry: Principles of Structure and Reactivity*, 4th Edn. Harper Collins, New York, 1993, Ch. 18, pp. 861–875; Jacobsen, H. and Ziegler, T., *Comm. Inorg. Chem.* 1995, **17,** 301.
11. Hay-Motherwell, R. S., Wilkinson, G., Hussain-Bates, B. and Hursthouse, M. B., *Polyhedron*, 1993, **12,** 2009.
12. Mayer, J. M., *Comm. Inorg. Chem.* 1988, **8,** 125.
13. For a recent review describing the electronic structures of metal–oxo complexes, see: Miskowski, V. M., Gray, H. B. and Hopkins, M. D., *Adv. Trans. Met. Comp.* 1996, **1,** 159.
14. For further discussion of the influence of filled–filled repulsions in transition metal chemistry, see: Caulton, K. G., *New. J. Chem.* 1994, **18,** 25.
15. Parkin, G. and Bercaw, J. E., *J. Am. Chem. Soc.* 1989, **111,** 391; Parkin G. and Bercaw, J. E., *Polyhedron*, 1988, **7,** 2053.
16. A crude estimate of the relative number of studies on elements of the second and third transition series may be obtained by examining the number of papers that cite these elements themselves either in the title or abstract. For example, using the names of the elements as keywords, there are *ca* 25% more listings in the Science Citation Index (1982–1996) for the elements of the second transition series than for the third transition series.
17. As described in the text, the metal–chalcogenido interactions are a composite of three resonance structures with formal single $[\overset{+}{M}—\overset{-}{E}]$, double $[\overset{-}{M}=\overset{+}{E}]$, and triple $[\overset{-}{M}\equiv\overset{+}{E}]$ bonds. For simplicity, however, in this paper we use the representation [M=E] to refer generally to any terminal chalcogenido moiety, regardless of bond order.
18. Wood, P. T., Pennington, W. T., Kolis, J. W., Wu, B. and O'Connor, C. J., *Inorg. Chem.* 1993, **32,** 129.
19. The mean W—S single bond length (2.390 Å, with a range of 2.107–2.721 Å) is that for complexes in which sulfur is two-coordinate.
20. Lorenz, I.-P., Walter, G. and Hiller, W., *Chem. Ber.* 1990, **123,** 979.
21. Murphy, V. J. and Parkin, G., *J. Am. Chem. Soc.* 1995, **117,** 3522.
22. Some related problems in ligand assignment have been noted with the reformulation of complexes originally proposed to be alkoxides as, in fact, alcohol derivatives. See: Koch, S. A. and Lincoln, S., *Inorg. Chem.*, 1982, **21,** 2904.
23. For example, the Mo=O bond length in green *cis-mer*-$MoOCl_2(PEt_2Ph)_3$ [1.803(11) Å] is considerably longer than the mean value (1.678 Å) reported by Mayer for mono-oxo molybdenum complexes.
24. Chatt, J., Manojlovic-Muir, L. and Muir, K. W., *J. Chem. Soc., Chem. Commun.* 1971, 655; Manojlovic-Muir, L., *J. Chem. Soc. (A)* 1971, 2796; Manojlovic-Muir, L. and Muir, K. W., *J. Chem. Soc., Dalton Trans.* 1972, 686; Haymore, B. L., Goddard, III, W. A. and Allison, J. N., *Proc. Int. Conf. Coord. Chem.*, 23*rd* 1984, 535.
25. Jean, Y., Lledos, A., Burdett, J. K. and Hoffmann, R., *J. Am. Chem. Soc.* 1988, **110,** 4506; Jean, Y., Lledos, A., Burdett, J. K. and Hoffmann, R., *J. Chem. Soc., Chem. Commun.* 1988, 140.

26. Parkin, G., *Acc. Chem. Res.* 1992, **25,** 455; Parkin, G., *Chem. Rev.* 1993, **93,** 887.
27. Mayer has noted, however, that M=O bond lengths do increase slightly in the presence of a second multiply bonded ligand (e.g. oxo, nitrido, imido).
28. Rabinovich, D. and Parkin, G., *Inorg. Chem.* 1996, **34,** 6341.
29. L is a two-electron donor and X is a one-electron donor ligand. See: Green, M. L. H., *J. Organomet. Chem.* 1995, **500,** 127.
30. Howard, W. and Parkin, G., *J. Am. Chem. Soc.* 1994, **116,** 606.
31. See, for example the empirical Schomaker Stevenson equation, $d(A-B) = r(A)+r(B)-c|\chi(A)-\chi(B)|$. Schomaker, V. and Stevenson, D. P., *J. Am. Chem. Soc.* 1941, **63,** 37; Wells, A. F., *J. Chem. Soc.* 1949, 55; Wells, A. F., *Structural Inorganic Chemistry*, 5th edn, Oxford University Press, London, 1984, pp. 287–291.
32. Benson, M. T., Cundari, T. R., Lim, S. J., Nguyen, H. D. and Pierce-Beaver, K., *J. Am. Chem. Soc.* 1994, **116,** 3955; Benson, M. T., Cundari, T. R., Li, Y. and Strohecker, L. A., *Int. J. Quantum Chem.: Quantum Chemistry Symposium* 1994, **28,** 181; Gordon, M. S. and Cundari, T. R., *Coord. Chem. Rev.* 1996, **147,** 87.
33. The metallic radii of the transition elements are effectively identical to the covalent radii derived by consideration of the bond lengths (Å) in diatomic MH molecules: Ti (1.324), V (1.224), Cr (1.176), Mn (1.171), Fe (1.165), Co (1.162), Zr (1.454), Nb (1.342), Mo (1.296), Tc (1.271), Ru (1.246), Rh (1.252), Hf (1.442), Ta (1.343), W (1.304), Re (1.283), Os (1.260), Ir (1.265). Data taken from Pauling, L. *The Nature of the Chemical Bond*, 3rd edn, Cornell University Press, Ithaca, 1960, p. 256.
34. Page, E. M., Rice, D. A., Hagen, K., Hedberg, L. and Hedberg, K., *Inorg. Chem.* 1991, **30,** 4758.

Pergamon

PII: S0277-5387(96)00413-5

Polyhedron Vol. 16, No. 7, pp. 1047–1056, 1997
Copyright © 1997 Elsevier Science Ltd
Printed in Great Britain. All rights reserved
0277-5387/97 $17.00+0.00

Spectrophotometry and voltammetry of cobalt triethanolamine complexes in aqueous solutions in the absence and presence of oxygen

Sophia Teller,[a] Yizhak Marcus[a]* and Yaakov Tur'Yan[b]

[a]Department of Inorganic and Analytical Chemistry, The Hebrew University of Jerusalem, Jerusalem 91904, Israel

[b]National Physical Laboratory of Israel, Danciger Bldg. A, The Hebrew University of Jerusalem, Jerusalem 91904, Israel

(Received 3 April 1996; accepted 12 August 1996)

Abstract—The absorption spectra of solutions of Co^{II} and Co^{III} in the presence of triethanolamine (TEA) are reported. For the former complexes there is no evidence for chelation, but a bischelate is formed with the latter. Saturation of Co^{II}–TEA solutions with oxygen yields more than one new, dioxygen-containing, species that age slowly. The oxygen may be partly removed by bubbling nitrogen through the solutions. The electroreduction of cobalt–triethanolamine complexes in aqueous solutions in the presence of oxygen was followed voltammetrically on a stationary Pt disk electrode. Strong catalytic enhancement of the electroreduction current of oxygen involved with the complex was achieved. A mechanism for the formation of the electrochemically active species, involving OH- and O_2-bridged dimeric species of both Co^{II} and Co^{III}, was suggested. A pseudo first order was established for the reversible reaction of this complex formation. Relevant rate and equilibrium constants were obtained. Copyright © 1997 Elsevier Science Ltd

Keywords: oxygen; cobalt(II); cobalt(III); triethanolamine; spectra; electroreduction.

Complexed cobalt ions are known to catalyse the electroreduction of oxygen in aqueous solutions by forming coordination species with dioxygen. Most studies have been made with amine chelating ligands containing at least two nitrogen atoms (except for complexes with ammonia) forming well-characterized chelates [1, 2]. The formation, stability, properties and structure of the μ-peroxo and μ-superoxo complexes formed by such chelates with dioxygen have been reviewed [3–5]. Triethanolamine (TEA) as a ligand is an exception to this generalization, apparently not forming chelates (see below), although it permits well-catalysed electroreduction of oxygen, as is described in this paper. On the whole, aminoalcohol complexes of transition metals have not been studied extensively [6–9], in spite of the potential technological applications [7,8]. For instance, the catalase activity of cobalt–TEA complexes for the decomposition of hydrogen peroxide is higher than for some other cobalt–amine systems. The relative values are 50 for monoethanolamine, 140 for diethanolamine, 23–489 for ethylenediamine, 29–3350 for ammonia and as high as 24560 for TEA [10]. This is a result of coordination sites at the cobalt atom not being occupied by the TEA and available for the H_2O_2. TEA is, in a sense, unique among amine ligands in that, although it is potentially quadridentate (one N and three O donor atoms), it is reluctant to form chelates with metal ions in aqueous solutions, as is manifested by the known stability constants [6, 9] for complexes with TEA. For cobalt(II) ions this is illustrated by the following values of $\log K_1$ of the tripodant complexes with nitrilotriacetate (NTA) [11], $N(CH_2CO_2^-)_3$: 10.4, tris(2-aminoethyl)amine (tren) [12], $N(CH_2CH_2NH_2)_3$: 12.4, and triethanolamine (TEA) [13], $N(CH_2CH_2OH)_3$: 2.3.

The single species $CoTEA^{2+}$, with a stability constant $\log K_1 = 1.73$, was suggested [14] in a 0.5 M KNO_3 medium, whereas two species: $CoTEA^{2+}$, $\log K_1 = 2.70$, and $CoTEA_2^{2+}$, $\log K_2 = 1.65$ in a 0.43 M ethanolammonium nitrate medium were reported

* Author to whom correspondence should be addressed.

[15], in both cases at 25°C. The latter work appears to overestimate the tendency of Co^{II} to complex with triethanolamine, in view of the much lower $\bar{n}$ (mean ligand number) shown by this metal ion compared with that of, for example, Ni^{II}, with $\log K_1 \approx 2.9$ [6]. A more recent study [13] again reports only a single complex, $CoTEA^{2+}$ with $\log K_1 = 2.25$ in a 0.1 m $NaNO_3$ medium at 25°C.

An important feature of the chemistry of cobalt(II) ions in solution is their ready oxidation by molecular oxygen in the presence of a variety of complexing ligands, in particular those with hydrogen donor atoms. Owing to the instability of intermediates, the action of oxygen normally yields a binuclear peroxo species of cobalt(III) [1,2], but the initial step may well involve coordination of O_2 [3–5]. The activation of oxygen by transition metal complexes proceeds by the coordination interaction alone, without the need for external energy.

Whereas the spectra of the Ni^{II}–TEA species have been reported [6], this is not the case for the Co^{II} species, nor of the Co^{III} one. The octahedral hexaaquocobalt(II) ions, $Co(H_2O)_6^{2+}$, with cubic symmetry, have the ^4F level split into three, with the lowest one degenerate, $^4T_1$ ($t_{2g}^6 e_g^1$). The resulting weak bands peak at *ca* 1250 nm (*ca* 8000 cm^{-1}, $^4\Gamma_5$), 880 nm (11,300 cm^{-1}, $^2\Gamma_3$) and 625 nm (16,000 cm^{-1}, $^4\Gamma_3$), with $\varepsilon \leqslant 0.2$ M^{-1} cm^{-1}, whereas the stronger, still Laporte-forbidden bands, peak at 514 nm (19,400 cm^{-1}, $^4\Gamma_4$), $\varepsilon = 4.55$ M^{-1} cm^{-1}, and at 464 nm (21,550 cm^{-1}, $^4\Gamma_4$), $\varepsilon = 2.6$ M^{-1} cm^{-1} [16,17]. Nominally, octahedral cobalt(II) species with symmetry lower than a perfect cubic have enhanced absorptivities, as is the case, for instance, in ethanolic solutions [18] and as is shown here in aqueous TEA solutions. Replacement of the six oxygen donor atoms of the hexaaquocobalt(II) ion with six nitrogen atoms, as in the hexaamino or trisethylenediamino complexes leads to shifts of the main peaks to the red, as well as enhancement of the absorptivities [18].

The hexaaquocobalt(III) ion is unstable in aqueous solutions, oxidizing the solvent ($E^\circ[Co^{III}Co^{II}] = 1.841$ V at −5°C in a 6.5 M $NaClO_4$ medium [19], $E^\circ[Co^{III}Co^{II}] = 1.93 \pm 0.03$ V at 25°C) [20]. Still, the low-spin $Co(H_2O)_6^{3+}$ ion can be found in crystals of $CsCo(SO_4)_2 \cdot 12H_2O$ [20,21], and has been assigned two bands, peaking at 606 nm (16,500 cm^{-1}, $^1\Gamma_4$) and 405 nm (24,700 cm^{-1}, $^1\Gamma_5$) [17, 21]. Cobalt(III) in aqueous solutions is stabilized by complexation and the hexaamino and trisethylenediamino complexes, among others, have been well characterized. There are strong shifts to the blue, with $Co(en)_3^{3+}$ having peaks at 467 nm (21,400 cm^{-1}, $^1\Gamma_4$), $\varepsilon = 86$ M^{-1} cm^{-1}, and 338 nm (29,600 cm^{-1}, $^1\Gamma_5$), $\varepsilon = 80$ M^{-1} cm^{-1}, as well as a low intensity band at 730 nm (13,700 cm^{-1}, $^3\Gamma_4$), $\varepsilon = 0.3$ M^{-1} cm^{-1} [22].

The present paper examines the electrochemical and spectrophotometric behaviour of cobalt ions in solutions containing triethanolamine in the absence of oxygen and in its presence. In the former case only Co^{II} species are found, whereas in the latter both these (with coordinated oxygen) and Co^{III} species (again with coordinated oxygen) are found. Species responsible for the observed spectra and kinetics of reduction are suggested. The considerable enhancement of the rate of electroreduction of oxygen in these solutions at an inert cathode can be employed both as an analytical tool for oxygen in water and for fuel cells, where the cathode reaction is often rate limiting.

RESULTS

A solution containing 0.05 M cobalt(II) and 1.0 M TEA shows a much enhanced absorptivity relative to the hexaaquocobalt(II) species (Fig. 1), with the maxima shifted towards the red. The spectrum can be resolved into three bands with maxima ($\bar{\nu}/cm^{-1}$, ε/M^{-1} cm^{-1}) at 464 (21,550, 10.2), 534 (18,730, 21.8) and 555 nm (18,020, 2.5). At the concentrations employed and with the reported stability constants [13, 14], practically all the Co^{II} is converted to the monoligated complex. Its non-symmetrical structure explains the enhancement with respect to the spectrum of $Co(H_2O)_6^{+2}$, and the presence of one nitrogen donor atom instead of oxygen explains the red shift.

The absorption spectrum of a solution containing 0.05 M cobalt(III), obtained by anodic oxidation in 1.0 M TEA, 3.0 M sodium nitrate and in the absence of oxygen, is shown in Fig. 2. It has two main absorption peaks ($\bar{\nu}/cm^{-1}$, ε/M^{-1} cm^{-1}), at 348 (28,740, 68) and 527 nm (18,980, 27) and these are compared with those of $Co(H_2O)_6^{3+}$ and $Co(en)_3^{3+}$. The positions of the absorption maxima of the hexaaquocobalt(III) cations are indicated, but the molar absorptivity has not been reported [21, 23]. A blue shift of the two main peaks of the TEA-complexed cobalt(III) with respect of the hexaaquo ion is noted, but not as far as the shift of the trisethylenediamino complex [22]. The peak of the TEA complex of cobalt(III) at 527 nm, however, is sufficiently close to the position of the peak of the TEA–cobalt(II) complex, 534 nm, so that from the spectrum alone it is impossible to conclude that the anodic oxidation was complete. Polarographic reduction data [24] on the solution, see below, lend support to the observed peak in Fig. 2 at 527 nm being a result of the cobalt(III)–TEA complex. There is also some light absorption in the 730 nm region in the cobalt(III)–TEA solutions, which is some 5–10 times larger than in the tris-ethylenediamino complex, but the molar absorptivity could not be determined accurately owing to its low value, so it is not shown in Fig. 2.

When oxygen was bubbled through solutions containing cobalt(II) and TEA, absorption spectra were obtained similar in some respects to that of cobalt(III) complexed by TEA, but differing in others; typical spectra are shown in Fig. 3. The spectra evolved with time (up to a few days), depended on the pH of the solution and obeyed Beer's law only up to *ca* 0.1 M

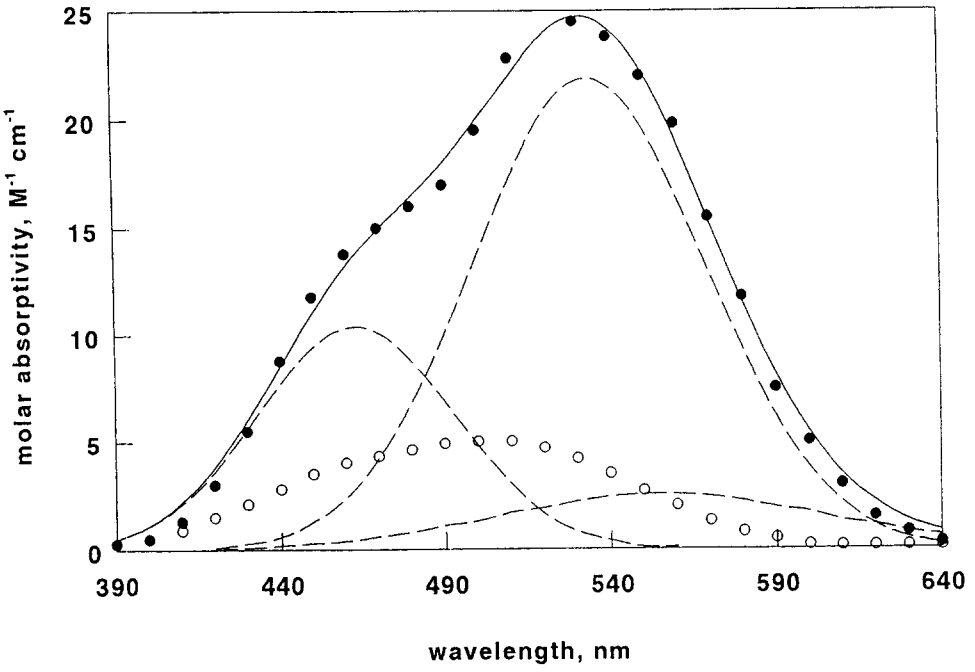


Fig. 1. The absorption spectra of cobalt(II) solutions: —, the observed $CoTEA(H_2O)_x^{2+}$ spectrum; ---, the component bands of this complex; ●, the spectrum calculated from these bands; ○, $Co(H_2O)_6^{2+}$ [11].

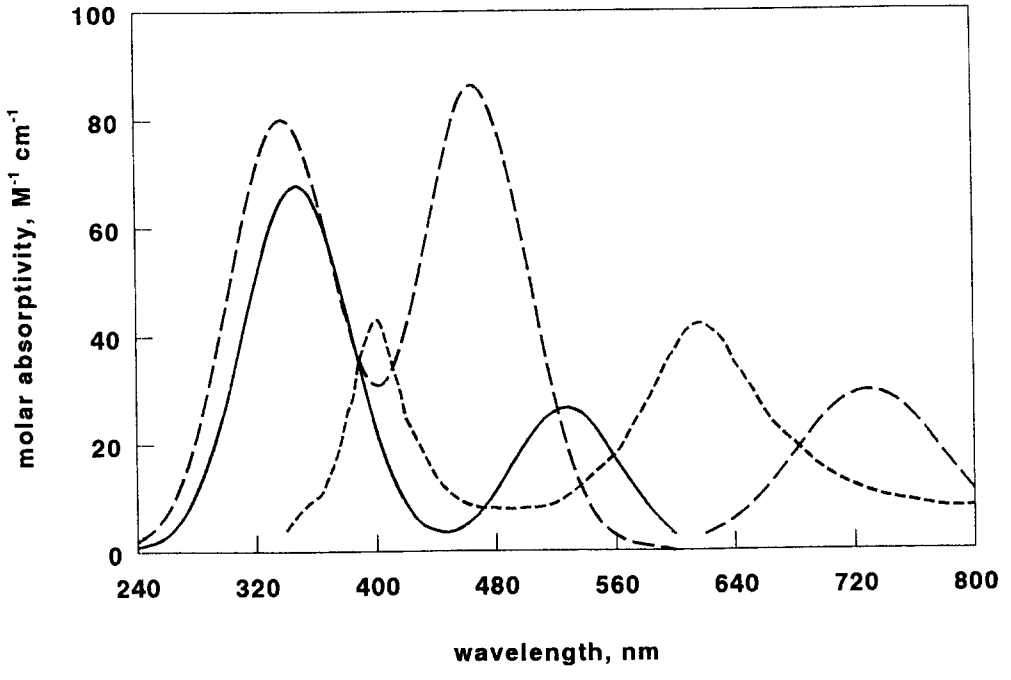


Fig. 2. The absorption spectra of cobalt(III) solutions: —, the observed $CoTEA(H_2O)_x^{3+}$ spectrum; ———, the spectrum of $Co(en)_3^{3+}$ [17], the absorptivity of the long wavelength part (630–800 nm) having been magnified a hundred fold; ---, the reflectance spectrum of $Co(H_2O)_6^{3+}$ in crystalline $CsCo(SO_4)_2 \cdot 12H_2O$ (arbitrary absorptivities) [21].

cobalt salt (in 1 M TEA) immediately after the preparation of the solution. After *ca* 1 h, however, Beer's law was obeyed up to 0.2 M cobalt, and only when the concentration was increased to 0.5 M (so that there were only 2 TEA molecules per cobalt ion) was there a sharp break in the curve (Fig. 4).

The spectrum of 0.05 M cobalt nitrate in 1.0 M TEA + 3.0 M $NaNO_3$ after 15 min of oxygen bubbling

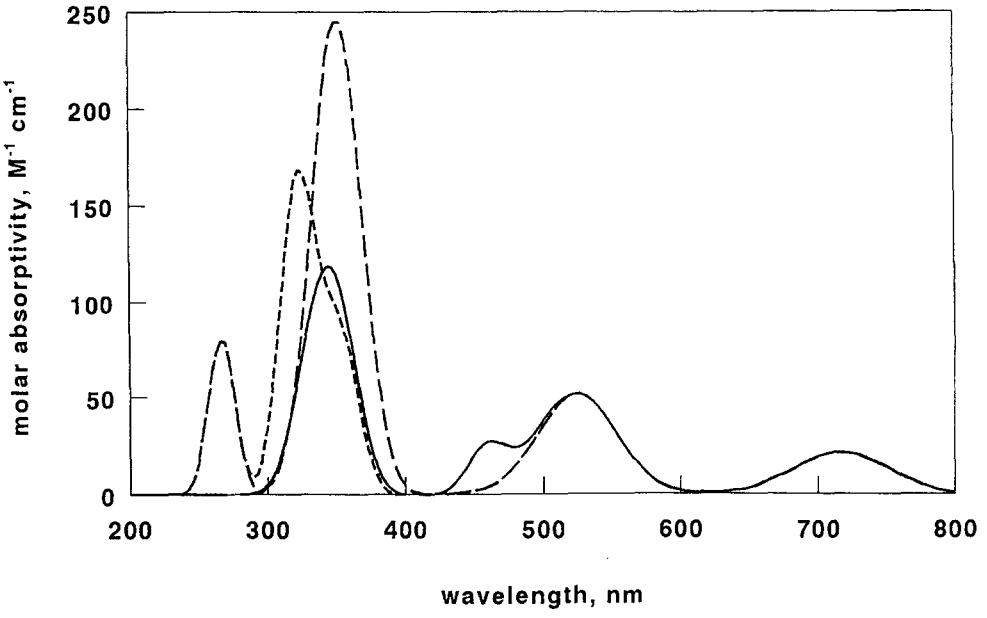


Fig. 3. The absorption spectra of initially 0.05 M cobalt(II) solutions saturated with oxygen in 1.0 M TEA+3.0 M $NaNO_3$: —, pH = 9.5; ----, pH = 11.0, 1 min after O_2 bubbling for 15 min; — — —, pH = 11.0, 24 h after O_2 bubbling for 15 min.

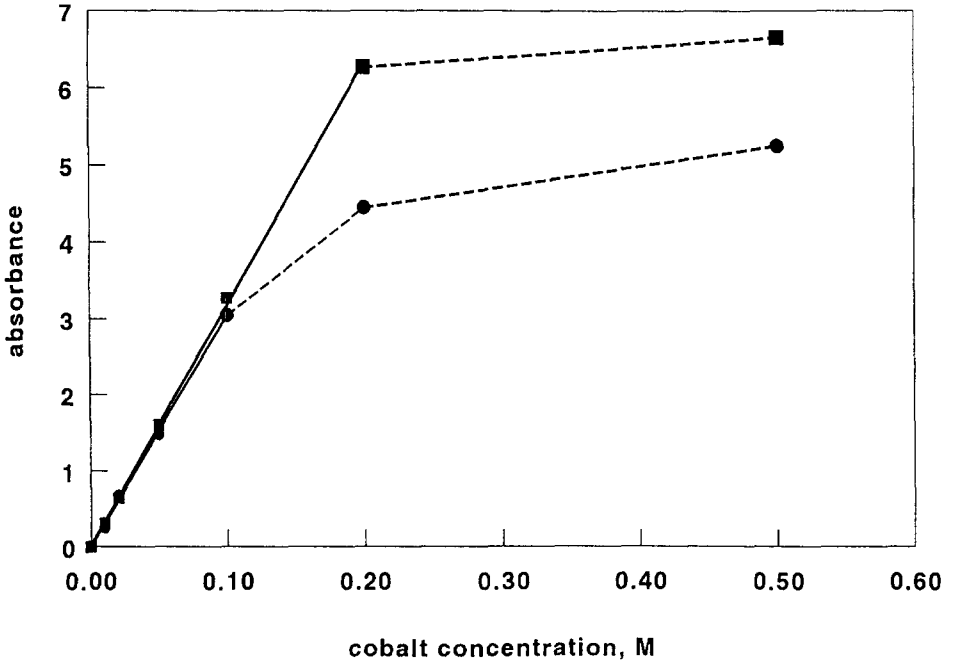


Fig. 4. The absorbance at 525 nm of cobalt(II) solutions in 1 M TEA + 3 M $NaNO_3$, pH = 9.8, through which oxygen was bubbled for 1 min (●) or 1 h (■).

at pH ≈ 9.5 showed a shoulder ($\bar{\nu}/cm^{-1}$, $\varepsilon/M^{-1}\,cm^{-1}$) at 333 nm (30,030, 68), and peaks at 353 (28,330, 83), 460 (21,740, 23), 525 (19,050, 52) and 717 nm (13,950, 21). Ageing of the solutions for 48 h caused a slight (0.2 units) decrease in pH when 0.5 M TEA was the ligand, no change at 1.0 M, and a slight increase in pH (0.2 units) with 2.0 M ligand. The spectra, however, were quite similar.

At pH ≥ 10, however, a band ($\bar{\nu}/cm^{-1}$, $\varepsilon/M^{-1}\,cm^{-1}$) at 267 (37,450, 83) grows in, the 333 nm shoulder becomes a band at 323 (30,960, 165) which shifts with time (within the first 30 min) to 351 nm (28,490 cm^{-1})

and increases in intensity, to $\varepsilon = 250\ M^{-1}\ cm^{-1}$. The 525 and 717 nm bands do not increase in intensity appreciably with time. The 460 nm band, however, is not observed at pH > 10. Further ageing of the solutions, after bubbling of oxygen was discontinued, caused further increases in the intensity of the 320–350 nm bands. If nitrogen is bubbled through the solutions the peak heights decrease appreciably, although the spectrum does not revert to that of Co^{II} in TEA.

Preliminary studies showed that the optimal composition of the solutions for the electroreduction of the cobalt/oxygen was 0.8–1.2 mol dm^{-3} TEA at pH of 9.5–12. In such solutions the catalytic effect for the oxygen electroreduction was most pronounced.

The electroreduction polarization curve of molecular oxygen in the absence of cobalt ions was measured in aerated aqueous 1 mol dm^{-3} TEA + 3 mol dm^{-3} $NaNO_3$ (Fig. 5, curve 2). The limiting current was 1.7 times lower than the corresponding current in aerated aqueous 0.1 mol dm^{-3} KCl (Fig. 5, curve 1), owing to the salting-out effect of the concentrated $NaNO_3$. In the absence of oxygen, in an inert atmosphere (N_2), the current was further decreased (Fig. 5, curve 3). In such freshly prepared, oxygen-free solutions the electroreduction current did not depend on the cobalt(II) concentration in the range 0.002–0.1 mol dm^{-3} (Fig. 5, curve 3). This means that the cobalt(II) triethanolamine complexes are not electroreduced in the given potential range.

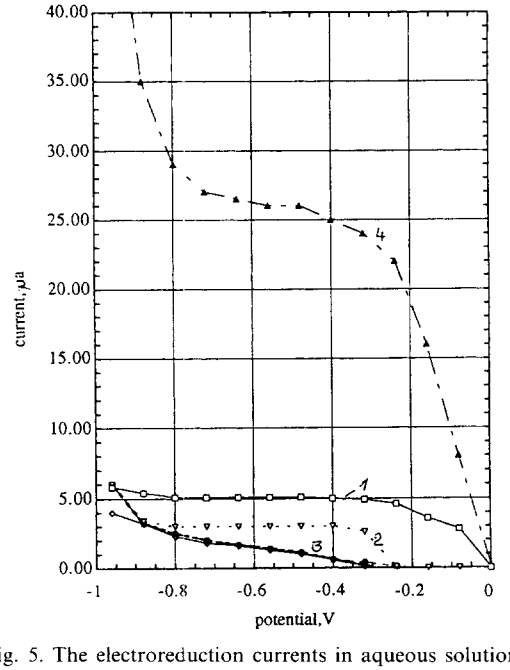


Fig. 5. The electroreduction currents in aqueous solutions containing: (1) 0.1 mol dm^{-3} KCl; (2) 1.0 mol dm^{-3} TEA + 3.0 mol dm^{-3} $NaNO_3$; (3) de-aerated (by N_2) 1.0 mol dm^{-3} TEA + 3.0 mol dm^{-3} $NaNO_3$ without and with 0.002 to 0.1 mol dm^{-3} $Co(NO_3)_2$; (4) as for curve (2) with 0.05 mol dm^{-3} $Co(NO_3)_2$ after bubbling air for 1 h at pH = 11.

When air was bubbled through the solutions to saturation the cobalt(II)–TEA complexes coordinated the oxygen readily, as the spectral results described above show. The electroreduction current increased many-fold (Fig. 5, curve 4, and Fig. 6) and depended on the bubbling time (Fig. 6). The formal redox potential shifted towards more positive values (*cf.* curves 2 and 4 in Fig. 5).

These observations coincide with the noted higher absorbance at 328 nm (Fig. 7) as well as at 267 nm (Fig. 3). The light absorption intensity of the 267 and 328 nm peaks depends not only on the concentration of the cobalt, but also on the rate and duration of the bubbling of air (Fig. 7). On the other hand, the 525 nm peak is a result of cobalt(II)–TEA complexes only.

The absorption of oxygen by the cobalt(II)–TEA complexes is slow (Fig. 6), the half-time being of the order of 0.5 h with equilibrium being substantially achieved in 3–4 h. Figures 6 and 8 show this for the limiting reduction current i_l at −0.40 V and the absorbance A at 333 nm, respectively. The equilibrium values of these quantities, i_{l_e} and A_e were obtained by extrapolation of the curves to *ca* 3 h. At longer times, ageing of the system takes place, leading to new species. During the first 3 h, however, the oxygen absorption reaction is completely reversible, and when nitrogen is bubbled after the saturation by air, oxygen evolution is observed.

DISCUSSION

Triethanolamine (TEA) is a unique ligand for Co^{II}, Co^{III} and $Co^{II,III}$–O_2 complexes in the sense that it has only one nitrogen donor atom but several oxygen donor atoms available for chelation in principle. In this respect it is similar to nitrilotriacetic acid (NTA), with the disadvantage that it is not charged at high pH values. The complex formed by TEA with Co^{II} is therefore fairly weak, although at the ligand concentrations employed in the present study practically all the cobalt is in the form of $CoTEA(H_2O)_x^{2+}$, in view of the reported stability constants [13–15]. That chelation may not take place in this complex can also be deduced from the similarity of K_1 for TEA and ammonia [13,25]. No data on the absorption spectrum of the corresponding $Co(NH_3)(H_2O)_x^{2+}$ species could be found. Only scant data are available for the spectrum of the mono-nitrilotriacetate chelate of cobalt(II) [26], which has one nitrogen and three oxygen donor atoms as has TEA, but the maximum of its absorption band appears to be at 510 nm ($\varepsilon \sim 21\ M^{-1}\ cm^{-1}$). This should be compared with the most intense component of the cobalt(II)–TEA complex, found here at 534 nm ($\varepsilon = 21.8\ M^{-1}\ cm^{-1}$, Fig. 1), which is more red shifted with respect to the hexaaquo complex that has perfect octahedral symmetry. The lower symmetry of the $CoTEA(H_2)_x^{2+}$ species causes removal of the degeneracy of the $^4T_1$ ground state level, and this explains the appearance of three bands, at 18,020,

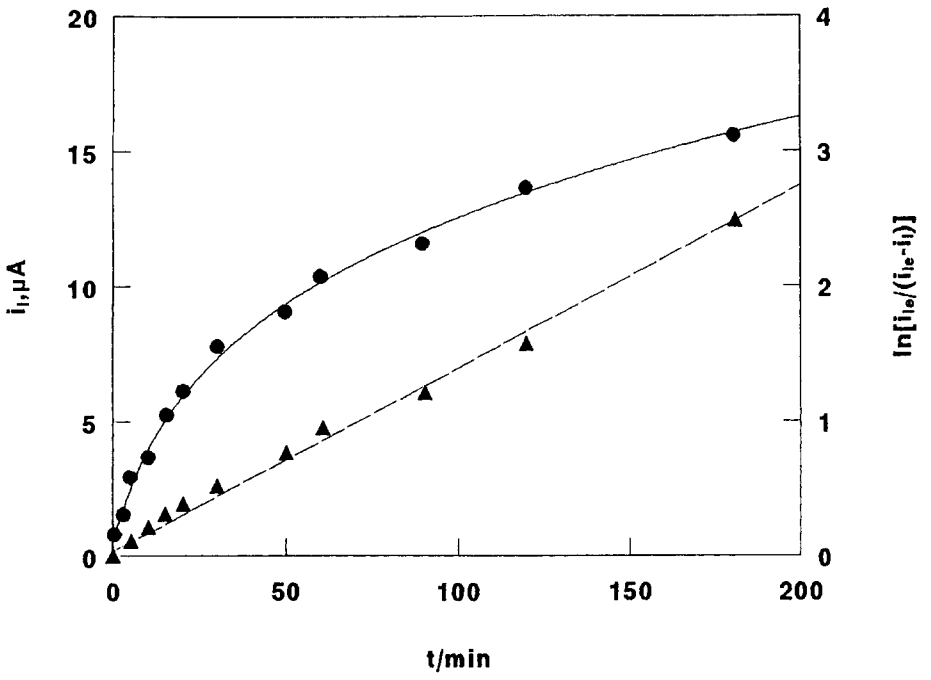


Fig. 6. The limiting currents i_r (●, left-hand ordinate) and the function $\ln [i_{re}/(i_{re} - i_r)]$ (▲, right-hand ordinate) in solutions containing 1.0 mol dm^{-3} TEA + 3.0 mol dm^{-3} $NaNO_3$ + 0.050 mol dm^{-3} $Co(NO_3)_2$ at pH = 9.6 as a function of time, t.

18,730 and 21,550 cm^{-1}, instead of the two, at 19,400 and 21,550 cm^{-1}, of $Co(H_2O)_6^{2+}$.

Cobalt(III) complexes with ligands having nitrogen and oxygen donor atoms are well known, but most have at least four nitrogen atoms in their octahedral coordination sphere (e.g. four ammonia or two ethylenediamine molecules, the other positions being occupied by water molecules). The apparent stability found here (Fig. 2) of a species with TEA ligands has not been observed previously. There being a 20-fold excess of TEA over Co^{III} in the solutions, and with the expected higher stability of the Co^{III} complexes with respect to the Co^{II} ones, it is conceivable that the species having the spectrum shown in Fig. 2 is $Co(TEA)_2(H_2O)_2^{3+}$ or $Co(TEA)_2^{3+}$, with each TEA ligand contributing one, respectively, two oxygen atoms towards chelation of the cobalt. Even so, the species have only two nitrogen atoms in the coordination shell. The appearance of just two bands, as is found in $Co(en)_6^{3+}$ (Fig. 2) or $Co(NH_3)_6^{3+}$, with maxima ($\bar{\nu}$/cm^{-1}, ε/M^{-1} cm^{-1}) at 339 (29,500, 55) and 475 nm (21,050, 60) [27], respectively, although with different molar absorptivities, indicates high symmetry for the species formed. The bands are assigned to the $^1A_{1g}$ to $^1T_{1g}$ and $^3T_{2g}$ transitions [20]. More bands are found for species with lower symmetry (e.g. $Co(NH_3)_5F^{2+}$ or $Co(NH_3)_4Cl_2^+$) [27], hence the presumed TEA species appears to be the more symmetric one of those assumed to be present. The spectrum of this species is quite different from the binuclear, dioxygen bridged Co^{III} complexes $L_5CoOOCoL_5$ or $L_4Co(O_2,OH)CoL_4$ formed with ligands having several nitrogen donor atoms, e.g. tren, in the presence of oxygen [28].

When oxygen is bubbled through alkaline cobalt salt solutions oxidation to cobalt(III) and/or formation of Co^{II}–ligand–dioxygen and/or Co^{III}–ligand–dioxygen complexes takes place, the latter being mononuclear and/or dinuclear [1,29]. Since so many species can be formed, and owing to the changes in the spectra with ageing, it is impossible to specify which ones are formed in the presence of TEA as the ligand. The spectra shown in Fig. 3, compared with that of the Co^{III}–TEA complex species in Fig. 2, do rule out the simple oxidation from Co^{II}–TEA to Co^{III}–TEA. The presence of oxygen in the species is thus established. The decrease of the absorbance when nitrogen is bubbled through the solutions shows, however, that some of the oxygen bound to the cobalt can be removed, but the remaining species is neither the Co^{II}–TEA nor the Co^{III}–TEA complex (Figs 1 and 2). Therefore, more than one dioxygen species must have been formed in the aged solutions.

The observed spectrophotometric (Figs 1–4) and electrochemical (Figs 6 and 7) data require a complicated mechanism for their explanation. Similar mechanisms have been invoked in the past for explaining kinetic and other results with ligands containing more than one nitrogen donor atom, such as tren and en [30,31]. However, the suggested mechanism must also explain the enhanced reactivity of the TEA-containing species (towards electroreduction and removal of some of the oxygen) compared with the relative inertness of species with ligands having more than

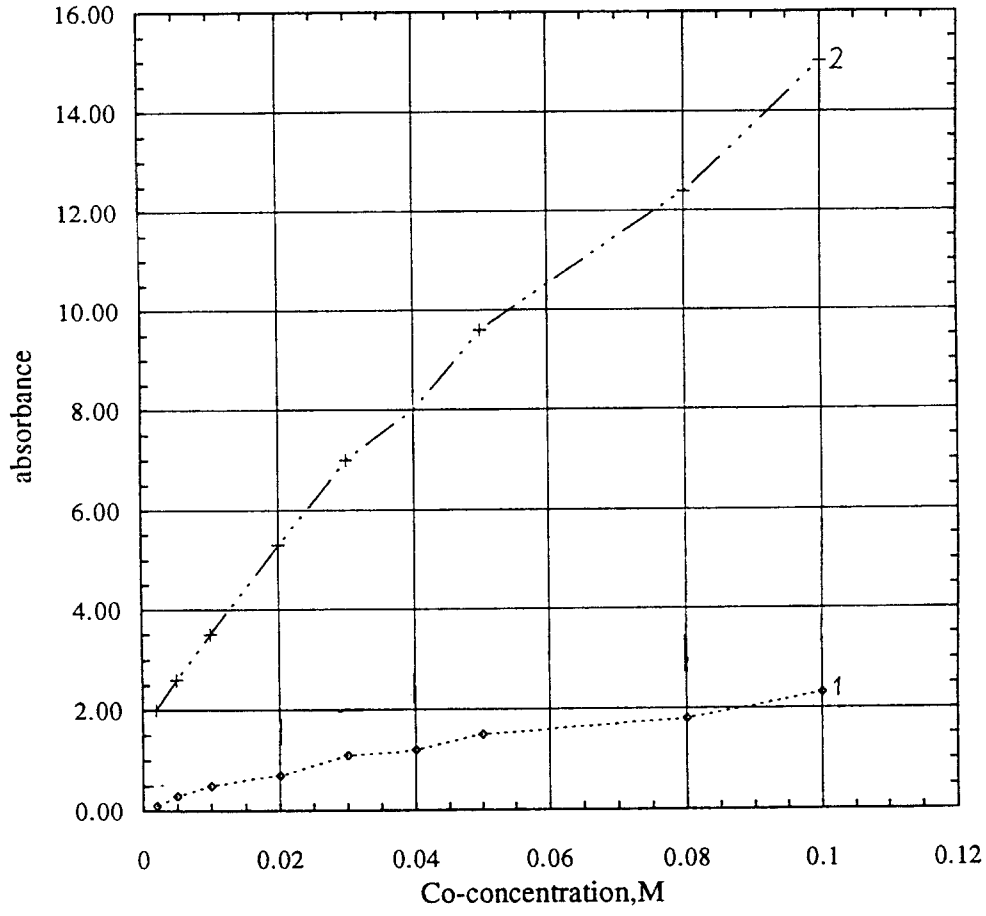


Fig. 7. Dependence of light absorbance at 328 nm on the cobalt concentration in 1.0 mol dm^{-3} TEA + 3.0 mol dm^{-3} $NaNO_3$ solutions: (1) exposed to a N_2 atmosphere for 3 h; (2) prepared similarly but after bubbling of air through the solution for 15 min.

one nitrogen donor atom. At the elevated pH values employed (9.5–12) deprotonation of the $CoTEA(H_2O)_x^{2+}$ complex ($x = 3$ or 4) is assumed to take place with simultaneous dimerization:

$$2CoTEA(H_2O)_x^{2+} + OH^- \rightleftarrows [(H_2O)_yTEACo\text{–}OH\text{–}CoTEA(H_2O)_y]^{3+} \quad (1)$$

The species on the right-hand side is designated $Co^{II,II}$ in short. On the basis of the stability constant of the Co^{II}–TEA complexes [13], the equilibrium of reaction (1) can be taken to lie considerably to the right, so that:

$$[Co(II,II)]_0 = c_{Co}^0/2 \quad (2)$$

where $[Co(II,II)]_0$ and c_{Co}^0 are the initial complexed and total (0.05 mol dm^{-3}) cobalt(II) concentrations, respectively.

The resulting species has such a distance between cobalt atoms that they can accommodate a coordinated oxygen molecule [1,2], in a reversible and slow reaction:

$$[(H_2O)_yTEACo\text{–}OH\text{–}CoTEA(H_2O)_y]^{3+} + O_2 \rightleftarrows [(H_2O)_yTEACo(\overset{OH}{\underset{O_2}{\diamond}})CoTEA(H_2O)_y]^{3+} \quad (3)$$

Subsequently and rapidly, an internal redox reaction takes place and an electron is transferred from one of the cobalt atoms to the oxygen molecule to produce Co^{III} and a superoxide ligand, rapidly reaching equilibrium:

$$[(H_2O)_yTEACo(II)(\overset{OH}{\underset{O_2}{\diamond}})Co(II)TEA(H_2O)_y]^{3+} \rightleftarrows [(H_2O)_yTEACo(II)(\overset{OH}{\underset{O_2^-}{\diamond}})Co(III)TEA(H_2O)_z]^{3+} + (y-z)H_2O \quad (4)$$

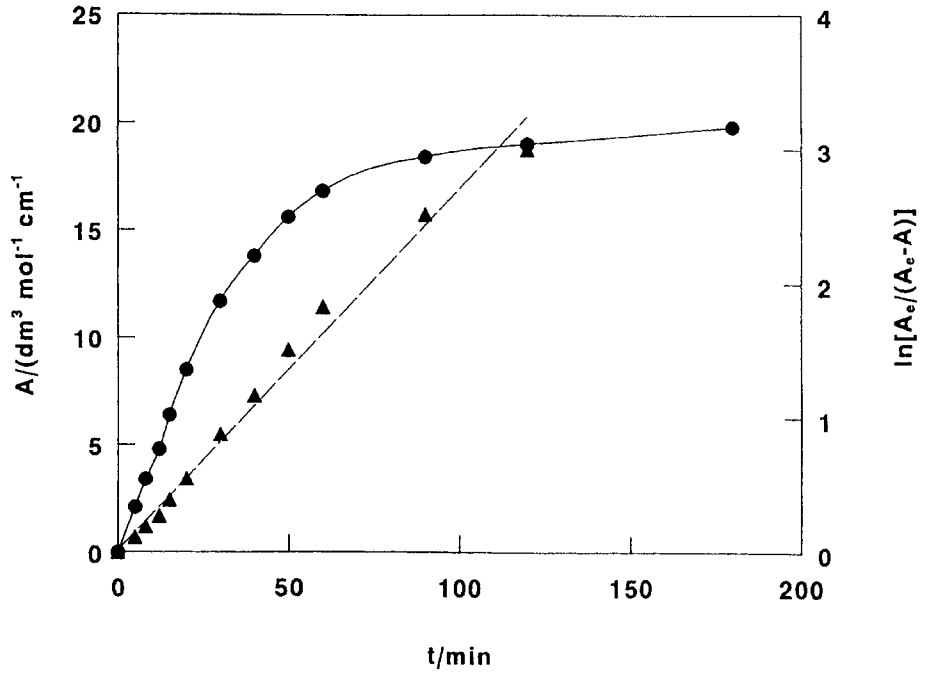


Fig. 8. The absorbance A at 330 nm (●, left-hand ordinate) and the function $\ln[A_e/(A_e-A)]$ (▲, right-hand ordinate) in solutions as in Fig. 6 as a function of time, t.

The species on the right-hand side is designated Co^{II,III,O_2^-} in short. Such a mechanism is suggested following studies of ethanolamine- and ethylenediamine-ligated complexes of cobalt binding with molecular oxygen [32–34]. It is noteworthy that the observed molar absorptivities (all $\varepsilon \leqslant 1000$ M^{-1} cm^{-1}) are considerably lower than those obtained for species with two Co^{III} centres, e.g. [31] $trenCo^{III}$ (μ-O_2,μ-OH)Co^{III})tren (with $\varepsilon > 6000$ M^{-1} cm^{-1}) [31]. The observed slow ageing reaction can be described by the overall scheme, combining reactions (1), (3) and (4):

$$Co^{II/II} + O_2 \underset{k_{-1}}{\overset{k_{+1}}{\rightleftharpoons}} Co^{II,III,O_2^-} \qquad (5)$$

At a constant concentration of oxygen in the solution, produced by bubbling air to saturation at a given temperature, the kinetics of the reversible reaction (5) are described by the pseudo first-order expression:

$$d[Co(II,III,O_2^-)]/dt = k_{+1}[Co(II,II)] - k_{-1}[Co(II,III,O_2^-)] \qquad (6)$$

The fact that at the potentials of this voltammetric study the $Co^{II,II}$ complex is electrochemically inactive (Fig. 5) was taken into account. The much enhanced electroreduction current of oxygen in the presence of the cobalt–TEA complex is therefore caused by the reduction of the $Co(II,III,O_2^-)$ complex:

$$Co(II,III,O_2^-) + 4e^- + 2H_2O \rightarrow Co(II,II) + 4OH^- \qquad (7)$$

Since the rate constant k_{+1} is relatively low (see below), the regeneration of the $Co(II,III,O_2^-)$ species according to reaction (3) on the electrode surface during reduction can be practically ignored. Therefore, the limiting current i_ℓ is diffusion controlled and:

$$i_\ell = k[Co(II,III,O_2^-)] \qquad (8)$$

On the basis of Eqs (2), (6) and (8) and that $[Co(II,II,O_2)] \ll [Co(II,III,O_2^-)]$, the kinetic equation for reaction (5) is:

$$\ln[i_{\ell e}/(i_{\ell e} - i_\ell)] = k_{+1}(i) \cdot c_{Co^0} \cdot t/2 \cdot [Co(II,III,O_2^-)]_e \qquad (9)$$

(see Fig. 8), where the subscript "e" designates the equilibrium condition. The values of $[Co(II,III,O_2^-)]_e$ is obtained from:

$$[Co(II,III,O_2^-)]_e = (i_{\ell e}/i_\ell{}^0)c_{O_2} \qquad (10)$$

where $i_\ell{}^0$ is the limiting current at $t = 0$. The solubility of oxygen in water at 25°C and 0.101 Mpa pressure is 1.274×10^{-3} mol dm^{-3} [27], so that air saturation of water should produce a concentration of 20.9% of this value (2.67×10^{-4} mol dm^{-3}) in view of the partial pressure of oxygen in air. Salting out by the 3 mol dm^{-3} sodium nitrate should decrease this concentration by $10^{3.0 \times 0.124}$ to $c_{O_2} = 1.13 \times 10^{-4}$ mol dm^{-3}, 0.124 being the Setchenow coefficient [35]. At the temperature of our experiments this concentration should be 2–4% higher, but this difference is ignored here. Hence, with the limiting currents $i_{\ell e}$ and $i_\ell{}^0$ read from

Fig. 2 and Eq. (10), $[Co(II,III,O_2^-)]_e = 2.3 \times 10^{-3}$ mol dm^{-3}. A large amount of oxygen is, thus, "stored" in the $Co(II,III,O_2^-)$ complex and is amenable to electroreduction.

Similarly, the absorbance data at 333 nm shown in Fig. 6 follow the expression:

$$\ln[A_e/(A_e - A)] = k_{+1}(A)c_{Co^0} \cdot t/2 \cdot [Co(II,III,O_2^-)]_e \quad (11)$$

where A is the absorbance of the $Co(II,III,O_2^-)$ species. The linear dependencies of $\ln[A_e/(A_e - A)]$, according to Eq. (11) (Fig. 6), and of $\ln[i_{/e}/(i_{/e} - i_/)]$, according to Eq. (9) (Fig. 8), on t require the values of $k_{+1}(A)$ and $k_{+1}(i)$ to be the same if the reducible species and absorbing species are the same. Within the imprecision of the measurements this is the case, the values being 2.4×10^{-3} min^{-1} and 1.4×10^{-3} min^{-1}, respectively.

The equilibrium constant of reaction (3) is:

$$K = [Co(II,III,O_2^-)]_e/[Co(II,II)]_e c_{O_2}$$

$$= [Co(II,III,O_2^-)]_e/\{c_{Co^0}/2 - [Co(II,III,O_2^-)]_e\}c_{O_2}$$

$$= 8.6 \times 10^2 \text{ dm}^3 \text{ mol}^{-1} \quad (12)$$

The rate constant for the reverse of reaction (4) is then $k_{-1} = k_{+1}/K \cdot c_{O_2} \approx 1.9 \times 10^{-3}/8.6 \times 10^2 \cdot 1.13 \times 10^{-4} = 1.9 \times 10^{-2}$ min^{-1} if the average of the voltammetrically and spectrophotometrically obtained forward rate constants is used.

The mechanism considered above is seen to be able to describe the kinetics and catalytic electroreduction current of oxygen in the cobalt(II)–TEA–O_2 system.

EXPERIMENTAL

The inorganic reagents used were of analytical grade: cobalt(II) chloride, nitrate and sulfate, sodium hydroxide and nitrate, and potassium chloride; and pure triethanolamine (Fluka, 99%) and triply distilled and deionized water were employed.

The spectra were measured on a Perkin–Elmer Lambda 5 spectrophotometer at ambient temperatures (23 ± 2°C). Owing to high absorptivities of some of the solutions, 1, 2, 5 and 10 mm light-path-length cells were used according to need. The wavelength range 240–800 nm was scanned. When nitrate solutions were used, the reference cell contained exactly the same concentration of nitrate in order to avoid complications from its charge transfer band.

Solutions containing cobalt(II) and TEA in the absence of oxygen were prepared in a glove-bag under nitrogen and the optical cells were stoppered tightly to avoid air oxidation. Solutions of cobalt(III) in the presence of TEA were made by anodic oxidation at a platinum electrode in the optical cell with a salt bridge to the cathode compartment, again in a glove-bag under nitrogen. This was done in order to avoid oxidizing reagents (such as air or hydrogen peroxide) that might leave oxygen in the solutions to form a complex with the cobalt.

Oxygenated solutions were prepared by bubbling air through them to saturation. In some cases, subsequent bubbling of nitrogen was used in order to (partly) decompose the dioxygen-containing complexes.

The electroreduction of cobalt ions in aqueous triethanolamine (TEA) solutions in the absence and presence of oxygen was studied voltammetrically and the bulk processes taking place were controlled spectrophotometrically. The pH of the solutions was controlled by a pH-meter with a glass electrode to ±0.01 units. The temperature was controlled at 23.0 ± 0.5°C by water flowing in the jacket of the cell from a Haake E-12 thermostat. Voltammetric measurements were made with a Polarecord E-261 instrument equipped with a stationary Pt disk electrode in an unstirred solution, except for comparative voltammograms (Fig. 5), when the solution was stirred with a magnetic stirrer. The reference electrode was Ag/AgCl/1 M KCl. The applied potential was varied at a rate of 5 mV s^{-1} and its interval was +0.2 to −1.0 V. The reproducibility of the electrode surface was checked by measurement of the current–voltage response for electroreduction of oxygen in 0.1 mol dm^{-3} KCl. As supporting electrolyte 3 mol dm^{-3} $NaNO_3$ was generally used.

Acknowledgements—The support of this work by the Ministries of Science and Technology and of Absorption of Immigrants is gratefully acknowledged. The latter Ministry is also thanked for the support of one of us (S.T.) throughout this work.

REFERENCES

1. Bratushko, Yu. I. and Yatsimirskii, K. B., *Progress in Coordination Compounds*, Naukova Dumka, Kiev, 1975, Part 1, pp. 16–18. [In Russian.]
2. Savitski, A. V. and Nelubin, V. I., *Adv. Chem.* 1975, XLIV, **2,** 214.
3. McLendon, G. L. and Martell, A. E., *Coord. Chem. Rev.* 1976, **19,** 1.
4. Jones, R. D., Summerville, D. A. and Basolo, F., *Chem. Rev.* 1978, **79,** 139.
5. Fallab, S., *Adv. Inorg. Bioinorg. Mech.* 1984, **3,** 311.
6. Agarwala, B. V. and Bjerrum, J., *Acta Chem. Scand.* 1982, **A36,** 459.
7. Khue Do Ngok, Tur'yan, Ya. J. and Pokhodzei, V. F., *USSR Certif. of Invention*, 1987, 1 484 091.
8. Tur'yan, Ya. J., Pokhodzei, V. F., Dravtseva, N. A. and Il'ina, L. P., *USSR Certif. of Invention*, 1988, 1 682 319.
9. Petit, G. and Petit, L. D., *IUPAC Stability Constants Database*, 1995, Release 2.
10. Reibel, J. M., *Khim. Perekisnykh Soedin., Akad. Nauk SSSR, Inst Obshch. i Neorg. Khim.* 1963, 68; *Chem. Abstr.* 1963, **61,** 2520f.

11. Schwarzenbach, G. and Gut, R., *Helv. Chim. Acta*, 1956, **34,** 1589.
12. Jellish, R. and Thompson, L., *J. Coord. Chem.* 1975, **4,** 199.
13. Hancock, R. D. and Nakani, B. S., *J. Coord. Chem.* 1984, **13,** 309.
14. Bjerrum, J. and Refn, S., *6 Nordiska Kemistmöte.* Lund, 1947, abstr. p. 227.
15. Sklenskaya, E. V. and Karapet'yants, M. Kh., *Zh. Neorg. Khim* 1966, **11,** 2749; *Russ. J. Inorg. Chem.* 1966, **11,** 1478.
16. Jørgensen, C. K., *Acta Chem. Scand.* 1954, **8,** 1495.
17. Jørgensen, C. K., *Absorption Spectra and Chemical Bonding in Complexes.* Pergamon, Oxford, 1962, pp. 285, 293.
18. Jørgensen, C. K., *Acta Chem. Scand.* 1954, **8,** 175.
19. Biedermann, G., Orecchio, S., Romano, V. and Zingales, R., *Acta Chem. Scand.* 1986, **A40,** 161.
20. Johnson, D. A. and Nelson, P. G., *J. Chem. Soc., Dalton Trans.* 1990, 1.
21. Johnson, D. A. and Sharpe, A. G., *J. Chem. Soc. (A)* 1966, 798.
22. Jørgensen, C. K., *Acta Chem. Scand.* 1954, **8,** 1502.
23. Jørgensen, C. K., *J. Inorg. Nucl. Chem.* 1958, **8,** 143, quoting data supplied by C. E. Schäffer.
24. Kim, H. A., *J. Korean Chem. Soc.* 1963, **7,** 34; *Chem. Abstr.* 1963, **59,** 14901f.
25. Luca, C., Magearu, V. and Popa, G., *J. Electroanal. Chem.* 1966, **12,** 45.
26. Kornev, V. I., Valyaeva, V. A. and Mukanov, I. P., *Zhur. Fiz. Khim.* 1978, **52,** 1132.
27. Linhard, M., *Z. Elektrochem.* 1944, **50,** 224; M. Linhard and H. Weigel, *Z. Anorg. Allg. Chem.* 1952, **271,** 101.
28. Fallab, S. and Zehnder, M., *Helv. Chim. Acta*, 1984, **67,** 392.
29. Buckingham, D. A. and Clark, C. R. in *Comprehensive Coordination Chemistry*, Vol. 4, ed. G. Wilkinson, Pergamon Press, Oxford, 1976, pp. 782–783.
30. Brüstrlein-Banks, P. and Fallab, S., *Helv. Chim. Acta* 1977, **60,** 1601.
31. Maecke, H., *Helv. Chim. Acta* 1981, **64,** 1579.
32. Konrad, D. and Vlček, A. A., *Coll. Czech. Chem. Commun.* 1963, **28,** 808.
33. Bartlet, H. and Skilandat, H., *J. Electroanal. Chem.* 1969, **23,** 407.
34. Palade, D. M., PhD. thesis, Donetsk, USSR, 1984.
35. Groisman, A. Sh. and Khomutov, N. E., *Uspekh. Khim.* 1990, **59,** 1217.

Pergamon

PII: S0277-5387(96)00391-9

Polyhedron Vol. 16, No. 7, pp. 1057–1068, 1997
Copyright © 1997 Elsevier Science Ltd
Printed in Great Britain. All rights reserved
0277-5387/97 $17.00+0.00

Homoscorpionates (hydridotris(1-pyrazolyl)borato complexes) of the trivalent 4*f* ions. The crystal and molecular structure of $[(HB(N_2C_3H_3)_3]_3Ln^{III}$, (Ln = Pr, Nd)†

C. Apostolidis,[a] J. Rebizant,[a] B. Kanellakopulos,[b]* R. von Ammon,[b] E. Dornberger,[b] J. Müller,[b] B. Powietzka[b] and B. Nuber[c]

[a]European Commission, Joint Research Centre, Institute for Transuranium Elements, Postfach 2340, D-76125 Karlsruhe, Germany

[b]Institut für Technische Chemie/CPV, Forschungszentrum Karlsruhe, Technik and Umwelt, Postfach 3640, D-76021 Karlsruhe, Germany

[c]Anorganisch-Chemisches Institut der Universität Heidelberg, Im Neuenheimer Feld 270, D-69120 Heidelberg, Germany

(Received 18 June 1996; accepted 8 August 1996)

Abstract—The compounds $[(\eta^3\text{-}HB(N_2C_3H_3)_3]_3M$ of scandium, yttrium, lanthanum and of the trivalent lanthanides from cerium to lutetium (with the exception of promethium) have been synthesized by the reaction of MCl_3 with $K[HB(N_2C_3H_3)_3]$ in tetrahydrofuran or in water. The crystal and molecular structures of the Pr and Nd compounds were determined by single-crystal X-ray diffraction. The crystal structure corresponds to the structure of the praseodymium trichloride ($LaCl_3$-type). The Pr^{3+} is nine-coordinate to the N atoms of the three Tp ligands. One N atom of each of the three Tp ligands and the Pr ion are almost coplanar with a Pr—N distance of 278.3 pm, while all other six N atoms are at a distance of 260.9 pm in a tricapped trigonal prismatic arrangement. The M—N distances in the Nd compound are 280.4 (3 ×) and 259.9 (6 ×) pm. IR spectroscopic studies have shown that the metal ion in the $LnTp_3$ compounds from La to Dy is nine-coordinate, while in the compounds of the heavier lanthanides from Ho to Lu, of Sc, and Y, the central ion is eight-coordinate.
Copyright © 1997 Elsevier Science Ltd

Keywords: lanthanide-trispyrazolyl borates; IR; NMR spectroscopy; magnetic susceptibility; structures.

Lanthanide trichlorides react with the [HB(pyrazol-1-yl)$_3$] ligand (=Tp^-)‡ to complexes of the type Tp_2LnCl, Tp_2LnL, Tp_3Ln^{III} and to several heteroleptic eight-coordinate complexes with oxybidentate ligands, such as oxalate, benzoate, tropolonate, β-diketonate, dipivalomethanido, trifluoroacetyl, etc. [1–6]. The crystal and molecular structure of several mixed lanthanide-complexes containing the Tp ligand have been investigated. Most of the compounds have a distorted square-antiprismatic geometry [3]. The structures of $Tp_2Y(H_2O)Cl$ [2] or $Tp_2Nd(H_2O)Cl$ [3], for example, show an eight-coordinate molecule with a *cis*-position of the water and chloride ligands. The divalent Sm in $(Tp^{t\text{-}But,Me})SmI(THF)$ is five-coordinate in a distorted trigonal-bipyramidal geometry with a N atom and the O atom of the tetrahydrofuran molecule occupying the axial sites [7]. The corresponding Yb

* Author to whom correspondence should be addressed.
† Dedicated to Professor Kenneth Winfield Bagnall.

compound also has been described [9]. Recently, six-coordinate complexes of the divalent lanthanides Sm, Eu and Yb with Tp^{Me_2} as the ligand were synthesized and investigated [10].

From the $LnTp_3$ series, nevertheless, prepared in aqueous solutions [11], only the crystal and molecular structure of the ytterbium compound has been determined by single-crystal X-ray diffraction so far [12]. In this compound the Yb is not, as expected nine-, but eight-coordinate, one of the three Tp ligands being bidentate, with a bicapped-trigonal prismatic coordination geometry [12].

After we had synthesized and investigated compounds of the type $Tp^{Me_2}MCl_2$ (M = Pr, Nd, Yb and Pu), which are dimeric [13], and compounds of the type Tp_2LnCl [14], we were interested in the synthesis of the Tp_3Ln class of the lighter lanthanides and/or of the lighter actinides in order to obtain single crystals and to investigate the coordination of the central 4*f*-ion for comparing and discussing their molecular structure with the known structure of the ytterbium compound [12]. In this contribution we present the synthesis and coordination of pure $[HB(N_2C_3H_3)_3]_3M$ compounds of Sc^{3+}, Y^{3+}, La^{3+} and some trivalent lanthanide ions.

EXPERIMENTAL

Materials

All chemicals were reagent grade. The chlorides used were prepared by dissolving the sesquioxides in hydrochloric acid. Anhydrous chlorides were obtained by chlorination of the sesquioxides with a Cl_2/CCl_4/argon stream at temperatures up to the melting point of the corresponding chloride.

Physical and analytical methods

IR spectra were obtained on a Perkin–Elmer 2000-FT-IR spectrometer. Solid-state UV–NIR spectra of the compounds embedded in potassium bromide or teflon [15] as matrix were taken on a Perkin–Elmer Lambda 9 spectrometer. Metal analysis was made by gravimetric measurement of the sesquioxide after oxidation of the compound and/or by AAS.

Magnetic susceptibilities of polycrystalline samples were measured with a Faraday-type magnetic balance with magnets with Henry-type pole caps (Bruker-Analytische Messtechnik) and an electrical microbalance (Sartorius type 4102) at eight different external magnetic fields from 190 to 15,000 kOe [16]. Mass spectra were obtained with a Finnigan MAT 4500 equipment.

^1H and ^{13}C NMR spectra in solution (mostly CD_2Cl_2, 99% D, Merck) were recorded on Bruker AC 250 or 200 spectrometers. TMS was used as internal standard. Paramagnetic shifts Δ^{iso} of the pyrazolyl ring protons were referred to an average of the respective signals of the diamagnetic Lu complex (3-H : 7.2 ppm ; 4-H : 6.0 ppm ; 5-H : 6.5 ppm).

Synthesis of the MTp_3 *compounds*

The general preparation method used for the synthesis of the $LnTp_3$ compounds was the reaction of the anhydrous metal trichlorides with a stoichiometric molar amount of KTp in tetrahydrofuran or the reaction of the trichlorides with a slight molar excess of KTp in water as first reported by Bagnall *et al.* [11]. In the first method a mixture of the anhydrous $LnCl_3$ in THF with a slight excess of KTp was heated under reflux for 2 days. After elimination of the solvent *in vacuo*, the solid residue was extracted with THF, benzene or toluene for several days. The extracted dried $LnTp_3$ was heated *in vacuo* to remove the solvent. When THF was used as extractant, the compound contained traces of KCl. Sublimation of the polycrystalline compound at 300–330°C (10 Torr Ar) gave a microcrystalline, chloride-free compound.

In the second method MCl_3- or $M(NO_3)_3$-hydrate was used as starting material. The metal salt was dissolved in distilled water, the solution filtered for elimination of oxychlorides or hydrolysed salt and an excess of KTp added with stirring. After centrifugation, KTp was added to the clear decantate and the procedure repeated in the case that new MTp_3 is formed. Due to the low solubility of the $LnTp_3$ compounds and the good solubility of KTp and KCl in water, the crude products can be purified easily by washing them with distilled water with stirring, followed by centrifugation and drying in a desiccator with P_2O_5. Reaction conditions, yields and metal analysis for all compounds are listed in Table 1.

Separation of lanthanides by solvent extraction

A 1 : 1 molar mixture of $LaCl_3$ and $YbCl_3$ in distilled water was treated with KTp and the mixed compound $(La_{0.5}Yb_{0.5})Tp_3$ was isolated, purified and characterized by metal analysis and IR spectroscopy. Samples of 2–3 mg of the compound were extracted with 5 cm^3 of different solvents (rigorous shaking at room temperature for 10 hours). After centrifugation and filtration (250 nm filter) the La and Yb ions were determined in the filtrates. The concentrations (g dm^{-3}) of $YbTp_3$ and boron in the used solvents were : toluene : 0.389 (B : 0.016) ; CH_2Cl_2 : 0.563 (B : 0.020) ; THF : 0.586 (B : 0.021), while the concentration of La in all solvents was found to be lower than 1 ppm (5 mg $LaTp_3$ per dm^3). In all solvents $YbTp_3$ has been quantitatively extracted with a separation factor of 50–100.

‡ The abbreviation Tp used in this paper is that proposed by Dr S. Trofimenko, see Reference [1]. The authors appreciate the helpful suggestions of Dr Trofimenko.

Table 1. On the preparation of MTp_3 compounds

M^{3+}	Preparation method	%Yield	Colour	%Metal Calc.	%Metal Found	B—H vibration[a] (cm^{-1})			$(I_{rel})^b$
La	c,d	88–92	White	17.8	17.8	2443	2405	2374	(2.0 : 1.5 : 1.0)
Ce	c,d,e	75–91	White	18.0	17.9	2442	2405	2375	(4.0 : 2.3 : 1.0)
Pr	c,d,e	45–99	Pale green	18.1	18.0	2442	2405	2375	(4.1 : 1.6 1.0):
Nd	c,d,e	42–98	Pale mauve	18.4	18.3	2442	2405	2375	(6.0 : 2.0 : 1.0)
Sm	d	89	Pale yellow	19.0	19.0	2443	2406	2375	(5.6 : 2.0 :1.0)
Eu	d	71	White	19.2	19.0	2443	2406	2375	(4.7 : 1.7 : 1.0)
Gd	c,d	68–72	White	19.7	19.7	2444	2408	2376	(4.3 : 1.7 : 1.0)
Tb	d	97	White	19.9	19.8	2444	2408	2376	(3.0 : 1.5 : 1.0)
Dy	d	86	White	20.3	20.3	2444	2408	2377	(3.3 : 1.5 : 1.0)
Ho	d	96	Pale pink	20.5	20.5	2459	2414	2378	(3.2 : 1.5 : 1.0)
Er	d	94	Pale rose	20.7	20.7	2458	2415	2378	(3.0 : 1.6 : 1.0)
Tm	c,d,e	71–96	White	20.9	20.9	2458	2415	2378	(2.2 : 1.1 : 1.0)
Yb	c,d	78–99	White	21.3	21.3	2459	2416	2379	(2.2 : 1.3 : 1.0)
Lu	d	94	White	21.5	21.4	2459	2416	2379	(5.0 : 2.0 : 1.0)
Sc	c	89	White	—	—	2458	2415	2379	(3.0 : 1.5 : 1.0)
Y	c,d	75–90	White	—	—	2459	2415	2379	(3.0 : 1.5 : 1.0)

[a]H—B vibration in KTp : 2437, 2402, 2372 cm^{-1} (2.0 : 1.50 : 1.0).
[b]By integration of the peak area.
[c]Reaction of MCl_3 with KTp in tetrahydrofuran.
[d]Reaction of MCl_3 with KTp in water.
[e]Sublimation.

Collection and analysis of X-ray data

Single crystals of the Pr compound were obtained by sublimation of polycrystalline Tp_2PrCl [14] or $PrTp_3$ in a glass tube sealed under low pressure of *ca* 10 Torr argon, at 300–310°C. The single crystals of the pale-green coloured compound were formed in the colder zone of the oven (*ca* 220°C) in a yield higher than 45%. Single crystals of the neodymium compound were obtained by prolonged extraction (several weeks) of the polycrystalline $NdTp_3$ with benzene. Attempts to grow single crystals of other compounds using different experimental methods failed [17].

The single crystals were mounted in quartz capillaries and transferred to an Siemens-Stoe AED II- and/or to a Enraf–Nonius CAD4 four-circle X-ray diffractometer. The unit-cell parameters were determined from 20–25 reflections in the region $4.5 < 2\theta < 22.0°$. The models were refined by using the SHELXTL PLUS program package [18] or with the Enraf–Nonius SDP program with a Microvax II computer [18]. Hydrogen atoms were included as fixed contributions in idealized positions. Structures were solved by standard Patterson, Fourier or direct-methods procedures. Atomic scattering factors were taken from the International tables for X-ray Crystallography [19]. A summary of the structure data, data collection and refinement are given in Table 2.

RESULTS AND DISCUSSION

Reaction of MCl_3 (M = Sc, Y, La, Lanthanide) with $K[HB(N_2C_3H_3)_3]$ (=KTp) in solution resulted in the spontaneous formation of MTp_3 compounds, which were insoluble in water. Through the tridentate ligand Tp the coordination sphere of the central ion is saturated and all of the synthesized compounds are stable in air when they are in crystalline form.

The colour of the compounds corresponds to that of the trichlorides, but it is somewhat brighter, due to the lower concentration of the trivalent ion compared with the corresponding concentration in the chloride. The compounds of the heavier lanthanides (Tb–Lu) are moderately soluble in toluene and more soluble in polar solvents, especially in those with electron-donor character, while the compounds of the lighter lanthanides (La to Gd) are practically insoluble. Thus, the heavier lanthanides can be easily separated from the lighter lanthanides in mixed $LnTp_3$ compounds by solvent extraction.

Although in the compounds of the second class the Ln^{3+} ion is eight-coordinate, the Ho–Lu compounds do not interact with Lewis bases, as nitriles, isonitriles, etc., to give isolable adducts.

All compounds can be sublimed *in vacuo* at temperatures above 180°C. Mass spectrometric investigations of the Pr compound show the molecular

Table 2. Summary of crystallographic data and data collection of the MTp_3 compounds

Parameter/compound	Pr	Nd
Formula	$C_{27}H_{30}B_3N_{18}Pr$, $M_r = 780.00$	$C_{27}H_{30}B_3N_{18}Nd$, $M_r = 783.33$
Space group	C_{6h}^2, $P6_3/m$ (no. 176)	C_{6h}^2, $P6_3/m$ (no. 176)
Temperature (°C)	20	20
Cell dimensions from	26 refl.; $2.25 < \theta < 11.0°$	20 refl.; $8.44 < \theta < 14.81°$
a (pm)	1184.4(6)	1174.5(5)
c (pm)	1374.2(7)	1383.4(9)
V (10^6 pm^3)	1669.5	1652(2)
d_{calcd} (Mg m^{-3})	1.55	1.574
Z	2	2
Crystal size (mm)	$0.10 \times 0.10 \times 0.35$	$0.15 \times 0.25 \times 0.60$
Habit	Pale green, needle	Transparent, pale mauve, needle
μ (mm^{-1})	1.50	1.62
Radiation	graphite-monochromated Mo-K_α ($\lambda = 71.073$ pm)	
Scan type	ω	θ–2θ
Decay corrections (min/max)		0.978/1.028
Absorption correction	Empirical, 6 reflections, $7.0 < \theta < 39.0°$	Psi-scans, 9 reflections, $5.62 < \theta < 8.87°$
Transmission factor (min/max)	0.95/1.00	0.73/1.00
θ region	$3.0 < 2\theta < 56.0°$	$4.0 < 2\theta < 46°$
Quadrant	$h = 0/16$; $k = -16/0$; $l = 0/19$	$h = -12/12$; $k = 12/12$; $l = 0/15$
Collected data	2988	4778
No. of unique data	2009 ($R_{int} = 0.041$)	803 ($R_{int} = 0.038$)
No. of observed data	972 with $I > 2.5\,\sigma(I)$	672 with $I > 3\,\sigma(I)$
Refinements		
Non-H atoms	All anisotropic	
H atoms	Calculated with C—H = 95 pm (B = 5.0)	
R_{merge}	0.041	0.061
Resolution electron density (max/min) (e Å^{-3})	0.86/−0.73	1.43/−1.451
R	0.048	0.061
Rw	0.038	0.079
$F(000)$	784	786
GoF	1.70	2.34
Extinction factor		4.80×10^{-7}
Shift/esd-max	0.002	0.00
Diffractometer	AED II (1)/Syntex R3 (2)	Enraf–Nonius CAD4

peak ($m/z = 780.00$, $I_{rel} = 1\%$). The strongest peak ($I_{rel} = 100\%$) corresponds to the species $PrTp_2^+$ (m/z = calc. 0.566.97, exp.: 568.5; I_{rel}: 26.0, 567.2, $I_{rel} = 100$; 566.3, $I_{rel} = 59.7$). Further main fragments were $Pr[HB(N_2C_3H_3)_3][N_2HC_3H_3]$ ($m/z = 421.0$, $I_{rel} = 63.7\%$), $Pr[HB(N_2C_3H_3)_3]_2[HB(N_2HC_3H_3)_2]$ ($m/z = 712.8$, $I_{rel} = 6.60\%$), $Pr(N_2C_3H_3)_2$ ($m/z = 275.04$, $I_{rel} = 15.0\%$). The double ionized molecular peak ($m/z = 390.0$) occurs with $I_{rel} = 5\%$. The fragmentation pattern of the mass spectrum demonstrates the tendency of the compound to moieties with a seven-coordinate central ion. This is reflected by the highest intensity of $PrTp_2^+$, which was recently established experimentally through the crystallographic characterization of several seven-coordinate triflate complexes of the type $LnTp_2^{Me_2}(OTf)$ [8].

IR spectroscopic investigations

The IR spectra of the $LnTp_3$ compounds show two different structures. In the compounds of the lanthanides from La to Dy the central ion is nine-coordinate. All compounds of this class are isostructural and have the structure of $PrTp_3$ ($LaCl_3$-type), which is discussed later in this paper. The compounds of the heavier lanthanides from Ho to Lu and of Sc and Y, with small ionic radii, show a different structure. In this class of compounds, the central ion is eight-coordinate, as in the case of $YbTp_3$ [12]. For the dysprosium complex, there is evidence that both structural types coexist in the sublimed crystalline material. While the bulky microcrystalline compound obtained by sublimation *in vacuo* is nine-coordinate (crystal habitus prismatic), small crystals of plateform, which crystallize orthorhombic (eight-coordinate), can be observed under the microscope. Although the size of the hexagonal crystals was not suitable for a full crystallographic analysis, the elementary cell and its dimensions have shown that the compound exhibits a hexagonal structure. The crystal structure of the eight-coordinate orthorhombic

compound was indubitably elucidated [17]. The eight Dy—N distances are: 259.0, 253.9, 253.3, 250.1, 248.6, 248.0, 246.3 and 240.4 pm. There is no doubt that $DyTp_3$ is dimorphic. Both structures have been identified by IR-spectroscopy in the far-IR region (Table 3).

The structural change which results from the contraction in ionic radius across the lanthanide series occurs in the region of $DyTp_3$ and $HoTp_3$. From the crystallographic investigations it can be assumed that the critical ionic size for the structural change is 89 to 91 pm.

The two classes of the MTp_3 compounds exhibit a B—H stretch vibration in two different regions. The nine-coordinate compounds of the first class show a B—H vibration at 2440–2447 cm^{-1}, while the B—H vibration of the members of the second class is shifted to higher energies and occurs at 2457–2458 cm^{-1} (Table 1). In both classes of compounds the B—H frequency is shifted to higher energies relatively to the corresponding main absorption band in KTp (2437 cm^{-1}). Through the bonding of the Tp anion to the metal ion, *via* the three nitrogen atoms of the pyrazole rings, the B atom becomes more electropositive, thus the B—H bond is stronger and the corresponding frequency of the B—H bond is shifted to higher energies.

There are two further regions in the IR spectra, where the two compound groups show a distinct difference in number and positions of the absorption bands: (a) in the region 800–650 cm^{-1} (Fig. 1). The nine-coordinate compounds exhibit six absorption bands at *ca* 780, 770, 750, 739, 724 and 672 cm^{-1}. The eight-coordinate compounds show only four absorption bands at 782, 759, 724 and 670 cm^{-1}. (b) The second difference between the two compound classes is in the far-IR region below 400 cm^{-1}, where the characteristic skeleton vibrations of the molecule appear (Fig. 2). The absorption bands in this region reflect the molecular symmetry of the compound and can give quick information on the coordination of the central ion, as it has been shown earlier in the case of organometallic complexes of the actinide and lanthanide ions [20].

The M—N stretching absorptions appear between 150 and 288 cm^{-1}. The complexes of the second group (Ho–Lu, Sc, and Y) exhibit new absorptions at 272 and 282 cm^{-1} and three absorption bands in the 202–245 cm^{-1} IR region, whose positions correspond to the absorptions of KTp (Table 3). Obviously the latter absorption bands are due to the eight-coordinate central ion and have their origin in the uncoordinated pyrazolyl ring of one Tp anion, as the compounds of the lighter lanthanides La–Dy do not exhibit absorption bands in the 200–250 cm^{-1} region. The three absorptions at 320, 334 and 337–335 cm^{-1} can be undoubtedly assigned as ligand modes, because they appear in all $M^{III}Tp_3$ compounds, in KTp, and in the thorium, uranium and neptunium complexes of the type Tp_2AnX_2, with X = Cl, Br [14]. Although no group-theoretical analysis of the low-frequency IR absorption bands of Tp metal complexes is available, our suggestions are supported by the results of Hutchinson, Hoffbauer and Takemoto, who have used

Table 3. Far-IR absorption bands of KTp and of the $M^{III}Tp_3$ compounds in the 100–400 cm^{-1} region (cm^{-1})

KTp	158	162		202/208	254	271	278	320		338
$M^{III}Tp_3$ (M =)										
La	156	176	184		259			319	330	337
Ce	155	176	185		260			319	331	339
Pr	155	178	187		260			320	334	340
Nd	155	178	189		260			320	334	340
Sm	155	178	191		259			320	331	338
Eu	154	178	192		262			323	332	339
Gd	152	178	193		265			323	333	339
Tb	152	178	194		264			324	333	339
Dy	151	178	194		264			322	332	339
Dy	153	168/176	195	206	248	270	279	323	331	343
Ho	152	167/174	194	202/208	247	271	281	323	334	343
Er	152	167/174	194	202/212	245	271	281	323	334	346
Tm	153	167/173	191	202/214	246	272	285	324	336	346
Yb	152	162/173	198	202/214	248	272	285	325	336	346
Lu	151	167/173	184	202/215	248	272	288	324	335	351
Sc	151	166/173	188	202/217	245	273	282	324	334	345
Y	152	164/174	188	202/215	245	274	282	324	334	346

Table 4. Selected bond lengths (Å)

Ln	Pr	Nd
Ln(1)—N(1)	2.783(6)	2.804(7)
Ln(1)—N(3)	2.609(6)	2.599(7)
N(2)—B(1)	1.522(16)	1.51(2)
N(1)—N(2)	1.367(10)	1.33(1)
N(1)—C(3)	1.320(14)	1.34(2)
N(2)—C(1)	1.307(10)	1.36(1)
N(3)—N(4)	1.380(9)	1.357(8)
N(4)—C(4)	1.353(8)	1.38(1)
N(3)—C(6)	1.353(8)	1.34(1)
N(4)—B(1)	1.558(7)	1.554(9)
C(1)—C(2)	1.326(18)	1.34(3)
C(2)—C(3)	1.369(11)	1.39(2)
C(4)—C(5)	1.367(10)	1.37(1)
C(5)—C(6)	1.398(11)	1.40(1)

the metal-isotope substitution method on Tp complexes of the light transition metals Fe, Co, Ni, Cu and Zn for the assignment of the low-frequency IR absorptions [21].

The crystal and molecular structure of MTp_3

The crystal structure of MTp_3 of the lighter lanthanides consists of discrete molecules in which the metal ion is nine-coordinate and displays tricapped trigonal prismatic geometry. The crystal lattice of the $PrTp_3$-type compounds has the same hexagonal structure ($LaCl_3$-type) as in the case of the trichlorides of the lighter lanthanides [22]. An ORTEP view with atom labeling and the coordination polyhedron of the hexagonal $LnTp_3$ compounds is shown in Fig. 3 and selected bond lengths are given in Table 4. Table 5 summarizes selected bond angles of the compounds.

The coordination polyhedron (Fig. 3) formed by the nine nitrogen atoms of the three Tp ligands about the lanthanide ion is an almost ideal tricapped trigonal prism. The six metal–apical N(3) bonds are exactly the same by symmetry (260.9 pm in the praseodymium and 259.9 pm in the neodymium compound), while the three equatorial N(1) atoms lie in the same plane with the central ion in a Ln–N(1) distance of 278.3 pm in the Pr and of 280.4 pm in the Nd compound. A D_{3h} site symmetry for the central can be stated.

Electronic absorption spectra

The almost identical magnetic behaviour of the two isostructural compounds $PrCl_3$ and $PrTp_3$ within the investigated temperature region between 1 and 330 K (see below) is certainly an experimental evidence for a comparable crystal field strength in the two compounds. In fact, the electronic absorption spectra of the two compounds are quite similar. Figure 4 shows the absorption spectra of the two isostructural compounds in the region 400–650 nm.

As can be seen from Fig. 4, the centres of gravity of the absorption bands for the ^3P, ^1J and ^1D terms of the two compounds have quite similar energies: $^3P_{1,2}$: 22,237 ($PrTp_3$) and 22,222 cm^{-1} ($PrCl_3$); $^1J_6$: 21,124 ($PrTp_3$) and 21,061 cm^{-1} ($PrCl_3$); $^3P_0$: 20,492 ($PrTp_3$) and 20,424 cm^{-1} ($PrCl_3$); $^1D_2$: 16,794 ($PrTp_3$) and 16,756 cm^{-1} ($PrCl_3$). The better resolution in the spectrum of $PrTp_3$ in Fig. 5 is due to the fact, that the sample in this case was prepared from powdered single

Table 5. Bond angles (°)

Ln	Pr	Nd		Pr	Nd
N(1)—Ln(1)—N(1A)	120.0(1)	120.0(3)	N(1)—N(2)—C(1)	110.4(9)	107(2)
N(1)—Ln(1)—N(1B)	120.0(1)	120.0(3)	N(2)—N(1)—C(3)	103.6(6)	108.9(8)
N(1)—Ln(1)—N(3)	66.8(1)	66.5(3)	N(3)—N(4)—C(4)	110.0(5)	110.0(5)
N(1)—Ln(1)—N(3C)	67.7(1)	68.1(2)	N(4)—N(3)—C(6)	105.4(5)	108.5(4)
N(3)—Ln(1)—N(3D)	134.4(1)	134.6(2)	N(1)—N(2)—B(1)	120.9(6)	122.6(8)
N(3A)—Ln(1)—N(3D)	78.5(2)	79.0(2)	N(3)—N(4)—B(1)	122.8(4)	125.0(9)
N(3B)—Ln(1)—N(3D)	134.4(1)	134.6(1)	N(2)—B(1)—N(4)	109.0(6)	107.4(9)
N(3C)—Ln(1)—N(3D)	84.3(2)	83.8(3)	N(4A)—B(1)—N(4B)	111.9(6)	112.0(8)
N(1)—Ln(1)—N(3E)	140.8(1)	140.5(2)			
N(3D)—Ln(1)—N(3E)	84.2(2)	83.8(3)	C(1)—N(2)—B(1)	128.7(8)	131.0(2)
			C(4)—N(4)—B(1)	127.0(6)	126.5(8)
Ln(1)—N(1)—N(2)	123.0(6)	122.1(5)			
Ln(1)—N(3)—N(4)	123.6(3)	122.7(4)	N(2)—C(1)—C(2)	109.5(8)	112(2)
Ln(1)—N(3)—C(6)	129.5(5)	129.5(4)	C(1)—C(2)—C(3)	104.7(9)	104(1)
			N(1)—C(3)—C(2)	111.8(1)	109(1)
			N(3)—C(6)—C(5)	110.7(6)	111.3(8)
			C(4)—C(5)—C(6)	105.4(6)	104(1)
			N(4)—C(4)—C(5)	108.6(7)	110.2(8)

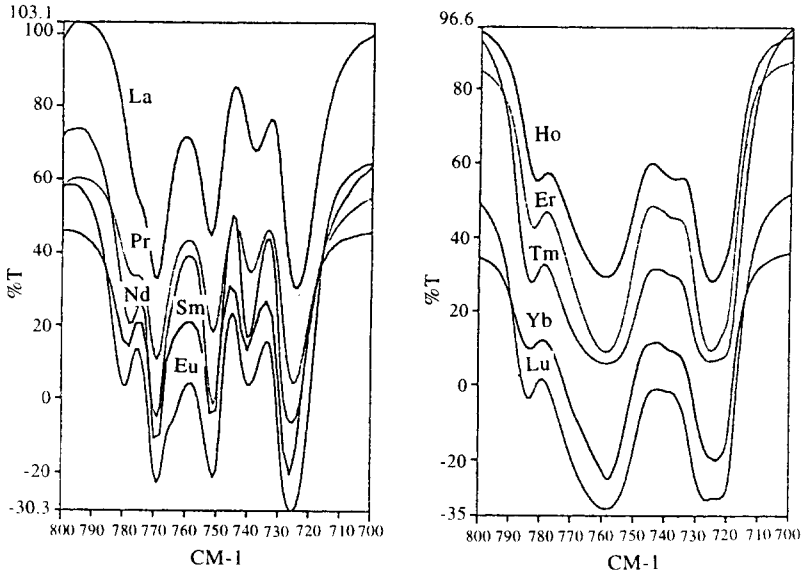


Fig. 1. IR spectra of $LnTp_3$ in the region 800–700 cm^{-1} (left: nine-coordinate compounds of La, Pr, Nd, Sm and Eu; right: eight-coordinate compounds of Ho, Er, Tm, Yb and Lu).

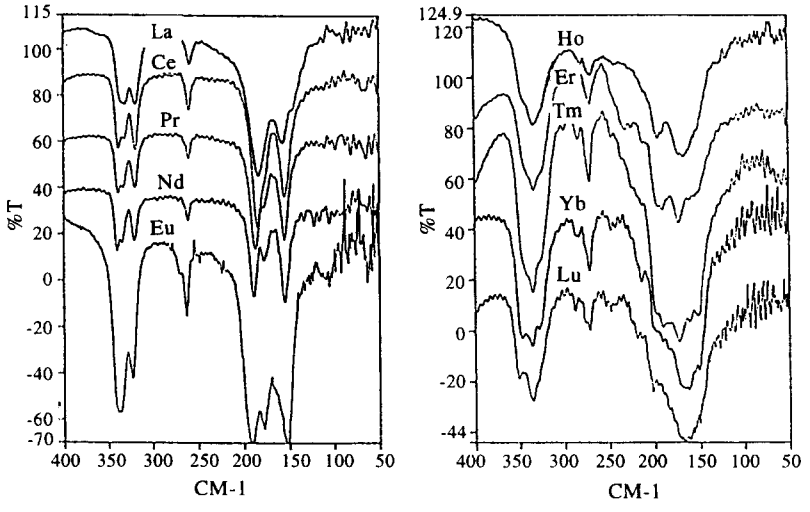


Fig. 2. Far IR spectra of $LnTp_3$ in the region 400–50 cm^{-1} (left: nine-coordinate-, right: eight-coordinate compounds).

crystals, while the $PrCl_3$ sample was a powdered polycrystalline compound, obtained from anhydrous $PrCl_3$ fused in a HCl stream.

As in the case of $PrTp_3$ the electronic absorption spectra of all $LnTp_3$ compounds are quite similar to those of the trichlorides.

Magnetic susceptibility of $PrTp_3$

The same structure of $PrCl_3$ and $PrTp_3$ is reflected in the magnetic susceptibilities of the two compounds, which are almost identical (Fig. 5).

Both compounds obey the Curie–Weiss law with the same Θ constant of -23 (± 0.5) K. The magnetic moment of both compounds at room temperature is quite close to the moment of $3.62\mu_B$, calculated for the free Pr^{3+} ion ($4f^2$) with $g_j = 4/5$. The ground state of the two compounds very likely is the same.

NMR spectra

The aim of the NMR study was to elucidate the molecular structure of the MTp_3 complexes in solution and compare them with the solid-state structures. However, it turned out that the solubility of the complexes of the lighter lanthanides (La–Gd) in not too polar solvents, where decomposition reactions can be excluded, is too low to obtain meaningful spectra.

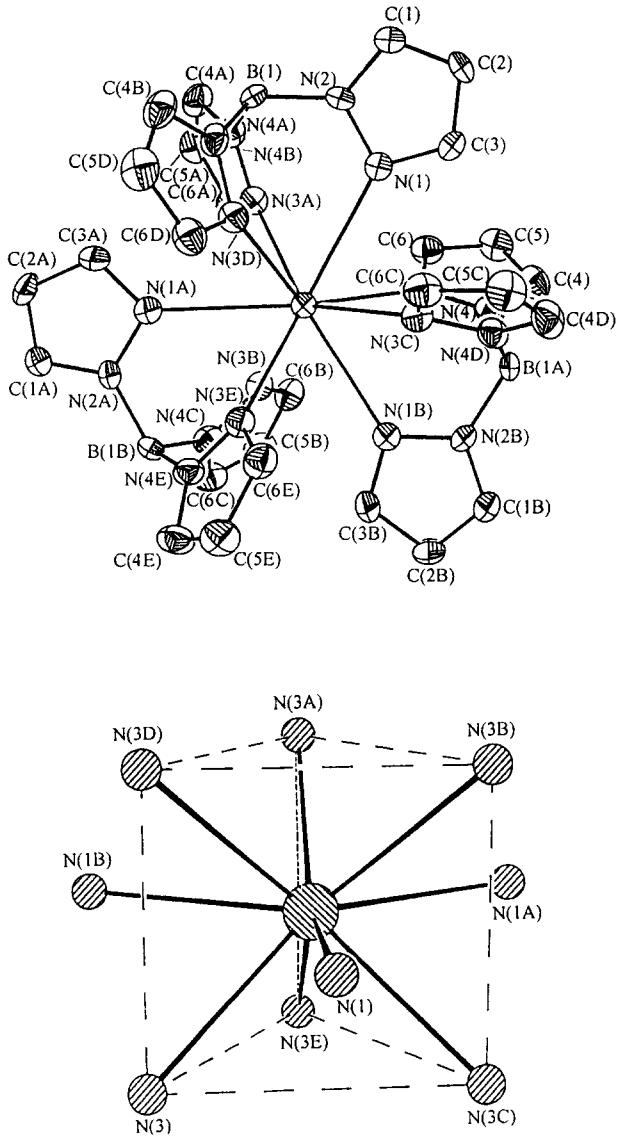


Fig. 3. ORTEP view of the molecular structure (top) and the coordination polyhedron of $LnTp_3$ (bottom); Ln = Pr, Nd.

Solution spectra could be obtained only for the complexes with M = Sc, Y and Tb–Yb.

The diamagnetic complexes MTp_3 (M = Lu, Sc, Y)

^1H and ^{13}C NMR spectra of $LuTp_3$ have been published by Stainer and Takats [23]. Assignment of the fairly complex ^1H spectrum (13 multiplets) was then only partially possible on the basis of the multiplicity of the signals (doublet of a doublet for the 3- and 5-protons, triplet for the 4-proton on each pyrazolyl ring). We have improved the assignment by two-dimensional ^1H-^1H Cosy spectra: of the 18 signals to be expected in the eight-coordinated structural case, 13 are resolved, so five overlap with others. From the Cosy spectrum (Fig. 6) it can definitely be deduced which three signals belong to the same ring. However, it is still not possible to assign the individual rings, e.g. the bidentate one.

The ^1H spectra of $ScTp_3$ and YTp_3 are practically identical with the spectrum of $LuTp_3$.

The same is true for the ^{13}C spectra, which consist of three groups of six lines each, from the C-4 carbons (centred at 104 ppm from TMS) and the C-3 and C-5 carbons (between 134 and 144 ppm).

The paramagnetic complexes (Ln = Tb, Dy, Ho, Er, Tm)

The ^1H spectra of the five complexes all show the expected 18 signals corresponding to the pyrazolyl rings; the broad signals of the three B—H protons,

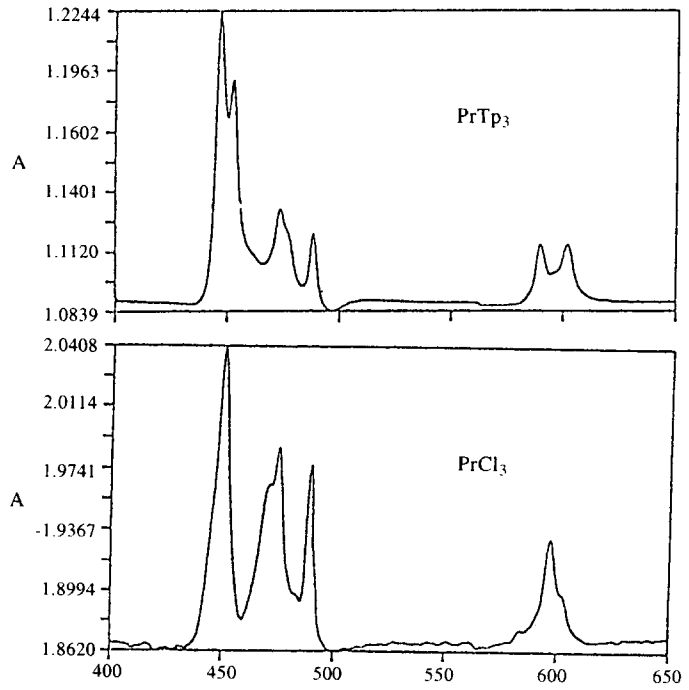


Fig. 4. Electronic absorption spectra of $PrTp_3$ and $PrCl_3$ in the region 400–650 nm.

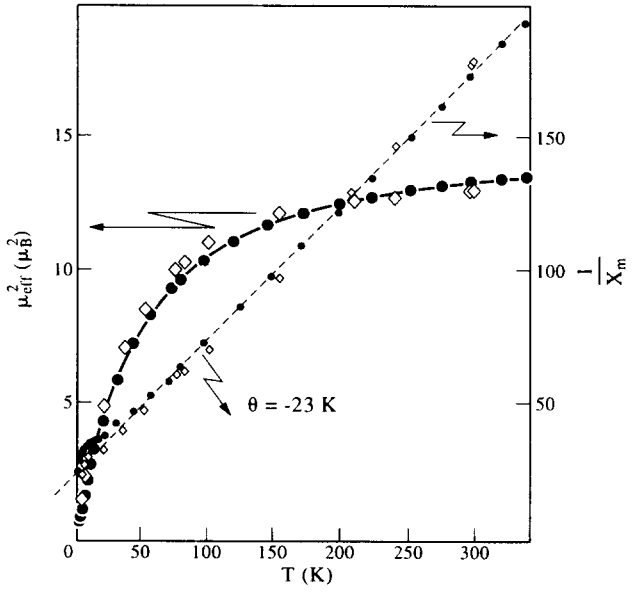


Fig. 5. Squared magnetic moment (left ordinate) and reciprocal molar susceptibility (right ordinate) of $PrTp_3$ (full symbols) and $PrCl_3$ (open symbols).

however, can be identified with certainty only in rare cases. If the assignment of the spectrum of the Yb complex [23] is taken as a basis, the spectra of the other complexes can also be assigned accordingly, with more or less certainty. Of course, the differing magnitude and sign of the magnetic anisotropy factors D_1 and D_2 in the equation for the dipolar shift [eq. (1)]:

$$\Delta^{dip} = D_1 \frac{(3\cos^2 \vartheta - 1)}{r^3} + D_2 \frac{\sin^2 \vartheta \cos^2 \omega}{r^3} \quad (1)$$

give rise to large shift variations, even if the geometry factors are considered to be constant (r, ϑ and ω are the polar coordinates of the respective nucleus with respect to the magnetic axis).

In Fig. 7 these variations are shown for several

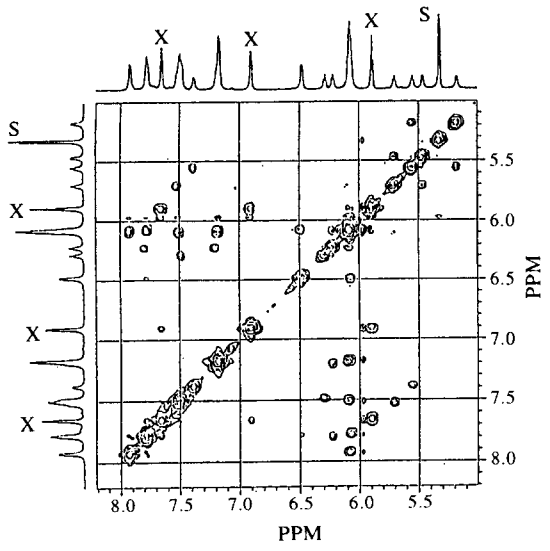


Fig. 6. Two-dimensional ^{1}H-^{1}H cosy spectrum of $LuTp_3$ in CD_2Cl_2 at 200 MHz (S = solvent, x = impurity, possibly of KTp, as the signals of pure KTp appear at 6.28, 6.49 and 7.62 ppm).

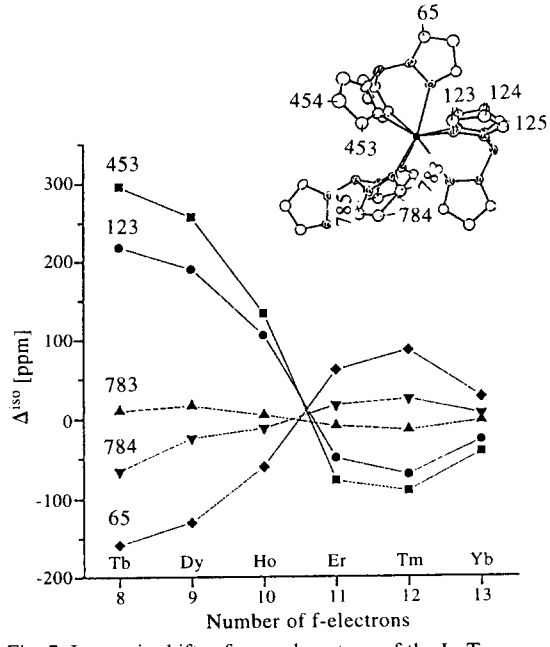


Fig. 7. Isotropic shifts of several protons of the $LnTp_3$ complexes (Ln = Tb–Yb); the numbers are the labels for the pyrazolyl ring protons according to [23].

protons whose assignment seems certain. The assignment labels were chosen according to Stainer and Takats [23], where the two-digit numbers 33, 34, 35, etc., refer to the three rings whose nuclei have intensity one and the three-digit numbers 123, 124, 125, etc., to the nuclei of two equivalent rings (intensity two). The last digit always refers to the ring position of the respective nucleus (see upper part of Fig. 7).

Tb causes the largest shifts: the H signals of $TbTp_3$ cover the range −190 (low field) to 288 ppm. The change of sign between Ho and Er is a phenomenon well known from other lanthanide complexes [24]. The spectrum most similar to that of the Yb complex and therefore easiest to assign is that of $TmTp_3$ (Fig. 8).

The signals of all 18 protons assigned by Stainer and Takats [23] appear in the same order with appropriate intensities. Except for the stronger anisotropy, the geometry factors seem to be almost identical to those in the Yb complex. The only uncertainty is the signal at 142.8 pm which should correspond to the B—H proton H3 (106.5 ppm in the Yb complex) but seems to have a too narrow line width for such a proton. The ratio $\Delta^{iso}(Tm)/\Delta^{iso}(Yb)$ for corresponding protons ranges between two and three or, in other words, the magnetic anisotropy of $TmTp_3$ is roughly two to three times as large as that of $YbTp_3$.

Quite similar to the spectrum of $TmTp_3$ is that of $ErTp_3$; we deduce therefrom that its structure essentially is still unchanged, resulting in nearly identical geometry factors of the various protons. The magnetic anisotropy of $ErTp_3$ is smaller than that of $TmTp_3$ by *ca* 15% (see Fig. 7).

The signal pattern observed in the spectra of $YbTp_3$, $TmTp_3$ and $ErTp_3$ is still retained in the ^{1}H spectra of the Ho, Dy and Tb complexes, but, apart from the fact that the magnetic anisotropy has changed its sign and is much larger than for the forementioned complexes (by a factor of about three for $TbTp_3$ compared with $TmTp_3$), assignments cannot be achieved with certainty for all signals. As an example, the spectrum of $DyTp_3$ is shown in Fig. 9.

Although assignment labels for all 18 non-equivalent protons are given, some of them must be considered tentative (especially in the region 35 to −21 ppm). Obviously, slight changes in the structure have been taken place, but there is no indication that the coordination number has changed from 8 to 9. In that case a much more profound change in the spectrum would have taken place. In the ideal case, when the highly symmetric X-ray structure of the solid phase is retained in solution, a pattern of three lines with intensity one and three lines with intensity two would result for the ring protons.

^{13}C *NMR*

The ^{13}C spectra which were recorded for the $LnTp_3$ compounds with Ln = Tb–Tm showed not nearly as good a signal-to-noise ratio than the spectrum of $YbTp_3$. This may be caused by a reduced solubility. Except for $ErTp_3$, where the line pattern resembles that of $YbTp_3$ fairly well, only part of the 18 signals to be expected could be identified. The anisotropy term in the shifts of $ErTp_3$ is approximately twice as large as for the Yb complex, in accordance with the ^{1}H case.

The NMR results of the Tb, Dy and Ho complexes

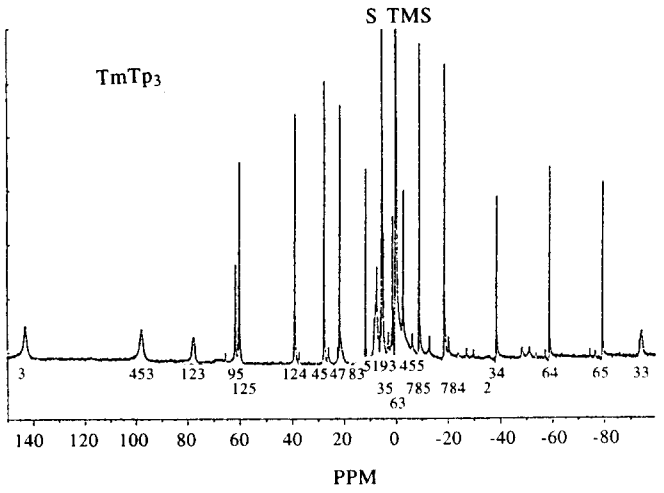


Fig. 8. ^{1}H NMR spectrum of $TmTp_3$ in CD_2Cl_2 at 300 K (250 MHz); assignments of the signals according to the spectrum of $YbTp_3$ [23].

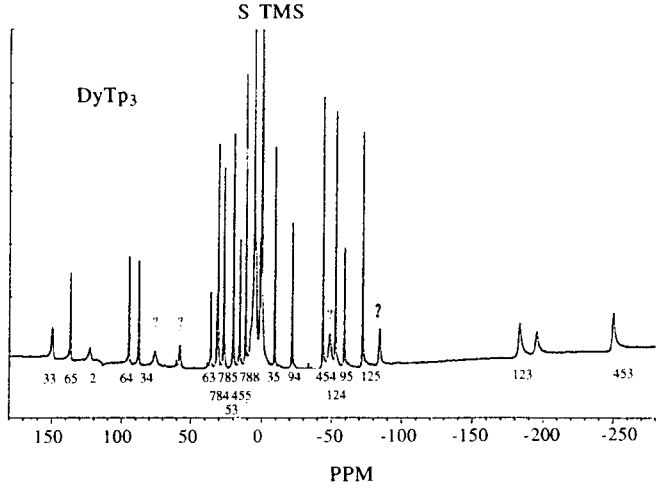


Fig. 9. ^{1}H NMR spectrum of $DyTp_3$ in CD_2Cl_2 at 300 K (250 MHz); assignment of the signals as in Fig. 8.

in solution seem to contradict the other measurements in the solid state reported above, where a change of the coordination number from 9 to 8 appears to take place between Ho and Dy. Two explanations for this discrepancy are possible:

(a) either the coordination number for the three complexes is different in the solid state (9) and in solution (8);
(b) or these complexes appear in dimorphic form (hexagonal and orthorhombic) in the solid state, as has been proven for $DyTp_3$. Only one of them (the orthorhombic form with eight-fold coordination) is soluble in CD_2Cl_2 and exhibits the spectrum of the more or less distorted structure of $YbTp_3$, whereas the other (hexagonal) insoluble form with nine-fold coordination is undetected by NMR.

Acknowledgements—We thank Mr W. Roth, ITC-CPV, for the MS investigations and Mr B. Fueger, WAK-GmbH Karlsruhe, for metal analysis of several compounds. Thanks are also due to Dr G. Schilling (University of Heidelberg) for recording some of the spectra, especially of the ^{1}H-^{1}H Cosy type. The authors are grateful to Professor H. H. Eysel, National Research Council, Winnipeg, Manitoba, Canada, for helpful discussions on the IR spectra.

REFERENCES

1. Trofimenko, S., *Chem. Rev.* 1993, **93,** 943, and refs cited therein.
2. Reger, D. L., Lindeman, J. A. and Lebioda, L., *Inorg. Chim. Acta* 1987, **139,** 71; *Inorg. Chem.* 1988, **27,** 1890; *ibid*, 1988, **27,** 3923.
3. Onishi, M., Nagaoja, N., Hiraki, K. and Itoh, K., *J. of Alloys and Compounds*, 1996, **236,** 6.
4. Reger, D. L., Knox, S. J., Lindeman, J. A. and Lebioda, L., *Inorg. Chem.* 1990, **29,** 416.

5. Moss, M. A. J. and Jones, J., *J. Chem. Soc., Dalton Trans.* 1990, 581.
6. (a) Santos, I. and Marques, N., *New J. Chem.* 1995, **19,** 551; (b) Lawrence, R. G., Jones, C. J., Kresinski, R. A., *J. Chem. Soc., Dalton Trans.* 1996, 501.
7. Hasinoff, L., Takats, J., Zhang, X. W., Bond, A. H. and Rogers, R. D., *J. Am. Chem. Soc.* 1994, **116,** 8833.
8. Liu, Sg.-Yg., Maunder, G. H., Sella, A., Stevenson, M. and Tocher, D. A., *Inorg. Chem.* 1996, **35,** 76.
9. Maunder, G. H., Sella, A. and Tocher, D. A., *J. Chem. Soc., Chem. Commun.* 1994, 2689.
10. (a) Moss, M. A., Kresinski, R. A., Jones, C. J. and Evans, W. J., *Polyhedron*, 1993, **12,** 1953; (b) Takats, J., Zhang, X. W., Day, V. and Ebersbacher, T. A., *Organometallics*, 1993, **12,** 4286; (c) Maunder, G., Sella, A. and Tocher, D. A., *J. Chem. Soc., Chem. Commun.* 1994, 885.
11. Bagnall, K. W., Tempest, A. C., Takats, J. and Masino, A. P., *Inorg. Nucl. Chem. Lett.*, 1976, **12,** 555.
12. Stainer, M. V. R. and Takats, J., *Inorg. Chem.* 1982, **21,** 4050.
13. Apostolidis, C., Kanellakopulos, B., Maier, R., Meyer, D., Marques, N. and Rebizant, J., 21*èmes Journées des Actinides*, Montechoro, Algarve/Portugal, April 28–May 1, 1991, Abstr. No. P4.8, p. 187.
14. Apostolidis, C. and Kanellakopulos, B., to be published.
15. Schmieder, H., Dornberger, E. and Kanellakopulos, B., *Appl. Spectrosc.* 1970, **24,** 499.
16. Kanellakopulos, B., Henrich, E., Kellèr, C., König, E., Baumgärtner, F. and Desai, V. P., *Chem. Phys.* 1980, **53,** 197.
17. Meanwhile single crystals of all other $LnTp_3$ compounds, as well as for the trivalent lighter actinide elements uranium, neptunium and plutonium, have been obtained and their molecular and crystal structure were analysed. In agreement with the IR spectroscopic investigations the actinide and the lanthanide ion up to Dy is ninefold-coordinate, while in the compounds from Ho to Lu the central ion is eightfold-coordinate. The full data will be published in this journal in a separate paper.
18. SHELXTL-PLUS. Siemens Analytical X-Ray Instruments Inc., Madison, WI, 1989; ENRAF-NONIUS SDP-Plus, Structure Determination Package, Enraf-Nonius, Delft, Netherlands (1987).
19. International Tables for X-ray Crystallography, Vol. IV. Kynoch Press, Birmingham, 1974.
20. Kanellakopulos, B., Maier, R. and Heuser, J., *J. of Alloys and Compounds*, 1991, **176,** 89.
21. Hutchinson, B., Hoffbauer, M. and Takemoto, J., *Spectrochim. Acta*, 1972, **32A,** 1785.
22. Wells, A. F., *Structural Inorganic Chemistry*, Clarendon Press, Oxford, 1962, p. 340; Zachariasen, W. H., *Acta Cryst.* 1948, **1,** 265.
23. Stainer, M. V. R. and Takats, J., *J. Am. Chem. Soc.* 1983, **105,** 410.
24. Fischer, R. D., *Fundamental and Technological Aspects of Organo-f-Element Chemistry*, ed. T. Marks, I. L. Fragalà, D. Reidel Publ. Comp., Dordrech/Boston/Lancaster, 1985, p. 277.

Pergamon

PII: S0277-5387(96)00412-3

Polyhedron Vol. 16, No. 7, pp. 1069–1079, 1997
Copyright © 1997 Elsevier Science Ltd
Printed in Great Britain. All rights reserved
0277-5387/97 $17.00+0.00

Kinetics of iron removal from monoferric and cobalt-labelled monoferric transferrins by ethylenediaminetetra(methylenephosphonic acid) and ethylenediaminetetraacetic acid

Wesley R. Harris* and Gang Bao

Department of Chemistry, University of Missouri-St. Louis, St. Louis, MO 63121, USA

(Received 4 March 1996; accepted 7 August 1996)

Abstract—The rates at which ferric ion is removed from the two metal binding sites of the serum iron transport protein transferrin by ethylenediaminetetra(methylenephosphonic acid) (EDTP) and ethylenediaminetetraacetic acid (EDTA) have been evaluated. Solutions were buffered at pH 7.4 by 0.1 M *N*-2-hydroxyethylpiperazine-*N'*-2-ethanesulfonic acid and maintained at 25°C. Pseudo first-order rate constants as a function of ligand concentration were measured for iron removal from diferric transferrin, from N- and C-terminal monoferric transferrin and from monoferric transferrins which had been labelled at the vacant site with kinetically inert cobalt(III). The data on iron removal from the cobalt-labelled monoferric transferrins provide accurate estimates of the rate constants for iron removal from diferric transferrin. A significant negative cooperativity is observed, in which occupancy of the C-terminal site slows the rate of iron release from the N-terminal site. Iron release from most of the transferrin complexes shows a combination of saturation and first-order kinetics which are interpreted in terms of parallel pathways for iron removal. The addition of 100 mM perchlorate to the samples accelerates iron removal through both pathways for the C-terminal site, but sharply decreases the rate of iron removal from the N-terminal site. The implications of these new results with respect to proposed mechanisms of iron release from transferrin are discussed. Copyright © 1997 Elsevier Science Ltd

Keywords: transferrin; monoferric transferrin; kinetics; phosphonic acids.

Serum transferrin (Tf) is the protein responsible for the transport of iron through the blood between sites of uptake, utilization and storage [1–4]. The protein consists of a single polypeptide chain, but it folds into a bilobal tertiary structure with a single high-affinity iron binding site located within each lobe [5,6]. The two sites are structurally very similar. Each ferric ion is six coordinate, ligated by the phenolic groups of two tyrosine residues, the imidazole side chain of a histidine residue, the carboxylate group of an aspartate residue and a bidentate carbonate anion [7–9]. This exogenous carbonate ligand is referred to as the synergistic anion, as it, or some suitable substitute, is required for strong metal binding to the protein.

Transferrin is a potential target for therapeutic chelating agents designed to treat the iron overload that accompanies long-term transfusion therapy for genetic diseases such as β-thalassaemia. A considerable amount of effort has been devoted to the elucidation of the mechanism of the exchange of iron between transferrin and low molecular weight chelating agents. Although several mechanisms have been proposed [10–14], the iron release process is still not well understood. Iron removal by some ligands follows simple saturation kinetics with respect to the ligand concentration [10,15,16]. In a few cases, iron removal has followed simple first-order kinetics with respect to the ligand [14,17], and in several cases the kinetics show a combination of saturation and linear dependence on the ligand [11,12,14,17–20].

Crystal structures of transferrin [5,8] and the closely related protein lactoferrin [6,9] have shown that the iron binding sites sit in a narrow cleft in the protein. When iron is removed to form apoTf, there is a major conformational change in which this cleft opens much wider [7,21]. This change, or possibly some intermediate step along the pathway of the overall con-

* Author to whom correspondence should be addressed.

formational change, is probably involved in regulating the rate of iron removal from the protein. It is also clear that the iron release process is strongly influenced by the binding of anions such as Cl^- or ClO_4^- from the solution [11–13,15,18,19,22–26]. In the case of charged ligands such as pyrophosphate, the chelating agent being used to remove the iron from the protein may also function as an allosteric anion [11,12,15].

We have previously reported on iron release by pyrophosphate and a series of aminophosphonic acids [14,17,20,24,27]. In all cases, the apparent first-order rate constant for iron removal shows a complex dependence on the ligand concentration, which appears to represent a combination of saturation and first-order kinetics. This paper extends these studies to include the kinetics of iron removal from both forms of monoferric transferrin by ethylenediaminetetra(methylenephosphonic acid) (EDTP). The expected complex ligand dependence is observed only at the C-terminal site. In addition, there is a surprising degree of negative cooperativity associated with iron release from the N-terminal site. The effect of sodium perchlorate on the iron removal kinetics has also been measured, and the data are discussed in terms of the current proposed mechanisms for iron removal.

EXPERIMENTAL

Materials

Human serum transferrin was purchased from Calbiochem and purified as previously described [28]. Simple monoferric transferrins and cobalt-labelled monoferric transferrins were prepared and purified as described previously [28]. Ethylenediaminetetra (methylenephosphonic acid) (EDTP) was purchased from TCI America in Portland, OR, and used as received.

Methods

Iron removal reactions were run in 0.1 M *N*-2-hydroxyethylpiperazine-*N'*-2-ethanesulfonic acid (HEPES) at pH 7.4. The reaction was followed by monitoring the decrease in the transferrin iron–phenolate charge transfer band at 465 nm with a Hewlett–Packard model 8452A diode array UV–vis spectrophotometer. The spectrophotometer was equipped with a six-position cell holder connected to an external constant temperature water bath to keep the cuvettes at 25°C during the iron removal reaction.

Rate constants were calculated using either the kinetics routines provided by Hewlett–Packard for the HP Chemstation computer or custom-written programmes based on the general non-linear least squares program ORGLS [29]. All iron removal reactions were run with a large excess of ligand over ferric transferrin and were treated as pseudo first-order, irreversible reactions. For kinetic studies on monoferric transferrins, the absorbance *vs.* time data were fit to Eq. (1)

$$A_t = (A_0 - A_\infty)\, e^{-k_{obs}t} + A_\infty \qquad (1)$$

where A_0, A_∞ and A_t are the absorbances at zero time, infinite time, and any intermediate time t during the reaction, and k_{obs} is the apparent first-order rate constant for a specified concentration of EDTP. For reactions that went to completion, A_0, A_∞ and k_{obs} were all treated as adjustable parameters, and data out to three or four half-lives were included in the calculation. In situations where iron removal did not go to completion, the value for A_∞ was fixed based on the values observed at higher ligand concentrations. The value for k_{obs} was calculated from the initial data collected before the back reaction of iron donation from EDTP to apoTf became a significant factor.

Iron removal from diferric transferrin was also followed by urea–polyacrylamide gel electrophoresis. The electrophoresis method was basically that originally reported by Makey and Seal [30] with the modifications described by Bali and Harris [28]. Gels were run using a BioRad Protean TM-11 16 cm vertical slab gel assembly with a BioRad Model 500/200 power supply. Gels were dried and scanned using a BioRad Model 620 Video densitometer. Peak areas were determined using the BioRad 1D software. In the kinetic studies, diferric transferrin was reacted with 100 mM EDTP. Sequential aliquots were removed from the reaction mixture, frozen in liquid nitrogen to stop further reaction, and later analysed by gel electrophoresis.

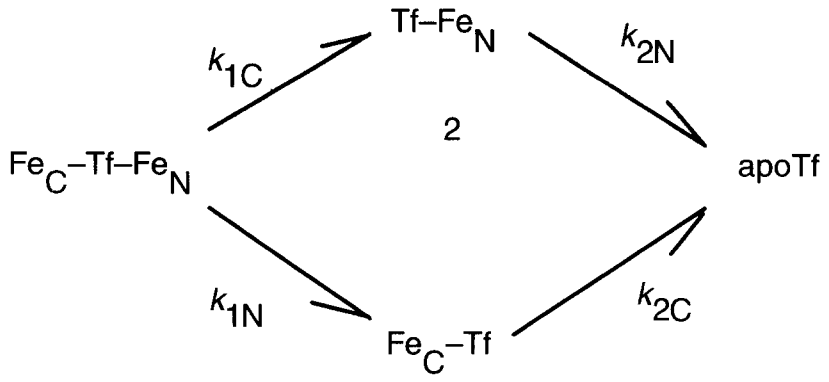
RESULTS

Because transferrin has two metal binding sites, there are four microscopic rate constants for iron removal from diferric transferrin as shown below. The subscript for each rate constant indicates the site from which iron is being removed (C-terminal or N-terminal) and whether it is the first or second iron to be removed from the transferrin molecule.

Based on Scheme 1, the exact function for absorbance *vs.* time during iron release from diferric transferrin is

$$A_t - A_\infty = (\varepsilon_C + \varepsilon_N) C_0\, e^{-(k_{1N}+k_{1C})t} + \left[\frac{\varepsilon_C C_0 k_{1N}}{k_{1N}+k_{1C}-k_{2C}}\left(e^{-k_{2C}t} - e^{-(k_{1N}+k_{1C})t}\right)\right] + \left[\frac{\varepsilon_N C_0 k_{1C}}{k_{1N}+k_{1C}-k_{2N}}\left(e^{-k_{2N}t} - e^{-(k_{1N}+k_{1C})t}\right)\right] \qquad (2)$$

where ε_C and ε_N are the molar extinction coefficients for ferric ion bound at each of the two binding sites,



Scheme 1.

and C_0 is the initial concentration of diferric transferrin [25]. Even though the two metal binding sites are about 40 Å apart [6], the occupancy of one site can affect the rate of iron removal at the other site [4,16,17,20,22], so one cannot routinely simplify the equation by assuming that $k_{1C} = k_{2C}$ or that $k_{1N} = k_{2N}$. Unfortunately, it can be extremely difficult to calculate reliable values for k_{1C}, k_{1N}, k_{2C} and k_{2N} from a four-parameter fit of absorbance *vs* time data on diferric transferrin to Eq. (2) [17,20]. Thus we have emphasized studies on purified N-terminal and C-terminal monoferric transferrins. This allows us to calculate values for k_{2N} and k_{2C} as a simple first-order process using Eq. (1).

Iron removal from monoferric transferrins

Pseudo first-order rate constants for the removal of ferric ion from both C-terminal and N-terminal monoferric transferrin have been measured at a series of EDTP concentrations. Plots of k_{obs} *vs* [EDTP] are shown in Fig. 1. These plots resemble saturation kinetics. However, it appears that the rate constant for iron removal from the C-terminal site continues to increase at high ligand concentrations. This more complex ligand dependence has been observed for several other ligands [11,14,17–20], and can be described empirically by the equation

$$k_{obs} = \frac{k'[L]}{1+k''[L]} + k'''[L] \qquad (3)$$

The data for both monoferric transferrins have been fit to Eq. (3) using k' and k'' only (two-parameter fit) and using k', k'' and k''' (three-parameter fit). The results for both two- and three-parameter fits are shown in Fig. 1. Each fit is characterized by an *R*-factor, R_x, where x denotes whether R corresponds to a two- or three-parameter fit. Since the addition of a third adjustable parameter should always improve the fit, the ratio of R_2/R_3 should always be greater than 1. One can test whether the improvement in the fit associated with the third adjustable parameter is statistically significant by comparing the ratio of R_2/R_3 with the test statistic

$$R_{b,n-p,\alpha} = \left(\frac{b}{n-p}F_{b,n-p,\alpha}+1\right)^{1/2} \qquad (4)$$

where p is the maximum number of parameters varied, b is the number of constants held fixed in the more restrictive two-parameter fit, n is the number of observations included in the fitting and α is the desired level of confidence [31]. One may conclude that the value of k''' makes a significant improvement in the fit of k_{obs} *vs* [EDTP] when the *R*-factor ratio exceeds $R_{b,n-p,\alpha}$.

This *R*-factor test has been applied to the data for both C- and N-terminal monoferric transferrin. For N-terminal monoferric transferrin, there is no significant improvement produced by including k''' in the calculation. Thus the N-terminal system follows simple saturation kinetics, and an excellent fit is obtained by setting k''' to zero and using only k' and k'' as adjustable parameters. However, for C-terminal monoferric transferrin, one obtains a significantly better fit with three parameters ($\alpha = 0.005$). Thus the C-terminal site shows complex kinetics that cannot be described as either first-order or saturation.

Equation (3) is an empirical description of the ligand dependence. The possible mechanisms that might explain this behaviour have been the subject of considerable debate [11,13–15,17–20,22]. We interpret the complex ligand dependence of k_{obs} in terms of two parallel pathways for iron removal, one which follows saturation kinetics and one which is simple first-order in ligand. In this model the parameter k'' describes the approach to saturation and has the units of an equilibrium constant. The ratio of k'/k'' gives k_{max}, the maximum rate constant for iron removal through the saturation pathway. The parameter k''' is the rate constant for the first-order pathway. Values of k_{max}, k'' and k''' for iron removal from the monoferric transferrins by EDTP are listed in Table 1.

To compare the behaviour of aminophosphonic acids *vs* aminocarboxylic acids, a more limited set of kinetic data were also collected for iron removal from

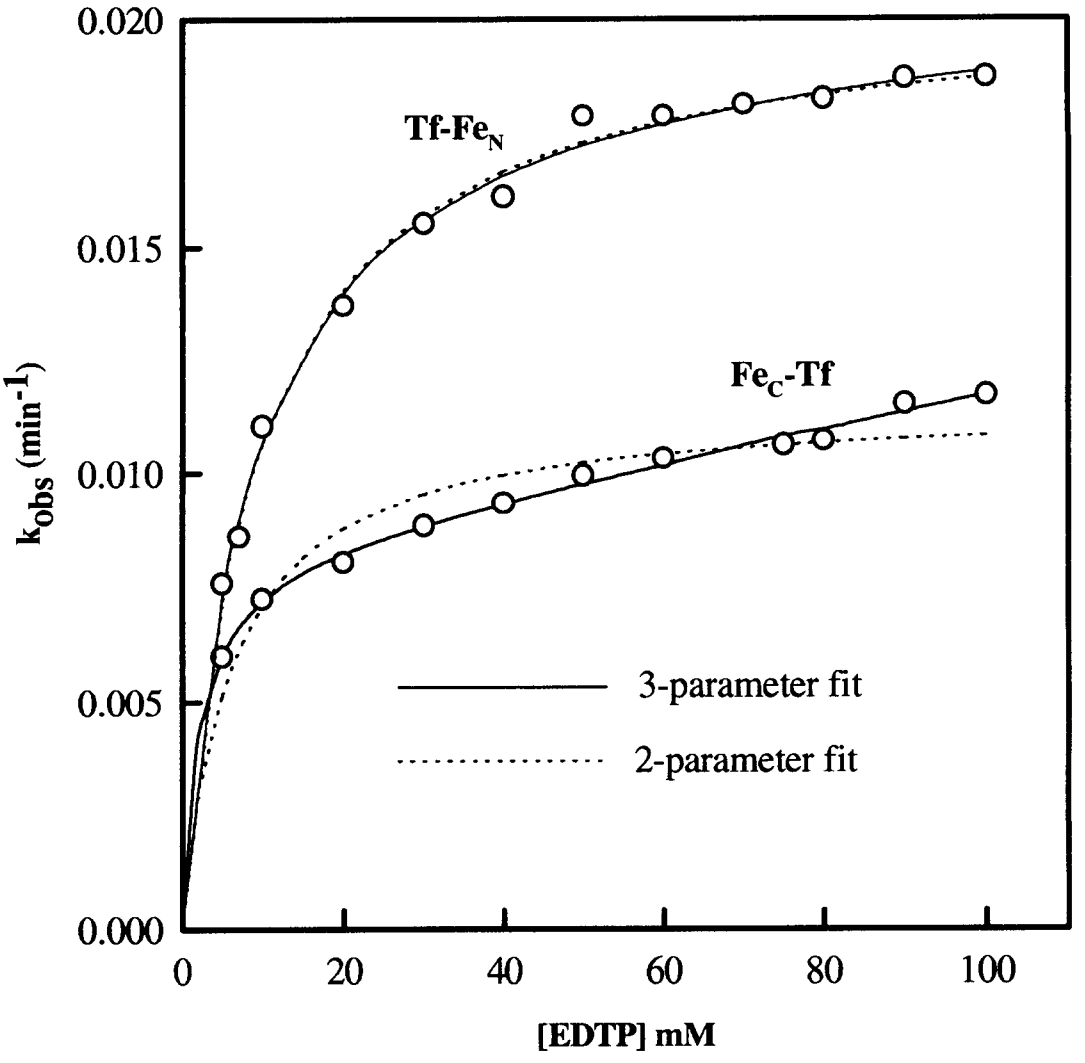


Fig. 1. Apparent first-order rate constants for iron removal from C- and N-terminal monoferric transferrins as a function of the concentration of EDTP. All solutions were buffered at pH 7.4 by 0.1 M HEPES and maintained at 25°C. The lines represent fits of the data to Eq. (3) using either k' and k'' only (two-parameter fit) or k', k'' and k''' (three-parameter fit).

Table 1. Kinetic parameters for iron removal from transferrins by EDTP and EDTA

Sample	$10^3\,k_{max}$ (min^{-1})	k'' (M^{-1})	$10^3\,k'''$ (M^{-1} min^{-1})
Without added perchlorate			
Fe$_C$–Tf + EDTP	8.3 ± 1.6	480 ± 70	36.0 ± 0.3
Fe$_C$–Tf–Co$_N$ + EDTP	11.4 ± 1.8	72 ± 9	0
Fe$_C$–Tf + EDTA	6.4 ± 1.6	118 ± 26	114 ± 6
Tf–Fe$_N$ + EDTP	20.4 ± 1.2	110 ± 5	0
Co$_C$–Tf–Fe$_N$ + EDTP	4.8 ± 1.7	210 ± 70	11.3 ± 4.9
Tf–Fe$_N$ + EDTA	24.9 ± 2.3	370 ± 30	27 ± 5
With 100 *mM* $NaClO_4$			
Fe$_C$–Tf + EDTP	40.7 ± 3.1	59 ± 4	148 ± 9
Tf–Fe$_N$ + EDTP	1.2 ± 0.7	73 ± 33	0

both forms of monoferric transferrin by EDTA. These data are plotted in Fig. 2. *R*-factor ratio tests indicate that three-parameter fits are appropriate for both sites, although the first-order component is much more prominent for the C-terminal site. Values for k_{max}, k'' and k''' are listed in Table 1.

Iron removal from cobalt-labelled monoferric transferrins

To assess the degree of cooperativity between the two transferrin binding sites, one needs to compare k_{1N} with k_{2N} and k_{1C} with k_{2C}. However, it can be difficult to calculate k_{1C} and k_{1N} simultaneously from data on iron removal from diferric transferrin. Thus we have developed the method of labelling one of the binding sites with the kinetically inert cobalt(III) ion [14,17,20]. This allows us to measure the rate of iron removal from one site while the other remains filled with a kinetically inert trivalent metal ion. The resulting rate constants are presented as estimates of k_{1C} and k_{1N} for diferric transferrin.

Both forms of monoferric transferrin have been labelled at the vacant binding site with cobalt(III) to give Fe_C–Tf–Co_N and Co_C–Tf–Fe_N. Dicobalt transferrin was also prepared. Preliminary studies on the reaction of dicobalt transferrin with EDTP showed that there was no significant removal of the kinetically inert cobalt(III) ion over the time period of the iron removal reactions. This is consistent with the recent report that the half-life for removal of Co^{3+} from transferrin by PP_i is over 20 h even at pH 6.5 [32].

Iron removal from Fe_C–Tf–Co_N by EDTP behaved as a simple pseudo first-order process described by Eq. (1). However, iron removal from Co_C–Tf–Fe_N unexpectedly showed two kinetic phases. There was a very rapid initial phase, which accounted for about 20% of the total absorbance change, followed by a larger, slower absorbance change. The first phase was

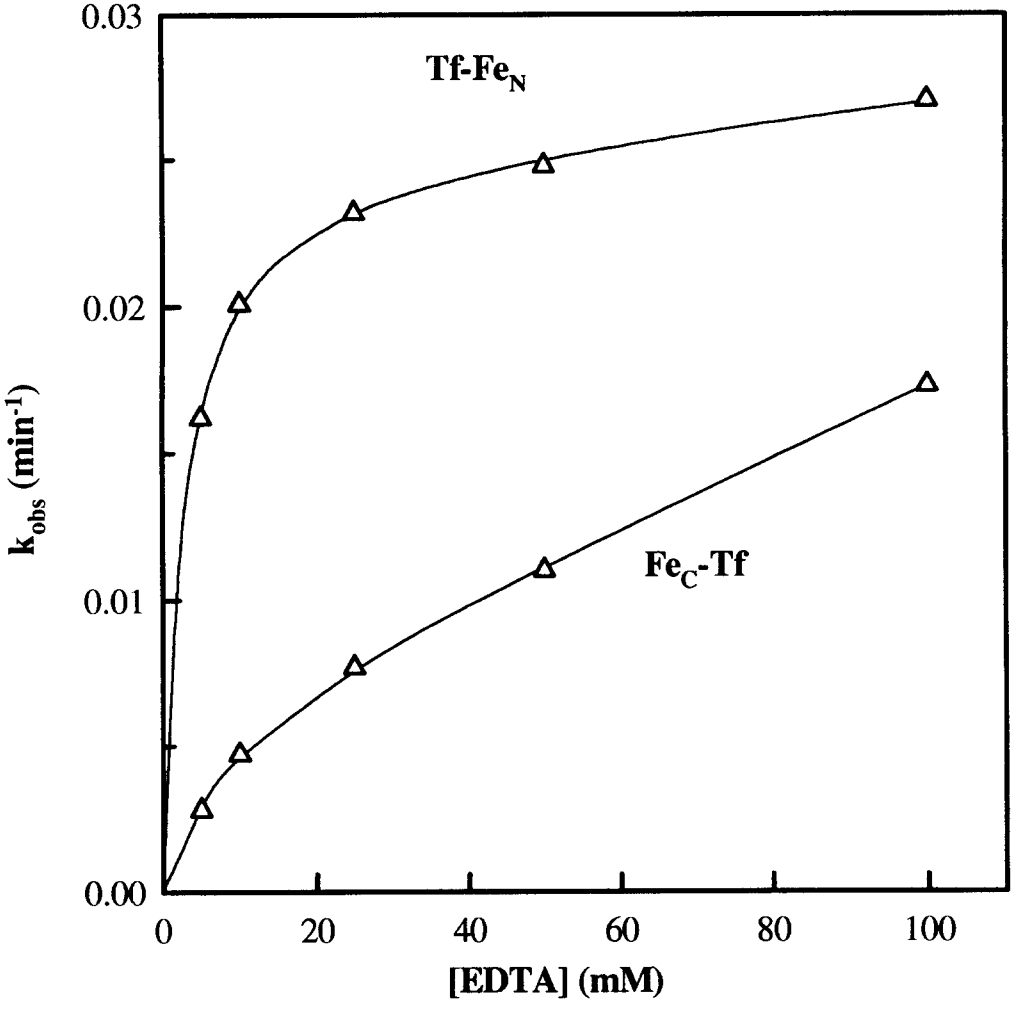


Fig. 2. Apparent first-order rate constants for iron removal from C- and N-terminal monoferric transferrins as a function of the concentration of EDTA. All solutions were buffered at pH 7.4 by 0.1 M HEPES and maintained at 25°C.

much more rapid than iron release from unlabelled monoferric transferrin, and the amplitude of the second phase coincided with the absorbance change expected for the iron removal reaction. Therefore, the rate constant for iron removal was calculated from the slow reaction phase. The origin of the initial faster phase is still not understood.

Rate constants for iron removal from the cobalt-labelled monoferric transferrins as a function of the EDTP concentration are presented in Fig. 3. The data have been treated by both two- and three-parameter fits. The *R*-factor ratio tests indicate that three parameters are required to fit the data for Co_C–Tf–Fe_N, but that iron removal from Fe_C–Tf–Co_N can be described by only two parameters. The resulting values for k_{max}, k'' and k''' are listed in Table 1. Adding cobalt to the N-terminal site has very little effect on the overall rate of iron removal from the C-terminal site. A small increase in k_{max} is offset by a decrease in k'''. In contrast, the addition of cobalt to the C-terminal site results in a sharp drop in the k_{max} for iron removal from the N-terminal site by EDTP. This type of negative cooperativity has not been observed in the previous studies on cobalt-labelled monoferric transferrins [14,17,20].

Iron removal from diferric transferrin

Two types of studies on iron removal from diferric transferrin were conducted to test the validity of using cobalt-labelled monoferric transferrins as a simple tool for measuring accurate values for k_{1C} and k_{1N}. In one set of experiments, iron removal was followed by electrophoresis. This method has the critical advantage that it can easily resolve diferric transferrin from monoferric and apotransferrin [30]. Thus, unlike the case with visible spectrophotometry, which only measures total iron removal, electrophoresis can directly follow the changes in the concentration of diferric transferrin.

The rate of disappearance of diferric transferrin is

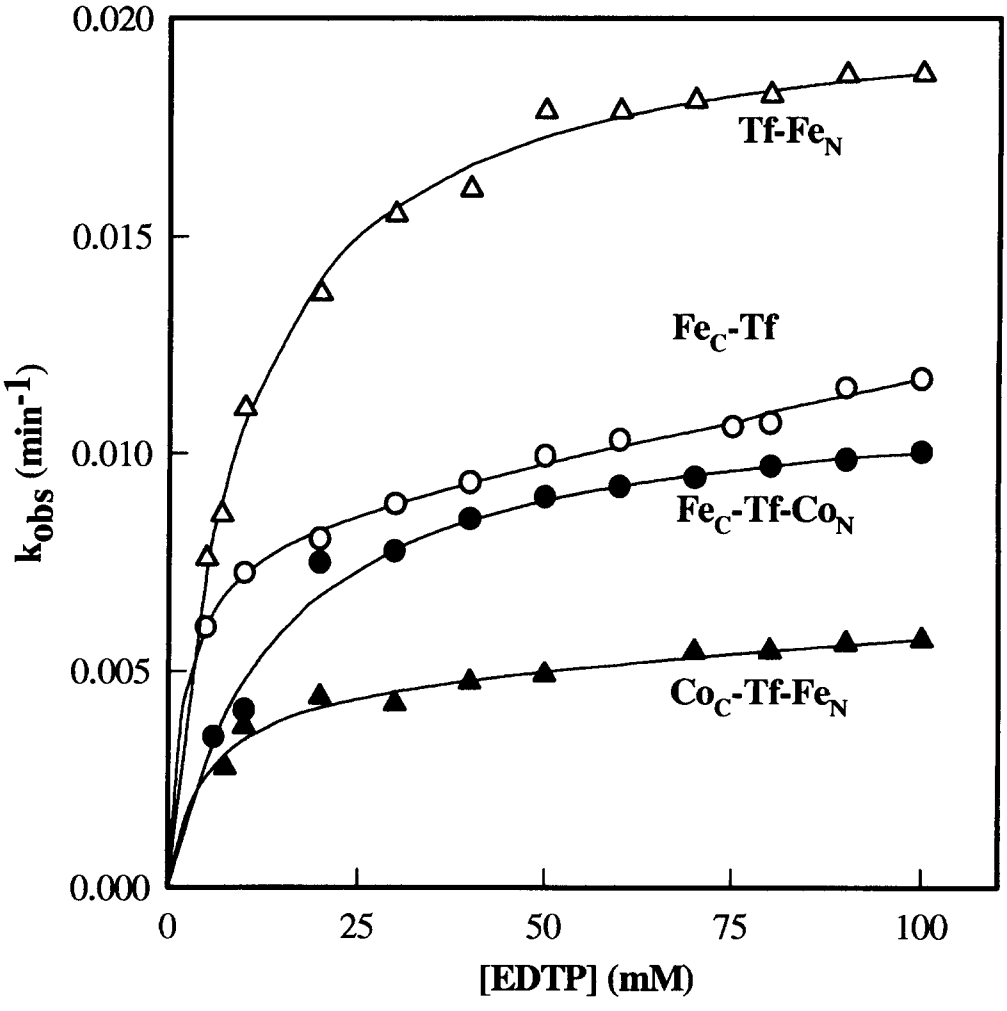


Fig. 3. Apparent first-order rate constants for iron removal from monoferric and cobalt-labelled monoferric transferrins as a function of the concentration of EDTP. All solutions were buffered at pH 7.4 by 0.1 M HEPES and maintained at 25°C.

first-order in diferric transferrin with an observed rate constant equal to the sum of $k_{1C}+k_{1N}$ [25,28]. The densitometry peak areas for diferric transferrin during iron removal by 100 mM EDTP were fit to a first-order equation to obtain $k_{obs} = 0.017 \pm 0.001$ min^{-1}. The sum of the k_{1C} and k_{1N} values for 100 mM EDTP from the spectrophotometric data on the cobalt-labelled monoferric transferrin is 0.016 ± 0.003 min^{-1}. Thus there is excellent agreement with the electrophoresis data on diferric transferrin and the spectrophotometric data on cobalt-labelled monoferric transferrins.

In a second set of experiments, iron removal from diferric transferrin by EDTP was followed spectrophotometrically for a series of EDTP concentrations from 10 to 100 mM. These data were analysed by several different computational methods. One method was to fit the data to Eq. (2) using all four site-specific rate constants as adjustable parameters. However, the parameters fluctuated widely during refinement, and the resulting values of k_{2C} and k_{2N} did not agree with the results on the purified monoferric transferrins. Even when k_{2C} and k_{2N} were both fixed at values determined for the monoferric transferrins, it was not possible to get a smooth, simultaneous refinement of k_{1C} and k_{1N}.

Since we were primarily interested in confirming that k_{1N} is smaller than k_{2N}, a third calculation was run in which k_{2C} and k_{2N} were fixed at the values for monoferric transferrin, k_{1C} was fixed at the value determined from studies on Fe_C–Tf–Co_N, and the data on differic transferrin were fit to Eq. (2) using only k_{1N} and A_∞ as adjustable parameters. Over the range of 20–100 mM EDTP, there was very good agreement between the values of k_{1N} calculated from data on diferric transferrin and from data on cobalt-labelled N-terminal monoferric transferrin. Below 20 mM EDTP, it became difficult to deal with the problem of incomplete iron removal from diferric transferrin. Nevertheless, the agreement between two sets of k_{1N} values confirms that the cobalt-labelled monoferric transferrins provide very good models for the kinetic behaviour of diferric transferrin, and that occupancy of the C-terminal site results in slower iron release from the N-terminal site by EDTP.

Owing to its complexity, Eq. (2) is often reduced to the two exponential Eq. (5)

$$(A - A_\infty) = C_0\varepsilon\left(\left(2 - \frac{m_1}{(m_1 - m_2)}\right)e^{-m_1 t} + \left(\frac{m_1}{m_1 - m_2}\right)e^{-m_2 t}\right) \quad (5)$$

where C_0 is the initial concentration of diferric transferrin, ε is the molar extinction coefficient of diferric transferrin and the rate constants are related back to Scheme 1 by the equations $m_1 = k_{1C}+k_{1N}$ and $m_2 = k_{2C} = k_{2N}$ [5,16,25]. The spectrophotometric data on iron removal from diferric transferrin by EDTP have been fit to Eq. (5) using m_1, m_2, C_0 and A_∞ as adjustable parameters. Equation (5) gives an excellent fit of the absorbance *vs* time data, and the resulting values of both m_1 and m_2 show simple saturation kinetics. However, the results are not consistent with the results on the monoferric transferrins. The value of m_2, which should approximate the average of k_{2C} and k_{2N}, levels off at only *ca* 0.006 min^{-1}, which is smaller than either k_{2C} (*ca* 0.010 min^{-1}) or k_{2N} (*ca* 0.018 min^{-1}). Conversely, the value of m_1 levels off at *ca* 0.022 min^{-1} and is greater than the sum of the k_{1C} and k_{1N} values determined from the cobalt-labelled monoferric transferrins.

Salt effects on iron removal

The ligand dependence of the apparent first-order rate constant for iron removal by EDTP has been measured in 0.1 M HEPES buffer which also contained 100 mM $NaClO_4$. At each ligand concentration, the reaction follows first-order kinetics. The apparent first-order rate constant is plotted as a function of the ligand concentration in Fig. 4 for both forms of monoferric transferrin. The presence of 100 mM perchlorate dramatically increases the rate of iron release from the C-terminal binding site. There is a highly significant improvement in the three-parameter fit for the C-terminal data. Thus the faster rate can be attributed to both an increase in k_{max} from 0.00824 to 0.0407 min^{-1} as well as an increase in k''' from 0.036 to 0.148 min^{-1}. These two factors combine to give an overall five-fold increase in the rate of iron removal by 100 mM EDTP. Perchlorate has a much different effect on iron release from the N-terminal binding site. There is a very sharp decrease in k_{max} from 0.020 min^{-1} to only 0.0012 min^{-1}. There is no first-order term either with or without perchlorate.

DISCUSSION

The rates of iron release by EDTP are generally similar to those reported previously for PP_i and other aminophosphonic acids [14,17,20]. However, the first-order component of the ligand dependence curves is less prominent for EDTP than for the related ligands nitrilotris(methlenephosphonic acid) (NTP) or diethylenetriaminepenta(methylenephosphonic acid) (DTPP). The value of k''' can be set to zero for iron removal from Tf–Fe_N and Fe_C–Tf–Co_N. Although the addition of k''' provides a statistically significant improvement in the fit for Co_C–Tf–Fe_N, the chemical significance of this added parameter is doubtful. The standard deviations for k'' and k''' are quite high, and the saturation pathway is still the dominant route of iron removal. The first-order pathway is most important for iron removal from Fe_C–Tf. In this case the improvement in the fit associated with the addition of k''' is highly significant, and the resulting value of k''' is well defined with a small standard deviation.

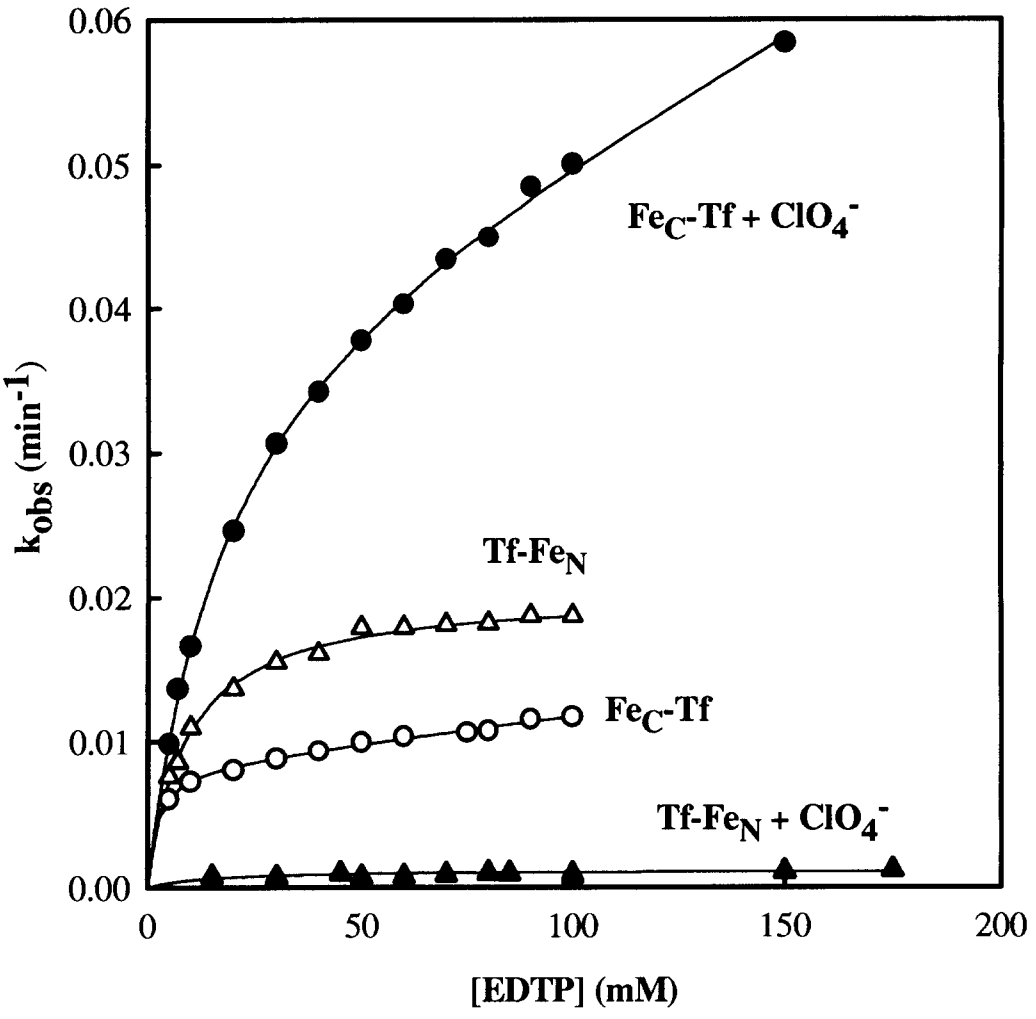


Fig. 4. The effect of $NaClO_4$ on the rates of iron removal from both forms of monoferric transferrin. Open symbols show apparent first-order rate constants in the absence of perchlorate, while closed symbols show the rate constants measured in the presence of 100 mM $NaClO_4$. All solutions were buffered at pH 7.4 by 0.1 M HEPES and maintained at 25°C.

In recent studies with both forms of monoferric transferrin, iron removal by the aminocarboxylates NTA and DTPA followed simple first-order kinetics with respect to the ligand concentration [14,17]. Iron removal from diferric transferrin by EDTA had been studied earlier and appeared to follow either saturation or complex kinetics [25]. In repeating the experiments on iron removal by EDTA using monoferric transferrins, we suspected that this apparent discrepancy between EDTA and the other aminocarboxylates reflected the difficulties of getting reliable two-exponential fits for diferric transferrin. Thus we expected that the monoferric transferrins would show simple first-order kinetics with EDTA as they had with NTA and DTPA. However, the results on the monoferric transferrins are in fact very similar to the earlier results on diferric transferrin [23,25]. It is quite clear that neither site follows simple first-order kinetics. It is not at all clear why EDTA behaves so differently from NTA and DTPA.

Cooperativity. In previous studies on iron removal by PP_i [20], NTP [17] and DTPP [14], cobalt-labelling has shown either no effect or a small positive cooperativity. This study on EDTP is the first example of significant negative cooperativity, in which cobalt-labelling of the C-terminal site substantially retards the rate of iron release from the N-terminal site. This is almost entirely owing to a sharp decrease in k_{max} from 0.020 to 0.0012 min^{-1}.

While the cooperativity effects in iron removal from the two transferrin binding sites tend to be rather modest, they are important in relation to attempts to simplify the fitting of the data on iron release from diferric transferrin. If there were no cooperativity between the two binding sites, then Eq. (2) would reduce to a simple two-exponential equation

$$A_t = (A_0 - A_\infty)(0.5\,e^{-k_C t} - +0.5\,e^{-k_N t}) + A_\infty \quad (6)$$

where k_C and k_N are the rate constants for the indi-

vidual binding sites. This equation was used with apparent success to fit the absorbance data on iron removal from diferric transferrin by high concentrations of EDTP and NTP [33]. However, Bali and Harris [20] showed that even though Eq. (6) gave an excellent fit to the experimental data on iron removal from diferric transferrin by PP_i, there were serious inconsistencies between the resulting rate constants for diferric transferrin and the rate constants measured for iron removal from the purified monoferric transferrins.

Equation (5) is also a two-exponential fit of the absorbance data, where it is assumed that k_{2C} and k_{2N} are similar to each other, and that each is much smaller than the sum of $k_{1C}+k_{1N}$ [25]. This equation is more flexible than Eq. (6), allowing for different pre-exponential terms and for cooperativity between the two sites. However, even these less restrictive assumptions are not valid for iron removal by EDTP. The values of k_{2C} and k_{2N} differ by almost a factor of 2, and the sum of $k_{1C}+k_{1N}$ is approximately equal to the average of k_{2C} and k_{2N}. Nevertheless, Eq. (5) still gives an excellent fit to the absorbance data reported here on iron removal from diferric transferrin by EDTP. The only indication that anything is wrong is the fact that the values of m_1 and m_2 are inconsistent with the results on the purified monoferric transferrins.

Similar discrepancies between m_1 and m_2 and corresponding data on monoferric transferrins have been reported for iron removal by NTP [17]. The critical point to be made here is not that Eq. (5) is necessarily invalid for all ligands, but that the quality of the fit of absorbance *vs* time is not a good criterion for judging the validity of the calculated values of m_1 and m_2. Thus one must be cautious in accepting results on iron removal from diferric transferrin based on two-exponential fits unless some corroborating data from monoferric transferrins is available.

Mechanisms for iron release. Iron removal from the N-terminal binding site by EDTP follows simple saturation kinetics. Similar results have been observed for LICAMS [16], AHA [10], mimosine [15] and tiron [15]. Such results are consistent with a rate-limiting conformational change during iron removal as first proposed by Cowart *et al.* [10]. This simple conformational change mechanism is shown below.

$$\text{Fe–CO}_3\text{–Tf} \underset{k_{-1}}{\overset{k_1}{\rightleftharpoons}} \text{Fe–CO}_3\text{–Tf*} \qquad (7)$$

$$\text{Fe–CO}_3\text{–Tf*} + \text{L} \underset{k_{-2}}{\overset{k_2}{\rightleftharpoons}} \text{L–Fe–CO}_3\text{–Tf*} \qquad (8)$$

$$\text{L–Fe–CO}_3\text{–Tf*} \underset{k_{-3}}{\overset{k_3}{\rightleftharpoons}} \text{HCO}_3\text{–Tf*} + \text{Fe–L} \qquad (9)$$

$$\text{apoTf*} + \text{HCO}_3 \overset{K_C}{\rightleftharpoons} \text{HCO}_3\text{–Tf*} \qquad (10)$$

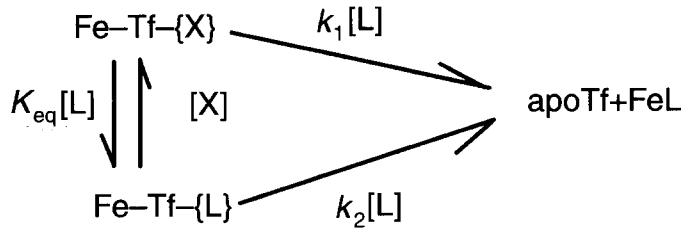
The asterisk is used to denote an "open", reactive form of the protein. At high ligand concentration, the forward reaction in Eq. (7) becomes rate limiting. Since this step does not involve the ligand, one observes saturation kinetics with respect to the free ligand concentration.

Kretchmar and Raymond [13] have shown that the rates of iron removal by LICAMS extrapolate essentially to zero at zero ionic strength, and they have proposed that a critical anion binding site on the protein must be occupied in order for iron removal to occur. This site is often referred to as the *ki*netically *s*ignificant *a*nion *b*inding (KISAB) site [12,19]. This nomenclature serves to distinguish clearly this site from the binding of the synergistic bicarbonate anion. In the absence of added salts, the KISAB site is presumably filled by an anion from the buffer or by an anionic ligand. Although the KISAB site has not been structurally characterized, it has been suggested, based on the transferrin crystal structure, that it may involve cationic amino acid side chains that project into the interdomain cleft near the metal binding site [7,9].

There have been several reports that the addition of perchlorate accelerates iron release from the C-terminal binding site, but retards the rate of iron release from the N-terminal binding site [11,12,18,19,23,24]. The present study shows that the addition of perchlorate produces a sharp decrease in k_{max} for the saturation pathway of Tf–Fe_N from 0.020 to 0.0012 min^{-1}. The value of k''' for the N-terminal site is zero with or without perchlorate. Thus one cannot regard occupancy of the KISAB site as a simple on/off switch between native and modified forms of the protein, since replacing an anion from the buffer with perchlorate alters the value of k_{max} of the modified form. These results are essentially consistent with the kinetic model of Bertini *et al.* [11], which contains two saturation pathways linked by an anion binding equilibrium. It is also noteworthy that with EDTP, the binding of a cobalt ion at the C-terminal site produces much the same shift from one saturation process to a second, much slower saturation pathway.

Iron removal from Fe_C–Tf by EDTP shows a complex combination of saturation and first-order kinetics. As Fig. 4 shows, perchlorate accelerates both the saturation and the first-order components of iron release. There is an increase in k_{max} for the saturation pathway from 0.0083 to 0.0407 min^{-1}, as well as an increase in the first-order rate constant k''' from 0.036 to 0.148 min^{-1}. These results are consistent with the existence of two independent pathways for iron release, one that shows saturation kinetics and one that is first order in ligand, each of which can be affected by added anions. Such a mechanism is flexible enough to explain the salt effects and to accommodate the observations that some ligands, such as LICAMS and AHA, follow simple saturation kinetics [10,16], while other ligands, such as NTA and DTPA, follow simple first-order kinetics [14,17].

We have suggested that the first-order pathway is related to a disruption of the binding of the synergistic



Scheme 2.

bicarbonate anion by an anionic functional group of the ligand. It is well known that many different ligands (e.g. NTA, EDTA and oxalate) can form weak Fe–L–Tf ternary complexes [34,35], which would be expected to dissociate quickly into FeL and apoTf. Recent studies on the R124K and R124S mutants of the transferrin N-terminal half-molecule have confirmed that modification of the binding site arginine residue significantly accelerates iron removal by pyrophosphate, although iron removal from R124K continues to follow saturation kinetics with respect to pyrophosphate [26].

Recent crystallographic data indicate a degree of structural flexibility in the binding of the synergistic anion. In dicupric transferrin the carbonate anion in the C-terminal site is bidentate, while the anion in the N-terminal site is only monodentate [36]. Thus it is also possible that the first-order pathway might involve a direct attack of the ligand on the metal and a shift in the mode of coordination of the anion from bidentate to monodentate. One potential weakness of these hypotheses for the first-order pathway is that to avoid the rate limitations of the conformational change, one must accept that ligands have direct access to the iron even in the closed form of the Fe–CO_3–Tf complex.

Another mechanism for iron removal has been proposed, which consists of two first-order processes linked by the pre-equilibrium binding of an anion to the KISAB site [12,18,19], as shown in Scheme 2, where the { } brackets are used to denote the KISAB anion binding site. At low ligand concentration, the KISAB site is presumably occupied by an inorganic anion (X) from the buffer or from added salts [13]. As the ligand concentration increases, the ligand competes with the original anion for occupancy of the KISAB site. The appearance of complex ligand dependence curves is attributed to the conversion of Fe–Tf–{X}, with a faster first-order rate constant for iron removal, to Fe–Tf–{L}, with a slower first-order rate constant, i.e. k_2 must be smaller than k_1.

Since k_2 reflects the rate of iron release when the KISAB site is occupied by the ligand, this mechanism requires that for a given chelating agent, k_2 must be independent of any added anion. Egan *et al.* [12] evaluated the effect of several anions on iron removal from the C-terminal site at a series of PP_i concentrations, and found that, as predicted, these anions had no effect on k_2. The rate constant k_2 from Scheme 2 is mathematically equivalent to k''' in Eq. (3). Thus it is significant that the results reported here on EDTP show that the addition of perchlorate results in a very substantial increase in k''' from 0.036 to 0.148 min^{-1}. This indicates that the observation made by Egan *et al.* [12] that the slope of the linear portion of complex kinetic ligand dependence curves is unaffected by added anions, may be true for PP_i but it cannot be accepted as a general statement for other ligands. In addition, it is difficult to account for systems that show simple saturation kinetics as a combination of two first-order pathways. We believe that the only way to account for the range of kinetic behaviours observed with different ligands is to allow for two independent pathways, one which shows saturation kinetics and the other of which is first-order in ligand. The results of this study require that this model be expanded to allow for the binding of anions to a KISAB site. This anion binding can affect both pathways and may either accelerate or retard the rates of iron removal.

Acknowledgement—This work was supported by grant no. DK R01 35533 from the National Institutes of Health.

REFERENCES

1. Harris, D. C. and Aisen, P., in *Iron Carriers and Iron Proteins*, ed. T. M. Loehr. VCH Publishers, New York, 1989, pp. 239–352.
2. Aisen, P., in *Iron Carriers and Iron Proteins*, ed. T. M. Loehr. VCH Publishers, New York, 1989, pp. 353–372.
3. Brock, J. H., in *Metalloproteins, Part II*, ed. P. Harrison. Macmillan, London, 1985, pp. 183–262.
4. Bates, G. W., Graybill, G. and Chidambaram, M. V., in *Control of Animal Cell Proliferation*, Vol. II, ed. A. L. Boynton and H. L. Leffert. Academic Press, New York, 1987, pp. 153–202.
5. Bailey, S., Evans, R. W., Garratt, R. C., Gorinsky, B., Hasnain, H., Horsburgh, C., Jhoti, H., Lindley, P. F., Mydin, A., Sarra, R. and Watson, J. L., *Biochemistry* 1988, **27**, 5804.
6. Anderson, B. F., Baker, H. M., Dodson, E. J., Norris, G. E., Rumball, S. V., Waters, J. M. and Baker, E. M., *Proc. Natl. Acad. Sci. U.S.A.* 1987, **84**, 1769.
7. Baker, E. N. and Lindley, P. F., *J. Inorg. Biochem.* 1992, **47**, 147.

8. Sarra, R., Garratt, R. C., Gorinsky, B., Jhoti, H. and Lindley, P. F., *Acta Cryst.* 1990, **B46,** 763.
9. Anderson, B. F., Baker, H. M., Norris, B. E., Rice, D. W., Baker, E. N., *J. Mol. Biol.* 1989, **209,** 711.
10. Cowart, R. E., Kojima, N. and Bates, G. W., *J. Biol. Chem.* 1982, **257,** 7560.
11. Bertini, I., Hirose, J., Kozlowski, H., Luchinat, C., Messori, L. and Scozzafava, A., *Inorg. Chem.* 1988, **27,** 1081.
12. Egan, T. J., Ross, D. C., Purves, L. R. and Adams, P. A., *Inorg. Chem.* 1992, **31,** 1994.
13. Kretchmar, S. A. and Raymond, K. N., *Inorg. Chem.* 1988, **27,** 1436.
14. Harris, W. R., Bali, P. K. and Crowley, M. M., *Inorg. Chem.* 1992, **31,** 2700.
15. Kretchmar Nguyen, S. A., Craig, A. and Raymond, K. N., *J. Am. Chem. Soc.* 1993, **115,** 6758.
16. Kretchmar, S. A. and Raymond, K. N., *J. Am. Chem. Soc.* 1986, **108,** 6212.
17. Bali, P. K., Harris, W. R. and Nesset-Tollefson, D., *Inorg. Chem.* 1991, **30,** 502.
18. Marques, H. M., Egan, T. J., Pattrick, G., *S. African J. Sci.* 1990, **86,** 21.
19. Marques, H. M., Watson, D. L. and Egan, T. J., *Inorg. Chem.* 1991, **30,** 3758.
20. Bali, P. K. and Harris, W. R., *J. Am. Chem. Soc.* 1989, **111,** 4457.
21. Anderson, B. F., Baker, H. M., Norris, G. E., Rumball, S. V. and Baker, E. N., *Nature* 1990, **344,** 784.
22. Williams, J., Chasteen, N. D. and Moreton, K., *Biochem. J.* 1982, **201,** 527.
23. Baldwin, D. A. and de Sousa, D. M. R., *Biochem. Biophys. Res. Com.* 1981, **99,** 1101.
24. Harris, W. R. and Bali, P. K., *Inorg. Chem.* 1988, **27,** 2687.
25. Baldwin, D. A., *Biochim. Biophys. Acta* 1980, **623,** 183.
26. Zak, O., Aisen, P., Crawley, J. B., Joannou, C. L., Patel, K. J., Rafiq, M. and Evans, R. W., *Biochemistry* 1995, **34,** 14428.
27. Harris, W. R., Rezvani, A. B. and Bali, P. K., *Inorg. Chem.* 1987, **26,** 2711.
28. Bali, B. K. and Harris, W. R., *Arch. Biochem. Biophys.* 1990, **281,** 251.
29. Busing, W. R. and Levy, H. A., Report ORNL-TM-271, Oak Ridge National Laboratories, Oak Ridge, TN, 1962.
30. Makey, A. G. and Seal, U. S., *Biochim. Biophys. Acta* 1976, **453,** 4457.
31. Hamilton, W. C., *Statistics in Physical Science.* Ronald Press, New York, 1964, pp. 157–162.
32. Regoeczi, E., Bolyos, M. and Nieboer, E., *Analyst* 1995, **120,** 733.
33. Harris, W. R., *J. Inorg. Biochem.* 1984, **21,** 263.
34. Schlabach, M. R. and Bates, G. W., *J. Biol. Chem.* 1975, **250,** 2182.
35. Dubach, J., Gaffney, B. J., More, K., Eaton, G. R. and Eaton, S. S., *Biophys. J.* 1991, **59,** 1091.
36. Shongwe, M. S., Smith, C. A., Ainscough, E. W., Baker, H. M., Brodie, A. M. and Baker, E. N., *Biochemistry* 1992, **31,** 4451.

Pergamon

PII: S0277-5387(96)00387-7

Polyhedron Vol. 16, No. 7, pp. 1081–1088, 1997
Copyright © 1997 Elsevier Science Ltd
Printed in Great Britain. All rights reserved
0277-5387/97 $17.00+0.00

Synthesis and X-ray crystal structures of imido and isodiazene complexes of vanadium, niobium and tantalum

Andreas A. Danopoulos,[a] Robyn S. Hay-Motherwell,[a] Geoffrey Wilkinson,✠ Tracy K. N. Sweet[b] and Michael B. Hursthouse[b]*

[a]Johnson Matthey Laboratory, Chemistry Department, Imperial College, London SW7 2AY, U.K.

[b]Department of Chemistry, University of Wales, Cardiff, PO Box 912, Cardiff CF1 3TB, U.K.

(Received 23 July 1996; accepted 6 August 1996)

Abstract—Interaction of $[M(NBu^t)(NHBu^t)(H_2NBu^t)Cl_2]_2$, M = Nb, Ta, with five equiv. of Bu^tNHLi gave $\{[M(NBu^t)_3(NHBu^t)]Li_2\}_2$, M = Nb (**2a**), M = Ta (**2b**), which showed the presence of three different *tert*-butylimido groups and resisted further metallation. Interaction of MCl_5, M = Nb, Ta, with 1-amino-2,2,6,6-tetramethylpiperidine, $C_9H_{18}NNH_2$, in the presence of Me_3SiCl–Et_3N gave $(Et_3NH)[M(C_9H_{18}N_2)_2Cl_4]$, M = Nb (**3a**), M = Ta (**3b**). A similar interaction with NH_4VO_3 gave low yields of $[(C_9H_{18}N_2)_2(OSiMe_3)_2V(\mu\text{-}O)V(O)(OSiMe_3)_2]$ (**4**). The X-ray crystal structures of (**2a**), (**3b**) and (**4**) have been determined. Copyright © 1997 Elsevier Science Ltd

Keywords: imido complexes; isodiazene complexes; vanadium; niobium; tantalum; crystal structures.

Anionic homoleptic *tert*-butylimido complexes $M(NBu^t)_4Li_2$, M = Mo, W [1a], Cr [1b], $Re(NBu^t)_4Li(tmed)$ [1c] and $Mn(NBu^t)_4Li_2(dme)_2$ [1d] were prepared by deprotonation of the complexes $M(NBu^t)_2(NHBu^t)_2$, M = Cr, Mo, W, $Re(NBu^t)_3(NHBu^t)$ and interaction of $Mn(NBu^t)_3Cl$ with $LiNHBu^t$ under specific conditions. This paper describes attempts to prepare homoleptic *tert*-butylimido complexes of niobium and tantalum.

Isodiazene complexes of tungsten and rhenium using the bulky hydrazine, 1-amino-2,2,6,6-tetramethylpiperidine, have been structurally characterized [2]. The extension of this chemistry to group 5 metals is also described.

RESULTS AND DISCUSSION

tert-*Butylimido complexes*

From the range of known *tert*-butylimido complexes of niobium and tantalum [3], $[M(NBu^t)(NHBu^t)(H_2NBu^t)Cl_2]_2$, M = Nb (**1a**), M = Ta (**1b**), seemed to be good starting materials for the synthesis of imido-amido complexes, which in turn could be deprotonated to anionic imido complexes by strongly basic alkyl lithiums. Interaction of **1a** or **1b** with 6 equiv. of $LiNHBu^t$ in diethyl ether gave, after work-up, oils, the ^1H NMR of which consisted of one broad and one sharp *tert*-butyl peaks in approximate ratio 3:1. Although a plausible formulation for these oils is $M(NBu^t)$ e.g. $(NHBu^t)_3$ (M = Nb, Ta), which is supported by their reactivity with $LiNHBu^t$ (see below), no attempt at further characterization was undertaken. Interaction of the dimers **1a** or **1b** with 10 equiv. of Bu^tNHLi in ether gave, after work-up, good yields of $\{[M(NBu^t)_3(NHBu^t)]Li_2\}_2$ M = Nb (**2a**); M = Ta (**2b**), as colourless, extremely air-sensitive prisms. Compounds **2a** and **2b** could also be obtained, but in lower yields, by reactions of the above mentioned oils with 3 equiv. of Bu^tNHLi. It is worth noting that neither higher $(Bu^tNHLi):\mathbf{1}$ ratios, nor interaction of **2a** or **2b** with Bu^nLi or MeLi, resulted in deprotonation of the remaining *tert*-butylamido group. An analogous situation was observed by Wigley [4] who reported the preparation of $[Li(thf)_2][M(Nmes)_3(NHmes)]$ M = Nb, Ta, mes = 2,4,6-trimethylphenyl.

* Author to whom correspondence should be addressed.

The crystal structure of **2a** has been determined by X-ray diffraction and is shown in Fig. 1; selected bond lengths and angles are in Table 1. There are two crystallographically independent centrosymmetric dimers in each of which two $Nb(NBu^t)_3(NHBu^t)$ units are linked by N···Li···N bridges. The four lithium cations of each dimer exhibit positional disorder and fractionally occupy six sites in the form of a cyclohexane-type ring (Fig. 1). A similar situation was observed in the related dimer $[W_2(NBu^t)_8Li_4]$ [5]. In the present case the amido function is presumed to be contained within the bridging system, since the terminal ligand is a normal, linear 6e *tert*-butylimido. The two imido groups on each niobium which are involved in the bridging are bent, presumably as a result both of the lithium coordination and the over availability of π-electrons for an 18e niobium count. Whilst there may be some disorder of the three bridged ligands, linked to the disorder of the lithiums, it would seem that the amide predominantly occupies the N(n4) site, which has the longest bond and the smallest Nb—N—C angle. The amide protons were not, however, located on a difference map. The lithium cations can formally be considered as four-coordinate. Three sites are occupied by nitrogen atoms with Li···N interactions ranging between 1.92(3) and 2.20(3) Å, and the fourth site taken up by an "agostic" interaction with a methyl group, with Li···C distances ranging from 2.50(2) to 2.66(2) Å.

Compounds **2a** and **2b** show identical spectroscopic (IR, NMR) behaviour. The ν(N—H) in the IR is at 3175 cm^{-1}, while in the ^1H NMR spectrum there are four inequivalent *tert*-butyl groups in the ratio 1 : 1 : 1 : 1. These are assigned to one linear *tert*-butylimido, one *tert*-butylamido and two *tert*-butylimido groups associated with lithium atoms. The chemical inequivalence of these four groups is consistent with an arrangement in which one lithium atom is bridging two imido groups, while the other is bridging one imido and one amido groups. Each lithium site connects the two NbN_4 tetrahedra by association with three nitrogen atoms, therefore, each cation is bound to two bridging imido nitrogen atoms and one amido nitrogen atom. This is further supported by the presence of two inequivalent lithium environments in the ^7Li NMR spectrum.

Compounds **2a** and **2b** reacted with C_6H_5SeBr in petroleum to give low yields of oily products which were characterized by EI mass spectra as $(Bu^tN)M(NHBu^t)(Bu^tNSePh)_2$, M = Nb, Ta, but crystalline compounds could not be obtained. Similar compounds have been obtained by interaction of $W(NBu^t)_4Li_2$ with C_6H_5SCl [6].

Isodiazene complexes

In a previous paper [2] we reported on the interaction of 1-amino-2,2,6,6-tetramethylpiperidine with tungsten and rhenium oxo-complexes to obtain com-

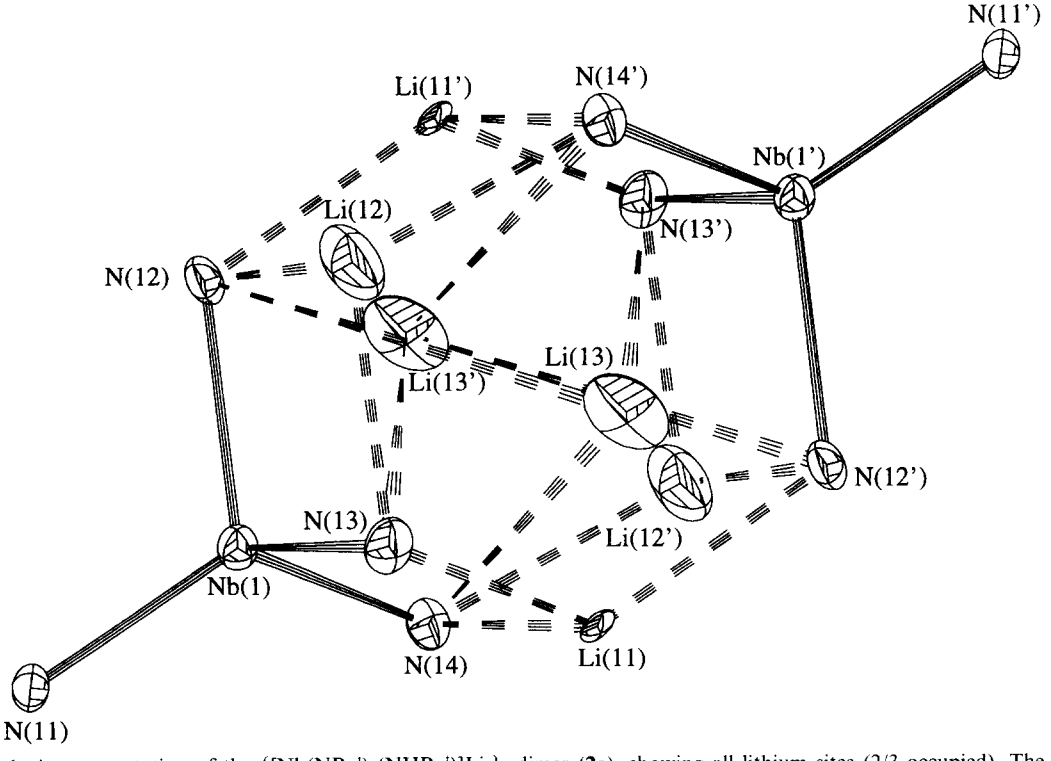


Fig. 1. A representation of the $\{[Nb(NBu^t)_3(NHBu^t)]Li_2\}_2$ dimer (**2a**), showing all lithium sites (2/3 occupied). The Bu^t carbon atoms have been omitted for clarity.

Table 1. Selected bond lengths (Å) and angles (°) for $\{[Nb(NBu^t)_3(NHBu^t)]Li_2\}_2$ (**2a**) with e.s.d.s in parentheses

	$n = 1$	$n = 2$
Nb(n)—N($n1$)	1.810(6)	1.782(6)
Nb(n)—N($n2$)	1.980(7)	1.949(6)
Nb(n)—N($n3$)	2.000(7)	2.011(7)
Nb(n)—N($n4$)	2.023(6)	2.029(7)
N($n1$)—C($n1$)	1.447(10)	1.489(9)
N($n2$)—C($n2$)	1.486(9)	1.485(9)
N($n3$)—C($n3$)	1.500(10)	1.522(10)
N($n4$)—C($n4$)	1.494(11)	1.478(10)
N($n1$)—Nb(n)—N($n2$)	117.9(2)	115.9(3)
N($n1$)—Nb(n)—N($n3$)	114.5(3)	116.5(3)
N($n1$)—Nb(n)—N($n4$)	116.1(3)	115.8(3)
N($n2$)—Nb(n)—N($n3$)	102.3(3)	103.0(3)
N($n2$)—Nb(n)—N($n4$)	102.3(3)	103.0(3)
N($n3$)—Nb(n)—N($n4$)	101.5(2)	100.5(3)
Nb(n)—N($n1$)—C($n1$)	175.5(5)	177.3(6)
Nb(n)—N($n2$)—C($n2$)	138.2(5)	135.0(5)
Nb(n)—N($n3$)—C($n3$)	133.4(6)	132.2(5)
Nb(n)—N($n4$)—C($n4$)	130.1(5)	132.1(5)
N($n2'$)—Li($n1$)—N($n3$)	116.8(11)	—
N($n2'$)—Li($n1$)—N($n4$)	115.6(10)	—
N($n3$)—Li($n1$)—N($n4$)	96.7(8)	—
N($n3''$)—Li($n1$)—N($n4$)	—	114.0(12)
N($n4$)—Li($n1$)—N($n2$)	—	92.8(9)
N($n3''$)—Li($n1$)—N($n2$)	—	115.3(12)
N($n3$)—Li($n2$)—N($n4'$)	112.6(10)	—
N($n3$)—Li($n2$)—N($n2$)	93.7(11)	—
N($n4'$)—Li($n2$)—N($n2$)	111.0(12)	—
N($n2''$)—Li($n2$)—N($n3$)	—	117.4(12)
N($n2''$)—Li($n2$)—N($n4$)	—	114.5(11)
N($n3$)—Li($n2$)—N($n4$)	—	92.1(8)
N($n3'$)—Li($n3$)—N($n2$)	117.4(14)	—
N($n3'$)—Li($n3$)—N($n4$)	116.7(12)	—
N($n2$)—Li($n3$)—N($n4$)	92.8(10)	—
N($n4''$)—Li($n3$)—N($n3$)	—	111.7(12)
N($n4''$)—Li($n3$)—N($n2$)	—	114.4(11)
N($n2$)—Li($n3$)—N($n3$)	—	94.7(10)

Where $n = 1$ (molecule 1) or 2 (molecule 2); ′ represents the symmetry transformation $-x+1, -y, -z+1$; ″ represents the symmetry transformation $-x+2, -y+1, -z$.

pounds which, on the grounds of structural data and oxidation state arguments, were classified as isodiazene complexes rather than hydrazido (2^-) species. Extension of this chemistry to group 5 metals led to isolation of anionic complexes $(Et_3NH)[M(N_2C_9H_{18})_2Cl_4]$ (**3a**), M = Nb; (**3b**) M = Ta. They were prepared in satisfactory yields in benzene from MCl_5 (M = Nb, Ta) in the presence of Et_3N/Me_3SiCl, which is thought to form *in situ* trimethylsilylhydrazine. They were crystallized from toluene as toluene solvates, which prevented informative and reproducible combustion analyses due to solvent loss.

The structure of **3b** was determined by X-ray crystallography and is shown in Fig. 2; selected bond lengths and angles are in Table 2. The tantalum centre has distorted octahedral geometry with *cis*-$C_9H_{18}N_2$ groups. Close intermolecular contacts are found between the octahedral face defined by Cl(2), Cl(3) and Cl(4) and the triethylammonium cation [N(3)···Cl distances range between 3.40(1) and 3.46(1) Å]. The Ta—N—N unit is nearly linear [176.5(5) and 176.4(5)°], while the *exo* nitrogen atoms N(11) and N(21) are planar [angle sum 357.5(2) and 357.2(2)°, respectively]. Their planes are approximately aligned with the meridional planes of the octahedron [i.e. plane of N(11) with that defined by N(1), Ta, Cl(1), Cl(3) and of N(21) with that defined by N(2), Ta, Cl(1) and Cl(3)]. There are two types of Ta—Cl distances, the longest being *trans* to the N ligands, indicative of a certain degree of *trans* influence exerted by the $C_9H_{18}N_2$ group. The Ta—N distances [1.865(7) and 1.882(6) Å] and the N—N distances [1.283(9) and 1.259(8) Å] are both within the range between single and double bonds. Thus, metrical data of the Ta—N—N moiety strongly support the presence of extensive π-interaction delocalized over the metal and nitrogen atoms. Various resonance forms have been invoked to describe the bonding in compounds of type MN_2R_4 [2], e.g.

$$M \leftarrow N^- {=}^+ NR_2 \quad M^- — \ddot{N} {=}^+ NR_2$$

$$M{=}\ddot{N}—\ddot{N}R_2 \quad M^- {\equiv}^+ N—NR_2$$

making the unambiguous assignment of formal metal oxidation states difficult. The two extreme models of hydrazido (2^-) and isodiazene (0) have been encountered in the literature [2]. In the present case an isodiazene formulation is preferred, since it gives a realistic oxidation state of (III) for the tantalum. In support of this is the observation of Ta—Cl(1) and Ta—Cl(3) distances [2.451(2) and 2.472(2) Å], which are longer than those reported for the tantalum(V) compounds [7] [2.317(2)–2.362(2) Å].

The diamagnetism of **3b** may be ascribed to pairing of the two *d*-electrons occupying the lowest energy single orbital resulting from π-perturbation because of the isodiazene ligands.

The identical ^1H NMR spectra of **3a** and **3b** suggest that they are isostructural.

Interaction of NH_4VO_3 with $H_2NNC_9H_{18}$ in neat Me_3SiCl/Et_3N (see Experimental) gave crystals of $[(C_9H_{18}N_2)_2(OSiMe_3)_2V(\mu\text{-}O)V(O)(OSiMe_3)_2]$ (**4**). This could not be obtained free of siloxanes even after repeated recrystallizations from petroleum.

The structure was unequivocally determined by X-ray crystallography and is shown in Fig. 3; selected bond lengths and angles are in Table 3. It is an asymmetric oxo-bridged dimer. The coordination geometry at V(1) can be best described as trigonal bypyramidal; the axial sites are occupied by one $C_9H_{18}N_2$ ligand and the bridging oxo atom, while an additional $C_9H_{18}N_2$ and two $OSiMe_3$ groups are in the equatorial position [coordination angles: N(1)—V(1)—O(1) = 171.97(11)°, the angles in the equatorial plane range between 117.68(12) and 120.22(11)°]. The coord-

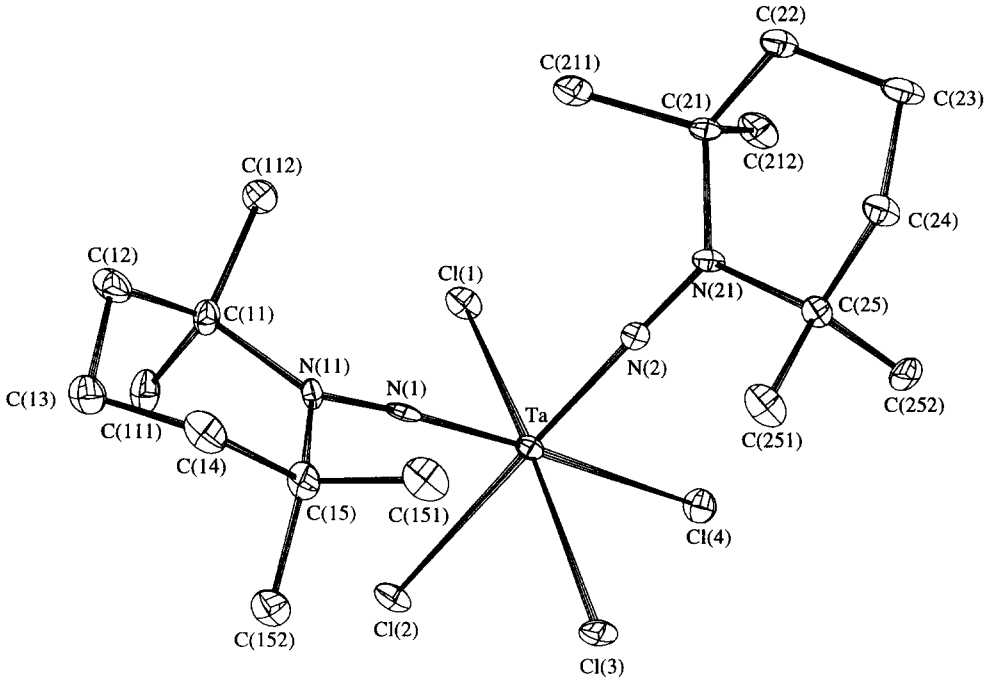


Fig. 2. The structure of the $[Ta(C_9H_{18}N_2)_2Cl_4]^-$ anion of **3b**.

Table 2. Selected bond lengths (Å) and (°) for the $[Ta(C_9H_{18}N_2)_2Cl_4]^-$ anion of **3b**, with e.s.d.s in parentheses

Ta—N(1)	1.865(7)
Ta—N(2)	1.882(6)
Ta—Cl(1)	2.451(2)
Ta—Cl(2)	2.553(2)
Ta—Cl(3)	2.472(2)
Ta—Cl(4)	2.535(3)
N(1)—N(11)	1.283(9)
N(2)—N(21)	1.259(8)
Cl(1)—Ta—Cl(2)	83.12(6)
Cl(1)—Ta—Cl(3)	163.64(7)
Cl(1)—Ta—Cl(4)	85.58(9)
Cl(1)—Ta—N(1)	96.3(2)
Cl(1)—Ta—N(2)	96.0(2)
Cl(2)—Ta—Cl(3)	84.23(6)
Cl(2)—Ta—Cl(4)	87.04(6)
Cl(2)—Ta—N(1)	91.2(2)
Cl(2)—Ta—N(2)	177.7(2)
Cl(3)—Ta—Cl(4)	83.44(9)
Cl(3)—Ta—N(1)	94.3(2)
Cl(3)—Ta—N(2)	96.2(2)
Cl(4)—Ta—N(1)	177.3(2)
Cl(4)—Ta—N(2)	90.8(2)
N(1)—Ta—N(2)	91.0(2)
Ta—N(1)—N(11)	176.5(5)
Ta—N(2)—N(21)	176.4(5)

ination geometry at V(2) is distorted tetrahedral comprising two $OSiMe_3$ groups, one terminal oxo and one bridging oxo atoms. The metrical data for the V—N—N moiety on V(1) observed here, e.g. short N—N [1.285(3)–1.245(4) Å], V—N [1.725(2)–1.781(3) Å] bonds and planar *exo*-nitrogen atoms [angle sums 356.6 and 359.9° around N(11) and N(21), respectively], resemble those already discussed above for **3b**, again pointing to an isodiazene as the best description of the nitrogen ligand. Of particular interest is the almost linear highly asymmetric oxo-bridge. In this V(2)—O(1) [1.650(2) Å] is only slightly longer than the terminal V(2)—O(6) [1.616(2) Å] and is in contrast with the long V(1)—O(1) bond [2.175(2) Å], the latter indicating weakening of the bond between V(1) and the bridging oxygen O(1). An explanation of this asymmetry could be found in the different electronic environment of the vanadium atoms: V(1), formally a V^{III} centre, is π-electron rich and, therefore, is not involved in any π-type interactions with the oxo-group. V(2) is more π-acidic, resulting in strong vanadium–oxygen bonds. The slight difference in V—$OSiMe_3$ distances between the two metal centres underlines the nature of siloxides as "spectator" ligands.

The same compound could be obtained when using $VOCl_3$, V_2O_5 or $VOCl_2(OSiMe_3)$ instead of NH_4VO_3, although purification was even more difficult. Replacement of the last oxo group from the vanadium proved impossible even after prolonged reaction times.

EXPERIMENTAL

Analyses were by the Imperial College microanalytical laboratory. All operations were carried out under purified Ar or N_2, or in a Vacuum Atmospheres

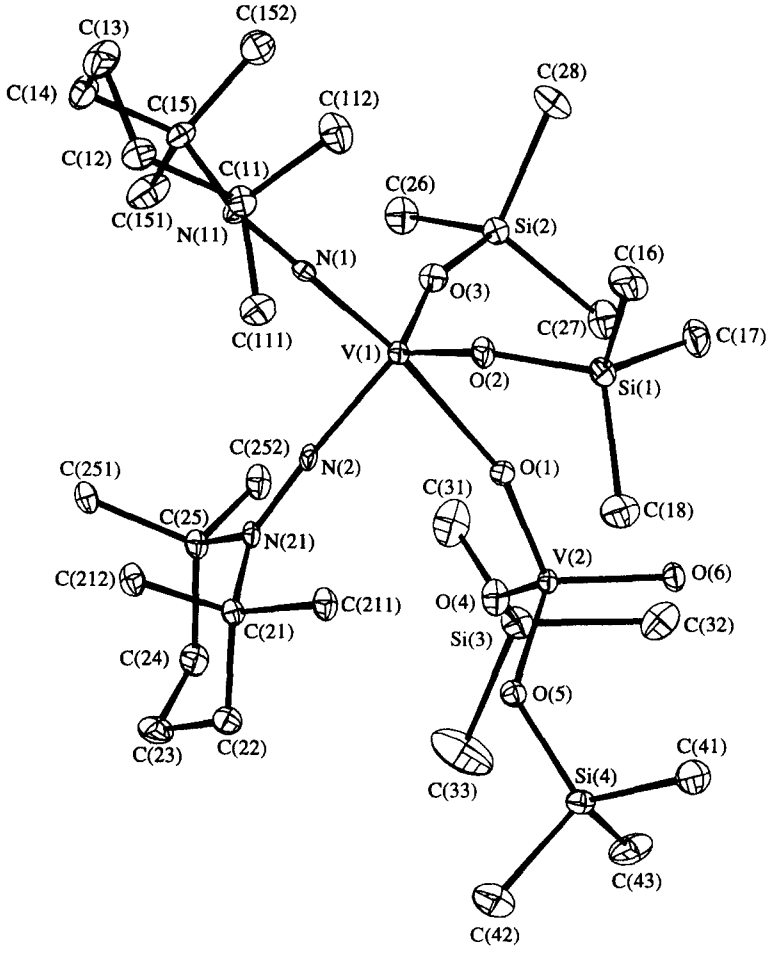


Fig. 3. The structure of $[(C_9H_{18}N_2)_2(OSiMe_3)_2V(\mu\text{-}O)V(O)(OSiMe_3)_2]$ (**4**).

glove-box. All solvents were degassed and distilled before use.

NMR data were obtained using a JEOL EX-270 or Bruker Avance DRX-300 spectrometer operating at 270 or 300 MHz (^1H), respectively, and referenced to the residual proton impurity in the solvent (δ 7.15 C_6D_6). Mass spectra were obtained on a VG-7070E or VG Autospec spectrometers.

Commercial chemicals were from Aldrich and Avocado Chemicals.

The following starting materials were prepared according to literature procedures: $[Nb(NBu^t)(HNBu^t)(H_2NBu^t)Cl_2]_2$ [8], $[Ta(NBu^t)(NHBu^t)(H_2NBu^t)Cl_2]_2$ [8] $H_2NNC_9H_{18}$ [9]. Bu^tNHLi was obtained by interaction of Bu^nLi with Bu^tNH_2 in hexanes. The petroleum used throughout had a boiling point of 40–60°C.

Dilithiumtris(tert-*butylimido*)(tert-*butylamido*) *niobate*(**2a**)

To a solution of $[(Bu^tN)Nb(HNBu^t)(H_2NBu^t)Cl_2]_2$ (0.76 g, 1 mmol) at −78°C in Et_2O (*ca* 50 cm^3) was added a suspension of Bu^tNHLi [0.79 g, 10 mmol in Et_2O (30 cm^3)]. The mixture was allowed to warm to room temperature and stirred overnight. Evaporation of volatiles under reduced pressure, extraction of residue with hot petroleum (5×30 cm^3), filtration and concentration of filtrate to *ca* 30 cm^3 and standing at room temperature overnight gave colourless prisms. Yield 0.55 g 70%; m.p. > 230°C (decomposition). X-ray quality crystals were obtained by slow cooling solutions in toluene. [Found (calc.): C, 49.2 (49.1); H, 9.4 (9.4); N, 15.0 (14.3)%]. NMR (C_6D_6): ^1H: δ 2.6 (s, br, 1H, N*H*CMe$_3$), 1.83, 1.62, 1.59 (s, 9H each, NC*Me*$_3$), 1.47 (s, 9H, NHC*Me*$_3$). ^7Li: δ 2.5 and 2.0.

Dilithiumtris(tert-*butylimido*)(tert-*butylamido*) *tantalate*(**2b**)

As for **2a**, but from $[(Bu^tN)Ta(HNBu^t)(H_2NBu^t)Cl_2]_2$ (0.94 g, 1 mmol) and Bu^tNHLi (0.79 g, 10 mmol). Yield 0.69 g, 75%; m.p. > 230°C (decomposition). [Found (calc.): C, 39.8 (40.0); H, 7.5 (7.7); N, 11.6 (11.7)%]. NMR (C_6D_6) ^1H: δ 2.6 (s, br, 1H, N*H*CMe$_3$), 1.73, 1.49, 1.47 (s, 9H each, NC*Me*$_3$), 1.37 (s, 9H, NHC*Me*$_3$). ^7Li: δ 2.5 and 2.0.

Table 3. Selected bond lengths (Å) and angles (°) for $[(C_9H_{18}N_2)_2(OSiMe_3)_2V(\mu\text{-}O)V(O)(OSiMe_3)]_2$ (**4**) with e.s.d.s in parentheses

V(1)—N(1)	1.725(2)
V(1)—N(2)	1.781(3)
V(1)—O(1)	2.175(2)
V(1)—O(2)	1.827(2)
V(1)—O(3)	1.813(2)
V(2)—O(1)	1.650(2)
V(2)—O(4)	1.806(2)
V(2)—O(5)	1.810(2)
V(2)—O(6)	1.616(2)
Si(1)—O(2)	1.626(2)
Si(2)—O(3)	1.619(2)
Si(3)—O(4)	1.633(2)
Si(4)—O(5)	1.645(2)
N(1)—N(11)	1.285(3)
N(2)—N(21)	1.245(4)
N(1)—V(1)—N(2)	91.86(12)
N(1)—V(1)—O(1)	171.97(11)
N(1)—V(1)—O(2)	96.72(11)
N(1)—V(1)—O(3)	98.91(12)
N(2)—V(1)—O(1)	80.32(10)
N(2)—V(1)—O(2)	117.68(12)
N(2)—V(1)—O(3)	119.00(12)
O(1)—V(1)—O(2)	85.42(9)
O(1)—V(1)—O(3)	86.59(9)
O(2)—V(1)—O(3)	120.22(11)
V(1)—N(1)—N(11)	176.4(2)
V(1)—N(2)—N(21)	174.3(2)
V(1)—O(1)—V(2)	162.93(13)
V(1)—O(2)—Si(1)	142.11(14)
V(1)—O(3)—Si(2)	162.89(14)
O(1)—V(2)—O(4)	111.07(11)
O(1)—V(2)—O(5)	110.42(11)
O(1)—V(2)—O(6)	109.64(12)
O(4)—V(2)—O(5)	108.46(11)
O(4)—V(2)—O(6)	110.34(11)
O(5)—V(2)—O(6)	106.81(11)
V(2)—O(4)—Si(3)	148.00(14)
V(2)—O(5)—Si(4)	128.22(13)

(Triethylammonium)[tetrachlorobis(2,2,6,6-tetramethylpiperid-1-ylnitrene)tantalate(III) (**3b**) *and niobate(III)* (**3a**)

To $TaCl_5$ (0.3 g, 0.84 mmol) in benzene (10 cm^3) was added sequentially Et_3N (0.58 g, 4.2 mmol), 1-amino-2,2,6,6-tetramethylpiperidine (0.32 g, 2.1 mmol) then Me_3SiCl (0.53 g, 4.2 mmol). The mixture was stirred and refluxed under N_2 overnight. After cooling and removal of all volatiles *in vacuo*, the residue was washed with petroleum (20 cm^3) and extracted with toluene (2×30 cm^3). After filtration, reduction of volume of toluene to *ca* 15 cm^3 and cooling to $-20°C$, orange–red crystals were obtained. Yield 0.36–0.48 g, 60–70%. Recrystallization from toluene yielded crystals of X-ray quality. The crystals decomposed on drying *in vacuo* due to facile removal of toluene. Consequently, no satisfactory analytical results were obtained. ^1H NMR of various samples showed the presence of toluene to varying concentrations. NMR (C_6D_6) ^1H: δ 9.42 (s, br, 1H, Et_3NH), 2.56 [pseudoquartet, br, 6H $(CH_3CH_2)_3NH$], 1.85 (s, 12H, $Me_4C_5H_6$), 1.77 (s, 12H, $Me_4C_5H_6$), 1.33 (m, 12H, $Me_4C_5H_6$), 0.78 (t, br, 9H, $(CH_3CH_2)_3NH$].

The corresponding niobium compound could be prepared in the same way with or without the presence of C_6H_6. However, toluene was lost more readily from the final crystalline material. NMR (C_6D_6) ^1H: δ 9.42 (s, br, 1H, Et_3NH), 2.56 [pseudoquartet, br, 6H $(CH_3CH_2)_3NH$], 1.85 (s, 12H, $Me_4C_5H_6$), 1.77 (s, 12H, $Me_4C_5H_6$), 1.33 (m, 12H, $Me_4C_5H_6$), 0.78 [t, br, 9H, $(CH_3CH_2)_3NH$].

[Bis(2,2,6,6-tetramethylpiperid-1-ylnitrene)bis(trimethylsiloxo)]vanadium(μ-oxo)[bis(trimethylsiloxo)oxo]vanadium (**4**)

This compound could be prepared using any of the following starting materials, $VOCl_3$, NH_4VO_3, V_2O_5, $VOCl_2(OSiMe_3)$ [prepared from $VOCl_3$ using $(Me_3Si)_2O$ in the presence of Et_3N and Me_3SiCl] without benzene as solvent. NH_4VO_3 gave the cleanest product. To NH_4VO_3 (0.6 g, 6 mmol) was added sequentially with stirring, Et_3N (8 g, 25 mmol), 1-amino-2,2,6,6-tetramethylpiperidine (2.3 g, 15 mmol) then Me_3SiCl (8 cm^3, 25 mmol) and the mixture refluxed overnight. After cooling the volatiles were removed under vacuum and the dark residue was extracted with petroleum (2×50 cm^3). After concentration of extracts *in vacuo* to *ca* 5 cm^3 and cooling to $-30°C$, dark violet crystals were obtained. X-ray quality crystals were obtained after recrystallization from petroleum. Yield: 0.25 g, 20–30%. Repeated recrystallization from petroleum did not yield crystals of analytical purity due to contamination by silicon-containing oils and starting piperidine, as proved by NMR. NMR (C_6D_6) ^1H: δ 1.47 (s, 12H, $Me_4C_5H_6$), 1.01, 0.89, 0.86, 0.82 (each s, 6H, $Me_4C_5H_6$), 0.35 (s, 18H, $OSiMe_3$), 0.28 (s, 18H, $OSiMe_3$).

X-ray crystallography

X-ray data for compounds **2a**, **3b** and **4** were collected at low temperature (see Table 4) using a FAST TV area detector diffractometer with Mo-K_α radiation ($\lambda = 0.71069$ Å), as previously described [10]. The structures were solved *via* direct methods procedures of SHELXS-86 [11], and refined by full-matrix least-squares on F_0^2, using the program SHELXL-93 [12]. All unique data used were corrected for Lorentz polarization factors and for absorption using the program DIFABS [13], with maximum and minimum correction factors listed in Table 4. The non-hydrogen atoms were refined with anisotropic thermal parameters and the hydrogen atoms of **2a** and **3b** were

Table 4. Crystal data and structure refinement details for compounds **2a**, **3b** and **4**

Compound	**2a**	**3b**	**4**
Formula	$C_{32}H_{74}Li_4N_8Nb_2$	$C_{18}H_{36}Cl_4N_4Ta \cdot C_7H_8 \cdot C_6H_{16}N$	$C_{50}H_{72}N_4O_6Si_4V_2$
Mr	784.56	825.59	799.16
Crystal system	Triclinic	Monoclinic	Triclinic
Space group	$P\bar{1}$	$P2_1/c$	$P\bar{1}$
a (Å)	10.22(2)	10.198(8)	10.087(3)
b (Å)	13.92(2)	25.180(10)	12.597(4)
c (Å)	15.916(7)	15.292(10)	18.823(2)
α(°)	92.26(13)	90	70.65(1)
β(°)	100.7(2)	106.46(7)	87.77(5)
γ(°)	90.81(4)	90	87.20(2)
U (Å^3)	2222(4)	3766(2)	2253(1)
Z	2	4	2
D_c (Mg m^{-3})	1.173	1.456	1.178
F(000)	824	1688	860
Crystal size (mm)	0.18 × 0.18 × 0.15	0.42 × 0.15 × 0.12	0.36 × 0.18 × 0.12
μ(Mo-K_α) (mm^{-1})	0.499	3.229	0.546
Reflections collected	9384	14662	9619
Independent reflections (R_{int})	6117 (0.0718)	5596 (0.0642)	6225 (0.0537)
Data, restraints, parameters	6112, 0, 465	5589, 0, 366	6215, 0, 483
Goodness of fit, F^2	1.035	1.067	0.965
Final *R* indices R_1, wR_2, [$I > 2\sigma(I)$]	0.0540, 0.1080	0.0504, 0.1215	0.0421, 0.1016
R_1, wR_2 (all data)	0.0923, 0.1196	0.0665, 0.1472	0.0574, 0.1400
Largest difference peak and hole (e Å^{-3})	0.753, −0.499	3.632, −0.885	0.581, −0.342

$S = [\Sigma(w(F_o^2 - F_c^2)^2/(n-p))]^{1/2}$; $R_1 = \Sigma[(F_o - F_c)]/\Sigma F_o$; $wR_2 = [\Sigma w(F_o^2 - F_c^2)^2/\Sigma w(F_o^2)^2]^{1/2}$; $w = 1/[\sigma^2(F_o^2) + (xP)^2 + gP]$; $P = [\max(F_o^2) + 2(F_c^2)]/3$.

Where n = number of reflections, p = total number of parameters, x = 0, 0.0716, 0.0527 and g = 0, 0, 0 for compounds **2a**, **3b** and **4**, respectively.

included in idealised positions. Due to the uncertainties in positioning, hydrogen atoms on the Bu^t methyl groups of **1** associated with the Li interactions were omitted. The methylene protons of **4** were experimentally located whilst the methyl hydrogen atoms were placed in calculated positions. The solvent of crystallization, toluene, within the lattice of **3b** was shown to exhibit positional disorder. The carbon atoms were refined in split sites with partial occupancy factors and consequently hydrogen atoms were ignored in the refinement. All crystal data and refinement details are summarized in Table 4.

Additional material available from the Cambridge Crystallographic Data Centre comprises fractional atomic co-ordinates, thermal parameters and remaining bond lengths and angles.

Acknowledgements—We thank the EPSRC for support (A.A.D. and R.S.H.-M.) and for provision of X-ray facilities.

REFERENCES

1. Danopoulos, A. A., Wilkinson, G., Hussain-Bates, B. and Hursthouse, M. B., (a) *J. Chem. Soc., Dalton Trans.* 1990, 2753; (b) Danopoulos, A. A. and Wilkinson, G., *Polyhedron*, 1990, **9**, 1009; (c) Danopoulos, A. A., Longley, C. J., Wilkinson, G., Hussain, B. and Hursthouse, M. B., *Polyhedron*, 1989, **8**, 1767; (d) Danopoulos, A. A., Wilkinson, G., Sweet, T. K. N. and Hursthouse, M. B., *J. Chem. Soc., Dalton Trans.* 1994, 1037.
2. Danopoulos, A. A., Wilkinson, G. and Williams, D. J., *J. Chem. Soc., Dalton Trans.* 1994, 907, and refs therein.
3. Wigley, D. E., *Prog. Inorg. Chem.* 1994, **42**, 239.
4. Smith, D. P., Allen, K. D., Carducci, M. D. and Wigley, D. E., *Inorg. Chem.* 1992, **31**, 1319.
5. Danopoulos, A. A., Wilkinson, G., Hussain, B. and Hursthouse, M. B., *J. Chem. Soc., Chem. Commun.* 1989, 896.
6. Hankin, D. M., Danopoulos, A. A., Wilkinson, G., Sweet, T. K. N. and Hursthouse, M. B., *J. Chem. Soc., Dalton Trans.* 1996, 1309.
7. (a) Cotton, F. A., Durag, S. A. and Roth, W. J., *Acta Cryst.* 1985, **C41**, 881; (b) Lavasseur, G. and Beauchamp, A. L., *Acta Cryst.* 1991, **C47**, 547, and refs therein.
8. Bates, P. A., Nielson, A. J. and Waters, J. M., *Polyhedron*, 1985, **4**, 1391.
9. Hinsberg III, W. D., Schultz, P. G. and Dervan, P. B., *J. Am. Chem. Soc.* 1982, **104**, 766.
10. Danopoulos, A. A., Wilkinson, G., Hussain-Bates, B. and Hursthouse, M. B., *J. Chem. Soc., Dalton Trans.* 1991, 1855.

11. Sheldrick, G. M., SHELXS-86, *Acta Cryst.* 1990, **A46,** 467.
12. Sheldrick, G. M., *SHELXL*-93, *Program for Crystal Structure Refinement.* University of Göttingen, Germany, 1993.
13. Walker, N. P. C. and Stuart, D., *Acta Cryst.* 1983, **A39,** 158 adapted for FAST geometry by A. Karaulov, University of Wales, Cardiff, 1991.

Pergamon

PII: S0277-5387(96)00386-5

Polyhedron Vol. 16, No. 7, pp. 1089–1094, 1997
Copyright © 1997 Elsevier Science Ltd
Printed in Great Britain. All rights reserved
0277-5387/97 $17.00+0.00

Cyclic S—N compounds and phosphorus reagents—XV [1]. Synthesis, spectral and X-ray structural characterization of (Ph)(DCA)(R)P=N—S_3N_3 [R=$(C_2H_5)_2N$—; $(n\text{-}C_4H_9)_2N$—]

Janarthanan Gopalakrishnan,[a] M. N. Sudheendra Rao,[a]* Janaswamy Srinivas[b] and G. Srinivasamurthy[b]

[a] Department of Chemistry, Indian Institute of Technology, Madras 600 036, India

[b] Department of Physics, Indian Institute of Technology, Madras 600 036, India

(Received 28 June 1996; accepted 6 August 1996)

Abstract—Room-temperature reactions of asymmetric phosphines, (Ph)(DCA)(R)P (R = Et_2N—, Bu^n_2N—) with S_4N_4 in acetonitrile afforded phosphiniminocyclotrithiazenes, (Ph)(DCA)(R)P=N—S_3N_3 (R = Et_2N—, **I**; Bu^n_2N—, **II**) in modest yields (*ca* 50%). The heterocycles have been characterized by spectroscopic [IR, UV–vis, NMR (^1H and ^{31}P) and mass] and single crystal X-ray diffraction methods. Strikingly, the angle at P—N(4)—S(1) is 135° in **I**, the largest observed so far and is 119.3° in **II**. This is also accompanied by the shortest exocyclic S(1)—N(4) bond length of 1.537 Å observed in the case of **I**. In the unit cell of **II**, two types of molecules with slightly differing degree of deviation of the tricoordinate sulfur (0.664 and 0.673 Å from the mean plane [N(1)—S(2)—N(2)—S(3)—N(3)] are observed. Copyright © 1997 Elsevier Science Ltd

Keywords: asymmetric phosphines; phosphiniminocyclotrithiazenes; synthesis; spectra; X-ray structure.

Recently, we have prepared a large variety of phosphiniminocyclotrithiazenes, →P=N—S_3N_3, which are stable examples of monosubstituted 8π-electron "—S_3N_3" ring systems. We have since then undertaken detailed investigations to evaluate the influence if any, of the changing substituents on phosphorus on the stability, properties, structure and chemical behaviour of this type of inorganic heterocyclic compounds. Exploiting the steric protection offered by the dicyclohexylamino group (DCA), we have recently prepared several such compounds namely (Ph)(DCA)(R)PN—S_3N_3, where "R" is a *cyclic amino* group, and characterized them structurally [2,3].

In this paper, we report the preparation and characterization of (i) the asymmetric phosphines, (Ph)(DCA)(R)P, (ii) (Ph)(DCA)(R)PN—S_3N_3, where "R" is an *acyclic amino* group [(a) diethylamino and (b) di-*n*-butylamino group] and (iii) single crystal X-ray structure determination of the heterocycles.

EXPERIMENTAL

General procedures and materials

All the reactions and subsequent work-up were performed under dry N_2 gas. Solvents C_6H_6, *n*-C_6H_{14}, CH_3CN and CH_2Cl_2 were purified as per prescribed procedures [4] before use. S_4N_4 prepared by the literature method [5] was recrystallized from toluene before use. $PhPCl_2$ (Fluka), dicyclohexylamine (E. Merck), diethylamine (Ranbaxy) and di-*n*-butylamine (Fluka) were used as received.

Spectral facilities and operations made use of for the characterization of compounds are the same as described elsewhere [6].

* Author to whom correspondence should be addressed

Preparation of the phosphines (Ph)(DCA)(R)P [R = (i) Et_2N—; (ii) Bu^n_2N—]

The intermediate, "(Ph)(DCA)PCl", was produced by employing the reported procedure and was subsequently converted to (Ph)(DCA)(Et_2N)P and (Ph)(DCA)(Bu^n_2N)P by its stoichiometric reaction (1 : 2) with the corresponding amines following the same procedure [7]. Their characterization data is given in Table 1.

Preparation of (Ph)(DCA)(R)P=N—S_3N_3 [R = (i) Et_2N—; (ii) Bu^n_2N—]

S_4N_4 and the corresponding phosphine taken in 1 : 2 molar ratio were reacted as per the previously reported procedure [8] to isolate the corresponding →P=N—S_3N_3 derivatives as red precipitates. They were recrystallized using CH_2Cl_2–CH_3CN mixture (3 : 1) at 0°C. Table 1 lists their characterization data.

X-ray crystallographic analyses

Single crystals of **I** and **II** suitable for X-ray analyses were grown from a mixture of dichloromethane and acetonitrile (3 : 1, v/v) at 0°C. The crystal data and experimental conditions are summarized in Table 2. The crystals were glued at their sharpest points on to glass fibre. The cell constants were obtained by least-squares refinement employing 25 carefully chosen reflections in the range $8 \leqslant \theta \leqslant 12°$. All the data were collected on an Enraf–Nonius CAD-4 diffractometer using Mo-K_α radiation ($\lambda = 0.71073$ Å) at 293 K and were corrected for Lorentz and polarization effects. The reflections were measured using the ω–2θ scan technique. Numerical absorption corrections were made using an in-built software of the diffractometer.

The structure was solved by direct methods using the SHELXS-86 [9] program and refined by full-matrix least-squares using the program SHELXL-93 [10]. All the hydrogen atoms could be located from the difference electron-density maps during the refinement. All the non-hydrogen atoms were refined with anisotropic thermal parameters and hydrogen atoms with isotropic temperature parameter. The quantity minimized was $\Sigma w(F_o^2 - F_c^2)^2$, where $w = 1/[\sigma(F_o^2 + aP^2 + bP]$, $P = [F_o^2 + 2F_c^2]/3$, and a and b are refinable parameters. All the atomic scattering factors were those incorporated in SHELXL-93.

Table 1. Characterization data for (Ph)(DCA)(R)P = N—S_3N_3[a,b] [R = Et_2N—, (**I**); Bu^n_2N—, (**II**)] and (Ph)(DCA)(R)P [R = Et_2N—, (**III**); Bu^n_2N—, (**IV**)

Sl. No.	Compound No.	Yield (%)	M. pt. (°C)	IR[c] (cm^{-1})	UV–vis (nm; $dm^3\ mol^{-1}\ cm^{-1}$)	^{31}P NMR (δ, ppm)	^1H NMR (δ, ppm)
1	**I**	52	115–17	1190, 1178, 1162, 1149, 1101, 1050, 1021, 928, 723 and 691	486.0 (3.98×10^3) 338.5 (3.06×10^3) 290.0,sh (3.06×10^3)	32.4	1.0–2.0 (m,26H); 3.0–3.3 (m,6H); 7.35–7.65 (m,3H); 7.83–8.05 (m,2H)
2	**II**	55	116–18	1360, 1133, 1094, 1053, 979, 966, 938, 918 and 746	486.0 (4.01×10^3) 338.0 (3.17×10^3) 290.0,sh (3.0×10^3)	32.3	0.9 (t,6H); 1.05–1.30 (m, 12H); 1.5–2.00 (m,3H); 7.91–7.98 (m,2H)
3	**III**	45	86–88	1450, 1370, 1170, 1110, 1060, 1010, 960, 920, 890, 850, 810, 790, 740 and 700		78.4	1.0–2.1 (m,26H); 2.75–3.15 (m,6H); 7.25–7.35 (m,3H); 7.37–7.45 (m,2H)
4	**IV**	49	89–91	1469, 1443, 1373, 1254, 1206, 1158, 1114, 1050, 1024, 966, 886, 746 and 694		79.8	0.9 (t,6H); 1.0–1.9 (m, 24H); 3.0–3.1 (m,6H); 7.35–7.45 (m,3H); 7.80–7.89 (m,2H)

[a] Recorded as KBr pellets.

[b] MS for **I**: *m/z*: 484 [$(M-N_2)^+$, 3]; 420 [$M\text{-}S_2N_2)^+$, 6]; 374 [Ph(DCA)(Et_2N)P=N^+,6]; 197 [PhP(Et_2N)NH_2^+, 29]; 181 [$(C_6H_{11})_2NH^+$, 18]; 180 [$(C_6H_{11})_2N^+$ or Ph(Et_2N)P^+, 100]; 124 [$PhPNH_2^+$, 42]; 77 [$C_6H_5^+$, 11]; 72 [$(C_2H_5)_2N^+$, 52%]. MS for **II**: *m/z*: 540 [$(M\text{-}N_2)^+$, 2]; 476 [$(M\text{-}S_2N_2)^+$,7]; 430 [Ph(DCA)(Bu^n_2N)P=N^+, 4]; 236 [Ph(Bu^n_2N)P^+, 21]; 181 [$(C_6H_{11})_2NH^+$, 16]; 180 [$(C_6H_{11})_2N^+$, 100]; 129 [$(Bu^n_2N)^+$, 48]; 124 [$PhPNH_2^+$, 42]; 77 [$C_6H_5^+$, 6%].

[c] 1600–600 cm^{-1}; characteristic and only strong peaks are given.

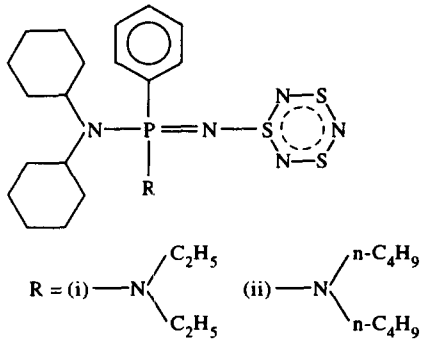
Table 2. Crystal and structure refinement data for **I** and **II**

Identification code	**I**	**II**
Empirical formula	$C_{22}H_{37}N_6PS_3$	$C_{26}H_{45}N_6PS_3$
Formula weight	512.73	568.83
Crystal system	Triclinic	Monoclinic
Space group	$P\bar{1}$	$P2_1/n$
a (Å)	9.8561 (5)	10.5450 (5)
b (Å)	10.5908 (8)	29.6030 (8)
c (Å)	14.0352 (13)	19.9265 (6)
α (°)	81.792 (7)	90.0
β (°)	77.369 (5)	100.94 (3)
γ (°)	66.204 (5)	90.0
V (Å^3)	1305.6(2)	6107.3(4)
Z	2	8
Density calc, (mg m^{-3})	1.304	1.237
Absorption coefficient. (mm^{-1})	0.368	0.321
F(000)	548	2448
Crystal dimensions (mm)	0.12 × 0.16 × 0.22	0.10 × 0.10 × 0.26
θ range scanned (°)	2–25	2–25
Reflections collected	3332	5953
Index ranges	$0 \leqslant h \leqslant 11$ $-12 \leqslant k \leqslant 12$ $-16 \leqslant l \leqslant 16$	$0 \leqslant h \leqslant 12$ $0 \leqslant k \leqslant 34$ $-23 \leqslant l \leqslant 23$
Independent reflections	3142 [R(int) = 0.0193]	5577 [R(int) = 0.0153]
No. of parameters refined	437	961
Final "R" indices [$I > 3\sigma(I)$]	$R_1 = 0.0439$ $wR_2 = 0.1175$	$R_1 = 0.0505$ $wR_2 = 0.1350$
GOF	1.085	0.907
Largest difference peak and hole (e Å^{-3})	0.374 and −0.477	0.595 and −0.223

RESULTS AND DISCUSSION

The phosphines, (Ph)(DCA)(R)P [R = (i) diethylamino; (ii) di-n-butylamino], similar to other tertiary phosphines such as $(C_6H_5)_3P$ [11], $(C_5H_{10}N)_3P$ [8] and $(C_6H_5)_2(C_5H_{10}N)P$ [12] react smoothly with S_4N_4 to give the corresponding phosphiniminocyclotrithiazenes, (Ph)(DCA)(Et_2N)PN—S_3N_3 (**I**) and (Ph)(DCA)(Bu^n_2N)PN—S_3N_3 (**II**) as stable red crystal-line solids.

The electronic spectra of compounds **I** and **II** show, besides the two characteristic absorptions of the cyclotrithiazene ring (—S_3N_3) [13,14], an additional absorption at 290 nm, as in the case of tertiary aminophosphines [8]. The phosphorus chemical shifts in **I** and **II** are considerably more shielded compared with the corresponding phosphines **III** and **IV**, a situation also found in the case of all the aminophosphines reported so far [8,12].



X-ray crystal structures of **I** *and* **II**

The ORTEP plots, packing diagrams and selected bond length, bond angle data for **I** and **II** are shown in Figs 1–4 and Tables 3 and 4, respectively. Compounds **I** and **II** can be regarded as very similar except for the ethyl groups of **I** replaced with *n*-butyl groups in the other. Interestingly, the structural difference between the two, first became evident from the observed difference in their crystal system, space group and the volume of the unit cell. In accordance with the previous observation, the tricoordianate sulphur, S(1) in **I** and **II** is substantially deviated from the approximate mean plane, N(1)—S(2)—N(2)—S(3)—N(3), of the heterocycle. It is 0.701 Å for **I**, the

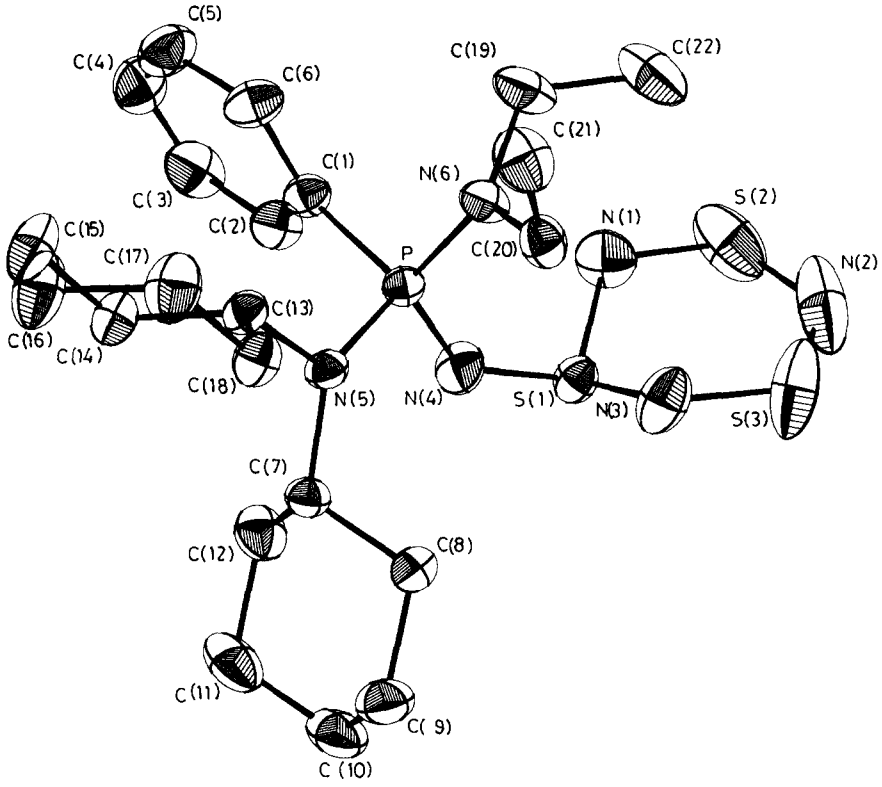


Fig. 1. ORTEP plot (50% probability ellipsoids) and atomic numbering scheme for (Ph)(DCA)(Et_2N)P=N—S_3N_3 (**I**).

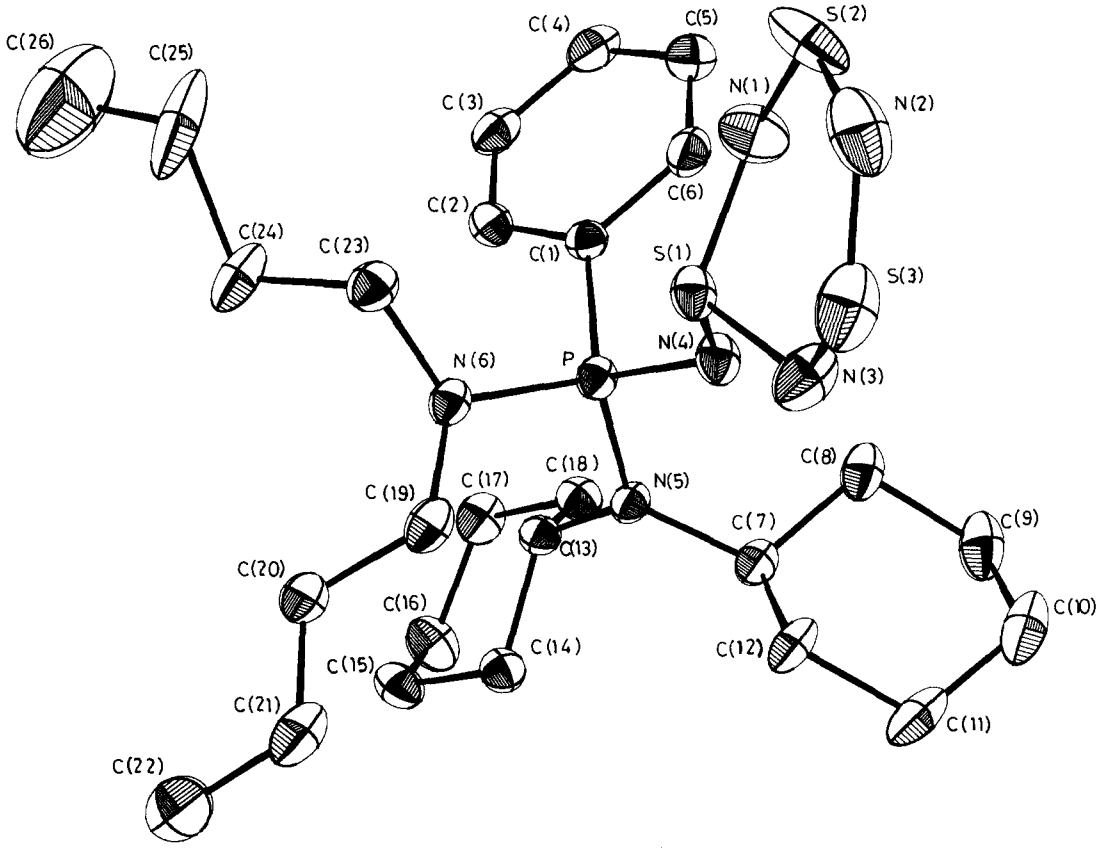


Fig. 2. ORTEP plot (50% probability ellipsoids) and atomic numbering scheme for (Ph)(DCA)(Bu^n_2N)P=N—S_3N_3 (**II**, molecule A).

Table 3. Selected bond lengths (Å) and bond angles (°) with ESDs in parentheses for (Ph)(DCA)(Et_2N)P=N—S_3N_3 (I)

P—N(4)	1.601 (3)	S(3)—N(3)	1.607 (4)
N(4)—S(1)	1.537(3)	N(3)—S(1)	1.647 (3)
S(1)—N(1)	1.641(3)	P—N(5)	1.640 (3)
N(1)—S(2)	1.592 (4)	P—N(6)	1.641 (2)
S(2)—N(2)	1.581 (6)	P—C(1)	1.808 (3)
N(2)—S(3)	1.604 (6)	P—S(1)	2.899(6)
P—N(4)—S(1)	135.0 (2)	S(3)—N(3)—S(1)	115.9 (2)
N(4)—S(1)—N(1)	105.3 (2)	N(4)—P—N(5)	120.0 (2)
N(4)—S(1)—N(3)	106.1 (2)	N(4)—P—N(6)	106.45 (14)
N(1)—S(1)—N(3)	107.2 (2)	N(5)—P—N(6)	107.75 (13)
S(1)—N(1)—S(2)	116.7 (2)	N(4)—P—C(1)	108.2 (2)
N(1)—S(2)—N(2)	115.6 (2)	N(5)—P—C(1)	105.94 (14)
S(2)—N(2)—S(3)	123.8 (3)	N(6)—P—C(1)	107.96 (13)
N(2)—S(3)—N(3)	114.5 (2)		

maximum observed so far and is found to be 0.664 and 0.673 Å for **II**, indicating that the compound **II** has two distinguishable types of molecules in the unit cell. Another strikingly different structural feature between **I** and **II** is that the angle at exocyclic nitrogen, P—N(4)—S(1), is significantly widened in **I** (135.0 *vs* 119.3°). This variation may be attributed to the stereochemical difference of the two chosen acyclic amino groups. This is further supported by the fact that the non-bonded P—S(1) distance is found to be *ca* 2.9 and 2.7 Å for **I** and **II** respectively. These values are sufficiently low compared with their van der Waals contact (3.65 Å), which indicates significant bonding interaction between "P" and "S(1)" in these compounds [8,15]. One of the angles at the tetrahedral phosphorus is distinctly larger than the rest in both **I** and **II**. While the dicy-

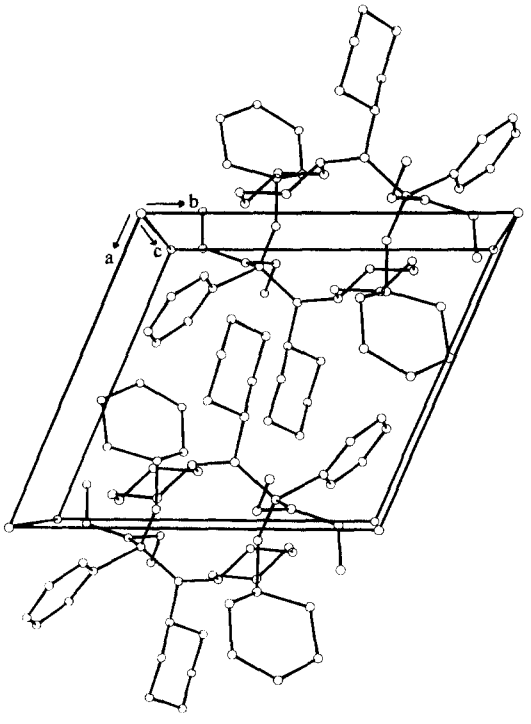


Fig. 3. Molecular packing of (Ph)(DCA)(Et_2N)P=N—S_3N_3 in the unit cell.

Table 4. Selected bond lengths (Å) and bond angles (°) with ESDs in parentheses for (Ph)(DCA)(Bu^n_2N)P=N—S_3N_3 (II)

	Molecule A	Molecule B
P—N(4)	1.618 (4)	1.612 (4)
N(4)—S(1)	1.569 (4)	1.573 (4)
S(1)—N(1)	1.642 (5)	1.642 (5)
N(1)—S(2)	1.615 (5)	1.595 (5)
S(2)—N(2)	1.593 (8)	1.583 (6)
N(2)—S(3)	1.582 (7)	1.609 (6)
S(3)—N(3)	1.604 (5)	1.626 (5)
N(3)—S(1)	1.649 (6)	1.655 (5)
P—N(5)	1.641 (4)	1.647 (4)
P—N(6)	1.654 (4)	1.656 (4)
P—C(1)	1.807 (5)	1.812 (6)
P—S(1)	2.750 (7)	2.765 (7)
P—N(4)—S(1)	119.3 (3)	120.5 (3)
N(4)—S(1)—N(1)	101.0 (3)	102.6 (3)
N(4)—S(1)—N(3)	102.9 (3)	101.0 (3)
N(1)—S(1)—N(3)	107.4 (3)	106.4 (3)
S(1)—N(1)—S(2)	115.9 (3)	120.4 (3)
N(1)—S(2)—N(2)	113.7 (3)	116.1 (3)
S(2)—N(2)—S(3)	124.6 (4)	123.1 (3)
N(2)—S(3)—N(3)	115.4 (3)	113.5 (3)
S(3)—N(3)—S(1)	118.4 (4)	114.2 (3)
N(4)—P—N(5)	106.7 (2)	106.4 (2)
N(4)—P—N(6)	117.4 (2)	117.6 (2)
N(5)—P—N(6)	107.1 (2)	107.3 (2)
N(4)—P—C(1)	109.7 (3)	109.3 (2)
N(5)—P—C(1)	109.7 (2)	111.7 (2)
N(6)—P—C(1)	106.2 (2)	104.6 (2)

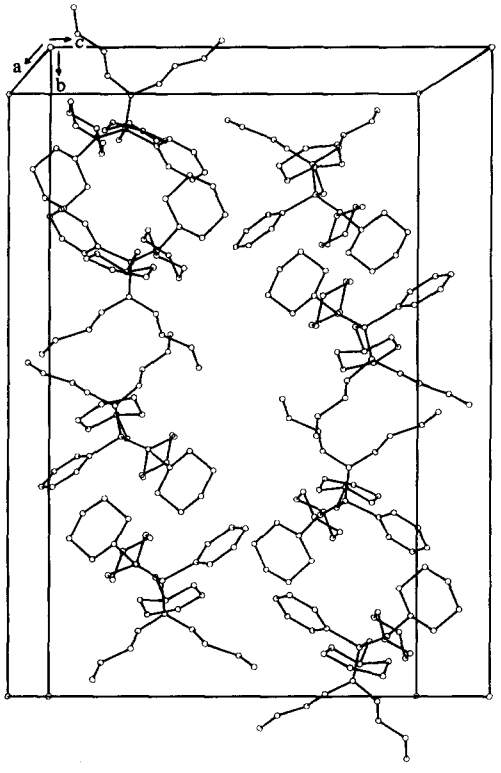


Fig. 4. Molecular packing of (Ph)(DCA)(Bu^n_2N)P=N—S_3N_3 in the unit cell.

clohexylamino group determines this angle in **I** (120°), the acyclic amino group, namely the di-*n*-butylamino moiety, contributes to the observed angle in the other (*ca* 117°), which clearly demonstrates the steric influence of the groups on phosphorus on the structure.

Although the exocyclic P—N(4) bond length is practically the same for both **I** and **II**, the adjoining N—S bond [N(4)—S(1)] is considerably shorter in **I** (1.537 *vs* 1.569 Å). The reason for the observed N(4)—S(1) bond length of 1.537 Å, much shorter than a typical N—S double bond (1.55 Å [16]), though it remains unclear, is suggestive of its interaction with both the endocyclic S—N bonds and the adjoining P—N bond. The trend in the endocyclic bond variation in **I** and **II** is found to be similar as in the reported cases [8,15].

The cyclohexyl groups of "DCA" are found to be in an approximately chair conformation and the cyclotrithiazene ring is found to be in a half-chair conformation in both cases.

Conclusion

The introduction of acyclic amino groups, namely, diethylamino and di-*n*-butylamino moieties for "R" in (Ph)(DCA)(R)PN—S_3N_3 derivatives bring subtle, but noticeable differences in their structures, as revealed by X-ray crystallography.

Acknowledgements—JG and JS thank IIT, Madras for financial support. RSIC, IIT, Madras is acknowledged for spectral facilities.

REFERENCES

1. Part XIV :Swarnalatha, U., Rao, M. N. S. and Udupa, M. R., *Thermochim. Acta* (communicated).
2. Mohan, T., Srinivas, J., Srinivasamurthy, G. and Rao, M. N. S., *Acta Cryst.* 1996, **C52,** 1250.
3. Mohan, T. and Rao, M. N. S., Unpublished results.
4. Perrin, D. D., Armarego, W. L. F. and Perrin, D. R., *Purification of Laboratory Chemicals*, 2nd edn. Pergamon Press, Oxford, 1980.
5. Villena Blanco, M. and Jolly, W. L., *Inorg. Synth.* 1967, **9,** 98.
6. Mohan, T., Senthivel, P. and Rao, M. N. S., *Indian J. Chem.* 1995, **34A,** 961.
7. Mohan, T., Rao, M. N. S. and Aravamudan, G., *Tetrahedron Lett.* 1989, **30,** 4871.
8. Elias, A. J., Rao, M. N. S. and Varghese, B., *Polyhedron*, 1990, **9,** 1433.
9. Sheldrick, G. M., *SHELXL*-93. *Acta Cryst.* 1990, **A46,** 467.
10. Sheldrick, G. M., *SHELXL*-93 *Program for the Refinement of Crystal Structure*. University of Göttingen, Germany, 1993.
11. Chivers, T., Cordes, A. W., Maclean, G. and Oakley, R. T., *Inorg. Chem.* 1981, **20,** 16.
12. Thomas, C. J., and Rao, M. N. S., *Heteroatom. Chem.* 1992, **3,** 321.
13. Chivers, T., *Chem. Rev.* 1985, **85,** 341.
14. Gmelins Handbook of Inorganic Chemistry, *Sulfur–Nitrogen Compounds*, Part 3, Verlag, Weinheim, 1987.
15. Holt, E. M. and Holt, S. L., *J. Chem. Soc., Dalton Trans.* 1974, 1990.
16. Bats, J. W., Coppens, P. and Koetzle, T. P., *Acta Cryst.* 1977, **B33,** 37.

Pergamon

PII: S0277-5387(96)00372-5

Polyhedron Vol. 16, No. 7, pp. 1095–1100, 1997
Copyright © 1997 Elsevier Science Ltd
Printed in Great Britain. All rights reserved
0277-5387/97 $17.00+0.00

Seven-coordinate Mo–Sn complexes containing bidentate PP-donor ligands

M. Cano,[a]* J. A. Campo[b] and M. Panizo[c]

[a] Departamento de Química Inorgánica I, Facultad de Ciencias Químicas, Universidad Complutense, 28040 Madrid, Spain

[b] Departamento de Química Inorgánica y Materiales, Facultad de Ciencias Experimentales y Técnicas, Universidad San Pablo-CEU, Urb. Montepríncipe, 28668-Boadilla del Monte, Madrid and Departamento de Química Inorgánica I, Facultad de Ciencias Químicas, Universidad Complutense, 28040 Madrid, Spain

[c] Departamento de Química, Facultad de Ciencias, Universidad Autónoma, 28049 Madrid, Spain

(Received 18 July 1996; accepted 2 August 1996)

Abstract—Two different routes have been studied to produce heterobimetallic Mo–Sn compounds containing bidentate PP-donor ligands. The first, involving the reaction of $[Mo(SnRCl_2)(Cl)(CO)_3(CH_3CN)_2]$ (R = Me, Ph) with PP-donor ligands [PP = 1,2-bis(diphenylphosphine)ethane, dppe; 1,3-bis(diphenylphosphine)propane, dppp] always gave rise to neutral seven-coordinate complexes of the type $[Mo(SnRCl_2)(Cl)(CO)_3(\eta^2\text{-PP})]$ (**I**). On the other band, three types of compounds were isolated from reactions of $[Mo(CO)_3(\eta^2\text{-LL})(L')]$ [LL = PP- or NN-donor ligand, PP = bis(diphenylphosphine)methane (dppm), NN = 2,2′-bipyridine (bpy), 1,10-phenanthroline (phen), 2,9-dimethyl-1,10-phenanthroline (dmp); L′ = CO or η^1-dppm] with $SnCl_4$ used as second synthetic route. So, the cationic six-coordinate complex $[Mo(SnCl_3)(CO)_3(\eta^2\text{-dppm})]^+$ (**II**) and neutral or cationic seven-coordinate complexes $[Mo(SnCl_3)(Cl)(CO)_3(\eta^2\text{-NN})]$ (**III**) and $[Mo(SnCl_3)(CO)_2(\eta^2\text{-NN})(\eta^2\text{-dppm})]^+$ (**IV**) are obtained depending on the solvent and the nature of the ligands. Copyright © 1997 Elsevier Science Ltd

Keywords: heterobimetallic Mo–Sn complexes; bidentate PP-donor ligands; cationic and neutral Mo–Sn compounds.

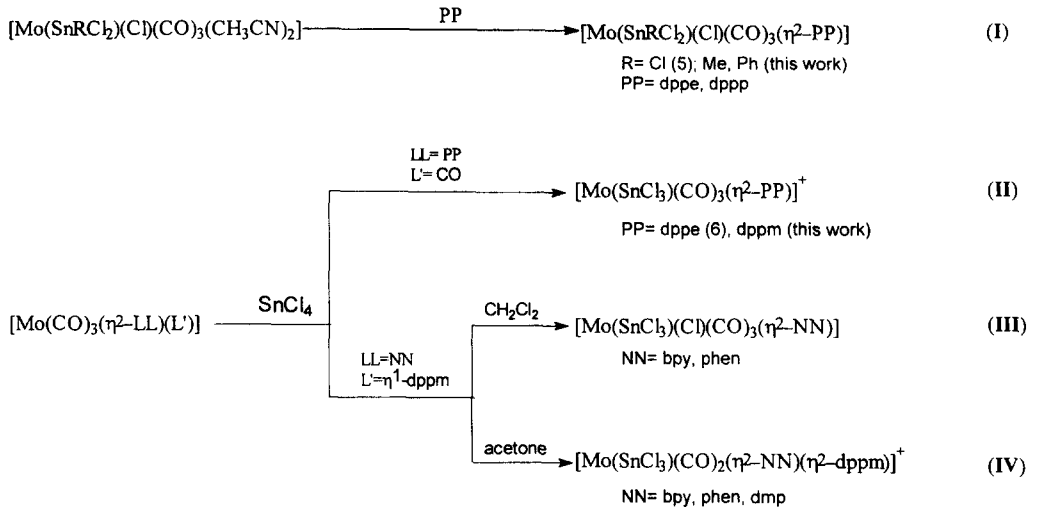
Seven-coordinate Mo complexes of the type $[Mo(X)_2(CO)_3(L)_2]$ (X = Cl, Br; L = PPh_3, $AsPh_3$) have been shown to exhibit important catalytic activity involving the dissociation of the L ligands as the rate determining step of that behaviour [1–3].

These precedents have encouraged research into related heterobimetallic compounds in which cooperative effects between dissimilar metals are also important from the point of view of their catalytic activity.

From previous results we now propose two potential synthetic routes in order to produce new seven-coordinate Mo–Sn compounds. The first consists of the displacement of acetonitrile ligands from $[Mo(SnRCl_2)(Cl)(CO)_3(CH_3CN)_2]$ (R = Cl, Me, Ph) by monodentate or bidentate P-donor ligands. Alternatively the oxidative addition of tin(IV) organohalides to $[Mo(CO)_3(\eta^2\text{-LL})(L')]$ (LL = NN- or PP-donor ligand; L′ = CO or monodentate P-donor ligand) is used as the second way to yield the desired species.

Some of these reactions have already been described. So, in a previous work [4] we have established that seven-coordinate complexes of the type $[Mo(L)(Cl)(CO)(CH_3CN)(PR'_3)]$, $[Mo(\mu\text{-Cl})(L)(CO)(PR'_3)]_2$ or $[Mo(L)(Cl)(CH_3COCH_3)_2(PR'_3)]$ [L = $(SnRCl_2)(CO)_2$, R = Me, Ph; R′ = 4-XC_6H_4, X = CH_3O, CH_3, H, F, Cl] are produced by reaction of $[Mo(SnRCl_2)(Cl)(CO)_3(CH_3CN)_2]$ with PR'_3 depending on several factors. The displacement of the two acetonitrile ligands in related complexes (R = Cl) by PP-donor ligands has also been established [5].

* Author to whom correspondence should be addressed.



Scheme 1.

Following these precedents we were interested to extend the above studies by using PP-donor ligands with different chain lengths.

So, the reactivity of $[Mo(SnRCl_2)(Cl)(CO)_3(CH_3CN)_2]$ (R = Me, Ph) towards 1,2-bis(diphenylphosphine)ethane(dppe) and 1,3-bis(diphenylphosphine)propane(dppp) is described in this work.

On the other hand, the reaction of complexes of the type $[Mo(CO)_3(\eta^2\text{-LL})(L')]$ (LL = bidentate NN- or PP-donor ligand; L′ = CO or monodentate P-donor ligand) with haloderivatives of Sn(IV) gave rise to tricarbonyl or dicarbonyl heterobimetallic complexes depending on the lability of the CO ligands towards to the other ligands [6–8]. Then, we think that $[Mo(CO)_3(\eta^2\text{-NN})(\eta^1\text{-dppm})]$ or $[Mo(CO)_3(\eta^2\text{-dppm})(CO)]$ [dppm = bis(diphenylphosphine)methane] should be appropriate starting compounds to react with tin(IV) derivatives in order to analyse the coordinative competence between CO and a P-donor atom of the dppm ligand, free in the former and coordinated in the latter, respectively.

On the above basis we also describe in this work the reactivity of $[Mo(CO)_3(\eta^2\text{-LL})(L')]$ [LL = 2,2′-bipyridine(bpy), 1,10-phenanthroline(phen), 2,9-dimethyl-1,10-phenanthroline(dmp), L′ = η^1-dppm; LL = dppm, L′ = CO] with $SnCl_4$.

RESULTS AND DISCUSSION

Scheme 1 summarizes the results of the reactions studied as well as the four types of heterobimetallic complexes (**I–IV**) isolated. Some literature results are included for comparative purposes.

Compounds of type I: Reactions of $[Mo(SnRCl_2)(Cl)(CO)_3(CH_3CN)_2]$ (R = Me, Ph) *with dppe and dppp* (**1–4**)

The reactions of $[Mo(SnRCl_2)(Cl)(CO)_3(CH_3CN)_2]$ (R = Me, Ph) with PP-donor ligands (dppe and dppp) in dichloromethane gave rise to the seven-coordinate complexes $[Mo(SnRCl_2)(Cl)(CO)_3(\eta^2\text{-PP})]$ (R = Me, Ph; PP = dppe, dppp; **1–4**), which were fully characterized by analytical and spectroscopic techniques (Table 1).

In these reactions the bidentate PP-donor ligands caused the elimination of the two acetonitrile molecules from the starting compounds, which were not displaced by two P-donor ligands of the type PR'_3 (R′ = 4-XC_6H_4; X = CH_3O, CH_3, H, F, Cl) [4]. A similar reaction had already been observed with dppm as the ligand [5]. Therefore, the different size or the steric characteristics of the PP-donor ligand does not modify the course of the reaction to produce seven-coordinate complexes **1–4**.

The IR spectra of **1–4** in the solid state show three bands in the carbonyl stretching region (Table 1), which suggests a *fac* distribution of the three carbonyl groups [9]. No absorptions in the $\nu(C{\equiv}N)$ region (2400–2200 cm^{-1}) are observed indicating the full substitution of the CH_3CN ligands.

The ^{31}P NMR spectra of **1–4** show signals in the range of coordinated phosphorus ligands, as deduced by the values of the coordination chemical shifts [$\Delta\delta(^{31}P)$], see Table 1. In all cases, with the exception of $[Mo(SnMeCl_2)(Cl)(CO)_3(\eta^2\text{-dppe})]$ (**1**), the presence of a single signal is consistent with an equivalence of the coordinate phosphorus atoms of the PP-donor ligand. The main feature comes from comparing the chelate ring size with the $\Delta\delta(^{31}P)$ values. So, com-

Table 1. Analytical and spectroscopic data of $[Mo(SnRCl_2)(Cl)(CO)_3(\eta^2\text{-PP})]$ (R = Me, Ph; PP = dppe, dppp) (**1–4**)

Compound	Analyses (%)[a] C	H	IR (cm^{-1}) $\nu(CO)$[b]	$\nu(CO)$[c]	$\nu(SnCl)$[c]	$\nu(MoCl)$[c]	^{31}P NMR (ppm)[d] δ	$\Delta\delta(^{31}P)$[e]
$[Mo(SnMeCl_2)(Cl)(CO)_3(\eta^2\text{-dppe})]$	44.1	3.3	1996	1996	308	295	53.8	66.3
(**1**)	(44.0)	(3.3)	1913	1908			47.2	59.7
			1845	1840				
$[Mo(SnMeCl_2)(Cl)(CO)_3(\eta^2\text{-dppp})]$	45.0	3.5	1999	1993	337	305	3.8	21.1
(**2**)	(44.7)	(3.5)	1936	1931				
			1842	1842				
$[Mo(SnPhCl_2)(Cl)(CO)_3(\eta^2\text{-dppe})]$	47.1	3.3	2002	2002	312	303	45.6	58.1
(**3**)	(47.7)	(3.3)	1910	1910				
			1837	1837				
$[Mo(SnPhCl_2)(Cl)(CO)_3(\eta^2\text{-dppp})]$	48.4	3.5	2003	1995	312	303	4.4[f]	21.7
(**4**)	(48.3)	(3.5)	1928br	1926				
				1904				

[a] Calculated in parentheses.
[b] In acetone solution.
[c] In Nujol suspension.
[d] In $CDCl_3$ solution at room temperature.
[e] $\Delta\delta(^{31}P) = \delta(^{31}P)_{complex} - \delta(^{31}P)_{free\ ligand}$ (chemical shifts of free ligands were taken from ref. [12]).
[f] $^2J(Sn—P) = 36.7$ Hz.

pounds with the dppe ligand show a substantially larger degree of deshielding than those with dppp. This fact, which could be related with the value of the P—M—P angle of the five- or six-membered rings produced in each type of compounds, had already been observed in other examples [10–12]. The higher P—M—P angle in the six-membered rings (compounds **2** and **4**) than in the five-membered rings (compounds **1** and **3**) appears to produce a less-favoured orbital overlap between the metal and the phosphorus atoms and consequently a higher shielding of them.

Compounds type II–IV: Reactions of $[Mo(CO)_3(\eta^2\text{-LL})(L')]$ (LL = *bpy, phen, dmp,* $L' = \eta^1$-*dppm*; LL = *dppm*, L′ = CO) *with* $SnCl_4$ (**5–11**)

In the second part of this study we discuss the reactivity of complexes $[Mo(CO)_3(\eta^2\text{-LL})(L')]$ with $SnCl_4$. Bidentate LL ligands were NN- or PP-donor (NN = bpy, phen, dmp; PP = dppm) and monodentate L′ ligands were η^1-dppm or CO, respectively. Table 2 lists the analytical, conductivity and spectroscopic (IR and NMR) data of the new complexes (**5, 8–11**).

When LL = dppm and L′ = CO, the $[Mo(CO)_3(\eta^2\text{-dppm})]$ group was bonded to a $SnCl_3$ group giving rise to the cationic complex $[Mo(SnCl_3)(CO)_3(\eta^2\text{-dppm})]^+$, which was isolated as the salt of $[SnCl_5]^-$ (compound type **II**). The analytical, conductivity and spectroscopic data (Table 2) are consistent with a formulation as $[Mo(SnCl_3)(CO)_3(\eta^2\text{-dppm})][SnCl_5]\cdot(CH_3CH_2)_2O$ (**5**). The IR spectrum in the solid state shows in the carbonyl stretching region three bands (two strong and the other broad) at 1965, 1940 and 1870 cm^{-1}, typical of a *fac*-distribution [4]. In the lower region, a broad band centred at 365 cm^{-1} is consistent with the presence of different Sn—Cl bonds in the complex.

In the above reaction we consider the insertion of the $[Mo(CO)_3(\eta^2\text{-dppm})]$ fragment into a Sn—Cl bond of $SnCl_4$, followed by the dissociation of the Cl ligand bonded to the Mo atom. This chloride atom should be bonded to a second $SnCl_4$ molecule producing the counterpart anion $[SnCl_5]^-$, in agreement with the proposed formulation. The isolated complex shows a low stability in solution, but in freshly prepared solutions it behaves as 1 : 1 electrolyte. The stereochemistry of this complex is related with that observed in other seven-coordinate Mo–Sn complexes [6].

On the other hand, new types of compounds (**III** and **IV**) are formed when LL = η^2-NN (NN = bpy, phen, dmp) and L′ = η^1-dppm in the starting compounds (Scheme 1).

From the experimental results we deduce that the reaction course depends on the solvent used and on the NN-donor ligand.

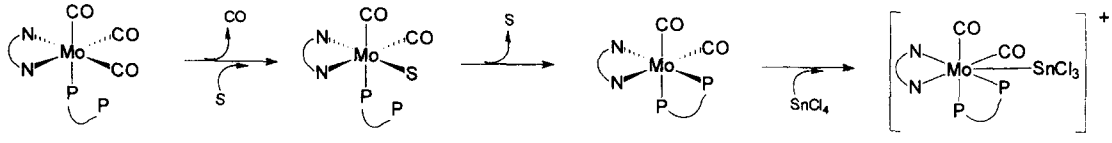
So, in dichloromethane the elimination of the PP-donor ligand occurs and consequently the 16 e^- intermediate $[Mo(CO)_3(\eta^2\text{-NN})]$ (NN = bpy, phen) fragment is inserted into a Sn—Cl bond of $SnCl_4$ yielding type **III** compounds $[Mo(SnCl_3)(Cl)(CO)_3(\eta^2\text{-NN})]$ (NN = bpy, **6**; phen, **7**), which have already previously been described [13]. The analogous complex $[Mo(SnCl_3)(Cl)(CO)_3(\eta^2\text{-dmp})]$ (**8**) was not obtained by this route, but it is produced by reaction of $[Mo(CO)_4(\eta^2\text{-dmp})]$ with $SnCl_4$ in dichloromethane (Table 2).

By contrast if the reaction was carried out in a coordinating solvent such as acetone, the dppm ligand

Table 2. Analytical and spectroscopic data for the complexes $[Mo(SnCl_3)(CO)_3(\eta^2\text{-dppm})][SnCl_5]\cdot Et_2O$ (**5**), $[Mo(SnCl_3)(Cl)(CO)_3(\eta^2\text{-dmp})]\cdot CH_2Cl_2$ (**8**) and $[Mo(SnCl_3)(CO)_2(\eta^2\text{-NN})(\eta^2\text{-dppm})][SnCl_5]\cdot Et_2O$ (NN = bpy, **9**; phen, **10**; dmp, **11**)

Compound	Analyses (%)[a]			IR (cm^{-1})				^{31}P NMR (ppm)[d]	
	C	H	N	ν(CO)[b]	ν(CO)[c]	ν(SnCl)[c]	$\Lambda_m(\Omega^{-1}\,cm^2\,mol^{-1})$[b]	δ	$\delta\Delta(^{31}P)$[e]
5	33.1	2.9	—		1965	365	60	*f*	
	(32.4)	(2.5)	—		1940				
					1870				
8	28.9	2.0	3.8		2000	330			
	(29.5)	(1.9)	(3.8)		1920	310			
					1890	270[g]			
9	38.3	2.9	2.4	1955	1952	320	129	38.6	60.4
	(38.2)	(3.1)	(2.2)	1892	1888				
10	40.1	2.9	2.4	1958	1950	350	132	40.0	62.2
	(39.4)	(3.1)	(2.1)	1892	1890				
11	40.7	3.4	2.2	1905	1900	330	130	42.5	64.3
	(40.3)	(3.3)	(2.1)	1828	1820	305			

[a] Calculated in parentheses.
[b] In acetone solution.
[c] In KBr pellets.
[d] In $CDCl_3$ solution at room temperature.
[e] $\Delta\delta(^{31}P) = \delta(^{31}P)_{complex} - \delta(^{31}P)_{free\ ligand}$ (chemical shifts of free ligands were taken from ref. [12]).
[f] Unstable.
[g] ν(MoCl).



PP= dppm, S= acetone, NN= bpy, phen

Scheme 2.

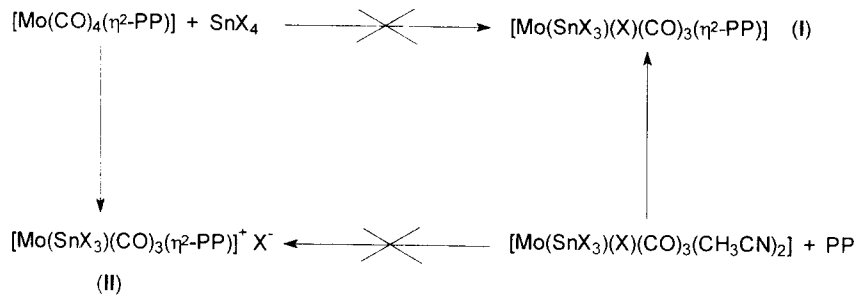
was coordinated in a bidentate fashion with the corresponding displacement of CO. A mechanism as depicted in Scheme 2 is proposed to explain the observed behaviour. The suggested intermediates $[Mo(CO)_2(\eta^2\text{-NN})(\eta^2\text{-dppm})]$ (NN = bpy, phen) are coordinatively and electronically saturated, therefore, only one $SnCl_3$ group is oxidatively added to produce the cationic seven-coordinate species $[Mo(SnCl_3)(CO)_2(\eta^2\text{-NN})(\eta^2\text{-dppm})]^+$ (type **IV**), which were isolated as salts of $[SnCl_5]^-$ (NN = bpy, **9**; phen, **10**; Table 2).

The same type of complex $[Mo(SnCl_3)(CO)_2(\eta^2\text{-dmp})(\eta^2\text{-dppm})][SnCl_5]$ (**11**) was formed by reaction of $[Mo(CO)_3(\eta^2\text{-dmp})(\eta^1\text{-dppm})]$ with $SnCl_4$ in dichloromethane at room temperature (Table 2). By contrast in acetone that complex is recovered as a side product together decomposition products.

The IR spectra of **9–11** in the solid state show two strong carbonyl bands centred at 1950 and 1890 cm^{-1}, typical of a *cis*-dicarbonyl disposition [14–15]. The ^{31}P NMR spectra in $CDCl_3$ solution of **9–11** show a single signal in the region of coordinate phosphine (Table 2), suggesting the presence of two equivalent phosphorus atoms. Complexes **9–11** show a low stability in solution, but they behave as 1 : 1 electrolytes in freshly prepared solutions.

The analytical, conductivity and spectroscopic data are consistent with the formulation $[Mo(SnCl_3)(CO)_2(\eta^2\text{-NN})(\eta^2\text{-dppm})][SnCl_3]\cdot(CH_3CH_2)_2O$ (NN = bpy, phen, dmp) for the new complexes. The $(CH_3CH_2)_2O$ molecule could be occupying the sixth position of coordination at the tin atom vacant on the $[SnCl_5]^-$ group. This fact is related with those observed in other relevant compounds containing Mo—Sn bonds [6].

In the light of the results of this work, the obtention of seven-coordinate Mo–Sn complexes is determined by the route of the preparation, independent of the nature of the PP-donor ligand used. As an illustrative



Scheme 3.

example. Scheme 3 shows this fact for type **I** and **II** complexes.

EXPERIMENTAL

General

All reactions were carried out under oxygen-free dinitrogen by standard Schlenk techniques. Commercial solvents were dried and degassed prior to use. $[Mo(SnRCl_2)(Cl)(CO)_3(CH_3CN)_2]$ (R = Me, Ph), $[Mo(CO)_3(\eta^2\text{-NN})(\eta^1\text{-dppm})]$ (NN = bpy, phen, dmp) and $[Mo(CO)_4(\eta^2\text{-dppm})]$ were prepared according to previously described methods [9,11,16] $SnCl_4$ was distilled prior to use. Other commercial reagents were used as supplied.

Elemental analyses for carbon, hydrogen and nitrogen were carried out by the Microanalytical Service of the Autónoma University of Madrid. IR spectra were recorded on Nicolet 5DX FT-IR or Perkin-Elmer 1300 spectometers. ^1H and ^{31}P NMR spectra were recorded on a Varian XL-300 spectrometer at room temperature in $CDCl_3$ solutions, operated at 299.95 MHz for ^1H and 121.42 MHz for ^{31}P (shifts are relative to internal tetramethylsylane and external 85% phosphoric acid, respectively). Conductance measurements were performed on freshly acetone solutions at room temperature with a Philips PW9526 conductivity bridge and a Philips PW9550/60 conductivity cell.

Reactions

Preparation of $[Mo(SnRCl_2)(Cl)(CO)_3(\eta^2\text{-PP})]$ (R = Me, Ph; PP = *dppe*, *dppp*) (**1–4**). To a solution of $[Mo(SnRCl_2)(Cl)(CO)_3(CH_3CN)_2]$ (0.7 mmol) in dichloromethane or acetone (15 cm^3) was added a stoichometric amount of the PP-donor ligand (0.7 mmol). The mixture was stirred under a slight stream of nitrogen for 2 h. Then the solvent was partially reduced and cold diethyl ether added. The solid formed was filtered off, washed with cold diethyl ether and dried *in vacuo*. The new complexes are air-sensitive solids and they are soluble in common polar solvents.

Preparation of $[Mo(SnCl_3)(CO)_3(\eta^2\text{-dppm})][SnCl_5]\cdot Et_2O$ (**5**). To a solution of $[Mo(CO)_4(\eta^2\text{-dppm})]$ (0.5 mmol) in acetone (20 cm^3) was added 3 drops of $SnCl_4$. The solution was stirred at 45°C for 4 h. Then the solvent was removed under reduced pressure, giving rise to an orange–brown oil which was treated with cold diethyl ether. The yellow solid formed was filtered off and dried *in vacuo*. The complex is very unstable even when stored under nitrogen in the dark and at low temperature. It is soluble in polar solvents but its solutions quickly decompose.

Preparation of $[Mo(SnCl_3)(Cl)(CO)_3(\eta^2\text{-NN})]$ (NN = *bpy*, *phen*) (**6**, **7**). To a solution of $[Mo(CO)_3(\eta^2\text{-NN})(\eta^1\text{-dppm})]$ (0.5 mmol) in dichloromethane (20 cm^3) was added 4 drops of $SnCl_4$. A change of the solution colour to yellow was immediately observed and after 5 min a yellow–orange solid precipitated. The mixture was stirred for 1 h and then the solid was filtered off, washed with cold diethyl ether and dried *in vacuo*.

Preparation of $[Mo(SnCl_3)(Cl)(CO)_3(\eta^2\text{-dmp})]\cdot CH_2Cl_2$ (**8**). $SnCl_4$ (4 drops) was added to a suspension of $[Mo(CO)_4(\eta^2\text{-dmp})]$ (0.5 mmol) in dichloromethane (15 cm^3) causing an immediate colour change to yellow–orange. The solution was stirred for 30 min and the solvent was then removed to dryness, and the orange oil formed treated with cold diethyl ether. The yellow–orange solid obtained was filtered off and dried *in vacuo*.

Preparation of $[Mo(SnCl_3)(CO)_2(\eta^2\text{-NN})(\eta^2\text{-dppm})][SnCl_5]\cdot Et_2O$ (NN = *bpy*, *phen*) (**9**, **10**). To a solution of $[Mo(CO)_3(\eta^2\text{-NN})(\eta^1\text{-dppm})]$ (0.5 mmol) in acetone (10 cm^3) was added an excess of $SnCl_4$ (4 drops). The solution quickly changed colour to red and later to yellow. The solution was stirred for 6 h and then cold diethyl ether added. The yellow–orange solid formed was filtered off, washed with cold diethyl ether and dried *in vacuo*. The new complexes are air-sensitive solids, which are soluble in polar solvents, but they show a low stability albeit enough to obtain good NMR spectra.

Preparation of $[Mo(SnCl_3)(CO)_2(\eta^2\text{-dmp})(\eta^2\text{-dppm})][SnCl_5]\cdot Et_2O$ (**11**). $SnCl_4$ (4 drops) was added to a solution of $[Mo(CO)_3(\eta^2\text{-dmp})(\eta^1\text{-dppm})]$ (0.5 mmol) in dichloromethane (20 cm^3). The solution colour quickly changed from violet to yellow. After 30

min of stirring, cold diethyl ether was added and then the orange solid formed was filtered off, washed with cold diethyl ether and dried *in vacuo*. The new complex shows the same behaviour as the related species **9–10**.

Acknowledgements—We thank the DGICYT and CICYT of Spain for financial support (Projects PB92-0213 and MAT95-0940-E).

REFERENCES

1. Bencze, L. and Krant-Vass, A., *J. Mol. Catal.* 1985, **28,** 369.
2. Bencze, L., Krant-Vass, A. and Prókai, L., *J. Chem. Soc., Chem. Commun.* 1985, 911.
3. Zhang, H. X., Guibé, F. and Balavoine, G., *J. Org. Chem.* 1990, **55,** 1857.
4. Cano, M., Campo, J. A., Panizo, M., Tornero, J. and Menéndez, N., *Polyhedron* 1994, **13,** 3309.
5. Baker, P. K. and Bury, A., *J. Organomet. Chem.* 1989, **359,** 189.
6. Cullen, W. R. and Pomeroy, R. K., *Inorg. Chem.* 1975, **14,** 939.
7. Panizo, M. and Cano, M., *J. Organomet. Chem.* 1985, **287,** 221.
8. Cano, M., Campo, J. A., Overjero, P. and Heras, J. V., *Inorg. Chim. Acta* 1990, **170,** 139.
9. Cano, M., Campo, J. A., Pérez-García, V., Gutiérrez-Puebla, E. and Alvarez-Ibarra, C., *J. Organomet. Chem.* 1990, **382,** 397, and refs therein.
10. Garrou, P. E., *Inorg. Chem.* 1975, **14,** 1435.
11. Grim, S. O., DelGaudio, J., Molenda, R. P., Tolman, C. A. and Jesson, J. P., *Inorg. Chem.* 1974, **13,** 1095.
12. Andrews, G. T., Colquhoun, I. J., McFarlane, W. and Grim, S. O., *J. Chem. Soc., Dalton Trans.* 1982, 2353.
13. Kummer, R. and Graham, W. A. G., *Inorg. Chem.* 1968, **7,** 1208.
14. Manning, A. R., *J. Chem. Soc. A*, 1967, 1984.
15. Cano, M., Panizo, M., Campo, J. A., Tornero, J. and Menéndez, N., *Polyhedron*, 1994, **13,** 1835.
16. Cano, M., Panizo, M., Campo, J. A., Tornero, J. and Menéndez, N., *J. Organomet. Chem.* 1993, **463,** 121.

Pergamon

PII: S0277-5387(96)00384-1

Polyhedron Vol. 16, No. 7, pp. 1101–1103, 1997
Copyright © 1997 Elsevier Science Ltd
Printed in Great Britain. All rights reserved
0277-5387/97 $17.00+0.00

Photochemical and thermal synthesis of metal carbonyl complexes of tetraalkyl diphosphine disulfides $[M(CO)_4(R_2P(S)P(S)R_2)]$ (M = Mo, W; R = Me, Et, Pr-n, Bu-n)

Matthew J. Almond,[a] Fadime Sarikahya[b]* and Ozan S. Senturk[b]

[a] Department of Chemistry, University of Reading, Whiteknights, Reading RG6 2AD, U.K.

[b] Ege University, Faculty of Science, Department of Chemistry, Bornova, 35100, Izmir, Turkey

(Received 18 July 1996; accepted 2 August 1996)

Abstract—The new complexes $[M(CO)_4(R_2P(S)P(S)R_2)]$, **1A–1D, 2A–2D,** (**1A**, M = Mo, R = Me; **1B**, M = Mo, R = Et; **1C**, M = Mo, R = Pr-n; **1D**, M = Mo, R = Bu-n; **2A**, M = W, R = Me; **2B**; M = W, R = Et; **2C**, M = W, R = Pr-n; **2D**, M = W, R = Bu-n) have been prepared either by the photochemical reaction of $M(CO)_6$ with $R_2P(S)P(S)R_2$, or by thermal displacement of coordinated norbornadiene in $C_7H_8Mo(CO)_4$ with $R_2P(S)P(S)R_2$, to give the complexes $[M(CO)_4(R_2P(S)P(S)R_2)]$. The complexes have been characterized by elemental analysis, IR and ^{31}P-[^1H]-NMR spectroscopy and FAB-Mass spectrometry; the spectroscopic studies suggest a *cis*-chelate bidentate coordination of the ligand. Copyright © 1997 Elsevier Science Ltd

Keywords: phosphorus; sulfur; diphosphine disulfide; molybdenum carbonyl; tungsten carbonyl; photochemistry.

Since preparation of the first tetraalkyldiphosphine disulfide complexes in 1965 [1,2], such compounds have continued to attract attention in part because of the different possible coordination geometries which the ligand may adopt. In most cases the ligand is presumed to adopt the expected *cis*-chelate bidentate coordination, although in certain cases, e.g. $[CuCl{\cdot}Me_4P_2S_2]_2$ [3], the ligand, while retaining a chelating bidentate structure, adopts the *gauche* conformation. In the copper(II) complex $[CuCl_2{\cdot}Me_4P_2S_2]_m$ [4] the ligands retain the *trans* structure seen for the uncoordinated molecule and act in a bridging bidentate manner to give an infinite polymer in which $CuCl_2$ groups are connected by $Me_4P_2S_2$ molecules to form long —Cu—S—P—P—S—Cu—S—P—P—S— chains. It is possible for the ligand to adopt a monodentate coordination such as in $[Au(PPh_3)(Et_4P_2S_2)][PF_6]$, where a single sulfur atom coordinates to the gold centre [5]. In certain reactions fragmentations of the dialkyldiphosphine disulfide has been observed. This certainly occurs when a number of square-planar platinum complexes react with $Et_4P_2S_2$. A single crystal X-ray diffraction study of $[Pt(SPEt_2)P(OC_6H_5)_3]_2$, formed in this way [6], shows that the core of the molecule consists of a Pt—Pt moiety and to Et_2PS units in which each Pt atom is bonded to the P atom of one Et_2PS unit and to the S atom of the other equivalent unit. In another intriguing reaction $Cp^*_2Yb(OEt_2)$($Cp^* = \eta$-C_5Me_5) reacts with $Me_4P_2S_2$ to yield $Cp^*Yb(Me_2PS_2)$ as the only metal-containing products [7]. This last reaction illustrates an interesting rearrangement of the dialkyldiphosphine disulfide to a dialkyldithiophosphine ligand.

We have recently discovered a photochemical reaction of the above type in which $Mm_2(CO)_{10}$ and $Me_4P_2S_2$ react to form the dimethyldithiophosphinate derivative $Me_2PS_2Mn(CO)_4$ [8]. Some years ago it was found that the mononuclear metal carbonyl $Fe(CO)_5$ reacts photochemically with $Me_4P_2S_2$ to cleave the P—P bond and form the complex $[(CO)_3Fe(Me_2PS)]_2$, in which each sulfur atom bridges the two Fe centres [9]. In this paper we report that, in contrast to the last

* Author to whom correspondence should be addressed.

two mentioned reactions, simple tetraalkyldiphosphine disulfide complexes of $M(CO)_4$(M = Mo or W) fragments may be prepared by straightforward thermal and photochemical reactions. The complexes are characterized by elemental analysis backed up by FAB mass spectrometry, IR and ^{31}P NMR spectroscopy. The spectroscopic studies, moreover, suggest that the ligands adopt the usual *cis*-chelate bidentate structure.

EXPERIMENTAL

All preparations were carried out under dry nitrogen by using Schlenk techniques. All the solvents used in synthesis were deoxygenated. The elemental analyses were carried out using a Perkin–Elmer 240B microanalyser by Medac Ltd at Brunel University. IR spectra were recorded on samples in KBr discs at the University of Reading using a Perkin–Elmer 1720-X Fourier Transform Spectrophotometer. NMR spectra were recorded on $(CD_3)_2CO$ solutions at the University of Reading using a Jeol JNM-EX 400FT spectrometer. FAB-Mass spectra were recorded at the EPSRC Mass Spectrometry Center at University College, Swansea, on a VG Autospec instrument using caesium ion bombardment at 25 kV of the sample dissolved in 3-nitrobenzyl alcohol. UV irridiations were performed with a medium-pressure 400 W Medium Pressure Mercury Lamp through a quartz-walled immersion wall reactor.

Norbornadiene (nbd), tetrahydrofuran, benzene, hexane, pentane, dichloromethane, acetone and diethylether were purchased from Merck; $Mo(CO)_6$ and $W(CO)_6$ from Aldrich. These reagents were used as supplied. The tetraalkyldiphosphine disulfides [10, 11] and $C_7H_8Mo(CO)_4$ [12] were prepared by literature methods.

The complexes **1A–1D** and **2A–2D** (**1A**, M = Mo, R = Me; **1B**, M = Mo, R = Et; **1C**, M = Mo, R = Pr-n; **1D**, M = Mo, R = Bu-n; **2A**, M = W, R = Me; **2B**, M = W, R = Et; **2C**, M = W, R = Pr-n; **2D**, M = W, R = Bu-n) were prepared by the photochemical reactions of $R_2P(S)P(S)R_2$ and $M(CO)_6$. Yields were typically in the range 50–70%. Complexes **1A–1D** were also prepared by the thermal reaction of $C_7H_8Mo(CO)_4$ with $R_2P(S)P(S)R_2$ in typically >60% yield. The following two procedures exemplify the synthetic methods adopted.

Method A. $Mo(CO)_6$ (0.264 g, 1 mmol) and $Me_2P(S)P(S)Me_2$ (0.186 g, 1 mmol) were dissolved in benzene (100 cm^3 reactions utilising the Et, Pr-n and Bu-n derivatives were performed in *n*-pentane) and the solution mixture irradiated in a UV cell for 1 h. During the irridiation a bright-yellow precipitate was formed. The yellow solid was filtered, washed with pure solvent and dried *in vacuo*. to give yellow microcrystals (0.24 g, 61% yield).

Method B. A solution of $C_7H_8Mo(CO)_4$ (0.12 g, 0.4 mmol, in 10 cm^3 of warm *n*-hexane) was treated with $Me_2P(S)P(S)Me_2$ (0.07 g, 0.4 mmol in 10 cm^3 of CH_2Cl_2). A bright yellow precipitate formed immediately which was filtered, washed with pentane and dried *in vacuo* to give yellow microcrystals (0.12 g, 76% yield).

RESULTS AND DISCUSSION

Analytical data

1A: Found C, 24.1; H, 3.0; S, 16.1; Calc. C, 24.4; H, 3.0; S, 16.2%. **1B**: Found C, 31.8; H, 4.5; S, 14.0; Calc. C, 32.0; H, 4.4; S, 14.2%. **1C**: Found C, 37.8; H, 5.6; S, 13.0; Calc. C, 37.9; H, 5.5; S, 12.6%. **1D**: Found C, 42.6; H, 6.25; S, 11.1; Calc. C, 42.7; H, 6.4; S, 11.4%. **2A**: Found C, 20.1; H, 2.7; S, 12.9; Calc. C, 19.9; H, 2.5; S, 11.3%. **2B**: Found C, 26.9; H, 3.7; S, 11.4; Calc. C, 26.8; H, 3.7; S, 11.9%. **2C**: Found C, 32.1; H, 4.9; S, 10.9; Calc. C, 32.3; H, 4.7; S, 10.8%. **2D**: Found C, 36.8; H, 5.4; S, 9.6; Calc. C, 36.9; H, 5.5; S, 9.9%.

Spectroscopic data

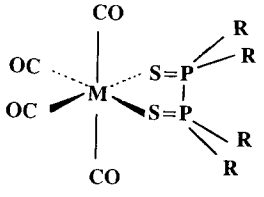
1A: ν(CO) 2019, 1919, 1847, 1794 cm^{-1}; ν_{sym}(PS) 588 cm^{-1}; ν_{as}(PS) 551 cm^{-1}; δ_P 41.00 ppm. **1B**: ν(CO) 2017, 1912, 1853, 1804 cm^{-1}; ν_{sym}(PS) 574 cm^{-1}; ν_{as}(PS) 533 cm^{-1}; δ_P 56.49 ppm. **1C**: ν(CO) 2015, 1899, 1862, 1816 cm^{-1}; ν_{sym}(PS) 595 cm^{-1}; ν_{as}(PS) 558 cm^{-1}; γ_P 51.75 ppm. **1D**: ν(CO) 2017, 1897, 1857, 1820 cm^{-1}; ν_{sym}(PS) 596 cm^{-1}; ν_{as}(PS) 560 cm^{-1}. **2A**: ν(CO) 2012, 1859, 1837, 1785 cm^{-1}; ν_{sym}(PS) 586 cm^{-1}; ν_{as}(PS) 549 cm^{-1}; δ_P 40.98 ppm. **2B**: ν(CO) 2010, 1893, 1843, 1798 cm^{-1}; ν_{sym}(PS) 588 cm^{-1}; ν_{as}(PS) 532 cm^{-1}; δ_P 56.49 ppm. **2C**: ν(CO) 2008, 1883, 1852, 1808 cm^{-1}; ν_{sym}(PS) 588 cm^{-1}; ν_{as}(PS) 569 cm^{-1}; δ_P 51.75 ppm. **2D**: ν(CO) 2010, 1884, 1850, 1812 cm^{-1}; ν_{sym}(PS) 591; ν_{as}(PS) 564 cm^{-1}; δ_P 52.66 ppm. $Me_4P_2S_2$: ν_{as}(PS) 571 cm^{-1}; δ_P 34.7–35.07 ppm. $Et_4P_2S_2$: ν_{as}(PS) 551 cm^{-1}; δ_P 49.4–52.5 ppm. $Pr_4P_2S_2$: ν_{as}(PS) 587 cm^{-1}; δ_P 46.65 ppm. $Bu_4P_2S_2$: ν_{as}(PS) 592 cm^{-1} [11, 13–15].

Mass spectrometric data. Relative intensities are given in parentheses; probable assignments in square brackets—for all assignments the most abundant isotopes of Mo and W have been selected: ^{98}Mo, 24.0% abundant; ^{184}W, 30.7% abundant.

M/z: **1A** (RMM = 396): 310(25) $[M^+ - 2CO - 2CH_3]$; 189(30) $[M^+ - 3CO + (CH_3)_2PS + 2CH_3]$. **1B** (RMM = 452): 425(10) $[M^+ - CO]$; 368(11) $[M^+ - 3CO]$; 340(10) $[M^+ - 4CO]$; 242(75) $[Et_4P_2S_2^+]$; 121(100) $[Et_2PS^+]$. **1C** (RMM = 508): 424 $[M^+ - 3CO]$; 298(50) $[Pr_4P_2S_2^+]$; 149(100)$[Pr_2PS^+]$. **1D** (RMM = 564); 536(13) $[M^+ - CO]$; 508(15) $[M^+ - 2CO]$; 480(65) $[M^+ - 3CO]$: 452(45) $[M^+ - 4CO]$; 354(100) $[Bu_4P_2S_2^+]$; 177(23) $[BuPs^+]$. **2A** (RMM = 484): 484(7) $[M^+]$; 400(7) $[M^+ - 3CO]$; 333(15) $[M^+ - CO + Me_2PS + 2Me]$; 298(20) $[M^+ - Me_4P_2S_2]$. **2B** (RMM = 540): 540(6) $[M^+]$; 512(4) $[M^+ - CO]$; 484(9)$[M^+ - 2CO]$;

456(7) [M^+-3CO]; 428(5) [M^+-4CO]; 242(100) [$Et_4P_2S_2^+$]; 121(70) [Et_2PS^+]. **2C** (RMM = 596): 596(10) [M^+]; 568(25) [M^+-CO]; 540(50) [M^+-2CO]; 512(20) [M^+-3CO]; 484 (75) [M^+-4CO]; 298(95) [$Pr_4P_2S_2^+$]; 149(100) [Pr_2PS^+]. **2D** (RMM = 652); 652 (10)[M^+]; 624(15) [M^+-CO]; 596(25) [M^+-2CO]: 540(35) [M^+-4CO]; 354(100) [$Bu_4P_2S_2^+$]; 177(18) [Bu_2Ps^+].

The photogeneration of the 16-electron fragments $M(CO)_5$ from $M(CO)_6$ (M = Mo or W) and their reaction with available donors to form $M(CO_5)L$ species have been extensively studied. When L is a ligand capable of chelating bidentate coordination rapid continuation to the $M(CO)_4L$ product may occur [16]. The photochemical reactions of $M(CO)_6$ with $R_2P(S)P(S)R_2$ proceed in this expected manner to yield the hitherto unknown series of complexes **1A–1D** and **2A–2D**. Likewise, thermal reactions of the $nbdMo(CO)_4$ complex (nbd = C_7H_8) with $R_2P(S)P(S)R_2$ proceed in an entirely expected manner by displacement of the nbd ligand to give the monometallic complexes **1A–1D**.



1 M = Mo
2 M = W
A R = Me
B R = Et
C R = *n*-Pr
D R = *n*-Bu

The IR spectra data for **1A–2D** show a decrease in ν_{as}(PS) on coordination. In the free ligand the IR active mode ν_{as}(PS) is at 567 cm^{-1} for tetramethyl diphosphine disulfide [13]. On coordination, two bands are observed: *ca* 590 [ν_{sym}(PS)] and *ca* 550 cm^{-1} [ν_{as}(PS)]. As expected four bands arising from ν(CO) vibrations are seen for each complex which presumably have *local* C_{2v} symmetry of the $M(CO)_4$ unit.

The ^{31}P-[^1H]-NMR spectra of $(CD_3)_2CO$ solutions of the complexes show one signal corresponding to the phosphorus atoms of the coordinated ligands. The δ_P values of the coordinated ligands are higher than those of free ligands. Only one signal is observed in accord with the symmetry of the complexes [17]. The FAB-mass spectra show fragmentation *via* successive loss of CO groups and fragmentation of the organic ligands.

The IR spectroscopic results are in accord with a *cis*-chelating bidentate coordination of the ligand [2]. The ^{31}P NMR data show that the P atoms of the $R_4P_2S_2$ ligands are somewhat deshielded with respect to the free ligand. The ν(CO) modes of **1A–2D** move to low wavenumber when compared with the starting $M(CO)_6$ molecules. These data suggest, as expected, that the $R_4P_2S_2$ ligand is acting principally as a σ-donor.

Acknowledgements—We thank BP (Turkey) for the provision of photochemical apparatus. We thank UK EPSRC for allocation of time at the Mass Spectrometry Service at University College, Swansea. We thank the British Council for financial support of O.S.S. and F.S. We are grateful to Mr P. Heath for obtaining the NMR data.

REFERENCES

1. Baker, K. and Fowles, G. W. A., *J. Less Common Met.* 1965, **8,** 45; Teichmann, H., *Angew. Chem., Int. Ed. Engl.* 1965, **4,** 785.
2. Meek, D. W. and Nicpon, P., *J. Am. Chem. Soc.* 1965, **87,** 4951.
3. Cotton, F. A., Frenz, B. A., Hunter, D. L. and Mester, Z. C., *Inorg. Chim. Acta*, 1974, **11,** 111.
4. Cotton, F. A., Frenz, B. A., Hunter, D. L. and Mester, Z. C., *Inorg. Chim. Acta*, 1974, **11,** 119.
5. Jones, G. C. H., Jones, P. G., Maddock, A. G., Mays, M. J., Vergano, R. A. and Williams, A. F., *J. Chem. Soc., Dalton Trans.*, 1977, 1440.
6. Wagner, K. P., Hess, R. W., Treichel, P. M. and Calabrese, J. C., *Inorg. Chem.*, 1975, **14,** 1121.
7. Berg, D. J., Andersen, R. C. and Zailkin, A., *Organometallics*, 1988, **7,** 1858.
8. Almond, M. J., Drew, M. G. B., Sarikahya, F. and Senturk, O. S., *Polyhedron*, 1995, **14,** 1433.
9. Kruger, G. J., Lotz, S., Linford, L., Van Dyk, M. and Raubenheimer, H. G., *J. Organomet. Chem.*, 1985, **280,** 241.
10. Moeller, T., Birch, H. J. and Nielson, N. C., *Inorg. Synth.*, 1953, **4,** 71; Butter, S. A. and Chatt, J., *Inorg. Synth.*, 1974, **15,** 186; Vogel, A. I., *Textbook of Practical Organic Chemistry*, 3rd edn, pp. 139–145, 163–179, 193 and 280–288. Longman, London, 1977; Issleib, K. and Tzschach, A., *Chem. Ber.* 1959, **92,** 704; Nierbergall, H. and Langenfeld, B., *Chem. Ber.*, 1962, **95,** 64.
11. Christen, P. J., Van der Linde, L. M. and Hooge, F. N., *Rec. Trav. Chim.*, 1959, **78,** 161.
12. King, R. B. and Fronzaglia, A., *Inorg. Chem.*, 1966, **5,** 1837.
13. McQuillan, G. P. and Oxton, I. A., *Spectrochim. Acta*, 1977, **33A,** 233; McQuillan, G. P. and Oxton, I. A., *Spectrochim. Acta*, 1978, **34A,** 33; McQuillan, G. P. and Oxton, L. A., *J. Chem. Soc., Dalton Trans.*, 1979, 895; Cowley, A. H. and White, W. D., *Spectrochim. Acta*, 1966, **22,** 1431.
14. Harris, R. K., Merwin, I. H. and Hagele, G., *J. Chem. Soc., Faraday Trans.* 1, 1987, **83,** 1055; Aime, S., Harris, R. K., McVicker, E. M. and Fild, M., *J. Chem. Soc., Dalton Trans.*, 1976, 2144; Moedritzer, K., Maier, L. and Groenweghe, L. D. C., *J. Chem. Eng. Data*, 1962, **7,** 307; Fluck, E. and Issleib, K., *Chem. Ber.*, 1965, **98,** 2674.
15. Gerding, H., Zijp, D. H., Hooge, F. N., Blasse, G. and Christen, P. J., *Rec. Trav. Chim.*, 1965, **84,** 1274; Park, P. J. D., Chambers, G., Wyn-Jones, E. and Hendra, P. J., *J. Chem. Soc. (A)*, 1967, 646.
16. See Cotton, F. A. and Wilkinson, G., *Advanced Inorganic Chemistry*, 5th edn, p. 1047, Wiley Interscience, New York, 1988.
17. Claver, C., Riuz, A., Masdeu, M. A., Vinas, J., Saballs, T., Lahoz, F. J. and Plou, F., *J. Organomet. Chem.*, 1989, **373,** 269.

Pergamon

PII: S0277-5387(96)00383-X

Polyhedron Vol. 16, No. 7, pp. 1105–1110, 1997
Copyright © 1997 Elsevier Science Ltd
Printed in Great Britain. All rights reserved
0277-5387/97 $17.00+0.00

Synthesis and crystal structure of zirconium complexes with fluorinated tetradentate β-ketoiminate ligands

A. Bastianini, G. A. Battiston, F. Benetollo,* R. Gerbasi and M. Porchia

Istituto di Chimica e Tecnologie Inorganiche e dei Materiali Avanzati-C.N.R., Corso Stati Uniti. I-35127 Padova, Italy

(Received 12 July 1996; accepted 2 August 1996)

Abstract—Two β-ketoiminato complexes of zirconium, di[bis-trifluoroacetylacetone-ethylenediiminato]zirconium $Zr(enTFA_2)_2$ (**1**), and di[bis-trifluoroacetylacetone-trimethylenediiminato]zirconium, $Zr(trimenTFA_2)_2$ (**2**), have been obtained in high yield from the reaction of $ZrCl_4$ and the sodium salt of the corresponding Schiff base. The compounds have been characterized by elemental analysis, NMR, mass spectrometry and X-ray structure determination. The coordination geometry around the zirconium atom is a dodecahedron in **1** and a square antiprism in **2**. The increase of the aliphatic bridging chain of the ligand does not produce significant changes in the Zr—O_{av} bond distances [2.101(2) in **1** and 2.086(4) Å in **2**] while the Zr—N_{av} bond distances are lengthened [2.432(4) in **1** and 2.491(5) Å in **2**]. Copyright © 1997 Elsevier Science Ltd

Keywords: zirconium; crystal structure; ketoimine ligands.

Tetradentate Schiff-base complexes of transition and main-group elements are well known and detailed studies have been reported on their synthesis and chemico-physical properties [1–4]. Moreover, due to the enhanced thermal stability of β-ketoiminato (or β-ketodiiminato) complexes with respect to the β-diketonates, their potential application in gas-chromatography for qualitative and quantitative metal analyses has been envisaged [5,6]. The recent development of MOCVD (metal organic chemical vapour deposition) technique for metal and metal oxides deposition and the related research aimed to find new metal precursors (thermally stable, air-stable, volatile and easy to handle) led to the "rediscovery" of some known classes of compounds such as alkoxides, diketonates and amides [7,8]. Among them β-ketoiminates and fluorinated β-ketoiminates of Cu^{I} and Cu^{II} and of Ni^{II} have been successfully used as precursors for copper and nickel deposition [9–11] and barium β-ketoiminate for $BaPbO_3$ MOCVD [12]. Such complexes, thermally stable and volatile, are interesting because, with respect to β-diketonates, an additional site, i.e. the imine nitrogen, can be exploited for tailoring their reactivity and their volatility. Few examples are reported on the synthesis and the crystal structure of complexes formed from $ZrCl_4$ with Schiff-base ligands [13–14]. In particular, studies on zirconium β-ketodiiminate are limited to the partially substituted Zr(β-ketodiiminate)Cl_2 [15]. Looking for suitable precursors for ZrO_2 chemical vapour deposition and having in mind the above reported results, we have synthesized and fully characterized two new zirconium compounds, namely di[bis-trifluoroacetylacetone-ethylenediiminato]zirconium, $Zr(enTFA_2)_2$, and di[bis-trifluoroacetylacetone-trimethylenediiminato]zirconium, $Zr(trimenTFA_2)_2$. Studies on their chemical-physical properties as well as their structural determination are reported and discussed.

EXPERIMENTAL

Synthesis of the complexes

Trifluoroacetylacetone (Htfac, Aldrich) was distilled prior to use. Ethylendiamine and 1,3-propanediamine were dried over potassium hydroxide and redistilled before use. Benzene, ethanol and n-hexane were dried and purified by standard

* Author to whom correspondence should be addressed.

procedures. ^1H and ^{13}C NMR spectra were recorded on a Bruker AC 200 spectrometer (solvent: C_6D_6 or $CDCl_3$, chemical shifts relative to TMS). Mass spectrometric measurements were performed on a VG ZAB 2F mass spectrometer (*EI* = 70 eV).

Tetradentate β-ketoimines. Both bis-trifluoroacetylacetone-ethylenediimine [H_2(enTFA$_2$)] and bis-trifluoroacetylacetone-trimethylenediimine [H_2(trimenTFA$_2$)] were synthesized according to the literature [1]. In particular, they were prepared by adding the diamine to an ethanolic solution of Htfac (Aldrich) at 0°C. After the addition, the mixture was allowed to warm up and refluxed for 3 h. Both the ketoamines (white, crystalline solids) are obtained by crystallization from water with a yield of *ca* 40%. Their purity was checked by elemental analysis, NMR, IR and mass spectroscopy.

Na *derivatives.* Na$_2$(enTFA$_2$) and Na$_2$(trimenTFA$_2$) were prepared by reaction of metallic sodium with the respective ketoimine in benzene at room temperature in dry-boxes [N_2 atmosphere, O_2 and H_2O < 2 ppm]. After 12 h excess sodium was eliminated by filtration and the natrium salt, obtained by evaporating the solvent, was characterized by ^1H NMR. Na$_2$(enTFA$_2$), ^1H NMR spectrum (C_6D_6): δ (ppm) 1.51 (s, 6H, CH_3), 5.28 (2, 2H, *CH*), 3.19 (s, 4H, N—CH_2); Na$_2$(trimenTFA$_2$), ^1H NMR spectrum (C_6D_6): δ (ppm) 1.49 (s, 6H, CH_3), 5.26 (s, 2H, *CH*), 3.02 (m, 4H, N—CH_2), 1.92 (m, 2H, CH_2).

Zr(enTFA$_2$)$_2$. A benzene solution of Na$_2$(enTFA$_2$) (3 g, 4 mmol) was added to $ZrCl_4$ (466 mg, 2 mmol) suspended in benzene. The mixture was refluxed for 3 h, NaCl was filtered and by crystallization from benzene and *n*-hexane, colourless, air-stable crystals of Zr(enTFA$_2$)$_2$ were obtained (decomposition starts at 170°C followed by melting at 220°C). Yield with respect to $ZrCl_4$: 80%. Found C, 37.8; H, 3.4; N, 7.0. Calc. for [$ZrN_4O_4C_{24}H_{24}F_{12}$]: C, 38.3; H, 3.2; N, 7.4%. ^1H NMR spectrum (C_6D_6): δ (ppm) 1.42 (s, 12H, CH_3), 5.38 (s, 4H, *CH*), 3.60 (s, 8H, N—CH_2); ^{13}C NMR spectrum ($CDCl_3$): δ (ppm) 22.47 (q, CH_3), 100.18 (d, *CH*), 51.04 (t, N—CH_2), 119.92 (q, CF_3, $^1J_{C-F}$ = 280 Hz), 154.42 (q, *CO*, $^2J_{C-F}$ = 33 Hz), 164.97 (s, *CN*).

Zr(trimenTFA$_2$)$_2$. $ZrCl_4$ (233 mg, 1 mmol) was slowly added, at room temperature, to a benzene solution of Na$_2$(trimenTFA$_2$) (692 mg, 2 mmol). After 3 h the mixture was filtered from NaCl, the solvent removed under vacuum and the white residue washed with *n*-hexane. By crystallization of the residue from a mixture of benzene/*n*-hexane, white air-stable crystals of Zr(trimenTFA$_2$)$_2$ were recovered. Yields with respect to $ZrCl_4$: 81%. It decomposes without melting at 210–220°C. Found: C, 40.0; H, 3.6; N, 7.0. Calc. for [$ZrN_4O_4C_{26}H_{28}F_{12}$]: C, 40.0; H, 3.6; N, 7.2%. ^1H NMR spectrum ($CDCl_3$): δ (ppm) 1.60 (s, 12H, CH_3), 4.97 (s, 4H, *CH*), 3.31 (m, 8H, N—CH_2), 1.96 (m, 4H, —CH_2—); ^{13}C NMR spectrum ($CDCl_3$): δ (ppm) 22.31 (q, CH_3), 102.55 (d, *CH*), 46.97 (t, N—CH_2), 26.24 (t, —CH_2—), 119.99 (q, CF_3, $^1J_{C-F}$ = 281 Hz), 153.87 (q, *CO*, $^2J_{C-F}$ = 36 Hz), 166.72 (s, *CN*).

X-ray measurements and structure determination

Crystal data, collected reflections and parameters of the final refinement for [Zr(enTFA$_2$)$_2$] and [Zr(trimenTFA$_2$)$_2$] are reported in Table 1. Reflections were collected using a Philips PW1100 diffractometer [16] with graphite-monochromated Mo-K_α radiation. The orientation matrix and cell dimensions were determined by least-squares refinement of the angular positions of 30 reflections. Data were collected at room temperature. Two standard reflections were monitored every 200 reflections and no significant decay was observed during data collection. The intensity data were corrected for Lorentz–Polarization effects and for absorption, as described by North *et al.* [17]. The structure was solved by heavy-atom methods [18]. All non-H atoms were located in the subsequent Fourier maps. The structures were refined by full-matrix least-squares using anisotropic temperature factors for all non-hydrogen atoms. The hydrogen atoms were introduced at calculated positions in their described geometries and during refinement were allowed to ride on the attached carbon atoms with fixed isotropic thermal parameters (1.2 U_{eq} of the parent carbon atom). Structure refinement and final geometrical calculations were carried out with SHELXL-93 [19] and PARST [20] programs, drawings were produced using ORTEP-II [21]. The significant bond lengths for the two compounds are reported in Table 2.

RESULTS AND DISCUSSION

The Schiff-base complexes were not straightforwardly prepared from H_2(enTFA$_2$) or H_2(trimenTFA$_2$) and $ZrCl_4$, but the sodium salt of the ligand was employed in order to better control the stoichiometry of the reaction. The complete replacement of the protic hydrogens and substitution with Na can be easily checked by NMR analysis, i.e. the signal of the enolic O—H proton disappears. The reaction of $ZrCl_4$ with the sodium salts gives **1** and **2** in high yield (80%). The new compounds are air-stable and easily crystallizable. Moreover, differently from other Schiff-base complexes, they are quite soluble in organic solvents and this allowed a complete spectroscopic characterization by ^{13}C and ^1H NMR.

The crystal structure of [Zr(enTFA$_2$)$_2$] consists of well separated molecules. An ORTEP view is shown in Fig. 1. The coordination polyhedron around Zr is a dodecahedron. The molecule possesses a two-fold crystallographic symmetry passing through the zirconium and half way of each ethylenic chain. The two independent six-membered chelation rings have the half-chair conformation and are twisted to form a dihedral angle of 61.0(2)°, while in the same ligand are approximately planar. The five-membered chelation

Table 1. Experimental data for the crystallographic analyses

Compound	$[Zr(enTFA_2)_2]$	$[Zr(trimenTFA_2)_2]$
Formula	$ZrN_4O_4C_{24}H_{24}F_{12}$	$ZrN_4O_4C_{26}H_{28}F_{12}$
Mol wt.	751.7	779.7
Crystal size (mm)	$0.26 \times 0.23 \times 0.25$	$0.18 \times 0.20 \times 0.16$
Crystal system	Tetragonal	Triclinic
Space group	$I4_1/a$	$P\bar{1}$
a (Å)	13.585(3)	8.996(3)
b (Å)		11.907(3)
c (Å)	33.025(4)	15.651(4)
α ( )		102.09(3)
β ( )		90.90(3)
γ ( )		107.11(3)
V (Å^3)	6095(2)	1561.4(8)
Z	8	2
D_c g cm^{-3}	1.64	1.66
$F(000)$	3008	784
2θ range ( )	3–28	3–28
Radiation (λ, Å)	Mo–K_α(0.71069)	Mo–K_α(0.71069)
μ (cm^{-1})	4.71	4.63
No. of reflections collected	7182	4992
No. of observed $[I \geqslant 3\sigma(I)]$	2543	4321
Weighting scheme, w	$1/[\sigma^2(F_o^2) + (0.0568P)^2 + 10.56P^*]^a$	$1/[\sigma^2(F_o^2) + (0.0000P)^2 + 6.11P]^a$
$R = \Sigma[\|F_o\| - \|F_c\|]/\Sigma\|F_o\|$	0.042	0.053
R_w (on F^2)	0.115	0.118
GOF	1.11	1.14

$^a P = \max(F_o^2 - 2F_c^2)^3$.

Table 2. Selected bond distances (Å)

	$Zr(enTFA_2)_2$	$Zr(trimenTFA_2)_2$
Zr—O(1)	2.095(2)	2.079(4)
Zr—O(2)	2.108(2)	2.091(3)
Zr—O(3)		2.092(4)
Zr—O(4)		2.081(3)
Zr—N(1)	2.422(3)	2.501(5)
Zr—N(2)	2.443(2)	2.478(5)
Zr—N(3)		2.482(5)
Zr—N(4)		2.502(4)
O(1)—C(1)	1.301(4)	1.298(8)
O(2)—C(7)	1.290(4)	1.304(7)
O(3)—C(18)		1.294(8)
O(4)—C(25)		1.298(7)
N(1)—C(3)	1.295(4)	1.297(9)
N(1)—C(5)	1.470(4)	1.475(8)
N(2)—C(9)	1.281(6)	1.295(8)
N(2)—C(11)	1.469(6)	1.488(8)
N(3)—C(14)		1.488(8)
N(3)—C(15)		1.297(8)
N(4)—C(21)		1.485(8)
N(4)—C(22)		1.293(7)
C(O)—C(H)(av.)	1.341(6)	1.336(9)
C(N)—C(H)(av.)	1.445(7)	1.440(9)
C—C(met)(av.)	1.518(8)	1.518(9)
CH_2—CH_2(av.)	1.520(9)	1.52(1)
C—C(F_3)(av.)	1.514(7)	1.51(1)
C—F(av.)	1.33(1)	1.30(1)

ring has again a half-chair conformation. The Zr—O distances are significantly shorter than the Zr—N distances [Zr—O_{av} 2.101(2)and Zr—N_{av} 2.432(3) Å] and follow the trend found in other zirconium β-ketoiminato derivatives such as $[Zr(acen)Cl_2(THF)]$ [15] and $[Zr(acen)Cl_2]$ [15] (acen = bis-acetylacetoneethylendiiminate). However, in these mono-acen derivatives of lower coordination numbers, seven and six, respectively, the Zr—O and Zr—N bond distances are shorter as expected and the difference between Zr—O_{av} and Zr—N_{av} is 0.264 and 0.245 Å, respectively, while in the bis ($enTFA_2$) derivative it is 0.331 Å. Increasing the length of the bridging aliphatic chain of the ligand of one member, the resulting $[Zr(trimenTFA_2)_2]$ derivative does not possess in the solid state any imposed crystallographic symmetry and the coordination polyhedron is a square antiprism where the two squares O(1), N(1), O(4), N(4) and O(2), N(2), O(3), N(3) are formed by the chelating hexaatomic ring belonging in both cases alternatively to each of the two "$trimenTFA_2$" ligands, as shown in Fig. 2; the twist angle between the two squares is about 43°. Also in this case the half-chair conformation is maintained and the two moieties in the same ligand are less planar with respect to the ethylene derivative, the dihedral angle being *ca* 8° in both ($trimenTFA_2$) ligands.

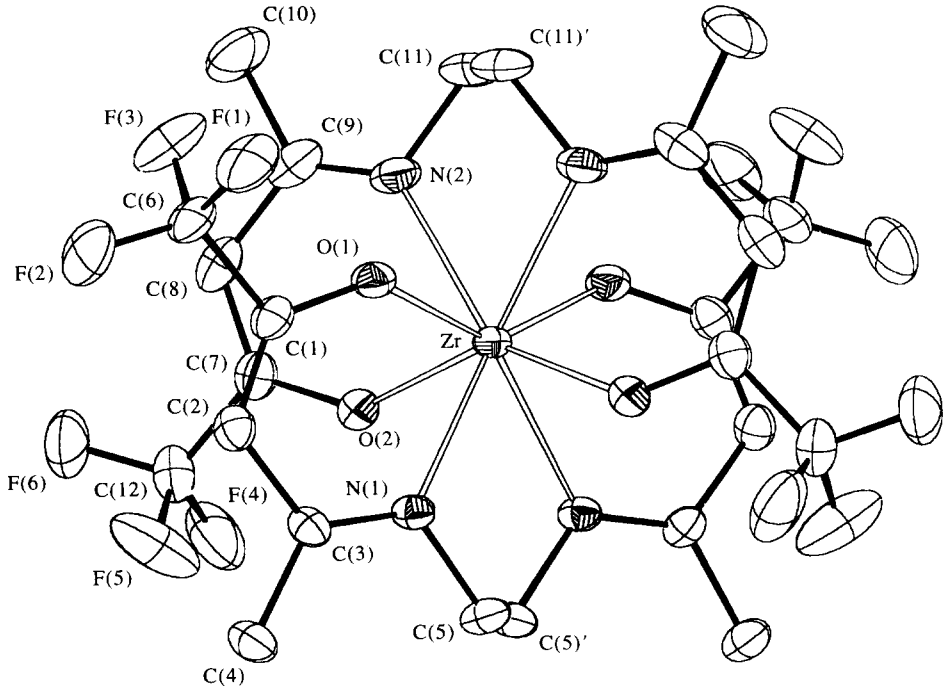


Fig. 1. ORTEP perspective view with the atom numbering scheme for $Zr(enTFA_2)_2$.

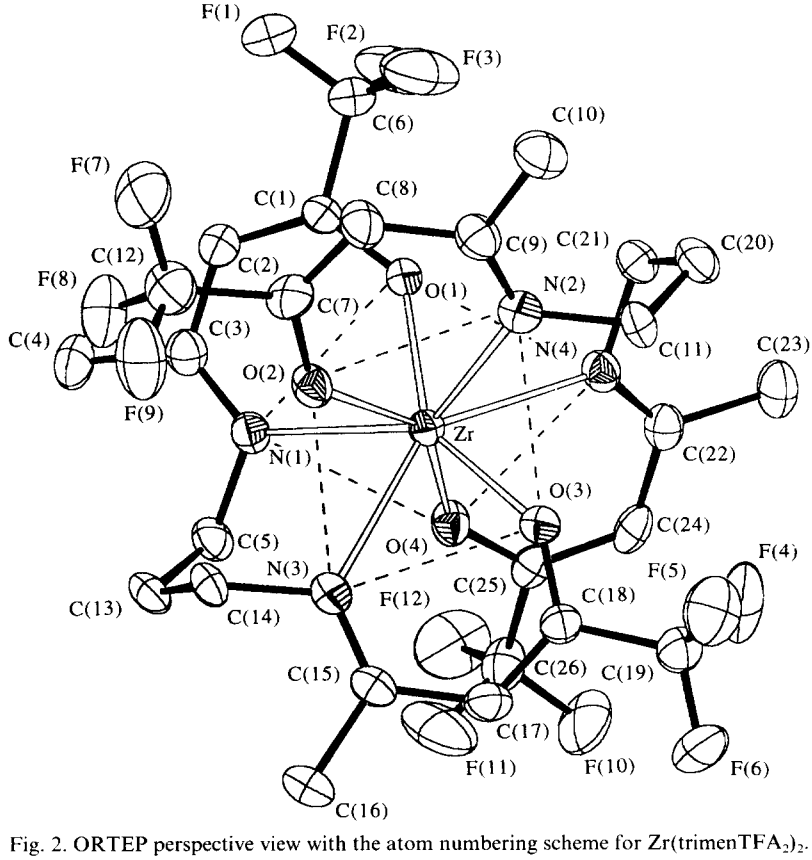


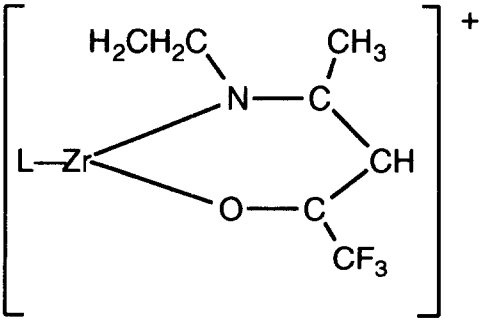
Fig. 2. ORTEP perspective view with the atom numbering scheme for $Zr(trimenTFA_2)_2$.

Table 3. 70eV mass spectra of $Zr(enTFA_2)_2$ and $Zr(trimenTFA_2)_2$

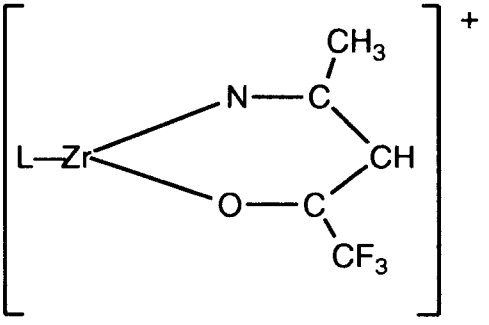
$Zr(enTFA_2)_2$			$Zr(trimenTFA_2)_2$		
m/z	Relative abundance	Assignments	*m/z*	Relative abundance	Assignments
751	35	M^+	778	100	M^+
732	4	$M^+ - F$	708	4	$M^+ - CF_3$
598	3	$M^+ - CF_3C(O)CHC(N)CH_3$	612	12	$M^+ - CF_3C(O)CHC(CH_3)NCH_3$
585	8	$M^+ - Ligand + F/2$	585	8	$M^+ - CF_3C(O)CHC(CH_3)NCH_2CH_2$
572	10	$M^+ - CF_3C(O)CHC(CH_3)NCH_2CH_2$	452	88	$M^+ - Ligand + F$
549	5	$M^+ - CF_3C(O)CHC(N)CH_3 - CF_2$	354	60	$M^+ - Ligand - CF_2 - 2CH_3$
440	100	$M^+ - Ligand + F$			
421	6	$M^+ - Ligand$			
391	6	$M^+ - Ligand - 2CH_3$			
369	22	$M^+ - Ligand - CF_2$			

The two hexaatomic rings formed with the propylene chain have a twisted conformation. The increased length of the aliphatic chain which should induce more flexibility to the ($trimenTFA_2$) ligand allows shorter Zr—O bond distances [Zr—O $2.086(4)_{av}$ *vs* 2.101(2) Å in the ($enTFA_2$) derivative], but unexpectedly the Zr—N_{av} [2.491(5) Å] length is significantly longer than Zr—N_{av} [2.432(4) Å] in the ($enTFA_2$) derivative; the change in the coordination polyhedron from dodecahedron to a square antiprism could be responsible for this lengthening, influencing the weaker Zr—N bonds.

The major ions in the mass spectra of complexes **1** and **2** are reported in Table 3. Molecular ions are detectable for both compounds and are the most abundant species in the case of **2**. Analogously to fluorinated β-diketone chelates, loss of radical species ($F^{\cdot}$, $CF_3^{\cdot}$) takes place from the molecular ions and loss of neutral species (CF_2) from the (M^+-Ligand) ion [22]. Cleavage of the ligand corresponding to the N—C bond in **1** and C—C of the bridging chain in **2** leave analogous metal-containing fragments of **1** (*m/z* 598) and **2** (*m/z* 612):



The ligand undergoes cleavage of the remaining nitrogen–carbon bond leading to the analogous species:



(*m/z* 572 for **1** and 585 for **2**). For **1** the peak corresponding to a symmetrical cleavage of the ligand is also present (M^+-L/2, *m/z* 585).

The main feature of both spectra is the presence of very intense peaks corresponding to species obtained by loss of one ligand and F rearrangement with the formation of a Zr—F bond [(M^+-Ligand + F) = *m/z* 440, 100% for **1**; *m/z* 452, 88% for **2**]. The migration of fluorine to the metal has already been noticed in the mass spectra of several fluorinated compounds, such as fluoroalkoxides of zirconium [23] and β-diketonates of different metals [22], and thermodynamic and kinetic explanations of such processes have been reported. In this case thermodynamics play a major role since the compounds **1** and **2** do not present intramolecular F···Zr interactions, which could provide a kinetic route to Zr···F, nor in the solid state, as demonstrated by X-ray analysis and presumable neither in the gas phase. Since the results obtained in the mass spectrometer by electron ionization generally give some clues about the preferential thermal decomposition pathways, the formation of ZrF_4 in CVD experiments using **1** and **2** must be taken into account; in fact, as the fluorides are thermodynamically more stable than oxides many

reported fluorinated systems thermally decompose giving metal fluorides instead of metal oxides [23–25].

Acknowledgements—The authors thank Mr F. Braga for NMR technical assistance.

REFERENCES

1. McCarthy, P. J., Hovey, R. J., Ueno, K. and Martell, A. E., *Inorg. Chem.*, 1955, **77,** 5820.
2. Ueno, K. and Martell, A. E., *J. Phys. Chem.*, 1955, **59,** 998.
3. Calligaris, M. and Randaccio, L., *Comprehensive Coordination Chemistry*, Vol. 2, ed. G. Wilkinson, R. D. Gillard and J. A. McCleverty. Pergamon Press, Oxford, 1987, p. 715.
4. Holm, R. H., Everett Jr, G. W. and Chakraworty, A., *Prog. Inorg. Chem.*, 1966, **7,** 83.
5. Belcher, R., Pravica, M., Stephen, W. I. and Uden, P. C., *J. Chem. Soc., Chem. Commun.*, 1971, 41.
6. Belcher, R., Blessel, K., Cardwell, T., Pravica, M., Stephen, W. I. and Uden, P. C., *J. Inorg. Nucl. Chem.*, 1973, **35,** 1127.
7. Hubert-Pfalzgraf, L. G., *Appl. Organomet. Chem.*, 1992, **6,** 627.
8. Bastianini, A., Battiston, G. A., Daolio, S., Gerbasi, R. and Porchia, M., *J. Physique Coll.*, 1995, **C5,** 525.
9. Shin, H.-K., Hampden-Smith, M. J., Kodas, T. T. and Rheingold, A. L., *J. Chem. Soc., Chem. Commun.*, 1992, 217.
10. Gerfin, T., Becht, M. and Dahmen, K.-H., *Materials Science and Engineering*, 1993, **B17,** 97.
11. Becht, M., Gallus, J., Hunziker, M., Atamny, F. and Dahmen, K.-H., *J. de Physique Coll.*, 1995, **C5,** 465.
12. Schulz, D. L., Hinds, B. J., Stern, C. L. and Marks, T. J., *Inorg. Chem.*, 1993, **32,** 249.
13. Bradley, D. C., Hursthouse, M. B. and Rendall, I. F., *J. Chem. Soc., Chem. Commun.*, 1970, 368.
14. Archer, R. D., Day, R. O. and Illingsworth, M. L., *Inorg. Chem.*, 1979, **18,** 2908.
15. Corazza, F., Solari, E., Floriani, C., Chiesi-Villa, A., and Guastini, C., *J. Chem. Soc., Dalton Trans.*, 1990, 1335.
16. Belletti, D., Internal Report 1/93. Centro di Studio per la Strutturistica Diffattometrica del CNR, Parma, 1993.
17. North, A. C. T., Philips, D. C. and Mathews, F. S., *Acta Cryst.*, 1968, **A24,** 351.
18. Sheldrick, G. M., *SHELXS*-86. *Acta Cryst.*, 1990, **A46,** 467.
19. Sheldrick, G. M., *SHELXL*-93. *Programme for the Refinement of Crystal Structures.*, University of Göttingen, Germany, 1993.
20. Nardelli, M., *Computing Chem.*, 1983, **7,** 95; *J. Appl. Cryst.*, 1995, **28,** 659.
21. Johnson, C. K., ORTEP-II. Report ORNL-5138. Oak Ridge National Laboratory Tennesse, USA, 1976.
22. Ballarin, B., Battiston, G. A., Benetollo, F., Gerbasi, R., Porchia, M., Favretto, D. and Traldi, P., *Inorg. Chim. Acta*, 1994, **217,** 71.
23. Samuels, J. A., Chiang, W.-C., Yu, C.-P., Apen, E., Smith, D. C., Baxter, D. V. and Caulton, K. G., *Chem. Mater.*, 1994, **6,** 1684.
24. Sato, H. and Sugawara, S., *Inorg. Chem.*, 1993, **32,** 1941.
25. Purdy, A. P., Berry, A. D., Holm, R. T., Fatemi, M. and Gaskill, D. G., *Inorg. Chem.*, 1989, **28,** 2799.

Pergamon

PII: S0277-5387(96)00381-6

Polyhedron Vol. 16, No. 7, pp. 1111–1117, 1997
Copyright © 1997 Elsevier Science Ltd
Printed in Great Britain. All rights reserved
0277-5387/97 $17.00+0.00

Synthesis and characterization of $[PPh_4][M(diod)_2]$, M = Ni, Pd, Cu or Au; crystal structure of $[PPh_4][Cu(diod)_2]$

Catherine F. Cleary,[a] Neil Robertson,[a] Masaki Takahashi,[a] Allan E. Underhill,[a]* David E. Hibbs,[b] Michael B. Hursthouse[b] and K. M. Abdul Malik[b]

[a] Department of Chemistry, University of Wales, Bangor, Gwynedd LL57 2UW, U.K.

[b] Department of Chemistry, University of Wales, Cardiff, P.O. Box 912, Park Place, Cardiff CF1 3TB, U.K.

(Received 12 July 1996; accepted 2 August 1996)

Abstract—The complexes $[P(C_6H_5)_4][M(diod)_2]$ [where M = Ni, Pd, Cu or Au (**2a, b, c, d**)] have been prepared and characterized spectroscopically, electrochemically and by X-ray structure determination for **2c**. Preparation of **2d** involved isolation of an intermediate complex with only one diod ligand. The Ni complex **2a** forms semi-conducting charge transfer complexes with TTF and BEDT-TTF. Copyright © 1997 Elsevier Science Ltd

Keywords: dithiolene; crystal structure; charge-transfer salt.

Metal bis-1,2-dithiolene complexes have been widely studied due to potential applications as molecular conductors [1,2], the observation of large third order optical non-linearities [3] and the occurrence of unusual magnetic properties [4,5] in salts of these compounds. In order to extend the range of such compounds available for study, we recently prepared and structurally characterized TBA[Ni(diod)$_2$] (diod = 1,4-dithia-6-oxa-2,3-dithiolate, Fig. 1) from which a charge-transfer complex with BEDT-TTF was prepared [6]. We have also reported preliminary studies on analogous Cu and Au complexes [7]. These complexes have a structure related to that of the organic donor molecule OTT [bis(2-oxatrimethylenedithio)tetrathiafulvalene or BOBMT-TTF] [8], which has been shown to be capable of forming conducting charge transfer salts.

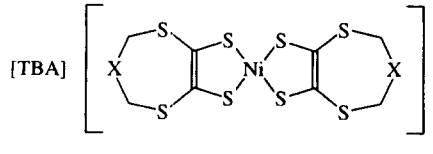


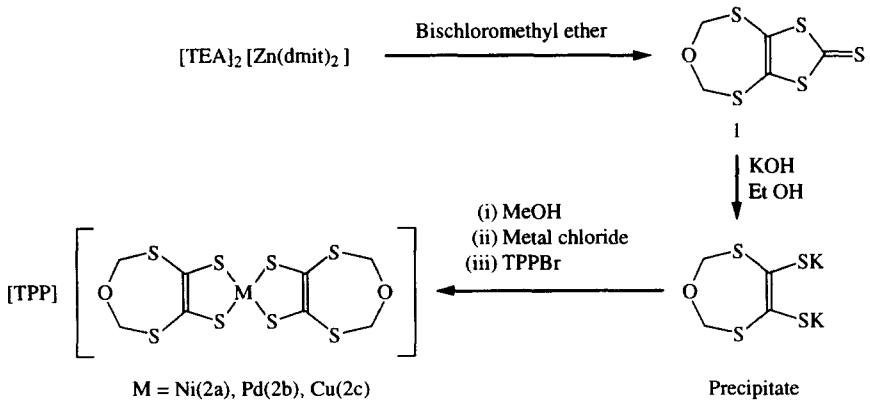
Fig. 1. X = O, TBA[Ni(diod)$_2$]; X = S, TBA[Ni(dtdt)$_2$].

We now report an improved synthesis of these compounds which has led to the isolation of TPP salts of Ni, Pd, Cu and Au complexes (**2a, b, c, d**) of the diod ligand and their spectroscopic and electrochemical characterization together with an X-ray structure determination of the Copper salt **2c**.

RESULTS AND DISCUSSION

The preparation of the complexes [TPP][M(diod)$_2$] (where M = Ni, Pd, Cu) is outlined in Scheme 1. The thione **1** was readily prepared by reaction of $[TEA]_2[Zn(dmit)_2]$ (dmit = 1,3-dithiol-2-thione-4,5-dithiolate), a convenient source of the $C_3S_5^{2-}$ unit, with bischloromethyl ether. The dipotassium salt of the ligand precursor was prepared by reaction of the thione **1** with KOH in warm ethanol and was obtained as a yellow precipitate which could be isolated. The potassium salt was allowed to react in methanol with the appropriate metal chloride and finally [TPP]Br was added to give a precipitate of the product. This procedure is analogous to that used by Kato *et al.* for the preparation of the analogous complex with a terminal sulfur rather than oxygen atom (Fig. 1) [9].

* Author to whom correspondence should be addressed.



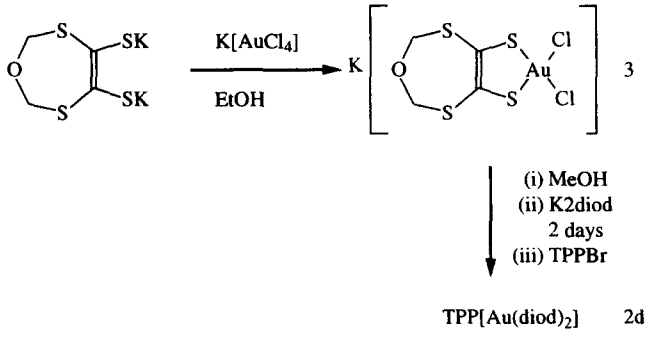
Scheme 1.

The analogous gold complex was not obtained by the above scheme due to formation of a brown precipitate after reaction of the ligand precursor with $K[AuCl_4]$. This product was believed to be $K[Au(diod)Cl_2]$ by analogy with the complex $K[Au(dtdt)Cl_2]$, which was isolated in a related study [10]. It was not possible to purify the product by recrystallization due to the almost complete lack of solubility, however, elemental analysis of the brown precipitate **3** was not inconsistent with this formula. Further evidence for the structure of **3** was obtained by the successful reaction of **3** with a further portion of K_2diod over 2 days in methanol to give the gold bis diod salt **2d** after addition of [TPP]Br (Scheme 2).

The synthesis of **2a, b, c, d** contrasts with the method used previously for the preparation of TBA[Ni(diod)$_2$] [6], in which the thione **1** was deprotected with refluxing NaOEt/EtOH and the soluble sodium salt formed reacted *in situ* with the metal chloride. This method was found to be unreliable over many repetitions as a mixture of products were often obtained which proved difficult to separate. It is believed that side products arose from the further degradation of the thione to $C_2S_4^{4-}$ fragments, which could bridge between metal centres to give rise to dimeric or polymeric products. This was supported by elemental analyses which showed a higher sulfur content and lower carbon content than that expected for the monomeric species and consistent with monoanionic salts of bridged species. In addition, an indication of interacting metal centres was detected electrochemically. The formation of the dipotassium salt of the ligand as a precipitate in the method described here, however, avoids the possibility of further degradation in solution.

The structure of $[PPh_4][Cu(diod)_2]$ (**2c**) was determined by single-crystal X-ray diffraction and consists of $[PPh_4]^+$ cations and $[Cu(diod)_2]^-$ anions held together by Van der Waals forces (Fig. 2). The shortest inter-ionic contact involving non-hydrogen atoms is 3.347 Å [O(1)$\cdots$C(8) at $1+y, z$], which indicates fairly close packing of the cationic and anionic species in the crystal. The anions are arranged in more or less parallel layers, but they are separated by the $[PPh_4]^+$ cations in a way that excludes any possibility of stacking interactions between them. The tetraphenylphosphonium cation is sited on a crystallographic two-fold axis with bond lengths and angles expected for this type of species. One of the angles at P(1) [C(5)—P(1)—C(5′)], however, is considerably narrowed compared with the others [104.5(3) *vs* 109.2(3)–111.1(2)°] probably as a result of packing requirements.

The $[Cu(diod)_2]^-$ moiety (Fig. 3) is centro-



Scheme 2.

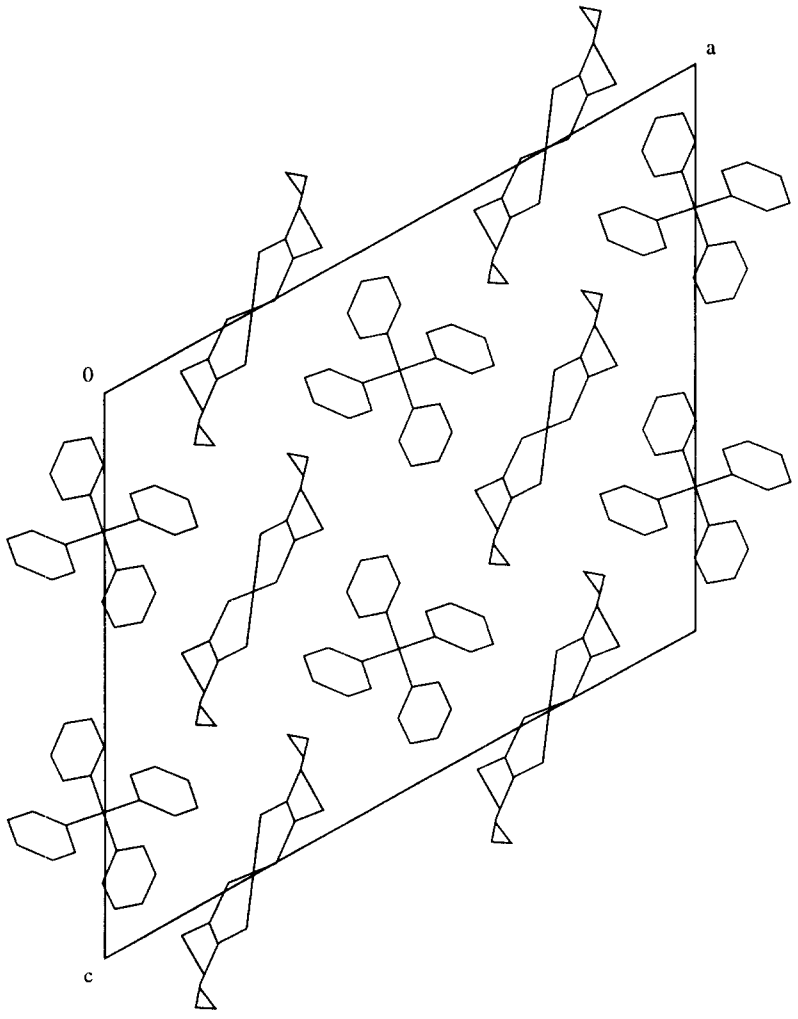


Fig. 2. The unit-cell contents of $[PPh_4][Cu(diod)_2]$ projected along *b*.

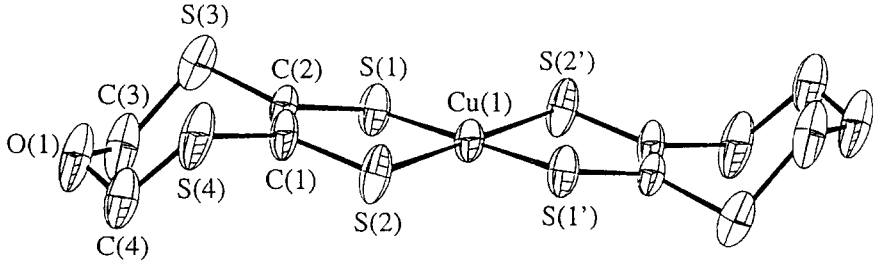


Fig. 3. The structure of the centrosymmetric $[Cu(diod)_2]^-$ anion showing the atom labelling scheme. The thermal ellipsoids are drawn at the 50% probability level. The hydrogen atoms are omitted for clarity.

symmetric with the Cu atom showing an exactly planar configuration. The unique Cu—S distances, 2.1800(13) and 2.1874(11) Å, are the same within experimental error. The *trans* angles are 180° by symmetry, whilst the *cis* angles show slight deviations (1.16°) from 90.0°, which may be attributed to the requirement of the bite angle of the chelating diod ligand. Similar angular distortions were also observed in the square planar $[Ni(diod)_2]^-$ anion in $[NBu_4][Ni(diod)_2]$ [6] and also in the complexes $[Ni(S_2C_2S_2R_2)_2]$ (R = butyl or hexyl) [11], $[Ni\{S_2C_2S_2(RR')\}_2]$ (R = Ph, R′ = Bu; R = Ph, R′ = cyclopentylmethyl) [12] and $[Ni(S_2C_2S_2(CH_2)_2C{=}CH_2)_2]$ [13]. Other geometrical parameters of the central $CuS_4C_4S_4$ core are typical for this class of compound [14]. The C—C bond length in

the chelate ring [1.331(5) Å] is comparable with those in other similar species and indicative of the delocalized nature of the bonding. The S(1)S(2)C(1)C(2) fragment of the diod ligand is planar within 0.009 Å, with the Cu(1), S(3) and S(4) atoms lying, respectively, −0.381, −0.071 and 0.014 Å away from this plane. As observed in $[NBu_4][Ni(diod)_2]$ [6], the seven-membered C_4OS_2 ring in the present case also has a chair conformation, with fold angles of 61.2 and 65.9° along the S(3)···S(4) and C(3)···C(4) lines, respectively. A similar conformation of the seven-membered C_5S_2 ring was also observed in $[Ni(dpdt)_2]$ [13], but in this case the two-fold angles above were nearly equal at 62.7 and 61.9° (see Tables 1 and 2).

The electrochemical properties of **2a, b, c, d** were studied by cyclic voltammetry against SCE in acetonitrile and the results are presented in Table 3.

The values obtained for the nickel complex **2a** are in agreement with those previously observed for the related TBA salt and show a 1−/0 couple similar to that of other metal dithiolene complexes with a proven ability to form molecular metals [6]. The separation between the 1−/0 and 2−/1− couples however, is large and indicates a poorer ability to delocalize charge than $[Ni(dmit)_2]^{x-}$. These observations are reflected in the inability to prepare molecular conductors with $[Ni(diod)_2]^{x-}$ as the sole conducting component, although the use of this complex as a counter ion for TTF or BEDT-TTF has shown greater utility towards the preparation of conducting solids. The palladium complex **2b** shows a similar reversible 1−/0 couple to **2a,** but differs in that the reduction to a dianionic state occurs irreversibly, again presumably reflecting the reduced ability of the diod ligand to delocalize charge. Compared with dmit therefore, the dianionic diod complex with Pd is destabilized such that no analogue of the isolable salts of $[Pd(dmit)_2]^{2-}$ is available.

The results obtained for the Cu and Au complexes **2c, d** reflect the double occupation of the HOMO for the monoanions of these complexes, which cause reduction to be disfavoured as it involves introduction of an electron into a higher energy molecular orbital. The Cu complex **2c** therefore, showed reduction at −1.4 V with an associated oxidation whose position and peak height was dependant on sweep rate, suggesting that this process would be chemically reversible if a high enough sweep rate could be attained. For the gold complex **2d,** no reduction was observed up to −1.5 V. The oxidation observed for **2d** occurred at +0.64 V and was irreversible. A recent study [15] has demonstrated that the oxidation process in related gold dithiolene complexes can become reversible at high sweep rates (50–2000 V s^{-1}). This, however, could not be investigated for **2d** due to instrumental limitations.

The UV–vis and near IR spectra of complexes **2a, b, c, d** were recorded in methylene chloride solution and results are presented in Table 4. The nickel complex **2a** shows an intense absorption at 950 nm typical for this class of compound and consistent with the results previously observed for the related TBA salt. The Pd complex **2b,** which also has a singly occupied HOMO displays a low energy band at 1200 nm. The large difference in the values observed for **2a** and **2b** indicates the strong influence of the central metal on the frontier orbitals of the complex. This is expected if the ligand is strongly electron-withdrawing and this may reflect the presence of the electron-withdrawing oxygen atom in the diod ligand. The Cu and Au analogues, however, possess an additional valence elec-

Table 1. Selected bond lengths (Å) and angles (°) for $[PPh_4][Cu(diod)_2]$

Cu(1)—S(1)	2.1800(13)	Cu(1)—S(2)	2.1874(11)
S(1)—C(2)	1.756(4)	S(2)—C(1)	1.754(5)
S(3)—C(2)	1.759(4)	S(3)—C(3)	1.814(5)
S(4)—C(1)	1.759(4)	S(4)—C(4)	1.799(5)
P(1)—C(5)	1.796(5)	P(1)—C(11)	1.800(4)
O(1)—C(3)	1.402(5)	O(1)—C(4)	1.407(6)
C(1)—C(2)	1.331(5)		
S(1)—Cu(1)—S(1′)^{i}	180.0	S(2)—Cu(1)—S(2)^{i}	180.0
S(1)—Cu(1)—S(2)	91.16(4)	S(1)—Cu(1)—S(2′)^{i}	88.84(4)
C(2)—S(1)—Cu(1)	102.77(13)	C(1)—S(2)—Cu(1)	102.56(14)
C(2)—S(3)—C(3)	102.3(2)	C(1)—S(4)—C(4)	103.5(2)
C(5′)^{ii}—P(1)—C(5)	104.5(3)	C(5′)^{ii}—P(1)—C(11)	111.1(2)
C(5)—P(1)—C(11)	110.4(2)	C(11)—P(1)—C(11′)^{ii}	109.2(3)
C(3)—O(1)—C(4)	113.9(4)	C(2)—C(1)—S(4)	124.5(3)
C(2)—C(1)—S(2)	120.9(3)	S(4)—C(1)—S(2)	114.6(2)
C(1)—C(2)—S(3)	125.3(4)	C(1)—C(2)—S(1)	120.3(3)
S(3)—C(2)—S(1)	114.3(2)	O(1)—C(3)—S(3)	116.1(4)
O(1)—C(4)—S(4)	116.5(4)		

The primed atoms are related to the unprimed ones by the symmetry: (i) $0.5-x, 0.5-y, -z$; (ii) $-x, y, 0.5-z$.

Table 2. Crystal data and details of data collection and structure refinement for $[PPh_4][Cu(diod)_2]$

Empirical formula	$[C_{24}H_{20}P][C_8H_8CuO_2S_8]$
Formula weight	795.53
Temperature (K)	298(2)
λ(Mo-K_α) (Å)	0.71069
Crystal system	Monoclinic
Space group	$C2/c$
Unit-cell dimensions	$a = 25.607(4)$ Å
	$b = 7.282(3)$ Å
	$c = 21.183(5)$ Å
	$\beta = 119.02(3)^\circ$
Volume (Å^3)	3454(2)
Z	4
Density (calculated) (Mg m^{-3})	1.530
Absorption coefficient (mm^{-1})	1.192
F(000)	1632
Crystal size (mm)	$0.32 \times 0.12 \times 0.10$
θ range for data collection (°)	2.06–24.88
Index ranges	$-29 \leqslant h \leqslant 16$, $-7 \leqslant k \leqslant 8$, $-20 \leqslant l \leqslant 24$
Total data collected	5752
Independent reflections	2252 [$R_{int} = 0.0788$]
Absorption correction factors	0.798–1.107
Refinement method	Full-matrix least-squares on F^2
Data/parameters	2252/201
Goodness-of-fit on F^2	0.857
Final R indices (all 2252 data)[a]	$R_1 = 0.0584$, $wR_2 = 0.0897$
R indices [1563 data with $I > 2\sigma(I)$][a]	$R_1 = 0.0383$, $wR_2 = 0.0871$
Largest diff. peak and hole (e Å^{-3})	0.494 and −0.284

[a] $R_1 = \Sigma(\Delta F)/\Sigma(F_0)$; $wR_2 = [\Sigma\{w(F_0^2 - F_c^2)^2\}/\Sigma\{w(F_0^2)^2\}]^{1/2}$; $w = [\sigma^2(F_0)^2 + (0.0325P)^2]$, where $P = [\mathrm{Max}(F_0)^2 + 2F_c^2]/3$.

Table 3.

Compound	1−/0 (V)	2−/1− (V)
[TPP][Ni(diod)$_2$]	+0.27 (reversible)	−0.65 (reversible)
[TPP][Pd(diod)$_2$]	+0.26 (reversible)	−1.24 (irreversible)
[TPP][Cu(diod)$_2$]	+0.56 (irreversible)	−1.40 (quasi-reversible)
[TPP][Au(diod)$_2$]	+0.64 (reversible)	not observed

Table 4.

Complex	λ (max)	ε (M^{-1} cm^{-1})
[TPP][Ni(diod)$_2$]	950	7300
	450	6610
	325	16,700
[TPP][Pd(diod)$_2$]	1200	4370
	315	16,700
[TPP][Cu(diod)$_2$]	450	28,400
	350	12,500
[TPP][Au(diod)$_2$]	500 (broad)	

tron and, therefore, have a fully occupied HOMO and cannot exhibit a low-energy excitation. These observations are consistent with the electrochemical behaviour of these species.

The copper complex **2c** shows a visible colour change from green to red upon dissolution in methylene chloride and comparison of the solid-state reflectance and solution spectra showed additional broad bands at 1350 and 650 nm in the solid state. As the crystal structure of this complex indicates no significant intermolecular interactions, it appears that the colour change arises from some intramolecular rearrangement. It has been previously observed that in the complex [*N*-ethyl pyridinium][Cu(dmit)$_2$] the dihedral angle between the ligand planes is 57.3° around the central metal in the solid state structure [16]. This suggests that copper complexes are able to adopt a tetrahedral arrangement of the sulfur donor atoms in solution and that the colour change in **2c** may be associated with a change from tetrahedral to square-planar geometry.

In the IR spectrum of **2a,** a band was observed at 1386 cm^{-1} corresponding to a weakened C=C bond. For **2b, c, d,** this band could not be unambiguously

assigned due to the presence of broad bands in this region associated with the TPP cation. C—S bond stretching was observed for complexes **2a, b, c, d** at around 1040 cm^{-1} and at around 905 cm^{-1}. The gold complex **3** showed bands at 1399 and 1048 cm^{-1}, consistent with the presence of a diod ligand in the proposed structure.

Electrochemical crystallization of the TPP, TBA and TMA salts of the nickel complexes were attempted in order to obtain partially oxidized salts of this complex with TPP, TMA or TBA present as counterion. These studies, however, seemed only to lead to isolation of the neutral complex $[Ni(diod)_2]$, which has also been previously prepared by reaction of **2a** with I_2 [6]. Electrocrystallizations were also attempted in the presence of TTF and BEDT-TTF in order to obtain charge-transfer complexes involving these organic donors. Highly conducting solid-state products were obtained from these experiments which appeared from elemental analysis data to have a composition approximate to that of neutral $[Ni(diod)_2]$, but clearly contained some other component as the conductivity was several orders of magnitude higher (Table 5). We postulate that these products contain a small ratio of the organic donor to the nickel complex although it is not possible to ascertain the true stoichiometry in the absence of better quality crystals which could lead to structural data.

Conclusions

A series of monanionic metal complex salts of the ligand diod have been prepared and characterized, including a crystal structure of the copper complex. Preparation of the gold complex involved isolation of an intermediate which appeared to contain only one diod ligand and may have potential as a precursor towards the preparation of asymmetric metal dithiolene containing complexes. Conducting charge-transfer complexes have been prepared from TTF or BEDT-TTF with $[Ni(diod)_2]^{x-}$, but a detailed understanding could not be obtained due to lack of high quality crystals.

EXPERIMENTAL

Bischloromethyl ether [17], $TEA_2[Zn(dmit)_2]$ [18] and thione [6] were prepared by previously described methods. $NiCl_2 \cdot 6H_2O$, $PdCl_2(NCPh)_2$, $CuCl_2$ and $K[AuCl_4]$ were used as purchased without further purification. Ethanol was distilled from Mg/I_2 prior to use and stored over molecular sieve. IR spectra of samples pressed as KBr discs were recorded on a Perkin–Elmer 1600 series FTIR spectrometer. Near IR, UV–vis and reflectance spectra were recorded on a Beckman DK-2A instrument. Electrocrystallization experiments were carried out by methods analogous to those described previously [6].

Table 5.

Complex	σ_{RT} (S cm^{-1})
$[Ni(diod)_2]$	9×10^{-6}
$[TTF]_x[Ni(diod)_2]$	2×10^{-3}
$[BEDT\text{-}TTF]_x[Ni(diod)_2]$	3×10^{-1}

Preparation of $TPP[M(diod)_2]$ **(2a, b, c)**

(i) **2a**: The thione **1** (1.078 g, 4.49 mmol) was stirred in dry ethanol (50 cm^3) with KOH (2.0 g, 36 mmol) for 2 h in a water bath at 45–50°C. A pale yellow precipitate was formed which was filtered off under nitrogen and washed with ethanol. The salt was dried *in vacuo* and dissolved in dry methanol (20 cm^3). $NiCl_2 \cdot 6H_2O$ (0.309 g, 1.30 mmol) dissolved in dry methanol (20 cm^3) was added and stirring continued for 16 h at room temperature under nitrogen. Air was bubbled through the solution for 20 min and the mixture filtered to remove a pale yellow residue. TPPBr (2.524 g, 6.02 mmol) dissolved in methanol was added to the filtrate dropwise with stirring. The brown precipitate formed was filtered off, washed with methanol and dried in air. The product was recrystallized by dissolving in acetone, filtering to remove any undissolved solid, addition of IPA and reduction of the volume until the solution became cloudy. The crystalline product was allowed to form over 2 h, filtered off, washed with IPA and dried in air. Yield = 0.37 g, 0.47 mmol, 36%. Found: N, 0.0; C, 46.9; H, 3.5; S, 32.4. Requires: N, 0.0; C, 46.6; H, 2.4% S, 31.1. IR: ν_{max}/cm^{-1} 3433, 1480, 1434, 1386, 1305, 1184, 1107, 1038.

(ii) **2b,c**: These were formed by a procedure identical to that for **2a** but substituting $NiCl_2 \cdot 6H_2O$ for $PdCl_2(NCPh)_2$ and $CuCl_2$, respectively.

2b: Yield = 5%. Found: N, 0.1; C, 46.0; H, 2.6; S, 24.9. Requires: N, 0.0; C, 45.9; H, 3.3; S, 30.6%. IR: ν_{max}/cm^{-1} 3446, 2361, 1702, 1482, 1436, 1301, 1108, 1043, 996, 972, 906.

2c: Yield = 7%. Found: N, 0.0; C, 48.1; H, 3.1; S, 31.8. Requires: N, 0.0; C, 48.3; H, 3.5; S, 32.2%. IR: ν_{max}/cm^{-1} 1481, 1434, 1305, 1108, 1035, 904.

Preparation of **3**

The thione **1** (0.411 g, 1.71 mmol) and KOH (0.856 g, 15.26 mmol) were dissolved in dry ethanol (20 cm^3) and stirred under nitrogen at 45°C for 2.5 h. A pale yellow precipitate was formed and filtered off under nitrogen. The yellow solid was stirred in methanol (20 cm^3) under nitrogen along with $K[AuCl_4]$ (0.20 g, 0.52 mmol) and stirred overnight. A dark brown solid was formed which was filtered off and washed with methanol. Found: N, 0.0; C, 7.3; H, 0.5; S, 24.2. Requires:

N, 0.0; C, 9.5; H, 0.8; S, 25.5%. IR: ν_{max}/cm^{-1} 1399, 1048.

Preparation of **2d**

The thione **1** (0.20 g) and KOH (0.41 g) were reacted in dry ethanol over 2.5 h and the resultant yellow precipitate filtered off, washed with ethanol and dried under nitrogen. This solid was dissolved in dry methanol (50 cm^3) and reacted with **3** over 2 days at 50°C under nitrogen then filtered to remove any undissolved solid. To the filtrate was added TPPBr (0.813 g) in dry methanol (20 cm^3) dropwise with stirring forming a yellow/brown precipitate. This was filtered off, washed with methanol and dried in air. Yield = 0.113 g, 0.12 mmol, 24%. Found: N, 0.0; C, 40.7; H, 2.9; S, 28.7. Requires: N, 0.0; C, 41.4; H, 3.0; S, 27.6%. IR: ν_{max}/cm^{-1} 3448, 1638, 1548, 1484, 1436, 1382, 1304, 1108, 1037, 905, 723, 688, 618.

X-ray structure determination of $[PPh_4][Cu(diod)_2]$

All crystallographic measurements were made at 298(2) K on a Delft Instruments FAST TV area detector diffractometer positioned at the window of a rotating anode generator using Mo-K_α radiation ($\lambda = 0.71069$ Å) by following procedures described elsewhere [19]. The structure was solved by Patterson methods (SHELXS86) [20] and difference syntheses, and refined on F^2 by full-matrix least-squares (SHELXL93) [21] using all unique data corrected for Lorentz and polarization factors and also for absorption effects (DIFABS) [22]. The non-hydrogen atoms were refined anisotropically, the hydrogen atoms were included in calculated positions (riding model) with U_{iso} tied to the U_{eq} of the parent carbons. Sources of scattering factors as in reference [21]. The diagrams were drawn with SNOOPI [23]. The calculations were done on a Pentium P5-90 personal computer. Important bond lengths and angles are given in Table 1, and the crystal data and details of data collection and structure refinement are presented in Table 2. The atomic coordinates, thermal parameters, full lists of bond lengths and angles, and structure factor tables have been deposited with the Editor as supplementary material.

Acknowledgement—We thank the EPSRC for financial support.

REFERENCES

1. Cassoux, P., Valade, L., Kobayashi, H., Clark, R. A. and Underhill, A. E., *Coord. Chem. Rev.* 1991, **110,** 115.
2. Le Narvor, N., Robertson, N., Weyland, T., Kilburn, J. D., Underhill, A. E., Webster, M., Svenstrup, N. and Becher, J., *J. Chem. Soc., Chem. Commun.* 1996, 1363.
3. Winter, C. S., Oliver, S. N., Rush, J. D., Hill, C. A. S. and Underhill, A. E., *J. Mater. Chem.* 1992, **2,** 433; Bjørnholm, T., Geisler, T., Petersen, J. C., Greve, D. R. and Schiødt, N. C., *Non-Linear Optics*, 1995, **10,** 129.
4. Coomber, A. T., Beljonne, D., Friend, R. H., Bredas, J. L., Charlton, A., Robertson, N., Underhill, A. E., Kurmoo, M. and Day, P., *Nature*, 1996, **380,** 144.
5. Awaga, K., Okuno, T., Maruyama, Y., Kobayashi, A., Kobayashi, H., Schenk, S. and Underhill, A. E., *Inorg. Chem.* 1994, 33.
6. Robertson, N., Parkin, D. L., Underhill, A. E., Hursthouse, M. B., Hibbs, D. E. and Abdul Malik, K. M., *J. Mater. Chem.* 1995, **5,** 1731.
7. Underhill, A. E., Robertson, N. and Parkin, D. L., *Syn. Met.* 1995, **71,** 1955.
8. Mori, T., Inokuchi, H., Kini, A. M. and Williams, J. M., *Chem. Lett.* 1990, 1279; Nakano, H., Yamada, K., Nogami, T., Shirota, Y., Miyamoto, A. and Kobayashi, H., *Chem. Lett.* 1990, 2129; Mueller, H. and Ueba, Y., *Bull. Chem. Soc. Jpn.* 1993, **66,** 1773.
9. Kato, R., Kobayashi, H., Kobayashi, A. and Sasaki, Y., *Bull. Chem. Soc. Jpn*, 1986, **59,** 627.
10. Takahashi, M., Robertson, N. and Underhill, A. E., unpublished results.
11. Charlton, A., Hill, C. A. S., Underhill, A. E., Malik, K. M. A., Hursthouse, M. B., Karaulov, A. I. and Moller, J., *J. Mater. Chem.* 1994, **4,** 1861.
12. Hill, C. A. S., Charlton, A., Underhill, A. E., Malik, K. M. A., Hursthouse, M. B., Karaulov, A. I., Oliver, S. N. and Kershaw, S. V., *J. Chem. Soc., Dalton. Trans.* 1995, 587.
13. Charlton, A., Underhill, A. E., Malik, K. M. A., Hursthouse, M. B., Jørgensen, T. and Becher, J., *Synthetic Metals*, 1995, **68,** 221.
14. Vance, C. T., Bereman, R. D., Bordner, J., Hatfield, W. E. and Helms, J., *Inorg. Chem.* 1985, **24,** 2905.
15. Schiødt, N. C., Sommer-Larsen, P., Bjørnholm, T., Former Nielson, M., Larsen, J. and Bechgaard, K., *Inorg. Chem.* 1995, **34,** 3688.
16. Matsubayashi, G., Takahashi, K. and Tanaka, T., *J. Chem. Soc., Dalton Trans.* 1988, 967.
17. Buc, S. R., *Org. Synth.* 1964, **36,** 1.
18. Steimecke, G., Sieler, H.-J., Kirmse, R. and Hoyer, E., *Phosphorus and Sulfur*, 1979, **7,** 49.
19. Darr, J. A., Drake, S. R., Hursthouse, M. B. and Malik, K. M. A., *Inorg. Chem.* 1993, **32,** 5704.
20. Sheldrick, G. M., *Acta Cryst.* 1990, **A64,** 467.
21. Sheldrick, G. M., *SHELXL93. Program for Crystal Structure Refinement*. University of Göttingen, Germany, 1993.
22. Walker, N. P. C. and Stuart, D., *Acta Cryst.* 1983, **A39,** 158; adapted for FAST geometry by Karaulov, A. I., University of Wales, Cardiff, 1991.
23. Davies, K., *SNOOPI Program for Crystal Structure Drawing*, University of Oxford, U.K., 1983.

Pergamon

PII: S0277-5387(96)00380-4

Polyhedron Vol. 16, No. 7, pp. 1119–1122, 1997
Copyright © 1997 Elsevier Science Ltd
Printed in Great Britain. All rights reserved
0277-5387/97 $17.00+0.00

Synthesis and crystal structure of a heterometallic chromium–potassium one-dimensional chain

Hui Li,[a] Zhuang Jin Zhong,[a]* Xiao-Zeng You[a] and Wei Chen[b]

[a] Coordination Chemistry Institute, Key Laboratory of Coordination Chemistry, Nanjing University, Nanjing 210093, P.R. China

[b] Department of Chemistry, University of Malaya, Lambah Pautai, 59100 Kuala Lumpur, Malaysia

(Received 12 July 1996; accepted 1 August 1996)

Abstract—A novel chain complex containing chromium(III) and alkali metal, namely, [Cr(salen)$(NCS)_2K \cdot H_2O$] [salen^{2-} = *N*,*N*′-ethylenebis(salicyldiminato)] was prepared and its crystal structure was determined by X-ray diffraction technique. Each chromium atom is six-coordinated with the tetradentate ligand salen^{2-} in the equatorial plane and two NCS ligands in the axial positions *via* the N atoms. The bond lengths of the Cr atom with the coordinating atoms are comparable with other Cr^{III} Schiff base complexes. Each K atom is also six-coordinated with five oxygen atoms and a sulfur atom. The bond lengths of K—O fall into the range of potassium complexes of cyclic polyethers. There are two kinds of bridging modes: water molecules link two K atoms and phenolato groups in the Schiff base ligand and NCS anions link Cr and K atoms, resulting in a chain running in the direction parallel to the a-axis. Copyright © 1997 Elsevier Science Ltd

Keywords: chromium(III); potassium; crystal structure; heterometallic complex; one-dimensional chain.

One-dimensional coordination polymers of metal complexes have been intensely studied for nearly 30 years as materials with unusual properties [1–4]. Molecular-based ferromagnets, synthetic metallic conductors, non-linear optical materials and ferroelectrics represent several applications of low-dimensional coordination polymers. Many efforts have been made to prepare this kind of complex. It remains a continuing challenge for the experimental chemists to assemble molecules. In this study we attempted to obtain a complex [Cr(salen)$(NCS)_2$]$^-$ [salen^{2-} = *N*,*N*′-ethylenebis(salicyldiminato)], since the two thiocyanato ligands in it may act as bridging ligands. So, the complex may act as a precursor of one-dimensional polymers, especially heterometallic one-dimensional polymers. To our surprise, the structure determination revealed the title complex [Cr(salen)$(NCS)_2K \cdot H_2O$] to be a one-dimensional chromium–potassium heterobimetallic polymer. This kind of complex is still rare so far [5].

* Author to whom correspondence should be addressed.

EXPERIMENTAL

Preparations

All the chemicals were analytical grade and used without further purification. [Cr(salen)$(H_2O)_2$]NO_3 was prepared according to the literature methods [6].

Synthesis of [Cr(salen)$(NCS)_2K \cdot H_2O$]. To a methanol solution (20 cm^3) of [Cr(salen)$(H_2O)_2$]NO_3 (2 mmol) was added a methanol solution (5 cm^3) of KSCN (8 mmol, molar ratio: 1:4) and the resultant mixture was refluxed for 4 h with stirring. Some insoluble solid appeared when cooled to room temperature. After filtration, the filtrate was allowed to stand for several days. Reddish-brown single crystals suitable for X-ray analysis were obtained. Found: C, 43.5; H, 2.9; N, 11.3. Calc. for $C_{18}H_{16}CrN_4O_3S_2K$: C, 44.0; H, 3.3; N, 11.4%.

Physical measurements

Elemental analyses were performed at the Analysis and Measurement Center of Nanjing University. The

Table 1. Crystal data and data collection parameters

Formula	$C_{18}H_{16}CrKN_4O_3S_2$
Formula weight	491.57
Crystal system	Monoclinic
Space group	$P2_1/n$
Unit-cell parameters	
a	8.538(6) Å
b	12.972(2) Å
c	19.180(2) Å
β	92.095(7)°
V	2122.8(4) Å^3
Z	4
D_{calc} (g cm^{-3})	1.538
Final R indices for $[I > 2\sigma(I)]$	$R_1 = 0.0428$, $wR_2 = 0.1006$
Weighting scheme	$w = 1/[\sigma^2\|F_0^2\| + (0.082p)^2 + 2.39p]$
Residual extrema in final difference map (e Å^{-3})	+0.503 to −0.418

FT-IR spectra were recorded in the 4000–400 cm^{-1} region using KBr pellets on a Nicolet 170 SX FTIR spectrometer.

X-ray structure determination

The crystal selected for X-ray diffraction was a reddish-brown parallelepiped of dimensions $0.5 \times 0.25 \times 0.18$ mm^3. Raw intensities were collected on a four-circle CAD4 diffractometer with Mo-K_α radiation at room temperature (27°C). The scan mode was ω-scan with a fixed speed of 3 s per reflection. The accurate unit-cell parameters were determined from automatic centring of 25 reflections ($1.90 \leqslant \theta \leqslant 24.98°$) and refined by least-squares methods. The crystallographic data, conditions retained for the intensity collection and some features of structure refinement are listed in Table 1.

7279 reflections were collected in the range $-10 \leqslant h \leqslant 10$, $0 \leqslant k \leqslant 15$, $-22 \leqslant l \leqslant 22$, and 3736 reflections were assumed as observed by applying the condition $I > 2\sigma(I)$. Absorption corrections based on 3 rather weak reflections were performed by means of the psi-scan technique. The structures were solved by

Table 2. Selected bond distances (Å) and bond angles (°)

Cr—O(2)	1.937(2)	Cr—O(1)	1.948(2)
Cr—N(2)	2.002(3)	Cr—N(1)	2.006(3)
Cr—N(3)	2.015(3)	Cr—N(4)	2.020(3)
K—O(2)1	2.738(2)	K—O	2.764(4)
K—O(1)1	2.854(2)	K—O(1)2	2.877(3)
K—O1	2.904(4)	K—N(3)2	3.228(3)
K—C(1)2	3.291(3)	K—S(2)	3.334(2)
K—C(17)2	3.528(4)	S(1)—C(17)	1.622(4)
S(2)—C(18)	1.622(4)	O(1)—C(1)	1.323(4)
O(2)—C(16)	1.319(4)	N(1)—C(7)	1.281(5)
N(1)—C(8)	1.465(4)	N(2)—C(10)	1.277(5)
N(2)—C(9)	1.479(4)	N(3)—C(17)	1.159(4)
N(4)—C(18)	1.144(4)	C(8)—C(9)	1.513(6)

O(2)—Cr—O(1)	96.34(10)	O(1)—Cr—N(1)	90.28(11)
O(2)—Cr—N(2)	91.83(11)	N(2)—Cr—N(1)	81.55(12)
O(1)—Cr—N(2)	171.83(11)	O(2)—Cr—N(3)	88.96(12)
O(2)—Cr—N(1)	173.37(11)	O(1)—Cr—N(3)	92.16(12)
N(3)—Cr—N(4)	178.14(12)	O(2)1—K—O	108.38(11)
O(2)1—K—O(1)1	62.32(7)	O—K—O(1)1	85.43(11)
O(2)1—K—O(1)2	99.33(8)	O—K—O(1)2	138.96(10)
O(1)1—K—O1	124.37(11)	O(1)2—K—O1	143.52(10)
C(17)—N(3)—Cr	163.9(3)	C(18)—N(4)—Cr	172.4(3)
N(3)—C(17)—S(1)	177.8(3)	N(4)—C(18)—S(2)	177.7(3)

Symmetry transformations used to generate equivalent atoms: (1) $-x+1, -y+2, -z+2$; (2) $x+1, y, z$; (3) $x-1, y, z$.

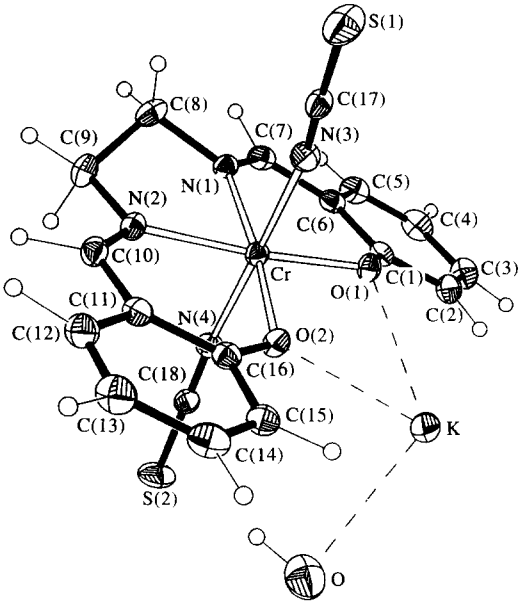


Fig. 1 The molecular structure of the crystallgraphic unique unit.

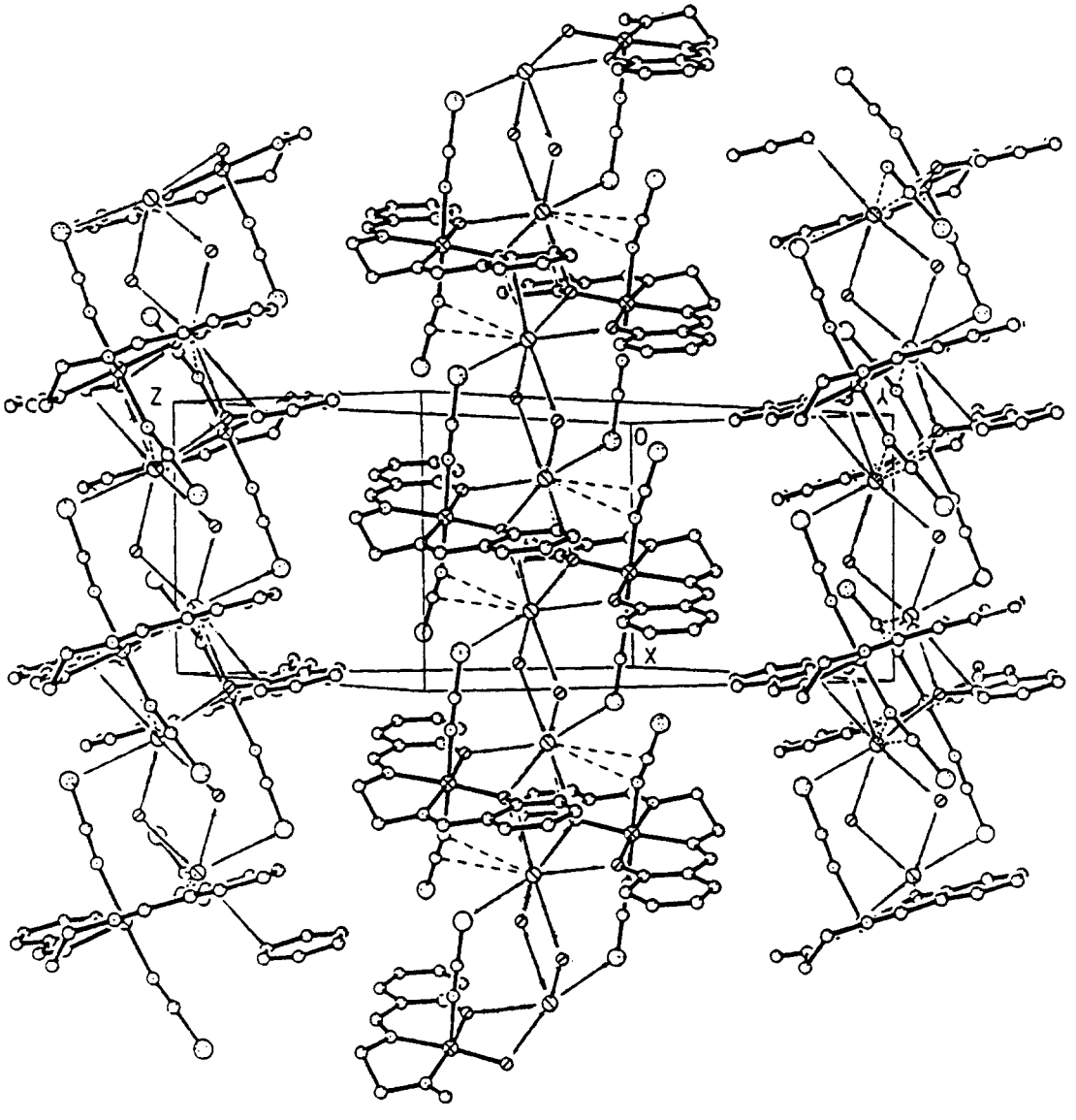


Fig. 2. Packing diagram viewed down the *b* axis.

the Patterson method using SHELXS-86 [7]. All H atoms (except one on H_2O) were located from the difference map. All non-H atoms were subjected to anisotropic refinements. Crystallographic computations were performed using the SHELXL-93 package [8] on a 486 PC computer. Selected bond lengths and angles are given in Table 2.

Additional material available from the Cambridge Crystallographic Data Center comprises H-atom coordinates, and remaining bond lengths and angles.

RESULTS AND DISCUSSION

Description of the structure

Figure 1 illustrates the geometry and labelling of the cell unit. The Cr atom is six-coordinate with the tetradentate ligand salen^{2-} in the equatorial plane and two NCS ligands in the axial positions *via* the N atoms. The bond distances Cr—O(1) [1.948(2)], Cr—O(2) [1.937(2)], Cr—N(1) [2.006(3)] and Cr—N(2) [2.002(3) Å] are close to those in other Cr^{III} complexes $[Cr(salen)(H_2O)_2]^+Cl^-$ [9] and $[Bu_4N][\{Cr(salen)CN\}_2CN]$ [10], in which Cr—N(imine) is *ca* 2.00 Å and Cr—O(phenolato) is *ca* 1.94 Å. The bond lengths of Cr—N(3) and Cr—N(4) are 2.015(3) and 2.020(3) Å, respectively. Similar distances were also seen in $[\{Cr(tmpa)(NCS)\}_2O]^{2+}$ [Cr—N (NCS) = 2.004(3) Å] [11]. The bond angles of O(1)—Cr—N(2) and O(2)—Cr—N(1) are 171.83(11) and 173.37(11)°, respectively, showing the Cr atom slightly out of the equatorial plane. The bond angle ∠NCS is *ca* 177°, indicating a linear NCS group, but the bond angle of C(17)—N(3)—Cr (163.9°) is smaller than that of C(18)—N(4)—Cr [172.4(3)°].

The K atom is coordinated by five oxygen atoms and a sulfur atom (Fig. 2). The oxygen atoms originate from two water molecules and the others from different phenolato groups of salen ligands in the complex anions. The bond distances of K—O are in the range 2.7–2.9 Å and are comparable with the K—O distances of 2.70–3.09 Å in potassium complexes of cyclic polyethers [12–14]. The bond length of K—S (from the SCN anion) is 3.334(2) Å, close to those K—S bond distances (3.20–3.35 Å) in the potassium dithiocarboxylate complex $[S_2CphCS_2]2K \cdot 2H_2O$ [15] and the potassium monothiocarboxylates complex $[SOCNHNHCOS]2K \cdot 2H_2O$ [16]. The distances of K—C(17)2, K—N(3)2 and K—C(1)2 are 3.528(2), 3.228(4) and 3.291(3) Å, respectively, suggesting some weak interaction may operate among them. Two further points merit attention. One is that the water molecules in the crystal act as bridging ligands linking two K atoms. The other is that the phenolato groups in the Schiff base ligand and the NCS anions bridge the K atoms and Cr atoms. As a result, a chain including the Cr^{III} and K atoms forms running in the direction parallel to the *a*-axis.

IR spectra

The IR spectra of the complex display a strong absorption at 2045 cm^{-1}. It is the characteristic C=N stretch for an N-coordinated thiocyanate ion. This is consistent with the results of X-ray analysis. IR spectra also show a strong absorption band at *ca* 1623 cm^{-1} which is assigned to a C=N stretching mode in the Schiff base. Comparing with the free H_2salen ligand (1635 cm^{-1}) the absorption band is slightly red-shifted.

Acknowledgements—This work was supported by grants from the State Science and Technology Commission and the National Natural Science Foundation of China.

REFERENCES

1. Sheats, J. E., Carraher Jr, C. E., Pittmen Jr, C. U., Zeldin, M. and Currell, B., (eds), *Inorganic and Metal-Containing Polymerials*. Plenum Press, New York 1990.
2. Harrod, J. F. and Laine, R. M., (eds), *Inorganic and Organometallic Oligomers and Polymers*. Kluwer, Dordrecht, 1991.
3. Laine, P. M., ed., *Inorganic and Organometalic Polymers with Special Properties*, Kluwer, Dordrecht, 1992.
4. Chen, C.-T. and Suslick, K. S., *Coord. Chem. Rev.* 1993, **128,** 293, and refs. therein.
5. Blake, A. J., Grant, C. M., Parsons, S., Rawson, J. M., Solan, G. A. and Winpenny, R. E. P., *J. Chem. Soc., Dalton Trans.* 1995, 2311.
6. Lloret, F., Julve, M., Mollar, M., Castro, I., Latorre, J. and Faus, J., *J. Chem. Soc., Dalton Trans.* 1989, 729.
7. Sheldrick, G. M., *Acta Cryst.* 1990, **A46,** 467.
8. Sheldrick, G. M., *SHELXL*-93. University of Gottingen, Germany, 1993.
9. Coggon, P., McPhail, A. T., Mabbs, F. E., Richards, A. and Thornley, A. S., *J. Chem. Soc. A.*, 1970, 3296.
10. Li, H., Zhong, Z. J., Chen, W. and You, X.-Z., submitted to *J. Coord. Chem.*
11. Gafford, B. G., Holverda, R. A., Schugar, H. J. and Potenza, J. A., *Inorg. Chem.* 1988, **27,** 1126.
12. Hubbersty, P., *Coord. Chem. Rev.* 1990, **102,** 1, and refs therein.
13. Dobler, M. and Phizackerley, R. P., *Acta Cryst.* 1974, **B30,** 2748.
14. Kamitori, S., Hirolsu, K. and Higuchi, T., *J. Am. Chem. Soc.* 1987, **109,** 2409.
15. Nikloweit, U. and Mattes, R., *Z. Anorg. Allg. Chem.* 1986, **532,** 145.
16. Fusser B. and Matters, R., *Z. Anorg. Allg. Chem.* 1987, **547,** 158.

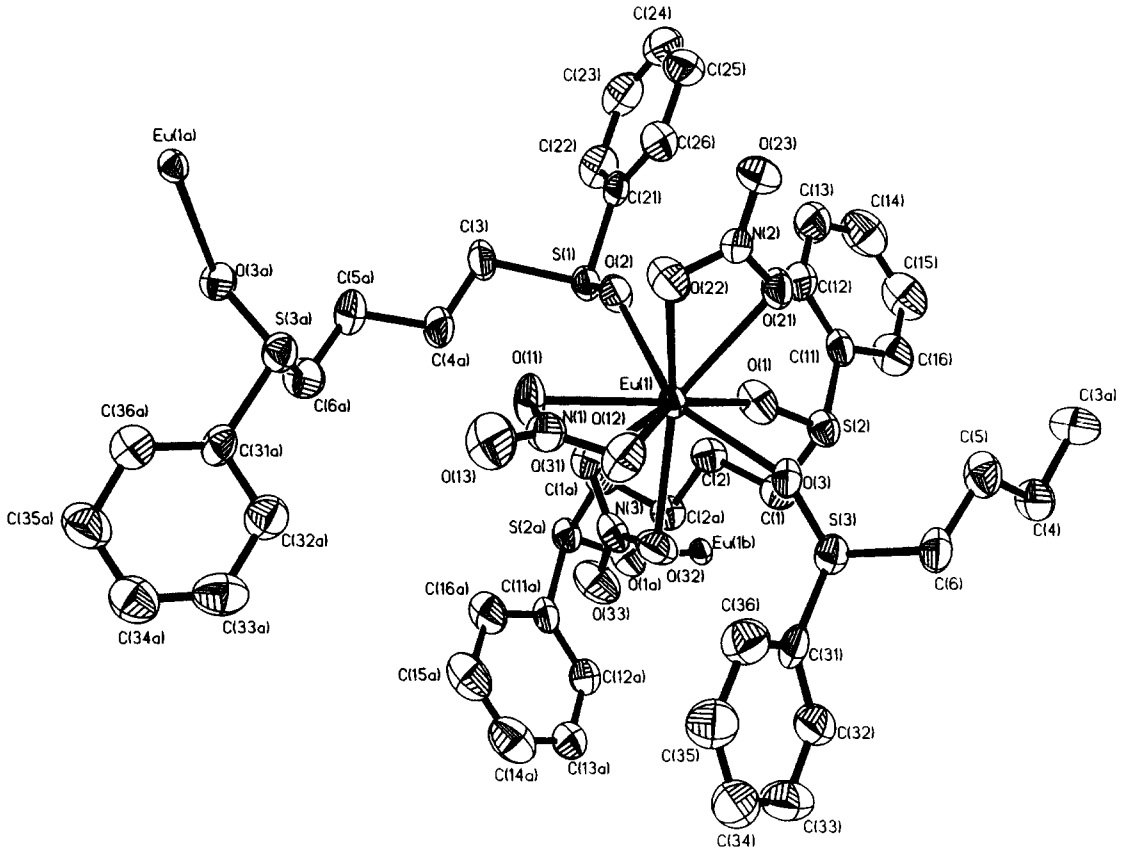


Fig. 1. The labelling scheme of the complex.

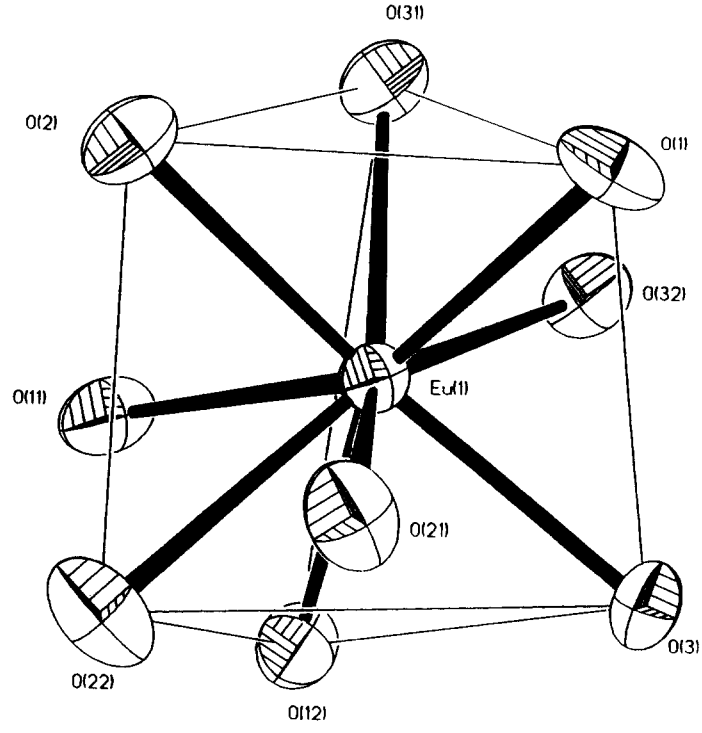


Fig. 2. The coordination around each Eu^{III}.

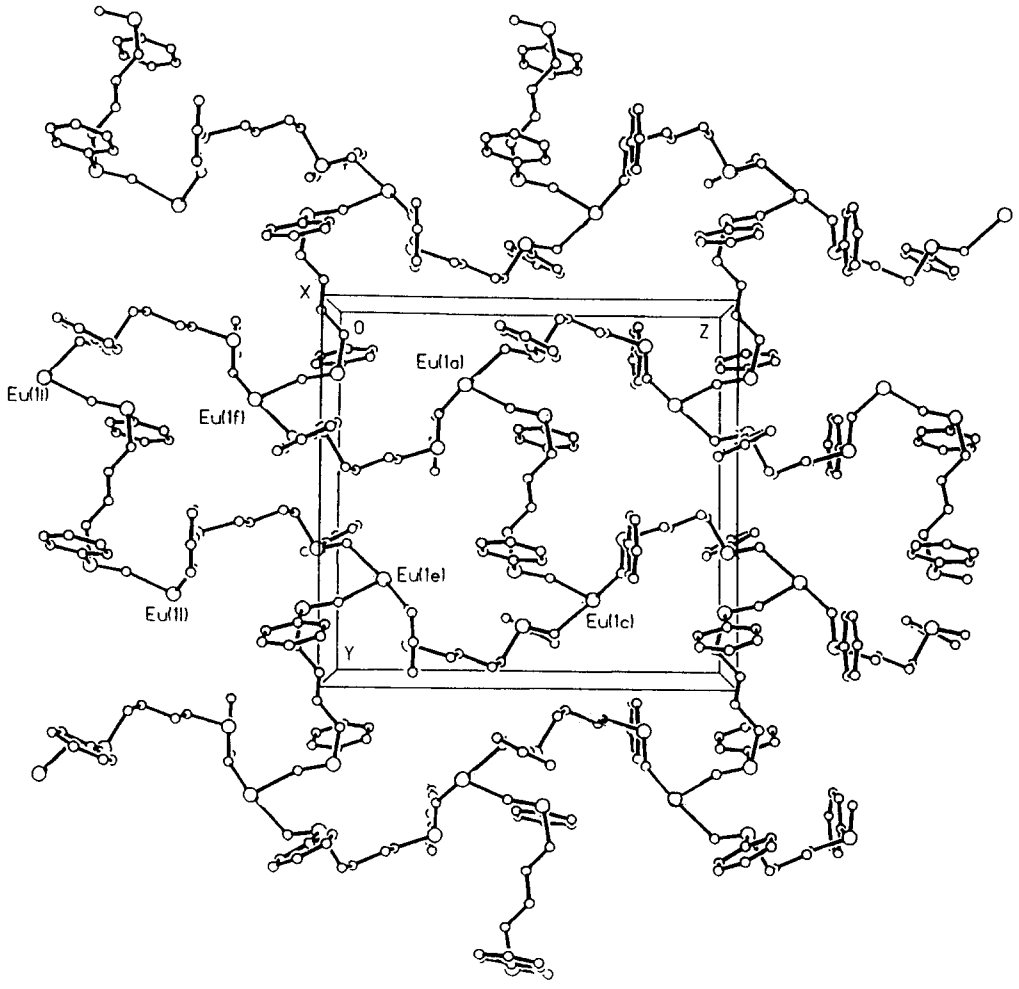


Fig. 3. Part of one of the sheet of linked 54-membered macrocycles in the structure of the complex (nitrate ions are not shown).

sheet (Fig. 3) in the y and z directions. The linkages between macrocycles are through one edge to form a chain of macrocycles extending along the z direction and bridged ligands along the y direction.

Molecular conductance and IR spectrum

The molar conductance value of the title complex in methanol is ~ 0 s mol^{-1} cm^2, which indicates the complex behaves as a nonelectrolyte.

The IR spectrum of the complex indicated that the bphsb binds metal ions through the oxygen atoms of sulfoxide moieties. The S=O bond stretching frequencies of the complex (988 cm^{-1}) are lower than the corresponding one in the free ligand (1040 cm^{-1}). IR data also indicate the presence of bidentate nitrate group [C_{2v}: $\nu_1(A_1)$ 1496, $\nu_4(B_1)$ 1290, $\nu_2(A_1)$ 1028, $\nu_3(A_1)$ 818, $\nu_5(B_1)$ 740 and $\nu_2+\nu_5$ 1765, $\nu_2+\nu_6$ 1725 cm^{-1}] [10]. Therefore, IR spectrum and molar conductance suggest that all nitrate ions are coordinated bidentately and the ligand bphsb acts as a neutral bidentate. These results are consistent with crystal structure analysis.

Absorption, excitation and emission spectra

The absorption spectrum of a methanol solution of the complex at room temperature shows three absorption bands: n–π^* band of the S=O group (213 nm) and two bands of the π–π^* transition (238, 270 nm).

The excitation spectrum at 610 nm emission presents a wide excitation band at 280–340 nm (absorption band of ligand) and some sharp bands in the range 360–500 nm (absorption bands of Eu^{3+}).

The emission spectrum of the complex shows a typical f–f transition of the $^5D_0$ state to ^7F_J stark levels of

Pergamon

PII: S0277-5387(96)00379-8

Polyhedron Vol. 16, No. 7, pp. 1123–1127, 1997
Copyright © 1997 Elsevier Science Ltd
Printed in Great Britain. All rights reserved
0277-5387/97 $17.00+0.00

A new framework structure polynuclear complex of europium nitrate with 1,4-bis(phenylsulfinyl)butane

Ruo-Hua Zhang,[a]* Bao-Qing Ma,[a] Xian-He Bu,[a] Hong-Gen Wang[b] and Xin-Kan Yao[b]

[a] Department of Chemistry, Nankai University, Tianjin 300071, P.R. China

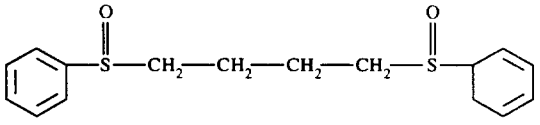
[b] Centre Laboratory, Nankai University, Tianjin 300071, P.R. China

(Received 5 July 1996; accepted 1 August 1996)

Abstract—A polynuclear europium(III) complex of the formula $[Eu(bphsb)_{1.5}(NO_3)_3]_n$ [bphsb = 1.4-bis(phenylsulfinyl)butane] has been prepared and its structure and luminescent properties have been determined by X-ray diffraction and spectral measurements. The structure consists of Eu^{III} ions bridged by bidentate bphsb ligands and coordinated by NO_3^- groups to make a polynuclear neutral complex. The europium ion is nine-coordinated and the geometry around the Eu^{III} is that of a distorted tricapped trigonal prism. The polynuclear complex has a framework structure with 54-membered macrocyclic rings, each containing six europium ions. The complex exhibits sensitized luminescence that originates from $^5D_0$ state to ^7F_J Stark levels. Copyright © 1997 Elsevier Science Ltd

Keywords: polynuclear europium(III) complex; framework structure; luminescent properties.

Polynuclear Ln^{III} complexes are important as novel light-conversion moleculear devices with potential application as probes and labels for a variety of chemical and biological systems [1–3]. Some polynuclear lanthanide complexes have been reported [4–5], but there is little information on lanthanide complexes with a framework structure [6]. During our studies on the coordinating ability of disulfoxide, we found 1,4-bis(phenylsulfinyl)butane (bphsb) was a good bridging ligand to generate polymers with unusual structures. To our knowledge, the bphsh ligand produces the first example of polynuclear complex with framework structure in the reported disulfoxide lanthanide complexes [7–8]. In this paper, we present the synthesis, structure and photophysical properties on the new polynuclear europium complex of bis(phenylsulfinyl)butane $[Eu(bphsb)_{1.5}(NO_3)_3]_n$, which is a new class of supramolecular compound.



ligand(bphsb)

Scheme 1. ligand(bphsb)

EXPERIMENTAL

Synthesis of polynuclear complex $[Eu(bphsb)_{1.5}(NO_3)_3]_n$

Hydrated eropium nitrate (0.5 mmol) in anhydrous methanol (5 cm^3) was dehydrated by the addition of triethylorthoformate (3 cm^3). The mixture solution was added dropwise to anhydrous methanol solution (4 cm^3) of ligand (bphsb, 1.5 mmol). The mixture was stirred at 70–80°C for 6 h. A small precipitate was filtered and the filtrate was allowed to evaporate slowly at room temperature; after a week, colorless single crystals were obtained. Found: Eu, 18.82. Calc. for $C_{24}H_{27}N_3O_{12}S_3Eu$: Eu, 19.1%.

Physical measurements

The IR spectrum of the complex in the 4000–400 cm^{-1} range (as KBr pellets) was recorded on a WHF-

* Author to whom correspondence should be addressed.

30 model spectrometer. Conductivity of the complex in the methanol solution (10^{-3} mol dm^{-3}) was measured at room temperature using a DDS-11A conductometer. Electronic spectrum of the methanol solution of the complex was recorded in the 190–325 nm range on a Shimadzu UV-240 spectrophotometer. Luminescence spectrum of the complex was recorded on a F111 AI Fluorolog-2 spectrofluorometer at room temperature.

Crystal structure determination and refinement

The data were collected using an Enraf–Nonius CAD4 diffractometer with Mo-K_α graphite-monochromated radiation ($\lambda = 0.071073$ nm) by using the ω–2θ scan method. A total of 4613 reflections were measured and 3303 observed reflections [$I > 3\sigma(I)$] used for the structure solution and refinement. The structure was solved by direct methods (MULTAN82). The final refinement by the full-matrix least-squares method with anisotropic thermal parameters for non-hydrogen atoms and gave the final unweighted and weighted agreement factors 0.039 and 0.05, respectively. All the calculation were carried out on a PDP11/44 computer using a SDP-PLUS computer program system.

The crystal data and additional details are as follows: $C_{24}H_{27}N_3O_{12}S_3Eu$: monoclinic, space group $P2_1/c$ $a = 1.0686(3)$, $b = 1.6365(6)$, $c = 1.7590(3)$ nm: $\beta = 91.28(3)^\circ$, $V = 3.075(2)$ nm^3, $M = 797.65$, $D_x = 1.723$ Mg m^{-3}, $\mu = 2.298$ mm^{-1}, $F(000) = 1596$, $Z = 4$.

RESULTS AND DISCUSSION

Description of the structure

Selected bond distances (nm) and angles (°) for the complex are listed in Table 1. Fig. 1. shows the structure and labeling scheme of the title complex.

The X-ray analysis of the title complex reveals the stoichiometry to be $[Eu(bphsb)_{1.5}(NO_3)_3]_n$. The europium(III) ion is nine-coordinated and is bound to one oxygen atom of each of three bphsb ligands and to three bidentate nitrates in a distorted tricapped trigonal prism configuration (Fig. 2). The Eu—O distances fall in two distinct groups with those to the bphsb oxygen atoms in the range: 0.2326(4)–0.2348(4) nm and those to the nitrate groups in the range: 0.2455(4)–0.2512(5) nm. The average Eu—O bond length is 0.2443(9) nm, a little smaller than the sum of the ionic radius of 0.247 nm (nine-coordinated Eu^{3+} 0.112 and O^{2-} 0.135 nm) [9]. This fact shows that the Eu—O bonds have some covalent character.

In the title complex, the bphsb ligands serve to bridge the adjacent metal centres forming a polynuclear structure with a macrocyclic array (Fig. 3). The resulting structure comprises 54-membered macrocyclic rings, each containing six europium atoms. Adjacent rings are in a "parquet-like" pattern to form a two-dimensional

Table 1. Selected bond distances (10^{-1} nm) and bond angles (°) for the title complex

Eu(1)—O(1)	2.326(4)	Eu(1)—O(22)	2.512(5)
Eu(1)—O(2)	2.348(4)	Eu(1)—O(31)	2.474(4)
Eu(1)—O(3)	2.346(4)	Eu(1)—O(32)	2.455(4)
Eu(1)—O(11)	2.499(4)	S(1)—O(2)	1.495(4)
Eu(1)—O(12)	2.501(4)	S(1)—C(3)	1.813(8)
Eu(1)—O(21)	2.491(4)	S(1)—C(21)	1.780(6)

O(1)—Eu(1)—O(2)	81.3(2)	O(3)—Eu(1)—O(22)	97.7(2)
O(1)—Eu(1)—O(3)	82.0(2)	O(22)—Eu(1)—O(31)	138.3(2)
O(1)—Eu(1)—O(11)	152.1(2)	O(22)—Eu(1)—O(32)	152.8(2)
O(1)—Eu(1)—O(12)	152.9(2)	O(31)—Eu(1)—O(32)	51.1(1)
O(1)—Eu(1)—O(21)	73.8(1)	O(3)—Eu(1)—O(31)	122.3(1)
O(1)—Eu(1)—O(22)	122.5(1)	O(3)—Eu(1)—O(32)	72.7(2)
O(1)—Eu(1)—O(31)	78.6(1)	O(11)—Eu(1)—O(12)	50.2(1)
O(1)—Eu(1)—O(32)	82.1(2)	O(11)—Eu(1)—O(21)	121.7(2)
O(2)—Eu(1)—O(3)	154.2(1)	O(11)—Eu(1)—O(22)	71.9(2)
O(2)—Eu(1)—O(11)	80.0(2)	O(11)—Eu(1)—O(31)	76.2(2)
O(2)—Eu(1)—O(12)	125.9(2)	O(11)—Eu(1)—O(32)	91.4(2)
O(2)—Eu(1)—O(21)	78.0(2)	O(12)—Eu(1)—O(21)	108.2(2)
O(2)—Eu(1)—O(22)	75.3(2)	O(12)—Eu(1)—O(22)	70.5(2)
O(2)—Eu(1)—O(31)	73.1(1)	O(12)—Eu(1)—O(31)	107.9(2)
O(2)—Eu(1)—O(32)	123.9(2)	O(12)—Eu(1)—O(32)	82.4(2)
O(3)—Eu(1)—O(11)	122.1(1)	O(21)—Eu(1)—O(22)	50.5(1)
O(3)—Eu(1)—O(12)	72.3(2)	O(21)—Eu(1)—O(31)	142.5(2)
O(3)—Eu(1)—O(21)	78.6(1)	O(21)—Eu(1)—O(32)	144.5(2)

Eu^{3+} (Fig. 4). The $^5D_0$–$^7F_0$ transition is weaker. There are two main transitions to $^7F_1$ level (585.5, 590.5 nm) and the transition to the $^7F_2$ level is comprised of three main bands (612.0, 616.0, 625.5 nm). The observed $^5D_0$–$^7F_4$ transition is split into three bands (688.0, 683.0, 698.5 nm). Overall the emission spectrum points to Eu^{III} ions having chemical and structural environment with a lower symmetry (not higher than C_3) [11].

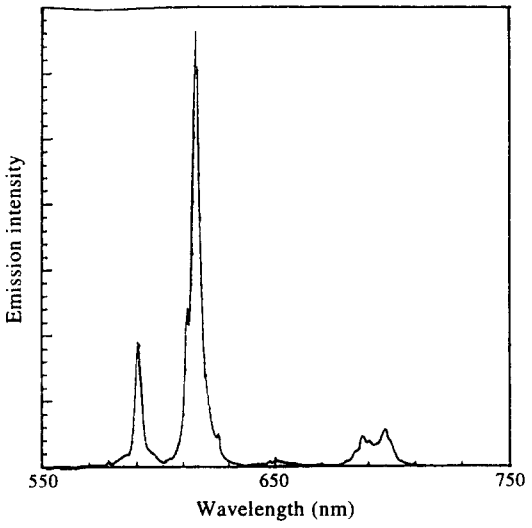


Fig. 4. The luminescent spectrum of the complex (room temperature, ED: 399 nm).

REFERENCES

1. Bunzli, J.-C. G., Froidevaux, P. and Harrowfield, J. M., *Inorg. Chem.* 1993, **32,** 3306.
2. Piguet, C., Bunzli, J.-C. G., Bernardinelli, G., Hopfgartner, G. and Williams, A. F., *J. Am. Chem. Soc.* 1993, **115,** 8197.
3. Matttews, K. D., Kahwa, I. A. and Williams, D. J., *Inorg. Chem.* 1994, **33,** 1382.
4. Goodgame, D. M. L., Hill, S. P. W. and Williams, D. J., *J. Chem. Soc., Chem. Commun.* 1993, 1019.
5. Zhou, D.-J., Huang, C.-H., Wang, K.-Z. and Xu, G.-X., *Polyhedron*, 1994, **13,** 987.
6. Doyle, G. A., Goodgame, D. M. L., Hill, S. P. W. and Williams, D. J., *J. Chem. Soc., Chem. Commun.* 1993, 207.
7. Zhang, R.-H., Zhan, Y.-L., Chen, J.-T., *Polyhedron*, 1994, **13,** 1881.
8. Zhang, R.-H., Zhan, Y.-L., Chen, J.-T., *Synth. React. Inorg. Met-Org. Chem.* 1995, **25,** 283.
9. Zhang, R.-H., *Rare Earth Element Chemistry* (in Chinese). Tianjin Press of Science and Technology, Tianjin, P.R. China, 1987, p. 40.
10. Rosenthal, M. R., *J. Chem. Educ.* 1973, **50,** 331; Foster R. J. and Hendricker, D. G., *Inorg. Chim. Acta.* 1972, **6,** 371.
11. Murray, G. M., Sarrio, R. V. and Peterson, J. R., *Inorg. Chim. Acta.* 1990, **176,** 233.

Pergamon

PII: S0277-5387(96)00378-6

Polyhedron Vol. 16, No. 7, pp. 1129–1136, 1997
Copyright © 1997 Elsevier Science Ltd
Printed in Great Britain. All rights reserved
0277-5387/97 $17.00+0.00

Facile thermal desolvation of $Ce_2(OPr^i)_8(Pr^iOH)_2$: Characterization and molecular structure of $Ce_4(\mu_4\text{-}O)(\mu_3\text{-}OPr^i)_2(\mu\text{-}OPr^i)_4(OPr^i)_8$

Christine Sirio,[a] Liliane G. Hubert-Pfalzgraf[a]* and Claudine Bois[b]

[a] Laboratoire de Chimie Moléculaire, URA-CNRS, Univeristé de Nice Sophia-Antipolis, Parc Valrose, 06 108 Nice Cédex 2, France

[b] Laboratoire de Chimie des Métaux de Transition, URA-CNRS, 4 Place Jussieu, 75 230 Paris, Cédex 05, France

(Received 5 July 1996; accepted 1 August 1996)

Abstract—Thermal treatment of $Ce_2(OPr^i)_8(Pr^iOH)_2$ yielded $Ce_4(\mu_4\text{-}O)(OPr^i)_{14}$ by desolvation under mild conditions. The tetranuclear oxoalkoxide has been characterized by elemental analysis, FT-IR, ^1H NMR and X-ray diffraction. The structure is described as $[Ce_4(\mu_4\text{-}O)(\mu_3\text{-}OPr^i)_2(\mu\text{-}OPr^i)_4(OPr^i)_8]$. The $Ce_4(\mu_4\text{-}O)$ core corresponds to a distorted flattened tetrahedron, with two hexa- and two hepta-coordinated metals. The Ce—O bond lengths spread over the range 2.03(2) to 2.54(1) Å and follow the order Ce—OR < Ce—μOR < Ceμ_3—OR. Copyright © 1997 Elsevier Science Ltd

Keywords: cerium; oxoalkoxides; desolvation.

Despite the implication of cerium in a variety of advanced materials such as high T_c superconductors, γ-scintillators, solid electrolytes or catalysts, only a few molecular precursors are available [1]. They are essentially represented by a dimeric isopropoxide solvate $Ce_2(OPr^i)_8(Pr^iOH)_2$ having a structure similar to that of the other tetravalent metals (zirconium, hafnium, tin) [2] and by a monomeric butoxide $Ce(OBu^t)_4(THF)_2$ [3]. While the latter has been reported to convert to $Ce_3O(OBu^t)_{10}$ in toluene solutions over 2 days at room temperature the isopropoxide was considered to be stable up to *ca* 200°C [4]. While the photoreduction of $Ce_2(OPr^i)_8(Pr^iOH)_2$ led to the mixed valency Ce^{III}–Ce^{IV} cluster $Ce_4O(OPr^i)_{13}(Pr^iOH)$ [5], no further indication on its thermal stability was provided. A non-solvated isopropoxide, $[Ce(OPr^i)_4]_m$, has been reported but without further characterization [4].

Studies of the reactivity of $Ce_2(OPr^i)_8(Pr^iOH)_2$ required us to reinvestigate its thermal stability, both in the solid state and in solution. We report herein these investigations which afforded a tetranuclear Ce^{IV} oxo cluster, $Ce_4O(OPr^i)_{14}$, characterized by single crystal X-ray diffraction.

EXPERIMENTAL

All manipulations were carried out under argon using Schlenk tubes and vacuum-line techniques. Solvents were purified by standard methods. $Ce_2(OPr^i)_8(Pr^iOH)_2$ was prepared as reported in the literature [2]. IR spectra were obtained as Nujol mulls on an IRFS 45 Bruker spectrometer, NMR spectra were registered with an AC-200 Bruker spectrometer. Analyses were performed at the Centre de microanalyses du CNRS.

Synthesis of $Ce_4(\mu_4\text{-}O)(OPr^i)_{14}$

$Ce_2(OPr^i)_8(Pr^iOH)_2$ (2 g, 2.3 mmol) was heated in the solid state for about 15 min (70°C/10^{-3} mm Hg). The yellow solid became pasty and was dissolved in

* Author to whom correspondence should be addressed.

DME-Pr^{i}OH (2/3 in volume). Orange crystals of $Ce_4O(OPr^i)_{14}$ (0.7 g, 43%) and $Ce_2(OPr^i)_8(Pr^iOH)_2$ were separated by crystallization at $-10°C$. The oxo species is soluble in common solvents including isopropanol and hexane. M.p. 145°C, decomposition at 170°C.

Analysis found: C, 37.5; 6.9 calc. for $C_{42}H_{98}O_{15}Ce_4$: C, 35.9; H, 7.0%. IR (cm^{-1}): 1456s, 1377s, 1359sh, 1328m, 1159sh, 1135s, 1125sh, 986s, 973m, 952m, 936m, 827sh, 557sh, 520m, 504w, 490w, 448m, 412w, 395w (νCe—O); ^1H NMR (C_7D_8, 25°C): 5.4m (1H, CH); 1.37d ($J = 6.5$ Hz, 6H, Me); ^1H NMR (C_7D_8, $-70°C$): 5.80, 5.32, 5.15m 3:2:2, CH); 1.8–1.7, 1.5–1.4 (overlapping of doublets, 18H, $J = 6.5$ Hz, 24H, Me).

The same compound was obtained by refluxing $Ce_2(OPr^i)_8(Pr^iOH)_2$ in toluene for *ca* 1.5 h. The yellow solution turns orange immediately. Yield ~ 25%.

Crystal structure determination of $Ce_4(\mu_4\text{-}O)(OPr^i)_{14}$

Intensity data were collected at $-100°C$ on an Enraf–Nonius CAD-4 diffractometer, using Mo-K_α radiation. Unit-cell dimensions with estimated standard deviations were obtained from least-squares refinements of the setting angles of 25 well-centered reflections. Two standard reflections were monitored periodically, they showed no change during data collection. Crystallographic data and other information are summarized in Table 1. Corrections were made for Lorentz and polarization effects. Empirical absorption corrections (Difabs) [6] and extinction correction were applied.

Computations were performed by using the PC version of CRYSTALS [7]. Atomic form factors for neutral Ce, O and C were taken from reference [8]. Real and imaginary parts of anomalous dispersion were taken into account. The structure was solved by direct methods (SHELXS-86) [9] and successive Fourier maps. Two crystallographically independent molecules are found in the unit cell. All atoms were anisotropically refined. Refinements were carried out in five blocks by minimizing the function $\Sigma w(|F_o|-|F_c|)^2$, where F_o and F_c are the observed and calculated structure factors. Models reached convergence with $R = \Sigma(|F_o|-|F_c|)/\Sigma wF_o$ and $Rw = [\Sigma w(|F_o|-|F_c|)^2/\Sigma w(F_o)^2]^{1/2}$ having the values listed in Table 1. The weighting scheme was unity. The structure was drawn using the program Cameron [10].

Tables of atomic coordinates, anisotropic temperature factors, non-essential bond lengths and angles have been deposited at the Cambridge Crystallographic Data Centre.

RESULTS AND DISCUSSION

Our initial investigations of the reactivity of the cerium isopropoxide solvate **1** were hampered by a poor reproducibility [11]. These observations prompted us to reconsider the basic characteristics of this starting material and especially its stability. While information on its photosensitivity has been provided [4], the compound has been considered as reasonably stable thermally.

Thermal stability of $Ce_2(OPr^i)_8(Pr^iOH)_2$

The transformation of **1** in the solid state is actually observed after a period of heating as short as 15 min at 50–70°C *in vacuo*. The yellow crystals of **1** became pasty while their FT-IR spectrum accounts for the disappearance of the absorption band of the νOH vibration at 3170 cm^{-1} and the appearance of absorption bands characteristic of disopropylether (1120, 945, 920, 840, 805 cm^{-1}). Recrystallization in DME/Pr^{i}OH gave orange crystals of a compound, (**2**), identified by X-ray diffraction as $Ce_4O(OPr^i)_{14}$ in ~ 43% yield.

An orange colour developed also by heating **1** in refluxing toluene and in the dark. The oxoalkoxide **2** was, however, obtained in lower yield (~20%) and the transformation is slower than in the solid state. Longer reaction times did not improve the yield of **2**, either in solution or in the solid state, but led to the formation of other species. A yellow compound **3**, characterized in the FT-IR by νCe—O absorption bands at 561, 525, 512 and 495 cm^{-1} is for instance obtained by heating **1** for 1–4 h at 70°C.

Molecular structure of $Ce_4(\mu_4O)(OPr^i)_{14}$

X-ray diffraction studies established that compound **2** is actually a tetranuclear oxo species, of the formula $[Ce_4(\mu_4\text{-}O)(\mu_3\text{-}OPr^i)_2(\mu\text{-}OPr^i)_4(OPr^i)_8]$. Two independent molecules **2a** and **2b** are found in the unit cell. The molecular structure of one of these molecules is depicted in Fig. 1. Pertinent bond lengths and angles are collected in Table 2. The M_4O_{15} core is based on a distorted tetrahedral framework assembled around a μ_4-oxo ligand. The metals are further connected *via* doubly bridging alkoxide ligands. The coordination sphere of each cerium atom is completed with two terminal OR, thus providing coordination numbers of six for two metals and coordination number seven for two others. The surrounding of the oxo ligand O(1) is severely distorted with angles varying from 97.3(4) to 154.0(5)°. Similar distortions of the μ_4-oxo ligand have been observed for $Ce_4(\mu_4\text{-}O)(OPr^i)_{13}(Pr^iOH)$, which has a butterfly core [4], $Al_4(\mu_4\text{-}O)(\mu\text{-}OPr^i)_5[H(OPr^i)_2]Cl_4$ [12] and for $Pb_2Ti_2(\mu_4\text{-}O)(OPr^i)_{10}$ [13] for instance. Despite the distorted surrounding around the oxo ligand, the tetrahedron is quite regular for isomer **2a** [Ce···Ce distances spread over the range 3.485(2)–3.888(2) Å], while for isomer **2b** one non-bonding Ce···Ce distance, Ce(53)—Ce(54) expands to 4.377(1) Å, thus illustrating the main difference between the two independent molecules. The Ce···Ce distances are slightly longer than for the

Table 1. Crystal data for $[Ce_4O(\mu_3\text{-}OPr^i)_2(\mu\text{-}OPr^i)_4(OPr^i)_8]$

$C_{42}H_{98}O_{15}Ce_4$	
Fw	1403.71
Crystal system	Triclinic
a (Å)	13.700(5)
b (Å)	20.663(6)
c (Å)	21.931(7)
α ( )	108.04(3)
β ( )	90.74(3)
γ ( )	93.33(3)
V (Å^3)	5890(4)
Z	4
Space group	$P\bar{1}$
Linear absorption coefficient μ (cm^{-1})	31.3
Density ρ (g cm^{-3})	1.58
Diffractometer	CAD4 Enraf–Nonius
Radition	Mo K_α (λ = 0.71069 Å)
Scan type	$\omega/2\theta$
Scan range ( )	$0.8+0.345\ \mathrm{tg}\theta$
θ limits ( )	2–17
Temperature of measurement (°C)	−100
Octants collected	*h*: 0, 11; *k*: −17, 16; *l*: −18, 18
No. of data collected	7398
No. of unique data collected	6837
No. of unique data used for refinement	5773 $(F_o)^2 > 3\sigma(F_o)^2$
R (int)	0.023
Decay of standards reflection (%)	0
$R = \Sigma\|\|F_o\| - \|F_c\|\|/\Sigma\|F_o\|$	0.043
$Rw = [\Sigma w(\|F_o\| - \|F_c\|)^2/\Sigma wF_o^2]^{1/2}$	0.045
Absorption correction	DIFABS (min = 0.856, max = 1.245)
Extinction parameter ($\times 10^{-6}$)	40.7
No. of variables	1101
$\Delta\rho$min (e Å^{-3})	−0.96
$\Delta\rho$max (e Å^{-3})	1.32

initial dimer **1** (3.473 Å). The Ce—O bond lengths range from 2.02(1) to 2.57(1) Å, the order of variation being Ce—OR < Ce—μ-OR < Ce—μ_3-OR. The distortion of the oxo ligand is also illustrated by the difference in the Ce μ_4-O distances, mean value 2.23(1) Å for the six-coordinated metals Ce(3) and Ce(4) and 2.50(1) Å for the hepta-coordinated metals. The various Ce—O bond distances are in agreement with the values from the literature [2,14], and as expected they are slightly longer for the seven-coordinated metals. The latter have a monocapped trigonal prism stereochemistry. No short contact between the various molecules is detected. The Ce—O—C angles of the terminal isopropoxide ligands are large: (171.5° average for the six-coordinate metals, 162.6° average for the hepta-coordinated ones), as usually observed for lanthanides and early transition metals.

The formation of the tetranuclear species **2** results from the assembly of the two desolvated $Ce_2(OPr^i)_8$ dimeric units as shown in Fig. 2. This assembly proceeds with the elimination of diisopropylether as evidenced by FT-IR. The initial dimeric species, **1**, can be seen as two octahedra having a common edge. The coordinative insaturation due to the loss of one isopropanol molecule can be filled by the sharing of a face between the two octahedra. Elimination of the second solvated isopropanol molecule and junction of two dinuclear units along edges with subsequent elimination of isopropylether results in the formation of the M_4O_{15} framework. Formally, the condensation of Ce_2 units into Ce_4 ones corresponds to the transformation of two terminal OR groups into doubly bridging ones and of two doubly bridging ones into μ_3-ones, thus allowing two metal centers to be heptacoordinated.

The ^{1}H NMR spectra of **2** in $CDCl_3$ or deuterated toluene show only one type of isopropoxide ligands at 25°C, thus suggesting fluxionality. At −70°C, three types of magnetically non-equivalent OPr^i groups are observed at 5.80, 5.15 and 5.32 ppm (integration ratio 6:4:4). According to the solid-state structure, four resonances in an integration ration 2:4:4:4 are expected for the CH groups. The NMR spectra of **2** are independent of the dilution and thus account for the presence of a single molecular species. The NMR data suggest that the tetranuclear solid state structure of **2** is retained in solution, the μ-OPr^i and μ_3-OPr^i groups being still in dynamic exchange at −70°C, while the exchange between the terminal isopropoxide ligands borne by the six- and seven-coordinated

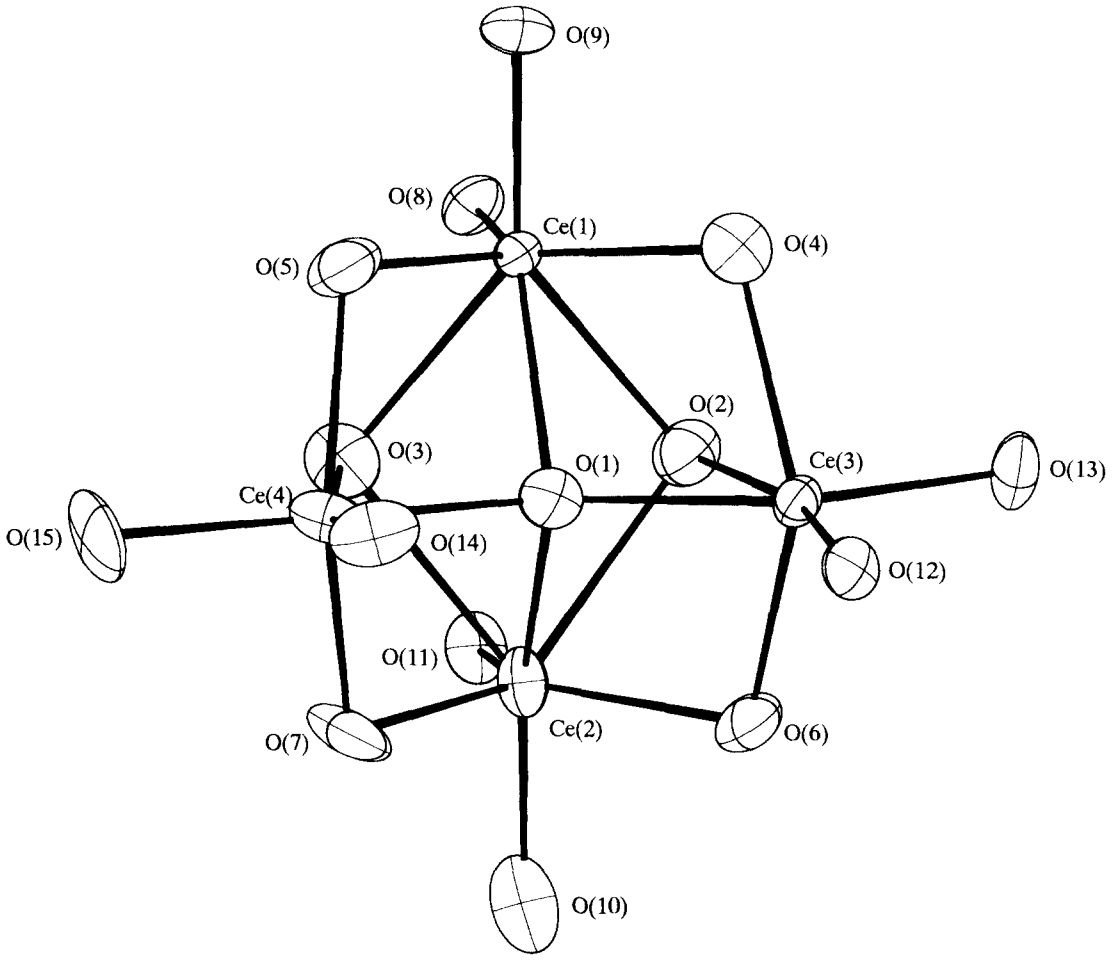


Fig. 1. CAMERON view of the Ce_4O_{15} core of the $Ce_4O(OPr^i)_{14}$ cluster.

cerium atoms is frozen out. At higher temperatures, coalescence between the two multiplets attributed to the terminal OR groups is observed, giving for instance at -30°C, a spectrum composed of two signals at 5.8 and 5.2 ppm corresponding to the bridging and terminal methine groups.

Oxoisopropoxides and more generally oxoalkoxides are a common feature in lanthanide alkoxide chemistry as a means to reach high coordination numbers [5] for the metals and thus stable species. The chemistry of structurally characterized Ce^{IV} oxoalkoxides has been limited to $Ce_3(\mu_3\text{-}O)(\mu\text{-}OBu^t)_3(OBu^t)_6$ obtained by decomposition of $Ce(OBu^t)_4(THF)_2$ or of $NaCe_2(OBu^t)_9$ [3]. Although a quite rich oxo chemistry has been observed for Ce^{IV} isopropoxides [11], no evidence could be obtained so far for a trinuclear $Ce_3O(OPr^i)_{10}$ moiety.

Oxoalkoxides derived from tetravalent metal alkoxides are essentially represented by the solvates $Sn_3(\mu_3\text{-}O)(\mu\text{-}OBu^t)_3(OBu^t)_7(Bu^tOH)_2$, resulting from the hydrolysis of $Sn(OBu^t)_4$ [15], and $[Hf_3(\mu_3\text{-}O)(\mu\text{-}OEt)_4(OEt)_6(EtOH)]_2$ [16], the latter corresponding to the compound formulated in the literature as $Hf(OEt)_4$. Unsolvated trinuclear oxoalkoxides based on large M^{IV} transition metals correspond to $[M_3(\mu_3\text{-}O)_3\text{-}OR)(\mu\text{-}OR)_3(OR)_6]$ M = Ce [3], Mo, W [17], U [18], Th). Hexa-coordination of the metals appears as a common feature. The $Zr_3O(OPr^i)_{10}$ moiety, which has been observed in mass spectrometry [19], has been stabilized in the $[PbZr_3O(OPr^i)_{10}(OAc)_2]$ mixed-metal species [20]. It is interesting to observe that these trinuclear units are generally derived from monomeric starting materials. The formation of $Ce_4O(OPr^i)_{14}$ rather than $Ce_3O(OPr^i)_{10}$ suggests that the dinuclear species **1** displays quite good stability with respect to dissociation into mononuclear fragments.

These studies establish that oxoalkoxides can be generated quite easily by desolvation reactions. Microhydrolysis experiments of **1** in toluene with an hydrolysis ratio $h = 0.5$ ($h =$ moles H_2O/ moles **1**) did not give access to **2** but afforded compound **3**. These observations are consistent with the fact that aggregates of higher nuclearity are generally obtained by hydrolysis [21] and in the absence of ancillary ligands such as β-diketones [1] or cyclopentadienyls [22], which can act as polymerization lockers. The overall results from thermal decomposition and microhydrolysis experiments indicate that cerium^{IV}

Table 2. Selected bond lengths and angles for $Ce_4O(OPr^i)_{14}$

Ce(1)—O(1)	2.52(1)	Ce(51)—O(51)	2.475(9)
Ce(1)—O(2)	2.50(1)	Ce(51)—O(52)	2.45(1)
Ce(1)—O(3)	2.46(1)	Ce(51)—O(53)	2.534(9)
Ce(1)—O(4)	2.33(1)	Ce(51)—O(54)	2.39(1)
Ce(1)—O(5)	2.34(1)	Ce(51)—O(55)	2.34(1)
Ce(1)—O(8)	2.06(1)	Ce(51)—O(58)	2.08(1)
Ce(1)—O(9)	2.06(1)	Ce(51)—O(59)	2.07(1)
Ce(2)—O(1)	2.52(1)	Ce(52)—O(51)	2.502(9)
Ce(2)—O(2)	2.54(1)	Ce(52)—O(52)	2.50(1)
Ce(2)—O(3)	2.57(1)	Ce(52)—O(53)	2.43(1)
Ce(2)—O(6)	2.32(1)	Ce(52)—O(56)	2.33(1)
Ce(2)—O(7)	2.29(1)	Ce(52)—O(57)	2.36(1)
Ce(2)—O(10)	2.03(2)	Ce(52)—O(60)	2.07(1)
Ce(2)—O(11)	2.08(1)	Ce(52)—O(61)	2.07(1)
Ce(3)—O(1)	2.22(1)	Ce(53)—O(51)	2.236(9)
Ce(3)—O(2)	2.47(1)	Ce(53)—O(52)	2.52(1)
Ce(3)—O(4)	2.32(1)	Ce(53)—O(54)	2.27(1)
Ce(3)—O(6)	2.24(1)	Ce(53)—O(56)	2.31(1)
Ce(3)—O(12)	2.07(1)	Ce(53)—O(62)	2.02(1)
Ce(3)—O(13)	2.06(1)	Ce(53)—O(63)	2.10(1)
Ce(4)—O(1)	2.19(1)	Ce(54)—O(51)	2.257(9)
Ce(4)—O(3)	2.48(1)	Ce(54)—O(53)	2.51(1)
Ce(4)—O(5)	2.26(1)	Ce(54)—O(55)	2.28(1)
Ce(4)—O(7)	2.25(1)	Ce(54)—O(57)	2.28(1)
Ce(4)—O(14)	2.05(1)	Ce(54)—O(64)	2.07(1)
Ce(4)—O(15)	2.08(1)	Ce(54)—O(65)	2.09(1)
Ce(1)—Ce(2)	3.888(2)	Ce(51)—Ce(52)	3.739(1)
Ce(1)—Ce(3)	3.594(1)	Ce(51)—Ce(53)	3.584(1)
Ce(1)—Ce(4)	3.570(1)	Ce(51)—Ce(54)	3.601(1)
Ce(2)—Ce(3)	3.577(1)	Ce(52)—Ce(53)	3.588(1)
Ce(2)—Ce(4)	3.575(2)	Ce(52)—Ce(54)	3.594(1)
Ce(3)—Ce(4)	3.485(2)	Ce(53)—Ce(54)	4.377(1)
O(1)—Ce(1)—O(2)	58.9(4)	O(51)—Ce(51)—O(52)	61.5(3)
O(1)—Ce(1)—O(3)	59.5(4)	O(51)—Ce(51)—O(53)	60.4(3)
O(2)—Ce(1)—O(3)	78.5(4)	O(52)—Ce(51)—O(53)	79.9(3)
O(1)—Ce(1)—O(4)	70.2(4)	O(51)—Ce(51)—O(54)	70.4(3)
O(2)—Ce(1)—O(4)	72.4(4)	O(52)—Ce(51)—O(54)	71.4(3)
O(3)—Ce(1)—O(4)	129.5(4)	O(53)—Ce(51)—O(54)	130.3(3)
O(1)—Ce(1)—O(5)	71.0(4)	O(51)—Ce(51)—O(55)	70.0(3)
O(2)—Ce(1)—O(5)	129.2(4)	O(52)—Ce(51)—O(55)	131.2(3)
O(3)—Ce(1)—O(5)	69.1(4)	O(53)—Ce(51)—O(55)	71.7(3)
O(4)—Ce(1)—O(5)	99.3(5)	O(54)—Ce(51)—O(55)	98.1(3)
O(1)—Ce(1)—O(8)	131.9(4)	O(51)—Ce(51)—O(58)	132.9(4)
O(2)—Ce(1)—O(8)	85.6(4)	O(52)—Ce(51)—O(58)	85.6(4)
O(3)—Ce(1)—O(8)	83.9(4)	O(53)—Ce(51)—O(58)	82.7(4)
O(4)—Ce(1)—O(8)	132.4(5)	O(54)—Ce(51)—O(58)	132.5(4)
O(5)—Ce(1)—O(8)	126.6(5)	O(55)—Ce(51)—O(58)	127.3(4)
O(1)—Ce(1)—O(9)	139.2(4)	O(51)—Ce(51)—O(59)	140.4(4)
O(2)—Ce(1)—O(9)	140.0(4)	O(52)—Ce(51)—O(59)	136.9(4)
O(3)—Ce(1)—O(9)	140.1(4)	O(53)—Ce(51)—O(59)	140.7(4)
O(4)—Ce(1)—O(9)	82.6(5)	O(54)—Ce(51)—O(59)	83.0(4)
O(5)—Ce(1)—O(9)	84.6(4)	O(55)—Ce(51)—O(59)	85.4(4)
O(8)—Ce(1)—O(9)	89.0(4)	O(58)—Ce(51)—O(59)	87.1(4)
O(1)—Ce(2)—O(2)	58.3(4)	O(51)—Ce(52)—O(52)	60.4(3)
O(1)—Ce(2)—O(3)	58.0(4)	O(51)—Ce(52)—O(53)	61.4(3)
O(2)—Ce(2)—O(3)	75.8(4)	O(52)—Ce(52)—O(53)	80.9(3)
O(1)—Ce(2)—O(6)	70.5(4)	O(51)—Ce(52)—O(56)	71.3(3)
O(2)—Ce(2)—O(6)	69.7(4)	O(52)—Ce(52)—O(56)	72.1(3)
O(3)—Ce(2)—O(6)	127.7(4)	O(53)—Ce(52)—O(56)	132.4(3)
O(1)—Ce(2)—O(7)	70.8(4)	O(51)—Ce(52)—O(57)	70.2(3)
O(2)—Ce(2)—O(7)	128.1(4)	O(52)—Ce(52)—O(57)	130.4(3)
O(3)—Ce(2)—O(7)	68.8(4)	O(53)—Ce(52)—O(57)	71.6(3)

Table 2. (*Continued*)

O(6)—Ce(2)—O(7)	104.1(6)	O(56)—Ce(52)—O(57)	97.2(3)
O(1)—Ce(2)—O(10)	140.1(4)	O(51)—Ce(52)—O(60)	142.7(4)
O(2)—Ce(2)—O(10)	141.3(4)	O(52)—Ce(52)—O(60)	141.2(4)
O(3)—Ce(2)—O(10)	141.4(5)	O(53)—Ce(52)—O(60)	134.5(4)
O(6)—Ce(2)—O(10)	85.4(5)	O(56)—Ce(52)—O(60)	87.0(4)
O(7)—Ce(2)—O(10)	85.6(5)	O(57)—Ce(52)—O(60)	83.5(4)
O(1)—Ce(2)—O(11)	131.0(4)	O(51)—Ce(52)—O(61)	131.2(4)
O(2)—Ce(2)—O(11)	85.5(4)	O(52)—Ce(52)—O(61)	81.1(4)
O(3)—Ce(2)—O(11)	83.3(4)	O(53)—Ce(52)—O(61)	85.4(4)
O(6)—Ce(2)—O(11)	130.0(5)	O(56)—Ce(52)—O(61)	126.3(4)
O(7)—Ce(2)—O(11)	124.9(5)	O(57)—Ce(52)—O(61)	134.5(4)
O(10)—Ce(2)—O(11)	89.0(5)	O(60)—Ce(52)—O(61)	86.1(4)
O(1)—Ce(3)—O(2)	63.3(5)	O(51)—Ce(53)—O(52)	63.5(3)
O(1)—Ce(3)—O(4)	75.9(4)	O(51)—Ce(53)—O(54)	76.8(4)
O(2)—Ce(3)—O(4)	73.0(4)	O(52)—Ce(53)—O(54)	71.8(3)
O(1)—Ce(3)—O(6)	77.8(5)	O(51)—Ce(53)—O(56)	76.6(3)
O(2)—Ce(3)—O(6)	72.1(5)	O(52)—Ce(53)—O(56)	72.0(3)
O(4)—Ce(3)—O(6)	143.0(5)	O(54)—Ce(53)—O(56)	141.9(4)
O(1)—Ce(3)—O(12)	106.3(5)	O(51)—Ce(53)—O(62)	98.5(4)
O(2)—Ce(3)—O(12)	168.1(4)	O(52)—Ce(53)—O(62)	161.9(4)
O(4)—Ce(3)—O(12)	111.2(5)	O(54)—Ce(53)—O(62)	104.7(4)
O(6)—Ce(3)—O(12)	100.8(5)	O(56)—Ce(53)—O(62)	105.8(4)
O(1)—Ce(3)—O(13)	158.5(5)	O(51)—Ce(53)—O(63)	161.5(4)
O(2)—Ce(3)—O(13)	95.6(4)	O(52)—Ce(53)—O(63)	98.1(4)
O(4)—Ce(3)—O(13)	94.5(5)	O(54)—Ce(53)—O(63)	99.9(4)
O(6)—Ce(3)—O(13)	100.6(5)	O(56)—Ce(53)—O(63)	96.7(4)
O(12)—Ce(3)—O(13)	95.1(5)	O(62)—Ce(53)—O(63)	100.0(4)
O(1)—Ce(4)—O(3)	63.6(5)	O(51)—Ce(54)—O(53)	63.4(3)
O(1)—Ce(4)—O(5)	78.7(4)	O(51)—Ce(54)—O(55)	75.2(3)
O(3)—Ce(4)—O(5)	69.8(5)	O(53)—Ce(54)—O(55)	73.0(3)
O(1)—Ce(4)—O(7)	78.0(5)	O(51)—Ce(54)—O(57)	76.1(3)
O(3)—Ce(4)—O(7)	70.9(5)	O(53)—Ce(54)—O(57)	71.3(3)
O(5)—Ce(4)—O(7)	140.1(5)	O(55)—Ce(54)—O(57)	141.4(4)
O(1)—Ce(4)—O(14)	101.6(5)	O(51)—Ce(54)—O(64)	103.4(4)
O(3)—Ce(4)—O(14)	163.5(5)	O(53)—Ce(54)—O(64)	165.8(4)
O(5)—Ce(4)—O(14)	101.4(5)	O(55)—Ce(54)—O(64)	110.0(4)
O(7)—Ce(4)—O(14)	114.8(5)	O(57)—Ce(54)—O(64)	101.3(4)
O(1)—Ce(4)—O(15)	160.1(5)	O(51)—Ce(54)—O(65)	159.2(4)
O(3)—Ce(4)—O(15)	96.9(5)	O(53)—Ce(54)—O(65)	96.2(4)
O(5)—Ce(4)—O(15)	99.0(5)	O(55)—Ce(54)—O(65)	95.8(4)
O(7)—Ce(4)—O(15)	92.3(5)	O(57)—Ce(54)—O(65)	102.2(4)
O(14)—Ce(4)—O(15)	98.3(6)	O(64)—Ce(54)—O(65)	97.3(4)
Ce(1)—O(1)—Ce(2)	100.9(5)	Ce(51)—O(51)—Ce(52)	97.4(3)
Ce(1)—O(1)—Ce(3)	98.6(4)	Ce(51)—O(51)—Ce(53)	98.9(3)
Ce(2)—O(1)—Ce(3)	97.8(5)	Ce(52)—O(51)—Ce(53)	98.3(3)
Ce(1)—O(1)—Ce(4)	98.5(5)	Ce(51)—O(51)—Ce(54)	99.0(3)
Ce(2)—O(1)—Ce(4)	98.5(5)	Ce(52)—O(51)—Ce(54)	98.0(3)
Ce(3)—O(1)—Ce(4)	153.6(7)	Ce(53)—O(51)—Ce(54)	154.0(5)
Ce(1)—O(2)—Ce(2)	101.1(4)	Ce(51)—O(52)—Ce(52)	98.1(3)
Ce(1)—O(2)—Ce(3)	92.7(4)	Ce(51)—O(52)—Ce(53)	92.2(3)
Ce(2)—O(2)—Ce(3)	91.2(4)	Ce(52)—O(52)—Ce(53)	91.1(3)
Ce(1)—O(3)—Ce(2)	101.2(5)	Ce(51)—O(53)—Ce(52)	97.7(3)
Ce(1)—O(3)—Ce(4)	92.5(4)	Ce(51)—O(53)—Ce(54)	91.0(3)
Ce(2)—O(3)—Ce(4)	90.0(4)	Ce(52)—O(53)—Ce(54)	93.2(3)
Ce(1)—O(4)—Ce(3)	101.1(5)	Ce(51)—O(54)—Ce(53)	100.5(4)
Ce(1)—O(5)—Ce(4)	101.8(5)	Ce(51)—O(55)—Ce(54)	102.3(4)
Ce(2)—O(6)—Ce(3)	103.3(5)	Ce(52)—O(56)—Ce(53)	101.3(4)
Ce(2)—O(7)—Ce(4)	104.0(5)	Ce(52)—O(57)—Ce(54)	101.5(4)
Ce(1)—O(8)—C(19)	156.7(15)	Ce(51)—O(58)—C(69)	173.2(11)
Ce(1)—O(9)—C(22)	172.7(14)	Ce(51)—O(59)—C(72)	153.5(11)
Ce(2)—O(10)—C(25)	156.7(14)	Ce(52)—O(60)—C(75)	162.2(13)
Ce(2)—O(11)—C(28)	173.4(11)	Ce(52)—O(61)—C(78)	152.6(14)
Ce(3)—O(12)—C(31)	171.3(11)	Ce(53)—O(62)—C(81)	173.1(13)
Ce(3)—O(13)—C(34)	173.1(16)	Ce(53)—O(63)—C(84)	169.0(14)
Ce(4)—O(14)—C(37)	176.8(17)	Ce(54)—O(64)—C(87)	174.5(11)
Ce(4)—O(15)—C(40)	165.7(16)	Ce(54)—O(65)—C(90)	168.2(11)

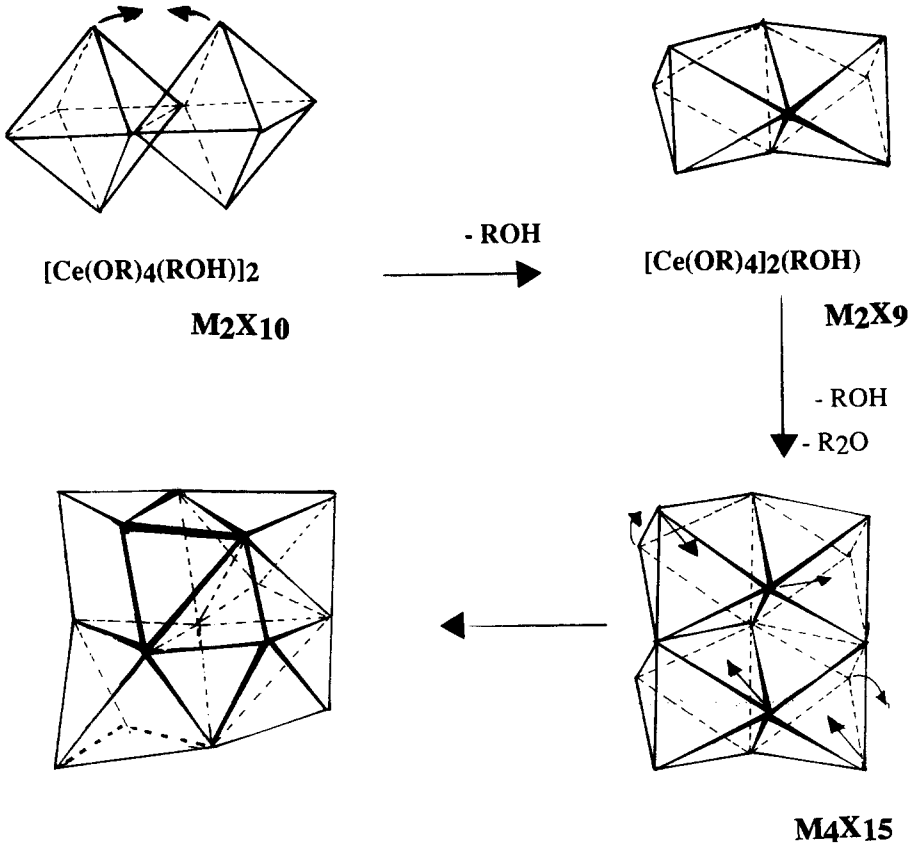


Fig. 2. Polyhedral view of the assembly of the dinuclear units into the $Ce_4O(OPr^i)_{14}$ species.

displays a quite rich chemistry of oxoisopropoxide derivatives and further studies on their characterization and reactivity are in progress [23].

REFERENCES

1. Hubert-Pfalzgraf, L. G., *New J. Chem.* 1995, **19,** 727.
2. Vaartstra, B. A., Huffman, J. C., Gradeff, P. S., Hubert-Pfalzgraf, L. G., Daran, J. C., Parraud, S., Yunlu, K. and Caulton, K. G., *Inorg. Chem.* 1990, **29,** 3126,
3. Evans, W. J., Deming, T. J., Olofson, J. M. and Ziller, J. W., *Inorg. Chem.* 1989, **28,** 4027.
4. Bradley, D. C., Mehrotra, R. C. and Gaur, D. P., *Metal Alkoxides* Academic Press, London, 1978.
5. Yunlu, K., Gradeff, P. S., Shalimoff, W. K., Streib, W. E., Vaartstra, B. A. and Caulton, K. G., *Inorg. Chem.* 1991, **30,** 2317.
6. Walker, N. and Stuart, D., *Acta Cryst.* 1983, **A39,** 158.
7. Watkin, D. J., Carruthers, J. R. and Betteridge, P. W., *Crystal User Guide*, Chemical Crystallography Laboratory, Oxford, 1988.
8. *International Tables for X-ray Crystallography*, Vol. IV. Kynoch Press, Birmingham, U.K., 1974.
9. Sheldrick, G. M. *SHELXS*-86. *Program for Crystal Structure Solution*, Univerität Göttingen, Germany, 1986.
10. Peace, L. J. and Watkin, D. J., *CAMERON*, Chemical Crystallography Laboratory, Oxford, U.K., 1992.
11. Sirio, C., Ph.D. thesis, Université de Nice, 1995, to be published.
12. Turova, N. Ya., Yanovskii, A. I., Kessler, V. G., Kozlova, N. I. and Struchkov, Yu. T., *Russ. Inorg. Chem.* 1991, **36,** 1404.
13. Daniele, S., Papiernik, R., Hubert-Pfalzgraf, L. G., Jagner, S. and Häkansson, M., *Inorg. Chem.* 1995, **34,** 628.
14. El Khokh, N., Hubert-Pfalzgraf, L. G. and Daran, J. C., *Polyhedron*, 1992, **11,** 59.
15. Reuter, H. and Kremser, M., *Z. Anorg. Allgm. Chem.* 1992, **615,** 137.
16. Turova, N. Ya. private communication.
17. Chisholm, M. H. L., Folting, K., Huffman, J. C. and Kirkpatrick, C. C., *Inorg. Chem.* 1984, **23,** 1021.
18. Cotton, F. A., Marler, D. O. and Schowtzer, W., *Inorg. chim. Acta*, 1984, **95,** 207.

19. Turevskaya, E. P., Kozlova, N. I., Turova, N. Ya., Belokon, A. I., Beralyev, D. V., Kessler, V. G. and Griskhin, Yu. K., *Russ. Chem. Bull.* 1995, **44,** 734.
20. Hubert-Pfalzgraf, L. G., *Better Ceramics through Chemistry V* 1972, **271,** 15; Hubert-Pfalzgraf, L. G., Daniele, S., Papiernik, R., Massiani, M. C., Septe, B., Vaissermann, J. and Daran, J. C., *J. Mater. Chem.*, in press.
21. Schmid, R., Mosset, A. and Galy, J., *J. Chem. Soc., Dalton Trans* 1992, 1999; Day, V. W., Eberspacher, T. A., Klemperer, W. G. and Park, C. W., *J. Am. Chem. Soc.* 1993, **115,** 8469.
22. Carofiglio, T., Floriani, C., Sgamellotti, A., Rosi, M., Chiesi-Villa, A. and Rizzoli, C., *J. Chem. Soc., Dalton Trans.* 1992, 1081, and refs therein.
23. Hubert-Pfalzgraf, L. G. and Sirio, C., to be published.

Pergamon

PII: S0277-5387(96)00377-4

Polyhedron Vol. 16, No. 7, pp. 1137–1142, 1997
Copyright © 1997 Elsevier Science Ltd
Printed in Great Britain. All rights reserved
0277-5387/97 $17.00+0.00

The coordination chemistry of (2-thiazolin-2-yl)hydrazine hydrochloride (TzHyHCl)—III. Study of its interaction with cobalt and crystal structure of $[Co(TzHy)_3]Cl_3 \cdot 2H_2O$

A. Bernalte-García,[a]* F. J. García-Barros,[a] F. J. Higes-Rolando,[a] A. M. Pizarro-Galán[a] and C. Valenzuela-Calahorro[b]

[a]Departamento de Química Inorgánica, Facultad de Ciencias, Universidad de Extremadura, 06071 Badajoz, Spain

[b]Departamento de Química Inorgánica, Facultad de Farmacia, Universidad de Granada, 18071 Granada, Spain

(Received 28 June 1996; accepted 30 July 1996)

Abstract—The complexation equilibria of (2-thiazolin-2-yl)hydrazine hydrochloride (TzHyHCl) with cobalt(II) have been studied in aqueous solution at 298 K and 0.1 M ionic strength in $NaClO_4$. The formation constants were determined and discussed in terms of the characteristics of the ligand. The compound $[Co(TzHy)_3]Cl_3 \cdot 2H_2O$ has been isolated and characterized by IR, UV–vis–NIR diffuse reflectance and thermal measurements, and its crystal and molecular structure determined by X-ray analysis. In this compound the complex cation shows a distorted octahedral geometry with the cobalt atom coordinated to three terminal hydrazine nitrogen atoms [average Co—N = 1.973 Å] and three thiazoline nitrogen atoms [average Co—N = 1.900 Å]. Angles N—Co—N for adjacent nitrogen donors are comprised between 94.9 and 82.8°. According to the position of the ligands, the complex can be described as a *facial* isomer. A hydrogen bond scheme is present in the structure interlinking TzHy ligands, water molecules and chloride ions. Copyright © 1997 Elsevier Science Ltd

Keywords: cobalt complexes; crystal structure; hydrazine; potentiometric study; thiazoline.

As part of our program on the coordination chemistry of (2-thiazolin-2-yl)hydrazine hydrochloride (TzHy HCl), we have reported its coordination behaviour and equilibria study with nickel(II) [1], zinc(II) and cadmium(II) [2] in aqueous solution. Likewise, the solid phases obtained by the reaction between the ligand and the aforementioned divalent cations have been characterized by elemental analysis and X-ray diffraction.

In the present paper we have set out to elucidate the behaviour of TzHyHCl with cobalt(II) ion in aqueous solution and we report the synthesis and characterization of the solid phase $[Co(TzHy)_3]Cl_3 \cdot 2H_2O$.

* Author to whom correspondence should be addressed.

EXPERIMENTAL

Reagents

The ligand (2-thiazolin-2-yl)hydrazine hydrochloride (TzHyHCl) was prepared according to a reported procedure [3], taking into account published modifications [4] and recrystallized from methanol.

Cobalt(II) stock solutions were prepared in double distilled freshly boiled water from its chloride and their concentrations were determined as usually [5]. Sodium hydroxide stock solutions were prepared by dilution of a concentrated solution of sodium hydroxide, according to Kolthoff *et al* [6]. These solutions were kept under CO_2-free atmosphere and standardized by titration against potassium hydrogen phthalate. All working solutions were prepared at

0.1 M ionic strength adjusted with sodium perchlorate. All the remaining chemicals used were commercial, analytical grade reagents.

Preparation of $[Co(TzHy)_3]Cl_3 \cdot 2H_2O$

The Co^{III} complex was isolated as follows: a freshly prepared aqueous solution of cobalt(II) chloride was added to an aqueous solution of TzHyHCl and the pH of the whole solution was then adjusted, by dropwise addition of NaOH, at appropriate pH according with the titration curves. By means of liquid–vapor diffusion of ethanol over this solution, red crystals were isolated, filtered off by suction, washed with ethanol, air-dried and stored in a desiccator containing silica gel. Found: C, 19.9; H, 4.4; N, 22.7; S, 18.1; Co, 9.9. Calc. for $C_9H_{25}Cl_3N_9S_3Co$: C, 19.6; H, 4.6; N, 22.8; S, 17.4; Co, 10.7%.

Instrumental procedures

Chemical analysis of carbon, hydrogen, nitrogen and sulfur were performed by means of microanalytical methods using a Perkin–Elmer 240C microanalyser. The metal content was estimated by thermogravimetry as Co_3O_4. A UV–vis–NIR reflectance spectrum of the complex in the 200–1200 nm range was obtained from a pellet of the sample, using a Shimadzu UV-3101PC spectrophotometer and $BaSO_4$ as a reference. IR spectra were recorded on a Perkin–Elmer FT-IR 1720 spectrophotometer, from KBr pellets in the 4000–400 cm^{-1} range and on a Perkin–Elmer FT-IR 1700X spectrophotometer, from polyethylene pellets in the 400–150 cm^{-1} range. A thermal study was carried out on a Mettler TA-4000 system, provided with a Mettler TG-50 thermobalance and a DSC-20 differential scanning calorimeter. The TG curve was obtained on heating a sample of the solid in a dynamic pure air atmosphere (200 cm^3 min^{-1}) in the 35–900°C temperature range, whereas the DSC plot was recorded under a static air atmosphere in the temperature range between 35 and 600°C. In both cases a heating rate of 10°C min^{-1} and samples varying in weight from 3 to 13 mg were utilized. The procedures and apparatus used for potentiometric measurements were described in detail previously [1]. Briefly, measurements were made at 25 ± 0.1°C and 0.1 M ($NaClO_4$) ionic strength. The electrode system was calibrated in terms of hydrogen ion concentration by performing strong acid *vs* strong base titrations [7]. The concentration of ligand in the experimental solutions was always 2×10^{-3} mol dm^{-3} and successive 1:1, 2:1 and 3:1 ligand-to-metal ratios were investigated. The numerical analysis of all the experimental e.m.f. data were carried out with the computer program SUPERQUAD [8]. All calculations were performed on an IBM RS/6000 computer (Computer Centre, University of Extramadura). X-ray powder diffraction was obtained through a Philips PW-1700 diffractometer using Cu-K_α radiation.

Crystal structure determination

Crystal data, data collection and refinement details for $[Co(TzHy)_3]Cl_3 \cdot 2H_2O$ are given in Table 1. Examination of three standard reflections, monitored after 97 scans, showed no sign of crystal deterioration. The data were corrected for Lorentz and polarization effects, and were also corrected for absorption effects using an empirical method based on azimuthal scan data. The structure was solved by direct methods and subsequent Fourier differences using the SHELXTL-IRIS program [9] and refined by full-matrix least-squares. The H atoms were located from a differential Fourier synthesis and included in the calculation with estimated isotropic displacement parameters without refinement (riding model). All calculations were performed with a Silicon Graphics Iris Indigo XS24.

Thermal parameters, atom coordinates and a listing of observed and calculated structure factors have been deposited with the Editor, from whom copies are available on request.

Table 1. Crystal data, data collection and refinement details for $[Co(TzHy)_3]Cl_3 \cdot 2H_2O$

Crystal shape	Prismatic
Size (mm)	$0.36 \times 0.36 \times 0.16$
Chemical formula	$C_9H_{25}Cl_3N_9O_2S_3Co$
Formula weight	552.8
Crystal system	Monoclinic
Space group	$P2_1/n$
Unit-cell dimensions	
a (Å)	9.788(1)
b (Å)	14.214(1)
c (Å)	15.639(1)
β ( )	91.46(2)
Cell volume (Å^3)	2175.1(6)
Z	4
D_x (g cm^{-3})	1.688
μ (cm^{-1})	14.71
F (000)	1136
Diffractometer	Siemens P4
Radiation	Mo-K_α ($\lambda = 0.71073$ Å)
Collection method	θ–2θ
2θ range	2.0–50
Index ranges	$-1 \leqslant h \leqslant 11$; $-1 \leqslant k \leqslant 16$; $-18 \leqslant l \leqslant 18$
Independent reflections	3828
Observed reflections	2748 [$F > 4\sigma(F)$]
No. of refined parameters	244
R	0.041
wR	0.042
w	$1/[\sigma^2(F) + 0.0002F^2]$
GOF	1.22
ρ_{max}, ρ_{min} (e Å^{-3})	0.41, −0.33

RESULTS AND DISCUSSION

Potentiometric studies

The final stoichiometries and formation constants of the complexes formed were determined by means of the computer program SUPERQUAD [8] to identify that which, according to χ^2, best fitted the experimental data. The titration curves were treated either as a single set or as separate entities without significant variation in the formation constants. Only experimental points in which variations in the degree of formation of the complexes occurred were processed in the last refinement. The chemical models yielding the best fits between the measured and calculated titration curves, together with the refined formation constants and statistical parameters (SIGMA and χ^2), are compiled in Table 2. The formation constants for the hydrolysis products produced by the reaction of the cobalt(II) with water [10] were included in the chemical modelling. In addition, it has been established and also incorporated models of dissociation processes of the ligand in which the possible existence of neutral [(TzHy)] and protonated [$(TzHyH)^+$] species were considered. It was verified that all the proposed species [denoted as $M_p(TzHy)_qH_r$] existed in significant concentrations over a reasonable range data.

It can be seen that while in the titration curve with a relation ligand : metal 1 : 1 the model chosen, formed by the apparently simple model of 110, resulted in a satisfactory numerical and graphical fitting, in the titrations with a relation ligand : metal 2 : 1 and 3 : 1 the existing experimental evidence was sufficient to determine with accuracy that 133 complex is present. In addition, in the titration curve 2 : 1 the combination of this species and 121 gave the best findings.

Study of the $[Co(TzHy)_3]Cl_3 \cdot 2H_2O$ *complex*

The analytical results agree with the molecular formula $C_9H_{25}Cl_3N_9S_3Co$ for the red Co^{III} complex.

The structure of $[Co(TzHy)_3]Cl_3 \cdot 2H_2O$ is built up by $[Co(TzHy)_3]^{3+}$ cations, chloride anions and water molecules of crystallization. Figure 1 shows the molecular structure of the cation complex. Selected bond lengths, angles and hydrogen-bond parameters are listed in Table 3.

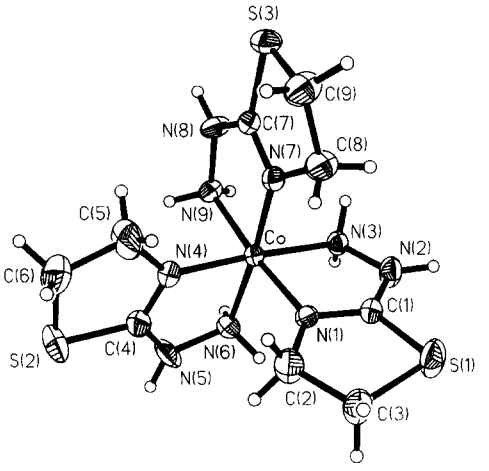


Fig. 1. Molecular structure of the $[Co(TzHy)_3]^{3+}$ cation, showing the atom-numbering scheme. The thermal ellipsoids are drawn at a 50% level.

Table 2. Formation constants (log β) at 25°C and $I = 0.1$ mol dm^{-3}

System	Species[a]	logβ	χ^2	Σ
$TzHyH^+/Co^{2+}$ (1/1)	$[Co(TzHy)]$	2.42(1)	10.29	2.4
$TzHy^+/Co^{2+}$ (2/1)	$[Co(TzHy)_2H]$	12.61(1)	11.90	1.4
	$[Co(TzHy)_3H_3]$	27.79(2)		
$TzHy^+/Co^{2+}$ (3/1)	$[Co(TzHy)_3H_3]$	28.93(1)	12.00	2.8

[a]Changes are omitted for the sake of clarity.

The coordination geometry around the cobalt atom is a distorted octahedron with bidentate TzHy ligands coordinated through thiazolinic nitrogens and terminal hydrazine nitrogens. According to the position of the ligands, the complex can be described as a *facial* isomer. Thus, the whole molecule exhibits pseudo-C_3 symmetry with the C_3 axis passing through the centres of the faces defined by N(1), N(4), N(7) and N(3), N(6), N(9).

In similar form to that observed in other complexes containing the TzHy ligand [1,2], and for analogous reasons, the Co—N(thiazoline) distances [average 1.900 Å] are appreciably shorter than the Co—N (hydrazine) distances [average 1.973 Å].

The chelate rings are essentially planar, with maximum deviation for N(3) (0.086 Å).

Bond lengths and angles in the ligands are similar and comparable with those observed in TzHyHCl [1] and the complexes with Ni^{II}, Zn^{II} and Cd^{II} [1, 2], and indicate that the organic moiety preserves the thiazoline–hydrazine form. However, it should be pointed out that the three thiazoline rings show different conformations. Thus, the values of the puckering parameters, calculated according to Cremer and Pople [11], are:

Ring A
[S(1)—C(1)—N(1)—C(2)—C(3)] $q_2 = 0.152$ Å $\phi_2 = 150.0$

Ring B
[S(2)—C(4)—N(4)—C(5)—C(6)] $q_2 = 0.011$ Å $\phi_2 = 90.0$

Ring C
[S(3)—C(7)—N(7)—C(8)—C(9)] $q_2 = 0.268$ Å $\phi_2 = 134.6$

These values indicate that ring A shows a conformation near to envelope with the apex at C(3).

Table 3. Selected bond lengths (Å), angles (°) and hydrogen bonds for $[Co(TzHy)_3]Cl_3 \cdot 2H_2O$

Co—N(1)	1.899(3)	Co—N(3)	1.972(3)
Co—N(4)	1.904(3)	Co—N(6)	1.977(3)
Co—N(7)	1.898(3)	Co—N(9)	1.969(3)
N(1)—Co—N(3)	82.8(1)	N(6)—Co—N(7)	175.4(1)
N(1)—Co—N(4)	94.9(1)	N(6)—Co—N(9)	93.3(1)
N(1)—Co—N(6)	90.7(1)	N(7)—Co—N(9)	83.3(1)
N(1)—Co—N(7)	92.9(1)	Co—N(3)—N(2)	108.3(2)
N(1)—Co—N(9)	174.3(1)	Co—N(6)—N(5)	108.4(2)
N(3)—Co—N(4)	176.3(1)	Co—N(9)—N(8)	108.6(2)
N(3)—Co—N(6)	93.7(1)	Co—N(1)—C(1)	113.4(3)
N(3)—Co—N(7)	89.6(1)	Co—N(1)—C(2)	131.9(3)
N(3)—Co—N(9)	93.0(1)	Co—N(4)—C(4)	113.3(3)
N(4)—Co—N(6)	83.4(1)	Co—N(4)—C(5)	132.6(3)
N(4)—Co—N(7)	93.4(1)	Co—N(7)—C(7)	113.6(3)
N(4)—Co—N(9)	89.5(1)	Co—N(7)—C(8)	132.9(3)

Bond A···H—D	Position of D	A···D (Å)	A···H—D (°)
Cl(2)···H(2)—N(5)	$1/2-x, -1/2+y, 1/2-z$	3.148(4)	176.5(1)
Cl(2)···H(7)—N(3)	$-x, 1-y, 1-z$	3.171(3)	166.5(1)
Cl(2)···H(5)—N(2)	x, y, z	3.122(4)	156.3(1)
Cl(2)···H(2w)—O(1)	$-1+x, y, z$	3.334(4)	166.3(1)
Cl(1)···H(13)—N(6)	$-1+x, y, z$	3.215(3)	144.3(1)
Cl(1)···H(20)—N(9)	$-1+x, y, z$	3.117(3)	147.9(1)
Cl(1)···H(6)—N(3)	$-1+x, y, z$	3.155(5)	133.6(1)
Cl(3)···H(14)—N(6)	$-1+x, y, z$	3.251(6)	176.0(1)
Cl(3)···H(21)—N(9)	$-1/2-x, -1/2+y, 1/2-z$	3.237(4)	161.6(1)
Cl(3)···H(3w)—O(2)	$1/2-x, -1/2+y, 1/2-z$	3.217(4)	170.3(2)
Cl(3)···H(1w)—O(1)	$1/2-x, 1/2+y, 1/2-z$	3.194(5)	163.2(3)
O(2)···H(19)—N(8)	$-x, 1-y, 1-z$	2.717(5)	160.3(2)
O(1)···H(4w)—O(2)	$1-x, -y, 1-z$	2.795(5)	151.5(2)

This atom is 0.233 Å out of the plant formed by S(1)—C(1)—N(1)—C(2) [maximum mean-plane deviation for N(1) = 0.008 Å]. Ring B is planar, with maximum mean-plane deviation for N(4) (0.007 Å). Ring C is puckered most and shows an intermediate form between envelope and half-chair conformations, with C(8) and C(9) deviating 0.151 and 0.298 Å above and below, respectively, the S(3)—C(7)—N(7) plane.

The crystal structure is stabilized by a very extensive hydrogen bond network in which hydrazinic nitrogen atoms act as donors, chloride anions act as acceptors and oxygen atoms of water of crystallization act as donors and acceptors. A view showing this network is given in Fig. 2.

The diffuse reflectance spectrum exhibits one band at 11,800 cm^{-1} and one triplet at 14,400, 14,900 and 16,000 cm^{-1}, all of low intensity, and two more intense bands at 19,650 and 26,750 cm^{-1}. These bands may be assigned as $^1A_{1g} \rightarrow {}^3T_{1g}$; $^1A_{1g} \rightarrow {}^3T_{2g}$; $^1A_{1g} \rightarrow {}^1T_{1g}$ and $^1A_{1g} \rightarrow {}^1T_{2g}$ transitions, respectively, in an idealized O_h symmetry. The position of the observed spectral bands permits to calculate the ligand field parameters, 10 Dq, B and C, using the following known relationships [12]:

$$E(^3T_{1g} \leftarrow {}^1A_{1g}) = 10\,Dq - 3C \quad (1)$$

$$E(^3T_{2g} \leftarrow {}^1A_{1g}) = 10\,Dq + 8B - 3C \quad (2)$$

$$E(^1T_{1g} \leftarrow {}^1A_{1g}) = 10\,Dq - C \quad (3)$$

$$E(^1T_{2g} \leftarrow {}^1A_{1g}) = 10\,Dq + 16B - C \quad (4)$$

in which, for the application of (2), the mean of the observed triplet has been considered. The calculated values of the ligand field parameters 10 Dq (~23,800 cm^{-1}), B (~430 cm^{-1}) and C (~4000 cm^{-1}) are consistent with the presence of a chromophore group $[Co^{III}N_6]$ [13].

The IR spectrum in the 4000–400 cm^{-1} region shows the presence of characteristic bands due to the thiazoline ring at 1630 (W_1), 970 (W_2), 880 (W_3), 800 (W_4), 680 (W_5), 615 (W_6), 560 (W_8), 480 (W_7) and 425 cm^{-1} (Γ_1) [14]. Moreover, other relevant bands are registered at 3505 and 3415 (ν_{H_2O}), 3160–3090 (ν_{NH_2},

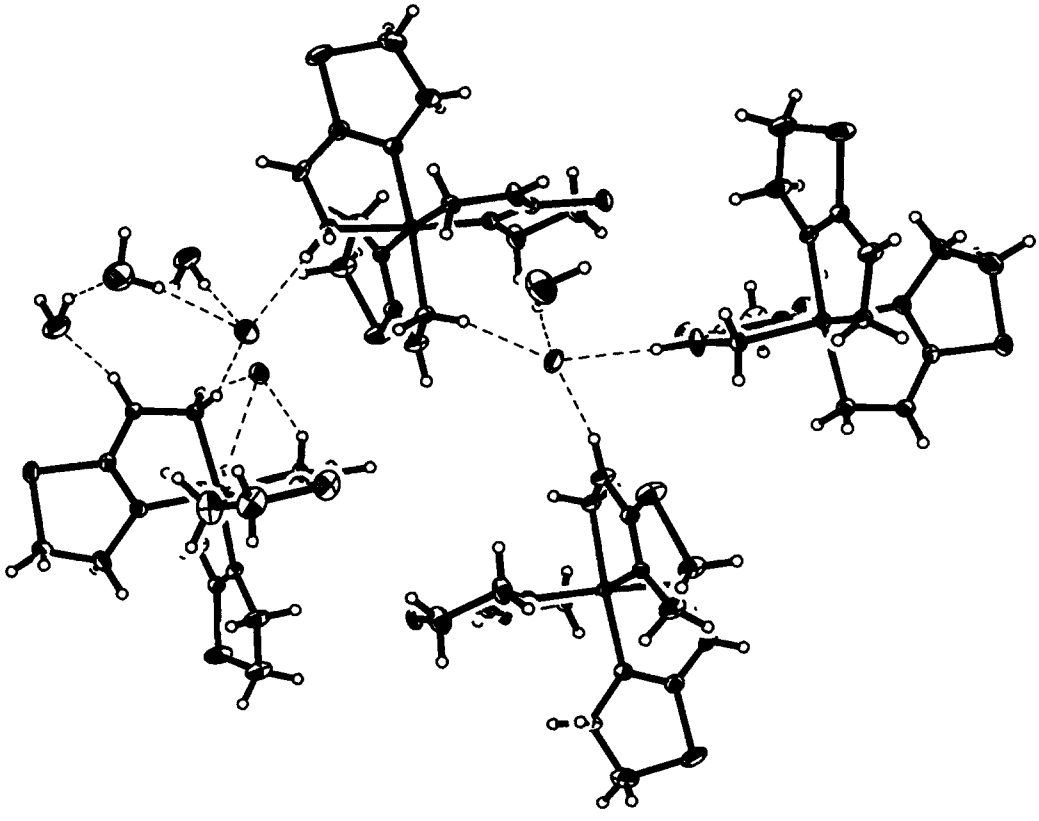


Fig. 2. View of the hydrogen-bond network of $[Co(TzHy)_3]Cl_3 \cdot 2H_2O$.

ν_{NH}), and 1040 cm^{-1} ($\nu_{N\ N}$). It is worth noting the absence of the bands observed at 2820 and 2790 cm^{-1} in the spectrum of TzHyHCl and assigned to ν_{NH^+} [15], which is according to the fact that the ligand acts in a deprotonated form.

The low-frequency region shows four bands assignable to Co–ligand stretching vibrations, concordantly with the pseudo-C_3 symmetry of the complex cation. In other complexes containing this ligand it is observed that $\nu_{M\text{-}N(hydrazine)}$ vibrations occur at upper frequencies than $\nu_{M\ N(thiazoline)}$ vibrations [15]. For that, the bands observed at 382 and 368 cm^{-1} are tentatively attributed to $\nu_{M\ N(hydrazine)}$, while the bands at 310 and 268 cm^{-1} could be assigned to $\nu_{M\ N(thiazoline)}$.

The study of thermal data obtained for $[Co(TzHy)_3]Cl_3 \cdot 2H_2O$ reveals that the decomposition takes place in three steps. In the first the complex becomes totally dehydrated in the 50–125°C range; at the last temperature the weight loss found (8.3%) could be assigned to moisture ($\sim$1.8%) and to the loss of two H_2O molecules (6.5%). This step is associated with an endothermic effect in the DSC plot (ΔH = 448 J g^{-1}). The anhydrous complex is stable up to 200°C. From this temperature onwards the decomposition starts with an intense effect of weight loss, in two overlapping steps ending at 430°C and corresponding to the pyrolytic degradation of the sample. These steps are reflected in the DSC plot by exothermic effects. At temperatures above this latter effect, combustion of the remaining sample takes place, finally giving Co_3O_4 that was characterized by IR spectroscopy and X-ray powder diffraction.

REFERENCES

1. Bernalte, A., Díaz, M. A., Barros, F. J. G., Higes, F. J., Pizarro, A. M., Romero, J. and Valenzuela, C., *Polyhedron*, 1996, **15**, 1691.
2. Bernalte, A., Díaz, M. A., Barros, F. J. G., Higes, F. J., Pizarro, A. M., Romero, J. and Valenzuela, C., *Polyhedron*, 1997, **16**, 297.
3. Ansell, M. F., ed., *Rodd's Chemistry of Carbon Compounds. Heterocyclic Compounds*, Vol. 4 C. Elsevier, Amsterdam, 1986.
4. Ávalos, M., Babiano, R., Cintas, P., Jiménez, J. L. and Palacios, J. C., *Heterocycles*, 1992, **33**, 973.
5. Bermejo, F. and Prieto, A., *Aplicaciones Analíticas del AEDT y Análogos*. Ser. Publ. Univ., Santiago de Compostela, 1960.
6. Kolthoff, I. M., Sandell, E. B., Meehan, E. J. and Bruckenstien, S., *Quantitative Chemical Analysis*. The Macmillan Company Collier-Macmillan Canada Ltd, Toronto, 1969.
7. Linder, P. W., Torrington, R. G. and Williams, D. R., *Analysis using Glass Electrodes*. Open University Press, Milton Keynes, 1984.
8. Gans, P., Sabatani, A. and Vacca, A., *J. Chem. Soc., Dalton Trans.* 1985, 1195.

9. Sheldrick, G. M., SHELXTL-IRIS. Release 4.2. Siemens Analytical X-ray Instruments Inc., Madison, Wisconsin, U.S.A. 1991.
10. Baes, C. F. Jr, and Mesmer, R. E., *The Hydrolysis of Cations*. John Wiley & Sons, New York, 1976.
11. Cremer, D. and Pople, J. A., *J. Am. Chem. Soc.* 1975, **97,** 1354.
12. Lever, A. B. P., *Inorganic Electronic Spectroscopy*. Elsevier, Amsterdam, 1968.
13. Jörgensen, C. K., *Absorption Spectra and Chemical Binding in Complexes*. Pergamon Press, Oxford, 1962.
14. Mille, G., Meyer, J. L. and Chouteau, J., *J. Mol. Struct.* 1978, **50,** 247.
15. Pizarro, A. M., Compuestos de coordinación de iones de metales de transición con clorhidrato de (2-tiazolin-2-il)hidrazina. Ph.D. Thesis, Universidad de Extremadura, Badajoz, 1996.

Pergamon

PII: S0277-5387(96)00375-0

Polyhedron Vol. 16, No. 7, pp. 1143–1147, 1997
Copyright © 1997 Elsevier Science Ltd
Printed in Great Britain. All rights reserved
0277-5387/97 $17.00+0.00

Spectroscopic properties and crystal structure of an oxovanadium(V) alkoxo complex with the ligand: 5-chloro-*o*-hydroxyacetophenone-salicylhydrazide

María S. Palacios,[a]✠ María J. Rocío,[a] Sixto Domínguez,[a] Pedro Gili,[a]* Catalina Ruiz-Pérez,[b] Fernando V. Rodríguez-Romero[b] and Jean-Michel Dance[c]

[a] Departamento de Química Inorgánica, Universidad de La Laguna, 38200 La Laguna, Tenerife, Canary Islands, Spain

[b] Departamento de Física Fundamental y Experimental, Universidad de La Laguna, E-38204, La Laguna, Canary Islands, Spain,

[c] Laboratoire de Chimie du Solide du CNRS, Université de Bordeaux I, 351 Cours de la Liberation, 33405 Talence Cédex, France

(Received 28 May 1996; accepted 30 July 1996)

Abstract—The preparation and characterization by means of IR and electronic spectroscopies, magnetic measurements and molecular structure by X-ray diffraction of a single-crystal are reported for a monomeric oxovanadium(V) complex: $[V^{V}O(5Cl\text{-}OHA\text{-}SHZ)(OCH_2CH_3)]$, where (5Cl-OHA-SHZ) is the dianionic tridentate ONO donor ligand 5-chloro-*o*-hydroxyacetophenone-salicylhydrazide. The vanadium atom is essentially five coordinate. Three ONO donor atoms of the (5Cl-OHA-SHZ) ligand and an oxygen atom from an alkoxide group form a distorted square-pyramidal geometry around the metal center. The basal coordination plane is formed by three donor atoms ONO (a phenolic oxygen, an imine nitrogen and an enolic oxygen) from the ligand and an oxygen atom from the alkoxide group. This structure is compared with the corresponding copper (II) complex with the same ligand. Copyright © 1997 Elsevier Science Ltd

Keywords: oxovanadium; alkoxo complex; *o*-hydroxyacetophenone; salicylhydrazide; monomeric complex; five-coordinate complex.

Within the general field of molecular recognition the selectivity of metal ions to binding by appropriate donor atoms of a receptor or ligand is important [1]. The metal cations are often viewed as hard spheres and the recognition is simply based on charge and size considerations [2]. This model works well for most metal cations, including transition metal cations, such as Cu^{II} and Ni^{II}, but for metal oxo cations, such as VO^{2+}, VO_2^+, UO_2^{2+}, the latter considerations are not satisfactory. In this case the ligands should include aspects which recognize the metal oxo moiety on the basis of geometrical properties (Stereognostic coordination chemistry [2]). Taking into account these considerations, a ligand that incorporates groups that can bind strongly to the equatorial positions of a square-based pyramid, for example, can be a candidate to form stable complexes with oxovanadium cations.

Also vanadium is receiving considerable attention as a biologically important metal due to the existence of vanadoenzymes [3,4]. Thus, work with model complexes to mimic the phenolate oxygen of tyrosine [5], so that alkoxide coordination may result from deprotonated serine or threonine residues [3] have been studied. In this paper we describe the synthesis, spectroscopic properties and the single-crystal X-ray structure of $[V^{V}O(5Cl\text{-}OHA\text{-}SHZ)(OCH_2CH_3)]$ com-

* Author to whom correspondence should be addressed

plex, where 5Cl-OHA-SHZ(5-chloro-*o*-hydroxyacetophenone-salicylhydrazide) is a dianionic tridentate ligand, which presents the ONO donor atoms (with a phenolate oxygen) that can bind strongly to the equatorial positions around the metal. This ligand forms a complex with Cu^{II} where the stereochemistry around the metal ion is distorted square planar incorporating an oxygen atom from a DMF solvent molecule in the fourth position [6]. We have also attempted the preparation of a complex of VO^{2+} with this ligand, but we have only been able to prepare a stable, mononuclear pentavalent vanadium complex. The pentavalent oxidation state rather than the tetravalent state is physiologically active [7], although the oxidation state within organisms seems to be highly variable [8].

EXPERIMENTAL

Synthesis of the compound

All chemicals were reagent grade and used as supplied. Salicylhydrazide and 5-chloro-2-hydroxyacetophenone were prepared following methods previously described [9,10]. 5Cl-OHA-SHZ was prepared by the procedure described in reference [6].

[$V^{V}O$(5Cl-OHA-SHZ)(OCH_2CH_3)]. To a magnetically stirred hot ethanolic solution (300 cm^3) of Schiff base 5Cl-OHA-SHZ (0.61 g, 2 mmol) was added an aqueous solution of $VOSO_4 \cdot 5H_2O$ (0.52 g, 2 mmol). The resulting green solution after 15 min turned reddish-brown and was then refluxed for 3 h. Evaporation of the solvent at room temperature yielded after several days a crystalline reddish-brown product, which was recrystallized twice from ethanol. The separated reddish-brown crystals, filtered off and air-dried, are slightly soluble in water and soluble in most common polar and nonpolar organic solvents. These crystals are stable up to 215°C, where decomposition begins to take place without melting. Found: C, 49.2; H, 3.9; N, 6.8; V, 12.2. $VOClC_{15}H_{12}N_2O_3 \cdot C_2H_5O$ requires: C, 48.9; H, 3.8; N, 6.7; V, 12.2%.

If it is recrystallized from methylene chloride the reddish-brown compound forms a green solution from which a green powder is precipitated. The redissolution of this latter compound in ethanol gave the initially prepared reddish-brown crystals of [$V^{V}O$(5Cl-OHA-SHZ)(OCH_2CH_3)] after several days.

Chemical analyses of C, H and N were performed on a Carlo Erba microanalyser. Vanadium was determined by thermogravimetric analysis, after decomposition and ignition of the sample to V_2O_5.

Physical measurements

Thermal analyses were carried out on a Perkin–Elmer TGS-1 thermobalance. Electronic spectra of the solid compound were run on a Beckman DU-2 spectrophotometer after dilution of the sample in $BaSO_4$, in the 400–1000 nm spectral range. IR spectra were recorded on a Nicolet 5PCFT spectrophotometer, using KBr as support, in the 4000–250 cm^{-1} spectral range. The magnetic susceptibility was measured on a Faraday type microbalance and the EPR spectra were recorded on a X-band Bruker spectrometer.

X-ray crystallography

Table 1 summarises crystal data, data collection and structure determination. Positions of the remaining non hydrogen atoms and the C_2H_5O group were located from the subsequent Fourier synthesis. The C(17) atom of the CH_3 group on C_2H_5O shows a statistical disorder which could be identified through a Fourier difference synthesis. The disorder problem was handled by refining the two carbon sites [C(171) and C(172)] with isotropic thermal parameters. In the final stages of the structure refinement, a Fourier difference synthesis revealed the locations of the hydrogen atoms except for the C_2H_5O group, which were subsequently refined with isotropic thermal parameters.

Additional material available from the Cambridge Crystallographic Data Centre comprises atom coordinates, thermal parameters, bond lengths and angles, torsion angles and least-squares mean planes.

RESULTS AND DISCUSSION

Molecular structure of [$V^{V}O$(5-Cl-OHA-SHZ)(OCH_2CH_3)]

Selected bond lengths and angles for this compound are shown in Table 2. An ORTEP [13] drawing of the structure including the atomic numbering scheme is given in Fig. 1. The asymmetric unit consists of a discrete molecule of the complex. The coordination around the vanadium can be described as distorted square pyramidal. The basal plane is made up by the phenolic oxygen O(1), [V(1)—O(1) = 1.856(4) Å], the enolic oxygen O(3), [V(1)—O(3) = 1.912(3) Å], the imine nitrogen N(2) [V(1)—N(2) = 2.136(3) Å] from the 5Cl-OHA-SHZ ligand and O(2) [V(1)—O(2) = 1.757(3) Å] from the deprotonated alkoxide oxygen. These values are in the range seen for other vanadium Schiff base complexes [3]. The 5Cl-OHA-SHZ acts as a tridente dianion ligand, presenting in the complex contiguous five and six-membered chelate rings as in the copper(II) complex [6]. If we compare these bond lengths with those found for copper(II) complex [6], [Cu(5Cl-OHA-SHZ)DMF], we observe that the largest difference corresponds to the imine nitrogen–copper distance [1.933(3) Å]. This is probably due to the presence of the terminal oxo ligand O(4) that produces a *cis* lengthening of the vanadium–nitrogen bond. There is

Table 1. Crystal data, data collection and structure determination summary for [V^{V}O(5Cl-OHA-SHZ)(OCH_2CH_3)]

Crystal data	
Formula	$VOClC_{15}H_{12}N_2O_3 \cdot C_2H_5O$
Colour habit	Reddish-brown, prismatic
Formula weight	415.73
Crystal size (mm)	$0.50 \times 0.40 \times 0.30$
Crystal system	Monoclinic
Space group	$C2/c$
Cell measurements reflections used	20
Cell measurement θ range (°)	8–12
Unit-cell dimensions	$a = 17.386(3)$; $b = 18.155(3)$; $c = 12.996(2)$ Å $\beta = 118.96(2)$
Volume (Å^3)	3588.9(3)
Z	8
Density (calc, g cm^{-3})	1.538
Absorption coefficient (mm^{-1})	6.254
$F(000)$	1704
Data collection and structure determination	
Diffractometer used	Syntex P1 four-circle
Radiation	Cu-$K\alpha$($\lambda = 1.54180$ Å)
Temperature (K)	293(2)
Monochromator	Graphite
θ range (°)	3.79–59.98
Scan type	2θ–θ
Scan speed (° min^{-1})	Variable
Standard reflections	2 measured every 60 min
Standard reflections decay (%)	< 10
Index range	$0 \leqslant h \leqslant 19$; $0 \leqslant k \leqslant 20$; $-13 \leqslant l \leqslant 12$
Reflections collected	2289
Observed reflections	2148 [$I \geqslant 2.0\sigma(I)$]
Absorption correction	None
Computing data collection	Siemens Diffractometer Software
System used	SHELXL-86 (Sheldrick [11])
Solution	Patterson
Structure refinement	SHELXS-93 (Sheldrick [12])
Refinement method	Full-matrix least-squares
Quantity minimized	F^2
Extinction correction	SHELXL-93 (Sheldrick [12])
Extinction coefficient	0.0004(3)
Weighting scheme	$w = 1/[\sigma^2(F_o^2) + P^2]$; $P = (F_o^2 + 2F_c^2)/3$
Number of parameters refined	262
Final R indices (obs. data)	0.0547
wR^2	0.2268
Goodness-of-fit	0.248
Largest and mean Δ/σ	−2.082, 0.261
Data-to-parameter ratio	8.2:1
Largest difference peak (e Å^{-3})	0.512
Largest difference hole (e Å^{-3})	−0.728

no significant distortion toward trigonal bipyramidal geometry, as demonstrated by the *trans*-O(3)—V(1)—O(1) and N(2)—V(1)—O(2) angles, 143.4(1) and 161.1(1)°, respectively. The same angles for the copper(II) complex [6] are 175.7(2) and 173.9(2)°, respectively, the coordination around the copper being essentially planar. The apical position is occupied by the terminal oxo group O(4), being the V(1)—O(4) distance 1.577(3)Å; this short distance (indicating a V=O strong double-bond character) is found in five-coordinate [2,3] and octahedral complexes [14] of vanadium(IV) and (V). The vanadium atom is displaced toward the apical oxo ligand O(4) by 0.402(1) Å from the best least-squares plane defined by O(1), O(3), N(2) and O(2). This deviation is between the values found for complexes [2, 3, 14] of vanadium(IV) and (V). The V(1)—N(2)—N(1)—C(9)—O(3) and V(1)—N(2)—C(7)—C(6)—C(1)—O(1) chelate rings do not deviate significantly from planarity, the dihedral angle formed by both planes being 162.5(1)°.

The shortest intermolecular contact was found for

Table 2. Interatomic distances (Å) and selected bond angles for [$V^{V}O$(5Cl-OHA-SHZ)(OCH_2—CH_3)]

V(1)—O(1)	1.856(4)	V(1)—O(2)	1.757(3)	V(1)—O(3)	1.912(3)
V(1)—O(4)	1.577(3)	V(1)—N(2)	2.136(3)	N(2)—N(1)	1.398(5)
N(1)—C(9)	1.306(6)	C(9)—O(3)	1.309(5)	O(1)—C(1)	1.354(5)
C(1)—C(6)	1.404(6)	C(6)—C(7)	1.467(6)	C(7)—N(2)	1.293(6)
C(9)—C(10)	1.454(6)	C(10)—C(15)	1.403(6)	C(15)—C(14)	1.385(8)
C(14)—C(13)	1.380(9)	C(13)—C(12)	1.378(9)	C(12)—C(11)	1.372(9)
C(11)—C(10)	1.398(7)	C(6)—C(5)	1.406(6)	C(5)—C(4)	1.368(7)
C(4)—C(3)	1.394(7)	C(3)—C(2)	1.367(7)	C(2)—C(1)	1.381(6)
O(2)—C(16)	1.447(7)	C(16)—C(171)	1.46(2)	C(16)—C(172)	1.52(2)
O(1)—V(1)—O(2)	100.2(2)	O(1)—V(1)—O(3)	143.4(1)	O(2)—V(1)—O(3)	93.7(1)
O(1)—V(1)—O(3)	93.7(1)	O(1)—V(1)—O(4)	103.9(2)	O(2)—V(1)—O(4)	103.7(2)
O(3)—V(1)—O(4)	105.4(2)	O(1)—V(1)—N(2)	81.6(1)	O(2)—V(1)—N(2)	161.1(1)
O(3)—V(1)—N(2)	74.9(1)	O(4)—V(1)—N(2)	94.0(2)	V(1)—O(1)—C(1)	124.9(3)
V(1)—O(2)—C(16)	131.5(3)	V(1)—O(3)—C(9)	119.7(3)	N(2)—N(1)—C(9)	109.6(3)
V(1)—N(2)—N(1)	114.1(3)	O(1)—C(1)—C(6)	121.4(4)	C(1)—C(6)—C(7)	122.2(4)
C(6)—C(7)—N(2)	118.5(4)	C(8)—C(7)—C(6)	120.1(4)	O(5)—C(15)—C(10)	122.6(4)
C(9)—C(10)—C(11)	120.0(4)	C(9)—C(10)—C(15)	121.7(4)	C(11)—C(10)—C(15)	118.3(4)

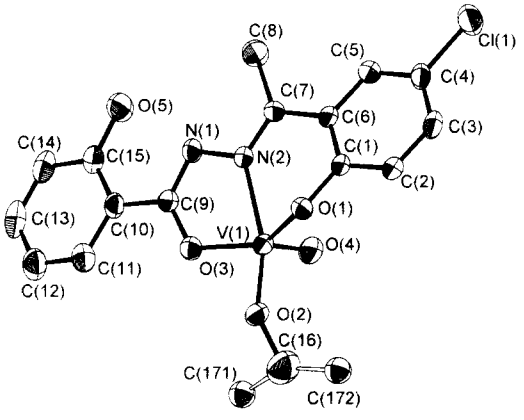


Fig. 1. ORTEP drawing and atom-numbering scheme for [$V^{V}O$(5Cl-OHA-SHZ)(OCH_2CH_3)] (50% probability ellipsoids, H atoms excluded)

V(1)—O(1′) 2.660(3) Å $(-x+1/2, -y+1/2-z)$. Through this phenolic oxygen, dimeric units as is found in vanadium(V) and (IV) complexes [3,14] could be formed.

The complex has a VO^{3+} core and the initial oxidation of VO^{2+} is due to aerobic conditions during the preparation of the complex. The change in color in a solution of methylene chloride from reddish-brown to green indicates a reduction to a vanadium(IV) complex. Unfortunately, we have not had success in preparing the dimer complex as well as isolating crystals of the green solution. The interconversion in solution of monomer–dimers, such as V^{IV}/V^{V} oxidative processes by dioxygen, are described in references [3,15], but not V^{V}/V^{IV} reductive processes in a nonpolar solvent such as CH_2Cl_2 as described in this paper.

The HO(5) atom is bonded to the N(1) atom in an intramolecular hydrogen bond 2.617(6) Å, the angle being 153.5(6) . One weak intramolecular hydrogen interaction is found between the C(11) atom and O(3), 2.785(6) Å, the angle being 101.2(3) .

Magnetic, EPR, electronic and IR spectroscopic measurements

The complex is diamagnetic, although a small amount of vanadium(IV) contaminant was detected only between 4.2 and 10 K with both EPR (a weak spectrum of eight-line pattern of a monomeric species ^{51}V, $I = 7/2$, 99.96% abundant) and magnetic susceptibility studies. Above 10 K the compound exhibits diamagnetic behavior.

The diffuse reflectance spectrum of the reddish-brown compound shows ligand–metal charge transfer (LMCT) bands at 405 and between 500 and 700 (weak) nm. These weak LMTC bands in this latter spectral region may be due to the existence of paramagnetic excited states of low energy [16].

The IR spectrum of the free ligand shows two strong bands at 3264 and 1630 cm^{-1}, which are assigned to ν(=N—H) and ν(>C=O) absorptions, respectively. In the complex these bands are not observed as a consequence of the coordination of the (=N—H)amide group through deprotonation and the enolization of the (>C=O) group. The bands appearing between 2500 and 3000 cm^{-1}, which are observed in both the free ligand and the complex spectra, although with lower intensity in the latter, which are associated with the presence of intramolecular hydrogen bonding OH ... N, already described. One band at 1602 cm^{-1} in the complex spectrum (not observed in the free ligand) is assigned to stretching frequency of the (>C=N—) [7].

Finally, the strong bands at 985 and 952 cm^{-1} which appear only in the complex spectrum are attributed

to V=O stretching frequencies. The splitting of the V=O band may be due to unit-cell group splitting or a crystal-packing effect [17].

REFERENCES

1. Lehn, J. M. *From Coordination Chemistry to Supramolecular Chemistry, Perspective in Coordination Chemistry*, Ed. A. L. Williams, F. Floriani and A. E. Merbach. Verlag Helvetica Chimica Acta, Basel, 1992, pp. 447–462.
2. Dewey, T. M., Bois, J. D. and Raymond, K. N. *Inorg. Chem.*, 1993, **32,** 1729.
3. Carrano, C. J., Nunn, C. M., Quan, R., Bonadies, J. A. and Pecoraro, V. L. *Inorg. Chem.*, 1990, **29,** 944.
4. Frausto da Silva, J. J. R. and Williams, R. J. P. *The Biological Chemistry of the Elements. The Inorganic Chemistry of Life.* Clarendon Press, Oxford, 1991, pp. 427–430.
5. Li, X., Lah, M. S. and Pecoraro, V. L. *Inorg. Chem.*, 1988, **27,** 4567.
6. Dance, J. M., Gambardella, M. T. D., Santos, R. H. A., Medina, E., Manrique, F. G. and Palacios, M. S. *Inorg. Chim. Acta*, 1989, **162,** 239.
7. Collinson, D., Eardley, D. R., Mabbs, F. E., Powell, A. K. and Turner, S. S. *Inorg. Chem.*, 1993, **32,** 664.
8. Bertini, I., Gray, H. B., Lippard, S. J. and Valentine, J. S. *Bioinorganic Chemistry*, University Science Books, Mill Valley, California, 1994, p. 10.
9. Kachhawaha, M. S. and Bhattacharya, A. K. *J. Inorg. Nucl. Chem.*, 1963, **25,** 361.
10. Blatt, A. H. *Organic Reactions*, Vol. 1, Wiley, New York, 1942, p. 342.
11. Sheldrick, G. M. *Acta Cryst.*, 1990, **A46,** 467.
12. Sheldrick, G. M. *Program for the Refinement of Crystal Structures.* University of Göttingen, Germany, 1993.
13. Johnson, C. K., Report ORNL-5138. Oak Ridge National Laboratory, Tennessee, U.S.A., 1978, Bruggemand, R. and Schmid, G., PC adaptation, University of Ulm, Germany, 1990.
14. Kojima, A., Okazaki, K., Ooi, S. and Saito, K. *Inorg. Chem.*, 1983, **22,** 1168.
15. Boas, L. V. and Pessoa, J. C. *Comprehensive Coordination Chemistry.* Ed. G. Wilkinson, R. D. Gillard and J. A. McCleverty, Vol. 3. Pergamon Press, London, 1987, pp. 453–569.
16. Frausto da Silva, J. J. R., Wooton, R. and Gillard, R. D. *J. Chem. Soc. (A)*, 1970, 3369.
17. Syamal, A., Carey, E. F. and Theriot, L. J. *Inorg. Chem.*, 1973, **12,** 245.

Pergamon

PII: S0277-5387(96)00374-9

Polyhedron Vol. 16, No. 7, pp. 1149–1156, 1997
Copyright © 1997 Elsevier Science Ltd
Printed in Great Britain. All rights reserved
0277-5387/97 $17.00+0.00

A structural change between the complexes of praseodymium and neodymium nitrates with (*Z*)-2,3-diphenyl-1,4,7,10,13-pentaoxacyclopentadec-2-ene(stilbeno-15-crown-5): synthesis and structures of $[Pr(NO_3)_3$ (stilbeno-15-crown-5)] and $[Nd(NO_3)_3(EO_5)]$ (EO_5 = tetraethyleneglycol)

Tongbu Lu,[a]* Liangnian Ji,[a] Minyu Tan,[b] Yu Liu[c] and Kaibei Yu[d]

[a] Department of Chemistry, Zhongshan University, Guangzhou 510275, P.R. China

[b] Department of Chemistry, Lanzhou University, Lanzhou 730000, P.R. China

[c] Department of Chemistry, Nankai University, Tianjin 310081, P.R. China

[d] Chengdu Center of Analysis and Measurement, Acdemia Sinica, Chengdu 610041, P.R. China

(Received 28 May 1996; accepted 30 July 1996)

Abstract—A structural change in $Ln(NO_3)_3 \cdot nH_2O$ complexes with stilbeno-15-crown-5 occurs between Ln = Pr and Ln = Nd. The unstable $Nd(NO_3)_3 \cdot L$ (L = stilbeno-15-crown-5) can react with formic acid to form stable $Nd(NO_3)_3 \cdot EO_5$. Under the same conditions the stable $Pr(NO_3)_3 \cdot L$ cannot be transformed into $Pr(NO_3)_3 \cdot EO_5$. X-ray crystallographic examinations of these two complexes have been carried out. There are two independent $Pr(NO_3)_3 \cdot L$ monomers in one asymmetric unit; in each the coordination number is 11. The tetraethyleneglycol ligand wraps around the neodymium(III) ion in $Nd(NO_3)_3 \cdot EO_5$ and all the three nitrate groups are bidentate. The coordination number is also 11. Copyright © 1997 Elsevier Science Ltd

Keywords: praseodymium nitrate; neodymium nitrate; stilbeno-15-crown-5; tetraethyleneglycol; synthesis; structural change.

The coordination power of the crown ethers depends on the number of donor atoms, the cavity diameter and the substituents. The crystal structures of $Ln(NO_3)_3 \cdot 12C4$ have revealed that 12-crown-4 can be coordinated directly to most of the lanthanide ions effectively, even though hydrated lanthanide nitrates are used as starting material [1,2]. 15-Crown-5, however, can only be coordinated directly to lighter lanthanide ions (La–Eu) [1], for the heavier lanthanide ions (Gd–Lu), second-sphere hydrogen-bonded complexes are obtained owing to the decreasing ionic radii [3,4]. (2-Methyl-1,3-xylyl)-15-crown-5 cannot be coordinated directly to all the lanthanide ions [1,5] due to the existence of the substituent.

Recently, we have reported the synthesis and properties of the solid complexes of stilbeno-15-crown-5 with lanthanide nitrates in anhydrous medium [6]. We found that only lighter lanthanide nitrate complexes (La–Nd) could be obtained and the yields changed from 75% for the praseodymium complex to 16% for the neodymium complex. In order to find out the reason of this change, we prepared the single crystals of these two complexes and the structural investigation shows some interesting results.

* Author to whom correspondence should be addressed.

EXPERIMENTAL

Reagents

Hydrated lanthanide nitrates were prepared by dissolving the corresponding oxides (Anala R) in 50% nitric acid. The ligand was prepared by the literature method [7]. All other chemicals were AnalaR grade. The complexes were prepared according to the method described in a previous paper [6].

Preparation

Single crystals of the praseodymium complex were obtained by dissolving the powdered solid complex in acetonitrile and leaving the solution in a desiccator over $CaCl_2$ at room temperature. After about 10 days, the crystals used for the X-ray experiment formed from the solution. Found: C, 38.7; H, 3.9; N, 7.3; Pr, 19.2%. Calc. for $C_{23}H_{27.5}PrN_{3.5}O_{14}$: C, 38.5; H, 3.8; N, 6.8; Pr, 19.6%.

Single crystals of the neodymium complex could not be obtained under the above preparation condition.

In order to obtain the single crystals of the neodymium complex, triethylorthoformate was added to the solution of $Nd(NO_3)_3 \cdot L$ in acetonitrile. The mixture was refluxed for 1 h and then filtered. The filtrate was cooled to room temperature and left in a desiccator over $CaCl_2$. After about 1 month, the crystals used for the X-ray experiment formed from the solution. Found: C, 18.7; H, 3.5; N, 7.9; Nd, 27.2%. Calc. for $C_8H_{18}NdN_3O_{14}$: C, 18.3; H, 3.4; N, 8.0; Nd, 27.5%.

We prepared the single crystals of the praseodymium complex using the same method as preparing the single crystals of the neodymium complex. The analytical data indicates that the composition of the crystals of the praseodymium complex is also $Pr(NO_3)_3 \cdot L$.

X-ray crystallography of $[Pr(NO_3)_3 \cdot L] \cdot 0.5CH_3CN$

Crystal data. $2[C_{22}H_{26}PrN_3O_{14}] \cdot CH_3CN$, $M = 1434.8$, monoclinic, space group $P2_1/a$, $a = 16.132(3)$, $b = 15.635(3)$, $c = 22.781(4)$ Å, $\beta = 94.82(1)^\circ$, $U = 5725(2)$ Å^3, $D_c = 1.66$ g cm^{-3}, $Z = 4$, $\lambda(\text{Mo-}K_\alpha) = 0.71073$ Å, $F(000) = 1968$.

Data collection. X-ray diffraction intensities were collected at 298 K from crystals of dimensions $0.28 \times 0.52 \times 0.52$ mm on an R3M/E four-circle X-ray diffractometer with graphite-monochromatized Mo-K_α radiation, using the $\theta/2\theta$ scan technique, scan rate 8° min^{-1}. Negligible change in the intensities of three standards monitored during the data collection indicated no crystal decomposition. Some 9566 independent reflections were collected in the range $2 \leqslant 2\theta \leqslant 48^\circ$ (h from 0 to 20, k from 0 to 19, l from -28 to 28). Of these, 7308 reflections with $I \geqslant 1.5\sigma(I)$ were used in the structure determination and refinement. The intensities were corrected for Lorentz–polarization effects and for empirical absorption.

Structure solution and refinement. The structure was solved by the Patterson method and subsequent difference-Fourier techniques, and refined by full-matrix least-squares methods with anisotropic thermal factors for all non-hydrogen atoms; the crown ether hydrogen atoms were placed in calculated positions. All calculations were performed by using the SHELXTL system of computer programs. The final values $R = 0.0516$ $(R = \Sigma \| F_o | - | F_c \| / \Sigma | F_o |)$, $R_w = 0.0479$ $(R_w = \Sigma \| F_o | - | F_c \| w^{1/2} / \Sigma | F_o | w^{1/2})$, with $w = [\sigma^2 | F_o | + 0.0001 | F_o |^2]^{-1} \times [1 - \exp\{-5 (\sin\theta/\lambda)\}]$ were obtained.

X-ray crystallography of $[Nd(NO_3)_3 \cdot EO_5]$

Crystal data. ($C_8H_{18}NdN_3O_{14}$, $M = 524.24$, monoclinic, space group $P2_1/n$, $a = 8.143(1)$, $b = 16.806(3)$, $c = 12.739(3)$ Å^3, $\beta = 101.01(1)^0$, U = 1711(1) Å^3, $D_c = 2.03$ g cm^{-3}, $Z = 4$, $\lambda(\text{Mo-}K_\alpha) = 0.71073$ Å, $\mu(\text{Mo-}K_\alpha) = 31.46$ cm^{-1}, $F(000) = 1028$.

Data collection. X-ray diffraction intensities were collected at 298 K from crystals of dimensions $0.20 \times 0.20 \times 0.32$ mm on an R3M/E four-circle X-ray diffractometer with graphite-monochromatized MoK_α radiation, by using the $\theta/2\theta$ scan technique, scan rate 8° min^{-1}. Negligible change in the intensities of three standards monitored during the data collection indicated no crystal decomposition. Some 2524 independent reflections were collected in the range $1 \leqslant 2\theta \leqslant 45^\circ$ (h from 0 to 9, k from 0 to 19, l from -14 to 14). Of these, 2018 reflections with $I \geqslant 1.5\sigma(I)$ were used in the structure determination and refinement. The intensities were corrected for Lorentz–polarization effects and for empirical absorption.

Structure solution and refinement. The structure solution and refinement were determined as described above for $[Pr(NO_3)_3 \cdot L] \cdot 0.5CH_3CN$. The final values $R = 0.0295$ and $R_w = 0.0248$ were obtained. The weighting scheme employed converged at $w = [\sigma^2 | F_o | + 0.0001 | F_o |^2]^{-1} \times [1 - \exp\{-5(\sin\theta/\lambda)\}]$.

RESULTS AND DISCUSSION

The selected bond lengths and bond angles for $Pr(NO_3)_3 \cdot L$ are given in Tables 1 and 2, respectively. Figure 1 shows the molecular structures of the Pr(1) and Pr(2) monomers in $Pr(NO_3)_3 \cdot L$. Figure 2 illustrates the molecular packing arrangement in the unit cell.

As with $[La(NO_3)_3 \cdot L]$ [6], the structure analysis shows there are two independent $Pr(NO_3)_3 \cdot L$ monomers in one asymmetric unit and the structures of these two monomers are similar. In each of the $Pr(NO_3)_3 \cdot L$ nonomers, the praseodymium(III) is 11-coordinated, being bonded to five crown ether oxygen atoms on one side and six oxygen atoms of three bidentate nitrate groups on the other side. The bond

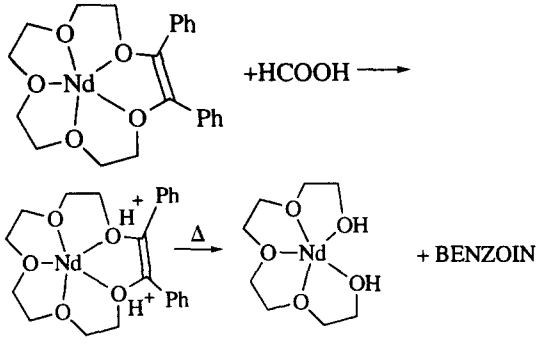
Table 1. Selected bond lengths (Å) for the Pr(1) and Pr(2) monomers

Pr(1)—O(1)	2.727(5)	Pr(2)—O(15)	2.261(4)
Pr(1)—O(2)	2.618(5)	Pr(2)—O(16)	2.583(5)
Pr(1)—O(3)	2.670(5)	Pr(2)—O(17)	2.671(6)
Pr(1)—O(4)	2.657(5)	Pr(2)—O(18)	2.698(5)
Pr(1)—O(5)	2.668(4)	Pr(2)—O(19)	2.822(5)
Pr(1)—O(6)	2.554(5)	Pr(2)—O(20)	2.544(5)
Pr(1)—O(7)	2.591(5)	Pr(2)—O(21)	2.521(5)
Pr(1)—O(9)	2.535(6)	Pr(2)—O(23)	2.602(5)
Pr(1)—O(10)	2.543(5)	Pr(2)—O(24)	2.530(6)
Pr(1)—O(12)	2.581(6)	Pr(2)—O(26)	2.515(6)
Pr(1)—O(13)	2.552(6)	Pr(1)—O(27)	2.645(6)

lengths lie in the ranges: Pr(1)—O(crown), 2.618(5)–2.727(5) [average 2.668(5)]; Pr(2)—O(crown), 2.583(5)–2.822(5) Å [average 2.679(5) Å]; Pr(1)—O(nitrate), 2.535(6)–2.591(5) [average 2.559(6) Å]; Pr(2)—O(nitrate), 2.515(6)–2.645(6) Å [average 2.556(6) Å]. From Table 1 it can be found that the Pr(1)—O(1) and Pr(2)—O(19) distances are significantly longer than other Pr—O(crown) distances. The reason is that the existence of the stibene group makes the flexibility of the crown ether become lower. The ligand is difficult to adopt to folded conformation to make O(1) and O(19) coordinate effectively to the praseodymium(III) ion. The shorter Pr(2)—O(15) and Pr(2)—O(16) distances suggested that the Pr(2) ion lies nearer the border of the crown ether than the Pr(1) ion. This arrangement makes the interaction of the Pr(1) and Pr(2) ions in the asymmetric unit decrease and the asymmetric unit becomes more stable.

Comparing the average Pr—O bond lengths with the corresponding average La—O bond lengths [6] [La(1)—O(crown) = 2.695(6), La(2)—O(crown) = 2.697(5), La(1)—O(nitrate) = 2.600(7), La(2)—O(nitrate) = 2.599(6) Å], it can be found that the Pr—O bond lengths are shorter than the La—O bond lengths due to the smaller Pr^{III} ionic radius. The decrease of Ln—O(nitrate) [La(1)—O–Pr(1)—O = 0.041 Å] is close to the expected decrease of La^{III} and Pr^{III} ionic radius [8] (0.05 Å, coordination number 11). However, the decrease of Ln—O(crown) [La(1)—O–Pr(1)—O = 0.027, La(2)—O–Pr(2)—O = 0.018 Å] is much smaller than the expected decrease of La^{III} and Pr^{III} ionic radius. This is also due to the rigidity of the stilbene group; the ligand cannot coordinate effectively to the praseodymium(III) ion. To the neodymium(III) ion with smaller ionic radius, a more folded conformation is needed in order to achieve the correct Nd—O distance. However, the more folded conformation makes the tensile force of the ligand in the complex become larger. The ligand is more difficult to be coordinated effectively to the neodymium(III) ion compared with the praseodymium(III) ion. So the neodymium complex can be obtained only with 16% yield and this complex is unstable owing to the larger tensile force in the complex. When triethylorthoformate is added to the solution of neodymium complex in acetonitrile at refluxing conditions, the following reactions occur:

$$HC(OC_2H_5)_3 + H_2O \text{ (trace in acetonitrile)} \longrightarrow HCOOH + C_2H_5OH \quad (1)$$



(2)

The stilbene group is dissociated from the crown ether by the action of acid catalyst and the flexible chain (EO_5) which can be coordinated effectively to the neodymium (III) ion is produced. $Nd(NO_3)_3 \cdot L$ is decomposed to stable $Nd(NO_3)_3 \cdot EO_5$. At the same condition, the stable $Pr(NO_3)_3 \cdot L$ complex cannot be transformed into $Pr(NO_3)_3 \cdot EO_5$. This transformation is testified by the results of elemental analysis and the crystal structure determination of neodymium complex.

Figure 3 shows the molecular structure of $Nd(NO_3)_3 \cdot EO_5$. Figure 4 illustrates the molecular packing arrangement in the unit cell. The selected bond lengths and bond angles are given in Tables 3 and 4, respectively.

As shown in Fig. 3, the 11-coordinate Nd^{3+} ion is coordinated to five oxygen atoms of EO_5 and six oxygen atoms of three bidentate nitrate groups. The five O(ligand) atoms form with one O(nitrate) [O(6)] atom a quasi regular hexagon around the metal ion in which the six O—Nd—O angles are comprised in a very small range of values (59.5–62.0°). The neodymium(III) ion and the above six oxygen atoms are coplanar. The two bidentate nitrates are coordinated axially above and below this plane, while the third nitrate is bonded to the Nd^{III} ion through the open side of the ligand chain. This coordination pattern is similar to that of $La(NO_3)_3 \cdot EO_5$ complex[9] and very different from that of another $Nd(NO_3)_3 \cdot EO_5$ complex reported by Hirashima *et al.*, in which the nitrate ion bonded through the open side of the ligand is monodentate. [10]

Five Nd—O(nitrate) distances lie in the range 2.551(4)–2.595(4) Å and average 2.620(4) Å, while the Nd—O(6) distance in which the oxygen atom is involved in the plane is considerably longer [2.859(4) Å]. A similar situation occurs for other 11-coordinate

Table 2. Selected bond angles (°) for $[Pr(NO_3)_3 \cdot L] \cdot 0.5CH_3CN$

O(1)—Pr(1)—O(2)	61.7(1)	O(1)—Pr(1)—O(3)	99.1(1)
O(2)—Pr(1)—O(3)	61.5(1)	O(1)—Pr(1)—O(4)	78.9(2)
O(2)—Pr(1)—O(4)	100.1(2)	O(3)—Pr(1)—O(4)	60.6(1)
O(1)—Pr(1)—O(5)	57.9(1)	O(2)—Pr(1)—O(5)	119.0(1)
O(3)—Pr(1)—O(5)	120.4(1)	O(4)—Pr(1)—O(5)	61.2(1)
O(1)—Pr(1)—O(6)	126.1(2)	O(2)—Pr(1)—O(6)	68.0(1)
O(3)—Pr(1)—O(6)	71.6(2)	O(4)—Pr(1)—O(6)	129.6(2)
O(5)—Pr(1)—O(6)	167.7(1)	O(1)—Pr(1)—O(7)	136.5(2)
O(2)—Pr(1)—O(7)	109.3(2)	O(3)—Pr(1)—O(7)	113.6(2)
O(4)—Pr(1)—O(7)	141.9(2)	O(5)—Pr(1)—O(7)	119.4(2)
O(6)—Pr(1)—O(7)	48.9(2)	O(1)—Pr(1)—O(9)	153.5(2)
O(2)—Pr(1)—O(9)	121.5(2)	O(3)—Pr(1)—O(9)	66.4(2)
O(4)—Pr(1)—O(9)	74.7(2)	O(5)—Pr(1)—O(9)	108.9(2)
O(6)—Pr(1)—O(9)	72.2(2)	O(7)—Pr(1)—O(9)	69.5(2)
O(1)—Pr(1)—O(10)	123.8(2)	O(2)—Pr(1)—O(10)	171.1(2)
O(3)—Pr(1)—O(10)	109.8(2)	O(4)—Pr(1)—O(10)	75.5(2)
O(5)—Pr(1)—O(10)	65.9(2)	O(6)—Pr(1)—O(10)	108.7(2)
O(7)—Pr(1)—O(10)	71.8(2)	O(9)—Pr(1)—O(10)	50.2(2)
O(1)—Pr(1)—O(12)	78.8(2)	O(2)—Pr(1)—O(12)	114.9(2)
O(3)—Pr(1)—O(12)	176.4(2)	O(4)—Pr(1)—O(12)	121.5(2)
O(5)—Pr(2)—O(12)	61.1(2)	O(6)—Pr(1)—O(12)	107.1(2)
O(7)—Pr(1)—O(12)	66.8(2)	O(9)—Pr(1)—O(12)	116.7(2)
O(10)—Pr(1)—O(12)	73.8(2)	O(1)—Pr(1)—O(13)	69.4(2)
O(2)—Pr(1)—O(13)	68.1(2)	O(3)—Pr(1)—O(13)	126.9(2)
O(4)—Pr(1)—O(13)	148.1(2)	O(5)—Pr(1)—O(13)	97.5(2)
O(6)—Pr(1)—O(13)	75.2(2)	O(7)—Pr(1)—O(13)	68.2(2)
O(9)—Pr(1)—O(13)	137.2(2)	O(10)—Pr(1)—O(13)	119.6(2)
O(12)—Pr(1)—O(13)	49.6(2)	O(15)—Pr(2)—O(16)	62.3(1)
O(15)—Pr(2)—O(17)	123.3(2)	O(16)—Pr(2)—O(17)	62.3(2)
O(15)—Pr(2)—O(18)	115.5(1)	O(16)—Pr(2)—O(18)	95.5(1)
O(17)—Pr(2)—O(18)	60.1(2)	O(15)—Pr(2)—O(19)	56.2(1)
O(16)—Pr(2)—O(19)	74.6(1)	O(17)—Pr(2)—O(19)	98.3(1)
O(18)—Pr(2)—O(19)	59.6(1)	O(15)—Pr(2)—O(20)	67.9(1)
O(16)—Pr(2)—O(20)	79.1(2)	O(17)—Pr(2)—O(20)	111.5(2)
O(18)—Pr(2)—O(20)	171.6(2)	O(19)—Pr(2)—O(20)	124.1(1)
O(15)—Pr(2)—O(21)	109.4(2)	O(16)—Pr(2)—O(21)	75.1(2)
O(17)—Pr(2)—O(21)	66.0(2)	O(18)—Pr(2)—O(21)	122.5(2)
O(19)—Pr(2)—O(21)	149.7(2)	O(20)—Pr(2)—O(21)	50.0(2)
O(15)—Pr(2)—O(23)	119.8(2)	O(16)—Pr(2)—O(23)	145.0(2)
O(17)—Pr(2)—O(23)	111.9(2)	O(18)—Pr(2)—O(23)	111.4(2)
O(19)—Pr(2)—O(23)	138.2(2)	O(20)—Pr(2)—O(23)	71.3(2)
O(21)—Pr(2)—O(23)	71.6(2)	O(15)—Pr(2)—O(24)	71.6(2)
O(18)—Pr(2)—O(24)	67.6(1)	O(19)—Pr(2)—O(24)	122.8(2)
O(20)—Pr(2)—O(24)	111.3(2)	O(21)—Pr(2)—O(24)	78.4(2)
O(23)—Pr(2)—O(24)	49.0(2)	O(15)—Pr(2)—O(26)	88.8(2)
O(16)—Pr(2)—O(26)	141.2(2)	O(17)—Pr(2)—O(26)	130.6(2)
O(18)—Pr(2)—O(26)	72.9(2)	O(19)—Pr(2)—O(26)	67.4(2)
O(20)—Pr(2)—O(26)	115.3(2)	O(21)—Pr(2)—O(26)	142.6(2)
O(23)—Pr(2)—O(26)	71.0(2)	O(24)—Pr(2)—O(26)	77.8(2)
O(15)—Pr(2)—O(27)	61.9(2)	O(16)—Pr(2)—O(27)	122.2(2)
O(17)—Pr(2)—O(27)	174.5(2)	O(18)—Pr(2)—O(27)	120.7(2)
O(19)—Pr(2)—O(27)	86.3(1)	O(20)—Pr(2)—O(27)	67.7(2)
O(21)—Pr(2)—O(27)	111.2(2)	O(23)—Pr(2)—O(27)	62.6(2)
O(24)—Pr(2)—O(27)	103.4(2)	O(26)—Pr(2)—O(27)	48.6(2)

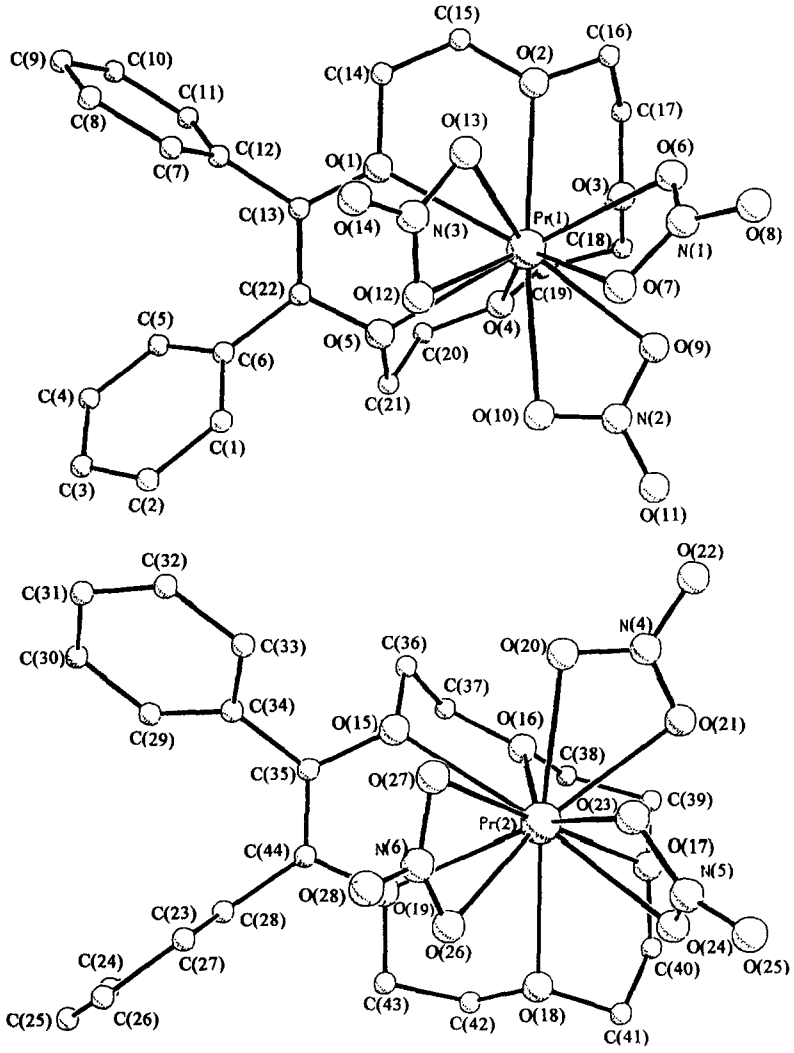


Fig. 1. The molecular structures of the two independent monomers, designated Pr(1) and Pr(2), in the asymmetric of $Pr(NO_3)_3 \cdot L$.

complexes of lanthanum(III) [6,9,11], cerium(III) [12] and europium(III) [13], in which one or two Ln—O(nitrate) bond lengths are significantly longer. The five Nd—O(ligand) distances [mean 2.620(4) Å] are of two types: the two terminal Nd—O(alcohol) distances [mean 2.537(4) Å] are significantly shorter than the three Nd—O(ether) ones [mean 2.675(4) Å]. This pattern is much different from that found in the structure of $Pr(NO_3)_3 \cdot L$, in which the Pr(1)—O(1) and Pr(2)—O(19) distances are significantly longer than other Pr—O(ether) ones.

Comparing the mean Nd—O(ligand) and Nd—O(nitrate) distances with the corresponding Ln—O distances listed in Table 5, it can be found that the mean Nd—O(ligand) of 11-coordinated $Nd(NO_3)_3 \cdot EO_5$ is the shortest in all the complexes. It is even shorter than those of 10-coordinated $Nd(NO_3)_3 \cdot EO_5$ and 11-coordinated $Eu(NO_3)_3 \cdot 15C5$. On the contrary, the mean Nd—O(nitrate) distance of 11-coordinated $Nd(NO_3)_3 \cdot EO_5$ is significantly longer than other Ln—O(nitrate) complexes. This exception indicates the property of $Nd(NO_3)_3 \cdot EO_5$ decomposed from the $Nd(NO_3)_3 \cdot L$ is much different from that prepared from the $Nd(NO_3)_3 \cdot nH_2O$ and EO_5.

Conclusions

A structural change in $Ln(NO_3)_3 \cdot nH_2O$ complexes with stilbeno-15-crown-5 occurs between Ln = Pr and Ln = Nd. With Ln = Nd the unstable $Nd(NO_3)_3 \cdot L$ tends to become stable $Nd(NO_3)_3 \cdot EO_5$ in the presence of acid catalyst (triethylorthoformate) and this transformation is due to the rigidity of the ligand and the decrease of lanthanide ionic radius. The large tensile force owing to the folded conformation of the ligand during the complexation makes the complex becomes

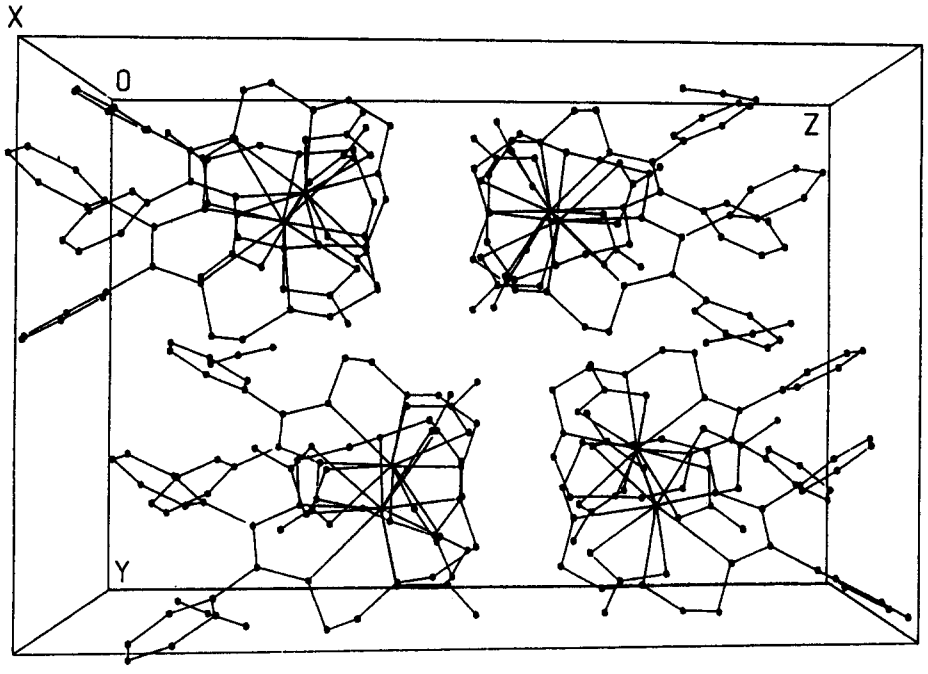


Fig. 2. The molecular packing arrangement in the unit cell for $[Pr(NO_3)_3 \cdot L] \cdot 0.5CH_3CN$.

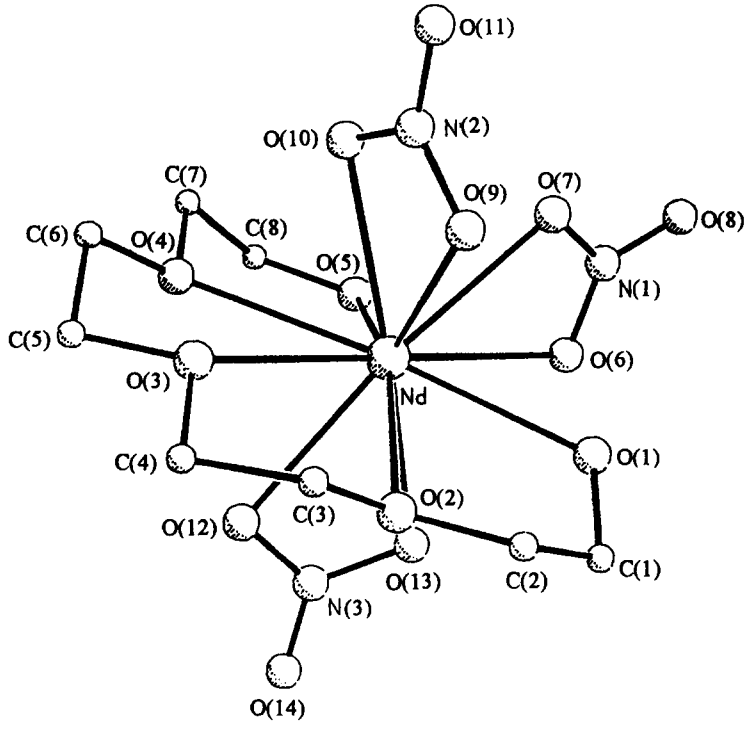


Fig. 3. The molecular structures of $Nd(NO_3)_3 \cdot EO_5$ decomposed from $Nd(NO_3)_3 \cdot L$.

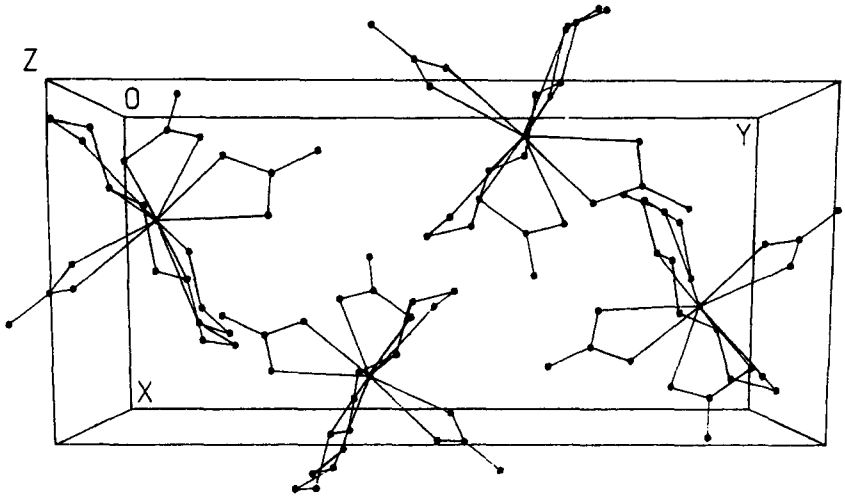


Fig. 4. The molecular packing arrangement in the unit cell for $Nd(NO_3)_3 \cdot EO_5$.

Table 3. Selected bond lengths (Å) for $[Nd(NO_3)_3 \cdot EO_5]$

Nd—O(1)	2.566(4)	Nd—O(6)	2.859(4)
Nd—O(2)	2.646(4)	Nd—O(7)	2.565(4)
Nd—O(3)	2.663(3)	Nd—O(9)	2.576(3)
Nd—O(4)	2.717(4)	Nd—O(10)	2.551(4)
Nd—O(5)	2.508(4)	Nd—O(12)	2.574(4)
		Nd—O(13)	2.595(4)

Table 4. Selected bond angles (°) for $[Nd(NO_3)_3 \cdot EO_5]$

O(1)—Nd—O(2)	62.0(1)	O(1)—Nd—O(3)	121.2(1)
O(2)—Nd—O(3)	60.6(1)	O(1)—Nd—O(4)	174.9(1)
O(2)—Nd—O(4)	117.4(1)	O(3)—Nd—O(4)	59.6(1)
O(1)—Nd—O(5)	119.2(1)	O(2)—Nd—O(5)	160.0(1)
O(3)—Nd—O(5)	119.0(1)	O(4)—Nd—O(5)	59.5(1)
O(1)—Nd—O(6)	59.7(1)	O(2)—Nd—O(6)	120.2(1)
O(3)—Nd—O(6)	179.1(1)	O(4)—Nd—O(6)	119.5(1)
O(5)—Nd—O(6)	60.1(1)	O(1)—Nd—O(7)	71.1(1)
O(2)—Nd—O(7)	121.6(1)	O(3)—Nd—O(7)	134.1(1)
O(4)—Nd—O(7)	112.2(1)	O(5)—Nd—O(7)	74.2(1)
O(6)—Nd—O(7)	46.1(1)	O(1)—Nd—O(9)	76.8(1)
O(2)—Nd—O(9)	70.7(1)	O(3)—Nd—O(9)	73.8(1)
O(4)—Nd—O(9)	107.9(1)	O(5)—Nd—O(9)	129.2(1)
O(6)—Nd—O(9)	106.8(1)	O(7)—Nd—O(9)	66.4(1)
O(1)—Nd—O(10)	120.5(1)	O(2)—Nd—O(10)	111.4(1)
O(3)—Nd—O(10)	71.8(1)	O(4)—Nd—O(10)	64.6(1)
O(5)—Nd—O(10)	85.7(1)	O(6)—Nd—O(10)	108.0(1)
O(7)—Nd—O(10)	65.4(1)	O(9)—Nd—O(10)	49.7(1)
O(1)—Nd—O(12)	106.9(1)	O(2)—Nd—O(12)	74.0(1)
O(3)—Nd—O(12)	68.0(1)	O(4)—Nd—O(12)	68.4(1)
O(5)—Nd—O(12)	87.3(1)	O(6)—Nd—O(12)	111.6(1)
O(7)—Nd—O(12)	156.2(1)	O(9)—Nd—O(12)	137.1(1)
O(10)—Nd—O(12)	129.0(1)	O(1)—Nd—O(13)	69.2(1)
O(2)—Nd—O(13)	82.5(1)	O(3)—Nd—O(13)	113.7(1)
O(4)—Nd—O(13)	105.8(1)	O(5)—Nd—O(13)	80.0(1)
O(6)—Nd—O(13)	66.2(1)	O(7)—Nd—O(13)	111.9(1)
O(9)—Nd—O(13)	143.8(1)	O(10)—Nd—O(13)	165.5(1)
O(12)—Nd—O(13)	48.9(1)		

Table 5. Some mean Ln—O distances (Å) for $Ln(NO_3)_3 \cdot L'$

L′	Ln	CN[a]	Ln—O(ligand)	Ln—O(nitrate)	Reference
EO_5	La	11	2.70(4)	2.64(8)	[9]
	Nd	10	2.65(4)	2.55(2)	[10]
	Nd	11	2.62(1)	2.62(1)	This work
15C5	Nd	11	2.65(4)	2.55(4)	[14]
	Eu	11	2.63(6)	2.53(8)	[15]
Stilbeno-15-Crown-5	La	11	2.70(1)	2.60(1)	[6]
	Pr	11	2.68(1)	2.56(1)	This work

[a] CN = coordination number.

unstable. The stilbene group is dissociated from the crown ether by the action of acid catalyst and the flexible chain (EO_5) which can be coordinated effectively to the neodymium(III) ion is produced. $Nd(NO_3)_3 \cdot L$ is transformed into stable $Nd(NO_3)_3 \cdot EO_5$ and the structure of this complex is different from that prepared from the $Nd(NO_3)_3 \cdot nH_2O$ and EO_5. At the same conditions, the stable $Pr(NO_3)_3 \cdot L$ can not be transformed into $Pr(NO_3)_3 \cdot EO_5$.

Acknowledgment—This work was supported by the Guangdong Provincial Natural Science Foundation.

REFERENCES

1. Bünzli, J.-C. G., *Handbook on the Physics and Chemistry of Rare Earths*, eds. K. A. Gschneidner and L. Eyring Jr, Vol. 9, Ch. 60. North Holland, Amsterdam, 1987, p. 362, and refs therein.
2. Rogers, R. D. and Kurihara, L. K., *Inclusion Phenom.* 1986, **4,** 351.
3. Rogers, R. D. and Kurihara, L. K., *Inorg. Chim. Acta*, 1986 **116,** 171.
4. Rogers, R. D. and Kurihara, L. K., *Inorg. Chem.* 1987, **26,** 2360.
5. Tomat, G. and Valle, G., *Inorg. Chim. Acta*, 1985, **110,** 113.
6. Lu, T. B., Tang, N., Tan, M. Y., Liu, Y., Yu, K. B., Inoue, Y. and Hakushi, T., *Aust. J. Chem*, 1993, **46,** 1817.
7. Merz, A., Eichner, M. and Tomahogh, R., *Tetrahedron Lett.* 1981, **22,** 1319.
8. Shannon, R. D., *Acta Cryst.* 1976, **32,** 751.
9. Casellato, U., Tomat, G., Bernardo, P. D. and Grazianni, R., *Inorg. Chim. Acta*, 1982, **61,** 181.
10. Hirashima, Y., Tsutsui, R. and Shiokawa, J., *Chem. Lett*, 1981, 1501.
11. Eriksson, B., Larsson, L. O., Niinisto, L. and Valkonen, J., *Inorg. Chem.* 1980, **19,** 1207.
12. Bukorwaka-strzyewska, M. and Tosik, A., *Inorg. Chim. Acta*, 1978, **30,** 189.
13. Bünzli, J.-C. G., Klein, B., Chapuis, G. and Schenk, K. J., *Inorg. Chem.* 1982, **21,** 808.

Pergamon

PII: S0277-5387(96)00373-7

Polyhedron Vol. 16, No. 7, pp. 1157–1160, 1997
Copyright © 1997 Elsevier Science Ltd
Printed in Great Britain. All rights reserved
0277-5387/97 $17.00+0.00

Influence of sodium dodecyl sulfate micelles on the kinetics of complex formation between $Pd(H_2O)_4^{2+}$ and glutathione

Mihajilo S.Tošić,[a] Vesna M. Vasić,[a] Jovan M. Nedeljković[a]* and Ljubomir A. Ilić[b]

[a]Institute of Nuclear Sciences "Vinča", P.O. Box 522, 11001 Belgrade, Yugoslavia

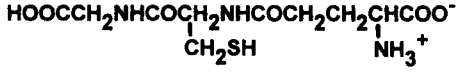
[b]Pharmaceutical and Chemical Industry "Zdravlje", 16000 Leskovac, Yugoslavia

(Received 24 May 1996; accepted 30 July 1996)

Abstract—The kinetics of the complex formation between $Pd(H_2O)_4^{2+}$ and glutathione was investigated in the presence of sodium dodecyl sulfate in the acidity range from 2 M $HClO_4$ to pH 5. Acceleration (from 2 M $HClO_4$ to pH 3.5) and retardation ($3.5 < pH < 5$) of the complex formation in the presence of anionic micelles was observed compared with the kinetic data in aqueous solution. These effects were explained by the electrostatic interaction of the reacting species with negatively charged micellar surface and their effective concentration and/or separation in the vicinity of micellar surface. Copyright © 1997 Elsevier Science Ltd

Keywords: palladium (II); glutathione; sodium dodecyl sulfate; stopped-flow; complex formation; micellar catalysis.

Glutathione (L-glutamyl-L-cysteinyl glycine, GSH) is a naturally occuring tripeptide containing a thioether group (see Scheme 1). GSH is a biological reducing agent in thiol-dependent enzyme reactions, recently reported to have anticancer activity [1].



GSH ($2.12 < pH < 3.53$)

Scheme 1.

Although complexes of Cr^{III} [2], Fe^{II} and Fe^{III} [3], and Zn^{II}, Cd^{II}, Hg^{II}, Pb^{II}, Co^{II}, Ni^{II} and Pd^{II} [4] with GSH have been synthesized and characterized, only a few studies have been published concerning the kinetics of the complex formation. So far, kinetics of the reactions of several Pt antitumor agents with GSH have been reported [5], as well as thiol exchange reaction between bis(thio)selenide of penicillamine and GSH [6].

In the present paper the influence of the anionic surfactant sodium dodecyl sulfate (SDS) on the rate of the complex formation between $Pd(H_2O)_4^{2+}$ and GSH in aqueous solution was studied. The mechanism of this reaction is already well understood in solutions containing no surfactant, in the broad acidity range from 2 M $HClO_4$ to pH 5 [7]. The effects of micellar systems on chemical reactions have been studied extensively, especially for organic reactions [8]. On the other hand, only a few studies have been done on inorganic reactions. Electron-transfer reactions involving metal complexes [9] and the complex formation of Ni^{II}, Mn^{II} and Pd^{II} with organic ligands have been investigated [10–15]. These studies are important not only from the viewpoint of inorganic reaction mechanisms, but also from biochemical aspects, i.e. as models of electron-transfer and ligand-exchange reactions on the surface of a biomembrane or at the interface of a globular protein.

EXPERIMENTAL

All reagents were commercial products of the highest purity available. The standard solution of 1×10^{-3} M $Pd(H_2O)_4^{2+}$ was prepared as described elsewhere

* Author to whom correspondence should be addressed.

[16]. The acidity of the solution was adjusted by addition of either NaOH ($2 < pH < 5$) or $HClO_4$ ($pH < 2$). The ionic strength was kept constant by the addition of $NaClO_4$ ($I = 0.1$), except for the measurements performed in concentrated perchloric acid. The acidity of the concentrated $HClO_4$ was characterized by the Hammet acidity function, H_0.

The absorption spectra were recorded on a Perkin–Elmer Lambda 5 UV–vis spectrophotometer. For the stopped-flow experiments, the universal rapid kinetic accessory HI-TECH model SFA 12 was fitted to a spectrophotometer. All the other reagents (surfactant, acid or inert salt) were added to the ligand and metal ion solutions at least 20 min prior to mixing. The kinetic experiments were performed by mixing equal volumes of GSH and $Pd(H_2O)_4^{2+}$ solutions at 25 ± 0.1°C. The rate of the complex formation was followed by monitoring the increase of the optical absorbance at 265 nm. All kinetic measurements were reproducible within the limits of error of $\pm 5\%$. The quoted values are the averages of at least five runs under identical experimental conditions.

The measurements of the relative light scattering intensity were performed using a Chomatix KMX-6 low-angle laser photometer operating at 633 nm. The optical purification of all solutions and solvent was carried out in the usual manner.

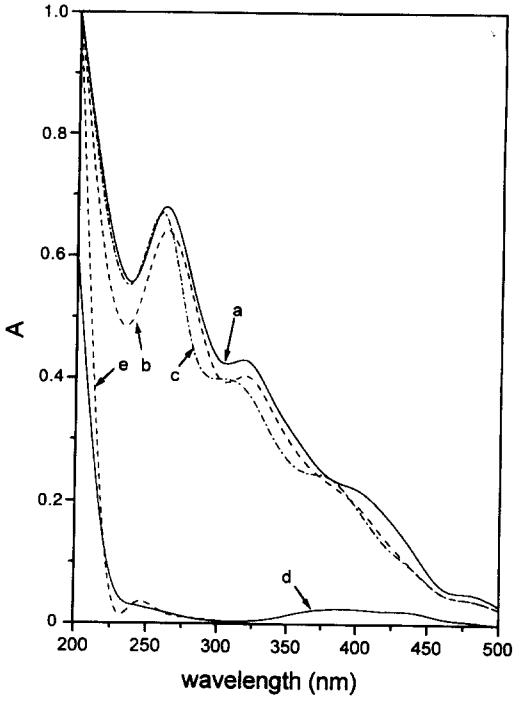


Fig. 1. Absorption spectra of solutions containing equal concentrations of $Pd(H_2O)_4^{2+}$ and GSH (2×10^{-5} M), and 1×10^{-2} M SDS at different acidities: (a) 2 M $HClO_4$; (b) pH 1; (c) pH 4.5. Absorption spectra of solutions containing (d) 2×10^{-5} M $Pd(H_2O)_4^{2+}$ and (e) 2×10^{-5} M GSH.

RESULTS AND DISCUSSION

Absorption spectra and stoichiometry of the Pd^{II}*–GSH complex in the presence of anionic micelles*

The complex formation between $Pd(H_2O)_4^{2+}$ and GSH in the presence of 1×10^{-2} M SDS was investigated in the acidity range from 2 M $HClO_4$ to pH 5. The absorption spectra of the solution containing equal concentration of $Pd(H_2O)_4^{2+}$ and GSH and 1×10^{-2} M SDS at different acidities are shown in Fig. 1. Clear isosbestic points were not observed indicating the existence of more than two absorbing species in the solution. The Pd^{II}–GSH complex in the presence of anionic micelles has the absorption maximum at 265 nm and the shoulders at 320 and 400 nm. For comparison, absorption spectra of the reacting species ($Pd(H_2O)_4^{2+}$ and GSH) are also given in Fig. 1.

The stoichiometry of the complex (Pd^{II}:GSH = 1:2) in the presence of 1×10^{-2} M SDS was determined at different acidities (2 M $HClO_4$, pH 1, 3 and 5) by continuous variation of the ratio between initial concentrations of $Pd(H_2O)_4^{2+}$ and GSH. Also, the absorption spectra at the constant $Pd(H_2O)_4^{2+}$/GSH ratio were followed as a function of the acidity. The absorption spectra indicated that the metal chelate structure was not affected by the change of acidity. The slight shift of the position of the absorption maximum is most likely due to the presence of different ionic forms of the ligand at different acidities ($pK_1 = 2.12$, $pK_2 = 3.53$) [17]. Similar effects were also noticed in the reactions of $Pd(H_2O)_4^{2+}$ and $PdCl_2$ with *S*-carboxymethyl-L-cysteine in aqueous [18] and micellar solutions [15].

The kinetics of complex formation between $Pd(H_2O)_4^{2+}$ *and GSH in the presence of SDS*

The kinetics of the complex formation between $Pd(H_2O)_4^{2+}$ and GSH in the presence of micelle forming surfactant SDS was followed in the acidity range from 2 M $HClO_4$ to pH 5. Under pseudo-first-order conditions (GSH $\gg$ Pd^{II}) the experimentally determined rate constants (k_{obs}) followed the simple rate expression:

$$k_{obs} = k_f C_{GSH} + k_r, \qquad (1)$$

where k_f and k_r are the forward and reverse pH-dependent rate constants, respectively. The collected values of k_{obs} as a function of C_{GSH} at constant acidity (see Table 1) indicated the absence of a measurable reverse reaction in the investigated range of acidity.

The pH dependence of k_f in the absence and in the presence of 1×10^{-2} M SDS is shown in Fig. 2. The presence of micelles has a two-fold effect on the rate of complex formation: (a) the complex formation is accelerated in the presence of micelles in the acidity range from 2 M $HClO_4$ to pH 3.5; (b) the complex formation is retarded in the pH range from 3.5 to

Table 1. Experimental rate constants (k_{obs}) of complex formation between GSH and $Pd(H_2O)_4^{2+}$ (2×10^{-5} M) as a function of the GSH concentration in the presence of 1×10^{-2} M SDS at different acidities

$C_{GSH} \times 10^5$	k_{obs} (s^{-1})					
pH	1	2	4	10	15	20
−0.8	0.020	0.039	0.095	0.198	0.350	0.470
1	0.030	0.050	0.114	0.280	0.400	0.540
2	0.014	0.034	0.088	0.195	0.250	0.450
3	0.015	0.034	0.078	0.175	0.210	0.390
3.5	0.015	0.028	0.070	0.150	0.205	0.320
4.5	0.0130	0.020	0.063	0.119	0.200	0.250

5, compared with the kinetic results obtained in the absence of SDS. It should be noticed that the pH value at which rates of complex formation in the absence and in the presence of SDS are equal coincide with the pK_2 of GSH.

Acceleration of the complex formation between Pd^{II} and GSH in the acidity range from 2 M $HClO_4$ to pH 3.5 can be explained as a result of the increased concentration of reagent molecules in the vicinity of the anionic micelles (see Fig. 2). The anionic micelles provide a dispersed negatively charged surface in solution. As a consequence, the positively charged $Pd(H_2O)_4^{2+}$ ions will partition out the bulk aqueous phase into the surface region of the micelles. The estimated binding constants for bivalent ions are in the range from 1.2×10^3 to 2.5×10^3 M^{-1} [19] and almost all the $Pd(H_2O)_4^{2+}$ ions are on the micellar surface. Also, the process of concentration of two times protonated (from 2 M $HClO_4$ to pH 2.12) and zwitter ion ligand species with net positive charge equal to one ($2.12 < pH < 3.53$), in the vicinity of anionic micellar surface, is an electrostatically favorable process. The net effect is an overal increase in the concentration of reacting species in the vicinity of the micellar surface and the complex formation is faster compared with the reaction in the absence of surfactant.

In the pH range from 3.5 to 5 complex formation between Pd^{II} and GSH in the presence of 1×10^{-2} M SDS was slower compared with the kinetic results in aqueous solutions (see Fig. 2). This can be explained as a consequence of the effective separation of the reacting species in the presence of anionic micelles. In this pH range both carboxylic groups of the hydrophilic ligand GSH are deprotonated and the ligand species exist as a zwitter ion with the net charge equal to zero. Although the net charge of the ligand is equal to zero in this pH range, due to the electrostatic repulsion between negatively charged micellar surface and negatively charged terminal carboxylic groups, the ligand is located solely in the bulk aqueous phase. Therefore, in the presence of anionic micelles the reacting species are effectively separated and the complex formation is slowed down. Similar effects of acceleration/retardation have been observed for the Pd^{II}/MONO-PACA [1,8-dihydroxy-2-(pyrazol-5-ylazo)naphthalene-3,6-disulfonic acid] and Pd^{II}/$SCMCH_2$ (*S*-carboxymethyl-L-cysteine) systems [14, 15].

Although the influence of SDS on the rate of complex formation between Pd^{II} and GSH is very small, the kinetic measurements can be used for the precise detection of the surfactant concentration at which the micelle formation occurs, which is generally considered to be the critical micellization concentration (CMC) of the surfactant. Typical dependencies of the rate constants (k_{obs}) on the concentration of SDS, at different acidities, are shown in Fig. 3. The increase and/or decrease of the rate constant indicates the first appearance of micelles or pre-micellar aggregates. The CMC values, at different acidities, were also determined by measuring the relative light scattering inten-

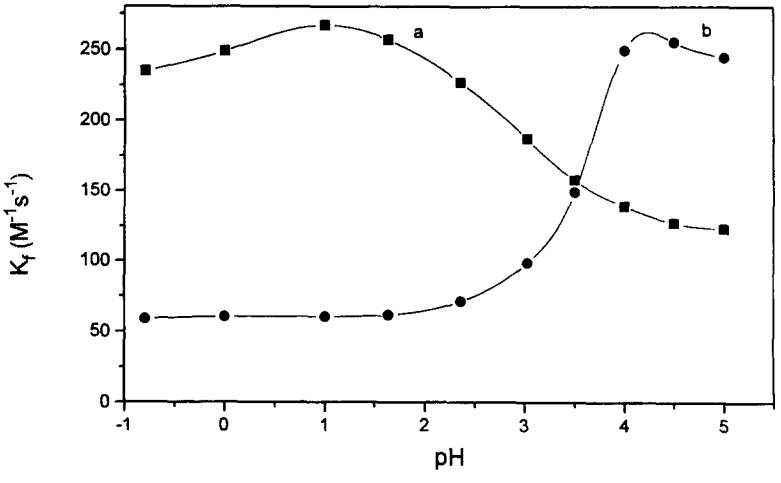


Fig. 2. pH profile of the forward rate constant (k_f) for the formation of the $Pd(H_2O)_4^{2+}$-GSH complex (a) in the presence and (b) in the absence of 1×10^{-2} M SDS at 298 K.

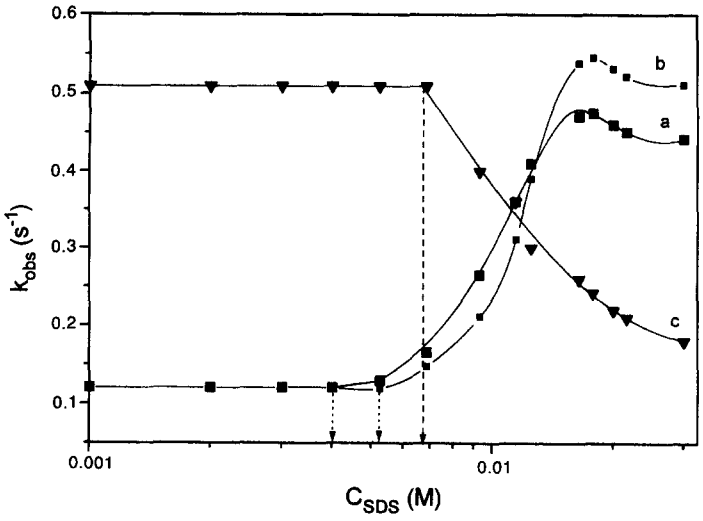


Fig. 3. Experimental rate constants (k_{obs}) of complex formation between 2×10^{-5} M $Pd(H_2O)_4^{2+}$ and 2×10^{-4} M GSH as a function of the SDS concentration at different acidities: (a) 2 M $HClO_4$; (b) pH 1; (c) pH 3; (d) pH 4.5. Temperature: 298 K.

sity as a function of the surfactant concentration. The agreement between the CMC values determined from light scattering and kinetic measurements was found. It should be noticed that the obtained CMC values (around 7×10^{-3}, 5×10^{-3} and 4×10^{-3} at pH 4.5 and 1, and in 2 M $HClO_4$, respectively) are smaller than the reported CMC value at zero ionic strength (7.75×10^{-3} M). This effect can be explained by the well-known fact that the addition of acids lowers the CMC of surfactants [20].

REFERENCES

1. Novi, A. M., *Science*, 1981, **212,** 541.
2. Abdullah, M., Barrett, J. and O'Brien, P., *J. Chem. Soc., Dalton Trans.* 1985, **10,** 2085.
3. Silver, J., Hamed, M. Y. and Morrison, I. E. G., *Inorg. Chim. Acta*, 1985, **107,** 169.
4. Mukherjee, H. G., Datta, S. K. and Shyamali, D., *J. Indian Chem. Soc.* 1986, **63,** 775.
5. Dedon, P. C. and Borch, R. F., *Biochem. Pharmacol.* 1987, **36,** 1955.
6. Nakagawa, T., Hasegawa, Y., Tanaka, H., Chikuma, M., Sakurai, H. and Nakayama, M., *Ganryu Aminosan*, 1985, **8,** 55.
7. Vasić, V. M., Tošić, M. S. and Nedeljković, J. M., to be submitted.
8. Fendler, H. J. and Fendler, E. J., *Catalysis in Micellar and Micromolecular Systems.* Plenum Press, New York, 1975.
9. Burgess, J., *Colloids and Surfaces*, 1990, **48,** 185.
10. James, A. D. and Robinson, B. H., *J. Chem. Soc., Faraday Trans.* 1 1978, **74,** 10.
11. Holzworth, J., Knoche, W. and Robinson, B. H., *Ber. Bunsen-Ges. Phys. Chem.* 1978, **82,** 1001.
12. Reinsborough, V. C. and Robinson, B. H., *J. Chem. Soc., Faraday Trans.* 1 1979, **75,** 2395.
13. Ficher, M., Knoche, W., Flecher, P. D. I. and Robsinon, B. H., *Colloid Polymer Sci.* 1980, **258,** 733.
14. Vasić, V. M. and Nedeljković, J. M., *J. Serb. Chem. Soc.* 1994, **54,** 157.
15. Vasić, V. M., Tošić, M. S. and Nedeljković, J. M., *J. Phys. Org. Chem.*, 1996, **9,** 398.
16. Vasić, V. M. and Muk, A. A., *Polyhedron*, 1992, **11,** 1597.
17. Edsall, D. V. and Wyman, J. M., *Biophysical Chemistry.* Academic Press, New York, 1958.
18. Nedeljković, J. M., Vasić, V. M., Vuković, V. V. and Jovanović, T. S., *J. Pharm. Biomed. Analysis*, 1995, **13,** 471.
19. Pellizzetti, E. and Pramuro, E., *Inorg. Chem.* 1980, **19,** 1407.
20. Perez-Benito, E. and Rodenas, E., *J. Colloid Interface Sci.* 1990, **139,** 87.

Pergamon

PII: S0277-5387(96)00369-5

Polyhedron Vol. 16, No. 7, pp. 1161–1167, 1997
Copyright © 1997 Elsevier Science Ltd
Printed in Great Britain. All rights reserved
0277-5387/97 $17.00+0.00

Vibrational spectra of solid, molten and matrix isolated antimony tribromide, $SbBr_3$

Aharon Loewenschuss,[a] Nicola-Irina Gerull,[b] Susanne Angermann[b] and Wolfgang Brockner[b]*

[a] Department of Inorganic and Analytical Chemistry, The Hebrew University of Jerusalem, Jerusalem 91904, Israel

[b] Institut für Anorganische und Analytische Chemie, Technische Universität Clausthal, D-38670 Clausthal-Zellerfeld, Germany

(Received 25 April 1996; accepted 30 July 1996)

Abstract—The condensed phase and matrix isolation IR and Raman spectra of antimony tribromide are reported. The solid-state spectrum comprises bands assignable to both molecular $SbBr_3$ and ionic $SbBr_6^-$ species. The frequency shifts and mode sequence in the melt spectrum indicate strong dipole–dipole interactions. The matrix isolation spectra show bands of monomeric $SbBr_3$ and of its centrosymmetric dimer, but no features of cooperative interactions. A "bond fluctuation" explanation, previously forwarded for antimony trichloride, is considered to be further substantiated by the present findings. Copyright © 1997 Elsevier Science Ltd

Keywords: $SbBr_3$; Raman; FIR/IR; matrix isolation; bond fluctuation; melt.

In a recent Raman spectroscopic investigation [1] of crystalline antimony trichloride the observed spectra were interpreted in terms of a "bond fluctuation", indicating a transition between the molecular and ionic forms, formally described by

$$2SbCl_3 \rightleftharpoons Sb^+ + SbCl_6^-.$$

This suggestion was based upon the fact that the number of the observed bands exceeded that expected for the monomeric molecular $SbCl_3$ and on coincidences of the recorded bands with modes of the ionic $SbCl_6^-$ species.

The phenomenon of molecular to ionic transition in the solid state is far less common than the parallel heterolytic dissociation of molecules to ions in polar solvents. In the absence of host environmental stabilization of the ionic products, the molecular to ionic transformation must then be interpreted in terms of a change in charge distribution, either intramolecularly or, more likely, intermolecularly, made feasible by bulk stabilization. Studies on the transition of molecular dinitrogen tetroxide to ionic nitrosonium nitrates investigated the intermolecularity, temperature and order/disorder dependence of the process in thin cryogenically deposited films [2]. Another well investigated system, showing both ionic and molecular solid forms, is phosphorus pentachloride [3], which can be deposited as either molecular PCl_5 or ionic $PCl_4^+ + PCl_6^-$.

The purpose of the present investigation is to study the vibrational spectrum of solid antimony tribromide in the solid [4–6] in comparison with that of the melt and of its matrix isolated species, to establish band assignments and to learn whether a molecular to ionic transition may also be proposed for this substance.

EXPERIMENTAL

Antimony tribromide used was prepared by synthesis from the elements with the bromine dissolved in CS_2 [7]. The crude product was refined by repeated distillations over metallic antimony and collected directly into glass tubes, which were then sealed. Inert gas techniques were used to avoid contamination and to exclude moisture and oxygen. Purity was checked thermo-analytically by establishing the melting point to be 96°C, in accordance with the literature value [7].

* Author to whom correspondence should be addressed.

Room-temperature Raman spectra, excited by a Spectra Physics model 165 krypton ion laser, were recorded on a Coderg PH1 spectrometer. The Raman scattering was observed perpendicular to the incident beam. The spectrometer and modified sample compartment were described previously [8,9]. Low-temperature and matrix isolation Raman spectra were excited by either krypton ion or argon ion Spectra Physics model 164/5 lasers and recorded on a Spex 1401 double monochromator equipped with a Third Monochromator (TTM) filter in tandem to reduce scattered light. Samples were produced by co-deposition of vapor and rare gas beams onto a gold plated oxygen-free copper (OFHC) plate cooled by closed cycle Air Products CS202A helium refrigerator.

Low-temperature infrared and matrix isolation IR spectra were recorded on a Bruker 113v FT-IR spectrometer using the helium refrigerator and the reflection–absorption method. Far-IR (FIR) room-temperature spectra were obtained from $SbBr_3$/paraffin oil grindings on a modified Beckman FS interferometer interfaced to a Kontron KAP 1000 computer.

RESULTS

The vibrational spectra of crystalline and molten antimony tribromide are shown in Figs 1 and 2, respectively, and those of matrix isolated $SbBr_3$ in Figs 3 and 4. Table 1 summarizes the observed Raman and FIR frequencies of solid antimony tribromide with their proposed assignment in comparison to literature data. The Raman frequencies of molten $SbBr_3$ are given in Table 2, the FIR frequencies of the matrix isolated $SbBr_3$ species in Table 3 and the matrix isolation Raman frequencies in Table 4.

DISCUSSION

Crystalline antimony tribromide

In crystalline antimony tribromide (α-$SbBr_3$, $P2_12_12_1$, $Z = 4$; β-$SbBr_3$, *Pnma*, $Z = 4$) [11], pyramidal $SbBr_3$ molecules of C_{3v} symmetry are stacked one on top of the other. Therefore, an $SbBr_3$ molecule vibrational spectrum may be expected. Such a spectrum is indeed observed for gaseous and dissolved antimony tribromide [4,10], but the observed condensed state spectra show additional bands as listed in Tables 1 and 2. The assignments of the fundamentals of crystalline antimony tribromide cannot, therefore, be based on distinct $SbBr_3$ molecules only. The spectrum of crystalline antimony tribromide is analogous to that of antimony trichloride and will be interpreted in similar terms.

The interpretation of the solid-state $SbBr_3$ spectrum may be approached from the crystal field, ionic and "bond fluctuation" points of view.

As pointed out for crystalline $SbCl_3$ [1], which is isotypic to $SbBr_3$ [11], site or factor group splitting could not provide a satisfactory interpretation for the observed spectra. Therefore, these same arguments should be valid for crystalline antimony tribromide and its vibrational spectrum.

An ionic interpretation would involve a process of auto-dissociation to form distinct cations and anions. Such ions are encountered in the formation of PCl_4^+ and PCl_6^- in phosphorus pentachloride [3,12] or in the transition of dinitrogen tetroxide into nitrosonium NO^+ and nitrate NO_3^- ions [2]. In the present case, no bands assignable to either $SbBr_2^+$ or $SbBr^{2+}$ have been observed, nor has there been spectral evidence for the existence of the known bromoantimonate(III)

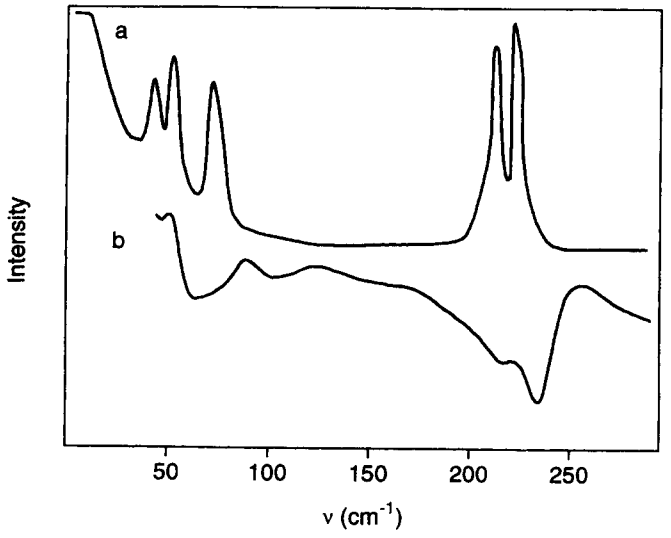


Fig. 1. (a) Raman and (b) FIR spectra of crystalline antimony tribromide recorded at room temperature.

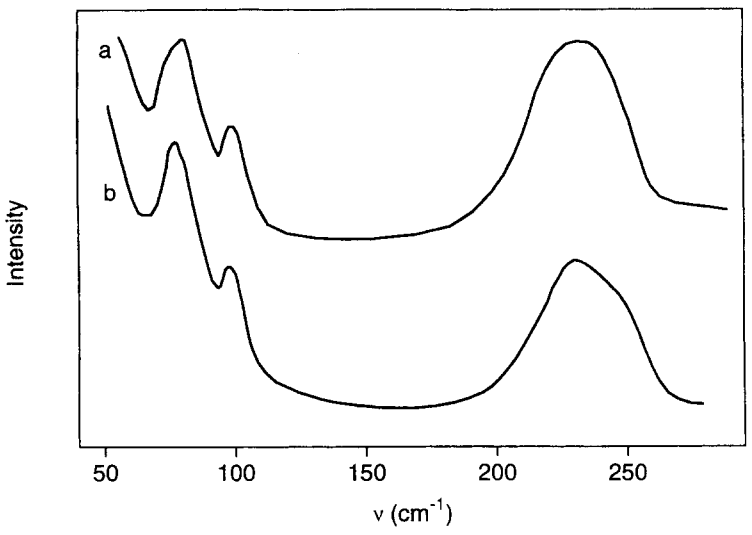


Fig. 2. (a) Raman spectrum of molten $SbBr_3$ ($T = 120$ C) with (b) polarization measurement.

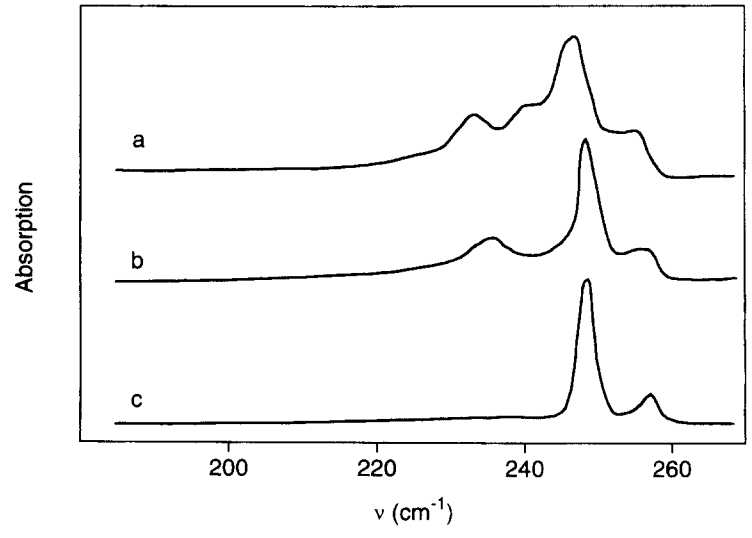


Fig. 3. Matrix isolation FIR spectra ($T = 10$ K) of (a) $SbBr_3$; (b) $SbBr_3$: Krypton = 1 : 10; (c) $SbBr_3$: Krypton = 1 : 100.

anions $SbBr_5^{2-}$, $SbBr_6^{3-}$, $Sb_2Br_7^-$ and $Sb_2Br_9^{3-}$ [6,13–20].

Only the "bond fluctuation" approach, involving an intermolecular charge delocalization and a transient existence of Sb^I and Sb^VBr_6 units in the lattice, may then provide a suitable interpretation of the spectrum, involving molecular $SbBr_3$ and ionic $SbBr_6^-$ species. The case for terming the phenomenon as "bond fluctuation" is even stronger for $SbBr_3$ than for $SbCl_3$. The vibrational modes of octahedral $SbBr_6^-$ ions [16,21,22] are not seen in the spectrum, in contrast to $SbCl_6^-$ modes in solid $SbCl_3$, which were observed in the spectrum of the solid [1]. In considering the $SbBr_3$ crystal structure (Fig. 5), a prismatic coordination of Sb is present in both the α- and β-modifications. Such a prismatic unit might be involved in a "bond fluctuation" in accordance with a formal equilibrium

$$2SbBr_3 \rightleftharpoons Sb^+ + SbBr_6^- \quad \text{(prism)}.$$

Such an $SbBr_6^-$ prism, of D_{3h} symmetry, existing due to this equilibrium, spans the following vibrational fundamentals [22]

$$\Gamma_{vib}(SbBr_6^- \text{ prism}/D_{3h}) = 2A_1'(R) + 3E'(R, IR) + A_1'' + 2A_2''(IR) + 2E''(IR),$$

with $A_1' + E' + A_2'' + E''$ being mostly stretching modes and $A_1' + 2E' + A_2'' + E''$, which are mostly bending frequencies. The assignment of the spectrum bands of crystalline antimony tribromide in Fig. 1, as given

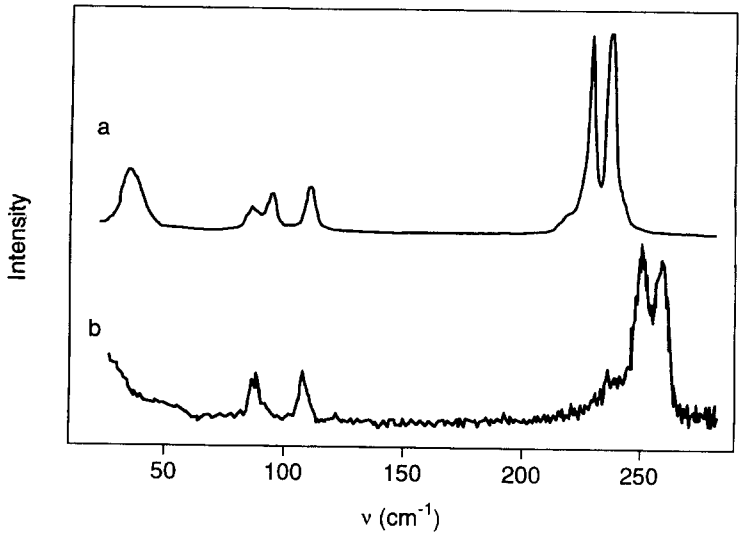


Fig. 4. Matrix isolation Raman spectra (T = 20 K) of (a) $SbBr_3$ and (b) $SbBr_3$: Krypton ≅ 1 : 10.

Table 1. Vibrational frequencies (cm^{-1}) with estimated intensities of crystalline antimony tribromide along with the proposed assignment (C_{3v}: $SbBr_3$ molecule; D_{3h}: prismatic units fixed in the lattice) and literature data for comparison

Raman [4][a]	Raman [5][a]	FIR [5]	Raman 20°C	Raman 20 K	FIR	Assignment C_{3v}	Assignment D_{3h}
					79w	ν_4(E)	
	89vw,sh						
86m	92w-m		82m	83.1	82vw		ν_7(E′)
94m-s	98m-s		95s	91.3	97s	ν_2(A_1)	
110m	113s		107s	107.6	108vw,sh		ν_2(A_1')
					130w-m		ν_5(A_2'')
			215w,sh	217.6sh	213vw,sh	ν_3(E)	
	223vw		222vw,sh				ν_9(E″)
230vs	229vs	228	226vs	227.3	226s	ν_1(A_1)	
238vs	234vs		234vs	235.5			ν_1(A_1')
243vw,sh	243vw,sh	242	242vw,sh	243sh	245vs		ν_6(E′)
	246	255					
		280-290					

[a] Estimated intensity. s = strong, m = medium, w = weak, v = very, sh = shoulder.

Table 2. Raman frequencies (cm^{-1}) of molten $SbBr_3$ with polarization data and estimated intensities along with the assignment (C_{3v}) in comparison to literature data

Raman [4][a] Melt, 100°C	Raman [10] Vapor phase	Raman Melt, 120°C	Assignment (C_{3v})
86s	76.2	76s,dp	ν_4(E)
105m	101.2	99m,p	ν_2(A_1)
	256.0	~224vs,p	ν_1(A_1)
~240vs,vbr			
	248.9	~243s,dp	ν_3(E)

[a] Estimated intensities. s = strong, m = medium, w = weak, v = very, br = broad, p = polarized, dp = depolarized.

Table 3. FIR frequencies (cm^{-1}) of matrix isolated $SbBr_3$ with estimated intensities and proposed assignment

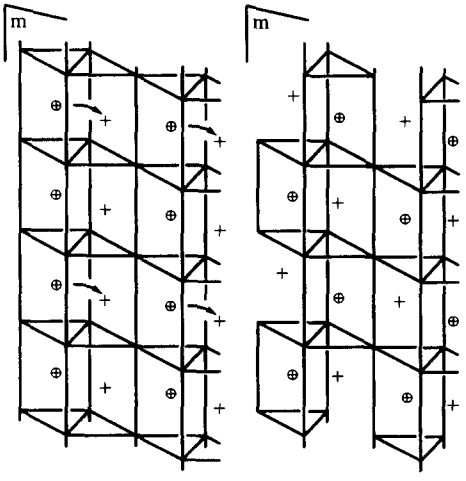
Matrix isolation-FIR/10 K			
$SbBr_3$[a]	$SbBr_3$: Kr = 1 : 10	$SbBr_3$: Kr = 1 : 100	Assignment
225w			$A_u(C_{2h})$
234m	234vw,sh		$B_u(C_{2h})$ with isotopic splitting
236vw,sh	236w-m		
241w,sh			$A_u(C_{2h})$
247vs	248vs	248vs	$E(C_{3v})$
252m			$B_u(C_{2h})$ with isotopic splitting
	255vw	254vw	
254vw,sh			
255w-m	257w-m	257m	$A_1(C_{3v})$

[a] Slow deposition.

Table 4. Raman frequencies (cm^{-1}) of matrix isolated $SbBr_3$ with estimated intensities and proposed assignment

Matrix isolation Raman/20 K[a] $SbBr_3$: Kr ≅ 1 : 10	Assignment (C_{3v})
80.2m	$\nu_4(E)$
100.2m	$\nu_2(A_1)$
231.6w	dimer/Ag stretch
246.1 vs	$\nu_1(A_1)$
254.8s-vs	$\nu_3(E)$

[a] Estimated intensities.



⊕ Site
\+ Unoccupied site
m Mirror plane

Fig. 5. Sections of the antimony tribromide crystal structure showing infinite chains in α-$SbBr_3$ (right) and β-$SbBr_3$ (left) [11].

in Table 1, is then based on a superposition of the vibrational modes of $SbBr_3$ molecules and $SbBr_6^-$ prisms.

The interpretation of the solid-state $SbBr_3$ vibrational spectrum, suggested here, involving the "bond fluctuation" approach is consistent with the spectral observation. Further substantiation of this interpretation may be expected from high-pressure low-temperature investigations.

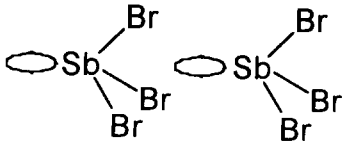
Molten antimony tribromide

The physical properties of $SbBr_3$ [23] favor a molecular melt with relatively strong intermolecular interactions. The Raman spectrum (Fig. 2, Table 2) of the antimony tribromide melt indeed exhibits no features indicating the existence of ionic species. Pyramidal $SbBr_3$ molecules, being of C_{3v} symmetry, span the vibrational modes [22]

$$\Gamma_{vib}(SbBr_3, C_{3v}) = 2A_1(R, IR) + 2E(R, IR),$$

with $A_1 + E$ contributions from both stretching and bending internal coordinates. Comparing the melt Raman spectrum with that of antimony tribromide in the gas phase or in solution, where the existence of isolated $SbBr_3$ molecules was confirmed [4,10], one notices a marked red shift of the stretching mode frequencies and a reversal in their order—$\nu_3(E) > \nu_1(A_1)$ for the melt compared with a $\nu_1(A_1) > \nu_3(E)$ sequence for isolated molecules. The fact that this reversal is observed in the melt, but in the more densely packed solid, where intermolecular interactions may be expected to be more evident, the normal sequence is retained, is taken as additional support for the interpretation of the spectrum of the latter, which is based on the existence of separated $SbBr_3$ entities.

The strong temperature dependence of the melt frequency values (Table 2) is indicative of a decrease in intermolecular dipole–dipole interactions with temperature increase. Due to these interactions the melt may be considered to be composed of aggregates, illustrated for the simplest case of two molecules as:



For such an arrangement, the repulsion between the bromide ion electron pairs with the Sb lone pair would cause an increase of the bond–bond angle in the melt and be responsible for the change of frequency sequence, discussed above, by bringing it closer to that of planar C_{3v} molecules and the frequency sequence characterizing them [24].

In this conjecture it is also instructive to compare the frequency sequences of antimony tribromide with those of other molecules of C_{3v} symmetry: NH_3 and PCl_3 present cases of $\nu_1(A_1) > \nu_3(E)$ and $\nu_3(E) > \nu_1(A_1)$, respectively [10,22,25], and in both the transition to condensed phase is accompanied with a red shift in frequencies. However, in both this shift is considerably larger for the E stretching mode than for the A_1 stretch. In PCl_3 $\Delta\nu_3(E)$ gas/liquid = 20 cm^{-1}, whereas $\Delta\nu_1(A_1) = 4$ cm^{-1}. In contrast, for $SbBr_3$ the corresponding values found are $\Delta\nu_3(E)$ gas/melt = 6 cm^{-1} and $\Delta\nu_1(A_1) = 32\,cm^{-1}$. It is reasonable that for molecular arrangement similar to that suggested, the concerted motion in the symmetric mode will be the more affected ones. As pointed out in the previous section, such an arrangement, promoting cooperative concerted vibrational motions, is also the basis for the assumption of the "bond fluctuation" stipulated there.

Matrix isolated antimony tribromide

The "bond fluctuation" model proposed above to explain the coexistence of molecular and ionic forms in a solid formed from a clearly molecular vapor relies on strong intermolecular interactions between the $SbBr_3$ species in condensed phase antimony tribromide. The major aim in studying the matrix isolation spectra of $SbBr_3$ species is then to corroborate this claim by recording spectra in a phase which, although condensed, provides for the separation of the molecules of interest. The nature of the molecular to ionic transition in thin films of dinitrogen tetroxide was established to be intermolecular on the basis of similar experiments [26].

In comparing the 20 K Raman spectra of matrix isolated $SbBr_3$ with that of solid antimony tribromide at the same temperature, it becomes immediately obvious that the 91.3 cm^{-1} band of the solid has no corresponding feature in the matrix isolation spectrum. However, this band does have its analog in the 170 cm^{-1} Raman band of solid antimony trichloride [1].

The matrix isolation IR and Raman spectra of antimony tribromide comprise more bands than expected for isolated monomeric $SbBr_3$ species. The assignment of the monomer bands in Tables 3 and 4 follows the accepted assignment for the gaseous molecule [10]. The existence of dimeric species of bridged structure in dihalide and trihalide matrix isolation spectra is well established and dimeric antimony bromide species would be the first to form along the monomers. The suggested assignment of the nonmonomeric bands is to these species. Three possible structures for the dimer are (Fig. 6)

(a) An Al_2Cl_6 analogous structure without any sterical activity of the lone pairs (D_{2h} symmetry), the vibrational modes spanning the symmetry species

$$\Gamma_{vib}(Sb_2Br_6/D_{2h}) = 4A_g(R) + 2B_{1g}(R) + 2B_{2g}(R) + B_{3g}(R) + A_{1u} + 3B_{1u}(IR) + 2B_{2u}(IR) + 3B_{3u}(IR)$$

with $A_g + B_{1g} + B_{2u} + B_{3u}$ contributions of the terminal bond stretches and $A_g + B_{2g} + B_{1u} + B_{3u}$ contributions of the bridging bond stretches.

(b) A *cis*-arrangement of the lone pairs (C_{2v} symmetry), the vibrational modes spanning the symmetry species

$$\Gamma_{vib}(Sb_2Br_6/C_{2v}) = 6A_1(R, IR) + 4A_2(R) + 4B_1(R, IR) + 4B_2(R, IR)$$

with $A_1 + A_2 + B_1 + B_2$ contributions from both the terminal and bridging stretches.

(c) A *trans*-arrangement of the lone pairs (C_{2h} symmetry), the vibrational modes spanning the symmetry species

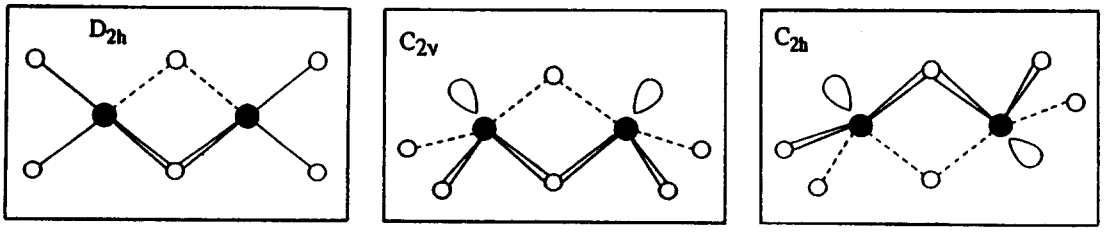


Fig. 6. Structures of Sb_2Br_6 species; (a) Al_2Cl_6 analog (D_{2h}), (b) *cis*-lone pair arrangement (C_{2v}), and (c) *trans*-lone pair arrangement (C_{2h}).

$$\Gamma_{vib}(Sb_2Br_6/C_{2h}) = 5A_g(R) + 4B_g(R) + 4A_u(IR) + 5B_u(IR)$$

with $A_g + B_g + A_u + B_u$ contributions from both the terminal and bridging stretches.

In $SbBr_3$ matrix isolation Raman spectrum only one weak sharp band at 231.6 cm^{-1} is discernible on top of a much broader feature, which is most probably due to the symmetric stretching mode of the outer nonbridging Sb—Br bonds. The fact that this band does not coincide with any of the observed IR bands confirms that the dimer is of centrosymmetric symmetry. Based on the stereochemical activity of the Sb^{III} lone pairs and their preferred *trans*-positions in Sb^{III} halogenocomplexes [27], it is concluded that the *trans*-Sb_2Br_6 species with C_{2h} symmetry is more likely. The broader background is caused by higher oligomeric and polymeric species, present in the matrix due to the experimental necessity to resort to higher concentration of guest molecules matrix isolation Raman experiments as compared to analogous IR investigation. While this preference of C_{2h} over a C_{2v} symmetry for these species cannot be considered to be fully conclusive, it would be compatible with the intermolecular interactions suggested here for the neat condensed phases. The other assignments, forwarded in Tables 3 and 4, are then in accordance with a C_{3v} symmetry of the monomer and the C_{2h} structure for the dimer.

CONCLUSIONS

We have reported the condensed phase and matrix isolation IR and Raman spectra of antimony tribromide. The solid-state spectrum exhibits both ionic and molecular features attributed to a "bond fluctuation". The strong intermolecular interactions evidenced by the frequency shifts and mode sequence in the spectrum of the melt are considered to be in support of this assumption. Additional support is found in the matrix isolation spectra where the bands due to cooperative interactions are absent, but features due to a centrosymmetric bridged dimer may be found.

Acknowledgment—Financial support by Niedersächsisches Ministerium für Wissenschaft und Kultur is gratefully acknowledged. We thank Dr A. Givan and Dr G. Blumberg for help with the low-temperature experiments.

REFERENCES

1. Friedewold, H. and Brockner, W., *Z. Naturforsch.* 1991, **46a,** 595, and refs therein.
2. Givan, A. and Loewenschuss, A., *J. Chem. Phys.* 1991, **94,** 7562, and refs therein.
3. Finch, A., Gates, P. N. and Muir, A. S., *J. Chem. Soc., Chem. Commun.* 1981, 812.
4. Evans, J. C., *J. Mol. Spectrosc.* 1960, **4,** 435.
5. Chemouni, E., *J. Inorg. Nucl. Chem.* 1971, **33,** 2317.
6. Angermann, S., Ph.D. thesis, Technical University Clausthal, 1993.
7. Brauer, G., *Handbuch der Präparativen Anorganischen Chemie*, Vol. 1, Enke Verlag, Stuttgart, 1975, p. 591.
8. Bues, W., Brockner, W. and Grünewald, D., *Spectrochim. Acta*, 1972, **28A,** 1519.
9. Øye, H. A. and Bues, W., *Inorg. Nucl. Chem. Lett.* 1972, **8,** 31.
10. Clark, R. J. H. and Rippon, D. M., *J. Mol. Spectrosc.* 1974, **52,** 58.
11. Galy, J. and Enjalbert, R., *J. Solid State Chem.* 1982, **44,** 1.
12. Wells, A. F., *Structural Inorganic Chemistry*, 5th edn. Clarendon Press, Oxford, 1984, p. 851.
13. Donaldson, J. D., Tricker, M. J. and Dale, B. W., *J. Chem. Soc.* 1972, 893.
14. Ahlijah, G. Y. and Goldstein, M., *J. Chem. Soc. (A)*, 1970, 326.
15. Cariati, F., Panzanelli, A., Antolini, L., Menabue, L., Pellacani, G. C. and Marcotrigiano, G., *J. Chem. Soc., Dalton Trans.* 1981, 909.
16. Adams, C. J. and Downs, A. J., *Chem. Commun.* 1970, 1699.
17. Allenand, G. C. and McKeeking, R. F., *Inorg. Chim. Acta*, 1977, **23,** 185.
18. Clark, R. J. H. and Trumble, W. R., *J. Chem. Soc., Dalton Trans.* 1976, 1145.
19. Robin, M. B. and Day, P., *Adv. Inorg. Chem. Radiochem.* 1975, 382.
20. Gerull, N.-I., Diploma work. Technical University Clausthal, Clausthal-Zellerfeld, Germany, 1992.
21. Adams, C. J. and Downs, A. J., *J. Inorg. Nucl. Chem.* 1972, **34,** 1829.
22. Weidlein, J., Müller, U. and Dehnicke, K., *Schwingunsspektroskopie*, Thieme, Stuttgart-New York, 1982; Wilson, E. B., Decius, J. C. and Cross, P. C., *Molecular Vibrations*. McGraw Hill Book Co., New York–Toronto–London, 1955.
23. D'Ans/Lax, *Taschenbuch für Chemiker und Physiker*, ed. E. Lax and C. Synowietz, 3. Aufl., Bd. 1. Springer-Verlag, Berlin–Heidelberg–New York, 1967.
24. Herzberg, G., *Molecular Spectra and Molecular Structure*; *Bd. II*: *Infrared and Raman Spectra of Polyatomic Molecules*. Van Nostrand Reinhold Co., New York–Toronto–London–Melbourne 1945.
25. Siebert, H., *Anwendungen der Schwingungsspektroskopie in der Anorganischen Chemie*. Springer-Verlag, Berlin–Heidelberg–New York 1966.
26. Givan, A. and Loewenschuss, A., *J. Chem. Phys.* 1989, **91,** 5126.
27. Greenwood, N. N. and Earnshaw, E., *Chemie der Elemente*. VCH, Weinheim, 1988.

Pergamon

PII: S0277-5387(96)00368-3

Polyhedron Vol. 16, No. 7, pp. 1169–1176, 1997
Copyright © 1997 Elsevier Science Ltd
Printed in Great Britain. All rights reserved
0277-5387/97 $17.00 + 0.00

Reactions of rhodium and iridium salts with multidentate *N*-heterocycles

V. Gayathri, E. G. Leelamani, N. M. N. Gowda* and G. K. N. Reddy

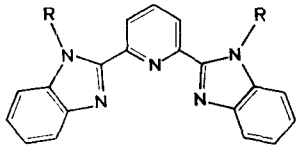
Department of Chemistry, Central College Campus, Bangalore University, Bangalore 560 001, India

(Received 23 February 1996; accepted 30 July 1996)

Abstract—Complexes of rhodium and iridium of the types MX_3L, $MX(CO)_2L$ and $MX_3(CO)L$ (X = halide) containing multidentate *N*-heterocycles (L), 2,6-bis(benzimidazolyl)pyridine ($bBzlH_2py$) and 2,6-bis(*N*-methylbenzimidazolyl)pyridine ($bBzlMe_2py$) have been prepared and characterized by IR, electronic and ^1H and ^{13}C NMR spectral data. $RhX(CO)_2L$, on treatment with alcoholic solvents or DMF undergoes reversible decarbonylation to produce $RhXL \cdot 2H_2O$. Passage of NO or O_2 through the carbonyl suspended in hot 2-methoxyethanol releases CO_2. Copyright © 1997 Elsevier Science Ltd

Keywords: rhodium; iridium; multidentate *N*-heterocycles; carbon monoxide; 2,6-bis(benzimidazolyl) pyridine; 2,6-bis(*N*-methylbenzimidazolyl)pyridine.

Development of new multidentate *N*-heterocycles, which produce organised supramolecules upon coordination to metal ions is of interest in the recent past [1]. They are quite promising in the design of stable light conversion devices and in the production of triple stranded helicates [2]. Further a wide variety of complexes associated with *N*-donor ligands are being actively considered for their catalytic activity [3]. We have been investigating metal complexes containing *N*-heterocycles as they are of potential relevance in such studies. Here, we describe the syntheses and characterization of complexes of rhodium and iridium containing polydentate benzimidazole derivatives (**I**), 2,6-bis(benzimidazolyl/*N*-methylbenzimidazolyl) pyridine ($bBzlH_2py$/$bBzlMe_2py$).



I

R	L
H	$bBzlH_2py$
CH_3	$bBzlMe_2py$

* Author to whom correspondence should be addressed.

EXPERIMENTAL

Hydrated rhodium trichloride and sodium hexahaloiridates were obtained from Arora Matthey, India and Johnson Matthey, England. Hydrated rhodium tribromide and rhodium(III) perchlorate were prepared as described elsewhere [4]. Polydentate *N*-heterocycles-2,6-bis(benzimidazolyl)pyridine and its *N*-methylated derivative were prepared according to literature methods [5–7]. The IR (nujol mull and KBr) and electronic (Nujol mull and DMF solution) spectra were recorded on Carl–Zeiss SPECORD 75-IR and Hitachi 150-20 spectrophotometers, respectively. The ^1H and ^{13}C NMR spectra in DMSO-d_6 were recorded at ambient temperatures on Bruker 270 and 400 MHz spectrometers with TMS as the internal reference. Conductivity measurements were carried out using a Toshniwal conductivity bridge type CL 01.02.

Preparation of the complexes

$RhX_3(bBzlH_2py/bBzlMe_2py)$ (X = Cl, Br *or* I). An ethanolic solution (10 cm^3) of rhodium trichloride/bromide (1 mmol) was treated with the *N*-heterocycle (1 mmol) dissolved in ethanol (10 cm^3) and the mixture was refluxed on a steam bath for 4 h during which yellow or orange solid separated. It was washed with alcohol and dried *in vacuo*.

Metathesis reaction of the chloro complex in ethanol with 15-fold excess of sodium iodide gave the iodo complex as a brown solid. Yield: 80–90%.

$[Rh(bBzlH_2py)_2(OClO_3)](ClO_4)_2$ *and* $[Rh(bBzlMe_2py)](ClO_4)_3$. The perchlorate complexes were prepared using the procedure described above by taking rhodium perchlorate and the heterocycle in the mole ratio 1 : 2. Yield: 65%.

$IrX_3(bBzlH_2py/bBzlMe_2py)$ (X = Cl *or* Br). The complexes were prepared in the same way (preceding method) starting from sodium hexahalo iridate(IV) using 2-methoxy ethanol as the solvent. Yield: 55–60%.

$RhX(CO)_2L \cdot nH_2O$ (X = Cl *or* Br, L = $bBzlH_2py$, n = 1.5; X = Cl, L = $bBzlMe_2py$, n = 1). CO was bubbled through an ethanolic solution (10 cm^3) of hydrated rhodium trihalide (1 mmol) at refluxing temperature until it turned yellow. To this was added the *N*-heterocycle (1 mmol) in ethanol (10 cm^3) and the passage of CO was continued for about half an hour when an amorphous green solid separated. The solid was washed with ether and dried *in vacuo*. Yield: 60–70%.

$Rh(bBzlH_2py)(CO)_2(OClO_3)$ *and* $[Rh(bBzlMe_2py)(CO)_2]ClO_4$. The complexes were prepared starting from the carbonylated rhodium perchlorate solution using the procedure described above. Yield: 60%.

$[RhX_2(CO)(bBzlH_2py)]X$ (X = Cl *or* Br). $RhX(CO)_2(bBzlH_2py) \cdot 1.5H_2O$ (1 mmol) was suspended in CCl_4 (10 cm^3) and to this was added the corresponding halogen in CCl_4 (2 mmol) followed by ethanol (5 cm^3). The mixture was stirred, when the green dicarbonyl gradually dissolved simultaneously precipitating yellow/orange solid. It was washed with CCl_4 followed by ether and dried *in vacuo*. Yield: 60%.

$IrX(CO)_2(bBzlH_2py) \cdot nH_2O$ (X = Cl, n = 1; X = Br, n = 1.5). CO was bubbled through sodium hexahalo iridate (1 mmol) in 2-methoxy ethanol (10 cm^3) at refluxing temperature until the solution turned yellow. The solution was cooled to room temperature and the *N*-heterocycle (1 mmol) dissolved in 10 cm^3 of 2-methoxyethanol was added and the passage of CO was continued for 2 h. The solvent was evaporated under CO atmosphere to nearly 5 cm^3 and cooled to ice temperature when a green or red solid separated. It was washed with ether and dried *in vacuo*. Yield: 55%.

RESULTS AND DISCUSSION

Reaction of rhodium trihalide or sodium hexahalo iridate with the *N*-heterocycle, $bBzlH_2py/bBzlMe_2py$ (**I**) in 1 : 1 mole ratio in alcohol/2-methoxyethanol produced yellow, orange and red complexes whose elemental analyses correspond to the formula MX_3L (M = Rh or Ir, X = Cl or Br, L = $bBzlH_2py$ or $bBzlMe_2py$). In the case of rhodium, the iodo analogs are prepared by stirring a mixture of rhodium trichloride with 15-fold excess of sodium iodide and the *N*-heterocycle in 1 : 1 mole ratio in methanol. The complexes are insoluble in common organic solvents, but dissolve in DMF in which they behave as non-electrolytes. The complexes containing $bBzlMe_2py$ are sparingly soluble in DMF.

Rhodium(III) perchlorate reacts with $bBzlH_2py$ and $bBzlMe_2py$ in the mole ratio 1 : 2 in methanol refluxing temperature to give yellow crystalline solids. The elemental analyses of the complexes correspond to the formula $RhL_2(ClO_4)_3$. While the $bBzlH_2py$ complex behaves as a 1 : 2 electrolyte in MeCN or DMF, the $bBzlMe_2py$ analog is a 1 : 3 electrolyte in the same solvents. However, the former displayed 1 : 3 electrolytic behavior in DMSO. Some physical properties and analytical data of the complexes are listed in Table 1.

Treatment of a carbonylated solution of rhodium trihalide/perchlorate with the multidentate *N*-heterocycles produced green solids of the composition $MX(CO)_2L \cdot nH_2O$ (M = Rh, X = Cl or Br, *n* = 1.5, L = $bBzlH_2py$; X = ClO_4, *n* = 0, L = $bBzlH_2py$ or $bBzlMe_2py$; X = Cl, *n* = 1, L = $bBzlMe_2py$). The halocarbonyl complexes are also obtained by the (i) carbonylation of RhX_3L in DMF (ii) halobridge cleavage of the carbonyl dimers, $[RhX(CO)_2]_2$ (X = Cl or Br) with the *N*-heterocycle. The bromocarbonyl complex containing $bBzlMe_2py$ is obtained in a low state of purity. Carbonylation reactions with sodium hexahalo iridate and the *N*-heterocycle yielded green/orange solids of the composition $IrX(CO)_2(bBzlH_2py)$. The $bBzlMe_2py$ analogs are yet to be properly characterized.

The chloro- and bromocarbonyl complexes of rhodium are diamagnetic and undergo decarbonylation on treatment with solvents like alcohol, 2-methoxy ethanol and DMF to produce yellow solids whose elemental analyses correspond to the formula $RhX(L) \cdot 2H_2O$. Carbonylation of the latter suspended in the same solvents produced the parent carbonyls. Further the passage of NO or O_2 through alcoholic (2-methoxy or 2-ethoxy ethanol) suspension of $RhX(CO)_2L$ or $RhXL \cdot 2H_2O$ around 100°C produced carbon dioxide. Thus, these complexes seem to be good candidates for the design of three-way catalysts for automobile exhaust emissions. This is in view of the fact that among platinum group metals, rhodium has displayed the best catalytic activity [8]. This work is being pursued.

The dicarbonyl $RhX(CO)_2(bBzlH_2py) \cdot 1.5H_2O$ (X = Cl or Br) on oxidative addition with the corresponding halogen in CCl_4 undergoes the loss of a CO ligand and affords yellow or orange products of the formula $[RhX_2(CO)(bBzlH_2py)]X$. Such an oxidative addition reaction did not proceed in the case of $RhCl(CO)_2(bBzlMe_2py) \cdot H_2O$.

The Nujol mull IR spectra of the complexes are similar to those of the uncoordinated *N*-heterocycles, except for the minor shifts in the positions of the

Table 1. Physical properties and analytical data of the complexes

Complex	Color	m.p. d.p. (°C)	IR spectral data (cm^{-1}) ν_{CO}	ν_{ClO_4}	Analytical data (%) Found (Calc) C	H	N
$RhCl_3(bBzlH_2py)$	Yellow	>250			43.9 (43.8)	2.2 (2.5)	13.4 (13.5)
$RhBr_3(bBzlH_2py)$	Orange	>250			34.6 (34.9)	2.2 (2.0)	10.3 (10.7)
$RhI_3(bBzlH_2py)$	Brown	>250			28.2 (28.7)	1.7 (1.7)	8.5 (8.8)
$[Rh(bBzlH_2py)_2(OClO_3)](ClO_4)_2$	Yellow	180		1143 1120 623	46.8 (44.6)	2.6 (2.6)	13.6 (13.7)
$RhCl(CO)_2(bBzlH_2py)\cdot 1.5H_2O$	Green	225	2021, 1987		47.4 (47.3)	3.0 (3.0)	13.9 (13.2)
$RhBr(CO)_2(bBzlH_2py)\cdot 1.5H_2O$	Green	180	2027 1193		43.1 (43.7)	2.6 (2.8)	12.6 (12.1)
$Rh(CO)_2(bBzlH_2py)(OClO_3)$	Green	200–210	2047, 1987	1141, 1113, 1100, 627	45.3 (44.3)	2.8 (2.3)	12.4 (12.3)
$RhCl(bBzlH_2py)\cdot 2H_2O$	Yellow	>250			46.9 (47.0)	3.3 (3.5)	13.7 (13.7)
$RhBr(bBzlH_2py)\cdot 2H_2O$	Yellow	>250			42.2 (43.0)	3.3 (3.2)	12.5 (13.2)
$[RhCl_2(CO)(bBzlH_2py)]Cl$	Yellow	>250	2119w 2068s		43.8 (43.8)	2.5 (2.4)	12.8 (12.7)
$[RhBr_2(CO)(bBzlH_2py)]Br$	Orange	>250	2100w, 2100s 2058s,	35.0	2.1 (35.2)	9.7 (1.9)	(10.3)
$RhCl_3(bBzlMe_2py)$	Yellow	>250	2060w		46.3 (46.0)	2.9 (3.1)	13.3 (12.8)
$RhBr_3(bBzlMe_2py)$	Orange	>250			36.9 (37.0)	2.4 (2.5)	11.1 (10.3)
$RhI_3(bBzlMe_2py)$	Brown	>250			29.8 (30.7)	2.0 (2.1)	8.3 (8.5)
$[Rh(bBzlMe_2py)_2](ClO_4)_3$	Yellow	>250		1052 630	46.4 (46.7)	3.2 (3.2)	13.1 (12.9)
$RhCl(CO)_2(bBzlMe_2py)\cdot H_2O$	Green	255–260	2060 1977		50.6 (50.1)	3.2 (3.5)	13.5 (12.7)
$[Rh(CO)_2(bBzlMe_2py)]ClO_4$	Green	235–240	1973	1093 627	46.6 (46.2)	3.1 (2.9)	12.6 (11.7)
$IrCl_3(bBzlH_2py)$	Orange	>250			37.1 (37.4)	2.6 (2.2)	10.9 (11.5)
$IrBr_3(bBzlH_2py)$	Orange	>250			30.8 (30.7)	2.0 (1.8)	9.5 (9.4)
$IrCl(CO)_2(bBzlH_2py)\cdot H_2O$	Brown	>250	2003 (2010 in KBr)		41.3 (41.1)	3.0 (2.5)	11.5 (11.4)
$IrBr(CO)_2(bBzlH_2py)\cdot 1.5H_2O$	Red	>250	2020 (2020 in KBr)		37.9 (37.8)	2.5 (2.4)	10.5 (10.5)
$IrCl_3(bBzlMe_2py)$	Red	>250			39.4 (39.5)	2.7 (2.7)	10.1 (11.0)
$IrBr_3(bBzlMe_2py)$	Orange	>250			32.5 (32.7)	2.1 (2.2)	8.2 (9.1)

peaks. The spectra of $MX_3(bBzlH_2py)$ exhibited a ν_{NH} band in the range 3150–3180 cm^{-1}, indicating the coordination of the heterocycle through the tertiary nitrogens. This is further supported by the shift of the $\nu_{C=N}$ band by 20 cm^{-1} to lower/higher wave-number in the complexed species. A band at 1412 cm^{-1} noticed in the spectra of $MX_3(bBzlMe_2py)$ complexes is assigned to the N—Me stretch [7,9].

The IR spectra of the complexes $RhL_2(ClO_4)_3$, in addition to the peaks due to *N*-heterocycle, displayed bands due to perchlorate groups around 1100 (ν_3) and 620 cm^{-1} (ν_4). In the spectrum of $Rh(bBzlH_2py)_2(ClO_4)_3$, the former band is split (1083, 1010 cm^{-1}), implying the coordination of at least one of the perchlorates. This is supported by 1:2 electrolytic behavior of the complex in MeCN/DMF. In the case of $Rh(bBzlMe_2py)_2(ClO_4)_3$, both the IR spectral and conductivity data indicate the ionic nature of the perchlorates [10].

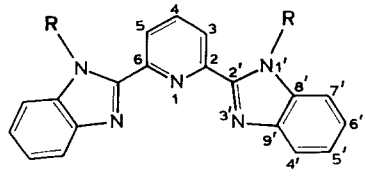
The IR spectra of Rh^I halocarbonyl complexes in KBr displayed a split peak at 1990 and 2030 cm^{-1} due to ν_{CO} and the intensities of the two peaks have been found to fluctuate with different preparations despite the elemental analysis being satisfactory. The IR spectra of $Rh(CO)_2(bBzlH_2py)(ClO_4)$ (ν_{CO}, 2047, 1987 cm^{-1}) and its $bBzlMe_2py$ analog (ν_{CO}, 1973 cm^{-1}), in addition to ν_{CO} peaks, displayed bands characteristic of coordinated (1113, 1110, 627 cm^{-1}) and ionic (1093, 627 cm^{-1}) perchlorates, respectively. The KBr pellet spectra of the monocarbonyls $[RhX_2(CO)(bBzlH_2py)]X$ (X = Cl or Br) exhibited two peaks, one around 2060 cm^{-1} and the other at 2100 cm^{-1} due to ν_{CO}, suggesting the presence of isomeric forms. For the chloro complex, the former band is more intense than the latter, whereas for the bromo analog the intensities of the two peaks varied with different preparations. The dicarbonyl complex of iridium $IrX(CO)_2(bBzlH_2py)$ (X = Cl or Br) displayed a strong IR peak around 2000 cm^{-1}, indicating a *trans* disposition of the carbonyl groups.

The ^1H NMR spectra of $bBzlH_2py$ and $bBzlMe_2py$ in DMSO-d_6 exhibited resonances due to phenylene and pyridine ring protons (Table 2) and the assignments are in consonance with those reported by Addison and coworkers [11]. The spectra of the complexes illustrated both positive and negative coordination induced shifts (c.i.s = $\delta_{complex}$-δ_{ligand}), the appreciable one being for H-4′. The resonance due

Table 2. Proton chemical shifts for the free ligands and their rhodium and iridium complexes in DMSO-d_6[a]

Compound	Benzimidazole ring protons				Pyridine ring protons		NH
	4′	5′	6′	7′	3,5	4	N—Me
$bBzlH_2py$	7.8m	7.3m	7.3m	7.8m	8.4d	8.2t	13.0s
$RhCl_3(bBzlH_2py)$	8.6d	7.5qn	7.5qn	7.8d	8.4d	8.5t	10.2s
	(0.8)	(0.2)	(0.2)			(0.3)	(−2.8)
$Rh(bBzlH_2py)_2(ClO_4)_3$	6.1d	7.2t	7.3t	8.8d	9.0d	9.3t	7.9br
	(−1.7)	(−0.1)		(1.0)	(0.6)	(1.1)	(−5.1)
$IrCl_3(bBzlH_2py)$	8.4d	7.5t	7.6t	7.8d	8.7d	8.2t	15.0s
	(0.6)	(0.2)	(0.3)		(0.3)		(2.0)
$RhCl(CO)_2(bBzlH_2py)$	7.6m	7.3m	7.3m	7.8m	8.4m	8.2t	
	(0.2)						
$RhBr(CO)_2(bBzlH_2py)$	7.7d	7.4m	7.4m	7.8m	8.4m	8.3t	
	(−0.1)	(0.1)	(0.1)			(0.1)	
$[RhCl_2(CO)(bBzlH_2py)]Cl$	8.4m	7.6t	7.5m	7.5m	8.7m	8.7m	15.4s
	(0.6)	(0.3)	(0.2)	(−0.3)	(0.3)	(0.5)	(2.4)
$[RhBr_2(CO)(bBzlH_2py)]Br$	8.7m	7.6t	7.6m	7.6m	8.8m	8.8m	15.3s
	(0.9)	(0.3)	(0.3)	(−0.2)	(0.4)	(0.6)	(2.3)
$bBzlMe_2py$	7.8d	7.4t	7.3t	7.7d	8.4d	8.2t	4.3s
$Rh(bBzlMe_2py)_2(ClO_4)_3$	6.1d	7.5t	7.3t	7.9d	9.4d	9.3t	4.6s
	(−1.7)	(0.1)		(0.2)	(1.0)	(1.1)	(0.3)

[a] Values in parentheses are coordination induced shifts: (c.i.s.) = $\delta_{complex} - \delta_{ligand}$.



R = H or Me

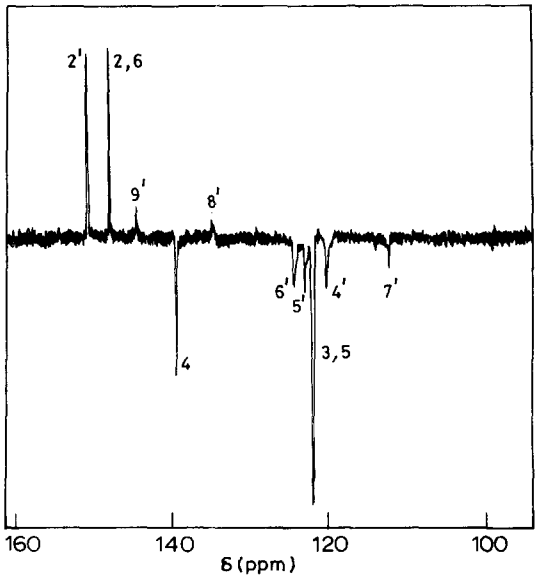


Fig. 1. ^{13}C SEFT NMR spectrum of $bBzlH_2py$

to the imine proton observed in the range 7–16 is concentration dependant. In the spectra of some of the complexes, the imine proton resonance is not observed, and probably it is too broad owing to rapid exchange with water protons present in the solvent. For the cationic complexes $[Rh(bBzlH_2py)_2(OClO_3)](ClO_4)_2$ and $[Rh(bBzlMe_2py)_2](ClO_4)_3$ only one set of proton resonances have been observed implying the magnetic equivalence of the corresponding protons in both the coordinated *N*-heterocycles. In the former complex, it is likely that the coordinated perchlorate becomes displaced by the uncoordinated N atom of the heterocycle. The spectra revealed c.i.s. and H-4′ has experienced a shielding effect.

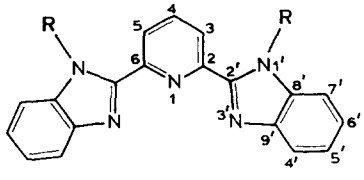
The ^{13}C NMR spectra of the uncoordinated *N*-heterocycles in DMSO-d_6 displayed 10 resonances as against eight signals reported by Addison and coworkers [11], and the assignments are given in Table 3. An additional resonance at δ 32.5 is observed for the N—Me group of $bBzlMe_2py$. According to the earlier report on $bBzlMe_2py$, the phenylene carbons 7′ and 4′ are magnetically equivalent, so also are the quaternary carbons 8′ and 9′. Thus, two resonances, one at δ 115.72 for C-7′,4′ and another at δ 139.23 for C-8′,9′, have been reported [11]. A similar finding has been made for $bBzlMe_2py$. Surprisingly in the present investigation, the four carbons 7′, 4′, 8′ and 9′ are seen to be magnetically nonequivalent in the same solvent and thus four resonances at δ 112.1, 119.9, 134.5 and 144.2, respectively, have been observed (Fig. 1). On complexation, the carbons have displayed both positive and negative c.i.s. The resonances have been identified by Spin Echo Fourier Transformation experiments (Fig. 2).

The electronic spectra of MX_3L (L = $bBzlH_2py$ or $bBzlMe_2py$, X = Cl, Br or I for M = Rh and X = Cl or Br for M = Ir), $RhL_2(ClO_4)_3$ (L = $BzlH_2py$ or $bBzlMe_2py$) and $RhX_3(CO)(bBzlH_2py)$ (X = Cl or Br) complexes in Nujol mull have exhibited an intense band in the range 400–450 nm and is assigned to metal-to-ligand charge transfer transition. Two more

Table 3. ^{13}C NMR chemical shifts for the free ligands and their complexes in DMSO-d_6[a]

Compound	Benzimidazole ring							Pyridine ring			N—Me
	2′	4′	5′	6′	7′	8′	9′	2,6	3,5	4	
$bBzlH_2py$	150.7	119.9	122.6	124.1	112.1	134.5	144.2	147.9	121.7	139.4	
$RhCl_3(bBzlH_2py)$	151.3	119.0	121.8	124.9	114.2	134.9	141.5	149.4	124.0	140.8	
	(0.6)	(−0.9)	(−0.8)	(0.8)	(2.1)	(0.4)	(−2.7)	(1.5)	(2.3)	(1.4)	
$Rh(bBzlH_2py)_2(ClO_4)_3$	151.5	116.3	124.8	125.8	113.4	135.3	138.4	149.0	126.3	145.7	
	(0.8)	(−3.6)	(2.2)	(1.7)	(1.3)	(0.8)	(−5.8)	(1.1)	(4.6)	(6.3)	
$IrCl_3(bBzlH_2py)$	153.6	118.4	121.6	125.2	113.8	132.5	141.5	150.5	125.6	140.4	
	(2.9)	(−1.5)	(−1.0)	(1.1)	(1.7)	(−2.0)	(−2.7)	(2.6)	(3.9)	(1.0)	
$bBzlMe_2py$	150.2	120.2	123.7	125.3	110.0	137.3	142.7	149.7	122.9	138.0	32.5
$Rh(bBzlMe_2py)_2(ClO_4)_3$	149.5	114.9	126.8	128.2	113.5	134.9	136.5	148.4	127.1	144.8	33.7
	(−0.7)	(−5.3)	(3.1)	(2.9)	(3.5)	(−2.4)	(−6.2)	(−1.3)	(4.2)	(6.8)	(1.2)

[a] Values in parentheses are coordination-induced shifts: c.i.s. = $\delta_{complex} - \delta_{ligand}$.



R = H or Me

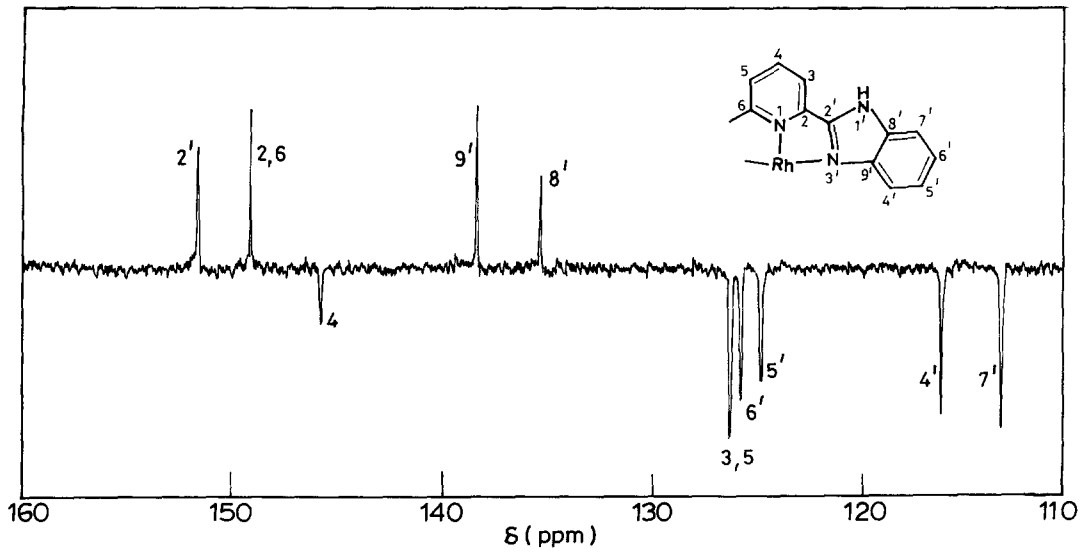


Fig. 2. ^{13}C SEFT NMR spectrum of $[Rh(bBzlH_2py)_2](ClO_4)_3$

peaks are observed around 500 (weak) and 550 nm (very weak) and are respectively assigned to the $^1A_{1g} \rightarrow {}^1T_{1g}$ and $^1A_{1g} \rightarrow {}^3T_{2g}$ transition of an octahedral low-spin d^6 system [12,13]. The $^1A_{1g} \rightarrow {}^1T_{2g}$ transition is probably obscured in the M → L charge transfer band. The electronic spectra of $MX_3(bBzlH_2py)$, $RhL_2(ClO_4)_3$ and $[RhX_2(CO)(bBzlH_2py)]X$ complexes in DMF are compiled in Table 4. In the case of carbonyl complexes of rhodium(I) and iridium(I) the metal ions have strong reducing character and hence their *d–d* transitions are probably obscured in the intense metal-to-ligand charge-transfer band in the range 400–450 nm [13].

Stereochemistry

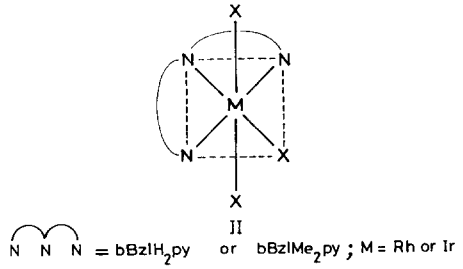
The *N*-heterocycles (L) are planar and each would function as chelating tridentate *via* the tertiary nitrogens. Hence, MX_3L complexes possess an octahedral meridional structure **II**. For the complex $[Rh(bBzlMe_2py)_2](ClO_4)_3$ an octahedral structure **III**, wherein each of the planar *N*-heterocycle would function as tridentate, is proposed, the two heterocycles' planes being mutually perpendicular [14]. In the case of $[Rh(bBzlH_2py)_2(OClO_3)](ClO_4)_2$ the solid-state IR spectrum indicated the presence of coordinated and ionic perchlorate and hence structure **IV** for the

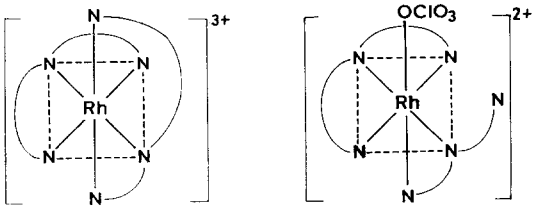
Table 4. Electronic spectral data in DMF (nm)

Compound	Observed electronic transitions[a]
$bBzlH_2py$	312(33058), 330(37645), 342(32686).
$RhCl_3(bBzlH_2py)$	325(49470), 346(48987), 364(44960), 430(5670).
$RhBr_3(bBzlH_2py)$	329(28590), 345(29496), 367(26990), 425(5071).
$RhI_3(bBzlH_2py)$	342(32540), 370(31230), 426(8975).
$[Rh(bBzlH_2py)_2(OClO_3)](ClO_4)_2$	336(50981), 357(44846), 374(45429), 414(10613), 435(6074), 450(1786).
$[Rh(CO)Cl_2(bBzlH_2py)]Cl$	322(26452), 343(27590), 363(24972), 419(5586).
$[Rh(CO)Br_2(bBzlH_2py)]Br$	329(26634), 344(25899), 366(20629), 424(3738)
$IrCl_3(bBzlH_2py)$	315(37960), 331(44060), 343(42910), 364(31740), 430(5647), 514(1091), 565(503).
$IrBr_3(bBzlH_2py)$	333(51810), 439(7980), 515(614), 571(288).
$bBzlMe_2py$	306(51495), 323(61747).
$[Rh(bBzlMe_2py)_2](ClO_4)_3$	326(41724), 368(31517), 401(14879), 421(10310), 441(2569), 484(65), 516(53), 577(15).

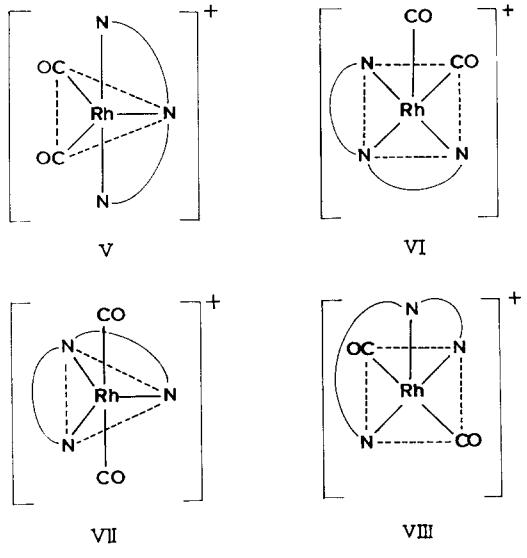
[a] ε values are in parentheses.

complex, wherein one of the *N*-heterocycles is tridentate and the other is bidentate with a pendant nitrogen. Such varied coordination behavior for the multidentate *N*-heterocycles have been observed in $[Cu(bBzlMe_2py)_2]ClO_4 \cdot 2H_2O$ [14], $[Co(bBzlH_2py)_2(OClO_3)]ClO_4$ and $[Co(bBzlMe_2py)_2](ClO_4)_2$ [7,15].

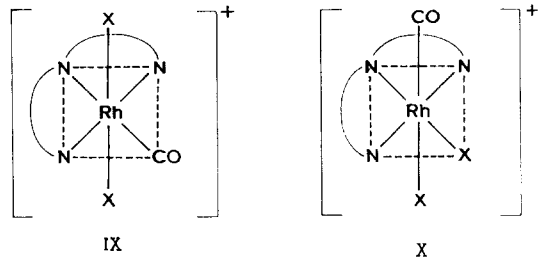




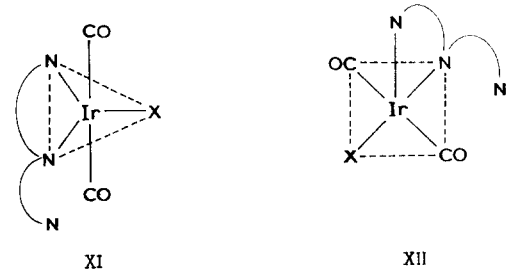
The halo/perchlorate dicarbonyl complexes of rhodium(I) are expected to be five-coordinate with the *N*-heterocycle behaving as chelating tridentate. Five-coordinate complexes of rhodium(I) generally conceive trigonal-bipyramidal (tbp) or square-pyramidal (sp) (**V**–**VIII**) configuration [16].



For the complex $[Rh(CO)_2(bBzlMe_2py)]ClO_4$ the 1 : 1 electrolytic behavior in nitrobenzene and a single ν_{CO} peak in the IR region suggest trans disposition of the carbonyls and hence structure **VII** or **VIII** for the cation. The trihalo carbonyl cations may be proposed to have configuration **IX** or **X**, wherein the *N*-heterocycle would serve as a chelating tridentate ligand. Here again it is likely that the complexes exhibit isomerism as the intensities of the two ν_{CO} peaks varied with different preparations.



The halodicarbonyls $[IrX(CO)_2(bBzlH_2py)]$ exhibit a single ν_{CO} peak and hence five-coordinate square pyramidal/trigonal bipyramidal *trans*-COs structures (**XI** or **XII**) with the *N*-heterocycle as chelating bidentate are proposed.



Acknowledgments—The authors are thankful to Professor C. L. Khetrapal, S.I.F., I.I.Sc., Bangalore, for the NMR spectra; UGC, New Dehli, for a DRS programme and CSIR, New Dehli, for a Research Associateship to VG.

REFERENCES

1. (a) Ruttimann, S., Bernardinelli, G. and Williams, A. F., *Angew. Chem. Int. Ed. Engl.* 1993, **32,** 392; (b) Lehn, J. M. and Rigault, A., *Angew. Chem. Int. Ed. Engl.* 1988, **27,** 1095; (c) Williams, A. F., Piguet, C. and Bernardinelli, G., *Angew. Chem. Int. Ed. Engl.* 1991, **30,** 1490; (d) Constable, E. C. and Ward, M.D., *J. Am. Chem. Soc.* 1990, **112,** 1256; (e) Ryabov, A. D., *Chem. Rev.* 1990, **90,** 403; (f) Dietrich-Buchecker, C. O., Guilhem, J., Pascard, C. and Sauvage, J. P., *Angew. Chem. Int. Ed. Engl.* 1990, **29,** 1154.
2. (a) Lehn, J. M., *Angew. Chem. Int. Ed. Engl.* 1990, **29,** 1304; (b) Piguet, C., Bernardinelli, G., Williams, A. F. and Bocquet, B., *Angew. Chem. Int. Ed. Engl.* 1995, **34,** 582; (c) Piguet, C., Bunzli, J. G., Bernardinelli, G., Bochet, C. G. and Froidevaux, P., *J. Chem. Soc. Dalton Trans.* 1995, 83.
3. (a) Uson, R., Gimeno, J., Oro, L. A., Valderama, M., Sariego, R. and Martinez, E., *Trans. Met. Chem.* 1981, **6,** 103; (b) Mahajan, D., Creutz, C. and Sutin, N., *Inorg. Chem.* 1985, **24,** 2063; (c)

Leelamani, E. G., Nanje Gowda, N. M., Gayathri, V. and Reddy, G. K. N., *Recent Advances in Catalytic Reaction Engineering*. RRL-IICT (CSIR), Hyderabad, India, 1986, p. 262; (d) Leelamani, E. G., Gayathri, V. and Reddy, G. K. N., *Indian J. Chem.* 1986, **25A,** 719; (e) Parameswaran, V. R. and Vancheesan, S., *Proc. Indian Acad. Sci. (Chem. Sci.)*, 1991, **103,** 99; (f) Lei, Y. and Hurst, J. K., *Inorg. Chem.* 1994, **33,** 4460; (g) Agrazzi, R., Bignozzi, C. A., Heimer, T. A., Cartellana, F. N. and Meyer, G. J., *Inorg. Chem.* 1994, **33,** 5741.

4. (a) Reddy, G. K. N. and Leelamani, E.G., *Current Science* 1965, **34,** 146; (b) Reddy, G. K. N. and Susheelamma, C. H., *J. Chem. Soc. D.* 1970, 54.
5. Addison, A. W. and Burke, P. J., *J. Heterocycl. Chem.* 1981, **18,** 803.
6. Addison, A. W., Burman, S., Wahlgren, C. G., Rajan, O. A., Rowe, T. M. and Sinn, E., *J. Chem. Soc. Dalton Trans.* 1987, 2621.
7. Gayathri, V., Shashikala, N., Gowda, N. M. N. and Reddy, G. K. N., *Indian J. Chem.* 1993, **32A,** 33.
8. Thompson, D., *Insights into Speciality Inorganic Chemicals*. The Royal Society of Chemistry, 1995.
9. Piguet, C., Bocquet, B., Muller, E. and Williams, A. F., *Helv. Chem. Acta* 1989, **72,** 323.
10. Gowda, N. M. N., Naikar, S. B. and Reddy, G. K. N., *Adv. Inorg. Chem. and Radiochem.* 1984, **28,** 41.
11. Xiaoming, X., Haga, M., Matsumura-Inoue, T., Ru, Y., Addison, A. W. and Kano, K., *J. Chem. Soc. Dalton Trans.* 1993, 2477.
12. Chandra, S. and Singh, R., *Indian J. Chem.* 1988, **27A,** 417.
13. Lever, A. P. B., *Inorganic Electronic Spectroscopy*. Elsevier, Amsterdam, 1984, p. 507.
14. Sanni, S. B., Behm, H. J., Beurskens, P. T., Van Alabada, G. A., Reedijk, J., Lenstra, A. T. H., Addison, A. W. and Palaniandavar, M., *J. Chem. Soc. Dalton Trans.* 1988, 1429.
15. Shklover, V., Eremenko, I. L., Berke, H., Nesper, R., Zakeeruddin, S. M., Nazeeruddin, Md. K. and Gratzel, M., *Inorg. Chim. Acta*, 1994, **219,** 11.
16. (a) Reddy, G. K. N. and Ramesh, B. R., *J. Organomet. Chem.* 1975, **87,** 347; (b) Collman, J. P. and Poper, W. R., *Adv. Organomet. Chem.* 1968, **7,** 57.

Pergamon

PII: S0277-5387(96)00366-X

Polyhedron Vol. 16, No. 7, pp. 1177–1191, 1997
Copyright © 1997 Elsevier Science Ltd
Printed in Great Britain. All rights reserved
0277-5387/97 $17.00+0.00

Metal-assisted unorthodox reactions of formamidines: coupling, cleavage and insertions

F. Albert Cotton,[a]* Lee M. Daniels,[a] John H. Matonic,[a] Xiaoping Wang[a] and Carlos A. Murillo[b]*

[a] Laboratory for Molecular Structure and Bonding, Department of Chemistry, Texas A&M University, College Station, TX 77843-3255, U.S.A.

[b] Department of Chemistry, University of Costa Rica, Ciudad Universitaria, Costa Rica; Department of Chemistry and Laboratory for Molecular Structure and Bonding, Texas A&M University, College Station, TX 77843-3255, U.S.A.

(Received 15 July 1996; accepted 25 July 1996)

Abstract—The purpose of this report is to call attention to the wide range of reactions that an amidine or amidinium may undergo in the presence of reduced metal ions, other than simple ligation of the metal ions. Crystal structures of five examples are presented. In (η-dmpm)Cl_2Ta(μ-NTol)(μ-η^2-HC=NTol)(μ-dmpm)TaCl(η^2-DTolF) (**I**), both fragments from a C—N bond cleavage of the di-*p*-tolylformamidinate anion, $DTolF^-$, namely tolylimido and tolylformimidoyl groups, are found forming bridges between the metal atoms. An amido group is also found in $TaCl_2$(NPh)(DPhF)(HDPhF) (**II**), in which a six-coordinated tantalum atom is surrounded also by two chlorine atoms, a chelating diphenylformamidinate, $DPhF^-$ and a neutral HDPhF molecule. A new neutral chelating ligand forms during the synthesis of $CoCl_2$(PhNCHNPhCHNPh) (**III**), in which the divalent cobalt atom is in a pseudo-tetrahedral environment. The six-membered metallocycle formed by the Co—N—C—N—C—N atoms is essentially planar. Reaction of K with crude $Ta_2(\mu_2$-η^4-$B_2H_6)(\mu$-$DTolF)_4$ produces [(B_2H_5)N(Tol)C(H)N(Tol)]Ta(μ_2-NTol)$_2$(μ_2-DTolF)$_2$Ta[(Tol)NC(H)N(Tol)B_2H_5]·$2Et_2O$ (**IV**), in which a ditantalum unit is bridged by two DTolF and two tolylimido groups. A new ligand formed by fusion of a $B_2H_5^-$ unit to a $DTolF^-$ anion chelates to each of the metal atoms. In the crystals, 50% of the B_2H_5 moieties are BH_3 groups. Coupling of two DPhF anions is observed in PhNC(H)N(Ph)C(H)(NPh)$_2$Ta(DPhF)$_3$·Et_2O (**V**). The new dianion chelates the metal center, to which three other DPhF groups are attached giving an eight-coordinated compound. Copyright © 1997 Elsevier Science Ltd

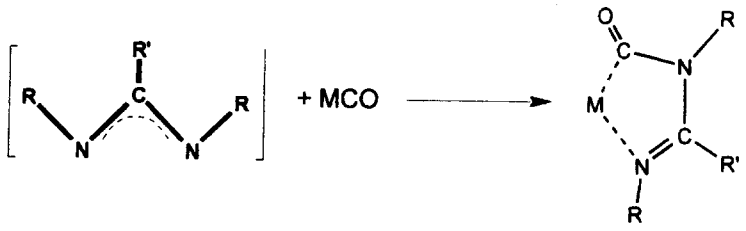
Keywords: tantalum and cobalt compounds; amidinate cleavage; coupling; borohydride insertion; crystal structure.

Amidinate anions of the type $[RNC(R')NR]^-$ have been widely used as ligands in coordination chemistry [1], where they are usually found intact in monodentate [2] and chelating [3] bonding modes, but also forming bridges between metal atoms [4]. It is in the latter field that many efforts have concentrated in the last few years [5]. Today more elements are known to form metal–metal bonded compounds with amidinate bridges than with the classical carboxylates or any other stereoelectronically similar type of ligand.

Up to now there have been few accounts of reactions in which an amidinate ligand reacted in the presence of a metal ion to lose its identity, either by adding another molecule or by losing some of its atoms to give a different ligand. The best studied reaction is the formation of carbamoyl complexes by insertion of a metal carbonyl into the amidinate ligand [6].

Kilner and collaborators have also studied the orthometalation of several compounds including

* Authors to whom correspondence should be addressed.



those of Pd and Pt with aryl amidinates [7]. Reports have appeared in which the amidinates are severed during the reaction to give imido-containing metal species [8]. Two reactions are also known in which benzonitrile has been a part of the reaction. In one case lithium benzamidinate was reacted with $Pt(PhCN)_2Cl_2$ to give $[Pt\{HNC(Ph)NC(Ph)NH\}_2]$, in which a different chelating mononegative anionic ligand was formed [9]. In the other case thermolysis of $C_6H_5C(NSiMe_3)_2Ti(OPri)_3$ promoted the elimination of C_6H_5CN to form an amide-containing species, namely $(SiMe_3)_2NTi(OPri)_3$ [10].

In this paper we show that the presence of metal species can modify the integrity of the amidinate moiety and thus lead to the subsequent isolation of many interesting but serendipitously obtained products. Most of the compounds were obtained in small yields as byproducts and a few crystals presented minor crystallographic problems such as slight twinning. Some of the structures were initially treated as oddities, but the continued appearance of transformed formamidinates has revealed a pattern of reactivity which can no longer be ignored. Consequently, we are reporting the structures of five compounds containing modified formamidinate species, with the intention of alerting others who may work with these useful ligands to the many unanticipated ways in which they can react.

EXPERIMENTAL

All operations were carried out under an argon atmosphere using standard Schlenk or dry-box techniques. Solvents were purified by conventional methods and distilled under nitrogen from Na/K. Tantalum(V) chloride (resublimed 99.99%) was obtained from Strem. Other chemicals, including HDPhF and $LiBH_4$ were purchased from Aldrich and were used as received. $CoCl_2(HDPhF)_2$ [2b] and $Ta_2(\mu_2\text{-}\eta^4\text{-}B_2H_6)(DTolF)_4$ [11] were prepared according to published procedures. Slightly modified literature procedures were used to synthesize HDTolF [12] and $Ta_2Cl_6(SMe_2)_3$ [13]. Potassium graphite (KC_8) was prepared by heating at 180°C a mixture of potassium metal and graphite with a potassium to carbon mole ratio of 1 : 8 [14].

Preparations

$(\eta\text{-dmpm})Cl_2Ta(\mu\text{-NTol})(\mu\text{-}\eta^2\text{-HC=NTol})(\mu\text{-dmpm})\ TaCl(\eta^2\text{-DTolF})$ (**I**). To a mixture of $Ta_2Cl_6(SMe_2)_3$ (0.38 g, 0.5 mmol) and LiDTolF (1.0 mmol) in toluene (15 cm^3) THF (1 cm^3) was added zinc powder (0.10 g, 1.5 mmol) and dmpm (0.18 cm^3, 1.1 mmol). The solution turned green upon addition of dmpm ligand. The mixture was allowed to react over a period of 4 h in a sonicator and then filtered. Crystals of compound **I** were obtained upon slow diffusion of hexanes (20 cm^3) into the filtrate. Yield 0.25 g, 21%.

$TaCl_2(NPh)(DPhF)(HDPhF)$ (**II**). $TaCl_5$ (1.46 g, 4.1 mmol) and $LiBH_4$ (0.29 g, 13.3 mmol) were mixed in toluene (20 cm^3) and heated to 105°C for 24 h. A dark solid formed. After distillation of most of the toluene, THF (20 cm^3) was added at room temperature. An exothermic reaction was observed. The brown suspension was stirred for 15 min and then cooled to −78°C. Then a solution of LiDPhF (8.2 mmol) in 15 cm^3 THF was transferred to the cold suspension, the mixture was slowly warmed to room temperature and stirred for 4 h. The solvent was removed *in vacuo* and the solid was extracted with benzene (30 cm^3)/hexane (5 cm^3). The solution was filtered through 3 cm Celite. Crystals of $Ta(NPh)(DPhF)_3$ were obtained after layering the solution with hexanes [8b].

To the remaining solid was added toluene (20 cm^3). The red–brown slurry was stirred for 2 h at 90°C. After cooling to room temperature, it was filtered through 3 cm Celite. The filtrate was then reduced to a volume of 15 cm^3 and layered with hexanes (20 cm^3). Red crystals of compound **II** were produced after slow diffusion of hexanes into the toluene solution. Yield 0.46 g, 15%.

$CoCl_2(PhNCHNPhCHNPh)$ (**III**). To a toluene solution of $CoCl_2(HDPhF)_2$ (0.40 g, 0.77 mmol) at −78°C was added 1.5 cm^3 of methyllithium (1.0 M in THF/cumene). After bubbling of methane ceased, the reaction mixture was warmed to room temperature. The solvent was then evaporated under vacuum and the residue was redissolved in a mixture of 10 cm^3 CH_2Cl_2/CH_3CN (1 : 1). Then, an acetonitrile solution of $NOBF_4$ (0.09 g, 0.77 mmol) was added by cannula and the mixture stirred for 1 h. The solvent was evaporated *in vacuo* and CH_2Cl_2 (10 cm^3) was added. After filtration, the solution was layered with hexanes to

produce large, blue needle-like crystals of **III**. Yield 0.035 g, 15%.

$[(B_2H_5)N(Tol)C(H)N(Tol)]Ta(\mu_2\text{-}NTol)_2(\mu_2\text{-}DTolF)_2Ta[(Tol)NC(H)N(Tol)B_2H_5]\cdot 2Et_2O$ (**IV**). To a solution of crude $Ta_2(\mu_2\text{-}\eta^4\text{-}B_2H_6)(DTolF)_4$ (0.80 g, 0.5 mmol) containing about 0.05 mmol of LiDTolF in toluene (30 cm^3) was added potassium metal (0.16 g, 4 mmol). The mixture was refluxed for 30 min and then stirred overnight at room temperature. After filtration the solvent was stripped off under reduced pressure and the solid obtained was extracted with diethyl ether (30 cm^3). A green–brown solution was obtained. After filtration it was placed in a freezer for 2 weeks. Crystals of **IV** suitable for single crystal X-ray analysis were obtained. Yield 0.10 g, 12%.

$PhNC(H)N(Ph)C(H)(NPh)_2Ta(DPhF)_3\cdot Et_2O$ (**V**). To a slurry of $TaCl_5$ (0.54 g, 1.51 mmol) and potassium graphite (0.62 g, 4.6 mmol) in THF (20 cm^3) was added LiDPhF (3 mmol) in THF (15 cm^3) at −30 C. After stirring for 4 h, the solvent was removed by syringe and the remaining dark green solid was dried *in vacuo*. It was extracted with ether (30 cm^3). The green–brown solution obtained after filtration was placed in a freezer for 2 weeks. The color of the solution changed to brown and brown crystals of compound **V** were obtained. Yield 0.095 g, 5%. The solid which remained after the extraction was then treated with 20 cm^3 toluene from which $Ta(DPhF)_4$ was isolated after layering with hexanes [8b].

X-ray structure determinations

Geometric and intensity data for compounds **I, II, III** and **V** were gathered at −60°C with an Enraf–Nonius FAST area detector system, utilizing the program MADNES [15]. Detailed procedures have previously been described [16]. Data for **IV** were collected on a Rigaku AFC5R diffractometer equipped with a Cu rotating anode.

Unit-cell indexing for **I, II, III** and **V** were performed on 50 reflections taken from three 10° ω rotations in the range $0 \leqslant \omega \leqslant 120°$ and unit-cell refinement used 250 reflections in the range $18 \leqslant 2\theta \leqslant 42°$. In each case, the cell dimensions and Laue group were confirmed by axial images. Unit-cell refinement for **IV** utilized 25 high-angle reflections. All data were corrected for Lorentz and polarization effects. An empirical absorption correction based on six ψ-scans was applied for **IV**. For compounds **I** and **V**, the program SORTAV was used to correct for absorption [17]. Data from the FAST diffractometer were processed into SHELX format using the program ABSURD [18]. Data for **IV** were processed using the TEXSAN package [19].

In all structures, the positions of the heavy atoms were found in direct methods E-maps produced by the software solution portion of SHELXTL [20]. Subsequent cycles of least-squares refinement followed by difference-Fourier syntheses revealed the positions of the remaining non-hydrogen atoms. For purposes of structure-factor calculations, hydrogen atoms were usually placed in idealized positions. In some cases, hydrogen atoms were located in difference Fourier maps and then refined isotropically. The positions of the two hydrogen atoms that bridge atoms Ta and B(1) in compound **IV** and the hydrogen atom that attaches to C(3) in compound **V** were obtained following this procedure.

In compound **I**, the two highest residuals of 1.3 and 1.9 e A^{-3} in the final difference Fourier map were found very close to the tantalum atoms. The highest peaks (1.3 and 1.4 e A^{-3}, respectively) in compounds **II** and **V** were 1.5 and 1.0 Å, respectively, from phenyl carbon atoms. The remainder of the final difference maps in these compounds were featureless.

Atom B(2) in compound **IV** was best refined anisotropically with an occupancy factor of 50%. This result indicates the existence of a mixture of $H_3BB(H)_2DTolF^-$ and hydrogen-substituted $HB(H)_2DTolF^-$ ligands. The terminal hydrogen atom in the $HB(H)_2DTolF^-$ moiety was refined with fixed coordinates at half occupancy. The refined model also includes two disordered molecules of diethyl ether either on a two-fold axis (56%) or a general position (44%).

Other details of data collection and refinement are given in Table 1. Selected bond distances and angles for compound **I** are given in Table 2 and a comparison with other coordinated formimidoyl and isocyanide ligands is presented in Table 3. For compounds **II–V**, selected bond distances and angles are found in Tables 4–7, respectively. Other crystallographic data are given as supplementary material.

RESULTS AND DISCUSSION

$(\eta\text{-dmpm})Cl_2Ta(\mu\text{-NTol})((\mu\text{-}\eta^2\text{-HC}{=}\text{NTol})(\mu\text{-dmpm})TaCl(\eta^2\text{-DTolF})$ (**I**)

The reduction of $Ta_2(\mu\text{-}SMe_2)_3Cl_6$ with Zn metal in the presence of bis(dimethylphosphino)methane (dmpm) and LiDTolF yields **I**, the structure of which is shown in Fig. 1. The dinuclear molecule is unsymmetric with six- and seven-coordinated tantalum atoms and has a long metal to metal separation of 2.948(1) Å. The dmpm ligands show two very different modes of bonding: one of them bridges the metal atoms in the usual way [21], while the other acts as a monodentate ligand, a mode which is not common but has also been observed in the solid state for dppm in $[Mo_2Cp_2(\mu\text{-}\eta\text{-}CNBu^t)(\eta\text{-}PPh_2CH_2PPh_2)(CO)_3$ [22] and in solution for dmpe compounds such as $Ru(\eta^2\text{-dmpe})(\eta^1\text{-dmpe})(CNPh)_2$ [23]. The most notable feature of **I** is the reduction and cleavage of a formamidine ligand which gives rise to bridging tolylimide and tolylformimidoyl fragments:

Table 1. Crystal data and structure refinement for (η-dmpm)Cl_2Ta(μ-NTol)(μ-η^2-HC=NTol)(μ-dmpm)TaCl(η^2-DTolF), **(I)**, $TaCl_2$(NPh)(DPhF)(HDPhF) **(II)**, $CoCl_2$(PhNCHNPhCHNPh) **(III)**, [(B_2H_5)N(Tol)C(H)N(Tol)]Ta(μ_2-NTol)$_2$(μ_2-DTolF)$_2$Ta[(Tol)NC(H)N(Tol)B_2H_5]·2Et_2O **(IV)** and (PhNC(H)N(Ph)C(H)(NPh)$_2$)Ta(DPhF)$_3$$Et_2O$ **(V)**

Empirical formula	$C_{40}H_{53}Cl_3N_4P_4Ta_2$	$C_{32}H_{25}Cl_2N_5Ta$	$C_{20}H_{17}Cl_2CoN_3$	$C_{82}H_{102}B_3N_{10}O_2Ta_2$	$C_{69}H_{65}N_{10}OTa$
Formula weight	1181.99	731.42	429.20	1543.83	1231.26
Space group	$P2_1/n$	$P2_1/c$	$I2/a$	$C2/c$	$P2_1/c$
a (Å)	18.822(9)	9.908(2)	10.162(2)	27.514(3)	13.932(3)
b (Å)	12.450(1)	21.844(6)	16.549(3)	12.8371(7)	19.855(2)
c (Å)	20.50(1)	14.436(1)	12.135(2)	24.426(4)	21.465(2)
α (°)	90	90	90	90	90
β (°)	102.75(2)	104.56(1)	107.70(3)	109.844(8)	95.81(1)
γ (°)	90	90	90	90	90
V (Å^3)	4686(3)	3024(1)	1944.2(7)	8115(2)	5907(2)
Z	4	4	4	4	4
d_{calc} (g cm^{-3})	1.675	1.607	1.466	1.354	1.384
Crystal size (mm)	0.28 × 0.20 × 0.12	0.19 × 0.21 × 0.23	0.35 × 0.20 × 0.10	0.45 × 0.24 × 0.18	0.26 × 0.23 × 0.21
Absorption coefficient (mm^{-1})	5.005	3.841	1.166	5.269	1.914
Data collection instrument	FAST	FAST	FAST	Rigaku, AFC5R	FAST
Radiation (monochromated in incident beam) Mo-K_α	0.71073 Å	0.71073 Å	0.71073 Å	1.54184 Å	0.71073 Å
Orientation reflections, number, range (θ)	250, 6.9–23.7	250, 9.05–20.8	250, 6.5–20.5	25, 15–30	250, 9.05–20.8
Temperature (K)	213(2)	213(2)	213(2)	293(2)	213(2)
Scan method	Frame data from ω scans	Frame data from ω scans	Frame data from ω scans	ω–2θ scans	Frame data from ω scans
Data collected range, θ (°)	2.33–21.00	2.32–21.50	2.15–22.50	3.42–60.00	2.17–22.50
No. unique data, total	4853	3331	1267	5683	7694
Number of parameters refined	482	361	154	451	736
Final R indices [$I > 2\sigma(I)$][a]	$R1$ = 0.062, $wR2$ = 0.143	$R1$ = 0.043, $wR2$ = 0.102	$R1$ = 0.048, wR = 0.104	$R1$ = 0.030, $wR2$ = 0.080	$R1$ = 0.042 ,$wR2$ = 0.099,
R indices (all data)[b]	$R1$ = 0.110, $wR2$ = 0.174	$R1$ = 0.057, $wR2$ = 0.120	$R1$ = 0.061, $wR2$ = 0.111	$R1$ = 0.040, $wR2$ = 0.085	$R1$ = 0.066, $wR2$ = 0.115
Quality-of-fit indicator[c]	0.857	1.116	1.096	1.075	1.076
Largest shift/e.s.d. final cycle	0.001	0.000	0.000	0.080	0.000
Largest peak, final cycle (e Å^{-3})	1.9(2)	1.3(1)	0.60(9)	0.70(8)	1.4(1)

[a] $R1 = \Sigma \| F_o| - |F_c \| / \Sigma | F_o|$.

[b] $wR2 = [\Sigma w(F_o^2 - F_c^2)^2 / \Sigma w(F_o^2)^2 / \Sigma w(F_o^2)^2]^{1/2}$, $w = 1/[\sigma^2(F_o^2) + (\mathbf{a}\cdot p)^2 + b\cdot p$, $p = [\max(F_o^2) + 2(F_c^2)]/3$. $a = 0.0$ and $b = 0.00$ for **I**; $a = 0.0385$ and $b = 23.1$ for **II**; $a = 0.0542$ and $b = 3.50$ for **III**; $a = 0.397$ and $b = 10.8$ for **IV**; $a = 0.0$ and $b = 0.0$ for **V**.

[c] Quality-of-fit = $[\Sigma w(|F_o^2| - |F_c^2|)^2 / (N_{obs} - N_{parameters})]^{1/2}$.

Table 2. Selected bond lengths (Å) and angles (°) for (η-dmpm)Cl_2Ta(μ-NTol)(μ-η^2-HC=NTol)(μ-dmpm)TaCl(η^2-DTolF) (**I**)

Ta(1)—N(4)	1.98(1)	Ta(2)—Cl(3)	2.503(5)
Ta(1)—N(3)	2.06(2)	Ta(2)—Cl(2)	2.549(5)
Ta(1)—C(40)	2.19(2)	Ta(2)—P(2)	2.589(6)
Ta(1)—N(1)	2.21(2)	Ta(2)—P(4)	2.616(6)
Ta(1)—N(2)	2.25(2)	N(1)—C	1.31(2)
Ta(1)—Cl(1)	2.419(6)	N(1)—C(11)	1.44(2)
Ta(1)—P(1)	2.640(6)	C—N(2)	1.32(2)
Ta(1)—Ta(2)	2.948(1)	N(2)—C(21)	1.40(3)
Ta(2)—C(40)	1.90(2)	N(4)—C(40)	1.37(2)
Ta(2)—N(3)	1.95(2)	N(4)—C(41)	1.40(2)
N(4)—Ta(1)—N(3)	119.0(6)	Cl(2)—Ta(2)—Ta(1)	131.8(1)
N(4)—Ta(1)—C(40)	38.0(7)	P(2)—Ta(2)—Ta(1)	95.1(1)
N(3)—Ta(1)—C(40)	81.3(7)	P(4)—Ta(2)—Ta(1)	96.9(2)
N(4)—Ta(1)—N(1)	148.7(6)	C—N(1)—C(11)	114(2)
N(3)—Ta(1)—N(1)	91.0(6)	C—N(1)—Ta(1)	95(1)
C(40)—Ta(1)—N(1)	163.7(7)	C(11)—N(1)—Ta(1)	148(1)
N(4)—Ta(1)—N(2)	90.9(6)	N(1)—C—N(2)	112(2)
N(3)—Ta(1)—N(2)	149.1(6)	N(1)—C—Ta(1)	56(1)
C(40)—Ta(1)—N(2)	127.0(7)	N(2)—C—Ta(1)	57(1)
N(1)—Ta(1)—N(2)	58.3(5)	C—N(2)—C(21)	123(2)
N(4)—Ta(1)—Cl(1)	96.1(5)	C—N(2)—Ta(1)	94(1)
N(3)—Ta(1)—Cl(1)	97.5(5)	C(21)—N(2)—Ta(1)	139(1)
C(40)—Ta(1)—Cl(1)	107.4(6)	C(5)—P(1)—C(1)	108(1)
N(1)—Ta(1)—Cl(1)	87.8(4)	C(5)—P(1)—C(4)	104(1)
N(2)—Ta(1)—Cl(1)	86.2(4)	C(1)—P(1)—C(4)	102(1)
N(4)—Ta(1)—P(1)	87.3(5)	C(5)—P(1)—Ta(1)	111.3(7)
N(3)—Ta(1)—P(1)	91.3(5)	C(1)—P(1)—Ta(1)	114.3(8)
C(40)—Ta(1)—P(1)	82.6(6)	C(4)—P(1)—Ta(1)	116.6(7)
N(1)—Ta(1)—P(1)	83.2(4)	C(1)—P(2)—C(2)	105(1)
N(2)—Ta(1)—P(1)	81.8(4)	C(1)—P(2)—C(3)	100(1)
Cl(1)—Ta(1)—P(1)	167.5(2)	C(2)—P(2)—C(3)	102(1)
N(4)—Ta(1)—Ta(2)	77.9(5)	C(1)—P(2)—Ta(2)	111.5(7)
N(3)—Ta(1)—Ta(2)	41.2(4)	C(2)—P(2)—Ta(2)	117.4(9)
C(40)—Ta(1)—Ta(2)	40.1(5)	C(3)—P(2)—Ta(2)	119.0(9)
N(1)—Ta(1)—Ta(2)	130.8(4)	P(2)—C(1)—P(1)	114(1)
N(2)—Ta(1)—Ta(2)	164.1(4)	C(31)—N(3)—Ta(2)	136(1)
Cl(1)—Ta(1)—Ta(2)	106.1(1)	C(31)—N(3)—Ta(1)	129(1)
P(1)—Ta(1)—Ta(2)	86.4(1)	Ta(2)—N(3)—Ta(1)	94.6(7)
C—Ta(1)—Ta(2)	159.3(4)	C(9)—P(3)—C(6)	101(1)
C(40)—Ta(2)—N(3)	92.2(7)	C(9)—P(3)—C(10)	97(2)
C(40)—Ta(2)—Cl(3)	97.4(6)	C(6)—P(3)—C(10)	99(1)
N(3)—Ta(2)—Cl(3)	169.3(5)	C(8)—P(4)—C(7)	104(1)
C(40)—Ta(2)—Cl(2)	172.2(7)	C(8)—P(4)—C(6)	105(1)
N(3)—Ta(2)—Cl(2)	88.2(5)	C(7)—P(4)—C(6)	105(1)
Cl(3)—Ta(2)—Cl(2)	83.0(2)	C(8)—P(4)—Ta(2)	115(1)
C(40)—Ta(2)—P(2)	94.0(7)	C(7)—P(4)—Ta(2)	114.4(9)
N(3)—Ta(2)—P(2)	92.3(5)	C(6)—P(4)—Ta(2)	112.7(7)
Cl(3)—Ta(2)—P(2)	82.3(2)	C(40)—N(4)—C(41)	125(2)
Cl(2)—Ta(2)—P(2)	93.8(2)	C(40)—N(4)—Ta(1)	79(1)
C(40)—Ta(2)—P(4)	90.3(7)	C(41)—N(4)—Ta(1)	156(1)
N(3)—Ta(2)—P(4)	99.8(6)	P(3)—C(6)—P(4)	118(1)
Cl(3)—Ta(2)—P(4)	85.0(2)	N(4)—C(40)—Ta(2)	153(1)
Cl(2)—Ta(2)—P(4)	81.9(2)	N(4)—C(40)—Ta(1)	62.5(9)
P(2)—Ta(2)—P(4)	167.0(2)	Ta(2)—C(40)—Ta(1)	91.9(7)
C(40)—Ta(2)—Ta(1)	48.0(6)	C(46)—C(41)—N(4)	119(2)
N(3)—Ta(2)—Ta(1)	44.2(5)	N(4)—C(41)—C(42)	123(2)
Cl(3)—Ta(2)—Ta(1)	145.2(1)		

Table 3. Structural parameters for some representative compounds containing formimidoyl ($HC{=}NR^-$) and isocyanide ($C{\equiv}NR$) ligands

Compound	Ligand	M—C—NC—N—R ( )		M—C (Å)	C—N (Å)	N—R (Å)	Reference
$[Cp_2Ln(\mu\text{-}\eta^2\text{-}HC{=}NCMe_3)]_2$ Ln = Y	$HC{=}NR^-$	155.3(4)	124.3(4)	2.545(5)	1.275(6)	1.504(6)	24a
Ln = Er[a]	$HC{=}NR^-$	155.6(4)	124.6(5)	2.527(6)	1.262(8)	1.505(7)	24a
Ln = Er[a]	$HC{=}NR$	154.8(4)	122.8(5)	2.544(6)	1.288(7)	1.489(7)	24a
$(\mu\text{-}H)(\mu\text{-}\eta^2\text{-}HC{=}NC_6H_5)Os_3(CO)_9(P(OCH_3)_3)$	$HC{=}NPh^-$	116.0(6)	123.0(6)	2.075(9) 1.842(6)	1.32(1)	1.43(1)	24b
$Cp_3^*Co_3(\text{-}H)(\mu\text{-}\eta^2\text{-}HC{=}NCMe_3)$	$HC{=}NR^-$	115.1(4)	120.7(4)	1.968(5) 1.839(4)	1.346(7)	1.509(7)	24c
$Cp_3^*Co_3(\mu\text{-}H)(\mu\text{-}\eta^2\text{-}HC{=}NCMe_2CH_2Me)$	$HC{=}NR$	116.0(3)	120.7(3)	1.966(5)	1.358(6)	1.498(6)	24c
$Cl_2(dmpm)Ta(\mu\text{-}NTol)(\mu\text{-}\eta^2\text{-}HC{=}NTol)(\mu\text{-}dmpm)Ta(DTolF)$	$HC{=}NTol^-$	153(1)	125(2)	1.90(2) 2.19(2)	1.37(2)	1.40(2)	this work
$(CpZrMe)_2(\mu\text{-}\eta^2\text{-}C{\equiv}N(Me_2C_6H_3)(C_{10}H_8)$	$C{\equiv}NPh$	173.8(5)	131.7(5)	2.363(6)	1.273(7)	1.450(8)	25a
$Mo_2(\mu\text{-}\eta^2\text{-}CNBu^t)(CO)_4Cp_2$	$C{\equiv}NR$	168.1(6)	136.3(7)	1.953(7)	1.21(1)	1.50(1)	25b
$Mo_2(\mu\text{-}\eta^2\text{-}CNPh)(CO)_4Cp_2$	$C{\equiv}NPh$	167.7(2)	135.2(2)	2.247(2)	1.244(3)	1.426(3)	25c
$(CpZrCl)_2(\mu\text{-}\eta^2\text{-}C{\equiv}NBu^t)(C_{10}H_8)$	$C{\equiv}NR$	168.0(1)	130.5(1)	2.180(2) 1.951(4)	1.249(2)	1.517(2)	25d
$Mo_2Cp_2(\mu\text{-}\eta^2\text{-}C{\equiv}NBu^t)(Ph_2PCH_2PPh_2)(CO)_3$	$C{\equiv}NR$	164.7(3)	136.7(4)	2.274(4)			22

[a] There are two crystallographically independent molecules.

$$[Tol{-}N{-}C(H){-}N{-}Tol]^- \xrightarrow{\text{reduction}} Tol{-}N^{2-} + Tol{-}N{=}C(H)^{\cdot}.$$

The formimidoyl anions must also be present in the reaction from which compound **III** is isolated (*vide infra*).

Since we did not locate the hydrogen atom from our structural study there is of course the possibility that such a fragment could be formulated as an isocyanide. Table 3 shows the structural parameters for some representative compounds in which the formimidoyl and isocyanide fragments bridge metal atoms in a comparable way to that found in **I** [24, 25]. The M—C—N and C—N—R angles are within narrow ranges of 165–174 and 130–137° for the isocyanide compounds, while they are significantly smaller for the formimidoyl compounds. The C—N—R angles of 125(2)° found in **I** are essentially the same as those of the latter. The M—C—N angles are very close to those found in the dinuclear compounds but deviate from those found in trinuclear compounds, as expected.

$TaCl_2(NPh)(DPhF)(HDPhF)$ (II)

From a high temperature reaction of $TaCl_5$ with $LiBH_4$ in the presence of $DPhF^-$, crystals of $Ta(DPhF)_3(NPh)$ and **II** are isolated [8b]. The oxidation state of the metal atom remains unaffected but a formamidinate group is reduced to phenylimide anion, which binds to the tantalum atom in a nearly linear manner as shown in Fig. 2. The Ta—N(5)—C(51) bond angle is 173.6(6)°. As expected, the shortest Ta—N bond distance of 1.778(7) Å corresponds to the $Ta{-}N_{(imide)}$ bond [26], while the longest [2.351(7) Å] is to the corresponding *trans* nitrogen atom which belongs to a chelating formamidine group. The other coordination sites of the six-coordinated molecule (**II**), are occupied by two *cis* Cl atoms and the nitrogen atom of a neutral formamidine molecule. The latter

Table 4. Selected bond lengths (Å) and angles (°) for $TaCl_2(NPh)(DPhF)(HDPhF)$ (**II**)

Ta—N(5)	1.778(7)	N(2)—C(1)	1.31(1)
Ta—N(3)	2.123(8)	N(2)—C(21)	1.42(1)
Ta—N(1)	2.206(7)	N(3)—C(2)	1.36(1)
Ta—N(4)	2.351(7)	N(3)—C(31)	1.41(1)
Ta—Cl(2)	2.392(2)	N(4)—C(2)	1.28(1)
Ta—Cl(1)	2.398(3)	N(4)—C(41)	1.40(1)
N(1)—C(1)	1.28(1)	N(5)—C(51)	1.39(1)
N(1)—C(11)	1.46(1)		
N(5)—Ta—N(3)	102.1(3)	C(2)—N(3)—C(31)	122.3(8)
N(5)—Ta—N(1)	91.5(3)	C(2)—N(3)—Ta	97.8(6)
N(3)—Ta—N(1)	84.7(3)	C(31)—N(3)—Ta	139.9(6)
N(5)—Ta—N(4)	159.8(3)	C(2)—N(4)—C(41)	123.7(8)
N(3)—Ta—N(4)	59.0(3)	C(41)—N(4)—Ta	146.7(6)
N(1)—Ta—N(4)	80.2(2)	C(51)—N(5)—Ta	173.6(6)
N(5)—Ta—Cl(2)	101.1(2)	N(1)—C(1)—N(2)	129.4(9)
N(3)—Ta—Cl(2)	92.6(2)	C(12)—C(11)—N(1)	119.0(8)
N(1)—Ta—Cl(2)	167.4(2)	C(16)—C(11)—N(1)	120.0(8)
N(4)—Ta—Cl(2)	87.8(2)	C(26)—C(21)—N(2)	119.2(9)
N(5)—Ta—Cl(1)	104.8(3)	C(22)—C(21)—N(2)	120.2(9)
N(3)—Ta—Cl(1)	151.3(2)	C(32)—C(31)—N(3)	120.8(9)
N(1)—Ta—Cl(1)	84.8(2)	C(36)—C(31)—N(3)	120.1(8)
N(4)—Ta—Cl(1)	92.9(2)	C(46)—C(41)—N(4)	125(1)
Cl(2)—Ta—Cl(1)	91.84(9)	C(42)—C(41)—N(4)	118.3(8)
C(1)—N(1)—C(11)	117.7(7)	N(5)—C(51)—C(52)	120.4(8)
C(11)—N(1)—Ta	118.5(6)	N(5)—C(51)—C(56)	121.4(8)
C(1)—N(2)—C(21)	125.4(8)		

Table 5. Selected bond lengths (Å) and angles (°) for $CoCl_2(PhNCHNPhCHNPh)$ (**III**)[a]

Co(1)—N(1)	1.998(3)	N(2)—C(21)	1.458(7)
Co(1)—Cl(1)	2.227(1)	N(1)—C(1)	1.283(5)
N(2)—C(1)	1.382(5)	N(1)—C(11)	1.444(5)
N(2)—C(1A)	1.382(5)		
N(1)—Co(1)—N(1A)	91.9(2)	C(1)—N(2)—C(21)	116.4(3)
N(1)—Co(1)—Cl(1)	107.4(1)	C(1)′—N(2)—C(21)	116.4(3)
N(1A)—Co(1)—Cl(1)	117.9(1)	C(1)—N(1)—C(11)	117.6(4)
N(1)—Co(1)—Cl(1A)	117.9(1)	C(1)—N(1)—Co(1)	125.2(3)
N(1A)—Co(1)—Cl(1A)	107.4(1)	C(11)—N(1)—Co(1)	117.0(3)
Cl(1)—Co(1)—Cl(1A)	113.03(7)	N(1)—C(1)—N(2)	125.3(4)
C(1)—N(2)—C(1A)	127.1(5)		

[a] Atoms labeled with an "A" are symmetry generated by a two-fold axis.

coordination mode has been observed in several compounds, examples of which are those of the divalent metal chloride, such as $MCl_2(amidine)_2$ for M = Fe, Co, Ni and Pt [2]. The ligand dimensions are comparable to those studied before.

$CoCl_2(PhNCHNPhCHNPh)$ (III)

If a reaction mixture containing $CoCl_2(HDPhF)_2$ and methyllithium, which is known to produce $Co_2(DPhF)_4$ and LiCl [27], is reacted with $NOBF_4$ in a mixture of CH_3CN and CH_2Cl_2, then compound **III** is isolated. The crystal structure of the blue compound contains a pseudotetrahedral cobalt atom as shown in Fig. 3. A two-fold axis bisects the Cl—Co—Cl angle and extends along the Co—N(2) vector. The neutral chelating N-[(phenylimino)methyl]methanimidamide ligand obtained can be thought of as formed from the reaction of a formamidine ligand and a phenylformimidoyl fragment from a ruptured formamidinate ligand (see discussion on compound **I**):

$$[PhN—C(H)—NPh]^- + HC{=}NPh^- \xrightarrow{\text{oxidation}} PhNC(H)N(Ph)C(H)NPh.$$

The six-membered metallocycle is planar as found in

Table 6. Selected bond lengths (Å) and angles (°) for $[(B_2H_5)N(Tol)C(H)N(Tol)]Ta(\mu_2\text{-}NTol)_2(\mu_2\text{-}DTolF)_2Ta[(Tol)NC(H)N(Tol)B_2H_5]\cdot 2Et_2O$ (**IV**)[a]

Ta—Ta(A)	2.6606(4)	B(1)—B(2)	1.58(1)
Ta—B(1)	2.534(5)	B(1)—H(1)	1.09(6)
Ta—H(1)	2.11(5)	B(1)—H(2)	1.16(4)
Ta—H(2)	2.18(4)	B(1)—H(3)	1.21(3)
Ta—N(1)	2.266(3)	B(1)—N(2)	1.535(6)
Ta—N(3)	2.247(3)	C(1)—N(2)	1.330(5)
Ta—N(4A)	2.252(4)	N(1)—C(1)	1.310(5)
Ta—N(5A)	2.028(3)	N(1)—C(11)	1.439(5)
Ta—N(5)	1.976(3)		
H(1)—B(1)—B(2)	104(3)	N(5)—Ta—N(3)	90.7(1)
H(1)—B(1)—H(2)	108(3)	N(5)—Ta—N(4A)	92.2(1)
H(1)—B(1)—H(3)	106(8)	N(5)—Ta—N(5A)	96.7(1)
H(1)—B(1)—N(2)	111(3)	Ta—N(5)—Ta(A)	83.3(1)
H(2)—B(1)—B(2)	110(2)	C(1)—N(1)—C(11)	113.0(3)
H(2)—B(1)—H(3)	110(8)	C(1)—N(1)—Ta	119.6(3)
H(2)—B(1)—N(2)	111(2)	C(1)—N(2)—B(1)	119.9(3)
H(3)—B(1)—N(2)	111(7)	C(1)—N(2)—C(21)	117.7(3)
H(3)—B(1)—Ta	144(7)	C(11)—N(1)—Ta	127.0(2)
N(1)—C(1)—N(2)	123.6(4)	C(2)—N(3)—Ta	119.5(3)
N(1)—Ta—Ta(A)	147.48(8)	C(2)—N(4)—C(41)	113.3(4)
N(2)—B(1)—B(2)	112.3(7)	C(2)—N(4)—Ta(A)	119.2(3)
N(3)—C(2)—N(4)	127.0(4)	C(21)—N(2)—B(1)	122.4(3)
N(3)—Ta—N(1)	90.3(1)	C(31)—N(3)—Ta	126.8(3)
N(3)—Ta—N(4A)	166.7(1)	C(41)—N(4)—Ta(A)	127.0(3)
N(4A)—Ta—N(1)	90.7(1)	C(51)—N(5)—Ta(A)	142.1(3)
N(5A)—Ta—N(1)	100.0(1)	C(51)—N(5)—Ta	134.5(3)
N(5A)—Ta—N(3)	84.1(1)	B(1)—H(1)—Ta	100(4)
N(5A)—Ta—N(4A)	82.7(1)	B(1)—H(2)—Ta	94(2)
N(5)—Ta—N(1)	163.3(1)	B(2)—B(1)—Ta	142.4(6)

[a] Atoms labeled with an "A" are generated by an inversion center.

two other compounds known for the benzyl substituted ligand, namely Cu(acetate)$_2$(BzN(CH)N(Bz)C(H)NBz) [28] and [Hg(BzNC(H)N(Bz)C(H)NBz)$_2$][Hg(C$_2$F$_3$O$_2$)$_4$] [29] and also in the hydrogen-substituted Cu(HNC(H)N(H)C(H)NH)$_2$(ClO$_4$)$_2$ compound [30]. The pattern of shorter bond distances between C(1)—N(1) and longer distance between C(1)—N(2) [1.283(5) and 1.382(5) Å, respectively] is essentially the same in the three compounds. Other compounds containing a planar M—N—C—N—C—N metallocycle or variations thereof are known [31]. However, variations in the nature of the substituents and the charge of the ligand do not allow a meaningful comparison of the molecular dimensions. The Co—N bond distances in **III** are very slightly shorter than those found in CoCl$_2$(HDTolF)$_2$ and CoCl$_2$(HDPhF)$_2$ as are the Co—Cl bond distances [2].

$[(B_2H_5)N(Tol)C(H)N(Tol)]Ta(\mu_2\text{-}NTol)_2(\mu_2\text{-}DTolF)_2Ta[(Tol)NC(H)N(Tol)B_2H_5]\cdot 2Et_2O$ (**IV**)

Reaction of potassium metal with crude $Ta_2(\mu_2\text{-}\eta^4\text{-}B_2H_6)(DTolF)_4$ produces compound **IV**. Fig. 4 shows the molecular structure. The dinuclear molecule possesses a crystallographically imposed inversion center. Two DTolF groups form bridges between the metal atoms which are separated by a distance of 2.6608(7) Å, which is consistent with the presence of a single bond. Two tolylimido groups also bridge the metal atoms. At opposite ends of the ditantalum unit a new type of ligand appears. It is formed by the insertion reaction of a $B_2H_5^-$ molecule into a DTolF group. This reaction is probably similar to the insertion reaction of metal carbonyls into amidinate groups to form carbamoyl units [6] or the reaction of BH_3 and diazaphosphates [32]. The refinement of the crystallographic data indicated that 50% of the molecules in the crystal are the product of insertion of a BH_3 group instead, in which case the third hydrogen atom resides where B(2) is shown in Fig. 5.

As expected, the Ta—N$_{(imide)}$ bond length of 1.976(3) Å found in **IV** is significantly shorter than the other three crystallographically independent Ta—N distances. The B(1)—N(2) distance of 1.535(6) Å compares well with those of other boron–nitrogen-containing species such as polypyrazolylborates [33]. The B(1)—B(2) separation of 1.58(1) Å is slightly shorter than those found in $Ta_2(\mu_2, \eta^4\text{-}B_2H_6)(DArF)_4$, Ar = phenyl and tolyl [1.72(2) and 1.68(2) Å, respectively] [11]. The reason for this shortening is likely to

Table 7. Selected bond lengths (Å) and angles ( ) for $PhNC(H)N(Ph)C(H)(NPh)_2Ta(DPhF)_3 \cdot Et_2O$ (V)

Ta—N(5)	2.080(5)	N(4)—C(41)	1.408(8)
Ta—N(6)	2.084(5)	N(5)—C(51)	1.396(8)
Ta—N(4)	2.202(5)	N(5)—C(3)	1.448(9)
Ta—N(2)	2.238(5)	C(3)—N(6)	1.440(9)
Ta—N(8)	2.244(5)	C(3)—N(10)	1.484(9)
Ta—N(1)	2.246(5)	N(6)—C(61)	1.430(8)
Ta—N(7)	2.273(6)	N(7)—C(4)	1.321(9)
Ta—N(3)	2.301(6)	N(7)—C(71)	1.402(8)
N(1)—C(1)	1.322(8)	C(4)—N(8)	1.321(9)
N(1)—C(11)	1.407(8)	N(8)—C(81)	1.417(9)
C(1)—N(2)	1.313(8)	N(9)—C(5)	1.287(9)
N(2)—C(21)	1.403(8)	N(9)—C(91)	1.414(9)
N(3)—C(2)	1.306(8)	C(5)—N(10)	1.368(9)
N(3)—C(31)	1.417(9)	N(10)—C(101)	1.428(9)
C(2)—N(4)	1.343(8)		

N(5)—Ta—N(6)	63.5(2)	N(3)—C(2)—N(4)	112.5(6)
N(5)—Ta—N(4)	86.9(2)	C(2)—N(4)—C(41)	119.7(6)
N(6)—Ta—N(4)	119.4(2)	C(2)—N(4)—Ta	96.1(4)
N(5)—Ta—N(2)	129.4(2)	C(41)—N(4)—Ta	144.0(4)
N(6)—Ta—N(2)	81.2(2)	C(32)—C(31)—N(3)	120.4(7)
N(4)—Ta—N(2)	80.0(2)	C(36)—C(31)—N(3)	121.3(6)
N(5)—Ta—N(8)	83.9(2)	C(42)—C(41)—N(4)	120.1(6)
N(6)—Ta—N(8)	136.1(2)	C(46)—C(41)—N(4)	121.7(6)
N(4)—Ta—N(8)	84.8(2)	C(51)—N(5)—C(3)	118.5(5)
N(2)—Ta—N(8)	141.9(2)	C(51)—N(5)—Ta	135.7(4)
N(5)—Ta—N(1)	143.1(2)	C(3)—N(5)—Ta	95.6(4)
N(6)—Ta—N(1)	86.0(2)	N(6)—C(3)—N(5)	98.7(5)
N(4)—Ta—N(1)	128.0(2)	N(6)—C(3)—N(10)	116.0(6)
N(2)—Ta—N(1)	58.6(2)	N(5)—C(3)—N(10)	114.1(6)
N(8)—Ta—N(1)	108.0(2)	C(61)—N(6)—C(3)	118.3(6)
N(5)—Ta—N(7)	80.1(2)	C(61)—N(6)—Ta	141.1(4)
N(6)—Ta—N(7)	86.4(2)	C(3)—N(6)—Ta	95.7(4)
N(4)—Ta—N(7)	141.7(2)	C(52)—C(51)—N(5)	124.2(6)
N(2)—Ta—N(7)	135.0(2)	N(5)—C(51)—C(56)	119.5(6)
N(8)—Ta—N(7)	58.2(2)	C(66)—C(61)—N(6)	120.8(6)
N(1)—Ta—N(7)	77.6(2)	C(62)—C(61)—N(6)	120.5(6)
N(5)—Ta—N(3)	138.8(2)	C(4)—N(7)—C(71)	120.7(6)
N(6)—Ta—N(3)	151.1(2)	C(4)—N(7)—Ta	94.0(4)
N(4)—Ta—N(3)	58.5(2)	C(71)—N(7)—Ta	142.4(4)
N(2)—Ta—N(3)	70.0(2)	N(8)—C(4)—N(7)	112.5(6)
N(8)—Ta—N(3)	72.3(2)	C(4)—N(8)—C(81)	120.2(6)
N(1)—Ta—N(3)	77.4(2)	C(4)—N(8)—Ta	95.3(4)
N(7)—Ta—N(3)	112.4(2)	C(81)—N(8)—Ta	142.6(5)
C(1)—N(1)—C(11)	120.0(5)	N(7)—C(71)—C(76)	122.2(6)
C(1)—N(1)—Ta	94.0(4)	N(7)—C(71)—C(72)	120.3(6)
C(11)—N(1)—Ta	145.5(4)	C(82)—C(81)—N(8)	121.5(7)
N(2)—C(1)—N(1)	112.7(6)	C(86)—C(81)—N(8)	120.5(7)
C(1)—N(2)—C(21)	123.5(5)	C(5)—N(9)—C(91)	119.4(6)
C(1)—N(2)—Ta	94.6(4)	N(9)—C(5)—N(10)	123.0(7)
C(21)—N(2)—Ta	139.4(4)	C(5)—N(10)—C(101)	117.4(6)
C(12)—C(11)—N(1)	120.8(6)	C(5)—N(10)—C(3)	120.1(6)
C(16)—C(11)—N(1)	120.6(6)	C(101)—N(10)—C(3)	121.9(6)
C(26)—C(21)—N(2)	124.5(6)	C(96)—C(91)—N(9)	117.3(7)
N(2)—C(21)—C(22)	117.9(6)	C(92)—C(91)—N(9)	125.0(7)
C(2)—N(3)—C(31)	120.8(6)	C(102)—C(101)—N(10)	121.1(6)
C(2)—N(3)—Ta	92.8(4)	C(106)—C(101)—N(10)	119.2(7)
C(31)—N(3)—Ta	145.4(4)		

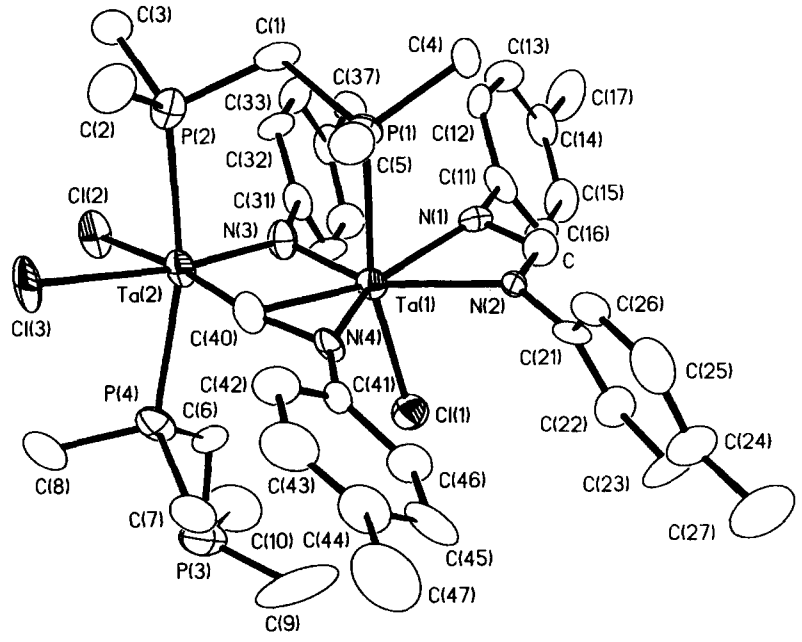


Fig. 1. A drawing of the molecular structure of **I** showing the atom numbering scheme. Atoms are represented by their 30% probability ellipsoids.

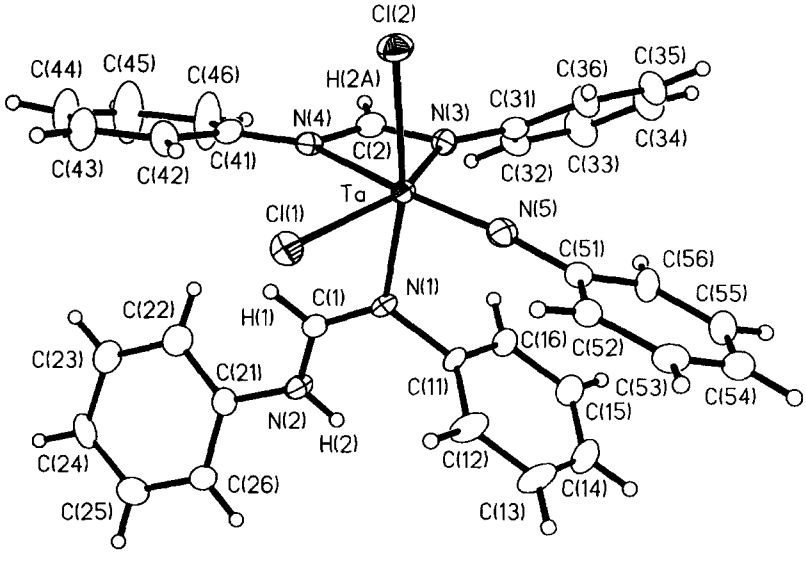


Fig. 2. Thermal ellipsoid plot of the X-ray structure of **II**. Non-hydrogen atoms are represented by their 30% probability ellipsoids.

be artificial and is probably due to the partial occupancy of the position close to B(2) by a hydrogen atom in the BH_3-substituted molecules. In $Ta_2(\mu_2,\eta^4\text{-}B_2H_6)(DArF)_4$ which also have Ta—H—B bonds, Ta—B separations range from 2.47(1) to 2.52(2) Å, which compares well with the Ta—B distance of 2.534(5) Å found in **IV**. All atoms in the B—N—C—N—Ta unit are essentially planar.

$PhNC(H)N(Ph)C(H)(NPh)_2Ta(DPhF)_3 \cdot Et_2O$ (**V**)

Reaction of $TaCl_5$ and potassium graphite with a cold THF solution of LiDPhF gave a green solid. Extraction with Et_2O yielded a green–brown precipitate whose color changed slowly to brown when placed in a freezer. From that solution brown crystals of compound **V** were obtained in small yield. From

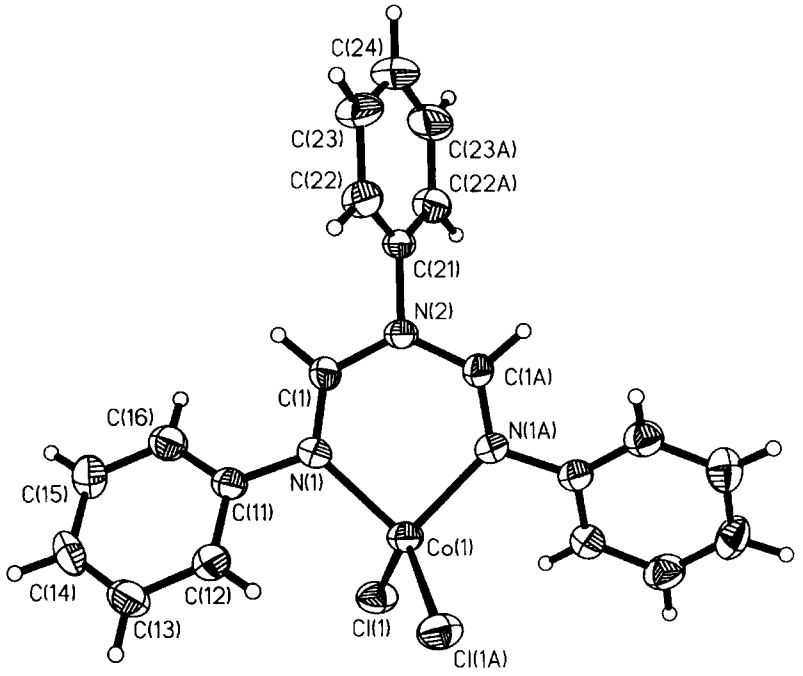


Fig. 3. A drawing of the structure of **III**. Atoms are represented by their 50% probability ellipsoids.

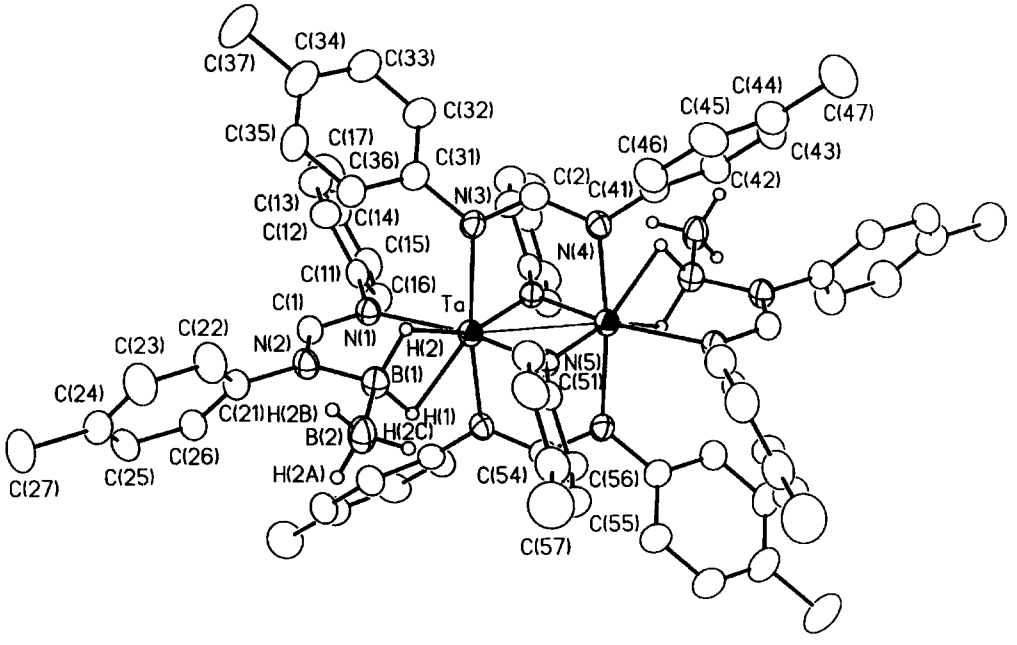


Fig. 4. A drawing of the centrosymmetric structure of **IV**. A disorder in the molecule imposes the partial occupancy at B(2), which is then substituted by a hydrogen atom. 30% probability ellipsoids are shown for non-hydrogen atoms.

the solid residue an extraction with toluene generated an orange solution from which orange crystals of $Ta(DPhF)_4$ were obtained [8b]. A drawing of the eight-coordinated mononuclear compound **V** is shown in Fig. 6. Three of the chelating groups surrounding the tantalum(IV) ion are typical DPhF anions. The fourth group, N,N′,N″-triphenyl-N-[(phenylamino)methyl]methanetriaminato(2-)-N′,N″, is unorthodox. It appears to be the product of a condensation of two DPhF anions, which produces a

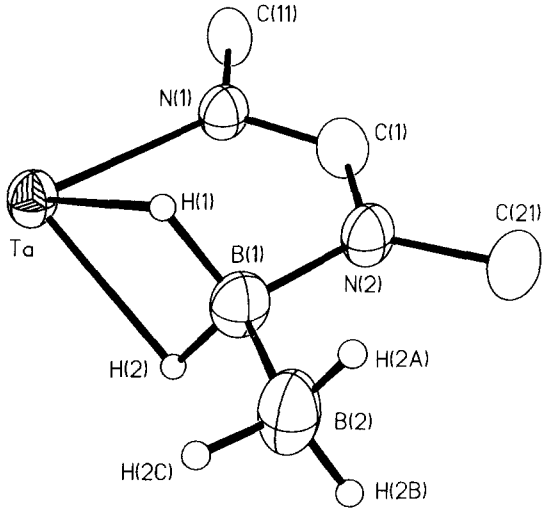


Fig. 5. Thermal ellipsoid plot of the core of the boron-containing formamidinate ligand in **IV**. Non-hydrogen atoms are represented by their 30% probability ellipsoids.

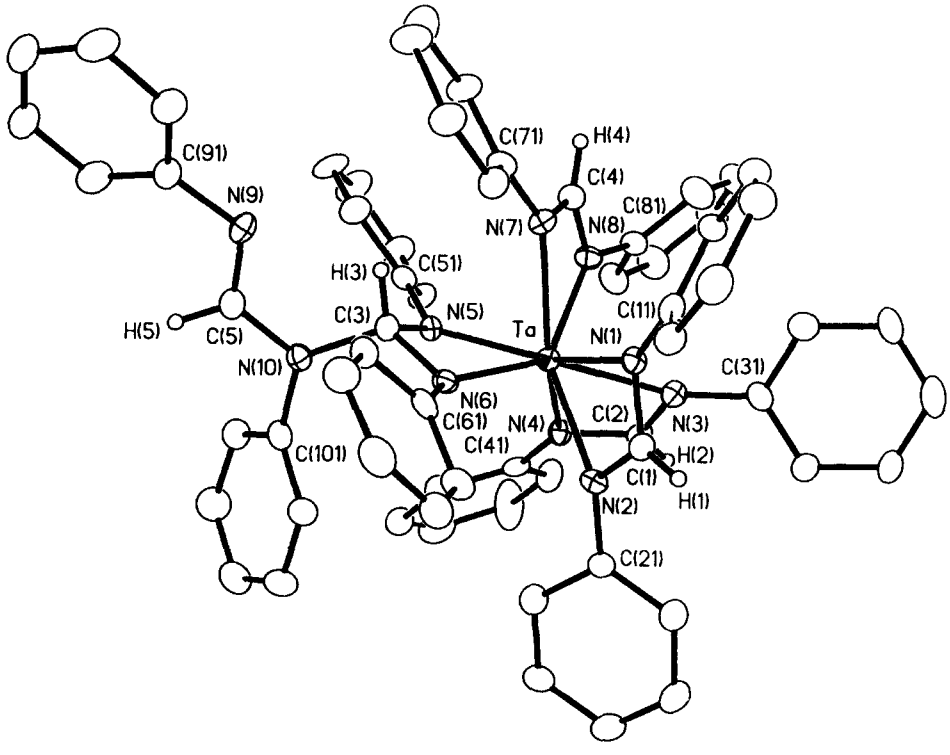


Fig. 6. A drawing of the molecular structure of **V**. Non-hydrogen atoms are represented by their 30% probability ellipsoids.

dianion that acts essentially as a diamide. The Ta—N distances to the dianion are shorter (0.12 to 0.22 Å) than those found in Ta—$N_{(DPhF)}$.

Figure 7 is a thermal ellipsoid drawing of the condensed ligand and shows some of the relevant interatomic dimensions. C(3) is clearly an sp^3 hybridized atom with long C—N bond lengths while C(5) is sp^2 hybridized. The C(5)—N(9) separation of 1.287(9) Å is typical for a C—N double bond.

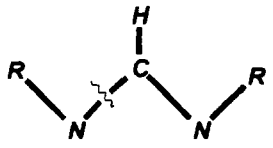
Summary

In the development of the field of metal to metal bonds, carboxylates have played an important role. The ability of amidinates to stabilize a variety of oxidation states throughout the transition series allows the formation of compounds for which no carboxylate analogs are known, as well as analogs of known carboxylate compounds.

As more reactions have been carried out with elements which require more drastic conditions to obtain an oxidation state which might give bonds between the metal atoms, the reactive nature of the amidinate ligand has become more and more evident.

Figure 8 summarizes reactions in which amidinate ligands are modified in the presence of metal-containing species. Examples have been observed of coupling of small molecules such as CO and $B_2H_5^-$ or BH_3 (derived from $B_2H_6^{2-}$ and BH_4^-, respectively) which give rise to N—C and N—B bond formation. Phenylnitrile may be inserted into the amidine or removed from a benzamidine. Classical orthometalation reactions are also known for aryl substituted amidines. An unusual reaction in which two amidinate ligands couple is evidenced by **V**.

Other reactions require cleavage of a formamidine carbon–nitrogen bond which gives imido and formimidoyl fragments.



Both of those entities are present as such in **I**. The imido group frequently finds its way to the metal center to form either M=N—R or $M_2(\mu$-NR) moieties, while the formimidoyl anion may form bonds to the metal atoms as in **I** and **II** or insert into a formamidine anion as in **III** to give a new neutral chelating ligand. Cleavage of carbon–nitrogen bonds has precedent in the coordination chemistry of tantalum [34].

In addition to the unorthodox reaction products reported here, we have also observed an attack on a methyl carbon atom of a chelated acetylacetonate group to produce the anion PhN(H)C(H)C(H)C(O)C(H)C(O)(CH_3) [35]. In still another reaction there is an insertion of two carbon atoms of an acetone molecule between the imido and formimidoyl fragments [36]. Both of these reactions are being studied further and full reports will appear later.

Note added in Proof—Recent evidence found in our laboratory strongly suggests that compound **I** is an isocyanide complex. The presence of arylformimidoyl groups has been established unambiguously in other tantalum complexes (F. A. Cotton, L. M. Daniels, C. A. Murillo and X. Wang, *Inorg. Chem.*, submitted).

Acknowledgements—We are grateful to the Vicerretoria de Investigación U. C. R. (Project 115-87-516) and the Depart-

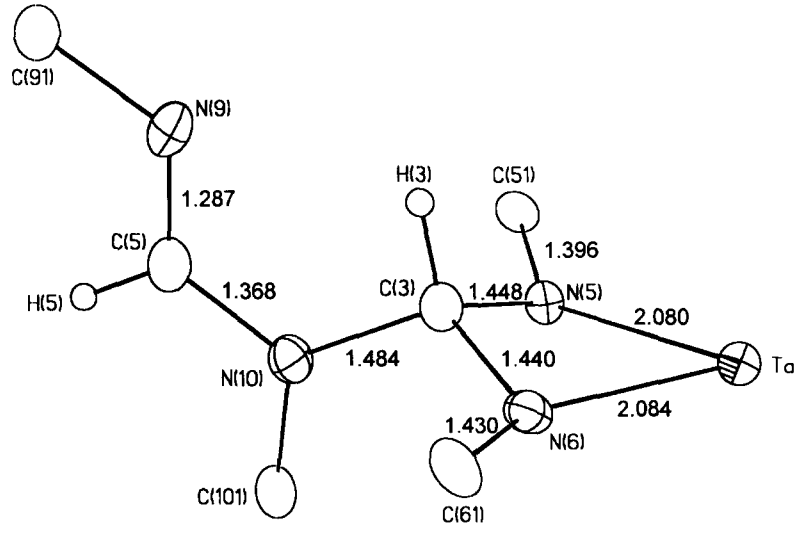


Fig. 7. Thermal ellipsoid plot of the skeleton of the coupled formimidinate dianion in **V** showing the interatomic distances in angstroms. (See Table 7 for estimated standard deviations.)

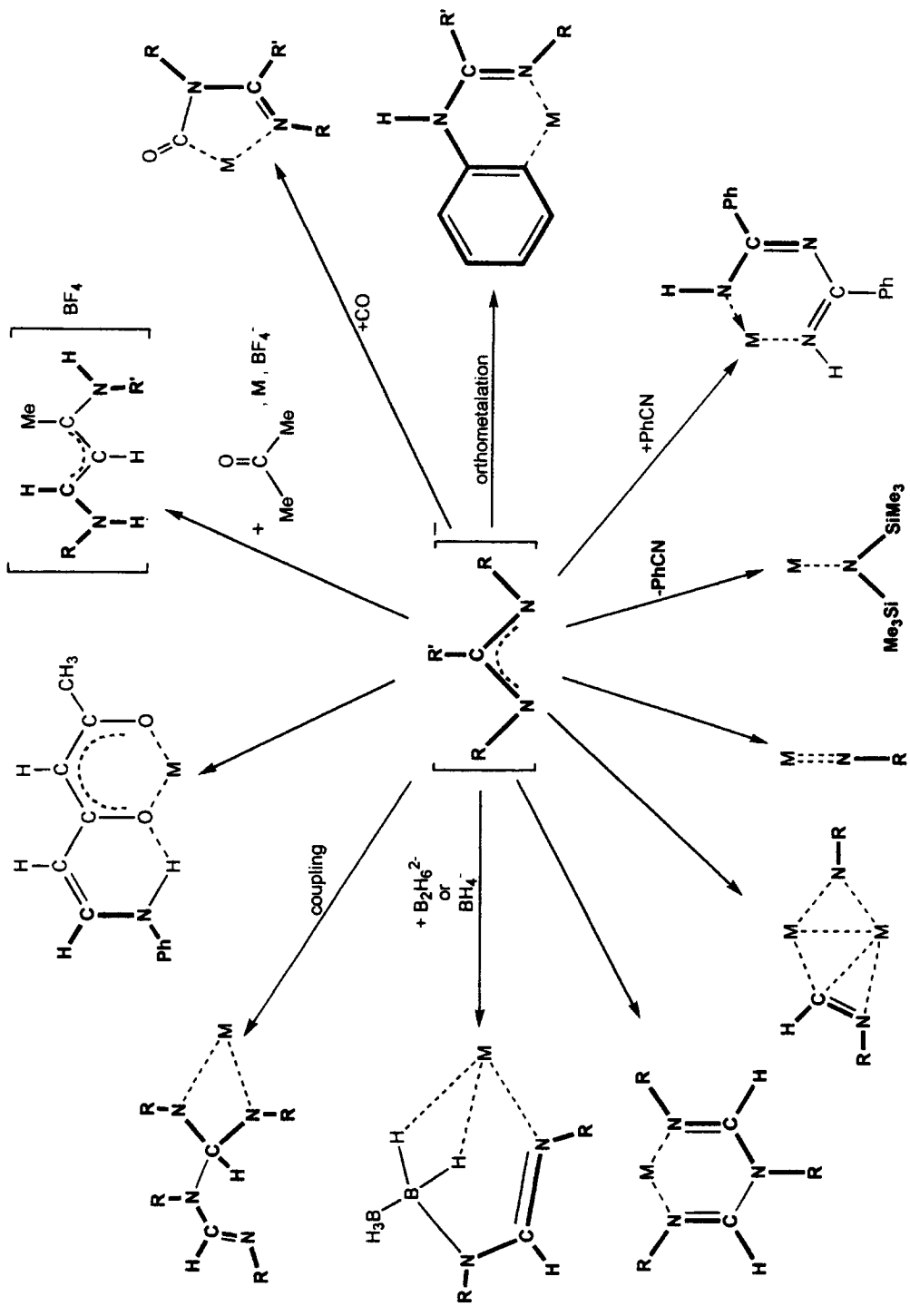


Fig. 8. A schematic representation of reactions in which amidinate ligands are modified in the presence of metal-containing species. For clarity the non-hydrogen atoms, which originated from an amidinate ligand are shown in bold and metal-to-ligand bonds as dotted lines. Other ligands bonded to the metal center are not shown.

ment of Chemistry for support of work at the University of Costa Rica and to the National Science Foundation for support of work at Texas A&M University.

REFERENCES

1. Barker, J. and Kilner, M., *Coord. Chem. Rev.* 1994, **133,** 219.
2. (a) Cotton, F. A., Daniels, L. M., Maloney, D. J., Matonic, J. H. and Murillo, C. A., *Polyhedron*, 1994, **13,** 815; (b) Arnold, D. I., Cotton, F. A., Maloney, D. J., Matonic, J. H. and Murillo, C. A., *Polyhedron*, 1997, **16,** 133.
3. Cotton, F. A., Daniels, L. M., Maloney, D. J. and Murillo, C. A., *Inorg. Chim. Acta*, 1996, **242,** 31.
4. Cotton, F. A. and Walton, R. A., *Multiple Bonds between Metal Atoms*, 2nd edn. Oxford University Press, Oxford, U.K. 1993.
5. See for example: (a) Cotton, F. A., Daniels, L. M. and Murillo, C. A., *Inorg. Chem.* 1993, **32,** 2881; (b) Cotton, F. A., Daniels, L. M., Falvello, L. R. and Murillo, C. A., *Inorg. Chim. Acta* 1994, **219,** 7.
6. (a) Inglis, T., Kilner, M., Reynoldson, T. and Robertson, E. E., *J. Chem. Soc. Dalton Trans.* 1975, 924; (b) Inglis, T. and Kilner, M., *J. Chem. Soc. Dalton Trans.* 1976, 562.
7. Barker, J., Cameron, N. D., Kilner, M., Mahmoud, M. M. and Wallwork, S. C., *J. Chem. Soc. Dalton Trans.* 1991, 3435.
8. (a) Cotton, F. A. and Wojtczak, W. A., *Polyhedron* 1994, **13,** 1337; (b) Cotton, F. A., Matonic, J. H., Murillo, C. A. and Wang, X., *Bull. Soc. Chim. France*, 1996, **133,** 711.
9. Barker, J., Kilner, M., Mahmoud, M. M. and Wallwork, S. C., *J. Chem. Soc. Dalton Trans.* 1989, 837.
10. Flores, J. C., Chien, J. C. W. and Rausch, M. D., *Organometallics* 1995, **14,** 1827.
11. Cotton, F. A., Daniels, L. M. and Murillo, C. A. and Wang, X., *J. Am. Chem. Soc.* 1996, **118,** 4830.
12. Roberts, R. M., *J. Org. Chem.* 1949, **14,** 277.
13. Cotton, F. A. and Najjar, R. C., *Inorg. Chem.* 1981, **20,** 2716.
14. (a) Fürstner, A. in *Active Metals* ed. A. Fürstner. VCH Publishers, New York, 1996, p. 381; (b) Schwindt, M. A., Lejon, T. and Hegedus, L. S., *Organometallics*, 1990, **9,** 2814; (c) Fürstner, A., *Angew. Chem. Int. Ed. Engl.* 1993, **32,** 164.
15. Pflugrath, J. and Messerschmitt, A., *MADNES*, Munich Area Detector (New EEC) System, Version EEC 11/1/89, with enhancements by Enraf–Nonius Corporation, Delft, The Netherlands. A description of MADNES appears in Messerschmitt, A. and Pflugrath, J., *J. Appl. Cryst.* 1987, **20,** 30.
16. (a) Bryan, J. C., Cotton, F. A., Daniels, L. M., Haefner, S. C. and Sattelberger, A. P., *Inorg. Chem.* 1995, **34,** 1875; (b) Scheidt, W. R. and Turowska-Turk, I., *Inorg. Chem.* 1994, **33,** 1314.
17. Blessing, R. H., *Acta Cryst.* 1995, **A51,** 31.
18. Evans, P. R., *ABSURD*—Absorption correction program, for the area detector. MRC Laboratory of Molecular Biology, Hills Road, Cambridge, U.K., 1990.
19. TEXSAN–TEXRAY Structure Analysis Package, Molecular Structure Corporation, 1985.
20. SHELXTL Version 5; Siemens Industrial Automation Inc., Madison, WI, U.S.A.
21. Puddephatt, R. J., *Chem. Soc. Rev.* 1983, **12,** 99.
22. Riera, V., Ruiz, M. A., Villafañe, F., Bois, C. and Jeannin, Y., *J. Organomet. Chem.* 1990, **382,** 407, and refs therein.
23. Jones, W. D. and Kosar, W. P., *Organometallics* 1986, **5,** 1823, and refs therein.
24. (a) Evans, J. W., Hanusa, T. P., Meadows, J. H., Hunter, W. E. and Atwood, J. L., *Organometallics*, 1987, **6,** 295; (b) Adams, R. A. and Golembeski, N. M., *J. Am. Chem. Soc.* 1979, **101,** 2579; (c) Casey, C. P., Widenhoefer, R. A., Hallenbeck, S. L., Hayashi, R. K. and Gavney, Jr., J. A., *Organometallics* 1994, **13,** 4720.
25. (a) Cuenca, T., Gómez, R., Gómez-Sal, P., Rodriguez, G. M. and Royo, P., *Organometallics*, 1992, **11,** 1229; (b) Adams, H., Bailey, N. A., Bannister, C., Faers, M. A., Fedorko, P., Osborn, V. A. and Winter, M. J., *J. Chem. Soc. Dalton Trans.* 1987, 341; (c) Adams, R. A., Katahira, D. A. and Yang, L.-W., *Organometallics*, 1982, **1,** 231; (d) Herrmann, W. A., Menjón, B. and Herdtweck, E., *Organometallics*, 1991, **10,** 2134.
26. (a) Maloney, D. J., dissertation, Texas A&M University, TX, 1995; (b) Cotton, F. A., Daniels, L. M., Maloney, D. J., Matonic, J. H. and Murillo, C. A., *Inorg. Chim. Acta*, 1997, accepted.
27. Compare for example with other Ta—$N_{(imide)}$ given in Table 5.3 in Nugent, W. A. and Mayer, J. M., *Metal–Ligand Multiple Bonds*. John Wiley & Sons, New York, NY, 1988.
28. Breuer, S. W. and Small, R. W. H., *Acta Cryst.* 1991, **C47,** 871.
29. Breuer, S. W. and Small, R. W. H., *Acta Cryst.* 1995, **C51,** 1784.
30. Turnbull, M. M., Wei, M. Y. and Wilett, R. D., *J. Coord. Chem.* 1995, **35,** 11.
31. See for example (a) Robinson, V., Taylor, G. E., Woodward, P., Bruce, M. I. and Wallis, R. C., *J. Chem. Soc. Dalton Trans.* 1981, 1169; (b) Bland, W. J., Kemmitt, R. D. W., Nowell, I. W. and Russell, D. R., *Chem. Commun.* 1968, 1065; (c) Pal, C. K., Chattopadhyay, S., Sinha, C. and Chakravorty, A., *Inorg. Chem.* 1996, **35,** 2442.
32. Alcaraz, G., Baceiredo, A., Nieger, M., Schoeller, W. W. and Bertrand, G., *Inorg. Chem.* 1996, **35,** 2458.
33. See for example (a) Cotton, F. A., Frenz, B. A. and Murillo, C. A., *J. Am. Chem. Soc.* 1975, **97,** 2118; (b) Cotton, F. A. and Murillo, C. A., *Inorg. Chim. Acta* 1976, **17,** 121; (c) Collins, D. M., Cotton, F. A. and Murillo, C. A., *Inorg. Chem.* 1976, **15,** 1861; (d) Reger, D. L., Mason, S. S., Reger, L. B., Rheingold, A. L. and Ostrander, R. L., *Inorg. Chem.* 1994, **33,** 1811.
34. Gray, S. D., Smith, D. P., Bruck, M. A. and Wigley, D. E., *J. Am. Chem. Soc.* 1992, **114,** 5462, and refs therein.
35. Arnold, D. I., Cotton, F. A., Matonic, J. H. and Murillo, C. A., *J. Chem. Soc., Chem. Commun.* 1996, 2113.
36. *Cotton, F. A., Daniels, L. M., Haefner, S. C. and Murillo, C. A., J. Chem. Soc., Chem. Commun.*, 1996, 2507.

Pergamon

PII: S0277-5387(96)00367-1

Polyhedron Vol. 16, No. 7, pp. 1193–1199, 1997
Copyright © 1997 Elsevier Science Ltd
Printed in Great Britain. All rights reserved
0277-5387/97 $17.00+0.00

Synthesis and structural characterization of Zintl anions containing the tris(ethylenediamine)-zinc cation: $[Zn(N_2C_2H_8)_3][Te_3] \cdot (0.5en)$ and $[Zn(N_2C_2H_8)_3]_2[Sn_2Te_6] \cdot (en)$

Julie L. Shreeve-Keyer, Christopher J. Warren, Sandeep S. Dhingra† and Robert C. Haushalter*

NEC Research Institute, 4 Independence Way, Princeton, NJ 08540, U.S.A.

(Received 4 April 1996; accepted 25 July 1996)

Abstract—Two Zintl anions which contain the [tris(ethylenediamine)-zinc]$^{2+}$ cation have been synthesized and structurally characterized by single-crystal X-ray diffraction. When a constant current of 1 mA is applied between a $ZnTe_{10}$ alloy cathode and a Ni plate anode, in a saturated solution of tetrapropylammonium bromide in ethylenediamine, a deep red–purple solution is generated around the cathode as polyanions are generated. After a few days, small, black crystals formed, which were identified by single crystal X-ray diffraction as $[Zn(N_2C_2H_8)_3][Te_3] \cdot 0.5(N_2C_2H_8)$ (**1**). The 1 : 1 : 1 stoichiometric reaction of the Zintl phase K_4SnTe_4 with $ZnCl_2$ in the presence of $(C_2H_5)_4NBr$ in ethylenediamine at 100°C for 1 day in a sealed evacuated quartz tube gave crystals of $[Zn(N_2C_2H_8)_3]_2[Sn_2Te_6] \cdot (en)$ (**2**). The structures of **1** and **2** consist of discrete anions which are surrounded in the solid state by the tris(ethylenediamine)-zinc cations. Copyright © 1997 Elsevier Science Ltd

Keywords: Zintl anion; crystal structure; zinc; tellurium; tin; electrochemical synthesis.

The chemistry of polytelluride complexes has become an increasingly active area of research [1]. This is partially due to the emerging uses of tellurides in industrial settings where they have found application as small-band gap semiconductors, in the preparation of photovoltaic materials and in IR detection devices [2]. There also exists a number of synthetic methodologies available to prepare these types of compounds, which not only circumvent the hazards associated with toxic substances such as H_2Te, but also produce a variety of new and interesting materials. By far, the most commonly used methods are those of the high temperature fusion of the elements [3] and the solvent extraction of alloy phases [4], although other less commonly used techniques such as the treatment of binary alloys with potassium (or other alkali metals) [4a], reactions carried out in molten salts [1d], solventothermal techniques [5] and chemical transport reactions [6] have been employed. We have also recently developed a novel electrochemical synthetic method which allows for the room-temperature generation of Zintl anion clusters from the cathodic dissolution of tellurium alloy electrodes [7]. This electrochemical method has been quite successful for generation of new polychalcogenides and has produced such species as $[Sb_9Te_6]^{3-}$ [8a], $[Sb_4Te_4]^{4-}$ [8a], $[Sb_2Te_5]^{4-}$ [8b], $[Sb_6Te_9]^{4-}$ [8b], $[Sn_2Te_3]^{2}$ [8c], $[Sn_2Te_6]^{4-}$ [8c], $[Au_3Te_4]^{3-}$ [8d], $[GaTe_2] \cdot (en)_2^{-1}$ [8e], $[In_2Te_4]^{2-}$ [8f], $[As_2Te_5]^{2-}$ [8g], $[Hg_3Te_7] \cdot (0.5en)^{4-}$ [8h] and $[Te_{12}]^{2-}$ [8i]. All of these techniques have produced an abundance of new and interesting molecular species, one-dimensional chain materials, layered compounds and even extended three-dimensional solid state structures. They have all been extremely successful as routes to the isolation of stable, solid derivatives of the homo- and heteropolyatomic anions of the heavier main group and

* Author to whom correspondence should be addressed.

† Current address: Mobil Research and Development Corporation, Central Research Division, Post Office Box 1025, Princeton, NJ 08540, U.S.A.

post-transition metals, and have helped to increase our understanding of the bonding modes and chemistry of these species.

In this paper we describe the synthesis and single-crystal X-ray structures of two polytellurides $[Zn(N_2C_2H_8)_3][Te_3]\cdot 0.5(N_2C_2H_8)$ (**1**) and $[Zn(N_2C_2H_8)_3]_2[Sn_2Te_6]\cdot(en)$ (**2**), with zinc-containing counter cations. The structures of both compounds **1** and **2** consist of discrete anions, which are surrounded in the solid state by the tris(ethylenediamine)-zinc cations.

EXPERIMENTAL

General techniques

All reactions and manipulations were performed with the careful exclusion of air and water under a high-purity He or Ar atmosphere. Ethylenediamine (Aldrich) was purified before use first by distillation from CaH_2 followed by multiple distillations from a red solution of K_4Sn_9. The electrochemical cells and quartz tube vessels were dried in an oven at 200°C for at least 2 h prior to use.

Preparation of $[Zn(N_2C_2H_8)_3][Te_3]\cdot 0.5(en)$ (**1**)

The synthesis of compound **1** was performed in a three-compartment, liquid-junction, air-tight electrochemical cell equipped with a Ni plate counter electrode in a saturated ethylenediamine (en) solution of tetrapropylammonium bromide (TPABr) as previously described [7], using a cathode of nominal composition $ZnTe_{10}$. The reaction was run at constant current using an external power supply which was connected to the leads of the cathode and anode and set to run at the maximum current allowed, 1 mA. Application of 1 mA of current resulted in the production of a dark purple stream of anions which surrounded the cathode and then slowly sank to the bottom of the cathode chamber. After approximately 4 days, small black crystals were found growing throughout the cathode chamber and were isolated in 38% yield [9].

Preparation of $[Zn(N_2C_2H_8)_3]_2[Sn_2Te_6]\cdot(en)$ (**2**)

The synthesis of compound **2** was accomplished by the reaction of the Zintl phase K_4SnTe_4 (0.10 g, 0.127 mmol) with $ZnCl_2$ (0.0173 g, 0.127 mmol) and $(C_2H_5)_4NBr$ (0.0267 g, 0.127 mmol) in ethylenediamine (1 cm^3) in a sealed quartz ampoule held at 100°C for 1 day. The K_4SnTe_4 was prepared by the high-temperature fusion reaction of KSn (2.00 g, 0.013 mol) and Te (1.62 g, 0.013 mol) in a quartz vessel under a constant pressure of argon (the KSn alloy was prepared by carefully reacting potassium metal with tin metal in a similar process). This rather violent reaction produces the congruently melting K_4SnTe_4 phase [10] and a tin plug which can be removed from the melt on grinding and recycled into the next reaction. Crystals of $[Zn(N_2C_2H_8)_3]_2[Sn_2Te_6]\cdot(en)$ (**2**) were isolated in approximately 40% yield [11]. The reaction also produces excess Te metal, which is required by the stoichiometry of the reaction and is observed as dark gray powder in the reaction vessel.

Since compound **2** does not contain the $(C_2H_5)_4N^+$ cation, attempts to grow crystals of **2** were tried in the absence of this cation. These reactions typically resulted in the formation of compound **2**, but with an overall decrease in the yield of the product. The role of the $(C_4H_5)_4NBr$ in the reaction process is not understood at this time.

X-ray diffraction analyses

$[Zn(N_2C_2H_8)_3][Te_3]\cdot 0.5(en)$ (**1**). A black block-shaped crystal of approximate dimensions $0.10\times 0.15\times 0.20$ mm was sealed into a glass capillary under an inert atmosphere of helium. X-ray intensity data were collected on a Rigaku AFC7R automatic four-cycle diffractometer equipped with Mo-K_α radiation and an RU300 18 kW rotating anode generator. Cell constants and an orientation matrix for data collection were obtained from the setting angles of 24 carefully centered reflections in the range $20.76 \leqslant 2\theta \leqslant 26.30°$ and corresponded to a primitive monoclinic cell with the unit cell dimensions given in Table 1. The systematic absences of $h0l$: $h+l \neq 2n$ and $0k0$: $k \neq 2n$ uniquely determined the space group to be $P2_1/n$ (no. 14).

The data collection consisted of scans of $(1.05+0.35\tan\theta)°$ in the range $5 \leqslant 2\theta \leqslant 50.1°$, which were made using the ω–2θ scan technique at a speed of 16.0° min^{-1} (in omega). The weak reflections $[I < 20\sigma(I)]$ were rescanned a maximum of four times and the counts were accumulated to ensure good counting statistics. The intensities of three standard reflections were measured after every 150 reflections and, over the course of data collection, decreased in intensity by 8.1%. A linear correction factor was supplied to the data to account for this phenomenon. An empirical absorption correction using the program DIFABS [12] was also applied in the final stages of refinement and resulted in transmission factors ranging from 0.88 to 1.00. The data were also corrected for Lorentz and polarization effects.

The structure was solved by direct methods [13] and refined by F by full-matrix least-squares using the *teXsan* crystallographic software package of Molecular Structure Corporation [14]. All of the non-hydrogen atoms in the structure were refined with anisotropic displacement coefficients. Hydrogen atoms were included in the final model, but were not refined. The final least-squares refinement was based on 1383 observed reflections $[I > 3.0\sigma(I)]$ and 163

Table 1. Crystallographic data for $[Zn(N_2C_2H_8)_3][Te_3]\cdot 0.5(en)$ (**1**) and $[Zn(N_2C_2H_8)_3]_2[Sn_2Te_6](en)$ (**2**)

Compound	**1**	**2**
Empirical formula	$C_7H_{28}N_7Te_3Zn$	$C_{14}H_{56}N_{14}Sn_2Te_6Zn_2$
Mol. wt (g mol^{-1})	658.53	1554.43
Temperature (K)	293	293
Crystal color, habit	Black, block	Black, prism
Crystal dimensions (mm)	$0.10\times0.15\times0.20$	$0.20\times0.15\times0.30$
Space group	$P2_1/n$ (no. 14)	$P2_1/n$ (no. 14)
a (Å)	8.502(1)	8.580(1)
b (Å)	15.554(2)	15.970(1)
c (Å)	15.046(1)	15.2466(9)
β (°)	102.25(1)	95.076(8)
Volume (Å^3)	1944.3(4)	2081.1(3)
Z	4	2
D_{calc} (g cm^{-3})	2.249	2.480
Scan type	ω–2θ	ω–2θ
Scan rate (e min^{-1})	16.0 (in ω)	32.0 (in ω)
2θ (max) (°)	50.1	50.1
μ (Mo-K_α) (cm^{-1})	56.74	64.76
Reflections collected	2944	4107
Unique reflections	2691	3839
Observed reflections	1383 [$I > 300\sigma(I)$]	3002 [$I > 3.00\sigma(I)$]
No. of variables	163	172
Final R, R_w	0.029, 0.028	0.036, 0.044

variable parameters and converged with $R(R_w) = 0.029(0.028)$, with GOF = 1.54 and $\rho(\max) = 0.58$ e Å^{-3}, $\rho(\min) = -0.46$ e Å^{-3}. Further details of the X-ray structural analysis of **1** are given in Table 1.

$[Zn(N_2C_2H_8)_3]_2Sn_2Te_6\cdot(en)$ (**2**). A black prism-shaped crystal of approximate dimensions $0.20\times0.15\times0.30$ mm was sealed into a glass capillary tube under an inert atmosphere of helium. X-ray intensity data were collected on a Rigaku AFC7R automatic four-circle diffractometer equipped with Mo-K_α radiation and an RU300 18 kW rotating anode generator. Cell constants and an orientation matrix for data collection were obtained from the setting angles of 25 carefully centered reflections in the range $20.04 \leqslant 2\theta \leqslant 30.26°$ and corresponded to a primitive monoclinic cell with the unit cell dimensions given in Table 1. The systematic absences of $h0l$: $h+l \neq 2n$ and $0k0$: $k \neq 2n$ uniquely determined the space group to be $P2_1/n$ (no. 14).

The data collection consisted of scans of $(1.37+0.35\tan\theta)°$ in the range $5 \leqslant 2\theta \leqslant 50.1°$, which were made using the ω–2θ scan technique at a speed of 32° min^{-1} (in omega). The weak reflections [$I < 20\sigma(I)$] were rescanned a maximum of four times and the counts were accumulated to ensure good counting statistics. The intensities of three standard reflections were measured after every 150 reflections and, over the course of data collection, decreased in intensity by 0.4%. A linear correction factor was applied to the data to account for this phenomenon. An empirical absorption correction using the program DIFABS [12] was also applied in the final stages of refinement and resulted in transmission factors ranging from 0.89 to 1.00. The data were also corrected for Lorentz and polarization effects.

The structure was solved by direct methods [15] and refined on F by full-matrix least-squares using the *teXsan* crystallographic software package of Molecular Structure Corporation [14]. All of the non-hydrogen atoms in the structure were refined with anisotropic displacement coefficients. Hydrogen atoms were included in the final model, but were not refined. The final least-squares refinement was based on 3002 unique reflections [$I > 3.0\sigma(I)$] and 172 variable parameters and converged with $R(R_w) = 0.036(0.044)$. Further details of the X-ray structural analysis of **2** are given in Table 1.

RESULTS AND DISCUSSION

Two Zintl anions which contain the [tris (ethylenediamine)-zinc]$^{2+}$ cation have been synthesized, one by electrochemical methods and the other by the reaction of K_4SnTe_4 and $ZnCl_2$ in ethylenediamine in a sealed tube at 100°C. Electrochemical dissolution of a $ZnTe_{10}$ cathode in a saturated solution of tetrapropylammonium bromide in ethylenediamine formed a very dark purple solution from which crystals of $[Zn(N_2C_2H_8)_3][Te_3]\cdot 0.5(N_2C_2H_8)$ (**1**) were obtained. The polytelluride **1** recrystallizes as black, block-shaped crystals which contain one Te_3^{2-} anion, one [tris(ethylenediamine)-zinc]$^{2+}$ cation and half a molecule of ethylenediamine in the crystal lattice, per formula unit. The structure of the cation and anion

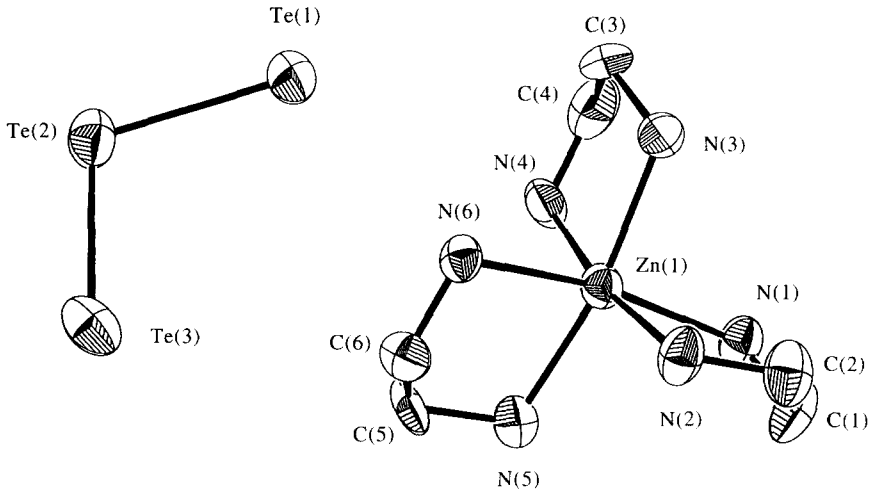


Fig. 1. The structure of $[Zn(N_2C_2H_8)_3][Te_3]\cdot 0.5(en)$ (**1**), showing the atomic numbering scheme and 50% probability ellipsoids. Selected bond distances and angles appear in Table 4.

of **1** are shown in Fig. 1. The Te_3^{2-} anion in **1** consists of three tellurium atoms which are connected by two Te—Te bonds. The anion has a bent structure with a Te—Te—Te angle of 105.24(5)° and Te—Te bond distances of 2.708(1) and 2.720(1) Å, which are similar to the 2.692(5)–2.805(3) Å range of distances and the 100.06–113.1(2)° range of angles found in other tritellurides [16].

A view of the unit cell of **1** down the *a* axis is shown in Fig. 2. This view shows the discrete Te_3^{2-} anions surrounded in the solid state by tris(ethylenediamine)-zinc cations and isolated ethylenediamine molecules. The ethylenediamine molecules of solvation are sufficiently far from the Te_3^{2-} anions, with the closest interaction being 3.68(1) Å, to rule out any interaction between the two, and can therefore be considered as simply solvates of crystallization.

The Zn^{2+} cations in both **1** and **2** are six-coordinate,

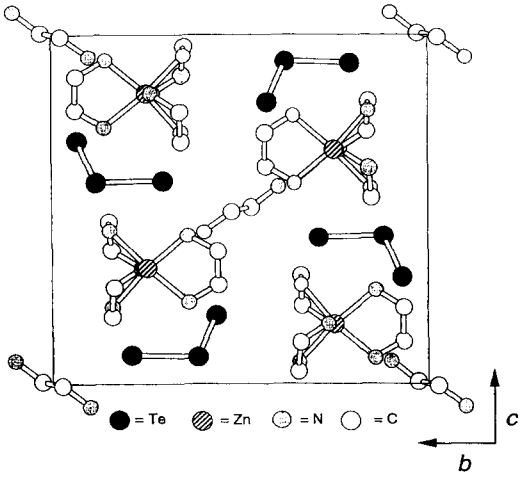


Fig. 2. Unit-cell view of the structure of $[Zn(N_2C_2H_8)_3][Te_3]\cdot 0.5(en)$ (**1**) down the crystallographic *a* axis.

with the Zn atom bonded to three bidentate ethylenediamine ligands. The structure of the [tris(ethylenediamine)-zinc]$^{2+}$ cation from compound **1** is shown in Fig. 1. The geometry around the Zn atoms is that of a slightly distorted octahedron with the N—Zn—N angles ranging from 79.8(4) to 96.4(3)° in **1** and 75.9(4) to 99.2(6)° in **2**.

The structure of compound **1** is most closely related to the structure of $[Ba(en)_3]Te_3$ [16], which also contains Te_3^{2-} anions. However, in the barium-containing structure, the coordination of the three ethylenediamine molecules about the barium is severely distorted by interactions between the Te_3^{2-} anion and the barium atom. This interaction causes the barium atom to be formally ten-coordinate, being bonded to three ethylenediamine molecules, three Te atoms from the Te_3^{2-} unit and one Te atom from an adjacent Te_3^{2-} moiety. This interaction is not seen between the Zn and Te atoms in **1**. This is most likely due, in part, to the large size of Ba^{2+} (effective ionic radius of 1.35 Å) [17] *vs* Zn^{2+} (effective ionic radius of 0.74 Å) [17] and therefore the ability of the barium atom to achieve a higher coordination number than zinc. The Te_3^{2-} anion has also been structurally characterized in K_2Te_3 [18], Rb_2Te_3 [19], Cs_2Te_3 [19], $BaTe_3$ [20] $[Ba(en)_{4.5}]Te_3$ [16] and $[K(2,2,2,\text{-crypt})]_2Te_3\cdot en$ [21], but never before with non-alkali or alkaline earth cations. Furthermore, the previously known Te_3^{2-} compounds were synthesized using more traditional thermal and extraction techniques, rather than using electrochemical methods. Selected bond distances and angles for compound **1** appear in Table 2.

Single crystals of the compound $[Zn(N_2C_2H_8)_3]_2Sn_2Te_6\cdot(en)$ (**2**) were prepared by the reaction of K_4SnTe_4 with $ZnCl_2$ and $(C_2H_5)_4NBr$ in ethylenediamine at 100°C. Compound **2** crystallizes as black prisms which contain the $Sn_2Te_6^{4-}$ anion, tris(ethylenediamine)-zinc cation, and one ethylenediamine molecule of crystallization per formula unit. The $Sn_6Te_6^{4-}$ anion con-

Table 2. Selected bond distances (Å) and angles (°) for $[Zn(N_2C_2H_8)_3][Te_3]\cdot 0.5(en)$ (**1**) and $[Zn(N_2C_2H_8)_3]_2[Sn_2Te_6]\cdot(en)$ (**2**)

Compound **1**			
Te(1)—Te(2)	2.708(1)	Te(1)—Te(2)—Te(3)	105.24(5)
Te(2)—Te(3)	2.720(1)		
Compound **2**			
Sn(1)—Te(1)	2.6830(9)	Te(1)—Sn(1)—Te(2)	110.34(3)
Sn(1)—Te(1*)	2.789(1)	Te(1)—Sn(1)—Te(2*)	115.08(3)
Sn(1)—Te(2)	2.7865(9)	Te(1)—Sn(1)—Te(3)	113.62(3)
Sn(1)—Te(3)	2.6817(9)	Te(2)—Sn(1)—Te(2*)	94.47(3)
Sn(1)···Sn(1*)	3.786	Te(2)—Sn(1)—Te(3)	110.83(3)
Te(1)···Te(1*)	4.093	Te(2)—Sn(1)—Te(3*)	110.94(3)
		Sn(1)—Te(2)—Sn(1*)	85.53(3)

sists of an essentially planar Sn_2Te_2 four-membered ring with four terminal Sn—Te bonds (Fig. 3). It can be described as two tetrahedral $SnTe_4$ units, which share an edge to form the $Sn_2Te_6^{4-}$ moiety. The $Sn_2Te_6^{4-}$ anion sits on an inversion center and although it is required to have only this crystallographic center of inversion, has effective *mmm* symmetry making it isostructural to diborane (B_2H_6). The $Sn_2Te_6^{4-}$ anion has been synthesized previously as the tetramethylammonium salt (by the methanol/$(CH_3)_4N^+$ extraction of the K_4SnTe_4Zintl phase) [10], the tetraethylammonium salt [by the reaction of Li_2Te, Te, $LiBH_4$ and $SnCl_2$ in DMF followed by extraction with a solution of $(C_2H_5)_4NCl$ in CH_3CN) [22], and in an electrochemical process involving the cathodic dissolution of a $SnTe_2$ alloy electrode in a saturated ethylenediamine solution of RbI and $(C_2H_5)_4NI$ [8c]. In all cases, the structure of the $Sn_2Te_6^{4-}$ anion retains its structural similarity to diborane.

The charge of 4− on the $Sn_2Te_6^{4-}$ anion is established by the presence of one crystallographically independent tris(ethylenediamine)-zinc^{2+} cation per $SnTe_3$ structural moiety in the asymmetric unit. In the structure of the anion, terminal Te atoms Te(1), Te(1*), Te(2) and Te(2*) each have only one bond and therefore can be considered to have a formal charge of −1. The two internal Te atoms [Te(2) and Te(2*)] are each two-coordinate and, as such, are neutral. This leads to an oxidation state of IV for the Sn atoms, which is expected for Sn in this tetrahedral environment.

The $Sn_2Te_6^{4-}$ anion has two sets of Sn—Te bond distances. The $Sn—Te_{terminal}$ bond distances are 2.6817(9) and 2.6830(9) Å. The $Sn—Te_{bridging}$ bond distances are significantly longer at 2.7865(9) and 2.789(1) Å. The Sn—Sn transannular non-bonded distance is 3.786 Å and that of the Te—Te bonded distance is 4.093 Å. These bond distances are essentially identical to those observed in the other two structurally characterized $Sn_2Te_6^{4-}$ anions.

A unit cell picture of the structure of $[Zn(N_2C_2H_8)_3]_2Sn_2Te_6\cdot(en)$ (**2**) is shown in Fig. 4. As can be seen from this figure, the compound consists

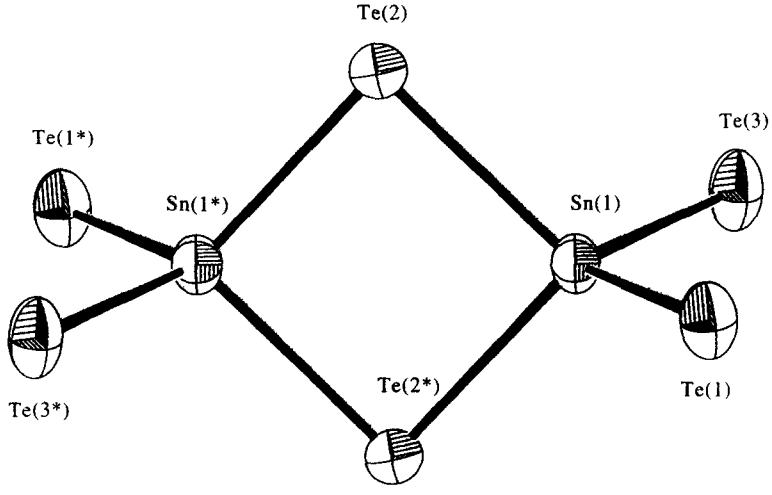


Fig. 3. The structure of the $[Sn_2Te_6]^{4-}$ anion showing the atomic numbering scheme and 50% probability thermal ellipsoids. Bond distances and angles for this anion appear in Table 4.

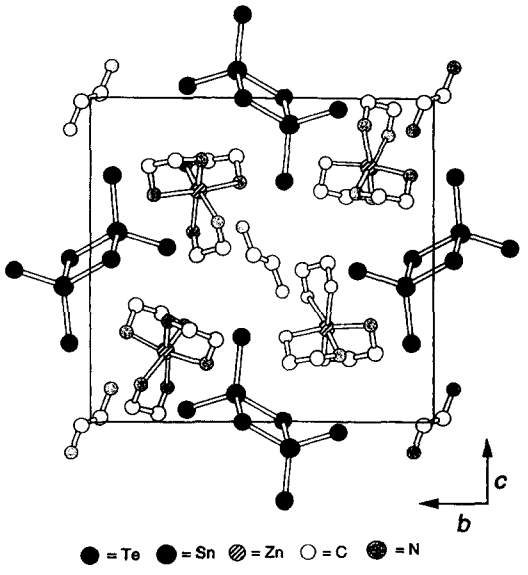


Fig. 4. Unit-cell view of the structure of $[Zn(N_2C_2H_8)_3]_2[Sn_2Te_6]\cdot(en)$ (**2**), down the crystallographic *a* axis.

of completely isolated $Sn_2Te_6^{4-}$ anions surrounded in the solid state by tris(ethylenediamine)-zinc cations and isolated ethylenediamine molecules. The ethylenediamine molecules in the structure are sufficiently distant from the Te atoms (closest N—Te bond distance = 3.881 Å) to preclude the possibility of any hydrogen bonding interactions. As in the crystal structure of **1**, they are present merely as solvates of crystallization.

Both the sulfur and selenium analogs to the $Sn_2Te_6^{4-}$ anion are known and have been prepared by methods involving the methanolothermal reactions of the alkali metal carbonates and the metal disulfides (or diselenides) [23]. All derivatives contain the edge-shared SnX_4 tetrahedra and display approximate *mmm* crystallographic symmetry. Selected bond distances and angles for compound **2** appear in Table 2.

In conclusion, two polychalcogenide Zintl anions containing the tris(ethylenediamine)-$zinc^{2+}$ cation have been synthesized by two entirely different processes, and both in reasonably good yield. The elctrochemical process is still relatively new and continues to yield new and interesting Zintl anions from a variety of main group systems. The second, a more traditional route to the synthesis of Zintl anions, has once again demonstrated its versatility by the synthesis of $[Zn(N_2C_2H_8)_3]_2Sn_2Te_6\cdot(en)$ (**2**).

Supplementary material

Complete tables of experimental crystallographic details, atomic coordinates, bond distances and angles, anisotropic displacement parameters and calculated and observed structure factors for **1** (9 pages) and **2** (10 pages) are available from author R.C.H.

REFERENCES

1. (a) Kanatzidis, M. G., *Comments Inorg. Chem.* 1990, **10,** 161; (b) Ansari, M. A. and Ibers, J. A., *Coord. Chem. Rev.* 1990, **100,** 223; (c) Kolis, J. W., *Coord. Chem. Rev.* 1990, **105,** 195; (d) Kanatzidis, M. G., *Chem. Mater.* 1990, **2,** 353; (e) Keane, P. M., Lu, Y.-J. and Ibers, J. A., *Acc. Chem. Res.* 1991, **24,** 223; (f) Böttcher, P., *Angew. Chem. Int. Ed. Engl.* 1988, **27,** 759; (g) Roof, L. C. and Kolis, J. W., *Chem. Rev.* 1993, **90,** 1037; (h) Ansari, M. A. and McConnachie, J. M. and Ibers, J. A., *Acc. Chem. Res.* 1993, **26,** 574.
2. (a) Kudryastev, A. A., *The Chemistry and Technology of Selenium and Tellurium*, 2nd ed.; trans. E. M. Elkin. Collet's Publishers, London, 1974; (b) Bube, R. H., *Ann. Rev. Mater. Sci.* 1990, **20,** 19; (c) Maier, H. and Hesse, J., *J. Cryst. Growth: Prop. Appl.* 1980, **4,** 145.
3. (a) Nesper, R., *Angew. Chem. Int. Ed. Engl.* 1991, **30,** 789; (b) Nesper, R., *Prog. Solid State Chem.* 1990, **20,** 1; (c) von Schnering, H. G. and Hönle, W., *Chem. Rev.* 1988, **88,** 243; (d) Böttcher, P., *Angew. Chem., Int. Ed. Engl.* 1988, **27,** 759; (e) Schäfer, H., *J. Solid State Chem.* 1985, **57,** 97; (f) Schäfer, H., *Ann. Rev. Mater. Sci.* 1985, **15,** 1; (g) Schäfer, H. and Eisenmann, B., *Reviews in Inorg. Chem.* 1981, **3,** 29; (h) von Schnering, H. G., *Angew. Chem. Int. Ed. Engl.* 1981, **20,** 33; (i) Schäfer, H., Eisenmann, B. and Müller, W., *Angew. Chem. Int. Ed. Engl.* 1973, **12,** 694, and refs therein.
4. Some examples include: (a) Haushalter, R. C., *J. Chem. Soc., Chem. Commun.* 1987, 196; (b) Haushalter, R. C., Eichhorn, B. W., Rheingold, A. L. and Geib, S. J., *J. Chem. Soc., Chem. Commun.* 1988, 1027; (c) Belin, C. and Mercier, H., *J. Chem. Soc., Chem. Commun.* 1987, 190; (d) Burns, R. C. and Corbett, J. D., *Inorg. Chem.* 1985, **24,** 1489; (e) Haushalter, R. C., Eichhorn, B. W., Rheingold, A. L. and Geib, S. J., *J. Chem. Soc., Chem. Commun.* 1985, 1207; (f) Corbett, J. D., *Chem. Rev.* 1985, **85,** 383; (g) Critchlow, S. C. and Corbett, J. D., *Inorg. Chem.* 1985, **24,** 979; (h) Haushalter, R. C., *Angew. Chem., Int. Ed. Engl.* 1985, **24,** 432, 433; (i) Haushalter, R. C., *Inorg. Chim. Acta*, 1985, **102,** L37; (j) Huffman, J. C., Haushalter, J. P. and Umarji, A. M., Shenoy, G. K. and Haushalter, R. C., *Inorg. Chem.* 1984, **23,** 2312; (k) Teller, R. G., Krause, L. J. and Haushalter, R. C., *Inorg. Chem.* 1983, **22,** 1809; (l) Corbett, J. D., Critchlow, S. C. and Burns, R. C., *Rings, Clusters and Polymers of the Main Group Elements*, ed. A. Cowley. ACS Symposium Series 232. ACS, Washington, DC, 1983, pp. 95–110, and refs therein.
5. Dhingra, S. S. and Haushalter, R. C., *Chem. Mater.* 1994, **6,** 2376.
6. (a) Glaum, R. and Gruehn, R., *Z. Kristallogr.* 1987, **178,** 72; (b) Florke, U. Z., *Z. Anorg. Allg. Chem.* 1983, **502,** 218; (c) Richardson, M. W. and Nolang, B., *J. Cryst. Growth* 1977, **42,** 90.
7. Warren, C. J., Haushalter, R. C. and Bocarsly, A. B., *J. Alloys and Compounds*, 1995, **229,** 175.
8. (a) Warren, C. J., Ho, D. M., Haushalter, R. C. and Bocarsly, A. B., *Angew. Chem. Int. Ed. Engl.*

1993, **32,** 1646; (b) Warren, C. J., Dhingra, S. S., Ho, D. M., Haushalter, R. C. and Bocarsly, A. B., *Inorg. Chem.* 1994, **33,** 2709; (c) Warren, C. J., Ph.D. Dissertation, Princeton University, June 1994; (d) Warren, C. J., Ho, D. M., Haushalter, R. C. and Bocarsly, A. B., *J. Am. Chem. Soc.* 1993, **115,** 6416; (e) Warren, C. J., Ho, D. M., Haushalter R. C. and Bocarsly, A. B., *J. Chem. Soc., Chem. Commun.* 1994, 361; (f) Warren, C. J., Dhingra, S. S., Haushalter, R. C. and Bocarsly, A. B., *J. Solid State Chem.* 1994, **112,** 340; (g) Warren, C. J., Haushalter, R. C. and Bocarsly, A. B., *Chem. Mater.* 1994, **6,** 780; (h) Dhingra, S. S., Warren, C. J., Haushalter, R. C. and Bocarsly, A. B., *Chem. Mater.* 1994, **6,** 2382; (i) Warren, C. J., Haushalter, R. C. and Bocarsly, A. B., *J. Alloys and Compounds* 1996, **223,** 23.

9. Compound **1** was isolated in 38% yield based on 0.389 g (0.290 mmol) of $ZnTe_{10}$ electrode dissolved after 7 days, which gave rise to 0.074 g (0.112 mmol) of $[Zn(N_2C_2H_8)_3][Te_3]\cdot 0.5(N_2C_2H_8)$ crystals that were collected from the cathode chamber. The yield was based on moles of Zn. Electrochemical Yield = moles product/moles e^- passed = 12%. The deep purple color of the solution suggests that some fraction of the polyanions produced are soluble and remain in solution. Qualitative microprobe analysis (Princeton Gamma Technology EDS detector on a Hitachi S-2700 SEM) confirmed the crystals contained Zn and Te in approximately 1 : 3 ratio.
10. Huffman, J. C., Haushalter, J. P., Umarji, A. M., Shenoy, G. K. and Haushalter, R. C., *Inorg. Chem.* 1984, **23,** 2312.
11. The reaction that produces $[Zn(N_2C_2H_8)_3]_2[Sn_2Te_6]\cdot$(en) (**2**) also produces a mixture of other products from which single crystals of **2** had to be mechanically separated to determine the overall yield. A yield of 41.6% was based on 0.0412 g of **2** and was calculated on the basis of moles of Sn.
12. DIFABS: Walker, N. and Stuart, N., *Acta Cryst.* 1983, **39A,** 158.
13. SAPI91: Hai-Fu, F. Structure Analysis Program with Intelligent Control, Rigaku Corporation, Tokyo, Japan, 1991.
14. TeXsan Single Crystal Analysis Software Package. Version 1.7-1. Molecular Structure Corporation, The Woodlands, TX 77381, U.S.A., 1995.
15. SHELX86: Sheldrick, G. M., in *Crystallographic Computing* 3, eds G. M. Sheldrick, C. Kruger and R. Goddard. Oxford University Press, Oxford, 1985, pp. 175–189.
16. Zagler, R., Eisenmann, B. and Schäfer, H., *Z. Naturforsch.* 1987, **42B,** 151.
17. Shannon, R. D., *Acta Cryst.* 1976, **32A,** 751.
18. Eisenmann, B. and Schäfer, H., *Angew. Chem.* 1978, **90,** 73.
19. Böttcher, *J. Less Common Met.* 1980, **70,** 263.
20. Cordier, G., Schwidetzky, C. and Schäfer, H., *Z. Naturforsch.* 1984, **39B,** 833.
21. Cisar, A. and Corbett, J. D., *Inorg. Chem.* 1977, **16,** 632.
22. Ansari, M. A., Bollinger, J. C. and Ibers, J. A., *Inorg. Chem.* 1993, **32,** 231.
23. (a) Sheldrick, W. S. and Braunbeck, H. G., *Z. Naturforsch,* 1989, **44B,** 851; (b) Krebs, B. and Uhlen, H., *Z. Anorg. Allg. Chem.* 1987, **549,** 35; (c) Krebs, B., Pohl, S. and Schiwy, W., *Angew. Chem., Int. Ed. Engl.* 1970, **9,** 897.

Pergamon

PII: S0277-5387(96)00364-6

Polyhedron Vol. 16, No. 7, pp. 1201–1209, 1997
Copyright © 1997 Elsevier Science Ltd
Printed in Great Britain. All rights reserved
0277-5387/97 $17.00+0.00

Studies on dinuclear metal complexes of macrocyclic ligands with varying chelate ring size

Chepuri. R. K. Rao and P. S. Zacharias*

School of Chemistry, University of Hyderabad, Hyderabad 500 046, India

(Received 28 June 1996; accepted 24 July 1996)

Abstract—Dinuclear $Cu^{(II)}$, $Ni^{(II)}$ and $Co^{(II)}$ complexes of macrocyclic Schiff-base ligands of 2,6-diformyl-4-methylphenol with α,ω-diamines have been synthesized and characterized. The effect of chelate ring size and saturation of azomethine groups of these ligands on stability, structure and electrochemical properties of the metal complexes has been investigated. Catalytic activity of the metal complexes in the oxidation reaction of 3,5-di-tert-butylcatechol to 3,5-di-tert-butylquinone by molecular oxygen is reported. Copyright © 1997 Elsevier Science Ltd

Keywords: macrocycle; Robson ligand; chelate ring; conproportion; antiferromagnetism; mixed valence.

Dinuclear complexes with two metal ions in close proximity show interesting magnetic, catalytic and electron transfer properties. Efforts to synthesize ligands capable of generating such dinuclear complexes have resulted in a large number of dinucleating ligands [1]. One such ligand system is obtained from [2+2] condensation of 2,6-diformyl-4-methylphenol with 1,3-diaminopropane [2]. The dinucleating ability of this ligand system stems from the readiness of phenol to deprotonate and bridge two metal ions in close proximity. Similar macrocyles, called "Robson-type ligands" have been used for studies on homo-, hetero- and mixed-valent [2–4] dinuclear complexes of 3*d* metal ions.

During our efforts to synthesize and study such systems, we have prepared and characterized a number of dinuclear $Cu^{(II)}$, $Ni^{(II)}$ and $Co^{(II/III)}$ metal complexes of unreduced ligands H_2L^1–H_2L^3 and reduced ligands H_2L^4–H_2L^6 (Fig. 1). These ligands have varying chelate ring sizes. The effect of ring size and the saturation of the azomethine groups on stability, structure, electrochemical and catalytic properties of these complexes has been investigated, and the results are presented and discussed here.

EXPERIMENTAL

All amines were distilled prior to use. The solvents methanol and ethanol were purified by standard methods [5–8]. Spectroscopic grade *N*,*N*-dimethylformamide (DMF) and, acetonitrile (SD fine chemicals) were used for spectral and electrochemical studies. Metal(II) perchlorates were prepared by treating perchloric acid with the relevant carbonates. CAUTION! All perchlorates are explosion prone and must be handled with care.

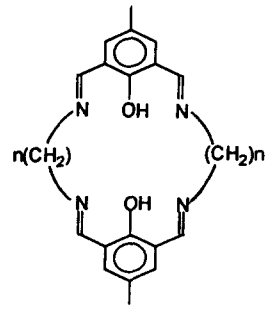
Synthesis of ligands and metal complexes

2,6-Diformyl-4-methylphenol was prepared according to the procedure given by Gagne *et al.* [3]. The reduced ligands H_2L^4–H_2L^6 were prepared by the procedure reported by Mandal and Nag [9]. All complexes derived from the ligands H_2L^1–H_2L^3 were prepared by the procedure adopted by Robson *et al.* [2] and complexes derived from reduce ligands H_2L^4–H_2L^6 were prepared by the procedure given by Mandal and co-workers [10,11].

Preparation of $Cu_2L(ClO_4)_2$ *complexes* [L = L^1–L^3, **(1)**–**(3)**]

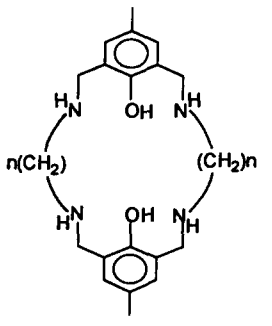
1,2-Diaminoethane (0.180 g, 3 mmol) dissolved in methanol (10 cm^3) was added to a solution of copper perchlorate (0.74 g, 2 mmol) in methanol (25 cm^3). 2,6-Diformyl-4-methylphenol (0.328 g, 2 mmol) in methanol (25 cm^3) was added while hot and the result-

* Author to whom correspondence should be addressed.



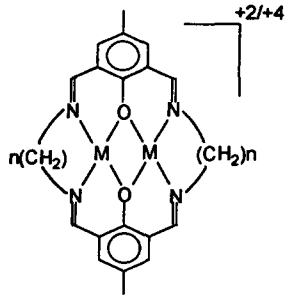
unreduced ligands

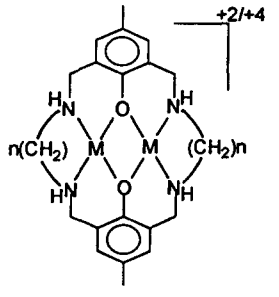
n = 2, H_2L^1; n = 4, H_2L^2; n = 6, H_2L^3



reduced ligands

n = 2, H_2L^4 ; n = 3, H_2L^5 ; n = 4, H_2L^6





1 = $[Cu_2\,L^1(ClO_4)_2]$
2 = $[Cu_2\,L^2(ClO_4)_2]$
3 = $[Cu_2\,L^3(H_2O)_2(ClO_4)_2]$
7 = $[Ni_2\,L^1]^{+2}$
8 = $[Ni_2\,L^2]^{+2}$
9 = $[Ni_2\,L^3]^{+2}$
13 = $[Co_2\,L^1(ClO_4)_4]$
14 = $[Co_2\,L^2(ClO_4)_2]$
15 = $[Co_2\,L^3(ClO_4)_2]$

4 = $[Cu_2\,L^4(ClO_4)_2]$
5 = $[Cu_2\,L^5(ClO_4)_2]$
6 = $[Cu_2\,L^6(ClO_4)_2]$
10 = $[Ni_2\,L^4]^{+2}$
11 = $[Ni_2\,L^5(MeOH)_2(ClO_4)_2]$
12 = $[Ni_2\,L^6(MeOH)_2(ClO_4)_2]$
16 = $[Co_2L^4(ClO_4)_4]$
17 = $[Co_2\,L^5(ClO_4)_2]$
18 = $[Co_2\,L^6(ClO_4)_2]$

Fig. 1. Structure of ligands and metal complexes.

ing, mixture was refluxed for 7 h with stirring. The green precipitate $[Cu_2L^1(ClO_4)_2]$ (**1**) was filtered and washed with water. This was recrystallized from a 1 : 1 methanol/water mixture. The complexes $Cu_2L^2(ClO_4)_2$ and $Cu_2L^3(ClO_4)_2$, (**2**) and (**3**), were prepared by similar methods.

Preparation of $Cu_2L'(ClO_4)_2$ *complexes* [L′ = L^4–L^6, (**4**)–(**6**)]

To the ligand H_2L^5 (0.41 g, 1 mmol) dissolved in methanol (10 cm^3) was added an aqueous (10 cm^3) solution of NaOH (0.08 g, 2 mmol). $Cu(ClO_4)_2 \cdot 6H_2O$ (0.74 g, 2 mmol) dissolved in water (10 cm^3) was added and the resulting mixture was refluxed for 3 h. The deep green crystals of **5** formed when cooled to room temperature were filtered and recrystallized from methanol. A similar procedure was adopted for the preparation of complexes **4** and **6** derived from the ligands H_2L^4 and H_2L^6. The resulting green products were recrystallized from methanol.

Preparation of $Ni_2L(ClO_4)_2$ *complexes* [L = L^1–L^3, (**7**)–(**9**)]

The nickel(II) complexes, $Ni_2L^1(ClO_4)_2$ (**7**), $Ni_2L^2(ClO_4)_2$ (**8**) and $Ni_2L^3(ClO_4)_2$ (**9**) were prepared by methods similar to those for corresponding copper(II) complexes. These complexes are orange and yellow in colour.

Preparation of $Ni_2L'(ClO_4)_2$ *complexes* [L′ = L^4–L^6, (**10**)–(**12**)]

To a methanol solution (15 cm^3) of the ligand H_2L^5 (0.41 g, 1 mmol), $Ni(ClO_4)_2 \cdot 6H_2O$ (0.731 g, 2 mmol) and triethylamine (0.3 cm^3, 98%) were added and

refluxed for 1 h. The resulting wine-red solution, on concentration over $CaCl_2$ afforded a pink crystalline compound, $Ni_2L^5(ClO_4)_2$ (**11**). This was filtered and recrystallized from methanol by diffusion of diethyl ether [11]. The complexes derived from H_2L^4 (**10**) and H_2L^6 (**12**) were pink and green, respectively, and were recrystallized from methanol and diethyl ether.

Preparation of cobalt(II/III) *complexes*

The cobalt complexes of unreduced ligands H_2L^1–H_2L^3 (**13–15**) and reduced ligands H_2L^4–H_2L^6 (**16–18**) were prepared by the same procedure as described for the preparation of $Cu_2L(ClO_4)_2$ (L = L′–L^3) and $Ni_2L'(ClO_4)_2$ (L′ = L^4–L^6) complexes, respectively, but under dry nitrogen.

Physical measurements

The C, H, N elemental analyses were performed on a Perkin–Elmer 240C elemental analyser. Conductivity measurements were done on a CM-82T Elico conductivity meter at 25°C in DMF at solution concentrations of *ca* 1×10^{-3} mol dm^{-3}. Infrared spectra were recorded as KBr pellets on a Perkin–Elmer 1310 spectrometer in the region 4000–600 cm^{-1}. Electronic spectra were recorded on a Perkin–Elmer Lamda 3B UV–vis and Cary 17D spectrophotometer. Proton NMR spectra were recorded on a Jeol JEL 980B JNM-FX–100 FT NMR spectrometer in $CDCl_3$ with tetramethylsilane (TMS) as internal standard. Magnetic susceptibility measurements were carried out by the Faraday technique on a Cahn magnetic susceptibility system equipped with a model 4600 adjustable gap electromagnet and Cahn 1000 electrobalance. $Hg[Co(SCN)_4]$ was used as standard. The resultant susceptibilities were corrected for diamagnetism. Cyclic voltammograms were recorded on a PAR electrochemistry system consisting of a model 174A polarographic analyser, a model 175 universal programmer and an RE 0074 X-Y recorder. A model 374 three-electrode cell system, consisting of a Metrohm E410 hanging mercury drop electrode (HMDE), BAS MF2013 Platinum or glassy carbon electrode as working electrodes, PAR model 9331 saturated calomel electrode (SCE) as reference electrode and Pt wire as auxiliary electrode were used. The experiments were carried out for 1×10^{-3} M solutions of the complexes under nitrogen using tetraethyl- or tetrabutylammonium perchlorates (TEAP or TBAP, 0.1 M) as supporting electrolytes at room temperature.

Catalysis experiments were carried out on a Shimadzu UV 200S double-beam, spectrophotometer in methanol using 3,5-di-t-butylcatechol (3,5-DTBC) as substrate. A methanol solution of 3,5-DTBC (1×10^{-3} M) and the respective copper(II), nickel(II) or cobalt(II/III) complexes (0.02×10^{-3} M) in a 10 cm^3 standard flask was kept under nitrogen. The characteristic absorbance band of 3,5-di-t-butylquinone (3,5-DTBQ) at 400 nm (ε/mol^{-1} dm^3 cm^{-1} = 1900 in methanol [12]) was taken as a measure of quinone formation. Absorbance was measured at regular intervals after exposing the solution to air.

RESULTS AND DISCUSSION

The ligands H_2L^1–H_2L^3 shown in Fig. 1 were generated *in situ* in the presence of metal perchlorates following the template synthesis procedure [2]. Complexes of these ligands exhibit characteristic IR bands at 1640 cm^{-1} due to —HC=N— and at 1100 and 620 cm^{-1} due to perchlorate ions. The reduced ligands H_2L^4–H_2L^6 are white crystalline compounds and are obtained in low yields. They are characterized by analytical, IR and NMR techniques. IR spectra of these ligands do not show the band at 1640 cm^{-1} indicating complete reduction of —HC=N— to —NH—CH_2—. In addition they show sharp bands at *ca* 3200 and 1600 cm^{-1} assignable to the ν_{NH} and δ_{NH} modes of the secondary amino group of the ligand. A broad band at *ca* 3500 cm^{-1} assigned to the ν_{OH} mode of phenol. The electronic absorption spectra of these ligands in DMF show two absorptions at *ca* 289 and 265 nm in the UV region. The $\pi \rightarrow \pi^*$ transition of azomethine (—HC=N—) group at *ca* 340 nm is absent.

Copper(II) *complexes*

Synthetic details of the complexes are given in the experimental section. The complex **1** is reported in the literature as the chloride salt [13], while complex **2** is known as the perchlorate salt [14], complex **1** is recrystallized from 50% aqueous methanol. Complex **2** is recrystallized from water and complex **3** is thoroughly washed with hot methanol to obtain pure compounds. The complexes of the ligands H_2L^4–H_2L^6 are green in colour and are recrystallized from methanol [15]. The purity of all these complexes was checked by C, H, N elemental analysis and the data are collected in Table 1. The complexes have the composition $[Cu_2L^n(ClO_4)_2]$ (n = 1–6) and the structure is shown in Fig. 1.

The positions of the characteristic peaks in the IR spectra and their assignments based on comparison to the related complexes [2] are presented in Table 2. Conversion of the aldehyde groups onto Schiff-base derivatives is indicated by the absence of the aldehyde HC=O stretching band at 1680 cm^{-1} and the appearance of a strong band at 1640 cm^{-1} assignable to the —HC=N— group. The complexes **1**, **3** and **4–6** exhibit a band centred between 3450 and 3500 cm^{-1} originating from ν_{OH} of water present. The ν_{NH} and δ_{NH} absorptions originating from the ligands are seen at *ca* 3200 and 1600 cm^{-1}, respectively. IR spectra show ν_3 and ν_4 absorptions of perchlorate ion at 1100 and 630 cm^{-1}, respectively. The band at 1100 cm^{-1}

Table 1. Analytical data of complexes

Complex	Analysis % (calculated) C	H	N
1·H_2O	37.0 (36.8)	3.5 (3.4)	7.7 (7.8)
2	41.4 (41.2)	4.1 (4.0)	7.3 (7.4)
3·$2H_2O$	42.5 (42.4)	5.0 (5.0)	6.8 (6.6)
4	35.4 (35.5)	4.7 (4.6)	7.4 (7.5)
5·$2H_2O$	37.1 (37.3)	5.0 (4.9)	7.0 (7.2)
6·$2H_2O$	39.0 (38.9)	5.1 (5.2)	7.1 (7.0)
7·H_2O	38.0 (37.3)	3.3 (3.4)	8.3 (7.9)
8·H_2O	40.3 (40.1)	4.3 (4.2)	7.5 (7.3)
9·MeOH	44.9 (44.6)	5.1 (5.0)	6.8 (6.7)
10	37.9 (37.8)	4.5 (4.3)	8.1 (8.0)
11·2MeOH	37.9 (38.2)	6.0 (6.2)	7.1 (7.0)
12·2MeOH	41.5 (41.1)	5.7 (5.6)	6.7 (6.8)
13·$2H_2O$	28.9 (28.8)	3.0 (2.8)	6.3 (6.1)
14·$2H_2O$	41.0 (39.8)	4.5 (4.4)	7.3 (7.2)
15·$2H_2O$	43.1 (42.9)	5.0 (5.0)	6.6 (6.7)
16·2MeOH	30.0 (29.9)	4.1 (4.0)	6.0 (5.9)
17·$3H_2O$	36.8 (36.9)	5.0 (5.1)	7.1 (7.2)
18·2MeOH	41.1 (41.0)	5.7 (5.6)	7.0 (6.8)

for these complexes is broad, indicating possible coordination of perchlorate ion in the solid state [16].

The μ_{eff} at room temperature for complexes **1**–**3** are 1.10, 0.77 and 1.34 B.M., respectively (Table 2). The reported magnetic moment of the known complex **2**, is 0.46 B.M. [14]. The experimental difficulty of measuring the susceptibilities of weakly paramagnetic, spin-coupled systems led to variations in the values reported by various groups. For example, the complex $[Cu_2L(X)_2]$ (X = Cl^-, ClO_4^-) is reported to exhibit μ_{eff} values of 0.47 [14], 0.6 [4] and 0.74 B.M. [17] at room temperature. The μ_{eff} values of the present complexes are less than the spin-only value for one unpaired electron and indicate antiferromagnetic interactions between the copper(II) centres. Antiferromagnetic interaction has already been established in complex **2** [14]. The μ_{eff} for complexes **4**–**6** fall in the range of 0.8–1.1 B.M. and suggest antiferromagnetic interaction in these complexes also.

Electronic spectra. The electronic spectra of the complexes are recorded in DMF and the data are collected in Table 2. The complexes exhibit one high intensity band in the range 360–420 nm in the UV region and another in the visible region 545–770 nm. The high intensity band in the UV region may be owing to a combination of a $\pi \rightarrow \pi^*$ transition of HC=N— and ligand to metal charge transfer transitions. The charge transfer may be from the *p* orbital of coordinated phenolic oxygen to the vacant *d* orbitals of copper(II). Similar charge transfer bands have been observed in several oxo-bridged copper(II) complexes [18]. In comparison with electronic spectral data of complexes of similar ligands [2,3,14,19–21],

Table 2. Spectral, magnetic and conductivity data of complexes

Complex	IR (cm^{-1}) —HC=N—	—NH—	$\lambda_{max}(\varepsilon)^a$ nm ($mole^{-1}$ dm^3 cm^{-1})	μ_{eff}/atom[b] B.M.	Λ_M[a] S cm^2 m^{-1}
1	1630	—	545 (264)	1.1	177
2	1620	—	770 (160), 640 sh, 400 sh,	0.77	175
3	1630	—	670 (171), 420 (2760)	1.34	175
4	—	3200, 1600	610 sh, 340 (4800)	1.1	220
5	—	3200, 1600	590 (270), 340 (2550)	0.80	225
6	—	3250, 1600	580 (192), 340 (2760)	1.07	222
7	1640	—	470 sh, 410 (5700), 390 (4575)	*c*	147
8	1640	—	570 (144), 405 sh,	*c*	135
9	1640	—	*d*	*c*	*d*
10	—	3150, 1600	1040 (24), 482 (98), 340 (361)	1.65	225
11	—	3250, 1610	840 (14), 776 (9), 496 (110), 360 (390)	3.10	230
12	—	3250, 1600	885 (15), 770 (12), 486 (17), 360 sh	3.31	230
13	1640	—	405 (7900)	*c*	185
14	1640	—	410 (3289)	4.67	176
15	1630	—	410 (2760)	4.62	180
16	—	3200, 1600	600 (540)	*c*	220
17	—	3200, 1620	620 sh, 360 (3096)	4.71	230
18	—	3150, 1620	370 (1670)	4.81	225

[a] In DMF.
[b] At room temperature.
[c] Diamagnetic.
[d] Insoluble.

the complex **1**, which has a ligand field band at 545 nm, could be square pyramidal. This geometry is achieved by the coordination of one perchlorate group each to the copper(II) atoms in a *trans* axial fashion in the solid state. The IR spectrum of this complex indicates coordinated perchlorate groups. Complex **2** is shown to have a distorted octahedral structure in the solid state [14] by the coordination of two perchlorate groups. The electronic spectrum of complex **2** in DMF shows two overlapping bands at *ca* 770 and 640 nm. Complex **3** has a band at 670 nm, which lies in between the band positions of the square pyramidal complex **1** and octahedral complex **2**. The IR spectrum of this complex shows a coordinated perchlorate group and analytical data indicate the presence of two water molecules. The red shift of the absorption band of **3** with respect to **1**, and the blue shift with respect to **2**, may arise through weak coordination of a water molecule to each copper centre, thereby providing an octahedral geometry wherein one of the axial positions is occupied by a coordinated water molecule and the other by a perchlorate group. The conductivity experiments show that these complexes are 1 : 2 electrolytes [22]. The two coordinated perchlorate groups of the complexes have been replaced by solvent DMF molecules in solution.

The ligand H_4L^5 is reported to form a copper(II) complex of composition $[Cu_2L^5(H_2O)_2](ClO_4)_2$ with square pyramidal geometry [23], with an electronic band at 574 nm. This complex is green and has a magnetic moment of 0.5 B.M. Complexes **4–6** are green in colour and exhibit *d–d* bands in the range 580–610 nm. Since IR spectra indicate perchlorate coordination, these complexes are suggested to possess a square-pyramidal structure with axial coordination of perchlorate ions to the copper(II) centres. The conductivity experiments for these complexes show that they are 1 : 2 electrolytes and indicate replacement of perchlorate groups in solution by solvent DMF molecules.

Electrochemistry. Redox properties of complexes **1**, **2** and **4–6** have been investigated in DMSO solvent using a glassy carbon electrode. Cyclic voltammograms of representative complexes **2** and **6** are shown in Fig. 2. The complexes undergo stepwise reductions at two different potentials. This is similar to the behaviour observed for related complexes [17]. The two redox couples are seen at *ca* −0.49, −1.07 V for complex **1**, and at *ca* −0.34, −0.76 V for **2** with reference to the SCE. Complex **3** gave only ill-defined peaks. A comparison of the first one-electron reduction potential for the two complexes indicates that the electron transfer is more facile in complex **2**. Ligand flexibility associated with the butylene bridge may be responsible for this. Such an effect has been noticed previously [14]. The ΔE_p values of the two redox couples are, 120 and 80 mV for complex **1** and 80 and 120 mV for complex **2**. These values show that redox couples involve quasi-reversible one-electron processes. The proposed mechanism involves $Cu^{II}/Cu^{II} \rightarrow Cu^{I}/Cu^{II}$ and $Cu^{I}/Cu^{II} \rightarrow Cu^{I}/Cu^{I}$ stepwise reductions. The stability of mixed-valence Cu^{I}/Cu^{II} complex intermediate expressed by the conproportionation constant, K_{con}, for the equilibrium

$$[Cu^{II}/Cu^{II}] + [Cu^{I}/Cu^{I}] \overset{K_{con}}{\rightleftharpoons} 2[Cu^{I}/Cu^{II}]$$

is given by $K_{con} = \exp(nF(\Delta E)/RT)$ where $\Delta E = E^1_{1/2} - E^2_{1/2}$. The larger the separation between the potentials of the couple (ΔE), the greater the stability of the mixed-valence species with respect to conproportionation. The K_{con} values have been estimated for the complexes. The higher value of K_{con} (6.5×10^9) for **1** compared with **2** (1.3×10^7) indicates that the intermediate species, Cu^{II}/Cu^{I} is more stable for complex **1**. The electrochemical data are given in Table 3.

The complexes **4–6** behaved in a similar way. The CV data are collected in Table 3. These complexes undergo stepwise one-electron reductions. Comparison of $E^1_{1/2}$ values of the complexes show that the first electron addition is facile for complex **6**. This trend is observed for the copper(II) complexes **1** and **2** (unreduced forms of **4** and **6**) and is also known from the literature [24]. Comparison of $E^1_{1/2}$ values shows a negative shift for complexes **4** and **6**. This indicates that Cu^{I} states are destabilized when the ligands are saturated. This may result from the ability of the unsaturated macrocycle to accept electrons from copper(I) through the antibonding orbital of C=N linkages, whereas the saturated macrocycle acts solely as an electron donor [15,25].

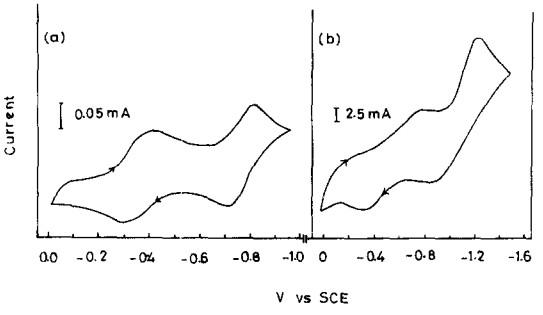


Fig. 2. Cyclic voltammograms of copper(II) complexes **2** (a) and **6** (b). The scan rate is 100 mV s^{-1}.

Nickel(II) complexes

The nickel(II) complexes **7–9** are obtained as orange and yellow solids. Complexes **10** and **11** are pink and complex **12** is green. These complexes are recrystallized from their methanol solutions by diffusion of diethyl ether. The analytical data for the complexes are collected in Table 1. Complexes **7–9** and **10** have the composition $[Ni_2L^n]^{2+}$, while the other complexes have the composition $[Ni_2L^n(MeOH)_2(ClO_4)_2]$. The structure of the complexes is shown in Fig. 1.

IR spectral data for the complexes are collected in

Table 3. Electrochemical data of copper(II) complexes

Complex	Cu^{II}/Cu^{II}–Cu^{II}/Cu^{I} $E^1_{1/2}$ (V)	ΔE_p (mV)	Cu^{II}/Cu^{I}–Cu^{I}/Cu^{I} $E^2_{1/2}$ (V)	ΔE_p (mV)	K_{con}
1	−0.490	120	−1.07	80	6.5×10^9
2	−0.34-	80	−0.760	120	1.3×10^7
4	−0.590	380	−1.150	200	2.96×10^9
5	−0.710	120	−1.060	100	8.3×10^5
6	−0.500	380	−0.950	200	4.09×10^7

Table 2. Broad bands are observed at *ca* 3400 cm^{-1} for complexes **7**–**9** indicative of lattice water and intense bands at *ca* 1640 cm^{-1} owing to HC=N— groups. The ν_3 absorption of the perchlorate group at *ca* 1100 cm^{-1} is seen as a sharp band and indicates the non-coordinated nature of the group, while the ν_4 absorption is seen at 630 cm^{-1}. The conductivity measurements in DMF show that the complexes behave as 1 : 2 electrolytes [22]. The conductivity data are collected in Table 2. All the complexes are diamagnetic which suggests a square-planar geometry. The IR spectra of complexes **11** and **12** exhibit a broad band centred at 3400 cm^{-1} indicating the presence of water or methanol. The C, H, N analytical data show two and three methanol molecules, respectively, are present in these complexes. The ν_3 band ofClO_4^- in complexes **11** and **12** at 1100 cm^{-1} is broad and indicates coordination to the metal centres. The ν_4 band is seen at 620 cm^{-1}. The ν_{NH} and δ_{NH} of the —NH— group are seen at *ca* 3200 and 1600 cm^{-1}, respectively, for complexes **10**–**12**. Conductivity experiments on these complexes show that they are 1 : 2 electrolytes.

Electronic spectra. The electronic spectra of the complexes **7** and **8** were measured in DMF solvent. Complex **9** is insoluble. The spectral data are collected in Table 2. The complexes show two high intensity bands in the range 360–410 nm in the UV region and one band in the 470–570 nm in the visible region.

The nickel(II) ion with a d^8 electronic configuration has a tendency to form four-coordinate, diamagnetic, planar complexes, especially with stronger ligands or where steric hindrance restricts higher coordination numbers. Such complexes exhibit a single *d*–*d* band in the range 400–550 nm and are often orange, yellow or red. The one *d*–*d* band in the diamagnetic, square-planar nickel(II) complexes is assigned to the $^1A_1(F) \rightarrow {}^1B_1$ transition [26,27]. The two high intensity bands at *ca* 370 and 400 nm for complexes **7** and **8** in the UV region can be interpreted as the intraligand $\pi \rightarrow \pi^*$ transition of the azomethine group and charge transfer from ligand to metal; similarly to the copper(II) complexes. It is noteworthy that the nickel(II) complex analogous to **7** with chloride as anion, $Ni_2L^1Cl_2 \cdot 3H_2O$, is also planar with a similar electronic spectrum [13].

Electronic spectra of the complexes **10**–**12** were measured in DMF and the data are collected in Table 2. The known complex **11** $[Ni_2L^5(CH_3OH)_2(ClO_4)_2]$, with distorted octahedral geometry exhibits electronic bands at 1160, 810, 750, 495, 375 nm. These bands are assigned to transitions from $^3B_{1g}$ to ^3E_g, $^3B_{2g}$, $^3A_{2g}$, ^3E_g, $^3A_{2g}$ and/or $^3E_g(P)$ in a tetragonally distorted octahedral field [11]. Complex **12** exhibits bands at 885, 770, 486 and 360 nm similar to complex **11**. Thus, this complex should also have a tetragonally distorted octahedral structure. This geometry is achieved by coordination of both methanol and perchlorate ions to each of the nickel centres. However, complex **10** exhibits bands at 1040 and 482 nm in DMF in the visible region, which is different from that of **11** and **12**. It has been established that [28] squeezing the macrocycle H_2L^5 by replacing one of the diaminopropane lateral chains [—NH—$(CH_2)_3$—NH—] with a diaminoethane chain [—NH—$(CH_2)_2$—NH—], generated a dinickel complex with one octahedral and one square-planar nickel centre. Since complex **10** has only diaminoethane as a bridging unit on both sides, two square-planar nickel(II) centres can be expected for this complex. The room temperature magnetic moment values for complexes **10**–**12** are given in Table 2. The μ_{eff} values for complexes **11** and **12** are in the range 3.1–3.31 B.M. and fall in the range usually observed for octahedral nickel(II) complexes and are comparable to related systems [11,28]. However, complex **10** is also paramagnetic, with a low μ_{eff} value (1.65 B.M. per nickel) at room temperature, which is contrary to the diamagnetism expected for square-planar complexes. This may be caused by the possible intermolecular interaction of nickel atoms with phenolic oxygens of other molecules in the solid state. Similar types of interactions have been reported in *N*,*N*′-polymethylenebis(salycilaldimine)nickel(II) complexes with a μ_{eff} value of 1.6 B.M. and electronic bands at 600 and 1000 nm [29].

Cobalt(II/III) *complexes*

The cobalt(II) complexes, **13** and **16,** are highly unstable and are obtained as black cobalt(III) complexes, while the other cobalt(II) complexes are stable and are brown in colour. Complexes **13–18** were recrystallized from methanol solutions by diffusion of diethyl ether. The cobalt(II) complexes have the general composition $[Co_2L''(ClO_4)_2]$. The general structure of the complexes is shown in Fig. 1.

IR spectra of these complexes indicate the presence of water or methanol as the ν_{OH} absorption is seen as a broad band at *ca* 3400 cm^{-1}. Sharp, intense bands are seen at 1640 cm^{-1} for complexes **13–15** and are assigned to —HC=N— groups. The analytical data in Table 1 suggest that two water molecules are present in the complexes. The broad bands centred at *ca* 1100 cm^{-1} are assignable to the ν_3 mode of the perchlorate group. The ν_4 absorption is seen as a sharp band at 630 cm^{-1}. The bands at *ca* 3200 and 1600 cm^{-1} are assigned to the ν_{NH} and δ_{NH} modes of the —NH— group.

Room temperature magnetic moments for complexes **13–18** are collected in Table 2. The cobalt(III) complex (**13**) is diamagnetic and presumably six-coordinated. The μ_{eff} values for **14** and **15** fall in the range expected for pseudo-tetrahedral or five-coordinate geometries. For complexes **14** and **15** a tetrahedral arrangement may not be favoured owing to the dinuclear nature of these complexes. An analogous dicobalt(II) complex [2] $[Co_2LCl_2]$ ($n = 3$, unreduced ligand), possesses a square-pyramidal geometry with a μ_{eff} value of 4.61 B.M. The μ_{eff} values for complexes **14** and **15** are 4.67 and 4.62 B.M., respectively. Square-pyramidal geometry appears to be reasonable for these complexes with two perchlorate groups coordinating to the two cobalt(II) ions [2, 27]. Room temperature magnetic moments for complexes **16–18** are given in Table 2. The cobalt(III) complex **16** is diamagnetic [30]. The other complexes, **17** and **18** exhibit μ_{eff} values in the range 4.7–4.8 B.M. per metal atom. The magnetic moment for high-spin, five-coordinate cobalt(II) complexes falls in the range 4.5–4.8 B.M. Thus, a square-pyramidal geometry with two perchlorate groups coordinating to each cobalt(II) ion is a distinct possibility [2] the conductivity measurements in DMF show that these complexes are 1 : 2 electrolytes (Table 2). This indicates that the perchlorate groups are replaced by solvent DMF molecules in solution.

Electronic spectra. The electronic spectra of these complexes were recorded in DMF and the data are collected in Table 2. The complexes show one high intensity band at *ca* 400 nm in the UV region and no bands are observed in the visible region. Because of intense UV bands tailing into the visible region, the *d–d* bands might have been masked. Dinuclear cobalt(II) systems have been reported where *d–d* bands are masked by such high intensity UV bands [31]. Therefore, electronic spectra in the visible region have not been effective in differentiating between square pyramidal or octahedral geometry for these complexes. The cobalt(III) complex **16** shows one band at 600 nm assignable to the $^1A_{1g} \rightarrow {}^1E_g$ transition, as expected for low-spin, six-coordinated cobalt(III) complexes [32]. The other complexes do not show any bands in the visible region.

Catalytic properties

It has been shown that magnetically interacting dinuclear complexes are catalytically active for the oxidation of two-electron donors such as 3,5-di-t-butylcatechol (3,5-DTBC) and ascorbic acid [33, 34]. The proposed pathway for the electron transfer between ascorbic acid and the dinuclear copper(II) complex involves a steric match between the donor and acceptor [33] and subsequent transfer of an electron, forming a Cu^I intermediate species. The formation of Cu^I species is generally evidenced by the disappearance of *d–d* bands in the visible absorption spectra. Although the complete mechanism of the catalytic process involved in oxidation of 3,5-DTBC is not yet established, it probably involves a 1 : 1 adduct between the complex and DTBC which requires a metal–metal distance of *ca* 3–4 Å. This adduct reacts with dioxygen to form the starting complex and 3,5-DTBQ.

The copper(II), nickel(II) and cobalt(II/III) complexes were examined for catalytic activity in the oxidation of 3,5-DTBC by molecular oxygen to the quinone, DTBQ. This is monitored by measurement of the 400 nm (ε/mol^{-1} dm^3 cm^{-1} = 1900 in methanol) [12] absorption band characteristic of 3,5-DTBQ. Catalytic activity is checked for a 50 : 1 molar ratio of catechol to the complex, except for the cobalt(III) complexes **13** and **16** for which it is 100 : 1. The results are summarized in Table 4. The reactions between ascorbic acid and the copper(II) complexes were also examined. These complexes failed to react with the acid.

The experiments on copper(II) complexes show that complexes with unreduced ligands (H_2L^1–H_2L^3) are more active than those with reduced ligands (H_2L^4–H_2L^6). The time-dependent growth of 3,5-DTBQ catalysed by copper(II) complex **4** is shown in Fig. 3 (a). The nickel(II) complexes are less active. The cobalt(III) complexes are found to be good catalysts. The Co^{III} complex **13** converts 97% in 3 h. Figure 3 (b) shows the time-dependent growth of 3,5-DTBQ catalysed by complex **13**. The other complex, **16,** converts 95% of 3,5-DTBC in 6 h. The catalytic efficiency of the complexes decreases in the order $Co^{III} > Co^{II} > Cu^{II} > Ni^{II}$.

Acknowledgements—Financial assistance from U.G.C and C.S.I.R, New Delhi is gratefully acknowledged by C. R. K. Rao.

Table 4. Percentage of conversion of DTBC in the catalytic experiments for Cu^{II}, Ni^{II} and $Co^{II/III}$ complexes

Complex	% of 3,5-DTBC conversion (time)
1	5.5 (0.5 h), 5.5 (1 h), 5.8 (3 h), 6.4 (8 h), 7.0 (20 h), 7.7 (24 h)
3	6.1 (0.5 h), 6.6 (1 h), 7.9 (3 h), 10.1 (8 h), 15.4 (20 h), 17.5 (24 h)
4	21 (1 h), 32 (2 h), 40 (3 h), 46 (4 h), 52 (5 h), 55 (6 h), 93 (23 h), 94 (24 h)
5	4.6 (1 h), 5.7 (2 h), 6.7 (3 h), 8.6 (4 h), 10.3 (5 h), 10.8 (6 h), 27 (23 h), 27 (24 h)
6	5.1 (1 h), 6.5 (2 h), 8.3 (3 h), 12.5 (4 h), 13.7 (5 h), 13.8 (6 h), 37 (23 h), 37 (24 h)
7	4.7 (0.5 h), 4.7 (1 h), 4.7 (3 h), 4.7 (8 h), 6.9 (20 h), 7.2 (24 h)
8	4.2 (0.5 h), 4.2 (1 h), 4.7 (3 h), 5.3 (8 h), 6.9 (20 h), 7.2 (24 h)
10	3.2 (1 h), 5.3 (2 h), 7.89 (5 h), 9.5 (7 h), 11.2 (9 h), 12.7 (11 h), 14.9 (13 h), 22.8 (24 h)
11	1.5 (1 h), 2.1 (2 h), 4.2 (5 h), 4.8 (7 h), 5.8 (9 h), 6.9 (11 h), 7.9 (13 h), 13.3 (24 h)
12	1.0 (1 h), 1.5 (2 h), 2.1 (5 h), 2.7 (7 h), 3.2 (9 h), 3.7 (11 h), 4.3 (13 h), 7.4 (24 h)
13	23 (5 m), 78.8 (30 m), 81.3 (1 h), 90.8 (2 h), 97 (3 h), 97 (24 h)
14	5.0 (0.5 h), 5.3 (1 h), 6.6 (3 h), 7.9 (8 h), 13.2 (20 h), 15.6 (24 h)
15	4.2 (0.5 h), 4.2 (1 h), 5.3 (3 h), 6.4 (8 h), 10.6 (20 h), 11.6 (24 h)
16	12 (10 m), 20 (20 m), 34 (40 m), 43 (50 m), 50 (1 h), 55 (1.1 h), 60 (1.2 h), 64 (1.3 h), 69 (1.4 h), 74 (2 h), 85 (3 h), 88 (4 h), 92 (5 h), 95 (6 h)
17	3.2 (1 h), 5.3 (2 h), 10.6 (5 h), 11.7 (6 h), 16 (8 h), 18.1 (9 h), 39 (22 h), 40 (23 h), 41.4 (24 h)
18	16.7 (1 h), 24 (2 h), 33.8 (5 h), 40.8 (6 h), 47.2 (8 h), 56 (9 h), 80 (22 h), 81.3 (23 h), 81.3 (24 h)

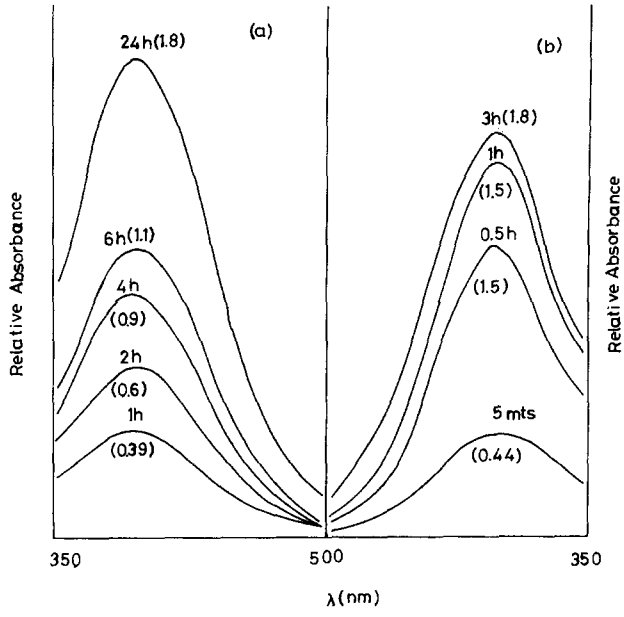


Fig. 3. Time-dependent growth of 3,5-DTBQ catalysed by (a) copper(II) complex **4** and (b) cobalt(III) complex **13**. Relative absorbance is given in brackets.

REFERENCES

1. Casellato, U., Vigato, P. A. and Vidali, M. *Coord. Chem. Rev.*, 1977, **23,** 31; Zanello, P., Tamburini, S., Vigato, P. A. and Mazzochin, G. A. *Coord. Chem. Rev.*, 1987, **77,** 165; Vigato, P. A., Tamburini, S. and Fenton, D. E. *ibid.*, 1990, **106,** 25; Guerriero, P., Tamburini, S. and Vigato, P. A. *ibid.*, 1995, **139,** 17.
2. Pilkington, N. H. and Robson, R. *Aust. J. Chem.*, 1970, **23,** 2225.
3. Gagne, R. R., Spiro, C. L., Smith, T. J., Hamann, C. A., Thies, W. R. and Shiemke, A. K. *J. Am. Chem. Soc.* 1981, **103,** 4073.
4. Gagne, R. R., Koval, C. A., Smith, T. J. and Cimolino, M. C. *J. Am. Chem. Soc.*, 1979, **101,** 4571.
5. Burfield, D. R. and Smithers, R. H. *J. Org. Chem.*, 1978, **43,** 3966.
6. Vogel, A. I. *Textbook of Practical Organic Chemistry*, 4th ed. ELBS and Longman, 1978, p. 264.
7. Riddick, J. A. and Burger, W. B. *Organic Solvents*, ed. A. Weissberger. Wiley Interscience, New York, 1970.

8. Perrin, D. D., Armarego, W. L. F. and Perrin, D. R. *Purification of Laboratory Chemicals*. Pergamon Press, London, 1966.
9. Mandal, S. K. and Nag, K. *J. Org. Chem.*, 1986, **51,** 3900.
10. Mandal, S. K., Thompson, L. K., Nag, K. and Charland, J. P. *Inorg. Chem.*, 1987, **26,** 1391.
11. Das, R. P. and Nag, K. *Inorg. Chem.*, 1991, **30,** 2831.
12. Flaig, W., Teil, B., Ploetz, Th. and Kullmer. A. *Z. Naturforsch.*, 1955, **10b,** 668.
13. Okawa, H. and Kida, S. *Bull. Chem. Soc. Jpn*, 1972, **45,** 1759.
14. Mandal, S. K., Thompson, L. K., Newlands, M. J. and Gabe, E. J. *Inorg. Chem.*, 1989, **28,** 3707.
15. Mandal, S. K., Thompson, L. K., Nag, K. and Charland, J. P. *Inorg. Chem.*, 1987, **26,** 1391.
16. Nakamato, K. *Infrared Spectra of Inorganic and Coordination Compounds*, 3rd edn. Wiley, New York, 1978.
17. Mandal, S. K. and Nag, K. *J. Chem. Soc., Dalton Trans.*, 1983, 2429.
18. Grzybowski, J. J., Merrell, R. H. and Urbach, F. L. *Inorg. Chem.*, 1978, **17,** 3078; Grzybowski, J. J., Merrell, R. H. and Urbach, F. L. *ibid.*, 1980, **19,** 2604; Nishida, Y. and Kida, S. *J. Inorg. Nucl. Chem.*, 1976, **38,** 451; Nishida, Y., Numata, Y. and Kida, S. *Inorg. Chim. Acta*, 1974, **11,** 189.
19. Adhikary, B., Mandal, S. K. and Nag, K. *J. Chem. Soc., Dalton Trans.*, 1988, 935.
20. Carlisle, W. Daniel, Fenton, D. E., Roberts, P. B., Casellato, U., Vigato, P. A. and Graziani, R. *Trans. Met. Chem.*, 1986, **11,** 292.
21. Mandal, S. K., Adhikari, B. and Nag, K. *J. Chem. Soc., Dalton Trans.*, 1986, 1175.
22. Geary, W. J. *Coord. Chem. Rev.*, 1971, **7,** 81.
23. Mandal, S. K., Thompson, L. K., Nag, K., Charland, J. P. and Gabe, E. J. *Can. J. Chem.*, 1987, **65,** 2815.
24. Mandal, S. K., Thompson, L. K., Newlands, M. J. and Gabe, E. J. *Inorg. Chem.*, 1989, **28,** 3707.
25. Okawa, H., Tadokoro, M., Aratake, Y., Ohba, M., Shindo K., Mitsumi, M., Koikawa, H., Tomono, M. and Fenton, D. E. *J. Chem. Soc., Dalton Trans.*, 1993, 253.
26. Holm, R. H. *J. Am. Chem. Soc.*, 1960, **82,** 5632.
27. Maki, G. *J. Chem. Phys.*, 1958, **29,** 1129.
28. Nanda, K. K., Das, R. P., Subramanian, K. V., Paul, P. and Nag, K. *J. Chem. Soc., Dalton Trans.*, 1993, 2515; Das, R. P., Nanda, K. K., Subramanian, K. V., Paul, P. and Nag, K. *J. Chem. Soc., Dalton Trans.*, 1992, 1253.
29. Hoyt, W. C. and Everett, Jr, G. W. *Inorg. Chem.*, 1969, **8,** 2013.
30. Figgis, B. N. and Lewis, J. *Progress in Inorganic Chemistry*, Vol. 6. Wiley Interscience, New York, 1964.
31. McFadyen, W. D., Robson, R. and Schaap, H. *Inorg. Chem.*, 1972, **11,** 1777; Srinivas, B. and Zacharias, P. S., *Trans. Met. Chem.*, 1991, **16,** 521.
32. Mahapatra, M., Chakravorthy, V. and Dash, K. C. *Polyhedron*, 1989, **8,** 1509 and references therein.
33. Oishi, N., Nishida, Y., Ida, K. and Kida, S. *Bull. Chem. Soc. Jpn*, 1980, **53,** 2847.
34. Casellato, U., Tamburini, S., Vigato, P. A., Destafeni, A., Vidali, M. and Fenton, D. E. *Inorg. Chim. Acta*, 1983, **69,** 45; Grzybowski, J. J., Merrell, P. H. and Urbach, F. L. *Inorg. Chem.*, 1978, **17,** 3078.

Pergamon

PII: S0277-5387(96)00362-2

Polyhedron Vol. 16, No. 7, pp. 1211–1221, 1997
Copyright © 1997 Elsevier Science Ltd
Printed in Great Britain. All rights reserved
0277-5387/97 $17.00+0.00

Structural and electronic effects of alkyl substituents on the main group dithiocarbamato complexes: crystal and molecular structures of tris(*N*,*N*′-iminodiethanoldithiocarbamato)metal(III) complexes (M = As, Sb and Bi) and cyclic voltammetric studies on substituted dithiocarbamates

V. Venkatachalam,[a] K. Ramalingam,[a]* U. Casellato[b] and R. Graziani[c]

[a]Department of Chemistry, Annamalai University, Annamalainagar 608 002, India

[b]Istituto di Chimica e Tecnologie Inorganiche e dei Materiali Avanzati del C.N.R., Area della Ricerca 35020, Padova, Italy

[c]Dipartimento di Chimica Inorganica, Metallorganica e Analitica, Universita' di Padova, Italy

(Received 17 April 1996; accepted 24 July 1996)

Abstract—Various dithiocarbamates of As^{III}, Sb^{III} and Bi^{III} with diethyldithiocarbamic acid (dedtc), *N*-methylaminoethanoldithiocarbamic acid (nmedtc) and *N*,*N*′-iminodiethanoldithiocarbamic acid were subjected to cyclic voltammetric reduction studies with a glassy carbon working electrode. One-electron reduction processes occurs around −1.0 V for As and Sb complexes and around −0.5 V for Bi complexes which are completely irreversible. Attachment of the polar ends of the molecule is indicated by the pre- and post-reduction adsorption processes. As the number of $—CH_2CH_2OH$ groups increases, the peak currents increase. In the case of Bi complexes, the reduction process tends to become reversible. In addition, the larger peak current associated with the third response indicates the possible reduction of $Bi(dtc)_2(DMF)_n$.

In all the complexes the dtc^- ion was lost from $M(dtc)_3^-$ species, with oxidization around +0.6 V in the reverse scans. The crystal structures of $As(deadtc)_3$ (**1**), $Sb(deadtc)_3$ (**2**) and $Bi(deadtc)_3$ (**3**) were determined by single crystal X-ray analysis.

The coordination polyhedron in $As(deadtc)_3$ is a distorted trigonal antiprism, with three strong (2.33–2.35 Å) and three weak (2.82–2.86 Å) As—S bonds. $Sb(deadtc)_3$ has a coordination polyhedron which can be described as a distorted pentagonal pyramid. One of the Sb—S bonds is very short (2.46 Å) and differences between others are not significant owing to the larger size of antimony compared with arsenic. The stereochemical requirement of the lone pair on Sb has a more pronounced effect in disturbing the neighbouring atoms than that observed in the corresponding As compounds. The binuclear $Bi_2(deadtc)_6$ complex is centrosymmetric, two bidentate ligands being bridged in such a way that each sulfur atom is simultaneously bonded to both metal ions. The resulting coordination polyhedron can be described as a distorted square antiprism. The asymmetry in the M—S (M = As, Sb, Bi) bonds is a consequence of the stereochemical requirement for the ligand and the lone pair of electrons on the metals. This is supported by the valence bond sums (VBS) calculated for the complexes. Copyright © 1997 Elsevier Science Ltd

Keywords: crystal structures; electronic effects; alkyl substituents; dithiocarbamates; cyclic voltammetry.

* Author to whom correspondence should be addressed.

Group VA elements, such as As, Sb and Bi, provide interesting variations in their reactivities related to the gradual increase in metallic character down the group [1]. Various compounds of these elements were extensively used as medicines in the treatment of syphilis, kala-azar, elephantiasis and yaws but their use has been discouraged because of their toxicity [2,3]. A recent discovery that colloidal bismuth subcitrate (CBS) was useful in treating peptic ulcers has increased interest in the chemistry of these elements [4–6], as has the use of these elements in high-temperature superconductors [7,8].

Recently, a few studies on dithiocarbamato complexes of As, Sb and Bi have been reported [9–13]. As a continuation of our interest in sulfur-containing ligands [14–16], we report here the synthesis and cyclic voltammetric studies of various $M(dtc)_3$ complexes [M = As^{III}, Sb^{III}, Bi^{III}; dtc = *N,N'*-diethyldithiocarbamate (dedtc), *N*-methylaminoethanoldithiocarbamate (nmedtc), *N,N'*-iminodiethanoldithiocarbamate (deadtc)] along with the X-ray crystal structures of $As(deadtc)_3$, $Sb(deadtc)_3$ and $Bi(deadtc)_3$.

EXPERIMENTAL

Materials

$AsCl_3$, Sb_2O_3, $BiONO_3$ and *N,N'*-iminodiethanol, *N*-methylaminoethanol, *N,N'*-diethylamine from BDH/E-Merck were used as received.

N,N'-Imminodiethanoldithiocarbamic acid (0.03 mol) was prepared from 2.8 cm^3 of *N,N'*-iminodiethanol and 1.8 cm^3 of carbon disulfide in methanol under cold conditions (5°C).

Tris(N,N'-*iminodiethanoldithiocarbamato*)*arsenic* (III), $As(deadtc)_3$

A freshly prepared yellow dithiocarbamic acid solution (0.03 mol) was added to arsenic chloride (0.8 cm^3, 0.01 mol) in methanol (10 cm^3) with continuous stirring. The white dithiocarbamato complex separated out on neutralization of the excess acid by passing ammonia. Yield 60%, m.p. 107–110°C. Crystals suitable for X-ray analysis were obtained from methanol.

Tris(N,N'-*iminodiethanoldithiocarbamato*)*antimony* (III), $Sb(deadtc)_3$

Antimony trioxide Sb_2O_3, (1.5 g, 0.05 mol) was dissolved in concentrated HCl solution (5 cm^3) and the volume of the solution was reduced to 50% by boiling. After cooling the freshly prepared *N,N'*-iminodiethanoldithiocarbamic acid solution (0.03 mol) was added with continuous stirring. The resulting pale yellow solution gave a pale yellow complex after passing ammonia gas. Yield 70%, m.p. 130–132°C. Suitable crystals for X-ray analysis were obtained from a methanolic solution of the compound.

Tris(N,N'-*iminodiethanoldithiocarbamato*)*bismuth* (III), $Bi(deadtc)_3$

Bismuth oxynitrate $BiONO_3$ (2.9 g, 0.01 mol) was dissolved in concentrated HCl solution (5 cm^3) and the volume of the solution was reduced to 50% by Patterson and Fourier methods, alternated with cycles of least-squares refinement of the atomic parameters. Hydrogen atoms were located on the Fourier difference maps but were generally introduced in the calculated positions with fixed C—H distances and isotropic temperature factors (C—H = 1.08 Å, U_{iso} = 0.08 $Å^2$). It was not possible to locate the H atoms of the terminal OH groups in the Bi compound because of the partial disorder in the chains. Anisotropy was introduced for all non-hydrogen atoms. Refinement of scale factor and positional and thermal parameters was performed, minimizing the function $\Sigma w(\Delta F)^2$ with $w = 1$. At convergence, the largest parameter shift among the refined parameters of the non-hydrogen atoms was 0.2 times the standard deviation. No significant residuals of electron density were observed in the final electron density maps. Scattering factors for the atoms were supplied internally by the SHELX program system [17]. Crystal and intensity data for compounds **1**, **2** and **3** are reported in Table 1. Bond distances and angles are reported in Tables 2–5. Diagrams of the molecular structures of **1**, **2** and **3** are shown in Figs 1–3, respectively. Atomic coordinates and anisotropic thermal parameters for non-hydrogen atoms are available as supplementary material.

RESULTS AND DISCUSSION

Electrochemical reduction of $M(dtc)_3$ *complexes*

CV studies on the dithiocarbamato complexes of As, Sb and Bi are sparse. Data obtained in the present study are given in Table 6. Typical voltammograms are shown in Fig. 4. All the dithiocarbamato complexes, $M(dtc)_3$, showed three responses which are completely irreversible in the case of As and Sb. For the Bi complexes, the response around −0.5 V tends to become reversible.

Under identical experimental conditions $AsCl_3$ and $BiCl_3$ showed a single response during the reduction process at −0.82 and −0.70 V, respectively. However, the same could not be proved for $BiCl_3$ because of its high insolubility. The appearance of more CV responses for the $M(dtc)_3$ complexes is a result of the inherent property of the glassy carbon electrode used. Glassy carbon can have the functional groups adsorbed on the surface, leading to chemically modified pathways.

Table 1. Crystallographic data for $As(deadtc)_3$ (**1**), $Sb(deadtc)_3$ (**2**) and $Bi_2(deadtc)_6$ (**3**)

Compound	$As(deadtc)_3$	$Sb(deadtc)_3$	$Bi_2(deadtc)_6$
Empirical formula	$C_{15}H_{30}N_3O_6S_6As$	$C_{15}H_{30}N_3O_6S_6Sb$	$C_{30}H_{60}N_6O_{12}S_{12}Bi_2$
M	615.7	662.5	1499.4
Crystal system	triclinic; $P\bar{1}$	triclinic; $P\bar{1}$	monoclinic; $P2_1/c$
a/Å	8.346(3)	9.973(3)	11.172(5)
b/Å	11.580(3)	11.113(3)	21.451(7)
c/Å	15.017(4)	12.489(4)	22.264(8)
α/Å	88.62(3)	104.23(3)	90
β/°	74.44(3)	75.06(3)	98.26(4)
γ/°	87.73(3)	85.71(3)	90
U/Å^3	1397(1)	1282(1)	5280(3)
D_c/g cm^3	1.46	1.71	1.89
Z	2	2	4
μ(Mo-K_α)/cm^{-1}	16	15	68.9
Scan mode	$\theta/2\theta$	$\theta/2\theta$	$\theta/2\theta$
Scan speed/° min^{-1}	2	2	2
Recorded reflections	3075	4731	4728
Observed reflections [$I > 3\sigma(I)$]	2820	3062	3913
Residual R, R_w	0.056, 0.062	0.028, 0.035	0.063, 0.070

Table 2. Selected bond distances (Å) and angles (°) for $As(deadtc)_3$ (**1**)

As—S(1)	2.353(2)	As—S(2)	2.820(2)
As—S(3)	2.339(2)	As—S(4)	2.853(2)
As—S(5)	2.334(2)	As—S(6)	2.863(2)
C(1)—S(1)	1.762(8)	C(1)—S(2)	1.65(1)
C(1)—N(1)	1.34(1)	N(1)—C(2)	1.48(1)
N(1)—C(4)	1.50(1)	C(6)—S(3)	1.760(9)
C(6)—S(4)	1.697(9)	C(6)—N(2)	1.33(1)
N(2)—C(7)	1.47(1)	N(2)—C(9)	1.46(1)
C(11)—S(5)	1.735(9)	C(11)—S(6)	1.694(9)
C(11)—N(3)	1.32(1)	N(3)—C(12)	1.46(1)
N(3)—C(14)	1.48(3)		
S(1)—As—S(2)	68.8(1)	S(1)—As—S(3)	88.5(1)
S(3)—As—S(4)	68.9(1)	S(1)—As—S(5)	90.6(1)
S(5)—As—S(6)	68.0(1)	S(3)—As—S(5)	87.0(1)
S(2)—As—S(4)	105.3(1)	As—S(1)—C(1)	91.9(3)
S(2)—As—S(6)	111.8(1)	As—S(2)—C(1)	79.1(3)
S(4)—As—S(6)	110.2(1)	As—S(3)—C(6)	93.9(3)
S(1)—C(1)—S(2)	119.4(5)	As—S(4)—C(6)	78.8(3)
S(3)—C(6)—S(4)	118.3(5)	As—S(5)—C(11)	94.9(3)
S(5)—C(11)—S(6)	118.0(5)	As—S(6)—C(11)	78.7(3)
S(1)—C(1)—N(1)	116.7(7)	S(2)—C(1)—N(1)	123.9(7)
C(1)—N(1)—C(2)	123.5(8)	C(1)—N(1)—C(4)	118.0(1)
C(2)—N(1)—C(4)	118.6(9)	S(3)—C(6)—N(2)	118.1(7)
S(4)—C(6)—N(2)	123.6(7)	C(6)—N(2)—C(7)	122.4(8)
C(6)—N(2)—C(9)	121.0(8)	C(7)—N(2)—C(9)	116.4(8)
S(5)—C(11)—N(3)	117.8(7)	S(6)—C(11)—N(3)	124.2(7)
C(11)—N(3)—C(12)	123.7(8)	C(11)—N(3)—C(14)	115.8(9)
C(12)—N(3)—C(14)	118.9(9)		

Surface attachment of the polar ends of the compounds has already been encountered [18,19]. Of the three responses, those around −1.0 V for As and Sb and those around −0.5 V for Bi are owing to one-electron metal-based reductions. The peak currents associated with this set of responses were relatively larger than those associated with the other two responses.

Other weaker responses lie in the ranges 0 to −0.4

Table 3. Selected bond distances (Å) and angles (°) for $Sb(deadtc)_3$ (**2**)

Sb—S(1)	2.645(2)	Sb—S(2)	2.763(2)
Sb—S(3)	2.463(2)	Sb—S(4)	2.878(2)
Sb—S(5)	2.673(2)	Sb—S(6)	2.849(2)
C(1)—S(1)	1.721(6)	C(1)—S(2)	1.720(6)
C(1)—N(1)	1.337(7)	N(1)—C(2)	1.470(8)
N(1)—C(4)	1.472(8)	C(6)—S(3)	1.753(6)
C(6)—S(4)	1.690(5)	C(6)—N(2)	1.336(6)
N(2)—C(7)	1.481(7)	N(2)—C(9)	1.472(8)
C(11)—S(5)	1.743(6)	C(11)—S(6)	1.708(6)
C(11)—N(3)	1.324(7)	N(3)—C(12)	1.478(8)
N(3)—C(14)	1.478(8)		
S(1)—Sb—S(2)	65.87(9)	S(1)—Sb—S(5)	76.9(1)
S(3)—Sb—S(4)	66.94(9)	S(2)—Sb—S(4)	78.68(8)
S(5)—Sb—S(6)	64.61(9)	S(4)—Sb—S(6)	74.74(8)
S(3)—Sb—S(1)	91.4(1)	Sb—S(1)—C(1)	89.0(2)
S(3)—Sb—S(2)	90.09(9)	Sb—S(2)—C(1)	85.2(2)
S(3)—Sb—S(5)	93.1(1)	Sb—S(3)—C(6)	92.4(2)
S(3)—Sb—S(6)	85.6(1)	Sb—S(4)—C(6)	80.3(2)
S(1)—C(1)—S(2)	117.5(3)	Sb—S(5)—C(11)	90.3(2)
S(3)—C(6)—S(4)	118.9(3)	Sb—S(6)—C(11)	85.2(2)
S(5)—C(11)—S(6)	117.8(4)	S(1)—C(1)—N(1)	121.3(4)
C(1)—N(1)—C(2)	121.3(5)	S(2)—C(1)—N(1)	121.2(4)
C(2)—N(1)—C(4)	116.7(5)	C(1)—N(1)—C(4)	113.4(5)
S(4)—C(6)—N(2)	122.7(4)	S(3)—C(6)—N(2)	118.4(4)
C(6)—N(2)—C(9)	121.5(5)	C(6)—N(2)—C(7)	121.4(5)
C(7)—N(2)—C(9)	117.0(4)	S(5)—C(11)—N(3)	120.2(4)
C(11)—N(3)—C(12)	121.3(5)	S(6)—C(11)—N(3)	122.0(5)
C(12)—N(3)—C(14)	117.6(5)	C(11)—N(3)—C(14)	121.2(5)

Table 4. Selected bond distances (Å) for $Bi_2(deadtc)_6$ (**3**)

Molecule 1		Molecule 2	
Bi(1)—S(1)	3.085(7)	Bi(2)—S(9)	3.080(7)
Bi(1)—S(2)	3.076(9)	Bi(2)—S(10)	3.139(8)
Bi(1)—S(1^{I})	3.130(7)	Bi(2)—S(9^{II})	3.137(7)
Bi(1)—S(2^{I})	3.179(9)	Bi(2)—S(10^{II})	3.129(7)
Bi(1)—S(3)	2.819(7)	Bi(2)—S(7)	2.671(7)
Bi(1)—S(4)	2.729(7)	Bi(2)—S(8)	2.790(7)
Bi(1)—S(5)	2.669(7)	Bi(2)—S(11)	2.691(6)
Bi(1)—S(6)	2.885(7)	Bi(2)—S(12)	2.822(7)
Bi(1)···Bi(1^{I})	3.893(4)	Bi(2)···Bi(2^{II})	3.807(4)
S(1)—C(1)	1.67(3)	S(9)—C(21)	1.74(3)
S(2)—C(1)	1.77(2)	S(10)—C(21)	1.72(2)
C(1)—N(1)	1.34(3)	C(21)—N(5)	1.34(3)
N(1)—C(2)	1.45(3)	N(5)—C(22)	1.51(3)
N(1)—C(4)	1.50(4)	N(5)—C(24)	1.45(3)
S(4)—C(6)	1.71(3)	S(11)—C(26)	1.79(3)
S(3)—C(6)	1.73(3)	S(12)—C(26)	1.71(2)
C(6)—N(2)	1.36(3)	C(26)—N(6)	1.28(3)
N(2)—C(7)	1.53(3)	N(6)—C(27)	1.52(3)
N(2)—C(9)	1.43(3)	N(6)—C(29)	1.45(3)
S(5)—C(11)	1.69(3)	S(7)—C(16)	1.72(3)
S(6)—C(11)	1.73(3)	S(8)—C(16)	1.69(3)
C(11)—N(3)	1.33(3)	C(16)—N(4)	1.40(3)
N(3)—C(12)	1.47(4)	N(4)—C(17)	1.44(3)
N(3)—C(14)	1.48(4)	N(4)—C(19)	1.44(3)

Table 5. Selected bond angles (°) for $Bi_2(deadtc)_6$ (3)

Molecule 1		Molecule 2	
S(3)—Bi(1)—S(4)	64.6(2)	S(7)—Bi(2)—S(8)	65.7(2)
S(5)—Bi(1)—S(6)	64.2(2)	S(11)—Bi(2)—S(12)	65.6(2)
S(1)—Bi(1)—S(2)	78.0(2)	S(9)—Bi(2)—S(10)	77.9(2)
$S(1^I)$—Bi(1)—$S(2^I)$	75.8(2)	$S(9^I)$—Bi(2)—$S(10^{II})$	78.9(2)
S(1)—Bi(1)—$S(2^I)$	75.9(2)	S(9)—Bi(2)—$S(10^{II})$	78.9(2)
S(2)—Bi(1)—$S(1^I)$	78.0(2)	S(10)—Bi(2)—$S(9^{II})$	77.9(2)
S(5)—Bi(1)—S(3)	82.5(2)	S(7)—Bi(2)—S(12)	81.9(2)
S(6)—Bi(1)—S(4)	86.4(2)	S(8)—Bi(2)—S(11)	83.7(2)
Bi(1)—S(1)—$Bi(1^I)$	77.5(1)	Bi(2)—S(9)—$Bi(2^{II})$	75.6(1)
Bi(1)—S(2)—$Bi(1^I)$	77.0(1)	Bi(2)—S(10)—$Bi(2^{II})$	74.8(1)
Bi(1)—S(1)—C(1)	83(1)	Bi(2)—S(9)—C(21)	85(1)
Bi(1)—S(2)—C(1)	84(1)	Bi(2)—S(10)—Bi(21)	83(1)
$Bi(1^I)$—S(1)—C(1)	89(1)	$Bi(2^I)$—S(9)—C(21)	84(1)
$Bi(1^I)$—S(2)—C(1)	85(1)	$Bi(2^I)$—S(10)—C(21)	84(1)
Bi(1)—S(3)—C(6)	85(1)	Bi(2)—S(7)—C(16)	88(1)
Bi(1)—S(4)—C(6)	89(1)	Bi(2)—S(8)—C(16)	85(1)
Bi(1)—S(5)—C(11)	92(1)	Bi(2)—S(11)—C(26)	89(1)
Bi(1)—S(6)—C(11)	84(1)	Bi(2)—S(12)—C(26)	86(1)
S(1)—C(1)—S(2)	118(1)	S(9)—C(21)—S(10)	119(1)
S(1)—C(1)—N(1)	123(1)	S(9)—C(21)—N(5)	121(2)
S(2)—C(1)—N(1)	119(2)	S(10)—C(21)—N(5)	120(2)
C(1)—N(1)—C(2)	124(2)	C(21)—N(5)—C(22)	123(2)
C(1)—N(1)—C(4)	120(2)	C(21)—N(5)—C(24)	121(2)
C(2)—N(1)—C(4)	115(2)	C(22)—N(5)—C(24)	115(2)
S(3)—C(6)—S(4)	120(2)	S(7)—C(16)—S(8)	121(2)
S(3)—C(6)—N(2)	117(2)	S(7)—C(16)—N(4)	119(2)
S(4)—C(6)—N(2)	122(2)	S(8)—C(16)—N(4)	120(2)
C(6)—N(2)—C(7)	118(2)	C(16)—N(4)—C(17)	121(2)
C(6)—N(2)—C(9)	124(2)	C(16)—N(4)—C(19)	119(2)
C(7)—N(2)—C(9)	118(2)	C(17)—N(4)—C(19)	118(2)
S(5)—C(11)—S(6)	119(2)	S(11)—C(26)—S(12)	117(1)
S(5)—C(11)—S(3)	122(2)	S(11)—C(26)—N(6)	120(2)
S(6)—C(11)—N(3)	119(2)	S(12)—C(26)—N(6)	122(2)
C(11)—N(3)—C(12)	124(3)	C(26)—N(6)—C(27)	122(2)
C(11)—N(3)—C(14)	120(2)	C(26)—N(6)—C(29)	121(2)
C(12)—N(3)—C(14)	117(3)	C(27)—N(6)—C(29)	117(2)

V and −1.5 to −2.4 V. For the less negative response (0 to −0.4 V) the maximum peak current was only 70 μA. This is probably owing to the attachment of polar ends of the molecule to the glassy carbon electrode. Data in Table 6 show that there is a significant linearity in the peak currents for the first response, in the order: $M(dedtc)_3 < M(nmedtc)_3 < M(deadtc)_3$. A large number of polar —CH_2CH_2OH groups increases the peak current. The reduced species $M(dtc)_3^-$ is highly unstable and could not be detected as observed earlier for other species [20]. Often, as an alternative to the stabilization of $M(dtc)_3^-$ species, dissociation takes place to give rise to dtc^-:

$$M(dtc)_3^- \rightarrow M(dtc)_2 + dtc^-.$$

Subsequently, dtc^- gets oxidised to disulfide [20, 21]. All $M(dtc)_3$ complexes showed three oxidation responses in the reverse scans: +0.60, +0.65 and +0.55 V for $dedtc^-$, $nmedtc^-$, and $deadtc^-$, respectively. The oxidation response appeared even if the potential scan was stopped after the second reduction responses in the complexes.

The third CV responses in the potential range −1.5 to −2.4 are of moderate peak currents. Variation in peak currents with respect to the number of —CH_2CH_2OH groups attached is regular for $As(dtc)_3$ complexes. Coulometry and controlled potential electrolysis gave no conclusive evidence of any conceivable species. Therefore, the third response should be attributed to the stabilization of $M(dtc)_2$ species on the electrode surface or to a second electron addition process on the solvated species $M(dtc)_2(DMF)_n$ [21]:

$$M(dtc)_2(DMF)_n + e^- \rightarrow M(dtc)_2(DMF)_n^-.$$

Stabilization of $M(dtc)_2$ on the electrode surface appears to be reasonable for As and Sb complexes. For the Bi analogues, the peak currents of the third responses are comparable to the second responses, therefore, the electron addition to the solvated species appears to be favoured.

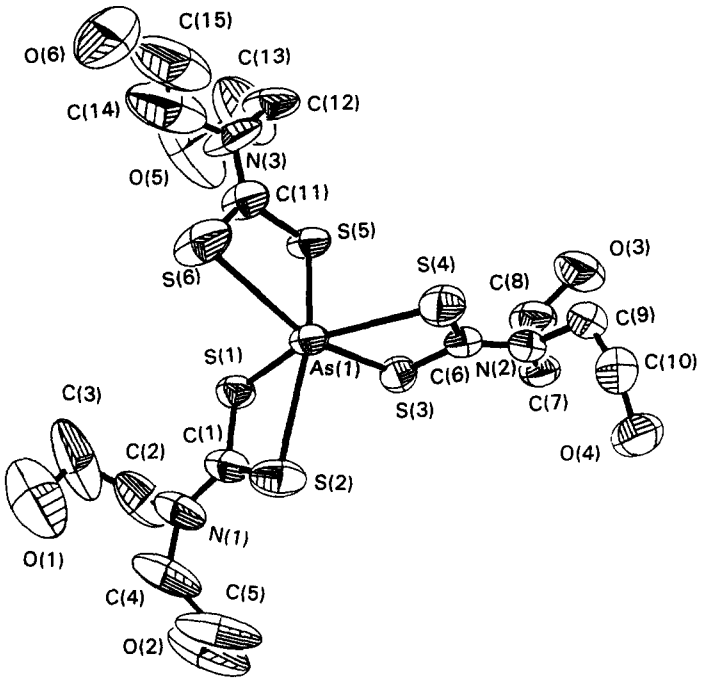


Fig. 1. ORTEP plot of As(deadtc)$_3$ (**1**) showing the labelling scheme.

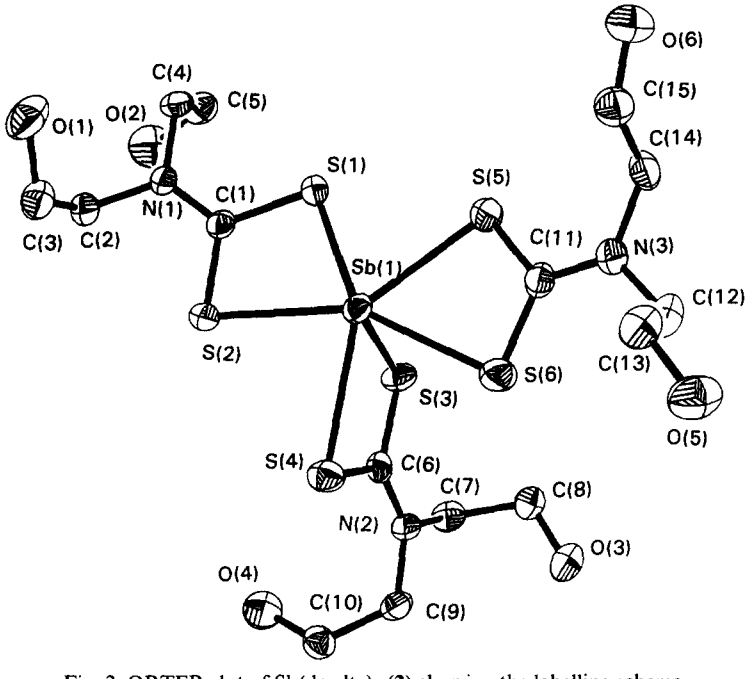


Fig. 2. ORTEP plot of Sb(deadtc)$_3$ (**2**) showing the labelling scheme.

In conclusion, the bismuth compound shows a lesser negative reduction potential compared with the other two complexes. The presence of polar —CH_2CH_2OH groups on the dithiocarbamate ligands increased the tendency to become stabilized on the glassy carbon electrode.

X-ray crystal structures

The structure of As(deadtc)$_3$ is shown in Fig. 1. The bidentate ligands are chelated to the As atom forming a polyhedron which can be described as a distorted trigonal antiprism. There are three short As—S bonds

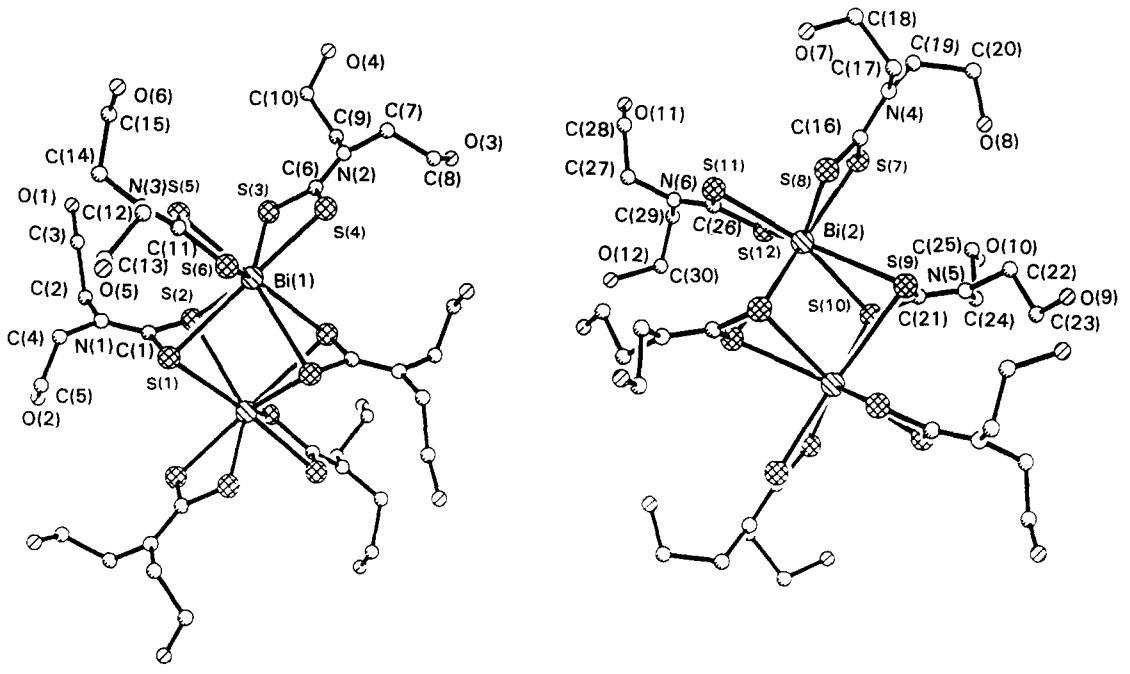


Fig. 3. Molecular structure of the two crystallographyically independent units of $Bi_2(deadtc)_6$ (**3**). Unlabelled atoms are related by symmetry operation to labelled atoms.

Table 6. Cyclic voltammetric data for $M(dtc)_3$ [M = As^{III}, Sb^{III}, Bi^{III}; dtc = dedtc, nmedtc, deadtc) in DMF [peak potentials (V) and peak currents (μA)]

Compound	E_{p_1}	i_{p_1}	E_{β}	i_{p_2}	E_{p_3}	i_{p_3}
$As(dedtc)_3$	−0.35	20	−1.14	220	−1.66	150
$As(nmedtc)_3$	−0.28	35	−1.25	225	−2.28	220
$As(deadtc)_3$	−0.36	70	−1.30	350	−2.35	350
$Sb(dedtc)_3$	−0.25	10	−0.7	220	−1.75	75
$Sb(nmedtc)_3$	−0.30	50	−0.65	320	−2.00	140
$Sb(deadtc)_3$	−0.35	60	−0.75	290	−2.02(qr)	90
$Bi(dedtc)_3$	−0.05	30	−0.46 (E_{p_r})	450	−2.00	400
			−0.15 (E_{p_a})	260		
$Bi(nmedtc)_3$	−0.25	50	−0.50 (E_{p_r})	250	−1.70	110
			−0.10 (E_{p_a})	90		
$Bi(deadtc)_3$	−0.10	70	−0.45 (E_{p_r})	130	−1.98	320
			−0.20 (E_{p_a})	20		

Concentration = 1×10^{-3} M.
Supporting electrolyte = 0.1 M of TBAP.
Working electrode = glassy carbon.
Reference electrode = Ag/AgCl.

and three long As—S bonds. All the three short bonds [mean As—S = 2.34(2) Å] indicate a strong "S" coordination while the other set corresponds to a weak interaction [mean As—S = 2.84(2) Å]. It is noticeable that in all ligands the C—S bond associated with the strong As—S bond is significantly longer [mean 1.77(9) Å] than that [mean 1.68(7) Å] associated with the weak As—S bond, showing clearly the localization of the double bonds. A remarkable feature concerns the N—C—S angles. Of the two sets of N—C—S angles [*viz.*, mean 123.9(7) Å and 118.2(7) Å] the larger value is as expected owing to the mutual repulsion between the double bond and the adjacent electronegative "N" atom. The strong As—S bonds are nearly at right angles to one another.

A schematic diagram of the coordination polyhedron showing the two trigonal faces of the antiprism is depicted in Figure 5. The plane defined by S(1), S(3) and S(5), which are the strongly coordinated sulfur atoms, is essentially parallel to that defined by S(2), S(4) and S(6) (the two planes are inclined by 2.2°) and As is displaced by 1.38 and 0.96 Å, respectively,

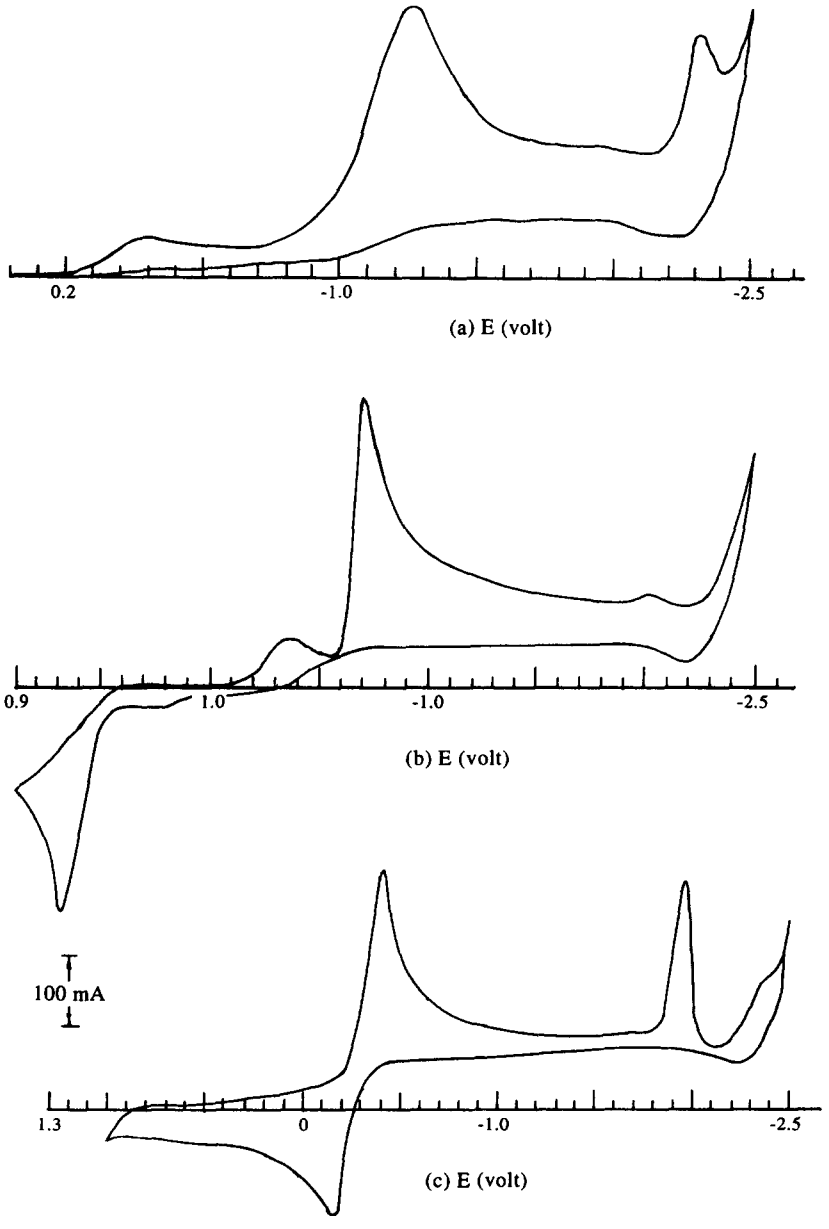


Fig. 4. Typical voltammograms of (a) $As(deadtc)_3$, (b) $Sb(nmedtc)_3$ and (c) $Bi(deadtc)_3$.

from the planes. Complexes of As^{III}, Sb^{III} and Bi^{III} with polydentate ligands occupying six coordination sites have been found to have a stereochemically active lone pair [22–25]. Of the two sets of S—As—S angles in the two trigonal prisms (Fig. 6), the large angle is 111.8(1)°, and this widening allows the lone pair to occupy the space.

The thioureide C—N bond [mean 1.33(1) Å] is comparable to that observed in the diethyldithiocarbamate analogue [11]. The presence of the electron-withdrawing $—CH_2CH_2OH$ group does not influence the thioureide distance significantly. However, the thioureide C—N bond is significantly shorter than the adjacent typical C—N single bond [mean 1.47(3) Å] indicating a partial double bond character as found earlier [15]. Two terminal C—C—O angles, C(12)—C(13)—O(5) and C(14)—C(15)—O(6) are 134(2) and 121(1)°, respectively. This is likely to be a result of the requirements of the terminal —OH groups and also the requirements of the lone pair on the arsenic atom.

The structure of $Sb(deadtc)_3$ is shown in Fig. 2 along with the numbering scheme. The coordination polyhedron can be described as a distorted pentagonal pyramid with S(3) as the apex. The relatively large size of the antimony, in addition to the establishment of metallic character by way of true coordinative interaction with the sulfurs of the deadtc, is responsible for comparable Sb—S bonds [10,12,13]. In the case of the arsenic analogue, the interaction is of a more covalent

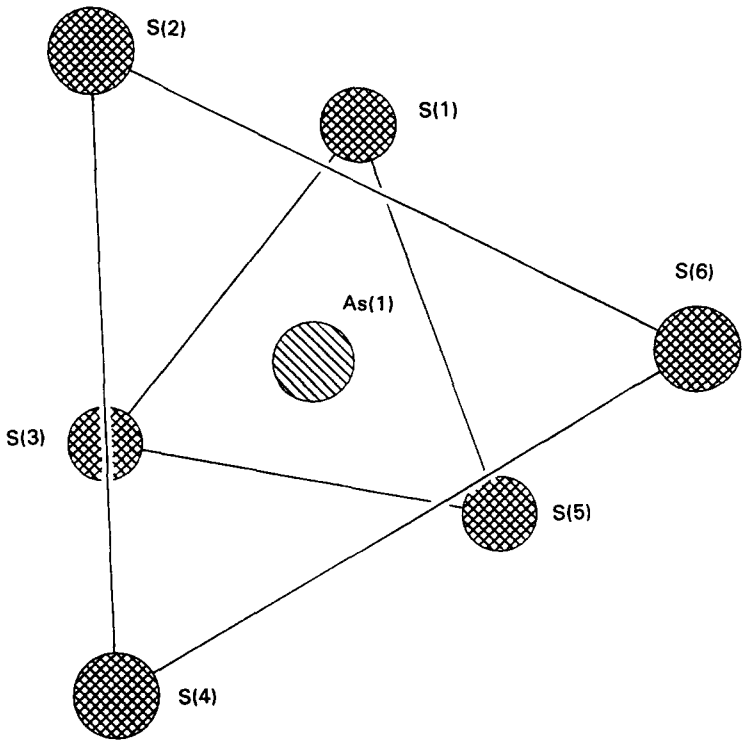


Fig. 5. A schematic diagram of the coordination polyhedron in $As(deadtc)_3$ showing the two trigonal faces of the antiprism.

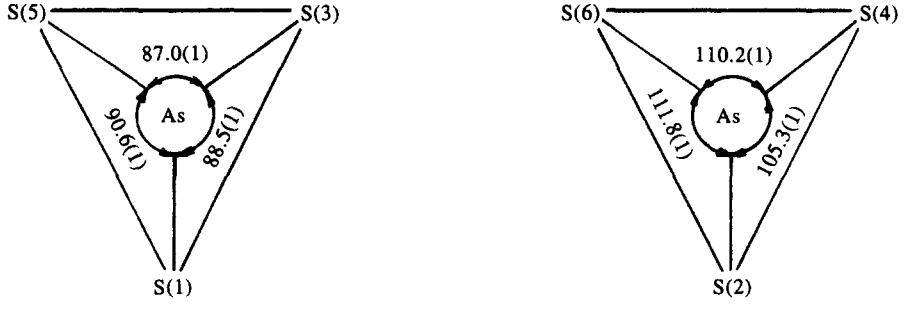


Fig. 6. Two sets of S—As—S angles in the two trigonal prisms of $As(deadtc)_3$.

nature leading to a trigonal antiprismatic polyhedron [9,11]. The strongest of all the Sb—S bonds is the apical Sb—S(3) bond with a bond distance of 2.46(2) Å. It is noteworthy that in the ligand where the two Sb—S bonds are similar, such as Sb—S(1) and Sb—S(2), the two C—S bonds are also roughly equivalent; while they are different when the difference between the Sb—S bonds is more pronounced, such as for Sb—S(5) and Sb—S(6). The difference becomes more significant in the third ligand where Sb—S(4) is the longest bond and Sb—S(3) is the shortest. In this context, the terminal C—C—O angles must also be considered. Of the six C—C—O angles, the C(9)—C(10)—O(4) angle is 128(1)°. Larger perturbations observed in the third ligand are likely to be a result of the position of the stereochemically active lone pair across S(2), S(4) [25]. The N—C—S angles are approximately equal in two ligands, while they differ significantly (122.7° *vs* 118.4°) in the third ligand, where the double bond character is more localized [on C(6)—S(4)]. The average thioureide C—N distance is 1.332(7) Å, which compares well with the value found in the diethyl analogue [10].

The molecular structure of $Bi_2(deadtc)_6$ is shown in Fig. 3. Two independent centrosymmetric molecules of the compound are present in the structure so that the asymmetric unit is formed by one half of both molecules, and a total of four molecules comprise the unit cell. In any case, although independent from a crystallographical point of view, all molecules have the same structure with comparable values for bond lengths and angles. Two of the six bidentate ligands are bridged in such a way that each sulfur atom is simultaneously bonded to both metal ions. As a result,

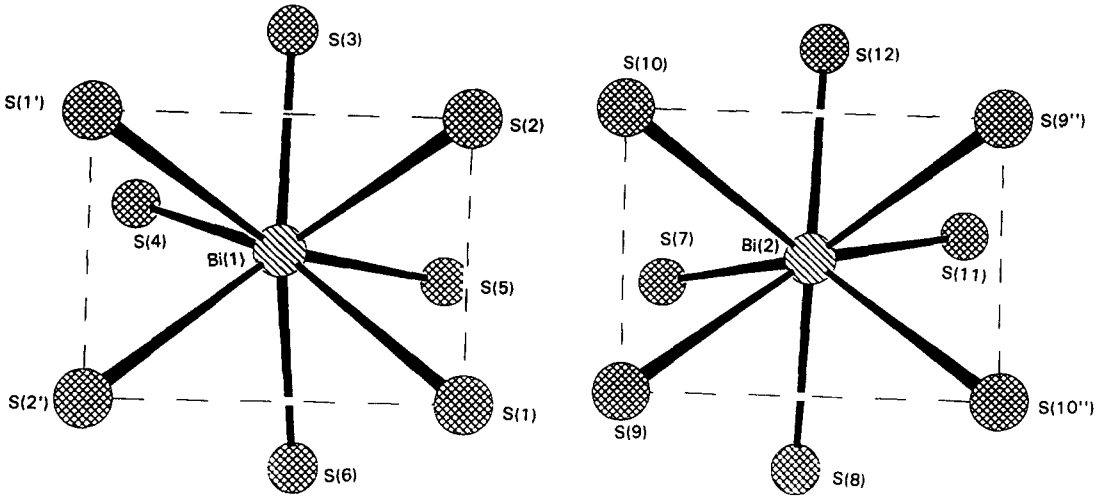


Fig. 7. Square antiprismatic environment of sulfurs around bismuth in $Bi_2(deadtc)_6$.

the metal is eight-coordinate in a coordination polyhedron that can be described as a distorted square antiprism (Fig. 7). Two sets of Bi—S distances are observed; mean Bi—S = 2.775(7) and 3.117(9) Å, and similarly two sets of S—Bi—S angles: 64.4(2) and 76.9(2)°. The two faces of the polyhedron are quasi parallel, with dihedral angles of 5.3 and 1.2°. The Bi atoms in the two molecules are displaced by 1.47 Å from the faces formed by the non-bridging S atoms, and by 1.94 and 1.90 Å from those of the bridging atoms. Inspection of bond lengths clearly shows that non-bridging S atoms form coordination bonds that are at least 0.35 Å shorter than those of the bridging S atoms. All Bi—S bond distances are generally longer than the sum of the corresponding covalent or atomic radii. In addition, one of the two Bi—S bonds of each non-bridging ligand is always significantly shorter than the other, whereas no systematic differences are found for the bridging ligands. Comparison of the structural parameters of $Bi_2(deadtc)_4$ with those of the diethyl analogue [10] clearly differentiates the characteristic dimer observed in the former.

In all three complexes, O···O non-bonded distances are observed of the order of 2.66 Å, indicating extensive intermolecular hydrogen bonding involving the alkyl chain. However, high esds associated with bond parameters and large thermal motions of the terminal oxygen atoms of the ligand molecules preclude detailed analysis. This is not surprising because the structure is strongly dominated by heavy As, Sb and Bi ions.

The formation of a complex of any metal ion with a multidentate ligand represents a compromise between steric interactions in the ligand and the steric and electronic requirements of the metal [3]. In particular, the anisobidenticity observed in the As, Sb and Bi dithiocarbamato complexes seems to be a consequence of the steric and electronic requirements. However, the valence bond sum (VBS) of the complexes [26, 27] determined from the bond valence parameters [28] accounts for the valence of the central ion irrespective of the number of bonds and the strength of interaction. In the present case, VBS-0B turns out to be 2.86, 2.99 and 3.11 for $As(deadtc)_3$, $Sb(deadtc)_3$ and $Bi(deadtc)_3$, respectively, and this clearly shows that charge neutralization is accomplished at the expense of anisobidenticity, In this study the valence bond sum should, theoretically, be equivalent to "3", in order to neutralize the charge on the central ion. The number of bonds attached to the metal and the variations in bond lengths observed in the complexes are only molecular adjustments to satisfy the requirements mentioned above. However, for all the complexes examined here, the VBS turns out to be close to 3, as expected, although the coordination polyhedra are different. The VBSs calculated for the As, Sb and Bi complexes are as shown in Table 7.

The VBS has been proposed to equal the valence or charge on an atom or ion and is calculated by summing $\exp[(r_c - r_o)/B]$ for each bond to the atom or ion in question, where r_c is a constant for a particular bond type, r_o is the observed bond length and B is a constant (taken as 0.37). The bond valence method has recently had considerable success in predicting and interpreting bond lengths in ionic solids.

Table 7. Valence bond sums for the complexes

Complex	R_{ij}[a]	VBS-OB[b]	VBS-BA[c]
$As(deadtc)_3$	2.272	2.86	3.12
$Sb(deadtc)_3$	2.474	2.99	3.18
$Bi(deadtc)_3$	2.570	3.11	3.27

[a] R_{ij} calculated for the atoms in a bond by the method of O'Keefe and Brese [26].
[b] VBS calculated by the method of O'Keeffe and Brese [26].
[c] VBS calculated by the method of Brown and Altermatt [27].

Acknowledgement—We gratefully acknowledge the Central Electrochemical Research Institute, Karaikudi, India for recording the cyclic voltammograms of our compounds.

REFERENCES

1. Cotton, F. A. and Wilkinson, G., *Advanced Inorganic Chemistry*, 5th edn. Wiley-Interscience, New York, 1988.
2. Reynolds, J. E. F. (ed.), Martindale, *The Extra Pharmacopoeia*, 20th edn. The Pharmaceutical Press, London, 1982.
3. Summers, S. P., Abboud, K. A., Farrah, S. R. and Palenik, G. J., *Inorg. Chem.*, 1994, **33,** 88.
4. Herrmann, W. A., Herdtweck, E. L. and Pajdla, Z., *Inorg. Chem.*, 1991, **30,** 2579.
5. Hermann, W. A., Herdtweck E. and Pajdla, L., *Z. Kristallogr.*, 1992, **198,** 257.
6. Asato, E., Driessen, W. L., deGraff, R. A. G., Hulsbergen, F. B. and Reedijik, J., *Inorg. Chem.*, 1991, **30,** 4210.
7. El-Issa, D., Pyykko, P. and Zanati, H. M., *Inorg. Chem.*, 1991, **30,** 2781.
8. Sleight, A. W., *Science*, 1990, **247,** 656.
9. Raston, C. L. and White, A. H., *J. Chem. Soc., Dalton Trans.*, 1975, 2425.
10. Raston, C. L. and White, A. H., *J. Chem. Soc., Dalton Trans.*, 1976, 791.
11. Colapietro, M., Domenicano, A., Scaramuzza, L. and Vaciago, A., *J. Chem. Soc., Chem. Commun.*, 1968, 302.
12. Kavounis, C. A., Kokkou, S. C., Rentzeperis, P. J. and Karangiannidis, P., *Acta Cryst.*, 1980, **B36,** 2954.
13. Kavounis, A. A., Kokkou, S. C., Rentzeperis P. J. and Karangiannidis, P., *Acta Cryst.*, 1982, **B38,** 2686.
14. Ramalingam, K., Aravamudan, G. and Seshasayee, M., *Inorg. Chim. Acta*, 1987, **128,** 231.
15. Ramalingam, K., Aravamudan, G. and Venkatachalam, V., *Bull. Chem. Soc. Jpn*, 1993, **66,** 1554.
16. Akilan, R., Sivakumar, K., Venkatachalam, V., Ramalingam, K., Chinnakali, K. and Fun, H. K., *Acta Cryst.*, 1994, **C51,** 368.
17. Sheldrick, G. M., SHELX 76, University of Cambridge, Cambridge, 1976.
18. Bond A. M. and Wallace, C. G., *Inorg. Chem.*, 1984, **23,** 1858.
19. Anderson, C. W. and Lung, K. G., *J. Electrochem. Soc.*, 1982, **129,** 2505.
20. Bond, A. M. and Martin, R. L., *Coord. Chem. Rev.*, 1984, **54,** 23.
21. Riechel, T. L., DeHayes, L. J. and Sawyer, D. T., *Inorg. Chem.*, 1976, **15,** 1900.
22. Poore, M. C. and Russell, D. R., *Chem. Commun.*, 1971, 18.
23. Nag, S. W. and Zuckerman, J., *Adv. Inorg. Chem. Radiochem.*, 1985, **29,** 302.
24. Thorp, H., *Inorg. Chem.*, 1992, **31,** 1585.
25. Lawton, S. L. and Kokotailo, G. T., *Inorg. Chem.*, 1972, **11,** 363.
26. O'Keeffe, M. and Brese, N. E., *J. Am. Chem. Soc.*, 1991, **113,** 3226.
27. Brown, I. D. and Altermatt, D., *Acta Cryst.*, 1985, **B41,** 244.
28. Ray, N. K., Samuels, L. and Par, N. G., *J. Chem. Phys.*, 1979, **70,** 3680.

Pergamon

PII: S0277-5387(96)00351-8

Polyhedron Vol. 16, No. 7, pp. 1223–1234, 1997
Copyright © 1997 Elsevier Science Ltd
Printed in Great Britain. All rights reserved
0277–5387/97 $17.00+0.00

Praseodymium alkoxide chemistry: synthesis and molecular structure of $[Pr_4(\mu_4\text{-}O)_2(\mu_3,\eta^2\text{-}OR)_2(\mu,\eta^2\text{-}OR)_4(\mu,\eta^1\text{-}OR)(OR)(OPMe_3)]_2$ ($R = C_2H_4OMe$) and $[Y_4Pr(\mu_5\text{-}O)(\mu_3\text{-}OR)_4(\mu\text{-}OR)_4(OR)_5]$ ($R = Pr^i$)

Liliane G. Hubert-Pfalzgraf,[a] * Stephane Daniele,[a] Abderrhamane Bennaceur,[a] Jean-Claude Daran[b]† and Jacqueline Vaissermann[b]

[a] Laboratoire de Chimie Moléculaire, URA-CNRS, Université de Nice-Sophia-Antipolis, 06108 Nice Cedex, France

[b] Laboratoire de Chimie des Métaux de Transition, URA-CNRS, 4 Place Jussieu, 75230 Paris Cedex 05, France

(Received 28 May 1996; accepted 15 July 1996)

Abstract—Various routes to praseodymium alkoxides have been investigated. Compounds such as $Pr_5O(OR)_{13}$ [$R = Pr^i$ (**1**), Am^t], $[Pr_4O_2(ONp)_8]_m$ (Np = neopentyl), $[Pr(OC_2H_4NMe_2)_3]_3$ were obtained by reaction of praseodymium turnings with the corresponding alcohols. Alcoholysis reactions of the bis-trimethylsilylamide afforded $[Pr_4O(ONp)_{10}]_m$, $[Pr_4O_2(ONp)_8]_m$, $Pr_3(OR)_9(ROH)_2$ [$R = Bu^t$, Am^t] and $[Pr_4O_2(OC_2H_4OMe)_8]_m$ (**2a**), the latter derivatives illustrating the trend for the formation of oxo species. The compounds were characterized by elemental analysis, FT-IR and NMR. Their reactivity has been investigated, the mixed-metal species $Pr_4TiO(OPr^i)_{14}$ and $Y_4PrO(OPr^i)_{13}$ were obtained. Ligand exchange reactions afforded $[Pr_4O_2(OR)_3(OR')_5]_m$ species ($R = Pr^i$, $R' = C_2H_4NMe_2$' $R = SiMe_3$, $R' = Pr^i$) and $[Pr(OC_2H_4NMe_2)(thd)_2]_2$. X-ray structure analysis of the adduct obtained by reaction of $[Pr_4O_2(OC_2H_4OMe)_8]_m$ with trimethylphosphine oxide reveals a centrosymmetric framework $[Pr_4(\mu_4\text{-}O)_2(\mu_3,\eta^2\text{-}OR)_2(\mu,\eta^2\text{-}OR)_4(\mu,\eta^1\text{-}OR)(OR)(OPMe_3)]_2$ (**2b**) of eight octa-coordinated praseodymium atoms, assembled by tetrahedral and square-planar oxo ligands. The M—O bond lengths spread over the range 2.246(6)–2.762(6) Å and to follow the order Pr—OR (terminal) < μ,η^2-Pr—OR < μ_3,η^2-Pr—OR < Pr—O(ether). The $Y_4PrO(OPr^i)_{13}$ species corresponds to a pentanuclear oxo aggregate similar to that of the parent homometallic species. Copyright © 1997 Elsevier Science Ltd

Keywords: alkoxides; praseodymium; lanthanides; sol–gel; MOCVD; mixed-metal alkoxides.

The alkoxide chemistry of the lanthanides remains confined to a few elements. Regarding praseodymium, only the tris-isopropoxide [1] and a methoxyethoxide derivative resulting from C—O bond cleavage of DME [2] have been mentioned for many years. Fluoroalkoxides $\{Pr[OCMe(CF_3)_2]_3(NH_3)_2\}_2$, $\{Pr[OCMe(CF_3)_2]_3\}_3$ [3], the aryloxide $[Pr(O\text{-}C_6H_2(CH_2NMe_2)_3\text{-}2,4,6]_3(H_2O)_2$ [4] and the mixed-metal species $[PrAl_2Cl(OPr^i)_8(Pr^iOH)]_2$ [5] and [Pr Cu(bdmmpH)(bdmmp)(μ-OH)(hfacac)$_3$] (bdmmpH = 2,6-bis[dimethylamino)-methyl-4-methylphenol, hfacacH = hexfluoroacetylacetone) [5b] have been structurally characterized recently. Praseodymium oxide, Pr_6O_{11}, is used as an additive in varistors [6] and in $PrBa_2Cu_3O_x$, an insulating material [7] which might be associated with high temperature superconductors of comparable lattice parameters such as $YBa_2Cu_3O_{7-x}$ in order to form heterostructures, or, in $Pr_{1.85}Ce_{0.15}CuO_{4-x}$, the only superconducting material based on praseodymium reported so far [8].

Various routes, such as direct attack of the metal,

* Author to whom correspondence should be addressed.

† *Present address*: Laboratoire de Chimie de Coordination, 205 Route de Norbonne, 31077 Toulouse, France.

alcoholysis of the bis-trimethylsilylamide and alcohol exchange reactions, were investigated in order to expand the range of praseodymium oxide precursors. We report here the synthesis of $Pr_5O(OR)_{13}$ (R = Pr^i, Am^i), $[Pr_3(OR)_9(ROH)_2]$ (R = Bu^t, Am^t) and $[Pr_3(OC_2H_4NMe_2)_9]$. The high tendency of the formation of oxo species is illustrated by the formation of $[Pr_4O(ON_p)_{10}]_m$, $[Pr_4O_2(ONp)_8]_m$ and $[Pr_8(\mu_4\text{-}O)_4(OC_2H_4OMe)_{16}(OPMe_3)]_2$, the latter having been structurally characterized. Stabilization of the isopropoxide derivative has been achieved through the formation of mixed-metal species, $[Pr_4TiO(OPr^i)_{14}]$ and $[PrY_4O(OPr^i)_{13}]$. $[Pr_4O_2(OR)_3(OR')_5]_m$ and $[Pr(OC_2H_4NMe_2)(thd)_2]_2$ were obtained by ligand exchange reactions. The various compounds have been characterized by elemental analysis, FT-IR, NMR and molecular weight data.

EXPERIMENTAL

Synthesis and characterization were carried out routinely under argon using Schlenk tubes and vacuum line techniques. Solvents were dried using standard procedures. Alcohols were dried over molecular sieves or $Al(OPr^i)_3$ and distilled. Me_3SiOH [9] and $Pr[N(SiMe_3)_2]_3$ [10] were obtained according to the literature. IR spectra were obtained as Nujol mulls on an FT-IR45S Bruker spectrometer. NMR spectra were registered on an AC-200 Bruker spectrometer. Molecular weight data were obtained by the Signer method [11]. TGA data were obtained with a Setaram system using a heating rate of 5°C min^{-1}. Analytical data were obtained from the Centre de Microanalyses du CNRS. Analytical and FT-IR data of the various homometallic compounds are summarized in Table 1.

Reaction between praseodymium chips and alcohols

Synthesis of $Pr_5O(OR)_{13}$ [R = Pr^i (**1**), Am^i]. A toluene : Pr^iOH (1 : 1) solution (250 cm^3) was added to praseodymium chips (12.05 g, 85.5 mmol). After refluxing for 1 h, 10 mg of catalyst [$HgCl_2$: $Hg(OAc)_2$, 1 : 1] were added and refluxing was maintained for 48 h. The hot reaction mixture was filtered over a Celite pad. The filtrate was cooled to −35°C. Yellow–green crystals of $Pr_5O(OPr^i)_{13}$ (**1**) were isolated by filtration and dried *in vacuo* (24.4 g, 90%).

The same procedure using isoamyl alcohol gives $Pr_5O(OAm^i)_{13}$ (85%).

Synthesis of $[Pr_4O_2(ONp)_8]$ *and* $[Pr(OC_2H_4NMe_2)_3]_3$. The same reactions using neopentyl alcohol or 2,2-dimethylaminoethanol gave $[Pr_4O_2(ONp)_8]_m$ (65%) and $[Pr(OC_2H_4NMe_2)_3]_3$ (96%), respectively. M.W. (C_6H_6) = 1180 (calc. 1214.72).

$Pr_5O(OAm^i)_{13}$ and $[Pr(OC_2H_4NMe_2)_3]_3$ are soluble in common organic solvents, including petroleum ether. $Pr_5O(OPr^i)_{13}$ is, like other $Ln_5O(OPr^i)_{13}$ derivatives (Ln = Y, La, Nd, Sm, Gd), soluble in toluene when freshly prepared, but its solubility decreases on ageing.

Alcoholysis of $Pr[N(SiMe_3)_2]_3$

Synthesis of $Pr_3(OR)_9(ROH)_2$ (R = Bu^t, Am^t). A solution of Bu^tOH (0.8 g, 10.8 mmol) in toluene (20 cm^3) was added dropwise to a solution of $Pr[N(SiMe_3)_2]_3$ (1.5 g, 2.4 mmol) in toluene (40 cm^3) at 0°C. The reaction was slightly exothermic and the reaction mixture was stirred for 12 h. After filtration, concentration and cooling at −20°C, green crystals analysing as $Pr_3(OBu^t)_9(Bu^tOH)_2$ (0.6 g, 62%) were obtained.

A similar procedure applied to $Pr[N(SiMe_3)_2]_3$ (1.5 g, 2.4 mmol) in toluene (40 cm^3) and 0.9 g (10.8 mmol) of tert-amyl alcohol in toluene (20 cm^3) offered $Pr_3(OAm^t)_9(Am^tOH)_2$ (0.75 g, 69%).

Synthesis of $[Pr_4O(ONp)_{10}]_m$ *and* $[Pr_4O_2(ONp)_9]_m$. The preceeding procedure applied to $Pr[N(SiMe_3)_2]_3$ (1.5 g, 2.4 mmol) in toluene (40 cm^3) and neopentyl alcohol (0.83 g, 9.4 mmol) in toluene (20 cm^3) afforded $Pr_4O(ONp)_{10}$ (0.37 g, 42%) as the first crop of crystals and $Pr_4O_2(ONp)_8$ (0.18 g, 23%) as the second crop after 4 days at −30°C.

$Pr_3(OR)_9(ROH)_2$ (R = Bu^t,Am^t), $[Pr_4O(ONp)_{10}]_m$ and $[Pr_4O_2(ONp)_8]_m$ are soluble in toluene and THF but insoluble in hexane.

Alcohol interchange reactions of $Pr_5O(OPr^i)_{13}$

Synthesis of $[Pr_4O_2(OC_2H_4OMe)_8]_m$ (**2a**). 2-Methoxyethanol (0.37 cm^3, 4.7 mmol) was added to a suspension of $Pr_5O(OPr^i)$ (467 mg, 0.314 mmol) in petroleum ether (15 cm^3). After dissolution, precipitation was observed. Addition of THF (10 cm^3) gave a homogeneous solution, which gave crystals of $Pr_4O_2(OC_2H_4OMe)_8$ (0.3 g, 64%) on cooling to −30°C. The compound is poorly soluble in common organic solvents, even polar ones such as THF, but it is more soluble in 2-methoxyethanol.

The same compound was obtained by reacting Pr chips with 2-methoxyethanol in refluxing toluene but its isolation as crystals required several recrystallizations in diethyl ether, thus leading to a low yield.

Synthesis of $[Pr_4O_2(OPr^i)_3(OC_2H_4NMe_2)_5]_m$ *and* $[Pr_4O_2(OPr^i)_5(OSiMe_3)_3]_m$. $Me_2NC_2H_4OH$ (1.26 g, 15.6 mmol) was added to a suspension of $Pr_5O(OPr^i)_{13}$ (2.8 g, 1.9 mmol) in toluene (30 cm^3). Complete dissolution was observed over 45 min. Evaporation to dryness left a light green powder of formula $[Pr_4O_2(OPr^i)_3(OC_2H_4NMe_2)_5]_m$ (3.4 g, 98%).

The same procedure using a solution of freshly prepared Me_3SiOH (5.9 g, 65 mmol) diethyl ether (10 cm^3) and applied to a suspension of $Pr_5O(OPr^i)_{13}$ (2.8 g, 1.88 mmol) in Et_2O (20 cm^3) led to immediate dissolution. 2.3 g (87%) of $[Pr_4O_2(OPr^i)_5(OSiMe_3)_3]_m$ were obtained after evaporation to dryness.

Table 1. Microanalytical and FT-IR data of various praseodymium alkoxides

Compound	Synthesis (yield, %)	Analytical data (%) Found (Calc.) C	H	N	IR ν(M—OR) cm − 1
$Pr_5O(OPr^i)_{13}$ (**1**)	[a] (90)	31.3 (31.5)	6.1 (6.1)		519s, 482s, 444s, 397sh
$Pr_5O(OAm^i)_{13}$	[a] (85)	42.4 (42.1)	8.2 (7.7)		497b, 489s, 458s, 422sh
$[Pr(OC_2H_4NMe_2)_3]_3$	[a] (96)	35.7 (35.5)	7.6 (7.4)	10.2 (10.4)	591s, 535s
$[Pr_4O(ONp)_{10}]_m$	[b] (42)	40.5 (41.4)	7.8(7.6)		596s, 558m, 400s, 364vs
$[Pr_4O_2(ONp)_8]_m$	[a] (65)	37.5 (37.2)	7.1 (6.8)		595s, 561m, 508s, 415vs, 364vs
	[b] (23)				514s, 488s, 464m, 381s [ν(OH) 3379]
$Pr_3(OBu^t)_9(Bu^tOH)_2$	[b] (62)	42.3 (43.0)	8.1 (8.2)		
$Pr_3(OAm^t)_9(Am^tOH)_2$	[b] (69)	47.1 (47.8)	8.8 (8.9)		544s, 501vs, 481vs, 377vs [ν(OH) 3382]
$[Pr_4O_2(OC_2H_4OMe)_8]_m$ (**2a**)	[c] (64)	23.5 (24.2)	4.6 (4.7)		563s, 516s, 474s, 453s, 412s, 393s
$[Pr_4O_2(OC_2H_4OMe)_8$ $(OPMe_3)]_2$ (**2b**)	[a] (10)	24.8 (25.2)	4.9 (5.0)	5.7 (5.8)	509s, 508s, 475m, 445m, 400sh, 309sh, 324m
$[Pr_4O_2(OPr^i)_3(OC_2H_4$ $NMe_2)_5]_m$	[c] (98)	27.8(28.6)	5.9 (5.9)		588m, 521m, 442sh, 403sh
$[Pr_4O_2(OPr^i)_5(OSiMe_3)_3]_m$	[c] (87)	23.4 (24.9)	5.4 (5.4)[d]		673m, 518sh, 484m
$[Pr(OC_2H_4NMe_2)(thd)_2]_2$	[c] (95)	52.0 (52.4)	7.9 (8.1)	2.5 (2.3)	594m, 467m, 459sh, 397w[e]

[a] From metal chips.
[b] Alcoholysis of $Pr[N(SiMe_3)_2]_3$.
[c] Alcohol interchange.
[d] *Si 6.3 (5.8) (%).
[e] ν(CO): 1590sh, 1537s, 1549s, 1503s.

Synthesis of $[Pr(OC_2H_4NMe_2)(thd)_2]_2$

A solution of 2,2,6,6-tetramethylheptane-3,5-dione (7.1 g, 38.5 mmol) in diethyl ether (20 cm^3) was added to a solution of $Pr(OC_2H_4NMe_2)_3$ (7.8 g, 19.23 mmol) in the same solvent (50 cm^3). After 1 h, the solution was evaporated to dryness. $Pr(OC_2H_4NMe_2)(thd)_2$ was obtained by sublimation at 170°C/10^{-3} mm of Hg (95%). M.p. = 105–110°C, $\mu = 3.30$ μB, M.W. (C_6D_6) = 1250 (calc. 678.9). TGA (N_2, 1 atm): 240–380°C sublimation, residue 18%.

The same product was obtained if the reaction was carried out in a 1:1 stoichiometry, although in a lower yield (40%). Cell parameters (−100°C) $a = 13.554(2)$, $b = 18.607(2)$, $c = 21.886(2)$ Å, $\beta = 25.05(3)°$, monoclinic, $P2_1$ or $P2_1/m$, but the structure could not be solved.

Synthesis of $Y_4PrO(OPr^i)_{13}$

$Pr_5O(OPr^i)_{13}$ (0.67 g, 0.45 mmol) was added to a solution of $Y_5O(OPr^i)_{13}$ (2.21 g, 1.8 mmol) in THF (40 cm^3). The reaction medium was stirred for 18 h at room temperature giving a light green solution. The resulting solid was recrystallized in toluene. $PrY_4O(OPr^i)_{13}$ (2.3 g, 80%) is soluble in all common solvents except petroleum ether. Found: C, 36.6; H, 7.1. Calc. for $C_{39}H_{91}O_{14}PrY_4$: C, 35.7; H, 6.4%. IR(cm^{-1}): 1337vs, 1171vs, 1130vs, 1009vs; 995s, 978s; 952s, 836m, 828m; 535s, 494s, 453s, 420s, 396s [ν(M—OR)]; ^1H NMR (C_6D_6): δ 4.45 (sept, $J = 6$ Hz, 13H), 1.63 (d, $J = 6$ Hz, CH_3, 48H), 1.48 (d, $J = 6$ Hz, CH_3, 30H); ^{13}C-{^1H} NMR (C_6D_6): δ 67.4, 68 (CH), 28.5, 27.8 br (CH_3).

Synthesis of $Pr_4TiO(OPr^i)_{14}$

$Pr_5O(OPr^i)_{13}$ (0.73 g, 0.5 mmol) in toluene (30 cm^3) were added to $Ti(OPr^i)_4$ (0.183 cm^3, 0.6 mmol). The reaction medium was stirred at room temperature for 48 h. A crop of green crystals, soluble in toluene, THF and isopropanol, but poorly soluble in hexane, analysing as $Pr_4TiO(OPr^i)_{14}$ (0.5 g, 71%), was obtained at −20°C. Found: Pr, 12.8; Ti, 16.6. Calc. for $C_{42}H_{98}O_{15}Pr_4Ti$: Pr, 12.0; Ti, 16.3%. IR [cm^{-1}]: 1332m, 1151vs, 1125vs [ν(C—O)]; 994vs, 987s, 954m, 850w, 834m, 830w, 824w, 645m, 613m, 555m, 517m, 473m, 445m [ν(M—O)].

Crystallography of $[Pr_8O_4(OC_2H_4OMe)_{16}(OPMe_3)_2]$ *and* $[YPr_4O(OPr^i)_{13}]$

Crystals of $[Pr_8O_4(OC_2H_4OMe)_{16}(OPMe_3)_2]$ (**2b**) and $[YPr_4O(OPr^i)_{13}]$ were grown from the reaction medium. Crystals of **2b** were obtained when the methoxethoxide derivative crystallized in the presence of $OPMe_3$. A selected crystal was mounted on an Enraf–Nonius CAD-4 diffractometer; cell parameters were obtained from the setting of 25 well-centred reflections. Crystallographic data and other pertinent information are given in Table 2.

Table 2. Crystallographic data for $[Pr_8O_4(OC_2H_4OMe)_{16}(OPMe_3)_2]$ and for $[YPr_4O(OPr^i)_{13}]$

Chemical formula	$C_{54}H_{130}O_{38}P_2Pr_8$	$C_{39}H_{91}O_{14}PrY_4$
F.w.	2576.81	1280.85
Crystal system	Monoclinic	Monoclinic
Space group	$P2_1/n$	$P2_1/n$
Z	2	4
a, Å	17.662(7)	12.773(5)
b, Å	17.660(3)	21.383(9)
c, Å	14.626(3)	21.434(14)
β, °	100.45(3)	91.31(4)
V, Å^3	4486	5853
ρ_{calc}, g cm^{-3}	1.90	1.45
μ(Mo-K_α), cm^{-1}	43.5	48
Scan type	$\omega/2\theta$	$\omega/2\theta$
Scan range θ, (°)	$1.2+0.34\tan\theta$	$1.2+0.34\tan\theta$
2θ range, (°)	4–44	4–38
Reflections collected	5478	4707
$R(F)$	0.036	0.059
$R_w(F)^a$	0.040	0.066

$^a R_w(F) = [\Sigma_i w_i(F_o - F_c)^2/\Sigma_i w_i F_o^2]^{1/2}$.

Data were collected for $[Pr_8O_4(OC_2H_4OMe)_{16}(OPMe_3)_2]$ and $[YPr_4O(OPr^i)_{13}]$ at low temperature (−100°C) using graphite-monochromated Mo-K_α radiation ($\lambda = 0.71073$ Å). Metal atoms were found using SHELXS [12]. All remaining non-hydrogen atoms were located on successive difference electron density maps. The structures were refined by least-squares techniques with approximation (in three blocks) to the normal matrix using CRYSTALS II [13]. The hydrogen atoms were not included in the refinement. 4168 and 2360 reflections with $I > 3\sigma(I)$ were used to solve and refine the structures of $[Pr_8O_4(OC_2H_4OMe)_{16}(OPMe_3)_2]$ ($R = 0.036$, $R_w = 0.040$, 461 variables) and of $[YPr_4O(OPr^i)_{13}]$ ($R = 0.059$, $R_w = 0.066$, 330 variables), respectively. Anomalous dispersion terms were applied. Empirical absorption corrections using DIFABS [14] were made. Atomic coordinates, non-essential bond lengths and angles and thermal parameters have been deposited at the Cambridge Crystallographic Data Centre.

RESULTS AND DISCUSSION

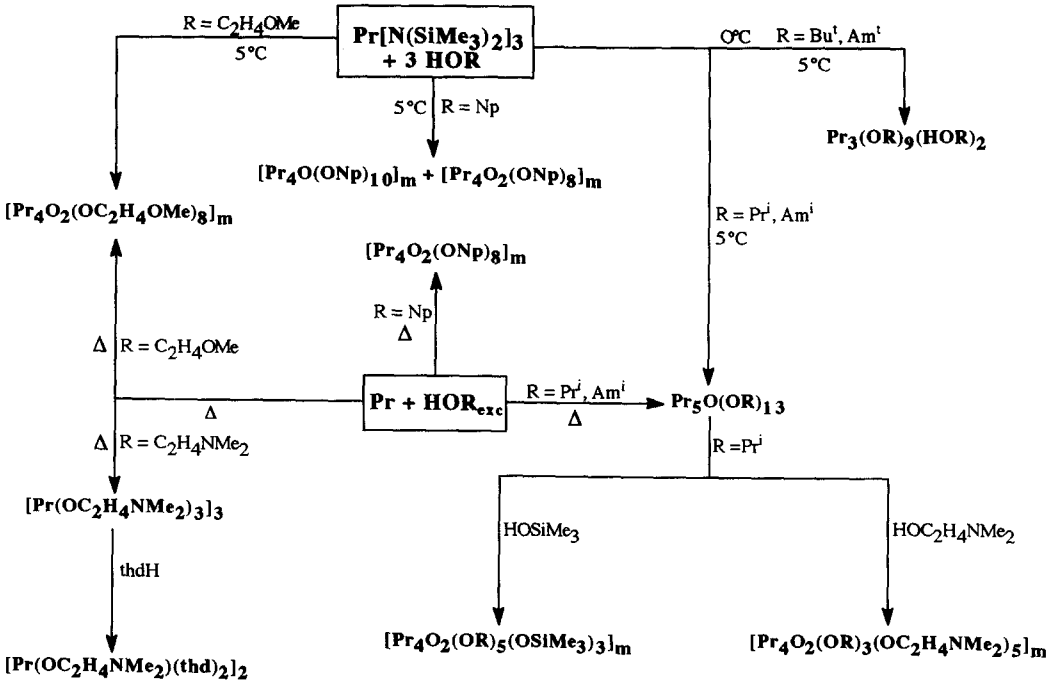
Synthesis and characterization

Various synthetic routes to praseodymium alkoxides have been investigated, namely reaction between the metal and alcohols, alcohol interchange reactions and alcoholysis of the bis-trimethylsilylamide derivative ($Pr[N(SiMe_3)_2]_3$) (Scheme 1). The various products, generally light yellow–green microcrystalline solids, have been characterized by elemental analysis, FT-IR, NMR, molecular weight data and X-ray diffraction for $[Pr_8O_4(OC_2H_4OMe)_{16}(OPMe_3)_2]$ and for $[PrY_4O(OPr^i)_{13}]$. Table 1 summarizes the most relevant characteristics of the novel praseodymium alkoxide derivatives.

The reaction between praseodymium chips and isopropanol proceeds as for yttrium and the lanthanides (samarium, gadolinium, ytterbium,...), with the formation of an oxo species $Pr_5O(OPr^i)_{13}$ (**1**) (see also ref. [15]). However in contrast with the derivatives of these lanthanides, **1** is sensitive to "ageing" and becomes progressively insoluble in non-polar as well as polar solvents. The formation of **1** proceeds *via* a soluble solvate which can be isolated as a crystalline material [ν(OH) 3358 cm^{-1}] but which is converted into **1** by loss of the labile Pr^iOH molecules during drying. The use of an alcohol with a longer carbon chain, isoamyl alcohol $Me_2CHC_2H_4OH$ for instance, leads to a compound having the same empirical formula but which appears to remain soluble over time. The presence of the M_5O core is supported by numerous M—OR vibrations in the IR spectra for the isopropoxide and isoamyloxide derivatives (519, 482, 444, 397 and 497, 489, 458, 422 cm^{-1}, respectively) and a pattern comparable to that observed for the well-characterized $M_5O(OPr^i)_{13}$ (M = Y, Yb) species [1b].

As a general feature, the work-up of the praseodymium derivatives resulting from direct reactions between the metal and alcohols appeared to be more tedious than for the other lanthanides investigated so far (formation of oily and/or insoluble products, metallic colloids difficult to separate, change in the colour promoted by O-donor solvents). These drawbacks are more important in the case of alcohols with high boiling points such as 2-methoxyethanol, and $[Pr_4O_2(OC_2H_4OMe)_8]_m$ (**2a**) could only by crystallized out in moderate yields (25%).

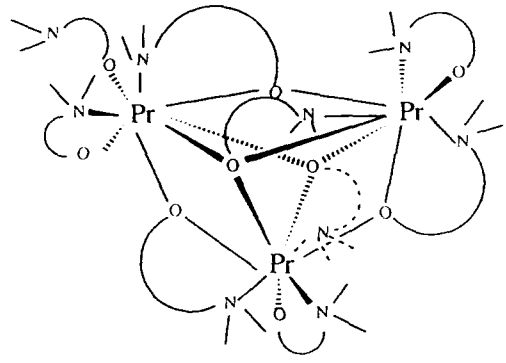
The formation of oxo species displaying mostly a poor solubility appears as another general trend for praseodymium. Thus, while the reaction between yttrium and 2-methoxyethanol gives a decamer,



Scheme 1. Various synthetic routes to praseodymium derivatives (all reactions in toluene at room temperature if not otherwise stated).

$Y_{10}(OC_2H_4OMe)_{30}$, soluble in petroleum ether [16], a similar reaction with praseodymium offers, after isolation from diethyl ether (no solubility in hexane), oxo clusters based on a $Pr_4O_2(OR)_8$ empirical formulation. Indeed, the generation of oxo ligands, shown to display a μ_4 coordination mode (see below) allows praseodymium to achieve large coordination numbers in molecular aggregates. In view of the limited solubility of most of these oxo species, bulky and/or functional alkoxide ligands were selected as a means to stabilize species of smaller nuclearity, soluble and/or volatile. This strategy allowed the isolation of $Pr(OC_2H_4NMe_2)_3$ shown to be trimeric by molecular weight measurements in benzene. A structure based on a bi-capped triangular unit analogous to that established for $Pr_3[\mu_3\text{-}OCMe(CF_3)_2]_2[\mu\text{-}OCMe(CF_3)_2]_3[OCMe(CF_3)_2]_4$ is likely [3]. The $\mu 3,\eta^2$ bridging-chelating coordination mode of the aminoalkoxide ligand has found precedent for $[Ba_5(OH)(\mu_3,\eta^2\text{-}OCHMeCH_2NMe_2)_4(thd)_5]$ and for $[Ba_2Cu(\mu_3,\eta^2\text{-}OCHMeCH_2NMe_2)_2(thd)_4(Pr^iOH)_2]$ [17]. The functionality of the $OC_2H_4NMe_2$ ligand allows praseodymium to be eight-coordinated without the presence of oxo ligands in the metal coordination sphere. However, despite its low nuclearity, this species remains non-volatile.

Alcoholysis reactions of bis-trimethylsilylamides generally represent an alternative, clean route to metal alkoxides and this synthetic procedure has allowed the isolation of praseodymium fluoroisopropoxides by Bradley *et al.* [3]. Indeed, this procedure facilitates the isolation of the derivatives and $Pr_3(OR)_9(ROH)_2$



($R = Bu^t, Am^t$) species have been isolated in high yields (70%) (see also ref. [15]). In the case of neopentyl alcohol, two types of oxo derivatives $[Pr_4O(ONp)_{10}]_m$ and $[Pr_4O_2(ONp)_8]_m$ were isolated successively over four days (yield 42 and 23%, respectively). One can notice that the latter was the only compound isolated from the reaction between the metal and the alcohol that proceeds at higher temperature. These observations illustrate again the trend of praseodymium to form oxo species. The reactions involving $Pr[N(SiMe_3)_2]_3$ appear more prone to side reactions than in the case of lanthanum or yttrium.

Reactivity

Various reactions aimed at obtaining stable and/or soluble praseodymium derivatives were investigated.

The reaction between **1** and 2-methoxyethanol (15 equivalents) proceeds quite easily at room temperature with formation of the oxo species $[Pr_4O_2(OC_2H_4OMe)_8]_m$ in about 65% yield. Introduction of trimethylsiloxide ligands in the metal coordination sphere generally offers more soluble compounds. Alcoholysis reactions of **1** were also achieved at room temperature with trimethylsilanol and dimethylaminoethanol. Dissolution was observed in both cases, the reactions proceed with formation of heteroleptic species of general formulae $[Pr_4O_2(OR)_3(OR')_5]_m$ ($R = SiMe_3$, $R' = Pr^i$; $R = Pr^i$, $R' = C_2H_4NMe_2$). Attempts to obtain trimethylsiloxide derivatives by reaction between **1** and Me_3SiOAc were less selective owing to the formation of acetato derivatives, evidenced in the FT-IR spectra by $\nu(CO_2)$ vibrations at 1559 cm^{-1} resulting from C—O bond cleavage reactions [1b].

Another aspect of the ageing phenomenon is the change in colour from green to reddish-green while solubility properties are retained. This colour change is favoured by oxygen donor solvents such as diethyl ether or THF and by heating, but was not further investigated.

Mixed-metal species are another means to achieve solubilization and/or stabilization [1b]. Such reactions were explored between **1** and $Ti(OPr^i)_4$. The reactions proceed with dissolution of the $Pr_5O(OPr^i)_{13}$ derivative and formation of new species in which the metals achieve a 4:1 stoichiometry. The 4:1 stoichiometry was anticipated for the reaction with titanium isopropoxide and a structure similar to that of $[Sm_4Ti(\mu_5\text{-}O)(\mu_3\text{-}OPr^i)_2(\mu\text{-}OPr^i)_6(OPr^i)_6]$ [18] is likely for $[Pr_4TiO(OPr^i)_{14}]$. This analysis is supported by the similarity of the FT-IR pattern observed for the ν(M—OR) region. IR and ^1H NMR data for $[PrY_4O(OPr^i)_{13}]$ are in favour of the formation of a new species, different from the starting metal alkoxides. X-ray diffraction studies on single crystals account for the presence in the solid of pentanuclear aggregates displaying a $[M_5(\mu_5\text{-}O)(\mu_3\text{-}OPr^i)_4(\mu\text{-}OPr^i)_4(OPr^i)_5]$ core (see below) but in which the different metals are disordered.

The reactions between $[Pr(OC_2H_4NMe_2)_3]_3$ and 2,2,6,6-tetramethyl-3,5-heptanedione (thdH) were considered as a means of achieving volatile derivatives, which could also be used as synthons for the build-up of heteroleptic mixed-metal species [17]. $Pr(OC_2H_4NMe_2)(thd)_2$ appears to be more stable than $Pr(OC_2H_4NMe_2)_2(thd)$ and is obtained independently of the stoichiometry, 1:1 or 1:2, of the reaction. It appears as a dimer by molecular weight data measurements. It sublimes at *ca* 170°C/10^{-3} mm of Hg and is thus less volatile than the homoleptic praseodymium tetramethylheptanedionate $[Pr(thd)_3]_2$ (180°C/10^{-2}). These observations were also confirmed by the TGA measurements. The thermograms (under 1 atmosphere of nitrogen) indicate that the sublimation of $Pr_2(thd)_6$ occurs between 220 and 310°C but only in the temperature range 240–380°C for $[Pr(OC_2H_4NMe_2)(thd)_2]_2$.

The FT-IR spectra of the homoleptic alkoxides, or their oxo analogues, display essentially the absorption bands of the organic groupings and those of the ν(M—OR) vibrations below 600 cm^{-1}. The molecules solvated by the parent alcohol are characterized by ν(OH) absorption bands around 3380 cm^{-1}. The β-diketonatoalkoxide shows the classic C=O absorptions around 1550–1600 cm^{-1}. The assignment of the M—oxo vibration in metal alkoxides is generally difficult owing to the versatility of the coordination modes of this ligand and the numerous absorption bands related to the organic groups. The spectra of $[Pr_4O(ONp)_{10}]_m$ and $[Pr_4O_2(ONp)_8]_m$ differ mainly in a strong band at 798 cm^{-1}, tentatively attributed to a μ_n-O—Pr vibration. The low frequency of the stretching C—H vibrations (2614 cm^{-1}) observed for the neopentyloxide derivative obtained by the direct route (from the metal), suggests agostic Pr···C—H bonding, as established by X-ray diffraction for $[Ln(OCH_2Bu^t)_3]_4$ [19]. The Pr_4O_2 or Pr_5O cores are characterized by more Pr—OR absorption bands than for the non-oxo $Pr_3(OR)_9(ROH)_2$ species.

The paramagnetism of the Pr^{3+} ion causes large pseudo-contact shifts, and the peaks observed are often quite broad. The dispersion of the chemical shifts might be observed over about 140 ppm, especially for the heteroleptic derivatives $[Pr_4O_2(OR)_3(OR')_5]_m$, but assignment is difficult in view of the various structures possible. (No molecular weight data by the Signer method, and therefore information of the nuclearity, could be obtained in view of the evolution of these structures during the measurements.) The ^1H NMR spectra of $Pr_5O(OPr^i)_{13}$ display a broad peak at δ 3.16 for the CH groups (hfw $\approx$ 120 Hz) while the CH_3 groups appear as broad singlets, at δ 1.35, 0.9 and 0.4 (integration ratio 5:4:4, hfw $\approx$ 60 Hz), confirming the retention of the M_5O_{14} core in solution.

Molecular structures of $[Pr_8O_4(OC_2H_4OMe)_{16}(OPMe_3)_2]$ (**2b**) *and* $[Y_4PrO(OPr^i)_{13}]$

The molecular structure of the methoxyethoxide adduct **2b** consists of discrete centrosymmetric aggregates of eight praseodymium atoms (Fig. 1), the metals all being eight coordinate. Selected bond lengths and angles are given in Table 3. The aggregate is formed by assembling two $[Pr_4(\mu_4\text{-}O)(\mu_2,\eta^2\text{-}OR)_3(\mu_2\text{-}OR)(OR)]$ units. These subunits, in which the metals form a nearly planar arrangement, are connected by two μ_4-oxo ligands, four triply bridging chelating μ_3,η^2 alkoxo groups and two doubly bridging chelating μ_2,η^2 ones. The two basic units, which are roughly parallel to each other, are slightly translated, thus giving the cluster represented in Fig. 1. The arrangement is quite regular with non-bonding metal–metal distances varying from 3.6031(9) to 3.9188(6) Å. These values are

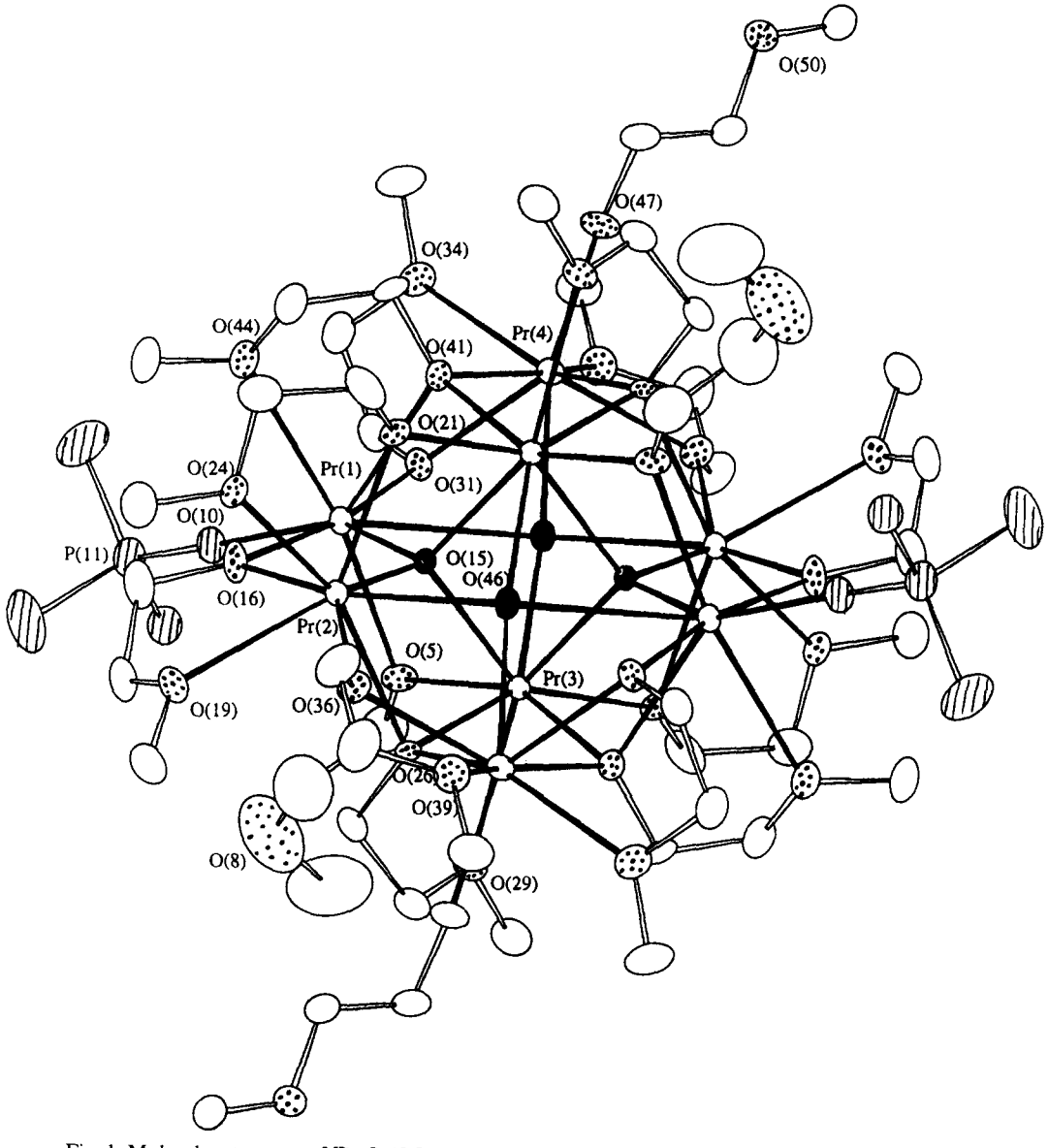


Fig. 1. Molecular structure of $[Pr_4O_2(OC_2H_4OMe)_8(OPMe_3)]_2$ (**2b**) showing the atom-labelling scheme.

in the range of these observed for $[Pr(OCMe(CF_3)_2]_3$ [3].

Metal–oxygen distances range from 2.224(6) to 2.762(6) Å. The O^{2-} ligands are of two types. The oxygens O(15), which connect the two building blocks, have a tetrahedral environment with quite regular Pr—O distances [2.276(5) −2.330(5) Å]. The other oxo ligands, O(46), have a less regular surrounding with Pr—O distances varying from 2.488(6) to 2.762(5) Å. Another feature is their distortion towards a planar geometry [O—Pr—O angles between 82.1(1) and 95.7(2)°] although the sum of the angles around the oxygen (354.4°) and the distance from the Pr(1)Pr(2)Pr(3)Pr(4) plane (0.415 Å) indicates possible pyramidal geometry. The octanuclear cluster displays four types of alkoxide ligand. The praseodymium alkoxide distances follow the pattern previously observed for 2-methoxyethoxide derivatives [6,20]: Pr—OR (terminal) < μ_2,η^2-Pr—OR < μ_3,η^2-Pr—OR < Pr—O(ether).

The metal–oxygen bond distances are quite large, as a result of the metal eight coordination, although the values are comparable with those observed for the other praseodymium alkoxide derivatives structurally characterized [3,5b]. The terminal Pr—OR bonds have a value of 2.224(6) Å, with large associated Pr—O—C angles [174.6(6)°]. Two praseodymium atoms bear trimethylphosphine oxide ligands; the Pr(1)—O(10) coordination bonds [2.292(6) Å] and the Pr(1)—O(10)—P(11) angle [174.0(4)°] are in agreement with the data available on other lanthanide–phosphoryl adducts [21]. The presence of

Table 3. Selected bond lengths (Å) and angles (°) for $[Pr_4O_2(OC_2H_4OMe)_8(OPMe_3)]_2$

Pr(1)—Pr(2)	3.8959(6)	Pr(1)—Pr(3)	3.7330(6)
Pr(1)—Pr(3)″	3.9188(6)	Pr(1)—Pr(4)	3.8463(6)
Pr(2)—Pr(3)	3.8006(6)	Pr(2)—Pr(3)′	3.6113(6)
Pr(2)—Pr(4)′	3.7105(6)	Pr(3)—Pr(3)′	3.6031(9)
Pr(1)—O(5)	2.421(6)	Pr(1)—O(10)	2.292(6)
Pr(1)—O(15)	2.330(5)	Pr(1)—O(16)	2.476(6)
Pr(1)—O(31)	2.467(5)	Pr(1)—O(41)	2.589(6)
Pr(1)—O(44)	2.704(6)	Pr(2)—O(15)	2.276(5)
Pr(2)—O(16)	2.390(6)	Pr(2)—O(19)	2.641(6)
Pr(2)—O(21)	2.464(6)	Pr(2)—O(24)	2.632(6)
Pr(2)—O(26)	2.541(5)	Pr(2)—O(36)	2.423(6)
Pr(2)—O(46)	2.519(5)	Pr(3)—O(5)	2.420(5)
Pr(3)—O(15)	2.326(5)	Pr(3)—O(15)′	2.295(5)
Pr(3)—O(21)′	2.436(5)	Pr(3)—O(26)	2.523(5)
Pr(3)—O(29)	2.649(6)	Pr(3)—O(41)′	2.591(5)
Pr(3)—O(46)′	2.762(6)	Pr(4)—O(26)′	2.513(5)
Pr(4)—O(31)	2.427(5)	Pr(4)—O(34)	2.672(6)
Pr(4)—O(36)′	2.455(6)	Pr(4)—O(39)′	2.719(6)
Pr(4)—O(41)	2.504(6)	Pr(4)—O(46)′	2.488(6)
Pr(4)—O(47)	2.224(6)		
O(10)—Pr(1)—O(5)	92.8(2)	O(15)—Pr(1)—O(10)	148.2(2)
O(15)—Pr(1)—O(5)	73.5(2)	O(16)—Pr(1)—O(5)	95.4(2)
O(16)—Pr(1)—O(10)	85.6(2)	O(31)—Pr(1)—O(5)	91.8(2)
O(31)—Pr(1)—O(10)	85.8(2)	O(41)—Pr(1)—O(5)	127.0(2)
O(41)—Pr(1)—O(10)	135.1(2)	O(44)—Pr(1)—O(5)	169.3(2)
O(44)—Pr(1)—O(10)	78.7(2)	O(16)—Pr(1)—O(15)	67.8(2)
O(31)—Pr(1)—O(15)	122.3(2)	O(31)—Pr(1)—O(16)	169.1(2)
O(41)—Pr(1)—O(15)	72.3(2)	O(41)—Pr(1)—O(16)	107.5(2)
O(41)—Pr(1)—O(31)	74.3(2)	O(44)—Pr(1)—O(15)	110.6(2)
O(44)—Pr(1)—O(16)	77.7(2)	O(44)—Pr(1)—O(31)	94.0(2)
O(44)—Pr(1)—O(41)	63.4(2)		
O(16)—Pr(2)—O(15)	70.2(2)	O(19)—Pr(2)—O(15)	125.8(2)
O(19)—Pr(2)—O(16)	64.8(2)	O(21)—Pr(2)—O(15)	74.2(2)
O(21)—Pr(2)—O(16)	97.3(2)	O(24)—Pr(2)—O(15)	133.5(2)
O(24)—Pr(2)—O(16)	92.8(2)	O(26)—Pr(2)—O(15)	75.2(2)
O(26)—Pr(2)—O(16)	101.6(2)	O(36)—Pr(2)—O(15)	136.3(2)
O(36)—Pr(2)—O(16)	144.5(2)	O(46)—Pr(2)—O(15)	70.2(2)
O(46)—Pr(2)—O(16)	140.4(2)	O(21)—Pr(2)—O(19)	138.6(2)
O(24)—Pr(2)—O(19)	78.1(2)	O(24)—Pr(2)—O(21)	65.3(2)
O(26)—Pr(2)—O(19)	85.7(2)	O(26)—Pr(2)—O(21)	135.7(2)
O(26)—Pr(2)—O(24)	151.2(2)	O(36)—Pr(2)—O(19)	79.8(2)
O(36)—Pr(2)—O(21)	111.6(2)	O(36)—Pr(2)—O(24)	81.6(2)
O(36)—Pr(2)—O(26)	72.2(2)	O(46)—Pr(2)—O(19)	145.0(2)
O(46)—Pr(2)—O(21)	72.2(2)	O(46)—Pr(2)—O(24)	115.0(2)
O(46)—Pr(2)—O(26)	67.6(2)	O(46)—Pr(2)—O(36)	71.0(2)
O(15)—Pr(3)—O(5)	73.6(2)	O(15)′—Pr(3)—O(5)	131.4(2)
O(21)′—Pr(3)—O(5)	99.7(2)	O(26)—Pr(3)—O(5)	93.1(2)
O(29)—Pr(3)—O(5)	76.7(2)	O(41)′—Pr(3)—O(5)	155.7(2)
O(46)′—Pr(3)—O(5)	67.6(2)	O(15)—Pr(3)—O(15)′	77.5(2)
O(21)′—Pr(3)—O(15)	134.5(2)	O(21)′—Pr(3)—O(15)′	74.4(2)
O(26)—Pr(3)—O(15)	74.7(2)	O(26)—Pr(3)—O(15)′	115.8(2)
O(26)—Pr(3)—O(21)′	150.4(2)	O(29)—Pr(3)—O(15)	128.5(2)
O(29)—Pr(3)—O(15)′	149.6(2)	O(29)—Pr(3)—O(21)′	91.0(2)
O(29)—Pr(3)—O(26)	66.0(2)	O(41)′—Pr(3)—O(15)	116.2(2)
O(41)′—Pr(3)—O(15)′	72.8(2)	O(41)′—Pr(3)—O(21)′	88.6(2)
O(41)′—Pr(3)—O(26)	70.1(2)	O(41)′—Pr(3)—O(29)	80.4(2)
O(46)′—Pr(3)—O(15)	67.5(2)	O(46)′—Pr(3)—O(15)′	65.5(2)
O(46)′—Pr(3)—O(21)′	68.5(2)	O(46)′—Pr(3)—O(26)	141.0(2)
O(46)′—Pr(3)—O(29)	134.1(2)	O(46)′—Pr(3)—O(41)′	136.3(2)

Table 3. (*Continued*)

O(31)—Pr(4)—O(26)′	130.2(2)	O(34)—Pr(4)—O(26)′	147.6(2)
O(34)—Pr(4)—O(31)	63.2(2)	O(36)′—Pr(4)—O(26)′	72.2(2)
O(36)′—Pr(4)—O(31)	109.3(2)	O(36)′—Pr(4)—O(34)	136.6(2)
O(39)′—Pr(4)—O(26)′	133.0(2)	O(39)′—Pr(4)—O(31)	83.2(2)
O(39)′—Pr(4)—O(34)	71.7(2)	O(39)′—Pr(4)—O(36)′	64.9(2)
O(41)—Pr(4)—O(26)′	71.6(2)	O(41)—Pr(4)—O(31)	76.5(2)
O(41)—Pr(4)—O(34)	86.6(2)	O(41)—Pr(4)—O(36)′	135.4(2)
O(46)′—Pr(4)—O(26)′	68.6(2)	O(46)′—Pr(4)—O(31)	65.7(2)
O(46)′—Pr(4)—O(34)	127.8(2)	O(46)′—Pr(4)—O(36)′	71.0(2)
O(47)—Pr(4)—O(26)′	85.5(2)	O(47)—Pr(4)—O(31)	139.2(2)
O(47)—Pr(4)—O(34)	76.0(2)	O(47)—Pr(4)—O(36)′	99.4(2)
O(41)—Pr(4)—O(39)′	155.3(2)	O(46)′—Pr(4)—O(39)′	112.1(2)
O(46)′—Pr(4)—O(41)	72.1(2)	O(47)—Pr(4)—O(39)′	83.4(2)
O(47)—Pr(4)—O(41)	102.9(2)	O(47)—Pr(4)—O(46)′	154.0(2)
Pr(1)—O(5)—Pr(3)	100.9(2)	Pr(1)—O(16)—Pr(2)	106.3(2)
Pr(1)—O(15)—Pr(2)	115.5(2)	Pr(1)—O(31)—Pr(4)	103.6(2)
Pr(1)—O(15)—Pr(3)	106.6(2)	Pr(1)—O(41)—Pr(3)	98.3(2)
Pr(1)—O(15)—Pr(3)′	115.8(2)	Pr(1)—O(41)—Pr(4)	98.1(2)
Pr(2)—O(15)—Pr(3)	111.3(2)	Pr(2)—O(26)—Pr(4)′	94.5(2)
Pr(2)—O(15)—Pr(3)′	104.4(2)	Pr(2)—O(36)—Pr(4)′	99.0(2)
Pr(2)—O(21)—Pr(3)′	95.0(2)	Pr(2)—O(46)—Pr(3)	86.2(2)
Pr(2)—O(26)—Pr(3)	97.3(2)	Pr(2)—O(46)—Pr(4)′	95.6(2)
Pr(3)—O(15)—Pr(3)′	102.5(2)	Pr(3)—O(41)—Pr(4)	104.8(2)
Pr(3)—O(26)—Pr(4)′	106.5(2)	Pr(3)—O(46)—Pr(4)′	161.7(2)
Pr(1)—O(10)—P(11)	174.0(4)		

[a] Atoms labelled ′ correspond to −x, −y, −z.

$OPMe_3$ is also confirmed by additional absorption bands in the FT-IR spectrum (with respect to **2a**) at 995 and 950 cm^{-1}.

Compound **2b** represents the first example of eight coordination for lanthanides in alkoxide chemistry (without carboxylates or β-diketonates as ancilliary ligands), the usual coordination number being generally six, with increase to seven for functional alkoxide groups [1]. The tendency for praseodymium to have larger coordination numbers than other lanthanides is also reflected by the seven coordination observed for the mixed-metal isopropoxide $[PrAl_2Cl(OPr^i)_8(Pr^iOH)]_2$ [5] and by $[Pr(OCMe(CF_3)_2)_3]_3$, in which the metals are seven and eight coordinated, depending on the number of secondary Pr···F bonds [3]. Tetranuclear lanthanide alkoxides have found precedent for isopropoxides as illustrated by $[Nd(OPr^i)_3(Pr^iOH)]_4$ [1b] or by $Ln_4(OCH_2Bu^t)_{12}$ (Ln = La, Nd) [19]. The presence of agostic Ln···H—C interactions in the solid for the latter, and of solvated alcohol molecules complementing the metal coordination sphere in the neodymium isopropoxide, allows the lanthanides to reach six coordination. Tetranuclear oxoalkoxide lanthanide moieties in which the lanthanides are six coordinated have been stabilized in mixed-metal alkoxides, namely $[Y_4(\mu_3\text{-}OBu^t)_2(\mu\text{-}OBu^t)_4(OBu^t)_4(\mu_4\text{-}O)\ (\mu\text{-}Cl)_2Li_4(\mu\text{-}OBu^t)_2]_2$ [22] and $Sm_4(\mu_4\text{-}O)(OPr^i)_{10}Ti(OPr^i)_4$ [18]. The metallic M_4 framework results from the assembly of two triangular subunits and so corresponds to a butterfly arrangement. The elimination of the solvated alcohol molecules of the lanthanide isopropoxide derivatives leads to oxo species as a means of retaining the six coordination [1b]. The compounds having the formulation $[Pr_4O_2(OR)_8]_m$ or $[Pr_4O_2(OR)_3(OR')_5]_m$ are likely to display metal oxygen frameworks related to that of **2b**. Octanuclear aggregates have been reported in lanthanide chemistry as well as in alkoxide chemistry. They result, generally, from hydrolytic polycondensation reactions. $[Er_8(\mu_4\text{-}O)(thd)_{10}(\mu_3\text{-}OH)_{12}]$ represents the first example of assembly *via* a planar

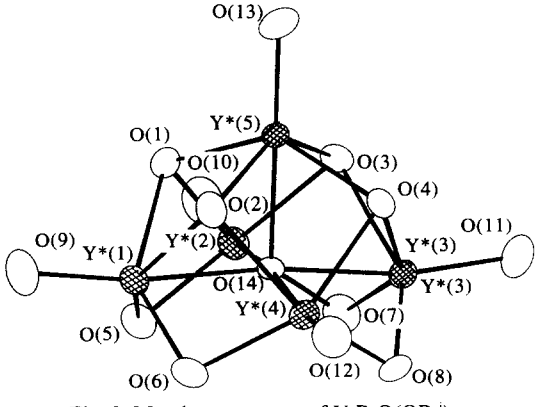


Fig. 2. Metal oxygen core of $Y_4PrO(OPr^i)_{13}$.

Table 4. Selected bond lengths (Å) and angles (°) for $[Y_4Pr(\mu_4\text{-}O)(\mu_3\text{-}O^iPr)_4(\mu\text{-}O^iPr)_4(O^iPr)_5]$

Y(1)*—Y(2)*	3.404(3)	Y(1)*—Y(4)*	3.410(3)
Y(1)*—Y(5)*	3.531(3)	Y(2)*—Y(5)*	3.539(3)
Y(2)*—Y(3)*	3.405(3)	Y(3)*—Y(4)*	3.402(3)
Y(3)*—Y(5)*	3.534(3)	Y(4)*—Y(5)*	3.538(3)
Y(1)*—O(1)	2.46(2)	Y(3)*—O(8)	2.25(2)
Y(1)*—O(2)	2.47(2)	Y(3)*—O(11)	2.07(2)
Y(1)*—O(6)	2.24(2)	Y(3)*—O(14)	2.40(2)
Y(1)*—O(5)	2.28(2)	Y(4)*—O(2)	2.46(2)
Y(1)*—O(9)	2.04(2)	Y(4)*—O(4)	2.49(2)
Y(1)*—O(14)	2.45(2)	Y(4)*—O(6)	2.27(2)
Y(2)*—O(1)	2.45(2)	Y(4)*—O(8)	2.26(2)
Y(2)*—O(3)	2.48(2)	Y(4)*—O(12)	2.01(2)
Y(2)*—O(5)	2.25(2)	Y(4)*—O(14)	2.38(2)
Y(2)*—O(7)	2.26(2)	Y(5)*—O(1)	2.35(2)
Y(2)*—O(10)	2.04(2)	Y(5)*—O(2)	2.36(2)
Y(2)*—O(14)	2.43(2)	Y(5)*—O(3)	2.35(2)
Y(3)*—O(3)	2.45(2)	Y(5)*—O(4)	2.33(2)
Y(3)*—O(4)	2.47(2)	Y(5)*—O(13)	2.03(2)
Y(3)*—O(7)	2.24(2)	Y(5)*—O(14)	2.41(1)
O(5)—Y(1)*—O(1)	77.2(6)	O(5)—Y(1)*—O(2)	141.2(6)
O(6)—Y(1)*—O(1)	141.6(6)	O(6)—Y(1)*—O(2)	76.6(6)
O(6)—Y(1)*—O(5)	106.0(7)	O(9)—Y(1)*—O(1)	107.4(8)
O(9)—Y(1)*—O(2)	106.6(7)	O(9)—Y(1)*—O(5)	109.1(7)
O(9)—Y(1)*—O(6)	107.3(8)	O(14)—Y(1)*—O(1)	66.4(5)
O(14)—Y(1)*—O(2)	65.7(5)	O(14)—Y(1)*—O(5)	77.0(6)
O(14)—Y(1)*—O(6)	76.9(6)	O(14)—Y(1)*—O(9)	170.6(7)
O(3)—Y(2)*—O(1)	77.4(5)		
O(5)—Y(2)*—O(1)	77.8(6)	O(5)—Y(2)*—O(3)	141.8(5)
O(7)—Y(2)*—O(1)	141.5(6)	O(7)—Y(2)*—O(3)	76.0(6)
O(7)—Y(2)*—O(5)	107.9(7)	O(10)—Y(2)*—O(1)	104.7(7)
O(10)—Y(2)*—O(3)	106.3(7)	O(10)—Y(2)*—O(5)	107.7(7)
O(10)—Y(2)*—O(7)	109.2(8)	O(14)—Y(2)*—O(1)	66.8(5)
O(14)—Y(2)*—O(3)	65.8(5)	O(14)—Y(2)*—O(5)	77.9(6)
O(14)—Y(2)*—O(7)	77.1(6)	O(14)—Y(2)*—O(10)	169.1(7)
O(4)—Y(3)*—O(3)	76.9(5)		
O(7)—Y(3)*—O(3)	77.0(6)	O(7)—Y(3)*—O(4)	141.5(6)
O(8)—Y(3)*—O(3)	141.9(6)	O(8)—Y(3)*—O(4)	77.5(6)
O(8)—Y(3)*—O(7)	107.8(7)	O(11)—Y(3)*—O(3)	104.9(7)
O(11)—Y(3)*—O(4)	105.2(8)	O(11)—Y(3)*—O(7)	108.6(8)
O(11)—Y(3)*—O(8)	108.7(7)	O(14)—Y(3)*—O(3)	66.7(5)
O(14)—Y(3)*—O(4)	65.7(5)	O(14)—Y(3)*—O(7)	78.1(6)
O(14)—Y(3)*—O(8)	77.2(6)	O(14)—Y(3)*—O(11)	168.4(7)
O(4)—Y(4)*—O(2)	76.8(5)		
O(6)—Y(4)*—O(2)	76.2(6)	O(6)—Y(4)*—O(4)	140.7(6)
O(8)—Y(4)*—O(2)	142.0(6)	O(8)—Y(4)*—O(4)	77.0(6)
O(8)—Y(4)*—O(6)	109.3(7)	O(12)—Y(4)*—O(2)	106.0(8)
O(12)—Y(4)*—O(4)	108.1(7)	O(12)—Y(4)*—O(6)	106.4(7)
O(12)—Y(4)*—O(8)	108.0(8)	O(14)—Y(4)*—O(2)	66.9(5)
O(14)—Y(4)*—O(4)	65.8(5)	O(14)—Y(4)*—O(6)	77.6(6)
O(14)—Y(4)*—O(8)	77.4(6)	O(14)—Y(4)*—O(12)	171.1(7)
O(2)—Y(5)*—O(1)	82.6(6)	O(3)—Y(5)*—O(1)	82.0(6)
O(3)—Y(5)*—O(2)	136.3(6)	O(4)—Y(5)*—O(1)	136.5(6)
O(4)—Y(5)*—O(2)	81.9(6)	O(4)—Y(5)*—O(3)	81.8(6)
O(13)—Y(5)*—O(1)	112.0(7)	O(13)—Y(5)*—O(2)	110.3(7)
O(13)—Y(5)*—O(3)	113.4(7)	O(13)—Y(5)*—O(4)	111.5(7)
O(14)—Y(5)*—O(1)	68.7(5)	O(14)—Y(5)*—O(2)	68.0(6)
O(14)—Y(5)*—O(3)	68.2(5)	O(14)—Y(5)*—O(4)	67.8(5)
O(14)—Y(5)*—O(13)	178.2(8)		

Table 4. (*Continued*)

Y(2)*—O(1)—Y(1)*	87.8(5)	Y(5)*—O(1)—Y(1)*	94.5(6)
Y(5)*—O(1)—Y(2)*	94.9(6)	Y(4)*—O(2)—Y(1)*	87.7(5)
Y(5)*—O(2)—Y(1)*	94.1(6)	Y(5)*—O(2)—Y(4)*	94.6(6)
Y(3)*—O(3)—Y(2)*	87.3(5)	Y(5)*—O(3)—Y(2)*	94.2(5)
Y(5)*—O(3)—Y(3)*	94.8(6)	Y(4)*—O(4)—Y(3)*	86.7(5)
Y(5)*—O(4)—Y(3)*	94.8(5)	Y(5)*—O(4)—Y(4)*	94.5(5)
Y(2)*—O(5)—Y(1)*	97.3(6)	Y(4)*—O(6)—Y(1)*	98.2(7)
Y(3)*—O(7)—Y(2)*	98.1(6)	Y(4)*—O(8)—Y(3)*	97.7(6)
Y(2)*—O(14)—Y(1)*	88.5(5)	Y(3)—O(14)—Y(1)*	172.0(7)
Y(3)*—O(14)—Y(2)*	89.6(5)	Y(4)*—O(14)—Y(1)*	89.9(5)
Y(4)*—O(14)—Y(2)*	170.7(7)	Y(4)*—O(14)—Y(3)*	90.7(5)
Y(5)*—O(14)—Y(1)*	93.3(5)	Y(5)*—O(14)—Y(2)*	94.0(5)
Y(5)*—O(14)—Y(3)*	94.6(5)	Y(5)*—O(14)—Y(4)*	95.2(5)
C(9)—O(9)—Y(1)*	164.3(22)	C(10)—O(10)—Y(2)*	167.6(22)
C(11)—O(11)—Y(3)*	161.7(23)	C(12)—O(12)—Y(4)*	170.6(25)
C(13)—O(13)—Y(5)*	164.2(20)		

oxo ligand [23]. $Nb_8O_{10}(OEt)_{20}$ [24], $Ti_8O_6(OBz)_{20}$ (Bz = benzyl) [24], and $[Mo_8O_8Cl_6(\mu_3\text{-}O)_4(OH)_2(\mu\text{-}OH)_4(\mu\text{-}OEt)_4(EtOH)_4$ [26] obtained by microhydrolysis of alkoxides, have *closo* structures, while the structure of $[Mo_8O_{16}(OMe)_8(PMe_3)_4$ [27], which is derived from the photo-oxidation of a molybdenum carbonyl derivative, is based on a puckered cycle.

$Y_4PrO(OPr^i)_{13}$ possess a M_5O_{14} core similar to that of $Y_5O(OPr^i)_{13}$ [28], the metals all being six coordinated (Fig. 2). The yttrium and praseodymium atoms could not however be distinguished and the electron density of the metal atoms corresponds in fact to the average value for four yttrium and one praseodymium atom, these atoms are depicted Y*. Selected bond lengths and angles for $[Y_4PrO(OPr^i)$ are collected in Table 4. The isopropoxide ligands are of three types, four of them are triply bridging, four doubly bridging and five terminal. Metal–oxygen distances range from 2.01(2) to 2.49(2) Å and follow the pattern previously observed for $Y_5O(OPri)_{13}$: Y*—OR (terminal) < Y*—μ-OR < Y*—μ_3-OR ~ Y*—(μ_5—O) with the terminal Y*—OR bond distances being shorter than the sum of the covalent radii (2.35 Å). The cluster is quite regular with non-bonding metal–metal distances varying from 3.402(3) to 3.539(3) Å; the μ_5-oxo ligand is near the centre of the basal plane. As expected, the Y*—O and Y*···Y* distances are slightly longer than for the homometallic yttrium derivative.

In conclusion it appears that praseodymium alkoxide chemistry displays specific features with respect to other lanthanides. While praseodymium shares with other lanthanides formulations such as $Pr_5O(OPr^i)_{13}$ and $Pr_3(OR)_9(ROH)_2$, it displays a trend for high coordination numbers and thus more condensed oxo species. Secondary bonds such as Pr···F, Pr···H—C might contribute to the increase in the coordination number, as well as the generation of several oxo ligands even by reaction in mild conditions.

Acknowledgements—We are grateful to A. Mari (Toulouse) for the magnetic susceptibility measurements and to the CNRS (Greco "Sol–gel inorganiques") for financial support.

REFERENCES

1. (a) Mehrotra, R. C., Singh, A. and Tripathi, A., *Chem. Rev.*, 1991, **91,** 1287; (b) Hubert-Pfalzgraf, L. G., *New J. Chem.*, 1995, **19,** 727.
2. Razuvaev, G. A., Kalinina, G. S. and Fedorova, E. A., *J. Organomet. Chem.*, 1980, **190,** 157.
3. Bradley, D. C., Chudzynska, H., Hammond, M. E., Hursthouse, M. B., Motevalli, M. and Ruowen, W., *Polyhedron* 1992, **11,** 375.
4. Daniele S., Hubert-Pfalzgraf, L. G. and Vaissermann, J., *Polyhedron*, 1995 **14,** 327.
5. (a) Tripathi, A., Singh, R. C., Mehrotra, R. C., Goel, S. C., Chiang, M. Y. and Buhro, W. E., *J. Chem. Soc., Chem. Commun.*, 1992, 152; (b) Wang, S., Pang, Z., Smith, K. D. L., Hua, Y. S., Deslippe, C. and Wagner, M. J., *Inorg. Chem.*, 1995, **34,** 908.
6. Kilbourn, B. T., *J. Less-Common Met.*, 1985, **111,** 1.
7. Engler, E. M., Lee, V. Y., Nazzal, A. I., Beyers, R. B., Lin, G., Grant, P. M., Parkin, S. S. P., Ramirez, M. L., Vazquez, J. E. and Savory, R. J., *J. Am. Chem. Soc.*, 1987, **109,** 2848; Tokura, Y., Takagi, H. and Uchida, S., *Nature*, 1989, **337,** 345.
8. Hiskes, R., Dicarolis, S. A., Jacowitz, R. D., Lu, Z., Feigelson, R. S., Route, R. K. and Young, J. L., *J. Cryst. Growth*, 1993, **128,** 781.
9. Saüer, J. G., *J. Am. Chem. Soc.*, 1944, **68,** 1707; Sommer, L. H., Pietrusza, E. W. and Whitmore, F. C., *J. Am. Chem. Soc.*, 1946, **68,** 2282.
10. Bradley, D. C., Ghotra, J. S. and Hart, F. A., *J. Chem. Soc., Dalton Trans.*, 1973, 1021.
11. Clark, E. P., *Inorg. Eng. Chem., Anal. Ed.*, 1941, **13,** 820.
12. Sheldrick, G. M., SHELXS-86, Program for

Crystal Structure Solution, University of Gôttingen, Germany, 1986.
13. Watkin, D. J., Carruthers, J. R. and Betteridge, P. W., CRYSTALS User Guide, Chemical Crystallography Laboratory, University of Oxford, 1986.
14. Walker, N. and Stuart, D., *Acta Cryst.*, 1983, **A39,** 158.
15. The compounds $[Pr_5O(OPr^i)_{13}]$ and $[Pr_3(OBu^t)_9(Bu^tOH)_2]$ were previously prepared and characterized by Ms Ruowen Wu, Ph.D. thesis, London University (1991). Personal communication from Professor D. C. Bradley.
16. Poncelet, O., Hubert-Pfalzgraf, L. G. and Daran, J. C., *Inorg. Chem.*, 1990, **29,** 2883; Poncelet, O., Hubert-Pfalzgraf, L. G., Daran, J. C. and Astier, R., *J. Chem. Soc., Chem. Commun.*, 1989, 1846.
17. (a) Labrize, F., Hubert-Pfalzgraf, L. G., Vaissermann, J. and Knobler, C., *Polyhedron*, 1996, **15,** 577; (b) Hubert-Pfalzgraf, L. G., Labrize, F., Bois, C. and Vaissermann, J., *Polyhedron*, 1994, **13,** 2163; (c) Hubert-Pfalzgraf, L. G. and Poncelet, O., unpublished work.
18. Daniele, S., Hubert-Pfalzgraf, L. G., Daran, J. C. and Halut, S., *Polyhedron*, 1994, **13,** 927.
19. Barnhart, D. M., Clark, D. L., Gordon, J. C., Huffman, J. C., Watkin, J. G. and Zwick, B. D., *J. Am. Chem. Soc.*, 1993, **115,** 8461.
20. Daniele, S., Hubert-Pfalzgraf, L. G. and Daran, J. C., *Polyhedron*, 1996, **15,** 1063.
21. Hart, F. A., *Comprehensive Coordination Chemistry*, Vol. 3, ed. G. S. Wilkinson. Pergamon Press, London, 1987, ch. 34.
22. Evans, W. J., Sollberger, M. S. and Hanusa, T. P., *J. Am. Chem. Soc.*, 1988, **110,** 1841.
23. Boeyens, J. C. A. and de Villiers, J. P. R., *J. Cryst. Mol. Struct.*, 1972, **2,** 197; Rambo, J. R., Huffman, J. C., Christou, G. and Eistenstein, O., *J. Am. Chem. Soc.*, 1989, **111,** 8027; Cotton, F. A. and Shang, M., *J. Am. Chem. Soc.*, 1990, **112,** 1584.
24. Turova, N. Ya., Turevskaya, E. P., Kessler, V. G., Yanovski, A. I. and Sruchkov, Y. T., *J. Chem. Soc., Chem. Commun.*, 1992, **31,** 4048.
25. Day, V. W., Eberspacher, T. A., Klemperer, W. G., Park, C. W. and Rosenberg, F. S., *J. Am. Chem. Soc.*, 1991, **113,** 8190.
26. Chae, H. K., Klemperer, W. G. and Marquart, T. A., *Coord. Chem. Rev.*, 1993, **128,** 209.
27. Blake, A. J., Downs, A. J., Limberg, C. and Parsons, S., *J. Chem. Soc., Dalton Trans.*, 1995, 3263.
28. Poncelet, O., Sartain, W., Folting, K., Hubert-Pfalzgraf, L. G. and Caulton, K. G., *Inorg. Chem.*, 1989, **28,** 263.

Pergamon

PII: S0277-5387(96)00329-4

Polyhedron Vol. 16, No. 7, pp. 1235–1240, 1997
Copyright © 1997 Elsevier Science Ltd
Printed in Great Britain. All rights reserved
0277-5387/97 $17.00+0.00

Interaction of phenylhydrazine with Ru^{III}–EDTA complexes: reduction of phenylhydrazine to ammonia and aniline in aqueous acidic conditions

Raju Prakash, Beena Tyagi, Debabrata Chatterjee and Gadde Ramachandraiah*

Reactive Polymers and Catalysis Divisions, Central Salt and Marine Chemicals Research Institute, Bhavnagar-364002, India

(Received 10 May 1996; accepted 1 July 1996)

Abstract—Reaction of the phenylhydrazinium ($PhN_2H_4^+$) ion with the labile aquo complexes of [Ru^{III}(HEDTA)(H_2O)] (EDTA = ethylenediaminetetraacetate) was studied electrochemically employing sampled DC, cyclic voltammetry and differential pulse techniques in 0.2 M CH_3COONa and H_2SO_4 mixture between pH 1.0 and 4.5 at 25°C. It produced two phenylhydrazinium complexes, namely [Ru^{III}(HEDTA)(N_2H_4Ph)]$^+$ and [Ru^{III}(EDTA)(N_2H_4Ph)] in the rapid aquo-substitution reactions. The second-order rate constants, k_1, for the formation of the former, and k_2 for the latter are 0.98 and 36.85 M^{-1} s^{-1}, respectively, as determined spectrophotometrically by following the intensity of the LMCT band at 420 nm. The complex, [Ru^{III}(HEDTA)(N_2H_4Ph)]Cl · $2H_2O$ was prepared and characterised by physicochemical methods. These phenlhydrazinium complexes were reduced by two electrons at $E_{1/2} = -0.175$ V *vs* SCE, producing one mole of NH_3 and the corresponding Ru^{III}–NH_2Ph complexes in subsequent rapid decomposition steps. The unstable Ru^{III}–NH_2Ph complexes were rapidly hydrolysed to one mole of NH_2Ph and the respective aquo complex. One-electron reduction steps for the regenerated aquo complex at ($E_{1/2}$) −0.254 V and the unhydrolysed Ru^{III}–NH_2Ph complex at −0.417 V were also observed. Phenylhydrazine was reduced to ammonia and aniline by constant potential coulometry at −0.200 V(Hg) *vs* SCE, in the presence of [Ru^{III}(HEDTA)(H_2O)] at 100 : 1 molar ratio. The turnover number (per mole of catalyst per hour) with respect to ammonia is 5.98 and 2.82 at pH 2.8 and 1.9, respectively. The probable mechanisms for the electroreduction of the above phenylhydrazinium complexes and the catalytic reduction of phenylhydrazine to NH_3 and NH_2Ph, are proposed. Copyright © 1997 Elsevier Science Ltd

Keywords: Ru^{III}–EDTA; phenylhydrazine; interaction; electrocatalysis; ammonia; aniline

We have studied the chemistry of Ru–EDTA complexes extensively [1–7] and the present work is a continuation of our efforts to develop a simple water-soluble metal complex for activating and reducing the N—N bonded molecules to ammonia and/or amines in order to elucidate the pathways for N—N bond reductions in homogeneous solution. Metal bound hydrazine is considered to be the active intermediate in nitrogen fixation by primitive organisms, e.g. *Azotobacter*, carrying a nitrogenase system [8–11]. Our earlier communications [8,12,13], revealed the reduction of hydrazinium [12] and azide [13] ions, surprisingly, at unexpected potentials of the Hg electrode catalysed by Ru–EDTA complexes in aqueous acidic conditions. To obtain more mechanistic details and to study the substitutional effect on the coordinated N of hydrazine in this intriguing N—N bond reduction, we have selected phenylhydrazine as a substrate in the present study. The results of spectrophotometric, kinetic and electrochemical studies of the interaction of phenylhydrazine with Ru^{III}–EDTA complexes in aqueous acidic solutions are reported. The results are correlated with the data reported for hydrazinium and azide ions.

* Author to whom correspondence should be addressed.

EXPERIMENTAL

Materials

$K[Ru^{III}(HEDTA)Cl]\cdot 2H_2O$ was prepared from $K_2[Ru^{III}Cl_5(H_2O)]$ by previously reported methods, and was characterised [14,15]. This complex, as evidenced earlier [12,16] by spectrophotometric and kinetic data, quickly changes to $[Ru^{III}(HEDTA)(H_2O)]$ ($pK_a = 2.37$) in aqueous solution of pH 1.0–4.5. Hence, $[Ru^{III}(HEDTA)(H_2O)]$ has been considered as the precursor in this study. Phenylhydrazine hydrochloride (N_2H_4PhCl) was obtained from Allied Chemicals, U.S.A. and used as a source for $N_2H_4Ph^+$ ion. All other chemicals used were of AR grade.

$[Ru^{III}(HEDTA)(N_2H_4Ph)]Cl\cdot 2H_2O$ was prepared by dissolving $K[Ru^{III}(HEDTA)Cl]\cdot 2H_2O$ (100 mg, 0.2 mmol) phenylhydrazine hydrochloride (30.66 mg, 0.21 mmol) in the minimum quantity of water. The resulting dark yellow solution was stirred for 2 h at 45° under Ar atmosphere. The product was precipitated with absolute alcohol, filtered and washed repeatedly with 9 : 1 acetone–water mixture and dried *in vacuo*. Found: C, 33.7; H, 4.4; N, 9.8. Calc. for $[Ru^{III}(HEDTA)(N_2H_4Ph)]Cl\cdot 2H_2O$: 33.5; H, 4.1; N, 9.4%. IR (cm^{-1}): 3210 (N—H stretching), 1750 (COOH), 1640 (coordinated COO^-), 1420 and 1080 (N—H deformations).

pH-metric titrations

N_2H_4PhCl was titrated with standard NaOH (0.1 M) solution as usual [14] and from the resulting pH data, the acid dissociation constant (pK_a) of $NHPh\cdot NH_3^+$ ion was calculated as 5.15 ± 0.01 at 25°C. Similar titrations were carried out with $[Ru^{III}(HEDTA)(H_2O)]$, in the absence and presence of one equivalent of N_2H_4PhCl. This data revealed that the acidic proton on the more basic nitrogen in $NHPh.NH_3^+$ is unaffected during its interaction with the Ru^{III} centre. This is sufficient to prove the coordination of $N_2H_4Ph^+$ at the sixth vacant position on Ru^{III} through its weak basic NHPh group.

Measurements and method

Electrochemical measurements such as sampled DC, differential pulse polarography (DPP), cyclic voltammetry (CV) and differential pulse voltammetry (DPV), were performed with EG&G Princeton Applied Research models: 174A polarographic analyzer, 175 universal programmer with a high-precision *X–Y* recorder. A three-electrode assembly of EG&G PAR model 303, comprising a Pt wire auxiliary, SCE reference and a dropping mercury electrode (DME) of 3.85 mg s^{-1} or a hanging mercury drop electrode (HMDE) of 0.021 cm^2 was used. All *E–i* plots were recorded under Ar in the potential range +0.2 to −0.8 V. The electrochemical cell was thermostatted to 25°C within ±0.1°C. Controlled potential coulometry (CPC) was carried out using a EG&G PAR model 173 galvanostat and 179 digital integrator in a three-compartment cell. The auxiliary Pt mesh and the reference SCE electrodes were separated from the main compartment cell by fine (G4) glass frits. The main compartment contained Hg-pool (1-inch convex surface diameter) as the working electrode with a glass disk agitator just above the mercury surface. A 30-ml solution containing 0.2 M CH_3COONa, 30 μmol $K[Ru^{III}(HEDTA)Cl]\cdot 2H_2O$ and 30 mmol N_2H_4PhCl, having the pH adjusted to the required value (1.9 or 2.8) with H_2SO_4 solution, was electrolysed for 10 h at −0.200 V under Ar. The quantity of ammonia produced was estimated at 1 h intervals using an Orion 940 ion analyser equipped with an ammonia-sensing electrode [12]. Aniline, produced along with ammonia, was tested using vanadium(V) salt [17].

The electronic absorption spectra were recorded at 25°C using a Shimadzu UV–vis NIR scanning spectrophotometer, model UV-3101 PC. Kinetic studies were carried out on a Hi-Tech stopped-flow spectrophotometer, SF-51 coupled to an Apple data processor. The observed rate data for the formation of the phenylhydrazinium complex were obtained by monitoring absorbance changes in the growth of the characteristic LMCT band at 420 nm. Experiments were conducted under pseudo-first-order conditions of excess phenylhydrazine hydrochloride concentration. The ionic strength of the kinetic solution was adjusted with 2 M KCl. The temperature was maintained to 25±0.1°C using a built-in thermostatic cell compartment.

RESULTS AND DISCUSSION

Voltammetry

The *E–i* responses of $[Ru^{III}(HEDTA)(H_2O)]$ species in the absence and presence of one equiv. N_2H_4PhCl at pH 2.8 were examined at the DME (sampled DC, DPP) and the HMDE (CV and DPV). In the absence of N_2H_4PhCl, the complex exhibited a cathodic wave at $E_{1/2} = -0.213$ V in sampled DC and a pair of cathodic (−0.236 V) and anodic (−0.173 V) peaks in CV, which conforms with the reported values assigned for the $Ru^{III/II}$ couple [12,13].

In the presence of N_2H_4PhCl, after 3–5 min of equilibration, $[Ru^{III}(HEDTA)(H_2O)]$ showed three closely separated reduction waves in sampled DC (Fig. 1a) at $E_{1/2} = -0.155$, −0.233 and −0.407 V. The overall wave height at −0.5 V is nearly three and a half times larger than that of the $[Ru^{III}(HEDTA)(H_2O)]$ one-electron wave. These changes are accounted for by the formation and subsequent participation of phenylhydrazinium complexes in the electrochemical processes. The $E_{1/4}-E_{3/4}$ values of these waves were measured as 30, 55 and 60 mV which indicated the first wave as a two-electron process and

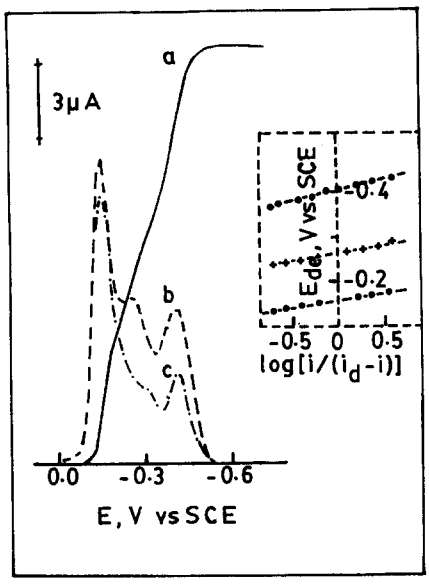


Fig. 1. Voltammetric responses of $[Ru^{III}(HEDTA)(H_2O)]$ (1 mM) in the presence 1 equiv. of N_2H_4PhCl. (a) Sample DC, (b) DPP, (c) DPV. pH = 2.8. Inset: Plots of E_{de} *vs* log $\{i/(i_d-i)\}$ for the polarographic steps shown in (a).

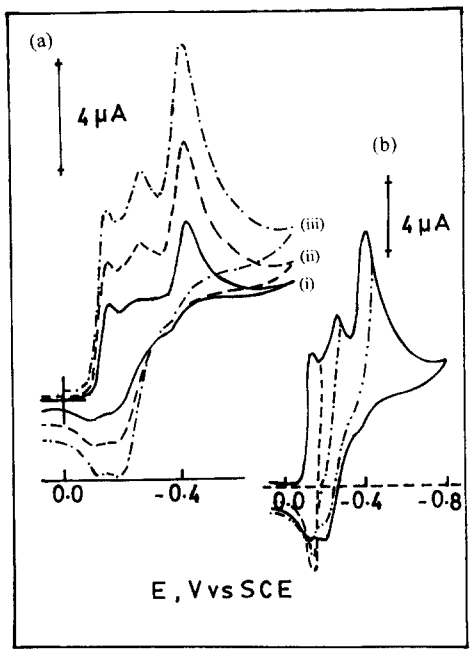


Fig. 2. Cyclic voltammograms of $[Ru^{III}(HEDTA)(H_2O)]$ (1 mM) in the presence of 1 equiv. N_2H_4PhCl at the potential scan speed (a) (i) 0.02, (ii) 0.05, (iii) 0.1 V s^{-1} and (b) 0.1 V s^{-1} at various switching potentials.

the last two as one-electron processes. The plots of E_{de} *vs* $\log i(i_d-i)$ were linear as seen in the inset of Fig. 1 indicating that all three waves in Fig. 1a are diffusion controlled and reversible at the DME.

The behaviour of $[Ru^{III}(HEDTA)(H_2O)]$ in the presence of 0.1–100 equiv. N_2H_4PhCl was also studied. The diffusion current at -0.5 V had increased linearly with the concentration of N_2H_4PhCl between 0.1–1.0 equivalent, whereas the changes in the overall total diffusion current and the $E_{1/2}$ values at higher equivalents of N_2H_4PhCl were inconspicuous. However, the height of the second wave had reached a minimum value at $[N_2H_4PhCl]/[Ru^{III}(HEDTA)(H_2O)] \geqslant 10$. A plot of the mole ratio of N_2H_4PhCl to the complex against the diffusion current at -0.5 V suggested the formation of monomeric phenylhydrazinium adducts; namely $[Ru^{III}(HEDTA)(N_2H_4Ph)]^+$ and $[Ru^{III}(EDTA)(N_2H_4Ph)]$, as was confirmed spectrophotometrically.

Figure 1 (b and c) shows the DPP and DPV responses of the above solution. While the position of these peaks correlated with the $E_{1/2}$ values of the corresponding waves in Fig. 1a, the second peak diminished and moved to cathodic potentials in DPV. Whilst, in CV, three cathodic peaks at -0.157, -0.270 and -0.456 V in the forward scan, and two anodic peaks at -0.118 and -0.185 V (counterparts of the first two) in the reverse scan (Fig. 2a), were observed. There was no anodic counterpart to the third cathodic response. Peak intensities of all three cathodic (CV) responses varied as a function of the square root of the scan speed, while peak positions remained static. Although, the two anodic peaks appeared closely separated at scan speeds <0.1 V s^{-1} (see Fig. 2a, part ii) or the potentials were switched to the foot of the second/third cathodic waves (see Fig. 2b), they diminished slowly as the scan approached 0.02 V s^{-1}.

The effect of pH on the $E_{1/2}$ of the waves in Fig. 1a, and the difference in diffusion current at -0.5 V in the absence and presence of 1 and 100 equiv. of N_2H_4PhCl, were measured. The half-wave potential of the waves in Fig. 1(a) was not shifted significantly. However, the enhanced current at -0.5 V changed considerably, as shown in Fig. 3. The rise in the diffusion current was a maximum in the pH range 2.0–3.5. The lowering of enhanced diffusion current between pH 1.0 and 2.0 is the result of the low rate of formation of $[Ru^{III}(HEDTA)(N_2H_4Ph)]^+$, while that at pH > 3.5 is owing to the stabilization of the $[Ru^{III}(EDTA)(N_2H_4Ph)]$ complex.

Spectrophotometry

The reaction of $[Ru^{III}(HEDTA)(H_2O)]$ with N_2H_4PhCl in 0.2 M CH_3COONa and H_2SO_4 mixture (pH 2.8) accompanied the spectral change producing a new absorption (ligand to metal charge transfer) band at 420 nm. Spectral changes that occurred immediately after the addition of N_2H_4PhCl to a solution of $[Ru^{III}(HEDTA)(H_2O)]$ in different molar ratio at pH 2.8 are shown in Fig. 4a. The kinetics of the reaction were studied as a function of $[N_2H_4PhCl]$ and pH under pseudo-first-order conditions at 25°C. The values of observed rate constant of formation (k_{obs})

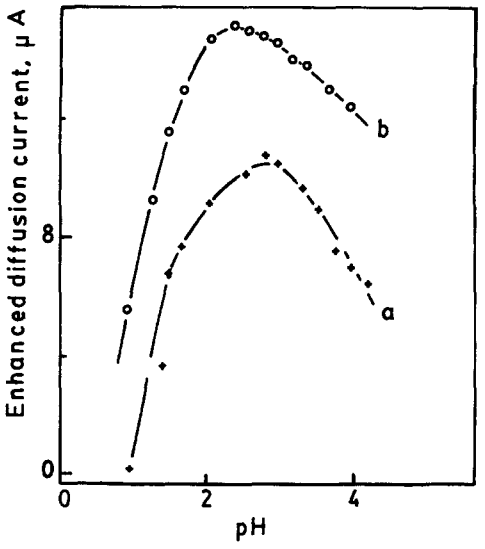


Fig. 3. Influence of solution pH on the enhanced diffusion current (Δi_d) at -0.45 V in the presence of (a) 1, (b) 100 equiv. of phenylhydraine. [Ru^{III}(HEDTA)(H_2O)], 1 mM.

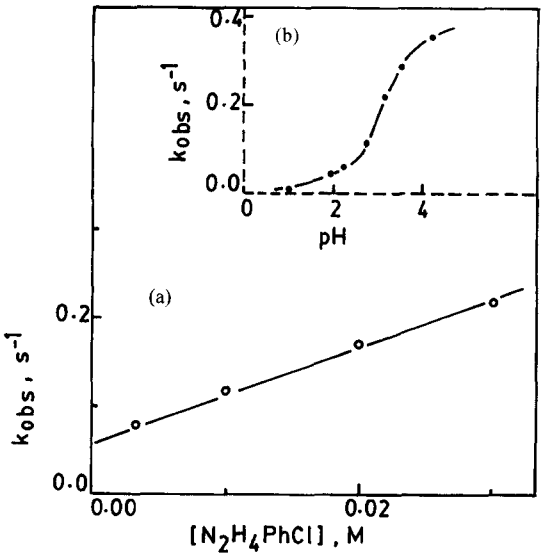


Fig. 5. (a) Plot of k_{obs} *vs* [N_2H_4PhCl]. [Ru^{III}(HEDTA)(H_2O)], 0.5 mM, pH 2.8. (b) Plot of k_{obs} *vs* pH: [Ru^{III}(HEDTA)(H_2O)], 0.5 mM; [N_2H_4PhCl], 0.02 M.

of the hydrazinium adduct changed linearly with [N_2H_4PhCl]. The plot of k_{obs} *vs* [N_2H_4PhCl] (Fig. 5a) showed an appreciable intercept which indicated the presence of reverse reaction of products. The ratio of intercept to slope was 94.1 which was in good agreement with the slope-to-intercept ratio, ($K_{eq.} = 77$) [16] obtained from the plot of $(\Delta A)^{-1}$ *vs* $[N_2H_4PhCl]^{-1}$ (Fig. 4b).

The pH-observed rate constant profile (k_{obs}), which

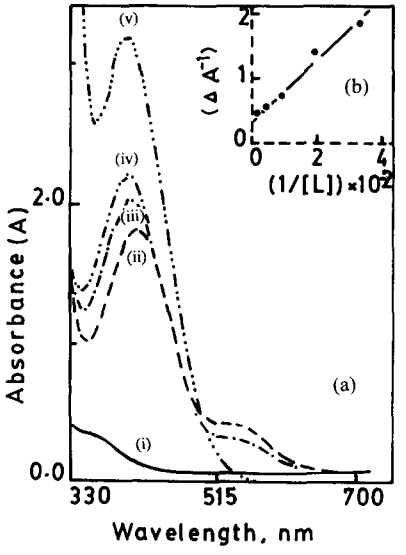


Fig. 4. (a) Absorption data of [Ru^{III}(HEDTA)(H_2O)] (2 mM) immediately after the addition of N_2H_4PhCl at 25°C. $10^3 \times$ [N_2H_4PhCl]: (i) 0.0, (ii) 0.5, (iii) 1.0, (iv) 2.0, (v) 10 M. pH 2.8. (b) Plot of the reciprocal absorbance change (ΔA^{-1}) at 420 nm *vs* the reciprocal N_2H_4PhCl concentration. [Ru^{III}(HEDTA)(H_2O)] (1 mM) was dissolved in 0.2 M CH_3COONa and H_2SO_4 mixture at 25°C. pH = 2.8.

is quite similar to those of the [Ru^{III}(HEDTA)(H_2O)] substitution reactions [6,18], is shown in Fig. 5b. A sharp increase in k_{obs} in the pH range 2.0–4.5 is attributed to the acid dissociation equilibrium of the carboxylic acid of the HEDTA ligand, since the dissociation of the proton of the bound $N_2H_4Ph^+$ in the pH range investigated here was not observed in the pH-metric titration of 1 : 1 K[Ru^{III}(HEDTA)Cl]·$2H_2O$ and [N_2H_4PhCl]. Thus, the pH dependence in Fig. 5b is attributed to the participation of two types of Ru^{III}–EDTA complexes in Eq. (1) as indicated in reactions (2) and (3).

$$[Ru^{III}(HEDTA)(H_2O)] \overset{K_a}{\rightleftharpoons} [Ru^{III}(EDTA)(H_2O)]^- + H^+ \quad (1)$$

$$[Ru^{III}(HEDTA)(H_2O)] + N_2H_4Ph^+ \overset{k_1}{\rightarrow} [Ru^{III}(HEDTA)(N_2H_4Ph)]^+ + H_2O \quad (2)$$

$$[Ru^{III}(EDTA)(H_2O)]^- + N_2H_4Ph^+ \overset{k_2}{\rightarrow} [Ru^{III}(EDTA)(N_2H_4Ph)] + H_2O \quad (3)$$

The rate expression for the above reactions can be expressed as

$$K_{obs} = \{k_1[H^+] + k_2K_a\}\{[N_2H_4Ph^+]\}/\{[H^+] + K_a\} \quad (4)$$

Where $K_a = 2.37$. From the plot of K_{obs} $\{[H^+] + K_a\}/[N_2H_4Ph^+]$ *vs* $[H^+]$, the second-order rate constants k_1 and k_2 were evaluated as 0.98 and 36.85 M^{-1} s^{-1}, respectively, which were found to be larger (about two orders of magnitude) than the

values of the corresponding hydrazinium complexes [12].

Mechanism of electroreduction of phenylhyrazinium complexes

Figure 6a depicts the voltammetric (sampled DC and CV) responses of $[Ru^{III}(HEDTA)(N_2H_4Ph)]Cl \cdot 2H_2O$, which showed the characteristic absorption band at 440 nm (Fig. 6b) in 0.2 M CH_3COONa and H_2SO_4 mixture at pH 2.8. Three reduction waves identical to those given in Fig. 1a were observed in sampled DC (Fig. 6a, part i). The first two waves at ($E_{1/2}$) −0.175 and −0.254 V were poorly resolved, while the third appeared as a low, intense wave at −0.417 V. The CV response in Fig. 6a part ii had further confirmed that the reduced species at −0.175, −0.254 and −0.417 V were coupled to some complex chemical reactions. In the exhaustive electrolysis at −0.5 V *vs* SCE, $[Ru^{III}(HEDTA)(N_2H_4Ph)]Cl \cdot 2H_2O$ consumed total charge equivalent to three electrons per Ru atom, which produced one equiv. ammonia and aniline. The CV of the reduced solution exhibited a pair of cathodic and anodic peaks close to those at −0.270 and −0.185 V, respectively, as shown in Fig. 4a part (ii) or those of the aquo complex. On the basis of these results, the mechanisms for the electroreduction of phenylhydrazinium adducts $[Ru^{III}(HEDTA)(N_2H_4Ph)]^+$ and $[Ru^{III}(EDTA)(N_2H_4Ph)]$ in Figs 1 and 2 are as shown in Scheme 1.

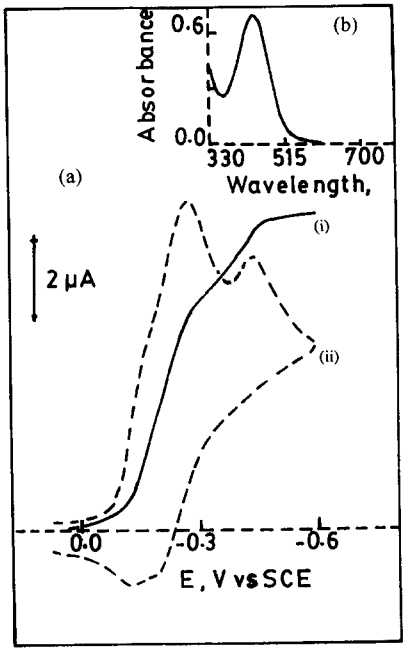


Fig. 6. Voltammetric responses: (i) sampled DC; (ii) CV at scan speed = 0.1 V s^{-1} and (b) absorption spectrum of $[Ru^{III}(HEDTA)(N_2H_4Ph)]Cl \cdot 2H_2O$ (1 mM) in 0.2 M CH_3COONa and H_2SO_4 mixture at 25°C, pH, 2.8.

It is significant to note that the addition of $PhNH_3Cl$ to a solution of $[Ru^{III}(HEDTA)(H_2O)]$ under the present experimental conditions showed no remarkable change in the voltammetric behaviour of the $Ru^{III/II}$ couple and the absorption spectra of the latter. In other words, this accounts for the very low stability of $LRu^{III}NH_2Ph$ and $LRu^{II}NH_2Ph^-$ complexes in solution, as predicted in Scheme 1.

Catalytic reduction of phenylhydrazine

Phenylhydrazine hydrochloride (100 equiv.) in 0.2 M CH_3COONa and H_2SO_4 mixture (pH 2.8 or 1.9) containing one equiv. $K[Ru^{III}(HEDTA)Cl] \cdot 2H_2O$ was electrolysed at −0.200 V *vs* SCE in order to estimate the catalytic activity of the Ru^I–EDTA complexes of phenylhydrazine. As expected, phenylhydrazine was reduced to give NH_3 and NH_2Ph, justifying the first reduction wave at ($E_{1/2}$) −0.175 V as a multi-electron wave. The quantity of ammonia produced in the 10-h reaction was linear (Fig. 7) and consistent with the mechanism shown in Scheme 2. The turnover number, with respect to moles of ammonia formed per mole of catalyst per hour, is 5.98 at pH 2.8 and 2.82 at pH 1.9, and the coulombic efficiency was 100%.

The reduced solution, after 10 h electrolysis, showed all the electrochemical features that are shown in Figs 1 and 2 and produced ammonia when electrolysis was continued further, at the turnover rate found before. This proved that the efficiency of the metal remained intact during the turnover of phenylhydrazine reduction.

The data presented here, and previously, attests to the excellent ability to ruthenium metal, in its EDTA complexes, in transferring electrons from the external electron source (Hg electrode) to the bound N—N bonds, and the superior electron conducting nature of the Ru—N bond of nitrogenous (hydrazines/azide)

$$LRu^{III}N_2H_4Ph \underset{-2e,-0.175}{\overset{+2e}{\rightleftharpoons}} LRu^{I}N_2H_4Ph^{2-} \xrightarrow[-NH_3]{+H^+} LRu^{III}NH_2Ph \xrightarrow[-NH_2Ph]{+H_2O} LRu^{III}H_2O$$

$$-0.417\downarrow + e \qquad\qquad -e \uparrow\downarrow {}^{+e}_{-0.254}$$

$$LRu^{II}NH_2Ph^- \xrightarrow[-NH_2Ph]{+H_2O} LRu^{II}H_2O^-$$

Where L = HEDTA or EDTA

Scheme 1.

$$LRu^{III}NHPhNH_3 \rightleftharpoons LRu^{I}NHPhNH_3^{2-}$$

$$LRu^{I}NHPhNH_3^{2-} \rightarrow LRu^{III}NHPh^{2-} + NH_3$$

$$LRu^{III}NHPh^{2-} + H^+ \rightarrow LRu^{III}NH_2Ph^-$$

$$LRu^{III}NH_2Ph^- \rightarrow LRu^{III}NHPhNH_3 + NH_2Ph$$

$$LRu^{III}NH_2Ph^- + H_2O \rightarrow LRu^{III}H_2O^- + NH_2Ph$$

$$LRu^{III}H_2O^- + N_2H_4Ph^+ \rightarrow LRu^{III}NHPhNH_3 + H_2O$$

Scheme 2.

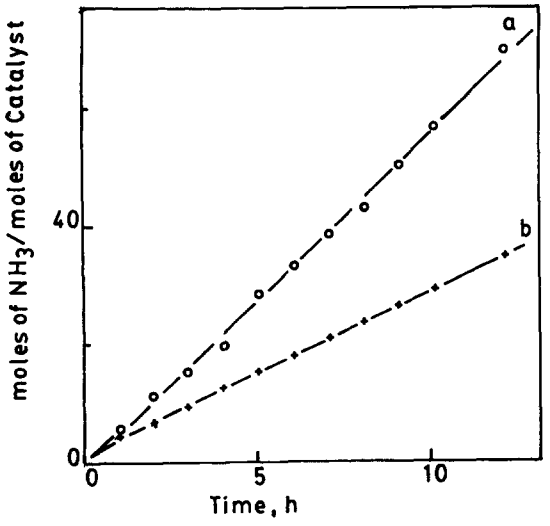


Fig. 7. Plot of moles of NH_3 per mole of $[Ru^{III}(HEDTA)(H_2O)]$ *vs* electrolysis time (h) at the initial pH (a) 2.8, (b) 1.9.

compounds. Apparently, these intrinsic properties of the metal were not altered by a change in the N—N bond order from 1.0 to 2.5, or phenyl ring substitution on the coordinated N of the $N_2H_5^+$ ion. However, the turnover rate of formation of NH_3 with N_2H_4PhCl was found to be less than the expected value (of one-half) of the turnover rate obtained with $N_2H_5HSO_4$ [12]. This slight deviation could be attributed to the combined effects of hydrophobic nature and steric and electrostatic repulsions in the reduced complexes, caused by the phenyl ring present on the bound NHPh group.

Acknowledgements—We thank the Department of Science and Technology, New Delhi for its financial support (No. SP/S1/F-12/95) and Prof. P. Natarajan, Director, CSMCRI for his constant encouragement throughout this work.

REFERENCES

1. M. M. Taqui Khan, M. R. H. Siddiqui, A. Hussain and M. A. Moiz, *Inorg. Chem.* 1986, **25,** 2765.
2. M. M. Taqui Khan, R. S. Shukla and A. P. Rao, *Inorg. Chem.* 1989, **28,** 452.
3. M. M. Taqui Khan, A. Hussain, G. Ramachandraiah and M. A. Moiz, *Inorg. Chem.* 1986, **25,** 3023.
4. M. M. Taqui Khan, D. Chatterjee, R. R. Marchant, P. Paul, S. H. R. Abdi, D. Srinivas, M. A. Moiz, M. M. Bhadbhade and K. V. Subramanian, *Inorg. Chem.* 1992, **31,** 2711.
5. D. Chatterjee, H. C. Bajaj and A. Das, *Inorg. Chem.* 1993, **32,** 4049.
6. D. Chatterjee, H. C. Bajaj and A. Das, *Inorg. Chim. Acta* 1994, **224,** 189.
7. D. Chatterjee, and H. C. Bajaj, *J. Chem. Soc., Dalton Trans.* 1995, 2497.
8. J. Chatt, J. R. Dilworth and R. L. Richards, *Chem. Rev.* 1978, **78,** 589.
9. B. K. Burgess, *Chem. Rev.* 1990, **90,** 1377.
10. M. Hidai and Y. Mizobe, *Chem. Rev.* 1995, **95,** 1115.
11. T. A. Bazhenova and A. E. Shilov, *Coord. Chem. Rev.* 1995, **144,** 69.
12. G. Ramachandraiah, *J. Am. Chem. Soc.* 1994, **116,** 6733.
13. G. Ramachandraiah, *Proc. Indian Acad. Sci. (Chem. Sci.)* 1995, **107,** 385. (Note: The potential axes of Figs 1 and 2 in this reference were wrongly marked. −0.1 V is to be added to read them correctly. Accordingly, the values in the text should be changed.)
14. M. M. Taqui Khan, A. Hussain, G. Ramachandraiah and M. A. Moiz, *Inorg. Chem.* 1986, **25,** 3023.
15. M. M. Taqui Khan, A. Kumar and Z. Shirin, *J. Chem. Res.* 1986, **5,** 1003.
16. T. Matsubara and C. Creutz, *Inorg. Chem.* 1979, **18,** 1956.
17. V. N. Alexeyev, *Qualitative Chemical Semimicro Analysis* (Edited by P. K. Agasyan), p. 475. Mir Publishers, Moscow (1975).
18. H. C. Bajaj and R. van Eldik, *Inorg. Chem.* 1988, **27,** 4052.

Pergamon

PII: S0277-5387(96)00182-9

Polyhedron Vol. 16, No. 7, pp. 1241–1245, 1997
Copyright © 1997 Elsevier Science Ltd
Printed in Great Britain. All rights reserved
0277-5387/97 $17.00+0.00

Synthesis and characterization of 2,4-disubstituted-5-imino-Δ^2-1,3,4-telluradiazolines and 1,4-dihydro-2-imino-3-telluraquinolines

Ali Z. Al-Rubaie* and Shakeer A. N. Al-Jadaan

Department of Chemistry, College of Science, University of Basrah, Basrah, Iraq

(Received 9 January 1996; accepted 9 April 1996)

Abstract—2,4-Disubstituted-5-imino-Δ^2-1,3,4-telluradiazolines were isolated together with α-tellurocyanatobenzaldehyde arylhydrazones when potassium tellurocyanate was reacted with hydrazidoyl bromides in DMSO solution. *N*-Acetyl derivatives were prepared by reaction of 5-imino-Δ^2-1,3,4-telluradiazolines with acetic anhydride. Reaction of 2-amino-benzyl iodide with KTeCN afforded the novel heterocyclic tellurium compound 1,4-dihydro-2-imino-3-telluraquinoline, which, on treatment with acetic anhydride, gave the acetyl derivative. The acetyl derivative was hydrolysed with HCl/H_2O to afford 1-*N*-acetyl-4-hydro-3-telluraquinolin-2-one. Copyright © 1997 Elsevier Science Ltd

Keywords: potassium tellurocyanate; telluradiazolines; telluraquinolines; hydrazidoyl halides; 2-aminobenzyl tellurocyanate; tellurides.

Potassium selenocyanate has been the object of much more intensive study by organic chemists than its less stable tellurium counterpart [1,2]. As is well known, the reaction of hydrazidoyl halides with KSeCN in ethanol gives the corresponding 5-imino-Δ^2-1,3,4-selenadiazolines [3,4], which are easily hydrolysed to their corresponding 5-oxo compounds [4]. The corresponding reaction of potassium tellurocyanate with hydrazidoyl halides has not previously been reported. It was, therefore, of interest for us to see whether hydrazidoyl bromide will undergo a similar cyclization reaction with potassium tellurocyanate. Reaction of 2-aminobenzyl iodide with potassium tellurocyanate is also reported.

EXPERIMENTAL

(*a*) *Physical measurements*

Melting points were determined on a Gallenkamp apparatus and are uncorrected. Infrared (KBr) spectra were recorded in the range 4000–200 cm^{-1} on a Pye–Unicam SP3-300s spectrophotometer. Elemental analyses were performed on an EA-1108 Carlo–Ebra elemental analyser. ^1H NMR spectra were recorded in $CDCl_3$ solution containing TMS as internal standard using a Jeol EX-90 instrument.

(*b*) *Synthesis*

All reactions were carried out under argon, α-bromobenzaldehyde phenylhydrazone and α-bromo-4-nitrobenzaldehyde-2,4-dinitrophenylhydrazone were prepared by mixing equimolar amounts of arylhydrazine and aldehyde in ethanol/acetic acid solution as previously described [5].

α-Tellurocyanatobenzaldehyde phenylhydrazone (**1**) *and* 2,4-*diphenyl*-5-*imino*-Δ^2-1,3,4-*telluradiazoline* (**2**)

A solution of potassium tellurocyanate was readily prepared by stirring together 5 mmol each of powdered tellurium and dry powdered KCN in dry DMSO (15 cm^3), at 100°C for 1 h under argon according to Spencer *et al.* [6]. To the resulting pale yellow solution, cooled to room temperature and diluted with dry

* Author to whom all correspondence should be addressed.

DMSO (15 cm^3), was added dropwise with stirring a solution of α-bromobenzaldehyde phenylhydrazone (1.4 g, 5 mmol) in dry DMSO (15 cm^3). The reaction mixture was stirred at room temperature for 4 h and filtered. The filtrate was poured into distilled water (200 cm^3), which was then extracted with dichloromethane (3×30 cm^3). The combined extracts were dried ($MgSO_4$) and then evaporated under reduced pressure to yield a red–brown oil consisting of two components according to TLC. Column chromatography [silica; toluene/methanol (19 : 1)] gave compound **1** as a red crystalline solid and compound **2** as a red–brown crystalline solid. Recrystallization of **1** from CCl_4 gave red crystals, m.p. 136–137°C. Recrystallization of **2** from carbon tetrachloride gave reddish brown crystals m.p. 169–170°C.

α-Tellurocyanato-4-nitrobenzaldehyde-2′,4′-dinitrophenylhydrazone (**3**) *and 5-imino-2-(4′-nitrophenyl)-4-(2′,4′-dinitrophenyl)-Δ²-1,3,4-telluradiazoline* (**4**)

The reaction of KTeCN with α-bromo-4-nitrobenzaldehyde-2′,4′-dinitrophenylhydrazone in dry DMSO was carried out as described in the above method. The resulting solution was poured into distilled water (200 cm^3), extracted with chloroform (3×50 cm^3) and dried ($MgSO_4$). The extracts were evaporated under reduced pressure to afford a brown precipitate consisting of two components. Extraction of the brown solid with THF using a Soxhlet extractor was continuous. The extract was evaporated to give an orange–yellow precipitate. Recrystallization from toluene/ethanol (9 : 1) gave orange–yellow crystals of α-tellurocyanto-4-nitrobenzaldehyde-2′,4′-dinitrophenylhydrazone.

The remaining residue was recrystallized from ethanol/THF (4 : 1) and gave a yellow precipitate, m.p. 290–292°C.

5-N-Acetylimino-2,4-diphenyl-Δ²-1,3,4-telluradiazoline (**5**) *and 5-N-acetylimino-2-(4′-nitrophenyl)-4-(2′,4-dinitrophenyl)-Δ²-1,3,4-telluradiazoline* (**6**)

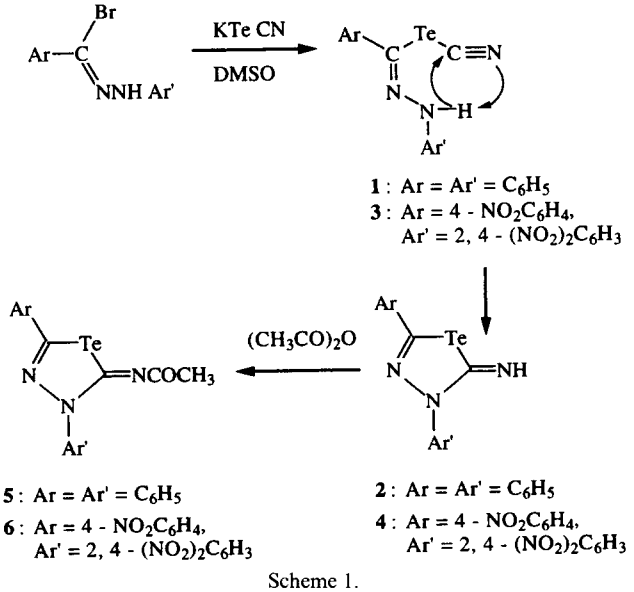
The corresponding 5-imino-1,3,4-telluradiazoline (11 mmol) was refluxed in acetic anhydride (20 cm^3) for 20 min. The resulting solution was cooled to room temperature, poured into iced distilled water, stirred for 30 min and then extracted with chloroform (3×25 cm^3). The combined extracts were washed with aqueous sodium bicarbonate and water, dried ($MgSO_4$) and evaporated under reduced pressure to yield a red–brown solid. Recrystallization from ethanol gave red crystals. Compound **5**, m.p. 75–76°C. Compound **6**, m.p. 272°C.

1,4-Dihydro-2-imino-3-telluraquinoline (**7**)

To 10 mmol of KTeCN in dry DMSO[6] was added 2-aminobenzyl iodide (2.32 g, 10 mmol) in 15 cm^3 of dry DMSO over 15 min. The yellow solution was stirred for 2 h. The resulting solution was filtered, poured into water (500 cm^3) and left overnight. A dark brown solid was formed, filtered and recrystallized from ethanol/hexane to give orange crystals, m.p. 75–77°C.

1-N-Acetyl-4-hydro-2-imino-3-telluraquinoline (**8**)

Compound **6** (1.04 g, 4 mmol) was refluxed in acetic anhydride (20 cm^3) for 20 min. The mixture was cooled to room temperature and then poured onto

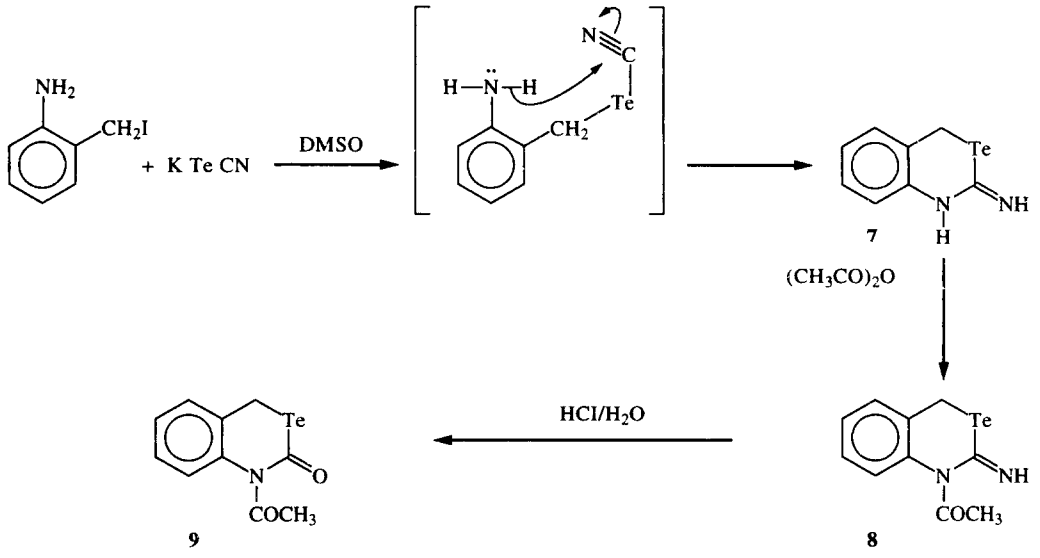


Scheme 1.

Table 1. Physical properties, analytical and IR data for compounds **1**–**9**

Compound	Colour	M.p.(°C)	Yield (%)	Analysis[a](%)			IR (cm^{-1})				
				C	H	N	ν(NH)	ν(TeCN)	ν(C—O)	ν(C—N)	ν(Te—C)
1	Red	136–137	28	48.1 (48.2)	3.1 (3.2)	11.9 (12.0)	3300m	2240s		1270m	540w 495m
2	Red–brown	169–170	56	48.1 (48.2)	3.0 (3.2)	11.8 (12.0)	3200mb			1265m	520w, 485w
3	Orange–yellow	148–150	18	39.0 (38.7)	3.2 (3.2)	17.2 (15.1)	3350w			1260m	535w, 480w
4	Yellow	290–292	62	34.5 (34.7)	1.6 (1.7)	17.1 (17.4)	3280m br	2230m		1270m	510w, 470w
5	Brown	76–77	87	48.9 (49.2)	3.3 (3.3)	10.5 (10.7)			1690s	1260m	520w, 480w
6	Red	272 (decomp.)	71	36.4 (36.5)	1.8 (1.9)	15.7 (16.0)			1720s	1270m	
7	Orange	75–77	56	36.8 (37.0)	2.9 (3.1)	10.6 (10.8)	3350m +3250m			1260s	535w, 480w
8	Red	90–92	60	39.5 (39.8)	3.1 (3.3)	8.9 (9.3)	3330m		1720s	1280s	530w, 460w
9	Yellow	131–133	84	39.4 (39.7)	2.9 (3.0)	4.5 (4.6)			1660s +1715s	1300s	530w, 470w

[a]Calculated values are in parentheses.



Scheme 2.

crushed ice. The orange precipitate was collected and washed several times with water and finally with ethanol. Recrystallization from ethanol gave orange crystals, m.p. 90–92°C.

1-*N*-*Acetyl*-4-*hydro*-2-*imino*-3-*telluraquinolin*-2-*one* (**9**)

A solution of **7** (0.7 g, 2.3 mmol) in 50 cm^3 of distilled water containing 15 cm^3 of 1 N HCl was refluxed for 2 h, then cooled to room temperature. The acidic solution was neutralized with NaOH solution, extracted with CH_2Cl_2 (3×25 cm^3), dried ($MgSO_4$), filtered and evaporated. Recrystallization from petroleum ether (60/80) gave yellow crystals, m.p. 131–133°C.

RESULTS AND DISCUSSION

Many selenadiazolines have been prepared by the action of sodium or potassium selenocyanate on hydrazidoyl halides [4]. It was therefore, of interest to determine whether or not the same reaction was operative in organic tellurocyanate chemistry. it was found that the reaction of KTeCN with hydrazidoyl bromides under argon gave a mixture of products from which a good yield of the desired telluradiazolines (**2** and **4** in 64 and 71% yields, respectively), together with a 29 and 18% yield of the corresponding organotellurocyanate (i.e. **1** and **3**, respectively) were obtained (Scheme 1). Reaction of **2** and **4** with acetic anhydride gave **5** and **6**, respectively, in good yields (Scheme 1).

The methods used for the preparation of all these new compounds are shown in Scheme 1. Yields, melting points, colour and C, H, N analytical data for the compounds are shown in Table 1. All compounds gave satisfactory elemental analyses. Compound **3** is exceptional and its elemental analysis is more in agreement with the presence of a residual diethyl ether molecule.

Distinction of the two products (**1** and **2**) and (**3** and **4**) by IR spectroscopy was relatively easy. Compounds **1** and **3** show strong bands at 2240 and 2230 cm^{-1}, respectively, which are attributed to ν(Te—CN) [7]. The bands assigned to ν(Te—CN) were absent from the spectra of **2** and **4**, Table 1.

In general, the IR spectra of compounds **1**–**6** gave characteristic bands. Compounds **2** and **4** showed bands assignable to the imino group at 3200 and 3280 cm^{-1}, respectively. The presence of an acetyl group in **5** and **6** was also confirmed from their IR data, (Table 1).

We expected that the reaction of 2-aminobenzyl iodide with potassium tellurocyanate would lead to the corresponding 2-aminobenzyl tellurocyanate, but instead we obtained the novel heterocycle **7**. The reaction may have first afforded the organic tellurocyanate intermediate, which then cyclized spontaneously to the new cyclic telluride (**7**) (Scheme 2). Treatment of **7** with acetic anhydride yielded the corresponding *N*-acetyl derivative (**8**) in 60% yield, which was subsequently hydrolysed by HCl/H_2O to give **9** in 84% yield (Scheme 2). This supports the acetylation of the amino group rather than the imino group.

The important IR frequencies are listed in Table 1. The spectrum of **9** reveals the appearance of two strong bands, one at 1660 cm^{-1} and another at 1715 cm^{-1} which are attributed to the stretching vibrations

of the ring and side chain carbonyl groups, respectively. The spectrum of **8** shows only one ν(C=O) at 1720 cm^{-1} as a strong band.

The ν(Te—$C_{aliphatic}$) vibrations in the IR spectra for all the compounds (**1**–**9**) are consistent with those reported previously for alkyltellurium compounds [8,9].

^{1}H NMR spectra for compounds **1**, **2** and **3** were measured in $CDCl_3$. These compounds gave complex aryl proton signals at *ca* δ 6.96–8.00 and a broad signal due to NH protons at δ 6.30 and 9.21 for **1** and **2**, respectively. The spectrum of **3** revealed an acetyl signal at δ 2.20.

In conclusion, a new and convenient one-pot synthesis of new cyclic tellurides containing nitrogen, using potassium tellurocyanate as a tellurating agent, has been described.

REFERENCES

1. A. Toshimitsu and S. Uemura, in *The Chemistry of Organic Selenium and Tellurium Compounds* (edited by S. Patai), Vol. 2, p. 541, John Wiley, New York (1987).
2. See, for example, K. J. Irgolic, *J. Organomet. Chem.*, 1978, **158**, 235; S. Ogawa, S. Ohara, K. Kawai and R. Sato, *Heterocycles*, 1994 **38**, 491.
3. R. Fusco and C. Musante, *Gazz. Chim. Ital.*, 1938, **68**, 665.
4. M. H. Hassaneen, A. Shetta and A. S. Shawali, *J. Heterocyc. Chem.*, 1980, **17**, 1185.
5. A. S. Shawali and H. M. Hassaneen, *Tetrahedron*, 1973, **29**, 121; A. S. Shawali and A. O. Abdelhamid, *Bull. Chem. Soc. Jpn.*, 1976, **49**, 321.
6. H. K. Spencer, M. V. Lakshmikantham and M. P. Cava, *J. Am. Chem. Soc.*, 1977, **99**, 1470.
7. S. J. Falcon and M. P. Cava, *J. Org. Chem.*, 1980, **45**, 1044; K. Maartmann, K. A. Sanderud and J. Songstad, *Acta Chem. Scand., Ser. A*, 1981, **35**, 151; L. Engman, *J. Org. Chem.*, 1983, **48**, 2920.
8. A. Z. Al-Rubaie and A. F. Hassan, *Polyhedron*, 1992, **11**, 3155.
9. A. Z. Al-Rubaie, S. Uemura and H. Masuda, *J. Organomet. Chem.*, 1991, **410**, 309.

Pergamon

PII: S0277-5387(96)00173-8

Polyhedron Vol. 16, No. 7, pp. 1247–1253, 1997
Copyright © 1997 Elsevier Science Ltd
Printed in Great Britain. All rights reserved
0277-5387/97 $17.00+0.00

Synthesis and characterization of oxovanadium(IV) and dichlorovanadium(IV) complexes of biologically active 4-aminoantipyrine derivatives

Ali El-Dissouky,* Aziza K. Shehata and Ghada El-Mahdey

Chemistry Department, Faculties of Science and Education, Alexandria University, Alexandria, Egypt

(Received 18 September 1995; accepted 4 April 1996)

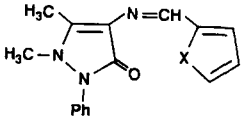
Abstract—A new series of oxovanadyl complexes of the Schiff base ligands 4-(2-pyrrolyl methylideneamino)antipyrine (PyAAP), 4-(2-thienylmethylideneamino)antipyrine (TAAP), 4-furfurylideneaminoantipyrine (FAAP) and 4-(2-hydroxybenzylideneamino)antipyrine (SAAP), have been synthesized and characterized by different physical techniques. The spectral and magnetic data indicate a distorted square pyramidal structure for all complexes. The selective deoxygenation of the oxovanadyl complexes $[(PyAAP\text{-}H)_2(VO)_2SO_4]$ and $[(SAAP\text{-}H)_2VO]$, which gave a good yield of the corresponding dichloro compounds $[L_2VCl_2]$, L = PyAAP-H or SAAP-H, is made by using different deoxygenating agents in different solvents and at various temperatures. The purity and the percentage yield of the products are found to be solvent, temperature and deoxygenating agent dependent. Spectral and magnetic studies are used to elucidate the structure of the dichloro derivatives. The solvent effects upon the electronic spectra of the oxovanadyl complexes and the corresponding dichloro derivatives are ascertained. Copyright © 1997 Elsevier Science Ltd

Keywords: antipyrine; vanadium(IV); spectra; synthesis; magnetism; chlorination.

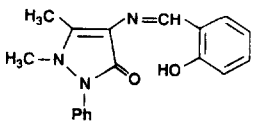
It is becoming increasingly apparent that the chemistry of vanadium is of great importance to a wide variety of biological and industrial systems. Recently, it was found that there is a series of nitrogenase metalloenzymes which have vanadium at the active site [1–8]. In these enzymes vanadium appears to shuttle between V^{2+} and V^{4+} and is possibly bound to an iron–sulfur cluster, as it is difficult for direct linking of iron–sulfur clusters [9] and V^{4+}. Furthermore, the role of vanadium in the biosphere is very important. It has been found that mammals require vanadium at the nano- to pico- molar level, and several lower organisms have a vanadium requirement at a much higher level [3,10].

Vanadium is also important in the fuel industry [9–11]. Vanadium occurs naturally and can be in high concentrations in heavier crude oil. It affects the industry because its necessary removal poisons the heterogeneous catalysis used in processing [12–14]. The intermediate species in the transformation of the naturally occurring VO^{2+} complexes to vanadium sulfide on the upgrading catalyst surface are not well characterized. Some evidence suggests that VO^{2+} is deoxygenated to V(IV) [13,15]. Vanadium compounds have also been used to generate slurry-type catalysts to upgrade heavy oils and assist in coal liquefaction. Clearly the activation of the V=O bond is a critical part in the fuel industry.

Due to the importance of vanadium compounds, we aimed to prepare and characterize some biologically active vanadyl complexes of antipyrine derivatives (I) followed by the deoxygenation of the isolated complexes to form dichloro derivatives.



X = NH, PYAAP
S, TAAP
O, FAAP



SAAP

* Author to whom correspondence should be addressed.

EXPERIMENTAL

Synthesis of the organic ligands

The organic ligands were prepared according to the following method: a solution of the corresponding aldehyde (1.0 or 1.1 g, 0.01 mol of furan-2-aldehyde or thiophene-2-aldehyde, respectively) in EtOH (20 cm^3) was added to a solution of 4-aminoantipyrine (2.1 g, 0.01 mol) in 50 cm^3 of the same solvent. The reaction mixture was refluxed on a water bath for 1–2 h. Upon cooling to room temperature the solid formed in each case was isolated by filtration and recrystallized from EtOH and dried *in vacuo* over P_4O_{10}.

Synthesis of oxovanadyl complexes

All vanadyl complexes of the 4-aminoantipyrine Schiff bases were prepared by the general method; namely, the salt $VOSO_4 \cdot 2H_2O$ (2.0 g, 0.01 mol) was dissolved in water (15 cm^3) and the solution was added to a warm, stirred solution of the corresponding organic compound (6.2, 6.5, 6.3 or 6.8 g; 0.022 mol of PyAAP, TAAP, FAAP or SAAP, respectively) in ethanol (50 cm^3). An aqueous solution (15–20 cm^3) of NaOAc (0.3 M solution) was added and the suspension was stirred for 2 h. The corresponding crystalline product was filtered off, washed with water, EtOH, diethyl ether and dried *in vacuo* over P_4O_{10}.

Synthesis of dichlorovanadium complexes, $[(PyAAP\text{-}H)_2VCl_2]$ *and* $[(SAAP\text{-}H)_2VCl_2]$

The synthesis was carried out under dry, purified dinitrogen gas. Different deoxygenating agents such as $SOCl_2$, PCl_5 or CH_3COCl and different solvents were used. The following procedure was applied, $[(PyAAP\text{-}H)_2(VO)_2SO_4]$ (2.0 g, 0.025 mol) or $[(SAAP\text{-}H)_2VO]$, (1.8 g, 0.0025 mol) was dissolved in 50 cm^3 of the appropriate solvent (toluene, CH_2Cl_2, bezene or dioxene). In all cases a dark green or dark brown solution was obtained. The solution was degassed and the deoxygenating agent (1.0, 1.8 or 0.6 g of $SOCl_2$, PCl_5 or CH_3COCl, respectively; 0.80 mol) was added while stirring at room temperature. In some cases a boiling condition was utilized. The reaction mixture was stirred at room temperature overnight and then layered with the appropriate solvent and placed in a freezer. The crystalline product in each case was filtered off and dried. Recrystallization from CH_2Cl_2 or $C_2H_4Cl_2$/hexane mixture lead to pure materials as determined from their physical measurements.

Elemental analysis

Carbon, hydrogen and nitrogen contents in each sample were estimated at the Microanalysis Unit, Cairo University. Vanadium content was determined by igniting a suitable accurate weight in silica crucible to a constant weight. The product was VO_2, in which the vanadium content was determined. Chlorine and sulfur contents were determined argentometrically and gravimetrically, respectively [16].

Physical measurements

Molecular weight for each sample was determined by the method of depression of freezing point. The other physical measurements and the elemental analyses were carried out as previously reported [16].

RESULTS AND DISCUSSION

The oxovanadyl complexes were found to be air stable, soluble in most common organic solvents, but insoluble in water. The formulation of the complexes was based on the elemental analysis, molecular weight determination and the molar conductivity values (Table 1).

The selective deoxygenation of the two complexes $[(PyAAP\text{-}H)_2(VO)_2SO_4]$ and $[(SAAP\text{-}H)_2VO]$ which gave pure and high percentage yields of the corresponding dichloro complex $[(L_2VCl_2]$, L = PyAAP-H or SAAP-H, was made by using $SOCl_2$, PCl_5 and CH_3COCl. It was found that both oxo-complexes react to a different extent with the three different deoxygenating agents. Furthermore, the purity of the reaction product and percentage yield were found to be solvent and temperature dependent (Table 2).

Under refluxing conditions, $SOCl_2$ reacts with the oxo-vanadyl complexes in dry benzene producing a pure and good yield of $[L_2VCl_2]$. This reaction may proceed according to eq. (1).

$$[L_2VO] + SOCl_2 \xrightarrow{\text{dry benzene}} [L_2VCl \cdot SO_2Cl] \rightarrow [L_2VCl_2] + SO_2 \quad (1)$$

In 1,4-dioxan, PCl_5 gives the best dichloro complexes at room temperature according to eq. (2).

$$2PCl_5 \rightleftharpoons PCl_4 \cdot PCl_6 + [L_2VO] \xrightarrow{\text{1,4 dioxan}} [LVCl \cdot ClPOCl_3] \rightarrow [LVCl_2] + POCl_3 \quad (2)$$

Acetyl chloride was found to be the best deoxygenating agent in toluene at room temperature, since it leads to the formation, in high yield, of dichloro derivatives. The reaction mechanism may proceed by electrophilic attack of the CH_3COCl on vanadyl oxygen, as shown in eq. (3).

$$[L_2VO] + 3CH_3COCl \xrightarrow{\text{toluene}} [L_2VCl_2] + (CH_3COO)_2O + CH_3{-}C_6H_4{-}COCH_3 \quad (3)$$

In all cases, 50% of the deoxygenating agent has been employed to minimize the extent of hydrolysis of $SOCl_2$, PCl_5 or CH_3COCl. This is in addition to the use of dry solvents. The above reactions would suggest

Table 1. Analytical data for the vanadyl complexes and some physical properties

Compound[a]	Colour	Λ_M^b	μ_{eff}^c	M.W. Found (Calc.)	% Found (% Calc.) C	H	N	V	X
$[L_2^1(VO)_2SO_4]$	pale green	1.30	1.61	796 (788)	48.5 (48.7)	4.0 (3.8)	14.0 (14.2)	13.1 (12.9)	4.3 (4.1)
$[L_2^1VCl_2]$	blue green	2.90	1.76	680 (680)	56.6 (56.5)	4.6 (4.4)	16.5 (16.5)	7.8 (7.5)	16.6 (10.4)
$[L_2^2VO]SO_4$	yellowish green	96.40	1.76	760 (757)	50.4 (50.7)	3.9 (4.0)	11.1 (11.1)	6.8 (6.7)	12.5 (12.7)
$[L_2^3VO]SO_4$	pale yellow	87.55	1.78	720 (725)	52.7 (53.0)	3.9 (4.1)	11.6 (11.6)	7.3 (7.0)	4.5 (4.4)
$[L_2^4VO]$	green	1.90	1.73	681 (679)	63.4 (63.6)	4.7 (4.7)	12.4 (12.4)	7.8 (7.5)	
$[L_2^4VCl_2]$	blue	2.05	1.75	736 (734)	58.8 (58.9)	4.5 (4.4)	11.3 (11.4)	7.2 (6.9)	10.0 (9.7)

[a] L^1 = PyAAP-H, L^2 = SAAP-H, L^3 = TAAP, L^4 = FAAP.
[b] Molar conductivity values of 10^{-3} M solutions at 25 ± 1 °C.
[c] Effective magnetic moment (B.M.) at room temperature.

Table 2. Products from the reaction of vanadyl complexes with the different deoxygenating agents as shown from the spectroscopic studies

Starting complex	Deoxygenating agent	Solvent	Temperature	Purified yield%[a] (1)	(2)
	$SOCl_2$	CH_2Cl_2	R.T.	28	22
		toluene	boiling	31	38
		benzene	boiling	38	36
		1,4-dioxane	R.T.	30	28
$[L_2^1(VO)_2SO_4]$	PCl_5	toluene	boiling	25	34
or		CH_2Cl_2	R.T.	34	40
$[L_2^4VO]$		1,4-dioxane	R.T.	36	42
	CH_3COCl	1,4-dioxane	R.T.	41	48
		CH_2Cl_2	R.T.	48	48
		benzene	boiling	52	46
		toluene	R.T.	63	70
		toluene	boiling	56	49

[a] (1) L^1 = PyAAP-H. (2) L^4 = SAAP-H.

the formation of a *cis* isomer as previously reported [17]. It was found that *cis/trans* isomerization is rapid, allowing for the formulation of the observed *trans* isomer [17]. Table 2 summarizes the products from the reaction of the vanadyl complexes with the different deoxygenating agents, as shown from the spectroscopic studies.

Vibrational spectra

Table 3 lists the most important and characteristic bands of the IR spectra of oxovanadyl and the dichloro derivatives. The absence of bands at 968 and 986 cm^{-1} characteristic of V=O in $[(PyAAP\text{-}H)_2(VO)_2SO_4]$ and $[(SAAP\text{-}H)_2VO]$, respectively, indicates the conversion to the dichloro complexes. This observation is taken as a good parameter for the completeness of the deoxygenation process. The low value of $\nu(V{=}O)$ for $[(PyAAP\text{-}H)_2(VO)_2SO_4]$ may be taken as evidence for the polymeric nature of this complex as shown from its IR spectrum. Its deoxygenation may proceed according to eq. (4)

$$[(PyAAP\text{-}H)_2(VO)_2SO_4) \rightleftharpoons [(PyAAP\text{-}H)_2VO] + VOSO_4$$

$$[(PyAAP\text{-}H)_2VO] + \begin{matrix}SOCl\\ \text{or } PCl_5\\ \text{or } Ch_3COCl\end{matrix} \rightarrow [(PyAAP\text{-}H)_2VCl_2] + \begin{matrix}SO_2\\ \text{or } POCl_3\\ \text{or } (CH_3CO_2)O\end{matrix} \quad (4)$$

Table 3. Infrared spectral data (ν cm^{-1}) for the vanadyl complexes

Compound[a]	ν(C=O)	ν(C=N)	ν(V=O)	ν(V—N)	ν(V=O)	ν(V—Cl)
HL^1	1659s	1600				
L^2	1942	1596				
L^3	1637	1603				
HL^4	1650	1592				
$[L^1_2(VO)_2SO_4]$	1639s	1589m	968vs	463m	360	
				334m		
$[L^1_2VCl_2]$	1660s	1579m	—	458m	—	364
				436m		
		1572m				
$[L^4_2VO]$	1649s		986s	448m	338m	
		1566s				
$[L^4_2VCl_2]$	1652s	1570m	—	432m	342	356
		1575s				
$[L^3_2VO]SO_4$	1621m		976s	449m	346m	
		1560s				
		1590m				
$[L^2_2VO]SO_4$	1616m		988s	468m	356m	
		1582s				

[a] L^1 = PyAAP-H, L^2 = FAAP, L^3 = TAAP, L^4 = SAAP-H.

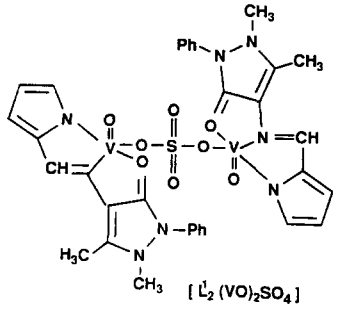
The ν(C=O) mode in the parent Schiff base, except SAAP, shifts to lower wavenumbers by *ca* 20 cm^{-1} in the case of their oxovanadyl complexes, indicating the bond of the amide oxygen to vanadium, but not in the case of complex [(SAAP-H)$_2$VO]. The band in the range 1613–1590 cm^{-1} in the free organic compounds due to ν(C=N) is shifted to 1590–1572 cm^{-1} upon complexation. This observation suggests that the C=N bond is weakened due to coordination of the azomethine-N to vanadium. The splitting of this band in the investigated complexes, except [(PyAAP-H)$_2$(VO)$_2$SO$_4$], suggests that the two azomethine groups are distorted below and above the horizontal plane. The broad band at 3434 cm^{-1} with a band width of 1660 cm^{-1} in the spectrum of SAAP, is assigned to hydrogen bonded OH. Furthermore, the existence of a broad weak band at 1915 cm^{-1} can be taken as evidence for the presence of intramolecular hydrogen bonding of the type O—H···N. This was also supported by the appearance of the ν(C—O) phenolic band at 1267 cm^{-1}. Upon complexation, the bands at 3434 and 1915 cm^{-1} disappeared and that at 1267 cm^{-1} was shifted to 1305 cm^{-1}, indicating the bonding of the ionized phenolic oxygen to vanadium.

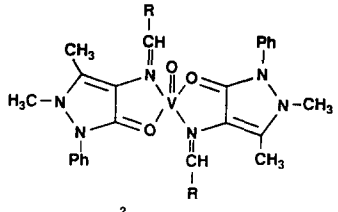
The spectrum of (PyAAP) shows a broad band at 2964–3156 cm^{-1} due to the different vibrational modes of –NH– of the pyrrole ring, and is absent in [(PyAAP-H)$_2$(VO)$_2$SO$_4$] indicating its deprotonation upon complexation. The spectra of FAAP and SAAP display bands at 1505 and 1332 cm^{-1} due to C—O—C and C—S—C, respectively. These bands were found to be largely unaffected upon complexation, indicating the non-bonding nature of the oxygen and sulphur in the heterocyclic rings.

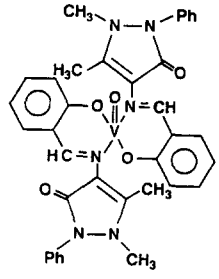
The far-IR spectra for all complexes except [(PyAAP-H)$_2$VCl$_2$] display a band at 338–360 cm^{-1} due to ν(V—O). The spectrum of [(PyAAP-H)$_2$VCl$_2$] exhibits a band at 1660 cm^{-1} due to ν(C=O) indicating that the amide oxygen is not bonded to vanadium. The band in the range 468–432 cm^{-1} is assigned to ν(V—N) of the azomethine group. In addition, the spectra of [(PyAAP-H)$_2$(VO)$_2$SO$_4$] and [(PyAAP-H)$_2$VCl$_2$] exhibit another band at 443 and 436 cm^{-1} assignable to ν(V—N)$_{pyrrole}$. The dichloro complexes exhibit bands at 303 and 309 cm^{-1} due to ν(V—Cl) in [(PyAAP-H)$_2$VCl$_2$] and [(SAAP-H)$_2$VCl$_2$], respectively.

The diagnostic IR band frequencies of the sulphate anions indicate its ionic nature in [(FAAP)$_2$VO]SO$_4$ and [(TAAP)$_2$VO]SO$_4$ and act as a bridging group in the case of [(PyAAP-H)$_2$(VO)$_2$SO$_4$] [18].

It appears, therefore, that PyAAP behaves as a monobasic tridentate ligand in [(PyAAP-H)$_2$(VO)$_2$SO$_4$] and as a monobasic bidentate ligand in [(PyAAP-H)$_2$VCl$_2$]. In the first complex the vanadyl group is coordinated to PyAAP *via* ketoamide oxygen, azomethine and pyrrole nitrogen atoms. In the second it is coordinated via the azomethine and pyrrole nitrogen atoms. The previously mentioned IR data indicate the bidentate nature of SAAP, through the azomethine nitrogen and the phenolate oxygen atoms. The other and ligands (FAAP and TAAP) appear to be neutral bidentate ligands coordinated to VO *via* the azomethine-N and ketoamide oxygen atoms. Accordingly, the following structures could be assumed.







One can observe that the ν(C=N) for the dichloro complexes appears at a lower wavenumber than that for the starting oxovanadyl complexes. This is consistent with the observations reported for *trans*-dihalo complexes of V(IV) [19–21], and can be rationalized by considering the metal complex symmetry and the nature of the ligands. ESR studies of several V(IV) dihalide complexes [22] revealed that on going from the vanadyl structure (where the metal is somewhat out of the plane of the equatorial ligands) to the *trans* structure (where the metal is in the plane of the ligands) stabilizes both the σ-bonding d_{xy} orbital, slightly, and the π-bonding $d_{x^2-y^2}$ orbital, greatly, due to increased orbital overlap. This, in turn, increases delocalization and effectively reduces the charge on the ligand. This results in a decrease in frequency of the diagnostic ligand bands. Contrary to the *trans* structure, the orbital overlap of the *cis* structure is reduced, because the deviation from the ligand plane is increased. This localizes the charge on the ligand, and results in increasing the frequencies of the diagnostic ligand bands. Furthermore, the geometry of $VCl_2(t\text{-}C_4H_9COCHCO)\text{-}t\text{-}C_4H_9)_2$ is determined by examining the V—Cl bands in the far IR [23]. The reported assignment of 362 cm^{-1} for the *trans* geometry matches ours of 364 and 356 cm^{-1} for $[(PyAAP\text{-}H)_2VCl_2]$ and $[(SAAP\text{-}H)_2VCl_2]$, respectively. The previously mentioned evidence indicates that $[(PyAAP\text{-}H)_2VCl_2]$ and $[(SAAP)_2VCl_2]$ also have a *trans* geometry.

Magnetic and electronic spectral data

The positive spin–orbit coupling [24] (λ) for oxovanadium(IV) complexes exhibits a room temperature magnetic moment very close to the spin only value (1.73 B.M.) [25]. The complexes under investigation, except $[(PyAAP\text{-}H)_2(VO)_2SO_4]$, also exhibit room temperature magnetic moments in the range 1.73–1.78 B.M. corresponding to one unpaired spin. The value for $[(PyAAP\text{-}H)_2(VO)_2SO_4]$ of 1.61 B.M. indicates the possibility of a magnetic exchange interaction between the vanadyl centres through the bridging sulphate group, or possibly some V(V) impurity.

The electronic spectral data of the oxovanadium complexes and the dichloro derivatives, either as solid or solution, are summarized in Table 4. No bands are found at lower energies, and splitting of the low energy band is found, as in the case of $[VO(N\text{-}CH_3)_3]Cl_2$ [26]. The large extinction coefficients for $[(SAAP\text{-}H)_2VO]$, $[(FAAP)_2VO]SO_4$ and $[(TAAP)_2VO]SO_4$ compared with $[(PyAAP\text{-}H)_2(VO)_2SO_4]$ may arise from a greater metal–ligand bond covalency and/or a larger distortion from the C_{2v} symmetry assumed for this type of complex. The bands with smaller molar extinction coefficients can be assigned to *d–d* transitions. The spectrum of $[(PyAAP\text{-}H)_2(VO)_2SO_4]$ exhibits two intense *d–d* transition at about 15,800 and 12,820 cm^{-1}, and a third one of lower intensity at 21,300 cm^{-1}, all of which are on the tail of a charge transfer band. In $CHCl_3$, three well-defined bands are observed, with no great change in position, indicating that no geometrical change in $CHCl_3$ took place. The increase in the intensities of these bands may be attributed to the disproportionation of the polymeric complex $[(PyAAP\text{-}H)_2(VO)_2SO_4]$ [eq. (5)], followed by the interaction of the solvent molecules, organized around $[(PyAAP\text{-}H)_2VO]$, with the dipole of the complex.

$$[(PyAAP\text{-}H)_2(VO)_2SO_4] \rightleftharpoons [(PyAAP\text{-}H)_2VO] + VOSO_4 \quad (5)$$

In the excited Frank–Condon state, the solvent molecules do not have enough time to rearrange in response to the dipole in the excited complex $[(PyAAP\text{-}H)_2VO]$. There is a possible hydrogen bonding formation between the oxovanadyl group and the active hydrogen in $CHCl_3$. This is confirmed from the red shift of the charge transfer band as given in Table 4. The effects of $CHCl_3$ on the band positions in the case of the other oxovanadium complexes (Table 4) are similar to those for $[(PyAAP\text{-}H)_2(VO)_2SO_4]$. The spectral features are consistent with those reported for square pyramidal oxovanadium complexes [27–29].

The spectral bands of all complexes in DMSO exhibit a drastic change in the positions and intensities of the *d–d* transitions as well as the charge transfer bands,

Table 4. Electronic spectral data for the vanadyl(IV) complexes

Compound[a]	Medium	ν(cm^{-1})(ε mol^{-1} l cm^{-1})			
		d–d transitions			C.T.
$[L^1_2(VO)_2SO_4]$	Nujol mull	21,300	15,800	12,800	29,400
	$CHCl_3$	21,500(32)	15,600(52)	12,700(54)	27,900(8200)
	DMSO		17,300(19)	14,200(10)	28,900(10300)
$[L^4_2VO]$	Nujol mull	21,600	16,500		28,400
	$CHCl_3$	20,800(44)	16,300(68)	13,200	27,300(7480)
	DMSO		17,200(18)	12,800(52)	
				13,900(11)	
$[L^3_2VO]SO_4$	Nujol mull	22,400	16,300		27,900
	$CHCl_3$	23,100(26)	16,000(68)	13,300	27,300(7620)
	DMSO		17,000(21)	13,200(36)	36,900(9700)
				14,000(12)	
$[L^2_2VO]SO_4$	Nujol mull	22,300	16,300		28,000
	$CHCl_3$	22,500(40)	16,100(98)	13,200	28,400(8050)
	DMSO		16,900(28)	12,900(60)	27,500(12300)
				13,800(16)	
$[L^1VCl_2]$	Nujol mull		16,400		27,000
	EtOH		16,200(16)	13,200	26,400(4760)
				13,000(45)	
$[L^4VCl_2]$	Nujol mull		17,000		27,100
	EtOH		17,100(19)	13,400	27,000(7000)
				13,100(42)	

[a] L^1 = PyAAP-H, L^2 = FAAP, L^3 = TAAP, L^4 = SAAP-H.

indicating solvent coordination to the sixth coordination site of the oxovanadyl complexes. These spectral features are consistent with those reported for similar compounds [27,28].

The energy level and MO calculations on square pyramidal oxovanadium complexes [28–31] revealed that the vanadium 3*d* orbital populations are $d_{x^2-y^2}$ (b_2) < d_{xz}, d_{yz} (e^*_π) < d_{z^2}(b^*_1) < d_{xy} (a^*_1). This ordering is consistent with the assignment of the $b_2(d_{xy}, d_{xz}) \rightarrow b_1(d_{z^2})$ transition for the lowest energy band (12,660–13,300 cm^{-1}). The band at 15,600–16,350 cm^{-1} is due to the $b_2 \rightarrow e^*_\pi$ transition, while that at 20,600–22,500 cm^{-1} is assigned to the $b_2 \rightarrow a^*_1$ transition. In DMSO, three *d–d* transitions in the range of 13,800–14,200, 16,800–17,480 and 22,030–24,000 cm^{-1} are assigned to $b_2 \rightarrow b^*_1$, $b_2 \rightarrow e^*_\pi$ and $b_2 \rightarrow a_1$ transitions, respectively, characteristic for a distorted octahedral oxovanadium complex [30,31]. On the basis of the data available, it appears that these complexes have a tetragonally distorted structure. The transition due to $b_2 \rightarrow b_1$ (16,800–17,480 cm^{-1}) is taken as 10 Dq. Therefore the ligands could be ordered according to their strengths as: SAAP > PyAAP > FAAP > TAAP. This ordering may be attributed to the effect of the moiety bonded to the azomethine group [C_4H_4O (FAAP); C_4H_5N (PyAAP); C_6H_4O (SAAP); C_4H_4S (TAAP)].

The spectra of $[(PyAAP\text{-}H)_2VCl_2]$ and $[(SAAP\text{-}H)_2VCl_2]$ as Nujol mulls and as $CH_2Cl_2/SOCl_2$ (19 : 1 V/V) solutions are identical and similar to those reported for various dichlorovanadium(IV) complexes in an octrahedral ligand field [32]. The Nujol mull spectra exhibit only two *d–d* transitional bands at 13,200, 13,400 and 16,100, 16,350 cm^{-1} for $[(PyAAP\text{-}H)_2VCl_2]$ and $[(SAAP\text{-}H)_2VCl_2]$, respectively. The third band may be buried under the intense absorption originating at 20,000 cm^{-1}. The two bands could be assigned to $b_2 \rightarrow b^*_1$ and $b_2 \rightarrow e^*_\pi$ transitions, respectively.

REFERENCES

1. R. L. Robson, R. R. Eady, T. H. Richardson, R. W. Miller, M. Hawkins and J. R. Postgate, *Nature* 1986, **322,** 388.
2. J. M. Arber, B. R. Dobson, R. R. Eady, P. Stephens, S. S. Hasanin, C. D. Garner and B. E. Smith, *Nature* 1987, **325,** 372.
3. C. N. Dennis (Ed.), *Vanadium in Biological Systems*, Kluwer Academic Publishers, Dordrecht, The Netherlands (1990).
4. A. Butler and C. J. Carrano, *Coord. Chem. Rev.* 1991, **61,** 109.
5. D. Rehdre, *Angew. Chem., Int. Ed. Engl.* 1991, **30,** 148.
6. J. Dai, S. Akiyama, M. Munakata and M. Mikuriya, *Polyhedron* 1994, **13,** 2495.
7. E. Alberico, G. Micera, D. Sanna and A. Dessi, *Polyhedron* 1994, **13,** 1763.
8. N. Azuma and T. Ozawa, *Inorg. Chim. Acta* 1994, **71,** 227.
9. E. L. Jones, J. G. Reynolds, J. C. Huffman and G. Christou, *Polyhedron* 1991, **10,** 1817.

10. C. A. Root, J. D. Hoeschele, C. R. Cornman, J. W. Kampf and V. L. Pecorare, *Inorg. Chem.* 1993, **32,** 3855.
11. H. S. Soedjak and A. Butler, *Biochemistry* 1990, **29,** 7974.
12. J. F. Branthaver, *ACS Symp. Ser.* 1987, **344,** 188.
13. J. G. Speight, *The Chemistry and Technology of Petroleum Chemical Industries*, Vol. 3, Marcel Dekker, New York (1983).
14. P. W. Tamm, H. F. Harnsberger and A. G. Bridge, *Ind. Eng. Chem. Proc. Res. Dev.* 1981, **20,** 262.
15. P. C. H. Mitchell and J. A. Valers, *Inorg. Chim. Acta* 1983, **71,** 179; *React. Kinet. Catal. Lett.* 1982, **20,** 219.
16. A. El-Dissouky and G. B. Mohammad, *Inorg. Chim. Acta* 1989, **162,** 263.
17. J. G. Reynolds, E. L. Jones, J. C. Huffmann and G. Christou, *Polyhedron* 1993, **12,** 407.
18. K. Nakamoto, *Infrared Spectra of Inorganic Coordination Compounds*, p. 156, John Wiley, New York (1963).
19. T. W. Hambley, C. J. Hawkins and T. A. Kabanos, *Inorg. Chem.* 1987, **26,** 3740.
20. K. Bahzadi and A. J. Thompson, *J. Less Comm. Met.* 1987, **128,** 281.
21. C. J. Hawkins and T. A. Kabanos, *Inorg. Chem.* 1989, **28,** 1084.
22. A. Jezierski and J. B. Raynor, *J. Chem. Soc., Dalton Trans.* 1981, 1.
23. R. B. Von Dreele and R. C. Fay, *J. Am. Chem. Soc.* 1972, **94,** 7935.
24. A. Syamal, *Coord. Chem. Rev.* 1975, **16,** 309.
25. B. N. Figgis, *Introduction to Ligand Fields*, p. 226. Wiley, New York (1966).
26. J. E. Drake, J. Vekris and J. S. Wood, *J. Chem. Soc. (A)* 1968, 1000.
27. S. H. Cheng, S. R. Sheen, C. P. Cheng and C. T. Chang, *Inorg. Chim. Acta* 1990, **21,** 171.
28. H. J. Stoklosa, J. R. Wasson and B. J. McCormick, *Inorg. Chem.* 1974, **13,** 592.
29. C. J. Ballhausen and H. B. Gray, *Inorg. Chem.* 1962, **1,** 111.
30. J. Selbin, *Chem. Rev.* 1965, **65,** 153; *Coord. Chem. Rev.* 1966, **1,** 293. J. Selbin and L. Morpurgo, *J. Inorg. Nucl. Chem.* 1965, **27,** 673.
31. R. Hoffmann, *J. Chem. Phys.* 1962, **39,** 1397.
32. W. E. Farrar, *Am. J. Med.* 1963, **34,** 134.

Pergamon

PII: S0277-5387(96)00409-3

Polyhedron Vol. 16, No. 7, pp. 1255 1257, 1997
Copyright © 1997 Elsevier Science Ltd
Printed in Great Britain. All rights reserved
0277-5387/97 $17.00+0.00

COMMUNICATION

Synthesis and structure of a monomeric magnesium phenylselenolate complex [Tp$^{p\text{-Tol}}$]MgSePh supported by tris (3-p-tolylpyrazolyl)hydroborato ligation

Prasenjit Ghosh and Gerard Parkin*

Department of Chemistry, Columbia University, New York, NY 10027, USA

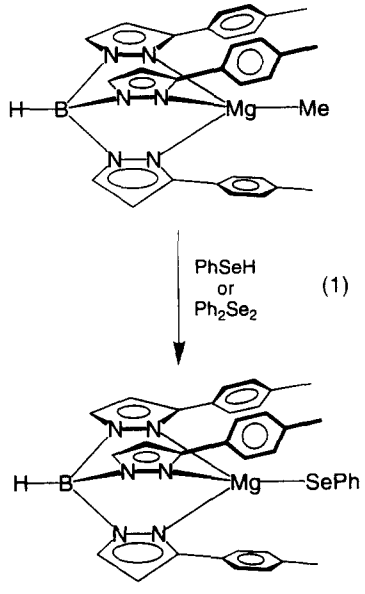
(Received 31 May 1996; accepted 12 August 1996)

Abstract—The magnesium phenylselenolate complex [Tp$^{p\text{-Tol}}$]MgSePh has been synthesized by the reactions of [Tp$^{p\text{-Tol}}$]MgMe with PhSeH and Ph_2Se_2. The molecular structure of [Tp$^{p\text{-Tol}}$]MgSePh has been determined by X-ray diffraction. Copyright © 1997 Elsevier Science Ltd

Keywords: magnesium; selenium; chalcogen; selenolate.

As recently noted by Arnold, the chemistry of selenolate and tellurolate complexes is poorly developed compared with that of their alkoxide and thiolate counterparts [1]. Indeed, we are aware of only three structurally characterized selenolate or tellurolate complexes for magnesium, namely $Mg[Se(C_6H_2Bu^t_3)]_2(THF)_2$ [2], $[\eta^2\text{-}Bu^tSi(CH_2PMe_2)_3]Mg[SeSi(SiMe_3)_3]_2$ [3] and $Mg[TeSi(SiMe_3)_3]_2(THF)_2$ [3], each of which is distinguished by the presence of a bulky substituent on the chalcogen [4]. In this paper, we describe the synthesis and structural characterization of a magnesium phenylselenolate complex supported by tris (pyrazolyl)hydroborato ligation [5,6].

Our previous studies have demonstrated that the tris(pyrazolyl)hydroborato ligand system allows facile access to a series of alkoxide complexes, e.g. [Tp$^{Bu^t}$]MgOR (R = Et, PR^i, Bu^t, Ph), *via* the alcoholysis reactions of the methyl derivative [Tp$^{Bu^t}$]MgMe [7,8]. The ability to synthesize such a series of alkoxide derivatives suggested that the heavier chalcogenolate analogues may also be isolated by adoption of a similar approach. Indeed, we have found that the phenylselenolate complex [Tp$^{p\text{-Tol}}$]MgSePh is formed instantaneously by the reaction of [Tp$^{p\text{-Tol}}$]MgMe [9] with PhSeH, and is accompanied by the elimination of methane [Eq. (1)].



Furthermore, [Tp$^{p\text{-Tol}}$]MgSePh is also obtained by treatment of [Tp$^{p\text{-Tol}}$]MgMe with Ph_2Se_2 [Eq. (1)], a

* Author to whom correspondence should be addressed.

Table 1. Comparison of Mg—Se bond lengths

	d(Mg—Se)/Å	Reference
[Tp$^{p\text{-Tol}}$]MgSePh	2.495(4)	This Work
[Tp$^{p\text{-Tol}}$]MgSeH	2.465(2)	9
{[Tp$^{p\text{-Tol}}$]Mg}$_2$Se	2.406(2)	9
Mg[Se(C$_6$H$_2$Bu$^t_3$)]$_2$(THF)$_2$	2.536(3)	2
	2.539(3)	
[η^2-Bu^{t}Si(CH$_2$PMe$_2$)$_3$]Mg[SeSi(SiMe$_3$)$_3$]$_2$	2.483(8)	3
	2.500(8)	

reaction that is accompanied by elimination of the selenoether PhSeMe [10]. A precedent for the latter transformation is provided by the reactions of Grignard reagents with diaryldiselenides. Specifically, the reactions of Ar_2Se_2 with RMgX have been employed in the syntheses of selenoethers ArSeR, with the presumption that the magnesium selenolate species ArSeMgX are formed as by-products [11]; however, the ArSeMgX complexes thus generated were neither isolated nor characterized.

The molecular structure of [Tp$^{p\text{-Tol}}$]MgSePh has been determined by X-ray diffraction, as illustrated in Fig. 1 [12]. The coordination environment is distorted tetrahedral, with average N—Mg—N and N—Mg—Se angles of 91 and 124°, respectively. The Mg—Se bond length of 2.495(4) Å in [Tp$^{p\text{-Tol}}$]MgSePh is close to the sum of the respective covalent radii (2.54 Å) [13] and lies within the range 2.41–2.54 Å observed for the rather limited number of structurally

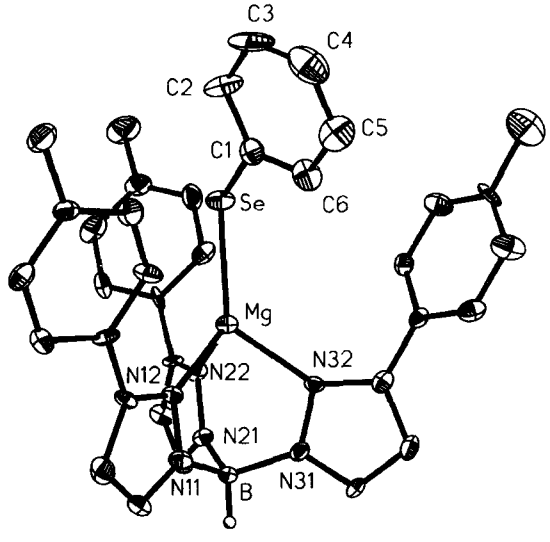


Fig. 1. Molecular structure of [Tp$^{p\text{-Tol}}$]MgSePh. Selected bond lengths (Å) and angles (°): Mg—Se 2.495(4), Mg—N(12) 2.129(14), Mg—N(22) 2.100(11), Mg—N(32) 2.098(9), Se—C(1) 1.927(14); Se—Mg—N(12) 131.1(3), Se—Mg—N(22) 112.5(5), Se—Mg—N(32) 128.0(4), N(12)—Mg—N(22) 93.0(5), N(12)—Mg—N(32) 90.5(5), N(22)—Mg—N(32) 90.8(4), Mg—Se—C(1) 109.7(7).

characterized magnesium selenolate and selenide complexes (Table 1).

The most relevant structural comparisons of [Tp$^{p\text{-Tol}}$] MgSePh are with its tris(pyrazolyl)hydrobraoto relatives, [Tp$^{p\text{-Tol}}$]MgSeH and {[Tp$^{p\text{-Tol}}$]Mg}$_2$Se [9]. Thus, the Mg—Se bond length in [Tp$^{p\text{-Tol}}$]MgSePh [2.495(4) Å] is marginally longer than that in [Tp$^{p\text{-Tol}}$] MgSeH [2.465(2) Å], a difference that is presumably a result of the greater steric demands of a phenyl versus hydrogen substituent. The Mg—Se bond length in [Tp$^{p\text{-Tol}}$]MgSePh is also considerably longer than that in the dinuclear complex {[Tp$^{p\text{-Tol}}$] Mg}$_2$Se [2.406(2) Å]; however, such a difference is not immediately rationalized in terms of steric demands since a phenyl substituent is considerably less sterically encumbered than a {[Tp$^{p\text{-Tol}}$]Mg} group. A possible explanation for the longer Mg—Se bond length in [Tp$^{p\text{-Tol}}$]MgSePh compared with that in {[Tp$^{p\text{-Tol}}$] Mg}$_2$Se resides with the bond angle at selenium: *viz.* the Mg—Se—Ph bond angle of 109.7(7)° [14] in [Tp$^{p\text{-Tol}}$]MgSePh sharply contrasts with the 180.0° bond angle at selenium in {[Tp$^{p\text{-Tol}}$]Mg}$_2$Se. Linear M—Se—M moieties are often attributed to the existence of π donation from Se to an electron-deficient metal centre [15], which may therefore provide a rationalization for the shorter Mg—Se bond length in {[Tp$^{p\text{-Tol}}$]Mg}$_2$Se. However, even if π donation is responsible for the shorter Mg—Se bond length in {[Tp$^{p\text{-Tol}}$]Mg}$_2$Se, it should be noted that the existence of π interactions may be merely a consequence of a linear geometry being dictated by steric interactions between the two bulky {[Tp$^{p\text{-Tol}}$]Mg} moieties. In other words, the linear geometry of {[Tp$^{p\text{-Tol}}$] Mg}$_2$Se is not a consequence of π donation, but rather that efficient π interactions are consequence of a linear geometry. In this regard, it should be noted that the linearity at tellurium in the scandium complex [Me$_2$Si(C$_5$H$_3$Bu^t)$_2$Sc(PMe$_3$)]$_2$Te has been rationalized in terms of a steric rather than electronic argument [16].

The phenylselenolate complex [Tp$^{p\text{-Tol}}$]MgSePh has also been studied by ^{77}Se NMR spectroscopy. Interestingly, [Tp$^{p\text{-Tol}}$]MgSePh is characterized by a ^{77}Se NMR signal at δ 9 ppm, significantly different from those observed for [Tp$^{p\text{-Tol}}$]MgSeH [δ −486] and {[Tp$^{p\text{-Tol}}$] MgSe}$_2$ [δ − 582]. Large ^{77}Se NMR chemical shift ranges for similar complexes are not unusual.

Indeed, it has previously been noted that selenolate complexes in general exhibit a very large ^{77}Se NMR chemical shift range [1].

In summary, $[Tp^{p\text{-}Tol}]MgSePh$, a rare example of a structurally characterized magnesium selenolate complex, has been synthesized by the reactions of $[Tp^{p\text{-}Tol}]MgMe$ with either PhSeH or Ph_2Se_2.

Acknowledgements—Acknowledgement is made to the National Science Foundation (Grant CHE 93-00398) and Kanagawa Academy of Science and Technology for support of this research. G.P. is the recipient of a Camille and Henry Dreyfus Teacher–Scholar Award (1991–1996) and a Presidential Faculty Fellowship Award (1992–1997).

REFERENCES

1. Arnold, J. *Prog. Inorg. Chem.* 1995, **43,** 353.
2. Ruhlandt-Senge, K. *Inorg. Chem.* 1995, **34,** 3499.
3. Gindelberger, D. E. and Arnold, J. *Inorg. Chem* 1994, **33,** 6293.
4. For some examples of magnesium selenolate complexes that have not been structurally characterized, see: Petragnani, N. *Chem. Ber.* 1963, **96,** 247; du Mont, W.–W., Kubinok, S., Lange, L., Pohl, S., Saak W., and Wagner, I. *Chem. Ber.* 1991, **124,** 1315.
5. Trofimenko, S. *Chem. Rev.* 1993, **93,** 943; Parkin, G. *Adv. Inorg. Chem.* 1995, **42,** 291; Kitajima, N. and Tolman, W. B. *Prog. Inorg. Chem.* 1995, **43,** 419.
6. The abbreviations adopted here for tris (pyrazolyl)hydroborato ligands are based on those described by Trofimenko (ref. 5). Thus, the tris(pyrazolyl)hydroborato ligands are represented by the abbreviation Tp, with the 3- and 5-alkyl substituents listed respectively as superscripts.
7. Han, R. and Parkin, G. *J. Am. Chem. Soc.* 1992, **114,** 748.
8. Chisholm has recently employed the ethoxide derivative as single-site catalyst for the ring-opening polymerization of poly(dilactide). See: M. H. Chisholm and N. W. Eilerts, *J. Chem. Soc., Chem. Commun.* 1996, 853.
9. Ghosh, P. and Parkin, G. *J. Chem. Soc., Chem. Commun.* 1996, 1239.
10. PhSeMe was identified by comparison of its ^1H NMR and ^{77}Se-$\{^1H\}$ NMR spectra with those of an authentic sample prepared according to the literature method [10a]. However, it should be noted that the ^1H NMR shifts that we observe [10b] differ slightly from those reported in the literature [10a,c]. (a) Davis, F. A., Stringer, O. D. and McCauley, J. P. Jr., *Tetrahedron*, 1985, **41,** 4747; (b) ^1H NMR (200 MHz) in $CDCl_3$: δ 2.34 (s, 3H, Me, $^2J_{Se\ H}$ = 11 Hz), 7.2–7.4 (m, 5H, Ph); ^{77}Se-$\{^1H\}$ NMR in C_6D_6: δ 200; (c) ^1H NMR in $CDCl_3$: δ 2.6 (s, 3H, Me), 7.1–7.6 (m, 5H, Ph)
11. Campbell, T. W. and McCullogh, J. D. *J. Am. Chem. Soc.* 1945, **67,** 1965.
12. $[Tp^{p\text{-}Tol}]MgSePh$ is monoclinic, $P2_1/n$ (No. 14), a = 17.646(3), b = 12.260(2), c = 19.691(4) Å, β = 111.20(2)°, V = 3974(2) Å^3 and Z = 4.
13. Pauling, L. *The Nature of the Chemical Bond*, 3rd edn. Cornell University Press, Ithaca, 1960, p. 246.
14. For comparison, the mean M—Se—aryl bond angle of complexes listed in the Cambridge Structural Database (version 5.11) is 105°.
15. For example, "16"-electron $[(dppe)(CO)_3V]_2Se$ [15a] is linear, while 18-electron $[(Me_3P)_2(CO)_3Re]_2Se$ is bent [116.1(1)°] [15b]. (a) Albrecht, N., Hübener, P., Behrens, U. and Weiss, E. *Chem. Ber.* 1985, **118,** 4059; (b) Küllmer, V., Röttinger, E. and Vahrenkamp, H. *Z. Naturforsch.* 1979, **34B,** 217.
16. Piers, W. E., Ferguson, G. and Gallagher, J. F. *Inorg. Chem.* 1994, **33,** 3784.

Pergamon

PII: S0277-5387(96)00359-2

Polyhedron Vol. 16, No. 7, pp. 1259–1261, 1997
Copyright © 1997 Elsevier Science Ltd
Printed in Great Britain. All rights reserved
0277-5387/97 $17.00+0.00

COMMUNICATION

Synthesis and X-ray crystal structure of a polymetallate with a metal complex cation as counter ion, $[Ag(PPh_3)_4]_2Mo_6O_{19} \cdot 3CH_2Cl_2$

De-Liang Long,[a] Xin-Quan Xin,[a]* Xiao-Ming Chen[b] and Bei-Sheng Kang[b]

[a]State Key Laboratory of Coordination Chemistry, Coordination Chemistry Institute, Nanjing University, Nanjing 210093, P.R. China

[b]Department of Chemistry, Zhongshan University, 135 Xingang Road W., Guangzhou 510275, P.R. China

(Received 25 April 1996; accepted 24 July 1996)

Abstract—The reaction of $Ag(PPh_3)_2NO_3$ and $K_4Mo(CN)_8$ in H_2O/CH_2Cl_2 gave an emulsion, from which light yellow crystals were obtained. Elemental analysis, IR spectra and X-ray diffraction verified that the compound is a hexamolybdate with two tetra(triphenylphosphine)silver cations acting as counter ions, $[Ag(PPh_3)_4]_2Mo_6O_{19} \cdot 3CH_2Cl_2$. Oxidation of Mo^{IV} to Mo^{VI} took place when $Mo(CN)_8^{4-}$ was hydrolysed.
Copyright © 1997 Elsevier Science Ltd

Keywords: synthesis; crystal structure; coordination compounds; hydrolysis reaction; polymetallate; phase-transfer process.

Octacyanides of molybdenum(IV) have been a subject of interest for many years from the point of view of structure, reactivity and photochemistry [1]. Recently, we have demonstrated that many inorganic clusters and coordination compounds derived from $MS_nO_{4-n}^{2-}$ (M = Mo and W) exhibit very interesting non-linear optical properties (NLO) [2,3]. Attempts at imitating $MS_nO_{4-n}^{2-}$ (M = Mo and W) with $Mo(CN)_8^{4-}$ to synthesize polynuclear coordination compounds resulted in the formation of polymolybdate. It is interesting to understand the formation process of the polymolybdate and its complex counter ions. A solution of $Ag(PPh_3)_2NO_3$ in CH_2Cl_2 was mixed with a solution of $K_4Mo(CN)_8$ in water giving a white emulsion. This emulsion was placed in air for several days and its colour remained unchanged. As the solvent was evaporated light yellow cubic crystals were produced. Elemental analyses, IR spectra† and X-ray diffraction verified that the compound comprises a polymolybdate and two tetra(triphenylphosphine) silver cations $[Ag(PPh_3)_4]_2Mo_6O_{19} \cdot 3CH_2Cl_2$ (**1**).

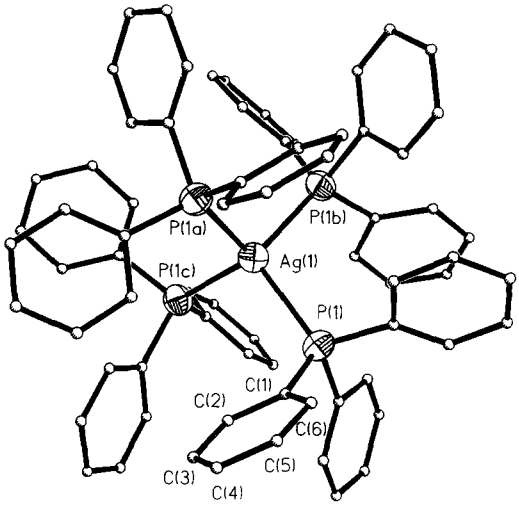
The X-ray structure‡ of **1** shows that the silver

* Author to whom correspondence should be addressed.

† Selected characterization data: IR (KBr): 1483m, 1433m, 1089m, 958vs, 802vs, 744s, 695s, 512m cm^{-1}. Found: C, 50.5; H, 3.6. Calc. for $C_{147}H_{126}Ag_2Cl_6Mo_6O_{19}P_8$: C, 50.3; H, 3.6%.

‡ *Crystal data*: $C_{147}H_{126}Ag_2Cl_6Mo_6O_{19}P_8$: cubic, space group *Fm3m*, $a = 24.500(3)$ Å, $Z = 4$, $V = 14707(7)$ Å^3, $D_c = 1.596$ g cm^{-3}, $F(000) = 6912$. A total of 712 independent reflections were collected using an Enraf–Nonius diffractometer with graphite-monochromated Mo-K_α radiation and ω scans. The structure was solved by direct methods using SAPI-91 and refined with a full-matrix least-squares technique using SHELXTL-PC program package to give $R = 8.32\%$ and $R_w = 8.82\%$ for 553 independent observed [$F > 6.0s(F)$]. An empirical absorption correlation was applied. The Mo, Ag and O atoms were refined anisotropically. The highly disordered phenyl rings of Ph_3P were refined isotropically as rigid hexagons. The solvate CH_2Cl_2 was derived from the difference Fourier map.

atom is coordinated by four triphenylphosphines in a tetrahedral geometry, in which the four phosphine ligands are identical (Fig. 1). This is unusual except for the report of $Ag(PPh_3)_4ClO_4$, in which the phosphine silver complex possesses a crystallographic threefold axis: four phosphine ligands are at two independent positions coordinating to the silver atom [4]. The Ag—P distance of 2.635(4) Å in the title compound is shorter than the Ag—P distances of 2.668(5) and 2.659(2) Å in $Ag(PPh_3)_4ClO_4$. The hexmolybdate anions lie at the origin and face-centre position of the cubic cell, and possess octahedral symmetry.



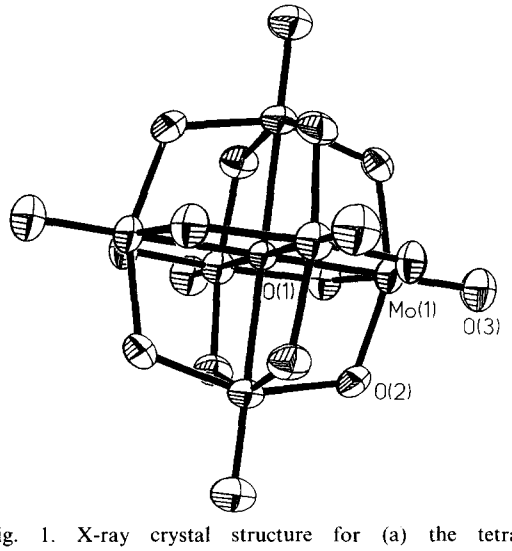


Fig. 1. X-ray crystal structure for (a) the tetra-(triphenylphosphine) silver cation and (b) the polymolybdate anion of **1**. Selected bond lengths (Å); Ag—P 2.635(4); Mo(1)—O(1) 2.316(2); Mo(1)—O(2) 1.921(5); Mo(1)—O(3) 1.618(16).

The formation of the product is reasonable. A number of studies have been made on the kinetics and mechanism of the photoreaction of octacyano complexes of Mo^{IV} and W^{IV} with or without organic base ligands, and some intermediates have been isolated and characterized [1]. In the first step, one of the cyano ligands in $Mo(CN)_8^{4-}$ is replaced by the hydroxyl ion, yielding $Mo(CN)_7(OH)^{4-}$. Further hydrolysis results in more cyano ligands being replaced. In addition, it is known that Ag^+ can ligate CN^- and enhance the hydrolysis process [5,6]. The interesting fact is that an oxidation reaction has taken place at the same time. The Mo^{IV} is oxidised to Mo^{VI}, which exists as molybdates. The oxidant is probably oxygen in the air or silver(I) in the solution, the mechanism of which is unknown at present. The MoO_4^{2-} ions can polymerize to polymolybdate in acidic solution. The overall reaction may be as follows:

$$6Mo(CN)_8^{4-} + 19H_2O - 12e^- \rightarrow Mo_6O_{19}^{2-} + 48CN^- + 38H^+.$$

The examples of hexamolybdate crystallizing with complex cations as counter ions are $[M_2(MeCN)_{10}][Mo_6O_{19}]_2$ (M = Re, Rh, Mo, W) [7,8], $[FeCl(DMF)_5][Mo_6O_{19}]$ [9], $[(PhC_5Me_5)Cl(MeCN)_2]_2Mo_6O_{19}$ [10], $[Mo_2(\eta\text{-}C_5H_5)_2(CO)_4(\mu\text{-}H)(\eta\text{-}Ph_2PCH_2PPh_2)]_2[Mo_6O_{19}]\cdot 4THF$ [11], $[Mo(CO)_2(\eta\text{-}Ph_2PCH_2P(Se)Ph_2)]_2[Mo_6O_{19}]\cdot 4CH_3NO_2$ [12], $[(18\text{-crown-}6)K]_2Mo_6O_{19}\cdot H_2O$ [13] and $[Mo_2(S_2CNEt_2)_4]_2Mo_6O_{19}$ [14]. These were all synthesized in organic solvents. In some cases, the $Mo_6O_{19}^{2-}$ anions are acquired by the anion exchange, while in others they are produced by the oxidation reaction of the corresponding low-valent molybdenum reactants. Recently, we synthesized $[MoS_4Cu_4(\gamma\text{-MePy})_4][Mo_6O_{19}]$ [15], in which a large cluster cation was obtained with the reaction of thiomolybdate and copper(I) in γ-methylpyridine and the hexamolybdate was produced by the oxidation of thiomolybdate. The title compound, on the contrary, is produced in a mixed solvent. It is interesting that a synthetic route to obtain crystals of polymetallates and large complex cations through a phase-transfer process may be derived. Polymolybdate anions are readily generated and dissolved in water, while organic phosphine complex cations are only soluble in organic solvents. Combination of these two species in mixed solvents results in crystallization of polymetallates with large complex cations.

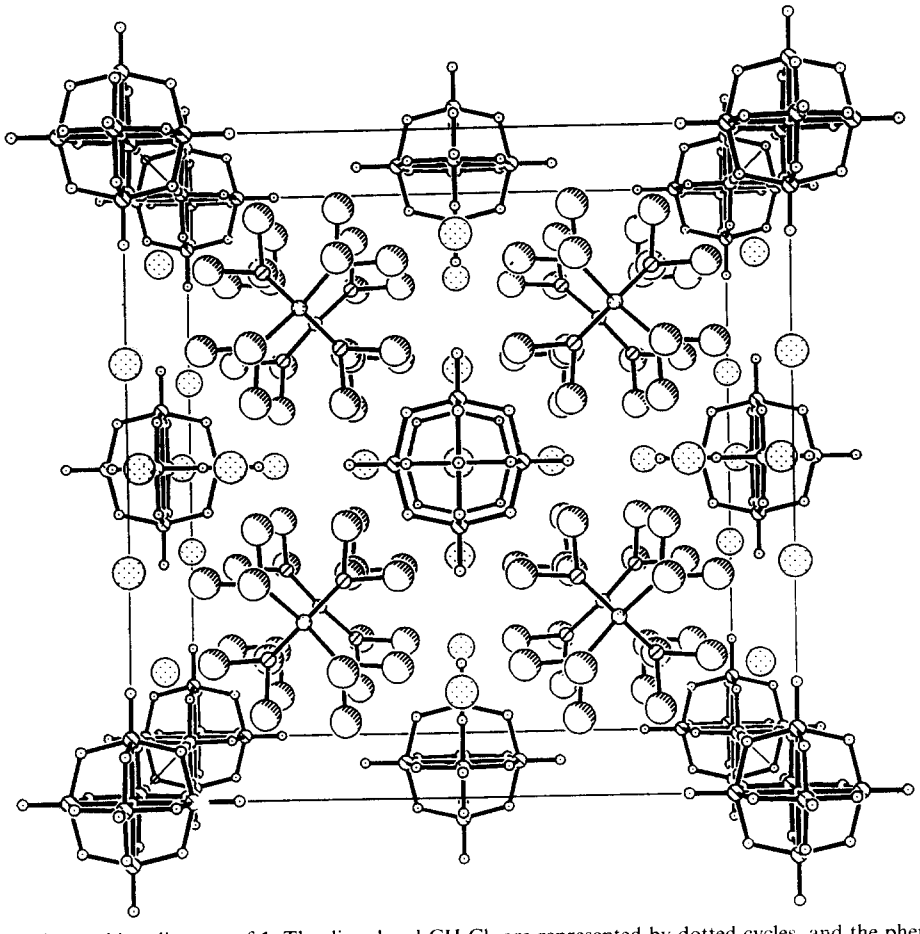


Fig. 2. Molecular packing diagram of **1**. The disordered CH_2Cl_2 are represented by dotted cycles, and the phenyl rings by hatched ones.

REFERENCES

1. Samotus, A. and Szklarzewicz, J., *Coord. Chem. Rev.*, 1993, **125,** 63.
2. Shi, S., Ji, W., Tang, S. H., Lang, J. P. and Xin, X. Q., *J. Am. Chem. Soc.*, 1994, **116,** 3615; Hou, H. W., Ye, X. R., Xin, X. Q., Liu, J., Chen, M. Q. and Shi, S., *Chem. Mater.*, 1995, **7,** 472.
3. Shi, S., Hou, H. W. and Xin, X. Q., *J. Phys. Chem.*, 1995, **99,** 4050; Sankane, G., Shibahara, T., Hou, H. W., Xin, X. Q. and Shi, S., *Inorg. Chem.*, 1995, **34,** 4785.
4. Engelhardt, L. M., Pakawatchai, C. and White, A. H., *J. Chem. Soc., Dalton Trans.*, 1985, 125.
5. Ali, S. I. and Kaur, H., *J. Photochem. Photobiol. A. Chem.*, 1991, **61,** 191; 1992, **68,** 147.
6. Ali, S. I. and Kaur, H., *Trans. Met. Chem.*, 1991, **16,** 450.
7. Bartley, S. L., Bernstein, S. N. and Dunbar, K. R., *Inorg. Chim. Acta*, 1993, **213,** 213.
8. Bernstein, S. N. and Dunbar, K. R., *Angew. Chem.*, 1992, **104,** 1412.
9. Lu, S., Huang, J. and Huang, Z., *Huaxue Xuebao*, 1992, **30,** 348.
10. Zhang, C., Ozawa, Y., Hayashi, Y. and Isobe, K., *J. Organomet. Chem.*, 1989, **373,** C21.
11. Riera, V., Ruiz, M. A., Villatane, F., Jeannin, Y. and Bois, C., *J. Organomet. Chem.*, 1988, **345,** C4.
12. Colton, R., Hoskins, B. F. and Panagiotidou, P., *Aust. J. Chem.*, 1988, **41,** 1295.
13. Nagano, O. and Sasaki, Y., *Acta Cryst.*, 1979, **B35,** 2387.
14. Jasin, K. S., Chieh, C. and Mak Thomas, C. W., *J. Crystallogr. Spectrosc. Res.*, 1985, **15,** 403.
15. Pope, M. T., Lang, J. P., Xin, X. Q. and Yu, K. B., *Chin. J. Chem.*, 1995, **13,** 40.

Pergamon

PII: S0277-5387(96)00357-9

Polyhedron Vol. 16, No. 7, pp. 1263–1265, 1997
Copyright © 1997 Elsevier Science Ltd
Printed in Great Britain. All rights reserved
0277-5387/97 $17.00+0.00

COMMUNICATION

Molecular recognition of organic non-linear optical material by bis(perchlorate)tris(phenanthroline)cadmium(II)

Ren-Gen Xiong, Cai-Ming Liu, Da Guang Li, Hong Wang and Xiao-Zeng You*

Coordination Chemistry Institute, State Key Laboratory of Coordination Chemistry, Nanjing University, Nanjing 210093, P.R. China

(Received 24 May 1996; accepted 15 July 1996)

Abstract—The crystallization of bis(perchlorate)tris(phenanthroline)cadmium(II) [$Cdphen_3 \cdot (ClO_4)_2$] in the presence of *para*-nitroaniline (PNA) yielded a co-crystal 1:2 adduct, $Cdphen_3(ClO_4)_2 \cdot 2PNA$ (**1**); which exhibits weak second-harmonic-generation activity even though it has a centrosymmetric space group. Copyright © 1997 Elsevier Science Ltd

Keywords: cadmium(II) complexes; phenanthroline-N^1,N^{10} complexes; crystal structures; second-harmonic-generation activity; molecule recognition; self-assembly.

Molecular recognition and self-assembly of molecules are generally based on a strong (O—H···O and N—H···O hydrogen bonds), weak (van der Waals, $\pi \cdots \pi$ stacking) and potentially weak (C—H···Y hydrogen bonds, Y=O, N) intermolecular interactions [1–3]. However, a massive research effort has recently been focused on the intermolecular interactions between organic molecules [4]. Few organic–metal complexes were used as a host to recognize an organic guest molecules through hydrogen bonds [5, 6]. On the other hand, chemists and physicists have endeavoured to search for a new method of removing crystalline centrosymetric geometry in guest molecules so that the criteria for SHG (second-harmonic generation) may also be satisfied in a centrosymmetric crystal structure [7, 8]. As we know, organic materials that have π-conjugate systems with an electron donor and acceptor are highly efficient non-linear optical (NLO) materials. Unfortunately, *para*-nitroaniline, having a centrosymmetric crystal structure, exhibits no SHG activity in bulk [9]. We report here the synthesis, characterization and crystal structure of bis(perchlorate)tris(phenanthroline-N^1,N^{10}) cadmium–bis(*para*-nitroaniline) (**1**), which displays weak SHG activity even though it has a centrosymmetric space group. As far as we are aware, this is the first example of crystal engineering design through hydrogen bond interaction between an organic NLO molecule and a metal complex and may give a new insight into NLO molecule recognition by an anion.

The reaction of $(phen)_3Cd(ClO_4)_2$ with two equiv. of *para*-nitroaniline in a solution of ethanol and water (v/v 1:1) yielded a yellow solution, from which pale yellow columnar crystals of **1** were isolated in 60–70% yield after evaporation of the solution at room temperature for a few days. The infrared spectrum of **1** exhibits a diagnostic band for perchlorate (1108 cm^{-1}) at a higher wavenumber compared with normal perchlorate (1080 cm^{-1}) probably owing to hydrogen bonds. Two absorption bands at 3450 and 3362 (m) cm^{-1} may be assigned to the ν_{NH} stretching frequency. In the far-IR spectrum of **1**, the ν_{Cd-N} (274 and 244 cm^{-1}) bands observed, were in the normal region. Moreover, thermogravimetric analysis (TGA) of **1** reveals that the first decomposition event takes place

* Author to whom correspondence should be addressed.

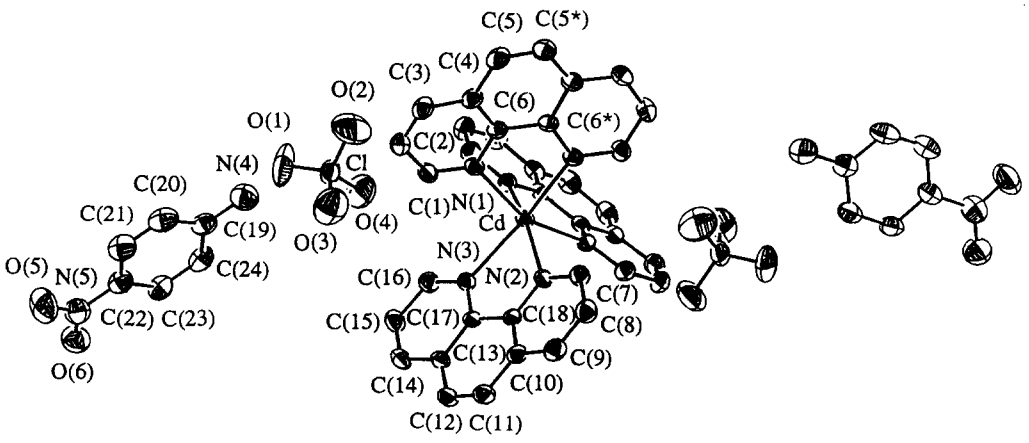


Fig. 1. A displacement ellipsoid plot (30% probability) of **1** showing the atom-numbering scheme. Selected bond distances (Å) and angles (°) are as follows: Cd—N(1) 2.340(3), Cd—N(1a) 2.340(3), Cd—N(2) 2.332(3), Cd—N(2a) 2.332(3), Cd—N(3) 2.366(3), Cd—N(3a) 2.366(3), Cl—O(1) 1.346(4), Cl—O(2) 1.390(5), Cl—O(3) 1.446(6), Cl—O(4) 1.406(4), N(5)—O(5) 1.225(6), N(5)—O(6) 1.227(6), N(5)—C(22) 1.446(7), C(22)—C(21) 1.384(7), C(21)—C(20) 1.366(8), C(20)—C(19) 1.403(7), C(19)—N(4) 1.357(6), C(19)—C(24) 1.400(7), C(24)—C(23) 1.368(7), C(23)—C(22) 1.386(6), N(1)—Cd—N(1a) 71.7(1), N(2)—Cd—N(3) 71.7(1), N(2a)—Cd—N(3a) 71.7(1), O(5)—N(5)—O(6) 123.0(5), O(5)—N(5)—C(22) 118.0(5), O(6)—N(5)—C(22) 119.0(4), N(5)—C(22)—C(23) 119.8(4), N(5)—C(22)—C(21) 120.1(4), N(4)—C(19)—C(20) 120.9(5), N(4)—C(19)—C(24) 121.8(4), O(3)···H(14)—N(4) 3.097(8)(177.9), O(4)···H(13b)—N(4b) 3.054(7)(159.8). Symmetry code (a): $1-x, y, \frac{3}{2}-z$, (b) $\frac{1}{2}-x, -\frac{1}{2}+y, \frac{3}{2}-z$.

at *ca* 247°C, suggesting that perchlorate ion is strongly hydrogen bonded to NH_2 in *para*-nitroaniline to form a stable composite, **1**. On the basis of weight changes, the first process of weight loss (23.9%) corresponds to the loss of two *para*-nitroaniline (theoretical loss: 24.4%), by an endothermal process.

The Cd atom in **1** (Fig. 1) exhibits a slightly distorted octabhedral geometry in which the Cd atom is coordinated to six N atoms from three phenanthrolines.* The Cd—N bond lengths are in the expected range. [10] A striking feature of **1** is that the perchlorate anion recognizes *para*-nitroaniline guest molecules through hydrogen bonds (Fig. 2). To our knowledge, organic non-linear optical material recognition by the anion in a metal complex through hydrogen bonding is unprecedented in the self-assembly process. It is found, somewhat surprisingly, that the perchlorate anion in **1** displays some shape selectivity in the recognition process. While *para* and *meta*-nitroaniline were efficiently assembled, the *ortho* isomer, was not recognized. This is different from that observed in $[Cd(4,4'\text{-bipy})_2 \cdot (NO_3)_2 \cdot (o\text{-}Br_2C_6H_4)_2]_\infty$ (only *ortho*-dibromobenzene included) [5] and $[Cd(4,4'\text{-bipy})_2 \cdot (H_2O)_2 \cdot (o\text{-}NO_2C_6H_4NH_2)_2 \cdot (4,4'\text{-bipy})](ClO_4)_2$(only *ortho*-nitroaniline included) [6]. It is noteworthy that when *para*- and *meta*-nitroaniline exists simultaneously in solution, *para*-nitroaniline is recognized preferentially to separate fom *meta*-nitroaniline. It is very interesting to note that **1** exhibits weak SHG response, probably owing to the perchlorate ion having a little disorder in the crystal (higher thermal parameter) [11] even though **1** has a centrosymmetric space group. Furthermore, as Eaton pointed out [8], when the structure with disorder was solved with a centrosymmetric space group, the observation of SHG is reliable and the structure may be assigned as an acentric space group. On the other hand, the disorder in the crystal may provide the local dissymmetry needed to support charge separation [11] while material having low-lying charge-transfer states,

*Crystal data for **1**: monoclinic, $C2/c$, a = 25.072(4), b = 10.752(3), c = 19.407(2) Å, β = 116.62(1)°, V = 4677(3) Å^3, Z = 4, D = 1.60 g cm^{-3}, F (000) = 2288, μ = 6.53 cm^{-1}. The intensity data were collected on an Enraf–Nonius CAD-4 diffractometer at 296 K, using graphite-monochromated Mo-K_α radiation (λ = 0.71069 Å), ω–2θ scan mode. 4439 reflections were measured in the range $2 \leqslant 2\theta \leqslant 50°$. 4347 unique reflections, 3675 of which, with $I > 3\sigma(I)$, were used for refinement. Intensities were corrected for Lorentz and polarization effects and empirical absorption. The structure was solved by direct methods using MITHRIL. The Cd atom was located in an E map and the remaining non-H atoms were located using DIRDIF. Hydrogen atoms were placed in geometrically calculated positions with C—H = 0.95 Å, but were not included in the refinement. The structure was refined by full-matrix least-squares techniques with anisotropic displacement parameters for all non-H atoms. All calculations were performed on a VAX3100 computer using the TEXSAN program package, refined on F, number of parameters 330, R = 0.048, R_w = 0.057, S = 1.66. Final difference maps showed no peaks >0.44 or < −0.93 Å. All Δ/ρ values <0.01. Atomic coordinates bond lengths and angles and thermal parameters have been deposited at the Cambridge Crystallographic Data Centre.

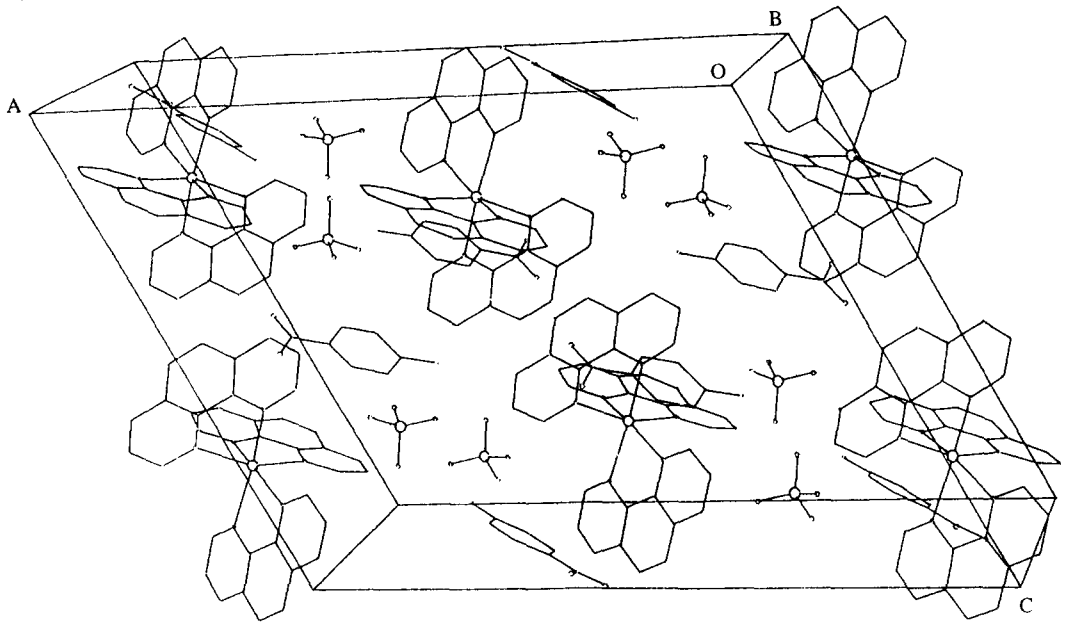


Fig. 2. Unit cell diagram of **1**.

or experiencing large changes in molecular dipole moment upon photo-excitation is potentially SHG active [12].

Acknowledgements—This research was funded by the State Science and Technology Commission, the National Nature Foundation of China and the Foundation of the Chinese Postdoctoral Fellowship as a major key research project.

REFERENCES

1. Whitesides, G. M., Mathisa, J. P. and Seto, C. T. *Science*, 1991, **254,** 1312; Yang, J., Fan, E., Geib, S. J. and Hamilton, A. D. *J. Am. Chem. Soc.*, 1993, **115,** 5314; Kotera, M., Lehn, J.-M. and Vigneron, J. P., *J. Chem. Soc., Chem. Commun.*, 1994, 197.
2. Hunter, C. A., *Angew. Chem., Int. Ed. Engl.*, 1993, **32,** 1584; Cochran, J. E., Parrott, T. J., Whitlock B. J. and Whitlock, H. W. *J. Am. Chem. Soc.*, 1992, **114,** 2269.
3. Keegstra, E. M. D., Spek, A. L., Zwikker, J. W. and Jenneskens, L. W., *J. Chem. Soc., Chem. Commun.*, 1994, 1633.
4. Kim, J., Whang, D., Lee, J. L. and Kim, K. *J. Chem. Soc., Chem. Commun.*, 1993, 1400; Harata, K., *J. Chem. Soc., Chem. Commun.*, 1993, 546.
5. Fugita, M., Kwon, Y. J., Washizu, S. and Ogura, K., *J. Am. Chem. Soc.*, 1994, **116,** 1151; Yaghi O. M. and Li, H., *J. Am. Chem. Soc.*, 1995, **117,** 10401.
6. Xiong, R.-G., Liu, C.-M., You, X.-Z. and Fun, H.-K., submitted to *J. Am. Chem. Soc.*; see also You, X.-Z., Xiong, R.-G., Liu, C.-M., Fun H.-K. and Sivakumar, K. 31st ICCC, Abstracts 106, Vancouver, Canada, August 18–23, 1996.
7. Eaton, D. F., Anderson, A. G., Tam, W. and Wang, Y., *J. Am. Chem. Soc.*, 1987, **109,** 1886.
8. Ashwell, G. L., Jefferles, G., Hamilton, D. G., Lynch, D. E., Roberts, M. P. S., Bahra G. S. and Brown, C. R., *Nature*, 1995, **375,** 385.
9. Tomaru, S., Zembutsu, S., Kawachi, M. and Kobayashi, M., *Proceedings of the Third International Symposium on Clathrate Compounds and Molecular Inclusion Phenomena and the Second International Symposium on Cyclodextrins*, eds J. L. Atwood, J. E. D. Davies and T. Osa, D. Reidel Publishing Co., Tokyo, Japan, July 23–27, 1984.
10. Wang, H., Xiong, R.-G., Chen, H.-Y. and Huang, X.-Y., *Acta Cryst.*, 1996, **C52,** 1658.
11. Rheingold, A. L. and King, W., *Inorg. Chem.*, 1989, **28,** 1715.
12. Oudar, J. L. and Chemla, D. S., *J. Chem. Phys.*, 1977, **66,** 2664.

Pergamon

Polyhedron Vol. 16, No. 7, p. 1267, 1997
Copyright © 1997 Elsevier Science Ltd
Printed in Great Britain. All rights reserved
0277-5387/97 $17.00+0.00

BOOK REVIEW

Gmelin Handbook of Inorganic and Organometallic Chemistry, 8th Edition, Supplement Volume B8. **Ternary Silicon–Fluorine–Hydrogen Compounds,** 212+xiii pp., Springer–Verlag, Berlin, 1996, Price 1330 DM, ISBN 3-540-93728-5.

This volume is the latest of the Gmelin Institute's comprehensive series on silicon compounds to appear. It picks up the story from 1959, and reviews the literature from all sources (including patents) right up to November 1995. As always, it is thorough, logically organized, reliable and critical: ambiguities, inconsistencies and errors in publications are noted and, where possible, resolved. Besides the compounds defined by the title, there is also a short section on silicon–fluorine–noble gas systems.

If a random group of inorganic chemists were asked to give some example of Si–F–H compounds, then no doubt most would choose hexafluorosilicic acid, H_2SiF_6, while some might suggest the fluorosilanes, SiH_3F, SiH_2F_2 ad $SiHF_3$. After that, there might be a long pensive pause. The coverage in this volume affords some support for these choices, since the SiH_xF_{4-x} (x = 1–3) compounds take up over 80 pages, while nearly 60 are devoted to H_2SiF_6. In both cases, it becomes clear that this is due in part to their industrial significance. Fluorosilanes, for example, have been widely proposed in patents (and actually used, which is not the same thing) as precursors for the deposition of amorphous solids comprising fluorinated and hydrogenated silicon (a-Si : F, H); these find application in solar cells and other electronic devices. Hexafluorosilicic acid is made on a large scale, often as a valuable by-product from environmental control of the SiF_4 and HF released when phosphate fertilizers are made from fluoride-containing rock. The acid is then used to synthesize a wide range of fluorine-containing chemicals, including ceramic glazes, insecticides, cryolite for aluminium production and (until recently) CFCs.

This volume goes on, however, to provide many surprises for that random group of inorganic chemists (and sometimes for this reviewer) because of the very large number of other Si–F–H compounds that appear. Not only are there simple molecules such as SiHF, SiH_2F and $SiHF_2$, together with positive and negative ions derived from them, but also di- and polysilane derivatives such as SiF_3SiH_3, $SiF_3SiH_2SiF_3$ and $(SiF_3)_3SiH$. In earlier years, it was part of the mythology of inorganic silicon chemists that such SiF_3 derivatives readily disproportionated, giving SiF_4; it now appears that this instability was due to small amounts of impurities.

In many cases, the species described have not been isolated, but are inferred from the results of more or less sophisticated computational procedures. Thus, for instance, the standard enthalpy of formation, preferred structure, fundamental vibrational modes and even the chemical reactivity of unknown $SiH_2F_3^-$ have been predicted. It appears too that small molecules such as SiHF provide a tempting test-bed for theoretical chemists, spectroscopists and physicists: for this particular compound, some five pages of the volume include detailed results of measurements or calculations of its rotational constants, molecular geometry of both ground and excited states, thermodynamic functions, time-resolved fluorescence, dissociation enthalpies, Zeeman effects, proton affinity and so on.

One of the rewarding aspects of reading a concentrated work of reference such as this is the discovery of intriguing facts, forgotten references, new associations of ideas, and interesting experiments which, surprisingly, have never been done. In the first few pages of this book, for example, it is noted that dissolution of crystalline silicon in HF leads to a surface terminated with Si—H and some Si—F bonds (a process utilized in the fabrication of electronic devices), while the last page tells of calculations performed on the experimentally unknown cluster $Si_{10}H_{13}F$. This cluster serves as a model for the surfaces of the pore walls in porous silicon, in which the ratio of H to F terminating atoms is similar—very different systems yielding interesting connections. Again, in the section dealing with Si–F compounds and noble gases, it is noted that in the gas phase there is only very weak interaction, denoted by small changes in the infrared spectrum. It therefore seems very strange that these systems have apparently never been studied by matrix isolation techniques at low temperature. On a lighter note, there is a reference to one publication describing the use of SiH_2F_2 to fluorinate, and presumably enhance, tooth enamel; it seems unlikely, however, that a spray for daily home use which delivered this HF-producing gas would be a great commercial success.

Once again, the authors of this series of volumes deserve the thanks of all those involved in silicon science and technology; like its predecessors, this book provides an invaluable resource of critically surveyed and authentic information.

B. J. AYLETT
Department of Chemistry,
Queen Mary & Westfield College,
London, U.K.

Pergamon

Polyhedron Vol. 16, No. 7, p. 1269, 1997
Elsevier Science Ltd. Printed in Great Britain

ERRATUM

Structural characterization of nitrosodicyanomethanide and dicyamide complexes of copper(II), nickel(II) and cobalt(II) with imidazole and 1-methylimidazole. X-ray crystallographic evidence of unusual nitrosodicyanomethanide O-bonding in $Cu\{ONC(CN)_2\}_2(1\text{-methylimidazole})_4$. M. Hvástijová, J. Kožíšek, J. Kohout, J. Mroziński, L. Jäger and I. Svoboda (*Polyhedron* Vol. 16, No. 3, pp. 463–471 (1997)).

The publishers regret that there were several errors in Table 5. The corrected Table appears below.

Table 5. Electronic spectral data for the compounds

Compound	ν_{max} (μm^{-1})[a]					Dq (cm^{-1})	B (cm^{-1})	β
$Cu\{ONC(CN)_2\}_2(iz)_2$	(1.66)	1.90	(2.05)	(2.65)		870		
$Cu\{ONC(CN)_2\}_2(meiz)_4$	1.74	2.25				[b]		
$Cu\{ONC(CN)_2\}_2(meiz)_2$	(1.34)	1.67	(2.22)	(2.70)		890		
$Ni\{ONC(CN)_2\}_2(iz)_4$	1.00	(1.69)	2.07	(2.58)	(2.68)	1000	783	0.76
$Ni\{ONC(CN)_2\}_2(meiz)_2$	1.05	(1.58)	(1.92)	(2.60)	(2.86)	1050	712	0.69
$Co\{ONC(CN)_2\}_2(iz)_4$	0.94	(1.67)	(2.01)	2.46		1060	792	0.82
$Co\{ONC(CN)_2\}_2(meiz)_2$	0.93	(1.91)	(2.47)			1040	728	0.75
$Cu\{N(CN)_2\}_2(meiz)_2$	(1.21)	(1.31)	1.54			860		
$Ni\{N(CN)_2\}_2(iz)_2$	1.07	(1.33)	1.74	2.82		1070	887	0.86
$Ni\{N(CN)_2\}_2(meiz)_2$	1.02	1.70	2.74			1020	968	0.94
$Co\{N(CN)_2\}_2(meiz)_2$	0.91	(1.87)	2.12			1035	889	0.92

[a] The data in parentheses are related to shoulders, whose positions are only approximately determined.
[b] Not calculated; see text.

Pergamon

Polyhedron Vol. 16, No. 7, p. 1271, 1997
Elsevier Science Ltd. Printed in Great Britain

CORRIGENDA

Metal–metal bond formation in the oxidative addition to dinuclear gold(I) species. Implications from dinuclear and trinuclear gold chemistry for the oxidative addition process generally. J. P. Fackler, Jr (*Polyhedron*, Vol. 16, No. 1, pp. 1–17 (1997)).

The author wishes to point out that there are two typographical errors in this *Polyhedron* Report.

1. Page 3, paragraph 2, the first sentence should read:

Although there are obvious features in common between the oxidative addition studies described in this report and studies involving open-shell ions such as Ir^{I} or Pt^{II}, the specific influence of **incompletely** filled electronic levels at the metal atom is different enough from system to system that electronic generalizations become less reliable.

2. Page 6, section 5, the second sentence should read:

This dicationic species has a short, **2.6** Å, metal–metal bond.

A voltammetric study of the aluminium complexes of catechol and 1,2-dihydroxyanthraquinone-3-sulfonic acid. A. J. Downard, B. O'Sullivan and K. J. Powell (*Polyhedron* Vol. 15, No. 20, pp. 3469–3479 (1996)).

The authors regret that there are two errors in this paper.

1. Reference 10 should read: J. A. Kennedy and H. K. J. Powell, *Aust. J. Chem.* 1985, **38,** 659.

2. Table 1 contained several wrong entries. A corrected copy is shown below.

Table 1. Calculated solution compositions for the catechol-Al^{III} system and measured concentration of free catechol and complexed catechol.[a]

Solution pH	Total Concentration (mM) Total catechol	Total Al^{III}	Free catechol	Calculated Concentration (mM) $[Al(cat)]^{+}$	$[Al(cat)OH]^{0}$	$[Al(cat)_2]^{-}$	$[Al(cat)_2OH]^{2-}$	$[Al(cat)_3]^{3-}$	Measured Concentration Free catechol	Complexed catechol
9.9	1.0	0.17	0.55	—	—	—	0.06	0.11	0.63	0.12
8.8	1.0	1.0	0.03	—	—	0.08	0.39	0.01	0.07	0.37
8.1	1.0	0.10	0.79	—	—	0.05	0.04	0.01	0.81	0.06
8.1	1.0	0.30	0.39	—	—	0.14	0.14	0.01	0.45	0.23
7.2	1.0	0.50	0.18	0.01	0.10	0.32	0.04	—	0.48	0.13
4.8	1.0	0.33	0.74	0.25	0.01	—	—	—	0.80	—

[a]Calculated concentrations were obtained using SOLGAWATER[16] and stability constants from ref. 10. Measured concentrations are from cyclic voltammetric peak heights, $v = 100$ mV s^{-1}, using a base-pretreated GC electrode. Measured concentrations of complexes assume that one catechol ligand per complex is electroactive.

Pergamon

PII: S0277-5387(96)00425-1

Polyhedron Vol. 16, No. 8, pp. 1273–1277, 1997
Copyright © 1997 Elsevier Science Ltd
Printed in Great Britain. All rights reserved
0277-5387/97 $17.00+0.00

Synthesis, crystal structure and magnetic properties of a manganese(III) complex with bound water and double hydrogen-bonding bridges

Xiang Shi Tan,[a] Dao Feng Xiang,[a] Wen Xia Tang[a]* and Min Qin Chen[b]

[a] State Key Laboratory of Coordination Chemistry, Coordination Chemistry Institute, Nanjing University, Nanjing 210093, P.R. China

[b] Research Center of Analysis & Measurement, Fudan University, Shanghai 200433, P.R. China

(Received 6 June 1996; accepted 22 August 1996)

Abstract—The new manganese(III) complex $\{[HimH]^+[Mn(sal)_2(py)H_2O]^-\}_2$ (sal = salicylate, $C_7H_4O_3$; py = pyridine, C_5H_5N; $[HimH]^+$ = imidazole cation, $C_3H_5N_2$) has been prepared and characterized by X-ray analysis and magnetic measurements. The structure of the title complex consists of imidazole cations and two types of mononuclear Mn^{III} complex anions of $[Mn(1)(sal)_2(py)(H_2O)]^-$ and $[Mn(2)(sal)_2(py)(H_2O)]^-$. Each manganese(III) ion displays elongated octahedral geometry with water and pyridine molecules occupying axial sites. The equatorial plane is defined by four oxygen atoms from salicylates. Each Mn^{III} complex unit is linked to its neighbors above and below by pairs of Ow—H···O hydrogen bonds between bound water and two noncoordinating carboxylate oxygens of salicylates of the adjacent Mn^{III} units forming an infinite chain running parallel to the crystallographic *c*-axis. The two types of chains are cross-linked by N—H···O hydrogen bonds with imidazolium bridges. The magnetic properties of the title complex are reported and discussed. Copyright © 1997 Elsevier Science Ltd

Keywords: manganese; manganese complexes; crystal structures; magnetism; syntheses; hydrogen bonds.

The chemistry of manganese in various oxidation states is currently receiving much attention owing to its importance in many biological systems, such as superoxide dismutation [1], and peroxide disproportionation [2]. The most important is the realization that manganese plays an essential and specific role in the water-oxidizing complex of photosystem II (PSII) [3]. We now report the preparation, structure and magnetic properties of the title manganese(III) complex with bound water, which are important to understand the photosynthetic water oxidation center (WOC), since the ligand of water and its hydrogen bonding to carboxylate groups may be providing a glimpse into how the WOC binds its substrate H_2O and activates it to deprotonation, a necessary step in water oxidation. The compound is also interesting for its novel hydrogen bonding character.

* Author to whom correspondence should be addressed.

EXPERIMENTAL

Preparations

$(NBu^n_4)MnO_4$ [4] was prepared as described previously. $[Mn_3O(O_2CPh)_6(Im)_2(H_2O)]$ was synthesized according to a similar method to that used for $[Mn_3O(O_2CPh)_6(py)_2(H_2O)]\cdot CH_3CN$ [5]. Other chemicals were reagent grade and used as received.

To a stirred brown solution of $[Mn_3O(O_2CPh)_6(Im)_2(H_2O)]$ (0.50 mmol) in CH_3CN was added solid salicylic acid (2.0 mmol). The acid soon dissolved and the brown solution turned deep black gradually. The resulting solution was stirring for 30 min and filtered in order to remove a green–gray precipitate. The black crystals of the title complex were grown by diffusion in pyridine/ether atmosphere at room temperature and collected by filtration, washed with CH_3CN and Et_2O, and dried *in vacuo*. The yield was 53.5% (based on Mn). The crystals were suitable for

X-ray crystallography. Found C, 53.5; H, 4.0; N, 8.4; Mn, 11.6. Calc. for $C_{44}H_{40}Mn_2N_0O_{14}$: C, 53.7; N, 3.9; N, 8.5; Mn, 11.2%.

X-ray crystallography

A suitable single crystal was mounted on glass fibre and aligned on an Enraf-Nonius CAD-4 diffractometer for data collection. Cell parameters were determined on the basis of 25 reflections with $12 < \theta < 13°$. Intensity data were obtained with graphite-monochromated Mo-$K\alpha$ radiation ($\lambda = 0.71073$ Å) and ω–2θ scan mode in the range $0 < 2\theta < 50°$ at room temperature. During data collection, the intensity of three standard reflections monitored at 3600 s of X-ray exposure time showed no significant decay. After taking into account Lorentz and polarization effects, an empirical absorption correlation based on a series of PSI scans was applied to the data. Relative transmission coefficients ranged from 0.706 to 0.997. The structure solution by the direct methods (MULTAN-86) revealed the metal-atom coordinates and subsequently difference Fourier methods yielded positions of all the remaining non-H atoms and most of the hydrogen atoms. All non-H atoms were refined anisotropically by unit-weight full-matrix least-squares, while the hydrogen atoms, located from the difference Fourier maps, were riding on the related carbon atoms with fixed isotropic thermal parameters in the refinement. Refinement converged at $R = 0.048$ and $Rw = 0.053$ for 2083 observed reflections with $I > 3\sigma(I)$ of 3839 unique ones. A final difference-Fourier map exhibited no significant peaks greater than 0.40(6) e Å^{-3}. Scattering factors were taken from International Table for X-ray crystallography (1974). All computations were performed on a Micro Vax II computer using SDP/VAX and ORTEP programs.

Physical measurements

Magnetic measurements on powder samples were measured by using a CAHN-2000 Faraday-type magnetometer in the 77–300 K temperature range. The apparatus was calibrated with $[Ni(en)_3]S_2O_3$ (en = ethylenediamine). Diamagnetic corrections were made using Pascal's constants.

RESULTS AND DISCUSSION

Description of the crystal structure

Parameters for data collection and refinement are given in Table 1. Selected bond distances and angles are listed in Table 2. Important hydrogen-bonding parameters are listed in Table 3. The structures for the title complex are showed in Fig. 1 and 2, respectively. The crystal structure consists of imidazolium cations and two types of independent mononuclear

Table 1. Crystallographic data for the title complex

Formula	$C_{44}H_{40}Mn_2N_6O_{14}$
Formula weight	986.72
Crystal system	Monoclinic
Space group	$P2/c$
a (Å)	15.576(2)
b (Å)	11.432(2)
c (Å)	12.268(3)
β (°)	90.11(2)
V (Å^3)	2184.5(1)
Z	2
Crystal size (mm)	$0.10 \times 0.10 \times 0.15$
d_{calc} (g cm^{-3})	1.50
μ(Mo-$K\alpha$) (mm^{-1})	6.27
No. of parameter refined	302
R^a	0.048
Rw^a	0.053
S	1.89

[a] $R + \Sigma|F_o - F_c|/\Sigma F_o$.
[b] $Rw = [\Sigma w(F_o - F_c)^2/\Sigma wF_o^2]^{1/2}$.

manganese(III) complex units, $[Mn(1)(sal)_2(py)(H_2O)]^-$ (Mn1 unit) [Fig. 1(a)] and $[Mn(2)(sal)_2(py)(H_2O)]^-$ (Mn2 unit) [Fig. 1(b)]. As illustrated in Fig. 1(a, b), each Mn^{III} ion is hexacoordinate and possesses and NO_5 ligand environment by virtue of two bidentate salicylate ligands that form an equatorial plane and two axial ligands of a pyridine and a H_2O molecule. Each Mn^{III} unit has C_2 symmetry, with the rotation axis passing through O(w1), Mn(1), N(11) and C(14) for the Mn(1) unit and O(w2), Mn(2), N(31) and C(34) atoms for the Mn(2) unit. In terms of angles within the coordination sphere, $MnNO_5$ is close to an octahedron. The ranges of *cis* and *trans* angles at the Mn^{III} centers are 88.1(2)–92.0(2)°, 178.0(2)–180.1(6)° for the Mn(1) unit and 88.1(2)–91.9(2)°, 177.8(2)–180.1(6)° for the Mn(2) unit, respectively. The equatorial Mn–phenolic oxygen (O_p) and Mn–carboxylate oxygen (O_c) bond lengths are 1.878(4) [Mn(1)—O(1)], 1.917(4) Å [Mn(1)—O(9)] for the Mn(1) unit and 1.871 Å [Mn(2)—O(21)], 1.910(4) Å [Mn(2)—O(29)] for the Mn(2) unit, respectively, and close to those in $[Mn_4(sal)_4(H_2O)_4(py)_8]_n[salH]_{2n}\cdot 4npy$ [Mn—O_p = 1.854(5)–1.874(6) Å, Mn—O_c = 1.883(6)–1.928(6) Å] [6]. The axial Mn—Ow distances are 2.213(7) [Mn(1)—O(w1)] and 2.225(7) Å [Mn(2)—O(w2)], respectively, which are distinctly longer than those in the equatorial plane and similar to that in [Mn(sal)(bpy)(MeOH)Cl]·MeOH [7]. Such marked axial elongation is typical for a high-spin d^4 system.

There is a significant hydrogen-bonding interaction between neighboring Mn(1) units of Mn(2) units, involving two Ow—How of the water on one Mn^{III} unit and two non-coordinating carboxylate oxygens of salicylates on the adjacent Mn^{III} units. These interactions lead to a chain structure running parallel to the crystallographic c-axis, as an example the Mn(2)

Table 2. Selected bond distances (Å) and angles (°) for the title complex

Mn(1)—O(1)	1.878(4)	Mn(1)—O(9)	1.917(4)
Mn(1)—N(11)	2.368(8)	Mn(1)—Ow(1)	2.213(7)
Mn(2)—O(21)	1.871(4)	Mn(2)—O(29)	1.910(4)
Mn(2)—N(31)	2.369(7)	Mn(2)—Ow(2)	2.225(7)
O(1)—Mn(1)—O(1′)	179.5(2)	O(1)—Mn(1)—O(9)	92.0(2)
O(1)—Mn(1)—O(9′)	88.1(2)	O(1)—Mn(1)—N(11)	90.2(2)
O(1)—Mn(1)—Ow(1)	89.8(2)	O(1′)—Mn(1)—O(9)	88.1(2)
O(1′)—Mn(1)—O(9′)	92.0(2)	O(1′)—Mn(1)—N(11)	90.2(2)
O(1′)—Mn(1)—Ow(1)	89.8(2)	O(9)—Mn(1)—O(9′)	178.0(2)
O(9)—Mn(1)—N(11)	89.0(1)	O(9)—Mn(1)—Ow(1)	91.0(1)
O(9′)—Mn(1)—N(11)	89.0(1)	O(9′)—Mn(1)—Ow(1)	91.0(1)
N(11)—Mn(1)—Ow(1)	180.1(6)	O(21)—Mn(2)—O(21′)	179.5(2)
O(21)—Mn(2)—O(29)	91.9(2)	O(21)—Mn(2)—O(29′)	88.1(2)
O(21)—Mn(2)—N(31)	90.3(2)	O(21)—Mn(2)—Ow(2)	89.7(2)
O(21′)—Mn(2)—O(29)	88.1(2)	O(21′)—Mn(2)—O(29)	91.9(2)
O(21′)—Mn(2)—N(3)	190.3(2)	O(21′)—Mn(2)—Ow(2)	89.7(2)
O(29)—Mn(2)—O(29′)	177.8(2)	O(29)—Mn(2)—N(31)	88.9(1)
O(29)—Mn(2)—Ow(2)	91.1(1)	O(29′)—Mn(2)—N(31)	88.9(1)
O(29′)—Mn(2)—Ow(2)	91.1(1)	N(31)—Mn(2)—Ow(2)	180.1(2)

Table 3. Hydrogen-bonding parameters for the title complex

A···H—D	A···H (Å)	H—D (Å)	A···D (Å)	<ADH°
O(10)···How(1)—Ow(1)	1676(4)	1.008(3)	2.666(5)	166.5(3)
O(30)···How(2)—Ow(2)	1.925(4)	0.793(2)	2.653(5)	152.2(4)
O(10)···H(42)—N(42)	2.042(4)	0.950(6)	2.979(7)	168.4(5)
O(30)···H(40)—N(40)	2.011(4)	0.990(6)	2.975(7)	164.3(5)

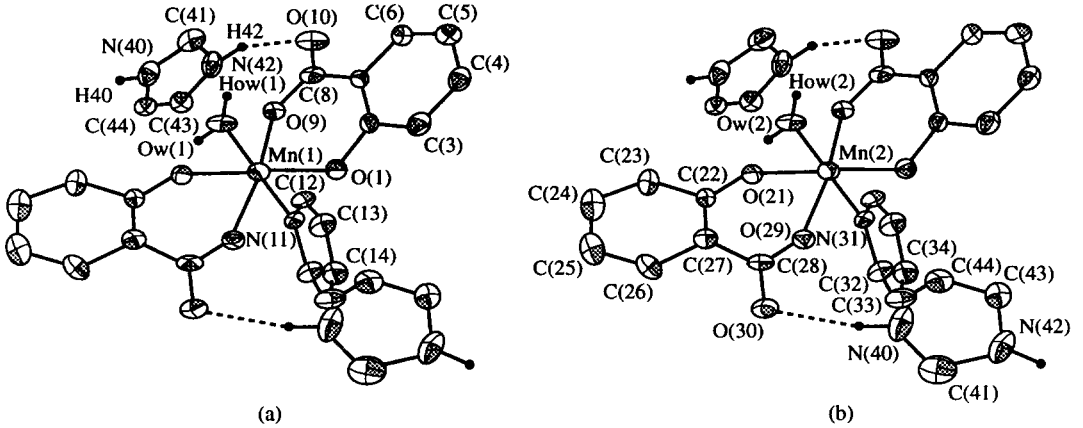


Fig. 1. Molecular structure for (a) the Mn(1) unit and (b) the Mn(2) unit of the title complex showing 25% probability displacement ellipsoids (except the H atoms of water and imidazolium, all other H atoms are omitted for clarity).

unit chain is depicted in Fig. 2. In the chain each Mn(2) unit is linked to its neighbors above and below by pairs of O(30)···H(ow2)—O(w2) hydrogen bonds. The O(30)···O(w2) and H(ow2)—O(w2) distances and O(30)···H(ow2)—O(w2) angle are 2.653(5), 0.793 Å and 152.2(4)°, respectively. Additionally, every $[HimH]^+$ cation is associated with two Mn^{III} complex units [Mn(1) unit and Mn(2) unit] through hydrogen bonds of N(42)—H(42)···O(10) and N(40)—H(40)···O(30), respectively. So the two

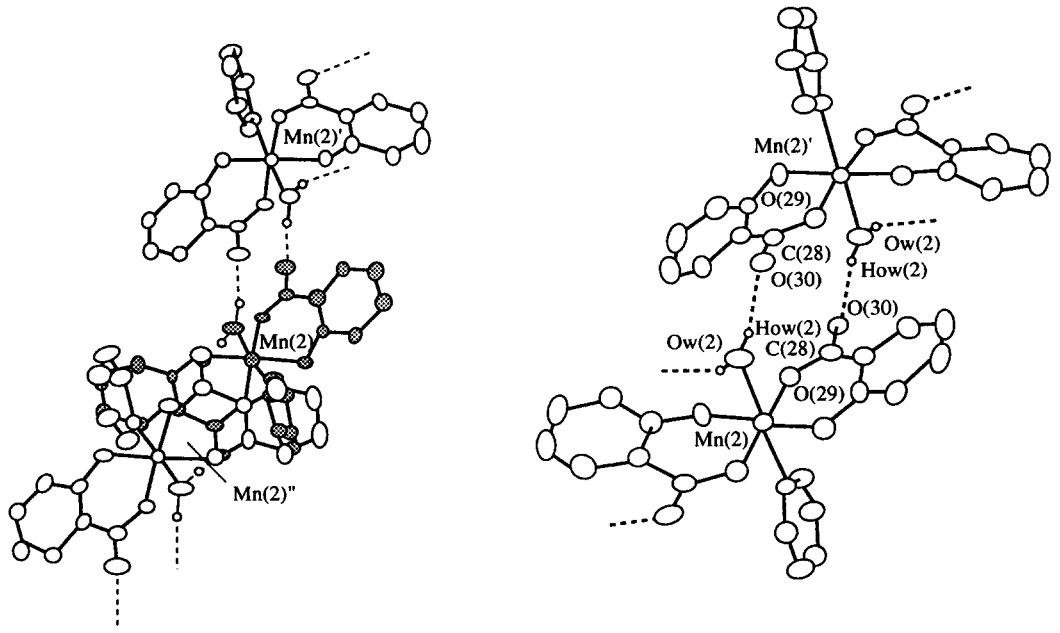


Fig. 2. Part of the Mn(2) unit chain showing the polymeric nature by double hydrogen-bonding bridges. Broken lines represent hydrogen bonds.

types of Mn^{III} unit chains are cross-linked by N—H···O hydrogen bonds with imidazolium bridges. All the hydrogen bonding parameters are listed in Table 3.

Magnetic properties

The temperature dependence of the magnetic susceptibility per $[HimH]^+[Mn(sal)_2(py)(H_2O)]^-$ for the title compound in the form of χ_M *vs* T is shown in Fig. 3. The magnetic moment of the compound per

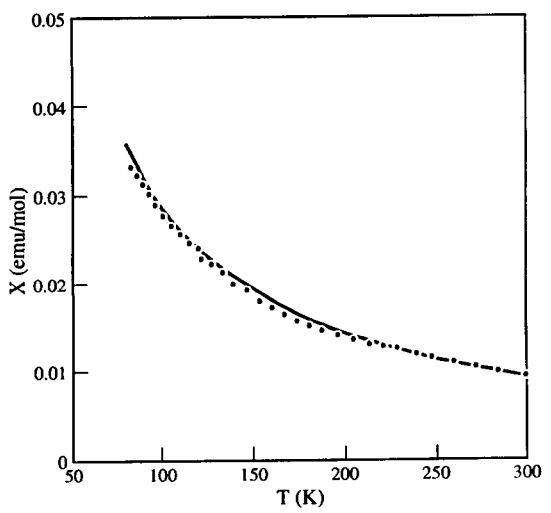


Fig. 3. Temperature dependence of the molecular magnetic susceptibility per $[HimH]^+$ $[Mn(sal)_2(py)(H_2O)]^-$ for the title complex.

$[HimH]^+[Mn(sal)_2(py)(H_2O)]^-$ for the title complex at 285 K is 4.88 B.M., which is close to spin-only value of 4.89 B.M. expected for one uncoupled high-spin Mn^{III} ion ($S = 2$). When the temperature is lowered, the magnetic moment of the title complex decreases slightly and reaches a value of 4.70 B.M. at 78 K, which may be due to zero-field splitting of the ground state and intermolecular magnetic interaction. The crystal structure of the title complex shows the Mn^{III} centre to exist in a distorted octahedral arrangement as a result of the Jahn–Teller effect. Due to the axial distortion and spin-orbit coupling, the $S = 2$ state is split into three zero-field split levels, $Ms = 0, \pm 1$ and ± 2, the separation between Ms = 0 and ± 1 and between Ms = 0 and ± 2 being D and $4D$, respectively. By use of spin-Hamiltonian formalism of the form [eq. (1)] [8] in which any rhombic splitting was ignored, D is the ZFS parameter).

$$H = DS_z^2 + g\beta H \cdot S \qquad (1)$$

the following equation for the principal magnetic susceptibility can be derived [8,9]:

$$X_{\parallel} = 2Ng^2\beta^2/KT \cdot (e^{-D/KT} + 4e^{-4D/KT})/(1 + 2e^{-D/KT} + 2e^{-4D/KT})$$

$$X_{\perp} = Ng^2\beta^2/3D \cdot (18 - 14e^{-D/KT} - 4e^{-4D/KT})/(1 + 2e^{-D/KT} + 2e^{-4D/KT})$$

$$X_M = (X_{\parallel} + 2X_{\perp})/3.$$

To describe the intermolecular interactions, a molecular field term [10] was added and the expression for the magnetic susceptibility becomes:

$$X'_M = X_M/(1\text{-}2xJ'X_M/Ng^2\beta^2). \qquad (2)$$

Using eq. (2) the data of the compound were analyzed at 77–300 K and the best fit parameters obtained are $g = 2.00$ $D = -4.51$ cm^{-1}, $zJ' = -0.83$ cm^{-1}, and $R = 8.23 \times 10^{-4}$, where $R = \Sigma(X_{calcd} - X_{obs})^2/\Sigma(X_{obs})^2$.

The D value found here is in agreement with the literature data in the range -1 to -8 cm^{-1} for some high-spin Mn^{III} complexes [6,7,11]. The zJ' value at -0.83 cm^{-1} reflects the possibility of weak antiferromagnetically intermolecular exchange interaction through hydrogen bonds and magnetic dipole–dipole interactions.

REFERENCES

1. Michelson, J. M., McCord, J. M. and Fridovich, I., *Superoxide and Superoxide Dismutase*. Academic: New York, 1977.
2. (a)Fronko, R. M. and Penner-Hahn, J. E., *J. Am. Chem. Soc.* 1988, **110,** 7554; (b) Beyer, W. F. and Fridovich, I., *Biochemistry*, 1985, **24,** 64607; (c) Kono, Y. and Fridovich, I., *J. Biol. Chem.* 1983, **258,** 6015.
3. Weighardt, K., *Angew. Chem. Int. Ed. Engl*, 1989, **28,** 115.
4. Sala, T. and Sargent, M. V., *J. Chem. Soc., Chem. Commun.* 1978, 253.
5. Vincent, J. B., Chang, H.-R., Folting, K., Huffman, J. C., Christou, G. and Hendrickson, D. N., *J. Am. Chem. Soc.* 1987, **109,** 5703.
6. Tan, X. S., Chen, J., Chen, Z. N., Zheng, P. J. and Tang, W. X., *Inorg. Chim. Acta*, 1995, **234,** 27.
7. Tan, X. S., Chen, J., Zheng, P. J. and Tang, W. X., *Polyhedron*, 1996, **15,** 2087.
8. Behere, D. V. and Mitra, S., *Inorg. Chem.* 1980, **19,** 992.
9. Klein, C. L., O'Connor, C. J., Majeste, R. J. and Trefonas, L. M., *J. Chem. Soc., Dalton Trans.* 1982, 2419.
10. Carlin, R. L., *Magnetochemistry*. Springer, Berlin, Heidelberg, 1986.
11. Kennedy, B. J. and Murray, K. S., *Inorg. Chem.* 1985, **24,** 1552.

Pergamon

PII: S0277-5387(96)00424-X

Polyhedron Vol. 16, No. 8, pp. 1279–1289, 1997
Copyright © 1997 Elsevier Science Ltd
Printed in Great Britain. All rights reserved
0277-5387/97 $17.00+0.00

Synthesis and structure of mono- and binuclear copper(II) complexes with polyfunctional nitroxide 4-(1′carboxy-2′-oxopropylidene)-2,2,5,5-tetramethyl-3-imidazolidine-1-oxyl, $[Cu(LH)_2(H_2O)_2]$ and $[Cu_2L_2(H_2O)_5]$. Caterpillar-like reaction

Victor I. Ovcharenko,[a]* Kira E. Vostrikova,[a] Alexei V. Podoplelov,[a] Galina V. Romanenko,[b] Vladimir N. Ikorskii[b] and Vladimir A. Reznikov[c]

[a] International Tomography Center, Russian Academy of Sciences, Siberian Branch, Institutskaya St. 3A, 630090 Novosibirsk, Russia

[b] Institute of Inorganic Chemistry, Russian Academy of Sciences, Lavrentiev Av. 3, 630090 Novosibirsk, Russia

[c] Institute of Organic Chemistry, Russian Academy of Sciences, Lavrentiev Av. 7, 630090 Novosibirsk, Russia

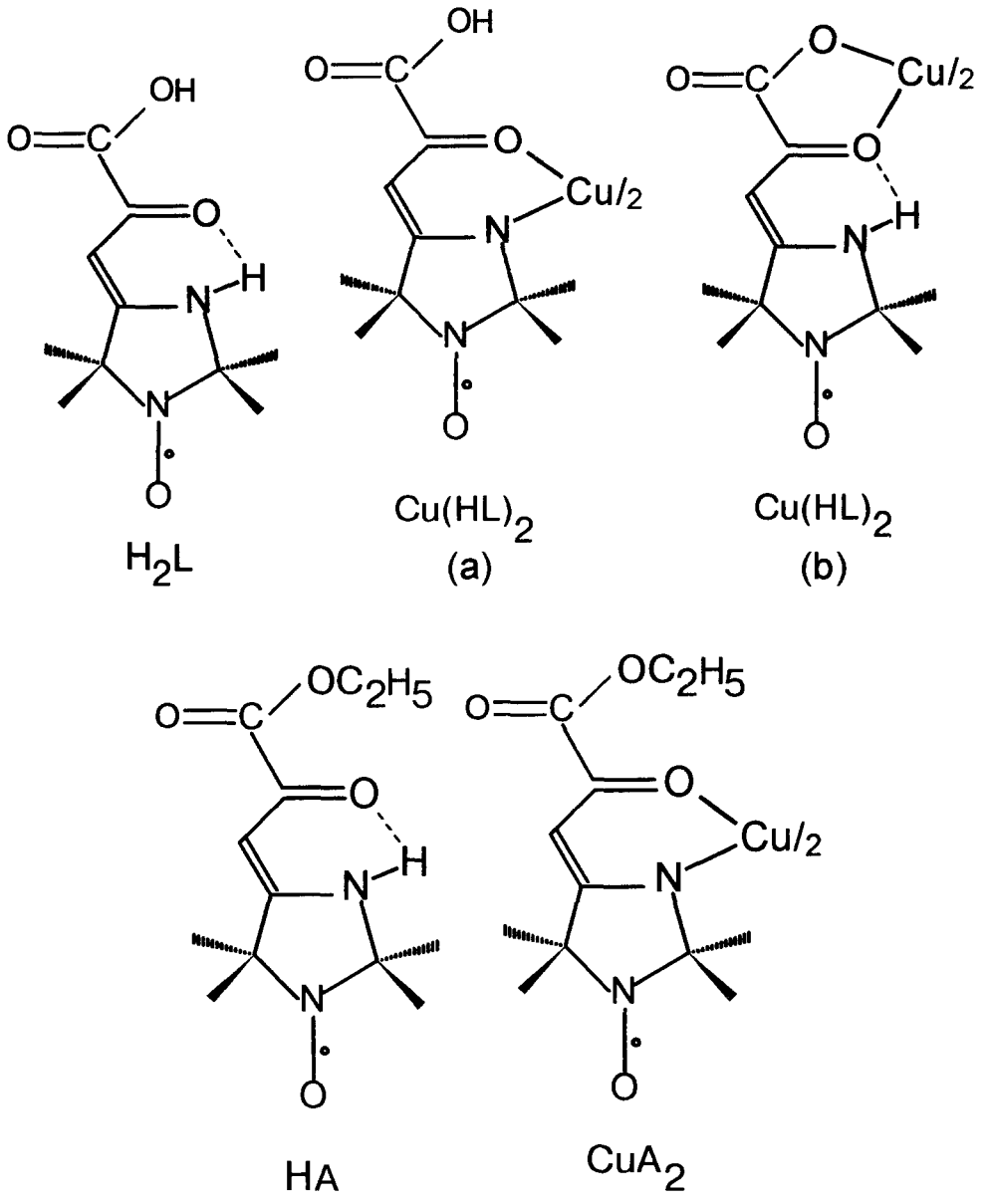
(Received 10 May 1996; accepted 22 August 1996)

Abstract—Cu^{II} reacted with the polyfunctional nitroxide 4-(1′-carboxy-2′-oxopropylidene)-2,2,5,5-tetramethyl-3-imidazolidine-1-oxyl (H_2L; $Cu/H_2L = 1:2$) to yield $Cu(LH)_2(H_2O)_2$, which was characterized by strong fixation of water molecules exclusively by hydrogen bonds. In the interaction of $Cu(LH)_2(H_2O)_2$ with an additional amount of Cu^{II} ($Cu/H_2L = 1:1$), the ligands moved towards each other in parallel directions to form the binuclear compound $Cu_2L_2(H_2O)_5$. This process is very unusual in coordination chemistry. Copyright © 1997 Elsevier Science Ltd

Keywords: complexes with nitroxides; structure; unusual reaction.

Many current studies of metal complexes with stable nitroxides are concerned with the search for the combinations of nitroxide functional groups that provide effective complexation in solutions and lead to the formation of metal-ion-induced self-assembly chain, layered and frame heterospin polymers in solids, which is favorable for the occurrence of cooperative magnetic phenomena [1–3]. This is a challenging problem, therefore, the nitroxide derivatives used in the syntheses become increasingly complicated, involving several functional groups [4–8]. In this work, we synthesized the Cu^{II} complexes with the polyfunctional nitroxide 4-(1′-carboxy-2′-oxopropylidene)-2,2,5,5-tetramethyl-3-imidazolidine-1-oxyl (H_2L). Since H_2L contains both enamineketone and α-ketocarboxylate functional groups and each of them is favorable to the formation of chelate rings [structures **a** and **b** in Scheme 1], it was difficult to predict which chelate ring would be formed preferably. Nevertheless, on both cases, there was a possibility of bonding to one more metal ion due to the free donor [carboxylate (**a**) or amino (**b**)] group, which is, in principle, favorable to the formation of polymeric compounds. This determined our choice of Cu^{II}. If the first step of the complex formation followed path (a), the additional Cu^{II} could be bonded through the carboxylate group. The resulting classical bridging copper carboxylates could form polymeric layers (Fig. 1). In path (b), the introduction of additional Cu^{II} should lead to the for-

* Author to whom correspondence should be addressed.



Scheme 1.

mation of polymeric structures due to bonding to the nitrogen of the secondary amino groups.

It should be noted that H_2L arises in the hydrolysis of the ethyl carboxylate HA, which was used to obtain layered polymeric CuA_2 capable of ferromagnetic ordering [9]. The layered polymeric structure of solid CuA_2 was formed due to the coordination of the N•—O oxygens of neighboring molecules by copper ions. We could not rule out a similar way of coordination of the nitroxide in the Cu^{II} complexes with H_2L (Scheme 1).

The above considerations seem to be quite reasonable. Therefore, it was rather unexpected that when the Cu : L proportion in the reaction mixture reached 1 : 1, the initially formed mononuclear complex transformed into the binuclear one. During this transformation the polyfunctional ligands moved toward each other, which is unusual for the chemistry of coordination compounds. This process can be presented by Scheme 2. The scheme shows that, in fact, one of the ligands creeps on copper ions like a caterpillar. Therefore, we designated this process as a caterpillar-like reaction. For metal complexes with paramagnetic organic ligands, this reaction is reported for the first time [10].

EXPERIMENTAL

Preparation of $Cu(HL)_2(H_2O)_2$

A solution of $Cu(CH_3COO)_2(H_2O)$ (0.88 g, 4.4 mmol) in water (40 cm^3) was added to a solution of H_2L (2 g, 8.8 mmol) in ethanol (40 cm^3). The resulting

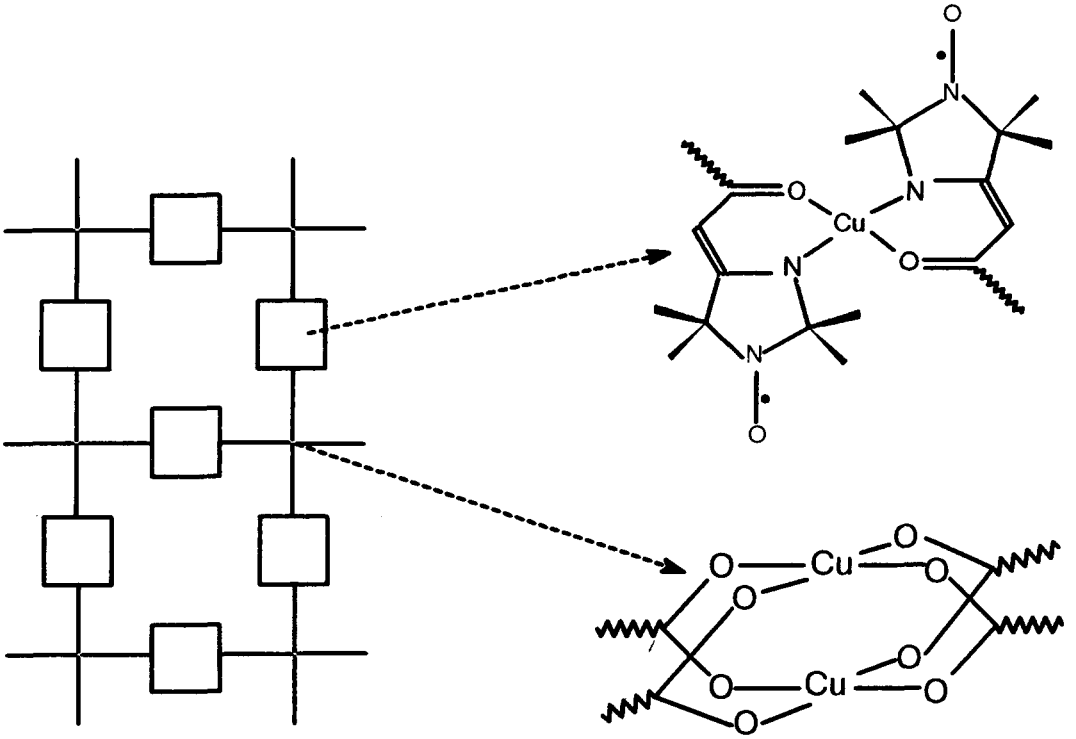
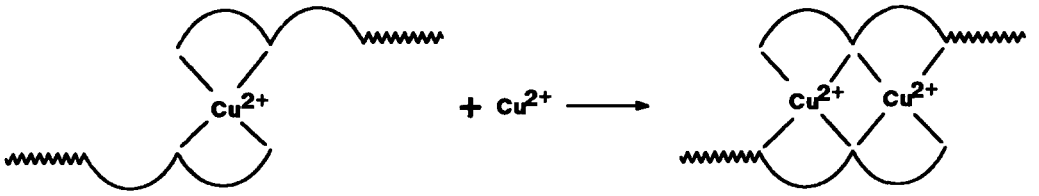


Fig. 1. Hypothetical scheme of the layered polymeric structure. Squares denote bischelate fragments; the intersection points of the straight lines correspond to binuclear carboxylate nodes.



Scheme 2.

mixture was stirred and refluxed for 5 min, then it was evaporated to a small bulk and the solid precipitate was filtered off, washed with water and dried *in vacuo* over $Mg(ClO_4)_2$. Recrystallization from an EtOH : H_2O mixture (1 : 1) afforded green octahedra of $Cu(HL)_2(H_2O)_2$ in 60% yield (1.7 g).

Noteworthy is that the recrystallization from hot absolute ethanol produces light green crystals of $Cu(HL)_2(C_2H_5OH)_2$ (75% yield), which are unstable in air, since the water molecules slowly replace the alcohol ones.

Preparation of $Cu_2L_2(H_2O)_5$ *and* Cu_2L_2

A solution of H_2L (0.45 g, 2 mmol) in ethanol (10 cm^3) was added to a solution of $Cu(CH_3COO)_2(H_2O)$ (0.4 g, 2 mmol) in water (10 cm^3). Then NaOH (0.14 g, 3.5 mmol) was added to the mixture. The reaction mixture was heated to boiling and ethanol was evaporated in a rotary evaporator. The water (10 cm^3) was added to the mixture and the solution was cooled to 0°C. The resulting deep green octahedra were filtered off, washed with water and dried *in vacuo* over $Mg(ClO_4)_2$. Recrystallization from an EtOH : H_2O mixture (1 : 1) afforded deep green crystals of $Cu_2L_2(H_2O)_5$ in 70% yield (0.47 g).

$Cu_2L_2(H_2O)_5$ can also be obtained by:

(a) heating an equimolar mixture of $Cu(HL)_2(H_2O)_2$ [or $Cu(HL)_2(C_2H_5OH)_2$)] and $Cu(CH_3COO)_2(H_2O)$ in a water : ethanol (1 : 1) solution, followed by adding a base and allowing the solution to stand for 24 h; or

(b) heating an ethanol–water solution of CuA_2 with NaOH, followed by adding $Cu(CH_3COO)_2(H_2O)$.

Cu_2L_2 was obtained in quantity by keeping $Cu_2L_2(H_2O)_5$ *in vacuo* at 70°C for 5–6 h.

Analytical data for $Cu(HL)_2(H_2O)_2$, $Cu(HL)_2(C_2H_5OH)_2$, $Cu_2L_2(H_2O)_5$ and Cu_2L_2 are in good agreement with the corresponding theoretical values.

Physical measurements

The IR spectra of the compounds tabletted in KBr were recorded on a UNICAM-75-IR spectrophotometer in the range 400–4000 cm^{-1}. The TG and DTA curves were obtained using a Paulik–Paulik–Erdey derivatograph for 50 mg samples in air at a heating rate of 2.5 K min^{-1}. The magnetic susceptibilities of the polycrystalline samples of the title complexes were measured by the Faraday technique over the temperature range 4.2–300 K. The samples were sealed in quartz ampoules. The molar magnetic susceptibilities were calculated as corrected for the atomic diamagnetism and temperature-independent paramagnetism of Cu^{2+}.

Crystal structure determination

Experimental data for the single crystals of $Cu(HL)_2(H_2O)_2$ and $Cu_2L_2(H_2O)_5$ were collected on the automatic four-circle diffractometers SYNTEX $P2_1$ and CAD4, respectively, using a standard procedure. The parameters of the monoclinic unit cells and the details of data collection and structure refinement are listed in Table 1. The structures were solved by direct methods (SHELXS-86) [11] and refined by the full-matrix least-squares procedure in the anisotropic approximation for all nonhydrogen atoms. For both structures hydrogen atoms were located on difference Fourier maps and included in the refinement in the isotropic approximation. All calculations concerning the structure refinement were performed using the SHELXL-93 programs [12]. Selected bond length distances and bond angles are given in Tables 2 and 3.

RESULTS

Mononuclear complex

$Cu(CH_3COO)_2(H_2O)$ interacts with H_2L (1 : 2) in a water : ethanol mixture to form the solvated bischelate $Cu(HL)_2$. In numerous attempts to obtain single crystals of this product we revealed the following. The second and third recrystallization of the product from water-containing ethanol yield green crystals of $Cu(HL)_2(H_2O)_2$ together with light green crystals of $Cu(HL)_2(C_2H_5OH)_2$. Increasing the H_2O/C_2H_5OH ratio in the solvent used for the recrystallization shar-

Table 1. Crystallographic data and some experimental details for $Cu(HL)_2(H_2O)_2$ (**1**) and $Cu_2L_2(H_2O)_5$ (**2**)

	1	**2**
Formula	$C_{20}H_{32}CuN_4O_{10}$	$C_{20}H_{36}Cu_2N_4O_{13}$
Fw	552.04	667.62
T (K)	293(2)	293(2)
λ (Å)	1.54180	0.71069
Crystal system	Monoclinic	Monoclinic
Space group, *Z*	$P2_1/c$, 2	$P2_1/c$, 4
Cell dimensions: *a* (Å)	5.862(2)	14.722(3)
b (Å)	11.843(2)	16.867(3)
c (Å)	18.423(8)	11.873(2)
β (°)	103.56(3)	102.97(3)
V (Å^3)	1243.3(7)	2873.0(9)
D_{calc} (g cm^{-3})	1.475	1.543
μ (mm^{-1})	1.773	1.547
F(000)	578	1384
Monochromator	Graphite	Graphite
Crystal size (mm)	$0.5 \times 0.4 \times 0.2$	$0.8 \times 0.18 \times 0.06$
θ range for data collection (°)	4.48–54.91	1.42–21.97
Index ranges	$0 \leqslant h \leqslant 6$,	$-15 \leqslant h \leqslant 15$
	$0 \leqslant k \leqslant 12$,	$-17 \leqslant k \leqslant 0$
	$-19 \leqslant l \leqslant 18$	$0 \leqslant l \leqslant 10$
I (meas)	1741	3033
I (uniq)	1560 (R_{int} = 0.0166)	2846 (R_{int} = 0.0573)
Data/restraints/parameters	1557/0/225	2846/0/497
GOOF	0.998	1.040
Final *R* indices [$I > 2\sigma(I)$]	R_1 = 0.0402,	R_1 = 0.0460
	wR_2 = 0.1064	wR_2 = 0.1283
R indices (all data)	R_1 = 0.0459,	R_1 = 0.0653
	wR_2 = 0.1100	wR_2 = 0.1468
Extinction coefficient	0.00030(12)	0.00029(10)
Largest difference peak and	0.231	0.742
hole (e Å^{-3})	−0.273	−0.877

Table 2. Selected bond lengths (Å) and angles (°) for $Cu(HL)_2(H_2O)_2$

Cu—O(111)	1.9131(6)	Cu—O(1)	1.9179(6)
O(111)—C(11)	1.291(1)	O(112)—C(11)	1.217(1)
C(11)—C(1)	1.534(1)	O(1)—C(1)	1.284(1)
C(1)—C(2)	1.368(1)	N(1)—C(3)	1.307(1)
N(1)—C(4)	1.469(1)	N(1)—H(1n1)	1.09(1)
C(2)—C(3)	1.412(1)	C(2)—H(1c2)	0.869(8)
C(3)—C(5)	1.503(1)	C(4)—N(11)	1.47(1)
C(4)—C(42)	1.507(2)	C(4)—C(41)	1.527(2)
N(11)—O(11)	1.252(1)	N(11)—C(5)	1.489(1)
C(5)—C(52)	1.518(2)	C(5)—C(51)	1.520(1)
O(1w)—H(1w)	0.671(9)	O(1w)—H(2w)	0.84(8)
O(111)—Cu—O(1)	85.05(3)	C(11)—O(111)—Cu	113.76(6)
O(112)—C(11)—O(111)	125.86(9)	O(112)—C(11)—C(1)	121.25(8)
O(111)—C(11)—C(1)	112.88(8)	C(1)—O(1)—Cu	112.13(6)
O(1)—C(1)—C(2)	123.82(8)	O(1)—C(1)—C(11)	115.26(7)
C(2)—C(1)—C(11)	120.87(8)	C(3)—N(1)—C(4)	115.99(7)
C(3)—N(1)—H(1n1)	129.0(8)	C(4)—N(1)—H(1n1)	114.3(8)
C(1)—C(2)—C(3)	121.63(8)	C(1)—C(2)—H(1c2)	120.8(5)
C(3)—C(2)—H(1c2)	117.5(5)	N(1)—C(3)—C(2)	125.68(7)
N(1)—C(3)—C(5)	110.74(8)	C(2)—C(3)—C(5)	123.54(8)
N(1)—C(4)—N(11)	98.61(7)	N(1)—C(4)—C(42)	110.88(8)
N(11)—C(4)—C(42)	111.65(8)	N(1)—C(4)—C(41)	110.82(8)
N(11)—C(4)—C(41)	110.83(9)	C(42)—C(4)—C(41)	113.17(9)
O(11)—N(11)—C(4)	121.93(8)	O(11)—N(11)—C(5)	123.29(7)
C(4)—N(11)—C(5)	114.74(7)	N(11)—C(5)—C(3)	99.74(7)
N(11)—C(5)—C(52)	110.39(8)	C(3)—C(5)—C(52)	112.45(8)
N(11)—C(95)—C(51)	109.40(8)	C(3)—C(5)—C(51)	113.28(8)
C(52)—C(5)—C(51)	111.02(8)	H(1w)—O(1w)—H(2w)	99(2)

ply increases the amount of the $Cu(HL)_2(H_2O)_2$ crystals. When the $H_2O : C_2H_5OH$ ratio is close to 1 : 1 and higher, only the $Cu(HL)_2(H_2O)_2$ crystals are isolated in the solid phase. Pure $Cu(HL)_2(C_2H_5OH)_2$ [without $Cu(HL)_2(H_2O)_2$ admixture] is obtained by the recrystallization of the complex from absolute ethanol. The $Cu(HL)_2(C_2H_5OH)_2$ crystals are unstable in air, since the water molecules slowly replace alcohol molecules [13]. In $Cu(HL)_2(H_2O)_2$, in contrast, water molecules are strongly bound. The complex does not lose water on heating (neither in air or *in vacuo*) up to the decomposition temperature ($\sim 120°C$). This is rather unusual since in $Cu(HL)_2(H_2O)_2$ the water molecules are not coordinated by the metal ion, being held in the solid complex due to hydrogen bonds (Fig. 2).

Crystal structure and magnetic properties of $Cu(HL)_2(H_2O)_2$

The $Cu(HL)_2(H_2O)_2$ complex has a molecular structure. A centrosymmetric molecule of the complex is shown in Fig. 2. The paramagnetic ligand is bonded in a bidentate fashion to the copper atom by the oxygens of the deprotonated carboxylate group and the keto group of the enamineketone fragment. In the resulting five-membered chelate ring, the Cu—O bond lengths are on the average 1.915 Å, the OCuO angle being 85.05(3)°. Thus, two coordinated LHs form a centrosymmetric square around the copper atom. The water molecules are outside the coordination sphere of the metal. The N—H hydrogen of the ligand forms the H(1n1)···O(1) bond (2.124 Å), with the coordinated enamineketone oxygen and the H(1n1)···O(1w) bond (1.906 Å) with the water molecule, which is also bonded to the noncoordinated carboxyl oxygen of the ligand of the neighboring molecule [H(1w)···O(112′) is equal to 2.196 Å]. As mentioned above, the involvement of the water molecules in several hydrogen bonds tends to hold them strongly in solid $Cu(HL)_2(H_2O)_2$.

In $Cu(HL)_2(H_2O)_2$ both intra- and intermolecular distances between the paramagnetic centers are rather large: within the molecules, the Cu···—•O distances are 7.900 Å, the shortest intermolecular distances Cu···O•— are no less than 5.152 Å and the shortest —•O···O•— and Cu···Cu distances are 5.862 Å. The large separation of the paramagnetic centers determines their weak interaction. Figure 3 shows the experimental and theoretical functions $\mu_{eff}(T)$ for $Cu(HL)_2(H_2O)_2$. The experimental data are adequately described by the theoretical curve, which was constructed according to the model of the isolated exchange cluster O•—N···Cu^{2+}···N—•O for $g_{Cu} = 2.07$, $J = -2.5\,cm^{-1}$ and $zJ' = -0.1\,cm^{-1}$. The analytical expressions used in calculating the exchange cluster O•—N···Cu^{2+}···N—•O are given elsewhere

Table 3. Selected bond lengths (Å) and angles (°) for $Cu_2L_2(H_2O)_5$

Cu(1)—O(2)	1.973(2)	Cu(1)—N(1)	1.969(2)
Cu(1)—O(611)	1.945(2)	Cu(1)—O(1)	1.927(1)
Cu(1)—O(1w)	2.213(2)	Cu(1)—Cu(2)	3.0588(7)
Cu(2)—O(1)	1.962(2)	Cu(2)—N(2)	1.963(2)
Cu(2)—O(2)	1.953(1)	Cu(2)—O(111)	1.971(2)
Cu(2)—O(2w)	2.300(2)	O(111)—C(11)	1.272(3)
Cu(11)—O(112)	1.234(2)	C(11)—C(1)	1.518(3)
C(1)—O(1)	1.312(2)	C(1)—C(2)	1.353(3)
C(2)—C(3)	1.419(3)	C(3)—N(1)	1.299(3)
C(3)—C(4)	1.519(3)	N(1)—C(5)	1.460(3)
C(4)—C(41)	1.537(4)	C(4)—N(11)	1.459(3)
C(4)—C(42)	1.516(4)	N(11)—O(11)	1.273(3)
N(11)—C(5)	1.471(3)	C(5)—C(52)	1.517(4)
C(5)—C(51)	1.514(4)	O(611)—C(61)	1.273(3)
C(61)—O(612)	1.227(3)	C(61)—C(6)	1.535(3)
C(6)—O(2)	1.334(3)	C(6)—C(7)	1.326(3)
C(7)—C(8)	1.439(3)	C(8)—N(2)	1.308(3)
C(8)—C(9)	1.523(4)	N(2)—C(10)	1.480(3)
C(9)—N(21)	1.459(3)	C(9)—C(91)	1.498(3)
C(9)—C(92)	1.541(4)	N(21)—O(21)	1.266(3)
N(21)—C(10)	1.473(3)	C(10)—C(101)	1.498(3)
C(10)—C(102)	1.522(4)		

O(1)—Cu(1)—N(1)	91.06(7)	N(1)—Cu(1)—O(611)	106.60(7)
O(2)—Cu(1)—O(1)	76.41(6)	O(611)—Cu(1)—O(1)	152.04(6)
O(1)—Cu(1)—O(1w)	96.62(6)	N(1)—Cu(1)—O(1w)	99.47(7)
N(1)—Cu(1)—O(2)	162.96(6)	O(1)—Cu(2)—N(2)	162.71(7)
O(611)—Cu(1)—O(1w)	101.47(6)	O(2)—Cu(1)—O(1w)	93.50(6)
O(2)—Cu(2)—N(2)	91.12(7)	O(1)—Cu(2)—O(2)	76.06(6)
N(2)—Cu(2)—O(111)	107.73(7)	O(1)—Cu(2)—O(111)	81.70(6)
O(1)—Cu(2)—O(2w)	86.89(6)	N(2)—Cu(2)—O(2w)	106.90(7)
O(2)—Cu(2)—O(2w)	99.34(6)	O(111)—Cu(2)—O(2w)	92.50(6)
C(11)—O(111)—Cu(2)	114.46(13)	O(112)—C(11)—O(111)	125.9(2)
O(112)—C(11)—C(1)	119.2(2)	O(111)—C(11)—C(1)	114.9(2)
O(1)—C(1)—C(2)	123.1(2)	O(1)—C(1)—C(11)	112.4(2)
C(2)—C(1)—C(11)	124.5(2)	C(1)—O(1)—Cu(1)	126.3(1)
C(1)—O(1)—Cu(2)	113.4(1)	Cu(2)—O(1)—Cu(1)	103.74(7)
C(1)—C(2)—C(3)	123.4(2)	N(1)—C(3)—C(2)	127.4(2)
N(1)—C(3)—C(4)	112.6(2)	C(2)—C(3)—C(4)	119.9(2)
C(3)—N(1)—C(5)	112.7(2)	C(3)—N(1)—Cu(1)	123.2(2)
C(5)—N(1)—Cu(1)	124.1(1)	C(41)—C(4)—N(11)	109.8(2)
C(41)—C(4)—C(3)	110.5(2)	N(11)—C(4)—C(3)	99.5(2)
C(41)—C(4)—C(42)	112.5(2)	N(11)—C(4)—C(42)	110.7(2)
C(3)—C(4)—C(42)	113.1(2)	O(11)—N(11)—C(4)	123.9(2)
O(11)—N(11)—C(5)	122.8(2)	C(4)—N(11)—C(5)	113.3(2)
N(1)—C(5)—C(52)	111.6(2)	N(1)—C(5)—C(51)	110.6(2)
C(52)—C(5)—C(51)	112.9(2)	N(1)—C(5)—N(11)	101.7(2)
C(52)—C(5)—N(11)	109.2(2)	C(51)—C(5)—N(11)	110.2(2)
C(61)—O(611)—Cu(1)	115.6(1)	O(612)—C(61)—O(611)	124.7(2)
O(612)—C(61)—C(6)	119.8(2)	O(611)—C(61)—C(6)	115.3(2)
O(2)—C(6)—C(7)	124.1(2)	O(2)—C(6)—C(61)	110.2(2)
C(7)—C(6)—C(61)	125.6(2)	C(6)—O(2)—Cu(1)	114.0(5)
C(6)—O(2)—Cu(2)	124.1(1)	Cu(1)—O(2)—Cu(2)	102.36(7)
C(6)—C(7)—C(8)	123.0(2)	N(2)—C(8)—C(7)	127.5(2)
N(2)—C(8)—C(9)	113.1(2)	C(7)—C(8)—C(9)	119.3(2)
C(8)—N(2)—C(10)	112.1(2)	C(8)—N(2)—Cu(2)	123.1(2)
C(10)—N(2)—Cu(2)	124.7(1)	N(21)—C(9)—C(91)	110.8(2)
N(21)—C(9)—C(8)	99.1(2)	C(91)—C(9)—C(8)	112.6(2)
N(21)—C(9)—C(92)	109.2(2)	C(91)—C(9)—C(92)	111.3(2)
C(8)—C(9)—C(92)	113.0(2)	O(21)—N(21)—C(9)	123.5(2)
O(21)—N(21)—C(10)	122.1(2)	C(9)—N(21)—C(10)	114.4(2)
C(101)—C(10)—N(21)	109.5(2)	C(101)—C(10)—N(2)	111.4(2)
N(21)—C(10)—N(2)	101.1(2)	C(101)—C(10)—C(102)	114.2(2)
N(21)—C(10)—C(102)	110.2(2)	N(2)—C(10)—C(102)	109.7(2)

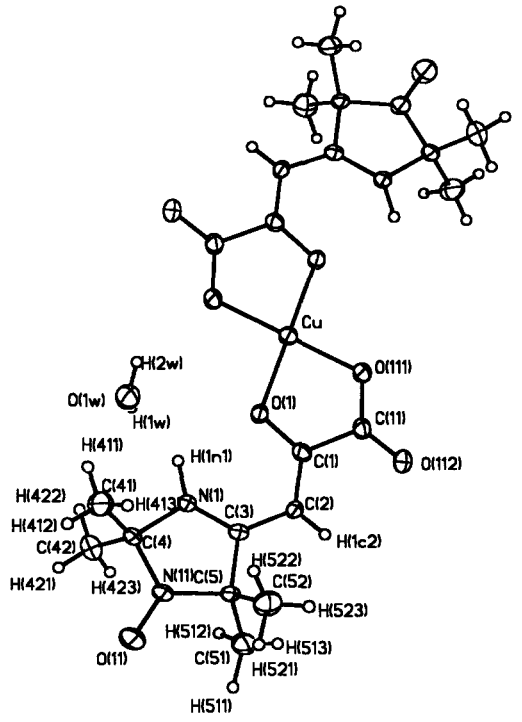


Fig. 2. Structure and atomic numbering of $Cu(HL)_2(H_2O)_2$.

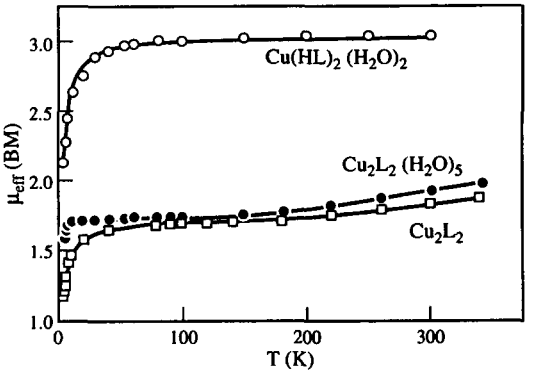


Fig. 3. Experimental magnetic data plotted as μ_{eff} *vs* temperature for $Cu(HL)_2(H_2O)_2$ (○), $Cu_2L_2(H_2O)_5$ (●) and Cu_2L_2 (□). The solid lines are the least-squares fits of the experimental data by the expressions given in the text. [For $Cu_2L_2(H_2O)_5$ and Cu_2L_2, μ_{eff} were calculated per half molecule, $CuL(H_2O)_{2.5}$ and CuL, respectively.]

[14]. The weak intramolecular exchange interaction ($-2.5\ cm^{-1}$) is in good agreement with the sufficiently large intramolecular distance between Cu^{2+} and the N—•O group. The very small value of zJ' accounts for the weak intercluster exchange interactions resulting from the very large intermolecular separation of the paramagnetic centers (> 5.1 Å).

Binuclear complex

Interaction between H_2L and $Cu(CH_3COO)_2(H_2O)$ (1 : 1) gave solid $Cu_2L_2(H_2O)_5$ in 40–50% yield. Addition of a base to the reaction mixture increased the yield to 70–85%. The enamineketone proton is much less acid than the carboxylate one ($pK_1 = 3.73 \pm 0.05$; $pK_2 = 11.85 \pm 0.05$) [15], therefore, the addition of a base shifts the equilibrium toward the formation of $Cu_2L_2(H_2O)_5$ and increases its yield. Without base, the yield of $Cu_2L_2(H_2O)_5$ is lower and the solid contains an insignificant admixture of $Cu(HL)_2(H_2O)_2$. However, since both $Cu_2L_2(H_2O)_5$ and $Cu(HL)_2(H_2O)_2$ appear as well-shaped single crystals of different colors and shapes, unit $Cu(HL)_2(H_2O)_2$ crystals can be mechanically separated from the bulk of $Cu_2L_2(H_2O)_5$. The $Cu_2L_2(H_2O)_5$ complex can also be obtained by the reaction between $Cu(HL)_2(H_2O)_2$ [or $Cu(HL)_2(C_2H_5OH)_2$] and $Cu(CH_3COO)_2(H_2O)$, followed by adding a base to the reaction mixture. The base hydrolysis of CuA_2, followed by the addition of $Cu(CH_3COO)_2(H_2O)$ to the resulting solution, also yielded $Cu_2L_2(H_2O)_5$. Thus, in all cases under consideration, when the Cu : L ratio approached 1 : 1, solid $Cu_2L_2(H_2O)_5$ was obtained.

Crystal structure and magnetic properties of $Cu_2L_2(H_2O)_5$

X-ray diffraction data for $Cu_2L_2(H_2O)_5$ suggest the binuclear structure of the complex (Fig. 4). In $Cu_2L_2(H_2O)_5$ the tridentate bridging L binds two copper atoms to form a five-membered chelate ring [similar to that in $Cu(HL)_2(H_2O)_2$] with one Cu atom and a six-membered chelate ring with the other Cu atom. The donor enamineketone oxygen acts as a bridge between the two metal atoms. The Cu—O and Cu—N bond lengths are, on average, 1.950 and 1.966 Å, respectively. In the five- and six-membered cycles, the average chelate angles are 81.37 and 91.09°, respectively. In the binuclear molecule, each copper atom coordinates one water molecule, i.e. the copper atom has a distorted trigonal bipyramidal environment. The equatorial planes of the bipyramids involve the O(111), O(2) and O(1w) atoms for Cu(1) and the O(611), O(1) and O(2w) atoms for Cu(2). The axial positions are occupied by O(1) and N(2) in the Cu(1) bipyramid and by O(2) and N(1) in the Cu(2) bipyramid.

It should be noted that all coordinated water molecules are located on one side of the $[Cu_2L_2]$ fragment and are far removed from the metal atoms (Table 3). Three noncoordinated water molecules form many different hydrogen bonds with the binuclear fragments $[Cu_2L_2(H_2O)_2]$ to bind them in a frame. In $Cu_2L_2(H_2O)_5$ the water molecules are held not as tightly as those in $Cu(HL)_2(H_2O)_2$. The TG and DTA curves show that heating $Cu_2L_2(H_2O)_5$ to 60–115°C leads to the complete one-step loss of water to form Cu_2L_2 quantitatively. Therefore, Cu_2L_2 can readily be obtained by keeping $Cu_2L_2(H_2O)_5$ *in vacuo* at 70–80°C for 5–6 h. Losing water molecules is a reversible

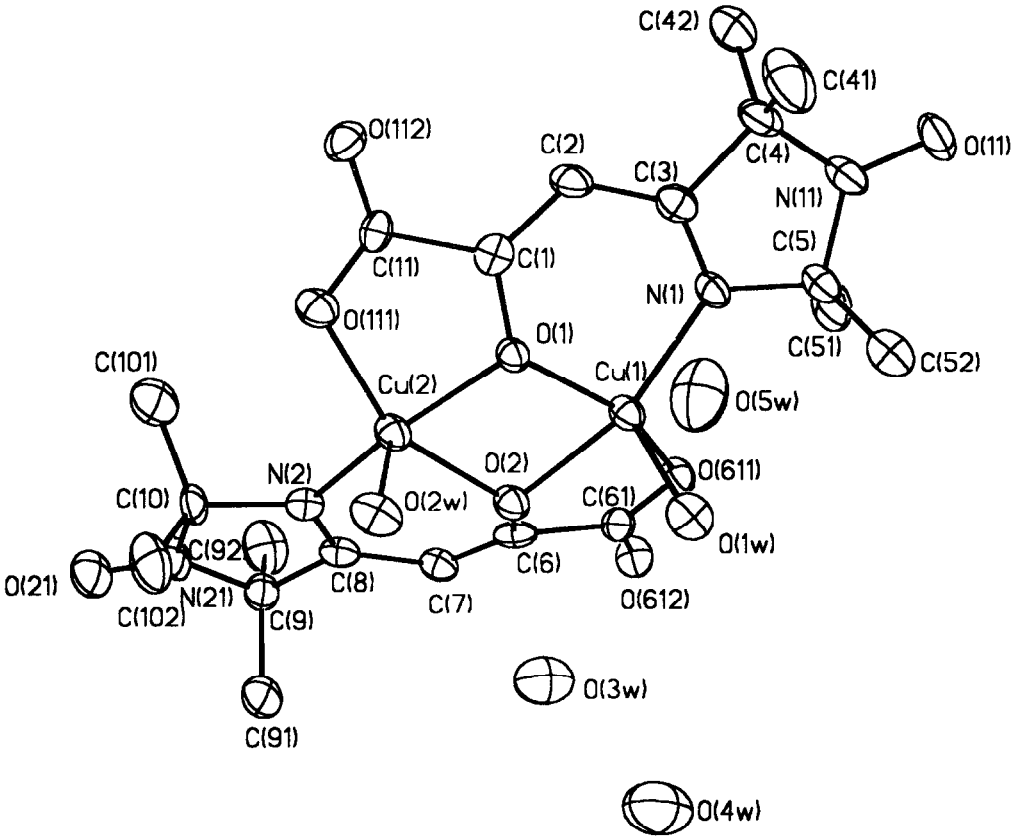


Fig. 4. Structure and atomic numbering of $Cu_2L_2(H_2O)_5$.

process. When stored in a moist atmosphere for 24 h, Cu_2L_2 transforms into $Cu_2L_2(H_2O)_5$. The $Cu_2L_2(H_2O)_5$ complex and the product of its thermolysis, saturated with water, have identical IR spectra. The IR spectrum of $Cu_2L_2(H_2O)_5$ exhibits an intense ν(OH) band at 3427 cm^{-1}, which corresponds to water molecules and is broadened due to the hydrogen bonds. In the IR spectrum of Cu_2L_2, this band is not observed. The presence/absence of this band allows one to easily monitor the presence/absence of water molecules in the solid compound.

In the intramolecular binuclear fragment, the Cu···Cu distance is 3.0588 Å. It is the shortest distance between the paramagnetic centers in $Cu_2L_2(H_2O)_5$. All intermolecular Cu···Cu distances are significantly longer. Within the binuclear molecule, the shortest Cu···—•O distance is 5.370 Å. The intermolecular distances —•O···O•— are not less than 6.542 Å. Therefore, the main exchange interactions occur in the Cu$\langle^{O}_{O}\rangle$Cu fragments. The $\mu_{eff}(T)$ and $\chi^{-1}(T)$ curves (Figs 3 and 5) suggest that both $Cu_2L_2(H_2O)_5$ and Cu_2L_2 exhibit two exchange interactions between the paramagnetic centers, which significantly differ in value. These are the strong antiferromagnetic exchange interactions (J) through the bridging oxygen atoms in the intramolecular fragments Cu$\langle^{O}_{O}\rangle$Cu and the much weaker exchange interactions between the N—•O groups (J_1). The condition $J \gg J_1$ allows the isolation of two temperature regions, $T < 150$ K and $T > 150$ K, on the $\mu_{eff}(T)$ and $\chi^{-1}(T)$ curves. In the low-temperature region the magnetic properties are determined mainly by the interactions between the unpaired electrons of the >N—•O groups, since at low temperatures the spins of metal ions in the Cu$\langle^{O}_{O}\rangle$Cu fragment are fully paired. In the low-temperature region, χ obeys the Curie–Weiss law $[C/(T-\theta)]$ and C is close to that for two weakly coupled electrons (Table 4, Fig. 5). At

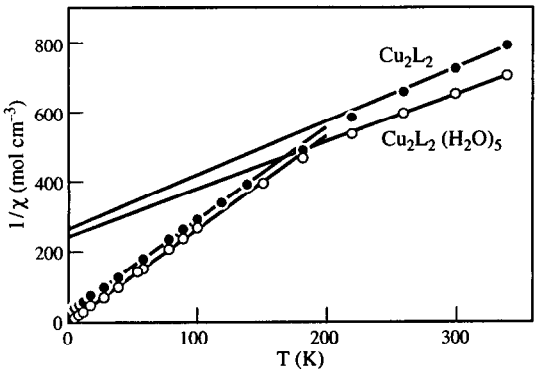


Fig. 5. $1/\chi$ as a function of temperature for $Cu_2L_2(H_2O)_5$ (○) and Cu_2L_2 (●) [$1/\chi$ were calculated per half molecule, $CuL(H_2O)_{2.5}$ and CuL, respectively.]

Table 4. Fitting parameters of the magnetic data

	C (cm^3 K mol^{-1})	θ (K)	g_{Cu}	J (cm^{-1})	zJ' (cm^{-1})
$Cu_2L_2(H_2O)_5$	0.757	−0.6	2.13	−292	−0.8
Cu_2L_2	0.749	−4.2	2.08	−360	−5.8

high temperatures, the strong antiferromagnetic exchange interaction in the Cu<O>Cu fragment, whose magnetic susceptibility is well described by the Bleaney–Bowers equation [16], makes a considerable contribution to the magnetic susceptibility of the compound. Thus, the magnetic susceptibility of each of the complexes can be represented as a sum of two contributions:

$$\chi_M(T) = \frac{C}{(T-\theta)} + \frac{2N\beta^2 g_{Cu}^2}{3kT}(1+\tfrac{1}{3}e^{-2J/kt})^{-1} + N\alpha,$$

where the second term is the Bleaney–Bowers equation and $N\alpha$ is the temperature-independent paramagnetism of Cu^{II}, which was taken equal to 60×10^{-6} cm^3 mol^{-1}. The optimal parameters obtained for $Cu_2L_2(H_2O)_5$ and Cu_2L_2 using the above equation are listed in Table 4. Table 4 also gives values for the parameter of the exchange interaction between the radical centers (zJ'), estimated by the equation $\theta = 2zJ'S(S+1)/3k$ [17] (where z is the number of the nearest neighbors of the radicals) in the molecular field approximation.

It can be seen from Table 4 that removing water from $Cu_2L_2(H_2O)_5$ contracts the magnetic system, which increases the energy of exchange interactions (zJ') between the nitroxides. This is consistent with the well known fact that in the complexes of transition metals with nitroxides the efficiency of H_2O molecules in the spin density transfer is extremely low [18–21]. In addition, removing water increases the value of $|J|$ in the exchange cluster, which points to a certain deformation of the exchange cluster Cu<O>Cu on going from $Cu_2L_2(H_2O)_5$ to Cu_2L_2. In the binuclear fragments, the value of J is determined by the Cu—O—Cu angle [22]. For $Cu_2L_2(H_2O)_5$, these angles are 102.36(7) and 103.74(7)°. The value of J determined for $Cu_2L_2(H_2O)_5$ is in good agreement with the familiar dependence of the exchange parameters on the Cu—O—Cu angle [22].

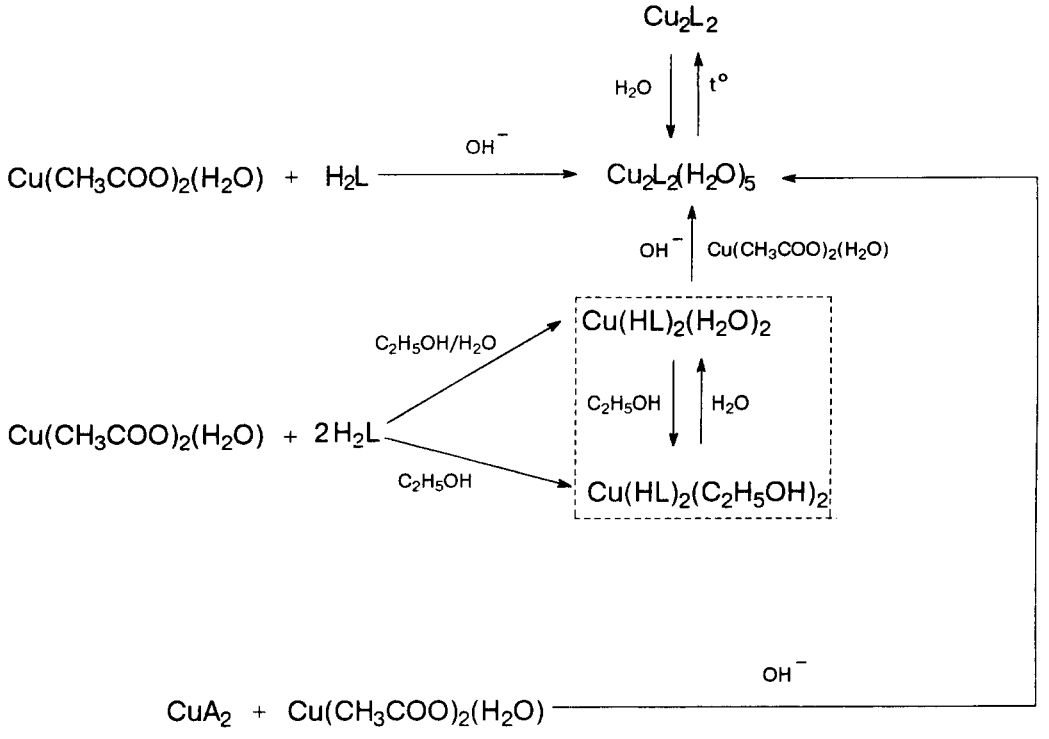
DISCUSSION

The general scheme of the complex formation in the interactions between Cu and H_2L at different Cu : L ratios and under different synthesis conditions could be presented as in Scheme 3.

The interaction of Cu^{II} with H_2L at a 1 : 2 ratio yields the solvated bischelate $Cu(HL)_2(H_2O)_2$ [or $Cu(HL)_2(C_2H_5OH)_2$]. The sufficiently high acidity of the pseudo-oxalate fragment of H_2L provides the formation of $Cu(HL)_2$ without adding a base. Thus, the first step of the complex formation involves the coordination of the nitroxide by type (b) (Scheme 1). It should be noted that in solid $Cu(HL)_2(H_2O)_2$ the water molecules are not coordinated by the metal ions, but form strong hydrogen bonds with the protons of the secondary amino groups and with the noncoordinated oxygens of the carboxylate groups of neighboring molecules. It is not unlikely that in $Cu(HL)_2(C_2H_5OH)_2$ the ethanol molecules are bonded in a similar manner. However, the low stability and twinning of the $Cu(HL)_2(C_2H_5OH)_2$ crystals did not allow us to determine the structure of this complex.

Changing the Cu^{II} : L ratio to 1 : 1 and increasing pH in the reaction mixture are favorable to the formation of the binuclear complex $Cu_2L_2(H_2O)_5$. The structure rearrangement observed in the transition from mononuclear $Cu(HL)_2$ to binuclear Cu_2L_2 is rather unexpected, since it involves the movement of the polyfunctional ligands toward each other (Scheme 2), which is an unusual process in the coordination chemistry. We designate this process as caterpillar-like reaction. For metal complexes with organic radicals, this process is reported for the first time. It should also be noted that in the available literature on metal complexes with diamagnetic organic ligands of a similar structure, we failed to find a description of a similar structural rearrangement of the mononuclear complex into the binuclear one. The Cambridge Structural Database [23] also contains no information about structural rearrangement of this type. However, a search through the above database has shown that the formation of polynuclear compounds in caterpillar-like reactions, which occur during interactions between polyfunctional organic ligands and metal ions, can be observed not only through processes traditional for the coordination chemistry, but also in biochemical processes [24–27].

It can be seen from Scheme 3 that binuclear $Cu_2L_2(H_2O)_5$ is formed regardless of the method of reaching that ratio Cu^{II} : L = 1 : 1. We would like to place particular emphasis upon the interaction between CuA_2 and copper acetate. In the first step of the reaction, the formation a six-membered enamineketone chelate ring through a direct interaction between Cu^{2+} and H_2L is impossible. Therefore, to synthesize the layered polymer by the scheme shown in Fig. 1, we used CuA_2 as an initial compound. (The presence of two six-membered enamineketone rings in CuA_2 was shown in the previous work [9].) However,



Scheme 3.

all interactions of CuA_2 with copper acetate, hydroxide and chloride (with and without base, in hydrated media, in anhydrous organic solutions, and in heterophase syntheses in water–chloroform mixtures) proceed to form the binuclear $Cu_2L_2(H_2O)_5$, which points to the high stability of the complex.

In the introduction we mentioned that the heterospin systems based on transition metal complexes with organic radicals are currently synthesized using progressively complicated nitroxide derivatives with several functional groups. In this context it is not impossible that caterpillar-like molecular processes will be observed more often. At least, they should be taken into account in developing the synthesis procedures for chain, layered and frame heterospin polymers in solid.

Acknowledgements—The authors gratefully acknowledge the financial support from INTAS (Grant 94-3508) and the Ministry of Science and Technical Policy of Russia. The gratitude is also expressed to the Cambridge Crystallographic Data Centre for the gift of the Cambridge Structural Database. The authors are grateful to Dr I. V. Mironov for providing the pK values of H_2L.

REFERENCES

1. Caneschi, A., Gatteschi, D. and Rey, P., *Prog. Inorg. Chem.* 1991, **39,** 331.
2. Caneschi, A., Gatteschi, D., Renard, J. P., Rey, P. and Sessoli, R., *J. Am. Chem. Soc.* 1989, **111,** 785.
3. Ovcharenko, V., Burdukov, A. and Musin, R., *Mol. Cryst. Liq. Cryst.* 1995, **273,** 89.
4. Luneau, D., Risoan, G., Rey, P., Grand, A., Caneschi, A., Gatteschi, D. and Laugier, J., *Inorg. Chem.* 1993, **32,** 5616.
5. Stumpf, H. O., Ouahab, L., Pei, Y., Bergerat, P. and Kahn, O., *J. Am. Chem. Soc.* 1994, **116,** 3866.
6. Pei, Y., Kahn, O. Aebersold, M. A., Ouahab, L., Le Berre, F., Pardi, L. and Tholence, J. L., *Adv. Mater.* 1994, **6**(9), 681.
7. Caneschi, A., David, L., Ferraro, F., Gatteschi, D. and Fabretti, A. C., *Inorg. Chim. Acta,* 1994, **217,** 7.
8. Luneau, D., Laugier, J., Rey, P., Ulrich, G., Ziessel, R., Legoll, P. and Drillon, M., *J. Chem. Soc. Chem. Commun.* 1994, 741.
9. Vostrikova, K. E., Ovcharenko, V. I., Romanenko, G. V., Ikorskii, V. N., Podberezskaya, N. V., Reznikov, V. A. and Volodarskii, L. B., *Zh. Neorg. Khim.* 1992, **37,** 1755.
10. It should be noted that in the Cambridge Structural Database we failed to find data on similar structurally characterized rearrangements during the transition from the mono- to binuclear structure for Cu^{II} complexes with diamagnetic organic ligands as well.
11. Sheldrick, G. M., *Acta Cryst.* 1990, **A46,** 467.
12. Sheldrick, G. M., *Acta Cryst.* 1993, **A49**(suppl), C53.

13. All $Cu(HL)_2(C_2H_5OH)_2$ crystals were twins, therefore we could not obtain reliable information about the structure of this complex.
14. Burdukov, A. B., Ovcharenko, V. I., Ikorskii, V. N., Pervukhina, N. V., Podberezdsakaya, N. V., Grigor'ev, I. A., Larionov, S. V. and Volodarsky, L. B., *Inorg. Chem.* 1991, **30,** 972.
15. We give the values of the effective constants obtained at 293 K for ethanol : water solutions of H_2L ($c = 10^{-2}$ M) at the 57.6% concentration of ethanol and 0.1 M of $NaClO_4$.
16. Bleaney, B. and Bowers, K. D., *Proc. Roy. Soc. London, Ser. A*, 1952, **214**(3), 451.
17. Selwood, P. W., *Magnetochemistry*. Interscience Publishers, Inc., New York, 1956.
18. Cotton, F. A. and Felthouse, T. R., *Inorg. Chem.* 1982, **21,** 2667.
19. Dickman, M. and Doedens, R. J., *Inorg. Chem.* 1983, **22,** 1591.
20. Luneau, D., Rey, P., Laugier, J., Belorizky, E. and Cogne, A., *Inorg. Chem.* 1992, **31,** 3578.
21. Ovcharenko, V. I., Vostrikova, K. E., Podoplelov, A. V., Sagdeev, R. Z., Romanenko, G. V. and Ikorskii, V. N., *Polyhedron*, 1994, **13,** 2781.
22. Hatfield, W. E., In *Theory and Application of Molecular Paramagnetism*, Ch. 7. Wiley, New York, 1976, p. 349.
23. Allen, F. H. and Kennard, O., *Chemical Design Automation News*, 1993, **8**(1), 1, 31.
24. Teintze, M., Hossain, M. B., Barnes, C. L., Leong, J. and van der Holm, D., *Biochemistry*, 1981, **20,** 6446.
25. Swanson, R., Ilsley, W. H. and Stanislowski, A. G., *J. Inorg. Biochem.* 1983, **18,** 187.
26. Shweky, I., Bino, I., Goldberg, D. P. and Lippard, S. J., *Inorg. Chem.* 1994, **33,** 5161.
27. Castro, S. L., Cass, M. E., Hollander, F. J. and Bartley, S. L., *Inorg. Chem.* 1995, **34,** 466.

Pergamon

PII: S0277-5387(96)00422-6

Polyhedron Vol. 16, No. 8, pp. 1291–1295, 1997
Copyright © 1997 Elsevier Science Ltd
Printed in Great Britain. All rights reserved
0277-5387/97 $17.00+0.00

Synthesis and spectroscopic characterization of binuclear thioazomethine palladacycles

P. Chattopadhyay, M. K. Nayak, S. P. Bhattacharyya and C. Sinha*

Department of Chemistry, The University of Burdwan, Burdwan 713 104, India

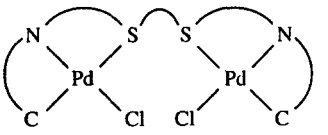
(Received 3 April 1996; accepted 22 August 1996)

Abstract—Several 1,2-bis(2-thio(*N*-benzylidene)anilines)ethane [$(RC_6H_4CH = NC_6H_4SCH_2)_2$] (**4**) and 1,3-bis(2-thio(N-benzylidene)anilines)propane [$(RC_6H_4CH = NC_6H_4SCH_2)_2CH_2$] (**5**), R = H (a), 11-CH_3 (b), 11-OCH_3 (c), 11-Cl (d) and 11-NO_2 (e)] have been synthesized and reacted with $Pd(OAc)_2$ in boiling benzene. The binuclear cyclopalladated acetato complexes (8/9) thus obtained reacted with LiCl, giving the chloro complexes having the coordination sphere $[Pd(C, N, S)Cl_2]_2$ (**10/11**). The mode of ligand binding was established using high-resolution ^1H NMR and IR data. Copyright © 1997 Elsevier Science Ltd

Keywords: thioazomethines; cyclopalladation; dinuclear.

Cyclometallated organopalladium compounds have been extensively studied [1,2] because of their potential utility in the activation of C—H bonds and several reviews on their synthesis and characterization have appeared [3–10]. Various applications of cyclopalladated complexes to organic synthesis are known [11]. Many such reactions are useful in the synthesis of regio- and stereo-selected organic and heterocyclic compounds [9,11], optically active molecules [1,2], resolution of chiral substrates [13], estimation of optical purity [14] and catalysts for hydrogenations.

Cyclopalladated complexes containing Pd—C σ-bonds stabilized by the additional coordination via a suitably substituted N-donor centre, *viz.* amines [1–3], imines [3,5,6], azobenzenes [7,8,11], arylhydrazones [16], are of particular interest. The imines bearing an additional donor group at a suitable position to maintain chelate structure provide extra stability to the cyclopalladated complexes [6]. Herein we describe binuclear organometallics of coordination type $Pd(C, N, S)Cl_2$ (**1**) of 1,2-bis(2-thio(N-benzylidene)anilines)ethane (**4**) and 1,3-bis(2-thio(N-benzylidene)anilines)propane (**5**). The ligand systems have been designed on our familiarity [7] with the binuclear cyclometallated platinum metal chemistry of hexadentate (C, N, S)-type azoligands.



1

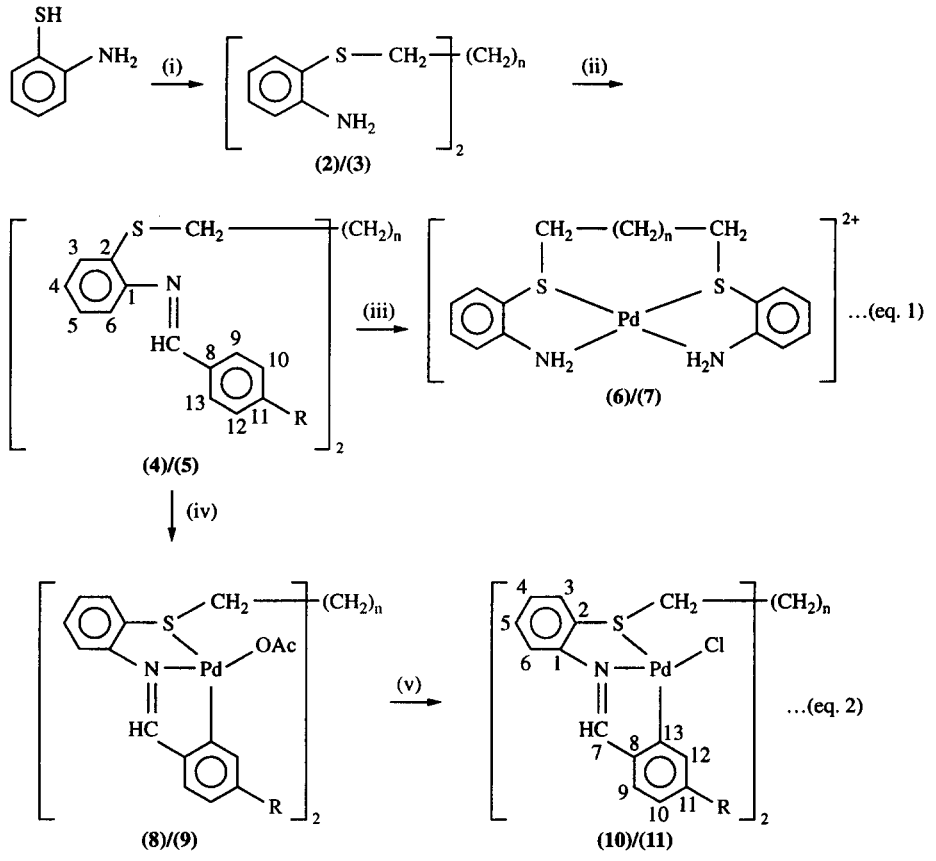
RESULTS AND DISCUSSION

Synthesis

The Schiff bases and their cyclopalladation described in this work are shown in Scheme 1 along with the methods used for synthesis and atom-numbering scheme. The ligands are of effective hexadentate (C, N, S)-type. They were synthesized in good yields by condensation of *para*-substituted benzaldehydes with 1,2-bis((2-aminophemyl)thio)ethane (**2**) or 1,3-bis((2-aminophemyl)thio)propane (**3**). These ligands are new and are systematically named as 1,2-bis(2-thio(*N*-benzylidene)anilines)ethane (**4**) or 1,3-bis(2-thio(*N*-benzylidene)anilines)propane (**5**). The reaction of Schiff bases with Na_2PdCl_4 in aqueous ethanol turns to a suspension and a brown salt is separated quickly by the addition of $NaClO_4$ into the solution, which is characterized as imine-hydrolysed thioamine palladium(II) perchlorate [eq. (1)].

A similar reaction using $Pd(OAc)_2$ in benzene in 1:2 mole proportion gave an orange–brown precipitate after refluxing for a period of 1 h or more. The

* Author to whom correspondence should be addressed.



R=	H	CH_3	OCH_3	Cl	NO_2		
	(a)	(b)	(c)	(d)	(e)	n=0	(**2**), (**4**), (**6**), (**8**), (**10**)
						n=1	(**3**), (**5**), (**7**), (**9**), (**11**)

(i) Na/EtOH / $Br(CH_2)_2Br$ or $Br(CH_2)_3Br$; (ii) p-R•C_6H_4CHO/EtOH, reflux; (iii) Na_2PdCl_4/EtOH-H_2O; (iv) $Pd(OAc)_2$/benzene,reflux; (v) $CHCl_3$-MeOG/LiCl

Scheme 1.

acetate derivatives (**8**/**9**) on metathesis in chloroform : acetone (1 : 1, v/v) by adding LiCl produced the chloro derivatives (**10**/**11**) [eq. (2)].

Spectral and binding mode

The appearance of sharp strong bands in IR spectra at 1600–1625 cm^{-1} in the ligands (**4**/**5**) is suggestive of the ν(C=N) mode [17]. This band is red shifted by $\Delta\nu$ = 20–25 cm^{-1} on complexation, suggesting coordination of the metal ions to the azomethine nitrogen [18]. The acetato complexes (**8**/**9**) exhibit strong bands ν_{as} (COO) at 1550–1560 cm^{-1} and ν_s (COO) 1320–1340 cm^{-1} ($\Delta\nu$ = 220–230 cm^{-1}), which correspond to the unidentate character of the bonded —COO groups [17–20]. The chloro complexes (**10**/**11**) are characterized by a sharp single (Pd—Cl) mode at 320–340 cm^{-1} [21].

The complexes are sparingly soluble in common organic solvent and the UV–vis spectra are recorded in DMSO. The absorptions around 450 nm (absent in free ligand) may be assigned to the characteristic of *ortho*-palladation and probably represent transitions localized on the metalated fragment [7,8]. Two other absorptions at 345–390 and 280–295 nm may be ascribed to intraligand charge transfer transitions [20]. The spectral data are collected in Table 1.

In the ^{1}H NMR spectra, all aromatic protons of the ligand (**4**/**5**) and cyclopalladated complexes (**10**/**11**) are unambiguously assigned on the basis of spin–spin structure and changes therein on substitution. The spectra of the ligands in $CDCl_3$ and the complexes in DMSO-d_6 are in complete agreement with the structures in which the halves of the molecule are magnetically equivalent to each other (e.g. 6 = 6′, etc.) The aromatic region displays a group of left–right symmetrical multiplet peaks (4-H_2, b–e) characterizing the four-spin AA′BB′ system (9-H, 13-H; 10-

Table 1. Microanalytical, UV–vis and IR spectral data

Compound	Melting point (°C)	Elemental analyses[a] C(%)	H(%)	N(%)	UV–vis λ_{max}	Spectral data[b] (ε ($dm^3\ mol^{-1}\ cm^{-1}$))	IR spectral data[c] ν(C=N) (cm^{-1})	ν(C—S) (cm^{-1})	ν(Pd—Cl) (cm^{-1})
4a	gum				350 (10,650)	280[d] (25,200)	1620	765	
4b	52±1	74.9 (75.0)	5.6 (5.8)	6.0 (5.8)	360 (8980)	285[d] (18,330)	1620	755	
4c	120±1	70.0 (70.3)	5.6 (5.5)	5.3 (5.5)	365 (11,857)	290[d] (31,663)	1605	770	
4d	135±1	64.3 (64.5)	4.1 (4.2)	5.3 (5.4)	345 (9153)	290[d] (12,399)	1620	780	
4e[e]	170±1	61.8 (62.0)	3.9 (4.0)	10.4 (10.3)	390 (7588)	290[d] (20,802)	1625	780	
5a	gum				370 (7850)	285[d] (19,180)	1610	755	
5b	44±1	75.1 (75.3)	6.2 (6.1)	5.4 (5.6)	375 (11,980)	290[d] (24,450)	1625	765	
5c	85±1	70.6 (70.7)	5.6 (5.7)	5.5 (5.3)	360 (7331)	285[d] (20,840)	1610	770	
5d	96±1	65.2 (65.0)	4.3 (4.5)	5.2 (5.2)	355 (8920)	280[d] (19,300)	1615	775	
5e[e]	138±1	62.4 (62.5)	4.4 (4.3)	10.2 (10.1)	390 (7994)	290[d] (23,493)	1630	775	
10a		45.6 (45.8)	3.1 (3.0)	3.7 (3.8)	450 (5850)	345 (12,300) 290[d] (18,390)	1600	820	320
10b		47.4 (47.2)	2.8 (2.6)	3.8 (3.7)	460 (6200)	350 (15,240) 245[d] (22,850)	1605	825	325
10c		45.3 (45.3)	3.3 (3.3)	3.4 (3.5)	455 (6850)	345 (20,340) 280[d] (31,750)	1595	820	325
10d		41.7 (41.8)	2.6 (2.5)	3.6 (3.5)	465 (5650)	350 (18,000) 290[d] (24,630)	1600	830	330
10e[e]		40.7 (40.8)	2.3 (2.4)	6.9 (6.8)	455 (8200)	3800 (19,300) 285[d] (33,800)	1605	840	340
11a		46.6 (46.5)	3.1 (3.2)	3.7 (3.7)	460 (6440)	375 (15,300) 285[d] (24,650)	1600	820	325
11b		48.1 (47.9)	3.7 (3.6)	3.5 (3.6)	465 (7080)	380 (18,400) 290[d] (26,300)	1610	815	330
11c		45.9 (46.0)	3.5 (3.5)	3.4 (3.5)	445 (7630)	365 (14,770) 295[d] (31,500)	1600	825	325
11d		42.5 (42.6)	2.6 (2.7)	3.5 (3.4)	460 (6650)	360 (17,300) 290[d] (26,800)	1600	830	330
11e[e]		41.4 (41.5)	2.5 (2.6)	6.8 (6.7)	465 (9800)	380 (22,600) 280 (35,350)	1605	835	335

[a] Calculated values are in parentheses.
[b] In $CHCl_3$ for **3**, **4** and in DMSO for **10** and **11**.
[c] In KBr disks.
[d] Shoulder.
[e] $\nu(NO_2)$: 1340–1345 cm^{-1}.

H, 12-H) at lower field. These signals vary considerably with different R substituents in the aromatic aldehyde. It is quite clear that the electron-releasing groups [Me (b), OMe (c)] shift the signal upfield and withdrawing groups [1 (d), NO_2 (e)] shift them downfield. These signal movements are in accord with the inductive and resonance effects of the R substituent [22]. The signals (4-H) at higher field correspond to *N*-phenyl protons and almost remain unperturbed on substitution. The imine proton (7-H) is expected to appear to the most downfield position as a sharp singlet and moves slightly in either direction depending on the nature of substitution at the C-phenyl ring. The aliphatic protons move to higher field; 14, 14′-H appear as triplet and 15-H as quintet protons. The *N*-phenyl protons are systematically deshielded on palladation: 3-H to 6-H protons are shifted downfield by 0.6–0.7 ppm. The substitution on the C-phenyl ring (11th position) has little influence on these protons.

Sulfur coordination to palladium is reflected by

Table 2. ^{1}H NMR spectral data[a]

Compound	δ (ppm)												
	3,3′-H[b]	4,4′-H[c]	5,5′-H[c]	6,6′-H[b]	7,7′-H[d]	9,9′-H[b]	10,10′-H	11,11′-H	12,12′-H	13,13′-H[b]	14,14′-H[c]	15,15′-H[e]	R
(1)	(2)	(3)	(4)	(5)	(6)	(7)	(8)	(9)	(10)	(11)	(12)	(13)	(14)
4a	6.70	7.01	7.01	7.21	8.31	7.82	7.62[c]	7.62[c]	7.62[c]	7.82	3.02	—	—
4b	6.71	7.01	7.01	7.20	8.27	7.78	7.42[b]	—	7.42[b]	7.78	3.03		2.38
4c	6.67	6.95	6.95	7.18	8.26	7.85	7.25[b]	—	7.25[b]	7.85	3.09		3.85
4d	6.73	7.04	7.04	7.27	8.32	7.92	7.69[b]	—	7.69[b]	7.92	3.06		
4e	6.79	7.08	7.08	7.32	8.48	8.05	8.24[b]	—	8.24[b]	8.05	3.08		
5a	6.66	7.02	7.02	7.14	8.29	7.90	7.58[c]	7.58[c]	7.58[c]	7.90	3.05	2.00	
5b	6.69	7.00	7.00	7.16	8.25	7.75	7.36[b]	—	7.36[b]	7.75	3.06	2.04	2.40
5c	6.67	6.96	6.96	7.13	8.29	7.88	7.20[b]	—	7.20[b]	7.88	3.08	2.03	3.85
5d	6.71	7.06	7.06	7.18	8.32	7.94	7.58[b]	—	7.58[b]	7.94	3.09	2.05	
5e	6.75	7.09	7.09	7.22	8.46	8.08	8.24[b]	—	8.24[b]	8.08	3.10	2.05	
10a	7.34	7.52	7.52	7.85	9.12	8.11	7.42[c]	7.42[c]	7.82[b]	—	3.33	—	—
10b	7.42	7.52	7.52	7.84	9.11	8.04	7.28[b]	—	7.61[d]	—	3.31	—	2.40
10c	7.43	7.52	7.52	7.78	9.09	7.92	7.18[b]	—	7.49[d]	—	3.33		3.86
10d	7.45	7.54	7.54	7.80	9.14	8.10	7.62[b]	—	7.91[d]	—	3.34		
10e	7.46	7.55	7.55	7.82	9.27	8.15	8.12[b]	—	8.47[d]	—	3.36		
11a	7.38	7.54	7.54	7.79	9.08	8.01	7.43[c]	7.43[c]	7.74[b]	—	3.42	2.78	—
11b	7.40	7.52	7.52	7.82	8.94	7.89	7.21[b]	—	7.56[d]	—	3.39	2.72	2.40
11c	7.43	7.54	7.54	7.81	9.02	8.02	7.11[b]	—	7.46[d]	—	3.33	2.68	3.85
11d	7.45	7.57	7.57	7.84	9.08	8.06	7.48[b]	—	7.74[d]	—	3.41	2.73	—
11e	7.47	7.60	7.60	7.86	9.14	8.14	8.16[b]	—	8.28[d]	—	3.44	2.75	

[a] In $CDCl_3$ for **3, 4** and DMSO-d_6 for **10** and **11**.
[b] Doublet.
[c] Triplet.
[d] Singlet.
[e] Multiplet.

downfield shifting of the —S—CH_2— signal from the free ligand position. In the complexes the signal of 14, 14′-H protons appear at 0.3 ppm downfield from those of the ligands and the 15-H signal is shifted downfield by 0.7 ppm. The azomethine proton (7-H) shows downfield shifting on metallation of *ca* 0.8 ppm. This accounts for the chelation of the imine nitrogen. On metallation all the protons suffer downfield shifts. The most perturbed protons are the *C*-phenyl protons and the significant feature is the loss of resonance due to 13-H of the *C*-phenyl ring from the NMR spectra and the appearance of new singlet in **10 b–e**. The spectral data are collected in Table 2.

EXPERIMENTAL

Disodium tetrachloropalladate was prepared by treating palladium(II) chloride with sodium chloride in water and evaporating the aqueous solution [7]. Palladium(II) acetate was recrystallized from benzene solution before use. All other chemicals were reagent grade and were used as received. The solvents used in the reactions were dried by reported procedures [23].

UV–vis spectra were recorded on a Shimadzu UV 160A spectrophotometer and IR (4000–200 cm^{-1}) spectra on a Perkin–Elmer 783 and 883 spectrometer. ^{1}H NMR spectra were recorded in $CDCl_3$ and DMSO-d_6 solution on varian Gemini 300 MHz FT NMR spectrometers. Elemental analyses were obtained using a Perkin–Elmer 240c elemental analyser.

Synthesis of ligands

1-2-*Bis*(2-*thio*(N-*benzylidene*)*aniline*)*ethane*, (**3a**). 1,2-Bis((2-aminophenyl)thio)ethane (**2**) was first synthesized by a reported procedure [7]. To a dry ethanolic solution (20 cm^3) of **2** (2 g, 7.25 mmol) was added benzaldehyde (1.54 g, 14.50 mmol) and the solution was refluxed for 2 h on a steam bath. The orange–yellow solution was cooled to room temperature and a dark-coloured gummy mass was separated slowly. The light-yellow supernatant was decanted off. The mass was further boiled with dry ethanol on a steam bath, cooled and the supernatant was decanted off twice as described earlier. It was evaporated at reduced pressure and dried over $CaCl_2$. The yield was 0.98 g (30%). Other Schiff bases were prepared similarly and the yield varied from 30–60%. The solid products obtained for **3c–e** and **4c–e** were purified by recrystallization from a chloroform : ethanol (1 : 4 v/v) mixture. The physical properties are set out in Table 1.

Synthesis of complexes

Dichloro [1,2-*bis*(2-*thio*(N-*benzylidene*)*aniline*) *ethane*)-C^{13}, N, S, $C^{13'}$, N', S',-*dipalladium* (II) (**10a**). To a benzene solution (10 cm^3) of **3a** (0.2 g, 0.48 mmol) was added slowly a warm benzene solution (5 cm^3) of $Pd(OAC)_2$ (0.24 g, 1.07 mmol) and the mixture was refluxed for 1 h. The deposited orange–brown solid was filtered and washed with cold benzene. The dry mass was dissolved in chloroform : acetone (8 cm^3, 1 : 1, v/v) and LiCl (2.5 mmol) was added with continuous stirring. The volume of the mixture was half reduced by slow evaporation at reduced pressure and the separated brown crystals were filtered, washed with a cold chloroform : acetone (1 : 1, v/v) mixture (5 $cm^3 \times 2$) and dried over $CaCl_2$. The yield was 0.18 g, 50%.

Other complexes were also prepared similarly and the yield varied between 45 and 55%. The physical properties are collected in Table 1.

Acknowledgements—The authors are thankful to Professor A. Chakravorty, Calcutta, for elemental analyses and spectral measurements. We thank Dr N. K. Bag, Michigan State University, and Dr P. Basu, Arizona State University, U.S.A., for recording the ^1H NMR spectra. Financial assistance from the Department of Science and Technology and University Grants Commission, New Delhi, is gratefully acknowledged.

REFERENCES

1. Omae, I., *Organometallic Intramolecular Coordination Compounds*. Elsevier, Amsterdam, 1966.
2. Wilkinson, G., Stone, F. G. A. and Abel, E. W., *Comprehensive Organometallic Chemistry*, Vol. 6, Pergamon Press, New York, 1982, p. 279.
3. Dunina, V. V., Zalevskaya, O. A. and Potapov, V. M., *Russ. Chem. Rev.* 1988, **57,** 434.
4. Rothwell, I. P., *Polyhedron*, 1985, **4,** 177.
5. Constable, E. C., *Polyhedron*, 1984, **3,** 1037.
6. Basuli, F., Chattopadhyay, P. and Sinha, C., *Polyhedron*, 1996, **15,** 2439.
7. Chattopadhyay, S., Sinha, C., Chowdhury, S. B. and Chakravorty, A., *J. Organomet. Chem.* 1992, **427,** 111.
8. Chattopadhyay, S., Sinha, C., Basu, P. and Chakravorty, A., *J. Organomet. Chem.* 1991, **414,** 421, and refs therein.
9. Braunstein, P., Carnerio, T. M. G., Matt, D., Balegroune, F. and Grandjean, D., *Organometallics*, 1989, **8,** 1737.
10. Yatsimirsky, A. K., Karankov, G. M. and Ryabov, A. D., *J. Chem. Soc. Perkin Trans.* 1992, **2,** 1295.
11. Ryabov, A. D., *Synthesis*, 1985, 233.
12. Albert, J., Granell, J., Sales, J., Bardia, M. F. and Solans, X., *Organometallics*, 1995, **14,** 1393.
13. Allen, L. G., McLaughlin, G. M. and Robertson, G. B., *Inorg. Chem.* 1982, **21,** 1007.
14. Ghedini, M., Armento, S., Neve, F. and Licoccia, S., *J. Chem. Soc., Dalton Trans.* 1988, 1565.
15. Mukherjee, D. K., Palit, B. K. and Saha, C. R., *Indian. J. Chem.* 1992, **31A,** 243.
16. Granell, J., Moragas, R., Sales, J., Bardia, M. F. and Solans, X., *J. Chem. Soc., Dalton Trans.* 1993, 1237.
17. Nakamoto, K., *Infrared and Raman Spectra of Inorganic and Coordination Compound*, 4th edn, Wiley, New York, 1986.
18. Ohoue, H., and Moritani, I., *J. Organomet. Chem.* 1972, **43,** 431.
19. Mukherjee, G., Poddar, S. N. and Dey, K., *Indian J. Chem.* 1986, **25A,** 275.
20. Chattopadhyay, P. and Sinha, C., *Indian J. Chem.* 1995, **34A,** 76.
21. Chattopadhyay, P. and Sinha, C., *Polyhedron*, 1994, **13,** 2689.
22. Jackman, L. M., *Applications of Nuclear Magnetic Resonance Spectroscopy in Organic Chemistry*, Pergamon Press, New York, 1959.
23. Vogel, A. I., *A Text Book of Practical Organic Chemistry*, 2nd edn. Longman, Green, London, 1959, p. 167.

Pergamon

PII: S0277-5387(96)00423-8

Polyhedron Vol. 16, No. 8, pp. 1297–1300, 1997
Copyright © 1997 Elsevier Science Ltd
Printed in Great Britain. All rights reserved
0277–5387/97 $17.00+0.00

Synthesis, characterization and X-ray crystal structure of Zn^{II} complex with poly-nitrogen ligand $[\eta^3\text{-HB(3,5-Me}_2\text{pz)}_3]_2\text{Zn}\cdot 2\text{C}_6\text{H}_5\text{CH}_3$

Ke-Wu Yang,[a] Yong-Zhen Wang,[a] Zhong-Xian Huang[a]* and Jie Sun[b]

[a] Department of Chemistry, Fudan University, Shanghai 200433, P. R. China

[b] Shanghai Institute of Organic Chemistry, Academia Sinica, Shanghai 200032, P. R. China

(Received 31 January 1996; accepted 22 August 1996)

Abstract—Di-hydrotris(3,5-dimethylpyrazol-1-yl)borate Zn^{II} was prepared from $KHB(3,5\text{-Me}_2\text{pz})_3$ and $Zn(NO_3)_2\cdot 6H_2O$ in acetone, characterized by elemental analysis and ^1H NMR. Crystal structure determination shows that the configuration around the Zn^{II} center is a slightly distorted octahedron. Copyright © 1997 Elsevier Science Ltd

Keywords: synthesis; characterization; crystal structure; zinc complex; poly-nitrogen ligand.

Zinc as an essential element has many physiological functions in living systems. There are more than 160 zinc enzymes which are now known. It is an integral component of many proteins which participate in various metabolic processes. Zinc is also known to be one of the essential inorganic ions which contribute to the catalytic activity and the stability of many metalloenzymes, polynucleotides and membranes [1]. It was of interest to study the model complexes of zinc with poly-nitrogen ligands. In the title compound, the ligand is hydrotris(3,5-dimethylpyrazol-1-yl)borate. It is favourable for the preparation of the transition metal complex [2]. Its geometry as well as strong electron-donating property are valuable in the synthesis of model compounds of several metalloproteins, since coordination of multi-histidyl nitrogen atoms is often observed in metalloproteins. In this paper we describe the preparation, characterization and crystal structure of the title complex.

EXPERIMENTAL

Preparation and analyses of the complex

All chemicals in the reaction were of reagent grade. The preparation of the title compound was in acetone. C, H, N were determined by a Cardo Erba 1106 Element analyser; ^1H NMR spectra were obtained on a Bruker MSL 300 MHz spectrometer using $CDCl_3$ as solvent and TMS as an internal reference. The ligand, potassium hydrotris(3,5-dimethylpyrazol-1-yl)borate, $KHB(3,5\text{-Me}_2\text{pz})_3$, was prepared according to the literature [3]. KBH_4 was reacted with 4.0 equiv. of 3,5-dimethylpyrazol at 204°C for 1 h, with the evolution of 3.0 equiv. of H_2, and filtration followed by washing with hot toluene several times. White crystalline $KHB(3,5\text{-Me}_2\text{pz})_3$ was obtained in 74% yield. $KHB(3,5\text{-Me}_2\text{pz})_3$ was reacted with 1 equiv. of $Zn(NO_3)_2\cdot 6H_2O$ in acetone for 2 h, then the precipitate was filtered, washed with water and acetone many times. The filtrate recrystallized from toluene and left standing for several days. Then the crystal was collected. Found: C, 55.1; N, 24.6; H, 7.0. Calc. for $C_{31.5}H_{47}B_2O_{0.5}N_{12}Zn$ (mol. wt. 688.0). C, 54.9; N, 24.4; H, 6.9%. ^1H NMR ($CDCl_3$): δ ppm 1.37 (s, 18H, Me); 2.42 (s, 18H, Me); 5.58 (s, 6H, pz). The peak at 2.42 ppm was assigned to the methyl near the zinc atom, while the peak at 1.37 ppm to the methyl near the boron atom.

Crystal structure determination

Crystals of the title compound were obtained by slowly cooling the hot toluene solution to room tem-

* Author to whom correspondence should be addressed.

Table 1. Crystal data

Formula	$C_{44}H_{60}N_{12}B_2Zn$
Formula weight	844.04
Crystal system	Triclinic
Space group	*P*[ol]1[/ol]
a (Å)	10.047(6)
b (Å)	14.206(3)
c (Å)	8.700(3)
α (°)	91.69(3)
β (°)	101.34(4)
γ (°)	109.47(2)
V (Å)	1141.9(9)
Z	1
D_c (g cm^{-3})	1.227
Crystal size (mm)	0.20 × 0.20 × 0.30
$F_{(000)}$	448.00
μ(Mo-$K\alpha$) (cm^{-1})	5.83

Table 2. Selected bond lengths (Å)

Zn—N(2)	2.160(4)	N(1)—N(2)	1.372(5)
Zn—N(4)	2.175(4)	N(3)—N(4)	1.381(5)
Zn—N(6)	2.197(4)	N(5)—N(6)	1.371(5)
N(1)—C(2)	1.340(6)	C(1)—C(2)	1.505(8)
C(2)—C(3)	1.373(8)	C(4)—C(5)	1.481(8)
C(3)—C(4)	1.386(8)	N(1)—B	1.554(8)
N(3)—B	1.552(8)	N(5)—B	1.534(7)

Table 3. Selected bond angles (°)

N(2)—Zn—N(2)	180.0	N(4)—Zn—N(4)	180.0
N(6)—Zn—N(6)	180.0	N(2)—Zn—N(4)	94.7(1)
N(2)—Zn—N(4)	85.3(1)	N(2)—Zn—N(6)	85.9(1)
N(2)—Zn—N(6)	94.1(1)	N(4)—Zn—N(6)	93.6(1)
N(4)—Zn—N(6)	86.4(1)	N(1)—N(2)—Zn	117.6(3)
C(4)—N(2)—Zn	135.8(3)	C(2)—N(1)—B	130.0(4)
C(12)—N(5)—B	130.7(4)	C(7)—N(3)—B	130.8(4)
N(1)—B—N(5)	109.3(4)	N(1)—B—N(3)	109.7(4)
N(3)—B—N(5)	108.6(4)	N(2)—N(1)—B	120.6(4)
N(4)—N(3)—B	120.0(4)	N(6)—N(5)—B	120.7(4)

perature and a colorless platelet of dimensions 0.2 × 0.2 × 0.3 mm was chosen for the measurement. All crystallographic data was collected with a Rigaku AFC7R diffractmeter using Mo-$K\alpha$ radiation (λ = 0.71069 Å) in the ω–2θ scan mode. Of the 2295 collected, 2133 reflections were independent and 1978 reflections with $I > 3.00\ \sigma\ (I)$ were used for the calculation after an empirical absorption based on ψ scans. The structure was solved by direct methods. The non-hydrogen atoms were refined anisotropically. The final cycle of full-matrix least-squares refinement was converged with $R = 0.052$, $Rw = 0.076$ (unweighted and weighted agreement factors resp.) for 269 parameters.

RESULTS AND DISCUSSION

The title compound was prepared according to the following equation:

$$2KHB(3,5\text{-}Me_2pz)_3 + Zn(NO_3)_2 \cdot 6H_2O$$
$$= 2KNO_3 + 6H_2O + [HB(3,5\text{-}Me_2pz)_3]_2Zn$$

The reaction was carried out in acetone and the zinc complex was recrystallized from toluene. The compound was transparent and thermally stable. It was characterized by elemental analysis and ^{1}H NMR spectra. The crystal cell of the complex consists of discrete monomeric molecules, each zinc complex being accompanied by two solvent molecules. The crystallographic data collections and refinement details are listed in Table 1, selected bond distances and angles are given in Tables 2 and 3. The ORTEP plot and unit packing diagram are presented in Figs 1 and 2, respectively.

The Zn atoms are coordinated by six nitrogen atoms of the six pyrazol rings. As evidenced by the N(2)—Zn—N(2) angle (180°), other angles of N—Zn—N (not in a line) are from 85.3(1) to 94.7(1)° and the bond lengths of Zn—N are between 2.160(4) and 2.197(4) Å. The coordination environment of the Zn is a slightly distorted octahedron. The deviation from the ideal configuration can be explained by the steric effect caused by the methyls of the ligands. The boron atoms was coordinated with three nitrogen atoms of the pyrazol rings. The three B—N bond lengths are almost the same (1.55 Å) and so are the N—B—N angle values (109°). It shows that the boron

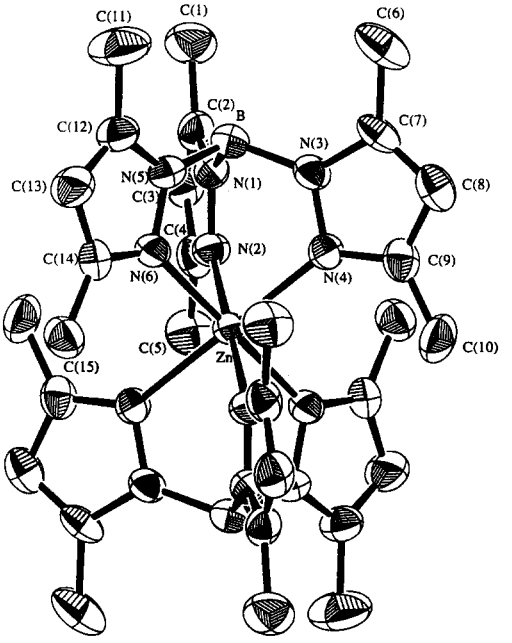


Fig. 1. The ORTEP plot of the crystal.

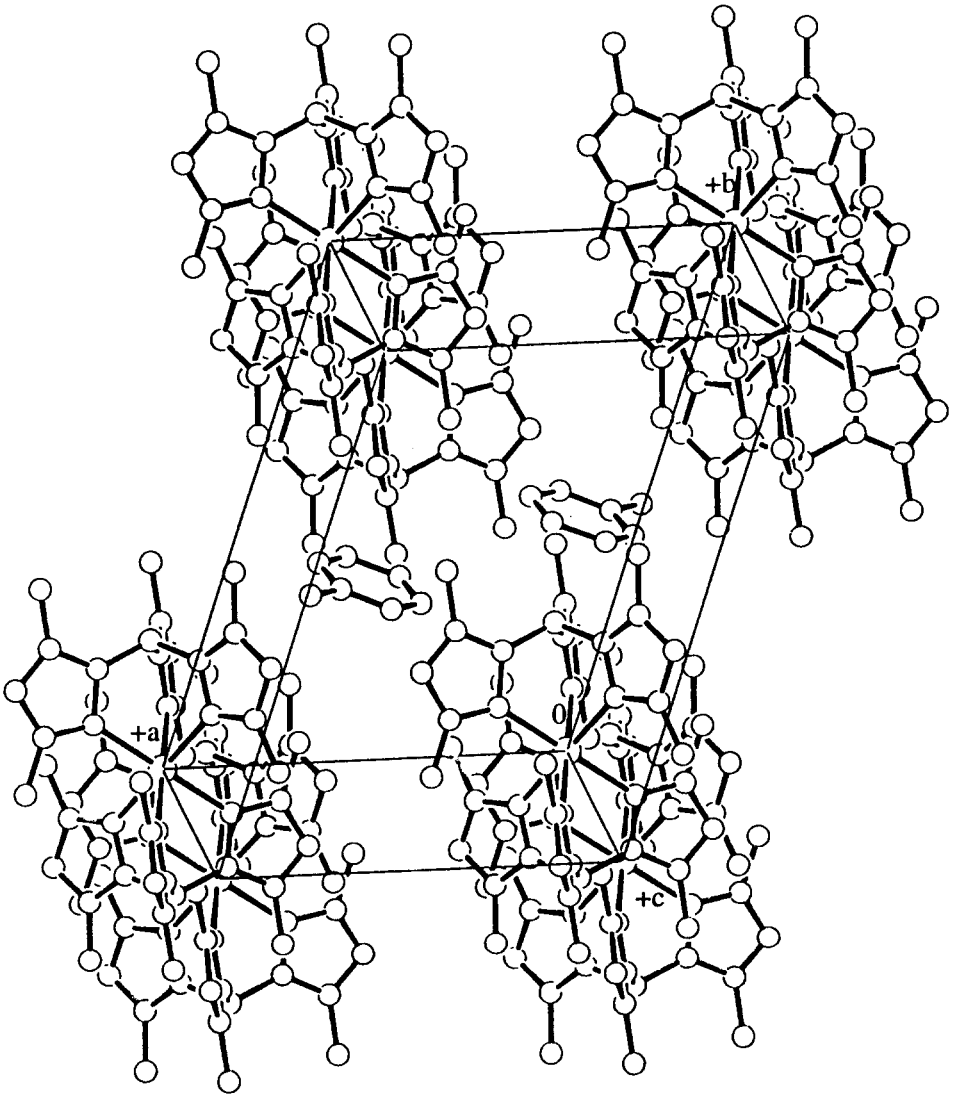


Fig. 2. The unit cell packing diagram of the crystal.

atom retains a strictly tetrahedral configuration. The three N—N lines are parallel, approximately, and the six-membered $B(NN)_2Zn$ ring takes the boat form.

The Zn—N bond distances [average 2.177(1) Å] are longer than the values found in $[\eta^3$-HB(3-Phpz)$_3]$ZnBr [4], [average 2.043(3) Å]. The Zn—N bond lengths are also longer than the Cu—N bond lengths of the compound $[HB(3,5\text{-}Me_2pz)_3CuPPh_3]$ [2.066(5)–2.092(5) Å] [5] and the compound $[pz_2\text{-}(\mu\text{-}pz)_2\text{-}Cu(PPh_3)_2]$ [2.051(3)–2.087(3) Å] [6]. The difference may be the result of the different coordination environments of the metal ions. It is remarkable that the configuration of the title compound is octahedral. Many of the zinc complexes with nitrogen-donor ligands adopt the tetrahedral configuration [7] with Zn—N bond distances (about 2.04 Å) which are shorter than in the title compound. In the title complex the Zn—N bond distances are typical for zinc in octahedral coordination [8] and they are within the ranges found in other octahedral zinc complexes [9].

There are six pyrazol rings in the complex, and they are almost planar. The maximum displacement is 0.001(6) Å for ring N(1)—C(2)—; 0.002(5) Å for

Table 4. Dihedral angles between planes (°)

Plane	1	2	3	4	5
2	121.59				
3	59.12	62.59			
4	150.28	29.36	91.26		
5	90.37	31.48	32.26	60.83	
6	31.77	90.59	28.17	118.56	60.37

Plane 1: N(1)—C(2) ring; 2: N(3)—C(7) ring; 3: N(5)—C(12) ring; 4: N(1)—N(2)—N(3)—N(4) ring; 5: N(3)—N(4)—N(5)—N(6) ring; 6: N(1)—N(2)—N(5)—N(6) ring.

ring N(3)—C(7)— and 0.005(6) Å for ring N(5)—C(13)—. The $(NN)_2$ are almostly in a plane, the maximum displacement is 0.028(4) Å [ring N(1)—N(2)—N(5)—N(6)]. The dihedral angles between the rings are listed in Table 4, in which the planes were defined in the way as the note shows. The biggest dihedral angle is the angle between plane 1 and 4 (150.28°), while the smallest one is the angle between plane 2 and 4 (29.36°).

Acknowledgements—This work was supported by the Postdoctoral Science Foundation of China, Postdoctoral Science Foundation of Shanghai Municipal and National Science Foundation of China.

REFERENCES

1. Tsuru, D., *"ZINC" in Bioactive Molecular*. Vol. 8, *Metalloproteins Chemical Properties and Biological Effects*, S. Otsuka; T. Yamanaka, Elsevier, Tokyo, p. 343, 1988.
2. Trofimenko, S., *Prog. Inorg. Chem.* 1986, **34,** 115.
3. Oulos, A. A., *J. Inorg. Nucl. Chem.* 1976, **38,** 435.
4. Kewu, Y., Yuanqi, Y. and Daosin, J., *Polyhedron*, 1995, **14,** 1021.
5. Kewu, Y., Yongzhen, W., Zhongxian, H. and Jie, S., To be submitted.
6. Cecchi, P., Bovio, B., Lobbia, G. G., Pettinari, C. and Leonesi, D., *Polyhedron*, 1995, **14,** 2441.
7. Donald, J. D., Matthew, W. H., Badana, K., Kevin, K. K. and Joseph, H. R., *Inorg. Chem.* 1995, **34,** 2389.
8. Brandt, W., Wirbser, J., Powell, A. K. and Vahrenkamp., *Z. Nat. Forsch. Teil. B*: *Chem. Sci.* 1991, **46,** 440.
9. Chaudhuri, P., Stockheim, C., Wieghardt, K., Gregorzik, R., Vahrenkamp, H., Nuber, B. and Weiss, J., *Inorg. Chem.* 1992, **31,** 1451.

Pergamon

PII: S0277-5387(96)00414-7

Polyhedron Vol. 16, No. 8, pp. 1301–1305, 1997
Copyright © 1997 Elsevier Science Ltd
Printed in Great Britain. All rights reserved
0277-5387/97 $17.00+0.00

Synthesis of μ_2-phenoxy-bridged binuclear cadmium(II) cryptates and X-ray crystal structure of one of them

Xin-You Xu,[a] Qin-Hui Luo,[a]* Meng-Chang Shen,[a] Xiao-Yun Huang[b] and Qiang-Jin Wu[b]

[a] Coordination Chemistry Institute, Coordination Chemistry State Key Laboratory, Nanjing University, Nanjing 210093, P.R. China

[b] Fuzhou State Key Laboratory of Structure Chemistry, Fuzhou 350002, P.R. China

(Received 4 June 1996; accepted 16 August 1996)

Abstract—Four binuclear cadmium(II) cryptates have been synthesized by [2+3] Schiff-base condensation of tris(3-aminopropyl)amine with sodium 2,6-diformyl-4-R-phenolates (R = OCH_3, CH_3, Br and Cl) in the presence of $Cd(ClO_4)_2 \cdot 6H_2O$. The crystal structure of the cryptate of macrocyclic L^3 (R = Br) $[CdL^3](ClO_4)$ was determined by X-ray diffraction. Each cadmium(II) atom is bonded to three μ_2-phenoxy oxygen atoms and three imine atoms. The coordination geometry of Cd^{II} is considered an irregular distorted octahedron.
Copyright © 1997 Elsevier Science Ltd

Keywords: cadmium(II); binuclear complexes; cryptates; crystal structure; oxygen bridge; irregular distorted octahedron.

The polyaza macrocycles have strong coordination ability and recognition functions for transition metal ions [1–5]. A new kind of macrocyclic ligand has been obtained [6] by template condensation of 2,6-diformyl-4-substituted-phenol with various diamines. These ligands have strong donor atoms, namely, phenoxy oxygen atoms as well as amine nitrogen atoms, and therefore play excellent roles in catalysis and biological simulation [7,8] owing to the special coordination ability with transition metal ions. Recently Gagne and co-workers [9], Nelson and co-workers [10] and others [11] have synthesized several transition metal cryptates by [2+3] condensation of tris(3-aminoethyl)amine (tren) with 2,6-diformyl-4-methylphenol (dmp) in the presence of transition metal ions. But so far there have been few reports of cryptates synthesized by condensation of tris(3-aminopropyl)amine (trpn, the analogue of tren) with dmp or its derivatives. It would be expected that these cryptates would have more plentiful host–guest properties as a result of the flexible long chain of trpn. For example, we have obtained an interesting pentanuclear silver(I) cluster [12] by condensation of trpn with dmp in the presence of silver(I). This paper reports four μ-oxo-bridged binuclear cadmium(II) cryptates synthesized by [2+3] Schiff-base condensation of trpn with 2,6-diformyl-4-R-phenol (R = OCH_3, CH_3, Br, Cl) in the presence of $Cd(ClO_4)_2 \cdot 6H_2O$. The X-ray crystal structure of the cryptate for R = Br shows that the coordination geometry of the Cd^{II} is an irregular distorted octahedron (Fig. 1), being different from the analogues reported up to now in which the coordination geometry of Cd^{II} is an irregular capped octahedron.

EXPERIMENTAL

Materials

2,6-Diformyl-4-R-phenols (R = CH_3O, CH_3, Br, Cl) were prepared by the literature method [13]. Sodium 2,6-diformyl-4-R-phenolates were obtained by mixing equimolar amounts of 2,6-diformyl-4-R-phenol and NaOH in ethanol. Tris(3-ami-

* Author to whom all correspondence should be addressed.

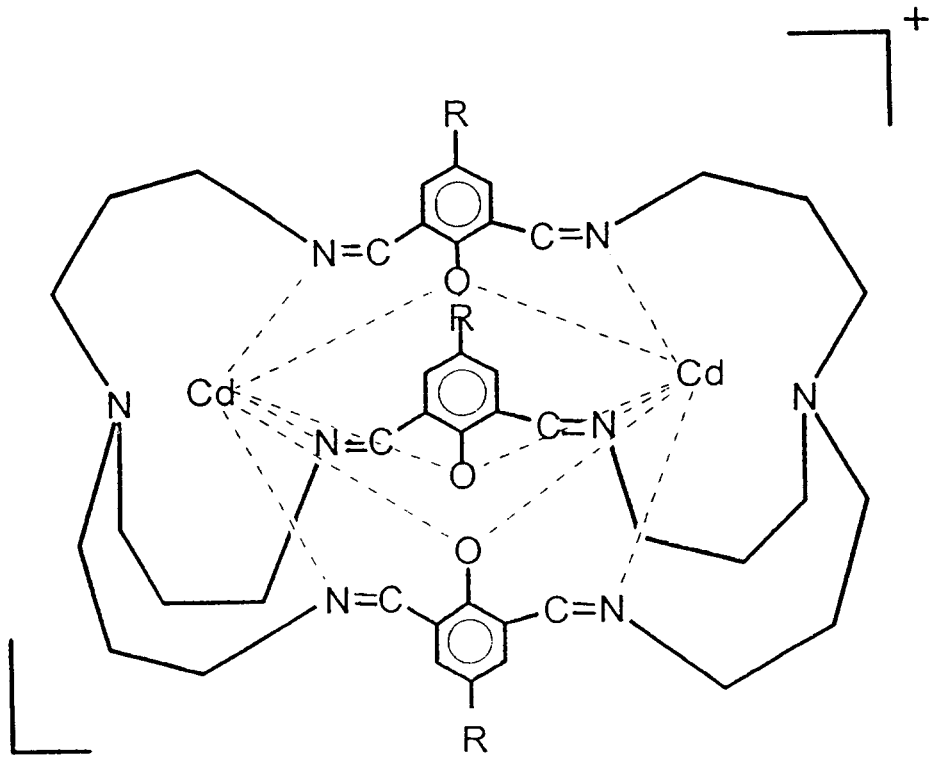


Fig. 1. The structures of the cryptate cations (R = OCH_3, L^1; CH_3, L^2; Br, L^3; Cl, L^4).

nopropyl)amine was prepared by a modified literature method [14] with a purity of over 99%. All starting materials were of chemical purity.

Physical measurements

The solution electrical conductivity was measured by a BDS-A numerical conductometer (Jiangsu, China) with solution concentrations of *ca* 10^{-4} mol dm^{-3} in acetonitrile. IR spectra were measured as KBr discs using a Nicolet 5DX FT-IR spectrophotometer. Electronic spectra were recorded on a Shimadzu UV-240 spectrophotometer.

Preparation of the cryptates

$[Cd_2L^1](ClO_4)\cdot H_2O$. To a stirred solution of sodium 2,6-diformyl-4-methoxylphenolate (0.1515 g, 0.75 mmol) and $Cd(ClO_4)_2\cdot 6H_2O$ (0.2621 g, 0.625 mmol) in absolute methanol (30 cm^3) was added dropwise a solution of tris(3-aminopropyl)amine (0.094 g, 0.5 mmol) in 15 cm^3 absolute methanol at 0°C. After stirring for 2 h at 35°C, yellowish microcrystals were precipitated and filtered off, washed with methanol and dried *in vacuo*, (yield 75%). Found: C, 47.3; H, 5.5; N, 9.7; Cd, 19.7. Calc. for $C_{45}H_{59}N_8O_{11}ClCd_2$: C, 47.2; H, 5.2; N, 9.8; Cd, 19.7%. IR (cm^{-1}, KBr): 3466 br, [$\nu_{(OH)}(H_2O)$]; 1630 s, ($\nu_{(C=N)}$); 1537 s, ($\nu_{(Ar\text{-}O)}$); 1103 s, ($\nu_{(ClO_4^-)}$). UV–vis [λ_{max} (nm), CH_3CN]: 240 (9310 mol^{-1} dm^3 cm^{-1}); 440 (2724). Λ_M (CH_3CN, 291 K): 104.6 S cm^2 mol^{-1}.

$[Cd_2L^2](ClO_4)\cdot 2CH_3OH$. Similar to $[Cd_2L^1](ClO_4)\cdot H_2O$, $[Cd_2L^2](ClO_4)\cdot 2CH_3OH$ was obtained as a yellowish crystalline product (yield, 65%). Found: C, 49.7; H, 5.2; N, 9.6; Cd, 19.3. Calc. for $C_{47}H_{65}N_8O_9ClCd_2$: C, 49.2; H, 5.7; N, 9.8; Cd, 19.6%. IR (cm^{-1}, KBr): 3452 br, [$\nu_{(OH)}(CH_3OH)$]; 1631 s, ($\nu_{(C=N)}$); 1539 s, ($\nu_{(Ar\text{-}O)}$); 1096 s ($\nu_{(ClO_4^-)}$). UV–vis [λ_{max} (nm), CH_3CN]: 240 (14,000 mol^{-1} dm^3 cm^{-1}); 430 (5000). Λ_M (CH_3CN, 301 K): 100 S cm^2 mol^{-1}.

$[Cd_2L^3](ClO_4)\cdot 3H_2O$. By a similar procedure, $[Cd_2L^3](ClO_4)\cdot 3H_2O$ was obtained as a yellowish crystalline product (yield, 80%). Found: C, 37.6; H, 4.0; N, 8.6; Cd, 17.5. Calc. for $C_{42}H_{54}N_8O_{10}Br_3ClCd_2$: C, 37.9; H, 4.1; N, 8.4; Cd, 16.9%. IR (cm^{-1}, KBr): 3450 br, [$\nu_{(OH)}(H_2O)$]; 1638 s, ($\nu_{(C=N)}$); 1537 s, ($\nu_{(Ar\text{-}O)}$); 1096 s ($\nu_{(ClO_4^-)}$). UV–vis [λ_{max} (nm), CH_3CN]: 420 (3643 mol^{-1} dm^3 cm^{-1}); 238 (15,178). Λ_M (CH_3CN, 291 K): 114 S cm^2 mol^{-1}. The yellowish crystals $[Cd_2L^3](ClO_4)$ suitable for X-ray structure determination were obtained by slow evaporation of the filtrate at ambient temperature.

$[Cd_2L^4](ClO_4)\cdot 0.5H_2O$. By a similar procedure, $[Cd_2L^4](ClO_4)\cdot 0.5H_2O$ was obtained as a yellowish crystalline product (yield, 69%). Found: C, 44.0; H, 4.6; N, 9.8; Cd, 19.2. Calc. for $C_{42}H_{49}N_8O_{7.5}Cl_4Cd_2$: C, 43.8; H, 4.3; N, 9.4; Cd, 19.5%. IR (cm^{-1}, KBr): 3480 br, [$\nu_{(OH)}(H_2O)$]; 1637 s, ($\nu_{(C=N)}$);

1539 s, ($\nu_{(Ar\text{-}O)}$); 1103 s ($\nu_{(ClO_4^-)}$). UV–vis [λ_{max} (nm), CH_3CN]: 410 (3428 mol^{-1} dm^3 cm^{-1}); 240 (9407). Λ_M (CH_3CN, 291 K): 90.7 S cm^2 mol^{-1}. ***CAUTION!*** Perchlorate salts of metal complexes with organic ligands are potentially explosive. Only small amounts of material should be prepared, and these should be handled with caution. The complexes described in this report have, so far, been found to be safe when used in small quantities.

X-ray crystal structure determination of $[Cd_2L^3](ClO_4)$

Crystal data. $C_{42}H_{48}N_8O_7Br_3ClCd_2$, F.W. = 1276.88, monoclinic, space group $C2/c$ (No. 15), a = 21.374(8), b = 12.340(2), c = 18.961(4) Å, β = 112.09(2)°, Z = 4, V = 4634(4) Å^3, $F(000)$ = 2520, D_c = 1.83 g cm^{-3}, μ = 35.91 cm^{-1}, R = 0.052, R_w = 0.063.

Data collection and refinement of the crystal structure. A single crystal of dimension 0.38 × 0.22 × 0.08 mm was mounted on a glass fibre. The crystal data were collected on an Enraf–Nonius CAD4 four circle diffractometer with graphite-monochromated Mo-K_α radiation (λ = 0.71073 Å, T = 296 K) using an ω–2θ scan mode with ω scan width, 0.50 + 0.350 tanθ, scan rate <5.49° min^{-1}; a total of 4304 independent reflections were collected in the range of $2 < 2\theta < 50°$, of which 2600 reflections with $I > 3\sigma(I)$ were used in the structure determination and refinement after Lp corrections. The structure was solved by the MITHRIL direct method. Additional non-hydrogen atoms were located from a difference Fourier map. Hydrogen atoms were introduced in calculated positions but not refined. The final least-squares cycle gave R = 0.052, R_w = 0.063 [w = $1\sigma^2(F)$]. The maximum and minimum residuals had values of 0.89 and −1.34 eÅ^{-3}, respectively. All calculations were performed using the programs contained in the TEXSAN package.

RESULTS AND DISCUSSION

Characterization of the cryptates

All the four cryptates possess similar spectral features. In the infrared spectra the strong peaks appeared at *ca* 1630 cm^{-1} corresponding to the stretching vibration of imino C=N bonds, and neither symmetric and asymmetric stretching frequencies at 3280 and 3330 cm^{-1} for NH_2 groups, nor strong peaks at 1650–1700 cm^{-1} for the carbonyl groups were present. This means that all the NH_2 and CO groups have been condensed into C=N bonds. A broad band at *ca* 3400 cm^{-1} characteristic of the OH group of CH_3OH or H_2O showed that CH_3OH or H_2O molecules existed in the cryptates, in agreement with the elemental analysis. But the three water molecules were lost during the growth of the single crystal of $[Cd_2L^3](ClO_4)$ for X-ray structure determination. The strong peak at *ca* 1090 cm^{-1}, without splitting, showed that the ClO_4^- did not take part in coordination with the Cd^{II} atom. This was also confirmed by the molar conductivity of the cryptates (Λ_M values are 90–114 S cm^2 mol^{-1}) which was attributable to 1 : 1 electrolytes [15]. It implies that the three phenol groups in the ligand lost hydrogen atoms during coordination. Two intense absorptions at about 240 and 400 nm in the electronic spectra of the cryptates were designated as π–π^* transitions of the K-band of the benzene rings and of the C=N groups [6], respectively. The substituents hardly gave any effects on the peak positions of the π–π^* transitions of the benzene rings, but positions of the maxima for the C=N bonds depended on the electron-attracting ability of the substituents. For the cryptates with different substituents, the values for the wavelengths of the C=N peaks have the following sequence: $OCH_3 > CH_3 > Br > Cl$; namely, the strong electron-attracting ability of substituents make the charge transfer require high energy, as a result, the peaks are blue-shifted.

Description of the structure of $[Cd_2L^3](ClO_4)$

A perspective view of the cation $[Cd_2L^3]^+$ and a packing diagram are shown in Figs 2 and 3, respectively. The selected bond distances and angles are given in Tables 1 and 2, respectively.

Figure 3 shows that each unit cell contains four molecular units, each consisting of one molecule of the cryptate cation $[Cd_2L^3]^+$ and one perchlorate anion. It may be seen from Fig. 2 that the cryptate cation has crystallographic C_2 symmetry. The C_2 axis passes through one of the benzene rings, the phenoxy group and the bromide. Each cadmium atom lies in the centre of an irregular distorted octahedron composed of three imino nitrogen atoms, N(2), N(3a), N(4), and three bridging phenoxy oxygen atoms, O(1), O(1a), O(2). Of these N(2) and O(1a) are located approximately at the axial sites and N(3a), O(1), O(2) and N(4) lie in equatorial positions of the octahedron. The

Table 1. Selected bond distances (Å) for the cryptate $[Cd_2L^3](ClO_4)$

Cd(1)—Cd(1a)	3.452(2)	C(4)—C(5)	1.46(1)
Cd(1)—O(1a)	2.320(6)	C(5)—C(6)	1.40(1)
Cd(1)—O(2)	2.323(5)	C(5)—C(10)	1.42(1)
Cd(1)—N(4)	2.325(7)	C(6)—C(7)	1.36(1)
Cd(1)—O(1)	2.329(6)	C(7)—C(8)	1.38(1)
Cd(1)—N(3a)	2.331(7)	C(8)—C(9)	1.39(1)
Cd(1)—N(2)	2.332(7)	C(9)—C(10)	1.43(1)
Br(1)—C(7)	1.895(8)	C(9)—C(11)	1.43(1)
Br(2)—C(18)	1.91(1)	C(12)—C(13)	1.51(1)
O(1)—C(10)	1.28(1)	C(13)—C(14)	1.55(2)
O(2)—C(15)	1.29(1)	C(15)—C(16)	1.42(1)
N(1)—C(1)	1.48(1)	N(2)—C(4)	1.27(1)
N(3)—C(11)	1.28(1)	N(4)—C(19)	1.29(1)

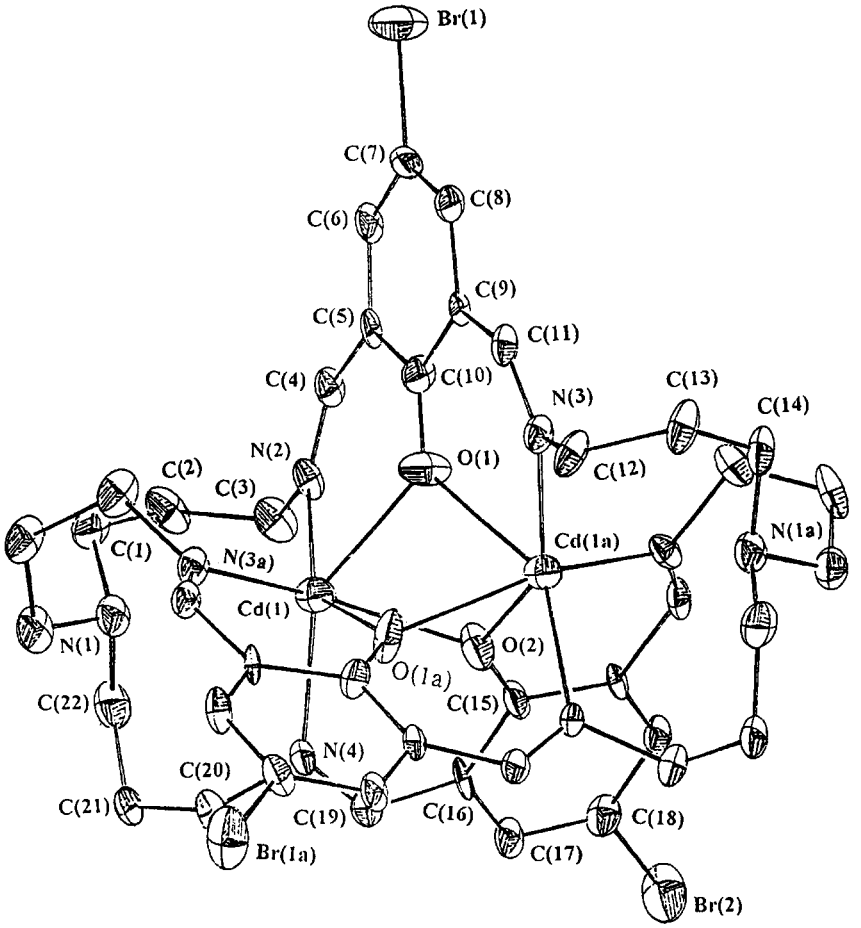


Fig. 2. A perspective view of the cation $[Cd_2L^3]^+$.

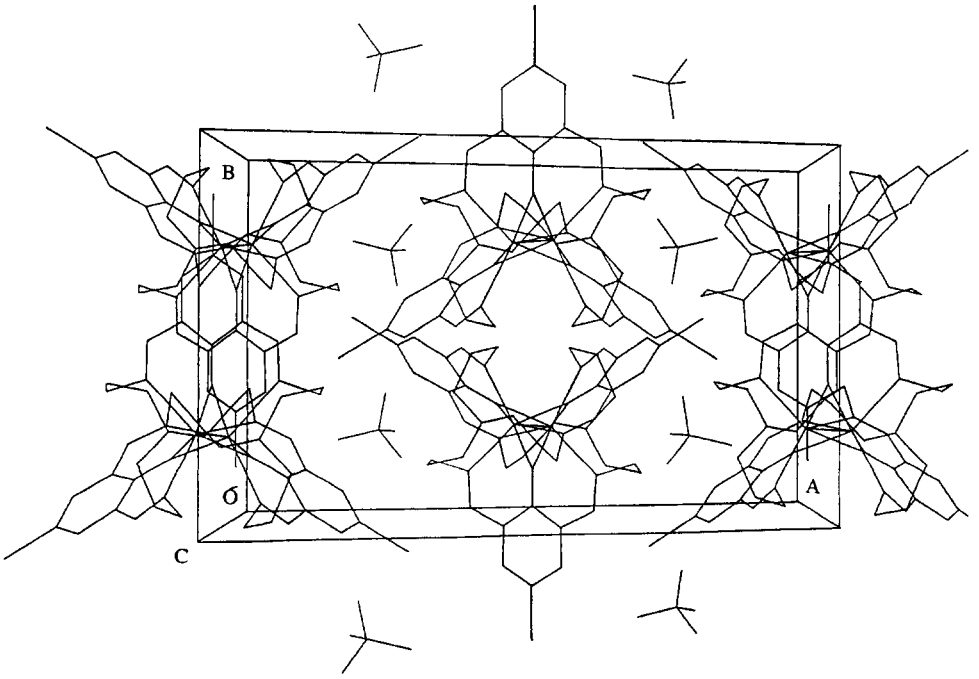


Fig. 3. A packing diagram of the cryptate $[Cd_2L^3]$ (ClO_4).

Table 2. Selected bond angles (°) for the cryptate $[Cd_2L^3](ClO_4)$

O(1a)—Cd(1)—Cd(1a)	42.1(1)	O(2)—Cd(1)—Cd(1a)	42.0(1)
N(4)—Cd(1)—Cd(1a)	107.8(2)	O(1)—Cd(1)—Cd(1a)	42.0(2)
N(3a)—Cd(1)—Cd(1a)	108.1(2)	N(2)—Cd(1)—Cd(1a)	107.6(2)
O(1a)—Cd(1)—O(2)	70.8(2)	O(1a)—Cd(1)—N(4)	97.0(3)
O(1a)—Cd(1)—O(1)	71.3(3)	O(1a)—Cd(1)—N(3a)	74.6(2)
O(1a)—Cd(1)—N(2)	145.5(2)	O(2)—Cd(1)—N(4)	74.4(2)
O(2)—Cd(1)—O(1)	70.6(2)	O(2)—Cd(1)—N(3a)	145.4(2)
O(2)—Cd(1)—N(2)	96.9(2)	N(4)—Cd(1)—O(1)	145.0(2)
N(4)—Cd(1)—N(3a)	110.6(2)	N(4)—Cd(1)—N(2)	110.8(2)
O(1)—Cd(1)—N(3a)	98.2(3)	O(1)—Cd(1)—N(2)	74.2(2)
N(3a)—Cd(1)—N(2)	111.7(2)	C(20)—N(4)—Cd(1)	113.9(5)
C(10)—O(1)—Cd(1)	131.5(5)	Cd(1)—O(1)—Cd(1a)	95.9(2)
C(15)—O(2)—Cd(1a)	132.0(1)	C(15)—O(2)—Cd(1)	132.0(1)
Cd(1)—O(2)—Cd(1a)	95.9(3)	C(1)—N(1)—C(22)	110(1)
C(4)—N(2)—C(3)	116.1(7)	C(4)—N(2)—Cd(1)	129.6(5)
C(3)—N(2)—Cd(1)	114.3(5)	C(11)—N(3)—Cd(1)	129.5(5)
C(12)—N(3)—Cd(1)	114.1(5)	C(19)—N(4)—C(20)	115.5(7)
C(19)—N(4)—Cd(1)	130.4(6)		

distances between Cd and each imino nitrogen are very close to each other, being about 2.33 Å. The Cd-μ-OPh distances are ranged from 2.32 to 2.30 Å. The distance Cd(1)···Cd(1a) is 3.452 Å and, apparently, there is no interaction between the two metals. The distance between Cd(1) and N(1) (tertiary nitrogen) is 3.051 Å, implying that there is no chemical bond between them. The Cd(1)···N(1) distance is longer than that of its analogue $[Cd_2L^2]^+$ in which the substituent on the benzene ring is a methyl group instead of the bromide and another analogue, whose ligand was synthesized by condensation of tren with dmp, their corresponding distances are 2.65 and 2.79 Å, respectively. Therefore, in our cryptate the substituent Br rendered the coordination environment of Cd^{II} different from that in the methyl substituent in which Cd^{II} is located in the centre of a seven-coordinate capped octahedron. The perchlorates are disordered and lie on a centre of inversion in the unit cell.

Acknowledgements—This project was supported by the Natural Science Foundation of China and the Fuzhou State Key Laboratory of Structure Chemistry.

REFERENCES

1. Lehn, J. M., *Angew. Chem., Int. Ed. Engl.* 1988, **27**, 89.
2. Jazwinskii, J., Lehn, J. M., Lillienbaum, D., Ziessel, R. and Guilheim, J., *J. Chem. Soc., Chem. Commun.* 1987, 1691.
3. Lu, Q., Latour, J.-M., Harding, C. J., Martin, N., Marrs, D. J., McKee, V. and Nelson, J., *J. Chem. Soc., Dalton Trans.* 1994, 1471.
4. Martell, A. E., in *Crown Compounds*, ed. S. R. Cooper. VCH, 1992, p. 99.
5. Yu, S.-Y., Luo, Q.-H., Shen, M.-C. and Huang, X.-Y., *Inorg. Chem.* 1994, **33**, 1251.
6. Pilkington, N. H. and Robson, R., *Aust. J. Chem.* 1970, **23**, 2225.
7. Zanello, P., Tamburini, S., Vigato, P. A. and Mazzocchim, G. A., *Coord. Chem. Rev.* 1987, **77**, 165.
8. Vigato, P. A., Tamburini, S. and Fenton, D. E., *Coord. Chem. Rev.* 1990, **106**, 105.
9. Timken, M. D., Marrit, W. A., Hendrickson, D. N., Gagne, R. A. and Sinn, E., *Inorg. Chem.* 1985, **24**, 4202.
10. Drew, M. G. B., Howarth, O. W., Morgan, G. G. and Nelson, J., *J. Chem. Soc., Dalton Trans.* 1994, 3149.
11. Chakraborty, P. and Chandra, S. K., *Polyhedron* 1994, **13**, 683.
12. Wang, J., Luo, Q. H., Shen, M. C., Huang, X. Y. and Wu, Q. J., *J. Chem. Soc., Chem. Commun.* 1995, 2373.
13. Taniguchi, S., *Bull. Chem. Soc. Jpn* 1984, **57**, 268.
14. Chin, J., Banaszczyk, M., Jubian, V. and Zou, X., *J. Am. Chem. Soc.* 1989, **111**, 186.
15. Geary, W. J., *Coord. Chem. Rev.* 1971, **7**, 81.
16. Yu, S. Y., Luo, Q. H., Shen, M. C., Huang, X. Y., *Inorg. Chim. Acta* 1994, **223**, 181.

Pergamon

PII: S0277-5387(96)00406-8

Polyhedron Vol. 16, No. 8, pp. 1307–1314, 1997
Copyright © 1997 Elsevier Science Ltd
Printed in Great Britain. All rights reserved
0277–5387/97 $17.00+0.00

Synthesis and spectroscopic studies of *trans* and *cis* rhodium(III) complexes of *o*-$C_6H_4(PMe_2)_2$ and *o*-$C_6H_4(AsMe_2)_2$. Crystal structures of *trans*-$[Rh\{o\text{-}C_6H_4(PMe_2)_2\}_2Cl_2]Cl$ and *trans*-$[Rh\{o\text{-}C_6H_4(AsMe_2)_2\}_2I_2]BF_4$

Angela M. Hill, William Levason,* Stephen R. Preece and Michael Webster

Department of Chemistry, University of Southampton, Southampton SO17 1BJ, U.K.

(Received 30 July 1996; accepted 12 August 1996)

Abstract—The rhodium(III) complexes *trans*-$[Rh(L\text{-}L)_2X_2]^+$ [L-L = *o*-$C_6H_4(PMe_2)_2$ or *o*-$C_6H_4(AsMe_2)_2$, X = Cl, Br or I] have been prepared from $RhX_3 \cdot nH_2O$ and L-L, and converted to the *cis*-$[Rh(L\text{-}L)_2X_2]^+$ by sequential treatment with Li_2CO_3 and HX. Both series of compounds have been characterized by analysis, UV–vis and multinuclear (^1H, $^{31}P\{^1H\}$ and ^{103}Rh) NMR spectroscopy. The trends in the ^{103}Rh chemical shifts with L-L, X and stereochemistry are discussed. The crystal structures of *trans*-$[Rh\{o\text{-}C_6H_4(PMe_2)_2\}_2Cl_2]Cl$ and *trans*-$[Rh\{o\text{-}C_6H_4(AsMe_2)_2\}_2I_2]BF_4$ have been determined. Copyright © 1997 Elsevier Science Ltd

Keywords: rhodium; NMR; diphosphine; diarsine.

The kinetic inertness of low-spin d^6 ions in pseudo-octahedral environments often allows the isolation of geometric isomers and for Rh^{III} many examples of *mer* and *fac* and *cis* and *trans* isomers with particular ligand sets have been characterized [1]. Despite a number of reports of *trans*-$[Rh(L\text{-}L)_2X_2]^+$ (L-L = diphosphine or diarsine, X = Cl or Br) [2–7], systematic studies of the *cis* isomers are lacking, little has been reported about the complexes with X = I and a recent paper [8] which characterized *cis*-$[Rh(L\text{-}L)_2Cl_2]^+$ [L-L = $Me_2P(CH_2)_nPMe_2$, n = 2 or 3] cast doubt on some previous reports of *cis* isomers. We report here a systematic study of the syntheses and properties of both *cis* and *trans* isomers of the structurally related ligands *o*-$C_6H_4(PMe_2)_2$ and *o*-$C_6H_4(AsMe_2)_2$ and show that ^{103}Rh NMR spectroscopy is a powerful way of identifying the isomers.

RESULTS AND DISCUSSION

The reaction of hydrated rhodium(III) trihalides $RhX_3 \cdot nH_2O$ (X = Cl, Br, or I; n usually *ca* 3)† with the ligands in ethanol–H_2O mixtures gave the rhodium(III) cations $[Rh(L\text{-}L)_2X_2]^+$ [L-L = *o*-$C_6H_4(PMe_2)_2$ or *o*-$C_6H_4(AsMe_2)_2$] isolated either as X^- or BF_4^- salts. Examination of the crude products by ^1H or in the case of the diphosphine complexes by $^{31}P\{^1H\}$ NMR spectroscopy showed that the *trans* isomer was the major product in each case, usually $\geqslant 80\%$, and pure *trans* isomers were easily obtained by recrystallization. The only exception was $[Rh\{o\text{-}C_6H_4(PMe_2)_2\}_2Br_2]^+$, where the *cis* isomer was present to $\leqslant 40\%$. The *cis* isomers were made from the *trans* by heating with excess Li_2CO_3 in aqueous ethanol for 48 h, which generates the η^2-carbonato complex, followed by treatment with aqueous HX. This method was developed by Bosnich *et al.* to prepare *cis*-$[Co(L\text{-}L)_2X_2]^+$ from the corresponding *trans* isomers [9]. The complexes are generally poorly soluble in chlorocarbons and alcohols, but more soluble in *N*, *N*-dimethylformamide or dimethylsulfoxide.

The ^1H NMR spectra (Table 1) of the *trans*-$[Rh\{o\text{-}C_6H_4(AsMe_2)_2\}_2X_2]^+$ isomers each show a single sharp

* Author to whom correspondence should be addressed.

† Commercial samples (Johnson Matthey Ltd) were used as received. ^{103}Rh NMR studies on the chloride have shown that mixtures of chloro-aquo complexes are present in varying amounts [10]. The bromide is probably similar. The black $RhI_3 \cdot nH_2O$ is very slightly soluble in water, but dissolves on heating with the ligands in EtOH–H_2O mixture.

Table 1. ^{1}H and $^{31}P\{^{1}H\}$ NMR data[a]

Complex	^{1}H	$^{31}P\{^{1}H\}$
trans-$[Rh\{o\text{-}C_6H_4(PMe_2)_2\}_2Cl_2]^+$	1.95[b]	41.0(d)[d], ^{1}J = 83 Hz
trans-$[Rh\{o\text{-}C_6H_4(PMe_2)_2\}_2Br_2]^+$	2.10[b]	34.2(d)[f], ^{1}J = 82 Hz
trans-$[Rh\{o\text{-}C_6H_4(PMe_2)_2\}_2I_2]^+$	2.45[c]	23.5(d)[f], ^{1}J = 78 Hz
cis-$[Rh\{o\text{-}C_6H_4(PMe_2)_2\}_2Cl_2]^+$	1.40, 1.75, 1.90, 2.25[d]	44.2(d.t)[f], $^{1}J_{Rh-P}$ = 84 Hz 51.1 (d.t), $^{1}J_{Rh-P}$ = 105 Hz $^{2}J_{P-P}$ = 18 Hz
cis-$[Rh\{o\text{-}C_6H_4(PMe_2)_2\}_2Br_2]^+$	1.56, 1.93, 2.18, 2.26[d]	38.3(d.t)[f], $^{1}J_{Rh-P}$ = 83 Hz 49.8(d.t), $^{1}J_{Rh-P}$ = 106 Hz $^{2}J_{P-P}$ = 15 Hz
cis-$[Rh\{o\text{-}C_6H_4(PMe_2)_2\}_2I_2]^+$	2.15, 2.22, 2.52, 2.60[c]	29.0(d.t)[f], $^{1}J_{Rh-P}$ = 83 Hz 42.5(d.t), $^{1}J_{Rh-P}$ = 104 Hz $^{2}J_{P-P}$ = 14 Hz
trans-$[Rh\{o\text{-}C_6H_4(AsMe_2)_2\}_2Cl_2]^+$	2.02[c]	
trans-$[Rh\{o\text{-}C_6H_4(AsMe_2)_2\}_2Br_2]^+$	2.20[c]	
trans-$[Rh\{o\text{-}C_6H_4(AsMe_2)_2\}_2I_2]^+$	2.35[c]	
cis-$[Rh\{o\text{-}C_6H_4(AsMe_2)_2\}_2Cl_2]^+$	1.95, 1.98, 2.00, 2.07[b]	
cis-$[Rh\{o\text{-}C_6H_4(AsMe_2)_2\}_2Br_2]^+$	2.05, 2.18, 2.19, 2.22[c]	
cis-$[Rh\{o\text{-}C_6H_4(AsMe_2)_2\}_2I_2]^+$	2.15, 2.29, 2.38, 2.48[c]	

[a] In solvent specified; $^{31}P\{^{1}H\}$ data relative to 85% H_3PO_4.
[b] CD_2Cl_2.
[c] $CDCl_3$.
[d] $(CD_3)_2SO$.
[e] CD_3NO_2.
[f] $HCONMe_2$.
The ^{1}H δ(Me) resonances of the diphosphine complexes are ill-defined second-order multiplets due to strong P—P couplings. d = doublet, d.t = doublet of triplets.

δ(Me) resonance, which shift to high frequency Cl < Br < I. Those of the diphosphines are similar, although the resonances are broader due to poorly resolved phosphorus couplings. The corresponding *cis* isomers exhibit four δ (Me) resonances of equal intensity. For the *trans*-$[Rh\{o\text{-}C_6H_4(PMe_2)_2\}_2X_2]^+$ the $^{31}P\{^{1}H\}$ NMR spectra are doublets with ^{1}J (^{31}P—^{103}Rh) = 80–85 Hz, whilst the *cis* isomers exhibit two doublets of triplets (Table 1) with the higher frequency d. of t. due to P_{transX} with ^{1}J (^{31}P—^{103}Rh) *ca* 105 Hz and ^{2}J (^{31}P—^{31}P) *ca* 15 Hz, whilst the second d. of t. is due to P_{transP} with ^{1}J (^{31}P—^{103}Rh) *ca* 83 Hz.

The ^{103}Rh NMR spectra are listed in Table 2 and Fig. 1 shows typical examples. The spectra were recorded by direct observation from saturated solutions of the complexes in $HCONMe_2$ or CH_2Cl_2 containing a free radical relaxation agent and with a 2 s pulse delay. For the diphosphine complexes relatively poor solubilities necessitated *ca* 70–100,000 scans to clearly resolve the couplings. The data in Table 2 reveal relatively systematic shifts with donor atoms and with the isomer present. Thus, for a particular ligand–halide combination the resonance of the *cis* isomer is always to low frequency of the *trans*, whilst for a particular geometric isomer the $\delta(^{103}Rh)$ of the diphosphine complexes are *ca* 400–500 ppm to low frequency of the diarsine analogues. The effect of changing the halide is also a systematic shift to low frequency Cl→Br→I. The literature data on ^{103}Rh NMR chemical shifts are very limited for group 15 donor complexes [10], but the trends in chemical shift observed in this work with isomer and donor atom are consistent with published data. It is, however, notable that the shifts observed in the present series of complexes are to low frequency of those observed for corresponding complexes of type *cis*- and *trans*-$[RhL_4X_2]^+$ (L = PMe_3 or $AsMe_3$) [10]

Table 2. $^{103}Rh\{^{1}H\}$ NMR data[a]

Complex	L-L = $o\text{-}C_6H_4(PMe_2)_2$	$o\text{-}C_6H_4(AsMe_2)_2$
trans-$[Rh(L\text{-}L)_2Cl_2]^+$	+628 (quintet)	+1130
cis-$[Rh(L\text{-}L)_2Cl_2]^+$	+99 (t. of t.)	+700
trans-$[Rh(L\text{-}L)_2Br_2]^+$	+387 (quintet)	+670
cis-$[Rh(L\text{-}L)_2Br_2]^+$	0 (t. of t.)	+410
trans-$[Rh(L\text{-}L)_2I_2]^+$	−364 (quintet)	−160
cis-$[Rh(L\text{-}L)_2I_2]^+$	−709 (t. of t.)	−300

[a] In $HCONMe_2$ at 300 K relative to Ξ = 3.16, all signals are singlets unless indicated otherwise. t. of t. = triplet of triplets.

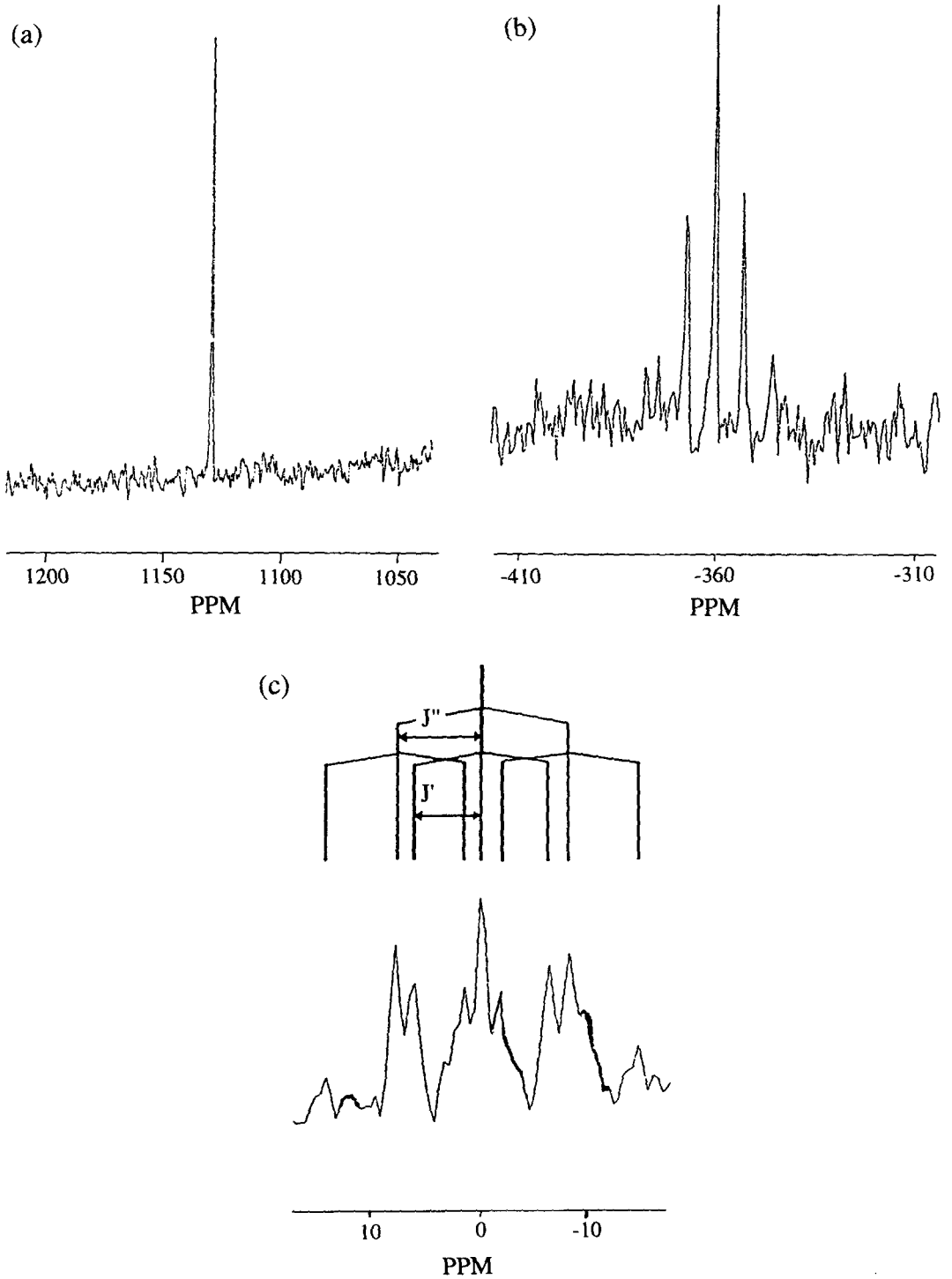


Fig. 1. ^{103}Rh $\{^1H\}$ NMR spectra in $HCONMe_2$ solutions at 300 K (δ relative to $\Xi = 3.16$) of (a) *trans*-$[Rh\{o\text{-}C_6H_4(AsMe_2)_2\}Cl_2]_2Cl$; (b) *trans*-$[Rh\{o\text{-}C_6H_4(PMe_2)_2\}_2I_2]$ I; (c) *cis*-$[Rh\{o\text{-}C_6H_4(PMe_2)_2\}_2Br_2]Br$, the relative intensities of the lines are predicted to be 1 : 2 : 2 : 1 : 4 : 1 : 2 : 2 : 1. $J'' = 105$ Hz, $J' = 83$ Hz.

or (*cis*-) $[Rh\{As(o\text{-}C_6H_4AsMe_2)_3\}X_2]^+$ [11]. The diphosphine and diarsine ligands used in the present study produce very large ligand fields [3] and since in the Ramsay equation the ^{103}Rh chemical shift varies inversely with the electronic exitation energy between the filled and empty *d*-orbitals [10], this correlates with the substantial low-frequency shifts observed. Comparisons can also be made with the ^{59}Co NMR shifts of the *trans*/*cis*-$[Co(L\text{-}L)_2X_2]^+$ [L-L = $o\text{-}C_6H_4(PMe_2)_2$ and $o\text{-}C_6H_4(AsMe_2)_2$] [12,13]. The broad lines

Table 3. UV–vis data $E_{max}/10^3$ cm^{-1} (ε_{mol}/cm^{-1} mol^{-1} dm^3)[a]

Complex	L-L = *o*-$C_6H_4(PMe_2)_2$	*o*-$C_6H_4(AsMe_2)_2$
trans-$[Rh(L\text{-}L)_2Cl_2]Cl$	33.1(2520), 25.9(270)	32.9(1780), 29.6(1370), 24.4(290)
trans-$[Rh(L\text{-}L)_2Br_2]Br$	29.4(4000), 21.2(460)	29.2(4000), 23.1(240)
trans-$[Rh(L\text{-}L)_2I_2]BF_4$	26.2(7600), 22.5(sh)	30.7(sh), 25.4(7110), 21.8(sh)
cis-$[Rh(L\text{-}L)_2Cl_2]Cl$	30.3(sh)	33.1(3940)
cis-$[Rh(L\text{-}L)_2Br_2]Br$	30.5(4260)	31.7(6040), 25.6(1600)sh
cis-$[Rh(L\text{-}L)_2I_2]I$	34.2(17450), 27.5(8150)	35.1(9460), 27.1(2770), 23.1(1420)

[a] CH_2Cl_2 solutions.

($W_{1/2} \leqslant 20{,}000$ Hz) resulting from the fast relaxation of the quadrupolar ^{59}Co nucleus ($I = 7/2$, 100%) limit the precision of the shifts to *ca* ±30 ppm, but whilst the same low frequency shift on replacing arsenic by phosphorus is found, the halide dependence is reversed with the iodide complexes having the highest frequency resonance and with chloride and bromide having similar shifts. The $\delta(^{59}Co)$ resonances of corresponding *cis* and *trans* isomers for X = Cl or Br are also the same within *ca* 50 ppm (*cis* isomers have not been made for X = I).

The UV–vis spectra of the complexes are listed in Table 3. The *d–d* spectra of low-spin d^6 ions in an octahedral L_6 environment are expected to contain two transitions from the $^1A_{1g}$ ground state to (in order of increasing energy) $^1T_{1g}$ and $^1T_{2g}$. In *trans*-L_4X_2 environments (local D_{4h} symmetry) the $^1T_{1g}$ splits into ^1E_g and $^1A_{2g}$, but the higher energy transition to $^1T_{2g}$ is rarely detectably split. The same states occur for the *cis* isomers, but the splitting of the $^1T_{1g}$ state is much smaller and often not resolved [14]. For the *trans*-$[Rh(L\text{-}L)_2X_2]^+$ (Table 3) the lowest energy band in each case is clearly the $^1A_{1g} \rightarrow {}^1E_g$ transition. Except for *trans*-$[Rh\{o\text{-}C_6H_4(PMe_2)_2\}_2Cl_2]^+$ all the complexes also show a second band $< 30{,}000$ cm^{-1} which are the $^1A_{1g} \rightarrow {}^1A_{2g}$ transition. The very high extinction coefficients reported are due to the fact that these bands lie in the tails of the very intense features $> 30{,}000$ cm^{-1} which are $\pi \rightarrow \pi^*$ of the Ph rings and $\pi(X) \rightarrow e_g(Rh)$ and σ (P/As) $\rightarrow e_g$ (Rh). The *d–d* transitions of the corresponding *cis* isomers, which are expected to lie at higher energy than those in the *trans* complexes, are mostly obscured by the charge transfer transitions.

Cyclic voltammetry studies in CH_2Cl_2 solutions containing 0.1 mol dm^{-3} $[Bu^n_4N][BF_4]$ revealed that all the complexes undergo completely irreversible reductions in the range −0.6 to −0.9 V (*vs* Fc/Fc^+ at +0.57 V) presumably to Rh^I, but no oxidative activity was seen out to the solvent limit at *ca* +2 V. The irreversibility no doubt reflects the change in coordination number, since Rh^I is likely to be four- or five-coordinate, whilst the great stability of the $4d\text{-}t_{2g}^6$ configuration with strong field ligands precludes oxidation to Rh^{IV} [15].

Crystallographic results

The structures of both complexes reported are of *trans* isomers, despite numerous attempts we were unable to obtain suitable crystals of the *cis* isomers. The structures of one cation in *trans*-$[Rh\{o\text{-}C_6H_4(AsMe_2)_2\}_2I_2]BF_4$ is shown in Fig. 2 and bond lengths and angles are given in Table 4. Despite some problem with the choice of crystal system (see Experimental),

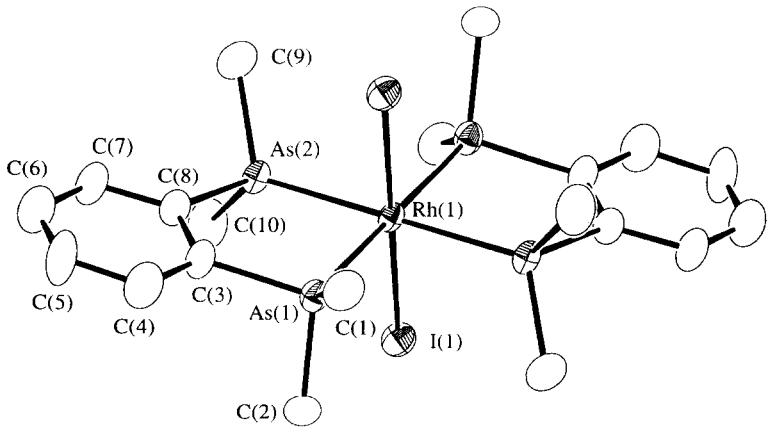


Fig. 2. One of the two cations in $[Rh\{o\text{-}C_6H_4(AsMe_2)_2\}_2I_2]BF_4$ with ellipsoids drawn at the 50% level. The second cation is very similar.

Table 4. Selected bond lengths (Å) and angles (°) for $[Rh\{o\text{-}C_6H_4(AsMe_2)_2\}_2I_2]BF_4$

Rh(1)—I(1)	2.679(1)	Rh(2)—I(2)	2.680(1)
Rh(1)—As(1)	2.426(2)	Rh(2)—As(3)	2.422(2)
Rh(1)—As(2)	2.424(2)	Rh(2)—As(4)	2.424(2)
	As—C	1.90(2)–1.96(2)	
	C—C	1.37(3)–1.43(2)	
	B—F	1.32(3)–1.61(3)	
As(1)—Rh(1)—As(2)	84.80(5)	As(3)—Rh(2)—As(4)	84.72(5)
I(1)—Rh(1)—As(1)	92.88(5)	I(2)—Rh(2)—As(3)	92.38(5)
I(1)—Rh(1)—As(2)	92.31(5)	I(2)—Rh(2)—As(4)	92.85(5)

in chemical terms the geometry is established. The cations lie on a centre of symmetry with Rh—I distances of 2.679(1) and 2.680(1) Å compared with 2.629(1)–2.755(1) Å in $[RhI_3(dppm)(CH_3CN)]$ [16] and Rh—As distances of 2.422(2)–2.426(2) compared with 2.345(4) to 2.454(4) Å in three $[Rh(L\text{-}L)_2Cl_2]^+$ [L-L = $Me_2As(CH_2)_3AsMe_2$] species [7]. The angles between the plane of the C_6 ring and the $RhAs_4$ residue are both 12°. The structure of the cation in *trans*-$[Rh\{o\text{-}C_6H_4(PMe_2)_2\}_2Cl_2]Cl$ is shown in Fig. 3 and bond lengths and angles are given in Table 5. Both *cis* and *trans* isomers of $[Rh(L\text{-}L)_2Cl_2]^+$ [L-L = $Me_2P(CH_2)_nPMe_2$, $n = 2$ or 3] species have been characterized [7,8] and the Rh—Cl [2.359(1) Å] and Rh—P distances [2.333(1), 2.328(1) Å] in the present compound can be compared with values from *trans*-$[Rh(Me_2P(CH_2)_3PMe_2)_2Cl_2]PF_6$, Rh—Cl 2.359(1), Rh—P 2.363(1), 2.364(1) Å] [8]. The Rh is positioned on a centre of symmetry and the angle between the C_6 ring and the RhP_4 residue is 9.1°.

EXPERIMENTAL

Physical measurements were made as described previously [17]. ^{103}Rh $\{^1H\}$ NMR data were recorded at

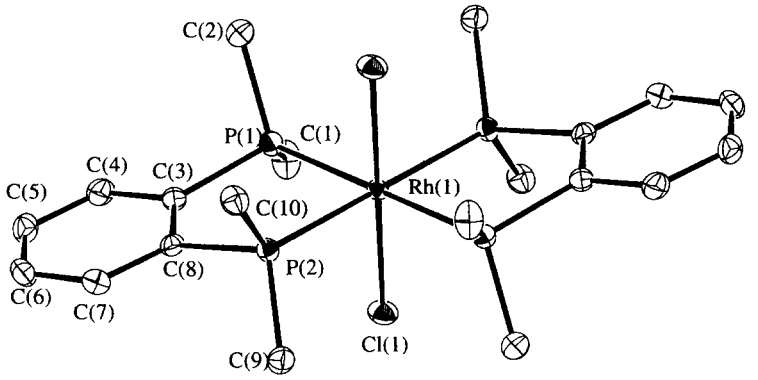


Fig. 3. The cation in $[Rh\{o\text{-}C_6H_4(PMe_2)_2\}_2Cl_2]Cl$ with ellipsoids drawn at the 50% level and with H atoms omitted for clarity.

Table 5. Selected bond lengths (Å) and angles (°) for $[Rh\{o\text{-}C_6H_4(PMe_2)\}_2Cl_2]Cl$

Rh(1)—P(1)	2.3330(7)	Rh(1)—Cl(1)	2.3590(7)
Rh(1)—P(2)	2.3284(8)		
P(1)—C(1)	1.809(3)	P(2)—C(8)	1.824(3)
P(1)—C(2)	1.817(3)	P(2)—C(9)	1.812(3)
P(1)—C(3)	1.825(3)	P(2)—C(10)	1.813(3)
	C—C	1.381(4)–1.401(4)	
	C—H	0.90(3)–1.01(3)	
Cl(1)—Rh(1)—P(1)	87.27(3)	P(1)—Rh(1)—P(2)	84.61(3)
Cl(1)—Rh(1)—P(2)	88.35(3)		
Rh(1)—P(1)—C(1)	117.2(1)	Rh(1)—P(2)—C(8)	108.3(1)
Rh(1)—P(1)—C(2)	117.9(1)	Rh(1)—P(2)—C(9)	116.0(1)
Rh(1)—P(1)—C(3)	107.9(1)	Rh(1)—P(2)—C(10)	118.3(1)

11.4 MHz on a Bruker AM360 spectrometer at 300 K, from concentrated solutions of the complexes in CH_2Cl_2 or $HCONMe_2$ in 10 mm o.d. tubes containing the free radical TEMPO as a relaxation agent and with a 2 s pulse delay. Typically 50–100,000 scans were accumulated. Due to the long accumulation times the temperature was maintained at 300 K *via* the variable temperature unit of the spectrometer, otherwise variations in room temperature broadened or split the resonances observed [10]. Chemical shifts are reported to high frequency of $\Xi = 3.16$ MHz [10]. Hydrated rhodium(III) halides were obtained from Johnson Matthey and used as received.

Preparations and characterizations

Trans-$[Rh\{o\text{-}C_6H_4(PMe_2)_2\}_2Cl_2]Cl$. To a solution of $RhCl_3 \cdot 3H_2O$ (0.26 g, 1.0 mmol) in aqueous ethanol (50 cm^3 1:2 H_2O: EtOH, v/v) was added the ligand (0.42 g, 2.1 mmol) under nitrogen. The mixture was refluxed for 2 h when a clear yellow solution formed. The solution was concentrated under reduced pressure and the pale yellow solid which separated was recrystallized from CH_2Cl_2/EtOH (0.36 g, 60%). Found: C, 39.9; H, 5.2. Calc. for $C_{20}H_{32}Cl_3P_4Rh$: C, 39.6; H, 5.3%.

Trans-$[Rh\{o\text{-}C_6H_4(PMe_2)_2\}_2X_2]X$ (X = Br or I) were made similarly. Found: C, 31.9; H, 4.1. Calc. for $C_{20}H_{32}Br_3P_4Rh$: C, 32.4; H, 4.3%. Found: C, 27.0, H, 3.5. Calc. for $C_{20}H_{32}I_3P_4Rh$: C, 27.3; H, 3.6%.

Trans-$[Rh\{o\text{-}C_6H_4(AsMe_2)_2\}_2Cl_2]BF_4$. To a solution of $RhCl_3 \cdot 3H_2O$ (0.39 g, 1.5 mmol) in ethanol (50 cm^3) was added the ligand (0.86 g, 3.0 mmol) under nitrogen and the mixture refluxed for 3 h. The solution was concentrated to 10 cm^3 and 40% HBF_4 (5 cm^3) added. The yellow precipitate was filtered off, rinsed with diethyl ether and recrystallized from hot ethanol (0.58 g, 70%). Found: C, 28.4; H, 3.8. Calc. for $C_{20}H_{32}As_4BCl_2F_4Rh$: C, 28.8; H, 3.8%.

Trans-$[Rh\{o\text{-}C_6H_4(AsMe_2)_2\}_2I_2]BF_4$ was made similarly. Found: C, 23.8; H, 3.3. calc. for $C_{30}H_{32}As_4BF_4I_2Rh$: C, 23.6; H, 3.1%. *trans*-$[Rh\{o\text{-}C_6H_4(AsMe_2)_2\}_2Br_2]Br$ was made by the same method but omitting the HBF_4. Found: C, 26.6; H, 3.4. Calc. for $C_{20}H_{32}As_4Br_3Rh$: C, 26.2; H, 3.5%.

Cis-$[Rh\{o\text{-}C_6H_4(PMe_2)_2\}_2Cl_2]Cl$. A slurry of the *trans* isomer (0.36 g, 0.6 mmol) in ethanol (30 cm^3) was treated with Li_2CO_3 (0.18 g, 2.4 mmol) in water (30 cm^3) and the mixture refluxed for 48 h under nitrogen. The resulting pale solution was cooled, filtered and then concentrated hydrochloric acid (3 cm^3) added slowly. The ethanol was removed *in vacuo* and the yellow precipitate filtered off, rinsed with distilled water and diethyl ether. It was recrystallized from ethanol/CH_2Cl_2 (0.16 g, 45%). Found: C, 40.1; H, 5.5. Calc. for $C_{20}H_{32}Cl_3P_4Rh$: C, 39.6; H, 5.3%. The corresponding bromide and iodide were made similarly. Found: C, 32.9; H, 4.5. Calc. for $C_{20}H_{32}Br_3P_4Rh$: C, 32.4; H, 4.3%. Found: C, 27.2, H, 3.6. Calc. for $C_{20}H_{32}I_3P_4Rh$: C, 27.3; H, 3.6%.

The *cis*-$[Rh\{o\text{-}C_6H_4(AsMe_2)_2\}_2X_2]X$ were made from the *trans* isomers and Li_2CO_3 (as above) yields *ca* 50%. (X = Cl) Found: C, 28.2; H, 3.8. Calc. for $C_{20}H_{32}As_4Cl_3Rh$: C, 28.8; H, 3.8%. (X = Br) Found: C, 26.7; H, 3.8. Calc. for $C_{20}H_{32}As_4Br_3Rh$: C, 26.2; H, 3.5%. (X = I) Found: C, 22.5; H, 3.1. Calc. for $C_{20}H_{32}As_4I_3Rh$: C, 22.7; H, 3.0%.

Crystal structure determinations

Diffracted intensities were recorded on a Rigaku AFC7S diffractometer fitted with Mo radiation and graphite monochromator. Crystals of $[Rh\{o\text{-}C_6H_4(AsMe_2)_2\}_2I_2]BF_4$ were obtained from CH_2Cl_2/Et_2O by slow evaporation and the intensity data recorded at 150 K. The initial unit cell [$a = 12.983(2)$, $b = 36.789(6)$, $c = 11.084(2)$ Å, $\alpha = 92.81(1)$, $\beta = 109.35(1)$, $\gamma = 84.00(2)°$] and measured intensities (18353) gave a solution containing the unusual number of six cations per unit cell ($Z = 6$). Inspection of a packing diagram of the unit cell and the atomic coordinates strongly suggested that the chosen cell was too large by a factor of three and that a smaller cell with $Z = 2$ could be chosen. An identical effect has been commented on before [18]. The transformation resulted in a large amount of discarded very weak reflection data and that remaining was used to obtain a structure from the crystal of less than ideal quality. It was noted that the Niggli matrix [19] for this smaller cell indicated that it could be transformed into a monoclinic C-lattice [18] and an alternative solution was explored in the higher symmetry system. The likely space groups are $C2/c$ or $C2/m$, both being centrosymmetric, the choice being governed by the $h0l$ reflections for which a number had $I \gg \sigma(I)$. No solution emerged in $C2/m$ and while $C2/c$ adequately described the cation it failed to produce a plausible BF_4^- anion. The structure solution was therefore described in terms of the triclinic ($Z = 2$) cell with details given in Table 6. The Rh atoms are positioned on a centre of symmetry; Rh, As, I and C atoms were given anisotropic thermal parameters; no H atoms were included in the model and the BF_4^- anion shows the commonly encountered disorder problems. The structure solution and refinement on F^2 were carried out using SHELXS86 [20] and SHELXL93 [21], respectively.

Crystals of $[Rh\{o\text{-}C_6H_4(PMe_2)_2\}_2Cl_2]Cl$ were obtained from CH_2Cl_2/Et_2O by slow evaporation and the intensity data recorded at 150 K. The structure emerged from the heavy atoms located using SHELXS86 [20], and subsequent atoms were found from structure factor and electron density calculations. The rhodium is positioned on a centre of symmetry; all the non-hydrogen atoms were given anisotropic thermal parameters and the H atoms were located in the electron-density maps. Hydrogen atom

Table 6. Crystallographic data

Mol formula	$C_{20}H_{32}As_4BF_4I_2Rh$	$C_{20}H_{32}Cl_3P_4Rh$
Mol wt	1015.68	605.63
Crystal system	triclinic	monoclinic
Space group	$P\bar{1}$ (no. 2)	$P2_1/c$ (no. 14)
a (Å)	12.983(2)	9.068(1)
b (Å)	12.980(2)	9.463(2)
c (Å)	11.084(2)	14.770(1)
α (°)	109.33(2)	90.0
β (°)	109.35(1)	98.94(1)
γ (°)	78.87(2)	90.0
V (Å^3)	1655.7(5)	1252.0(3)
T (K)	150	150
Density (calcd) (g cm^{-3})	2.037	1.606
Z	2	2
F (000) e	952	616
Crystal size (mm)	$0.2\times0.2\times0.3$	$0.15\times0.2\times0.6$
Type of data collection	$\omega/2\theta$	$\omega/2\theta$
Total no. of observations	6149	2514
Total no. of unique observations	5864	2358
Absorption correction	ψ-scan	ψ-scan
No. of data used in refinement	5840	1796
No. of parameters	267	179
Weighting scheme (w^{-1})	$\sigma^2(F_o^2)+(0.1029P)^2+71.56P$ $P=[\mathrm{Max}(F_o^2,0)+2F_c^2]/3$	$\sigma^2(F_o)$
λ, Å (Mo-K_α)	0.71069	0.71069
μ (cm^{-1})	63.8	12.6
max 2θ (°)	50.0	50.0
hkl limits	0 to 15, −15 to 15, −13 to 12	0 to 11, 0 to 11, −18 to 18
S	1.11	1.49
max shift /e.s.d	0.06	0.01
R [$F > n\sigma(F)$]	0.068 (n = 4, 4658 refs)	0.022 (n = 3, 1796 refs)
R (all data)	0.086	—
wR_2 (all data)	0.265	—
wR [$F > n\sigma$ (F)]	—	0.023 (n = 3, 1796 refs)

$R=[\Sigma\|F_o|-|F_c\|/\Sigma|F_o|]$; $wR_2=[\Sigma w(F_o^2-F_c^2)^2/\Sigma wF_o^4]^{1/2}$; $wR=[\Sigma w(F_o-F_c)^2/\Sigma wF_o^2]^{1/2}$.

positions were refined with a common refined thermal parameter. Full-matrix least-squares refinement [22] on F converged to $R = 0.022$ and details are given in Table 6.

Acknowledgements—We thank the EPSRC for financial support (A.M.H. and S.R.P) and for funds to purchase the X-ray diffractometer.

REFERENCES

1. Jardine, F. H. and Sheridan, P. S., in *Comprehensive Coordination Chemistry*, Vol. 4, ed. G. Wilkinson, J. A. McCleverty and R. D. Gillard. p. 901, Pergamon Press, Oxford, 1987.
2. Nyholm, R. S., *J. Chem. Soc.*, 1950, 857.
3. Warren, L. F. and Bennett, M. A., *Inorg. Chem.*, 1976, **15,** 3126.
4. Butter, S. A. and Chatt, J., *J. Chem. Soc. (A)*, 1970, 1411.
5. Levason, W. and McAuliffe, C. A., *Inorg. Chim. Acta*, 1976, **16,** 176.
6. Simonsen, K. P., Suzuki, N., Hamada, M., Kojima, M., Ohba, S., Saito, Y. and Fujita, J., *Bull. Chem. Soc. Jpn*, 1989, **62,** 3790.
7. Simonsen, K., Hamada, M. Suzuki, N., Kojima, M., Ohba, S., Galsbøl, F., Saito, Y. and Fujita, J., *Bull. Chem. Soc. Jpn*, 1990, **63,** 2904.
8. Suzuki, T., Isobe, K. and Kashiwabara, K., *J. Chem. Soc., Dalton Trans.* 1995, 3609.
9. Bosnich, B., Jackson, W. G. and McLaren, J. W., *Inorg. Chem.* 1974, **13,** 1133.
10. Mann, B. E., in *Transition Metal NMR*, ed. P. S. Pregosin. Elsevier, New York, 1991, p. 177; Goodfellow, R. J., in *Multinuclear NMR*, ed. J. Mason. Plenum Press, New York, 1987, Ch. 20.
11. Hill, A. M., Levason, W., Preece, S. R. and Frampton, C. S., *Inorg. Chim. Acta*, in press.
12. Levason, W., Preece, S. R. and Frampton, C. S., *Polyhedron* 1996, **15,** 2719.
13. Jewiss, H. C., Levason, W. and Webster, M., *Inorg. Chem.* 1986, **25,** 1997.

14. Lever, A. B. P., *Inorganic Electronic Spectroscopy*, 2nd. ed. Elsevier, Amsterdam, 1984.
15. Cipriano, R. A., Levason, W., Pletcher, D., Powell, N. A., and Webster, M., *J. Chem. Soc., Dalton Trans.* 1987, 1901.
16. Cotton, F. A., Dunbar, K. R., Eagle, C. T., Falvello, L. R., Kang, S.-J., Price, A. C. and Verbruggen, M. G., *Inorg. Chim. Acta*, 1991, **184,** 35.
17. Cipriano, R. A., Levason, W., Mould, R. A. S., Pletcher, D. and Webster, M., *J. Chem. Soc., Dalton Trans.* 1990, 2609.
18. Marsh, R. E., *Acta Cryst.* 1995, **B51,** 879.
19. de Wolff, P. M. and Gruber, B., *Acta Cryst.* 1991, **A47,** 29; Mighell, A. D. and Rodgers, J. R., *Acta Cryst.* 1980, **A36,** 321.
20. Sheldrick, G. M., *SHELXS*86, *Program for the Solution of Crystal Structures.* University of Göttingen, Germany, 1985.
21. Sheldrick, G. M., *SHELXL*93, *Program for the Refinement of Crystal Structures.* University of Göttingen, Germany, 1993.
22. teXsan, Crystal Structure Analysis Package, Version 1.7-1. Molecular Structure Corporation, 3200 Research Forest Drive, The Woodlands, TX 77381, U.S.A., 1995.

Pergamon

PII: S0277-5387(96)00407-X

Polyhedron Vol. 16, No. 8, pp. 1315–1322, 1997
Copyright © 1997 Elsevier Science Ltd
Printed in Great Britain. All rights reserved
0277–5387/97 $17.00+0.00

Metal supported macrocycles: synthesis and characterization of some new 1,3-bis(benzimidazol-1-yl-methylene)benzene and 1,4-bis(benzimidazol-1-yl-methylene)benzene-bridged metal(II) cation complexes

Sukhvinder K. Chawla* and Beerpal K. Gill

Department of Chemistry, Guru Nanak Dev University, Amritsar 143005, India

(Received 30 July 1996; accepted 12 August 1996)

Abstract—Two new non-chelating bidentate ligands 1,3-bis(benzimidazol-1-yl-methylene)benzene, hereafter 1,3-BIX, and 1,4-bis[benzimidazol-1-yl-methylene]benzene, hereafter 1,4-BIX, have been synthesized and their complexes with M^{II} salts (M = Co, Ni, Cu, Zn, Pd and Pt) have been prepared and characterized using elemental analysis, magnetic moment measurement, IR, UV–vis and ^{13}C NMR and FAB-MS (in some cases) studies. Cu^{II}, Pd^{II} and Pt^{II} metal ions yield dinuclear square-planar complexes *viz.* $[enM(BIX)]_2X_4$ (en = 1,2 diaminoethane; M = Pd or Pt, X = NO_3; M = Cu, X = ClO_4, BIX = 1,3- or 1,4-BIX). Co^{II} chloride forms dimeric tetrahedral $[Co(BIX)Cl_2I_2$, whereas Ni^{II} and Zn^{II} chlorides yield polymeric $[M(BIX)Cl_2]_n$ complexes.
Copyright © 1997 Elsevier Science Ltd

Keywords: non-chelating; macrocycle; metal supported; supramolecule.

Currently there has been particular interest in the synthesis of macrocycles by the self-assembly of ligands around the metal ion in which the metal → ligand coordinate bond replaces the conventional covalent C—C or C—X bond of organic macrocycles. Access to supramolecules *via* non-covalent interactions is presently at the forefront of modern chemistry. Moreover, metal supported macrocycles can be conveniently generated *via* one pot synthesis in contrast to their organic counterparts which involve cumbersome multistep synthesis.

In the past two decades, there have been scattered accounts of the late transition metal ions forming di-, tri-, and tetranuclear complexes enclosing a cavity in the middle. For example, bis-pyrazoles, imidazoles, pyridazines and 3,5-bis[2-pyridyl]pyridazine form multinuclear complexes with Co^{II}, Ni^{II}, Cu^{I}, Cu^{II} and Au^{I} metal ions [1–5]. All these ligands have one thing in common that they disfavour binding to the same metal centre. However, Fujita *et al.* [6] were the first to recognize the potential of such molecules to act as inorganic hosts and used them for molecular recognition. These and other workers have prepared a series of cationic dimeric and tetrameric complexes by interaction of square-planar metal ion species *viz.* $[L_2MX_2]$ [L_2 = en or 1,3-bis(diphenylphosphino)propane or bis-triphenylphosphine; X = OSO_2CF_3, NO_3 or ClO_4] by reacting a variety of linear bidentate ligands such as 4,4′-bipyridine [6], diazapyrene, dicyanobenzene [7], 1,2-bis(4-pyridyl)ethane, 1,4-bis[4-pyridylmethylene]-2,3,5,6-tetrafluorobenzene [8] and 1,4-bis(4-pyridylmethylene)benzene [9] and evaluated some of these complexes for charged and neutral organic guests.

We are interested in linear biosimulating nitrogen-based potentially bidentate ligands because of the ease with which one can achieve variation in pre-organization, cavity size, rigidity and electronic effects of macrocycle. Complexes of 1,3-BIX and 1,4-BIXX (Fig. 1) have been prepared and characterized with a variety of metal ions *viz.* Co^{II}, Ni^{II}, Cu^{II}, Zn^{II}, Pd^{II} and Pt^{II}.

* Author to whom correspondence should be addressed.

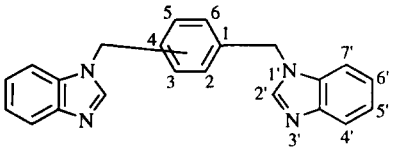


Fig. 1. 1,3- or 1,4-BIX ligand.

EXPERIMENTAL

Physical measurement

Elemental analysis of the complexes were carried out by Regional Sophisticated Instrumentation Centre of Punjab University, Chandigarh, on a Carlo Erba Model 1106. The FAB-MS studies on some complexes were made on POS FAB NBA at the Department of Biochemistry, Washington State University, U.S.A. The ^1H and ^{13}C NMR spectra of ligands and their Pd^{II} and Pt^{II} complexes were recorded on a Bruker A.C. 200 MHz instrument. Mass spectra of the ligands were obtained on Shimadzu-GCMS-OP 2000A. UV–vis spectra of the complexes as solutions were recorded in the range 200–1100 nm using UV-160A recording type Shimadzu spectrophotometer. IR spectra of complexes were recorded on FTIR 8101 M Shimadzu and SP3-300 spectrophotometers as KBr pallets. The ESR spectra of the Cu^{II} complexes were studied at room temperature on an FE-3XG JEOL X-band instrument. The magnetic field in the range 3000 ± 2500 G at a constant microwave frequency of 9.44 GHz was applied. The magnetic susceptibility measurements were made on powdered samples using Evan's method on the magnetic susceptibility balance, Johnson Matthey Engineered Products, England.

Materials

Benzoyl peroxide, *m*-and p-xylenes, *N*-bromo-succinimide were procured from Loba, Bombay. Benzimidazole and metal salts were purchased from Glaxo Laboratories, Bombay or Ranbaxy Chandigarh.

Solvent ether was dried over sodium metal, while acetonitrile was distilled over phosphorus pentoxide immediately before use. All other materials and solvents were used as such without further purification.

m-xylene dibromide and *p*-xylene dibromide were prepared by a reported method [10].

Preparation of 1,3-*bis*(*benzimidazol*-1-*yl-methylene*) *benzene*

A mixture of benzimidazole (3.57 g, 0.03 M), potassium-*tert*-butoxide (3.57 g, 0.032 M) and the catalyst 18-crown-6 (3–4 mg) was stirred for 15 min in dry ether and *m*-xylene dibromide (4 g, 0.015 M) was quickly added to the reaction mixture. The contents were stirred for 25 h (TLC monitored) and filtered. The residue was washed twice with dry ether and refluxed with acetonitrile (30 cm^3) for 1 h to extract the product. It was then filtered and washed with two portions of acetonitrile (10 cm^3). The combined filtrate was concentrated to half its volume, which on cooling gave crystals of the product. The crude product was further purified by recrystallization from acetonitrile; m.pt 109°C, yield 61%. MS data *m/z* 338 (M^+). ^1H NMR (d_6-DMSO-$CDCl_3$-TMS); δ 7.28–7.13 (m, 10H) and 8.16–7.69 (m, 4H) (heterocyclic/phenylene protons), 5.11 (s, 4H, —CH_2 protons).

Preparation of 1,4-*bis*(*benzimidazol*-1-*yl-methylene*) *benzene*

It was prepared by the analogous method discussed above; m.p. = 124°C, yield = 60%. MS data *m/z* 338 (M^+). ^1H NMR (d_6-DMSO-$CDCl_3$-TMS): δ 7.40–7.19 (m, 10H) and 8.49–7.9 (m, 4H) (heterocyclic/phenylene protons), 5.12 (s, 4H, —CH_2 protons).

Preparation of complexes

Preparation of $[M(BIX)Cl_2]_n$, [(BIX) = 1,3-BIX *and* 1,4-BIX; M = Co, n = 2; *and* M = Zn, n = x]. Treatment of aqueous solutions (10.0 cm^3) of metal (II) chloride (0.002 M) with a methanolic solution (10.0 cm^3) of the ligand (675 mg, 0.002 M) at room temperature resulted in the immediate separation of a quantitative precipitate of the complex, which was filtered off and washed several times with water, followed by methanol and dried *in vacuo*. Yield: *ca* 90%.

Repeated attempts to prepare $[Cu(BIX)Cl_2]_2$ under the above conditions resulted in the formation of polymer of stoichiometry $[(BIX)_2Cu_3Cl_6]$.

Preparation of $[Ni(BIX)Cl_2]_n$. The reaction mixture obtained by mixing methanolic solution (15.0 cm^3) of 1,3-BIX (675 mg, 0.002 M) and aqueous solution of nickel(II) chloride (237 mg, 0.002 M in 10 cm^3) was refluxed for 1 h, which on concentration yielded a mixture of two components which were separated by dissolving in CH_3OH. The insoluble green component A (*ca* 80%) could be easily separated from soluble pale brownish component B (*ca* 20%). The component A was washed several times with water and methanol and dried *in vacuo*.

However, repeated attempts to prepare 1,4-BIX analogue of the above complex in the pure state under similar experimental conditions failed and only an impure green product could be isolated.

Preparation of $[enCu(BIX)]_2(ClO_4)_4$. The solutions of $Cu(ClO_4)_2 \cdot 6H_2O$, [0.02 M (standardized against EDTA)], ethylenediamine (0.02 M) and BIX ligands (0.02 M) were prepared in acetonitrile. $Cu(ClO_4)_2 \cdot 6H_2O$ and ethylenediamine solutions were mixed in equal volumes (20 cm^3 each) to prepare

$[enCu(H_2O)_4](ClO_4)_2$ as a bright blue solution *in situ*, which on addition of either ligand (20 cm^3, 0.02 M) turned dark blue. The reaction mixture on standing at room temperature for 2–3 days yielded blue precipitate of the complex, which was filtered off, washed several times with acetonitrile and dried *in vacuo*. Yield *ca* 80%.

Preparation of $[enM(BIX)]_2(NO_3)_4$ [M = Pd *and* Pt]. The complexes $[enPdCl_2]$ [11] and $[enPtCl_2]$ [12] were prepared by the reported methods starting from $PdCl_2$ and H_2PtCl_6, respectively.

An aqueous suspension (5 cm^3) of $[enMCl_2]$ (0.002 M) was treated with a solution of $AgNO_3$ (680 mg, 0.004 M in 5 cm^3 of water). The reaction mixture was stirred for 10 min, and the white precipitate of AgCl was filtered off and a pale brownish solution of $[enM(NO_3)_2]$ was used for the preparation of the complexes. The methanolic solution (10 cm^3) of 1,3-BIX (675 mg, 0.002 M) was added to the above solution of $[enM(NO_3)_2$ and stirred for 10 min. The pale yellow precipitate of $[enM(1,3\text{-}BIX)_2]$ $(NO_3)_4$ separated out on concentration, which was filtered off, washed twice with methanol and dried *in vacuo*. Yield 75%.

The analogous complexes $[enM(1,4\text{-}BIX)]_2(NO_3)_4$ were prepared following the above procedure. Yield 75%.

RESULTS AND DISCUSSION

Cobalt(II) *complexes*

Treatment of $CoCl_2 \cdot 6H_2O$ with either ligand (1 : 1) in $H_2O : CH_3OH$ at room temperature resulted in the separation of an immediate blue precipitate of the complex, which corresponds to $[(BIX)CoCl_2]$ stoichiometry, as indicated by CHN analysis (Table 1). Both the complexes are insoluble in H_2O, CH_3OH, $CHCl_3$ and CH_3CN, but moderately soluble in DMF, DMA and DMSO. The magnetic moment values for $[Co(1,3\text{-}BIX)Cl_2]$ and $[Co(1,4\text{-}BIX)Cl_2]$ complexes are found to be 4.3 and 4.4 B.M., respectively [13], which are suggestive of tetrahedral stereochemistry around the Co^{II} ion.

The visible spectral studies on the complexes as DMF solutions record a broad band at *ca* 635 nm (15,748 cm^{-1}) with a shoulder on the higher energy side *ca* 575 nm (17,391 cm^{-1}) (Table 2, Fig. 2). The position of the band corresponds to the $^4A_2 \rightarrow {}^4T_1(P)$ transition of the tetrahedral complex. The spectra of the complexes in the present case closely resemble tetrahedral Co (imidazole)$_2Cl_2$ [14]. A peak at 615 nm (16,260 cm^{-1}) with shoulders at 585 (17,090 cm^{-1}) and 630 nm (15,070 cm^{-1}) is observed. However, the spectra are vastly different from octahedral Co (imidazole)$_6Cl_2$, which records a band at 487 nm [20,500 cm^{-1}, $^4T_{1g}(F) \rightarrow {}^4T_{1g}(P)$] with a very weak shoulder *ca* 613 nm (16,300 cm^{-1}) due to the spin forbidden $^4T_{1g}(F) \rightarrow {}^2T_{1g}$ transition. Hence, the visible spectral studies of both complexes support the tetrahedral stereochemistry of the Co^{II} ion. The other two transitions *viz.* $^4A_2 \rightarrow {}^4T_1(P)$ and $^4A_2 \rightarrow {}^4T_2(F)$, could not be assigned because these transitions occur beyond the range of the instrument used (above 1000 nm). Furthermore, as the ligands are deliberately designed not to bind to the same metal centre, a ligand-bridged dimeric tetrahedral structure is assigned to these complexes (Fig. 3).

The FAB-MS of $[Co(1,4\text{-}BIX)Cl_2]_2$ in 3-nitrobenzyl alcohol shows a pair of peaks corresponding to $[M^+ + H - Cl]$ at m/z values 900 and 902 (Scheme 1), which first loses HCl (m/z = 864) and then Co (m/z = 806), HCl (m/z = 770) and Cl (m/z = 735) generating $(BIX)_2Co$. This fragment further loses a molecule of ligand (m/z = 397) and Co (m/z = 338) to record the fragment of the ligand at m/z 338 as a base peak. Hence, FAB-MS strongly support the given structural assignment to these complexes.

Table 1. CHN analysis, colour and magnetic moment of the complexes

Complex	Colour	%C Found (Calc.)	%H Found (Calc.)	%N Found (Calc.)	Magnetic moment (B.M.)
(1) $[Co(1,3\text{-}BIX)Cl_2]_2$	Royal blue	56.6 (56.5)	3.6 (3.8)	12.4 (12.0)	4.3
(2) $[Co(1,4\text{-}BIX)Cl_2]_2$	Royal blue	55.4 (56.5)	3.4 (3.8)	12.7 (12.0)	4.4
(3) $[Ni(1,3\text{-}BIX)Cl_2]_n$	Light green	55.9 (56.4)	4.3 (3.8)	11.9 (11.9)	3.6
(4) $[Ni(1,4\text{-}BIX)Cl_2]_n$	Light green	Not obtained in pure form			3.7
(5) $[Cu_3(1,3\text{-}BIX)_2Cl_6]_n$	Light green	49.6 (48.9)	3.2 (3.3)	9.9 (10.3)	2.1
(6) $[Cu_3(1,4\text{-}BIX)_2Cl_6]_n$	Light green	49.3 (48.9)	3.1 (3.3)	11.2 (10.3)	2.3
(7) $[enCu(1,3\text{-}BIX)]_2(ClO_4)_4$	Light blue	43.2 (43.5)	4.1 (3.9)	15.1 (14.5)	2.1
(8) $[enCu(1,4\text{-}BIX)]_2(ClO_4)_4$	Light blue	43.8 (43.5)	4.2 (3.9)	15.3 (14.5)	1.9
(9) $[Zn(1,3\text{-}BIX)Cl_2]_n$	White	53.4 (53.6)	—	11.0 (11.4)	—
(10) $[Zn(1,4\text{-}BIX)Cl_2]_n$	White	53.2 (53.6)	3.1 (4.1)	12.0 (11.4)	—
(11) $[enPd(1,3\text{-}BIX)]_2(NO_3)_4$	Pale yellow	45.6 (45.8)	4.4 (4.1)	16.8 (17.8)	—
(12) $[enPt(1,3\text{-}BIX)]_2(NO_3)_4$	Pale white	41.1 (40.2)	3.1 (3.6)	15.3 (15.6)	—
(13) $[enPt(1,4\text{-}BIX)]_2(NO_3)_4$	Pale white	41.9 (40.2)	3.2 (3.6)	15.0 (15.6)	—

Table 2. UV-vis spectral data of the some complexes

Complex	Solvent	λ_{max} (nm)
(1) $CoCl_2 \cdot 6H_2O$	DMF	527 [$^4A_{1g}(F) \rightarrow {}^4T_1(P)$]
(2) $[Co(1,3\text{-BIX})Cl_2]_2$	DMF	575 (sh), 640 [$^4A_2 \rightarrow {}^4T_1(P)$]
(3) $[Co(1,4\text{-BIX})Cl_2]_2$	DMF	572 (sh), 635 [$^4A_2 \rightarrow {}^4T_1(P)$]
(4) $Co(imidazole)_2Cl_2$	Solid	585 (sh), 615, 630 (sh)
(5) $NiCl_2 \cdot 6H_2O$	Methanol	366 [$^3A_{2g} \rightarrow {}^3T_{1g}(P)$] 660 (sh), 740 [$^3A_{2g} \rightarrow {}^3T_{1g}(F)$]
(6) $[Ni(1,3\text{-BIX})Cl_2]_n$	Methanol	350 [$^3A_{2g} \rightarrow {}^3T_{1g}(P)$] 650, 735 (sh), [$^3A_{2g} \rightarrow {}^3T_{1g}$]
(7) $[Ni(1,4\text{-BIX})Cl_2]_n$	Methanol	350 [$^3A_{2g} \rightarrow {}^3T_{1g}(P)$] 650, 738 (sh), [$^3A_{2g} \rightarrow {}^3T_{1g}$]
(8) $[enCu(H_2O)_4](ClO_4)_2$	Acetonitrile	663 [$d \rightarrow d$ transition]
(9) $[enCu(1,3\text{-BIX})]_2(ClO_4)_4$	Acetonitrile	580 [$d \rightarrow d$ transition]
(10) $[enCu(1,4\text{-BIX})]_2(ClO_4)_4$	Acetonitrile	580 [$d \rightarrow d$ transition]
(11) $[Cu(benzimidazole)_4]X_2$	Solid	580, 710 (sh)

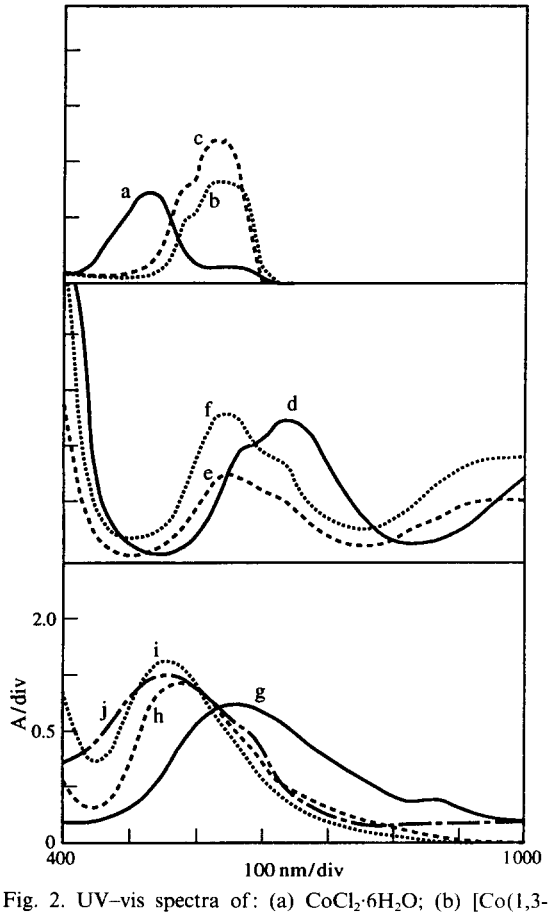


Fig. 2. UV–vis spectra of: (a) $CoCl_2 \cdot 6H_2O$; (b) $[Co(1,3\text{-BIX})Cl_2]_2$; (c) $[Co(1,4\text{-BIX})Cl_2]_2$; (d) $NiCl_2 \cdot 6H_2O$; (e) $[Ni(1,3\text{-BIX})Cl_2]_n$; (f) $[Ni(1,4\text{-BIX})Cl_2]_n$; (g) $[enCu(H_2O)_4](ClO_4)_2$; (h) $[enCu(1,3\text{-BIX})]_2(ClO_4)_4$; (i) $[enCu(1,4\text{-BIX})]_2(ClO_4)_4$; (j) $Cu(benzimidazole)_4X_2$.

Nickel(II) *complexes*

$NiCl_2 \cdot 6H_2O$ does not react with either ligand at room temperature. However, refluxing a 1 : 1 mixture of metal salt and 1,3-BIX ligand in $CH_3OH : H_2O$ (1 : 1) for 1 h, on concentration yielded a mixture of two components. The insoluble green component A was separated from the soluble brown component B by treating the mixture with methanol. However, prior to isolation both the components are completely soluble in the reaction mixture. However, once isolated, component A becomes highly insoluble. The CHN analysis of this component corresponds to 1:1 (L/M) stoichiometry (Table 1). Its magnetic moment value has been found to be 3.6 B.M. The component B was not studied further.

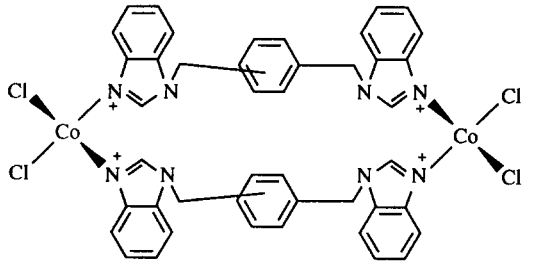
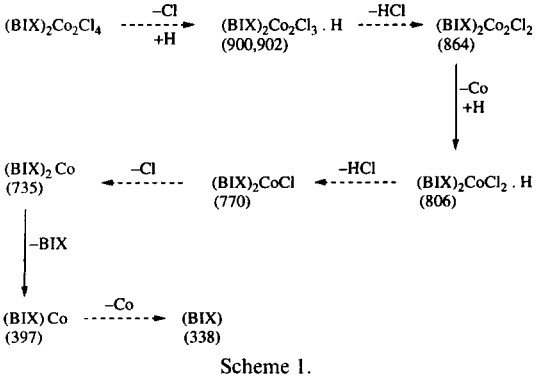


Fig. 3. Co^{III} driven self-assembly of 1,3- and 1,4-BIX ligands.

Reaction of 1,4-BIX with $NiCl_2 \cdot 6H_2O$ under analogous conditions yielded an insoluble green complex,



Scheme 1.

which, however could not be isolated in an analytically pure state. The magnetic moment of the crude product was found to be 3.7 B.M. The tetrahedral ground state $^3T_1(F)$ has much inherent orbital angular momentum and, therefore, the magnetic moment of a truly tetrahedral Ni^{II} complex should be around 4.2 B.M. However, small distortion reduces the μ value to 3.5–4.0 B.M. For all the octahedral and more distorted tetrahedral complexes the range is 3.0–3.5 B.M. [15]. Hence, the magnetic moment values suggest either distorted tetrahedral or octahedral structure for the complexes.

The VIS spectra of the reaction solutions were recorded before isolation of the product. Both spectra show transitions at *ca* 350 nm (28,571 cm^{-1}), a second band in the region of 650 nm (15,385 cm^{-1}) with a shoulder at 735 nm (13,605 cm^{-1}) and another band above 1100 nm (90,909 cm^{-1}, beyond the range of the instrument used), (Table 2, Fig. 2). These transitions correspond to $^3A_{2g} \rightarrow {}^3T_{1g}(P)$, $^3A_{2g} \rightarrow {}^3T_{1g}(F)$ and $^3A_{2g} \rightarrow {}^3T_{2g}(F)$, respectively, of octahedral complexes [16]. The blue shift of the visible transition in the present case compared with the octahedral $[Ni(H_2O)_6]Cl_2$ complex [715 nm, (13,986 cm^{-1})] is a consequence of the replacement of H_2O by N donors which lie towards the stronger end of the spectrochemical series.

Hence, it is concluded that these complexes exist as dimers (because the bidentate ligand is non-chelating) with octahedral stereochemistry around each nickel(II) ion in solution (the other two ligands may be H_2O), which became converted into ligand-bridged polymers in the solid state. The high insolubilities of these complexes in various solvents further support polymeric nature of these complexes.

Copper(II) *complexes*

Reactions of both ligands with $CuCl_2 \cdot 2H_2O$ in $CH_3OH : H_2O$ in a 1 : 1 molar ratio resulted in the immediate separation of a green precipitate of the complexes. Both the complexes correspond to 2 : 3 (L/M) stoichiometry (Table 1). These complexes are found to be highly insoluble in all common solvents and their structure has been discussed elsewhere [17].

To prepare dimeric Cu^{II} complexes, the $[enCu(H_2O)_4](ClO_4)_2$ complex was used as a source of Cu^{II} ions. As expected, the reaction of $[enCu(H_2O)_4](ClO_4)_2$ with 1,3-BIX or 1,4-BIX under highly dilute conditions in acetonitrile generated the square-planar $[enCu(BIX)]_2(ClO_4)_4$ (Fig. 4). The magnetic moment values for 1,3-BIX and 1,4-BIX complexes are found to be 2.1 and 1.9 B.M., respectively. As the magnetic moment values of all the Cu^{II} complexes lacking Cu—Cu interactions fall in the range 1.75–2.20 B.M. [18], the μ values, therefore, do not give any clue regarding the stereochemistries of the complexes, but indicate that the Cu—Cu interaction is absent in the present case.

The visible spectra of these complexes in acetonitrile

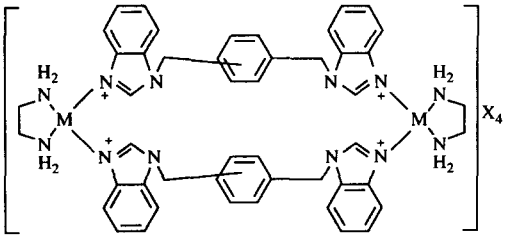


Fig. 4. Metal(II) assisted self-assembly of 1,3- and 1,4-BIX ligands (M = Cu^{II}, Pd^{II} and Pt^{II}).

(Fig. 2, Table 2) record a broad unsymmetrical band in the region *ca* 580 and 590 nm (17,214 and 16,949 cm^{-1}) for the 1,3- and 1,4-BIX complexes, respectively. This band position is of the general type found for planar or tetragonally distorted octahedral copper(II) complexes [19]. Here the four N atoms lie approximately in the plane and bulky ClO_4 anions are placed out of the plane. As in the case of $Cu(benzimidazole)_4(ClO_4)_2$, here again the ClO_4 anions are uncoordinated. Due to the steric reasons the benzimidazole ring and en ring are forced to lie at an angle with the CuN_4 plane, which offer steric hindrance to the approach of large ClO_4 anions. The positions and shapes of IR spectral bands [1100 cm^{-1} (ν_3) unsplit and 620 cm^{-1} (ν_1)] again support that the ClO_4 are uncoordinated (Table 3) [20].

The g_x and g_y values of Cu^{II} complexes which have usual $d_x^2 - y^2$ ground state typically lie between 2.04 and 2.07, while the g_z value falls in the 2.15–2.40 range. In contrast, one of the g values of g_z is close to 2.002, which is indicative of d_z^2 ground state [21]. In the present case the ESR spectrum of $[enCu(1,3\text{-}BIX)]_2(ClO_4)_4$ shows three peaks corresponding to the g values *viz.* $g_1 = 2.01$, $g_2 = 2.075$ and $g_3 = 2.12$ (Fig. 5), which suggest a rhombic elongated structure with $d_x^2 - y^2$ ground state. The $[enCu(1,4\text{-}BIX)]_2(ClO_4)_4$ complex records $g_\parallel$ at 2.43 and shows evidence of a nuclear hyperfine splitting (A = 120 G which can be accounted for due to the presence of the large ClO_4 anion) and $g_\perp = 2.10$. The range of g values again supports an axially enlongated structure with $d_{x^2-y^2}$ ground state [22,23]. As the phenyl rings of the xylene spacer are expected to be planar, some distortion of the CuN_4 chromophore towards tetrahedral may be expected.

Zinc(II) *complexes*

Highly insoluble material separated out on mixing either ligand with $ZnCl_2 \cdot H_2O$. The CHN analysis of the complexes correspond to 1 : 1 (M/L) stoichiometry (Table 1). A ligand-bridged tetrahedral polymeric structure has been proposed for the complexes.

Palladium(II) *and Platinum*(II) *complexes*

As discussed previously for the Cu^{II} complexes, *cis*-$[enM(NO_3)_2]$, [M = Pd or Pt], complexes were reacted

Table 3. Selected IR data of Cu^{II}, Pd^{II} and Pt^{II} complexes

Complex	en	ClO_4	NO_3	M—N
(1) $[enCu(1,3\text{-}BIX)]_2(ClO_4)_4$	3400, 3150 (νNH_2) 1620 (δ_d NH_2) 890 (ρ_r)	1100 (ν_3) 620 (ν_1)	— —	— —
(2) $[enCu(1,4\text{-}BIX)]_2(ClO_4)_4$	3400, 3100 (νNH_2) 1610 (δ_d NH_2) 1200 (δ_s) 800 (ρ_r)	1100 (ν_3) 620 (ν_1)		
(3) $[enPd(1,3\text{-}BIX)]_2(NO_3)_4$	3400, 3100 (νNH_2) 1600 ($\delta_d NH_2$) 1200 (δ_s), 800 (ρ_r)		1380 (ν_3), 1045 (ν_1) 720 (ν_4)	480
(4) $[enPd(1,4\text{-}BIX)]_2(NO_3)_4$	3400, 3250 (νNH_2) 1600 ($\delta_d NH_2$) 920 (ρ_r)		1345 (ν_3), 1080 (ν_1) 740 (ν_4)	480
(5) $[enPt(1,3\text{-}BIX)]_2(NO_3)_4$	3450 (νNH_2) 1600 ($\delta_d NH_2$) 1125 ($\delta_s NH_2$), 860 (ρ_r)		1300 (ν_3), 1105 (ν_1) 740 (ν_4)	550
(6) $[enPt(1,4\text{-}BIX)]_2(NO_3)_4$	3400 (νNH_2) 1600 ($\delta_d NH_2$) 1120 ($\delta_s NH_3$) 870 (ρ_r)		1320 (ν_3), 1080 (ν_1) 720 (ν_4)	

δ_s = Symmetric deformation; δ_d = degenerate deformation; ρ_r N—H rocking.

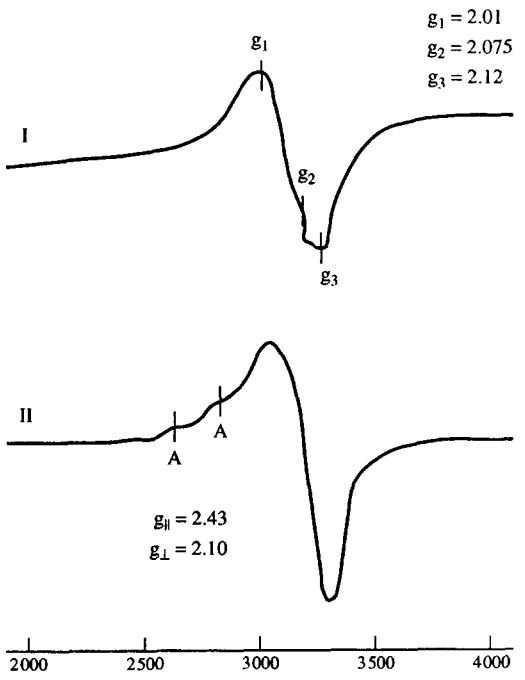


Fig. 5. ESR spectra of (I) $[enCu(1,3\text{-}BIX)]_2(ClO_4)_4$; (II) $[enCu(1,4\text{-}BIX)]_2(ClO_4)_4$.

with 1,3- or 1,4-BIX in CH_3OH–H_2O in 1 : 1 molar ratio to generate dinuclear square $[enM(BIX)]_2(NO_3)_4$ (Fig. 4) complexes. These complexes are soluble in hot water, DMSO, DMF and DMA.

IR spectral data (Table 3) corresponds to vibrational bands for the ethylene diamine at 3450, 3100 [ν NH_2, 1620–1600 ($\delta_d NH_2$) 1200–1120 (δ_s) and 920–800 cm^{-2} (ρ_r)]. The bands due to the uncoordinated nitro group appear at 1380–1320 (ν_3), 1105–1045 (ν_1) [20]. These bands are in addition to various vibrational bands due to benzimidazole ligands.

^{13}C NMR data for the ligands as well as complexes are reported in Table 4. In the complexes the positions of the C-2 carbon is shifted downfield, confirming the coordination of the benzimidazole N atom to the metal ion.

The FAB-mass study of $[enPd(1,4\text{-}BIX)]_2(NO_3)_4$ confirms the macrocyclic dinuclear structure for these complexes. It shows a parent ion peak at m/z 1258 $[M^+ + 2H]$. A peak for $[en_2(BIX)_2Pd_2]$ due to the loss of all the four NO_3 $[M^+ - 4NO_3]$ groups is recorded at m/z 1008, which further loses both molecules of ethylene diamine to generate a peak at m/z 888 corresponding to the fragment $(BIX)_2Pd_2$. Successive loss of Pd, BIX and Pd from $(BIX)_2Pd_2$ yields fragments at m/z 782.444 and 338, respectively. In another series of fragmentation pattern, first the loss of both ethylene diamines and then $4NO_3$ is observed to give a peak at m/z at 888 corresponding to $(BIX)_2Pd_2$ (Scheme 2). A base peak for $(BIX)Pd_2$ is shown at m/z 550 from which one Pd dissociates to give (BIX)Pd at m/z 444. Loss of the second Pd gives a free ligand at m/z 338.

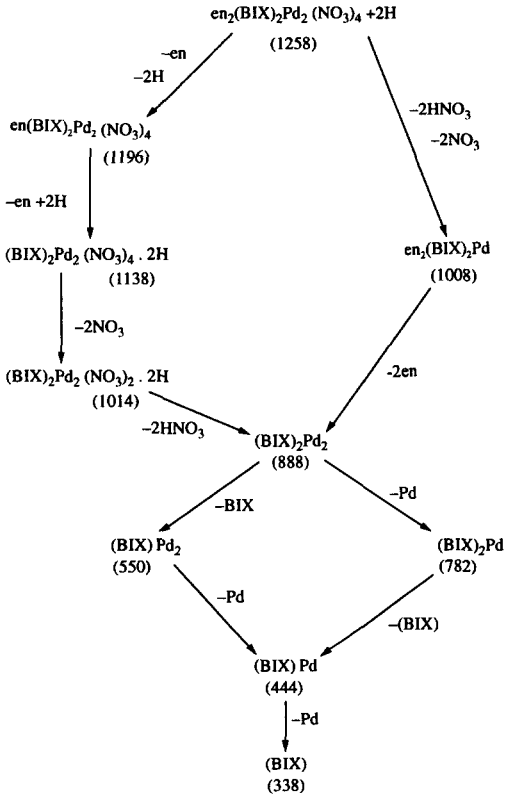
CONCLUSION

The formation of these unique complexes clearly shows the success achieved in the self-assembly of the ligands around the metal ion by reacting appropriately designed ligands and carefully selected the metal ion species.

Table 4. ^{13}NMR chemical shifts (ppm) of ligands, Pd^{II} and Pt^{II} complexes

S. No.	Compound	C—2	C—4	C—5	C—6	C—7	Phenylene Carbon	en $-CH_2$ Carbons	
(1)	1,3-BIX[a]	143.5	110.2	122.0	122.4	115.2	136.7, 133.5 129.4, 126.9 126.3, 122.8 119.7	48.2	—
(2)	1,4-BIX[a]	142.2	109.0	120.3	120.9	113.5	135.9, 126.5, 131.0, 134.5 118.3	45.8	—
(3)	$[enPd(1,3\text{-}BIX)]_2(NO_3)_4$[a]	148.4	110.5	121.4	124.0	117.9	140.3, 134.0, 126.7 125.3, 115.3 109.5	48.0 46.9	21.9
(4)	$[enPd(1,4\text{-}BIX)]_2(NO_3)_4$[a]	148.5 144.2	109.5	121.5	124.9	115.3	140.4, 135.0 126.9, 117.9 115.3, 111.6	48.1 46.0	21.8
(5)	$[enPt(1,3\text{-}BIX)]_2(NO_3)_4$[b]	147.8	—	120.0	124.5	115.3	142.4 134.3, 132.1, 127.6 127.1, 126.9, 124.6	52.7	17.6, 20.0
(6)	$[enPt(1,4\text{-}BIX)]_2(NO_3)_4$[b]	146.6 144.3	107.8	121.9	120.7 118.7	—	139.5, 134.7 134.4, 130.8 112.1		17.6

[a] d_6-DMSO-$CDCl_3$ was used as solvent.
[b] DMF-$CDCl_3$ was used as solvent, TMS was used as internal reference.



Scheme 2.

REFERENCES

1. Andew, J. E., Ball, P. W. and Blake, A. B., *Chem. Commun.* 1969, 143.
2. (a) Ball, P. W. and Blake, A. B., *J. Chem. Soc. A.* 1969, 1415; (b) Blake, A. B., Ewing, D., Hamin, J. E. and Lockyer, J. M., *J. Chem. Soc., Dalton Trans.* 1977, 1897.
3. Chaudhuri, P., Karpenstein, I., Winter, M., Lengen, M., Butzlaff, C., Bill, E., Trautwein, A. X., Florke, U. and Haupt, H. J., *Inorg. Chem.* 1993, **32,** 888.
4. Kolks, G., Lippard, S. J., Waszczak, J. U. and Lilienthal, H. R., *J. Am. Chem. Soc.* 1982, **104,** 717.
5. (a) Bonati, F., Minghetti, G. and Banditelli, G., *J. Chem. Soc., Chem. Commun.* 1974, 88; (b) Minghetti, G., Banditelli, G. and Bonati, F., *Inorg. Chem.* 1979, **18,** 658.
6. (a) Fujita, M., Yazaki, J. and Ogura, K., *J. Am. Chem. Soc.* 1990, **112,** 5645; (b) Fujita, M., Yazaki, J. and Ogura, K., *Tetrahedron Lett.* 1991, **32,** 5589; (c) Fujita, M., Yazaki, J. and Ogura, K., *Chem. Lett.* 1991, 1031.
7. Stang, J., Cao, D. H., Saito, S. and Arif, A. M., *J. Am. Chem. Soc.* 1995, **117,** 6273.
8. Fujita, M., Nagao, S., Iida, M., Ogata, K. and Ogura, K., *J. Am. Chem. Soc.* 1993, **115,** 1574.
9. Fujita, M., Nagao, S. and Ogura, K., *J. Am. Chem. Soc.* 1995, **117,** 4175.
10. Wenner, W., *J. Org. Chem.* 1952, 523.
11. Drew, H. D. K., Pinkard, F. W., Preston, G. H. and Wardlaw, W., *J. Chem. Soc.* 1932, 1895.
12. (a) *Handbook of Preparative Inorganic Chemistry,*

Ed. G. Brauer. Academic Press, New York, 1965, 1572; (b) Basolo, F., Bailar Jr, J. C., Tarr, B. R., *J. Am. Chem. Soc.* 1950, **72,** 2433.
13. Goodgame, M. and Cotton, F. A., *J. Am. Chem. Soc.* 1962, **84,** 1543.
14. Eilbeck, W. J., Holmes, F. and Underhill, A. E., *J. Chem. Soc. A.* 1967, 757.
15. Cotton, F. A. and Wilkinson, G., *Advanced Inorganic Chemistry*, 5th Edn, John Wiley, New York, 1988, p. 743.
16. Lever, A. B. P., *Inorganic Electronic Spectroscopy*. 2nd edn, Amsterdam, Elsevier, 1984, p. 507.
17. Chawla, S. K., *Polyhedron*, 1997, accepted.
18. (a) Earnshaw, A., *An Introduction to Magnetochemistry*. Academic Press, London, 1968; (b) Mabbs, F. E. and Machin, D. J., *Magnetism and Transition Metal Complexes*. Chapman and Hall, London, 1973.
19. Goodgame, M. and Haines, L. I. B., *J. Chem. Soc. A.* 1966, 174.
20. Nakamoto, K., *Infrared Spectra of Inorganic and Coordination Compounds*. Wiley Interscience, London, 1970.
21. Mcpherson, G. L. and Anderson, C. P., *Inorg. Chem.* 1974, **13,** 677.
22. Hathaway, B. J., *Comprehensive Coordination Chemistry*, ed. G. Wilkinson, R. D. Gillard and J. A. McCleverty, Pergamon Press, Oxford, 1987, Vol. 5, p. 662.
23. Hathaway, B. J., Hodgson, D. G. and Power, P. C., *Inorg. Chem.* 1974, **13,** 2009.

Pergamon

PII: S0277-5387(96)00405-6

Polyhedron Vol. 16, No. 8, pp. 1323–1329, 1997
Copyright © 1997 Elsevier Science Ltd
Printed in Great Britain. All rights reserved
0277-5387/97 $17.00+0.00

Second and third row transition metal complexes of 1,1′-bi-2-naphthol and the X-ray crystal structures of $(Bu^n_4N)[MoO_2(acac)(BINO)]$ (1) and $(Bu^n_4N)_2(H_2BINO)_2[Mo_2O_7]$ (2)

William P. Griffith,* Helena I. S. Nogueira, Andrew J. P. White and David J. Williams*

Inorganic Chemistry and Chemical Crystallographic Research Laboratories, Department of Chemistry, Imperial College of Science, Technology and Medicine, London SW7 2AY, U.K.

(Received 23 July 1996; accepted 12 August 1996)

Abstract—The new complexes $[MoO_2(BINO)(acac)]^-$ (H_2BINO = 1,1′-bi-2-naphthol and acac = acetylacetonate), $[Mo_2O_5(BINO)_2]^{2-}$, $[MO_2(BINO)_2]^{2-}$ (M = Mo, W, Os) and $[M(PPh_3)_2(BINO)]$ (M = Pd, Pt) have been prepared. The X-ray crystal structures of the title compounds **1** and **2** are described and the vibrational spectra of the complexes reported. Copyright © 1997 Elsevier Science Ltd

Keywords: molybdenum; 1,1′-bi-2-napthol; X-ray crystal structure; Raman spectra.

The ligand 1,1′-bi-2-naphthol (H_2BINO) has potential uses as a chiral auxiliary in oxidation catalysis [1]. In the course of our work on peroxometalates as epoxidation catalysts [2] we have prepared a number of new complexes containing BINO for possible use as chiral epoxidation catalysts. In this paper we report the X-ray crystal structures of $(Bu^n_4N)[MoO_2(acac)(BINO)]$ (**1**) and $(Bu^n_4N)_2(H_2BINO)_2[Mo_2O_7]$ (**2**), and also the syntheses and vibrational spectra of other new complexes of BINO with tungsten, osmium, palladium and platinum.

Four X-ray crystal structures of H_2BINO complexes with titanium and lanthanides have been reported, for [Ti{ethylene-bis(4,5,6,7-tetrahydro-(*S*)-1-indenyl)}((*S*)-BINO)] [3] and $Na_3[Ln((S)\text{-}BINO)_3]\cdot 6THF\cdot H_2O$ [4] (Ln = Pr, Nd or Eu). A number of BINO complexes of tungsten [5,6,7] and titanium [3,8,9] have been isolated, including $[W_2(BINO)_2(OBu^t_2)_2]$ [7], $[W_2(BINO)_3]$ [7] and $[W(BINO)_2Cl_2]\cdot H_2O$ [5], the latter having been used as a catalyst for the ring opening polymerization of alkenes. The complex $[W(BINO)_3]$ was used as a precatalyst in polymerization catalysis [6].

RESULTS AND DISCUSSION

Preparations and X-ray crystallography

Synthesis of the complexes. The molybdenum complexes were made from the tetrabutylammonium or tetramethylammonium salts of 1,1′-bi-2-naphthol and *cis*-$[MoO_2(acac)_2]$ (acac = acetylacetonate); the tungsten complex from 1,1′-bi-2-naphthol and $Na_2[WO_4]$ with tetrabutylammonium chloride; the osmium complex from *trans*-$K_2[OsO_2(OCH_3)_4]$ and 1,1′-bi-2-naphthol; and the palladium and platinum complexes from $[M(PPh)_3)_2Cl_2]$ and 1,1′-bi-2-naphthol with triethylamine.

X-ray crystal structure of **1**. Orange crystals of the compound, suitable for X-ray analysis, were obtained after recrystallization in acetonitrile.

The X-ray analysis of **1** reveals a MoO_2 *cis*-dioxo coordination, the remaining coordination sites being occupied by *cis*-coordinated binaphthol and acetylacetonate ligands, as shown in Fig. 1. The octahedral coordination at molybdenum is severely distorted with angles at Mo ranging between 78.3(1) to 104.5(2)°, and 162.4(1) to 169.2(1)°. The bite angles associated with the chelating ligands are markedly reduced from orthogonal to 82.8(1) and 81.1(1)° for the binaphthol and acetylacetonate groups, respec-

* Authors to whom correspondence should be addressed.

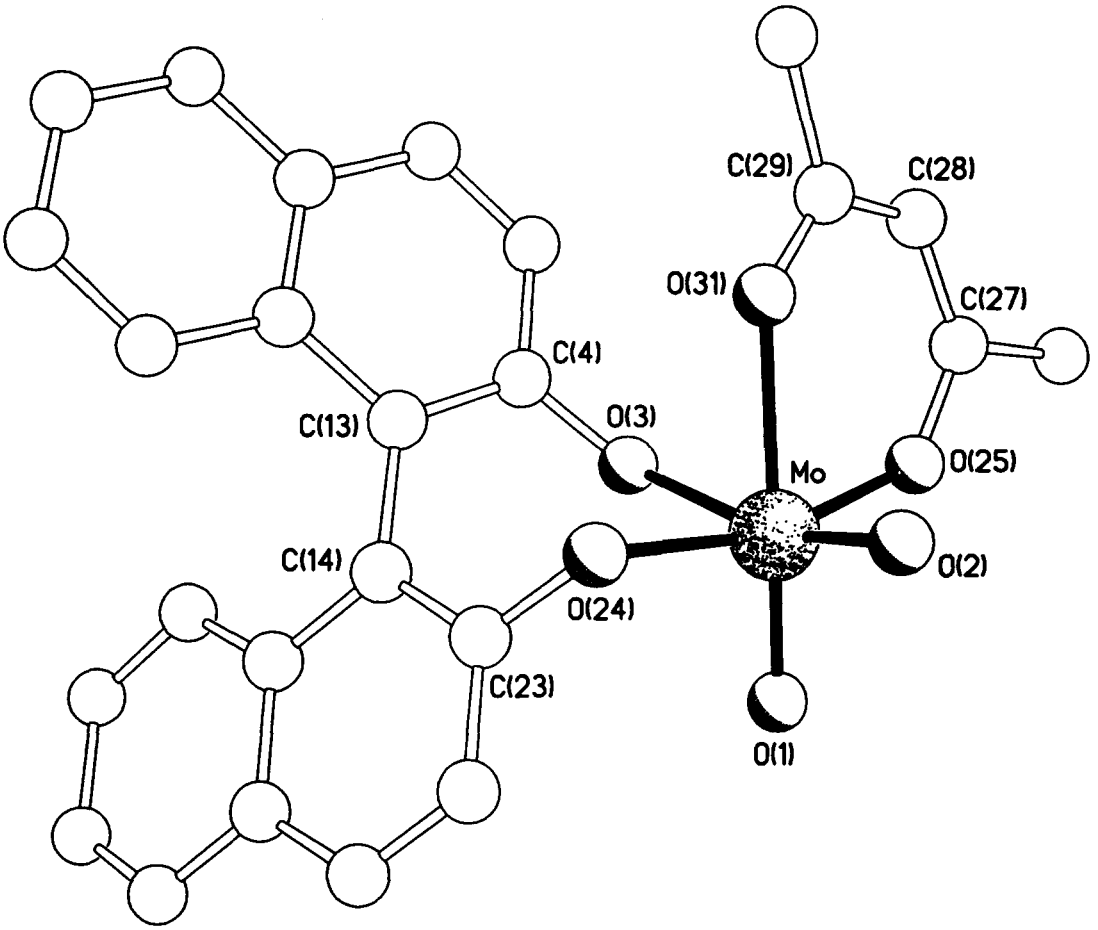


Fig. 1. The molecular structure of the anion in **1**.

tively. There are characteristic displacements of the molybdenum atom towards the oxo substituents out of the plane of the atoms normal to these directions of 0.25 and 0.17 Å for O(1) and O(2), respectively; the two associated Mo—O distances, 1.698(3) [O(1)] and 1.701(3) Å [O(2)], are normal with the O—Mo—O angle being 104.5(2)°.

For both chelating ligands there is a noticeable asymmetry in their Mo—O coordination distances reflecting the powerful *trans* influence of the oxo ligands. In the case of the binaphthol unit [which exhibits a mean torsional twist of *ca* 58° about the C(13)—C(14) linkage] the two Mo—O distances differ by 0.13 Å and in the acetylacetonate moiety the difference is 0.16 Å. Furthermore, these asymmetries extend to include the adjacent C—O bonds in both ligands (Table 1); indeed in the acetylacetonate ligand a pattern of alternation of bond lengths extends throughout the whole ligand (with the exception of the terminal methyl groups), which maintains a coplanar geometry (to within 0.04 Å) with the molybdenum atom.

The only significant non van der Waals packing interaction is a C—H···O hydrogen bond between one of the binaphthol C—H groups in one molecule and the O(1) oxo atom of a *c*-glide-related molecule, thereby forming a loosely-linked chain that extends in the crystallographic *c* direction [C···O, H···O distances 3.26, 2.34 Å; C—H···O angle 176°], Fig. 2.

X-ray crystal structure of **2**. Recrystallization of the orange crystals of **1** from acetonitrile gave beige crystals which were found by X-ray analysis to be $(Bu^n_4N)_2(H_2BINO)_2[Mo_2O_7]$ (**2**). The structure comprises an Mo_2O_7 core hydrogen-bonded to two binaphthol units (*vide infra*), Fig. 3. Thus, unlike **1** where the binaphthol acts as a bidentate ligand, here no coordination has occurred. Initial analysis of the structure indicated a linear geometry for the Mo—O—Mo linkage (with somewhat short Mo—O distances), the bridging oxygen atom being positioned on a crystallographic inversion centre. However, the bridging atom exhibited significant thermal anisotropy normal to the Mo···Mo direction, indicating that a more realistic model is one in which there is a superimposition of two half occupancy non-linear geometries related by the centre of symmetry. Splitting of the position of this bridging oxygen atom resulted in more realistic thermal parameters, and bridging

Table 1. Selected bond lengths (Å) and angles (°) for **1**

Mo—O(1)	1.698(3)	Mo—O(2)	1.701(3)
Mo—O(24)	1.955(3)	Mo—O(25)	2.060(3)
Mo—O(3)	2.087(3)	Mo—O(31)	2.222(3)
O(3)—C(4)	1.335(5)	C(4)—C(13)	1.392(5)
C(13)—C(14)	1.488(5)	C(14)—C(23)	1.384(5)
C(23)—O(24)	1.364(4)	O(25)—C(27)	1.284(6)
C(27)—C(28)	1.369(8)	C(28)—C(29)	1.394(7)
C(29)—O(31)	1.254(5)		
O(1)—Mo—O(2)	104.5(2)	O(1)—Mo—O(24)	99.51(13)
O(2)—Mo—O(24)	94.45(13)	O(1)—Mo—O(25)	91.79(14)
O(2)—Mo—O(25)	94.56(14)	O(24)—Mo—O(25)	163.32(12)
O(1)—Mo—O(3)	93.10(12)	O(2)—Mo—O(3)	162.41(13)
O(24)—Mo—O(3)	82.79(10)	O(25)—Mo—O(3)	84.39(11)
O(1)—Mo—O(31)	169.22(13)	O(2)—Mo—O(31)	84.21(14)
O(24)—Mo—O(31)	85.94(11)	O(25)—Mo—O(31)	81.03(12)
O(3)—Mo—O(31)	78.28(11)	C(4)—O(3)—Mo	126.2(2)
O(3)—C(4)—C(13)	121.3(3)	C(4)—C(13)—C(14)	119.0(3)
O(24)—C(23)—C(14)	121.0(3)	C(23)—O(24)—Mo	120.3(2)
C(27)—O(25)—Mo	133.5(3)	O(25)—C(27)—C(28)	125.3(5)
C(27)—C(28)—C(29)	125.5(5)	O(31)—C(29)—C(28)	123.9(5)
C(29)—O(31)—Mo	130.4(3)		

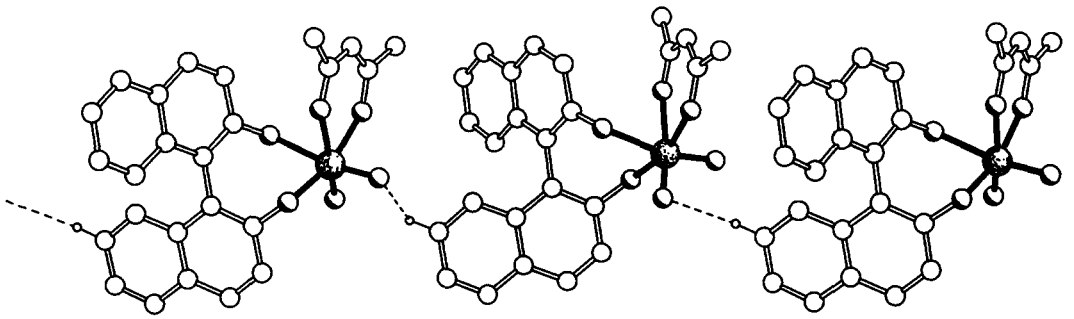


Fig. 2. Part of one of the loosely hydrogen-bonded chains present in the crystal structure of **1**.

Mo—O distances and a Mo—O—Mo angle [155(2)°] comparable to those found in other related systems such as $(Bu^n_4N)_2[Mo_2O_7]$ [10] and $[(\eta\text{-}C_5H_4CH_3)Mo(CO)_2(\mu\text{-dppm})Pt(dppm)]_2[Mo_2O_7]$ [11]. The remaining Mo—O distances are unexceptional, Table 2. A detailed analysis of the angular geometry at molybdenum is not justified in view of the disorder described above. The binaphthol unit exhibits a characteristic skewed geometry with a mean torsional twist about the bond linking the two naphthalene rings of *ca* 85°, a value substantially larger than that observed for the coordinated counterpart of **1**.

An inspection of the packing shows that the pattern of hydrogen-bonding between the binaphthol units and the Mo_2O_7 core alluded to above extends to form chains of molecules, which propagate in the crystallographic *a* direction (O···O distances 2.68 and 2.70 Å), Fig. 4. Adjacent chains are interleaved and stabilized by T-type edge to face aromatic–aromatic interactions between naphthyl rings (centroid··· centroid distance between C_6H_4 rings 5.02 Å).

Vibrational and ^{1}H *NMR spectra*

IR and Raman spectroscopic data for the free ligand and the complexes are listed in Table 3. General assignments of the IR spectrum of 1,1′-bi-2-naphthol have been reported [12,13]. The existence of two bands of the O—H stretch, ν(O—H), at 3485 and 3401 cm^{-1}, was ascribed [12] to the asymmetry of 1,1′-bi-2-naphthol in the solid state, since the two naphthyl rings lie in two different planes. In the IR spectra of our BINO complexes the band corresponding to ν(O—H) was not observed due to loss of protons on coordination and the ν(C—O) band is shifted from 1382 cm^{-1} in H_2BINO to approximately 1366 cm^{-1} in the complexes, suggesting coordination through the oxygen atoms of the hydroxyl groups (similar effects are noted for the IR spectra of catecholato complexes [14,15]). The C—C stretch bands of H_2BINO are only slightly shifted in the complexes. A new band at approximately 1557 cm^{-1}, assigned to ν(C—C), is also seen in the Raman spectrum of **1**, together with

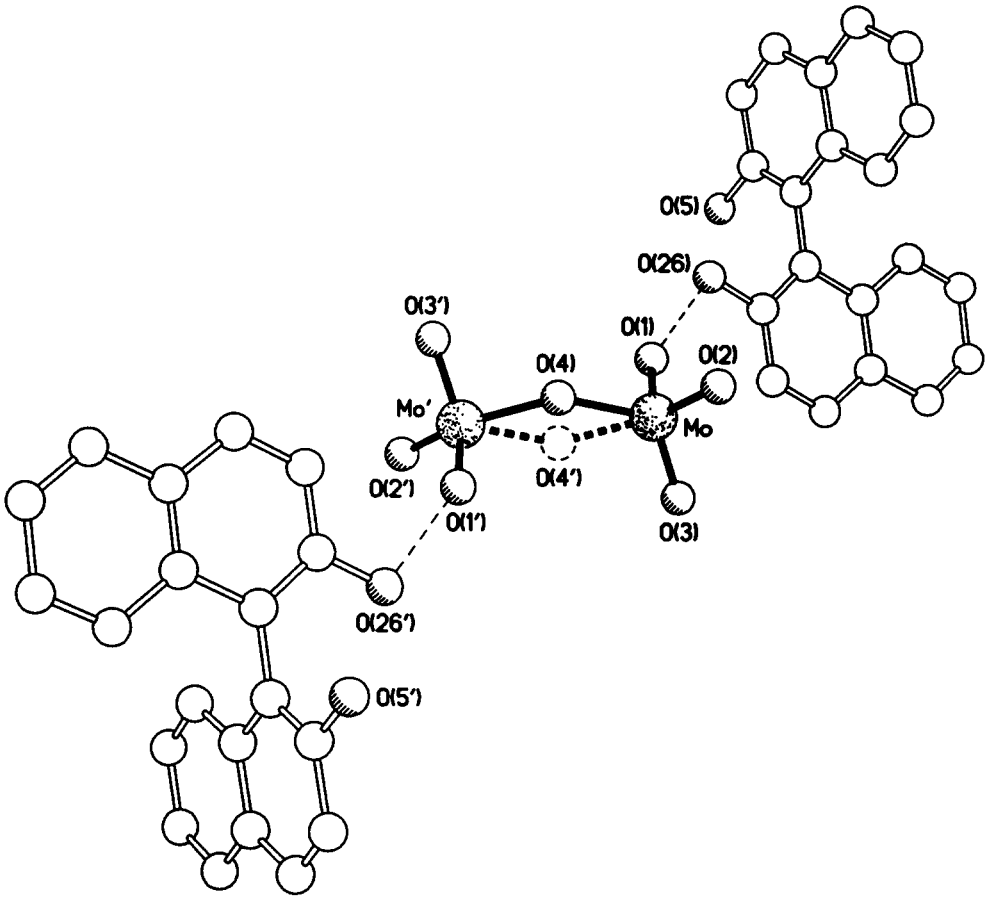


Fig. 3. The Mo_2O_7 core and adjacent hydrogen-bonded binaphthol units in the structure of **2**; the broken bonds correspond to the alternative orientation of the Mo—O—Mo bridge.

Table 2. Selected bond lengths (Å) for **2**

Mo—O(1)	1.693(9)	Mo—O(2)	1.718(7)
Mo—O(3)	1.647(14)	Mo—O(4)	1.90(2)
Mo'—O(4)	1.88(2)	Mo···Mo'	3.701(2)

acetylacetonate bands in both IR and Raman spectra. In **2** the O—H stretch of 1,1'-bi-2-naphthol is shifted from 3485 and 3401 cm^{-1} to 3124 cm^{-1}. In this compound the ν(C—O) band is shifted to 1370 cm^{-1}, an intermediate position between the values for the complexes (shifted to lower wave-numbers) and for H_2BINO.

^1H NMR data for H_2BINO were measured and the data agree well with those of Puga *et al.* [16], there was, however, relatively little change in the spectra on complexation.

EXPERIMENTAL

All starting materials were supplied by Aldrich and used without further purification. The complexes $[MoO_2(acac)_2]$ [17], *trans*-$K_2[OsO_2(OCH_3)_4]$ [18], $[Pd(PPh_3)_2Cl_2$ [19] and $[Pt(PPh_3)_2Cl_2]$ [20] were made by the cited literature procedures. The salts (Bu^n_4N)(HBINO) and (Me_4N)(HBINO) were prepared by refluxing ethanolic solutions of H_2BINO and Bu^n_4NCl or Me_4NCl in equimolar proportions, filtered and cooled.

Preparation of $(Bu^n_4N)[MoO_2(acac)(BINO)]$

To a solution of $[MoO_2(acac)_2]$ (0.16 g, 0.5 mmol) in acetone (5 cm^3) was added a solution of (Bu^n_4N)(HBINO) (0.26 g, 0.5 mmol) in acetone (10 cm^3). The yellow precipitate formed was filtered, washed with acetone and dried in a desiccator over silica gel. Yield = 0.32 g, 0.24 mmol, 49%. Orange crystals of the compound were obtained by recrystallization in acetonitrile.

Preparation of $(Bu^n_4N)_2(H_2BINO)_2[Mo_2O_7]$

The orange crystals obtained by recrystallization of $(Bu^n_4N)[MoO_2(acac)(BINO)]$ were left in acetonitrile for a week. The colour faded and beige crystals of $(Bu^n_4N)_2(H_2BINO)_2[Mo_2O_7]$ were obtained.

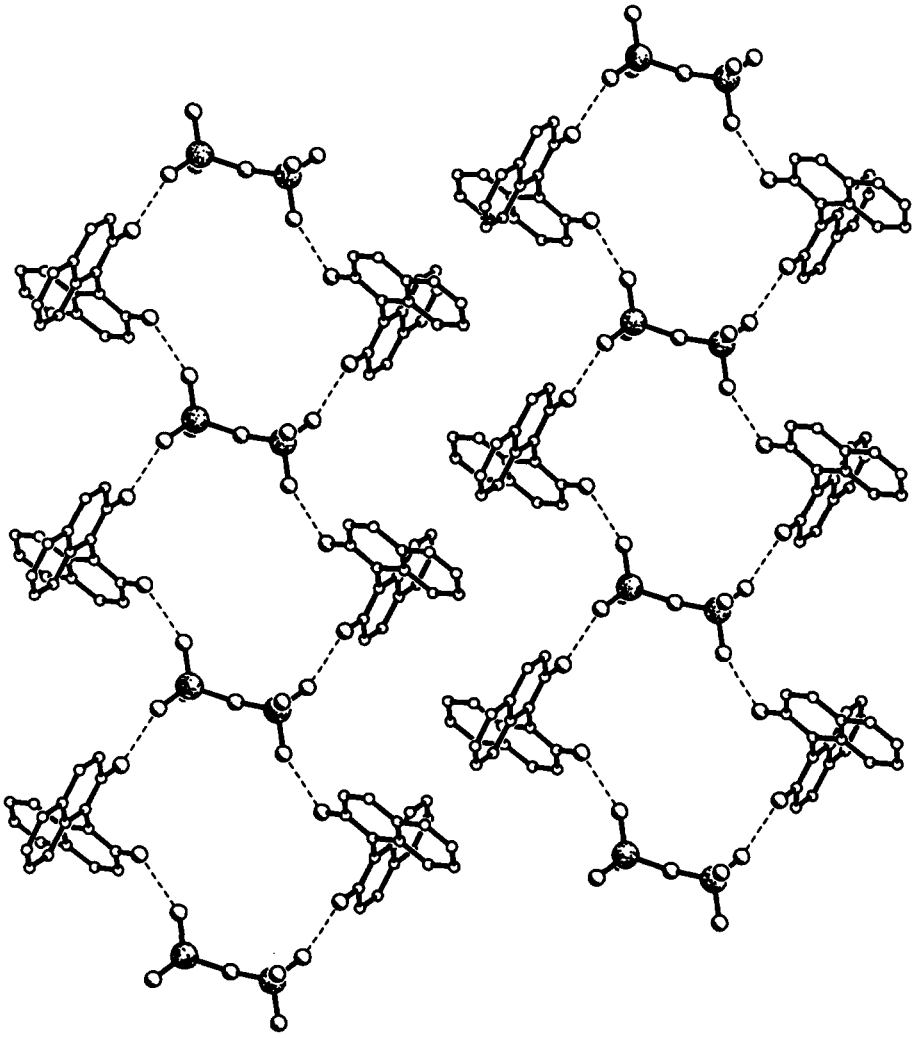


Fig. 4. Part of a pair of interleaved hydrogen-bond chains of Mo_2O_7 and binaphthol molecules in the structure of **2**.

Preparation of $(Me_4N)_2[MoO_2(BINO)_2]\cdot 2MeOH$

To a solution of $[MoO_2(acac)_2]$ (0.16 g, 0.5 mmol) in methanol (20 cm^3) was added 1,1′-bi-2-naphthol (0.29 g, 1.0 mmol) and tetramethylammonium chloride (0.11 g, 1.0 mmol). The resulting yellow solution was heated to reflux for 2 h, filtered hot and reduced to approximately half of the volume by rotary evaporation. Beige crystals were obtained after refrigeration for 4 days, filtered and dried in a desiccator with silica gel. Yield = 0.050 g, 0.055 mmol, 11%.

Preparation of $(Me_4N)_2[Mo_2O_5(BINO)_2]$

To a solution of $[MoO_2(acac)_2]$ (0.082 g, 0.25 mmol) in acetone (3 cm^3) was added a solution of $(Me_4N)(HBINO)$ (0.18 g, 0.5 mmol) in acetone (10 cm^3). The yellow suspension obtained was stirred for 1 h. The yellow precipitate was filtered and dried in a desiccator over silica gel. Yield = 0.13 g, 0.24 mmol, 49%.

Preparation of $(Bu^n_4N)_2[WO_2(BINO)_2]\cdot 2H_2O$

To an aqueous solution of sodium tungstate (0.17 g, 0.5 mmol, 10 cm^3 of water) was added an ethanolic suspension of 1,1′-bi-2-naphthol (0.29 g, 1.0 mmol, 20 cm^3 of ethanol) and an aqueous solution of tetrabutylammonium chloride (0.28 g, 1.0 mmol, 2 cm^3 of water). The resulting light yellow solution (with some 1,1′-bi-2-naphthol suspended) was heated at reflux for 3 h and filtered. Beige crystals were obtained after refrigeration for 3 days, filtered, washed with ethanol and dried in a desiccator with silica gel. Yield = 0.279 g, 0.21 mmol, 43%.

Preparation of $K_2[OsO_2(BINO)_2]\cdot 6H_2O$

To a stirred solution of *trans*-$K_2[OsO_2(OCH_3)_4]$ (0.20 g, 0.47 mmol) in methanol (15 cm^3) was added a methanolic solution of 1,1′-bi-2-naphthol (0.29 g, 1.0 mmol, 5 cm^3 of methanol). The resulting dark green solution was left stirring for *ca* 10 min, a dark-

Table 3. Analytical and IR and Raman spectroscopic data for complexes of 1,1′-bi-2-naphthol

Compound	Analysis[a] (%) C	H	N	Vibrational spectra[b,c] (cm^{-1}) ν(C—C)	ν(C—O)	$\nu^{s}(MO_2)$[d]	$\nu^{as}(MO_2)$
1,1′-Bi-2-naphthol				1618 vs/1596 vs	1381 vs	—	—
				1620 (2)/1592 (3)	*1381 (10)*	—	—
$(Bu^n_4N)[MoO_2(acac)(BINO)]$	64.6	7.3	2.1	1612 vs/1590 vs	1365 m	920 vs	892 vs
	(65.3)	(7.3)	(2.1)	*1616 (2)/1591 (2)*	*1366 (10)*	*921 (4)*	*896 (2)*
$(Bu^n_4N)_2(H_2BINO)_2[Mo_2O_7]$	63.2	7.3	2.0	1624 s/1584 m	1379 m	933 m	872 vs
	(63.5)	(7.4)	(2.1)	*1622 (3)/1584 (5)*	*1370 (9)*	*937 (10)*	*866 (4)*
$(Me_4N)_2[MoO_2(BINO)_2]\cdot 2MeOH$	66.3	6.6	3.2	1620 s/1583 m	1370 s	950 s	871 m
	(66.1)	(6.2)	(3.1)	*1623 (3)/1584 (8)*	*1367 (10)*	*957 (2)*	—
$(Me_4N)_2[Mo_2O_5(BINO)_2]$	57.9	5.8	3.2	1624 vs/1584 s	1360 sh	896 s	808 vs
	(58.3)	(4.9)	(2.8)	*1624 (2)/1584 (6)*	*1366 (10)*	*900 (6)*	*804 (2)*
$(Bu^n_4N)_2[WO_2(BINO)_2]\cdot 2H_2O$	66.0	6.5	1.4	1618 vs/1593 vs	1365 sh	945 s	878 m
	(66.3)	(7.7)	(2.2)	*1618 (2)/1590 (3)*	*1370 (10)*	*951 (1)*	—
$K_2[OsO_2(BINO)_2]\cdot 6H_2O$	49.3	2.0	—	1615 s/1586 s	1360 m	—	844 vs
	(49.2)	(3.7)	—				
$[Pd(PPh_3)_2(BINO)]\cdot EtOH$	72.4	5.3	—	1619 s/1594 s	1370 sh	—	—
	(72.5)	(5.0)	—	*1615 (1)/1585 (10)*	*1368 (8)*		
$[Pt(PPh_3)_2(BINO)]\cdot EtOH$	65.6	4.0	—	1615 m/1587 m	1368 m	—	—
	(66.3)	(4.6)	—	*1613 (2)/1586 (7)*	*1368 (4)*		

[a] Calculated values in parentheses.
[b] Raman data in italics.
[c] ν indicates a stretching mode; intensity of bands: vs = very strong, s = strong, m = medium, sh = shoulder.
[d] ν(Mo—O) for Mo_2O_7.

brown precipitate started to form and then diethyl ether (20 cm^3) was added. The solution turned darker and upon filtration a brown solid was isolated. The solid was washed with diethyl ether and dried in a desiccator with silica gel. Yield = 0.23 g, 0.23 mmol, 50%.

Preparation of $[Pd(PPh_3)_2(BINO)]\cdot EtOH$

To a stirred suspension of $[Pd(PPh_3)_2Cl_2]$ (0.35 g, 0.5 mmol) in ethanol (10 cm^3) was added a methanolic solution of 1,1′-bi-2-naphthol (0.29 g, 1.0 mmol, 4 cm^3 of methanol) and triethylamine (0.6 cm^3, 4.0 mmol). The resulting yellow suspension was stirred for 7 days and a suspension of a yellow solid in a red solution was obtained. It was centrifuged and the red solution isolated. To this solution was added the same volume of water and an orange solid was formed. It was centrifuged and the orange solid isolated and dried in a desiccator over silica gel. Yield = 0.13 g, 0.14 mmol, 27%.

Preparation of $[Pt(PPh_3)_2(BINO)]\cdot EtOH$

To a stirred suspension of $[Pt(PPh_3)_2Cl_2]$ (0.40 g, 0.5 mmol) in ethanol (10 cm^3) was added a methanolic solution of 1,1′-bi-2-naphthol (0.29 g, 1.0 mmol, 4 cm^3 of methanol) and triethylamine (0.6 cm^3, 4.0 mmol). The resulting white suspension was stirred for 7 days and a yellow suspension was obtained. It was centrifuged and the yellow solid isolated and dried in a desiccator over silica gel. Yield = 0.39 g, 0.37 mmol, 74%. Yellow crystals of the compound were obtained by recrystallization in acetonitrile.

Crystal structure determinations

Crystal data for **1**. $[C_{25}H_{19}O_6Mo][(C_4H_9)_4N]$, $M = 753.8$, monoclinic, space group $P2_1/c$, $a = 10.708(2)$, $b = 18.451(2)$, $c = 19.439(3)$ Å, $\beta = 91.92(1)°$, $V = 3838(1)$ Å^3, $Z = 4$, $D_c = 1.30$ g cm^{-3}, μ(Cu-K_α) = 31.6 cm^{-1}, $F(000) = 1592$. An orange/yellow plate of dimensions $0.33 \times 0.20 \times 0.05$ mm was used.

Data collection and processing. Data were measured on a Siemens P4/PC diffractometer with Cu-K_α radiation (graphite monochromator) using ω-scans. 5351 independent reflections were measured ($2\theta \leqslant 116°$) of which 4443 had $|F_o| > 4\sigma(|F_o|)$ and were considered to be observed. The data were corrected for Lorentz and polarization factors, and a Gaussian absorption correction (face-indexed numerical) was applied; the maximum and minimum transmission factors were 0.851 and 0.539, respectively.

Structure analysis and refinement. The structure was solved by the heavy atom method and the non-hydrogen atoms were refined anisotropically. The hydrogen atoms of the methyl groups attached to sp^2 centres were located from ΔF maps and subsequently optimized. The positions of the remaining hydrogens were

idealized, assigned isotropic thermal parameters, [U(H) = 1.2U_{eq}(C); U(H) = 1.5U_{eq}(C—Me)], and allowed to ride on their parent carbon atoms. Refinement was by full-matrix least-squares based on F^2 to give $R_1 = 0.042$, $wR_2 = 0.105$ for the observed data and 443 parameters. The maximum and minimum residual electron densities in the final ΔF map were 0.58 and −0.64 e Å^{-3}, respectively. The mean and maximum shift/error ratios in the final refinement cycle were 0.003 and −0.023, respectively.

Crystal data for **2**. $[Mo_2O_7][(C_4H_9)_4N]_2 \cdot [C_{20}H_{14}O_2]_2$, M = 1361.4, triclinic, space group $P\bar{1}$, a = 10.371(3), b = 10.759(3), c = 16.759(5) Å, α = 103.84(2), β = 102.89(2), γ = 92.73(2)°, V = 1759.9(8) Å^3, Z = 1 (the molecule has crystallographic C_i symmetry), D_c = 1.29 g cm^{-3}, μ(Cu-K_α) = 33.8 cm^{-1}, F(000) = 718. A clear prismatic plate of dimensions 0.21 × 0.12 × 0.01 mm was used.

Data collection and processing. Data were measured on a Siemens P4/PC diffractometer with Cu-K_α radiation (graphite-monochromator) using ω-scans. 2851 independent reflections were measured ($2\theta \leqslant 120°$), of which 2177 had $|F_o| > 4\sigma(F_o|)$ and were considered to be observed. The data were corrected for Lorentz and polarization factors and a Gaussian absorption correction (face-indexed numerical) was applied; the maximum and minimum transmission factors were 0.961 and 0.729, respectively.

Structure analysis and refinement. The structure was solved by the heavy-atom method and the non-hydrogen atoms were refined anisotropically. The hydroxyl hydrogen atoms were located from a ΔF map and were refined isotropically subject to an O—H distance constraint. The positions of the remaining hydrogens were idealized, assigned isotropic thermal parameters, [U(H) = 1.2U_{eq}(C), U(H) = 1.5U_{eq}(C—Me)] and allowed to ride on their parent carbon atoms. Refinement was by full-matrix least-squares based on F^2 to give $R_1 = 0.061$, $wR_2 = 0.149$ for the observed data and 405 parameters. The maximum and minimum residual electron densities in the final ΔF map were 0.53 and −0.66 e Å^{-3}, respectively. The mean and maximum shift/error ratios in the final refinement cycle were 0.000 and 0.000, respectively.

For both structures, computations were carried out on 50 MHz 486 PC computers using the SHELXTL-PC program system [21]. Additional material available from the Cambridge Crystallographic Data Centre comprises fractional atomic coordinates, H-atom coordinates, thermal parameters and remaining bond lengths and angles.

Characterization

IR spectra were measured as KBr discs on a Perkin–Elmer 1720 FT instrument. Raman spectra were recorded on as powders on a Perkin–Elmer 1760 X FT-IR instrument fitted with a 1700 X NIR FT-Raman accessory (Spectron Nd:YAG laser, 1064 nm excitation). ^{1}H NMR spectra were measured on a Jeol EX-270 spectrometer (^{1}H, 270.05 MHz). Microanalyses were measured by the Microanalytical Department, Imperial College.

Acknowledgements—We thank the Calouste Gulbenkian Foundation for a postgraduate grant to HISN, the University of London Intercollegiate Research Service for the Raman spectrometer and the EPSRC for the X-ray diffractometer. We thank Johnson Matthey Ltd for loan of platinum group metals.

REFERENCES

1. Ojima, I., *Catalytic asymmetric synthesis*. VCH Publishers, New York, 1993, pp. 421–423.
2. Gresley, N. M., Griffith, W. P., Parkin, B. C., White, A. J. P. and Williams, D. J., *J. Chem. Soc., Dalton Trans.* 1996, 2039.
3. Wild, F. R. W. P., Zsolnai, L., Huttner, G. and Brintzinger, H. H., *J. Organomet. Chem.* 1982, **232,** 233.
4. Sasai, H., Suzuki, T., Itoh, N., Tanaka, K., Date, T., Okamura, K. and Shibasaki, M., *J. Am. Chem. Soc.* 1993, **115,** 10372.
5. Hamilton, J. G., Ivin, K. J., McCann, G. M. and Rooney, J. J., *Makromol. Chem.* 1985, **186,** 1477.
6. Dietz, S. D., Eilerts, N. W., Heppert, J. A. and Morton, M. D., *Inorg. Chem.* 1993, **32,** 1698.
7. Dietz, S. D., Eilerts, N. W., Heppert, J. A. and Velde, D. V., *Inorg. Chem.* 1993, **32,** 1689.
8. Schnutenhaus, H. and Brintzinger, H. H., *Angew. Chem., Int. Ed. Engl.* 1979, **18,** 777.
9. Boyle, T. J., Barnes, D. L., Heppert, J. A., Morales, L. and Takusagawa, F., *Organometallics*, 1992, **11,** 1112.
10. Day, V. W., Fredrich, M. F., Klemperer, W. G. and Shum, W., *J. Am. Chem. Soc.* 1977, **99,** 6146.
11. Braunstein, P., Bellefon, C. M., Lanfranchi, M. and Tiripicchio, A., *Organometallics*, 1984, **3,** 1772.
12. Didi, M. A., Maki, A. K. T. and Mostafa, M. M., *Spectrochim. Acta*, 1991, **47A,** 667.
13. Szymanski, H. A., *Interpreted Infrared Spectra*. Plenum Press, Data Division, New York, 1967.
14. Griffith, W. P., Nogueira, H. I. S., Parkin, B. C., Sheppard, R. N., White, A. J. P. and Williams, D. J., *J. Chem. Soc., Dalton Trans.* 1995, 1775.
15. Griffith, W. P., Pumphrey, C. A. and Rainey, T. J., *J. Chem. Soc., Dalton Trans.* 1986, 1125.
16. Puga, G. M., Horák, V. and Svoronos, P., *Collect. Czech. Chem. Commun.* 1993, **58,** 77.
17. Chen, G. J. J., McDonald, J. W. and Newton, W. E., *Inorg. Chem.* 1976, **15,** 2612.
18. Criegee, R., Marchand, B., and Wannowius, H., *Leibigs Ann. Chem.* 1942, **550,** 99.
19. Cookson, R. C. and Jones, D. W., *J. Chem. Soc.* 1965, 1881.
20. Bailar Jr, J. C. and Itatani, H., *Inorg. Chem.* 1965, **4,** 1618.
21. SHELXTL PC, Version 5.03. Siemens Analytical X-Ray Instruments, Inc., Madison, WI, 1994.

Pergamon

PII: S0277-5387(96)00404-4

Polyhedron Vol. 16, No. 8, pp. 1331–1336, 1997
Copyright © 1997 Elsevier Science Ltd
Printed in Great Britain. All rights reserved
0277–5387/97 $17.00+0.00

Synthesis and characterization of (μ-oxalato)nickel(II) complexes

František Březina,[a]* Zdeněk Smékal,[a] Zdeněk Trávníček,[a] Zdeněk Šindelář,[a] Richard Pastorek[a] and Jaromír Marek[b]

[a]Department of Inorganic and Physical Chemistry, Palacký University, Křížkovského 10, Olomouc 77147, Czech Republic

[b]Department of Inorganic Chemistry, Masaryk University, Kotlářská 2, Brno 61137, Czech Republic

(Received 18 July 1996; accepted 12 August 1996)

Abstract—Three new nickel(II) dinuclear oxalato-bridged compounds Ni(TAA)(ClO_4)·0.5ox (**1**), Ni_2(APO-sal_2)ox·$2H_2O$ (**2**) and Niphen$_2$oxNiacac$_2$·$4H_2O$ (**3**) have been characterized [TAA = $N(CH_2CH_2NH_2)_3$ ox = oxalate, phen = 1,10-phenanthroline, acac = acetylacetonate and APO-sal_2 is the Schiff base formed by the condensation of salicylaldehyde and 1,3-diamino-2-propanol]. The crystal structure of **1** has been determined by a single-crystal X-ray analysis. The nickel atom is coordinated by two oxygen atoms of an oxalato ligand and four nitrogen atoms belonging to TAA in an octahedral arrangement. The intermetallic distance of Ni(1)—Ni(2) is 5.412(1) Å. Magnetic measurements (77–300 K) show that three compounds are antiferromagnetically coupled, $J = -14.4$, -11.25 and -19.3 cm^{-1} for **1**, **2** and **3**, respectively. Copyright © 1997 Elsevier Science Ltd

Keywords: nickel(II) complexes; (μ-oxalato) complexes; magnetic properties.

The magnetic behaviour of nickel(II) dimers, in which the oxalate anion acts as a bis-bidentate bridging ligand, is a well-known subject and the general trends of their magnetic properties are well established, the oxalato bridge is very efficient in propagating antiferromagnetic interactions between the two paramagnetic centres of dinuclear compounds. In these compounds the nickel(II) shows octahedral coordination in all the [Ni–ox–Ni] pairs reported to date and the Ni–oxalao–Ni fragment is rigid and planar, and only small differences in the bond parameters can be found in the bridge fragment. However, this generalization should be assumed only for compounds in which four remaining coordination positions of the nickel atom have similar properties—such as aminate ligands (NiN_4O_2 environment). The NiN_4O_2 nickel–oxalato dinuclear compounds contain tetraaza macrocycles, tetraaza amines or two diamines [1–5]. The aim of this study is to characterize the nickel–oxalato dimer with tetraaza amine (TAA) and to compare the magnetic properties of this compound with those of [phen$_2$Ni–ox–Niacac$_2$] with NiN_4O_2 and NiO_6 environment. In fact, linear trimeric bis(acetylacetonato)nickel(II) has been reported [6] to have both ferromagnetic coupling ($J = +26$ cm^{-1}) between adjacent nickel atoms and antiferromagnetic coupling ($J = -7$ cm^{-1}) between the terminal nickel atoms. The third studied compound is a monomeric binuclear nickel(II) complex based on Schiff base derivative of 1,3-diaminopropan-2-ol with oxalate as bridging ligand.

EXPERIMENTAL

All chemicals were of reagent grade and used as purchased from commercial sources. Niphen$_2$$Cl_2$·$4H_2O$ [7] and Niacac$_2$ [8] were prepared according to literature methods.

Preparation of Ni(TAA)(ClO_4)·0.5ox

$N(CH_2CH_2NH_2)_3$ (1.66 mmol, 0.25 cm^3) was added to a solution of $Ni(ClO_4)_2$·$6H_2O$ (1.6 mmol, 0.6 g) in water (5 cm^3). After stirring for a few minutes, a

* Author to whom correspondence should be addressed.

solution of Na_2ox (0.8 mmol, 0.11 g) in water (5 cm^3) was added. The reaction mixture was stirred at 80°C for 15 min, then filtered and the blue solution was allowed to stand for 5 days. The precipitated deep blue crystals were filtered off and washed with cold water. Found: C, 24.3; H, 5.1; N, 15.9; Cl, 10.4. Calc. for $C_7H_{18}ClN_4O_6Ni$: C, 24.1; H, 5.2; N, 16.1; Cl, 10.2%.

Preparation of $Ni_2(APO\text{-}sal_2)ox \cdot 2H_2O$

Salicylaldehyde (5 mmol, 0.52 cm^3) and 1,3-diamino-2-propanol (2.5 mmol, 0.15 g) were refluxed in methanol (8 cm^3) for 2 h. After cooling to room temperature triethylamine (14 mmol, 2 cm^3) was added. Then the solution of $NiCl_2 \cdot 6H_2O$ (5 mmol, 1.2 g) in 10 cm^3 methanol and oxalic acid (2.8 mmol, 0.25 g) in 10 cm^3 methanol was added while stirring. The mixture was heated under reflux for 1 h and then was allowed to stand overnight. The solids formed were filtered off and washed with ethanol and ether. Found: C, 41.8; H, 4.15; N, 5.1; Ni, 22.2. Calc. for $C_{19}H_{20}N_2O_9Ni_2$: C, 42.4; H, 3.8; N, 5.2; Ni, 21.8%.

Preparation of $Niphen_2oxNiacac_2 \cdot 4H_2O$

Separated methanolic solutions (10 cm^3) of $Niphen_2Cl_2 \cdot 4H_2O$ (1 mmol, 0.6 g) and oxalic acid (1 mmol, 0.09 g) were added to a hot ethanolic solution (15 cm^3) of $Niacac_2$ (1.2 mmol, 0.3 g) under continuous stirring. Triethylamine (4.4 mmol, 0.6 cm^3) was after 5 min added to this solution and the resulting reaction mixture was left to stand at room temperature. Blue microcrystals, which were not suitable for X-ray analysis, were deposited in a few hours. Found: C, 51.4; H, 4.3; N, 7.1; Ni, 14.5. Calc. for $C_{36}H_{38}N_4O_{12}Ni_2$: C, 51.7; H, 4.6; N, 6.7; Ni, 14.0%.

Physical measurements

The carbon, hydrogen and nitrogen analyses were determined on an EA1108 instrument (Fisons). IR spectra were measured on a Specord M80 (Carl Zeiss, Jena) using Nujol mulls within the region ν = 4000–400 cm^{-1}. Electronic absorption spectra were obtained on a Specord M40 (Carl Zeiss, Jena). The magnetic susceptibility of powdered complexes were measured by the Faraday method in the temperature range 77–300 K. The apparatus was calibrated with $HgCo(NCS)_4$. Corrections for the diamagnetism were estimated from Pascal's constants [9]. Thermal decomposition was studied with a Q1500 Derivatograph (MOM Budapest) with a sample weight of 130–180 mg over a temperature range 20–800°C at a heating rate of 2.5°C min^{-1}.

Structural characterization

Crystals suitable for a single-crystal X-ray analysis were obtained by recrystallization of the studied complex from a water solution.

Data collection and processing. The intensity data were collected on a KUMA KM-4 diffractometer at 153(2) K using graphite monochromated Mo-K_α radiation and an ω–2θ scan technique. From 2483 measured reflections, 2093 with $I > 2\sigma(I)$ were considered observed. Lattice parameters and orientation matrix for data collection were obtained from least-squares refinement on setting angles for 25 reflections ($17.1 < 2\theta < 26.1°$). Periodics checks on two standard reflections indicated no crystal instability during data collection. Absorption and extinction effects were ignored.

Structure analysis and refinement. The structure was solved by heavy-atom method (SHELXS-86) [10] and refined anisotropically by full-matrix least-squares procedure (SHELXL-93) [11] with weight: $w = 1/[\sigma^2(F_0^2) + (0.0636P)^2 + 0.7843P]$, where $P = (F_0^2 + 2F_c^2)/3$. The H atoms were located from difference-Fourier maps and all their parameters were refined. Largest differences in the peak and hole on a final difference electron density map were 0.611 and -0.876 e $Å^{-3}$, respectively. All structure determination calculations were carried out on IBM RS/6000 98F and PC AT 486 computers. Crystal data and refinement parameters for $Ni(TAA)(ClO_4) \cdot 0.5ox$ are summarized in Table 1.

RESULTS AND DISCUSSION

Structure of $Ni(TAA)(ClO_4) \cdot 0.5ox$

The structure consists of the binuclear $[(TAA)Ni\text{–}ox\text{–}Ni(TAA)]^{2+}$ cation and perchlorate anions. A view of the cation is shown in Fig. 1. Principal bond distances are listed in Table 2. The binuclear cation consists of two $(TAA)Ni^{II}$ units bridged by a bis-bidentate oxalate anion. The geometry at the two nickel(II) centres is octahedral, with ligation provided by the four nitrogen atoms of the TAA ligand and the oxygen atoms of the bridging oxalate. As usual the Ni—C_2O_4—Ni fragment is practically planar, deviations from the least-square plane fitted through the Ni(1)—C(1)—O(1)—O(2)—C(1a)—O(1a)—O(2a)—Ni(1a) atoms are lower than 0.010 Å. The Ni(1)···Ni(2) separation of 5.412(1) Å falls within the range found for similarly coordinated μ-oxalato-nickel(II) complexes.

Spectroscopic and magnetic properties of $Ni(TAA)(ClO_4) \cdot 0.5ox$

The electronic spectrum in water solution shows the three characteristic absorptions of octahedral nickel(II) at 27,950, 17,700 and 10,000 cm^{-1}.

Table 1. Crystal data and structure refinement for Ni(TAA)(ClO_4)·0.5ox

Empirical formula	$C_{14}H_{36}Cl_2N_8Ni_2O_{12}$
Formula weight	696.83
Temperature (K)	153(2)
Wavelength (Å)	0.71073
Crystal system, space group	Triclinic, $P\bar{1}$
Unit cell dimensions	$a = 7.311(2)$ Å $\alpha = 79.55(2)°$ $b = 8.407(2)$ Å $\beta = 89.905(14)°$ $c = 10.8207(14)$ Å $\gamma = 85.04(2)°$
Volume (Å^3)	651.5(3)
Z	1
Density (calculated) (Mg m^{-3})	1.776
Absorption coefficient (mm^{-1})	1.723
$F(000)$	362
Crystal size (mm)	0.60 × 0.40 × 0.15
Theta range for data collection (°)	1.91–25.06
Index ranges	$-8 \leqslant h \leqslant 8$, $-10 \leqslant k \leqslant 0$, $-12 \leqslant l \leqslant 12$
Reflections collected	2483
Independent reflections	2310 [$R_{int} = 0.0194$]
Data/parameters	2310/244
Goodness-of-fit on F^2	1.009
R_{obs} [$I > 2\sigma(I)$]	$R_1 = 0.0336$, $wR_2 = 0.0898$
R_{eff}	$R_1 = 0.0380$, $wR_2 = 0.0942$
Largest difference peak and hole (e Å^{-3})	0.611 and −0.876

The IR spectrum of the complex is consistent with the structural data presented above. It shows the sharp bands at 3200 (s), 3180 (s) and 3120 (s) cm^{-1} assigned to the N—H stretching vibrations. The band at 1625 cm^{-1} (s) is attributed to the antisymmetric NH_2-bending vibration and NH_2-twisting vibrations which appear at 1040 (s) and 1000 (s) cm^{-1}. The absorptions at 880 (m) and 906 cm^{-1} (m) may be assigned to the

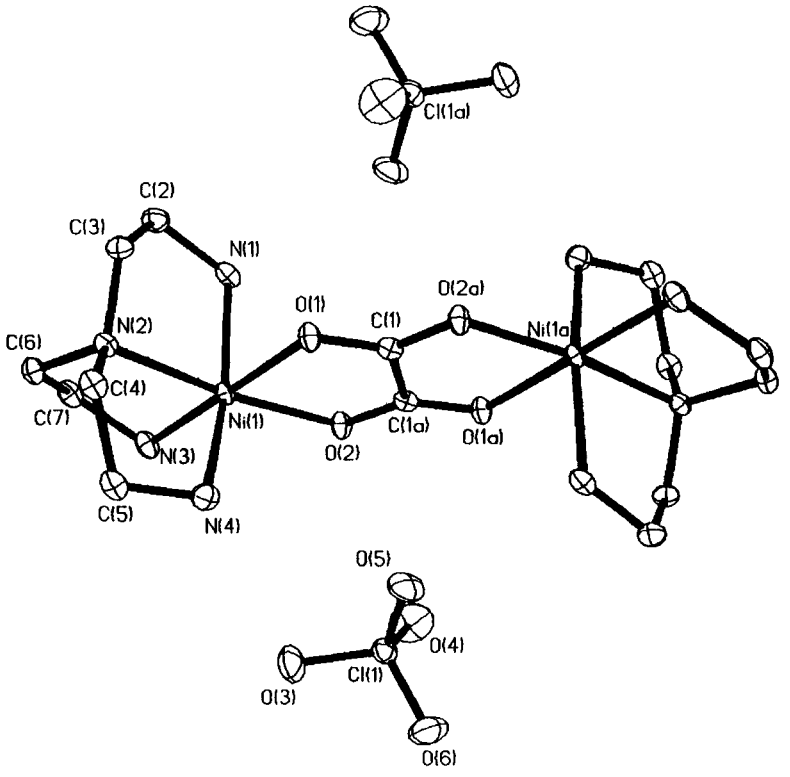


Fig. 1. Structure of Ni(TAA)(ClO_4)·0.5ox.

Table 2. Selected bond lengths (Å) and angles (°) for Ni(TAA)(ClO_4)·0.5ox

Vicinity of the central atom			
Ni(1)—O(1)	2.112(2)	O(2)—Ni(1)—O(1)	80.39(7)
Ni(1)—O(2)	2.049(2)	N(3)—Ni(1)—N(2)	84.20(9)
Ni(1)—N(1)	2.139(2)	N(3)—Ni(1)—N(4)	93.75(11)
Ni(1)—N(2)	2.077(2)	N(2)—Ni(1)—N(4)	84.40(9)
Ni(1)—N(3)	2.066(2)	N(3)—Ni(1)—N(1)	93.73(10)
Ni(1)—N(4)	2.113(3)	N(2)—Ni(1)—N(1)	82.74(9)
		N(4)—Ni(1)—N(1)	164.38(10)
		O(1)—Ni(1)—N(3)	179.08(8)
		O(2)—Ni(1)—N(2)	173.23(8)
Oxalate bridge			
O(1)—C(1)	1.248(3)	O(1)—C(1)—O(2a)[a]	126.3(2)
O(2)—C(1a)[a]	1.256(3)	O(1)—C(1)—C(1a)[a]	116.8(3)
C(1)—O(2a)[a]	1.256(3)	O(2a)—C(1)—C(1a)[a]	116.9(3)
C(1)—C(1a)[a]	1.554(5)		
Perchlorate anion			
Cl(1)—O(3)	1.436(2)	O(4)—Cl(1)—O(3)	109.6(2)
Cl(1)—O(4)	1.431(2)	O(4)—Cl(1)—O(6)	109.0(2)
Cl(1)—O(5)	1.438(2)	O(3)—Cl(1)—O(6)	109.0(2)
Cl(1)—O(6)	1.439(2)	O(4)—Cl(1)—O(5)	110.5(2)
		O(3)—Cl(1)—O(5)	108.93(14)
		O(6)—Cl(1)—O(5)	109.72(14)

Symmetry transformations used to generate equivalent atoms: (a) $-x+1$, $-y$, $-z+1$.

CH_2-rocking, at 1268 cm^{-1} (w) to the CH_2-wagging and at 1382 cm^{-1} (s) to the CH_2-bend vibrations [12]. The occurrence of tetradentate oxalate is clearly observed in the IR spectrum of the title compound: the ν_{asym}(CO) 1644 (s), ν_{sym}(CO) 1355 (s), 1312 (s), δ(CO) 796 cm^{-1} bands agree very well with those reported [13] for Nitrien(ClO_4)·0.5ox (trien = triethylenetetramine). The bands at 1090 (s) and 624 (s) cm^{-1} belong [14] to anion ClO_4^-.

The effective magnetic moment of 2.94 B.M. at 297 K per Ni^{2+} is typical for octahedrally coordinated nickel(II). The variable-temperature magnetic moment and magnetic susceptibility in the range 78–300 K for a solid sample of the title compound is shown in Fig. 2. The magnetic moment is temperature dependent and decreases from 4.23 B.M. mol^{-1} (2.94 B.M. per Ni^{2+}) at 297 K to 3.57 B.M. at 77.9 K. This proves that there is antiferromagnetic coupling across the oxalate bridge. The magnetic behaviour of the title complex could be interpreted using isotropic spin Hamiltonian $H = -2JS_1S_2$, where $S_1 = S_2 = 2/2$ and J is the exchange integral. The experimental data have been fitted to the expression [2]:

$$\chi_M = \frac{\mu_0 N g^2 \beta^2}{3kT} \times \left(\frac{30\exp(6J/kT) + 6\exp(2J/kT)}{5\exp(6J/kT) + 3\exp(2J/kT) + 1} \right) + N_\alpha \quad (1)$$

by using Klička's program [15] for the HDVV-dimer model. In this expression N, β, k and T have their usual meaning, J is the exchange integral and it is assumed that $g_x = g_y = g_z = g$. The last term in this equation, N_α, is the temperature-independent paramagnetism (TIP). The best fit parameters obtained are: $J = -14.4\ cm^{-1}$, $g = 2.25$. For Ni^{II} complexes in octahedral geometry, the metal x^2-y^2 orbital is half occupied and is aligned to allow overlap with the oxalate σ-orbitals. For present complex, the observed J value of $-14.4\ cm^{-1}$ is very similar to those of [Ni_2trien_2ox](ClO_4)$_2$ ($J = -15.1\ cm^{-1}$, our result, or [2] $J = -15.7\ cm^{-1}$) or [3] [Ni_2en_4ox](NO_3)$_2$ ($J = -16\ cm^{-1}$).

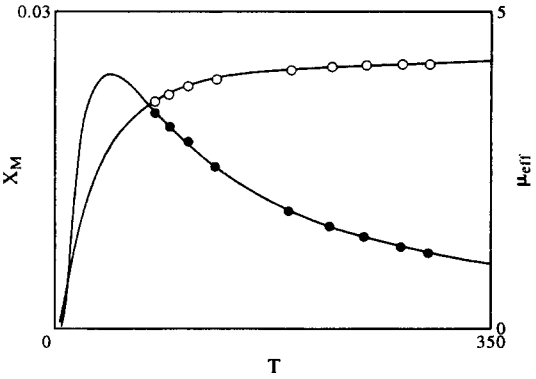


Fig. 2. The paramagnetic susceptibility (●—in cgs) and effective moment (○—B.M.) *vs* temperature curves for Ni(TAA)(ClO_4)·0.5ox. The circles are the experimental points, the solid lines are theoretical lines.

Properties of $Ni_2(APO\text{-}sal_2)ox \cdot 2H_2O$

The binuclear nickel(II) oxalato-bridged complex of the ligand (APO-sal_2) precipitates from the solution as a brown powder, which was not suitable for X-ray study. The thermal behaviour of the compound has been deduced from its TG and TGA curves. The removal of the water molecules starts at 75°C and the corresponding small endothermic peak at approximately 150°C is broad. The weight loss continues in the temperature range 210–400°C with two exothermic peaks at 290 and 340°C. A constant mass is achieved at 400°C. The last observed solid product was identified by its X-ray powder diffraction pattern as NiO (Δm_{th} 72.2%, Δm_{exp} 72.5%).

The IR spectrum shows a strong absorption band at 1620 cm^{-1}. This frequency corresponds to the ν(C=N), which is typical for Schiff bases. The (C=O) at 1670 cm^{-1} of the salicylaldehyde disappears as a result of condensation. The phenolic (C—O) band (1270 cm^{-1}) of the ligand shifts to a higher frequency [1290 cm^{-1} (s)] in the complex due to the bonding [16] to nickel. The occurrence of oxalate is observed in the IR spectrum of this complex at 1640 (m) – ν_{asym}(CO), 1365 (s), 1300 (s) – ν_{sym}(CO) and δ(C—O) at 755 cm^{-1} (m).

The effective magnetic moment at room temperature (296 K) is 4.00 B.M. mol^{-1}; i.e. 2.79 B.M. per Ni^{II}. The temperature dependence of the magnetic moment of this compound is displayed in Fig. 3. On lowering of the temperature, μ_{eff} decreases from 4.00 B.M. at 296 K to 3.47 B.M. at 77.5 K. This magnetic behaviour is characteristic of an antiferromagnetically coupled Ni^{II}–Ni^{II}. The value of the exchange parameter $J = -11.25$ cm^{-1} ($g = 2.04$) based on Eq. (1) is a little smaller than that in the previous compound.

Properties of $Niphen_2oxNiacac_2 \cdot 4H_2O$

This compound was obtained as blue microcrystals almost insoluble in organic solvents.

The thermal analysis shows that the compound starts its decomposition above 60°C, losing its water molecules in an endothermic process. A weight loss of 8.5% in the TG curve corresponds to the loss of four water molecules (Δm_{th} 7.5%). The anhydrous salt is stable from 120 up to 210°C, above this temperature the thermal decomposition continued in one step. A constant mass is achieved at 440°C, at which temperature the weight of the residue was in accordance with this calculated for NiO (NiO was identified by X-ray powder diffraction pattern).

The IR data of this complex show the characteristic bands of the oxalate bridging ligands. Three peaks ν_{asym}(C—O), ν_{sym}(C—O) and δ(C—O) of oxalate are found at 1652 (w), 1312 (s) and 770 (w) cm^{-1}. The ν(C=C) and ν(C=O) bands of the acetylacetone ion [17,18] are found at 1592 (m) and 1520 (m) cm^{-1}, respectively, and for phenanthroline complexes are found following typical peaks [19] 1442 (s), 1345 (s), 1156 (m) and 850 (w) cm^{-1}.

At 295 K the magnetic moment μ_{eff}/molecule is 4.61 B.M., the μ_{eff}/Ni^{2+} is 3.18 B.M., which is in the range expected for an octahedral Ni^{II} atom. The thermal dependence of χ_M and μ_{eff} for this complex in the temperature range 78.5–295 K is shown in Fig. 4. From room temperature, the μ_{eff} value decreases to 3.54 B.M. mol^{-1} at 78.5 K. The value of $J = -19.4$ cm^{-1} and $g = 2.38$ have been evaluated from the best fit of the experimental data to Eq. (1). This value is a bit higher value, but not greatly deviated from this ($J = -14.3$ cm^{-1}) reported [17] for μ-oxalato-bis[(acetylacetonato)(*N*,*N*,*N*′,*N*′-tetramethylethylenediamine)nickel(II)].

The exchange integrals J found for all three compounds studied are in the -11.25 to -19.4 cm^{-1} range. The data obtained in this study show that the main factor influencing the strength of the antiferromagnetic coupling is the extent of overlap between the magnetic orbitals of the paramagnetic nickel ions and those of the μ-oxalato bridging ligand. In other words, there is only small influence of the

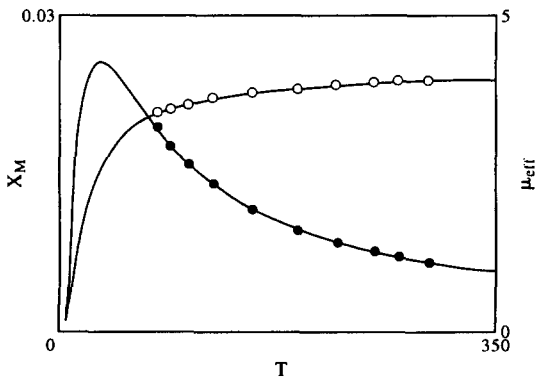


Fig. 3. The paramagnetic susceptibility (●—in cgs) and effective moment (○—B.M.) *vs* temperature curves for $Ni_2(APO\text{-}sal_2)ox \cdot 2H_2O$. The circles are the experimental points, the solid lines are theoretical lines.

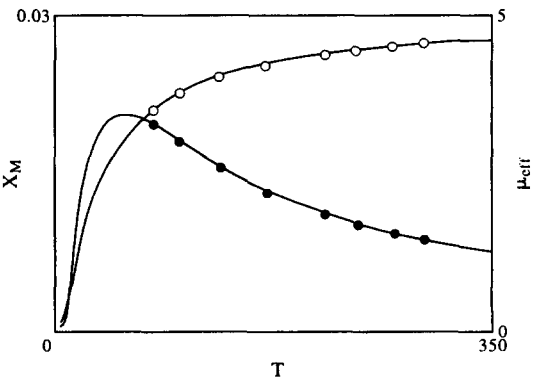


Fig. 4. Temperature dependence of χ_M (●—in cgs) and μ_{eff} (○—B.M.) for $Niphen_2oxNiacac_2 \cdot 4H_2O$. The circles are the experimental points, the solid lines correspond to the best theoretical fits.

change in the remaining terminal ligands to the magnetic interaction between the two nickel(II) ions in binuclear μ-oxalato complexes.

Acknowledgement—This work was financially supported by the Grant Agency of the Czech Republic (203/96/0440; 203/95/1190; 203/96/0111).

REFERENCES

1. Curtis, N. F., McCormick, J. R. N. and Waters, T. N., *J. Chem. Soc., Dalton Trans.* 1973, 1537.
2. Duggan, D. M., Barefield, E. K. and Hendrickson, D. N., *Inorg. Chem.* 1973, **12,** 985.
3. Ball, P. N. and Blake, A. B., *J. Chem. Soc. A*, 1969, 1415.
4. Glerup, J., Goodson, P. A., Hodgson, D. J. and Michelsen, K., *Inorg. Chem.* 1995, **34,** 6255.
5. Escuer, A., Vicente, R., El Fallah, M. S. and Jaud, J., *Inorg. Chim. Acta*, 1995, **232,** 151.
6. Ginsberg, A. P., Martin, R. L. and Sheerwood, R. C., *Inorg. Chem.* 1968, **7,** 932.
7. Basolo, F., Hayes, J. C. and Neumann, H. M., *J. Am. Chem. Soc.* 1953, **75,** 5102.
8. Gach, F., *Monatsh. Chem.* 1990, **21,** 98.
9. König, E., *Magnetic Properties of Coordination and Organometallic Transition Metal Compounds.* Springer, Berlin, 1966.
10. Sheldrick, G. M., *Acta Cryst.* 1990, **A46,** 467.
11. Sheldrick, G. M., *SHELXL*-93, *Program for Crystal Structure Refinement.* University of Göttingen, Germany, 1993.
12. Buckingham, D. A. and Jones, D., *Inorg. Chem.* 1965, **4,** 1387.
13. Curtis, N. F., *J. Chem. Soc.* 1963, 4109.
14. Hathaway, B. J. and Underhill, A. E., *J. Chem. Soc.* 1961, 3091.
15. Klička, R. and Šindelář, Z., *Chem. Listy*, 1993, **87,** 89.
16. Zhang, X.-M., You, X. Z. and Wang, X., *Polyhedron*, 1996, **15,** 1793.
17. Yamada, K., Fukuda, Y., Kawamoto, T., Kushi, Y., Mori, W. and Unoura, K., *Bull. Chem. Soc. Jpn*, 1993, **66,** 2758.
18. Fukuda, Y. and Sone, K., *J. Inorg. Nucl. Chem.* 1972, **34,** 2315.
19. Inskeep, R. N., *J. Inorg. Nucl. Chem.* 1962, **24,** 763.

Pergamon

PII: S0277-5387(96)00418-4

Polyhedron Vol. 16, No. 8, pp. 1337–1341, 1997
Copyright © 1997 Elsevier Science Ltd
Printed in Great Britain. All rights reserved
0277-5387/97 $17.00+0.00

Synthesis and structural studies of four- and five-coordinated monomeric alkylaluminum O,N-chelate compounds derived from 2-aminoacetophenone. Crystal and molecular structure of the five-coordinated $MeAl[O{=}C(Me)C_6H_4\text{-}2\text{-}NH]_2$ complex

Janusz Lewiński,* Janusz Zachara, Tomasz Kopeć and Zbigniew Ochal

Department of Chemistry, Warsaw University of Technology, Noakowskiego 3, 00-664 Warsaw, Poland

(Received 28 June 1996; accepted 12 August 1996)

Abstract—The reaction of Me_3Al with 1 and 2 equiv. of 2-aminoacetophenone yielded $Me_2Al[O{=}C(Me)C_6H_4\text{-}2\text{-}NH]$ (**1**) and $MeAl[O{=}C(Me)C_6H_4\text{-}2\text{-}NH]_2$ (**2**), respectively. Compound **2** was also obtained in the reaction of **1** with 1 equiv. of 2-aminoacetophenone. The addition of 4-methylpyridine (py-Me) to **1** produced the Lewis acid–base adduct $Me_2Al[O{=}C(Me)C_6H_4\text{-}2\text{-}NH]\cdot$ py-Me (**3**). The resulting compounds have been characterized by elemental analysis, cryometric molecular weight determination and ^1H and ^{27}Al NMR spectroscopy. These studies revealed that compound **1** has a four-coordinated chelate structure in solution, while **2** and **3** are five-coordinated monomeric complexes. The molecular structure of **2** has been confirmed by single-crystal X-ray crystallography. Copyright © 1997 Elsevier Science Ltd

Keywords: organoaluminum compound; O,N-chelate complex.

The reactions of organoaluminum compounds with O,O′-bidentate ligands, and the structure and reactivity of alkylaluminum chelate complexes, have been the subject of intense studies recently [1–5]. We succeeded in synthesizing and structural characterizing of the first simple five-coordinated alkylaluminum chelate complex, $RAl(O,O')_2$, [3] and also characterized a number of new $R_2Al(O,O')$-type complexes and showed that the structure of dialkylaluminum chelate compounds in solution depends on the nature of the O,O′-chelate ligand [4,5]. For example, if both chelating oxygen atoms are involved in the conjugated bond system of the O,O′-chelate, the $R_2Al(O,O')$ complexes occur as monomeric compounds in solution. Studies have been carried out by us on the reactions of monohydroxy O.O′-bidentate ligands. Similarly, the structurally characterized dialkylaluminum O,N-chelate complexes described in the literature concerned only the derivatives of the O,N-bidentate ligands bearing a hydroxy group [6–10].

In this paper we report the interactions of trimethylaluminum with 2-aminoacetophenone as an O,N-bidentate ligand bearing an acidic proton bonded to a nitrogen atom, and structural studies of the four- and five-coordinated monomeric alkylaluminum O,N-chelate complexes.

RESULTS AND DISCUSSION

The interaction of Me_3Al with 1 and 2 equiv. of 2-aminoacetophenone (amketH) leads to the formation of $Me_2Al(amket)$ (**1**) and $MeAl(amket)_2$ (**2**), respectively, and evolution of methane [Eqs. (1) and (2)], Compound **2** may also be prepared directly from the reaction of **1** with 1 equiv. of amketH [Eq. (3)].

* Author to whom correspondence should be addressed.

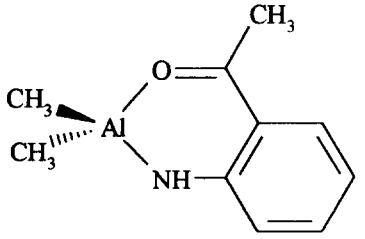
$$Me_3Al + amketH \rightarrow Me_2Al(amket) + MeH \quad (1)$$

$$Me_3Al + 2\,amketH \rightarrow MeAl(amket)_2 + 2\,MeH \quad (2)$$

$$Me_2Al(amket) + amketH \rightarrow MeAl(amket)_2 + MeH \quad (3)$$

Compound **1** is a deep-red solid and is soluble in hydrocarbon solvents, while **2** is an orange solid and is soluble in methylene chloride and aromatic solvents.

Elemental analysis, cryometric molecular weight determinations, ^{27}Al and ^1H NMR and IR spectroscopy are consistent with the formulae of compound **1** and **2** as given, and the monomeric chelate structures in solution. The ^{27}Al NMR spectrum of **1** consists of one resonance at δ 152.0, indicative of a four-coordinated aluminum atom. This is in the same range as the signals for monomeric $R_2Al(O,O')$ chelate compounds recently reported [4,5]. In the ^1H NMR spectrum three singlets corresponding to Me—Al, Me—C and N—H amide protons, as well as four multiplets of aromatic protons are observed, which is consistent with the tetrahedral chelate structure **I**.



I

The results concerning structure **I** in solution are in agreement with those of our earlier findings for $R_2Al(O,O')$ complexes; namely that the presence of a conjugated bond system in the chelating ligand favours the formation of monomeric dialkylaluminum chelate complexes [4,5]. Unfortunately, we have been unable to perform X-ray diffraction studies on **1** at ambient temperature.

The ^{27}Al NMR shift for **2** (δ 74) is similar to that previously observed by us for the monomeric five-coordinated methylaluminum O,O'-chelate compound [3]. In the ^1H NMR spectrum one methylaluminum peak and a single set of resonances for the amket ligands are observed. The structure of **2** has been confirmed by X-ray crystallography.

The molecular structure of **2** is shown in Fig. 1 and selected bond lengths and angles are given in Table 1. The complex comprises a five-coordinated aluminum atom with an idealized trigonal bipyramid coordination sphere. The aluminum atom lies exactly in the $CAlN_2$ equatorial plane determined by the methyl group carbon atom and two amide nitrogen atoms. The angles between the bonds in this plane are close to 120°. The carbonyl group oxygen atoms of the chelating ligand are in axial positions.

Simultaneously, the deviation of the axial bonds from an ideal position, as shown in Fig. 2, probably results from strains in the O,N-chelating ligand. Chelating ligands form deformed six-membered AlNCCCO heterocyclic rings in the shape of an open envelope with a dihedral angle defined by NAlO and NCCCO atoms equal to 14.4°. The mean length of the Al—N bonds is 1.865 Å and is comparable with corresponding bond lengths in five-coordinated alkylaluminum complexes with O,N-macrocyclic ligands [11,12]. The lengths of the axial Al—O bonds are comparable with those observed for axial bonds lengths in an analogous compound with an O,O'-ligand, $MeAl(mesal)_2$ [3]. The structurally characterized compound **2** is the first simple five-coordinated alkylaluminum chelate complex with an O,N-bidentate ligand.

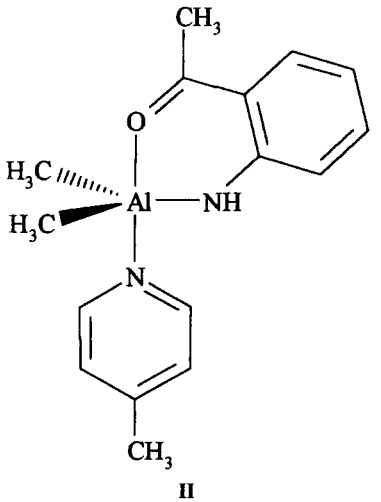
The reaction of **1** with 4-methylpyridine (py-Me) results in the formation of the Lewis acid–base adduct $Me_2Al(amket)(py\text{-}Me)$ (**3**) in quantitative yield [Eq. (4)].

$$Me_2Al(amket) + py\text{-}Me \rightarrow Me_2Al(amket) \cdot py\text{-}Me \quad (4)$$

Compound **3** is a deep red liquid insoluble in hydrocarbon solvents and soluble in methylene chloride and aromatic solvents. It is unstable at ambient temperature and slowly decomposes within 1–2 days to yield **2** and $Me_3Al \cdot py\text{-}Me$ [Eq. (5)].

$$Me_2Al(amket) \cdot py\text{-}Me \rightarrow MeAl(amket)_2 + Me_3Al \cdot py\text{-}Me \quad (5)$$

Compound **3** has been characterized by elemental analysis, cryometric molecular weight determinations and ^{27}Al and ^1H NMR spectroscopy. The ^{27}Al NMR spectrum of **3** consists of one resonance at δ 73 with a chemical shift similar to that observed for **2** indicative of a five-coordinated aluminum atom.



II

The ^1H NMR spectrum of this complex shows four singlets in an intensity ratio of 6:3:3:1, which can be easily assigned to Me—Al, Me—C, Me-py and N—H protons, respectively. The data obtained for **3**

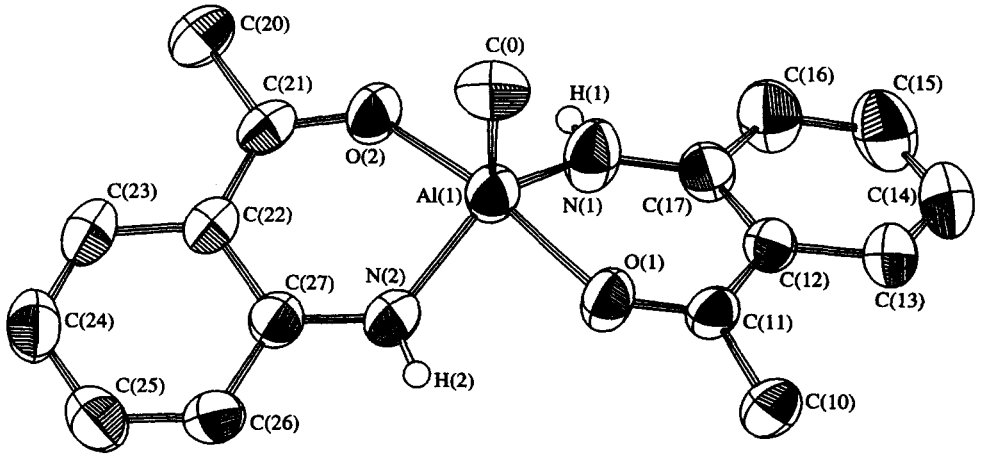


Fig. 1. Molecular structure of $MeAl[O{=}C(Me)C_6H_4\text{-}2\text{-}NH]_2$ (**2**) with the atom labelling scheme. Thermal ellipsoids are drawn at the 50% level. Hydrogen atoms, except NH groups, have been omitted for clarity.

are therefore consistent with the monomeric Lewis acid–base adduct and its structure can be described as depicted in **II**. Adduct **3** is the first example of a monomeric five-coordinated dialkylaluminum compound to be isolated and spectroscopically characterized. Further studies on the structure and reactivity of alkylaluminum O,N -chelate complexes are under way.

EXPERIMENTAL

All operations were carried out under nitrogen. Solvents were purified and dried by standard techniques. Me_3Al and 2-aminoacetophenone were distilled before use. Standard Schlenk line techniques were employed. NMR spectra were recorded on a Varian VXR-300 spectrometer.

Preparation of $Me_2Al[O{=}C(Me)C_6H_4\text{-}2\text{-}NH]$ (**1**)

2-Aminoacetophenone was dissolved in toluene (8 cm^3) and Me_3Al (0.44 g, 3.3 mmol) was added dropwise at −78°C. After the addition was completed the reaction mixture was allowed to warm up to room temperature. The solvent was then removed *in vacuo*, leaving an orange solid that was crystallized from a toluene/hexane solution at 0°C. Yield: 85%. Found: C, 62.5; H, 7.6; N, 7.0. Calc. for $C_{10}H_{14}NOAl$: C, 62.8; H, 7.4; N, 7.3; Al, 14.1%. Molecular weight

Table 1. Selected bond lengths (Å) and angles (°) for $MeAl[O{=}C(Me)C_6H_4\text{-}2\text{-}NH]_2$

Al(1)—N(1)	1.863(3)	Al(1)—N(2)	1.867(3)
Al(1)—O(1)	1.929(2)	Al(1)—O(2)	1.947(2)
Al(1)—C(0)	1.958(3)		
O(1)—C(11)	1.262(3)	O(2)—C(21)	1.257(3)
N(1)—C(17)	1.355(4)	N(2)—C(27)	1.349(4)
C(10)—C(11)	1.498(4)	C(20)—C(21)	1.496(4)
C(11)—C(12)	1.423(4)	C(21)—C(22)	1.429(4)
C(12)—C(17)	1.418(4)	C(22)—C(27)	1.422(4)
N(1)—Al(1)—N(2)	124.8(2)	O(1)—Al(1)—O(2)	164.94(10)
N(1)—Al(1)—O(1)	87.08(13)	N(2)—Al(1)—O(2)	86.03(13)
N(2)—Al(1)—O(1)	86.28(13)	N(1)—Al(1)—O(2)	86.70(13)
N(1)—Al(1)—C(0)	115.9(2)	N(2)—Al(1)—C(0)	119.28(14)
O(1)—Al(1)—C(0)	98.75(13)	O(2)—Al(1)—C(0)	96.30(13)
C(11)—O(1)—Al(1)	133.4(2)	C(21)—O(2)—Al(1)	131.7(2)
C(17)—N(1)—Al(1)	130.7(3)	C(27)—N(2)—Al(1)	129.6(3)
O(1)—C(11)—C(12)	122.1(3)	O(2)—C(21)—C(22)	122.4(3)
C(17)—C(12)—C(11)	121.0(3)	C(27)—C(22)—C(21)	120.6(3)
N(1)—C(17)—C(12)	122.3(3)	N(2)—C(27)—C(22)	122.1(3)

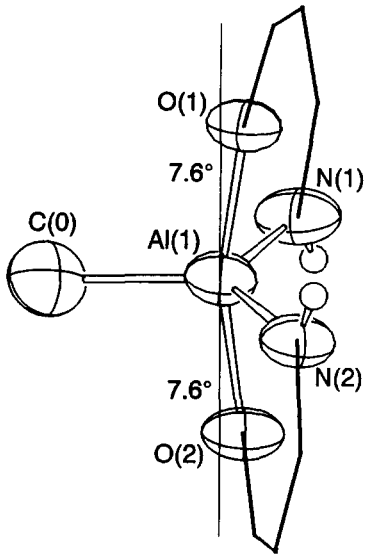


Fig. 2. View of the coordination sphere of the aluminum atom in MeAl[O=C(Me)C_6H_4-2-NH]$_2$ (**2**).

calc. for $C_{10}H_{14}NOAl$: 191.2; found: 210. ^{1}H NMR (C_6D_6, ppm): δ −0.21 (6H, s, Al—CH_3), 1.71 (3H, s, $COCH_3$), 4.40 (1H, s, NH), 5.88 (1H, d, 3-CH), 5.97–6.76 (4H, m, CH_{arom}). ^{27}Al NMR (C_6D_6, ppm): δ 152 ($\Delta H_{1/2}$ = 2280 Hz).

Preparation of MeAl[O=C(Me)C_6H_4-2-NH]$_2$ (**2**)

Compound **2** was prepared in a manner similar to that for **1**, using 2-aminoacetophenone (0.68 g, 5.0 mmol) and Me_3Al (0.18 g, 2.5 mmol) to give a yellow solid. Yield: 90%. Found: C, 65.7; H, 6.2; N, 9.0. Calc. for $C_{17}H_{19}N_2O_2Al$: C, 65.8; H, 6.2; N, 9.0; Al, 8.7%. Molecular weight calc. for: $C_{17}H_{19}N_2O_2Al$: 310.3; found: 311. ^{1}H NMR (C_6D_6, ppm): δ −0.07 (3H, s, Al—CH_3), 1.99 (6H, s, $COCH_3$), 5.05 (2H, s, NH), 6.13–7.05 (8H, m, CH_{arom}). ^{27}Al NMR (C_6D_6, ppm): δ 74 ($\Delta H_{1/2}$ = 4790 Hz).

Preparation of Me_2Al[O=C(Me)C_6H_4-2-NH] · py-Me (**3**)

To a solution of **1** (0.038 g, 0.2 mmol) in hexane (2 cm^3), 4-methylpyridine (0.036 g, 0.4 mmol) was added at room temperature. After stirring for 5 min, the solvent and excess of 4-methylpyridine were removed *in vacuo* to leave quantitatively a deep red liquid. Found: C, 67.9; H, 7.7; N, 9.9. Calc. for $C_{16}H_{21}N_2OAl$: C, 67.6; H, 7.4; N, 9.8; Al, 9.5%. Molecular weight calc. for $C_{16}H_{21}N_2OAl$; found: 293. ^{1}H NMR (C_6D_6, ppm): δ −0.18 (6H, s, Al—CH_3), 1.71 (3H, s, $COCH_3$), 2.00 (3H, s, CH_3), 5.07 (1H, s, NH), 6.14–8.35 (8H, m, CH_{arom}). ^{27}Al NMR (C_6D_6, ppm): δ 73 ($\Delta H_{1/2}$ = 5100 Hz).

X-ray crystal structure determination of **2**

A yellow crystal of compound **2** was sealed inside a Lindemann capillary and mounted on the goniometer head of a Siemens P3 diffractometer employing graphite-monochromated Mo-K_α, radiation. Crystal data, data collection and refinement parameters are summarized in Table 2. The cell parameters were obtained by least-squares refinement of measured setting angles of 28 randomly selected reflections with $7 < 2\theta < 30°$. Intensity data were collected using the ω–2θ technique with variable scan speed. Two check reflections (2 0 0; 0 1 3) measured every 70 reflections revealed drastic crystal decay of 60% and intensities were corrected accordingly. Lorentz and polarization corrections were applied to the data set; no corrections were applied for absorption.

The crystal of **2** was monoclinic and assigned to the $P2_1/c$ (No. 14) space group on the basis of systematic absences. The structure was solved by direct methods using SHELXS-86, [13] which revealed the positions of all non-hydrogen atoms. Refinement was per-

Table 2. Crystal data and structure refinement for MeAl[O=C(Me)C_6H_4-2-NH]$_2$

Empirical formula	$C_{17}H_{19}N_2O_2Al$
Formula weight	310.32
Temperature/K	293(2)
Radiation (Å)	Mo-K_α (λ = 0.71073 Å)
Crystal system	Monoclinic
Space group	$P2_1/c$
Unit cell dimensions:	
a/Å	8.1672(9)
b/Å	14.474(3)
c/Å	13.903(2)
β/°	96.675(12)
Volume/Å^3	1632.4(4)
Z	4
Density (calculated)/Mg m^{-3}	1.263
Absorption coefficient/mm^{-1}	0.132
F(000)	656
Crystal size/mm	0.42 × 0.40 × 0.34
2θ range for data collection/°	4.0–50.0
Index ranges	$0 \leqslant h \leqslant 9$, $0 \leqslant k \leqslant 17$, $-16 \leqslant l \leqslant 16$
Reflections collected	3319
Independent reflections	2486 (R_{int} = 0.0185)
Refinement method	Full-matrix least squares on F^2
Data/restraints/parameters	2483/0/223
Goodness-of-fit on F^2	1.092
Final R indices [$I > 2\sigma(I)$]	R_1 = 0.0535, wR_2 = 0.0957
R indices (all data)	R_1 = 0.0996, wR_2 = 0.1144
Extinction coefficient	0.0103(10)
Largest diff. peak/hole/eÅ^{-3}	+0.155/−0.156

formed by the full-matrix least-squares method on F^2 using the SHELXL-93 program. [14] All non-hydrogen atoms were refined with anisotropic thermal parameters. The aromatic and methyl H-atoms were placed in calculated positions and refined isotropically with a riding model. Hydrogen atoms of the methyl group bonded to the Al atom were refined as a disordered group with two positions rotated from each other by 60°. It was possible to identify on the difference Fourier map and successfully refine the positions of hydrogen atoms of both amide NH groups. An extinction correction was applied to all data during the final stages of refinement, and the extinction coefficient x was refined by leastsquares according to the equation $F_c^* = kF_c[1+0.001xF_c^2\lambda^3/\sin(2\theta)]^{-1/4}$, where k was the overall scale factor. Refinement of the structure led to convergence, and the maximum shift of the parameter was less than 0.01 of its estimated standard deviation. The largest peak in the final difference Fourier map had an electron density of 0.155 eÅ^{-3}, and the lowest excursion -0.156 eÅ^{-3}. The weighting scheme was of the form $w^{-1} = \sigma^2(F_o^2)+(0.365P)^2+0.6559P$, where $P = (2F_c^2+F_o^2)/3$. Residuals are defined as $wR_2 = \{\Sigma[w(F_o^2-F_c^2)^2]/\Sigma[w(F_o^2)^2]\}^{1/2}$ for all data and conventional $R_1 = \Sigma||F_o|-|F_c||/\Sigma|F_o|$ for reflections with $F_o^2 > 2\sigma(F_o^2)$, the latter for comparison with conventional refinements based on F values. Full lists of atomic coordinates, thermal parameters, bond lengths and bond angles have been deposited at the Cambridge Crystallographic Data Centre.

Acknowledgement—This work was supported by a grant from the Warsaw University of Technology.

REFERENCES

1. Lewiński, J., Zachara, J. and Grabska, E., *J. Am. Chem. Soc.* 1996, **118,** 6794.
2. Lewiński, J. and Pasynkiewicz, S., *J. Organomet. Chem.* 1985, **290,** 15.
3. Lewiński, J., Zachara, J., Mańk B. and Pasynkiewicz, S., *J. Organomet. Chem.* 1993, **454,** 5.
4. Lewiński, J. and Zachara, J., *Organometallics*, submitted for publication.
5. Lewiński, J., Zachara, J. and Starowieyski, K. B., *Organometallics*, submitted for publication.
6. Van Vliet, M. R. P., Buysingh, P., van Koten, G., Vrieze, K., Kojic-Prodic, B. and Spek, A. L., *Organometallics* 1985, **4,** 1701.
7. Dzugan, S. T. and Goedken, V. L., *Inorg. Chim. Acta* 1988, **154,** 169.
8. Sierra, M. L., de Mel, V. S. J. and Oliver, J. P., *Organometallics* 1989, **8,** 2486.
9. Van Steen, F. H., van Mier, G. P. M., Spek, A. L., Kroon, J. and van Koten, G., *J. Am. Chem. Soc.* 1991, **113,** 5742.
10. Kumar, R., Sierra, M. L. and Oliver, J. P., *Organometallics* 1994, **13,** 4285.
11. Zugan, S. J. and Goedken, V. L., *Inorg. Chem.* 1986, **25,** 2858.
12. Atwood, D. A., Jegier, J. A., Martin, K. J. and Rutherford, D., *Organometallics*, 1995, **14,** 1453.
13. Sheldrick, G. M., *Acta Cryst.* 1990, **A46,** 467.
14. Sheldrick, G. M., *SHELXL93*; *Program for the Refinement of Crystal Structures*, University of Göttingen, Germany, 1993.

Pergamon

PII: S0277-5387(96)00390-7

Polyhedron Vol. 16, No. 8, pp. 1343–1349, 1997
Copyright © 1997 Elsevier Science Ltd
Printed in Great Britain. All rights reserved
0277-5387/97 $17.00+0.00

A four-membered C,O-chelate: two families of ruthenium organometallics incorporating N···O hydrogen bonding

Prasanta Ghosh

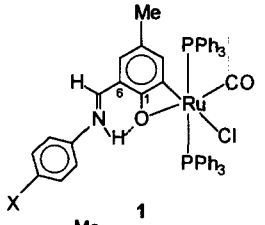
Department of Inorganic Chemistry, Indian Association for the Cultivation of Science, Calcutta 700 032, India

(Received 6 June 1996; accepted 6 August 1996)

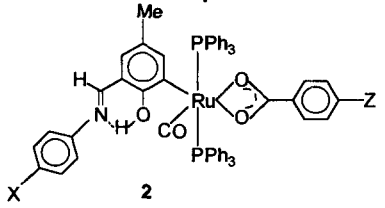
Abstract—The reaction of mono-Schiff bases of 4-methyl-2,6-diformylphenol and primary amines (p-$XC_6H_4NH_2$, X = OMe, Cl, CO_2Et and NO_2) with $Ru(PPh_3)_3Cl_2$ in boiling ethanol afforded violet diamagnetic complexes, $[Ru(\eta^2\text{-}p\text{-}XC_6H_4L)(PPh_3)_2(CO)Cl]$ (η^2-p-XC_6H_4L = [4-methyl-6-(*N*-p-Xphenyliminiomethyl) phenolato-C^2,O] incorporating the unprecedented orthoruthenated phenolato function, which is hydrogen-bonded with the uncoordinated imine nitrogen. These complexes were found to react with sodium benzoates (p-ZC_6H_4COO, Z = Me, Cl) to generate the new aryl complexes of ruthenium, $[Ru(\eta^1\text{-}p\text{-}XC_6H_4L)(PPh_3)_2(CO)(\eta^2\text{-}p\text{-}ZC_6H_4COO)]$. The spectral (IR, UV–vis and ^1H NMR) features of these two types of complexes and the effect of the X substituent on electronic and ^1H NMR spectra are scrutinized. The effect of PPh_3 ring currents on the chemical shifts of the metallated ring protons is semiquantitatively estimated. In these complexes different types of novel intramolecular N···O interaction and the conformational orientation of p-XC_6H_4L ligands are noted. The redox behaviour of these complexes is reported. The $E_{1/2}$ values of Ru^{III}/Ru^{II} couple correlate linearly with the Hammett constants (σ) of X substituent in the halo complexes. A spectro-electrochemical correlation in these complexes is also observed. Copyright © 1997 Elsevier Science Ltd

Keywords: ruthenium; decarbonylation; C,O-chelation; carboxylate chelation; N···O hydrogen bonding; spectroelectrochemical correlation.

Recently it has been reported that the reaction of $Ru(PPh_3)_3Cl_2$ with 4-methyl-2,6-diformylphenol in the presence of primary amines affords the novel organometallics of type **1** (X = H, Me) [1]. Complex **1** was found to react with carboxylates affording **2** (X = H, Me; Z = H) [2].



1



2

In this work the synthesis and characterization of a more complete series of compounds (X = OMe, Cl, CO_2Et and NO_2; Z = Me and Cl) and their spectral (IR, UV–vis and ^1H NMR), redox and the intramolecular N···O hydrogen-bonding features are reported. This has provided an opportunity for studying the substituent effects in a logical manner.

EXPERIMENTAL

Materials

The starting materials $Ru(PPh_3)_3Cl_2$ [3] and the 4-methyl-2,6-diformylphenol [4] were prepared by the reported procedures. The reactions of 4-methyl-2,6-diformylphenol and the aromatic primary amines (p-$XC_6H_4NH_2$) in 1:1 and 1:2 ratios in boiling ethanol affords, respectively, the Schiff bases **4** and **5**. The sodium benzoates (Na-p-ZC_6H_4COO) were prepared by neutralizing the corresponding acid with 0.1 N

NaOH solution. The purification of dichloromethane and the preparation of tetraethylammonium perchlorate (TEAP) for electrochemical work were carried out as before [5]. All other chemicals and solvents were of analytical grade and used without further purification.

Preparation of complexes

The complexes **1** were synthesized in excellent yields by reacting $Ru(PPh_3)_3Cl_2$ with the Schiff mono-bases **4**. The reaction of **1** with sodium benzoates generated **2** in high yields. Details are given for representative cases.

Carbonylchloro[4-*methyl*-6-(N-p-*chlorophenyliminiomethyl*)*phenolato-C*^{2},*O*]*bis*(*triphenylphosphine*) *ruthenium*(II), **1** (*X* = Cl). To a solution of 2-formyl-4-methyl-6-(*N*-*p*-chlorophenylimine)phenol (**4**, X = Cl; 45 mg, 0.15 mmol) in hot ethanol (30 cm^3) was added $Ru(PPh_3)_3Cl_2$ (100 mg, 0.10 mmol). The mixture was heated to reflux for 1 h and then cooled. A dark violet solid separated which was collected by filtration. It was washed thoroughly with cold ethanol and dried *in vacuo*. Yield: 80 mg [82% on the basis of $Ru(PPh_3)_3Cl_2$]. Found: C, 65.5; H, 4.5; N, 1.4. Calc. for $C_{51}H_{41}NO_2P_2Cl_2Ru$: C, 65.5; H, 4.4; N, 1.5%.

Complexes **1** with X = OMe, CO_2Et and NO_2 were synthesized similarly in 80–85% yields. Found: C, 67.2; H, 4.8; N, 1.4. Calc. for $C_{52}H_{44}NO_3P_2ClRu$ (**1**, X = OMe): C, 67.2; H, 4.7; N, 1.5%. Found: C, 66.7; H, 4.7; N, 1.4. Calc. for $C_{54}H_{46}NO_4P_2ClRu$ (**1**, X = CO_2Et): C, 66.7; H, 4.8; N, 1.4%. Found: C, 64.8; H, 4.4; N, 2.9. Calc. for $C_{51}H_{41}N_2O_4P_2ClRu$ (**1**, X = NO_2): C, 64.8; H, 4.4; N, 3.0%.

Carbonyl(p-*chlorobenzoato*)[4-*methyl*-6(N-p-*tolyiminomethyl*)*phenol-C*^{2}]*bis*(*triphenylphosphine*) *ruthenium*(II), **2** (*X* = Me; *Z* = Cl). To a vigorously stirred solution of **1** (X = Me) [6] (50 mg, 0.05 mmol) in dichloromethane (20 cm^3) and acetone (20 cm^3) was added dropwise an aqueous solution of Na-*p*-ClC_6H_4COO (60 mg, 0.34 mmol). The mixture was stirred for 0.5 h. The dark violet solution turned yellow. The organic solvents were then removed under reduced pressure, leaving an aqueous suspension of a yellow residue. This was isolated by filtration, washed thoroughly with water and dried *in vacuo*. Yield: 48 mg (85% on the basis of chloro precursor). Found: C, 68.5; H, 4.7; N, 1.3. Calc. for $C_{59}H_{48}NO_4P_2ClRu$: C, 68.5; H, 4.7; N, 1.3%.

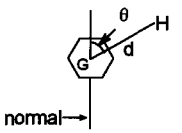
Complexes **2** with X = H, Z = Cl and X = H, Me, Z = Me, were similarly prepared in high yields (85–90%). Found: C, 68.3; H, 4.5; N, 1.4. Calc. for $C_{58}H_{46}NO_4P_2ClRu$ (**2**, X = H; Z = Cl): C, 68.3; H, 4.5; N, 1.4. Found: 70.8; H, 4.9; N, 1.4. Calc. for $C_{59}H_{49}NO_4P_2Ru$ (**2**, X = H; Z = Me): C, 70.9; H, 4.9; N, 1.4%. Found: C, 71.0; H, 5.1; N, 1.3. Calc. for $C_{60}H_{51}NO_4P_2Ru$ (**2**, X = Me; Z = Me): C, 71.1; H, 5.1; N, 1.4%.

Physical measurements

Electronic and IR spectra were recorded on Hitachi 330 and Perkin–Elmer 783 IR spectrophotometers. For ^{1}H NMR spectra a Bruker 270-MHz FT NMR spectrometer was used (tetramethylsilane as internal standard). Microanalyses (C, H, N) were obtained using a Perkin–Elmer 240C elemental analyser. The diamagnetic behaviour of the samples was established using a PAR 155 vibrating-sample magnetometer fitted with a Walker Scientific magnet. Electrochemical measurements were performed under nitrogen on a PAR 370-4 electrochemistry system, as reported earlier [5]. All the reported potentials are uncorrected for junction contributions. Solution ($\sim 10^{-3}$) electrical conductivities were measured with the Philips PR 9500 bridge. The following Hammett σ values [7] for *para*-substituents were used: H, 0.00; Me, −0.17; OMe, −0.27; Cl, +0.23; CO_2Et, +0.45; NO_2, +0.78.

Computation of chemical shift due to PPh_3 *ring currents*

The crystallographic data of **1** (X = Me) have been used [1b]. The computed parameters are d and θ. These are defined in **3**: d = distance of the concerned



3

proton from the centroid (G) of each PPh_3 phenyl ring and θ = angle between d vector and the normal to the plane of the phenyl ring at G. From these distances (d) and angle (θ) parameters, the cylindrical coordinates [8] ρ and z of the concerned proton were calculated in units of the radius of the benzene hexagon [9] as follows:

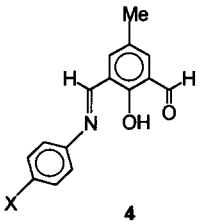
$$\rho = d\cos(90-\theta)/1.39 \quad z = d\sin(90-\theta)/1.39.$$

The ρ and z values were then used to compute the shift with the help of available isoshielding plots [9]. The net shift was estimated by summing up individual contributions.

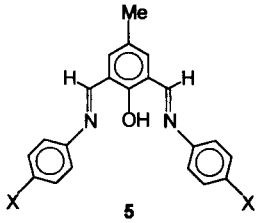
RESULTS AND DISCUSSION

Synthesis and characterization

Complexes **1** and **2** will be abbreviated as [Ru(η^2-*p*-XC_6H_4L)$(PPh_3)_2$(CO)Cl] and [Ru(η^1-*p*-XC_6H_4L)$(PPh_3)_2$(CO)(η^2-*p*-ZC_6H_4COO)], respectively. The [Ru(η^2-*p*-XC_6H_4L)$(PPh_3)_2$(CO)Cl] complexes were synthesized in excellent yields by the stoichiometric reaction of the mono-Schiff bases **4** and $Ru(PPh_3)_3Cl_2$ in boiling ethanol [eq. (1)]. The Schiff bases **4** were



4



5

obtained by reacting 4-methyl-2,6-diformylphenol with the appropriate amine in ethanol. The reaction of eq. (1) affords **1** when

$$Ru(PPh_3)_3Cl_2 + \mathbf{4} \rightarrow Ru(\eta^2\text{-}p\text{-}XC_6H_4L)(PPh_3)_2(CO)Cl + HCl + PPh_3 \quad (1)$$

1

$$\mathbf{1} + Na\text{-}p\text{-}ZC_6H_4COO \rightarrow [Ru(\eta^1\text{-}p\text{-}XC_6H_4L)(PPh_3)_2(CO)(\eta^2\text{-}p\text{-}ZC_6H_4COO)] + NaCl \quad (2)$$

2

the di-Schiff base **5** was used in place of **4**. This proceeds *via* hydrolysis of **5** by the water present in the solvent.

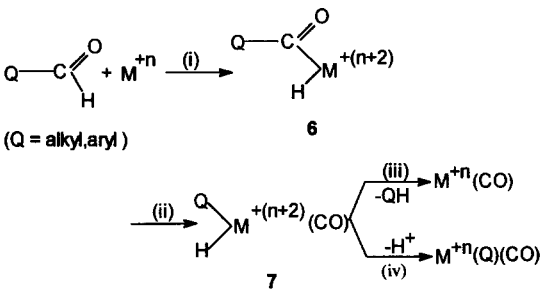
The reaction of the complexes **1** with the aqueous substituted sodium benzoates in dichloromethane–acetone mixture at room temperature afforded the $[Ru(\eta^1\text{-}p\text{-}XC_6H_4L)(PPh_3)_2(CO)(\eta^2\text{-}p\text{-}ZC_6H_4COO)]$ (Z = Me and Cl) complexes in nearly quantitative yields [eq. (2)]. The transformation causes a complete colour change from dark violet to yellow.

The complexes synthesized in this work are listed in Table 1. Complexes **1** and **2** are violet and yellow crystalline solids, respectively.

All the complexes are diamagnetic and non-electrolytic in organic polar solvents. They are soluble in dichloromethane, chloroform, benzene and acetone.

Formation path

Ruthenium [10] and rhodium [11] promoted decarbonylation reaction of aldehydes generally proceeds by the following steps [(i), (ii) and (iii)] [12]. However, in this reaction step (iii) does not occur. The inherently unstable Ru^{IV} carbonyls [13] with two PPh_3 ligands



(Q = alkyl,aryl)

6

7

easily eliminate the hydride from **7** as H^+ and are reduced to stable Ru^{II} carbonyl complexes [14], incorporating the four membered C,O-chelate ring (**1**). Step IV leading to the final product is a complete novelty for decarbonylative metallation reactions. The eliminated proton from **7** is then unsymmetrically bridged by the imine nitrogen and the phenolate to form the zwitter-ionic iminium-phenolato function.

Table 1. UV–vis spectral data and cyclic voltammetric reduction potentials at 298 K

Compound	UV–vis data[a] λ_{max}, nm(ε^b, M^{-1} cm^{-1})			Ru^{III}–Ru^{II} $E^c_{1/2}$, V (ΔE_p, mV)
1 (X = OMe)	525(4660),	405(11,000),	330[s](6620)	0.64(150)
1 (X = Cl)	545(4800),	410(13,090),	330[s](9360)	0.71(160)
1 (X = CO_2Et)	560(4160),	420(12,080),	310[s](9680)	0.75(140)
1 (X = NO_2)	580(3090),	430(10,940),	350[s](9330)	0.78(160)
2 (X = H, Z = Me)	400(5760),	330(15,936)		0.60(140)
2 (X = H, Z = Cl)	400(2750),	330(12,583)		0.62(150)
2 (X = Me, Z = Me)	400(3301),	330(16,505)		0.62(140)
2 (X = Me, Z = Cl)	400(2550),	330(11,600)		0.63(150)

[a] In CH_2Cl_2.

[b] Extinction coefficient.

[c] Conditions: solvent, dichloromethane; supporting electrolyte, TEAP (0.1 M); working electrode, platinum; reference electrode, SCE; solute concentration, $\sim 10^{-3}$ M; $E_{1/2} = 0.5(E_{pa} + E_{pc})$ at scan rate 50 mV s^{-1}, where E_{pa} and E_{pc} are anodic and cathodic peak potentials respectively; $\Delta E_p = E_{pa} - E_{pc}$.

In the absence of the imine function the reaction does not occur implying the formation of the iminium-phenolato motif makes the reaction feasible. No considerable effect of the substituent (X) is observed in the yield and the time of the reaction.

UV–vis spectra

The four-membered chelate chromophore in **1** displays characteristic spectral features in the visible region. Three allowed bands are observed in the range 300–700 nm (Table 1, Fig. 1). The band around 550 nm is obviously due to the metal-to-ligand charge-transfer (MLCT). The value of the λ_{max} of this band increases (red-shifted) with increasing order of electronegativity of X, i.e. $\lambda_{max}(NO_2) > \lambda_{max}(CO_2Et) > \lambda_{max}(Cl) > \lambda_{max}(H) > \lambda_{max}(Me) > \lambda_{max}(OMe)$, and correlates linearly with the Hammett constant (σ) of the X substituent [6]. This significant and systematic effect of p-XC_6H_4 substituent strongly suggests that the acceptor antibonding orbital has significant iminium character.

In this region the dramatic change of the spectral feature is noted when the hapticity of the p-XC_6H_4L ligand changes from η^2 to η^1 in the [Ru(η^1-p-XC_6H_4L)(PPh_3)$_2$(CO)(η^2-p-ZC_6H_4COO)] complexes. These benzoato complexes display two bands near 400 and 330 nm in dichloromethane solution (Fig. 1). The latter band is more intense than the former. The maxima of these bands are not shifted either varying the X or the Z substituents.

IR spectra

In the [Ru(η^2-p-XC_6H_4L)(PPh_3)$_2$(CO)Cl] complex the Ru—Cl stretching vibration occurs near 340 cm^{-1} with medium intensity. In [Ru(η^1-p-XC_6H_4L)(PPh_3)$_2$(CO)(η^2-p-ZC_6H_4COO)] the asymmetric and symmetric stretching vibrations of the carboxyl function appear as distinct bands of medium intensity in the region 1450–1530 cm^{-1}. The relatively low separation between the two stretching modes is consistent with the presence of chelated carboxyl function [15]. The C≡O stretching vibration in these complexes occurs in the region 1910–1920 cm^{-1}.

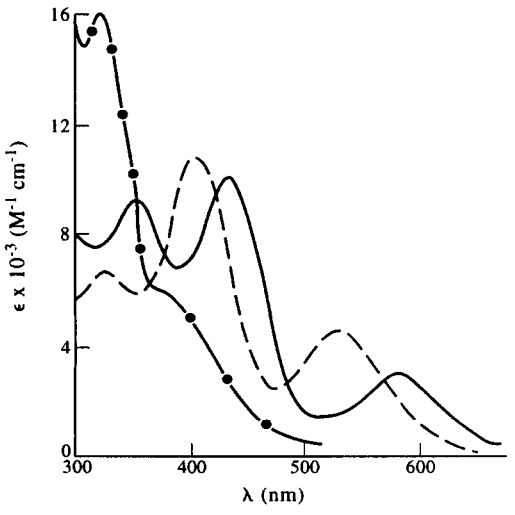


Fig. 1. Electronic spectra of [Ru(η^2-p-$O_2NC_6H_4L$)(PPh_3)$_2$(CO)Cl](——), [Ru(η^2-p-$MeOC_6H_4L$)(PPh_3)$_2$(CO)Cl] (– – –) and [Ru(η^1-PhL)(PPh_3)$_2$(CO)(η^2-p-MeC_6H_4COO)] (–·–·–) in dichloromethane.

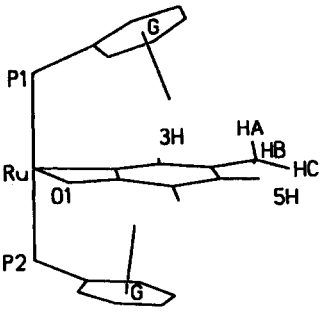
^{1}H *NMR spectra*

Free ligands. The 3-H (*ortho* to —CHO) and the 5-H protons in **4** (X = Cl) resonate as sharp singlets at 7.85 ppm and 7.51 ppm (Table 2).

The 4-Me and the aldimine (—CH=N—) signals appear at ~2.40 and ~8.7 ppm, respectively. The phenolic OH signal arises as a relatively sharp peak at ~13.7 ppm.

Complexes **1**. In **1** the —CHO (in **4**) or —CH=N— (in **5**) function *ortho* to the 3-H in free ligands is replaced by the ruthenium centre, which is bonded to PPh_3 ligands. C2 is potentially a carbanionic centre in these complexes. Due to the shielding effects of the C2 centre and the ring currents of the PPh_3 phenyls [1,16], the chemical shifts of the metallated ring protons are significantly low (Table 2). The signal at ~5.9 is assigned to 3-H which lies *ortho* to C2. The 5-H singlet appears at ~6.06 ppm. The azomethine function lying *ortho* to 5-H is attached to the p-XC_6H_4 substituent. This substituent has a small but significant effect on the 5-H resonance. The resonance shifts to lower field as the X substituent becomes more electron-withdrawing (Table 2). The chemical shift (~1.7 ppm) of the 4-Me signal is also considerably low. The effect of the PPh_3 ring currents to this group and the 3-H and 5-H proton signals may be interpreted by the following observations on the [Ru(η^2-p-MeC_6H_4L)(PPh_3)$_2$(CO)Cl] structure [1b].

In [Ru(η^2-p-MeC_6H_4L)(PPh_3)$_2$(CO)Cl] two phenyl rings of the PPh_3 ligands orient nearly parallel to the metallated benzene ring (**8**). The distances of 3-H, 5-



8

Table 2. ^{1}H NMR data in $CDCl_3$ [a]

Compound	3-H[s]	5-H[s]	4-Me[s]	δ ppm (J, Hz) =N$^+$H/OH	—CH=N$^+$/CH=N—	Others
4 (X = Cl)	7.85	7.51	2.40	13.81[rs]	8.65	Ar-H: 7.25(8.1)[d], 7.41(8.1)[d]; —CH=O, 10.55[s]
5 (X = Cl)	7.27	7.27	2.40	13.65[rs]	8.82	Ar-H: 7.22(8.1)[d], 7.39(8.2)[d]
1 (X = OMe)	5.88	6.02	1.69	13.10[br]	7.54	Ar-H: 6.97(7.5)[d], 7.24(7.6)[d]; MeO, 3.87[s]
1 (X = Cl)	5.89	6.05	1.69	13.20[br]	7.59	Ar-H: 6.99(8.5)[d], 7.40(8.6)[d]
1 (X = CO_2Et)	5.90	6.07	1.69	13.25[br]	7.26	Ar-H: 7.08(8.6)[d]m 8.10(8.4)[d]; —CO_2—CH_2—Me, 4.42(7.0)[q], —CO_2—CH_2—Me, 1.44(7.2)[t]
1 (X = NO_2)	5.93	6.10	1.70	13.28[br]	7.26	Ar-H: 7.13(8.9)[d], 8.30(8.8)[d]
2 (X = Me, Z = Me)	6.22	—	2.02	12.65[rs]	8.08	Me, 2.38[s] and 2.17[s]
2 (X = Me, Z = Cl)	6.23	—	2.04	12.75[rs]	8.08	Me, 2.39[s]

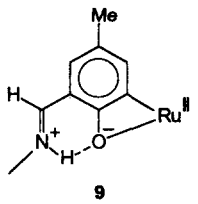
[a] TMS internal standard, PPh_3 signals at 7.23 and 7.66 ppm. Abbreviations: s = singlet; rs = relatively sharp singlet; br = broad; d = doublet; t = triplet; q = quartet; in **2**, aromatic signals (Ar—H) are non-resolvable.

H and 4-Me protons from the centroids (*G*) of the two rings and the angles at *G* with distance vectors show that these protons lie in the shielding region of the rings. Using these distance and angle parameters and the isoshielding ρ-*z* plots [9] the estimated upfield shielding of these protons are: 3-H, 1.00; 5-H, 0.75; 4-Me, 0.50 ppm.

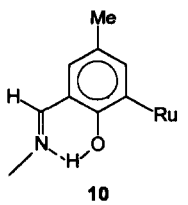
In the carboxylates rotation of the RL (here, R = *p*-XC_6H_4) ligand around the Ru—C axis is not restricted and in solution the effective shielding due to the PPh_3 ring currents is low. The 5-H signal merges with the other aromatic signals and the 3-H and 4-Me protons appear at ~6.2 ppm and 2.0 ppm respectively (Table 2).

Intramolecular $N^+H\cdots O^-$ *and* $OH\cdots N$ *hydrogen bonding*

The heteronuclear asymmetric $NH\cdots O$ hydrogen bonding plays an important role in the amide and peptide chemistry [17]. The reported $OH\cdots N$ interaction is rare [18]. However, both are important in enzyme catalytic phenomena [19]. The $N\cdots O$ interaction in the chloro complexes is illustrated in **9** in which the H atom is unsymmetrically bridged. In the IR spectra the N^+—H vibration is observed as a relatively broad band in the region 3400–3450 cm^{-1} (Table 1), indicating the presence of weak hydrogen bonding [20]. In ^{1}H NMR the N^+—H proton displays characteristically broad band (width at half height ~0.5 ppm) at ~12 ppm (Table 2).



9



10

Transformation of the complexes **1** to **2** leads to a tautomeric change of the hydrogen-bonded iminium-phenolato function (**9**) to the asymmetrically hydrogen-bonded imine-phenol function (**10**). In IR and ^{1}H NMR spectra this is clearly observable. In contrast to the presence of the N^+—H vibration in **9**, **10** displays a very broad feature in the region 3200–3600 cm^{-1} as observed in the case of free ligands (**4** and **5**). Instead of having any nitrogen quadrupole broadened N^+—H signal, **10** shows a relatively sharp O—H signal (width at half height ~0.1 ppm) at 12.6 ppm in the ^{1}H NMR spectra. The feature of this OH signal compares very well with the O—H signal in free ligands.

The intrinsic difference of the ^{1}H NMR signal of the aldimine proton in **1** and **2** is also consistent with the two forms of interactions. The aldimine proton of the —CH=N$^+$ function is expected to appear at higher field [21]. In **9** it appears at ~7.4 ppm, but in **10** it occurs at ~8.1 ppm. As expected [20a,22], the C=N stretching frequency is higher in **9** (~1630 cm^{-1}) than that (~1590 cm^{-1}) in **10**.

X-ray structure determination of [Ru(η^2-*p*-MeC_6H_4L)$(PPh_3)_2$(CO)Cl] [1b] and [Ru(η^1-*p*-MeC_6H_4L)$(PPh_3)_2$(CO)(η^2-$MeCO_2$)] [2], in which bridged H atoms have been located directly by difference Fourier maps, provide us the distance and angle parameters of $N^+H\cdots O^-$ and $OH\cdots N$ units, respectively [$N^+H\cdots O^-$: $N\cdots O$, 2.665(12) Å; N—H, 0.99(6) Å; $H\cdots O$, 1.75(5) Å; N—$H\cdots O$, 144(1)° and for $OH\cdots N$: $O\cdots N$, 2.592(10) Å; O—H, 1.14(3) Å; $H\cdots N$, 1.52(3) Å and O—$H\cdots N$, 156(1)°]. It shows that the O—$H\cdots N$ interaction in the tautometer **10** is stronger and the O—$H\cdots N$ angle is more close to 180°. However, the $N^+H\cdots O$ bridge (in **9**) is more unsymmetrical.

Conformational reorganization

The CO molecule in **1** lies *trans* to the phenolate, but in **2** it is positioned *cis* to that. In the transformation

1 → **2** the coordinated phenolate and the chloride are displaced by the benzoato oxygens. To avoid strong repulsive interaction [2] between the phenolic oxygen and one of the benzoato oxygens, the monodentate RL ligand rotates ~180° around the Ru—C axis resulting in the orientation as in **2**.

These two distinct orientations of the RL ligand having different modes of binding with the ruthenium centre incorporate the distinctive N···O interaction (**9** and **10**). However, these are easily interconvertible. The ruthenium centre with RL, CO and PPh_3 ligands has strong affinity towards

$$\mathbf{2} \underset{R'COO^-}{\overset{Cl^-}{\rightleftharpoons}} \mathbf{1} \qquad (3)$$

the chloride as well as the carboxylate, eq. (3). Upon treating with excess chloride **2** transforms to **1** and in the presence of HCl the carboxylate displacement is very fast and quantitative.

Interestingly it is noted that the tautomerization of the —CH=N$^+$H···O$^-$ to the —CH=N···HO$^-$ with a concomitant geometrical isomerization is the crucial occurrence in the photochemically induced cycle in the chromophore of the visual and bacterial rhodopsins [20a].

Metal redox and spectroelectrochemical correlation

In dichloromethane solution the [Ru(η^2-*p*-XC_6H_4L)$(PPh_3)_2$(CO)Cl] and the [Ru(η^1-*p*-XC_6H_4L)$(PPh_3)_2$(CO)(η^2-*p*-ZC_6H_4COO)] complexes display a characteristic quasi-reversible cyclic voltammetric response corresponding to the Ru^{III}/Ru^{II} couple, eqs (4) and (5). Current height data suggests that

$$\mathbf{1}^+ + e \rightarrow \mathbf{1} \qquad (4)$$

$$\mathbf{2}^+ + e \rightarrow \mathbf{2} \qquad (5)$$

the process involves the transfer of one electron. The high instability of the oxidized species did not permit their isolation.

In ^{1}H NMR it is observed that the X substituent has significant electronic influence on the metallated ring. It also has a measurable effect on the $E_{1/2}$ values (Table 1; Fig. 2). The reduction potential ($E_{1/2}$) of the couple, eq. (4), increases as the electron-withdrawing character of X increases [6]. A linear correlation of the $E_{1/2}$ values with the Hammett constants (σ) of X was found. No significant effect of the Z substituent on the couple of eq. (5) was noted. The $E_{1/2}$ values of the benzoates are lower than those of the chloro complexes.

The ease of charge transfer (MLCT) from the ruthenium(II) centre to the acceptor antibonding orbital of the metallated ring is a measure of the stability of the ruthenium(II) valence in the C,O-chelate. With the higher electronegative substituent (X), the acceptor orbital is more stabilized and the energy of the MLCT band becomes lower. This charge delocalization stabilizes the filled t_2-shell of ruthenium(II) in higher extent and it is reflected in the $E_{1/2}$ values of the Ru^{III}/Ru^{II} couple. The lower the energy of the band maxima $t_2 \rightarrow \pi^*$ the higher is the $E_{1/2}$ value and these two parameters have a linear spectroelectrochemical correlation [23].

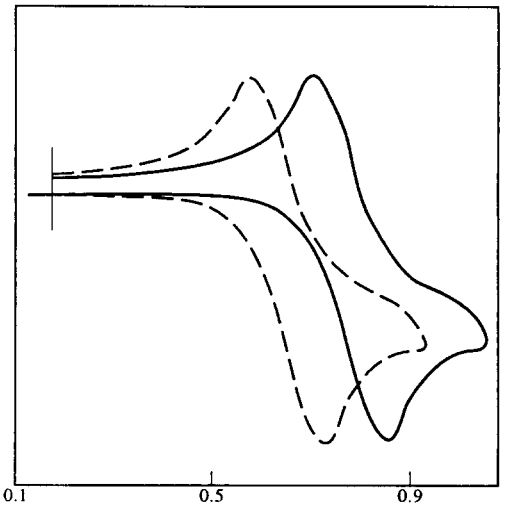


Fig. 2. Cyclic voltammograms of ~10^{-3} mol dm^{-3} solutions in dichloromethane for [Ru(η^2-*p*-$MeOC_6H_4L$)$(PPh_3)_2$(CO)Cl] (– – –) and [Ru(η^2-*p*-$O_2NC_6H_4L$)$(PPh_3)_2$(CO)Cl] (——).

In this work, a new family of *ortho*-ruthenated phenolates has been synthesized. The inherently unstable four-membered C,O-chelate ring of this type is stabilized in these complexes in the presence of two PPh_3, CO, Cl as coligands and a crucial —CH=NR (R = *p*-XC_6H_4) function (*ortho* to OH group) which is hydrogen-bonded (NH$^+$···O$^-$) to the coordinated phenolato oxygen. The *p*-XC_6H_4 substituent has indirect but considerable electronic influence on the chelate chromophore and the metal centre. The Hammett constants of X correlate linearly with the energy of the MLCT band and the $E_{1/2}$ values of the Ru^{III}–Ru^{II} couple. Expectedly the spectroelectrochemcial correlation is linear.

The new arylbenzoato complexes generated from these halo precursors incorporate the uncoordinated phenolic group and the substituents of imine and benzoato functions have no significant effect on the metal centre. In these benzoates the OH···N hydrogen bonding a tautometer of NH$^+$···O$^-$ constitutes a rare example.

Acknowledgements—I am thankful to Professor A. Chakravorty for providing facilities and useful suggestions. Financial support from the DST, New Dehli, is acknowledged.

REFERENCES

1. (a) Ghosh, P., Bag, N. and Charavorty, A.,

Organometallics, 1996, **15,** 3042; (b) Bag, N., Choudhoury, S. B., Pramanik, A., Lahiri, G. K. and Chakravorty, A., *Inorg. Chem.* 1990, **29,** 5013; (c) Bag, N., Choudhoury, S. B., Lahiri, G. K. and Chakravorty, A., *J. Chem. Soc., Chem. Commun.* 1990, 1626.

2. Ghosh, P., Pramanik, A. and Chakravorty, A., *Organometallics*, 1996, **15,** 4147.
3. Stephenson, T. A. and Wilkinson, G., *J. Inorg. Nucl. Chem.* 1966, **28,** 945.
4. (a) Ullmann, F. and Brittner, K., *Chem. Ber.* 1909, **42,** 2539; (b) Cagne, R. R., Spiro, C. L., Smith, T. J., Hamann, C. A., Thies, T. J. and Shiemke, A. K., *J. Am. Chem. Soc.* 1981, **103,** 4073.
5. Ghosh, P., Pramanik, A., Bag, N., Lahiri, G. K. and Chakravorty, A., *J. Organomet. Chem.* 1993, **454,** 237.
6. Complexes **1** (X = Me and H) were prepared by reported procedures [1]. UV–vis spectral data: λ_{max}, X = H; 535 (5650), 405 (13,900), 325^s (10,000) and λ_{max}, X = Me; 530 (4560), 405 (11,430), 320^s (7700). $E_{1/2}$, V(ΔE_p, mV) for the Ru^{III}/Ru^{II} couple: X = H; 0.68 (150) and X = Me; 0.65 (150).
7. Hammett, L. P., *Physical Organic Chemistry*, 2nd edn. McGraw-Hill, New York, 1970.
8. Margenau, H. and Murphy, G. M., *The Mathematics of Physics and Chemistry*. D. Van Nostrand Company, Inc., Princeton, New Jersey, 1956.
9. Johnson Jr, C. E. and Bovey, F. A., *J. Chem. Phys.* 1958, **29,** 1012.
10. (a) Prince, R. H. and Raspin, K. A., *J. Chem. Soc. A*, 1969, 612; (b) Chaudret. B. N., Cole-Hamilton, D. J., Nohr, R. S. and Wilkinson, G., *J. Chem. Soc, Dalton Trans.* 1977, 1549; (c) Domazetis, G., Tarpey, B., Dolphin, D. and James, B. R., *J. Chem. Soc., Chem. Commun.* 1980, 939.
11. (a) Suggo, J. W., *J. Am. Chem. Soc.* 1978, **100,** 640; (b) Milstein, D., *Acc. Chem. Res.* 1984, **17,** 221; (c) James, B. R. and Young, C. G., *J. Organomet. Chem.* 1985, **285,** 321; (d) Bianchini, C., Meli, A., Peruzzini, M., Ramirez, J. A., Vacca, A., Vizza, F. and Zanobini, F., *Organometallics*, 1989, **8,** 337; (e) Song, L., Arif, A. M. and Stang, P. J., *Organometallics*, 1990, **9,** 2792.
12. (a) Sahajpal, A., Robinson, S. D., Mazid, M. A., Matevalli, M. and Hursthouse, M. B., *J. Chem. Soc., Dalton Trans.* 1990, 2119; (b) Doughty, D. H. and Pignolet, L. H., *Homogeneous Catalysis with Metal Phosphine Complexes*; ed. L. H. Pignolet. Plenum Press, New York, 1983.
13. (a) Knox, G. R., *Organometallic Compounds of Ruthenium and Osmium*. Chapman and Hall, London, 1985; (b) Bruce, M. I., *Comprehensive Organometallic Chemistry*, ed. G. Wilkinson. Pergamon Press, Oxford, 1982., p. 661.
14. Pearson, R. G., *Chem. Rev.* 1985, **85,** 41.
15. (a) Kavanagh, B., Steed, J. W. and Tocher, D. A., *J. Chem. Soc., Dalton Trans.* 1993, 327; (b) Tocher, D. A., Gould, R. O., Stephenson, T. A., Bennett, M. A., Ennet, J. P., Matheson, T. W., Sawyer, L. and Shah, U. K., *J. Chem. Soc., Dalton Trans.* 1983, 1571; (c) Deacon, G. B. and Phillips, R. J., *Coord. Chem. Rev.* 1980, **33,** 227; (d) Moore, D. S. and Robinson, S. D., *Inorg. Chem.* 1979, **18,** 2307; (e) Robinson, S. D. and Uttley, M. F., *J. Chem. Soc., Dalton Trans.* 1973, 1912.
16. (a) Jia, G., Rheingold, A. L., Haggerty, B. S. and Meek, D. W., *Inorg. Chem.* 1992, **31,** 900; (b) Jia, G., Meek, D. W. and Gallucci, J. C., *Organometallics*, 1990, **9,** 2549.
17. (a) Taylor, R., Kennard, O. and Versichel, W., *J. Am. Chem. Soc.* 1984, **105,** 244; (b) MacDonald, J. C. and Whitesides, G. M., *Chem. Rev.* 1994, **94,** 2383.
18. (a) Camilleri, P., Marby, C. A., Odell, B., Rzepa, H. S., Sheppard, R. N., Stewart, J. J. P. and Williams, D. J., *J. Chem. Soc., Chem. Commun.* 1989, 1722; (b) Hibbert, F. and Emsley, J., *Adv. Phys. Org. Chem.* 1990, **26,** 255.
19. Cleland, W. W. and Kreevoy, M. M., *Science*, 1994, **264,** 1887.
20. (a) Sandorfy, C. and Vocelle, D., *Mol. Phys. Chem. Biol.* 1989, **IV,** 195; (b) Chevalier, P. and Sandorfy, C., *Can. J. Chem.* 1960, **38,** 2524.
21. Sharma, G. M. and Roels, O. A., *J. Org. Chem.* 1973, **38,** 3648.
22. Bohme, H. and Haake, M., *Advances in Organic Chemistry*, ed. H. Bohme and H. G. Viehe; Part 1, Vol. 9. Interscience Publications, New York, 1976, p. 1.
23. (a) Goswami, S., Mukherjee, R. N. and Chakravorty, A., *Inorg. Chem.* 1983, **22,** 2825; (b) Mukherjee, R. N. and Chakravorty, A., *J. Chem. Soc., Dalton Trans.* 1983, 2197.

Pergamon

PII: S0277-5387(96)00401-9

Polyhedron Vol. 16, No. 8, pp. 1351–1355, 1997
Copyright © 1997 Elsevier Science Ltd
Printed in Great Britain. All rights reserved
0277-5387/97 $17.00+0.00

X-ray absorption spectroscopic (XAS) study of nickel bisdithiolenes, $(n\text{-}Bu_4N)_x[Ni(dmbit)_2]$ ($x = 2, 1, 0.29$) and $(n\text{-}Bu_4N)[Ni(dmbbip)_2]$

Dong-Youn Noh,[a]* Masagi Mizuno,[b] Dong-Kuk Kim,[c] Joo-Byong Yoon[c] and Jin-Ho Choy[c]

[a] Department of Chemistry, Seoul Woman's University, Seoul 139-774, Korea

[b] National Institute of Materials and Chemical Research, Tsukuba, Ibaraki 305, Japan

[c] Department of Chemistry, Seoul National University, Seoul 151-742, Korea

(Received 4 June 1996; accepted 6 August 1996)

Abstract—X-ray absorption near-edge structure (XANES) and extended X-ray absorption fine structure (EXAFS) studies on the tetra(*n*-butyl)ammonium salt of $[Ni(dmbit)_2]^{x-}$ ($x = 2, 1$ and 0.29) and $[Ni(dmbbip)_2]^-$ have been performed in order to reveal the structural parameters of the $[NiS_4]^{x-}$ core along with the chemical state. The central nickel ion is confirmed to have coordination number four with square-planar geometry. The [Ni—S] bond distance in $[Ni(dmbit)_2]^-$ (2.154 Å) is identical with that of $[Ni(dmbbip)_2]^-$, but shorter than those of $[Ni(dmbit)_2]^{2-}$ (2.178 Å) and $[Ni(dmbit)_2]^{0.29-}$ (2.165 Å). Copyright © 1997 Elsevier Science Ltd

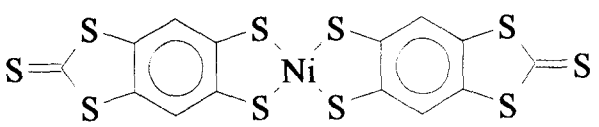
Keywords: X-ray absorption near-edge structure (XANES); extended X-ray absorption fine structure (EXAFS); molecular-based organic conductor; nickel-1,2-dithiolene.

Recently we have studied the synthesis, magnetic and electrical properties of $Ni(dmbit)_2$ and $Ni(dmbbip)_2$ complexes [1–5] (dmbit: 5,6-dithio-benzo[*d*]-1,3-dithiole-2-thione; dmbbip: 1,2-di(isopropylthio) benzene-4,5-dithiole) which have ligands with an expanded π-electron system (Scheme 1): Dmbit and dmbbip ligands can be regarded in the family of bdt (benzene-1,2-dithiolate) with a peripheral isotrithione [$(—S)_2C{=}S$] and isopropylthiol [$—SCH(CH_3)_2$] groups, respectively. Alternatively, the dmbit ligand can be considered as an analogue of the dmit ligand in which the C=C bond is substituted with the benzene ring. The bdt type ligand, however, behaves differently to the ethylenedithiolate type ligands, such as dmit (4,5-dimercapto-1,3-dithiole-2-thione) and mnt (maleonitriledithiolate), because the resonance energy of benzene is much higher than that of the isolated double bond in ethylenedithiolate (Scheme 2). Hence, there is a difference in stability between the dianionic ligands ($dmit^{2-}$ and bdt^{2-}) relative to the dithioketo forms, which are derived by a reversible oxidation of dianionic ligands.

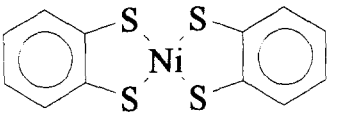
Monoanionic salts of $Ni(dmbit)_2$ and $Ni(dmbbip)_2$, which are insulators with pressed pellet conductivities of 10^{-9} and 10^{-11} S cm^{-1}, respectively, at room temperature, [1] show the antiferromagnetic coupling among nickel ions and the magnetic moments of 1.74 and 1.75 B.M., respectively, corresponding to low-spin d^7 state of nickel(III) [2]. The partially oxidized complex, $[Ni(dmbit)_2]^{0.29-}$, shows a metallic behaviour from 300 to 220 K at which it has the maximum conductivity of 1.35 S cm^{-1}. This is not a single crystal conductivity because attempts to grow single crystals suitable for electrical conductivity measurement were unsuccessful. X-ray crystal structure analysis has not been performed due to the same reason.

Extended X-ray absorption fine structure (EXAFS) spectroscopy using a synchrotron radiation source is a useful method for determining the local environment of a selected atom (e.g. interatomic distance, coordination number), although it is limited to the information with the near-neighbouring atoms. X-ray absorption near-edge structure (XANES) spec-

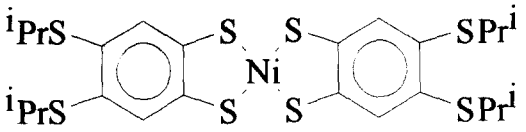
* Author to whom correspondence should be addressed.



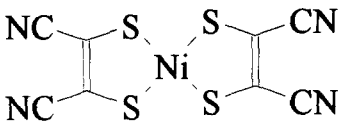
Ni(dmbit)2



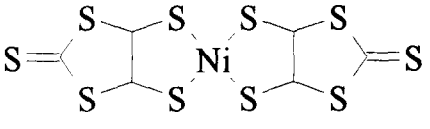
Ni(bdt)2



Ni(dmbbip)2

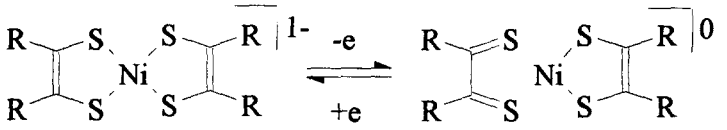


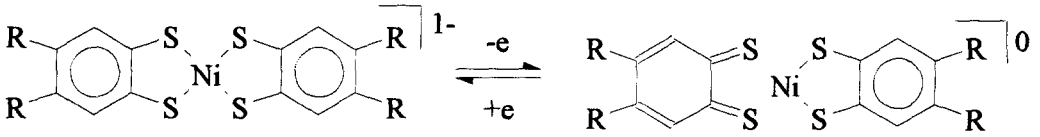
Ni(mnt)2



Ni(dmit)2

Scheme 1.





Scheme 2.

troscopy also gives valuable data on the oxidation state and local geometry of a selected atom. Above all, these techniques are applicable to the powdered samples as in our case [4]. Here we report the results of EXAFS and XANES studies on $[Ni(dmbit)_2]^{2-}$ and its oxidized complexes, $[Ni(dmbit)_2]^{x-}$ ($x = 1$ and 0.29), along with its analogue $[Ni(dmbbip)_2]^{-}$.

EXPERIMENTAL

Sample preparation

$(n\text{-}Bu_4N)_x[Ni(dmbit)_2]$ ($x = 2$, 1 and 0.29) and $(n\text{-}Bu_4N)[Ni(dmbbip)_2]$ complexes were prepared and confirmed as described in the previous paper, [1–2] in which the partial oxidation was performed by chemical method using $(n\text{-}Bu_4N)Br_3$ in CH_3CN.

XAS measurements

XANES and EXAFS experiments have been carried out on the beam-line 10B at the Photon Factory of the National Laboratory for High Energy Physics (2.5 GeV, 260 ~ 360 mA) by using a Si(311) channel-cut monochromator. Data were collected at room temperature in the transmission mode using ionization chambers filled with N_2 and $N_2(75\%) + Ar(25\%)$ gas for the measurements of incident X-ray intensity (I_0) and transmitted (I), respectively. Powder samples were finely ground with Nujol in a mortar and suspended homogeneously onto adhesive tape and the folded appropriately in order to be free from the thickness effect ($\Delta\mu t \cong 1$). Ni metal foil ($\phi = 0.5$ μm) was used as a standard to calibrate the energy of the samples. The inherent background in the data was removed by fitting a polynomial to the pre-edge

region, and extrapolated through the entire spectrum, from which it was subtracted.

Data reduction

The data were normalized to an edge jump of unity for comparing the XANES features directly. The energy positions of the edge features were determined from the positions of the half-width at half-maximum of the second derivatives. The data reduction of raw EXAFS spectra was carried out as described elsewhere [6]. The EXAFS function $\chi(k)$ is given by the equation, $\chi(k) = \{\mu(k) - \mu_0(k)\}/\mu_0(k)$, where k is the photoelectron wave-vector ejected given as $\{8\pi m(E-E_0)\}^{1/2}/h$. E represents the energy of the incident X-rays and E_0 is the threshold energy of a k-shell electron. A curve fitting procedure in the k space for the refinements of structure parameters was applied to the Fourier filtered $k^3\chi(k)_{obs}$ values to minimize the following error-squares sum, $\Sigma\ k^6(\chi(k)_{obs} - \chi(k)_{calc})^2/n$, where n represents the number of data points.

The model function $\chi(k)_{calc}$ was obtained according to the single-electron and single-scattering theory:

$$\chi(k)_{calc} = \Sigma\{n_j/(kr_j^2)\}F_j(\pi,k)\exp(-2\sigma_j^2k^2) \times \exp(-2r_j/\lambda)\sin(2kr_j+\phi_j(k)).$$

Here for the backscattering amplitude $F_j(\pi,k)$, the total scattering phase shift $\phi_j(k)$ and the mean free path of a photoelectron λ were used the values of the FEFF code (version 5.03). The interatomic distance r, the Debye–Waller factor σ_j the coordination number n and E_0 were optimized as variables in the course of the structural analysis.

RESULTS AND DISCUSSION

The Ni K-edge XANES spectra for $(n\text{-}Bu_4N)_x[Ni(dmbit)_2]$ ($x = 2, 1$ and 0.29) and $(n\text{-}Bu_4N)[Ni(dmbbip)_2]$ are shown in Fig. 1, in which the changes of peak position and intensity upon oxidation, $[Ni(dmbit)_2]^{2-} \rightarrow [Ni(dmbit)_2]^{-} \rightarrow [Ni(dmbit)_2]^{0.29-}$, are clearly shown and comparable with $[Ni(dmbbip)_2]^{-}$. The overall shape of spectra is very similar to that of coordination complexes with square-planar local symmetry around central metal, such as metalloporphyrin [7] and M[B(3-isopropylpyrazole-1-yl)$_4$]$_2$ (M = Fe, Co, Ni, Cu and Zn) [8]. Four peaks labelled A, B, C and D are recognized in the near-edge absorption region and the first EXAFS oscillation is followed at higher energy region. The energy positions of these peaks are estimated from their second derivatives and listed in Table 1. Among these, peak A at 8330 eV in the pre-edge region corresponds to the transition of the nickel 1s electron to its empty 3d-orbitals. Their intensities are very small compared with the other peaks, because this transition is principally forbidden by dipole selection rule ($\Delta l = \pm 1$). Peaks C and D correspond to the $1s \rightarrow 4p_\pi$ and $1s \rightarrow 4p_0$ transitions, respectively, and are also characteristics of the transition metal complexes with square-planar local symmetry. In addition, the second peak (B) in the spectra shows the most apparent difference in its intensity as well as the chemical shift among four peaks. This peak is attributed to the transition from the initial state, $|1s^2 3d^n 4p_\pi^0\rangle$, to the final state, $|1s^1 3d^{n+1} 4p_\pi^1 L\rangle$, where l denotes the ligand hole, and a simultaneous shake-down process through the ligand-to-metal charge-transfer (LMCT), which gives the core-hole screening effect in the final state. Therefore, this peak might be well modified by the electronic environment such as the ligand field and the chemical bonding because d-orbitals are most susceptible to the bonding nature of the ligands. If the nickel ion is located in the square-planar local geometry and therefore its electronic configurations of 3d-orbitals could be written as $(xz)^2(yz)^2(z^2)^2(xy)^2(x^2-y^2)^0$ and $(xz)^2(yz)^2(z^2)^2(xy)^1(x^2-y^2)^0$ for $[Ni(dmbit)_2]^{x-}$, where $x = 2$ and 1, respectively, a charge-transfer should occur from 3p-orbitals of ligating sulfur to the lowest empty orbitals of nickel, $(x^2-y^2)^0$ and $(xy)^1$, for $[Ni(dmbit)_2]^{2-}$ and $[Ni(dmbit)_2]^{1-}$, respectively. However, a charge-transfer to the $(xy)^1$-orbital for the compound $[Ni(dmbit)_2]^{1-}$ needs an additional spin-pairing energy, which might result in the lowering of transition probability and, as a consequence, the depression of peak intensity of B. Upon partial oxi-

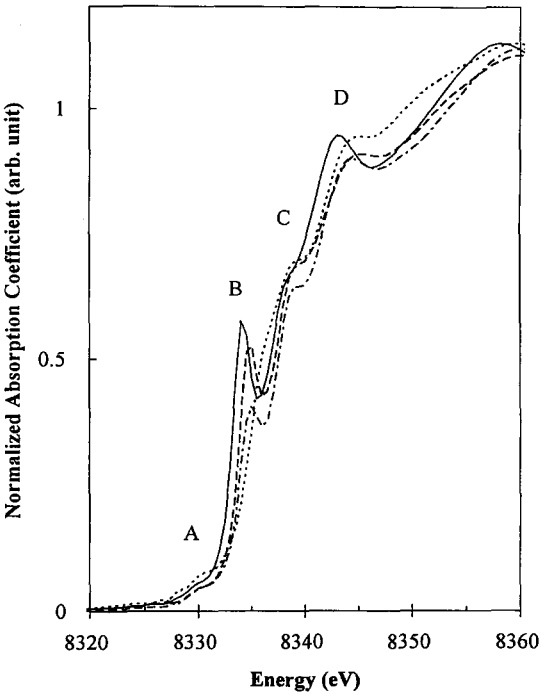


Fig. 1. Ni K-edge absorption spectra of $(n\text{-}Bu_4N)[Ni(dmbbip)_2]$ (dashed line), $(n\text{-}Bu_4N)[Ni(dmbit)_2]$ (one dotted–dashed line), $(n\text{-}Bu_4N)_2[Ni(dmbit)_2]$ (solid line) and $(n\text{-}Bu_4N)_{0.29}[Ni(dmbit)_2]$ (dotted line).

Table 1. The energies (eV) of the XANES transitions

Complex	Transition Peaks A	B	C	D
$(n\text{-}Bu_4N)_1[Ni(dmbbip)_2]$	8330	8335.0	8339.0	8344.0
$(n\text{-}Bu_4N)_2[Ni(dmbit)_2]$	8330	8334.5	8338.5	8343.2
$(n\text{-}Bu_4N)_1[Ni(dmbit)_2]$	8330	8335.3	8339.0	8344.0
$(n\text{-}Bu_4N)_{0.29}[Ni(dmbit)_2]$	8330	8336.2	8339.0	8344.0

dation of the monoanionic complex, only peak B related to the LMCT process shifts to higher energy by 0.9 eV, while peaks C and D remain unchanged in energy. These three peaks, however, shift by 0.5–0.8 eV due to the oxidation of the dianionic complex (Table 1). XANES transition energies of the $[Ni(dmbbip)_2]^-$ complex are almost the same as those of $[Ni(dmbit)_2]^-$, indicating that the electronic state of $[NiS_4]^{1-}$ core is nearly unaffected by the peripheral groups on the ligand and therefore could be considered with as almost identical electronic state in both monoanionic complexes [9].

The k^3-weighted EXAFS oscillations are shown in Fig. 2 and the magnitudes of Fourier transform of $k^3\chi(k)$ are in Fig. 3, where the first peak corresponds to the shell of the nearest-neighbour (ligating sulfur) around nickel. In order to compare the change of the [Ni—S] bond distance upon oxidation of $[Ni(dmbit)_2]^{2-}$, EXAFS curve fits were performed in the Fourier-filtered oscillation of the [Ni—S] shell (Fig. 3), using the curved-wave XAFS simulation program (FEFF). The fitting results are summarized in Table 2. Nickel ions in these complexes have the coordination number 4 within a typical error range, indicating the square-planar local symmetry. $[Ni(dmbit)_2]^{1-}$ exhibits a shorter [Ni—S] bond distance than that for $[Ni(dmit)_2]^{2-}$, as can be seen in the X-ray crystallographic analysis of nickel dithiolene complexes such as $[Ni(dmbit)_2]^{x-}$, where [Ni—S] bond distances are 2.156 ($x = 1$) [10] and 2.216 Å ($x = 2$) [11] and $[Ni(mnt)_2]^{x-}$, 2.146 ($x = 1$) [12] and 2.166 Å ($x = 2$) [13]. As for $[Ni(dmbbip)_2]^{1-}$, it is also identical with those of $[Ni(dmbit)_2]^{1-}$ (2.154 Å), and $[Ni(bdt)_2]^{1-}$ (2.151 Å) [14], which can be easily understood from the fact that three ligands (dmbit, dmbbip

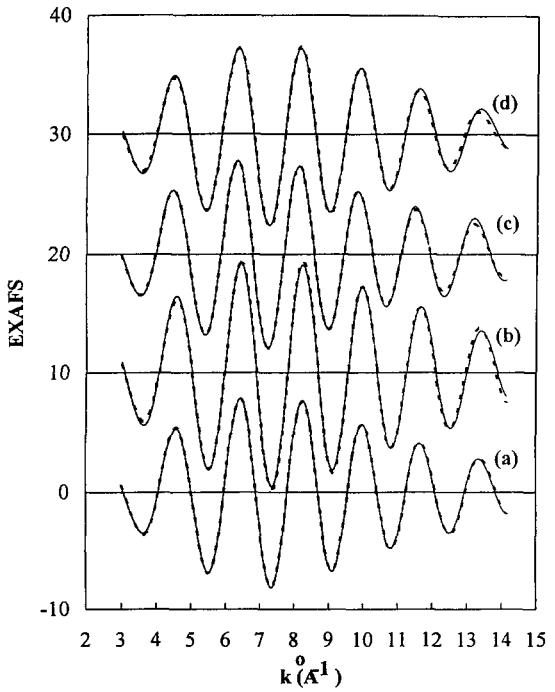


Fig. 2. Fourier transformed k^3-weighted Ni K-edge EXAFS data of (a) $(n\text{-}Bu_4N)[Ni(dmbbip)_2]$, (b) $(n\text{-}Bu_4N)[Ni(dmbit)_2]$, (c) $(n\text{-}Bu_4N)_2[Ni(dmbit)_2]$ and (d) $(n\text{-}Bu_4N)_{0.29}[Ni(dmbit)_2]$. The solid lines show the k^3-weighted raw EXAFS data and the dotted lines the results of the least-squares fit.

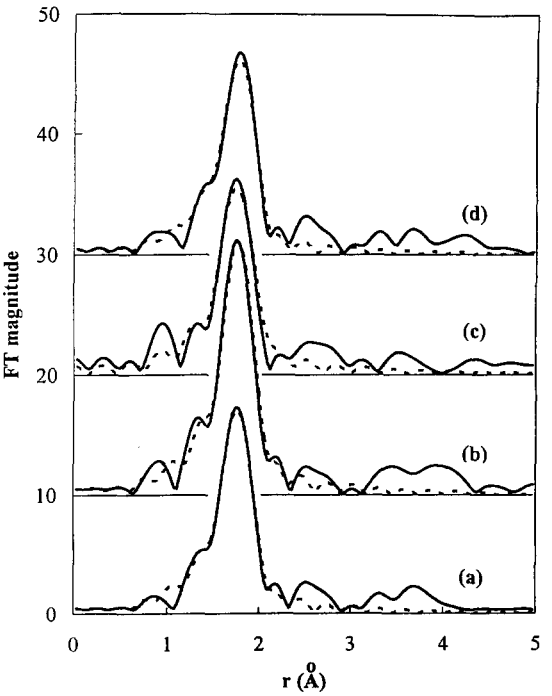


Fig. 3. Fourier filtered k^3-weighted Ni K-edge EXAFS data in the R range of 0.8–2.3 Å for (a) $(n\text{-}Bu_4N)[Ni(dmbbip)_2]$, (b) $(n\text{-}Bu_4N)[Ni(dmbit)_2]$, (c) $(n\text{-}Bu_4N)_2[Ni(dmbit)_2]$ and (d) $(n\text{-}Bu_4N)_{0.29}[Ni(dmbit)_2]$. The solid lines show the k^3-weighted EXAFS data and the dotted lines the results of the least-squares fit.

Table 2. Curve fitting results of Fourier-filtered EXAFS spectra for the first shell[a]

Complex	R(Å)[b]	C.N.[c]	σ^2(Å^2)[d]	ΔE_0(eV)
$(n\text{-}Bu_4N)_1[Ni(dmbbip)_2]$	2.154	4.1	3.53	−4.7
$(n\text{-}Bu_4N)_2[Ni(dmbit)_2]$	2.178	4.1	4.11	−5.3
$(n\text{-}Bu_4N)_1[Ni(dmbit)_2]$	2.154	4.2	2.82	−4.0
$(n\text{-}Bu_4N)_{0.29}[Ni(dmbit)_2]$	2.165	3.5	3.11	−6.3

[a] Typical accuracies are ±0.02 Å for R and ±25% for coordination number and Debye–Waller factor. A curve fitting procedure in the k space for the refinements of structure parameters was applied to the Fourier filtered $k^3\,\chi(k)_{obsd.}$ values over the k range 3.0–14.2 Å^{-1} of dk = 1.0 Å^{-1} and the R range 1.4–2.3 Å of dr = 1.0 Å.

[b] R is the [Ni—S] bond distance.

[c] Coordination number (C.N.) corresponds to the values when amplitude reduction factor is fixed to unit.

[d] Debye–Waller factor ($\times 10^{-3}$).

and bdt) belong to benzene-1,2-dithiolate group with the same $[NiS_4]^{1-}$ core.

Consequently, it is clear that the redox process is mainly centred on the $[NiS_4]^{x-}$ core during the oxidation of $[Ni(dmbit)_2]^{2-}$. The [Ni—S] bond distance of the partially oxidized complex (2.165 Å), however, is in between those of mono- and dianionic Ni-dmbit complexes. The metal–sulfur bond distance of conductive nickel-dithiolene is not easy to predict, but it could be assumed with these data that nickel(IV) was not generated by the partial oxidation; if so, the [Ni—S] distance should become shorter after partial oxidation, because the radius of the nickel(IV) ion is shorter than nickel(III) [15]. Therefore, the dmbit ligand can be thought to be oxidized in this step so that conducting electrons are delocalized all over the metal complex, which may cause the [Ni—S] bond distance to be longer than that of monocationic complex. Upon oxidation of $[Ni(dmbit)_2]^{2-}$, the Debye–Waller factor (σ^2), which contains information on the disorder of the interatomic distances, decreases by 31% associated with the decrease of the [Ni—S] bond distance and an increase up to 110% was observed in the partially oxidized complex, as can be expected in [Ni—S] bond distance variation.

CONCLUSIONS

The central nickel ion within the $[NiS_4]^{x-}$ core of the $[Ni(dmbit)_2]^{x-}$ and $[Ni(dmbbip)_2]^{1-}$ complexes is confirmed to have coordination number four with square-planar geometry. The LMCT process and electronic transition in the nickel ion were affected by the oxidation of $[Ni(dmbit)_2]^{2-}$ to $[Ni(dmbit)_2]^{1-}$ accompanying the [Ni—S] bond distance decrease (*ca* 0.024 Å). It seems that the oxidation process is mainly centred at the $[NiS_4]^{2-}$ core and therefore an insulator $[Ni(dmbit)_2]^{1-}$ was produced. Upon partial oxidation, however, only the LMCT process was affected (peak B) and the [Ni—S] bond distance became longer (*ca* 0.013 Å), resulting in the conductive $[Ni(dmbit)_2]^{0.29-}$ complex.

Acknowledgements—We thank the Photon Factory, National Laboratory for High Energy Physics (92G196). D.-Y. Noh would like to thank the Korean Science and Engineering Foundation (KOSEF) for support.

REFERENCES

1. Noh, D.-Y., Mizuno, M. and Choy, J.-H., *Synth. Metals*, 1993, **55–57**, 1705.
2. Noh, D.-Y., Mizuno, M. and Choy, J.-H., *Inorg. Chim. Acta*, 1994, **216**, 147.
3. Noh, D.-Y. and Choy, J.-H., *Synth. Metals*, 1995, **70**, 1059.
4. Noh, D.-Y., Mizuno, M., Hur, N. H., Kim, D.-K. and Choy, J.-H., *Synth. Metals*, 1995, **70**, 1057.
5. Noh, D.-Y., Kang, M.-J., Lee, H.-J., Kim, J.-H. and Choy, J.-H., *Bull. Korean Chem. Soc.* 1996, **17**, 46.
6. Teo, B. K., *EXAFS: Basic Principles and Data Analysis*. Springer-Verlag, Berlin, 1986.
7. Cartier, C., Momenteau, M., Dartyge, E., Fontaine, A., Tourillon, G., Michalowicz, A. and Verdaguer, M., *J. Chem. Soc., Dalton Trans.* 1992, 609.
8. Hannay, C., Thissen, R., Briois, V., Hubin-Franskin, M., Grandjean, F., Long, G. J. and Trofimenko, S., *Inorg. Chem.* 1994, **33**, 5983.
9. Schidt, N. C., Sommer-Larsen, P., Bjørnholm, T., Nielsen, M. F., Larsen, J. and Bechgaard, K., *Inorg. Chem.* 1995, **34**, 3688.
10. Lindquist, O., Andersen, L., Sieler, J., Steimecke, G. and Hoyer, E., *Acta Chem. Scand. Ser. A.*, 1982, **855**, A36(10).
11. Lindquist, O., Sjölin, L., Sieler, J., Steimecke, G. and Hoyer, E., *Acta Chem. Scand. Ser. A.*, 1979, **445**, A33(6).
12. Fritchie, J. E., *Acta Cryst.* 1966, **107**, 20.
13. Eisenberg, R. and Ibers, J. A., *Inorg. Chem.* 1965, **4**, 605.
14. Mahadevan, C., Seshasayee, M., Kuppusamy, P. and Manoharan, P. T., *J. Crystallogr. Spectros. Res.* 1985, **15**, 305.
15. Higgins, S. J., Levason, W., Feiters, M. and Steel, A. T., *J. Chem. Soc., Dalton Trans.* 1986, 317.

Pergamon

PII: S0277-5387(96)00399-3

Polyhedron Vol. 16, No. 8, pp. 1357–1360, 1997
Copyright © 1997 Elsevier Science Ltd
Printed in Great Britain. All rights reserved
0277-5387/97 $17.00+0.00

Synthesis and crystal structure of a heteronuclear copper and yttrium complex with alanine: $[CuY(Ala)_4(H_2O)_5](ClO_4)_5 \cdot 3H_2O$

Feng Gao,[a] Rui-Yao Wang,[a] Tian-Zhu Jin,[a]* Guang-Xian Xu,[a] Zhong-Yuan Zhou[b] and Xiang-Ge Zhou[b]

[a] State Key Laboratory of Rare Earth Materials Chemistry and Applications, Peking University, Beijing 100871, P.R. China

[b] Chengdu Institute of Organic Chemistry, The Chinese Academy of Science, Chengdu 610041, P.R. China

(Received 28 May 1996; accepted 6 August 1996)

Abstract—The title complex was synthesized in aqueous solution and its crystal structure was determined by X-ray diffraction. The complex is binuclear, with copper and yttrium ions connected by four bridging carboxyl groups from four alanine molecules. The yttrium ion is coordinated by four oxygen atoms from four carboxyl groups and four oxygen atoms of four water molecules with the coordination number eight, taking a square antiprism arrangement. Copyright © 1997 Elsevier Science Ltd

Keywords: copper and yttrium; crystal structure; alanine complex.

Lanthanide ions are often used as spectroscopic probes for calcium ions in the studies of biological systems, dyeing promoters in the textile dyeing industry and additive elements of fertilizers in agriculture [1–3]. Since these applications are related to the interactions between lanthanide ions and biological ligands, the study of the bond models of lanthanide ions with amino acids is of interest. Recently, the crystal data of a series of lanthanide complexes with alanine have been reported [4–9]. Here we present the X-ray diffraction data for a heteronuclear complex of copper and yttrium with alanine.

EXPERIMENTAL

Preparation

The title complex was prepared by mixing $Cu(ClO_4)_2$ and $Y(ClO_4)_3$ in an aqueous solution of alanine at pH 4 in a 1 : 1 : 4 molar ratio. A blue single crystal was then obtained by slow evaporation at room temperature. After washing with water and air-drying, the composition of the crystal was determined by elemental analysis. Found: N, 5.1; C, 13.1; H, 4.0. Calc. for $[CuY(Ala)_4(H_2O)_5](ClO_4)_5 \cdot 3H_2O$: N, 4.9; C, 12.5; H, 3.9%. This formula is approximately consistent with the result of diffraction analysis.

IR spectra

IR spectra of the complex and alanine were obtained from KBr pellets at room temperature using a Nicolet Magna-IR 750 spectrophotometer. Compared with the IR spectrum of alanine, the ν_s(carboxyl) band at 1431 cm^{-1} of the complex is shifted 21 cm^{-1} to higher wavenumbers from 1410 cm^{-1}. This shows that the carboxyl groups of the ligand have been coordinated with the metal ion [10]. A broad absorption band for ν(hydroxyl) appears at 3400 cm^{-1} after complexation, showing the presence of water molecules in the complex.

* Author to whom correspondence should be addressed.

X-ray analysis

In air, the crystals quickly turn opaque due to the loss of water molecules. For this reason, a crystal of approximate dimension $0.26 \times 0.28 \times 0.36$ mm was mounted in a thin-walled capillary for structure determination. Intensity data were collected on a Siemens P4 diffractometer. 4487 independent reflections were collected, of which 3451 reflections with $F > 4.0(F)$ were used for structure refinement. Intensities were not corrected for absorption. All calculations were performed in the Siemens SHELXTL P4/PC system. The structure was solved by direct methods and difference-Fourier syntheses, respectively. Crystal data, details of data collection and refinement are listed in Table 1.

Table 1. Crystal data, details of data collection and refinement

Empirical formula	$C_{12}H_{44}N_4O_{36}Cl_5CuY$
Colour	Blue
Crystal size (mm)	$0.26 \times 0.28 \times 0.36$
Crystal system	Monoclinic
Space group	$P2_1$
a (Å)	14.370(4)
b (Å)	8.920(1)
c (Å)	16.651(2)
β (°)	91.36(2)
V (Å^3)	2133.7(7)
Z	2
M	1150.26
D_c (g cm^{-3})	1.790
Absorption coefficient (mm^{-1})	2.262
$F(000)$	1170
λ (Å) (Mo-K_α)	0.71073
Monochromator	Graphite
Scan type	2θ–θ
2θ range (°)	3.0–50.0
Scan speed (° min^{-1})	4.00–15.00
Standard reflections	3/97
Index range h; k; l	−1–17; −1–10; −19–19
Reflections collected	5048
Independent reflections	4487 ($R_{int} = 4.64\%$)
Observed reflections	3451 [$F > 4.0\sigma(F)$]
Absorption correction	N/A
Quantity minimized	$\Sigma\, \omega\, (F_o - F_c)^2$
Hydrogen atoms	Riding model, fixed isotropic U
Weighting scheme	$W^{-1} = \sigma^2(F) + 0.0018F^2$
Number of parameters refined	532
Final R	0.0728
Final Rw	0.0912
Goodness-of-fit	1.94
Maximum, Δ/ρ	0.011
Max., min. residual peak (e Å^{-3})	0.61, −0.92

RESULTS AND DISCUSSION

The crystal structure of the title complex and its coordination polyhedra are shown in Figs 1 and 2, respectively. Selected bond lengths and bond angles are listed in Table 2.

The complex exists as binuclear molecules with copper and yttrium ions connected by four bridging carboxyl groups from four alanine molecules. The yttrium ion is coordinated by four oxygen atoms from four alanine molecules and four oxygen atoms from four water molecules. Thus, the coordination number of yttrium ion is eight and the coordination polyhedron is a square antiprism. The copper ion, with coordination number 5, is coordinated by one oxygen atom from a water molecule and four oxygen atoms from the four bridging carboxyl groups, giving a square-pyramidal coordination polyhedron. The average bond lengths of Y—O(carboxyl) and Y—O(water) are 2.325 and 2.386 Å, respectively. The distance between Cu^{2+} and Y^{3+} is 3.491 Å. The perchlorate anions reside in the cavities of the crystal and stabilize the crystal packing by forming hydrogen bonds (Fig. 3).

The crystal structure of the complex $[CuY(Ala)_4(H_2O)_5](ClO_4)_5 \cdot 3H_2O$ has some similarities with the complexes $[Ln_2(Ala)_4(H_2O)_8](ClO_4)_6 \cdot nH_2O$ (Ln = Y, Ho, Er) [4–6]. They are all dimeric molecules and completely different from $[Dy(Ala)(H_2O)_6]Cl_3$, which is a one-dimensional infinite chain [8].

Acknowledgement—This work was supported by the Climbing Programme, a national key project for fundamental research.

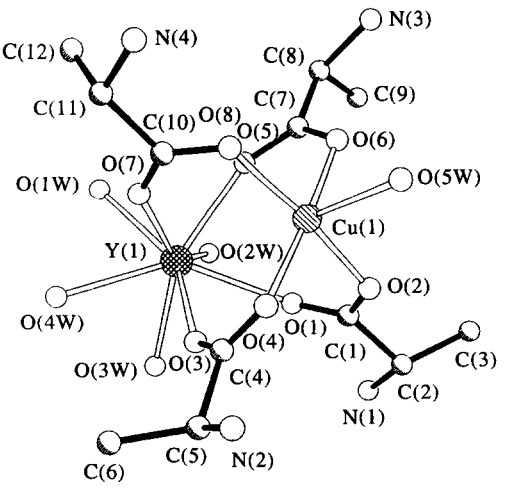


Fig. 1. Structure of $[CuY(Ala)_4(H_2O)_5](ClO_4)_5 \cdot 3H_2O$.

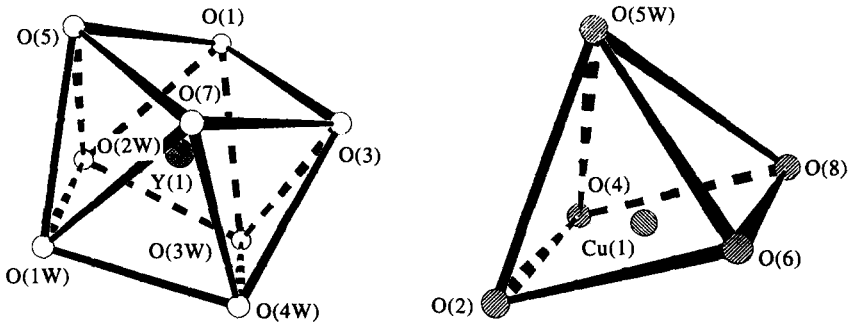


Fig. 2. Coordination polyhderons of Y^{3+} and Cu^{2+} in $[CuY(Ala)_4(H_2O)_5](ClO_4)_5 \cdot 3H_2O$.

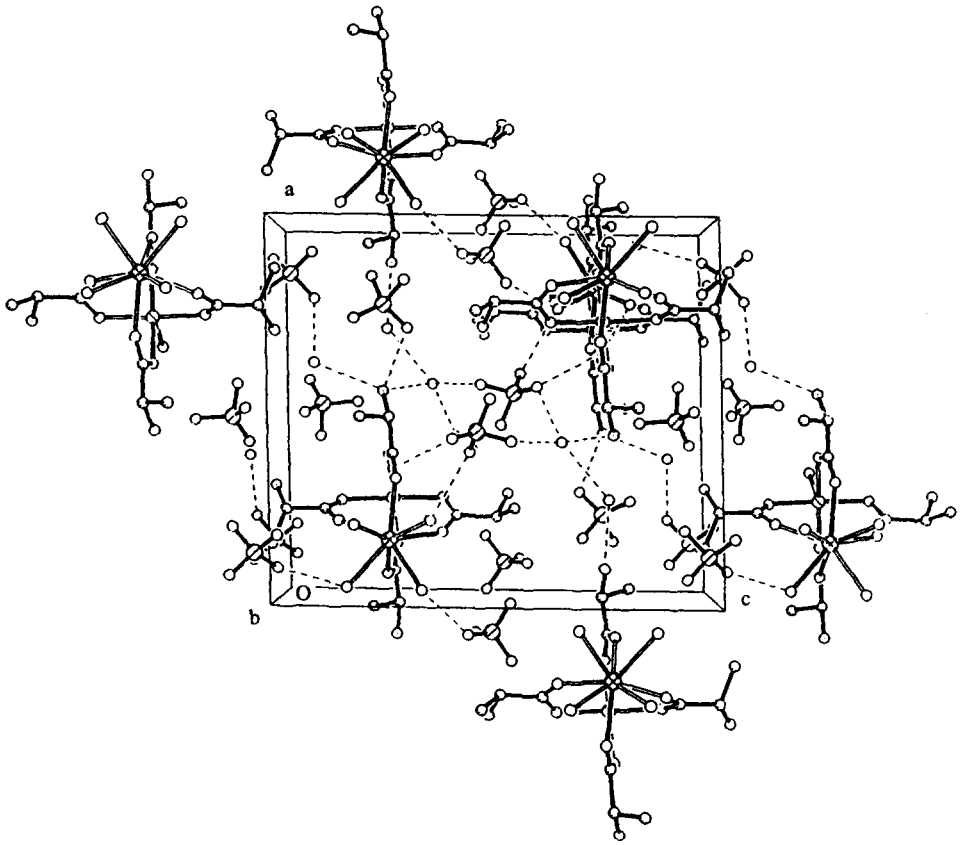


Fig. 3. Arrangement of $[CuY(Ala)_4(H_2O)_5](ClO_4)_5 \cdot 3H_2O$ in unit cell.

Table 2. Selected bond lengths (Å) and angles (°)

Y(1)—O(1)	2.337(3)	Y(1)—O(3)	2.319(3)
Y(1)—O(5)	2.308(3)	Y(1)—O(7)	2.292(3)
Y(1)—O(1w)	2.356(3)	Y(1)—O(2w)	2.412(3)
Y(1)—O(3w)	2.371(3)	Y(1)—O(4w)	2.406(3)
Cu(1)—O(2)	1.919(3)	Cu(1)—O(4)	1.941(4)
Cu(1)—O(6)	1.944(4)	Cu(1)—O(8)	1.933(3)
Cu(1)—O(5w)	2.272(3)		

O(1)—Y(1)—O(3)	72.2(1)	O(1)—Y(1)—O(5)	76.5(1)
O(1)—Y(1)—O(7)	119.5(1)	O(1)—Y(1)—O(1w)	139.8(1)
O(1)—Y(1)—O(2w)	72.6(1)	O(1)—Y(1)—O(3w)	79.3(1)
O(1)—Y(1)—O(4w)	142.2(1)	O(3)—Y(1)—O(5)	116.9(1)
O(3)—Y(1)—O(7)	76.1(1)	O(3)—Y(1)—O(1w)	148.0(1)
O(3)—Y(1)—O(2w)	137.1(1)	O(3)—Y(1)—O(3w)	79.3(1)
O(3)—Y(1)—O(4w)	77.1(1)	O(5)—Y(1)—O(7)	74.2(1)
O(5)—Y(1)—O(1w)	79.7(1)	O(5)—Y(1)—O(2w)	77.1(1)
O(5)—Y(1)—O(3w)	144.6(1)	O(5)—Y(1)—O(4w)	138.6(1)
O(7)—Y(1)—O(1w)	83.5(1)	O(7)—Y(1)—O(2w)	144.3(1)
O(7)—Y(1)—O(3w)	141.1(1)	O(7)—Y(1)—O(4w)	72.2(1)
O(1w)—Y(1)—O(2w)	70.8(1)	O(1w)—Y(1)—O(3w)	103.1(1)
O(1w)—Y(1)—O(4w)	73.4(1)	O(2w)—Y(1)—O(3w)	70.9(1)
O(2w)—Y(1)—O(4w)	120.6(1)	O(3w)—Y(1)—O(4w)	73.3(1)
O(2)—Cu(1)—O(4)	87.7(1)	O(2)—Cu(1)—O(6)	92.6(1)
O(2)—Cu(1)—O(8)	173.2(1)	O(2)—Cu(1)—O(5w)	97.3(1)
O(4)—Cu(1)—O(6)	174.9(1)	O(4)—Cu(1)—O(8)	91.4(1)
O(4)—Cu(1)—O(5w)	95.9(1)	O(6)—Cu(1)—O(8)	87.7(1)
O(6)—Cu(1)—O(5w)	89.1(1)	O(8)—Cu(1)—O(5w)	89.5(1)

REFERENCES

1. Britain, H. B., Richardson, F. S. and Martin, R. B., *J. Am. Chem. Soc.* 1978, **98,** 8255.
2. Britain, H. G., *Inorg. Chem.* 1979, **18,** 1740.
3. Fang, J. Y., Jin, T. Z. and Xu, G. X., *J. Chin. Rare Earth. Soc.* 1987, **5,** 47.
4. Jin, T. Z., Gao, S., Huang, C. H., Han, Y. Z. and Xu, G. X., *J. Chin. Rare Earth. Soc.* 1987, **5**(3), 1.
5. Dao, C. N., Glowiak, T., Huskowska, E. and Legendziewicz, J., *J. Less-Comm Metals*, 1988, **136,** 339.
6. Zeng, H. D. and Pan, K. Z., *J. Struct. Chem.* 1992, **11,** 393.
7. Wang, X. Q., Jin, T. Z. and Jin, Q. R., *Polyhedron*, 1994, **13,** 2333.
8. Glowiak, T. G., Legendziewicz, J., Dao, C. N. and Huskowska, E., *J. Less-Comm Metals*, 1991, **168,** 237.
9. Wang, X. Q., Jin, Q. R. and Jin, T. Z., *J. Chin. Rare Earth Soc.* 1994, **12,** 294.
10. Nakamoto, K., *Infrared Spectra of Inorganic and Coordination Compounds*, 4th edn. John Wiley & Sons Inc., New York, 1986, p. 258.

Pergamon

PII: S0277-5387(96)00400-7

Polyhedron Vol. 16, No. 8, pp. 1361–1364, 1997
Copyright © 1997 Elsevier Science Ltd
Printed in Great Britain. All rights reserved
0277-5387/97 $17.00+0.00

Synthesis and crystal structure of the potassium lanthanum complex with triethylenetetraaminehexaacetic acid (H_6TTHA): $K[KLa(HTTHA)(H_2O)]\cdot 8H_2O$

Rui-Yao Wang,[a] Jun-Ran Li,[a] Tian-Zhu Jin,[a]* Guang-Xian Xu,[a] Zhong-Yuan Zhou[b] and Xiang-Ge Zhou[b]

[a] State Key Laboratory of Rare Earth Materials Chemistry and Applications, Peking University, Beijing 100871, P.R. China

[b] Chengdu Institute of Organic Chemistry, The Chinese Academy of Science, Chengdu 610041, P.R. China

(Received 24 May 1996; accepted 6 August 1996)

Abstract—The title complex, $K[KLa(HTTHA)(H_2O]\cdot 8H_2O$, was synthesized in aqueous solution and its crystal structure was determined by X-ray diffraction. In the complex, the ten-coordinated lanthanum ion is bonded by four nitrogen atoms and six carboxyl oxygen atoms of the same triethylenetetraaminehexaacetic acid (H_6TTHA) molecule. The coordination polyhedron of lanthanum can be described as a distorted bicapped square antiprism. The crystal is composed of one dimensional infinite chains. Copyright © 1997 Elsevier Science Ltd

Keywords: lanthanum complex; crystal structure; triethylenetetraaminehexaacetic acid.

Paramagnetic metal ion complexes are finding many applications in biomedicine, especially as bioconjugates for monoclonal antibody radioisotope labeling and as magnetic resonance imaging (MRI) agents [1,2]. Polyaminecarboxylic acids and their derivatives are very important chelating agents for metal ions. They form stable complexes with trivalent lanthanide metal ions and the diethylenetriaminepentaacetic acid (H_5DTPA) complex with gadolinium has been used as a MRI agent in the NMR diagnosis of tumors [3,4]. Having similar coordination ability with H_5DTPA towards lanthanide ions, triethylenetetraaminehexaacetic acid (H_6TTHA) can also strongly chelate with lanthanides and its complex with gadolinium may also be used as an image enhancing agent. So far, studies on lanthanide complexes with H_6TTHA in solution have been carried out to determine the thermodynamic stability constants [5,6] and there is no crystallographic study on them. Here we report the synthesis and crystal structure of the title complex.

EXPERIMENTAL

Preparation

Lanthanum oxide (La_2O_3) and triethylenetetraaminehexaacetic acid (H_6TTHA) were mixed in a 1:2 molar ratio in water. The mixed solution was refluxed for *ca* 5 h under stirring. Then the solution was neutralized with KOH solution to *ca* pH6 and filtrated. The filtrate was concentrated on a water bath and the clear solution obtained was allowed to evaporate slowly at room temperature, yielding colorless prismatic crystals suitable for X-ray diffraction. The composition of the complex was deduced from the elemental analysis. Found: N, 6.4; C, 24.5; H, 3.9. Calc. for $K[KLa(HTTHA)(H_2O]\cdot 8H_2O$: N, 6.5; C, 24.9; H, 4.9%. The formula is approximately consistent with the results of diffraction analysis. The

* Author to whom correspondence should be adressed.

Table 1. Crystal data and details of data collection and refinement

Empirical formula	$C_{18}H_{43}N_4O_{21}K_2La$
Color	Colorless
Crystal size (mm)	$0.32 \times 0.36 \times 0.38$
Crystal system	Monoclinic
Space group	$P2_1/c$
a (Å)	9.501(2)
b (Å)	22.596(3)
c (Å)	15.678(2)
β (Å)	96.090(10)
V (Å^3)	3346.8(8)
Z	4
M	868.67
D_c (g/cm^{-3})	1.686
Absorption coefficient (mm^{-1})	1.611
$F(000)$	1768
λ (Å) (Mo$K\alpha$)	0.71073
Monochromator	Graphite
Scan type	2θ–θ
2θ range (°)	3.0–50.0
Scan speed (° min^{-1})	6.00
Standard reflections	3/97
Index ranges h; k; l	−1–11; −1–26; −18–18
Reflections collected	7409
Independent reflections	5886 (R_{int} = 1.16%)
Observed reflections	4937 [$F > 4.0\sigma(F)$]
Absorption correction	Semi-empirical
Quantity minimized	$\Sigma\omega(F_o - F_o)^2$
Hydrogen atoms	Riding model, fixed isotropic U
Weighting scheme	$w^{-1} = \sigma^2(F) + 0.0005F^2$
Number of parameters refined	415
Final R	0.0322
Final Rw	0.0446
Goodness-of-fit	1.84
Max., min. residual ρ (e/Å^{-3})	0.62, −0.81

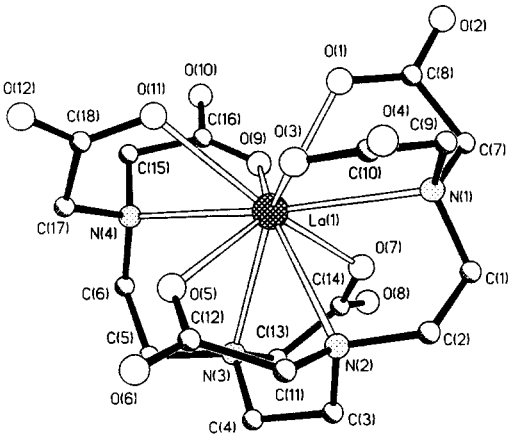


Fig. 1. Structure of K[KLa(HTTHA)(H_2O)]·8H_2O.

hydrogen content found is a little lower than that of the real composition of the complex. This may be caused by the efflorescent of the crystal before elemental determination.

IR spectra

IR spectra of the complex and free ligand were obtained from KBr pellets at room temperature using a Nicolet Magna-IR 750 spectrophotometer. Compared with the IR spectrum of free ligand, the ν_{as} (carboxyl) band of the complex is shifted 44 cm^{-1} to lower wave-numbers from 1642 cm^{-1} and the ν_s (carboxyl) band of the complex is shifted 6 cm^{-1} to higher frequency from 1398 cm^{-1}. This indicates that the carboxyl groups of the ligand have been coordinated with the metal ion [7,8]. A broad absorption band for ν(hydroxyl) appears at 3400 cm^{-1} after complexation, showing the presence of water molecules in the complex.

X-ray analysis

A colorless crystal of the title compound was mounted in a thin-walled capillary for structure determination. The reflections were collected on a Siemens P4 diffractometer. There were some small crystallites on the surface of the main crystal, so we used the program CHDU to calculate the cell parameters (CHDU is programmed by us, which is used to eliminate the influence of the small crystallites on the calculation of the cell parameters). Intensities were corrected for absorption by a semi-empirical method. The structure was solved by the heavy-atom method. Lanthanum-ion coordinates were determined by analysis of the Patterson map and all non-hydrogen atoms were determined by Fourier syntheses. Hydrogen atoms were located either from difference Fourier

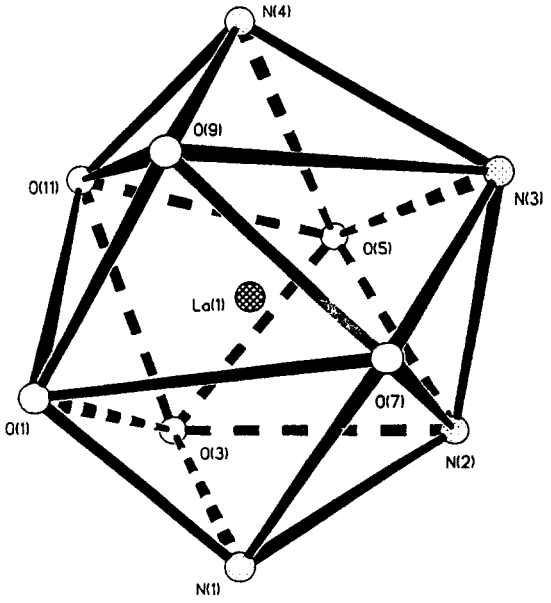


Fig. 2. Coordination polyhedron of K[KLa(HTTHA)(H_2O]·8H_2O.

Table 2. Selected bond lengths (Å) and angles (°)

La(1)—O(1)	2.547(2)	La(1)—O(3)	2.555(2)
La(1)—O(5)	2.502(2)	La(1)—O(7)	2.469(2)
La(1)—O(9)	2.711(2)	La(1)—O(11)	2.560(2)
La(1)—N(1)	2.791(2)	La(1)—N(2)	2.806(2)
La(1)—N(3)	2.788(3)	La(1)—N(4)	2.843(2)
K(1)—O(1)	2.713(3)	K(1)—O(11)	2.813(2)
K(1)—O(1w)	2.889(3)	K(1)—O(3a)	2.838(2)
K(1)—O(10a)	2.704(2)	K(1)—O(11a)	2.867(3)
K(1)—O(12a)	2.762(2)	K(2)—O(2w)	2.648(3)
K(2)—O(3wa)	3.040(3)	K(2)—O(3wb)	2.736(3)
K(2)—O(5wa)	2.689(3)	K(2)—O(6wa)	3.067(3)
K(2)—(9wa)	2.798(2)		

O(1)—La(1)—O(3)	79.1(1)	O(1)—La(1)—O(5)	142.9(1)
O(3)—La(1)—O(5)	69.3(1)	O(1)—La(1)—O(7)	87.5(1)
O(3)—La(1)—O(7)	129.2(1)	O(5)—La(1)—O(7)	127.5(1)
O(1)—La(1)—O(9)	66.9(1)	O(3)—La(1)—O(9)	143.2(1)
O(5)—La(1)—O(9)	134.2(1)	O(7)—La(1)—O(9)	65.1(1)
O(1)—La(1)—O(11)	80.3(1)	O(3)—La(1)—O(11)	72.5(1)
O(5)—La(1)—O(11)	72.2(1)	O(7)—La(1)—O(11)	152.7(1)
O(9)—La(1)—O(11)	87.6(1)	O(3)—La(1)—N(1)	62.5(1)
O(1)—La(1)—N(1)	60.3(1)	O(7)—La(1)—N(1)	68.3(1)
O(5)—La(1)—N(1)	116.8(1)	O(11)—La(1)—N(1)	123.7(1)
O(9)—La(1)—N(1)	108.7(1)	O(3)—La(1)—N(2)	71.7(1)
O(1)—La(1)—N(2)	124.9(1)	O(7)—La(1)—N(2)	77.0(1)
O(5)—La(1)—N(2)	62.9(1)	O(11)—La(1)—N(2)	129.8(1)
O(9)—La(1)—N(2)	140.2(1)	O(1)—La(1)—N(3)	145.6(1)
O(3)—La(1)—N(3)	132.3(1)	O(5)—La(1)—N(3)	71.2(1)
O(7)—La(1)—N(3)	62.4(1)	O(9)—La(1)—N(3)	84.4(1)
O(11)—La(1)—N(3)	118.6(1)	O(1)—La(1)—N(4)	110.5(1)
O(3)—La(1)—N(4)	126.8(1)	O(5)—La(1)—N(4)	76.0(1)
O(7)—La(1)—N(4)	103.9(1)	O(9)—La(1)—N(4)	58.5(1)
O(11)—La(1)—N(4)	59.0(1)	N(1)—La(1)—N(3)	116.5(1)
N(1)—La(1)—N(2)	64.9(1)	N(1)—La(1)—N(4)	167.2(1)
N(2)—La(1)—N(3)	67.1(1)	N(3)—La(1)—N(4)	65.3(1)
N(2)—La(1)—N(4)	124.5(1)		

Symmetry operation: (a) $x, -y, 0.5-z$; (b) $x, 0.5-y, 0.5+z$.

syntheses or by theoretical method. The refinement was made by full-matrix least-squares. Crystal data, details of data collection and refinement are listed in Table 1.

RESULTS AND DISCUSSION

The crystal structure of the title complex and its coordination polyhedron are shown in Figs 1 and 2, respectively. Selected bond lengths and bond angles are listed in Table 2.

In the complex, each La^{3+} ion is encapsulated by one H_6TTHA molecule and coordinated by six oxygen atoms from the six carboxyl groups and four nitrogen atoms of the H_6TTHA molecule with coordination number 10, making a distorted bicapped square antiprism arrangement. The average bond lengths of La—O and La—N are 2.557 and 2.807 Å, respectively. There are two kinds of potassium ions in the crystal, K(1) and K(2). K(1), with coordination number seven, is coordinated by six oxygen atoms from two neighboring H_6TTHA molecules and one oxygen atom from a water molecule. Completely different from K(1), K(2), with coordination number 6, is coordinated by six water molecules only.

The crystal structure can be described as having a one-dimensional infinite chain, where the metal atoms are arranged in the order K(1)···La(1)··· K(1a)···La(1a)···. The connecting diagram of the metal ions is shown in Fig 3. K(1)···La(1)···K(1a) are connected by four carboxyl groups. Two bridging

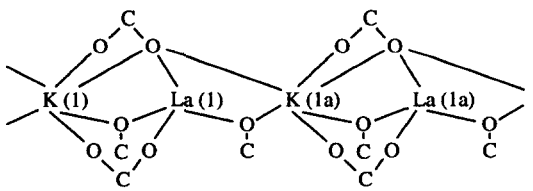


Fig. 3. Sketch map of the metal connection in K[KLa(HTTHA)(H2O)]·8H2O.

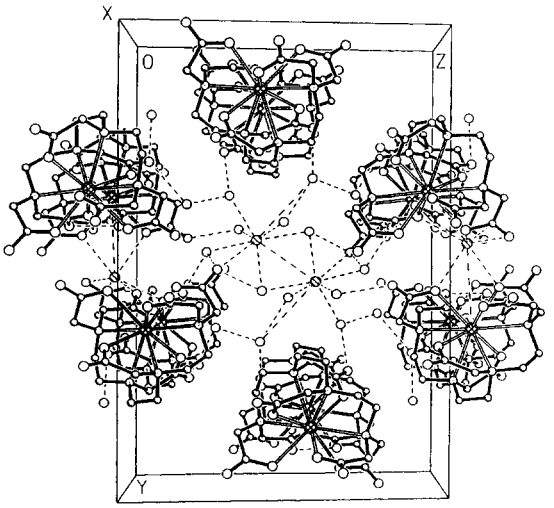


Fig. 4. Arrangement of K[KLa(HTTHA)(H_2O)·8H_2O.

carboxyl groups and a μ_2-O from a third carboxyl group connected to K(1) and La(1). One of the bridging carboxyl groups has an oxygen atom, acting as μ_3-O and bonding with La(1), K(1) and also K(1a). In contrast to the connection of K(1)···La(1), La(1) and K(1a) are connected only by the μ_3-O and a μ_2-O from the fourth carboxyl group. Therefore, there are two carboxyl bridges and two oxygen bridges between La(1) and K(1), but only two oxygen bridges between La(1) and K(1a). This is in good agreement with the distance data: K(1)···La(1), 4.154; K(la)···La(1), 4.378 Å.

In addition to the six-coordinated water molecules, there are still two uncoordinated water molecules in the crystal. They reside in the cavities of the crystal and stabilize the crystal packing through hydrogen bonds (Fig. 4).

Acknowledgement—This work was supported by the Climbing Programme, a national key project for fundamental research.

REFERENCES

1. Lauffer, R. B., *Chem. Rev.* 1987, **87,** 901.
2. Tweedle, M. F., *Lanthanide probes in life, Chemical and Earth Science*, Ch. 1 and 5, eds J.-C. G. Bunzliand and G. R. Choppin. Elsevier, Amsterdam, 1989.
3. Paul-Roth, C. and Raymond, K. N., *Inorg. Chem.* 1995, **34,** 1408.
4. Alexander, V., *Chem. Rev.* 1995, **95,** 273.
5. Martell, A. E. and Smith, R. M., *Critical Stability Constants*, Vol. 1. Plenum Press, New York, 1974, P. 286.
6. Harju, L., *Anal. Chim. Acta*, 1970, **50,** 475.
7. Sievers, R. E. and Bailar, J. C., *Inorg. Chem.* 1962, **1** 174.
8. Nakamoto, K., *Infrared Spectra of Inorganic and Coordination Compounds*, 4th edn. John Wiley & Sons Inc., New York, 1986, p. 231.

Pergamon

PII: S0277-5387(96)00398-1

Polyhedron Vol. 16, No. 8, pp. 1365–1370, 1997
Copyright © 1997 Elsevier Science Ltd
Printed in Great Britain. All rights reserved
0277-5387/97 $17.00+0.00

Synthesis and crystal structure of a novel manganese(III)–molybdenum(IV) hetero-octametallic cluster, $Na_2Mn_2[Mo_3O_4(O_2CEt)_8]_2$

Li Xu,* Zaofei Li and Jinshun Huang*

State Key Laboratory of Structural Chemistry and Fujian Institute of Research on the Structure of Matter, Chinese Academy of Sciences, Fuzhou, Fujian 350002, P.R. China

(Received 24 May 1996; accepted 6 August 1996)

Abstract—A mixture of $Na_2MoO_4{\cdot}2H_2O$, $Mo(CO)_6$, $Mn(CH_3CO_2)_3{\cdot}2H_2O$ and $(EtCO)_2O$ was heated at 120°C to produce the novel manganese(III)–molybdenum(IV) hetero-octanuclear cluster $Na_2Mn_2[Mo_3O_4(O_2CEt)_8]_2$ (**1**) as green–black crystals in *ca* 15% yield. The X-ray structure determination reveals the presence of the two incomplete cubane-type cluster units, $[Mo_3O_4(O_2CEt)_8]^{4-}$ bridged by two Mn^{III} ions. The centrosymmetric octanuclear dianions are linked by Na^+ into infinite chains. It is surprising that each Mn^{III} ion has a rather regular O_6 octahedral coordination sphere with O—Mn—O angles within 5° of the expected octahedral value and six similar Mn—O bond lengths [1.963(4)–2.001(5) Å], showing little Jahn–Teller distortion. Copyright © 1997 Elsevier Science Ltd

Keywords: cluster; manganese complex; molybdenum complex; octanuclear complex; crystal structure; Jahn–Teller effect.

This is the continuing study of the chemistry of the hetero-octametallic cluster series $Na_2M'_2[M_3O_4(O_2CR)_8]_2$ established in this laboratory [1–5]. Such species consist of the two incomplete cubane-type cluster units $[M^{IV}_3O_3O_4(O_2CR)_8]^{4-}$ (M = Mo, W) bridged by two trivalent metal ions (M′), such triangular metal–metal bonded clusters having been extensively studied over the past two decades [6–8]. Bridging oxides and carboxylate oxygen atoms from the two trinuclear units just constitute two rather regular O_6 octahedra for the M′ bridging metal ions. We have reported V^{III}-, Cr^{III}-, Fe^{III}-, Mo^{III}- and Al^{III}-bridged clusters **2**–**13** of this series. Herein we present the new Mn^{3+}-bridged derivative, $Na_2Mn^{III}_2[Mo^{IV}_3O_4(O_2CEt)_8]_2$ (**1**). As will be illustrated later, it provides an unprecedented example of little Jahn–Teller distortion for octahedral Mn^{III} complexes [9,10].

EXPERIMENTAL

Preparative reactions were carried out in the air. $Mn(CH_3CO_2)_3{\cdot}2H_2O$ was prepared according to [11]. Other reagents were used as supplied without special purification.

Synthesis of $Na_2Mn_2[Mo_3O_4(O_2CEt)_8]_2$ (1)

A mixture of $Na_2MoO_4{\cdot}2H_2O$ (0.63 g, 2.60 mmol), $Mo(CO)_6$ (0.40 g, 1.50 mmol), $Mn(CH_3CO_2)_3{\cdot}2H_2O$ (0.35 g, 1.30 mmol) and propionic anhydride (60 cm^3) was heated at 120°C for 3 days. After cooling to room temperature, well-formed black crystals of **1** were obtained (0.20 g, 15%).

X-ray crystallography

The crystallographic data for cluster **1** are summarized in Table 1. The reflection intensities were collected on a Rigaku AFC5R diffractometer, using graphite-monochromated Mo K_α radiation (λ = 0.71069 Å) at room temperature and $\omega/2\theta$ scan mode ($3 < 2\theta < 50°$) with scan speed 8° min^{-1}. The structures were solved by direct methods using MULTAN11/82 and refined by full-matrix least-squares with all nonhydrogen atoms anisotropic. The weighting scheme w was $1/[\sigma(F_o)^2 + (0.02 \times F_o)^2 + 1.000]$. All

* Authors to whom correspondence should be addressed.

Table 1. Crystallographic data for $Na_2Mn_2[Mo_3O_4(O_2CEt)_8]_2$

Formula	$[C_{48}H_{80}Mn_2Mo_6O_{40}]^{2-}2Na^+$
Mol. wt	2028.64
Space group	$P\bar{1}$
a (Å)	12.965(7)
b (Å)	14.007(7)
c (Å)	12.349(9)
α (°)	109.89(6)
β (°)	117.47(4)
γ (°)	90.43(5)
V (Å^3)	1834
Z	1
D_c (g cm^{-3})	1.84
R^a, R_w^b	0.043, 0.055

$^a R = \Sigma||F_o| - |F_c||/|F_o|$.
$^b R_w = [\Sigma w(||F_o| - |F_c||^2/\Sigma w(|F_o|)^2]^{1/2}$.

Table 2. Selected bond lengths (Å) for $Na_2Mn_2[Mo_3O_4(O_2CEt)_8]_2$

Mo(1)—Mo(2)	2.5096(9)	Mo(3)—O(3)	1.948(5)
Mo(1)—Mo(3)	2.5324(9)	Mo(3)—O(4)	1.922(4)
Mo(2)—Mo(3)	2.5172(9)	Mo(3)—O(31)	2.011(5)
Mo(1)—O(1)	2.006(4)	Mo(3)—O(32)	2.118(5)
Mo(1)—O(2)	1.944(5)	Mo(3)—O(33)	2.120(5)
Mo(1)—O(3)	1.941(5)	Mn—O(2)	1.993(4)
Mo(1)—O(11)	2.004(4)	Mn—O(3)	1.963(4)
Mo(1)—O(12)	2.103(4)	Mn—O(41)	1.970(5)
Mo(1)—O(13)	2.125(5)	Mn—O(42)	1.982(5)
Mo(2)—O(1)	2.011(4)	Mn—O(43)	2.001(5)
Mo(2)—O(2)	1.959(5)	Mn—O(44)	1.983(5)
Mo(2)—O(4)	1.900(4)	O(1)—Na(1)	2.318(5)
Mo(2)—O(21)	2.015(4)	O(14)—Na(1)	2.283(7)
Mo(2)—O(22)	2.099(5)	O(24)—Na(1)	2.407(6)
Mo(2)—O(23)	2.133(5)	O(2)—Na(1)	2.316(6)
Mo(3)—O(1)	2.041(4)	O(3)—Na(1)	2.254(8)

calculations were performed on a PC-486 using the Molen-PC program package with scattering factors taken from the International Tables.

RESULTS AND DISCUSSION

Synthesis

The synthesis of the Mn–Mo hetero-octametallic cluster **1** is convenient and straightforward. The redox reaction of MoO_4^{2-} and $Mo(CO)_6$ in propionic anhydride in the presence of $Mn(O_2CCH_3)_3$ produced the trinuclear unit $[Mo_3O_4(O_2CEt)_8]^{4-}$, which is trapped by Mn^{3+} ions to form the hetero-octanuclear anion $Mn_2[Mo_3O_4(O_2CEt)_8]^{2-}$. The dianion is further linked by Na^+ ions in the reaction into the insoluble infinite chain cluster **1**, which is believed to be essential to the successful preparation of this type of cluster. It should

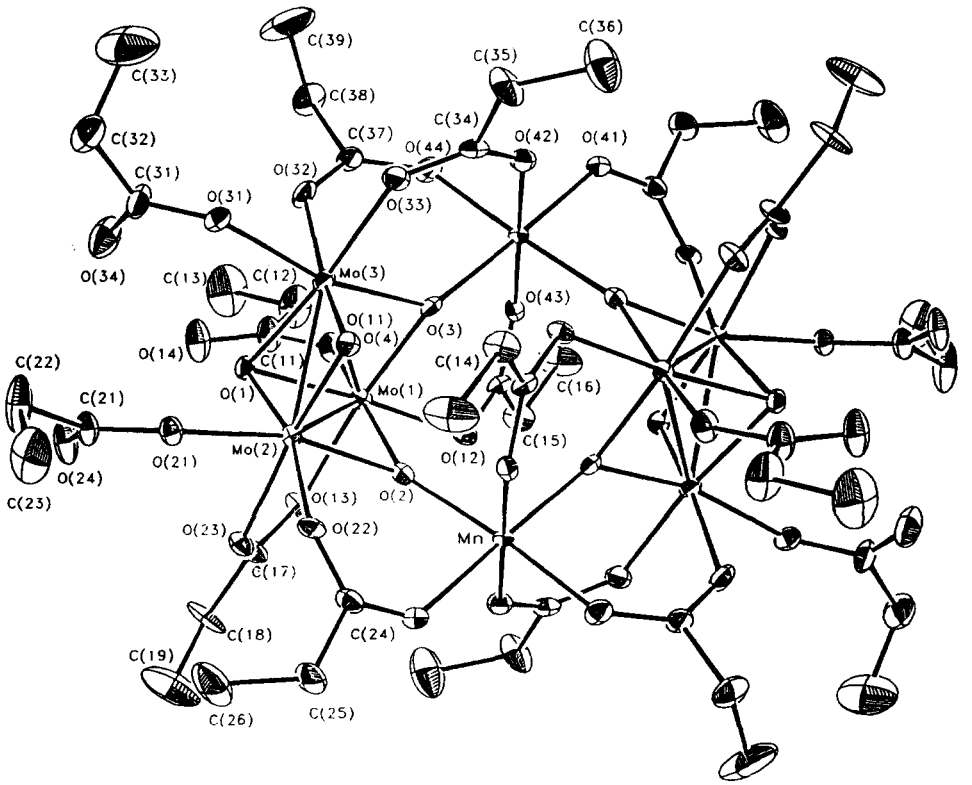


Fig. 1. ORTEP drawing of the cluster dianion of **1**, $Mn_2[Mo_3O_4(O_2CEt)_8]_2^{2-}$, with 50% thermal probability ellipsoids.

Table 3. Selected bond angles (°) for $Na_2Mn_2[Mo_3O_4(O_2CEt)_8]_2$

Mo(2)—Mo(1)—Mo(3)	59.90(2)	O(4)—Mo(3)—O(31)	94.3(2)
Mo(1)—Mo(1)—Mo(3)	60.50(2)	O(4)—Mo(3)—O(32)	170.3(2)
Mo(1)—Mo(3)—Mo(2)	59.60(2)	O(4)—Mo(3)—O(33)	84.1(2)
O(1)—Mo(1)—O(2)	101.4(2)	O(31)—Mo(3)—O(32)	81.5(3)
O(1)—Mo(1)—O(3)	100.7(2)	O(31)—Mo(3)—O(33)	83.8(2)
O(1)—Mo(1)—O(11)	89.1(2)	O(3)—Mo(3)—O(33)	86.7(3)
O(1)—Mo(1)—O(12)	166.9(2)	O(2)—Mn—O(3)	94.6(2)
O(1)—Mo(1)—O(13)	84.8(2)	O(2)—Mn—O(41)	88.7(2)
O(2)—Mo(1)—O(3)	90.5(2)	O(2)—Mn—O(42)	88.3(2)
O(2)—Mo(1)—O(11)	165.3(2)	O(2)—Mn—O(43)	90.0(2)
O(1)—Mo(1)—O(12)	88.3(2)	O(2)—Mn—O(44)	175.8(2)
O(2)—Mo(1)—O(13)	85.9(2)	O(3)—Mn—O(41)	176.2(2)
O(3)—Mo(1)—O(11)	97.7(2)	O(3)—Mn—O(42)	89.6(2)
O(3)—Mo(1)—O(12)	87.9(2)	O(3)—Mn—O(43)	89.0(2)
O(3)—Mo(1)—O(13)	173.9(2)	O(3)—Mn—O(44)	89.6(2)
O(11)—Mo(1)—O(12)	79.9(2)	O(41)—Mn—O(42)	92.5(2)
O(11)—Mo(1)—O(13)	84.9(2)	O(41)—Mn—O(43)	89.0(2)
O(12)—Mo(1)—O(13)	87.1(2)	O(41)—Mn—O(44)	87.2(3)
O(1)—Mo(2)—O(2)	100.8(2)	O(42)—Mn—O(43)	177.7(2)
O(1)—Mo(2)—O(4)	100.2(2)	O(42)—Mn—O(44)	91.3(2)
O(1)—Mo(2)—O(21)	87.9(2)	O(43)—Mn—O(44)	90.6(3)
O(1)—Mo(2)—O(22)	165.4(2)	Mo(1)—O(1)—Mo(2)	77.3(1)
O(1)—Mo(2)—O(23)	86.7(2)	Mo(1)—O(1)—Mo(3)	77.5(1)
O(2)—Mo(2)—O(4)	94.1(2)	Mo(2)—O(1)—Mo(3)	76.8(1)
O(2)—Mo(2)—O(21)	165.1(2)	Mo(1)—O(2)—Mo(2)	80.0(2)
O(2)—Mo(2)—O(22)	87.9(2)	Mo(1)—O(2)—Mn	147.6(2)
O(2)—Mo(2)—O(23)	83.2(2)	Mo(2)—O(2)—Mn	131.2(2)
O(4)—Mo(2)—O(21)	96.2(2)	Mo(1)—O(3)—Mo(3)	81.3(2)
O(4)—Mo(2)—O(22)	90.8(2)	Mo(1)—O(3)—Mn	133.6(2)
O(4)—Mo(2)—O(23)	173.0(2)	Mo(3)—O(3)—Mn	132.7(2)
O(21)—Mo(2)—O(22)	81.3(2)	Mo(2)—O(4)—Mo(3)	82.4(2)
O(21)—Mo(2)—O(23)	85.3(2)	O(1)—Na(1)—O(14)	80.4(2)
O(22)—Mo(2)—O(23)	82.7(2)	O(1)—Na(1)—O(24)	81.8(2)
O(1)—Mo(3)—O(3)	99.2(2)	O(1)—Na(1)—O(24)	156.0(3)
O(1)—Mo(3)—O(4)	98.3(2)	O(1)—Na(1)—O(34)	82.4(2)
O(1)—Mo(3)—O(31)	90.2(2)	O(14)—Na(1)—O(24)	146.7(3)
O(1)—Mo(3)—O(32)	90.4(2)	O(14)—Na(1)—O(24)	101.9(2)
O(1)—Mo(3)—O(33)	173.6(2)	O(14)—Na(1)—O(34)	116.0(3)
O(3)—Mo(3)—O(4)	97.9(2)	O(24)—Na(1)—O(24)	83.9(3)
O(3)—Mo(3)—O(31)	163.3(2)	O(24)—Na(1)—O(34)	89.0(3)
O(3)—Mo(3)—O(32)	84.6(2)	O(24)—Na(1)—O(34)	116.6(2)
O(3)—Mo(3)—O(33)	86.2(2)	Na(1)—O(24)—Na(1)	96.1(3)

be mentioned that the use of the freshly prepared Mn^{III} acetate [11] is necessary, otherwise, the yield of **1** will be substantially lowered presumably due to the facile disproportionation of Mn^{III} to Mn^{III} and Mn^{IV}. All attempts to prepare the Mn^{IV} derivative using Mn^{4+} compounds in place of $Mn(O_2CCH_3)_3$ were unsuccessful. This indicates that the correspondingly required 7e (metal *d* electrons are counted only) $[Mo_3O_4(O_2CEt)_8]^{5-}$ is unstable. In fact, the electrochemical reduction of the 6e $[Mo_3O_4(O_2CEt)_8]^{4-}$ always afforded 2e- or 3e-reduced derivatives [8]. It was also not possible to prepare Mn^{II} derivatives such as $Mg_2Mn^{II}[Mo_3^{IV}O_4(O_2CEt)_8]$ using $Mn(O_2CCH_3)_2$ to replace the Mn^{III} complex.

X-ray crystal structure

The structure of the cluster dianion of **1**, $Mn_2[Mo_3O_4(O_2CCH_3)_8]_2^{2-}$, is shown in Fig. 1. Selected bond lengths and angles in **1** are given in Tables 2 and 3 and a comparison of structural parameters in **1** and 12 related compounds are listed in Table 4. The structure consists of the two incomplete cubane-type cluster units, $[Mo_3O_4(O_2CCH_3)_8]^{4-}$, which is depicted in Fig. 2, with two Mn^{III} ions. An unusual feature in the cuboidal units shown in Fig. 2 is the single bridging ligand μ-$EtCO_2$, which has not been found in previously reported $[Mo_3O_4]^{4+}$-type species [6–8]. As shown in Table 3, the Mo—Mo and Mo—O bond

Table 4. A comparison of mean bond lengths in clusters **1–13** and related compounds

Compound	M—M	M—O_b[a]	M—O_b^*[b]	M—O_t[c]	M—O_{cp}[d]	M—O_{ba}[e]	M′—O_b^*	M′—O_{ba}	Reference
$Na_2Mn_2[Mo_3O_4(O_2CEt)_8]_2$ (**1**)	2.5197(9)	1.911(4)	1.948(5)	2.020(5)	2.019(4)	2.116(5)	1.978(4)	1.984(5)	This work
$Na_2Fe_2[Mo_3O_4(O_2CEt)_8]_2$ (**2**)	2.517(1)	1.915(7)	1.957(7)	2.010(8)	2.027(7)	2.121(8)	1.992(8)	1.993(8)	[3]
$Na_2Cr_2[Mo_3O_4(O_2CEt)_8]_2$ (**3**)	2.5198(9)	1.907(4)	1.952(5)	2.010(4)	2.026(4)	2.114(5)	1.947(4)	1.973(5)	[1,2]
$Li_2Cr_2[Mo_3O_4(O_2CEt)_8]_2$ (**4**)	2.519(2)	1.904(4)	1.952(5)	2.024(4)	2.020(4)	2.116(5)	1.949(4)	1.973(5)	[5]
$K_2Cr_2[Mo_3O_4(O_2CEt)_8]_2$ (**5**)	2.520(2)	1.911(6)	1.950(6)	2.033(6)	2.018(6)	2.114(6)	1.946(6)	1.970(6)	[5]
$Na_2V_2[Mo_3O_4(O_2CEt)_8]_2$ (**6**)	2.519(1)	1.905(6)	1.953(6)	2.005(6)	2.026(7)	2.119(8)	1.985(6)	1.989(8)	[2]
$Na_2Al_2[Mo_3O_4(O_2CMe)_8]_2$ (**7**)	2.518(1)	1.908(7)	1.957(7)	2.022(7)	2.023(7)	2.121(7)	1.901(8)	1.877(8)	[4]
$Na_2Al_2[Mo_3O_4(O_2CEt)_8]_2$ (**8**)	2.511(2)	1.895(8)	1.948(8)	2.010(8)	2.011(8)	2.113(8)	1.896(8)	1.885(8)	[4]
$Na_2Mo_2[M_3O_4(O_2CEt)_8]_2$ (**9**)	2.520(1)	1.909(9)	1.959(9)	2.011(9)	2.034(9)	2.104(9)	2.028(6)	2.079(9)	[3]
$Na_2Fe_2[W_3O_4(O_2CEt)_8]_2$ (**10**)	2.535(1)	1.92(1)	1.98(2)	2.02(2)	2.04(2)	2.11(2)	1.98(2)	2.02(2)	[3]
$Na_2Cr_2[W_3O_4(O_2CEt)_8]_2$ (**11**)	2.5313(9)	1.927(9)	1.972(8)	2.012(9)	2.059(9)	2.110(9)	1.929(8)	1.986(9)	[1,2]
$Na_2V_2[W_3O_4(O_2CEt)_8]_2$ (**12**)	2.5328(6)	1.926(6)	1.974(6)	2.013(6)	2.057(6)	2.107(7)	1.962(6)	2.012(6)	[2]
$Na_2Mo_2[W_3O_4(O_2CEt)_8]_2$ (**13**)	2.530(2)	1.90(2)	1.97(2)	1.99(2)	2.06(2)	2.10(3)	2.03(2)	2.10(2)	[3]
$[Mo_3O_4(C_2O_4)_3(H_2O)_3]^{2-}$	2.493(3)	1.915(7)			2.020(3)				[7]
β-[Mn(acac)$_3$]								1.891(8)	[9]
γ-[Mn(acac)$_3$]								1.994(4)	[10]
$[Mn_3O(O_2CH)_9]^{2-}$							1.90(2)	2.05(2)	[13]

[a] Bridging M atom.
[b] Bridging M and M′ atom.
[c] Terminal $C_2H_5Co_2$.
[d] Capping O atoms.
[e] Bridging $C_2H_5CO_2$.

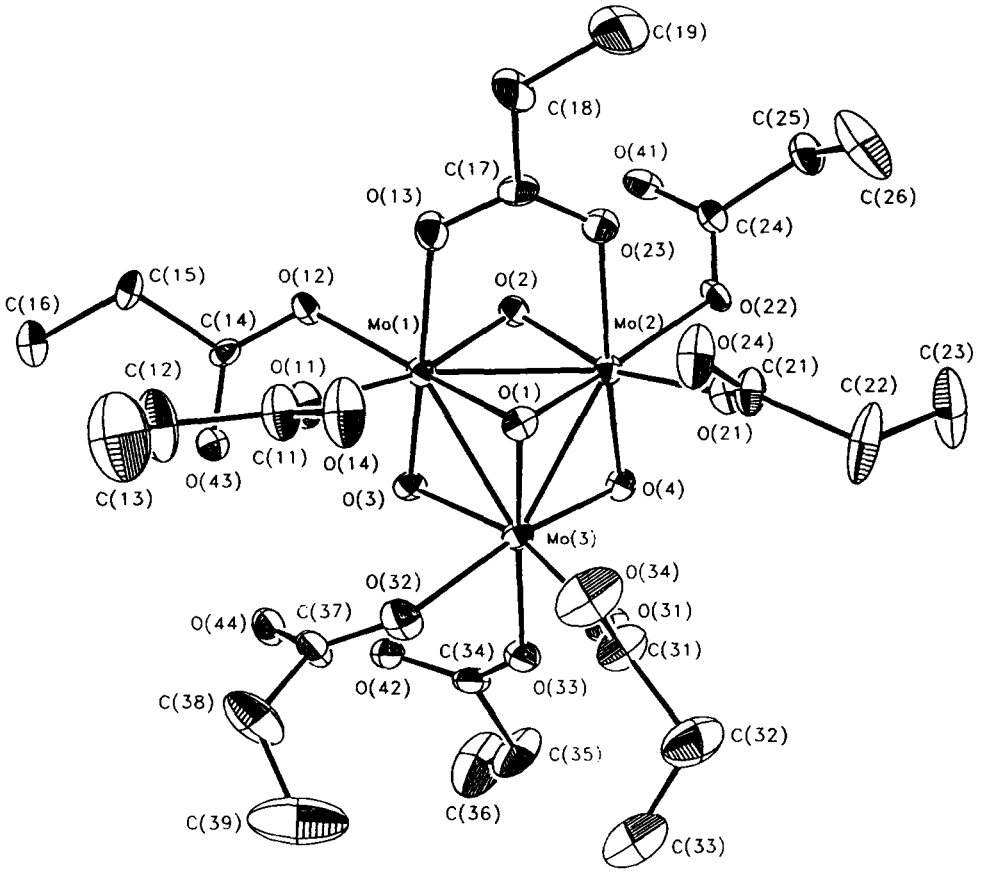


Fig. 2. Structure of the incomplete cubane-type cluster unit of **1**, $[Mo_3O_4(O_2CEt)_8]^{4-}$.

lengths in the $[Mo_3O_4(O_2CEt)_8]^{4-}$ unit of **1** and **2–8** are almost the same, indicating that the same oxidation state +4 of the Mo atoms in these species. By deduction, Mn has the oxidation state of +3 rather than +4, which requires a corresponding lowering of Mo oxidation states and thus change of the bond lengths about the Mo, in agreement with the experimental results described above. As shown in Fig. 1, each Mn is bound to two bridging oxides and four propionate oxygen atoms from the two trinuclear units in an octahedral arrangement. It can be seen from Table 2 that the resultant MnO_6 octahedron is rather regular with the O—Mn—O angles within 5° of the expected octahedral values. It is surprising that the anticipated tetragonal distortion has not occurred in the MnO_6 octahedron, as indicated by the six similar Mn—O bonds [1.963(4), 1.970(5), 1.982(5), 1.983(5), 1.993(4), 2.001(5) Å] given in Table 2. The averaged value of 1.989(5) Å for the six Mn—O bond lengths in the present cluster is close to the 1.981(8) and 1.994(3) Å in β-Mn(acac)$_3$ [9] and γ-Mn(acac)$_3$ [10], respectively. The reason for the lack of Jahn–Teller distortion in **1** is not clear, but the resulting instability of the MnO_6 octahedral is believed to be responsible for the low yield of **1**.

The mean Mn—O_b^* (bridging Mo and Mn) bond length [1.978(4) Å] which is close to the averaged Mn—O_{ba} (O_2CEt) distance [1.984(5) Å] is remarkably longer than the Mn—μ_3O bond in $[Mn_3O(O_2CH)_9]_2$ [av. 1.90(2) Å] [12], indicating very weak Mn—O_b^* d–p π-bonds. This is similar to the cases in the V, Fe and Al clusters, but unlike those in the Cr clusters where significant Cr—O_b^* d–p π-bonding has been observed.

As shown in Fig. 3, the octanuclear cluster dianions are linked by Na^+ ions into an infinite chain structure with the mean Na—O bond of 2.315(8) Å, responsible for the insolubility in water and common organic solvents and easy formation.

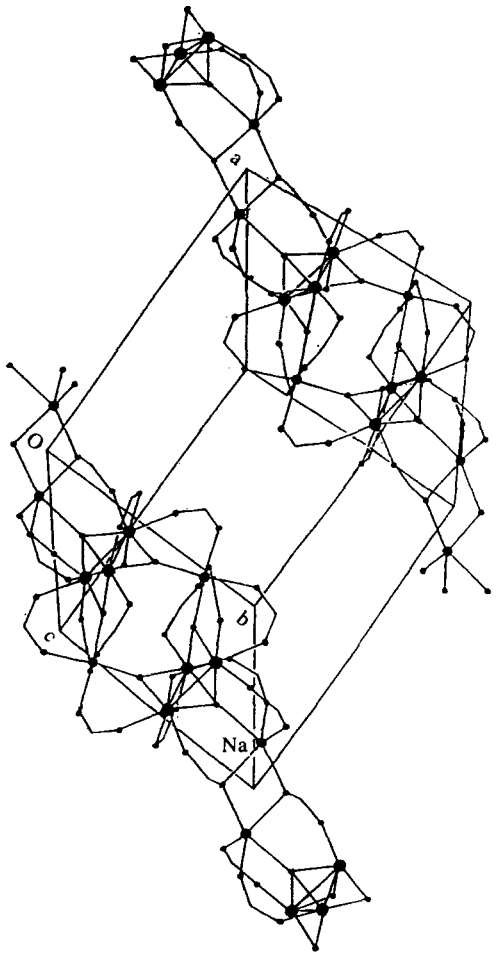


Fig. 3. Perspective view of the infinite chain of **1** with the Et groups omitted for clarity.

Acknowledgement—This work was supported by grants from the National Science Foundation of China.

REFERENCES

1. Xu, L., Liu, H., Yan, D. C., Huang, J. S. and Zhang, Q. E., *J. Chem. Soc., Chem. Commun.* 1993, 1509.
2. Xu, L., Liu, H., Yan, D. C., Huang, J. S. and Zhang, Q. E., *J. Chem. Soc., Dalton Trans.* 1994, 2099.
3. Xu, L., Liu, H., Huang, J. S., Yan, D. C. and Zhang, Q. E., *Chem. Eur. J.*, 1997, **3,** 140.
4. Xu, L., Li, Z. F. and Huang, J. S., *Inorg. Chem.* 1996, **35,** 5097.
5. Liu, H., Xu, L., Huang, J. S., Cheng, W. D., Huang, X. Y. and Huang, X., *Polyhedron*, 1996, **15,** 2003.
6. Cotton, F. A., *Polyhedron*, 1986, **5,** 3.
7. Benory, E., Bino, A., Cotton, F. A. and Dori, Z., *Inorg. Chim. Acta*, 1985, **99,** 137.
8. (a) Richens, D. T. and Sykes, A. G., *Inorg. Chem.* 1982, **21,** 418; (b) Paffet, M. T. and Anson, F. C., *Inorg. Chem.* 1983, **22,** 1347; (c) Ooi, B. L., Petrou, A. L. and Sykes, A. G., *Inorg. Chem.* 1988, **27,** 3626.
9. Fackler Jr, J. P. and Avdeef, A., *Inorg. Chem.* 1974, **13,** 1864.
10. Stults, B. R., Marianelli, R. and Day, V. W., *Inorg. Chem.* 1979, **18,** 1853.
11. Bush Jr, J. B. and Finkbeiner, H., *J. Am. Chem. Soc.* 1868, **90,** 5903.
12. Walker, N. G. and Stuart, D., *Acta Cryst.* 1983, **A39,** 158.

Pergamon

PII: S0277-5387(96)00388-9

Polyhedron Vol. 16, No. 8, pp. 1371–1375, 1997
Copyright © 1997 Elsevier Science Ltd
Printed in Great Britain. All rights reserved
0277-5387/97 $17.00+0.00

Crystal structure and magnetic properties of a new oxo-centred basic benzoate bridging heterotrinuclear compound $[Cr_2MnO(PhCOO)_6Py_3][CrO_3Cl]$

Hao Xu,[a] Jinyu Li,[a] Jianzhong Zou,[a] Zheng Xu,[a]* Xiaozeng You,[a] Guocong Guo,[b] Jinshun Huang[b] and Honghui Zhuang[b]

[a] Coordination Chemistry Institute, State Key Laboratory of Coordination Chemistry, Nanjing University, Nanjing 210093, P.R. China

[b] State Key Laboratory of Structural Chemistry, Fujian Institute of Research on the Structure of Matter, Academia Sinica, Fuzhou, P.R. China

(Received 21 April 1996; accepted 6 August 1996)

Abstract—A new oxo-centred heterotrinuclear complex $[Cr_2MnO(PhCOO)_6Py_3][CrO_3Cl]$ was synthesized, which exhibited weak antiferromagnetic interaction between three atoms Cr^{III}, Cr^{III} and Mn^{III}. The J values for Cr^{III}—Mn^{III} and Cr^{III}—Cr^{III} have been estimated; the central O atom provides the main superexchange pathway. It indicated that the distance of M—(μ_3-O) is an important factor for metal–metal superexchange interaction. Copyright © 1997 Elsevier Science Ltd

Keywords: crystal structure; magnetic susceptibility; heteronuclear complex; chromium–manganese complex; oxo-centred complex; trinuclear complex.

Oxo-centred trinuclear complexes were the first polynuclear complexes to be investigated magnetically [1–2] and the first [2] in which the magnetic interactions were found. X-ray crystal structure [3] demonstrated that they contained an essentially equilateral triangle of metal ions surrounding a central O atom. Trinuclear complexes [4–7] $M_3O(RCOO)_6L_3$ and $[M_3O(RCOO)_6L_3]X$ were known for a wider range of metal ions, such as V, Cr, Mn, Fe, Co, Ni, Ru, Rh and Ir. The mixed-metal clusters [8–12] have attracted particular attention because spin-coupling interactions between different metal atoms may be investigated in almost the same geometric framework. It was possible to answer such questions as: is the exchange interaction mediation by the central atom, the bridging ligand or both? Although heterotrinuclear complexes had been known for more than half a century, $[Fe_2^{III}M^{II}O(MeCOO)_6L_3]$ complexes (L: H_2O, M: Co, Ni or Zn; L: Py, M: Co, Ni) were originally prepared in 1928 by Weinland and Holtmeier [8] and the structure was proved in 1980 by Yokubov [9]. The complexes of $Cr_2^{III}M^{II}$, $Cr^{III}Fe^{III}Mn^{II}$ analogues were reported in 1982 [10], these heterotrinuclear complexes exhibited antiferromagnetic exchange interactions and the central O atom provided the main superexchange pathway [13], in which p-orbitals of oxygen atom in the M_3O plane were especially effective. It is apparent that the number of d-electrons in $M_2^{III}M'^{III}O$ compounds is one less than that in $M_2^{III}M'^{II}O$ compounds, so the magnetic properties of those complexes may appear quite different, but few heterotrinuclear $M_2^{III}M'^{III}O$ complexes [14] have been studied. In this paper we report the synthesis of a new heterotrinuclear compound $[Cr_2MnO(PhCOO)_6Py_3][CrO_3Cl]$ and the crystal structure and magnetic properties of the compound.

EXPERIMENTAL

Preparation of materials

Preparation of NBu_4MnO_4. *Described by T. Sale* [15].

$[Cr_2MnO(PhCOO)_6Py_3][CrO_3Cl] \cdot 2/3Py$.

* Author to whom correspondence should be addressed.

$CrCl_3 \cdot 6H_2O$ (2.17 g) and benzonic acid (7.5 g) were dissolved in pyridine (20 cm^3), while stirring NBu_4MnO_4 (1.14 g) was slowly added. After stirring for 30 min, pyridine was evaporated under reduced pressure and a viscous slurry was obtained, then absolute alcohol (50 cm^3) was added and stirred, then the precipitate was produced. The mixture was filtered, washed three times with a little absolute alcohol. The product was a brown solid, yield 80% (calculated according to Cr).

The brown solid was redissolved in a little acetonitrile and brown–black single crystals were obtained after evaporating slowly in the air for several days. Found: C, 54.8; H, 3.8; N, 4.0; Cr, 11.8; Mn, 4.4. Calc. for $C_{60.3}H_{48.3}N_{3.7}O_{16}ClCr_3Mn$: C, 54.6; H, 3.7; N, 3.9; Cr, 11.7; Mn, 4.1%.

Identification of the anion $[CrO_3Cl]^-$. There are three Cr atoms and one Mn atom in the title compound. It must be confirmed which metal atom (Cr or Mn) is in the anion. A single crystal structure analysis cannot distinguish this, because the atomic numbers of Cr and Mn are very close. In this case chemical methods are useful.

The acetonitrile solution containing KPF_6 was added with stirring to the acetonitrile solution of the title compound and the yellow precipitate obtained was then filtered out and washed three times with CH_3CN. The filter liquor was evaporated at room temperature and a few days later brown crystals were obtained. The data from the inductively coupled plasma atomic emission spectrum showed that the yellow precipitate contained the elements Cr and K and the brown crystals contained the elements Mn, Cr and P. These results with X-ray crystal structure analysis data indicated that the yellow precipitate is $KCrO_3Cl$, composed of the coordination anion CrO_3Cl^- and K^+ ion and the brown crystals were composed of PF_6^- anion and the large cation $[Cr_2MnO(PhCOO)_6Py_3]^+$.

Crystallographic studies

A deep black–brown single crystal (dimensions: $0.30 \times 0.50 \times 0.90$ mm^3) was mounted on a Rigaku AFC 5R diffractometer.

X-ray diffraction data were collected at 296 K with Mo-K_α radiation (0.71073 Å) and ω–2θ scan mode in the range $0 < 2\theta < 49.9°$. Of the 1881 independent reflections collected, 1119 reflections with $I > 3\sigma$ were used in structure calculation. All data were corrected for Lp factors and empirical absorption. The structure was solved by direct methods.

$[Cr_2MnO(PhCOO)_6Py_3][CrO_3Cl] \cdot 2/3Py$, M = 1326.69, hexagonal, space group $P6_3/m$, $a = b$ = 12.92(1), c = 21.35(2) Å, V = 3089(4) $Å^3$, Z = 2, D_x = 1.43 g cm^{-3}, $F(000)$ = 1356, μ = 8.02 cm^{-1}. The refinement converged at the final R = 0.050 and R_ω = 0.063. $R = \Sigma \| F_o | - | F_c \| / \Sigma | F_o |$; $R_\omega = [\Sigma\varepsilon(| F_o | / | F_c |)^2 / \Sigma\omega | F_o |^2]^{1/2}$; $\omega = 1/\sigma^2 F$.

RESULTS AND DISCUSSION

Structural description

The compound consists of a cation and an anion. The cation structure is shown in Fig. 1. Selected bond distances and angles of the compound are given in Table 1. In the cation unit three metal atoms form an equilateral triangle with μ_3-O located at the centre of this planar triangle and the three-fold axis is normal to the plane and through the μ_3-O atom. The bond distances of M(2)—(μ_3-O) are 1.903(2) Å, in agreement with the M—(μ_3-O) distance in $[M_3O(RCOO)_6]^+$, which lie within a fairly narrow range (1.90 ± 0.01 Å) [13]. The distance is longer than that of Cr—(μ_3-O) in the Cr_3O complex (1.89 Å) [5] and shorter than that of Mn—(μ_3-O) in the Mn_3O complex (1.936 Å) [16]. It is reasonable that the M(2)—(μ_3-O) distance in the title compound is the average value of two Cr—O bonds and one Mn—O bond. It means that two Cr^{III} ions and one Mn^{III} ion occupy the three M(2) ions sites, statistically. As compared with neutral M_3—(μ_3-O) type compounds, in which the formal oxidation numbers were II, III and III, the bond distances of M—(μ_3-O) in the title compound are shorter than the neutral one, because the formal oxidation number is higher in the latter (+3) than in the former (+2.7); both the ionic radius and static electronic contribute to a shorter bond distance of M—(μ_3-O). In the complex, the coordination geometry of each metal ion is a slightly distorted octahedral with five oxygen atoms from bridging benzonic acid groups and μ_3-O and a nitrogen atom from a terminal pyridine. The pyridine rings are almost perpendicular to the M_3O plane, probably due to greater steric interactions with the benzoate groups. The M(2)—N distance is 2.109(6) Å, which is shorter than that of the heterotrinuclear $Cr^{III}_2Ni^{II}O$ complex (2.137–2.149 Å) [11],

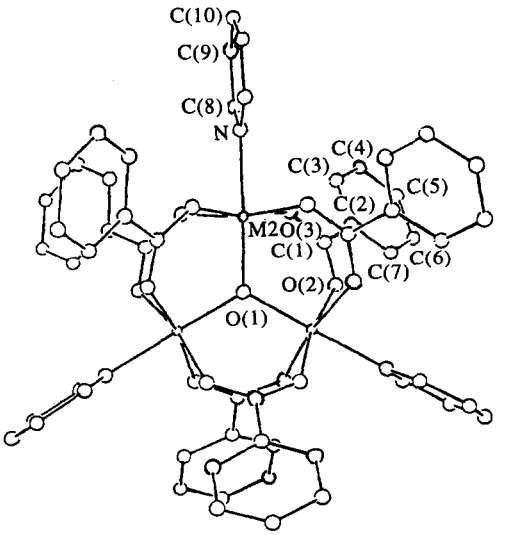


Fig. 1.

Table 1. Selected intramolecular distances (Å) and bond angles (°)

M(1)—O(4)	1.554(8)	M(1)—M(1)	2.145(5)
M(2)—O(1)	1.903(2)	M(2)—O(2)	1.981(4)
M(2)—O(3)	1.984(4)	M(2)—N	2.109(6)
C(1)—C(2)	1.492(7)	O(2)—C(1)	1.257(6)
O(3)—C(1)	1.247(6)	N—C(8)	1.333(6)
O(4)—M(1)—O(4)	112.2(3)	O(2)—M(2)—N	84.7(1)
O(4)—M(1)—M(1)	106.6(3)	O(2)—M(2)—O(3)	169.9(2)
O(1)—M(2)—O(2)	94.8(1)	O(2)—M(2)—O(3)	87.8(2)
O(1)—M(2)—O(3)	95.3(1)	O(3)—M(2)—O(3)	91.4(2)
O(1)—N(2)—N	179.4(2)	O(3)—M(2)—N	85.2(1)
O(2)—M(2)—O(2)	91.2(3)	M(2)—O(1)—M(2)	120.0003(8)
O(2)—M(2)—O(3)	87.8(2)	M(2)—O(1)—M(2)	120.00
O(2)—M(2)—O(3)	169.9(2)	M(2)—O(1)—M(2)	119.9996(7)

M(1) = 1/2Cr+1/2Cl, M(2) = 2/3Cr+1/3Mn.

because the positive charge in M(2) is higher than in the latter. The M(2)—M(2) distances are all 3.296(3) Å, so there are no M—M bonds between the metal ions. As a comparison, selected data of $Cr_3O(CF_2HCOO)_6Py_3$ (**A**) [17], $[Cr_3O(CH_3COO)_6(H_2O)_3]^+$ (**B**) [17] and $[Cr_2MnO(PhCOO)_6Py_3]^+$ (**C**) are listed in Table 2.

As we can see in Table 2, there are some composition differences between compound **A** and cations **B** and **C**. The different bridging ligands CH_3COO, CHF_2COO and PhCOO only have small effects. The equatorial ligands and formal oxidation numbers of the metals are more important. H_2O is a weaker base than pyridine, so the Cr—(μ_3-O) bond is stronger in cation **B** than in cation **C**. The formal oxidation number is +3 in cations **B** and **C**, but +2.67 in compound **A**. This is the reason that the distance between atoms are shorter in cations **B** and **C** than in compound **A**.

The structure of the anion $[CrO_3Cl]^-$ is shown in Fig. 2. The existence of $[CrO_3Cl]^-$ was proved by the chemical method as above. In the unit cell the CrO_3Cl ion is disordered over a centre of inversion, such that an ethane-like structure is produced (Fig. 3), with the Cl and Cr atoms half occupying the M(1) site, Fig. 2. The M(1)—M(1A) length appears to be shorter [2.145(5) *vs* 2.16 Å] and the M—O distances longer [1.554(8) *vs* 1.53 Å] than in $KCrO_3Cl$ [16], probably as a consequence of the disorder. The geometry of the anion is a pyramidal with Cl and three oxygen atoms located on the each apexes.

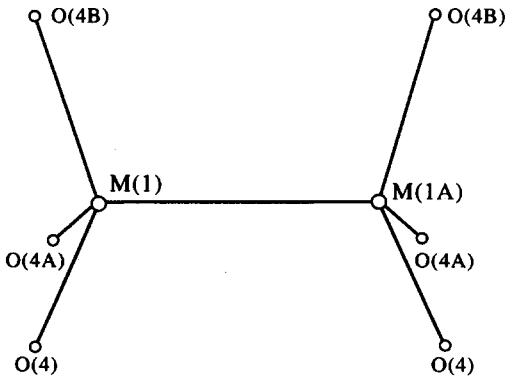


Fig. 2.

The solvent pyridine molecule is disordered about the three-fold axis parallel to the C direction and the C and N atoms are statistically distributed over all sites.

IR spectroscopy

Canon *et al.* [12] have convincingly assigned the IR spectra of a series of trinuclear Cr^{III} acetate and for-

Table 2. Selected bond lengths (Å) of compounds **A**, **B** and **C**

	Compound **A**	Compound **B**	Compound **C**
Formal oxidation number	+2.67	+3.0	+3.0
Cr—Cr	3.356(2)	3.274	3.296(3)
Cr—(μ_3-O)	1.938(1)	1.89(2)	1.903(2)
Cr—N	2.158(7)		2.109(6)
Cr—O(carboxy)	2.013(4), 2.054(5)	1.98	1.98(4), 1.984(4)
Cr—O(H_2O)		2.05	

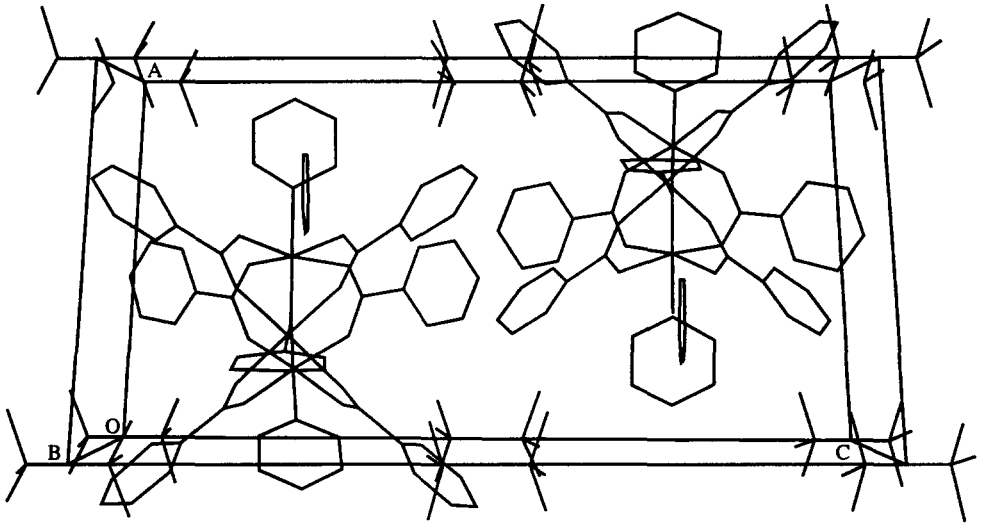


Fig. 3.

mate complexes and identified the vibrational modes of the central Cr_3O model, and found that when one of the Cr^{III} ions is replaced with Fe^{III} the band at 640–660 cm^{-1} splits.

As shown in Table 3, there are similar IR spectra for complexes $[Cr_3O(PhCOO)_6Py_3]ClO_4$ (**1**) [17], $[Cr_3O(PhCOO)_6Py_3]Cl$ (**2**) [17] and $[Cr_2MnO(PhCOO)_6Py_3][CrO_3Cl]^-$ at 935 cm^{-1} appears.

Magnetic properties

Variable-temperature (1.5–300 K) magnetic susceptibility data were recorded for powder samples of the compound using a CF-1 ESM magnetic balance. The effective magnetic moment (μ_{eff}) per molecule decreased slowly down to 54 K (6.9μ_B), below which it decreased quite rapidly (5.6μ_B at 51 K to 2.9μ_B at 1.5 K).

As can be seen in Fig. 4, the variable-temperature magnetic susceptibility of the sample follows the Curie–Weiss law with a slight deviation at the lower temperature. The Weiss constant $\theta = -37$ K and the Curie constant $C = 5.90$. There is an antiferromagnetic exchange interaction in the compound.

The spin-Hamiltonian which describes the isotropic magnetic exchange interaction in a triangular trinuclear complex is given in eq. (1).

$$H = -2[J_{12}(s_1s_2)+J_{23}(s_2s_3)+J_{31}(s_3s_1)] \quad (1)$$

here, $J_{12} = J_{31} = J_1$, $J_{23} = J_2$.

With the assumption that the g values of Cr^{III} and Mn^{III} are equal to 2.00, HDVV model leads to the expression of the molar magnetic susceptibility as follows

Table 3. IR spectra (cm^{-1}) of selected complexes

Compound **1**	Compound **2**	Compound **3**	Assignment
1620(br, vs)	1615(br, vs)	1613(vs)	PhCOO/Py
1570(vs)	1580(vs)	1573(vs)	PhCOO
1310(w)	1330(w)	1314(w)	PhCOO
1225(m)	1225(m)	1217(m)	Py
1185(m)	1185(m)	1177(m)	PhCOO
1050(w)		1047(m)	Py
1030(m)	1020(m)	1025(m)	Py
		953(s)	CrO_3Cl
850(m)	850(m)	844(w)	PhCOO
755(s)	755(s)	759(m)	Py/CO_2
720(vs)	720(vs)	717(vs)	PhCOO
700(vs)	700(s)	699(s)	Py
690(vs)	680(s)	684(s)	PhCOO
650(vs)	640(vs)	658(s), 635(s)	M_2O
610(m)	610(sh)	593(m)	Py

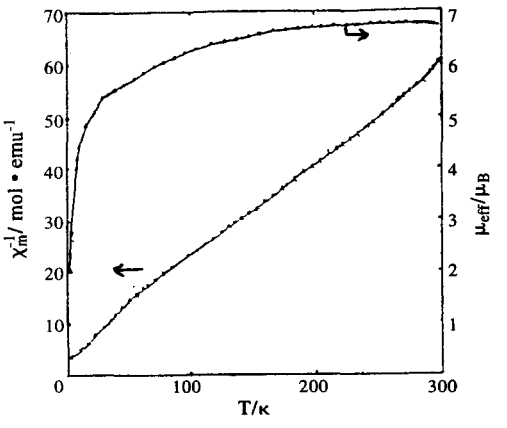


Fig. 4.

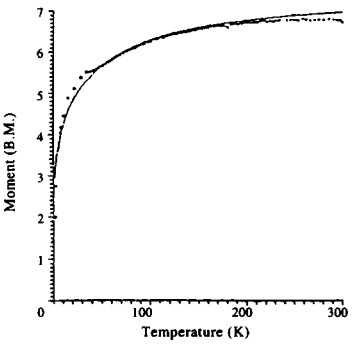


Fig. 5.

$$\chi_m = \frac{Ng^2\mu_B^2}{12kT}\cdot\frac{A}{B}. \quad (2)$$

Here, $A = 330\exp(18x+12y)+180\exp(8x+12y)+180\exp(14x+6y)+84\exp(12y)+84\exp(6x+6y)+84\exp(10x+2y)+30\exp(-6x+12y)+30\exp(6y)+30\exp(4x+2y)+30\exp(6x)+6\exp(-10x+12y)+6\exp(-4x+6y)+6\exp(2y)$; $B = 11\exp(18x+12y)+9\exp(14x+6y)+9\exp(8x+12y)+7\exp(12x)+7\exp(6x+6y)+7\exp(10x+2y)+5\exp(-6x+12y)+5\exp(6y)+5\exp(4x+2y)+5\exp(6x)+3\exp(-10x+12y)+3\exp(-4x+6y)+3\exp(2y)+\exp(-6x+6y)$; $x = J_1/kT$, $y = J_2/kT$.

The magnetic susceptibility data for the complex is fitted to eq. (2) with the fitting parameters $J_1 = -7.03$, $J_2 = -13.4$ cm^{-1} and Curie constant $C = 6.06$, the solid line in Fig. 5 represents this fitting.

It is indicated that there are weak antiferromagnetic interactions between three metal atoms, Cr, Cr and Mn, and the interaction of Cr—Cr is almost twice as large as that of Cr—Mn. According to the molecular structure, there are no M—M bonds between the metal ions and two possible superexchange pathways in the complex: the central O atom and the bridging benzoate groups. Vincent *et al.* [15] recently reported the oxo-centred trinuclear Mn^{III} complex, with J values of -10.2 cm^{-1} and the majority of this interaction is propagated by the central oxygen atom, not by the acetate bridges. It can be seen in Table 4 that the distance of M—(μ_3-O) is a very important factor.

The shorter the M^{III}—O distance, the larger is the J value. The short M^{III}—O distance could raise the energy of the dz^2 orbital directed along the M^{III}—O bond vector. In the Cr_2MnO complex the M^{III}—O bond length is an average value in crystallography, but they are different at the molecular level, so the J_1 and J_2 values are not equal.

Acknowledgement—This work was supported by a grant for key research project from the State Science and Technology Commission and the National Nature Science Foundation of China.

REFERENCES

1. Welo, L. A., *Philos. Mag.* 7 *ser.* 1928, **6,** 481.
2. Kamb, K. *J. Phys. Soc. Jpn*, 1950, **5,** 48; Foex, G., Tsai, B. and Wucher, J., *C. R. Hebd. Seances Acad. Sci.* 1951, **233,** 1432; Abragamand, A. and Yvon, J., *J. Phys.* 1952, **13,** 485.
3. Figgis, B. N. and Robertson, G. B., *Nature*, 1965, **205,** 694; Chang, S. C. and Jeffrey, S. A., *Acta Cryst.* 1970, **B26,** 673.
4. Catterick, J. and Thornton, P., *Adv. Inorg. Chem. Radiochem.* 1977, **20,** 291.
5. Chretien, A. and Lous, E., *Bull. Soc. Chim. Fr.* 1944, **11,** 446.
6. Baikie, A. R. E., Hursthouse, M. B., New, D. B. and Thornton, P., *J. Chem. Soc., Chem. Commun.* 1978, 62.
7. Cotton, F. A. and Norman, J. G., *Inorg. Chim. Acta*, 1972, **6,** 411.
8. Weinland, R. and Holtmeier, H., *Z. Anorg. Allg. Chem.* 1928, **173,** 49.
9. Yakubov, K. M., Zelentsov, V. V., Zhemchuzhnikova, T. A. and Fisher, V. R., *Dokl. Akad. Nuak. SSSR*, 1980, **250,** 402.
10. Blake, A. B. and Yavari, A., *Dokl. Akad. Nauk. SSSR*, 1982, 1247.
11. Yu, S. F. and Yuan, R. S., *Sci. Lett.* (*China*), 1987, **4,** 269.
12. Cannon, R. D., Jayassooriya, U. A., Montri, L. and Blake, A. B., *J. Chem. Soc., Dalton. Trans.* 1993, 2005.
13. Sale, T. and Sargent, M. V., *J. Chem. Soc., Chem. Commun.* 1978, 253.
14. Helmholz, L. and Foster, W. R., *J. Am. Chem. Soc.* 1950, **72,** 4971.
15. Vincent, J. B., Chang, H.-R. and Herdrickson, N., *J. Am. Chem. Soc.* 1987, **109,** 5703.
16. Harton, A., Nagi, M. K. and Vincent, J. B., *Inorg. Chim. Acta*, 1994, **217,** 171.
17. Cotton, F. A. and Wang, W., *Inorg. Chem.* 1982, **21,** 2675.

Table 4. M—O bond lengths and values of J in some trinuclear complexes

Complex	M—(μ_3-O) distance (Å)	J (cm^{-1})	References
$Cr_2^{III}Mn^{III}$—O	1.981(4)	−7.03 and −13.4	This work
Mn_3^{III}—O	1.936	−10.2	[15]
Cr_3^{III}—O	1.89	−11	[13]
Fe_3^{III}—O	1.862–1.867	−30	[13]

Pergamon

PII: S0277-5387(96)00389-0

Polyhedron Vol. 16, No. 8, pp. 1377–1380, 1997
Copyright © 1997 Elsevier Science Ltd
Printed in Great Britain. All rights reserved
0277–5387/97 $17.00+0.00

Crystal structure and magnetic properties of a new oxo-centred basic benzoic bridging mixed-valence trinuclear complex $Mn^{III}Co^{III}Mn^{II}O(PhCOO)_6Py_3$

Hao Xu,[a] Jian-Zhong Zou,[a] Jin-Yu Li,[a] Zheng Xu,[a]* Xiao-Zeng You,[a] Guo-Chong Guo[b] and Jin-Shun Huang[b]

[a] Coordination Chemistry Institute, the State Key Laboratory of Coordination Chemistry, Nanjing University, Nanjing 210093, P. R. China

[b] State Key Laboratory of Structure Chemistry, Fujian Institute of Research on the Structure of Matter, Academia Sinica, Fuzhou, P. R. China

(Received 6 October 1995; accepted 6 August 1996)

Abstract—A new mixed-valence heterotrinuclear complex [Mn^{III} Co^{III} $Mn^{II}O(PhCOO)_6Py_3$] was first synthesized by using NBu_4MnO_4 as the oxidizer. In the reaction, Co^{II} ions were oxidized to Co^{III}, while Mn^{VII} were reduced to Mn^{II} and Mn^{III}. The oxidation number of three metal ions were +3, +3 and +2, which was proved by the electrical conductivity. There are two types of trinuclear species in the single cell. One is valence delocalized in which the bond distance Co(2)—O(2) is 1.85(2) Å and the distance M—O is 1.933(9) Å, which is an average value of Mn^{II}—O and Mn^{III}—O; another is valence-localized in which the bond distance of Co^{III}—O is 1.84(1), Mn^{III}—O, 1.86(1), Mn^{II}—O, 1.99(1) Å. Variable temperature (1.5–300 K) magnetic susceptibility indicated that there is antiferromagnetic exchange interaction among the three metal ions.
Copyright © 1997 Elsevier Science Ltd

Keywords: crystal structure; mixed-valence complex; heteronuclear complex; manganese–cobalt complex; magnetic properties; oxo-centred complex.

Trinuclear, oxo-centred carboxylate complexes of transition metals have been of interest for several years [1]. The oxo-centred [2] heterotrinuclear complexes have special interests, because the magnetic exchange interaction of different nuclei could be studied under almost same geometry, but little work has been done. Blake [3] previously reported magnetic and spectroscopic properties of some heterotrinuclear basic acetic acids of $Cr_2^{III}M^{II}$ and $Fe_2^{III}M^{II}$ (M = Mg, Fe, Co, Ni, Mn). A series of mixed-metal and mixed-valence compounds, $[Cr_2MnO(PhCOO)_6Py_3][CrO_3Cl]$ [4], $Cr_2^{III}Mn^{II}O(CH_3COO)_6Py_3$ and $Mn_2^{III}M^{II}O(CH_3COO)Py_3$ [5], had been reported recently. These compounds had the similar oxo-centred structure and weak antiferromagnetic interaction between the metal ions.

Using Bu_4NMnO_4 as an oxidizer, the heterotrinuclear mixed-valence complex [$Mn^{III}Mn^{II}Co^{III}O$] was synthesized and the molecular structure and variable-temperature susceptibility were determined.

EXPERIMENTAL

Preparation of materials

Benzoic acid, $Co(OAc)_2$, pyridine, absolute ethanol and CH_3CN were used as received. The elemental analyses for carbon, hydrogen and nitrogen were determined on a Perkin–Elmer 240C analyser. X-ray photoelectron spectra (XPS) was performed on a VG MK II spectrometer using Mg-K_α radiation and charge-transfer correction referred to the binding energy of C_{1s}. The variable-temperature (1.5–300 K) magnetic susceptibility measurement of the title

* Author to whom correspondence should be addressed.

complex was obtained on a CF-1 ESM magnetic balance at 1.2T magnetic field.

Preparation of NBu_4MnO_4. Followed reference [6]. $Mn_2Co(PhCOO)_6(Py)_3$. $Co(OAc)_2$ (2.88 g) and benzoic acid (15 g) dissolved in pyridine (40 cm^3) forming a violet–red solution, to which NBu_4MnO_4 (2.28 g) was slowly added with stirring. After reacting for 10 min, pyridine was evaporated under reduced pressure and a brown oily slurry was obtained. Then, 200 cm^3 of absolute alcohol was added with stirring and some precipitates were deposited, filtered and washed three times with a little absolute alcohol. The brown solid was obtained and redissolved in a minimum amount of acetonitrile, then filtered. The filtrate was evaporated at room temperature for a few days, then black crystals were obtained. Found: C, 59.6; H, 3.9; N, 4.0; Mn, 8.5; Co, 5.0. Calc. for $C_{57}H_{45}N_3O_{13}Mn_2Co$: C, 59.6; H, 4.0; N, 3.7: Mn, 9.6; Co, 5.1%.

Variable-temperature (1.5–300 K) magnetic susceptibility data have been recorded for the microcrystal sample of the title complex using a CF-1 ESM magnetic balance.

Determination of electrical conductivity

The title compound and Et_4NBr were dissolved in acetonitrile, which was treated with CaH_2, P_2O_5 and K_2CO_3 before use. The conductivity data were determined using a DDS-11A electrical conductivity instrument at 20.00 ± 0.02°C.

The molar conductivity of the title compound (in CH_3CN) is 3.15 $\omega^{-1}cm^{-2}mol$, which corresponds to non-electrolytic behaviour. This means that the valences of three metal ions were +3, +3 and +2.

Table 1. Summary of crystal and intensity collection parameters

Formula	$C_{57}H_{45}O_{13}Mn_2Co$
Fw	1148.80
Crystal system	monoclinic
Space group	*C*2/*c*
Unit-cell constants	
a (Å)	58.62(2)
b (Å)	11.782(2)
c (Å)	24.839(7)
β (°)	100.56
V (Å^3)	16864
Z	12
D_c (Mg m^{-3})	1.36
F (000)	7068
$2\theta_{max}$(°)	50
Scan speed (° min^{-1})	8
ω-scan width	$1.38+0.35tg\theta$
Residuals (*R*, ωR)	0.083, 0.095
No. of variables	646

X-ray crystallography

A black prism crystal ($0.5 \times 0.3 \times 0.3$ mm) was used for X-ray diffraction (see Table 1). Data were collected on a Rigaku AFC5R diffractometer at 296 K using graphite-monochromatic Mo-K_α (0.71073 Å) radiation and $\omega/2\theta$ scan mode. 3790 observed reflections with $I > 3\sigma(I)$ were used in structure calculation and all data were corrected for Lp factors and empirical absorption. The structure was solved by direct methods. Successive Fourier syntheses gave the coordinates of all the non-hydrogen atoms refined with anisotropic thermal parameters. All calculations were performed on a Micro-VAX II computer using TEXSAN programs. Atomic coordinates and thermal parameters, together with observed and calculated structure factors, have been deposited with the Editor, from whom copies are available on request.

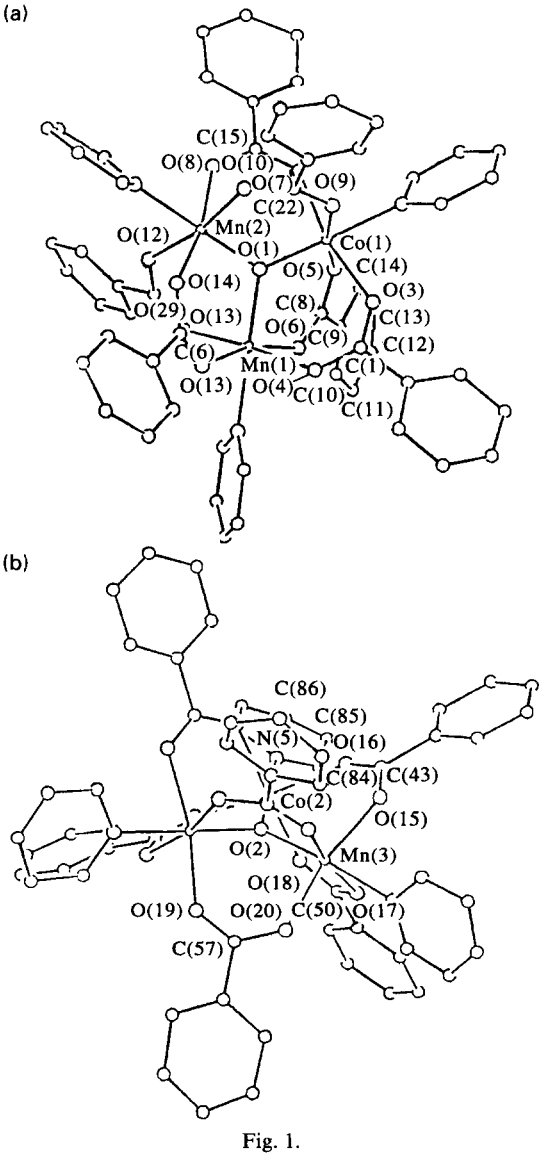


Fig. 1.

Table 2. Selected bond lengths (Å) and bond angles (°)

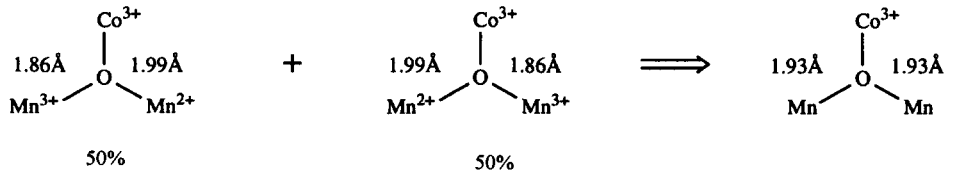
Co(1)—O(1)	1.84(1)	Co(1)—O(3)	2.06(1)
Co(1)—O(7)	2.04(1)	Co(1)—O(9)	2.08(1)
Co(1)—O(5)	2.08(1)	Co(1)—N(1)	2.09(1)
Co(2)—O(2)	1.85(2)	Co(2)—O(18)	2.04(1)
Co(2)—O(16)	2.06(1)	Co(2)—N(5)	2.14(3)
Mn(1)—O(1)	1.99(1)	Mn(1)—O(13)	2.08(1)
Mn(1)—O(10)	2.08(2)	Mn(2)—O(4)	2.09(1)
Mn(1)—O(11)	2.09(2)	Mn(1)—N(2)	2.15(2)
Mn(2)—O(1)	1.86(1)	Mn(2)—O(6)	2.01(1)
Mn(2)—O(12)	2.01(2)	Mn(2)—O(14)	2.08(1)
Mn(2)—O(8)	2.10(2)	Mn(2)—N(3)	2.11(2)
Mn(3)—O(2)	1.933(9)	Mn(3)—O(20)	2.02(1)
Mn(3)—O(15)	2.05(1)	Mn(3)—O(19)	2.09(1)
Mn(3)—N(4)	2.12(2)	Mn(3)—O(17)	2.15(1)

O(1)—Co(1)—O(7)	95.9(6)	O(1)—Co(1)—O(3)	97.8(5)
O(1)—Co(1)—O(9)	94.9(6)	O(1)—Co(1)—O(5)	94.5(6)
O(1)—Co(1)—N(1)	177.6(6)	O(2)—Co(2)—O(18)	93.7(4)
O(2)—Co(2)—(16)	98.0(4)	O(2)—Co(2)—N(5)	180.3(3)
O(1)—Mn(1)—O(13)	98.6(6)	O(1)—Mn(1)—O(10)	94.4(5)
O(1)—Mn(1)—O(4)	93.7(5)	O(1)—Mn(1)—O(11)	91.2(5)
O(1)—Mn(1)—N(2)	177.8(7)	O(1)—Mn(2)—O(6)	95.4(5)
O(1)—Mn(2)—O(12)	94.8(6)	O(1)—Mn(2)—O(14)	96.3(5)
O(1)—Mn(2)—O(8)	95.1(6)	O(1)—Mn(2)—N(3)	179.1(7)
O(2)—Mn(3)—O(20)	93.1(5)	O(2)—Mn(3)—O(15)	98.0(5)
O(2)—Mn(3)—O(19)	94.2(5)	O(2)—Mn(3)—N(4)	175.8(6)
O(2)—Mn(3)—O(17)	96.0(5)	Co(1)—O(1)—Mn(2)	122.0(6)
Co(1)—O(1)—Mn(1)	119.8(6)	Mn(1)—O(1)—Mn(2)	118.1(6)
Co(2)—O(2)—Mn(3)	119.7(4)	Mn(3)—O(2)—Mn(3)	120.6(9)

RESULTS AND DISCUSSION

The acetate bridging $Mn_2^{III}Co^{II}O$ species had been prepared by Cannon [5] recently using oxygen as the oxidizer. The title compound $Mn^{III}Co^{III}Mn^{II}$ was synthesized by using Bu_4NMnO_4 as oxidizer. The Co^{II} ion was oxidized to Co^{III}, while Mn^{VII} ions were reduced to Mn^{II} and Mn^{III}. X-ray photoelectron spectra of the title complex have been determined and display two peaks at 781.7 and 642.4 eV. The former belongs to $Co2P_{3/2}$ and the latter belongs to $Mn2P_{3/2}$.

The molecular structure is shown in Fig. 1, and selected bond distances and angles are given in Table 2. Every metal atom has a slightly distorted octahedral coordination geometry with four oxygen atoms from bridging benzoate groups, the μ_3-oxygen atom and a nitrogen atom of terminal pyridine. The pyridine rings are essentially perpendicular to the trinuclear complex, probably as a result of increased steric interactions between the pyridine rings and the benzoate phenyl group. There are two kinds of Mn_2CoO species in the unit cell. One is valence localized, in which the distances of three metal atoms to μ-O atom are 1.84(1), 1.86(1) and 1.99(1) Å, respectively [Fig. 1(a)]. Considering the oxidation state of the metal atoms in the title compound and the bond distances of M—O in references [7]–[9], we could classify three bonds of M—O as follows: 1.84(1) Å belongs to the bond distance of Co^{III}—O, 1.86 Å to Mn^{III}—O and 1.99 Å to Mn^{II}—O. Another one is valence delocalized (Fig. 1(b)), in which the distance Co(2)—O(2) is 1.85(2) Å and the distance Mn(3)—O(2) [1.933(9) Å] is a statistical average value of Mn^{III}—O [1.86(1) Å] and Mn^{II}—O [1.99(1) Å]. This is disorder stack as shown below:



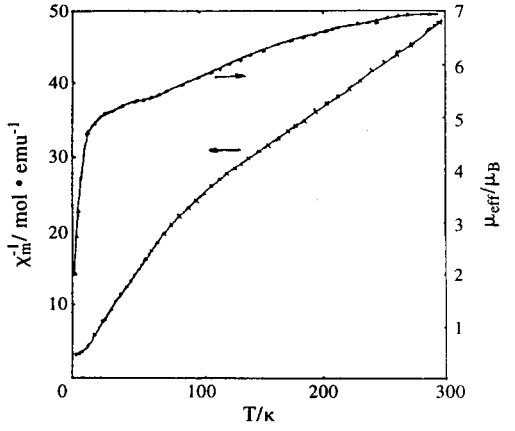


Fig. 2.

There are eight asymmetry units in a single cell and each unit contains 1.5 trinuclear complex units, $[Mn_2CoO(PhCOO)_6Py_3]$, of which the complete molecule has a bond delocalized structure [Fig. 1(b)] and the other 'half' which is part of a molecule sited on a two-fold axis has a bond localized structure [Fig. 1(a)].

Magnetic properties

As can be seen in Fig. 2, the effective magnetic moment (μ_{eff}) per molecule decreased 7.0μ_B at 300 K, 5.0μ_B at 80 K, 4.8μ_B at 17 K and 1.95μ_B at 1.5 K. This suggests that there is an antiferromagnetic exchange among the three metal atoms: Co^{III}, Mn^{III} and Mn^{II}.

Acknowledgements—This work was supported by a grant for key research projects from the state Science and Technology Commission and the National Nature Science Foundation of China and Beijing Zhongguancun Associated Centre of Analysis and Measurement.

REFERENCES

1. Welo, L. A., *Philos. Mag.* 7 *Ser.*, 1928, 481; Figgis, B. N. and Robertson, G. B., *Nature(London)*, 1965, **2051**, 694; Earnshaw, A., Figgis, B. N. and Lewis, J., *J. Chem. Soc.* (*A*), 1966, 1656; Chang, S. C. and Jeffrey, G. A., *Acta Crysta.* 1970, **B26,** 677; Vemura, S., Spencer, A. and Wilkinson, G., *J. Chem. Soc., Dalton. Trans.* 1973, 2565; Cotton, F. A. and Wang, W., *Inorg. Chem.* 1982, **21,** 2675; Cannon, R. D. and White, R. P., *Prog. Inorg. Chem.* 1988, **36,** 195.
2. Weinland, R. and Holtmeier, H., *Z. Anorg. Allg. Chem.* 1928, **173,** 49; Yakabov, K. M., Zelentsov, V. V., Zhemchuzhnikova, T. A., Abdullaev, S. K. and Fisher, R., *Dokl. Akad. Nauk. SSSR*, 1980, **250,** 402; Balke, A. B. and Yavari, A., *ibid*, 1982, 1247.
3. Blake, A. B., Yavari, A., Haffield, W. E. and Sethulekshmi, C. N., *J. Chem. Soc.,Dalton. Trans.* 1985, 2509.
4. Xu, H., Li, J., Zou, J., Xu, Z., You, X. and Gou, G., *Polyhedron*, in press.
5. Cannon, R. D., Jayassooriya, V. A., Montri, L., Bollen, S. K., Sanderson, W. R., Powell, A. K. and Blake, A. R., *J. Chem. Soc., Dalton. Trans.* 1993, 2006.
6. Sale, T. and Sargent, M. V., *J. Chem. Soc., Chem. Commun.* 1978, 253.
7. Baikie, A. R. E., Hursthouse, M. B., New, L., Thornton, P. and White, R. G., *J. Chem. Soc., Chem. Commun.* 1980, 684.
8. Vincent, J. B., Chang, H. R., Folting, K., Huffman, J. C., Christou, G. and Hendrickson, D. N., *J. Am. Chem. Soc.* 1987, **109,** 5703.
9. Charles, E. S. J. and Guy, R. S., *J. Am. Chem. Soc.* 1985, **107,** 6124.

Pergamon

PII: S0277-5387(96)00382-8

Polyhedron Vol. 16, No. 8, pp. 1381–1389, 1997
Copyright © 1997 Elsevier Science Ltd
Printed in Great Britain. All rights reserved
0277–5387/97 $17.00+0.00

Room-temperature fluorescence, phosphorescence and crystal structure of 4-acyl pyrazolone lanthanide complexes: $Ln(L)_3 \cdot 2H_2O$

Dejian Zhou,[a] Qin Li,[a] Chunhui Huang,[a]* Guangqing Yao,[a] Shigeo Umetani,[b] Masakazu Matsui,[b] Liming Ying,[c] Anchi Yu[c] and Xinsheng Zhao[c]

[a]State Key Laboratory of Rare Earth Materials Chemistry and Applications, Peking University, Beijing 100871, P.R. China

[b]Institute for Chemical Research, Kyoto University, Uji, Kyoto 611, Japan

[c]College of Chemistry and Molecular Engineering, Peking University, Beijing 100871, P.R. China

(Received 12 July 1996; accepted 2 August 1996)

Abstract—A series of ternary mixed ligand 4-acyl pyrazolone lanthanide complexes: $Ln(L)_3 \cdot 2H_2O$ [where Ln = Tb^{3+} or Gd^{3+}, L = 1-phenyl-3-methyl-4-acetyl-pyrazolone-5 (PMAP), 1-phenyl-3-methyl-4-propionyl-5-pyrazolone (PMPP), 1-phenyl-3-methyl-4-isobutyryl-5-pyrazolone (PMIP), 1-phenyl-3-methyl-4-neovaleryl-pyrazolone-5 (PMNP) and 1-phenyl-3-methyl-4-benzoyl-pyrazolone-5 (PMBP)] were synthesized and characterized by FT-IR spectra, UV–vis spectra and DTA-TG analysis. Room-temperature phosphorescence was observed from the Gd^{3+} complexes by excitation of the sample with the fourth harmonic frequency of a Nd: YAG laser beam (λ = 266 nm) and the triplet energies of the pyrazolone ligands were evaluated. Both the fluorescence intensity and fluorescence lifetime of the Tb^{3+} complexes depend on the structure of the ligands and explanations are presented. The crystal structure $[Tb(PMPP)_3 \cdot 2H_2O] \cdot EtOH$ was determined by X-ray diffraction. The structure was refined to $R = 0.064$ ($R_w = 0.073$). The complex is mononuclear and the central terbium ion is coordinated by eight oxygen atoms to form a square-antiprism coordination polyhedron, six of which are from the three bidentate pyrazolone ligands and the other two are from the two coordination water molecules. Copyright © 1997 Elsevier Science Ltd

Keywords: fluorescence; pyrazolone lanthanide; crystal structure; ligand; β-diketones.

β-Diketones have received extensive attention as important lanthanide extractants in solvent extraction. Among them, 1-phenyl-3-methyl-4-benzoyl-5-pyrazolone (HPMBP) was one of the most commonly used [1]. In recent years several other pyrazolones were synthesized, such as halogen substituted 4-acyl pyrazolones [2], bis-4-acyl pyrazolones [3] and these substituted pyrazolones have been found to be good chelating extractants in the separation of trivalent lanthanide ions [4]. Despite intense attempts, however, very few crystal structure of pyrazolone lanthanide extractants have been reported. Bombieri reported the crystal structure of tris(1-phenyl-3-phenyl-4-acetyl-5-pyrazolone)ytterbium dihydrate, $Yb(DPAP)_3 \cdot 2H_2O \cdot 3EtOH$ [5], while Huang *et al.* reported several trifluoro substituted 4-acyl pyrazolone lanthanide complexes [6]. The crystal structure of a lanthanide 4-acyl pyrazolone complex has not yet been reported. In this paper, we report the synthesis and crystal structure of tris(1-phenyl-3-methyl-4-propionyl-5-pyrazolone) terbium dihydrate, $[Tb(PMPP)_3 \cdot 2H_2O] \cdot EtOH$.

Some of the lanthanide β-diketonate complexes have interesting luminescence properties [7,8]. When irradiated with ultraviolet light, these lanthanide β-diketonate complexes exhibit narrow line emissions in the visible region characteristic of the metal ion. This phenomenon enables them to have many important

* Author to whom correspondence should be addressed.

practical applications, such as their use as fluorescence probes in biochemistry [9], and in the determination of trace amounts of trivalent lanthanide ions in solution [10]. Fluorescence methods are also used to obtain information about the structure of lanthanide complexes, their formation constants, symmetry, etc. [11]. Recently, they have been used in electroluminescent devices [12] and also as thresholdless microcavity laser materials [13]. Although there have been studies on the fluorescence properties of lanthanide β-diketonate complexes, there are still very few studies on 4-acyl pyrazolone lanthanide complexes of lanthanides [14]. The most commonly used pyrazolone (PMBP) complex with Tb^{3+} or Eu^{3+} was found to exhibit only very weak fluorescence and so it was supposed that the triplet energy of PMBP is too low to transfer energy efficiently to the central ion to obtain lanthanide fluorescence [14b]. We believe that the substitution of the benzoyl group with acyl can minimize the conjugation in the ligand, which may lead to a higher triplet energy such that a much higher fluorescence efficiency may be achieved. Room-temperature phosphorescence measurements on samples of Gd^{3+} with 4-acyl pyrazolone ligands confirmed our suggestion and as expected, strong green fluorescence from the 4-acyl pyrazolone terbium complexes was observed.

EXPERIMENTAL

Material and synthesis

The four 4-acyl pyrazolone ligands: 1-phenyl-3-methyl-4-acetyl-pyrazolone-5 (HPMAP), 1-phenyl-3-methyl-4-propionyl-pyrazolone-5 (HPMPP), 1-phenyl-3-methyl-4-iso-butyryl-pyrazolone-5 (HPMIP) and 1-phenyl-3-methyl-4-neovaleryl-pyrazolone-5 (HPMNP) were synthesized according to the procedure of Jensen [1]. 1-Phenyl-3-methyl-4-benzoyl-pyrazolone-5 (HPMBP) was analytical grade product purchased from the Beijing Chemical Factory (Beijing, China). Tb_4O_7 (>99.9%) and Gd_2O_3 (>99.9%) were purchased from Yuelong Chemical Factory (Shanghai, P.R. China). Aqueous solutions of $Tb(ClO_4)_3$ and $Gd(ClO_4)_3$ were prepared by dissolving Tb_4O_7 or Gd_2O_3 in perchloric acid to obtain a concentration of 0.40 M, (pH = 4.0). Other reagents were all analytical grade chemicals from the Beijing Chemical Factory.

The lanthanide complexes $Ln(L)_3 \cdot 2H_2O$ (where Ln = Tb, Gd and L = 4-acyl pyrazolones) were all synthesized by a similar method. A typical example for $Tb(PMAP)_3 \cdot 2H_2O$ is given as follows: A solution of HPMAP (3.00 mmol) in ethanol (30 cm^3) was neutralized by NaOH (3.00 mmol) aqueous solution under heating and stirring, then an aqueous solution of $Tb(ClO_4)_3$ (1.00 mmol) was added dropwise and refluxed for 20 min. When the resulting solution was cooled to room temperature, white solids were formed and filtered out. The crude product was recrystallized from mixed solvents of ethanol and water to obtain the sample as small crystals, then it was filtered and dried at 80°C for 4 h. Found: C, 51.4; H, 4.6; N, 9.8; Tb, 19.0. Calc. for $Tb(PMAP)_3 \cdot 2H_2O$ ($C_{36}H_{37}N_6O_8Tb$, denoted as compound **A**): C, 51.2; H, 4.8; N, 10.0; Tb, 18.8%. Found **C**: 53.0; H, 4.8; N, 9.5; Tb, 18.2. Calc. for $Tb(PMPP)_3 \cdot 2H_2O$ ($C_{39}H_{43}N_6O_8Tb$, denoted as compound **B**): C, 52.9; H, 5.2; N, 9.5; Tb, 17.9%. Found: C, 54.5; H, 5.2; N, 9.0; Tb, 17.3. Calc. for $Tb(PMIP)_3 \cdot 2H_2O$ ($C_{42}H_{49}N_6O_8$, denoted as compound **C**). C, 54.4; H, 5.65; N, 9.16; Tb, 17.19. Found: C, 56.0; H, 5.7; N, 8.6; Tb, 16.35. Calc. for $Tb(PMNP)_3 \cdot 2H_2O$ ($C_{45}H_{55}N_6O_8Tb$, denoted as compound **D**): C, 55.7; H, 6.0; N, 8.7; Tb, 16.4.). Found: C, 59.5; H, 4.1; N, 7.9; Tb, 15.6. Calc. for $Tb(PMBP)_3 \cdot 2H_2O$ ($C_5H_{43}N_6O_8Tb$, denoted as compound **E**): C, 59.5; H, 4.5; N, 8.2; Tb, 15.4.

Single crystals of $[Tb(PMPP)_3 \cdot 2H_2O] \cdot EtOH$ were obtained by dissolving the solid powder of $Tb(PMPP)_3 \cdot 2H_2O$ in a mixture of ethanol and water to obtain a clear solution. Then the solution was allowed to evaporate slowly and after 1 week, colorless single crystals suitable for X-ray diffraction studies were obtained. The crystals are stable and no changes were observed after storing under ambient atmosphere for 3 days.

Instruments and measurements

IR spectra of the ligands and complexes were recorded on a Magna 750 FT-IR spectrophotometer, using the KBr pellets in the range of 4000–400 cm^{-1}. Thermoanalysis measurements were carried out on a LCT-1 type DTA and TG analyser system under an air atmosphere. α-Al_2O_3 was used as the reference and the temperature was raised at a rate of 10°C min^{-1}. The UV–vis spectra were recorded on a Shimadazu UV-3100 spectrophotometer with a slit width of 2 nm. Fluorescence excitation and emission spectra were recorded on a Hitachi 850 fluorescence spectrophotometer, using a 430 nm excitation cut-off filter. Excitation and emission bandwidths of 5 nm were employed and the fluorescence spectra were corrected for nonlinear instrumental response and blank solvents [15].

The fluorescence lifetime determination was performed on a SLM 48000 Multi-Frequency Phase Fluorometer, using the frequency-domain method with glycogen as the reference. A 540 nm interference filter was placed in the emission path to eliminate interference from solvent and stray light. The modulated frequency used ranges from 200 to 5000 Hz. At each frequency both the phase shift and the relative modulation values were measured six times and the average values were used to evaluate the fluorescence lifetime in order to minimize the experimental error. A total of 10 different frequencies were used and the final fluorescence lifetime was determined by least-squares analysis of the 10 data that lead to the minimum value of R [16,17].

$$R = (1/2)\{\Sigma((\phi_\omega - \phi_\omega^c)/\delta_\phi)^2 + \Sigma((M_\omega - M_\omega^c)/\delta_M{}^2\}, \quad (1)$$

where ϕ_ω and ϕ_ω^c are the measured and the calculated phase shift, M_ω and ξM_ω^c are the measured and the calculated modification, and δ_ϕ and δ_M are the average phase error (0.5°) and modulation error (0.005).

The room-temperature phosphorescence of the $Gd(L)_3 \cdot 2H_2O$ samples, where L = 4 acyl pyrazolones, was measured by excitation of the samples with the fourth harmonic of the pulsed GCR-4 Nd : YAG laser (λ = 266 nm) with 30 Hz repetition rate and 6 ns pulse width. The laser irradiated on the powder samples with energy of 10 μJ pulse^{-1} at an area of 0.15 cm^2. The emissions from the samples were collected by a set of focus lenses, dispersed by the 500 nm focal length monochromator with a 1200 grooves mm^{-1} grating and detected by the R955 photomultiplier tube (Hamamatsu). To reduce the laser scattering light, a BG40 filter (Schott) was placed in front of the slit of the monochromator. The output of the photomultiplier was sent to the 4100 boxcar system (EG & G) for averaging, then transferred to the 286 personal computer *via* GPIB bus. The HP54510A digital oscilloscope was employed and the averaged real-time signal was transferred to a 386 SX/25 computer *via* GPIB bus in lifetime measurement [18].

X-ray data collection, structure solution and refinement

The crystal and refinement data of $[Tb(PMPP)_3 \cdot 2H_2O] \cdot C_2H_5OH$ are summarized in Table 1. A single crystal having approximate dimensions 0.2 × 0.2 × 0.2 mm^3 was mounted on an Enraf–Nonius CAD4 diffractometer. Data were collected in the ω–2θ scan mode at room temperature (26 ± 1°C) in the range $2 \leqslant \theta \leqslant 23°$. All the intensities were corrected for Lorentz and polarization effects and an absorption correction was also used. The crystal structure was solved by direct methods (MULTAN 82), the coordinates of the terbium atom were determined from an *E*-map and the coordinates of other nonhydrogen atoms were defined by successive Fourier synthesis. The coordinates of all nonhydrogen atoms and their anisotropic thermal parameters were refined by full-matrix least-squares and the structure converged to yield R and R_W factors of 0.064 and 0.073, respectively. All the calculations were carried out on a PDP 11/44 computer using a SDS-PLUS computer program package [19,20].

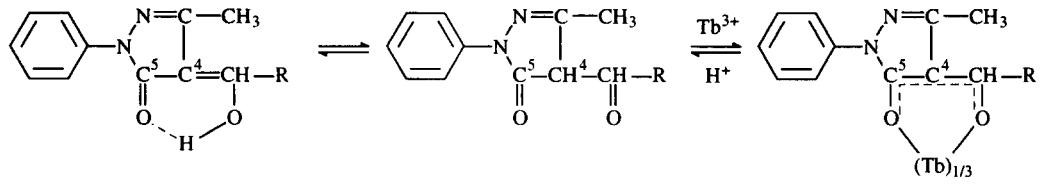
Table 1. Crystal data for $[Tb(PMPP)_3 \cdot 2H_2O] \cdot EtOH$

Formula	$C_{41}H_{49}N_6O_9Tb$
F. wt	928.82
Crystal system	Monoclinic
Space group	$P2_1/c$
a (Å)	17.481(7)
b (Å)	12.837(3)
c (Å)	18.397(9)
β (°)	101.04(3)
V (Å^3)	4052(2)
Z	4
D_x (Mg m^{-3})	1.526
F (000)	1908
Radiation, Mo-k_α, λ (nm)	0.071073
Reflections measured	6158
Independent reflections	4912
Unique observed reflections [$I \geqslant 3\sigma(I_0)$]	2820
Scan method	$\omega/2\theta$
Scan speed (°min^{-1})	0.92–5.49
Scan width (°)	$0.6 + 0.35 \times \tan\theta$
θ_{max} (°)	23
Refinement method	Full-matrix least-squares
Quantity minimized	$\Sigma w(\|F_o\| - \|F_c\|)^2$
R	0.064
R_w	0.073
μ (Mo-K_α) (mm^{-1})	1.824
Maximum residual peak, $\Delta\sigma_{max}$ (e Å^{-3})	1.16
Maximum residual hole, $\Delta\sigma_{min}$ (e Å^{-3})	−1.12

RESULTS AND DISCUSSION

Characterization of the complexes

All free pyrazolone ligands exhibit two types of strong C=O bond stretching vibrations in their FT-IR spectra. The positions of these two peaks differ slightly from ligand to ligand as listed in Table 2. The higher-frequency peak shifts to lower wavenumber and *vice versa* upon complexation. The stretching frequency difference ($\Delta\nu$) between the two carbonyl bands is smaller in the metal complex than that in the corresponding free ligands. The former (higher energy) peak is assigned to $\nu_{C=O}$ vibration at the 5-position of the pyrazolone ring. The coordination of the terbium ion to the oxygen atom of this carbonyl group weakens the C=O bond, resulting in a red shift. The latter (low-energy) peak is assigned to the vibration of the acyl carbonyl in the 4-position of the pyrazolone ring, which has some single bond character due to keto–enol tautomerization of the β-diketone group. The acyl carbonyl group is strengthened by equalization of single-double bond length upon complexation, leading to an increase in vibrational frequency. This assignment is supported by the crystal structure analysis of $Tb(PMPP)_3 \cdot 2H_2O$, in which the average bond length of the 5-pyrazolone carbonyls (1.276 Å) is slightly longer than that of the 4-acyl carbonyls (1.230 Å). The C=O band at the 5-position is weaker than in the 4-position, in agreement with our assignment. The process can be diagrammatically described as follows [21]:



(Enol) (Keto) (Complex)

The five ligands in ethanol solution all exhibit two broad strong absorption bands around 230–240 and 260–280 nm, with absorption maxima differing slightly from ligand to ligand in the UV–vis spectra (Table 2). The two bands are assigned to the $\pi \rightarrow \pi^*$ electronic transitions of the conjugated carbonyl and the phenyl ring group [21]. The absorption maximum of the first band in HPMBP is red-shifted by *ca* 6 nm compared with other 4-acyl pyrazolones. The second band is further red-shifted by *ca* 15 nm (except for HPMNP, whose position is also the same as HPMBP). The difference may be caused by the electron-donating ability of the alkyl groups and a lowering of conjugation caused by substitution of the benzoyl group with acyl groups. The complexes also exhibit two absorption bands in ethanol solution. It is clear that these two absorption bands are contributed by the ligands. In addition, the molar absorption coefficiencies of the complexes are *ca* three times larger compared with those of the free ligands, but this is expected since one mole of the complex contains three moles of the ligands.

The DTA-TG curves of compounds **B** and **D** are similar. Their TG curves both exhibit a weight loss around 120°C and the corresponding DTA curves exhibit an endothermic peak. This process corresponds to the complexes losing two water molecules. The weight loss percentages (experimental/theoretical) are 6.7/4.1 for **B** and 6.0/3.7 for **D**. An endothermic peak at 191°C for **B** and 220°C for **D** appears in their DTA curves, however, no weight loss appears in the corresponding TG curves. The peaks may be assigned to the melting point of the dehydrated complex. The dehydrated complexes undergo a series of complex oxidation and decomposition reactions and finally form Tb_4O_7 in the 310–550°C region. The DTA curves exhibit a small and large exothermic band around 330 and 500°C, while the TG curves exhibit a series of weight loss. There are no changes both in the TG and DTA curves when the temperature is higher than 550°C. The overall weight loss percentages are 80.0/78.8% for **B** and 75.7/80.6% for **D**, respectively. The experimental values are in agreement with the theoretical ones within the experimental error.

Room-temperature fluorescence and phosphorescence

The shapes of the fluorescence excitation spectra of the five terbium complexes are similar. They all exhibit a broad excitation band from 250 to 370 nm with maxima varying from sample to sample for powdered samples (Table 3). The excitation spectra of the complexes in dimethylformamide (DMF) solution, however, are quite different from those of the powdered samples. In DMF solution, they all exhibit a weak band around 260 nm and a strong band around 340 nm, with the intensity of the former band being only *ca* 1/15 of the latter. The excitation peak intensities for **A, B** or **C** are much stronger than that for **D** or **E**. A typical fluorescence excitation spectra for compound **A** in these two states are shown in Fig. 1. We

Table 2. The major C=O stretching peaks in the IR spectra (cm^{-1}) and the absorption maxima in the UV–vis spectra of the ligands and the complexes

	Stretching peaks in FT(s)IR spectra			Absorption maxima in UV–vis spectra			
Compound	Peak position		$\Delta\nu$ (cm^{-1})	λ_1 (nm)	ε (10^4)	λ_2 (nm)	ε (10^4)
HPMAP	1622(vs)	1567(vs)	55	230	1.59	265	1.43
HPMPP	1610(vs)	1571(vs)	39	232	1.52	265	1.96
HPMIP	1621(vs)	1560(vs)	61	233	1.52	263	2.10
HPMNP	1644(vs)	1596(s)	48	233	2.24	279	1.26
HPMBP	1645(vs)	1597(s)	48	239	1.35	278	1.12
$Tb(PMAP)_3 \cdot 2H_2O$	1627(vs)	1585(s)	42	233	3.16	262	6.89
$Tb(PMPP)_3 \cdot 2H_2O$	1618(vs)	1583(vs)	35	234	3.30	262	6.94
$Tb(PMIP)_3 \cdot 2H_2O$	1614(vs)	1583(s)	31	235	3.45	262	7.14
$Tb(PMNP)_3 \cdot 2H_2O$	1607(vs)	1578(s)	29	238	3.56	263	6.84
$Tb(PMBP)_3 \cdot 2H_2O$	1610(vs)	1584(s)	26	237	4.98	253	5.14

Table 3. The fluorescence parameters of the five terbium complexes at powderous states and in DMF solutions

Complex (State)	λ^{ex} max (nm)	λ^{em} max (nm)	I (a.u.)	τ (μs)
$Tb(PMAP)_3 \cdot 2H_2O$(powder)	323	544.8	647	220
$Tb(PMAP)_3 \cdot 2H_2O$(in DMF)	340	545	95	362
$Tb(PMPP)_3 \cdot 2H_2O$(powder)	314	544.7	776	215
$Tb(PMPP)_3 \cdot 2H_2O$(in DMF)	340	545	12	436
$Tb(PMIP)_3 \cdot 2H_2O$(powder)	324	545.2	740	198
$Tb(PMIP)_3 \cdot 2H_2O$(in DMF)	340	545.1	132	483
$Tb(PMNP)_3 \cdot 2H_2O$(powder)	266, 334	547.2	109	130
$Tb(PMNP)_3 \cdot 2H_2O$(in DMF)	266, 332	546.2	0.21	[a]
$Tb(PMBP)_3 \cdot 2H_2O$(powder)	264, 332	547.8	0.66	0.32
$Tb(PMBP)_3 \cdot 2H_2O$(in DMF)	304	558.9	0.015	[a]

[a] The fluorescence lifetime of $Tb(PPMNP)_3 \cdot 2H_2O$ and $Tb(PMBP)_3 \cdot 2H_2O$ in DMF cannot be measured correctly due to their weak fluorescence intensity. The concentration of the DMF solutions were all 1.00×10^3 mol l^{-1}.

consider the difference in excitation as the result of the difference environments between the two states. In solution the complex molecules are isolated, so the effects between the complex molecules are weak, but they may have strong interactions with the solvent molecules. In the solid state the molecules are closely packed so that they have a much stronger interaction [22].

The fluorescence emission spectra of the complexes are very similar and are all characteristic of Tb^{3+} ion emission spectra. They all exhibit five emission bands at 496, 546, 587, 624 and 655 nm, corresponding to the $^5D_0 \rightarrow {}^7F_j (j = 6, 5, 4, 3, 2)$ electronic transitions. Among these transitions, that which is located around 546 nm ($^5D_0 \rightarrow {}^7F_5$) is the strongest, in accordance with the spectra of other Tb^{III} complexes. Although the shapes of the emission spectra are similar, however, the fluorescence intensities are quite difference, as listed in Table 3. The emission intensity for compounds **A, B** or **C** are three orders of magnitude stronger than that for compound **E,** either in the solid state or in DMF solution. We believe that this is due to the different triplet energy level of the ligands. The PMBP ligand has a relatively low triplet energy level and thus it cannot efficiently transfer UV excitation energy to the lowest excited state of the terbium ion ($^5D_4$) to obtain the characteristic emission of Tb^{3+} [14]. The substitution of the benzoyl group with an acyl group may decrease the electron conjugate system to yield a ligand with a higher triplet energy level, so that ligand-to-metal energy transfer may proceed much more easily.

The above expectation was confirmed by the room-temperature phosphorescence spectra of the

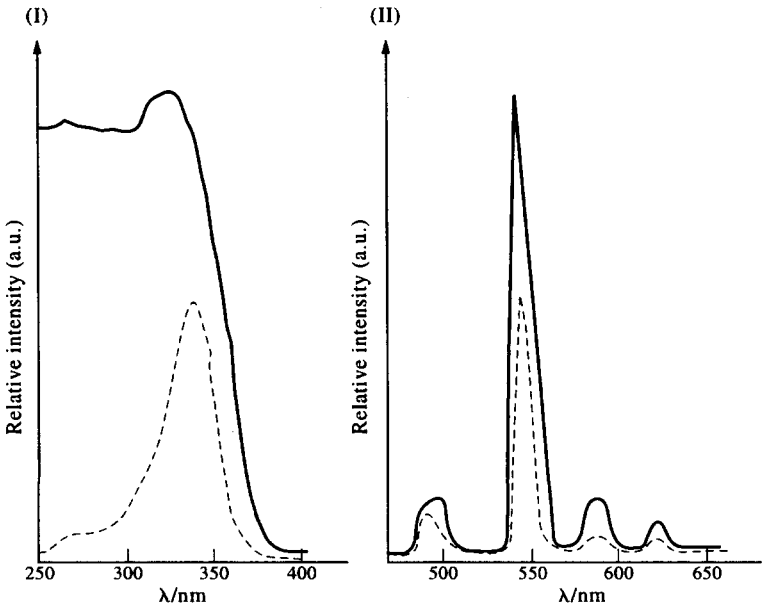


Fig. 1. The fluorescence excitation (**I**) and emission spectra (**II**) of $Tb(PMAP)_3 \cdot 2H_2O$ in the solid powderous state (solid line) and in DMF solution (broken line).

$Gd(L)_3 \cdot 2H_2O$ samples. It is well known that intramolecular energy transfer from the triplet state to the resonance level of a lanthanide ion is spin-forbidden. The energy is transferred by resonant exchange and the role of the triplet state is very important. Although there have been many reports on the phosphorescence of lanthanide complexes at low temperature (77K) [23], at room temperature phosphorescence of a lanthanide complex is very rare. The phosphorescence spectra of the $Gd(L)_3 \cdot 2H_2O$ complexes excited by a 266 nm laser beam are shown in Fig. 2. The phosphorescence spectra were obtained by setting the delay at 300 ns with a gate width of 1000 ns, except for $Gd(PMPB)_3 \cdot 2H_2O$, which was obtained by setting the gate delay at 300 ns with a gate width of 200 ns. All five spectra are very broad and structureless. The shapes of the former three ligands (PMAP, PMPP and PMIP) are similar both in intensity and peak position. However, when the methyl group in PMAP is substituted by a tert-butyl group (PMNP) or a phenyl group (PMBP), the spectra are red-shifted significantly. This indicates that the latter two ligands have much lower triplet energies. The triplet energies of the five ligands are estimated to be 20,580 cm^{-1} for PMAP, 20,750 cm^{-1} for PMPP, 20,370 cm^{-} for PMIP, 19,340 cm^{-1} for PMNP and 18,180 cm^{-1} for PMBP by choosing the positions of the emission maxima as the triplet energy level. In good agreement with expectations, the substitution of the benzoyl group with acyl groups increases the triplet energy in the pyrazolone ligands, which then strongly affects the fluorescence properties of the complexes. It is well known that the $^5D_4$ excited state of Tb^{3+} is *ca* 20,500 cm^{-1} [7]. The triplet energies of PMAP, PMPP and PMIP are slightly higher or almost the same as the $^5D_4$ excited state of Tb^{3+}, thereby increasing the efficiency of energy transfer and yielding strong Tb^{3+} ion fluorescence. However, the triplet energies of PMNP and PMBP are significantly lower than the $^5D_4$ excited state, thus the energy transfer cannot proceed smoothly (because of the width of the band, the phosphorescence spectra of PMNP and PMBP have some overlap with the $^5D_4$ excited state of Tb^{3+}). This leads to a much weaker fluorescence intensity, in good agreement with the fluorescence data.

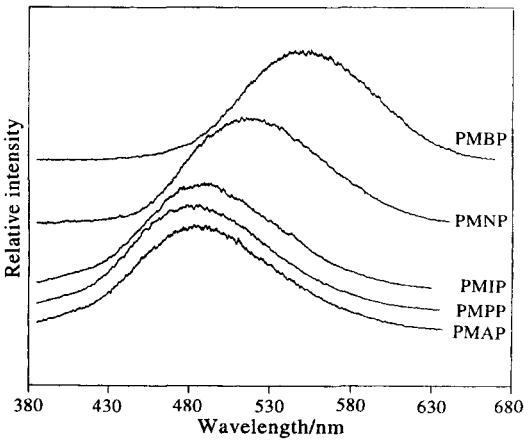


Fig. 2. Room-temperature phosphorescence spectra of $Gd(L)_3 \cdot 2H_2O$ excited by a 266 nm laser beam. L = PMAP, PMPP, PMIP, PMNP, PMBP.

Due to the time lag between absorption and emission, the emission is delayed to the modulated excitation. The fluorescence lifetime could be evaluated by measuring the phase shift and the relative modulation of the samples at different modulated excitation frequency. The basic equations in the frequency-domain method to determine the fluorescence lifetime are as follows [16,17]:

$$\tau_\phi = \tan\phi/\omega, \tag{2}$$

where ϕ is the phase shift caused by a sample of lifetime τ_ϕ and ω is the circular frequency of excitation (equals 2π times the excitation frequency in Hz)

$$\tau_M = (1/\omega)([1/D^2]-1)^{0.5}, \tag{3}$$

where D is the ratio of the relative modulation of the fluorescent sample and the glycogen reference solution.

By measuring the phase shift and the relative modulation of the samples at different frequency and using the methods described above, least-squares analysis of the 10 sets of data showed that the fluorescence lifetimes of the complexes are quite different at different states, as given in Table 3. All the samples exhibit only one fluorescent component. The lifetimes of **D** and **E** cannot be determined exactly due to their weaker fluorescence intensity. In the solid powdered states **A, B** and **C** have almost the same lifetime of *ca* 200 μs, much longer than for **D** or **E**. It is noteworthy that the lifetimes of **A, B** and **C** in DMF solution are much longer than those of the solid powders. This may be due to the strong coordination effect of the DMF molecules, which can substantially replace the two coordinated water [24]. The replacement can avoid the high-frequency O—H bond vibration and thus greatly decrease the energy loss through the coordination water to obtain a much longer fluorescence lifetime. All these emphasize that the triplet energy of the ligand is the key factor in determining the fluorescence intensity and lifetime of the complex, but the coordination environment also plays an important role.

Description of the structure of $[Tb(PMPP)_3 \cdot 2H_2O] \cdot EtOH$

Selected bond lengths and bond angles for $Tb(PMPP)_3 \cdot 2H_2O$ are listed in Table 4. The molecular structure is shown in Fig. 3. The complex is mononuclear, as expected. The central terbium ion is coordinated with eight oxygen atoms, six of which are from the three bidentate PMPP ligands and the other two are from the two coordinated water molecules. The eight oxygen atoms form a square-antiprism coordination

Table 4. Selected bond lengths (Å) and angles (°) for $Tb(PMPP)_3 \cdot 2H_2O$

Selected bond lengths between Tb^{III} and the ligands					
Tb(1)—O(1)	2.304(12)	Tb(1)—O(2)	2.345(11)	Tb(1)—O(3)	2.313(12)
Tb(1)—O(4)	2.362(14)	Tb(1)—O(5)	2.332(14)	Tb(1)—O(6)	2.372(12)
Tb(1)—O(7)	2.487(13)	Tb(1)—O(8)	2.412(12)	C(21)—O(1)	1.271(20)
C(25)—O(2)	1.241(22)	C(41)—O(3)	1.273(22)	C(45)—O(4)	1.233(24)
C(61)—O(5)	1.284(21)	C(65)—O(6)	1.216(22)	C(21)—C(22)	1.385(21)
C(22)—C(25)	1.442(24)	C(41)—C(42)	1.381(24)	C(42)—C(45)	1.411(26)
C(61)—C(62)	1.389(24)	C(62)—C(65)	1.463(27)		

Selected bond angles around the Tb^{III} coordination environment			
O(1)—Tb(1)—O(2)	76.4(4)	O(1)—Tb(1)—O(3)	141.5(4)
O(2)—Tb(1)—O(3)	118.5(4)	O(1)—Tb(1)—O(4)	74.9(4)
O(2)—Tb(1)—O(4)	142.2(4)	O(3)—Tb(1)—O(4)	75.4(4)
O(1)—Tb(1)—O(5)	75.6(4)	O(2)—Tb(1)—O(5)	77.6(4)
O(3)—Tb(1)—O(5)	140.4(4)	O(4)—Tb(1)—O(5)	115.4(4)
O(1)—Tb(1)—O(6)	140.0(4)	O(2)—Tb(1)—O(6)	73.6(4)
O(3)—Tb(1)—O(6)	76.3(4)	O(4)—Tb(1)—O(6)	142.8(4)
O(5)—Tb(1)—O(6)	74.5(4)	O(1)—Tb(1)—O(7)	112.9(5)
O(2)—Tb(1)—O(7)	140.87(5)	O(3)—Tb(1)—O(7)	80.6(5)
O(4)—Tb(1)—O(7)	72.8(4)	O(5)—Tb(1)—O(7)	68.2(5)
O(6)—Tb(1)—O(7)	79.3(5)	O(1)—Tb(1)—O(8)	80.2(4)
O(2)—Tb(1)—O(8)	73.0(4)	O(3)—Tb(1)—O(8)	71.0(4)
O(4)—Tb(1)—O(8)	80.3(4)	O(5)—Tb(1)—O(8)	145.8(4)
O(6)—Tb(1)—O(8)	112.3(4)	O(7)—Tb(1)—O(8)	144.9(5)

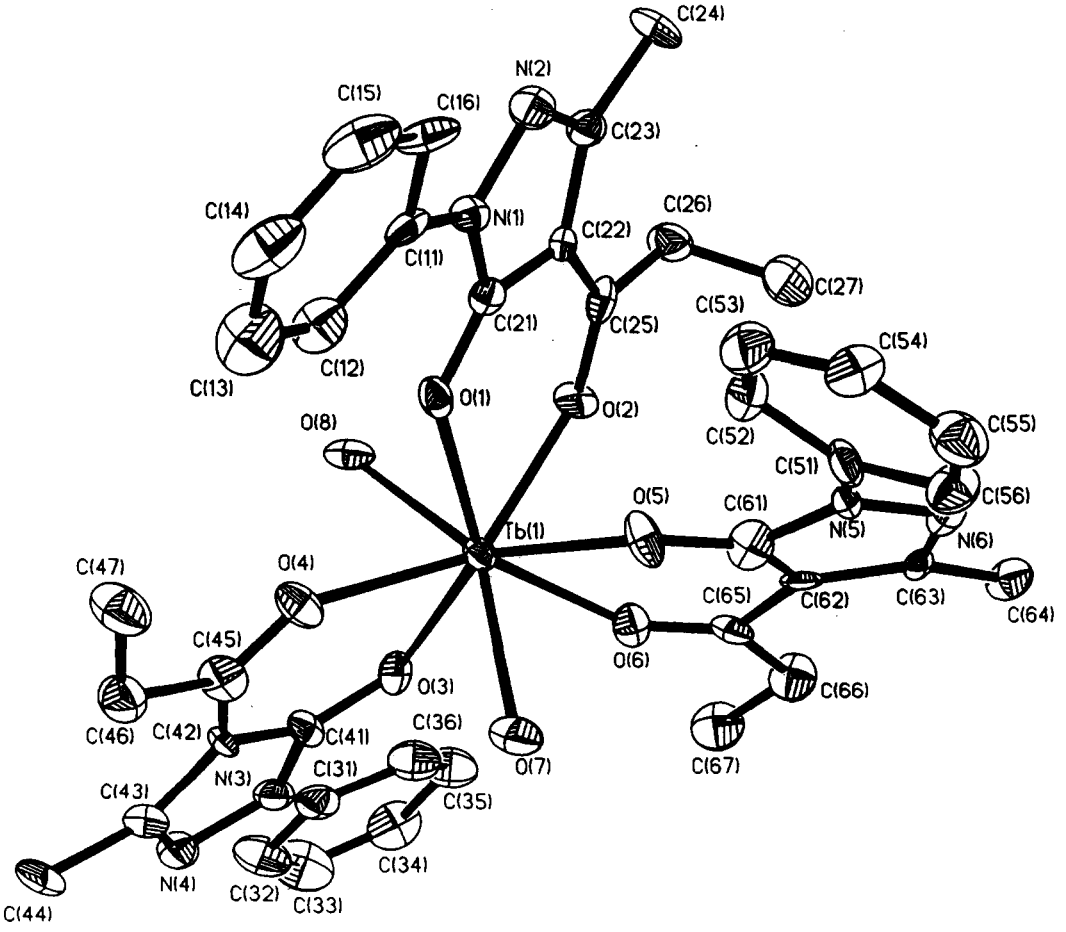


Fig. 3. The molecular structure of $Tb(PMPP)_3 \cdot 2H_2O$.

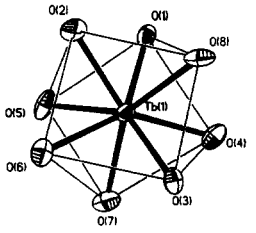


Fig. 4. The coordination polyhedron around the central terbium atom.

polyhedron around the central terbium ion (Fig. 4). The O(2), O(8), O(3) and O(4) oxygen atoms form the upper plane and the O(1), O(4), O(7) and O(5) atoms form the bottom plane. The distances of the oxygen atoms from the planes are less than 0.13 (10) Å and the dihedral angle between the two planes is 2.86(9)°, reflecting the fact that the deviation from the ideal square-antiprism coordination polyhedron is very small. The average bond length between the terbium ion and the pyrazolone oxygen atom is 2.338 Å, which is slightly shorter than that between the terbium and water oxygen atom (2.450 Å). This may be the result of the negative charge of the pyrazolone oxygen, which could be more strongly coordinated to the terbium ion due to electrostatic effects. The PMPP chelating mode is rather asymmetric, the terbium-to-carbonyl-oxygen distances being systematically longer on the side adjacent to the ethyl group (2.360 Å) than those from the pyrazolone ring (2.316 Å). This asymmetric chelation is similar to those found in the structures of lanthanide β-diketonate complexes, such as $Yb(acac)_3 \cdot H_2O$ [25], $Yb(DPAP)_3 \cdot 2H_2O$ [5]. The close proximity of the ethyl group to a coordinated oxygen atom could be consistent with the observed lengthening if electronic factors cannot in principle be ruled out. The PMPP ligands coordinate to the terbium ion in the enol form to form stable six-membered rings and the sum of the internal angles of the six-membered ring for the three ligands are 716.5, 717.6 and 718.8°, respectively. These angles are very close to 720°, suggesting that the six-membered rings are almost planar. The average C=C bond distance of the enol anion in the complex is 1.385 Å, a value which falls between the typical C=C double bond distance (1.33 Å) and C—C single bond distance (1.54 Å), reflecting a certain amount of electron delocalization upon complexation. All of the five-membered pyrazolone rings and the phenyl rings are planar and the dihedral angles between the pyrazolone ring and the phenyl ring are quite different in the three ligands, ranging from 9.28 to 145.06°.

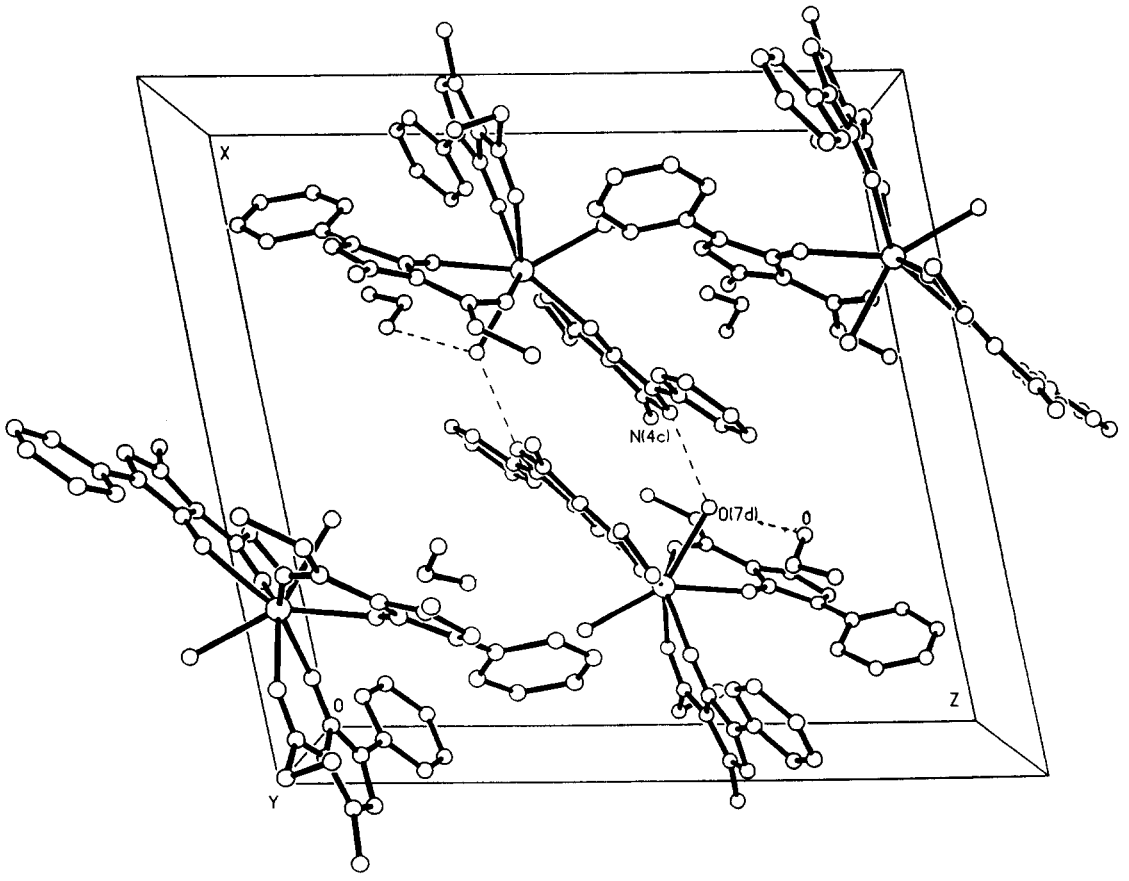


Fig. 5. The molecular packing diagram in the unit cell.

The molecular packing diagram of the unit cell is shown in Fig. 5. There are no disordered ethanol solvent molecules in the crystal, even though the ethanol oxygen atoms do not coordinate to the central terbium atom. This is different compared with the structure of $Yb(DPAP)_3 \cdot 2H_2O \cdot 3EtOH$, in which there are some disordered ethanol molecules in the unit cell, in agreement with the observation that the crystal does not lose solvent under ambient atmosphere. The distance between the coordinated water oxygen O(7d) and the ethanol oxygen is 2.884 Å and that between O(7d) and the pyrazolone nitrogen N(4) is 2.820 Å, indicating that the ethanol is connected to the complex molecule *via* hydrogen bonding [26]. The angles of N(4c)—O(7d)—O, N(4c)—O(7d)—Tb and Tb—O(7d)—O are 119.0, 129.0 and 108.0°, respectively. The crystal contains mainly isolated complex molecules, except for hydrogen bonding.

Supplementary materials. Tables of the atomic coordinates, equivalent isotropic and isotropic displacement coefficients of non hydrogen atoms, the bond distances and bond angles of the complex, the observed and calculated structure factors and the table of least-square planes and the dihedral angles between the planes are all submitted as supplementary materials.

Acknowledgements—The authors thank Professor X. K. Yao and H. G. Wang from the Central Laboratory of Nankai University (Tianjin, P.R. China) for their help in the crystal structure determination. We thank the Climbing Program (A National Fundamental Research Key Project of China) and the National Natural Science Foundation of China for financial support.

REFERENCES

1. Jensen, B. S., *Acta Chem. Scand.* 1959, **13,** 1668.
2. Huang, C. H. and Freiser, H., *Solv. Extr. Ion Exch.* 1986, **4,** 41.
3. Yang, L. and Yang, R., *Lanzhou Daxue Xue Bao*, 1988, **24,** 134.
4. (a) Stary, J., *The Solvent Extraction of Metal Chelates*. Pergamon Press, Oxford, 1964; (b) Sasaki, Y. and Freiser, H., *Inorg. Chem.* 1983, **22,** 2289.
5. Bombieri, C., Polo, A., Wang, J. F., Wu, J. G. and Xu, G. X., *Inorg. Chim. Acta*, 1987, **132,** 263.
6. (a) Huang, C. H., Zhang, S. W., Deng, A. P., Tang, H. T. and Xu, G. X., *Chin. J. Chem.* 1990, **1,** 29; (b) Huang, C. H., Deng, A. P., Xu, G. X., Liao, F. M. and Liu, X. L., *Chin. Sci. Bull.* 1989, 1077.
7. Moeller, T. and Schleitzer-Rust, E., ed. *Gmelin Handbook of Inorganic Chemistry*, 8th edn. Springer-Verlag, Berlin, 1981. Part D3, pp. 65–246.
8. (a) Buono-Core, G. E., Li, H. and Marciniak, B., *Coord. Chem. Rev.* 1990, **99,** 55; (b) Sweeting, L. M. and Rheingold, A. L., *J. Am. Chem. Soc.* 1987, **109,** 2652; (c) Melby, L. R., Rose, N. J., Abramson, E. and Caris, J. C., *J. Am. Chem. Soc.* 1964, **86,** 5117.
9. (a) Beddard, G. S. and West, M. A., ed. *Fluorescent Probes*. Academic Press, London, 1981; (b) Richardson, F. S., *Chem. Rev.* 1982, **82,** 541.
10. Parker, C. A., *Photoluminescence of Solutions*. Elsevier, Amsterdam, 1968, pp. 470–499.
11. (a) Mehrotra, R. C., Bohra, R. and Gaur, D. P., *Metal-Diketones and Applied Derivatives*. Academic Press, New York, 1978; (b) Bünzli, J. C. G. and Choppin, G. R., *Lanthanide Probes in Life, Chemical and Earth Science*, Elsevier, Amsterdam, 1989.
12. Kido, J., Hayase, H., Hongawa, K. and Nagai, K., *Appl. Phys. Lett.* 1994, **65,** 2124.
13. (a) Ebina, K., Okada, Y., Yamasaki, A. and Ujihara, K., *Appl. Phys. Lett.* 1995, **66,** 2783; (b) Yokoyama, Y., *Science*, 1992, **256,** 66.
14. (a) Li, Q., Zhou, D. J., Zhou, Y. F., Huang, C. F., Umetani, S. and Matsui, M., *Acta. Sci. Nat. Univ. Pekin.*, (in Chinese), 1996, **41,** in press; (b) Hu, J. M., Chen, G. Q. and Zeng, Y., *Chem. J. Chin. Univ.*, (in Chinese), 1990, **11,** 817.
15. (a) Zhou, D. J., Yao, G. Q., Huang, C. H., Bai, J. and Li, T. K., *Chin. Chem. Lett.* 1995, **6,** 903; (b) Zhou, D. J., Gan, L. B., Tan, H. S., Luo, C. P., Huang, C. H., Yao, G. Q. and Zhang, B. *Chin. Sci. Bull.*, (in Chinese), 1995, **40,** 2053; (c) Zhou, D. J., Gan, L. B., Tan, H. S., Luo, C. P., Huang, C. H. and Yao, G. Q., *Chem. J. Chin. Univ.* (in Chinese), 1995, **16,** 1512.
16. (a) Zhou, D. J., Gan, L. B., Luo, C. P., Tan, H. S., Huang, C. H., Yao, G. Q., Zhao, X. S., Liu, Z. F., Xia, X. H. and Zhang, B., *J. Phys. Chem.* 1996, **100,** 3150; (b) Zhou, D. J., Tan, H. S., Gan, L. B., Luo, C. P., Huang, C. H. and Yao, G. Q., *Chem. Lett.* 1995, 549.
17. Lakowicz, J. R. and Gryczynski, I., *Topics in Fluorescence Spectroscopy*, Vols 1 and 2, ed.J. R. Lakowicz, Plenum Press, New York, 1991.
18. Ying, L. M., Yu, A. C., Zhao, X. S., Li, Q., Zhou, D. J., Huang, C. H., Umetani, S. and Matasu, M., *J. Phys. Chem.* 1996, **100,** 18387.
19. (a) Zhou, D. J., Huang, C. H., Wang, K. Z. and Xu, G. X., *Polyhedron*, 1994, **13,** 997; (b) Gan, L. B., Xu, L. B., Luo, C. P., Huang, C. H., Umetani, S. and Matsui, M., *Polyhedron*, 1994, **13,** 3167; (c) Wang, K. Z., Huang, C. H., Xu, G. X. and Wang, R. J., *Polyhedron*, 1995, **14,** 3669.
20. Walker, N. and Stuart, D., *Acta Cryst.* 1993, **A39,** 158.
21. Huang, C. H., Wang, K. Z., Xu, G. X., Zhao, X. S., Xie, X. M., Xu, Y., Liu, Y. Q., Zhu, D. B., Xu, L. G. and Li, T. K., *J. Phys. Chem.* 1995, **99,** 14397.
22. Zhou, D. J., Huang, C. H., Yao, G. Q., Bai, J. and Li, T. K., *J. Alloys Compd.* 1996, **235,** 156.
23. (a) Matsuda, Y., Makishima, S. and Shinoya, S., *Bull. Chem. Soc. Jpn.* 1968, **41,** 1513; (b) Sato, S. and Wada, M., *Bull. Chem. Soc. Jpn.* 1970, 43, 1955.
24. (a) Sun, H. Y., Huang, C. H., Xu, G. X. and Ma, Z., *Polyhedron*, 1995, **14,** 947; (b) Yang, L. and Yang, R., *J. Coord. Chem.* 1994, **33,** 303.
25. Richardson, M. F., Corfield, P. W. R., Sands, D. E. and Sievers, R. E., *Inorg. Chem.* 1970, **9,** 1632.
26. The symmetry transformations are as follows: (c) $1-x, 0.5+y, 0.5-z$; (d) $x, 0.5-y, 0.5+z$.

Pergamon

PII: S0277-5387(96)00392-0

Polyhedron Vol. 16, No. 8, pp. 1391–1397, 1997
Copyright © 1997 Elsevier Science Ltd
Printed in Great Britain. All rights reserved
0277-5387/97 $17.00+0.00

Hydrotris(pyrazolyl)borate molybdenum chemistry: spin triplet 16-electron carbonyl derivatives of molybdenum(II), and the X-ray structure of the Mo(V) oxo compound $\{HB(3,5\text{-}Me_2C_3N_2H)_3\}MoOI_2$

Akila A. Saleh,‡ Brett Pleune, James C. Fettinger and Rinaldo Poli†

Department of Chemistry and Biochemistry, University of Maryland, College Park, MD 20742, U.S.A.

(Received 23 May 1996; accepted 31 July 1996)

Abstract—The hydrotris(3,5-dimethylpyrazolyl)borate complexes $Tp^*Mo(CO)_2X$ (X = Cl, I) are rare examples of 16-electron carbonyl derivatives with a spin triplet ground state, which exhibit relatively sharp contact-shifted ^1H NMR spectra. Oxidation of $Tp^*MoI(CO)_2$ led to the isolation and crystallographic characterization of Tp^*MoOI_2. Copyright © 1997 Elsevier Science Ltd

Keywords: molybdenum; hydrotris(pyrazolyl)borate; paramagnetic organometallic compounds.

The hydrotris(pyrazolyl)borate (Tp) ligand provides a structurally rigid and chemically inert capping ligand, which in many respects resembles (but in many other aspects it differs from) the ubiquitous cyclopentadienyl ring. We were interested in extending some of the chemistry we have recently explored for intermediate oxidation state cyclopentadienylmolybdenum compounds to the Tp ligand system. Although Tp systems of Mo have been studied extensively in low-oxidation states [1–10], much less work has been carried out in high oxidation states [11–13] and the only reported compound of Mo^{III} appears to be a salt of $[Tp^*MoCl_3]^-$[Tp* = hydrotris(3,5-dimethylpyrazolyl)borate] [14].

We have focused our attention on the sterically more demanding Tp*. In an attempt to access higher-valent Tp*Mo halide derivatives by oxidative decarbonylation of lower-valent derivatives, a technique which successfully provides an entry into higher-valent CpMo halides ($Cp = \eta^5-C_5H_5$)[15], we have investigated the reaction of excess halogen with $[Tp^*Mo(CO)_3]^-$. During the course of this study we have been able to isolate and fully characterize the product of partial oxidation, $[Tp^*MoX(CO)_2]$ (X = Cl, I). Such a compound (for X = I) was first mentioned by Templeton, but neither it nor the corresponding tricarbonyl derivative were isolated nor spectroscopically characterized other than by *in situ* IR spectroscopy [4]. More recently, the compound $Tp^*MoI(CO)_2$ has been isolated from the reaction between $[MoI_2(CO)_3(MeCN)_2]$ and KTp*, and has been described as a diamagnetic compound, showing well-defined ^1H NMR spectroscopic properties [16]. The latter publication prompted us to submit the results of our own investigations, since they substantially differ from those therein reported. We also describe here the X-ray structure of Tp^*MoI_2O, a product of further aerobic oxidation of $Tp^*MoI(CO)_2$.

EXPERIMENTAL

General data

All operations were carried out under dinitrogen with standard Schlenk-line techniques. Solvents were distilled directly from the drying agent (toluene and heptane from Na, THF from Na/K/benzophenone,

† Author to whom correspondence should be addressed.
‡ Permanent address: Department of Chemistry, Faculty of Education, Ain Shams University, Cairo, Egypt.

CH_2Cl_2 from P_4O_{10}) under argon prior to use. FT-IR spectra were recorded with KBr cells on a Perkin–Elmer 1800 spectrophotometer. ^1H NMR spectra were recorded on Bruker WP200 and AF200 spectrometers; the peak positions are reported with positive shifts downfield of TMS as calculated from the residual solvent peaks. The magnetic susceptibility measurements were carried out with a Johnson Matthey magnetic balance, which operates by a modified Gouy method whereupon the effect of the immersion of a sample in the magnetic field gradient is measured by a change of the magnet weight rather than by a change of the sample weight. The magnetic moments were calculated by the formula $\mu_b = 2.828 \cdot (\chi_M T)^{-1}$, the molar susceptibility χ_m being corrected by the diamagnetism of the ligands by using Pascal's constants. The elemental analyses were carried out by M-H-W Laboratories, Phoenix, AZ. Compounds KTp* [17] and $PhICl_2$ [18,19] were prepared as previously described. $Mo(CO)_6$ (Aldrich) was used without any further purification.

Preparation of Tp*MoI(CO)$_2$

A solution of $[Tp^*Mo(CO)_3]^-$ was prepared *in situ* by refluxing $Mo(CO)_6$ (2.63 g, 10.0 mmol) and KTp* (3.36 g, 10.0 mmol) in THF (85 cm^3). To this solution I_2 (2.54 g, 10.0 mmol) was added. Immediately after the I_2 addition, the IR spectrum of the reaction mixture exhibited CO stretching vibrations at 2025 (s), 1998 (m), 1937 (s) and 1922 (s) cm^{-1}. After stirring overnight at room temperature, the absorptions at 2025 and 1937 cm^{-1} had disappeared, while those at 1937 and 1922 cm^{-1} had grown in intensity. The mixture was concentrated to *ca* 20 cm^3 and *n*-heptane (50 cm^3) was added. The red–brown precipitate was filtered off, washed with heptane and dried *in vacuo*. Yield: 4.26 g (74%). Found: C, 35.2; H, 4.0; N, 14.5. Calc. for $C_{17}H_{22}BIMoN_6O_2$: C, 35.4; H, 3.8; N, 14.6% IR (THF, cm^{-1}): 1999 s, 1920 s. ^1H NMR ($CDCl_3$, δ, 298 K): 87.8 (s, CH_3, 3H), 70.5 (s, CH_3, 3H), 47.2 (s, CH_3, 6H), 34.8 (s, CH_3, 6H), 8.6 (s, CH, 2H), −2.3 (br, BH, 1H), −7.2 (s, CH, 1H). $\mu_{eff} = 3.00$ μ_B.

Preparation of Tp*MoCl(CO)$_2$

By a procedure analogous to that reported above, a solution of KTp*Mo(CO)$_3$ (2.83 mmol) was prepared from $Mo(CO)_6$ and KTp* in THF (50 cm^3). To this solution $PhICl_2$ (0.779 g, 2.83 mmol) was added. Immediately after the addition of $PhICl_2$, the IR spectrum of the reaction mixture exhibited CO stretching vibrations at 2007 (s) and 1923 (s) cm^{-1}. After stirring overnight at room temperature, the IR spectrum had not changed. The mixture was concentrated to *ca* 10 cm^3 and *n*-heptane (30 cm^3) was added. The orange precipitate was filtered off, washed with heptane and dried *in vacuo*. Yield: 0.869 g (63%). IR (THF, cm^{-1}): 2007 s, 1923 s. ^1H NMR ($CDCl_3$, δ, 298 K): 96.9 (s, CH_3, 3H), 71.5 (s, CH_3, 3H), 41.9 (s, CH_3, 6H), 31.7 (s, CH_3, 6H). $\mu_{eff} = 2.81$ μB.

Reaction of Tp*MoI(CO)$_2$ *with* I_2

Formation of Tp*MoI$_2$O. Tp*MoI(CO)$_2$ (0.542 g, 0.941 mmol) and I_2 (0.239 g, 9.42 mmol) were dissolved in toluene (30 cm^3). The mixture was stirred at room temperature overnight. Monitoring by IR spectroscopy revealed the complete loss of the CO stretching absorptions. The mixture was evaporated to dryness and the residue was used for several recrystallization attempts. A small amount (< 20 mg) of single crystals which were suitable for an X-ray structural determination was obtained from a toluene/*n*-heptane layer. Found: C, 31.5; H, 3.6; N, 11.6. Calc. for $C_{18.5}H_{26}BI_2MoN_6O$ ($Tp^*MoOI_2 \cdot 1/2C_7H_8$): C, 31.3; H, 3.7; N, 11.8%.

X-ray crystallography for Tp*MoI$_2$O·C_7H_8

A dark purple, nearly black colored crystal with dimensions $0.400 \times 0.125 \times 0.100$ mm was placed on the Enraf–Nonius CAD-4 diffractometer. The cell parameters and crystal orientation matrix were determined form 25 reflections in the range $35.2 < 2\theta < 40.64°$ and confirmed with axial photographs. Data were collected [Mo−K_α] with $\omega/2\theta$ scans over the range $2.23 < \theta < 24.98°$ with a scan width of $(0.64 + 0.56 \tan\theta)°$ and a variable scan speed of 2.3–2.7° min^{-1} with each scan recorded in 96 steps with the outermost 16 steps on each end of the scan being used for background measurement. The diffractometer was controlled with a Digital Equipment Corporation Micro VAX II (MVII) computer and the automated Enraf–Nonius control program Express (version 5.1). Three nearly orthogonal standard reflections were monitored at 1 h intervals of X-ray exposure with minimal variations in intensity being observed. Data were collected with the indices *-hkl*; resulting in the measurement of 2461 unique reflections. Data were corrected for Lorentz and polarization factors, and for absorption based on nine ψ-scan reflections in the range $5.1 < \theta < 15.3°$, with transmission factors ranging from 0.3809–0.5015. Systematic absences indicated the centrosymmetric space group *Pnma* (no. 62) or the noncentrosymmetric space group $Pna2_1$ (no. 33); intensity statistics clearly favored the centric case. The structure was determined by direct methods, with the successful location of the three heavy atoms and several carbon and nitrogen atoms. The remaining nonhydrogen atoms were found from two subsequent difference-Fourier maps. The toluene molecule was found to be disordered with two of the atoms nearly overlapping with their symmetry equivalents that represented other positions of the ring, namely, the C12, C16 pair and the C11 and C17 pair. AFIX commands were used to impose the

molecular geometry as a six-membered ring with C17 as the methyl group. Hydrogen atoms were placed in calculated positions, these being dependent on both the type of bonding at the carbon atom, with the aromatic hydrogen atoms calculated with d(C—H) = 0.950 Å and U_H set equal to $1.2U_{(parent)}$, whereas the methyl hydrogen atoms were initially determined with a rotational difference-Fourier map about the central carbon atom that was further optimized for tetrahedral geometry with d(C—H) = 0.980 Å and U_H set equal to $1.5U_{(parent)}$. The hydrogen atom attached to the boron atom was placed in an idealized tertiary position with d(B—H) = 1.00 Å and U_H set equal to $1.2U_{(parent)}$. All nonhydrogen atoms were refined anisotropically during the final series of cycles and to convergence [$\delta/\sigma \leqslant 0.001$] with $R(F) = 4.47\%$, $wR(F^2) = 7.23\%$ and GOF = 1.075 for all 2460 unique reflections [$R(F) = 3.10\%$, $wR(F^2) = 6.67\%$ for those 2000 data with $F_0 > 4\sigma(F_0)$]. A final difference-Fourier map was essentially featureless with the largest peaks being within 1 Å from a heavy atoms and $|\Delta\rho| \leqslant 0.65$ e Å^{-3}. The function minimized during the full-matrix least-squares refinement was $\Sigma w(F_0^2 - F_0^2)$, where $w = 1/[\sigma^2(F_0^2) + (0.0320*P)^2 + 4.4833*P]$ and $P = (\max(F_0^2, 0) + 2*F_0^2)/3$. An empirical correction for extinction was also attempted but found to produce a negative value and was not applied.

Crystal data and refinement parameters are listed in Table 1, and selected bond distances and angles are collected in Table 2 (the atomic positions have been deposited with the Cambridge Crystallographic Data Centre).

RESULTS

The reaction between $Tp^*Mo(CO)_3^-$ and the halogenating agents $PhICl_2$ and I_2 provide a simple and high yield synthesis of the Mo^{II} 16-electron derivatives $Tp^*MoX(CO)_2$(X = Cl, I), see Eqs (1) and (2). Both derivatives have been isolated as crystalline solids and characterized by elemental analysis (C, H, N, for X = I only), ^{1}H NMR, IR and magnetic susceptibility.

$$Tp^*Mo(CO)_3^- + PhICl_2 \rightarrow Tp^*MoCl(CO)_2 + Cl^- + PhI \quad (1)$$

$$Tp^*Mo(CO)_3^- + I_2 \rightarrow Tp^*MoI(CO)_2 + I^- \quad (2)$$

The iodo derivative has already been reported twice in the literature, but in one case it was not isolated [4], whereas in the other case it has been mischaracterized [16]. Templeton *et al.* carried out the same reaction reported here and reported the initial formation of the tricarbonyl derivative, $Tp^*MoI(CO)_3$, which is characterized by IR absorptions at 2025 and 1937 cm^{-1} in THF [4]. Upon further stirring for 20 h in THF, a gradual conversion to the dicarbonyl compound, which is characterized by absorptions at lower energy (i.e. 1998 and 1921 cm^{-1}) [4],

Table 2. Selected bond distances (Å) and angles (°) for compound $Tp^*MoOI_2 \cdot C_7H_8$

Mo(1)—I(1)	2.7368 (5)
Mo(1)—N(1)	2.150 (3)
Mo(1)—N(3)	2.358 (5)
Mo(1)—O(1)	1.695 (5)
I(1)—Mo(1)—I(1)#	94.56 (2)
I(1)—Mo(1)—O(1)	96.21 (11)
I(1)—Mo(1)—N(1)	90.55 (9)
I(1)—Mo(1)—N(1)#	167.63 (9)
I(1)—Mo(1)—N(3)	86.51 (8)
N(1)—Mo(1)—O(1)	94.4 (2)
N(1)—Mo(1)—N(1)#	82.3 (2)
N(1)—Mo(1)—N(3)	82.55 (13)
O(1)—Mo(1)—N(3)	176.0 (2)

Table 1. Crystal and refinement parameters for compound $Tp^*MoOI_2 \cdot C_7H_8$

Empirical formula	$C_{22}H_{30}BI_2MoN_6O$
Formula weight	755.07
Temperature (K)	153(2)
Wavelength (Å)	0.71073
Crystal system	Orthorhombic
Space group	*Pnma*
Unit cell dimensions	$a = 18.1680(11)$ Å $\alpha = 90°$
	$b = 18.2579(11)$ Å $\beta = 90°$
	$c = 8.1580(3)$ Å $\gamma = 90°$
Volume (Å), Z	2706.1(3), 4
Density (calculated) (Mg m^{-3})	1.853
Absorption coefficient (mm^{-1})	2.792
F(000)	1460
Data/restraints/parameters	2460/4/181
Final R indices [$I > 2\sigma(I)$]	$R_1 = 0.0310$, $wR_2 = 0.0667$[2000 data]
R indices (all data)	$R_1 = 0.0447$, $wR_2 = 0.0723$
Largest difference peak and hole (eÅ^{-3})	0.655 and −0.413

was reported by these authors. It was also reported that the CO loss process is inhibited by a CO atmosphere. No further characterization data were provided in that work. Our IR observations fully match those reported in the above mentioned contribution. The IR absorptions of the isolated solid, which was crystallized from the THF solution by addition of *n*-heptane, are 1999 and 1920 cm^{-1} in THF. We have also established that the exposure of $Tp^*MoI(CO)_2$ to an atmosphere of CO does not produce any observable amounts of the tricarbonyl derivative.

Cano and coworkers on the other hand, have prepared the compound by an alternative route, namely the reaction of KTp* with $MoI_2(CO)_3(MeCN)_2$. They have obtained a crystalline solid, for which they report satisfactory C, H, N analyses for the formulation $Tp^*MoI(CO)_2 \cdot 2MeCN$, directly from the reaction medium (MeCN) after only 30 min stirring at room temperature [16]. The formulation of this product was based on the observation of only two IR stretching vibrations (at 2000 and 1850 cm^{-1} in KBr pellet), whereas a tricarbonyl derivatives with a four-legged piano stool structure and C_s symmetry should exhibit three absorptions ($2A' + A$), as is indeed observed for the related $TpMoI(CO)_3$ complex [2]. This assignment is, however, dubious because broad and sometimes shifted bands are usually observed in polycrystalline samples; the lower frequency absorption does not match either of those observed by Templeton *et al.* for the tricarbonyl and dicarbonyl complexes. Although mention is made of the solubility of the isolated product in common organic solvents, no IR data in solution were reported.

The most critical discrepancy between the previously reported [16] characterization of $Tp^*MoI(CO)_2$ and ours is related to the ^1H NMR properties. The previously reported spectrum [16] was characterized by the expected pattern for a Tp* ligand sitting on a mirror plane, the resonances being in a region of the spectrum which is typical for *diamagnetic* compounds. However, the compound isolated by us is paramagnetic, the solid-state magnetic moment being 3.00 μ_B in agreement with a spin triplet state and shows relatively sharp but highly contact-shifted resonances in the ^1H NMR spectrum, see Fig. 1. The simplest explanation that we can advance is that the relatively rapid precipitation and isolation of the product from MeCN by the previous workers [16] did not allow a complete conversion of the tricarbonyl derivative to the dicarbonyl derivative. Although the composition of the reported product may indeed be close to that of the dicarbonyl, the observed resonances in the diamagnetic region are probably due to residual amounts of the diamagnetic tricarbonyl derivative.

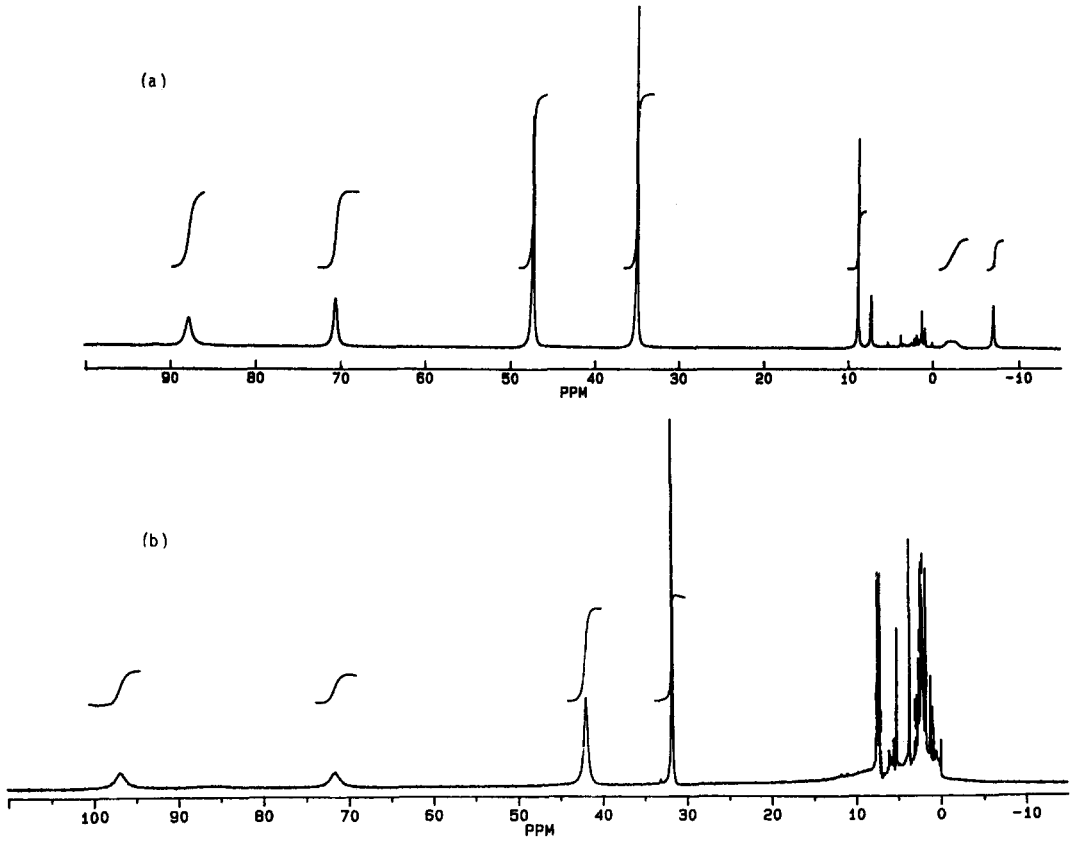


Fig. 1. Room-temperature ^1H NMR spectra of compounds $Tp^*MoX(CO)_2$ [(a) X = I; (b) X = Cl]. Solvent = $CDCl_3$.

The ^{1}H NMR spectrum of Tp*MoI(CO)$_2$ clearly shows two sets of resonances in a 2 : 1 ratio for each type of TP* proton, consistent with the structural rigidity of the C_s pseudo-octahedral structure. There is greater spin density transmitted to the unique pyrazole ring with respect to the other two, the resonance for each type of proton of this ring being shifted to a much greater extent (δ 87.8 and 70.5 for the two ME groups and -7.2 for the ring H, with respect to 47.2, 34.8, and 8.6 for the corresponding protons of the two equivalent rings). A much broader resonance at δ -2.3 is assigned to the B—H proton. Resonances in the diamagnetic region are quite small, attesting to the purity of the compound, and resonances that may be assigned to the tricarbonyl derivative, equivalent to those reported by Cano and coworkers are not visible [16].

The spectroscopic properties of the chloro compound, which has not been described before, parallel those of the iodo analog. The magnetic moment of this derivative is 2.81 μ_B. The ^{1}H NMR resonances are broader relative to those of the iodo analogue, a phenomenon which is commonly observed in the ^{1}H NMR spectra of paramagnetic halide derivatives [20]. The pyrazole ring CH and the BH protons are not visible in this case (see Fig. 1).

Further diiodine oxidation of compound Tp*MoI(CO)$_2$ in THF afforded, after workup and crystallization from toluene/heptane, single crystals of compound Tp*MoOI$_2$, the oxygen atom being possibly provided by adventitious moisture or air. This reaction was monitored by ^{1}H NMR spectroscopy, showing a complex behavior with the formation of several reaction intermediates, none of which has been isolated to date. A similar process has been described in the literature for the oxidation of Tp*Mo(CO)$_3^-$ with thionyl chloride, followed by exposure to air, to afford Tp*MoOCl$_2$ [13,14].

Compound Tp*MoOI$_2$ exhibits a broad EPR resonance ($w_{1/2}$ = 57 G at the X-band; g = 2.045), in agreement with its d^1 configuration. The formulation of this oxo product is confirmed by X-ray crystallography (see Fig. 2). The geometry parallels that established for the related TpMoOCl$_2$. There is no

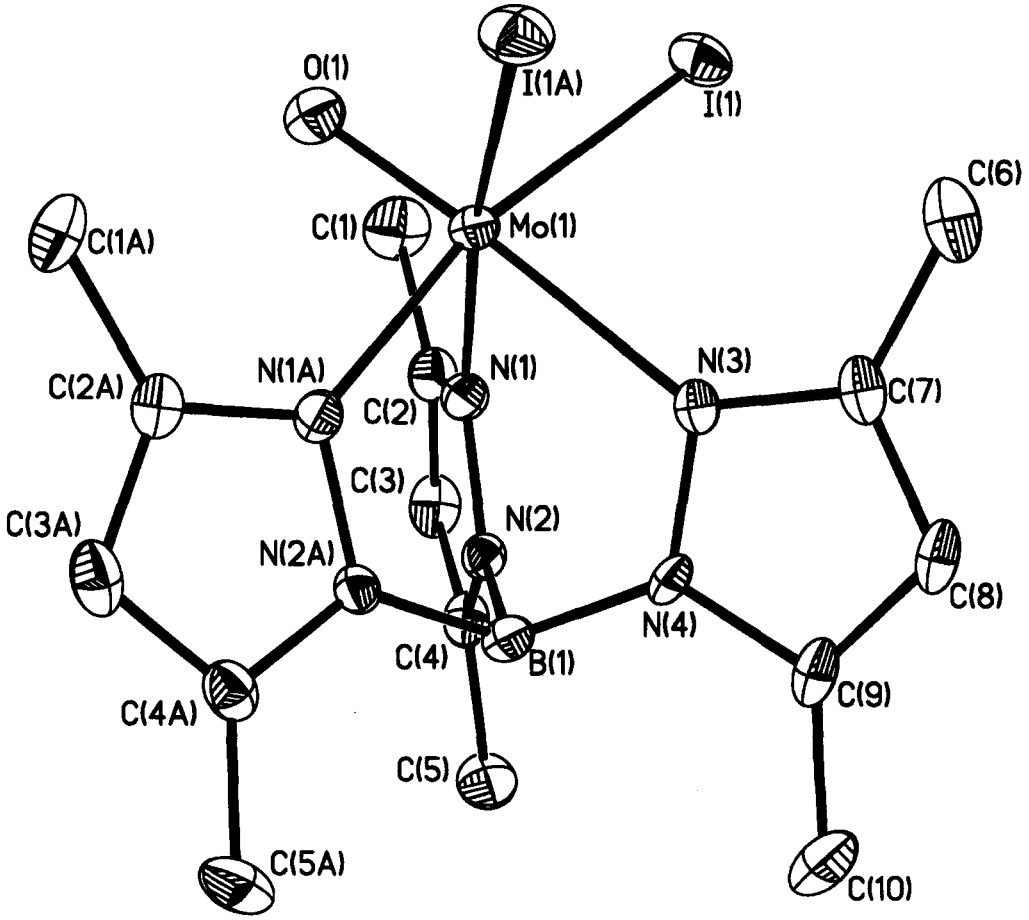


Fig. 2. An ORTEP view of the Tp*MoOI$_2$ molecule with the numbering scheme used. Ellipsoids are shown at the 40% probability level.

sign of positional disorder between the smaller oxygen and the bigger iodine atoms, whereas a O/Cl positional disorder was observed for $TpMoOCl_2$ [12]. The oxygen atom exerts a greater *trans* influence than the iodine atoms, lengthening the Mo—N(3) distance by *ca* 0.2 Å with respect to the Mo—N(1) distance. The other distances in the molecule are quite typical, including the short Mo—O distance, which is close to that reported for the terminal Mo—O bonds in $[TpMoOCl]_2O$ [1.67(4) Å] [12]. The I—Mo—I and I—Mo—O angles are slightly greater and all N—Mo—N angles are smaller than the ideal octahedral angle.

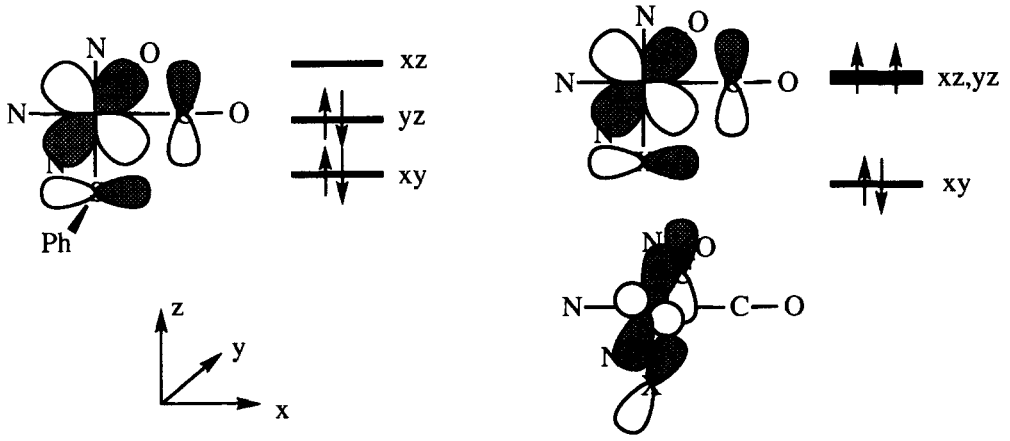
DISCUSSION

The spontaneous CO loss from hydrotris (pyrazolyl)boratotricarbonylhalomolybdenum(II) is a phenomenon first observed by Templeton for $Tp^*MoI(CO)_3$. No analogous process has been reported for the corresponding $TpMoX(CO)_3$ at room temperature, while mild thermolysis of $TpMoI(CO)_3$ in MeCN has been shown to lead to disproportionation products [2]. These observations suggest that the greater steric encumbrance of the Tp* ligand contributes significantly to the thermodynamics of the CO dissociation process. The $Tp^*WI(CO)_3$ compound, on the other hand, yielded the decarbonylated $Tp^*WI(CO)_2$ product only upon reflux for several hours in THF [21,22], attesting to the stronger W—CO bond relative to the Mo—CO bond. Another related literature report concerns compound $\{HB(3,5\text{-}Me_2C_2N_3)_3\}MoI(CO)_3$, i.e. a system completely analogous to $Tp^*MoI(CO)_3$, except for the formal substitution of the pyrazole rings CH groups with N atoms to yield 1,2,4-triazole rings. This compound was isolated from the I_2 oxidation of $[\{HB(3,5\text{-}Me_2C_2N_3)_3\}Mo(CO)_3]^-$ in MeCN and gas evolution was observed upon dissolution in other organic solvents [9]. The decarbonylated product, however, was not isolated or characterized.

Stable low-oxidation state organometallic compounds with an open-shell configuration are rare, especially for metals of the 4*d* and 5*d* series. Compounds with a 16-electron configuration are often stabilized by ligands that are capable of providing two additional electrons from a lone pair *via* a π-donation mechanism [23]. In order for this interaction to be most effective, the lone pair must interact with an empty metal orbital, thus leading to a spin-paired (diamagnetic) configuration. Half-sandwiched Mo(II) compounds such as $CpMo(CO)_2(AsBu^t_2)$ [24], $CpW(CO)_2[P(OCMe_2CMe_2O)]$ [25] and $Cp^*Mo(PPh_2)(PMe_3)_2$ [26] ($Cp^* = \eta^5-C_5Me_5$), can be rationalized in this light. We have recently provided the first example of a spin triplet analogue of the above compounds, namely $Cp^*MoCl(PMe_3)_2$ [27]. The chloride ligand is apparently a less efficient π-donor than phosphido or arsenido groups. Analogous complexes with carbonyl ligands, however, have always been found to be diamagnetic, even with weak π-donors such as halides. Examples are $MoBr_2(CO)_2(PPh_3)_2$ [28], $Mo(OBu^t)_2(CO)_2(py)_2$ [29] and $Mo(S_2CNPr^i_2)_2(CO)_2$ [30]. Octahedral complexes of d^4 centers can in principle adopt two spin configurations: a high-spin (quintet) $t^3_{2g}e^1_g$ or a low-spin (triplet) t_{2g} [4]. Both are observed for complexes of Cr(II) and the spin triplet configuration is adopted by carbonyl-free Mo^{II} complexes, e.g. $MoCl_2(PMe_3)_4$ [31]. In carbonyl complexes, however, the Jahn–Teller unstable (for d^4) octahedral geometry undergoes remarkable distortions to maximize the π-interactions and lead to diamagnetic ground states [32]. The $Tp^*MoX(CO)_2$(X = Cl, I) compounds described here are the first reported examples of octahedral carbonyl derivatives of Mo^{II} with a spin triplet ground state. They are also rare examples of spin triplet carbonyl complexes for any element, especially heavier metals of the 4*d* and 5*d* series. The only other magnetically characterized example known to us is $ReI_3(CO)_3$ [33]. The compound $Tp^*WI(CO)_2$, i.e. a W(II) analog of the Mo compounds discussed here, has also been described as paramagnetic [22], but no magnetic susceptibility nor NMR data for this compound have been reported. Given that severe distortions of the octahedral coordination geometry for Mo^{II} complexes are related to the electrons being paired in a singlet state, we postulate that the geometry of the $Tp^*MoX(CO)_2$ should describe a relatively undistorted octahedron (e.g. bond angles close to 90°). We were unfortunately unable to grow suitable single crystals of this compound.

It is interesting to compare the paramagnetism of $Tp^*MoX(CO)_2$(X = Cl, I) with the diamagnetism of the related $Tp^*M(SPh)(CO)_2$(M = Mo, W) [1,22] and other W^{II} derivatives, e.g. $Tp^*W(NR_2)(CO)_2$ [34]. The halide on one side, and the thiolato and amido ligands on the other side, differ in the strength and symmetry of the π-interactions. While SPh (if bent) and NR_2 are single-sided π-donors, a halide ligand has two equivalent and orthogonal lone pairs. Thus, in an undistorted octahedral structure, the SPh and NR_2 ligands will be able to remove the degeneracy of the metal d_{xz} and d_{yz} orbitals (see Scheme 1, left) and lead to a spin paired ground state, while the halide ligands, even if they engage in a significant π interaction, will not (Scheme 1, right). The imido ligand in complex $[Tp^*W(NPh)(CO)_2]^+$ also has the ability of participating in M—N π-bonding with both lone pairs. The structure shows a linear W—N—Ph moiety and a relatively undistorted octahedral geometry, but the reported NMR properties of the compound indicate diamagnetism [34].

Acknowledgement—We gratefully acknowledge the National Science Foundation (CHE-9508521) for support of this work.



Scheme 1.

REFERENCES

1. Trofimenko, S., *Inorg. Chem.* 1971, **10,** 504.
2. Curtis, M. D. and Shiu, K.-B., *Inorg. Chem.* 1985, **24,** 1213.
3. Lincoln, S., Soong, S.-L., Koch, S. A., Sato, M. and Enemark, J. H., *Inorg. Chem.* 1985, **24,** 1355.
4. Gamble, A. S., White, P. S. and Templeton, J. L., *Organometallics*, 1991, **10,** 693.
5. Protasiewicz, J. D. and Theopold, K. H., *J. Am. Chem. Soc.* 1993, **115,** 5559.
6. Skagestad, V. and Tilset, M., *J. Am. Chem. Soc.* 1993, **115,** 5077.
7. MacNeil, J. H., Roszak, A. W., Baird, M. C., Preston, K. F. and Rheingold, A. L., *Organometallics*, 1993, **12,** 4402.
8. Ward, Y. D., Villanueva, L. A., Allred, G. D., Payne, S. C., Semones, M. A., and Liebeskind, L. S., *Organometallics*, 1995, **14,** 4132.
9. Macleod, I. T., Tiekink, E. R. T. and Young, C. G., *J. Organomet. Chem.* 1996, **506,** 301.
10. Mauthner, K., Slugovc, C., Mereiter, K., Schmid, R., and Kirchner, K., *Organometallics*, 1996, **15,** 181.
11. Koch, S. A. and Lincoln, S., *Inorg. Chem.* 1982, **21,** 2904.
12. Lincoln, S. and Koch, S. A., *Inorg. Chem.* 1986, **25,** 1594.
13. Lincoln, S. and Loehr, T. M., *Inorg. Chem.* 1990, **29,** 1907.
14. Millar, M., Lincoln, S. and Koch, S. A., *J. Am. Chem. Soc.* 1982, **104,** 288.
15. Gordon, J. C., Lee, V. T. and Poli, R., *Inorg. Chem.* 1993, **32,** 4460.
16. Cano, M., Campo, J. A., Heras, J. V. and Pinilla, E., *Polyhedron*, 1996, **15,** 1705.
17. Trofimenko, S. *J. Am. Chem. Soc.* 1967, **89,** 6288.
18. Vogel, A., *Vogel's Textbook of Practical Organic Chemistry*. Longman, London, 1978, p. 638.
19. Lucas, H. J. and Kennedy, E. R., *Org. Synth.* 1942, **22,** 69.
20. Poli, R. and Mui, H. D., *Inorg. Chem.* 1991, **30,** 65.
21. Pérez, P. J., Luan, L., White, P. S., Brookhart, M. and Templeton, J. L., *J. Am. Chem. Soc.* 1992, **114,** 7928.
22. Philipp, C. C., Young, C. G., White, P. S. and Templeton, J. L., *Inorg. Chem.* 1993, **32,** 5437.
23. Caulton, K. G., *New J. Chem.* 1994, **18,** 25.
24. Luksza, M., Kimmer, S. and Malisch, W., *Angew. Chem., Int. Ed. Engl.* 1983, **22,** 416.
25. Gross, E., Jörg, K., Fiederling, K., Göttlein, A., Malisch, W. and Boese, R., *Angew. Chem., Int. Ed. Engl.* 1984, **23,** 738.
26. Baker, R. T., Calabrese, J. C., Harlow, R. L., and Williams, I. D., *Organometallics*, 1993, **12,** 830.
27. Abugideiri, F., Keogh, D. W. and Poli, R., *J. Chem. Soc., Chem. Commun.* 1994, 2317.
28. Drew, M. G. B., Tomkins, I. B. and Colton, R., *Aust. J. Chem.* 1970, **23,** 2517.
29. Chisholm, M. H., Huffman, J. C. and Kelly, R. L., *J. Am. Chem. Soc.* 1979, **101,** 7615.
30. Templeton, J. L., and Ward, B. C., *J. Am. Chem. Soc.* 1980, **102,** 6568.
31. Carmona, E., Marín, J. M., Poveda, M. L., Atwood, J. L. and Rogers, R. D., *Polyhedron*, 1983, **2,** 185.
32. Kubácek, P. and Hoffman, R., *J. Am. Chem. Soc.* 1981, **103,** 4320.
33. Calderazzo, F., Marchetti, F., Poli, R., Vitali, D. and Zanazzi, P. F., *J. Chem. Soc., Dalton Trans.* 1982, 1665.
34. Powell, K. R., Pérez, P. J., Feng, S. G., White, P. S., Brookhart, M. and Templeton, J. L., *Organometallics*, 1994, **13,** 1851.

Pergamon

PII: S0277-5387(96)00402-0

Polyhedron Vol. 16, No. 8, pp. 1399–1402, 1997
Copyright © 1997 Elsevier Science Ltd
Printed in Great Britain. All rights reserved
0277-5387/97 $17.00+0.00

COMMUNICATION

Preparation and characterization of the seven coordinate cadmium(II) complex $[Cd(3,4\text{-}H_2dhb)_2(H_2O)_3]\cdot HCl\cdot(3,4\text{-}H_3dhb)\cdot 2.5H_2O$; the first structural determination of a complex containing the 3,4-dihydroxybenzoato(-1)(3,4-H_2dhb^-) ligand

Vasilis Aletras,[a] Nick Hadjiliadis,[a]* Despina Stabaki,[b] Alexandra Karaliota,[b] Maria Kamariotaki,[b] Ian Butler,[c] John C. Plakatouras[d] and Spyros Perlepes[d]

[a]Department of Chemistry, University of Ioannina, 451 10 Ioannina, Greece

[b]Department of Chemistry, University of Athens, Panepistimiopolis, Kouponia, 157 01 Athens, Greece

[c]Department of Chemistry, McGill University, 801 Sherbrooke Street West, Montreal, Que., Canada H3A 2K6

[d]Department of Chemistry, University of Patras, 265 00 Patras, Greece

(Received 23 July 1996; accepted 12 August 1996)

Abstract—The 1:2:1 reaction of $CdCl_2\cdot 2.5H_2O$ with 3,4-dihydroxybenzoic acid ($3,4\text{-}H_3dhb$) and KOH in Pr^nOH–H_2O gave the unique, seven-coordinate cadmium(II) complex $[Cd(3,4\text{-}H_2dhb)_2(H_2O)_3]\cdot HCl\cdot(3,4\text{-}H_3dhb)\cdot 2.5H_2O$ as one of the products. Crystal structure and ^{113}Cd NMR studies showed that $3,4\text{-}H_2dhb^-$ behaves as a bidentate chelate with ligated atoms being the carboxylate oxygens, but that seven-coordination is not retained in aqueous solution. Copyright © 1997 Elsevier Science Ltd

Keywords: Cd^{II} complex; seven-coordinate complex; ^{113}Cd NMR; 3,4-dihydroxybenzoato(-1) Cd^{II} complex; crystal structure.

Several groups have been exploring the coordination chemistry of dihydroxybenzoic acids [1–7] and related ligands [8–10]. They have been motivated chiefly by the fact that in living systems, like plants or microorganisms, simple aromatic compounds bearing phenolic and carboxylic groups serve as versatile ligands to chelate toxic and nutrient metal ions. Many of these compounds are also present in the natural environment as by-products of degradation and metabolic processes and they act as nonspecific ligands toward metal ions in terrestrial and aquatic systems [11]. This family of ligands can provide an efficient chelating ability through several potential donor sets, e.g., of salicylato or catecholato type; mixed coordination modes are also possible. Polynuclear or polymeric species may also be formed with ligands able to bind a metal ion through a donor set while retaining further donor groups to coordinate another metal; these complexation processes may be significant due to their involvement in the natural processes leading to the formation of humic and fulvic matter [11]. Recently,

* Author to whom correspondence should be addressed.

we have developed an interest in cadmium complexes of dihydroxybenzoic acids, an area hitherto unexplored for this otherwise well studied metal and we report herein the preparation and characterization of $[Cd(3,4\text{-}H_2dhb)_2(H_2O)_3]\cdot HCl\cdot(3,4\text{-}H_3dhb)\cdot 2.5H_2O$ ($3,4\text{-}H_3dhb$ = 3,4-dihydroxybenzoic acid), a seven-coordinate cadmium(II) complex presenting a bidentate carboxylato-type coordination of $3,4\text{-}H_2dhb^-$. The X-ray structure of this complex is the first such reported for metal complexes containing any anionic form of $3,4\text{-}H_3dhb$.

The Cd^{II} complex is one of the two products from the 1 : 2 : 1 reaction* between $CdCl_2$, $3,4\text{-}H_3dhb$ and KOH in Pr^nOH–H_2O. Crystals suitable for a crystal structure analysis were obtained by slow cooling of a concentrated solution of the complex in H_2O.

Crystallographic studies† indicated the formula $[Cd(3,4\text{-}H_2dhb)_2(H_2O)_3]\cdot HCl\cdot(3,4\text{-}H_3dhb)\cdot 2.5H_2O$. The structure of the $[Cd(3,4\text{-}H_2dhb)_2(H_2O)_3]$ molecule (Fig. 1) proves conclusively that the $3,4\text{-}H_2dhb^-$ anion functions as a bidentate chelate with ligated atoms being the carboxylate oxygens [O(1), O(2) and O(11), O(12)]; the oxygen atoms [O(5), O(6), O(7)] from three terminal H_2O molecules complete seven-coordination at the metal atom. The chelating $3,4\text{-}H_2dhb^-$ anions are asymmetrically ligated [Cd(1)—O(1) 2.513(4), Cd(1)—O(2) 2.304(4); Cd(1)—O(11) 2.481(4), Cd(1)—O(12) 2.314(4) Å], while the Cd(1)—O_{aquo} bond lengths are similar [2.290(5), 2.309(4) and 2.291(4) Å]. The geometry around Cd(1) can be described as distorted pentagonal bipyramidal. Atoms O(1), O(2), O(6), O(11) and O(12) comprise the equatorial plane around Cd(1), while atoms O(5) and O(7) form the pyramidal apices [O(5)—Cd(1)—O(7) 170.5(2)°]. Cd(1) lies 0.061(3) Å above the least-squares equatorial plane [from which the maximum deviation of atoms concerned is 0.096(7) Å by O(11) towards O(5)]. The regularity of the arrangement is necessarily broken by the chelation angles subtended at Cd(1) by the rigid four-membered chelate rings [54.0(1), 54.3(1)°], the regular pentagon value being 72°. The present compound joins a relatively small family of seven-coordinate Cd^{II} species [13–19]. It is interesting to note that the coordination of each atom is not forced by the geometry of other coordinating atoms, although there are examples of apparent seven-coordination forced by geometrical demands of polydentate ligands [13,15–17]. The crystal structure is stabilized through a complex scheme of intra- and intermolecular hydrogen bonds involving the coordinated and lattice H_2O molecules, —OH groups, chloride ion and the carboxylic group of the noncoordinated $3,4\text{-}H_3dhb$ molecule.

In the IR spectrum, complex $[Cd(3,4\text{-}H_2dhb)_2(H_2O)_3]\cdot HCl\cdot(3,4\text{-}H_3dhb)\cdot 2.5H_2O$ exhibits bands at 3480, ~3350, 3190, ~2900, 1661, 1554, 1480, 1448, 1404, 1287 and 1265 cm^{-1}, assignable‡ to $\nu(O—H)_{bound\ H_2O}$, $\nu(O—H)_{lattice\ H_2O}$, $\nu(O—H)_{phenolic}$, $\nu(O—H)_{-COOH}$, $\nu(C{=}O)_{-COOH}$, ν_{asym} (CO_2), a ring stretching mode characteristic of free catechole-type ligands and their metal complexes, ν_{sym} (CO_2), $\delta(OH)_{-COOH}$, $\nu(C—O)_{-COOH}$ and $\nu(C—O)_{phenolic}$, respectively [1,3,4]. The small ν_{asym} (CO_2)-ν_{sym} (CO_2)

* To a stirred solution of $CdCl_2\cdot 2.5H_2O$ (0.34 g, 1.5 mmol) in Pr^nOH (25 cm^3) was added solid $3,4\text{-}H_3dhb$ (0.46 g, 3.0 mmol). Addition of a solution of KOH (0.084 g, 1.5 mmol) in H_2O (10 cm^3) led to the rapid precipitation of a Cd^{II}-containing cream microcrystalline material. After *ca* 15 min, the mixture was filtered and the essentially colorless mother liquor soon began to deposit well-formed crystals of the product. The crystals were collected by filtration, washed with Pr^nOH–H_2O (1 : 1) and acetone, and dried in air; yield *ca* 21% based on available Cd. Found: C, 35.8; H, 4.1; Cl, 4.8; Cd, 16.3. $C_{21}H_{28}ClCdO_{17.5}$ requires: C, 35.6; H, 4.0; Cl, 5.0; Cd, 15.9%).

† Crystal data: $C_{21}H_{28}ClCdO_{17.5}$, M = 708.31, monoclinic, space group $C2/c$, a = 27.925(14), b = 11.484(2), c = 19.908(6) Å, β = 126.49(2)°, U = 5133(3) Å^3 (by least-squares refinement of the setting angles of 24 automatically centered reflections in the 2θ range 30–40°, λ = 0.70930 Å), Z = 8, $F(000)$ = 2872, D_c = 1.83 g cm^{-3}, T = 296 K, colorless crystals, 0.47 × 0.21 × 0.14 mm, μ = 1.04 mm^{-1}, 9231 reflections measured, 4526 unique, giving 3389 with $I > 2.0\sigma(I)$ [R_{int} = 0.041], 366 refined parameters, $[\Delta/\sigma]_{max}$ = 0.060, $[\Delta\rho]_{max}$, $[\Delta\rho]_{min}$ = 1.690, −0.630 e Å^{-3}, $R(=\Sigma\|F_o|-|F_c\|/\Sigma|F_o|)$ = 0.047, $R'(=[\Sigma w(|F_o|-|F_c|)^2/\Sigma w|F_o|^2]^{1/2})$ = 0.043 for 3389 independent observed reflections, weights based on counting-statistics.

Intensity data, collected on a Rigaku AFC6S diffractometer using the $\omega/2\theta$ scan mode to $2\theta_{max}$ = 50°, were corrected for decay (−1.08%) and absorption (Ψ scans, transmission factors range: 0.684951–0.795685). The structure was solved by direct methods and refined on $|F|$ by full-matrix least-squares. The main molecule as well as two of the H_2O molecules and the extra neutral ligand are in general position giving eight of each in the unit cell. The chlorine atom Cl(1) sits on the two-fold axis (Z = 4), chlorine atom Cl(2) and H_2O molecule OW(3) are disordered about an inversion center and have site occupancy factors of 1/2. While chlorine is present on one side of the inversion center, water is present on the opposite side. The two partial chlorines cannot be present simultaneously, since they would be too close to one another. Hence, there are 2.5 solvation H_2O molecules per Cd^{II} atom and two half Cl atoms. The extra proton required to balance the charge could not be located; hydrogens on OW(3) and —OH hydrogens on free ligand were not found either and have not been included in the model. Nonhydrogen atoms were refined with anisotropic thermal parameters, except disordered atoms which were kept isotropic. Hydrogen atoms were located in difference maps, distances being normalized to 0.95 Å. Residual electron density in the area of the disordered atoms likely reflects extra components to the disorder that were not resolved. Attempts were made to introduce partial Cl or O atoms on that side, but standard uncertainties in bond lengths and angles as well as R factors did not improve; solution described above was retained. All computing was done using the NRCVAX system of crystallographic software [12]. Atomic coordinates, thermal parameters and bond lengths and angles have been deposited at the Cambridge Crystallographic Data Center.

‡ Details will be reported in the full paper.

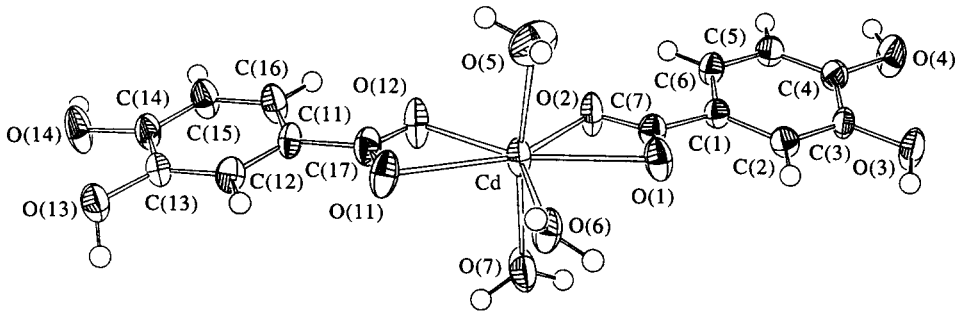


Fig. 1. An ORTEP [21] representation of the molecule $[Cd(3,4\text{-}H_2dhb)_2(H_2O)_3]$ in complex $[Cd(3,4\text{-}H_2dhb)_2(H_2O)_3]\cdot HCl\cdot(3,4\text{-}H_3dhb)\cdot 2.5H_2O$: Cd (1)—O(1) 2.513(4), Cd(1)—O(2) 2.304(4), Cd(1)—O(5) 2.290(5), Cd(1)—O(6) 2.309(4), Cd(1)—O(7) 2.291(4), Cd(1)—O(11) 2.481(4), Cd(1)—O(12) 2.314(4), C(7)—O(1) 1.251 (7), C(7)—O(2) 1.272(7), C(17)—O(11) 1.257(8), C(17)—O(12) 1.268(8) Å; O(5)—Cd(1)—O(7) 170.5(2), O(5)—Cd(1)—O(1) 84.6(2), O(5)—Cd(1)—O(6) 90.3(1), O(1)—Cd(1)—O(2) 54.0(1), O(1)—Cd(1)—O(12) 144.5(1), O(2)—Cd(1)—O(11) 144.9(1), O(2)—Cd(1)—O(6) 130.9(1), O(11)—Cd(1)—O(12) 54.3(1), O(6)—Cd(1)—O(11) 83.8(1), O(6)—Cd(1)—O(12) 137.6(1), O(7)—Cd(1)—O(11) 92.6(1), O(7)—Cd(1)—O(12) 91.7(2), O(6)—Cd(1)—O(7) 82.6(2)°.

separation is as expected for the bidentate chelating mode of the carboxylate ligation of $3,4\text{-}H_2dhb^-$ [20].

^{13}Cd NMR is a very useful tool for the study of Cd^{II} complexes due to the sensitivity of the ^{113}Cd chemical shift to the nature of donor atoms, their coordination geometry and bond length [22]. The complex reported here has an isotropic chemical shift at 45.9 ppm in D_2O solution (Fig. 2). The coordination number of Cd^{II} in complexes with exclusively oxygen ligation is six, seven or eight, while the isotropic chemical shifts span the range δ 140 to −115 [23,24]. From these systematic studies, a pattern has emerged [23] showing that six-coordinate Cd^{II} has a chemical shift ranging from δ 140 to −70, seven-coordinate cadmium(II) spans the range δ 0 to −70, and eight-coordinate cadmium(II) a range δ 0 to −115. Based on such data, the chemical shift at δ 45.9 is assigned to a six-coordinate cadmium(II) atom, indicating that the

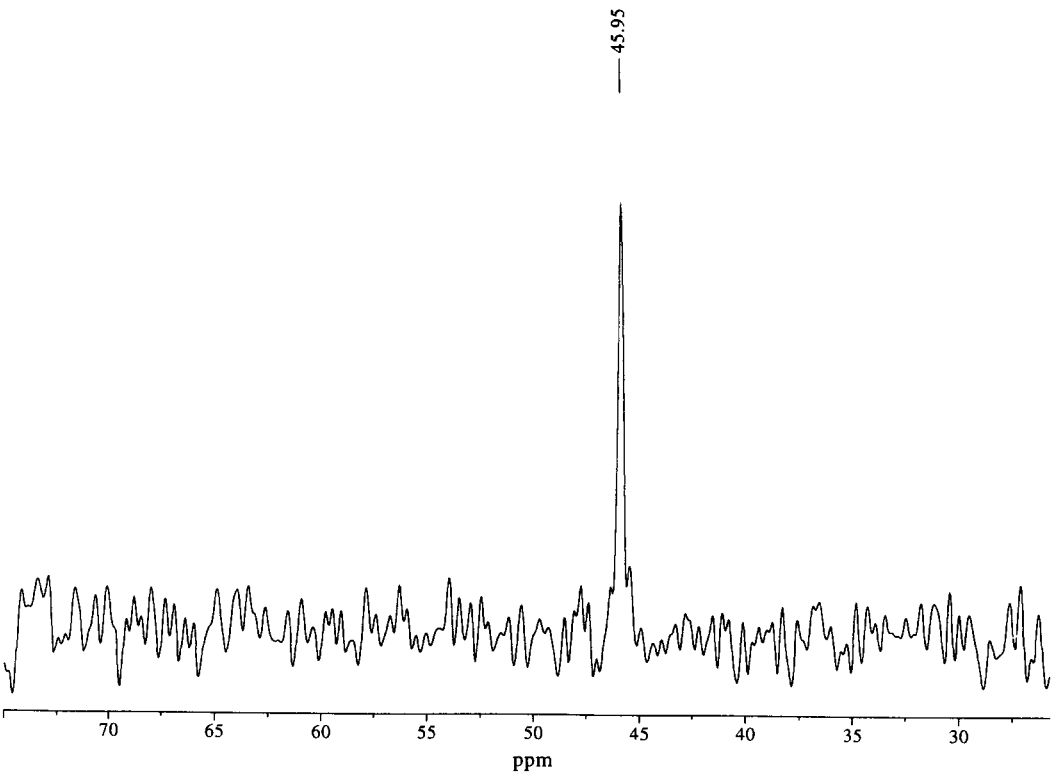


Fig. 2. ^{113}Cd NMR spectrum (88.7 MHz) of $[Cd(3,4\text{-}H_2dhb)_2(H_2O)_3]\cdot HCl\cdot(3,4\text{-}H_3dhb)\cdot 2.5H_2O$ in D_2O; chemical shift is referenced to an external sample of 0.1 M $Cd(ClO_4)_2$ in D_2O at 23°C.

solid-state structure of the $[Cd(3,4\text{-}H_2dhb)_2(H_2O)_3]$ molecule does not persist in solution. We are studying this and related complexes by solid-state ^{113}Cd NMR in order to determine the shifts of the individual tensors and anticipate direct structure/shielding correlations from these experiments.

A better understanding of the course of the reaction reported here must await identification of the other major product, the initial cream microcrystalline precipitate. This material seems to contain (IR evidence) doubly deprotonated 3,4-dihydroxybenzoic acid. Additional Cd^{II}-dihydroxybenzoato species—including high nuclearity clusters—are under investigation.

REFERENCES

1. Griffith, W. P., Nogueira, H. I. S., Parkin, B. C., Sheppard, R. N., White, A. J. P. and Williams, D. J., *J. Chem. Soc., Dalton Trans.* 1995, 1775, and refs therein.
2. Bodini, M., Osorio, C., Valle, M. A. D., Arancibia, V. and Munoz, G., *Polyhedron*, 1995, **14,** 2933.
3. Anbalagan, V. and Srivastava, T. S., *Polyhedron*, 1994, **13,** 291.
4. Kamariotaki, M., Karaliota, A., Stabaki, D., Bakas, T., Papaefthymiou, V., Perlepes, S. P. and Hadjiliadis, N., *Trans. Met. Chem.* 1994, **19,** 241.
5. Glowiak, T., Kozlowski, H., Erre, L. S., Micera, G. and Gulinati, B., *Inorg. Chim. Acta*, 1992, **202,** 43, and refs therein.
6. Jezowska-Bojczuk, M., Kozlowski, H., Zubor, A., Kiss, T., Branca, M., Micera, G. and Desi, A., *J. Chem. Soc., Dalton Trans.* 1990, 2903.
7. Kiss, T., Kozlowski, H., Micera, G. and Erre, L. S., *Polyhedron*, 1989, **8,** 647.
8. Erre, L. S., Micera, G., Gulinati, B. and Cariati, F., *Polyhedron*, 1992, **11,** 101.
9. Erre, L. S., Micera, G., Cariati, F., Ciani, G., Sironi, A., Kozlowski, H. and Baranowski, J., *J. Chem. Soc., Dalton Trans.* 1988, 363.
10. Erre, L. S., Micera, G., Piu, P., Cariati, F. and Ciani, G., *Inorg. Chem.* 1985, **24,** 2297.
11. Kiss, T., Micera, G., Sanna, D. and Kozlowski, H., *J. Chem. Soc., Dalton Trans.* 1994, 347, and refs therein.
12. Gabe, E. J., Le Page, Y., Charland, J.-P., Lee, F. I. and White, P. S., *J. Appl. Cryst.* 1989, **22,** 384.
13. Saalfrank, R. W., Burak, R., Reihs, S., Löw, N., Hampel, F., Stachel, H. D., Lentmaier, J., Peters, K., Peters, E.-M. and von Schnering, H. G., *Angew. Chem., Int. Ed. Engl.* 1995, **34,** 993.
14. Fujita, M., Kwon, Y. J., Miyazama, M. and Ogura, K., *J. Chem. Soc., Chem. Commun.* 1994, 1977.
15. Byriel, K. A., Dunster, K. R., Gahan, L. R., Kennard, C. H. L., Latten, J. L., Swann, I. L. and Duckworth, P. A., *Inorg. Chim. Acta*, 1993, **205,** 191.
16. Adam, K. R., Donnelly, S., Leong, A. J., Lindoy, L. F., McCool, B. J., Bashall, A., Dent, M. R., Murphy, B. P., McPartlin, M., Fenton, D. E. and Tasker, P. A., *J. Chem. Soc., Dalton Trans.* 1990, 1635.
17. Adam, K. R., Dancey, K. P., Leong, A. J., Lindoy, L. F., McCool, B. J., McPartlin, M. and Tasker, P. A., *J. Am. Chem. Soc.* 1988, **110,** 8471.
18. Post, M. L. and Trotter, J., *J. Chem. Soc., Dalton Trans.* 1974, 1922, and refs therein.
19. Kepert, D. L., in *Inorganic Chemistry Concepts*, Vol. 6, Ch. 10 and 11, ed C. K. Jorgensen, M. F. Lappert, S. J. Lippard, J. L. Margreave, K. Niedenzu, H. Nöth, R. W. Parry and H. Yamatera, Springer-Verlag, Berlin, 1982, pp. 117–151.
20. Deacon, G. B. and Phillips, R. J., *Coord. Chem. Rev.* 1980, **33,** 227.
21. Johnson, C. K., *ORTEP.* Report ORNL-5138. Oak Ridge National Lanoratory, Oak Ridge, TN, 1976.
22. Summers, M. F., *Coord. Chem. Rev.* 1988, **86,** 43.
23. Chung, K. H., Hong, E., Do, Y. and Moon, C. H., *J. Chem. Soc., Chem. Commun.* 1995, 2333, and refs therein.
24. Honkonen, R. S., Doty, F. D. and Ellis, P. D., *J. Am. Chem. Soc.* 1983, **105,** 4163.

Pergamon

PII: S0277-5387(96)00396-8

Polyhedron Vol. 16, No. 8, pp. 1403–1406, 1997
Copyright © 1997 Elsevier Science Ltd
Printed in Great Britain. All rights reserved
0277-5387/97 $17.00+0.00

COMMUNICATION

The production of hydrogen peroxide from dioxygen using hydroxylamine as substrate catalysed by Mn^{2+}-exchanged montmorillonite clay

Bhupinder Hothi, Virginie Lechene, Joseph Robinson and Tippu S. Sheriff*

Inorganic Research Laboratories, Department of Physical Sciences, University of Hertfordshire, College Lane, Hatfield, Hertfordshire AL10 9AB, U.K.

(Received 24 May 1996; accepted 6 August 1996)

Abstract—Mn^{2+}-exchanged montmorillonite clay, in milligramme quantities, efficiently catalyses the production of hydrogen peroxide from dioxygen (or air) and hydroxylamine at pH 8.0 in aqueous solution; concentrations of hydrogen peroxide > 0.40 mol dm^{-3} (~1.5% w/v H_2O_2, ~86% based on hydroxylamine) in 50 min and turnover numbers $[H_2O_2]/[Mn^{2+}] > 10^5$ were obtained. The mechanism for hydrogen peroxide production in this system is discussed together with the possibilities of developing a dual system to use the *in situ* generated hydrogen peroxide to effect some organic oxidation transformations. Copyright © 1997 Elsevier Science Ltd

Keywords: hydrogen peroxide; dioxygen; manganese; clay; catalysis; hydroxylamine.

Hydrogen peroxide is seen as the ideal oxidant from an environmental point of view, producing only water as a byproduct. It has been estimated [1] that of the 900,000 tonne per annum production of hydrogen peroxide, only 10% is used in the synthetic organic industry, mostly for epoxidation reactions and the paucity of practical applications contrasts with the clear environmental advantages. Solutions to the problems of the activation of hydrogen peroxide which results in this under-use are being found [2] and it is envisaged that the use of hydrogen peroxide will increase markedly in the coming decade.

The oxidation of organic molecules usually requires the use of fairly concentrated solutions of hydrogen peroxide or organic peroxides (30%), but recently dilute solutions of hydrogen peroxide (~2%) have been used to epoxidise alkyl-substituted alkenes [3]. Other important potential applications in the generation of dilute solutions of hydrogen peroxide from air or dioxygen in aqueous solution include the formulation of liquid laundry detergents and the disinfection of process waters and water used for air-conditioning etc. The *in situ* generation of hydrogen peroxide has additional environmental advantages in terms of the transport, storage and handling problems associated with hydrogen peroxide.

There has been a number of reports of the production of hydrogen peroxide by reaction of dioxygen and transition metal ions or complexes, although in the majority of these systems the peroxide rapidly disappears by further reaction or catalytic decomposition. In the presence of a reducing substrate, catalytic production of hydrogen peroxide is possible. Thus, it has been shown by one of us that manganese(II)/4,5-dihydroxybenzene-1,3-disulfonate (Tiron) provides an efficient homogeneous catalyst for the reduction of dioxygen to hydrogen peroxide with hydroxylamine in the pH range 7.5–8.6 [4]. Peroxide concentrations greater than 0.20 mol dm^{-3} and

* Author to whom correspondence should be addressed.

turnover numbers $[H_2O_2]/[Mn^{2+}] > 10^4$ were obtained. Unpublished data suggest that the overall process can be represented as follows:

$$O_2(air) + 2NH_2OH = H_2O_2 + N_2 + 2H_2O \quad (1)$$

Preparation of modified clay

Sodium bentonite (MPS-1), a montmorillonite supplied by Volclay, was dried for several hours at 105°C and then cooled in a desiccator. A 5% (w/v) suspension of the clay (20 g) in a 0.1 M aqueous solution of $MnCl_2 \cdot 4H_2O$ was stirred overnight, the supernatent liquid discarded and the clay washed several times with distilled water. The clay was isolated by centrifugation and again washed with distilled water until all the excess $MnCl_2$ had been removed (tested with $AgNO_3$). The Mn^{2+}-exchanged clay was dried (as before) and then crushed and powdered and sieved through a 500 micron mesh. Analysis of both Mn^{2+}-exchanged clay and sodium bentonite for manganese content was achieved by ICP with XRD being used to provide basal spacings data.

Hydrogen peroxide production and analysis

Accurately weighed portions of the clay were added to a Dreschel bottle (in a water bath) containing deionized water (100.0 cm^3) containing ACS grade $NH_2OH \cdot HCl$ (0.5 or 1.0 mol dm^{-3}) and Tiron (6×10^{-4} mol dm^{-3}), buffered using 4-(2-hydroxyethyl)-l-piperazinepropanesulfonic acid (EPPS, 0.1 mol dm^{-3}) to pH 8.0 using semiconductor grade, carbonate-free aqueous NaOH. A good supply of dioxygen from a cylinder or air *via* a vacuum created by a water pump were supplied to the stirred solution. Aliquots of the solution were removed at defined periods and analysed for hydrogen peroxide concentration using the colorimetric method based on titanium (IV) sulfate [5,6]. A Philips UV–vis spectrophotometer PU 8720 was used for colorimetric measurements.

The results are shown in Fig. 1. The yields of H_2O_2 produced with Mn^{2+}-clay, ~0.23 mol dm^{-3} (~90% based on NH_2OH) were consistent with earlier results using homogeneous catalysis [4], but the rate of production of hydrogen peroxide, $[H_2O_2]_{max}$ in ~30 min, was found to be a marked improvement. With NH_2OH (1.0 mol dm^{-3}) and using Mn^{2+}-clay (0.0074 g), remarkable concentrations of H_2O_2 of ~0.43 mol dm^{-3} (~1.5% w/v H_2O_2, ~86% based on NH_2OH) could be obtained in only *ca* 50 min.

In the absence of added clay (Fig. 1) only slow formation of H_2O_2 was observed which can probably be attributed to catalysis by adventitious traces of Mn^{2+} [7]. With sodium bentonite, there is also a slow (but slightly higher) formation of H_2O_2, which presumably results from catalysis by small quantities of manganese present within the clay, measured by ICP to be 0.15 mmol of total manganese per 100 g of clay. The Mn^{2+}-exchanged clay is catalytic in milligramme quantities with "saturation" being observed at weights of exchanged clay of 5 mg (per 100 cm^3 of reaction solution). The amount of Mn^{2+} exchanged in the clay was determined by ICP to be 33.95 mmol per 100 g of clay, corresponding to a cation exchange capacity (CEC) of the clay of 67.6 meq (mmol) per 100 g, giving turnovers of $[H_2O_2]/[Mn^{2+}] \sim 10^5$.

Previously "saturation" was achieved at levels of 1×10^{-4} mol dm^{-3} when using aqueous $MnCl_2$ [4], corresponding to a weight of manganese(II) of *ca* 50 mg. This clearly shows the greater efficiency of Mn^{2+} within the clay support to catalyse the process. This result can be either explained by the effect of the restricted two-dimensional space within a layered clay structure, thus allowing a greater probability for reactants to meet [8], or the effect of the reactants proximity adsorbed on the outer surface of the modified clay.

X-ray powder diffraction (XRD) analysis of sodium bentonite (undried) and Mn^{2+}-clay both produced sharp peaks implying an interlayer structure with basal spacings (d_{001}) of 1263 and 1281 pm, respectively. These results would give an interlayer (interlamellar) spacing of approximately 300 pm and 320 pm for the Na^+- and Mn^{2+}-clay, respectively [9]. In the aqueous reaction medium used, it would be expected that the Mn^{2+}-clay would fully hydrate, increasing the interlayer space to approximately 800 pm and this space would be important in especially enabling the intercalation and binding of the ligand (Tiron), and also the substrate (hydroxylamine) and dioxygen.

The rate of formation of hydrogen peroxide in air using Mn^{2+}-exchanged clay was approximately 1/5 that in pure dioxygen, indicating that dioxygen is involved in the rate-determining step. A mechanism for the homogeneous process has been proposed [4], whereby both dioxygen and hydroxylamine become bound to a square-planar assembly of manganese(II) and catecholate ligand with the resulting complex acting as an "electron sink" for the transfer of electron density from the bound substrate to dioxygen. The faster rates of hydrogen peroxide production with this partial heterogeneous system imply that the presence of manganese(II) adsorbed either onto the surface or within the interlamellar space of the clay facilitates this process.

Recently Uemura and *et al.* have reported the use of Mn^{2+}-clay to catalyse the oxidation of alkanes with *tert*-butyl hydroperoxide [10]. With the system described here, there is the possibility of developing a dual process which cannot only generate hydrogen peroxide *in situ*, but also catalyse important organic oxidation processes. Work is also continuing to search for alternative substrates to hydroxylamine to make this process more economically viable and for which some success has been achieved. This system is also of

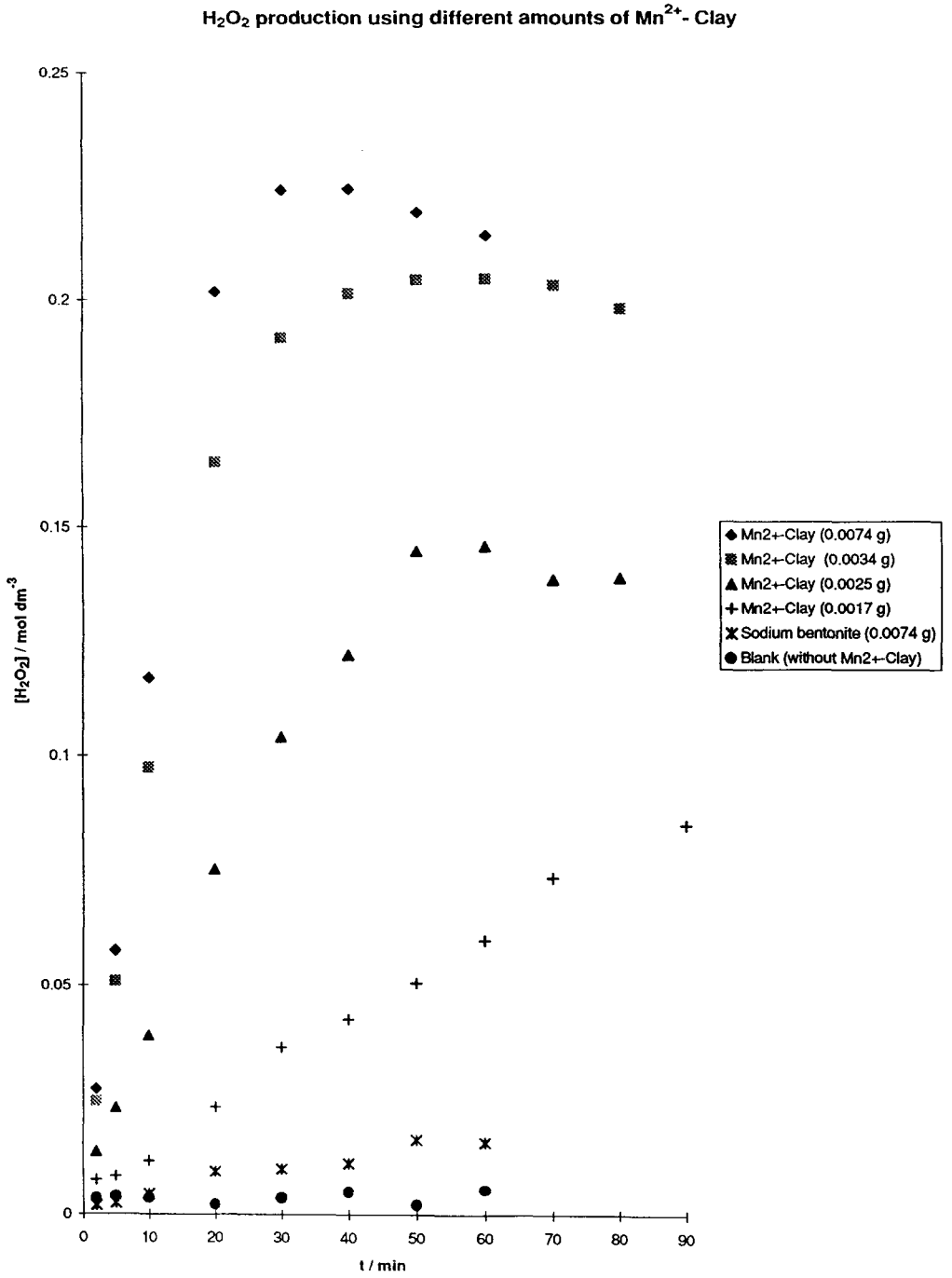


Fig. 1. The production of H_2O_2 in the Mn^{2+}-clay/Tiron/NH_2OH system in the presence of O_2 at $25 \pm 0.5°C$ and different weights of Mn^{2+}-clay. In all runs, the [Tiron] was 6×10^{-4} mol dm^{-3}, the initial [NH_2OH] was 0.5 mol dm^{-3} and the pH was 8.0 [0.1 mol dm^{-3}, 4-(2-hydroxyethyl)-l-piperazinepropanesulfonate (EPPS) buffer].

interest in modelling natural systems such as galactose oxidase [11].

Acknowledgements—B.H. would like to thank The Nuffield Foundation for the provision of a research bursary (NUF-URB95); J.R. would like to thank the Society of Chemical Industry for the provision of a maintenance grant under the Messel Fund. A gifted supply of sodium bentonite MPS-1 from Volclay Ltd is acknowledged with gratitude.

REFERENCES

1. Buchner, W., Schliebs, R., Winter, G. and Bucher, K. H., *Industrial Inorganic Chemistry*. VCH, Weinheim, 1989, p. 21.
2. Strukel, G., *Catalytic Oxidations With Hydrogen Peroxide As Oxidant*. Kluwer Academic Publishers, Dordrecht, 1992; Wilson, S. L., *Performance Chemicals*, October/November, 1993, 39.
3. Al-Ajlouni, A. M. and Espenson, J. H., *J. Org. Chem.* 1996, **61,** 3969.
4. Sheriff, T. S., *J. Chem. Soc., Dalton Trans.* 1992, 1051.
5. Egerton, A. C., Everett, A. J., Minkoff, G. J., Rudrakanchana, S. and Salooja, K. C., *Anal. Chim. Acta*, 1954, **10,** 422.
6. Clapp, P. A., Evans, D. F. and Sheriff, T. S., *Anal. Chim. Acta*, 1989, **218,** 332.
7. Ottoway, J. M. and Hale, D. J., *Pure Appl. Chem.* 1986, **58,** 1308; Gretzinger, K., Kotz, L., Tols, G. and Tschopel, P., *Talanta*, 1982, **29,** 1011.
8. Laszlo, P., *Acc. Chem. Res.* 1986, **19,** 121.
9. Clark, J. H., Kybett, A. P. and Macquarrie, D. J., *Supported Reagents: Preparation, Analysis and Applications*. VCH Publishers, New York, 1992, p. 51.
10. Tateiwa, J., Horiuchi, H. and Uemura, S., *J. Chem. Soc., Chem. Commun.* 1994, 2567.
11. Malmstrom, G., *Annu. Rev. Biochem.* 1982, **51,** 42.

Pergamon

PII: S0277-5387(96)00395-6

Polyhedron Vol. 16, No. 8, pp. 1407–1409, 1997
Copyright © 1997 Elsevier Science Ltd
Printed in Great Britain. All rights reserved
0277-5387/97 $17.00+0.00

COMMUNICATION

$Na_2[Mo_3O(O_2CCH_3)_8(H_2O)] \cdot 2H_2O$, an unusual monooxo-capped triangular carboxylate cluster of molybdenum

Li Xu,* Jinshun Huang and Qianer Zhang

State Key Laboratory of Structural Chemistry, Fujian Institute of Research on the Structure of Matter, Chinese Academy of Sciences, Fuzhou, Fujian 350002, P.R. China

(Received 24 May 1996; accepted 6 August 1996)

Abstract—The monooxo-capped trimolybdenum carboxylate cluster $Na_2[Mo_3O(O_2CCH_3)_8(H_2O)] \cdot 2H_2O$, with an unusual set of Mo—Mo bonds [2.441(5), 2.786(5), 2.808(6) Å] has been synthesized and structurally characterized. Copyright © 1997 Elsevier Science Ltd

Keywords: molybdenum; carboxylate; cluster; trinuclear complex; crystal structure.

Triangular metal–metal bonded cluster compounds of molybdenum have been extensively studied over the past two decades [1–9]. Three Mo—Mo bonds in all these reported species are, however, similar with the differences less than 0.1 Å. Herein we wish to present the novel monooxo-capped trimolybdenum carboxylate cluster $Na_2[Mo_3O(O_2CCH_3)_8(H_2O)] \cdot 2H_2O$ (**1**) with an unusual set of Mo—Mo bonds. It is also the first monooxo-capped hexacarboxylato-bridged cluster of molybdenum, while such clusters of tungsten have been reported more than 10 years ago [3,8].

Cluster **1** has been characterized by X-ray crystallography [10]. The structure of the cluster anion, $[Mo_3O(O_2CCH_3)_8(H_2O)]^{2-}$, is shown in Fig. 1. Its most important structural feature is an unprecedented set of Mo—Mo distances, one short [2.441(5) Å] and two long [2.786(5), 2.808(6) Å], the former being the shortest Mo—Mo bond length in reported trinuclear molybdenum clusters. The Mo—Mo bond difference of up to 0.356(5) Å is surprising because the greatest difference thus far reported for trimolybdenum clusters is less than 0.1 Å [2,9]. To understand this, a comparison of M—M bonds in **1** and the tritungsten cluster $[W_3O(O_2CMe)_5(OCMe)(H_2O)_3]^{2+}$ (**2**) [2.495(1), 2.684(1), 2.687(1) Å] [8b], may be helpful due to the structural similarity and almost the same bond radius. According to the compositions, **1** and **2** have 10 and 8 electrons, respectively, available for M—M bonding. The two more electrons in the former cluster function as shortening the short M—M bond and lengthening the long ones. This indicates that they occupy a Mo—Mo molecular orbital of Mo(1)—Mo(2) π-bonding and Mo(1) [or

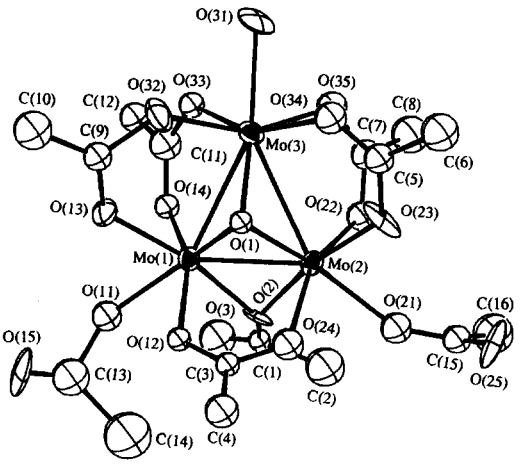


Fig. 1.

* Author to whom correspondence should be addressed.

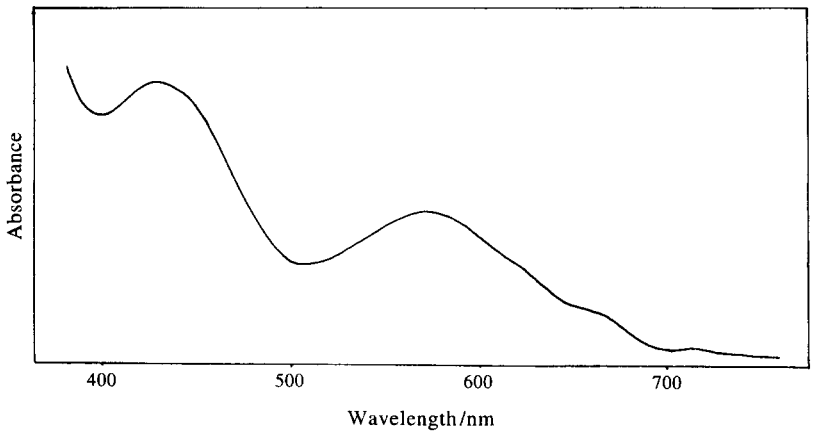


Fig. 2.

Mo(2)]—Mo(3) antibonding character. The asymmetry of the structure caused by the unidentate bridging acetate, η^1, μ_2-O_2CMe, is believed to be responsible for the occurrence of such an unusual set of Mo—Mo bonds, since the other symmetric 10e Mo_3 clusters $Mo_3HI_7L_3$ possess three almost equal Mo—Mo bonds [7].

The preparation of the crystalline **1** was as follows. A solution obtained by refluxing $Na_2MoO_4 \cdot 2H_2O$ in $(EtCO)_2O$ was added with Et_2O to produce a precipitate. A mixture of the precipitate, $Mo(CO)_6$ and Ac_2O was heated for 2 days to yield the green–black crystals of **1**. It is noteworthy that, by similar methods, we have prepared a novel series of hetero-octanuclear clusters of the formula $A_2M'_2[M_3O_4(O_2CR)_8]_2$ (A = Li, Na, K, M′ = V^{3+}, Cr^{3+}, Mn^{3+}, Fe^{3+}, Al^{3+}, Mo^{3+}, M = Mo, W, R = Me, Et) [11–16]. Cluster **1** is extremely sensitive to air. It dissolves in water or organic solvents (e.g. MeCN, EtOH) to give a green solution whose UV–vis spectrum is shown in Fig. 2. In the case of water, the solution becomes red in color after exposure to air for several hours. When added with a mixture of HBr and $ZnBr_2$, one can readily obtain red crystals of the oxidized product with the composition $[Mo_3O_2(O_2CCH_3)_6(H_2O)_3]ZnBr_4 \cdot 8H_2O$ [17].

Acknowledgement—This work was supported by a grant from National Science Foundation of China.

REFERENCES

1. Muller, A., Jostes, R. and Cotton, F. A., *Angew. Chem. Int. Ed. Engl.* 1980, **19,** 875.
2. Jiang, Y. S., Tang, A., Hoffmann, R., Huang, J. L. and Lu, J. X., *Organometallics*, 1985, **4,** 27.
3. Cotton, F. A., Shang, M. Y. and Sun, Z. S., *Inorg. Chim. Acta*, 1993, **212,** 95.
4. Cotton, F. A., *Polyhedron*, 1986, **5,** 3.
5. (a) Chisholm, M. H., Hoffman, D. M. and Huffman, J. C., *Inorg. Chem.* 1984, **23,** 3684, 17; (b) Chisholm, M. H., Cock, C. M. and Folting, K., *J. Am. Chem. Soc.* 1992, **114,** 2721.
6. Cotton, F. A., Shang, M. Y. and Sun, Z. S., *J. Am. Chem. Soc.* 1991, **113,** 6917.
7. Cotton, F. A. and Poli, R., *J. Am. Chem. Soc.* 1988, **110,** 830.
8. (a) Ardon, M., Cotton, F. A., Dori, Z., Fang, A., Kapon, M., Reisner, G. M. and Shaia, M., *J. Am. Chem. Soc.* 1982, **104,** 5394; (b) Bino, A., Cotton, F. A., Dori, Z., Gottlieb, M. S. and Kapon, M., *Inorg. Chem.* 1988, **27,** 3592.
9. Huang, J., Shang, M., Lu, S. and Lu, J., *J. Sci. Sin. (Engl. Transl.)*, 1982, **25,** 1270.
10. Crystal data for **1**: Fw = 876.21, hexagonal, space group $P6_1$, a = 21.259(14), c = 15.799(19) Å, V = 6183.5 Å^3, Z = 6, D_c = 1.36 g cm^{-3}, μ = 9.5 cm^{-1}, $F(000)$ = 2604, λ(Mo-K_α) = 0.71069 Å, $2\theta_{max}$ = 50°, RIGAKU AFC5R diffractomer, $\omega/2\theta$ scan, scan speed 8° min^{-1}, a total of 4105 reflections were collected with 3608 unique reflections. The structure analysis is based on 1302 observed reflections with $I > 3\sigma(I)$; the intensities were corrected for absorption using empirical scan data (0.879–0.952) and Lorentz and polarization factors. The structure was solved by direct methods using MULTAN11/82 and refined by full-matrix least-squares techniques with anisotropic thermal parameters for molybdenum and some oxygen atoms (229 variables), final R = 0.080, R_w = 0.094, where the weighting scheme is $w = 1/[\sigma(F_o)^2 + (0.020 \times F_o)^2 + 1.00]$. $(\Delta/\sigma)_{max}$ = 0.06, $(\Delta/\rho)_{max}$ = 0.90 e Å^3.
11. Xu, L., Liu, H., Yan, D. C., Huang, J. S. and Zhang, Q. E., *J. Chem. Soc., Chem. Commun.* 1993, 1507.
12. Xu, L., Liu, H., Yan, D. C., Huang, J. S. and Zhang, Q. E., *J. Chem. Soc., Dalton Trans.* 1994, 2099.

13. Liu, H., Xu, L., Huang, J. S., Cheng, W. D., Huang, X. Y. and Huang, X., *Polyhedron*, 1996, **15,** 2003.
14. Xu, L., Li, Z. F., Liu, H., Huang, J. S. and Zhang, Q. E., submitted.
15. Xu, L., Li, Z. and Huang, J. S., *Inorg. Chem.*, in press.
16. Xu, L., Li, Z. F. and Huang, J. S., *Polyhedron*, submitted.
17. Xu, L. and Huang, J. S., unpublished result.

Pergamon

PII: S0277-5387(96)00453-6

Polyhedron Vol. 16, No. 9, pp. 1411–1415, 1997
Copyright © 1997 Elsevier Science Ltd
Printed in Great Britain. All rights reserved
0277-5387/97 $17.00+0.00

Synthesis, crystal structure and magnetic properties of an isophthalate-bridged manganese(II) chain complex

Xiang Shi Tan,[a] Dao Feng Xiang,[a] Wen Xia Tang[a]* and Kai Bei Yu[b]

[a] State Key Laboratory of Coordination Chemistry, Coordination Chemistry Institute, Nanjing University, Nanjing 210093, P. R. China

[b] Crystal Structure Laboratory, Chengdu Institute of Organic Chemistry, Chinese Academy of Sciences, Chengdu 610041, P. R. China

(Received 25 June 1996; accepted 12 September 1996)

Abstract—An isophthalate-bridged manganese(II) chain complex of the formula $[Mn_2(bipy)_4(m\text{-phth})]_n[ClO_4]_{2n}\cdot 4nH_2O$, where bipy is 2,2′-bipyridine and *m*-phth is isophthalate (dianion of benzene-1,3-dicarboxylic acid), has been prepared and characterized by X-ray crystallography and magnetic measurements. The structure consists of cationic isophthalate-bridged $[Mn_2(bipy)_4(m\text{-phth})]^{2+}$ chains, non-coordinated perchlorate anions and water molecules of crystallization. Each isophthalate ligand is bound to four manganese atoms through carboxylate oxygens with the *syn–syn* bridging mode, affording manganese(II) pairs that are linked by the isophthalate group to yield a one-dimensional chain running along the *c*-axis. The manganese(II) ion displays a distorted octahedral coordination being linked to four nitrogen atoms of two bipy ligands and two oxygen atoms of two carboxylate groups from two isophthalate ligands. The variable temperature magnetic susceptibility of the title complex in the temperature range 4–300 K has been interpreted in terms of a Mn^{II} dimer with a molecular field approximation, and the values obtained for J, g(fixed) and zJ' being -0.98 cm^{-1}, 2.00 and -0.03 cm^{-1}, respectively, indicating a weakly antiferromagnetic exchange coupling between the Mn^{II} ions.
© 1997 Elsevier Science Ltd. All rights reserved.

Keywords: manganese complexes; chain complexes; crystal structures; magnetism; isophthalate; 2,2′-bipyridine.

Magnetic properties of polynuclear transition metal complexes with extended bridging ligands have been of interest for some years [1–8]. Many papers have been published on binuclear and chain copper(II) complexes containing the bridging benzene dicarboxylate ligands [2–6], but polynuclear manganese(II) complexes with bridging benzene dicarboxylate ligands have been very rare up to now [7–9]. In the present paper we describe the synthesis, crystal structure and magnetic properties of another manganese(II) chain complex with a bridging isophthalate ligand, $[Mn_2(bipy)_4(m\text{-phth})]_n[ClO_4]_{2n}\cdot 4nH_2O$, where bipy and *m*-phth correspond to 2,2′-bipyridine and isophthalate (dianion of benzene-1,3-dicarboxylic acid).

* Author to whom correspondence should be addressed.

EXPERIMENTAL

Preparations

2,2′-Bipyridine and other common chemicals were purchased from Sigma Chemical Co. and used as received. The piperidinium salt of isophthalic acid was prepared in a similar method to the piperidinium salt of terephthalic acid [4].

A methanolic solution (20 cm^3) of bipyridine (0.8 mmol) and piperidinium isophthalate (0.2 mmol) was slowly added to a solution (20 cm^3) of manganese(II) perchlorate hexahydrate (0.4 mmol) in the same solvent with continuous stirring. The light yellow powder separated during the addition was filtered off. Small yellow rectangular crystals of the title complex suitable for X-ray analysis were obtained after a month by slow evaporation of the mother liquor at 280±2

K. These were filtered off and air dried. Found: C, 49.5; H, 3.8; N, 9.8; Mn, 9.8. Calc. for $C_{24}H_{22}N_4O_8ClMn$: C, 49.3; H, 3.8; N, 9.6; Mn, 9.4%.

Physical measurements

Magnetic measurements on powder samples were carried out with a CF-1 type extracting sample magnetometer in the temperature range 4–300 K. The apparatus was calibrated with $Hg[Co(NCS)_4]$. Corrections for diamagnetism were estimated from Pascal's constants.

X-ray crystallography

Diffraction data were collected at 290±2 K on a P4 four-circle diffractometer with graphite-monochromated Mo-K_α radiation ($\lambda = 0.71073$ Å) by using the ω–2θ scan technique. Details of the crystal data are listed in Table 1. The lattice parameters were obtained from a least-squares refinement using the setting angles of 20 carefully centred reflections in the 2θ range 5.92–28.3°. Intensity data were collected in the 2θ range 3.32–48°. A total of 4252 reflections were collected and 3587 of them were considered as observed [$I > 2\sigma(I)$] and used for refinement of the structure. The intensities were corrected for Lorentz-polarization and absorption. The structure was solved by heavy-atom Patterson methods and expanded using Fourier techniques. The six oxygen atoms in the ClO_4 group from O(3) to O(6) and O(7) and O(8) of two crystallization water molecules, were found to exhibit locally positional disorder. All hydrogen atoms except H(19) and H(19) were created using Fourier techniques, while H(18) and H(19) were set in calculated positions. Hydrogen atoms were refined isotropically. Four hydrogen atoms of the two crystallization H_2O molecules were included but not refined. The final cycle of full-matrix least-squares refinement on F^2 was based on 3587 observed reflections [$I > 2\sigma(I)$] and 408 variable parameters and converged with unweighted and weighted agreement factors of $R = \Sigma||F_o| - |F_c||/\Sigma|F_o| = 0.059$, $R_w = [(\Sigma w(|F_o| - |F_c|)^2/\Sigma wF_o^2] = 0.1474$; $GOF = 0.867$ (on F^2). The maximum and minimum peaks on the final difference Fourier map corresponded to 0.501 and −0.356 e Å^{-3}, respectively. Selected bond distances and angles are given in Table 2.

Table 1. Crystal data for $[Mn_2(bipy)_4(m\text{-phth})]_n[ClO_4]_{2n}\cdot 4nH_2O$

Formula	$C_{24}H_{22}N_4O_8MnCl$
M_r	584.85
Crystal size/mm	0.60 × 0.14 × 0.14
Crystal system	Monoclinic
Space group	$C2/c$
a/Å	25.065(5)
b/Å	12.530(2)
c/Å	16.523(3)
U/Å^3	5077(2)
α/°	90
β/°	101.970(10)
γ/°	90
Z	8
D_c/g cm^{-1}	1.530
μ(Mo-K_α)/cm^{-1}	6.82

RESULTS AND DISCUSSION

Description of the crystal structure

The structure of the complex consists of polymeric cationic chains composed of $[Mn_2(bipy)_4(m\text{-phth})]^{2+}$ units, non-coordinated perchlorate anions and crystallization water molecules. One of the independent structural units is shown in Fig. 1 together with the atom-numbering scheme. The isophthalate group acts as a tetrakis(monodentate) ligand which is bound on each side to two manganese(II) ions through the carboxylate oxygens in a *syn–syn* configuration, yielding a chain that runs parallel to the *c*-axis, as shown in Figs 1 and 2. The interchain metal–metal separations are 4.84, 9.72 and 7.06 Å for Mn···Mn(A), Mn···Mn(B) and Mn(A)···Mn(B), respectively (see Fig. 1).

The Mn ion is six coordinate and possesses an N_4O_2 environment by virtue of two carboxylate oxygen atoms [O(1) and O(2)] from two isophthalate ligands that occupy *cis* positions, and four nitrogen atoms [N(1), N(2), N(3) and N(4)] from two chelating bipy groups. The Mn—N (bipy) average bond length is 2.265 Å while the Mn—O(carboxylate) average bond length is 2.125 Å. These bond distances are in agreement with those in the structures of $[Mn_2(bipy)_4(ta)]_n[ClO_4]_{2n}$ (bipy = 2,2′-bipyridine; ta = terephthalate) [10], and $[Mn_4(o\text{-phth})_2(bipy)_8][ClO_4]_4\cdot 3H_2O$ (*o*-phth = phthalate) [9]. Large deviations of bond angles from 90° of the idealized octahedral geometry are found for angles N(1)—Mn(1)—N(2) [71.8(2)°] and N(3)—Mn(1)—N(4) [72.4(2)°] which are restricted by the bipy five-membered chelate ring. So the Mn ion has a distorted octahedral coordination sphere. The best equatorial plane is defined by atoms O(1), N(2), N(3) and N(4). The largest deviation from the mean plane is 0.216 Å for N(4) and the Mn atom is 0.109 Å out of this plane. The dihedral angle between the benzene ring of the isophthalate and the equatorial plane of the Mn octahedron is 83.68°. The Mn atom and all atoms of the bridging isophthalate are coplanar [largest deviation from the mean plane 0.61 Å for O(1A)]. Each bipy ligand is coplanar, and the dihedral angle between two bipy mean planes is 91.74°.

The perchlorate groups have their expected tetrahedral geometry.

Table 2. Selected bond lengths (Å) and angles (°) for $[Mn_2(bipy)_4(m\text{-phth})]_n[ClO_4]_{2n} \cdot 4nH_2O$

Mn—O(1)	2.145(4)	Mn—O(2)	2.104(4)
Mn—N(1)	2.295(5)	Mn—N(2)	2.242(5)
Mn—N(3)	2.283(5)	Mn—N(4)	2.239(5)
Cl—O(3)	1.317(9)	Cl—O(4)	1.332(8)
Cl—O(5)	1.339(8)	Cl—O(6)	1.392(8)
O(2)—Mn—O(1)	93.3(2)	O(2)—Mn—N(4)	94.4(2)
O(1)—Mn—N(4)	90.0(2)	O(2)—Mn—N(2)	100.2(2)
O(1)—Mn—N(2)	94.0(2)	N(4)—Mn—N(2)	164.6(2)
O(2)—Mn—N(3)	81.9(2)	O(1)—Mn—N(3)	161.2(2)
N(4)—Mn—N(3)	72.4(2)	N(2)—Mn—N(3)	104.7(2)
O(2)—Mn—N(1)	163.2(2)	O(1)—Mn—N(1)	101.8(2)
N(4)—Mn—N(1)	92.8(2)	N(2)—Mn—N(1)	71.8(2)
N(3)—Mn—N(1)	85.9(2)	O(3)—Cl—O(4)	113.6(9)
O(3)—Cl—O(5)	106.8(8)	O(4)—Cl—O(5)	110.3(6)
O(3)—Cl—O(6)	102.9(7)	O(4)—Cl—O(6)	109.3(7)
O(5)—Cl—O(6)	113.7(7)	C(21)—O(2)—Mn	138.0(4)
C(5)—N(1)—Mn	117.7(4)	C(1)—N(1)—Mn	123.6(5)
C(10)—N(2)—Mn	123.1(5)	C(6)—N(2)—Mn	118.5(4)
C(15)—N(3)—Mn	116.0(5)	C(1)—N(3)—Mn	125.2(5)
C(16)—N(4)—Mn	117.5(5)	C(20)—N(4)—Mn	123.5(5)

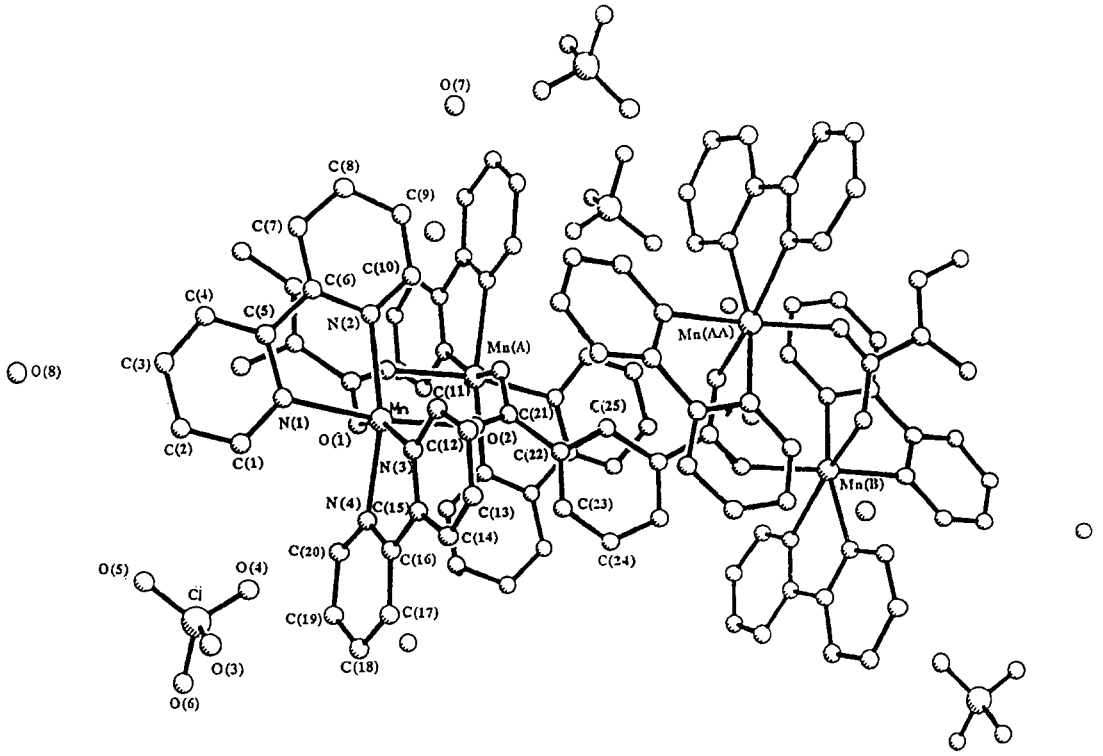


Fig. 1. The part structure of $[Mn_2(bipy)_4(m\text{-phth})]_n[ClO_4]_{2n} \cdot 4nH_2O$ showing the bridging mode of isophthalate ligand and one of hte independent structural units with the atom-numbering scheme. Symmetry transformations used to generate equivalent atoms: A $-X+1, -Y+1, -Z+1$; b $-X+1, Y, -X+1/2$; AA x, $-y+1, z-1/2$.

Magnetic properties

The temperature dependence of the molar magnetic susceptibility and magnetic moment per two Mn^{II} ions unit of the title complex in the form of χ_M versus T and μ_{eff} versus T are shown in Fig. 3a and b. The effective magnetic moment per two Mn^{II} ions unit of $[Mn_2(bipy)_4(m\text{-phth})][ClO_4]_2 \cdot 4H_2O$ at 300 K is 8.34 B.M. which is close to the spin-only value of 8.36 B.M. expected for two uncoupled high-spin Mn^{II} ions.

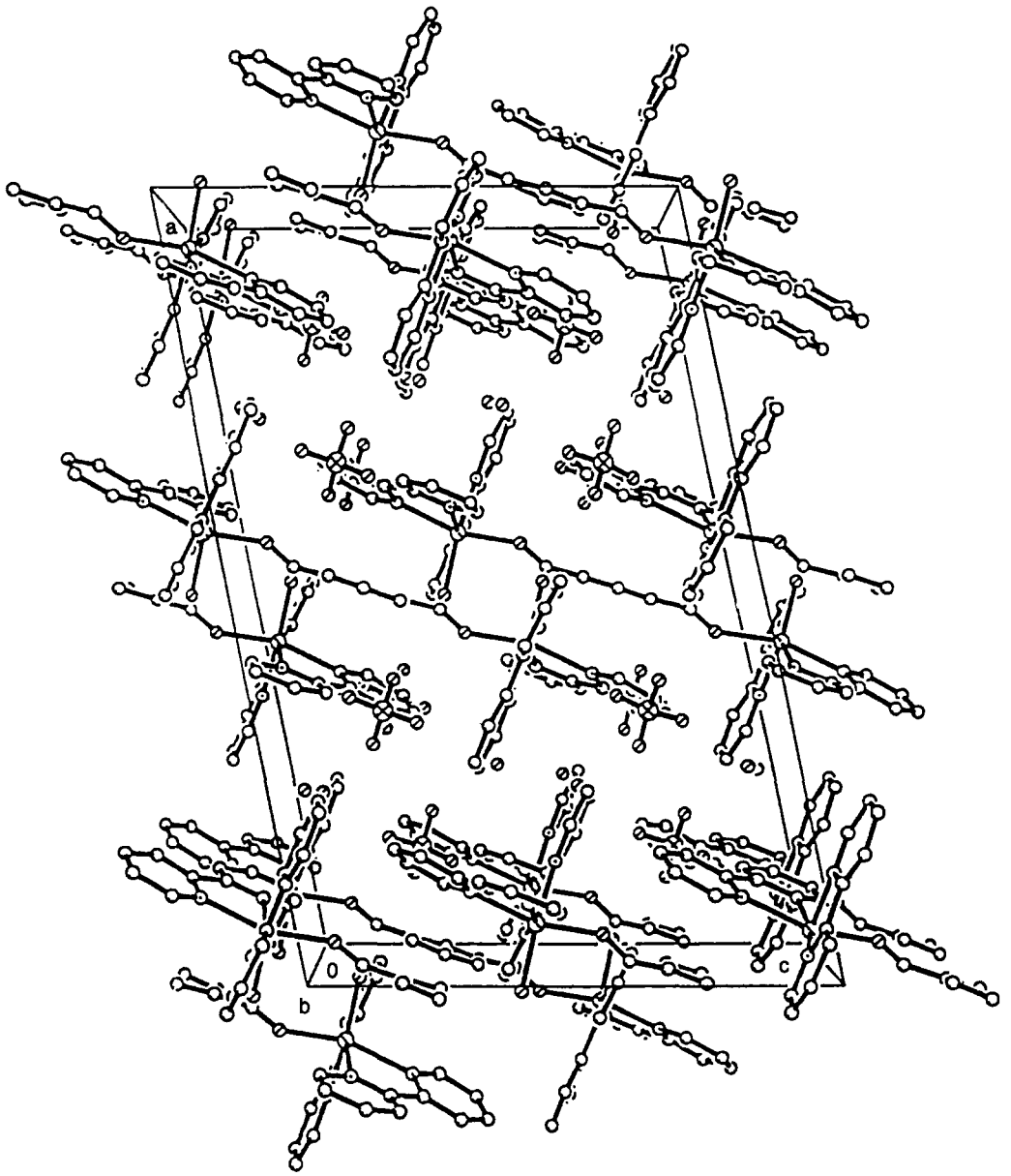


Fig. 2. Unit cell and packing diagram for $[Mn_2(bipy)_4(m\text{-phth})]_n[ClO_4]_{2n} \cdot 4nH_2O$.

When the temperature is lowered, the magnetic moment value decreases steadily from 8.34 B.M. at 300 K to 7.05 B.M. at 28.17 K and to 3.46 B.M. at 4.54 K, showing the presence of weak antiferromagnetic spin-exchange interactions between high-spin Mn^{II} ions through the double carboxylate and the extended isophthalate bridges.

The magnetic behaviour of the chain manganese(II) complex is quite complicated by exchange interactions, low-symmetry ligand field and g-tensor anisotropy. As can be seen in other cases, the single-ion zero-field splitting D and rhombic splitting parameter E for Mn^{II} ions are small and can be negligible [8,9,11]. We attempted to interpret this magnetic system for the title complex by using the Heisenberg–Dirac–Van Vleck $S_A = S_B = \frac{5}{2}$ spin-coupled dimer model ($H = -JS_AS_B$). For the two Mn^{II} dimers bridged by two carboxylate groups respectively, there must be separated J values, but to the first approximation, they were considered as the same. The expression of magnetic susceptibility [12] of the title complex is

$$\chi_M = 2Ng^2\beta^2/kT[(e^x + 5e^{3x} + 14e^{6x} + 30e^{10x} + 55e^{15x})/(1 + 3e^x + 5e^{3x} + 7e^{6x} + 9e^{10x} + 11e^{15x})] \quad (1)$$

where N, g, β, x are the Avogardro's number, g-factor, Bohr magneton, and $x = J/kT$, respectively, and J is the exchange coupling constant within the Mn^{II} dimer with double carboxylates in the *syn–syn* conformation.

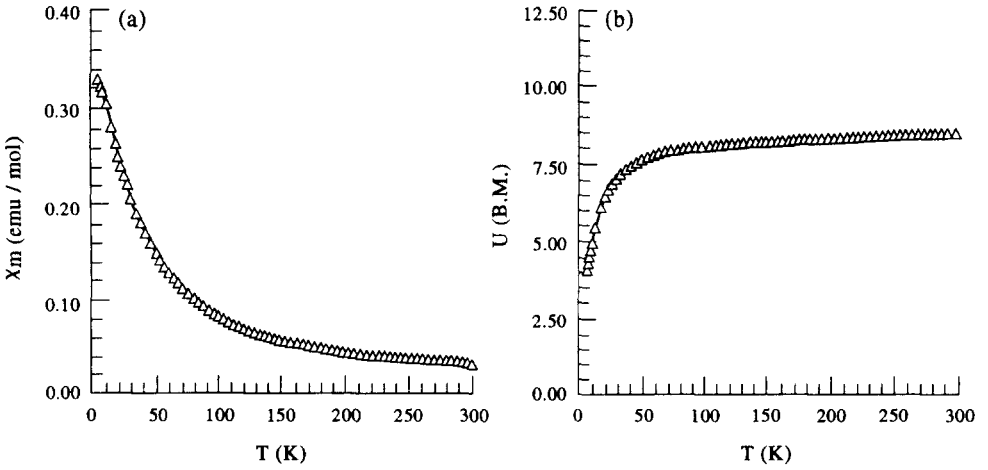


Fig. 3. Experimental (△) and calculated (-) temperature dependent molar magnetic susceptibility (a) and effective magnetic moment (b) per two Mn^{II} ions unit of $[Mn_2(bipy)_4(m\text{-path})][ClO_4]_2 \cdot 4H_2O$.

A molecular field (zJ') [8,13], representing intrachain Mn^{II} ions (through the extended bridging isophthalate) and interchain Mn^{II} ions magnetic interactions, was added to account for the actual nature of the compound. Thus the expression for the magnetic susceptibility of the title complex becomes

$$\chi_M' = \chi_M/[1-2zJ'\chi_M/Ng^2\beta^2] \quad (2)$$

Using Eq. (2), the least-squares fit to the magnetic susceptibility data gives the parameters: $J = -0.98$ cm^{-1}, $zJ' = -0.03$ cm^{-1} and $R = 2.9 \times 10^{-4}$ $[R = \Sigma(\chi_{calc}-\chi_{obs})^2/\Sigma(\chi_{obs})^2]$, assuming $g = 2.0$. The J value indicates a weakly antiferromagnetic exchange coupling within the manganese(II) dimer while the zJ' value reflects very weakly antiferromagnetic interactions.

The nature of the magnetic coupling within the Mn^{II} dimer for the title complex is similar to that of the Mn^{II} chain complex bridged by terephthalate (weak antiferromagnetic, $J = -1.35$ cm^{-1}) and most other triply and doubly bridged carboxylate Mn^{II} complexes [10].

Acknowledgement—Funding for this work was provided by the National Natural Science Foundation of China.

REFERENCES

1. Willet, R. D., Gatteschi, D. and Kahn, O., *Magneto-Structural Correlations in Exchange Coupled Systems*, NATO ASI Series. Reidel, Dordrecht, 1985.
2. Xanthopoulos, C. E., Sigalas, M. P., Katsoulos, G. A., Tsipis, C. A., Terzis, A., Mentzafos, M. and Hountas, A., *Inorg. Chem.*, 1993, **32,** 5433.
3. Bakalbassis, E. G., Bergerate, P., Kahn, O., Jeannin, S., Jeannin, Y., Dromzel, Y. and Guillot, M., *Inorg. Chem.*, 1992, **31,** 625.
4. Verdaguer, M., Gouteron, J., Jeannin, S., Jeannin, Y. and Kahn, O., *Inorg. Chem.*, 1984, **23,** 4291.
5. Bakalbassis, E. G., Bozopoulos, A. P., Mrozinski, J., Pentzeperis, P. J. and Tsipis, C. A., *Inorg. Chem.*, 1988, **27,** 529.
6. Chaudhuri, P., Oder, K., Wieghardt, K., Gehring, S., Haase, W., Nuber, B. and Weiss, J., *J. Am. Chem. Soc.*, 1988, **110,** 3657.
7. Jiang, Z. H., Ma, S.-L., Liao, D.-Z., Yan, S.-P., Wang, G.-L., *Science in China (Series B)*, 1993, **23,** 1009.
8. Cano, J., Munno, G. D., Sanz, J., Ruiz, R., Lloret, F., Faus J. and Julve, M., *J. Chem. Soc., Dalton. Trans.*, 1994, 3465.
9. Jiang, Z. H., Ma, S. L., Liao, D. Z., Yan, S. P., Wang, G. L., Yao, X. K. and Wang, R. J., *J. Chem. Soc., Chem. Commun.*, 1993, 745.
10. Yu, S.-R., Wang, C.-P., Day, E. P. and Holm, R. H., *J. Am. Chem. Soc.*, 1991, **30,** 4067.
11. Kennedy, B. J. and Murray, K. S., *Inorg. Chem.*, 1985, **24,** 1552.
12. Kahn, O., *Molecular Magnetism*. VCH Publisher, Inc., New York, 1993.
13. Ginsberg, A. P. and Lines, M. E., *Inorg. Chem.*, 1972, **11,** 2289.

Pergamon

PII: S0277-5387(96)00452-4

Polyhedron Vol. 16, No. 9, pp. 1417–1424, 1997
Copyright © 1997 Elsevier Science Ltd
Printed in Great Britain. All rights reserved
0277-5387/97 $17.00+0.00

Lanthanide(III) complexes with bidentate biheterocyclic ligands

P. Thakur, V. Chakravortty and K. C. Dash*

Department of Chemistry, Utkal University, Bhubaneswar 751004, India

(Received 24 May, 1996; accepted 12 September 1996)

Abstract—Eight lanthanide thiocyanate complexes of the type $[Ln(NCS)_3(PBH)_2]$ and $[Ln(NCS)_3(MPB)_2]$, where Ln = La, Pr, Nd, Sm, Eu, Gd, Dy and Y and PBH and MPB are 2-(2-pyridylbenzimidazole) and 1-methyl-2-(2′-pyridyl)benzimidazole, respectively, have been synthesized and characterized by various physicochemical techniques such as conductance and thermogravimetric studies, electronic, IR, NMR (^1H and ^{13}C), EPR, CV and fluorescence spectral investigations. The $\nu(C{\equiv}N)$ of the thiocyanate group indicates N coordination in all cases. © 1997 Elsevier Science Ltd. All rights reserved.

Keywords: lanthanide complexes; EPR; NMR; fluorescence spectra; thermogravimetric analysis; cyclic voltammetry.

The trivalent lanthanide ions have very specific spectroscopic and magnetic properties which make them ideal as probes in studies of a wide variety of chemical, biological and environmental systems [1,2]. Imidazole and its derivatives are biologically significant. The ligand 2-(2′-pyridyl)benzimidazole (PBH) has aroused considerable interest because of its structural similarity to the widely studied 2,2′-bipyridine, 1,10-phenanthroline, 2,2′-biimidazole, *etc.*, in containing the —N=C—C=N— group. The ligand acts as a powerful bidentate chelating agent [3,4] and has been found to form stable complexes with various transition metal ions [5–7]. However, the literature is quite scarce in dealing with the various aspects involving different physicochemical properties and complexation behaviour of its N-methylated analogue 1-methyl 2-(2′-pyridyl)benzimidazole (MPB). Substituted pyridyl benzimidazoles can act as very good coordinating agents [8]. Substituents in the ring effect the electronic distribution and consequently the coordinating ability of its derivatives. The ligand 1-methyl-2-(2′-pyridyl)benzimidazole (MPB) was synthesized by condensation of *N*-methyl-*o*-phenylene diamine with picolinic acid in polyphosphoric acid (PPA) or by refluxing in HCl [9]. The ligand has been recommended as a suitable reagent for the spectrophotometric determination of Fe^{II} [10]. MPB has a lower melting point than its unsubstituted derivative PBH, owing to the absence of intermolecular hydrogen bonding. The fluorescence spectra [11] in ethanol and prototropic equilibria [12] in aqueous solution of MPB have been reported. The lanthanide complexes of PBH and MPB have not hitherto been reported. Earlier work from this laboratory dealt with complexes of U^{VI} and Th^{IV} with related 1,2-diamine ligands such as PBH [13], 2,2′-bi-imidazole (H_2Biim) [14] and 1,1′-dimethyl-2,2′-biimidazole (DMBIm) [15]. In order to understand the coordination chemistry of lanthanides, we report here the synthesis and characterization of complexes with the novel bidentate biheterocyclic ligands PBH and MPB.

EXPERIMENTAL

Hydrated metal nitrates (Indian Rare Earths Ltd; 99.90% pure) were used as received. Methanolic solutions of metal thiocyanates were obtained by metathesis of the respective metal nitrates with stoichiometric amounts of KNCS. Physical measurements were carried out as reported earlier [13,14]. ^1H and ^{13}C NMR spectra of the ligand and its coordination complexes were obtained using Bruker 400 MHz AMX and 270 MHz FTNMR instruments, respectively. Fluorescence spectra of the complexes were recorded using a Shimadzu spectrofluorophotometer RF-510. Electronic spectra were

* Author to whom correspondence should be addressed.

recorded on a Beckmann DU-640B spectrophotometer; EPR and CV were recorded on Varian E-4 spectrometer and Polarecord E-506 (Metrohm), respectively. The metal ion was determined by EDTA titration using xylenol-orange as indicator.

Syntheses of ligands PBH and MPB

The ligand PBH was prepared as reported earlier [9]. The preparation of MPB from PBH is as follows: 1.5 cm^3 (15 mmol) of dimethyl sulfate (DMS) was added dropwise to a well stirred suspension of powdered NaOH (2.357 g, 60 mmol), PBH (1.95 g, 10 mmol) and tetrabutyl ammonium bromide (0.19 g, 4 mol%), (TBAB, used as a phase transfer catalyst) in dioxane (25 cm^3). Stirring at room temperature was continued for 30 min and the reaction was monitored by TLC. The mixture was filtered, washed with ethyl acetate and the combined washings along with the filtrate were treated with a 1:1 aqueous ammonia solution to remove excess DMS. The volume of the resultant solution was reduced to 5–10 cm^3 and was stored at 4°C for about 2 h. The orange-red oily liquid was washed with hexane and the light yellow washings were cooled to give colourless crystals of MPB. These were filtered, washed with the minimum amount of hexane and finally dried in air. Yield: 1.01 g (48%). M.p. 62°C (lit. 64–65°C) [11]. Found: C, 74.3; H, 5.2; N, 19.9; Calc. for MPB ($C_{13}H_{11}N_3$): C, 74.6; H, 5.3; N, 20.1%: MS: *m/z* 209.

Syntheses of complexes

Both types of complexes $[Ln(NCS)_3(PBH)_2]$ and $[Ln(NCS)_3(MPB)_2]$, were synthesized by refluxing methanolic solutions of the ligands (PBH or MPB) and the corresponding metal salts in stoichiometric amounts at 70–80°C for 4 h. The solid complexes were filtered off and washed with small aliquots of methanol followed by diethyl ether, recrystallized from methanol and finally dried *in vacuo*.

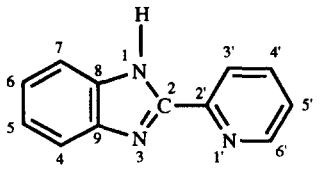
RESULTS AND DISCUSSION

The bidentate chelating ligand 2-(2′-pyridyl) benzimidazole (**I**) and 1-methyl-2-(2′-pyridyl) benzimidazole (**II**) interact with lanthanide ions to form well-defined complexes which are presented in Tables 1 and 2 along with relevant characterizing data. The IR and ^1H NMR spectra of the complexes suggest coordination of the ligands in a bidentate manner. The complexes are sparingly soluble in common organic solvents and the molar conductances of the complexes show them to be non-electrolytes [16,17]. A higher conductivity value for the complexes is observed in MeOH or Me_2SO, which may be owing to solvolysis of the complexes. The increase in molar conductivity of the complexes in the presence of added TOPO (trioctyl phosphine oxide) further suggests coordination of the anion to the metal ions.

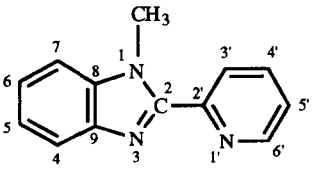
The reported coordination complexes are insoluble in organic solvents such as benzene, nitrobenzene, bromoform, c-hexane, *etc.* with which cryoscopic measurements are usually done and hence, molecular mass determination of these complexes could not be made. These complexes are, however, soluble in methanol, acetone, acetonitrile, *etc.* It is speculated that they are monomeric in nature in which case the lanthanide ion would be seven coordinate and possible structures are monocapped octahedron [18], monocapped trigonal prism [19] or pentagonal bipyramid [20].

Electronic and IR spectra

The electronic spectra of all the complexes were recorded in methanol. In the UV region an intense band at 302–308 nm with one shoulder at 274–280 nm was attributable to an intraligand π–π^* transition. Visible spectra indicate that in lanthanide ions the 4*f* orbitals are effectively shielded by $5s^25p^6$ electrons and lines that appear in the absorption spectra arise from electronic transitions within the 4*f* levels. These transitions are normally forbidden, but become allowed when degeneracy in the 4*f* orbitals is removed by applying an external crystal field [21,22]. The absorption bands in the Pr^{III}, Nd^{III}, Sm^{III} and Dy^{III} complexes were recorded at 1×10^{-3} mol dm^{-3} in absolute methanol. The spectra of the complexes (Table 3) show a shift of the bands towards lower energy, compared with those of the aqua ions [23] owing to the nephelauxetic effect. The bonding parameter ($b^{\frac{1}{2}}$), the covalency parameter (δ) and the nephelauxetic parameter ($\bar{\beta}$) are less than unity, while Sinha's parameter (δ) is positive, indicating a moderate covalent character for the bond between the metals and ligands [24].



I



II

Table 1. Analytical, magnetic and conductivity data of lanthanide thiocyanate complexes of PBH (calculated values in parentheses)

Complex	Colour	M.p. (°C)	Analysis(%)					μ_{eff}[a] (B.M.)	Molar conductivity[b]	
			M	C	H	N	S		In acetonitrile	In acetone
$La(NCS)_3(PBH)_2$	White	>300	19.5 (19.8)	46.0 (46.1)	2.6 (2.6)	17.8 (17.9)	13.0 (13.6)	0.00 (0.00)	48.56	69.44
$Pr(NCS)_3(PBH)_2$	Greenish white	>300	20.0 (20.0)	46.0 (46.0)	2.5 (2.6)	17.8 (17.9)	13.5 (13.6)	3.25 (3.58)	45.71	39.98
$Nd(NCS)_3(PBH)_2$	Pale violet	290d	20.0 (20.3)	45.7 (45.8)	2.5 (2.5)	17.8 (17.8)	13.5 (13.5)	3.58 (3.62)	46.80	33.96
$Sm(NCS)_3(PBH)_2$	White	274d	21.0 (21.0)	45.3 (45.4)	2.5 (2.5)	17.6 (17.6)	13.0 (13.4)	1.52 (1.65)	47.24	60.70
$Eu(NCS)_3(PBH)_2$	White	268d	21.2 (21.2)	45.1 (45.2)	2.5 (2.5)	17.6 (17.6)	13.3 (13.4)	3.32 (3.40)	46.58	67.86
$Gd(NCS)_3(PBH)_2$	White	>300	21.5 (21.8)	44.6 (44.9)	2.5 (2.5)	17.5 (17.5)	13.2 (13.3)	7.92 (7.97)	45.92	47.50
$Dy(NCS)_3(PBH)_2$	White	>300	22.3 (22.3)	44.6 (44.6)	2.4 (2.5)	17.3 (17.3)	13.1 (13.2)	10.25 (10.70)	48.89	46.82
$Y(NCS)_3(PBH)_2$	White	>300	13.6 (13.6)	49.6 (49.6)	2.7 (2.7)	19.2 (19.3)	14.7 (14.7)	0.00 (0.00)	48.30	48.32

d: Decomp. temp.

[a] Calculated using the Van Vleck formula.

[b] Ω^{-1} cm^2; the concentration $\sim 10^{-3}$ M.

Table 2. Analytical, magnetic and conductivity data of lanthanide thiocyanate complexes of MPB (calculated value in parentheses)

Complex	Colour	M.p. (°C)	Analysis(%)					μ_{eff}[a] (B.M.)	Molar conductivity[b]	
			M	C	H	N	S		In acetonitrile	In acetone
$La(NCS)_3(MPB)_2$	White	280d	19.0	47.2	3.0	17.2	13.3	0.00	24.06	70.69
			(19.0)	(47.6)	(3.0)	(17.2)	(13.1)	(0.00)		
$Pr(NCS)_3(MPB)_2$	Greenish white	285d	19.0	47.3	3.0	17.2	13.1	3.52	28.95	23.50
			(19.2)	(47.5)	(3.0)	(17.2)	(13.1)	(3.58)		
$Nd(NCS)_3(MPB)_2$	Pale violet	>300	19.5	47.2	3.0	17.1	13.1	3.56	45.96	74.56
			(19.6)	(47.3)	(3.0)	(17.1)	(13.0)	(3.62)		
$Sm(NCS)_3(MPB)_2$	White	>300	20.0	46.3	3.0	17.0	13.0	0.98	48.25	42.84
			(20.1)	(47.0)	(3.0)	(17.0)	(13.0)	(1.65)		
$Eu(NCS)_3(MPB)_2$	White	290d	20.2	47.0	3.0	17.0	12.5	3.25	72.53	29.98
			(20.4)	(47.0)	(3.0)	(17.0)	(13.0)	(3.40)		
$Gd(NCS)_3(MPB)_2$	White	>300	21.0	46.4	3.0	16.5	13.0	7.82	68.29	46.67
			(21.0)	(46.5)	(3.0)	(17.0)	(13.0)	(7.97)		
$Dy(NCS)_3(MPB)_2$	White	>300	22.0	46.0	3.0	16.5	12.3	10.45	65.45	48.92
			(21.5)	(46.2)	(3.0)	(16.7)	(13.0)	(10.70)		
$Y(NCS)_3(MPB)_2$	White	>300	13.0	51.0	3.0	18.2	14.0	0.00	62.09	25.29
			(13.0)	(51.1)	(3.2)	(18.5)	(14.0)	(0.00)		

d: Decomp. temp.

[a] Calculated using the Van Vleck formula.

[b] Ω^{-1} cm^2; the concentration $\sim 10^{-3}$ M.

Table 3. Important *f–f* bands and their tentative assignments[a]

Complex	λ_{max} (cm^{-1})	Tentative assignments	Calculated spectral parameters
$[Pr(NCS)_3(MPB)_2]$	22,421	$^3H_4 \rightarrow {}^3P_2$	$\bar{\beta} = 0.997$
	21,276	$^3H_4 \rightarrow {}^3P_1$	$b_{\frac{1}{2}} = 0.041$
	20,661	$^3H_4 \rightarrow {}^3P_0$	$\delta = 0.341$
	16,778	$^3H_4 \rightarrow {}^1D_2$	
	13,297	$^3H_4 \rightarrow {}^1G_4$	
$[Nd(NCS)_3(MPB)_2]$	19,531	$^4I_{\frac{9}{2}} \rightarrow {}^2G_{\frac{9}{2}}$	$\bar{\beta} = 0.992$
	19,083	$^4I_{\frac{9}{2}} \rightarrow {}^2G_{\frac{7}{2}}$	$b_{1/2} = 0.063$
	17,182	$^4I_{\frac{9}{2}} \rightarrow {}^4G_{\frac{5}{2}}, {}^2G_{\frac{7}{2}}$	$\delta = 0.81$
	13,495	$^4I_{\frac{9}{2}} \rightarrow {}^4F_{\frac{9}{2}}$	
	13,333	$^4I_{\frac{9}{2}} \rightarrow {}^4F_{\frac{5}{2}}$	
	12,468	$^4I_{\frac{9}{2}} \rightarrow {}^4F_{\frac{3}{2}}$	
$[Sm(NCS)_3(MPB)_2]$	24,875	$^6I_{\frac{5}{2}} \rightarrow {}^4P_{\frac{9}{2}}$	$\bar{\beta} = 0.987$
	20,746	$^6I_{\frac{5}{2}} \rightarrow {}^4I_{\frac{9}{2}}$	$b_{1/2} = 0.08$
	15,197	$^6I_{\frac{5}{2}} \rightarrow {}^4I_{\frac{11}{2}}$	$\delta = 0.50$
$[Dy(NCS)_3(MPB)_2]$	20,491	$^6I_{\frac{15}{2}} \rightarrow {}^6F_{\frac{11}{2}}$	$\beta = 0.995$
	15,197		$b_{1/2} = 0.062$
			$\delta = 0.72$

[a]The covalence factors were calculated by the relations $\bar{\beta} = \nu$ (complex)/ν (aqua), $b_{1/2} = [1/2(1-\beta)]^{1/2}$ and $\delta = 100(1-\bar{\beta})/\beta$.

The IR spectra of ligands PBH and MPB and its complexes were recorded and prominent vibrations are presented in Tables 4 and 5. The spectra of the ligands and complexes are virtually identical except for the appearance of additional bands owing to the coordinated anion. The absorption bands in the region 3400–3045 cm^{-1} of the free ligand (PBH) and its metal complexes are assigned to N—H stretching frequencies [25]. Bands observed in the region 3170–3200 cm^{-1} and 2930–2860 cm^{-1} are assigned to the aromatic ν(C—H) and ν(C—H) of the N—CH_3 group, respectively. An intense band observed at *ca* 1637 cm^{-1} is due to the ν(C=N) stretching of the ligand. Appearance of this band at a lower frequency region in the complexes suggests coordination of the ligands through the nitrogen atom. Pyridine ring vibrations are observed as a weak band in the region 1500–1560 cm^{-1}. The in-plane deformation mode of the pyridine ring appears at *ca* 645 cm^{-1} [26,27] which indicates that the pyridine nitrogen and the nitrogen of the benzimidazole rings coordinate to lanthanide(III) ions.

The highly intense ν(C≡N) band in the region 2080–2040 cm^{-1} and ν(C—S) at *ca* 825 cm^{-1} [28,29] suggest the presence of a nitrogen-bonded isothiocyanate. A new band at *ca* 365 cm^{-1} in the far-IR

Table 4. Significant IR absorptions (cm^{-1}) of PBH and its complexes

Complex	—N—H (str.)	—C—H (str.)	—C≡N (str.)	Py ring vibration	C—H out-of-plane deformation	ν(L n—N)	Anion vibration
PBH	3400m	3150s	1637m	1568m	742s	—	—
$La(NCS)_3(PBH)_2$	3346m	3150s	1620m	1500m	745s	357w	2070sh, 810m
$Pr(NCS)_3(PBH)_2$	3269m	3145s	1618m	1500m	742s	355w	2069sh, 815m
$Nd(NCS)_3(PBH)_2$	3200m	3120s	1610m	1490m	770s	352w	2070sh, 810m
$Sm(NCS)_3(PBH)_2$	3240m	3140s	1620m	1500m	750s	362w	2068sh, 810m
$Eu(NCS)_3(PBH)_2$	3245m	3145s	1595m	1520m	772s	356w	2080sh, 810m
$Gd(NCS)_3(PBH)_2$	3356m	3120s	1618m	1512m	745s	359w	2068sh, 810m
$Dy(NCS)_3(PBH)_2$	3369m	3150s	1620m	1525m	672s	360w	2068sh, 810m
$Y(NCS)_3(PBH)_2$	3251m	3145s	1618m	1535m	670s	357w	2078sh, 825m

Table 5. Significant IR absorptions (cm^{-1}) of MPB and its complexes

Complex	Aromatic C—H (str.)	Methyl C—H (str.)	C=N (str.)	Pyridine ring vib.	C—H out-of-plane deformation	ν(Ln—N)	Anon vibrations
MPB	3150m	2926s 2856s	1600m	1151m	748s	—	—
$La(NCS)_3(MPB)_2$	3155m	2920s	1590m	1150m	740s	365w	2060sh, 820m
$Pr(NCS)_3(MPB)_2$	3145m	2852s	1590m	1160m	742s	360w	2060sh, 820m
$Nd(NCS)_3(MPB)_2$	3170m	2856s	1595m	1159m	742s	359w	2091sh, 821m
$Sm(NCS)_3(MPB)_2$	3140m	2962s	1597m	1159m	742s	354w	2069sh, 823m
$Eu(NCS)_3(MPB)_2$	3145m	2866s	1597m	1159m	794s	363w	2069sh, 823m
$Gd(NCS)_3(MPB)_2$	3173m	2854s	1597m	1157m	646s	365w	2069sh, 820m
$Dy(NCS)_3(MPB)_2$	3145m	2952s	1597m	1157m	742s	361w	2065sh, 821m
$Y(NCS)_3(MPB)_2$	3151m	2965s	1585m	1157m	746s	358w	2081sh, 828m

region of the complexes may be assigned to the metal–nitrogen stretching vibrations [30].

NMR spectra

The NMR (^1H and ^{13}C) spectra of the ligands and complexes in DMSO-d_6 and acetone-d_6 provide evidence in favour of bonding of the ligand to Ln^{3+}. The aromatic protons were observed as a complex multiplet in the region δ 7.22–8.68 in the ligand, which was shifted to δ 7.26–8.22 in the complexes. The observed downfield shift of the signals is a good indication of complex formation [31]. No pseudo-contact shift was, however, observed for paramagnetic lanthanide complexes.

The ^1H NMR spectrum of the ligand MPB in acetone-d_6 showed a multiplet in the region δ 7.26–8.67 [9]. The signal observed at δ 7.3 corresponded to the 5, 6, 3′ and 5′ protons. The signal corresponding to H(4) and H(7) was observed at δ 7.8. The doublets observed at δ 8.3 and 8.6 corresponds to H(4′) and H(6′), respectively. The methyl proton observed at δ 4.3 was shifted to δ 3.92 in the complexes. However, when the spectra were taken in DMSO-d_6 the N—CH_3 proton signal appeared at δ 4.3; i.e. there was no shift in the complexes.

The ^{13}C NMR chemical shifts of the ligands at δ 152.51, 143.40, 138.71, 124.62, 123.59, 123.23 and 122.51 correspond to the C(2), C(9), C(8), C(5), C(6), C(4) and C(7) atoms of the benzimidazole moiety, whereas the signals observed at δ 151.14, 149.54, 120.89 and 110.81 are assigned to C(2′), C(6′), C(3′, 5′) and C(4′) of the pyridine moiety of the ligand. The signal owing to 1—CH_3 is observed at δ 33.58. In DMSO-d_6 the corresponding ^{13}C signals are observed at δ 152.25, 143.02, 138.45, 124.34, 123.28, 122.27, 151.01, 149.36, 120.49, 110.38 and 33.42 and undergo a downfield shift.

Thermal behaviour

The TG technique has been used to follow the thermal behaviour of the ligand and the complexes. According to the results obtained, the complexes are not volatile and their decomposition commences only above 200°C, which indicates the absence of coordinated or lattice water. The final product of the decomposition was the lanthanide(III) oxide in all cases.

Fluorescence spectra

The solid fluorescence spectra of the complexes of Sm^{3+}, Eu^{3+} and Dy^{3+} with MPB are shown in Table 6 along with their assignments. These spectra exhibit the following attributes: in the spectra of $Eu(NCS)_3(MPB)_2$, the $^5D_0 \rightarrow {}^7F_0$ transition observed as a weak band at 575 nm existing as a single peak indicates the presence of only one site for the Eu^{3+} ion [2] the $^5D_0 \rightarrow {}^7F_1$ transition around 593 nm is separated into two bands (585.0, 590.0 nm) and the strong band appearing at *ca* 602 nm is assigned to the $^5D_0 \rightarrow {}^7F_2$ transition. The transition $^5D_0 \rightarrow {}^7F_3$ at 650 nm is of low intensity and can be reasonably taken as forbidden and the $^5D_0 \rightarrow {}^7F_4$ transition appears at 698 nm. The electric dipole transition $^5D_0 \rightarrow {}^7F_2$ is clearly stronger than the magnetic dipole transition $^5D_0 \rightarrow$

Table 6. The fluorescence data for solid Sm^{III}, Eu^{III} and Dy^{III} complexes with MPB

Complex	E_x (nm)	E_m (nm)	Assignments
MPB	308	425	
$[Sm(NCS)_3(MPB)_2]$	305	580	$^5D_0 \rightarrow {}^7F_2$
		620	$^5D_0 \rightarrow {}^7F_1$
		640	$^5D_0 \rightarrow {}^7F_4$
$[Eu(NCS)_3(MPB)_2]$	305	575	$^5D_0 \rightarrow {}^7F_0$
		593	$^5D_0 \rightarrow {}^7F_1$
		602	$^5D_0 \rightarrow {}^7F_2$
		698	$^5D_0 \rightarrow {}^7F_4$
$[Dy(NCS)_3(MPB)_2]$	305	574	$^4D_{\frac{7}{2}} \rightarrow {}^6F_{\frac{5}{2}}$
		481	$^4D_{\frac{7}{2}} \rightarrow {}^6F_{\frac{13}{2}}$

$^7F_1$ and this indicates the absence of inversion symmetry at the Eu^{3+} site.

The Sm complex shows weak metal ion luminescence and its emission spectrum exhibits three bands (Table 6). It is found that the fluorescence properties are in tune for each lanthanide ion.

Magnetic susceptibility and cyclic voltammetry

The observed magnetic moments of the complexes are close to those given by the Van Vleck equation indicating that the lanthanides in the complexes remain in the +3 oxidation state and the 4*f* electrons are little influenced by the ligands.

The cyclic voltammetry of the MPB complexes in acetonitrile solution shows two reduction waves, as illustrated in Fig. 1. For the Sm complex the first wave at −1.349 versus ($Ag/AgCl_{(s)}$, Cl^-) is reversible and has been assigned to the complexes Sm^{III}/Sm^{II} couple (see Table 7). The second wave is presumed to be a ligand-based reduction. The other redox potential values are attributed to the redox behaviour of the ligands.

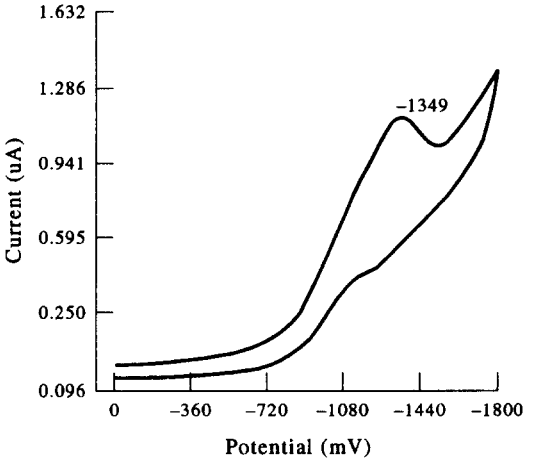


Fig. 1. Cyclic voltammograms of Sm–MPB complex.

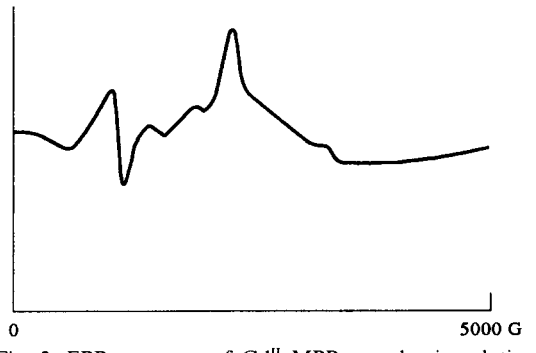


Fig. 2. EPR spectrum of Gd^{II}–MPB complex in solution (DMSO) at liquid nitrogen temp. (77 K).

Table 7. *E* (in volts) against Ag/AgCl(s) Cl^-

Complex	*E*	*E*
$[Nd(NCS)_3(MPB)_2]$	1.649	1.033
	1.574	0.834
	1.649	1.033
	2.00	1.574
	−0.942	
	1.413	0.926
$[Sm(NCS)_3(MPB)_2]$	1.636	0.972
	−1.119	−1.206
	1.533	1.127
	−1.349	
$[Dy(NCS)_3(MPB)_2]$	−1.489	
	−1.535	

Table 8. g_{eff} values of Gd^{III} complexes of PBH and MPB

Complex	g_{eff}
$[Gd(NCS)_3(PBH)_2]^a$	1.64
$[Gd(NCS)_3(PBH)_2]^b$	1.58
$[Gd(NCS)_3(PBH)_2]^c$	1.99
$[Gd(NCS)_3(MPB)_2]^a$	1.67
$[Gd(NCS)_3(MPB)_2]^b$	1.96
$[Gd(NCS)_3(MPB)_2]^c$	1.49

[a] Polycrystalline solid at room temperature.
[b] Polycrystalline solid at liquid nitrogen temperature.
[c] Solution (DMSO) at liquid nitrogen temperture.

EPR spectra

The EPR spectra of the Gd^{3+} complexes in the solid state and in solution (DMSO) were recorded both at room (303 K) and liquid nitrogen temperature (77 K). The "*g*" values calculated from the spectra are presented in Table 8. The following conclusions can be drawn from the spectra.

1. Each formula unit contains one Gd^{3+} ion with spin–spin interactions that cause excessive Gaussian broadening of the EPR lines in the solid phase, both at low temperature and room temperature. It is impossible to extract the zero field splitting features.
2. The high concentration of Gd^{3+} in the solution gives rise to line broadening due to spin–spin relaxation.
3. The intensity of the low field line, being almost the same as that of the high field line, indicates a large zero-field splitting [2,32].
4. In some cases two types of spectra are observed: those with relatively narrow symmetric peaks and those with broad symmetric peaks, in accordance with the work of Geraldes and Williams [33].

Acknowledgements—K.C.D. thanks the Jawaharlal Nehru Centre for Advanced Scientific Research, IISC Campus,

Bangalore for a visiting assignment. Grateful thanks are due to CSIR, New Delhi for funding this project.

REFERENCES

1. Richardson, F. S., *Chem. Rev.*, 1982, **82,** 541.
2. Bunzli, J. C. G. and Choppin, G. R., *Lanthanide Probes in Life, Chemical and Earth Sciences*. Elsevier, Amsterdam, 1989.
3. Mohanty, R. N., Chakravortty, V. and Dash, K. C., *Indian J. Chem.*, 1991, **30A,** 454.
4. Rout, K. C., Mohanty, R. R., Jena, S. and Dash, K. C., *Polyhedron*, 1996, **15,** 1023.
5. Ghosh, S. P., Bhattacharjee, P. and Mishra, L. K., *J. Indian Chem. Soc.*, 1974, **51,** 308.
6. Nath, P. K., Mishra, N. C., Chakravortty, V. and Dash, K. C., *Polyhedron*, 1987, **6,** 455.
7. Mishra, P. K., Chakravortty, V. and Dash, K. C., *Indian J. Chem.*, 1989, **28A,** 581.
8. Addison, A. W., Burman, S., Wahlgren, C. G., Rajan, O. A., Rowe, T. M. and Sinn, E., *J. Chem. Soc., Dalton Trans.*, 1987, 2621.
9. Addison, A. W., Rao, T. N. and Wahlgren, C. G., *J. Heterocyclic Chem.*, 1983, **20,** 1481.
10. Walter, J. L. and Freiser, H., *J. Am. Chem. Soc.*, 1956, **78,** 260.
11. Kondo, M., *Bull Chem. Soc. Jpn*, 1978, **51,** 3027.
12. Novo, M., Mosquera, M. and Prieto, F. R., *Can. J. Chem.*, 1992, **70,** 823.
13. Dash, K. C. and Mohanta, H. N., *J. Inorg. Nucl. Chem.*, 1978, **40,** 499.
14. Mohanty, R. R., Rout, K. C., Jena, S. and Dash, K. C., *Polyhedron*, 1994, **13,** 559.
15. Mohanty, R. R., Rout, K. C., Jena, S. and Dash, K. C., *Polyhedron*, 1994, **13,** 2945.
16. Geary, W. J., *Coord. Chem. Rev.*, 1971, **7,** 81.
17. Savan, V. V. and Patel, C. C., *J. Inorg. Nucl. Chem.*, 1972, **34,** 1462.
18. Zalkin, A., Templeton, D. H. and Karraker, D. G., *Inorg. Chem.*, 1968, **8,** 2680.
19. Wasson, S. J. S., Sands, D. E. and Wagner, R. F., *Inorg. Chem.*, 1973, **12,** 187.
20. Dyer, D. S., Cunningham, J. A., Brooks, J. J., Sievers, R. E. and Randeau, R. E., *Nuclear Magnetic Shift Reagents*, ed. R. E. Sievers. Academic Press, New York, 1973, p. 21.
21. Yost, D. M., Russel, H. and Garner, C. S., *The Rare Earths Elements and their Compounds*. Wiley, New York, 1947.
22. Lapitakaya, A. V. and Pirkes, S. B., *Zh. Neorg. Khim.*, 1971, **16,** 369.
23. Carnall, W. T., Fields, P. R. and Rajnak, K., *J. Chem. Phys.*, 1961, **49,** 4424.
24. Tandan, S. P. and Mehta, P. C., *J. Chem. Phys.*, 1970, **72,** 4896.
25. Jain, M. C., Srivastava, A. R. and Jain, P. C., *Inorg. Chim. Acta*, 1977, **23,** 199.
26. Radecka-Paryzek, W., *Inorg. Chim. Acta*, 1980, **45,** L147.
27. Radecka-Paryzek, W., *Inorg. Chim. Acta*, 1981, **52,** 261.
28. Pecile, C., *Inorg. Chem.*, 1966, **5,** 210.
29. Bailey, R. A., Kozak, S. L., Michelsen, T. W. and Mills, W. N., *Coord. Chem. Rev.*, 1971, **6,** 407.
30. Wang, S., Luo, Q., Zhou, X. and Zeng, Z., *Polyhedron*, 1993, **12,** 1939.
31. Carlson, R. H. and Brown, T. L., *Inorg. Chem.*, 1966, **5,** 268.
32. O'Hara, P. B. and Koenig, S. H., *Biochemistry*, 1986, **25,** 1445.
33. Geraldes, E. C. N. F. and Williams, D. J. P., *J. Chem. Soc., Dalton Trans.*, 1971, 1721.

Pergamon

PII: S0277-5387(96)00454-8

Polyhedron Vol. 16, No. 9, pp. 1425–1431, 1997
Copyright © 1997 Elsevier Science Ltd
Printed in Great Britain. All rights reserved
0277-5387/97 $17.00+0.00

A novel pentanuclear Co–S raft cluster compound consisting of fused $Co_3(\mu_3\text{-}S)$ units: X-ray crystal structure of $Co_5(CO)_2S_3(SC_5H_4N)_7$

Botao Zhuang,* Peihua Yu, Liangren Huang, Lingjie He and Guohua Pan

Fujian Institute of Research on the Structure of Matter, Chinese Academy of Sciences, State Key Laboratory of Structural Chemistry, Fuzhou, Fujian 350002, P. R. China

(Received 5 July 1996; accepted 10 September 1996)

Abstract—The reaction of $Na[Co(CO)_4]$ with PyS–(2-mercapto-pyridine) in THF at room temperature gave a dark crystalline product $[Co_5(CO)_2(\mu_3\text{-}S)_3(SC_5H_4N)_7]$ (**1**). The crystal structure of **1** determined by single crystal X-ray diffraction, revealed a pentanuclear metallic core, $Co_5(\mu_3\text{-}S)_3(\mu\text{-}S)_4(\mu\text{-}C)$, which can be described as a skeleton comprising three incomplete cubane-like structural units, two SCo_3S_3 and a SCo_3S_2C, in an inversion arrangement sharing two rhombic CoS_2Co faces or, in other words, as a raft-type structure consisting of fused $Co_3(\mu\text{-}S)$ units. The geometry around each Co atom is a distorted octahedron and the octahedra are divided into four types according to the different coordination environments. The three Co—Co bond distances of 2.72–2.80 Å indicate weak metal–metal interactions. The formal oxidation states of the five cobalt atoms are one Co^{I} and four Co^{III}. The formation of **1** is discussed and the cyclic voltammetry of **1** has been measured. Interestingly, **1** contains three inorganic μ_3-S atoms notwithstanding the absence of inorganic S^{2-}source in the synthetic reaction system, implying a process related to desulfurization of 2-mercaptopyridine in the preparative reaction. © 1997 Elsevier Science Ltd. All rights reserved.

Keywords: cobalt–sulfur; raft cluster; $Co_3(\mu_3\text{-}S)$ unit; structure; cyclic voltammetry.

The chemistry of cobalt–sulfur compounds has been significant with regard to hydrogenation, hydroformylation and hydrodesulfurization catalysis. As part an investigation of the effect of various organosulfur compounds on both hydrogenation and hydroformylation of olefins, a large number of unusual polymeric cobalt carbonyl sulfur complexes [1–18] have been produced by the reaction of dicobalt octacarbonyl with sulfur or sulfur-containing reagents and characterized by X-ray crystallography; most of the complexes contain $Co_3(\mu_3\text{-}S)$, $Co_4(\mu_4\text{-}S)$ and $Co_2(\mu\text{-}S)$ units. As part of our studies on the chemistry of transition metal–sulfur complexes containing low- and mixed-valence metal atoms, we report herein a novel pentanuclear cobalt–sulfur cluster compound with a raft-type structure consisting of fused $Co_3(\mu_3\text{-}S)$ units.

*Author to whom correspondence should be addressed.

EXPERIMENTAL

Materials and methods

THF was distilled from $LiAlH_4$, $Co_2(CO)_8$ and PySH were purchased from Aldrich. All the procedures were carried out under nitrogen using the Schlenk technique.

IR spectra were recorded on a Perkin–Elmer 577 IR spectrometer.

Cyclic voltammetry (CV) measurements were carried out with a three-electrode cell using 0.1 M Bu_4NF_4 as the supporting electrolyte and MeCN as solvent. The working electrode was a glassy carbon and the reference electrode was an aqueous SCE separated from the sample solution by a salt bridge. Solutions were deoxygenated and blanketed with nitrogen and the potentiostat was a CV-1B from BAS (Bioanalytical System).

Synthesis of $Co_5(\mu_3\text{-}S)_3(CO)_2(SC_5H_4N)_7$ **(1)**

A mixture of $Co_2(CO)_8$ (0.34 g, 1 mmol), NaOH (0.40 g, 10 mmol) in THF (40 cm^3) was stirred at room temperature overnight, resulting in a light yellow solution with a purple precipitate. After filtering off the precipitate, to the filtrate was added Et_4NCl (0.33 g, 2 mmol) and PySH (0.22 g, 2 mmol) and the reaction mixture was stirred at room temperature giving a bright yellow solution with a white precipitate. The reaction mixture was stirred at 40°C for another 2 h, resulting in a brown–yellow solution. After filtering off the white residue and removing the solvent by pumping nearly to dryness, the nearly dry residue was dissolved in EtOH (30 cm^3) giving a brown solution. A small amount (0.1 g) of dark brown crystals was obtained after cooling the solution at 4°C for several weeks. The IR spectrum of **1** (KBr pellet) showed besides the characteristic absorptions of the PyS ligands, two strong bands at 1810 and 1930 cm^{-1} indicating the existence of carbonyls and a weak band at 450 cm^{-1} which might be the stretching vibrational frequency of a metal-bridging sulfur bond. In fact, the X-ray crystal structure determination verifies that **1** contains two carbonyl ligands and three μ_3-S atoms. After filtering off the crystalline product **1**, a little air was added to the filtrate and the resulting filtrate was cooled at 4°C for 24 h, and another crystalline product, $[Et_4N][Co(PyS)_3]$ **(2)**, was obtained which has been previously characterized by X-ray crystallography [19].

X-ray crystal structure determination of **1**

A single crystal of **1** having dimensions of $0.30 \times 0.30 \times 0.40$ mm^3 was mounted on a glass fibre with epoxy cement. Data collection was performed on an Enraf–Nonius CAD4 computer-controlled kappa diffractometer utilizing graphite-monochromated Mo-K_α radiation ($\lambda = 0.71073$ Å) at room temperature. All calculations were performed on a VAX computer using the MOLEN program [20]. Compound **1** crystallizes in the monoclinic space group $P2_1/n$ with $a = 12.852(2)$, $b = 20.991(3)$, $c = 19.691(3)$ Å; $\beta = 100.14(4)°$; $V = 5229.3$ $Å^3$; $Z = 4$; $D_{calc} = 1.55$ g cm^{-3}. A total of 9926 reflections, of which 9903 reflections were unique, were collected in the range $0 \leqslant 2\theta \leqslant 50°$ using ω–2θ scan technique. Lorentz and polarization corrections were applied to the data and the linear absorption coefficient is 19.7 cm^{-1} for Mo-K_α radiation. No absorption correction was made. The structure was solved by direct methods. A total of eight atoms were located from an *E*-map and the remaining atoms were located in succeeding difference Fourier syntheses. Hydrogen atoms were not included in the calculations. The structure was refined in full-matrix least-squares where the function minimized was $w(\Sigma[F_o] - [F_c])$ and the weight w is defined as by the Killean and Lawrence method with terms of 0.020 and 1.0 [21]. Only the 7197 reflections having $I \geqslant 3\sigma(I)$ were used in the refinements. The final cycle of refinement included 550 variable parameters and converged with unweighted and weighted agreement factors of $R = \Sigma(|[F_o] - [F_c]|)/\Sigma[F_o] = 0.042$ and $R_w = [\Sigma w(F_o - F_c)^2/\Sigma w(F_o)^2]^{1/2} = 0.058$.

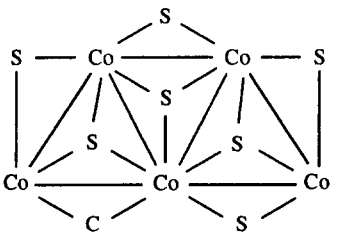
The estimated standard deviation of observation of unit weight was 1.04 and the highest peak in the final difference Fourier map was 0.71 e $Å^{-3}$.

A list of atomic coordinates and calculated thermal parameters have been deposited at the Cambridge Crystallographic Data Centre.

RESULTS AND DISCUSSION

The structure and mixed-valence metal atoms of $[Co_5(\mu_3\text{-}S)_3(CO)_2(SC_5H_4N)_7]$ **(1)**

The bond distances and angles of complex **1** are listed in Tables 1 and 2, and the molecular structure of **1** is depicted in Fig. 1. As shown in Tables 1 and 2 and Fig. 1, the molecule of **1** contains a pentanuclear Co—S skeleton, $[Co_5(\mu_3\text{-}S)_3(\mu\text{-}S)_4(\mu\text{-}C)]^{3+}$ **(A)** consisting of three incomplete cubane-like cluster units, two Co_3S_4 and a Co_3S_3C, in an inversion arrangement to each other, sharing two rhombic CoS_2Co faces. Around the skeleton can be found four bridging PyS (five-electron donor), three terminal PyS (three-electron donor) and one terminal carbonyl ligand, resulting in six coordination of each cobalt atom. Interestingly, the five cobalt atoms in the molecule are in a raft geometry, where three Co_3 triangles are aligned linearly sharing their edges. Each Co_3 triangle is capped by an inorganic sulfur atom and each peripheral Co—Co edge is bridged by a sulfur atom from PyS except for one which is bridged by a carbon atom from a bridging carbonyl.



A

Although the three Co_3 triangles are not exactly coplanar (the dihedral angles between Co(1), Co(2), Co(5) and Co(5), Co(3), Co(2) and between Co(5), Co(3), Co(4) and Co(5), Co(3), Co(2) are 9.6 and 2.5°, respectively), it is obvious that the two capping sulfur atoms of the two terminal Co_3 triangles [Co(1), Co(2), Co(5) and Co(3), Co(4), Co(5)] are located at the opposite side of the capping sulfur atom of the central Co_3 triangle [Co(2), Co(3), Co(5)]. The capping and bridging atoms form two layers and the

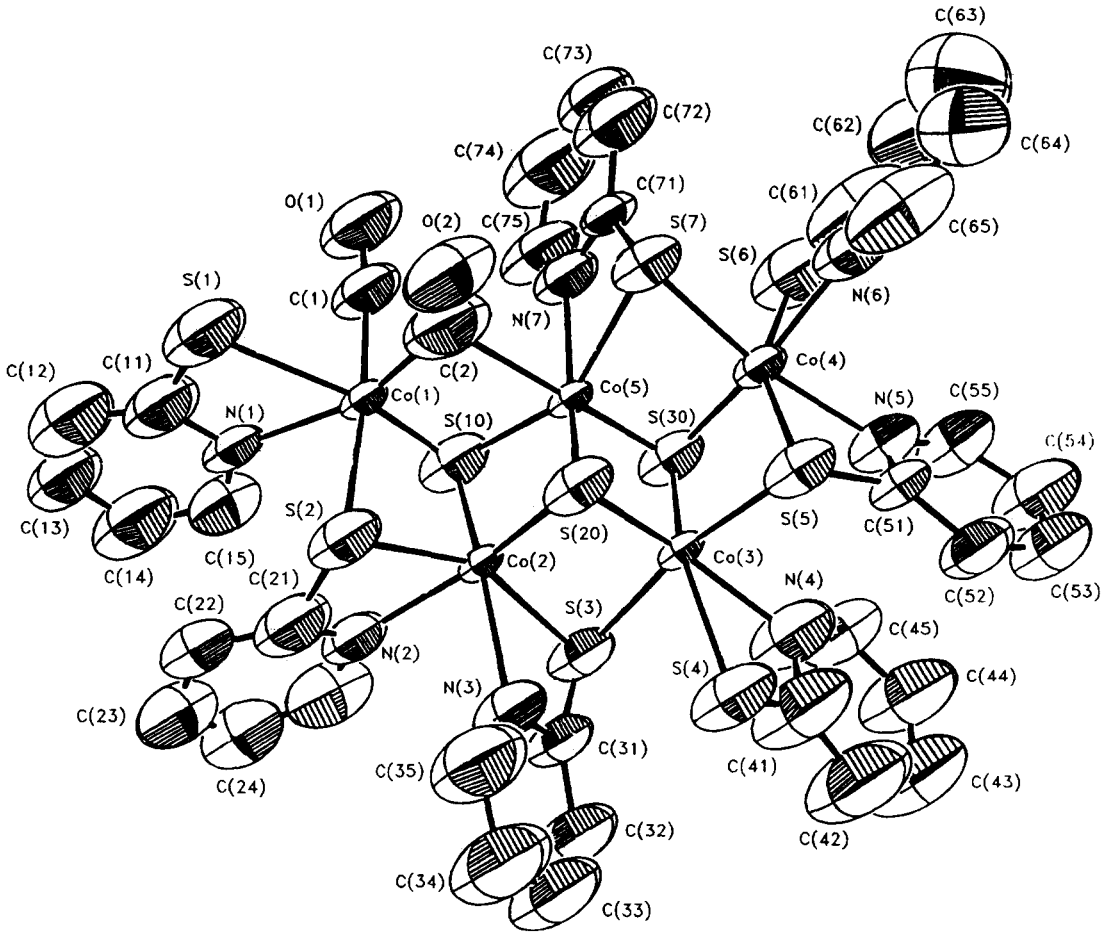


Fig. 1. The structure of $Co_5(\mu_3\text{-}S)_3(CO)_2(PyS)_7$ (**1**).

Table 1. Selected bond distances (Å) for $Co_5(\mu_3\text{-}S)_3(CO)_2(PyS)_7$ (**1**)

Co(1)—Co(2)	2.8883(9)	Co(4)—Co(5)	2.8076(10)
Co(1)—Co(5)	3.0329(10)	Co(4)—S(5)	2.452(2)
Co(1)—S(1)	2.565(3)	Co(4)—S(6)	2.490(3)
Co(1)—S(2)	2.512(2)	Co(4)—S(7)	2.453(2)
Co(1)—S(10)	2.357(2)	Co(4)—S(30)	2.383(2)
Co(1)—C(1)	1.955(9)	Co(4)—N(5)	2.138(7)
Co(1)—C(2)	1.91(1)	Co(4)—N(6)	2.158(8)
Co(2)—Co(3)	2.9121(10)	Co(5)—S(7)	2.443(2)
Co(2)—Co(5)	2.7207(9)	Co(5)—S(10)	2.354(2)
Co(2)—S(2)	2.464(2)	Co(5)—S(20)	2.362(2)
Co(2)—S(3)	2.446(2)	Co(5)—S(30)	12.336(2)
Co(2)—S(10)	2.321(2)	Co(5)—C(2)	2.53(1)
Co(2)—S(20)	2.349(2)	Co(5)—N(7)	2.204(6)
Co(2)—N(2)	2.250(6)	S(1)—C(11)	1.79(1)
Co(2)—N(3)	2.266(7)	S(2)—C(21)	1.84(1)
Co(3)—Co(4)	2.8975(10)	S(3)—C(31)	1.666(7)
Co(3)—Co(5)	2.7274(9)	S(4)—C(41)	1.69(1)
Co(3)—S(3)	2.510(2)	S(5)—C(51)	1.764(6)
Co(3)—S(4)	2.580(3)	S(6)—C(61)	1.74(1)
Co(3)—S(5)	2.476(2)	S(7)—C(71)	1.752(6)
Co(3)—S(20)	2.362(2)	O(1)—C(1)	1.207(9)
Co(3)—S(30)	2.368(2)	O(2)—C(2)	1.26(1)
Co(3)—N(4)	2.204(9)		

Numbers in parentheses are estimated standard deviations.

Table 2. Selected bond angles (°) for $Co_5(\mu_3\text{-}S)_3(CO)_2(PyS)_7$ (**1**)

S(1)—Co(1)—S(2)	90.07(8)	Co(5)—Co(3)—S(20)	54.73(5)
S(1)—Co(1)—S(10)	150.72(9)	Co(5)—Co(3)—S(30)	54.02(5)
S(1)—Co(1)—C(1)	83.8(2)	Co(5)—Co(3)—N(4)	146.1(2)
S(1)—Co(1)—C(2)	99.3(4)	S(3)—Co(3)—S(4)	88.53(8)
S(2)—Co(1)—S(10)	101.69(7)	S(3)—Co(3)—S(5)	169.36(7)
S(2)—Co(1)—C(1)	173.8(2)	S(3)—Co(3)—S(20)	103.54(7)
S(2)—Co(1)—C(2)	97.0(3)	S(3)—Co(3)—S(30)	82.91(7)
S(10)—Co(1)—C(1)	84.3(2)	S(3)—Co(3)—N(4)	83.4(2)
S(10)—Co(1)—C(2)	105.7(4)	S(4)—Co(3)—S(5)	81.20(8)
C(1)—Co(1)—C(2)	82.9(4)	S(4)—Co(3)—S(20)	95.21(8)
Co(5)—Co(2)—S(2)	110.10(6)	S(4)—Co(3)—S(30)	155.85(8)
Co(5)—Co(2)—S(3)	95.65(5)	S(4)—Co(3)—N(4)	64.3(2)
Co(5)—Co(2)—S(10)	54.98(6)	S(5)—Co(3)—S(20)	80.31(7)
Co(5)—Co(2)—S(20)	54.95(5)	S(5)—Co(3)—S(30)	105.44(7)
Co(5)—Co(2)—N(2)	140.0(2)	S(5)—Co(3)—N(4)	89.6(2)
Co(5)—Co(2)—N(3)	139.1(2)	S(20)—Co(3)—S(30)	108.73(7)
S(2)—Co(2)—S(3)	154.23(7)	S(20)—Co(3)—N(4)	158.5(2)
S(2)—Co(2)—S(10)	104.18(8)	S(30)—Co(3)—N(4)	92.2(2)
S(2)—Co(2)—S(20)	88.81(7)	S(5)—Co(4)—S(6)	154.5(1)
S(2)—Co(2)—N(2)	67.4(2)	S(5)—Co(4)—S(7)	98.33(7)
S(2)—Co(2)—N(3)	93.3(2)	S(5)—Co(4)—S(30)	105.76(7)
S(3)—Co(2)—S(10)	91.14(7)	S(5)—Co(4)—N(5)	68.1(2)
S(3)—Co(2)—S(20)	105.92(7)	S(5)—Co(4)—N(6)	99.3(2)
S(3)—Co(2)—N(2)	93.6(2)	S(6)—Co(4)—S(7)	99.80(9)
S(3)—Co(2)—N(3)	65.1(2)	S(6)—Co(4)—S(30)	86.8(1)
S(10)—Co(2)—S(20)	108.90(8)	S(6)—Co(4)—N(5)	89.3(2)
S(10)—Co(2)—N(2)	86.0(2)	S(6)—Co(4)—N(6)	66.0(2)
S(10)—Co(2)—N(3)	151.1(2)	S(7)—Co(4)—S(30)	104.67(7)
S(20)—Co(2)—N(2)	154.8(2)	S(7)—Co(4)—N(5)	159.5(2)
S(20)—Co(2)—N(3)	94.1(1)	S(7)—Co(4)—N(6)	81.6(2)
N(2)—Co(2)—N(3)	79.5(2)	S(30)—Co(4)—N(5)	94.1(2)
Co(5)—Co(3)—S(3)	94.02(5)	S(30)—Co(4)—N(6)	152.8(2)
Co(5)—Co(3)—S(4)	149.60(7)	N(5)—Co(4)—N(6)	85.5(3)
Co(5)—Co(3)—S(5)	96.24(5)	Co(2)—Co(5)—Co(3)	64.62(3)
Co(2)—Co(5)—S(7)	144.12(6)	Co(3)—S(5)—C(51)	99.6(2)
Co(2)—Co(5)—S(10)	53.85(6)	Co(4)—S(5)—C(51)	79.7(2)
Co(2)—Co(5)—S(20)	54.50(5)	Co(4)—S(6)—C(61)	82.9(6)
Co(2)—Co(5)—S(30)	96.45(6)	Co(4)—S(7)—Co(5)	69.83(6)
Co(2)—Co(5)—C(2)	84.6(2)	Co(4)—S(7)—C(71)	96.4(2)
Co(2)—Co(5)—N(7)	143.0(2)	Co(5)—S(7)—C(71)	81.9(2)
Co(3)—Co(5)—S(7)	106.75(6)	Co(1)—S(10)—Co(2)	76.24(7)
Co(3)—Co(5)—S(10)	102.16(6)	Co(1)—S(10)—Co(5)	80.14(7)
Co(3)—Co(5)—S(20)	54.75(5)	Co(2)—S(10)—Co(5)	71.16(7)
Co(3)—Co(5)—S(30)	55.12(5)	Co(2)—S(20)—Co(3)	76.35(6)
Co(3)—Co(5)—C(2)	129.3(2)	Co(2)—S(20)—Co(5)	70.55(6)
Co(3)—Co(5)—N(7)	139.4(2)	Co(3)—S(20)—Co(5)	70.52(6)
S(7)—Co(5)—S(10)	151.01(8)	Co(3)—S(30)—Co(4)	75.16(6)
S(7)—Co(5)—S(20)	91.28(7)	Co(3)—S(30)—Co(5)	70.86(6)
S(7)—Co(5)—S(30)	106.42(7)	Co(4)—S(30)—Co(5)	72.86(6)
S(7)—Co(5)—C(2)	75.0(2)	Co(1)—C(1)—O(1)	174.9(7)
S(7)—Co(5)—N(7)	66.9(2)	O(1)—C(1)—C(2)	133.2(7)
S(10)—Co(5)—S(20)	107.35(8)	Co(1)—C(2)—Co(5)	84.9(4)
S(10)—Co(5)—S(30)	88.29(8)	Co(1)—C(2)—O(2)	141(1)
S(10)—Co(5)—C(2)	88.5(2)	Co(5)—C(2)—O(2)	133.0(8)
S(10)—Co(5)—N(7)	89.6(2)	Co(5)—C(2)—C(1)	86.1(4)
S(20)—Co(5)—S(30)	109.84(7)	O(2)—C(2)—C(1)	126.6(8)
S(20)—Co(5)—C(2)	74.7(2)	S(1)—C(11)—C(12)	126.6(8)
S(20)—Co(5)—N(7)	155.9(2)	S(1)—C(11)—C(13)	161.6(6)
S(30)—Co(5)—C(2)	175.1(2)	S(2)—C(21)—C(22)	127.6(7)
S(30)—Co(5)—N(7)	87.1(2)	Co(1)—S(1)—C(11)	83.7(3)
C(2)—Co(5)—N(7)	89.2(3)	Co(1)—S(2)—Co(2)	70.96(6)
Co(1)—S(2)—C(21)	100.6(3)	Co(2)—N(2)—C(21)	101.2(5)
Co(2)—S(2)—C(21)	81.6(3)	Co(2)—N(2)—C(25)	139.0(6)

Table 2. *continued*

Co(2)—S(3)—Co(3)	71.96(6)	C(21)—N(2)—C(25)	119.2(8)
Co(2)—S(3)—C(31)	84.2(3)	S(3)—C(31)—C(32)	131.9(7)
Co(3)—S(3)—C(31)	100.6(3)	S(3)—C(31)—N(3)	112.2(5)
Co(3)—S(4)—C(41)	80.6(5)	Co(2)—N(3)—C(31)	97.8(5)
Co(3)—S(5)—Co(4)	72.02(6)	Co(2)—N(3)—C(35)	131.9(7)
S(4)—C(41)—C(45)	141.7(8)	S(4)—C(41)—C(42)	128.(1)
Co(3)—N(4)—C(41)	102.2(7)	S(6)—C(61)—N(6)	107.(1)
Co(3)—N(4)—C(45)	136.8(8)	Co(4)—N(6)—C(61)	104.1(8)
S(5)—C(51)—C(52)	125.5(6)	Co(4)—N(6)—C(65)	139.5(9)
S(5)—C(51)—N(5)	110.1(5)	C(61)—N(6)—C(65)	116.(1)
Co(4)—N(5)—C(51)	100.9(4)	Co(5)—N(7)—C(71)	100.7(4)
Co(4)—N(5)—C(55)	139.1(6)	Co(5)—N(7)—C(75)	140.9(6)
S(6)—C(61)—C(62)	129.(2)	C(71)—N(7)—C(75)	118.3(7)
S(2)—C(21)—N(2)	109.0(7)		

Numbers in parentheses are estimated standard deviations.

cobalt atoms are sandwiched between them. This is the first example of a Co—S compound containing a raft geometry consisting of fused $Co_3(\mu_3\text{-}S)$ units, although a similar geometry of Mo atoms has been found in the Mo—S cluster compound, $[Mo_6S_{10}(SH)_2(PEt_3)_6]$ [22]. The Co—Co distances are 2.72, 2.73, 2.80, 2.89, 2.90, 2.91 and 3.03 Å. The three shorter Co—Co distances [Co(5)—Co(4), Co(5)—Co(3) and Co(5)—Co(2)] seem to indicate a somewhat weak metal–metal interaction although the 90 skeletal electrons have occupied the whole 45 orbitals of the five Co atoms. The Co—μ_3-S bond distances are 2.321(2)–2.382(2) Å, the Co—μ_2-S(PyS) bond lengths are 2.443(2)–2.512(2) Å and the Co—S(PyS) distances are 2.490(3)–2.580(3) Å. The irregularity of the Co—S and Co—Co bond distances implies the complicated electron structure of the cobalt atom centres and the possibility of the existence of mixed-valence cobalt atoms in the cluster compound. Carefully inspecting the coordination environment of each cobalt atom in the molecule it is evident that all the five cobalt atoms are different from each other. However, considering the sort of atoms around the cobalt atoms, the five cobalt atoms in the cluster could be divided into three groups: (i) Co(2), Co(3) and Co(4) atoms (which contain S and N as surrounding atoms); (ii) Co(5) which has a bridging C atom from a carbonyl ligand besides the S and N atoms as surrounding atoms; and (iii) Co(1), which possesses a carbon atom from a terminal carbonyl ligand in addition to bridging C, S and N atoms as surrounding atoms. Considering the unsymmetric bridging carbonyl between the Co(1) and Co(5) atoms [Co(1)—C(2) and Co(5)—C(2) bond distances are 1.91(1) and 2.53(1) Å, respectively] then Co(5) should be included in the group of Co(2), Co(3) and Co(4) atoms. However, it is worth pointing out that because of the existence of an unsymmetric bridging carbonyl ligand leading to the transfer of a pair of electrons on the Co(5) atom to the carbon atom, the Co(5) atom may vacate its one orbital to form metal–metal bonds with neighbouring Co atoms. This is probably the reason why the bond distances of Co(5)—Co(2), Co(5)—Co(3) and Co(5)—Co(4) are shorter than the others and could be considered as being a result of metal–metal interaction. This fact, perhaps, implies the existence of some electron transfer of Co → μ_3-S.

In connection with the different coordination environments of the cobalt atoms and the electric charge equilibrium of the neutral molecule there are, at least, two oxidation states of Co atoms in the molecule and, reasonably, the Co(2), Co(3), Co(4) and Co(5) atoms are in the oxidation state +3 and the Co(1) atom is in the +1 state. The fact that the Co(1) atom contains two carbonyls for stabilizing its low oxidation state supports the above suggestion.

Interestingly, the incomplete cubane-like Co_3S_4 structural units in **1** are configurationally similar to Fe_3S_4 units [23], which are of special interest owing to the more general significance of the 3 Fe sites in the Fe—S protein, *D. gigas* ferredoxin II [24] and are similar to the Mo_3S_4 units [25], which exhibits some aromaticity with d–p π conjugation like benzene and special reactivities [25–28].

Formation and cyclic voltammetry of **1**

According to the X-ray crystal structure of **1**, there are several conspicuous features: (i) the oxidation states of the cobalt atoms in **1** are higher than that in the starting material, cobalt carbonyls; (ii) there are three inorganic sulfur atoms, μ_3-S, in **1**. This implies that the formation of **1** involves the oxidation of cobalt atoms and hydrodesulfurization of 2-mercapto-pyridine(PyS) because of the lack of an in-

organic sulfur source of S^{2-} or S^{2-}-containing compound as starting material in the preparative reaction. As a reactant, the yellow solution obtained from the reaction of $Co_2(CO)_8$ with NaOH in THF at room temperature is, in fact, the $Na[Co(CO)_4]$ [29] with a lower oxidation state of the cobalt atom. Thus the formation of **1** is mainly due to the reaction of $[Co(CO)_4]^-$ with PySH. However, it cannot be excluded that existence of the higher valence cobalt compound with PySH is a result of the $Co_2(CO)_8$ in THF leading to the formation of $Co(THF)_6[Co(CO)_4]_2$ [30–32]. The synthetic reaction, beyond doubt, is so complicated that the yield of **1** is low and there are other products besides **1** in the reaction mixture. However, in the light of the structural features of **1** and the formation of the Co^{II} compound, $[Co(PyS)_3]^-$, by addition of a little air into the synthetic reaction solution [19], it appears that the precursor compounds are $[Co(CO)_x(PyS)_y]^{n-}$ ($x = 1$–4; $y = 1$–4 and $n = 0$–3), formed by reaction of different valent Co compounds with PySH, and the hydrodesulfurization of PyS^- is completed by cooperation of certain precursor compounds resulting in the formation of polynuclear cluster compounds containing inorganic μ_3-S atoms. Interestingly, a similar result, whereby the reaction of iron pentacarbonyl with PySH or dithiocarbamate results in a trinuclear iron–sulfur–carbonyl complex containing an inorganic μ_3-S atom, $[Fe_3S(CO)_9]^{2-}$, has been found [33]. This seems to imply that the formation of μ_3-S, containing cluster compounds is essential to hydrosulfurization. These μ_3-S-containing cluster compounds formed following the hydrodesulfurization would be advantageous to understanding the hydrodesulfurization and looking for highly effective hydrodesulfurization catalysts.

The cyclic voltammograms of **1** in acetonitrile are shown in Fig. 2. There is a redox couple at *ca* −0.12 V *vs* SCE (−0.09 V/−0.15 V) (Fig. 2a). With reference to the electrochemical data of the cobalt ion and PySH [34], it is apparent that this event is not the redox of the simple cobalt ion or PyS ligand and should reflect the electrochemical behaviour of the whole cluster compound **1** as in Eq. (1),

$$[Co_5(\mu_3\text{-}S)_3(CO)_2(SC_5H_4N)_7]^0 \underset{-e}{\overset{+e}{\rightleftharpoons}} [Co_5(\mu_3\text{-}S)_3(CO)_2(SC_5H_4N)_7]^- \quad (1)$$

However, the redox couple at −0.12 V *vs* SCE disappeared and oxidation peaks at +0.56 and 0.81 V *vs* SCE appeared when the positive scan went to +1.4 V *vs* SCE (Fig. 2b). This indicated that **1** decomposed and chemical reaction took place in the solvent under this higher potential.

Acknowledgements—We would like to acknowledge the NNSFC (National Nature Science Foundation of China) and CP-NKPFR (Climbing Program–National Key Project for Fundamental Research) for support of this research.

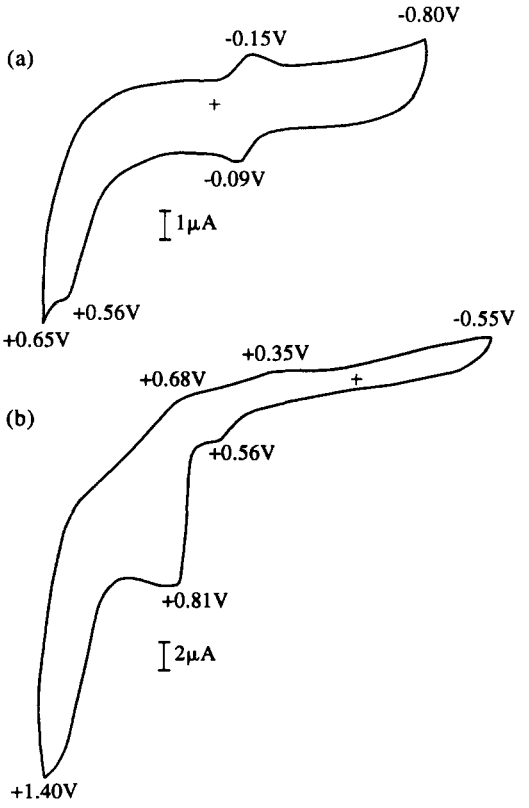


Fig. 2. Cyclic voltammograms of **1** in MeCN; concentration of the sample, 0.0004 M; scan rate, 200 mV s^{-1}.

REFERENCES

1. Marko, L., Bor, G. and Almasy, G., *Chem. Ber.* 1961, **94,** 847.
2. Marko, L., Bor, G. and Klumpp, E., *Chem. Ind(Lond.)*, 1961, 1491.
3. Marko, L., Bor, G., Klumpp, E., Marko, B. and Almasy, B., *Chem. Ber.* 1963, **96,** 955.
4. Marko, L., Bor, G. and Klumpp, E., *Angew. Chem.* 1963, **75,** 248.
5. Klumpp, E., Marko, L. and Bor, G., *Chem. Ber.* 1964, **97,** 926.
6. Stenvenson, D. L., Magnuson, V. R. and Dahl, L. F., *J. Am. Chem. Soc.* 1967, **89,** 3727.
7. Wei, C. H. and Dahl, L. F., *J. Am. Chem. Soc.* 1968, **90,** 3960.
8. Wei, C. H. and Dahl, L. F., *J. Am. Chem. Soc.* 1968, **90,** 3969.
9. Wei, C. H. and Dahl, L. F., *J. Am. Chem. Soc.* 1968, **90,** 3977.
10. Brumer, H., Janietz, N., Meier, W., Wachter, J., Herdtweck, E., Herrmann, W. A., Serhadli, O. and Ziegler, M. L., *J. Organomet. Chem.* 1988, **347,** 237.
11. Brumer, H., Janietz, N., Meier, W., Sergson, G., Wachter, J., Zahn, T. and Ziegler, M. L., *Angew. Chem. Int. Ed. Engl.* 1985, **24,** 1060.
12. Uchtman, V. A. and Dahl, L. F., *J. Am. Chem. Soc.* 1969, **91,** 3756.

13. Simon, G. L. and Dahl, L. F., *J. Am. Chem. Soc.* 1973, **95,** 2164.
14. Hagen, K. S., Christon, G. and Holm, R. H., *Inorg. Chem.* 1983, **22,** 309.
15. Gervasio, G., Resseto, R., Stanghellini, P. L. and Bor, G., *Inorg. Chem.* 1984, **23,** 2073.
16. Vahrenkamp, H. and Wucherer, E. J., *Angew. Chem. Int. Ed. Engl.* 1981, **20,** 680.
17. Jiang, F., Lei, X., Huang, Z., Hong, M., Kang, B., Wu, D. and Liu, H., *J. Chem. Soc., Chem. Commun.* 1990, 1655.
18. Muller, A., Jostes, R., Hellman, W., Romer, C., Bogge, H., Schimanski, U., Zhuang, B., Rosenheim, L. D., McDonald, J. W. and Newton, W. E., *Z. Anorg. Allg. Chem.* 1986, **533,** 125.
19. Yu, P., Zhuang. B., Huang. L. and Pan, B., *Acta Cryst.* 1996, **C52,** 630.
20. Molen, *An Interactive Structure Solution Procedure*, Enraf–Nonius, Delft, The Netherlands, 1990.
21. Killean, R. C. G. and Lawrence, J. L., *Acta Cryst.* 1960, **B25,** 1750.
22. Tsuge, K., Imoto, H. and Saito, T., *Inorg. Chem.* 1992, **31,** 4716.
23. Strasdeit, H., Krebs, B. and Henkel, G., *Inorg. Chem.* 1984, **23,** 1816.
24. Antonio, M. L., Averill, B. A., Moura, L., Moura, J. J. G., Orme-Johnson, W. H., Teo, B. K. and Xavier, A., *J. Biol. Chem.* 1982, **257,** 6646.
25. Huang, J.-L., Huang, J.-Q., Shang, M., Lu, S., Lin, X., Lin, Y., Huang, M., Zhuang. H. and Lu, J., *Pure Appl. Chem.* 1988, **60,** 1185.
26. Huang, J., Lu, S., Shang, M., Lin, X., Huang, M., Lin, Y., Wu, D., Zhuang. H. and Lu, J., *Jiegou Huaxue*, 1987, **4,** 219.
27. Lu, J. and Chen, Z., *Int. Rev. Phys. Chem.* 1994, **13,** 85.
28. Li, J., Liu, C.-W. and Lu, J., *Polyhedron*, 1994, **13,** 1841.
29. Edgell, W. F. and Lypord, J., *Inorg. Chem.* 1970, **9,** 1932.
30. Wender, I., Sternberg, H. W. and Orehin, M., *J. Am. Chem. Soc.* 1952, **74,** 1216.
31. Heiber, W. and Sedlmeier, J., *Chem. Ber.* 1954, **87,** 25.
32. Heiber, W., Abeck, W. and Sedlmeier, J., *Angew. Chem.* 1952, **64,** 480.
33. Zhuang, B., Yu, P. and Pan, G., unpublished data.
34. Yao, Y.-B., Xie, T. and Gao, Y.-M., *Handbook of Physical Chemistry*. Shanghai Science and Technology Publishing House, Shanghai, 1983, pp. 1132–1152.

Pergamon

PII: S0277-5387(96)00449-4

Polyhedron Vol. 16, No. 9, pp. 1433–1437, 1997
Copyright © 1997 Elsevier Science Ltd
Printed in Great Britain. All rights reserved
0277-5387/97 $17.00+0.00

Syntheses and spectroscopic properties of complexes with the cubane-like core $\{MoCu_3Se_3X\}$ (X = Cl, Br, I). Crystal structure of $[\{MoCu_3Se_3Cl\}(PPh_3)_3Se]$

Qianfeng Zhang, Maochun Hong,* Weiping Su, Rong Cao and Hangin Liu

State Key Laboratory of Structural Chemistry, Fujian Institute of Research on the Structure of Matter, Chinese Academy of Sciences, Fuzhou, Fujian 350002, P.R. China

(Received 10 April 1996; accepted 5 September 1996)

Abstract—Mo–Cu–Se complexes with cubane-like cores $\{MoCu_3Se_3X\}$, $[\{MoCu_3Se_3X\}(PPh_3)_3Se]$ (X = Cl, Br, I) have been synthesized from CuX, $MoSe_4^{2-}$ and PPh_3 in appropriate conditions and characterized by IR, ^{31}P NMR, ^{95}Mo NMR and UV–vis electronic spectra. The structure of $[\{MoCu_3Se_3Cl\}(PPh_3)_3Se]$ has been determined by X-ray single crystal diffraction analysis. The structure contains a strongly distorted cubane-like $\{MoCu_3Se_3Cl\}$ core. Each Cu centre is bonded tetrahedrally to one P, one Cl and two Se atoms and the Mo centre is bonded tetrahedrally to four Se atoms. The mean Mo—Cu distance is 2.749(5) Å. The ^{95}Mo NMR spectra of the title compounds along with $[Ph_4P]_2MoSe_4$ consist of one single resonance in the range of δ = 1303–3145 ppm. © 1997 Elsevier Science Ltd. All rights reserved.

Keywords: Mo–Cu–Se complexes; cubane-like; syntheses; crystal structure; NMR spectra; IR and UV–vis spectra.

Transition metal cluster compounds that contain sulfur donor ligands have been an active area of research for many years, especially in the chemistry of thiometalates [1]. Much of this interest is generated by efforts to model both biological systems [2] and industrial catalysts used for hydrodesulfurization processes [3]. However, the research on the corresponding chemistry of transition metal selenides has been carried out only in the last few years [4,5]. That some of the coordination chemistry of metal selenides parallels that of metal sulfides has been confirmed by several recent results [4].

Because of the lone-pair electrons and unsaturated coordination in the complex ion MS_4^{2-} (M = Mo, W), several different structural types of polynuclear complexes have been obtained from soft acids, such as the coinage-metal cations Cu^+ and Ag^+, and thiometalates in the presence of ligands like PPh_3, R_2NCS_2. Several interesting structural types such as linear, cage, cubane-like and double cubane-like have been studied in detail [6–10]. However, studies of their selenium analogues are limited. In the Cu(Ag)/WSe_4^{2-} system, a few compounds have been reported [11–15]. However, in the Cu(Ag)/$MoSe_4^{2-}$ system, surprisingly few complexes have been characterized [15–17]. As part of our interest in Mo(W)–Cu(Ag) cluster compounds, we have isolated a series of Mo(W)–Cu–S compounds with different structural types, such as $[M(CuL)_nS_4]^{2-}$ (M = Mo, W; n = 1–3) [8–20], $[M_2Cu_4S_6E_2(L)_2]^{2-}$ [21], $[M_2Cu_5S_6E_2(L)_3$ [2–10,22] (L = R_2dtc) and $[MoCu_{10}S_4Cl_{12}]^{4-}$ [23]. Recently, we have begun to explore the chemistry of the Mo(W)–Cu(Ag)–Se system, and obtained a cubane-defect or so-called "string bag" cluster compound, $[Ph_4P]_2\{MoCu_3Se_3Cl_3(Py)\}O$ [24]. In this paper, we report the syntheses and spectroscopic properties of cubane-like cluster compounds, $[\{MoCu_3Se_3X\}(PPh_3)_3Se]$, X = Cl, (**1**); X = Br, (**2**); X = I, (**3**), and the crystal structure of (**1**) is also described.

EXPERIMENTAL

All operations were carried out under dinitrogen. Solvents and reagents were degassed by repeated

* Author to whom correspondence should be addressed.

evacuation and flushing with pure dinitrogen before use. $Cu(PPh_3)_3Br$ was prepared according to literature methods [25]. The reagents and solvents used were purchased as AR grade. Elemental analyses were carried out by the Elemental Analysis Laboratory in our Institute. The visible and UV electronic spectra were recorded on a Shimadzu UV-3000 spectrophotometer. IR spectra were obtained on a Digilab FTS-40 spectrophotometer. ^{31}P and ^{95}Mo NMR data were measured on a Varian Unity-500 spectrometer, relative to 85% H_3PO_4 acid and 2 mol dm^{-3} Na_2MoO_4 in D_2O, respectively.

Preparation of $[Ph_4P]_2MoSe_4$

$[Ph_4P]_2MoSe_4$ was prepared by a modification of the literature method [26]. $Mo(CO)_6$ (1.32 g, 5 mmol) was added to the fresh slurry of Na_2Se_x, prepared from heating selenium powder (1.58 g, 20 mmol) and sodium (0.25 g, 10 mmol) in 50 cm^3 of DMF solution. After the reaction solution was heated at about 80°C for 0.5 h, Ph_4PBr (4.19 g, 10 mmol) was added, and the solution filtered. An equal volume of THF was added, and, after storage at 4°C overnight, the product as blue–purple crystals was isolated. Yield: 3.28 g (60.2%). IR (KBr, cm^{-1}): 341.2(s): ^{95}Mo NMR (ppm): δ 3145.

Synthesis of $[\{MoCu_3Se_3Cl\}(PPh_3)_3Se]$ (**1**)

A suspension of CuCl (0.075 g, 0.75 mmol) in CH_2Cl_2 (10 cm^3) was added with stirring to a solution of $[PPh_4]_2MoSe_4$ (0.28 g, 0.25 mmol) in CH_2Cl_2 (10 cm^3). The deep blue solution turned brown immediately and a precipitate formed. Then an excess of PPh_3 (0.53 g, 2.0 mmol) was added to bring the resulting precipitate into solution. After the reaction mixture was stirred for *ca* 1 h at room temperature, a reddish brown filtrate was collected. The filtrate was diffused by diethyl ether vapour and X-ray-quality crystals of **1** as dark-red blocks were obtained after several days. Yield: 0.218 g (59.6%). Found: C, 45.3; H, 3.1; P, 7.0; Cu, 13.8; Mo 7.1. Calc. for $C_{54}H_{45}ClCu_3MoP_3Se_3$: C, 45.5; H, 3.2; P, 6.5; Cu, 13.4; Mo, 6.7%. IR (KBr, cm^{-1}): 1479.1 vs, 1434.6 vs, 1095.5 vs, 744.2 vs, 703.9 vs, 691.5 vs, 512. 6 vs, 505.8 vs, 492.6 vs, 383.3 s, 329.9 s.

Synthesis of $[\{MoCu_3Se_3Br\}(PPh_3)_3Se]$ (**2**)

$Cu(PPh_3)_3Br$ (0.70 g, 0.75 mmol) in CH_2Cl_2 (10 cm^3) was added to a CH_2Cl_2 solution (10 cm^3) of $[Ph_4P]_2MoSe_4$ (0.28 g, 0.25 mmol). The resulting brown solution was stirred for 1 hour at room temperature and subsequently filtered to afford a reddish brown filtrate. Black–red crystals of **2** were obtained over several days by layering the filtrate with THF. Yield: 0.157 g (41.6%). Found: C, 43.8; H, 3.2; P, 6.9; Cu, 13.5; Mo, 6.5. Calc. for $C_{54}H_{45}BrCu_3MoP_3Se_3$: C, 44.1; H, 3.1; P, 6.3; Cu, 13.0; Mo, 6.5%. IR (KBr, cm^{-1}): 1478.8 vs, 1434.4 vs, 1095.1 vs, 744.2 vs, 703.8 vs, 691.3 vs, 521.3 vs, 505.5 vs, 491.8 vs, 384.8 s, 329.3 s.

Synthesis of $[\{MoCu_3Se_3I\}(PPh_3)_3Se]$ (**3**)

A clear CH_2Cl_2 (10 cm^3) solution of CuI (0.15 g, 0.75 mmol) and PPh_3 (0.59 g, 2.25 mmol) was slowly added to a solution of $[PPh_4]_2MoSe_4$ (0.28 g, 0.25 mmol) in CH_3CN (10 cm^3), then stirred for a while. After filtering, Pr^iOH (2 cm^3) was added. The filtrate was kept at the room temperature and black–red crystals of **3** were obtained the next day. Field: 0.176 g (45.2%). Found: C, 42.3; H, 3.1; P, 6.4; Cu, 13.1; Mo, 7.1. Calc. for $C_{54}H_{45}ICu_3MoP_3Se_4$: C, 42.7; H, 3.0; P, 6.1; Cu, 12.6; Mo, 6.3%. IR (KBr, cm^{-1}): 1479.3 vs, 1432.3 vs, 1095.5 vs, 740.9 vs, 704.7 vs, 691.4 vs, 521.3 vs, 503.9 vs, 489.1 vs, 381.4 s, 323.9 s.

Crystallographic structure determination

A selected single crystal of compound **1** with dimensions $0.4 \times 0.15 \times 0.15$ mm^3 was mounted on a glass fibre and the cell dimensions were obtained by a least-squares fit of setting angles for 25 reflections. Diffraction data were collected on an Enraf–Nonius CAD4 diffractometer using graphite-monochromated Mo-K_α ($\lambda = 0.71073$ Å) radiation. The scan mode was ω–2θ. A total of 5156 independent reflections were collected in the range $1 \leqslant \theta \leqslant 25°$ and 2943 observed reflections with $I \geqslant 3\sigma(I)$ were used for further computation.

All calculations were performed on a COMPAQ 486 computer with MOLEN/PC program package [27] and the hydrogen atoms were not included in the calculations. Non-hydrogen scattering factors were taken from Cromer and Waber [28]. Intensity data were corrected for Lorentz and polarization effects and empirical absorption based on Ψ-scans. The coordinates of the metal atoms were determined by direct methods and all the remaining non-hydrogen atoms were located from successive difference Fourier syntheses. The structure was refined by full-matrix least-squares techniques with anisotropic thermal parameters for the non-hydrogen atoms. The crystal and refinement data for the complex are shown in Table 1, together with some experimental details.

The important bond lengths and bond angles for the complex are given in Tables 2 and 3, respectively.

RESULTS AND DISCUSSION

Synthesis

In the present reaction system of $MoSe_4^{2-}$, CuX and phosphine in CH_2Cl_2, the neutral complexes CuX (X = Cl, Br, I) coordinate to the $MoSe_4^{2-}$ anion in a

Table 1. Crystal data for $[\{MoCu_3Se_3Cl\}(PPh_3)_3Se]$

Chemical formula	$C_{54}H_{45}ClCu_3MoP_3Se_4$
Formula weight	1424.7
Crystal system	Orthorhombic
Space group	$D_4^2/P2_12_12_1$
a (Å)	12.970(2)
b (Å)	17.825(5)
c (Å)	22.774(6)
V (Å^3)	5264.9
Z	4
μ(Mo-K_α) (cm^{-1})	43.42
F(000)	2636
D_{calc} (g cm^{-3})	1.80
Temp. (K)	296
No. of refl. collected	5156
No. of refl. observed	2943
R	0.071
R_w	0.080
Largest different peak (e Å^{-3})	1.23
Max. shift	0.08

$R = \Sigma||F_o| - |F_c||/\Sigma|F_o|$.
$R_w = [\Sigma(|F_o| - |F_c|)^2/\Sigma F_o^2]^{1/2}$.

Table 2. Selected bond distances (Å) for $[\{MoCu_3Se_3Cl\}(PPh_3)_3Se]$

Mo—Se(1)	2.388(4)	Cu(1)—P(1)	2.200(9)
Mo—Se(2)	2.382(4)	Cu(2)—Cl	2.430(9)
Mo—Se(3)	2.359(4)	Cu(2)—P(2)	2.219(8)
Mo—Se(4)	2.184(6)	Cu(3)—Cl	2.733(9)
Mo—Cu(1)	2.736(5)	Cu(3)—P(3)	2.232(9)
Mo—Cu(2)	2.768(5)	P(1)—C(11)	1.81(3)
Mo—Cu(3)	2.743(5)	P(1)—C(21)	1.84(3)
Se(1)—Cu(1)	2.381(6)	P(1)—C(31)	1.79(4)
Se(1)—Cu(3)	2.386(5)	P(2)—C(41)	1.84(3)
Se(2)—Cu(1)	2.376(5)	P(2)—C(51)	1.83(3)
Se(2)—Cu(2)	2.426(5)	P(2)—C(61)	1.84(3)
Se(3)—Cu(2)	2.426(6)	P(3)—C(71)	1.83(4)
Se(3)—Cu(3)	2.379(6)	P(3)—C(81)	1.82(3)
Cu(1)—Cl	2.682(9)	P(3)—C(91)	1.85(4)

Mo : Cu ratio of 1 : 3 to yield the Mo–Cu–Se–X compounds as the first step:

$$[Ph_4P]_2MoSe_4 + 2CuX \rightarrow (Ph_4P)_2[MoSe_4(CuX)_3] \quad (1)$$

The reaction occurred very rapidly and the resulting compound was nearly insoluble in CH_2Cl_2. Addition of a phosphine to the reaction system caused the products to dissolve at the second step. It is possible that the PPh_3 ligands, which are highly soluble in CH_2Cl_2, substitute Cl^- ions and that the $\{MoSe_4Cu_3(PPh_3)_3\}^+$ produced is dissolved. In the presence of the released Cl^- ion, the distorted cubane-like complexes are formed:

$$(Ph_4P)_2[MoSe_4(CuX)_3] + PPh_3 \longrightarrow [MoSe_4(CuPPh_3)_3X] + 2Ph_4PX \quad (2)$$

From the reaction mechanism mentioned above based on experimental phenomena, excess PPh_3 ligands should increase the yield of the title compound.

Moreover, when a phosphine-substituted Cu^+ species is added to $[Ph_4P]_2MoSe_4$ in a similar or identical condition, the same results can be obtained, the reaction requiring only one step:

$$[Ph_4P]_2MoSe_4 + 3Cu(PPh_3)_3X \longrightarrow [MoSe_4(CuPPh_3)_3X] + 2Ph_4PX + 6PPh_3 \quad (3)$$

However, the yield of the title complexes is much lower than that in the two-step reaction.

Structure of $[\{MoCu_3Se_3Cl\}(PPh_3)_3Se]$ (**1**)

The molecular structure of compound **1** is shown in Fig. 1. The structure is the same as that previously reported SOWKEU [17] but with an improvement. The compound possesses a stronger distorted cubane-like core $\{MoCu_3Se_3Cl\}$. Examples of related cubanes containing different MoS_4^{2-} moieties are known [6,7,11,15,16]. In the core of $\{MoCu_3Se_3Cl\}$, both the Cu and Mo atoms are tetrahedrally coordinated. Each Cu centre is bonded tetrahedrally to one P, one Cl and two Se atoms, and the Mo centre is bonded tetrahedrally to four Se atoms. The title compound presents two kinds of Cu—Cl bond distance, one short Cu—Cl bond [2.430(9) Å] and two long Cu—Cl bonds [av. 2.708(9) Å], which is different from the $\{MoAg_3S_3Cl\}(PPh_3)_3E'$ (E′ = O,S) cluster [8,9], with three long Ag—X bonds. The Mo—Cu interactions of 2.736(5), 2.768(5) and 2.743(5) Å with an average value of 2.749 Å, are approximately the same as those for $\{MoCu_3S_3Cl\}(PPh_3)_3S$ [8]. In general, the trends in bond distances and angles in Tables 2 and 3 parallel those observed in earlier analogous structures [7,11].

Spectroscopy

In the Mo(W)–Cu(Ag)–S compounds, both infrared and electronic spectroscopy was of use in characterization of products, but their usefulness in the Mo(W)–Cu(Ag)–Se compounds was more limited. The small differences in the bond distances of the three Cu—P [2.200(9), 2.219(8), 2.232(9) Å] are shown in the IR spectra, in which the vibrational stretches appear at 513, 506 and 493 cm^{-1}. The Mo—Se and Cu—Se vibrations are observed in the IR spectra in the range 280–385 cm^{-1} and cannot be easily distinguished from one another. The terminal Mo—Se absorption at 385 cm^{-1} of the title compound is blue shifted, compared with that of Mo—Se in $MoSe_4^{2-}$ (ν = 341 cm^{-1}): however, the bridge Mo—Se vibrations at 330 cm^{-1} are red shifted compared with

Table 3. Selected bond angles (°) for $[\{MoCu_3Se_3Cl\}(PPh_3)_3Se]$

Se(1)—Mo—Se(2)	108.4(1)	Se(2)—Cu(1)—Cl	98.3(2)
Se(1)—Mo—Se(3)	109.1(1)	Se(2)—Cu(1)—P(1)	116.4(3)
Se(1)—Mo—Se(4)	112.0(3)	Cl—Cu(1)—P(1)	101.5(3)
Se(2)—Mo—Se(3)	108.2(1)	Se(2)—Cu(2)—Se(3)	104.6(2)
Se(2)—Mo—Se(4)	110.7(3)	Se(2)—Cu(2)—Cl	104.2(2)
Se(3)—Mo—Se(4)	108.4(2)	Se(2)—Cu(2)—P(2)	123.8(3)
Mo—Se(1)—Cu(1)	70.0(1)	Se(3)—Cu(2)—Cl	102.9(2)
Mo—Se(1)—Cu(3)	70.1(1)	Se(3)—Cu(2)—P(2)	112.0(3)
Cu(1)—Se(1)—Cu(3)	87.6(2)	Cl—Cu(2)—P(2)	107.2(3)
Mo—Se(2)—Cu(1)	70.2(1)	Se(1)—Cu(3)—Se(3)	108.4(2)
Mo—Se(2)—Cu(2)	70.3(1)	Se(1)—Cu(3)—Cl	95.2(2)
Cu(1)—Se(2)—Cu(2)	79.7(2)	Se(1)—Cu(3)—P(3)	122.4(3)
Mo—Se(3)—Cu(2)	70.7(1)	Se(3)—Cu(3)—Cl	95.7(2)
Mo—Se(3)—Cu(3)	70.7(1)	Se(3)—Cu(3)—P(3)	120.7(3)
Cu(2)—Se(3)—Cu(3)	82.0(2)	Cl—Cu(3)—P(3)	107.2(3)
Se(1)—Cu(1)—Se(2)	108.8(2)	Cu(1)—Cl—Cu(2)	73.8(2)
Se(1)—Cu(1)—Cl	96.6(2)	Cu(1)—Cl—Cu(3)	75.1(2)
Se(1)—Cu(1)—P(1)	127.6(3)	Cu(2)—Cl—Cu(3)	75.0(3)

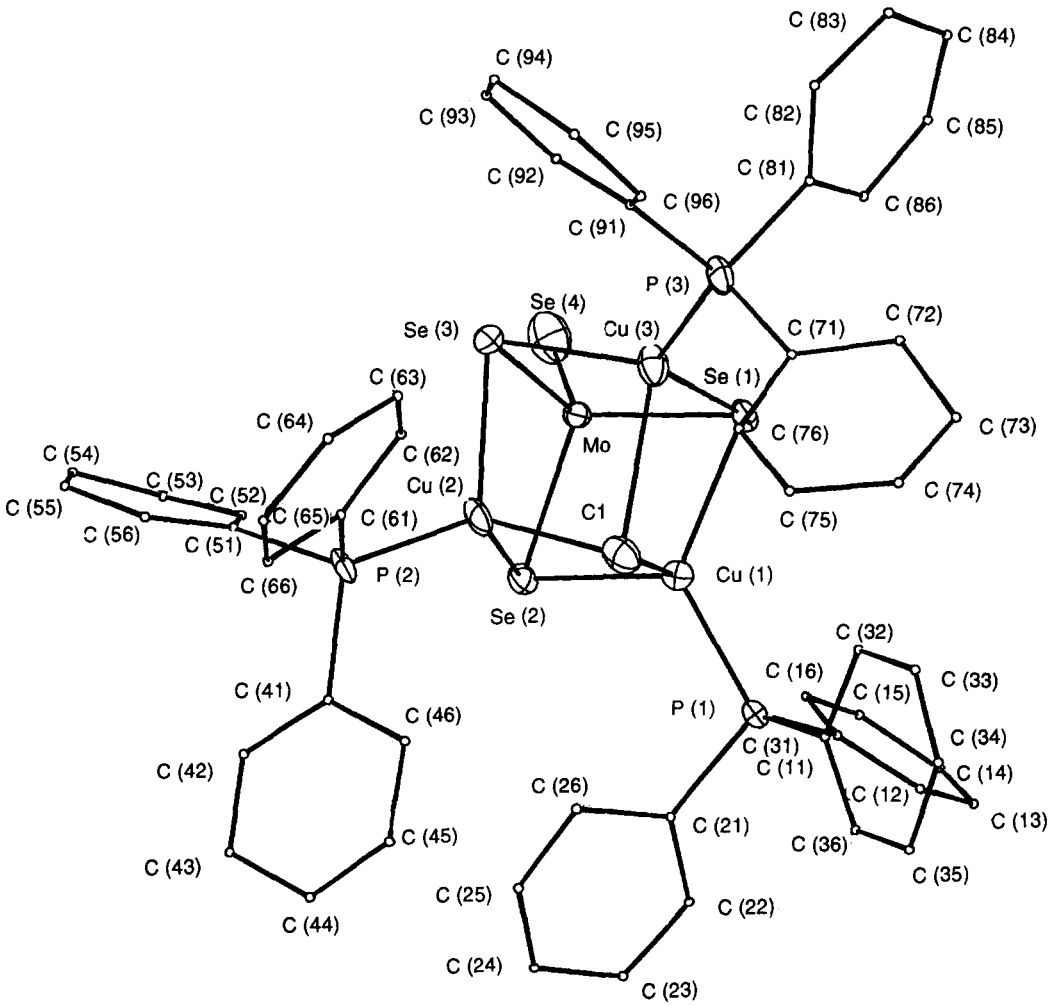


Fig. 1. Molecular structure of compound **1**.

Table 4. Electronic spectra, ^{31}P NMR chemical shifts and IR vibrational frequencies for the compounds

Complex	λ_{max}/nm (10^{-3} ε/dm^3 mol^{-1} cm^{-1})[a]	δ/ppm[b]	ν_{Mo-Se}/cm^{-1}
$[Ph_4P]_2MoSe_4$			341
1	268 (29.7), 373 (6.8)	14.01	385, 330
2	260 (32.1), 382 (7.2)	12.74	385, 329
3	269 (31.4), 385 (7.4)	9.38	382, 324

[a] In DMF.
[b] In CH_2Cl_2.

that in $MoSe_4^{2-}$, which is owing to coordination of the Cu atoms to $MoSe_4^{2-}$. The title compound in solution has an intense band at 200–500 nm in its absorption spectra, typically a very intense peak at 268 nm ($\varepsilon = 2.9 \times 10^4$ M^{-1} cm^{-1}) and a broad peak at 373 nm ($\varepsilon = 6.8 \times 10^3$ M^{-1} cm^{-1}). The charge transfer bands inferred in the region are owing to π(Se) $\rightarrow$ d(Mo) arising from the $MoSe_4^{2-}$ moiety and a relatively weak ligand $d(MoSe_4^{2-}) \rightarrow d(Cu^+)$ interaction [11]. Very similar results can be found in the other two compounds.

As opposed to electronic and infrared spectra, both ^{95}Mo and ^{31}P NMR spectra provide useful characterization of the Se present in the compounds. Since Cu^+ is a d^{10} system, the deshielding effect may result from orbital overlap. As the radius of the Se atom is larger than that of S, the orbital overlap between Cu and Se, Mo and Se can increase. The chemical shift in the ^{95}Mo NMR spectrum changes from δ 3145 in $MoSe_4^{2-}$ to δ 1302 for the title compound in CH_2Cl_2 solution. The chemical shift upfield from anion to complex in selenium is larger than that for the sulfido complex. The ^{31}P NMR resonances (Table 4) for the title complexes shows a single peak downfield from that of the free PPh_3 ligand, and the ^{31}P resonances shift upfield on going from Cl^- to I^-, a trend that can again be ascribed to a smooth increase in orbital overlap.

Acknowledgements—We acknowledge grants from the National Nature Science Foundation of China and the Natural Science Foundation of The State Key Laboratory of Structural Chemistry.

REFERENCES

1. Ansari, M. A. and Ibers, J. A., *Coord. Chem. Rev.*, 1990, **100,** 223; Whitmire, K. H., *J. Coord. Chem. B*, 1988, **17,** 95.
2. Conconvanis, D., *Acc. Chem. Res.*, 1991, **24,** 1; Holm, R. H., Cinrli, S. and Weighl, J. A., *Prog. Inorg. Chem.*, 1990, **38,** 1.
3. Rakowski, D. M., *Chem. Rev.*, 1989, **89,** 1.
4. Roof, L. C. and Kolis, J. W., *Chem. Rev.*, 1993, **93,** 103.
5. Kolis, J. W., *Coord. Chem. Rev.*, 1990, **115,** 195.
6. Ahlborn, E. K. and Muller, A., *Angew. Chem., Int. Ed. Engl.*, 1976, **15,** 680.
7. Muller, A., Bogge, H. and Schimanski, U., *Inorg. Chim. Acta*, 1983, **69,** 5.
8. Zhu, N. Y., Wu, J. H., Du, S. W., Wu, X. T. and Lu, J. X., *Inorg. Chim. Acta*, 1992, **191,** 65.
9. Du, S. W., Zhu, N. Y., Chen, P. C. and Wu, X. T., *Polyhedron*, 1992, **11,** 2489.
10. Liu, H. Q., Cao, R., Lei, X. J., Wu, D. X., Wei, G. W., Huang, Z. Y., Hong, M. C. and Kang, B. S., *J. Chem. Soc., Dalton Trans.*, 1990, 1023.
11. Christuk, C. C., Ansari, M. A. and Ibers, J. A., *Inorg. Chem.*, 1992, **31,** 4365.
12. Christuk, C. C., Ansari, M. A. and Ibers, J. A., *Angew. Chem., Int. Engl.*, 1992, **31,** 1477.
13. Christuk, C. C. and Ibers, J. A., *Inorg. Chem.*, 1993, **32,** 5105.
14. Ansari, M. A., Bollinger, J. C., Christuk, C. C. and Ibers, J. A., *Acta. Cryst.*, 1994, **C50,** 869.
15. Du, S. W., Wu, X. T. and Lu, J. X., *Polyhedron*, 1994, **13,** 841.
16. Muller, A., Wienboker, U. and Penk, M., *Chimia*, 1989, **43,** 50.
17. Pref. SOWKEU, *Cambridge Crystallographic Data Base*, Adat 902908, Mdat 930827.
18. Lei, X. J., Liu, Q. T. and Liu, H. Q., *Jiegou Huaxue*, 1988, **7,** 99.
19. Huang, Z. Y., Lei, X. J., Kang, B. S., Liu, J. N., Liu, Q. T., Hong, M. C. and Liu, H. Q., *Inorg. Chim. Acta*, 1990, **169,** 25.
20. Cao, R., Lei, X. J., Hong, M. C., Huang, Z. Y. and Liu, H. Q., *Jiegou Huaxue*, 1992, **11,** 34.
21. Lei, X. J., Huang, Z. Y., Hong, M. C. and Liu, H. Q., *Chinese J. Chem.*, 1993, **11,** 40.
22. Lei, X. J., Huang, Z. Y., Liu, Q. T., Hong, M. C. and Liu, H. Q., *Inorg. Chem.*, 1989, **28,** 4303.
23. Wu, D. X., Hong, M. C., Cao, R. and Liu, H. Q., *Inorg. Chem.*, 1996, **35,** 1080.
24. Wu, M. H., Huang, X. Y., Hong, M. C. and Liu, H. Q., unpublished results.
25. Stephens, R. D., *Inorg. Synth.*, 1972, **19,** 88.
26. O'Neal, S. C. and Kolis, J. W., *J. Am. Chem. Soc.*, 1988, **110,** 1971.
27. MOLEN, *An Interactive Structure Solution Procedure*, Enraf–Nonius, Delft, The Netherlands, 1990.
28. Cromer, D. T. and Waber, T. (ed.), *International Tables for X-ray Crystallography*, Vol. IV. Kynoch Press, Birmingham 1974.

Pergamon

PII: S0277-5387(96)00448-2

Polyhedron Vol. 16, No. 9, pp. 1439–1446, 1997
Copyright © 1997 Elsevier Science Ltd
Printed in Great Britain. All rights reserved
0277-5387/97 $17.00+0.00

Trimetallic complexes containing nickel or palladium and two molybdenum nitrosyl groups

Stanley M. Kagwanja,* Christopher J. Jones† and Jon A. McCleverty‡

School of Chemistry, University of Bristol, Cantocks Close, Bristol BS8 1TS, U.K.

(Received 20 August 1996; accepted 3 September 1996)

Abstract—The reaction of $[Mo(NO)\{HB(dmpz)_3\}Cl_2]$ [$HB(dmpz)_3$ = tris(3,5-dimethylpyrazolylborate] with nickel(II) and palladium(II) Schiff-base complexes derived by condensation of two mole equivalents of 2,5-dihydroxybenzaldehyde with α,ω-diamines [1,2-$C_6H_4(NH_2)$, $NH_2(CH_2)_nNH_2$, n = 2–4 for Ni, n = 2 for Pd) affords trimetallic species. From cyclic, square wave and differential pulse voltammetric data it is shown that the species may be reduced to a dianion and that the sites of reduction are probably the two molybdenum nitrosyl fragments. From the electrochemical and limited EPR spectral data obtained from reduced species, it is clear that there is very weak electronic and minimal magnetic interaction between the redox centres. © 1997 Elsevier Science Ltd. All rights reserved.

Keywords: tris(pyrazolyl)borate; nitrosyl; molybdenum; redox-active; trimetallic.

In oxidizable and/or reducible complexes where the two metal centres are connected by a multiatom bridge, the redox behaviour of the two centres can be very strongly mediated by the coligands, be they bridging or peripheral. This is particularly so in compounds containing bipyridyls or quinones, where the ligands themselves are capable of redox activity [1]. Such redox behaviour offers the opportunity to study unusual mixed-valence compounds, and to generate electron-rich or -poor species with relevance to biomimetic and/or molecular electronic behaviour [2]. The now well-characterized and readily manipulated tris(3,5-dimethylpyrazolyl)molybdenum nitrosyls, $[Mo(NO)\{HB(dmpz)_3\}XY]$ afford a particularly convenient vehicle for generating binuclear species exhibiting interesting photochemical, second-order nonlinear optic or unusual but controllable magnetic properties [3]. However, there are relatively few studies of the redox behaviour of trinuclear species, particularly heterometallic systems, especially those in which one of the three metal centres is part of a multiatom bridge between the other two. We have described some compounds derived from the ferrocenyl group with two molybdenum nitrosyls centres [4], and recently reported the construction and characterization of complexes containing a single copper(II) centre attached to two $\{Mo(NO)\{HB(dmpz)_3\}Cl\}^+$ groups [5]. In this last study, we found that the copper atom had a small but detectable influence on the redox behaviour of molybdenum centres, which themselves were only weakly interacting electrochemically. This trimetallic system was based on a near-planar Schiff-base ligand system derived from 2,4-dihydroxybenzaldehyde and α,ω-diamines [**1**, M = Cu, M′ = $Mo(NO)\{HB(dmpz)_3\}Cl$; B = hydrocarbyl]. A possible reason why the electrochemical interaction between the two remote molybdenum nitrosyl centres was not substantially enhanced by the implantation of the copper ion in the centre of the ligand array could be that there is a slight distortion of these copper Schiff-base complexes from planarity, thereby perturbing the potential delocalization across the trimetallic species. In order to probe this view, we have prepared a series of analogous nickel(II) and palladium(II) species, where planar coordination is more likely to be maintained and potential delocalization is maximised.

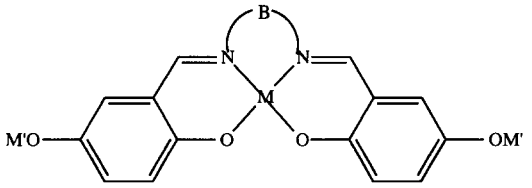
EXPERIMENTAL

The compound $[Mo(NO)\{HB(dmpz)_3\}Cl_2]$ and the Schiff-base ligands were prepared as described pre-

* Present address: Department of Chemistry, Egerton University, PO Box 536, Njoro, Keyna.

† Present address: School of Chemistry, The University of Birmingham, Edgbaston, Birmingham, B15 2TT, U.K.

‡ Author to whom correspondence should be addressed.



{**1**; M = Ni or Pd, M' = H or Mo(NO){HB(dmpz)$_3$Cl; B = hydrocarbyl}

viously, and all general work-up and spectroscopic procedures were also as previously reported [5]. FAB-mass spectral data were obtained using a NOBA matrix. Cyclic voltammetry, differential pulse and square wave voltammetry were carried out using an EC & G PAR 273A galvanostat and potentiostat. Solutions in acetonitrile and dichloromethane were *ca* 1×10^{-3} mol dm^{-3} in the complex, with [Bu$^n_4$N][PF$_6$] (0.1 mol dm^{-3}) as the base electrolyte and the saturated calomel electrode (SCE) as the reference electrode. The working and counter electrode was a Pt bead and Pt wire, respectively, and all formal potentials were taken as the average of anodic and cathodic peak potentials. Differential pulse voltammetry was carried out using a pulse amplitude of 10 mV and the Δi *vs* E relationship was recorded. To obtain ΔE_f values from these waves, the separation between the two reduction potentials was calculated using the graphical method developed by Richardson and Taube [6].

Synthesis of nickel and palladium Schiff-base precursors (**1**, M = Ni *or* Pd; M' = H; B = *hydrocarbyl*)

In general, the nickel complexes were prepared by refluxing a mixture of nickel chloride hexahydrate or nickel acetate with the Schiff base in absolute ethanol. The palladium compounds were obtained similarly, using palladium acetate, either in methanol or ethanol.

[**1**, M = Ni; M' = H; B = C_6H_4]. A dark red precipitate formed immediately when $NiCl_2 \cdot 6H_2O$ (0.21 g, 0.86 mmol) dissolved in ethanol (10 cm^3) was refluxed with the appropriate Schiff base (0.3 g, 0.86 mmol) in ethanol (20 cm^3). Refluxing was maintained for 3 h, and the mixture was then cooled, the red precipitate filtered off and washed thoroughly with ethanol and diethyl ether and dried *in vacuo* (0.19 g, 52%). Mass spectrum (FAB): Found m/z = 405. Calc. for compound 405. IR (KBr disc, cm): 1610 ($\nu_{C=N}$). ^{1}H NMR [$(CD_3)_2SO$]: δ 8.83 (C*H*=N, s, 2H), 8.73 (O*H*, s, 2H), 8.15 (C_6H_4, dd, 2H), 7.30 (C_6H_4, dd, 2H), 6.93 (part of C_6H_3, m, 4H), 6.57 (part of C_6H_3, m, 4H, J_{HH} = 9.9 Hz). UV–vis (DMSO): λ_{max} nm (ε) 263 (2699), 298 (1449), 385 (1786), 519 (704).

[**1**, M = Ni; M' = H; B = CH_2CH_2]. This compound was prepared similarly, using $NiCl_2 \cdot 6H_2O$ (0.12 g, 0.5 mmol) and the appropriate Schiff base (0.15 g, 0.5 mmol). The brown product was collected, washed as before and dried *in vacuo* (0.13 g, 66%). Mass spectrum (FAB): Found m/z = 357. Calc. for compound 357. IR (KBr disc, cm^{-1}): 1629 ($\nu_{C=N}$). ^{1}H NMR [$(CD_3)_2SO$]: δ 8.63 (C*H*=N, s, 2H), 8.5 (O*H*, s, 2H), 7.84 (part of C_6H_3, s, 2H), 6.76 (part of C_6H_3, d, 2H, J_{HH} = 7.42 Hz), 6.60–6.53 (part of C_6H_3 and hydrogen-bonded H of OH, distorted t, 4H), 3.38 (CH_2CH_2, s, 4H).

[**1**, M = Ni; M' = H; B = $CH_2CH_2CH_2$]. This compound was prepared in the same way as (**1**, M = Ni; M' = H; B = C_6H_4), using $NiCl_2 \cdot 6H_2O$ (0.23 g, 0.96 mmol) and the appropriate Schiff base (0.3 g, 0.96 mmol). The mixture was refluxed for 2 days and the red–brown solution was filtered, cooled and the filtrate evaporated *in vacuo*. The brown residue was treated with diethyl ether and the precipitate formed was filtered off, washed with diethyl ether and dried *in vacuo* (0.25 g, 71%). Mass spectrum (FAB): Found m/z = 371. Calc. for compound 371. IR (KBr disc, cm^{-1}): 1608 ($\nu_{C=N}$). ^{1}H NMR [$(CD_3)_2SO$]: δ 8.63 (C*H*=N, s, 2H), 8.50 (O*H*, s, 2H), 6.90 (part of C_6H_3, d, 2H, J_{HH} = 6.53 Hz), 6.56 (part of C_6H_3, s, 2H), 6.48 (part of C_6H_3, d, 1H, J_{HH} = 9.1 Hz), 6.45 (part of C_6H_3, d, 1H; J_{HH} = 9.1 Hz), 4.37 (CH_2N, s, 2H), 4.76 (CH_2N, s, 2H), 1.79 ($CH_2CH_2CH_2$, s, 2H).

[**1**, M = Ni; M' = H; B = $(CH_2)_4$]. This compound was prepared in a way similar to that of (**1**, M = Ni; M' = H; B = C_6H_4), but using nickel acetate (0.22 g, 0.88 mmol) and the Schiff base (0.29 g, 0.88 mmol) in ethanol (50 cm^3). The mixture was refluxed overnight, filtered while hot and the filtrate cooled and evaporated *in vacuo*. The green–yellow solid that precipitated was washed thoroughly with ethanol and diethyl ether and dried *in vacuo* (0.25 g, 66%). Mass spectrum (FAB): Found m/z = 385. Calc. for compound 385. IR (KBr disc, cm^{-1}): 1616 ($\nu_{C=N}$). The compound was paramagnetic and no ^{1}H NMR spectrum could be recorded.

[**1**, M = Pd; M' = H; B = C_6H_4]. A solution of palladium acetate (0.32 g, 1.41 mmol) in methanol (20 cm^3) was added to a solution of the appropriate Schiff base (0.49 g, 1.41 mmol) in methanol (40 cm^3). This mixture was refluxed, and after 15 min a red precipitate had formed. Refluxing was continued for a further 5 h, whereupon the mixture was cooled and the red solid that had formed was filtered off, washed thoroughly with methanol and then diethyl ether and dried *in vacuo* (0.52 g, 82%). Mass spectrum (FAB): Found m/z = 452. Calc. for compound 452. IR (KBr disc, cm^{-1}): 1603 ($\nu_{C=N}$). ^{1}H NMR [$(CD_3)_2SO$]: δ = 9.07 (O*H*, 2, 2H), 8.87 (C*H* = N, s, 2H), 8.34 (C_6H_4, dd, 2H), 7.41 (C_6H_4, dd, 2H), 7.06–6.88 (C_6H_3, m, 6H).

[**1**, M = Pd; M' = H; B = CH_2CH_2]. This compound was prepared in a way similar to that of (**1**, M = Pd; M' = H; B = C_6H_4), using palladium acetate (0.31 g, 1.37 mmol) and the appropriate Schiff base (0.41 g, 1.37 mmol) in ethanol (80 cm^3). The mixture was refluxed for 1 h, and after the usual work-up afforded a yellow solid (0.36 g, 65%). Mass spec-

trum (FAB): Found m/z = 405. Calc. for compound 404. IR (KBr disc, cm^{-1}): 1627 ($\nu_{C=N}$). ^1H NMR [$(CD_3)_2SO$]: δ 8.60 (O*H*, s, 2H), 8.09 (C*H* = N, s, 2H), 6.87 (part of C_6H_3, s, 2H), 6.70 (part of C_6H_3, d, 2H, J_{HH} = 11.97 Hz), 6.70 (part of C_6H_3, s, 2H), 3.79 (CH_2CH_2, s, 4H).

Bis-molybdenum complexes, [**1**, M = Ni *or* Pd; M′ = Mo(NO){HB(dmpz)$_3$}Cl; B = *hydrocarbyl*]

In general, these complexes were prepared by treatment of one mole equivalent of the nickel or palladium Schiff-base complexes, i.e. (**1**, M = Ni or Pd; M′ = H; B = hydrocarbyl) with [Mo(NO){HB(dmpz)$_3$Cl$_2$] in dry toluene to which a few drops of triethylamine had been added. The mixture was then refluxed either overnight (when M = Ni) or for several days (M = Pd). On evaporation of the solvent *in vacuo* followed by chromatography of the residue over silica gel (60, 70–230 mesh) using dichloromethane and/or dichloromethane/THF mixtures as eluant, various fractions could be collected, the solvent partially evaporated *in vacuo* and the desired compound precipitated as a solid on addition of n-hexane. Details of particular compounds are given below.

[**1**, M = Ni; M′ = Mo(NO){HB(dmpz)$_3$}Cl; B = C_6H_4]. A suspension of (**1**, M = Ni; M′ = H; B = C_6H_4) (0.09 g, 0.22 mmol) in dry toluene (50 cm^3) containing some triethylamine and [Mo(NO){HB(dmpz)$_3$}Cl$_2$] (0.22 g, 0.45 mmol) was treated as described in the general discussion, affording a blue solution. On chromatography using dichloromethane, three fractions were collected, the first yellow and the second green ([{Mo(NO){HB(dmpz)$_3$}Cl}$_2$O] identified by mass spectrometry) being discarded, the third and major blue fraction being completely eluted using dichloromethane containing 1% THF. On partial reduction of the volume *in vacuo* to *ca* 10 cm^3, and on addition of n-hexane, the compound was precipitated as a blue solid (0.09 g, 31%). Mass spectrum (FAB): Found m/z = 1321. Calc. for complex 1320. IR (KBr disc, cm^{-1}): 2553 (ν_{BH}), 1677 (ν_{NO}), 1602 ($\nu_{C=N}$), 1574 ($\nu_{C=C}$). ^1H NMR (CD_2Cl_2): δ 8.434 (C*H* = N, s, 2H), 7.56 (C_6H_4, distorted A_2B_2 multiplet, 4H), 7.56 (part of C_6H_3, d 2H, J_{HH} = 8.8 Hz); 7.18 (part of C_6H_3, d, 2H, J_{HH} = 2.5 Hz), 7.15 (part of C_6H_3, s, 2H), 5.93 ($Me_2C_3HN_2$, s, 2H), 5.88 ($Me_2C_3HN_2$, s, 2H), 5.78 ($Me_2C_3HN_2$, s, 2H), 2.63 [$(CH_3)_2HN_2$ s, 6H], 2.42–2.40 [$(CH_3)_2C_3HN_2$), m, 18H], 2.23 [$(CH_3)_2C_3HN_2$, s, 6H], 2.04 [$(CH_3)_2C_3HN_2$, s, 6H].

[**1**, M = Ni; M′ = Mo(NO){HB(dmpz)$_3$}Cl; B = CH_2CH_2]. Prepared similarly to the compound above, using (**1**, M = Ni; M′ = H; B = CH_2CH_2) (0.09 g, 0.31 mmol), toluene (20 cm^3), triethylamine and [Mo(NO){HB(dmpz)$_3$}Cl$_2$] (0.31 g, 0.62 mmol). A green–blue mixture was formed which was worked-up as described above, affording the compound as a blue solid (0.15 g, 45%). Mass spectrum (FAB): Found m/z = 1272. Calc. for complex 1272. IR (KBr disc, cm^{-1}): 2553 (ν_{BH}), 1667 (ν_{NO}), 1614 ($\nu_{C=N}$), 1584 ($\nu_{C=C}$). ^1H NMR (CD_2Cl_2): δ 7.75 (C*H* = N, s, 2H), 7.43 (part of C_6H_3, t, 3H), 7.04 (part of C_6H_3, m, 6H), 5.93 ($Me_2C_3HN_2$, s, 2H), 5.86 ($Me_2C_3HN_2$, s, 2H), 5.76 ($Me_2C_3HN_2$, s, 2H), 3.48 NCH_2CH_2N, s, 4H), 2.60 [$(CH_3)_2C_3HN_2$, s, 6H], 2.41–2.31 [$(CH_3)_2C_3HN_2$, m, 18H], 2.20 [$(CH_3)_2C_3HN_2$, s, 6H], 2.02 [$(CH_3)_2C_3HN_2$, s, 6H].

[**1**, M = Ni; M′ = Mo(NO){HB(dmpz)$_3$}Cl; B = $CH_2CH_2CH_2$]. Prepared as above, using (**1**, M = Ni; M′ = H; B = $CH_2CH_2CH_2$) (0.17 g, 0.45 mmol), toluene (40 cm^3), triethylamine and [Mo(NO){HB(dmpz)$_3$}Cl$_2$] (0.45 g, 0.91 mmol). The blue solution that formed afforded, on chromatography, red, green–yellow and blue fractions, and after work-up as described above, the desired compound was isolated as a blue solid (0.32 g, 54%). Mass spectrum (FAB): Found m/z = 1285. Calc. for complex 1286; 1227 ([M − Ni]$^+$). IR (KBr disc, cm^{-1}): 2554 (ν_{BH}), 1668 (ν_{NO}), 1617 ($\nu_{C=N}$), 1586 ($\nu_{C=C}$). ^1H NMR (CD_2Cl_2): δ 7.47 (C*H* = N, s, 2H), 7.39 (part of C_6H_3, d, 2H, J_{HH} = 2.54 Hz), 6.99 (part of C_6H_3, m, 4H), 5.92 ($Me_2C_3HN_2$, s, 2H), 5.86 ($Me_2C_3HN_2$, s, 2H), 5.76 ($Me_2C_3HN_2$, s, 2H), 3.60 (NCH_2, s, 4H), 2.60 [$(CH_3)_2C_3HN_2$, s, 6H], 2.40–2.38 [$(CH_3)_2C_3HN_2$ and CH_2CH_2N, m, 22 H, 6H], 2.18 [$(CH_3)_2C_3HN_2$, s, 6H], 2.04 [$(CH_3)_2C_3HN_2$, s, 6H].

[**1**, M = Ni; M′ = Mo(NO){HB(dmpz)$_3$}Cl; B = $(CH_2)_4$]. Prepared as described above using [**1**, M = Ni; M′ = H; B = $(CH_2)_4$] (0.14 g, 0.32 mmol), toluene (40 cm^3), triethylamine and [Mo(NO){HB(dmpz)$_3$}Cl$_2$] (0.32 g, 0.64 mmol). The purple solution that formed was chromatographed as described previously, giving red, purple and blue fractions, and the desired compound was isolated from the blue fraction as a blue solid (0.2 g, 44%). Mass spectrum (FAB): Found m/z = 1303. Calc. for complex 1300; 1243 ([M − Ni]$^+$). IR (KBr disc, cm^{-1}): 2554 (ν_{BH}), 1672 (ν_{NO}), 1623 ($\nu_{C=N}$), 1581 ($\nu_{C=C}$). The complex was paramagnetic and did not afford a ^1H NMR spectrum.

[**1**, M = Pd; M′ = Mo(NO){HB(dmpz)$_3$}Cl; B = C_6H_4]. A suspension of (**1**, M = Pd; M′ = H; B = C_6H_4) (0.13 g, 0.28 mmol) in dry toluene (40 cm^3) containing some triethylamine and [Mo(NO){HB(dmpz)$_3$}Cl$_2$] (0.28 g, 0.57 mmol) was refluxed for 3 days. The purple mixture was filtered while hot and the filtrate cooled and evaporated *in vacuo*, affording a purple powder. This was dissolved in the minimum volume of dichloromethane and chromatographed on alumina. The first red fraction was eluted with hexane (40% v/v) in dichloromethane, but the second fraction, which contained a mixture of green and red species, was discarded. The third major blue fraction was eluted with pure dichloromethane. This last was concentrated to *ca* 10 cm^3 and n-hexane added to precipitate a blue solid which was filtered off, thoroughly washed with hexane and dried *in vacuo* (0.12 g, 31%). Mass spectrum (FAB): Found m/z = 1368. Calc. for complex 1367. IR (KBr disc,

cm^{-1}): 2550 (ν_{BH}), 1672 (ν_{NO}), 1649 ($\nu_{C=N}$), 1587 ($\nu_{C=C}$). ^1H NMR (CD_2Cl_2): δ 8.42 (CH = N, s, 2H), 7.84 (C_6H_4, A_2B_2 multiplet, 4H), 7.54 (part of C_6H_3, d, 2H, J_{HH} = 2.91 Hz), 7.19 (part of C_6H_3, m, 4H), 5.99 ($Me_2C_3HN_2$, s, 2H), 5.94 ($Me_2C_3HN_2$, s, 2H), 5.94 ($Me_2C_3HN_2$, s, 2H), 2.59 [$(CH_3)_2C_3HN_2$, s, 6H], 2.44–2.43 [$(CH_3)_2C_3HN_2$, m, 18H], 2.19 [$(CH_3)_2C_3HN_2$, s, 6H], 2.08 [$(CH_3)_2C_3HN_2$, s, 6H].

[**1**, M = Pd; M′ = Mo(NO){HB(dmpz)$_3$}Cl; B = CH_2CH_2]. Prepared as described above, using (**1**, M = Pd; M′ = H; B = CH_2CH_2) (0.15 g, 0.38 mmol), toluene (20 cm^3), triethylamine and [Mo(NO){HB(dmpz)$_3$}Cl_2] (0.37 g, 0.75 mmol), the mixture being refluxed for 3 days. The purple solution that formed afforded, on chromatography, two purple and one blue fraction. The latter gave the desired compound as a blue solid (0.23 g, 46%). Mass spectrum (FAB): Found m/z = 1321. Calc. for complex 1319. IR (KBr disc, cm^{-1}): 2552 (ν_{BH}), 1668 (ν_{NO}), 1624 ($\nu_{C=N}$), 1587 ($\nu_{C=C}$). ^1H NMR (CD_2Cl_2): δ 8.01 (CH = N, s, 2H), 7.48 (part of C_6H_3, d, 2H, J_{HH} = 2.90 Hz), 7.30 (part of C_6H_3, dd, 2H), 7.05 (part of C_6H_3, d, 2H, J_{HH} = 9.44 Hz), 5.98 ($Me_2C_3HN_2$, s, 2H), 5.93 ($Me_2C_3HN_2$, s, 2H), 5.82 ($Me_2C_3HN_2$, s, 2H), 3.88 (NCH_2CH_2N, s, 4H), 2.57 [$(CH_3)_2C_3HN_2$, s, 6H], 2.44–2.42 [$(CH_3)_2C_3HN_2$, m, 18H], 2.17 [$(CH_3)_2C_3HN_2$, s, 6H], 2.06 [$(CH_3)_2HN_2$, s, 6H].

RESULTS AND DISCUSSION

Synthetic studies

The trimetallic species [**1**, M = Ni, M′ = Mo(NO){HB(dmpz)$_3$}Cl; B = C_6H_4, $(CH_2)_n$, n = 2–4] and [**1**, M = Pd, M′ = Mo(NO){HB(dmpz)$_3$}Cl; B = C_6H_4 or CH_2CH_2] were obtained by reaction of the preformed nickel or palladium Schiff base complexes (**1**, M = Ni or Pd, M′ = H) with [Mo(NO){HB(dmpz)$_3$}Cl_2] in a 1:2 molar ratio in the presence of triethylamine. The amine can act in two ways: either by reduction of [Mo(NO){HB(dmpz)$_3$}Cl_2] to a labile monoanion that readily undergoes substitution [7], or by facilitating elimination of HCl in the reaction. The reaction mixture was refluxed overnight (Ni species) or for 2–3 days (Pd), and purification of the compounds was achieved by column chromatography using dichloromethane as eluant. There was evidence for the formation of other compounds during these reactions, and we know from other work that these can be [Mo(NO){HB(dmpz)$_3$}$(OH)_2$] and/or [{Mo(NO){HB(dmpz)$_3$}$(\mu$-OH)$\}_2$], and [{Mo(NO){HB(dmpz)$_3$}Cl$\}_2(\mu$-O)] [8]. The first two species are coloured pink/red and the last green. None were specifically isolated for purification, and there is probably also decomposition of the Schiff base species, although we did not isolate identifiable fragments. The trimetallic species were obtained as blue solids in yields ranging from 31–54%. Elemental analyses (Table 1) and FAB mass spectral data (Experimental section) are in general agreement with our formulations.

Spectroscopic studies and magnetic properties

The IR spectra of the new complexes contain absorptions consistent with the presence of the tetradentate ligands and, where appropriate, the HB(dmpz)$_3$ ligands (ν_{BH} 2250–2254 cm^{-1}). The NO stretching frequencies of the trimetallic nickel complexes occur in the range 1667–1677 cm^{-1} and those of their palladium analogues fall in the range 1668–1672 cm^{-1}, whereas those in the copper species occurs at 1678–1685 cm^{-1} [5]. The very slight increase in ν_{NO} of [**1**, M = Cu; M′ = Mo(NO){HB(dmpz)$_3$Cl;

Table 1. Analytical data obtained from mono- and tri-metallic Schiff-base complexes [**1**, M = Ni or Pd; M′ = H or Mo(NO){HB(dmpz)$_3$}Cl; B = hydrocarbyl}] · xH_2O

Compound				Elemental analysis (%)					
				Calculated			Found		
M	M′	B	xH_2O	C	H	N	C	H	N
Ni	H	C_6H_4	1.0	56.8	3.8	6.6	56.6	3.2	6.7
Ni	H	$(CH_2)_2$	0.5	52.5	4.1	7.7	52.5	4.1	7.6
Ni	H	$(CH_2)_3$	0.5	53.7	4.5	7.4	53.9	5.1	6.9
Ni	H	$(CH_2)_4$	2.0	51.3	5.2	6.7	51.8	5.2	6.0
Pd	H	C_6H_4	0.5	52.0	3.3	6.1	52.3	3.6	6.1
Pd	H	$(CH_2)_2$	0.5	46.4	3.6	6.8	46.8	3.7	6.9
Ni	Mo(NO){HB(dmpz)$_3$}Cl	C_6H_4	0	45.5	4.2	17.0	45.3	4.4	16.7
Ni	Mo(NO){HB(dmpz)$_3$}Cl	$(CH_2)_2$	0	43.4	4.4	17.6	43.6	4.9	16.8
Ni	Mo(NO){HB(dmpz)$_3$}Cl	$(CH_2)_3$	0	43.9	4.5	17.4	43.9	4.9	17.4
Ni	Mo(NO){HB(dmpz)$_3$}Cl	$(CH_2)_4$	0	44.3	4.6	17.2	44.6	4.8	17.4
Pd	Mo(NO){HB(dmpz)$_3$}Cl	C_6H_4	0	43.9	4.1	16.4	44.7	4.4	16.7
Pd	Mo(NO){HB(dmpz)$_3$}Cl	$(CH_2)_2$	0	41.8	4.2	17.0	42.7	4.6	16.7

B = hydrocarbyl] is not thought to be significant, and so the central metal atom has little effect on ν_{NO} of the molybdenum fragments. The NO stretching frequencies fall in a region typical of a {Mo(NO){HB(dmpz)$_3$}Cl} fragment bonded to a phenolic ligand although they occur at values slightly lower than those in simple related monophenolate complexes [9]. The stretching frequency of azomethine —C=N— linkages decreases on complexation of the Schiff base ligand by nickel or palladium as expected, and on incorporation of the {Mo(NO){HB(dmpz)$_3$}Cl} fragments, $\nu_{C=N}$ occurs in the range 1602–1623 cm^{-1} for the Ni complexes and 1649–1624 cm^{-1} for the Pd complexes.

The majority of the complexes are diamagnetic and their ^1H NMR spectra details are recorded in the Experimental section. However [**1**, M = Ni, M′ = H, B = $(CH_2)_4$] and [**1**, M = Ni, M′ = Mo(NO){HB(dmpz)$_3$}Cl; B = $(CH_2)_4$] are paramagnetic (see below). The ^1H NMR spectra of the diamagnetic nickel and the two palladium complexes are broadly consistent with our formulations, and require no special comment. It should be noted that the azomethine resonances occur as singlets, indicating the symmetrical nature of these complexes. In the molybdenated complexes [**1**, M = Ni; M′ = Mo(NO){HB(dmpz)$_3$}Cl; B = C_6H_4, $(CH_2)_n$, n = 2, 3] and [**1**, M = Pd; M′ = H; B = C_6H_4, $(CH_2)_2$], the 4-H protons of the pyrazolyl rings in HB(dmpz)$_3$ appear as three closely equivalent resonances of relative area six, owing to the overall symmetry of the trimetallic species and to the lack of a plane of symmetry within each octahedral {Mo(NO){HB(dmpz)$_3$}Cl(O—)} fragment.

The electronic spectra were recorded in the range 1100–200 nm. The monometallic diamagnetic nickel complexes (**1**, M = Ni; M′ = H; B = C_6H_4 and CH_2CH_2), exhibit relatively weak absorptions at 519 and 550 nm in DMSO. Similar Ni^{II} Schiff base complexes have absorptions between 540 and 585 nm [10], which are assigned to *d–d* transitions. The spectrum of [**1**, M = Ni; M′ = H; B = $(CH_2)_3$] is somewhat different, with a broad shoulder at *ca* 600 nm, and while this complex is diamagnetic in DMSO, its analogue [**1**, M = Ni; M′ = H; B = $(CH_2)_4$] has a similar spectrum but is paramagnetic both in solution (DMSO) and the solid state. A magnetic susceptibility measurement of [**1**, M = Ni; M′ = H; B = $(CH_2)_4$] confirmed that it is paramagnetic in the solid state (μ_{eff} = 1.53 B.M.). The value of μ_{eff} is significantly lower than that expected for a six- or five-coordination, or pseudo-tetrahedral Ni^{II} centre, although there are two water molecules of crystallization present in the compound (Table 1). The species analyses well, but the electronic spectrum is ambiguous, is not consistent with a NiN_2O_4 or NiN_2O_3 chromophore and cannot be used to determine the nature of this Ni species in solution or the solid state. However, it is possible that the length of B is sufficient to permit some flexibility within the tetradentate ligand system, leading to some distortion either towards a tetrahedral geometry or by formation of a five-coordinate species (in DMSO). Such distortions would cause some perturbation of magnetic properties without substantial electronic spectral changes, and this has been detected in other Ni^{II} Schiff-base complexes [10]. Some evidence of distortion from planar towards tetrahedral or five-coordinate species was detected in the electronic spectra of the related copper(II) complexes (**1**, M = Cu; M′ = H; B = hydrocarbyl) [5].

The electronic spectra of the trimetallic species [**1**, M = Ni or Pd; M′ = Mo(NO){HB(dmpz)$_3$Cl; B = C_6H_4, $(CH_2)_n$, n = 2–4] are dominated by two moderately intense absorptions. In the nickel complexes these occur in the ranges 740–750 nm and 612–630 nm, both somewhat stronger than expected for *d–d* transitions in Ni^{II}. We have observed an absorption associated with the molybdenum fragment in the region 600–750 nm before, and believe that it is due to a ligand-to-metal charge transfer [11]. The palladium complexes exhibit broadly similar spectra. The ^1H NMR spectrum showed that [**1**, M = Ni; M′ = Mo(NO){HB(dmpz)$_3$}Cl; B = $(CH_2)_4$] is paramagnetic in solution, but insufficient material was available for solid state susceptibility measurements.

Electrochemical studies

The complexes (**1**, M = Ni or Pd; M′ = H; B = hydrocarbyl) have relatively low solubility in dichloromethane and acetonitrile and so their electrochemical properties were investigated by cyclic (CV) and square wave voltammetry (SWV) in DMSO. The CV of all the nickel compounds, with the exception of (**1**, M = Ni; M′ = H; B = CH_2CH_2), exhibited an irreversible reduction process between −1.47 and −1.60 V as shown by detection of a cathodic peak (E_p^c) in their CVs and by SWV. Only (**1**, M = Ni; M′ = H; B = C_6H_4), exhibited a second reduction process, at −2.05 V, which was detected by SWV. On reverse sweep, the CVs of these complexes exhibited one or two anodic peaks, the first of which may have been associated with reoxidation of a species generated by reductive decomposition of the complexes near −1.50 V. Some of the complexes exhibited a further oxidation process, E_p^a varying from +0.43 to +0.65 V. For comparison purposes, we investigated the electrochemistry of (**1**, M = Ni; M′ = Me; B = C_6H_4), in order to determine whether the presence of the hydroxyl groups in (**1**, M = Ni; M′ = H; B = C_6H_4) had any influence on the electrode behaviour of this compound (for example, oxidation to quinone fragments). Again, an irreversible reduction was observed, at −1.54 V, but in the CV the anodic sweep showed only one oxidative electrode reaction, at −0.65 V, so methylation of the hydroxyl groups has little influence on the electrode reactions of the nickel Schiff-base complex. The CVs of the palladium complexes (**1**, M = Pd; M′ = H; B = C_6H_4 and CH_2CH_2) showed

that they underwent quasi-reversible (B = C_6H_4) or reversible (B = CH_2CH_2) reductions at −0.52 V. Their SWVs similarly revealed reduction, at −0.56 V (B = C_6H_4) and −0.51 V (B = CH_2CH_2). From these data, it is not possible to establish precisely what these electrode processes represent, although the reductions may be owing to formation of M^I from M^{II}.

The CVs of the molybdenated species, [**1**, M = Ni or Pd; M′ = Mo(NO){HB(dmpz)$_3$}; B = hydrocarbyl] were determined in acetonitrile and revealed only one significant electrode process, an apparent two-electron reduction at *ca* −0.50 V. This is due to reduction of the molybdenum centres, the E_f values for the Ni complexes occurring at −0.52 to −0.53 V, those of the Pd analogues being slightly more anodic, at −0.49 and −0.45 V; the E_f values being consistent with those obtained from other phenoxy-substituted Mo(NO){HB(dmpz)$_3$} fragments [11]. No other significant electrode behaviour was detected in these compounds. That this electrochemical behaviour is a result of a two-electron reduction was not determined directly by coulometry but by comparison of the electrode behaviour of related bimetallic species such as [{Mo(NO){HB(dmpz)$_3$}Cl$_2$(OC$_6$H$_4$CH=NC$_6$H$_4$N=CHC$_6$H$_4$O)] [12] and [**1**, M = Cu; M′ = Mo(NO){HB(dmpz)$_3$Cl; B = hydrocarbyl] [5]. The difference in peak potentials, ΔE_f ($E_f^c - E_f^a$), in acetonitrile fell in the range 100–137 mV for the nickel complexes and 106–117 mV for the palladium species, the values being virtually independent of scan rate. For a reversible one-electron process ΔE_f should be 59 mV, and for a two-electron transfer process it should either be of the order of 120 mV for sequential electrode reactions ($E_f^1 < E_f^2$ or $E_f^1 > E_f^2$, where < means less cathodic than) or 29 mV for a synchronous process. ΔE_f for the oxidation of ferrocene, used as internal reference in all the species studied, varies from 62 to 122 mV, a deviation from the ideal indicating that there is uncompensated solution resistance and a non-ideal electrochemical cell configuration. However, ΔE_f for the trimetallic complexes is reasonably close to the theoretical value for two sequential electron transfers, in which there is very weak interaction between the two redox centres. This is consistent with the previously observed behaviour of the copper analogues [5]. The data in Table 2 show that the reduction potential for the molybdenum nitrosyl fragments is influenced only slightly by the central metal, the palladium complexes (*ca* −0.47 V) being reduced at a potential *ca* 60 mV more anodic than their nickel counterparts (*ca* −0.53 V). The reduction potentials of the related copper complexes [**1**, M = Cu; M′ = Mo(NO){HB(dmpz)$_3$}}Cl; B = hydrocarbyl] average −0.46 V, showing that while the LUMO in this class of complexes is influenced by M, that influence is small. The reduction potentials of the molybdenated nickel complexes, like their copper analogues, show no significant dependence on the nature of B.

Because of the suggestion of two sequential one-electron reductions in the cyclic voltammograms of [**1**, M = Ni or Pd; M′ = Mo(NO){HB(bmpz)$_3$}Cl; B = hydrocarbyl], we conducted pulse voltammetry (DPV) in the range −0.4 to −0.6 V. Richardson and Taube [6] have derived a relationship between E_f and the width at half-height ($w_{1/2}$) of a differential pulse voltammetric peak for systems where the interaction between two redox centres in the same molecule is small. In the complexes described here, this interaction is going to be between 36 mV (the theoretically calculated separation of E_f^1 and E_f^2 for two non-interacting centres is 35.6 mV) and *ca* 180 mV. The data in Table 3 shows ΔE_f for the trimetallic species varying between 68 and 90 mV, broadly comparable to that in the copper analogues, consistent with weakly interacting redox sites. The coproportionation constants (K_c) for the equilibrium

[**1**, M = Ni, Pd; M′ = Mo(NO){HB(dmpz)$_3$}Cl]

+ [**1**, M = Ni, Pd; M′ = Mo(NO){HB(dmpz)$_3$}Cl]$^{2-}$

$\rightleftharpoons$ 2[**1**, M = Ni, Pd; M′ = Mo(NO){HB(dmpz)$_3$}Cl]$^-$

determined using the relationship $\Delta E_f = 59.16 \log K_c$, show that the monoreduced species have small but significant stabilities, the general electrochemical behaviour being consistent, as stated already, with weak interaction between the two molybdenum nitrosyl centres. The K_c data are broadly similar to the copper analogues [5] and it appears that the reduced species containing palladium are marginally more stable than their nickel analogues.

We had previously attempted to reduce [**1**, M = Cu; M′ = Mo(NO){HB(dmpz)$_3$}Cl; B = hydrocarbyl], primarily with the intention of generation a dianion containing, in principle, three unpaired electrons, one owing to Cu^{II} and two associated with the monoreduced [Mo(NO){HB(dmpz)$_3$}Cl] fragments. This was unsuccessful because the reduced species decomposed [5].

However, cobaltocene reduction of [**1**, M = Ni; M′ = Mo(NO){HB(dmpz)$_3$}Cl; B = $(CH_2)_n$, n = 3 and 4] in dichloromethane afforded EPR-active species that exhibited g = 1.97, consisting of a sextet (A_{Mo} = 50 ± 1 G; *ca* 25% of molybdenum atoms have nuclear spin I = 5/2) superimposed on a central singlet. This spectrum is not inconsistent with a dianion, [**1**, M = Ni; M′ = Mo(NO){HB(dmpz)$_3$}Cl; B = $(CH_2)_n$, n = 3 and 4)]$^{2-}$ in which the two unpaired spins on the molybdenum nitrosyl centres do not correlate with each other. Non-correlation of the two unpaired spins in paramagnetic binuclear molybdenum nitrosyl species containing dipyridyl bridging ligands is rare but has been observed [13], and seems to be mainly a function of twist within the dipyridyl fragment separating the isolated electrons. The complexes described here are not significantly twisted, nor are the two reduced molybdenum centres particularly far apart (minimum separation of 13 bonds) although the electrochemical interaction between them is very small. However, since the

Table 2. Electrochemical data obtained from mono- and tri-metallic Schiff base complexes [**1**, M = Ni or Pd; M′ = H or Mo(NO){HB(dmpz)$_3$}Cl; B = hydrocarbyl]

			Cyclic voltammetry (V)[a]		Square wave voltammetry (V)[b]		Cyclic voltammetry (reduction) (V)[c]		
M	B	M′	Red[d]	Oxid[e]	E_1	E_2	E_f^f	ΔE_f^g	ΔE^h
Ni	C_6H_4	H	−1.53[i]	+0.43[j]	−1.47	−2.05			
Ni	C_6H_4	Me	−1.54[k]	+0.48[l]	−1.50				
Ni	$(CH_2)_2$	H	−1.15[l]	+0.65[l]	−1.05				
Ni	$(CH_2)_3$	H	−1.57[m]		−1.55				
Ni	$(CH_2)_4$		n.d.[n]	n.d.[n]	−1.60[o]				
Pd	C_6H_4	H	−0.52[p]		−0.56				
Pd	$(CH_2)_2$	H	−0.52[q]		−0.51				
Ni	C_6H_4	Mo(NO){HB(dmpz)$_3$}Cl			n.d.[n]		−0.53	137	122
Ni	$(CH_2)_2$	Mo(NO){HB(dmpz)$_3$}Cl			n.d.[n]		−0.52	102	74
Ni	$(CH_2)_3$	Mo(NO){HB(dmpz)$_3$}Cl			n.d.[n]		−0.53	100	78
Ni	$(CH_2)_4$	Mo(NO){HB(dmpz)$_3$}Cl			n.d.[n]		−0.52	106	77
Pd	C_6H_4	Mo(NO){HB(dmpz)$_3$}Cl			n.d.[n]		−0.49	117	100
Pd	$(CH_2)_2$	Mo(NO){HB(dmpz)$_3$}Cl			n.d.[n]		−0.45	106	62

[a] Obtained using Pt bead electrode *vs* SCE, 0.1 mol dm^{-3} [Bu$^n_4$N][PF$_6$] in DMSO, scan rate 200 mV s^{-1}.
[b] First and second reduction processes recorded in DMSO where appropriate.
[c] Obtained using a Pt bead electrode *vs* SCE, 0.1 mol dm^{-3} [Bu$^n_4$N][PF$_6$] in acetonitrile, scan rate 200 mV s^{-1}.
[d] Peak detected on cathodic sweep.
[e] Peak detected on return anodic sweep.
[f] Reduction processes, measured in acetonitrile.
[g] $\Delta E_f = E_f^c - E_f^a$, in mV.
[h] Difference between cathodic and anodic peak potentials for ferrocene: 59 mV for a reversible one-electron transfer process.
[i] E_p^c, reverse sweep, E_p^a at −0.14 V.
[j] Irreversible oxidation peak +0.48 V.
[k] E_p^c; reverse sweep, E_p^a at −0.65 V.
[l] E_p^c; reverse sweep; E_p^a at −0.23 V; irreversible oxidation peak +0.65 V.
[m] Irreversible process, E_p^c = −1.66 V, E_p^a = −1.47 V.
[n] Not determined.
[o] Poorly soluble compound, approximate peak position.
[p] Quasi-reversible process, ΔE_f = 116 mV, further irreversible reduction process at −1.99 V.
[q] Reversible process, ΔE_f = 82 mV, further irreversible reduction process at −1.82 V.

Table 3. Differential pulse voltammetric data and coproportion constants obtained from trimetallic complexes [**1**, M = Ni or Pd; M′ = Mo(NO){HB(dmpz)$_3$}Cl; B = hydrocarbyl]

M	B	E (V)[a]	$w_{1/2}$ (mV)[b]	ΔE_f (mV)[c]	$E_f(1)$[d]	$E_f(2)$[d]	K_c[e]
Ni	C_6H_4	−0.510	155	77	−0.468	−0.543	18.5
Ni	$(CH_2)_2$	−0.512	153	74	−0.470	−0.544	17.8
Ni	$(CH_2)_3$	−0.512	140	67.5	−0.473	−0.541	13.8
Ni	$(CH_2)_4$	−0.514	148	72.5	−0.473	−0.546	16.8
Pd	C_6H_4	−0.462	173	90	−0.412	−0.502	33.2
Pd	$(CH_2)_2$	−0.448	167	85	−0.401	−0.486	27.4

[a] Centre of DPV curve in acetonitrile *vs* SCE using a Pt bead electrode.
[b] Peak width at half-height of DPV curve; theoretical value for a one-electron reversible process 90.4 mV.
[c] Separation between $E_f(1)$ and $E_f(2)$ determined graphically from ref. [6]; for two one-electron reversible processes in non-interacting systems within the same molecule, ΔE_f = 36.5 mV, probable error ±10 mV.
[d] Obtained from $E_f = E + \Delta E_f + E_{pulse}$; E_{pulse} = pulse potential −10 mV.
[e] Coproportion constant.

reduced species are very unstable in solution, we cannot rule out the possibility that decomposed fragments give rise to EPR signals consistent with *monometallic* paramagnetic ($S = \frac{1}{2}$) molybdenum nitrosyl species whose spectra are similar to that detected here.

CONCLUSIONS

We have shown that the diamagnetic trimetallic species [**1**, M = Ni or Pd; M′ = Mo(NO){HB(dmpz)$_3$}Cl; B = hydrocarbyl] are very similar to their paramagnetic copper analogues, undergoing detectable redox behaviour localized on the molybdenum nitrosyl fragments. The central metal atom (Ni or Pd) has a small influence on the peripheral molybdenum nitrosyl groups, leading to a slight increase in charge density on them. However, there is only a weak interaction between the two molybdenum redox centres, detected primarily by differential pulse voltammetry. The EPR spectra of the reduced trimetallic species [**1**, M = Ni; M′ = Mo(NO){HB(dmpz)$_3$}Cl; B = $(CH_2)_n$, $n = 3$ and 4]$^{2-}$, are consistent with unpaired spins isolated on each molybdenum nitrosyl centre.

Acknowledgements—We are grateful to the Association of Commonwealth Universities for support to (S.M.K.), and to Messrs T. Green (Birmingham), A. Stevenson and D. Taylor (Bristol) for extensive technical help.

REFERENCES

1. Roffia, S., Paradiso, C. and Bignozzi, C. A., in *Molecular Electrochemistry of Inorganic, Bioinorganic and Organometallic Compounds*, ed. Pombeiro, A. J. L. and McCleverty, J. A. Kluwer Academic Publishers, The Netherlands, 1993, 217; Espinet, P. and Garcia-Herbosa, G., *ibid.* p. 247; Bruns, W., Kaim, W., Ladwig, M., Olbrich-Deussner, B., Roth, T. and Schwederski, B., *Ibid.*, p. 255.
2. Trofmenko, S., *Chem. Rev.*, 1993, **93,** 943; Kitajima, N. and Tolman, W. B., *Prog. Inorg. Chem.*, 1995, **43,** 419; McCleverty, J. A., *Molecular Electrochemistry of Inorganic, Bioinorganic and Organometallic Compounds*, NATO ASI Series C, Vol. 385, ed. Pombeiro, A. J. L. and McCleverty, J. A. Kluwer Academic Publishers, The Netherlands, 1992, p. 77; McCleverty, J. A., *Transition Metals in Supramolecular Chemistry*, NATO ASI Series C, Vol. 448, Ed. Fabrizzi, L. and Poggi, A. Kluwer Academic Publishers, The Netherlands, 1994, p. 261.
3. Rowley, N. M., Kurek, S. S., Foulon, J.-D., Hamor, T. A., Jones, C. J., McCleverty, J. A., Hubig, S. M., McInnes, E. J. L., Payne, N. N. and Yellowlees, L. J., *Inorg. Chem.*, 1995, **34,** 4414; Coe, B. J., Hamor, T. A., Jones, C. J., McCleverty, J. A., Bloor, D., Cross, G. H. and Axon, T. L., *J. Chem. Soc., Dalton Trans.*, 1995, 673; Cargill Thompson, A. M. W., Gatteschi, D., Maher, J. P., McCleverty, J. A., Rentschler, E. and Ward, M. D., *Inorg. Chem.*, 1996, **35,** 2701.
4. Beer, P. D., Jones, C. J., McCleverty, J. A. and Sidebotham, R. P., *J. Organomet. Chem.*, 1987, **325,** C19; Murr, N. El., Sellami, A. and McCleverty, J. A., *New J. Chem.*, 1988, **12,** 209; Sidebotham, R. P., Beer, P. D., Hamor, T. A., Jones, C. J. and McCleverty, J. A., *J. Organomet. Chem.*, 1989, **371,** C31; Bhadbhade, M. M., Das, A., Jeffery, J. C., McCleverty, J. A., Navas, J. A. and Ward, M. D., *J. Chem. Soc., Dalton Trans.*, 1995, 2769.
5. Kagwanja, S. M., Jones, C. J., Maher, J. P. and McCleverty, J. A., *Polyhedron*, 1994, **13,** 2615.
6. Richardson, D. E. and Taube, H., *Inorg. Chem.*, 1981, **20,** 1278.
7. McWhinnie, S. L. W., Jones, C. J., McCleverty, J. A., Collison, D. and Mabbs, F. E., *Polyhedron*, 1992, **11,** 2639.
8. Włodarczyk, A., private communication.
9. McCleverty, J. A., *Chem. Rev.*, 1983, **12,** 331.
10. Sacconi, L., Mani, F. and Bencini, A., in *Comprehensive Coordination Chemistry*, ed. Wilkinson, G., Gillard, R. D. and McCleverty, J. A. Pergamon Press, 1987, Ch. 50, p. 188 *et seq.*
11. Obaidi, N. Al., Chaudhury, M., Clague, D., Jones, C. J., Pearson, J. C., McCleverty, J. A. and Salam, S. S., *J. Chem. Soc., Dalton Trans.*, 1987, 1733; Sharsley, S. M., Jones, C. J., McCleverty, J. A., Neaves, B. D., Reynolds, S. J. and Denti, G., *ibid.*, 1988, 293; Sharsley, S. M., Jones, C. J., McCleverty, J. A., Neaves, B. D. and Reynolds, S. J., *ibid.*, 1988, 301.
12. Kagwanja, S., Jeffery, J. C., Jones, C. J. and McCleverty, J. A., *Polyhedron*, 1996, **15,** 2959.
13. Jouaiti, A.-A., McCleverty, J. A., Shonfield, P. and Ward, M. D., work to be published.

Pergamon

PII: S0277-5387(96)00451-2

Polyhedron Vol. 16, No. 9, pp. 1447–1451, 1997
Copyright © 1997 Elsevier Science Ltd
Printed in Great Britain. All rights reserved
0277–5387/97 $17.00+0.00

A niobium(V) complex with mixed O,S-donor ligands. Synthesis, structure and properties of the anion tris(2-mercapto-4-methylphenolato)niobate(V)

Paul R. Challen,[a]* Diane H. Peapus[b] and Karen A. Magnus[b]

[a] Department of Chemistry, John Carroll University, Cleveland, OH 44118, U.S.A.

[b] Department of Biochemistry, Case Western Reserve University, Cleveland, OH 44106, U.S.A.

(Received 23 April 1996; accepted 3 September 1996)

Abstract—Reaction of $Nb(OEt)_5$ with 2-mercapto-4-methylphenol ($mmpH_2$) in the presence of triethylamine gave the mononuclear tris complex $(Et_3NH)[Nb(mmp)_3]$ which was structurally characterized. The coordination geometry around the niobium is between octahedral and trigonal prismatic, with a twist angle of 41.5°. The mercaptophenolate ligands are arranged around the metal in a "propeller" fashion. $(Et_3NH)[Nb(mmp)_3]$ was characterized by IR, ^1H NMR and UV–vis spectroscopies, and cyclic voltammetry. A reversible reduction wave found at −1.03 V is for reduction to the Nb^{IV} complex. © 1997 Elsevier Science Ltd. All rights reserved.

Keywords: niobium; mercaptophenolate; 2-mercapto-4-methylphenol.

The coordination of V, Nb and Ta to sulfur donors, either inorganic sulfide or thiolate, is no longer considered especially unusual, in view of the range of such molecular complexes prepared and structurally characterized in the past 10 years [1]. We have recently reported [2] the structure and properties of the mononuclear V^{IV} complex of 2-mercapto-4-methylphenol ($mmpH_2$, $mmp^{2-} = CH_3C_6H_3OS^{2-}$), a mixed O,S-donor ligand related to catechol [o-$C_6H_4(OH)_2$] and to benzene-1,2-dithiol [o-$C_6H_4(SH)_2$]. Catecholate [3] and dithiolene [4] complexes of both main group and transition metals have attracted much attention on account of their intriguing structural, electronic and redox properties, and their numerous applications. Tris-dithiolene complexes display a range of geometries from octahedral to trigonal prismatic [5], as well as other distorted polyhedra [6], and the factors influencing these geometries have been vigorously debated in the literature [7].

Wishing to extend our studies of the complexes of the mercaptophenolate ligand to the heavier congeners of vanadium we have synthesized the niobium(V) tris complex anion, $Nb(mmp)_3^-$. While a brief report of $HNb(mp)_3$ (mp = 2-mercaptophenolate) has appeared [8], no structural or spectroscopic characterization was included. This paper describes the synthesis, X-ray structure, ^1H NMR, IR, UV–vis and cyclic voltammetry of $[Et_3NH][Nb(mmp)_3]$.

EXPERIMENTAL

All operations were carried out under purified nitrogen or argon using standard inert atmosphere techniques. 2-Mercapto-4-methylphenol was prepared by a literature synthesis [9]. Reagents niobium(V) ethoxide and triethylamine, were purchased from Aldrich Chemical Co. and used as received. Solvents were distilled under nitrogen using conventional drying agents [MeOH over $Mg(OMe)_2$, MeCN and CH_2Cl_2 over CaH_2, Et_2O over sodium/benzophenone].

Elemental analyses (C, H and N) were performed by Oneida Research Services, Whitesboro, NY. Metal analysis was performed in-house using ICP-AES on acidic aqueous digests.

* Author to whom correspondence should be addressed.

Preparation of $(Et_3NH)[Nb(mmp)_3]$

A solution of $Nb(OEt)_5$ (1.0 g, 3.1 mmol) in MeOH (5 cm^3) was added to a solution containing 2-mercapto-4-methylphenol (1.35 g, 9.6 mmol) and Et_3N (0.61 g, 6.0 mmol) in MeOH (1 cm^3). The orange–brown mixture was stirred for 1 h, and the solvent subsequently removed *in vacuo* to leave a brown oil. This was stirred vigorously with Et_2O for several hours, then the mixture was filtered, affording 1.9 g of brown solid, $(Et_3NH)[Nb(mmp)_3]$. The product was recrystallized from $MeCN/Et_2O$ to yield 1.3 g of analytically pure dark brown microcrystalline solid (67% yield), which was used for subsequent measurements. Found: C, 52.7; H, 5.5; N, 2.3; Nb, 15.4. Calc. for $C_{27}H_{34}NO_3S_3Nb$: C, 53.2; H, 5.6; N, 2.3; Nb, 15.2%. ^1H NMR (CD_3CN, 300 MHz): δ 6.3–6.9 (arom. $CH_3C_6H_2OS$), 2.2 (s, 9H, $CH_3C_6H_2OS$), 1.2 [t, 9H, $(CH_3CH_2)_3NH$], 3.1 [q, 6H, $(CH_3CH_2)_3NH$]. Slow diffusion of Et_2O into a MeCN solution of the product afforded dark brown crystals suitable for X-ray diffraction measurements.

Physical measurements

Infrared spectra were obtained as KBr pellets on a Nicolet 5PC FTIR spectrometer. Electronic spectra were obtained on MeCN solutions in gas-tight quartz cuvettes using a HP 8453 spectrophotometer. ^1H NMR measurements were conducted on a Varian Gemini 300 spectrometer with TMS as internal standard. Electrochemical measurements were performed on CH_2Cl_2 solutions (*ca* 4 mM) using a BAS 100B electrochemical analyser; a glassy carbon working electrode was used in conjunction with a platinum wire auxiliary electrode and a saturated calomel reference electrode. The solutions contained 0.1 M tetra-n-butylammonium perchlorate as supporting electrolyte. IR compensation was employed. The ferrocene/ferrocenium couple was used as internal standard.

X-ray diffraction and structure solution

A single black crystal of dimensions $1.3 \times 0.5 \times 0.5$ mm was mounted in a glass capillary under an inert atmosphere. Intensity data were taken at room temperature (293 K) using a Rigaku AFC6 diffractometer on a Rigaku R200X rotating anode with Cu-K_α radiation ($\lambda = 1.5418$ Å) at 50 kW, and were corrected for absorption empirically using psi-scans, and for Lorentzian and polarization effects. Three standard reflections were monitored every 100 data points, showing less than 1% variation. Direct methods using SHELX-86 [10] revealed only the Nb, S, O and some of the aromatic ring carbons; however, no clear distinction between the sulfur and oxygen atoms was evident at this point. Therefore, initial phases were determined based on the Nb atom alone and F^2 difference Fourier analysis using SHELX-93 [11] revealed the rest of the structure, including a two-fold disorder of the cationic methylene group. All non-hydrogen atoms, including the disordered methylene, were refined anisotropically. Hydrogen atom positions were idealized and allowed to ride on the atoms to which they were attached. Hydrogen atoms were assigned an isotropic U value corresponding to the atoms of attachment.

Crystal data. $C_{27}H_{34}NO_3S_3Nb$, $M = 609.64$, trigonal, space group $P\bar{3}$, $a = b = 13.122(4)$, $c = 9.591(2)$ Å, $V = 1430.2(7)$ Å^3, $Z = 2$, $D_{calc} = 1.416$ g cm^{-3}, $F(000) = 632$, $\mu = 5.698$ mm^{-1}, scan type $\omega, 2\theta$ range 3.5–45°, reflections collected = 817, unique reflections = 686, observed reflections [$F_0 > 2\sigma(F_0)$ = 650], refinement parameters = 114, final R (on F) = 0.0496, R_w (on F^2; all data) = 0.1414, goodness-of-fit (all data) = 1.312.

The asymmetric unit consists of one-third of the formula, with the Nb and N atoms found on special positions along the triad, and the nitrogen H constrained to the threefold axis. The unit cell, therefore, contains two $(Et_3NH)[Nb(mmp)_3]$ units, with the anion and cation clearly separated.

Atomic coordinates have been deposited at the Cambridge Crystallographic Data Centre.

RESULTS AND DISCUSSION

Synthesis of $(Et_3NH)[Nb(mmp)_3]$

The synthesis of $(Et_3NH)[Nb(mmp)_3]$ was accomplished by the reaction of $Nb(OEt)_5$ with the protonated form of the ligand, $mmpH_2$, in the presence of mild base, Et_3N, to provide the Et_3NH^+ countercation, as in the equation below:

$$Nb(OEt)_5 + 3mmpH_2 + Et_3N \rightarrow [Nb(mmp)_3]^- + Et_3NH^+ + 5EtOH$$

This simple, clean acid–base procedure avoids potential side reactions which might ensue from reaction of niobium(V) halides with the ligand or salts of the ligand, and generates the product in high yield with minimal work-up. There was no evidence for oxo or sulfido niobium species, nor for reduced niobium complexes, all of which have been previously observed in reactions of niobium halides with thiolates [12].

$(Et_3NH)[Nb(mmp)_3]$ is sensitive to oxygen in solution, but no visible decomposition occurs in crystals exposed to the air over several days.

Structure of $(Et_3NH)[Nb(mmp)_3]$

The molecular structure and atomic-numbering scheme for the anion $[Nb(mmp)_3]^-$ are shown in Fig. 1. The view is along the crystallographic threefold axis; this axis generates two of the three mmp ligands

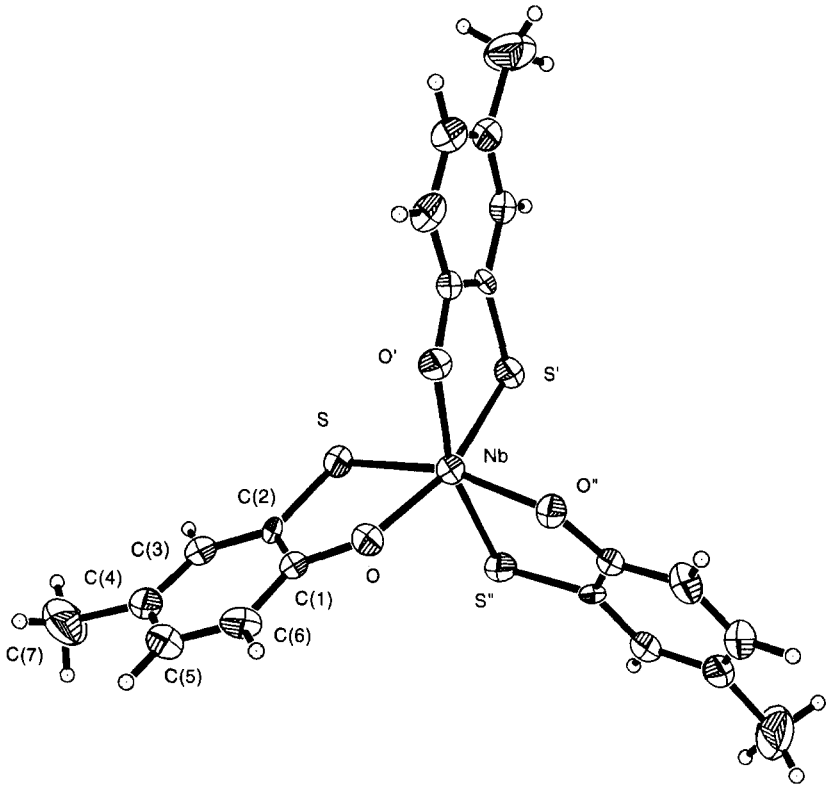


Fig. 1. Structure and numbering scheme of the anion in $(Et_3NH)[Nb(mmp)_3]$. Thermal ellipsoids are drawn at the 50% probability level.

from the asymmetric unit. Selected bond lengths and angles are in Table 1.

The complex anion consists of three bidentate chelating mmp ligands coordinated to niobium through three oxygen and three sulfur atoms in a facial arrangement, with crystallographically imposed C_3 symmetry. As a result of the symmetry the two triangular planes defined by the three sulfur atoms and three oxygen atoms are rigorously parallel. The twist angle between these S_3 and O_3 planes is 41.5°, indicating a geometry intermediate between octahedral (twist angle of 60°) and trigonal prismatic (twist angle of 0°). An assignment of distorted octahedral geometry is also supported by the *trans* angle of 160.6°, which is between the values of 136° for a trigonal prism and 168.1° for an octahedron (corrected for a bite angle of 78.1°). The geometry of $[Nb(mmp)_3]^-$ is close to that of $[V(mmp)_3]^{2-}$ [2], but differs from the dithiolene $[Nb(S_2C_6H_4)_3]^-$ [5], which is a slightly distorted trigonal prism with a twist angle of only 0.7°. While no structural information on simple tris-catecholates of Nb^V could be found in the literature for comparison with $[Nb(mmp)_3]^-$, such complexes are generally [13] octahedral or distorted octahedral in the absence of ligand constraints that favour another coordination geometry. In $[Nb(S_2C_6H_4)_3]^-$ the three ligand aromatic rings are in a "paddle-wheel" [5] arrangement around the central metal atom, with the ring planes lined up with the pseudo-threefold axis. In contrast, in $Nb(mmp)_3$ the twist towards octahedral geometry causes the three ligand planes to rotate into a "propeller" arrangement around the Nb, with an angle of 62.7° between the threefold axis and the normal to the aromatic ring planes (this angle would be 90° in a "paddle-wheel" arrangement). The Nb falls almost exactly in the projected planes of the aromatic rings, with only a very slight bending of 4.2° about the O–S vectors. This is substantially less than the bending observed in $[V(mmp)_3]^{2-}$ (average of 10.0°) and trigonal prismatic

Table 1. Selected bond lengths (Å) and angles (°)

Nb—O	1.943(5)	Nb—S	2.475(2)
O—C(1)	1.356(8)	S—C(2)	1.754(7)
C(1)—C(2)	1.402(10)	C(2)—C(3)	1.378(9)
C(3)—C(4)	1.377(10)	C(4)—C(5)	1.386(11)
C(5)—C(6)	1.396(10)	C(6)—C(1)	1.359(9)
C(4)—C(7)	1.532(10)		
O—Nb—S	78.14(15)	O—Nb—S′	160.56(15)
O—Nb—S″	99.45(14)	O—Nb—O′,O″	99.9(2)
S—Nb—S′,S″	83.07(7)	C(2)—S—Nb	98.3(3)
C(1)—O—Nb	129.9(5)	twist angle[a]	41.5

[a] Owing to the symmetry, the calculation of the twist angle reduces to the angle between O—Nb—S when all are projected onto the same *xy*-plane.

dithiolenes [5] such as $[Nb(S_2C_6H_4)_3]^-$ (22.4°) and $Mo(S_2C_6H_4)_3$ (21.4°).

The Nb—S distance in $[Nb(mmp)_3]^-$ is unusually long at 2.475(2) Å, in comparison with averaged values of 2.441 Å in $[Nb(S_2C_6H_4)_3]^-$ [5] 2.405 Å in $[Nb(SPhMe\text{-}p)_6]^-$ [1g] and 2.450 Å in $[Nb(SCH_2CH_2S)_3]^-$ [14], all of which contain Nb^V. It is not much shorter than the Nb^{IV}—S distance in $[Nb(SPh)_6]^{2-}$ [1g], at 2.488 Å. However, the C—S, C—O and C(1)—C(2) distances indicate that the ligands are in a fully reduced state and are not consistent with a Nb^{IV} + semiquinone/thione formulation. Furthermore, the Nb—O distance at 1.943 Å is short, and in keeping with other Nb^V—O bond lengths, such as in Nb(HTrencam) [15] (Nb—O_{av} = 2.03 Å). The long Nb—S distance in $[Nb(mmp)_3]^-$ may be a consequence of optimization of the Nb—O bond strengths at the expense of the Nb—S bonds. The bite angle of 78.1° is similar to that in $[V(mmp)_3]^{2-}$ (82.0°) and other six-coordinate complexes of mercaptophenolate [16].

^{1}H *NMR, IR and UV–vis spectroscopies*

The mid-IR spectrum of $[Nb(mmp)_3]^-$ displays ligand vibrations at 1467 (C—C ring stretch) and 1236 cm^{-1} (C—O). A sharp band at 3122 cm^{-1} is assigned to the cation N—H stretch. In $(Et_3NH)(PNP)[V(mmp)_3]$, where the Et_3NH^+ cation is hydrogen bonded to the anion, this band appears at lower frequency (3053 cm^{-1}) and is of lower intensity. The shift to higher frequency and intensity in $(Et_3NH)[Nb(mmp)_3]$ is consistent with the lack of hydrogen bonding shown in the X-ray structure.

Intense LMCT bands occur in the UV–vis spectrum at 288 nm (ε = 26,800 M^{-1} cm^{-1}), 367 (ε = 11,400) and *ca* 430 (sh; *ca* 7600 M^{-1} cm^{-1}). These are at higher energy than the charge transfer bands seen in $[V(mmp)_3]^{2-}$ reflecting the higher energy of the Nb unoccupied orbitals compared with V. The bands are also of higher energy than LMCT bands in dithiolenes [5,17] such as $[Nb(S_2C_6H_3CH_3)]^-$ and $[Nb(DDDT)_3]^-$, suggesting a greater stability of ligand orbitals in the mixed O,S ligand as compared to the S,S analogues.

The diamagnetic nature of the complex is established by the observation of an NMR spectrum (see Experimental section), with ^{1}H signals observed from the ligand and cation.

Cyclic voltammetry

Figure 2 shows the cyclic voltammogram of $[Nb(mmp)_3]^-$. The reversible reduction at $E_{1/2}$ = −1.03 V (*vs* SCE; −1.49 V *vs* Fc^+/Fc internal standard [18]. $E_{pa} - E_{pc}$ = 90.0 mV for the $[Nb(mmp)_3]^-/[Nb(mmp)_3]^{2-}$ wave; $E_{pa} - E_{pc}$ = 62.0 mV for the Fc^+/Fc wave) corresponds to conversion to the Nb^{IV} complex, while the irreversible oxidation

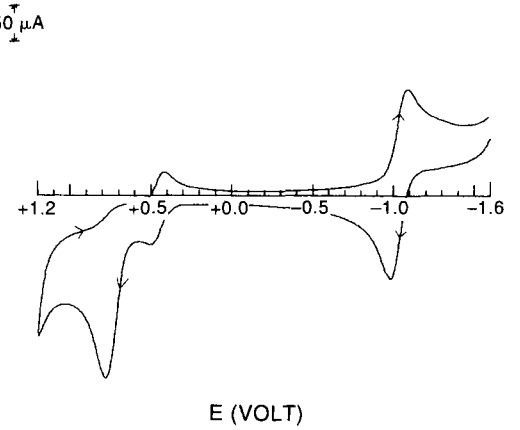


Fig. 2. Cyclic voltammetry of $(Et_3NH)[Nb(mmp)_3]$ in CH_2Cl_2 solution at room temperature (scan speed 200 mV s^{-1}; reference electrode SCE). Wave at +0.46 V is the ferrocene internal standard.

waves at positive potentials are ligand-based processes. These latter irreversible oxidation waves are also seen in the electrochemistry of $[V(mmp)_3]^{2-}$. The $[V(mmp)_3]^-/[V(mmp)_3]^{2-}$ couple [2] is at a more positive potential (−0.27 V *vs* Ag/AgCl) than that of $[Nb(mmp)_3]^-/[Nb(mmp)_3]^{2-}$, consistent with the well-known greater stability of higher oxidation states for the second transition metal series.

Acknowledgements—We thank Professor Fred L. Urbach and Shawn Swavey for assistance with electrochemical measurements.

REFERENCES

1. (a) Dance, I. G., *Polyhedron*, 1986, **5,** 1037; (b) Lee, S. C., Li, J., Mitchell, J. C. and Holm, R. H., *Inorg. Chem.*, 1992, **31,** 4333; (c) Christou, G., Heinrich, D., Money, J. K., Rambo, J. R., Huffman, J. C. and Folting, K., *Polyhedron*, 1989, **8,** 1723; (d) Halbert, T. R., Hutchings, L. L., Rhodes, R. and Stiefel, E. I., *J. Am. Chem. Soc.*, 1986, **108,** 6437; (e) Woodward, S., Curtis, M. D., Rheingold, A. L. and Haggerty, B. S., *Organometallics*, 1992, **11,** 2140; (f) Curnow, O. J., Curtis, M. D., Rheingold, A. and Haggerty, B. S., *Inorg. Chem.*, 1991, **30,** 4043; (g) Koo, S. M., Bergero, R., Salifoglou, A. and Coucouvanis, D., *Inorg. Chem.*, 1990, **29,** 4844; (h) Tatsumi, K., Kawaguchi, H., Matsubara, I., Nakamura, A., Miki, K. and Kasai, N., *Inorg. Chem.*, 1993, **32,** 2604.
2. Klich, P. R., Daniher, A. T., Challen, P. R., McConville, D. B. and Youngs, W. J., *Inorg. Chem.*, 1996, **35,** 347.
3. Pierpont, C. G. and Lange, C. W., *Prog. Inorg. Chem.*, 1994, **41,** 331.
4. Eisenberg, R., *Prog. Inorg. Chem.*, 1970, **12,** 295 and references cited therein.
5. Cowie, M. and Bennett, M. J., *Inorg. Chem.*, 1976, **15,** 1589.

6. Koenemann, M., Stueer, W., Kirschbaum, K. and Giolando, D., *Polyhedron*, 1994, **13,** 1415.
7. Martin, J. L. and Takats, J., *Can. J. Chem.*, 1989, **67,** 1914.
8. Andrae, K. and Rollka, W., *Z. Anorg. Allg. Chem.*, 1972, **391,** 19.
9. Cabiddu, S., Maccioni, A. and Secci, M., *Gazz. Chim. Ital.*, 1969, **99,** 1095.
10. Sheldrick, G. M., in *Crystallographic Computing* 3, ed. G. M. Sheldrick, C. Kruger and R. Goddard. Oxford University Press, London, 1985, pp. 175–189.
11. Sheldrick, G. M., SHELXL-93, *A Program for the Refinement of Crystal Structures*. University of Göttingen, Germany, 1993.
12. Coucouvanis, D., Al-Ahmad, S., Kim, C. G. and Koo, S. M., *Inorg. Chem.*, 1992, **31,** 2996; Seela, J. L., Huffman, J. C. and Christou, G., *J. Chem. Soc., Chem. Commun.*, 1987, 1258; (c) Tatsumi, K., Kawaguchi, H., Matsubura, I., Nakamura, A., Miki, K. and Kasai, N., *Inorg. Chem.*, 1993, **32,** 2604.
13. Karpishin, T. B., Stack, T. D. P. and Raymond, K. N., *J. Am. Chem. Soc.*, 1993, **115,** 182.
14. Tatsumi, K., Sekiguchi, Y., Cramer, R. E. and Rupp, J. J., *Angew. Chem., Int. Ed. Engl.*, 1986, **25,** 86.
15. Evans, D. F., Slawin, A. M. Z., Williams, D. J., Wong, C. Y. and Woollins, J. D., *Polyhedron*, 1993, **12,** 1103.
16. Weng, L. H., Kang, B. S., Chen, X. T., Hong, M. C., Lei, X. J., Hu, Y. H. and Liu, H. Q., *Chin. J. Chem.*, 1993, **11,** 30.
17. Welch, J. H., Bereman, R. D. and Singh, P., *Inorg. Chem.*, 1990, **29,** 68.
18. Gagné, R. R., Koval, C. A. and Lisensky, G. C., *Inorg. Chem.*, 1980, **19,** 2854.

Pergamon

PII: S0277-5387(96)00450-0

Polyhedron Vol. 16, No. 9, pp. 1453–1459, 1997
Copyright © 1997 Elsevier Science Ltd
Printed in Great Britain. All rights reserved
0277-5387/97 $17.00+0.00

High-pressure synthesis of $[Ru_2(\mu\text{-dppm})_2(\mu\text{-CO})(CO)_4]$, $Ru_2(\mu\text{-dppm})(\mu\text{-dmpm})(\mu\text{-CO})(CO)_4]$, and $[Ru(dcypm)(CO)_3]$ from $Ru_3(CO)_{12}$ and the diphosphines: $R_2PCH_2PR_2$; R = CH_3(dmpm), C_6H_5 (dppm) and C_6H_{11} (dcypm). Crystal and molecular structures of $[Ru_2(\mu\text{-dppm})_2(\mu\text{-CO})(CO)_4]$, and $[Ru(dcypm)(CO)_3]$

Gregory M. Ferrence,[a]† Phillip E. Fanwick,[a]* Clifford P. Kubiak[a]‡ and Raymond J. Haines[b]

[a] Department of Chemistry, 1393 Brown Laboratory, Purdue University, West Lafayette, IN 47907, U.S.A.

[b] Department of Chemistry, University of Natal, PO Box 375, Pietermaritzburg 3200, South Africa

(Received 17 June 1996; accepted 29 August 1996)

Abstract—The high-pressure (1300 psi CO, 120°C) reactions of $Ru_3(CO)_{12}$ with the diphosphines $R_2PCH_2PR_2$; R = CH_3 (dmpm), C_6H_5 (dppm), and C_6H_{11} (dcypm), are reported. In the case of dppm, the disphosphine-bridged dinuclear ruthenium complex $[Ru_2(\mu\text{-dppm})_2(\mu\text{-CO})(CO)_4]$ was obtained. The corresponding reaction with dcypm afforded the mononuclear chelated diphosphine complex $[Ru(dcypm)(CO)_3]$. The mixed ligand system $[Ru_2(\mu\text{-dppm})(\mu\text{-dmpm})(\mu\text{-CO})(CO)_4]$ was obtained by employing a 1 : 1 mixture of dppm and dmpm. The crystal and molecular structures of $[Ru_2(\mu\text{-dppm})_2(\mu\text{-CO})(CO)_4]$ and $[Ru(dcypm)(CO)_3]$ were also determined. © 1997 Elsevier Science Ltd. All rights reserved.

Keywords: dinuclear ruthenium; complex; diphosphine; high-pressure synthesis; crystal structure.

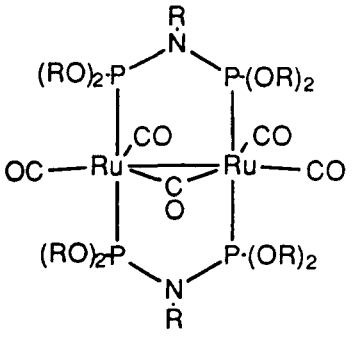
Diphosphine and diphosphazane-bridged dinuclear ruthenium complexes have been the subject of considerable study [1–10]. The chemistry of dinuclear ruthenium diphosphazane complexes, **1** (R = Me, tPr[i] or Ph), has been pursued extensively in the laboratories of Haines and co-workers [1–6]. The study of these complexes has led to a detailed model system for the stepwise oxidation of CO to CO_2 [6] as well as to a novel photochemical Michaelis–Arbuzov-type rearrangement [11]. We have therefore sought to expand the scope of this class of dinuclear transition metal complexes.

The high-pressure synthesis of the bis(dimethylphosphino)methane (dmpm)-bridged complex **2** was reported by Johnson and Gladfelter [7]. The bis(diphenylphosphino)methane (dppm)-bridged complex $[Ru_2(\mu\text{-dppm})_2(\mu\text{-CO})(CO)_4]$ (**3**) was first synthesized by the photochemical reaction of $Ru_3(CO)_{12}$ with dppm [8]. More recently, **3** was also prepared by the reduction of ruthenium acetate in the presence of carbon monoxide, although the structure of this material has yet to be reported [9]. We report studies of the high-pressure (1300 psi CO, 120°C) reactions of $Ru_3(CO)_{12}$ with the diphosphines $R_2PCH_2PR_2$; R = CH_3 (dmpm), C_6H_5 (dppm) and C_6H_{11} (dcypm), including the preparation of the mixed-ligand system

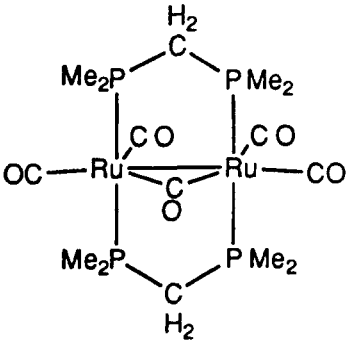
* Address correspondence pertaining to crystallographic studies to this author.

† *Present address*: Department of Chemistry, Amherst College, Amherst, MA 01002-5000, USA.

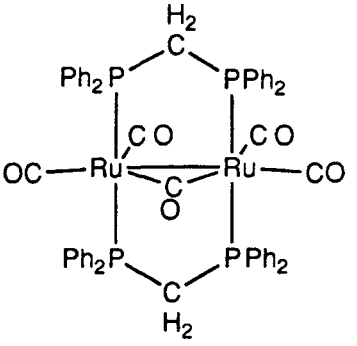
‡ Author to whom correspondence should be addressed.



1



2



3

$[Ru_2(\mu\text{-dppm})(\mu\text{-dmpm})(\mu\text{-CO})(CO)_4]$ (**4**) and the mononuclear complex $[Ru(dcypm)(CO)_3]$ (**5**). The crystal and molecular structures of **3** and **5** are also described.

EXPERIMENTAL

All manipulations were carried out under nitrogen in a VAC glove-box, or using standard Schlenk techniques. Toluene was distilled from sodium prior to use. Hexane was used as purchased from Fisher Scientific. $Ru_3(CO)_{12}$ and dmpm [bis(dimethyl-phosphino) methane] were purchased from Strem. Dppm [bis (dimethylphosphino)methane] was purchased from Aldrich. Dcypm [bis(dicyclohexylphosphino)methane] was obtained from Dr. I. P. Rothwell (Purdue University). The complex $[Ru_2(\mu\text{-dmpm})_2(\mu\text{-CO})(CO)_4]$ was prepared according to the literature procedure [7]. IR spectra of compounds as KBr pellets were recorded using a Perkin–Elmer 1710 Fourier transform infrared spectrometer. ^1H and ^{31}P-[^1H] NMR spectra were recorded on either Varian XL-200 or General Electric 300 spectrometers.

Preparation of $[Ru_2(\mu\text{-dppm})_2(\mu\text{-CO})(CO)_4]$ (**3**)

Complex **3** was prepared by a modification of Gladfelter's method [7] for the synthesis of $[Ru_2(\mu\text{-dmpm})_2(\mu\text{-CO}(CO)_4]$. $Ru_3(CO)_{12}$ (0.940 g, 1.47 mmol) and dppm (1.697 g, 4.41 mmol) were placed in a 500 cm^3 high-pressure Parr reactor to which 100 cm^3 of toluene was added. The reactor was charged and sealed in the dry-box and then placed in a heating well and pressurized with CO to *ca* 1000 psi. Upon heating to 120°C, the reactor pressure rose to *ca* 1300 psi. The reaction was stirred under these conditions using a mechanical stirrer for 16 h, after which it was cooled to room temperature and vented. The reactor was then returned to the dry-box where the reaction contents were transferred to a round-bottomed flask and reduced in volume under vacuum to *ca* 50 cm^3 and precipitated with *ca* 200 cm^3 hexane. A yellow solid was recovered by filtration, rinsed with hexane and dried *in vacuo*. Yield: 2.06 g (84%). ^1H NMR (200 MHz, C_6D_6): δ_H 3.4 (4H, m, CH_2), 6.7–7.7 (40H, m, CH). ^{31}P-[^1H] NMR (81 MHz, C_6D_6): δ_P 39.9 (s). IR (KBr) ν(CO) cm^{-1}: 1964 s, 1918 vs, 1894 vs, 1872 s, 1700 s.

Preparation of $[Ru_2(\mu\text{-dppm})(\mu\text{-dmpm})(\mu\text{-CO})(CO)_4]$ (**4**)

Complex **4** was prepared by a similar method to that for **3** but equimolar amounts of dppm and dmpm were used; $Ru_3(CO)_{12}$ (470 g, 736 mmol), dmpm (0.18 cm^3, 1.1 mmol) and dppm (425 g, 1.11 mmol). The final reaction mixture contained essentially a statistical mixture of **4**, **3** and $[Ru_2(dmpm)_2(CO)_5]$.

Reducing the solution volume to *ca* 30 cm^3 resulted in precipitation of $[Ru_2(dmpm)_2(CO)_5]$. This was removed by filtration and then through successive addition of hexane and filtration, **4** and then **3** were isolated and dried *in vacuo*. For **4**: Yield: 0.33 g (30%). $^{31}P-\{^1H\}$ NMR (81 MHz, C_6D_6(: δ(AA'BB') 15.3 (m), 39.4 (m). IR (KBr)ν(CO) cm^{-1}: 1951 s, 1912 vs, 1895 vs, 1867 s, 1682 s.

Preparation of [Ru(dcypm)$(CO)_3$] (**5**)

Complex **5** was prepared by a similar method to that for **3**, but dcypm was substituted for dppm; $Ru_3(CO)_{12}$ (266 mg, 416 mmol) and dcypm (510 mg, 1.25 mmol). Light yellow needles of **5** crystallized upon reducing solvent volume. For **5**: ^1H NMR (200 MHz, C_6D_6) : δ_H 2.7 (2H, t, CH_2), 1.0–2.1 (44H, broad overlapping m, cyclohex). $^{31}P-\{^1H\}$ NMR (81 MHz, C_6H_6): δ_P −3.30 (s) ppm. IR (KBr) ν(CO) cm^{-1}: 1981 vs, 1899 vs, 1880 vs.

Crystal data for [$Ru_2(\mu$-dppm$)_2(\mu$-CO)$(CO)_4$] (**3**)

X-ray quality crystals of $\mathbf{3}\cdot 2CH_3CN$, ($C_{59}H_{50}N_2O_5P_4Ru_2$), were grown by slow evaporation from CH_3CN. An orange plate having approximate dimensions of $0.24\times0.20\times0.13$ mm^3 was mounted in a glass capillary. Data collection were performed at 293 ± 1 K with Cu-K_α radiation (λ = 1.54184 Å) on an Enraf–Nonius CAD4 computer-controlled kappa-axis diffractometer equipped with a graphite crystal, incident beam monochromator. The crystal data and data collection parameters are given in Table 1. Cell constants and an orientation matrix for data collection were obtained from least-squares refinement, using the setting angles of 25 reflections in the range $24 < \theta < 47°$, measured by the computer-controlled diagonal slit method of centring. As a check on the crystal quality, omega scans of several intense reflections were measured; the width at half-height was 0.40° with a take-off angle of 6.0°, indicating good crystal quality. Lorentz and polarization corrections were applied to the data. The linear absorption coefficient is 63.8 cm^{-1} for Cu-K_α radiation. An empirical absorption correction based on the method of Walker and Stuart was applied [12]. Relative transmission coefficients ranged from 0.478 to 1.000 with an average value of 0.639. The structure was solved using the structure solution program SHELX-86 [13]. The remaining atoms were located in succeeding difference Fourier syntheses. Hydrogen atoms were located and added to the structure factor calculations but their positions were not refined. The structure was refined in full-matrix least-squares where the function minimized was $\Sigma w\ (|F_o|-|F_c|)^2$ and the weight w is defined as by the Killean and Lawrence method with terms of 0.020 and 1.0 [14]. Scattering factors were taken from Cromer and Waber [15]. Anomalous dispersion effects were included in F_c [16]; the values for f' and f'' were those of Cromer [17]. All calculations were performed on a VAX computer. Refinement was done using MolEN [18]. Crystallographic drawings were done using programs ORTEP [19].

Crystal data for [Ru(dcypm)$(CO)_3$] (**5**)

X-ray quality crystals of **5**, ($C_{28}H_{46}O_3P_2Ru$), were grown by solvent evaporation from toluene. A colourless needle having approximate dimensions of $0.50\times0.35\times0.25$ mm^3 was mounted in a glass capillary. The crystal data and data collection parameters are given in Table 1. Structural analysis was similar to that described for **3** with the following modifications. Cell constants and an orientation matrix for data collection were obtained from least-squares refinement, using the setting angles of 25 reflections in the range $17 < \theta < 21°$, measured by the computer-controlled diagonal slit method of centring. As a check on the crystal quality, omega scans of several intense reflections were measured; the width at half-height was 0.43° with a take-off angle of 3.0°, indicating good crystal quality. The structure was solved using the Patterson heavy-atom method which revealed the position of the Ru atom.

RESULTS AND DISCUSSION

The reaction of $[Ru_3CO_{12}]$ with dppm under 1000 psi CO in toluene led to the formation of [$Ru_2(\mu$-dppm$)_2(\mu$-CO$)(CO)_4$] (**3**). In the presence of a 1 : 1 mixture of dppm and dmpm the mixed-ligand system [$Ru_2(\mu$-dmpm$)(\mu$-dppm$)(\mu$-CO$)(CO)_4$] (**4**) was formed in essentially a statistical yield, along with **2** and **3**. Complex **4** was isolated by fractional crystallization from toluene/hexane solutions. Upon continued addition of hexane, complex **2** crystallizes first, followed by **4** and then **3**.

Table 2 compares the carbonyl infrared stretching frequencies of complexes **2–4** and the related diphosphazanes. As expected, increasing the basicity of the ligand from phosphazane to phosphine leads to a decrease in carbonyl stretching frequencies owing to increased π backbonding. Similarly, the less basic **3** shows higher stretching frequencies than **2**. The mixed ligand system **4** exhibits ν(CO) bands at frequencies that are intermediate between the bis(dmpm) and bis(dppm) compounds, **2** and **3**. Complex **3**, like **2**, shows a singlet in the ^{31}P NMR spectrum while the mixed-ligand system, **4**, shows an AA'BB' pattern owing to the different phosphorus chemical environments of dmpm and dppm.

An ORTEP view of [$Ru_2(\mu$-dppm$)_2(\mu$-CO$)(CO)_4$] (**3**) is shown in Fig. 1, and crystal data and data collection parameters are summarized in Table 1. Selected bond distances and angles are given in Table 3. the structure consists of two five-coordinate ruthenium centres separated by a Ru—Ru distance of

Table 1. Crystal data and data collection parameters

Compound	**3**·2CH_3CN	**5**
Formula	$C_{59}H_{50}N_2O_5P_{84}Ru_2$	$C_{28}H_{46}O_3P_2Ru$
Formula weight	1193.10	596.70
Space group	$P2_{1/n}$ (No. 14)	$P2_{1/c}$ (No. 14)
a, Å	12.3250(9)	10.176(1)
b, Å	19.690(3)	21.649(3)
c, Å	22.1109(9)	14.261(3)
β, °	103.1(3)	106.74(1)
V, Å^3	5226(7)	3008(2)
Z	4	4
d_{calc}, g cm^{-3}	1.516	1.311
Crystal dimensions, mm	0.24 × 0.20 × 0.13	0.50 × 0.35 × 0.25
Temperature, K	293	293
Radiation (wavelength)	Cu-K_α (1.54184 Å)	Mo-K_α (0.71073 Å)
Monochromator	Graphite	Graphite
Linear abs coeff, cm^{-1}	63.83	6.39
Absorption correction applied	Empirical[a]	None
Diffractometer	Enraf–Nonius CAD4	Enraf–Nonius CAD4
Scan method	ω–2θ	ω–2θ
2θ range, °	4.88–124.60	4.00–45.00
Scan width, °	0.40 + 0.26tan θ	0.43 + 0.35tan θ
Take-off angle, °	6.00	2.95
Programs used	Enraf–Nonius MolEN	Enraf–Nonius MolEN
F (000)	2424.0	1248.0
p-factor used in weighting	0.040	0.040
Data collected	8998	40.54
Unique data	8559	4054
Data with $I > 3.0\sigma$ (I)	4118	2719
Number of variables	649	307
Largest shift-esd in final cycle, e Å^{-3}	0.04	0.12
R	0.041	0.032
R_w	0.048	0.041
Goodness-of-fit	1.125	1.172

[a] See ref. [15].

Table 2. Comparison of IR carbonyl stretching frequencies, ν(CO), of [$Ru_2(\mu$-$R_2PYPR_2)(\mu$-$R'_2PYPR'_2)(\mu$-CO)$(CO)_4$]

R	R′	Y	ν(CO)				
OPh	OPh	NEt	2021	1987	1948	1932	1720[a]
OMe	OMe	NEt	1999	1960	1929	1913	1703[a]
Ph	Ph	CH_2	1964	1918	1894	1872	1700[b]
Me	Me	CH_2	1953	1904	1881	1855	1686[b]
Ph	Me	CH_2	1951	1912	1895	1867	1682[b]

[a] Cyclohexane solution sample [5].
[b] KBr pellet.

2.9073(9) Å, as compared with 2.8928(8) for **2** [7]. Similarly Ru—C and Ru—P bond distances are rather similar for **3** and **2**. Generally, core bond distances are longer in **3** than in the related diphosphazane, [$Ru_2\{\mu$-$(MeO)_2PN(Et)P(OMe)_2\}_2(\mu$-CO$)(CO)_4$] [5].

Substituting dcypm in the high-pressure synthesis resulted in the formation of the mononuclear ruthenium complex [Ru(dcypm)$(CO)_3$] (**5**). This is likely to be the result of the steric bulk of the cyclohexyl rings. Dinuclear dcypm-bridged complexes do, however, exist [20]. Complex **5** shows a singlet in the ^{31}P NMR at $\delta -3.3$ and three ν(CO) bands in the IR at 1981, 1899 and 1880 cm^{-1}. This is characteristic of axial, equatorial coordinated ruthenium bis(phosphine) complexes [21–23]. The ν(CO) bands occur lower in energy than the similar bis(diphenylphosphino)ethane (dppe) complex, [Ru(dppe)$(CO)_3$ (ν(CO) = 1997, 1942, 1885 cm^{-1}) [21] owing to the increased basicity of dcypm. The large shift of the ^{31}P NMR signal of **5** higher field (−3.3 ppm) compared with the bridging diphosphine complexes **2**–**4** is characteristic of the four-membered RuP_2C ring of a chelating methylene diphosphine. The ring contributions, Δ_R, to the ^{31}P chemical shifts of chelating methylene diphosphine complexes can be greater than −50 ppm [24].

An ORTEP view of [Ru(dcypm)$(CO)_3$] (**5**) is shown in Fig. 2. Crystal data and data collection parameters are given in Table 1. Selected bond distances and angles are given in Table 4. The complex is mononuclear and five-coordinated about ruthenium. The Ru—C bond distances are 1.884(7), 1.894(6) and

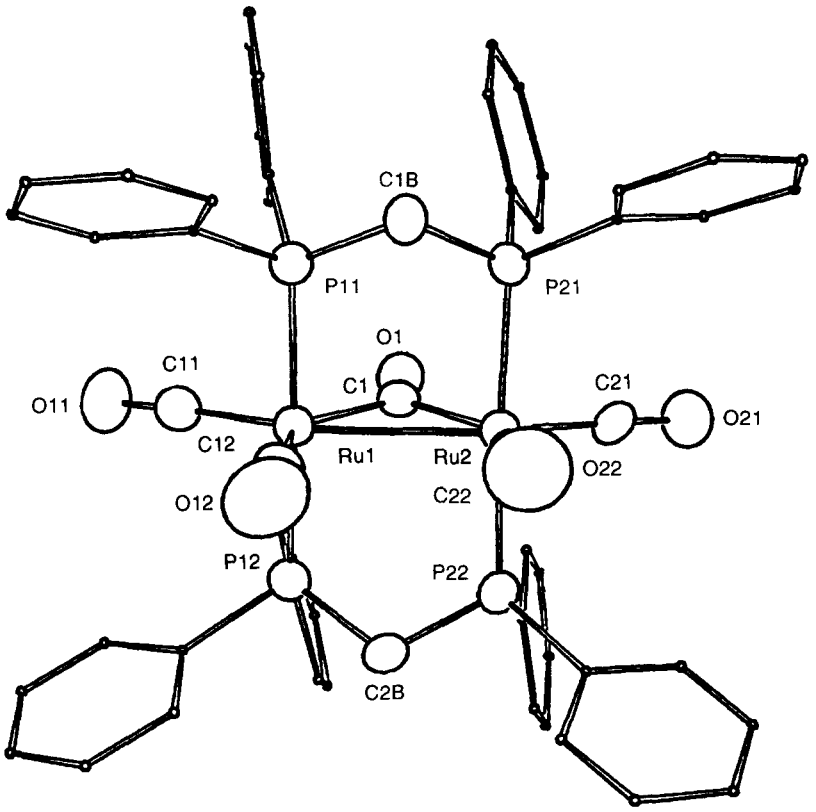


Fig. 1. An ORTEP view of $[Ru_2(\mu\text{-dppm})_2(\mu_2\text{-CO})(CO)_4]$ (**3**)

Table 3. Selected bond distances (Å) and angles (°) for $[Ru_2(dppm)_2(\mu\text{-CO})(CO)_4]\cdot 2CH_3CN$ (**3**)

Ru(1)—Ru(2)	2.9073(9)	Ru(2)—C(1)	2.139(9)
Ru(1)—P(11)	2.331(2)	Ru(1)—C(21)	1.86(1)
Ru(1)—P(12)	2.339(2)	Ru(2)—C(22)	1.93(1)
Ru(1)—C(1)	2.132(9)	O(1)—C(1)	1.16(1)
Ru(1)—C(11)	1.86(1)	O(11)—C(11)	1.15(1)
Ru(1)—C(12)	1.92(1)	O(12)—C(12)	1.15(1)
Ru(2)—P(21)	2.340(3)	O(21)—C(21)	1.15(1)
Ru(2)—P(22)	2.349(2)	O(22)—C(22)	1.14(1)
P(11)—Ru(1)—P(12)	176.33(9)	P(21)—Ru(2)—C(21)	89.1(3)
P(11)—Ru(1)—C(1)	92.1(2)	Ru(1)—C(1)—Ru(2)	85.8(3)
P(11)—Ru(1)—C(11)	89.5(3)	P(21)—Ru(2)—C(22)	89.8(3)
P(11)—Ru(1)—C(12)	90.9(3)	P(22)—Ru(2)—C(1)	93.1(2)
P(12)—Ru(1)—C(1)	88.2(2)	P(22)—Ru(2)—C(21)	87.7(3)
P(12)—Ru(1)—C(11)	87.0(3)	P(22) Ru(2)—C(22)	92.4(3)
P(12)—Ru(1)—C(12)	91.3(3)	C(1)—Ru(2)—C(21)	106.1(4)
C(1)—Ru(1)—C(11)	107.6(4)	C(1)—Ru(2)—C(22)	141.8(4)
C(1)—Ru(1)—C(12)	139.9(4)	C(21)—Ru(2)—C(22)	111.9(4)
C(11)—Ru(1)—C(12)	112.3(4)	Ru(1)—C(1)—O(1)	137.3(8)
P(21)—Ru(2)—P(22)	176.58(9)	Ru(2)—C(1)—O(1)	136.9(8)
P(21)—Ru(2)—C(1)	86.8(2)		

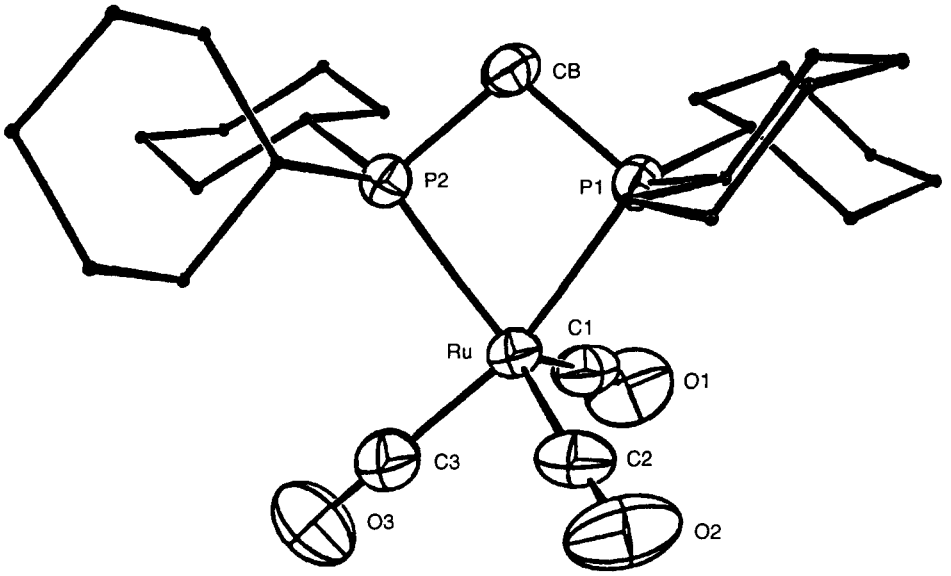


Fig. 2. An ORTEP view of [Ru(dcypm)$(CO)_3$] (**5**)

Table 4. Selected bond distances (Å) and angles (°) for [Ru(dcypm)$(CO)_3$] (**5**)

Ru—P(1)	2.370(1)	Ru—C(3)	1.909(7)
Ru—P(2)	2.378(1)	O(1)—C(1)	1.160(7)
Ru—C(1)	1.884(7)	O(2)—C(2)	1.152(6)
Ru—C(2)	1.894(6)	O(3)—C(3)	1.137(7)

P(1)—Ru—P(2)	70.71(4)	C(1)—Ru—C(2)	116.8(2)
P(1)—Ru—C(1)	95.3(2)	C(1)—Ru—C(3)	92.6(3)
P(1)—Ru—C(2)	92.8(2)	C(2)—Ru—C(3)	93.6(3)
P(1)—Ru—C(3)	166.4(2)	Ru—P(1)—C(B)	96.5(2)
P(2)—Ru—C(1)	119.7(2)	Ru—P(2)—C(B)	96.2(2)
P(2)—Ru—C(2)	122.1(2)	P(1)—C(B)—P(2)	96.3(2)
P(2)—Ru—C(3)	95.7(2)		

1.909(7) Å and the Ru—P distances are 2.370(1) and 2.378(1) Å, not significantly different from those reported for [Ru$(PMe_3)_2(CO)_3$] and [Ru$(PPh_3)_2(CO)_3$] [13,14]. The P—Ru—P angle is quite narrow at 70.71(4)°.

We have thus shown the generality of the high-pressure synthesis of mono- and di-nuclear ruthenium complexes from [Ru$(CO)_{12}$] and bis(dialkylphosphino)- or bis(diarylphosphino)-methanes. The novel mixed-ligand complex [Ru_2(μ-dmpm)(μ-dppm)(μ-CO)$(CO)_4$] has also been prepared by this method. The selectivity of this method for preparing mononuclear *vs* dinuclear products appears to depend on the steric requirements of the diphosphine ligand.

Acknowledgements—We are grateful to NSF(CHE-9319173) for support of this work. We thank Dr I. P. Rothwell for supplying dcypm. G. M. F. thanks the US Department of Education for a National Needs Fellowship.

REFERENCES

1. Field, J. S., Haines, R. J., Stewart, M. W., Sundermeyer, J. and Woollam, S. F., *J. Chem. Soc., Dalton Trans.* 1993, 947.
2. Field, J. S., Haines, R. J., Honrath, U., Sundermeyer, J. and Woollam, S. F. *J. Organomet. Chem.* 1990, **395**. C9.
3. Engel, D. W., Field, J. S., Haines, R. J., Honrath, U., Horsfield, E. C., Sundermeyer, J. and Woollam, S. F., *J. Chem. Soc., Dalton Trans.* 1994, 1131.
4. Field, J. S., Francis, A. M. A. and Haines, R. J., *J. Organomet. Chem.* 1988, **356**, C23.
5. Leeuw, G. D., Field, J. S., Haines, R. J., McCulloch, B., Meintjies, E., Monberg, C., Oliver, G. M., Ramdial, P., Sampson, C. N., Sigwarth, B., Steen, N. D. and Moodley, K. G., *J. Organomet. Chem.* 1984, **275**, 99.
6. Haines, R. J., *Comprehensive Organometallic Chemistry II*, Vol. 7, eds in chief E. W. Abel, F.

G. A. Stone and G. Wilkinson, 1995, pp. 625–68, Pergamon, Oxford.
7. Johnson, K. A. and Gladfelter, W. L., *Organometallics*, 1989, **8,** 2866.
8. Engel, D. W., Moodley, K. G., Subramony, L. and Haines, R. J., *J. Organomet. Chem.* 1988, **349,** 393.
9. Mirza, H. A., Vittal, J. J. and Puddephatt, R. J., *Inorg. Chem.* 1993, **32,** 1327.
10. Johnson, K. A. and Gladfelter, W. L., *Organometallics*, 1990, **9,** 2101.
11. Granger, R. M., Fanwick, P. E., Haines, R. J. and Kubiak, C. P., *Inorg. Chem.* 1993, **32,** 3570.
12. Walker, N. and Stuart, D., *Acta Cryst.* 1983, **A39,** 158.
13. Sheldrick, G. M., Institut für Anorganische Chemie der Universitat Gottingen, Germany, 1986.
14. Killean, R. C. G. and Lawrence, J. L., *Acta Cryst.* 1969, **B25,** 1750.
15. Cromer, D. T. and Waber, J. T., *International Tables for X-Ray Crystallography* Vol. IV. Table 2.2B. Kynoch Press, Birmingham (1974).
16. Ibers, J. A. and Hamilton, W. C., *Acta Cryst.* 1964, **17,** 781.
17. Cromer, D. T., *International Tables for X-Ray Crystallography*, Vol. IV. Table 2.3.1. Kynoch Press, Birmingham (1974).
18. Fair, C. K., MolEN Structure Determination System, Delft Instruments, Delft, The Netherlands (1990).
19. Johnson, C. K., ORTEPII, Report ORNL-5138, Oak Ridge National Laboratory, Tennessee, USA (1976).
20. Morgan, C. A., Fanwick, P. E. and Rothwell, I. P., *Inorg. Chim. Acta*, 1994, **224,** 105.
21. Sanchez-Delgado, R. A., Bradley, J. S. and Wilkinson, G., *J. Chem. Soc., Dalton Trans.* 1976, 339.
22. Dahan, F., Sabo, S. and Chaudret, B., *Acta Cryst.* 1984, **C40,** 786.
23. Jones, R. A., Wilkinson, G., Galas, A. M. R., Hursthouse, M. B. and Malik, K. M. A., *J. Chem. Soc., Dalton Trans.* 1980, 1771.
24. Garrou, P. E., *Chem. Rev.* 1981, **81,** 229.

Pergamon

PII: S0277-5387(96)00422-1

Polyhedron Vol. 16, No. 9, pp. 1461–1464, 1997
Copyright © 1997 Elsevier Science Ltd
Printed in Great Britain. All rights reserved
0277-5387/97 $17.00+0.00

Crystal and molecular structure of bis(niflumato)bis(3-pyridylmethanol)copper(II)

Fedor Valach,[a]* Miroslav Tokarčík,[a] Pavol Kubinec,[a] Milan Melník[b] and L'ubov Macášková[b]

[a] Department of Chemical Physics, Faculty of Chemical Technology, Slovak Technical University, SK-812 37 Bratislava, Slovakia

[b] Department of Inorganic Chemistry, Faculty of Chemical Technology, Slovak Technical University, SK-812 37 Bratislava, Slovakia

(Received 29 July 1996; accepted 27 August 1996)

Abstract—The crystal and molecular structure of the first copper(II) complex of (2-{[3-(trifluoromethyl) phenyl]amino}-3-pyridinecarboxylate with 3-pyridylmethanol as neutral ligand was determined by X-ray analysis. © 1997 Elsevier Science Ltd. All rights reserved.

Keywords: fenamate; copper(II) niflumate; 3-pyridylmethanol; crystal structure; X-ray diffraction analysis; bond valences.

(2 - {[3 - (Trifluoromethyl)phenyl]amino} - 3 - pyridinecarboxylic acid (niflumic acid) and other fenamates (flufenamic acid and mefenamic acid) are believed to act through the inhibition of prostaglandin biosynthesis, like other anti-inflammatory analgesics [1]. The interaction of the copper(II) atom, which plays a vital role in a number of quite different biological processes, with therapeutically administrated drugs is a subject of considerable interest.

X-ray crystallographic studies of the 1 : 1 complex between niflumic acid and ethanolamine showed deprotonation of one carboxylic oxygen atom [2]. The bond valences [3] of the niflumate anion calculated by the formula $s = (R_0/R)^N$ are shown in Fig. 1. R is the bond length, R_0 and N are fitted constants. Available atom valences of the terminal atoms were calculated as the difference between the theoretical atomic valence and the sum of bond valences around the atom. The greatest available valence of one oxygen atom indicates the preferred coordination of niflumate ligand to the metal cation through one carboxylic oxygen atom. On the basis of spectroscopic and magnetic properties of $Cu(nif)_2(3\text{-pyMe})_2$ (nif = niflumate, 3-pyMe = 3-pyridylmethanol) the polymeric structure with a pseudo-octahedral environment about the Cu^{II} atom was proposed.

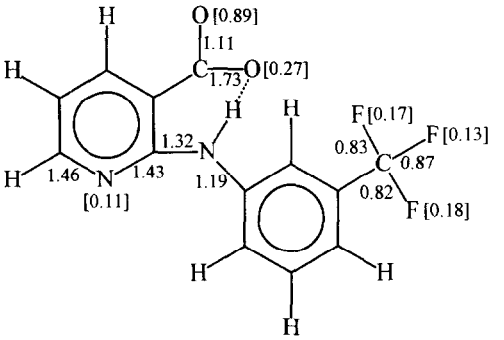


Fig. 1. Bond valences (in valence units, v.u.) of niflumic acid anion. Valences of C—C bonds are in the range 1.20–1.71 v.u. Available valences of the terminal atoms are enclosed in square brackets.

In order to understand better some aspects of metal ion–drug interactions, we have studied the structure of the title compound at room temperature.

EXPERIMENTAL

The copper(II) niflumate was prepared as described elsewhere [4]. The 3-pyridylmethanol adduct of cop-

* Author to whom correspondence should be addressed.

per(II) niflumate was prepared by adding the ligand 3-pyMe (2.73 g, 0.025 mol) to 100 cm^3 of a methanol suspension of $Cu(nif)_2$ (3.43 g, 0.01 mol). After heating to boiling, a solution was obtained which was left to cool and stand at room temperature. The precipitated product was isolated, washed with cold methanol and then dried at room temperature. The crude product was recrystallized from hot methanol to yield green crystals. Found (Calc.) for $Cu(nif)_2(3\text{-pyMe})_2$: Cu, 7.5 (7.5); C, 53.5 (54.0); H, 3.9 (3.9); N, 5.5 (5.6)%.

Crystal data for $Cu(nif)_2(3\text{-pyMe})_2$, $C_{38}H_{30}F_6N_6O_6Cu$

The density of the crystals measured by flotation in CCl_4/benzene mixture is $D_m = 1.52\ g\ cm^{-3}$, calculated $D_x = 1.53\ g\ cm^{-3}$. $M_r = 844.23$, monoclinic, $a = 11.806(3)$, $b = 22.856(6)$, $c = 7.101(8)$ Å, $\beta = 106.7(3)^\circ$; $V = 1835(2)$ Å^3, space group $P2_1/n$, $Z = 2$, $F(000) = 862$, $\mu(\text{Mo-}K_\alpha) = 0.68\ mm^{-1}$. A crystal of dimensions *ca* $0.25 \times 0.20 \times 0.20\ mm^3$ was measured on a Syntex $P2_1$ diffractometer, with graphite-monochromated Mo-K_α radiation ($\lambda = 0.71069$ Å). The cell parameters were refined by least squares for 15 reflections in the range $11.0 \leqslant 2\theta \leqslant 32.1^\circ$. 3308 reflections in total were measured using the $\omega/2\theta$ scan technique, $2\theta_{max} = 110^\circ$, time per reflection *ca* 60 s, index range $0 \leqslant h \leqslant 15$, $0 \leqslant k \leqslant 25$, $-9 \leqslant l \leqslant 8$, two standard reflections with variation 2%, $R_{int} = 0.036$. Correction for empirical absorption was applied. The maximum and minimum transmission factor values were 1.0 and 0.825, respectively. 2219 unique reflections obeying the condition $F > 3\sigma(F)$ were estimated. All non-hydrogen atoms were localized by direct methods, using the SHELXS86 program [5]. The atom-scattering factors and f', f'' values were obtained from *International Tables for X-ray Crystallography* [6]. The structure was refined by the least-squares method, using the SHELX76 program [7]. After the anisotropic refinement all hydrogen atoms were located from difference maps, but not refined. The final values were $R = 0.048$ and $Rw = 0.048$, $w = 0.3802/[\sigma(F_o) + 0.001(F_o)^2]$. Goodness-of-fit, S, was 0.06. The maximum and minimum heights in the final difference Fourier map were 0.5 and -0.3 e Å^{-3}, respectively. All calculations were performed on a PC 386 computer.

RESULTS AND DISCUSSION

The molecular structure of $[Cu(nif)_2(3\text{-pyMe})_2]$ is shown in Fig. 2. Selected bond lengths and bond angles are summarized in Table 1. *Trans* coordination of the Cu atom is formed by two carboxylic oxygen atoms from two niflumic ligands and two nitrogen atoms from two 3-pyridylmethanol ligands. This almost square-planar coordination of the Cu atom is supplemented by two methanolic oxygen atoms of the neighbouring structural units, forming a pseudo-octahedral coordination connecting the units $[Cu(nif)_2(3\text{-pyMe})_2]$ into infinite chains along the Z-direction (Fig. 3). The chains are held mutually by the van de Waals forces.

Using the data in refs [8,9] for Cu—N(1) bond valence, according to Brown and Shannon [10] the predicted bond length Cu^{II}—O(3) is 2.61 Å, which is very close to the observed value (Table 1). The coordination of the Cu^{II} atom may therefore be described as pseudo-octahedral and the Cu···O(2) contact, being 3.231(3) Å, should be regarded as non-bonding. The dihedral angle between the rigid car-

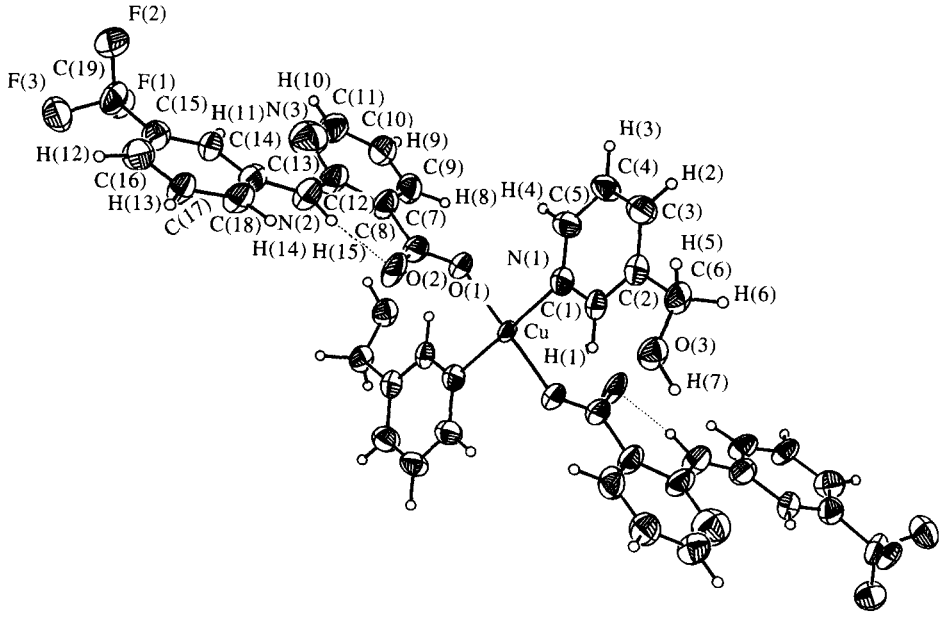


Fig. 2. A perspective view of the molecular structure of $Cu(nif)_2(3\text{-pyMe})_2$.

Table 1. Bond lengths (Å) and bond angles (°) with e.s.d.s in parentheses

Cu—N(1)	2.038(3)	C(2)—C(3)	1.400(7)
Cu—O(1)	1.946(3)	C(2)—C(6)	1.526(7)
Cu—O(3)	2.573(3)	C(3)—C(4)	1.398(8)
N(1)—C(1)	1.359(6)	C(4)—C(5)	1.384(6)
N(1)—C(5)	1.361(6)	C(7)—C(8)	1.489(8)
N(2)—C(12)	1.361(7)	C(8)—C(9)	1.388(7)
N(2)—C(13)	1.389(6)	C(8)—C(12)	1.423(6)
N(3)—C(11)	1.329(8)	C(9)—C(10)	1.426(8)
N(3)—C(12)	1.367(9)	C(10)—C(11)	1.420(6)
O(1)—C(7)	1.252(5)	C(13)—C(14)	1.423(8)
O(2)—C(7)	1.253(6)	C(13)—C(18)	1.422(7)
O(3)—C(6)	1.429(6)	C(14)—C(15)	1.390(6)
F(1)—C(19)	1.285(6)	C(15)—C(16)	1.391(8)
F(2)—C(19)	1.272(5)	C(15)—C(19)	1.480(8)
F(3)—C(19)	1.330(5)	C(16)—C(17)	1.424(8)
C(1)—C(2)	1.392(6)	C(17)—C(18)	1.386(6)
N(1)—Cu—O(1)	89.9(1)	C(9)—C(8)—C(12)	118.7(5)
N(1)—Cu—O(3)	96.4(1)	C(8)—C(9)—C(10)	120.0(4)
O(1)—Cu—O(3)	85.1(1)	C(9)—C(10)—C(11)	115.2(5)
Cu—N(1)—C(5)	120.5(3)	N(3)—C(11)—C(10)	126.7(5)
Cu—N(1)—C(1)	120.2(3)	N(3)—C(12)—C(8)	122.8(5)
C(1)—N(1)—C(5)	119.4(4)	N(2)—C(12)—C(8)	119.2(5)
C(12)—N(2)—C(13)	130.5(4)	N(2)—C(12)—N(3)	118.0(5)
C(11)—N(3)—C(12)	116.4(6)	N(2)—C(13)—C(18)	115.6(4)
Cu—O(1)—C(7)	129.9(3)	N(2)—C(13)—C(14)	125.0(4)
C(6)—O(3)—Cu	127.6(2)	C(14)—C(13)—C(18)	119.4(4)
N(1)—C(1)—C(2)	122.1(4)	C(13)—C(14)—C(15)	117.7(5)
C(1)—C(2)—C(6)	122.0(4)	C(14)—C(15)—C(19)	117.5(4)
C(1)—C(2)—C(3)	118.7(4)	C(14)—C(15)—C(16)	123.5(5)
C(3)—C(2)—C(6)	119.2(4)	C(16)—C(15)—C(19)	119.0(4)
C(2)—C(3)—C(4)	118.6(4)	C(15)—C(16)—C(17)	119.0(5)
C(3)—C(4)—C(5)	120.2(5)	C(16)—C(17)—C(18)	118.9(5)
N(1)—C(5)—C(4)	121.0(5)	C(13)—C(18)—C(17)	121.6(5)
O(3)—C(6)—C(2)	110.4(4)	F(3)—C(19)—C(15)	113.3(4)
O(1)—C(7)—O(2)	123.6(5)	F(2)—C(19)—C(15)	113.8(4)
O(2)—C(7)—C(8)	119.9(4)	F(2)—C(19)—F(3)	103.3(4)
O(1)—C(7)—C(8)	116.4(4)	F(1)—C(19)—C(15)	115.2(4)
C(7)—C(8)—C(12)	124.3(5)	F(1)—C(19)—F(3)	100.4(4)
C(7)—C(8)—C(9)	117.0(4)	F(1)—C(19)—F(2)	109.5(4)

boxylate group [the sum of the bond angles around the C(7) atom is 359.93(7)°] and the equatorial plane of the copper coordination sphere is 93.5(2)°. The intramolecular ligand hydrogen bond N(2)—H(15)···O(2) [the interatomic distances are N(2)···O(2) 2.657(5) and H(15)···O(2) 1.851(3) Å, and the bond angle N(2)—H(15)···O(2) is 135.4(3)°] encloses a pseudo-ring in the niflumic ligand (Fig. 2).

Both benzene and pyridine rings of the niflumic ligand deviate significantly from planarity (χ^2 values of 45.0 and 84.4, respectively). The dihedral angle created by the least-squares planes of both rings is 11.7(1)°. The torsion angle C(8)—C(12)—N(2)—C(13) (Table 2) does not differ from the corresponding angle for the niflumic acid anion (174.1°) [2]. The other two torsion angles defining the conformation of the niflumic ligand differ significantly from the values for niflumic acid (−177.2 and −4.5°). Such deformation is in agreement with the stabilization effect of the hydrogen bond N(2)—H(15)···O(2) occurring in the niflumic acid anion, too. The pyridine ring of the 3-pyridylmethanol ligand is planar. Mean C—C and C—N bond lengths in the niflumic and 3-pyridylmethanol ligands exhibit no significant differences from mean bond lengths of the same type in the structures of morpholinoethyl niflumate [11] and bis(salicylato)-bis(3-pyridylmethanol)copper(II) [12]. The dihedral angle between the plane of pyridine ring and the equatorial plane of the copper atom coordination is 97.3(1)°.

Acknowledgements—We thank Professor G. M. Sheldrick and Dr E. Irmer from the University of Göttingen, Germany, for useful discussions. This work was supported by the

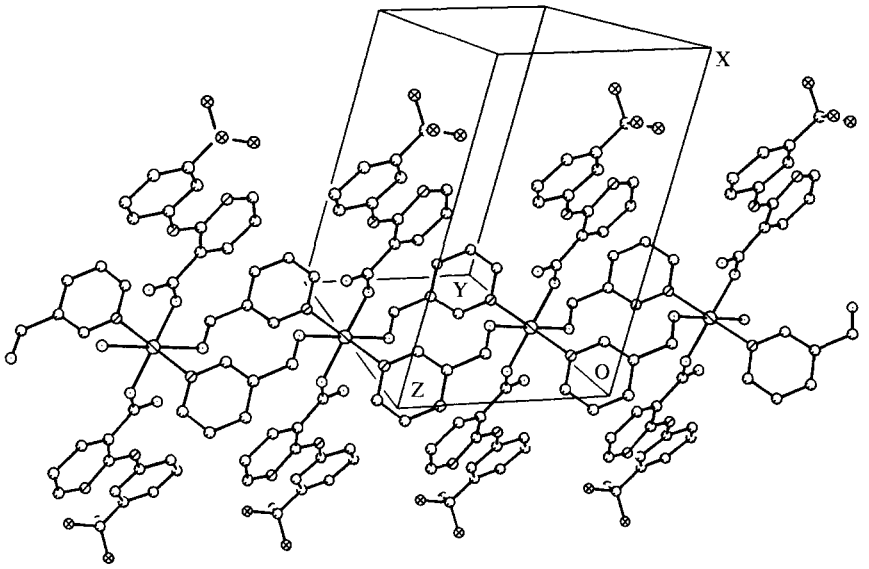


Fig. 3. Structure of the chain in the crystal structure of $Cu(nif)_2(3\text{-}pyMe)_2$. Hydrogen atoms are omitted for clarity.

Table 2. Torsion angles (°)

O(2)—C(7)—C(8)—C(9)	−175.1(5)	C(8)—C(12)—N(2)—C(13)	174.3(5)
C(12)—N(2)—C(13)—C(14)	6.2(9)	C(1)—C(2)—C(6)—O(3)	−22.1(6)

Slovak Ministry of Education and Science (Research Project No. 1/3201/96).

REFERENCES

1. Flower, R. J., *Pharm. Rev.*, 1974, **22,** 33.
2. Dhanaraj, V. and Vijayan, M., *Acta Cryst.*, 1983, **C39,** 1398.
3. Brown, I. D., in *Structure and Bonding in Crystals*, Vol. 2, ed. M. O'Keeffe and A. Navrotsky. Academic Press, New York, 1981, pp. 1–30.
4. Melník, M., Macášková, L'. and Holloway, C. E., *J. Coord. Chem.*, 1993, **30,** 145.
5. Sheldrick, G. M., *Acta Cryst.*, 1990, **A46,** 467.
6. *International Tables for X-ray Crystallography*, Vol. IV. Kynoch Press, Birmingham, 1974, pp. 99–101.
7. Sheldrick, G. M., *SHELX76. Program for Crystal Structure Determination.* University of Cambridge, England, 1976.
8. Valach, F., Contributions to the development of coordination chemistry, in *Proceedings 14th Conference on Coordination Chemistry*, Smolenice, Slovakia, 1993, pp. 59–64.
9. Valach, F., *DrSc. Thesis*, Slovak Technical University, Bratislava, 1994.
10. Brown, I. D. and Shannon, R. D., *Acta Cryst.*, 1973, **A29,** 266.
11. Toffoli, P., Coquillay, M., Rodier, N., Ceolin, R., Teulon, J. M. and Guechot, C., *Acta Cryst.*, 1988, **C44,** 547.
12. Hoang, N. N., Valach, F., Macášková, L'. and Melník, M., *Acta Cryst.*, 1992, **C48,** 1933.

Pergamon

PII: S0277-5387(96)00428-7

Polyhedron Vol. 16, No. 8, pp. 1465–1469, 1997
Copyright © 1997 Elsevier Science Ltd
Printed in Great Britain. All rights reserved
0277-5387/97 $17.00+0.00

Syntheses and properties of the neutral nickel complexes of 1,2-dithiolates MEDT and PHDT. The crystal structure of [Ni(MEDT)$_2$]

Jing-Lin Zuo,[a] Fei You,[a] Xiao-Zeng You[a]* and Hoong-Kun Fun[b]

[a] Coordination Chemistry Institute and the State Key Laboratory of Coordination Chemistry, Nanjing University, Center for Advanced Studies in Science and Technology of Microstructure, Nanjing 210093, P.R. China

[b] X-ray Crystallography Unit, School of Physics, Universiti Sains Malaysia, 11800 USM, Penang, Malaysia

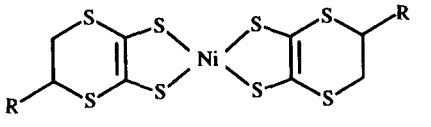
(Received 28 June 1996; accepted 27 August 1996)

Abstract—Two neutral nickel complexes of multi-sulfur 1,2-dithiolenes, [Ni(MEDT)$_2$], **1** (MEDT = 5,6-dihydro-5-methyl-1,4-dithiin-2,3-dithiolate), and [Ni(PHDT)$_2$], **2** (PHDT = 5,6-dihydro-5-phenyl-1,4-dithiin-2,3-dithiolate) have been prepared and characterized. The X-ray structure analysis of **1** reveals that the molecules are arranged as two different oriented "stacks" along the *a* axis. The shortest intrastack S···S contact is 3.9312 Å. © 1997 Elsevier Science Ltd. All rights reserved.

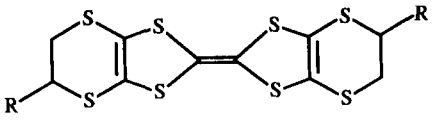
Keywords: crystal structures; nickel complexes; 1,2-dithiolenes; conductors.

Since the metal complexes DMIT ligand (DMIT = 4,5-dimercapto-1,3-dithiole-2-thionate) were first reported to exhibit superconduction, a massive research effort has centred on the design and synthesis of similar complexes [1–2]. The crystal structures of these complexes reveal that intermolecular interactions through the sulfur–sulfur interatomic contact is the basic requirement for high conductivity. Following this, the multi-sulfur 1,2-dithiolene complexes $[Ni(DDDT)_2]^-$ [3] (DDDT = 5,6-dihydro-1,4-dithiin-2,3-dithiolate) and $[Ni(PDDT)_2]^-$ [4] (PDDT = 6,7-dihydro-5H-1,4-dithiepin-2,3-dithiolate) have been synthesized and studied. In our previous work we reported the syntheses, properties of the nickel complexes of MEDT and PHDT ligands (MEDT = 5,6-dihydro-6-methyl-1,4-dithiin-2,3-dithiolate; PHDT = 5,6-dihydro-5-phenyl-1,4-dithiin-2,3-dithiolate) and the crystal structure of $[Bu_4N][Ni(MEDT)_2]$ [5].

In a continuation of this work, we have synthesized the two neutral complexes of MEDT and PHDT ligands, [Ni(MEDT)$_2$] (**1**) and [Ni(PHDT)$_2$] (**2**, see Scheme 1), which are "inorganic analogues" of the organic donor molecules BMeDT-TTF [6] and BPhDT-TTF [7] (BMeDT-TTF = bis(5,6-dihydro-5-methyl-1,3-dithiol-[4,5-*b*][1,4]-dithiocyclohexen-2-ylidene); BPhDT-TTF = bis(5,6-dihydro-5-phenyl-1,3-dithiol-[4,5-*b*][1,4]-dithiocyclohexen-2-ylidene). We also report the crystal structure of [Ni(MEDT)$_2$] (**1**).



1. R=Me **2. R=Ph**



1'. R=Me **BMeDT-TTF**

2'. R=Ph **BPhDT-TTF**

Scheme 1.

* Author to whom correspondence should be addressed.

Table 1. Single-crystal X-ray crystallographic analysis

Formula	$C_{10}H_{12}NiS_8$
Molecular weight	447.39
Crystal size (mm)	$0.28 \times 0.28 \times 2.00$
Crystal colour	Black
Crystal habit	Needle
Crystal system	Monoclinic
Space group	$P2_1/c$
Cell dimensions	$a = 5.273(3)$ Å
	$b = 15.206(7)$ Å
	$c = 10.224(4)$ Å
	$\beta = 90.34(4)^\circ$
Volume (Å^3)	819.8(7)
Z	2
D_{calc} (g cm^{-3})	1.812
$F(000)$	456
Temperature (K)	293(2)
Absorption coefficient (cm^{-1})	21.83
2θ range ($^\circ$)	4.80–55.0
Scan type	θ–2θ
Reflections collected	2651
Independent reflections	1873
Unique reflections [$I > 2\sigma(I)$]	1872
Variables	111
Goodness of fit on F^2	1.227
R	0.0809
$wR(F^2)$	0.02521

EXPERIMENTAL

Reagents

$[Bu_4N][Ni(MEDT)_2]$ and $[Bu_4N][Ni(PHDT)_2]$ were prepared according to the literature method [3]. All the chemicals used were analytically pure without further purification.

Syntheses

$[Ni(MEDT)_2]$ (**1**) and $[Ni(PHDT)_2]$ (**2**) were prepared by I_2 oxidation of $[Bu_4N][Ni(MEDT)_2]$ and $[Bu_4N][Ni(PHDT)_2]$ in acetone, respectively.

The black needle-shaped crystals of $[Ni(MEDT)_2]$ were obtained by recrystallization in CS_2 through slow evaporation. Found: C, 27.0; H, 2.8. Calc. for $C_{10}H_{12}S_8Ni$: C, 26.9; H, 2.7%. IR (KBr): 1257(s), 1214(s), 1144(s), 1076(m), 873(m), 483(m) Cm^{-1}.

$[Ni(PHDT)_2]$ was recrystallized from CS_2 or benzene. Found: C, 42.3; H, 3.1. Calc. for $C_{20}H_{16}S_8Ni$: C, 42.0; H, 2.8%. IR (KBr): 1234(s), 1174(s), 1134(m), 886(m), 469(m) cm^{-1}.

Physical measurements

IR spectra were measured on a Nicolet FT-IR 170SX spectrophotometer using KBr pellets. UV–vis and NIR spectra were recorded on a UV3100 spectrophotometer. Elemental analyses were performed using a Perkin–Elmer 240 analytical instrument.

Single-crystal analysis

A representative crystal of $[Ni(MEDT)_2]$ (**1**) was surveyed. A data set was collected using a Siemens P4 diffractometer equipped with graphite-monochromated Mo-K_α radiation ($\lambda = 0.71073$ Å). A psi-scan was used for an empirical absorption correction [8]. Pertinent crystal survey, data collection and structure refinement are summarized in Table 1.

The structure was solved by direct method using SHELXL-86 [9] and refined by full-matrix least-squares method on F^2 using SHELXL-93 [10]. The H atoms located from difference maps and refined isotropically.

RESULTS AND DISCUSSION

The neutral complexes of $[Ni(DDDT)_2]$ [11], $[Ni(DMIT)_2]$ [12] and $[Ni(PDDT)_2]$ [13] are very insoluble in CS_2, benzene and other organic solvents. Attachment of a bulky group, such as phenyl in **2** and methyl in **1**, did indeed increase the solubility in CS_2 and benzene enabling us to obtain good crystals of **1** and **2** for structure determination.

The complexes **1** and **2** in benzene solution show strong broad absorption at 1029 ($\varepsilon = 36{,}000$) and 1028 nm ($\varepsilon = 43{,}000$), respectively. This low energy near-IR absorption is due to the $\pi \rightarrow \pi$ transition of

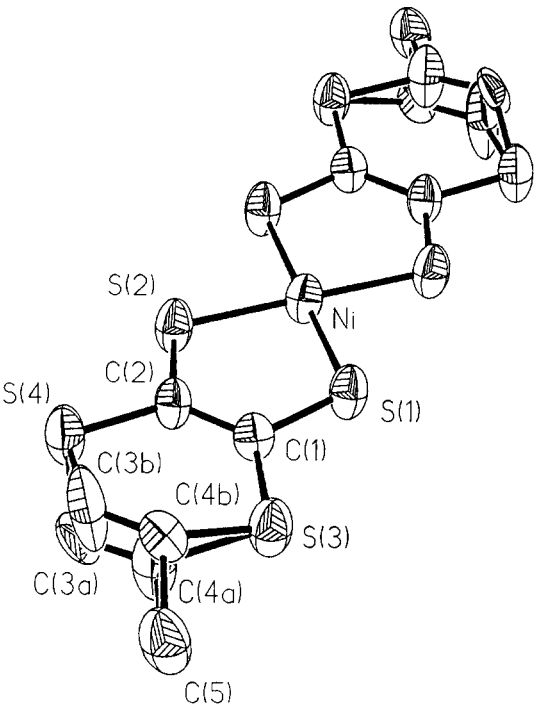


Fig. 1. Structure of $[Ni(MEDT)_2]$ with the numbering scheme.

the delocalized ligand. While the monoanion, $[Ni(MEDT)_2]^-$ and $[Ni(PHDT)_2]^-$, exhibit this band at 1177 and 1172 nm, respectively [5].

The three IR absorption bands of **1** at 1257, 1274 and 873 cm^{-1} are ascribed to ν(C=C), ν(C—S) and ν(R—C≪), respectively. While in complex **2,** these bands are around 1234, 1174 and 840 cm^{-1}.

Figure 1 shows the structure and labelling scheme of [Ni(MEDT)$_2$ (**1**). Selected bond lengths and angles for the complex are listed in Table 2. A comparison of the structural features of [Ni(MEDT)$_2$] to other selected monoanionic and neutral nickel dithiolenes is shown in Table 3.

The four sulfur atoms surrounding the nickel atom yield a square-planar environment with an average S—Ni—S angle of 91.30(9)°. The average Ni—S, C—S and C=C bond lengths in the five-membered ring containing the nickel atom are 2.128(3), 1.703(5) and 1.399(12) Å, respectively, while in the monoanion, $[Bu_4N][Ni(MEDT)_2]$, these values are 2.126, 1.73 and 1.34 Å, respectively. The shorter C—S bond lengths in [Ni(MEDT)$_2$] are indicative of double-bond character. This is the same in other similar complexes, as [Ni(PDDT)$_2$ [13] [1.711(4) Å], [Ni(PHDT)$_2$ [14] (1.706 Å) and [Ni(DDDT)$_2$] [1.68(2) Å]. It suggests that oxidation occurs essentially on the 1,2-multi-sulfur dithiolene ligand rather than the metal centre.

The external —$CH_2CH(Me)$— groups exist in a *trans* configuration. C(3), C(4) and C(5) are highly uncharacteristic, which are certainly due to the conformational disorder of the non-planar outer ring. The partial occupancies for C(3A), C(3B), C(4A) and C(4B) are 0.5, respectively.

A stereoview of the unit cell packing of the [Ni(MEDT)$_2$] molecules viewed down the *b* axis (Fig. 2) shows the molecules forming a layered structure along the *c* axis. From Fig. 3 we can see the molecules are arranged as two differently oriented "stacks" along the *a* axis. This is similar to the structure of [Ni(PHDT)$_2$ [14].

The shortest intrastack S···S contact in this structure is 3.9312 Å, occurring between S(3) and S(3) $(-X+1, -Y+1, -Z+1)$. There is no close S···S

Table 2. Selected bond distances (Å) and angles (°) in [Ni(MEDT)$_2$]

Ni—S(1)	2.127(3)	Ni—S(1)^a	2.127(3)
Ni—S(2)	2.129(3)	Ni—S(2)^a	2.129(3)
S(1)—C(1)	1.703(9)	S(2)—C(2)	1.702(10)
S(3)—C(1)	1.730(9)	S(3)—C(4A)	1.814(11)
S(4)—C(2)	1.743(9)	S(4)—C(3A)	1.753(12)
C(1)—C(2)	1.399(12)	C(3A)—C(4A)	1.32(2)
C(4A)—C(5)	1.521(13)		

S(1)—Ni—S(1)^a	180.0	S(1)^a—Ni—S(2)^a	91.30(9)
S(1)—Ni—S(2)^a	88.70(9)	S(1)^a—Ni—S(2)	88.70(9)
S(1)—Ni—S(2)	91.30(9)	S(2)^a—Ni—S(2)	180.0
C(1)—S(1)—Ni	10.5.5(3)	C(2)—S(2)—Ni	105.4(3)
C(1)—S(3)—C(4A)	104.9(5)	C(2)—S(4)—C(3A)	105.6(7)
C(2)—C(1)—S(1)	118.8(7)	C(2)—C(1)—S(3)	126.6(7)
S(1)—C(1)—S(3)	114.6(5)	C(1)—C(2)—S(2)	119.0(7)
C(1)—C(2)—S(4)	126.5(7)	S(2)—C(2)—S(4)	114.5(5)
C(4A)—C(3A)—S(4)	125.2(13)	C(3A)—C(4A)—C(5)	127.9(12)
C(5)—C(4A)—S(3)	106.0(8)		

^{a} Symmetry transformations used to generate equivalent atoms: $-X, -Y+1, -Z$.

Table 3. Distances (Å) and angles (°) of some multi-sulfur 1,2-dithiolene complexes

Ligand	*n*	Ni—S	S—C	C=C	S—Ni—S	Ni—S—C	S—C—C	Reference
MEDT	1	2.126	1.73	1.34	88.7(2)	104.6(1)	120(1)	5
MEDT	0	2.128(3)	1.703(5)	1.399(12)	91.30(9)	105.5(3)	118.9(7)	This work
DDDT	1	2.148(2)	1.735(8)	1.339(11)	91.2(1)	104.5(2)	119.9(5)	3
DDDT^a	0 A	2.119(5)	1.68(2)	1.34(2)	90.9(2)	105(1)	120(2)	11
	B	2.123(6)	1.70(6)	1.40(3)	91.3(2)	106(1)	119(2)	
PDDT	1	2.142	1.726(3)	1.357(4)	91.4(1)	104.5(6)	119.6(2)	4
PDDT	0	2.132(1)	1.711(4)	1.395(5)	90.89(4)	105.7(6)	118.7(3)	13
PHDT	0	2.126	1.706	1.384	91.57(3)	105.01(11)	119.2(2)	14
DMIT	1	2.156(3)	1.72(1)	1.35(1)	93.2(1)	102.1(4)	121.4(8)	12

^{a} There are two crystallography independent molecules in the unit cell of [Ni(DDDT)$_2$].

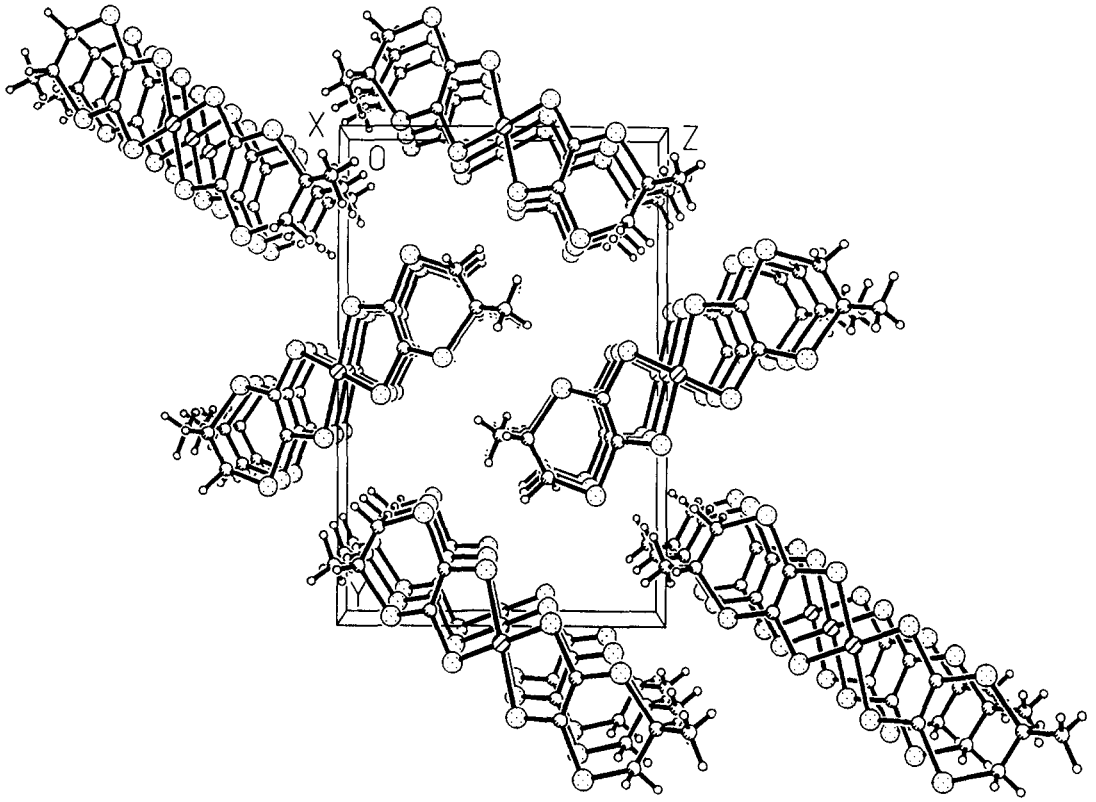


Fig. 2. Packing diagram of the unit cell of [Ni(MEDT)$_2$] looking down the *b* axis.

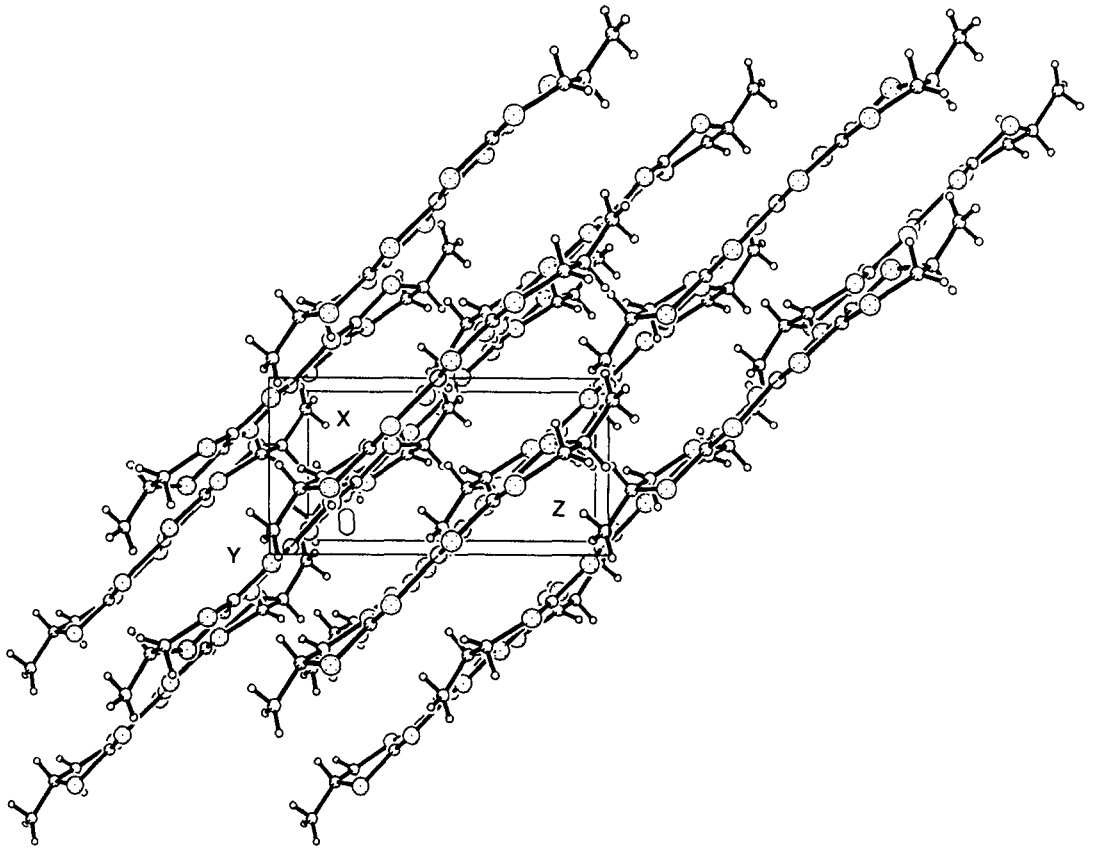


Fig. 3. Packing diagram of the unit cell of [Ni(MEDT)$_2$] looking down the *a* axis.

contact less than 3.70 Å. The nearest Ni···Ni contact is 5.273(3) Å, which is the length of the *a* axis. This is the intermediate value between the corresponding value of [Ni(DDDT)$_2$] (4.672 Å) and [Ni(PHDT)$_2$] (6.977 Å).

Acknowledgements—This work was supported by grants for key search project in climbing program from the State Science and Technology Commission and National Nature Science Foundation of China. Hoong-Kun Fun would like to thank the Malaysia Government and Universiti Sains Malaysia for research grant R&D No. 190-9609-2801.

REFERENCES

1. Cassoux, P., Valade, L., Kobayashi, H., Kobayashi, A., Clark, R. A. and Underhill, A. E., *Coord. Chem. Rev.* 1991, **110,** 115.
2. Bosseau, M., Valade, L., Legros, J. P., Cassoux, P., Garbauskas, M. and Interrante, L. V., *J. Am. Chem. Soc.* 1986, **108,** 1908.
3. Vance, C. T., Bereman, R. D., Bordner, J., Haffield, W. E. and Helms, J. H., *Inorg. Chem.* 1985, **24,** 2905.
4. Bereman, R. D. and Lu, H., *Inorg. Chim. Acta*, 1993, **204,** 53.
5. Yao, T. M., Zuo, J. L., You, X. Z. and Huang, X. Y., *Polyhedron*, 1996, **14,** 1487.
6. Singh, J. D. and Singh, H. B., *J. Chem. Soc., Perkin Trans.* 1992, 2913.
7. Varma, K. S., Evans, J., Edge, S., Underhill, A. E., Bojesen, G. and Becher, J., *J. Chem. Soc., Chem. Commun.* 1989, 257.
8. Siemens. XSCANS Users Manual Version 2.1. Siemens Analytical X-ray Instruments Inc., Madison, Wisconsin, U.S.A. 1994.
9. Sheldrick, G. M., *Acta Cryst.* 1990, **A46,** 467.
10. Sheldrick, G. M., *SHELXL*-93. *Program for Crystal Structure Refinement*. University of Göttingen, Germany, 1993.
11. Kim, H., Kobayashi, A., Sasaki, Y., Kato, R. and Kobayashi, H., *Bull. Chem. Soc. Jpn*, 1988, **61,** 579.
12. Valade, L., Legros, J. P., Bosseau, M. and Cassoux, P., *J. Chem. Soc., Dalton Trans.* 1985, 783.
13. Geiser, U., Tytko, S. F., Allen, T. J., Wang, H. H., Kini, A. M. and Williams, J. M., *Acta Cryst.* 1991, **C47,** 1164.
14. Zuo, J. L., Yao, T. M., You, F., You, X. Z., Fun, H. K. and Yip, B. C., *J. Mater. Chem.* 1996, **6**(10), 1633.

Pergamon

PII: S0277-5387(96)00439-1

Polyhedron Vol. 16, No. 9, pp. 1471 1475, 1997
Copyright © 1997 Elsevier Science Ltd
Printed in Great Britain. All rights reserved
0277-5387/97 $17.00+0.00

A mesoscopic molecular superparamagnet: preparation, crystal structure and magnetic properties of $[Mn_{12}O_{12}(O_2CMe)_4(O_2CEt)_{12}(H_2O)_4]\cdot 2H_2O\cdot 4EtCO_2H$ with an $S = 9$ ground state

Yong-Ge Wei, Shi-Wei Zhang,* Mei-Cheng Shao and You-Qi Tang

Department of Chemistry, Peking University, Beijing 100871, P.R. China

(Received 18 June 1996; accepted 27 August 1996)

Abstract—The first dodecanuclear manganese aggregate containing heterocarboxylate ligands $[Mn_{12}O_{12}(O_2CMe)_4(O_2CEt)_{12}(H_2O)_4]$ (**1**) has been prepared and structurally characterized. The single crystal X-ray diffraction of **1** shows that it is similar to $[Mn_{12}O_{12}(O_2CR)_{16}(H_2O)_4]$ (**2a**, R = Me or **2b**, R = Ph) in its skeletal structure but it has a different crystal structure. Primary magnetism studies imply that **1** has an $S = 9$ spin ground state. A clear hysteresis loop was also observed for a polycrystalline sample of $\mathbf{1}\cdot 2H_2O\cdot 4EtCOOH$, but there was no anomaly in susceptibility down to 1.5 K. The cluster **1** represents another example of nanometre-sized molecular superparamagnets without particle size distribution. © 1997 Elsevier Science Ltd. All rights reserved.

Keywords: manganese-oxo cluster; nanomolecule; molecular bistability; superparamagnet; molecular magnetism; mesoscopic physics and chemistry.

An important development in molecular magnetism is the progress from the study of the paramagnetic properties of isolated molecules to the design and synthesis of the so-called molecular ferromagnets—molecular materials exhibiting spontaneous magnetization below a critical temperature [1,2]. A fundamental step in the preparation of molecular ferromagnets is the synthesis of molecular species possessing large spin ground states, which are ferromagnetically arranged in the solid structure. Recently, synthetic methodologies for clusters of increasing complexity [3–10] have opened a new road to preparing this kind of molecule, with large spin ground state, because high nuclearity spin clusters could stabilize high-spin ground states. To date, several aggregates with high-spin ground states have been reported [9,11–18] and superparamagnetic-like behaviour has been proven in some of these aggregates [9,14,19]. Our research group began work on this project in 1993 and a ferromagnetic transition at $T_c = 3.3$ K in a manganese-containing high-spin cluster was observed in our laboratory and communicated in this journal recently [20]. In this communication, we report a manganese-containing mesoscopic molecular superparamagnet **1** with an $S = 9$ spin ground state.

To a clear solution of $Mn(O_2CMe)_2\cdot 4H_2O$ (2 g, 8.15 mmol) in 20 cm^3 60% (v/v) $EtCO_2H/H_2O$ was slowly added, dropwise, $KMnO_4$ (0.5 g, 3.15 mmol) with caution, followed by slow heating to 60°C. On cooling to room temperature, the resulting black-brown solution was filtered and allowed to stand in air without disturbance. After about 3 weeks, black crystals of $\mathbf{1}\cdot 2H_2O\cdot 4EtCO_2H$, were deposited in 60% yield based on Mn^{VII}. Elemental analyses of this sample are in agreement with the indicated formulation.

Cluster **1** crystallizes in the space group $I\bar{4}$ with two water and four propionic acid molecules and the corresponding crystallographic data for $\mathbf{1}\cdot 2H_2O\cdot 4EtCO_2H$ are given in Table 1. Unlike the cluster **2** [13,21], there are two discrete molecules of **1** in the asymmetric unit with essentially identical structures. As shown in Fig. 1, cluster **1** has a dimension of 1 nm owing to the longest metal–metal distance of 8.49 Å,

* Author to whom all correspondence should be addressed.

Table 1. Crystallographic data for $1 \cdot 2H_2O \cdot 4EtCO_2H$

Formula	$C_{56}H_{108}Mn_{12}O_{58}$
M_r	2368.7
Colour, habit	Black, capped prism
Crystal dimensions, mm	$0.15 \times 0.3 \times 0.4$
Crystal system	Tetragonal
Space group	$I\bar{4}$
Temp., °C	22
a, Å	26.645(10)
c, Å	13.608(5)
V, Å^3	9661(13)
Z	4
D (calc), g cm^{-3}	1.629
Absorption coeff., mm^{-1}	1.545
Radiation type (λ, Å)	0.71073
Goodness-of-fit	2.74
2θ range, °	3.0, 46.0
No. of total data	3757
No. of unique data	3702
No. of observed data	2956
$R(F)$, %	6.79
$wR(F)$, %	7.21

and is made up of a central $Mn^{IV}_4O_4$, almost ideal, cubane held within a non-planar ring of eight Mn^{III} atoms by μ_3-oxide atoms. However, peripheral ligation is by twelve μ_2-propionate, four μ_2-acetate and four H_2O groups. Besides μ_3-oxide bridges, the four Mn(1) and four Mn(2) atoms are linked by four μ_2-acetate bridges, but the four Mn(2) and four Mn(3) atoms are linked by eight μ_2-propionate bridges instead of the acetate groups as in **2a**. Octahedral Mn^{III} should be Jahn–Teller distorted, and this is apparent in the Mn(2) atoms with tetragonal elongation along the axes parallel to the principal molecular $\bar{4}$ axis. The Jahn–Teller effect also occurs in the Mn(3) atoms but this is probably an orthorhombic distortion. The four H_2O ligands are located on the four Mn(3) atoms to complete their octahedral coordination.

Variable-temperature magnetic susceptibility data were recorded at 10 kG in the range 1.5–300 K for a polycrystalline sample of cluster **1**, and are presented in Fig. 2. In Fig. 3 the effective magnetic moment per molecule versus temperature is shown. From this figure we find that the effective magnetic moment per molecule drops slightly from $12.03\mu_B$ at 300 K to $11.65\mu_B$ at 195 K, then it steadily increases with decreasing temperature to reach a maximum of $22.70\mu_B$ at 9.2 K, below which it drops again sharply to $5.17\mu_B$ at 1.5 K. This behaviour clearly indicates that there are appreciable intramolecular magnetic exchange interactions in this cluster and not all of the spin states of the cluster are equally thermally populated, because if there were no magnetic exchange interactions present in a mixed valency $Mn^{IV}_4Mn^{III}_8$ aggregate, or all the spin states were equally thermally populated, the spin-only effective magnetic moment with $g = 2$ should be equal to $15.87\mu_B$. Apparently, the principal interaction in this cluster is ferromagnetic, owing to the increase in effective moment per molecule with decreasing temperature below 195 K and the cluster has a maximum average spin state of 11 at 9.2 K. However, there must be some competing antiferromagnetism as well, owing to the decrease in the effective moment per molecule and the smaller values than $15.87\mu_B$ with decreasing temperature in the range from 300–195 K. Furthermore, the shape of Fig. 3 and the average spin state of 11 at 9.2 K suggest that all of the clusters are populated in some large spin ground states which are net ferromagnetic at low temperature. The decline in effective magnetic moment below 9 K reflects zero-field splitting in the ground state which is associated with the single-ion anisotropy of the Jahn–Teller-distorted manganese(III) ions.

In order to determine the spin of the ground state, bulk magnetization (M) measurements were performed for this compound at 1.5 K in fields in the range 0–70 kG. The bulk reduced magnetization ($M/N\beta$) is shown in Fig. 4, plotted as a function of H/T. This curve should follow a Brillouin function [22], and at large H/T (i.e. spin saturation), $M/N\beta$ approaches a maximum value of $2S$ with $g = 2$. Figure 4 shows clearly that the cluster **1** has an $S = 9$ ground state because the value of $2S$ goes towards 18 when H/T is greater than 2. Additionally, a break was observed in this curve at $H/T \approx 1$, which suggests that there should be a transition of molecular origin relative to the applied magnetic field and temperature in this cluster.

Interestingly, this cluster exhibits a clear hysteresis loop below 3 K, as shown in Fig. 5, although its curve of initial magnetization is not surrounded by this loop. This hysteresis effect is totally different from that of a three-dimensional ordered ferromagnet, which shows an anomaly in the susceptibility (see Fig. 2) and specific heat curves at the Curie temperature, and appears to be of molecular origin. We feel that this magnetic hysteresis may result from the applied field-induced molecular states transition between the two stable states $M_S = \pm 9$ of this cluster and this kind of transition could indeed be observed in the initial magnetization curve near the "coercive" field, where there is a break in this curve (Figs 2 and 5). Similarly to cluster **2a**, a superparamagnetic-like property should be responsible for the magnetic behaviour of this cluster.

To conclude, the present results indicate that cluster **1** represents the first example of a dodecanuclear manganese aggregate containing mixed carboxylate ligands structurally characterized by single crystal X-ray diffraction and is another interesting compound with mesoscopic structure, which is a new field between micro- and macroscopic structures, and has a dimension of several to hundreds of nanometres, and molecular superparamagnetic properties. Since there is no molecular weight distribution, it is a better model system for mesoscopic physics and chemistry.

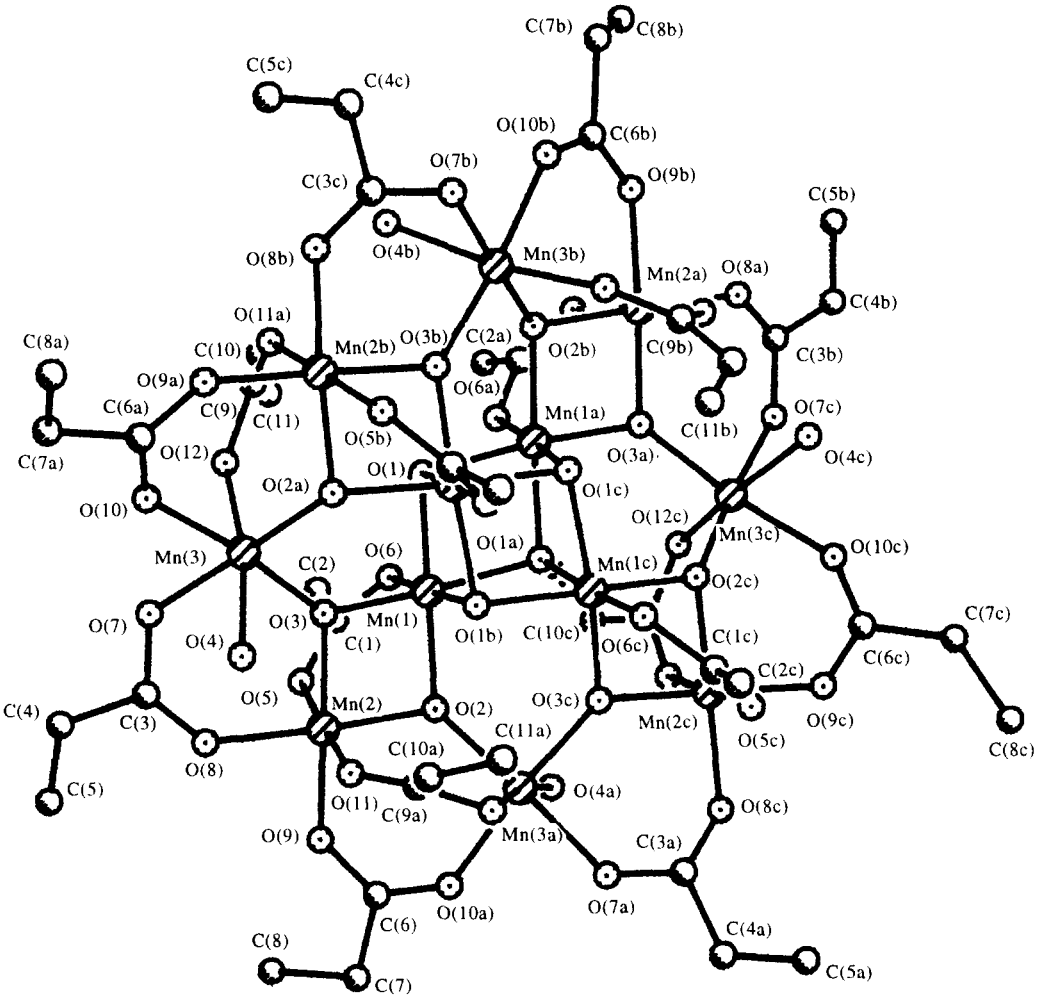


Fig. 1a. The structure of cluster 1. Selected distances (Å): Mn(1)...Mn(1a), 2.943(5); Mn(1)...Mn(1b), 2.828(5); Mn(1)...Mn(2), 2.775(4); Mn(1)—O(1), 1.917(10); Mn(1)—O(1a), 1.966(10); Mn(1)—O(1b), 1.901(13); Mn(1)—O(2), 1.909(10); Mn(1)—O(3), 1.827(10); Mn(1)—O(6), 1.871(15); Mn(2)—O(3), 1.894(10); Mn(2)—O(11), 2.127(14); Mn(2)—O(5), 2.243(13); Mn(2)—O(2), 1.887(11); Mn(2)—O(8), 1.916(11); Mn(2)—O(9), 1.931(12); Mn(3)—O(3), 1.921(10); Mn(3)—O(7), 1.963(11); Mn(3)—O(10), 2.006(11); Mn(3)—O(12), 2.082(13); Mn(3)—O(2a), 1.902(10).

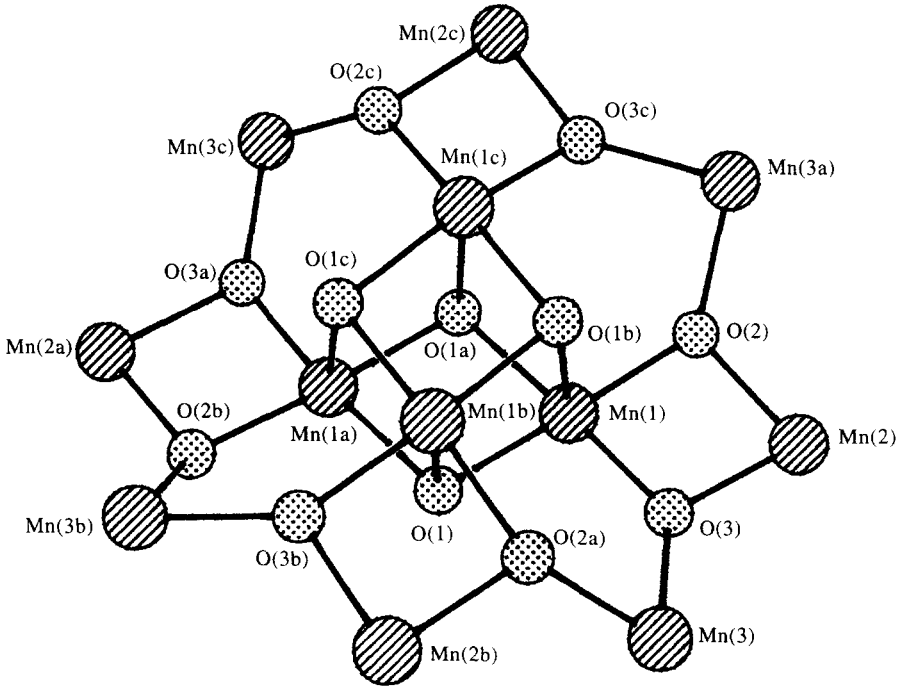


Fig. 1b. A view of the $[Mn_{12}O_{12}]^{16+}$ core.

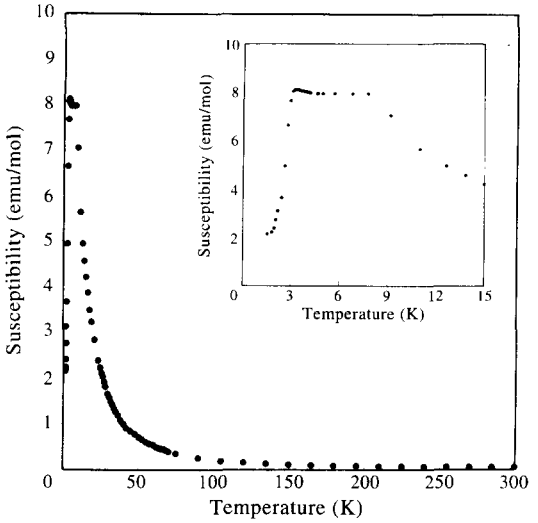


Fig. 2. Plot of magnetic susceptibility per mole (χ_M) measured at 10 kG versus temperature for $1 \cdot 2H_2O \cdot 4EtCO_2H$.

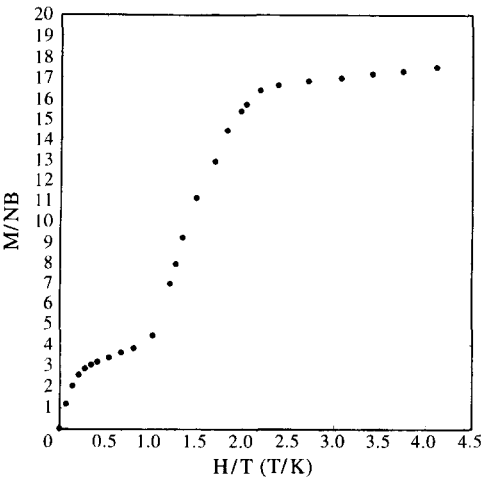


Fig. 4. Plot of reduced magnetization, $M/N\beta$ versus H/T for $1 \cdot 2H_2O \cdot 4EtCO_2H$, where N is Avogadro constant number, β is the Bhor magneton, and H is the magnetic field.

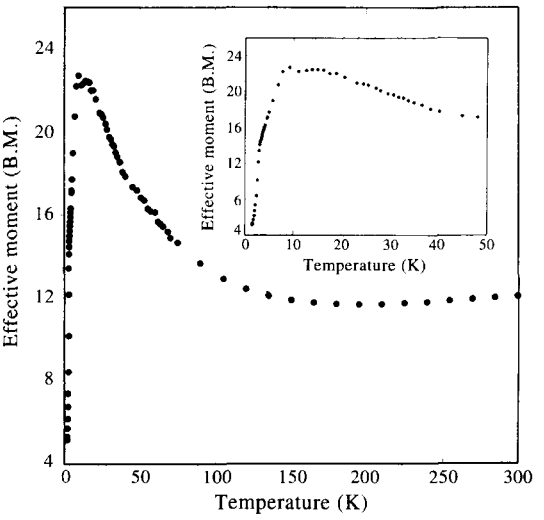


Fig. 3. Plot of effective magnetic moment per molecule (μ_{eff}/molecule) measured at 10 kG versus temperature for $1 \cdot 2H_2O \cdot 4EtCO_2H$.

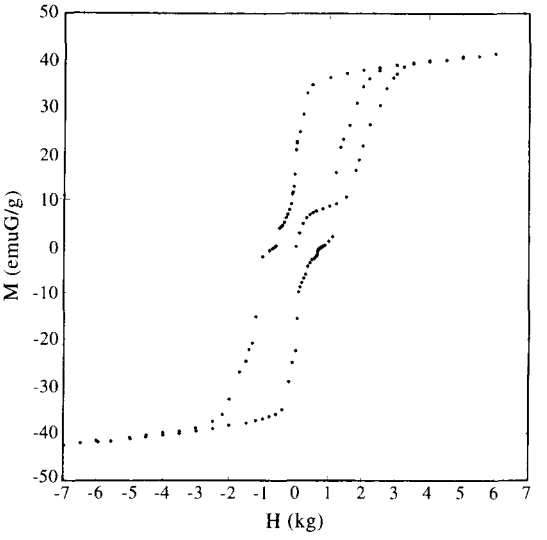


Fig. 5. Hysteresis loop of a powder sample of $1 \cdot 2H_2O \cdot 4Et$-CO_2H at 1.5 K.

In addition, the observed hysteresis for individual molecules implies that there are two stable states in some molecular systems which could be frozen under an applied magnetic field. This molecular bistability opens a new road to store information at the molecular level.

Acknowledgements—Financial support from the National Natural Science Foundation of China, the Key Project in Climbing Program from the State Science and Technology Commission and the Doctorial Foundation of the State Educational Committee are gratefully acknowledged. We also thank Professor Wen-Sheng Zhou for helpful discussions in magnetism and the editors and the referees for revision of this manuscript.

REFERENCES

1. Miller, J. S. and Dougherty, D. A. (Eds), *Mol. Cryst. Liq. Cryst.*, 1989, 176.
2. Gatteschi, D., Khan, Ö., Miller, J. S. and Palacio, F., *Magnetic Molecular Materials*, NATO ASI Series. Kluwer, Dordrecht, 1991.
3. Wieghardt, K., Pohl, K., Jibril, I. and Huttner, G., *Angew. Chem., Int. Ed. Engl.*, 1984, **23,** 77.
4. Gorun, S. M., Papaefthymiou, G. C., Frankel, R. B. and Lippard, S. J., *J. Am. Chem. Soc.*, 1987, **109,** 3337.
5. Micklitz, W. and Lippard, S. J., *J. Am. Chem. Soc.*, 1989, **111,** 6856.
6. Heath, S. L. and Powell, A. K., *Angew. Chem., Int. Ed. Engl.*, 1992, **31,** 191.
7. Goldberg, D. P., Caneschi, A. and Lippard, S. J., *J. Am. Chem. Soc.*, 1993, **115,** 9299.

8. Dimitrou, K., Folting, K., Streib, W. E. and Christou, G., *J. Chem. Soc., Chem. Commun.*, 1994, 1385.
9. Taft, K. L., Papaefthymiou, G. C. and Lippard, S. J., *Inorg. Chem.*, 1994, **33,** 1510.
10. Squire, R. C., Aubin, S. M. J., Folting, K., Streib, W. E., Hendrickson, D. N. and Christou, G., *Angew. Chem., Int. Ed. Engl.*, 1994, **34,** 887.
11. Caneschi, A., Gatteschi, D., Laugier, J., Rey, P., Sessoli, R. and Zanchini, C., *J. Am. Chem. Soc.*, 1988, **110,** 2795.
12. Caneschi, A., Gatteschi, D. and Sessoli, R., *J. Am. Chem. Soc.*, 1991, **113,** 5873.
13. Sessoli, R., Tsai, H.-L., Schake, A. R., Wang, S., Vincent, J. B., Folting, K., Gatteschi, D., Christou, G. and Hendrickson, D. N., *J. Am. Chem. Soc.*, 1993, **115,** 1804.
14. Eppley, H. J., Tsai, H.-L., de Vries, N., Folting, K., Christou, G. and Hendrickson, D. N., *J. Am. Chem. Soc.*, 1995, **117,** 301.
15. Tsai, H.-L., Wang, S., Folting, K., Streib, W. E., Hendrickson, D. N. and Christou, G., *J. Am. Chem. Soc.*, 1995, **117,** 2503.
16. Taft, K. L., Caneschi, A., Pence, L. E., Delfs, C. D., Papaefthymiou, G. C. and Lippard, S. J., *J. Am. Chem. Soc.*, 1993, **115,** 11753.
17. Goldberg, D. P., Caneschi, A., Delfs, C. D., Sessoli, R. and Lippard, S. J., *J. Am. Chem. Soc.*, 1995, **117,** 5789.
18. Mallah, T., Auberger, C., Verdaguer, M. and Veillet, P., *J. Chem. Soc., Chem. Commun.*, 1995, 61.
19. Sessoli, R., Gatteschi, D., Caneschi, A. and Novak, M. A., *Nature*, 1993, **365,** 141.
20. Zhang, S.-W., Wei, Y.-G., Liu, Q., Shao, M.-C. and Zhou, W.-S., *Polyhedron*, 1996, **15,** 1040.
21. Lis, T., *Acta Cryst.*, 1980, **B36,** 2042.
22. Carlin, R. L., *Magnetochemistry*. Springer-Verlag, Berlin, 1986.

Pergamon

PII: S0277-5387(96)-00441-X

Polyhedron Vol. 16, No. 9, pp. 1477–1482, 1997
Copyright © 1997 Elsevier Science Ltd
Printed in Great Britain. All rights reserved
0277-5387/97 $17.00+0.00

Copper complexes derived from 1-(2-carboxybenzoyl)thiosemicarbazide (H_3L): syntheses, characterization and crystal structure of $[Cu_3L_2(Py)_6](HIm)(H_2O)_2$

Xu Shen,[a]* Daxu Wu,[a] Xiaoying Huang,[a] Qiutian Liu,[a] Zhishu Huang and Beisheng Kang[b]*

[a] State Key Laboratory of Structural Chemistry and Fujian Institute of Research on the Structure of Matter, Chinese Academy of Sciences, Fuzhou 350002, P.R. China

[b] Department of Chemistry, Zhongshan University, Guangzhou 510275, P.R. China

(Received 12 July 1996; accepted 23 August 1996)

Abstract—The reaction of $CuCl_2 \cdot 2H_2O$ with 1-(2-carboxybenzoyl)thiosemicarbazide (H_3L) and imidazole (HIm) in NaOH gave a Cu^{II} complex, which was crystallized from pyridine (Py) to give complex **1**, $[Cu_3L_2(Py)_6(HIm)](H_2O)_2$. The complex molecule contains a linear Cu_3 array in which the central copper atom at the crystallographic inversion centre has an octahedral environment and the other two Cu atoms are square pyramidal, each bridged to the central Cu atom *via* the L group, with the atoms O(1) and N(2) chelating to Cu(1), and the atoms N(1), S and O(2) to Cu(2). The carboxylate groups coordinate to the metal atoms in a unidentate fashion. Complex **2**, $[Cu_2(H_3L)_2Cl_2](H_2O)_3$, obtained by the reaction of $CuCl_2 \cdot 2H_2O$ with H_3L has been characterized by IR, UV, NMR (^1H and ^{13}C) spectra, and TGA and molar conductance measurements. The ESR and magnetic moment measurements show that the Cu atoms in complex **2** are in the Cu^I oxidation state. © 1997 Elsevier Science Ltd. All rights reserved.

Keywords: syntheses; crystal structure; Cu^{II} complex; Cu^I complex; 1-(2-carboxybenzoyl)thiosemicarbazide; pyridine.

Substituted phthalamidic acids are important for their many kinds of pharmacological activities and analytical uses [1,2]. It has been reported that their metal complexes could exhibit more efficient actions. Up to now, many substituted phthalamidic acids and their transition metal complexes have been reported [3]. However, most of the published work has focused on ligands with only oxygen and nitrogen donor atoms. In recent years, metal complexes with sulfur-containing ligands such as thiosemicarbazone and its derivatives have been given great attention because of their biological and magnetic properties [4,5]. It is also thought that the N,N,S-tridentate ligand system is a common feature for carcinostatic potency. In particular, the copper complexes of pyridine-2-carbaldehyde thiosemicarbazone have been shown to be stable in biological systems [4] and have *in vitro* cytotoxic effects against Ehrlich cells, and a second mechanism of interaction has been suggested involving the binding of the copper(II) drug to the nitrogen bases of DNA or RNA [6].

In our previous work, a series of lanthanide complexes with an amido acid derived from 4-pheynylthiosemicarbazide were reported [7], and the biological activity studies showed that some of them (Ce, Sm and Tm) demonstrated definite antiarthritic activities *in vivo*. However, no X-ray crystallographic data on such complexes have yet been reported. In order to study the structural properties of complexes with these kinds of ligands, and to extend the study on the relationship between the coordination behaviour and the biological activities, we have synthesized two copper complexes with a new ligand derived from thiosemicarbazide (Fig. 1).

* Authors to whom correspondence should be addressed.

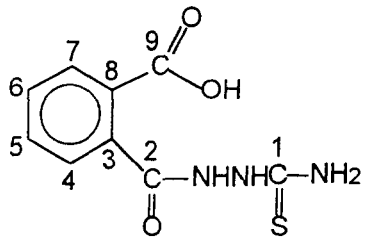


Fig. 1. 1-(2′-carboxybenzoyl)thiosemicarbazide (H_3L) (m.f. $C_9H_9O_3N_3S$) (the numbers in the figure are denoted for ^{13}C NMR assignments).

EXPERIMENTAL

All the chemicals are of A.R. grade and used without further purification.

Synthesis of the ligand H_3L

To 100 cm^3 of acetonitrile solution containing phthalic anhydride (3.8 g, 25.3 mmol) was added thiosemicarbazide (2.3 g, 25.3 mmol). This reaction mixture was stirred at 60–70°C for 2 h, then was refluxed for one more hour. The precipitate formed was filtered and recrystallized from methanol–ethanol (2:1, v/v), and dried *in vacuo*. Yield, 1.54 g (85%). Found: C, 45.1; H, 4.1; N, 17.7. Calc. for $C_9H_9N_3O_3S$: C, 45.2; H, 3.8; N, 17.6%.

Synthesis of complex **1** $[\{Cu_3L_2(Py)_6\}(HIm(H_2O)_2]$

To 30 cm^3 of an aqueous solution of NaOH (0.1 g, 3.0 mmol) and H_3L (0.3 g, 1.0 mmol) was added $CuCl_2 \cdot 2H_2O$ (0.3 g, 1.5 mmol). After stirring at room temperature for 1 h, imidazole (0.1 g, 1.5 mmol) was added. The mixture was then stirred continuously for two more hours. The brown solid precipitated was isolated by filtration, washed repeatedly with water and anhydrous methanol and dried *in vacuo*. After slow evaporation of the pyridine solution of the solid (0.2 g in 10 cm^3 of pyridine) over a period of a few weeks (the volume was reduced to about 3 cm^3), deep green crystals deposited, which were filtered and dried in air. Yield, 0.1 g. Found: C, 49.1; H, 4.5; N, 16.2. Calc. for $C_{51}H_{50}N_{14}O_8S_2Cu_3$: C, 49.3; H, 4.0; N, 15.8%.

Synthesis of complex **2** $[\{Cu_2(H_3L)_2Cl_2\}(H_2O)_3]$

To 25 cm^3 of an anhydrous methanolic solution containing H_3L (0.6 g, 2.5 mmol) was added $CuCl_2 \cdot 2H_2O$ (0.4 g, 2.5 mmol). After stirring for 3–4 h at room temperature, a white product precipitated and was collected, washed thoroughly with anhydrous methanol and dried *in vacuo*. Yield, 0.5 g (57%). Found: C, 29.4; H, 3.0; Cl, 10.1; N, 11.4; S, 9.2. Calc. for $C_{18}H_{24}N_6O_9S_2Cu_2Cl_2$: C, 29.6; H, 3.3; Cl, 9.7; N, 11.5; S, 8.8%.

Physical measurements

Elemental analyses (C, H and N) were performed on a Carlo–Erba 1106 elemental analyser. The contents of Cl and S were analysed in our group. IR spectral data were recorded on a Magna 750 spectrometer as KBr disks in the range of 4000–200 cm^{-1}. UV spectra were collected by a Shimadzu UV-300 spectrophotometer. NMR (^1H and ^{13}C) spectra were recorded on a Bruker AM 500 spectrometer in DMSO-d_6 solution. ESR spectra were measured with a Bruker 2000-SRC spectrometer. Magnetic susceptibility measurements were carried out at room temperature with a CTP-F_{82} Faraday balance, and by the Guoy method with $CuSO_4 \cdot 5H_2O$ ($\chi_g = 6.06 \times 10^{-6}$ c.g.s. μ) as calibrant. Molar conductance values were collected on a Shanghai-11A molar conductometer in DMSO solution. TGA data were recorded in nitrogen between room temperature and 450°C by a Shimatzu TGA 50 thermogravimetric analyser.

Crystal structure determination

Crystallographic details for complex **1** are listed in Table 1. The unit-cell parameters were determined by a least-squares treatment obtained with $10.09 < \theta < 10.93°$. The single crystal was mounted on an Enraf–Nonius CAD4 diffractometer for data collection. Three reflections were chosen as intensity standards and were remeasured every 400 reflections. No significant intensity decay was found during the data collection. Data were corrected for Lorentz, polarization and absorption effects. All the calculations were performed on a VAX 785 computer using the TEXSAN program package. The structure was solved by heavy-atom methods with some of the non-hydrogen atoms located by successive difference Fourier syntheses, and was refined by the full-matrix least-squares method with anisotropic thermal parameters for all the non-hydrogen atoms. Hydrogen atoms were included as fixed contributions and not refined. The solvent imidazole molecule was disordered over two positions and atom N(8) is the statistical distribution of C and N atoms. The occupancy percentage for H(25), which would be attached to the C atom is 50%.

RESULTS AND DISCUSSION

The syntheses of the two complexes can be described by the following two equations:

$$2H_3L + 3CuCl_2 \cdot 2H_2O \xrightarrow[2.Py]{1.NaOH/H_2O} \text{Complex } \mathbf{1}$$

$$H_3L + CuCl_2 \cdot 2H_2O \xrightarrow{MeOH} \text{Complex } \mathbf{2}$$

Complex **1** is a deep green crystalline solid, while complex **2** is a white powder. Both are insoluble in common solvents such as alcohol, chloroform and

Table 1. Summary of crystallographic data and parameters for complex **1**

Formula	$C_{51}H_{50}N_{14}O_8S_2Cu$
M	1241.80
Crystal size/mm	$0.6 \times 0.25 \times 0.25$
Crystal colour and habit	Deep green hexagonal prism
Crystal system	Monoclinic
Space group	$C2/c$(No. 15)
Cell constants	
a/Å	33.69(1)
b/Å	9.018(4)
c/Å	18.044(5)
β/°	91.04(3)
V/Å^3	5481(3)
Z	4
D_c/g cm^{-3}	1.50
Radiation/Å	Mo-K_α(λ = 0.71069) Graphite-monochromated
F(000)	2548
μ/cm^{-1}	12.93
Range of hkl	±40, 0–10, 0–21
2θ max./°	49.9
Scan width/°	$0.95+0.35\tan\theta$
Scan speed/min.$^{-1}$	< 5.41
No. of reflections measured	5332
No. of unique reflections	5275
No. of reflections with $I > 3\sigma(I)$	2395
No. of variables	354
Temperature/°C	23
R	0.057
R_w	0.062
GOF	1.31
Max. shift in final cycle	0.68
$\Delta\rho$ max., min./eÅ^{-3}	0.56, −0.40

acetonitrile, but soluble in DMF, DMSO and Py. The low molar conductance values of 13.58 $\mu s \cdot cm^{-1}$ for complex **1** and 7.32 $\mu s \cdot cm^{-1}$ for complex **2** imply a non-electrolytic nature for these neutral complexes.

The TGA data show that complex **2** began to lose three water molecules at about 53–70°C, corresponding to the weight loss of 7.82% (Calc. 7.40%). Because of the low temperature, such water molecules can be regarded as lattice water. At about 296°C, this complex tends to decompose.

For complex **1**, the ESR spectrum at 286 K consists of one band with $g = 2.0866$, $\Delta H = 178.2$ G, and at 77 K, it is composed of one band with $g = 2.0910$, $\Delta H = 177.0$ G, showing that the copper ions in complex **1** remain in the 2+ oxidation state. For complex **2**, there are no signals in the ESR spectra at the above two temperatures, and the result of the magnetic susceptibility measurement at room temperature showed that complex **2** was diamagnetic in nature, confirming that the Cu ions in complex **2** are in the Cu^I state.

Description of the structure of complex **1**

The molecular structure and packing in the unit cell for complex **1** are depicted in Figs 2 and 3, respectively. Selected bond distances and angles are summarized in Table 2.

As shown in Fig. 1, the three copper atoms are linked together linearly by two μ_2-bridged L groups. The central Cu(1) atom is located on the crystallographic inversion centre with either of the other two copper atoms located 4.738(2) Å away. The Cu(1) atom is in a six-coordinated octahedral geometry with the two pyridine molecules in axial positions and the two amido-carbonyl oxygen atoms [O(1), O(1a)] in the equatorial plane. The terminal Cu(2) atom is coordinated in a trigonal-bipyramidal geometry composed of two nitrogen atoms from two pyridine molecules and one sulfur atom from the thiourea, as well as one oxygen atom from the carboxylate. Thus, the L group forms two five-membered chelate rings with the Cu atoms, ring Cu(1)O(1)C(1)N(1)N(2) and ring Cu(2) SC(9)N(2)N(1), with a dihedral angle of 7.5(1)°. A third seven-membered ring, Cu(2)O(2)C(8)C(7)C(2) C(1)N(1), is puckered along atoms N(1) and C(8), with a dihedral angle of 106.9(4)° between the two least-squares planes N(1)C(1)C(2)C(7)C(8) and C(8)O(2)Cu(2)N(1). Therefore, the ligand L is η^2(O,N)-chelated to Cu(1) and η^3(N,S,O)-chelated to Cu(2).

The steric congestion of the pyridine molecules in

Table 2. Selected atomic distances (Å) and bond angles (°) for complex **1**

Cu(1)—O(1)	1.960(5)	Cu(2)—N(4)	2.234(8)	Cu(2)—N(6)	2.024(7)	C(1)—O(1)	1.292(9)
Cu(1)—N(2)	1.991(7)	Cu(2)—N(1)	1.974(6)	Cu(2)—S	2.277(3)	N(1)—N(2)	1.415(8)
Cu(1)—N(5)	2.50(1)	Cu(2)—O(2)	1.992(6)	C(1)—N(1)	1.29(1)	N(2)—C(9)	1.33(1)
						S—C(9)	1.718(8)

O(1)—Cu(1)—N(2)	80.7(2)	N(1)—Cu(2)—O(2)	91.5(3)	N(6)—Cu(2)—N(4)	90.2(3)
O(1)—Cu(1)—N(5)	91.7(3)	N(1)—Cu(2)—N(6)	177.9(3)	N(6)—Cu(2)—S	93.2(2)
N(2)—Cu(1)—N(5)	91.6(3)	N(1)—Cu(2)—N(4)	90.7(3)	O(2)—Cu(2)—N(6)	89.8(3)
		N(1)—Cu(2)—S	84.7(2)	O(2)—Cu(2)—N(4)	117.3(3)
		N(4)—Cu(2)—S	112.4(2)	O(2)—Cu(2)—S	130.3(2)

O(1w)···O(3)	2.91(1)	O(1w)···N(3)	2.96(1)

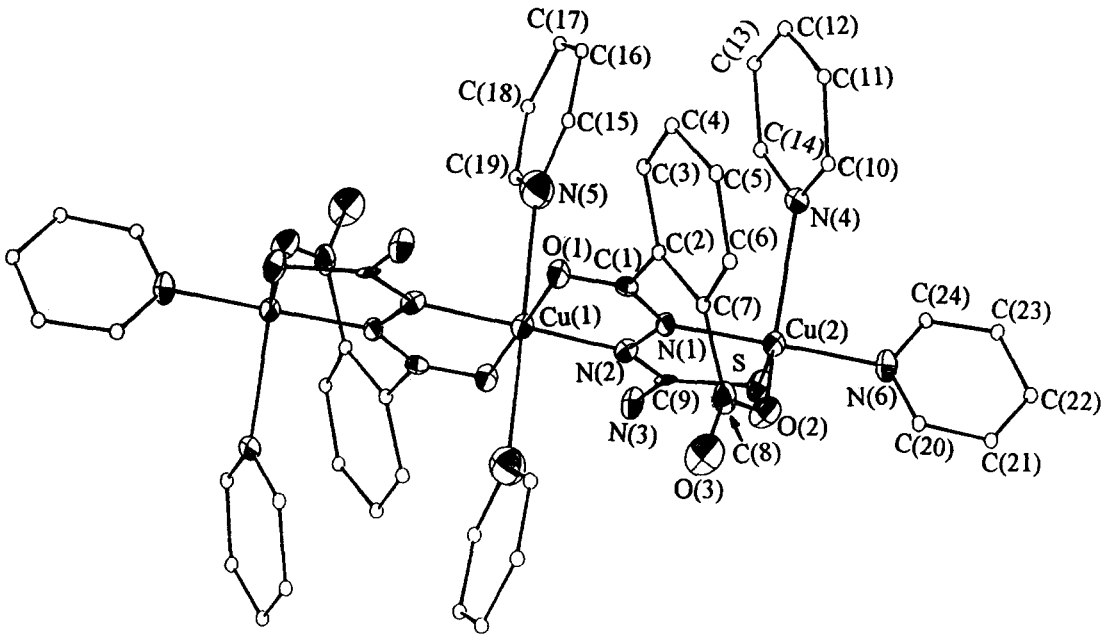


Fig. 2. Structure of the $[Cu_3L_2(Py)_6]$ core of complex **1** with the hydrogen atoms omitted for clarity.

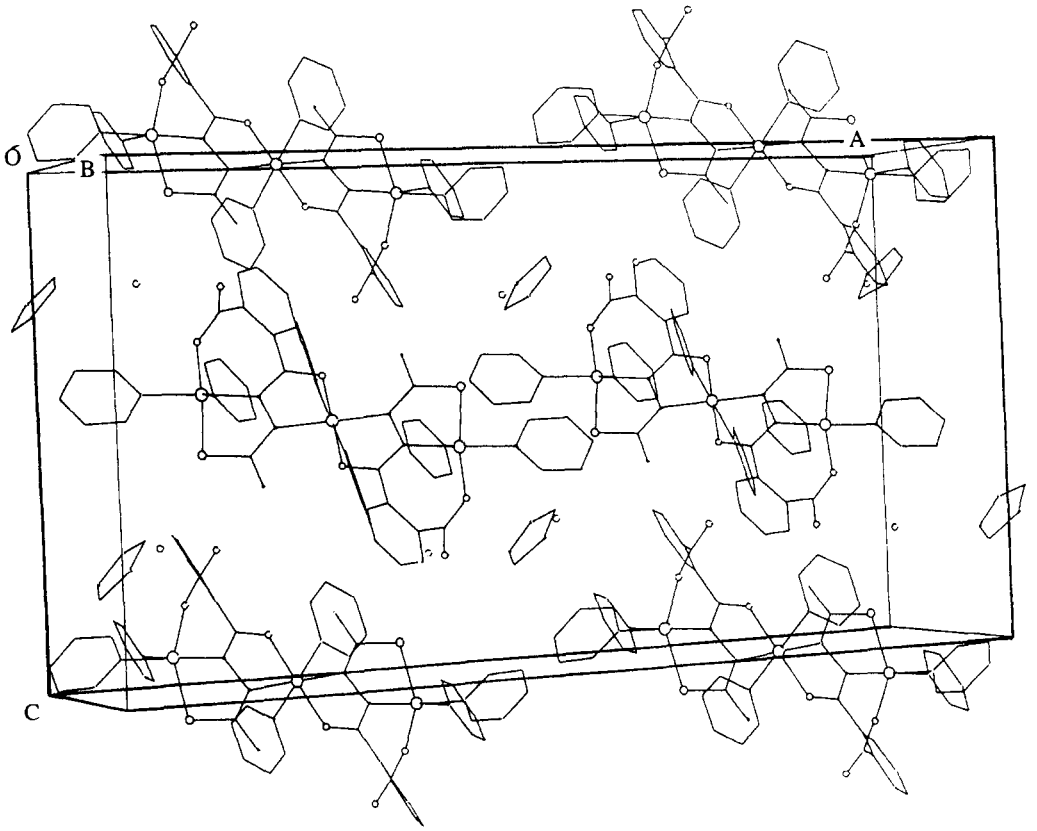


Fig. 3. The unit cell packing of complex **1** $[\{Cu_3L_2(Py)_6\}(HIm)(H_2O)_2]$.

the complex is: Py(5) > Py(4) > Py(6) as shown by the order of the Cu—N_{Py} distances Cu(1)—N(5) > Cu(2)—N(4) > Cu(2)—N(6). The Cu(1)—O(1) and Cu(1)—N(2) distances are 1.960(5) and 1.991(7) Å, respectively, both of which are slightly longer than those in a previously reported dinuclear copper(II)

semicarbazone compound with a similar coordination mode [8], probably owing to the steric effect of the pyridine molecules. The distances Cu(2)—S [2.277(3) Å] and Cu(2)—N(1) [1.974(6) Å] agree well with the corresponding bonds in the Cu^{II} complexes containing thiosemicarbazone ligands [5]. The bond Cu(2)—O(2) [1.992(6) Å] involving the carboxylate group is within the normal range of unidentate coordination of a carboxylate to Cu^{II} [9]. The bonds C(1)—N(1), N(2)—C(9), O(1)—C(1) and C(9)—S are well within the range of published results for thiosemicarbazone complexes [5], indicating the existence of C(1)=N(1), N(2)=C(9), O(1)—C(1) and C(9)—S bonds. It is noted that the N—N bond distance of 1.415(8) Å is slightly longer than those reported in the literature for thiosemicarbazone copper(II) compounds [5,10], which might be owing to their different coordination mode. The non-coordinated carboxylate oxygen atom O(3) is hydrogen-bonded with both the solvate water molecule [O(1w)···O(3) = 2.91(1) Å, O(1w)—H_{23}—O(3) = 156.0(1)°] and the NH_2 group [O(3)···N(3) = 2.96(1) Å, O(3)—H_2—N(3) = 166.9(1)°]. The imidazole molecule adopts a space-filling role only.

NMR (^1H, ^{13}C)

Because of the strong paramagnetic nature of complex **1**, it is hard to interpret its NMR spectral data.

In the ^1H NMR spectrum of the free ligand H_3L, the proton signal at δ 13.73 is attributed to OH(COOH), while the two peaks at δ 10.36 and 9.44 are ascribed to NH[1H, C(O)NH] and NH[1H, NHC(S)], respectively. The proton signals for the phenyl ring are found at δ 8.23, 7.90, 7.68 and 7.60. The peak for NH(2H, C(S)NH_2) appears at δ 7.43.

In the ^1H NMR spectrum of complex **2**, most of its proton signals are observed shifted downfield relative to those of the free ligand H_3L. The peak at δ 13.63 is ascribed to OH(1H, COOH), which is much closer to that of the ligand H_3L, suggesting that in complex **2** the carboxylate group is not involved in coordination to the metal ion. In comparison with the free ligand H_3L, the two slightly downfield-shifted proton signals of NH[1H, C(O)NH] and NH[1H, NHC(S)] at δ 10.68 and 10.24, respectively, indicate that neither of these two nitrogen atoms binds to the metal atom, and the slightly downfield shift effect might be due to the coordination of the S and the O atom of the amido-carbonyl group to the metal ion, which can be confirmed further by the IR spectra. Unlike for the free ligand, two proton signals at δ 8.89 and 7.54 appear for C(S)NH_2 in complex **2**.

In the ^{13}C NMR spectrum of the ligand H_3L, the signal at δ 182.94 is ascribed to C_1 (atom labelling is given in Fig. 1), and δ 168.32 to C_2 and C_9. The other six peaks at δ 137.36, 132.80, 130.24, 130.17, 129.33 and 128.62 are attributed to C_3, C_5, C_7, C_6, C_8 and C_4, respectively.

With respect to complex **2**, all the signals have been found to shift to higher fields compared with those of the ligand. The signal for C_1 is observed to shift to a higher field at δ 179.01, such a high-field shift effect may be ascribed to the existence of the M → S back donation in complex **2**. Unlike in the free ligand H_3L, C_2 and C_9 are found separately at δ 167.60 and 167.95, respectively. The signals for the phenyl ring are observed at δ 136.26 (C_3), 132.31 (C_5), 129.89 (C_7), 129.74 (C_6), 128.88 (C_8) and 128.16 (C_4).

IR and UV spectra

For all three compounds (H_3L, **1** and **2**) bands in the region 3390–3180 cm^{-1} are usually attributed to the stretching frequencies ν(NH), and bands in the region 3530–3540 cm^{-1} in the two complexes can be assigned to ν(OH) from water. The intense band arising from the amide-I stretching vibration at 1655 cm^{-1} in the free ligand undergoes changes in frequency and intensity when compared with those of the two complexes. In complex **1**, it shifts to 1548 cm^{-1}, while in complex **2**, it appears at 1630 cm^{-1}, suggesting the complexation of the oxygen atom of the amido-carbonyl to the metal ion in these two complexes. As regards the mode of the C=S group, this band at 840 cm^{-1} in the free ligand H_3L has changed to 735 cm^{-1} in complex **1**, suggesting coordination *via* the thiolate sulphur atom, which is also indicated by the presence of a band of 345 cm^{-1} assignable to ν(Cu—S) [11]. For complex **2**, the ν(C=S) band has shifted to 785 cm^{-1}, indicating engagement of the thionyl sulfur atom in the complex formation, and the band at 257 cm^{-1} is assigned to ν(Cu—S) [12]. Additionally, in complex **1**, coordination of the nitrogen and oxygen atoms to Cu atoms is observed by the presence of bands at 450–480 cm^{-1}, assignable to ν(Cu—N) [13] and ν(Cu—O) [4].

The UV spectral diagrams of the ligand H_3L and the two complexes are shown in Fig. 4. The absorption at about 272 nm for the compounds is assigned to the $^1L(a)$ absorption of the aromatic ring. The absorption peak at 330.4 nm for the free ligand H_3L is attributed to a $\pi \rightarrow \pi^*$ transition. In the case of the spectra of the two complexes, there is no absorption above 300 nm, implying coordination of the oxygen atom of the amido-carbonyl to the metal ion in the complexes. The absorption band at 300 nm in complex **1** is ascribed to $^1L(b)$ of the aromatic ring.

Therefore, based on the aforementioned facts and known preference of Cu^I for the tetrahedral structure [15], the proposed structure of complex **2** can be tentatively described as that shown in Fig. 5.

Acknowledgements—The financial support from the Postdoctoral Science Foundation (XS) and NNSF of China are greatly appreciated as well as the Natural Science Foundation of Guangdong Province.

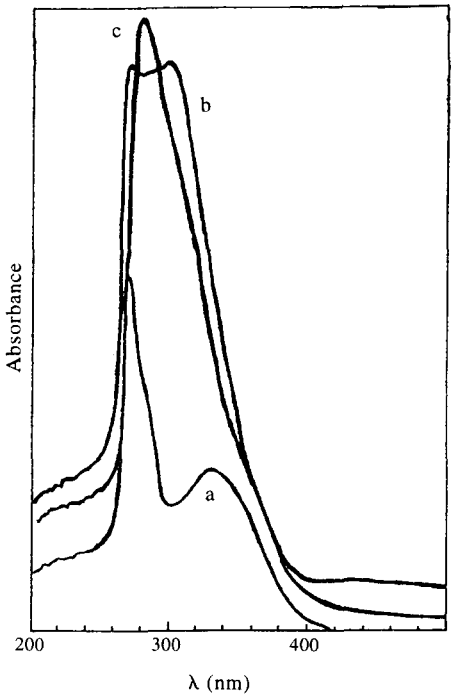


Fig. 4. UV spectral diagrams of the ligand H_3L (**a,** 0.081 mg/cm^3), complex **1** (**b,** 0.069 mg/cm^3), and complex **2** (**c,** 1.075 mg/cm^3) in DMSO solution.

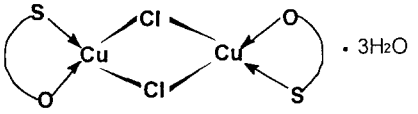


Fig. 5. Proposed structure of complex **2,** $[Cu_2(H_3L)Cl_2]\cdot 3H_2O$ ($\widehat{OS} = H_3L$).

REFERENCES

1. Malcolm, S. and Pressman. D., *J. Am. Chem. Soc.*, 1954, **76,** 2863.
2. Datta, S. K., *Z. Anal. Chem.*, 1955, **148,** 259, 267, 335.
3. Sigel, H. and Martin, R. B., *Chem. Rev.*, 1982, 385; Agarwal, R. C. and Singh, N. K., *Inorg. Chem.*, 1981, **20,** 2794; Ravindar, V., Swamy, S. J., Srihari, S. and Lingaiah, P., *Polyhedron*, 1985, **4,** 1511; Chauhan, H. P. S., Chourasia, S., Agrawal, N. and Rao, R. J., *Synth. React. Inorg. Met.-Org. Chem.*, 1994, **24,** 325; Shi, J., Yang, B. and Ma, H., *Chem. J. Chinese Univ.*, 1991, **12,** 1157; idem. 1995, **16,** 1003.
4. Saryan, L. A., Ankel, E., Krishnamuti, C., Petering, D. H. and Elford, H., *J. Med. Chem.*, 1979, **22,** 2218.
5. Garcia-Tojal, J., Karmele Urtiaga, M., Cortes, R., Lezama, L., Arriortua, M. I. and Rojo, T., *J. Chem. Soc., Dalton Trans.*, 1994, 2233; Bingham, A. G., Bogge, H., Muller, A., Ainscough, E. W. and Brodie, A. M., *J. Chem. Soc., Dalton Trans.*, 1987, 493.
6. Enthioline, W. E., Knight, J., Whelan, H. and Petering, D. H., *Mol. Pharmacol.*, 1977, **13,** 89; bid., *J. Med. Chem.*, 1976, **19,** 339.
7. Shen, X., Xie, Y. and Geng, H., *Synth. React. Inorg. Met.-Org. Chem.*, 1994, **24,** 1351.
8. Koziol, A. E., Palenik, R. C. and Palenik, G. J., *J. Chem. Soc., Chem. Commun.*, 1989, 650.
9. Li, S., Liu, D., Meng, F., Zhou, J. and Yang, Z., *Chinese J. Struct. Chem.*, 1995, **14,** 55.
10. West, D. X., Yang, Y., Klein, T. L., Golberg, K. I. and Liberta, A. E., *Polyhedron*, 1995, **14,** 1681; Butcher, R. J. and West, D. X., *Trans. Met. Chem.*, 1993, **18,** 449; Ferrari, M. B., Fava, G. G., Peiizzi, C., Tarasconi, P. and Tosi, G., *J. Chem. Soc., Dalton Trans.*, 1987, 227; 1989, 361.
11. Roy, R., Chaudhury, M., Mondai, S. K. and Nag, K., *J. Chem. Soc., Dalton Trans.* 1984, 1681.
12. Sen, D., Panda, A. K., Banerjee (Dutta), B. and Sen, S. S., *Indian J. Chem.*, 1982, **21A,** 1096.
13. Ferraro, J. R. and Walkers, W. R., *Inorg. Chem.*, 1965, **4,** 1382.
14. Ferraro, J. R., *Low Frequency Vibrations of Inorganic and Coordination Compounds*, Plenum Press, New York, 1971.
15. Bailar, J. C., *The Chemistry of Coordination Compounds*, Vol. 354. Reinhold, New York, 1956, p. 371.

Pergamon

PII: S0277-5387(96)00437-8

Polyhedron Vol. 16, No. 9, pp. 1483–1486, 1997
Copyright © 1997 Elsevier Science Ltd
Printed in Great Britain. All rights reserved
0277-5387/97 $17.00+0.00

Mutagenic activity of rhodium(III) complexes with 2,2′-biquinoline and 2-(2′-pyridyl)quinoline

May. F. Sadiq[a] and Mukarram H. Zaghal[b]*†

[a]Department of Biological Sciences, Yarmouk University, Irbid, Jordan

[b]Department of Chemistry, Yarmouk University, Irbid, Jordan

(Received 12 August 1996; accepted 22 August 1996)

Abstract—The mutagenic activity of the rhodium(III) complexes with 2,2′-biquinoline(biq) and 2-(2′-pyridyl)quinoline(pq) namely, *mer*- and *fac*-$[Rh(pq)Cl_3(H_2O)]$, *cis*-$[Rh(NN)_2X_2]X$ (NN = biq or pq; X = Cl, Br) and *cis*-$[Rh(pq)_2Cl_2]$ $[Rh(CO)_2Cl_2]\cdot H_2O$, was investigated in strains of *Salmonella typhimurium* TA1530 (hisG46, Δgal, Δuvr, R^-) and TA98 (hisD3052, ΔuvrB, rfa, R^+). All of the complexes studied appear to be active in inducing both base substitution and frame shift mutations. The complex *cis*-$[Rh(biq)_2Cl_2]Cl$ exhibits the highest activity in both strains and has the lowest toxicity. © 1997 Elsevier Science Ltd. All rights reserved.

Keywords: mutagenic activity; rhodium(III); 2,2′-biquinoline; 2-(2′-pyridyl)quinone; *Salmonella typhimurium* TA1530 and TA98; base substitution; frame shift mutations.

In 1969 complexes of rhodium(III) of the type *trans*-$[RhL_4X_2]Y$ (L = substituted pyridine; X = Cl, Br; Y = Cl, Br, NO_3, ClO_4) were reported to have high levels of antibacterial activity [1]. During the same year, Rosenberg *et al.* reported that cisplatin, *cis*-$[Pt(NH_3)_2Cl_2]$, was a potential antitumour complex [2]. Since that time, the biological properties of many complexes of Group VIIIB metals, especially rhodium, ruthenium, iridium and palladium, in addition to platinum have been investigated (for example, see [3–10]).

The antitumour property of cisplatin was based upon the observation that this complex induced filamentous growth in strains of *Escherichia coli* [8]. When this microbiological property was used to test the biological activity of a series of platinum-group metal complexes, rhodium(III) complexes were found to be the most active [8].

Complexes of rhodium(III) of the type *cis*-$[Rh(NN)_2X_2]X$ (NN = 2,2′-bipyridine (bpy) or 1,10-phenanthroline (phen) and X = Cl, Br, I) have also attracted great interest for their possible use as antibacterial and antitumour agents [11]. Moreover, complexes of rhodium(III) with 2,6-diaminopyridine and its substituted derivatives have been reported to exhibit biological properties [12]. The biological activity of rhodium(III) complexes with *N*-heterocyclic ligands has been suggested to be due to the generation of rhodium(I) species [13]. In fact, rhodium(I) complexes have also been found to produce filamentous growth of *E. coli* and to induce lamda prophage in lysogenic bacteria [7, 14].

All these considerations prompted us to investigate the biological properties of rhodium(III) complexes with *N*-donor ligands. We have recently reported the synthesis and characterization of a series of rhodium(III) complexes with 2,2′-biquinoline(biq) and 2-(2′-pyridyl)quinoline(pq) [15–19]. We now report the mutagenic activity of some of these complexes on *S. typhimurium* TA1530 and TA98.

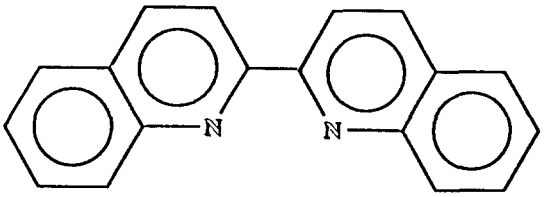
EXPERIMENTAL

Materials

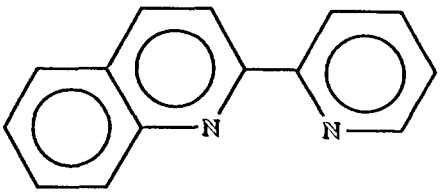
All solvents used were AR grade. The chemicals used were purchased from Laborat, Aldrich, Fluka or BDH. The ligands biq and pq were recrystallized from PhMe and CH_3OH, respectively. The rhodium(III)

* Author to whom correspondence should be addressed.

† Present address: Department of Chemistry, Sultan Qaboos University, 36-Al Khod, 123-Muscat, Sultanate of Oman.



biq



pq

complexes used are: *mer*- and *fac*-$[Rh(pq)Cl_3(H_2O)]$, *cis*-$[Rh(NN)_2X_2]X$ (NN = pq, bis; X = Cl, Br) and *cis*-$[Rh(pq)_2Cl_2][Rh(CO)_2Cl_2]\cdot H_2O$. They were prepared as described earlier [15–19].

The rhodium(III) complexes were dissolved in small amounts (200–500 μL) of dimethylsulfoxide then mixed with deionized water up to 1 cm^3 and filter sterilized before use.

Bacterial strains

The strains of *S. typhimurium* TA1530 (hisG46, Δgal, Δuvr, R^-) and TA98 (hisD3052, ΔuvrB, rfa, R^+) used were a generous gift from Bruce Ames, Berkeley, U.S.A.

Mutagenesis assay

The mutagenicity of the rhodium(III) complexes was tested without metabolic activation, according to Ames *et al.* [20]. The tester strains were cultured daily from frozen permanents [21] and were incubated overnight on a gyratory shaker at 37°C.

The test was briefly carried out as follows: an appropriate amount of each rhodium complex solution and 0.1 cm^3 of the bacterial culture were gently mixed with 2 cm^3 of molten top agar and spread over a Petri dish containing 20 cm^3 of Vogel–Bonner agar [20]. Each treatment was carried out in duplicate. Plates were allowed to solidify, incubated at 37°C for 48 h and then screened for colonies of histidine revertants. Control plates were prepared using the proper concentrations of the solvents.

The number of revertants per plate, expressed as the mean value of at least two independent experiments, was used as an indication of the mutagenic activity of the tested complexes. A complex was considered mutagenic whenever the number of revertant colonies was at least double that of the spontaneous revertants in the control plates. The mutagenic effects were also confirmed by demonstrating a dose–response relationship whereby various concentrations (10–400 μg complex/plate) were used.

RESULTS AND DISCUSSION

The mutagenic activity of some rhodium(III) complexes with biq and pq was tested on *S. typhimurium* TA1530 and TA98. The results are presented in Table 1. It can be concluded that all the complexes tested are able to raise the number of histidine revertants over the spontaneous level when both bacterial strains are used. This means that the rhodium(III) complexes used possess mutagenic activity for bacteria; they induce both base substitution and frame shift mutations. They appear, however, to have different levels of biological activity.

Based on their activity to induce base substitution mutations, the complexes may be arranged in the following order:

cis-$[Rh(biq)_2Cl_2]Cl$ > *cis*-$[Rh(pq)_2Br_2]Br$ > *cis*-$[Rh(pq)_2Cl_2]Cl$ > *cis*-$[Rh(biq)_2Br_2]Br$ > *fac*-$[Rh(pq)Cl_3(H_2O)]$ > *cis*-$[Rh(pq)_2Cl_2][Rh(CO)_2Cl_2]\cdot H_2O$ > *mer*-$[Rh(pq)Cl_3(H_2O)]$.

The complexes *cis*-$[Rh(biq)_2Cl_2]Cl$ and *cis*-$[Rh(pq)_2Br_2]Br$ are highly mutagenic; *cis*-$[Rh(pq)_2Cl_2]Cl$ and *cis*-$[Rh(biq)_2Br_2]Br$ are moderately mutagenic while *fac*- and *mer*-$[Rh(pq)Cl_3(H_2O)]$ and *cis*-$[Rh(pq)_2Cl_2][Rh(CO)_2\ Cl_2]\cdot H_2O$ are slightly mutagenic.

However, when *S. typhimurium* TA98 was used, the complexes *cis*-$[Rh(pq)_2Cl_2]Cl$, *cis*-$[Rh(pq)_2Cl_2][Rh(CO)_2Cl_2]\cdot H_2O$ and *cis*-$[Rh(biq)_2X_2]X$ (X = Cl, Br) were found to be highly mutagenic *via* frame shifts, while *mer*-$[Rh(pq)Cl_3(H_2O)]$ and *cis*-$[Rh(pq)_2Br_2]Br$ were moderately mutagenic.

It seems that the complexes used in this study (Table 1) are more active *via* frame shift than base substitution mechanisms. Complexes of platinum with bidentate amines have been reported to show the same behaviour [6]. The absence of detailed reports on the structural aspects of the interactions of biologically active rhodium(III) compounds with bacterial DNA makes it difficult to relate the activity of our complexes to their structures. However, some conclusions can be drawn since both rhodium and platinum are heavy transition metals and bind to similar types of ligands [22, 23]. One has to keep in mind, however, that the majority of rhodium(III) and platinum(IV) complexes are octahedral, while those of platinum(II) are square-planar [22,23].

It has been reported that most biologically active platinum complexes, whether octahedral or square-planar, have two moderately labile *cis* leaving groups

Table 1. Mutagenic activity of rhodium(III) complexes on *S. Typhimurium* TA1530 and TA98

	Histidine revertants[a] at various concentrations (μg complex/plate)							
	0	10	20	25	50	100	200	400
mer-[Rh(pq)$Cl_3(H_2O)$]	94±15	83±23	130±12	-	137±15	156±9	203±7	226±29
					(78±12)[b]		—	(110±20)[b]
fac-[Rh(pq)$Cl_3(H_2O)$]	66±29	—	99±10	—	84±1	136±9	171±2	—
cis-[Rh(pq)$_2Cl_2$]Cl	78±12	126±6	134±3	—	206±93	259±59	270±25	—
					(320±40)[b]	(317±45)[b]	(91±3)[b]	—
cis-[Rh(pq)$_2Br_2$]Br	74±15	144±5	132±1	198±6	219±2	302±52	354±53	—
						(93±16)[b]	—	(0±0)[b]
cis-[Rh(pq)$_2Cl_2$][Rh $(CO)_2Cl_2$]·H_2O	89±5	—	—	—	111±28	174±21	222±29	313±5
					(151±25)[b]	(620±24)[b]	—	(596±27)[b]
cis-[Rh(biq)$_2Cl_2$]Cl	89±5	—	—	—	305±35	352±18	480±6	512±16
						(144±32)[b]	—	(>1500)[b]
cis-[Rh(biq)$_2Br_2$]Br	89±5	—	—	167±8	224±29	271±42	166±3	—
							(427±35)[b]	(>1000)[b]

[a] Histidine revertants are counted and calculated as the average number of colonies/plate after a 48 h incubation at 37 C in the presence of the indicated amounts of complexes. Each data is an average of at least two independent experiments, each of which included duplicate plates.

[b] These values refer to revertants of *S. typhimurium* TA98; control value = 28±2.

and two *cis* nitrogen donor amine ligands [24]. All the bis-biq and -pq rhodium(III) complexes used have *cis* configurations [15–19]. The *mer*- and *fac*- isomers also satisfy this requirement.

The toxicity of the complexes used in this study (Table 1) seems to depend on the bacterial strains used. The complex *cis*-[Rh(biq)$_2Br_2$]Br is toxic to strains TA1530; *cis*-[Rh(pq)$_2X_2$]X (X = Cl, Br) are highly toxic to strains TA98, while all the other complexes are not significantly toxic to both strains within the concentration range used (Table 1).

The toxicity of cisplatin, *cis*-[Pt$(NH_3)_2Cl_2$], has been related to its ease of hydrolysis; the hydrolysis products were found to oligomerize and form toxic products [8]. Complexes with bidentate amine ligands, such as ethylenediamine or 1,2-diaminocyclohexane, have been reported to be less toxic than cisplatin. The complexes used in this study have the advantage of containing bidentate N-donor chelating agents (biq and pq). Moreover, platinum(II) and platinum(IV) have been reported to form their most stable complexes with the most polarizable ligands (I > Br > Cl > N ~ O) [5]. The toxicity of *cis*-[Rh$(NN)_2Br_2$]Br (NN = biq, pq) could be due to their instability in solution, which is caused by the repulsions between the bulky biq or pq and the Br ligands.

Finally, it can be concluded from this study that the chloro complex *cis*-[Rh(biq)$_2Cl_2$]Cl exhibits the highest mutagenic activity and the lowest toxicity among all complexes tested and is expected to be the most promising candidate for further biological studies.

Acknowledgements—The partial financial support from the Deanship of Research and Graduate Studies at Yarmouk University (Jordan) is greatly appreciated.

REFERENCES

1. Bromfield, R. J., Dainty, R. H., Gillard, R. D. and Heaton, B. T., *Nature*, 1969, **223,** 735.
2. Rosenberg, B., VanCamp, L., Trosko, J. E. and Mansour, V. H., *Nature*, 1969, **222,** 385.
3. Connors, T. A., Jones, M., Ross, W. C. J., Braddock, P. D., Khokhar, A. R. and Tobe, M. L., *Chem. Biol. Interactions*, 1972, **5,** 415.
4. Meischen, S. J., Gale, G. R., Lake, L. M., Frangakis, C. J., Rosenblum, M. G., Walker, Jr, E. M., Atkins, L. M. and Smith, A. B., *J. Natl. Cancer Inst.* 1976, **57,** 841.
5. Roberts, J. J. and Thomson, A. J., *Prog. Nucleic Acid Res. Mol. Biol.* 1979, **22,** 71.
6. Coluccia, M., Correale, M., Giordano, D., Mariggio, M. A., Moscelli, S., Fanizzi, F. P., Natile, G. and Maresca, L., *Inorg. Chim. Acta*, 1986, **123,** 225.
7. Monti-Bragadin, C., Giacca, M., Dolzani, L. and Tamaro, M., *Inorg. Chim. Acta*, 1987, **137,** 31.
8. Umapathy, P., *Coord. Chem. Rev.* 1989, **95,** 129, and refs therein.
9. Tsubomura, T., Ogawa, M., Yano, S., Kobayashi, K., Sakurai, T. and Yoshikawa, S., *Inorg. Chem.* 1990, **29,** 2622, and refs therein.
10. Bednarski, P. J., *J. Inorg. Biochem.* 1995, **80,** 1.
11. Ramesh, B. R., Mallikarjuna, B. S. S. and Reddy, G. K. N., *Nat. Acad. Sci. Lett.* 1978, **1,** 24, and refs therein.

12. Vassilian, A., Bikhazi, A. B. and Tayim, H. A., *J. Inorg. Nucl. Chem.* 1979, **41,** 775.
13. Gillard, R. D., Harrison, K. and Mather, I. H., *J. Chem. Soc., Dalton Trans.*, 1975, 133.
14. Dutta, D. K. and Singh, M. M., *Trans. Met. Chem.* 1979, **4,** 230, and refs therein.
15. Zaghal, M. H. and Qaseer, H. A., *Inorg. Chim. Acta*, 1989, **163,** 193.
16. Zaghal, M. H. and Shatnawi, M. Y., *Dirasat* (University of Jordan, Amman, Jordan), 1989, **16,** 27.
17. Zaghal, M. H. and Shatnawi, M. Y., *Mu'tah J. for Research and Studies* (University of Mu'tah, Al-Karak, Jordan), 1991, **6,** 51.
18. Zaghal, M. H. and Qaseer, H. A., *Trans. Met. Chem.*, 1991, **16,** 39.
19. Zaghal, M. H. and Ali, B. F., *Polyhedron*, 1995, **14,** 1011.
20. Ames, B. N., McCann, J. and Yamasaki, E., *Mutat. Res.*, 1975, **31,** 347.
21. Maron, D. M. and Ames, B. N., *Mutat. Res.*, 1983, **113,** 173.
22. Cotton, F. A. and Wilkinson, G., *Advanced Inorganic Chemistry*, 4th edn. Wiley, New York, 1980, pp. 934–965.
23. Greenwood, N. N. and Earnshaw, A., *Chemistry of the Elements*, Pergamon Press, Oxford, 1984, pp. 1309–1354.
24. Sherman, S. E. and Lippard, S. J., *Chem. Rev.*, 1987, **87,** 1153.

Pergamon

PII: S0277-5387(96)00431-7

Polyhedron Vol. 16, No. 9, pp. 1487–1490, 1997
Copyright © 1997 Elsevier Science Ltd
Printed in Great Britain. All rights reserved
0277-5387/97 $17.00+0.00

Direct synthesis and crystal structure of tetrameric copper(I) iodide with trimethylamine $[CuI(NMe_3)]_4$

Olga A. Babich and Vladimir N. Kokozay*

Department of Chemistry, Kiev Shevchenko University, 252033 Kiev, Ukraine

(Received 23 July 1996; accepted 22 August 1996)

Abstract—The tetrameric cluster $[CuI\{N(CH_3)_3\}]_4$ has been synthesized directly from copper powder and trimethylammonium iodide in non-aqueous solutions (acetonitrile, *N*,*N*-dimethylformamide) and characterized by X-ray crystallography. The compound $[CuI\{N(CH_3)_3\}]_4$ possesses a molecular structure. A tetrahedral Cu_4 cluster with short Cu—Cu distances (2.67 Å) is surrounded by an I_4 tetrahedron, thus each face of the Cu_4 tetrahedron is centred by a μ_3-bridging iodine atom. © 1997 Elsevier Science Ltd. All rights reserved.

Keywords: tetrameric copper(I) complex; crystal structure; direct synthesis.

Direct synthesis involving metal powder provides an opportunity to prepare various types of coordination compounds [1]. In this paper we report the details of the preparation and the results of the structure determination of the first compound of cluster type obtained by direct method. Tetrameric copper(I) compounds of stoichiometry $[CuI(L)]_4$ (where L = Lewis base) have been described previously in the literature [2–5], but the cluster compound $[CuI\{N(CH_3)_3\}]_4$ is the first one prepared by the direct synthesis.

EXPERIMENTAL

All chemicals were commercial products of reagent grade and used without further purification. Trimethylammonium iodide was synthesized from trimethylammonium chloride and potassium iodide in methanol solution by exchange reaction and recrystallized from isopropanol. All experiments were carried out in air.

Synthesis of $[CuI\{N(CH_3)_3\}]_4$

The following method was used for the preparation of the complex: Cu (0.63 g, 10 mmol), $(CH_3)_3N \cdot HI$ (3.71 g, 20 mmol) and acetonitrile (70 cm^3) were placed in a flask in the above order. The mixture was stirred at ambient temperature over 5–6 h and left overnight. Next morning the colourless crystals were separated from the pale brown solution. Yield: 0.95 g (76%). Found: C, 13.9; H, 3.2; N, 6.0; Cu, 25.1; I, 51.0. Calc. for $C_{12}H_{36}Cu_4I_4N_4$: C, 14.4; H, 3.6; N, 5.6; Cu, 25.5; I, 50.8%.

Crystal structure determination

Crystallographic measurements were obtained at 20°C using an Enraf–Nonius CAD-4 diffractometer operating in the ω–2θ scan mode (the ratio of the scanning rates was $\omega/\theta = 1.2$). The intensity data were collected within the range $1.60 \leqslant \theta \leqslant 21.97°$ using graphite-monochromated Mo-K_α radiation. The accurate unit-cell constants and the orientation matrix for data collection were obtained from least-squares refinement, using the setting angles of 24 reflections in the range $13 < \theta < 15°$. The structures were solved by direct methods and refined by full-matrix least-squares techniques on F^2 in the anisotropy approximation using SHELX-93 [6]. The positions of the hydrogen atoms were idealized and included in the calculations of the structure factors as the fixed contributions. The non-centrosymmetric space group $P\bar{4}3n$ was chosen during the structure solution. Transition to the centrosymmetric space group $Pm3n$ is impossible because the molecule of complex does not

* Author to whom correspondence should be addressed.

Table 1. Crystallographic data and parameters for $[CuI\{N(CH_3)_3\}]_4$

Compound	$[CuI\{N(CH_3)_3\}]_4$
Colour	Colourless
Formula weight	998.21
Crystal system	Cubic
Space group	$P\bar{4}3n$
a (Å)	17.976(2)
Cell volume (Å^3)	5808.7(11)
Formula units	8
T (K)	293
D_c (g cm^{-3})	2.283
D_m (gm)	2.27
Radiation (Å)	Mo-K_α (λ = 0.71073)
$F(000)$	3712
Number of unique data	673
Data used in refinement	491 [$I > 2\sigma(I)$]
Refinement method	Full matrix least-squares on F^2
R	0.0335 (wR_2 = 0.0845)[a]
GOF	1.011
Absolute structure parameter	0.2(2)

[a] The inverted structure gave R = 0.034, wR_2 = 0.0855, GOF = 1.019, absolute structure parameter = 0.6(2).

possess the symmetry centre. The density measured by the floatation method is 2.27 g cm^{-3} and to be compared with the calculated density of 2.283 g cm^{-3}. The crystallographic data are summarized in Table 1. Convergence was reached at the agreement factor listed in Table 1.

Selected bond distances and angles are given in Table 2. A fragment of the unit-cell packing of $[CuI\{N(CH_3)_3\}]_4$ is shown in Fig. 1. Atomic coordinates, anisotropic thermal parameters, full list of bond distances and angles are given in the supplementary material.

DISCUSSION

The crystal of $[CuI\{N(CH_3)_3\}]_4$ complex consists of the discrete tetrameric molecules. Two independent complex molecules are present in the unit cell. Figure 2 shows the labelling scheme for atoms in one of the two molecules, and a view of the Cu_4I_4 core. The coordination environments of Cu(1) and Cu(2) atoms are topologically similar, but differ somewhat from each other geometrically (Table 2). The Cu(2), N(2) and I(2) atoms occupy special positions at three-fold axes, while the other atoms occur in general positions.

The base of the complex molecule is a tetrahedral Cu_4 cluster surrounded by a tetrahedron of iodine atoms, thus each face of the Cu_4 tetrahedron has been centred by a μ_3-bridging iodine atom [Fig. 1(b)]. The significant distortion of the Cu_4I_4 core from regular cubic geometry involves symmetric and opposing distortions of the Cu—I—Cu and I—Cu—I angles (the average value I—Cu—I = 112.86° and Cu—I—Cu = 60.5°) and it may be caused by the repulsion between the iodine atoms [7]. The iodine $\cdots$ iodine contacts within the $[CuI\{N(CH_3)_3\}]_4$ molecule range from 4.392 to 4.505 Å, which is similar to the I $\cdots$ I contacts in the corresponding $[CuI(L)]_4$ complexes with the nitrogen-donor ligands [2,5].

The coordination environment of the copper(I) atoms is formed by three iodine atoms and one nitrogen atom of the trimethylamine molecule

Table 2. Selected bond lengths (Å) and angles (°) for $[CuI\{N(CH_3)_3\}]_4$

Cu(1)—I(1)	2.688(3)	Cu(2)—I(2)	2.690(2)
Cu(1)b—I(1)	2.685(3)	Cu(2)—N(2)	2.13(5)
Cu(1)c—I(1)	2.678(3)	Cu(2)—Cu(2)d	2.678(7)
Cu(1)—N(1)	2.09(2)	N(2)—C(4)	1.43(3)
Cu(1)—Cu(1)b	2.676(5)		
N(1)—C(1)	1.47(4)		
N(1)—C(2)	1.50(3)		
N(1)—C(3)	1.45(3)		
Cu(1)b—I(1)—Cu(1)	59.83(10)	Cu(2)—I(2)—Cu(2)f	59.7(2)
Cu(1)c—I(1)—Cu(1)	59.75(10)	I(2)—Cu(2)—I(2)f	113.04(8)
Cu(1)b—I(1)—Cu(1)c	61.31(10)	N(2)—Cu(2)—I(2)	105.61(10)
I(1)b—Cu(1)—I(1)	113.96(11)	Cu(2)f—Cu(2)—Cu(2)e	60.0
I(1)c—Cu(1)—I(1)	114.18(11)	Cu(2)—N(2)—C(4)	108(2)
I(1)c—Cu(1)—I(1)b	109.95(9)		
N(1)—Cu(1),I(1)	104.8(6)		
N(1)—Cu(1)—I(1)b	106.6(7)		
Cu(1)b—Cu(1)—Cu(1)c	61.44(11)		
Cu(1)b—Cu(1)—Cu(1)a	59.28(6)		
Cu(1)—N(1)—C(1)	108(2)		

Symmetry transformations used to generate equivalent atoms: (a) $-x, 1-y, z$; (b) $1/2-y, 1/2+x, 1/2-z$; (c) $-1/2+y, 1/2-x, 1/2-z$; (d) $1-x, 1-y, +z$; (e) $1-x, +y, 1-z$; (f) $+x, 1-y, 1-z$.

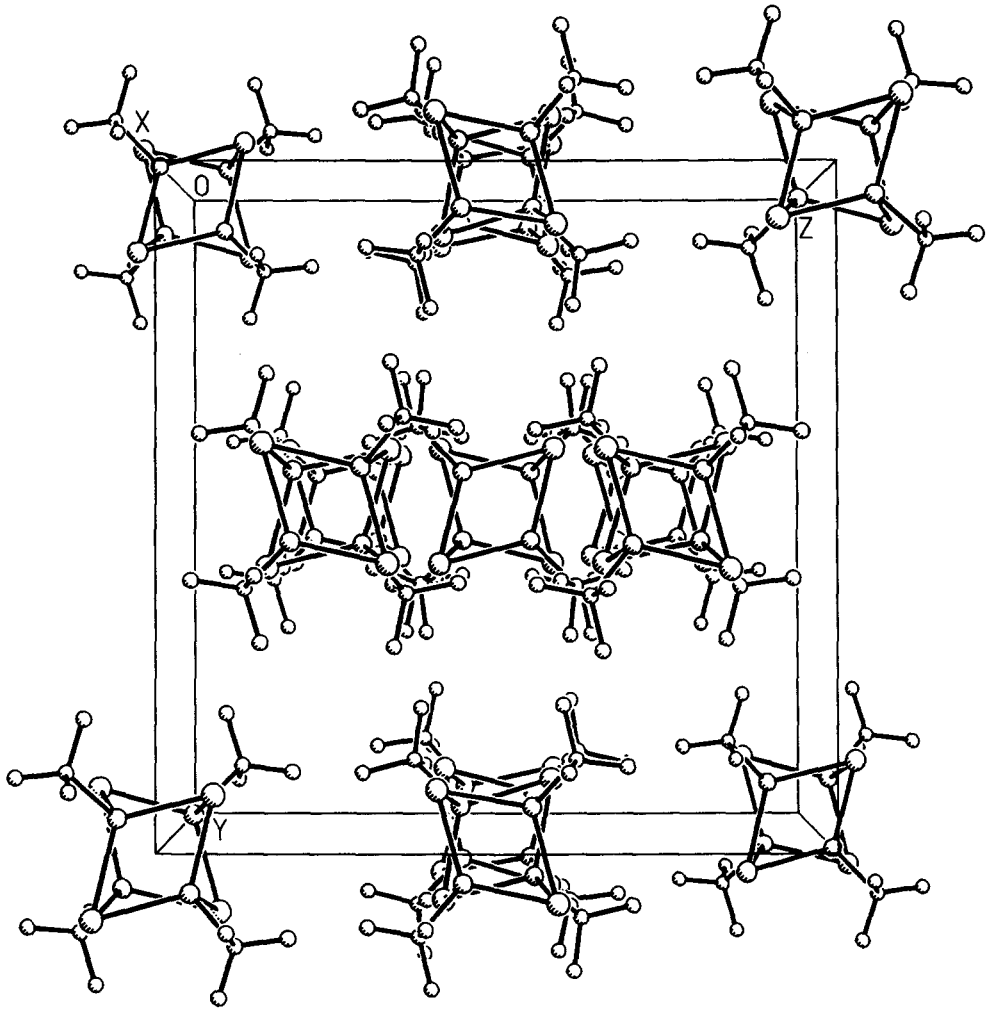


Fig. 1. Fragment of the unit-cell packing of $[CuI\{N(CH_3)_3\}]_4$.

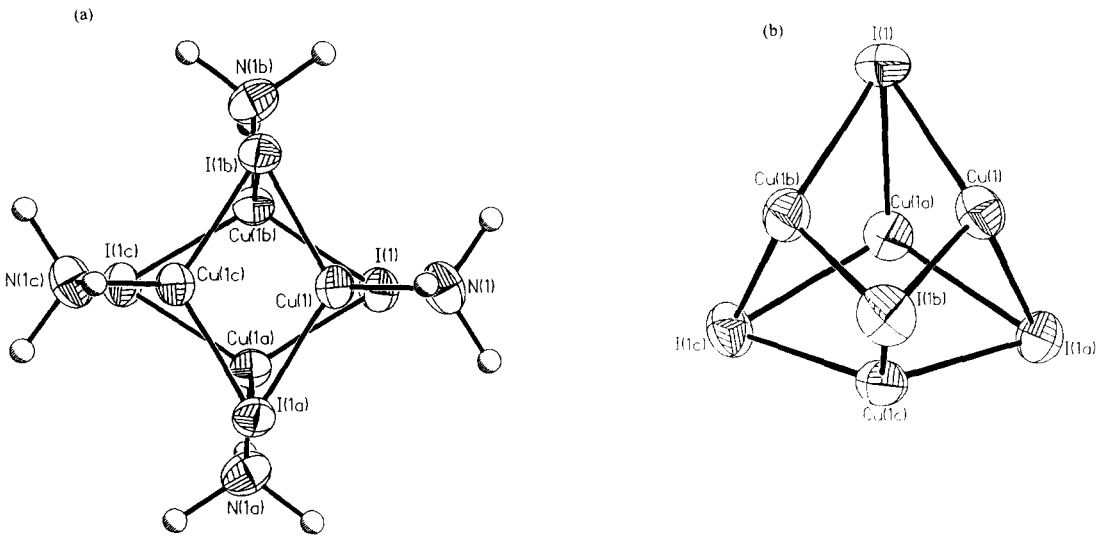


Fig. 2. (a) One of the two complex molecules in $[CuI\{N(CH_3)_3\}]_4$ with the atom-labelling scheme ("a", "b" and "c" refer to the $-x, 1-y, z$; $1/2-y, 1/2+x, 1/2-z$; $-1/2+y, 1/2-x, 1/2-z$, respectively; the carbon atoms are unlabelled) and (b) a view of the Cu_4I_4 core.

[Cu—N = 2.09(2)–2.13(5) Å] and represents a slightly distorted tetrahedron.

The average distance between copper atoms (2.678 Å) is greater than the value for standard copper–copper bonds (2.56 Å). However, it is significantly shorter than the average Cu···Cu distance in complexes with phosphine or arsine-donor ligands and comparable to those found in other nitrogen-donor cubic $[CuI(L)]_4$ structures [8]. Investigation of the emission spectra [4] has shown that if the copper···copper distance in $[CuI[L]]_4$ systems is less than 2.8 Å some metal–metal interaction may be assumed.

The local geometry of each nitrogen atom corresponds to C_{3v} symmetry. N—C bond lengths range from 1.43(3) to 1.50(3) Å; C—N—C angles vary from 107(2) to 111(2)°.

Acknowledgements—This work has been partly financed by the International Soros Program of Support of Education in the Field of natural Sciences (ISSEP), grant no. PSU063004.

REFERENCES

1. Skopenko, V. V., Kokozay, V. N. and Pavlenko, V. A., *Ukr. Khim. Zh. (Russ. Ed.)*, 1993, **59,** 485.
2. Schramm, V., *Inorg. Chem.* 1978, **17,** 714.
3. Churchill, M. and Youngs, W., *Inorg. Chem.* 1979, **18,** 1133.
4. Rath, N., Holt, E. and Tanimura, K., *Inorg. Chem.* 1985, **24,** 3934.
5. Toth, A., Floriani, C., Chiesi-Villa, A. and Guastini, C., *Inorg. Chem.* 1987, **26,** 3897.
6. Sheldrick, G. M., *SHELX*93. *A System of Computer Programs for X-ray Structure determination.* University of Göttingen, Germany, 1993.
7. Campbell, J. A., Raston, C. L. and White, A. H., *Aust. J. Chem.* 1977, **30,** 1937.
8. Harrison, P. G., in *Comprehensive Coordination Chemistry*, Vol. 5, ed. G. Wilkinson, R. D. Gillard and J. A. McCleverty. Pergamon Press, Oxford, 1987, p. 560.

Pergamon

PII: S0277-5387(96)00429-9

Polyhedron Vol. 16, No. 9, pp. 1491–1495, 1997
Copyright © 1997 Elsevier Science Ltd
Printed in Great Britain. All rights reserved
0277-5387/97 $17.00+0.00

Synthesis and crystal structure of complexes of erbium(III) picrate with N,N,N′,N′-tetraphenyl-3,6,9-trioxaundecanediamide

Shi-Xia, Liu,[a] Wei-Sheng Liu,[a]* Min-Yu Tan[a] and Kai-Bei Yu[b]

[a] Department of Chemistry, Lanzhou University, Lanzhou 730000, P.R. China

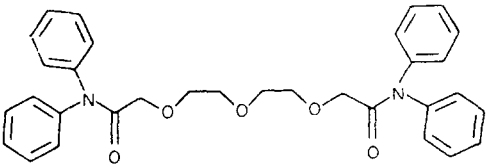
[b] Chengdu Centre of Analysis and Determination, Academia Sinica, Chengdu 610041, P.R. China

(Received 5 July 1996; accepted 22 August 1996)

Abstract—Reaction of erbium picrate with N,N,N′,N′-tetraphenyl-3,6,9-trioxaundecanediamide (TTD) yielded [Er(Pic)$_3$(TTD)]. Its crystal structure shows that the Er^{III} ion is coordinated to five oxygen atoms of TTD, three oxygen atoms of two picrates and one oxygen atom of H_2O giving a coordination number of nine. The TTD molecule acts as a multidentate ligand forming a ring-like coordination structure similar to those of crown compounds. © 1997 Elsevier Science Ltd. All rights reserved.

Keywords: erbium picrate; TTD; complex; synthesis; structure.

Noncyclic polyethers show a high complexation selectivity which makes them suitable reagents for the extraction and analysis (ion-selective electrodes) of the lanthanide ions [1–5]. The extraction of fission products by N,N,N′,N′-tetraphenyl-3,6,9-trioxaundecanediamide (TTD) has been studied by an isotopic tracer technique and the extractability of alkaline earths and lanthanide ions by nitrobenzene solution of TTD is very high when picrate is used as an accompanying ion [5]. In addition, TTD was used as an active material for barium ion-selective electrode, showing an excellent electromotive force stability [6,7]. In this work, we describe the synthesis and crystal structure of the Er^{III} picrate complexes with TTD.



Structure 1. N,N,N′,N′-Tetraphenyl-3,6,9-Trioxaundecanediamide (TTD)

EXPERIMENTAL

Erbium(III) picrate [8] and TTD [9] were prepared according to the literature methods. All solvents used were purified by standard methods.

Synthesis of [Er(Pic)$_3$(TTD)]

A solution of TTD (0.1 mmol) in anhydrous ethanol (15 cm^3) was added dropwise to a solution of

* Author to whom correspondence should be addressed.

erbium(III) picrate (0.1 mmol) in anhydrous ethanol (20 cm^3). The mixture was stirred at room temperature for 2 h. The precipitated solid complex was filtered, washed with anhydrous ethanol and dried *in vacuo* over P_4O_{10} for 48 h. Found: C, 43.7; H, 2.8; N, 11.3; Er, 12.5. Calc. for $[Er(Pic)_3(TTD)]$: C, 43.6; H, 2.8; N, 11.2; Er, 12.2%. The solid complex was recrystallized from a solution of MeCN by slow evaporation to obtain the transparent yellow crystals of $[Er(Pic)_2(TTD)\cdot H_2O]\cdot Pic\cdot CH_3CN$.

X-ray diffraction analysis for $[Er(Pic)_2(TTD)\cdot H_2O]\cdot Pic\cdot CH_3CN$

Data collection was performed on an R3M/E four-circle diffractometer with Mo-K_α radiation ($\lambda = 0.71073$ Å) using the $\omega/2\theta$ scan mode. Correction for LP factors was applied. The structure was solved by the Patterson method and subsequent difference Fourier techniques and refined by full-matrix least-squares procedures based on F. All non-hydrogen atoms were refined anisotropically. The coordinates of the hydrogen atoms were fixed by theoretical models and refined only with isotropic thermal factors. All calculations were performed on an Eclipse S/140 computer with the SHELXTL program. Crystal data and a summary of intensity data collection and structure refinement parameters are listed in Table 1.

Positional parameters, anisotropic displacement parameters, hydrogen atom coordinates, a full list of bond lengths and angles and observed and calculated structure factors have been deposited as supplementary material with the Cambridge Crystallographic Data Centre. Selected bond lengths and bond angles are given in Table 2.

Table 1. Crystallographic data and processing parameters

Empirical formula	$C_{52}H_{43}ErN_{12}O_{27}$
Formula weight	1435.24
Crystal color	yellow
Crystal size (mm)	$0.5\times0.5\times0.5$
Crystal system	Triclinic
Space group	$P\bar{1}$
a (Å)	12.715(1)
b (Å)	12.796(1)
c (Å)	19.860(2)
α (°)	73.27(1)
β (°)	82.73(1)
γ (°)	70.54(1)
V (Å^3)	2916.0(4)
Z	2
D_{calc} (Mg m^{-3})	1.64
μ (mm^{-1})	1.539
$F(000)$	1446
Reflections collected	8971
Reflections used [$I > 2\sigma(I)$]	8503
$2\theta_{max}$(°)	24
GOF	1.089
R	0.027
wR	0.079
Largest residue	0.50

RESULTS AND DISCUSSION

The structure for $[Er(Pic)_2(TTD)\cdot H_2O]\cdot Pic\cdot CH_3CN$ is illustrated in Fig. 1. Figure 2 shows the molecular packing arrangement in the unit cell.

The crystal structure is composed of a $[Er(Pic)_2(TTD)(H_2O)]^+$ cation, one picrate anion and one MeCN molecule linked by electrostatic attraction and weak van der Waals forces. The Er^{III} ion is nine-coordinated by oxygen atoms, five from TTD, three from one bidentate and one unidentate picrates and one from H_2O. The coordination polyhedron is a monocapped tetragonal antiprism (Fig. 3). The TTD molecule wraps around the metal ion with its oxygen atoms and forms a ring-like coordination structure together with the bidentate picrate [O(14)] situated at the open side of the TTD chain (Fig. 4). The four oxygen atoms of TTD [O(2), O(3), O(4), O(5)] are not quite coplanar, their deviations from the mean plane being in the range of 0.0345–0.9754 Å. O(1) lies out of this plane by 1.5036 Å and the erbium atom by 0.2867 Å. Obviously TTD is distorted to some extent in order to maintain the Er—O distances at suitable lengths for coordination.

The average distance between the erbium atom and the coordinated oxygen atoms is 2.393 Å, where the Er—O(7) distance is the shortest probably due to the higher electron density on the oxygen anion of the picrate, while the Er—O [phenolic, O(14)] distance is shorter than the Er—O [nitro, O(15)] one in the bidentate picrate. The Er—O (C=O) distances (mean 2.344 Å) are significantly shorter than the Er—O (C—O—C) ones (mean 2.471 Å). This suggests that the Er—O (C=O) bond is stronger than the Er—O (C—O—C) one.

In conclusion, the TTD molecule acts as a multidentate ligand forming a ring-like coordination structure. The internal cavity formed by coordinating oxygen atoms is suited for the uptake of a cation, while the nonpolar groups (CH_2 groups, aliphatic rings) form a lipophilic shell around the coordination sphere. The TTD molecule, therefore, shows high selectivity complexation and lipophilicity, which make it a useful extract of lanthanide ions and a component in sensors for Ba^{2+}.

Acknowledgements—This work was supported by a grant from the Climb Plan Foundation of the State Science and Technology Commission of China, National Natural Science Foundation of China and the Doctoral Point Foundation of the State Education Commission of China.

Table 2. Selected bond lengths (Å) and angles (°)

Er—O(1)	2.364(2)	Er—O(6)	2.338(3)
Er—O(2)	2.561(3)	Er—O(7)	2.245(3)
Er—O(3)	2.410(3)	Er—O(14)	2.258(3)
Er—O(4)	2.441(3)	Er—O(15)	2.599(3)
Er—O(5)	2.325(3)		

O(1)—Er—O(2)	62.78(9)	O(2)—Er—O(3)	65.63(9)
O(1)—Er—O(3)	90.78(10)	O(2)—Er—O(6)	70.14(9)
O(1)—Er—O(7)	76.20(10)	O(2)—Er—O(14)	71.60(9)
O(1)—Er—O(14)	81.78(9)	O(3)—Er—O(4)	65.72(9)
O(1)—Er—O(15)	68.49(10)	O(3)—Er—O(6)	77.13(10)
O(4)—Er—O(5)	64.54(9)	O(3)—Er—O(7)	83.07(10)
O(4)—Er—O(6)	72.11(10)	O(4)—Er—O(7)	73.34(9)
O(5)—Er—O(6)	80.62(10)	O(5)—Er—O(7)	90.37(10)
O(5)—Er—O(14)	79.86(10)	O(5)—Er—O(15)	67.45(9)
O(6)—Er—O(14)	75.67(10)	O(7)—Er—O(15)	71.70(9)
O(14)—Er—O(15)	65.17(9)		

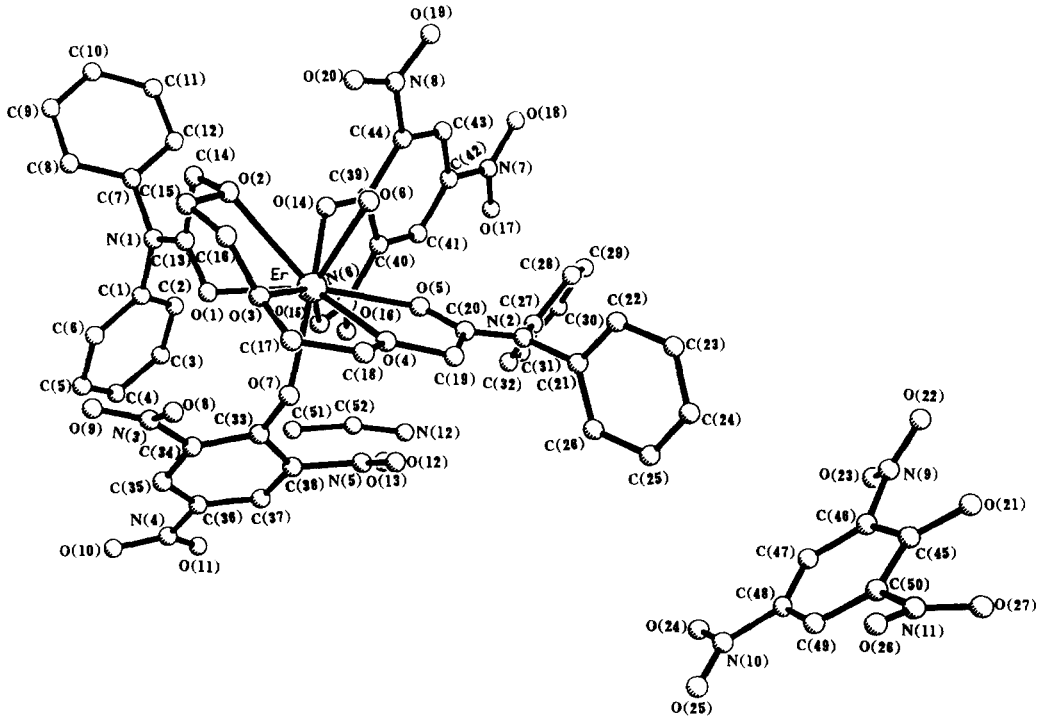


Fig. 1. Molecular structure of $[Er(Pic)_2(TTD)\cdot H_2O]\cdot Pic\cdot CH_3CN$.

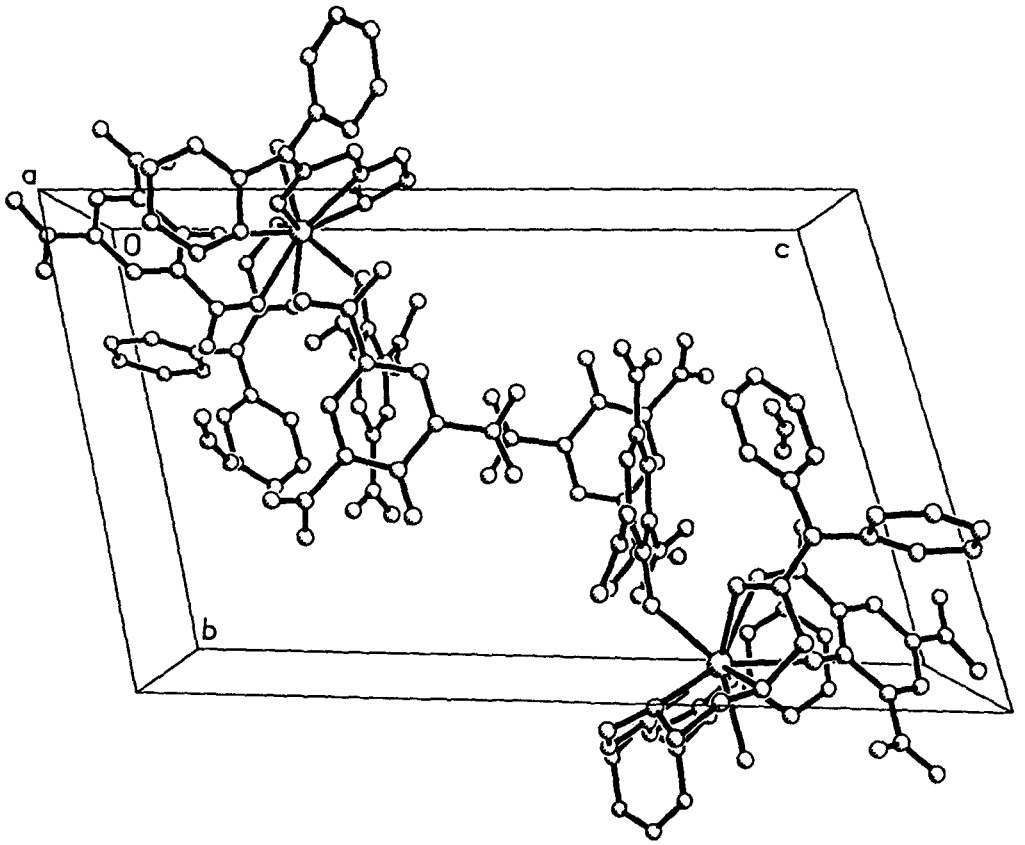


Fig. 2. Unit-cell contents for $[Er(Pic)_2(TTD)\cdot H_2O]\cdot Pic\cdot CH_3CN$.

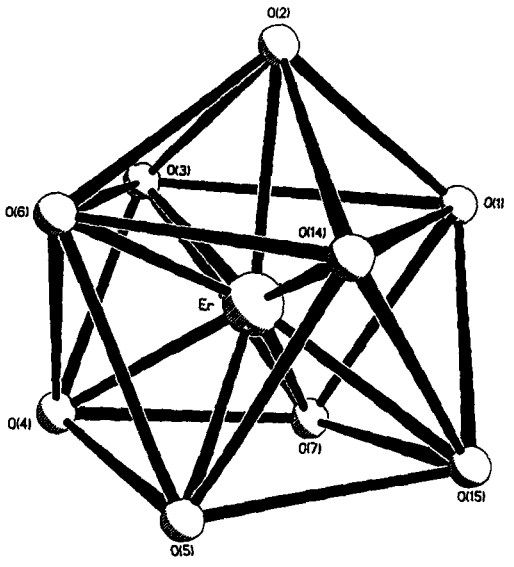


Fig. 3. The coordination polyhedron about the erbium atom.

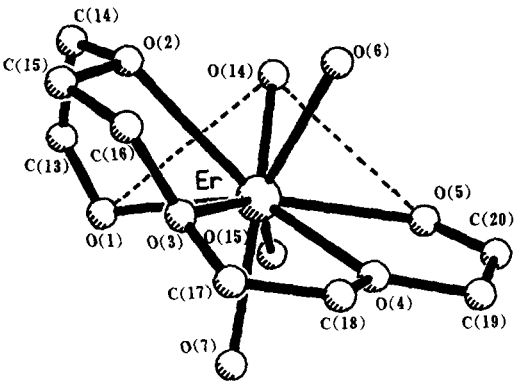


Fig. 4. The ring-like coordination structure of $[Er(Pic)_2(TTD)\cdot H_2O]\cdot Pic\cdot CH_3CN$.

REFERENCES

1. Bünzli, J.-C. G., Pfefferlé, J.-M., Ammann, B., Chapuis, G. and Zuniga, F.-J., *Helv. Chim. Acta*, 1984, **67,** 1121.
2. Yang, Y.-S. and Ding, Y.-Z., *J. Nucl. Radiochem.* 1982, **4,** 21.
3. Ding, Y.-Z., Lu, J.-C., Yang, Y.-S., Tan, G.-Z. and Xu, J.-Z., *Huaxue Shiji*, 1986, **8,** 201.
4. Yang, Y.-S. and Cai, S.-H., *Huaxue Shiji*, 1985, **6,** 133.
5. Yang, Y.-S., Ding, Y.-Z., Tan, G.-Z., Xu, J.-Z., Yiao, Z.-Q. and Zhang, F.-S., *J. Nucl. Radiochem.* 1984, **6,** 196.
6. Güggi, M., Pretsch, E. and Simon, W., *Anal. Chim. Acta*, 1977, **91,** 107.
7. Levins. R. J., *Anal. Chem.* 1971, **43,** 1045; 1972, **44,** 1544.
8. Tian, Y.-C., Liang, Y.-Q. and Ni, J.-Z., *Chem. J. Chin. Univ.* 1988, **9,** 113.
9. Tan, G.-Z., Xu, J.-Z., Yiao, Z.-Q. and Zhang, F.-S., *Huaxue Shiji*, 1983, **5,** 100.

Pergamon

PII: S0277-5387(96)00427-5

Polyhedron Vol. 16, No. 9, pp. 1497–1503, 1997
Copyright © 1997 Elsevier Science Ltd
Printed in Great Britain. All rights reserved
0277-5387/97 $17.00+0.00

High activity for oxidation reaction by peroxide adduct of binuclear iron(III) compound with (μ-η^1 : η^1)-coordination mode

Tetsuya Akamatsu, Teruyuki Kobayashi, Yumiko Sasaki, Sayo Ito and Yuzo Nishida*

Department of Chemistry, Faculty of Science, Yamagata University, Yamagata 990, Japan

(Received 28 June 1996; accepted 22 August 1996)

Abstract—Reactivities of the peroxide adducts of the iron(III) compounds with binucleating ligands, $Fe_2(HPTP)(OH)(NO_3)_2^{2+}$, $Fe_2(HPTB)(OH)(NO_3)_2^{2+}$ and $Fe_2(HXTA)(CH_3COO)_2^{-}$, were compared in the reaction with hydrogen peroxide (catalase-like function) and in the oxidation reactions of phenols and 2′-deoxyribose, (where H(HPTP), H(HPTB) and H_5(HXTA) denote N,N,N′,N′-tetrakis(2-pyridylmethyl)-1,3-diamino-propane-2-ol, N,N,N′,N′-tetrakis(2-benzimidazolylmethyl)-1,3-diamino-propane-2-ol and N,N′-2-hydroxy-5-methyl-1,3-xylylenebis[*N*-(carboxymethyl)]glycine, respectively). The peroxide adduct of the H(HPTP) complex exhibited the highest activity in all the reactions described above and the origin of the results are discussed in terms of the electrophilic nature of the peroxide adduct, electronic structure of the reactant, Lewis acidity of an iron(III) ion, orbital correlationship between metal peroxide adduct and the substrate and the steric hindrance of the ligand system. Based on these facts, we have proposed a new scheme for the catalase-like function catalysed by a binuclear iron(III) complex. © 1997 Elsevier Science Ltd. All rights reserved.

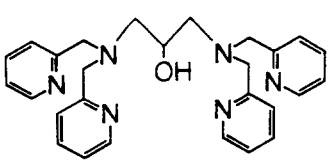
Keywords: binuclear iron(III); peroxide adduct; oxidative reaction; electrophilic peroxide adduct.

The reaction of the O_2 molecule at a diiron(II) center to give a binuclear iron(III)-peroxide adduct is sometimes observed in biological systems and several proteins known or believed to share this functional motif include hemerythrin (the O_2 carrier protein of certain marine invertebrates), methane monooxygenase from methanotrophic bacteria and stearoyl-CoA Δ9 desaturase from yeast and plants, and ribonucleotide reductase (DNA synthesis) [1–6]. For each of the diiron proteins, the chemical outcome of the O_2-reaction is distinct; in hemerythrin O_2 is reversibly bound in a hydroperoxidediferric complex [7–9], in methane monooxygenase O_2 is activated for the two-electron oxidation (hydroxylation) of an unactivated hydrocarbon [10,11], in stearoyl-CoA Δ9 desaturase O_2 is activated for the unhydrogenation of stearoylthioether [12], and in ribonucleotide reductase (RR), O_2 is activated for the one-electron oxidation of an endogenous tyrosine residue [13]. An objective which is central to the study of these diiron proteins is to identify structural and electronic features of the iron clusters and their protein chelators, which allow similar centers to mediate very different reactions with O_2.

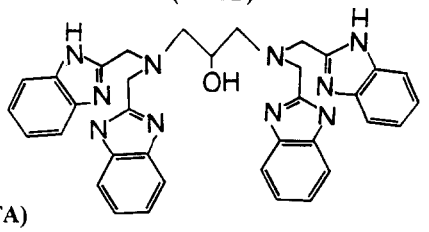
In our previous papers we have pointed out that the metal-peroxides play an important role in some biological systems [14] and proposed a meaningful understanding of structure–function relationships in these peroxide adducts, which may require knowledge of both the structure and chemical mechanism [15]. Until now, three diiron(III) compounds are known to give a peroxide adduct in the reaction with hydrogen peroxide; there are those with H(HPTB) [16], H(HPTP) [17] and H_5(HXTA) [18], where H(HPTP), H(HPTB) and H_5(HXTA) represent N,N,N′,N′-tetrakis(2-pyridylmethyl)-1,3-diaminopropane-2-ol, N,N,N′,N′-tetrakis(2-benzimidazolylmethyl)-1,3-diaminopropane-2-ol and N,N′-2-hydroxy-5-methyl-1,3-xylylenebis[N-(carboxymethyl)glycine], respectively [see Scheme 1]. For the case of $[Fe_2(HPTB)(OH)(NO_3)_2]^{2+}$, two possible structures

* Author to whom correspondence should be addressed.

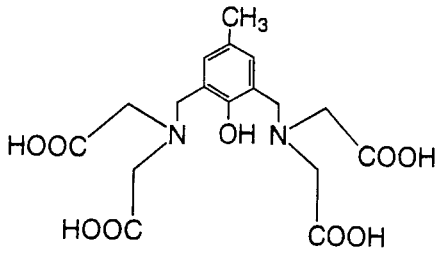
H(HPTP)



H(HPTB)



H_5(HXTA)

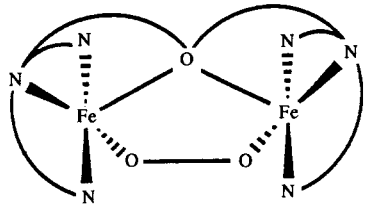


Scheme 1

have been postulated as a peroxide adduct, (a) and (b) as illustrated in Fig. 1 [19], and recent studies have suggested that the former, *cis*-μ-$\eta^1:\eta^1$ mode, should be most likely [20]. We have already reported that the peroxide adduct with H(HPTP) exhibited much higher activity for the formation of a phenoxo radical in the reaction with phenols [21], which is a model reaction for tyrosine radical formation observed in ribonucleotide reductase, however, the origin for the negligible activity of the other compounds, H(HPTB) and H_5(HXTA), is unknown.

In our recent papers we have observed that the oxidation and oxygenation reactions catalysed by the binuclear iron(III)-peroxide adduct are carried out by a different peroxide adduct and different reactivity (oxidation and oxygenation) is attributed to the different orbital phase-relationship between the metal-peroxide adduct and reactant [15,22]. In this study we have compared the reactivities of three peroxide adducts of H(HPTP), H(HPTB) and H_5(HXTA) compounds in the reaction of hydrogen peroxide, i.e. catalase-like function, and in oxidation reactions of phenols and 2′-deoxyribose. Based on these results, we propose a new scheme for the reactivity of the peroxide adduct of the binuclear iron(III) compound, and attempt to give a clear understanding of the origin of high activity for oxidation reaction by the peroxide adduct of binuclear iron(III) compounds with the (μ-$\eta^1:\eta^1$)-coordination mode.

(a)



(b)

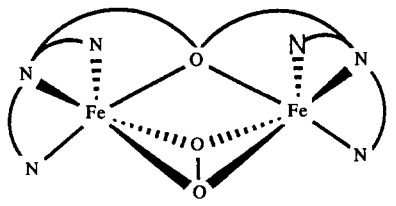


Fig. 1. Two possible structures for peroxide adduct of binuclear iron(III) compound.

EXPERIMENTAL

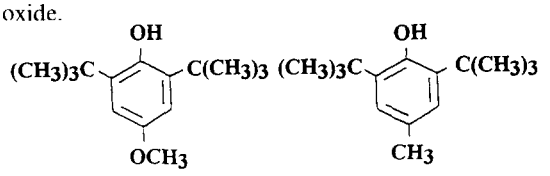
Materials

The binuclear iron(III) complexes used in this study were prepared according to the published methods [16–18].

ESR signal due to the formation of phenoxo radical

ESR spectra of the reaction mixture containing the iron(III) compound (1 cm^3, 1/500 mol dm^3 of ethanol/water = 1/1 solution), phenol (1 cm^3, 1/25 mol dm^{-3} ethanol/water = 1/1 solution) and hydrogen peroxide (1 cm^3, 1/50 mol cm^{-3} ethanol/water = 1/1 solution) were measured at 298K. The intensity of the ESR signal was normalized in terms of that of MnO used as an internal standard. Phenols used in this study were 2,6,di-*tert*-butyl-4-hydroxy-anisole (DTBHA) and 2,6-di-*tert*-butyl–4-methylphenol (BHT), and the ESR study on these phenoxo radicals has already been reported [23]. In addition to these

cases, we have also measured the ESR signal due to the phenoxo radical by adding NADH (1cm^3, 3/500 mol dm^{-3} aqueous solution) instead of hydrogen peroxide.



DTBHA BHT

Catalase-like function

All reactions were performed at 25°C in a 10 cm^3 reactor containing a stirring bar under air. The flask containing a binuclear iron(III) compound (10μmol) solution (5 cm^3) was closed with a rubber septum. Hydrogen peroxide solution (1 cm^3, commercial 30% aqueous solution was diluted to 1 M solution by water) was injected through the septum with a syringe. The reactor was connected with a graduated burette filled with water and the dioxygen evolved was measured at appropriate times by volumetry. In the case of MnO_2 as a catalyst, *ca* 16 cm^3 of dioxygen evolved under our experimental conditions.

TBARS (thiobarbituric acid reactive substance) formation in the reaction mixture containing 2′-deoxyribose [24]

To an iron(III) compound solution (20 cm^3 aqueous solution of $[Fe^{3+}] = 5 \times 10^{-2}$ mol dm^{-3} containing 2′-deoxyribose (50 mg) was added hydrogen peroxide solution (10cm^3 1×10^{-1} mol dm^{-3}) and the resulting solution was treated with 2-thiobarbituric acid (TBA, 20 mg), as described in the previous paper [25], and the absorbance at 532 nm of the mixture was measured according to the usual work-up. In this case, the pink material should be due to the formation of malondialdehyde in the solution, which should be derived from oxidative degradation of 2′-deoxyribose [24].

RESULTS

Phenoxo radical formation

As shown in Fig. 2, the solution of DTBHA and hydrogen peroxide gives a negligible ESR signal (trace A) and it is thus clear that the formation of phenoxo radical (g-value, 2.0039 and peak-to-peak separation, 0.082 mT) [23] observed in the reaction mixture of hydrogen peroxide and binuclear iron(III) complexes (see Fig. 2, traces B, C and D) should be due to its reaction with the peroxide adduct of a binuclear iron(III) compound. This radical formation is greatly enhanced by the presence of a binuclear iron(III) complex with H(HPTP), which are much stronger than those of H(HPTB) and H_5(HXTA). The ESR signal strength of the phenoxo radical observed in this experiment is generally time-dependent, one of the examples observed for the H(HPTP) complex being illustrated in Fig. 3 and schematically shown in Fig. 4. This shows that the phenoxo radical formed may be quenched by a phenoxo radical or peroxide adduct of the iron(III) complex. The results obtained for the BHT are also

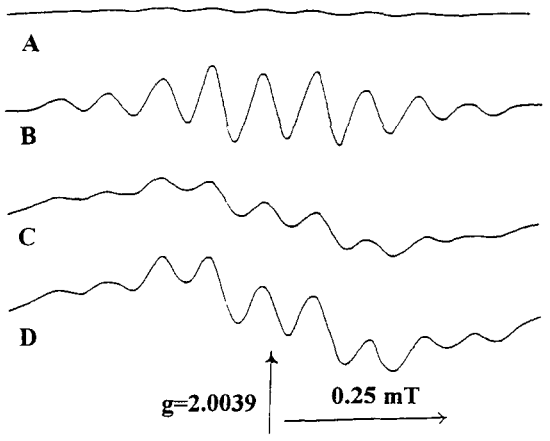


Fig. 2. ESR spectra of solution containing iron(III) complex, hydrogen peroxide and DTBHA (X-band, 25°, measured at 10 min after addition of hydrogen peroxide). (A) No iron(III), gain ×100; (B) Fe_2(HPTP)(OH)$(NO_3)_2^{2+}$, gain ×1; (C) Fe_2(HPTB)(OH)$(NO_3)_2^{2+}$, gain ×20; (D) Fe_2(HXTA)$(CH_3COO)_2^-$, gain ×100.

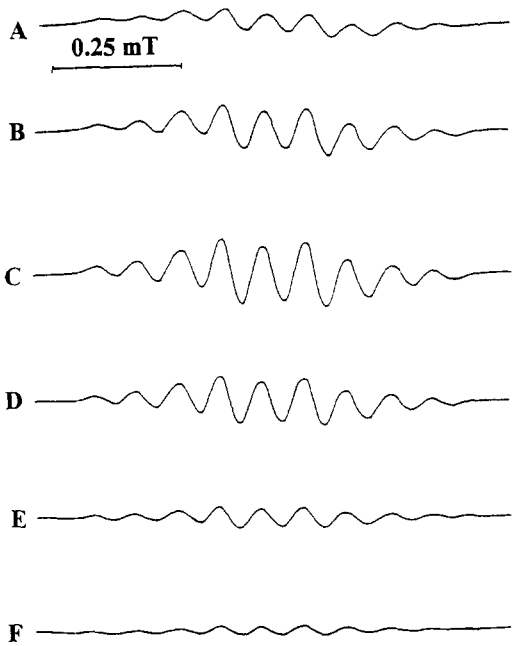


Fig. 3. Time course of the ESR spectra of solution containing Fe_2(HPTP)(OH)$(NO_3)_2^{2+}$, hydrogen peroxide and DTBHA (X-band, 25°C, gain ×1). Measured after addition of hydrogen peroxide at (A) 1, (B) 2, (C) 10, (D) 15, (E) 20 and (F) 25 min.

represented in Fig. 5; in these cases, the H(HPTP) also shows the highest activity for the formation of the radical as observed for the DTBHA system.

In Fig. 6, the ESR signal due to the phenoxo radical formation by the addition of NADH is shown, in this case, the activity of compound with H(HPTP) is also the highest, suggesting that an active species for phenoxo radical formation should be similar to that in the binuclear iron(III)/hydrogen peroxide system. Thus, it seems quite likely that in solution the following reaction proceeds and the formation of the peroxide adduct is responsible for the radical formation:

$$Fe_2^{II}(HPTP)(OH)^{4+} \xrightarrow[NADH]{} Fe_2^{III}(HPTP)^{3+} \xrightarrow[O_2]{}$$

Peroxide adduct of binuclear Fe^{III}

The last process has been investigated by Lippard and co-workers in detail [26].

Catalase-like function

In Fig. 7, the time course of dioxygen evolution in the presence of binuclear iron(III) compound and hydrogen peroxide is shown. It should be noted here that among the three compounds, the H(HPTP) complex exhibits the highest activity and that of the H(HPTB) complex is negligible in water.

Activity for TBARS Formation

In Fig. 8 the absorption spectra of the solutions treated by TBA are shown. It is well known that TBA reacts with malondialdehyde to give the following substance (see the figure below) [25], which shows a strong absorption band at 532 nm; these are called the thiobarbituric acid reactive substances, abbreviated as TBARS. Figure 8 shows that the iron(III) complex with H(HPTP) produced a much larger quantity of TBARS than those of the H(HPTB) and H_5(HXTA); this suggests that the former compound exhibits much

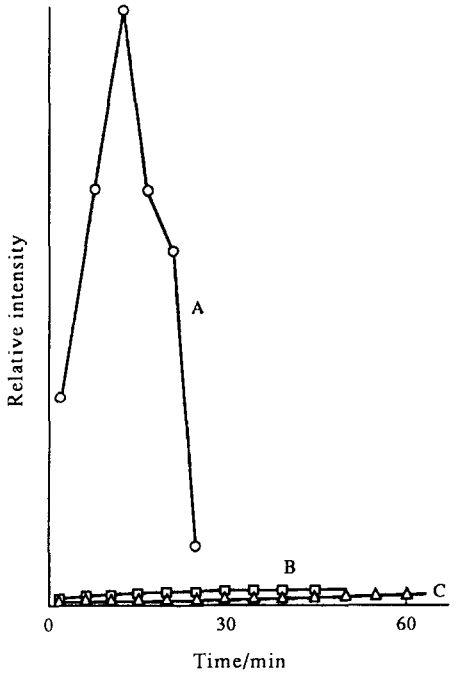


Fig. 4. Relative strength of ESR signal observed for the DTBHA system. (A) $Fe_2(HPTP)(OH)(NO_3)_2^{2+}$; (B) $Fe_2(HPTB)(OH)(NO_3)_2^{2+}$; (C) $Fe_2(HXTA)(CH_3COO)_2^-$.

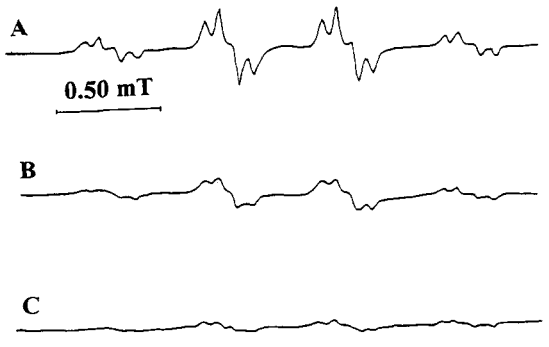


Fig. 5. ESR spectra of the solution containing the iron(III) complex, hydrogen peroxide and BHT (X-band, 25°C, measured at 6 min after mixing). (A) $Fe_2(HPTP)(OH)(NO_3)_2^{2+}$, gain ×100; (B) $Fe_2(HPTB)(OH)(NO_3)_2^{2+}$, gain ×200; (C) $Fe_2(HXTA)(CH_3COO)_2^-$, gain ×200.

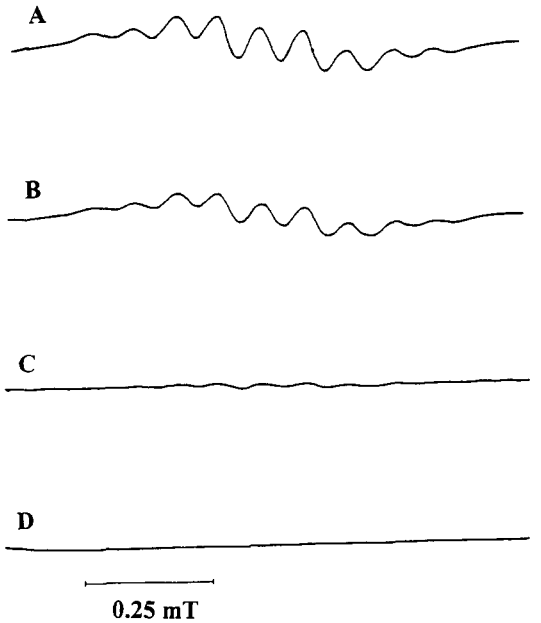


Fig. 6. ESR spectra of the solution containing the iron(III) complex, DTBHA and NADH (X-band, 25°C, gain ×50, measured at 2 min after mixing). (A) $Fe_2(HPTP)(OH)(NO_3)_2^{2+}$; (B) $Fe_2(HPTB)(OH)(NO_3)_2^{2+}$; (C) $Fe_2(HXTA)(CH_3COO)_2^-$; (D) no iron(III) ion.

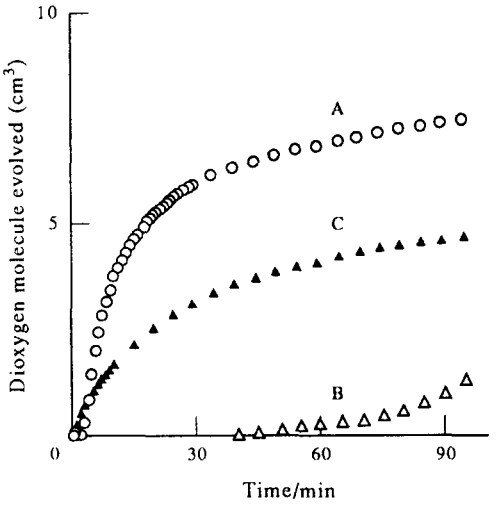


Fig. 7. Time course of dioxygen evolution from the solution containing the iron(III) complex and hydrogen peroxide. (A) $Fe_2(HPTP)(OH)(NO_3)_2^{2+}$; (B) $Fe_2(HPTB)(OH)(NO_3)_2^{2+}$; (C) $Fe_2(HXTA)(CH_3COO)_2^-$.

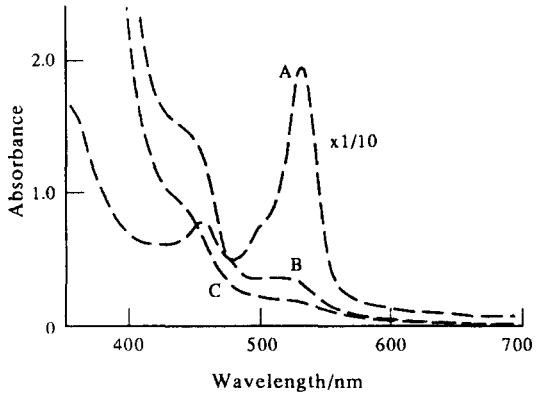


Fig. 8. Absorption spectra of the solution containing the iron(III) complex, hydrogen peroxide and 2′-deoxyribose, treated by TBA. (A) $Fe_2(HPTP)(OH)(NO_3)_2^{2+}$; (B) $Fe_2(HPTB)(OH)(NO_3)_2^{2+}$; (C) $Fe_2(HXTA)(CH_3COO)_2^-$.

higher activity for oxidative degradation of 2′-deoxyribose in the presence of hydrogen peroxide.

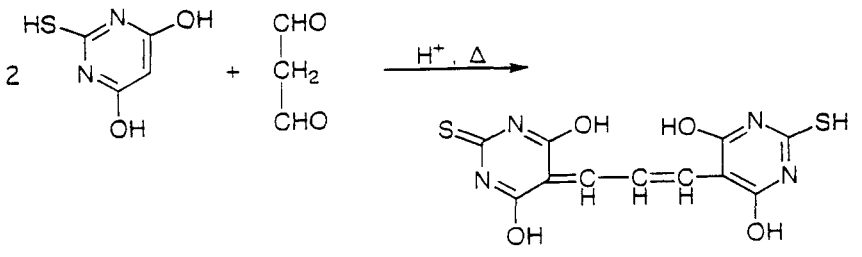
DISCUSSION

Active species for oxidation of phenols

It is well known that the binuclear iron(III) compound with H(HPTB), $[Fe_2(HPTB)(OH)(NO_3)_2]^{2+}$ reacts with hydrogen peroxide, to give a blue peroxide adduct [16]. At present, although the precise structure of the peroxide adduct is not established, it may be of *cis*-μ-η^1:η^1 type, as shown in Fig. 1 (a) [19]. A similar peroxide adduct formation was already pointed out for the compound with H(HPTP) and H_5(HXTA).

As shown in Fig. 2, this peroxide adduct should be an intrinsically active species for the oxidation of phenol, because no radical formation was observed in the presence of only free hydrogen peroxide or an iron(III) compound. This shows that some binuclear iron(III)-peroxide adducts exhibit an oxidation activity. Oxidation activity should be due to its electron acceptor power and thus it seems quite likely that the formation of a phenol radical should be due to the electrophilic nature of the peroxide adduct, as emphasized in the previous papers [21,22], and the occurrence of the electrophilic nature of the metal-peroxide adducts has been rationalized in terms of the MO scheme of the compounds [14,15]. A few years ago, several authors have reported that an active species for the formation of tyrosine radical observed in ribonucleotide reductase should be an FE^{IV}-oxo-species, which is derived from the binuclear iron(III)-peroxide adduct [27,28]. However, the above consideration seems unlikely on the basis of the discussion that the negligible activity of the Fe_2(HXTA) compound for the formation of phenoxo radical clearly excludes the possible participation of an Fe^{IV} =oxo species in the reaction, because the formation of an Fe^{IV}=oxo species is expected to be more preferable for the H_5(HXTA) complex than those of the H(HPTP) and H(HPTB) complexes according to the electrochemical data [17]. Our conclusion is quite consistent with the recent discussion developed for the ribonucleotide reductase [13].

The electrophilic nature of the peroxide adduct should be enhanced when the energy of the orbital which interacts with the occupied orbital of the substrate is lower; the energy of the MO containing *d*-orbital and orbital of the peroxide adduct may be controlled by the Lewis acidity of an iron(III) ion [14], which may be evaluated in terms of the reduction potential of the metal ion observed in the CV data. CV data shows that reduction potential ($Fe^{III} \rightarrow Fe^{II}$) of the iron(III) ions are similar to each other in the compounds with H(HPTP) and H(HPTB), but more negative in the H_5(HXTA) compound [17]; this predicts simply that the electrophilic nature of the peroxide adduct should be in the order



H(HPTP) ≈ H(HPTB) > H_5(HXTA). On the basis of the above discussion, much of the difference observed in the activity for phenoxo radical formation of H(HPTP) and H_5(HXTA) compounds can be rationalized. The different reactivity observed for the H(HPTP) and H(HPTB) compounds should be due to the large steric hindrance due to the benzimidazole moiety in the H(HPTB) compound, which may prevent the approach of the phenol, leading to the lower activity for the formation of a phenoxo radical.

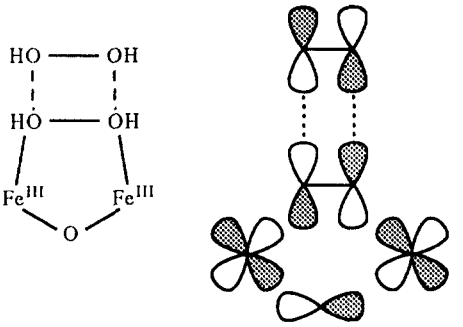


Fig. 10. Orbital relationship for facile electron transfer between the peroxide ion and the peroxide adduct of the binuclear iron(III) complex.

Chemical mechanism in catalase-like function

There may be two pathways for the evolution of dioxygen in the reaction mixture of hydrogen peroxide and a binuclear iron(III) compound; (1) electron transfer from the peroxide to an iron(III) ions through the formation of the peroxide adduct and (2) electron transfer from a peroxide ion to the peroxide adduct of binuclear iron(III) complex, as depicted in Fig. 9. In pathway (1) the oxidation–reduction cycle between Fe^{II} and Fe^{III} occurs, and in the latter case, the oxidation state of the Fe^{III} is settled throughout the reaction. As the reduction potential of the H(HPTB) and the H(HPTB) compounds are essentially the same, the results in Fig. 7 completely exclude the possibility of pathway (1), because negligible activity of the H(HPTB) compound cannot be explained by this pathway. This also excludes the possible participation of an iron(IV)=oxo species in the catalase-like function. The above discussion leads to the conclusion that the evolution of dioxygen observed in the present systems should proceed *via* pathway (2). In pathway (2), the coincidence between the orbital phases of the electron donor and acceptor, as depicted in Fig. 10, should be very important. In the case of the H(HPTB) compound, the steric hindrance as described above should also be responsible for the negligible activity observed and the lower activity of the (HXTA) compound should also be explained in terms of the lower Lewis acidity of an iron(III) ion than that in the H(HPTP) compound.

Origin for high activity for oxidation reaction

We already reported that the reactivity of the peroxide adduct of the metal complex with side-on coordination mode is highly dependent on the electronic structure of the reactants [22], for example, the Mn^{III}-peroxide adduct exhibits high reactivity for the acid anhydride, on the other hand, its reactivity towards the acid ester is almost negligible. Based on these facts, the importance of the electrophilic nature of the peroxide adduct and of the orbital correlationship between the peroxide adduct (unoccupied) and the substrate (occupied) were pointed out. This con-

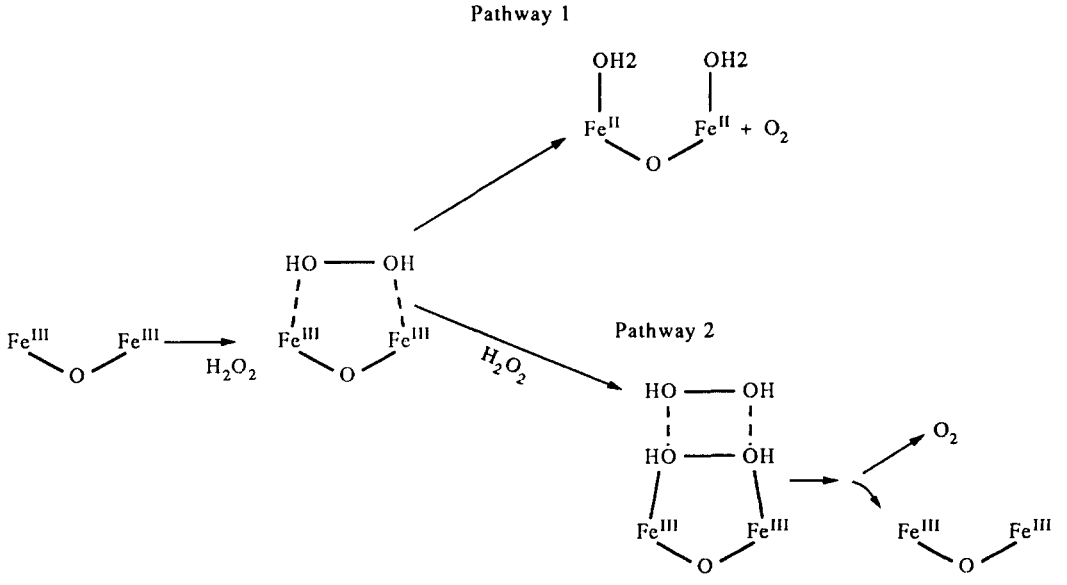


Fig. 9. Two possible pathways for dioxygen evolution.

sideration may give a reasonable explanation for the facts that in general these peroxide adducts exhibit much lower activity for alkane functionalization and for high activity for catalase-function of the (HPTP) complex as shown in Fig. 10. The oxidation reaction of phenol should proceed with the loss of a hydrogen atom from phenolic group *via* electron transfer and thus the orbital relationship between donor and acceptor does not control the reaction, which may explain the high activity of the peroxide adduct of the (HPTP) complex for oxidation reactions of phenols and 2′-deoxyribose and may support our previous conclusion that oxidation and oxygenation reactions are carried out by a different peroxide adduct than described before; peroxide adducts with an end-on η^1-coordination mode are proposed to be active for the oxygenation reaction [29].

REFERENCES

1. Feig, A. L. and Lippard, S. J. *Chem. Rev.* 1994, **94,** 759.
2. Stubbe, J., *Curr. Opin. Struct. Biol.* 1991, **1,** 788.
3. Que, Jr, L. and True, A. E., *Prog. Inorg. Chem.* 1990, **38,** 97.
4. Vincent, J. B., Lilley, G. L. O. and Averill, B. A., *Chem. Rev.* 1990, **90,** 1447.
5. Kurtz, D. M., *Chem. Rev.* 1990, **90,** 585.
6. Loher, J. S., *Iron Carriers and Iron Proteins*, ed. T. M. Loher, VCH Publishers Inc, Weinheim, 1989, pp. 375–466.
7. Shiemke, A. K., Loher, T. M. and Loher, J. S., *J. Am. Chem. Soc.* 1984, **106,** 4951.
8. Stenkampe, R. E., Sieker, L. C., Jensen, L. H., McCallum, J. D. and Loher, J. S., *Proc. Natl. Acad. Sci. U.S.A.*, 1985, **82,** 713.
9. Shiemke, A. K., Loher, T. M. and Loher, J. S., *J. Am. Chem. Soc.* 1986, **108,** 2437.
10. Lipscomb, J. D., *Ann. Rev. Microbiol.* 1994, **48,** 371.
11. Liu, K. E., Valentine, A. M., Wang, D., Huynh, B. H., Edmondson. D. E., Salifgolou, A. and Lippard, S. J., *J. Am. Chem. Soc.* 1995, **117,** 10174.
12. Fox, B. G., Shanklin, J., Somerville, C. and Munck, E., *Proc. Natl. Acad. Sci. U.S.A.*, 1993, **90,** 2486.
13. Ravi, N., Bollinger, Jr, J. M., Huynh, B. H., Edmondson, D. E. and Stubbe, J., *J. Am. Chem. Soc.* 1994, **116,** 8007; Bollinger, Jr, J. M., Tong, W. H., Ravi, N., Huynh, B. H., Edmondson, D. E. and Stubbe, J., *ibid.* 1994, **116,** 8015; Bollinger, Jr, J. M., Tong, W. H., Ravi, N., Huynh, B. H., Edmondson, D. E. and Stubbe, J., *ibid.* 1994, **116,** 8024.
14. Nishida, Y. and Takeuchi, M., *Z. Naturforsch.* 1987, **42B,** 52; Nishida, Y. and Yokomizo, T., *Inorg. Chim. Acta*, 1989, **163,** 9; Nishida, Y., Yoshizawa, K., Takahashi, S. and Watanabe, I., *Z. Naturforsch.* 1992, **47C,** 290; Nishida, Y., Itoh, H. and Yamazaki, A., *Polyhedron*, 1994, **13,** 2473.
15. Nishida, Y. and Ito, S., *Z. Natursforsch.* 1995, **50C,** 205; *ibid.* 1995, **50C,** 571.
16. Nishida, Y., Takeuchi, M., Shimo, H. and Kida, S., *Inorg. Chim. Acta*, 1984, **96,** 115.
17. Nishida, Y., Nasu, M. and Akamatsu, T., *Z. Naturforsch.* 1992, **47B,** 115.
18. Murch, B. P., Bradley, F. C. and Que, Jr, L., *J. Am. Chem. Soc.* 1986, **108,** 5027.
19. Brenann, B. A., Chen, Q., Garcia, C. J., True, A. E., O'Connor, C. J. and Que, Jr, L., *Inorg. Chem.* 1991, **30,** 1937.
20. Yoshizawa, K. and Hoffmann, R., *Inorg. Chem.* 1996, **35,** 2409.
21. Nishida, Y., Akamatsu, T. and Nasu, M., *Chem. Lett.*, 1991, 1703.
22. Nishida, Y., Takahashi, S., Watanabe, I., Yamazaki, A., Itoh, H. and Sakamoto, M., *Polyhedron*, 1994, **13,** 1539.
23. Valoti, M., Sipe, H. J., Sgaragli, G. and Mason, R. P., *Arch. Biochem. Biophys.* 1989, **269,** 423.
24. Halliwell, B. and Gutteridge, J. M. C., *Free Radicals in Biology and Medicine*, Ch. 4. Oxford University Press, London, 1985.
25. Nishida, Y. and Ito, S., *Polyhedron*, 1995, **14,** 2301.
26. Feig, A. L., Becker, M., Schinder, S., van Eldik, R. and Lippard, S. J., *Inorg. Chem.* 1996, **35,** 2590.
27. Fontecave, M., Gerez, C., Atta, M. and Jeunet, A., *Biochem. Biophys. Res. Commun.* 1990, **168,** 659.
28. Sahlin, M., Sjoberg, B. M., Backes, G., Loher, T. M. and Loher, J. S., *Biochem. Biophys. Res. Commun.* 1990, **167,** 813.
29. Ito, S., Suzuki, M., Kobayashi, T., Itoh, H., Harada, A., Ohba, S. and Nishida, Y., *J. Chem. Soc., Dalton Trans.* 1996, 2579.

Pergamon

PII: S0277-5387(96)00426-3

Polyhedron Vol. 16, No. 9, pp. 1505–1512, 1997
Copyright © 1997 Elsevier Science Ltd
Printed in Great Britain. All rights reserved
0277-5387/97 $17.00+0.00

X-ray crystal structure of copper(II) and silver(I) complexes with the new ligand 1,4-bis(5′-methyl-2,2′-bipyridine-5-ethyl)-benzene: the effects of substituent and linking position on the assembly of helical complexes

You-Jun Fu,[a] Hao Yang,[a] De-Fen Wang,[a] Wen-Xia Tang,[a]* Bo-Mu Wu[b] and Thomas C. W. Mak[b]

[a]State Kay Lab of Coordination Chemistry, Coordination Chemistry Institute, Nanjing University, Nanjing 210093, P. R. China

[b]Department of Chemistry, Hong Kong Chinese University, Hong Kong

(Received 25 June 1996; accepted 22 August 1996)

Abstract—A new tetradentate ligand 1,4-bis(5′-methyl-2,2′-bipyridine-5-ethyl)-benzene(p-bpy) and its Cu^{II} and Ag^{I} complexes were synthesized. In complex **1**, $Cu(p\text{-bpy})[ClO_4]_2 \cdot 0.5MeCN$, the four nitrogen atoms of the ligand coordinate with one Cu^{II} to form a flattened tetrahedron. The metal ion also has weak interactions with two ClO_4^- ions, which link the Cu^{II} ions in a one dimensional fashion to make an infinite chain. In complex **2**, $Ag(p\text{-bpy})[ClO_4]$, the coordination geometry of Ag^{I} is flattened tetrahedron. © 1997 Elsevier Science Ltd. All rights reserved.

Keywords: helical complex; molecular assembly; copper(II) complex; silver(I) complex; substituted bipyridene.

There is considerable interest in molecular topology, with particular emphasis being placed on the ability of metal ions to control the configuration of organic ligands [1]. Several groups have been involved in studies on the formation of helical complexes [2–5]. It was reported that oligobipyridines containing 6,6′-disubstituted bpy units spaced by $—CH_2OCH_2—$ and $—CH_2CH_2—$ form with Cu^{I} and Ag^{I} double helical complexes [6,7,8], while the ligand 1,2-bis(2,2′-bipyridyl-6-yl)ethane (*o*-bpy) forms with both Cu^{II} and Cu^{I} only mononuclear complexes [9]. The mononuclear complexes of Ru^{II} and Re^{V} of *o*-bpy has also been studied recently [10,11] on the interest of photochemistry. Nevertheless, Lehn and coworkers [8,12] observed that a slight modification of the steric effects by shifting from a 6,6′- to a 5,5′-disubstitution results in the formation of triple helical complexes and a 4,4′-disubstitution results in a triply bridged dinuclear Fe^{II} complex [13]. In order to further illustrate the effects by the linking positions and properties of spacer groups (flexibility and length), we combined the effects of preparing a new tetradentate ligand based on 5,5′-disubstituted bpy using $—CH_2CH_2—C_6H_4—CH_2CH_2—$ as the spacer. The results showed that the coordinating behaviour of the ligand are unexpectedly not similar to the above 6,6′- or 5,5′ disubstituted bpy-based ligands, but similar to *o*-bpy, forming mononuclear complexes with Ag^{I} and Cu^{II}. The synthesis of the tetradentate ligand 1,4-bis(5′-methyl-2,2′-bipyridine-5-ethyl)-benzene(*p*-bipy), the preparation, X-ray structure and properties of its Cu^{II} and Ag^{I} complexes are reported.

* Author to whom correspondence should be addressed.

EXPERIMENTAL

Preparation of the ligand (p-*bpy*)

1,4-Bis(bromomethyl)benzene was prepared according to the literature [13], 50%, m.p. 142.5–144.5°C.

5,5′-Dimethyl-2,2′-bipyridine was prepared according to the literature [14,15], m.p. 115.5–116.5°C (literature value 114.5–115°C), ^{1}H NMR results: δ2.39 (6H,s,-CH_3), δ7.62 (2H,d,H_4,$H_{4'}$), δ8.26 (2H,d,H_3,$H_{3'}$), δ8.49 (2H,s,H_6,$H_{6'}$).

1,4-Bis(5′-methyl-2,2′-bipyridine-5-ethyl)-benzene (*p*-bpy): Lithium diisopropylamide was prepared by addition of butyllithium (14.4 mmol, 1.7 M solution in ether) to diisopropylamine (2.10 cm^3, 14.86 mmol) in dry THF (40 cm^3) under argon at −78°C. This solution was added slowly by cannula to 5,5′-dimethyl-2,2′-bipyridine (2.66 g, 14.44 mmol) in dry THF (40 cm^3) at −78°C. The dark reddish brown reaction mixture was stirred for about 2.5 h. 1,4-Bis(bromomethyl)benzene (1.85 g, 6.8 mmol) in THF (60 cm^3) was added dropwise with stirring within *ca* 40 min, during the period the temperature was allowed to increase slowly but not above 0°C. Stirring at 0°C was continued for 30 min and then water (20 cm^3) was added to quench the reaction. THF was removed *in vacuo* and the yellow precipitate filtered off, suspended in MeOH (50 cm^3) and filtered again. The remaining solid was chromatographed on a silica column with chloroform/methanol = 95 : 5. Colourless crystal needles were obtained with condensation. Yield 900 mg (30%), m.p. 242.0–244.0°C, FAB+, *m/z* 471. Found: C, 82.1; H, 6.7; N, 12.1. Calc. for $C_{32}H_{30}N_4$: C, 81.7; H, 6.4,N,11.9%, ^{1}H NMR results: δ2.39 (6H,s,—CH_3), δ2.94 (8H,m,—CH_2—), δ7.07 (4H,s,—C_6H_4—), δ7.55 (2H,d,H_4), δ7.62 (2H,d,$H_{4'}$), δ8.26 (4H,d,H_3, $H_{3'}$), δ8.45 (2H,s,H_6), δ8.49 (2H,s,$H_{6'}$). All results indicate that the title ligand has been obtained.

Preparation of the complexes

Cu(*p*-bpy) $[ClO_4]_2 \cdot 0.5MeCN$ (**1**) was prepared by refluxing a suspension solution of *p*-bpy (25.4 mg, 0.054 mmol) in methanol (20 cm^3) containing an equivalent of $Cu(ClO_4)_2 \cdot 6H_2O$ (20 mg, 0.054 mmol) for *ca* 2 h. Green precipitates were obtained upon concentration. The micro-elemental analysis of the dried powder sample is consistent with the unsolvated formula: Found: C, 51.6; H, 4.3; N, 7.4. Calc. for $C_{32}H_{30}N_4CuCl_2O_8$: C, 52.4; H, 4.1; N, 7.6%. Suitable crystals were recrystallized from a acetonitrile/toluene (1 : 1) solution of the precipitates at room temperature by slow evaporation of the solvent.

Ag(*p*-bpy) $[ClO_4]$ (**2**): Refluxing of the suspension solution of the ligand *p*-bpy (27.8 mg, 0.059 mmol) in methanol with an equivalent of $AgNO_3$ (10 mg, 0.059 mmol) gave a colourless solution. Precipitates were obtained upon the addition of saturated methanolic $LiClO_4$ solution and filtration. Suitable crystals were recrystallized from a methanolic solution of the complex by slow evaporation of the solvent. The micro-elemental analysis is consistent with the unsolvated formula: Found: C, 56.2; H, 4.1; N, 8.5. Calc. for $C_{32}H_{30}N_4AgClO_4$: C, 56.8; H, 4.4; N, 8.3%.

X-ray crystallography

Crystals of the complexes were mounted on a Rigaku RAXIS IIc diffractometer equipped with highly oriented graphite-monochromatized Mo-K_α radiation (λ = 0.71073 Å). Reflection data were collected at 292 K using an imaging plate system in the variable ω-scan technique. The refinement of the coordinates and anisotropic thermal parameters of the non-hydrogen atoms was carried out by the full-matrix least-squares analysis. The hydrogen atoms of the ligands were placed in their calculated positions and assigned fixed isotropic thermal parameters and allowed to ride on their respective parent atoms. Analytic expressions of atomic scattering factors were employed and anomalous dispersion corrections were incorporated [16–18]. All calculations were performed on a PC 486 computer.

Summary of data collection and crystal data for both complexes are listed in Table 1. Selected bond lengths and bond angles are listed in Tables 2 and 3 for complex **1** and complex **2**, respectively.

ESR spectrum

The ESR spectrum were recorded at 110 K on a Bruker 2000-SRC spectrometer operating at 9.4884 GHz in frozen acetonitrile.

RESULTS AND DISCUSSION

Structural description and discussion

The structure of complex **1** is characterized by a half occupancy of the solvent acetonitrile molecule. Two crystallographically non-equivalent complex molecules are observed (Fig. 1). Copper(II) was found to coordinate with only one ligand molecule in a flattened tetrahedral geometry. The two terminal pyridine nitrogen atoms in each ligand have shorter bonds with the metal ion Cu(1): Cu(1)—N(1) = 1.968(1), Cu(1)—N(4) = 1.948(2), Cu(1)—N(2) = 1.995(2), Cu(1)—N(3) = 1.991(1) Å, similar to the complex of *o*-bpy [8]; but the situation is different in the case of Cu(2): Cu(2)—N(5) = 1.996(2) Å is the longest and Cu(2)—N(6) = 1.972(2), Cu(2)—N(8) = 1.974(2) Å, while the shortest is Cu(2)—N(7) = 1.945(2) Å. The pyridine rings within the 2,2′-bipy subunits are not completely coplanar, with dihedral angles 1/2, 8.4°; 3/4, 13.8°; 5/6, 11.8°; 7/8, 7.5° (the pyridyl rings are

Table 1. Crystallographic data for the complexes

Compounds	Complex **1**	Complex **2**
Chemical formula	$C_{65}H_{61.5}Cl_4Cu_2N_{8.5}O_{16}$	$C_{32}H_{30}AgN_4O_4Cl$
Crystal dimensions (mm^3)	$0.10 \times 0.40 \times 0.60$	$1.00 \times 0.20 \times 0.10$
Reflections measured	11290	19189
Unique reflections	7952	11498
R_{int} (%)	4.66	6.04
Observed reflections [$F > 6.0\sigma(F)$]	5468	7964
Variable number	873	728
fw	1486.6	677.9
a (Å)	28.358(1)	28.678(1)
b (Å)	15.105(1)	8.414(1)
c (Å)	15.822(1)	28.703(1)
β (°)	102.52(1)	119.35(1)
V ($Å^3$)	6622(3)	6037(3)
Z	4	8
Space group	Cc	$P2_1/n$
$F(000)$	3060	2768
D_c ($g\,cm^{-3}$)	1.491	1.492
μ (Mo-K_α) (cm^{-1})	8.79	7.99
R_1 (obs. data)	0.069	0.0682
wR (obs. data)	0.068	0.0736
w^{-1}	$\sigma^2 \lvert F_o \rvert + 0.00004 \lvert F_o \rvert^2$	$\sigma^2 \lvert F_o \rvert + 0.000005 \lvert F_o \rvert^2$

Table 2. Selected bond lengths (Å) and angles (°) for **1**

Cu(1)—N(1)	1.968(1)	Cu(1)—N(2)	1.995(2)
Cu(1)—N(3)	1.991(1)	Cu(1)—N(4)	1.948(2)
Cu(2)—N(5)	1.996(2)	Cu(2)—N(60	1.972(2)
Cu(2)—N(7)	1.945(2)	Cu(2)—N(8)	1.974(2)
Cu(1)···O(11)	3.303(3)	Cu(1)···O(13)	3.169(3)
Cu(1)···O(22a)	3.310(3)	Cu(1)···O(23a)	2.962(3)
Cu(2)···O(12)	3.263(3)	Cu(2)···O(14)	3.143(3)
Cu(2)···O(21)	3.117(3)	Cu(2)···O(24)	3.213(3)

N(1)—Cu(1)—N(2)	83.6(1)	N(1)—Cu(1)—N(3)	151.0(1)
N(2)—(1)—N(3)	105.3(1)	N(1)—Cu(1)—N(4)	104.2(1)
N(2)—Cu(1)—N(4)	149.4(1)	N(3)—Cu(1)—N(4)	82.3(1)
N(5)—Cu(2)—N(6)	84.1(1)	N(5)—Cu(2)—N(7)	150.2(1)
N(6)—Cu(2)—N(7)	106.1(1)	N(5)—Cu(2)—N(8)	102.2(1)
N(6)—Cu(2)—N(8)	151.3(1)	N(7)—Cu(2)—N(8)	82.5(1)
O(22a)···Cu(1)···O(23a)	42.3(1)	O(13)···Cu(1)···O(11)	41.6(1)
O(21)···Cu(2)···O(24)	42.9(1)	O(12)···Cu(2)···O(14)	43.8(1)

Table 3. Selected bond lengths (Å) and angles (°) for **2**

Ag(1)—N(1)	2.265(2)	Ag(1)—N(2)	2.419(2)
Ag(1)—N(3)	2.332(2)	Ag(1)—N(4)	2.295(2)
Ag(2)—N(5)	2.253(2)	Ag(2)—N(6)	2.342(2)
Ag(2)—N(7)	2.303(2)	Ag(2)—N(8)	2.293(2)

N(1)—Ag(1)—N(2)	71.4(1)	N(1)—Ag(1)—N(3)	134.0(1)
N(2)—Ag(1)—N(3)	100.4(1)	N(1)—Ag(1)—N(4)	137.3(1)
N(2)—Ag(1)—N(4)	146.8(1)	N(3)—Ag(1)—N(4)	71.8(1)
N(5)—Ag(2)—N(6)	72.7(1)	N(5)—Ag(2)—N(7)	151.0(1)
N(6)—Ag(2)—N(7)	112.7(1)	N(5)—Ag(2)—N(8)	123.4(1)
N(6)—Ag(2)—N(8)	139.5(1)	N(7)—Ag(2)—N(8)	72.1(1)

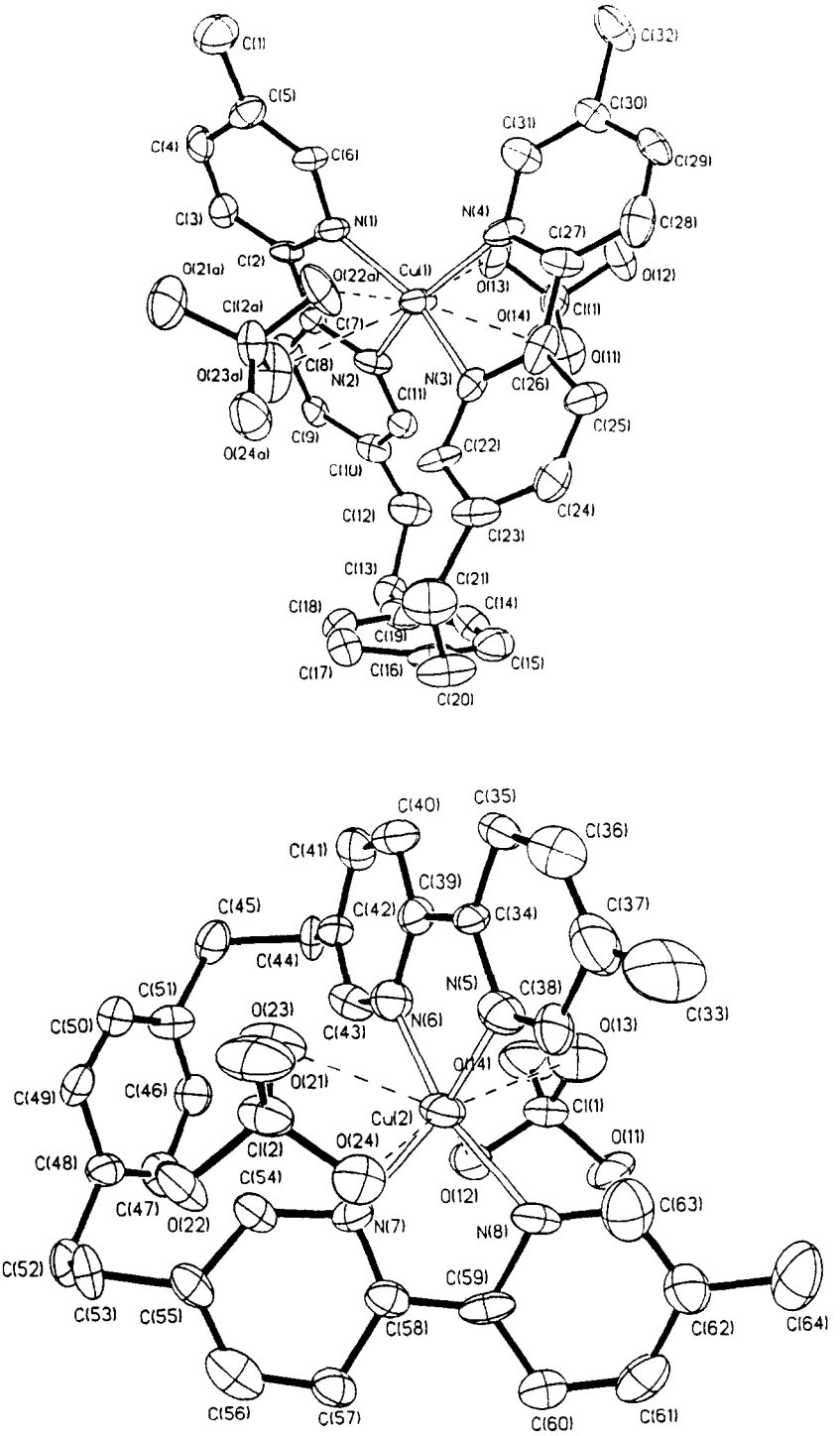


Fig. 1. The molecular structure of complex **1** with atom numbering scheme.

numbered after the nitrogen atoms they contain). The bond angles involving the five-membered chelation, N(1)—Cu(1)—N(2) = 83.6°, N(3)—Cu(1)—N(4) = 82.3°, N(5)—Cu(2)—N(6) = 84.1°, N(7)—Cu(2)—N(8) = 82.5° are slightly larger than the value of 81.6° reported for the *o*-bpy complex. The Cu(1)—Cu(2) distance is 7.605 Å. The angle between intramolecular plane normals of the two bipyridines is *ca* 60° in both molecules and the phenyl ring has dihedral angles of *ca* 61° with both bipy normals in molecules containing Cu(1), but in the second molecule the dihedral angles are different: 64 and 55°, respectively, for normals containing N(5), N(6) and N(7), N(8). The phenyl plane of the ligand and the coordination least-squares plane are perpendicular to each other with a dihedral angle of 89.3°.

The molecular structure of complex **2** is depicted in Fig. 2 with atom numbering scheme. Similar to complex **1**, two independent mononuclear molecules of the formula Ag(*p*-bpy)ClO_4 are identified in the lattice. No aromatic stacking is observed between them. The coordination geometry of silver(I) is a flattened tetrahedron. The major difference between the two unique molecules is the different bond angles (see Table 3). The dihedral angle values in the same molecules between pyridyl rings are Ag(1): 1/2 13.9° ; 3/4, 2.3 ; Ag(2): 5/6, 3.7°; 7/8, 2.9° (the pyridine ring planes numbered after the nitrogen atoms they contain). The distance Ag(1)—Ag(2) = 15.247 Å and the angle between intramolecular plane normals of the two bipyridine(bpy) is 69 and 60°, respectively, for that containing Ag(1) and Ag(2).

Several ligands that have comparable structures have been reported. For 6,6′-disubstituted 2,2′-bipyridine-based ligands, 1,2-bis(6′-methyl-2,2′-bipyridyl-6-yl)ethane(*o*-dmbpy) forms with a Cu^{I} double helical complex, as does the ligand using 1,10-phenanthroline as a replacement of the bipyridyl segments [8]. The other series of ligands using —CH_2OCH_4— as the spacer can also form with Cu^{I} and Ag^{I} double helical complexes [7]. The literature [19,20] reports the syntheses of several knotted molecules in which the key step is the synthesis of Cu^{I} dinuclear double helical complexes. A flexible spacer as long as —CH_2CH_2 CH_2CH_2— was used in the synthesis. However, when the 6′-methyl group is removed, the ligand 1,2-bis(2,2′-bipyridyl-6-yl)ethane(*o*-bpy) can only form with Cu^{II} and Cu^{I} mononuclear complexes [9]. Lehn and co-workers found that a slight steric modification from 6,6′- to 5,5′-disubstituents results in the formation of a triple helical complex of 1,2-bis(5′-methyl-2,2′-bipyrid-5-yl)ethane with Fe^{II} [8]. And the tris-(bipyridyl) ligand 5,5′-bis(5′-methyl-2,2′-bipyridyl-5-ethyl)-2,2′-bipyridine forms with Ni^{II} a trinuclear triple helical complex, the X-ray structure of which has been determined [12].

It can be seen that the structures of both of the Ag^{I} and Cu^{II} complexes with the newly synthesized ligand *p*-bpy in this paper are different from all the above two cases of 6,6′- and 5,5′-disubstituted bpy based ligands. On the first hand, these facts indicate the steric effects of the 6′-methyl in *o*-dmbpy is most important in the formation of the Cu^{I} double helix for 6,6′-disubstituted bpy-based ligands. The methyl substitution of *p*-bpy at the 5′-position, not at the crucial 6′-position, creates no steric repulsion when the ligand adopts the near planar all-*cis* conformation to form a ring cavity. On the other hand, the significant difference between the 6,6′- and 5,5′-disubstituted ligands spaced by —CH_2CH_2— is perhaps

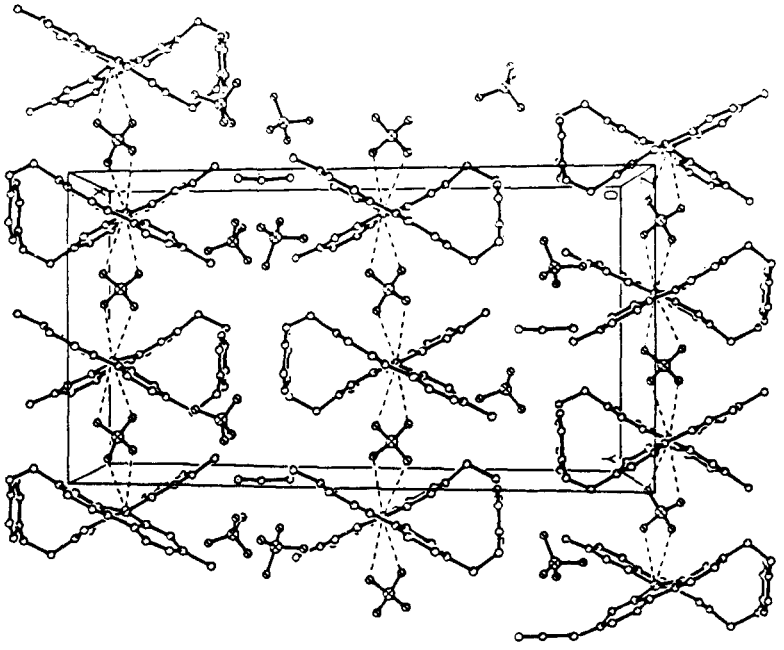


Fig. 2. The crystal packing of complex **1**.

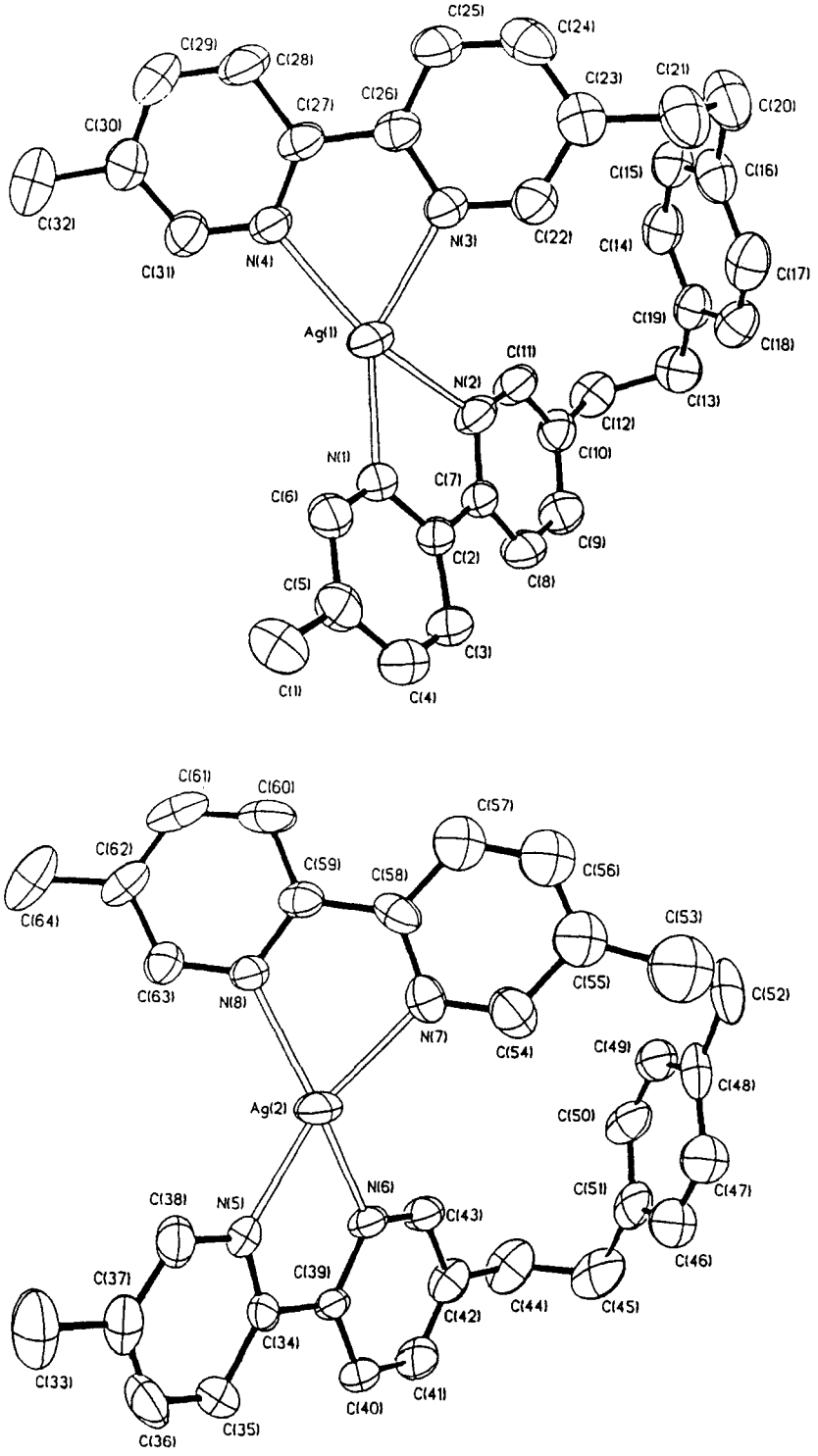


Fig. 3. The molecular structure of complex **2** with atom numbering scheme.

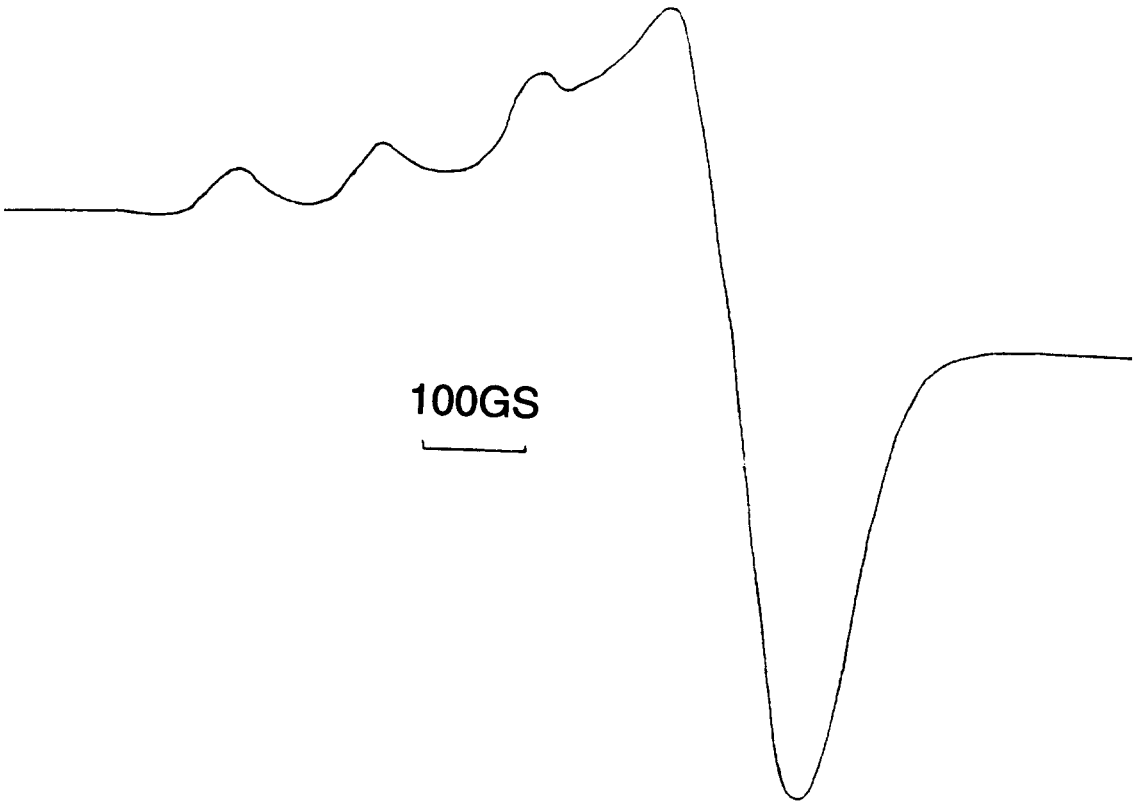


Fig. 4. ESR spectrum of complex **1** in solvent acetonitrile at 110 K.

caused by the facts that the 5,5′-disubstituted ligands has a larger planar cavity than the 6,6′-disubstituted ones and the metal ions with smaller ionic radius, such as Ni^{II} and Fe^{II}, cannot fit in. However, when a helical conformation was adopted by the ligand molecules, they can coordinate simultaneously with two metal ions to establish the octahedral geometric requirement of the cations and form a triple helix. However, the change of the spacer from $—CH_2CH_2—$ to $—CH_2CH_2—C_6H_4—CH_2CH_2—$ also disfavours the formation of multiple helicates, because the length and flexibility of the spacer made is possible for the ligand to act as a tetradentate ligand coordinating with only one Cu^{II} or Ag^{I} ion.

Therefore, it can be concluded that for ligands based on substituted bpy, both flexibility, length of the spacer group and the steric groups at crucial positions can control the formation of helical complexes. The flexibility, the longer spacer group and the absence of steric groups at the terminal 6′-positions are responsible for the failure in forming double or triple helixes in this paper.

The structure of the two complexes are essentially similar apart from the weak coordination of perchlorate ions in complex **1**. This difference results from the tendency of Cu^{II} to form six-coordinate octahedral geometry. In complex **1**, the ClO_4^- anions act as bidentate ligands and occupy positions relative to the CuN_4 chromophore, such that four long Cu—O distances (ranging from 2.962 to 3.303 Å) are present to yield a distorted eight-coordinate CuN_4O_4 dodecahedral chromophore. The Cu—O distances are longer than that in Cu(*o*-bpy) $(ClO_4)_2$ (2.7 Å), but shorter than that of Cu—F in $Cu(bpy)_2(PF_6)_2$ (3.3 Å). As the Cu—O distances are too long [21], the copper stereochemistry is best considered as compressed tetrahedral in the title complex **1**. The longest reported bond length of Cu—O, to our knowledge is 2.932 Å in a bis(2-pyridylcarbonyl)amido complex [22]. Most recently weak $Cu\cdots OClO_3$ bonds were observed ranging from 2.992 to 3.348 Å [23]. Therefore, it is appropriate to say that ClO_4^- has weak coordinating interactions with Cu^{II}. The structure is in a one-dimensional infinite chain form (Fig. 3). The crystal packing is perhaps the main cause of the existence of the two molecules with a different coordination situation in both complexes.

ESR spectrum

The ESR spectrum (Fig. 4) can best be described as isotropic with a weak $g_{\|}$ component located at 2.268 and a $g_{\perp}$ located at 2.081. The spectrum is similar to that of $[Cu(o\text{-bpy})](ClO_4)_2$ [8].

Acknowledgements—This work was supported by the China

National Science Foundation and Hong Kong Research Grants council Earmarked Grant CUHK 311/94P.

REFERENCES

1. Lawrence, D. S., Jiang, T. and Levett, M., *Chem. Rev.* 1995, 33.
2. Potts, K. T., Keshavarzk, M., Tham, F. S, Abruna, H. D. and Arana, C. R., *Inorg. Chem.* 1993, **32,** 4422; 4436.
3. Constable, E. C., *Tetrahedron*, 1992, **48,** 10013.
4. Piguet, C., Hopfgartner, G., Bocquet, B., Schaad, O. and Williams, A. F., *J. Am. Chem. Soc.* 1994, **116,** 9092.
5. Fu, Y., Sun, J., Li, Q., Dai, W., Wang, D., Mak, T. C. W., Tang, W. and Hu, H., *J. Chem. Soc., Dalton Trans.* 1996, 2309.
6. Lehn, J. M., Rigault, A., Siegel, J., Harrowfield, J., Chevrier, B. and Moras, D., *Proc. Acad. Sci. (U.S.A.)*, 1987, **27,** 2565.
7. Lehn, J.-M. and Rigault, A., *Angew. Chem., Int. Ed. Engl.* 1988, **27,** 1095.
8. Youinou, M. T., Ziessel, R. and Lehn, J.-M., *Inorg. Chem.* 1991, **30,** 2144.
9. Garber, T., Wallendael, S. V., Rillema, D. P., Kirk, M., Hatfield, W. E., Welch, J. H. and Singh, P., *Inorg. Chem.* 1990, **29,** 2863.
10. Masood, Md. A., Sullivan, B. P. and Hodgson, D. J., *Inorg. Chem.* 1994, **33,** 4611.
11. Masood, Md. A., Sullivan, B. P. and Hodgson, D. J., *Inorg. Chem.* 1993, **32,** 5360.
12. Kramer, R., Lehn, J.-M., Cian, A. D. and Fischer, J., *Angew. Chem., Int. Ed. Engl.* 1993, 703.
13. Wenner, W., *J. Org. Chem.* 1952, **17,** 523.
14. Sasse, W. H. F. and Whittle, C. P., *J. Chem. Soc.* 1961, 1347.
15. Badger, G. M. and Sasse, W. H. F., *J. Chem. Soc.* 1956, 616.
16. Tanner, J. and Krause, K., *The Rigaku Journal*, 1994, **11,** 4; 1990, **7,** 28.
17. Krause, K. L. and Phillips, G. N. Jr., *J. Appl. Cryst.* 1992, **25,** 146.
18. Sato, M., Yamamoto, M., Imada, K., Katsube, Y., Tanaka, N. and Higashi, T., *J. Appl. Cryst.* 1992, **25,** 348.
19. Dietrich-Buchecker, C. O. and Sauvage, J. P., *Angew Chem., Int. Ed. Engl.* 1989, **28,** 189.
20. Dietrich-Buchecker, C. O., Nierengarten, J.-F., Sauvahe, J.-P., Armaroli, N., Balzani, V. and De Cola, L., *J. Am. Chem. Soc.* 1993, **115,** 11237.
21. Foley, J., Tyagi, S. and Hathaway, B. J., *J. Chem. Soc., Dalton Trans.* 1984, 1.
22. Castro, I., Sletten, J., Faus, J., Julve, M., Journaux, Y., Lloret, F. and Alvarez, S., *Inorg. Chem.* 1992, **31,** 1889.
23. Burger, K. S., Chandhuri, P., Wieghardt, K. and Nuber, B., *Chem. Eur. J.* 1995, **1,** 583.

Pergamon

PII: S0277-5387(96)00438-X

Polyhedron Vol. 16, No. 9, pp. 1513–1516, 1997
Copyright © 1997 Elsevier Science Ltd
Printed in Great Britain. All rights reserved
0277-5387/97 $17.00+0.00

Organometallic compounds as complexing agents: a rare example of a crystalline alkali metal podate

Ulrich Siemeling

Fakultät für Chemie, Universität Bielefeld, Universitätsstraße 25, D-33615 Bielefeld, Germany

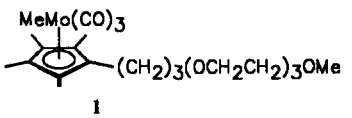
(Received 12 August 1996; accepted 21 August 1996)

Abstract—The tentacle-bearing ferrocenes $[Fe\{R_4C_5SiMe_2(OCH_2CH_2)_nOMe\}_2]$ (**4a**: R = H, $n = 2$; **4b**: R = Me, $n = 2$; **4c**: R = H, $n = 3$; **4d**: R = Me, $n = 3$) and $[Fe\{Me_4C_5(CH_2)_3(OCH_2CH_2)_3OMe\}_2]$ (**5**) act as podands for alkali metal cations; **4b, 4d,** and **5** are much better podands than **4a** and **4c**. Compound **5** and $[(C_5H_5)Fe\{Me_4C_5(CH_2)_3(OCH_2CH_2)_3OMe\}]$ (**8**) are oxidized to $\mathbf{5}^+$ $[PF_6]^-$ and $\mathbf{8}^+$ $[PF_6]^-$, respectively, which both show no tendency to crystallize. The cobaltocenium species $[Co\{Me_4C_5(CH_2)_3(OCH_2CH_2)_3OMe\}_2]^+[PF_6]^-$ ($\mathbf{11}^+$ $[PF_6]^-$) is a selective podand, which prefers potassium over lithium cations; its potassium podate $\mathbf{11}^+$ $[PF_6]^- * K^+[PF_6]^-$ is the first example of a crystalline oligoethylene glycol ether podate, whose crystallinity does not rely on the rigid end-group principle. © 1997 Elsevier Science Ltd. All rights reserved.

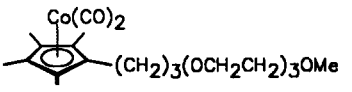
Keywords: cyclopentadienyl ligand, functionalized; ferrocene, functionalized; oligoethylene glycol ether; podate; crystalline; organometallic chemistry, supramolecular; tentacle.

We have recently described a series of cyclopentadienes of the type HR_4C_5-Z-$(OCH_2CH_2)_nOMe$ (Z = spacer group) functionalized with a pendent oligoethylene glycol ether "tentacle" [1]. These compounds have been utilized for the preparation of a wide variety of cyclopentadienyl complexes such as, for example, the carbonyl complexes **1** [2] and **2** [1b], the titanium half-sandwich complex **3** [2] and the ferrocenes **4a–d** [3] and **5** [1b], which show extraordinarily high solubilities in organic solvents of all polarities due to the amphiphilic nature of the tentacle substituent.

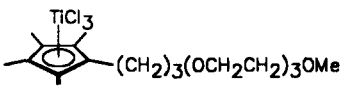
We have also been able to synthesize rather unusual compounds such as, for example, the half-sandwich iron(II) chloride complex **6** [4] and the primary α-ferrocenyl carbocation $\mathbf{7}^+$ [5]; the stabilising influence of the tentacle on these otherwise very unstable species is based on a predominantly intramolecular coordination of the tentacle to the unsaturated position present in these compounds.



1

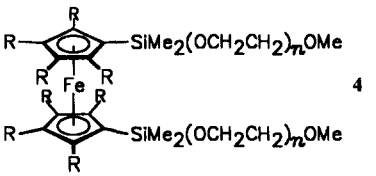


2

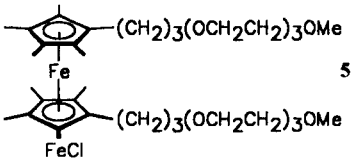


3

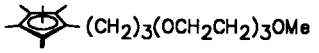
	R	n
a	H	2
b	Me	2
c	H	3
d	Me	3



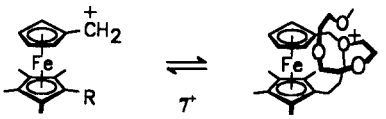
4



5



6



R = $(CH_2)_3(OCH_2CH_2)_3OMe$

This paper focuses on a supramolecular aspect of tentacle-functionalized cyclopentadienyl compounds, which is based on the well-known ability of oligoethylene glycol ether units to act as podands [6].

RESULTS AND DISCUSSION

The podand abilities of the ferrocenes **4a–d** and **5** towards alkali metal cations were determined by using the well-established picrate extraction method developed by Peterson [7]. The results of this investigation are summarised in Table 1.

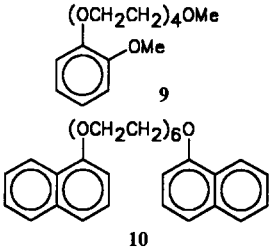
Two effects can be made out quite clearly. The first effect is based on the ring substitution of the ferrocenes: The ferrocenes with permethylated cyclopentadienyl rings (**4b, 4d** and **5**) are much better podands than the unmethylated ferrocenes **4a** and **4c**. The second effect is based on the tentacle length: Considering the ferrocenes of type **4**, it is evident that among the pairs with identical ring methylation the ferrocene with the longer tentacle is the better podand. Not surprisingly, the podand abilities of **4d** and **5**, which have the same ring methylation and tentacle length, are almost identical.

Generally, tentacle-bearing molecules are oils which show no tendency to crystallize [8]. This is even true for ionic compounds such as $[Fe\{Me_4C_5(CH_2)_3(OCH_2CH_2)_3OMe\}_2]^+[PF_6]^-$ (**5**$^+[PF_6]^-$), which is a viscous oil, and $[(C_5H_5)Fe\{Me_4C_5(CH_2)_3(OCH_2CH_2)_3OMe\}]^+[PF_6]^-$ (**8**$^+[PF_6]^-$), which is a waxy semi-solid (this may reflect the presence of only one tentacle in this species); both compounds were obtained in essentially quantitative yields by oxidation of **5** and $[(C_5H_5)Fe\{Me_4C_5(CH_2)_3(OCH_2CH_2)_3OMe\}]$ (**8**) [5], respectively, with 1 equiv. of ferrocenium hexafluorophosphate in acetonitrile.

Table 1. Relative extractabilities (in %) of alkali metal cations from the aqueous into the organic phase by the ferrocenes **4a–d** and **5**. Concentrations: 10^{-2} M for **4a–d** and **5** (in dichloromethane); 7×10^{-5} for picric acid and 10^{-1} M for the alkali metal chlorides (in water)

	Li	Na	K	Rb	Cs
4a	0.2	2.2	3.1	2.5	2.3
4b	12.6	20.2	21.1	20.2	18.2
4c	2.3	3.0	3.8	4.4	5.4
4d	76.1	85.6	87.2	88.5	89.5
5	72.0	84.8	89.7	89.7	89.5

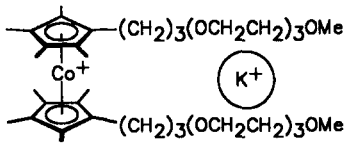
The great reluctance of such compounds to crystallize is due to the high flexibility of the tentacles, which is substantially reduced upon complexation of metal cations. Crystalline podates of simple oligoethylene glycol ethers $Me(OCH_2CH_2)_nOMe$ are indeed known for a variety of transition metal and alkaline earth metal cations [6b], but not for alkali metal cations, for which crystalline podates could be obtained only with oligoethylene glycol ethers such as **9** [9] and **10** [10], which bear rigid aromatic end-groups.



9

10

Owing to the presence of a spacer group between the tentacle and the ferrocenyl nucleus the ferrocenes **4a–d** and **5** cannot be regarded as oligoethylene glycol ethers bearing a rigid aromatic end-group. Not unexpectedly, attempts to crystallize their alkali metal podates failed. Surprisingly, however, **11**$^+$, which is the isoelectronic cobaltocenium analogue of **5**, yielded a beautifully crystalline potassium podate. Complex **11**$^+$ was synthesized by air oxidation of an acidified THF solution of the corresponding cobaltocene $[Co\{Me_4C_5(CH_2)_3(OCH_2CH_2)_3OMe\}_2]$ (**11**) prepared *in situ* from $Li[Me_4C_5(CH_2)_3(OCH_2CH_2)_3OMe]$ and cobalt(II) chloride in THF. Precipitation of the cobaltocenium species with an excess of potassium hexafluorophosphate afforded yellow crystals of the stoichiometry **11**$^+[PF_6]^- * K^+[PF_6]^-$ in good yield. Remarkably, lithium cations, which were also present in the solution in approximately the same concentration as potassium cations, could not be detected in the solid complex. Complex **11**$^+$ therefore appears to be a selective podant with a pronounced preference for potassium over lithium cations in aqueous solution. The podate **11**$^+[PF_6]^- * K^+[PF_6]^-$ is very soluble in acetone, acetonitrile and nitromethane. It may be recrystallized quite conveniently from aqueous acetone by slow evaporation of the organic solvent. Obviously, the cooperation of an increased ionicity with respect to the potassium podates of the ferrocenes **4a–d** and **5** and a decreased flexibility of the two tentacles with respect to the ferrocenium salt **5**$^+[PF_6]^-$ leads to facile crystallization. Crystals suitable for a single-crystal X-ray diffraction study could not be obtained so far, because the compound forms very thin platelets. It is therefore as yet uncertain whether each potassium ion is coordinated by the two tentacles of one cobaltocenium ion (as shown in Fig. 1) or whether they are coordinated by one tentacle each of two



$11^+[PF_6]^- * K^+[PF_6]^-$

Fig. 1. Possible structure of the podate $11^+[PF_6]^- * K^+[PF_6]^-$.

cobaltocenium units leading to a polymeric arrangement.

The compound $11^+[PF_6]^- * K^+[PF_6]^-$ is the first example of a crystalline alkali metal podate which does not rely on the rigid end-group principle. The cooperative behaviour of the two tentacles present in this species seems to be facilitated by the cobaltocenium hinge, which reduces the flexibility of the system by allowing only rotational motion around the C_5 ring centroid-C_5 ring centroid axis; the closely related di(O_4-tentacle) species $MeO(CH_2CH_2O)_3$-$(CH_2)_5(OCH_2CH_2)_3OMe$ has an association constant of less than 1.25 for the complexation of K^+ and no corresponding podate can be isolated.

EXPERIMENTAL

All reactions were performed in an inert atmosphere (purified argon or dinitrogen) by using standard Schlenk techniques unless stated otherwise. Solvents and reagents were appropriately dried and purified by using standard procedures. NMR spectra were recorded at 300 K with a Bruker DRX 500 instrument operating at 500.13 MHz for ^1H. Elemental analyses were performed by Mikroanalytisches Laboratorium Beller, Göttingen, and the Microanalytical Laboratory of the University of Bielefeld.

Synthesis of $5^+[PF_6]^-$

A solution of ferrocenium hexafluorophosphate (364 mg, 1.10 mmol) in acetonitrile (10 cm^3) was added to a solution of **5** [1b] (777 mg, 1.10 mmol) in acetonitrile (10 cm^3). The solution was stirred for 14 h. The solvent was removed *in vacuo*. Ferrocene was removed by sublimation (70°C/10^{-3} mbar) leaving $5^+[PF_6]^-$ (936 mg, 100%) as a dark green, viscous oil. Found: C, 53.7; H, 7.9. $C_{38}H_{66}F_6FeO_8P$ requires: C, 53.6; H, 7.8.

Synthesis of $8^+[PF_6]^-$

A solution of ferrocenium hexafluorophosphate (364 mg, 1.10 mmol) in acetonitrile (10 cm^3) was added to a solution of **8** [3] (491 mg, 1.10 mmol) in acetonitrile (10 cm^3). The solution was stirred for 14 h. The solvent was removed *in vacuo*. Ferrocene was removed by sublimation (70°C/10^{-3} mbar) leaving $8^+[PF_6]^-$ (650 mg, 100%) as a dark green, waxy semi-solid. Found: C, 48.7; H, 6.6. $C_{24}H_{38}F_6FeO_4P$ requires: C, 48.7; H, 6.5%.

Synthesis of $11^+[PF_6]^- * K^+[PF_6]^-$

Bu*n*Li (5.00 cm^3 of a 1.58 M solution in hexane, 7.90 mmol) was added dropwise with stirring to a solution of $HMe_4C_5(CH_2)_3(OCH_2CH_2)_3OMe$ [1b] (2.58 g, 7.90 mmol) in THF (30 cm^3) cooled to 0°C. The resultant solution of $Li[Me_4C_5(CH_2)_3(OCH_2CH_2)_3OMe]$ was added dropwise with stirring to a solution of $CoCl_2$ (520 mg, 4.00 mmol) in THF (50 cm^3) cooled to −60°C. The mixture was allowed to warm to room temperature overnight. Hydrochloric acid (0.1 N; 80 cm^3, 8.00 mmol) was added to the dark brown solution of the cobaltocene **11** thus obtained. A stream of air was passed through the mixture over a period of 2 h. The aqueous layer was separated, extracted with diethyl ether (2 × 20 cm^3) and was subsequently filtered into a solution of $K^+[PF_6]^-$ (1.47 g, 8.00 mmol) in water (30 cm^3). The solution was allowed to stand in a large Petri dish overnight. The yellow crystals of $11^+[PF_6]^- * K^+[PF_6]^-$ (2.58 g, 62%) were collected by filtration, washed with cold water (2 × 5 cm^3) and dried *in vacuo*. Found: C, 44.0; H, 6.5; Co, 5.5; F, 22.0. $C_{38}H_{66}CoF_{12}KO_8P_2$ requires: C, 43.9; H, 6.4; Co, 5.7; F, 21.9%. ^1H NMR (CD_3NO_2): δ 1.70 ("t", 4H, $CH_2CH_2CH_2$), 1.80 and 1.82 (2s, 24H, C_5Me_4), 2.32 (t, J = 7.2 Hz, 4H, $C_5Me_4CH_2CH_2CH_2OR$), 3.32 (s, 6H, OMe), 3.45 (t, J = 6.4 Hz, 4H, $C_5Me_4CH_2CH_2OR$), 3.50–3.61 [m, 24H, $(OCH_2CH_2)_3$]; $^{13}C\{^1H\}$ NMR (CD_3NO_2): δ 8.4 (C_5Me_4), 20.7 and 29.6 ($C_5Me_4CH_2CH_2CH_2OR$), 59.2 (OMe), 71.0, 71.1, 71.3 and 72.8 [$CH_2(OCH_2CH_2)_3$], 95.4, 96.4 and 98.5 (C_5Me_4); ^{19}F NMR (CD_3NO_2): δ −72.6 [d, J(PF) = 707 Hz]; $^{31}P\{^1H\}$ NMR (CD_3NO_2): δ −143.2 [sept, J(PF) = 707 Hz].

Determination of the relative extractabilities of alkali metal cations from the aqueous into the organic phase by the ferrocenes **4a–d** and **5**

Equal volumes (5 cm^3) of a solution of the respective ferrocene (10^{-2} M) in dichloromethane and of picric acid (7×10^{-5} M) and the respective alkali metal chloride (10^{-1} M) in water were equilibrated at room temperature by vigorous shaking. The respective aqueous solutions and pure dichloromethane were equilibrated likewise. The extinction of each equilibrated aqueous phase was determined at λ = 357 nm (absorption maximum of picrate). The relative extractability (in %) for a specific alkali metal cation by a specific ferrocene corresponds to the value $[(E_0 - E)/E_0] \times 100$ (E_0: extinction for the extraction of the aqueous solution of the respective alkali metal chloride and picric acid with pure dichloromethane; E: extinction for the corresponding extraction with

10^{-2} M of the respective ferrocene in dichloromethane).

Acknowledgements—Financial support by the Deutsche Forschungsgemeinschaft, the Fonds der Chemischen Industrie and the University of Bielefeld is gratefully acknowledged.

REFERENCES

1. (a) Siemeling, U., *J. Organomet. Chem.* 1992, **429,** C14; (b) Siemeling, U., *J. Chem. Soc., Chem. Commum.* 1992, 1335.
2. Siemeling, U., Habilitation thesis, University of Bielefeld, 1996.
3. Siemeling, U. Neumann, B. and Stammler, H.-G., *Chem. Ber.* 1993, **126,** 1311.
4. Siemeling, U., *Chem. Ber.* 1995, **128,** 1135.
5. Siemeling, U. and Hüffmann, G., *J. Organomet. Chem.* 1994, **475,** 229.
6. For relevant reviews, see (a) Vögtle, F., *Supramolekulare Chemie*, 2nd edn. Teubner, Stuttgart, 1992; (b) Vögtle, F. and Weber, E., in *Crown and Analogs*, Ch. 4, ed. S. Patai and Z. Rappoport. Wiley, Chichester, 1989, Ch. 4, p. 207; (c) Vögtle, F. and Weber, G., *Angew. Chem.* 1979, **91,** 813. (*Angew. Chem., Int. Ed. Engl.* 1979, **18,** 753).
7. Pedersen, C. F., *Fed. Proc.* 1968, **27,** 1305.
8. An instructive example is the barium bis(alkoxide) $Ba[(OCH_2CH_2)_3OMe]_2$, which is a liquid at room temperature; see Rees, Jr, W. S. and Morena, D. A., *J. Chem. Soc., Chem. Commun.* 1991, 1759.
9. Heimann, U. and Vögtle, F., *Angew. Chem.* 1978, **90,** 211 (*Angew. Chem., Int. Ed. Engl.* 1978, **17,** 197).
10. Sieger, H. and Vögtle, F., *Angew. Chem.* 1978, **90,** 212 (*Angew. Chem., Int. Ed. Engl.* 1978, **17,** 198).
11. Chaput, G., Jeminet, G. and Juillard, J., *Can. J. Chem.*, 1975, **53,** 2240.

Pergamon

PII: S0277-5387(96)00436-6

Polyhedron Vol. 16, No. 9, pp. 1517–1528, 1997
Copyright © 1997 Elsevier Science Ltd
Printed in Great Britain. All rights reserved
0277-5387/97 $17.00+0.00

New tetradentate Schiff bases, their oxovanadium(IV) complexes, and some complexes of bidentate Schiff bases with vanadium(III)

Nosheen Choudhary,[a] David L. Hughes,[b] Uwe Kleinkes,[b] Leslie F. Larkworthy,[c] G. Jeffery Leigh,[a]* Michael Maiwald,[b] Celine J. Marmion,[c] J. Roger Sanders,[b] Gallenius W. Smith[a] and Claas Sudbrake[b]

[a]School of Chemistry and Molecular Sciences, University of Sussex, Brighton, BN1 9QJ, U.K.

[b]John Innes Centre, Chatt Laboratory, Norwich Research Park, Colney, Norwich NR4 7UH, U.K.

[c]Department of Chemistry, University of Surrey, Guildford GU2 5XH, U.K.

(Received 6 August 1996; accepted 21 August 1996)

Abstract—New vanadyl(IV) complexes of tetradentate Schiff-base dianions containing one, two or three carbon atoms between the two iminato-nitrogen atoms are described. The compounds are either mononuclear or polymeric, as shown by the value of $\nu(V{=}O)$, and depending upon the Schiff-base dianion. There is no evidence for electron delocalization along the polymeric chains. Some vanadium(III) complexes of bidentate Schiff-base monoanions have also been isolated; the crystal structure of $[VO(2\text{-}OC_6H_4CHNH)_2]$ and preliminary data on the structure of $[V(Prhap)_3]\cdot$toluene [HPrhap = $2\text{-}HOC_6H_4C(Me)NCH_2CH_2Me$] are reported. © 1997 Elsevier Science Ltd. All rights reserved.

Keywords: vanadium; Schiff bases; low oxidation states; complexes; X-ray structures; preparations.

We have recently described [1,2] preparations and structures of cations consisting of vanadium–oxygen chains, all containing the tetradentate $(salen)^{2-}$, $(OC_6H_4CH:NCH_2CH_2N:CHC_6H_4O)^{2-}$. We have now extended the scope of these reactions to oxovanadium(IV) complexes with similar Schiff base ligands. In the course of this work we have prepared several new Schiff bases and their oxovanadium(IV) complexes which present several features of interest. We have also attempted, without much success, to reduce vanadyl(IV) and dichlorovanadium(IV) complexes of tetradentate Schiff base anions to vanadium(III) complexes, but we succeeded in preparing vanadium(III) complexes of bidentate Schiff-base monoanions, using sodium or lithium reduction.

* Author to whom correspondence should be addressed.

RESULTS AND DISCUSSION

Complexes of vanadium(IV) *and tetradentate Schiff-base dianions*

Most of the tetradentate Schiff bases described here have either ethylene (—CH_2CH_2—) or 2,2-dimethyl-(trimethylene) (—$CH_2CMe_2CH_2$—) bridges between their two nitrogen atoms. Metal complexes derived from these two types of Schiff base will have five- or six-membered central chelate rings, respectively. All the Schiff bases used are detailed in Table 1. The new vanadyl(IV) complexes are listed in Table 2.

Ethylene-bridged complexes

Oxovanadium(IV) complexes with ethylene bridges may be divided into two classes. A typical example of

Table 1. New and known Schiff bases

Amine	Aldehyde/ketone	Abbreviated symbols and formula		Yield%	C%	H%	N%
$NH_2CH_2CH_2NH_2$	2-OH-4,6-$(MeO)_2C_6H_2CHO$	$H_2\{(MeO)_4salen\}$	$C_{20}H_{24}N_2O_6$	51	60.8(61.9)	6.4(6.2)	7.0(7.2)
$NH_2CH_2CH_2NH_2$	2-OH-5-ClC_6H_3CHO	H_2Cl_2salen	$C_{16}H_{14}Cl_2N_2O_2$	89	57.4(57.6)	4.1(4.2)	8.2(8.3)
$NH_2CH_2CH_2NH_2$	2-OH-5-BrC_6H_3CHO	H_2Br_2salen	$C_{16}H_{14}Br_2N_2O_2$	92	45.4(45.1)	3.1(3.3)	6.2(6.6)
$NH_2CH_2CH_2NH_2$	2-OH-3,5-$Cl_2C_6H_2CHO$	H_2Cl_4salen	$C_{16}H_{12}Cl_4N_2O_2$	87	53.7(53.6)	3.9(3.9)	15.6(15.6)
$NH_2CH_2CH_2NH_2$	2-OH-3,5-$Br_2C_6H_2CHO$	H_2Br_4salen	$C_{16}H_{12}Br_4N_2O_2$	91	47.3(47.3)	2.7(3.0)	6.6(6.9)
$NH_2CH_2CH_2NH_2$	2-OH-5-$NO_2C_6H_3CHO$	$H_2\{(NO_2)_2salen\}$	$C_{16}H_{14}N_4O_6$	80	32.4(32.9)	1.9(2.1)	4.5(4.8)
$NH_2CH_2CH_2NH_2$	2-OH-C_6H_4COMe	H_2hapen[a]	$C_{18}H_{20}N_2O_2$	95	73.0(73.0)	6.8(6.8)	9.5(9.5)
$NH_2CHMeCH_2NH_2$	2-OH-C_9H_4CHO	H_2sal-1,2-pn[a]	$C_{17}H_{19}N_2O_2$	68	72.0(72.3)	(6.4)	
$NH_2CH_2CMe_2CH_2NH_2$	2-OH-3-$MeOC_6H_3CHO$	$H_2\{(MeO)_2salnptn\}$	$C_{21}H_{26}N_2O_4$	45	68.4(68.1)	7.0(7.0)	7.6(7.6)
$NH_2CH_2CMe_2CH_2NH_2$	2-OH-$C_{10}H_6CHO$	H_2nalnptn	$C_{27}H_{26}N_2O_2$	20	78.5(79.0)	6.3(6.3)	6.9(6.8)
$NH_2CH_2CMe_2CH_2NH_2$	2-OH-C_6H_4COMe	H_2hapntn	$C_{21}H_{26}N_2O_2$	58	74.5(74.5)	8.1(7.6)	8.4(8.2)
$NH_2CH_2CH_2CH_2NH_2$	2-OH-4,6-$(MeO)_2C_6H_2CHO$	$H_2\{(MeO)_4salpn\}$	$C_{21}H_{26}N_2O_6$	48	62.6(62.7)	6.6(6.5)	7.2(7.0)
$NH_2CH_2CH_2CH_2NH_4$	2-OH-C_6H_4COMe	H_2happn	$C_{19}H_{22}N_2O_2$	56	72.6(73.5)	6.9(7.1)	8.8(9.0)
$NH_2CH_2NH_2$	2-OH-C_6H_4CHO	H_2salmn	$C_{15}H_{14}N_2O_2$	62	70.7(70.9)	5.5(5.5)	10.9(11.0)
NH_3	2-OH-C_6H_4CHO	Hydrosalicylamide	$C_2H_{18}N_2O_3$	72	72.4(72.8)	5.2(5.2)	8.1(8.1)
$NH_2CH_2C_6H_5$	2-OH-C_6H_4CHO	Hbzsal[a]	$C_{14}H_{13}NO$	95	79.4(79.6)	6.1(6.2)	6.6(6.6)
$NH_2CH_2C_6H_5$	2-OH-$C_6H_4COCH_3$	Hbzhap	$C_{15}H_{15}NO$	93	80.0(80.0)	6.7(6.7)	6.2(6.2)
$NH_2C_6H_4Me$-4	2-OH-$C_6H_4COCH_3$	HMebzhap	$C_{16}H_{17}NO$	89	80.3(80.3)	7.2(7.2)	5.9(5.9)
$NH_2CH_2CH_2CH_3$	2-OH-$C_9H_4COCH_3$	HPrhap	$C_{11}H_{16}NO$	94	74.5(74.5)	8.7(8.5)	7.9(7.9)

[a] These have been reported previously, but all the data are from our preparations. Analytical figures in parentheses are calculated values.

Table 2. Schiff base complexes of vanadyl(IV)

Formulae		Yield%	Analyses[a] C%	H%	N%	Colour	ν(V=O) (cm^{-1})	μ_{eff}/μ_B
[VO(salen)]·MeOH	$C_{17}H_{18}N_2O_4V$	81	55.3(55.9)	4.7(4.9)	7.7(7.7)	Green	972	1.80
[VO(salen)] [3][b]	$C_{16}H_{14}N_2O_3$	87	57.6(57.7)	4.2(4.2)	8.4(8.4)	Green	977	1.83
[VO{$(MeO)_2$salen}] [18][b]	$C_{19}H_{18}N_2O_5V$	92	53.3(55.0)	4.7(4.6)	8.3(7.1)	Green	978	1.85
[VO(nalen)] [19][b]	$C_{24}H_{18}N_2O_3V$	89	67.1(66.6)	3.7(4.1)	6.0(6.4)	Green	984	1.77
[VO{$(MeO)_4$salen}]	$C_{20}H_{22}N_2O_7V$	76	53.3(53.0)	4.9(4.9)	6.3(6.2)	Green	983	1.83
[VO(Cl_2salen)]	$C_{16}H_{12}Cl_2N_2O_3V$	85	47.9(47.8)	2.8(3.0)	6.8(7.0)	Green	980	1.80
[VO(Br_2salen)]	$C_{16}H_{12}Br_2N_2O_3V$	90	39.3(39.1)	2.2(2.4)	5.3(5.7)	Green	980	1.86
[VO(Cl_4salen)]	$C_{16}H_{10}Cl_4N_2O_3V$	91	41.4(40.8)	2.3(2.1)	5.8(6.0)	Red	881	1.81
[VO(Cl_4salen)]	$C_{16}H_{10}Cl_4N_2O_3V$	90	40.9(40.8)	1.9(2.1)	5.8(6.0)	Green	992	1.65
[VO(Br_4salen)]	$C_{16}H_{10}Br_4N_2O_3V$	90	29.6(29.6)	1.5(1.5)	4.2(4.3)	Orange	880	1.74
[VO{$(NO_2)_2$salen}]	$C_{16}H_{12}N_4O_7V$	78	45.1(45.3)	3.0(2.8)	13.0(13.2)	Red	879	1.75[c]
[VO(salnptn)] [11][b]	$C_{19}H_{20}N_2O_3$	59	60.4(60.8)	5.3(5.3)	7.2(7.5)	Orange	868	1.83[c]
[VO(sal-1,2-pn)]	$C_{17}H_{16}N_2O_3V$	79	58.1(58.8)	4.5(4.6)	7.9(8.1)	Green	977	1.77
[VO(hapen)]	$C_{18}H_{18}N_2O_3V$	83	59.3(59.8)	4.9(5.0)	7.6(7.8)	Green	971	1.77
[VO{$(MeO)_2$salnptn}]	$C_{21}H_{24}N_2O_5V$	—	57.2(57.9)	5.5(5.5)	6.3(6.4)	Brown	858	2.07
[VO(nalnptn)]	$C_{27}H_{24}N_2O_3V$	77	67.2(68.2)	4.5(5.1)	5.9(5.9)	Yellow	877	1.71
[VO{$(MeO)_4$salpn}]	$C_{21}H_{24}N_2O_7V$	82	54.5(54.0)	5.1(5.1)	6.0(6.0)	Yellow	860	1.88
[VO(salmn)]·MeOH	$C_{16}H_{16}N_2O_4V$	40	54.3(54.7)	4.1(4.6)	7.8(8.0)	Yellow	986	1.73
[VO($OC_6H_4CHNH)_2$]	$C_{14}H_{12}N_2O_3V$	62	55.0(54.7)	4.1(3.9)	9.2(9.1)	Green	981	1.73

[a] Required values in parentheses.

[b] These have been previously reported in the given references, but all the data are from our preparations.

[c] No deviation from ideal behaviour down to 87 K.

the first class is [VO(salen)], which forms green crystals, is fairly soluble in solvents such as acetonitrile and dichloromethane, has ν(V=O) in its solid-state IR spectrum at 980 cm^{-1} and is monomeric in the solid state [3,4]. The class also includes a complex with a ligand derived from ethylenediamine and 2-hydroxybenzophenone, which has ν(V=O) at 981 cm^{-1} [5]. The only difference from the salen complex is that the CH=N motif is replaced by CPh=N. However, an analogous complex made in the same way with a ligand derived from ethylenediamine and 2-hydroxy-5-chlorobenzophenone is gold, not green, relatively insoluble and has ν(V=O) at 881 cm^{-1}. This is representative of the second class, with ν(V=O) *ca* 100 cm^{-1} to lower frequency compared with the first. These are all apparently polymeric in the solid state, forming chains $\cdots V{=}O \rightarrow V{=}O \rightarrow \cdots$. The shift of *ca* 100 cm^{-1} in ν(V=O) between apparently similar compounds is also found in the chemistry of vanadyl(IV) complexes with bidentate and tridentate ligands and at least one compound is known which exists in both forms with different crystal shapes [6]. The two forms are apparently isomers.

If we assume that the green vanadyl(IV) complexes are all square pyramidal and five-coordinate, as in [VO(salen)] [3], the difference between the ν(V=O) values can easily be rationalized [7] in terms of the infinite chain polymerization of the orange or gold compounds in the solid state. No structural studies showing such polymeric chains in ethylene-bridged complexes (except [1] for the cation [V(salen)OV(salen)O]$^+$ with ν(V=O) at 880 cm^{-1}) have been reported, although [VO{$OC_6H_4CH:N(CH_2)_3N:CHC_6H_4O$}] has a chain structure and a low value of ν(V=O) [7].

The reason for the changeover from "normal" ν(V=O) values at 980 cm^{-1} "low" values at 880 cm^{-1} must be in part electronic, because substitutions in the phenyl rings should not influence sterically the geometry round the vanadium atom [5]. The electronic effects of aromatic substituents might most simply be assessed using the pK_A values of the related 3- and 4-substituted benzoic acids; pK_A values in acetonitrile (the solvent most frequently used in this work) include 20.7 for benzoic acid, 19.5 for 3-bromobenzoic acid, 19.2 for 3-nitrobenzoic acid and 18.7 for 3,5-dichlorobenzoic acid [8].

We have therefore made [VO{$(MeO)_4$salen}], [VO(Cl_2salen)], [VO(Br_2salen)], [VO(Cl_4salen)], [VO(Br_4salen)] and [VO{$(NO_2)_2$salen}] using Schiff bases prepared from ethylenediamine and 4,6-dimethoxysalicylaldehyde, 5-chlorosalicylaldehyde, 5-bromosalicylaldehyde, 3,5-dichlorosalicylaldehyde, 3,5-dibromosalicylaldehyde and 5-nitrosalicylaldehyde, respectively. The first three form green crystals with higher ν(V=O), the last two form insoluble powders with low ν(V=O). The sixth complex, derived from Cl_4salen is unique among tetradentate Schiff base derivatives in being apparently obtainable in both polymeric and monomeric forms, although we were unable to confirm this by X-ray structure analysis. The green solid, ν(V=O) = 991 cm^{-1}, was isolated from acetonitrile after heating the preparative reaction mixture in acetonitrile for 20 min at reflux. Upon prolonged exposure to acetonitrile solution or upon exposure to solvents such as diethyl ether, acetone, dichloromethane and methanol, or even upon heating the solid *in vacuo*, the green form changes to the orange form, with ν(V=O) = 868 cm^{-1}. We believe that the only other example of such isomerism is the complex bis[(*N*-(4-chlorophenyl)salicylideneaminato) oxovanadium(IV)] [6,7].

The data seem to suggest that within a given class of compound (monomeric or polynuclear) some lowering of ν(V=O) is favoured by electron-withdrawing substituents such as chloro, bromo and nitro. The known [VO{$(MeO)_2$salen}] has a high ν(V=O) and is presumably monomeric. There are no intermediate values of ν(V=O), which suggests a sudden switch in structure induced by the electronic effects of the substituents and the change between monomeric and polymeric structures seems a reasonable explanation.

However, this may not be in the whole story. Kuska and Yang [5] studied a series of analogous complexes based on the Schiff base 4,5-$R^1R^2C_6H_2$(OH)CPh=N-CH_2CH_2—N=CPhC_6H_2(OH)R^1R^2-4,5. They plotted ν(V=O) against the Hammett σ factors for R^1 and R^2, and showed that ν(V=O) increases with the electron-withdrawing power of the substituents within the "high-frequency" group, which is observed for: R^1 = H, R^2 = Cl; R^1 = CH_3, R^2 = Cl; R^1 = R^2 = H and R^1 = H, R^2 = CH_3 in solution in $CHCl_3$. However, in Nujol mulls, the first two compounds are in the "low-frequency" group. Our data, within the "high-frequency" and "low-frequency" groups, show that electron-withdrawing substituents have no consistent effect on ν(V=O), but the overall effect, as with Kuska and Yang, is hardly significant and certainly not comparable with the effect of polymerization on ν(V=O). However, the observations do imply that steric effects have a secondary influence. The fact that heavily substituted aromatic rings and bridges other than ethylene tend to favour polymerization hints at a crystal-packing effect. However, the low solubility of the polymeric compounds has prevented sensible solution studies.

The magnetic moments of all the complexes are close to the spin-only values for vanadium(IV) complexes. As the unpaired electron is believed to be in an orbital orthogonal to the V=O axis [9], it should not be affected by polymerization along V—O—V—O chains. The effective magnetic moment of [VO{$(NO_2)_2$salen}] exhibits normal Curie–Weiss behaviour down to 87 K.

2,2-*Dimethyl(trimethylene)-bridged complexes*

Alone among compounds of formula [VO($OC_6H_4CH:N(CH_2)_nN:CHC_6H_4O$)] ($n$ = 2–10) the complex

with $n = 3$ has a "low" ν(V=O) [4] and that with $n = 4$ shows two values of ν(V=O). The X-ray structure for $n = 3$ shows that this material is polymeric [7]. This may be a consequence of distortions in the coordination sphere of the vanadium atom upon lengthening the bridge rather than electronic factors, since there are no substituents on phenyl rings.

We report here syntheses of several dimethyl (trimethylene)-bridged complexes which also contain six-membered central chelate rings, with a geometry about the vanadium atom similar to that of trimethylene-bridged complexes. All these complexes, i.e. [VO(salnptn)], [VO{$(MeO)_2$salnptn}], [VO(nalnptn)] and [VO{$(MeO)_4$salpn}] from 2,2-dimethylpropane-1,3-diamine and salicylaldehyde, 3-methoxysalicylaldehyde and 2-hydroxy-1-naphthaldehyde, respectively, and from 4,6-dimethoxysalicyaldehyde and propane-1,3-diamine show a "low" ν(V=O) value and are presumably polymeric. This was confirmed for [VO(salnptn)] by an X-ray study [10]. Unlike its trimethylene-bridged analogue, the dimethyl(trimethylene) derivative [VO(salnptn)] is soluble in common organic solvents and several protonation, oxidation and reduction reactions of it have been carried out. Details of these reactions are being published separately. The effective magnetic moment of [VO(salnptn)] was found to be virtually independent of field and temperature from 293 K down to 87 K and the compound exhibits normal Curie–Weiss behaviour. Even though the compound is apparently polymeric, there is no indication of electron delocalization, consistent with the unpaired electron being in the d_{xy} orbital and orthogonal to the V—O chain.

Yields of dimethyl(trimethylate)-bridged complexes were usually considerably smaller than those of ethylene-bridged complexes made by the same route. The attempted synthesis of [VO($OC_6H_4CMe:NCH_2CMe_2CH_2N:CMeC_6H_4O$)] and of its trimethylene-bridged analogue from [VO(acac)$_2$] and the Schiff base failed altogether, while the synthesis of its ethylene-bridged analogue by the same route proceeded in good yield.

Methylene-bridged complexes

A Schiff base with a methylene bridge would be accessible from methylenediamine if this existed. A compound derived from this Schiff base with molybdenum, but synthesized from hexamethylenetetramine, salicylaldehyde and, presumably, traces of water, has recently been reported [11]. Unexpectedly, the tetradentate Schiff base is dinucleating. We have, however, prepared $HOC_6H_4CH:NCH_2N:CHC_6H_4OH$ (H_2salmn) for the first time by reaction of salicylaldehyde, methylenediamine dihydrochlorine and triethylamine.

Treatment of H_2salmn with [VO(acac)$_2$] or with $VOSO_4$ under various conditions gave products which could not be characterized. However, treatment of H_2salmn with [{VO(OMe)(acac)}$_2$] under very mild conditions gave a yellow powder, soluble in dichloromethane and acetonitrile, analysing for [VO(salmn)] · MeOH with an IR band at 986 cm^{-1} characteristic of a terminal ν(V=O) and a magnetic moment of 1.73 BM. Due to the colour it seems unlikely that this is the simple monomer of its empirical formula and a crystal structure analysis is needed to elucidate its nature.

Attempted synthesis compounds of vanadium(II) with tetradentate Schiff-base dianions

Attempts were made to prepare vanadium(II) complexes of $(hapen)^{2-}$ and $(happn)^{2-}$ by reaction of the sodium or lithium salts of the Schiff bases with $VCl_2(thf)_2$ [12], $VBr_2(MeOH)(thf)$ [13] or [$VCl_2(py)_4$] [14]. In no case was an unequivocal vanadium(II) product obtained. Attempts were also made to reduce the vanadium(IV) complexes [VCl_2(hapen)] and [VCl_2(sal-1,2-pn)] with sodium sand. These dihalides were prepared from the corresponding vanadyl species by standard routes. This method was also unsuccessful, although in the latter case a vanadium(III) complex, [{VCl(sal-1,2-pn)}$_2$], was obtained and characterized. All these halo-compounds are detailed in Table 3. This formulation is based upon the usual analytical and spectroscopic data and analogy with [{VCl(salen)}$_2$], which has been suggested to be dinuclear [15].

Compounds of vanadium(IV) with bidentate Schiff-base monoanions

Schiff bases are made in 1 : 1 reactions between aldehydes and primary amines.

$$ArCHO + RNH_2 \longrightarrow ArCH:NR$$

However, when R = H (i.e. with ammonia), three molecules of aromatic aldehyde react with two molecules of ammonia giving hydroamides, whereas aliphatic aldehydes yield polymers (aldol condensation) and/or aldehyde-ammonias.

$$3ArCHO + 2NH_3 \longrightarrow ArCH:NCHArN:CHAr$$

$$AlkCHO + NH_3 \longrightarrow AlkC(H)(OH)(NH_2)$$

We made hydrosalicylamide (Ar = C_6H_4OH), from salicylaldehyde and ammonia, to react with $VOSO_4$. We hoped to obtain an analogue of [VO(salmn)] substituted in the methylene bridge by a —C_6H_4OH group, but we isolated green crystals analysing as $C_{14}H_{12}N_2O_3V$ with a strong IR band at 980 cm^{-1}, ν(V=O), and sharp bands at 3360 and 3240 cm^{-1} ν(NH). We assign the structure [VO($OC_6H_4CH:NH)_2$] to this compound; it contains a sali-

Table 3. Halo complexes of vanadium(III) and vanadium(IV)

Formulae		Yield%	Analyses[a] C%	H%	N%	Colour	μ_{eff}/μ_B 295 K
$[VCl_2(sal\text{-}1,2\text{-}pn)]$	$C_{17}H_{16}Cl_2N_2O_2V$	86	50.8(50.8)	4.0(4.0)	7.1(7.0)	Blue	1.72
$[VBr_2(sal\text{-}1,2\text{-}pn)]$	$C_{17}H_{16}Br_2N_2O_2V$	74	41.1(41.6)	3.3(3.3)	5.7(5.7)	Blue	1.79
$[VI_2(sal\text{-}1,2\text{-}pn)]$	$C_{17}H_{16}I_2N_2O_2V$	18	33.9(34.9)	2.8(2.8)	4.7(4.8)	Tan	1.87
$[\{VCl(sal\text{-}1,2\text{-}pn)\}_2]$	$C_{34}H_{32}Cl_2N_4O_4V_2$	—	56.2(55.8)	6.1(4.1)	8.5(7.7)	Dark red	
$[VCl_2(hapen)]\cdot 2H_2O$	$C_{18}H_{22}Cl_2N_2O_4V$	71	47.4(47.8)	4.3(4.9)	6.7(6.2)	Blue	
$[VBr_2(hapen)]$	$C_{18}H_{18}Br_2N_2O_2V$	59	45.1(42.8)	3.7(3.6)	6.2(5.4)	Blue	

[a] Analytical figures in parentheses are calculated values.

cylideneiminato-ligand whose free acid (salicylaldeimine, $HOC_6H_4CH:NH$) is unknown, and it is the previously unreported parent compound of all oxovanadium(IV) bis(bidentate) Schiff base complexes.

X-ray studies of similar complexes $[VO(OC_6H_4CH:NR)_2]$ [16] ($R \neq H$) show that the two N donor atoms take *trans* positions to one another to minimize interactions between their R groups. In our compound where R = H these interactions would be small and there seems no reason why these two atoms should not be *cis* to one another, with one N—H group above and one below the plane formed by the N_2O_2 atom donor set, as happens to the methylene groups in [VO(salen)]. This would result in two slightly different N—H stretching frequencies. In fact, the NH groups are indeed *trans*, but different. An X-ray structure analysis has clarified the situation. The structure is shown in Fig. 1 and selected bond lengths and angles are in Table 4.

The vanadium atom is five-coordinate with the expected square pyramidal pattern, similar to that in [VO(salen)] [3], the vanadyl oxygen O(3) is in the apical position and the two bidentate ligands form the base plane. However, whereas in [VO(salen)] the two halves are related by pseudo-mirror plane symmetry, here the two ligands are related by a pseudo-two-fold symmetry axis along the V—O(3) bond. The difference in the two imido groups, at opposite corners of the square base plane, arises from their contacts with adjacent molecules; H(29) forms a good hydrogen bond with the vanadyl oxygen atom of the next molecule down the *a* axis (thus linking the molecules in infinite chains parallel to this axis); in contrast, H(19) has no close neighbours.

Dimensions around the V atom are as expected. The V—O(3) vanadyl distance is short, at 1.589(4) Å. The two V—O distances in the base plane are virtually identical, as are the two V—N distances. All the distances are very similar to those found in [VO(salen)].

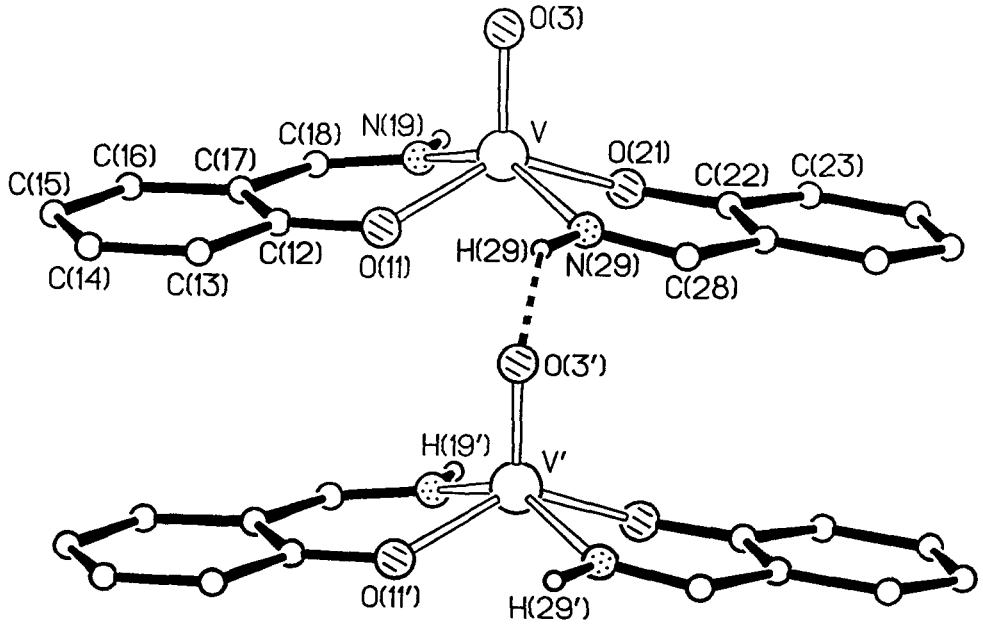


Fig. 1. Representation of the molecular structure of $[VO(OC_6H_4CHNH)_2]$ showing the single intermolecular hydrogen bond.

Table 4. Molecular dimensions in $[VO(OC_6H_4CHNH)_2]$. Bond lengths are in Å, angles in (°), e.s.d.s are in parentheses

(a) About the V atom			
V—O(11)	1.919(4)	V—N(29)	2.058(6)
V—N(19)	2.056(6)	V—O(3)	1.589(4)
V—O(21)	1.917(4)		
O(11)—V—N(19)	86.2(2)	O(21)—V—N(29)	86.4(2)
O(11)—V—O(21)	139.2(2)	O(11)—V—O(3)	111.6(2)
N(19)—V—O(21)	84.6(2)	N(19)—V—O(3)	102.4(3)
O(11)—V—N(29)	83.7(2)	O(21)—V—O(3)	109.2(2)
N(19)—V—N(29)	152.3(2)	N(29)—V—O(3)	105.3(2)
(b) In the OC_6H_4CHNH ligands			
O(11)—C(12)	1.323(7)	O(21)—C(22)	1.322(7)
C(12)—C(13)	1.407(9)	C(22)—C(23)	1.399(9)
C(12)—C(17)	1.403(9)	C(22)—C(27)	1.417(10)
C(13)—C(14)	1.381(10)	C(23)—C(24)	1.382(9)
C(14)—C(15)	1.384(12)	C(24)—C(25)	1.389(11)
C(15)—C(16)	1.365(11)	C(25)—C(26)	1.362(10)
C(16)—C(17)	1.406(8)	C(26)—C(27)	1.420(9)
C(17)—C(18)	1.428(9)	C(27)—C(28)	1.427(9)
C(18)—N(19)	1.281(9)	C(28)—N(29)	1.281(8)
N(19)—H(19)	0.82(8)	N(29)—H(29)	0.94(9)
V—O(11)—C(12)	129.2(4)	V—O(21)—C(22)	130.9(4)
O(11)—C(12)—C(13)	118.3(6)	O(21)—C(22)—C(23)	118.6(6)
O(11)—C(12)—C(17)	124.0(5)	O(21)—C(22)—C(27)	123.0(6)
C(13)—C(12)—C(17)	117.7(6)	C(23)—C(22)—C(27)	118.4(6)
C(12)—C(13)—C(14)	121.0(8)	C(22)—C(23)—C(24)	121.2(7)
C(13)—C(14)—C(15)	120.9(7)	C(23)—C(24)—C(25)	120.5(7)
C(14)—C(15)—C(16)	119.2(6)	C(24)—C(25)—C(26)	119.8(6)
C(15)—C(16)—C(17)	121.4(7)	C(25)—C(26)—C(27)	121.3(7)
C(12)—C(17)—C(16)	119.8(6)	C(22)—C(27)—C(26)	118.8(6)
C(12)—C(17)—C(18)	121.4(5)	C(22)—C(27)—C(28)	121.7(6)
C(16)—C(17)—C(18)	118.7(6)	C(26)—C(27)—C(28)	119.4(6)
C(17)—C(18)—N(19)	125.4(6)	C(27)—C(28)—N(29)	125.1(6)
V—N(19)—C(18)	126.4(5)	V—N(29)—C(28)	128.0(5)
V—N(19)—H(19)	127(5)	V—N(29)—H(29)	113(5)
C(18)—N(19)—H(19)	105(5)	C(28)—N(29)—H(29)	119(5)
(c) In the hydrogen bond			
N(29)···O(3′)	3.145(8)	N(29)—H(29)···O(3′)	146(7)
H(29)···O(3′)	2.32(10)		

N.B. O(3′) is at $x-1, y, z$.

Complexes of vanadium(II) *and vanadium*(III) *with bidentate Schiff-base anions*

An attempt to prepare a vanadium(II) complex from $VCl_2(thf)_2$ and the sodium salt of the Schiff base formed from 2-hydroxyacetophenone and *n*-propylamine, Na(Prhap), gave, instead of $[V(Prhap)_2]$, $[V(Prhap)_3]$ (see Experimental). This has been characterized as an octahedral vanadium(III) complex with a tris(chelate) structure by a single-crystal X-ray determination. The resolution obtained was finally only to $R = 0.10$ and therefore serves only to confirm the essential octahedral structure nature of the material (Fig. 2). We include experimental details below only for the record and do not propose to discuss the structure further.

Since considerable care was taken to exclude adventitious oxygen during this work, the oxidation of vanadium(II) to vanadium(III) might have been due to the Schiff base. However, reactions of saturated compounds, such as $[VCl_2(py)_4]$, with heavily substituted bidentate Schiff base anions, in the hope that the pyridine would block otherwise reactive sites, gave only poorly characterized blue materials. We cannot claim to have prepared with certainty any vanadium(II) compounds.

The vanadium(III) complexes (Table 5) presumably all have a structure similar to that of $[V(Prhap)_3]$. Their effective magnetic moments are close to the spin-only value at room temperature (2.83 μ_B), and they decrease considerably with temperature. This is the usual behaviour of mononuclear, distorted,

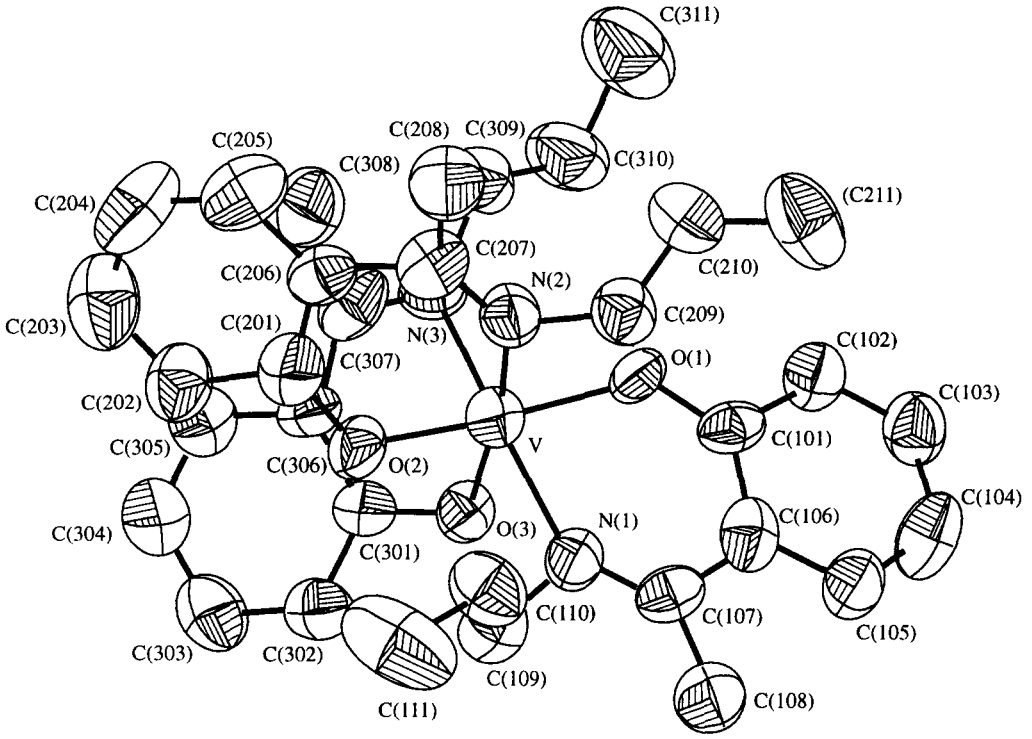


Fig. 2. Structure of the vanadium complex in $[V(Prhap)_3] \cdot C_7H_8$. Thermal ellipsoids are drawn at 50% probability.

octahedral six-coordinate vanadium(III) complexes [17].

EXPERIMENTAL

Reactions involving vanadium complexes were carried out using standard Schlenk techniques in dried solvents under N_2. C,H,N analyses were carried out at the Universities of Sussex and Surrey, or by Butterworth Microanalytical Laboratories. IR spectra were obtained using a Perkin–Elmer 883 spectrometer and magnetic moments at 20°C were determined by the Faraday method using $Hg[Co(CNS)_4]$ as standard and making diamagnetic corrections using Pascal's constants. Variable-temperature magnetic moments on two compounds were made on a Gouy balance. Aldehydes, amines, $VOSO_4$ and $[VO(OCMeCHCOMe)_2]$, and $[VO(acac)_2]$ were purchased from Aldrich or Lancaster Synthesis. $[VCl_2(py)_4]$ [14], $VCl_2(thf)_2$ [12] and $VBr_2(MeOH)(thf)$ [13] were prepared by literature methods.

Schiff bases (Table 1) were generally prepared by mixing boiling methanol solutions of aldehydes and amines and their vanadium compounds (Table 2) by ligand exchange with $[VO(acac)_2]$, as described [3]. All exceptions to this are given below. Analyses, yields, colours, V—O stretching frequencies $\nu(V{=}O)$ and magnetic moments (μ_B) are given in the Tables.

Ethylene-N,N′-*bis*(*salicylideneiminato*)*oxovanadium* (IV)–*methanol*(1/1)

The Schiff base H_2salen (0.53 g, 2 mmol) and $[VO(acac)_2]$ (0.53 g, 2.0 mmol) were dissolved in dichloromethane (20 cm^3) and methanol (20 cm^3) was added. After 24 h the volume was slowly reduced *in vacuo* to ~10 cm^3, when green crystals (0.59 g, 81%) were formed, washed with methanol and diethyl ether and dried *in vacuo*.

Methylene-N,N′-*bis*(*salicylideneimine*)

Methylenediamine bishydrochloride (3.0 g, 25 mmol) dissolved in methanol (40 cm^3) was cooled to −60°C. Salicylaldehyde (6.1 g, 50 mmol) and triethylamine (10 cm^3, ~75 mmol) were added and the solution allowed to warm with stirring overnight, giving a light yellow crystalline precipitate which was filtered off, washed with diethyl ether and dried in air, yield 4.0 g, 62%.

Methylene-N,N′-*bis*(*salicylideneiminato*)*oxovanadium* (IV)–*methanol*(1/1)

The Schiff base H_2salen (0.51 g, 2 mmol) and $[\{VO(OMe)(acac)\}_2]$ (0.78 g, 2 mmol) were dissolved in dichloromethane (20 cm^3) and methanol (20 cm^3) was added. The volume was reduced *in vacuo* after 24

Table 5. Bidentate Schiff base complexes of vanadium(III)

Formulae	Yield%	Analyses[a] C%	H%	N%	Colour	μ_{eff}/μ_B 293 K	89 K	θ (K)
$[V(bzhap)_3]$	—	74.8 (74.8)	5.8 (5.9)	5.2 (5.8)	Flame red	2.97	2.69	20
$[V(Mebzhap)_3]$—LCl (2/1)	47	73.3 (73.3)	6.4 (6.2)	5.4 (5.3)	Red–brown	2.93	2.74	18
$[V(bzsal)_3]$—LiCl (4/1)	—	72.0 (71.9)	5.3 (5.2)	6.1 (6.0)	Red			
$[V(Prhap)_3]\cdot C_7H_8$	—	71.5 (71.5)	7.6 (7.5)	6.4 (6.3)	Red	2.93	2.63	30
$C_{45}H_{42}N_3O_3V$								
$C_{48}H_{48}Cl_{1/2}Li_{1/2}N_3O_3V$								
$C_{42}H_{36}Cl_2Li_2N_3O_3V$								
$C_{40}H_{34}N_3O_3V$								

[a] Required values in parentheses.

h to ~10 cm³ when a yellow powder precipitated. This was filtered off and dried *in vacuo*; yield 0.31 g, 44%.

Hydrosalicylamide

Ammonia (2.0 M in methanol, 20 cm³, 40 mmol) was added to salicylaldehyde (7.3 g, 60 mmol) giving a yellow solid. The mixture was warmed briefly to 60°C when all dissolved to give a clear solution and then allowed to cool giving yellow crystals (5.0 g, 72%).

Oxobis(salicylideneiminato)vanadium(IV)

$VOSO_4\cdot H_2O$ (0.9 g, 5 mmol), hydrosalicylamide (1.8 g, 5 mmol) and methylamine (2 cm³, 15 mmol) were heated under reflux in aqueous ethanol (1 : 1, 50 cm³) for 1 h giving a green solid which was filtered off, washed with water, ethanol and diethyl ether and recrystallized from acetonitrile (100 cm³).

Tris(2-*phenolato*-N-*benzylacetophenoneimine*)*vanadium*(III)

Toluene (150 cm³) was added to Hbzhap (3.44 g, 15.27 mmol) under nitrogen forming a clear yellow solution. This was cooled in an ice-bath and LiMe (11.0 cm³, 1.4 M solution in diethyl ether) was syringed in forming a red solution after much effervescence. After stirring for 5 min, $[VCl_3(MeCN)_3]$ (1.43 g, 5.10 mmol) was added producing a mixed suspension of the green starting material and the white lithium salt Li(bzhap), but on stirring a deep red solution formed and the $[VCl_3(MeCN)_3]$ slowly dissolved. The mixture was heated under reflux for 3 h, allowed to cool and then the white precipitate (LiCl) was filtered off and the deep red solution was reduced slightly in volume. Flame red microcrystals separated, which were filtered off and dried *in vacuo*.

Tris(2-*phenolato*-N-4-*methylbenzylacetophenoneimine*)*vanadium*(III)

To an ice-cold solution of the Schiff base HMebzhap (3.40 g, 14.2 mmol) in toluene (100 cm³), LiMe (10.2 cm³, 14.2 mmol, 1.4 M solution in diethyl ether) was added. Much efferverscence occurred and the yellow solution became dark red, but upon complete addition of the LiMe a white precipitate formed with a pale orange solution. Then $[VCl_3(MeCN)_3]$ (1.33 g, 4.73 mmol) was added and the mixture heated under reflux for 1 h. The red–brown microcrystals which appeared from the deep red solution on cooling were filtered off on a sintered disc and extracted with the mother liquor. A white solid (LiCl) remained on the sinter and the red filtrate was held at −15°C. Very little solid precipitated, so the solution was taken to

dryness and the red–brown solid washed with and finally suspended in diethyl ether. The solid was filtered off and dried *in vacuo*. The analyses suggest that some LiCl is associated with the complex.

Tris(salicylaldehydatobenzylimine)vanadium(III)

The Schiff base Hbzsal (3.35 g, 15.9 mmol) was dissolved in toluene (100 cm^3) to give a clear yellow solution. This was cooled in solid CO_2 ice/acetone and LiMe (11.4 cm^3, 47.6 mmol, 1.4 M solution in diethyl ether) added slowly, forming a white precipitate in an opaque solution. On warming to room temperature and after much effervescence the colour of the solution had changed to pink but the white precipitate remained. $[VCl_3(MeCN)_3]$ (1.33 g, 4.73 mmol) was added and the suspension stirred overnight. Next day a red precipitate had formed; this was filtered off and extracted from the sintered disc by the mother liquor. The red product which appeared on cooling was filtered off and dried *in vacuo*.

Tris(2-*phenolato*-N-n-*propylacetophenoneimine*)*vanadium*(III)–*toluene*(1/1)

Na(Prhap) was prepared by the careful addition of sodium hydride (2.21 g, 92.1 mmol) to a solution of HPrhap (16.1 g, 90.8 mmol) in thf (70 cm^3). The white product which precipitated after much effervescence was filtered off and dried *in vacuo*.

To a yellow solution of Na(Prhap) (1.85 g) in thf (100 cm^3) was added the vanadium(II) species $VBr_2(MeOH)(thf)$ (0.93 g, 2.62 mmol). On stirring, a red solution formed almost immediately and stirring was continued at room temperature overnight. The white solid (NaCl) which precipitated was filtered off and the deep red filtrate was concentrated to dryness yielding a dark red product.

Toluene (70 cm^3) was added to give a deep red solution. A little toluene was pumped off until some solid began to form. Then the mixture was left to stand at room temperature for *ca* 3 weeks during which time bright red crystals appeared. They were filtered off and dried *in vacuo*. The crystals changed to green on exposure to air.

Halocomplexes of vanadium(III) *and vanadium*(IV)

Dichloro[*propan*-1,2-*diyl*-N,N′-*bis*(*salicylideneiminato*)]*vanadium*(IV) The HCl gas used in this preparation was prepared by the careful dropwise addition of concentrated H_2SO_4 to concentrated HCl. The vanadyl derivative [VO(sal-1,2-pn)] (2.01 g, 5.79 mmol) was dissolved in acetonitrile (50 cm^3) forming a green solution. The HCl gas was bubbled through this solution, which changed rapidly from green to deep blue, for *ca* 30 min. The deep blue microcrystalline solid which formed on standing at 4°C overnight was filtered off, washed with methanol and dried in a vacuum desiccator.

Dibromo[*propan*-1,2-*diyl*-N,N′-*bis*(*salicylideneiminato*)]*vanadium*(IV). The HBr gas used in this preparation was generated from bromine and tetralin. The HBr gas was bubbled through a green acetonitrile of [VO(sal-1,2-pn)] (0.5 g, 1.4 mmol) which became blue–purple within 5 min. The gas was bubbled through the reaction mixture for a further 25 min. The deep blue solid which formed on standing at 4°C overnight was filtered off, washed with methanol and dried in a vacuum desiccator.

Diiodo[*propan*-1,2-*diyl*-N,N′-*bis*(*salicylideneiminato*)]*vanadium*(IV). A flask containing [VO(sal-1,2-pn)] (1.74 g, 5.01 mmol) was evacuated, dinitrogen was admitted and the solid dissolved in freshly distilled dichloromethane (100 cm^3), forming a green solution. Trimethylsilyl iodide (1.43 cm^3, 10.0 mmol) was added forming a brown–black solution with the rapid precipitation, on stirring, of a tan solid. This was filtered off and dried *in vacuo*.

Chloro[*propan*-1,2-*diyl*-N,N′-*bis*(*salicylideneiminato*)]*vanadium*(III). The dark blue crystalline $[VCl_2(sal\text{-}1,2\text{-}pn)]$ (0.7 g, 1.7 mmol) was added to thf (30 cm^3) forming a blue–black suspension in a blue solution. An excess of sodium sand (0.13 g, 5.6 mmol) was added and after stirring the mixture at room temperature for 3 days, a dark red solution and white precipitate resulted. The white solid, presumably NaCl, was filtered off and the filtrate was taken to dryness, yielding a dark red semicrystalline solid.

Dichloro[*ethylene*-N,N′-*bis*(*acetophenoneiminato*)]*vanadium*(IV). A green solution of [VO(hapen)] (0.5 g, 1.4 mmol) in acetonitrile (50 cm^3) was treated with HCl gas. The solution changed rapidly from green to deep blue and gas was bubbled through the reaction mixture for a further 25 min. The deep blue microcrystalline solid which formed on standing at 4°C overnight was filtered off, washed with methanol and dried in a vacuum desiccator.

Dibromo[*ethylene*-N,N′-*bis*(*acetophenoneiminato*)]*vanadium*(IV). This was made by bubbling HBr gas through an acetonitrile solution (50 cm^3) of [VO(hapen)] (0.5 g, 1.4 mmol) until the colour changed from green to a deep blue. On standing at 15°C overnight, a dark grey–blue solid precipitated which was filtered off, washed with methanol and dried in a desiccator.

Crystal structure analysis of $[VO(OC_6H_4CHNH)_2]$

Crystal data. $C_{14}H_{12}N_2O_3V$, $M = 307.2$. Orthorhombic, space group $P2_12_12_1$ (no. 19), $a = 5.5475(6)$, $b = 11.797(1)$, $c = 20.494(3)$ Å, Vol. = 1341.1 $Å^3$. $Z = 4$, $D_c = 1.521$ g cm^{-3}, $F(000) = 628$, μ(Mo-K_α) = 7.2 cm^{-1}, λ(Mo-K_α) = 0.71069 Å.

Crystals are very long, fine, grey needles. One, cut down to *ca* 0.36 × 0.13 × 0.04 mm, was mounted on a glass fibre and, after photographic examination, was

transferred to an Enraf–Nonius CAD4 diffractometer (with monochromated radiation) for determination of accurate cell parameters (by refinement from the settings of 25 reflections, having θ in the range 10–12°, each reflection centred in four orientations) and measurement of diffraction intensities (to $\theta_{max} = 25°$).

During processing, the intensity data were corrected for Lorentz–polarization effects and were adjusted to eliminate negative net intensities (by Bayesian statistical methods). There was no deterioration of the crystal during examination. Of the 1410 unique reflections input to the SHELX program system for structure analysis, 1196 had $I > 2\sigma_I$.

The structure was determined by the heavy atom method and refined by full-matrix least-squares procedures. All the non-hydrogen atoms were allowed anisotropic thermal parameters. The two imido hydrogen atoms were located in difference maps and their coordinates were refined independently; the remaining H atoms were included in idealized positions. The isotropic thermal parameters of all the H atoms were refined freely. Refinement converged with $R = 0.060$ and $R_g = 0.073$ [20] for all 1410 reflections weighted $w = (\sigma_F^2 + 0.00341\,F^2)^{-1}$. In a final difference map, the largest peaks, at *ca* 0.7 e Å^{-3}, were around the vanadium atom.

Refinement of the opposite enantiomeric structure produced R and R_g [20] values of 0.064 and 0.077 and slightly higher e.s.d.s throughout. We are confident, therefore, that we are reporting the absolute configuration for that particular crystal.

Scattering factors for neutral atoms were taken from reference [21]. Computer programs used in this analysis have been noted above and in Table 4 of reference [22], and were run on a DEC MicroVAX 3600 machine currently in the Chatt Laboratory.

Crystal structure determination of $[V(Prhap)_3] \cdot C_7H_8$

Crystal data. $C_{33}H_{42}N_3O_3V \cdot C_7H_8$, $M = 671.8$. Monoclinic, space group $P2_1/c$ (no. 14), $a = 12.434(27)$, $b = 18.418(25)$, $c = 16.529(11)$ Å, $\beta = 101.16(12)°$, Vol. = 3714 Å^3. $Z = 4$, $D_c = 1.201$ g cm^{-3}, $F(000) = 1432$, μ(Mo-K_α) = 2.9 cm^{-1}, $T = 295$ K. λ(Mo-K_α) = 0.71073 Å.

The intensity data were collected from a crystal with dimensions $1 \times 0.45 \times 0.45$ mm using an Enraf–Nonius CAD4 diffractometer with graphite monochromated Mo-K_α radiation. The resulting unit cell, obtained from 25 reflections, had larger than usual errors, probably as a result of the crystal size but also arising from a lack of crystal quality due to the disorder present in the structure. This has been reflected in the relatively high final R value ($R = 0.10$) at the end of the refinement.

The Lorentz–polarization correction was applied to the diffraction intensities. An empirical absorption correction based upon Ψ-scan data gave minimum/maximum corrections of 0.30/0.99, average 0.66, which so badly distorted the intensity data that refinement was impeded. The correction was later ignored and this is justified as the absorption coefficient is only 2.9 cm^{-1}.

The position of the V atom together with four oxygen atoms was obtained from the Patterson map. The usual heavy atom method produced the remainder of the molecule, now identified as $[V(Prhap)_3]$, together with some disordered atoms indicative of a solvent molecule. Convergence was slow, reaching an R value of 0.22 with difficulty. The decision was made at this stage to ignore the empirical absorption corrected data and to use the uncorrected set, when R improved to 0.18. At the same time, effort was expended to establish the exact nature of the solvent molecule and whether it was only a fractional molecule or a full molecule. It was concluded after trial refinements of the occupancy factors that the solvent was that of a full toluene molecule. Hydrogen atoms were also added to the atoms list, but not refined, in calculated positions using $d_{C-H} = 1.0$ Å.

Anisotropic refinement of the vanadium complex, the toluene molecule remaining isotropic, allowed R to converge to 0.10, $R_w = 0.14$ and $S = 1.291$ using a weighting scheme $w^{-1} = [\sigma_F^2 + (0.08F)^2 + 8.0]$. The highest peak in the final difference map was 0.55 electrons. The isotropic temperature factors, B_{iso}, of the toluene atoms are very high, ranging from 16 to 34 Å^2, indicating substantial disorder in the structure.

Acknowledgements—We acknowledge the award of a CASE studentship to C.J.McG., an EPRSC Studentship to N.C. and financial support under the Erasmus programme to U.K., M.M. and C.S.

REFERENCES

1. Hills, A., Hughes, D. L., Leigh, G. J. and Sanders, J. R., *J. Chem. Soc., Dalton Trans.* 1991, 61.
2. Hills, A., Hughes, D. L., Leigh, G. J. and Sanders, J. R., *J. Chem. Soc., Chem. Commun.* 1991, 827.
3. Riley, P. E., Pecoraro, V. L., Carrano, C. J., Bonadies, J. A. and Raymond, K. N., *Inorg. Chem.* 1986, **25,** 154; Selbin, J., Manning, H. and Cessac, G., *J. Inorg. Nucl. Chem.* 1963, **25,** 1253.
4. Kolawole, G. A. and Patel, K. S., *J. Chem. Soc., Dalton Trans.* 1981, 1241.
5. Kuska, H. A. and Yang, P.-H., *Inorg. Chem.* 1977, **16,** 1938.
6. Hamilton, D. E., *Inorg. Chem.* 1991, **30,** 1670.
7. Mathew, M., Carty, A. J. and Palenik, G. J., *J. Am. Chem. Soc.* 1970, **92,** 3197.
8. Kolthoff, I. M. and Chantooni, M. K. Jr, *J. Am. Chem. Soc.* 1971, **93,** 3843; *idem, J. Phys. Chem.* 1966, **70,** 856.
9. Ballhausen, C. J. and Gray, H. B., *Inorg. Chem.* 1962, **1,** 111.
10. Fairhurst, S. A., Hughes, D. L., Kleinkes, U., Leigh, G. J. and Sanders, J. R., unpublished data.
11. Xu, X., Wang, X., Liu, H. and You, X., *J. Chem. Soc., Dalton Trans.* 1993, 1377.

12. Cotton, F. A., Duraj, S. A., Extine, M. W., Lewis, G. E., Roth, W. J., Schmulback, C. D. and Schwotzer, W., *J. Chem. Soc., Chem. Commun.* 1983, 1377; Cotton, F. A., Duraj, S. A. and Roth, W. J., *Inorg. Chem.* 1985, **24,** 913; Bouma, R. J., Teuben, J. H., Beukema, W. R., Bansemer, R. L., Huffman, J. C. and Caulton, K. G., *Inorg. Chem.* 1984, **23,** 2715.
13. Holt, D. G. L., Larkworthy, L. F., Povey, D. C., Smith, G. W. and Leigh, G. J., *Inorg. Chim. Acta*, 1993, **207,** 11.
14. Khamar, M. M., Larkworthy, L. F., Patel, K. C., Phillips, D. J. and Beech, G., *Aust. J. Chem.* 1974, **27,** 41.
15. Mazzanti, M., Gambarotta, S., Floriani, C., Chiesi-Villa, A. and Guastini, C., *Inorg. Chem.* 1986, **25,** 2308.
16. Pasquali, M., Marchetti, F., Floriani, C. and Merlino, S., *J. Chem. Soc., Dalton Trans.* 1977, 139.
17. Mabbs, F. E. and Machin, D. J., *Magnetism and Transition Metal Complexes.* Chapman and Hall, London, 1973.
18. Patel, K. S., Kolawole, G. A. and Earnshaw, A., *J. Inorg. Nucl. Chem.* 1981, **43,** 3107.
19. Patel, K. S. and Kolawole, G. A., *J. Coord. Chem.* 1982, **12,** 231.
20. Sheldrick, G. M., *SHELX. Program for Crystal Structure Determination.* University of Cambridge, U.K., 1976.
21. *International Tables for X-ray Crystallography*, Vol. 4, Kynoch Press, Birmingham, 1974, pp. 99 and 149.
22. Anderson, S. N., Richards, R. L. and Hughes, D. L., *J. Chem. Soc., Dalton Trans.* 1986, 245.

Pergamon

PII: S0277-5387(96)00435-4

Polyhedron Vol. 16, No. 9, pp. 1529–1534, 1997
Copyright © 1997 Elsevier Science Ltd
Printed in Great Britain. All rights reserved
0277-5387/97 $17.00+0.00

Coordination of d^{10}-metal cations by thiacycloalkynes

Francesca M. Kerton, G. Farouq Mohmand, Julian D. Webb and Michael J. Went*

Department of Chemistry, University of Kent, Canterbury, Kent CT2 7NH, U.K.

(Received 2 August 1996; accepted 21 August 1996)

Abstract—A range of complexes has been prepared by reaction of thiacycloalkynes with Ag^{I}, Cu^{I} and Hg^{II} cations and cationic MPR_3 (M = Ag, Cu, Hg) fragments. ^1H NMR studies reveal that coordination of 1,4,7-trithiacycloundec-9-yne (L^1) to Ag^{I} results in a change of ligand conformation from exodentate in the free ligand to endodentate in the coordinated ligand implying involvement of the thioether functionalities in coordination. Participation of the alkyne linkage in coordination is less certain and a polymeric structure is suggested in the solid state. Reaction of $AgSbF_6$ with L^1 and PPh_3 or PMe_2Ph afforded complexes in which the silver is coordinated by a phosphine and an endodentate η^3-L^1. Similar studies with Cu^{I} and Hg^{II} showed a reduced tendency for thioether coordination reflected in a reduced denticity of L^1. Studies with a range of dithiacycloalkynes and a tetrathiacyclodiyne show that Ag^+ and Cu^+ can be successfully coordinated by ligands containing a combination of two thioether donors and one alkyne. © 1997 Elsevier Science Ltd. All rights reserved.

Keywords: silver; copper; mercury; thioether; alkyne; phosphine.

The ability of polythioether macrocycles to coordinate metal ions and metal–ligand fragments has been extensively studied in recent years [1,2]. Interest has focused on 1,4,7-trithiacyclononane (9S3), which forms a remarkable range of stable complexes due to its endodentate conformation, but several other thiacrown ethers which are not preorganized for facial coordination, such as 2,5,8-trithia[9]-*o*-benzenophane (TTOB), display good ligating properties and useful selectivity [3]. We have reported the synthesis of 1,4,7-trithiacycloundec-9-yne (L^1) *via* decomplexation from a hexacarbonyldicobalt fragment [4] or *via* a high dilution method [5]. Several other ligands L^2–L^7 have also been prepared by the high dilution method [5,6]. Selective coordination of the alkyne functionality in such systems has been illustrated by their reactions with $[Co_2(CO)_8]$ to form monoalkynehexacarbonyldicobalt complexes [5,6] and with $[Mo(CO)_2(S_2CNMe_2)_2]$ to afford bisalkynebis(dithiocarbamate)molybdenum complexes [5]. In this paper we report the complexation of the soft metal centres Cu^{I}, Ag^{I} and Hg^{II} by thiacycloalkynes L^1–L^7.

* Author to whom correspondence should be addressed.

EXPERIMENTAL

All reactions were carried out under nitrogen using standard Schlenk tube and vacuum line techniques, and all solvents were freshly distilled under nitrogen and over appropriate drying agents. Light petroleum (boiling point 40–60°C) and acetonitrile were distilled over calcium hydride and tetrahydrofuran and diethyl ether were distilled over potassium. The ligands were prepared by literature methods [5]. Fast atom bombardment (FAB) mass spectra were recorded from a NOBA matrix by the EPSRC mass spectrometry service at the University of Swansea with a VG ZAB-E instrument. Raman spectra were recorded with an SA multichannel Raman spectrometer model HF640 with a CCD detector. NMR spectra were recorded with a JEOL GX 270 instrument. Molecular-mechanics calculations were carried out using HYPERCHEM (Release 3) [7]. Structures were minimized with conjugate gradients (Polak–Ribiere algorithm) using the MM+ force field until the gradients were less than 0.01 kcal mol^{-1} $Å^{-1}$. Elemental analyses were performed by Mr A. J. Fassam at the University of Kent. Analytical and physical data for the new compounds is given in Table 1.

Table 1. Analytical and physical data

Compound	Appearance	Yield (%)	[a]ν(C≡C) (cm^{-1})	[b]Analysis (%) C	H	[c]*m/z*
1[AgL^1][BF_4]	White solid	99	—	24.0 (24.1)	3.0 (3.0)	313 ($M-BF_4$)
2[AgL^1][SbF_6]	White solid	67	2231	18.4 (17.5)	2.2 (2.2)	517 ($M+L^1-SbF_6$), 313 ($M-SbF_6$)
3[AgL^1][O_3SCF_3]	White solid	92	2238	24.3 (23.4)	2.7 (2.6)	—
4[$AgL^1(PPh_3)$][SbF_6]	White solid	85	2252, 2222	40.5 (38.5)	3.3 (3.4)	575 ($M-SbF_6$)
5[$AgL^1(PMe_2Ph)$][SbF_6]	White solid	67	2225	28.0 (28.0)	3.3 (3.4)	451 ($M-SbF_6$)
6[CuL^1][PF_6]	White solid	100	—	22.8 (23.2)	2.9 (2.9)	266 ($M-H-PF_6$)
7[$CuL^1(PPh_3)$][PF_6]	White solid	55	2228, 2223	47.6 (46.3)	4.1 (4.0)	529 ($M-PF_6$)
8[$CuL^1(PMe_2Ph)$][PF_6]	White solid	17	2225	35.2 (34.9)	4.2 (4.2)	405 ($M-PF_6$)
9[HgL^1_2]Cl_2	Off-white solid	87	2226	29.5 (28.3)	3.9 (3.6)	—
10[$HgL^1(PPh_3)$]Cl_2	White solid	69	—	41.4 (42.3)	5.1 (3.7)	761 ($M+Na-2Cl$)
11[Ag_2L^2][BF_4]$_2$	White solid	100	—	22.2 (21.3)	2.4 (2.4)	504 ($M-2BF_4$)
12[Cu_2L^2][PF_6]$_2$	White solid	100	—	20.2 (20.4)	2.3 (2.3)	415 ($M-2PF_6$)
13[AgL^3][BF_4]	White solid	100	—	23.9 (23.8)	2.6 (2.9)	265 ($M-BF_4$)
14[CuL^3][PF_6]	White solid	100	—	22.4 (22.9)	2.9 (2.8)	—
15[AgL^4][BF_4]	White solid	100	—	25.9 (26.2)	3.1 (3.3)	—
16[CuL^4][PF_6]	White solid	100	—	24.7 (25.2)	3.3 (3.2)	—
17[AgL^5][BF_4]	White solid	93	—	27.8 (28.4)	3.3 (3.7)	—
18[CuL^5][PF_6]	White solid	60	—	—	—	249 ($M-PF_6$)
19[AgL^6][BF_4]	White solid	100	—	—	—	283 ($M-BF_4$)
20[CuL^6][PF_6]	White solid	93	—	21.2 (22.0)	2.8 (2.6)	—
21[AgL^7][BF_4]	White solid	100	—	25.2 (25.1)	3.3 (3.2)	297 ($M-BF_4$)
22[CuL^7][PF_6]	White solid	100	—	23.8 (24.2)	3.2 (3.1)	251 ($M-PF_6$)

[a] Raman spectroscopy.
[b] Calculated values are given in parentheses.
[c] Fast atom bombardment (FAB) mass spectroscopy.

Preparation of [AgL^1][BF_4](**1**)

To a solution of $AgBF_4$ (0.162 g, 0.83 mmol) in THF (50 cm^3) was added 1 equiv of L^1 (0.17 g, 0.83 mmol), which caused the immediate formation of a white precipitate. After stirring for 3 h, Et_2O (50 cm^3) was added and the mixture left overnight at −25°C before the product was isolated by filtration and dried *in vacuo* to afford [AgL^1][BF_4] (0.33 g, 99%). Compounds **2**, **3**, **11**, **13**, **15**, **17**, **19** and **21** were prepared by similar procedures.

Preparation of [$AgL^1(PPh_3)$][SbF_6] (**4**)

To a stirred solution of L^1 (0.10 g, 0.49 mmol) and PPh_3 (0.13 g, 0.49 mmol) in THF (20 cm^3) was gradually added $AgSbF_6$ (0.17 g, 0.49 mmol). After 3 h the solution was filtered and the product precipitated by addition of light petroleum (60 cm^3). The white precipitate was isolated by filtration and dried *in vacuo* to afford [$AgL^1(PPh_3)$][SbF_6] (0.34 g, 85%).

Preparation of [$AgL^1(PMe_2Ph)$][SbF_6] (**5**)

$AgSbF_6$ (0.34 g, 0.98 mmol) was gradually added to a stirred solution of L^1 (0.20 g, 0.98 mmol) in THF (30 cm^3) followed by addition of PMe_2Ph (0.14 cm^3, 0.98 mmol). After 3 h the solution was filtered and the product precipitated by addition of light petroleum (60 cm^3). The white precipitate was isolated by filtration and dried *in vacuo* to afford [$AgL^1(PMe_2Ph)$][SbF_6] (0.45 g, 67%).

Preparation of [CuL^1][PF_6] (**6**)

To a suspension of [$Cu(NCMe)_4$][PF_6] (0.20 g, 0.54 mmol) in THF (50 cm^3) was added 1 equiv of L^1 (0.11 g, 0.54 mmol), which caused the immediate formation of a white precipitate. After stirring for 5 h, Et_2O (50 cm^3) was added and the mixture left overnight at −25°C before the product was isolated by filtration and dried *in vacuo* to afford [CuL^1][PF_6] (0.22 g, 100%). Compounds **12**, **14**, **16**, **18**, **20** and **22** were prepared by similar procedures.

Preparation of [$CuL^1(PPh_3)$][PF_6] (**7**)

To a stirred solution of L^1 (0.10 g, 0.49 mmol) and PPh_3 (0.12 g, 0.49 mmol) in MeCN (15 cm^3) was added [$Cu(NCMe)_4$][PF_6] (0.18 g, 0.49 mmol). Stirring was continued overnight and then the solvent removed *in vacuo*. The residue was dissolved in hot THF (15 cm^3)

and filtered before precipitation of the product by addition of light petroleum (50 cm^3). The white precipitate was isolated by filtration and dried *in vacuo* to afford $[CuL^1(PPh_3)][PF_6]$ (0.18 g, 55%). Compound **8** was prepared in a similar manner except PMe_2Ph was added to a solution of L^1 and $[Cu(NCMe)_4][PF_6]$.

Preparation of $[Hg(L^1)_2]Cl_2$ (**9**)

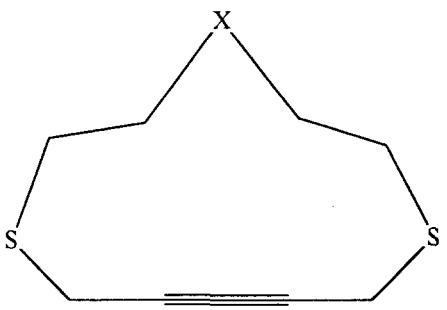
$HgCl_2$ (0.13 g, 0.49 mmol) was added to a stirred solution of L^1 (0.20 g, 0.98 mmol) in THF (20 cm^3). After 3 h the solvent was removed *in vacuo* and the residue precipitated from THF (15 cm^3) by addition of light petroleum (60 cm^3) to afford $[Hg(L^1)_2]Cl_2$ (0.58 g, 87%).

Preparation of $[HgL^1(PPh_3)]Cl_2$ (**10**)

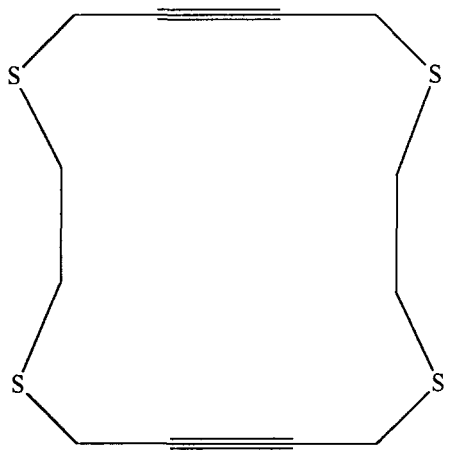
A solution of L^1 (0.10 g, 0.49 mmol) and PPh_3 (0.13 g, 0.49 mmol) in 1 : 1 MeCN : Et_2O (20 cm^3) was mixed with a solution of $HgCl_2$ (0.13 g, 0.49 mmol) in 1 : 1 MeCN : Et_2O (10 cm^3). A precipitate formed immediately which after 2 h was collected by filtration, washed with light petroleum (60 cm^3) and dried *in vacuo* to afford $[HgL^1(PPh_3)]Cl_2$ (0.25 g, 69%).

RESULTS AND DISCUSSION

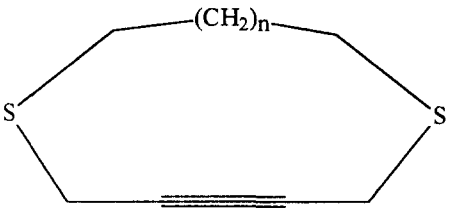
Treatment of a THF solution of $AgBF_4$ with L^1 affords $[AgL^1][BF_4]$ (**1**) in quantitative yield. Its formulation was confirmed by elemental analysis and by FAB mass spectrometry with observation of an isotope envelope at m/z 313 corresponding to $[AgL^1]^+$ (Table 1). The formation of a 1 : 1 product contrasts with the 1 : 2 products formed between Ag^+ and TTOB[3] and 9S3, although a 1 : 1 trimer $[Ag_3(9S3)_3]^{3+}$ has also been characterized [8]. The ^1H NMR spectrum of **1** contains a singlet at 3.42 ppm assigned to the four acetylenic methylene protons and a single AA′BB′ pattern due to the $CH_2CH_2SCH_2CH_2$ fragment. Simulation and iterative fitting of the spectrum using LAOCOON PC [9] resulted in values for the vicinal coupling of $J = 8.34(4)$ and $J' = 3.27(4)$, which indicates an equilibrium containing pre-



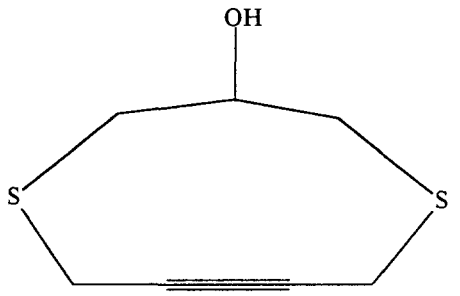
L^1 X = S
L^7 X = O



L^2



L^3 n = 1
L^4 n = 2
L^5 n = 3



L^6

dominantly *gauche* S—C—C—S fragments [10]. This can be compared with the NMR spectrum of L^1 in the same solvent (CD_3CN), which has values of $J = 11.14(2)$ and $J' = 5.13(2)$, indicating an equilibrium of containing predominantly *anti* S—C—C—S fragments in accord with the solid-state structure of L^1 as determined by X-ray crystallography [4]. It appears that L^1 adopts an endodentate conformation to coordinate to Ag^+, but **1** is highly fluxional with both sides of the ring being made equivalent on the NMR timescale. Molecular-mechanics calculations suggest that an endodentate conformation of L^1 is accessible with an energy of 8.97 kcal mol^{-1} compared with the exodentate conformation observed in the free ligand which has an energy of 8.29 kcal mol^{-1}. The ^{13}C NMR spectrum of **1** is very simple and contains four resonances corresponding to the four different carbon environments in the complex. The acetylenic carbon resonance at 84.5 ppm is shifted to the lower field by 4.8 ppm compared with L^1, while the other resonances are shifted by *ca* 3–4 ppm. Relatively few alkyne complexes of silver have been reported [11–15]. The interaction is typically weak and causes only small chemical shift changes to the alkyne carbons so a shift of 4.8 ppm could indicate an interaction between the triple bond and silver in solution. Unfortunately we were unable to grow crystals suitable for X-ray crystallography to determine the solid-state structure of **1**. Coordination of the alkyne would be expected to reduce the tripe bond strength and hence its stretching frequency. For example, coordination of silver(I) triflate to 1,6-cyclodecadiyne results in a change of $\nu(C{\equiv}C)$ from 2282, 2224 cm^{-1} to 2230, 2160 cm^{-1} [14]. The triple bond of L^1 gives a strong absorption in the Raman spectrum at 2227 cm^{-1}, but unfortunately the corresponding resonance for **1** could not be observed in either the IR spectrum, presumably because it is very weak, or in the Raman spectrum, due to fluorescence. However, the spectra did indicate that the counter-ion BF_4^- was not coordinated. In order to gain further information complexes $[AgL^1][SbF_6]$ (**2**) and $[AgL^1][O_3SCF_3]$ (**3**) were prepared containing different counter-ions. Both complexes gave NMR spectra similar to **1** and also produced poor Raman spectra, but resonances could be observed at 2231 and 2238 cm^{-1}, suggesting negligible interaction of the alkyne with the metal. The FAB mass spectrum of **2** contains an isotope envelope at m/z 517 corresponding to $[Ag(L^1)_2]^+$ suggesting a polymeric structure in the solid state. Figure 1 illustrates a possible polymeric solid-state structure for compounds **1–3** involving μ-η^3-η^1-L^1 ligands. A similar bonding mode is exhibited by 9S3 in $[Ag_3(9S3)_3]^{3+}$ [8].

Reaction of $AgSbF_6$ with L^1 and PPh_3 affords the complex $[AgL^1(PPh_3)][SbF_6]$ (**4**). The mass spectrum shows an isotope envelope at m/z 575 corresponding to $[AgL^1PPh_3]^+$. The vicinal coupling constants (Table 2) reveal that the ring is adopting an endodentate confirmation similar to that observed in

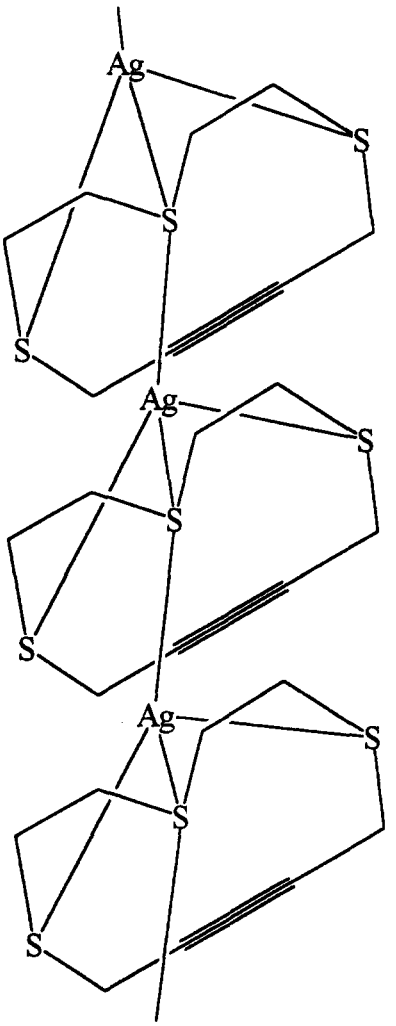


Fig. 1. Proposed structure for compounds **1–3**.

$[Co_2(CO)_6L^1AgPPh_3]$ [16]. Strong absorptions are observed in the Raman spectrum at 2252 and 2222 cm^{-1}, possibly indicating two different environments for the alkyne linkage in the solid state but neither indicating a significant weakening of the bond as might be expected if metal coordination had occurred. Similar results were obtained with PMe_2Ph in the formation of $[AgL^1(PMe_2Ph)][SbF_6]$ (**5**). Both **4** and **5** display only a single resonance at room temperature in the ^{31}P NMR spectra at 14.1 and −21.5 ppm, respectively. The spectrum of **5** was also recorded at 212 K and appears as a four line pattern due to coupling to ^{107}Ag and ^{109}Ag [J(AgP) = 600 and 690 Hz], indicating that phosphine exchange is rapid at room temperature.

Reaction of L^1 with $[Cu(NCMe)_4][PF_6]$ affords $[CuL^1][PF_6]$ (**6**). Elemental analysis supports the formulation and confirms that no acetonitrile ligands remain coordinated to the copper centre. In acetonitrile the vicinal coupling constants indicate an equilibrium containing equal amounts of *anti* and *gauche* S—C—C—S segments, suggesting that L^1 is acting as

Table 2. ^{1}H and ^{13}C NMR data[a]

Compound	H (δ)	$^{13}C\{^{1}H\}$ (δ)
L^1	3.47 (s, 4H, CCH_2), 2.918, 2.896 [AA'BB', 8H, J = 11.10(3), J' = 5.16(3), J_{gem} = −13(2)]	79.6 (C_2), 30.9, 29.6 (SCH_2), 19.1 (CCH_2)
1	3.42 (s, 4H, CCH_2), 3.121, 3.094 [AA'BB', 8H, J = 8.34(4), J' = 3.27(4), J_{gem} = −13(3)]	84.5 (C_2), 33.7, 32.4 (SCH_2), 23.3 (CCH_2)
2	3.40 (s, 4H, CCH_2), 3.12–3.11 (m, 8H, SCH_2)	84.5 (C_2), 33.6, 32.4 (SCH_2), 23.3 (CCH_2)
3	3.39 (s, 4H, CCH_2), 3.11–3.10 (m, 8H, SCH_2)	84.5 (C_2), 33.6, 32.4 (SCH_2), 23.2 (CCH_2)
4	7.50 (m, 15H, Ph), 3.23 (s, 4H, CCH_2), 3.189, 3.148 [AA'BB', 8H, J = 8.33(4), J' = 3.86(4), J_{gem} = −15(4)]	133.3–129.0 (Ph), 82.3 (C_2), 31.9, 31.4 (SCH_2), 21.5 (CCH_2)
5	7.50 (m, 5H, Ph), 3.31 (s, 4H, CCH_2), 3.14 (s, 8H, SCH_2), 1.71 (s, 6H, Me)	132.2–129.9 (Ph), 83.4 (C_2), 32.9, 32.7 (SCH_2), 22.8 (CCH_2), 14.8 (d, Me, J_{pc} = 20)
6	3.52 (s, 4H, CCH_2), 3.040, 2.996 [AA'BB', 8H, J = 8.31(4), J' = 6.25(4), J_{gem} = −8(7)]	81.5 (C_2), 32.8, 32.4 (SCH_2), 22.2 (CCH_2)
7	7.5–7.3 (m, 15H, Ph), 3.46 (s, 4H, CCH_2), 2.934, 2.911 [AA'BB', 8H, J = 10.34(3), J' = 5.52(3), J_{gem} = −13(4)]	—
8	7.7–7.4 (m, 5H, Ph), 3.47 (s, 4H, CCH_2), 2.953, 2.928 [AA'BB', 8H, J = 9.87(3), J' = 5.66(3), J_{gem} = −14(5)]	131.7–129.7 (Ph), 81.2 (C_2), 32.5, 31.6 (SCH_2), 21.1 (CCH_2), 14.1 (d, Me, J_{pc} = 20)
9	3.47 (s, 4H, CCH_2), 2.928, 2.904 [AA'BB', 8H, J = 10.81(9), J' = 5.43(9), J_{gem} = −21(17)]	79.2(C_2), 30.3, 29.1 (SCH_2), 18.6 (CCH_2)
11	3.58 (s, 8H, CCH_2), 3.13 (s, 8H, SCH_2)	81.2 (C_2), 32.2 (SCH_2), 21.6 (CCH_2)
12	3.47 (s, 8H, CCH_2), 2.99 (s, 8H, SCH_2)	80.4 (C_2), 31.7 (SCH_2), 20.6 (CCH_2)
13	3.43 (s, 4H, CCH_2), 3.10 (t, 4H, SCH_2, J_{HH} = 6), 2.08–1.98 (m, 2H, CH_2)	87.2 (C_2), 33.5 (CH_2), 30.1 (SCH_2), 23.0 (CCH_2)
14	3.35 (s, 4H, CCH_2), 3.03 (t, 4H, SCH_2, J_{HH} = 6), 1.86 (m, 2H, CH_2)	87.7 (C_2), 32.6 (CH_2), 29.3 (SCH_2), 22.5 (CCH_2)
15	3.50 (s, 4H, CCH_2), 2.94–2.84 (m, 4H, SCH_2), 1.99–1.87 (m, 4H, CH_2)	81.6 (C_2), 32.3 (CH_2), 28.6 (SCH_2), 23.2 (CCH_2)
16	3.38 (s, 4H, CCH_2), 2.86–2.72 (m, 4H, SCH_2), 2.00–1.94 (m, 4H, CH_2)	81.6 (C_2), 31.8 (CH_2), 28.2 (SCH_2), 22.2 (CCH_2)
17	3.39 (s, 4H, CCH_2), 2.95–2.86 (m, 4H, SCH_2), 1.88–1.72 (m, 6H, CH_2)	82.2 (C_2), 33.8, 23.2 (CH_2), 27.9 (SCH_2), 22.4 (CCH_2)
18	3.26 (s, 4H, CCH_2), 2.84–2.76 (m, 4H, SCH_2), 1.88–1.68 (m, 6H, CH_2)	82.0 (C_2), 33.0, 23.3 (CH_2), 28.2 (SCH_2), 21.4 (CCH_2)
19	4.00–3.89 (m, 1H, CH), 3.47–2.70 (m, 9H, CCH_2, SCH_2 and OH)	87.7 (C_2), 73.2 (CH), 35.7 (SCH_2), 22.1 (CCH_2)
20	4.09–3.97 (m, 1H, CH), 3.48–2.88 (m, 9H, CCH_2, SCH_2 and OH)	87.2 (C_2), 73.2 (CH), 36.1 (SCH_2), 22.4 (CCH_2)
21	3.76 (t, 4H, OCH_2, J_{HH} = 5), 3.40 (s, 4H, CCH_2), 3.08 (t, 4H, SCH_2, J_{HH} = 5)	86.6 (C_2), 66.0 (OCH_2), 35.0 (SCH_2), 22.4 (CCH_2)
22	3.75 (t, 4H, OCH_2, J_{HH} = 5), 3.32 (s, 4H, CCH_2), 2.88 (t, 4H, SCH_2, J_{HH} = 5)	82.0 (C_2), 70.6 (OCH_2), 34.4 (SCH_2), 22.7 (CCH_2)

[a] Chemical shifts (δ) in ppm, coupling constants in Hz, e.s.d.s in parenthesis. Measured in CD_3CN.

a didentate (η^2) ligand with possibly rapidly exchanging acetonitrile as a co-ligand.

Reaction of L^1 and PPh_3 or PMe_2Ph with $[Cu(NCMe)_4][PF_6]$ affords compounds $[CuL^1(PPh_3)][PF_6]$ (**7**) and $[CuL^1(PMe_2Ph)][PF_6]$ (**8**). The vicinal coupling constants (Table 2) indicate that in both compounds the ligand has maintained its exodentate conformation. Raman spectroscopy (Table 1) shows changes of less than 4 cm^{-1} in $\nu(C{\equiv}C)$ consistent with no interaction between the alkyne and the metal centre. A possible structure of **7** and **8** would be linear with L^1 coordinated in a unidentate (η^1) fashion *via* the central sulfur atom.

Reaction of L^1 with $HgCl_2$ affords compound $[HgL^1_2]Cl_2$ (**9**). Again the vicinal coupling constants indicate an exodentate conformation and the Raman spectrum suggests that the alkyne is not involved in coordination, so a linear two-coordinate structure is suggested. Reaction of L^1 and PPh_3 with $HgCl_2$ affords **10**, which was too insoluble for NMR measurements and is formulated as $[HgL^1(PPh_3)]Cl_2$ on the basis of FAB mass spectroscopy (Table 1).

The reactions of several other thiacycloalkynes (L^2–L^7) were investigated in less detail and the results tabulated in Tables 1 and 2. The results indicate that Ag^+ and Cu^+ can be successfully coordinated by ligands containing a combination of two thioether donors and one alkyne. Ligand L^2 with four thioethers and two alkynes can coordinate two metal ions simultaneously.

Acknowledgements—We thank Dr J. A. Creighton for recording the Raman spectra and H. A. Bower for experimental assistance. The EPSRC provided a studentship (GFM) and access to the mass spectrometry service.

REFERENCES

1. Blake, A. J. and Schröder, M., *Adv. Inorg. Chem.* 1990, **35**, 1.
2. Cooper, S. R. and Rawle, S. C., *Struct. Bonding (Berlin)*, 1990, **72**, 1.
3. de Groot, B., Jenkins, H. A. and Loeb, S. J., *Inorg. Chem.* 1992, **31**, 203.
4. Mohmand, G. F., Thiele, K. and Went, M. J., *J. Organomet. Chem.* 1994, **471**, 241.
5. Kerton, F. M., Mohmand, G. F., Tersteegen, A., Thiel, M. and Went, M. J., *J. Organomet. Chem.* 1996, **519**, 17.
6. Meier, H. and Dai, Y., *Tetrahedron Lett.* 1993, **33**, 5277.
7. Pazun, J. L., *J. Chem. Inf. Comput. Sci.* 1993, **33**, 931.
8. Küppers, H.-J., Wieghardt, K., Tsay, Y.-H., Krüger, C., Nuber, B. and Weiss, J., *Angew. Chem. Int. Ed. Engl.* 1987, **26**, 575.
9. Clark, M. and Thrasher, J. S., *J. Chem. Educ.* 1990, **67**, 235.
10. Lockhart, J. C. and Tomkinson, N. P., *J. Chem. Soc., Perkin Trans.* 1992, **2**, 533.
11. Lang, H., Köhler, K. and Blau, S., *Coord. Chem. Rev.* 1995, **143**, 113.
12. Chi, K.-M., Lin, C.-T., Peng, S.-M. and Lee, G.-H., *Organometallics* 1996, **15**, 2660.
13. Lewandos, G. S., Gregston, D. K. and Nelson, F. R., *J. Organomet. Chem.* 1976, **118**, 363.
14. Gleiter, R., Karcher, M., Kratz, D., Ziegler, M. L. and Nuber, B., *Chem. Ber.* 1990, **123**, 1461.
15. Ferrara, J. D., Djebli, A., Tessier-Youngs, C. and Youngs, W. J., *J. Am. Chem. Soc.* 1988, **110**, 647.
16. Demirhan, F., Gelling, A., Irisli, S., Jeffery, J. C., Salek, S. N., Sentürk, O. S. and Went, M. J., *J. Chem. Soc. Dalton Trans.* 1993, 2765.

Pergamon

PII: S0277-5387(96)00434-2

Polyhedron Vol. 16, No. 9, pp. 1535–1541, 1997
Copyright © 1997 Elsevier Science Ltd
Printed in Great Britain. All rights reserved
0277–5387/97 $17.00+0.00

The reactivity of CuX_2 ($X^- = Cl^-$, Br^-, $MeCO_2^-$) salts towards *tris*-pyrazolyl-borates of differing steric requirements. The single crystal X-ray structure of $[CuCl(pz^{Ph}H)(HB\{pz^{Ph}\}_3)] \cdot CH_2Cl_2$

Malcolm A. Halcrow,* John E. Davies and Paul R. Raithby

Department of Chemistry, University of Cambridge, Lensfield Road, Cambridge CB2 1EW, U.K.

(Received 31 July 1996; accepted 20 August 1996)

Abstract—Treatment of CuX_2 ($X^- = Cl^-$, Br^-) with one molar equivalent of $K[HB\{pz^{Ph}\}_3]$ ($pz^{Ph}H$ = 3-phenylpyrazole) in CH_2Cl_2 : MeCN (4 : 1) at room temperature afforded $[CuX(pz^{Ph}H)(HB\{pz^{Ph}\}_3)]$ ($X^- = Cl^-$, **I**; $X^- = Br^-$, **II**) in moderate to good yields. The crystal structure of the title compound shows a square-pyramidal copper(II) centre, with Cu—Cl = 2.2740(13) Å and Cu—N = 2.010(3), 2.031(3), 2.038(3), 2.241(3) Å. The complex exhibits an intramolecular N—H···Cl hydrogen bond, with N···Cl = 3.034(4) Å, N—H···Cl = 119.4°, and an intramolecular graphitic interaction between the $pz^{Ph}H$ pyrazole ring and a phenyl group from the tripodal ligand. Steric repulsions between this phenyl group and the bound Cl^- cause substantial distortions from an ideal square-pyramidal geometry. Reaction of $K[HB\{pz^{Ph}\}_3]$ with $Cu_2(O_2CMe)_4 \cdot 2H_2O$ yields $[Cu(O_2CMe)(HB\{pz^{Ph}\}_3)]$ (**III**). The EPR and UV-vis spectroscopic properties of **I**–**III** are consistent with a $\{d_{x^2-y^2}\}^1$ configuration at copper. © 1997 Elsevier Science Ltd. All rights reserved.

Keywords: copper; *tris*-pyrazolylborate; B—N cleavage; crystal structure.

There has been widespread use of *tris*-pyrazolylborates as protecting ligands in synthetic inorganic chemistry [1]. This popularity has resulted from their ease of preparation and the facility with which their steric and electronic properties can be varied by use of different pyrazole ring substituents [1c]. We report here the syntheses of $[CuX(pz^{Ph}H)(HB\{pz^{Ph}\}_3)]$ ($pz^{Ph}H$ = 3-phenylpyrazole; $X^- = Cl^-$, Br^-), which we have encountered while preparing starting materials for our biomimetic copper coordination chemistry studies [2], and the crystal structure of the chloro complex. These compounds are different from the previously reported products of reactions of CuX_2 salts with other *tris*-pyrazolylborates and offer a good example of how the coordination chemistries of these ubiquitous ligands can vary with their steric bulk.

* Author to whom correspondence should be addressed.

EXPERIMENTAL

All manipulations were carried out in air. All solvents, $CuCl_2$ and $CuBr_2$ were used as supplied, while $pz^{Ph}H$ and $K[HB\{pz^{Ph}\}_3]$ were prepared by the literature procedure [3]. $Cu_2(O_2CMe)_4 \cdot 2H_2O$ was prepared from $CuCO_3$ and acetic acid and recrystallized from hot water.

Synthesis of (hydrido-tris-{3-phenylpyrazol-1-yl}borato)(5-phenylpyrazole)chlorocopper(II) (I)

Anhydrous $CuCl_2$ (0.28 g, 2.08×10^{-3} mol) and $K[HB\{pz^{Ph}\}_3]$ (1.00 g, 2.08×10^{-3} mol) were stirred in CH_2Cl_2 : MeCN (4 : 1; 50 cm^3) at room temperature for 16 h, yielding a deep green solution and pale green precipitate. The mixture was filtered and the filtrate reduced to an oil. Trituration with a minimum volume of Et_2O immediately yielded green microcrystals; after

addition of an equal volume of hexanes and overnight storage at −30°C, the product was filtered and dried *in vacuo* (yield 1.0 g, 70%). Found: C, 62.5; H, 4.43; N, 16.4. Calc. for $C_{36}H_{30}N_8BClCu$: C, 63.2; H, 4.42; N, 16.4%. IR (cm^{-1}): 3223m, 2518w, 1556w, 1524w, 1493s, 1458m, 1424w, 1362m, 1298w, 1259m, 1195s, 1139m, 1119w, 1094m, 1072m, 1046m, 1028w, 960m, 918w, 792m, 760s, 737m, 727w, 694m, 661w, 509w. UV–vis ($CHCl_3$): λ_{max} = 244 nm (ε_{max} = 48,800 M^{-1} cm^{-1}), 248 (sh), 313 (sh), 708 (103), 925 (sh). FAB mass spectrum (fragment, %): 776 ($[^{63}Cu_3(H^{11}B\{pz^{Ph}\}_3)(pz^{Ph}H)]^+$, 6), 711 ($[^{63}Cu_2(H^{11}B\{pz^{Ph}\}_3)(pz^{Ph}H)]^+$, 5), 648 ($[^{63}Cu(H^{11}B\{pz^{Ph}\}_3)(pz^{Ph}H)]^+$, 17), 604 ($[^{63}Cu_2(H^{11}B\{pz^{Ph}\}_3)^{35}Cl]^+$, 12), 567 ($[^{63}Cu_2(H^{11}B\{pz^{Ph}\}_3)]^+$, 17), 539 ($[^{63}Cu(H^{11}B\{pz^{Ph}\}_3)^{35}Cl]^+$, 4), 504 ($[^{63}Cu(H^{11}B\{pz^{Ph}\}_3)]^+$, 10), 361 ($[^{63}Cu(H^{11}B\{pz^{Ph}\}_2)]^+$, 100), 207 ($[^{63}Cu(pz^{Ph}H)]^+$, 45) with correct isotropic distributions.

Synthesis of (*hydrido*-tris-{3-*phenylpyrazol*-1-*yl*}*borato*)-5-*phenylpyrazole*)*bromocopper*(II) (**II**)

Method as for **I**, employing $CuBr_2$ (0.47 g, 2.08×10^{-3} mol). The product formed green microcrystals from Et_2O/hexanes (yield 0.52 g, 34%). Found: C, 58.9; H, 4.10; N, 15.2. Calc. for $C_{36}H_{30}N_8BBrCu$: C, 59.3; H, 4.15; N, 15.4%. IR (cm^{-1}): 3191m, 2512w, 1557w, 1524w, 1489s, 1458s, 1426w, 1364m, 1307w, 1261m, 1196s, 1137m, 1118w, 1096m, 1072m, 1050s, 1029w, 960m, 942w, 910w, 790m, 762s, 736m, 727m, 692s, 662w. UV–vis ($CHCl_3$): λ_{max} = 244 nm (ε_{max} = 43,200 M^{-1} cm^{-1}), 251 (sh), 306 (2,950), 352 (sh), 715 (148), 964 (sh). FAB mass spectrum (fragment %): 865 ($[^{63}Cu_2(H^{11}B\{pz^{Ph}\}_2)(H^{11}B\{pz^{Ph}\}_3)]^+$, 9), 726 ($[^{63}Cu(H^{11}B\{pz^{Ph}\}_3)(pz^{Ph}H)^{79}Br-H]^+$, 4), 711 ($[^{63}Cu_2(H^{11}B\{pz^{Ph}\}_3)(pz^{Ph}H)]^+$, 5), 659 ($[^{63}Cu(H^{11}B\{pz^{Ph}\}_2)_2]^+$, 12), 648 ($[^{63}Cu(H^{11}B\{pz^{Ph}\}_3)(pz^{Ph}H)]^+$ and $[^{63}Cu_2(H^{11}B\{pz^{Ph}\}_3)^{79}Br]^+$, 21), 583 ($[^{63}Cu(H^{11}B\{pz^{Ph}\}_3)^{79}Br]^+$, 6), 567 ($[^{63}Cu_2(H^{11}B\{pz^{Ph}\}_3)]^+$, 8), 505 ($[^{63}Cu(H^{11}B\{pz^{Ph}\}_3)+H]^+$, 47), 439 ($[^{63}Cu(H^{11}B\{pz^{Ph}\}_2)^{79}Br-H]^+$, 10), 361 ($[^{63}Cu(H^{11}B\{pz^{Ph}\}_2)]^+$, 100), 207 ($[^{63}Cu(pz^{Ph}H)]^+$, 48) with correct isotopic distributions.

Synthesis of (*hydrido*-tris-{3-*phenylpyrazol*-1-*yl*}*borato*)*acetatocopper*(II) (**III**)

Method as for **I**, employing $Cu_2(O_2CMe)_4 \cdot 2H_2O$ (0.42 g, 1.04×10^{-3} mol). The product formed green microcrystals from Et_2O/hexanes (yield 0.82 g, 53%). Found: C, 61.9; H, 4.50; N, 15.0. Calc. for $C_{29}H_{25}N_6O_2BCu$: C, 61.8; H, 4.47; N, 14.9%. IR (cm^{-1}): 2473w, 1568w, 1514m, 1493s, 1470s, 1416w, 1368m, 1311w, 1282w, 1257w, 1190s, 1117w, 1092w, 1074m, 1055s, 1012w, 957w, 945w, 910w, 886w, 819w, 796m, 784m, 764m, 756s, 723m, 698s, 690s, 676m, 616w, 528w. UV–vis ($CHCl_3$): λ_{max} = 247 nm (sh), 253 (sh), 296 (sh), 735 (ε_{max} = 78 M^{-1} cm^{-1}), 975 (sh). FAB mass spectrum (fragment, %): 711 ($[^{63}Cu_2(H^{11}B\{pz^{Ph}\}_3)(pz^{Ph}H)]^+$, 10), 648 ($[^{63}Cu(H^{11}B\{pz^{Ph}\}_3)(pz^{Ph}H)]^+$, 8), 567 ($[^{63}Cu_2(H^{11}B\{pz^{Ph}\}_3)]^+$, 8), 564 ($[^{63}Cu(H^{11}B\{pz^{Ph}\}_3)(O_2CMe)]^+$, 14), 504 ($[^{63}Cu(H^{11}B\{pz^{Ph}\}_3)]^+$, 17), 420 ($[^{63}Cu(H^{11}B\{pz^{Ph}\}_2)(O_2CMe)]^+$, 55), 361 ($[^{63}Cu(H^{11}B\{pz^{Ph}\}_2)]^+$, 100), 207 ($[^{63}Cu(pz^{Ph}H)]^+$, 45) with correct isotopic distributions.

X-ray structure determination of **I** · CH_2Cl_2

Slow diffusion of hexanes into a CH_2Cl_2 solution of **I** yielded X-ray quality crystals, which lost solvent upon exposure to air. Experimental details of the structure determination are given in Table 1. The structure was solved by direct methods (SHELXTL-PLUS [4]) and refined by full-matrix least-squares on F^2 (SHELXL-93 [5]). During refinement, the CH_2Cl_2 molecule was found to be disordered over three equally occupied orientations, which were modelled using a common C—Cl distance and tetrahedral Cl—C—Cl angle; one Cl atom, Cl(52), is common to two of these fragments. All non-H atoms except the C atoms of the disordered solvent were refined anisotropically, and all hydrogen atoms were included in calculated positions.

Other measurements

IR spectra were obtained as Nujol mulls pressed between KBr windows between 400 and 4000 cm^{-1} using a Perkin–Elmer Paragon 1000 spectrophotometer. UV–vis spectra were obtained with a Perkin–Elmer Lambda 12 spectrophotometer operating between 200 and 1100 nm, in 1 cm quartz cells. Positive-ion fast atom bombardment (FAB) mass spectra were performed on a Kratos MS50 spectrometer using a 3-NOBA matrix. CHN microanalyses were performed by the University of Cambridge Department of Chemistry microanalytical service. X-band EPR spectra were obtained using Varian E103E and Bruker ECS160 instruments. All electrochemical measurements were carried out using an Autolab PGSTAT20 voltammetric analyser, in CH_2Cl_2 containing 0.5 M $Bu^n_4NPF_6$ (prepared from Bu^n_4NOH and HPF_6) as supporting electrolyte. Cyclic voltammetric experiments involved the use of a double platinum working/counter electrode and a silver wire reference electrode; all potentials quoted in the text are referenced to an internal ferrocene/ferrocenium standard and were obtained at a scan rate of 100 mV s^{-1}.

RESULTS AND DISCUSSION

Treatment of CuX_2 ($X^- = Cl^-$, Br^-) with one molar equivalent of $K[HB\{pz^{Ph}\}_3]$ [3] in 4:1 CH_2Cl_2:MeCN at room temperature afforded a blue–

Table 1. Experimental details for the single crystal structure determination of $\mathbf{I}\cdot CH_2Cl_2$

Formula	$C_{36}H_{30}N_8BClCu\cdot CH_2Cl_2$
Crystal habit	Green block
Crystal size (mm)	$0.3\times0.2\times0.2$
Crystal system	Triclinic
Space group	$P\bar{1}$
a (Å)	12.063(3)
b (Å)	13.544(4)
c (Å)	12.049(4)
α (°)	98.75(3)
β (°)	113.48(2)
γ (°)	79.82(2)
U (Å^3)	1769.9(9)
Z	2
No. of data for lattice parameters	25
θ range for lattice parameters (°)	$40.0\leqslant\theta\leqslant50.0$
T (K)	156(2)
Diffractometer	Rigaku AFC 7-R
Radiation	Graphite-monochromated Mo-K_α
λ (Å)	0.71069
Scan type	ω–2θ
Measured reflections	6561
Independent reflections	6234
R_{int}	0.026
Absorption correction	Empirical (Ψ-scans)
Min. transmission	0.72
Max. transmission	0.99
Observed reflections	4635
Criteria for observed	$I>2\sigma(I)$
Range in 2θ (°)	$5\leqslant2\theta\leqslant50$
Standards	3 every 200 reflections
Variation during data collection	0.5% decay
Range in h	$0\leqslant h\leqslant14$
Range in k	$-15\leqslant k\leqslant16$
Range in l	$-14\leqslant l\leqslant13$
No. of parameters	482
No. of restraints	9
$R(F)^a$	0.049
$wR(F^2)^b$	0.126
GOF	1.038
Weighting scheme^c	$w=1/[\sigma^2(F_o^2)+(0.0601P)^2+1.3098P]$
Max. shift/e.s.d.	0.013
$\Delta\rho_{min}$ (e Å^{-3})	−0.49
$\Delta\rho_{max}$ (e Å^{-3})	0.67

$^aR=\Sigma[|F_o|-|F_c|]/\Sigma|F_o|$.
$^bwR=[\Sigma w(F_o^2-F_c^2)/\Sigma wF_o^4]^{1/2}$.
$^cP=(F_o^2+2F_c^2)/3$.

green solution and pale green precipitate, from which a green microcrystalline solid was isolated after filtration, evaporation of the filtrate to an oil and extraction with Et_2O. The yields of these reactions are 70% ($X^-=Cl^-$) or 34% ($X^-=Br^-$) based on the amount of $K[HB\{pz^{Ph}\}_3]$ employed; lower yields of the same products were obtained from analogous reactions carried out in MeOH or acetone. The IR spectra of these new compounds show, in addition to the expected weak ν_{B-H} absorption at *ca* 2515 cm^{-1}, a medium intensity band close to 3200 cm^{-1} attributable to a N—H or O—H stretching vibration, while microanalysis suggests their formulation as $[CuX(pz^{Ph}H)(HB\{pz^{Ph}\}_3)]$ ($X^-=Cl^-$, **I**; $X^-=Br^-$, **II**). The FAB mass spectra of **I** and **II** are complex, containing many peaks assignable to mono-, di- and tri-copper molecular ions, but confirm the presence of $[HB\{pz^{Ph}\}_3]^-$, $pz^{Ph}H$ and X^-.

The EPR spectra of **I** and **II** in CH_2Cl_2, which are very similar, are distinct from those of tetrahedral copper(II)/*tris*-pyrazolylborate complexes [6,7] and exhibit the pseudoaxial symmetry typical of a tetragonal $\{d_{x^2-y^2}\}^1$ electronic structure [8] (for **I** at 77 K; $g_\parallel=2.26$, $A_\parallel\{^{63,65}Cu\}=163$ G, $g_\perp=2.08$; at 293 K; $\langle g\rangle=2.14$, $\langle A\rangle=62$ G: for **II** at 77 K; $g_\parallel=2.24$, $A_\parallel\{^{63,65}Cu\}=167$ G, $g_\perp=2.09$; at 293 K; $\langle g\rangle=2.16$, $\langle A\rangle=65$ G). The spectra of **II** are rather broad, however, suggesting the presence of fluxionality and/or multiple species in solution. Superhyperfine coupling to ^{14}N or halogen nuclei was not detectable under these conditions. The UV–vis spectra of **I** and **II** in $CHCl_3$ show *d*–*d* maxima at 708 and 715 nm, respectively, both bands exhibiting shoulders at higher wavelength; this is again typical of tetragonal copper(II) centres [8]. In addition to these bands, both complexes exhibit absorptions close to 310 nm. For **I** this region forms a broad and undefined shoulder, but in the spectrum of **II** it is resolved into two distinct bands at $\lambda_{max}=352$ (sh) and 306 nm ($\varepsilon_{max}=2{,}950$ M^{-1} cm^{-1}). We assign these peaks to $X\rightarrow Cu$ ($X^-=Cl^-$, Br^-) LMCT bands [8,9]. Intra-pz^{Ph} $\pi\rightarrow\pi^*$ transitions are observed at $\lambda_{max}=251$ and 244 nm [10].

The source of $pz^{Ph}H$ in the syntheses of **I** and **II** is not an impurity in the $K[HB\{pz^{Ph}\}_3]$ starting material employed, which contains <5% free $pz^{Ph}H$ by ^1H NMR. Rather, the formation of these compounds involves the Cu^{2+}-assisted cleavage of the $[HB\{pz^{Ph}\}_3]^-$ B—N bonds. Such Lewis or Brønsted acid-catalysed degradations of pyrazolylborates to their parent pyrazoles are well known and present a common decomposition pathway for their metal complexes [11]. The feasibility of such a process in this system is suggested by the FAB mass spectra of **I**–**III** (*vide infra*) and other $Cu/[HB\{pz^{Ph}\}_3]^-$ complexes that we have examined [2], which uniformly show a very intense peak at $m/z=361$, corresponding to $[^{63}Cu(H^{11}B\{pz^{Ph}\}_2)]^+$. The syntheses of the related compounds $[MCl(pz^{i\text{-}Pr2}H)(HB\{pz^{i\text{-}Pr2}\}_3)]$ ($pz^{i\text{-}Pr2}H$ = 3,5-di-iso-propylpyrazole; M = Mn, Fe) have been reported, although these preparations involve the addition of excess pyrazole to the reaction mixture [12]. Addition of 1 molar equivalent of $pz^{Ph}H$ to preparations of **I** and **II** increases the rate of reaction (which is now complete in 15 min), but only marginally improves the final yield of products in terms of the amount of CuX_2 employed.

The isolation of **I** and **II** contrasts with previous reports of reactions of other *tris*-pyrazolylborates with $CuCl_2$. Thus, treatment of $CuCl_2$ with one molar equi-

valent of $Na[HBpz_3]$ (pzH = pyrazole) yields $[Cu(HBpz_3)_2]$ [6] or the dimer of square pyramidal copper(II) ions $[Cu(\mu\text{-}Cl)(HBpz_3)]_2$ [13], depending on reaction conditions, while analogous reactions employing $K[HB\{pz^{i\text{-}Pr2}\}_3]$ or $K[HB\{pz^{t\text{-}Bu}\}_3]$ ($pz^{t\text{-}Bu}H$ = 3-*tert*-butylpyrazole) give tetrahedral complexes of form $[CuCl(HB\{pz^R\}_3)]$ ($pz^RH = pz^{i\text{-}Pr2}H$, $pz^{t\text{-}Bu}H$) [1b,6,14]. The driving force for the formation of **I** and **II** presumably arises from a combination of several factors, namely: the high Lewis acidity of the Cu^{2+} ion; the desire of the copper(II) centre to maximize its coordination number; the intermediate steric properties of the $[HB\{pz^{Ph}\}_3]^-$ ligand, which permit five-coordination at copper; and the steric bulk of the pendant pyrazolyl phenyl substituents, which prevents the dimerization of the $[CuCl(HB\{pz^{Ph}\}_3)]$ unit.

A single crystal X-ray structure determination of $\mathbf{I}\cdot CH_2Cl_2$ shows that **I** adopts an irregular five-coordinate geometry in the solid state (Fig. 1, Table 2), which might be described as trigonal bipyramidal with N(3) and N(25) as axial donors [N(3)—Cu(1)—N(25) = 171.40(12)° or as square pyramidal with N(36) apical. Given the observed pattern of Cu—N distances [Cu(1)—N(3) = 2.010(3), Cu(1)—N(14) = 2.031(3), Cu(1)—N(25) = 2.038(3), Cu(1)—N(36) = 2.241(3) Å] and the spectroscopic data described above, the latter description of the complex seems more justified. By comparison with the related square pyramidal complex $[CuCl(DMF)(HB\{pz^{i\text{-}Pr2}\}_3)]$ [6], **I** exhibits a rather distorted molecular structure. Firstly, Cl(2) is displaced from the least squares plane of the three basal N-donors by 1.23 Å, although the Cu(1)—Cl(2) bond is only lengthened by 0.014 Å compared with the literature compound. Secondly, there is a weak intramolecular N—H···Cl hydrogen bond between the chloride ligand and $pz^{Ph}H$ pyrrolic proton [Cl(2)···N(4) = 3.034(4) Å, Cl(2)···H(4)—N(4) = 119.4°]. Thirdly, the orientation of the $pz^{Ph}H$ ligand in the molecule is fixed by a graphitic interaction between the $pz^{Ph}H$ pyrazole ring and a phenyl substituent from the tripodal ligand, which lie 3.17 Å apart at their closest approach (the dihedral angle between the planes of the two groups is 10.5°). Finally, Cu(1) is displaced from the basal N-donor plane by 0.097 Å *away* from the apical N-donor.

The origin of the molecular distortions in $\mathbf{I}\cdot CH_2Cl_2$ is evident from examination of a space-filling diagram of the complex (Fig. 2). The apical phenyl group, which is fixed in orientation by the aforementioned graphitic interaction with the $pz^{Ph}H$ ligand, is twisted so that one edge is in close contact with the bound chloride [Cl(2)···C(42) = 3.450(4) Å]. It is the steric demands of this interaction, rather than the N—H···Cl hydrogen bond, that force Cl(2) out of the ligand basal plane.

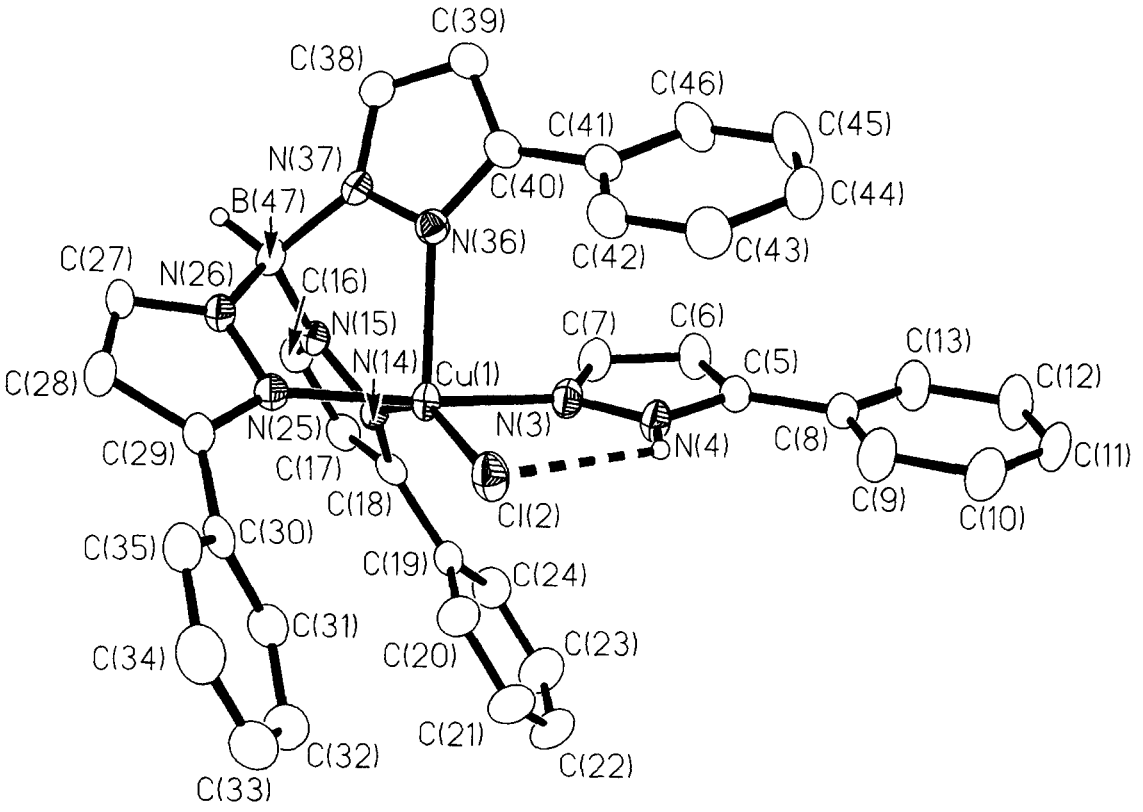


Fig. 1. Solid-state structure of $[CuCl(pz^{Ph}H)(HB\{pz^{Ph}\}_3)]$ (**I**), showing the atom numbering scheme employed. Thermal ellipsoids are at the 50% probability level. For clarity, all carbon-bound hydrogen atoms have been omitted.

Table 2. Selected bond lengths (Å) and angles (°) for $\mathbf{I}\cdot CH_2Cl_2$

Cu(1)—Cl(2)	2.2740(13)	C(17)—C(18)	1.398(5)
Cu(1)—N(3)	2.010(3)	C(18)—C(19)	1.476(5)
Cu(1)—N(14)	2.031(3)	N(25)—N(26)	1.364(4)
Cu(1)—N(25)	2.038(3)	N(25)—C(29)	1.347(4)
Cu(1)—N(36)	2.241(3)	N(26)—C(27)	1.351(5)
N(3)—N(4)	1.351(4)	N(26)—B(47)	1.538(5)
N(3)—C(7)	1.330(5)	C(27)—C(28)	1.366(5)
N(4)—C(5)	1.350(5)	C(28)—C(29)	1.404(5)
C(5)—C(6)	1.377(5)	C(29)—C(30)	1.470(5)
C(5)—C(8)	1.464(5)	N(36)—N(37)	1.360(4)
C(6)—C(7)	1.387(5)	N(36)—C(40)	1.347(5)
N(14)—N(15)	1.364(4)	N(37)—C(38)	1.353(5)
N(14)—C(18)	1.349(5)	N(37)—B(47)	1.538(5)
N(15)—C(16)	1.346(5)	C(38)—C(39)	1.368(5)
N(15)—B(47)	1.558(5)	C(39)—C(40)	1.403(5)
C(16)—C(17)	1.372(5)	C(40)—C(41)	1.475(5)

Cl(2)—Cu(1)—N(3)	90.75(9)	C(17)—C(18)—C(19)	128.5(3)
Cl(2)—Cu(1)—N(14)	152.73(9)	N(14)—C(18)—C(19)	122.3(3)
Cl(2)—Cu(1)—N(25)	97.73(9)	Cu(1)—N(25)—N(26)	114.1(2)
Cl(2)—Cu(1)—N(36)	113.72(8)	Cu(1)—N(25)—C(29)	138.2(2)
N(3)—Cu(1)—N(14)	88.22(12)	N(26)—N(25)—C(29)	106.9(3)
N(3)—Cu(1)—N(25)	171.40(12)	N(25)—N(26)—C(27)	109.4(3)
N(3)—Cu(1)—N(36)	86.24(12)	N(25)—N(26)—B(47)	122.7(3)
N(14)—Cu(1)—N(25)	84.90(12)	C(27)—N(26)—B(47)	127.8(3)
N(14)—Cu(1)—N(36)	93.41(11)	N(26)—C(27)—C(28)	108.8(3)
N(25)—Cu(1)—N(36)	89.01(11)	C(27)—C(28)—C(29)	105.5(3)
Cu(1)—N(3)—N(4)	124.1(2)	N(25)—C(29)—C(28)	109.3(3)
Cu(1)—N(3)—C(7)	129.6(3)	N(25)—C(29)—C(30)	123.6(3)
N(4)—N(3)—C(7)	105.2(3)	C(28)—C(29)—C(30)	126.9(3)
N(3)—N(4)—C(5)	112.1(3)	Cu(1)—N(36)—N(37)	113.0(2)
N(4)—C(5)—C(6)	105.9(3)	Cu(1)—N(36)—C(40)	138.1(2)
N(4)—C(5)—C(8)	123.7(3)	N(37)—N(36)—C(40)	106.5(3)
C(6)—C(5)—C(8)	130.3(3)	N(36)—N(37)—C(38)	109.7(3)
C(5)—C(6)—C(7)	105.9(3)	N(36)—N(37)—B(47)	119.6(3)
N(3)—C(7)—C(6)	110.8(3)	C(38)—N(37)—B(47)	130.6(3)
Cu(1)—N(14)—N(15)	116.1(2)	N(37)—C(38)—C(39)	108.8(3)
Cu(1)—N(14)—C(18)	136.4(2)	C(38)—C(39)—C(40)	105.0(3)
N(15)—N(14)—C(18)	107.4(3)	N(36)—C(40)—C(39)	110.0(3)
N(14)—N(15)—C(16)	109.0(3)	N(36)—C(40)—C(41)	121.8(3)
N(14)—N(15)—B(47)	120.7(3)	C(39)—C(40)—C(41)	128.2(3)
C(16)—N(15)—B(47)	130.1(3)	N(15)—B(47)—N(26)	107.3(3)
N(15)—C(16)—C(17)	109.1(3)	N(15)—B(47)—N(37)	109.5(3)
C(16)—C(17)—C(18)	105.4(3)	N(26)—B(47)—N(37)	108.7(3)
N(14)—C(18)—C(17)	109.1(3)		

Intramolecular N—H···X hydrogen bonds have been previously observed in the solid-state structures of pyrazole complexes of formula *trans*-$[MX_2(pzH)_4]$ [15] (e.g. for M = Ni and $X^- = Cl^-$; N···Cl = 3.10(1), 3.17(1) Å [15a,b]). Such interactions have also been described for the square pyramidal species $[MnX(pz^{i\text{-}Pr2}H)(HB\{pz^{i\text{-}Pr2}\}_3)]$ ($X''^- = \eta^1$-$PhCO_2^-$, η^2-O_2^{2-}) [16]. The manganese complex with $X^- = Cl^-$ has been suggested not to show such an interaction, however, although its IR spectrum shows a $\nu_{N\text{-}H}$ absorbance close to those of **I** and **II** and no structural study was reported [16a]. Intramolecular graphitic interactions of the type found in $\mathbf{I}\cdot CH_2Cl_2$ are also reported in the solid-state structures of the octahedral complexes $[M(HB\{pz^{Ph}\}_3)_2]$ (M = Mn, Fe) [3b].

Attempts to synthesize other complexes of the formula $[CuX(pz^{Ph}H)(HB\{pz^{Ph}\}_3)]$ ($X^- = N_3^-$, NCS^-) by reacting $K[HB\{pz^{Ph}\}_3]$ with $Cu(BF_4)_2\cdot xH_2O$ in the presence of one molar equivalent of NaX were unsuccessful, affording dark green microcrystalline solids consisting of at least two different $[HB\{pz^{Ph}\}_3)]^-$ and X^--containing products by IR, which we were unable to separate by crystallization. While we have not unambiguously identified the products of these reactions, it is possible that dimerization competes with the $[HB\{pz^{Ph}\}_3]^-$ cleavage reaction under these conditions as a method of achieving five-coordination at

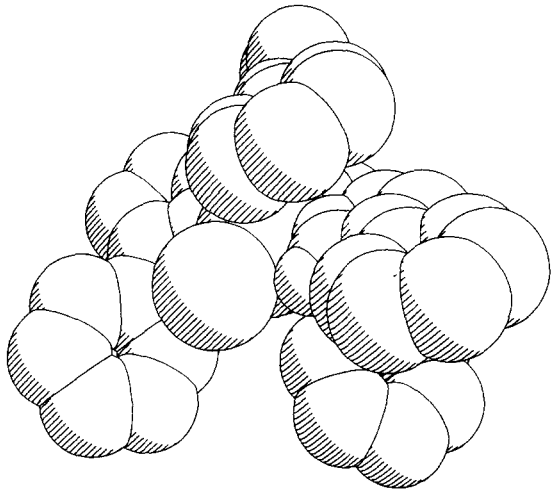


Fig. 2. Space-filling model of the solid-state structure of **I** showing the steric interactions between Cl(2) and the apical phenyl substituent, and the N(4)—H(4)···Cl(2) hydrogen bond. For clarity, all carbon-bound hydrogen atoms have been omitted. The view is approximately parallel to the Cu···B vector, with B(47) lying directly behind Cu(1).

copper. It is notable in this regard that the single crystal structure (but not the synthesis or spectroscopic properties) of $[Cu_2(\mu\text{-}N_3)_2(HB\{pz^{i\text{-}Pr2}\}_3)_2]$ has been reported [17]. However, reaction of $K[HB\{pz^{Ph}\}_3]$ with $Cu_2(O_2CMe)_4 \cdot 2H_2O$ cleanly yields green microcrystals analysing as $[Cu(O_2CMe)(HB\{pz^{Ph}\}_3)]$ (**III**). The IR spectrum of **III** shows ν(O—C—O) at 1514 and 1470 cm^{-1}, consistent with the presence of a chelating acetato ligand [18], while UV–vis ($CHCl_3$) and EPR (CH_2Cl_2) spectroscopies are similar to those of other reported $[Cu(O_2CR)(HB\{pz\}_3)]$ complexes [19] and again suggest a $\{d_{x^2-y^2}\}^1$ configuration at copper (at 77 K; $g_\parallel = 2.29$, $A_\parallel\{^{63,65}Cu\} = 148$ G, $g_\perp = 2.08$: at 293 K; $\langle g \rangle = 2.16$, $\langle A\{^{63,65}Cu\} \rangle = 44$ G). We therefore assign **III** as a square pyramidal complex, containing a (probably asymmetric) bidentate acetate ligand.

The cyclic voltammogram (CV) of **I** in CH_2Cl_2/0.5M $Bu^n_4NPF_6$ at 293 K shows a *quasi*-reversible couple at $E_{1/2} = -0.44$ V *vs* ferrocene/ferrocenium ($\Delta Ep = 380$ mV at 100 mV s^{-1}) assignable to the $Cu^{II/I}$ couple. The oxidative wave of this process is considerably sharper than the reductive peak, suggesting a significant kinetic barrier to the reductive process, which presumably involves concomitant decoordination of Cl^- or $Pz^{Ph}H$ to afford a tetrahedral copper(I) centre. This oxidation exhibits minimal decay upon repeated scanning, while $Ip_c : Ip_a$ is almost invariant between scan rates of 10 and 1000 mV s^{-1}. The CVs of **II** and **III** under identical conditions, while still showing *quasi*-reversible $Cu^{II/I}$ reductions at $E_{1/2} = -0.36$ (**II**) and -0.20 V (**III**), exhibit additional minor peaks indicative of the presence of several species at the electrode. In addition to these processes, **I**–**III** exhibit an additional, irreversible reduction at $Ep_c = -1.11$ (**I**), -1.31 (**II**) and -1.02 V (**III**), which does not have a detectable daughter wave or desorption spike; the identity of this process is unclear.

Acknowledgements—We thank the Royal Society (London) for a University Research Fellowship to M.A.H., the E.P.S.R.C. for purchase of a diffractometer, the University of Cambridge and St Catharine's College for support. We also thank Dr G. Reid (University of Southampton) for the EPR spectrum of **II**.

REFERENCES

1. (a) Trofimenko, S., *Prog. Inorg. Chem.* 1986, **34,** 115; (b) Trofimenko, S., *Chem. Rev.* 1993, **93,** 943; (c) Kitajima, N. and Tolman, W. B., *Prog. Inorg. Chem.* 1995, **43,** 419; (d) Parkin, G., *Adv. Inorg. Chem.* 1995, **42,** 291.
2. Halcrow, M. A., unpublished data.
3. (a) Trofimenko, S., Calabrese, J. C. and Thompson, J. S., *Inorg. Chem.* 1987, **26,** 1507; (b) Eichhorn, D. M. and Armstrong, W. H., *Inorg. Chem.* 1990, **29,** 3607.
4. Sheldrick, G. M., *SHELXTL PLUS.* PC version Siemens analytical X-ray instruments Inc., Madison, WI, U.S.A. (1990).
5. Sheldrick, G. M., *SHELXL93. Program for the Refinement of Crystal Structures.* University of Göttingen, Germany, 1993.
6. Kitajima, N., Fujisawa, K. and Moro-oka, Y., *J. Am. Chem. Soc.* 1990, **112,** 3210.
7. Ruggiero, C. E., Carrier, S. M., Antholine, W. E., Whittaker, J. W., Cramer, C. J. and Tolman, W. B., *J. Am. Chem. Soc.* 1993, **115,** 11285.
8. Hathaway, B. J., in *Comprehensive Coordination Chemistry*, Vol. 5, Ch. 53, ed. G. Wilkinson, R. D. Gillard and J. A. McCleverty. Pergamon Press, Oxford, 1987, pp. 674–680.
9. Solomon, E. I., Penfield, K. W. and Wilcox, D. E., *Struct. Bonding (Berlin)*, 1983, **53,** 1.
10. Elguero, J., Jacquier, R. and Duc, H.C.N.T., *Bull. Soc. Chim. Fr.* 1966, 3744.
11. See e.g. (a) Hubert-Pfalzgraf, L. G. and Tsunoda, M., *Polyhedron*, 1983, **2,** 203; (b) Bradley, D. C., Hursthouse, M. B., Newton, J. and Walker, N. P. C., *J. Chem. Soc., Chem. Commun.* 1984, 188; (c) Cotton, F. A., Dori, Z., Llusar, R. and Schwotzer, W., *Inorg. Chem.* 1986, **25,** 3529; (d) Hughes, D. L., Leigh, G. J. and Walker, D. G., *J. Chem. Soc., Dalton Trans.* 1988, 1153; (e) Kime-Hunt, E., Spartalian, K., DeRusha, M., Nunn, C. M. and Carrano, C. J., *Inorg. Chem.* 1989, **28,** 4392; (f) Abbaidi, N., Jones, C. J. and McCleverty, J. A., *Polyhedron*, 1989, **8,** 1033; (g) Taqui Kahn, M. M., Roy, P. S., Venkatasubramanian, K. and Kahn, N. H., *Inorg. Chim. Acta*, 1990, **176,** 49; (h) Jalon, F. A., Otero, A. and Rodríguez, A., *J. Chem. Soc., Dalton Trans.* 1995, 1629.
12. (a) Kitajima, N., Singh, U. P., Amagai, H., Osawa, M. and Moro-oka, Y., *J. Am. Chem. Soc.* 1991, **113,** 7757; (b) Kitajima, N., Tamura, N., Amagai, H., Fukui, H., Moro-oka, Y., Mizutani,

Y., Kitagawa, T., Mathur, R., Heerwegh, K., Reed, C. A., Randall, C. R., Que Jr, L. and Tatsumi, K., *J. Am. Chem. Soc.* 1994, **116,** 9071.
13. Roundhill, S. G. N., Roundhill, D. M., Bloomquist, D. R., Landee, C., Willett, R. D., Dooley, D. M. and Gray, H. B., *Inorg. Chem.* 1979, **18,** 831.
14. Han, R., Looney, A., McNeill, K., Parkin, G., Rheingold, A. L. and Haggerty, B. S., *J. Inorg. Biochem.* 1993, **49,** 105.
15. (a) Reimann, C. W., Mighell, A. D. and Mauer, F. A., *Acta Cryst.* 1967, **23,** 135; (b) Reimann, C. W. and Santoro, A., *Acta Cryst.* 1969, **B25,** 595; (c) Reedijk, J., Stork-Blaisse, B. A. and Verschoor, G. C., *Inorg. Chem.* 1971, **10,** 2594; (d) Dapporto, P. and Mani, F., *J. Chem. Res. (M)*, 1979, 4201.
16. (a) Kitajima, N., Osawa, M., Tamura, N., Moro-oka, Y., Hirano, T., Hirobe, M. and Nagano, T., *Inorg. Chem.* 1993, **32,** 1879; (b) Kitajima, N., Komatsuzaki, H., Hikichi, S., Osawa, M. and Moro-oka, Y., *J. Am. Chem. Soc.* 1994, **116,** 11596.
17. Fujisawa, K. and Kitajima, N., unpublished results. Cited in ref. 1(c)
18. Nakamoto, K., *Infra-red and Raman Spectra of Inorganic and Coordination Compounds*, 4th edn. Wiley, New York, 1986.
19. (a) Kitajima, N., Fujisawa, K. and Moro-oka, Y., *Inorg. Chem.* 1990, **29,** 357; (b) Tolman, W. B., *Inorg. Chem.* 1991, **30,** 4877; (c) LeCloux, D. D., Keyes, M. C., Osawa, M., Reynolds, V. and Tolman, W. B., *Inorg. Chem.* 1994, **33,** 6361.

Pergamon

PII: S0277-5387(96)00432-9

Polyhedron Vol. 16, No. 9, pp. 1543–1548, 1997
Copyright © 1997 Elsevier Science Ltd
Printed in Great Britain. All rights reserved
0277-5387/97 $17.00+0.00

Syntheses and crystal structures of two heterometallic incomplete cubane-like clusters: $[\{MoAg_2S_3C_5H_5NS\}(PPh_3)_2(S)]\cdot CH_2Cl_2$ and $[\{WAg_2Se_3C_5H_5NS\}(PPh_3)_2(Se)]\cdot CH_2Cl_2$

Quanming Wang, Xintao Wu,* Qun Huang, Tianlu Sheng and Ping Lin

State Key Laboratory of Structural Chemistry, Fujian Institute of Research on the Structure of Matter, Chinese Academy of Sciences, Fuzhou, Fujian 350002, P.R. China

(Received 30 July 1996; accepted 20 August 1996)

Abstract—Two incomplete cubane-like clusters, $[\{MoAg_2S_3C_5H_5NS\}(PPh_3)_2(S)]\cdot CH_2Cl_2$ (**I**) and $[\{WAg_2Se_3C_5H_5NS\}(PPh_3)_2(Se)]\cdot CH_2Cl_2$ (**II**), were obtained from the reaction of $MoS_4Ag_2(PPh_3)_3$ and $WSe_4Ag_2(PPh_3)_3$ with excess C_5H_5NS in CH_2Cl_2 solvent. The X-ray crystallography analysis shows that **I** and **II** have incomplete cubane-like structures, in which the Mo(W) and Ag atoms are tetrahedrally coordinated.
© 1997 Elsevier Science Ltd. All rights reserved.

Keywords: incomplete cubane-like cluster; crystal structure; molybdenum; tungsten; pyridine-2-thiol.

The incomplete cubane-like cluster compounds have attracted much attention, due to their relationship to the novel quasi-aromaticity [1] and the nitrogenase models [2,3]. Many molybdenum and tungsten compounds with incomplete cubane-like M_3S_4 cores have been reported [4], for instance, $Mo_3S_4(dtp)_4\cdot(H_2O)$ and $W_3S_4(dtp)_4\cdot(H_2O)$ [5,6]. However, only a few heterometallic compounds with incomplete cubane-like structure are known, such as MoW_2 and Mo_2W cores [7]. During the past few years, some incomplete cubane-like clusters with M_2Cu (M = Mo, W) and M_2Ag (M = Mo, W) cores have been synthesized in our laboratory [8–10]. Here we report the syntheses and crystal structures of two heterometallic incomplete cubane-like compounds with $MoAg_2$ and WAg_2 cores. It is interesting that these two clusters crystallize in an acentric space group on which is the essential condition for nonlinear optical frequency doubling materials.

* Author to whom correspondence should be addressed.

EXPERIMENTAL

Synthesis

All chemical reagents are of A.R. grade and used as purchased. $MoS_4Ag_2(PPh_3)_3$ and $WSe_4Ag_2(PPh_3)_3$ are prepared according to the literature methods [11]. IR spectra were recorded on FTS-40 and Magna 750 spectrophotometers and UV–vis electronic spectra on a Shimadzu UV-3000 spectrophotometer.

Preparation of $[\{MoAg_2S_3C_5H_5NS\}(PPh_3)_2(S)]\cdot CH_2Cl_2$. $MoS_4Ag_2(PPh_3)_3$ 0.2 g, 0.163 mmol was dissolved in CH_2Cl_2 (10 cm^3) and to the solution C_5H_5NS (0.15 g, 1.35 mmol, excess) was added. After stirring for *ca* 5 min, the resulting solution was filtered. Then *i*-propanol (1 cm^3) was added to the orange filtrate, it was allowed to stand at ambient temperature for 2 days, when 0.05 g of black needle crystals were obtained (yield: 26.4%). Found: C, 43.7; H, 3.3; N, 1.4. Calc. for $C_{42}H_{37}Ag_2Cl_2MoNP_2S_5$: C, 43.5; H, 3.2; N, 1.2% IR (KBr pellet, cm^{-1}): 1562.1, 1496.5, 1477.2, 1432.9, 1126.2, 1093.5, 744.4, 723.2, 692.3, 516.8, 503.3, 490.2, 482.1, 459.0, 451.3, 410.8. UV–vis

(in DMF) $\lambda(\varepsilon)$(nm/10^{-3} M^{-1} cm^{-1}): 485(7.0), 320(18), 270(35).

Preparation of $[\{WAg_2Se_3C_5H_5NS\}(PPh_3)_2(Se)]\cdot CH_2Cl_2$ (**II**). The preparing procedure is similar to the synthetic method for **I**, using $WSe_4Ag_2(PPh_3)_3$ (0.2 g) rather than $MoS_4Ag_2(PPh_3)_3$; 0.07 g of black block crystals were obtained (yield: 36.6%). Found: C, 35.4; H, 2.6; N, 1.0. Calc. for $C_{42}H_{37}Ag_2Cl_2Se_4NP_2SW$: C, 35.1; H, 2.6; N, 1.0%. IR (KBr pellet, cm^{-1}): 1560.3, 1496.1, 1477.5, 1432.9, 1123.7, 1093.4, 741.8, 722.7, 693.0, 518.7, 492.3, 445.1, 333.1, 303.1, 292.9. UV–vis (in DMF) $\lambda(\varepsilon)$(nm/10^{-3} M^{-1} cm^{-1}): 475(4.9), 350(25), 290(36), 270(35).

X-ray structure determinations

The crystal data for compounds **I** and **II** are summarized in Table 1, together with some experimental details. Data were collected on an Enraf–Nonius CAD4 diffractometer using Mo-K_α radiation (λ = 0.71073 Å) at 296 K. Three standard reflections were measured every 120 min.

The structures were solved by direct methods; the Mo(W) atom was located in the E map. The remaining atoms were located in succeeding difference-Fourier syntheses. Hydrogen atoms were not included. The structures were refined by the full-matrix least-squares technique with anisotropic thermal parameters, except for the phenyl C atoms. Final $R = \Sigma||F_o| - |F_c||/\Sigma|F_o| = 0.049$ (0.055), $wR = [\Sigma w(|F_o - F_c|)^2/\Sigma wF_o^2]^{1/2} = 0.055$ (0.057) and $S = [\Sigma w(|F_o - F_c|)^2/(N_o - N_v)]^{1/2} = 1.37$ (1.30); N_o = number of observations, N_v = number of variables) for cluster **I** (cluster **II**). The weighting scheme was $w = 1/\sigma^2(F_o)$ for **I** and **II**. All calculations were performed on a COMPAQ PL4/50 computer using the MoLEN/PC program package [12]. Scattering factors were taken from Cromer and Waber [13].

RESULTS AND DISCUSSION

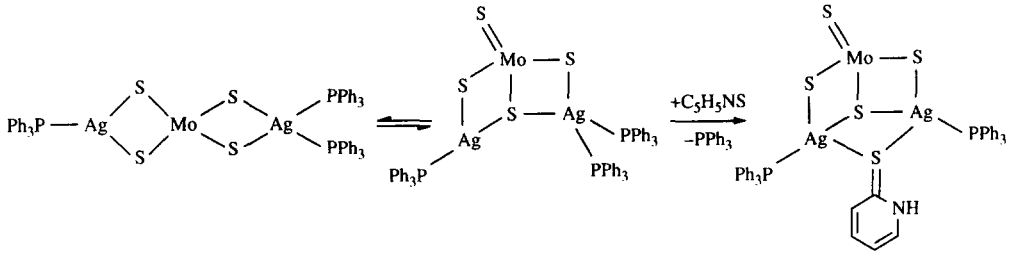
Synthesis

The precursors for synthesizing the clusters have the linear configuration and have been used to prepare some single cubane-like and double cubane-like clusters [14]. Here, two incomplete cubane-like clusters were obtained from these two precursors. The reactions are easily performed in CH_2Cl_2 with excess C_5H_5NS. The possible reaction pathway is illustrated in Scheme 1.

The linear precursor can have a reversible butterfly configuration; as C_5H_5NS attaches to the framework, one PPh_3 ligand is detached, which results in the formation of the incomplete cubane structure.

Table 1. Crystallographic data and some experimental details for clusters **I** and **II**

Compound	**I**	**II**
Chemical formula	$C_{42}H_{37}Ag_2Cl_2MoNP_2S_5$	$C_{42}H_{37}Ag_2Cl_2Se_4NP_2SW$
Formula weight	1160.62	1436.12
$F(000)$	2304	2720
Crystal dimensions (mm)	0.65 × 0.15 × 0.15	0.20 × 0.15 × 0.10
Crystal system	Orthorhombic	Orthorhombic
Space group	$P2_12_12_1$	$P2_12_12_1$
a (Å)	9.037(3)	9.173(2)
b (Å)	19.579(3)	19.698(9)
c (Å)	25.265(4)	25.398(8)
V (Å^3)	4470.5	4588.8
Z	4	4
D_{calc} (g cm^{-3})	1.72	2.08
μ (cm^{-1})	15.8	68.0
Scan type	ω–2θ	ω–2θ
Scan rate (° min^{-1})	1–7	1–5
$2\theta_{max}$	50.0	52.0
hkl range	−10, 0; −23, 0; −30, 0	−11, 0; 0, 24; 0, 31
No. of reflections measured	4440 total, 4440 unique	5063 total, 5063 unique
Corrections	Lp, ψ	Lp, ψ
T_{max}/T_{min}	0.84/1.00	0.88/1.00
Least-squares weights	$1/\sigma^2(F_o)$	$1/\sigma^2(F_o)$
No. of observed reflections, $I > 3\sigma(I)$	3277	3357
Parameters refined	301	301
Residuals: R, Rw	0.049, 0.055	0.055, 0.057
Goodness of fit, S	1.37	1.30
Largest shift	0.01	0.01
Largest/smallest peaks in final difference map (e Å^{-3})	0.85/−0.17	1.73/−0.32



Scheme 1.

Table 2. Selected bond lengths for cluster **I**

Mo—Ag(1)	2.972(1)	Ag(2)—S(3)	2.632(3)
Mo—Ag(2)	2.966(1)	Ag(2)—S	2.774(3)
Mo—S(1)	2.128(4)	Ag(2)—P(2)	2.416(4)
Mo—S(2)	2.204(4)	S—C(1)	1.70(1)
Mo—S(3)	2.264(3)	P(1)—C(111)	1.82(1)
Mo—S(4)	2.195(4)	P(1)—C(121)	1.84(1)
Ag(1)—S(3)	2.595(3)	P(1)—C(131)	1.83(1)
Ag(1)—S(4)	2.519(4)	P(2)—C(211)	1.83(1)
Ag(1)—S	2.714(3)	P(2)—C(221)	1.83(1)
Ag(1)—P(1)	2.408(3)	P(2)—C(231)	1.84(1)
Ag(2)—S(2)	2.543(4)		

Table 4. Selected bond lengths for cluster **II**

W—Ag(1)	3.017(2)	Ag(2)—Se(3)	2.728(3)
W—Ag(2)	3.011(2)	Ag(2)—S	2.760(6)
W—Se(1)	2.264(3)	Ag(2)—P(2)	2.429(7)
W—Se(2)	2.339(2)	S—C(1)	1.72(2)
W—Se(3)	2.398(3)	P(1)—C(111)	1.80(2)
W—Se(4)	2.330(2)	P(1)—C(121)	1.81(2)
Ag(1)—Se(3)	2.672(3)	P(1)—C(131)	1.85(2)
Ag(1)—Se(4)	2.607(3)	P(2)—C(211)	1.81(3)
Ag(1)—S	2.712(6)	P(2)—C(221)	1.82(3)
Ag(1)—P(1)	2.420(6)	P(2)—C(231)	1.85(2)
Ag(2)—Se(2)	2.642(3)		

Table 3. Selected bond angles for cluster **I**

Ag(1)—Mo—Ag(2)	76.15(4)	Mo—Ag(2)—S(2)	46.38(8)
Ag(1)—Mo—S(1)	129.6(1)	Mo—Ag(2)—S(3)	47.24(7)
Ag(1)—Mo—S(2)	121.4(2)	Mo—Ag(2)—S	92.15(8)
Ag(1)—Mo—S(3)	57.53(8)	Mo—Ag(2)—P2	164.5(1)
Ag(1)—Mo—S(4)	56.0(1)	S(2)—Ag(2)—S(3)	91.0(2)
Ag(2)—Mo—S(1)	142.3(1)	S(2)—Ag(2)—S	110.2(2)
Ag(2)—Mo—S(2)	56.7(1)	S(2)—Ag(2)—P2	124.3(1)
Ag(2)—Mo—S(3)	58.60(9)	S(3)—Ag(2)—S	89.7(1)
Ag(2)—Mo—S(4)	110.9(2)	S(3)—Ag(2)—P2	132.9(1)
S(1)—Mo—S(2)	108.9(2)	S—Ag(2)—P2	103.3(1)
S(1)—Mo—S(3)	108.0(1)	Mo—S(2)—Ag(2)	77.0(1)
S(1)—Mo—S(4)	106.8(2)	Mo—S(3)—Ag(1)	75.07(9)
S(2)—Mo—S(3)	111.5(1)	Mo—S(3)—Ag(2)	74.15(9)
S(2)—Mo—S(4)	108.5(1)	Ag(1)—S(3)—Ag(2)	88.9(1)
S(3)—Mo—S(4)	113.0(1)	Mo—S(4)—Ag(1)	77.8(1)
Mo—Ag(1)—S(3)	47.40(8)	Ag(1)—S—Ag(2)	83.7(1)
Mo—Ag(1)—S(4)	46.22(9)	Ag(1)—S—C(1)	100.3(4)
Mo—Ag(1)—S	93.23(7)	Ag(2)—S—C(1)	103.5(4)
Mo—Ag(1)—P(1)	159.69(9)	Ag(1)—P(1)—C(111)	114.5(4)
S(3)—Ag(1)—S(4)	93.2(1)	Ag(1)—P(1)—C(121)	116.0(4)
S(3)—Ag(1)—S	91.8(1)	Ag(1)—P(1)—C(131)	112.8(4)
S(3)—Ag(1)—P(1)	131.8(1)	Ag(2)—P2—C(211)	117.6(4)
S(4)—Ag(1)—S	99.1(2)	Ag(2)—P2—C(221)	115.4(5)
S(4)—Ag(1)—P(1)	125.4(1)	Ag(2)—P2—C(231)	111.1(4)
S—Ag(1)—P(1)	106.9(2)		

Crystal structure

The important bond lengths and bond angles for the two compounds are given in Tables 2–5, respectively.

The crystal structure of cluster **I** consists of a neutral molecule $[\{MoAg_2S_3C_5H_5NS\}(PPh_3)_2(S)]$ and a solvent CH_2Cl_2. Figure 1 gives the ORTEP drawing of $[\{MoAg_2S_3C_5H_5NS\}(PPh_3)_2(S)]$. The cluster core $\{MoAg_2S_3C_5H_5NS\}$ is an incomplete cubane-like type structure, which contains a terdentate MoS_4^{2-}, two

Table 5. Selected bond angles for cluster **II**

Ag(1)—W—Ag(2)	74.95(5)	W—Ag(2)—Se(2)	48.35(6)
Ag(1)—W—Se(1)	128.72(8)	W—Ag(2)—Se(3)	49.10(5)
Ag(1)—W—Se(2)	122.75(8)	W—Ag(2)—S	92.8(1)
Ag(1)—W—Se3	57.79(6)	W—Ag(2)—P(2)	164.1(2)
Ag(1)—W—Se4	56.61(7)	Se(2)—Ag(2)—Se(3)	93.71(9)
Ag(2)—W—Se(1)	144.45(8)	Se(2)—Ag(2)—S	113.6(1)
Ag(2)—W—Se(2)	57.56(7)	Se(2)—Ag(2)—P(2)	121.7(2)
Ag(2)—W—Se(3)	59.29(6)	Se(3)—Ag(2)—S	90.5(1)
Ag(2)—W—Se(4)	108.60(8)	Se(3)—Ag(2)—P(2)	130.6(2)
Se(1)—W—Se(2)	108.5(1)	S—Ag(2)—P(2)	103.1(2)
Se(1)—W—Se(3)	107.32(9)	W—Se(2)—Ag(2)	74.09(8)
Se(1)—W—Se(4)	106.9(1)	W—Se(3)—Ag(1)	72.81(7)
Se(2)—W—S(3)	111.61(8)	W—Se(3)—Ag(2)	71.61(7)
Se(2)—W—Se(4)	108.35(9)	Ag(1)—Se(3)—Ag(2)	85.55(8)
Se(3)—W—Se(4)	113.98(8)	W—Se(4)—Ag(1)	75.11(8)
W—Ag(1)—Se(3)	49.40(5)	Ag(1)—S—Ag(2)	84.1(2)
W—Ag(1)—Se(4)	48.27(6)	Ag(1)—S—C(1)	99.9(6)
W—Ag(1)—S	93.6(1)	Ag(2)—S—C(1)	104.7(7)
W—Ag(1)—P(1)	158.4(2)	Ag(1)—P(1)—C(111)	113.6(8)
Se(3)—Ag(1)—Se(4)	97.37(9)	Ag(1)—P(1)—C(121)	116.7(7)
Se(3)—Ag(1)—S	92.7(1)	Ag(1)—P(1)—C(131)	113.8(7)
Se(3)—Ag(1)—P(1)	129.3(2)	Ag(2)—P(2)—C(211)	117.8(7)
Se(4)—Ag(1)—S	98.0(1)	Ag(2)—P(2)—C(221)	114.4(7)
Se(4)—Ag(1)—P(1)	123.6(2)	Ag(2)—P(2)—C(231)	109.5(6)
S—Ag(1)—P(1)	107.9(2)		

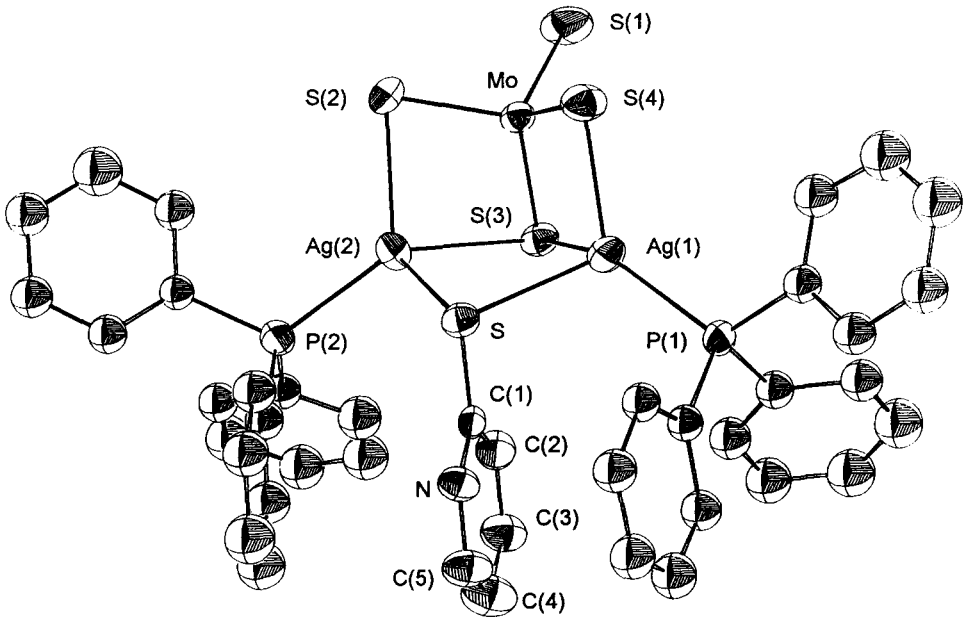


Fig. 1. The ORTEP drawing of $[\{MoAg_2S_3C_5H_5NS\}(PPh_3)_2(S)]$ with 50% probability level.

Ag atoms and a C_5H_5NS ligand. Two PPh_3 ligands are terminally attached to the two Ag atoms, respectively. The S atom of C_5H_5NS bridges the two Ag atoms. The Mo atom maintains its tetrahedral coordination geometry, with the S—Mo—S bond angles ranging from 106.8(2) to 113.0(1)°. The bond lengths of Mo—S range from 2.128(4) to 2.264(3) Å. The two Ag atoms have distorted tetrahedral coordination, with each Ag coordinated by one P and three S atoms. The S—Ag—S(P) bond angles are in the range 89.7(1)–132.9(1)°. The Mo—Ag distances are slightly different, one is 2.972(1) and the other is 2.966(1) Å.

Cluster **II** is isomorphous to cluster **I**. Figure 2 shows the ORTEP drawing of $[\{WAg_2\ Se_3C_5H_5NS\}(PPh_3)_2(Se)]$. Cluster **II** has the same molecular structure as cluster **I**, but the W and Se atoms replace the

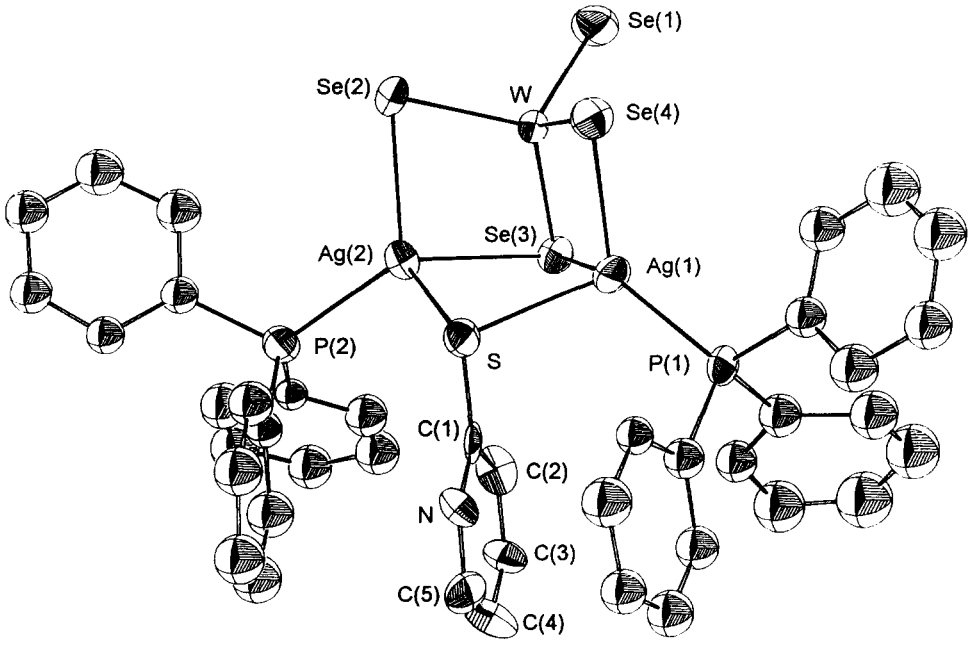


Fig. 2. The ORTEP drawing of [{$WAg_2Se_3C_5H_5NS$}$(PPh_3)_2$(Se)] with 50% probability level.

Mo and S atoms, respectively, which results in a slight increase in bond lengths. The mean bond lengths of cluster **II** are compared with that of the cubane-like cluster $[WAg_3Se_3I](Se)(Ph_3P)_3$ in Table 6; The W—Ag distances of cluster **II** are almost the same as that of $[WAg_3Se_3I](Se)(Ph_3P)_3$ [15], but the W—μ_3-Se and Ag—μ_3-Se bond lengths are a little longer than those of $[WAg_3Se_3I](Se)(Ph_3P)_3$.

The average bond lengths of clusters **I** and **II** as well as some related clusters are provided in Table 6.

As listed in Table 6, the average bond lengths Mo—μ_3-S and Mo—μ-S of **I** are shorter than those of $Mo_3S_4(dtp)_4\cdot(H_2O)$ and $[Et_4N]\{Mo_2AgS_4\}(S_2C_2H_4)_2(PPh_3)$, but the Ag—$\mu_3$-S mean bond length is longer than that of $Mo_3S_4(dtp)_4\cdot(H_2O)$ and $[Et_4N]\{Mo_2AgS_4\}(S_2C_2H_4)_2(PPh_3)$, which indicates that compared with the cores Mo_3 and Mo_2Ag, the incomplete cubane corner S atom of $MoAg_2$ is closer to the Mo atom.

As is well known C_5H_5NS exists in two tautomeric forms: the thione tautomer and the thiol tautomer. For cluster **I** and **II**, S—C bond lengths are 1.70(1) and 1.72(1) Å, respectively, which is fully in accord with thione tautomeric form [16]. The bridging mode of thione C_5H_5NS, has been reported by Constable *et al.* [17].

It is worth noting that these two clusters crystallized in an acentric space group. Recently, much attention has been paid to the study of nonlinear optical properties of W(Mo)—Cu(Ag)—S clusters [18,19], nonlinear absorption and nonlinear refraction have been observed in some W(Mo)—Cu(Ag)—S compounds, but the second harmonic generation (SHG) has not been studied in W(Mo)—Cu(Ag)—S system, because the requirement of a noncentrosymmetric lattice is not easy for the synthetic chemist to achieve. As the title clusters are acentric in the lattice, we intend to study the SHG property with these clusters in the future.

Acknowledgements—This research was supported by grants from the State Key Laboratory of Structural Chemistry, Fujian Institute of Research on the Structure of Matter,

Table 6. The comparison of mean bond lengths with some related compounds

	Mo(W)—Ag	Mo(W)—μ-S(Se)	Mo(W)—μ_3-S(Se)	Ag—μ-S(Se)	Ag—μ_3-S(Se)	Reference
$Mo_3S_4(dtp)_4(H_2O)$	—	2.281(3)	2.346(2)	—	—	5
$[Et_4N]\{Mo_2AgS_4\}(S_2C_2H_4)_2(PPh_3)$	3.064(4)	2.24(1)	2.35(1)	2.65(1)	2.55(1)	9
I	2.969(1)	2.200(4)	2.264(3)	2.631(4)	2.614(3)	This work
II	3.014(2)	2.335(2)	2.398(3)	2.625(3)	2.700(3)	This work
$[WAg_3Se_3I](Se)(Ph_3P)_3$	3.011(3)	—	2.372(4)	—	2.646(5)	15

Chinese Academy of Sciences and the National Science Foundation of China.

REFERENCES

1. Lu, J. X. and Chen, Z. D., *Int. Rev. Phys. Chem.* 1994, **13,** 85.
2. Chan, M. K., Kim, J. and Rees, D. C., *Science*, 1993, **260,** 792.
3. Bolin, J. T., Campobasso, N., Muchmore, S. W., Morgan, T. V. and Mortenson, L. E., in *Molybdenum Enzymes, Cofactors and Model Systems*, ed. E. I. Stiefel, D. Coucouvanis and W. E. Newton. ACS, Washington, D.C.; 1993, pp. 186–195.
4. Shibahara, T., *Adv. Inorg. Chem.* 1991, **37,** 143.
5. Lin, X.-T., Lin, Y.-H., Huang, J.-L. and Huang, J.-Q., *Chinese Sci. Bull.* 1986, **7,** 509.
6. Zhan, H.-Q., Zheng, Y.-F., Wu, X.-T., and Lu, J.-X., *J. Mol. Struct.* 1989, **196,** 241.
7. Shibahara, T. and Yamasaki, M., *Inorg. Chem.* 1991, **30,** 1687.
8. Zhu, N.-Y., Zheng, Y.-F. and Wu, X.-T., *Inorg. Chem.* 1990, **29,** 2707.
9. Zhu, N.-Y., Wu, X.-T. and Lu, J.-X., *J. Chem. Soc., Chem. Commun.* 1991, 235.
10. Wang, Q. M., Wu, X. T., Huang, Q. and Sheng, T. L., *J. Cluster. Sci.* 1996, **7,** 371.
11. (a) Müller, A., Bögge, H. and Schimanski, U., *Inorg. Chim. Acta*, 1983, **69,** 5; (b) Müller, A., Schimanski, U. and Schimanski, J., *Inorg. Chim. Acta*, 1983, **76,** L-245.
12. *MoLEN, An Interactive Structure Solution Procedure*. Enraf-Nonius, Delft, The Netherlands, 1990.
13. Cromer, D. T. and Waber, J. T., *International Tables for X-ray Crystallography*, Vol. IV. Kynoch Press, Birmingham, 1974.
14. (a) Du, S.-W., Zhu, N.-Y., Chen, P.-C. and Wu, X.-T., *J. Mol. Struct.* 1993, **291,** 167; (b) Du, S.-W. and Wu, X.-T., *J. Coord. Chem.* 1993, **30,** 183.
15. Du, S. W., Wu, X. T. and Lu, J. X., *Polyhedron*, 1994, **13,** 841.
16. Mura, P., Olby, B. G. and Robinson, S. D., *J. Chem. Soc. Dalton Trans.* 1985, 2101.
17. Constable, E. C. and Raithby, P. R., *J. Chem. Soc. Dalton Trans.* 1987, 2281.
18. Shi, S., Ji, W., Tang, S. H., Lang, J. P. and Xin, X. Q., *J. Am. Chem. Soc.* 1994, **116,** 3615.
19. Shi, S., Hou, H. W. and Xin, X. Q., *J. Phys. Chem.* 1995, **99,** 4050.

Pergamon

PII: S0277-5387(96)00433-0

Polyhedron Vol. 16, No. 9, pp. 1549–1554, 1997
Copyright © 1997 Elsevier Science Ltd
Printed in Great Britain. All rights reserved
0277-5387/97 $17.00+0.00

Metal substitution in the cluster $(\mu\text{-H})_2Fe_3(\mu_3\text{-Te})(CO)_9$—III.† Crystal and molecular structure of $[FeMo_2(\mu_3\text{-Te})(CO)_7(\eta^5\text{-}C_5H_5)_2]$

Sergei N. Konchenko,* Alexander V. Virovets, Sergei V. Tkachev and Nina V. Podberezskaya

Institute of Inorganic Chemistry, Siberian Division of RAS, Acad. Lavrentyev str. 3, Novosibirsk 630090, Russia

(Received 26 July 1996; accepted 20 August 1996)

Abstract—The reaction of $[(\mu\text{-H})_2Fe_3(\mu_3\text{-Te})(CO)_9]$ with $[CpM(CO)_3]_2$ (M = Mo, W; Cp = η^5-C_5H_5) complexes causes substitution of one and two $HFe(CO)_3$ groups with isolobal $CpM(CO)_2$ fragments. The first-stage substitution derivative $[(\mu\text{-H})Fe_2W(\mu_3\text{-Te})(CO)_8Cp]$ reacts with $[CpMo(CO)_3]_2$ resulting in the heterotrimetal $[FeMoW(\mu_3\text{-Te})(CO)_7Cp_2]$ cluster. The structure of $[FeMo_2(\mu_3\text{-Te})(CO)_7Cp_2]$ has been determined by X-ray analysis. The structures of the other products have been suggested based on ^1H, ^{77}Se and ^{125}Te NMR and IR spectroscopy. © 1997 Elsevier Science Ltd. All rights reserved.

Keywords: iron; molybdenum; selenium; tellurium; tungsten; heterometal clusters; synthesis; crystal and molecular structure.

The reaction of $[(\mu\text{-H})_2Fe_3(\mu_3\text{-Se})(CO)_9]$ (**Ia**) with the dimeric $[CpM(CO)_3]_2$ (M = Mo, W) complexes was recently shown to be a convenient method for the synthesis of two types of heterometal clusters: $[(\mu\text{-H})Fe_2M(\mu_3\text{-Se})(CO)_8Cp]$ [M = Mo(**IIa**),‡ W(**IIIa**)] and $[FeM_2(\mu_3\text{-Se})(CO)_7Cp_2]$ [M = Mo (**IVa**), W (**Va**)] [1,3]. Moreover, compound **IIIa** was shown to react with $[CpMo(CO)_3]_2$ resulting in the heterotrimetal $[FeMoW(\mu_3\text{-Se})(CO)_7Cp_2]$ (**VIa**) cluster [2]. These reactions mentioned previously [2] can be regarded as a cooperative decomposition of the initial polynuclear complexes resulting in the spontaneous formation of new compounds, whose structures cannot be predicted *a priori*. After the metal substitution in **Ia** had been studied it became possible to propose the reactions of this type as a general approach to the directed synthesis of a sufficiently large series of parent heterometal derivatives, not only cluster **Ia**, but its telluride analog $[(\mu\text{-H})_2Fe_3(\mu_3\text{-Te})(CO)_9]$ (**Ib**) as well. This work is devoted to an experimental verification of this proposition.

EXPERIMENTAL

All reactions were carried out under argon; the other manipulations were performed in air. All solvents were distilled from appropriate drying agents. The IR spectra were recorded on a Bruker IFS85 spectrometer. The NMR spectra were recorded on Bruker SXP-4-100 (^1H at 90 MHz) and CXP-300 (^{125}Te at 96.4 MHz) spectrometers. The chemical shift of ^{125}Te (positive downfield) was referenced to the 1 M water solution of H_6TeO_6 [δ = 712 ppm from $(CH_3)_2Te$ [4]] as an external standard and counted relative to dimethyltelluride. $[(\mu\text{-H})_2Fe_3(\mu_3\text{-Te})(CO)_9]$ (**Ib**) was obtained by the same procedure as used previously for **Ia** [3]. The NMR spectra parameters are given in Table 1.

Reactions of $[(\mu\text{-H})_2Fe_3(\mu_3\text{-Te})(CO)_9]$ (**Ib**) *with* $[CpM(CO)_3]_2$ (M = Mo, W)

In a typical manner compound **Ib** (0.82 g, 1.5 mmol) and $[CpM(CO)_3]_2$ (1.0 mmol) in *m*-xylene (15 cm^3)

* Author to whom correspondence should be addressed.

† See [1] and [2] for the previous communications.

‡ Cluster **IIa** was not isolated earlier, but it was obtained in the reaction of **Ia** with $[CpM(CO)_3]_2$ described recently [3].

Table 1. The NMR spectra parameters[a] of the telluride clusters obtained in this work and their selenide analogs described previously [1,2,3]

Cluster core	X = Te			X = Se		
	Compound	^1H	^{125}Te	Compound	^1H	^{77}Se
Fe_3X	Ib	−23.60	758	Ia	−24.20	651
Fe_2MoX	IIb	5.29	481	IIa	5.35	528
		−20.24			−21.38	
Fe_2WX	IIIb	5.39	64	IIIa	5.43	249
		−19.95	(168 ± 3)[b]		−20.08	(52 ± 3)[b]
		(39.7 ± 0.7)[b]			(39.0 ± 1.5)[b]	
$FeMo_2X$	IVb	5.22	61	IVa	5.28	421
FeMoWX	VIb	5.20	−284	VIa	5.28	183[c]
		5.28	(131 ± 3)[b]		5.32	
FeW_2X	Vb	5.25	−576	Va	5.31	−51
			(132 ± 3)[b]			(37.4 ± 1.2)[b]

[a] ^1H NMR: δ, ppm, related to TMS, $CDCl_3$ as a solvent; ^{125}Te NMR: δ, ppm, related to $(CH_3)_2Te$, CD_2Cl_2 as a solvent; ^{77}Se NMR: δ, ppm, related to $(CH_3)_2Se$, CD_2Cl_2 as a solvent.

[b] $J(^1H, ^{183}W)$, $J(^{125}Te, ^{183}W)$ and $J(^{77}Se, ^{183}W)$ in Hz.

[c] $J(^{77}Se, ^{183}W)$ has not yet been measured.

were refluxed for 4 h and the volatiles then removed in high vacuum. The solid residue was extracted with several portions of $CHCl_3$ and concentrated *in vacuo*. The soluble mixture of products thus obtained was separated by a column chromatography (20 × 40 cm, silica, hexane : benzene in a 3 : 2 ratio). Three major fractions were collected in every case:

(1) Small amounts of unreacted $[CpM(CO)_3]_2$.

(2) A first-step substituted product $[(\mu\text{-H})Fe_2M(\mu_3\text{-Te})(CO)_8Cp]$: M = Mo (**IIb**), yield 0.096 g (10%).* Found: C, 25.1; H, 0.87. Calc. for $C_{13}H_6Fe_2O_8TeMO$: C, 24.9; H, 0.96%. IR ($CHCl_3$, ν_{co}, cm^{-1}): 2069 s; 2059; 2031 sh; 2018 vs, 1998 vs; 1971 sh; 1959 sh; 1915 m, br. M = W (**IIIb**), yield 0.292 g (27%). Found: C, 21.8; H, 0.76. Calc. for $C_{13}H_6Fe_2O_8$ TeW: C, 21.9; H, 0.84%. IR ($CHCl_3$, ν_{co}, cm^{-1}): 2068 sh; 2059 s; 2019 vs; 1995 s; 1970 sh; 1957 sh; 1915 m, br.

(3) A second-step substituted product $[FeM_2(\mu_3\text{-Te})(CO)_7Cp_2]$: M = Mo (**IVb**), yield 0.245 g (23%). Found: C, 29.8; H, 1.6. Calc. for $C_{17}H_{10}FeMo_2O_7Te$: C, 29.1; H, 1.4%. IR ($CHCl_3$,ν_{co}, cm^{-1}): 2021 vs; 1975 s; 1951 vs; 1938 sh; 1886 w, br; 1849 w, br. M = W (**Vb**), yield 0.274 g (21%). Found: C, 23.4; H, 0.9. Calc. for $C_{17}H_{10}FeO_7TeW_2$: C, 23.3; H, 1.1% IR ($CHCl_3$, ν_{co}, cm^{-1}: 2018 vs; 1970 s; 1947 vs; 1931 sh; 1879 w, br; 1849 w, br.

Synthesis of 1,1,2,2,3,3,3-*heptacarbonyl*-1,2-*bis*-(η^5-*cyclopentadienyl*)-(1,2,3-μ_3-*tellurido*)*triangulo-tungsten-molybdenum-iron*

Compound **IIb** (0.128 g, 0.18 mmol) and $[CpMo(CO)_3]_2$ (0.17 g, 0.35 mmol) in *m*-xylene (5 cm^3) were refluxed for 8 h and the volatiles then removed in high vacuum. The solid residue was extracted with several portions of $CHCl_3$ and concentrated *in vacuo*. The mixture of soluble products thus obtained was separated by TLC on "Silufol" plates (hexane : benzene in a 2 : 3 ratio). Four major fractions were collected:

(1) The red fraction—small amounts of unreacted $[CpMo(CO)_3]_2$.

(2) The red–brown fraction—trace amounts of **IVb**.

(3) The red–violet fraction—$[FeMoW(\mu_3\text{-Te})(CO)_7Cp_2]$ (**VIb**), yield 0.054 g (38%). Found: C, 25.7; H, 1.3. Calc. for $C_{17}H_{10}FeMoO_7TeW$: C, 25.9; H, 1.3%. IR ($CHCl_3$, ν_{co}, cm^{-1}): 2020 vs; 1973 s; 1950 vs; 1933 sh; 1879 w, br; 1849 w, br.

(4) The dark red fraction—trace amounts of **Vb**.

X-ray structure determination of **IVb**

Crystal data: $C_{17}H_{10}FeMo_2O_7Te$, mol. weight 701.58, triclinic, space group $P\bar{1}$, $a = 7.296(1)$, $b = 8.207(1)$, $c = 16.434(2)$ Å, $\alpha = 96.77(1)$, $\beta = 76.07(1)$, $\gamma = 111.33(1)^\circ$, V = 889.2(2) Å^3, $D_c = 2.620$ g cm^{-3}, a "Syntex $P2_1$" diffractometer, λ(Cu-K_α), room temperature, $\theta/2\theta$ scans with $V_{min} = 3.5^\circ$ min^{-1} up to $2\theta_{max} = 110^\circ$. Total 1967 (1789 independent, $R_{int} = 0.0518$) reflections were measured. An absorption correction ($\mu = 308.97$ cm^{-1}) was applied using the integration method on a crystal shape: faces ±(100), a perpendicular distance 0.330 mm, ±(010), 0.320, ±(001), 0.056; transmission factors varied from 0.21715 to 0.01331. The structure was solved by direct method (SHELXS-86

* All yields are based on **Ib**.

[5]) and refined by the full-matrix least-squares method on F^2 (SHELXL-93 [6]). The H atoms were calculated geometrically and refined in the rigid body approximation (C—H = 0.96 Å). Final R values: $R(F) = 0.0431$, $wR(F) = 0.1135$ for 1546 $F_{hkl} > 4\sigma(F)$, $R(F) = 0.0489$, $wR(F^2) = 0.1186$ for all 1789 independent reflections used. Atomic coordinates and thermal parameters are deposited in the Cambridge Crystallographic Database.

RESULTS AND DISCUSSION

Synthesis

Cluster **Ib** reacts with dimeric complexes $[CpM(CO)_3]_2$ (M = Mo, W) resulting in metal substituted derivatives, which are analogous to the selenide complexes described previously [1,3] (Scheme 1).

It should be noted that the reactions were performed following the procedure used for the analogous selenide clusters previously described [1,3]. Therefore, one can compare yields of metal substituted products and make some conclusions.

For the first time a difference in reactivity of **Ia** and **Ib** with $[CpMo(CO)_3]_2$ has occurred: the first-step substituted product **IIb** was obtained by the general procedure, but its selenide analog **IIa** was not obtained [3]. In one experiment, **IIa** was isolated in a low yield from the reaction mixture when the process was interrupted after 2 h. In our opinion the difference mentioned reflects that telluride clusters are more stable at the reaction temperature used than selenide and exhibit the lower substitution rate.

An analogous conclusion can be made when the reactions of **Ib**(**Ia**) with the molybdenum dimer complex and with the tungsten one are compared. In contrast to molybdenum clusters, the yield of the first-step tungsten substituted derivative is higher than that of the second-step one. This observation gives evidence suggesting substitution of the $HFe(CO)_3$ fragments with $[CpMo(CO)_2]$ is faster than that with $[CpW(CO)_2]$.

Based on this conclusion the reaction of **IIIB** and $[CpMo(CO)_3]_2$ was chosen to prepare the $[FeMoW(\mu_3\text{-Te})(CO)_7Cp_2]$ (**VIb**) cluster (Scheme 2).

An inversion of the reaction partners (when **IIb** and $[CpW(CO)_3]_2$ were used) required an increased reaction time. It results in the **VIb** yield decreasing, probably, due to the decomposition of the initial complexes and products.

Spectroscopy

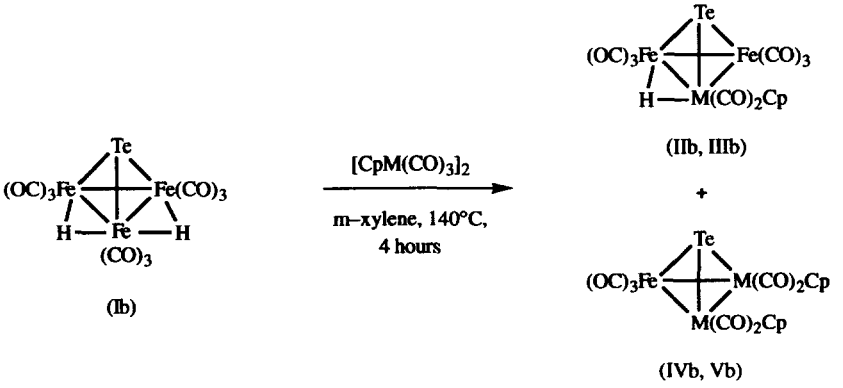
A single crystal sample of **IVb** was obtained by the slow diffusion of pentane into the toluene solution of the cluster and its structure has been determined by X-ray crystallography. Single crystals of the other heterometal complexes have not yet been obtained, so their structures are suggested on the basis of spectroscopy (see Experimental).

It was previously mentioned that the conclusion about a number of tungsten atoms in a cluster molecule can be made on the basis of the NMR spectra if the coupling on the ^{187}W nuclei is observed [1]. Based on the natural abundance and the statistical distribution of the ^{187}W isotope one can predict that the ^{125}Te NMR spectra will exhibit three peaks (a superposition of the singlet and the doublet with the same center) in a 1:12:1 ratio for the clusters containing one tungsten atom and in a 1:6:1 ratio for the clusters containing two tungsten atoms [1]. The spectra recorded confirm the number of the W atoms proposed for **IIB, Vb** and **VIb** (Table 1).

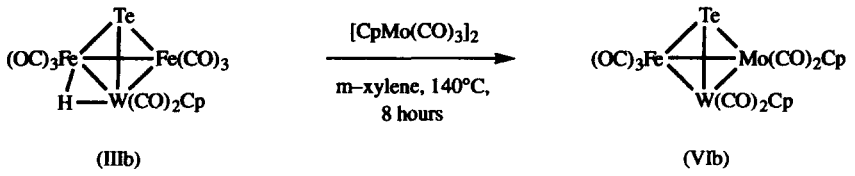
The IR spectra of **IVb, Vb** and **VIb** are very similar with only slight differences in the position of the peaks. This is supporting evidence in favour of **Vb** and **Vib** having core structures analogous to **IVb**.

The ^1H NMR spectra of **IVb** and **Vb** exhibit the singlet signals for the Cp ligand protons. In contrast the spectrum of **VIb** exhibits two singlet signals for Cp ligands linked to W and Mo atoms, respectively (Table 1). The fact that **VIb** is an individual compound and not a mixture of **IVb** and **Vb** is confirmed by chromatography (see Experimental).

The ^1H NMR spectra of the first-step substituted products **IIb** and **IIb** exhibit signals for μ-H and Cp



Scheme 1.



(IIIb) (VIb)

Scheme 2.

ligand protons in a 1 : 5 ratio. In the case of **IIIb**, the coupling on the ^{187}W nuclei was observed for the μ-H proton (Table 1). The IR spectrum of **IIb** is very similar to **IIIb**.

The additive decrease of the ^{125}Te chemical shift was observed in the **IVb, VIb, Vb** set as well as the ^{77}Se one in the **IVa, VIa, Va** set [2] (Table 1). The clusters forming each of the sets can be considered formally as the products obtained by the sequential substitution of $CpMo(CO)_3$ with $CpW(CO)_3$.

Ia, IIA and **IVa**; **Ia, IIa** and **Va**; **Ib, IIb** and **IVb**; **Ib, IIIb** and **Vb** represent the sets of the clusters obtained by the sequential substitution of $HFe(CO)_3$ with $CpM(CO)_2$ (M = Mo, W). Both in the case of the selenide clusters and the telluride ones there is no accurate additivity in the chalcogenide chemical shift variation in these rows, but the variation tendencies are very similar (Table 1).

The data mentioned in this section allow one to be sure in the correctness of the structures proposed (Schemes 1 and 2).

Crystal and molecular structures of **IVb**

Compound **IVb** has a molecular structure, as shown in Fig. 1. The crystal packing is illustrated in Fig. 2

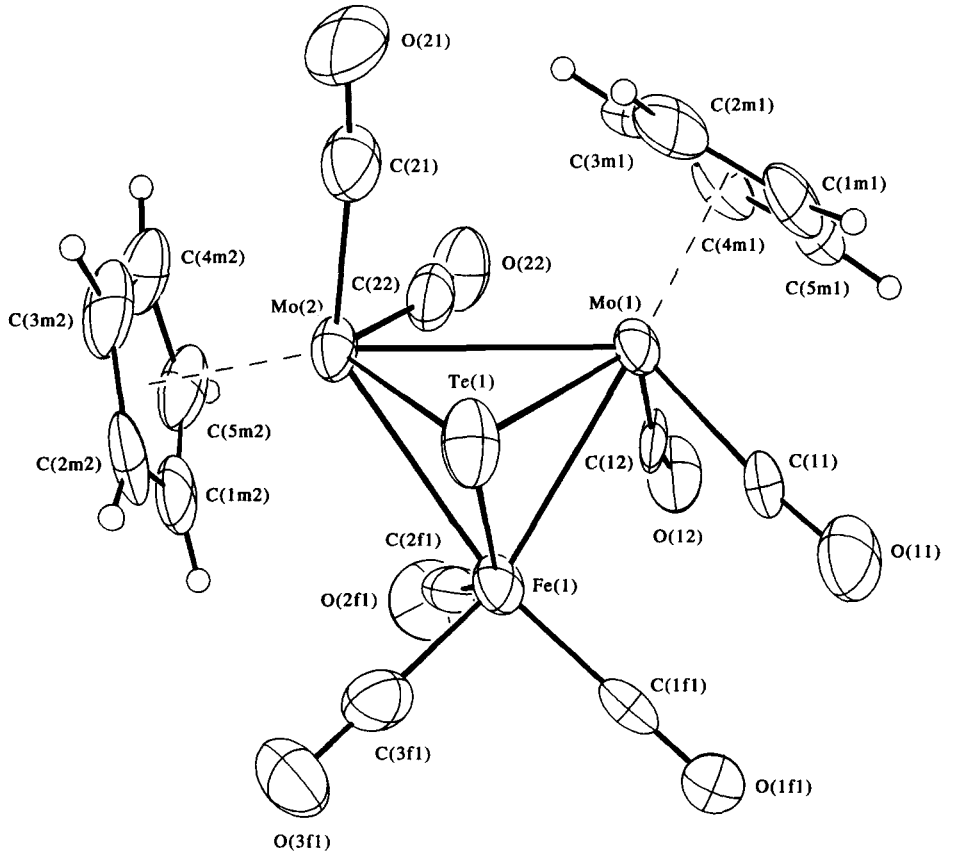


Fig. 1. Molecule **IVb** (50% probability level thermal ellipsoids). Short nonvalence contacts of Te atom are shown by dashed lines. The selected bond distances (Å): Mo(1)—Mo(2), 3.002(1), Mo(1)—Fe(1), 2.704(2), Mo(2)—Fe(1), 2.837(2), Mo(1)—Te(1), 2.700(1), Mo(2)—Te(1), 2.551(1), Fe(1)—Te(1), 2.410(2), Mo(1)—C(11), 1.95(2), Mo(1)—C(12), 1.90(1), Mo(1)—C(1m1), 2.14(1), Mo(1)—C(2m1), 2.24(1), Mo(1)—C(3m1), 2.37(1), Mo(1)—C(4m1), 2.33(1), Mo(1)—C(5m1), 2.22(1), Mo(2)—C(21), 1.89(2), Mo(2)—C(22), 1.94(2), Mo(2)—C(1m2), 2.22(1), Mo(2)—C(2m2), 2.34(1), Mo(2)—C(3m2), 2.28(1), Mo(2)—C(4m2), 2.20(1), Mo(2)—C(5m2), 2.12(1), Fe(1)—C(1f1), 1.78(2), Fe(1)—C(2f1), 1.65(2), Fe(1)—C(3f1), 1.74(2).

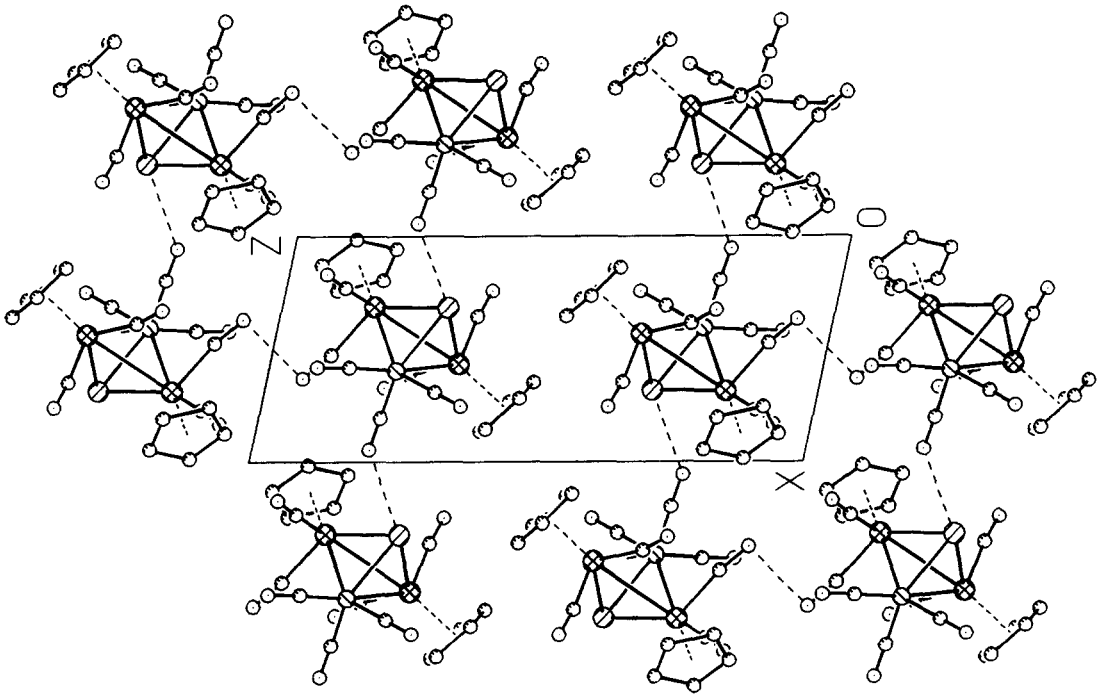


Fig. 2. Crystal packing of **IVb** (view along the *y* axis). Short intermolecular contacts of Te atom are shown by dashed lines.

and selected bond distances are given in the caption of Fig. 1.

In general the molecule of **IVb** seems to be similar to the selenide analogs **IVa** [3] and **Va** [1]. The main difference consists in an unexpected asymmetry of the **IVb** core: the cluster cores of **Va** and **IVa** have almost C_S symmetry [1,3], but the **IVb** core has no mirror plane. The Mo(2)—Te(1) bond length is shorter than Mo(1)—Te(1) by 0.149(1) Å and there is a large difference [0.133(2) Å] in the two Mo—Fe bond lengths.

From our point of view, two reasons are responsible for the core symmetry difference of the telluride clusters from the selenide analogs:

(1) *An asymmetric ligand arrangement of two* Mo atoms. The Cp ligands of Mo(1) and Mo(2) atoms have different orientations relative to the Mo(1)—Mo(2) bond (Fig. 1). This causes some difference in the electronic state of Mo *atoms* and, therefore, the difference in the Mo—Te and Mo—Fe bonding. An analogous asymmetry of the ligand environment takes place in the selenide complexes [1,2,3] also but Te seems to be more "soft" than Se.

(2) *Short non-valence contacts between* Te *and C (intramolecular) and between* Te *and* O *(intermolecular).** It is known that the tellurium atom exhibits a tendency to increase the coordination number by means of this type of contact [8,9]. In the structure of **IVb** the Te atom has only three covalent bonds, but its coordination number is 7 due to four additional nonvalence contacts. The selenium atom exhibits this tendency to a lesser degree. This may explain the core asymmetry of **IVb** and its crystal packing difference from the compounds **IVa** and **Va** (the structures of **IVa** and **Va** are monoclinic, the structure of **IVb** is triclinic).

CONCLUSION

This work and the previous ones [1,2,3] show that the metal substitution in the $[(\mu\text{-H})_2Fe_3(\mu_3\text{-X})(CO)_9]$ (X = Se, Te) clusters is a convenient method of a large-scale heterometal complex preparation.

REFERENCES

1. Konchenko, S. N., Virovets, A. V., Tkachev, S. V., Alekseev, V. I. and Podberezskaya, N. V., *Polyhedron*, 1996, **15**, 1221.
2. Konchenko, S. N., Virovets, A. V., Tkachev, S. V. and Podberezskaya, N. V., *Polyhedron*, 1997, **16**, 707.
3. Konchenko, S. N., Virovets, A. V., Varnek, V. A., Tkachev, S. V., Podberezskaya, N. V. and

*The short contacts are marked by the dashed lines in Figs 1 and 2: Te(1)···C(3f1) of 2.88(1), Te(1)···C(11) of 3.07(1) and Te(1)···C(21) of 3.18(1) Å (Fig. 1); Te(1)···O(2f1) $(1+x,y,z)$ of 3.17(1) A[faAn] (Fig. 2). The sum of van der Waals radii of Te and O is 2.15+1.5 = 3.65 Å, Te and C—2.15+1.7 = 3.85 Å [7].

Maksakov, V. A., *Zh. Strukt. Khim.*, 1996, **37,** 337 (in Russian).
4. Fedotov, M. A., *Yadernyi Magnitnyi Resonans v Rastvorakh Neorganicheskikh Veschestv* (in Russian). Nauka, Novosibirsk, 1986.
5. Sheldrick, G. N., *Acta Cryst.*, 1990, **A46,** 467.
6. Sheldrick, G. M., *Acta Cryst.*, 1993, **A49** (Suppl.), C53.
7. Batsanov, S. S., *Zhurnal Neorganich. Khimii*, 1991, **36,** 3015 (in Russian).
8. Bogan, L. E., Rauchfuss Jr, T. B. and Rheingold, A. L., *J. Am. Chem. Soc.*, 1985, **107,** 3843.
9. Zheng, B., Huang, J. and Lu, Q. Zh. J., *Acta Cryst.*, 1991, **C47,** 1090.

Pergamon

PII: S0277-5387(96)00393-2

Polyhedron Vol. 16, No. 9, pp. 1555–1561, 1997
Copyright © 1997 Elsevier Science Ltd
Printed in Great Britain. All rights reserved
0277-5387/97 $17.00+0.00

A search for the elusive red form in substituted Pt^{II} bipyridine complexes

Sudhir Achar and Vincent J. Catalano*

Department of Chemistry/216, University of Nevada, Reno, Reno, NV 89557, U.S.A.

(Received 17 June 1996; accepted 6 August 1996)

Abstract—An expedient method for the synthesis of $[Pt(bu_2bpy)Cl_2]$, **1**, (bu_2bpy) = 4,4′-di-*tert*-butyl-2,2′-bipyridine, is reported. The X-ray crystal structure determination of the complex **1** revealed that the monomers stack in a head-to-tail fashion with the interplanar separation of 3.7 Å. The platinum centers are 5.643 Å apart and the bipyridine portion of the ligands are *anti* to each other and offset. X-ray crystal structure analyses were performed for the complexes $[PtMe_2(bu_2bpy)]$ (**2**), $[PtMe_2(Me_2bpy)]$ (**3**), (Me_2bpy) = 4,4′-dimethyl-2,2′-bipyridine and $[PtMe_2(bpy)]$ (**4**), (bpy) = 2,2′-bipyridine, and various aspects of these structures are discussed.
© 1997 Elsevier Science Ltd. All rights reserved.

Keywords: Pt stacking, π–π stacking; red form bipyridine.

Bipyridine and phenanthroline complexes of platinum(II) have drawn considerable attention in the past 25 years because of the tendency of the platinum centers to aggregate in the solid state forming linear chains [1]. These resulting stacks often possess very short platinum–platinum separations (< 3.5 Å) resulting in intensely colored absorptions and emissions. Often these complexes are polymorphic and can be classified into three categories, *viz.* monomers that show no metal–metal interaction, linear chains with Pt^{II} centers stacked equidistant along an axis and discrete dimers dominated by short Pt^{II}–Pt^{II} interactions or by strong π–π stacking of the diimine ligands. For example, the dimorphic nature of the complex $[Pt(bpy)Cl_2]$ (bpy = 2,2′-bipyridine) has generated tremendous interest [2]. The monomer form (yellow) can be converted to the linear chain form (red) either by boiling with HCl or by heating it in pyridine [3]. Further, it is generally accepted that it is possible to control the morphology by altering the nature of the substituent on the auxiliary ligands. In an attempt to understand these factors, we have recently begun to investigate sterically encumbered *cis*-chelating diimine ligands coordinated to the Pt^{II} centers. Central to this study is the role of steric factors over electronic factors in determining the stacking motif.

In this paper we wish to report a convenient method for the synthesis of $[Pt(bu_2bpy)Cl_2]$ (**1**), (bu_2bpy) = 4,4′-di-*tert*-butyl-2,2′-bipyridine [4]. Also reported are the unusual solid-state structure of **1** and the previously unreported structures of $[PtMe_2(bu_2bpy)]$ (**2**) $[PtMe_2(Me_2bpy)]$ (**3**) and (Me_2bpy) = 4,4′-di-methyl-2,2′-bipyridine and $[PtMe_2(bpy)]$ (**4**).

EXPERIMENTAL

The ^1H NMR spectrum was recorded employing a General Electric QE 300 spectrometer. Chemical shifts are reported with respect to TMS. The UV–vis spectrum was recorded using a Perkin–Elmer Lambda 11 UV–Vis spectrometer in acetonitrile. The ligand (bu_2bpy) [5] and the complexes $[Pt(SMe_2)_2Cl_2]$ [6], $[PtMe_2(bu_2bpy)]$ [7], $[PtMe_2(Me_2bpy)]$ and $[PtMe_2(bpy)]$ [8] were prepared by literature methods.

$[Pt(bu_2bpy)Cl_2]$ (1)

To a stirred solution of (bu_2bpy) (0.15 g) in chloroform (10 cm^3) was added a solution of $[Pt(SMe_2)_2Cl_2]$ (0.22 g) in chloroform (10 cm^3), and the yellow solution was heated to reflux for 1 h after which the solvent volume reduced to nearly 3 cm^3 by distillation. On standing at room temperature, the product was precipitated as a yellow microcrystalline solid which was filtered, washed with hexane and dried *in vacuo*. Yield 85%. ^1H NMR in $CDCl_3$ (300 MHz): δ 1.46 (s, 18H,

* Author to whom correspondence should be addressed.

tert-butyl hydrogens), 7.48 [d, 2H, $^3J(H^5,H^6) = 6$ Hz, $^4J(H^5,H^{3'}) = 2$ Hz, $H^5,H^{5'}$ of bu_2bpy], 7.89 (s, 2H, $H^3,H^{3'}$ of bu_2bpy), 9.46 [d, 2H, $^3J(H^6,H^5) = 6$ Hz, $^3J(PtH) = 38$ Hz, $H^6,H^{6'}$ of bu_2bpy]. UV–vis λ_{max}: 376 nm.

X-ray structures

Crystals of $[Pt(bu_2bpy)Cl_2]$ were glued on a glass fiber and mounted on a Siemens P4 four-circle goniometer. Unit-cell parameters were determined from automatic machine centering of 46 reflections ($6.86 < 2\theta < 24.96°$) and refined by least-squares methods. Intensities were collected at 293 K with graphite-monochromated Mo-K_α radiation using ω scanning techniques. 3362 total reflections were collected between $1.89 < \theta < 22.5°$ and merged ($R_{int} = 0.054$) to yield 2437 unique reflections. Two check reflections showed only random fluctuations (<1%) during the data collection. The data were corrected for Lorentz and polarization effects. An empirical absorption correction using azimuthal (Ψ) scans of reflections was applied. Crystal data are provided in Table 1.

The structure was solved using direct methods and refined on F^2 using SHELXTL 5.1 [9] computer programs. All nonhydrogens were refined with anisotropic thermal parameters. Hydrogen atoms were added in calculated positions and refined by use of a riding model and fixed isotropic thermal parameters.

Crystals of **2, 3** and **4** were mounted as described above. Unit-cell parameters were determined by machine centering of 24 reflections for **2** ($9.71 < 2\theta < 24.77°$), 27 reflections for **3** ($9.94 < 2\theta < 24.97$) and 37 reflections for **4** ($5.48 < 2\theta < 24.97°$). For **2,** 3457 reflections were collected ($1.89 < \theta < 22.5°$) and merged to yield 2563 unique data ($R_{int} = 0.0410$), and 2534 ($2.18 < \theta < 22.5°$) reflections were collected for **3** and merged to give 1752 unique data ($R_{int} = 0.0303$). 1049 reflections ($1.89 < \theta < 22.5°$) were collected for **4** and merged to give 548 unique data ($R_{int} = 0.0548$). The data were treated as described above, except for **3** which was corrected for absorption using XABS2.

The structures were solved and refined as described above. The final coordinates, complete bond distances and angles, average temperature factor (U_{eq}), and packing diagrams for all compounds are given in the supporting information (34 pages).

RESULTS AND DISCUSSION

The synthesis of $[Pt(bu_2bpy)Cl_2]$ (**1**) was conveniently accomplished in chloroform by the reaction of (bu_2bpy) with $[Pt(SMe_2)_2Cl_2]$. Using low boiling, easily manipulated solvents makes the present method advantageous over earlier methods, and the product is obtained in high yield after only 2 h. The product was readily characterized by ^1H NMR and by single-crystal structure determination. The ^1H NMR spectrum exhibits a single resonance for the *tert*-butyl protons at $\delta = 1.46$ ppm followed by three peaks at the downfield region characteristic of the bipyridyl ring resonances. In addition, the *ortho*-protons ($H^6,H^{6'}$) also show platinum satellites with $^3J(PtH) = 36$ Hz. The assignments are given in the experimental section and are in close agreement with the reported values [10]. The dimethylplatinum(II) complexes $[PtMe_2(bu_2bpy)]$, $[PtMe_2(Me_2bpy)]$ and $[PtMe_2(bpy)]$ were prepared by the reaction of appro-

Table 1. Crystal data

Compound	**1**	**2**	**3**	**4**
Formula	$C_{18}H_{24}Cl_2N_2Pt$	$C_{20}H_{30}N_2Pt$	$C_{14}H_{18}N_2Pt$	$C_{12}H_{14}N_2Pt$
fw	534.38	493.55	409.39	381.34
a (Å)	7.480(1)	7.797(1)	6.908(1)	17.593(3)
b (Å)	19.219(2)	19.396(2)	17.678(2)	9.529(1)
c (Å)	13.044(2)	13.060(1)	11.094(2)	7.177(2)
β (°)	94.93(1)	97.95(1)	97.70(1)	110.84(3)
V (Å^3)	1868.2(4)	1956.1(4)	1342.6(3)	1124.4(3)
Space group	$P2_1/c$	$P2_1/c$	$P2_1/c$	$C2/c$
Z	4	4	4	4
D_{calc} (g cm^{-3})	1.900	1.676	2.025	2.253
Crystal size	$0.14 \times 0.18 \times 0.08$	$0.38 \times 0.18 \times 0.05$	$0.40 \times 0.08 \times 0.06$	$0.42 \times 0.12 \times 0.10$
μ(Mo-K_α) (mm^{-1})	7.797	7.175	10.431	12.446
Radiation (λ, Å)	Graphite-monochromated Mo-K_α (0.71093)	Graphite-monochromated Mo-K_α (0.71093)	Graphite-monochromated Mo-K_α (0.71093)	Graphite-monochromated Mo-K_α (0.71093)
Temperature (K)	293	293	293	293
Transmission factors:	0.957, 0.806	1.0/.633		
R,[a] R_w,[b] [$I > 2\sigma(I)$]	0.0497, 0.0731	0.0432, 0.0665	0.0573, 0.1484	0.0241, 0.0508

[a] $R = \Sigma|F_o - F_c|/\Sigma F_o|$.

[b] $R_w = \{[\Sigma w(F_o - F_c)^2]/[\Sigma w(F_o)^2]\}^{1/2}$.

priate diimine ligands with $[Pt_2Me_4(\mu\text{-}SMe_2)_2]$ according to the reported methods [6,7].

As shown in Fig. 1 the asymmetric unit contains one molecule of $[Pt(bu_2bpy)Cl_2]$. Selected bond distances and angles are listed in Table 2. The platinum center adopts a nearly square-planar geometry with the sum of the Pt containing angles equaling 360.1°. The contraction of N(1)—Pt—N(2) angle at 78.7(5)° from the ideal 90° is typical for *cis*-chelating bipyridines as is the expansion of the Cl(1)—Pt—N(1) [96.1(4)°] and Cl(2)—Pt—N(2) [96.5(4)°] from 90°. However, the *trans* angles show little deviation from linearity with N(1)—Pt—Cl(2) and N(2)—Pt—Cl(1) being nearly equal at 174.8(4) and 174.6(4)°, respectively. The Pt—Cl distances are nearly equal [Pt—Cl(1), 2.293(3); Pt—Cl(2), 2.287(4) Å] as are the Pt—N separations [Pt—N(1), 2.010(12); Pt—N(2) 2.019(10) Å]. These distances are consistent with other Pt^{II}—Cl and Pt^{II}—N separations and are unremarkable.

Excluding the *tert*-butyl group, the molecule is remarkably planar. The average deviation from planarity is only 0.05 Å. The angle between the least squares planes of the two pyridine subunits is only 4.4° and the $PtCl_2$ fragment is canted only by 2.2°. The most remarkable feature of this structure is the intermolecular interactions shown in Fig. 1. The Pt monomers stack in a head to tail fashion with a separation of 3.7 Å between the two planes. In this arrangement the Pt centers are offset and 5.643 Å apart. The bipyridine portion of the ligand are anti to each other and offset. This arrangement is fairly typical since most π-stacking involves groups which are offset from each other to maximize overlap [11]. There is no evidence of hydrogen bonding between the chlorides and the methyl hydrogens of the *tert*-butyl groups. It appears that a second geometry where Pt—Pt stacking predominates is possible. This would only require a translation of the two Pt centers towards each other. However, such an arrangement would eliminate the possibility of any π–π stacking from the bipyridine groups. The present arrangement may offer a higher packing efficiency by placing the *tert*-butyl groups on opposite sides of each other. This factor alone appears to be more important than Pt···Pt aggregation.

Similar results are seen in the solid state structures of **2, 3** and **4**. These structures are depicted in Figs 2, 3 and 4. For **2** the structure is remarkably similar to that of **1**. The Pt—N(1) and Pt—N(2) separations in **2** are slightly longer at 2.092(8) and 2.093(9) Å owing to the larger *trans* influence of Me over Cl. The corresponding N(1)—Pt—N(2) angle is 77.1(4)°. The sum of the angles around Pt in **1** is 360.1°, while in **2** that number is relaxed to 357.2°. Both are very close to the ideal for a square planar center of 360°.

Table 2. Selected bond distances (Å) and angles (°) for **1, 2, 3,** and **4**

		1	
Pt—N(1)	2.010(12)	Pt—N(2)	2.019(10)
Pt—Cl(1)	2.293(3)	Pt—Cl(2)	2.287(4)
N(1)—Pt—N(2)	78.7(5)	Cl(1)—Pt—Cl(2)	88.8(2)
N(1)—Pt—Cl(2)	174.8(4)	N(2)—Pt—Cl(1)	174.6(4)
N(1)—Pt—Cl(1)	96.1(4)	N(2)—Pt—Cl(2)	96.5(4)
Pt···Pt′	5.643		
		2	
Pt—N(1)	2.092(8)	Pt—N(2)	2.093(9)
Pt—C(19)	2.042(12)	Pt—C(20)	2.011(10)
N(1)—Pt—N(2)	77.1(4)	C(19)—Pt—C(20)	85.5(5)
N(1)—Pt—C(20)	175.4(4)	N(2)—Pt—C(19)	173.9(4)
N(1)—Pt—C(19)	98.5(4)	N(2)—Pt—C(20)	99.1(5)
Pt···Pt′	5.873		
		3	
Pt—N(1)	2.098(13)	Pt—N(2)	2.072(13)
Pt—C(1)	2.04(2)	Pt—C(2)	2.03(2)
N(1)—Pt—N(2)	78.2(6)	C(1)—Pt—C(2)	86.8(8)
N(1)—Pt—C(2)	97.2(7)	N(2)—Pt—C(1)	97.9(7)
N(1)—Pt—C(1)	176.0(7)	N(2)—Pt—C(2)	174.2(7)
Pt···Pt′	6.562		
		4	
Pt—N(1)	2.091(10)		
Pt—C(1)	2.021(7)		
N(1)—Pt—N(1)′	77.6(4)	C(1)—Pt—C(1)′	86.4(7)
N(1)—Pt—C(1)	98.0(4)	N(1)—Pt—C(1)′	175.5(4)
Pt···Pt′	5.526		

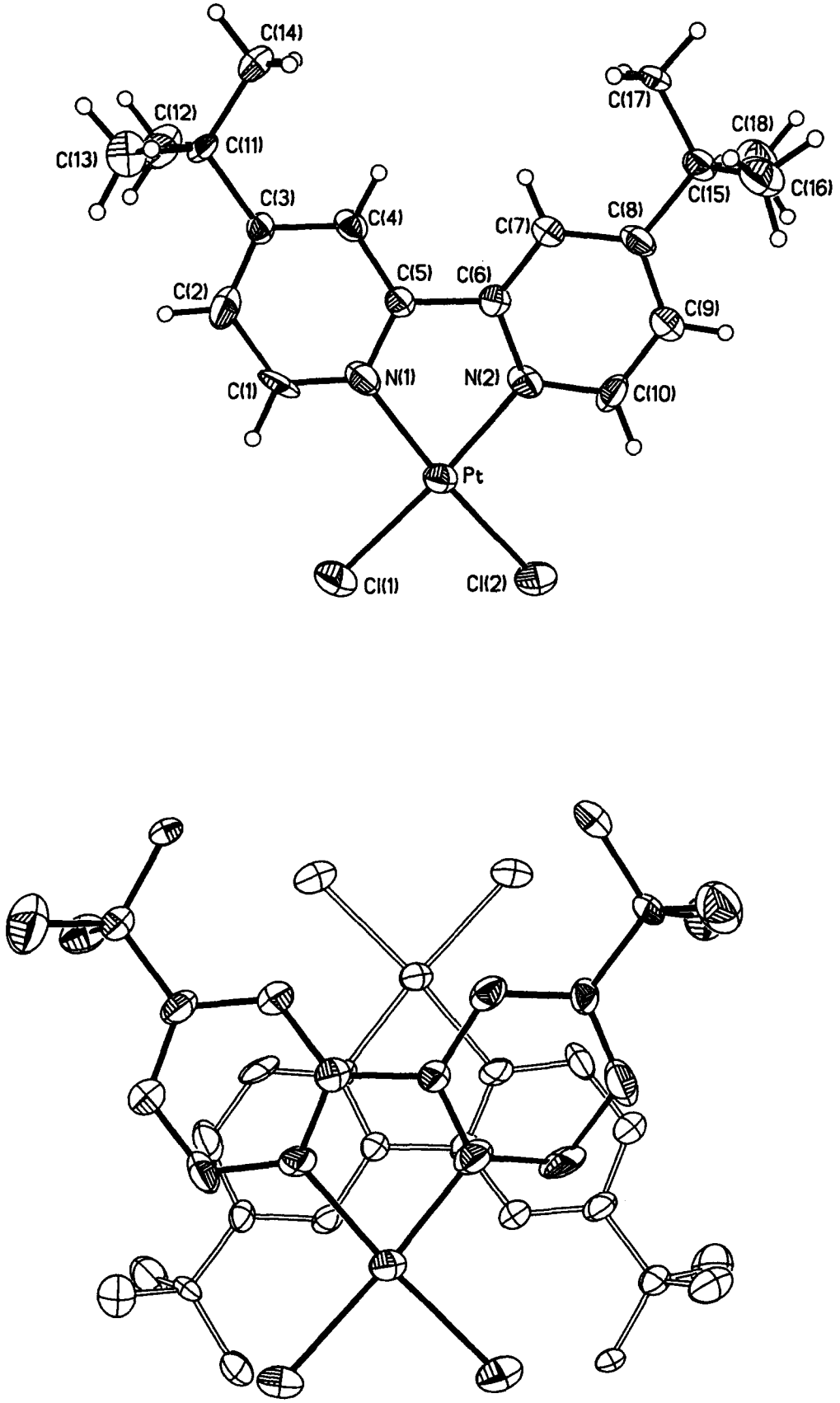


Fig. 1. Thermal ellipsoid (40% probability) drawing of **1** with numbering scheme (top) and plot emphasizing the stacking (bottom).

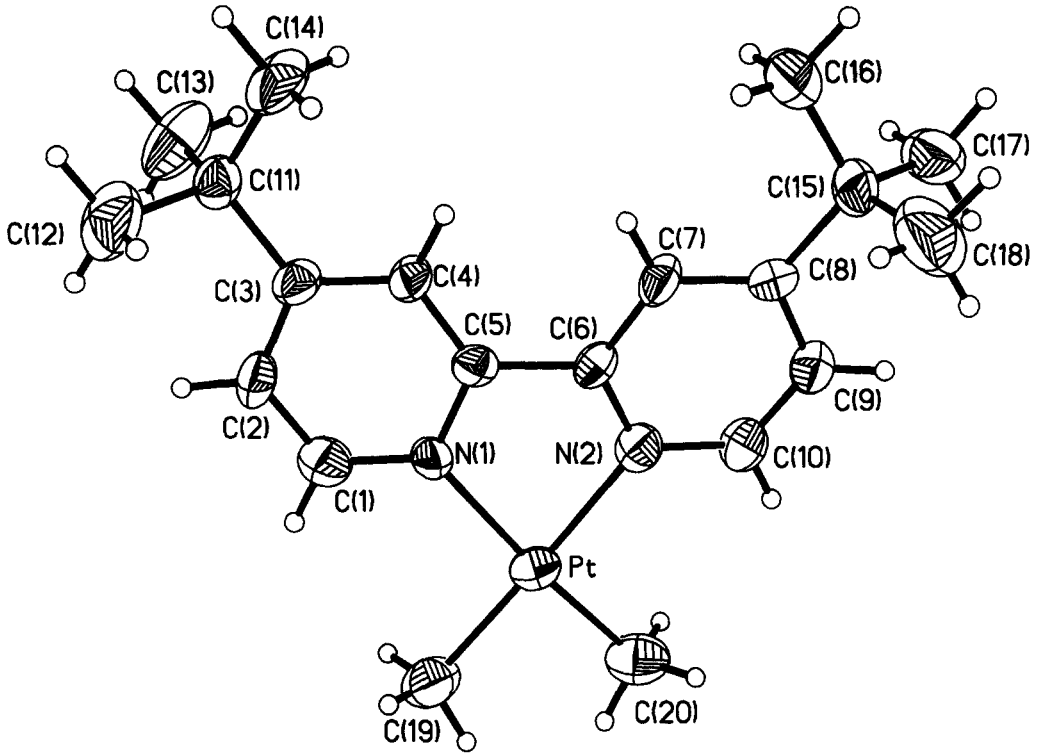


Fig. 2. Thermal ellipsoid (40% probability) drawing of **2** with numbering scheme.

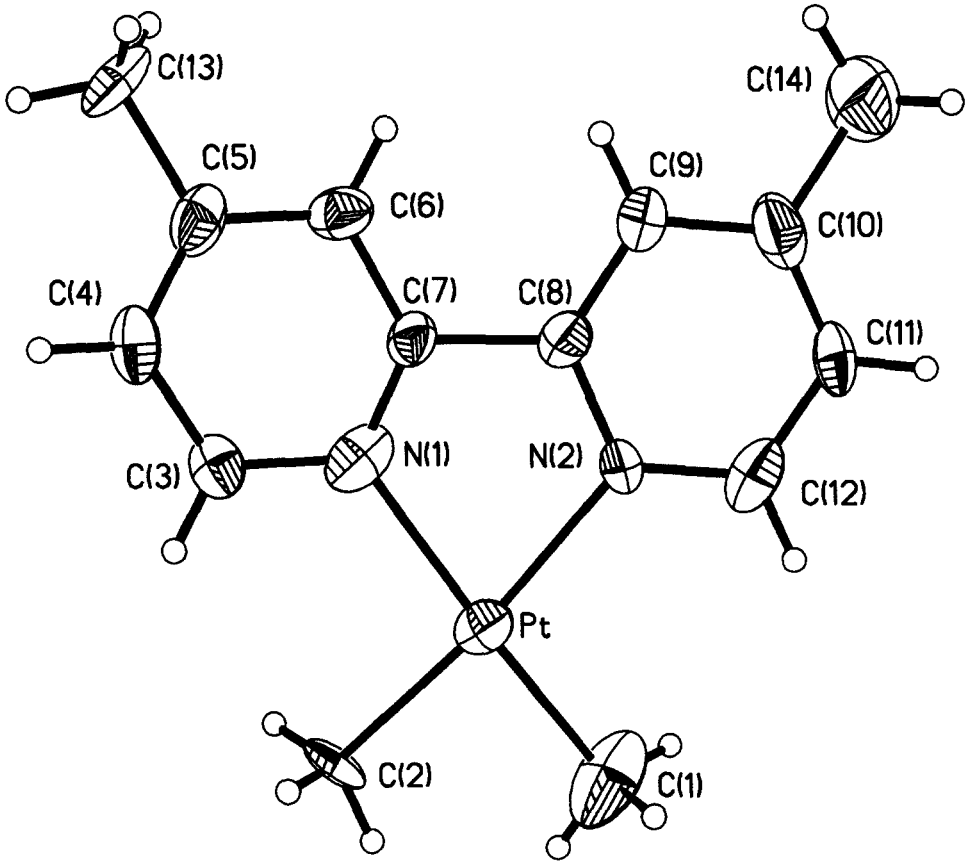


Fig. 3. Thermal ellipsoid (40% probability) drawing of **3** with numbering scheme.

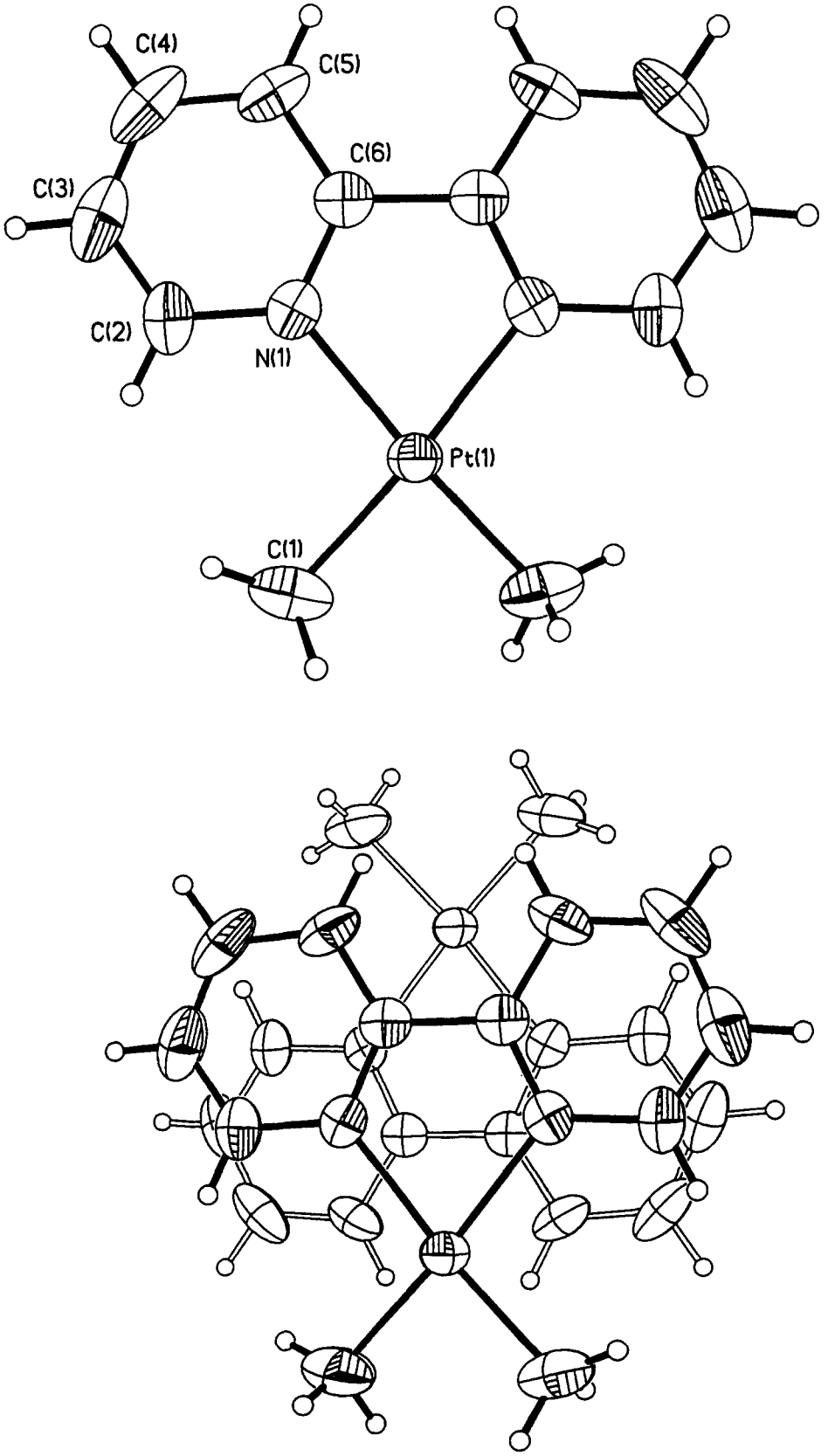


Fig. 4. Thermal ellipsoid (40% probability) drawing of **4** with numbering scheme (top) and plot emphasizing the stacking (bottom).

The structures of **3** and **4** are typical of non-Pt stacked complexes and are remarkable only in their absence of a strong Pt···Pt interaction. The Pt···Pt separations for **3** and **4** are 6.562 and 5.526 Å, respectively. The Pt atom of **4** is situated on a two-fold axis making this structure more rectilinear. Selected bond distances and angles can be found in Table 2. The average interplanar distances for **2, 3** and **4** are 3.7, 3.4 and 3.5 Å, respectively. Clearly the *tert*-butyl groups influence the interplanar separations. Packing diagrams for all compounds are provided in the supporting information.

There was no evidence for formation of the platinum stacked complexes in any of the compounds reported. It is apparent that the elusive red form is very sensitive to even subtle change in ligand sterics and perhaps electronics. $[PtMe_2(bpy)]$ and $[PtMe_2(bu_2bpy)]$ are naturally red from an intense MLCT transition and showed only a single nonstacked morphology [7]. This result is rather surprising since there is very little difference in sterics between **4** and its chloro analog for which the red form is known. From this it appears that electronics must also play a role in the Pt—Pt self association; however, it would seem that the more electron rich Pt center in **4** would be the better candidate for Pt stacking, but none was observed. Attempts to convert the unstacked forms into "red" forms all met with failure.

Acknowledgements—Acknowledgement is made to the donors of the Petroleum Research Fund, administered by the American Chemical Society, for their support of this research and to Johnson Matthey Ltd for their generous loan of platinum salts.

REFERENCES

1. (a) Gliemann, G. and Yersin, H., *Struct. Bonding*, 1985, **62,** 87; (b) Houlding, V. H. and Miskowski, V. M., *Coord. Chem. Rev.* 1991, **111,** 145; (c) Kato, M., Sasano, K., Yamazaki, M., Yano, S. and Kimura, M., *Inorg. Chem.* 1996, **35,** 116; (d) Miskowski, V. M. and Houlding, V. H., *Inorg. Chem.* 1989, **28,** 1529.
2. (a) Osborn, R. S. and Rogers, D., *J. Chem. Soc. Dalton Trans.* 1974, 1004; (b) Herber, R. H., Croft, M., Coyer, M. J., Bilash, B. and Sahiner, A., *Inorg. Chem.* 1994, **33,** 2422.
3. (a) Roulet, R. and Barbey, C., *Helv. Chim. Acta*, 1973, **567,** 2179; (b) Cox, E. G., Saenger, H. and Wardlaw, W., *J. Chem. Soc.* 1934, 182; (c) Morgan, G. T. and Burstall, F. H., *J. Chem. Soc.* 1934, 965.
4. Recently Puddephatt *et al.* have reported the synthesis of $[Pt(bu_2bipy)Br_2]$ by the reaction of $[PtBr_2(SMe_2)_2]$ with (bu_2bipy) in acetone [10].
5. Bager, G. M. and Sasse, W. H. F., *J. Chem. Soc.* 1956, 616.
6. Scott, J. D. and Puddephatt, R. J., *Organometallics*, 1983, **2,** 1643.
7. Achar, S. and Puddephatt, R. J., *Organometallics*, 1993, **12,** 4592.
8. Monaghan, P. K. and Puddephatt, R. J., *Organometallics*, 1984, **3,** 444.
9. Sheldrick, G. M., *Program for Crystal Structure Refinement*. University of Göttingen, Germany, 1993.
10. Levy, C. J., Vittal, J. J. and Puddephatt, R. J., *Organometallics*, 1996, **15,** 2108.
11. Hunter, C. A. and Sanders, J. K. M., *J. Am. Chem. Soc.* 1990, **112,** 5525.

Pergamon

PII: S0277-5387(96)00458-5

Polyhedron Vol. 16, No. 9, pp. 1563–1566, 1997
Copyright © 1997 Elsevier Science Ltd
Printed in Great Britain. All rights reserved
0277–5387/97 $17.00+0.00

COMMUNICATION

A novel $MNOP_3$ metallacycle. Crystal and molecular structure of *cis*-$[PtCl_2\{Ph_2POP(Ph)_2NPPh_2\text{-}P,P'\}]$

Alexandra M. Z. Slawin, Martin B. Smith and J. Derek Woollins*

Department of Chemistry, Loughborough University, Loughborough, Leics, LE11 3TU, U.K.

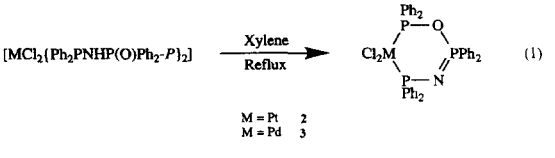
(Received 29 August 1996; accepted 18 September 1996)

Abstract—Thermolysis of *cis*-$[PtCl_2\{Ph_2PNHP(O)Ph_2\text{-}P\}_2]$ (**1**) in refluxing xylene gives *cis*-$[PtCl_2\{Ph_2POP(Ph)_2NPPh_2\text{-}P,P'\}]$ (**2**) containing the first example of an $MNOP_3$ metallacycle. Compound **2** has been characterized by multinuclear NMR spectroscopy (^1H, $^{31}P\text{-}\{^1H\}$ and $^{195}Pt\text{-}\{^1H\}$), IR spectroscopy and X-ray crystallography. The related palladium(II) complex *cis*-$[PdCl_2\{Ph_2POP(Ph)_2NPPh_2\text{-}P,P'\}]$ (**3**) was similarly prepared. © 1997 Elsevier Science Ltd. All rights reserved.

Keywords: metallacycle; synthesis; X-ray structure; mixed P(III)–P(V) ligand.

We recently reported the synthesis of the heterofunctional phosphine $Ph_2PNHP(O)Ph_2$ and described some coordination chemistry of this ligand with various late transition metals [1–3]. In particular we have successfully prepared new five-membered metallacycles of $MN(H)OP_2$ (Type **I**) and $MNOP_2$ (Type **II**) (M = Rh, Ir, Pd and Pt) [1,3] containing the P,O-chelating ligands $Ph_2PNHP(O)Ph_2$ and $[Ph_2PNP(O)Ph_2]^-$, respectively. The $[Ph_2PNP(O)Ph_2]^-$ anion can also behave as a P,O-bridging ligand forming a novel ten-membered $Pd_2N_2O_2P_4$ metallacycle (Type **III**) [2]. Furthermore, we found that refluxing a methanol suspension of *cis*-$[PtCl_2\{Ph_2PNHP(O)Ph_2\text{-}P\}_2]$ (**1**) affords an unsymmetrical complex *cis*-$[PtCl_2\{Ph_2PNHP(O)Ph_2\text{-}P\}(Ph_2POMe)]$ in which one Ph_2P—N bond has been cleaved [4]. Here we describe the first examples of metallacycles of $[MCl_2\{Ph_2POP(Ph)_2NPPh_2\text{-}P,P'\}]$ (M = Pt **2**; Pd **3**) (Type **IV**) of which **2** has been structurally characterized. The coordinated $Ph_2POP(Ph)_2NPPh_2$ ligand is closely related to $[Ph_2PNP(Ph)_2NPPh_2]^-$ (Type **V**) of which only a few examples of transition metal complexes are known [5–7].

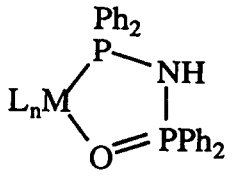
Refluxing a suspension of **1** in xylene for 40 min under nitrogen gave, after recrystallization from CH_2Cl_2/Et_2O, the platinum(II) complex *cis*-$[PtCl_2\{Ph_2POP(Ph)_2NPPh_2\text{-}P,P'\}]$ in 82% yield [Eq. (1)]. Compound **2** has the expected $^{31}P\text{-}\{^1H\}$ NMR spectrum (Fig. 1) together with the other anticipated spectroscopic and analytical data. The $^{31}P\text{-}\{^1H\}$ NMR



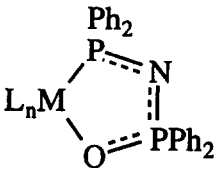
(1)

spectrum is particularly informative and reveals three unique phosphorus environments consistent with an unsymmetrical $Ph_2POP(Ph)_2NPPh_2$ ligand. The high frequency doublet at δ_P 83.5 [^1J(PtP) 4460 Hz] is typical for a metal-ligated phosphinite group [*cf* *cis*-$[PtCl_2(Ph_2POMe)_2]$ δ_P 85.6, ^1J(PtP) 4175 Hz].

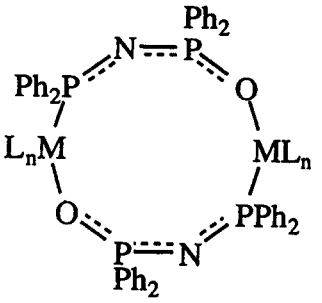
* Author to whom correspondence should be addressed, e-mail: j.d.woollins@lboro.ac.uk.



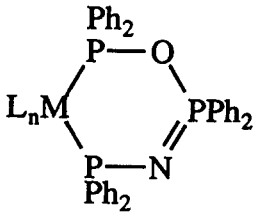
Type I



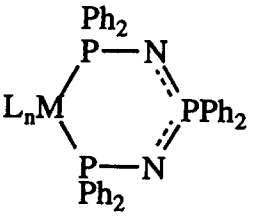
Type II



Type III



Type IV



Type V

Furthermore, the small ^3J(PtP) value of 194 Hz associated with the resonance at δ_P 36.7 is assigned to the central $OP(Ph)_2N$ moiety. A small J(PP) coupling constant is indicative of a mutual *cis* arrangement of phosphorus ligands and is further supported by the presence of two ν(Pt—Cl) stretches at 310 and 279 cm^{-1} in the IR spectrum (KBr disc). Examination of the xylene filtrate by ^{31}P-$\{^1H\}$ NMR revealed a major phosphorus species, which has been identified as the elimination product $Ph_2P(O)NH_2$ as anticipated from this thermal transformation. The corresponding palladium(II) analogue *cis*-$[PdCl_2\{Ph_2POP(Ph)_2NPPh_2$-$P,P'\}]$ (**3**) was synthesized from $[PdCl_2\{Ph_2PNHP(O)Ph_2$-$P\}_2]$ and has the expected spectroscopic data.†

Suitable crystals of **2** were grown by slow diffusion of Et_2O into a $CDCl_3$ solution. The X-ray structure‡ of **2** (Fig. 2) reveals the platinum to be almost perfectly square planar [the Pt atom lies 0.07 Å out of the plane of its substituent atoms]. The ring is puckered slightly and could be described as being "boat-like". The central P(1)—O(3)—N(1)—P(3) atoms are approximately planar [mean deviation 0.10 Å] with the prow and stern Pt(1) and P(2) atoms lying 0.43 and 0.48 Å, respectively, from this mean plane. Although the identity of the O and N atoms cannot be established unequivocally from the X-ray study, the evidence is excellent. A number of refinements with O,O; O,N; N,O and N,N were attempted. The lowest R factor was obtained in the O,N case as shown in

† Compounds **2** and **3** gave satisfactory carbon, hydrogen and nitrogen microanalysis. IR spectra (KBr discs), ^1H, ^{31}P-$\{^1H\}$ and ^{195}Pt-$\{^1H\}$ NMR spectra ($CDCl_3$). Selected spectroscopic data: For **2**: ^{31}P-$\{^1H\}$: δ_P 83.5 [^1J(PtP) 4460 Hz, (—PPh_2O)], 36.7 [^3J(PtP) 194 Hz ($OPPh_2N$)], 18.4 [^1J(PtP) 3506 Hz (—$NPPh_2$)]; ^{195}Pt-$\{^1H\}$: δ_{Pt} −4296; ^1H: δ_H 7.91–7.74, 7.56–7.30 (arom. H); IR: 310, 279 cm^{-1} [ν(Pt—Cl)]. For **3**: ^{31}P-$\{^1H\}$: δ_P 106.5 (—PPh_2O), 45.3 (—$NPPh_2$), 36.2 ($OPPh_2N$), 16, 28 Hz [J(PP)]; ^1H: δ_H 7.98–7.80, 7.53–7.28 (arom. H); IR: 305, 277 cm^{-1} [ν(Pd—Cl)].

‡ Crystal data for compound **2**: $C_{36}H_{30}Cl_2NOP_3Pt$, M = 851.56, monoclinic, space group $P2_1/n$, a = 12.351(2), b = 15.669(1), c = 17.507(2) Å, β = 97.007(10)°, U = 3363 Å^3, Z = 4, T = 293 K, D_c = 1.68 g cm^{-3}, $F(000)$ = 1672, λ = 1.54178 Å, μ(Cu-K_α) 11.0 mm^{-1}. Rigaku AFC 7S diffractometer, ω-scans ($2\theta_{max}$ = 120.1°). Crystal dimensions 0.12 × 0.21 × 0.22 mm^3. Of 5279 unique data, 3380 were observed and corrected for absorption [$I > 3.0\sigma(I)$]. The structure was solved by heavy-atom Patterson methods and refined to give R = 0.042 and R_w = 0.043. The structure was refined anisotropically using teXsan [12]. Atomic coordinates, bond lengths and angles and thermal parameters have been deposited at the Cambridge Crystallographic Data Centre.

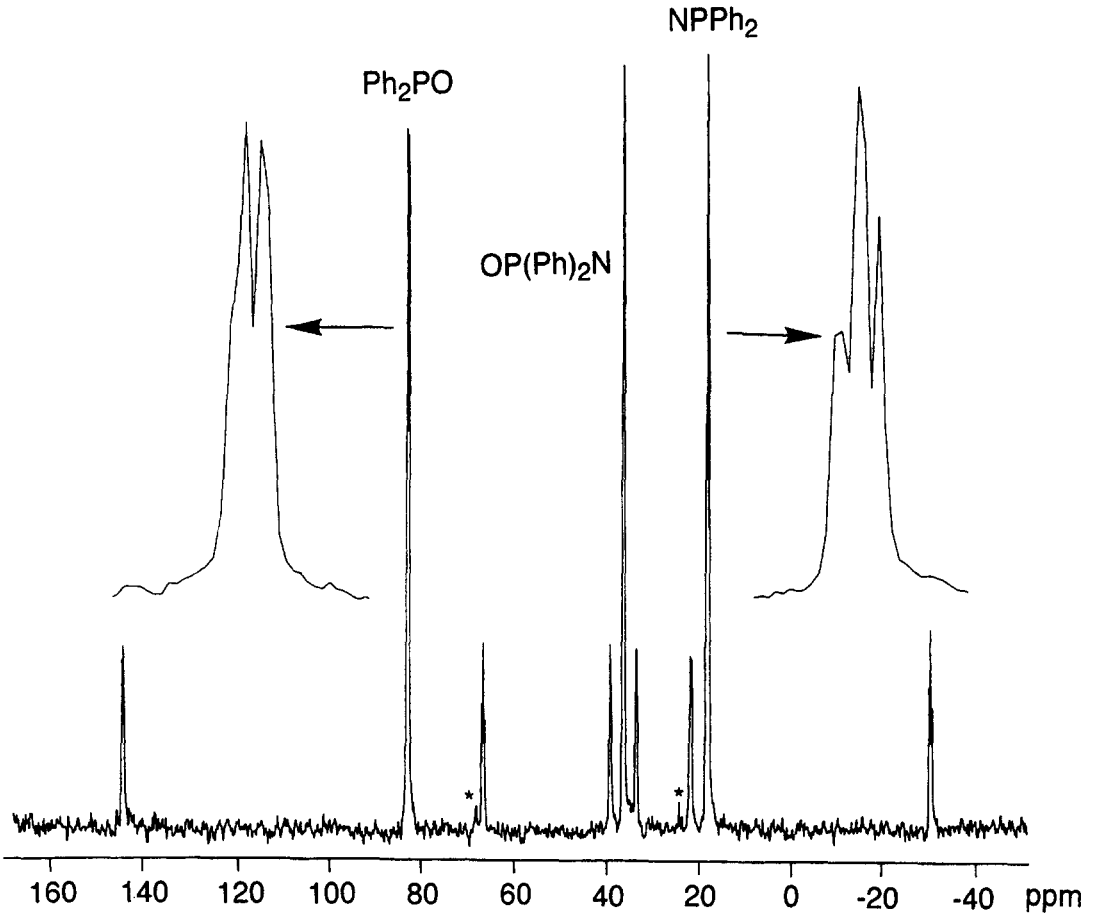
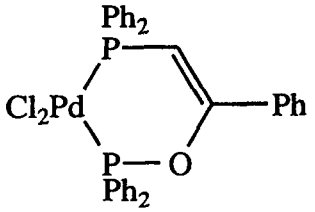


Fig. 1. The $^{31}P-\{^{1}H\}$ NMR spectrum (36.2 MHz) of **2** (*denotes impurity).

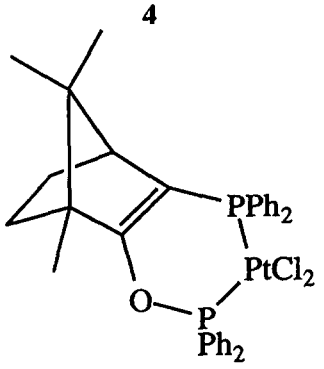
Fig. 2, which is supported by the microanalysis and NMR results. The P—O and P—N bond lengths are statistically indistinguishable, however the P(1)—O(3)—P(2) and P(2)—N(1)—P(3) angles [129.8(4) and 125.5(4)°, respectively] differ markedly. In the structures of $[M\{Ph_2PNP(Ph)_2NPPh_2\text{-}P,P'\}]$ (M = Ni, Pd) [5,6] seven of the eight P—N—P angles lie in the range 122.5(4)–125.2(4)° with one exception of 128.2(4)°. A comparison of equivalent P—N—P and P—O—P angles is not easy but a good example would be $Ph_2P(Se)EP(Se)Ph_2$ [for E = O, 135.8(2); E = NH, 132.3(2)°] [8,9] in which the angle for nitrogen is smaller than that for oxygen, again in agreement with our assignment here. The Pt(1)—P bond lengths are not significantly different but the Pt(1)—Cl bond lengths reflect the difference in *trans* groups with Pt(1)—Cl(2) [2.378(2) Å] being larger than Pt(1)—Cl(1) [2.351(3) Å] illustrating the better π acceptor ability of P(1) as a consequence of its oxygen substituent. Within the $PtNOP_3$ ring there is a substantial degree of localized bonding with the P—O/N bonds at P(2) being appreciably shorter than those at P(1) and P(3). The angles within the ring reflect the puckered geometry. The P(1)—Pt(1)—P(3) angle is slightly enlarged at 95.8(1)° whilst the Pt—P—O/N angles are *ca* 117°. The P(2) centre is close to tetrahedral whilst P(1) and P(3) are quite distorted from ideal geometries. There are no significant intermolecular interactions.

Attempts to liberate $Ph_2POP(Ph)_2NPPh_2$ from **3** with KCN/MeOH were unsuccessful and reflect the instability of this ligand. Several degradation products were identified by $^{31}P-\{^{1}H\}$ NMR spectroscopy, the major products are Ph_2POMe and $Ph_2PNHP(O)Ph_2$.

Palladium(II) and platinum(II) complexes of β-ketophosphines undergo similar transformations to give the phosphine–phosphinite complexes **4** and **5** [10,11]. A possible mechanism for the formation of **2** involves an intramolecular coupling reaction of the two *cis* ligands in **1**. The initial step is Ph_2P—N bond cleavage of one coordinated ligand. The base $[Ph_2P(O)NH]^-$ could rapidly deprotonate the amine of the second $Ph_2PNHP(O)Ph_2$ ligand with concomittant formation of **2** and $Ph_2P(O)NH_2$.



4



5

The M—P—O—P—N—P metallacycle is the first example of a new ring system closely related to the six-membered M—P—N—P—N—P rings of which only a few examples have been documented [5–7]. Further synthetic studies are currently in progress.

Acknowledgements—We are grateful to EPSRC for funding and to Johnson Matthey plc for loans of precious metals.

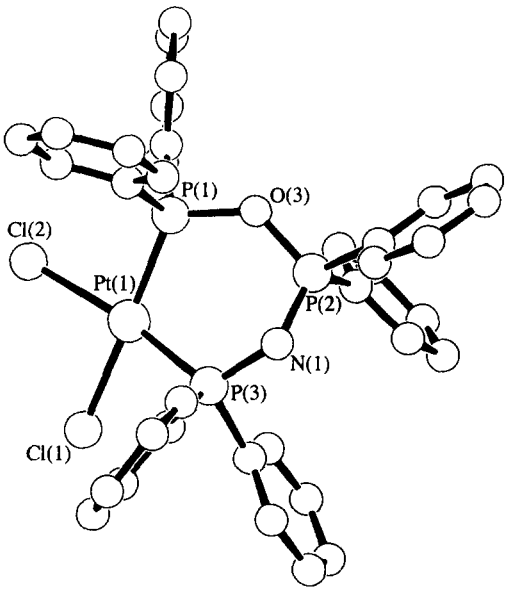


Fig. 2. The X-ray structure of **2**, selected bond lengths (Å) and angles (°): Pt(1)—Cl(1) 2.351(3), Pt(1)—Cl(2) 2.378(2), Pt(1)—P(1) 2.224(3), Pt(1)—P(3) 2.233(3), P(1)—O(3) 1.643(6), P(2)—O(3) 1.573(7), P(2)—N(1) 1.570(7), P(3)—N(1) 1.643(7); Cl(1)—Pt(1)—Cl(2) 88.51(9), Cl(1)—Pt(1)—P(1) 176.94(10), Cl(1)—Pt(1)—P(3) 86.84(9), Cl(2)—Pt(1)—P(1) 89.13(9), Cl(2)—Pt(1)—P(3) 170.5(1), P(1)—Pt(1)—P(3) 95.77(9), Pt(1)—P(1)—O(3) 116.9(3), O(3)—P(2)—N(1) 112.4(4), Pt(1)—P(3)—N(1) 117.5(3), P(1)—O(3)—P(2) 129.8(4), P(2)—N(1)—P(3) 125.5(4).

REFERENCES

1. Slawin, A. M. Z., Smith, M. B. and Woollins, J. D., *J. Chem. Soc., Dalton Trans.*, 1996, 1283.
2. Slawin, A. M. Z., Smith, M. B. and Woollins, J. D., *Polyhedron*, 1996, **15**, 1579.
3. Bhattacharyya, P., Slawin, A. M. Z., Smith, M. B. and Woollins, J. D., *Inorg. Chem.*, 1996, **35**, 3675.
4. Slawin, A. M. Z., Smith, M. B. and Woollins, J. D., *J. Chem. Soc., Dalton Trans.*, in press.
5. Ellermann, J., Sutter, J., Knoch, F. A. and Moll, M., *Angew. Chem., Int. Ed. Engl.*, 1993, **32**, 700.
6. Ellermann, J., Sutter, J., Schelle, C., Knoch, F. A. and Moll, M., *Z. Anorg. Allg. Chem.*, 1993, **619**, 2006.
7. Slawin, A. M. Z., Smith, M. B. and Woollins, J. D., *J. Chem. Soc., Chem. Commun.*, 1996, 2095.
8. Pilkington, M. J., Slawin, A. M. Z., Williams, D. J. and Woollins, J. D., *Main Group Chem.*, 1995, **1**, 145.
9. Bhattacharyya, P., Novosad, J., Phillips, J., Slawin, A. M. Z., Williams, D. J. and Woollins, J. D., *J. Chem. Soc., Dalton Trans.*, 1995, 1607.
10. Bouaoud, S.-E., Braunstein, P., Grandjean, D., Matt, D. and Nobel, D., *Inorg. Chem.*, 1986, **25**, 3765.
11. Knight, D. A., Cole-Hamilton, D. J. and Cupertino, D. C., *J. Chem. Soc., Dalton Trans.*, 1990, 3051.
12. TeXsan, Crystal Structure Analysis Package, Molecular Structure Corporation, Woodlands, TX, 1985, 1992.

Pergamon

PII: S0277-5387(96)00457-3

Polyhedron Vol. 16, No. 9, pp. 1567–1571, 1997
Copyright © 1997 Elsevier Science Ltd
Printed in Great Britain. All rights reserved
0277-5387/97 $17.00+0.00

COMMUNICATION

Dinuclear and tetranuclear oxo-bridged iron(III) complexes of the ambidentate ligand 3-(2-pyridyl)-pyrazole

Peter L. Jones, John C. Jeffery, Jon A. McCleverty* and Michael D. Ward*

School of Chemistry, University of Bristol, Cantock's Close, Bristol BS8 1TS, U.K.

(Received 20 August 1996; accepted 18 September 1996)

Abstract—The crystal structures of $[Fe_4^{III}(HL)_2(L)_6(\mu\text{-}O)_2[PF_6]_2\cdot 4MeCN$ (**1**·4MeCN) and $[Fe_2^{III}(HL)_4(OSO_3)_2(\mu\text{-}O)]\cdot 2MeOH\cdot 3H_2O$ (**2**·MeOH·$3H_2O$) have been determined [HL is the ambidentate, potentially terdentate ligand 3-(2-pyridyl)-pyrazole]: complex **2** is a conventional μ-oxo-diiron(III) complex in which HL acts as a bidentate chelate and the sulfate ligands are monodentate, but **1** is effectively a dimer containing two μ-oxo-diiron(III) cores linked by deprotonated ligands L^- which are bridging *via* the two N atoms of the pyrazolate rings. © 1997 Elsevier Science Ltd. All rights reserved.

Keywords: iron–oxo complexes; pyrazolate bridge; polynuclear complexes; crystal structures.

As part of our recent studies on the hexadentate podand ligand tris[{3-(2-pyridyl)-pyrazol-1-yl}hydroborate] (Tp^{Py}) [1, 2], which contains three *N,N'*-bidentate chelating arms linked by an apical boron atom, we observed formation of unusual tetrameric complexes $[M_4^{II}(Tp^{Py})_4]^{4+}$ with first-row transition metal dications (Mn, Fe, Co, Ni, Zn) [2]. Of these the Mn^{II} and Zn^{II} complexes have been crystallographically characterized. Whilst attempting to crystallize the Fe^{II} complex of this series we have observed formation of an unusual tetranuclear Fe^{III} complex **1**, arising from decomposition of the parent Tp^{Py} ligand with concomitant liberation of 3-(2-pyridyl)-pyrazole (HL). HL has been known for a while to be able to act as a simple bidentate chelate in mononuclear, octahedral iron(II) and nickel(II) complexes [3]. There is also the possibility of it being able to act as a terdentate bridging ligand *via* deprotonation of the pyrazolyl NH group and coordination of the pyrazolyl N^1 atom to a second metal ion. This coordination mode for L^- has not been observed until now, although pyrazolate anions are well known to be able to act as bis-monodentate bridges in other contexts [4].

Reaction of $K(Tp^{Py})$ with $FeSO_4\cdot 7H_2O$ in methanol (1 : 1 ratio) followed by precipitation of the complex with KPF_6 afforded a yellow solid†. Electrospray mass spectrometry indicated that it was the desired tetramer $[Fe_4^{II}(Ty^{Py})_4][PF_6]_4$, and an IR spectrum showed the characteristic $\nu_{B\text{-}H}$ band at *ca* 2450 cm^{-1}, con-

* Authors to whom correspondence should be addressed.

† *Preparations*. **1**: A mixture of KTp^{Py} (0.24 g, 0.5 mmol) and $FeSO_4\cdot 7H_2O$ (0.14 g, 0.5 mmol) in MeOH (20 cm^3) was stirred at room temperature to afford a yellow solution. Addition of excess aqueous KPF_6 afforded a yellow precipitate of $[Fe_4^{II}(Tp^{Py})_4][PF_6]_4$ which was filtered off, washed with water and dried *in vacuo*. Slow recrystallization by diffusion of diethyl ether vapour into an MeCN solution of the complex afforded brown crystalline blocks of **1**·4MeCN in 30% yield (based on Fe). FABMS: $m/z = 1555$ $\{M-PF_6^-\}$, 1410 $\{M-2PF_6^-\}$, 1264 $\{M-2PF_6^- - L\}$, 1120 $\{M-2PF_6^- - 2HL\}$, 976 $\{M-2PF_6^- - 2HL-L^-\}$.

2: Addition of a solution of HL (0.29 g, 2.0 mmol) in MeOH (20 cm^3) to a solution of $FeSO_4\cdot 7H_2O$ (0.25 g, 0.9 mmol) in MeOH (20 cm^3) immediately afforded a yellow precipitate. The suspension was stirred for 30 minutes in air, then the solid was filtered off, washed with methanol and dried *in vacuo*. Yield based on Fe: 85%. Recrystallization from $MeOH/H_2O$ afforded X-ray quality crystals. FABMS: $m/z = 924$ $\{M+Na^+\}$, 698 $\{M-Fe-HL\}$, 345 $\{Fe(HL)_2\}$.

Both complexes gave satisfactory elemental analyses. Unambiguous assignment of the asymmetric Fe—O—Fe stretch in the IR spectrum was not possible owing to the large number of other bands in the expected region (*ca* 770–850 cm^{-1}; ref. [7]).

firming that the Tp^{Py} ligand was intact. Recrystallization from MeCN diethyl ether (in air) over several days afforded brown crystals, which on X-ray analysis, were shown to be $[Fe_4^{III}(HL)_2(L)_6(\mu\text{-}O)_2][PF_6]_2\cdot 4MeCN$ (**1**·4MeCN)‡. Mass spectroscopic and analytical characterization of these crystals was in agreement with the crystal structure‡: also, the $\nu_{B\ H}$ band had disappeared from the IR spectrum.

The centrosymmetric complex cation of **1** is depicted in Figs 1 and 2, and has many unusual features. Each metal centre is coordinated by the bidentate pocket of two ligands L (pyridyl N and pyrazolyl N^2), one pyrazolate N^1 atom which acts as a bridge from an adjacent metal and an oxo ligand which acts as a bridge to a different metal, giving a pseudo-octahedral N_5O coordination sphere. The four bridging ligands, L^-, are all terdentate and deprotonated. The remaining four bidentate ligands, one on each metal ion, form two hydrogen-bonded pairs [Fig. 2a]. The separation between N(11) and N(71) [also N(11A) and N(71A)] is 2.78 Å, which is far too short for there to be two N—H bonds. Instead this short N···N separation is consistent with a weak N—H···N hydrogen bond between deprotonated (anionic) and protonated (neutral) pyrazole rings [5]. This was confirmed by the location of *two* very small, closely spaced peaks between N(11) and N(71) in the final Fourier difference map, consistent with the proton being disordered over two positions N—H···N and N···H—N. The formulation of **1** is therefore $[Fe_4(HL)_2(L)_6(\mu\text{-}O)_2][PF_6]_2$, which means that the metal ions must have a combined charge of +12, i.e. four Fe^{III} centres. This oxidation state assignment is confirmed by inspection of the Fe—O distances, which are all 1.77 Å: in contrast, the only structurally characterized $Fe^{II}(\mu\text{-}O)Fe^{III}$ complex has Fe—O distances of 1.999 and 2.069 Å [6]. The structural parameters of the metal–oxo core are in fact entirely typical of high-spin dinuclear Fe^{III} complexes linked by a single oxo bridge [7]. Aromatic π-stacking interactions between overlapping ligand segments are apparent, with inter-ring separations in the range 3.3–4 Å (Fig. 2b). This complex therefore provides an interesting example of a self-assembly process in which aromatic π-stacking and hydrogen bonding interactions, in addition to the normal metal–ligand bonding, contribute to the structure: the ability of L^- to be either bidentate and mononucleating, or terdentate and dinucleating, is also significant.

We attempted to prepare **1** deliberately by reaction of HL with $FeSO_4\cdot 7H_2O$ in methanol†. This afforded a yellow solid in good yield, but its spectroscopic data were not consistent with formation of **1** and accordingly its crystal structure was also determined (Fig. 3)‡. The product of this reaction was shown to be $[Fe_2^{III}(HL)_4(OSO_3)_2(\mu\text{-}O)]$ (**2**), which crystallized as **2**·2MeOH·$3H_2O$. The complex lies on a C_2 axis which passes through the oxo bridge [O(10)]. The two ligands HL on each iron(III) centre are simple bidentate chelates with protons attached to the non-coordinated pyrazolyl N^1 atoms. The structural parameters of the metal–oxo core are again entirely typical of high-spin dinuclear Fe^{III} complexes linked by a single oxo bridge [7]. There is again an aromatic π stacking interaction between two of the HL ligands, which are near-parallel and overlapping with separations of 3.2–3.6 Å from the atoms in one ligand to the mean plane of the other. The most unusual feature of this complex is that the sixth coordination site of each metal is occupied by a monodentate sulfate ion, which is to our knowledge the first time this has been observed in an oxo-bridged diferric complex. The only other structurally characterized $Fe_2^{III}(\mu\text{-}O)$ complex containing sulfate ligands is $[\{(Me_3tacn)Fe\}_2(\mu\text{-}O)(\mu\text{-}1,3\text{-}SO_4)_2]$ (Me_3tacn = *N*,*N*′,*N*″-trimethyl-1,4,7-triazacyclononane) in which the two sulfate ions bridge the iron centres [8]; similarly, $[\{Fe(NN)_2\}_2(\mu\text{-}O)(SO_4)_2]$ (NN = 2,2′-bipyridine or 1,10-phenanthroline) were proposed to have one sulfate ion bridging the two metal centres and one free sulfate, on the basis of their IR spectra [9]. Complex **2** is therefore a typical oxo-bridged diferric complex [7], albeit slightly unusual in having monodentate sulfate ligands.

‡ *Crystal data.* **1**·4MeCN: $C_{72}H_{62}F_{12}Fe_4N_{28}O_2P_2$, M = 1864.8, brown blocks, crystal size 0.8 × 0.5 × 0.3 mm³; triclinic, space group $P\bar{1}$; a = 10.101(3), b = 13.769(3), c = 16.227(5) Å; α = 96.51(2), β = 94.06(2), γ = 105.58(2)°; U = 2147.7(11) Å³; Z = 1; D_c = 1.442 g cm⁻³; $F(000)$ = 948; μ(Mo-$K\alpha$) = 0.786 mm⁻¹. The crystal was mounted in a sealed glass capillary tube with some of the mother liquor present to prevent solvent loss. 8410 data were collected with $2\theta_{max}$ = 46.5° at 293 K using a Siemens SMART diffractometer (Mo-$K\alpha$ radiation, graphite monochromator, λ = 0.71073 Å); after merging these gave 5971 unique data with R_{int} = 0.039.

2·2MeOH·$3H_2O$: $C_{34}H_{42}Fe_2N_{12}O_{14}S_2$, M = 1018.6, yellow blocks, crystal size 0.45 × 0.40 × 0.25 mm³; monoclinic, space group $C2/c$; a = 12.533(3), b = 19.612(2), c = 18.956(3) Å; β = 108.03(1)°; U = 4450.1(11) Å³; Z = 4; D_c = 1.520 mm⁻¹. The crystal was mounted in a sealed glass capillary tube with some of the mother liquor present to prevent solvent loss. 10,552 data were collected with $2\theta_{max}$ = 50° at 293 K using a Siemens SMART diffractometer (Mo-$K\alpha$ radiation, graphite monochromator, λ = 0.71073 Å); after merging these gave 3921 unique data with R_{int} = 0.052.

Both structures were solved by direct methods and refined on all F^2 data using the SHELX suite of programs [11]. All non-hydrogen atoms were refined with anisotropic thermal parameters; hydrogen atoms were included in calculated positions with isotropic thermal parameters. For **1**·4MeCN, refinement of 543 parameters converged at R_1 = 0.065, wR_2 = 0.190. The tetranuclear complex is centrosymmetric so each asymmetric unit contains half of the complex (two independent metal atoms) as well as one hexafluorophosphate anion and two molecules of MeCN. For **2**·2MeOH·$3H_2O$, refinement of 304 parameters converged at R_1 = 0.039, wR_2 = 0.111. The dinuclear complex lies on a C_2 axis so each asymmetric unit contains half of the complex (one independent metal atom) as well as one methanol molecule and 1.5 water molecules (of which the half molecule lies on the C_2 axis).

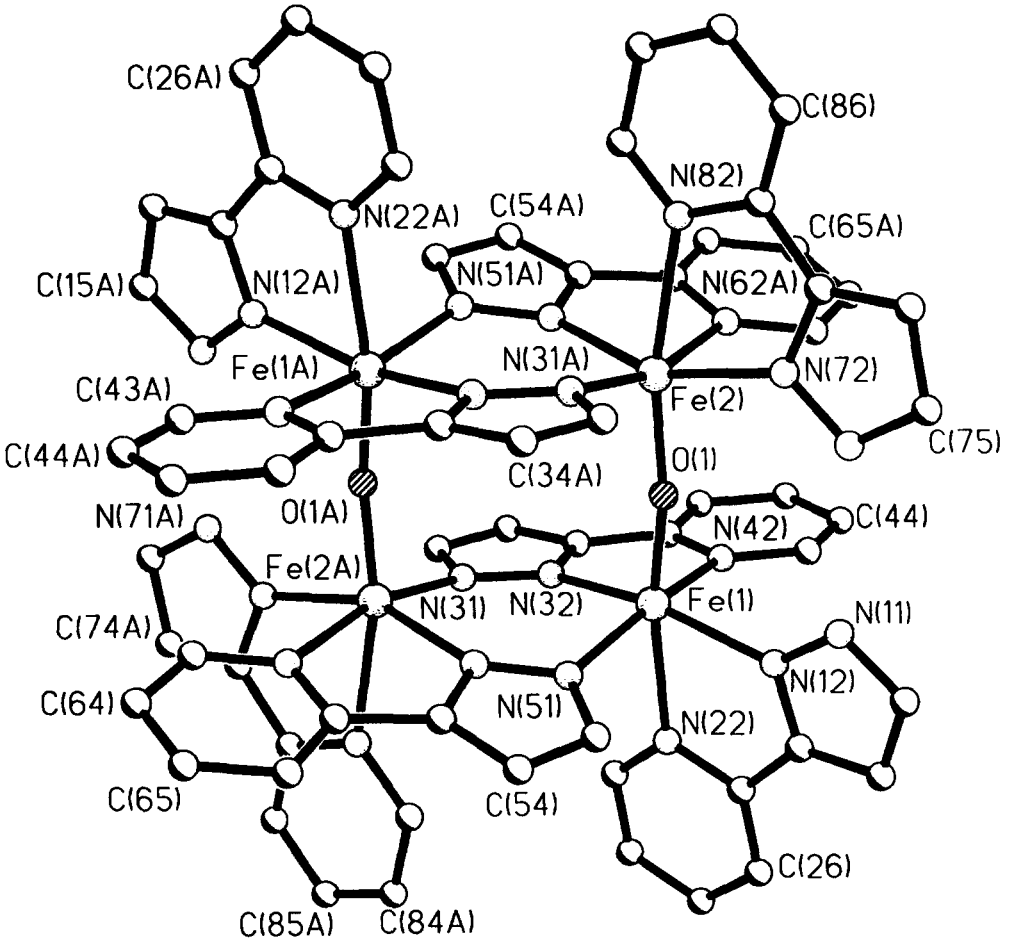


Fig. 1. Crystal structure of the dication of **1**. Selected bond lengths (Å) and angles (°): Fe(1)—O(1) 1.770(3), Fe(1)—N(12) 2.067(4), Fe(1)—N(32) 2.103(4), Fe(1)—N(51) 2.107(4), Fe(1)—N(42) 2.208(5), Fe(1)—N(22) 2.329(4), Fe(2)—O(1) 1.770(3), Fe(2)—N(31A) 2.096(4), Fe(2)—N(72) 2.094(5), Fe(2)—N(52A) 2.099(4), Fe(2)—N(62A) 2.204(5), Fe(2)—N(82) 2.339(5), Fe(1)...Fe(2) 3.517, Fe(1)...Fe(2A) 4.091; N(12)—Fe(1)—N(22) 73.7(2), N(32)—Fe(1)—N(42) 75.9(2), O(1)—Fe(1)—N(22) 169.6(2), O(1)—Fe(1)—N(12) 96.8(2), O(1)—Fe(1)—N(42) 94.4(2), O(1)—Fe(1)—N(32) 101.3(2), O(1)—Fe(1)—N(51) 99.4(2), N(72)—Fe(2)—N(82) 72.5(2), N(52A)—Fe(2)—N(62A) 76.0(2), O(1)—Fe(2)—N(82) 167.2(2), O(1)—Fe(2)—N(72) 94.9(2), O(1)—Fe(2)—N(62A) 95.7(2), O(1)—Fe(2)—N(52A) 106.0(2), O(1)—Fe(2)—N(31A) 98.1(2), Fe(1)—O(1)—Fe(2) 166.8(2).

We tried further to prepare **1** from direct reaction of HL with other iron salts not containing strongly coordinating anions, but without success: so far the only reliable preparation of **1** is by decomposition of $[Fe_4^{II}(Tp^{Py})_4][PF_6]_4$ in air during crystallization. Complex **2** may be considered as half of complex **1**, derived by breaking the bonds between the metal ions and the pyrazolate N^1 atoms, and filling the gaps with monodentate sulfate ligands: alternatively **1** is a dimer of **2**, derived from removal of the sulfate ligands and then allowing the vacancy at each metal site to be filled by a deprotonated bridging pyrazole from one of the ligands on an adjacent metal centre.

These complexes are of interest owing to their possible relevance as models for the active sites of non-heme iron proteins, which are widespread in nature [10]. Very many model complexes have been prepared that mimic the active sites of these metalloproteins, which has resulted in a very thorough understanding of the spectroscopic, electronic and magnetic properties of complexes containing the $Fe_2^{III}(\mu\text{-O})$ core [7]. We are attempting to prepare **1** in larger amounts because its magnetic properties are potentially interesting, with two oxo bridges and two pyrazolate bridges—both of which are known to be highly effective at mediating magnetic exchange interactions—linking the four Fe^{III} centres.

Acknowledgement—We thank Unilever Research and EPSRC for financial support.

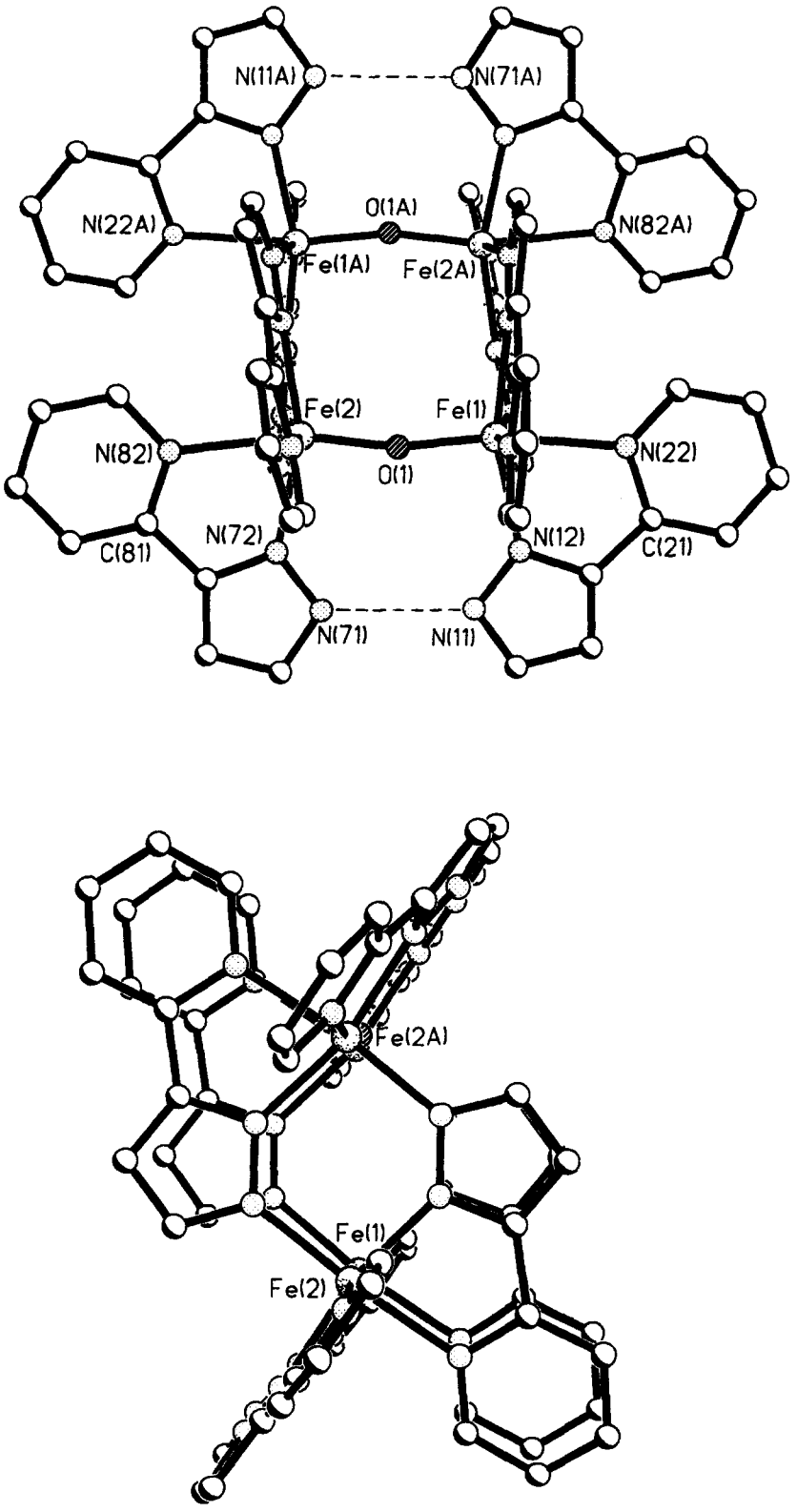


Fig. 2. Two alternative views of **1**, showing (a) the peripheral hydrogen bonding, and (b) the aromatic π stacking.

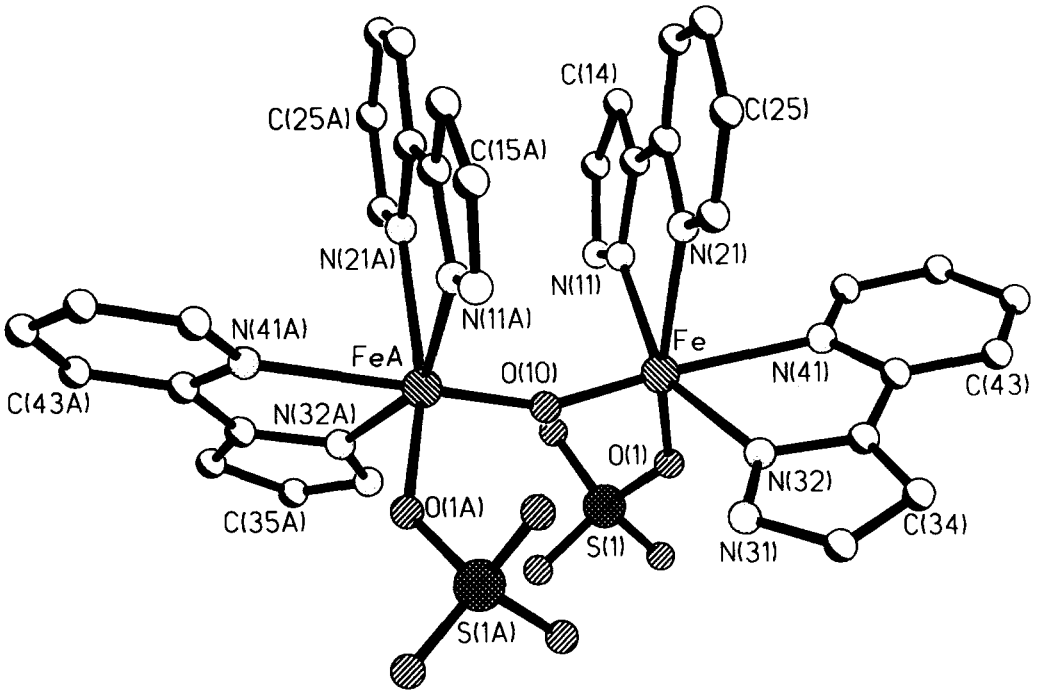


Fig. 3. Crystal structure of **2**. Selected bond lengths (Å) and angles (°): Fe—O(10) 1.7903(7), Fe—O(1) 1.973(2), Fe—N(32) 2.102(2), Fe—N(12) 2.125(2), Fe—N(21) 2.243(3), Fe—N(41) 2.312(3), Fe···Fe(A) 3.513; O(10)—Fe—O(1) 104.14(10), O(10)—Fe—N(32) 95.83(8), O(10)—Fe—N(12) 103.75(9), O(10)—Fe—N(21) 94.55(10), O(10)—Fe—N(41) 167.38(7), N(32)—Fe—N(41) 72.62(10), N(12)—Fe—N(21) 73.46(10), Fe—O(10)—Fe(A) 157.8(2).

REFERENCES

1. Amoroso, A. J., Cargill Thompson, A. M. W., Jeffery, J. C., Jones, P. L., McCleverty, J. A. and Ward, M. D., *J. Chem. Soc., Chem. Commun.*, 1994, 2751; Amoroso, A. J., Jeffery, J. C., Jones, P. L, McCleverty, J. A., Psillakis, E. and Ward, M. D., *J. Chem. Soc., Chem. Commun.*, 1995, 1175; Amoroso, A. J., Jeffery, J. C., Jones, P. L., McCleverty, J. A., Rees, L., Rheingold, A. L., Sun, Y., Takats, J., Trofimenko, S., Ward, M. D. and Yap, G. P. A., *J. Chem. Soc., Chem. Commun.*, 1995, 1881; Amoroso, A. J., Jeffery, J. C., Jones, P. L., McCleverty, J. A. and Ward, M. D., *Polyhedron*, 1996, **15,** 2023; Bardwell, D. A., Jeffery, J. C., Jones, P. L., McCleverty, J. A. and Ward, M. D., *J. Chem. Soc., Dalton Trans.*, 1995, 2921; Jones, P. L., Amoroso, A. J., Jeffery, J. C., McCleverty, J. A., Psillakis, E., Rees, L. and Ward, M. D., *Inorg. Chem.*, in press.
2. Amoroso, A. J., Jeffery, J. C., Jones, P. L., McCleverty, J. A., Thornton, P. and Ward, M. D., *Angew. Chem., Int. Ed. Engl.*, 1995, **34,** 1443.
3. Sugiyarto, K. H. and Goodwin, H. A., *Aust. J. Chem.*, 1988, **41,** 1645.
4. Some representative recent examples: Pinillos, M. T., Elduque, A., Martín, E., Navarro, N., Lahoz, F. J., López, J. A. and Oro, L. A., *Inorg. Chem.*, 1995, **34,** 111: Ehlert, M. K., Rettig, S. J., Storr, A., Thompson, R. C. and Trotter, J., *Inorg. Chem.*, 1993, **32,** 5176; Ehlert, M. K., Rettig, S. J., Storr, A., Thompson, R. C. and Trotter, J., *Acta Cryst.*, 1994, **C50,** 1023; Maekawa, M., Munakata, M., Kuroda, T. and Nozaka, Y., *Inorg. Chim. Acta*, 1993, **208,** 243; Carmona, D., Lamata, M. P., Ferrer, J., Modrego, J., Perales, M., Lahoz, F. J., Atencio, R. and Oro, L. A., *J. Chem. Soc., Chem. Commun.*, 1994, 575.
5. Novak, A., *Struct. Bonding (Berlin)*, 1974, **18,** 177.
6. Arena, F., Floriani, C., Chiesi-Villa, A. and Guastini, C., *J. Chem. Soc., Chem. Commun.*, 1986, 1369.
7. Kurtz, D. M., *Chem. Rev.*, 1990, **90,** 585.
8. Wieghardt, K., Drüeke, S., Chaudhuri, P., Flörke, U., Haupt, H.-J., Nuber, B. and Weiss, J., *Z. Naturforsch.*, 1989, **B44,** 1093.
9. Jezowska-Trzebiatowska, B., Ozarowski, A., Kozlowski, H., Cukierda, T. and Hanuza, J., *J. Inorg. Nucl. Chem.*, 1976, **38,** 1447.
10. Stenkamp, R. E., *Chem. Rev.*, 1994, **94,** 715; Rosenzweig, A. C., Frederick, C. A., Lippard, S. J. and Nordlund, P., 1993, **366,** 537; Lippard, S. J., *Angew. Chem., Int. Ed. Engl.*, 1988, **17,** 344; Doi, K., Antanaitis, B. C. and Aisen, P., *Struct. Bonding (Berlin)*, 1988, **70,** 1.
11. SHELXTL 5.03 Program System: Siemens Analytical X-Ray Instruments, Madison, WI, USA, 1995.

Pergamon

PII: S0277-5387(96)00444-5

Polyhedron Vol. 16, No. 9, pp. 1573–1576, 1997
Copyright © 1997 Elsevier Science Ltd
Printed in Great Britain. All rights reserved
0277-5387/97 $17.00+0.00

COMMUNICATION

Observations on the constitution of some "dithiocarbamato-bridged heterobimetallic complexes"

George Exarchos and Stephen D. Robinson*

Department of Chemistry, King's College London, Strand, London WC2R 2LS, U.K.

(Received 21 August 1996; accepted 3 September 1996)

Abstract—Some dithiocarbamato-bridged heterobimetallic complexes $[M'\{M(S_2CNR_2)_3\}_2]$ and $[\{M'M(S_2CNR_2)_4\}_n]$, obtained by successive addition of stoichiometric amounts of bivalent metal salts MX_2 (M = Zn, Cd or Hg) and $M'Y_2$ (M′ = VO, Mn, Fe, Co, Ni, Cu or Zn) to a solution of a sodium dithiocarbamate, are reformulated as mixtures of homonuclear complexes involving, in some instances (M′ = Mn, Fe or Co), trivalent $[M'(S_2CNR_2)_3]$ species. © 1997 Elsevier Science Ltd. All rights reserved.

Keywords: dithiocarbamate; bimetallic; transition metals.

In a series of papers Aggarwal [1], Johri [2], Singh [3] and Sodhi [4] and their colleagues have reported that tri- and poly-nuclear dithiocarbamato-bridged complexes of the general forms **I** and **II** precipitate when stoichiometric amounts of divalent metal salts MX_2 (M = Zn, Cd or Hg; X = $MeCO_2$, NO_3) and $M'Y_2$ (M′ = VO, Mn, Fe, Co, Ni, Cu or Zn; Y = NO_3, Cl, $1/2SO_4$) in 4:1 acetone/water solution are added successively to a solution of a sodium dithiocarbamate salt in the same solvent mixture. The underlying reactions may be formulated as shown in Schemes 1 and 2.

$$3Na(S_2CNR_2) + MX_2 \rightarrow Na[M(S_2CNR_2)_3] + 2NaX$$
$$2Na[M(S_2CNR_2)_3] + M'Y_2 \rightarrow [M'\{M(S_2CNR_2)_3\}_2] + 2NaY$$

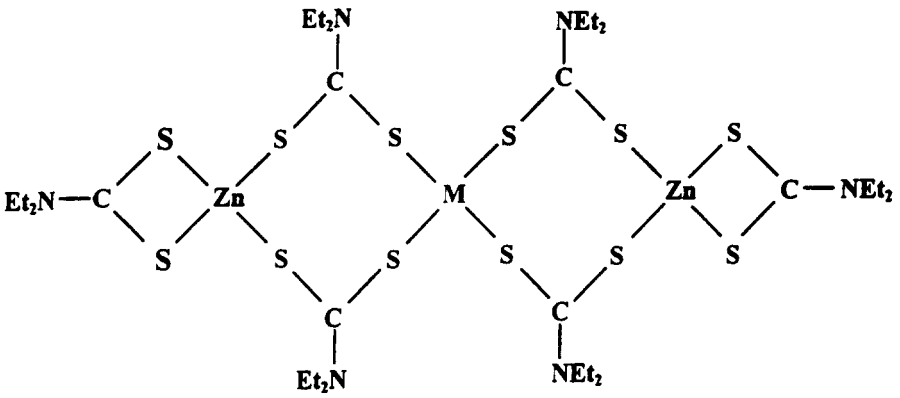
Scheme 1.

$$4Na(S_2CNR_2) + MX_2 \rightarrow Na_2[M(S_2CNR_2)_4] + 2NaX$$
$$Na_2[M(S_2CNR_2)_4] + MY_2 \rightarrow [\{M'M(S_2CNR_2)_4\}_n] + 2NaY$$

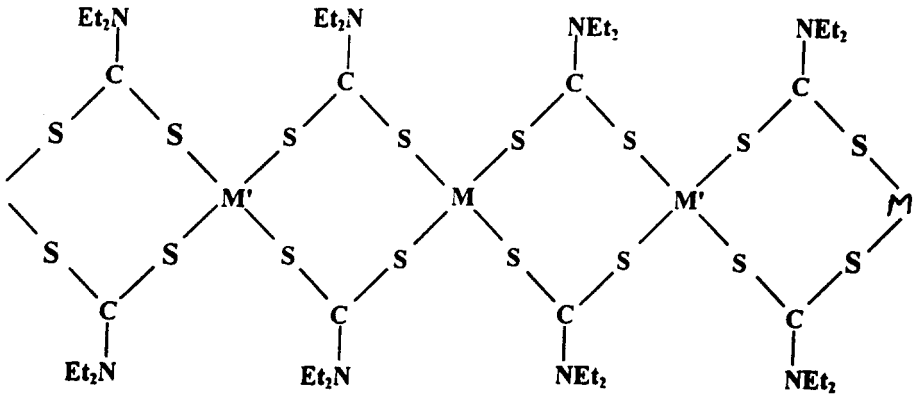
Scheme 2.

We have re-investigated these reactions and find that, contrary to the conclusions of the previous authors [1–4], the products precipitated are essentially mixtures of bis(dithiocarbamato) complexes $[\{M(S_2CNR_2)_2\}_n]$, $[\{M'(S_2CNR_2)_2\}_n]$ (n = 1 or 2) and, in some instances, the heterobinuclear species $[MM'(S_2CNR_2)_4]$. Furthermore, we find that when divalent salts of manganese, iron or cobalt are involved spontaneous oxidation to the trivalent state occurs leading to the formation of tris(dithiocarbamato) complexes $[M'(S_2CNR_2)_3]$ (M′ = Mn, Fe or Co). Our concerns regarding these reactions were first raised by the novel structures proposed for the products, none of which was supported by X-ray crystallographic evidence. In particular there is no obvious thermodynamic reason why heterometallic dithiocarbamato complexes involving divalent metal ions should adopt tri- or poly-nuclear structures **I** and **II**, respectively, when the corresponding simple divalent metal dithiocarbamates $[\{M(S_2CNR_2)_2\}_n]$ and $[\{M'(S_2CNR_2)_2\}_n]$ (n = 1 or 2) are monomers or dimers [5,6], with the latter tending to dissociate in solution [6–9]. Furthermore, the structural differences can hardly be attributed to kinetic factors since our ^1H NMR studies on the mixed systems $[M(S_2CNEt_2)_2]$/$[M'(S_2CNPr^i_2)_2]$ confirm previous reports [10] that the

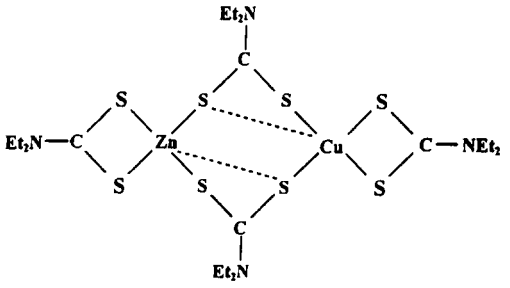
* Author to whom correspondence should be addressed.



(I)



(II)



(III)

dithiocarbamates of divalent transition metal ions are generally labile with respect to ligand exchange.

In order to confirm our belief that these "heterobimetallic" complexes are simple mixtures, samples of "$[Ni\{Zn(S_2CNEt_2)_3\}_2]$" prepared in the prescribed manner [3] were examined by NMR and X-ray powder diffraction methods. The sharp, well-resolved ^1H and $^{13}C-\{^1H\}$ NMR spectra of "$[Ni\{Zn(S_2CNEt_2)_3\}_2]$" were found to be identical with composite spectra of $[Ni(S_2CNEt_2)_2]$ and $[\{Zn(S_2CNEt_2)_2\}_2]$. Given that the chemical shifts recorded for these two homonuclear species display very significant differences (^1H *ca* δ 0.1–0.3, $^{13}C-\{^1H\}$ δ 5) it is highly unlikely that the NMR spectra of a heterobimetallic dithiocarbamato-bridged species could not be demonstrably different from those observed for the simple complexes. Likewise, we find that the X-ray powder pattern of "$[Ni\{Zn(S_2CNEt_2)_3\}_2]$" is essentially identical with the combined patterns of $[Ni(S_2CNEt_2)_2]$ and $[\{Zn(S_2CNEt_2)_2\}_2]$. We have also investigated the first product deposited from a synthesis of "$[Cu\{Zn(S_2CNEt_2)_3\}_2]$". Here, because of the paramagnetic nature of d^9 copper(II), only broad NMR resonances are observed from which little can be concluded. We therefore sought evidence from X-ray crystallographic data. The X-ray powder photographs of the copper/zinc product do indeed indicate the presence of a single phase. However, the unit cell parameters derived therefrom lie essentially midway between the closely related sets of data reported for $[\{Cu(S_2CNEt_2)_2\}_2]$ and $[\{Zn(S_2CNEt_2)_2\}_2]$. Given that *both* copper [9] and zinc [8] bis(dithiocarbamates) exist as dimers in the solid state we suggest that the lines present in the pattern of the precipitated product are attributable to the mixed *binuclear* species $[CuZn(S_2CNEt_2)_4]$(**III**) which is preferentially deposited because of lower solubility. Such binuclear species have been detected and characterized by Ivanov and co-workers [11–13] in the course of their ESR studies on paramagnetic copper(II) dithiocarbamates doped in low concentrations into the corresponding zinc dithiocarbamate lattices using preparative procedures similar to those employed by Aggarwal [1], Johri [2] and Singh [3] and colleagues.

A second and more serious reservation arises in the case of the species "$[\{MM'(S_2CNR_2)_4\}_\infty]$" (M′ = Mn, Fe or Co). These products, which purport to contain four-coordinate manganese(II), iron(II) and cobalt(II), respectively, were all apparently prepared in open vessels without protection from atmospheric oxygen [1,2]. Given that the simple bis(dithiocarbamato) complexes of manganese(II) [14,15] iron(II) [16] and cobalt(II) [17] are notoriously air sensitive, readily undergoing oxidation to the trivalent state and, in the case of manganese(II), reported pyrophoric [14], it seems highly improbably that heterometallic dithiocarbamato complexes containing these metals in the divalent state would be stable with respect to aerobic oxidation. Indeed, it has been reported that cobalt(II) salts, on treatment with aqueous sodium diethyldithiocarbamate, undergo spontaneous oxidation to the trivalent state *even under strictly anaerobic conditions* [14]. Our belief that oxidation occurs in the syntheses involving manganese, iron and cobalt and that the products are merely mixtures of $[\{M(S_2CNEt_2)_2\}_2]$ (M = Zn, Cd or Hg) and $[M'(S_2CNEt_2)_3]$ (M′ = Mn, Fe or Co) is strongly supported in the case of manganese by the observation that the products isolated are all reported [1,2] to display the violet colour associated with the relatively air-stable manganese(III) dithiocarbamates, rather than the bright yellow characteristic of their very air-sensitive manganese(II) counterparts [15]. Moreover, the electronic spectra (700–200 nm, CH_2Cl_2 solution) of the products "$M'\{Zn(S_2CNEt_2)_2\}_2]$" (M′ = Mn, Fe or Co) are essentially the same as those obtained by combining the spectra of $[\{Zn(S_2CNEt_2)_2\}_2]$ and the corresponding trivalent complexes $[M(S_2CNEt_2)_3]$.

In the case of the cobalt/zinc product "$[Co\{Zn(S_2CNEt_2)_3\}_2]$" the NMR spectra recorded by the previous authors [3] and confirmed in our present work display no evidence of the paramagnetic shifts or line broadenings expected for complexes containing d^7 cobalt(II) [17,18]. On the contrary, they are identical to those obtained by superimposing the spectra of $[Co(S_2CNEt_2)_3]$ and $[\{Zn(S_2CNEt_2)_2\}_2]$. In particular the ^1H NMR spectrum of the supposed heterobimetallic product displays the AB part of an ABX_3 pattern arising from the diastereotopic methylene protons [19], identical to that observed for an authentic sample of octahedral $[Co(S_2CNEt_2)_3]$.

Preliminary studies suggest that a parallel series of "heterobimetallic xanthates" reported by the same authors [20–22] should likewise be reformulated in many instances as mixtures of essentially homometallic complexes. A fuller study of these and some related systems will be reported in due course.

Acknowledgements—We thank Dr I. Abrahams of Queen Mary and Westfield College for X-ray powder photographs.

REFERENCES

1. Aggarwal, R. C., Singh, B. and Singh, M. K., *J. Ind. Chem. Soc.*, 1982, **59,** 269.
2. Johri, K. N., Kaushik, N. K., Bajaj, R. K. and Sharma, A. K., *Acta Chim. Hung.*, 1983, **113,** 325.
3. Singh, N. K., Kaw, C. and Singh, N., *Bull. Chem. Soc. Jpn*, 1991, **64,** 1440.
4. Sodhi, G. S. and Kaur, J., *Z. Naturforsch*, 1992, **47b,** 1297.
5. Eisenberg, R., *Prog. Inorg. Chem.*, 1970, **12,** 295.
6. Iwasaki, H., *Acta Cryst.*, 1973, **B29,** 2115.
7. Domenicano, A., Torelli, L., Vaciago, A. and Zambonelli, L., *J. Chem. Soc. A.*, 1968, 1351.
8. Bonamico, M., Mazzone, G., Vaciago, A. and Zambonelli, L., *Acta Cryst.*, 1965, **19,** 898.
9. Bonamico, M., Dessy, G., Mugnoli, A., Vaciago, A. and Zambonelli, L., *Acta Cryst.*, 1965, **19,** 886.

10. Moriyasu, M. and Hashimoto, Y., *Bull. Chem. Soc. Jpn*, 1980, **53,** 3590.
11. Ivanov, A. V., Solozhenkin, P. M., Khamkar, M. Z., Klyashtornyi, V. B. and Shvengler, F. A., *Russ. J. Coord. Chem.*, 1989, **15,** 699.
12. Ivanov, A. V. and Solozhenkin, P. M., *Russ. J. Inorg. Chem.*, 1990, **35,** 871.
13. Ivanov, A. V. and Klyashtornyi, V. B., *Russ. J. Inorg. Chem.*, 1992, **37,** 815, and references cited therein.
14. Fackler, J. P. and Holah, D. G., *Inorg. Nucl. Chem. Lett.*, 1966, **2,** 251.
15. Hill, D. M., Larkworthy, L. F. and O'Donoghue, M. W., *J. Chem. Soc., Dalton Trans.*, 1975, 1726.
16. Larkworthy, L. F., Fitzsimmons, B. W. and Patel, R. R., *J. Chem. Soc., Chem. Commun.*, 1973, 902, and references cited therein.
17. Fitzgerald, R. J. and Brubaker, G. R., *Inorg. Chem.*, 1969, **8,** 2265.
18. De, W., Horrocks, W. and Greenberg, E. S., *Inorg. Chem.*, 1971, **10,** 2190.
19. Golding, R. M., Healy, F. C., Newman, P. W. G., Sinn, E. and White, A. H., *Inorg. Chem.*, 1972, **11,** 2435.
20. Aggarwal, R. C., Singh, N. and Singh, S., *Ind. J. Chem.*, 1982, **21A,** 268.
21. Aggarwal, R. C., Singh, N. and Singh, S., *Polyhedron*, 1985, **4,** 343.
22. Singh, N., Singh, N. K. and Kaw, C., *Bull. Chem. Soc. Jpn*, 1989, **62,** 3328.

Pergamon

PII: S0277-5387(96)00440-8

Polyhedron Vol. 16, No. 9, pp. 1577–1580, 1997
Copyright © 1997 Elsevier Science Ltd
Printed in Great Britain. All rights reserved
0277–5387/97 $17.00+0.00

COMMUNICATION

Synthesis and characterization of the first gold(I) complex of reduced epidithiopiperazine-2,5-dione

Christina L. L. Chai,* David C. R. Hockless and K. D. Vinindra Weerasuria

Department of Chemistry and the Research School of Chemistry, The Australian National University, ACT 0200, Australia

(Received 12 August 1996; accepted 27 August 1996)

Abstract—1,4-Diethyl-3,6-dithiopiperazine-2,5-dione reacted with triphenylphosphine gold chloride to form the corresponding gold complex, the structure of which was determined by X-ray crystallography. The gold(I) complex reacted with iodine to form 5,7-diethyl-2,3-dithia-5,7-diazabicyclo-[2.2.2]octan-6,8-dione. © 1997 Elsevier Science Ltd. All rights reserved.

Keywords: gold(I) complex; epidithiopiperazine-2,5-dione.

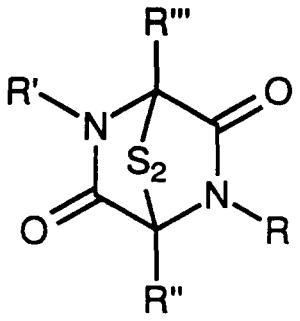
Compounds of many transition metals have proved to have medicinal value in both diagnosis and therapy [1]. Metal complexes such as cisplatin and its analogue carboplatin are capable of acting as selective cytotoxic agents [2], whereas auranofin and myocrisin are important gold drugs for the treatment of rheumatoid arthritis [3]. In other cases, biologically active compounds complexed with transition metals have enhanced biological properties [4].

Epidithiopiperazine-2,5-diones (**1**) are a class of compound that displays a wide range of biological activities [5]. For example, sporidesmin (**2**) is a toxin that causes the disease facial eczema in sheep and cattle, whereas gliotoxin (**3**) is a potent immunosuppressant. Studies have shown that the reduced form of the disulfide (i.e. dithiol) is also biologically active but thioalkylation of the sulfurs or desulfurization renders these compounds inactive [6]. The biological effects of these compounds can be abrogated with the use of metals such as zinc, mercury and cadmium and this has been attributed to the formation of metal thiolato complexes [7]. Recently, the detection of sporidesmin dianionic dithiolato complexes with zinc and cadmium by electrospray mass spectrometry was reported [8]. In this paper, we report the first isolated and fully characterized transition metal complex of 1,4-diethyl-3,6-dithiopiperazine-2,5-dione (**4**), the reduced form of a synthetic epidithiopiperazine-2,5-dione. It is hoped that the chemistry and biological properties of this metal complex will provide further insight into the biological mechanism of action of this class of compounds.

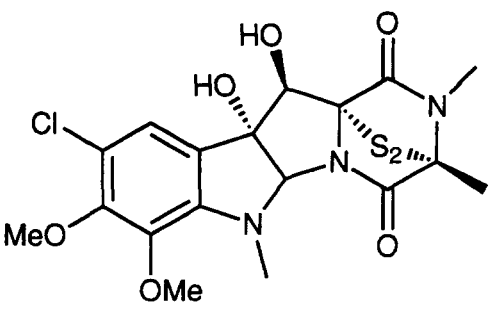
1,4-Diethyl-3,6-dithiopiperazine-2,5-dione (**4**) was synthesised following a modification of Trown's synthesis [9]. 1,4-Diethylpiperazine-2,5-dione was brominated with 2 equivalents of *N*-bromosuccinimide, followed by conversion of the corresponding dibromide to the dithioacetate at 0°C. Only the *cis* diastereomer was observed and hydrolysis (HCl/MeOH) gave the corresponding *cis*-dithiol in excellent yields. After extensive drying to remove water and residual acid, the dithiol was treated with triethylamine (2 equiv.) in dichloromethane, followed by the addition

* Author to whom correspondence should be addressed.

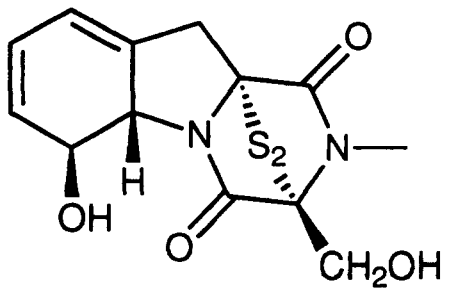
† M.p. = 193–196°C; ^{1}H NMR: δ 1.10(t, 2x 3H), 3.25 (m, 2x H), 3.85 (m, 2x1 H), 5.39 (s, 2x1H), 7.2–7.6 (m, aromatic H); ^{13}C NMR: δ 12.4, 39.3, 59.9, 129.1, 129.3, 130.1, 130.8, 131.6, 131.6, 134.5, 134.7, 166.6; ^{31}P NMR: δ 37.6; Found: C, 45.9; H, 3.7; N, 2.2; S, 5.2. Calc. for $C_{44}H_{42}N_2O_2P_2S_2Au_2$: C, 45.9; H, 3.7; N, 2.4; S, 5.6%. IR (KBr): 530, 690, 750, 1100, 1435, 1655 cm^{-1}.



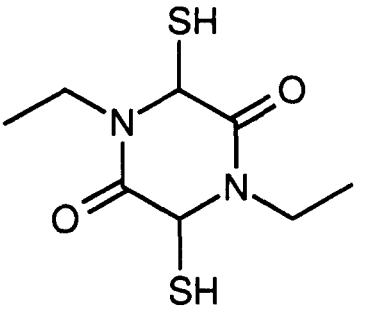
(1)



(2)



(3)



cis-

(4)

of triphenylphosphine gold chloride (2 equiv.) in dichloromethane. After work-up, the gold(I) dithio complex (**5**) was isolated in excellent yields (95%).†The ^{1}H NMR spectra showed a shift of the methine signal from δ 5.04 in the dithiol derivative to δ 5.4 in the gold complex. The sulfhydryl proton for the dithiol (δ 3.15) also disappeared upon complexation with triphenylphosphine gold chloride. ^{31}P NMR of the complex showed only one signal at δ 37.6. Other spectral data (IR, ^{13}C NMR), as well as combustion analysis, confirms the proposed structure. In addition, recrystallization from dichloromethane/ether gave crystals suitable for X-ray crystal structure analysis.‡

‡Crystal data for compound **5**: $C_{44}H_{42}N_2O_2P_2S_2Au_2$, M = 1150.83, T = 296(1) K, monoclinic, space group $C2/c$; a = 23.854(1), b = 11.812(3), c = 16.768(2) Å, β = 117.067(6)°, U = 4207(1) Å^3, D_c (Z = 4) = 1.82 g cm^{-3}, F(000) = 2224, μ(Cu-K_α) = 150.6 cm^{-1}, semi-empirical absorption correction; 3302 unique data ($2\theta_{max}$ = 120.1°), 2466 with $I > 3\sigma(I)$; R = 0.045, wR = 0.048, GOF = 2.56. Data were measured on a Rigaku AFC6R rotating anode diffractometer (graphite crystal monochromator, λ = 1.54180 Å). Refinement was by full-matrix least squares analysis on F using the teXsan structure analysis software of Molecular Structure Corporation [18].

The structure of the gold dithiolato complex is shown in Fig. 1. The piperazinedione ring is characterized by a boat conformation consistent with conformations observed for *cis*-α,α′-disubstituted piperazinediones [10]. The dithio functionalities adopt pseudoaxial positions and the molecule on the whole possesses a twofold axis of rotation. The conformational parameters [11] were as follows: ψ[N(1*)—C(1)—C(2)—N(1)] −23.8 (15)°, φ[C(1)—C(2)—N(1)—C(1*)] 26.7 (16)°, ω[C(2)—N(1)—C(1*)—C(2*)] −2.5 (17)°. The latter value shows that the deviation from planarity is small. The Hooker parameter β [12], measuring the degree of folding of the piperazinedione ring, is 26°.

The gold complex also possesses a short Au—Au bond distance of 3.0440(9) Å. Typically, short intramolecular Au^I—Au^I distances are observed for complexes in which two 1,2- or 1,3-difunctional bidentate ligands hold a pair of gold(I) atoms, and values as short as 2.76 Å have been reported [13]. For the gold complex **5**, Au—S and Au—P bond lengths of 2.308(3) and 2.267(3) Å are observed. The former is slightly longer than the observed Au—S bond length for auranofin (2.29 Å) [14]. The C—S bond length of 1.85(1) Å is slightly longer than the normal C—S value of 1.82 Å, but is shorter than the C—S bond distances found in gliotoxin (**3**) (1.89 Å) [15] and

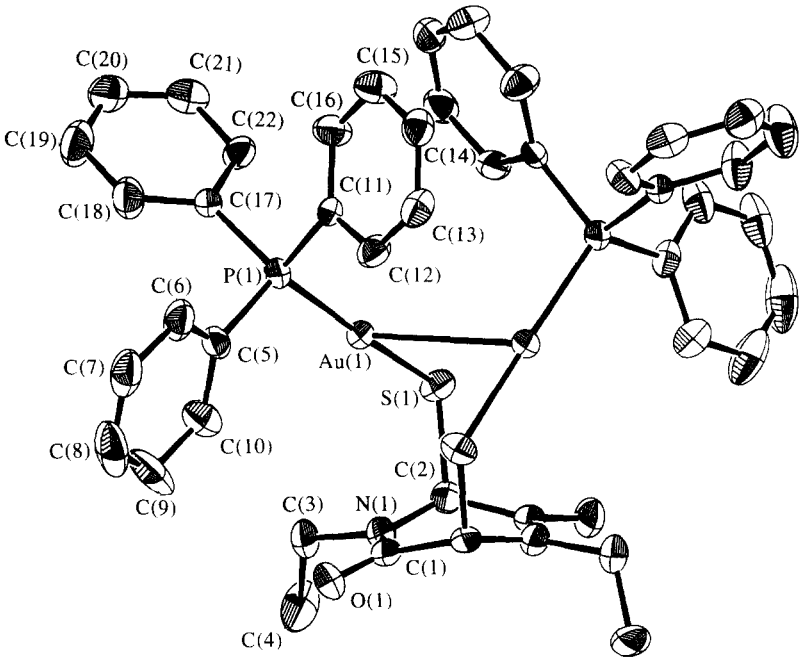


Fig. 1. A perspective view of the gold(I) dithiolato complex (**5**). Selected bond lengths (Å) and angles (°): Au(1)—Au(1) 3.044(9), Au(1)—P(1) 2.267(3), Au(1)—S(1) 2.308(3), S(1)—C(2) 1.85(1), O(1)—C(1) 1.22(1), N(1)—C(1) 1.36(1), N(1)—C(2) 1.45(1), N(1)—C(3) 1.45(1), C(1)—C(2) 1.51(1). Au(1)—Au(1)—S(1) 79.04(9). S(1)—Au(1)—P(1) 172.4(1), Au(1)—Au(1)—P(1) 106.27(8), Au(1)—S(1)—C(2) 107.2(4), C(1)—N(1)—C(2) 124.0(10), N(1)—C(1)—C(2) 117(1), S(1)—C(2)—N(1) 114.5(8), S(1)—C(2)—C(1) 110.0(8), N(1)—C(2)—C(1) 113(1).

sporidesmin (**2**) (1.90 Å) [16]. In addition, it is important to note that the coordination about gold(I) is slightly bent, with P—Au—S angles of 172.4(1) . This value is close to the observed angle for auranofin of 173.6°, but deviates significantly from the ideal value of 180° for linearity.

The ease of oxidative addition of gold centres has been reported [17]. In our studies, dropwise addition of I_2 in chloroform as monitored by NMR spectroscopy did not yield the corresponding Au^{I}/Au^{III} systems, nor Au^{II}/Au^{II} systems. Instead, formation of the disulfide, the epidithiopiperazine-2,5-dione was observed. The ease of oxidation of the gold dithiolato derivative to the disulfide is noted by the quantitative conversion with excess I_2.

The studies here have demonstrated that stable gold(I) dithio derivatives of piperazine-2,5-diones can be synthesized. Owing to the biological importance of these derivatives, it is interesting to examine the biological properties of these new metal piperazinedione complexes. Such studies could lead to the discovery of new and more selective therapeutic drugs, as well as further elucidation into the mechanism of action of epidithiopiperazinedione derivatives.

Acknowledgements—The authors thank Mr H. Neumann for his invaluable technical advice and the Australian Research Council for financial assistance.

REFERENCES

1. Burgess, J., *Trans. Met. Chem.*, 1993, **18,** 439; Sigel, H., (Ed.), *Metal Ions in Biological Systems*, Vol 11. Marcel Dekker, New York, 1980.
2. Green, M., Garner, M. and Orton, D. M., *Trans. Met. Chem.*, 1992, **17,** 164 and references therein.
3. Puddephatt, R. J., in: *Comprehensive Coordination Chemistry*, Vol. 5, ed. G. Wilkinson. Pergamon Press, Oxford, 1987, pp. 861–925, and references cited therein; Lippard, S. J., (Ed.), *Platinum, Gold and Other Metal Chemotherapeutic Agents: Chemistry and Biochemistry*, ACS Symposium Series: 209. American Chemical Society, Washington, D.C., 1983.
4. Kirschener, S., Wei, Y.-K., Francis, D. and Bergman, J. G., *J. Med. Chem.*, 1966, **9,** 369.
5. Waring, P., Eichner, R. D. and Müllbacher, A., *Med. Res. Rev.*, 1988, **8,** 499.
6. For example, see Middleton, M. C., *Biochem. Pharmacol.*, 1974, **23,** 811.
7. Munday, R., *J. Appl. Toxicol*, 1984, **4,** 182.
8. Henderson, W., Miles, C. O. and Nicholson, B. K., *J. Chem. Soc., Chem. Commun.*, 1995, 889.
9. Trown, P. W., *Biochem. Biophys. Res. Commun.*, 1968, **33,** 402.
10. Karle, I. L., *The Peptides*, Vol. 4, ed. E. Gross and J. Meienhofer. Academic Press, Inc., New York, 1981, pp. 4–8.
11. IUPAC-IUB Commission on Biochemical Nomenclature, *Biochemistry*, 1970, **9,** 347.

12. Hooker, T. M., Jr., Bayley, P. M., Radding, W. and Schellman, J. A., *Biopolymers*, 1974, **13,** 549.
13. Hesse, R. and Jennische, P., *Acta Chem. Scand.*, 1972, **26,** 3855.
14. Hill, D. T. and Sutton, B. M., *Cryst. Struct. Commun.*, 1980, **9,** 679.
15. Fridrichsons, J. and Mathieson, A. McL., *Acta Cryst.*, 1967, **23,** 439.
16. Fridrichsons, J. and Mathieson, A. McL., *Acta Cryst.*, 1965, **18,** 1043.
17. Manzany, A. M. and Fackler, J. P., *J. Am. Chem. Soc.*, 1984, **106,** 801.
18. *teXsan*: *Single Crystal Structure Analysis Software*, Version 1.7–1. Molecular Structure Corporation, The Woodlands, TX 77381, 1995.

Pergamon

PII: S0277-5387(96)00410-X

Polyhedron Vol. 16, No. 9, pp. 1581–1584, 1997
Copyright © 1997 Elsevier Science Ltd
Printed in Great Britain. All rights reserved
0277–5387/97 $17.00+0.00

COMMUNICATION

Lower rim alkylammonium-substituted calix[4]arenes as "proton-switchable" extractants for chromate and dichromate anions

Emil M. Georgiev,[a] Nicholas Wolf[b] and D. Max Roundhill[b]*

[a] Department of Chemistry, Tulane University, New Orleans, Louisiana 700118, U.S.A. and
[b] Department of Chemistry and Biochemistry, Texas Tech University, Lubbock, TX 79409-1061, U.S.A.

(Received 16 June 1996; accepted 12 August 1996)

Abstract—The compound 5,11,17,23-tetra-tert-butyl-25,27-bis(2-aminoethoxy)-26,28-dihydroxycalix[4]arene (**2**) has been synthesized by the borane reduction of 5,11,17,23-tetra-tert-butyl-25,27-bis(2-dicyanomethoxy)-26,28-dihydroxycalix[4]arene (**1**). The protonated alkylammonium form of **2** is an effective extractant for transferring the anions CrO_4^{2-} and $Cr_2O_7^{2-}$ from an aqueous into a chloroform layer. The monoanions Cl^-, $CH_3CO_2^-$ and NO_3^-, and dianions SO_4^{2-}, MoO_4^{2-} and WO_4^{2-} have little effect on the extraction of CrO_4^{2-} and CrO_7^{2-}. Deprotonation of the dialkylammonium cation results in reversal with CrO_4^{2-} and $Cr_2O_7^{2-}$ migrating back into the aqueous layer. © 1997 Elsevier Science Ltd. All rights reserved.

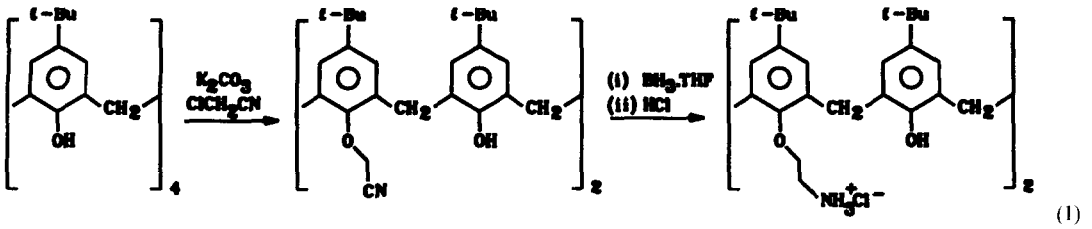
Keywords: calixarene; amino; chromate; dichromate.

The synthesis of complexants and hosts for specific metals is an important goal, especially if the metal is a commercially valuable one that is currently an environmental problem. For cations the metal can be directly bound to a ligating group on the host, but for anions or uncharged molecules there may be no direct interaction between the metal centre and the host. Although there are numerous examples of molecules that act as hosts and complexants for cations, there are fewer examples of molecules that act as hosts for anions [1–4]. Recently, however, a number of chemically modified calixarenes have been synthesized that can be used as hosts for simple anions [5]. From an environmental viewpoint, two important anions for which a selective host would be useful are chromate and dichromate. These particular ions are important because of their high toxicity [6–11] and because of their presence in soils and waters [12].

In designing complexants for these particular guest anions a number of structural features can be incorporated into the host molecule that may be important in achieving selective binding. For such a molecule to be effective as a host it is necessary that its structural features are compatible with those of the guest anion. Although there have been some recent reports of chemically modified calixarenes acting as host molecules for simple anions, none has yet been used as host for CrO_4^{2-} and $Cr_2O_7^{2-}$ [13]. Because the periphery of a chemically modified calixarene can be made structurally compatible with these ions we have targeted the synthesis of an extractant for them based on a calix[4]arene framework.

The chromate and dichromate ions CrO_4^{2-} and $Cr_2O_7^{2-}$ are dianions with oxide functionalities at their periphery. Since the metal centre does not bind to additional ligands there is no advantage in designing a host that can act as a complexant to it. Nevertheless, since the periphery of the anions have oxide moieties, these are potential sites for hydrogen bonding to the host molecule. We now report the synthesis of a chemically modified calix[4]arene that is an extractant for both CrO_4^{2-} and $Cr_2O_7^{2-}$ from an aqueous solution into a chloroform layer. This compound is

* Author to whom correspondence should be addressed.



1 2 (1)

5,11,17,23-tetra-tert-butyl-25,27-bis(2-aminoethoxy)-26,28-dihydroxycalix[4]arene bis hydrochloride. This particular calix[4]arene is a dication for the formation of a neutral ion-paired complex with CrO_4^{2-} and $Cr_2O_7^{2-}$, and it also has both hydroxyl and alkylammonium functionalities that can potentially form hydrogen bonds with these anions.

The synthetic route to this extractant follows that used for other 2-aminoethoxy-substituted calix[4]arenes and is shown in Eq. (1) [14]. The initial compound, 5,11,17,23-tetra-tert-butyl-25,27-bis(2-dicyanomethoxy)-26,28-dihydroxycalix[4]arene (**1**), has been prepared according to the literature procedure [15]. Reduction with a solution of borane in THF, followed by conversion to the amine hydrochloride salt with HCl, gives the product **2**. The compounds **1** and **2** show the following characteristic spectroscopic features: **1**, ^{1}H NMR ($CDCl_3$): δ 0.88 (s, Bu^t), 1.32 (s, Bu^t), 3.45 [d, CH_2, ^2J(HH) = 13.6 Hz], 4.23 [d, CH_2, ^2J(HH) = 13.6 Hz], 4.81 (s, CH_2), 5.57 (s, OH), 6.73 (s, ArH), 7.12 (s, ArH). **2**, ^{1}H NMR (DMSO-d_6): δ 1.12 (s, Bu^t), 1.17 (s, Bu^t), 3.50 [d, CH_2, ^2J(HH) = 12.4 Hz], 4.10 (d, CH_2, ^2J(HH) = 12.4 Hz], 3.51 [t, CH_2, ^3J(HH) = 7 Hz], 4.25 [t, CH_2, ^3J(HH) = 7 Hz], 7.18 (s, ArH), 8.54 (br s, OH + NH_3). Mass spectrum: m/z 735 (M − 2HCl).

Aqueous solutions of Na_2CrO_4 and $K_2Cr_2O_7$ show no extraction into a chloroform layer in the absence of a complexant. Furthermore, the alkylammonium salts of butylamine, *N*,*N*-dimethylbutylamine, tributylamine, ethylenediamine and *N*,*N*,*N*′,*N*′-tetramethylethylenediamine also show no extraction for these anions. However, when the protonated alkylammonium salt of **2** is added, extraction of CrO_4^{2-} and $Cr_2O_7^{2-}$ into the chloroform layer occurs. At ratios of CrO_4^{2-} : **2** of 1 : 0, 1 : 1, 1 : 2 and 1 : 20 the respective partition coefficients ($CHCl_3$: water) are 0, 0.5, 1.0 and 80, showing that the protonated form of **2** is an effective host. The absorption spectra of the guest CrO_4^{2-} and $Cr_2O_7^{2-}$ molecules and the ^{1}H NMR spectrum of the host **2** are unchanged, indicating that no chemical reaction has occurred between them. The extraction of CrO_4^{2-} and $Cr_2O_7^{2-}$ into chloroform by **2** in the presence of a ten-fold excess of Cl^-, SO_4^{2-}, $CH_3CO_2^-$, HPO_4^-, NO_3^-, MoO_4^{2-} and WO_4^{2-}, themselves potential guest anions for **2**, has been inves-

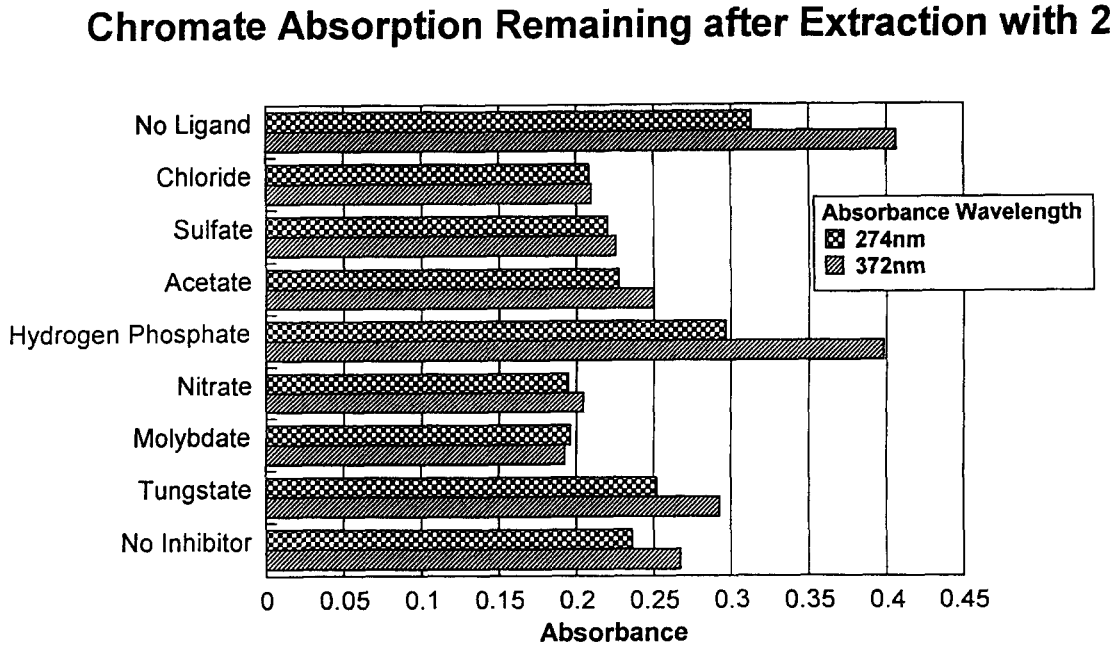


Fig. 1. Quantity of CrO_4^{2-} remaining in aqueous solution after extraction with **2** in chloroform in the presence of potential inhibitors. In each case the ratio of CrO_4^{2-} : **2** is 1 : 1, and the ratio of CrO_4^{2-} : inhibitor is 1 : 10.

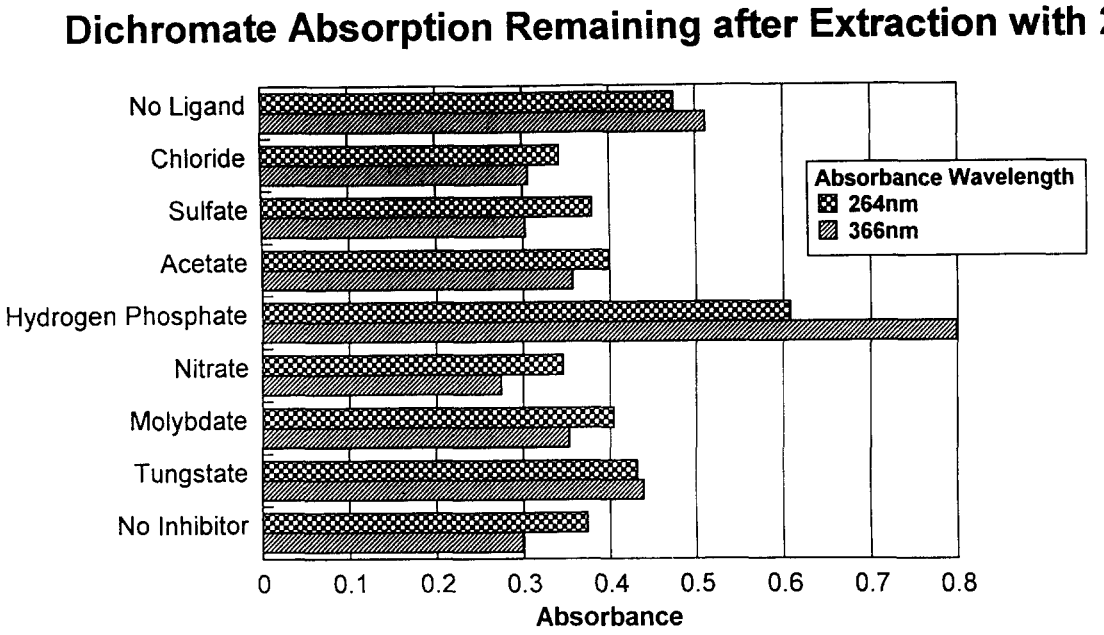
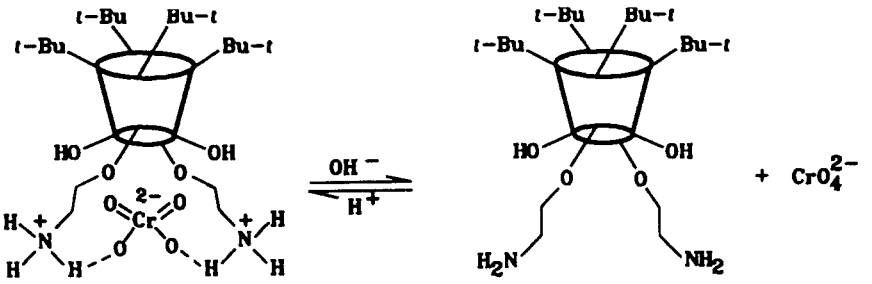


Fig. 2. Quantity of $Cr_2O_7^{2-}$ remaining in aqueous solution after extraction with **2** in chloroform in the presence of potential inhibitors. In each case the ration of $Cr_2O_7^{2-}$: **2** is 1 : 1, and the ratio of $Cr_2O_7^{2-}$: inhibitor is 1 : 10.



(2)

tigated. The data in Figs 1 and 2 show that the monoanions Cl^-, $CH_3CO_2^-$ and NO_3^-, with the exception of HPO_4^-, and the dianions, have little effect on the extraction of CrO_4^{2-} and $Cr_2O_7^{2-}$ [16].

Upon addition of NaOH to the aqueous layer, the deprotonated calixarene in the chloroform is no longer an effective host molecule for CrO_4^{2-} and the dianion then migrates back into the aqueous layer in a reversible process [Eq. (2)] [17].

Acknowledgements—We thank the National Institute of Environmental Health Sciences, the U.S. Army Research Office and the Center for Bioenvironmental Research at Tulane University for financial support.

REFERENCES

1. D. H. Busch, *Chem. Rev.* 1993, **93,** 847.
2. L. F. Lindoy, *The Chemistry of Macrocyclic Ligand Complexes*. Cambridge University Press, Cambridge, 1989.
3. G. Gokel, *Crown Ethers and Cryptands*, Monographs in Supramolecular Chemistry, ed. J. Fraser Stoddart. Royal Society of Chemistry, London, 1991.
4. F. C. J. M. van Veggel, W. Verboom and D. N. Reinhoudt, *Chem. Rev.* 1994, **94,** 281.
5. H. C. Visser, D. M. Rudkevich, W. Verboom, F. de Jong and D. N. Reinhoudt, *J. Am. Chem. Soc.* 1994, **116,** 11554.
6. D. Burrows, *Chromium: Metabolism and Toxicity*. CRC Press, Boca Raton, 1983.
7. J. A. H. Waterhouse, *Br. J. Cancer* 1975, **32,** 262.
8. S. Bonatti, M. Meini and A. Abbondandolo, *Mutat. Res.* 1976, **39,** 147.
9. V. Bianchi, A. Zantedeschi, A. Montaldi and J. Majone, *Toxicol. Lett.* 1984, **8,** 279.
10. S. De Flora and K. E. Wetterhahn, *Life Chem. Rep.* 1989, **7,** 169.
11. D. M. Stearns, L. J. Kennedy, K. D. Courtney, P. H. Giangrande, L. S. Phieffer and K. E. Wetterhahn, *Biochemistry* 1995, **34,** 910.
12. P. R. Wittbrodt and C. D. Palmer, *Environ. Sci. Technol.* 1995, **29,** 255.
13. Among the methods presently available for the extraction of Cr^{VI} are extraction methods with carbonate or phosphate buffers, and sonication

with hydroxide solution, see: B. R. James, J. C. Petura, R. J. Vitale and G. R. Mussoline, *Environ. Sci. Technol.* 1995, **29,** 2377.
14. D. M. Roundhill, E. Georgiev and A. Yordanov, *J. Incl. Phenom. Mol. Recogn. Chem.* 1194, **19,** 101.
15. E. M. Collins, M. A. McKervey, E. Madigan, M. B. Moran, M. Owens, G. Ferguson and S. J. Harris, *J. Chem. Soc., Perkin Trans* 1 1991, 3137.
16. The high absorbance of $Cr_2O_7^{2-}$ in the presence of HPO_4^- is owing to its conversion to CrO_4^{2-} at the pH of this solution.
17. This is a particularly important feature if it is desirable to recover the particular metal in pure form and re-use the extractant.

Pergamon

PII: S0277-5387(96)00484-6

Polyhedron Vol. 16, No. 10, pp. 1585–1594, 1997
Copyright © 1997 Elsevier Science Ltd
Printed in Great Britain. All rights reserved
0277-5387/97 $17.00+0.00

Paramagnetic charge transfer complexes: new molecular composites *via* intercalation of thiazole and benzothiazole derivatives within the cavities of the 3D host polymers $[(Me_3E)_3Fe(CN)_6]_\infty$; E = Sn or Pb

Amany M. A. Ibrahim[a] and Safaa El Din H. Etaiw[b]*

[a]Department of Chemistry, Faculty of Science, Ain Shams University, Cairo, Egypt

[b]Department of Chemistry, Faculty of Science, Tanta University, Tanta, Egypt

(Received 3 April 1996; accepted 30 September 1996)

Abstract—The three-dimensional (3D) polymers $[(Me_3Sn)_3Fe(CN)_6]_\infty$ (**I**) and $[(Me_3pb)_3Fe(CN)_6]_\infty$ (**II**) which have wide internal cavities capable of incapsulating voluminous organic compounds behave as host acceptors forming charge transfer complexes (CTC). Thiazole and benzothiazole derivatives acting as guest donor species are encapsulated within the cavities of the 3D polymeric hosts **I** or **II** forming yellow to green or red CTC having, in some cases, semiconducting properties. Some of the donors containing an amino group undergo polymerization within the cavities of the host polymers forming new molecular composites having pronounced electrical conductivity when doped in 2 M HCl solution. The interesting feature of these composites is the enhanced electronic conductivities exhibited by encapsulation of the conductive polymers within the cavities of the host 3D polymers. © 1997 Elsevier Science Ltd. All rights reserved.

Keywords: change transfer complexes; thiazole; benzothiazole; molecular composites; 3D-host polymers.

The novel supramolecular polymers of the type $[(R_3E)_nM(CN)_6]_\infty$ (where R = alkyl or phenyl, E = Sn or pb and M = Fe, Co or Ru) have different potential applications as they act as ion exchangers [1–3], oxidative materials [4] and 3D-hosts which serve as templates within which guest molecules are assembled and also as acceptors forming CTC [5–8]. Their structure is based on a 3D network of the octahedral $M(CN)_6$ building blocks and the trigonal bipyramidal (R_3E) connecting units. The octahedral $M(CN)_6$ building blocks are linked to each other *via* the trigonal bipyramidal [···CN—E(R_3)—NC···] configuration. The framework structures create wide parallel channels or cavities with diameters typically of *ca* 9.5 Å [7,9] into which many interesting reactions including electron or charge transfer have been explored.

In this article the reactions involving the intercalation of thiazole and benzothiazole derivatives acting as electron donors within the cavities of the 3D polymers $[(Me_3E)_3Fe(CN)_6]_\infty$, where E = Sn or Pb acting as electron acceptors, have been studied to obtain novel CTC. Thiazoles and benzothiazoles have wide applications in the fields of pharmaceutical, analytical and industrial chemistry [10]. However, although electronically conducting heteroatamic polymers such as polypyrrole and polythiophene have received considerable attention because of their remarkable electronic, magnetic and optical applications, there have been no such studies on thiazoles and benzothiazoles. The present report also reveals the formation of paramagnetic CTCs having conducting properties.

EXPERIMENTAL

Materials and preparations

All reagents used in this study were of the purest grade and purchased from either Aldrich or Sigma

*Author to whom correspondence should be addressed.

and used without further purification. However, thiazole and benzothiazole derivatives were purified by sublimation (solid materials) *in vacuo* or by recrystallization from ethanol and by distillation (liquids) *in vacuo*, and kept under nitrogen while thiazole was used as received. The orange precipitate of the host polymers **I** and **II** were obtained by mixing aqueous solutions of Me_3SnCl or Me_3PbCl, respectively, and $K_3Fe(CN)_6$ in 3 : 1 molar ratio under nitrogen in the dark. Each precipitate was filtered off, washed with water and then CH_2Cl_2. The purity and identity of **I** and **II** were checked by elemental analysis and IR spectroscopy (Tables 1 and 2). The CTCs were prepared by adding the dry freshly prepared **I** or **II** to an excess of the donor, thiazole or benzothiazole derivative, with continuous grinding at 5°C or at room temperature. The reaction rate was greatly increased by addition of a few drops of ethanol, while in the case of thiazole no solvent was added. After the addition of thiazole to **I** or **II** a deep red colour appeared which faded in time (*ca* 24 h) giving a stable yellow product. Thus, the red product was kept under nitrogen while all measurements were carried out directly after preparation. On the other hand, the CTCs **3′**, **8′**, **10′**, **14′** and **16′** were prepared by the method described above in the presence of a few drops of 2 M HCl solution. Also, the 2-aminothiazole and 2-aminobenzothiazole derivatives were subjected to oxidation by the addition of ammonium persulfate in the presence of 2 M HCl at 5°C to produce the corresponding polymers.[11] Only, 2 aminothiazole (**3″**), 2-aminobenzothiazole (**8″**) and 2-amino-6-methylbenzothiazole (**10″**) underwent polymerization under these experimental conditions giving brown or greenish-brown polymers. Since **I** and **II** are photo-and air-sensitive [12] all manipulations were carried out in the dark under nitrogen. The products were washed with ethanol several times and dried *in vacuo*. The colour and the composition of the CTC depended on the type of the donor, the reaction time and grinding (Table 1).

Instruments

All the analytical, spectroscopic and conductivity measurements as well as the instruments are as previously described [5,6].

RESULTS AND DISCUSSION

Analytical data

The stoichiometry of the CTC [moles donor (x) per mole acceptor polymer] was deduced from chemical analysis (Table 1). The results reveal that most of the donor molecules can intercalate within the channels of the polymers **I** and **II** with an amount less than 1 mol ($x < 1$) per mol of polymer while thiazole (compound **2**) reacts in the ratio 1 : 1 ($x = 1$). On the other hand, thiazole and some of the amino derivatives (compounds **1, 3, 8, 10, 13** and **16**) reacted in the ratio 3 : 2 ($x = 1.5$). The results revealed in addition that several samples contained some ethanol amounting to more or less the quantity of the donor species interca-

Table 1. Analytical data of the CTC

No.	Compound	Colour	Elemental analysis: Calc. (Found) (%)			
			C	H	N	Fe
I	$[(Me_3Sn)_3Fe(CN)_6]_x$	Orange	25.6(25.8)	3.9(4.9)	11.9(11.3)	7.9(7.9)
II	$[(Me_3Pb)_3Fe(CN)_6]_x$	Orange	18.6(18.3)	2.8(3.0)	8.7(8.4)	5.8(5.7)
1	$[(\text{Thiazole})_{1.5} + \text{I})_x$	Red	28.2(27.8)	3.8(3.7)	12.1(11.6)	6.7(6.6)
2	$[(H^+)\ (\text{Thiazole}) + \text{I})_x$	Canary yellow	27.4(27.1)	3.8(3.8)	12.4(11.9)	7.1(7.0)
3	$[(\text{2-Aminothiazole})_{1.5} + \text{I}]_x$	Brown	27.4(27.1)	3.9(3.7)	14.8(13.8)	6.5(6.6)
4	$[\text{2-Amino-4-methylthiazole})_{0.85} + \text{I}] \cdot 0.5\text{EtOH}$	Green	28.3(28.1)	4.3(4.3)	13.1(12.6)	6.8(6.7)
5	$[(\text{2-Amino-4 phenylthiazole})_{0.80} + \text{I}] \cdot 0.6\text{EtOH}$	Green	32.2(32.0)	4.2(4.2)	12.2(11.9)	6.4(6.3)
6	$[\text{2-Amino-5-nitrothiazole})_{0.65} + \text{I}] \cdot 0.5\text{EtOH}$	Greenish-yellow	26.2(26.1)	3.9(3.8)	13.6(12.9)	6.8(6.7)
7	$[(\text{Benzothiazole})_{0.80} + \text{I}] \cdot 0.8\text{EtOH}$	Green	31.4(31.2)	4.2(4.0)	11.2(10.8)	6.6(6.5)
8	$[(\text{2-Aminobenzothiazole})_{1.5} + \text{I}]_x \cdot 0.3\text{EtOH}$	Brown	33.2(33.2)	4.0(4.1)	13.4(12.9)	5.9(5.9)
9	$[(\text{2-Methylbenzothiazole})_{0.75} + \text{I}] \cdot 0.7\text{EtOH}$	Dark green	31.7(31.2)	4.3(4.3)	11.1(10.3)	6.6(6.5)
10	$[(\text{2-Amino-6-methylbenzothiazole})_{1.5} + \text{I}] \cdot 0.3\text{EtOH}$	Dark green	34.4(34.1)	4.3(4.1)	13.1(12.9)	5.8(5.7)
11	$[(\text{2-Amino-6-chlorobenzothiazole})_{0.65} + \text{I}]$	Greenish-yellow	28.5(28.1)	3.7(3.6)	12.4(11.8)	6.8(6.7)
12	$[(\text{2-Amino-6-nitrobenzothiazole})_{0.6} + \text{I}] \cdot 0.5\text{EtOH}$	Green	28.7(28.5)	3.9(3.9)	12.9(12.1)	6.6(6.6)
13	$[(\text{Thiazole})_{1.5} + \text{II})_x$	Red	21.3(21.2)	2.9(2.9)	9.6(9.1)	5.1(5.0)
14	$[(\text{2-Aminothiazole})_{1.5} + \text{II})_x$	Brown	20.9(20.6)	3.0(2.8)	11.3(10.8)	5.0(4.9)
15	$[(\text{Benzothiazole})_{0.75} + \text{II}] \cdot 0.7\text{EtOH}$	Green	23.6(23.3)	3.2(3.1)	8.6(8.0)	5.1(5.1)
16	$[(\text{2-Aminobenzothiazole})_{1.5} + \text{II}] \cdot 0.4\text{EtOH}$	Brown	26.0(25.9)	3.2(3.1)	10.4(10.1)	4.6(4.5)

Table 2. IR spectral data (cm^{-1}) of **I, II** and their CTCs, **1–16**

Compound	ν_{OH}	ν_{NH_2} ν_{NH}	ν_{C-H} (Aromatic)	$\nu_{(Fe^{III}CN)}$	$\nu_{(Fe^{II}CN)}$	$\nu_{C=N}$	ν_{Sn-C} ν_{Pb-C}	$\nu_{Fe^{III}C}$	$\nu_{Fe^{II}C}$
I				2146,2110			556	410	
II				2122,2115			495*	410	
1			3097		2075,2040	1625	553	411	462
2			3084		2080	1620	555	410	460
3		3280*	3074		2066,2020	1626	553	415	450
4	3480	3432	3032	2186,2135	2076	1624	552	409	465
5	3490	3420	3080	2180,2130	2065	1625	555	410	450
6	3500	3370	3075	2185,2136	2070	1615	555	412	455
7	3430		3048	2180,2142	2086	1628	553	408	452
8	3480	3289*	3079		2085,2048	1623	548	405	455
9	3432		3075	2180,2125	2062	1620	550	410	450
10	3460	3220*	3050		2070,2025	1622	552	408	460
11		3400	3078	2180,2122	2080	1618	555	412	450
12	3435	3380	3053	2184,2144	2075	1640	558	410	447
13			3062	2180,2115	2070	1622	490*	410	450
14		3275*	3070		2075,2055	1620	500*	412	445
15	3430		3080	2180,2110	2075	1624	495*	410	455
16	3420	3240*	3068		2080,2035	1625	495*	408	452

lated. Although the significance of the presence of the solvent molecules in these CTCs is not clear, it is worth noting that such results have been previously found for several other intercalates of the present polymers and of FeOCl [6,13].

IR spectra

The IR spectra of the CTC exhibit the characteristic bands of the corresponding donor and the acceptor polymer. These bands suffer some changes from those of the free donors [14] and the acceptor polymers (Table 2). The IR spectra of the CTCs **4, 5, 6, 11** and **12** showed broad bands at 3370–3420 cm^{-1} corresponding to ν_{NH}. The solvent molecules absorb around 3430 cm^{-1} due to ν_{OH}. The presence of the solvent molecules in the composition of most of the CTC was also confirmed by TGA where a stoichiometric ratio of one ethanol molecule per mole of the acceptor polymer (Table 1) was released in the temperature range 80–100°C. The ν_{CH} bands of the thiazole and benzothiazole moieties appear at 3048–3097 cm^{-1}, while those of $\nu_{C=N}$ and $\nu_{C=C}$ are located around 1625 and 1520 cm^{-1}. Generally, the IR bands due to the thiazole or benzothiazole donors suffer a shift to lower wavenumbers on CT complexation. On the other hand, the IR spectra of the polymers **I** and **II** exhibit drastic changes on CT complexation. A new strong band appears at 2065–2086 cm^{-1} due to $\nu_{Fe^{II}-CN}$ while the band due to $\nu_{Fe^{III}-CN}$ suffers a shift to lower wavenumbers with a dramatic decrease in relative intensity. Also, a new medium-to-weak band appears at 2180–2190 cm^{-1}, which may be attributed to the stretching frequency of some free terminal cyanide groups. In addition to the medium band at 410 cm^{-1} due to $\nu_{Fe^{III}-CN}$, a weak-to-medium band appears at 445–465 cm^{-1} corresponding to $\nu_{Fe^{III}-CN}$, indicating partial reduction of Fe^{III} to Fe^{II} by the thiazole or benzothiazole donor forming CTC.

In the case of thiazole, 2-aminothiazole, 2-aminobenzothiazole and 2-amino-6-methylbenzothiazole (compounds **1, 3, 8, 10, 13, 14** and **16**) the host polymer **I** or **II** was completely reduced to the isostructural, but anionic homologue $[(Me_3E)_3Fe^{II}(CN)_6]^-$. This is gathered by the disappearance of the bands at 2146–2122, 2110–2115 and 410 cm^{-1} due to $Fe^{III}CN$ building blocks and the appearance of strong-to-medium bands at 2075, 2040 and 450 cm^{-1} due to $Fe^{II}CN$ building blocks. Also the broad band due to ν_{NH_2} disappears and instead a sharp band appears at 3220–3289 cm^{-1}, corresponding to ν_{NH} indicating polymerization of these donors within the channels of the polymers **I** and **II** forming stable 3:2 molecular composites.

Upon intercalation, the acceptor polymers remain having channels as wide as the donor molecules can accommodate forming CTC as gathered from the presence of the characteristic bands of the (Me_3E) connecting units at 2980, 2900, 2800 and 780 cm^{-1} due to different modes of vibrations of the methyl groups and at 550 and 495 cm^{-1} due to ν_{Sn-C} and ν_{Pb-C}, respectively. The presence of two ν_{CH} bands at 2980 and 2900 cm^{-1} could arise from crystallographic non-equivalence of methyls in the distorted trigonal-bipyramidal structure of the zigzag chains and from methyls in linear chains [15].

NMR spectra

The ^1H NMR spectra of the CTCs were measured in alkaline NaOD solution. The CTCs dissociate after

heating the solution according to the following equation:

$$[(D^+)_x(Me_3E)_3Fe^{II}_xFe^{III}_{1-x}(CN)_6]_\infty \xrightarrow[\text{heating}]{\text{NaOD}} x(D^+)_{solv} + 3[Me_3E(OD)_2]^-_{solv} + x[(Fe(CN)_6]^{4-} + 1 - x[Fe(CN)_6]^{3-}.$$

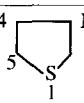
The NMR spectra of the CTCs (Table 3 and Fig. 1), reveal the signals characteristic of the thiazole and benzothiazole moieties as well as that of the methyl protons of the (Me_3E) connecting units. It is observed that the signals of the donors appear at more or less the same positions as the signals due to the protons of the free donors in DMSO [16]. The NMR spectra of **1, 2** and **13** indicate the polymerization of thiazole *via* the positions 2 and 5 and of 2-aminothiazole (compounds **3** and **14**) *via* position 5, since the signals due to the protons at these positions disappear while that of the proton at position 4 suffers a shift to higher field. The polymerization of 2-aminobenzothiazole and 2-amino-6-methylbenzothiazole was also confirmed by the shift of the multiplet due to the protons of the phenyl moiety to higher field relative to those of the corresponding monomers [16]. These results indicate the intercalation of thiazole and benzothiazole donors within the channels of the 3D polymers **I** and **II** forming CTCs, while the donors of **1, 3, 8, 10, 13, 14** and **16** undergo polymerization forming molecular composites.

Magnetic properties

The EPR spectra of the polymers **I** and **II** show the same behavior exhibiting five absorption signals with g values 1.9784, 2.2003, 2.5005, 2.9164, 3.147 and 4.5872. [5] The first four signals correspond to low-spin iron(III), which has a $(dE)^5$ electronic configuration with one unpaired electron in the d_{yz} orbital forming with the cyanide ions a distorted octahedral structure. [17–20] The last signal at 4.5872 is weak and corresponds to the trace amounts of high-spin iron(III) [21–23].

The EPR spectra of the molecular composites **1, 3, 8, 10, 13, 14** and **16** exhibit one strong symmetrical signal with g value $\sim$2.0 accompanied by the disappearance of the signals of the polymers **I** and **II** (Fig. 2). This signal corresponds to the free radical cation of the corresponding poly-donor and resembles that observed in the EPR spectrum of polyaniline [24,25] and its derivatives [5]. This argument was also supported by the presence of a strong signal at $g \simeq 2.0$ of the authentic samples of the polyaminothiazole and benzothiazole derivatives prepared by the oxidation of the monomers by ammonium persulfate. The polymerization of these donor molecules within the channels of the polymers **I** and **II** yields extremely paramagnetic molecular composites. However, the molecular composite **2** is EPR silent and diamagnetic. On the other hand, the EPR spectra of the CTCs also show a strong signal around g 2.0, in addition to weak signals at g values corresponding to the acceptor polymer **I** or **II**. The presence of the strong signal at

Table 3. The ^{1}H NMR[a] (δ ppm) and the magnetic[b] (μB) data of CTCs

	Signals of 4  N_3 moiety					
CTC	2	4	5	Signals of the phenyl moiety	Signals of the CH_3 group	μ_{eff}
1	9.30	8.15	7.82			1.55
2	9.20	8.10	7.85			Diamagnetic
3		6.7				1.25
4			5.95		2.0	1.20
5			5.80	7.35–8.0		1.10
6		7.90		—		1.50
7	9.0			6.40–7.85		1.15
8				6.25–7.0		1.60
9				6.30–7.25	2.0	1.45
10				6.30–7.10	2.40	1.30
11				6.75–7.45		1.75
12				6.80–7.60		1.83
13	9.25	8.05	7.85			1.58
14		6.75				1.61
15	8.95			6.40–7.50		1.30
16				6.35–7.15		1.22

[a]The signals due to $[Me_3E(OD_2)]^-_{solv}$ appear at 0.65–0.80 ppm.
[b]$\mu_{eff.}$ of **I** = 2.18 μB and of **II** = 2.56 μB.

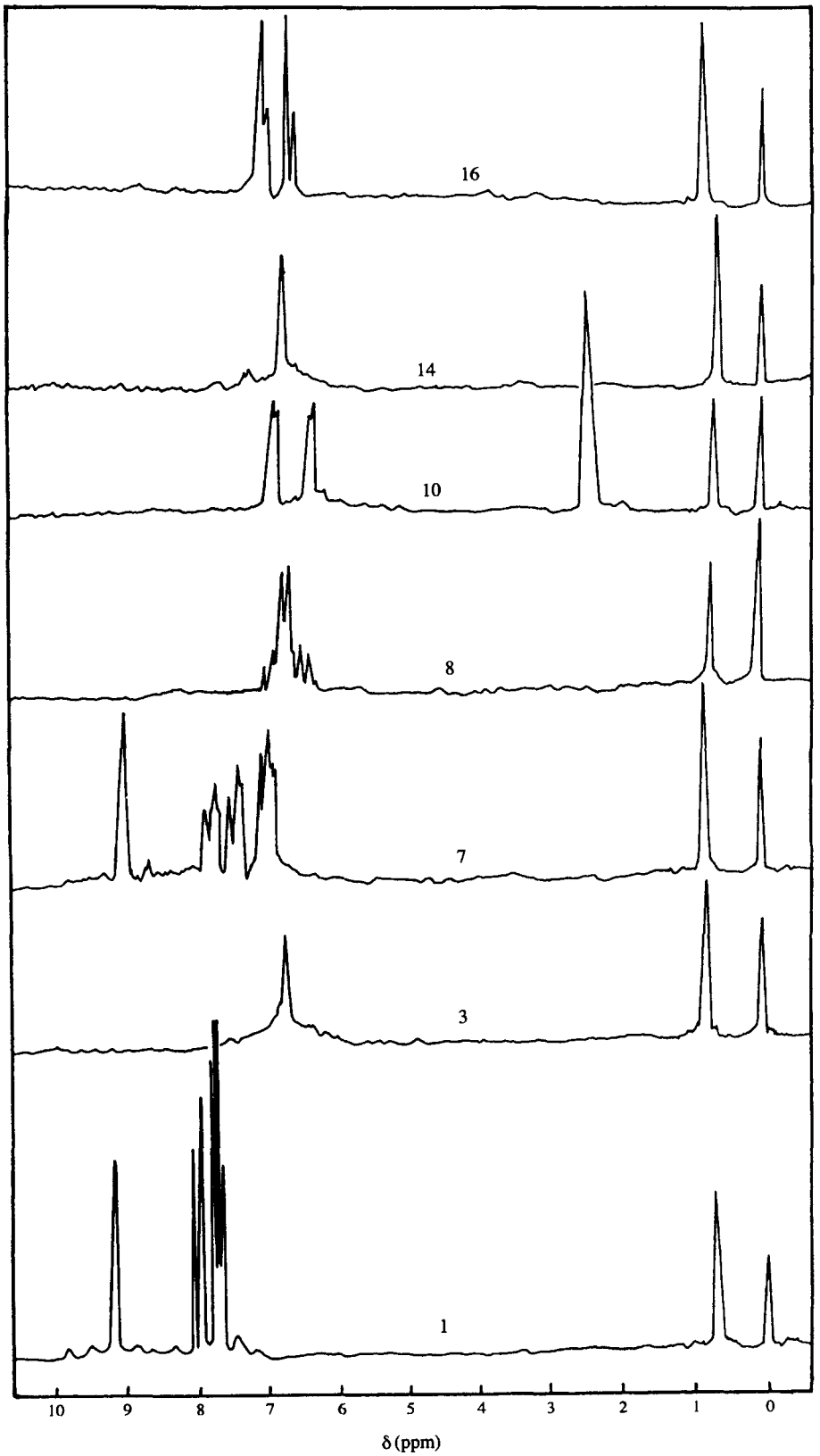


Fig. 1. ^{1}H NMR spectra of some CTCs.

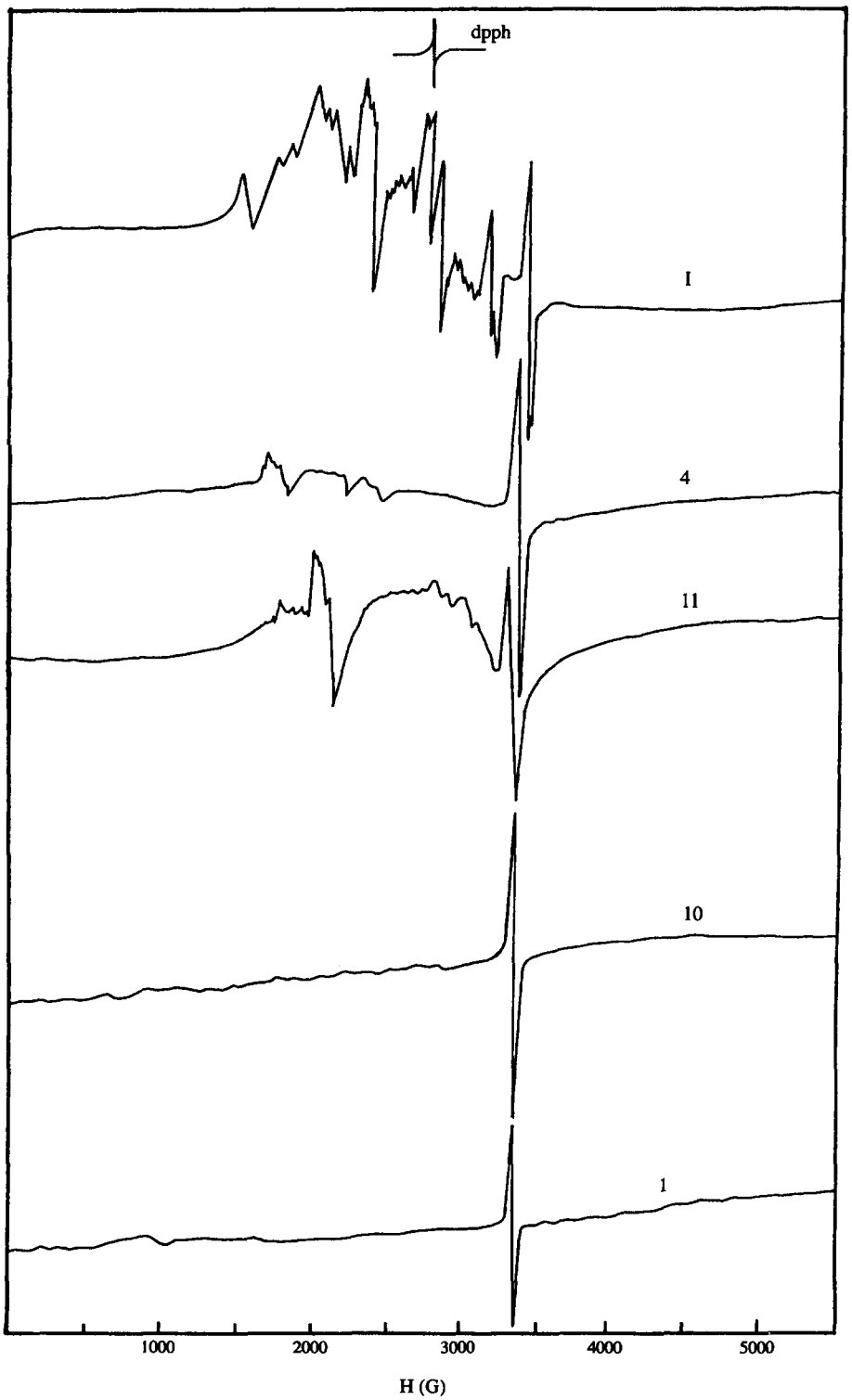


Fig. 2. EPR spectra of **I** and some CTCs.

Table 4. The electronic absorption spectral data (nm) of **I, II** and their CTCs

Compound	^1L_a-^1A phenyl	^1L_b-^1A thiazole	^1L_b-^1A phenyl	Π–Π* Fe^{II}-CN	Π–Π* Fe^{III}-CN	Π–Π* neutral oligomers	CT	Π Π* cation radicals + CT
I					300,430			
II					350,410			
1				315		285,387	360	530
2		235		312		285	370	
3		258		320				490
4		262		320	410		465	
5	220	260	280	318	410		468	
6		250		315	415		435	
7	218	255	285	300	415		470	
8	220	260	285	320				495
9	222	250	295	315	400		465	
10	220	255	290	310				476
11	225	265	275	300	390		445	
12	225	245	350	300	410		455	
13				320		285,385	344	530
14		260		320				492
15	220	255	290	310	412		445	
16	225	264	295	315				485

~2.0 is good evidence for the paramagnetic nature of these CTCs, while the weak intensity and the disappearance of some signals of the polymer **I** or **II** substantiate the intercalation of these donors within the cavities of **I** and **II**. Also the magnetic susceptibilities of the CTC (Table 3) confirm their paramagnetic nature.

The electronic absorption spectra

The electronic absorption spectra of the CTC in Nujol mulls (Table 4 and Fig. 3) show the characteristic bands of thiazole derivatives at 248–262 nm ($^1L_b \leftarrow {}^1A$) and those of benzothiazole derivatives at 220, 275–350 nm ($^1L_a \leftarrow {}^1A$ and $^1L_b \leftarrow {}^1A$ of the phenyl ring) and at 245–264 nm ($^1L_b \leftarrow {}^1A$ of the thiazole moiety) [14]. These bands exhibit pronounced blue shifts relative to those of the free donors. The spectra of the CTCs with $X < 1$ reveal a band at 390–415 nm (Π–Π* transitions of the ($Fe^{III}CN$) building blocks) with the appearance of a new broad band at 300–320 nm (Π–Π* transitions of the ($Fe^{II}CN$) building blocks) [5], indicating the partial reduction of iron(III) to iron(II). In the spectra of the CTCs within $X = 1$, the former band disappears due to complete reduction of iron(III) to iron(II). These results indicate the formation of CTC with $\sigma \leqslant 1$, the case which is further supported by the appearance of a new broad band at 430–470 nm corresponding to CT transitions. The Π–Π* nature of this CT band is shown from the photoelectron spectroscopic studies of thiazole deriva-

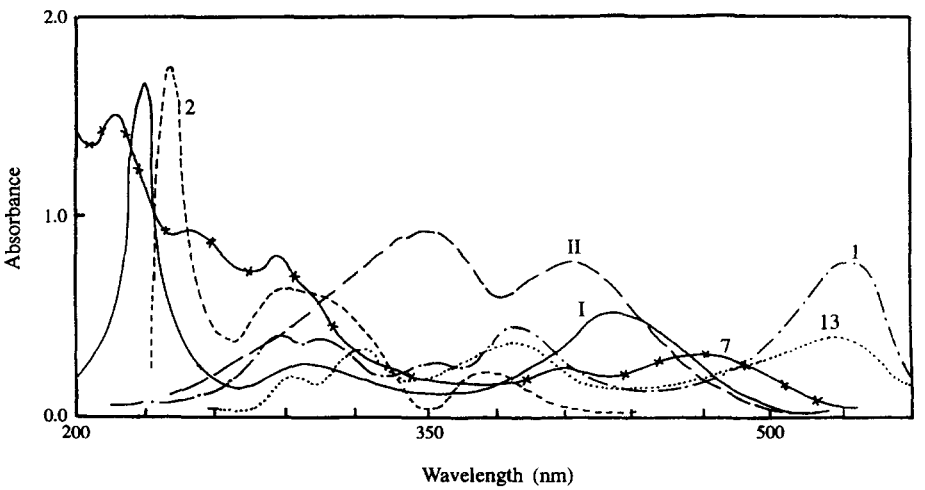


Fig. 3. Electronic absorption spectra of **I, II** and some CTCs.

Table 5. Electrical conductivity and spectral data of some molecular composites

Compound	λ_{max} (nm)	E_{max} (eV)	E_{CT} (eV) calculated	λ_{CT} (nm)	Compound	λ_{max} (nm)	E_{max} (eV)	$\sigma \times 10$ (300 K, S cm^{-1})	Compound	$\sigma \times 10^2$ (300 K, S cm^{-1})
3	490	2.53	2.71	458	**3′**	700	1.77	2.6	**3″**	1.4
8	495	2.51	2.62	473	**8′**	710	1.74	5.1	**8″**	2.5
10	476	2.60	2.74	453	**10′**	670	1.85	0.32	**10″**	0.65
14	492	2.52	2.90	428	**14′**	680	1.82	0.82		
16	485	2.56	2.81	442	**16′**	690	1.79	0.90		

tives [10]; I_p (Π_3–thiazole) = 9.50 eV and I_p (Π_3–2-aminothiazole) = 9.45 eV, which indicate that the CT transitions are from the highest occupied Π-orbitals of thiazoles as electron donors to the LUMO of the polymer **I** or **II** as an acceptor. On the other hand, HMO calculations of benzothiazale derivatives confirm that the cloud of the phenyl ring has more charge density than in the thiazole moiety. Therefore, in the case of benzothiazoles the Π-donation is from the phenyl ring. Also, the spectra of the CTC in Nujol mulls after the addition of 1 M HCl reveal the CT bands at the same position confirming their Π–Π* nature.

The electron affinity of the polymers **I** and **II** as novel acceptors can be calculated by the equation: $h\upsilon_1 - h\upsilon_2 = E_{A1} - E_{A2}$. Using the reported values of electron affinities E_{A1}, of 1,3-dinitrobenzene (1.26 eV), 2,4-dinitrotoluene (1.17 eV) and 1,3,5-trinitrobenzene (1.73 eV) [26,27] and the energies of the CT bands, $h\upsilon_1$, of these acceptors with some thiazole and benzothiazole derivatives [28]. The electron affinities of the polymers **I** and **II** are equal to 1.52 ± 0.05 and 1.45 ± 0.06 eV, respectively. Using the reported values of the adiabatic ionization potentials of thiazole and benzothiazole derivatives [10,28]. The energy of the CT band can be calculated according to the relation given by Briegleb [29].

$$E_{CT} = I_p - E_A + C_1$$

The mean calculated values of the Coulombic factors, C_1, of the polymers **I** and **II** are equal to 4.5 ± 0.18 and 4.4 ± 0.16 eV. The calculated values of E_{CT} (*ca* 2.56–2.90 eV) are reproducible and satisfactory compared with the experimental ones (*ca* 2.52–2.88 eV), except those of molecular composites where a pronounced deviation was observed between the calculated and the experimental E_{CT} values (Table 5). The broad band observed at the longer wavelength in the spectra of **3, 8, 10, 14** and **16** corresponds to two transitions. The first one can be attributed to CT from the donor to the host polymer acting as an acceptor and is located at positions corresponding to the calculated E_{CT} (Table 5). The second transition at 476–495 nm is due to a charge transfer exciton from the benzonoid [—HN—(C_7H_3NS)—NH—] to the quinoid [—N=(C_7H_3NS)=N—] structures, which is similar to that of polyaniline observed at 510 nm (*ca* 2.43 eV).[11] The presence of this band provides evidence for the polymerization of 2-aminothiazole, 2-aminobenzothiazole and 2-amino-6-methylbenzothiazole within the channels of the host polymers **I** and **II**. On the other hand, the spectra of the protonated molecular composites **3′**, **8′**, **10′**, **14′** and **16′** revealed a broad band at 670–718 nm (1.85–1.74 eV) (Fig. 4 and Table 5), corresponding to polaron lattice with the disappearance of the localized quinoid structure as the band at 476–495 nm disappears. This band resembles the broad band observed at 760 nm (1.6 eV) in the optical spectrum of protonated polyaniline [11,30].

The absorption spectra of the CTCs of thiazole as donor are quite different from those of the remaining donors. Thiazole itself absorbs in Nujol mull at 235 nm, while the spectra of **1** and **13** show bands in the region 285–530 nm (Table 4). The band at 235 nm disappears, indicating that the monomer species are not present and instead polymerization occurs. The new bands at 285 and 385 nm are attributed to neutral oligomers [31] formed within the channels of the host 3D polymers **I** and **II**, which are reduced to the isostructural anionic homologue. The bands are rather broad, which may be composed of contributions from several species. However, the band at 285 nm was definitely considered to be the absorbance of neutral oligomers since its intensity increases upon reduction of the species formed during electrochemical oxidation of thiazole [31] and the band at 385 nm disappears in the spectrum of **2**. The absorbance at 530 nm is due to the absorption of the cation radicals as also indicated by EPR spectra and magnetic results of the molecular composites **1** and **13**. On the other hand, the band at 530 nm is absent in the spectrum of **2**, indicating the formation of neutral oligomers which are EPR silent and diamagnetic. The CT band is observed at 360 and 344 nm for **1** and **13**, where the calculated (*ca* 3.48 and 3.65 eV) and the experimental (*ca* 3.45 and 3.60 eV) E_{CT} values are quite concordant. The CTCs behave as very weak semiconductors or insulators (Table 6), while the protonated forms of the molecular composites have good semiconducting

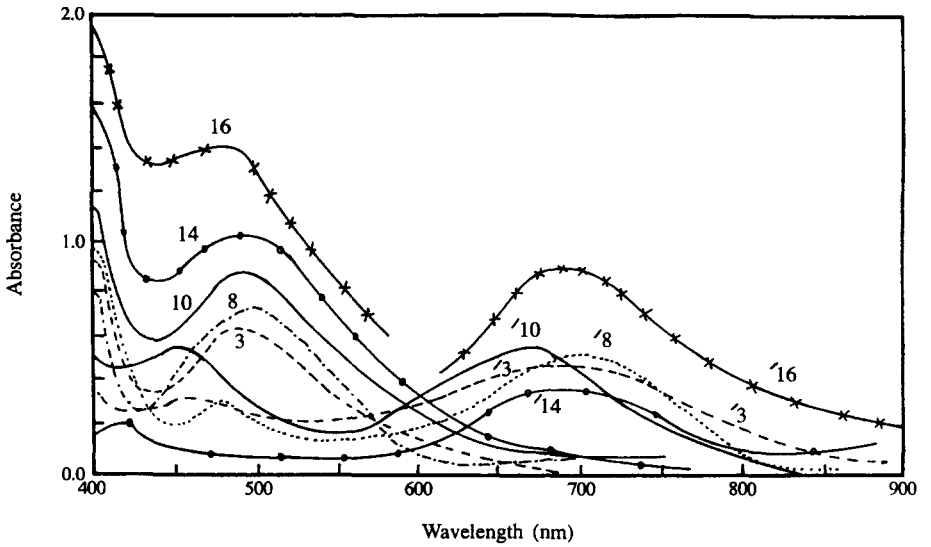


Fig. 4. Electronic absorption spectra of the molecular composites **3**, **8**, **10**, **14** and **16** and their protonated forms **3'**, **8'**, **10'**, **14'** and **16'**.

Table 6. Electrical conductivity (S cm $^{-1}$) at 300 K of **I**, **II** and their CTCs

Compound	σ	Compound	σ	Compound	σ
I	4.2×10^{-8}	**5**	3.0×10^{-6}	**11**	2.8×10^{-7}
II	0.9×10^{-9}	**6**	6.1×10^{-7}	**12**	1.1×10^{-7}
1	2.1×10^{-5}	**7**	4.5×10^{-7}	**13**	1.5×10^{-5}
2	1.2×10^{-7}	**8**	2.5×10^{-5}	**14**	5.7×10^{-6}
3	7.8×10^{-6}	**9**	4.6×10^{-6}	**15**	2.4×10^{-11}
4	3.1×10^{-6}	**10**	5.7×10^{-6}	**16**	1.9×10^{-5}

properties with conductivity higher than the unprotonated ones and than the corresponding authentic samples (Table 5).

This research has shown that the physical properties of the CTC could be varied by changing the host polymer, the donor and conditions of the reaction. Therefore, these CTCs can be tailored to meet specific properties.

REFERENCES

1. S. Eller, P. Schwarz, A. K. Brimah and R. D. Fischer, *Organometallics*. 1993, **12,** 3232.
2. S. Eller, P. Brandt, A. K. Brimah, P. Schwarz and R. D. Fischer, *Angew. Chem.* 1989 **101,** 1274; *Angew. Chem., Int. Edn Engl* 1989, **28,** 1263.
3. S. Eller, M. Adam and R. D. Fischer, *Angew. Chem.* 1990, **102,** 1157; *Angew. Chem., Int. Edn (Engl)* 1990, **29,** 1126.
4. M. Hassanein, and S. E. H. Etaiw, *Eur. Polym. J.* 1993, **29** 47.
5. S. E. H. Etaiw and A. M. A. Ibrahim, *J. Organomet. Chem.* 1993, **456,** 229.
6. A. M. A. Ibrahim, T. M. Soliman, S. E. H. Etaiw and R. D. Fischer, *J. Organomet. Chem.* 1994, **468,** 93.
7. U. Behrens, A. K. Brimah, T. M. Soliman, R. D. Fischer, D. C. Apperley, N. A. Davies and R. K. Harris, *Organometallics* 1992, **11,** 1718.
8. D. C. Apperley, N. A. Davies, R. K. Harris, S. Eller, P. Schwarz and R. D. Fischer, *J. Chem. Soc., Chem. Commun.* 1992, 740.
9. T. M. Soliman, S. E. H. Etaiw, G. Fendesak and R. D. Fischer, *J. Organomet. Chem.* 1991, **415,** C 5.
10. J. V. Metzger, *Comprehensive Heterocyclic Chemistry*, Vol. 6, Part 4B, pp. ed. A. R. Katritzky, W. Rees and K. T. Potts. Pergamon Press, Oxford, 1984 pp. 328–331.
11. E. M. Geniés, A. Boyle, M. Lapkowski and C. Tsintavis, *Synth. Met.* 1990, **36,** 139.
12. S. E. H. Etaiw and A. M. A. Ibrahim, *J. Organomet. Chem.* 1996, **522,** 77.
13. R. H. Herber and Y. Maeda, *Inorg. Chem.* 1981, **20,** 1409.
14. S. E. H. Etaiw, R. S. Farag, A. M. El-Atrash and A. M. A. Ibrahim, *Spec. Chim. Acta* 1992, **48,** 1025.

15. D. C. Apperley, N. A. Davies, R. K. Harris, A. K. Brimah, S. Eller and R. D. Fischer, *Organometallics* 1992, **9,** 2672.
16. A. M. A. Ibrahim, *Can. J. Chem.* 1993, **71,** 318.
17. J. M. Baker, B. Bleaney and K. D. Bowers, *Proc. R. Soc* 1956, **69,** 1205.
18. Y. Nishida, S. Oshio and S. Kida, *Inorg. Chim. Acta.* 1977, **23,** 59.
19. P. Beardwood and F. J. Gibson, *J. Chem. Soc., Dalton Trans.* 1983, 737.
20. H. Hori, *Biochim. Biophys. Acta* 1971, **251,** 227.
21. J. Peisach, W. E. Blumberg, E. T. Lode and M. J. Coon, *J. Biol. Chem.* 1971, **246,** 5877.
22. S. A. Cotton and J. F. Gibson, *J. Chem. Soc. A,* 1971, 803.
23. R. Aasa, S. P. J. Albracht, K. E. Falk, B. Lanne and T. Vanngaed, *Biochim. Biophys. Acta* 1976, **422,** 260.
24. J. M. Ginder, A. F. Richter, A. G. MacDiarmid and A. J. Epstein, *Solid State Commun.* 1987, **63,** 97.
25. E. M. Genies and M. Lapkowski, *J. Electroanal. Chem.* 1987, **236,** 199.
26. M. Batley and L. E. Lyons, *Nature* (*London*), 1962, **196,** 573.
27. G. Briegleb, *Angew. Chem., Int. Edn Engl.* 1964, **76,** 326.
28. R. M. Ramadan, A. M. El-Atrash and A. M. A. Ibrahim, *Spectrochim. Acta,* 1990, **46A,** 1305.
29. G. Briegleb, J. Zekalla and A. Hauser, *Z. Physik. Chem* 1959, **21,** 99.
30. V. Mehrotra and E. P. Gianneiis, *Solid State Commun.* 1991, **77,** 155.
31. M. Olbrich-Stock, J. Posdorfer and R. N. Schindler, *J. Electroanal. Chem.* 1994, **368,** 173, and ref therein.
32. R. Schollhorn, *Angew. Chem.* 1980, **92,** 1015.
33. V. Mehrotra and E. P. Gianneiis, *Solid State Commun.* 1991, **77,** 155.
34. M. S. Whittingham and A. J. Jacobson, (ed.), *Intercalation Chemistry.* Academic press, New York, 1982.

Pergamon

PII: S0277-5387(96)00476-7

Polyhedron Vol. 16, No. 10, pp. 1595–1598, 1997
Copyright © 1997 Elsevier Science Ltd
Printed in Great Britain. All rights reserved
0277-5387/97 $17.00+0.00

Synthesis and crystal structure of copper(II) 2,2,6,6-tetramethylheptan-3,5-dionate adduct with o-phenanthroline

S. I. Troyanov,[a] O. Yu. Gorbenko[a]* and A. A. Bosak[b]

[a]Chemistry Department, Moscow State University, 119899 Moscow, Russia

[b]High School of Material Science, Moscow State University, 119899 Moscow, Russia

(Received 19 September 1995; accepted 25 September 1996)

Abstract—The X-ray crystal structure of $Cu(thd)_2 \cdot Phen$, which is the first adduct of $Cu(thd)_2$ reported to be stable in the vapor phase, was determined. A *cis*-octahedral arrangement of chelate ligands around copper is of low symmetry due to Jahn-Teller distortion and the rigidity of the ligands. Peculiarities of the $Cu(thd)_2 \cdot Phen$ synthesis are discussed. © 1997 Elsevier Science Ltd. All rights reserved.

Keywords: copper; β-diketones; adducts; structure; MOCVD; precursors.

2,2,6,6-Tetramethylheptan-3,5-dionates of metals (thd-complexes) have attracted much attention recently as volatile precursors suitable for application in the MOCVD of complex oxides like high T_c superconductors [1,2]. Perspective single source versions of MOCVD require powder mixtures or organic solutions containing some different thd-complexes [3–5]. $Ba(thd)_2 \cdot 2Phen$ (Phen = o-phenanthroline) [6] is essentially more stable to the hydrolysis and polymerization than $Ba(thd)_2$ and is preferable for the application in MOCVD [7]. No chemical interaction in the system $Ba(thd)_2 \cdot 2Phen$-$Y(thd)_3$-$Cu(thd)_2$ used to deposit $YBa_2Cu_3O_{7-x}$ thin films has been reported so far. It is noteworthy that $Y(thd)_3 \cdot Phen$ was described as thermally unstable [8]. Adducts of $Cu(thd)_2$ with Phen have not been reported so far. At the same time, our preliminary study has shown that some chemical interaction involving $Cu(thd)_2$ occurred in the powder mixture under air or after heating *in vacuo* (XRD patterns of $Cu(thd)_2$ disappear, color changes from deep blue to green).

Only a few adducts of $Cu(thd)_2$ with monodentate N-donors have been isolated in the solid state [9]. All the complexes decomposed at room temperature to form $Cu(thd)_2$. The same was valid for adducts of $Cu(acac)_2$ (acac = acetylacetone) or other unfluorinated β-diketonates of copper(II) [10]. On the contrary $Cu(hfa)_2$ (hfa = hexafluoracetylacetonate) gave rise to various adducts stable at room temperature [11–13]. Only fluorinated β-diketonates have been known to form adducts $CuL_2 \cdot Phen$ and $CuL_2 \cdot 2,2'$-Dipy, where L is a β-diketonate [13].

We present here the synthetic procedures related to the preparation of $Cu(thd)_2 \cdot Phen$ as well as results of its crystal structure determination.

EXPERIMENTAL

Synthetic procedures

Two paths were proposed to synthesize the adduct of $Cu(thd)_2$ with Phen: (1) reaction of $Cu(thd)_2$ with Phen; (2) interaction between $Cu(NO_3)_2 \cdot n$Phen with Nathd. Only the former path was successful.

$Cu(thd)_2$ was synthesized by the reaction of stoichiometric amounts of water solution of $Cu(CH_3COO)_2 \cdot H_2O$ and Hthd and purified by vacuum sublimation (160 C).

$Cu(thd)_2 \cdot Phen$. The solution of anhydrous Phen (5 mmole) and $Cu(thd)_2$ (5 mmole) in 35 cm^3 of dry benzene was prepared. Then benzene was evaporated under aspiration. The green precipitate formed was purified by vacuum sublimation (130 C). Needle-like single crystals of $Cu(thd)_2 \cdot Phen$ were grown by slow cooling of a hot benzene solution.

*Author to whom correspondence should be addressed.

A similar procedure with $Cu(acac)_2$ and Phen was carried out. But only some Phen was collected after heating the powder mixture obtained *in vacuo*. No copper was detected in the sublimate.

$Cu(NO_3)_2 \cdot$Phen and $Cu(NO_3)_2 \cdot$2Phen were prepared from ethanol solutions of $Cu(NO_3)_2 \cdot 6H_2O$ and Phen$\cdot H_2O$ according to the procedure described in [14]. $Cu(NO_3)_2 \cdot$2Phen was formed by dehydration of $Cu(NO_3)_2 \cdot$2Phen$\cdot H_2O$ *in vacuo* (120°C).

Benzene solutions of Nathd were mixed with the copper compounds ($Cu(NO_3)_2 \cdot$Phen or $Cu(NO_3)_2 \cdot$2Phen) in the molar ratio 2:1 with subsequent heating and stirring for 3 h. Partial interaction was presumed for both systems judging by color variation of the solution and precipitate (from deep blue to light blue or greenish blue). However, no $Cu(thd)_2 \cdot$Phen was isolated from the benzene solutions.

Crystal structure determination

A crystal selected with approximate dimensions $0.2 \times 0.2 \times 0.6$ mm was not of good quality, being twinned parallel to the needle axis. The data were collected on a STADI4 (Stoe) diffractometer using Mo-K_α radiation with a graphite monochromator (θ-2θ scan method, $\theta_{max} = 21°$). A wide range of scanning (about 2°) was used due to the twinning so that reflections from both components of the twin could be measured. The cell parameters of triclinic crystals are $a = 10.00(1)$ Å, $b = 11.54(2)$ Å, $c = 16.21(2)$ Å, $\alpha = 71.91(8)°$, $\beta = 85.59(8)°$, $\gamma = 68.20(7)°$, $V = 1650$ Å^3, sp. gr. $P\bar{1}$, $Z = 2$, $d_{calc} = 1.229$ g cm^{-3}. From 3203 reflections measured 2349 were with $I \geqslant 2\sigma(I)$. The crystallographic calculations were performed using the SHELXS-86 and SHELXSL-93 program packages [15]. The structure was solved using a combination of direct and Fourier methods and refined by the full-matrix least-squares technique with anisotropic thermal parameters for all non-hydrogen atoms. The position of the hydrogen atoms were calculated and refined as riding atoms. The final R-values were $R_1 = 0.079$ and $wR_2 = 0.201$. Selected bond lengths and angles are listed in Table 1.

RESULTS AND DISCUSSION

In $CuL_2 \cdot Q$, where Q is a monodentate ligand, Cu has square pyramidal coordination [11,16,17]. According to EPR data Q can occupy an apical position (Q = acetonitrile, DMSO, THF) or basal position (Q = Py, PPh_3) in the structure of $Cu(hfa)_2 \cdot Q$. In a similar way octahedral $CuL_2 \cdot Q$ complexes can adopt *cis* or *trans* positions of the monodentate Q. The former takes place for $Cu(tta)_2 \cdot 2\gamma$-pic [18] and $Cu(hfa)_2 \cdot$2Py [19], the latter for $Cu(tta)_2 \cdot$2Py [20] (Table 2).

There are three possible positions for donor atoms of the bidentate Q′ in $CuL_2 \cdot Q'$ with tetragonally distorted octahedral Cu^{II} system (Fig. 1, Table 2): (a) *trans* coordination leading to the chain-like structure $Cu(acac)_2 \cdot$4,4′-Dipy [21,22], (b) *cis*-coordination in the equatorial plane resulting in equal Cu—N distances and equivalent β-diketonate-anions in $Cu(hfa)_2 \cdot$2,2′-Dipy [23], (c) *cis*-coordination not in the equatorial plane with non-equivalent β-diketonate-anions due to Jahn–Teller distortion. No structural data has been available for the latter possibility. So $Cu(thd)_2 \cdot$Phen is the first example of coordination of type (c) for $CuL_2 \cdot Q'$ (Fig. 2). Average values of Cu—O and Cu—N bond lengths are close to the values for complexes of type (b), as can be seen from Table 2, where the basic structural data for $CuL_2 \cdot Q'$ and $CuL_2 \cdot 2Q$ are presented.

Another feature of copper coordination is the shift of donor atoms from the equatorial plane (~0.11 Å) resulting in a very small tetrahedral distortion of the square.

The type (c) possesses the lowest symmetry among Cu coordination types in $CuL_2 \cdot Q'$ due to (1) Jahn–Teller distortion; (2) rigidity of ligands. As a result of the second factor angles D—Cu—D (D is a donor atom) in chelate rings are all markedly below 90°

Table 1. Selected bond lengths (Å) and angles (°) for $Cu(thd)_2 \cdot$Phen

Cu—O(4)	1.924(6)	O(4)—Cu—O(1)	175.5(3)
Cu—O(1)	1.950(5)	O(4)—Cu—O(3)	91.1(2)
Cu—O(3)	1.960(6)	O(1)—Cu—O(3)	91.8(2)
Cu—N(2)	2.052(7)	O(4)—Cu—N(2)	85.0(3)
Cu—O(2)	2.301(6)	O(1)—Cu—N(2)	92.8(3)
Cu—N(1)	2.393(7)	O(3)—Cu—N(2)	170.0(3)
O(1)—C(3)	1.298(10)	O(4)—Cu—O(2)	93.9(2)
O(2)—C(5)	1.277(10)	O(1)—Cu—O(2)	82.3(2)
O(3)—C(14)	1.288(10)	O(3)—Cu—O(2)	97.1(2)
O(4)—C(16)	1.267(10)	N(2)—Cu—O(2)	92.3(3)
C(3)—C(4)	1.392(12)	O(4)—Cu—N(1)	105.8(2)
C(4)—C(5)	1.399(13)	O(1)—Cu—N(1)	77.3(2)
C(14)—C(15)	1.381(13)	O(3)—Cu—N(1)	97.4(3)
C(15)—C(16)	1.408(12)	N(2)—Cu—N(1)	75.0(3)
		O(2)—Cu—N(1)	155.2(2)

Table 2. Structural data for adducts $CuL_2 \cdot 2Q$ and $CuL_2 \cdot Q'$

N	Compound	Type of O_4N_2 polyhedron (Fig. 1)	Bond lengths (Å)		Reference
			Cu—O	Cu—N	
1	$Cu(tta)_2 \cdot 2Py$	a	2.067(5) 2.143(6)	2.053(9) 2.098(10)	[20]
2	$Cu(acac)_2 \cdot 4,4'$-Dipy	a(t)	1.948(3) 1.949(3) 1.951(3) 1.965(3)	2.449(3) 2.452(3)	[21]
3	$Cu(hfa)_2 \cdot DAO$	a(t)	1.954(5) 1.958(5)	2.566(7)	[22]
4	$Cu(hfa)_2 \cdot Pyz$	a(t)	1.924(7) 2.004(7)	2.529(9)	[17]
5	$Cu(tta)_2 \cdot 2\gamma$-pic	b	1.977(4) 2.125(5)	2.174(5)	[18]
6	$Cu(hfa)_2 \cdot 2Py$	b(t)	1.994(5) 2.002(6) 2.266(6) 2.300(6)	2.003(6) 2.021(7)	[19]
7	$Cu(hfa)_2 \cdot 2,2'$-Dipy	b(t)	1.967 2.296	1.998	[23]
8	$Cu(thd)_2 \cdot Phen$	c(t)	1.924(6) 1.950(5) 1.960(6) 2.301(6)	2.052(7) 2.393(7)	This work

Pyz = pyrazine, DAO = 1,4-diazabicyclo-[2,2,2]-octane, tta = thenoyltrifluoroacetone, γ-pic = 4-methylpyridine, (t)-tetragonal distortion.

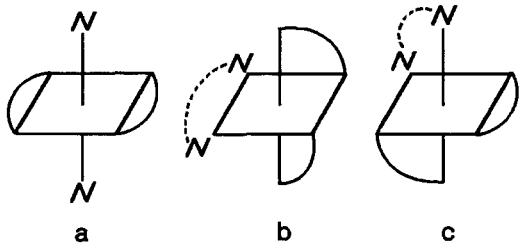


Fig 1. Possible positions for donor atoms in $CuL_2 \cdot Q'$ with tetragonally distorted octahedral Cu^{II} system.

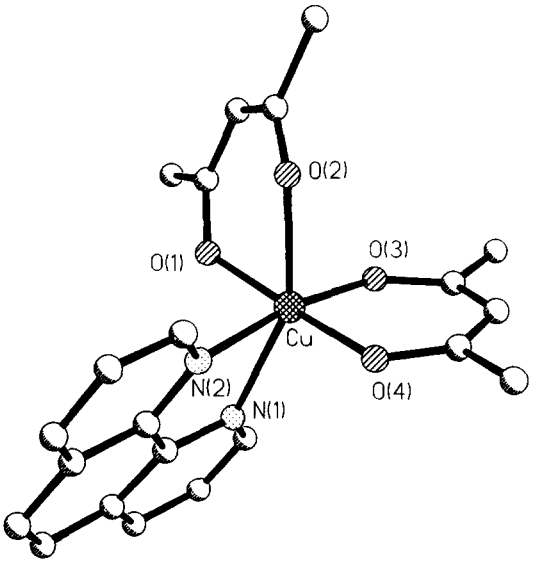


Fig 2. Molecular structure of $Cu(thd)_2 \cdot Phen$.

(especially N(1)—Cu—N(2), 75°). The contribution of the first factor can be demonstrated by comparison with the structure of $Mg(thd)_2 \cdot Phen$ [24] which is without Jahn–Teller distortion. In $Mg(thd)_2 \cdot Phen$ the Mg—O bonds have nearly the same length as Mg—N bonds. Angle distortions are similar too, except those due to the rigidity of ligands. In terms of the same labeling scheme as for $Cu(thd)_2 \cdot Phen$, the maximum deviations are for angles O(1)—Mg—N(2), 100.8° and O(3)—Mg—N(2), 161.2° instead of 90° and 180° respectively for the regular octahedron. The maximal deviating angles in $Cu(thd)_2 \cdot Phen$ are 77° and 155° for *cis* and *trans* positions (Table 1).

It should be also noted that all chelate rings are not planar and bent around D···D lines: 7.8° for Phen-Cu cycle, 11.6° and 30.8° for thd-Cu cycles. The latter value is higher than the usually observed swivel of β-diketonate–metal chelate rings [25].

The knowledge of the molecular structure of $Cu(thd)_2 \cdot Phen$ allows a better understanding of the stability and synthesis of $CuL_2 \cdot Q'$.

Among 3 bidentate chelate ligands in the distorted

tetragonally *cis*-octahedral arrangement around copper atom (types (b) and (c) only one ligand can place both its donor atoms in the equatorial plane. For π-donating ligand this position is most preferable [18] so the competition of ligands for such a position could be expected in the system under investigation. The complex would be stable if one of the competitive configurations is markedly preferable. If no configuration is preferable then both (b) and (c) structures would be unstable. This consideration conforms to the experimental data.

Really Phen or 2,2′-Dipy occupies *cis*-positions in the equatorial plane in octahedral Cu-complexes if other ligands are weaker donors (hfa [23] (Table 2, N7), salicylate [26], anions of inorganic acids [27–29]). On the contrary, stronger donor (thd^-) substitutes Phen in *cis* position of the equatorial plane ($Cu(thd)_2 \cdot Phen$). Judging by the increase of acidity in the sequence Hthd-Hacac-Hhfa one can expect the intermediate behavior for $acac^-$. Actually complexes of (b) or (c) types were not obtained for $Cu(acac)_2$, only (a) type. Moreover stable complexes of general formula $Cu(acac)X \cdot Phen$ (X = anion of strong inorganic acid like NO_3^- or ClO_4^-) with square pyramidal Cu coordination are known with donor atoms of both $acac^-$ and Phen in the basal plane [30].

The idea of competition of π-donating chelate ligands for position in the equatorial plane works well for the choice of synthetic paths to $CuL_2 \cdot Q'$. If the strongest π-donating chelate ligand of $CuL_2 \cdot Q'$ has both its donor atoms in the equatorial plane of the molecular precursor then the synthesis is expected to be successful. If the position is initially occupied by other chelate ligand the kinetic obstacles are possible. Actually $Cu(thd)_2$ with square coordination of copper(II) [31] forms $Cu(thd)_2 \cdot Phen$ easily but $Cu(NO_3)_2 \cdot x Phen$ is not suitable for preparation of the complex.

CONCLUSIONS

The stable complex $Cu(thd)_2 \cdot Phen$ of (c) type has been obtained. The possibility to prepare the adduct $CuL_2 \cdot Phen$ with structure (b) or (c) is determined by competition of π-donating chelate ligands for the position in the equatorial plane of tetragonally distorted octahedral Cu^{II} system.

Some new aspects following from this work are worth further study: (1) possibility of synthesis of adducts of $Cu(thd)_2$ with other chelate bidentate N-donor ligands (2,2′-Dipy, en *et al.*); (2) behavior of $Cu(pta)_2$ (pta = pivaloyltrifluoracetone) to such chelate ligands. Is it similar to $Cu(thd)_2$ or $Cu(hfa)_2$?

REFERENCES

1. H. Yamane and T. Hirai, *High TC Superconductor Thin Films* (Edited by L. Correra), p. 301. Elsevier, North Holland (1992).
2. T. Ozawa, *Thermochimica Acta* 1991, **174,** 185.
3. O. Yu. Gorbenko, V. N. Fuflyigin, Yu. Yu. Erokhin, A. R. Kaul and G. Wahl, *J. Mater. Chem.* 1994, **4,** 1585.
4. W. J. Lackey, W. B. Carter and J. A. Hanigofsky *Appl. Phys. Lett.* 1990, **56,** 1175.
5. A. R. Kaul and B. V. Seleznev, *J. de Physique IV*, 1993, Coll. C3, suppl. *J. de Physique II*, **3,** 375.
6. N. Kuzmina, V. Ivanov, S. Troyanov and L. Martynenko, *J. CVD* 1994, **3,** 32.
7. S. Aoki, T. Yamaguchi, A. Kagawa and O. Kohno, *Phase Transitions* 1993, **42,** 123.
8. E. M. Gavrishuk, N. G. Dzubenko and L. I. Martynenko, *Theoretical and Applied Chemistry of Metal β-Diketonates* Edited by V. I. Spytsin and L. I. Martynenko), p. 86. Moscow, Nauka (1985).
9. P. E. Rakita, S. J. Kopperl and J. P. Fackler, *J. Inorg. Nucl. Chem.* 1968, **30,** 2139.
10. D. P. Graddon and E. C. Watton, *J. Inorg. Nucl. Chem.* 1961, **21,** 49.
11. D. R. McMillin, R. S. Drago and J. A. Nusz, *J. Am. Chem. Soc.* 1976, **98,** 3120.
12. L. L. Funch and T. R. Ortolano, *Inorg. Chem.* 1968, **7,** 567.
13. V. J. Zub, E. A. Mazurenko and S. V. Volkov, *Koord. khim.* 1989, **15,** 623.
14. F. M. Jaeger and J. A. van Dijk, *Z. anorg. allg. Chem.* 1936, **227,** 273.
15. G. M. Sheldrick, SHELXL-93, *Program for Crystal Structure Refinement*. Goettingen University (1986).
16. J. Parimala, O. Shun'ichiro and F. Quintus, *J. Inorg. Nucl. Chem.* 1969, **31,** 1971.
17. R. C. E. Belford, D. E. Fenton and M. R. Truter, *J. Chem. Soc., Dalton. Trans.* 1974, 17.
18. J. A. Pretorius and J. C. A. Boeyens, *J. Inorg. Nucl. Chem.* 1978, **40,** 407.
19. J. Pradilla-Sorzano and J. P. Fackler, *Inorg. Chem.* 1973, **12,** 1174.
20. J. A. Pretorius and J. C. A. Boeyens, *J. Inorg. Nucl. Chem.* 1978, **40,** 1745.
21. Yuanzhi Xu and Shu Shi, *Acta Chim. Sin.* 1986, **44,** 336.
22. R. C. E. Belford, D. E. Fenton and M. R. Truter, *J. Chem. Soc., Dalton. Trans.* 1972, 2208.
23. M. V. Veidis, G. H. Schreiber, T. E. Gough and G. J. Palenic, *J. Am. Chem. Soc.* 1969, **91,** 1859.
24. I. E. Soboleva, N. P. Kuzmina, S. I. Troyanov and L. I. Martynenko, *Koord. khim.*, 1995, **15,** 688.
25. L. M. Shkol'nikova and M. A. Porai-Koshitz, *Itogi Nauki i Techniki* 1982, **16,** 117.
26. X. Solans, *Acta Cryst.* 1987, **C43,** 428.
27. R. J. Majeste and E. A. Meyers, *J. Phys. Chem.* 1970, **74,** 3497.
28. A. Benchini, A. C. Fabretti, C. Zanchini and P. Zannini, *Inorg. Chem.* 1987, **26,** 1445.
29. P. C. Healy, J. M. Patrici and A. H. White, *Austral. J. Chem.* 1984, **37,** 1111.
30. S. I. Troyanov, A. N. Grigor'ev, A. A. Drozdov and L. I. Martynenko, *Zh. neorg. khimii* 1992, **37,** 107.
31. N. I. Kirillova, Yu. T. Struchkov, L. I. Martynenko and N. G. Dzubenko, *β-Diketonates of Metals*, p. 41. Moscow, Nauka (1978).

Pergamon

PII: S0277-5387(96)00483-4

Polyhedron Vol. 16, No. 10, pp. 1599–1603, 1997
Copyright © 1997 Elsevier Science Ltd
Printed in Great Britain. All rights reserved
0277-5387/97 $17.00+0.00

Solid state structure and spectroscopic properties of $[WCl(SnCl_3)(CO)_3(\eta^4\text{-NBD})]$, NBD = norbornadiene

Teresa Szymańska-Buzar* and Tadeusz Głowiak

Faculty of Chemistry, University of Wrocław, 50-383 Wrocław, Poland

(Received 10 September 1996; accepted 25 September 1996)

Abstract—The heterobimetallic complex $[WCl(SnCl_3)(CO)_3(NCMe)_2]$(**1**) reacts with norbornadiene (NBD) at room temperature, liberating two acetonitrile ligands to form the seven-coordinate complex $[WCl(SnCl_3)(CO)_3(\eta^4\text{-NBD})]$(**2**). The compound **2** is the first structurally characterized example of monomeric, halocarbonyls with a tungsten–tin bond in which a diene ligand is present on tungsten. The IR, ^{13}C NMR spectra of **2** are also described and can be correlated with the crystallographically observed geometry. The structure of **2** provides a good model for comparing the *trans* influence of the chlorine and carbon monoxide ligands in this molecule. © 1997 Elsevier Science Ltd. All rights reserved.

Keywords: tungsten; tin; norbornadiene; crystal structure; seven-coordinate complex.

There is currently considerable interest in seven-coordinate complexes of tungsten(II), in particular the complexes $[WCl_2(CO)_3L_2]$, L = phosphine, arsine, which have recently been found to be catalysts for the metathesis of alkenes and polymerization of alkenes or alkyne [1–5]. These complexes require Lewis acid activation to be metathesis or polymerization catalysts at room temperature [4,5].

In the course of our investigation of the $W(CO)_6$–Lewis acid interaction we developed a new photochemical method for the preparation of tungsten(II)-Lewis acid adducts. This method has been successfully applied to the preparation of the highly versatile compound $[(CO)_4W(\mu\text{-}Cl)_3W(SnCl_3)(CO)_3]$ [6], which reacts with substances (L) containing nitrogen or phosphorus as donor atoms, to give products of the type $[WCl(SnCl_3)(CO)_3L_2]$ and $[WCl_2(CO)_3L_2]$ [7]. In a previous paper [7,8] we described a new high-yield synthesis of the acetonitrile complex $[WCl(SnCl_3)(CO)_3(NCMe)_2]$(**1**). Studies are in progress to explore the reactivity of that and the other tungsten(II) carbonyl complexes. Olefin binding to the metal centre has often been suggested and tungsten–alkene complexes have been proposed as key intermediates in several catalytic reactions; however, only a few examples of stable tungsten(II) alkene complexes have been reported [9,10].

The first tungsten(II) diene, e.g. norbornadiene, compound was prepared by Davidson and Vasapollo [9] in reaction of the tungsten(II) complex $[WBr_2(CO)_4]_2$ with norbornadiene. Next, from an X-ray crystallographic study, the compound was shown to be $[WBr_2(CO)_2(NBD)]$ [10]. The small number of tungsten(II) alkene complexes known is almost certainly due to the instability of alkene compounds. We now report a new high-yield synthesis of the complex $[WCl(SnCl_3)(CO)_3(\eta^4\text{-NBD})]$(**2**), from the reaction of **1** with norbornadiene. The unknown coordination geometry of the diene compound **2** together with the fact that compounds of this class can be used as a model of a catalytic centre make it an interesting problem for X-ray structure analysis.

Although many studies of seven-coordinate molybdenum(II) compounds of the general formula $MoCl(SnR_nCl_{3-n})(CO)_3(NCMe)_2$, (R = Me, Bu, Ph) have been carried out [11–17] to date there has been no report of these compounds reacting with an alkene or diene. For these reasons we consider it unusually interesting that tungsten(II) species of the $[WCl(SnCl_3)(CO)_3(\eta^4\text{-NBD})]$(**2**) type can be prepared directly from **1**.

*Author to whom correspondence should be addressed.

EXPERIMENTAL

All reactions were carried out under nitrogen by standard Schlenk line techniques. The solvents and reagents applied were dried, distilled and deoxygenated.

IR spectra were recorded on a Nicolet FT-IR Model-400 spectrometer by means of KBr pellets. Far-IR spectra were recorded (600–100 cm^{-1}) with a Brüker IFSv instrument in a Nujol mull on a polyethylene film. ^1H and $^{13}C\{^1H\}$ NMR spectra were recorded on AMX 300 Brüker spectrometer. An UV-vis absorption spectra were recorded on a Hewlett Packard 8452A spectrophotometer.

$[WCl(SnCl_3)(CO)_3(NCMe)_2]$(**1**) was prepared by a reaction of $[(CO)_4W(\mu\text{-}Cl)_3W(SnCl_3)(CO)_3]$ in acetonitrile according to the literature method [7,8]. To **1** (0.15 g, 0.25 mmol) dissolved in CH_2Cl_2 (25 cm^3) with continuous stirring under a stream of nitrogen a ten-fold excess of norbornadiene (0.3 cm^3, 2.5 mmol) was added *via* syringe. The mixture was stirred for 4 days during which time an orange solution of **1** gradually changed to a reddish-brown colour, while the ν(CO) frequencies of **1** disappeared. After the completion of the reaction, the solution was separated from some insoluble green powder by filtration. The isolation of the product by precipitation with heptane produced the analytically pure yellow crystalline complex of **2** (yield = 0.12 g, 80%).

IR(KBr): ν(C≡O) 2087w, 2040s(sh), 2021s(sh) and 2006 vs cm^{-1}; (Nujol): ν(C≡O) 2085w, 2040s(sh), 2020sh and 2003vs; ν(Sn—Cl) 351, 336, ν(W—Cl) 307w. ^1H NMR (CD_2Cl_2) δ 5.04(t, 2H, J = 2.5 Hz, =C*H*), 3.97(s, broad, 2H, C*H*), 3.71(t, 2H, J = 2.5 Hz, =C*H*), 1.50(t, 1H, J = 1.29 Hz, C*H*H), 1.48(t, 1H, J = 1.50 Hz, CH*H*) ppm; $^{13}C\{^1H\}$ NMR (CD_2Cl_2) δ 202.28 and 193.47 (*C*O), 81.81(=*C*H), 64.00(*C*H_2), 44.24(*C*H), 43.11(=*C*H), ppm; ^{13}C NMR (CD_2Cl_2) δ 82.9, 80.48 ppm ($J_{^{13}C\text{-}^1H}$ = 182 Hz, =*C*H), 65.7, 63.9 ppm ($J_{^{13}C\text{-}^1H}$ = 135 Hz, *C*H_2), 45.1, 43.0 ppm ($J_{^{13}C\text{-}^1H}$ = 157 Hz, *C*H), 44.2, 41.7 ppm ($J_{^{13}C\text{-}^1H}$ = 188 Hz, =*C*H). Abs.max.(CH_2Cl_2): λ, nm (ε, L mol^{-1} cm^{-1}): 384(278), 292(7973), 254(7882).

Crystallography

The yellow crystals of **2** were grown from a CH_2Cl_2/heptane (10:1) solution. The crystals were stable enough when handled in an inert atmosphere or coated with a light hydrocarbon oil to protect them from the atmosphere.

Crystallographic data were obtained using a KM4 κ-axis computer-controlled [18] four-circle diffractometer operating in the ω-2θ scan mode with graphite-monochromated Mo-K_α radiation (λ = 0.71069 Å). Cell dimensions were obtained by a least-squares refinement on setting angles of 36 well-spaced reflections in the range $19.8 < \theta < 35.6°$. The details of the crystal data intensity measurement are given in Table 1.

The structure was solved by heavy-atom methods with the SHELXS-86 program [19] and refined by a full-matrix least-squares method, using the SHELXL program [20]. Neutral atomic scattering factors were taken from the SHELXL-93 program [20]. For non-hydrogen atoms, refinement with anisotropic temperature factors converged to $R_1 = 0.0319$ and $wR_2 = 0.0815$. H atoms were fixed in trigonal or tetrahedral positions at 0.98 or 0.97 Å from the C atoms to which they were bonded.

Supplementary publication material includes positional parameters, remaining dimensions, torsion angles, anisotropic thermal parameters, and hydrogen positions.

RESULTS AND DISCUSSION

The tungsten(II) bis(acetonitrile) complex **1** [7,8] was synthesized by the reaction of $[(CO)_4W(\mu\text{-}Cl)_3W(SnCl_3)(CO)_3]$ [6] with CH_3CN in toluene at room temperature. Upon addition of diene to an orange solution of **1** in CH_2Cl_2 the colour gradually changes to reddish-brown, while the ν(CO) frequencies (2040s, 2020s, 1970m(sh) and 1930vs(br) cm^{-1}) of **1** disappear and the ν(CO) band at about 2080 cm^{-1} characteristic of norbornadiene complex **2** reaches a maximum. In order to drive the reaction to completion a ten-fold excess of the diene was necessary. After the completion of the reaction, isolation

Table 1. Crystal data and details of refinement for **2**

Chemical formula	$C_{10}H_8Cl_4O_3SnW$
Molecular weight	620.50
Crystal system	monoclinic
Space group	$P2_1/c$
a (Å)	8.718(2)
b (Å)	14.252(3)
c (Å)	13.134(3)
β(°)	106.91(3)
V(Å^3)	1561.3(6)
Z	4
T(K)	291(2)
Crystal size (mm)	0.10 × 0.10 × 0.12
D_c (g cm^{-3})	2.640
μ(Mo-K_α) (cm^{-1})	96.43
F(000)	1136
Method of collection	$\omega/2\theta$ scan
Index ranges	$0 \leqslant h \leqslant 10$
	$0 \leqslant k \leqslant 18$
	$-16 \leqslant l \leqslant 16$
2θ range (°)	$4 < 2\theta < 54$
No. of unique data	2840
No. of data with $I \geqslant 4\sigma(I)$	2155
Residuals R_1, wR_2	0.0319, 0.0815
Extinction coefficient	0.0092
Quality of fit	1.101
Final ($\Delta\rho$)e(Å^{-3})	−2.974/2.250

of the product by precipitation with heptane yields moderately air-stable yellow crystals of **2** in an 80% yield. The compound **2** is slowly hydrolysed on exposure to air, but no special precautions seem necessary to exclude air from the solvents to prepare crystals.

The molecule $[WCl(SnCl_3)(CO)_3(\eta^4\text{-NBD})]$(**2**), is shown in Fig. 1 together with the atomic numbering scheme. Table 2 contains selected bond distances and bond angles. The environment of the tungsten atom is a distorted capped trigonal prism with the tin atom occupying the unique capping position above the centre of the quadrilateral face defined by the chlorine and three carbonyl groups, two double bonds of norbornadiene making up the remaining edge. The square face that is capped by the $SnCl_3$ group is distorted. The major distortions from regularity of the prism appear to be associated with the presence of the chlorine atom in the capped quadrilateral face and with the fact that the W—Cl bond, at 2.454(2) Å, is considerably longer than the three W—CO distances (2.04 Å av). The angles subtended at the tungsten atom by the four atoms determining the capped face are in the range 82.1(3)–93.8(4) , whereas the angle subtended at the tungsten atom by the midpoints of the norbornadiene carbon–carbon double bonds is only 63.6(2) . Two CO groups in the capped face are mutually *cis* with C(2)—W—C(3) angle 92.4(4) and almost the same W—C distances, 2.029(9) and 2.032(9) Å, but the third CO group is in a *trans* position with a longer W—C(3) distance equal 2.06(1) Å. The *trans*-$W(CO)_2$ unit is slightly bent at the metal atom, the C—W—C angle being 166.8(4) .

The coordination of norbornadiene ligand is arranged in two types; the C=C *trans* to CO and the C=C *trans* to Cl. This gives rise to a slight difference between the W—C distances; such that W—C(6) = 2.326(8) Å and W—C(7) = 2.306(9) Å are almost 0.1 Å shorter than W—C(4) = 2.407(9) Å and W—C(5) = 2.413(8) Å. The two shorter bonds are both *trans* to chlorine ligand and longer *trans* to carbonyl. The above bond lengths are in excellent agreement with the degree of electron back-donation from the $d\pi$-orbitals of tungsten to the ligands whose π acidity is taken into account. As CO is a better π acid than C=C, back-donation to CO is much preferred. For the C=C and its *trans* Cl pair, the electron density due to back-donation is almost wholly accepted by C=C, resulting in shortened W—C(6) and W—C(7) distances and in a lengthened C(6)—C(7) distance compared to W—C(4), W—C(5) and C(4)—C(5) distances.

The structure of **2** thus provides a good model for comparing the *trans* influence of the chlorine and carbon monoxide ligands in this molecule.

The tungsten–tin bond is short at 2.764(1) Å compared to the sum of the relevant covalent radii of 2.97 Å [21, 22] but the longest of those observed previously. The W—Sn distances of 2.731(1),[6] 2.710(1),[8] 2.711(1) [23] and 2.737(1) [23], 2.759(3) [24] Å have been observed.

The tin atom is four-coordinate with a geometry that is best described as distorted tetrahedral; the mean W—Sn—Cl angle (118.78 av.) is greater than the mean Cl—Sn—Cl angle (98.79 av.), which is consistent with Bent's rule [25] that atomic *p* character

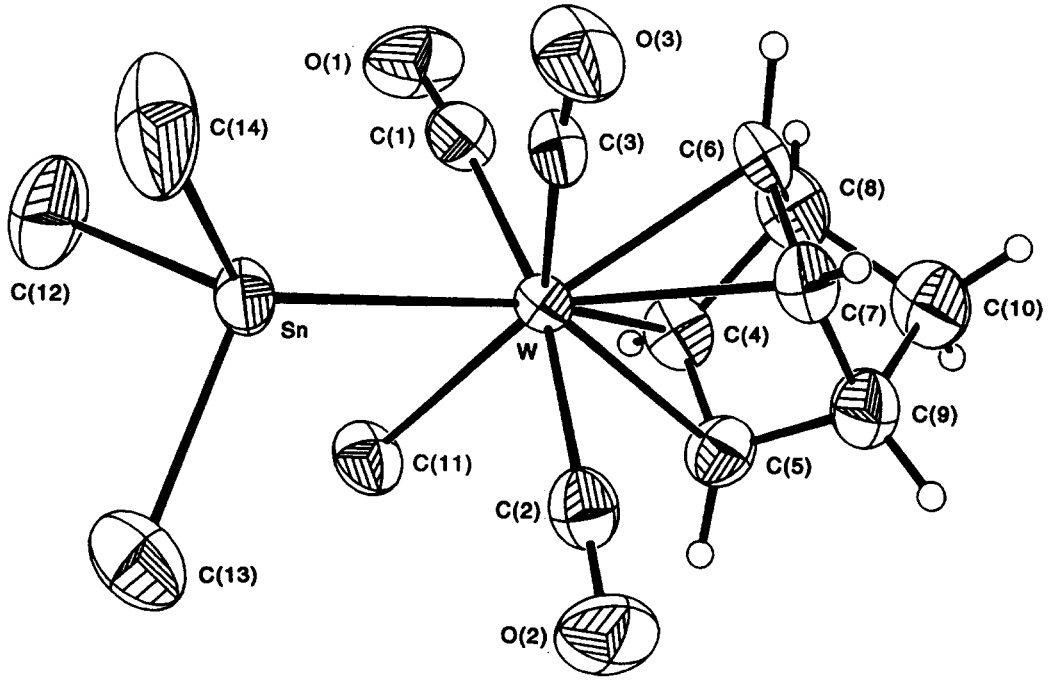


Fig. 1. An ORTEP drawing of $[WCl(SnCl_3)(CO)_3(\eta^4\text{-NBD})]$(**2**) molecule, giving the atomic labeling scheme.

Table 2. Bond lengths (Å) and angles (°) for **2**

W—Sn	2.764(1)	C(4)—C(5)	1.348(13)
W—C(1)	2.06(1)	C(6)—C(7)	1.388(13)
W—C(2)	2.029(9)	O(1)—C(1)	1.119(12)
W—C(3)	2.032(9)	O(2)—C(2)	1.127(11)
W—C(4)	2.407(9)	O(3)—C(3)	1.120(10)
W—C(5)	2.413(8)	C(4)—C(8)	1.568(13)
W—C(6)	2.326(8)	C(5)—C(9)	1.515(13)
W—C(7)	2.306(9)	C(6)—C(8)	1.522(13)
W—Cl(1)	2.454(2)	C(7)—C(9)	1.559(13)
Sn—Cl(2)	2.321(3)	C(8)—C(10)	1.527(15)
Sn—Cl(4)	2.344(3)	C(9)—C(10)	1.527(14)
Sn—Cl(3)	2.344(3)		
C(1)—W—Sn	86.0(3)	C(2)—W—C(6)	112.3(3)
C(2)—W—Sn	84.9(2)	C(3)—W—C(6)	74.5(3)
C(3)—W—Sn	72.1(2)	C(7)—W—C(6)	34.9(3)
Cl(1)—W—Sn	69.32(6)	C(2)—W—C(7)	77.4(3)
C(4)—W—Sn	147.8(2)	C(3)—W—C(7)	73.8(3)
C(5)—W—Sn	146.2(2)	C(7)—W—Cl(1)	142.2(2)
C(6)—W—Sn	142.9(2)	C(6)—W—Cl(1)	141.1(2)
C(7)—W—Sn	140.6(2)	C(4)—W—Cl(1)	81.6(2)
C(1)—W—C(2)	166.8(4)	C(5)—W—Cl(1)	82.5(2)
C(1)—W—C(3)	93.8(4)	Cl(2)—Sn—Cl(3)	101.83(12)
C(1)—W—Cl(1)	82.1(3)	Cl(2)—Sn—Cl(4)	97.85(13)
C(1)—W—C(4)	76.5(3)	Cl(4)—Sn—Cl(3)	96.69(13)
C(1)—W—C(5)	108.7(4)	Cl(2)—Sn—W	117.21(9)
C(1)—W—C(6)	80.6(3)	Cl(4)—Sn—W	123.30(8)
C(1)—W—C(7)	115.5(3)	Cl(3)—Sn—W	115.84(8)
C(2)—W—C(3)	92.4(4)	O(1)—C(1)—W	173.6(8)
C(2)—W—Cl(1)	85.9(3)	O(2)—C(2)—W	176.5(8)
C(3)—W—Cl(1)	141.4(2)	O(3)—C(3)—W	175.6(7)
C(2)—W—C(4)	106.9(3)	C(5)—C(4)—W	74.0(5)
C(3)—W—C(4)	135.0(3)	C(8)—C(4)—W	96.5(5)
C(6)—W—C(4)	60.6(3)	C(4)—C(5)—W	73.5(5)
C(7)—W—C(4)	71.5(3)	C(9)—C(5)—W	97.2(5)
C(2)—W—C(5)	74.6(3)	C(7)—C(6)—W	71.8(5)
C(3)—W—C(5)	134.1(3)	C(8)—C(6)—W	101.2(5)
C(4)—W—C(5)	32.5(3)	C(6)—C(7)—W	73.4(5)
C(6)—W—C(5)	70.7(3)	C(9)—C(7)—W	100.4(6)
C(7)—W—C(5)	60.5(3)		

concentrates in orbitals directed towards electronegative substituents. The Sn—Cl distances, one shorter (2.321(3) Å), and two longer (2.344(3) Å), observed in **1** are much shorter than in uncoordinated trichlorostannate: 2.53 Å in $CsSnCl_3$ [26]. This can be explained by coordination of the trichlorostannate to tungsten which removes electron density from tin. This loss of electron density is compensated by π bonding between the tin and the chloride, thus shortening the tin–chlorine bond [27].

A common feature of the structures reported for seven-coordinate complexes containing W—Sn or Mo—Sn bond such as $[WCl(SnCl_3)(CO)_3(NCMe)_2]$ [8] $[WCl(MeSnCl_2)(CO)_3(C_4H_{10}S_2)]$ [24], $[MoCl(SnCl_3)(CO)_3(C_4H_{10}S_2)](CH_2Cl_2)$ [28] and $[MoCl(MeSnCl_2)(CO)_3(C_{10}H_8N_2)]$ [29] is a distorted capped octahedron geometry and the presence of a tin atom in the unique capping position and a chlorine atom bridging the W—Sn or Mo—Sn bond with Sn—μ—Cl distances in the range 2.781–2.958 Å and M—Sn—Cl angles in the range 52.1–55.2°. In contrast, in the structure of **2** the chlorine atom bonded to W is very far from the Sn atom (2.979(2) Å) and W—Sn—Cl angle is only 50.4(2)°. The geometrical arrangement of the seven ligand atoms around the tungsten atom in **2** more closely approximates a capped trigonal prism.

A noticeable feature of **2** is the exceptionally high ν(CO) frequency (2087 cm^{-1}), which is among the highest known for seven-coordinate $[WX_2(CO)_3L_2]$ type compounds, comparable only with that for halocarbonyls $[WX_2(CO)_4]_2$ [6]. This frequency is significantly higher than that of analogous $[WBr_2(CO)_2NBD]$ (2063 cm^{-1} [10]). This indicates that smaller electron density is being back donated into empty π^*-orbitals of the CO ligands. This implies that $SnCl_3^-$ is more electronegative and capable of acting as a more effective π-acceptor than Cl or Br

and as a result there is smaller W—CO back donation in **2**.

The lower frequency region of the infrared spectrum is dominated by the principal absorptions at 352, 336 cm^{-1}, which can be regarded as ν_s and ν_{as} (Sn—Cl) vibration. Tin-halide frequencies of the $[SnCl_3]^-$ ion were observed in, for example, $[Et_4N][SnCl_3]$ at 295(A_1) and 259 cm^{-1} (E) [30] but increase upon coordination of $SnCl_3^-$ to metal or other ligand. The band at 307 cm^{-1} is assigned to the W—Cl stretching vibration.

The ^1H NMR spectrum of **2** shows five well-separated groups of signals consistent with the solid structure of **2**. The absorption at δ 5.04 is protons attached on the same double bond, while the peaks at 3.71 are protons attached to the other double bond. The resonance of olefin protons is at a higher field than that of the free norbornadiene by 1.77 and 3.10 ppm but lower by 0.41 and higher by 0.92 ppm than that of the tungsten(0) complex $[W(CO)_4NBD]$ (4.63 ppm [31]). The ^{13}C NMR spectrum shows two carbonyl resonances at δ 202.28 and 193.47 ppm, in an intensity ratio of 1 : 2 in keeping with the symmetry of **2** in the solid state. The resonance at δ 193.47 ppm can be assigned to the carbonyls that are mutually *trans*. This resonance is slightly highfield compared to the signal of the CO group that is *trans* to the C=C unit of norbornadiene. Carbon signals of coordinated NBD were correctly assigned by observing the $^{13}C-^1H$ coupling constants. One of the double bond resonances (43.11 ppm) shifts more upfield than other carbon signals, yet the coupling constant stays in the range characteristic of double bond carbons (188 Hz). As the most remarkable feature we note the large difference between the two C=C units of norbornadiene, which are separated by 38.7 ppm: $\Delta\delta = 100.1$ and 61.39 ppm. The coordination shift for $[W(CO)_4(NBD)]$ [32] is 74.4 ppm. Thus, we assign the lower field norbornadiene signal of **2** to the two carbons of the C=C unit in the *trans* position to the CO group and the signal at higher field to the two carbons of the double bond *trans* to the chlorine. With regard to the origin of this effect, the coordination shift correlates with the W—C bond distance and with the degree of metal ($d\pi$) → olefin(π^*) back-donation.

Acknowledgements—The authors thank the KBN (Grant No. 3T09A 094 10) for financial support of this work.

REFERENCES

1. L. Bencze, K. J. Ivin, and J. J. Rooney, *J. Chem. Soc., Chem. Comm.* 1980, 834.
2. L. Bencze and A. Kraut-Vass, *J. Mol. Catal.* 1984, **28,** 369; *J. Organomet. Chem.* 1984, **270,** 211.
3. L. Bencze, A. Kraut-Vass and L. Prókai, *J. Chem. Soc., Chem. Comm.* 1985, 911.
4. T. Szymańska-Buzar, *J. Mol. Catal.* 1991, **28,** 369.
5. T. Szymańska-Buzar, *J. Mol. Catal.* 1994, **93,** 137.
6. T. Szymańska-Buzar, T. Głowiak, *J. Organomet. Chem.* 1995, **489,** 207.
7. T. Szymańska-Buzar, *J. Organomet. Chem.* 1995, **492,** 241.
8. T. Szymańska-Buzar, T. Głowiak, unpublished results.
9. J. L. Davidson and G. Vasapollo, *J. Organomet. Chem.* 1983, **241,** C24.
10. F. A. Cotton and J. H. Meadows, *Inorg. Chem.* 1984, **23,** 4688.
11. P. K. Baker and A. Bury, *J. Organomet. Chem.* 1989, **359,** 189;
12. P. K. Baker and A. Bury, *Polyhedron* 1989, **8,** 917.
13. P. K. Baker and A. J. Quinlan, *Inorg. Chim. Acta* 1989, **162,** 179.
14. D. Miguel, J. A. Pérez-Martinez, V. Riera and S. Garcia-Granda, *Polyhedron* 1991, **10,** 1717;
15. D. Miguel, J. A. Pérez-Martinez, V. Riera and S. Garcia-Granda, *J. Organomet. Chem.* 1993, **455,** 121.
16. G. Barrado, D. Miguel, J. A. Pérez-Martinez, V. Riera and S. Garcia-Granda, *J. Organomet. Chem.* 1993, **463,** 127.
17. M. Cano, M. Panizo, J. A. Campo, J. Tornero and N. Menéndez, *J. Organomet. Chem.* 1993, **463,** 121.
18. *KUMA KM4 Software, User's Guide, Version* 3.1, KUMA DIFFRACTION, Wrocław, Poland (1989).
19. G. M. Sheldrick, *Acta Cryst.* 1990, **A46,** 467.
20. G. M. Sheldrick, SHELXL-93. *Program for the Refinement of Crystal Structure.* University of Göttingen, Germany (1993).
21. V. A. Siemion, Y. A. Chapovskii, Yu. T. Struchkov and A. N. Nesmeyanov, *Chem. Commun.* 1968, 666.
22. J. E. O'Connor and E. R. Corey, *J. Am. Chem. Soc.* 1967, **89,** 3930.
23. A. L. Balch and D. E. Oram, *Organometallics* 1988, **7,** 155.
24. M. Elder and D. Hall, *Inorg. Chem.* 1969, **8,** 1273.
25. H. A. Bent, *Chem. Rev.* 1961, **61,** 275.
26. P. G. Harrison, B. J. Haylett and T. J. King, *Inorg. Chim. Acta.* 1983, **75,** 265.
27. M. S. Holt, W. L. Wilson, and J. N. Nelson, *Chem. Rev.* 1989, **89,** 11.
28. R. A. Anderson and F. W. B. Einstein, *Acta Cryst.* 1976, **B32,** 966.
29. M. Elder and D. Hall, *Inorg. Chem.* 1969, **8,** 1268.
30. R. J. H. Clark, L. Maresca and P. J. Smith, *J. Chem. Soc. A* 1970, 2687.
31. R. B. King, A. Fronzaglia, *Inorg. Chem.* 1966, **5,** 1837.
32. F.-W. Grevels and J. Jacke, P. Betz, C. Krüger and Y.-H. Tsay, *Organometallics* 1989, **8,** 293.

Pergamon

PII: S0277-5387(96)00482-2

Polyhedron Vol. 16, No. 10, pp. 1605–1614, 1997
Copyright © 1997 Elsevier Science Ltd
Printed in Great Britain. All rights reserved
0277-5387/97 $17.00+0.00

A family of mixed ligand complexes of Ru^{II}-L [L = N-aryl-pyridine-2-aldimine], their reactions, isolation and characterization. X-ray crystal structure of $[Ru(pic)(L^1)_2][ClO_4] \cdot CH_2Cl_2$ [pic = 2-picolinate ion]

Kedar Nath Mitra,[a] Subrata Choudhury,[a] Sreebrata Goswami[a]* and Shie-Ming Peng[b]

[a]Department of Inorganic Chemistry, Indian Association for the Cultivation of Science, Calcutta 700 032, India

[b]Department of Chemistry, National Taiwan University, Taipei, Taiwan, R. O. C.

(Received 6 August 1996; accepted 25 September 1996)

Abstract—Synthesis of the tris-chelated complexes $[Ru(L)_n(L^3)_{3-n}]^{2+}$ (L = *N*-aryl-pyridine-2-aldimine, L^3 = 2-(*m*-tolylazo)pyridine) based on silver(I) assisted *trans*-metallation is described. The complexes, $[Ru(L)_3]^{2+}$ and $[Ru(L)(L^3)_2]^{2+}$ afford $[Ru(pic)(L)_2]^+$ and $[Ru(pic)(L^3)_2]^+$ (pic = 2-picolinate ion) respectively, on hydrolysis and subsequent oxidation. When $RuCl_2(L)_2$ was reacted with two moles of $[Ag(L^3)_2]^+$, a pink complex of composition $[Ru(L)(L^3)(L^4)]^+$ [L^4 = *N*-aryl-2-picolinamide] was isolated along with the expected brown complex, $[Ru(L^3)(L)_2]^{2+}$. Initial oxidation of the metal ion favours L → L^4 conversion. The complexes have been characterized using spectroscopy and X-ray crystallography. The X-ray structure of $[Ru(pic)(L^1)_2]ClO_4 \cdot CH_2Cl_2$ is reported. The metal oxidation as well as ligand reductions for the complexes have been studied voltammetrically in acetonitrile using platinum as the working electrode. It has been observed that the oxidation of the transformed complexes, *viz.* $[Ru(pic)(L)_2]^+$, $[Ru(pic)(L^3)_2]^+$ and $[Ru(L)(L^3)(L^4)]^+$ occur at lower potentials as compared to their parent $[Ru(L)_n(L^3)_{3-n}]^{2+}$ complexes. All the complexes show metal-to-ligand charge transfer transitions in the visible range and absorption energies linearly correlate with the differences between the metal oxidation and the first ligand reduction potentials. © 1997 Elsevier Science Ltd. All rights reserved.

Keywords: ruthenium; Schiff-base; structure; ligand transformations; redox and redox-spectra correlation.

This work stems from our interest in the ruthenium-diimine complexes. This class of compounds is important [1] due to their rich redox and optical properties. In this respect, we have been working [2–4] on the synthesis and reactivities of ruthenium complexes of *N*-aryl-pyridine-2-aldimine (**1**, L). These complexes [2–6] are intensely coloured, undergo multiple electron transfer and most importantly, they show interesting patterns of chemical as well as photochemical reactivities.

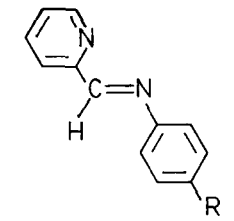
Herein we report the synthesis and characterization of the tris-chelated ruthenium complexes involving L and L^3. These may be conveniently synthesized starting from ruthenium bis-chelated dichlorides by the use of silver(I) assisted *trans* metallation reaction route. The study of reactions of ruthenated L in the above complexes forms an important part of the present work. Interestingly, different products were obtained from apparently similar types of reactions. All the relevant species have been fully characterized. The reason for transformation selectivity of L is discussed on the basis of the present findings and other results [3,4] from this laboratory and elsewhere.

*Author to whom correspondence should be addressed.

RESULTS AND DISCUSSION

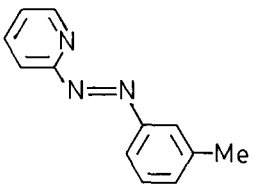
A. *The synthetic reactions*

In the process of synthesizing [2, 7–9] mixed ligand tris-chelated ruthenium complexes of L (**1**) and 2-(*m*-tolylazo)pyridine (L^3, **2**) some unusual products were



R = H : L^1
R = Me : L^2

1, L



L^3

2

obtained along with the expected products, which are elaborated below. The general reaction which has been studied may be represented as follows:

$$cis\text{-}RuCl_2L'_2 + 2AgL''_2 \xrightarrow[\substack{L',L''\\ L' = L,L^3\\ L'' = L,L^3}]{EtOH} RuL_2L'' + 2AgCl + 3L'$$

(a) (i) *Reaction of cis-*$RuCl_2(L)_2$ *and two moles of* $Ag(L)_2^+$

The bluish green *cis* isomer [3] of $RuCl_2(L)_2$ was reacted with two moles of silver complex [10], $Ag(L)_2^+$, in 1 : 1 aqueous ethanol. In addition to the expected [2] brown tris-chelate, $Ru(L)_3^{2+}$ (**3**), a pink compound was also formed. Interestingly, an aqueous ethanolic solution of pure $Ru(L)_3^{2+}$ in the presence of dilute aqueous $AgNO_3$ quantitatively produced the pink compound. The pink product was purified on a silica gel column eluting with 1 : 5 CH_3CN-CH_2Cl_2 mixture. The brown product was obtained from the column using a more polar solvent (2 : 3 CH_3CN-CH_2Cl_2 mixture) as an eluent.

(ii) *Characterization*

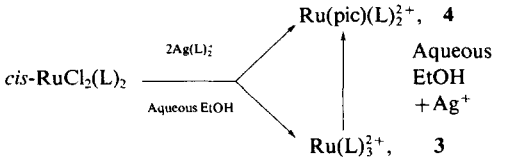
The brown compound was identified as the known [2] $[Ru(L)_3](ClO_4)_2 \cdot H_2O$ (**3**) which we do not discuss any further. The pink compound which analyzed as $[Ru(pic)(L)_2]ClO_4 \cdot CH_2Cl_2$ (**4**) (pic = 2-picolinate anion) is diamagnetic and a 1 : 1 electrolyte in CH_3CN. The IR spectrum showed all the characteristic features [2, 3] of coordinated L and ionic ClO_4^-. Interestingly, it also displayed a moderately strong band at 1650 cm^{-1} indicating the presence [11] of a carboxylic function. Selected characterization data are collected in Table 1.

Fortunately, single crystals of **4** (L = L^1) could be grown as solvates: **4**·CH_2Cl_2 and its structure was successfully solved crystallographically. Molecular views of the complex excluding the solvent of crystallization and the counter anion, ClO_4^- are shown in Fig. 1. Selected bond distances and bond angles are collected in Table 2. The structure solution of **4** unequivocally confirms the composition of **4** as $Ru(pic)(L^1)_2^+$. The geometry of the $Ru(L^1)_2$ fragment in **4** is *trans*, *cis* (*trans* with respect to two N^1(py) and *cis* with in the N^2 (imine) pair). The carboxylic function lies *trans* to one of the two imine nitrogens. In this manner the three pyridine nitrogens are positioned meridionally. We note here that the parent complex **3** exists [2] in the meridional geometry. Therefore, the transformation **3** → **4** is stereoretentive.

In the above structure, Ru—N(5) length agrees [12] well with the Ru—N lengths in $Ru(pic)_2(PPh_3)_2$. Interestingly, the four Ru—N lengths in the $Ru(L^1)_2$ fragment of **4** are not equal. The Ru—N(4) length is notably shorter than other three Ru—N lengths. This must be due to stronger $d\pi$–$p\pi$ interactions [13] between Ru^{II} and π^* of the imine function containing N(4), which lies *trans* to the strong σ-donor carboxylic acid function. Moreover, the average Ru—N (imine) length in **4** is shorter [4] by *ca* 0.03 Å compared to that in *trans*-$Ru^{III}(L^1)(L^4)Cl_2$ (L^4 = N-phenyl-2-picolinamide). This may be attributed to the superior back-bonding in ruthenium(II) complexes.

Finally, it may be noted that the reaction of hydrated $RuCl_3$ and $Ag(L)_2^+$ in 1 : 3 mole ratio also resulted in the formation of a mixture of **3** and **4**. The yield of **4** increases with the increase of the duration of the reaction.

The reactions, described above, are schematically presented in Scheme I.



Scheme I

Table 1. Characterization data

Compound	IR(cm^{-1})[a] $\nu_{C=O}$ (carboxylic acid)	$\nu_{C=O}$ (amide)	$\nu_{C=N}$	Λ_m[b] (ohm $^{-1}cm^2mol^{-1}$)	δMe[c] (ppm)
$[Ru(L^1)_3](ClO_4)_2 \cdot H_2O$			1610	210	
$[Ru(pic)(L^1)_2]ClO_4 \cdot CH_2Cl_2$	1650		1610	115	
$[Ru(L^2)_3](ClO_4)_2 \cdot H_2O$			1610	219	2.18, 2.08
$[Ru(pic)(L^2)_2]ClO_4 \cdot CH_2Cl_2$	1650		1610	120	2.15, 2.05
$[Ru(L^2)(L^3)_2](ClO_4)_2 \cdot H_2O$			1600, 1610	221	2.12, 2.21
$[Ru(pic)(L^3)_2]ClO_4 \cdot CH_2Cl_2$	1660		1610	126	2.21, 2.13
$[Ru(L^3)(L^2)_2](ClO_4)_2 \cdot H_2O$			1595, 1610	205	2.21, 2.16
$[Ru(L^2)(L^3)(L^4)]ClO_4 \cdot CH_2Cl_2$		1620	1595	105	2.30, 2.25, 2.16

[a] In KBr dist.
[b] In MeCN at 298 K with a solute concentration of *ca* 10^{-3} mol.
[c] In $CDCl_3$ using $Si(Me)_4$ as the internal standard.

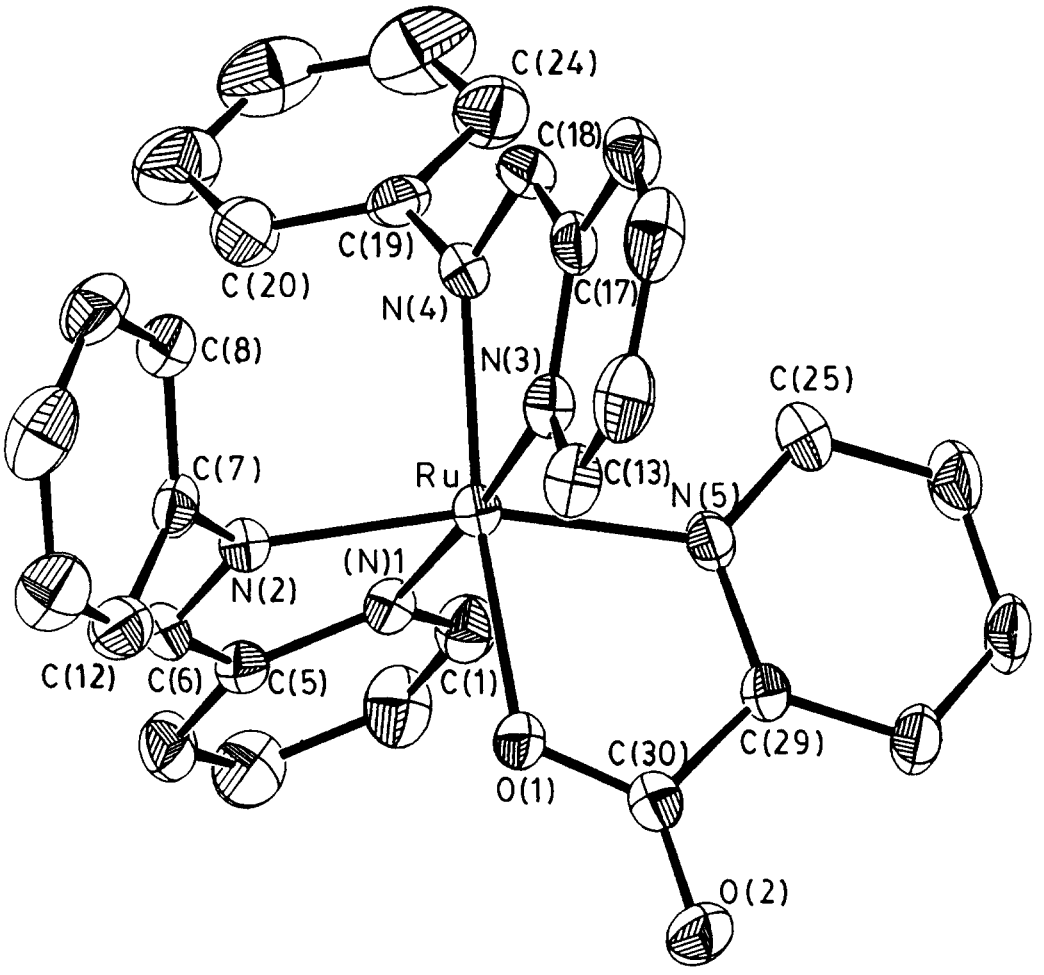


Fig. 1. ORTEP plot and atom labelling scheme for $Ru(pic)(L^1)_2$ in $[Ru(pic)(L^1)_2]ClO_4 \cdot CH_2Cl_2$.

Table 2. Selected bond distances (Å) and angles (°) and their estimated standard deviations for $[Ru(pic)(L^1)_2]ClO_4 \cdot CH_2Cl_2$

Ru—N(1)	2.046(5)	N(2)—C(6)	1.301(8)
Ru—N(2)	2.045(5)	N(4)—C(18)	1.316(8)
Ru—N(3)	2.048(5)	O(1)—C(30)	1.285(8)
Ru—N(4)	2.022(5)	O(2)—C(30)	1.225(8)
Ru—N(5)	2.079(5)	N(2)—C(7)	1.435(8)
Ru—O(1)	2.073(4)	N(4)—C(19)	1.435(8)
N(1)—Ru—N(2)	78.34(21)	N(2)—Ru—O(1)	87.29(18)
N(1)—Ru—N(3)	176.18(20)	N(3)—Ru—N(4)	78.91(21)
N(1)—Ru—N(4)	99.63(20)	N(3)—Ru—N(5)	90.37(20)
N(1)—Ru—N(5)	93.29(20)	N(3)—Ru—O(1)	93.83(19)
N(1)—Ru—O(1)	87.92(19)	N(4)—Ru—N(5)	95.60(20)
N(1)—Ru—N(3)	98.33(21)	N(4)—Ru—O(1)	171.27(19)
N(2)—Ru—N(4)	98.48(20)	N(5)—Ru—O(1)	79.47(18)
N(2)—Ru—N(5)	164.63(20)		

(b)(i) *Reaction of cis-*$RuCl_2(L^3)_2$ *and two moles of* $Ag(L)_2^+$

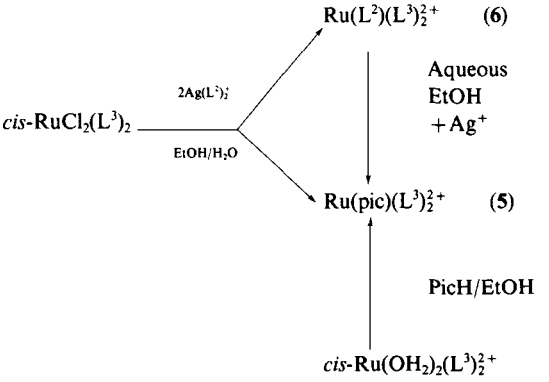
Similar to the prior reaction, this reaction also resulted in the formation of two major products, one of which is violet and the other one is brown in colour. The compounds were purified on a silica gel column by eluting with solvent mixtures of different polarities. The violet compound may be generated by boiling the brown product in aqueous ethanol in the presence of dilute $AgNO_3$ solution. Interestingly, the reaction [11] of *cis*-$Ru(OH_2)_2(L^3)_2^{2+}$ with PicH in ethanol instantaneously produces the violet product in a high yield.

(ii) *Characterization*

The first moving violet band was eluted with 5:2 CH_2Cl_2-CH_3CN mixture and it analyzed as $[Ru(pic)(L^3)_2]ClO_4 \cdot CH_2Cl_2$ (**5**). The brown product, which was eluted with 1:1 CH_2Cl_2–CH_3CN mixture, analyzed as $[Ru(L^2)(L^3)_2](ClO_4)_2 \cdot H_2O$, (**6**). The compound **5** is a 1:1 electrolyte whereas the compound **6** is 1:2 electrolyte in CH_3CN. The compound **5** displayed a moderately strong absorption at 1660 cm^{-1} in the IR spectrum. This band is conspicuously absent in the IR spectrum of **6**. Evidently, the 1660 cm^{-1} absorption indicates the presence [11] of a carboxylic function in **5** (Table 1).

The ^1H NMR spectra of the compounds **5** and **6** were examined. In this case we have used only methyl substituted ligand, L^2 to take advantage of monitoring the methyl resonances in the less crowded region of the ^1H NMR spectrum. The aromatic region of both the spectra are complex due to serious overlapping. Therefore, we concentrated only on the methyl resonances (Table 1). The compound **5** displayed two equally intense resonances at 2.15 and 2.05 δ. The intensities of two resonances correspond to six protons. The compound **6** also displayed two methyl resonances at 2.21 and 2.12 δ, but the ratio of signal intensities is 1:2. Moreover, the total area covered by the two methyl signals of **6** corresponded to nine protons. Therefore, it may be concluded that the two equally intense methyl resonances in **5** is due to the presence of two L^3 ligands. In the spectrum of **6** there are three methyl resonances, two of which are overlapping which are attributed [14] to methyl groups of L^3, and the second signal is due [2] to the *p*-tolyl group of L^2. The spectral data, presented above, clearly demonstrate that the hydrolytic oxidative cleavage of an imine function occurs in the formation of **5**.

Thus, the reaction is similar to the reaction which is described in Section (a).



Scheme II

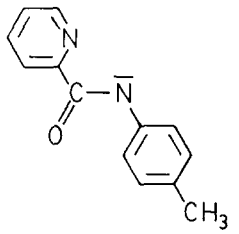
(c) (i) *Reaction of cis-*$RuCl_2(L^2)_2$ *and two moles of* $Ag(L^3)_2^+$

In this reaction bluish green *cis* isomer of $RuCl_2(L^2)_2$ was reacted with two moles [15] of $Ag(L^3)_2^+$ in aqueous ethanol. This reaction also yielded two major products. One of the two products is pink whereas the other one is brown. Unlike the two previously described reactions, the brown product is quite stable in boiling aqueous ethanol. Both the

products were purified by using the column chromatography technique.

(ii) *Characterization*

The pink product was eluted with 1:9 CH_3CN-CH_2Cl_2 solvent mixture and analyzed as $[Ru(L^2)(L^3)(L^4)](ClO_4)_2 \cdot 0.5CH_2Cl_2$ (L^4 = N-*p*-tolyl-2-picolinamide), (**7**). The brown product was then eluted with 1:1 CH_3CN-CH_2Cl_2 mixture. Based on the elemental analyzes the composition was ascertained as $[Ru(L^3)(L^2)_2](ClO_4)_2 \cdot H_2O$ (**8**). The characterization of **7** and **8** were unambiguously made based on their physical data.

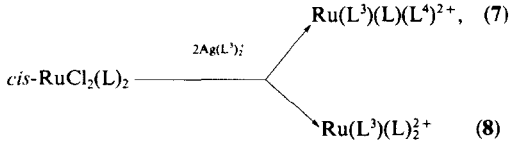


L^4

The compounds **7** and **8** are 1:1 and 1:2 electrolytic, respectively, in acetonitrile. Unlike monopicolinates, the compound **7** did not show any characteristic absorption of carboxylic function. Instead, a moderately strong band at 1620 cm^{-1} in the IR spectrum of **7** confirms the presence [4, 13] of an amide function. Fortunately, this compound (**7**) displayed highly resolved ^1H NMR spectrum (Fig. 2) which was conveniently used for its characterization. The spectrum consists of well separated, equally intense three methyl resonances between 2.1–2.3 δ. This clearly reveals the presence of three tolyl groups in **7**. Moreover, there are four doublets of 2H intensities in the range 7.0 to 5.5 δ. Such doublets of two proton intensities can only arise from *p*-tolyl groups in this compound. The rest of the spectrum is complex due to overlapping peaks. The ^1H NMR spectrum of **8**, as expected, consists of two methyl resonances, one of which is double the intensity of the other. The spectral data collectively taken with the analytical data do conform to the proposed composition of the above compounds.

The reaction, described above, may then be summarized below in Scheme III.

We note that a tris-chelated compound with three different bidentate ligands as in **7** is extremely rare [16].



Scheme III

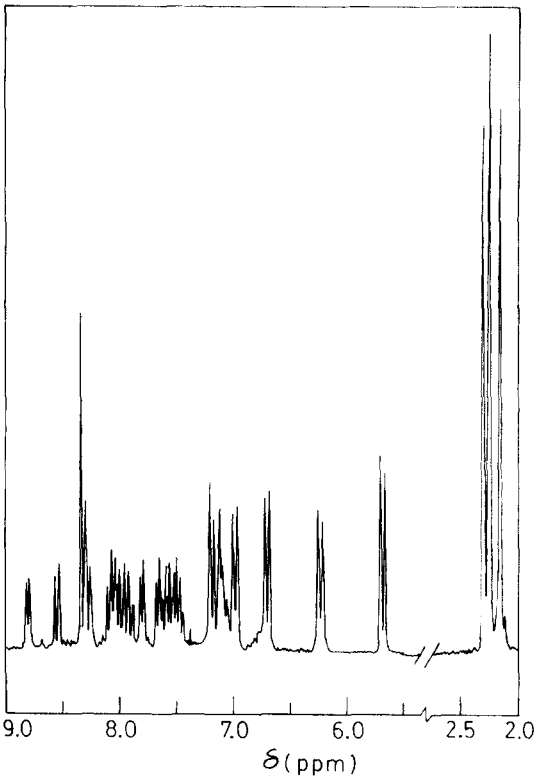


Fig. 2. ^1H NMR spectrum of $[Ru(L^2)(L^3)(L^4)]ClO_4 \cdot CH_2Cl_2$ in $CDCl_3$.

B. *The origin of transformations*

The reactions described above may be broadly classified in two categories: type (i) L → pic (reactions (a) and (b)); type (ii) L → L^4 (reaction (c)). We first consider the reaction (b) of type (i). In this reaction the starting ruthenium compound does not contain L. Therefore, the formation of $[Ru(pic)(L^3)_2]^+$ could, in principle, occur in two ways. Once the coordinated chlorides are precipitated as insoluble AgCl, the solution mixture then contains bis-solvento complex, $RuS_2(L^3)_2^{2+}$ (S = solvent) and four moles of free L. Coordination of L to $Ru(L^3)_2^{2+}$ moiety would produce $Ru(L)(L^3)_2^{2+}$ (**6**). Furthermore, hydrolysis [17] of an imine function in a hydroxylic solvent is a common phenomenon. Thus, hydrolysis of free L followed by oxidation of the aldehyde function would produce PicH in solution which may then react with the labile bis-solvento species to form the monopicolinate, **5**. The second possibility is the same transformation of L occurring after coordination to $Ru(L^3)_2^{2+}$ moiety. We note here that **6** can be easily transformed to **5** and the electrophilicity of L increases upon coordination, which is primary for the hydrolysis of an imine function. Out of the above two possibilities, we therefore propose that L → pic transformation presumably occurs *via* coordination of L. This proposal also applies to the reaction (a).

Table 3. Cyclic voltammetric data[a]

Compound	Metal-centred oxidation $E_{1/2}$(V)[E_p(mV)]	Ligand-based reductions $-E_{1/2}$(V)[ΔE_p(mV)]
$[Ru(L^1)_3](ClO_4)_2 \cdot H_2O$	1.43(75)	0.93(90), 1.16(100), 1.49(110)
$[Ru(pic)(L^1)_2]ClO_4 \cdot CH_2Cl_2$	1.00(75)	1.15(100), 1.48(90)
$[Ru(L^2)_3](ClO_4)_2 \cdot H_2O$	1.44(70)	0.90(90), 1.19(110), 1.52(110)
$[Ru(pic)(L^2)_2]ClO_4 \cdot CH_2Cl_2$	1.00(80)	1.16(100), 1.48(100)
$[Ru(L^2)(L^3)_2](ClO_4)_2 \cdot H_2O$	2.00[b]	0.15(90), 0.65(100), 1.56(170)
$[Ru(pic)(L^3)_2]ClO_4 \cdot CH_2Cl_2$	1.56(70)	0.28(100), 0.85(100), 1.71(180)
$[Ru(L^3)(L^2)_2](ClO_4)_2 \cdot H_2O$	1.81[b]	0.40(90), 1.05(100), 1.57(120)
$[Ru(L^2)(L^3)(L^4)](ClO_4)_2 \cdot CH_2Cl_2$	0.98(70)	0.92(100), 1.27(100)

[a] Cyclic voltammetric experiments were carried out in MeCN at 298 K using 0.1 mol NBu_4ClO_4 as supporting electrolyte and platinum as working electrode. The reported data correspond to scan rate $v = 50$ mV s^{-1}.

[b] Irreversible response, the potential corresponds to E_{pa}.

The other type of transformation, $L \rightarrow L^4$ (type (ii)) must occur with the coordinated L since both L are already coordinated in the starting material. This type of transformation of an imine function has been exemplified [4,13] very recently, in two other ruthenium systems. One such example is the oxidative transformation of *trans*-$Ru^{II}Cl_2(L)_2$ to *trans*-$Ru^{III}Cl_2(L)(L^4)$. It has been shown that initial oxidation of the metal ion followed by partial hydrolysis of coordinated L^1 and subsequent oxidation of the hydrolyzed L are the steps involved in the above transformation. At this stage, comparison of oxidation power of different reactants of reaction (c) is necessary for further discussion. We note that L^3 is a very strong [14] π-acceptor. Consequently, $Ag(L^3)_2^+$ should be a strong oxidant. Furthermore, the oxidation of *cis*-$RuCl_2(L)_2$ may be easily achieved [3] ($E_{1/2}$: 0.32 V). In the reaction (c), initial oxidation of $RuCl_2(L)_2$ by $Ag(L^3)_2^+$ is, therefore, the most plausible one. The oxidation of the metal ion then leads to an identical situation where coordinated $L \rightarrow L^4$ transformation was shown [4] to occur by the oxidation of the metal centre. In contrast to the previously reported examples [4,13], initial oxidation of the metal ion in reaction (c) is not reflected in the oxidation state of the same in the final product. In the present case (**7**) beside being coordinated to L^4, ruthenium is also bound to a very strong π-acceptor, L^3 and a moderate acceptor L. In the environment of L, L^3 and L^4, ruthenium is preferably stabilized in the bivalent state ($E_{1/2}$: Ru^{III}/Ru^{II} 1.0 V *vide infra*).

It may, therefore, be concluded, from the foregoing discussion, that hydrolysis followed by oxidation of coordinated L results in the formation of pic, whereas oxidation of the compound followed by hydrolysis would preferentially transform L to L^4.

C. *Electrochemical properties and redox-spectra correlation*

Electrochemical properties of the compounds **3**–**8** were studied cyclic voltammetrically in CH_3CN using tetrabutyl ammonium perchlorate (TBAP) as supporting electrolyte and platinum as a working electrode. The measurements were carried out in the range 2.2 V to −1.6 V versus SCE (saturated calomel electrode). All the complexes are electroactive, the electrochemical data are presented in Table 3. Representative voltammograms are displayed in Fig. 3.

We first consider the three parent chelates *viz.* **3**, **6** and **8**. Cyclic voltammogram [2] of the reported compound **3** is already discussed. Both **6** and **8** displayed an irreversible oxidation wave at a very high oxidation potential (> 1.6 V) due to $Ru^{II} \rightarrow Ru^{III}$ oxidation. Metal mediated oxidation of coordinated L has recently been discussed in the literature [4]. For the present complexes the oxidation potentials are very high and consequently the chemical reaction succeeding the electrochemical formation of Ru^{III}-L is expected to be very fast and thus the reverse waves were absent in the voltammograms of **6** and **8**. Both the complexes also display reversible, multiple electron transfer reductive responses on the negative of SCE. These are attributed to the reductions of the coordinated ligands. It may be noted that on moving from **3** to **8** *via* **6**, the metal oxidation potential increases in a parallel direction whereas a reverse trend was observed for the ligand reduction. The above trend is as expected, since L^3 stabilizes Ru^{II} better than L due to enhance $d\pi$–$p\pi$ back bonding and also undergoes reduction more easily due to the presence of lower acceptor orbital.

The two monopicolinates **4** and **5** showed reversible oxidative and reductive responses on both positive and negative of SCE. Their metal centered redox potentials are systematically lower than those for the parent diimine compounds. The picolinate ion which is a hard ligand, stabilizes [11] the higher valent state and thus the above shift of redox potential is observed. Moreover, on moving from **4** to **5** the $E_{1/2}$ of Ru^{III}/Ru^{II} couple shifts by about 0.56 V, presumably due to the better stabilisation of lower valent state by L^3 as noted before. For a similar reason, the ligand reductions in

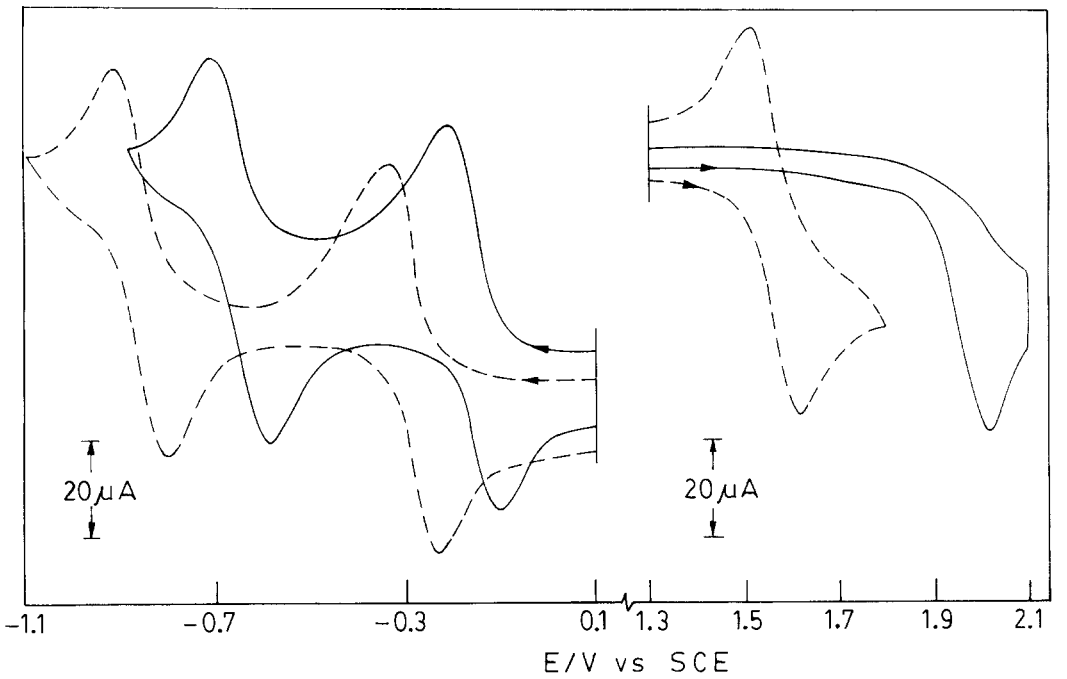


Fig. 3. Cyclic voltammograms of $[Ru(L^2)(L^3)_2](ClO_4)_2 \cdot H_2O$ (——) and $[Ru(pic)(L^3)_2]ClO_4 \cdot CH_2Cl_2$ ( ) in acetonitrile.

5 is easier than that in **4**. The cyclic voltammogram of the monopicolinamide **7** consists of a reversible oxidative response at 1.0 V attributed to Ru^{III}/Ru^{II} couple and two more reductive couples on the negative of SCE due to the ligand reductions.

Interestingly, the metal redox of **4, 5** and **6** are all reversible whereas those of their parents, **3, 6** and **8,** are either irreversible or quasireversible. Irreversibility in the latter group of complexes is due to metal assisted L oxidation reaction. In spite of the fact that both **4** and **6** contain L as coligand their metal redox responses are reversible. It may, therefore, be concluded that partially transformed products, even if they contain additional L, are resistant to further oxidation of L at least in the CV time scale.

The solution absorption spectra of the complexes were recorded in CH_2Cl_2. Representative spectra of the complexes are displayed in Fig. 4 and the data are collected in Tables 4 and 5. Although the complexes retain fairly intense intraligand transitions in the UV region, the key feature is the intense lower energy transitions occurring in the visible region (520–480 nm) those are assigned [2] to $Ru(d\pi) \rightarrow$ ligand (π^*) MLCT transitions. These transition energies for the parent complexes **3, 6** and **8** are systematically higher than those for the monopicolinates **4, 5** and monopicolinamide, **7**. The MLCT absorption energies for all the above complexes, (**3–8**), interestingly, show a linear correlation [2] with ΔE [where, $\Delta E = E_{1/2}(Ru^{III}/Ru^{II}) - E_{1/2}$ (ligand 0/−1)] (Table 5). This correlation, in other words, justifies our assignment of MLCT transitions for the complexes.

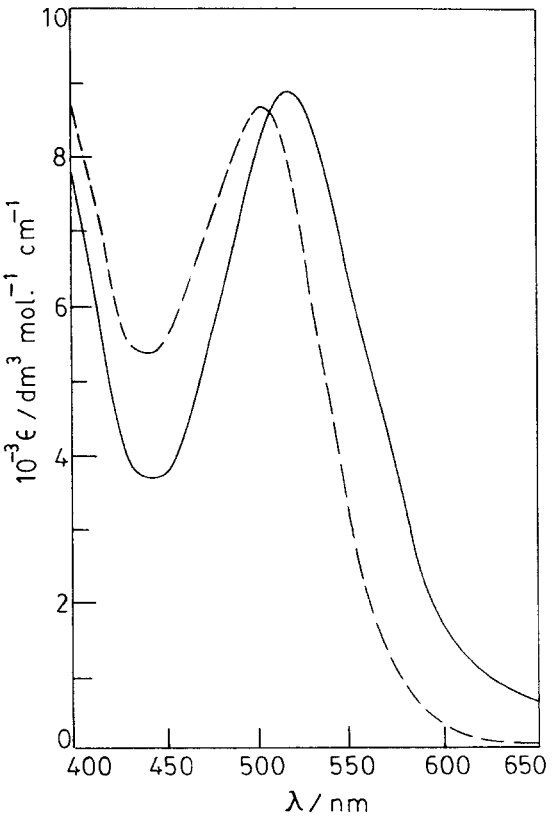


Fig. 4. Visible range absorption spectra of $[Ru(L^2)(L^3)(L^4)]ClO_4 \cdot CH_2Cl_2$ (——) and $[Ru(L^3)(L^2)_2](ClO_4)_2 \cdot H_2O$ (– – –) in CH_2Cl_2.

Table 4. UV–vis spectral data

Compound	Absorption[a] λ_{max} (nm)[δ(mol^{-1}cm^{-1})]
$[Ru(L^1)_3](ClO_4)_2 \cdot H_2O$	480(13760), 445[b](10 880), 300(25 600), 270(25 040)
$[Ru(pic)(L^1)_2]ClO_4 \cdot CH_2Cl_2$	515(10 950), 470[b](7300), 315(23 400), 270(19 040)
$[Ru(L^2)_3](ClO_4)_2 \cdot H_2O$	480(14 310), 445[b](11 120), 315(27 380), 270(25 120)
$[Ru(pic)(L^2)_2]ClO_4 \cdot CH_2Cl_2$	515(11 100), 470[b](7180), 310(23 660), 265(19 175)
$[Ru(L^3)(L^3)_2](ClO_4)_2 \cdot H_2O$	515(7400), 490[c], 370(17270), 320(15 790), 270(15 800)
$[Ru(pic)(L^3)_2]ClO_4 \cdot CH_2Cl_2$	545(11 980), 360(18 620), 310(21 250), 250[b](18 200)
$[Ru(L^3)(L^2)_2](ClO_4)_2 \cdot H_2O$	500(8700), 320(22 960), 265(23 540)
$[Ru(L)(L^3)(L^4)]ClO_4 \cdot CH_2Cl_2$	520(8850), 360[c], 315(23 720)

[a]In MeCN.
[b]Shoulder.
[c]Ill defined shoulder

Finally we wish to mention here that preliminary luminescence studies on the above complexes reveal that the picolinates and the amides have much stronger emission than their parent diimines in the visible region. Our work in this area is continuing.

EXPERIMENTAL

Materials

The salt, $RuCl_3 \cdot nH_2O$ was obtained from Arora Matthey, Calcutta and was digested thrice with concentrated HCl before use. The silver complexes, $[Ag(L)_2]ClO_4$ (L = L^1 or L^2) and $[Ag(L^3)_2]ClO_4$ were synthesized as before [10, 15]. The complexes *cis*-$[RuCl_2(L)_2]$ and *cis*-$[RuCl_2(L^3)_2]$ were prepared [3] by published procedures. The purification of dry solvents for electrochemical and spectral work was performed as described earlier. All other chemicals and solvents used for the preparative work were of reagent grade and were used as received.

Physical measurements

Spectra were recorded on the following equipment: UV–vis, Hitachi 330 spectrophotometer; NMR spectra, Varian XL 200 MHz FT NMR spectrometer. Electrochemical measurements were performed under nitrogen atomosphere on a PAR 370-4 electrochemistry system as described previously [14]. All potentials reported in this work are uncorrected for junction contribution. Solution (*ca* 1 mmol) electrical conductivity measurements were performed on an Elico CM 82T conductivity bridge.

Reactions

(a) Reaction of *cis*-$RuCl_2(L)_2$ (L = L^1 and L^2) and $[Ag(L)_2]ClO_4$. To a sample of bluish green *cis* isomer of $RuCl_2(L)_2$ (0.5 mmol) suspended in ethanol–water mixture (5 : 1) was added a solution of $[Ag(L)_2]ClO_4$ (1 mmol) in ethanol (10 cm^3) and the mixture was heated to reflux for 1 h. The solution was cooled and filtered through a G-4 sintered glass funnel. The filtrate was evaporated to dryness. The crude mass was then dissolved in CH_2Cl_2 and subjected to column chromatography on a silica gel column eluting with different mixtures of CH_2Cl_2-CH_3CN. A pink band of $[Ru(pic)(L)_2]^+$ was eluted with CH_2Cl_2-CH_3CN (5 : 1) followed by a brown band of $[Ru(L)_3]^{2+}$ eluted with CH_2Cl_2-CH_3CN (3 : 2). These were evaporated and crystallized from CH_2Cl_2-C_6H_{14} (1 : 1). The compounds were obtained as solvates. The yields and analyzes were as follows.

Table 5. Redox spectral data

Compound	$E_{1/2}$(V) Metal oxidation	$-E_{1/2}$(V) First ligand reduction	ΔE(V) Ox/Red	*vc.t.* (cm^{-1})
$[Ru(L^1)_3](ClO_4)_2 \cdot H_2O$	1.43	0.93	2.36	20833
$[Ru(pic)(L^1)_2]ClO_4 \cdot CH_2Cl_2$	1.00	1.15	2.15	19417
$[Ru(L^2)_3](ClO_4)_2 \cdot H_2O$	1.44	0.90	2.34	20833
$[Ru(pic)(L^2)_2]ClO_4 \cdot CH_2Cl_2$	1.00	1.16	2.16	19417
$[Ru(L^2)(L^3)_2](ClO_4)_2 \cdot H_2O$	2.00	0.15	2.15	19417
$[Ru(pic)(L^3)_2]ClO_4 \cdot CH_2Cl_2$	1.50	0.28	1.84	18348
$[Ru(L^3)(L^2)_2](ClO_4)_2 \cdot H_2O$	1.81	0.40	2.21	20000
$[Ru(L^2)(L^3)(L^4)]ClO_4 \cdot CH_2Cl_2$	0.98	0.92	1.90	19230

$[Ru(pic)(L^1)_2]ClO_4 \cdot CH_2Cl_2$: yield 35%. (Found: C, 48.3; H, 3.4; N, 9.1. Calc. for $C_{31}N_5H_{26}O_6Cl_3Ru$: C, 48.2; H, 3.4; N, 9.1%).

$[Ru(L^1)_3](ClO_4)_2 \cdot H_2O$: yield 25%. (Found: C, 50.2; H, 3.7; N, 9.6. Calc. for $C_{36}N_6H_{32}O_9Cl_2Ru$: C, 50.0; H, 3.7; N, 9.7%).

$[Ru(pic)(L^2)_2]ClO_4 \cdot CH_2Cl_2$: yield 37%. (Found: C, 49.3; H, 3.7; N, 8.9. Calc. for $C_{33}N_5H_{30}O_6Cl_3Ru$: C, 49.5; H, 3.7; N, 8.7%).

$[Ru(L^2)_3](ClO_4)_2 \cdot H_2O$: yield 26%. (Found: C, 51.5; H, 4.2; N, 9.3. Calc. for $C_{39}N_6H_{38}O_9Cl_2Ru$: C, 51.6; H, 4.2; N, 9.3%).

(b) Conversion of $[Ru(L^1)_3](ClO_4)_2$ to $[Ru(pic)(L^1)_2]ClO_4$. To a solution of 0.25 mmol of $[Ru(L^1)_3](ClO_4)_2$ in ethanol–water mixture (5:1) was added an aqueous solution of $AgNO_3$ (1 mmol in 5 cm^3 of water) and the mixture was heated to reflux for 2 h. It was then evaporated to dryness and subjected to column chromatography on a silica gel column eluting with different mixtures of CH_2Cl_2-CH_3CN as described in Section (a).

The yields were as follows: $[Ru(pic)(L^1)_2]ClO_4 \cdot CH_2Cl_2$: 76%; $[Ru(L^1)_3](ClO_4)_2 \cdot H_2O$: 19%.

(c) Reaction of *cis*-$RuCl_2(L^3)_2$ and $[Ag(L^2)_2]ClO_4$. This reaction was similarly performed as the reaction described in Section (a) starting from *cis*-$RuCl_2(L^3)_2$ and $[Ag(L^2)_2]ClO_4$. The yields and analyzes of the isolated products are as follows:

$[Ru(pic)(L^3)_2]ClO_4 \cdot CH_2Cl_2$: yield 42%. (Found: C, 46.3; H, 3.5; N, 12.2. Calc. for $C_{31}N_7H_{28}O_6Cl_3Ru$: C, 46.4; H, 3.5; N, 12.2%).

$[Ru(L^2)(L^3)_2](ClO_4)_2 \cdot H_2O$: yield 20%. (Found: C, 49.0; H, 3.9; N, 12.4. Calc. for $C_{37}N_8H_{36}O_9Cl_2Ru$: C, 48.9; H, 4.0; N, 12.3%).

(d) Conversion of $[Ru(L^2)(L^3)_2](ClO_4)_2$ to $[Ru(pic)(L^3)_2]ClO_4$. This was similarly performed as described in Section (c) starting from $[Ru(L^2)(L^3)_2](ClO_4)_2$. The yields were as follows: $[Ru(pic)(L^3)_2]ClO_4 \cdot CH_2Cl_2$: yield 85%; $[Ru(L^2)(L^3)_2](ClO_4)_2 \cdot H_2O$: yield 9%.

(e) Reaction of $[Ru(L^3)_2(OH_2)_2]^{2+}$ and PicH was performed as described previously [11].

(f) Reaction of *cis*-$RuCl_2(L^2)_2$ and $[Ag(L^3)_2]ClO_4$. The above reaction was also similarly performed as described in Section (a) starting from *cis*-$RuCl_2(L^2)_2$ and $[Ag(L^3)_2]ClO_4$. The yields and analyzes were as follows:

$[Ru(L^2)(L^3)(L^4)](ClO_4) \cdot CH_2Cl_2$: yield 40%. (Found: C, 52.3; H, 4.0; N, 11.3. Calc. for $C_{39}N_7H_{36}O_5Cl_3Ru$: C, 52.6; H, 4.0; N, 11.0%).

$[Ru(L^3)(L^2)_2](ClO_4)_2 \cdot H_2O$: yield 17%. (Found: C, 50.5; H, 4.1; N, 10.9. Calc. for $C_{38}N_7H_{37}O_9Cl_2$: C, 50.3; H, 4.1; N, 10.8%).

Crystallography

Single crystals of $[Ru(pic)(L^1)_2]ClO_4 \cdot CH_2Cl_2$ were grown at 298 K by slow diffusion of hexane into dichloromethane solution of the compound. Diffraction measurements were carried out on a Nonius CAD4 fully automated four-circle diffractometer. The unit cell was determined and refined using setting angles of 25 reflections, with 2θ angles in the range 11.60 to 20.82°. The unit cell dimensions are listed in Table 6. Data were collected by $\theta - 2\theta$ scans within the angular range 3–45°. All data reduction and structure refinement were performed using the NRCC-SDP-VAX packages. The structure was solved by the Patterson method. Final cycles of least square refinement converged with discrepancy indices of $R_f = 0.045$ and $Rw = 0.035$. Tables containing full listings of atom positions, anisotropic thermal parameters and hydrogen atom locations are available as supplementary material.

Table 6. Crystallographic data for $[Ru(pic)(L^1)_2]ClO_4 \cdot CH_2Cl_2$

Formula	$RuC_{31}H_{26}N_5Cl_3O_6$
fw	772.00
Crystal system	Triclinic
Space group	*P*-1
a (Å)	11.3737(23)
b (Å)	12.527(3)
c (Å)	13.255(3)
α (°)	71.978(20)
β (°)	66.052(19)
γ (°)	75.476(18)
V (Å^3)	1624.1
Z	2
D_{calc} (gm cm^{-3})	1.579
μ (cm^{-1})	7.028
Crystal size (mm)	$0.05 \times 0.05 \times 0.30$
λ (Å)	0.7107
T (K)	298
R_f, *Rw*	0.045, 0.035
GOF	1.61

Acknowledgement—Financial support received from the University Grants Commission, New Delhi is gratefully acknowledged.

REFERENCES

1. See, for Example, E. A. Seddon and K. R. Seddon, *The Chemistry of Ruthenium*, pp 414, 1173. Elsevier, New York (1984); G. Wilkinson, R. D. Gillard and J. A. McCleverty, *Comprehensive Coordination Chemistry*, vol. 4, p. 277. Pergamon, Oxford (1987); T. J. Meyer, *Pure Appl. Chem.* 1986, **58,** 1193; A. Juris, V. Balzani, F. Barigelletti, S. Campagna, P. Belser and A. von. Zelewsky, *Coord. Chem. Rev.* 1988, **84,** 85; H. Masui, A. B. P. Lever and E. S. Dodsworth, *Inorg. Chem.* 1993, **22,** 258; R. M. Berger and J. R. Holcombe, *Inorg. Chim. Acta* 1995, **232,** 217; F. Hartl, T. L. Snoeck, D. J. Stufkens and A. B. P. Lever, *Inorg. Chem.* 1995, **34,** 3887; M. Maruyama, H. Matsuzawa and Y. Kaizu, *Inorg. Chem.* 1995, **34,** 3232.

2. S. Choudhury, A. K. Deb and S. Goswami, *J. Chem. Soc., Dalton Trans.* 1994, 1305.
3. S. Choudhury, M. Kakoti, A. K. Deb and S. Goswami, *Polyhedron* 1992, **11,** 3183.
4. M. Menon, S. Choudhury, A. Pramanik, A. K. Deb, S. K. Chandra, N. Bag, S. Goswami and A. Chakravorty, *J. Chem. Soc., Chem. Commun.* 1994, 57.
5. E. V. Dose and L. J. Wilson, *Inorg. Chem.* 1978, **17,** 2600.
6. P. Belser and A. von Zelewsky, *Helv. Chim. Acta* 1980, **63,** 1675.
7. M. Kakoti, A. K. Deb and S. Goswami, *Inorg. Chem.* 1992, **31,** 1302.
8. A. K. Deb, M. Kakoti and S. Goswami, *J. Chem. Soc., Dalton Trans.* 1991, 3249.
9. S. Choudhury, A. K. Deb, W. Kharmawphlang and S. Goswami, *Proc. Indian Acad. Sci. (Chem. Sci.).* 1994, **106,** 665.
10. S. Choudhury, A. K. Deb and S. Goswami, *Polyhedron* 1994, **13,** 1063.
11. N. Chatak and S. Bhattacharya, *Polyhedron* 1994, **13,** 2999; N. Ghatak, J. Chakravarty and S. Bhattacharya, *Trans. Met. Chem.* 1995, **20,** 138.
12. M. C. Barral, R. J. Aparicio, E. C. Royer, M. J. Saucedo, F. A. Urbanos, E. G. Puebla, C. R. Valero, *J. Chem. Soc., Dalton Trans.* 1991, 1609.
13. M. Menon, A. Pramanik and A. Chakravorty, *Inorg. Chem.* 1995, **34,** 3310.
14. S. Goswami, R. N. Mukherjee and A. Chakravorty, *Inorg. Chem.* 1983, **22,** 2825.
15. A. K. Deb, S. Choudhury and S. Goswami, *Polyhedron* 1990, **9,** 2251.
16. G. F. Strouse, P. A. Anderson, J. R. Schoonover, T. J. Meyer and F. R. Keene, *Inorg. Chem.* 1995, **31,** 3004.
17. R. H. Keyser and R. M. Pollack, *J. Am. Chem. Soc.* 1977, **99,** 3379.

Pergamon

PII: S0277-5387(96)00481-0

Polyhedron Vol. 16, No. 10, pp. 1615–1619, 1997
Copyright © 1997 Elsevier Science Ltd
Printed in Great Britain. All rights reserved
0277-5387/97 $17.00 + 0.00

The first complex with TeI_2 ligands: synthesis and structure of $[Re_6Te_8(TeI_2)_6]I_2$

Vladimir P. Fedin,[a]* Vladimir E. Fedorov,[a] Hideo Imoto[b] and Taro Saito[b]

[a]Institute of Inorganic Chemistry of the Russian Academy of Sciences, pr. Lavrentjeva 3, 630090 Novosibirsk, Russia

[b]Department of Chemistry, School of Science, The University of Tokyo, Hongo, Bunkyo-ku, Tokyo 113, Japan

(Received 30 July 1996; accepted 25 September 1996)

Abstract—The tellurium-rich compound $[Re_6Te_{14}I_{14}]$ (**1**) was obtained in high yield by high-temperature reaction (400°C) of the octahedral cluster complex Re_6Te_{15} with I_2 in a 1 : 9 ratio. Compound **1** is diamagnetic, air-stable and insoluble in most common organic solvents. The structure of **1** has been determined by single-crystal X-ray diffraction. The $[Re_6Te_8(TeI_2)_6]^{2+}$ structure is characterized by the presence of the octahedral Re_6 cluster with Re—Re distances at 2.690(1)–2.700(1) Å; the Re—μ_3—Te distances are 2.689(1)–2.698(1) Å. Each Re atom is ligated by neutral TeI_2 group. The Re—TeI_2 distances are 2.670(1)–2.672(1) Å. The Te—I distances in the TeI_2 ligands range from 2.756(2) to 2.785(2) Å. The I—Te—I bond angles are 89.29(5)–92.67(5)° and the Re—Te—I angles span 104.19(4) to 106.56(3)°. © 1997 Elsevier Science Ltd. All rights reserved.

Keywords: rhenium tellurium cluster compound; crystal structure.

The chemistry of Te^{IV} halides is well developed, but much less is known about Te^{II} halides. It has not been possible yet to prepare the halides of Te^{II} as pure phases [1]. However, they do exist in solution or in the gas phase as dissociation products of Te^{IV} halides. Tellurium(II) halides demonstrate a very high tendency to be stabilized in solution through the formation of complexes with anionic or with neutral Lewis bases; for halochalcogenate(II) anionic species examples are (i) series of tetrahalotellurates(II), TeX_4^{2-} (X = Cl, Br, I) [2,3], (ii) the dinuclear planar $Te_2I_6^{2-}$ ion [1]. During attempts to prepare transition-metal derivatives of halotellurates(II) only the tetranuclear $Te_4I_{14}^{2-}$ complex was obtained [4].

Recently the first examples of the metal cluster complexes $[Nb_2Te_8I_{12}]$ [5] and $[Mo_3Te_{10}I_{10}]$ [6] containing $Te_2I_6^{2-}$ and TeI_3^- ligands have been described. It is remarkable that halotellurate(II) ions can be obtained in complex form from high-temperature reactions. In 1996 Strähle *et al.* described the synthesis and structure of $Re_4Te_4(TeBr_2)_4Br_8$ [7]. The complex was obtained from the elements at 550°C and contains $TeBr_2$ ligands. Hexanuclear Re_6 tellurohalide cluster compounds $[Re_6Te_6Cl_6(TeCl_2)_2]$ and $[Re_6Te_8(TeBr_2)_6]Br_2$ have been obtained by high-temperature reaction of rhenium halides with elemental Te [8].

In this paper, we report the use of a high-temperature reaction of octahedral tellurium-rich compound Re_6Te_{15} with I_2 for the synthesis of the octahedral cluster compound $Re_6Te_{14}I_{14}$ (**1**) containing terminal TeI_2 ligands coordinated to the rhenium atoms of the $[Re_6(\mu_3\text{-}Te)_8]^{2+}$ cluster fragment.

The inorganic ligands $TeCl_2$, $TeBr_2$ and TeI_2 are new. The number of known complexes with related SCl_2 and $SeCl_2$ ligands is limited and examples are (i) $PdCl_2(QCl_2)_2$ (Q = S, Se) [9, 10], (ii) $PtCl_4(SCl_2)_2$ [10], (iii) $Ru_2Cl_5(SCl_2)_4$ [11], and (iv) $AuCl_3(SCl_2)$ [12].

EXPERIMENTAL

Preparation of $Re_6Te_{14}I_{14}$ (1)

Re_6Te_{15} was prepared by the literature method [13b]. A mixture of Re_6Te_{15} (1.5155 g, 0.50 mmol) and I_2 (1.1548 g, 4.55 mmol) was heated (400°C, 48 h) in an evacuated fused silica tube. The tube was cooled

*Author to whom correspondence should be addressed.

Table 1. Crystal Data and Refinement Results for $[Re_6Te_8(TeI_2)_6]I_2$

Formula	$I_{14}Re_6Te_{14}$
a(Å)	10.770(2)
b(Å)	12.230(2)
c(Å)	10.677(2)
α(°)	104.32(2)
β(°)	118.42(1)
γ(°)	86.90(2)
V(Å^3)	1195.0(4)
Z	1
Formula weight	4680.3
Space group	$P\bar{1}$ (No. 2)
Crystal size (mm^3)	$0.3 \times 0.4 \times 0.06$
T(K)	295
λ(Å)	0.7107
ρ_{calcd} (g cm^3)	6.50
μ(mm^{-1})	32.6
R[a]	0.036
R_w[b]	0.029

[a] $R = \Sigma||F_o| - |F_c||/\Sigma|F_o|$ for 4064 reflections.
[b] $R_w = [\Sigma w(|F_o| - |F_c|)^2/\Sigma w|F_o|^2]^{1/2}$.

at 10°C h to promote crystal growth. Excess of iodine and TeI_4 were evaporated *in vacuo* at 160°C, allowing the isolation of hexagonal well-formed crystals of **1**. Yield: 2.25 g (96%). Found: Re, 23.8; Te, 38.2. Calc for $I_{14}Re_6Te_{14}$: Re, 23.9; Te, 38.2%.

In order to ensure product homogeneity, the X-ray powder diffraction diagram of the product was obtained and found to be identical with the one calculated from the single-crystal data.

X-ray data collection and structure solution

Reflection data of $Re_6Te_{14}I_{14}$ (**1**) were collected at 295 K on a Rigaku AFC-5R diffractometer with graphite monochromated Mo-K_α radiation ($\lambda = 0.7107$ Å). The ψ-scan data showed very large absorption effect (relative transmission factor: 0.232–0.983), and an empirical absorption correction was applied. Such a large absorption was inevitable because the crystals grew as hexagonal plates, and the compound had a large μ value ($\mu = 32.6$ mm^{-1}) due to the heavy atoms. The structure could be successfully solved by direct methods (SHELXS86). Successive refinements gave reasonable interatomic distances and angles. However, the R values were high for a crystal with a good quality ($R = 0.126$ and $Rw = 0.124$ for 6035 reflections with $|F_o| > 3\sigma(F_o)$). No large residual peak was found on the Fourier maps. Examination of the discrepancies between $|F_o|$ and $|F_c|$ values revealed that strongly absorbed reflections had larger differences, which indicated that strongly absorbed reflections had not been accurately corrected with the empirical ψ-scan method. Therefore, the accuracy of the atomic parameters was substantially determined by the accuracy of the absorption correction. To obtain more accurate atomic parameters, we removed reflections with the calculated transmission factor less than 0.45 because their intensities were corrected less accurately than those of other reflections. After these reflections were removed, the reflections that could be used for refinements were still abundant. The ratio of the number of reflections to the number of variables was 26.2, and enough to determine the structure accurately. The refinements with the reduced reflection data set gave reasonable R values ($R = 0.036$, $Rw = 0.029$ for 4064 reflections). The differences between the parameters obtained from the refinement with all reflections and the corresponding parameters obtained with reduced reflection data were very small: the ratios of the difference to the estimated standard deviation were all less than 2.0.

Crystal data and refinement results for **1** are given

Table 2. Selected bond distances (Å) and angles (°)[a]

Re(1)—Re(2)	2.692(1)	Re(3)—Te(3)	2.689(1)
Re(1)—Re(2′)	2.693(1)	Re(3)—Te(4)	2.690(1)
Re(1)—Re(3)	2.690(1)	Re(3)—Te(7)	2.664(1)
Re(1)—Re(3′)	2.699(1)	I(1)—Te(5)	2.758(2)
Re(1)—Te(1)	2.692(1)	I(2)—Te(5)	2.758(2)
Re(1)—Te(2)	2.697(1)	I(3)—Te(6)	2.757(2)
Re(1)—Te(3′)	2.694(1)	I(4)—Te(6)	2.756(2)
Re(1)—Te(4)	2.691(1)	I(5)—Te(7)	2.768(1)
Re(1)—Te(5)	2.672(1)	I(6)—Te(7)	2.785(2)
Re(2)—Re(3)	2.695(1)	Re(1)—Te(5)—I(1)	106.56(3)
Re(2)—Re(3′)	2.700(1)	Re(1)—Te(5)—I(2)	105.85(3)
Re(2)—Te(1)	2.694(1)	I(1)—Te(5)—I(2)	89.29(5)
Re(2)—Te(2)	2.698(1)	Re(2)—Te(6)—I(3)	104.91(3)
Re(2)—Te(3)	2.694(1)	Re(2)—Te(6)—I(4)	104.83(4)
Re(2)—Te(4′)	2.696(1)	I(3)—Te(6)—I(4)	93.56(5)
Re(2)—Te(6)	2.670(1)	Re(3)—Te(7)—I(5)	104.19(4)
Re(3)—Te(1)	2.692(1)	Re(3)—Te(7)—I(6)	105.67(3)
Re(3)—Te(2′)	2.700(1)	I(5)—Te(7)—I(6)	92.67(5)

[a] Symmetry operation: $-x, -y, -z$.

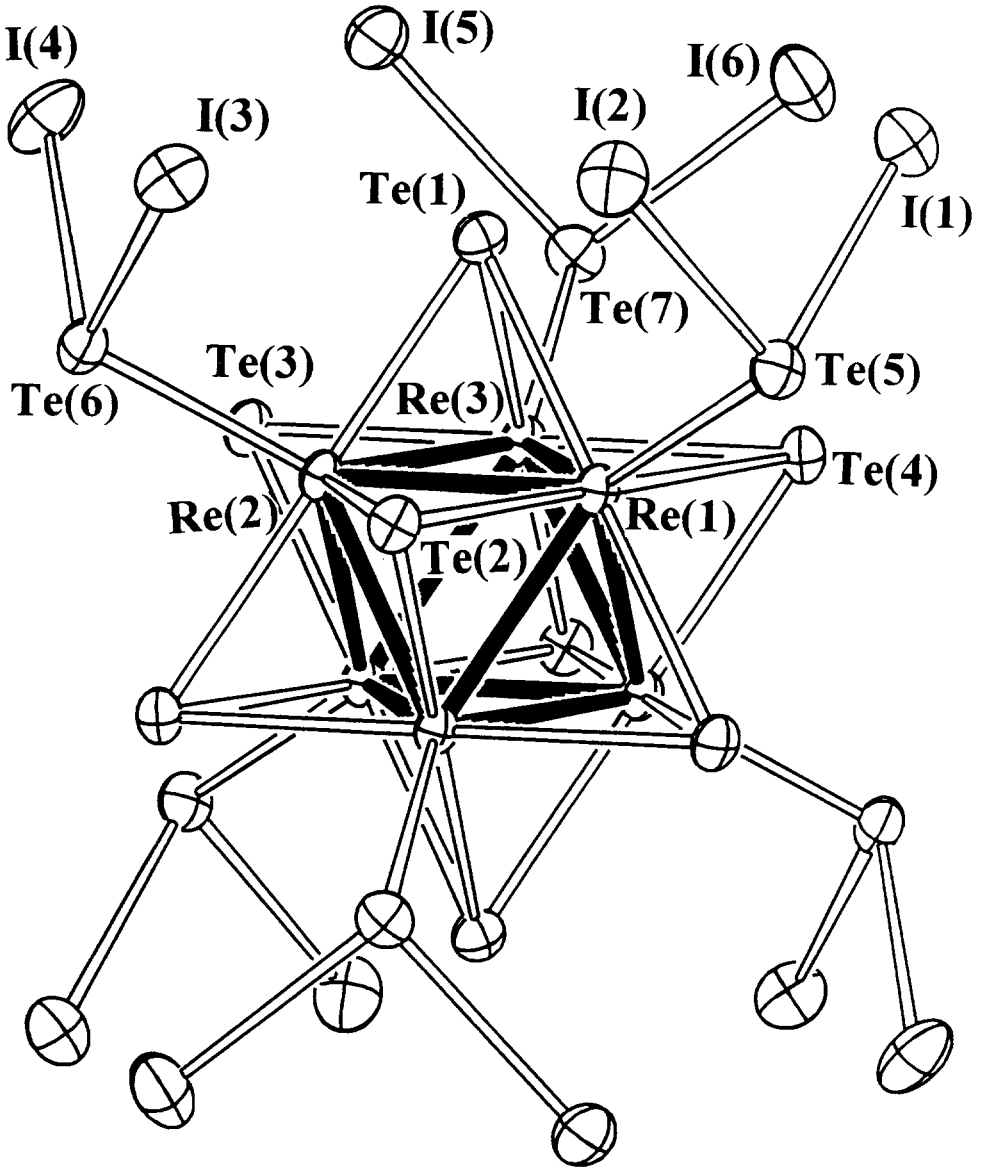


Fig. 1. ORTEP drawing of a $[Re_6Te_8(TeI_2)_6]^{2+}$ cluster. Thermal ellipsoids are drawn at the 50% probability level.

in Table 1. Selected interatomic distances and angles are given in Table 2.

RESULTS AND DISCUSSION

The hexanuclear Re_6 telluride Re_6Te_{15} is well known [13]. The cluster cores $[Re_6(\mu_3-Te)_8]$ of the compound are connected with each other *via* almost planar butterfly-like $Te_7 \equiv [Te(Te_3)_2]$ units. At room temperature Re_6Te_{15} reacts with Br_2 to form a molecular compound $Re_6Te_4Br_{10} \equiv [Re_6(\mu_3-Te)_4(\mu_3-Br)_4]Br_6$ with terminal Br atoms bonded to each rhenium atom [13b,14]. During the course of our study of controlled reaction of Re_6Te_{15} with I_2 we have obtained complex $[Re_6Te_{14}I_{14}]$ (**1**) containing terminal TeI_2 ligands coordinated to the rhenium atoms of the $[Re_6(\mu_3-Te)_8]^{2+}$ cluster fragment. Complex **1** is the first complex with TeI_2 ligands.

The tellurium-rich compound $[Re_6Te_{14}I_{14}]$ was obtained in high yield by the high-temperature reaction of the octahedral cluster complex Re_6Te_{15} with I_2 in a 1 : 9 ratio. The relevant equation is as in (1).

$$Re_6Te_{15} + 9I_2 \longrightarrow Re_6Te_{14}I_{14} + TeI_4 \qquad (1)$$

Compound **1** is diamagnetic, air-stable and insoluble in most common organic solvents. The structure of **1** has been determined by single-crystal X-ray diffraction. The $[Re_6Te_8(TeI_2)_6]^{2+}$ structure (Fig. 1) is characterized by the presence of the octahedral Re_6 cluster with Re—Re distances at 2.690(1)–2.700(1) Å, which are similar to those of Re_6Te_{15} (2.667(2)–2.682(2) Å) [15]. Each triangular face of the octa-

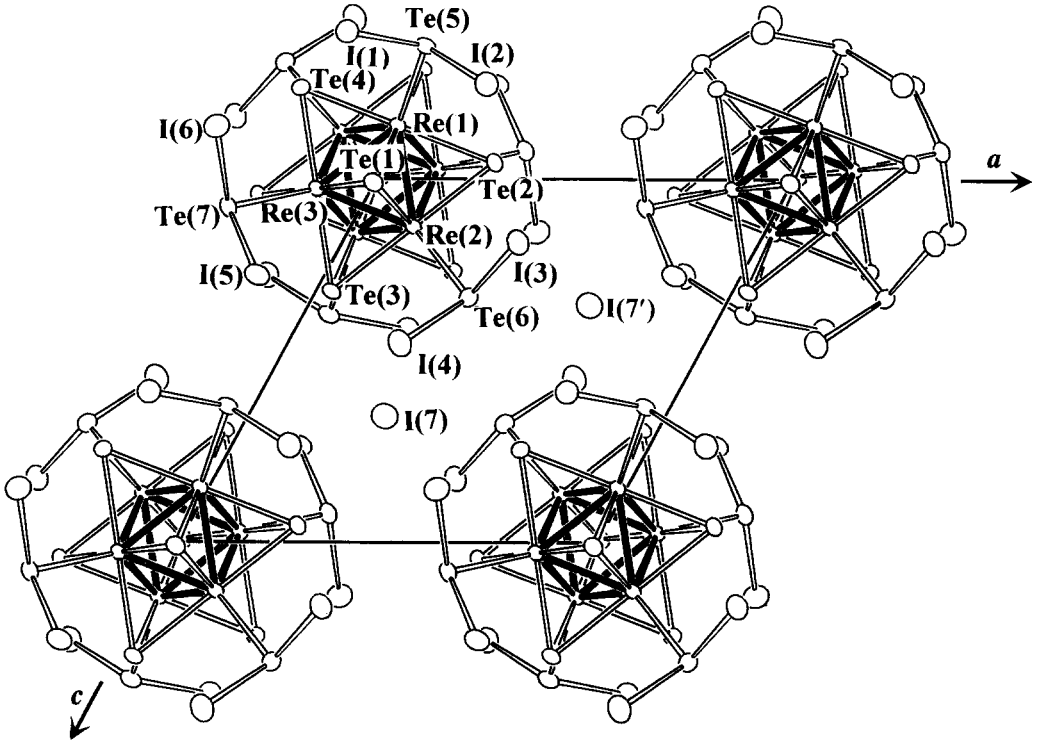


Fig. 2. ORTEP drawing of a cell of $[Re_6Te_8(TeI_2)_6]I_2$ projection on the *a*-*c* plane. Thermal ellipsoids are drawn at the 50% probability level.

hedron Re_6 is capped almost symmetrically by triply bridging telluride ions; the Re—μ_3—Te distances are 2.689(1)–2.698(1) Å. Each Re atom is further ligated by the neutral TeI_2 group. The Re—TeI_2 distances at 2.670(1)–2.672(1) Å are comparable to the Re—μ_3—Te distances. The Te—I distances in the TeI_2 ligands range from 2.756(2) to 2.785(2) Å. The I—Te—I bond angles are 89.29(5)–92.67(5)° and the Re—Te—I angles span 104.19(4) to 106.56(3)°. Tellurium atoms of the neutral ligands TeX_2 (X = Cl, Br, I) of the complexes $Re_6Te_6Cl_6(TeCl_2)_2$, $[Re_6Te_8(TeBr_2)_6]Br_6$ [8], $Re_4Te_4(TeBr_2)_4Br_8$ [7], and $[Re_6Te_8(TeI_2)_6]I_2$ have pyramidal geometry as predicted from VSEPR model consideration. The distortion of the polyhedron around the Te atom is caused by coordination to Re and by stereochemically active lone pairs directed from the Te atoms toward a vertex of tetrahedral polyhedrons.

The bonding in diamagnetic **1** can be rationalized in a straightforward manner. Counting iodine and μ_3-Te ligands as I^- and Te^{2-}, the TeI_2 groups as neutral ligands leads to the formulation $[(Re^{3+})_6(Te^{2-})_8(TeI_2)_6](I^-)_2$, where 24 electrons are shared by six Re atoms. In fact, the Re—Re bond distances in **1** are in good agreement with formal Re—Re single bond distances of the other 24 electron hexanuclear telluro, seleno and thio cluster complexes [15].

In the structure of $[Re_6Te_8(TeI_2)_6]I_2$, the clusters make close-packed layers along the *ac* plane (Fig. 2). All of the triangles in a close-packed layer are centered by iodide anions. Though a single layer has a pseudo-three-fold symmetry, the neighboring layer is shifted approximately along the *c*-axis by 0.3 c, and the whole crystal structure does not have pseudo-three-fold symmetry. A pseudo-three-fold axis passes Te1 atoms in a $[Re_6Te_8(TeI_2)_6]^{2+}$ cluster.

Acknowledgements—Dr A. V. Virovets is thanked for preliminary experiments. This work was supported by the Russian Foundation for Basic Research (research grant 96-03-33018).

REFERENCES

1. B. Krebs and F.-P. Ahlers, *Adv. Inorg. Chem.* 1990, **35,** 235.
2. S. Pohl, W. Saak and B. Krebs, *Z. Naturforsch.* 1985, **40b,** 251.
3. S. Pohl, A. Schäffer and B. Krebs, *Z. Kristallograph.* 1982, **162,** 180.
4. E. Erpenstein, Ph.D. thesis, Universität Münster, (1986), cited in: B. Krebs and F.-P. Ahlers, *Adv. Inorg. Chem.* 1990, **35,** 235.
5. A. Leist and W. Tremel, *Angew. Chem., Int. Ed. Engl.* 1993, **32,** 1751.
6. V. P. Fedin, H. Imoto and T. Saito, *J. Chem. Soc., Chem. Commun.* 1995, 1559.
7. E. S. Lang, U. Abram and J. Z. Strähle, *Anorg. Allg. Chem.* 1996, **622,** 251.

8. Y. V. Mironov, M. A. Pell and J. A. Ibers, *Inorg. Chem.* 1996, **35,** 2709.
9. V. B. Rybakov, L. A. Aslanov, S. V. Volkov, A. V. Grafov, V. I. Pekhno and Z. A. Fokina, *Russ. J. Inorg. Chem.* (*Engl. Transl.*) 1991, **36,** 680.
10. M. Paulus and G. Thiele, *Z. Anorg. Allg. Chem.* 1990, **588,** 69.
11. M. Paulus and G. Thiele, *Z. Naturforsch., B: Anorg. Chem., Org. Chem.* 1992, **47,** 253.
12. V. B. Rybakov, L. A. Aslanov, S. V. Volkov, Z. A. Fokina and V. F. Larko, *Russ. J. Inorg. Chem.* (*Engl. Transl.*) 1991, **36,** 1423.
13. (a) F. Klaiber, W. Petter and F. Hulliger, *J. Solid State Chem.* 1983, **46,** 112; (b) V. E. Fedorov, N. V. Podberezskaya, A. V. Mischenko, G. F. Khudorozko and I. P. Asanov, *Mat. Res. Bull.* 1986, **21,** 1335.
14. A. A. Opalovskii, V. E. Fedorov, E. U. Lobkov and B. G. Erenburg, *Russ. J. Inorg. Chem.* (*Engl. Transl.*) 1971, **16,** 1685.
15. (a) A. Perrin and M. Sergent, *New J. Chem.* 1988, **12,** 337; (b) S. C. Lee and R. H. Holm, *Angew. Chem., Int. Ed. Engl.* 1990, **29,** 840; (c) V. E. Fedorov, A. V. Mishchenko and V. P. Fedin, *Russ. Chem. Rev.* (*Engl. Transl.*) 1985, **54,** 408; (d) J. R. Long, A. S. Williamson and R. H. Holm, *Angew. Chem., Int. Ed. Engl.* 1995, **34,** 226.

Pergamon

PII: S0277-5387(96)00479-2

Polyhedron Vol. 16, No. 10, pp. 1621–1628, 1997
Copyright © 1997 Elsevier Science Ltd
Printed in Great Britain. All rights reserved
0277-5387/97 $17.00 + 0.00

Intramolecular benzoate exchange in benzoato *meso*-tetra (4-methoxyphenylporphyrinato) thallium(III), Tl(tmpp)($C_6H_5CO_2$)

Yeong-Horng Sheu,[a] Tay-Ning Hong,[a] Jyh-Horung Chen,[a]* Feng-Ling Liao,[b] Sue-Lein Wang,[b] Shin-Shin Wang[c] and Thomas C. Yang[d]

[a]Department of Chemistry, National Chung-Hsing University, Taichung 40227, Taiwan, R.O.C.

[b]Department of Chemistry, National Tsing-Hua University, Hsin-Chu 30043, Taiwan, R.O.C.

[c]Union Chemical Laboratories, Hsin-Chu 30043, Taiwan, R.O.C.

[d]Department of Chemistry, National Kaohsiung Normal University, Kaohsiung, Taiwan, R.O.C.

(Received 18 July 1996; accepted 25 September 1996)

Abstract—The new compound benzoato *meso*-tetra(4-methoxyphenylporphyrinato)thallium(III), Tl(tmpp)($C_6H_5CO_2$), has been synthesized and its molecular structure determined by X-ray analysis. The coordination sphere of the Tl^{3+} ion is an approximate square-based pyramid in which the apical site is occupied by an asymmetric-bidentate $C_6H_5CO_2^-$ group. The average Tl—N bond distance is 2.24(1) Å and the Tl atom is displaced 0.811 Å from the porphyrin plane. The Tl(1)—O(5) and Tl(1)—O(6) distances are 2.57(2) and 2.27(2) Å, respectively. Variable temperature ^{13}C NMR measurements show that the benzoato group of Tl(tmpp)($C_6H_5CO_2$) in CD_2Cl_2 solvent undergoes intramolecular exchange. In the slow exchange region, the carbonyl and $C_{1'}$ carbons of the benzoato group are separately located at 167.8 ppm [with ^2J(Tl-^{13}C) coupling constant 212 Hz] and 128.3 ppm [with ^3J(Tl-^{13}C) coupling constant 282 Hz] for Tl(tmpp)($C_6H_5CO_2$) in CD_2Cl_2 at −90°C. In the fast exchange region, the C*OO and $C_{1'}$ carbons of the $C_6H_5CO_2^-$ ligand in CD_2Cl_2 at 21°C are singlets at 168.4 and 130.3 ppm, respectively. The comparison of the ring current effect ($\Delta\delta$) for the benzoate ligand of Tl(tmpp)($C_6H_5CO_2$) and benzoato *meso*-tetra(4-methoxyphenylporphyrinto)tin(IV), Sn(tmpp)($C_6H_5CO_2$)$_2$, is also reported. © 1997 Elsevier Science Ltd. All rights reserved.

Keywords: crystal structure; thallium porphyrin complexes; intramolecular exchange; low temperature ^{13}C NMR; benzoato ligand; asymmetric bidentate ligand.

Previously, the synthesis, characterization and dynamic NMR studies of acetato *meso*-tetra(4-methoxyphenylporphyrinto) thallium(III), Tl(tmpp)(OAc), were reported by our group [1]. It turned out that the acetato ligand exchange for Tl(tmpp)(OAc) in CD_2Cl_2 solvent was intramolecular. When the OAc^- of Tl(tmpp)(OAc) was replaced by a bulkier and heavier benzoate group, $C_6H_5CO_2^-$, the complex Tl(tmpp)(OAc) became benzoato *meso*-tetra(4-methoxyphenylporphyrinto)thallium(III) Tl(tmpp)($C_6H_5CO_2$) (**1**). The acetato exchange of Tl(tmpp)(OAc) encouraged us to investigate a similar benzoato exchange for Tl(tmpp)($C_6H_5CO_2$) in CD_2Cl_2 by ^{13}C dynamic NMR method.

Smith *et al.* [2] reported the crystal structure of benzoato *meso*-tetra(4-methoxyphenylporphyrinto) tin(IV), Sn(tpp)($C_6H_5CO_2$)$_2$. Sn(tpp)($C_6H_5CO_2$)$_2$ is a tin(IV) complex with the benzoate, $C_6H_5CO_2^-$, being unidentately coordinated to the Sn atom. When the tpp was substituted by *meso*-tetra-(4-methoxyphenyl)porphyrin (tmpp), it became benzoato-*meso*-tetra-(4-methoxyphenylporphyrinato)tin(IV), Sn(tmpp)($C_6H_5CO_2$)$_2$ (**2**). The synthesis, ^{13}C and ^1H NMR spectroscopic studies of the new complex, Sn(tmpp)($C_6H_5CO_2$)$_2$ (**2**), are also reported.

In this paper, ^1H and X-ray analysis of Tl(tmpp)($C_6H_5CO_2$) (**1**) are reported. The ^{13}C NMR spectra at low temperature are examined to infer the intramolecular apical ligand, $C_6H_5CO_2^-$, exchange for Tl(tmpp)($C_6H_5CO_2$) in CD_2Cl_2. The comparison of

*Author to whom correspondence should be addressed.

the ring current shielding effect for compounds (**1**), (**2**) is an interesting subject and is also investigated in this paper.

EXPERIMENTAL

Synthesis

Tl(tmpp)($C_6H_5CO_2$) (**1**). Tl(tmpp)Cl (95.5 mg, 0.1 mmoles) [1] in $CHCl_3$ (20 cm^3) was treated with sodium benzoate (155.8 mg) in CH_3OH (10 cm^3) and stirred under reflux for ~13 h. After concentrating, it was dissolved in CH_2Cl_2 and extracted three times with distilled water to remove the excess $C_6H_5CO_2Na$. The CH_2Cl_2 layer was concentrated to dryness and gave purple prisms (91.8 mg, 87.9%). The crystals were grown by diffusion of ether vapour into a $CHCl_3$ solution. It was dissolved in CD_2Cl_2 (99.95% from Aldrich) for ^1H (Table 1, at 21°C) and ^{13}C (Table 2, at 21 and −90°C) NMR measurement.

Sn(tmpp)($C_6H_5CO_2$)$_2$ (**2**). Free base (tmpp; 150 mg, 0.204 mmoles, from Aldrich) and powdered $SnCl_2 \cdot 2H_2O$ (92 mg, 0.408 mmoles) were stirred and refluxed in pyridine (30 cm^3) for 3 h. The solution was cooled to 50°C, then saturated $C_6H_5CO_2H$ (12 cm^3, 32% in NH_3) was added, and heating and stirring were continued for another 3 h. After the solution was cooled, water (150 cm^3) was added, and the solid collected by vacuum filtration, washed with water, and dried by suction. The filter cake was digested *in situ* with CH_2Cl_2, dried with anhydrous Na_2SO_4 and filtered. The filtrate was taken to dryness under reduced pressure by rotatory evaporation and the product obtained was recrystallized from CH_2Cl_2/*n*-hexane yielding blue crystals (181 mg, 81%). It was dissolved in $CDCl_3$ for NMR measurement at 21°C (shown in Tables 1 and 2).

Spectroscopy

^1H and ^{13}C NMR spectra were recorded at 400.13 (or 600.20) and 100.61 (or 150.93) MHz, respectively, on a Bruker AM-400 spectrometer (or Bruker DMX-600) in $CDCl_3$ or CD_2Cl_2. ^{13}C NMR data are relative to the centre line of $CDCl_3$ at 77.0 ppm (or CD_2Cl_2 at 53.6 ppm). ^1H NMR data are relative to $CDCl_3$ at 7.24 ppm (or CD_2Cl_2 at 5.30 ppm).

Table 1. ^1H (400.13) MHz NMR data for compounds Tl(tmpp)($C_6H_5CO_2$) (**1**) in CD_2Cl_2 and Sn(tmpp)($C_6H_5CO_2$)$_2$ (**2**) in $CDCl_3$ at 21°C,[a] and the ring current effect ($\Delta\delta$) in ppm for the benzoate ligand in the complex[b]

Compound	β-H	$H_{2,6}$ (*ortho* H)		$H_{3,5}$ (*meta* H)		$H_{4''}$	$H_{3'',5''}$	$H_{2'',6''}$	*p*-O-CH_3
Tl(tmpp)($C_6H_5CO_2$)	9.09	8.25	8.06	7.32	7.27	6.93	6.69	6.39	4.06
(**1**) in CD_2Cl_2	(64.3)[c]	(7.5)[b]	(7.7)	(7.6)	(6.2)	t[d](7.4)	t(7.9)	d(7.6)	
						$\Delta\delta = -0.68$	$\Delta\delta = -0.78$	$\Delta\delta = -1.73$	
Sn(tmpp)($C_6H_5CO_2$)$_2$	9.23	8.16		7.32		6.67	6.33	4.91	4.11
(**2**) in CD Cl_3	(7.5)[e]	(8.9)		(8.9)		t(7.2)	t(7.8)	d(7.4)	
						$\Delta\delta = -0.94$	$\Delta\delta = -1.14$	$\Delta\delta = -3.21$	

[a] Chemical shifts are reported in ppm relative to $CHCl_3$ at 7.24 ppm or to CH_2Cl_2 at 5.30 ppm. Values in parentheses beneath were ^3J(H—H) coupling constants in Hz unless it was specified.

[b] $\Delta\delta = \delta$(coord) − δ(free), ^1H chemical shift difference between the coordination and the free benzoic acid.

[c] ^4J(Tl—H) coupling constants.

[d] Key: d = doublet, t = triplet.

[e] ^4J(Sn—H) coupling constants.

Table 2. ^{13}C NMR data for compound Tl(tmpp)($C_6H_5CO_2$) (**1**) in CD_2Cl_2 at 21 and −90°C and compound Sn(tmpp)($C_6H_5CO_2$)$_2$ (**2**) in $CDCl_3$ at 21°C. Values in parentheses beneath are J (Tl—^{13}C) coupling constant in Hz

Compound	Temp (°C)	COO	C_4	C_α	$C_{2,6}$ ($C_{2,2'}$)		C_1	C_β	$C_{4''}$	$C_{1''}$	$C_{2'',6''}$	$C_{3'',5''}$	C_m	$C_{3,5}$ ($C_{3,3'}$)	O—Me
Tl(tmpp)($C_6H_5CO_2$)	21	168.4	160.0	150.6	136.4	135.6	134.5	132.6	131.3	130.3	129.1	127.2	122.2	112.6	55.8
(**1**) in CD_2Cl_2				(20)	(24)	(24)	(29)	(121)					(150)	112.5	
	−90	167.8	158.1	149.1	135.6	135.2	132.7	132.1	130.9	128.3	128.0	126.6	121.4	111.4	55.3
		(212)		(18)	(18)	(18)	(29)	(122)		(282)			(150)	111.0	
Sn(tmpp)($C_6H_5CO_2$)$_2$	21	162.9	159.9	147.5	135.9		133.4	132.6	129.5	128.1	127.3	126.2	121.4	112.5	55.6
(**2**) in $CDCl_3$															

Crystallography

Crystal data and other information for [Tl(tmpp)($C_6H_5CO_2$)·$CHCl_3$] are given in Table 3. Measurements were made on a Siemens SMART CCD diffractometer using monochromatized Mo-K_α radiation ($\lambda = 0.71073$ Å) *via* the $\omega:2\theta$ scan technique. Absorption correction was based on 3516 symmetry-equivalent reflections using the SHELXTL-PC program package ($T_{min,max} = 0.482, 0.906$). The structure was solved by direct methods (SHELXTL PLUS) and refined by full-matrix least-squares. All non-hydrogen atoms were refined with anisotropic thermal parameters, whereas all hydrogen atom positions were calculated using a riding model and included in the structure factor calculation. Selected bond distances and angles for [Tl(tmpp)($C_6H_5CO_2$)·$CHCl_3$] are given in Table 4.

RESULTS AND DISCUSSION

Molecular structure of [Tl(tmpp)($C_6H_5CO_2$)·$CHCl_3$]

The skeletal framework of the complex [Tl(tmpp)($C_6H_5CO_2$)·$CHCl_3$], with $P2_1/C$ symmetry, is illustrated in Fig. 1. It reveals the six-coordination of the thallium atom with four nitrogen atoms of the porphyrinato group and the asymmetric bidentate $C_6H_5CO_2^-$ ligand; bond distances (shown in Table 4) are: Tl(1)—O(5) = 2.57(2), Tl(1)—O(6) = 2.27(2), O(5)—C(49) = 1.31(3), O(6)—C(49) = 1.17(2), C(49)—C(50) = 1.50(3) and the mean Tl(1)—N = 2.24(1) Å. The $CHCl_3$ molecule C(56)H(56a)Cl(1)Cl(2)Cl(3), in [Tl(tmpp)($C_6H_5CO_2$)·$CHCl_3$] arose from the solvent trapped during the crystal growth.

The thallium atom lies 0.789 and 0.811 Å from the four porphyrin nitrogens and the 24-atom porphyrin plane ($C_{20}N_4$), respectively. The dihedral angles between the mean planes of the skeleton ($C_{20}N_4$) and the planes of the phenyl group are 63.1° [C(24)], 80.7° [C(31)], 70.6° [C(38)] and 71.1° [C(45)].

The radius of the central "hole" ($C_t\cdots N$, the distance from the geometrical centre of the mean plane of the 24-atom core to the porphyrinato-core N atoms) in [Tl(tmpp)($C_6H_5CO_2$)·$CHCl_3$] is 2.096 Å which is larger than 2.01 Å suggested by Collins *et al.* [3]. The thallium(III) atom is bonded in a highly expanded porphyrinato core ($C_{20}N_4$) in [Tl(tmpp)($C_6H_5CO_2$)·$CHCl_3$] and the porphyrin ($C_{20}N_4$ and Tl) can be viewed as a domed shape. The net doming is 0.02 Å (= 0.811–0.789). Figure 2 shows the displacement (in Å) of each atom of the porphyrin ($C_{20}N_4$ and Tl) from the porphyrin mean plane ($C_{20}N_4$).

^{13}C and ^1H NMR for Tl(tmpp)($C_6H_5CO_2$) (**1**) *in* CD_2Cl_2 *and* Sn(tmpp)($C_6H_5CO_2$)$_2$ (**2**) *in* $CDCl_3$ *solution*

Figure 3 shows the representative broad band ^{13}C spectra of Tl(tmpp)($C_6H_5CO_2$) (**1**) in CD_2Cl_2 solvent

Table 3. Crystal data for [Tl(tmpp)($C_6H_5CO_2$)·$CHCl_3$]

Formula	$C_{56}H_{42}Cl_3N_4O_6Tl$
Formula weight	1177.7
a (Å)	12.4443(4)
b (Å)	33.313(1)
c (Å)	12.0870(4)
β(°)	99.853(1)
V(Å^3)	4937(1)
Z	4
D_c(g cm^{-3})	1.584
Space group	$P2_1/C$
F(000)	2344
μ(cm^{-1})	34.90
R^a	7.79%
$R_w{}^b$	10.68%
GOF	0.87
A^b	1
B^b	3.19×10^{-2}
Crystal size (mm^3)	$0.45\times0.31\times0.21$
Data collected	17980
$2\theta_{max}$(°)	51.4
Temperature (K)	296
Data used	6511 ($R_{int} = 0.0345$ after abs. cor.)
Discrimination	$I > 3.0\sigma(I)$

[a] $R = [\Sigma\|\|F_0| - |F_c\|/\Sigma|F_0|]$

[b] $R_w = [\Sigma w(\|F_0| - |F_c\|)^2/\Sigma w(|F_0|)^2]^{1/2}$; $w = A/(\sigma^2F_0 + BF_0^2)$

Table 4. Selected bond distance (Å) and angle (°) for [Tl(tmpp)($C_6H_5CO_2$)·$CHCl_3$]

Tl(1)—O(5)	2.57(2)	Tl(1)—N(1)	2.24(1)
Tl(1)—O(6)	2.27(2)	Tl(1)—N(2)	2.28(1)
O(5)—C(49)	1.31(3)	Tl(1)—N(3)	2.20(1)
O(6)—C(49)	1.17(2)	Tl(1)—N(4)	2.24(1)
C(49)—C(50)	1.50(3)		
O(5)—Tl(1)—N(1)	122.1(5)	O(6)—Tl(1)—N(1)	103.5(5)
O(5)—Tl(1)—N(2)	80.7(6)	O(6)—Tl(1)—N(2)	129.2(5)
O(5)—Tl(1)—N(3)	90.7(5)	O(6)—Tl(1)—N(3)	113.9(5)
O(5)—Tl(1)—N(4)	140.3(6)	O(6)—Tl(1)—N(4)	93.9(5)
N(1)—Tl(1)—N(2)	82.4(4)	N(2)—Tl(1)—N(3)	82.6(4)
N(1)—Tl(1)—N(3)	140.9(5)	N(2)—Tl(1)—N(4)	136.6(5)
N(1)—Tl(1)—N(4)	83.1(4)	N(3)—Tl(1)—N(4)	83.3(4)
O(5)—Tl(1)—O(6)	53.1(6)	C(50)—C(49)—O(5)	116(2)
C(49)—O(5)—Tl(1)	83(1)	C(50)—C(49)—O(6)	120(2)
C(49)—O(6)—Tl(1)	100(1)	O(5)—C(49)—O(6)	123(2)

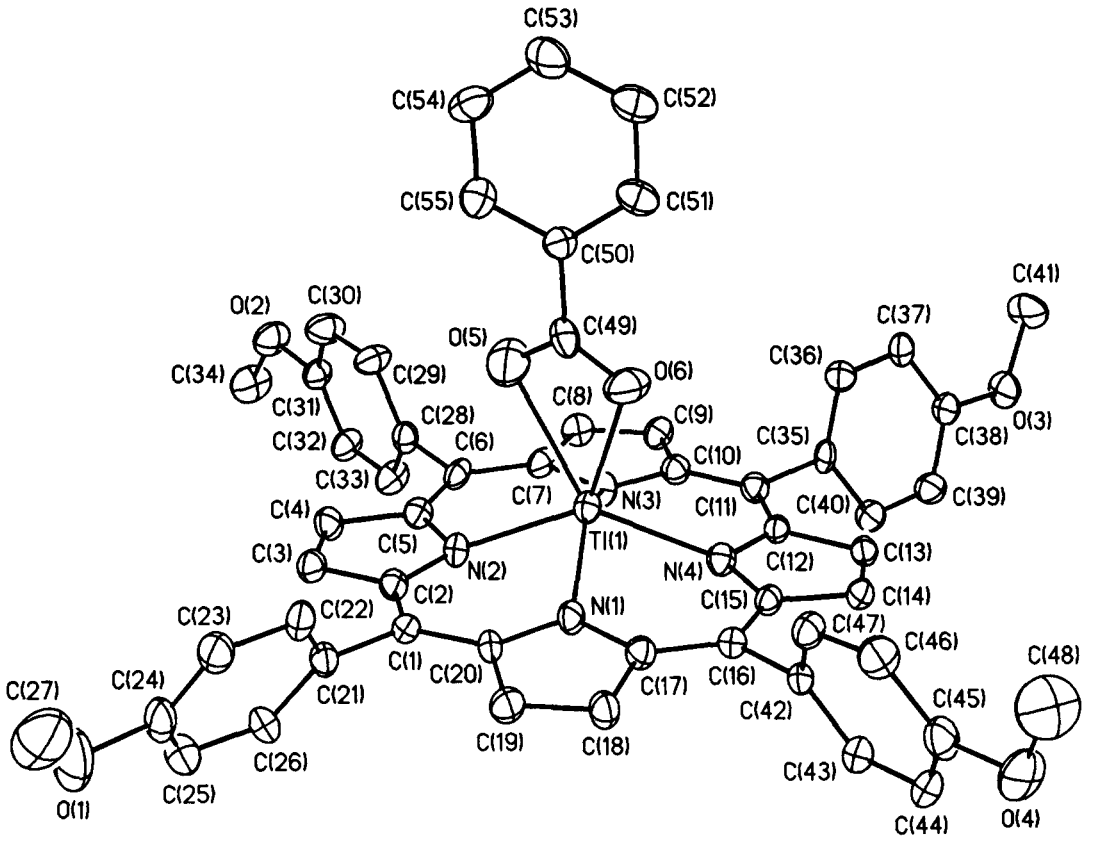


Fig. 1. Molecular configuration and atom labelling scheme for [Tl(tmpp)($C_6H_5CO_2$)·$CHCl_3$]. Hydrogen atoms and solvent C(56)H(56a)Cl(1)Cl(2)Cl(3) are omitted for clarity.

at 21°C and −90°C, respectively, and their ^{13}C data appear in Table 2. At 21°C, intramolecular exchange of the $C_6H_5CO_2^-$ group is rapid, indicated by singlet signals due to carbonyl carbons at 168.4 ppm and $C_{1''}$ carbons at 130.3 ppm shown in Fig. 3(a). At −90°C, the rate of the intramolecular exchange of $C_6H_5CO_2^-$ for Tl(tmpp)($C_6H_5CO_2$) (**1**) in CD_2Cl_2 is slow comparable with the coupling frequency of Tl-^{13}C, i.e. 247 ± 35 Hz. Hence, C*O and $C_{1''}$ carbons of $C_6H_5CO_2^-$ shown in Fig. 3(b) are observed at 167.8 ppm [with ^2J(Tl-^{13}C) = 212 Hz] and 128.3 ppm [with ^3J(Tl-^{13}C) = 282 Hz], respectively.

The intramolecular exchange of the $C_6H_5CO_2^-$ group is rapid for Tl(tmpp)($C_6H_5CO_2$) (**1**) in CD_2Cl_2

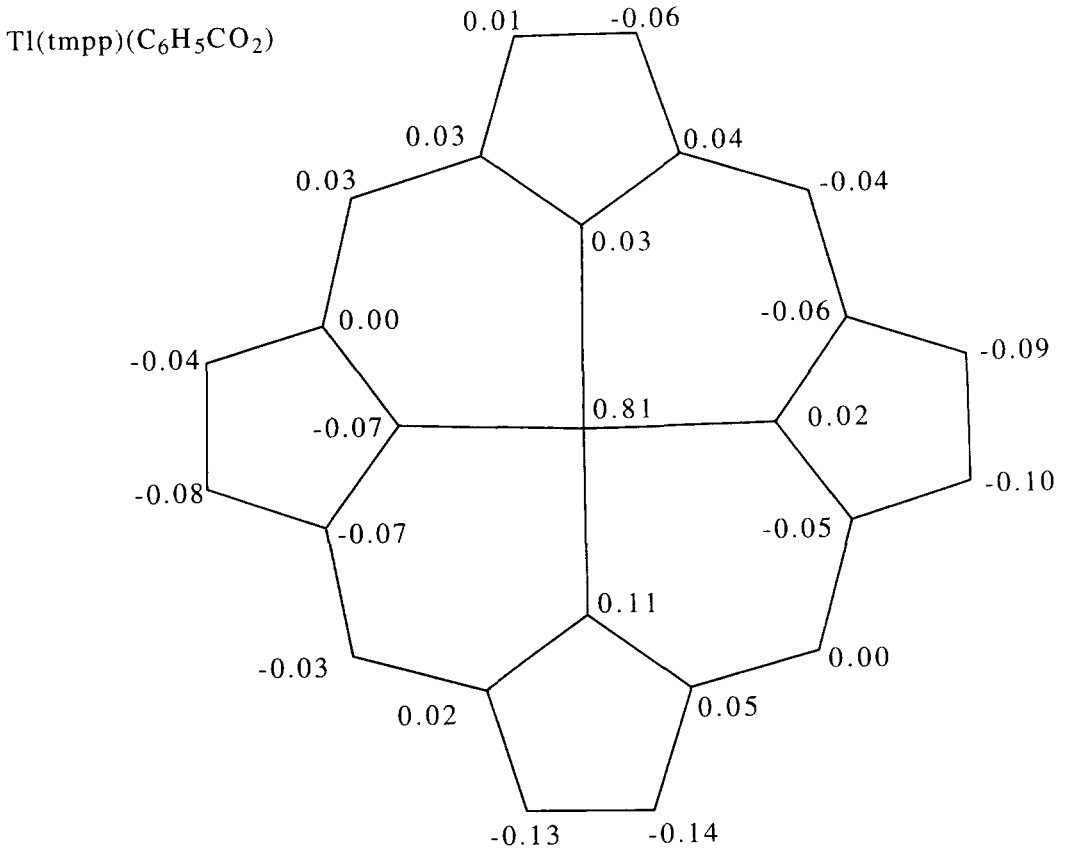


Fig. 2. Formal diagram of the porphyrin core ($C_{20}N_4$ and Tl) of [Tl(tmpp)($C_6H_5CO_2$)·$CHCl_3$] in which each atom symbol is replaced by a number showing the displacement (in Å) of that atom from the mean plane of porphyrin ($C_{20}N_4$).

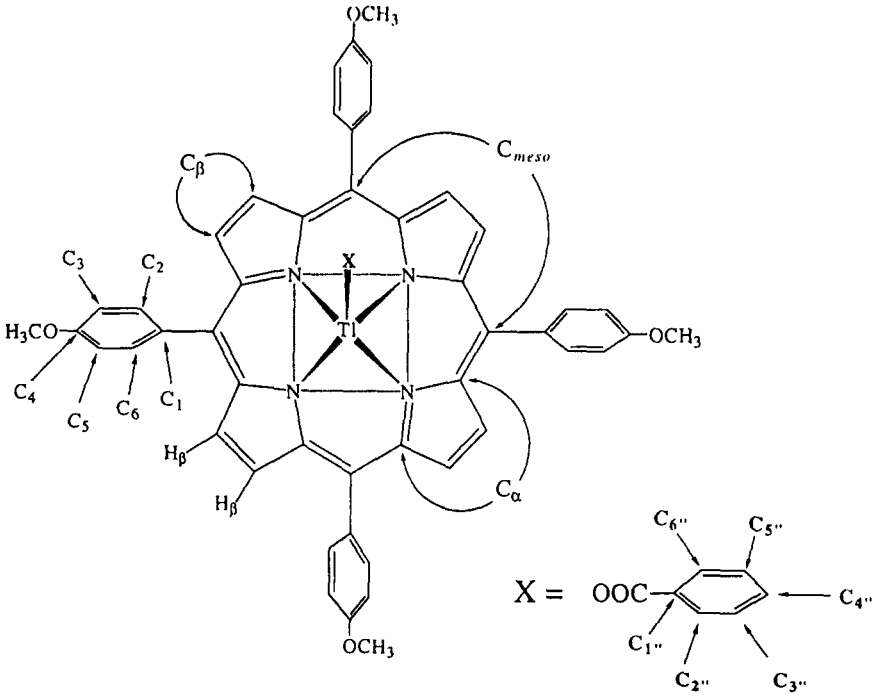
at 21 C, whereas the rotation of anisole group along C_1—C_{meso} bond is slow at the same temperature on the NMR time-scale. It is supported by both the assignment of 136.4, 135.6 ppm to the $C_{2,6}$ carbons and 112.6, 112.5 ppm due to the $C_{3,5}$ carbons (shown in Table 2) and by the assignment of 8.25, 8.06 ppm to $H_{2,6}$ protons (or *ortho*-H) and 7.32, 7.27 ppm due to $H_{3,5}$ protons (or *meta*-H, shown in Table 1).

The singlet signals for carbonyl carbons at 162.9 ppm and $C_{1''}$ carbons at 128.1 ppm (shown in Table 2) for Sn(tmpp)($C_6H_5CO_2$)$_2$ (**2**) in $CDCl_3$ at 21 and −50 C indicates no $C_6H_5CO_2^-$ exchange in compound (**2**). The benzoate might be, as in the case of Sn(tpp)($C_6H_5CO_2$)$_2$ [2], unidentately coordinated to the Sn atom for compound (**2**), and the tin(IV) atom is centered in an expanded porphyrinato core ($C_{20}N_4$).

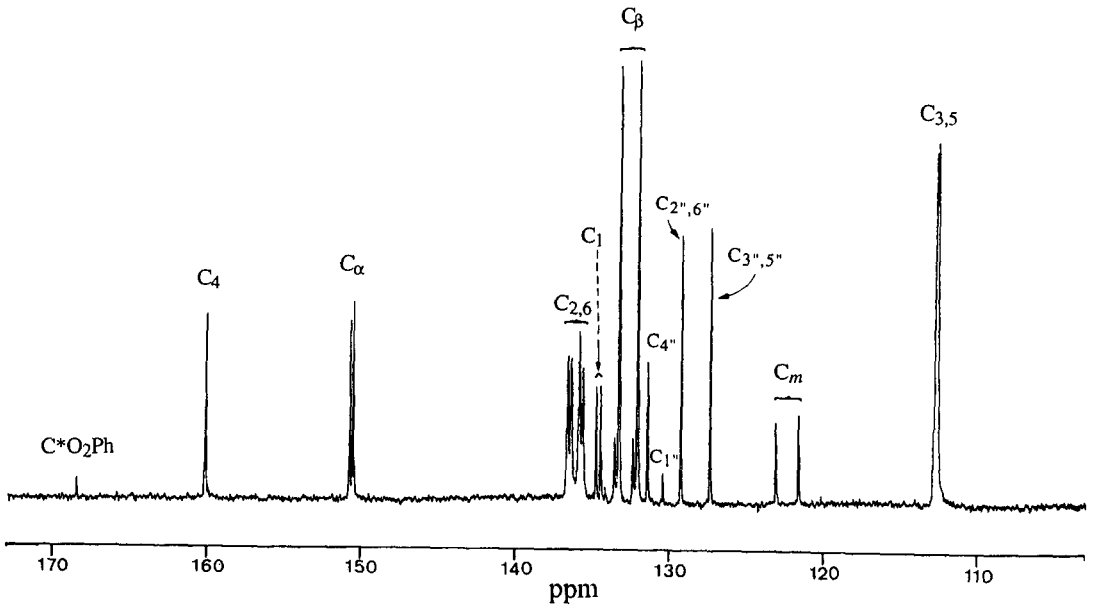
Compared with compound (**1**), the rotation of the anisole group along C_1—C_{meso} for compound (**2**) is fast at 21°C on the NMR time-scale. It is supported by both the assignment of 135.9 ppm to $C_{2,6}$ carbons and 112.5 ppm due to the $C_{3,5}$ carbons (shown in Table 2) and by the assignment of 8.16 ppm to $H_{2,6}$ protons and 7.32 ppm due to $H_{3,5}$ protons (shown in Table 1).

Due to the ring current effect, upfield shifts for the ^{1}H resonances of $H_{4''}$, $H_{3'',5''}$ and $H_{2'',6''}$ in Tl(tmpp)($C_6H_5CO_2$) (**1**) are $\Delta\delta = -0.68$ [from 7.61 (obtained from C_6H_5COOH) to 6.93 ppm], −0.78 (from 7.47 to 6.69 ppm) and −1.73 ppm (from 8.12 to 6.39 ppm), respectively (shown in Table 1). From the same effect, upfield shifts for the ^{1}H resonances of $H_{4''}$, $H_{3'',5''}$ and $H_{2'',6''}$ in Sn(tmpp)($C_6H_5CO_2$)$_2$ (**2**) are $\Delta\delta = -0.94$ (from 7.61 to 6.67 ppm), −1.14 (from 7.47 to 6.33 ppm) and −3.21 ppm (from 8.12 to 4.91 ppm), respectively (shown in Table 1). All indicate that as the protons of the benzoate ligand become closer to the $C_{t'}$, the shielding gets larger. The porphyrin ($C_{20}N_4$ and Tl) of compound (**1**) is viewed as domed shape whereas that ($C_{20}N_4$ and Sn) of compound (**2**) is planar. $C_{t'}$ (1.3391, 0.14134, 0.13389), of compound (**1**) is different from Tl(1), (1.38291, 0.14291, 0.09151), atom whereas $C_{t'}$ of compound (**2**) is Sn atom. The distances between $H_{4''}$, $H_{3'',5''}$, $H_{2'',6''}$ and $C_{t'}$ are longer in compound (**1**) than in compound (**2**). Hence the ring-current effect $\Delta\delta$ is larger in compound (**2**) than in compound (**1**) with (−0.94 *vs* −0.68 ppm) for $H_{4''}$, (−1.14 *vs* −0.78 ppm) for $H_{3'',5''}$ and (−3.21 *vs* −1.73 ppm) for $H_{2'',6''}$.

In summary, although the bulky benzoate group is asymmetrically and bidentately coordinated to the thallium atom in compound (**1**), it still undergoes the


OCH3
Cβ
Cmeso
C3
C2
X
N
N
H3CO
Tl
OCH3
C4
C5
C6
C1
N
N
Hβ
Hβ
Cα
OCH3
X =
OOC
C6"
C5"
C4"
C1"
C2"
C3"

(a) 21°C


Cβ
C3,5
C2",6"
C1
C3",5"
C4
Cα
C2,6
C4"
Cm
C*O2Ph
C1"
170
160
150
140
130
120
110
ppm

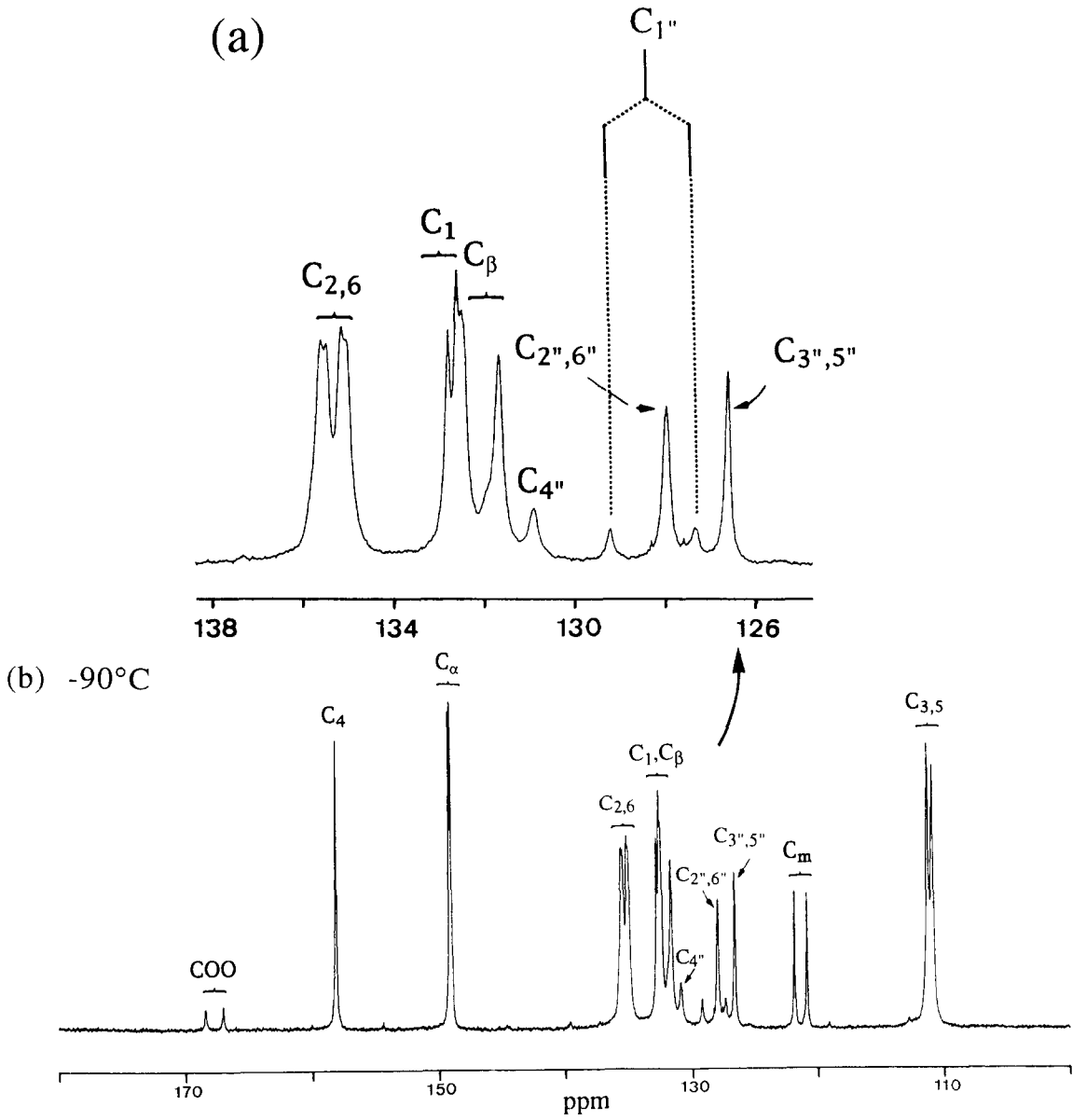


Fig. 3. ^{13}C broad band NMR spectra for Tl(tmpp)($C_6H_5CO_2$) (**1**) in CD_2Cl_2 (a) at 21°C (100.61 MHz) and (b) at −90°C (150.92 MHz).

intramolecular $C_6H_5CO_2^-$ exchange in CD_2Cl_2 solvent.

Acknowledgement—Financial support from the National Research Councils of the Republic of P. R. China under Grant NSC 86-2113-M-005-008 is gratefully acknowledged.

REFERENCES

1. Y. H. Sheu, T. N. Hong, C. C. Lin, J. H. Chen and S. S. Wang, *Polyhedron* 1996, in press.
2. G. Smith, D. P. Arnold, C. H. L. Kennard and T. C. W. Mak, *Polyhedron* 1991, **10,** 509.
3. D. M. Collins and J. L. Hoard, *J. Am. Chem. Soc.* 1970, **92,** 3761.

Pergamon

PII: S0277-5387(96)00480-9

Polyhedron Vol. 16, No. 10, pp. 1629–1635, 1997
Copyright © 1997 Elsevier Science Ltd
Printed in Great Britain. All rights reserved
0277-5387/97 $17.00+0.00

Structure and magnetism of tetra acetato bridged binuclear Nd^{III} complex

Shuyun Niu,[a]* Zhongzhi Yang,[a] Qingchuan Yang,[b] Bing Yang,[c] Jinquan Chao,[c] Guangdi Yang[c] and Er Zhong Shen[c]

[a]Department of Chemistry, Liaoning Normal University, Dalian 116029, P.R. China

[b]Department of Chemistry, Peking University, Beijing 100871, P.R. China

[c]Department of Chemistry and Institute of Theoretical Chemistry, Jilin University, Changchun 130023, P.R. China

(Received 18 July 1996; accepted 25 September 1996)

Abstract—A binuclear Nd^{III} complex of formula $[Nd_2(phen)_2(ONO_2)_2(CH_3COO)_4]$ (phen = phenanthroline) has been prepared and its structure and magnetism have been studied by X-ray diffraction and magnetic susceptibility measurements. The structure consists of two Nd^{III} ions bridged by four-bidentate CH_3COO^- groups and coordinated by two phen and two ONO_2 groups to give a binuclear $[Nd_2(phen)_2(ONO_2)_2(CH_3COO)_4]$ unit. This molecule possesses C_2 point group symmetry and the Nd atom is 9-coordinated in an irregular polyhedron. The average Nd—N distance (2.649 Å) is longer than the average Nd—O(2.493 Å). All four CH_3COO^- groups are bidentate ligands which connect to Nd as bridges while the O(4) atom is the μ_3 bridge oxygen and links two Nd atoms. The Nd—Nd distance is relatively short (3.974 Å). Cryomagnetic investigations (4.5–300 K) reveal a weak antiferromagnetic coupling with $J = -0.16$ cm^{-1}. © 1997 Elsevier Science Ltd. All rights reserved.

Keywords: neodymium; acetato; binuclear complex; synthesis; structure; magnetism.

Recently, the study of molecular-based magnets involving transition metals has been an active research field [1–9]. Introduction of lanthanide elements into these magnets might have great prospect since their **f** orbitals can accommodate more unpaired electrons than the **d** orbitals of transition metals. In fact, it has been demonstrated that lanthanides play an important function in permanent magnetism [10]. There are, however, only very few reports on this [11]. In addition, when lanthanides react with carboxylic acids and their derivatives, due to different ligand-bridging fashions, the structures of the resultant complexes are various and give rise to important effects on their optical, electronic and magnetic properties [12,13]. Investigations in this field may provide the basis for applying these sort of complexes.

EXPERIMENTAL

Preparation of $[Nd_2(phen)_2(ONO_2)_2(CH_3COO)_4]$

0.15 g phen., 0.2 g 8-hydrocyquinoline, 3 cm^3 water, 0.4 g CH_3COOH and 20 cm^3 acetone were fully mixed and 0.3 g $Nd(NO)_3 \cdot 6H_2O$ was resolved in 20 cm^3 acetone. Afterwards, the two solutions prepared above were mixed with stirring at room temperature, giving immediately a yellow solution which was kept at room temperature, and after one week pale yellow-pink crystals separated out. Found: C, 38.3; H, 2.8; N, 8.3; Nd, 28.3. Calc. for $C_{32}H_{28}N_6Nd_2O_{14}$, C, 38.1; H, 2.8; N, 8.3 and Nd, 28.6%.

Structure determination and refinement

Crystallographic data for the complex are given in Table 1. The treatment of the data was carried out on a VMS Computer using SHELXTL-Plus programs. The structure was solved by direct methods and refined with full matrix least-squares. The function minimized was $\Sigma\omega(F_o - F_c)^2$, where weighting scheme $\omega^{-1} = \sigma^2(F) + 0.0002F^2$ was used. At the same time, the extinction correction was made. An anisotropic thermal motion model was used for all non-hydrogen atoms, whilst the hydrogen atoms were placed in the

*Author to whom all correspondence should be addressed.

Table 1. Data collection and structure determination summary

Crystal data	
Empirical formula	$C_{32}H_{28}N_6Nd_2O_{14}$
Color; habit	Yellow block
Crystal size	0.10 × 0.10 × 0.27
Crystal system	Monoclinic
Space group	C_2
a (Å)	15.370(3)
b (Å)	12.259(2)
c (Å)	11.727(2)
β (°)	125.99(3)
V (Å^3)	1787.9(5)
Z	2
Formula weight	1009.1
D_c (Mg/m^3)	1.874
Absorption coefficient	2.957 mm^{-1}
F(000)	988
Data collection	
Diffractometer used	Rigaku AFC6S
Radiation	Mo-K_α (λ = 0.71073 Å)
Temperature (°C)	23
Monochromator	Highly oriented graphite crystal
2θ range	3.5–50.0°
Scan type	2 θ-θ
Scan speed	Variable; 4.00 to 32.00° min. in w
Scan range (w)	1.20° plus K_α-Separation
Standard reflection	3 measured every 150 reflections
Index ranges	$-14 \leqslant h \leqslant 18$, $-14 \leqslant k \leqslant 14$, $-13 \leqslant l \leqslant 0$
Reflections collected	3327
Independent reflections	3164 (R_{int} = 1.59%)
Absorption correction	Semi-empirical
Observed reflections	2744 ($F > 4.0\sigma$ (F))
Solution and refinement	
Quantity minimized	$\Sigma w(F_o - F_c)^2$
Absolute structure	N/A
Extinction correction	$X = -0.000004(15)$, where $F^* = F[1 + 0.002XF^2/\sin(2\theta)]^{-1/4}$
Weighting scheme	$w^{-1} = \sigma^2(F) + 0.0002F^2$
Number of parameters refined	250
Final R indices (obs. data)	R = 2.63%, wR = 2.98%
R indices (all data)	R = 3.46%, wR = 3.10%
Goodness-of-fit	1.01
Largest and mean W/S	1.104, 0.246
Data-to-parameter ratio	11.0 : 1
Largest difference peak	0.84 e Å^{-3}
Largest difference hole	−0.71 e Å^{-3}

calculated positions which fixed the isotropic thermal parameters.

Magnetic measurements

Magnetic susceptibilities were measured with a MPMS-7 type Superconducting Quantum Magnetometer in the temperature range 4.5–300 K and in a field of 10 KGS. The effective magnetic moments were calculated from the equation $\mu_{eff} = 2.828(\chi_m T)^{1/2}$, where χ_m is the molar magnetic susceptibility corrected for diamagnetism of constitutional atoms. The final data corrections were made using Pascal's constants.

RESULTS AND DISCUSSION

Description and discussion of the structure

The selected bond lengths and bond angles of complex $[Nd_2(phen)_2(ONO_2)_2(CH_3COO)_4]$ are listed in Table 2. The molecular structure and the packing of the molecules in unit cell of the complex are shown in Figs 1 and 2. The structure analysis demonstrates that

Table 2. Selected bond lengths (Å) and angles ( )

Nd—N(1)	2.709(19)	Nd—N(2)	2.589(19)
Nd—O(1)	2.600(15)	Nd—O(2)	2.485(19)
Nd—O(4)	2.707(3)	Nd—O(5)	2.496(5)
Nd—O(6)	2.439(12)	Nd—O(7)	2.355(14)
Nd—O(4)A	2.370(5)	O(4)—NdA	2.370(5)
N(1)—C(8)	1.340(22)	N(1)—C(9)	1.201(30)
N(2)—C(1)	1.359(24)	N(2)—C(10)	1.522(32)
N(3)—O(1)	1.213(26)	N(3)—O(2)	1.338(27)
N(3)—O(3)	1.248(10)	O(4)—C(13)	1.281(10)
O(4)—NdA	2.370(5)	O(5)—C(13)	1.252(6)
O(6)—C(15)	1.224(18)	O(7)—C(17)	1.292(20)
C(13)—C(14)	1.493(11)	C(15)—C(16)	1.402(33)
C(15)—O(6)A	1.224(18)	C(17)—C(18)	1.619(40)
C(17)—O(7)A	1.292(20)		

N(1)—Nd—N(2)	61.7(5)	N(1)—Nd—O(1)	71.8(6)
N(2)—Nd—O(1)	98.2(5)	N(1)—Nd—O(2)	97.8(5)
N(2)—Nd—O(2)	73.8(7)	O(1)—Nd—O(2)	50.2(5)
N(1)—Nd—O(4)	141.6(5)	N(2)—Nd—O(4)	141.1(5)
O(1)—Nd—O(4)	117.6(4)	O(2)—Nd—O(4)	117.0(5)
N(1)—Nd—O(5)	140.7(6)	O(2)—Nd—O(5)	141.2(7)
O(1)—Nd—O(5)	73.0(4)	O(2)—Nd—O(5)	72.0(5)
O(4)—Nd—O(5)	49.9(1)	N(1)—Nd—O(6)	133.7(7)
N(2)—Nd—O(6)	74.9(5)	O(1)—Nd—O(6)	132.9(6)
O(2)—Nd—O(6)	84.0(5)	O(4)—Nd—O(6)	69.7(5)
O(5)—Nd—O(6)	84.0(7)	N(1)—Nd—O(7)	76.1(5)
N(2)—Nd—O(7)	134.6(7)	O(1)—Nd—O(7)	82.7(5)
O(2)—Nd—O(7)	130.9(6)	O(4)—Nd—O(7)	69.0(6)
O(6)—Nd—O(7)	135.1(4)	O(5)—Nd—O(7)	82.7(7)
N(1)—Nd—NdA	115.7(4)	N(2)—Nd—NdA	114.8(5)
O(1)—Nd—NdA	146.0(3)	O(2)—Nd—NdA	145.7(4)
O(4)—Nd—NdA	35.6(1)	O(5)—Nd—NdA	85.4(1)
O(6)—Nd—NdA	67.9(3)	O(7)—Nd—NdA	68.4(3)
N(1)—Nd—O(4)A	80.2(5)	N(2)—Nd—O(4)A	79.6(6)
O(1)—Nd—O(4)A	148.9(6)	O(2)—Nd—O(4)A	150.4(6)
O(4)—Nd—O(4)A	77.2(2)	O(5)—Nd—O(4)A	127.0(1)
O(6)—Nd—O(4)A	76.9(7)	O(7)—Nd—O(4)A	77.6(7)
NdA—Nd—O(4)A	41.6(1)	Nd—N(1)—C(8)	122.6(14)
Nd—N(1)—C(9)	116.2(12)	Nd—N(2)—C(1)	121.4(15)
Nd—N(2)—C(10)	122.2(11)	O(1)—N(3)—O(2)	115.5(12)
O(1)—N(3)—O(3)	131.6(22)	O(2)—N(3)—O(3)	112.9(22)
Nd—O(1)—N(3)	96.2(10)	Nd—O(2)—N(3)	98.2(10)
Nd—O(4)—C(13)	89.0(3)	Nd—O(4)—NdA	102.8(2)
C(13)—O(4)—NdA	167.2(8)	Nd—O(5)—C(13)	99.7(5)
Nd—O(6)—C(15)	138.1(14)	Nd—O(7)—C(17)	137.0(15)
O(4)—C(13)—O(5)	120.8(7)	O(4)—C(13)—C(14)	118.7(5)
O(5)—C(13)—C(14)	120.4(8)	O(6)—C(15)—C(16)	117.5(12)
O(6)—C(15)—O(6)A	124.9(24)	C(16)—C(15)—O(6)A	117.5(12)
O(7)—C(17)—C(18)	124.1(26)	O(7)—C(17)—O(7)A	124.7(25)
C(18)—C(17)—O(7)A	111.0(24)	O(7)A—C(17)—C(18)	124.1(26)

A: $1-x, y, -z$

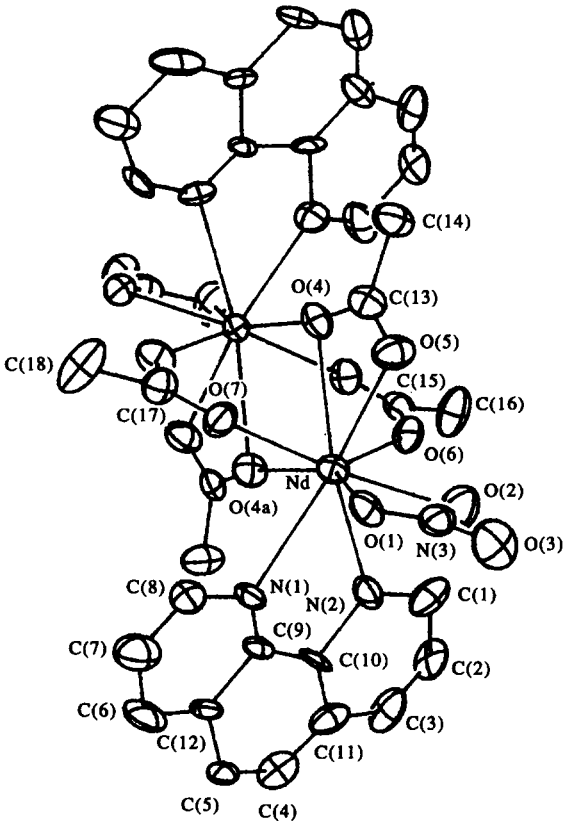


Fig. 1. The molecular structure of $[Nd_2(phen)_2(ONO_2)_2(CH_3COO)_4]$.

the $[Nd_2(phen)_2(ONO_2)_2(CH_3COO)_4]$ molecule is a binuclear Nd complex in which there are four CH_3COO^- group bridges. This molecule possesses C_2 symmetry, where the two-fold axis pass through atoms C(15), C(16) and C(17), and is parallel to the *b* axis of the cell. The C(18) atom is distributed on the both sides of this two-fold axis with occupancy factor of 0.5. The molecule contains two 9-coordinate (N_2O_7) irregular polyhedra with Nd at the center. The two ligand N atoms come from the phen ligands, with Nd—N bond lengths of 2.589(2) and 2.709(2) Å respectively. Two ligand O atoms come from a bidentate ONO_2 ligand, another five O atoms come from four CH_3COO^- groups, and the range of Nd—O bond lengths is 2.355(4)–2.707(3) Å. The four CH_3COO^- groups may be classified into two cases: two of them are simple bidentate bridges for each of which two oxygen atoms connect two Nd atoms respectively, but the other two chelate in such a way that one oxygen atom connects one Nd atom while the other O(4) or O(4a) connects two Nd atoms simultaneously becoming a μ_3-O atom. Therefore the coordination number of each Nd atom is 9. The separations of Nd—O(4) and Nd(A)—O(4) are 2.707(3) and 2.370(5) Å, respectively. So that Nd—Nd is relatively short, only 3.974(1) Å. This structure character of the title complex probably favors the magnetic coupling between the parallel electrons located on the two Nd^{3+} (f^3) ions which may contribute to the magnetism of the whole molecule.

The 8-membered ring constituted by two CH_3COO^- groups and two Nd atoms forms the molecular equatorial plane. The NO_3^- plane is approximately parallel to the equatorial plane (the dihedral angle is 20.0°) and another two CH_3COO^- and phen groups which are normal to each other with the dihedral angle 88.7°, are almost perpendicular to the equatorial plane with the respective dihedral angles of 83.3 and 99.3°.

Magnetic studies

The temperature dependence of molar magnetic susceptibility, χ_m, the magnetic moment, μ_{eff}, and χ_m^{-1} are depicted in Figs 3, 4 and 5. From Fig. 3 it is clearly seen that at room temperature χ_m is very small and varies very slowly with decreasing *T*. It is only at very low temperature ($T \sim 8$ K) where the magnetic susceptibility shows a dramatic change. In the complex two Nd^{3+} have the same coordination-surroundings, their *f* orbitals are occupied by 3 spin-parallel electrons respectively, i.e., their spin $S_1 = S_2 = 3/2$. Therefore, the magnetism of the complex arises from the Nd^{3+}—Nd^{3+} magnetic coupling. From Fig. 4 it can be seen that as *T* decreases the μ_{eff} decreases, which demonstrates that there is an antiferromagnetic coupling between the Nd^{3+} ions. Furthermore, if we treat $\chi_m^{-1} \sim T$ curve (in Fig. 5) as linear and extrapolate it intersecting the *T* axis; the crossing will be at the side of $-T$, which agrees with the $1/\chi = (T + \theta)/C$ [14]. All of these phenomena show that this complex possesses the character of the anti-ferromagnetic material.

In terms of the isotropic Heisenberg model, the Hamiltonian representing the magnetic interaction between two paramagnetic ions can be written as $\hat{H} = -2J\hat{S}_1\hat{S}_2$ where $\hat{S}_1$ and $\hat{S}_2$ stand for the spins of two Nd^{3+}, and *J* is the exchange integral between them. As $J > 0$, their interaction is ferromagnetic, and as $J < 0$ it is antiferromagnetic. By means of the model, the title complex has two Nd^{3+} ions of $S_1 = 3/2$ and $S_2 = 3/2$ so that the following expression of molar magnetic susceptibility can be deduced theoretically [15]:

$$\chi_m(\text{theor.}) = \frac{Ng^2\beta^2}{KT} \times \left[\frac{e^{-5J/KT} + 5e^{-3J/KT} + 14}{e^{-6J/KT} + 3e^{-5J/KT} + 5e^{-3J/KT} + 7}\right]$$

where *N* denotes Avogadro constant, *K* is Boltzmann constant, β is Bohr magnetron, *J* and *g* is magnetic parameter for evaluation, *T* is the absolute temperature. By using the least-squares method, a program is made in order to make χ_m(exp.) better simulate χ_m (theory.), shown in Fig. 3. After the simulation is optimized, the obtained magnetic parameter

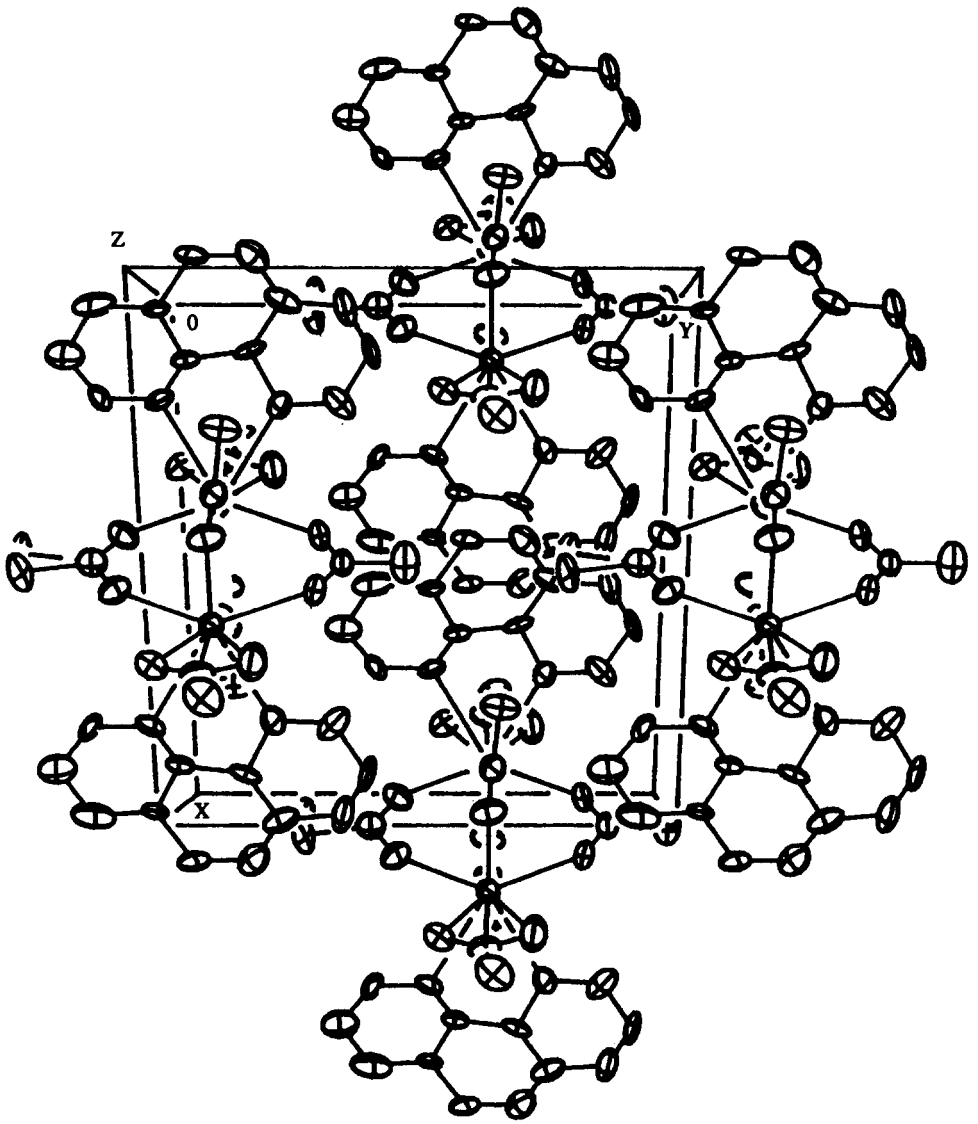


Fig. 2. The packing of the molecules in unit cell.

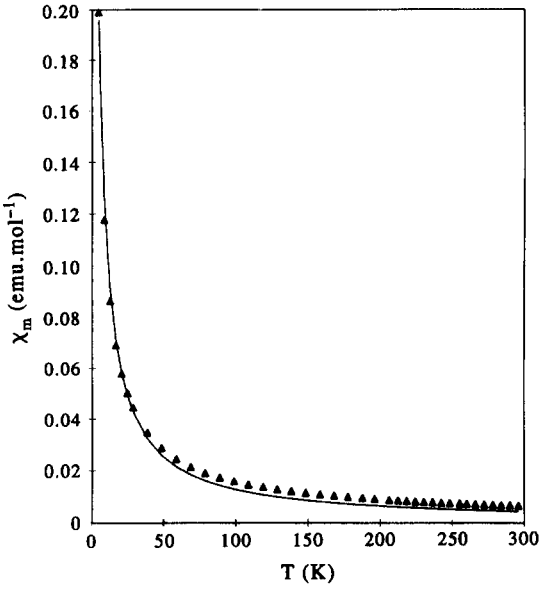


Fig. 3. Temperature dependence of χ_m (triangle is observed, line is calculated).

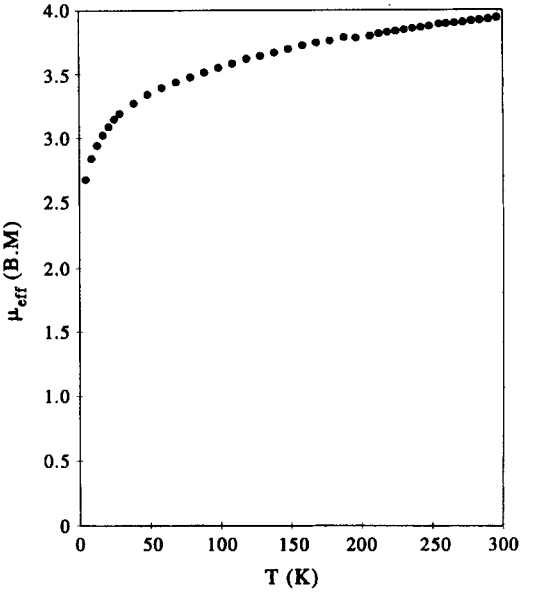


Fig. 4. Temperature dependence of μ_{eff}.

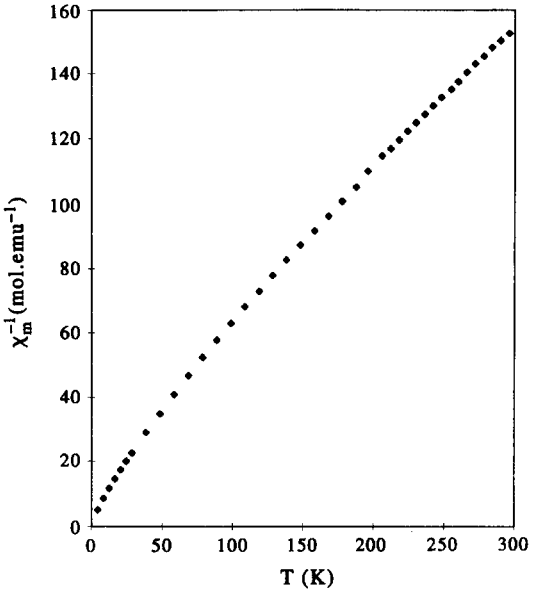


Fig. 5. Temperature dependence of $1/\chi_m$.

$J = -0.16$ cm^{-1} and the $g = 1.7$. The value of J reveals that a weak antiferromagnetic coupling between Nd—Nd ions in the complex.

Acknowledgement—Project supported by National Science Foundation of P.R. China.

REFERENCES

1. P. J. Koningsbruggen, O. Kahn, K. Nakatani, Y. Pei, J. P. Renard, M. Drillon and P. Legoll, *Inorg. Chem.* 1990, **29,** 3325.
2. A. Bencini, S. Midollini and C. Zanchini, *Inorg. Chem.* 1992, **31,** 2132.
3. H. O. Stumpf, L. Ouahab, Y. Pei, D. Grandjean and O. Kahn, *Science* 1993, **261,** 447.
4. M. Ohba, H. Tamaki, N. Matsumoto and H. Okawa, *Inorg. Chem.* 1993, **32,** 5358.
5. M. Monfort, J. Ribas and X. Solans, *Inorg. Chem.* 1994, **33,** 4271.
6. A. W. Graham, M. Kurmoo and P. Day. *J. Chem. Soc., Chem. Commun.* 1995, 2061.

7. B. Cheng, F. Cukiernik, P. H. Fries, J. C. Marchon and W. R. Scheidt, *Inorg. Chem.* 1995, **34,** 4627.
8. J. Manzur, A. M. Garcia, M. T. Garland, V. Acuna, O. Gonzalez, O. Pena, A. M. Atria and E. Spodinf, *Polyhedron* 1996, **15,** 5–6, 821.
9. D. M. Hong, Y. Y. Chu and H. H. Wei, *Polyhedron*, 1996, **15,** 447.
10. G. X. Xu and J. Z. Ni, *Fundamental Research on Rare-Earth Material*, p. 42. Hunan Science Technology Press, Changcha (1995).
11. O. Guillou, P. Bergerat, O. Kahn, E. Bakalbassis, K. Boubekeur, P. Batail and M. Guillot, *Inorg. Chem.* 1992, **31,** 110.
12. M. Frechette and C. Bensimon, *Inorg. Chem.* 1995, **34,** 3520.
13. L. P. Jin, M. Z. Wang, G. L. Chai, S. X. Liu, J. L. Huang and R. F. Wang, *Science in China* (*series B*), 1994, **24,** 6577.
14. A. J. Dekker, *Solid State Physics*, p. 523. Prentice Hall Inc. (1957).
15. E. König, *Inorg. Chem.* 1969, **8,** 6, 1278.

Pergamon

PII: S0277-5387(96)00478-0

Polyhedron Vol. 16, No. 10, pp. 1637–1641, 1997
Copyright © 1997 Elsevier Science Ltd
Printed in Great Britain. All rights reserved
0277-5387/97 $17.00+0.00

A novel tris (Lewis base) adduct. [(Dimercaptomethylene) propane-dinitrilato-S, S′] tris (3-methyl-pyridine) zinc(II)

Ren-Gen Xiong,[a] Cai-Ming Liu,[a] Xiao-Zeng You[a]* and Xiao-Ying Huang[b]

[a]Coordination Chemistry Institute, State Key Laboratory of Coordination Chemistry, Nanjing University, Centre for Advanced Studies in Science and Technology of Microstructure, Nanjing 210093, P. R. China

[b]State Key Laboratory of Structural Chemistry, Fujian Institute of Research on the Structure of Matter, Chinese Academy of Science, Fuzhou 350002, P. R. China

(Received 5 July 1996; accepted 25 September 1996)

Abstract—The zinc isomaleonitrile dithiolate (Zn(*i*-MNT)) reacts with 3-methylpyridine(3-mpy) to form a novel and stable adduct containing three coordinated 3-mpy molecules which was characterized by elemental analyses, IR and ^{1}H NMR. The crystal structure determination reveals that the Zn atom in tris(3-methylpyridine)[(dimercaptomethylene)propanedinitrilato-S,S′)] zinc(II) is in a distorted trigonal bipyramidal geometry with the N(1)S(1)N(3) occupying the equatorial plane and the N(2)S(1) occupying the apical positions. © 1997 Elsevier Science Ltd. All rights reserved.

Keywords: crystal structure; adduct; 3-methylpyridine; isomaleonitrile dithiolate; zinc(II) complex.

Recently, zinc complexes containing S_4, S_3N, or S_2N ligand cores have continued to receive increasing attention, owing to them acting as structural models of the immediate ligand environment of zinc in DNA-binding proteins and certain zinc-containing enzymes [1,2]. Furthermore, the volatile zinc thiolato and nitrogen containing ligand complexes are also very important MOCVD precursors for semiconducting materials, because zinc sulfides are widely used as phosphors, long-wavelength windows and catalysts [3]. Also, metal isomaleonitrile dithiolate(*i*-MNT) complexes and their reaction products with a variety of Lewis bases have been extensively investigated [4]. Like most of the bidentate complexes containing dithiolates such as dithiocarbamate, dialkyldithiophosphate and carbonadithiolate, Singh *et al.* suggested that the reaction of M(*i*-MNT)(M = Zn, Cd, Hg) with Lewis bases also destroyed the original polymeric structure to yield the mono-, bis- and tetrakis-(Lewis base) adducts [5,6]. To our knowledge, no metal(II) complexes have been found to form a stable tris (Lewis base) adduct. However, surprisingly it is found here that Zn(*i*-MNT) reacts with 3-methylpyridine to yield an adduct with three molecules of coordinated 3-methylpyridine. We report here the synthesis, spectral properties and X-ray crystal structure of [(dimercaptomethylene) propane dinitrilato-S, S′] tris (3-methypyridine) zinc(II) [Zn(*i*-MNT)(3-mpy)$_3$].

EXPERIMENTAL

Synthesis of Zn(*i*-MNT)(3-mpy)$_3$

Zinc chloride (1 mmol) was dissolved in 20 cm^3 absolute ethanol, to the clear solution was slowly added 20 cm^3 EtOH and $CHCl_3$ (1 : 1) solution of 1 mmol of [dimercaptomethylene propanedinitrilato-S, S′] dipotassium [K_2(*i*-MNT)]. Then excess 4-methylpyridine (4-mpy) was added dropwise to the yellow solution. The yellow columnar single crystal suitable for X-ray structure determination were obtained after the solution evaporated at room temperature for a few weeks. Yield 73.8%. Found: C, 54.4; H, 4.3; N,

*Author to whom correspondence should be addressed.

Table 1. Crystal data and data collection parameters for [Zn(*i*-MNT)(3-mpy)$_3$]

Formula	$C_{22}H_{21}N_5S_2Zn$
Formula weight	484.94
Crystal system	triclinic
Space group	$P\bar{1}$
a(Å)	8.884(2)
b(Å)	11.506(3)
c(Å	11.870(3)
α(°)	105.15(2)
β(°)	102.64(2)
γ(°)	93.74(2)
V(Å^3)	1133.1(5)
Z	2
T(K)	296
D_{calc}(g cm^{-3})	1.42
F(000)	500
μ(Mo K_α)(cm^{-1})	13.03
Collection range	$0 < 2\theta < 50°$
No. of observations ($I > 3\sigma(I)$)	3460
No. of variables	334
R	0.040
Rw	0.050
Goodness of fit indicator	1.61
Maximum shift in final cycle	0.17
Smallest/largest peak in final difference (e Å)	−0.69/0.33

14.4. Calc. for $C_{22}H_{21}N_5S_2Zn$: C, 54.3; H, 4.2; N, 14.2%.

Physical measurements

The IR spectrum was recorded on KBr pellets in the 4000–400 cm^{-1} and 500–100 cm^{-1} in Nujol mull modes using a Nicolet 170SXFTIR spectrophotometer. ^{1}H NMR spectrum (pyridine-d_5) was obtained using a Bruker AM 500 spectrometer at room temperature.

Crystallographic analysis

A yellow column single crystal with the approximate dimension 0.50 × 0.50 × 0.50 mm was mounted on an Enraf-Nonius CAD-4 diffractometer. X-ray data were collected with graphite-monochromated Mo-K_α radiation ($\lambda = 0.71069$ Å) at room temperature using the ω-2θ scan technique. Cell-parameters and an orientation matrix for data collection were obtained from least-square refinement, using the setting angles of 21 reflections in the range $20.02 \leqslant 2\theta \leqslant 29.68°$. A total of 3981 independent reflections ($R_{int} = 0.015$) were measured in the range $0 \leqslant 2\theta \leqslant 50°$ (h = 0–10, k = −13–13, l = −14–14), 3460 of which, with $I > 3\sigma(I)$, were used in the development and refinement of the structure. No significant intensity decay of three standard reflections recorded after every 300 reflections was observed. The intensity data were corrected for Lorentz and polarization effects. An empirical absorption correction based on a series of ψ-scans with minimum and maximum correction coefficient 0.9161 and 1.000, respectively, was applied [7].

The structure was solved by direct methods using MITHRIL [7]. The heavy atom Zn was located in an E map and the remaining non-H atoms were located using DIRDIF [8]. H atoms were placed in geometrically calculated positions (C—H = 0.95 Å) and were included in the structure factor calculations but not refined. The structure was refined by full-matrix least-squares techniques with anisotropic displacement parameters for all atoms. All calculations were performed on a VAX3100 computer using the TEXSAN program package [9]. The maximum and minimum peak values in the final difference Fourier map are 0.33 and −0.69 e Å^3, respectively. Crystal data and data collection parameters are summarized in Table 1. The atomic coordinates, thermal parameters and structure factors have been deposited with the editor as supplementary data.

RESULTS AND DISCUSSION

The results of elemental analyses, IR, and ^{1}H NMR spectra have shown that the reaction of Zn(*i*-MNT) with 3-methylpyridine forms the adduct. In the IR spectra of Zn(*i*-MNT)(3-mpy)$_3$, the characteristic absorption band of $\nu_{C\equiv N}$ (2175 cm^{-1}) was observed, in good accord with that of M(*i*-MNT) (M = Zn, Cd and Hg) [4]. Also, many bands at 3041(w), 1610(m), 1583(m), 1486(m), 1455(m), 1357(s), 1225(m), 1194(m), 1129(m), 1105(m), 1053(m), 984(w, sh),

Table 2. Selected bond distances (Å) and angles (°) for [Zn(*i*-MNT)(3-mpy)$_3$]

Zn—N(1)	2.053(2)	Zn—N(2)	2.260(3)
Zn—N(3)	2.050(2)	Zn—S(1)	2.308(1)
Zn—S(2)	2.698(1)		
S(1)—Zn—S(2)	71.86(3)	N(1)—Zn—N(2)	92.3(1)
N(1)—Zn—N(3)	115.6(1)	N(1)—Zn—S(1)	119.19(7)
N(1)—Zn—S(2)	98.40(7)	N(2)—Zn—N(3)	90.1(1)
N(2)—Zn—S(1)	94.93(7)	N(2)—Zn—S(2)	165.93(7)
N(3)—Zn—S(1)	124.62(7)	N(3)—Zn—S(2)	93.46(7)

947(s), 876(s), 787(m) and 704(s) cm^{-1}, respectively, were found. It is interesting to note that in the far-IR spectrum of Zn(*i*-MNT)(3-mpy)$_3$, a new medium absorption band appeared at 409 cm^{-1}, quite different from that found in Zn$_2$(*i*-MNT)$_2$(3-mpy)$_4$ [10]. Similarly, the ν_{Zn-N} (368(m) and 319(w) cm^{-1}) and ν_{Zn-S} (249(s) and 231(s) cm^{-1}) modes were also observed in the title adduct, in good agreement with those in Zn(en)(*i*-MNT) [4]; three medium bands were found at 190(m), 170(m) and 133(m) cm^{-1}, respectively. Furthermore, in the ^{1}H NMR spectrum of Zn(*i*-MNT)(3-mpy)$_3$, four group signals at 8.58(s, 2H, o-

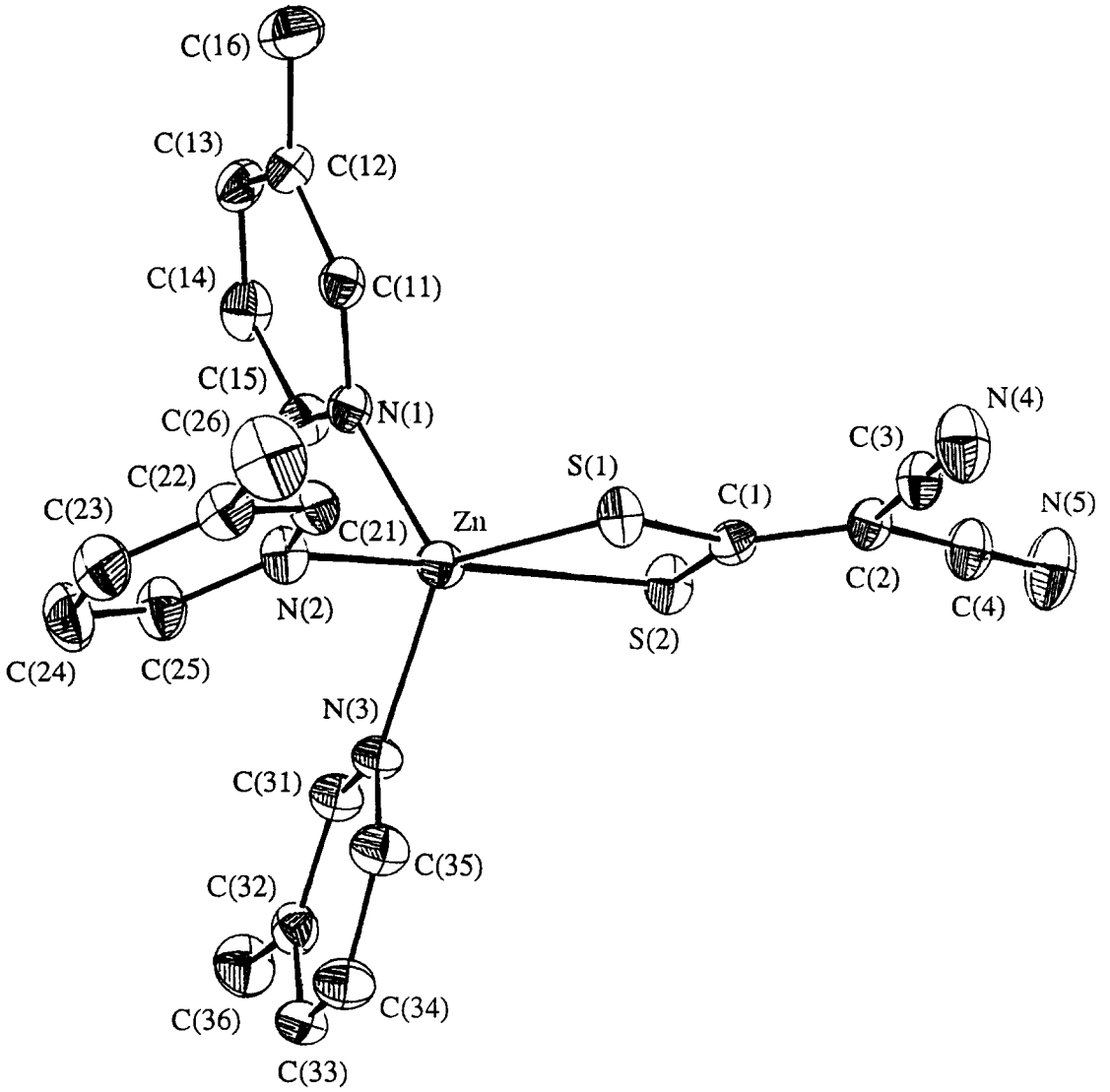


Fig. 1. ORTEP plot (30% probability thermal ellipsoids) of the [Zn(*i*-MNT)(3-mpy)$_3$] with the numbering scheme.

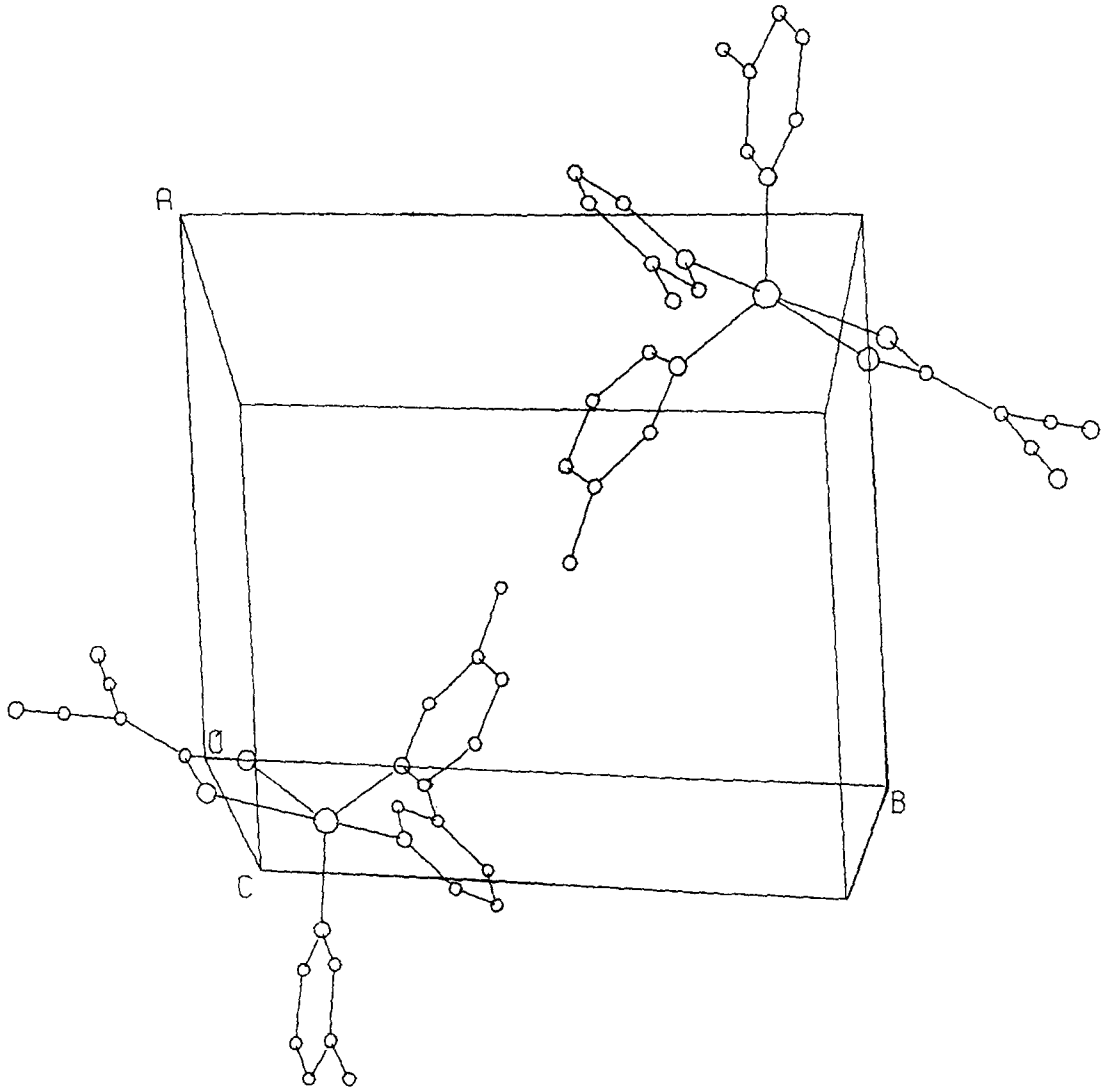


Fig. 2. Unit plot of the [Zn(*i*-MNT)(3-mpy)$_3$].

py), 7.37(d, 1H, p-py), 7.14(m, 1H, m-py) and 2.12(s, 3H, —CH_3) ppm, were observed, in agreement with the structure of Zn(*i*-MNT)(3-mpy)$_3$.

The selected bond distances and angles are listed in Table 2. The structure of Zn(*i*-MNT)(3-mpy)$_3$ is shown in Fig. 1, and stereoview of the molecular packing Zn(*i*-MNT)(3-mpy)$_3$ is depicted in Fig. 2. The crystal structural determination of Zn(*i*-MNT)(3-mpy)$_3$ (Fig. 1) reveals that the Zn atom is in a distorted trigonal bipyramidal environment with the N(1)S(1)N(3) occupying the equatorial plane and the N(2)S(1) occupying the two apical positions. A unique feature in the title adduct is that Zn(*i*-MNT) reacts with three nitrogen base molecules to form a novel and stable tris(3-methylpyridine) adduct (Fig. 2). As far as we know, this is the first crystallographically characterized example of the reaction of metal(II) complex with Lewis base forming stable adduct with three molecules of coordinated Lewis base. Generally speaking, the metal(II) complexes react with Lewis bases to yield the adducts with mono-, bis- and tetrakis-(Lewis base). Furthermore, a similar phenomenon in the low-valent coordination chemistry of the element groups 4 and 5 has also been observed [5]. It is worth noting that the lanthanide(III) complexes and other M(III) complexes (M = Nb, Ta, Cr etc.) have recently been found to be examples of structurally characterized adducts with three molecules of Lewis base [11]. Additionally, the Zn(*i*-MNT)(3-mpy)$_3$ having a monomeric structure is quite different from that of Zn_2(*i*-MNT)$_2$(4-mpy)$_4$ in which Zn(*i*-MNT) reacts with 4-methylpyridine to yield an eight-membered ring dimer and still remains dithiolato μ-bridge mode even though an adduct has effectively been formed [4]. The Zn—N (2.050(2)–2.260(3) Å) and Zn—S(2.308(1)–2.698(1) Å) bond distances exhibit much great variations, probably due to the Zn atom adopting a distorted trigonal bipyr-

amidal geometry in which three atoms, N(1), S(1) and N(3), describe an approximate equatorial plane and the two apical sites are occupied by the N(2) and S(2) atoms from an asymmetrically coordinating *i*-MNT ligand. The two Zn—N bond lengths from the equatorial plane are in good agreement with those of (2.064(3) Å, 2.045(4) Å, 2.057(6) ~ 2.037(6) Å and 2.035(4)–2.077(3) Å) found in $Zn(S_6)(py)_2$ [12], $Zn(S_6)(N\text{-}Melm)_2$ [1], $Zn(S\text{-}2,3,5,6\text{-}Me_4C_6H)_2(1\text{-}Me\text{-}imid)_2$ [13] and $Zn_2(i\text{-}MNT)_2(4\text{-}mpy)_4$ [10], respectively. Similarly, no significant difference of the Zn—S bond distances is observed, compared with $Zn(S_6)(py)_2$ (2.286(1) Å) [12], $Zn(S_6)(N\text{-}Melm)_2$ (2.317(1) Å) [1], $Zn(S\text{-}2,3,5,6\text{-}Me_4C_6H)_2(1\text{-}Me\text{-}imid)_2$ (2.301(2) ~ 2.298(2) Å) [13] and $Zn_2(i\text{-}MNT)_2(4\text{-}mpy)_4$(2.317(1)–2.321(1) Å [10], respectively. On the other hand, the bond angle of S(1)—Zn—S(2) is 71.86(3)°, significantly smaller than that of S(1)—Zn—S(2)′ (110.80(5)°), probably due to the dithiolato ligand in the latter bridging the two zinc atoms [10]. As expected, the bond distances of C—N, C—C and C—S are unexceptional.

Acknowledgements—This work was supported by a major project from the State Science and Technology Commission and the National Science Foundation of P. R. China, as well as the Foundation of the Chinese Postdoctoral Fellowship.

REFERENCES

1. D. T. Corwin Jr and S. A. Koch, *Inorg. Chem.* 1988, **27,** 493.
2. M. Bochmann and K. J. Webb, *J. Chem. Soc., Dalton Trans.* 1991, 2325.
3. K. Osakada and T. Yamamoto, *J. Chem. Soc., Chem. Commun.* 1987, 1117; S. Wang and J. P. Fackler Jr, *Acta Cryst.* 1990, **C46,** 2253; D. Zhu, X. C. Xing, P. J. Wu, P. Wang, D. M. Zhang and D. L. Yang, *Synth. Met.* 1991, **42,** 2541.
4. M. K. Singh, R. C. Aggarwal and B. Singh, *Synth. React. Inorg. Met-Org. Chem.* 1985, **15,** 459.
5. R.-G. Xiong, J.-L. Zuo, X.-Z. You, Q.-J. Wu and X.-Y. Huang, *Trans. Met. Chem.* 1995, **20,** 498; M. A. Araya, F. A. Cotton, J. H. Matonic and C. A. Murillo, *Inorg. Chem.* 1995, **34,** 5424.
6. D. M. Barnhar, D. L. Clark, J. C. Gordon, J. C. Huffman, J. G. Watkin and B. Md. Zwick, *Inorg. Chem.* 1995, **34,** 5416; X.-Y. Huang, R.-G. Xiong, J.-X. Dong and X.-Z. You, *Acta Cryst.* 1995, **C51,** 587.
7. R.-G. Xiong, X.-Y. You, Q.-J. Wu and X.-Y. Huang, *Acta Cryst.* 1995, **C51,** 1978; R.-G. Xiong, X.-Z. You, J.-X. Dong and X.-Y. Huang, *Acta Cryst.* 1995, **C51,** 835; C. J. Gilmore, *MITHRIL, Computer Program for the Automatic Solution of Crystal Structure from X-ray data.* Department of Chemistry, University of Glasgow, Scotland (1983).
8. P. T. Beurskens, *DIRDIF*, 1984, *Direct methods for Difference Structures—an Automatic Procedure for Phase Extension and Refinement of Difference Structure Factors. Technical Report* 1984/1. Crystallography Laboratory, Toernooiveld, 6526 ED Nijmegen, The Netherlands (1984).
9. Molecular Structure Corporation, *TEXSAN, TEXRAY Structure Analysis Package*, MSC3200 Research Forest Drive, The Woodlands, TX 77381, U.S.A. (1985).
10. R.-G. Xiong, J.-L. Zuo, X.-Z. You and X.-Y. Huang, *Inorg. Chem.* (in press).
11. J. Lee, B. Brewer, M. Berardini and J. G. Brennan, *Inorg. Chem.* 1995, **34,** 3215.
12. H.-J. Li, S.-W. Du and X.-T. Wu, *Acta Cryst.* 1994, **C50,** 498.
13. S. Der, E. Ramli, T. B. Rauchfuss, C. L. Stern, *J. Am. Chem. Soc.* 1990, **112,** 6385.

Pergamon

PII: S0277-5387(96)00477-9

Polyhedron Vol. 16, No. 10, pp. 1643–1650, 1997
Copyright © 1997 Elsevier Science Ltd
Printed in Great Britain. All rights reserved
0277-5387/97 $17.00+0.00

Synthesis, structure and spectroscopic properties of dimethylammonium lanthanide tetrakis(*N*,*N*-dimethyldithiocarbamate)

Chengyong Su,[a]* Minyu Tan,[a]† Ning Tang,[a] Xinmin Gan,[a] Zefu Zhang,[b] Qunji Xue[b] and Kaibei Yu[c]

[a]Department of Chemistry, Lanzhou University, Lanzhou 730000, P. R. China

[b]Lanzhou Institute of Chemistry Physics, Academia Sinica, Lanzhou 730000, P. R. China

[c]Chengdu Centre of Analysis and Measurement, Academia Sinica, Chengdu 610041, P. R. China

(Received 24 May 1996; accepted 25 September 1996)

Abstract—Trivalent lanthanide complexes of the type $[Ln(Me_2Dtc)_4]H_2NMe_2$ (Ln = La, Pr—Nd, Sm—Ho; Me_2Dtc = *N*,*N*-dimethyldithiocarbamate) have been prepared and characterized by means of elemental analyses, IR spectra, electronic spectra, ^1H NMR spectra and conductivity measurements. The X-ray crystal and molecular structure of the neodymium complex has been determined from diffractometer data. There are two independent $[Nd(Me_2Dtc)_4]H_2NMe_2$ monomers in each unit cell; the metal coordination number is 8. Spectroscopic properties of the complexes are discussed. © 1997 Elsevier Science Ltd. All rights reserved.

Keywords: lanthanide(III); *N*,*N*-dimethyldithiocarbamate; complex; synthesis; spectroscopic property; crystal structure.

The first well-characterized trivalent lanthanide dithiocarbamate was reported by Brown [1] and further confirmed by Ciampolini [2] by X-ray single crystal structure determination. In recent years some new lanthanide dithiocarbamates have been prepared [3–7] but crystal structures were few [6,7]. Common to all these earlier works is the observation that the lanthanide dithiocarbamate complexes under study were unstable to moist conditions and atmosphere; anhydrous lanthanide salts must be used and water must be excluded during preparation. Siddall [8] had managed to prepare the light lanthanide complexes $[Ln(^tBu_2Dtc)_4]$ $HNEt_3$ (Ln = La,Pr,Nd,Sm) using hydrated lanthanide nitrates and thought that the steric effect in R_2NCSS^- should play an important role in the stability of this kind of complex. We now report the synthesis and structure of $[Ln(Me_2Dtc)_4]$ H_2NMe_2 complexes which are sufficiently stable to be prepared and handled in the ordinary laboratory atmosphere.

EXPERIMENTAL

Materials

Dimethylammonium dimethyldithiocarbamate ($Me_2Dtc \cdot H_2NMe_2$) was prepared according to literature procedure [9]. Hydrated lanthanide chlorides (or perchlorates) were prepared by dissolving lanthanide oxides (AnalaR) in 1:1 chloric (or perchloric) acid. All other chemicals were AnalaR grade and were used without further purification.

Synthesis

To a solution of 0.18 mmol of hydrated lanthanide chlorides (or perchlorates) in 5 cm^3 of ethanol was added a solution of 0.72 mmol of $Me_2Dtc \cdot H_2NMe_2$ in 10 cm^3 of ethanol. The mixture was stirred at room temperature for about 30 min

*Present address: Department of Chemistry, Zhongshan University, Guangzhou 510275.

†Author to whom correspondence should be addressed.

when a precipitate appeared. The precipitate was filtered, washed several times with ethanol and dried *in vacuo* over P_4O_{10}-$CaCl_2$ for 48 h. The yield was about 80%.

A single crystal of the neodymium complex was obtained by the following procedure: $Nd(ClO_4)_3 \cdot nH_2O$ (0.18 mmol) and $Me_2Dtc \cdot H_2NMe_2$ (0.72 mmol) were dissolved in 20 cm^3 acetonitrile. To this clear solution was slowly added 5 cm^3 ether. The mixture was left standing overnight and a single crystal suitable for X-ray crystal determination appeared. The complex contains one acetonitrile molecule which is apt to escape and the crystal effloresces quickly once it is removed from the mother liquor.

X-ray measurements and structure determination

The crystal used for the structure determination was about $0.48 \times 0.50 \times 0.60$ mm in size. It was mounted in a sealed quartz capillary containing some mother liquor. X-ray diffraction intensity were collected at 21°C on an R3M/E diffractometer with graphite-monochromated Mo-K_α radiation, using the $\theta/2\theta$ scan technique. Two standard reflections were measured every 98th scan. A total of 9531 reflections which were collected in the range $2 \leqslant 2\theta \leqslant 46°$ yielded 9338 unique data in which 5884 had $I \geqslant 3\sigma(I)$. Data were corrected for Lorentz-polarization factors, but no correction was made for absorption. The intensities of the reflections decayed about 12% during the data collection period, and the data were corrected for this effect.

The structure was solved using direct methods followed by Fourier difference syntheses, and refined by full-matrix least-squares methods with anisotropic thermal factors for all non-hydrogen atoms and with hydrogen atoms in calculated position; weighting scheme: $w = [1-\exp(-5)(\sin(\theta/\lambda)^2]/[\sigma^2(F) + 0.00015F^2]$; final $R = 0.0309$, $Rw = 0.0308$. The maximum and minimum residual electron densities in the final difference map were 0.555 and -0.438 e $Å^{-3}$. All calculations were carried out on an Eclipse S140 computer using the SHELXTL (1985) program. Data collection and refinement parameters are summarized in Table 1.

Other measurements

Carbon, nitrogen and hydrogen analyses were determined using a Carlo-Erba 1106 elemental analyser, while metal ion contents were estimated with EDTA using xylenol orange as the indicator. IR spectra were recorded on a Nicolet-170 SX FT-IR spectrophotometer using KBr discs in the range 4000–220 cm^{-1}. Electronic spectra were recorded on a Shimadzu UV-260 spectrophotometer in the 190–900 nm region in the acetonitrile solution. ^1H NMR spectra were measured on an FT-80A spectrometer in $CDCl_3$ solution with TMS as internal standard. Conductivity measurements were carried out with a DDS-11A type conductivity bridge using 10^{-3} mol cm^{-3} solution in acetonitrile at 25°C.

RESULTS AND DISCUSSION

Hydrated lanthanide chlorides or perchlorates can be used directly for preparation of the complexes without any precaution against instability. Complexes prepared in this manner give satisfactory elemental analyses for La, Pr—Nd, Sm—Ho (Table 2). The pink powder of the Er^{3+} complex and yellow powder of the Yb^{3+} complex can also be obtained but they hydrolyse easily, confirming the suggestion that this kind of complex becomes progressively less stable with increasing atomic number [8]. Attempts to synthesize $[Ce(Me_2Dtc)_4]H_2NMe_2$ were accompanied by oxidation to Ce^{4+} [8]. All the complexes thus obtained are stable in air for several months; however, the characteristic colour of the corresponding complex in solution disappears in several hours suggesting that the complexes decompose readily in the solution.

The molar conductances of $[Ln(Me_2Dtc)_4]H_2NMe_2$ measured in aectonitrile at 25°C lie in the range 119–142 Ω^{-1} cm^2 mol^{-1}, indicating that all the complexes are 1 : 1 electrolytes, which is consistent with the formulation obtained from the elemental analyses. The complexes are readily soluble in CH_3CN, CH_2Cl_2, DMSO, DMF, soluble in MeOH, $CHCl_3$, THF, slightly soluble in EtOH, $ClCH_2CH_2Cl$ and insoluble in non-polar organic solvents.

X-ray structure of $[Nd(Me_2Dtc)_4]H_2NMe_2$

Selected bond lengths and angles are given in Tables 3 and 4. Figure 1 shows the structure for the complex; Fig. 2 shows the packing arrangement in the unit cell and Fig. 3 shows the coordination polyhedra of the Nd(1) and Nd(2) atoms in the complex.

As shown in Fig. 1, the structure contains two independent $[Nd(Me_2Dtc)_4]^-$ anions, two $H_2N^+Me_2$ cations and two uncoordinated acetonitrile molecules. In each of the $[Nd(Me_2Dtc)_4]^-$ monomers, the neodymium ion is coordinated to eight sulfur atoms of four Me_2Dtc ligands. A similar structure was found for $V((Me_2Dtc)_4$ [10]. In its crystal structure there are two non-equivalent $V(Me_2Dtc)_4$ monomers also. The coordination polyhedra of both Nd^{3+} atoms can be described as D_2 dodecahedra according to the rule of Blight and Kepert [11], for the calculated value of b is 1.23 for both monomers. However, when comparing the bond angles of two monomers carefully, slight differences can be found. The 16th, 17th and 18th lowest S—Nd(1)—S angles are 90.4°, 92.3° and 104.8°; whilst those of S—Nd(2)—S are 93.2°, 94.6° and 95.7°. So according to the criteria of Haigh [12], the structure of Nd(2) is "normal" dodecahedron

Table 1. Crystal data, data collection and refinement parameters

Formula	$C_{16}H_{35}N_6S_8Nd$
Formula weight	712.27
Crystal size (nm)	$0.48 \times 0.50 \times 0.60$
System	monoclinic
Space group	$P2_1/a$
Temperature (°C)	21 ± 1.5
a (Å)	19.514(3)
b (Å)	15.240(2)
c (Å)	20.770(3)
β (°)	90.38(1)
V (Å^3)	6176(2)
Z	8
D (Calc.) (g cm^{-3})	1.53
μ (cm^{-1})	22.2
Radiation (graphite monochromator)	Mo K_α (λ = 0.71073 Å)
Standard reflection	8, 0, 4; 6, 3, −8
Scan type and range	$2 \leqslant 2\theta \leqslant 46°$
Unique data	9338
Observable data with $I \geqslant 3.0\sigma(I)$	5884
R	0.0309
Rw	0.0308
S	0.953
Residual extrema in final difference map	−0.438–0.555

Table 2. Analytical data, colours and molar conductance data

Compound	Colour	Found (Calc.) % C	H	N	M	Λm (Ω^{-1}cm^{2}mol^{-1})
[La(Me$_2$Dtc)$_4$]H$_2$NMe$_2$	White	25.2	4.7	10.3	20.6	
		(25.2)	(4.8)	(10.5)	(20.9)	123
Pr(Me$_2$Dtc)$_4$]H$_2$NMe$_2$	Pale green	25.0	4.7	10.1	21.2	
		(25.2)	(4.8)	(10.5)	(21.1)	120
Nd(Me$_2$Dtc)$_4$]H$_2$NMe$_2$	Pale blue	25.0	4.6	10.4	21.4	
		(25.0)	(4.8)	(10.4)	(21.5)	122
Sm(Me$_2$Dtc)$_4$]H$_2$NMe$_2$	Pale yellow	24.7	4.7	10.1	22.0	
		(24.8)	(4.8)	(10.3)	(22.2)	119
Eu(Me$_2$Dtc)$_4$]H$_2$NMe$_2$	Orange red	24.5	4.7	10.0	22.1	
		(24.8)	(4.7)	(10.3)	(22.4)	121
Gd(Me$_2$Dtc)$_4$]H$_2$NMe$_2$	White	24.4	4.5	9.9	22.9	
		(24.6)	(4.7)	(10.2)	(23.0)	119
Tb(Me$_2$Dtc)$_4$]H$_2$NMe$_2$	White	24.6	4.6	9.8	22.9	
		(24.5)	(4.7)	(10.2)	(23.2)	124
Dy(Me$_2$Dtc)$_4$]H$_2$NMe$_2$	White	24.0	4.6	9.7	23.8	
		(24.4)	(4.7)	(10.2)	(23.6)	121
Ho(Me$_2$Dtc)$_4$]H$_2$NMe$_2$	Pale yellow	24.0	4.5	9.9	24.1	
		(24.3)	(4.7)	(10.1)	(23.8)	122

while that of Nd(1) has a distortion towards the bicapped prism.

The bond lengths of Nd(1)—S are 2.885–2.936 Å (mean 2,914 Å) and those of Nd(2)—S are 2.886–2.939 Å). They are nearly identical within the measurement error, approximately the same as found for $[Nd(S_2CNC_4H_6)_4]^-$ (mean 2.908 Å) [6] and are comparable with the La—S bond lengths of Na[La-($Et_2Dtc)_4$] [2] and La[$(S_2CNC_4H_8)_3$ ($C_4H_8O11\cdot H_2O$)] [6] (mean 2.97 Å) taking account of the difference in their ionic radii (La = 1.160, Nd = 1.109 Å).

All the S—C bond lengths of both two monomers are almost equal; in addition, all the bond lengths of N—C(SS) have more double bond character (N—C, 1.47 Å, N=C, 1.30 Å), denoting that the S=C double bond of the ligand is delocalized in the complex.

Table 3. Selected bond lengths (Å) with e.s.d.s in parentheses

Nd(1)—S(1)	2.920(2)	Nd(1)—S(2)	2.919(2)
Nd(1)—S(3)	2.939(2)	Nd(1)—S(4)	2.911(2)
Nd(1)—S(5)	2.903(2)	Nd(1)—S(6)	2.919(2)
Nd(1)—S(7)	2.917(2)	Nd(1)—S(8)	2.885(2)
Nd(2)—S(9)	2.886(2)	Nd(2)—S(10)	2.920(2)
Nd(2)—S(11)	2.936(2)	Nd(2)—S(12)	2.912(2)
Nd(2)—S(13)	2.923(2)	Nd(2)—S(14)	2.888(2)
Nd(2)—S(15)	2.927(2)	Nd(2)—S(16)	2.940(2)
S(1)—C(1)	1.720(6)	S(2)—C(1)	1.713(6)
S(3)—C(4)	1.725(6)	S(4)—C(4)	1.723(6)
S(5)—C(7)	1.706(6)	S(6)—C(7)	1.698(6)
S(9)—C(13)	1.718(6)	S(10)—C(13)	1.719(6)
S(11)—C(16)	1.723(6)	S(12)—C(16)	1.715(6)
S(13)—C(19)	1.722(6)	S(14)—C(19)	1.703(6)
S(15)—C(22)	1.708(6)	S(16)—C(22)	1.705(6)
N(1)—C(1)	1.324(7)	N(2)—C(4)	1.320(7)
N(3)—C(7)	1.336(8)	N(4)—C(10)	1.333(7)
N(5)—C(13)	1.328(8)	N(6)—C(16)	1.331(7)
N(7)—C(19)	1.319(8)	N(8)—C(22)	1.321(8)

Table 4. Selected bond angles (°)

S(1)—Nd(1)—S(2)	60.7(1)	S(1)—Nd(1)—S(3)	82.1(1)
S(2)—Nd(1)—S(3)	124.9(1)	S(1)—Nd(1)—S(4)	84.2(1)
S(2)—Nd(1)—S(4)	75.6(1)	S(3)—Nd(1)—S(4)	60.7(1)
S(1)—Nd(1)—S(5)	134.8(1)	S(2)—Nd(1)—S(5)	74.8(1)
S(3)—Nd(1)—S(5)	134.2(1)	S(4)—Nd(1)—S(5)	92.3(1)
S(1)—Nd(1)—S(6)	163.8(1)	S(2)—Nd(1)—S(6)	132.6(1)
S(3)—Nd(1)—S(6)	82.0(1)	S(4)—Nd(1)—S(6)	90.4(1)
S(5)—Nd(1)—S(6)	60.5(1)	S(1)—Nd(1)—S(7)	84.1(1)
S(2)—Nd(1)—S(7)	84.9(1)	S(3)—Nd(1)—S(7)	132.8(1)
S(4)—Nd(1)—S(7)	160.3(1)	S(7)—Nd(1)—S(5)	84.8(1)
S(6)—Nd(1)—S(7)	104.8(1)	S(1)—Nd(1)—S(8)	87.7(1)
S(2)—Nd(1)—S(8)	136.3(1)	S(3)—Nd(1)—S(8)	73.6(1)
S(8)—Nd(1)—S(4)	134.2(1)	S(5)—Nd(1)—S(8)	123.5(1)
S(6)—Nd(1)—S(8)	85.1(1)	S(7)—Nd(1)—S(8)	60.9(1)
S(9)—Nd(2)—S(10)	61.0(1)	S(9)—Nd(2)—S(11)	89.8(1)
S(10)—Nd(2)—S(11)	85.1(1)	S(9)—Nd(2)—S(12)	131.9(1)
S(10)—Nd(2)—S(12)	78.5(1)	S(11)—Nd(2)—S(12)	60.4(1)
S(9)—Nd(2)—S(13)	128.8(1)	S(10)—Nd(2)—S(13)	169.9(1)
S(11)—Nd(2)—S(13)	91.8(1)	S(12)—Nd(2)—S(13)	91.6(1)
S(9)—Nd(2)—S(14)	68.5(1)	S(10)—Nd(2)—S(14)	128.3(1)
S(11)—Nd(2)—S(14)	84.2(1)	S(12)—Nd(2)—S(14)	135.1(1)
S(13)—Nd(2)—S(14)	60.7(1)	S(9)—Nd(2)—S(15)	135.3(1)
S(10)—Nd(2)—S(15)	95.7(1)	S(11)—Nd(2)—S(15)	128.1(1)
S(12)—Nd(2)—S(15)	69.0(1)	S(15)—Nd(2)—S(13)	78.5(1)
S(14)—Nd(2)—S(15)	129.5(1)	S(9)—Nd(2)—S(16)	81.1(1)
S(10)—Nd(2)—S(16)	89.6(1)	S(11)—Nd(2)—S(16)	170.8(1)
S(12)—Nd(2)—S(16)	125.8(1)	S(13)—Nd(2)—S(16)	94.6(1)
S(14)—Nd(2)—S(16)	93.2(1)	S(15)—Nd(2)—S(16)	59.8(1)
S(1)—C(1)—S(2)	118.4(3)	S(3)—C(4)—S(4)	117.9(3)
S(5)—C(7)—S(6)	119.1(3)	S(7)—C(10)—S(8)	118.5(3)

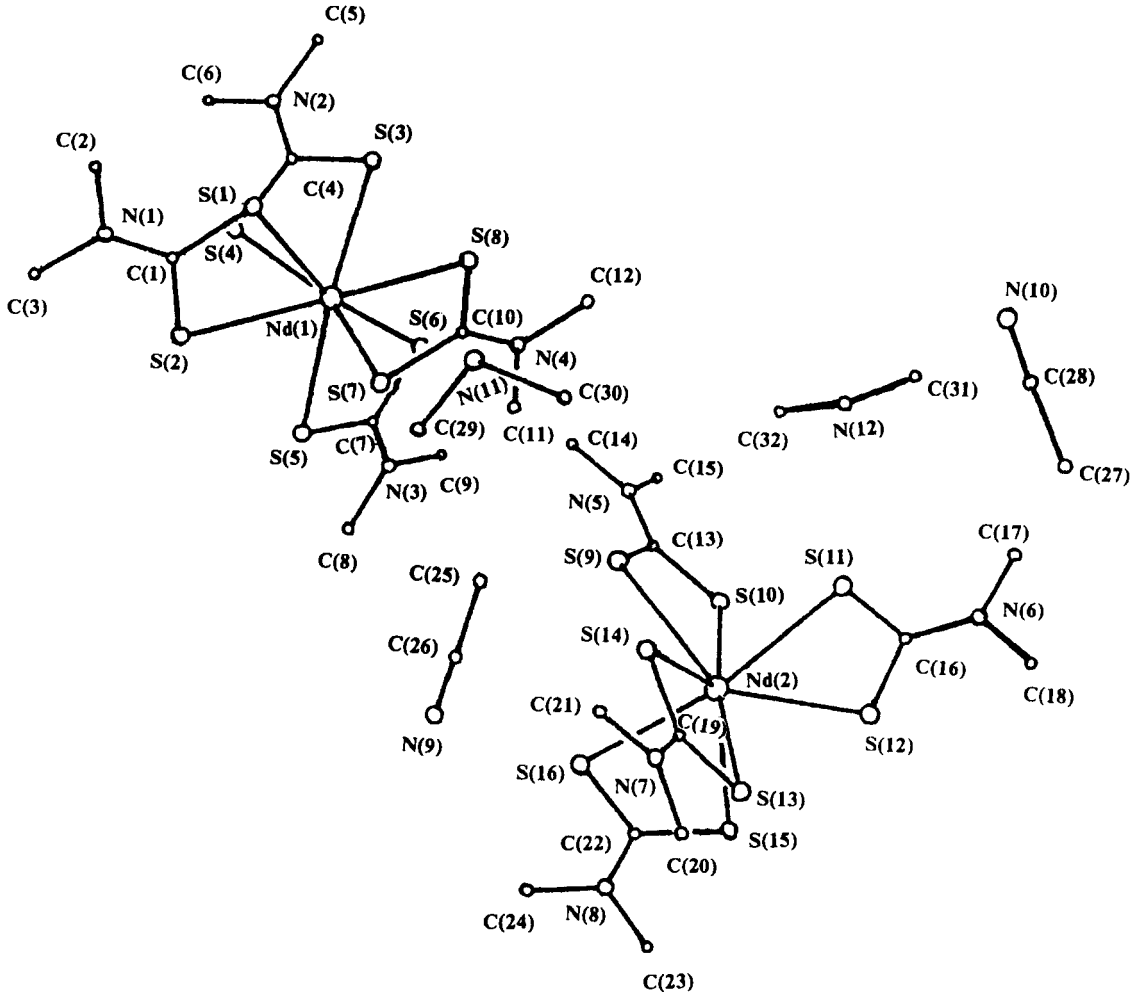


Fig. 1. Molecular structure for $\{[Nd(Me_2Dtc)_4]H_2NMe_2CH_3CN\}_2$.

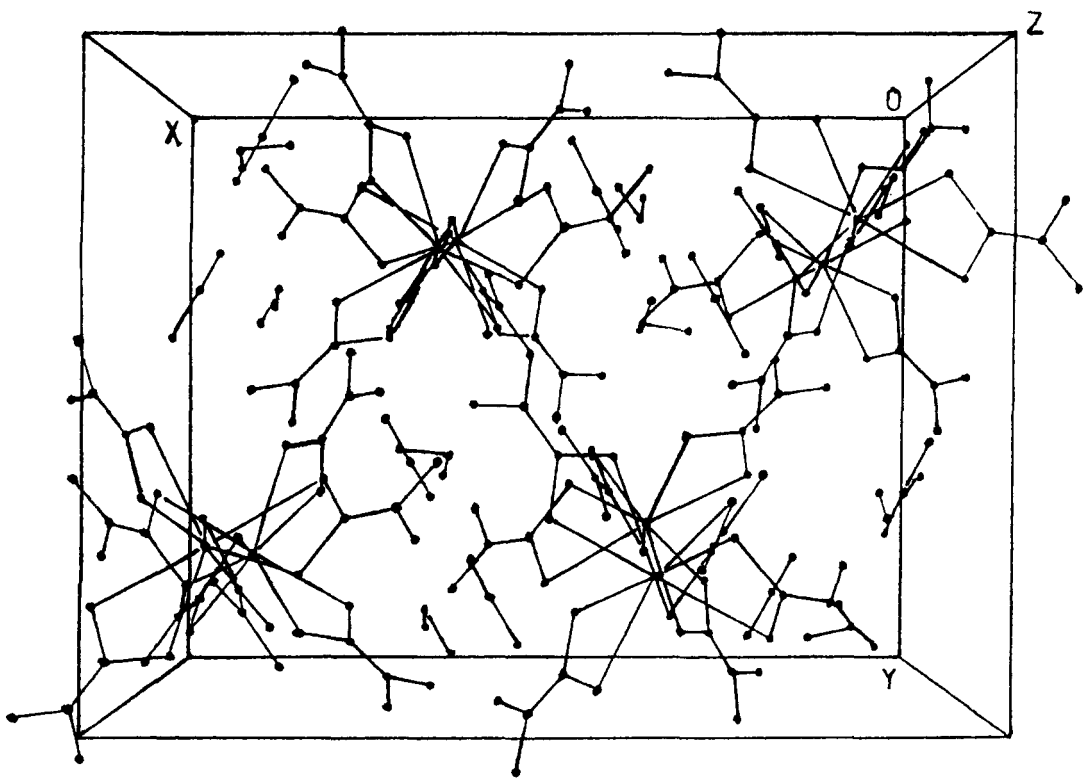


Fig. 2. Molecular packing arrangement in the unit cell.

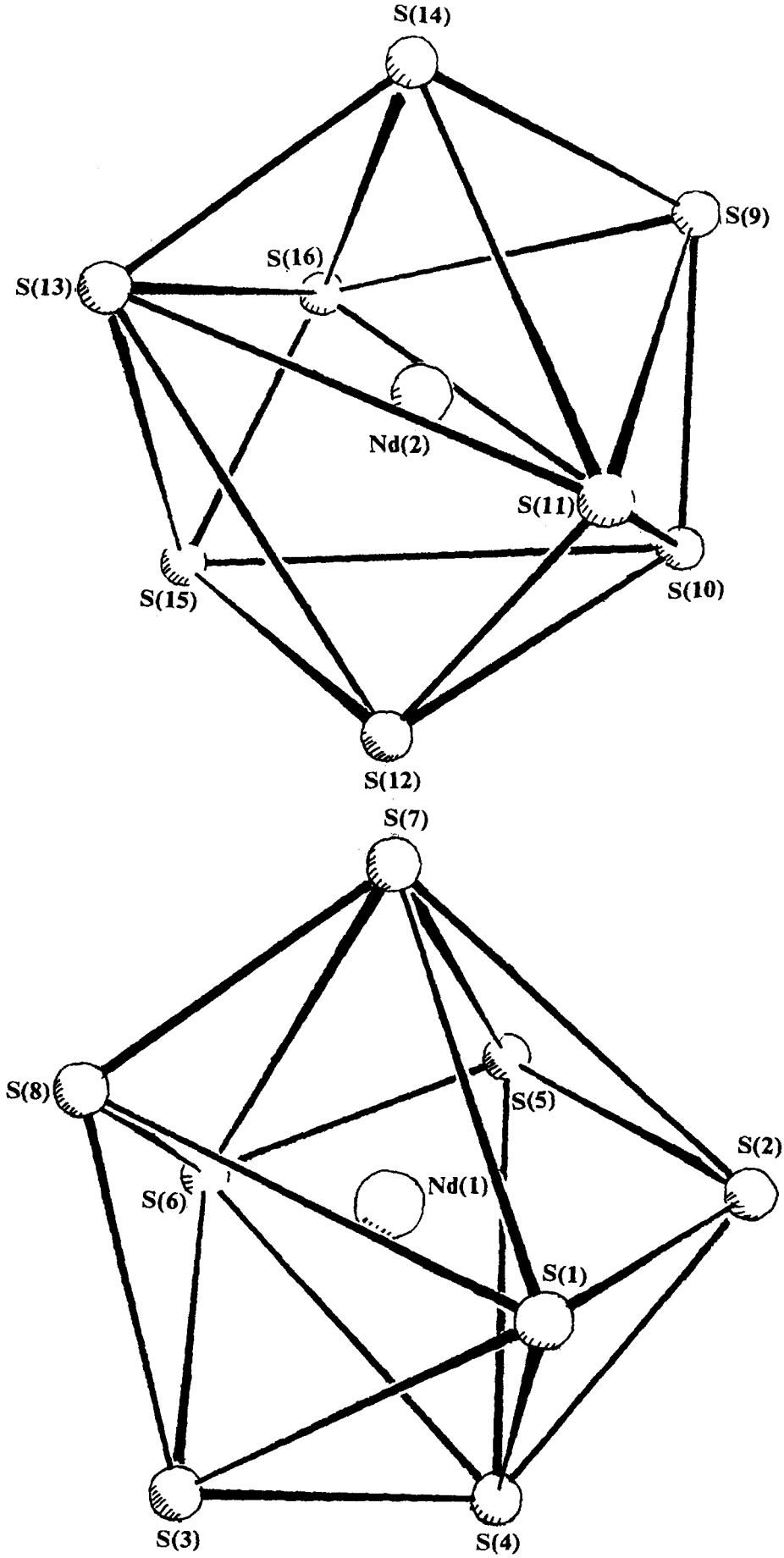


Fig. 3. The coordination polyhedron of Nd(1) and Nd(2) ions in complex.

Table 5. Electronic spectral data and covalent parameters

Compound[a]	Frequency (cm^{-1})	Assignment	Covalent parameters
$[Pr(Me_2Dtc)_4]H_2NMe_2$	16469	$^3H_4 \rightarrow {}^1D_2$	$\beta = 0.9680$
	20012	$\rightarrow {}^3P_0$	$\delta = 3.3058$
	20691	$\rightarrow {}^3P_1$	$b^{1/2} = 0.1265$
	21133	$\rightarrow {}^1I_6$[b]	
	21839	$\rightarrow {}^3P_2$	
$[Nd(Me_2Dtc)_4]H_2NMe_2$	11358	$^4I_{9/2} \rightarrow {}^4F_{3/2}$	$\beta = 0.9836$
	12346	$\rightarrow {}^4F_{5/2}, {}^2H_{9/2}$	$\delta = 1.6670$
	13262	$\rightarrow {}^4S_{3/2}, {}^4F_{7/2}$	$b^{1/2} = 0.0906$
	14599	$\rightarrow {}^4F_{9/2}$	
	15848	$\rightarrow {}^2H_{11/2}$	
	16892	$\rightarrow {}^4G_{5/2}, {}^2G_{7/2}$[b]	
	18762	$\rightarrow {}^4G_{7/2}, {}^2K_{13/2}$[b]	
	19194	$\rightarrow {}^4G_{9/2}$	
	20887	$\rightarrow {}^2G_{9/2}, {}^2(P,D)_{3/2}$	
	21367	$\rightarrow {}^4G_{11/2}$	
	23041	$\rightarrow {}^2P_{1/2}$	
$[Sm(Me_2Dtc)_4]H_2NMe_2$	18797	$^6H_{5/2} \rightarrow {}^4F_{3/2}$	$\beta = 0.9957$
	19920	$\rightarrow {}^4G_{7/2}$	$\delta = 0.4318$
	20833	$\rightarrow {}^4I_{9/2}, {}^4M_{15/2}$	$b^{1/2} = 0.0464$
	21469	$\rightarrow {}^4I_{13/2}$	
	22075	$\rightarrow {}^4F_{5/2}$	
	22620	$\rightarrow {}^4M_{17/2}, {}^4G_{9/2}$	
	23310	$\rightarrow {}^4M_{19/2}$	
	23923	$\rightarrow ({}^6P,{}^4P)_{5/2}$	
	25707	$\rightarrow {}^4L_{15/2}$	
$[Eu(Me_2Dtc)_4]H_2NMe_2$	21413	$^7F_0 \rightarrow {}^5D_2$	$\beta = 0.9954$
	24390	$\rightarrow {}^5D_3$	$\delta = 0.4621$
	25189	$\rightarrow {}^5L_6$	$b^{1/2} = 0.0479$
$[Ho(Me_2Dtc)_4]H_2NMe_2$	15314	$^5I_8 \rightarrow {}^5F_5$	$\beta = 0.9950$
	18399	$\rightarrow {}^5S_2, {}^5F_4$	$\delta = 0.5025$
	20491	$\rightarrow {}^5F_3$	$b^{1/2} = 0.0500$
	20920	$\rightarrow {}^5F_2$	
	21277	$\rightarrow {}^3K_8$	
	22075	$\rightarrow {}^5G_6$[b], ${}^5F_1$	
	23078	$\rightarrow ({}^5G, {}^3G)_5$	
	25640	$\rightarrow {}^5G_4$	
	25974	$\rightarrow {}^3K_7$	
	27548	$\rightarrow ({}^5G, {}^3H)_6, {}^3H_6$[b]	

[a]Acetonitrile.
[b]Hypersensitive bands.

Spectroscopic studies

The IR spectra of all the complexes showing a single ν_{C-S} absorption in the range 980–993 cm^{-1}, whilst the free ligand shows a doublet (962, 987 cm^{-1}). This finding is strongly indicative of the bidentate behavior of the ligand in the complexes [13, 14]. The presence of one strong ν_{C-N} band (1492–1504 cm^{-1}) at higher wavenumbers than in the free ligand (1453 cm^{-1}) gives further confirmation of the above suggested behaviour [15]. The new bands present in the 343–347 cm^{-1} range in the far-IR region may be assigned as the ν_{Ln-S} stretching frequency [15,16].

^1H NMR spectra of $Me_2Dt \cdot H_2NMe_2$ and the lanthanum complex (obtained similar to the preparation of single crystal of neodymium complex) were recorded. δ ($Me_2Dtc \cdot H_2NMe_2$), 2.77 (s, 6H, $H_2N(CH_3)$, 3.58 (s, 6H, $(CH_3)_2NCSS$), 8.06 (s, 2H, H_2NMe_2); δ ($[La(Me_2Dtc)_4]H_2NMe_2$), 2.78 (s, 6H, $H_2N(CH_3)$, 3.51 (s, 24H, $(CH_3)_2N$-CSS), 5.94 (s, 2H, H_2NMe_2), 2.02 (s, 3H, CH_3CN). The proton chemical shift of the ligand shows no significant shift after coordination to the diamagnetic lanthanum ion. However, the similar proton signals and its integral changes confirm the formation of the complexes. The presence of acetonitrile proton signal denotes that there is an acetonitrile molecule in the complex, which is in agreement with the result of the crystal structure determination.

The electronic spectra of the complexes present a

number of interesting features. The dithiocarbamates are strongly reducing ligands, so, as expected, the broad charge transfer band of $[Eu(Me_2Dtc)_4]H_2NMe_2$ in which Eu^{3+} is easily reduced to Eu^{2+} is observed in the visible region (415 nm). It settles the value of the optical electronegativity of Me_2Dtc at about 2.57, in agreement with that obtained for Et_2Dtc by Jörgensen [17].

Additionally, a number of *f–f* transitions are observed in the visible region of the electronic spectra. The relative energy and *J* level and assignment are given in Table 5. They are interesting in two respects [2,18]. First, the oscillator strengths of *f–f* transitions for these lanthanide dithiocarbamates are usually 2–5 times higher than that of the corresponding aqua-ions, especially for those of hypersensitive transitions, they are even up to 9–20 times more intense than the corresponding transitions in the aqua-ions. Second, a general red shift is found for most *f–f* transitions, which is known as the nephelauxetic effect.

The presence of the easily polarizable sulfur donor atoms allows one to expect more covalent character between the soft ligand and the hard lanthanide ions relative to the more common oxygen donor system [19,20]. It has been generally agreed that the nature of the red shift may be conveniently used as a measure of the metal ligand covalent bonding, assessed by Sinha's parameter (δ) and the bonding parameter $(b)^{1/2}$ [21,22]. These parameters have been calculated and compiled also in Table 5. The positive values of bonding parameters and β less than one support the existence of covalent character in the metal–ligand bond. Moreover, covalent bonds increase the configuration interaction which relaxes the selection rule for *f–f* transitions, thus increasing their intensity [23].

Acknowledgements—We are grateful to the Climb Plan Foundation of The State Science and Technology Commission of P. R. China and the Doctoral Point Foundation of the State Education Commission of P. R. China for financial support.

REFERENCES

1. D. Brown and D. G. Holah, *Chem. Comm.* 1968, 1545; D. Brown, D. G. Holah and C. E. F. Rickard, *ibid.* 1969, 280; *J. Chem. Soc.* (*A*) 1970, 786.
2. M. Ciampolini, N. Nardi, P. Colamarino and P. Orioli, *J. Chem. Soc., Dalton. Trans.* 1977, 379.
3. N. Tang, X. Gan, H. Zhu and M. Tan, *Polyhedron* 1990, **9,** 859.
4. H. Zhu, N. Tang, X. Gan, W. Zhang, M. Tan and A. Wang, *Polyhedron* 1993, **12,** 945.
5. W. Lu, X. Wang, X. Han and M. Chen, *Polyhedron* 1992, **11,** 1815.
6. J. Huang, S. Liu, M. Wang, Q. Zhang and J. Lu, *J. Inorg. Chim. Sin.* 1986, **3(1)**, 1; **3(2)**, 1.
7. N. Tang, H. Zhu, M. Tan, X. Gan and X. Wang, *Acta. Chim. Sin.* 1991, **49,** 42.
8. T. H. Siddall III, and W. E. Stewart, *J. Inorg. Nucl. Chem.* 1970, **32,** 1147.
9. G. D. Thorn and R. A. Ludwig, *The Dithiocarbamates and Related Compounds* Elsevier, New York (1962).
10. L. Fanfani, A. Nunai, P. F. Zanazzi and A. R. Zanzari, *Acta. Cryst.* 1972, **B28,** 1298.
11. D. G. Blight and D. L. Kepert, *Inorg. Chem.* 1972, **11,** 1556.
12. C. W. Haigh, *Polyhedron* 1995, **14,** 2871.
13. F. Bonati and K. Ugo, *J. Organomet. Chem.* 1967, **10,** 257.
14. T. N. Srivastava and V. Kumar, *J. Organomet. Chem.* 1976, **107,** 55.
15. D. Perry and R. A. Geanangel, *Inorg. Chim. Acta.* 1975, **13,** 185.
16. C. Preti, G. Tosi and P. Zannini, *J. Mol. Struct.* 1980, **65,** 283.
17. C. K. Jorgensen, *Mol. Phys.* 1962, **5,** 171.
18. A. A. Pinkerton, Y. Meseri and C. Rieder, *J. Chem. Soc., Dalton Trans.* 1978, 85.
19. S. Spiliadis and A. A. Pinkerton, *J. Chem. Soc., Dalton Trans.* 1982, 1815.
20. G. W. Rabe, G. P. A. Yap and A. L. Rheingold, *Inorg. Chem.* 1995, **34,** 4521.
21. S. P. Sinha, *Spectrochim. Acta.* 1966, **22,** 57.
22. D. E. Henrie and G. R. Choppin, *J. Chem. Phys.* 1968, **49,** 477.
23. A. A. Pinkerton and W. Earl, *J. Chem. Soc., Dalton Trans.* 1979, 1347.

Pergamon

PII: S0277-5387(96)00471-8

Polyhedron Vol. 16, No. 10, pp. 1651–1654, 1997
Copyright © 1997 Elsevier Science Ltd
Printed in Great Britain. All rights reserved
0277-5387/97 $17.00+0.00

The crystal and molecular structure of [bis(aquo)-bis(2-(methylamino)pyridine) copper(II)] dichloride

Antonis G. Hatzidimitriou* and Monir Uddin†

Department of Chemistry, University of Thessaloniki, 54006 Thessaloniki, Greece

(Received 29 July 1996; accepted 23 September 1996)

Abstract—Spectroscopic features of [bis(aquo)bis(2-aminomethylpyridine)copper(II)] dichloride, $[Cu(ampy)_2(H_2O)_2]Cl_2$, are presented and its X-ray crystal structure is described. The IR spectra, ligand field spectra and conductivity measurements confirmed that the chloride anions were not coordinated to the metal ion. The copper(II) cation is coordinated by two water and two bidentate 2-aminomethylpyridine molecules. The chloride anions are rather strongly hydrogen-bonded to two hydrogen atoms of water molecules and two hydrogen atoms of the primary amino group in a distorted tetrahedral arrangement. © 1997 Elsevier Science Ltd. All rights reserved.

Keywords: bis(aquo)bis(2-aminomethylpyridine)copper(II)] dichloride; bis(aquo)copper(II) chelate; axial aquo ligands in a copper(II) chelate; tetragonal mixed-ligand copper(II) chelate.

In a number of coordination compounds of 1,2-diamines, α-diimines and related nitrogenous bases that upon chelation form five-membered chelate rings, solvent molecules were found to act as coligands [1,2]. The importance of solvent molecules is exemplified, for instance, in the case of certain iron(II) chelates of 2-aminomethylpyridine (α-picolylamine), ampy, lying near the high spin–low spin crossover [3]. The magnetic behaviour of these chelates was found to be susceptible not only to changes in temperature, pressure and counteranion, but also to occluded solvent molecules. Complexes containing water as a ligand are readily used as precursors for the synthesis of more complicated compounds by replacing coordinated water with another ligand. As the literature examples of copper(II) compounds containing coordinated water are relatively few [2, 4–10] and their importance as precursors of complicated compounds remains great, anhydrous copper(II) dichloride was reacted with ampy in various solvents. The composition of the compound obtained from the reaction in wet ethanol was found to correspond to $CuCl_2 \cdot 2ampy \cdot 2H_2O$. Reaction with $AgNO_3$ and electrochemical measurements indicated the existence of chloride counteranions, while spectoscopic measurements provided evidence that the nitrogenous base and the water molecules were coordinated. The indications that the compound was the [bis(aquo)bis(2-aminomethylpyridine)copper(II)] dichloride, $[Cu(ampy)_2(H_2O)_2]Cl_2$, were confirmed by an X-ray diffraction study of a single crystal. The results of the investigation related to the [bis(aquo)bis(2-aminomethylpyridine)copper (II)] dichloride are presented and discussed in this work.

EXPERIMENTAL

Reagents and preparation of $[Cu(ampy)_2(H_2O)_2]Cl_2$

The synthesis of [bis(aquo)bis(2-aminomethylpyridine)copper(II)] dichloride, $[Cu(ampy)_2(H_2O)_2]Cl_2$, was achieved by dissolving copper(II) dichloride in wet ethanol and reacting it with a stoichiometric amount of 2-aminomethylpyridine (Aldrich). The crystals (mp 175–178°C) were developed by slow evaporation of the solvent under refrigeration. Found: C, 37.3; N, 14.5; H, 5.2%. Required for $C_{12}H_{20}Cl_2CuN_4O_2$: C, 37.3; N, 14.5; H, 5.2%.

*Author to whom correspondence should be addressed.
†Permanent address: Department of Chemistry, University of Chittagong, Chittagong, Bangladesh.

Physical measurements and determinations

Carbon, hydrogen and nitrogen were determined by microanalysis using a Perkin–Elmer 240B elemental analyser. Magnetic susceptibility measurements in powdered samples were performed at 25°C employing the Faraday method on a home-build balance calibrated against $Hg[Co(SCN)_4]$. Diamagnetic corrections were estimated from Pascal's constants. Electronic spectra in solution were measured on a Shimatzu 160 A spectrophotometer using 10 mm teflon stoppered quartz cells. The solid-state electronic spectra were obtained from Nujol mulls. IR spectra were obtained by the KBr disc technique and were recorded on a Perkin–Elmer 1600 FT-IR instrument. Additional instruments and techniques mentioned in this work have been described elsewhere [11].

X-ray crystallographic analysis of $[Cu(ampy)_2(H_2O)_2]Cl_2$

Intensities were collected by using a four-circle CAD4-F automatic X-ray diffractometer and graphite-filtered Mo-K_α radiation employing the $\omega/2\theta$ technique. The orientation matrix and refined unit-cell dimensions were obtained from 25 independent reflections of high intensity ($12 \leqslant \theta \leqslant 15°$). Three standard reflections were monitored periodically to detect intensity changes during the course of the data acquisition. The crystal was perfectly stable in the X-ray beam over the period of intensity measurements. The unique reflections were 1172 out of a total of 1799 with $0 \leqslant h \leqslant 9$, $0 \leqslant k \leqslant 8$, $-13 \leqslant l \leqslant 13$. 1005 reflections satisfied the acceptance criterion $I \geqslant 2\sigma(I)$. Systematic absences led to space group $P2_1/c$. Details of crystal data are given in Table 1. All intensities were corrected as usual for Lorentz and polarization effects.

Table 1. Crystal data and experimental details for the structural study of $[Cu(ampy)_2(H_2O)_2]Cl_2$

Formula	$C_{12}H_{20}N_4O_2CuCl_2$
Molecular mass, M_r	386.76
Crystal parameters	
Crystal shape	Blue rectangular prisms
Crystal size (mm)	0.27 × 0.29 × 0.24
Crystal system	Monoclinic
Space group	$P2_1/c$
Unit-cell dimensions	
a (Å)	8.306(1)
b (Å)	7.779(1)
c (Å)	12.287(2)
β (°)	92.39(2)
V_c (Å^3)	793.2(3)
Molecules per cell, Z	4
D_x (Mg m^{-3})	1.32
Linear absorption coefficient, μ (cm^{-1})	13.82

The copper position was deduced employing the SHELX-86 program [12] and used to compute a first-approximation electron-density synthesis, which revealed the position of all remaining atoms except the hydrogens. After least-squares refinements with the non-hydrogen atoms, the hydrogen atoms were also located in the difference Fourier map and those of the aromatic carbon atoms were in their expected position to which they were positioned geometrically after each refinement cycle. The positions of the hydrogen atoms of the methylamino group were also determined from difference Fourier maps and their coordinates were refined using slack constraints, N—H, C—H = 1.09(4) Å and angles around the carbon and the nitrogen atoms 109(3)°. All pertient calculations were performed using the CRYSTALS program [13]. The figures of the clinographic projections were produced with the ORTEPII program [14]. Refinement was carried out by full-matrix least-squares, with unit weight to all reflections. At the end of the isotropic stage of the refinement the DIFABS [15] absorption correction method was applied with an average coefficiency of 0.998. The function minimized in the least-squares refinement was $\Sigma w(|F_0| - |F_c|)^2$, where $|F_0|$ and $|F_c|$ are the observed and calculated structure factor amplitudes. Final $\Delta(\rho)\text{max}/\Delta(\rho)\text{min} = 0.25/-0.22$ e Å^{-3}. Agreement factors are defined as $R = \Sigma(|F_0| - |F_c|)/\Sigma(|F_0|) = 0.0258$ and $R_w = |\Sigma w(|F_0| - |F_c|)^2/\Sigma w(|F_0|)^{21/2} = 0.0272$. Further experimental details are deposited with the Editor.

RESULTS AND DISCUSSION

The stoichiometry of the compound resulting from the reaction of copper(II) dichloride with 2-(aminomethyl)pyridine in wet ethanol indicated the presence of water molecules, while the electrical conductivity in aqueous solution ($\Lambda_M = 196$ S cm^2 mol^{-1}) suggested [16] that the chloride anions do not interact covalently with copper(II). The broad ligand-field band with maximum at 1.70 μm^{-1} suggested the presence of a CuN_4O_2 chromophore [2,17], implying that the water molecules are bonded to copper. Additional information on the nature of interactions of the nitrogenous base and the water molecules with the metal, if any, were sought from the IR spectrum of the compound.

The bands emanating from the stretching vibrations of the primary amino group [18] are shifted appreciably to lower frequencies in relation to the free nitrogenous base and are observed at 3203 and 3117 cm^{-1}. On the other hand, the band present in the spectrum of the ligand at 1591 cm^{-1} and assigned to the stretching vibration of the aromatic C=N bond is shifted to higher frequency and in the spectrum of the complex occurs at 1608 cm^{-1}, suggesting that the

electronic density of the aforementioned bond has increased after coordination. A broad band peaking at 3381 cm^{-1} in conjunction with the absence of a band in the region 381 to 261 cm^{-1} attributable to free water, suggested that the water is coordinated [19,20], as has been observed in copper(II) chelates in which water displaces a halide anion that becomes the counteranion [4–10]. Further evidence of the ligation of ampy as bidentate ligand and the coordination of water was obtained from the X-ray diffraction analysis.

In the unit cell of the compound $[Cu(ampy)_2(H_2O)_2]Cl_2$ there are four copper atoms. The distance separating the metal atoms is greater than 6 Å and precludes copper–copper bonding interactions. The copper atom is surrounded by four nitrogen and two oxygen atoms symmetrically disposed in a distorted octahedral environment. Actually, in the immediate vicinity of copper are found only the four nitrogen atoms that lie in a plane encompassing the copper centre (plane 1, $3.128x - 6.503y - 5.094z = 1.564$) and the copper–nitrogen distances fall in the range usually observed for Cu—N(heterocyclic) ligands [2]. The intraligand distance separating the nitrogen atoms of the ligated 2-aminomethylpyridine [2.656(3) Å] indicated [3] that the nitrogenous base acts as a bidentate ligand forming five-membered chelate rings, the bite angle being 82.9(1)° (Table 2). The aromatic part of the methylaminopyridine ligand is perfectly planar and in the same plane also lies the carbon atom that links the pyridine ring with the amino group. The deviation of the C(6) carbon atom from the pyridine plane is smaller than the error. The terminal nitrogen atom N(2) is found 0.23(5) Å below the pyridine plane and the heteroaromatic plane forms with the coordination plane a dihedral angle of 6.4(4)°. The primary amine nitrogen and the sp^2 hybridized nitrogen atoms occupy, respectively, positions *trans* to each other and the interatomic distances indicated that the Cu—N(sp^2) bond is slightly longer than the observed length of the Cu—N(sp^2) bond (Table 2).

While the nitrogens of the bidentate ligand occupy equatorial positions, the oxygen atoms of the water molecules rather than the electronegative chloride anions are placed in axial positions. In the doubly charged bis(aquo)bis(2-aminomethylpyridine)copper(II) cation, $[Cu(ampy)_2(H_2O)_2]^{2+}$, the distance of the two oxygen atoms from copper is 2.562(3) Å and is within the range of bonding interactions termed "semicoordination" [2]. The long Cu—O bonds indicate appreciable tetragonal distortion ($T = 0.783$). Charge neutralization is effected by the chloride anions that are distanced 4.242(1) Å from the copper atom and are symmetrically disposed so that the metal atom becomes an inversion centre. A clinographic projection of the molecule is shown in Fig. 1.

The chlorine counteranions are placed in such a way so as to interact rather strongly with hydrogen atoms of the amino groups and the water molecules. Actually the interatomic distances of Cl(1) from H(10) and the symmetry related H(9)′, H(7)″ and H(8)# are: 2.35(4), 2.40(4), 2.45(4) and 2.52(4) Å, respectively. The corresponding nonbonding chlorine–oxygen and chlorine–nitrogen distances are: Cl(1)···O(1) 3.166(3), Cl(1)···O(1)′ 3.184(3), Cl(1)···N(2)″ 3.293(3), Cl(1)···N(2) 3.307(3) Å. It seems that these hydrogen-bonding interactions enfeeble the axial interaction of the water molecules with the copper ion and this weakening further contributes to the removal of the degeneracy of the ^2E_g ground state of copper(II) and results in a Jahn–Teller stabilization by splitting in $^2A_{1g}$ and $^2B_{1g}$. The hydrogen bonding is probably responsible for the low solubility of the compound in most solvents but the strongly polar ones.

Table 2. Selected interatomic distances (Å) and bond angles (°) of $[Cu(ampy)_2(H_2O)_2]Cl_2$

Cu(1)—N(1)	2.021(2)
Cu(1)—N(2)	1.992(3)
Cu(1)—O(1)	2.562(3)
N(1)—C(1)	1.332(4)
N(1)—C(5)	1.358(4)
C(1)—C(2)	1.396(4)
C(1)—C(6)	1.497(4)
C(2)—C(3)	1.380(5)
C(3)—C(4)	1.373(5)
C(4)—C(5)	1.384(4)
C(6)—N(2)	1.477(4)
N(1)—Cu(1)—N(1a)	180.00
N(2)—Cu(1)—N(1)	82.9(1)
N(2)—Cu(1)—N(1a)	97.1(1)
N(2a)—Cu(1)—N(1)	97.1(1)
N(2a)—Cu(1)—N(1a)	82.9(1)
N(2)—Cu(1)—N(2a)	180.00
O(1)—Cu(1)—N(1)	92.45(9)
O(1)—Cu(1)—N(1a)	87.55(9)
O(1)—Cu(1)—N(2)	91.8(1)
O(1)—Cu(1)—N(2a)	88.2(1)
O(1a)—Cu(1)—N(1)	87.55(9)
O(1a)—Cu(1)—N(1a)	92.45(9)
O(1a)—Cu(1)—N(2a)	88.2(1)
O(1a)—Cu(1)—N(2a)	91.8(1)
O(1)—Cu(1)—O(1a)	180.00
C(1)—N(1)—Cu(1)	114.5(2)
C(5)—N(1)—Cu(1)	126.7(2)
C(5)—N(1)—C(1)	118.8(3)
C(2)—C(1)—N(1)	122.3(3)
C(6)—C(1)—N(1)	116.9(3)
C(6)—C(1)—C(2)	120.8(3)
C(3)—C(2)—C(1)	118.5(3)
C(4)—C(3)—C(2)	119.3(3)
C(5)—C(4)—C(3)	119.6(3)
C(4)—C(5)—N(1)	121.3(3)
N(2)—C(6)—C(1)	111.2(3)
C(6)—N(2)—Cu(1)	112.0(2)

The atoms marked "a" are related to the corresponding atoms by a centre of symmetry located on Cu(1).

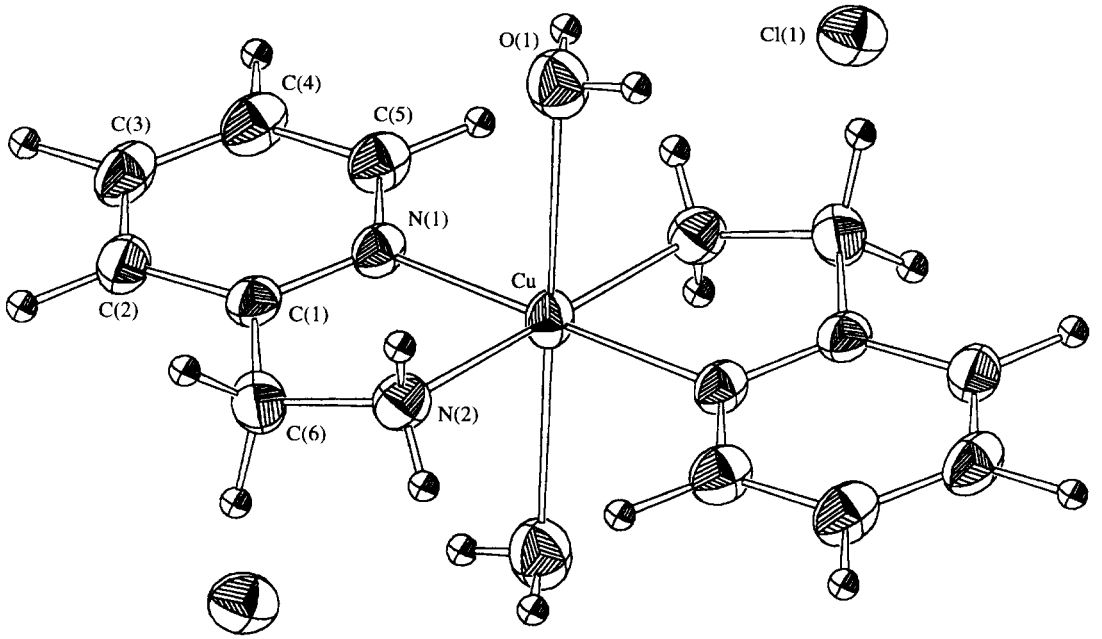


Fig. 1.

Acknowledgements—Thanks are due to Professor Chris Tsiamis for making available the facilities of his laboratory and for useful suggestions. M.U. wishes to thank the Consulate General of Bangladesh in Greece for financial support given to complete this project.

REFERENCES

1. D. A. House, in *Comprehensive Coordination Chemistry*, ed. G. Wilkinson, R. D. Gillard and J. A. McCleverty, Vol. 2. Pergamon Press, Oxford, 1987, p. 23.
2. B. J. Hathaway, in *Comprehensive Coordination Chemistry*, ed. G. Wilkinson, R. D. Gillard and J. A. McCleverty, Vol. 5, Pergamon Press, Oxford, 1987, p. 533.
3. A. M. Greenaway, C. J. O'Connor, A. Schrock and E. Sinn, *Inorg. Chem.*, 1979, **18,** 2692.
4. R. D. Ball, D. Hall, C. E. F. Rickard and T. N. Waters, *J. Chem. Soc.* (*A*), 1967, 1435.
5. D. Wester and G. J. Palenik, *J. Am. Chem. Soc.*, 1974, **96,** 7565.
6. J. Balvich, K. P. Fivizzani, S. F. Pavkovic and J. N. Brown, *Inorg. Chem.*, 1976, **15,** 71.
7. W. Vreugdenhil, P. J. M. W. L. Birker, R. W. M. ten Hoedt, G. C. Verschoor and J. Reedijk, *J. Chem. Soc., Dalton Trans.*, 1984, 429.
8. J. Emsley, M. Arif, P. A. Bates and M. B. Hursthouse, *J. Chem. Soc., Chem. Commun.*, 1988, 1387.
9. W. Clegg, J. R. Nicholson, D. Collison and C. D. Garner, *Acta Cryst.*, 1988, **C44,** 453.
10. J. Balvich, K. P. Fivizzani, S. F. Pavkovic and J. N. Brown, *Inorg Chem.*, 1992, **31,** 284.
11. M. Uddin, A. Hatzidimitriou, M. Lalia-Kantouri and C. Tsiamis, *Struct. Chem.*, 1997, **8,** in press.
12. G. M. Sheldrick, *Acta Cryst.*, 1993, **A46,** 467.
13. D. J. Watkin, J. R. Carruthers and P. W. Betteridge, *CRYSTALS*. Chemical Crystallographic Laboratory, Oxford University, 1993.
14. C. K. Johnson, ORTEPII, Report ORNL-5138. Oak Ridge National Laboratory, Tennessee, USA, 1976.
15. J. R. Carruthers and D. J. Watkin, *Acta Cryst.*, 1979, **A36,** 698.
16. W. J. Geary, *Coord. Chem. Rev.*, 1971, **7,** 81.
17. E. D. McKenzie, *J. Chem. Soc.*(*A*), 1970, 3095.
18. E. Sacher, *Spectrochim. Acta*, 1987, **A43,** 747.
19. M. Falk, *Spectrochim. Acta*, 1984, **A40,** 43.
20. J. Tomkinson, *Spectrochim. Acta*, 1992, **A48,** 329.

Pergamon

PII: S0277-5387(96)00470-6

Polyhedron Vol. 16, No. 10, pp. 1655–1661, 1997
Copyright © 1997 Elsevier Science Ltd
Printed in Great Britain. All rights reserved
0277-5387/97 $17.00+0.00

Effect of coexisting alkaline metal ions on the extraction selectivity of lanthanide ions with calixarene carboxylate derivatives

Keisuke Ohto,[a]* Masayuki Yano,[a] Katsutoshi Inoue,[a] Takeshi Nagasaki,[b] Masahiro Goto,[c] Fumiyuki Nakashio[c] and Seiji Shinkai[c]

[a]Department of Applied Chemistry, Faculty of Science and Engineering, Saga University, Honjo, Saga 840, Japan

[b]Department of Bioapplied Chemistry, Faculty of Engineering, Osaka City University, Sugimoto, Osaka 558, Japan

[c]Department of Chemical Science and Technology, Faculty of Engineering, Kyushu University, Hakozaki, Fukuoka 812-81, Japan

(Received 8 December 1995; accepted 23 September 1996)

Abstract—Extraction behavior of nine types of trivalent lanthanide ions from three types of aqueous solutions containing an alkaline metal ion such as lithium, sodium or potassium ion into chloroform was investigated with three types of extractants: 37,38,39,40,41,42-hexakis(carboxymethoxy)-5,11,17,23,29,35-hexakis(1,1,3,3-tetramethylbutyl)calix[6]arene and the cone conformational type of 25,26,27,28-tetrakis(carboxymethoxy)-5,11,17,23-tetrakis(1,1,3,3-tetramethylbutyl)calix[4]arene as well as *p*-(1,1,3,3-tetrametylbutyl)phenoxyacetic acid as the monomeric analog of their calixarene derivatives. The uptake behaviors of the three types of coexisting alkaline metal ions with the calix[4]arene carboxylate derivative and the monomeric analog were also investigated by measuring the chemical shifts of proton NMR spectra. It was found that the calix[4]arene derivative selectively extracted sodium ions, while lithium and potassium ions were hardly extracted, and also found that when sodium ion is contained in the feed solution, the order of extraction selectivity for rare earth metal ions with the calix[4]arene derivative was much changed from an ordinary system containing no sodium ion. That is, in the absence of sodium ion, the calix[4]arene derivative preferentially extracted the light lanthanides with greater ionic radii while in the presence of sodium ion it extracts the heavy lanthanides with smaller ionic radii. It was suggested that the cyclic tetramer preferentially extracts sodium ion at first and then the sodium-loaded calix[4]arene extract lanthanide ions, as a "preorganized" extractant. © 1997 Elsevier Science Ltd. All rights reserved.

Keywords: calixarene carboxylate; extraction; lanthanide; selectivity; preorganized; co-extraction.

Calixarene derivatives have been attracting much attention as novel types of macrocyclic host compounds [1–3]. Their high recognition as an ionophore is one of their remarkable features as a specific receptor. Their features as a receptor are as follows: [3,4] (1) macrocyclic phenolic oligomer; (2) having cyclic phenolic hydroxyl groups which are useful for the building-up of the functionalized host molecules; (3) having several-sized cavities for including the guest molecules.

In a previous study, we synthesized 37,38,39,40,41,42-hexakis(carboxymethoxy)-5,11,17,23,29,35-hexakis(1,1,3,3-tetramethylbutyl)calix[6]arene and 25,26,27,28-tetrakis(carboxymethoxy)-5,11,17,23-tetrakis(1,1,3,3-tetramethylbutyl)calix[4]arene as well as *p*-(1,1,3,3-tetramethylbutyl)phenoxy acetic acid as their monomeric analog to investigate their extraction behavior for lanthanide ions from the aqueous solution prepared by mixing nitric acid and glycine and found only a small difference in the selectivity among lanthanide ions even by the two types of cyclic extractants with different ring sizes [5].

A number of studies have been reported on the

* Author to whom correspondence should be addresssed.

extraction of alkaline metal ions with calixarenepolyols and calixarene derivatives having ester-, amide- and ketone groups [6–15]. Ferguson *et al.* reported that a cone conformational type of calix[4]arene derivative selectively gives rise to a complex with sodium ions, while calix[6]arenes forms complexes not only with a sodium ion but also with a potassium ion [11]. Therefore, it was suggested that calixarene derivatives with an ionizable functional group have a high possibility to form complexes with alkaline metal ions. In addition, other studies have been also reported on the extraction of multivalent metal ions with calixarene derivatives [5, 16–18]. In the majority of these studies, an alkaline metal ion was added to an aqueous solution to keep the ionic strength constant. However, there has been no paper discussing the effect of coexisting alkaline metal ions on the extraction behavior of multivalent metal ions.

In a previous study, cone coformation types of 25,27-bis(carboxypropoxy)-26,28-bis(carboxymethoxy)-5,11,17,23-tetrakis(1,1,3,3-tetramethylbutyl)calix[4]arene and 25,26,27,28-tetrakis(carboxymethoxy)-5,11,17,23-tetrakis(1,1,3,3-tetramethylbutyl)calix[4]arene were synthesized to investigate the extraction of the copper(II) ion in the absence or presence of sodium ions [18] and we found that these extractants co-extracted sodium ions together with copper ions in the presence of the former ion, and that the uptake of sodium ion accompanied the structural change of the extractants resulting in the enhancement of extractability of the copper ion.

In the present paper, we report the effect of three types of coexisting alkaline metal ion, lithium, sodium or potassium ion, on the extraction behavior of lanthanide ions with calixarene carboxylate derivatives. Complex formation was elucidated by utilizing the chemical shift of proton NMR for the cyclic tetramer as well as the monomeric analog in the absence or presence of an alkaline metal ions. The chemical shifts of proton NMR were also utilized to obtain information regarding the complexation of calix[4]arene derivatives with alkaline metal ions [10, 12].

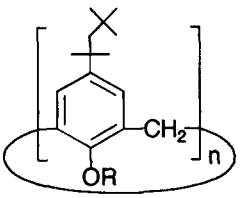
EXPERIMENTAL

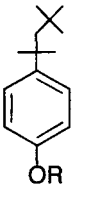
Reagents

The chemical structures of the calixarene carboxylate derivatives employed in the present work are shown in Fig. 1. The synthesis of these compounds was reported in a previous paper [5].

Distribution study

An organic solution was prepared by diluting each extractant into analytical grade of chloroform to desired concentrations ($\mathbf{1}_6$ and $\mathbf{1}_4$; 5 mM, $\mathbf{1}_1$; 20 mM). The following three types of aqueous stock solutions of rare earth metal ions were prepared by dissolving





$\mathbf{1}_n$: R = CH_2COOH (n = 4 (cone conformation) / 6)

$\mathbf{1}_1$: R = CH_2COOH

Fig. 1. Chemical structures of the extractants.

analytical-grade rare earth chlorides into 0.1 mol dm^{-3} nitric acid solution or into the aqueous mixture of 0.1 mol dm^{-3} glycine and 0.1 mol dm^{-3} alkaline hydroxide. (When a precipitate was formed in the solution, the former one was added.) The first stock solution contains La, Pr and Nd, the second contains Sm, Eu and Gd, and the third contains Ho, Er and Y. The initial pH was adjusted by mixing the stock solutions at an arbitrary volume ratio. An equal volume of organic and aqueous phases (10 cm^3) was mixed and shaken vigorously for 16 h at 30°C. After the phase separation, the equilibrium concentrations of lanthanide ions in the aqueous phase were measured by an inductively coupled plasma atomic emission spectrometer (Seiko model SPS 1200AR). The equilibrium pH in the aqueous solutions were measured by a pH meter (Beckmann model Ø45).

Study of proton NMR

The study of proton NMR was conducted for the complexes of alkaline metal ions with $\mathbf{1}_4$ and $\mathbf{1}_1$. The condition for the preparation of the sample solutions was similar to those of distribution study. The organic solution was prepared by diluting $\mathbf{1}_4$ or $\mathbf{1}_1$ into chloroform-*d* to the same concentrations as those used in the distribution study, i.e. the concentrations of $\mathbf{1}_4$ and $\mathbf{1}_1$ were 5 and 20 mol m^{-3}, respectively. The aqueous solutions were prepared by dissolving analytical-grade lithium, sodium or potassium nitrate into deuterium oxide. The concentration of alkaline metal ions was 0.1 mol dm^{-3}. Organic phase 0.8 cm^3 and 0.5 cm^3 of the aqueous phase were mixed and shaken vigorously for 16 h at 30°C. After the phase separation, the proton NMR of the organic phase was measured at 50°C for $\mathbf{1}_4$ and at 20°C for $\mathbf{1}_1$ (Jeol model GX-270).

RESULTS AND DISCUSSION

Distribution study

The effect of pH on the distribution of lanthanide ions in the extraction with $\mathbf{1}_6$ in the presence of lithium ions and with $\mathbf{1}_4$ in the presence of sodium ions is

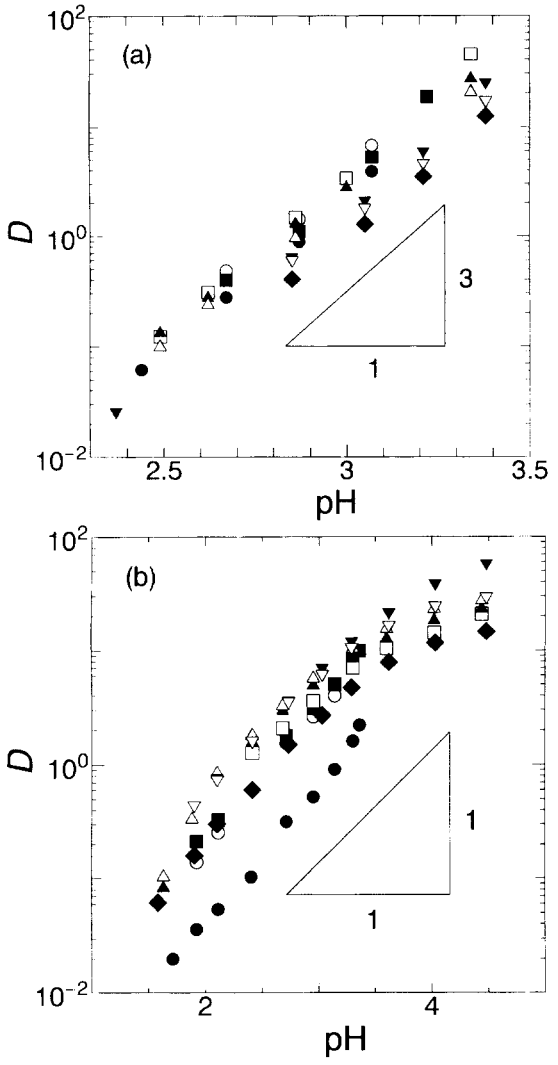


Fig. 2. Effect of pH on distribution ratio: (a) with $\mathbf{1}_6$ in the system containing lithium ions; (b) with $\mathbf{1}_4$ in the system containing sodium ions; La(●), Pr(○), Nd(■), Sm(□), Eu(▲), Gd(△), Ho(▼), Er(▽), Y(◆).

shown in Figs. 2(a) and (b), respectively, as typical experimental results. All plots in Fig. 2(a) lie on straight lines with the slope of 3, whereas those in Fig. 2(b) appear to lie on straight lines with the slope of 1. In the other extraction systems from an aqueous phase containing each alkaline metal ion with each extractant, a similar linear relationships to Fig. 2(a) was observed between the logarithm of the distribution ratio and pH. Table 1 summarizes the values of the slopes for the linear relationship observed in all the extraction systems in the present study. For a comparison, those observed in the absence of an alkaline metal ion are also listed. In the extraction of trivalent lanthanides based on a cation-exchange mechanism, the slope of pH dependency should be equal to 3. Actually, those observed in the extraction system without alkaline metal ions are close to 3, which is consistent with the above consideration. However, in some extraction systems, large deviations of the slopes from 3 were observed. The following should be taken into consideration to clarify the reason why the slopes are not consistent with the valence of lanthanide ions:

(1) Lanthanides are extracted accompanied by anionic species in the aqueous phase such as nitrate anion, partly neutralizing the positive charge of the lanthanide ion.
(2) Lanthanides give rise to complexes with glycine in the aqueous phase, suppressing the extraction.
(3) The extractants co-extract alkaline metal ion during the extraction of the lanthanides. In the third case, the extraction of alkaline metal ion might affect the extraction behavior of lanthanide ions.

The possibility of the first and second reasons can be excluded, because lanthanide ions hardly form a complex with nitrate anion [19] and glycine existing as a zwitterion, which is also difficult to form a complex with a metal cation under the present acidic condition. Concerning the third reason, the coextraction of alkaline metals has been confirmed by the previous study on the extraction of copper(II) with $\mathbf{1}_4$ [18]. For the extraction with $\mathbf{1}_4$, the possibility of the following four reactions may be inferred:

$$Ln^{3+} + \overline{(H_4R)_2} \rightleftarrows \overline{Ln(HR)(H_2R)} + 3H^+ \quad (1)$$

Table 1. Slope values of pH dependency in each system

Involved alkali metal	Extractant	La	Pr	Nd	Sm	Eu	Gd	Ho	Er	Y
None	$\mathbf{1}_6$	2.85	2.91	3.09	3.24	3.08	2.86	2.93	3.01	2.96
	$\mathbf{1}_4$	3.05	2.88	2.81	3.07	2.90	3.12	2.97	3.03	2.84
Li	$\mathbf{1}_6$	2.98	3.00	3.04	2.90	2.72	2.70	2.90	2.52	2.60
	$\mathbf{1}_4$	4.09	4.14	4.03	3.82	3.97	4.45	3.69	4.02	4.41
Na	$\mathbf{1}_6$	2.30	2.39	2.28	2.44	2.50	2.45	2.04	1.96	1.98
	$\mathbf{1}_4$	1.22	1.23	1.19	0.83	0.95	1.12	0.99	0.99	1.10
K	$\mathbf{1}_6$	2.94	3.15	3.02	2.45	2.34	2.34	2.00	1.99	2.04
	$\mathbf{1}_4$	4.12	3.80	4.31	4.19	3.92	3.06	2.82	2.85	2.10

$$2M^+ + \overline{(H_4R)_2} \rightleftarrows 2\overline{(M \cdot R_3H)} + 2H^+ \quad (2)$$

$$Ln^{3+} + 2M^+ + \overline{(H_4R)_2} \rightleftarrows \overline{Ln \cdot 2M \cdot (R)(HR)} + 5H^+ \quad (3)$$

$$Ln^{3+} + M^+ + \overline{(H_4R)_2} \rightleftarrows \overline{Ln \cdot M(HR)_2} + 4H^+ \quad (4)$$

where Ln, M and H_4R denote lanthanide metal, alkaline metal and $\mathbf{1}_4$, respectively. The extractant $\mathbf{1}_4$ was confirmed to exist mainly as a dimeric species in chloroform in the previous paper [5].

In the absence of alkaline metal ion, the complexation formation is considered to proceed through the reaction (1), while in the presence of alkaline metal ions, all of the reactions (1)–(4) should be taken into account. If the extraction of lanthanides takes place preferentially to an alkaline metal ion, only eq. (1) which takes place in the absence of alkaline metal ions and gives the pH dependency with the slope of 3 has to be taken into account. These are the cases observed in the extraction of all lanthanides with $\mathbf{1}_6$ in the presence of lithium and in that of light lanthanides in the presence of potassium with $\mathbf{1}_6$, as well as that of heavy lanthanides with $\mathbf{1}_4$. On the contrary, if the extraction of alkaline metals takes place preferentially to those of lanthanides, the release of three protons caused by the extraction of the lanthanide can be neglected, because the concentration of the lanthanide ion is much lower than those of alkaline metal ion and the extractant. Consequently, in the pH region where lanthanide ion was extracted, reaction (2) has only to be taken into account and the apparent slope of pH dependency should be 1. Actually, this interpretation satisfies the experimental results for the extraction of all lanthanides with $\mathbf{1}_4$ in the presence of sodium ions. The extraction in the other systems is considered to take place according to the simultanious reactions of all of the four reactions, which gives the complicated dependency of slopes with pH.

The selectivity series among lanthanides in the present work was evaluated in terms of $pH_{0.5}$, the pH at which 50% extraction is achieved, owing to the extremely complicated extraction reactions as mentioned above. The relations between the $pH_{0.5}$ with each extractant and the reciprocal of ionic radius of the lanthanide element (in hexa-coordination) in the presence of lithium, sodium and potassium ions are shown in Figs 3(a)–(c), respectively. Furthermore, the result in the absence of an alkaline metal observed in the previous work is also shown in Fig. 3(d) for comparison. The plots all lie on convex curves with maximum points. For the extraction in the absence of alkaline metal ion, the maximum point for $\mathbf{1}_6$ is located at praseodymium. In the presence of lithium or sodium, it is also located at praseodymium, whereas for that in the presence of potassium, it is shifted toward heavier lanthanides and is located at samarium, whose ionic radius is smaller than that of praseodymium. In the extraction with $\mathbf{1}_4$, the maximum points were also located at praseodymium, regardless of whether lithium or potassium is present or not, whereas in the presence of sodium it was located at gadolinium, which is smaller than praseodymium. Especially, the shift for the extraction with $\mathbf{1}_4$ in the presence of sodium was the most significant among all cases. The reasons why the drastic change in the selectivity to lanthanides took place in the extraction with $\mathbf{1}_4$ in the presence of sodium can be interpreted in relation to our recent study on the extraction of copper with calix[4]arene derivatives [18]. That is, in the co-extraction of sodium ion together with copper (II) ions by 25,27-bis(carboxymethoxy)-26,28-bis(carboxypropoxy)-5,11,17,23-tetrakis(1,1,3,3-tetramethylbutyl)calix[4]arene, we reached the following conclusions:

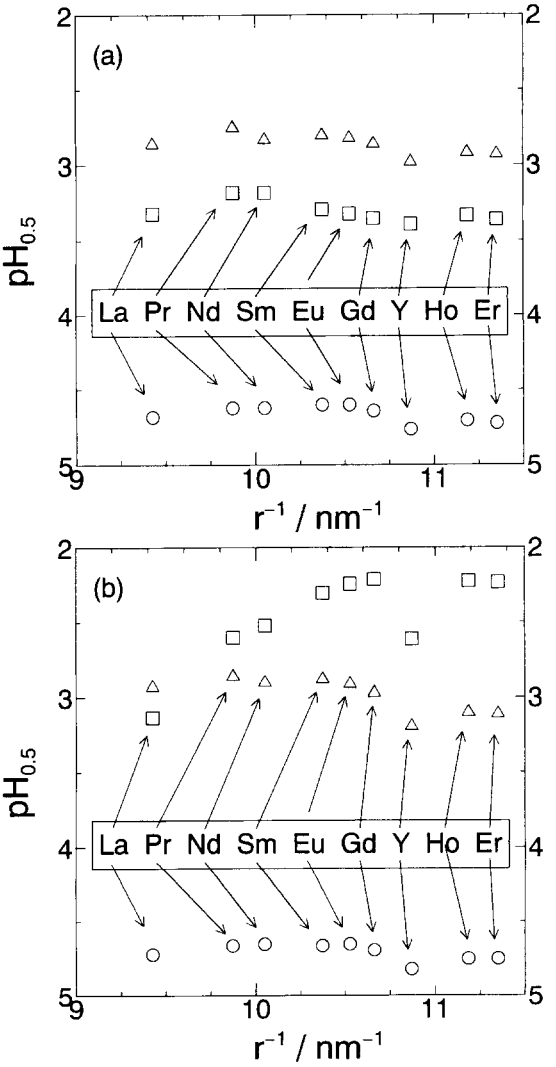


Fig. 3. Relation between $pH_{0.5}$ and reciprocal of ionic radius of each lanthanide element: △: $\mathbf{1}_6$, □:$\mathbf{1}_4$, ○:$\mathbf{1}_1$. (a) in the system containing lithium, (b) sodium, (c) potassium and (d) no alkali metal ion.

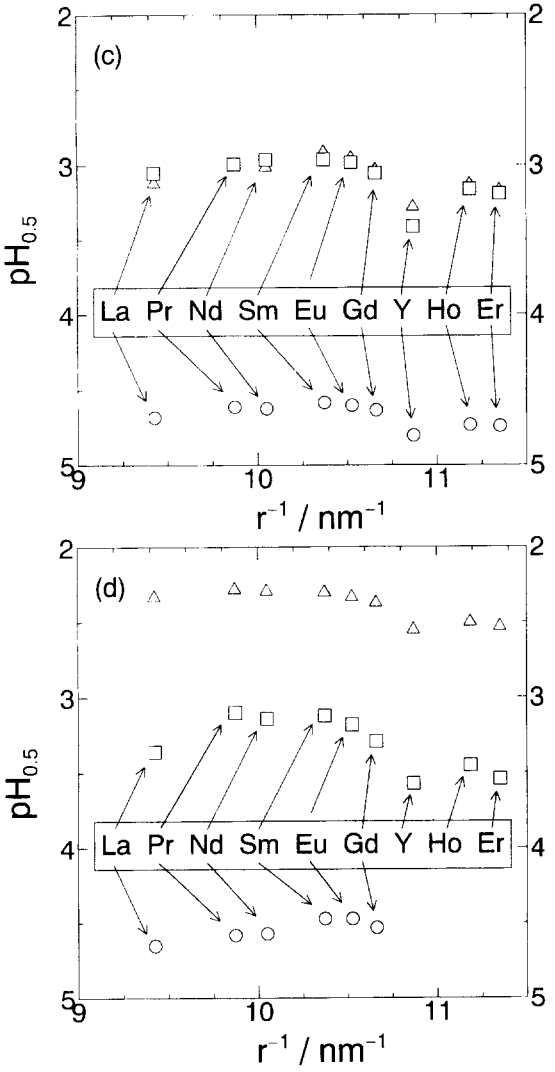


Fig. 3—*Continued.*

(1) Calix[4]arene derivatives exibit the sodium-selectivity (i.e. the ionic diameter of sodium ion fits the cavity size of the calix[4]arene).
(2) In the presence of sodium, the extractant $\mathbf{1}_4$ co-extracts a sodium ion together with a divalent copper ion.
(3) The uptake of sodium ions with the cyclic tetramer gives rise to a structural change, that is, it increases structural "rigidity" and provides "preorganization" in the structure of the extractant.
(4) The extractability is much enhanced due to the chelate effect regardless of the electric repulsion between sodium and copper ions.

Based on these points of view concerned with the extraction of copper, it is reasonable to consider that the similar co-extraction also takes place in the extraction of the lanthanides. The uptake of sodium ions causes a structural change and preorganizes the extractant $\mathbf{1}_4$, which results in the change of the selectivity to the lanthanides.

On the other hand, the change of the selectivity to lanthanides with $\mathbf{1}_6$ was smaller than that with $\mathbf{1}_4$ and, in addition, no change was observed in all the cases in the extraction with $\mathbf{1}_1$, which are interpreted as follows:

(1) The flexibility of $\mathbf{1}_6$ is higher than that of $\mathbf{1}_4$ owing to its greater ring size.
(2) The ring inversion of $\mathbf{1}_6$ is not suppressed and the ring conformation is not fixed on the cone type, whereas $\mathbf{1}_4$ is fixed on the cone conformation.
(3) Since the extractant $\mathbf{1}_1$ is a monomeric and acyclic derivative it is, therefore, the most flexible among all the extractants.
(4) The coordination ability of its phenoxy oxygen is considered to be very weak and the co-extraction with $\mathbf{1}_1$ may be difficult.

The pH region where lanthanides are extracted was considered as follows. In the extraction with $\mathbf{1}_6$, the addition of alkaline metals shifted the $pH_{0.5}$ to higher pH region compared with that in the absence of alkaline metal ions. This means that the extraction of lanthanide ion was suppressed due to the extraction of alkaline metal ion based on the acidic dissociation. Contrarily, in the extraction with $\mathbf{1}_4$, the $pH_{0.5}$ in the presence of lithium or potassium was the same with that in the absence of alkaline metal ion, while in the presence of sodium, the significant shift of the $pH_{0.5}$ to lower pH was observed in comparison with the other systems. The extractant $\mathbf{1}_4$ specifically extracts the sodium ion since its ionic diameter fits to the cavity size of $\mathbf{1}_4$. It is considered that the uptake of the sodium ion makes the extractant rigid and preorganized to change it so as to specifically accept other metal ions whose ionic diameter fits with the preorganized ring size. In the extraction with $\mathbf{1}_1$, the $pH_{0.5}$ in the presence of alkaline metals was the same as that in their absence, because $\mathbf{1}_1$ preferentially extracts the lanthanides than those of the alkaline metal ions.

Study of proton NMR

The results mentioned above suggest that coexisting alkaline metal ions might participate in the extraction of lanthanide ions with $\mathbf{1}_6$ and $\mathbf{1}_4$. In order to confirm the participation of alkaline metal ions in the lanthanide extraction, proton NMR studies were conducted.

Figure 4 shows proton NMR spectra for cone-type of $\mathbf{1}_4$ in deuterated chloroform and for the organic phase after being contacted with the aqueous phase containing a lithium, sodium or potassium ion. For the peaks in the system of lithium or potassium, an evident chemical shift cannot be observed, although slight indications were present. On the other hand, for all peaks in the system with sodium ions, evident shifts

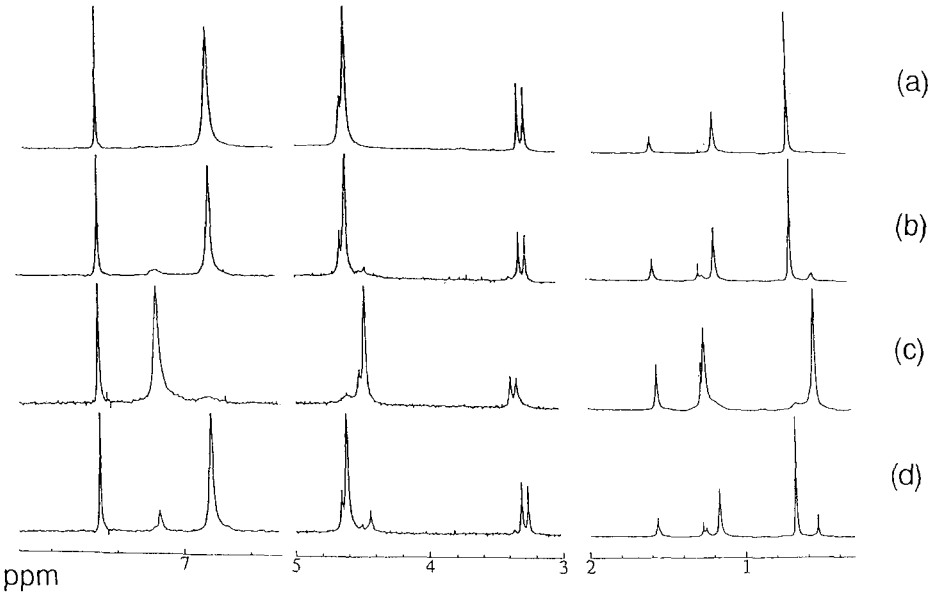


Fig. 4. ^{1}H NMR spectra of $\mathbf{1}_4$: (a) original, (b) in the system containing lithium, (c) sodium, (d) potassium ions.

were observed; these shifts are ascribable to the ring current of the benzene ring and symmetry change [10, 12]. These results clearly indicate that $\mathbf{1}_4$ extracts the sodium ion while lithium and potassium ions are not extracted.

The proton NMR spectra of $\mathbf{1}_1$ were not observed. That is, the peaks of all systems in the presence of alkaline metal ions were the same as the original peaks. Any chemical shift of the peaks cannot be observed in all the systems, which means that $\mathbf{1}_1$ does not extract the three kinds of alkaline metal ion.

For $\mathbf{1}_6$, clear spectra were not obtained in deuterated

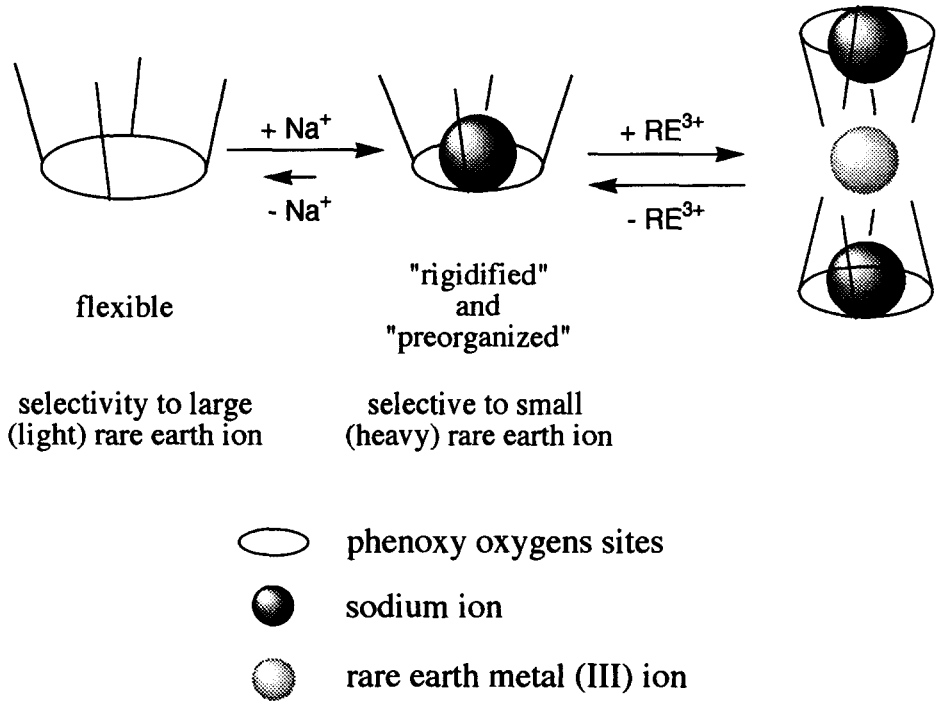


Fig. 5. Extraction models of $\mathbf{1}_4$ in the system in the presence of sodium ions.

chloroform around room temperature, owing to the flexible conformation of $\mathbf{1}_6$.

Extraction model of calix[4]*arene derivative in the system containing sodium ions*

Similar to the extraction model of the copper(II) ion with the calix[4]arene derivative in the presence of sodium ions, the extraction model for lanthanide ions with $\mathbf{1}_4$ in the presence of sodium ions can be schematically shown in Fig. 5. Since the lowering of $pH_{0.5}$ was observed during the extraction of sodium ion with $\mathbf{1}_4$, it is considered that the uptake of the sodium ion takes place according to an ion-exchange mechanism where one positive charge of the sodium ion is neutralized with one carboxylic group of $\mathbf{1}_4$ and the other coordination sites of the sodium ion are saturated with other carbonyl groups and phenoxy oxygens. As a result, all of the carboxyl groups of $\mathbf{1}_4$ might be combined at the near position with sodium ion, rigidifying and preorganizing the extractant. The resulting assembly of carboxyl groups results in the change of selectivity from light lanthanides with a large ionic radii to heavy ones with small ionic radii. (The results for $\mathbf{1}_6$ in the potassium system may support the above consideration.)

From the result of the present work, we have found that a preorganized extractant might have a high separation efficiency for lanthanides due not only to the rigidity, but also the chelate effect. This concept may be able to apply to the molecular design of novel types of extractants and to a separation of difficult separative series of metals.

Acknowledgement—The authors are grateful to Government Industrial Research Institute, Kyushu, for measurement of the concentrations of rare earth metal ions by using ICP-AES. This work was financially supported in part by a Grant-in-Aid for Scientific Research No. 06650886 from the Ministry of Education, Science and Culture.

REFERENCES

1. C. D. Gutsche, *Calixarenes*. Royal Society of Chemistry, Cambridge, 1989.
2. J. Vicens and V. Bohmer, *Calixarenes: A Versatile Class of Macrocyclic Compounds*. Kluwer Academic Publisher, The Netherlands, 1991.
3. T. Takeshita and S. Shinkai, *Bull. Chem. Soc. Jpn.* 1995, **68,** 1088.
4. Y. Masuda, T. Sawano and E. Sekido, *Anal. Sci.* 1991, suppl. **7,** 31.
5. K. Ohto, M. Yano, K. Inoue, T. Yamamoto, M. Goto, F. Nakashio, S. Shinkai and T. Nagasaki, *Anal. Sci.* 1995, **11,** 893.
6. R. M. Izatt, J. D. Lamb, R. T. Hawkins, P. R. Brown, S. R. Izatt and J. J. Christensen, *J. Am. Chem. Soc.*, 1983, **105,** 1782.
7. S. R. Izatt, R. T. Hawkins, J. J. Christensen and R. M. Izatt, *J. Am. Chem. Soc.* 1985, **107,** 63.
8. S. K. Chang and I. Cho, *Chem. Lett.* 1984, 477.
9. M. A. Mckervey, E. M. Sward, G. Ferguson, B. Ruhl and S. J. Harris, *J. Chem. Soc., Chem. Commun.*, 1985, 318.
10. A. Arduini, A. Pochini, S. Reverberi and R. Ungaro, *Tetrahedron*, 1986, **42,** 2089.
11. G. Ferguson, B. Kaitner, M. A. Mckervey and E. M. Seward, *J. Chem. Soc., Chem. Commun.* 1987, 584.
12. T. Arimura, M. Kubota, T. Matsuda, O. Manabe and S. Shinkai, *Bull. Chem. Soc. Jpn.* 1989, **62,** 1674.
13. I. Yoshida, S. Fujii, K. Ueno, S. Shinkai and T. Matsuda, *Chem. Lett.* 1989, 1535.
14. S. Shinkai, T. Ohtsuka, K. Fujimoto and T. Matsuda, *Chem. Lett.* 1990, 835.
15. K. Iwamoto and S. Shinkai, *J. Org. Chem.* 1992, **57,** 7066.
16. T. Nagasaki and S. Shinkai, *Bull. Chem. Soc. Jpn.* 1992, **65,** 471.
17. R. Ludwig, K. Inoue and T. Yamato, *Solv. Extr. Ion Exch.*, 1993, **11,** 311.
18. K. Ohto, K. Shiratsuchi, K. Inoue, M. Goto, F. Nakashio, S. Shinkai and T. Nagasaki, *Solv. Extr. Ion Exch.*, 1996, **14,** 459.
19. L. G. Sillen, *Stability Constants of Metal-ion Complexes*, p. 93. Supplement 1. The Chemical Society Burlington House, London, 1971.

Pergamon

PII: S0277-5387(96)00475-5

Polyhedron Vol. 16, No. 10, pp. 1663–1677, 1997
Copyright © 1997 Elsevier Science Ltd
Printed in Great Britain. All rights reserved
0277-5387/97 $17.00+0.00

Platinum(II)- and palladium(II)-amide complexes $[M\{NC(O)CH_2CH_2\}_2L_2]$ derived from 2-azetidinone (β-propiolactam); a synthetic, electrospray mass spectrometric and X-ray crystallographic study

William Henderson[a]* and Michal Sabat[b]

[a]Department of Chemistry, University of Waikato, Private Bag 3105, Hamilton, New Zealand

[b]Department of Chemistry, University of Virginia, McCormick Road, Charlottesville, Virginia, U.S.A.

(Received 3 September 1996; accepted 20 September 1996)

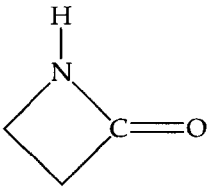
Abstract—A number of platinum(II) and palladium(II) complexes **3** and **4** containing amido ligands derived from β-propiolactam (2-azetidinone, Haz) have been synthesised in high yield by the silver(I) oxide-mediated reactions of the complexes *cis*-$[MCl_2L_2]$ [M = Pt, L = cycloocta-1,5-diene (COD) or PPh_3; M = Pd, L = 2,2′-bipyridine (BIPY) or 1,10-phenanthroline (PHEN)] with 2-azetidinone. Displacement of the COD ligand allowed the synthesis of a number of other derivatives containing phosphine, phosphite and isocyanide ligands. Electrospray mass spectrometry has also been used to further characterize these complexes, to probe the strength of binding of the amide ligands and to investigate the ability of the complexes to act as metallo-ligands towards other mono-, di- and trivalent cations. A detailed study on the bis(triphenylphosphine) platinum complex **3b** shows that fragmentation, induced by higher cone voltages, proceeds initially *via* loss of a deprotonated azetidinone monoanion (az^-) ligand, yielding $[Pt(az)(PPh_3)_2]^+$. Upon further increasing the cone voltage, cyclometallation of one of the triphenylphosphine ligands occurs. Complex **3b** readily forms adducts with a range of alkali-metal cations, Ag^+, divalent cations (Ba^{2+}, Cu^{2+}, Zn^{2+} and Pb^{2+}) and a trivalent cation (Pr^{3+}). Complex **3b** shows selectivity for Na^+ ions over other alkali-metal cations in forming a dipositively charged aggregate of the type $[2M + 2Na]^{2+}$ at low cone voltages. The X-ray structure of complex **3b** is also reported. © 1997 Elsevier Science Ltd. All rights reserved.

Keywords: platinum; palladium; amide; azetidinone; electrospray.

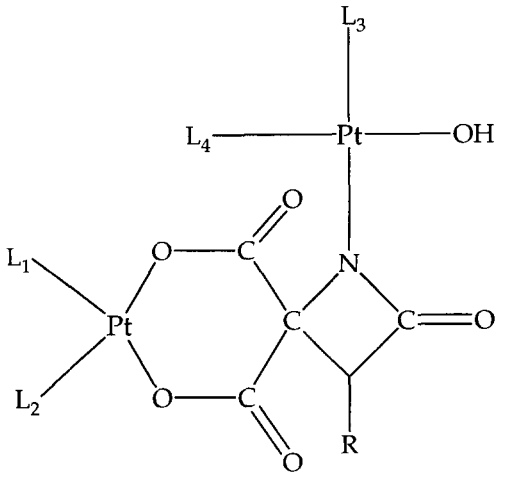
The interactions of small-ring organic molecules with metal complexes is of fundamental interest, since the metal may participate in ring-opening reactions, forming metallacyclic and other complexes [1]. As a specific example, the oxidative addition of propiolactone to low-valent platinum, rhodium and iridium complexes has been found to give five-membered ring metallalactone complexes [2]. Organic lactams may also coordinate to metal centres as the monoanion, *via* the amide nitrogen [3,4]. In view of the general interest in the chemistry of late transition-metal amide complexes [5] we wished to synthesize platinum and palladium complexes derived from the four-membered ring lactam 2-azetidinone (β-propiolactam) **1** [6]. Compounds containing derivatives of this ring system form the important class of β-lactam antibiotics. Since a number of transformations of azetidinone ring systems are catalysed by palladium complexes [7], understanding the different possible interactions of such ring systems with metal centres may provide valuable information on the role of the metal centre.

Mercury(II) complexes containing the monoanion of 2-azetidinone have been described previously and found to be precursors for the construction of supramolecular coordination assemblies [3]. Transition-metal amide complexes containing the M—NRC(O)—moiety are of some interest for their ability to act as ligands towards other metal centres, generating novel polymeric and macrocyclic structures [4].

*Author to whom correspondence should be addressed.



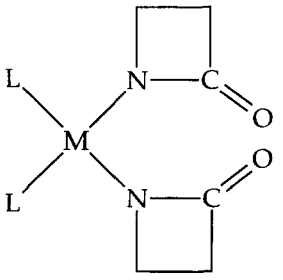
1



2

L_1-L_4 = NH_3, primary or secondary amine

R = H, alkyl, aryl etc



Compound	M	L
3a	Pt	COD
3b	Pt	PPh_3
3c	Pt	$P(CH_2CH_2CN)_3$
3d	Pt	DPPM
3e	Pt	$P(OPh)_3$
3f	Pt	2,6-XyNC
3g	Pt	^tBuNC
4a	Pd	BIPY
4b	Pd	PHEN

The only platinum or palladium derivatives of **1** which have been reported to data appear to be the binuclear ammine complexes **2**. These have been demonstrated to have good antitumour activity against mouse leukemia [8], offering a further impetus for studying the chemistry of platinum-group metal amide complexes [9]. In this work, the synthesis and electrospray mass spectrometric characterisation of amide complexes derived from 2-azetidinone is described, together with an X-ray crystal structure determination on one derivative.

RESULTS AND DISCUSSION

The reactions between the platinum(II) and palladium(II) halide complexes $[PtCl_2(COD)]$ (COD = cycloocta-1,5-diene) or *cis*-$[PtCl_2(PPh_3)_2]$ with 2-azet-

Table 1. Characterization data for the azetidinone complexes **3** and **4**

Compound	Mp (°C)	$\nu_{(C=O)}$ (cm^{-1})	Microanalytical data[a]		
			C	H	N
3a	165–167	1676(vs)	37.7(37.9)	4.6(4.5)	6.3(6.3)
3b	262–264	1667(vs)	57.7(58.7)	4.6(4.4)	3.2(3.3)
3c	195–205	Not determined	40.3(39.9)	4.9(4.5)	14.6(15.5)
3d	246–250	1666(vs)	51.8(51.7)	4.2(4.2)	4.1(3.9)
3e	156–158	1686(vs)	53.0(52.8)	4.0(4.0)	2.9(2.9)
3f	175	Not determined	47.6(48.2)	4.3(4.4)	9.2(9.4)
4a · $2H_2O$	>320 (decomp.)	1629(vs)	43.8(43.8)	4.6(4.6)	12.5(12.8)
4b	decomp. >260	1656(vs)	46.7(46.7)	4.3(4.4)	11.9(12.1)

[a]Calculated values in parentheses.

idinone (β-propiolactam) **1** in refluxing dichloromethane mediated by silver(I) oxide afforded high yields of the amido complexes **3a** and **b**, respectively, as white, air-stable crystalline solids. In analogous fashion, reaction of $[PdCl_2L_2]$ [L_2 = 2,2′-bipyridine (BIPY), or 1,10-phenanthroline (PHEN)] gave the palladium(II) complexes **4a** and **b** as yellow microcrystalline solids. The complexes have been fully characterized by multinuclear NMR and IR spectroscopies, elemental microanalysis and electrospray mass spectrometry.

Silver(I) oxide has been demonstrated to be a useful reagent for the synthesis of platinum-group metal amide complexes [10–12], providing that an electron-withdrawing substituent is present on the nitrogen atom. Advantages of the silver(I) oxide method include ease of product workup (the byproducts are silver chloride and water), and the non-necessity for dried solvents.

The labile COD ligand of **4a** can be readily displaced by other tertiary phosphines [$P(CH_2CH_2CN)_3$ and $Ph_2PCH_2PPh_2$ (DPPM)], triphenyl phosphite, 2,6-xylylisocyanide (XyNC), or *tert*-butylisocyanide giving a series of ligand-substituted derivatives **3c–g**. No reaction was observed between **4a** and triphenylarsine, and the COD complex was recovered unreacted. Microanalytical data and selected additional characterization data (melting points and IR spectroscopic data) for the azetidinone complexes are summarized in Table 1.

NMR spectroscopy

The ^1H and $^{13}C\{^1H\}$ NMR spectra of complexes **3** and **4** are consistent with their formulation as complexes containing the N-bonded azetidinone monoanion. In the ^1H NMR spectrum of the COD Pt complex **3a** two CH_2 resonances are observed, at δ 3.16 and 3.01, with the former assigned as the CH_2 adjacent to the more electron-withdrawing carbonyl group. Both CH_2 groups appear as triplets due to $^3J(H,H)$ coupling of 4.1 Hz. By comparison, the parent 2-azetidinone shows a triplet at δ 3.27 [$^3J(H,H)$-4.3 Hz] due to the CH_2CO protons, but a doublet of triplets at δ 2.98 for the CH_2N protons, due to additional coupling [$^3J(H,H)$-1.7 Hz] to the amide NH proton. A broad signal at δ 6.2 in 2-azetidinone due to the NH proton was not observed in any of the complexes **3** or **4**. The $^{13}C\{^1H\}$ NMR spectrum of **3a** showed singlets due to the $CH_2C(O)$ and CH_2N carbons at δ 41.1 and 38.5, respectively, and a singlet due to the two amide carbonyl groups at δ 174.1. The corresponding values for 2-azetidinone are δ 38.5, 35.2 and 169.1, respectively.

For the complexes containing phosphine ligands, typified by **3b**, the ^1H spectra were slightly more complex, although two CH_2 resonances were again observed for each complex. One, at δ 2.40, appeared as a slightly broadened triplet [$^3J(H,H)$-7.3 Hz] and is assigned as the CH_2CO protons, while the other (due to the CH_2N protons) was a broad unresolved singlet, as a result of additional four-bond coupling to the phosphine ligand(s). Confirmation of the above spectral assignment in complex **3b** was achieved by a ^{13}C–^1H correlation spectrum.

The $^{31}P\{^1H\}$ NMR spectrum of complex **3b** showed a single resonance with satellites due to coupling to ^{195}Pt, with $^1J(Pt,P)$-3054 Hz. This compares well with other platinum(II)-amide complexes [10,13].

Assignment of the NMR spectra of the palladium complexes was based on the assignment for the platinum complexes. Interestingly, for the BIPY Pd complex **4a**, the chemical shift difference between the two types of CH_2 protons was relatively small, and in the PHEN complex **4b**, these protons appeared as a somewhat broad unresolved singlet, due to coincidental chemical shifts. Upon examination of the carbon spectrum for this complex two separate CH_2 resonances were observed, at δ 40.9 and 39.0.

Electrospray mass spectrometry (ESMS) study

ESMS is a relatively recent mass spectrometric ionisation technique, ideally suited to the study of polar, high molecular weight molecules [14]. The technique

typically gives strong parent ions, which may be multiply charged and, therefore, can be used as an additional means of characterization, supplementary to more traditional spectroscopic and crystallographic techniques. However, the ability to select the amount of fragmentation in the ESMS system allows the potential to study the stability of coordination complexes. In addition, since the sample is introduced as a solution, *in situ* reactions of the complexes with various reagents is readily facilitated, using small quantities of material. Accordingly, the azetidinone complexes **3** and **4** have been investigated by electrospray mass spectrometry, using a CH_3CN/H_2O mobile phase; ESMS data are summarized in Table 2. For all major ions observed there was excellent agreement between the observed and calculated isotope patterns.

A detailed study on the triphenylphosphine platinum complex **3b** has been carried out in order to study the fragmentation patterns in this class of compound. ES spectra of **3b** recorded at three different cone voltages (20, 40 and 80 V) are shown in Fig. 1 (a–c, respectively). At 20 V the major peak was the "parent" ion $[M + H]^+$ (*m/z* 860), although there was an additional reasonably intense peak at *m/z* 1737, which is assigned to the aggregate $[2M + NH_4]^+$. One possible structure for this aggregate is given by **5a,** where two bidentate bis(amide) complexes hydrogen-bond with the NH_4^+ ion. The presence of "basic" carbonyl groups thus provide a mechanism for chemical ionisation *via* protonation or aggregation with NH_4^+ ions. Aggregate formation involving ammonium ions is reasonably frequently observed, although for this particular case it is interesting that only exceedingly weak corresponding species $[2M + H]^+$ (*m/z* 1720) and $[M + NH_4]^+$ (*m/z* 877) are observed. The larger aggregate ion $[3M + 2NH_4]^{2+}$ was observed as a weak peak at *m/z* 1306. The source of the NH_4^+ ions in this system is undoubtedly the acetonitrile mobile phase, since traces of NH_3 and NH_4^+ are ubiquitous in this solvent.

Upon increasing the cone voltage to 40 V, fragmentation of complex **3b** occurs. The principal change is loss of one of the azetidinone ligands as a monoanion (az^-) giving $[M - az]^+$ as the principal ion at *m/z* 789, i.e. $[Pt\{NC(O)CH_2CH_2\}(PPh_3)_2]^+$. It is noteworthy that the $[3M + 2NH_4]^{2+}$ aggregate ion was not observed at 40 V, though the aggregate ion $[2M + NH_4]^+$ was observed together with $[2M + H]^+$, these two peaks being of approximately equal intensity. Upon further increasing the cone voltage to 80 V, Fig. 1(c), the aggregate ions were only of low intensity, the species $[M - az]^+$ was the principal ion, and a new ion at *m/z* 718 was observed. The latter is assigned as the complex **6** containing a cyclometallated triphenylphosphine ligand. We have previously observed similar behaviour for a number of platinum complexes containing triphenyl-phosphine or -phosphite ligands [11,15]. Cyclometallation thus appears to provide a mechanism for loss of the second azetidinone amide ligand; the observation that the

Table 2. Electrospray mass spectrometric data for the azetidinone complexes **3** and **4**[a,b]

Complex	Cone voltage (V)	Principal Ions (*m/z*, %)
3a	20	$[M + H]^+$ (444, 100%), $[2M - az]^+$ (816, 45%), $[2M + NH_4]^+$ (905, 40%)
3b	20	$[M + H]^+$ (860, 100%), $[3M + 2NH_4]^{2+}$ (1306, 6%), $[2M + NH_4]^+$ (1737, 48%)
	40	$[M - az]^+$ (789, 100%), $[M + H]^+$ (860, 40%), $[2M + H]^+$ (1720, 25%), $[2M + NH_4]^+$ (1737, 30%)
	80	$[Pt(o\text{-}C_6H_4PPh_2)(PPh_3)]^+$ **6** (718, 40%), $[M - az]^+$ (789, 100%), $[M + H]^+$ (860, 17%), $[2M + H]^+$ (1720, 2%), $[2M + NH_4]^+$ (1737, 3%)
3d	20	$[M + H]^+$ (720, 100%), $[2M - az]^+$ (1369, 8%), $[2M + H]^+$ (1439, 11%), $[2M + NH_4]^+$ (1456, 3%)
3e	20	$[M + H]^+$ (956, 100%), $[2M + NH_4]^+$ (1928, 37%)
	40	$[M - az]^+$ (885, 100%), $[M + H]^+$ (956, 79%), $[2M + H]^+$ (1912, 10%), $[2M + NH_4]^+$ (1928, 39%)
4a	20	$[M + H]^+$ (403, 100%), $[2M + H]^+$ (807, 5%), $[2M + NH_4]^+$ (824, 10%)
4b	20	$[M + H]^+$ (427, 100%), $[2M - az]^+$ (783, 2%), $[2M + H]^+$ (855, 10%), $[2M + NH_4]^+$ (872, 9%)

[a]Species are identified by the major peak in the isotope distribution pattern.
[b]Haz = 2-azetidinone.

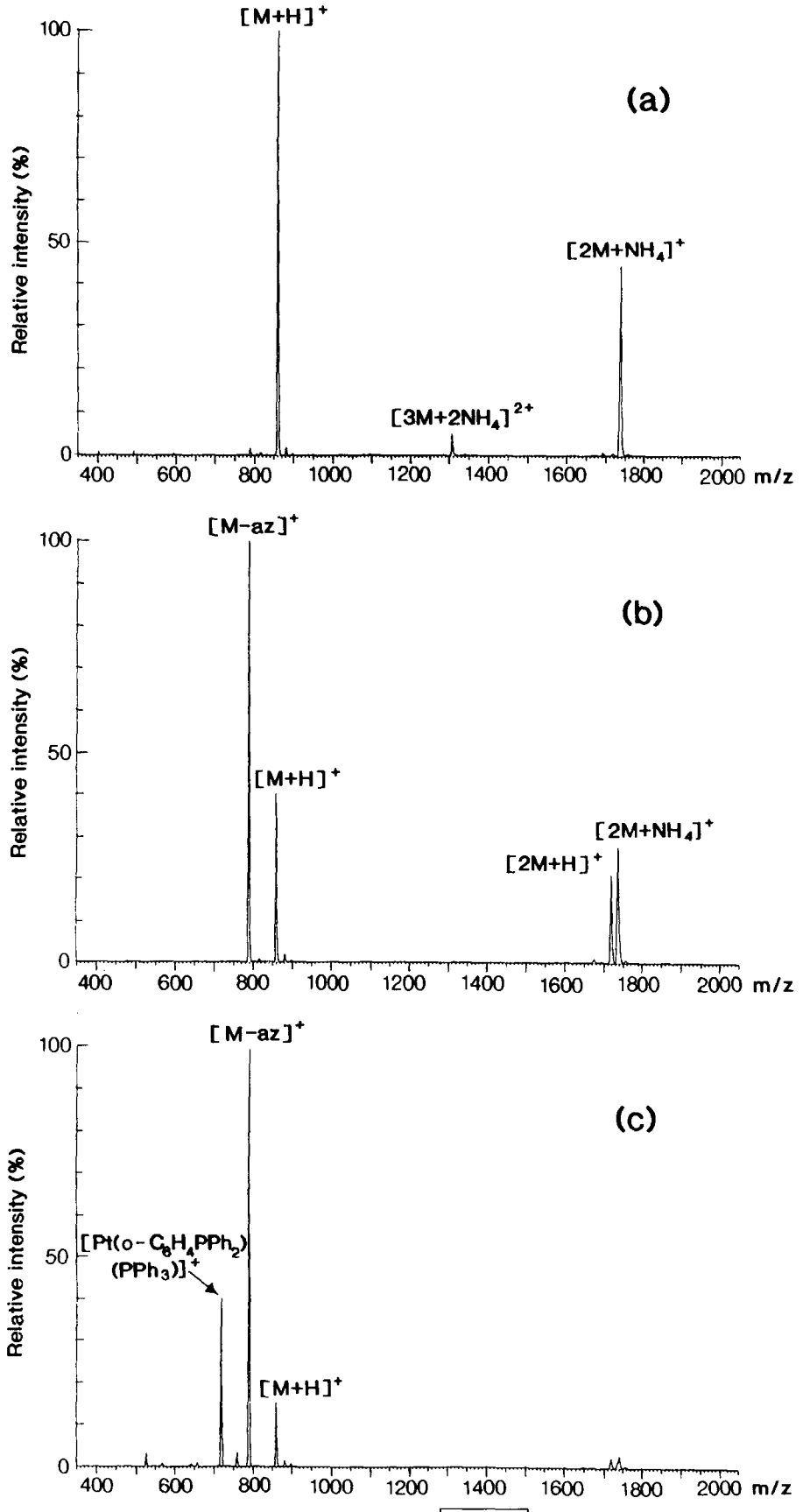
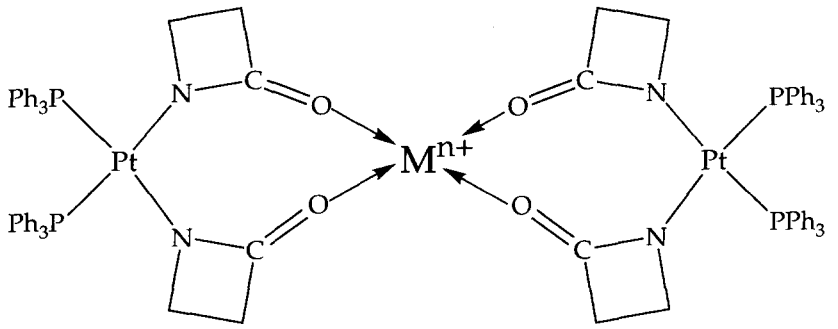
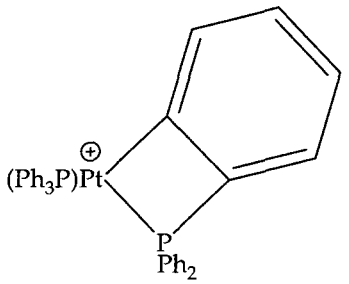


Fig. 1. Positive-ion electrospray spectra of the complex *cis*-[Pt{$\overline{NC(O)CH_2CH_2}$}$_2$(PPh$_3$)$_2$] (**3b**) (= M) recorded at cone voltages of (a) 20 V, (b) 40 V and (c) 80 V. The anion [$\overline{CH_2CH_2NC(O)}$]$^-$ is abbreviated as az.



5a; M = NH_4, n = 1
5b; M = Ba, n = 2



6

monoamide complex $[M - az]^+$ is stable to relatively high cone voltages (e.g. 80 V) which suggests that the platinum–nitrogen bond possesses significant stability.

In a similar fashion to **3b**, the positive-ion spectrum for the triphenylphosphite complex **3e** gave intense $[M + H]^+$ (*m/z* 956) and $[2M + NH_4]^+$ (*m/z* 1928) ions, again with no evidence of the corresponding $[M + NH_4]^+$ or $[2M + H]^+$ ions. As result of the strong signal intensity, and spectral simplicity, is it suggested that triphenylphosphite ligands may facilitate ESMS analysis of coordination complexes, particularly when other "basic" functional groups are absent. For the other complexes, aggregate ions of the type $[2M + H]^+$, $[2M + NH_4]^+$ and from time to time $[2M - az]^+$ were observed, as indicated in Table 1. The relative intensities of these appeared to vary somewhat with the complex and from day to day.

Complexes **3** and **4** readily add adventitious quantities of Na^+ (most likely leached from glassware) and the spectra often showed a small peak for $[M + Na]^+$ in addition to the peak for $[M + H]^+$. These observations suggested that the *cis*-diamide groups may be suitably disposed for coordination towards metal centres. Electrospray mass spectrometry was used to evaluate the possibilities for undertaking coordination chemistry with these new complexes, using the triphenylphosphine platinum complex **3b** as a typical example. There are a number of advantages to using ESMS to probe coordination chemistry; very small quantities of material may be used and once promising metal–ligand combinations have been identified, then the ESMS results can be used to subsequently direct synthetic studies on the macroscopic scale. ESMS has been used previously for the *in situ* study of coordination chemistry. Applications include studies of metal-binding peptides and proteins [16], metal complexes of ascidian-derived peptides [17] and ligand exchange processes of coordination complexes [18].

Complexation studies with added metal salts

Mass spectra of the triphenylphosphine platinum complex **3b** were recorded with addition of small quantities of various metal salts; results are sum-

marized in Table 3. Experiments were carried out with added LiCl, NaCl, KCl, CsCl, $AgNO_3$, $Cu(NO_3)_2$, $Ba(NO_3)_2$, $Pb(NO_3)_2$, $Pb(OAc)_2$, $Zn(OAc)_2$, $BeSO_4$ and $Pr(NO_3)_3$. In all cases, excellent agreement was obtained between the observed and calculated isotope pattern for all major ions.

(a) *With monovalent cations.* For mixtures of **3b** and the alkali metal cations ($cat^+ = Li^+$, Na^+, K^+ and Cs^+) a large peak for $[M + cat]^+$ was typically observed, often with other species. As a typical example, the positive-ion ES spectrum of **3b** with added NaCl is shown in Fig. 2, which shows $[M + Na]^+$ as the main platinum-containing species. Other ions observed were $[M + H]^+$, $[3M + 2Na]^{2+}$ and $[2M + Na]^+$. Examination of the isotope distribution patterns for the $[M + cat]^+$ ions at relatively high cone voltages (e.g. 40 V) yields only the pattern for the $[M + cat]^+$ ion. However, for the $[M + Na]^+$ ion, upon recording the isotope pattern at cone voltages of 20 V or less, additional peaks at half-mass separation grew in, as illustrated in the inset to Fig. 2. These are assigned to the dication $[2M + 2Na]^{2+}$. What is particularly noteworthy is that such a dication was *only observed in the case of sodium*; no $[2M + 2cat]^{2+}$ ions were observed for Li^+, K^+ or Cs^+ even at very low cone voltages (5 V). While of the origin of this selectivity is uncertain, it is possible that the bite angle of the two *cis* amide carbonyls is optimized for coordination to an ion the size of Na^+.

It is worth noting that the use of added alkali metal salts as an ionization reagent has been employed previously, for example in the analysis of polyethers by addition of lithium ions [19], and in the use of anhydrous KI for a range of organic compounds in aprotic solvents [20]. Coordination chemistry of metal complexes with alkali-metal cations has been studied previously by ESMS, for example for the tripodal oxygen and nitrogen ligands $[(\eta^5\text{-}C_5H_5)Co\{P(O)(OR)_2\}_3]$ and $[HB(pz)_3]^-$ (pz = pyrazolyl) [21] and Schiff bases [22]. The attachment of an alkali-metal cation is promoted by the presence of hard, basic oxygen (or nitrogen) atoms in the molecule. The Li^+ ion readily formed an adduct with **3b**, and, as a result of the high charge density of this ion, the mono acetonitrile solvate $[M + Li(MeCN)]^+$ is observed up to moderate cone voltages (40 V).

When $AgNO_3$ is added to a solution of **3b**, in addition to the expected $[Ag(NCMe)_x]^+$ ions ($x = 1$ or 2), the main platinum species observed was the expected $[M + Ag]^+$ at m/z 967. An additional peak at m/z 1138 could be assigned as the dimeric species

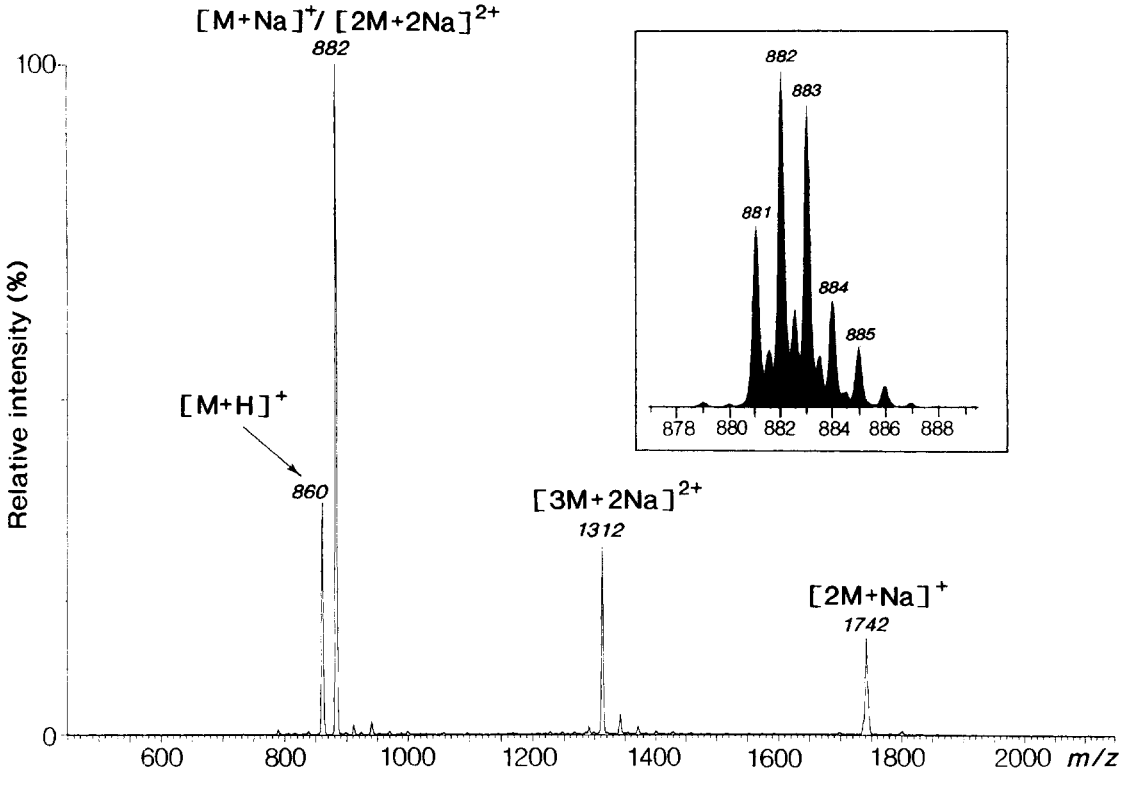


Fig. 2. Positive-ion electrospray spectrum of $[Pt\{NC(O)CH_2CH_2\}_2(PPh_3)_2]$ (**3b**) (= M) at a cone voltage of 20 V, with added NaCl, showing peak assignments. The inset shows the isotope distribution pattern for the m/z 882 ion, indicating the presence of the $[M + Na]^+$ and $[2M + 2Na]^{2+}$ ions.

Table 3. Electrospray mass spectrometric data for complexes of **3b** with added metal salts[a,b]

Mixture	Cone voltage (V)	Principal ions (m/z)
3b + LiCl	5	$[M + Li]^+$ (866), $[M + Li(MeCN)]^+$ (907)
3b + NaCl	20	$[M + H]^+$ (860), $[M + Na]^+$ (882), $[3M + 2Na]^{2+}$ (1312), $[2M + Na]^+$ (1742)
3b + KCl	20	$[M + H]^+$ (860), $[M + K]^+$ (898), $[3M + 2K]^{2+}$ (1328), $[2M + K]^+$ (1758)
3b + CsCl	20	$[M + H]^+$ (860), $[M + Cs]^+$ (992), $[M + 2Cs + Cl]^+$ (1161), in addition to peaks due to Cs^+, $[Cs_2Cl]^+$, $[Cs_3Cl_2]^+$ etc.
3b + $AgNO_3$	20	$[M + Ag]^+$ (967), $[2M + 2Ag + NO_3]^+$ (1138)
3b + $Ba(NO_3)_2$	20	$[Ba(MeCN)_3]^{2+}$ (130), $[Ba(MeCN)_4]^{2+}$ (151), $[Ba(MeCN)_5]^{2+}$ (171), $[Ba(MeCN)_6]^{2+}$ (191), $[BaNO_3(MeCN)]^+$ (241), $[BaNO_3(MeCN)_2]^+$ (282), $[BaNO_3(MeCN)_3]^+$ (323), $[M + Ba]^{2+}$ (498), $[M + Ba(MeCN)]^{2+}$ (519), $[M + Ba(MeCN)_2]^{2+}$ (539), $[M - az]^+$ (789), $[M + H]^+$ (860), $[2M + Ba]^{2+}$ (928), $[M + BaNO_3]^+$ (1058), $[3M + Ba]^{2+}$ (1357)
3e + $Ba(NO_3)_2$	20	$[M + Ba]^{2+}$ (546.5), $[M + Ba(MeCN)]^{2+}$ (566.5), $[M + Ba(MeCN)_3]^{2+}$ (587.5), $[M + H]^+$ (956), $[2M + Ba]^{2+}$ (1024), $[M + BaNO_3]^+$ (1155), $[3M + Ba]^{2+}$ (1502), $[2M + BaNO_3]^+$ (2110), together with Ba-MeCN-NO_3 species as indicated for **3b** above.
3b + $Pb(NO_3)_2$	20	$[M - az]^+$ (789), $[M - az + MeCN]^+$ (830), $[M + H]^+$ (860), $[M + PbNO_3]^+$ (1129)
3b + $Pb(OAc)_2$	20	$[M - az]^+$ (789), $[M + H]^+$ (860), $[2M + Pb]^{2+}$ (963), $[M + PbOAc]^+$ (1126), $[3M + Pb]^{2+}$ (1393), $[2M + NH_4]^+$ (1738), $[2M + PbOAc]^+$ (1985)
3b + $Cu(NO_3)_2$	20	$[M + Cu(MeCN)]^{2+}$ (482), $[M + Cu(MeCN)_2]^{2+}$ (502), $[M - az]^+$ (789), $[M - az + MeCN]^+$ (830), $[M + H]^+$ (860), $[2M + Cu]^{2+}$ (891), $[2M + 2H + NO_3]^+$ (923), $[M + CuNO_3]^+$ (985)
3b + $Zn(OAc)_2$	20	$[M + Zn(MeCN)]^{2+}$ (483), $[M + Zn(MeCN)_2]^{2+}$ (503), $[M + H]^+$ (860), $[2M + Zn]^{2+}$ (892), $[M + Zn(OAc)]^+$ (982)
3b + $BeSO_4$	5	$[M - az + MeCN]^+$ (830), $[M + H]^+$ (860)
3b + $Pr(NO_3)_3$	20	$[M + Pr(MeCN)_4]^{3+}$ (388), $[M + Pr(NO_3)]^{2+}$ (531), $[M + Pr(NO_3)(MeCN)]^{2+}$ (551.5), $[M + Pr(NO_3)(MeCN)_2]^{2+}$ (572), $[M + Pr(NO_3)(MeCN)_3]^{2+}$ (592.5), $[M - az]^+$ (789), $[M + H]^+$ (860), $[2M + Pr(NO_3)]^{2+}$ (961), $[M + Pr(NO_3)_2]^+$ (1124), $[M + Pr(NO_3)_2(MeCN)]^+$ (1165)

[a]Species are identified by the major peak in the isotope distribution pattern.
[b]Haz = 2-azetidinone.

$[2M + 2Ag + NO_3]^+$; analogous species were not observed for the alkali-metal cations.

(b) *With divalent cations.* Somewhat more complex spectra resulted upon addition of divalent metal ions to solutions of **3b,** although with some common features. As a typical example, the positive-ion spectrum obtained for a mixture of **3b** and $Ba(NO_3)_2$ is shown in Fig. 3. Overall, very similar results were obtained when a mixture of the triphenylphosphite complex **3e** and $Ba(NO_3)_2$ was investigated, indicating that the triphenylphosphite ligands do not confer any special coordinating properties. The predominant species in the spectra are the dications $[M + Ba(MeCN)_x]^{2+}$ ($x = 0$–2), $[2M + Ba]^{2+}$ and $[3M + Ba]^{2+}$. The monocations $[M + BaNO_3]^+$ and $[2M + BaNO_3]^+$ can also be observed as weak ions, and residual $[M + H]^+$ is also observed. A number of solvated barium cations, including $[Ba(MeCN)_x]^{2+}$ ($x = 2$–6) and $[BaNO_3(MeCN)_y]^+$ ($y = 1$–3) were additionally observed. One possibility for the structure of the barium complex $[2M + Ba]^{2+}$ is given by **5b,** analogous to the possible structure proposed for the ammonium ion aggregate **5a**.

Two lead salts were investigated with complex **3b**; $Pb(NO_3)_2$ and $Pb(OAc)_2$. Only limited success was achieved with the nitrate, the major peaks in the spectrum being $[M - az]^+$ and $[M - az + MeCN]^+$. Presumably these arise due to degradation of the parent complex, possibly by protonolysis from HNO_3 in the metal salt. In this case, the ion $[M + PbNO_3]^+$ was only observed as a weak ion. For $Pb(OAc)_2$, however, similar species to those with Ba^{2+} were found, *viz.* $[2M + Pb]^{2+}$, $[3M + Pb]^{2+}$, $[M + Pb(OAc)]^+$ and $[2M + Pb(OAc)]^+$.

With **3b** and $Zn(OAc)_2$ or $Cu(NO_3)_2$ ($= AX_2$) similar features to those found for Ba^{2+} and Pb^{2+} were again observed, with $[M + AX]^+$ being the major ion observed, followed by $[2M + A]^{2+}$, $[M + A(MeCN)]^{2+}$ and $[M + A(MeCN)_2]^{2+}$, as indicated in Table 3. It is significant that the ions $[3M + Zn]^{2+}$ and $[3M + Cu]^{2+}$ were small for these metals. This appears to be consistent with coordination of the

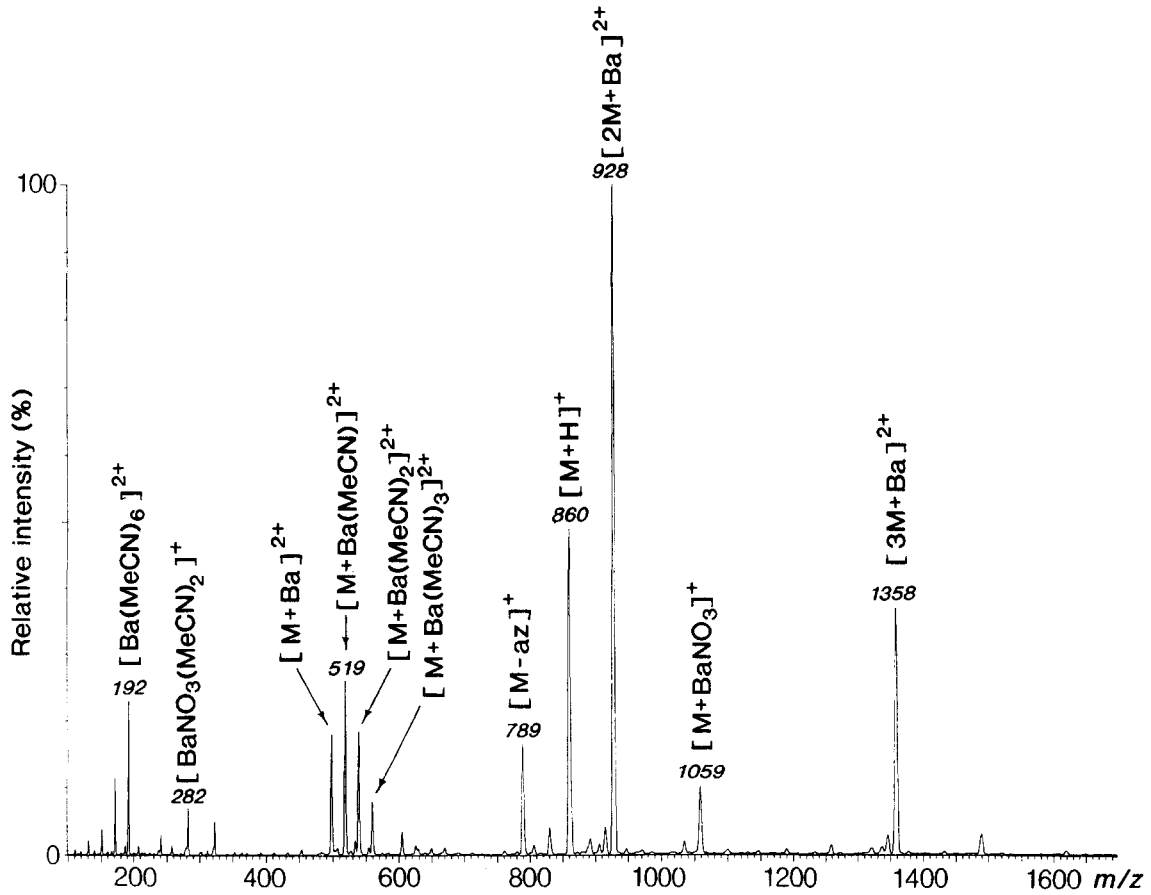


Fig. 3. Positive-ion electrospray spectrum of a mixture of complex **3b** and $Ba(NO_3)_2$ (cone voltage 20 V), showing the peak assignments.

azetidinone complexes to the added metal ions, since it would be anticipated that the larger Pb^{2+} and Ba^{2+} ions would adopt higher coordination numbers than Zn^{2+} or Cu^{2+}.

$BeSO_4$ showed markedly different behaviour, with no Be^{2+} adducts being detected. Instead, the spectrum yielded the $[M + H]^+$ species and the ion $[M - az + MeCN]^+$, presumably as a result of the expected hydrolysis of the aquated Be^{2+} ion generating H^+, with subsequent protonolysis of a platinum–amide bond. No further studies were carried out with this ion.

(*c*) *With a trivalent cation* Pr^{3+}. As a representative example of a trivalent cation salt, $Pr(NO_3)_3$ was studied with **3b**. A lanthanide ion was chosen, since these are less acidic than other tripositive cations such as Al^{3+} and Fe^{3+}. As anticipated, the spectra were rather more complex than those for divalent cations, and appeared to be much more variable. Some of the identifiable ions are listed in Table 3. The observed ions generally conform to the type predicted based on the divalent cation complexes, for example, $[2M + Pr(NO_3)_2]^{2+}$, $[M + Pr(NO_3)_2]^+$, $[M + PrNO_3]^{2+}$ and $[M + Pr(MeCN)_4]^{3+}$.

X-ray structure determination on the platinum complex **3b**

A single-crystal X-ray diffraction study has been carried out on the triphenylphosphine complex **3b**.

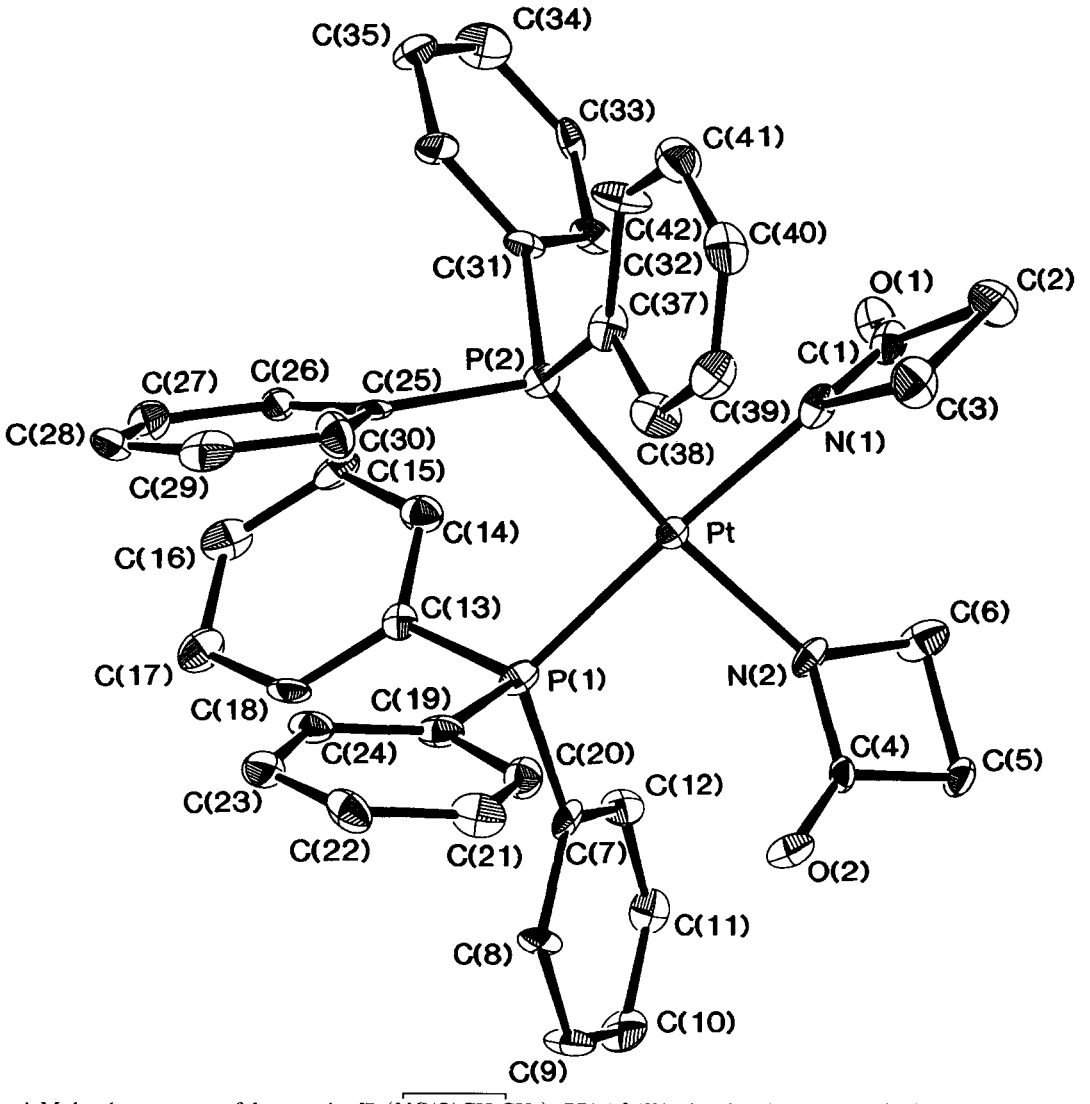


Fig. 4. Molecular structure of the complex $[Pt\{\overline{NC(O)CH_2CH_2}\}_2(PPh_3)_2]$ (**3b**), showing the atom numbering scheme. Thermal ellipsoids are shown at the 30% probability level. All hydrogen atoms and the dichloromethane molecule of crystallization have been omitted.

The molecular structure is shown in Fig. 4, together with the atom numbering scheme, while Table 4 gives bond distances and angles. The crystal of **3b** also contains one dichloromethane molecule per molecule of platinum complex. Elemental microanalytical data for this complex suggest that part of this solvent of crystallization is lost upon vacuum drying. Additionally, crystals of **3b** slowly turn opaque upon standing at room temperature in air.

The complex contains the expected approximately square-planar platinum atom, coordinated in *cis*-fashion to two triphenylphosphine ligands and two deprotonated 2-azetidinone ligands, bonded *via* the lactam nitrogens. The N(1)—Pt—N(2) bond angle [85.8(4)°] is slightly reduced from the idealized 90°, while the P(1)—Pt—P(2) angle is slightly larger [96.6(1)°], reflecting the steric bulk of the triphenylphosphine ligands. The platinum–amide bonds are equal in length [Pt—N(1) 2.05(1); Pt—N(2) 2.03(1) Å].

The planes of the two four-membered rings are twisted away from each other, resulting in one carbonyl group pointing above and the other below the platinum coordination plane. Thus, should both carbonyl ligands be involved in coordination to metal ions, rotation about the platinum–amide bonds is required. The carbonyl bonds [C(1)—O(1) 1.28(1); C(4)—O(2) 1.25(1) Å] are somewhat longer than in the parent 2-azetidinone, 1.226(1) Å [6(a)]. Additionally, the CH_2—N bond distances of **3b** [N(2)—C(6) and N(1)—C(3) both 1.52(2)Å] appear longer than in 2-azetidinone [1.467(2) Å], although the N—C(O) bond distances are comparable, within experimental error. An analogous distortion was not observed in an N-mercurated derivative of 2-azetidinone, which has been crystallographically characterized as a complex with erbium nitrate [3a].

In conclusion, a number of platinum and palladium complexes containing the deprotonated 2-azetidinone ligand have been prepared. Electrospray mass spectrometry indicates that these complexes interact with metal cations and we are currently investigating the chemistry of these complexes as metalloligands.

EXPERIMENTAL

^1H and ^{13}C ^1H NMR spectra were recorded in $CDCl_3$ solution on a Bruker AC300P spectrometer at 300.13 and 75.47 MHz, respectively, with $SiMe_4$ (δ 0.0) as reference. ^{31}P ^1H NMR spectra were recorded in $CDCl_3$ solution on a JEOL JNM FX-90Q spectrometer with 85% H_3PO_4 (δ 0.0) as external reference. IR spectra were recorded as KBr discs on a

Table 4. Selected bond lengths (Å) and angles (°) for the complex [Pt{NC(O)CH_2CH_2}$_2$(PPh_3)$_2$] (**3b**). CH_2Cl_2, with estimated standard deviations in parentheses

Pt—P(1)	2.266(3)	Pt—P(2)	2.291(3)
Pt—N(1)	2.05(1)	Pt—N(2)	2.03(1)
O(1)—C(1)	1.28(1)	O(2)—C(4)	1.25(1)
N(1)—C(1)	1.31(2)	N(1)—C(3)	1.52(2)
N(2)—C(4)	1.33(2)	N(2)—C(6)	1.52(2)
C(1)—C(2)	1.52(2)	C(2)—C(3)	1.54(2)
C(4)—C(5)	1.52(2)	C(5)—C(6)	1.54(2)
P(1)—C(7)	1.83(1)	P(1)—C(13)	1.83(1)
P(1)—C(19)	1.82(1)	P(2)—C(25)	1.84(1)
P(2)—C(31)	1.81(1)	P(2)—C(37)	1.81(1)
P(1)—Pt—P(2)	96.6(1)	P(1)—Pt—N(1)	175.6(3)
P(1)—Pt—N(2)	91.2(3)	P(2)—Pt—N(1)	86.6(3)
P(2)—Pt—N(2)	171.1(3)	N(1)—Pt—N(2)	85.8(4)
Pt—P(1)—C(7)	117.1(4)	Pt—P(1)—C(13)	113.4(4)
Pt—P(1)—C(19)	112.0(4)	C(7)—P(1)—C(13)	98.3(5)
C(7)—P(1)—C(19)	105.4(6)	C(13)—P(1)—C(19)	109.6(6)
Pt—P(2)—C(25)	123.7(4)	Pt—P(2)—C(31)	114.1(4)
Pt—P(2)—C(37)	107.4(4)	C(25)—P(2)—C(31)	100.8(5)
C(25)—P(2)—C(37)	101.2(6)	C(31)—P(2)—C(37)	108.3(6)
Pt—N(1)—C(1)	132.2(8)	Pt—N(1)—C(3)	133.6(8)
C(1)—N(1)—C(3)	91(1)	Pt—N(2)—C(4)	136.9(8)
Pt—N(2)—C(6)	130.3(8)	C(4)—N(2)—C(6)	92.9(9)
O(1)—C(1)—N(1)	132(1)	N(1)—C(1)—C(2)	97(1)
C(1)—C(2)—C(3)	83(1)	N(1)—C(3)—C(2)	88(1)
O(2)—C(4)—N(2)	130(1)	O(2)—C(4)—C(5)	135(1)
N(2)—C(4)—C(5)	95(1)	C(4)—C(5)—C(6)	85.2(9)
N(2)—C(6)—C(5)	86.9(9)	O(1)—C(1)—C(2)	131(1)

BioRad FTS40 spectrometer and melting points were determined using a Reichert Hotstage apparatus, and are uncorrected.

Electrospray mass spectra were obtained in positive-ion mode using a VG Platform II mass spectrometer and a 1:1 v/v acetonitrile: water mobile phase. The compounds were dissolved in the mobile phase to give a solution typically of approximate concentration 0.1 mM and spectra were recorded on the freshly prepared solutions. The diluted solution was injected into the spectrometer *via* a Rheodyne injector fitted with a 0.1 cm^3 sample loop. A Thermo Separation Products SpectraSystem P1000 LC pump delivered the solution to the mass spectrometer source (60 °C) at a flow rate of 0.01 $cm^3\ min^{-1}$, and nitrogen was employed both as a drying and nebulizing gas. Cone voltages were typically varied from 5 to 80 V, in order to investigate the effect of higher voltages on fragmentation of parent ions. Confirmation of all species in this ESMS study is aided by comparison of the observed and predicted isotope distribution patterns. Theoretical isotope distribution patterns were calculated using the *Isotope* computer program [23].

The complexes described are all air-stable and reactions were carried out in reagent grade dichloromethane with no further purification or drying. Light petroleum refers to the fraction boiling in the range 40–60 °C. The compounds $[PtCl_2(COD)]$ [24], $[PdCl_2(BIPY)]$ [25], $[PdCl_2(PHEN)]$ [26], $P(CH_2CH_2CN)_3$ [27] and 2,6-xylylisocyanide [28] were prepared *via* literature procedures. 2-Azetidinone (Aldrich), triphenylarsine (Fluka), triphenylphosphine (Pressure Chemical Co.), bis(1,2-diphenylphosphino)methane (Aldrich), silver(I) oxide (BDH), 2,2′-bipyridine (BDH), 1,10-phenanthroline (BDH) and triphenylphosphite (BDH) were used as received. Metal salts used in the electrospray study were of AR grade. The complex *cis*-$[PtCl_2(PPh_3)_2]$ was prepared *via* ligand displacement of COD from $[PtCl_2(COD)]$ using 2 mol equiv. of PPh_3 in dichloromethane solution.

Synthesis of $[Pt\{\overline{NC(O)CH_2CH_2}\}_2(COD)]$ (**3a**). A solution of $[PtCl_2(COD)]$ (200 mg, 0.535 mmol) and 2-azetidinone (77 mg, 1.083 mmol) in dichloromethane (20 cm^3) with silver(I) oxide (700 mg, excess) was refluxed for 4 h. Filtration to remove the insoluble silver salts afforded a colourless solution which was reduced in volume to *ca* 5 cm^3. Addition of light petroleum (*ca* 60 cm^3) gave a white microcrystalline solid which was filtered off, washed with a small quantity of light petroleum and dried *in vacuo* to give complex **3a** (220 mg, 93%). NMR: $^{13}C\ ^1H$, δ(C) 174.1 (s, CO), 97.5 [s, PtCH, ^1J(Pt,C)-121.1 Hz], 41.1 [s, CH_2CO, ^3J(Pt,C)-17.4 Hz], 38.5 [s, CH_2N, ^1J(Pt,C)-42.7 Hz] and 30.3 (s, CH_2, COD); ^1H, δ(H) 5.90 [s, 4 H, COD CH, ^2J(Pt,H)-55.5 Hz], 3.16 [t, 4 H, CH_2CO, ^3J(H,H)-4.1 Hz], 3.10 [t, 4 H, CH_2N, ^3J(H,H)-4.1 Hz], 2.6–2.2 (m, 8 H, COD CH_2).

Synthesis of cis-$[Pt\{\overline{NC(O)CH_2CH_2}\}_2(PPh_3)_2]$. (**3b**). A solution of *cis*-$[PtCl_2(PPh_3)_2]$ (400 mg, 0.506 mmol) and 2-azetidinone (37 mg, 0.521 mmol) in dichloromethane (25 cm^3) with silver(I) oxide (800 mg, excess) was refluxed for 8 h. Filtration to remove the silver salts afforded a pale brown solution, which was reduced in volume to *ca* 20 cm^3. Addition of light petroleum (*ca* 60 cm^3) gave pale pink prisms of **3b**, which were dried *in vacuo*. Yield (310 mg, 71%). Several recrystallizations from dichloromethane-light petroleum gave colourless microcrystals. NMR: $^{13}C\ ^1H$, δ 174.6 (s, CO), 134.6–127.8 (m, Ph), 53.5 (s, CH_2Cl_2), 40.2 [s, CH_2CO, ^3J(Pt,C) not resolved], and 37.8 [*pseudo*-t, CH_2N, $|^3J(P,C)_{trans} + {}^3J(P,C)_{cis}|$-4.4; ^2J(Pt,C)-*ca* 74 Hz]; ^1H, δ 7.54–7.15 (m, 30 H, Ph), 5.26 (s, 1 H, CH_2Cl_2), 2.40 [t, 2 H, CH_2CO, ^3J(H,H)-7.3 Hz] and 2.32 (s, br, CH_2N). Relative assignment of the CH_2 resonances was confirmed by means of a ^{13}C–^1H correlation spectrum. $^{31}P\ ^1H$, δ(P) 9.0 [s, ^1J(Pt,P)-3054 Hz].

Synthesis of $[Pd\{\overline{NC(O)CH_2CH_2}\}_2(BIPY)]$ (**4a**). A suspension of $[PdCl_2(BIPY)]$ (100 mg, 0.300 mmol) and 2-azetidinone (44 mg, 0.619 mmol) in dichloromethane (30 cm^3) with silver(I) oxide (0.6 g, excess) was refluxed for 4 h. Filtration to remove the silver salts afforded a yellow solution. The silver salts were extracted with an additional 30 cm^3 of dichloromethane and the solutions combined. Reduction in the volume of the solution to *ca* 40 cm^3, followed by addition of diethyl ether (*ca* 100 cm^3) gave pale lemon-yellow microcrystals of **4a**, which were filtered off and dried *in vacuo*. Yield 52 mg, 43%. NMR: ^1H, δ(H) 8.53 [d, 2 H, BIPY, J(H,H)-4.5 Hz], 8.37 [d, 2 H, BIPY, J(H,H)-8.0 Hz], 8.08 [dt, 2 H, BIPY, J(H,H)-7.9, 1.2 Hz], 7.35 [t, br, 2 H, BIPY, J(H,H)-6.2 Hz], 3.09 [m, second-order, 8 H, CH_2] and 2.1 (s, br, 4 H, H_2O).

Synthesis of $[Pd\{\overline{NC(O)CH_2CH_2}\}_2(PHEN)]$ (**4a**). A suspension of $[PdCl_2(PHEN)]$ (150 mg, 0.420 mmol) and 2-azetidinone (59.6 mg, 0.838 mmol) in dichloromethane (30 cm^3) with silver(I) oxide (0.6 g, excess) was refluxed for 3 h. The silver salts were removed by filtration and the volume of the filtrate reduced to *ca* 25 cm^3, whereupon crystallization commenced. Diethyl ether (50 cm^3) was added and the pale lemon–yellow microcrystals filtered off, washed with ether (10 cm^3) and dried *in vacuo*. Yield 135 mg (70%). NMR: ^1H, δ(H) 9.02 [d, 2 H, PHEN, J(H,H)-5.1 Hz], 8.52 [d, 2 H, PHEN, J(H,H)-8.2 Hz], 7.98 [d, 2 H, PHEN, J(H,H)-0.5 Hz], 7.76 [dd, 2 H, PHEN, J(H,H)-5.2, 5.6 Hz], 3.17 (s, 8 H, CH_2); $^{13}C\ ^1H$, δ(C) 177.6 (s, CO), 152.7, 146.2, 138.4, 129.7, 127.1, 125.4 (s, phen), 40.9 (s, CH_2CO), 39.0 (s, CH_2N).

Ligand substitution reactions with **3a**—*general method*

To a solution of complex **3a** in dichloromethane (1 cm^3) was added an excess of the ligand (as indicated), followed by light petroleum (5 cm^3) and the product allowed to crystallize. The solid was filtered off and

washed with two 5 cm^3 portions of light petroleum and dried *in vacuo*.

With tris(2-cyanoethyl)phosphine. Complex **3a** (60.0 mg, 0.135 mmol) and $P(CH_2CH_2CN)_3$ (54.0 mg, 0.280 mmol) gave a white powder of **3c** (98 mg, 100%). The product is sparingly soluble in all common organic solvents.

With DPPM. Complex **3a** (41.5 mg, 0.094 mmol) and DPPM (38 mg, 0.099 mmol) gave pale yellow needles of **3d** (36.0 mg, 54%). NMR: ^1H, δ(H) 7.77–7.37 (m, 20 H, Ph), 4.31 [t, 2 H, CH_2, DPPM, ^2J(P,H)-9.9, ^3J(Pt,H)-45.9 Hz], 3.21 [t, 4 H, CH_2CO, ^3J(H,H)-4.0 Hz] and 2.91 [t, br, 4 H, CH_2N, ^3J(H,H)-3.9 Hz]; ^{13}C ^1H, δ(C) 174.8 (s, CO), 133.2–128.5 (m, Ph), 53.5 [t, CH_2, DPPM, J(P,C)-31.5 Hz, J(Pt,C) not discernible], 41.8 (s, CH_2CO) and 37.1 [*pseudo*-t, $|^3J(P,C)_{trans} + {}^3J(P,C)_{cis}|$-4.8, ^2J(Pt,C)-52.2 Hz]; ^{31}P ^1H δ(P)-58.8 [s, ^1J(Pt,P)-2678 Hz].

With P(OPh)$_3$. Complex **3a** (42 mg, 0.095 mmol) and $P(OPh)_3$ (4 drops, excess) gave white crystals of **3e** (85 mg, 94%). NMR: ^{13}C ^1H, δ(C), 174.3 (s, CO), 151.0, 129.8, 125.3, 120.6 (s, Ph), 40.1 [s, br, CH_2CO, J(Pt,C) not discernible], 37.5 [*pseudo*-t, $|J(P,C)_{trans} + J(P,C)_{cis}|$-14.6 Hz, J(Pt,C) not discernible]. ^1H, δ(H) 7.33–7.17 (m, 30 H, Ph), 2.42 (s, br, 4 H, CH_2N), 2.10 [t, br, 4 H, CH_2CO, ^3J(H,H)-7.8 Hz]. ^{31}P ^1H, δ(P) 76.5 [s, ^1J(Pt, P)-4761 Hz].

With 2,6-xylyl isocyanide (XyNC). Complex **3a** (39 mg, 0.088 mmol) with XyNC (36 mg, 0.27 mmol) gave colourless crystals of **3f** (42.8 mg, 81%). NMR: ^{13}C ^1H, δ(C) 175.2 (s, CO), 135.9, 130.0, 128.2, 126.2 (s, Xy), 40.9 [s, CH_2CO, J(Pt,C)-21.4 Hz], 37.5 [s, CH_2N, J(Pt,C)-65.8 Hz] and 18.6 (s, Me). ^1H, δ(H) 7.26–7.08 (m, 3 H, Xy), 3.24 [t, 4 H, CH_2CO, ^3J(H,H) 4.1] 3.03 [t, 4 H, CH_2N, ^3J(H,H) 4.1, J(Pt, H)-*ca* 14 Hz].

With tert-butyl isocyanide. In a similar fashion to the synthesis of **3f,** reaction of **3a** (46 mg) with excess Bu^tNC gave 21 mg of **3g**. NMR: ^{13}C ^1H, δ(C) 175.2 (s, CO), 97.5 (m, CPt), 40.8 [s, CH_2CO, J(Pt, C)-20.2 Hz], 37.4 [s, CH_2N, J(Pt, C)-63.4 Hz] and 29.9 [s, Bu^t, J(Pt, C)-*ca* 5 Hz]. ^1H, δ(H) 3.14 [t, 4 H, CH_2CO, ^3J(H,H)-4.1 Hz], 2.97 [t, 4 H, CH_2N, ^3J(H,H)-4.1 Hz], 1.54 (s, 18 H, Bu^t).

With triphenylarsine. No reaction was observed at room temperature and the COD complex was recovered unreacted, as evidenced by ^1H NMR.

X-ray structure determination of **3b**

Prismatic pale pink crystals were obtained by slow recrystallization from dichloromethane–light petroleum. All X-ray measurements were carried out on a Rigaku AFC6S diffractometer using Mo-K_α radiation (λ = 0.71069 Å). Calculations were performed on a VAXstation 3500 computer by using the TEXSAN 5.0 software [29] and in the later stages on a Silicon Graphics Personal Iris 4D35 computer with the teXsan 1.7 package [30].

Relevant crystallographic data are listed in Table 5. Unit-cell dimensions were determined by applying the setting angles of 25 high-angle reflections. Three standard reflections were monitored during the data collection and showed no significant variance. The intensities were corrected for absorption by applying ψ scans of several reflections with the transmission factors ranging from 0.73–1.00.

Table 5. Summary of crystal data and intensity collection for $[Pt\{\overline{NC(O)CH_2CH_2}\}_2(PPh_3)_2]$ (**3b**) · CH_2Cl_2

Empirical formula	$C_{43}H_{40}Cl_2N_2O_2P_2Pt$
Formula weight	944.74
Crystal dimensions (mm)	0.26 × 0.22 × 0.32
Crystal system	Monoclinic
Lattice parameters	a = 19.321(2) Å
	b = 9.764(2) Å
	c = 21.746(4) Å
	β = 108.64(1)°
	V = 3887(2) Å^3
Space group	$P2_{1/n}$ (no. 14)
Z	4
D_{calc} (g cm^{-3})	1.61
Radiation	Mo-K_α (λ = 0.71069 Å)
μ(Mo-K_α) (cm^{-1})	39.04
Absorption corrections	ψ scans (transmission factors: 0.73–1.00)
Temperature (°C)	−120
$2\theta_{max}$ (°)	46
No. of reflections measured	Total: 5975
	Unique: 5780 (R_{int} = 0.027)
No. of reflections [$I > 3\sigma(I)$]	3472
No. of variables	469
Residuals R, R_w	0.044, 0.058
Goodness of fit	1.63
Maximum peak in final difference map (e Å^{-3})	1.0

The structure was solved by direct methods in SIR88 [31]. Full-matrix least-squares refinement with anisotropic displacement parameters for all non-hydrogen atoms yielded the final R of 0.044 ($R_w = 0.058$). All hydrogen atoms were found in difference-Fourier maps and included in calculations without further refinement. The final difference map was essentially featureless with the highest peak of 1.0 e $Å^{-3}$ close to the Pt atom. The results of the refinement are presented in Table 5.

Further details of the structure investigation, together with lists of final atomic coordinates, thermal parameters, and complete bond distances and angles, and structure factors may be obtained from the Cambridge Crystallographic Data Centre, or from the authors on request.

Acknowledgements—The Universities of Waikato and Virginia and the New Zealand Lottery Grants Board are acknowledged for financial support. Thanks are also extended to Dr Ralph Thomson for the NMR correlation spectrum and to A. Upreti and W. Jackson for technical assistance.

REFERENCES

1. See, for example, and references therein: D. Astruc, F. H. Jardine, K. Tamao, and M. Kumada, in *The Chemistry of the Metal–Carbon Bond*, ed. F. R. Hartley, vol. 4 chs. 7–9; Wiley, New York, 1987; K. Khumtaveeporn, and H. Alper, *Acc. Chem. Res.*, 1995, **28,** 414; P. W., Jennings, and L. L. Johnson, *Chem. Rev.*, 1994, **94,** 2241; H. Alper, *Aldrichimica Acta*, 1991, **24,** 3; K. A. Jørgensen, and B. Schiøtt, *Chem. Rev.*, 1990, **90,** 1483; S. D. Chappell, and D. J. Cole-Hamilton, *Polyhedron*, 1982, **1,** 739; R. J. Puddephatt, *Coord. Chem. Rev.*, 1980, **33,** 149.
2. T. Mizutani, T. Uesaka, and H. Ogoshi, *Organometallics*, 1995, **14,** 341; K.-T. Aye, G. Ferguson, A. J. Lough, and R. J. Puddephatt, *Angew. Chem. Int. Ed. Engl.*, 1989, **28,** 767; K.-T. Aye, D. Colpitts, G. Ferguson, and R. J. Puddephatt, *Organometallics*, 1988, **7,** 1454; A. A. Zlota, F. Frolow, and D. Milstein, *Organometallics*, 1990, **9,** 1300.
3. (a) D. M. L. Goodgame, A. M. Khaled, C. A. O'Mahoney, and D. J. Williams, *J. Chem. Soc., Chem. Commun.*, 1990, 851; (b) D. M. L. Goodgame, S. P. W. Hill, and D. J. Williams, *Polyhedron*, 1992, **11,** 1841.
4. A. J. Blake, C. M. Grant, S. Parsons, J. M. Rawson, G. A. Solan, and R. E. P. Winpenny, *J. Chem. Soc., Dalton Trans.*, 1995, 2311; L. H. Carrad, D. M. L. Goodgame, S. P. W. Hill, and D. J. Williams, *J. Chem. Soc., Dalton Trans.*, 1993, 1003; D. M. L. Goodgame, C. A. O'Mahoney, S. D. Plank, and D. J. Williams, *Polyhedron*, 1993, **12,** 2705; D. M. L. Goodgame, D. J. Williams, and R. E. P. Winpenny, *J. Chem. Soc., Dalton Trans.*, 1989, 1439.
5. D. M. Roundhill, *Chem. Rev.*, 1992, **92,** 1; H. E. Bryndza, and W. Tam, *Chem. Rev.*, 1988, **88,** 1163; M. D. Fryzuk, and C. D. Montgomery, *Coord. Chem. Rev.*, 1989, **95,** 1.
6. (a) Q.-C. Yang, P. Seiler, and J. D. Dunitz, *Acta Cryst.* 1987, **C43,** 565; (b) H. R. Pfaendler, and H. Hoppe, *Heterocycles*, 1985, **23,** 265.
7. A. Satake, H. Ishii, I. Shimizu, Y. Inoue, H. Hasegawa, and A. Yamamoto, *Tetrahedron*, 1995, **51,** 5331.
8. S. Masao, Y. Ichihara, and T. Kobayashi, *Japanese Patent* JP 03, 271, 297, 1991, *Chem. Abstr.*, 1991, **116,** 267958.
9. For references on anticancer active platinum-amide complexes see: J. Matsunami, H. Urata, and K. Matsumoto, *Inorg. Chem.*, 1995, **34,** 202.
10. A. D. Burrows, D. M. P. Mingos, A. J. P. White, and D. J. Williams, *J. Chem. Soc., Dalton Trans.*, 1996, 149.
11. J. Fawcett, W. Henderson, R. D. W. Kemmitt, D. R. Russell, and A. Upreti, *J. Chem. Soc., Dalton Trans.*, 1996, 1897.
12. W. Henderson, J. Fawcett, R. D. W. Kemmitt, C. Proctor, and D. R. Russell, *J. Chem. Soc., Dalton Trans.*, 1994, 1836; W. Henderson, B. K. Nicholson, and A. G. Oliver, *Polyhedron*, 1994, **13,** 3099; W. Henderson, and M. B. Dinger, *J. Chem. Soc., Chem. Commun.*, 1996, 211; W. Henderson, and B. K. Nicholson, *Polyhedron*, **15,** 4015.
13. R. D. W. Kemmitt, S. Mason, M. R. Moore, and D. R. Russell, *J. Chem. Soc., Dalton Trans.*, 1992, 409.
14. J. B. Fenn, M. Mann, C. K. Meng, S. F. Wu, and C. M. Whitehouse, *Mass Spectrom. Rev.*, 1990, **9,** 37; M. Mann, and M. Wilm, *Trends Biochem. Sci.*, 1995, 219; M. Mann, *Org. Mass Spectrom.*, 1990, **25,** 575; C. M. Whitehouse, R. N. Dreyer, M. Yamashita, and J. B. Fenn, *Anal. Chem.*, 1985, **57,** 675.
15. W. Henderson, unpublished observations.
16. P. Hu, and J. A. Loo, *J. Am. Chem. Soc.*, 1995, **117,** 11314; P. Hu, and J. A. Loo, *J. Mass Spectrom.*, 1995, **30,** 1076; C. Q. Jiao, B. S. Freiser, S. R. Carr, and C. J. Cassady, *J. Am. Soc. Mass Spectrom.*, 1995, **6,** 521.
17. A. L. van den Brenk, D. P. Fairlie, L. R. Gahan, G. R. Hanson, and T. W. Hambley, *Inorg. Chem.*, 1996, **35,** 1095; A. L. van den Brenk, K. A. Byriel, D. P. Fairlie, L. R. Gahan, G. R. Hanson, C. J. Hawkins, A. Jones, C. H. L. Kennard, B. Moubaraki, and K. S. Murray, *Inorg. Chem.*, 1994, **33,** 3549.
18. See for example: A. M. Bond, R. Colton, Y. A. Mah, and J. C. Traeger, *Inorg. Chem.*, 1994, **33,** 2548; J. M. Curtis, P. J. Derrick, A. Schnell, E. Constantin, R. T. Gallagher, and J. R. Chapman, *Inorg. Chim. Acta*, 1992, **201,** 197; A. M. Bond, R. Colton, A. D'Agostino, J. Harvey, and J. C. Traeger, *Inorg. Chem.*, 1993, **32,** 3952.
19. R. P. Lattimer, *J. Am. Soc. Mass Spectrom.*, 1992, **3,** 225.
20. R. Saf, C. Mirtl, and K. Hummel, *Tetrahedron Lett.*, 1994, **35,** 6653.
21. R. Colton, A. D'Agostino, J. C. Traeger, and W. Kläui, *Inorg. Chim. Acta*, 1995, **233,** 51.

22. T. J. Cardwell, R. Colton, S. Mitchell, and J. C. Traeger, *Inorg. Chim. Acta*, 1994, **216,** 75.
23. L. J. Arnold, *J. Chem. Educ.*, 1992, **69,** 811.
24. J. X. McDermott, J. F. White, and G. M. Whitesides, *J. Am. Chem. Soc.*, 1976, **98,** 6521.
25. B. J. McCormick, E. N. Jaynes Jr, and R. I. Kaplan, *Inorg. Synth.*, 1972, **13,** 216.
26. F. L. Wimmer, S. Wimmer, and P. Castan, *Inorg. Synth.*, 1992, **29,** 185.
27. W. J. Vullo, *Ind. Eng. Chem. Prod. Res. Dev.*, 1966, **5,** 346.
28. I. Ugi, R. Meyr, M. Lipinski, F. Bodesheim, and F. Rosendahl, *Org. Synth. Coll.*, 1973, **5,** 300.
29. *TEXSAN* 5.0. *Single Crystal Structure Analysis Software*. Molecular Structure Corp., The Woodlands, TX 77381, U.S.A., 1989.
30. *teXsan* 1.7. *Single Crystal Structure Analysis Software*. Molecular Structure Corp., The Woodlands, TX 77381, U.S.A. 1995.
31. M. C. Burla, M. Camalli, G. Cascarano, C. Giacovazzo, G. Polidori, R. Spagna, and D. Viterbo, *J. Appl. Cryst.*, 1989, **22,** 389.

Pergamon

PII: S0277-5387(96)00474-3

Polyhedron Vol. 16, No. 10, pp. 1679–1687, 1997
Copyright © 1997 Elsevier Science Ltd
Printed in Great Britain. All rights reserved
0277-5387/97 $17.00+0.00

Polymeric metal complexes of the "extended reach" ligand N_1,N_1'-*p*-phenylenedimethylene-bis(pyrazole)

Juxiang Chen, David M. L. Goodgame,* Stephan Menzer and David J. Williams

Chemistry Department, Imperial College of Science, Technology and Medicine, London SW7 2AY, U.K.

(Received 29 August 1996; accepted 20 September 1996)

Abstract—The preparation is reported of the "extended reach" ligand N_1,N_1'-*p*-phenylenedimethylene-bis(pyrazole) (*p*-XBPZ) and a range of its complexes with Mn^{II}, Co^{II}, Ni^{II}, Cu^{II}, Zn^{II} and Cd^{II}, for which pertinent spectroscopic data are also given. The compounds $Co(p\text{-XBPZ})(NO_3)_2$ (**1**) and $Cd_2(p\text{-XBPZ})_3(NCS)_4$ (**2**) have been studied by X-ray crystallography. Compound **1** has a chain structure in which octahedrally coordinated cobalt centres are linked by *p*-XBPZ ligands, with the nitrate groups being bonded in asymmetric bidentate fashion. In compound **2**, pairs of Cd atoms are linked by both NCS and *p*-XBPZ bridges so as to form ladder-like tapes which, in turn, are cross-linked by further *p*-XBPZ ligands resulting in a complex sheet polymeric structure comprising an array of 8-, 30- and 44-membered rings. © 1997 Elsevier Science Ltd. All rights reserved.

Keywords: X-ray structures; polymeric complexes; bis(pyrazole) ligand; cadmium thiocyanate.

There is currently appreciable interest in metal complexes which form extended networks, because of the prospects they offer for the development of new materials with useful chemical or physical properties. A variety of synthetic approaches has been employed, exploiting changes in, *inter alia*: (a) the nature of the donor atoms or groups bonded to the metal ions; (b) the length, flexibility, and conformational preferences of the 'spacer' bridges connecting the donor groups; (c) the coordination geometry at the metal centres or, in some cases, combinations of metal centres [1].

Extended reach ligands with pyridine rings as the donor groups have been shown to be particularly useful for forming networks [1a,b,2], catenanes [3], macrocyclic squares [4] and macrobicyclic cages [5]. In contrast, although there is a well-established coordination chemistry of simple pyrazoles, and of chelating pyrazolylborates and bispyrazoles, less attention appears to have been paid to the network-forming capabilities of ligands containing pyrazole donor groups, linked through their nitrogen atoms by spacer units designed to achieve more extended arrays. The ligand N_1,N_1'-ethylenebis(3,5-dimethylpyrazole) has been shown to bridge three $PdCl_2$ units to form a 21-membered trimetallic macrocycle.[6] We report here some complexes with the ligand N_1,N_1'-*p*-phenylenedimethylenebis(pyrazole) (**I**, *p*-XBPZ). The results of full X-ray characterization of two of them—$Co(p\text{-XBPZ})(NO_3)_2$ (**1**) and $Cd_2(p\text{-XBPZ})_3(NCS)_4$ (**2**)—demonstrate that extended chains or sheets of metallocyclic rings can be obtained with pyrazole ligands of this type.

*Author to whom correspondence should be addressed.

EXPERIMENTAL

Preparation of compounds

N_1,N_1'-p-*phenylenedimethylenebis(pyrazole)*. This was prepared by the method previously used for N,N'-*p*-phenylenedimethylenebis(pyridin-4-one) [1g] with pyrazole in place of pyridin-4-one. The product was recrystallized from methanol from which it formed a hemi-methanol solvate (38% yield, mp = 103–105°C). Found: C, 68.7; H, 5.9; N, 22.7. Calc. for $C_{14}H_{14}N_4 \cdot 0.5MeOH$: C, 68.7; H, 6.0; N, 22.1%. MS 238 (M+). (The constitution of the ligand is also confirmed by the structures of complexes **1** and **2**.)

Metal complexes of p-XBPZ

In most cases, the complexes were obtained by mixing solutions of the appropriate, hydrated metal halide or nitrate salt (AR or reagent grade) and *p*-XBPZ in 1:2 mole ratio (*ca* 0.08 mmol in metal salt) in hot ethanol. A 1:1 mol ratio of *p*-XBPZ and metal salt was used in the preparation of $Co(p\text{-XBPZ})(NCS)_2$ and a 3:1 ratio was employed for $Co(p\text{-XBPZ})X_2$ (X = Cl, Br, I, NO_3), $Ni_2(p\text{-XBPZ})_3(NO_3)_4$ and $Ni(p\text{-XBPZ})Br_2$, with a mixed ethanol/2,2-dimethoxypropane solvent system being used for the nickel bromide complex. Solutions of the metal thiocyanates were prepared metathetically from the stoichiometric amounts of the appropriate metal nitrate and sodium thiocyanate in ethanol followed by removal of the sodium nitrate. The solid complexes which separated on slow concentration of the solutions at room temperature were collected, washed with a small amount of the solvent used for the reaction and air-dried.

Analytical data (Microanalytical Laboratory, Imperial College) are given in Table 1.

Crystallography

Crystal data. For $Co(p\text{-XBPZ})(NO_3)_2$ (**1**): $C_{14}H_{14}CoN_6O_6$, $M = 421.2$, orthorhombic, space group *Pbca*, $a = 14.878(4)$, $b = 13.883(2)$, $c = 17.288(3)$ Å, $U = 3570.9(13)$ Å^3, $Z = 8$, $D_c = 1.567$ Mg m^{-3}, μ(Mo-K_α) = 1.006 mm^{-1}, $\lambda = 0.71073$ Å, $F(000) = 1720$. Violet block, crystal dimensions 0.20 × 0.34 × 0.40 mm.

For $Cd_2(p\text{-XBPZ})_3(NCS)_4$ (**2**): $C_{23}H_{21}CdN_8S_2$, $M = 586.0$, triclininic, space group $P\bar{1}$, $a = 9.1177(9)$, $b = 9.784(2)$, $c = 15.4728(14)$ Å, $\alpha = 90.038(10)$, $\beta = 105.549(7)$, $\gamma = 111.489(11)^\circ$, $U = 1229.8(3)$ Å^3, $Z = 2$, $D_c = 1.583$ Mg m^{-3}, μ(Mo-K_α) = 1.086 mm^{-1}, $\lambda = 0.71073$ Å, $F(000) = 590$. Colourless plate, crystal dimensions 0.10 × 0.33 × 0.40 mm.

Data collection and processing

Siemens P4/PC diffractometer, ω-scan method ($4.66 < 2\theta < 45^\circ$ for **1**, $4.5 < 2\theta < 50^\circ$ for **2**), graphite-monochromated Mo-K_α radiation, room temperature. For compounds **1** and **2** 2336 and 4339 independent reflections, respectively, were measured; 1710 [$|F_o| > 4\sigma(|F_o|)$] and 3928 [$|F_o| > 4\sigma(|F_o|)$] were considered observed and were corrected for Lorentz and polarization factors.

Structure analysis and refinement

Both structures were solved by the heavy-atom method. All non-hydrogen atoms were refined anisotropically. The hydrogen atoms were idealized (C—H 0.96 Å), assigned isotropic thermal parameters, $U(H) = 1.2_{eq}(C)$, and allowed to ride on their parent carbon atoms. Refinements were by full-matrix least-

Table 1. Analytical data for the compounds formed by **I** (= L)

Complex	Colour	Analysis (%)[a] C	H	N
$MnL_2Cl_2 \cdot H_2O$	Pale pink	54.3(54.2)	4.7(4.9)	18.1(18.1)
MnL_2Br_2	Pale pink	48.4(48.7)	4.2(4.1)	16.0(16.2)
$CoLCl_2$	Deep blue	45.1(45.7)	3.8(3.8)	14.8(15.2)
$CoLBr_2$	Deep blue	36.6(36.8)	2.8(3.1)	12.2(12.3)
$CoLI_2$	Prussian blue	30.8(30.5)	2.5(2.6)	10.2(10.2)
$CoL(NCS)_2$	Deep blue	46.4(46.5)	3.2(3.4)	20.1(20.3)
$CoL(NO_3)_2$	Violet	39.9(39.9)	3.0(3.4)	19.7(20.0)
$NiLBr_2$	Deep blue	36.7(36.8)	2.8(3.1)	12.0(12.3)
$NiL_2(NCS)_2$	Green	55.1(55.3)	4.4(4.3)	21.3(21.5)
$Ni_2L_3(NO_3)_4$	Green	46.7(46.7)	3.9(3.9)	20.1(20.7)
$CuLCl_2$	Dark green	45.3(45.1)	4.0(3.8)	15.7(15.0)
$CuLBr_2$	"Black"[b]	36.2(36.4)	2.9(3.1)	12.0(12.1)
$CuL(NO_3)_2$	Blue	39.8(39.5)	3.3(3.3)	19.4(19.7)
$ZnLCl_2$	White	44.4(44.5)	3.7(3.8)	14.3(15.0)
$ZnLBr_2$	White	36.2(36.3)	2.8(3.0)	11.7(12.1)
$ZnLI_2$	White	30.4(30.2)	2.7(2.5)	9.7(10.1)
$CdLCl_2$	White	40.0(39.9)	3.2(3.4)	13.2(13.3)
$CdLBr_2$	White	33.1(32.9)	2.6(2.8)	11.1(11.0)
$CdLI_2$	White	28.2(27.8)	2.2(2.3)	9.3(9.3)
$Cd_2L_3(NCS)_4$	White	47.0(47.1)	3.7(3.6)	18.9(19.1)
$CdL(NO_3)_2$	White	35.2(35.4)	2.9(3.0)	17.2(17.7)

[a] Calculated values are given in parentheses.

[b] This compound is "black" in the bulk state, but gives a very dark khaki–green "streak" when smeared on a white surface.

Table 2. Selected bond lengths (Å) and angles (°) for **1**

Co—N(18)	2.044(4)	Co—O(25)	2.047(3)
Co—O(19)	2.048(3)	Co—N(1)	2.067(4)
Co—O(21)	2.302(4)	Co—O(23)	2.309(3)
N(18)—Co—O(25)	111.39(14)	N(18)—Co—O(19)	94.04(14)
O(25)—Co—O(19)	138.14(14)	N(18)—Co—N(1)	94.40(14)
O(25)—Co—N(1)	104.76(13)	O(19)—Co—N(1)	105.81(14)
N(18)—Co—O(21)	152.5(2)	O(25)—Co—O(21)	91.88(14)
O(19)—Co—O(21)	58.43(13)	N(1)—Co—O(21)	93.56(14)
N(18)—Co—O(23)	89.66(14)	O(25)—Co—O(23)	58.66(12)
O(19)—Co—O(23)	90.19(13)	N(1)—Co—O(23)	163.13(13)
O(21)—Co—O(23)	90.30(13)		

squares on F^2 to give: for **1**, $R_1 = 0.0433$, $wR_2 = 0.0950$; for **2**, $R_1 = 0.0337$, $wR_2 = 0.0858$. The maximum and mean shift/errors in the final refinement were 0.005 and 0.001, respectively, for **1** and 0.002 and 0.000 respectively, for **2**, and the maximum and minimum residual electron densities in the final ΔF map were 0.245 and -0.250 e Å^{-3}, respectively, for **1** and 0.871 and -0.959 e Å^{-3}, respectively, for **2**. Computations were performed using the SHELXTL-PC system version 5.03 [7]. Important bond lengths and angles for compound **1** are listed in Table 2 and those for compound **2** are given in Table 3.

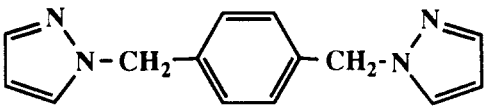
Spectroscopy

Spectroscopic measurements were made as described previously[8].

RESULTS AND DISCUSSION

Our principal objective in the present work was the synthesis of crystalline complexes of **I** so that its capacity for forming extended arrays could be determined by single crystal X-ray diffraction methods. Ligand **I** readily gave a range of solid compounds with the halides, nitrates or thiocyanates of Mn^{II}, Co^{II}, Ni^{II}, Cu^{II}, Zn^{II} and Cd^{II} (Table 1). In most cases the products isolated had the stoichiometry ML_2X_2 even when the reactants employed were in a 2:1 or 3:1 L:M mole ratio, but a few compounds of the types $M_2L_3X_4$ or ML_2X_2 were also formed.

Despite the range of compounds prepared, it proved difficult to obtain crystals of the appropriate quality for single crystal X-ray study, but in two cases, $Co(p\text{-XBPZ})(NO_3)_2$ (**1**) and $Cd_2(p\text{-XBPZ})_3(NCS)_4$ (**2**), this was achieved and their structures are discussed below. Some further, more limited, information about the coordination geometry of the metal ions in the other complexes was obtained by spectroscopic methods



I

Table 3. Selected bond lengths (Å) and angles (°) for **2**

Cd—N(28)	2.272(3)	Cd—N(31)	2.282(3)
Cd—N(1)	2.386(3)	Cd—N(27)	2.453(3)
Cd—N(10)	2.497(3)	Cd—S(30)#1	2.7384(9)
N(28)—Cd—N(31)	171.89(10)	N(28)—Cd—N(1)	88.93(10)
N(31)—Cd—N(1)	94.81(10)	N(28)—Cd—N(27)	81.22(10)
N(31)—Cd—N(27)	91.53(10)	N(1)—Cd—N(27)	90.72(9)
N(28)—Cd—N(10)	83.78(10)	N(31)—Cd—N(10)	103.64(10)
N(1)—Cd—N(10)	85.90(9)	N(27)—Cd—N(10)	164.68(9)
N(28)—Cd—S(30)#1	95.35(8)	N(31)—Cd—S(30)#1	82.82(7)
N(1)—Cd—S(30)#1	165.21(7)	N(27)—Cd—S(30)#1	103.90(7)
N(10)—Cd—S(30)#1	80.52(7)		

Symmetry transformations used to generate equivalent atoms: #(1) $-x+1, -y+1, -z+1$.

and this is summarised after the discussion of the X-ray results.

Structure of $Co(NO_3)_2$(p-XBPZ) (**1**)

The X-ray structure of $Co(NO_3)_2$(*p*-XBPZ) (**1**) confirms the 1 : 1 stoichiometry and reveals a *catena*-structure, wherein octahedrally coordinated cobalt centres are linked *via cis*-coordinated *p*-XBPZ ligands (Fig. 1). The nitrate groups are bonded in bidentate fashion but, consistent with their small 'bite' angle [58.4(1) and 58.7(1)° at N(22) and N(26), respectively], the geometry at Co is severely distorted. Whereas the Co—N distances to the two pyrazole groups are similar [2.044(4) and 2.067(4) Å to N(18) and N(1) respectively], subtending an angle of 94.4° at cobalt, there is a marked asymmetry in the Co—O bond lengths for each nitrate. The bonds *trans* to N(1) and N(18) are significantly longer, by *ca* 0.25 Å, than those *trans* to the oxygen atoms (Table 2).

Analysis of the *p*-XBPZ ligand conformation reveals a skewed relationship between the pyrazole and *p*-xylyl rings, with mean torsional twists about the N(5)—C(6) and C(6)—C(7) bonds of 22 and 51° and about C(10)—C(13) and C(13)—N(14) of 21 and 81°, respectively. Accompanying this geometry is a noticeable enlargement from tetrahedral of the angle at C(6) and C(13) to *ca* 114° in each case, indicating an element of strain in the polymer chain. This is further demonstrated by a bowing of the *p*-xylyl spacer, with the C(6)—C(7) and C(10)—C(13) bonds subtending an angle of *ca* 12°.

The polymer chain propagates *via* a *c*-glide to produce zigzag chains that extend in the *c*-direction (Fig. 2). Adjacent chains in the crystallographic *b*-direction pack in register with each other ("V in V") to form pseudo-sheets. Adjacent "sheets" are offset so as to produce an approximately antiphase relationship

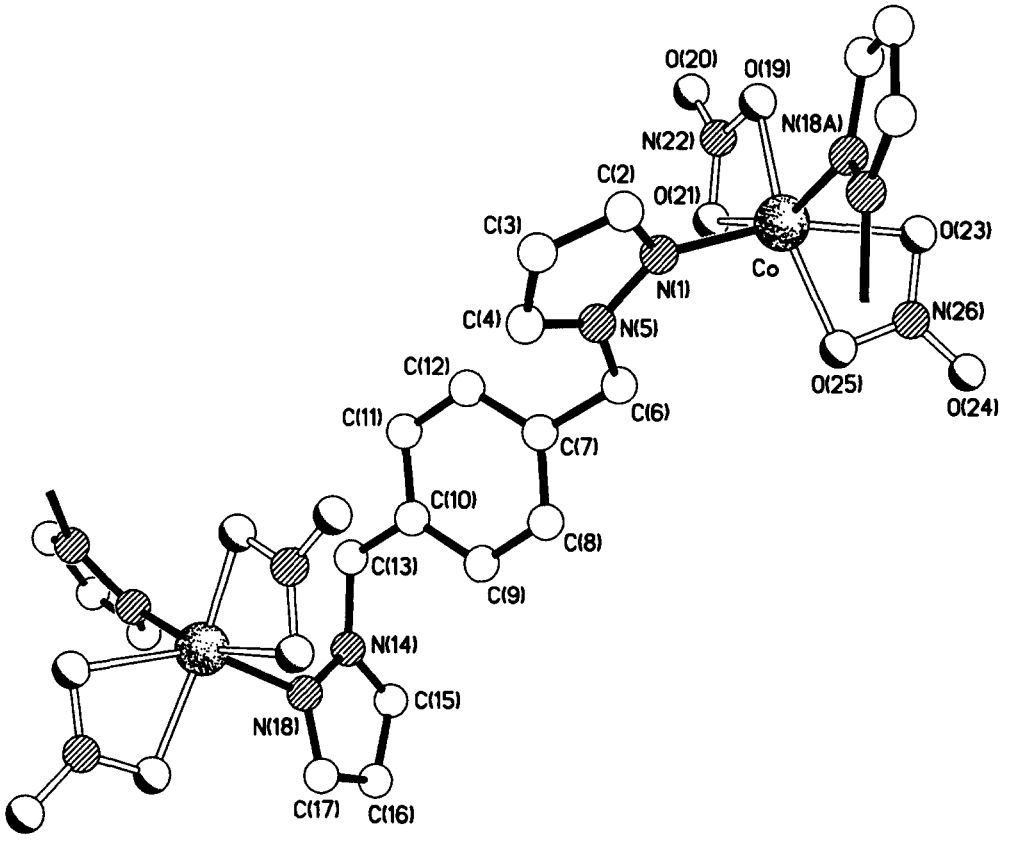


Fig. 1. The coordination geometry about Co in the structure of **1** showing also the form of the *p*-XBPZ ligand binding between adjacent Co centres.

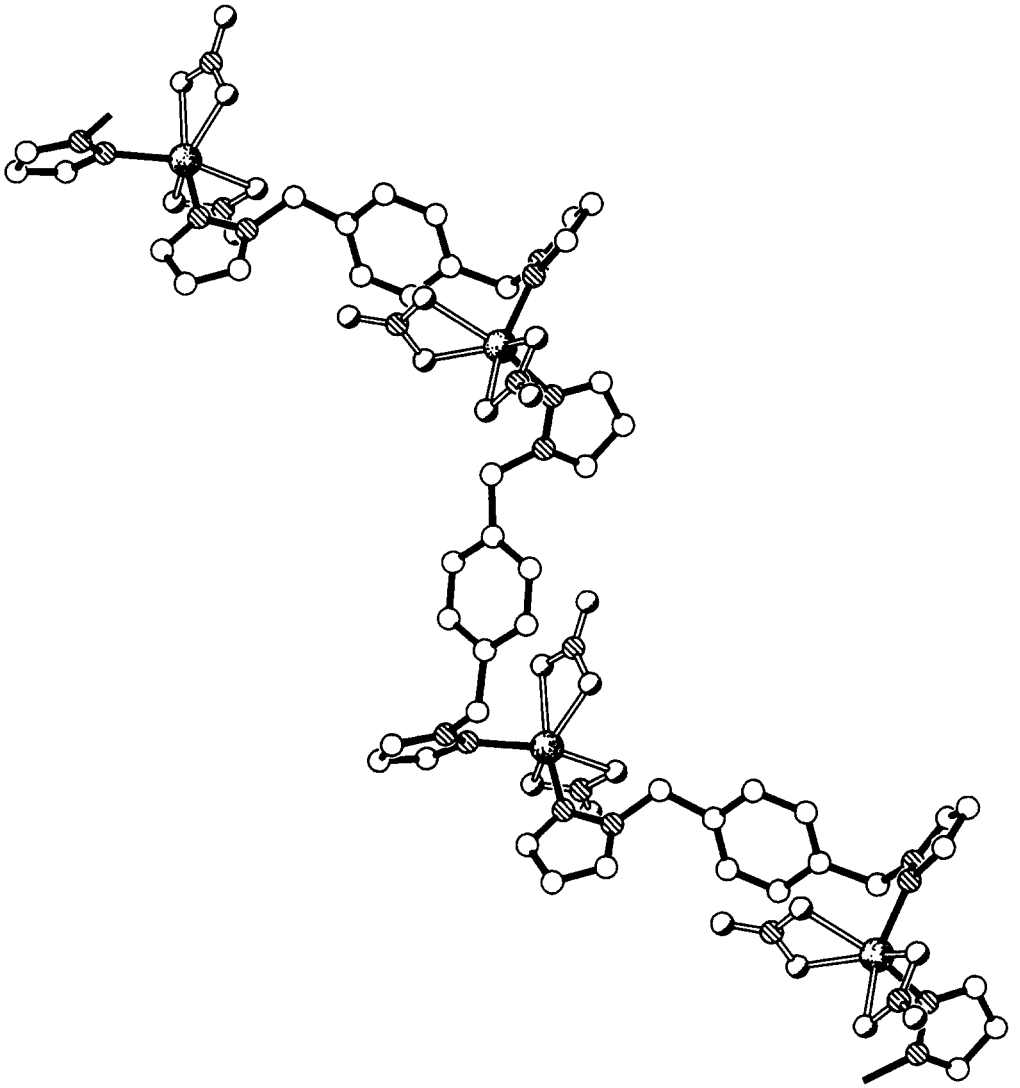


Fig. 2. Part of the polymer chain structure adopted by **1** in the solid state.

when viewed down the *a*-direction. There appear to be no important inter-chain interactions other than normal van der Waals.

Structure of $Cd_2(NCS)_4$(p-XBPZ)$_3$ (**2**)

The X-ray analysis of $Cd_2(NCS)_4$(*p*-XBPZ)$_3$ (**2**) (Fig. 3) shows the coordination environment about the cadmium atom to be essentially square pyramidal with the basal sites occupied by two *trans*-disposed independent isothiocyanate ligands and by two nitrogen atoms, one from each of two *p*-XBPZ ligands. The axial site is occupied by a nitrogen atom of a third *p*-XBPZ ligand. Approaching the "vacant" octahedral site at a noticeably longer distance (2.74 Å) is the S atom of a symmetry-related NCS group.

Within the basic square pyramid, the angles at Cd are in the ranges 81.2(1)–103.6(1) and 164.7(1)–174.9(1)° (Table 3). The Cd—N distances fall into three distinct groups: the longest are those to the *trans*-disposed pyrazole nitrogen atoms [2.453(3) and 2.497(3) Å], of intermediate length, 2.386(3) Å, is that to the axial pyrazole N atom, whilst the shortest distances are to the two *trans*-isothiocyanates.

With the exception of one of the NCS groups [that associated with N(31) and S(33)] the remaining ligands serve to link the Cd centres to create a polymeric array. One linkage in this process is the formation of two thiocyanate bridges between pairs of

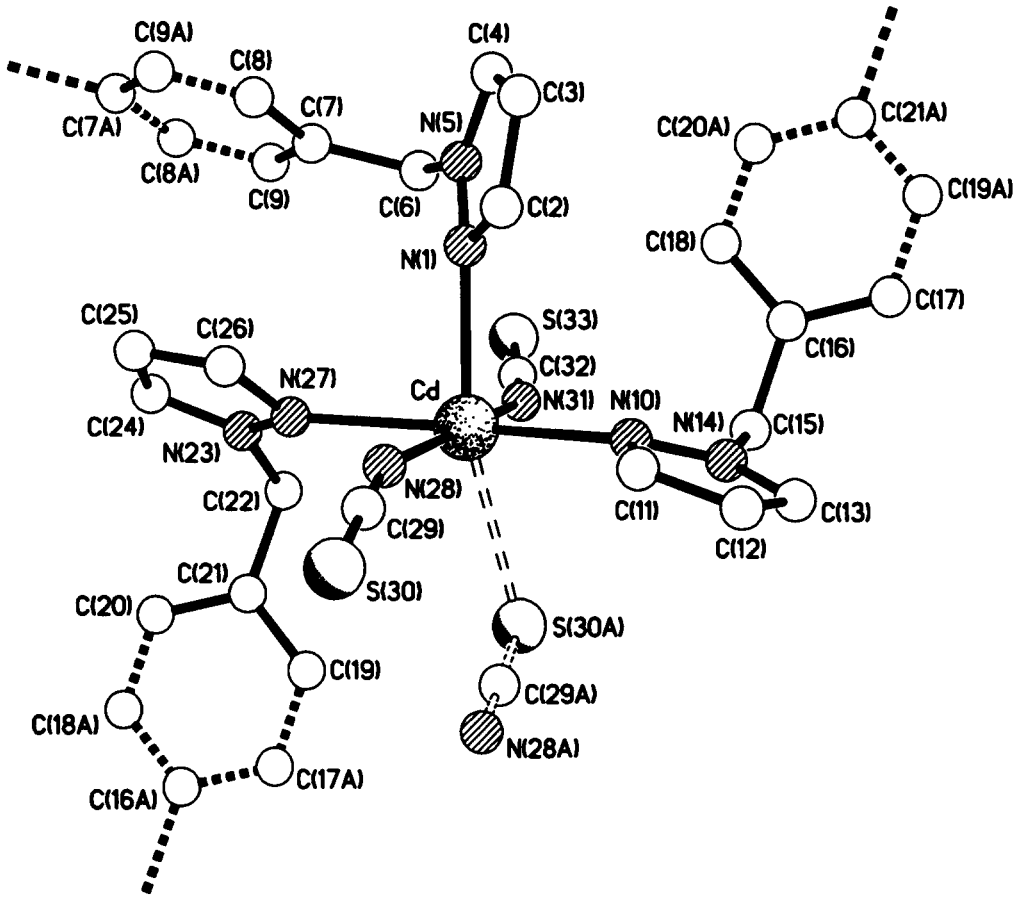


Fig. 3. The square-pyramidal coordination geometry at Cd in **2**, showing also the approach of a symmetry-related NCS ligand to the "vacant" coordination site.

C_i symmetrically related Cd atoms (Fig. 4). The associated non-bonded Cd···Cd separation is 5.81 Å.

Although the complex has a 2 : 3 Cd : *p*-XBPZ stoichiometry, there are only two crystallographically independent types of *p*-XBPZ ligand (A and B). Each of these plays a different role in generating the overall polymer structure. Pairs of A-type ligands bridge lattice-translated Cd centres to form extended ladder-like tapes as depicted in Fig. 4. Type B ligands then cross-link adjacent tapes to form the two-dimensional polymeric array illustrated in Fig. 5; this array extends in the 011 plane.

In forming this array the *p*-XBPZ ligand adopts two distinctly different comformations, both of which again differ from that observed in the structure of **1**. Within the ladder-like tapes the pyrazole and *p*-xylyl rings are in an "open-book" conformation with the

coordinated nitrogen atoms *anti*-disposed with respect to each other. The cross-linking ligands (type B) are C_i symmetric, with the pyrazole and *p*-xylyl rings being approximately orthogonal; the mean torsional twist about the N(5)—C(6) bond is *ca* 77°.

Spectroscopic studies

The electronic spectra of the deep blue compounds Co(*p*-XBPZ)X_2 (X = Cl, Br, I, NCS) in the solid state are characteristic [9] of a "tetrahedral" MN_2X_2 coordination geometry, showing (Table 4) three strong, overlapping bands in the range 6000–9000 cm^{-1} [transitions to components of $^4T_1(F)$] and a strong, multicomponent band in the visible region [transitions to components of $^4T_1(P)$]. The electronic spectrum of Ni(*p*-XBPZ)Br_2 (Table 4) also indicates a tetrahedral geometry.[9] For the compounds Co(*p*-XBPZ)Cl_2 and Zn(*p*-XBPZ)Cl_2 further evidence [10] for tetrahedral coordination geometry is afforded by their low frequency IR spectra, which have ν(M—Cl) bands at 330 and 305 cm^{-1} for M = Co and at 313 and 294 cm^{-1} for M = Zn. [Our instrumental low-frequency limit of 250 cm^{-1} precluded reliable assignment of the analogous ν(M—Br) and ν(M—I) bands in the other complexes of this type.] However, in the absence of full X-ray characterization, we cannot determine whether the *p*-XBPZ ligand connects these tetrahedrally coordinated metal centres into chains or individual rings, as we have made a number of examples of both of those structure types with "extended reach" O-donor [1f,11] or S-donor [12] ligands.

As expected from the results of the X-ray study, the electronic spectrum of Co(*p*-XBPZ)$(NO_3)_2$ (**1**) is typical of distorted octahedral coordination geometry about Co^{II}. A basically octahedral geometry is also clearly indicated by the electronic spectra of Ni(*p*-XBPZ)$_2(NCS)_2$ and Ni_2(*p*-XBPZ)$_3(NO_3)_4$ (Table 4). From its IR spectrum, the former of these two complexes contains N-bonded non-bridging thiocyanates [ν(CN) 2077 cm^{-1}] and it is likely that the *p*-XBPZ ligand serves to bridge *trans*-Ni(*p*-XBPZ)$_2(NCS)_2$ units into a sheet polymer.

The X-band EPR spectra of polycrystalline samples of Mn(*p*-XBPZ)$_2Cl_2\cdot H_2O$ and Mn(*p*-XBPZ)$_2Br_2$ show the presence of very pronounced zero-field splitting (Fig. 6). They are of the type found for simple Mn^{II} compounds containing tetragonally distorted octahedral MnN_4X_2 chromophores, where N represents a ligand such as 4-methylpyridine [13], so we conclude that they comprise arrays of *trans*-MnN_4X_2 (X = Cl or Br) units linked into sheets by the bridging capacity of the *p*-XBPZ ligand. Interestingly, the Mn···Mn distances in such arrays are sufficient to avoid any significant magnetic interaction between the Mn centres, which would lead to loss of the EPR spectral fine structure, as found for short bridges such as halide bridges.[14]

The X-band EPR spectra of polycrystalline samples of Cu(*p*-XBPZ)X_2 (X = Cl, NO_3) are of the axial type with $d_{x^2-y^2}$ ground state; the g values are g_{xy} = 2.057 and g_z = 2.271 for the chloride and g_{xy} = 2.059 and g_z = 2.304 for the nitrate. For both compounds the g_{xy} and g_z bands are very clearly resolved indicating that, as with the manganese(II) complexes referred to above, the bridging action of the *p*-XBPZ ligand separates the copper centres sufficiently to avoid any significant magnetic interaction between them. The EPR spectrum of a powdered sample of Cu(*p*-XBPZ)Br_2, however, simply gave a broad band centred on g_{eff} = 2.13 suggesting that bromide bridges are present in this case.

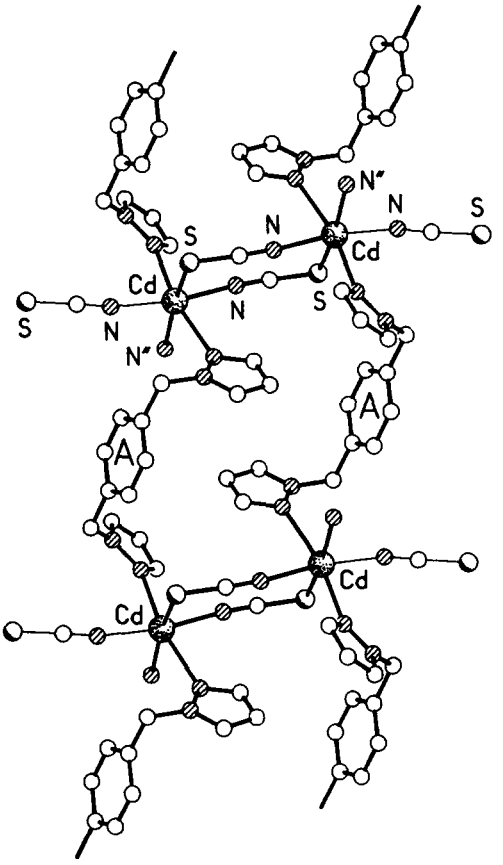


Fig. 4. Part of the ladder-like "tapes" of molecules in **2**, the "rungs" being formed by pairs of NCS bridges and the "uprights" by type A *p*-XBPZ ligands.

In summary, the results of this work show the ability of the *p*-XBPZ ligand to form both linear and sheet polymers. However, the X-ray studies additionally revealed an absence of a consistent conformational relationship between the pyrazole and *p*-xylyl rings and this renders it difficult reliably to predict the type of networks that may be constructed using this ligand as a bridging unit.

Acknowledgements—We thank the BBSRC for a post-doctoral fellowship (to S.M.) and the EPSRC for equipment.

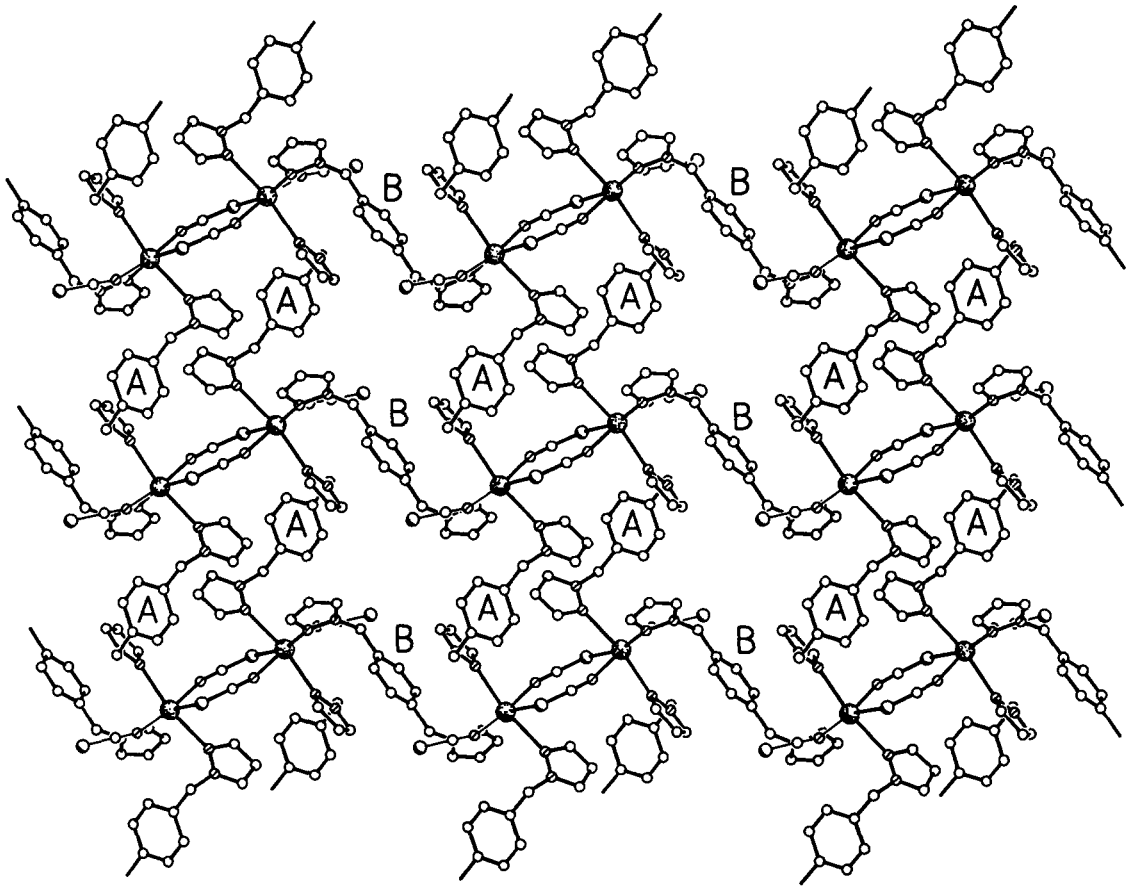


Fig. 5. Part of one of the two-dimensional polymer sheets formed by **2** in the solid state showing the cross-linking of the ladder-like tapes by type B *p*-XBPZ ligands.

Table 4. Electronic spectra (cm^{-1})[a] for some complexes formed by **I** (= L)

$CoLCl_2$	6410, 7410, 9260sh, 17,300
$CoLBr_2$	6250sh, 7350, 8850sh, 16,750
$CoLI_2$	5880sh, 6990, 8400, 16,100
$CoL(NCS)_2$	9090br,[b] 18,200
$CoL(NO_3)_2$	8660, 9570sh, 15,250w,sh, 19,500
$NiLBr_2$	~6900br, 10,300, 11,400sh, 17,700
$NiL_2(NCS)_2$	9900, 16,000, 25,600
$Ni_2L_3(NO_3)_4$	9130br, 16,100, 25,800
$CuLCl_2$	15,350[c]
$CuLBr_2$	15,150[d]
$CuL(NO_3)_2$	14,000, 17,400sh

[a] By reflectance method.
[b] Broad band, components not clearly resolved.
[c] Band asymmetric to higher energy.
[d] Overlapping with strong, parity-allowed absorption to high energy.

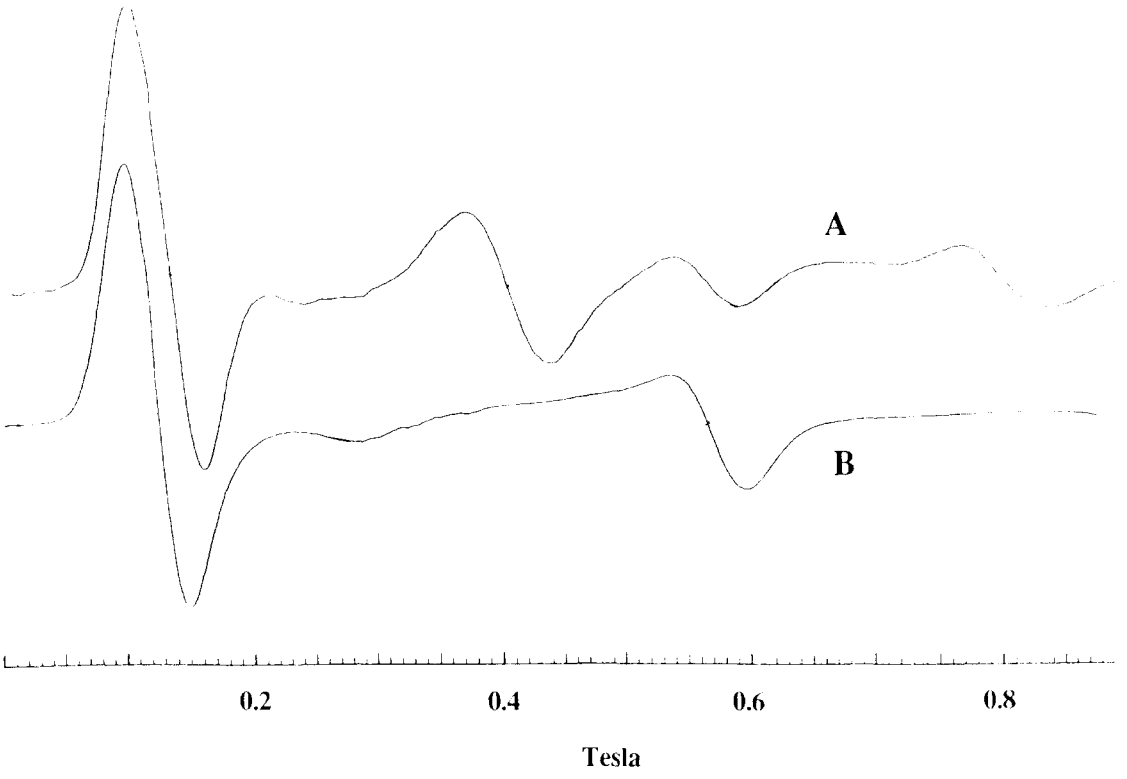


Fig. 6. X-band EPR spectra of polycrystalline: (A) $Mn(p\text{-}XBPZ)_2Cl_2 \cdot H_2O$; (B) $Mn(p\text{-}XBPZ)_2Br_2$.

REFERENCES

1. For lead-in references to various design strategies see: (a) M. Fujita, Y. J. Kwon, O. Sasaki, K. Yamaguchi and K. Ogura, *J. Am. Chem. Soc.* 1995, **117,** 7287; (b) S. R. Batten, B. F. Hoskins and R. Robson, *J. Am. Chem. Soc.* 1995, **117,** 5385; (c) S. R. Batten, B. F. Hoskins and R. Robson, *Angew. Chem., Int. Ed. Eng.* 1995, **34,** 820; (d) B. F. Hoskins, R. Robson and N. V. Y. Scarlett, *Angew. Chem., Int. Ed. Eng.* 1995, **34,** 1203; (e) T. Soma and T. Iwamoto, *Chem. Lett.* 1995, 271; (f) G. A. Doyle, D. M. L. Goodgame, S. P. W. Hill, S. Menzer, A. Sinden and D. J. Williams, *Inorg. Chem.* 1995, **34,** 2850; (g) D. M. L. Goodgame, S. Menzer, A. M. Smith, and D. J. Williams, *Angew. Chem., Int. Ed. Eng.* 1995, **34,** 574, and refs therein.
2. (a) R. W. Gable, B. F. Hoskins, and R. Robson, *J. Chem. Soc., Chem. Commun.* 1990, 1677; (b) L. R. MacGillivray, S. Subramanian, and M. J. Zaworotko, *J. Chem. Soc., Chem. Commun.* 1994, 1325; (c) D. M. L. Goodgame, S. Menzer, A. T. Ross, and D. J. Williams, *J. Chem. Soc., Chem. Commun.* 1994, 2605; (d) M. Fujita, Y. J. Kwon, S. Wahizu and K. Ogura, *J. Am. Chem. Soc.*, 1995, **117,** 7287.
3. (a) M. Fujita, F. Ibukuro, H. Hagihara and K. Ogura, *Nature*, 1994, **367,** 720; (b) M. Fujita, F. Ibukuro, K. Yamaguchi and K. Ogura, *J. Am. Chem. Soc.* 1995, **117,** 4175; (c) A. F. Williams and B. Brequet, *Angew. Chem., Int. Ed. Eng.* 1995, **34,** 582.
4. P. J. Stang, D. H. Cao, S. Saito and A. M. Arif, *J. Am. Chem. Soc.* 1995, **117,** 6273, and refs therein.
5. E.g. M. Fujita, S. Nagao and K. Ogura, *J. Am. Chem. Soc.* 1995, **117,** 1649.
6. A. T. Baker, J. K. Crass, M. Maniska and D. C. Craig, *Inorg. Chim. Acta* 1995, **230,** 225.
7. G. M. Sheldrick, SHELXTL, Version 5.03, University of Göttingen, Germany, 1995.
8. L. H. Carrad, D. M. L. Goodgame, S. P. W. Hill and D. J. Williams, *J. Chem. Soc., Dalton Trans.* 1994, 859.
9. D. M. L. Goodgame and M. Goodgame, *Inorg. Chem.* 1965, **4,** 139.
10. K. Nakamoto, *Infrared and Raman Spectra of Inorganic and Coordination Compounds*, 3rd edn. Wiley, New York, 1977, pp. 317–324, and refs therein.
11. D. M. L. Goodgame, S. P. W. Hill, A. M. Smith and D. J. Williams, *J. Chem. Soc., Dalton Trans.* 1994, 859.
12. Z. Atherton, D. M. L. Goodgame, D. A. Katahira, S. Menzer and D. J. Williams, *J. Chem. Soc., Chem. Commun.* 1994, 1423.
13. R. D. Dowsing, J. F. Gibson, M. Goodgame and P. J. Hayward, *J. Chem. Soc. (A)* 1969, 187.
14. R. D. Dowsing, J. F. Gibson, D. M. L. Goodgame, M. Goodgame and P. J. Hayward, *Nature* 1968, **219,** 1037.

Pergamon

PII: S0277-5387(96)00473-1

Polyhedron Vol. 16, No. 10, pp. 1689–1691, 1997
Copyright © 1997 Elsevier Science Ltd
Printed in Great Britain. All rights reserved
0277-5387/97 $17.00+0.00

Metal substitution reaction in the cluster $(\mu\text{-H})_2Fe_3(\mu_3\text{-Se})(CO)_9$—IV.† Crystal and molecular structure of $[Fe_2W_2(\mu_3\text{-Se})_2(\mu_3\text{-CO})(\mu\text{-CO})(CO)_5(\eta^5\text{-}C_5H_5)_2]$

Sergei N. Konchenko,* Alexander V. Virovets and Nina V. Podberezskaya

Institute of Inorganic Chemistry, Siberian Division of RAS, Acad. Lavrentyev str. 3, Novosibirsk 630090, Russia

(Received 20 August 1996; accepted 20 September 1996)

Abstract—The reaction of $[(\mu\text{-H})_2Fe_3(\mu_3\text{-Se})(CO)_9]$ with $[CpW(CO)_3]_2$ (Cp = η^5-C_5H_5) has been reinvestigated. In addition to tetrahedral heterometal clusters described previously the minor product $[Fe_2W_2(\mu_3\text{-Se})_2(\mu_3\text{-CO})(\mu\text{-CO})(CO)_5Cp_2]$ has been isolated. Its crystal and molecular structure has been determined by X-ray methods. © 1997 Elsevier Science Ltd. All rights reserved.

Keywords: iron; selenium; tungsten; heterometal clusters; synthesis; crystal and molecular structure.

The reactions of $(\mu\text{-H})_2Fe_3(\mu_3\text{-X})(CO)_9$ (X = Se, Te) with $[CpM(CO)_3]_2$ (M = Mo, W) have been determined previously to result in the heterometal cluster complexes $(\mu\text{-H})Fe_2M(\mu_3\text{-X})(CO)_8Cp$ and $FeM_2(\mu_3\text{-X})(CO)_7Cp_2$ (X = Se, Te) as the major products.[1–4] However, in addition to these there have been detected some minor products which have not been isolated yet. In this work one of the minor products has been obtained and its structure has been determined by X-ray analysis.

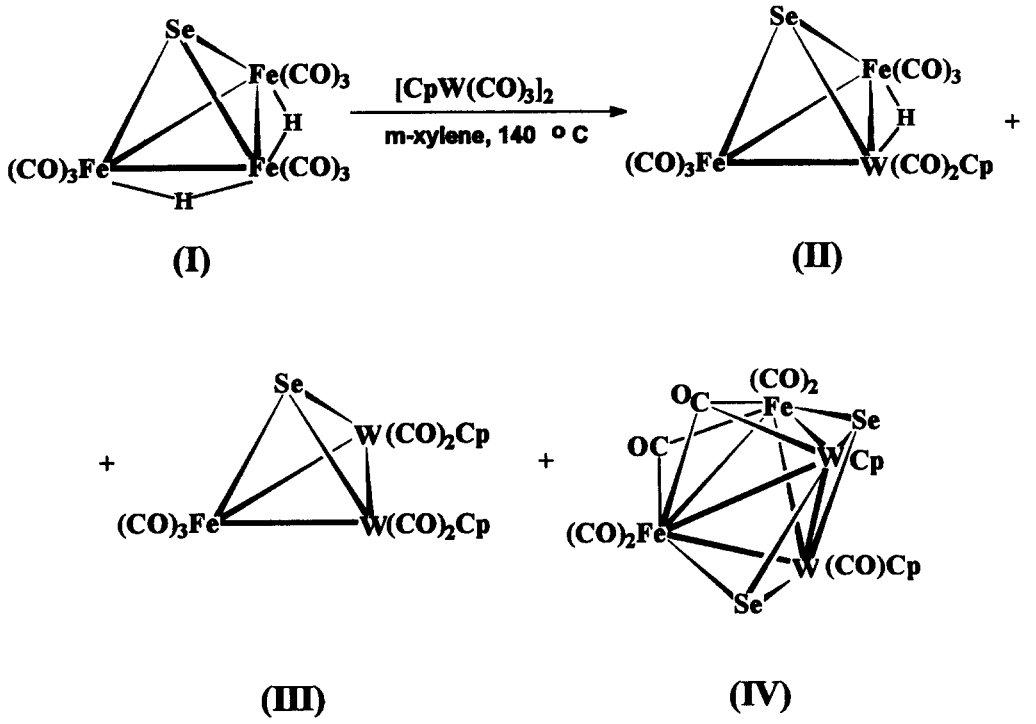
EXPERIMENTAL

The reaction of $(\mu\text{-H})_2Fe_3(\mu_3\text{-Se})(CO)_9$ (**I**) with $[CpW(CO)_3]_2$ was carried out as described previously [1]. After separation of the $(\mu\text{-H})Fe_2W(\mu_3\text{-Se})(CO)_8Cp$ (**II**) and $FeW_2(\mu_3\text{-Se})(CO)_7Cp_2$ (**III**) complexes the residue on the top of the chromatography column was eluted with benzene, resulting in an additional brown fraction which was collected and evaporated *in vacuo*. The solid thus obtained was extracted with toluene and an excess of pentane was layered on the solution. Two days later several crystals of $[Fe_2W_2(\mu_3\text{-Se})_2(\mu_3\text{-CO})(\mu\text{-CO})(CO)_5Cp_2]$ (**IV**) were isolated.

X-ray structure determination

The composition and the structure of **IV** were determined by X-ray analysis from an octahedrally shaped single crystal obtained by a slow diffusion of pentane to a toluene solution of the cluster. Crystallographic data: $C_{17}H_{10}Fe_2O_7Se_2W_2$, Mol. wt 963.57, orthorhombic, $Pna2_1$, $a = 13.276(1)$, $b = 11.999(1)$, $c = 12.990(2)$ Å, $V = 2069.3(4)$ Å^3, CAD-4 diffractometer, λ(Mo-K_α), room temperature, $\theta/2\theta$ scans with $V_{2\theta} = 2.5$–$19.5°$ min^{-1} up to $2\theta_{max} = 50°$. A total of 1895 independent reflections (1802 without systematic absences) was measured. An absorption correction was applied by using the azimuthal scan curve around the (222) reflection. The structure was solved by direct methods (SHELXS-86 [5]) and refined by the full-matrix least-squares method on F^2 (SHELXL-93 [6]).

*Author to whom correspondence should be addressed.
†See Refs [1–3] for the previous communications.



Scheme 1.

The hydrogen atoms were refined in the rigid-body approximation (C—H 0.96 Å). Final R values: $R(F) = 0.0259$, $wR(F^2) = 0.0584$ for 1629 $F_{hkl} > 4\sigma(F)$, $R(F) = 0.0310$, $wR(F^2) = 0.0594$ for all 1802 reflections used. Atomic coordinates and thermal parameters are deposited in the Cambridge Crystallographic Database.

RESULTS AND DISCUSSION

Synthesis

It was previously mentioned [2,3] that the reactions of $(\mu\text{-H})_2Fe_3(\mu_3\text{-X})(CO)_9$ with $[CpM(CO)_3]_2$ (X = Se, Te; M = Mo, W) can be described as a cooperative decomposition of the initial complexes following a spontaneous condensation of active intermediate products to more stable heterometal cluster compounds. The set of the products now determined for the reaction of **I** with $[CpW(CO)_3]_2$ (Scheme 1) allows one to propose possible ways of intermediate fragmentation of the initial complexes.

Probably, the intermediate thermal decomposition derivatives of **I** are the products of a stepwise mononuclear iron carbonyl group elimination, i.e. the unstable diiron selenide and/or monoiron selenide carbonyl complexes.

For $[CpW(CO)_3]_2$ one can propose two activated pathways: a dissociation of the dimer complexes to mononuclear derivatives and an elimination of two carbonyl groups resulting in a highly reactive $[CpW(CO)_2]_2$ complex containing a triple W≡W bond.

If this is really so, the cluster **II** can be considered as the product of the addition of the mononuclear tungsten intermediate complexes to the diiron selenide species. Compounds **III** and **IV** can be described as the products of a sequential addition of the monoiron selenide species [for example, $(CO)_3FeSe$] to a triple W≡W bond following an elimination of some CO ligands.

Crystal and molecular structure of **I**

The molecular structure is shown in Fig. 1. Selected bond distances are given in the Fig. 1 caption. Cluster **IV** is revealed to be isostructural with $[Fe_2Mo_2(\mu_3\text{-}Te)_2(\mu_3\text{-}CO)(\mu\text{-}CO)(CO)_5Cp]$ (**V**), taking into account the difference between $Pna2_1$ and $Pn2_1a$ cell settings [7–9]. A molecule of **IV** is also very similar to a molecule of **V**. It contains the Fe_2W_2 tetrahedron and two μ_3-Se atoms on the FeW_2 faces, the μ_3-carbonyl ligand on the Fe_2W face and the μ-carbonyl on the Fe—Fe edge (Fig. 1). In **IV** as well as in **V** the μ_3-CO ligand is coordinated non-symmetrically: Fe—C bonds are rather longer than the W—C (Mo—C) bond. The μ-CO ligand is coordinated symmetrically in both compounds. No short non-bonding contacts have been found in the molecular crystal packing of **IV**.

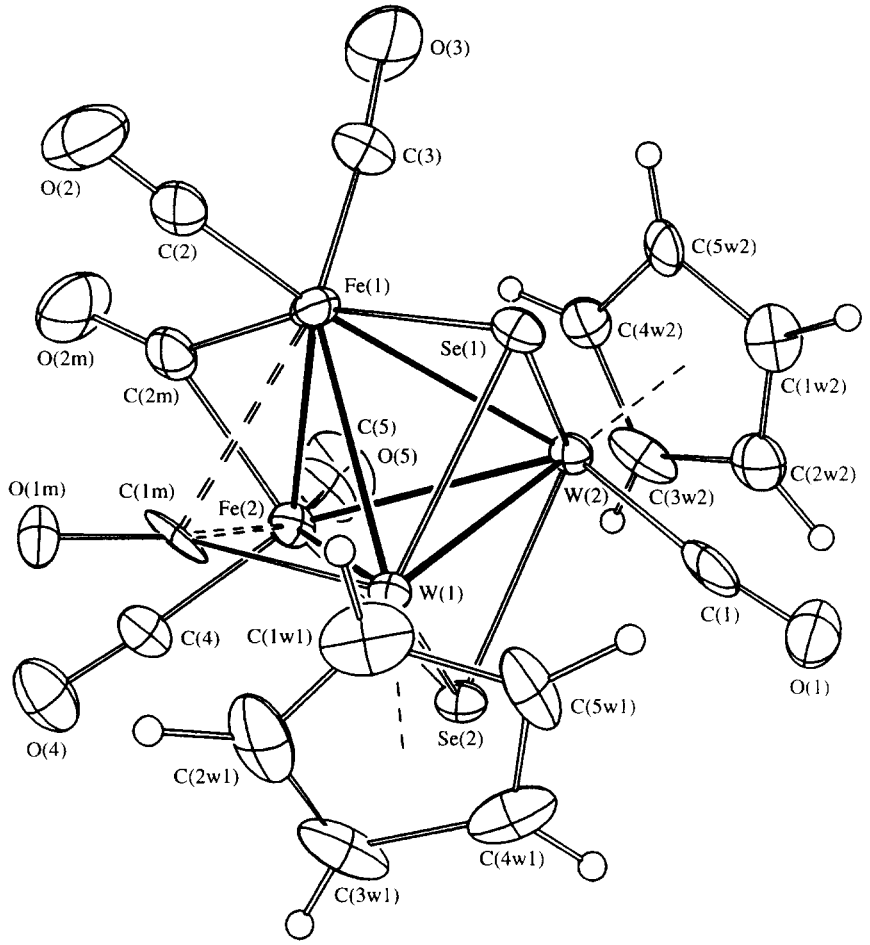


Fig. 1. The molecule of **IV** (40% probability ellipsoids). Cluster core is emphasized by solid lines. Long C(1m)—Fe(1) and C(1m)—Fe(2) bonds are shown by dashed lines. Selected bond distances (a): W(1)—W(2), 2.804(1), W(1)—Se(1), 2.503(2), W(1)—Se(2), 2.505(2), W(1)—Fe(1), 2.813(3), W(1)—Fe(2), 2.812(2), W(1)—C(1M), 1.97(2), W(1)—C(1W1), 2.35(2), W(1)—C(2W1), 2.31(2), W(1)—C(3W1), 2.33(2), W(1)—C(4W1), 2.35(2), W(1)—C(5W1), 2.35(2), W(2)—Se(1), 2.498(2), W(2)—Se(2), 2.503(2), W(2)—Fe(1), 2.805(3), W(2)—Fe(2), 2.790(3), W(2)—C(1), 1.97(3), W(2)—C(1W2), 2.29(2), W(2)—C(2W2), 2.31(2), W(2)—C(3W2), 2.38(2), W(2)—C(4W2), 2.38(2), W(2)—C(5W2), 2.36(2), Fe(1)—Fe(2), 2.449(4), Fe(1)—Se(1), 2.314(3), Fe(2)—Se(2), 2.316(3), Fe(1)—C(1M), 2.49(2), Fe(1)—C(2M), 1.93(2), Fe(1)—C(2), 1.79(2), Fe(1)—C(3), 1.76(2), Fe(2)—C(1M), 2.49(2), Fe(2)—C(2M), 1.95(2), Fe(2)—C(4), 1.77(2), Fe(2)—C(5), 1.77(2).

REFERENCES

1. S. N. Konchenko, A. V. Virovets, S. V. Tkachev, V. I. Alekseev and N. V. Podberezskaya, *Polyhedron*, 1996, **15,** 1221.
2. S. N. Konchenko, A. V. Virovets, S. V. Tkachev and N. V. Podberezskaya, *Polyhedron*, **16,** 707.
3. S. N. Konchenko, A. V. Virovets, S. V. Tkachev and N. V. Podberezskaya, *Polyhedron*, **16,** 1549.
4. S. N. Konchenko, A. V. Virovets, V. A. Varnek, S. V. Tkachev, N. V. Podberezskaya and V. A. Maksakov, *Zh. Strukt. Khim.*, 1996, **37,** 337 (in Russian).
5. G. M. Sheldrick, *Acta Cryst.*, 1990, **A46,** 467.
6. G. M. Sheldrick, *Acta Cryst.*, 1993, **A49** (Suppl.), C53.
7. L. E. Bogan Jr, T. B. Rauchfuss and A. L. Reingold, *J. Am. Chem. Soc.*, 1985, **107,** 3843.
8. X. Yang, J. Huang and J. Huang, *Jiegou Huaxue, Chinese J. Struct. Chem.*, 1985, **4,** 50.
9. X. Yang, J. Huang and J. Huang, *Jiegou Huaxue, Chinese J. Struct. Chem.*, 1987, **6,** 257.

Pergamon

PII: S0277-5387(96)00472-X

Polyhedron Vol. 16, No. 10, pp. 1693–1699, 1997
Copyright © 1997 Elsevier Science Ltd
Printed in Great Britain. All rights reserved
0277-5387/97 $17.00+0.00

Structure of six- and seven-membered cyclic-β-diketones and their metal(II) complexes

Margarita Kashchieva,[a] Neyko Stoyanov,[b] Venelin Enchev,[c] Stoyan Minchev,[d] Panayot R. Bontchev[e] and Mariana Mitewa[e]*

[a]Department of Chemistry, Higher Pedagogical Institute, 9700 Shoumen, Bulgaria

[b]Institute of Chemical Technology and Biotechnology, 7200 Razgrad, Bulgaria

[c]Institute of Organic Chemistry, Bulgarian Academy of Sciences, 1113 Sofia, Bulgaria

[d]Department of Chemistry, Economic University, 9000 Varna, Bulgaria

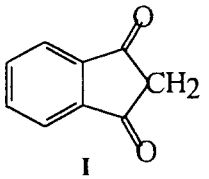
[e]Department of Chemistry, University of Sofia, 1126 Sofia, Bulgaria

(Received 19 August 1996; accepted 20 September 1996)

Abstract—Two new copper(II) complexes with physiologically active ligands containing both pyridine ring and cyclic β-diketones with different ring members were obtained with the metal to ligand ratio 1 : 2. The structure and coordination mode of both complexes were studied using IR and EPR methods. The AM1 method was applied for calculating the structure of 5,7-dioxo-6-(2-pyridyl)-6,7-dihydro-5H-dibenzo (a,c)cycloheptene and its Zn^{II} complex. It is shown that the structure of both complexes is a tetragonal one and the coordination is realized *via* the hydroxy O and N of the pyridine ring. © 1997 Elsevier Science Ltd. All rights reserved.

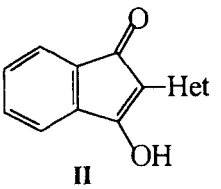
Keywords: metal(II) complexes; cyclic-β-diketones; structure; AM1 calculations; EPR.

The physiological activity of many heterocyclic derivatives of 1,3-indandione (**I**), namely phthalones (**II**), is well documented and some of them (especially pyrophthalone **III**) are used as therapeutic agents.[1–3] They exhibit mainly anticoagulant [4–6] but also antiinflammatory and analgesic activity [7,8]. In addition they have proved to be excellent complexating agents [9–15].



I

In the present paper the results obtained on the Cu^{II} complexes with the related ligands containing six- and seven-membered rings, namely 2-(2-pyridyl)-2,3-dihydrophenalene-1,3-dione (**IV**, L_1) and 5,7-dioxo-6-(2-pyridyl)-6,7-dihydro-5H-dibenzo(a,c)cycloheptene (**V**, L_2) are reported, as it is shown that the physiological activity of the cyclic β-diketones depends strongly on the ring dimension. It is proved that five- and six-membered ring compounds **III** and **IV** are anticoagolants, while compound **V** on the contrary shows coagulant action [16].



II

EXPERIMENTAL

Synthetic procedures

Synthesis of 2-(2-*pyridyl*)-2,3-*dihydrophenalene*-1,3-*dione* (**IV**, L_1). The compound was obtained using the literature method [17] with some modification in the

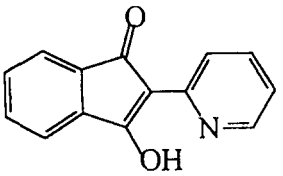
*Author to whom correspondence should be addressed.

procedure. For the purpose the anhydride (25 g, 0.126 mol) of naphthalic acid (finely ground), anhydrous $ZnCl_2$ (12 g, 0.088 mol), freshly finely ground, and 2-methylpyridine (14 g, 0.15 mmol) were mixed and refluxed (230°C) with stirring for 10 h. After cooling the reaction mixture was ground finely and mixed with 200 cm^3 1% HCl solution. After filtration the residue was washed repeatedly with water and heated again with 200 cm^3 25% HCl solution to boiling. The reaction mixture was filtered off and the extract dried with anhydrous Na_2SO_4, then evaporated to dry residue and recrystallized from dioxane. M.p. 273–274°C, yield 24%.

Anal. data for $C_{18}H_{11}NO_2$ (mol. wt 273.28): Calc. (Found): C, 79.1 (78.7); H, 4.1 (4.3); N 5.1 (5.4)%.

^{1}H NMR [$CDCl_3$, 300 K, δ (ppm), J (Hz)]: 19.8 (OH); 9.68 (d, 1H, J = 9, H-11); 8.62 (dd, 2H, J = 7.3; 1.0, H-4); 8.15 (dd, 1H, J = 7.1, H-14); 8.10 (dd, 2H, J = 8.2, 1.0, H-6); 8.01 (ddd, 1H, J = 9.0, 7.3; 1.8, H-12); 7.71 (t, 2H, J = 7.8, H-5); 7.24 (ddd, 1H, J = 7.0, 5.8, 1.0, H-13).

^{13}C NMR [DMSO-d_6, 350 K, δ(ppm)]: 180.91 (C-2); 153.72 (C-9); 142.11 (C-11); 137.41 (C-13); 132.40 (C-5); 131.30 (C-7); 128.63 (C-8); 127.64 (C-4); 126.83 (C-3); 126.48 (C-6); 122.93 (C-14); 119.40 (C-12); 102.80 (C-1).



III

Synthesis of 5,7-*dioxo*-6-(2-*pyridyl*)-6,7-*dihydro*-5H-*dibenzo*(*a*,*c*)*cycloheptene* (**V**, L_2). The compound was obtained as described in the literature [18] by reflux at 240°C of α-picoline diphenic anhydride and anhydrous $ZnCl_2$ for 10 h. The dark green product was washed with dilute HCl solution and water and recrystallized from ethanol. M.p. 201–202°C, yield 30%.

Anal. data for $C_{20}H_{13}NO_2$ (mol.wt 299.31) Calc. (Found): C, 80.2 (79.9); H, 4.4 (4.5); N, 4.7 (4.2)%.

^{1}H NMR [$CDCl_3$, 360 K, δ (ppm), J (Hz)]: 18.53 (1H, OH); 8.24 (tt, 1H, J = 9.7, 1.4, 1.0, H-11); 8.09 (dd, 1H, J = 5, 0.5, H-14), 7.89 (d, 2H, J = 7.3, H-4,4′); 7.76 (dtd, 1H, J = 8, 1.8, 1.6, 1.7, H-13); 7.65 (d, 2H, J = 7.5, H-7,7′); 7.47 (5d, 4H, J = 8, 1.5, H-5,5′, 6,6′); 7.04 (dtd, 1H, J = 6.5, 1, H-12).

Synthesis of Cu^{II} *complexes.* Ethanolic solutions (1×10^{-3} M) of the ligands were mixed with a water solution of $Cu(NO_3)_2$ (5×10^{-3} M) in 1 : 2 metal-to-ligand ratio and then 0.1 M NaOH solution was added to the reaction mixture to give pH 5. Brown and green precipitates were formed with L_1 and L_2, respectively. After filtration the complexes were washed repeatedly with ethanol and dried over P_4O_{10} for a week.

Anal. data for $Cu(L_1)_2$ ($C_{36}H_{20}N_2O_4Cu$) (mol. wt 608.08): Calc. (Found): C, 71.1 (70.9); H, 3.3 (3.6); N, 4.6 (4.9); Cu, 10.4 (10.0)%.

Anal. data for $Cu(L_2)_2$ ($C_{40}H_{24}N_2O_4Cu$) (mol. wt 660.15): Calc. (Found): C, 72.8 (72.4); H, 3.7 (3.9); N, 4.2 (4.3); Cu, 9.6 (9.8)%.

Analytical procedures

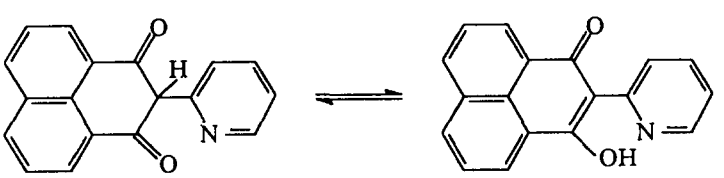
Nitrogen was determined by the Kjeldahl method (treatment for 12 h). Copper was determined complexometrically at pH 8 (indicator murexide) after ashing the samples and dissolving the residue in 2 HNO_3 : 1 H_2O solution.

Physical measurements

The solid-state IR spectra were obtained using a "Specord 75 IR" (Carl-Zeiss, Jena; 4000–400 cm^{-1} range) and this of L_2 in $CHCl_3$ solution—on an FT-IR spectrometer "Bruker Vector 22". The NMR spectra were taken on a "Bruker DRX 250" FT-NMR spectrometer (TMS as internal reference) and the EPR spectra—on an X-band spectrometer "ERS-220" (Carl-Zeiss, Jena; g-marker DPPH).

Quantum-chemical calculations

The semiempirical AM1 method [19] was used during the study of the different tautomeric forms of 5,7-



IV (L_1)

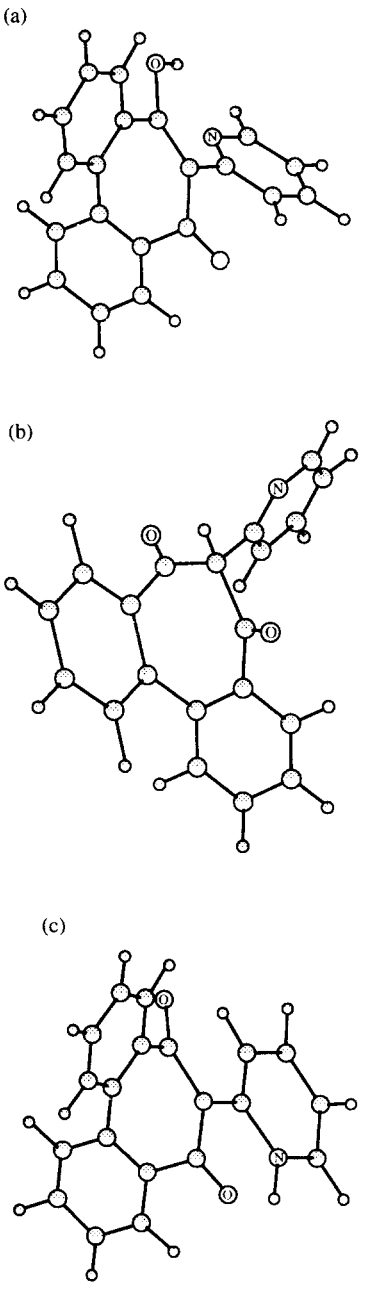


Fig. 1. AM1-calculated structures of the three tautomeric forms of 5,7-dioxo-6-(2-pyridyl)-6,7-dihydro-5H-dibenzo (a,c)cycloheptene (V, L_2): A (hydroxy), B (dioxo) and C (dioxo-imino).

dioxo-6-(2-pyridyl)-6,7-dihydro-5H-dibenzo(a,c) cycloheptene and its Zn^{II} complex. The AM1 parameters of the zinc atom reported by Dewar and Merz [20] were used. AM1 calculations were performed using the program GAMESS [21]. The geometry of the tautomers and the complex were completely optimized without any geometrical restrictions using algorithms [22,23] implemented in GAMESS for geometry searches. The gradient optimizations were terminated when the gradient length over all optimized

Table 1. AM1-calculated heats of formation H_f (kcal mol^{-1}) and dipole moments μ (in D) for tautomers of L_2 (Fig. 1) and its Complex $Zn(L_2)_2$ (Fig. 2). ΔH_f indicates relative stabilities of the three tautomeric forms of L_2

Compound	Tautomers	H_f	ΔH_f	μ
L_2	A	36.69	0.00	0.96
	B	37.60	0.91	2.97
	C	38.64	1.95	3.16
$Zn(L_2)_2$		128.05		0.73

parameters was reduced to 1.0×10^{-4} Hartree Bohr^{-1}.

RESULTS AND DISCUSSION

Calculated structure of 5,7-dioxo-6-(2-pyridyl)-6,7-dihydro-5H-dibenzo(a,c)cycloheptene

The 2,3-dihydrophenalene-1,3-dione part of L_1 being a conjugated aromatic system is expected to be planar, while the structure of the seven-membered ring system 5,7-dioxo-6-(2-pyridyl)-6,7-dihydro-5H-dibenzo(a,c)cycloheptene should be nonplanar. For that reason AM1 calculations were performed in order to obtain structural information and to elucidate the most stable tautomer in solution. L_2 may exist in three tautomeric forms, A (hydroxy), B (dioxo) and C (oxo-imino), as shown in Fig. 1. It can be seen from results listed in Table 1 that AM1 calculations predict the "hydroxy" tautomer A as most stable. As it was expected strong deviations from planarity were observed for the seven-membered ring (Fig. 1). The torsional angle between both benzene rings in the biphenyl fragment of L_2 was calculated to be 42.2°. This result is very close to AM1 calculated (40.6°) [24] and experimental value determined in the vapor phase (44.4°) in biphenyl [25].

The comparison of the calculated and experimentally obtained ($CHCl_3$ solution) IR spectrum of L_2 (Table 2) proved the existence of L_2 in its "hydroxy" tautomeric form (A).

Structure of metal(II) complexes with L_1 and L_2

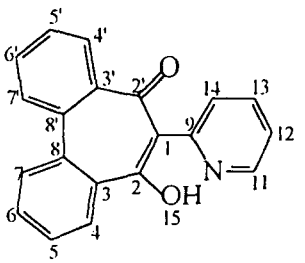
The analytical data obtained show the formation of Cu^{II} complexes with an M : L ratio of 1 : 2.

Structural information concerning the coordination mode and geometry of the complexes was obtained using IR and EPR spectroscopic data. In Table 2 selected IR data for both the free ligands and their Cu^{II} complexes are given.

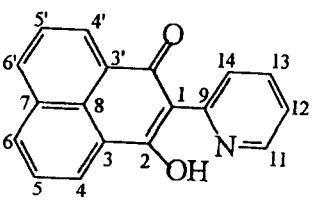
The IR data for the $Cu(L_1)_2$ complex indicate coordination *via* the hydroxy group as the ν_{OH} is not observed in the complex spectrum. On the other side two $\nu_{C=O}$ bands were observed. One of them is with higher frequency similar to other Cu^{II} complexes with cyclic β-diketones,[11] thus indicating the presence of an uncoordinated C=O group. The second $\nu_{C=O}$ band with lower frequency is likely due to a C=O group engaged in hydrogen bonding.

It seems very likely that chelation with the hydroxy group and the pyridine nitrogen atom (**VI**) is realized.

The EPR data obtained are in agreement with this supposition. The powder sample of the complex shows a two-component anisotropic EPR spectrum both at low and ambient temperatures ($g_\parallel = 2.215$, $g_\perp = 2.067$). Such a spectrum with $g_\parallel > g_\perp$ is typical of a Cu^{II} complex with rhombic (or distorted tetrahedral) structure [26]. Additional information was obtained from the frozen HMPA solution spectrum of the complex. It also shows a two-component anisotropic spectrum with $g_\parallel = 2.291$ and $g_\perp = 2.072$. In this spectrum the parallel component exhibits a four-component hfs



V(L_2)



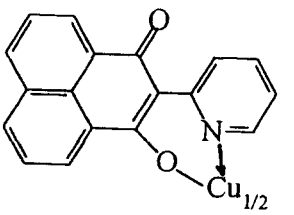


Table 2. Selected IR data (cm^{-1}) for the ligands and their Cu^{II} complexes (KBr disks); AM1 calculated values are in parentheses

Compound	ν_{OH}	$\nu_{C=O}$	$\nu_{C=C}$	$\nu_{skeletal}$ (seven-membered ring)	Aromatic system[a]
L_1	~3400 v.br.	~1620 sh; 1625	—		~1580 sh; 1560; 1540; 1490; 1380; 1370 sh
$Cu(L_1)_2$		1630; 1605	—	--	1570; 1510; 1490; 1410; 1380; 1340
L_2	~3400 v.br.	1640; ~1630	~1620 sh	1470; 1448	1595; 1585; 1565; 1545 br.; 1500; 1490
L_2[b]	—	1637	1613	1482; 1443	1596; 1562; 1541; 1496
	(3032)	(1832)	(1666)	(1510) (1465)	(1584) (1582) (1573) (1547)
$Cu(L_2)_2$	—	1620 br.	~1600 sh	1480; 1450 br	1550; 1430; 1400; 1375 br.

[a]Assignment according to Neiland and Kazen [9].
[b]$CHCl_3$ solution.

due to $^{63,65}Cu$ ($I = 3/2$, $A_{2,3}^{Cu} = 146$ Oe), while the perpendicular component shows a partially resolved shfs of five lines ($A^N \sim 14$ Oe) due to two ^{15}N ($I = 1$), thus confirming the coordination of two pyridine N atoms to Cu^{II} (coordination number 4).

EPR studies on the $Cu(L_2)_2$ complex in a broad temperature range (−160–40°C) also provided structural information (Table 3).

The polycrystalline sample data show significant temperature dependence. At low temperatures (−160 to −40°C) an isotropic EPR spectrum was obtained, showing a realization of tetrahedral structure for this 1:2, M:L complex. At higher temperatures (above −40°C) a two-component anisotropic EPR signal was observed, indicating a strong deviation from the regular structure.

In order to check the supposition for N-coordination solution EPR spectra of the $Cu(L_2)_2$ complex were recorded and the data obtained are shown in Table 4. All solution spectra exhibit three-component anisotropic signals, the only exception being the signal in acetonitrile (An, two-component anisotropy).* The g_3 ($g_\parallel$) component shows four-component hfs due to $^{63,65}Cu$ ($I = 3/2$) and the g_3 ($g_\perp$)—a partially resolved shfs due to two N atoms ($I = 1$) from the pyridine rings, thus confirming the coordination of the N atoms to Cu^{II}. Also at ambient temperature the chloroform spectrum of $Cu(L_2)_2$ ($g_{iso} = 2.082$) shows both four-component hfs due to $^{63,65}Cu$ ($I = 3/2$) ($A_{iso}^{Cu} = 82$ Oe) and five-component shfs due to 2 N atoms ($A^N = 12$ Oe).

The IR data available (Table 2) are in agreement with this supposition. In the $Cu(L_2)_2$ spectrum no band due to ν_{OH} is observed, while this at 1620 nm is ascribed to $\nu_{C=O}$ engaged in hydrogen-bonding.

It is also evident that no significant solvent effect on the EPR parameters is observed (Table 4, with the exception of An), although the solvents used ($CHCl_3$, DMSO and HMPA) possess quite different donor ability [27]. These data rule out the possibility of solvent coordination at the 5th and 6th sites (along the z-axis), indicating a significant steric hindrance of the ligand. All these experimental data suggest the realization of a distorted tetrahedral structure.

Table 3. EPR data for the $Cu(L_2)_2$ complex (powder sample) at different temperatures

T(°C)	$g_{iso} \pm 0.002$	$g_{II} \pm 0.002$	$g_\perp \pm 0.002$
−160	2.045	—	—
−120	2.042	—	—
−80	2.045	—	—
−40	2.045	—	—
0	(2.058)[a]	2.045	2.083
+40	(2.061)[a]	2.042	2.100

[a]Calculated according to the relation $g_{iso} = 2/3\, g_\perp + 1/3\, g_{II}$.

Since the AM1 method could not be used for calculating copper(II) complexes (no Cu parameters are available), the corresponding Zn^{II} complex was calculated although all attempts to synthesize the $Zn(L_2)_2$ complex failed. The structural data obtained are presented in Fig. 2 and Table 5. Not surprisingly, the calculated $Zn(L_2)_2$ structure proved to be tetrahedral, supporting the suggestion for a tetrahedral structure of the $Cu(L_2)_2$ complex. The dihedral angle O—Zn—O—C was calculated to be 113°. The bond lengths Zn—O and Zn—N were found to be 2.086 and 2.040 Å, respectively. Similar bond lengths (Zn—O 2.15 and Zn—N 2.03 Å) were determined for other Zn^{II} complexes with bidentate O, N-ligand using X-ray diffraction analysis [28], thus supporting the reliability of the structural data obtained using the AM1 method. It should be mentioned that a ligand-to-metal dative bond is formed as electron-density transfer from Zn to ligand was found.

Supplementary material. All structural data (bond lengths and angles) of both calculated structures are available on request.

*Evidently in this case the specific solvent effect is observed.

Acknowledgments—Financial support from Sofia University Foundation "Scientific Researches" (Project N 175/95) is greatfully acknowledged. We thank Dr S. Simova from Insti-

Table 4. EPR data for the frozen solutions of the $Cu(L_2)_2$ complex (−160°C) in different solvents

Solvent	g_{iso} (Calc.)[a]	$g_1 \pm 0.002$	$g_2 \pm 0.002$	$g_3 \pm 0.002$	$A^{Cu}_{2,3} \pm 2$ Oe	$A^{N} \pm 2$ Oe
$CHCl_3$	2.097	2.007	2.060	2.223	176	16
An	2.084	$g_\perp = 2.014$	$g_{II} = 2.223$		184	—
DMSO	2.101	2.016	2.063	2.223	166	12
HMPA	2.100	2.017	2.061	2.223	172	12

[a]According to the relation $g_{iso} = 1/3\, g_1 + 1/3\, g_2 + 1/3\, g_3$.
An ≡ Acetonitrile; DMSO ≡ dimethylsulfoxide; HMPA ≡ hexamethylphosphotriamide.

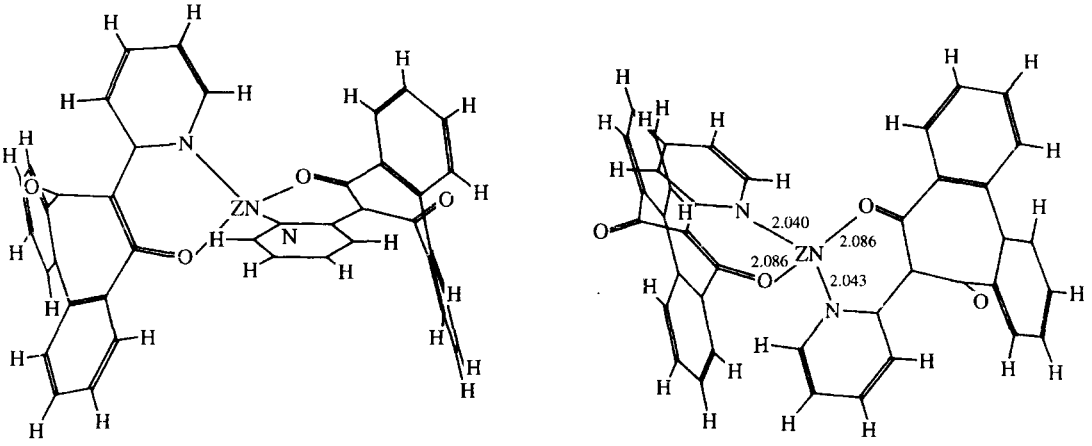


Fig. 2. AM1-calculated structure of complex $Zn(L_2)_2$. The bond distances Zn—O and Zn—N are in Å.

Table 5. Selected AM1 calculated structural parameters for L_2 (A form) and its Zn^{II} complex. Bond lengths are in Å, bond angles in °, Δ—differences between the corresponding parameters of the ligand and complex (for numbering of atoms see structure V)

Parameters	L_2	$Zn(L_2)_2$	Δ	Atom No.	Net L_2	Charge[a] $Zn(L_2)_2$
Bond lengths						
C(2')—O	1.234	1.233	−0.001	C(2)	0.19	0.36
C(2)—C(3)	1.471	1.493	0.022	C(1)	−0.25	−0.42
C(1)—C(2)	1.360	1.403	0.043	C(9)	0.03	0.20
C(1)—C(9)	1.472	1.438	−0.034	N(10)	−0.16	−0.24
C(9)—N(10)	1.361	1.371	0.010	O(15)	−0.25	−0.43
C(2)—O(15)	1.370	1.296	−0.074	Zn		0.72
Bond angles						
O(15)—C(2)—C(1)	125.0	127.1	2.1			
C(2)—C(1)—C(9)	124.4	126.1	1.7			
N(10)—C(9)—C(1)	119.3	122.3	3.0			
H—O(15)—C(2)	110.1					
Zn—O(15)—C(2)		126.4	6.3			

[a]Net atomic charges of the selected atoms are in e^-.

tute of Organic Chemistry, Bulgarian Academy of Sciences for recording and interpretation of the NMR spectra.

REFERENCES

1. D. C. Manley, A. Richardson, A. M. Stock, C. H. Tilford and E. D. Amstutz, *J. Org. Chem.*, 1958, **23,** 373.
2. M. Miloshev and B. Aleksiev, *Chem. Ber.*, 1969, **102,** 2869.
3. E. D. Amstutz and G. L. Kruger, U.S.A. Patent No. 2894952, 1959.
4. J. P. Solier and J. C. R. Gueguen, *Seancs Soc. Biol. Sec. Fil.*, 1974, **141,** 1007.
5. S. L. Sapiro, K. Gieger and L. Fredman, *J. Org. Chem.*, 1960, **25,** 1860.
6. B. Bourbon and A. Jules, English Patent No. 1033529, 1964.
7. J. Ploquin, L. Sparfel, G. le Baut, L. Welin, I. Y. Petit and N. Henry, *Chim Ther.*, 1973, 350.
8. G. le Baut, L. Sparfel, J. Ploquin, I. Y. Petit, N. Henry and L. Welin, *Bull. Soc. Pharm. de l'Quest*, 1973, **15,** 43.
9. O. I. Neiland and J. J. Kazen, *Khim. Geterotsikl. Soedin.*, 1975, 435; *Chem. Abstr.*, 1975, **83,** 78731.
10. J. R. Cook and D. F. Martin, *J. Inorg. Nucl. Chem.*, 1964, **26,** 571.
11. P. R. Bontchev, M. Mitewa, S. Minchev, M. Kashchieva and D. Mechandjiev, *J. Prakt. Chem.*, 1983, **325,** 803.
12. M. Mitewa, P. R. Bontchev, V. Enchev, S. Minchev and M. Kashchieva, *J. Prakt. Chem.*, 1985, **327,** 516.
13. M. Mitewa, P. R. Bontchev, M. Kashchieva, S. Minchev, V. Bardarov and G. Werner, *Polyhedron*, 1986, **5,** 1983.
14. M. Mitewa, P. R. Bontchev, E. Zhecheva, D. Mechandjiev, S. Minchev, M. Kashchieva and K. Kabassanov, *J. Prakt. Chem.* 1990, **32,** 99.
15. N. Stoyanov, M. Kashchieva, S. Minchev and M. Mitewa, *Synth. React. Inorg. Met-Org. Chem.*, 1996, **26,** 147.
16. M. Miloshev, B. Aleksiev, M. Nikolova and O. Angelova, *Pharmazie*, 1972, **27,** 520.
17. A. Taurins, *J. Prakt. Chem.* 1939, **153,** 177.
18. B. Aleksiev and M. Miloshev, *Pharmazie*, 1969, **24,** 291.
19. M. J. S. Dewar, E. G. Zoebish, E. F. Healy and J. J. P. Stewart, *J. Am. Chem. Soc.*, 1985, **107,** 3902.
20. M. J. S. Dewar and K. M. Merz, *Organometallics*, 1988, **7,** 522.
21. M. W. Schmidt, K. K. Baldridge, J. A. Boatz, S. T. Elbert, M. S. Gordon, J. H. Jensen, S. Koseki, N. Matsunaga, K. A. Nguyen, S. J. Su, T. L. Windus, M. Dupuis and J. A. Montgomery, *J. Comp. Chem.*, 1993, **14,** 1347.
22. J. Baker, *J. Comp. Chem.*, 1986, **7,** 385.
23. P. Gudot, G. Dive, V. H. Nguyen and J. M. Ghuysen, *Theor. Chim. Acta*, 1992, **82,** 189.
24. T.-H. Tang, M. Nowakowska, J. E. Guiller and T. G. Csizmalia, *J. Mol. Str. (Theochem.)*, 1991, **232,** 133.
25. A. Almenningen, O. Bastiansen, L. Fernholt, B. N. Cyvin, S. L. Cyvin and S. Samdal, *J. Mol. Struct.*, 1985, **128,** 59.
26. B. J. Hathaway and D. E. Billing, *Coord. Chem. Rev.*, 1970, **5,** 143.
27. V. Gutmann, *The Donor–Acceptor Approach to Molecular Interactions*. Plenum Press, New York, 1978.
28. J. M. Newman, C. A. Bear, T. W. Hambley and H. C. Freeman, *Acta Cryst.* 1990, **C46,** 44.

Pergamon

PII: S0277-5387(96)00466-4

Polyhedron Vol. 16, No. 10, pp. 1701–1706, 1997
Copyright © 1997 Elsevier Science Ltd
Printed in Great Britain. All rights reserved
0277-5387/97 $17.00+0.00

Synthesis and characterization of copper(II) coordination compounds with acyclovir: crystal structure of triaquabis [9-{(2-hydroxyethoxy)methyl}guanine] copper(II) nitrate(V) hydrate

Iztok Turel,[a]* Nataša Bukovec,[a] Margaret Goodgame[b] and David J. Williams[b]

[a] Faculty of Chemistry and Chemical Technology, University of Ljubljana, Aškerčeva 5, 1000 Ljubljana, Slovenia

[b] Department of Chemistry, Imperial College of Science and Technology, London SW7 2AY, U.K.

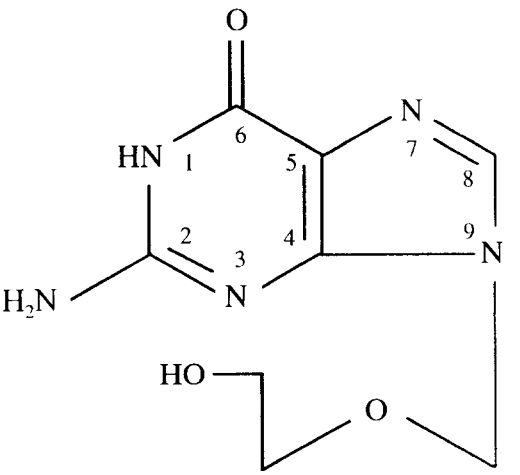
(Received 10 September 1996; accepted 18 September 1996)

Abstract—The coordination compounds $[Cu(acv)_2(H_2O)_3](NO_3)_2 \cdot H_2O$ (**I**) (acv = acyclovir) and $CuCl_2 \cdot acv$ (**II**) have been prepared. Different techniques (IR, electronic reflectance, ESR spectroscopy, thermal analysis, magnetic measurements) have been used to determine the properties of these compounds and also to elucidate the bonding in **II**. The molecular structure of **I** has been determined by X-ray crystallography and shows the coordination geometry at copper to be square pyramidal with two acv molecules bound through N-7 in *trans* basal positions, the other coordination sites being occupied by aqua ligands. The oxygen atom of the carbonyl group is not involved in intramolecular hydrogen bonding to the coordinated aqua ligands. There is a pattern of base-pair recognition between C_i symmetrically related molecules. A comparison of the properties of the new compounds (**I** and **II**) with previously isolated $[Cu(acv)_2(Cl)_2(H_2O)_2]$ (**III**) is also reported. © 1997 Elsevier Science Ltd. All rights reserved.

Keywords: 2′-deoxyguanosine analogue; acyclovir—antiherpes agent; copper(II) complexes; crystal structure; molecular recognition.

There is an increasing interest in the stereochemistry of nucleic acid component–metal ion interactions. The development of nucleoside analogues such as acv (Scheme 1) [1,2], which inhibits specific processes in herpes-infected cells, has encouraged the study of new compounds which may possess antiviral properties by affecting enzymes in infected cells. The majority of enzymes in infected and uninfected cells require metal ions for activity and this is one source of the potential antiviral properties in metal chelating agents [3].

The majority of our work is concerned with the copper(II) ion and we have already reported the crystal structure of **III** as well as that of Cu–acvmp (acvmp = acyclovir monophosphate) complex [4–6].



Scheme 1.

* Author to whom correspondence should be addressed. Fax: +386 61 1258 220; e-mail: iztok.turel@uni-lj.si

In the first of these compounds, $[Cu(acv)_2Cl_2(H_2O)_2]$, the copper(II) atom is bonded to two *trans* positioned acv ligands monodentately through N-7, the other two coordination sites being occupied by water molecules. Water molecules are hydrogen bonded to O-6. Two transversal bonds to Cl atoms are longer, thus forming distorted centrosymmetrical octahedral molecules [4,5]. In the other complex, $[Cu(acvmp)_2(H_2O)_2]\cdot H_2O$, the coordination geometry at copper is again slightly distorted octahedral [6]. The copper atom occupies an inversion centre and is coordinated to N-7 of the acvmp ligand, the oxygen of a water molecule and the oxygen of the phosphate group of an adjacent ligand molecule thus forming a polymeric structure.

Some platinum complexes with acv and its acetylated derivatives have also been reported [7,8].

Several copper(II) complexes of nucleotides, nucleosides and their analogues have also been examined by X-ray crystallography [9–17]. A variety of different coordination modes are found in these structures.

Here we report the crystal structure of the newly synthesized compound **I** which is distinctively different from **III**. The synthesis of **II** is reported and also a comparison of the physical and chemical properties of these compounds are given.

EXPERIMENTAL

Syntheses

Compound **I**. Copper(II) nitrate (0.215 g) was dissolved in distilled water and acv (0.100 g) was added slowly to the stirring solution. The green solution was kept at room temperature and after a few days green crystals were formed. The crystals were filtered off, washed and air dried.

Compound **II**. Copper(II) chloride dihydrate (0.152 g) was dissolved in absolute ethanol. After addition of acv (0.100 g) a green precipitate formed immediately. The precipitate was filtered, washed and air dried. The results were the same if methanol was used instead of ethanol.

Compound **III**. This was prepared as reported elsewhere [5].

Analyses and physical measurements

The analyses of carbon, hydrogen and nitrogen were carried out on a Perkin–Elmer 204C microanalyser.

Copper(II) ion was determined volumetrically using 0.010 M EDTA and Murexid indicator. Calculated (found) for **I**: C 27.1 (26.8); H 4.2 (4.3); N 23.7 (23.7); Cu 9.0 (9.3), and for **II**: C 26.7 (26.5); H 3.1 (3.2); N 19.5 (19.1); Cu 17.7 (17.3%). IR spectra were recorded in the solid state (KBr pellets), some samples were recorded on Nujol mulls between CsI windows on a Perkin–Elmer 1720X FT-IR spectrometer. Conditions: range 4000–220 cm^{-1}, resolution 2 cm^{-1}, number of scans 10. TG-DTG data were recorded in the temperature range from 25–500°C (300°C) in a stream of dry air on Mettler TA-3000 and TA-2000 thermobalances. Heating rate was 5°C/min. Reflectance spectra were recorded on a Beckman spectrophotometer D.K.2 in the range 300–2600 nm. Room temperature magnetic susceptibility measurements were carried out by a Sherwood Scientific balance, Cambridge Research Laboratory, England. *Q*-band ESR spectra were obtained with a Bruker ER 200D-SCR spectrometer and *X*-band ESR spectra with Varian E 12 spectrometer. All samples were measured as polycrystalline solids.

Crystallographic determination

A green crystal of dimensions $0.20\times0.30\times0.50$ mm^3 was used for the single-crystal determination. Data were collected on a Siemens P4/PC diffractometer with graphite-monochromated Mo-K_α radiation, using ω-scans ($3.0 < 2\theta < 50.0°$). 4815 independent reflections were measured, of which 4029 had $|F_o| > 3\sigma(|F_o|)$ and were considered to be observed. The data were corrected for Lorentz and polarization factors but not for absorption. The crystallographic parameters were as follows: $C_{16}H_{30}CuN_{12}O_{16}$, $M_r = 710.1$, triclinic, $a = 8.250(2)$, $b = 10.158(2)$, $c = 18.299(4)$ Å, $\alpha = 94.65(2)$, $\beta = 97.89(2)$, $\gamma = 113.95(2)°$, $V = 1372.1(4)$ Å^3, space group $P\bar{1}$, $Z = 2$, $D_c = 1.719$ g cm^{-3}, $\mu(Mo-K_\alpha) = 8.95$ cm^{-1}, $F(000) = 734$.

The structure was solved by direct methods and the non-hydrogen atoms were refined anisotropically. The positions of the hydroxy, amino and aqua hydrogen atoms were determined from a ΔF map and refined isotropically subject to N—H and O—H distance constraints. The positions of the remaining H atoms were idealized C—H = 0.96 Å, assigned isotropic thermal parameters $U(H) = 1.2\ U_{eq}(C)$ and allowed to ride on their parent carbon atoms. Refinement was by full-matrix least squares based on F to give $R = 0.0395$, $R_w = 0.073$ [$w^{-1} = \sigma^2(F) + 0.0004F^2$]. The mean and maximum shift/error ratios in the final refinement were 0.013 and 0.279, respectively, and the maximum and minimum residual electron densities in the final ΔF map were 0.47 and -0.37 e Å^{-3}, respectively.

Computations were carried out on a 386 PC using the SHELXTL PC program system [18]. Atomic coordinates, bond lengths and angles and thermal parameters have been deposited at the Cambridge Crystallographic Data Centre.

RESULTS AND DISCUSSION

Crystal structure of **I**

The copper(II) ions have a slightly distorted square-pyramidal coordination (*cf.* distorted octahedral in

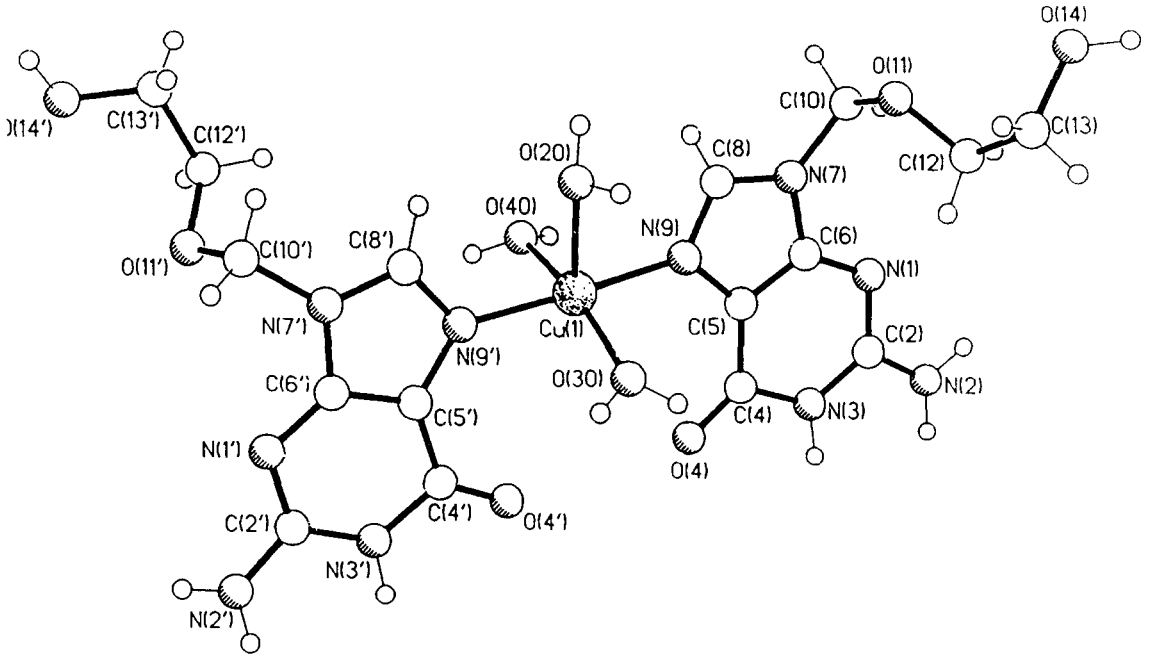


Fig. 1. View of compound **I** with atomic labelling. Note that crystallographic numbering is different from the conventional chemical numbering scheme.

III) (Fig. 1) with two acyclovir ligands bonded monodentately to copper(II) *via* N-7 in *trans* basal positions; Cu—N distances are 2.002(2) and 1.995(2) Å, respectively. The three other coordination sites are occupied by aqua ligands with Cu—O distances of 1.961(3) and 2.002(3) (basal) and 2.220(2) Å (axial). There is only a small departure from linearity for the N—Cu—N angle [177.7(1)°], the two *trans* aqua ligands representing the principal distortion from an ideal square-pyramidal geometry, the O(40)—Cu(1)—O(30) angle being 164.7(1)°. The Cu atom lies 0.12 Å above the mean plane of the four basal atoms in the direction of the axial aqua ligand. Table 1 gives selected bond lengths and bond angles of the compound.

The guanine rings are practically coplanar with a molecular torsion angle C(5)N(9)...N(9')C(5') of 0.3° and are in a *syn* conformation. They are both rotated by *ca* 70° out of the basal coordination plane thus precluding any intramolecular hydrogen bonding between the O(4) carbonyl groups and the coordinated aqua ligands. The closest approach of one of the aqua hydrogen atoms [on O(30)] to the carbonyl oxygen atoms [O(4)] is 2.67 Å. Both acyclic chains are folded with a *gauche* conformation.

The absence of any intramolecular hydrogen bonding is in striking contrast to the interactions observed in the majority of the related complexes [11–14,16].

Inspection of the packing of the molecules reveals a pattern of base-pair recognition with centrosymetrically related complexes hydrogen bonded *via* a series of donor–acceptor interactions (Fig. 2). These hydrogen-bonding interactions extend to include the acv hydroxyl groups to form tapes that propagate in the (101) direction in the crystals. Adjacent parallel and overlapping tapes are cross-linked by additional hydrogen bonds involving the aqua ligands, the included water molecules and the nitrate anions.

IR spectra

Previous work on similar compounds [5,19,20] permits us to assign some potentially informative bands. Thus, for free acv the reasonably pure C=O stretching vibration appeared at 1715 cm^{-1}, and the C—O of the acyclic chain at 1106 cm^{-1}, while the band at 1610 cm^{-1} is due essentially to the purine ring vibrations (Table 2). In compound **I** the shift of the C=O stretching vibration was very small and could be ascribed to hydrogen bonding of the carbonyl group. The very similar frequency found in compound **II** suggests a similar role of the carbonyl group in the structure.

In both compounds the shifts in the acyclic C—O and the purine ring vibrations are very small. Indeed, the order of the purine ring frequencies (acv > **I** > **II**) is the same as the order of the C=O frequencies, and may reflect changes in the coupling of these modes, as well as the direct effect of the coordination. The small changes in the C—O frequency are attributed to differences in conformation [21].

Thermal analysis

The thermal decomposition of compound **III** starts at approximately 100°C. The first stage of decompo-

Table 1. Selected bond lengths (Å) and angles (°)

Cu(1)—O(20)	2.220(2)	Cu(1)—O(30)	1.961(3)
Cu(1)—O(40)	2.002(3)	Cu(1)—N(9)	2.002(2)
Cu(1)—N(9′)	1.995(2)	N(1)—C(2)	1.320(4)
N(1)—C(6)	1.356(4)	C(2)—N(2)	1.334(4)
C(2)—N(3)	1.369(4)	N(3)—C(4)	1.404(4)
C(4)—O(4)	1.223(4)	C(4)—C(5)	1.418(4)
C(5)—C(6)	1.373(4)	C(5)—N(9)	1.390(4)
C(6)—N(7)	1.369(4)	N(7)—C(8)	1.360(4)
C(8)—N(9)	1.314(4)	N(1′)—C(2′)	1.335(4)
N(1′)—C(6′)	1.351(3)	C(2′)—N(2′)	1.328(4)
C(2′)—N(3′)	1.364(4)	N(3′)—C(4′)	1.398(4)
C(4′)—O(4′)	1.223(4)	C(4′)—C(5′)	1.420(4)
C(5′)—C(6′)	1.375(4)	C(5′)—N(9′)	1.394(4)
C(6′)—N(7′)	1.375(4)	N(7′)—C(8′)	1.362(4)
C(8′)—N(9′)	1.317(4)		

O(20)—Cu(1)—O(30)	94.4(1)	O(20)—Cu(1)—O(40)	100.8(1)
O(30)—Cu(1)—O(40)	164.7(1)	O(20)—Cu(1)—N(9)	90.6(1)
O(30)—Cu(1)—N(9)	90.6(1)	O(40)—Cu(1)—N(9)	90.7(1)
O(20)—Cu(1)—N(9′)	88.3(1)	O(30)—Cu(1)—N(9′)	91.5(1)
O(40)—Cu(1)—N(9′)	87.5(1)	N(9)—Cu(1)—N(9′)	177.7(1)
C(2)—N(1)—C(6)	112.7(2)	N(1)—C(2)—N(2)	120.3(3)
N(1)—C(2)—N(3)	123.3(3)	N(2)—C(2)—N(3)	116.4(3)
C(2)—N(3)—C(4)	125.6(3)	N(3)—C(4)—O(4)	121.9(3)
N(3)—C(4)—C(5)	110.9(2)	O(4)—C(4)—C(5)	127.2(3)
C(4)—C(5)—C(6)	119.5(3)	C(4)—C(5)—N(9)	130.7(3)
C(6)—C(5)—N(9)	109.7(2)	N(1)—C(6)—C(5)	127.9(3)
N(1)—C(6)—N(7)	125.9(2)	C(5)—C(6)—N(7)	106.1(2)
C(6)—N(7)—C(8)	106.8(2)	N(7)—C(8)—N(9)	112.5(3)
Cu(1)—N(9)—C(5)	130.2(2)	Cu(1)—N(9)—C(8)	124.9(2)
C(5)—N(9)—C(8)	104.9(2)	C(2′)—N(1′)—C(6′)	112.5(2)
N(1′)—C(2′)—N(2′)	119.4(3)	N(1′)—C(2′)—N(3′)	123.0(3)
N(2′)—C(2′)—N(3′)	117.6(3)	C(2′)—N(3′)—C(4′)	126.0(3)
N(3′)—C(4′)—O(4′)	120.9(3)	N(3′)—C(4′)—C(5′)	110.9(2)
O(4′)—C(4′)—C(5′)	128.2(3)	C(4′)—C(5′)—C(6′)	119.5(2)
C(4′)—C(5′)—N(9′)	131.2(2)	C(6′)—C(5′)—N(9′)	109.4(2)
N(1′)—C(6′)—C(5′)	128.1(3)	N(1′)—C(6′)—N(7′)	125.6(3)
C(5′)—C(6′)—N(7′)	106.3(2)	C(6′)—N(7′)—C(8′)	106.9(2)
N(7′)—C(8′)—N(9′)	112.2(2)	Cu(1)—N(9′)—C(5′)	131.3(2)
Cu(1)—N(9′)—C(8′)	123.3(2)	C(5′)—N(9′)—C(8′)	105.3(2)

Table 2. Selected infrared data for acv and its copper(II) coordination compounds (cm^{-1}) with possible assignments

	ν(C=O)	$\nu(C_4—N_3)$, $\nu(C_4—C_5)$, $\nu(C_5—N_7)$	ν(C—O) (acyclic chain)
acv	1715	1610	1106
I	1710	1605	1102
II	1702	1601	1107

sition indicates the loss of two molecules of water. Both estimated (5.55%) and calculated (5.80%) mass losses are in reasonable agreement. The dehydrated compound is stable in a short temperature interval (148–165°C) only and after that decomposes slowly. The dehydration of compound **I** is similar to ordinary nitrate(V) salts. The process is obscured by simultaneous decomposition of nitrate(V) ion.

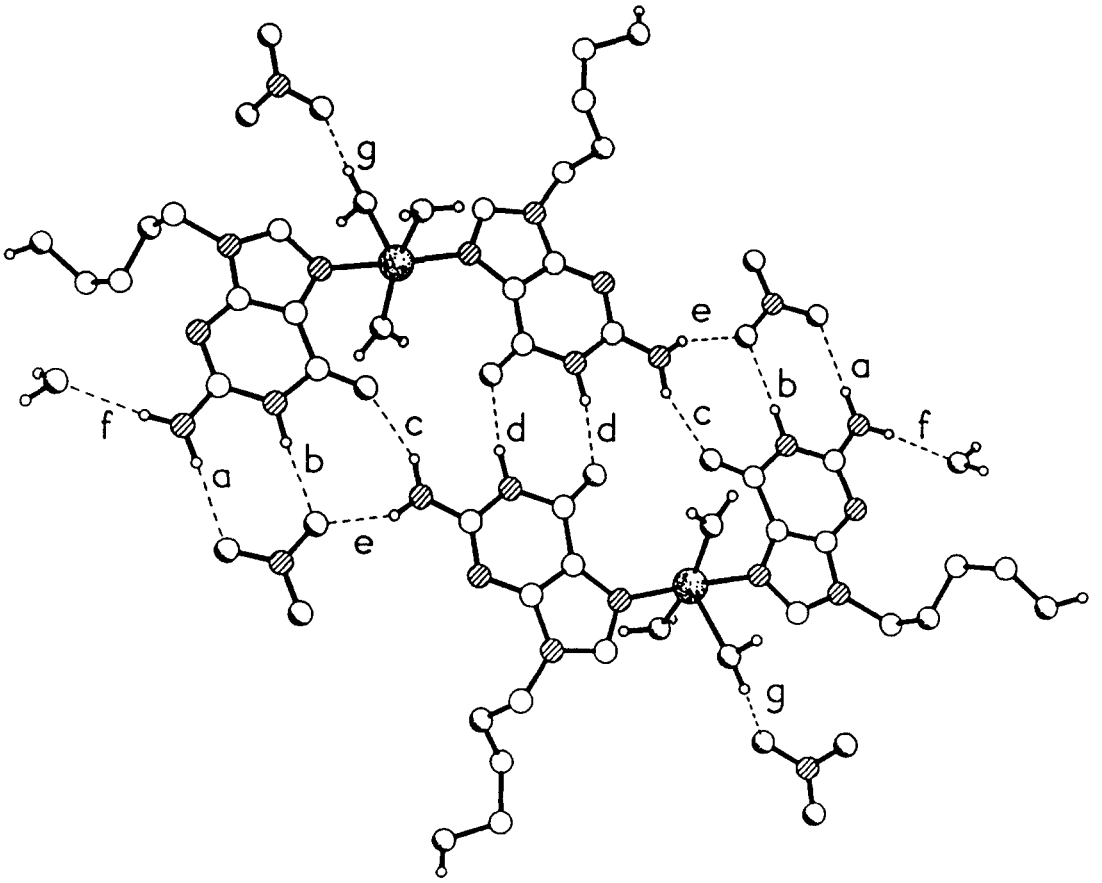


Fig. 2. The pattern of base recognition between centrosymmetrically related molecules of **I**. Hydrogen bonding geometries: N···O, N—H, H···O distances (Å), N—H···O angles (°); (a) 2.95, 0.90, 2.05, 176; (b) 2.94, 0.90, 2.04, 175; (c) 2.82, 0.90, 2.00, 149; (d) 2.79, 0.90, 1.90, 171; (e) 2.95, 0.90, 2.10, 157; (f) 3.00, 0.90, 2.11, 173; O···O, H—O, H···O distances (Å), O—H···O angle (°); (g) 2.75, 0.90, 1.90, 156.

TG analysis confirmed the absence of water in compound **II**. We have calculated the contents of the copper(II) ion in this compound from the end mass loss. This value was in good agreement with volumetrically determined copper(II) contents.

Electronic spectra

The diffuse reflectance spectra of the three compounds are very similar and only pure *d–d* transitions have been assigned (Fig. 3). The results for both compounds, the crystal structures of which were solved, suits perfectly the published data of structurally related complexes [22]. It is hard to predict anything in the case of compound **II**, except that a tetrahedral geometry is unlikely.

Magnetic susceptibility data and ESR spectroscopy

All values of μ_{eff} lie between 1.80 and 1.95 which is the characteristic range of magnetically dilute complexes. This means that individual copper(II) ions are well separated from each other and the interactions between them cannot occur.

ESR spectra of all the compounds were obtained at *X*- and *Q*- band. The *Q*-band spectra of all of them, showed some separation of g_x and g_y, with an essentially rhombic coordination geometry, which is in agreement with the crystal structures (Table 3). No firm prediction could be made about the structure of **II**, except that, as shown by the electronic spectrum.

Table 3. ESR g values for some coordination compounds of copper(II) and acv

	g_z	g_y	g_x
I	2.33	2.09	2.05
II	2.26	2.07	2.04
III	2.32	2.10	2.07

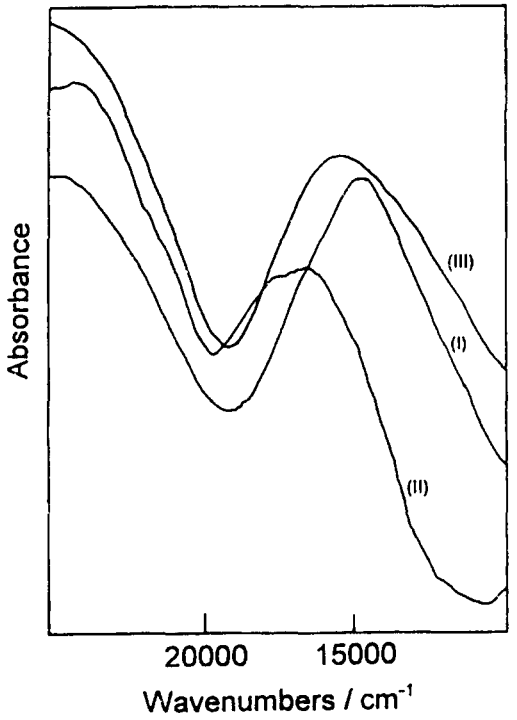


Fig. 3. Electronic reflectance spectra of compounds **I–III**. The region of *d–d* transitions only is shown.

it is unlikely to be tetrahedral. Since the infrared spectrum shows that the C=O is probably not coordinated, the most likely structure would seem to involve unsymmetrical halide bridging between copper ions.

Acknowledgement—We thank the Ministry of Science and Technology of the Republic of Slovenia for a Research Studentship (to I.T.).

REFERENCES

1. Elion, G. B., Furman, P. A., Fyfe, J. A., de Miranda, P., Beauchamp, L. and Schaeffer, H. J., *Proc. Natl. Acad. Sci. USA*, 1977, **74,** 5716.
2. Schaeffer, H. J., Beauchamp, de Miranda, P., Elion, G. B., Bauer D. J. and Collins, P., *Nature*, 1978, **272,** 583.
3. Williams, R. J. P., *Pure Appl. Chem.*, 1983, **55,** 35.
4. Blažič, B., Bukovec, N., Bukovec, P. and Lazarini, F., *Z. Kristall.*, 1988, **185,** 355.
5. Blažič, B., Turel, I., Bukovec, N., Bukovec, P. and Lazarini, F., *J. Inorg. Biochem.*, 1993, **51,** 737.
6. Turel, I., Leban, I. and Gruber, K., *J. Inorg. Biochem.*, 1996, **63,** 41.
7. Cavallo, L., Cini, R., Kobe, J., Marzili, L. G. and Natile, G., *J. Chem. Soc., Dalton Trans.*, 1991, **8,** 1867.
8. Sinur, A. and Grabner, S., *Acta Cryst.*, 1995, **C51,** 1769.
9. Hodgson, D. J., *Prog. Inorg. Chem.*, 1977, **23,** 211.
10. Sletten, E. and Fløgstad, N. F., *Acta Cryst.*, 1976, **B32,** 461.
11. de Meester, P., Goodgame, D. M. L., Jones, T. J. and Skapski, A. C., *Biochem. J.*, 1974, **139,** 791.
12. de Meester, P., Goodgame, D. M. L., Jones, T. J. and Skapski, A. C., *C. R. Acad. Sci. Paris*, 1974, **C667**, 279.
13. de Meester, P., Goodgame, D. M. L., Skapski, A. C. and Smith, B. T., *Biochim. Biophys. Acta*, 1974, **340,** 113.
14. Aoki, K., *Acta Cryst.*, 1976, **B32,** 1454.
15. Sletten, E. and Lie, B., *Acta Cryst.*, 1976, **B32,** 3301.
16. Kindberg, B. L., Griffith, E. A. H., Amma, E. L. and Jones Jr., E. R., *Cryst. Structr. Commun.*, 1976, **5,** 533.
17. Cingi, M. B., Lanfredi, A. M. M. and Tiripicchio, A., *Acta Cryst.*, 1983, **C39,** 1523.
18. Sheldrick, G. M., SHELXTL, An Integrated System for Solving, Refining and Displaying Crystal Structures from Diffraction Data, University of Göttingen, FRG, revision 4.1, August, 1983.
19. Tsuboi, M., Takahoshi, S. and Horada, I., in *Physicochemical Properties of Nucleic Acid*, Vol. **2,** ed. J. Duchense. Academic Press, New York, 1973, p. 91.
20. Tajmir-Riahi, H. A. and Theophanides, T., *Inorg. Chim. Acta*, 1983, **80,** 223.
21. Theophanides, T. and Tajmir-Raihi, H. A., *Spectroscopy of Biological Molecules*. D. Reidel Publishing Company, Dordrecht, 1982.
22. Lever, A. B. P., *Inorganic Electronic Spectroscopy*, 2nd edn. Elsevier, Amsterdam, 1984, p. 554.

Pergamon

PII: S0277-5387(96)00465-2

Polyhedron Vol. 16, No. 10, pp. 1707–1711, 1997
Copyright © 1997 Elsevier Science Ltd
Printed in Great Britain. All rights reserved
0277-5387/97 $17.00+0.00

Electrochemical synthesis and crystal structures of bis{4-methyl-*N*-(2-pyridin-2-yl-ethyl) benzenesulfonamide}copper(II) and bis {4-methyl-*N*-(2-pyridin-2-yl-ethyl) benzenesulfonamide}nickel(II)

María L. Durán,[a] Jose A. García-Vázquez,[a] Jaime Romero,[a] Alfonso Castiñeiras,[a] Antonio Sousa,[a]* Alexander D. Garnovskii[b]* and Dimitri A. Garnovskii[b]

[a] Departamento de Química Inorgánica, Universidad de Santiago de Compostela, Santiago de Compostela, Spain

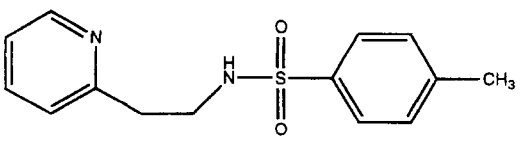
[b] Research Institute of Physical and Organic Chemistry, Rostov State University, Rostov-na-Donu, Russia

(Received 18 July 1996; accepted 18 September 1996)

Abstract—The complexes $[ML_2]$ (M = Cu and Ni) were prepared by electrochemical oxidation of the appropriate metal in a solution of 2-(2-pyridyl)-*N*-tosylethylamine in acetonitrile. The crystal and molecular structures of bis{4-methyl-*N*-(2-pyridin-2-yl-ethyl)benzenesulfonamide}copper(II) and bis{4-methyl-*N*-(2-pyridin-2-yl-ethyl)benzenesulfonamide}nickel(II) were determined by X-ray diffraction. Both compounds are isotypical and crystallize in the triclinic space group $P\bar{1}$ with one molecule in the unit cell. In both structures the metal atoms are in a distorted square-planar environment defined by two amide and two pyridyl nitrogen atoms. © 1997 Elsevier Science Ltd. All rights reserved.

Keywords: electrochemical synthesis; copper complex; nickel complex; amide complex; X-ray.

Previous work from our laboratories has shown that electrochemical methods can be used to prepare metal complexes of ligands having acid donor groups. The nature of the acid groups studied ranges from O—H (carboxylic acids, phenols, alcohols, enolizable carbonylic compounds) [1–3], N—H (pyrrole, imidazole) [1,4] to S—H (thiols) [1,5–10] or Se—H [1]. This paper extends this work to the case of secondary amides, in particular, ligands containing tosyl amide groups, as shown in the figure.



* Authors to whom correspondence should be addressed.

EXPERIMENTAL

Acetonitrile, 2-aminoethylpyridine, tosyl chloride and all other reagents were commercial products and were used as supplied. Metals (Ega Chemie) were used as *ca* 2×2 cm^2 plates.

The ligand (HL) was prepared by the reaction of equimolar amounts of the amine and the tosyl chloride in dichloromethane. A diluted solution of NaOH was added to the mixture until pH 8 and a white product was obtained and filtered at the pump upon a sintered glass funnel. The ligand was recrystallized from dichloromethane and dried *in vacuo*. Its purity was checked by recording its IR and ^{1}H NMR spectra.

Electrochemical synthesis

The electrochemical method was similar to that described by Tuck and co-workers [11]. The cell was

a 100-cm^3 tall-form beaker fitted with a rubber bung through which the electrochemical lead entered the cell. The anode was suspended from a platinum wire. The tosyl derivative was dissolved in acetonitrile, and a small amount (*ca* 20 mg) of tetraethylammonium perchlorate was added to the solution as a current carrier. Direct current was obtained from a purpose-built d.c. power supply. In both cases, hydrogen was evolved at the cathode. The cells can be summarized as:

$$Pt_{(-)}/CH_3CN + HL/M_{(+)} \quad M = Cu, Ni.$$

[CuL_2]. The electrochemical oxidation of copper metal in a solution of the ligand (0.2 g) in CH_3CN (50 cm^3) for 2 h at 20 mA resulted in the loss of 94 mg of metal from the anode ($E_f = 1.0$ mol F^{-1}). The reaction mixture was filtered to remove any precipitated particles of metal, and the filtrate was left to concentrate by evaporation at room temperature. A crystalline product identified as [CuL_2] was isolated: Found: C, 54.5; H, 4.6; N, 9.1; S, 9.3. Calc. for $C_{28}H_{30}N_4O_4S_2Cu$: C, 54.7; H, 4.9; N, 9.1; S, 10.4%.

[NiL_2]. The oxidation of nickel in a solution of the ligand (0.42 g) in acetonitrile (50 cm^3) for 2 h at 20 mA led to the dissolution of 45 mg of the metal ($E_f = 0.51$). Crystals of a compound identified as [NiL_2] were isolated by evaporation of the solution: Found: C, 55.0; H, 5.2; N, 9.3; S, 10.7. Calc. for $C_{28}H_{30}N_4O_4S_2Ni$: C, 55.2; H, 5.0; N, 9.2; S, 10.5%.

Physical measurements

The C, N, H and S analyses of the complexes were determined on a Carlo–Erba EA 1108 microanalyser. IR spectra were recorded as KBr mulls on a Perkin–Elmer 180 spectrophotometer. The proton NMR spectra were recorded on Bruker WM 250 MHz spectrometer using CD_3CN as solvent. Chemical shifts were referenced to TMS as internal standard.

Crystal structure determination

Crystal data for [CuL_2] (**1**). $C_{28}H_{30}CuN_4O_4S_2$, $M = 614.22$, triclinic, space group $P\bar{1}$, $a = 7.427(2)$, $b = 8.442(2)$, $c = 11.988(3)$ Å, $\alpha = 84.00(2)$, $\beta = 74.135(10)$, $\gamma = 72.221(10)°$; $Z = 1$, $D_c = 1.485$ g cm^{-3}. Prismatic greenish caramel crystals with dimensions $0.10 \times 0.30 \times 0.35$ mm^3.

Crystal data for [NiL_2] (**2**). $C_{28}H_{30}N_4NiO_4S_2$, $M = 609.39$, triclinic, space group $P\bar{1}$, $a = 7.428(2)$, $b = 8.314(2)$, $c = 11.950(3)$ Å, $\alpha = 83.54(2)$, $\beta = 73.26(1)$, $\gamma = 72.82(1)°$, $Z = 1$, $D_c = 1.500$ g cm^{-3}. Amber prismatic crystal with dimensions $0.10 \times 0.15 \times 0.25$ mm^3.

Data collection and processing. Enraf–Nonius CAD4 diffractometer fitted with graphite-monochromatized Mo-K_α radiation, $\lambda = 0.71073$ Å. The $\omega/2\theta$ scan technique was employed to measure the intensities for 5244 and 5171 reflections up to a maximum Bragg angle of 31° in both compounds. Cell parameters were refined by least-squares procedure on the setting angles of 25 reflections ($8.1 < \theta < 15.0°$ for **1** and $8.1 < \theta < 15.2°$ for **2**) [12]. No decomposition of the crystals occurred during the data collection. Corrections were applied for Lorentz and polarization effects and for absorption ($\mu = 0.99$ and 0.91 mm^{-1} for **1** and **2**, respectively) [13]. A total of 5244 and 5171 reflections were collected, respectively, of which 4345 (**1**) and 4285 (**2**) were unique ($R_{int} = 0.030$ and 0.057), and of these 4345 for **1** and 4285 for **2** satisfied the $I > 2.0\sigma(I)$ criterion of observability and were used in the subsequent analysis.

Structure analysis and refinement

The structures were solved by direct methods [14] and refined by a full-matrix least-squares procedure based on F^2 [15]. Non-hydrogen atoms were refined with anisotropic displacement parameters. Hydrogen atoms were located from difference Fourier synthesis and refined with isotropic displacement parameters, except those of the methyl group of the copper compound. The refinement proceeded smoothly to convergence with a maximum, Δ/σ of 0.001 when $R = 0.055$, $R_w = 0.118$ and $GOF = 1.024$ (goodness-of-fit) for 227 variables for the copper complex; $R = 0.072$, $R_w = 0.11$ and $GOF = 1.011$ for 239 variables for the nickel complex. Correction for extinction was made in the last cycle of refinement [16]. The analysis of variance showed no special features and the maximum and minimum residual electron density peaks in the final difference map were +0.64 and −0.51 e Å^{-3}, respectively for the copper complex and +0.50 and −0.42 e Å^{-3}, respectively for the nickel complex.

Atomic scattering factors and anomalous dispersion corrections for all atoms were taken from ref. [17]. The atomic positions, full lists of bond lengths and angles and other crystallographic data have been deposited as Supplementary Publication No. CSD. Copies can be obtained through the Fachinformationszentrum Karlsruhe, D-76344 Eggenstein-Leopoldshafen, Germany.

RESULTS AND DISCUSSION

The electrochemical oxidation of Cu and Ni in acetonitrile in the presence of 2-(2-pyridyl)-*N*-tosylethylamine (HL) proved to be a simple, direct route to compounds of general formula [ML_2]. The reaction can be represented as:

$$M + 2HL \rightarrow [ML_2] + H_2.$$

In both cases the electrolysis gave dark solutions

from which crystalline products were isolated by concentration. These compounds are air stable and insoluble in common organic solvents but soluble in CH_3CN.

In the case of the copper complex, the value of the electrochemical efficiency (moles of metal dissolved per Faraday of charge, E_f) was 1.0 mol F^{-1}. This, together with the formation of H_2 at the cathode, is compatible with the formation of Cu^I at the anode and subsequent oxidation to Cu^{II} in the solution.

$$\text{cathode:}\quad HL + e^- \rightarrow \tfrac{1}{2}H_2(g) + L^-$$

$$\text{anode:}\quad Cu + L^- \rightarrow [CuL] + e^-$$

$$[CuL] + HL \rightarrow [CuL_2] + \tfrac{1}{2}H_2(g).$$

These oxidation steps have been observed in other electrochemical processes involving copper as anode [18].

With Ni the value of E_f, 0.51 mol F^{-1}, is compatible with the process:

$$\text{cathode:}\quad 2HL + 2e^- \rightarrow H_2(g) + 2L^-$$

$$\text{anode:}\quad Ni + 2L^- \rightarrow [NiL_2] + 2e^-.$$

The molecular structures of $[CuL_2]$ *and* $[NiL_2]$

The crystals contain individual $[ML_2]$ (M = Cu, Ni) neutral molecules. ORTEP [19] drawings of the molecular structures of both complexes are presented in Fig. 1 together with the atomic-labelling system adopted. Selected bond distances and angles are listed in Tables 1 and 2.

Both structures are isotypic. In the complexes, the metal atom is located on a crystallographic symmetry centre and is coordinated to the sulphonamide nitrogen and pyridine nitrogen atoms of two symmetry-related moities.

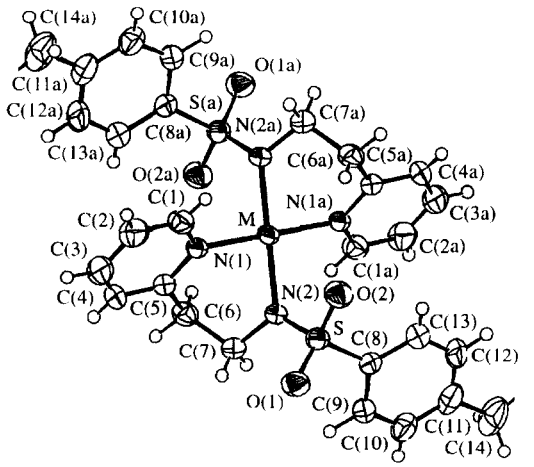


Fig. 1. The molecular structure of bis{4-methyl-N-(2-pyridin-2-yl-ethyl)benzenesulfonamide}M^{II}, where M = Ni, Cu.

The coordination geometry around the copper is square planar. Bond angles involving the copper atom and adjacent nitrogen atoms are 87.66(10) and 92.34(10)°.

The Cu—N bond distances are similar. The average value for the Cu—N_{py} bond distance, 2.002(5) Å, is similar to those reported for a number of four-coordinated square-planar copper complexes of pyridine and pyridine derivatives; for instance, 1.982(6) Å (average value) in dibromobis(2-methylpyridine) copper(II) [20] or 2.028(3) Å (average value) in bis[2-(2-aminoethyl)pyridine]copper(II) iodide [21]. Similarly, the average value for the Cu—N_{amide} bond distance, 1.922(2) Å, is very similar with the value 1.931(2) Å observed in bis-(*N*-phenylpyridine-2-carboxamido)copper(II) [22].

The configuration around the nickel atom is slightly distorted square planar with bond distances Ni—N_{py} 1.897(3) and Ni—N_{amide} 1.904(3) Å. These bond distances are similar to those found in related nickel square-planar complexes with both pyridine and amide nitrogen atoms as donors [23].

The ligand geometry in both complexes is similar to other substituted aminoethylpyridines, with the chelating portion of the group retaining the six-membered ring boat conformation.

The pyridine ring is approximately planar, with no atom deviating from the least-squares plane by more than 0.06 Å. Bond distances and angles are similar to those reported for other substituted pyridines.

Spectroscopic studies

None of the IR spectra of the complexes show bands assignable to ν(NH) at 3050 cm^{-1} in the spectrum of the free ligand, indicating that the amide hydrogen atom is lost during the electrochemical process. The bands attributable to the pyridine ring are shifted to higher frequencies as a consequence of the coordination through the pyridine nitrogen atom.

The ^1H NMR spectra for the ligand and Ni complex were recorded in CD_3CN as the solvent and the data reinforce the above conclusions. Thus the spectrum of the free ligand shows a peak around δ 6.1 assignable to the NH hydrogen. This signal is absent in the spectrum of the nickel complex, indicating the deprotonation of the ligand in the electrochemical process. The peak assignable to the α hydrogen of the pyridine ring is shifted downfield in the spectrum of the complex, in accordance with coordination of the ligand to the nickel atom through the pyridine nitrogen atom.

Acknowledgement—We thank the Russian Science Foundation (grant no. 960332026a) for financial support.

Table 1. Selected bond lengths (Å) and angles (°) for bis{4-methyl-*N*-(2-pyridine-2-yl-ethyl) benzenesulfonamide}copper(II)

Cu—N(2)#1	1.922(2)	Cu—N(2)	1.922(2)
Cu—N(1)	2.002(2)	Cu—N(1)#1	2.002(2)
S—O(1)	1.419(2)	S—O(2)	1.444(3)
S—N(2)	1.614(3)	S—C(8)	1.773(3)
N(1)—C(5)	1.338(4)	N(1)—C(1)	1.356(4)
N(2)—C(7)	1.456(4)		

N(2)#1—Cu—N(2)	180.0	N(2)#1—Cu—N(1)	92.34(10)
N(2)—Cu—N(1)	87.66(10)	N(2)#1—Cu—N(1)#1	87.66(10)
N(2)—Cu—N(1)#1	92.34(10)	N(1)—Cu—N(1)#1	180.0
O(1)—S—O(2)	115.3(2)	O(1)—S—N(2)	111.9(3)
O(2)—S—N(2)	109.0(2)	O(1)—S—C(8)	106.7(2)
O(2)—S—C(8)	107.2(2)	N(2)—S—C(8)	106.3(2)
C(5)—N(1)—C(1)	119.3(3)	C(5)—N(1)—Cu	118.6(2)
C(1)—N(1)—Cu	122.0(2)	C(7)—N(2)—S	120.5(2)
C(7)—N(2)—Cu	119.8(2)	S—N(2)—Cu	115.8(2)
N(1)—C(1)—C(2)	123.1(4)		

Symmetry transformations used to generate equivalent atoms: #1 $-x, -y, -z$.

Table 2. Selected bond lengths (Å) and angles (°) for bis{4-methyl-*N*-(2-pyridine-2-yl-ethyl) benzenesulfonamide}nickel(II)

Ni—N(1)#	1.897(3)	Ni—N(1)	1.897(3)
Ni—N(2)#1	1.904(3)	Ni—N(2)	1.904(3)
S—O(1)	1.440(3)	S—O(2)	1.443(3)
S—N(2)	1.582(3)	S—C(8)	1.777(4)
N(1)—C(1)	1.335(6)	N(1)—C(5)	1.358(5)
N(2)—C(7)	1.469(5)		

N(1)#1—Ni—N(1)	180.0	N(1)#1—Ni—N(2)#1	87.65(14)
N(1)—Ni—N(2)#1	92.35(14)	N(1)#1—Ni—N(2)	92.35(14)
N(1)—Ni—N(2)	87.65(14)	N(2)#1—Ni—N(2)	180.0
O(1)—S—O(2)	117.8(2)	O(1)—S—N(2)	111.0(2)
O(2)—S—N(2)	107.5(2)	O(1)—S—C(8)	105.8(2)
O(2)—S—C(8)	107.0(2)	N(2)—S—C(8)	107.2(2)
C(1)—N(1)—C(5)	118.9(4)	C(1)—N(1)—Ni	122.2(3)
C(5)—N(1)—Ni	118.8(3)	C(7)—N(2)—S	118.3(3)
C(7)—N(2)—Ni	119.2(3)	S—N(2)—Ni	120.6(2)
N(1)—C(1)—C(2)	123.3(5)		

Symmetry transformations used to generate equivalent atoms: #1 $-x, -y, -z$.

REFERENCES

1. Garnovskii, A. D., Kharisov, B. I., Gojon-Zorrilla, G. and Garnovskii, D. A., *Russ. Chem. Rev.*, 1995, **64,** 201, and references cited therein.
2. Labisbal, E., García-Vázquez, J. A., Romero, J., Picos, S., Sousa, A., Castiñeiras, A. and Maichle-Mössmer, C., *Polyhedron*, 1995, **14,** 663.
3. Luaces, L., Bermejo, M. R., García-Vázquez, J. A., Romero, J., Picos, S., Sousa, A., Mugnier, M., McAuliffe, C. A., Pritchard, R. G. and Helliwell, M., *Polyhedron*, 1996, **15,** 1375.
4. Castro, J. A., Romero, J., García-Vázquez, J. A., Sousa, A. and Castiñeiras, A., *J. Chem. Cryst.*, 1994, **24,** 469.
5. Castro, R., García-Vázquez, J. A., Romero, J., Sousa, A., Pritchard, R. G. and McAuliffe, C. A., *J. Chem. Soc., Dalton Trans.* 1994, 1115.
6. Tallón, J., García-Vázquez, J. A., Romero, J., Louro, M. S., Sousa, A., Chen, Q., Chang, Y. D. and Zubieta, J., *Polyhedron*, 1995, **14,** 2309.
7. Castro, J. A., Romero, J., García-Vázquez, J. A., Castiñeiras, A., Sousa, A. and Zubieta, J., *Polyhedron*, 1995, **14,** 2841.
8. Castro, R., García-Vázquez, J. A., Romero, J., Sousa, A., Chang, Y. and Zubieta, J., *Inorg. Chim. Acta*, 1995, **237,** 143.
9. Castro, R., Romero, J., García-Vázquez, J. A., Sousa, A., Chang, Y. D. and Zubieta, J., *Inorg. Chim. Acta*, 1996, **345,** 119.
10. Pérez-Lourido, P. A., García-Vázquez, J. A., Romero, J., Louro, M. S., Sousa, A., Chen, Q.,

Chang, Y. D. and Zubieta, J., *J. Chem. Soc., Dalton Trans.*, 1996, 2047.
11. Habeeb, J. J., Tuck, D. G. and Walters, F. H., *J. Coord. Chem.*, 1978, **8,** 27.
12. Frenz, B. A., in *Computing in Crystallography*, Vol. 2.2, ed. H. Schenk, R. Olthof-Hazekamp, H. van Koningsveld and G. C. Bassi. Delft Univ. Press, The Netherlands, 1985, pp. 64–71.
13. Walker, N. and Stuart, D., *Acta Cryst.*, 1983, **A39,** 158.
14. Sheldrick, G. M., SHELXS86, Program for the solution of crystal structures. Univ. of Göttingen, Germany, 1986.
15. Sheldrick, G. M., SHELXS93, Program for the refinement of crystal structures. Univ. of Göttingen, Germany, 1993.
16. Zachariasen, W. H., *Acta Cryst.*, 1963, **16,** 1139.
17. *International Tables for X-ray Crystallography*, Vol. IV. Kynoch Press, Birmingham, 1974. (Present distributor Kluwer Academic Publishers, Dordrecht.)
18. Atherton, N. M., Fenton, D. E., Hewson, G. J., McLean, C. H., Bastida, R., Romero, J., Sousa, A. and Castellano, E., *J. Chem. Soc., Dalton Trans.* 1988, 1059.
19. Johnson, C. K., ORTEPII, Report ORNL-5138, Oak Ridge National Laboratory, Tennessee, USA, 1976.
20. Singh, P., Jeter, D. Y., Hatfield, W. E. and Hodgson, D. J., *Inorg. Chem.*, 1972, **11,** 1657.
21. Copeland, V. C. and Hodgson, D. J., *Inorg. Chem.*, 1973, **12,** 2157.
22. Ray, M., Mukherjee, R., Richardson, J. F., Mashuta, M. A. and Buchanan, R. M., *J. Chem. Soc., Dalton Trans.*, 1994, 965.
23. Stephens, F. S. and Vagg, R. S., *Inorg. Chim. Acta*, 1982, **57**, 9.

Pergamon

PII: S0277-5387(96)00462-7

Polyhedron Vol. 16, No. 10, pp. 1713–1718, 1997
Copyright © 1997 Elsevier Science Ltd
Printed in Great Britain. All rights reserved
0277-5387/97 $17.00+0.00

Synthesis and properties of some 1,1′-bis [*N*-formyl-*N*′-substituted thiourea]ferrocene derivatives: crystal structure of 1,1′-bis [*N*-formyl-*N*′-*p*-chlorophenylthiourea]ferrocene

Yao-Feng Yuan,* Su-Ming Ye, Ling-Yun Zhang, Bin Wang and Ji-Tao Wang

Department of Chemistry, National Key Laboratory of Elemento-Organic Chemistry, Nankai University, Tianjin 300071, P.R. China

(Received 25 June 1996; accepted 18 September 1996)

Abstract—A series of 1,1′-bis[*N*-formyl-*N*′-substituted thiourea]ferrocene derivatives was synthesized through the reaction of 1,1′-bis[formyl isothiocyanate]ferrocene and various primary amines, with high yields after simple and convenient purification. All the compounds were characterized by elemental analysis, IR and ^{1}H NMR spectra. Intramolecular hydrogen bonding between the formyl carbonyl group and the proton attached to N′ was found to be common in this kind of compound. Cyclic voltammetric analysis revealed that the substituents on the N′ atom affect the electrochemical behaviour of the ferrocenyl group *via* the intramolecular hydrogen bonded ring. The crystal structure of 1,1′-[*N*-formyl-*N*′-*p*-chlorophenylthiourea]ferrocene was determined showing the character of the intramolecular hydrogen bonding. © 1997 Elsevier Science Ltd. All rights reserved.

Keywords: ferrocene; acyl thiourea; intramolecular hydrogen bonding; electrochemistry.

Many acyl thiourea compounds have been widely studied for their insecticidal, antibacterial and pesticidal activities and promoting effect on plant growth [1,2]. It has been found that intramolecular hydrogen bonding is common in *N*-ferrocenoyl-*N*′-monosubstituted thiourea derivatives, which form a novel kind of polychelate ligand ready to complex with transition metal ions [3,4]. Whether intramolecular hydrogen bonding exists in 1,1′-disubstituted acyl thiourea ferrocene compounds is still another question to be investigated. In an extensive study, 1,1′-bis[*N*-formyl-*N*′-substituted thiourea]ferrocene derivatives were synthesized through the reaction of 1,1′-bis[formyl isothiocyanate]ferrocene with various primary amines. The existence of intramolecular hydrogen bonding was confirmed by IR ^{1}H NMR spectra and single crystal X-ray diffraction.

EXPERIMENTAL

All reagents and solvents were of analytical or chemical grade quality. Acetone was dried by refluxing with P_2O_5 for 3–4 hours after treatment with anhydrous potassium carbonate. KSCN was baked before use. Aromatic amines were vacuum distilled or recrystallized. Aliphatic amines were used directly without further purification.

Elemental analysis (C, H, N) were performed on a CHN-Corderm7-3 autoanalyser. Melting points were determined on a PHMK melting point apparatus (from Germany) and are uncorrected. ^{1}H NMR spectra were recorded on a Jeol FX-90QNMR, spectrometer, using $CDCl_3$ or DMSO-d_6 as solvent and TMS as internal standard. IR spectra were carried out with a Nicolet-FT-IR5-DX infrared spectrophotometer. X-ray diffraction data were obtained using an Enraf Nonius CAD4 diffractometer with graphite-monochromated Mo-K_α radiation ($\lambda = 0.071073$ nm). The crystal belongs to the monoclinic, space group $P2_1/n$, $a = 8.435(1)$, $b = 23.088(8)$, $c = 13.307(3)$ Å, $\beta = 95.70(1)°$, $V = 2597(2)$ Å^3, $z = 4$, $D_c = 1.575$ g cm^{-3}, $\mu = 9.804$ cm^{-1} and $F(000) = 1248$. A total of 3240 independent reflections was collected in the range $4.0 < \theta < 46.0°$ by 2θ–θ scan, at room temperature (299 ± 1 K), of which 1690 were accepted as observable [$I \geqslant 3\sigma(I)$]. The intensities were fully corrected

*Author to whom correspondence should be addressed.

for Lp factors and empirical absorption. The crystal structure was solved by direct phase determination method (MULTAN82). One independent Fe atom was located on an E map. The other non hydrogen atoms were found in the successive difference Fourier syntheses. The hydrogen atoms were not included in the refinement and calculations of structure factors. The coordinates and anisotropic thermal parameters of non-hydrogen atoms were refined by full-matrix least-squares methods and converged to $R = 0.053$ and $R_w = 0.061$ with unit weights. The highest electron density on the final difference Fourier map was found to be 0.45 e $Å^{-3}$. All calculations were performed on a PDP11/44 computer using the SDP-PLUS program system.

Cyclic voltammetric experiments were performed on a BAS-100B electrochemical analyser equipped with a three electrode assembly with 0.1 mol dm^{-3} TBAFB (Bu_4NBF_4) as support electrolyte and CH_2Cl_2 as solvent. The working electrode was a ϕ 1.5 mm platinum disk embedded in a cobalt glass seal and was polished consecutively with polishing alumina and diamond suspensions between runs. The 0.1 M $AgNO_3$/Ag (in 0.1 M Bu_4NBF_4-DMSO) was the reference electrode. A platinum filament was used as an auxiliary electrode.

Synthesis of 1,1′-*bis(formyl isothioncyaate)ferrocene* (**I**)

KSCN (0.533 g, 5.5 mmol) was dissolved in acetone (15 cm^3) and added dropwise to the 20 cm^3 acetone solution of 2.5 mmol $Fc(COCl)_2$ and refluxed for 30 min. The red acetone solution of $Fc(CONCS)_2$ was obtained on filtration of KCl and used *in situ* for the following reactions without further separation and purification.

Reaction of aromatic amines and aminoferrocene with **I**

Taking *p*-chloroaniline as an example. *p*-Chloroaniline (0.65 g, 5 mmol) dissolved in acetone (20 cm^3) was added dropwise to the acetone solution of 2.5 mmol $Fc(CONCS)_2$ and a red solid rapidly appeared. The mixture was refluxed for 2 h and the red powder obtained by filtration was washed with acetone. A total of 1.39 g was collected, yield 91%.

Reaction of aliphatic amines with **I**

Taking isopropyl amine as an example. An acetone solution of isopropyl amine (5 mmol) was added to the aforesaid acetone solution of $Fc(CONCS)_2$ and refluxed for 5 h. After removal of acetone by distillation, the residue was dissolved in the minimum amount of $CHCl_3$, and 0.96 g orange–red crystal was eluted from a neutral Al_2O_3 (200–300 mesh) chromatographic, column, yield 81%.

RESULTS AND DISCUSSION

General characterization

Analytical and physical data for the 11 compounds are given in Table 1. Compounds **1**–**3** are very soluble in acetone, diethyl ether, chloroform and dichloromethane and are soluble in benzene and hot alcohol, but are insoluble in petroleum ether. Compounds **4**–**9** can be dissolved in DMF, DMSO and other non-protic solvents.

Reactivity of **I** *towards primary amines*

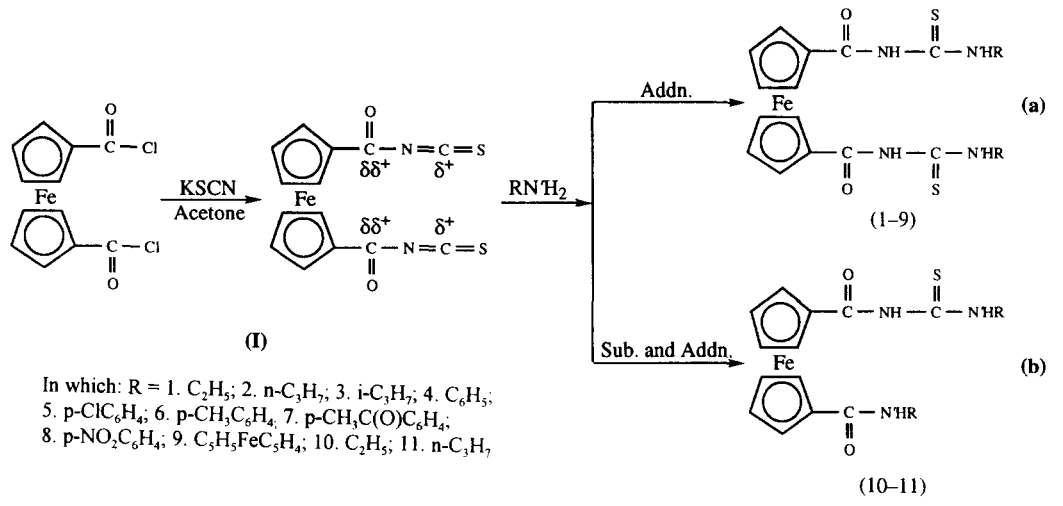
The intermediate 1,1′-bis[formyl isothiocyanate] ferrocene (**I**) was synthesized and reacted with aliphatic amines *in situ* under mild condition. There are two competing reactive sites in **I** as shown in Scheme 1.

If RNH_2 attacks the carbon atom in the isothiocyanate group ($C^{\delta+}$), addition of RNH_2 to the C=N double bond takes place, resulting in the thiourea product. An alternative site for RNH_2 to attack is

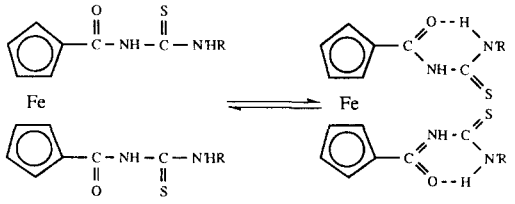
Table 1. Physical properties and elemental analysis for compounds **1**–**11**

Compound	M.p. (°C)	Yield (%)	Colour	Elemental analysis (%)[a]		
				C	H	N
1	178–9	70	orange-red	48.4(48.4)	5.0(5.0)	12.4(12.5)
2	88–9	68	red	50.8(50.6)	5.6(5.5)	11.8(11.8)
3	165–6	81	orange-red	50.6(50.6)	5.8(5.5)	11.8(11.8)
4	192–4	89	red	57.4(57.6)	4.1(4.1)	10.2(10.3)
5	195–7	91	orange-red	51.2(51.1)	3.4(3.3)	8.9(9.2)
6	198–9	92	orange-red	58.8(58.9)	4.6(4.6)	9.9(9.8)
7	196–8	88	orange-red	57.8(57.1)	4.2(4.2)	8.7(8.4)
8	212(dec.)	85	red	49.2(49.4)	3.2(3.2)	13.5(13.3)
9	184(dec.)	84	orange-yellow	53.8(54.0)	3.8(3.7)	7.4(7.4)
10	139–40	-	red	52.7(52.7)	6.5(6.5)	10.8(10.8)
11	148–50	-	red	54.9(54.9)	6.1(6.1)	9.9(10.1)

[a] Calculated values are given in parentheses.



Scheme 1.



Scheme 2.

the carbonyl carbon atom ($C^{\delta\delta+}$). In this case, the isothiocyanate group is substituted by the amino group, thus the amide product is anticipated. Unlike its monosubstituted ferrocene derivative analogue, whose reaction with primary amines gave only the addition product, the reaction of (**I**) with aliphatic amines involved competition between addition and substitution. Both products were isolated through column chromatography. In the case of aromatic primary amines, owing to their lower nucleophilicity, they were reacted with (**I**) under reflux. The products precipitated from the solution directly. No substitution took place and only the addition form was collected.

IR spectra

The medium–strong $\nu_{C=O}$ band in the IR spectra of all the compounds appears at about 1671 cm^{-1}, apparently decreasing in wavenumber compared with the ordinary carbonyl absorption (1710 cm^{-1}) (see Table 2). This is interpreted as being a result of its conjugate resonance with the ferrocenyl group and the possible formation of intramolecular hydrogen bonding with N′—H. In addition, the abnormal intensity ratio between $\nu_{C=O}$ and δ_{CNH} (1515–1550 cm^{-1}, vs) bands revealed that intramolecular hydrogen bonding might exist in this kind of compound (as shown in Scheme 2) [5]. No $\nu_{S\ H}$ absorption was observed in the region 2600–2500 cm^{-1}, indicating that the compounds do not exist in the thioenol form. The $\nu_{C=N}$ band appears at about 1269 cm^{-1} and is much weaker than $\nu_{C=O}$ and δ_{CNH} in intensity. It is presumed to be the mixed vibration of δ_{OCN} and ν_{N-H}. A strong band at about 1319–1355 cm^{-1} is assigned to the stretching vibration of the thione group. There is a weak or medium intensity singlet peak at 3300 cm^{-1} in the IR spectra of compounds **1–9**, indicating the presence of the secondary amino group. It is attributed to ν_{N-H}, whereas the $\nu_{N'-H}$ band shifts to 3010–3230 cm^{-1} and becomes broad and weak because of the intramolecular hydrogen bond formation. In the IR spectra of compounds **10** and **11**, there are three ν_{N-H} absorptions at 3279, 3246 and 3164 cm^{-1}, respectively, and two $\nu_{C=O}$ bands, one very strong at 1630 cm^{-1} and the other comparatively weak at about 1671 cm^{-1}. With respect to other regions, there is little difference compared with compounds **1–9**. All of the above facts support structure (b) in Scheme 1, in which one side chain gives the addition product while the other undergoes substitution.

Nujol IR spectra were also recorded and it was shown that there are no ν_{O-H} and ν_{S-H} bands. This indicates that compounds **1–11** exist in the keto-thione form.

^{1}H *NMR spectra*

In the ^{1}H NMR spectra of compounds **1–9** (Table 3), the signals of the cyclopentadienyl protons shift downfield owing to their proximity to the carbonyl group with δ_{ortho} (4.74–5.46) > δ_{meta} (4.48–4.78), displaying the characteristics of AA′BB′ coupling, since the two Cp rings are in the same chemical environment. There are two kinds of Cp rings in compound **9**, with four being monosubstituted and two unsubstituted. The former gives AA′BB′ coupling and altogether five Cp bands are observed. δ_{N-H} appears at 8 9 ppm. The downfield δ 12.50 peak is assigned to

Table 2. IR spectral data (cm^{-1}) for **1–11**

Compound	ν_{N-H}	$\nu_{N'-H}$	δ_{CHN}	$\nu_{C=O}$	$\nu_{C=S}$	ν_{C-N} C(O)—N	ν_{C-N} —C(S)—N
1	3263m	3200–3164w	1516vs 1548vs	1671s	1355w	1269m	1171s
2	3263m	3200–3100w	1507vs 1548vs	1671s	1335w	1269m	1171s
3	3312m	3222–3156w	1515vs 1548vs	1663s	1340m	1269m	1146s
4	3312s	3010w	1524vs	1671s	1351m	1269s	1163vs
5	3304m	3017w	1524vs	1663s	1327m	1269s	1155s
6	3312m	3100w	1524vs	1671m	1352m	1269m	1163vs
7	3279m	3107w	1530vs	1671s	1335m	1269s	1146s
8	3263m	3115w	1516vs	1671s	1335s	1278m	1155s
9	3271w	3148w	1507vs	1663s	1319w	1269m	1155s
10	3279m 3246w	3164m	1557vs 1507vs	1671s 1622vs	1352w	1269m	1179s
11	3279m 3246s	3164m	1557vs 1507vs	1680s 1630vs	1352w	1269m	1155m

vs: very strong; s: strong; m: middle; w: weak.

Table 3. ^1H NMR data (δ, ppm) for compounds **1–11**

Compound	Fc—H	N—H	N′—H	R
1	4.56 (s, 4H); 4.80 (s, 4H)	8.64 (s, 2H)	10.60 (s, 2H)	1.36 (t, 6H); 3.72 (q, 4H)
2	4.50 (s, 4H); 4.74 (s, 4H)	8.96 (s, 2H)	10.56 (s, 2H)	3.60 (d, 4H); 1.61 (m, 4H); 1.04 (t, 6H)
3	4.60 (s, 4H); 4.84 (s, 4H)	8.64 (s, 2H)	10.56 (s, 2H)	1.32 (d, 12H); 4.60 (m, 2H)
4	4.72 (s, 4H); 4.96 (s, 4H)	8.84 (s, 2H)	12.56 (s, 2H)	7.28-7.70 (m, 10H)
5	4.72 (s, 4H); 4.96 (s, 4H)	8.84 (s, 2H)	12.55 (s, 2H)	7.32-7.80 (m, 8H)
6	4.72 (s, 4H); 4.96 (s, 4H)	8.78 (s, 2H)	12.44 (s, 2H)	7.32-7.80 (m, 8H); 2.40 (s, 6H)
7[a]	4.78 (s, 4H); 5.44 (s, 4H)	10.90 (s, 2H)	13.30 (s, 2H)	7.92 (b, 8H); 3.52 (s, 6H)
8[a]	4.78 (s, 4H); 5.46 (s, 4H)	11.16 (s, 2H)	13.36 (s, 2H)	8.10 (b, 8H)
9[a]	4.00 (s, 4H); 4.08 (s, 10H) 4.48 (s, 4H); 4.56 (s, 4H) 4.92 (s, 4H)	9.72 s, 2H)	12.00 s, 2H)	
10	4.46–4.72 (m, 8H)	9.00 (s, 1H)	6.20 (s, 1H) 10.66 (s, 1H)	1.28 (m, 6H) 3.46 (q, 2H) 3.76 (q, 2H)
11	4.32–4.56 (m, 8H)	8.82 (s, 1H)	6.10 (s, 1H) 10.56 (s, 1H)	0.96 (t, 6H) 1.60 (m, 4H) 3.24 (t, 2H) 3.58 (t, 2H)

s: singlet; d: doublet; t: triplet; q: quartet; m: multiplet; b: broad.
[a] DMSO-d_6 as solvent.

$\delta_{N'-H}$ owing to the deshielding effect of intramolecular hydrogen bond formation. In compounds **7** and **8,** δ_{N-H} and $\delta_{N'-H}$ approach δ 11.00 and 13.00 owing to the electron-withdrawing groups on the phenyl ring. All of this evidence tallies with the structures drawn from their IR spectra.

Three amino protons were observed in the ^1H NMR spectra of compounds **10** and **11,** two of which are similar to those of the aforesaid compounds, while the other appears at δ 6.00, belonging to the amide proton. Besides, the cyclopentadienyl proton signals are too complicated to differentiate. With the aid of elemental analysis data, the structures of **10** and **11** are presumed to be (b). This further confirmed the conclusion derived from the IR spectra.

To demonstrate the existence of intramolecular hydrogen bond, ^1H NMR spectra of compounds **1** and **10** at different concentrations with $CDCl_3$ as solvent were recorded. It was found that the most downfield peak remains unchanged.

Electrochemistry

Cyclic voltammetric data of compounds **1–9** and ferrocene are listed in Table 4. The CV curves of compounds **2** and **9** are depicted in Figs 1 and 2.

One pair of reversible redox peaks was observed in compounds **1–8,** indicating that they undergo a one-electron redox reaction. Their $\bar{E}_p$ values at about 0.85

Table 4. Cyclic voltammetric data

Compound	r (mV s^{-1})	E_{Pa} (V)	E_{Pc} (V)	$\bar{E}_p$ (V)	$I_{Pa} \times 10^{7}$ (A)	$I_{Pc} \times 10^{7}$ (A)	I_{Pa}/I_{Pc}
Fc—H	100	0.431	0.092	0.262	11.135	10.238	1.0876
1	200	0.969	0.714	0.842	7.9757	5.0220	1.5882
2	200	0.992	0.702	0.847	9.6806	5.6394	1.7166
3	100	0.971	0.691	0.832	9.3665	6.4629	1.4493
	200	1.006	0.701	0.854	11.376	6.5971	1.7244
4	300	0.914	0.697	0.806	2.4778	1.7375	1.4261
5	200	1.018	0.738	0.878	7.8158	5.2249	1.4959
6	600	0.991	0.736	0.864	5.7196	3.0481	1.8764
	400	0.979	0.735	0.857	5.0934	2.6940	1.8906
7	600	0.984	0.719	0.852	3.8643	2.1636	1.7861
8	400	0.949	0.823	0.886	0.7469	0.2062	3.6229
9	300	0.302	0.171	0.237	2.0645	2.8886	0.7147
		0.698	0.650	0.674	1.1214	0.1803	6.2214

[a] $\bar{E}_p = 1/2(E_{pa} - E_{pc})$.

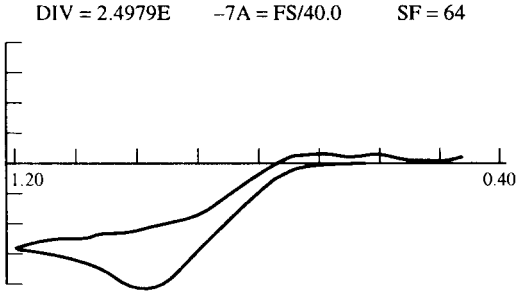


Fig. 1. Cyclic voltammogram of compound **2**.

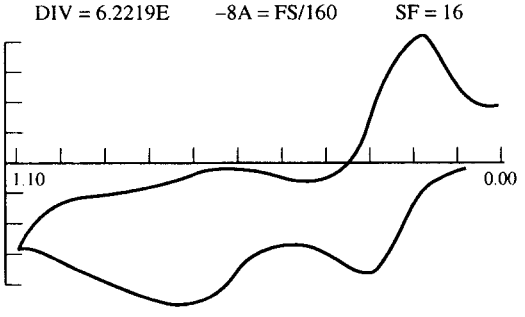


Fig. 2. Cyclic voltammogram of compound **9**.

V are higher than that of ferrocene (0.262 V), thus revealing that the acyl thiourea group is an electron-withdrawing group. In addition, at the same rate of scanning, their redox potentials are influenced by the properties of the substituents on the N′ atom. The more electron withdrawing the substituent is, the higher the $\bar{E}_p$ value becomes. For example, at the same scanning rate of 400 mV s^{-1}, $\bar{E}_p$ of compound **8** (*p*-NO_2) is 0.886 V, while that of compound **6** (*p*-CH_3) is 0.857 V. This is explained as follows: the strong electron-withdrawing property of *p*-NO_2 ($\sigma = 0.78$) and electron-donating property of *p*-CH_3 ($\sigma = -0.17$) can affect the electrochemical behaviour of the ferrocenyl group *via* the intramolecular hydrogen bonding planes.

There are two pairs of redox peaks in the CV curve of compound **9**, showing the characteristics of a multi-component redox system [6]. This is interpreted as resulting from two different kinds of ferrocenyl groups. The two monosubstituted ferrocenyls are electrochemically identical and are oxidized at the same potential, releasing two electrons at the same time. Their E_p (0.237 V) is lower than that of ferrocene, owing to the electron-donating properties of the amino group. Whereas the E_p value of the disubstituted ferrocenyl group (0.674 V) is higher than that of ferrocene, again confirming the electron-withdrawing properties of the acyl thiourea group.

Single crystal X-ray diffraction

To further confirm the existence of intramolecular hydrogen bonding the crystal structure of compound **5** was determined. X-ray analysis reveals that in each molecule there exist two independent intramolecular hydrogen bonds between the carbonyl oxygen and the hydrogen atom on N′ in either —C(O)—NH—C(S)—N′H— moiety, forming two parallel six-membered rings. The planar rings are approximately in the same plane as the cyclopentadienyl rings to which they are attached. The two phenyl rings are basically parallel as well. The molecular structure of compound **5** is depicted in Fig. 3. Table 5 lists the least squares planes of relevant groups and the dihedral angles

Table 5. Least-squares planes

Equation of plane 1 : $0.852(2)x-0.447(3)y-0.271(5)z+5.77(4)=0$

Atoms	N(1)	C(17)	N(2)	C(18)	O(1)
Distances to Plane (Å)	0.02(1)	−0.01(1)	−0.02(1)	0.04(1)	−0.03(1)

Equation of plane 2 : $-0.680(3)x+0.668(3)y-0.300(4)z+0.29(4)=0$

Atoms	C(11)	C(12)	C(13)	C(14)	C(15)	C(16)
Distances to plane (Å)	−0.00(8)	0.00(9)	0.00(6)	0.00(2)	0.00(1)	0.00(1)

Equation of plane 3 : $0.725(4)x-0.578(4)y-0.373(5)z+7.16(6)=0$

Atoms	C(21)	C(22)	C(23)	C(24)	C(25)
Distances to plane (Å)	−0.00(1)	0.00(1)	−0.00(1)	0.00(6)	−0.00(1)

Equation of plane 4 : $0.874(2)x-0.341(3)y-0.343(5)z+3.09(4)=0$

Atoms	N(3)	C(37)	N(4)	C(38)	O(2)
Distances to plane (Å)	−0.02(1)	0.05(1)	0.06(1)	0.04(1)	0.01(1)

Equation of plane 5 : $-0.739(3)x+0.606(4)y-0.290(4)z+3.32(3)=0$

Atoms	C(31)	C(32)	C(33)	C(34)	C(35)	C(36)
Distances to plane (Å)	0.00(1)	0.00(1)	0.00(1)	0.00(1	0.00(1)	0.00(1)

Equation of plane 6 : $0.758(4)x-0.536(5)y-0.370(5)z+3.63(6)=0$

Atoms	C(41)	C(42)	C(43)	C(44)	C(45)
Distances to plane (Å)	0.00(1)	0.00(1)	0.01(1)	0.00(1)	0.00(1)

Planes	1–2	1–3	1–4	1–5	1–6	2–3	2–4	2–5
Dihedral angle (°)	142.87	11.98	7.45	145.35	9.32	140.16	136.10	4.91
Planes	2–6	3–4	3–5	3–6	4–5	4–6	5–6	
Dihedral angle (°)	139.78	16.20	141.14	3.05	138.98	13.15	141.16	

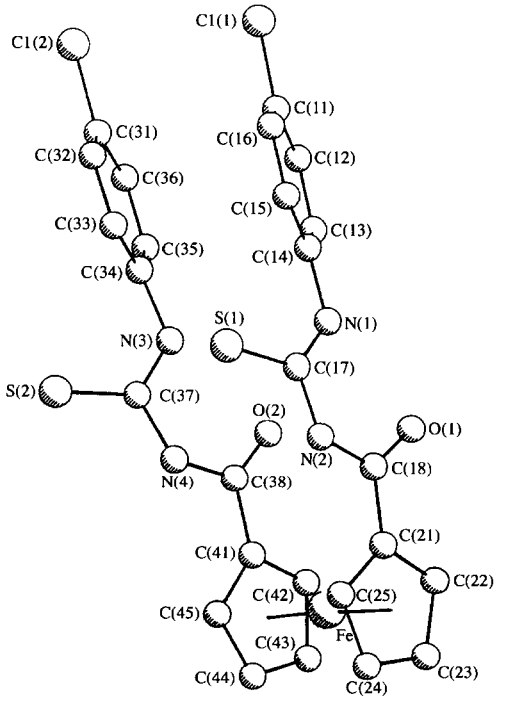


Fig. 3. X-ray diffraction single-crystal structure of compound **5**.

between them. This crystal consists of discrete molecules and the contact distances between the molecules are normal van de Waals' distances.

Acknowledgement—This work is supported by the National Natural Science Foundation of China.

REFERENCES

1. Sarkis, G. Y. and Faisal, E. D., *J. Heterocycl. Chem.* 1985, **22,** 137.
2. Wang, Ji-tao, Zhang, Yun-wen, Xu, Yu-ming, Yuan, Yao-feng and Gao, Sheng-hua, *Chem. J. Chin. Univ.*, 1993, **14,** 801.
3. Wang, Ji-tao, Yuan, Yao-feng, Xu, Yu-ming and Zhang, Yun-wen, *J. Organomet. Chem.*, 1994, **481** 211.
4. Wang, Ji-tao, Yuan, Yao-feng, Xu, Yu-ming and Zhang, Yun-wen, *Acta Chim. Sinica*, 1996, **54,** 32.
5. Bellamy, L. T., *The Infrared Spectra of Complex Molecules*. John Wiley, London, 1958. Translated into Chinese by Wei-yuan Huang and Chong-shi Nie, Science Press, Beijing 1975.
6. Benito, A., Cano, J. and Ramon, M. M., *Inorg. Chem.*, 1993, **32,** 1197.

Pergamon

PII: S0277-5387(96)00464-0

Polyhedron Vol. 16, No. 10, pp. 1719–1722, 1997
Copyright © 1997 Elsevier Science Ltd
Printed in Great Britain. All rights reserved
0277-5387/97 $17.00+0.00

Synthesis and crystal structure of a novel oxo-centred trinuclear manganese complex $[Mn_3O(C_6H_5COO)_6(py)_3]\cdot 2CH_3CN$

Zhuang Jin Zhong,[a]* Jian-Qing Tao,[a] Hui Li,[a] Xiao-Zeng You[a] and Thomas C. W. Mak[b]

[a] Coordination Chemistry Institute, State Key Laboratory of Coordination Chemistry, Nanjing University, Nanjing 210093, P.R. China

[b] Department of Chemistry, The Chinese University of Hong Kong, Shatin, New Territories, Hong Kong

(Received 12 July 1996; accepted 16 September 1996)

Abstract—The title complex, $[Mn_3O(C_6H_5COO)_6(py)_3]\cdot 2CH_3CN$ (py = pyridine), has been prepared. Single-crystal X-ray analysis revealed a μ_3-oxo-bridged $Mn_2^{III}Mn^{II}$ structure, in which each manganese atom has a distorted octahedral environment. The Mn(1) atom is readily assigned as a Mn^{III} centre from the Mn—(μ_3-O) distance [1.819(5) Å]. The remaining Mn(2) and Mn(3) atoms are essentially equivalent in crystallography, indicating an electronic delocalization between Mn^{II} and Mn^{III} atoms. © 1997 Elsevier Science Ltd. All rights reserved.

Keywords: crystal structure; trinuclear complex; manganese complex; μ_3-oxo centred metal carboxlate; mixed-valence complex; electronic delocalization.

The study of manganese polynuclear complexes has been important for understanding the structure and reactivity of manganese sites in biological systems [1,2], and in the quest to obtain molecular species with large spin ground states [3]. Trinuclear complexes of the general formulation of $[Mn_3O(RCO_2)_6L_3]^{0,1+}$ (L = py, H_2O) are known as good starting materials for synthesizing manganese polynuclear complexes [4]. In previous work, we have established that treatment of $[Mn_3O(CH_3COO)_6(py)_3]\cdot py$ (**1**) with 2,2′-bipyridyl-3,3′-dicarboxylic acid (H_2bpc) and triethylamine gave a novel linear trinuclear manganese(II) complex [5]. In this study, the title complex was isolated unexpectedly under the same conditions using $[Mn_3O(C_6H_5COO)_6(py)_2(H_2O)]\cdot 0.5CH_3CN$ (**2**) instead of the acetate derivative **1**. The crystal structure has been investigated.

EXPERIMENTAL

Preparations

All chemicals were obtained from commercial sources and used without further purification. $[Mn_3O(C_6H_5COO)_6(py)_2(H_2O)]\cdot 0.5CH_3CN$ (**2**) was prepared according to the literature method [6].

$[Mn_3O(C_6H_5COO)_6(py)_3]\cdot 2CH_3CN$. An acetonitrile solution containing 0.1 mmol of both H_2bpc and triethylamine was added to an acetonitrile solution of 0.2 mmol of **2** in a total volume of 15 cm^3, and the mixture was allowed to stand for several days to give black prisms. Found: C, 59.3; H, 4.4; N, 5.3. Calc. for $C_{61}H_{51}Mn_3N_5O_{13}$: C, 59.7; H, 4.2; N, 5.7%.

X-ray structure determination

Intensity data were collected on a Siemens R3m/V diffractometer using Mo-K_α radiation at 293 K. Although the unit cell has tetragonal geometry, on the basis of extinction conditions and correct structure solution, the orthorhombic space group $P2_12_12_1$ was chosen. Crystal parameters and details of the data collection and refinement are given in Table 1. The structure was solved by direct phase determination and refined by the blocked-diagonal least-squares method. Hydrogen atoms were placed in their calculated positions. All calculations were carried out using the SHELXTL-PC program package. The final

* Author to whom correspondence should be addressed.

Table 1. X-ray crystal data collection and processing parameters

Molecular formula	$C_{61}H_{51}Mn_3N_5O_{13}$
Molecular weight	1226.9
Colour and habit	Black, prism
Crystal size/mm	$0.36 \times 0.40 \times 0.46$
Crystal system	Orthorhombic
Space group	$P2_12_12_1$ (No. 19)
Unit-cell parameters	$a = 17.758(3)$ Å
	$b = 17.761(2)$ Å
	$c = 18.688(2)$ Å
	$V = 5894(1)$ Å^3
	$Z = 4$
	$F(000) = 2524$
Density (calcd)/g cm^{-3}	1.383
Radiation	graphite-monochromated Mo-K_α, $\lambda = 0.71073$ Å
Standard reflections	(0, 1, 3); (1, 3, 2)
Intensity variation	±1.1%
R_{int} (from merging of equiv. reflections)	0.000
Absorption coefficient/mm^{-1}	0.70
Mean μr	0.11
Transmission factors	0.841–0.905
Scan type and rate	ω–2θ scan; 3.50–29.30° min^{-1}
Scan range/°	1.00 below K_{α_1} to 1.00 above K_{α_2}
Background counting	Stationary counts for 1/5 of scan time at each end of scan range
Collection range	$0 \leqslant h \leqslant 21$, $0 \leqslant k \leqslant 21$, $0 \leqslant l \leqslant 22$; $2\theta_{max} = 50°$
Unique data measured	5663
Obs. data with $\|F_o\| \geqslant 4\sigma(\|F_o\|)$, n	2793
No. of variables, p	487
Weighting scheme	$w = [\sigma^2\|F_o\| + 0.0010\|F_o\|^2]^{-1}$
$R_F = \Sigma \|\|F_o\|-\|F_o\|\|/\Sigma\|F_o\|$	0.045
$wR = [\Sigma w^2(\|F_o\|-\|F_c\|)^2/\Sigma w^2\|F_o\|^2]^{1/2}$	0.049
$S = [\Sigma w(\|F_o\|-\|F_c\|)^2/(n-p)]^{1/2}$	0.96
Largest and mean Δ/σ	0.004, 0.000
Residual extrema in final difference map/e Å^{-3}	+0.76 to −0.40

R values and other parameters are displayed in Table 1 and selected bond lengths and angles are given in Table 2. Tables of atomic coordinates, thermal parameters, bond lengths and angles have been deposited at the Cambridge Crystallographic Data Centre.

RESULTS AND DISCUSSION

The crystal consists of trinuclear $[Mn_3O(C_6H_5COO)_6(py)_3]$ units and contains CH_3CN as solvent of crystallization in a 1:2 ratio. As shown in Fig. 1, the title complex features a μ_3-oxo-bridged trinuclear manganese structure, where each manganese atom has a distorted octahedral environment composed of the μ_3-oxo O(1) atom and four oxygen atoms from bridging benzoate groups and a terminal pyridine nitrogen atom. Such a structure is often seen in transition metal basic carboxylates [6,7]. The molecule approximates to C_{2v} symmetry and the geometry around Mn(2) and Mn(3) is very similar. The distances Mn(1)—Mn(2), Mn(1)—Mn(3) and Mn(2)—Mn(3) are 3.284, 3.285 and 3.403 Å, respectively, showing that the [Mn(1)Mn(2)Mn(3)] is an isosceles triangle. The central O(1) atom lies slightly above the Mn_3 plane (0.0085 Å). The charge on the complex necessitates a mixed-valence $Mn^{III}_2Mn^{II}$ description. The Mn(1) atom is readily assigned as an Mn^{III} centre, since the Mn(1)—O(1) distance [1.819(5) Å] is the shortest of the Mn—O distances. Thus, one of Mn(2) and Mn(3) is an Mn^{II} atom, the other a Mn^{III} atom. However, these two Mn atoms are essentially equivalent crystallographically, suggesting an electronic delocalization between them. In fact, the distances Mn(2)—O(1) 1.972(5) Å, Mn(3)—O(1) 1.966(5) Å are just close to the average value [1.975 Å of Mn^{II}, Mn^{III}—(μ_3-O)] distances observed in the valence-trapped complex **2**, in which Mn^{II}, Mn^{III} atoms are distinguished from each other [6]. Averaging of Mn^{II}, Mn^{III}—(μ_3-O) distances is also observed in complex **1**, which shows an electronic delocalization between all three Mn atoms [6]. It is interesting that the delocalization occurs only between two Mn atoms in the title complex in contrast to the valence-trapped complex **1** and non-valence-trapped complex **2**. Such a μ_3-oxo-centred metal carboxylate has not been reported so far to our knowledge.

Table 2. Selected bond distances (Å) and angles (°)

Mn(1)—O(1)	1.819(5)	Mn(1)—O(2)	2.002(6)
Mn(1)—O(7)	2.000(6)	Mn(1)—O(9)	2.127(7)
Mn(1)—O(13)	2.135(7)	Mn(1)—N(1)	2.077(7)
Mn(2)—O(1)	1.972(5)	Mn(2)—O(5)	2.113(7)
Mn(2)—O(6)	2.113(7)	Mn(2)—O(8)	2.097(7)
Mn(2)—O(10)	2.108(7)	Mn(2)—N(2)	2.194(10)
Mn(3)—O(1)	1.966(5)	Mn(3)—O(3)	2.123(7)
Mn(3)—O(4)	2.112(7)	Mn(3)—O(11)	2.112(7)
Mn(3)—O(12)	2.092(7)	Mn(3)—N(3)	2.199(11)
O(1)—Mn(1)—O(2)	95.2(3)	O(1)—Mn(1)—O(7)	95.3(2)
O(2)—Mn(1)—O(7)	169.5(3)	O(1)—Mn(1)—O(9)	97.2(3)
O(2)—Mn(1)—O(9)	88.5(3)	O(7)—Mn(1)—O(9)	90.2(3)
O(1)—Mn(1)—O(13)	96.8(3)	O(2)—Mn(1)—O(13)	90.6(3)
O(7)—Mn(1)—O(13)	88.1(3)	O(9)—Mn(1)—O(13)	166.0(3)
O(1)—Mn(1)—N(1)	179.8(4)	O(2)—Mn(1)—N(1)	84.6(3)
O(7)—Mn(1)—N(1)	84.9(3)	O(9)—Mn(1)—N(1)	82.8(3)
O(13)—Mn(1)—N(1)	83.2(3)	O(1)—Mn(2)—O(5)	94.6(2)
O(1)—Mn(2)—O(6)	91.9(2)	O(5)—Mn(2)—O(6)	88.8(3)
O(1)—Mn(2)—O(8)	98.6(2)	O(5)—Mn(2)—O(8)	166.7(3)
O(6)—Mn(2)—O(8)	89.1(3)	O(1)—Mn(2)—O(10)	92.8(3)
O(5)—Mn(2)—O(10)	89.4(3)	O(6)—Mn(2)—O(10)	175.1(3)
O(8)—Mn(2)—O(10)	91.6(3)	O(1)—Mn(2)—N(2)	177.0(3)
O(5)—Mn(2)—N(2)	83.7(3)	O(6)—Mn(2)—N(2)	90.6(3)
O(8)—Mn(2)—N(2)	83.1(3)	O(10)—Mn(2)—N(2)	84.7(3)
O(1)—Mn(3)—O(3)	92.1(2)	O(1)—Mn(3)—O(4)	92.8(3)
O(3)—Mn(3)—O(4)	174.9(3)	O(1)—Mn(3)—O(11)	94.7(2)
O(3)—Mn(3)—O(11)	88.2(3)	O(4)—Mn(3)—O(11)	89.6(3)
O(1)—Mn(3)—O(12)	98.7(3)	O(3)—Mn(3)—O(12)	89.6(3)
O(4)—Mn(3)—O(12)	91.4(3)	O(11)—Mn(3)—O(12)	166.5(3)
O(1)—Mn(3)—N(3)	177.0(3)	O(3)—Mn(3)—N(3)	90.0(3)
O(4)—Mn(3)—N(3)	85.1(3)	O(11)—Mn(3)—N(3)	83.1(3)
O(12)—Mn(3)—N(3)	83.5(3)	Mn(1)—O(1)—Mn(2)	120.0(3)
Mn(1)—O(1)—Mn(3)	120.4(3)	Mn(2)—O(1)—Mn(3)	119.6(3)

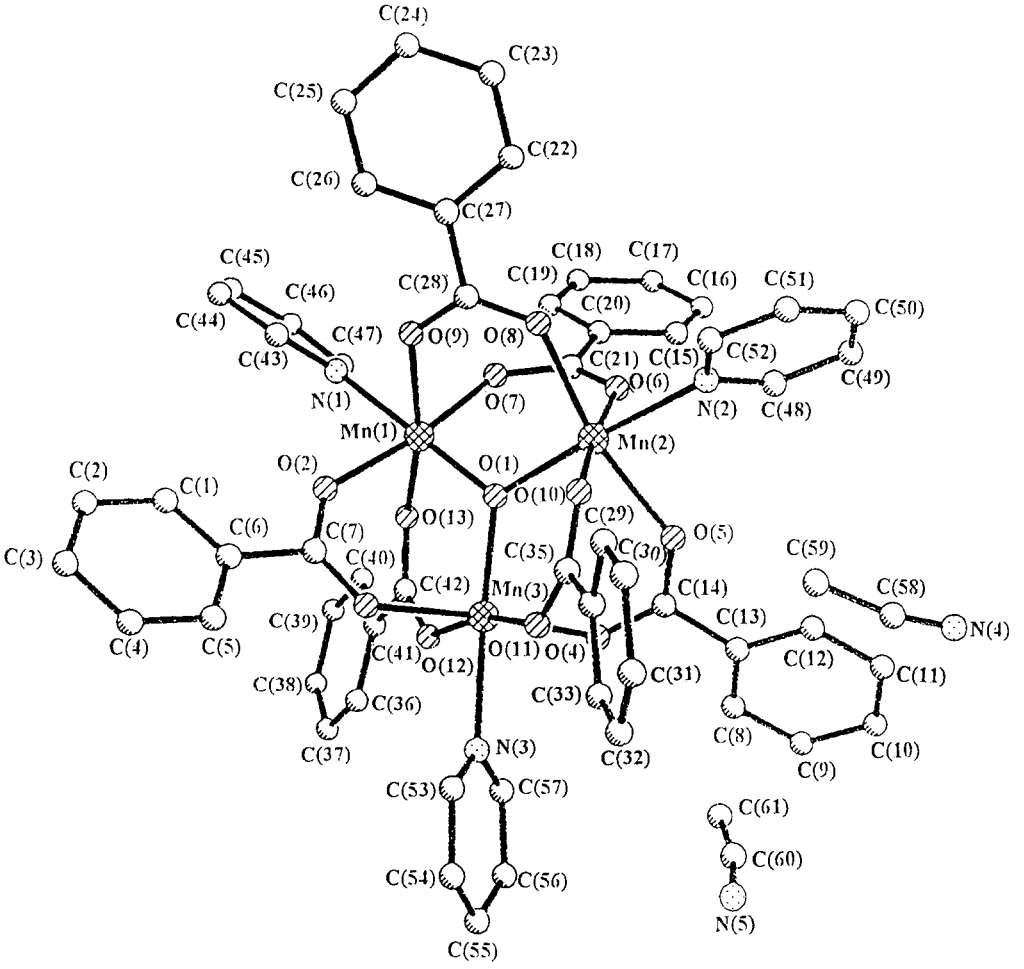


Fig. 1. Perspective view of the title complex with the atomic-numbering scheme.

Acknowledgements—This work was supported by a grant for Key Research Project from the State Science and Technology Commission and National Nature Science Foundation of China.

REFERENCES

1. Wieghardt, K., *Angew. Chem., Int. Ed. Engl.*, 1989, **28,** 1153.
2. Pal, S., Olmstead, M. M. and Armstrong, W. H., *Inorg. Chem.*, 1995, **34,** 4708.
3. Boyd, P. D. W., Li, Q., Vincent, J. B., Folting, K., Chang, H. R., Streib, W. E., Huffman, J. C., Christou, G. and Hendrickson, D. N., *J. Am. Chem. Soc.*, 1988, **110,** 8637.
4. Christou, G., *Acc. Chem. Res.*, 1989, **22,** 328.
5. Zhong, Z. J., You, X.-Z. and Mak, T. C. W., *Polyhedron*, 1994, **14,** 2157.
6. Vincent, J. B., Chang, H.-R., Folting, K., Huffman, J. C., Christou, G. and Hendrickson, D. N., *J. Am. Chem. Soc.*, 1987, **109,** 5703.
7. Woehler, S. E., Wittebort, R. J., Oh, S. M., Kambara, T., Hendrickson, D. N., Inniss, D. and Strouse, C. E., *J. Am. Chem. Soc.*, 1987, **109,** 1063.

Pergamon

PII: S0277-5387(96)00463-9

Polyhedron Vol. 16, No. 10, pp. 1723–1729, 1997
Copyright © 1997 Elsevier Science Ltd
Printed in Great Britain. All rights reserved
0277-5387/97 $17.00+0.00

Synthesis and structure of diaqua-bis(ethylenediamine)copper(II) salts with anions of carbamic acids

Larisa A. Kovbasyuk,[a] Igor O. Fritsky,[a]* Vladimir N. Kokozay[a]* and Turganbay S. Iskenderov[b]

[a] Department of Chemistry, Shevchenko University, Kiev 252033, Ukraine

[b] Department of Chemistry, Karakalpak University, 1a Universitetskaya Str., Nukus 742000, Uzbekistan

(Received 12 July 1996; accepted 16 September 1996)

Abstract—Two complexes of diaqua-bis(ethylenediamine)copper(II) with anions of *N*-carboxyglycine and ethylenediaminebiscarboxylic acid $[Cu(en)_2(H_2O)](OOCCH_2NHCOO)\cdot H_2O$ (**1**) and $[Cu(en)_2(H_2O)_2](OOCNHCH_2CH_2NHCOO)\cdot 2H_2O$ (**2**) were synthesized and investigated by single-crystal X-ray analysis and IR spectroscopy. Compound **1** was obtained by direct synthesis upon interaction of copper powder with glycine hydrochloride in methanol solution upon heating in air. Compound **2** was isolated as a result of a reaction between a copper(II) anionic complex with pyruvoylamide oxime (H_2pox) of composition K[Cu(pox)(Hpox)] with ethylenediamine and formaldehyde in methanol solution. In both cases formation of carbamate anions is connected with uptake of atmospheric carbon dioxide by the reaction mixtures. The crystal structures of **1** and **2** comprise $[Cu(en)_2H_2O)_2]^{2+}$ cations, carbamic acids anions and solvate water molecules. The complex cations of **1** and **2** consist of two ethylenediamine molecules coordinated in the equatorial plane [Cu—N = 2.007(3)–2.024(3) Å for **1** and 1.996(2) and 2.022(2) Å for **2**], and water molecules occupying the apical positions of distorted octahedra [Cu—O = 2.591(3) and 2.741(3) Å for **1** and 2.556(3) Å for **2**]. The extended hydrogen bond system in **1** and **2** unites the elements of the structures. © 1997 Elsevier Science Ltd. All rights reserved.

Keywords: carbon dioxide; direct synthesis; copper(II) complexes; carbamates; crystal structure; IR spectroscopy.

Removal of carbon dioxide from gaseous streams is an important procedure in different industrial technologies. One of the ways used in industry to eliminate carbon dioxide from gas mixtures is its absorption by liquid amines or their solutions [1] with formation of carbamates. As a rule, such interactions take place upon cooling to 0°C because CO_2 is liberated at higher temperatures owing to dissociation of the carbamates [2]. Most synthetic methods for aliphatic carbamates suggest the interaction of carbon dioxide with amines in alcoholic solutions at −10 to 0°C [3–5]. Recently, a method of CO_2 absorption on a silica gel containing 3-aminopropyl groups bonded to surface atoms of silicon at room temperature was reported [6] which led to the formation of surface carbamate groups.

Studying the results of direct synthesis of metal complexes with amines [7–9] and reactions of template condensation of amide-containing anionic complexes [10] with primary amines and formaldehyde, we noted that in some cases, when the reactions proceed in methanol solutions in air, unexpected products form owing to the uptake of carbon dioxide from the air. It is important that CO_2 absorption proceeds at room temperature or even upon heating. In order to study the nature and structure of these carbamate-containing products, and taking into account the fact that carbamates derived from primary amines and their metal complexes are poorly structurally characterized, we performed the X-ray single crystal and IR investigation of two new compounds. The present paper reports these results.

EXPERIMENTAL

All chemicals were commercial products of reagent grade and used without further purification. IR

* Authors to whom correspondence should be addressed.

spectra (KBr pellets) were recorded on an UR-20 spectrometer (Carl Zeiss Jena) in the region 400–4000 cm^{-1}.

Synthesis of $[Cu(en)_2(H_2O)_2](OOCCH_2NHCOO) \cdot H_2O$

Copper powder (0.63 g, 10 mmol) and glycine hydrochloride (1.1g, 1 mmol) were placed into the reactor, then 25 cm^3 of methanol and 2 cm^3 (30 mmol) of ethylenediamine were added. The reaction mixture was heated at 50–60°C upon continuous stirring for 20–25 min in the air until the complete dissolution of the copper powder was achieved. The solution formed was cooled and set aside in the air at room temperature for 24 h. Then isopropanol (20 cm^3) was added, and the blue crystalline product formed was filtered off and dried. Single crystals suitable for X-ray analysis were obtained by recrystallization from methanol. Yield 0.8 g (47%). Found: C, 23.9; H, 6.8; N, 20.2; Cu, 18.3. Calc. for $C_7H_{25}N_5O_7Cu$: C, 23.7; H, 7.1; N, 19.7; Cu, 17.9%.

Synthesis of $[Cu(en)_2(H_2O)_2](OOCNH_2CH_2NHCOO) \cdot 2H_2O$

K[Cu(pox)(Hpox)] (0.304 g, 1 mmol) prepared according to the literature method [11] was suspended in methanol (15 cm^3), then paraformaldehyde (0.060 g, 2 mmol) dissolved in methanol (10 cm^3) was added with the addition of 1 drop of 10% KOH in methanol and ethylenediamine (0.060, 1 mmol). The mixture obtained was heated at 60°C upon continuous stirring for 2 h in the air, then cooled and set aside for crystallization. The brown oil, after 3–4 weeks in the air, produced blue crystals of the title complex which were separated by hand from the bulky oil, washed with ethanol and dried in a dessicator. Yield 0.15 g (37%). Found: C, 24.2; H, 7.2; N, 20.8; Cu, 16.0. Calc. for $C_8H_{30}N_6O_8Cu$: C, 23.9; H, 7.5; N, 20.9; Cu, 15.8%.

Crystallographic data collection and structure determination

Crystal data and experimental details are presented in Table 1. The accurate unit-cell parameters and the orientation matrix were calculated from the setting angles of 24 reflections using the least-squares technique. Intensities were collected using an Enraf–Nonius CAD-4 diffractometer in the ω–2θ scan mode using Cu-K_α (for **1**) and Mo-K_α (for **2**) radiation. The intensities of three standard reflections, monitored every 100 intensity scans showed no evidence of crystal decay. Corrections for Lp effects, but not for absorption, were applied.

The positions of copper atoms and some non-hydrogen atoms were determined by direct methods, then the remaining non-hydrogen atoms were located in subsequent Fourier syntheses and refined by the full-matrix least-square technique using the SHELXL 93 program [12]. Neutral atom scattering factors and anomalous dispersion terms used in the refinement were taken from reference [13], real and imaginary components of anomalous dispersion were included for all non-hydrogen atoms. All the hydrogen atoms were localized from a difference Fourier map and their positional and isotropic displacement parameters were included in the final stage of the refinement. A weighting scheme of the form $w = 1/\sigma^2(F_0^2) + (0.0523P)^2 + 1.23P$ and $w = 1/\sigma^2(F_0^2) + (0.0417P)^2 + 1.05P$ [where P is defined as $F_0^2 + 2F_c^2)/3$] was applied for **1** and **2**, respectively. The bond distances and angles are listed in Tables 2 and 3.

RESULTS AND DISCUSSION

The structures of the complexes **1** and **2** are presented in Figs 1 and 2, respectively. The packing diagrams are presented in Figs 3 and 4. Both structures are ionic and consist of the complex cations $[Cu(en)_2(H_2O)_2]^{2+}$, anionic carbamic acid residues and the solvate water molecules. Complex **1** contain the anion of *N*-carboxyglycine, complex **2**, the anion of ethylenediaminebiscarbonic acid. The elements of the structure are joined to each other in the crystal packing by means of extended systems of hydrogen bonds where the protons belonging to the water molecules or NH_2 and NH groups act as donors (Figs 3 and 4). Parameters for the hydrogen bonds are listed in Tables 4 and 5.

The complex cations in **1** and **2** consist of two ethylenediamine molecules that coordinate the central atom in the equatorial plane in chelate mode, and two water molecules occupying the apical positions of the severely elongated octahedra (Figs 1 and 2). The Cu—N distances in both complexes are in the range of 1.996(2)–2.024(3) Å which is normal for Cu—N-(amine) bonds. The bite angles are decreased to 83.73(11)–84.78(7)°. Similar geometrical parameters for the coordination sphere have been reported for other diaqua-bis(ethylenediamine)copper(II) salts [14–17]. As the copper atom in **2** occupies the partial position ($\frac{1}{4}$, $\frac{1}{4}$, $\frac{1}{2}$) the coordination polyhedron is centrosymmetric (symmetry D_{4h}), the central and the donor atoms lie in the same plane. In **1** the donor atoms lie in the same plane (the maximal deviations do not exceed 0.01 Å), the copper atom is situated 0.05 Å above the plane of best fit towards the closer axial donor atom O(1). In **2** the long axial contact Cu—O(4) of 2.556(2) Å is in fact coincident with those found in other structures containing the centrosymmetric $[Cu(en)_2(H_2O)_2]^{2+}$ cation (2.580 Å [14] and 2.572 Å [15]). In compound **1** these distances are different [Cu—O(1) 2.591(3) and Cu—O(2) 2.741(3) Å]. This is probably owing to non-equivalence of the hydrogen bonds formed by the O(1) and O(2) atoms. The latter is involved in an additional acceptor hydro-

Table 1. Crystal data and structure refinement for **1** and **2**

	1	**2**
Empirical formula	$C_7H_{25}N_5O_7Cu$	$C_8H_{30}N_6O_8Cu$
M	354.86	401.92
Temperature/K	293(2)	293(2)
Wavelength/Å	1.54178	0.71073
Crystal system	Monoclinic	Monoclinic
Space group	$P2_1/n$	$C2/c$
a/Å	12.303(7)	19.310(3)
b/Å	9.462(5)	9.694(1)
c/Å	12.614(5)	10.172(1)
α/°	90.0	90.0
β/°	99.07(4)	113.74(1)
γ/°	90.0	90.0
U/Å^3	1450.0(13)	1743.0(4)
Z	4	4
D_c/Mg m^{-3}	1.625	1.532
μ/mm^{-1}	2.513	1.301
$F(000)$	748	852
Crystal size/mm	0.24 × 0.18 × 0.12	0.2 × 0.2 × 0.4
θ range/°	4.67–56.96	2.30–24.98
Range hkl	0 to 13, 0 to 10, −13 to 13	0 to 22, 0 to 11, −12 to 11
Reflections collected	2057	1573
Indpendent reflections (R_{int})	1939	1506
Data/parameters	1393/281	1506/166
Goodness-of-fit on F^2	1.067	1.063
Final R indices [$I > 2\sigma(I)$]	$R_1^a = 0.0345$, $wR_2^b = 0.0888$	$R_1^a = 0.0252$, $wR_2^b = 0.0674$
R indices (all data)	$R_1^a = 0.0448$, $wR_2^b = 0.1060$	$R_1^a = 0.0356$ $wR_2^b = 0.0804$
Max Δ/σ/Å	0.007	0.002
Max., min. electron density/e Å^{-3}	0.383, −0.576	0.438, −0.223

[a] $R_1 = \Sigma(F_o - F_c)/\Sigma F_o$.
[b] $wR_2 = \{\Sigma[w(F_o^2 - F_c^2)^2]/\Sigma[w(F_o^2)^2]\}^{1/2}$.

Table 2. Selected bond lengths (Å) and angles (°) for complex **1**

Cu—N(3)	2.007(3)	O(7)—C(7)	1.271(4)
Cu—N(1)	2.015(3)	N(1)—C(1)	1.470(4)
Cu—N(4)	2.021(3)	N(2)—C(2)	1.469(4)
Cu—N(2)	2.024(3)	N(3)—C(3)	1.471(4)
Cu—O(1)	2.591(3)	N(4)—C(4)	1.473(4)
Cu—O(2)	2.741(3)	N(5)—C(7)	1.376(4)
O(4)—C(5)	1.260(4)	N(5)—C(6)	1.437(5)
O(5)—C(5)	1.242(4)	C(1)—C(2)	1.490(5)
O(6)—O(7)	1.251(4)	C(3)—C(4)	1.497(5)
		C(5)—C(6)	1.484(4)

N(3)—Cu—N(1)	176.56(12)	O(1)—Cu—O(2)	177.37(8)
N(3)—Cu—N(4)	84.18(11)	C(7(—N(5)—C(6)	120.4(3)
N(1)—Cu—N(4)	95.59(11)	N(1)—C(1)—C(2)	107.5(3)
N(3)—Cu—N(2)	96.36(11)	N(2)—C(2)—C(1)	107.3(3)
N(1)—Cu—N(2)	83.73(11)	N(3)—C(3)—C(4)	107.7(3)
N(4)—Cu—N(2)	177.56(12)	N(4)—C(4)—C(3)	106.8(3)
N(3)—Cu—O(1)	87.98(11)	O(5)—C(5)—O(4)	124.7(3)
N(1)—Cu—O(1)	95.46(11)	O(5)—C(5)—C(6)	119.1(3)
N(4)—Cu—O(1)	96.42(12)	O(4)—C(5)—C(6)	116.2(3)
N(2)—Cu—O(1)	85.99(12)	N(5)—C(6)—C(5)	115.6(3)
N(3)—Cu—O(2)	92.42(11)	O(6)—C(7)—O(7)	124.9(2)
N(1)—Cu—O(2)	84.14(11)	O(6)—C(7)—N(5)	118.3(3)
N(4)—Cu—O(2)	86.21(12)	O(7)—C(7)—N(5)	116.7(3)
N(2)—Cu—O(2)	91.38(12)		

Table 3. Selected bond lengths (Å) and angles (°) for complex **2**

Cu—N(2)	1.996(2)	N(2)—C(2)	1.478(3)
Cu—N(1)	2.022(2)	N(3)—C(4)	1.345(3)
Cu—O(4)	2.556(2)	N(3)—C(3)	1.438(3)
O(1)—C(4)	1.267(2)	C(1)—C(2)	1.488(3)
O(2)—C(4)	1.267(2)	C(3)—C(3^{ii})	1.512(4)
N(1)—C(1)	1.463(3)		

N(2^{i})—Cu—N(2)	180.0	C(4)—N(3)—C(3)	125.4(2)
N(2^{i})—Cu—N(1)	95.22(7)	N(1)—C(1)—C(2)	109.0(2)
N(2)—Cu—N(1)	84.78(7)	N(2)—C(2)—C(1)	108.1(2)
N(2^{i})—Cu—O(4)	94.07(8)	N(3)—C(3)—C(3^{ii})	115.3(2)
N(2)—Cu—O(4)	85.93(8)	O(1)—C(4)—O(2)	123.7(2)
N(1)—Cu—O(4)	92.13(8)	O(1)—C(4)—N(3)	117.6(2)
N(1^{i})—Cu—O(4)	87.87(8)	O(2)—C(4)—N(3)	118.7(2)

Symmetry transformations used to generate equivalent atoms: (i) $-x+\frac{1}{2}, -y+\frac{1}{2}, -z+1$; (ii) $-x, y, -z-\frac{1}{2}$.

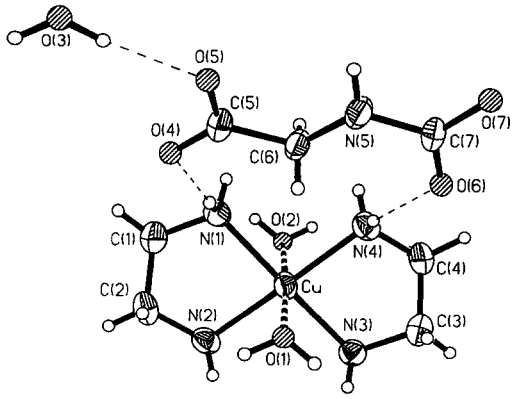


Fig. 1. Structure and numbering scheme for complex **1**.

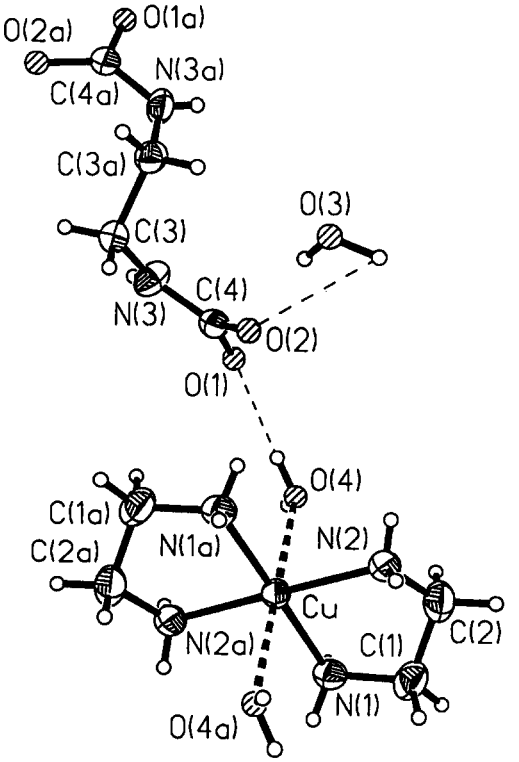


Fig. 2. Structure and numbering scheme for complex **2**.

gen bond, N(5)—H···O(2) (Table 4), which leads to elongation of the Cu—O(2) axial contact. Somewhat shorter values of Cu—O distances were seen in the only reported structure containing the non-centrosymmetric cation (2.514 and 2.674 Å) [17]. The five-membered chelate rings in both cations possess the *gauche* conformation with the carbon atoms deviating from the CuNN planes by 0.27–0.40 Å.

In the anion of ethylenediaminebiscarbonic acid (compound **2**) the C—O distances of the carboxylic moieties C(4)—O(1) and C(4)—O(2) are equal [1.267(2) Å], the angle O(1)—C(4)—O(2) is 123.7(2)°. In compound **1** one can observe the differences in C—O distances in the carboxylic moieties [1.242(2)–1.271(4) Å] which arise probably as a result of the non-equivalence of hydrogen bonds involving the carboxylic oxygen atoms. The values of the corresponding bond angles are: O(4)—C(5)—O(5) 124.7(3); O(6)—C(7)—O(7) 124.9(2)°. Such values for the geometrical parameters are typical of free deprotonated carboxylic groups [18]. The angular geometry around the nitrogen atoms in both anions approaches trigonal planar. The N—C(carboxyl) bond distances (in **1**: N(5)—C(7) 1.376(4); in **2**: N(3)—C(4) 1.345(3) Å] indicate their partly double bonded nature. This is because of the participation of the nitrogen atom in the delocalization of the electron density from the C—O bonds, which is characteristic of amides [19]. As a result, the CH_2—NH—COO^- moieties in both anions are nearly planar (the deviations of the atoms from the mean planes do not exceed 0.03 Å). In the case of ethylenediaminibiscarbaminate complex (**2**) the anion consists of two such planar fragments related by a two-fold axis and linked by the C(3)—C(3a) bond with a tor-

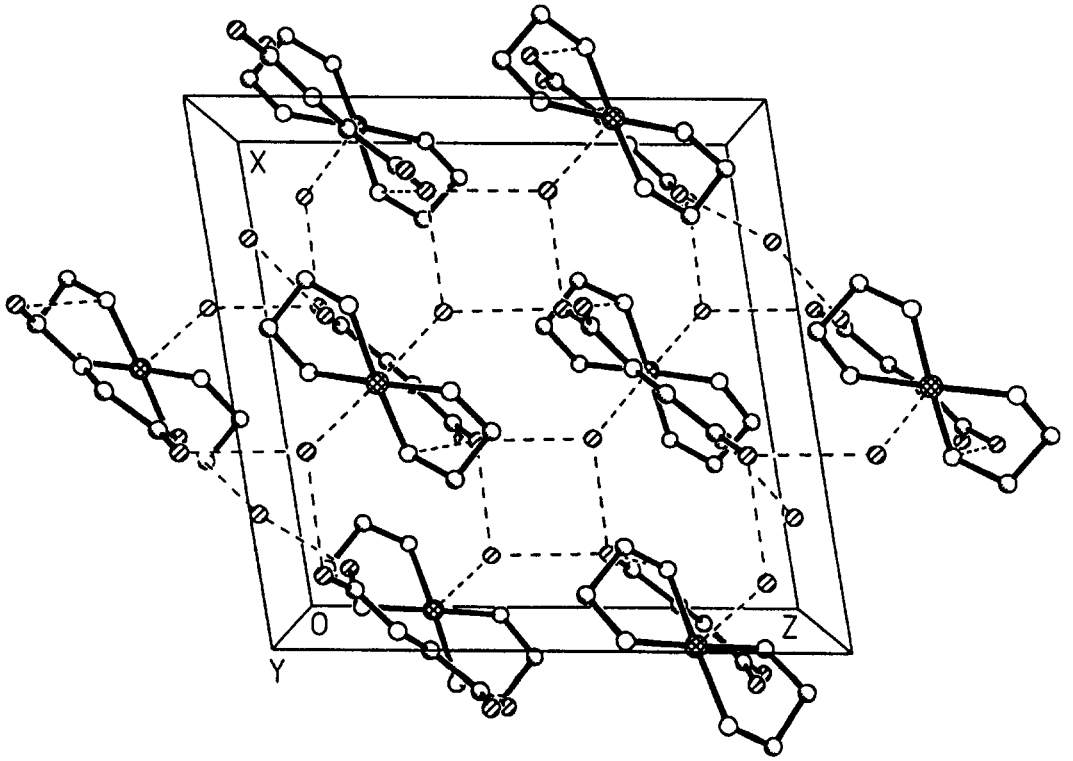


Fig. 3. Perspective view of the unit-cell packing for **1**.

Table 4. Hydrogen-bond parameters in the structure **1**

Donor (A)	Acceptor (B)	Symmetry of B	A···B (Å)	A—H (Å)	H···B (Å)	Angle A—H···B ( )
O(3)	O(5)	x, y, z	2.688(4)	0.82	1.89(5)	165
O(3)	O(6)	$x-\frac{1}{2}, -y+\frac{3}{2}, z+\frac{1}{2}$	2.680(4)	0.82	1.89(5)	164
O(1)	O(7)	$-x+\frac{1}{2}, y-\frac{1}{2}, -z+\frac{1}{2}$	2.844(4)	0.77	2.08(4)	173
O(1)	O(4)	$-x, -y+1, -z+1$	2.856(4)	0.81	2.06(4)	167
O(2)	O(7)	$-x, -y+1, -z$	1.825(4)	0.77	2.06(4)	172
N(1)	O(4)	x, y, z	2.931(4)	0.91	2.05(4)	163
N(2)	O(5)	$x, y-1, z$	3.008(4)	0.85	2.21(4)	156
N(3)	O(6)	$-x+\frac{1}{2}, y-\frac{1}{2}, -z+\frac{1}{2}$	3.031(4)	0.79	2.30(4)	154
N(3)	O(7)	$x, y-1, z$	2.911(4)	0.86	2.07(4)	163
N(4)	O(6)	x, y, z	3.051(4)	0.80	2.31(4)	155
N(5)	O(2)	$x, y+1, z$	3.187(4)	0.82	2.39(4)	166

Table 5. Hydrogen bond parameters in the structure **2**

Donor (A)	Acceptor (B)	Symmetry of B	A···B (Å)	A—H (A)	H···B (Å)	Angle A—H···B ( )
O(4)	O(1)	x, y, z	2.726(3)	0.79	1.94(4)	176
O(3)	O(2)	$-x+\frac{1}{2}, -y+\frac{1}{2}, -z$	2.764(2)	0.87	1.90(3)	171
O(3)	O(2)	x, y, z	2.772(2)	0.73	2.04(3)	172
N(1)	O(2)	$-x+\frac{1}{2}, -y+\frac{1}{2}, -z+1$	3.150(3)	0.84	2.34(3)	162
N(1)	O(3)	$-x+\frac{1}{2}, y-\frac{1}{2}, -z+\frac{1}{2}$	2.969(3)	0.79	2.20(3)	163
N(2)	O(1)	$-x+\frac{1}{2}, y+\frac{1}{2}, -z+\frac{1}{2}$	2.973(3)	0.84	2.17(3)	161
N(2)	O(3)	$-x+\frac{1}{2}, -y+\frac{1}{2}, -z$	2.948(3)	0.81	2.14(3)	175
N(3)	O(1)	$-x, -y, -z$	3.004(3)	0.69	2.33(3)	168

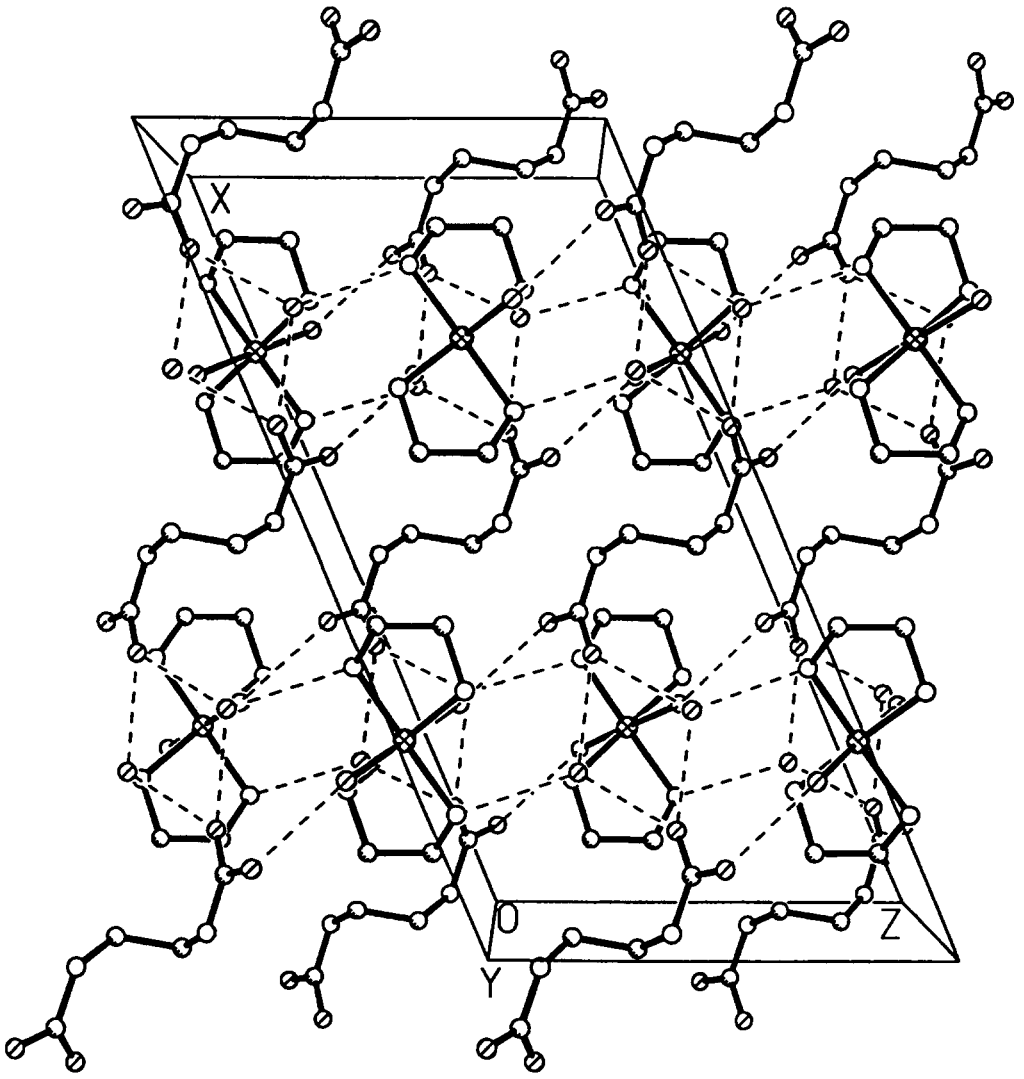


Fig. 4. Perspective view of the unit-cell packing for **2**.

sion angle N(3)—C(3)—C(3a)—N(3a) of 54.5°. Note, that the values of the bond distances and angles for both carbamate anions are close to those reported for N-(2-ammonioethyl)carbamate [20].

In the IR spectra of compounds **1** and **2** the bands corresponding to the ν_s and ν_{as} modes of the COO^- group are seen (**1**: 1418 and 1585 cm^{-1}; **2** 1421 and 1582 cm^{-1}, respectively). In compound **1**, however, these bands carry noticeable shoulders (at 1410 and 1575 cm^{-1}) which are probably a result of non-equivalence of two carboxylic groups in *N*-carboxyglycinate. In the region of 2850–3000 cm^{-1} the small bands for the ν(C—H) vibrations are observed: the intensive bands for the ν(C—N) vibrations are indicated at 1040 (**1**) and 1052 (**2**) cm^{-1}. The positions of the IR bands are close to those reported for the ethylenediaminebiscarbonic acid disodium salt [21].

Acknowledgements—This work was supported, in part, by the International Soros Science Education Program through Grant No. GSU 053068 (to L.A.K.). We also thank Edward B. Rusanov (Institute of Organic Chemistry, National Academy of Sciences of Ukraine) for collecting the X-ray data.

REFERENCES

1. Volkamer, K. and Wagner, U., *Fertilizer*, 1983, 139.
2. Caplow, M., *J. Am. Chem. Soc.*, 1958, **90,** 6795.
3. Katchalski, E., Berliner-Klibanski, C. and Berger, A., *J. Am. Chem. Soc.*, 1951, **73,** 1829.
4. Hoewe, B. D., Malone, L. J. and Manley, R. M., *Inorg. Chem.*, 1971, **10,** 930.
5. Gaines, G. L., *J. Org. Chem.*, 1985, **50,** 410.
6. Leal, O., Bolivar, C., Ovalles, C., Garcia, J. J. and Espidel, Y., *Inorg. Chim. Acta*, 1995, **240,** 183.

7. Vasilyeva, O. Yu., Kokozay, V. N. and Simonov, Yu. A., *Zh. Neorg. Khim.*, 1991, **36,** 3119.
8. Pavlenko, V., Kokozay, V. and Babich, O., *Z. Naturforsch.*, 1993, **48b,** 1321.
9. Kokozay, V. N. and Sienkiewicz, A. V., *Polyhedron*, 1995, **14,** 1547.
10. Fritsky, I. O. and Soukhan, V. V., International Symposium on Molecular Reaction Mechanisms involving Transition Metals: Experimental and Theoretical Aspects, 163. Book of Abstracts, Florence, Italy, 1994.
11. Simonov, Yu. A., Kravtsov, V. Kh., Fritskii, I. O., Gubina, E. E., Lampeka, R. D., Iskenderov, T. S. and Zhumabaev, A. Zh., *Koord. Khim.*, 1995, **21,** 407.
12. Sheldrick, G. M., SHELXL 93, University of Göttingen, Germany, 1993.
13. *International Tables for X-ray Crystallography*, vol. C., Kluwer, Dordrecht, Netherlands, 1992, Tables 4.2.6.8 and 6.1.1.4.
14. Fridman, A. Ya., Dyatlova, N. M., Trunov, V. K., Agre, V. M., Borkhanova, N. N. and Sisoeva, T. F., *Koord. Khim.*, 1981, **7,** 1638.
15. Emsley, J., Arif, M., Bates, P. A. and Hursthouse, M. H., *J. Chem. Soc., Chem. Commun.*, 1988, 1387.
16. Gomez-Romero, P., Jameson, G. B., Borras-Almenar, J. J., Escriva, E., Coronado, E. and Beltran, D., *J. Chem. Soc., Dalton Trans.*, 1988, 2747.
17. Shakibaie-Moghadam, M., Timper, U. and Heller, G., *Z. Naturforsch.*, 1994, **49,** 627.
18. Poray-Koshits, M. A., *Itogi Natuki I Tekhniki. Kristallografija (USSR)*, 1981, **15,** 3.
19. Sigel, H. and Martin, R. B., *Chem. Rev.*, 1982, **82,** 385.
20. Garbauskas, M. F., Goehner, R. P. and Davis, A. M., *Acta Cryst.*, 1983, **C39,** 1684.
21. Sevost'yanova, N. I., Martynenko, L. I. and Spitsyn, V. I., *Izv. Akad. Nauk. SSSR, Ser. Khim.*, 1972, **21,** 792.

Pergamon

PII: S0277-5387(96)00461-5

Polyhedron Vol. 16, No. 10, pp. 1731–1737, 1997
Copyright © 1997 Elsevier Science Ltd
Printed in Great Britain. All rights reserved
0277-5387/97 $17.00+0.00

Syntheses and X-ray structural characterization of phosphine cobalt(II) complexes with 2-mercaptobenzothiazole†

Bei-Sheng Kang,[a]* Zhong-Ning Chen,[a] Ye-Xiang Tong,[a] Han-Qin Liu,[a] Han-Rong Gao,[b] Bo-Mu Wu[b] and Thomas C. W. Mak[b]

[a] Department of Chemistry, Zhongshan University, Guangzhou, Guangdong 510275, P.R. China

[b] Department of Chemistry, Chinese University of Hong Kong, Shatin, New Territory, Hong Kong

(Received 18 June 1996; accepted 16 September 1996)

Abstract—Mononuclear cobalt(II) complexes $Co(mbt\text{-}N)_2(PBu^n_3)_2$ (**1**) (Hmbt = 2-mercaptobenzothiazole; PBu^n_3 = tri-n-butyphosphine) and $Co(mbt\text{-}S,N)_2(dppe)\cdot MeCN$ (**2**) [dppe = 1,2-bis(diphenylphosphino) ethane] were synthesized and characterized by X-ray crystallography, IR and EPR spectra, cyclic voltammetric data and magnetic susceptibility measurements. The Co atom in (**1**) exhibits an approximate square-planar geometry with the heterocyclic N-donors from mbt bonding to the cobalt atom in a monodentate mode. Complex (**2**) has a distorted octahedral environment of Co with both the exocyclic-S and the hetero-N donors of mbt bound to the cobalt atom in a bidentate chelating mode. The Co atom in both complexes shows spin state of $S = \frac{3}{2}$ with μ_{eff} of 4.25 and 4.40 μ_B for **1** and **2**, respectively. © 1997 Elsevier Science Ltd. All rights reserved.

Keywords: ternary cobalt complex; 2-mercaptobenzothiazole ligand; X-ray structure; tertiary phosphine.

Although metal complexes of thiolates with the participation of phosphine have been actively investigated and a broad variety of compounds with a great degree of complexity and nuclearity has been obtained [1–14], the area of phosphine cobalt complexes with heterocyclic thiolates as coligands has scarcely been touched. As a heterocyclic thiolato ligand with potential S and N donors, 2-mercaptobenzothiazole (Hmbt) is interesting not only because of the structural chemistry of its multifunctional coordination modes (unidentate-N, unidentate-$S_{exocyclic}$ or bidentate-N:S) [15], but also because of the formation of complexes with biological activities and with practical applications such as anticorrosion and as accelerators in the rubber vulcanization process [16–18]. Until now, the only Co–mbt complex with a known structure has been $Co(mbt)(py)_2$ [19], despite the fact that complexes of Zn [20,21], Cd [21–24], and Cu [25] are known. Our interest in phosphine-participated Co complex formation has been extended to mixed mbt and tertiary phosphines. Herein we report the syntheses of two complexes with different coordination geometries: four-coordinate, square-planar $Co(mbt\text{-}N)_2(PBu^n_3)_2$ (**1**) and six-coordinate, distorted octahedral $Co(mbt\text{-}N:S)_2(dppe)\cdot MeCN$ (**2**), by using monodentate and 1,2-bidentate phosphines, respectively.

EXPERIMENTAL

All operations were carried out under pure dinitrogen with Schlenk type apparatus. Reagents 2-mercaptobenzothiazole (Hmbt), tri-n-butyphosphine

* Author to whom correspondence should be addressed.

† Part III of 'Reaction of Transition Metal Thiolato Units'. Part I: Kang, B. S., Chen, Z. N., Zhou, Z. Y., Tong, Y. X. and Yu, X. L., *Acta Sci. Natur. Univ. Sunyatseni*, 1996, **35**, 127. Part II: Kang, B. S., Zhang, H. X., Gao, H. R., Zhou, Z. Y., Wu, B. M., Mak, T. C. W., Lin, Z. and Chen, Z. N., *Acta Chim. Sinica*, 1997, in press.

(PBu^n_3) and 1,2-bis(diphenylphosphino)ethane (dppe) were purchased from Aldrich and used as obtained. Anhydrous cobaltous chloride was prepared by refluxing $CoCl_2 \cdot 6H_2O$ in $SOCl_2$ according to the literature method [26]. Acetonitrile, DMF and MeOH were dried, distilled and flushed with pure dinitrogen or argon for 5 min before use.

Synthesis

Co(mbt-*N*)$_2$(PBu^n_3)$_2$ (**1**). To a mixture of Hmbt (0.34 g, 2 mmol), Na metal (0.046 g, 2 mmol) and PBu^n_3 (1 cm^3, 4 mmol) in 20 cm^3 of MeOH was added 0.26 g (2 mmol) of anhydrous $CoCl_2$ with stirring. After stirring for 3 h at room temperature, the solution was filtered and the dark green filtrate kept at 5°C for several days to given 0.15 g (9.0% yield based on Co) of dark brown cubic crystals of **1**. IR (KBr, cm^{-1}): 1585w, 1456s, 1423s, 1410s, 1392s, 1251m, 1088s, 1038s, 1014s, 969s, 905w, 891w, 754s, 724m, 690m, 656w, 615w, 592w, 503w, 432w and 424w.

Co(mbt-*N*:*S*)$_2$(dppe) (**2**). To a mixture of Hmbt (0.34 g, 2 mmol), Na metal (0.046 g, 2 mmol) in 1.5 cm^3 of MeOH and dppe (0.80 g, 2 mmol) in 20 cm^3 of MeCN was added 0.26 g (2 mmol) of anhydrous $CoCl_2$ with stirring. After refluxing for 3 h, the solution was filtered and the dark filtrate was kept at room temperature for one week to give 0.34 g (21.6% yield based on Co) of dark brown block crystals of **2**. IR (KBr, cm^{-1}): 1584m, 1562w, 1484w, 1456m, 1434s, 1377s, 1275w, 1249m, 1173s, 1159s, 1122m, 1093s, 1029s, 1014s, 999s, 876w, 843w, 829w, 750s, 727s, 690vs, 609w, 552w, 530s, 509m, 492m and 428w.

Crystal structure determination

Single crystals of compounds **1** and **2** with suitable dimensions were mounted on glass fibres and data collections were performed on diffractometers as shown in Table 1 using graphite-monochromated Mo-K_α radiation ($\lambda = 0.71073$ Å). The crystallographic data, data collection and structure refinement parameters are summarized in Table 1.

The coordinates of the metal atoms were determined by direct methods and the remaining non-hydrogen atoms were located from successive Fourier difference syntheses. The structures were refined by full-matrix least-square techniques with anisotropic thermal parameters for the non-hydrogen atoms. The positions of the hydrogen atoms were isotropically added to the structural factor calculation but not refined. All calculations were performed on an IBM PC/486 computer with the Siemens SHELXTL-PC program package [27]. Selected atomic distances and bond angles are presented in Tables 2 and 3 for **1** and **2**, respectively.

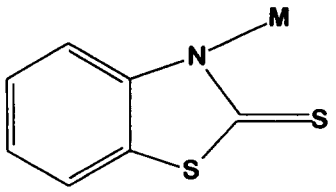
Physical measurements

Infrared spectra were recorded on a Nicolet 510 FT-IR spectrophotometer. Powder EPR spectra were recorded on a Bruker 2000-SRC spectrometer. Cyclic voltammetric measurements were performed on a HDV-7B potentiostat equipped with a DCD-3 low frequency–super low frequency functional generator and a LZ32-204 X-Y recorder in a three-electrode cell with platinum working and auxiliary electrodes and a saturated calomel electrode (SCE) as reference. The supporting electrolyte was $NBu^n_4BF_4$ (0.1 mol dm^{-3}) and the scan rate was 100 mV s^{-1}. Magnetic susceptibilities were measured on a model CF-1 superconducting extracting sample magnetometer at a magnetic field of 1.0 T.

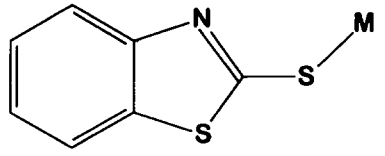
RESULTS AND DISCUSSION

As a versatile heterocyclic thiolato ligand with S and N donors, 2-mercaptobenzothiazole exhibits three different coordination modes known to date, bonding to metal ions through N or exocyclic S donors in monodentate terminal mode, or bidentate chelating mode, as shown in **I–III**.

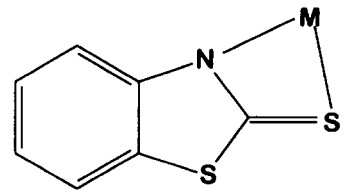
So far, modes **I–III** have all been found in Zn complexes [20,21], while no Cd complex has been found in mode **I** [21–24]. However, no regularities have been found and no rules can be followed so as to predict which mode will occur in a transition metal complex. The aforementioned complexes usually contain N-base or dialkyldithiocarbamate as coligands. No previous report has been made involving a phosphine



I



II



III

Table 1. Crystallographic data and data collection parameters for complexes **1** and **2**

	1	**2**
Formula	$C_{38}H_{62}N_2P_2S_4Co$	$C_{42}H_{35}N_3P_2S_4Co$
Formula weight	796.0	830.8
Crystal system	Monoclinic	Monoclinic
Space group	$P2_1/n$	$P2_1/n$
a (Å)	10.102(2)	12.047(1)
b (Å)	15.871(3)	19.392(1)
c (Å)	13.472(3)	17.663(1)
β ( )	97.51(3)	107.83(1)
V (Å^3)	2141.5(11)	3928(2)
Z	2	4
D_{calc} (g cm^{-3})	1.23	1.405
μ (cm^{-1})	6.98	7.66
$F(000)$	850	1716
Crystal dimensions (mm^3)	$0.35 \times 0.35 \times 0.50$	$0.30 \times 0.40 \times 0.50$
Diffractometer	Rigaku AFC 7R	Rigaku RAXIS
T (K)	293	293
Reflections independent	4386	8068
Reflections observed with $F > 8.0\ \sigma\ (F)$	3279	6361
R_{int}	0.0452	0.0399
Largest Δ/σ	0.001	0.048
R	0.0435	0.037
R_w	0.0545	0.045
Goodness-of-fit	1.05	0.92
Largest difference peak (e Å^{-3})	0.38	0.36

Table 2. Selected bond distances (Å) and bond angles ( ) for complex **1**

Co(1)—P(1)	2.312(1)	Co(1)—N(1)	1.938(2)
P(1)—C(8)	1.852(2)	P(1)—C(12)	1.833(3)
P(1)—C(16)	1.893(3)	S(1)—C(1)	1.684(2)
S(2)—C(1)	1.753(3)	S(2)—C(2)	1.743(3)
N(1)—C(1)	1.323(3)	N(1)—C(7)	1.388(3)
P(1)—Co(1)—N(1)	89.3(1)	N(1)—Co(1)—P(1a)	90.7(1)
Co(1)—P(1)—C(8)	116.0(1)	Co(1)—P(1)—C(12)	115.1(1)
Co(1)—P(1)—C(16)	116.0(1)	Co(1)—N(1)—C(1)	109.4(2)
Co(1)—N(1)—C(7)	137.2(2)	C(1)—S(2)—C(2)	90.2(1)
C(1)—N(1)—C(7)	113.3(2)	S(1)—C(1)—S(2)	125.9(1)
S(1)—C(1)—N(1)	121.0(2)	S(2)—C(1)—N(1)	113.0(2)
S(2)—C(2)—C(3)	129.6(2)	S(2)—C(2)—C(7)	109.8(2)

as coligand. When mono- and bi-dentate phosphines were used in this work, four- and six-coordinate complexes **1** and **2** were obtained respectively, with different coordination modes for Hmbt.

The structures of **1** and **2** are depicted in Figs 1 and 2, respectively. Complex **1** possesses a square-planar CoP_2N_2 core with the donor atoms P supplied by two PBu^n_3 ligands and N by two mbt ligands, where the latter are in the monodentate-N form, **I**. To our knowledge this is the first example containing mbt in a square-planar configuration as confirmed by X-ray analysis, although complexes with tetrahedral, square pyramidal, trigonal bipyramidal and octahedral geometries have all been reported previously [15–25]. Interestingly, when the monodentate tertiary phosphine is substituted by a 1,2-bidentate diphosphine, dppe, the six-coordinated Co^{II} complex **2** with a $CoP_2N_2S_2$ core in a distorted octahedron was formed.

Table 3. Selected bond distances (Å) and bond angles (°) for complex **2**

Co(1)—P(1)	2.241(1)	Co(1)—P(2)	2.227(1)
Co(1)—N(1)	2.000(2)	Co(1)—S(1)	2.470(1)
Co(1)—N(2)	2.024(2)	Co(1)—S(3)	2.682(1)
N(1)—C(27)	1.321(3)	N(1)—C(33)	1.394(3)
S(1)—C(27)	1.685(2)	S(2)—C(27)	1.750(2)
S(2)—C(28)	1.742(3)	N(2)—C(34)	1.321(3)
N(2)—C(40)	1.398(3)	S(3)—C(34)	1.688(2)
S(4)—C(34)	1.750(2)	S(4)—C(35)	1.744(2)

P(1)—Co(1)—P(2)	85.0(1)	P(1)—Co(1)—N(1)	90.8(1)
P(2)—Co(1)—N(1)	173.2(1)	P(1)—Co(1)—S(1)	90.6(1)
P(2)—Co(1)—S(1)	109.6(1)	N(1)—Co(1)—S(1)	65.0(1)
P(1)—Co(1)—N(2)	172.6(21)	P(2)—Co(1)—N(2)	92.3(1)
N(1)—Co(1)—N(2)	92.4(1)	S(1)—Co(1)—N(2)	96.8(1)
P(1)—Co(1)—S(3)	107.0(1)	P(2)—Co(1)—S(3)	86.0(1)
N(1)—Co(1)—S(3)	100.3(1)	S(1)—Co(1)—S(3)	157.7(1)
N(2)—Co(1)—S(3)	65.9(1)	Co(1)—N(1)—C(27)	104.8(1)
Co(1)—N(1)—C(33)	142.7(1)	Co(1)—S(1)—C(27)	69.4(1)
Co(1)—N(2)—C(34)	103.0(1)	Co(1)—N(2)—C(40)	144.6(1)
Co(1)—S(3)—C(34)	70.7(1)	N(1)—C(27)—S(1)	120.9(1)
N(1)—C(27)—S(2)	113.5(2)	S(1)—C(27)—S(2)	125.6(1)
N(2)—C(34)—S(3)	120.4(2)	N(2)—C(34)—S(4)	113.9(2)
S(3)—C(34)—S(4)	125.7(1)		

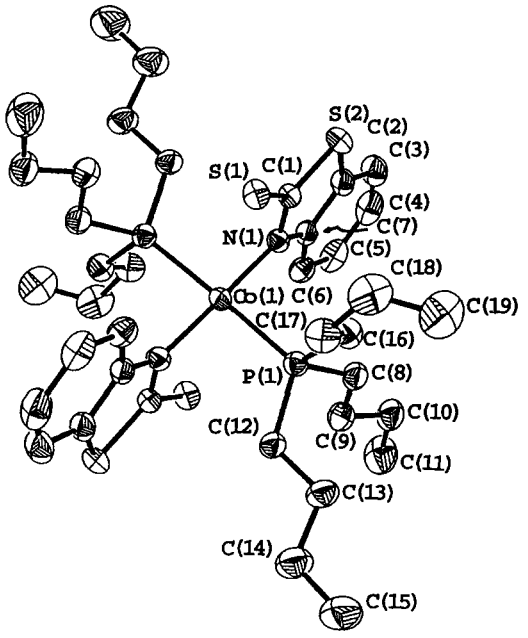


Fig. 1. Structure of Co(mbt-*N*)$_2$(PBu$^n_3$)$_2$ (**1**).

In this complex, the two mbt ligands coordinate to Co^{II} in bidentate-*N*:*S* form **III** with the S atoms in *trans* [S(1)—Co—S(3) 157.7(1)°] and N atoms in *cis* orientations [N(1)—Co—N(2) 92.4(1)°]. It is worthwhile noting that whether in **1** or **2**, with or without Co—S ligation, the C—S$_{exocyclic}$ distances remain within the range 1.68–1.69 Å, indicating that even with chelation of S to Co in **2**, the Co—S bond must be rather weak. This weak ligation is indeed shown by the longest average Co—S distance of 2.711 Å being found in **2**, of all the mbt-ligated complexes shown in Table 4. In general, the mbt ligand remains in the thione form after coordination.

The evidence for the formation of the four-membered chelate ring CoSCN in complex **2** comes from the decrease of the M—N—C(S) angle from 109.4° in **1** to 103.9°. The thiazole rings do not vary much between the two complexes, with N—C (to sulfur) averaging 1.32 Å, possessing a certain degree of double bond character and with N—C (to benzylidene) averaging 1.39 Å, more of a single bond. Since the N—C bond distance is 1.35 Å in the free ligand benzothiazole-2-thione [28] this is also considered evidence for delocalization in the ring system. The Co—P distance is shorter (by 0.08 Å) and Co—N longer (by 0.06 Å) in **2** compared with the corresponding bonds in **1**, probably owing to the different electronic effects of P and N atoms in square-planar or octahedral coordination sites. A definitive explanation for this result would be difficult before more complexes have been obtained for comparison. Comparing with the similarly octahedrally N:S-coordinated Cd complexes [Cd(mbt)$_3$] [24], Cd(mbt)$_2$(py)$_2$ [21], or Cd(mbt)$_2$(bipy) [22], complex **2** possesses the smallest M—S—C chelate angle (average 70.1°) and the largest M—N—C chelate angle (average 103.9°) within the four-membered chelate ring, as shown in Table 4.

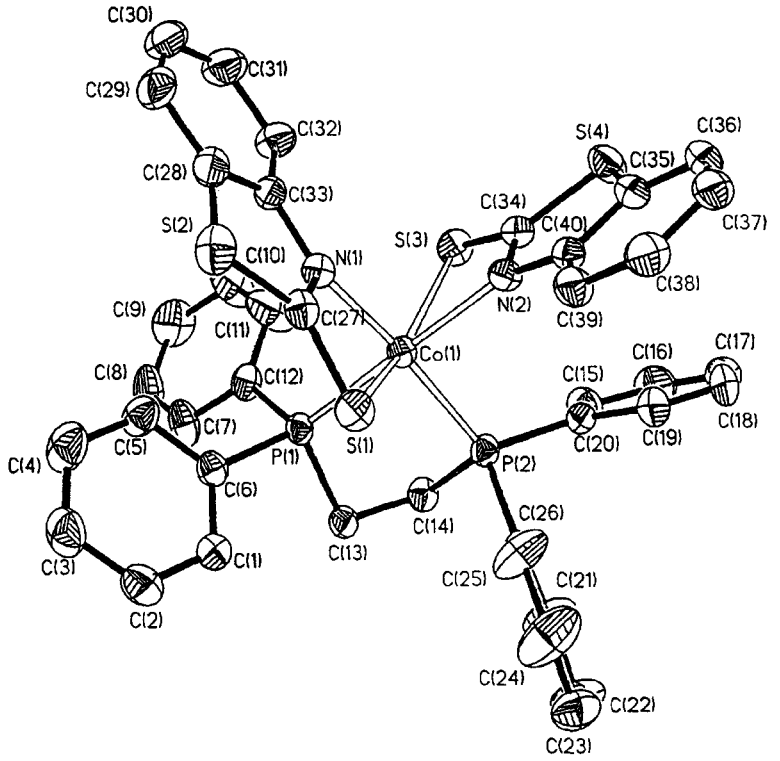


Fig. 2. Structure of Co(mbt-*N*:*S*)$_2$(dppe) (**2**).

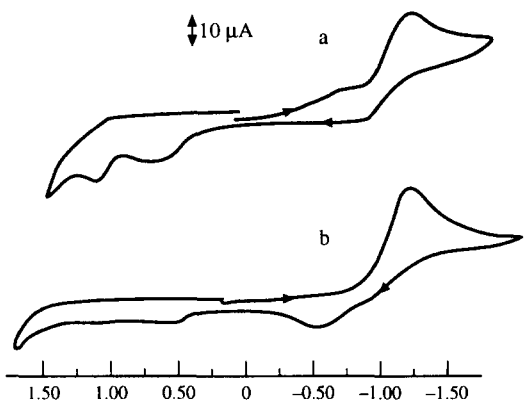


Fig. 3. Cyclic voltammograms of Co(mbt-*N*)$_2$(PBu^n_3)$_2$ (**1**) in (a) DMF and (b) MeCN at room temperature with 0.1 M of $Bu^n_4NBF_4$ as electrolyte at Pt electrode and SCE reference electrode.

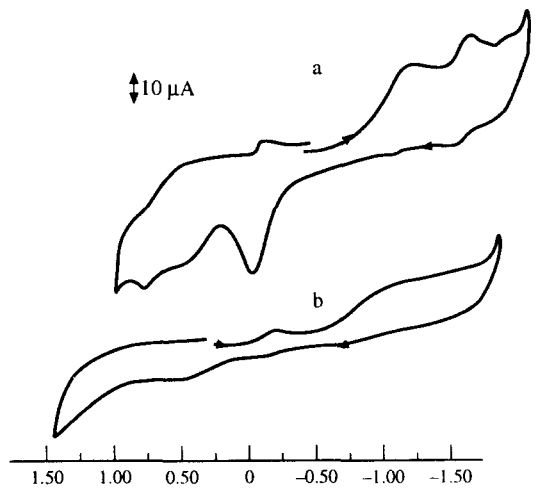


Fig. 4. Cyclic voltammograms of Co(mbt-N:S)$_2$(dppe) (**2**) in (a) DMF and (b) MeCN at room temperature with 0.1 M of $Bu^n_4NBF_4$ as electrolyte at Pt electrode and SCE reference electrode.

Table 4. Comparison of the structural data of the M–mbt ligation (or chelation) in complexes with 2-mercaptobenzothiazole

Compound	Geometry	Mode	M—N	M—S_e^a	C—N^b	C—S_e^a	M—N—C^c	M—S_e—C^a	Ref.
1	Square planar	**I**	1.938		1.323	1.684	109.4		This work
2	Octahedral	**III**	2.012	2.711	1.321	1.687	103.9	70.0	This work
$Co(mbt)_2(py)_2$	Octahedral	**III**	2.158	2.595	1.304	1.709	98.9	74.4	19
$[Zn(mbt)_3(H_2O)]^-$	Tetrahedral	**III**	2.019	3.125	1.331	1.690	112.9	*d*	20
		II		2.338	1.301	1.725		105.6	
$[Zn(mbt)(Me_2dtc)_2]^-$	Square pyramidal	**I**	2.061		1.328	1.679	121.3		20
$[Zn(mbt)_2(Me_2dtc)]$	Tetrahedral	**I**	1.997		1.316	1.681	115.3		20
$Zn(mbt)_2(py)_2$	Tetrahedral	**II**		2.324	*d*	*d*		*d*	21
$Zn(mbt)_2(2,2'\text{-bipy})$	Tetrahedral	**II**		2.310	*d*	*d*		*d*	21
$[Cd(mbt)_3]^-$	Trigonal prismatic	**III**	2.474	2.667	1.303	1.6903	94.5	79.5	24
$Cd(mbt)_2(py)_2$	Octahedral	**III**	2.422	2.706	*d*	*d*	*d*	*d*	21
$Cd(mbt)_2(2,2'\text{-bipy})$	Trigonal prismatic	**III**	2.529	2.618	1.320	1.704	92.3	81.3	22

[a] S_e indicates the exocyclic sulfur atom.
[b] $C—N_{bond\ to\ Se}$.
[c] $M—N—C_{bond\ to\ Se}$.
[d] Not reported.

The cyclic voltammograms of complexes **1** and **2** in both DMF and MeCN are depicted in Figs 3 and 4, respectively. The CV data are summarized in Table 5. Complex **1** in DMF showed two rather weak reductions (E_1 and E_2) probably caused by some impurities in addition to a strong reduction wave (E_3) at -1.25 V, which shifted 200 mV to -1.45 V and grew higher if the CV was measured after allowing the solution to stand under argon for 20 h. This phenomenon is presumably an indication of coordination of the complex by the coordinating solvent DMF, as complex **1** has the Co atom in a square-planar environment with two vacant sites available. Similarly, complex **1** in MeCN also showed a strong reduction peak (E_3) at -1.25 V which grew with time. This solvated, reduced species $[Co(mbt)\text{-}N)_2(PBu^n_3)_2(solvent)_2]$ underwent oxidation to give two waves (E_4 and E_5) at $+0.63$ and $+1.10$ V (in DMF) and -0.56 and $+0.54$ V (in MeCN), respectively. The electrochemical process could be expressed as follows:

$$[Co(mbt)_2(PBu^n_3)_2]^0 \xrightarrow{E_3}$$

$$[Co(mbt)_2(PBu^n_3)_2(solvent)_2]^{1-} \xrightarrow{E_4}$$

$$[Co(mbt)_2(PBu^n_3)_2(solvent)_2]^0 \xrightarrow{E_5}$$

$$[Co(mbt)_2(PBu^n_3)_2(solvent)_2]^{1+}$$

The six-coordinated complex **2** showed three pseudo-reversible redox couples in DMF with the two high potential couples (E_2 and E_3) merged into a broad irreversible reduction wave when the solvent is changed to the less polar MeCN, in which **2** is less soluble. In addition, two irreversible oxidation waves were observed similarly to **1**, in which the one near $+0.50$ V could be caused by dppe, as the free ligand has a similar wave in this region. The CV patterns of both complexes change with time, indicating that the redox behaviours are quite complicated in these solvating solvents, and also that decomposition or oxidation of complexes might also complicate the matter.

At 300 K, the effective magnetic moments μ_{eff} are 4.25 and 4.40 μ_B for **1** and **2**, respectively, both values are greater than the $S = \frac{3}{2}$ spin-only value (3.87 μ_B) and therefore indicate a fair amount of orbital contribution to both compounds. Upon decreasing the temperature, the μ_{eff} remains almost unchanged. Obviously, no appreciable intermolecular magnetic interactions or zero-field splitting effects are present in the two mononuclear cobalt(II) complexes. The EPR spectra of both complexes exhibit two signals with the g values being 2.03 and 4.75 for **1** and 2.16 and 5.32 for **2**, which are characteristic of square-planar and octahedral cobalt(II) ions with $S = \frac{3}{2}$, respectively [29].

Acknowledgements—Thanks are due to the financial support of the NNSF of China, the Hong Kong Research Council Earmarked Grant No. CUHK 311/94P and the NSF of Guangdong Province.

Table 5. CV data of complexes **1** and **2** in DMF and MeCN at room temperature

	Co(mbt-*N*)$_2$(PBu$^n_3$)$_2$ (**1**)				Co(mbt-*N*:*S*)$_2$(dppe) (**2**)					
	DMF		MeCN		DMF			MeCN		
E	$E_{p,c}$ (V)	$E_{p,a}$ (V)	$E_{p,c}$ (V)	$E_{p,a}$ (V)	$E_{p,c}$ (V)	$E_{p,a}$ (V)	$E_{1/2}$ (mV)	$E_{p,c}$ (V)	$E_{p,a}$ (V)	$E_{1/2}$ (mV)
E_1	−0.50		—	—	−0.13	−0.01	60	−0.18	−0.10	35
E_2	−0.70		—	—	−1.24	−1.11	65	−0.93		
E_3	−1.25		−1.25		−1.68	−1.55	65			
E_4		+0.63	—	−0.56	—	+0.48			+0.50	
E_5		+1.10		+0.54	—	+0.76		—		

REFERENCES

1. Kang, B. S., Xu, Y. J., Peng, J. H., Wu, D. X., Chen, X. T., Hu, Y. H., Hong, M. C. and Lu, J. X., *Polyhedron*, 1993, **12,** 871.
2. Wei, G. W., Hong, M. C., Huang, Z. Y. and Liu, H. Q., *J. Chem. Soc., Dalton Trans.* 1991, 3145.
3. Wei, G. W., Liu, H. Q., Huang, Z. Y., Hong, M. C., Huang, L. R. and Kang, B. S., *Polyhedron*, 1991, **10,** 553.
4. Wei, G. W., Liu, H. Q., Huang, Z. Y., Huang, L. R. and Kang, B. S., *J. Chem. Soc., Chem. Commun.*, 1989, 1839.
5. Kang, B. S., Peng, J. H., Hong, M. C., Wu, D. X., Chen, X. T., Weng, L. H., Lei, X. J. and Liu, H. Q., *J. Chem. Soc., Dalton Trans.*, 1991, 2897.
6. Jiang, F. L., Huang, Z. Y., Wu, D. X., Kang, B. S., Hong, M. C. and Liu, H. Q., *Inorg. Chem.*, 1993, **32,** 4971.
7. Kang, B. S., Xu, Y. J., Xie, X. L., Chen, C. N., Liu, Q. T., Liu, H. Q. and Lu, J. X., *Inorg. Chem.*, 1994, **33,** 3770.
8. Xu, Y. J., Kang, B. S., Chen, X. T., Cai, Y. B., Hu, Y. H. and Lu, J. X., *J. Cluster Sci.*, 1992, **3,** 167.
9. Jiang, F. L., Hong, M. C., Xie, X. L., Cao, R., Kang, B. S., Wu, D. X. and Liu, H. Q., *Inorg. Chim. Acta*, 1995, **231,** 153.
10. Jiang, F. L., Wei, G. W., Huang, Z. Y., Lei, X. J., Hong, M. C., Kang, B. S. and Liu, H. Q., *J. Coord. Chem.*, 1992, **25,** 183.
11. Cao, R., Hong, M. C., Jiang, F. L., Xie, X. L. and Liu, H. Q., *J. Chem. Soc., Dalton Trans.*, 1994, 3459.
12. Kita, M., Okuno, M., Kashiwabara, K. and Fujita, J., *Bull. Chem. Soc. Jpn*, 1992, **65,** 3042.
13. Kang, B. S., Hong, M. C., Wen, T. B., Liu, H. Q. and Lu, J. X., *J. Cluster Sci.* 1995, **6,** 379.
14. Chen, Z. N., Kang, B. S., Lin, Z., Wu, B. M., Zhou, Z. Y., Mak, T. C. W., Chen, C. N. and Liu, Q. T., *J. Chem. Soc., Dalton Trans.*, 1996, 177.
15. Raper, E. S., *Coord. Chem. Rev.*, 1985, **61,** 115.
16. Auerbach, I., *Ind. Eng. Chem. Ind.*, 1953, **45,** 1526.
17. Jeannin, S., Jeannin, Y. and Lauigne, G., *Trans. Met. Chem.*, 1976, **1,** 186.
18. Grassitti, R. D., Murray, J. F., Brooke, M. E. and Gutman, D., *J. Med. Chem.*, 1970, **13,** 273.
19. Dance, I. G. and Issac, D., *Aust. J. Chem.*, 1977, **30,** 2425.
20. McCleverty, J. A., Morrison, N. J., Spencer, N., Ashworth, C. A., Bailey, N. A., Johnson, M. R., Smith, J. M. A., Tabbiner, B. A. and Taylor, C. R., *J. Chem. Soc., Dalton Trans.*, 1980, 1945.
21. Baggio, R., Garland, M. T. and Perec, M., *J. Chem. Soc., Dalton Trans.*, 1993, 3367.
22. Baggio, R. F., Perec, M. and Garland, M. T., *Acta Cryst.*, 1994, **C50,** 1594.
23. Khullar, I. P. and Agarwala, U., *Can. J. Chem.*, 1975, **53,** 1165.
24. McCleverty, J. A., Gill, S. A., Kowalski, R. S. Z., Bailey, N. A., Adams, H., Lumbard, K. W. and Murphy, M. A., *J. Chem. Soc., Dalton Trans.*, 1982, 493.
25. Jeannin, S., Jeannin, Y. and Javigne, I. G., *Inorg. Chem.*, 1979, **18,** 3528.
26. Rochow, E. G., *Inorg. Synthesis*, 1960, **6,** 172.
27. Sheldrick, G. M., SHELXTL-PC. Siemens Analytical X-ray Instruments, Inc., Madison, Wisconsin, USA, 1990; Sheldrick, G. M., in *Computational Crystallography*, ed. D. Sayre. Oxford University Press, New York, 1982.
28. Chesick, J. P. and Eonohue, J., *Acta Cryst.*, 1971, **B27,** 1441.
29. Wertz, J. E. and Bolton, J. R., *Electron Spin Resonance, Elementary Theory and Practical Application*. McGraw-Hill, New York, 1973.

Pergamon

PII: S0277-5387(96)00459-7

Polyhedron Vol. 16, No. 10, pp. 1739–1745, 1997
Copyright © 1997 Elsevier Science Ltd
Printed in Great Britain. All rights reserved
0277-5387/97 $17.00+0.00

Crystal and molecular structures of *mer* (*N*)-dinitro-{*N*,*N*-bis(3-aminopropyl)glycinato} cobalt(III) and of bromide, perchlorate and nitrate salts of *mer* (*N*)-aquachloro-{*N*,*N*-bis(3-aminopropyl)glycinato} cobalt(III)

Y. Kitamura,* N. Azuma and T. Ozawa

Department of Chemistry, Faculty of Science, Ehime University, Matsuyama 790, Japan

(Received 24 May 1996; accepted 16 September 1996)

Abstract—X-ray structural analyses have been made on single crystals of *mer*(*N*)-[Co(5-dptma)$(NO_2)_2$] (**A**), *mer*(*N*)-[CoCl(5-dptma)(H_2O)] Br (**B**), *mer*(*N*)-[CoCl(5-dptma)(H_2O)]ClO_4 (**C**) and *mer*(*N*)-[CoCl(5-dptma)(H_2O)] NO_3 (**D**), where H(5-dptma) is *N*, *N*-bis(3-aminopropyl)glycine. Complex **A** crystallizes in the monoclinic space group $P2_1/c$ as a racemate; complex **B** in the monoclinic space group $P2_1/n$ as a racemate; complex **C** in the orthorhombic space group $P2_12_12_1$ as a conglomerate; and complex **D** in the orthorhombic space group $Pna2_1$ as a racemate. In these complexes, the tripod quadridentate 5-dptma coordinates to cobalt(III) with its three nitrogen atoms on a meridian of the coordination octahedron and with the six-membered chelate rings assuming the chair conformation. In **A** the molecular planes of the NO_2 ligands are anchored by intramolecular and intermolecular hydrogen bonds to the amine protons. The molecular planes of the aqua ligands in **B, C** and **D** are anchored by two intermolecular hydrogen bonds; one with the carbonyl oxygen atom and the other with the counter anion. © 1997 Elsevier Science Ltd. All rights reserved.

Keywords: crystal structure; aquachloro cobalt(III) complex; dinitro cobalt(III) complex; *N*,*N*-bis(3-aminopropyl)glycinato chelate; conglomerate; spontaneous resolution.

In our recent paper, we have described the preparation of several cobalt(III) complexes bearing the new quadridentate ligand 5-dptma, where 5-dptma is *N*,*N*-bis(3-aminopropyl)glycine, $(H_2NCH_2CH_2CH_2)_2NCH_2COOH$ [1]. In this report, we describe the X-ray crystal structures of four complexes: *mer*(*N*)-[Co(5-dptma)$(NO_2)_2$] (**A**), *mer*(*N*)-[CoCl(5-dptma)(H_2O)]Br (**B**), *mer*(*N*)-[CoCl(5-dptma)(H_2O)]ClO_4 (**C**), *mer*(*N*)-[CoCl(5-dptma)(H_2O)]NO_3 (**D**). We are interested in the chiral property of these crystals. It is well known that cobalt(III) complexes often dissolve spontaneously or crystallize as a conglomerate. For the positively charged dinitrotetraaminecobalt(III) complex, it has been pointed out that intramolecular hydrogen bonds between the NO_2 ligands and the adjacent amine proton lead to conglomerate formation, whereas blocking of such hydrogen bonds by counter anions leads to racemate formation [2]. In the present paper, we investigate the crystallization behaviour of the non-electrolyte dinitrocobalt(III) complex **A**, which is not accompanied by a counter anion. On the other hand we have recently reported the spontaneous resolution of two aquachloro complexes bearing tripod quadridentate ligands: *trans*(*O*)-[Co(aeida)Cl(H_2O)] and *mer*(*N*)-[CoCl(i-dtma)(H_2O)]ClO_4 (**E**), where H_2aeida is *N*-(2-aminoethyl)-*N*-(carboxymethyl)glycine and H(i-dtma) is *N*,*N*-bis(2-aminoethyl)glycine [3]. We expected additional examples of this type of complex to form a

* Author to whom correspondence should be addressed.

conglomerate. Our present complex, **C**, is of similar constitution to **E**. The 5-dptma ligand is composed of two aminopropyl side chains and the i-dtma ligand is composed of two aminoethyl side chains. We have compared the crystallization behaviour of **C** and **E** and examined the effect of the variation of the counter anion on the crystallization behaviour of the *mer*(*N*)-$[CoCl(5\text{-dptma})(H_2O)]^+$.

EXPERIMENTAL

Preparation of the complexes

The complexes were prepared as described previously [1].

Structure determination

These were carried out as described elsewhere [3]. The refinement details are shown in Table 1. In the case of complex **C**, the maximum residual electron density in the difference Fourier map of the final model is rather high. However, it cannot be ascribed to a solvated water molecule, because the peak is only 1.5 Å from Cl(2). The oxygen atoms in the perchlorate ion have equivalent temperature factors (B_{eq}) greater than 12 Å^2, which suggested disorder or pseudo-rotation of the perchlorate ion. The rather large R (R_w) factor and S value may be attributed to this disorder or rotation.

Observation on the conglomerate for the crystal of **C**

Because of the D_2 crystal point group and $Z = 4$, the chirality has been examined by the test of the R factor ratio [4]. The R_w factor for the structure refinement without anomalous dispersion effects was 0.060 for 119 variables and 1445 observations. Inclusion of the anomalous dispersion gave the R_w factors of 0.0606 and 0.0667 for this and its enantiomeric structure, respectively, which yielded the R_{w_1}/R_{w_2} ratio of 1.10. The corresponding significance point is $R_{b,N,\ \alpha} = R_{1,1326,0.005} = 1.003$, so that the enantiomeric structure can be rejected with a probability greater than 99.5% [5]. This result has encouraged us to examine the spontaneous resolution. Selected 21 Bijvoet pairs (2θ range about 20°) were remeasured carefully within a scan speed of 4° min^{-1} (in ω), in which the equivalent reflections ($hkl, h-k-l, -hk-l, -h-kl$ and $-h-k-l, -hkl, h-kl, hk-l$) were averaged. A table for comparison of the intensities of the 21 Bijvoet pairs was prepared. Then, a second single crystal from the same batch was subjected to the same measurement and comparison. The signs of inequality for all the Bijvoet pairs of the second crystal have been reversed compared with

Table 1. Crystal data, experimental conditions and refinement details of *mer*(*N*)-$[Co(5\text{-dptma})(NO_2)_2]$ (**A**), *mer*(*N*)-[CoCl(5-dptma)(H_2O)]Br (**B**), *mer*(*N*)-$[CoCl(5\text{-dptma})(H_2O)](ClO_4)$ (**C**), *mer*(*N*)-$[CoCl(5\text{-dptma})(H_2O)]NO_3$ (**D**)

	A	**B**	**C**	**D**
Formula	$C_8H_{18}N_5O_6Co$	$C_8H_{20}N_3O_3ClCoBr$	$C_8H_{20}N_3O_7Cl_2Co$	$C_8H_{20}N_4O_6ClCo$
Formula weight	339.19	380.55	400.10	362.66
Crystal system	Monoclinic	Monoclinic	Orthorhombic	Orthorhombic
a (Å)	8.375(1)	8.284(3)	11.600(2)	21.537(5)
b (Å)	14.074(3)	7.261(1)	17.944(2)	8.836(1)
c (Å)	11.580(1)	22.639(4)	7.2610(9)	7.277(2)
β (°)	110.679(9)	99.52(2)		
V (Å^3)	1277.0(4)	1343.0(6)	1511.4(3)	1384.8(9)
Space group	$P2_1/c$	$P2_1/n$	$P2_12_12_1$	$Pna2_1$
Z	4	4	4	4
D_c (g cm^{-3})	1.764	1.882	1.758	1.739
$F(000)$	704	768	824	752
Colour of crystal, Habit	Red, plate	Deep blue, block	Deep blue, prismatic	Deep blue, prismatic
Size of crystal (mm)	$0.330 \times 0.300 \times 0.130$	$0.430 \times 0.280 \times 0.200$	$0.380 \times 0.180 \times 0.150$	$0.420 \times 0.180 \times 0.200$
μ (Mo-K_α) (cm^{-1})	13.73	44.23	15.22	14.60
2θ range (°)	4.7–55	4.7–55	4.7–55	4.7–55
No. of unique reflections measured	3060	3340	2028	1878
No. of reflections observed [$I > 3\sigma(I)$]	2151	2148	1445	1288
R; R_w	0.031; 0.033	0.031; 0.031	0.052; 0.058	0.036; 0.035
S (goodness-of-fit)	1.23	1.37	1.91	1.22
Range of (Δ/ρ) (e Å^{-3})	−0.30–0.27	−0.46–0.59	−0.56–1.26	−0.35–0.35

those of the first one. Thus, we have concluded that this complex salt crystallizes as a conglomerate.

RESULTS AND DISCUSSION

The molecular structures of *mer*(*N*)-[Co(5-dptma)$(NO_2)_2$] (**A**), *mer*(*N*)-[CoCl(5-dptma)(H_2O)]Br (**B**), *mer*(*N*)-[CoCl(5-dptma)(H_2O)]ClO_4 (**C**) and *mer*(*N*)-[CoCl(5-dptma)(H_2O)]NO_3 (**D**) are shown in Figs 1–4, respectively, with atomic-numbering systems. The bond lengths and angles are given in Table 2, with important hydrogen bonds listed in Table 3. In complexes **A**, **B**, **C** and **D**, the tripod quadridentate 5-dptma coordinates to cobalt(III) with its three nitrogen atoms on a meridian of the coordination octahedron [*mer*(*N*) coordination mode]. For complexes **A** and **C**, it conforms with the previous *mer*(*N*) assignment on the glycinato proton resonance spectra [1]. Complexes **A**, **B** and **D** crystallize as racemates, whereas **C** is a conglomerate.

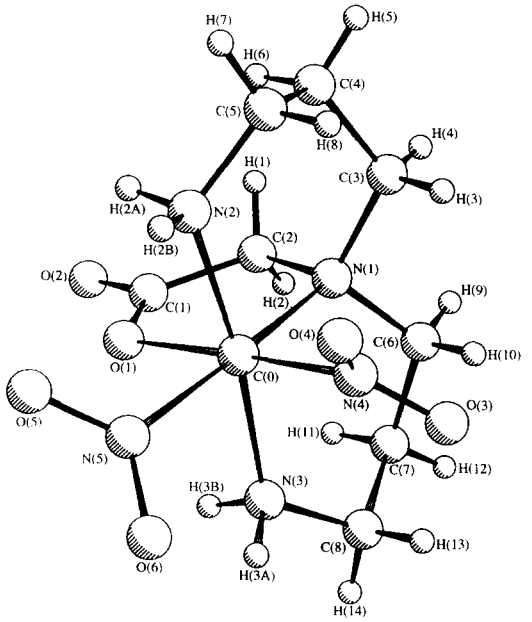


Fig. 1. Molecular structure of *mer*(*N*)-[Co(5-dptma)$(NO_2)_2$] (**A**) and the atomic numbering system.

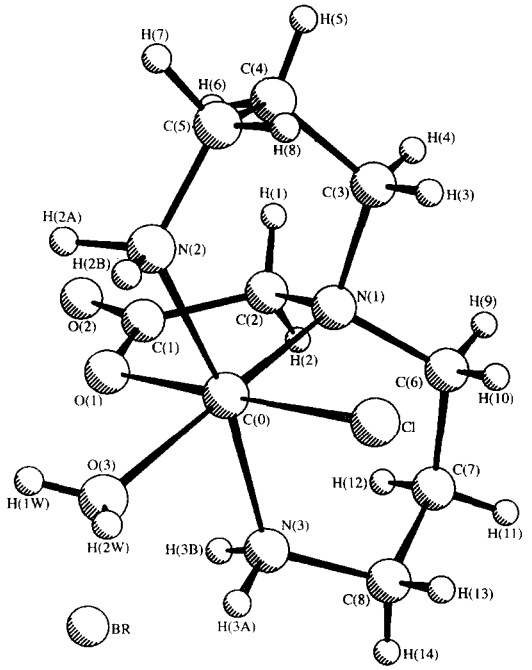


Fig. 2. Molecular structure of *mer*(*N*)-[CoCl(5-dptma)(H_2O)]Br (**B**) and the atomic numbering system.

In the crystal of **A**, the two NO_2 ligand planes are anchored through three intramolecular and two intermolecular hydrogen bonds to the amine protons (Table 3). Of the three aquachloro complex salts **B**, **C** and **D**, only the perchlorate salt **C** crystallizes as a conglomerate. In this case, the variation of the counter anion affects the crystallization behaviour. It is interesting that *mer*(*N*)-[CoCl(i-dtma)(H_2O)]ClO_4 (**E**) is also a perchlorate salt. Both **C** and **E** crystallize in the $P2_12_12_1$ space group as conglomerates, in spite of the different chelate ring constitution: a six-membered ring in **C** and a five-membered ring in **E**. All the six-membered chelate rings formed by the coordinating 5-dptma ligand assume the chair conformation in **A**–**D**. In **A**–**D**, the corresponding coordination bond lengths are of similar magnitudes to one another (Table 2). In **A** the Co—N(5) bond length is longer by 0.05 Å than the Co—N(4) length. The former bond, in the *trans* position to the Co tertiary amine bond, is weak. In this connection the derivation process of **C** from the dichloro precursor can be explained as follows [1]. In complex **C** the aqua ligand exists at the *trans* position to the tertiary amine (Fig. 3). One infers that the chloro ligand at the *trans* position to the tertiary amine may be labile in *mer*(*N*)-[$CoCl_2$(5-dptma)]. In complexes **A**–**D**, the corresponding bond lengths of the 5-dptma ligand are of similar magnitudes to one another. The N(1)—Co—N(2) angle (*ca* 93°) in **A** differs significantly from the corresponding angles (*ca* 98°) in **B**, **C** and **D**. However, these magnitudes are within the experimentally found N—Co—N angles 90–100° for a six-membered chair chelate [6–8]. The Co—N(1), Co—N(2) and Co—N(3) bond lengths in **C** are *ca* 0.04 Å longer than the corresponding ones in **E** [3]. This may be ascribed to the bulky six-membered chelate rings in **C**. In compensation for this the Co—O(3) bond length in **C** is shorter by *ca* 0.03 Å than the corresponding one in **E** [3]. The N(2)—Co—N(3) angle (167.4°) in **C** differs significantly from the corresponding angle (186.4°) in **E**, which may also be ascribed to the bulkiness of the six-membered chelate in **C**.

The molecular planes of the aqua ligands in **B**, **C** and **D** are anchored by two intermolecular hydrogen bonds; one with the carbonyl oxygen O(2) and the other with the counter anion (Table 3). In relation to these hydrogen bonds, O(3) atoms in **B**, **C** and **D** deviate by 0.16, 0.07 and 0.18 Å, respectively, from the plane defined by the Co, Cl, N(1) and O(1) atoms.

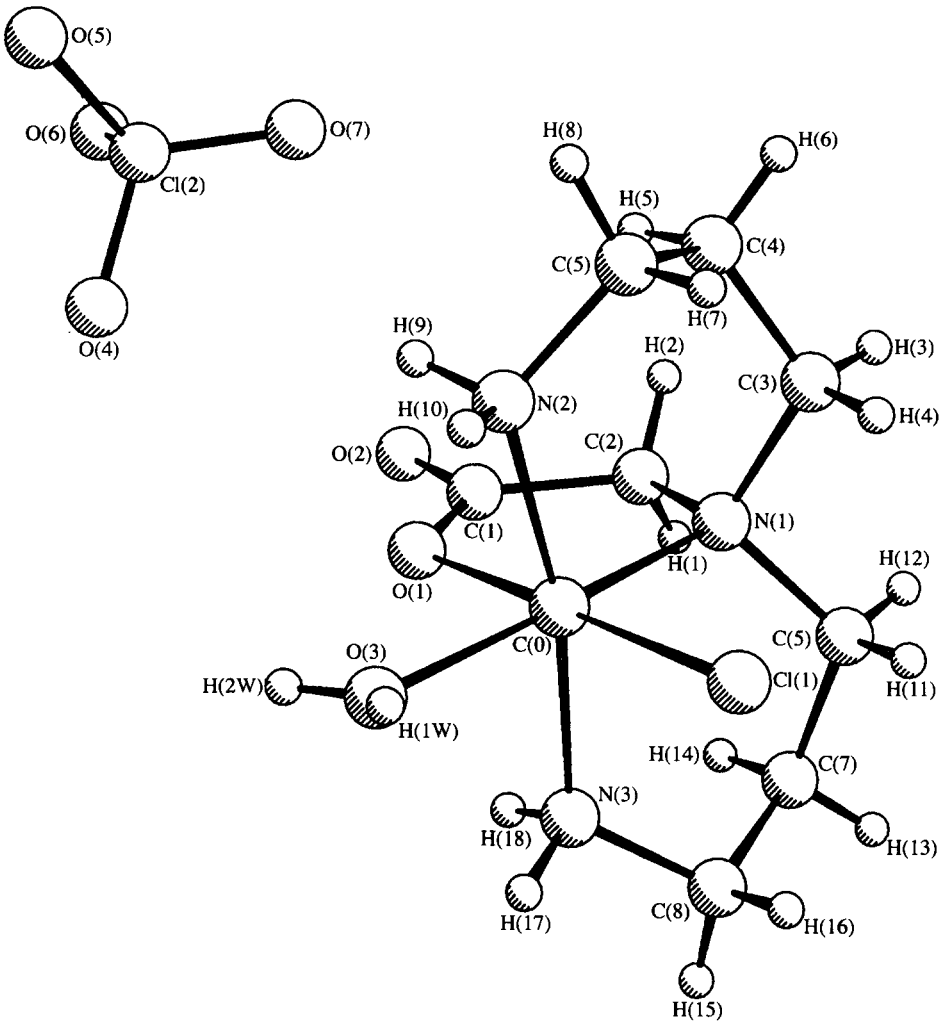


Fig. 3. Molecular structure of *mer*(*N*)-[CoCl(5-dptma)(H_2O)](ClO_4) (**C**) and the atomic numbering system.

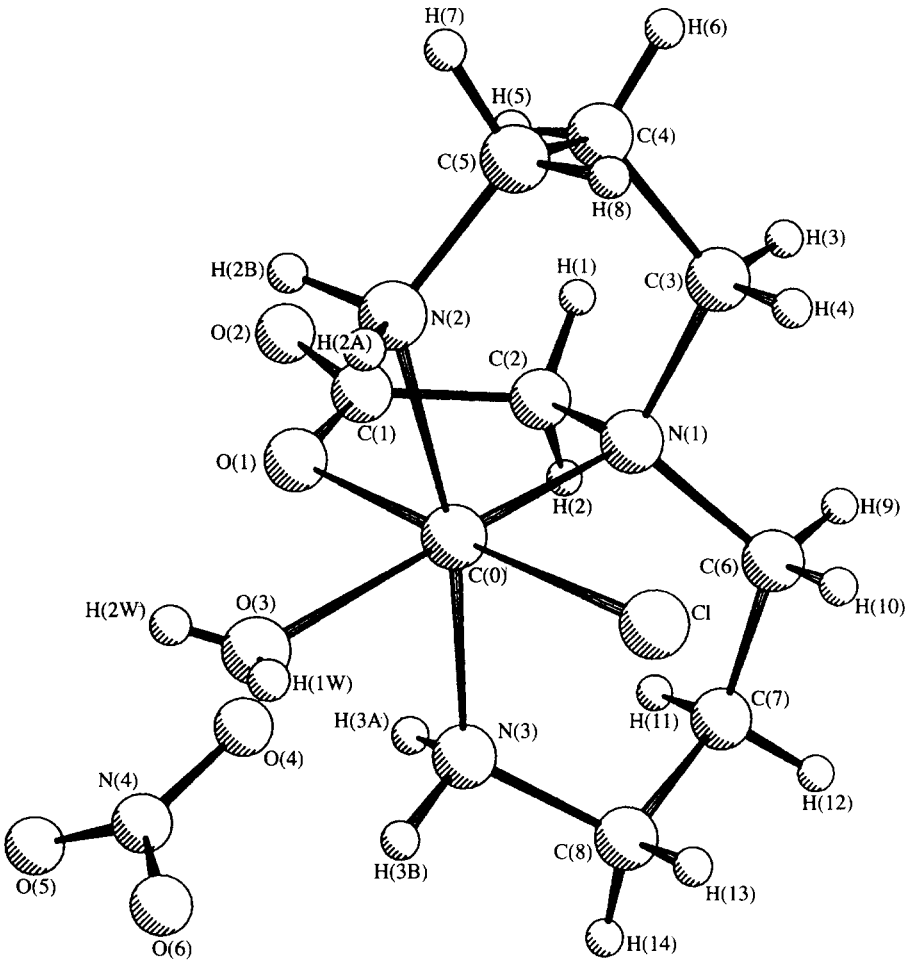


Fig. 4. Molecular structure of *mer*(*N*)-[CoCl(5-dptma)(H_2O)]NO_3 (**D**) and the atomic numbering system.

Table 2. Bond lengths (Å) and angles (°) for complexes **A**–**D**

	A	**B**	**C**	**D**
Co—O(1)	1.913(2)	1.891(2)	1.889(6)	1.901(3)
Co—N(1)	2.048(2)	1.996(3)	1.985(8)	1.993(4)
Co—N(2)	1.975(2)	1.964(3)	1.974(9)	1.975(5)
Co—N(3)	1.987(2)	1.973(3)	1.971(8)	1.968(5)
Co—O(3)		1.934(3)	1.933(8)	1.944(4)
Co—Cl		2.232(1)	2.224(3)	2.232(2)
Co—N(4)	1.911(2)			
Co—N(5)	1.958(2)			
O(1)—C(1)	1.286(3)	1.283(4)	1.30(1)	1.296(6)
O(2)—C(1)	1.222(3)	1.238(4)	1.21(1)	1.229(6)
N(1)—C(2)	1.512(3)	1.499(4)	1.51(1)	1.509(6)
N(1)—C(3)	1.515(4)	1.508(4)	1.51(1)	1.518(7)
N(1)—C(6)	1.514(4)	1.511(4)	1.52(1)	1.523(7)
N(2)—C(5)	1.479(4)	1.468(6)	1.50(1)	1.460(8)
N(3)—C(8)	1.483(4)	1.473(5)	1.47(1)	1.478(8)
C(1)—C(2)	1.505(4)	1.498(5)	1.51(1)	1.488(7)
C(3)—C(4)	1.507(4)	1.493(6)	1.49(2)	1.495(9)
C(4)—C(5)	1.499(4)	1.512(6)	1.48(2)	1.495(9)
C(6)—C(7)	1.510(4)	1.510(6)	1.49(2)	1.502(9)
C(7)—C(8)	1.504(4)	1.500(6)	1.48(2)	1.520(9)
O(3)—N(4)	1.231(3)			
O(4)—N(4)	1.237(3)			
O(5)—N(5)	1.235(3)			
O(6)—N(5)	1.232(3)			
O(1)—Co—N(1)	86.46(8)	86.9(1)	87.1(3)	87.0(2)
O(1)—Co—N(2)	88.85(9)	86.7(1)	88.3(3)	86.0(2)
O(1)—Co—N(3)	86.92(8)	90.2(1)	89.5(3)	88.9(2)
O(1)—Co—N(4)	176.11(9)			
O(1)—Co—N(5)	87.79(9)			
N(1)—Co—N(2)	92.95(9)	98.2(1)	97.9(4)	99.2(2)
N(1)—Co—N(3)	93.73(9)	92.5(1)	94.4(4)	91.5(2)
N(1)—Co—N(4)	97.29(9)			
N(1)—Co—N(5)	174.22(9)			
N(2)—Co—N(3)	171.86(9)	168.7(1)	167.4(4)	168.3(2)
N(2)—Co—N(4)	89.9(1)			
N(2)—Co—N(5)	87.50(9)			
N(3)—Co—N(4)	93.8(1)			
N(3)—Co—N(5)	85.39(9)			
N(4)—Co—N(5)	88.5(1)			
Cl—Co—O(1)		177.52(8)	178.4(2)	176.7(1)
Cl—Co—O(3)		90.60(9)	91.2(3)	89.9(1)
Cl—Co—N(1)		94.32(8)	94.5(2)	94.3(1)
Cl—Co—N(3)		91.9(1)	90.7(3)	93.1(2)
Cl—Co—N(2)		91.0(1)	91.1(2)	90.8(1)
O(1)—Co—O(3)		88.4(1)	87.2(3)	89.1(2)
O(3)—Co—N(1)		173.4(1)	173.9(3)	173.6(2)
O(3)—Co—N(2)		86.1(1)	84.0(4)	85.6(2)
O(3)—Co—N(3)		83.0(1)	83.5(5)	83.4(2)
Co—O(1)—C(1)	117.4(2)	115.9(2)	116.8(6)	115.7(3)
Co—N(1)—C(2)	105.1(2)	106.7(2)	107.2(5)	105.9(3)
Co—N(1)—C(3)	114.6(2)	113.4(2)	113.2(6)	112.1(3)
Co—N(1)—C(6)	115.0(2)	114.3(2)	113.9(7)	114.4(3)
C(2)—N(1)—C(3)	109.4(2)	108.4(3)	109.6(7)	108.8(4)
C(2)—N(1)—C(6)	109.1(2)	109.3(3)	107.9(8)	109.7(4)
C(3)—N(1)—C(6)	103.5(2)	104.6(3)	104.8(8)	105.9(4)
Co—N(2)—C(5)	123.5(2)	122.9(3)	121.7(7)	123.2(4)
Co—N(3)—C(8)	125.2(2)	122.8(2)	122.1(7)	121.8(4)
Co—N(4)—O(3)	120.8(2)			
Co—N(4)—O(4)	119.5(2)			
O(3)—N(4)—O(4)	119.6(2)			
Co—N(5)—O(5)	119.7(2)			
Co—N(5)—O(6)	120.5(2)			

Continued.

Table 2. (*Continued*)

	A	B	C	D
O(5)—N(5)—O(6)	119.8(2)			
O(1)—C(1)—O(2)	124.0(3)	123.6(3)	123.6(8)	123.7(5)
O(1)—C(1)—C(2)	115.9(2)	117.2(3)	115.6(8)	116.1(4)
O(2)—C(1)—C(2)	120.1(3)	119.2(3)	120.9(8)	120.1(5)
N(1)—C(2)—C(1)	115.0(2)	112.2(3)	113.1(7)	113.0(4)
N(1)—C(3)—C(4)	116.8(2)	115.7(3)	115.8(8)	116.5(5)
C(3)—C(4)—C(5)	112.9(2)	112.7(3)	114(1)	113.0(5)
N(2)—C(5)—C(4)	111.3(2)	110.6(3)	111.4(9)	111.3(5)
N(1)—C(6)—C(7)	115.6(2)	116.7(3)	116.7(9)	116.7(5)
C(6)—C(7)—C(8)	113.6(3)	113.3(3)	113(1)	112.6(6)
N(3)—C(8)—C(7)	110.4(2)	110.0(3)	109.4(9)	109.1(5)

Table 3. Selected hydrogen bond distances (Å)

A		B		C		D	
Intermolecular							
O(3)···H(3A)	2.38	O(3)—H(1W)···O(2)	2.60	O(3)—H(1W)···O(4)	2.88	O(33)—H(1W)···O(4)	2.76
O(5)···H(2A)	2.23	O(3)—H(2W)···Br	3.23	O(3)—H(2W)···O(2)	2.62	O(3)—H(2W)···O(2)	2.63
		N(2)—H(2A)···Br	3.58	N(2)—H(9)···O(7)	3.22	N(2)—H(2A)···O(2)	3.03
		N(2)—H(2B)···O(2)	3.07			N(3)—H(3A)···O(6)	3.10
Intramolecular							
O(4)···H(2B)	2.49						
O(5)···H(2B)	2.38						
O(6)···H(3A)	2.11						

Analogous hydrogen bonds and the deviation of the aqua oxygen from the corresponding plane have been observed in the case of complex **E** [3].

REFERENCES

1. Shibata, A., Kitamura, Y. and Tanabe, Y., *Polyhedron*, 1996, **15,** 1225.
2. Bernal, I., *Inorg. Chim. Acta*, 1985, **96,** 99.
3. Kitamura, Y., Shibata, A., Azuma, N. and Ozawa, T., *Polyhedron*, 1994, **13,** 2477.
4. Hamilton, W. C., *Acta Cryst.*, 1965, **18,** 502.
5. *International Tables for X-ray Crystallography*, Vol. 4, Kluwer Academic Publishers, Dordrecht, 1989, p. 288.
6. Bernal, I., Myrczek, J., Cetrullo, J. and Massoud, S. S., *J. Coord. Chem.*, 1993, **29,** 287.
7. Mali, T. N., Wade, P. W. and Hancock, R. D., *J. Chem. Soc., Dalton Trans.*, 1992, 67.
8. Cetrullo, J. and Bernal, I., *J. Coord. Chem.*, 1991, **23,** 257.

Pergamon

PII: S0277-5387(96)00455-X

Polyhedron Vol. 16, No. 10, pp. 1747–1753, 1997
Copyright © 1997 Elsevier Science Ltd
Printed in Great Britain. All rights reserved
0277-5387/97 $17.00+0.00

A new cyano-bridged one-dimensional polymeric mixed-valence Cu^{II}/Cu^{I} complex formed from reduction of a binuclear Cu^{II} complex with sodium cyanide

S. F. Huang,[a] H. H. Wei[a]* and Yu Wang[b]

[a] Department of Chemistry, Tamkang University, Tamsui, Taiwan, R.O.C.

[b] Department of Chemistry, National Taiwan University, Taipei, Taiwan, R.O.C.

(Received 6 August 1996; accepted 12 September 1996)

Abstract—A new cyano-bridged polymeric mixed-valence Cu^{II}/Cu^{I} complex, $[Cu(dien)_2(CN)_2Cu(CN)]_n$ (**2**) (dien = diethylenetriamine) has been prepared by the partial reduction of the OH-bridged binuclear complex $[Cu_2(dien)_2(OH)](ClO_4)_3$ (**1**) with sodium cyanide. The X-ray crystal structure shows that **1** is a polymeric, linear mixed-valence Cu^{I}/Cu^{II} complex and consists of a one-dimensional three-coordinated $[Cu^{I}(CN)]_n$ chain, in which the Cu^{I} atoms are linked by two disordered CN bonding groups. The structure of each Cu^{II} atom consists of a square-pyramidal five-coordinate environment, in which the basal plane is formed by the three nitrogen atoms of the dien ligands and one carbon atom of the terminal cyanide group, and the apical position is occupied by the nitrogen atom of a bridging cyano ligand. This is the first example of one Cu^{II} centre coordinating with two different bonding types of the terminal Cu^{II}—CN and the bridging Cu^{II}—NC in a polymeric complex. The cryomagnetic behaviour has been investigated in the temperature range 4.2–300 K. There is a weak antiferromagnetic interaction between two intrachain copper(II) ions with $J = -0.47\ cm^{-1}$.
© 1997 Elsevier Science Ltd. All rights reserved.

Keywords: Copper complexes; mixed-valence Cu^{I}/Cu^{II} complexes; polymeric copper complexes; X-ray structure; magnetic property.

It is well known that in aqueous solution copper(II) is easily reduced to copper(I) by cyanide and that simple C-bonded cyano complexes of copper(II) are unstable at normal temperatures with respect to reduction and cannot be isolated [1]. Nevertheless, it has been shown that by choosing ligands (e.g. amines) that have good σ-electron donor character and strongly prefer to coordinate to Cu^{II} rather than Cu^{I} ions, it is possible to stabilize the Cu^{II}—CN coordination bonding. To date, several such complexes have been reported: the mononuclear, $[Cu^{II}(phen)(CN)](NO_3)$ [2], $[Cu(bipy)_2(CN)])NO_3]$ [3], [Cu(cyclps)(CN)] [4], $[Cu(Me_6tren)(CN)](ClO_4)$ [5], the CN-bridged binuclear, $[Cu_2([14]\text{-}4,11,\text{-dien-}N_4)(CN)](ClO_4)$ [6], $[Cu_2(tren)(CN)_2](BPh_4)_2$ [7], and $[(Cu(Me_6tren))_2(CN)](ClO_4)$ [5], and the CN-bridged polynuclear $[Cu(Me_5\text{-dien})(CN)]_n(CF_3SO_3)_n$ [5]. In addition, a few cyano-bridged Cu^{I}/Cu^{II} mixed-valence complexes of $[Cu(en)_2][Cu_2(CN)_5H_2O]$ [8] $[Cu^{II}(en)_2]_3[Cu^{I}_6(CN)_6(SeCN)_6]$ [9], and $[Cu_2(L)(CN)](ClO_4)_2$ (L = N,S-containing macrocyclic ligand) [10] have been reported, but there are no cyanide groups directly coordinated to the Cu^{II} ion as C-bonded Cu^{II}—CN in these complexes. Most recently, a series of model molecular complexes of cytochrome-*c* oxidase containing the $[Fe^{III}$—CN—$Cu^{II}]$ bridge unit has been prepared by Holm *et al.* [5,11] and structurally characterized, but there are no stable C-bonded Cu^{II}—CN of $[Fe^{III}$—CN—$Cu^{II}]$ fragments reported in this series. Furthermore, to the best of our knowledge, only one example of a Cu^{II}/Cu^{I} mixed-valence stable polymer complex, $[Cu^{I}_4(CN)_6Cu^{II}(NH_3)_2]_n$ with cyano-bridged Cu^{I}—CN—Cu^{II} prepared from the reaction of $[Cu^{I}CN]$ with $[Cu^{II}(NH_3)_4]^{2+}$, has been reported [12]. In this example the two copper(I) units, a linear

* Author to whom correspondence should be addressed.

$[Cu(CN)_2]$ chain and a trigonal $[Cu(CN)_3]$ chain are bridged by cyanide ligands and there was no magnetic interaction between the Cu^{II} ions.

Undoubtedly the stable copper(II)–cyanide linkage formation is dependent on the chemical reduction process and the types of ligands that will stabilize coordination of cyanide [1]. The aim of this paper is to deal with the first example of the cyano-bridged polymeric mixed-valence complex $[Cu^{II}(dien)(CN)_2Cu^{I}(CN)]_n$ (**2**) (dien = diethylenetriamine) with a very unusual five-coordination of Cu^{II} containing a terminal C-bond Cu^{II}—CN and a bridging Cu^{II}—NC—Cu^{I} bonding. This compound was prepared by the reduction of the known OH-bridged binuclear complex $[Cu^{II}(dien)_2(OH)](ClO_4)_3$ (**1**) with sodium cyanide in methanol. The preparation, structural and cryomagnetic studies of this binuclear complex **1** have been reported [13,14]. The structure of $[Cu^{II}(dien)_2(OH)](ClO_4)_3$ consists of a discrete binuclear molecule where the two copper(II) atoms are bridged by a single OH group with Cu^{II}—OH—Cu^{II} angles of 128° and an intramolecular Cu^{II}—Cu^{II} distance of 3.43 Å and weaker interactions with oxygens from three perchlorate ions, with a strong antiferromagnetic interaction between two copper(II) ions. We chose this OH-bridged binuclear copper(II) complex for reduction with NaCN since from the viewpoint of the dien ligand in **1** it has the capability to stabilize Cu^{II}—CN bonding and also because such a complex would be relevant to the development of model systems for active sites of biological interest [15]. Additionally, cyanide is an irreversible inhibitor of the copper-oxidized enzymes; specifically, its toxicity has been traced to bimetallic oxidases such as cytochrome-*c* oxidase [16] and a haemocyanin [17]. Herein the preparation, X-ray crystal structure, spectroscopic and magnetic properties of the complex **2** are reported. In addition, for comparison, the structure of the OH-bridged binuclear complex **1** was reconfirmed by X-ray crystallographic analysis.

EXPERIMENTAL

Preparation of complexes

$[Cu_2(dien)_2(OH)](ClO_4)_3$ (**1**) was prepared following the method initially described by Curtis and Powell [13]. To a solution of $Cu(ClO_4)\cdot 6H_2O$ (1 mmol) in water (10 cm^3) were added diethylenetriamine (dien) in ethanol (15 cm^3). The resulting blue solution changed to blue-violet on adding of $Na_2CO_3\cdot 10H_2O$ (5 mmol). Deep blue-violet crystals of $[Cu_2(dien)_2(OH)](ClO_4)_3$ were obtained by slow evaporation at room temperature. These were collected by filtration, washed with water and air dried. Found: C, 15.0; H, 4.0; N, 12.9. Calc. for $C_8H_{17}N_6O_{13}Cl_3Cu_2$: C, 14.8; H, 4.2, N, 13.0%.

$[Cu(dien)(CN)_2Cu(CN)]_n$ (**2**). To a solution of $[Cu_2(dien)_2(OH)](ClO_4)_3$ (**1**) (30 mg, 0.04 mmol) in methanol were added 15 cm^3 of methanol containing an excess amount (18 mg) of NaCN. During the addition of NaCN the solution turned to light blue with subsequent precipitation of a white substance. The mixture was filtered off and the light blue filtrate was transferred to a beaker and allowed to stand at ambient temperature. After several days well-formed light blue crystals suitable for X-ray analysis were isolated, filtered off and dried *in vacuo*. Found: C, 31.4; H, 4.1; N, 22.6. Calc. for $C_7H_{13}N_6Cu_2$: C, 31.4; H, 4.3; N, 22.6%.

Physical measurements

Infrared spectra were recorded on a Bio-Rad FTS-40FTIR spectrophotometer as KBr pellets in the 4000–400 cm^{-1} region. *X*-band (9.8 GHz) EPR spectra at 298 K were recorded on a Bruker ECS-106 spectrometer. Cryomagnetic susceptibilities of the polycrystalline samples were measured between 4.2 and 300 K at a field of 1 T using a Quantum Design Model MPMS computer-controlled SQUID magnetometer. Diamagnetic corrections were made using Pascal's constants.

Crystal structure determinations for **1** *and* **2**

The X-ray crystallographic data of a dark blue crystal (0.40 mm × 0.45 mm × 0.60 mm) of **1** and a light blue plate (0.35 mm × 0.45 mm × 0.45 mm) of **2**, were collected with graphite-monochromatized Mo-K_α radiation at 25°C using an Enraf–Nonius CAD-4 diffractomer, and are given in Table 1. Cell parameters were calculated from the least-squares fitting of setting angles for 25 reflections. The ω–2θ scan technique to

Table 1. Crystallographic data for **1** and **2**

Formula	$C_8H_{17}N_6Cl_3O_{13}Cu_2$	$C_8H_{13}N_5Cu_2$
F.w.	638.70	306.317
Size, mm	0.4 × 0.45 × 0.60	0.35 × 0.45 × 0.45
Temp., K	298	298
Crystal system	Monoclinic	Orthorhombic
Space group	$P2_1$	*Pnma*
a, Å	11.4382(20)	19.184(6)
b, Å	9.402(3)	8.6917(24)
c, Å	11.849(3)	7.124(3)
β, °	117.928(20)	
V, Å^3	1125.9(5)	1187.9(7)
D_c, g cm^{-3}	1.884	1.578
Z	2	4
F(000)	640	616
μ, cm^{-1}	23.22	35.685
N	2736	1830
N_0 [$I > 2.0\sigma(I)$]	2156	1367
R^a	0.054	0.026
$R_w{}^b$	0.065	0.026

$^a R_f = \Sigma[|F_o| - |F_c|]/\Sigma|F_o|$.
$^b R_w = [\Sigma w(|F_o| - |F_c|)^2/\Sigma w|F_o|^2]^{1/2}$.

Table 2. Bond distances (Å) and angles (°) for **1**

Cu(1)—O(1)	1.893(10)	Cu(1)—O(7)	2.894(21)
Cu(1)—N(1)	2.180(14)	Cu(1)—N(2)	2.004(8)
Cu(1)—N(3)	1.993(10)	Cu(2)—O(1)	1.960(11)
Cu(2)—O(2)	2.481(9)	Cu(2)—O(7)	2.746(14)
Cu(2)—N(4)	2.158(15)	Cu(2)—N(5)	2.014(8)
Cu(2)—N(6)	1.960(11)	Cu(1)—Cu(2)	3.420(17)
Cu(1)—O(1)—Cu(2)	129.1(4)	Cu(1)—O(7)—Cu(2)	74.9(4)
N(1)—Cu(1)—N(3)	163.5(5)	N(1)—Cu(1)—O(1)	94.8(9)
N(3)—Cu(1)—O(1)	96.6(8)	N(4)—Cu(2)—O(1)	91.7(9)
O(1)—Cu(2)—O(2)	93.7(3)	Cu(2)—O(2)—Cl(1)	128.1(7)

Table 3. Selected bond distances (Å) and angles (°) for **2**

Cu(1)—C(4)	1.919(3)	Cu(1)—NC	1.9358(22)
Cu(2)—N(1)	2.0517(21)	Cu(2)—C(3)	1.971(3)
Cu(2)—N(4)	2.171(3)	NC—NCb	1.138(4)
C(4)—N(4)	1.127(4)	C(3)—N(3)	1.133(5)
C(4)—Cu(1)—NC	120.36(17)	NC—Cu(1)—NC	119.08(10)
N(4)—Cu(2)—C(3)	98.77(13)	N(1)—Cu(2)—C(3)	94.81(6)
N(1)—Cu(2)—N(1)	158.84(18)	N(2)—Cu(2)—C(3)	163.12(12)
Cu(1)—C(4)—N(4)	178.1(3)	Cu(2)—N(4)—C(4)	171.3(3)
Cu(2)—C(3)—N(3)	177.9(3)	Cu(1)—NC—NCb	176.84(21)

a $2\theta_{max}$ value of 55.0° for **1** and 160.0° for **2** was used. A total of 2736 reflections for **1** and 1830 for **2** were measured, of which 2730 for **1** and 1830 for **2** with $I > 2.0\sigma(I)$, were used in further calculations. The structures were solved by the heavy-atom method. Full-matrix least-squares anisotropic refinement for all non-hydrogen atoms yielded $R_f = 0.054$, $R_w = 0.065$ and *GOF* (goodness-of-fit) = 2.11 for **1** and $R_f = 0.026$, $R_w = 0.026$ and $GOF = 16$ at convergence. All calculations were performed using the NRCVAX computer crystallographic software package [18]. Disorder was observed in the chain-bridging cyano groups of **2**. Selected bond distances and angles for **1** and **2** are given in Tables 2 and 3, respectively. Complete crystal data, atomic coordinates, full listings of bond distances and angles and the anisotropic thermal parameters for **1** and **2** are available as supplementary material, and have been deposited at the Cambridge Crystallographic Data Centre.

RESULTS AND DISCUSSION

The chemical reduction of $[Cu_2(dien)_2(OH)](ClO_4)_3$ (**1**) in excess methanolic solution of NaCN yielded a one-dimensional chain structured Cu^{I}/Cu^{II} mixed-valence complex, $[Cu^{II}(dien)(CN)_2Cu^{I}(CN)]_n$ (**2**) and some white solid identified as $NaClO_4$. Complex **2** was isolated in low yield (*ca* 20%), but was air stable in solution and in the solid state for a long period.

IR spectra

The most relevant IR feature is the presence of bridging and terminally bound CN stretching vibrations. In general, the ν(CN) frequency should be significantly greater for the bridging case than for the terminal one. Therefore, complex **2** exhibits very sharp double ν(CN) bands at 2133 and 2118 cm^{-1} in KBr, suggestive of the absorptions for the bridging CN and the terminal CN stretching vibrations, respectively [5–7,11].

Description of the structures

The structure of **1** (as shown in Fig. 1) consists of a binuclear $[Cu_2(dien)_2(OH)]^{3+}$ cation with three ClO_4^- anions, which is the same as previously found [14]. Nevertheless, in our system, only one ClO_4^- group oxygen atom was coordinated to the Cu^{II} centre with a Cu(2)—O(2) bond distance of 2.481(9) Å and the oxygens of the other two ClO_4^- groups interact

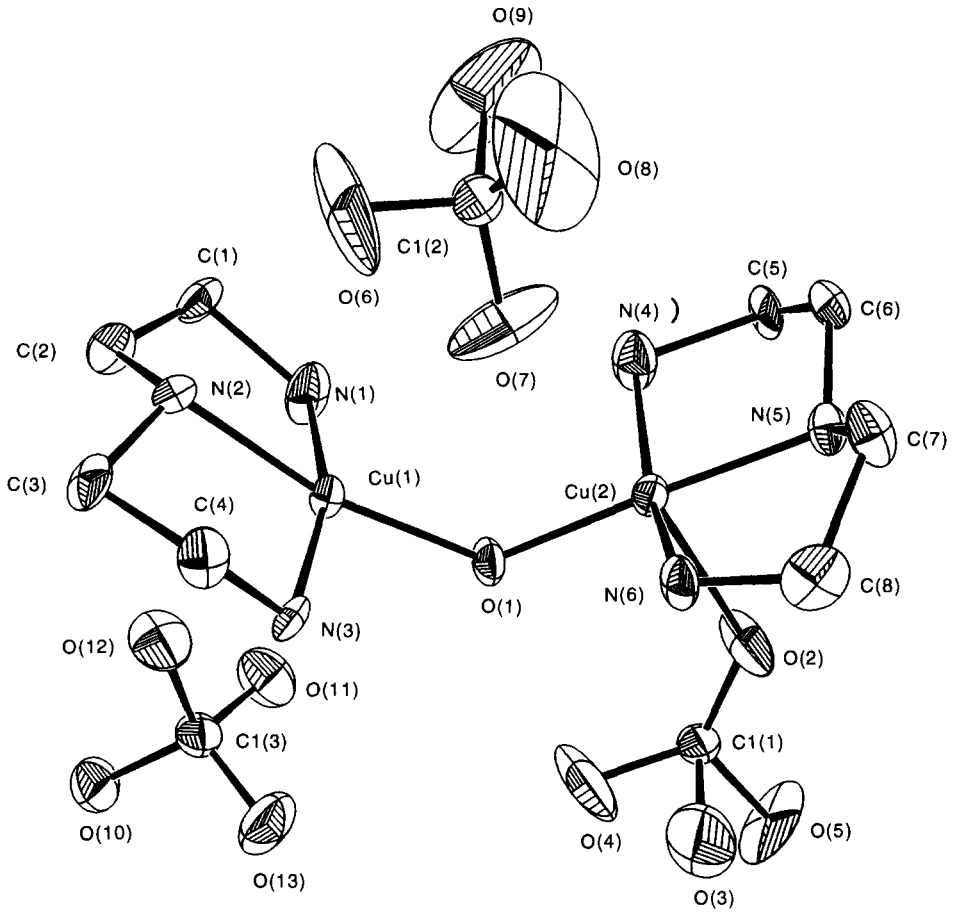


Fig. 1. ORTEP stereoview of $[Cu_2(dien)_2(OH)](ClO_4)_3$ (**1**) with atom-numbering scheme and vibrational ellipsoids at the 30% probability level.

only with Cu^{II}. These $Cu\cdots OClO_3$ interactions are very weak, at 2.608(10) [Cu(1)—O(12)], 2.746(14) [Cu(2)—O(7)] and 2.894(21) Å [Cu(1)—O(7)], and are probably electrostatic rather than covalent. The two copper atoms are bridged by a hydroxo group with the Cu(1)—OH—Cu(2) angle of 129.1(4)° and the intermolecular Cu(1)—Cu(2) separation of 3.4320(17) Å being close to those previously reported by Julve and co-workers [14]. The bridging Cu—O distances of 1.893(10) and 1.960(7) for Cu(1)—O(1) and Cu(2)—O(1), respectively agree closely with those previously reported [14].

The structure of the title compound $[Cu^{II}(dien)(CN)_2Cu^{I}(CN)]_n$ (**2**) consists of a one-dimensional skeleton formed by the polymeric mixed-valence Cu^{I}/Cu^{II} chain through the cyanide bridges as shown in Figs 2 and 3. The layer structure of this polymer is illustrated in Fig. 4. As shown in Fig. 2, the copper(II) atom, Cu(2), takes a distorted square-pyramidal coordination with three nitrogen atoms of the dien ligand, one carbon atom of the terminal CN ion and a nitrogen atom of CN in the apical position, which is linked with the copper(I) atom of the polymer chain. In the polymer chain, the copper atom, Cu(1), is in trigonal-planar coordination (three C—Cu^{I}—C bond angles are 120°) with D_{3h} symmetry.

It is important to note that due to static disorder, in the bridging CN groups with Cu^{I} the Cu^{I} atom bonded as Cu—CN, and the other bonded as Cu—NC, are almost identical; this means that discrimination between the N and C atoms of the N group linking the Cu^{I} centres is impossible, and they are assumed to have 50% probability for each of the C and N designated as NC, in the structure refinement. The bond length of NC—NCb 1.138(4) Å is slightly longer than that of 1.127(4) Å for C(4)—N(4) which link with the Cu^{II} atom. In the Cu^{II} site, the Cu^{II}—C(3) distance of 1.971(3) Å found here compares favourably with the distances found in the other C-bond Cu^{II}—CN complexes mentioned above [2–7]. The Cu(2)—N(CN) bond length of 2.171 Å is significantly longer than the mean Cu(2)—N(dien) bond length

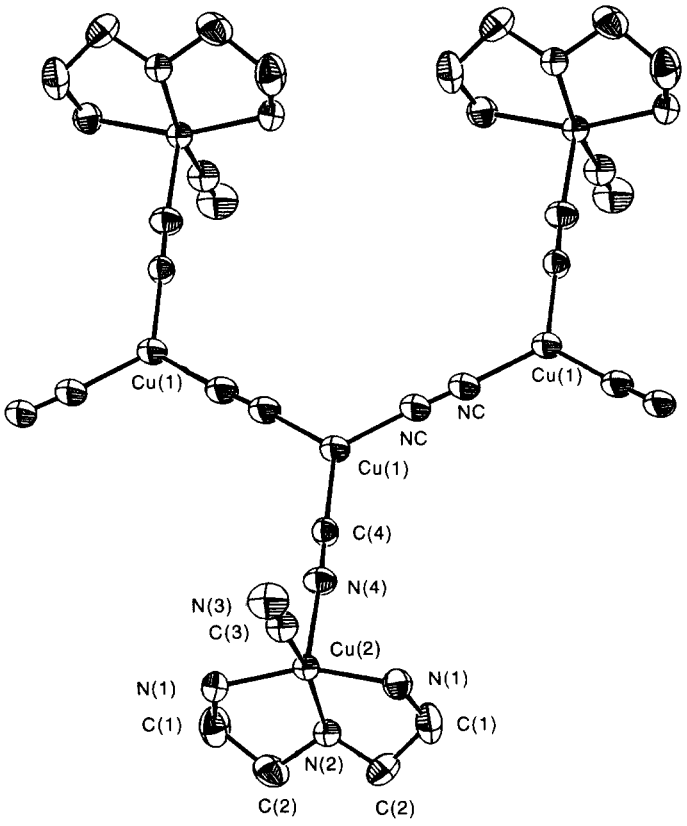


Fig. 2. ORTEP stereoview of $[Cu(dien)(CN)_2Cu(CN)]_n$ (**2**) with atom-numbering scheme and vibrational ellipsoids at the 30% probability level.

of 2.038 Å, which is within the normal range. The C(3)—N(3) bond length of 1.133(5) Å of the bridging CN is slightly longer than the terminal N(4)—C(4) distance of 1.127(4) Å. The nearest intrachain and interchain Cu^{II}—Cu^{II} separations are 6.2214(13) and 7.124(3) Å, respectively, and are likely to cause a very weak magnetic interaction between two copper(II) ions.

Magnetic properties

The *X*-band (9.8 GHz) polycrystalline EPR spectrum at 298 K for **2** was found to exhibit an axially elongated pyramidal copper(II) centre, with $g_{\parallel} = 2.21$ and $g_{\perp} = 2.03$. Magnetic susceptibility measurements from 300 to 4.2 K have been made for complex **2** as shown in Fig. 5, as the effective moments μ_{eff} and χ_m *vs.* *T*. In the temperature range studied, the μ_{eff} value of 2.10 μ_B at 300 K is slightly lower than the value of 2.45 μ_B expected for a non-coupled, two $S = \frac{1}{2}$ spin system, and decreases slowly with decreasing temperature, reaching 1.44 μ_B at 4.2 K. This decrease can be owing to intramolecular and/or intermolecular antiferromagnetic exchange interactions between the nearest Cu^{II} ions. Although there is not a detailed model for our complex mixed-valence system, we tried to reproduce the susceptibility of this compound by a modified Bleaney–Bowers susceptibility expression for the two-spin systems of $S = \frac{1}{2}$

$$\chi_m = 2Ng^2\beta^2/k(T-\theta)[\{1/(3+x^{-1})](1-\rho)\} + \rho/4] + N, \quad (1)$$

$x = \exp(-J/kT)$, the parameter θ is the Curie–Weiss constant, which accounts the intermolecular interaction between Cu^{II}—Cu^{II} of the interchain, let $\theta = zJ'$ (interchain coupling parameter) [19], ρ is the fraction of mononuclear paramagnetic impurity, N_z is the temperature-independent paramagnetism and the other symbols have their usual meaning. Where we have assumed the isotropic g value in calculation, the best result of the least squares fitting to Eq. (1) gives $g_i = 2.12$ (obtained from averaged g value of EPR data), $J = -0.47\ cm^{-1}$, $zJ' = -0.26\ cm^{-1}$, $\rho = 0.06$ and $N_z = 200 \times 10^{-6}\ cm^3\ mol^{-1}$. Figure 5 illustrates a plot of χ_m and μ_{eff} *vs.* *T* for **2**, with the solid line corresponding to the fitted parameters quoted above. The values of $J = -0.47\ cm^{-1}$ and $zJ' = -0.26\ cm^{-1}$

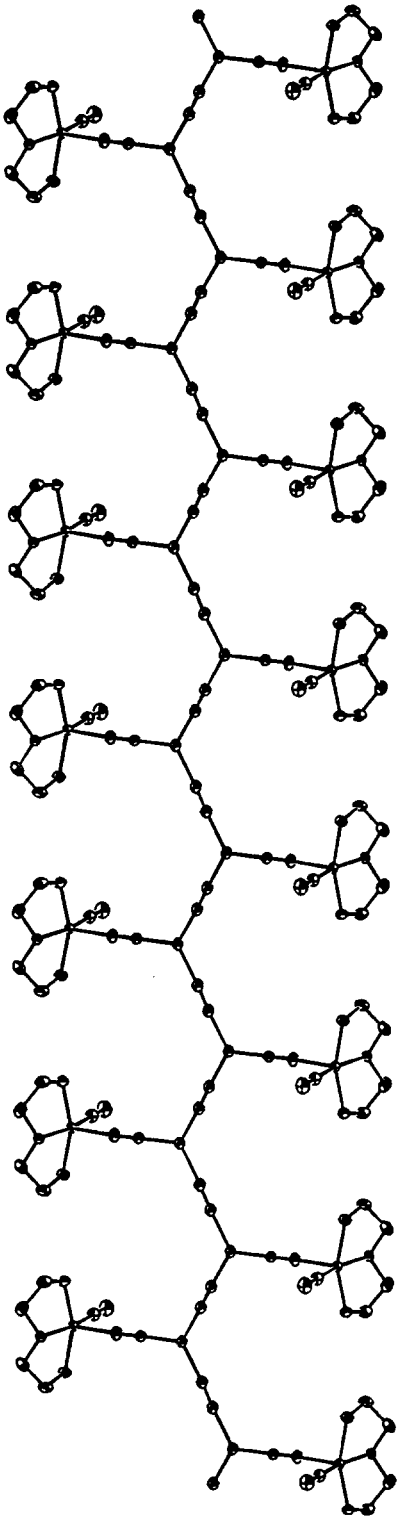


Fig. 3. View of the one-dimensional polymeric chain of **2**.

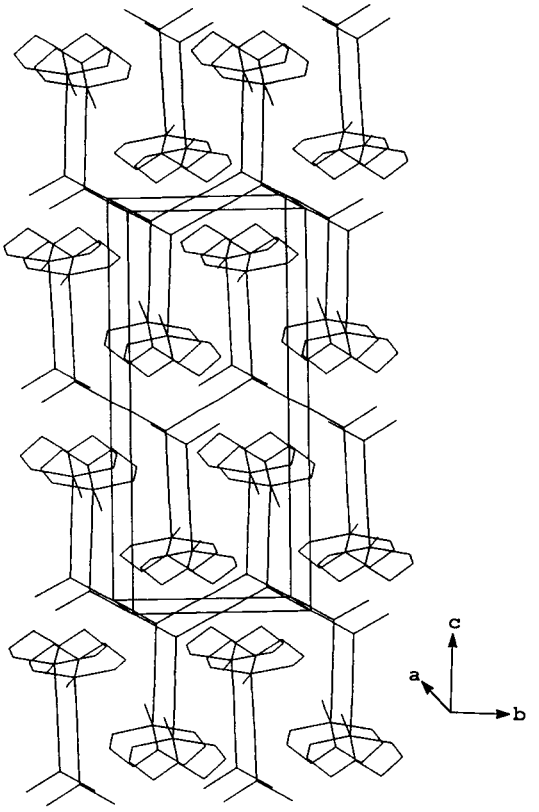


Fig. 4. Interchain molecular arrangement in the crystal of **2**, showing the layer structure.

are relatively much smaller, these may be due to a large separation, 6.22 and 7.12 Å, of the nearest magnetic Cu^{II} ions of the intrachain (through —NC—Cu^{I}—CN—bridge) and the interchain [through Cu^{II}—CN···NH(dien)Cu^{II} interaction] respectively, in **2**.

In summary, **2** is a new example of a mixed-valence Cu^{I}/Cu^{II} polymeric complex with the stable Cu^{II}—CN and Cu^{II}—NC bondings that resulted from the direct partial reduction of the OH-bridged binuclear copper(II) complex **1** by NaCN. The terminal C-bonded Cu^{II}—CN is stabilized by three nitrogen atoms of the dien ligand and one nitrogen atom of the bridged NC—Cu^{I}. Although the detailed mechanistic aspects for the partial reduction for the present system and related systems were not elucidated at present, this work is in progress.

Acknowledgement—This work was supported by a grant from the National Science Council of Taiwan (NSC85-2113-M-032-010).

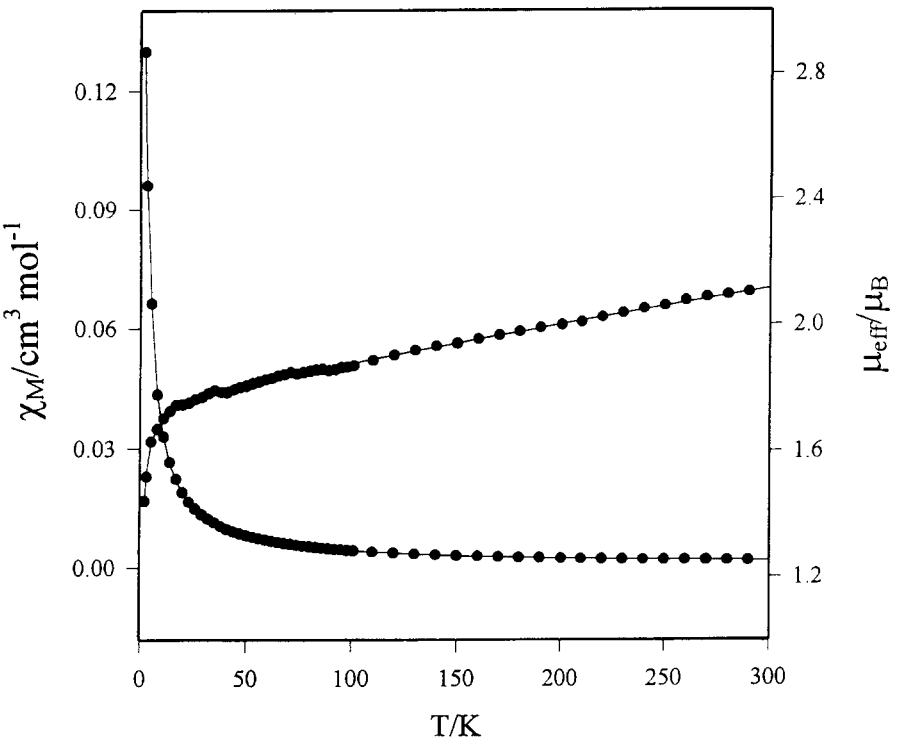


Fig. 5. Temperature dependence of the molar magnetic susceptibility and magnetic moment for **2**. The solid lines represent a fit based on Eq. (1).

REFERENCES

1. Hathaway, B. J., in *Comprehensive Coordination Chemistry*, ed. G. Wilkinson, Vol. 5. Pergamon Press, Oxford, 1987, p. 729.
2. Anderson, O. P., *Inorg. Chem.*, 1975, **14,** 730.
3. Tyagi, S. and Hathaway, B. J., *J. Chem. Soc., Dalton Trans.*, 1983, 199.
4. Anderson, O. P. and Packard, A. B., *Inorg. Chem.*, 1980, **19,** 2941.
5. Scott, M. J., Lee, S. C. and Holm, R. H., *Inorg. Chem.*, 1994, **33,** 4651.
6. Duggen, D. M., Jungst, R. G., Mann, K. R., Stucky, G. D. and Hendrickson, D. N., *J. Am. Chem. Soc.*, 1974, **96,** 3443.
7. Duggen, D. M. and Hendrickson, D. N., *Inorg. Chem.*, 1974, **13,** 1911.
8. Koziskova, Z., Dunaj-Jurco, M. and Gazo, J., *J. Chem. Zuesti*, 1984, **83,** 583.
9. Vrabel, V., Kellö, E. and Garaj, J., *Acta. Cryst.*, 1995, **C51,** 1286.
10. Agnus, Y., Gisselbrecht, J. P., Louis, R. and Metz, B., *J. Am. Chem. Soc.*, 1989, **111,** 1494.
11. Lee, S. C., Scott, M. J., Kauffmann, K., Münck, E. and Holm, R. H., *J. Am. Chem. Soc.*, 1994, **116,** 401; Scott, M. J. and Holm, R. H., *J. Am. Chem. Soc.*, 1994, **116,** 11357.
12. Kappenstein, C. and Schubert, U. J., *J. Chem. Soc., Chem. Commun.*, 1980, 1116.
13. Curtis, N. F. and Powell, H. K., *J. Chem. Soc. (A)*, 1968, 3069.
14. Casro, I., Faus, J., Julve, M., Floret, F., Verdaguer, M., Khan, O., Jeannin, Y. and Vaisserman, J., *J. Chem. Soc., Dalton Trans.*, 1990, 2207.
15. Fox, S., Potenzu, J. A., Knapp, S. and Schuger, H. J., in *Bioinrganic Chemistry of Copper*, ed. K. D. Karlin and Z. Tyklar. Chapman & Hall, New York, 1993.
16. Lablanca, D. A., *J. Chem. Educ.*, 1979, **56,** 788. This article provides some references about cyanide poisoning.
17. Himmelwright, R. S., Eickman, N. C. and Solomon, E. I., *J. Am. Chem. Soc.*, 1979, **101,** 1576; Himmelwright, R. S., Eickman, N. C., LuBien, C. D. and Solomon, E. I., *J. Am. Chem. Soc.*, 1980, **102,** 5378.
18. Gate, E. J., Le Page, Y., Cherland, J. P., Lee, F. L. and White, P. S., *J. Appl. Cryst.* 1989, **22,** 384.
19. Kahn, O., *Molecular Magnetism*. VCH, New York, 1993.

Pergamon

PII: S0277-5387(96)00416-0

Polyhedron Vol. 16, No. 10, pp. 1755–1761, 1997
Copyright © 1997 Elsevier Science Ltd
Printed in Great Britain. All rights reserved
0277-5387/97 $17.00+0.00

Chemistry of ruthenium phenolates. Synthesis, characterization and redox properties of a group of salicylaldiminato complexes of ruthenium

Nimai Chand Pramanik and Samaresh Bhattacharya*

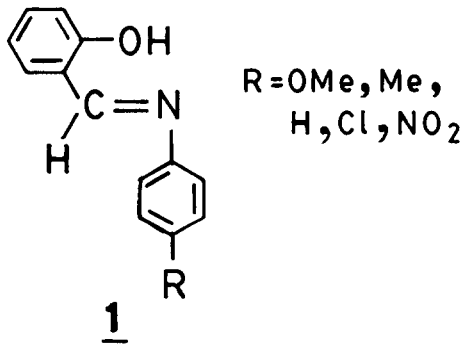
Department of Chemistry, Inorganic Chemistry Section, Jadavpur University, Calcutta 700 032, India

(Received 18 June 1996; accepted 16 August 1996)

Abstract—A group of five mixed ligand ruthenium(II) complexes of general formula $[Ru(bpy)(sal\text{-}R)_2]$ (bby = 2,2′-bipyridine, sal-R = salicylaldiminate anion) has been synthesized and characterized. The complexes are diamagnetic (low spin d^6, $S = 0$) and show intense MLCT transitions in the visible region in solution. In acetonitrile solution they all show a reversible ruthenium(II)–ruthenium(III) oxidation in the range −0.3 to 0.04 V versus SCE, followed by another reversible ruthenium(III)–ruthenium(IV) oxidation in the range 1.1 to 1.3 V versus SCE. The potential of these two oxidations is sensitive to the nature of the substituent R in the sal-R ligand. A reversible bpy reduction is also observed near −1.9 V versus SCE. The five $[Ru^{III}(bpy)(sal\text{-}R)_2]^+$ complexes have been synthesized by chemical oxidation of their respective ruthenium(II) precursors by iodine, and isolated as perchlorate salts. These oxidized complexes are paramagnetic (low spin d^5, $S = 1/2$) and show rhombic ESR spectra at 77 K. They show intense LMCT transitions in the visible region in acetonitrile solution, together with weak ligand-field transitions at lower energies. Chemical reduction of these ruthenium(III) complexes by hydrazine gives back the parent ruthenium(II) complexes. © 1997 Elsevier Science Ltd. All rights reserved.

Keywords: ruthenium salicylaldiminates; synthesis; characterization; redox properties.

The present work has originated from our interest in the chemistry of ruthenium in different coordination environments in general [1], and the chemistry of ruthenium phenolates in particular [2]. In the present study we have used salicylaldimine, abbreviated in general as Hsal-R (**1**; where H stands for the dissociable phenolic proton), as the principal ligand.



1

The two donor atoms of this ligand are of opposite natures. The phenolate oxygen is a hard donor and is known to stabilize the higher oxidation states of ruthenium [3], whereas the imine nitrogen is relatively much softer and is a recognized stabilizer of the lower oxidation states of this metal [4]. It is interesting to note that the chemistry of ruthenium salicylaldiminates has not been much explored [2c–e,5]. However, in all known ruthenium salicylaldiminate complexes, the effect of phenolate oxygen coordination is seen to win over that of imine nitrogen coordination. For example, in the tris-salicylaldiminate complexes, the trivalent state of ruthenium is highly stabilized, which is reflected in the low ruthenium(III)–ruthenium(II) reduction potential [5a]. This also indicates that chelation by salicylaldiminate alone can not stabilize the +2 state of ruthenium, and in order to have a stable salicylaldiminate complex of ruthenium(II) at least one of the three salicylaldiminate ligands of $[Ru(sal\text{-}R)_3]$ needs to be replaced by a strong π-acid ligand. In this context we wish to report here the chemistry of some

* Author to whom correspondence should be addressed.

bis-salicylaldiminate complexes of ruthenium. To satisfy the remaining two coordination sites of the $Ru(sal\text{-}R)_2$ moiety, 2,2′-bipyridine (bpy), which is a familiar stabilizer of ruthenium(II), has been used as the coligand. The synthesis, characterization and redox properties of a group of $[Ru(bpy)(sal\text{-}R)_2]$ complexes are described in this paper.

EXPERIMENTAL

Materials

Commercial ruthenium trichloride, purchased from Arora Matthey, Calcutta, India, was converted to $RuCl_3 \cdot 3H_2O$ by repeated evaporation to dryness with concentrated hydrochloric acid. 2,2′-Bipyridine was purchased from Loba, Bombay, India. $[Ru(bpy)Cl_3]$ was synthesized following a reported procedure [6]. The salicylaldimine ligands were prepared by reacting equimolar amounts of salicylaldehyde and the respective amine in hot ethanol. Purification of acetonitrile and preparation of tetraethylammonium perchlorate (TEAP) for electrochemical work were performed as reported in the literature [7]. All other chemicals and solvents were reagent grade commercial materials and were used as received.

Preparation of complexes

The $[Ru^{II}(bpy)(sal\text{-}R)_2]$ and $[Ru^{III}(bpy)(sal\text{-}R)_2]ClO_4$ complexes were synthesized following two general methods. Details are given for two representative cases only.

$[Ru^{II}(bpy)(sal\text{-}H)_2]$. $[Ru(bpy)Cl_3]$ (100 mg, 0.28 mmol) was suspended in ethanol (40 cm^3) and Hsal-H (135 mg, 0.69 mmol) was added to it, followed by an ethanolic solution of NaOH (28 mg, 0.70 mmol). The mixture was refluxed for 3 h under nitrogen. The solvent was then evaporated and the solid mass thus obtained was washed thoroughly with water followed by hexane, and dried *in vacuo* over P_4O_{10}. Recrystallization from a 1:1 dichloromethane/hexane solution gave $[Ru(bpy)(sal\text{-}H)_2]$ as a dark brown crystalline solid. Yield: 140 mg, 72%.

CAUTION ! Perchlorate salts of metal complexes are potentially explosive. Care should be taken in handling such samples.

$[Ru^{III}(bpy)(sal\text{-}H)_2]ClO_4$. $[Ru(bpy)(sal\text{-}H)_2]$ (100 mg, 0.154 mmol) was dissolved in acetonitrile (30 cm^3) and to it was added a solution of iodine (40 mg, 0.16 mmol) in acetonitrile. The resulting solution was stirred for 15 min. The initial dark brown colour turned to deep green within 5 min. A saturated aqueous solution of $NaClO_4$ (10 cm^3) was then added and the solution was kept in the refrigerator for 24 h. $[Ru(bpy)(sal\text{-}H)_2]ClO_4$ precipitated as a deep green microcrystalline solid which was collected by filtration, washed with cold water and dried *in vacuo* over P_4O_{10}. Yield 80 mg, 69%.

Physical measurements

Microanalyses (C, H, N) were performed using a Perkin–Elmer 240C elemental analyser. IR spectra were obtained on a Perkin–Elmer 783 spectrometer with samples prepared as KBr pellets. Electronic spectra were recorded on a Hitachi U-3400 spectrophotometer. Magnetic susceptibilities were measured using a PAR 155 vibrating sample magnetometer. ^1H NMR spectra were obtained on a Hitachi R-60 FT-NMR spectrometer using TMS as the internal standard. X-band ESR spectra were recorded on a Varian E-109C spectrometer fitted with a quartz Dewar for measurement at 77 K (liquid nitrogen) and the spectra were calibrated with DPPH ($g = 2.0037$). Solution electrical conductivities were measured using a Philips PR9500 bridge with a solute concentration of 10^{-3} M. Electrochemical measurements were made using the PAR model 370-4 electrochemistry system incorporating the following components: 174A polarographic analyser, 175 universal programmer, RE0074 X-Y recorder, 173 potentiostat, 179 digital coulometer, 377 cell system. All electrochemical experiments were performed under dinitrogen. A planar Beckman 39273 platinum inlay working electrode, a platinum wire auxiliary electrode and an aqueous saturated calomel reference electrode (SCE) were used in a three-electrode configuration. A platinum wire gauge working electrode was used in the coulometric experiments. All electrochemical data were collected at 298 K and are uncorrected for junction potentials.

RESULTS AND DISCUSSION

Synthesis and characterization

The reaction of $[Ru(bpy)Cl_3]$ with the salicylaldimines proceeds smoothly in refluxing ethanol in the presence of NaOH to afford the $[Ru(bpy)(sal\text{-}R)_2]$ complexes in good yields [Eq. (1)]. It may be noted here that during the course of this synthetic reaction, ruthenium undergoes a one-electron reduction.

$$[Ru(bpy)Cl_3] \xrightarrow[EtOH]{HL,NaOH} [Ru(bpy)(sal\text{-}R)_2] \quad (1)$$

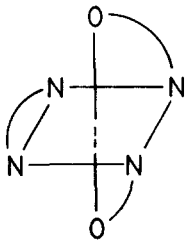
The solvent may serve as the reductant. Using five different Hsal-R ligands, five such complexes have been synthesized. The compositions of these complexes have been confirmed by their elemental (C, H, N) analytical data (Table 1). Magnetic susceptibility measurements show that all these complexes are diamagnetic, as expected for complexes of ruthenium(II) (low spin d^6, $S = 0$).

As the salicylaldiminate ion is an unsymmetrical bidentate ligand, $[Ru(bpy)(sal\text{-}R)_2]$ complexes may exist in three different geometrical isomeric forms, **2**, **3** and **4**. Both **2** and **3** have a C_2 axis, which indicates

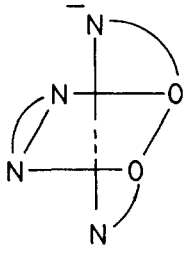
Table 1. Microanalytical, electronic spectral and cyclic voltammetric data

Compound	Analytical data[a] (%) C	H	N	Electronic spectral data[b] λ_{max}, nm (ε, M^{-1} cm^{-1})	Cyclic voltammetric data[c] E^0_{298}, V(ΔE_p, mV) $Ru^{III,IV}$	$Ru^{II,III}$	Ligand reduction
[Ru(bpy)(sal-OMe)$_2$]	64.0 (64.3)	4.4 (4.5)	8.1 (7.9)	705 (2800); 567 (4200); 440[d] (4900); 352 (12,300)	1.11 (90)	−0.26 (90)	−1.91 (90)
[Ru(bpy)(sal-Me)$_2$]	67.6 (67.3)	4.9 (4.7)	8.0 (8.3)	700 (2500); 570 (3600); 440[d] (4900); 352 (12,200)	1.13 (80)	−0.21 (90)	−1.90 (80)
[Ru(bpy)(sal-H)$_2$]	66.3 (66.6)	4.0 (4.3)	8.4 (8.6)	565 (6800); 440 (11,700); 340 (12,300)	1.16 (80)	−0.17 (90)	−1.88 (70)
[Ru(bpy)(sal-Cl)$_2$]	60.5 (60.2)	3.8 (3.6)	7.5 (7.8)	550 (6300); 442 (6900); 350 (9600)	1.20 (70)	−0.10 (70)	−1.86 (80)
[Ru(bpy)(sal-NO_2)$_2$]	58.3 (58.5)	3.7 (3.5)	11.2 (11.4)	580 (4900) 460 (5300); 350 (13,300)	1.29 (85)	0.04 (70)	−1.84 (75)

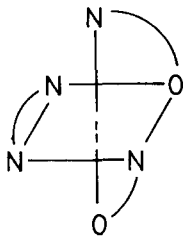
[a] Calculated values are in parentheses.
[b] In acetonitrile solution.
[c] Conditions: solvent, acetonitrile; supporting electrolyte, TEAP (0.1 M); working electrode, platinum; reference electode, SCE; solute concentration, ~ 10^{-3} M; $E^0_{298} = 0.5\ (E_{pa} + E_{pc})$, where E_{pa} and E_{pc} are anodic and cathodic peak potentials, $\Delta E_p = E_{pa} - E_{pc}$; scan rate 50 mV s^{-1}.
[d] Shoulder.



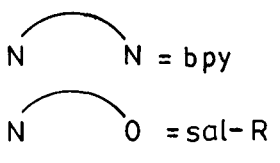
2



3



4



that the two sal-R ligands and the two pyridine rings of bpy are equivalent. In the case of **4**, there is no C_2 axis and hence all the hydrogens present in the complex may give rise to separate ^{1}H NMR signals (provided no overlap of signals occur). The ^{1}H NMR spectrum of [Ru(bpy)(sal-OMe)$_2$], recorded in $CDCl_3$ solution, shows two methyl signals of equal intensity at δ 3.58 and 3.74. This clearly shows that this complex has structure **4**. Similarly, two equally intense methyl signals are observed at δ 1.83 and 2.08 in the ^{1}H NMR spectrum of [Ru(bpy)(sal-Me)$_2$], indicating the same stereochemistry, **4**, for this complex. Therefore we assume structure **4** for all five [Ru(bpy)(sal-R)$_2$] complexes.

The [Ru(bpy)(sal-R)$_2$] complexes are soluble in acetonitrile, dichloromethane, chloroform, *etc.*, producing intense brown solutions. Conductivity measurements show that these complexes are non-electrolytes in solution, as expected. The electronic spectra have been recorded in acetonitrile solution and spectral data are given in Table 1 and selected spectrum is shown in Fig. 1. All five complexes show several intense absorptions in the visible region, which are due to allowed metal-to-ligand charge-transfer transitions. Multiple charge-transfer transitions in these complexes may result from lower symmetry splitting of the metal level, the presence of different acceptor orbitals and the mixing of singlet and triplet configurations in the excited state through spin–orbit coupling [8]. Such spectral behaviour has been observed before in similar mixed ligand complexes [1d].

Cyclic voltammetric studies

The electron transfer properties of the [Ru(bpy)(sal-R)$_2$] complexes have been studied in acetonitrile solution by cyclic voltammetry. Vol-

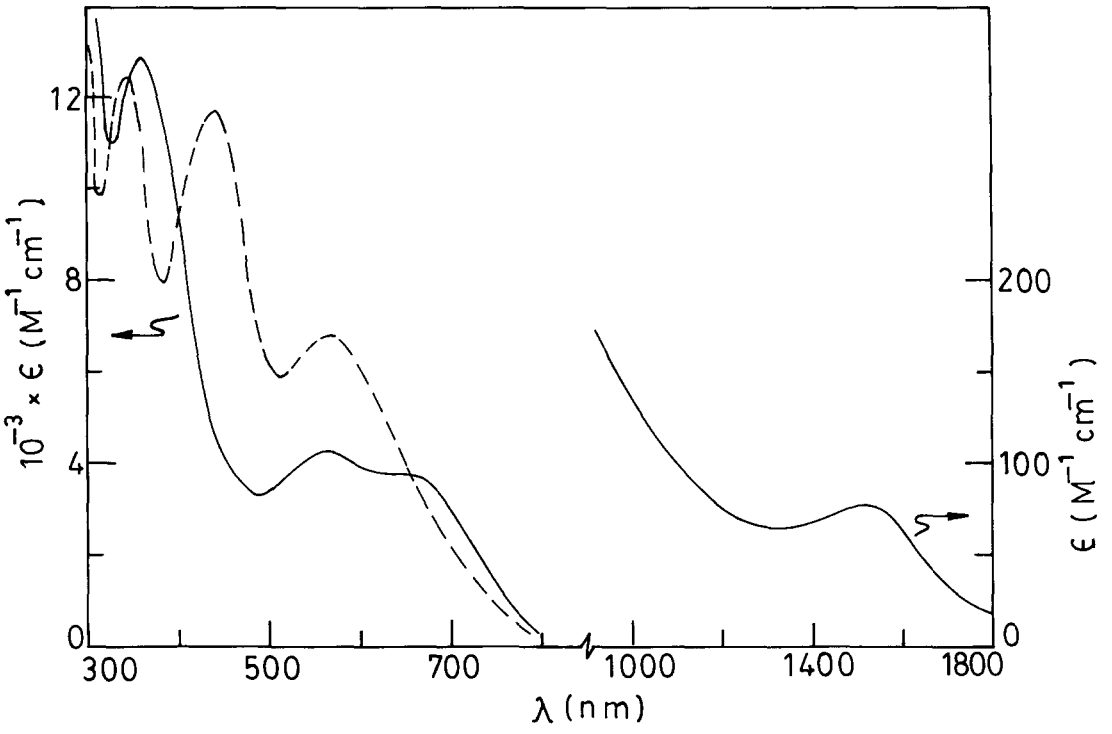


Fig. 1. Electronic spectra of $[Ru^{II}(bpy)(sal\text{-}H)_2]$ (– – –) and $[Ru^{III}(bpy)(sal\text{-}H)_2]ClO_4$ (——) in acetonitrile solution.

tammetric data are presented in Table 1 and a representative voltammogram is shown in Fig. 2. All these complexes show three voltammetric responses, two metal-centred oxidations and one ligand (bpy)-based reduction. We shall first consider the ligand-based reduction. A one-electron reduction near −1.9 V (all potentials are referenced to SCE) is displayed by all these complexes which is assigned to the reduction of the coordinated bpy [Eq. (2)].

$$[Ru^{II}(bpy)(sal\text{-}R)_2] + e^- \rightleftharpoons [Ru^{II}(bpy)(sal\text{-}R)_2]^- \quad (2)$$

The one-electron nature of this couple has been established by comparing its current heights with those of the ruthenium(II)–ruthenium(III) couple displayed by all these complexes near −0.1 V (see below). It is well known [9] that each bpy can successively accept two electrons in its lowest unoccupied molecular orbital. Hence, in these [Ru (bpy)(sal-$R)_2$] complexes two successive one-electron reductions are expected of which only the first reduction is actually observed. The second reduction, which is expected to occur at much more negative potentials, is not observed owing to solvent cut-off.

The metal-centred oxidations will now be

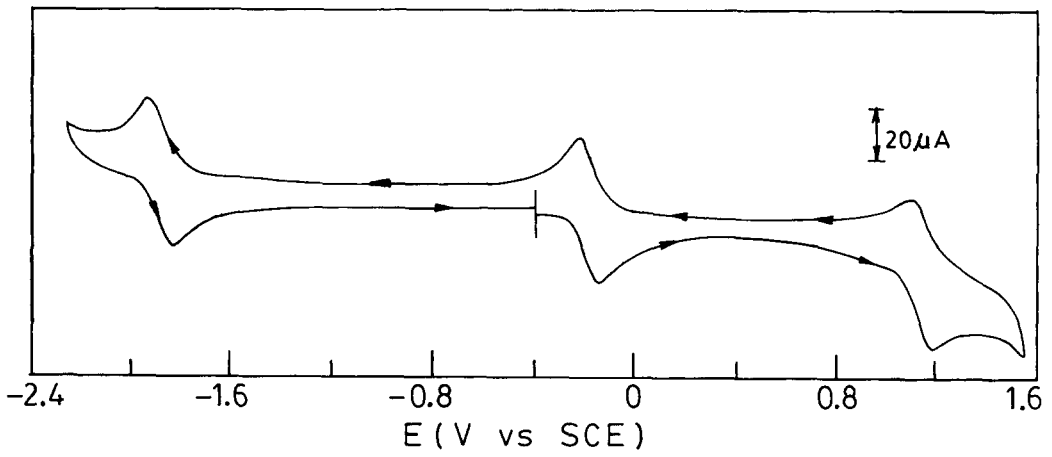


Fig. 2. Cyclic voltammogram of $[Ru^{II}(bpy)(sal\text{-}H)_2]$ in acetonitrile solution (0.1 M TEAP) at a scan rate of 50 mV s^{-1}. The solute concentration was 1×10^{-3} M.

considered. All these complexes show a reversible one-electron oxidation in the range −0.26 to 0.04 V, which is assigned to the ruthenium(II)–ruthenium(III) oxidation [Eq. (3)].

$$[Ru^{II}(bpy)(sal\text{-}R)_2] \rightleftharpoons [Ru^{III}(bpy)(sal\text{-}R)_2]^+ + e^- \quad (3)$$

Therefore the replacement of only one sal-R ligand of $[Ru(sal\text{-}R)_3]$ by bpy has indeed caused a significant increase in the stability of the +2 state of ruthenium. For example, the ruthenium(II)–ruthenium(III) couple is observed at −0.83 V in $[Ru(sal\text{-}H)_3]$ [5a], while the same couple appears at −0.17 V in $[Ru(bpy)(sal\text{-}H)_2]$. The positive shift of 660 mV reflects the ability of bpy to stabilize the bivalent state of ruthenium. It is interesting to note here that a gradual decrease in the potential of the ruthenium(II)–ruthenium(III) couple is observed in the series: $[Ru(bpy)_3]^{2+}$, 1.30 V [10]; $[Ru(bpy)_2(sal\text{-}H)]^+$, 0.63 V [2d]; $[Ru(bpy)(sal\text{-}H)_2]$, −0.17 V; $[Ru(sal\text{-}H)_3]$, −0.83V [5a]. The plot of these E^0_{298} values versus the number of bpy ligands in these $[Ru(bpy)_n(sal\text{-}H)_{3-n}]$ ($n = 0, 1, 2, 3$) complexes is linear (Fig. 3). A similar linear plot is obtained in any other $[Ru(bpy)_n(sal\text{-}R)_{3-n}]$ series. This correlation shows the relative ability of the sal-R and bpy ligands to stabilize the +3 and +2 states of ruthenium.

The potential of the ruthenium(II)–ruthenium(III) couple in the $[Ru(bpy)(sal\text{-}R)_2]$ complexes is found to be sensitive to the nature of the substituent R in the salicylaldiminate ligand. The formal potential (E^0_{298}) increases with increasing electron withdrawing character of R. The plot of E^0_{298} versus 2σ [σ = Hammett constant of R [11]; OMe = −0.27, Me = −0.17, H = 0.0, Cl = 0.23 and NO_2 = 0.78] is linear (Fig. 4) with $\rho = 0.14$ V (ρ = reaction constant of this couple [12]). It is clear from this plot that a single substituent on the sal-R ligand, which is six bonds away from the electroactive metal centre, can influence the metal oxidation potential in a predictable manner.

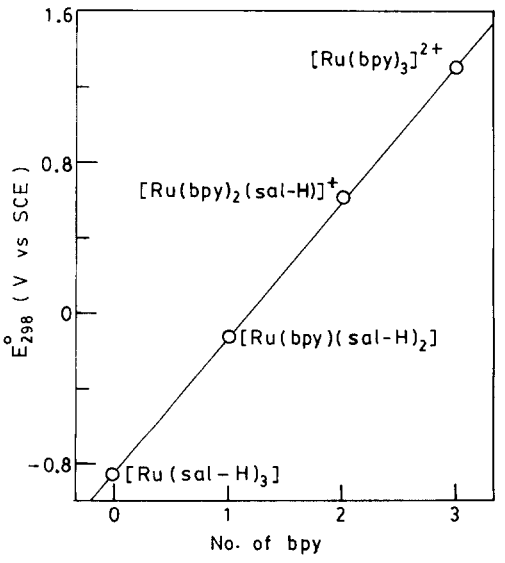


Fig. 3. Variation of ruthenium(II)–ruthenium(III) potential in $[Ru(bpy)_n(sal\text{-}H)_{3-n}]$.

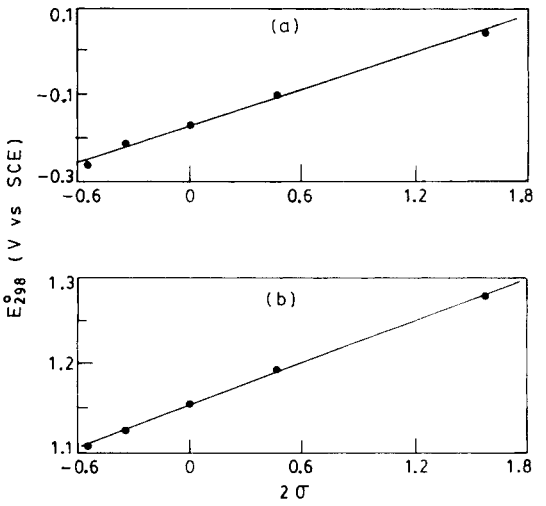


Fig. 4. Least-squares plot of E^0_{298} values of (a) Ru^{II}/Ru^{III} couple *versus* 2σ and (b) Ru^{III}/Ru^{IV} couple *versus* 2σ.

All the $[Ru(bpy)(sal\text{-}R)_2]$ complexes show a second, reversible one-electron oxidation in the range 1.1–1.3 V which is assigned to the ruthenium(III)–ruthenium(IV) oxidation [Eq. (4)].

$$[Ru^{III}(bpy)(sal\text{-}R)_2]^+ \rightleftharpoons [Ru^{IV}(bpy)(sal\text{-}R)_2]^{2+} + e^- \quad (4)$$

The potential of this oxidation is *ca* 500 mV more positive than that in the respective $[Ru(sal\text{-}R)_3]$ complexes [5a], which is owing to the strong π-acidity of the bpy ligand, as discussed above. The potential of this oxidation also correlates linearly with the Hammett constant (σ) of R (Fig. 4). The slope in this case is $\rho = 0.09$ V, which indicates that this ruthenium(III)–ruthenium(IV) oxidation potential is relatively less sensitive to the nature of R than the ruthenium(II)–ruthenium(III) oxidation potential.

$[Ru^{III}(bpy)(sal\text{-}R)_2]^+$ *complexes*

The reversibility of the ruthenium(II)–ruthenium(III) couple in the $[Ru(bpy)(sal\text{-}R)_2]$ complexes, and its relatively low potential, point to the possibility of the oxidized complex, $[Ru^{III}(bpy)(sal\text{-}R)_2]^+$, being stable on a much longer time-scale. To investigate this, the $[Ru(bpy)(sal\text{-}R)_2]$ complexes have been oxidized in acetonitrile solution (0.1 M TEAP) by constant-potential coulometry near 0.3 V. The oxidations have been smooth and quantitative [n (number of electron-transfer) = 0.97] affording deep green solutions of $[Ru^{III}(bpy)(sal\text{-}R)_2]^+$ which show similar cyc-

lic voltammograms to their respective precursors, except that the ruthenium(II)–ruthenium(III) couple now appears as a reductive response. Upon coulometric reduction of the green solutions near −0.5 V, deep brown solutions of $[Ru(bpy)(sal\text{-}R)_2]$ are obtained. The $[Ru^{III}(bpy)(sal\text{-}R)_2]^+$ complexes have also been synthesized by chemical oxidation of $[Ru^{II}(bpy)(sal\text{-}R)_2]$ in acetonitrile solution by iodine and the complex cations have been isolated as perchlorate salts in the solid state. Microanalytical data (Table 2) agree well with the compositions of these complexes. Conductivity measurements in acetonitrile solution show that these complexes behave as 1 : 1 electrolytes (Table 2), as expected. Electronic spectra recorded in acetonitrile solution show intense absorptions in the visible region together with a weak absorption at lower energies (Table 2, Fig. 1). The intense absorptions in the visible region are probably owing to ligand-to-metal charge-transfer transitions. The low intensity absorptions in the near-IR region are discussed below. Addition of hydrazine hydrate to the deep green solution of $[Ru(bpy)(sal\text{-}R)_2]ClO_4$ in acetonitrile brings about an instantaneous reduction affording a deep brown solution of $[Ru(bpy)(sal\text{-}R)_2]$.

The $[Ru(bpy)(sal\text{-}R)_2]ClO_4$ complexes are one-electron paramagnetic (Table 2), which corresponds to the +3 oxidation state of ruthenium (low spin d^5, $S = \frac{1}{2}$) in these complexes. ESR spectra of these complexes have been recorded in 1 : 1 dichloromethane/toluene solution at 77 K. All five complexes show rhombic ESR spectra with three distinct g-values (Fig. 5, Table 3). The rhombic nature of the spectra indicates the asymmetry of the electronic environment around ruthenium in these complexes. This asymmetry is understandable in terms of the stereochemistry of these complexes (**4**, *vide supra*) which has no C_2 axis. The observed spectra may be considered as pseudo-axial, consisting of a rather isolated signal near 1.90 ($g_\parallel$ in the axial case) and two relatively close signals near 2.25 and 2.10 (rhombic

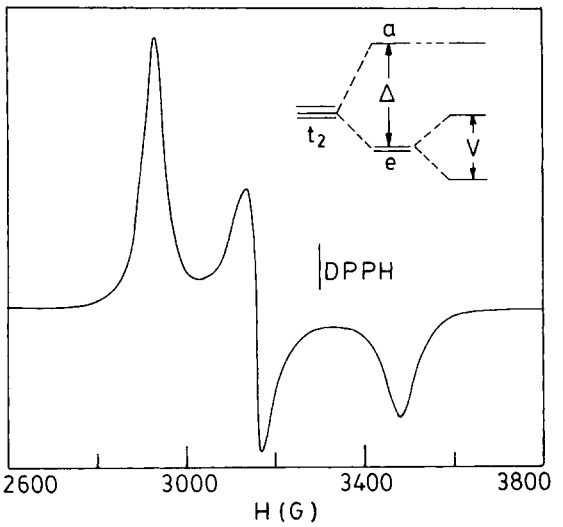


Fig. 5. ESR spectrum in 1 : 1 dichloromethane/toluene solution at 77 K and t_2 splittings of $[Ru^{III}(bpy)(sal\text{-}H)_2]ClO_4$.

Table 2. Microanalytical, molar conductivity, magnetic susceptibility and electronic spectral data

Compound	Analytical data[a] (%) C	H	N	Molar conductivity data[b] Λ_M (Ω^{-1} cm^2 M^{-1})	μ_{eff} (BM)	Electronic spectral data[c] λ_{max}, nm (ε, M^{-1} cm^{-1})
$[Ru(bpy)(sal\text{-}OMe)_2]ClO_4$	56.7	4.2	7.1	155	1.90	1550[d](80); 700[d](2600) 575 (4400); 350 (21,000)
	(56.4)	(4.0)	(6.9)			
$[Ru(bpy)(sal\text{-}Me)_2]ClO_4$	58.5	4.3	7.4	151	1.88	1550(68); 670[d](1800); 570 (2600); 355 (25,300)
	(58.3)	(4.1)	(7.2)			
$[Ru(bpy)(sal\text{-}H)_2]ClO_4$	57.5	3.5	7.2	144	1.82	1520(80); 675 (3500); 566 (4300); 355 (12,800)
	(57.7)	(3.7)	(7.5)			
$[Ru(bpy)(sal\text{-}Cl)_2]ClO_4$	53.1	3.5	6.4	148	1.85	1500 (60); 650[d](3200); 570 (4500); 360 (17,900)
	(52.8)	(3.2)	(6.8)			
$[Ru(bpy)(sal\text{-}NO_2)_2]ClO_4$	51.8	3.3	9.8	138	1.81	1450 (85); 600 (4800); 360 (15,700)
	(51.5)	(3.1)	(10.0)			

[a] Calculated values are in parentheses.
[b] In acetonitrile solution.
[c] In acetonitrile solution
[d] Shoulder

Table 3. ESR g-values[a] and derived energy parameters[b]

Compound	g_1	g_2	g_3	Δ/λ	v/λ	$\Delta E_1/\lambda$	$\Delta E_2/\lambda$
$[Ru(bpy)(sal\text{-}OMe)_2]ClO_4$	2.264	2.092	1.903	6.24	4.07	4.31	8.45
$[Ru(bpy)(sal\text{-}Me)_2]ClO_4$	2.259	2.091	1.902	6.17	3.95	4.30	8.33
$[Ru(bpy)(sal\text{-}H)_2]ClO_4$	2.257	2.092	1.900	6.07	3.80	4.27	8.15
$[Ru(bpy)(sal\text{-}Cl)_2]ClO_4$	2.226	2.099	1.900	5.77	2.89	4.42	7.43
$[Ru(bpy)(sal\text{-}NO_2)_2]ClO_4$	2.232	2.119	1.901	5.73	2.46	4.57	7.17

[a] In 1 : 1 dichloromethane/toluene solution at 77 K.

[b] Spin–orbit coupling constant (λ) for complexed ruthenium(III) is *ca* 1000 cm^{-1}.

component of g_1). Accordingly, the axial distortion (Δ) that splits the t_2 level into a and e components is expected to be larger than the rhombic distortion (V), which splits e (Fig. 5). Spin–orbit coupling causes further changes in the energy gaps. Thus, two electronic transitions (transition energies ΔE_1 and ΔE_2; $\Delta E_1 < \Delta E_2$) are possible within these three levels. All these energy parameters have been computed (Table 3) using the observed g-values, the g-tensor theory of low spin d^5 complexes [13] and a reported method [14]. The axial distortion is indeed larger than the rhombic one. The ΔE_2 transition has been observed in the spectra of all $[Ru(bpy)(sal\text{-}R)_2]^+$ complexes near the predicted energies (Table 2). However, the ΔE_1 transition could not be detected because the solvent (acetonitrile) itself is not transparent in this region.

Acknowledgements Financial assistance received from the Department of Science and Technology, (SR/OY/C-08/93), New Delhi, is gratefully acknowledged. The authors thank Professor Animesh Chakravorty of the Indian Association for the Cultivation of Science, Calcutta, and Professor Rabindranath Mukherjee of the Indian Institute of Technology, Kanpur, for their help. Thanks are also due to the referee for his suggestions at the revision stage.

REFERENCES

1. (a) Chakravarty, J. and Bhattacharya, S., *Polyhedron* 1994, **13,** 2671; (b) Ghatak, N. and Bhattacharya, S., *Polyhedron* 1994, **13,** 2999; (c) Ghatak, N., Chakravarty, J. and Bhattacharya, S., *Trans. Met. Chem.* 1995, **20,** 138; (d) Ghatak, N., Chakravarty, J. and Bhattacharya, S., *Polyhedron* 1995, **14,** 3591; (e) Chakravarty, J. and Bhattacharya, S., *Proc. Indian Acad. Sci. (Chem. Sci.)* 1995, **107,** 361; (f) Ghatak, N. and Bhattacharya, S., *Trans. Met. Chem.* 1996, **21,** 158.
2. (a) Bhattacharya, S., *Polyhedron* 1993, **12,** 235; (b) Bhattacharya, S., *Polyhedron* 1994, **13,** 451; (c) Chakravarty, J. and Bhattacharya, S., *Polyhedron* 1996, **15,** 257; (d) Chakravarty, J. and Bhattacharya, S., *Polyhedron* 1996, **15** 1047; (e) Sinha, P. K., Chakravarty, J. and Bhattacharya, S., *Polyhedron* 1996, **15,** 2931.
3. (a) Lahiri, G. K., Bhattacharya, S., Mukherjee, M., Mukherjee, A. and Chakravorty, A., *Inorg. Chem.* 1987, **26,** 3359; (b) Bhattacharya, S., Boone, S. R., Fox, G. K. and Pierpont, C. G., *J. Am. Chem. Soc.* 1990, **112,** 1088; (c) Bardwell D. A., Black, D., Jeffery, J. C., Schatz, E. and Ward, M. D., *J. Chem. Soc., Dalton Trans.* 1993, 2321.
4. (a) Reinhold, J., Beuedix, R., Birner, P. and Henning, H., *Inorg. Chim. Acta* 1979, **33,** 209; (b) Goswami, S., Chakravarty, A. R. and Chakravorty A., *Inorg. Chem.* 1981, **20,** 2246.
5. (a) Lahiri, G. K., Bhattacharya, S., Ghosh, B. K. and Chakravorty, A., *Inorg. Chem.* 1987, **26,** 4324; (b) El-Hendawy, A. M., El-Ghany, A., El-Kourashy and Shanab, M. M., *Polyhedron* 1992, **11,** 523; (c) El-Hendawy, A. M., Alkubaisi, A. H., El-Ghany, A., El-Kourashy and Shanab, M. M., *Polyhedron* 1993, **12,** 2343.
6. Anderson, S. and Seddon, K. R., *J. Chem. Res. (S)* 1979, 74.
7. (a) Sawyer D. T. and Roberts J. L. Jr, *Experimental Electrochemistry for Chemists.* John Wiley, New York, 1974, pp. 167–215; (b) Walter M. and Ramaley, L., *Anal. Chem.* 1973, **45,** 165.
8. (a) Pankuch, B. J., Lacy, D. E. and Grosby, G. A., *J. Phys. Chem.* 1980, **84,** 2061; (b) Ceulemans, A. and Vanquickenborne, L. G., *J. Am. Chem. Soc.* 1981, **103,** 2238; (c) Decurtius, S., Felix, F., Ferguson, J., Gudel, H. U. and Ludi, A., *J. Am. Chem. Soc.* 1980, **102,** 4102; (d) Kober, E. M. and Meyer, T. J., *Inorg. Chem.* 1982, **21,** 3967.
9. (a) Vleck, A. A., *Coord. Chem. Rev.* 1982, **43,** 39; (b) Kahl, J. L., Hanck, K. W. and DeArmond, K., *J. Phys. Chem.* 1978, **82,** 540.
10. Tokel-Takvorian, N. E., Hemingway, R. E. and Bard, A. J., *J. Am. Chem. Soc.* 1973, **95,** 6582.
11. Hammett, L. P., *Physical Organic Chemistry*, 2nd edn. McGraw Hill, New York, 1970.
12. Mukherjee, R. N., Rajan, O. A. and Chakravorty, A., *Inorg. Chem.* 1982, **21,** 785.
13. (a) Bleany B. and O'Brien, M. C. M., *Proc. Phys. Soc., London, Sect. B* 1956, **69,** 1216; (b) Griffith, J. S., *The Theory of Transition Metal Ions.* Cambridge University Press, London, 1961, p. 364.
14. Bhattacharya S. and Chakravorty, A., *Proc. Ind. Acad. Sci. (Chem. Sci.)* 1985, **95,** 159.

Pergamon

PII: S0277-5387(96)00394-4

Polyhedron Vol. 16, No. 10, pp. 1763–1766, 1997
Copyright © 1997 Elsevier Science Ltd
Printed in Great Britain. All rights reserved
0277-5387/97 $17.00+0.00

Solid-state structure of $[(Bu^t)_2In(\mu\text{-}Cl)]_\infty$: an unusual saw-tooth polymeric chain

Sarah L. Stoll,[a]† Simon G. Bott[b]* and Andrew R. Barron[a]*

[a]Department of Chemistry, Rice University, Houston, TX 77005, U.S.A.

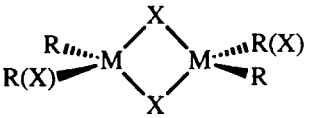
[b]Department of Chemistry, University of North Texas, Denton, TX 76203, U.S.A.

(Received 27 June 1996; accepted 7 August 1996)

Abstract—The solid-state structure of di-*tert*-butyl indium chloride, $[(Bu^t)_2In(\mu\text{-}Cl)]$, has been determined by X-ray diffraction and consists of polymeric $[—In—Cl—]_\infty$ chains arranged in an unusual saw-tooth pattern motif. The indium atom is in a severely distorted coordination environment approximated as a capped trigonal-planar geometry. The structure of $[(Bu^t)_2In(\mu\text{-}Cl)]_\infty$ is compared with $[(Me)_2In(\mu\text{-}Cl)]_2$. © 1997 Elsevier Science Ltd. All rights reserved.

Keywords: indium; chloride; polymer; Group 13.

The alkyl halide compounds, R_2MX and RMX_2, of the Group 13 metals are almost exclusively dimeric in solution and the gas phase (**I**) [1,2]. This structure is ordinarily continued in the solid state for aluminum and gallium. In contrast, the alkyl halide compounds of indium exist in a wide variety of solid-state structures. The alkyl indium dihalides are predominantly polymers [3], while the structures observed for the dialkyl indium halides range from simple halide bridged dimers [4–7] to infinite chain [8] and three-dimensional [9–12] structures. We have previously suggested that the solid-state structure of alkyl indium halides is controlled by both the desire of the indium to maximize its coordination number and the intermolecular interactions of the alkyl (and aryl) ligands [5]. As part of our continuing investigations aimed at gaining a fundamental understanding of the factors that determine the structure and bonding in Group 13 compounds, we report the unusual polymeric structure of $[(Bu^t)_2In(\mu\text{-}Cl)]_\infty$.



M = Al, Ga, In, X = Cl, Br, I

(I)

RESULTS AND DISCUSSION

The dialkyl indium chloride $[(Bu^t)_2In(\mu\text{-}Cl)]_\infty$ was prepared according to the literature methods [13] and recrystallized from CH_2Cl_2. The structure consisting of $(Bu^t)_2InCl$ moieties arranged to form infinite $[—In—Cl—]_\infty$ chains along the crystallographic *b*-axis, is shown in Fig. 1; selected bond lengths and angles are given in Table 1. The In(1)—Cl(1)—In(1a) angle [126.5(6)°] is significantly larger than those observed in $In(\mu\text{-}Cl)_2In$ units [4–7]. The *tert*-butyl groups are positioned above and below the plane defined by the indium and chlorine atoms. While the '$(Bu^t)_2In$' moieties have a fixed position, the chlorine atoms exhibit disorder along the polymer chain, resulting in a reversal of the conformation of the indium center, see Fig. 2.

* Authors to whom correspondence should be addressed.
† Present Address: Department of Chemistry, Oberlin College, Oberlin, OH 44074, U.S.A.

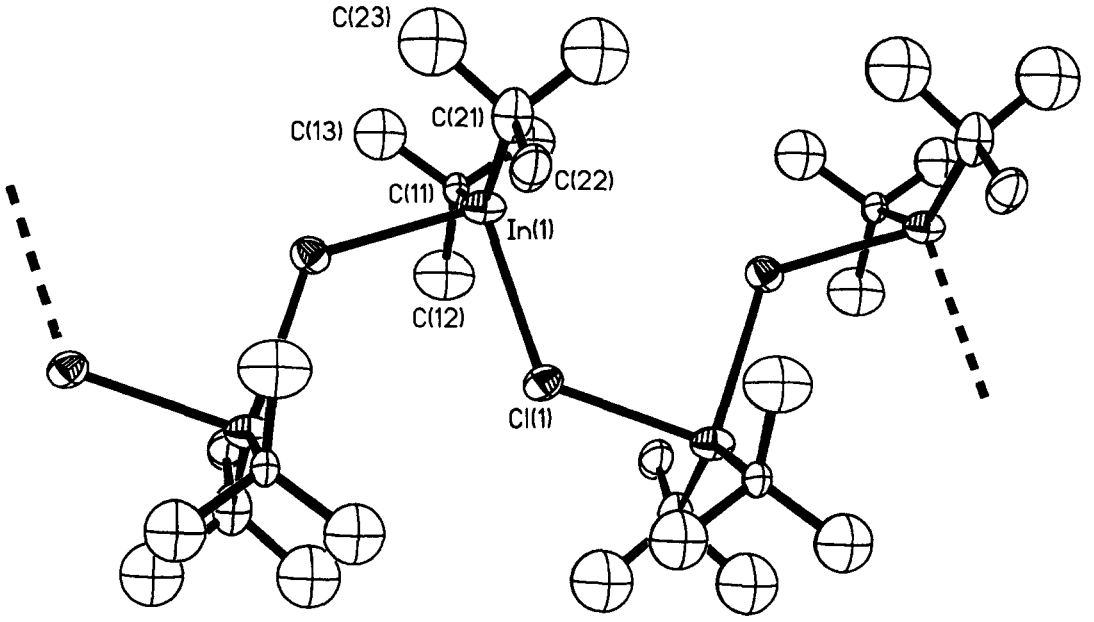


Fig. 1. Solid-state structure of the $[(Bu^t)_2In(\mu\text{-}Cl)]_\infty$. Only one of the positions for the disorder of the chlorine atoms is shown and all hydrogen atoms are omitted for clarity.

Table 1. Selected bond lengths (Å) and angles (°) for $[(Bu^t)_2In(\mu\text{-}Cl)]_\infty$

In(1)—Cl(1)	2.58(1)	In(1)—Cl(1a)	2.52(1)
In(1)—C(11)	2.19(4)	In(1)—C(21)	2.21(4)
Cl(1)—In(1)—Cl(1a)	90.2(4)	Cl(1)—In(1)—C(11)	109 (1)
Cl(1)—In(1)—C(21)	109 (1)	C(11)—In(1)—C(21)	139 (1)
In(1)—Cl(1)—In(1a)	126.5(6)		

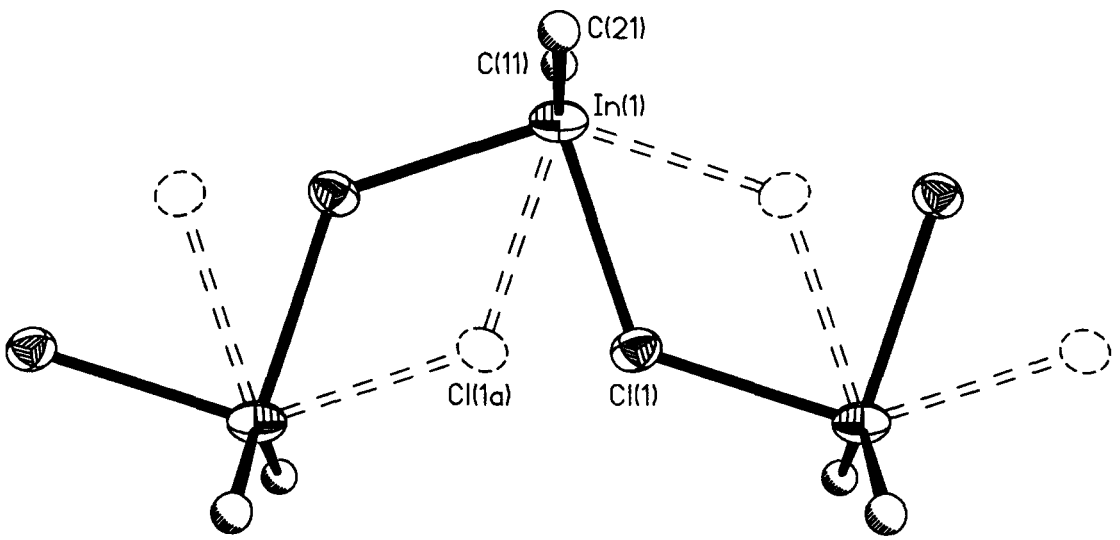
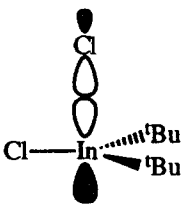


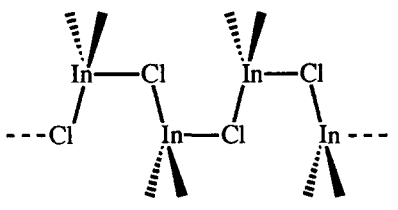
Fig. 2. Partial coordination sphere of one of the $[(Bu^t)_2In(\mu\text{-}Cl)]_\infty$ chains viewed perpendicular to the $(In—Cl)_\infty$ plane, showing the disordered chloride ligands. The *tert*-butyl methyl groups have been omitted for clarity.

While the indium center is four-coordinate, its coordination geometry is unusually distorted from idealized tetrahedral. In fact, the sum of the intraligand angles for C(1), C(2) and Cl(1) (357°) is what would be expected for a trigonal planar environment (i.e. 360°) rather than the base of a tetrahedral environment (328.5°). The coordination of the indium is therefore best described as capped trigonal planar or trigonal bipyramidal with a vacant coordination site. In either description the capped or axial In—Cl bond one would expect to be the longest. For example, in the case of a trigonal bipyramid structure the axial In—Cl bond would be significantly longer based upon a consideration of the relative In *s* and *p* character in the respective In—Cl bonds; axial (*p*) *vs* equatorial (sp^2). This is counter to that observed for the relative In—Cl bond lengths; In(1)—Cl(1) = 2.58(1) and In(1)—Cl(1a) = 2.523(1) Å. One rationalization for the shorter 'axial' In—Cl bond can be derived by consideration of the bonding orbitals for a trigonal bipyramidal structure in which only a single axial ligand is present (**II**). The lack of a *trans*-ligand should result in an unusually strong and therefore short 'axial' bond.

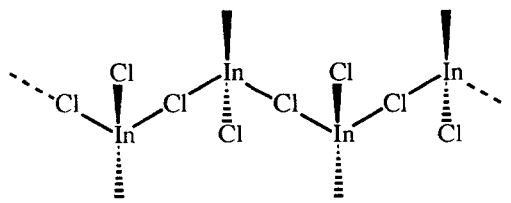


(II)

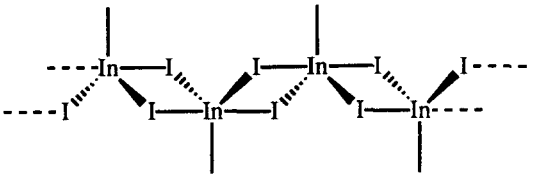
Polymeric chain structures have been reported for the alkyl (and aryl) indium dihalides, $[(R)In(\mu\text{-}X)_2]_x$, however, no polymeric chain structures have been reported for the mono halides. The shape of the —In—Cl— chain is unusual in having a saw-tooth pattern (**III**) unlike the zigzag (**IV**) or double chain (**V**) motifs previously observed for the dihalides [1,5].



(III)



(IV)



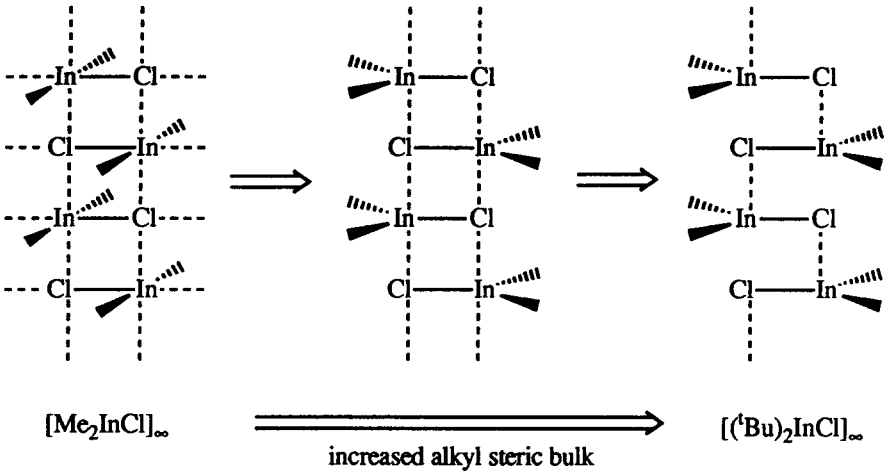
(V)

The solid-state structure of $[Me_2In(\mu\text{-}Cl)]_x$ as determined by X-ray crystallography consists of an infinite sheet-like lattice which may be considered as infinite [In—Cl] ladders linked together. Although the structure of $[(Bu^t)_2In(\mu\text{-}Cl)]_x$ and $[Me_2In(\mu\text{-}Cl)]_x$ appear disparate, they are in fact related as shown in Scheme 1. Examination of a space filling structure suggests that the steric bulk of the *tert*-butyl groups in $[(Bu^t)_2In(\mu\text{-}Cl)]_x$ precludes the inter-ladder interactions present in $[Me_2In(\mu\text{-}Cl)]_x$. Furthermore, the ladder structure is disrupted by intrachain steric interactions. Thus, the structure of $[(Bu^t)_2In(\mu\text{-}Cl)]_x$ may be considered as being derived from that of $[Me_2In(\mu\text{-}Cl)]_x$ as a result of being stretched like a concertina (*cf.* Scheme 1). The observation of a dimeric structure for $[(Mes)_2In(\mu\text{-}Cl)]_2$ indicates that the polymeric chain structure is destabilized completely with sterically demanding substituents [4]. It is interesting to speculate the continuum of structures for $[R_2In(\mu\text{-}Cl)]_n$ with increasing steric bulk of the alkyl groups. In particular, the cross over points between infinite sheets, ladders, polymeric chains and dimeric structures.

EXPERIMENTAL

A crystal of $[(Bu^t)_2In(\mu\text{-}Cl)]_x$ was sealed in a glass capillary under argon and mounted on the goniometer of an Enraf–Nonius CAD-4 automated diffractometer. Data collection and cell determinations were performed in a manner previously described [14]. The location of the majority of non-hydrogen atoms were obtained by using a Patterson, while the remaining atomic coordinates were determined through the generation of difference-Fourier maps using *MolEN* [15]. The chloride atoms were shown to have a disorder and were therefore refined with 50% occupancy. Attempts to solve the structure in either *C*2 or *Cm* also resulted in a disordered structure (the former results in two 0.5 occupancy chlorines and the latter in extra In positions). All non-hydrogen atoms [except C(13) and C(23)] were refined anisotropically. Hydrogen atoms were included and constrained to 'ride' upon the appropriate atoms [d(C—H) = 0.95 Å, U(H) = 1.2 B_{eq}(C)]. A summary of cell parameters, data collection and structure solution is given in Table 2. Scattering factors were taken from [16].

Acknowledgements – Financial support for this work is provided by the National Science Foundation (A. R. B.) and the Robert Welch Foundation (S. G. B.)



Scheme 1.

Table 2. Summary of X-ray diffraction data.

Compound	$[(Bu^t)_2In(\mu\text{-}Cl)]_\infty$
Empirical formula	$C_8H_{18}ClIn$
Crystal size (mm)	$0.42 \times 0.57 \times 0.58$
Crystal system	Monoclinic
Space group	$C2/m$
a (Å)	18.009(3)
b (Å)	6.419(6)
c (Å)	10.130(5)
β (°)	100.67
V (Å^3)	1151(1)
Z	4
D(calcd) (g cm^{-3})	1.531
μ (mm^{-1})	2.209
Radiation	Mo-K_α ($\lambda = 0.71073$ Å) graphite monochromator
Temperature (K)	298
2θ range (°)	2.0–44.0
No. of collected reflections	1004
No. of independent reflections	779
No. of observed reflections	421 ($\|F_0\| > 5.0\sigma\|F_0\|$)
Weighting scheme	$w^{-1} = 0.04(\|F_0\|)^2 + \sigma(\|F_0\|)^2$
R	0.0837
R_w	0.0959
Largest difference peak (e Å^{-3})	0.57

REFERENCES

1. Leman, J. T. and Barron, A. R., *Encyclopedia of Inorganic Chemistry*. Wiley, New York, 1995.
2. Tuck, D. G., *Comprehensive Organometallic Chemistry*, Vol. 1, Ch. 7., Ed. G. Wilkinson, F. G. A. Stone and E. W. Abel. Pergamon Press, Oxford, 1982.
3. Miller, S. B., Jelus, B. L. and Brill, T. B., *J. Organomet. Chem.* 1975, **96,** 1.
4. Leman, J. T. and Barron, A. R., *Organometallics*, 1989, **8,** 2214.
5. Leman, J. T., Ziller, J. W. and Barron, A. R., *Organometallics*, 1991, **10,** 1766.
6. Norman, N. C., Compton, N. A., Fisher, G. A. and Webster, P. M., Abstracts of Papers 200th National Meeting of the American Chemical Society, Washington DC, 1990, INOR 512.
7. See for example (a) Haupt, H. J., Wolfes, W. and Preut, H., *Inorg. Chem.* 1976, **15,** 2920; (b) Haupt, H. J., Preut, H. and Wolfes, W. Z., *Anorg. Allg. Chem.* 1979, **448,** 93.
8. Beachley Jr, O. T., Spiegel, E. F., Kopasz, J. P. and Rogers, R. D., *Organometallics*. 1989, **8,** 1915.
9. Hausen, H. D., Mertz, K., Veigel, E. and Weidlein, J., *Z. Anorg. Allg. Chem.* 1974, **410,** 156.
10. Hausen, H. D., Mertz, K., Weidlein, J. and Schwarz, W., *J. Organomet. Chem.* 1975, **93,** 291.
11. Patterson, D. B. and Carnevale, A., *Inorg. Chem.* 1974, **13,** 1479.
12. Miller, S. B., Jelus, B. L. and Brill, T. B., *J. Organomet. Chem.* 1975, **96,** 1.
13. Bradley, C. B., Frigo, D. M., Hursthouse, M. B. and Hussain, B., *Organometallics*, 1988, **7,** 1112.
14. Mason, M. R., Smith, J. M., Bott, S. G. and Barron, A. R., *J. Am. Chem. Soc.* 1993, **115,** 4971.
15. Enraf–Nonius, *MolEN. An Interactive Structure Solution Procedure*. Enraf–Nonius, Delft, The Netherlands, 1990.
16. *International Tables for X-ray Crystallography*, Vol. IV. Kynock Press, Birmingham, U.K. 1974. pp. 99, 149.

Pergamon

PII: S0277-5387(96)00469-X

Polyhedron Vol. 16, No. 10, pp. 1767–1770, 1997
Copyright © 1997 Elsevier Science Ltd
Printed in Great Britain. All rights reserved
0277-5387/97 $17.00+0.00

COMMUNICATION

First polymer-supported organogermanium hydrides and their reduction of organic halides

Kunio Mochida,* Hideo Sugimoto and Yasuo Yokoyama

Department of Chemistry, Faculty of Science, Gakushuin University, 1-5-1 Mejiro, Toshima-ku, Tokyo 171, Japan

(Received 4 September 1996; accepted 20 September 1996)

Abstract—Polystyrene-supported organogermanium hydrides were prepared by functionalization of a polystyrene or by functionalization of a styrene followed by polymerization. The germyl groups were separated from the aromatic ring of polystyrene by methylene units in the polymeric germanium hydrides. The germanium hydrides reduced organic halides with catalyst under mild conditions in the order: C—I > C—Br > C—Cl. © 1997 Elsevier Science Ltd. All rights reserved.

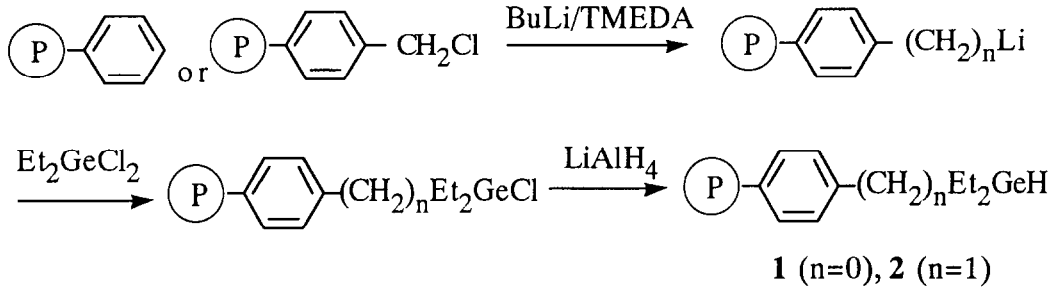
Keywords: polystyrene-supported; hydrogermane; reduction.

Reduction of organic halides involving halogen abstraction reaction by silyl and stannyl radicals has been investigated extensively and the synthetic utility of these reductions, especially with organotin hydrides, has been widely established [1–7]. Recently, reduction of organic halides by organogermanium hydrides has been also of considerable interest in a point of moderate reactivity combined with high selectivity and no toxic character as compared with silicon and tin hydrides [8,9]. In the course of our investigations on germyl radicals [4,10–15] we required polymer-supported germanium hydrides. The insoluble polymer-supported germanium hydrides in common organic solvents would easily be separated after use simply by filtering and would be recyclable. The polymer-supported germanium hydrides would also retain their integrity during chemical reactions. Several syntheses and their application of polymer-supported tin hydrides have been reported [16–21], but there is no study of polymeric germanium hydrides so far.

In this paper, we report the synthesis of polystyrene-supported germanium hydrides (**1**–**3**) and their reduction of organic halides.

The preparation of polystyrene-supported germanium hydrides, **1**–**3** is outlined below (Schemes 1 and 2). Polystyrene was lithiated with butyllithium/TMEDA and then reacted with diethyldichlorogermane to give poly(*p*-diethylchlorogermyl)styrene. The poly(*p*-diethylhydrogermyl) styrene **1** was obtained by treating the poly(*p*-diethylchlorogermyl)styrene with excess lithium aluminum hydride (LAH) in reflux THF for 1 h. The polystyrene-supported germanium hydride **1** was analysed by solid-state NMR, FT-IR (νGe—H: 2018 cm^{-1}) and XPS spectra (Ge content: 3.8 mmol g^{-1}, degree of functionalization = 0.28). The second polystyrene-supported germanium hydride **2**, in which the germyl moiety was separated from the aromatic ring by methylene, was prepared by similar method of **1**. Thus, polystyrene was chloromethylated [21], lithiated with butyllithium/TMEDA and reacted with diethyldichlorogermane to afford poly(*p*-diethylchlorogermylmethylene)styrene. The target polystyrene-supported germanium hydride **2** was obtained by reduction of the diethylchlorogermane polymer with excess LAH in reflux THF. The polymer **2** was iden-

*Author to whom correspondence should be addressed.



Scheme 1.

tified with solid NMR, FT-IR (νGe—H: 2015 cm^{-1}) and XPS spectra (Ge content: 3.8 mmol g^{-1}, degree of functionalization = 0.28).

The third polystyrene-supported germanium hydride **3**, in which the germyl group was separated from the aromatic ring by two methylene units, was prepared by polymerization of a substituted styrene.[19] *p*-Vinylphenethyldiethylchlorogermane was obtained by hydrogermylation of *p*-divinylbenzene with diethylchlorogermane under free-radical conditions. The germyl-substituted styrene was polymerized directly without the need for any further operations such as stabilization. The polystyrene-supported chlorogermane was reduced with LAH to give the poly(*p*-diethylhydrogermylethylene)styrene **3**. The polymeric germanium hydride **3** was identified by NMR, FT-IR and XPS analysis (νGe—H: 2000 cm^{-1}, Ge content: 4.0 mmol g^{-1}, degree of functionalization = 0.30).

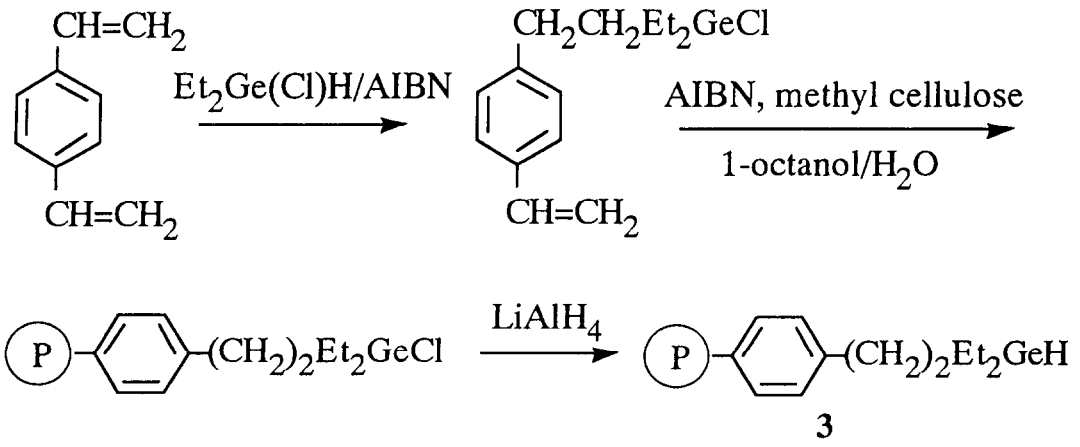
The polymer-supported germanium hydrides **1**–**3** are insoluble in organic solvents. Therefore, the reagents can easily be separated after use simply by filtering and can be regenerated after their reactions with organic substrates.

Polystyrene-supported germanium hydrides **1**–**3** are capable of reducing organic halides simply by heating with free-radical initiators. Table 1 summarizes the results in the reduction of alkyl and aryl halides as determined by GPC.

Tables 1 and 2 show the results of reduction of octyl and phenyl halides with the polymer **1**–**3** catalysed by DTBP. Organic halides were clearly reduced to the corresponding reduction products. No coupling products were detected. The observed order of reactivity falls in the order **3** > **2** > **1**. This is because decreasing steric crowding around the germanium atoms, as the number of methylene groups is increased, will cause a rise in the reactivity of the germanium hydride. The reactivity of the halogen atoms falls in the sequence: I > Br > Cl for **1**–**3**. The ease of reaction decreasing in the order: RX > PhX for organic halides. These features are in accord with those found in homolytic reduction of organic halides with trialkylgermyl hydrides previously reported [11].

Polyhalobenzenes are reduced stepwise, which makes it possible to carry out the selective reduction of polyhalides. *o*-Bromochlorobenzene and *o*-dibromobenzene are reduced with **1**–**3** stepwise to afford chlorobenzene and bromobenzene, respectively. The order of reactivity is **3** > **2** > **1**.

A typical procedure is as follows. A mixture of poly(*p*-diethylhydrogermane)styrene **1** (0.11 g, 0.16 mmol), octyl iodide (0.25 g, 1.03 mmol) and DTBP (0.003 g, 0.02 mmol) was placed in a Pyrex tube. The tube was degassed by evacuation and then filled with argon. After heating for 20 h at 135°C, the mixture was filtered and washed twice with ether (10 cm^3). The organic layer was analysed by GC and GC-MS.



Scheme 2.

Table 1. Reduction of octyl halides with polystyrene-supported hydrogermanes **1**–**3** initiated by DTBP[a]

Run	Polymer	Organic halide	Product (Yield/%)[b]
1	**1**	$C_8H_{17}I$	C_8H_{18} (54)
2	**1**	$C_8H_{17}Br$	C_8H_{18} (17)
3	**1**	$C_8H_{17}Cl$	C_8H_{18} (10)
4	**2**	$C_8H_{17}I$	C_8H_{18} (45)
5	**2**	$C_8H_{17}Br$	C_8H_{18} (20)
6	**2**	$C_8H_{17}Cl$	C_8H_{18} (trace)
7	**3**	$C_8H_{17}I$	C_8H_{18} (60)
8	**3**	$C_8H_{17}Br$	C_8H_{18} (60)
9	**3**	$C_8H_{17}Cl$	C_8H_{18} (34)

[a]At 135° C, for 20 h.
[b]GC yield.

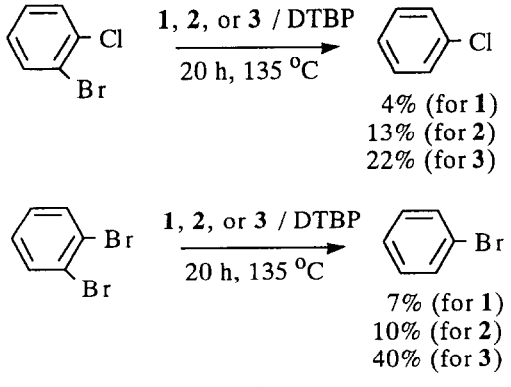
Table 2. Reduction of phenyl halides with polystyrene-supported hydrogermanes **1**–**3** initiated by DTBP[a]

Run	Polymer	Organic halide	Product (Yield/%)[b]
1	**1**	PhI	PhH (38)
2	**1**	PhBr	PhH (13)
3	**1**	PhCl	PhH (0)
4	**2**	PhI	PhH (44)
5	**2**	PhBr	PhH (trace)
6	**2**	PhCl	PhH (0)
7	**3**	PhI	PhH (55)
8	**3**	PhBr	PhH (45)
9	**3**	PhCl	PhH (trace)

[a]At 135 C, for 20 h.
[b]GC yield.

Regeneration of the used polymer: the polymer washed twice with ether and reduced with LAH in refluxing THF for 1 h.

The extent of regeneration of polymer-supported germanium hydrides **1**–**3** several times later is 90%.



Equation 1.

The yield of the first regeneration for polystyrene-supported tin hydrides has been reported to be 30 40% [17].

In conclusion, polystyrene-supported germanium hydrides **1**–**3** reduce organic halides under mild conditions. An advantage to the polymer is easier process, clean and simple work-up of the products and recyclable reagents.

Acknowledgments—The authors thank Dr Riichi Niside of Nissan Auto Co. Ltd for measuring the XPS of polymer-supported germanium hydrides. We also thank Mitsubishi Material Co. Ltd for a gift of tetrachlorogermane.

REFERENCES

1. H. G. Kuivila, *Adv. Organomet. Chem.*, 1964, **1**, 47.
2. H. G. Kuivila, *Acc. Chem. Res.*, 1968, **1**, 299.
3. W. P. Neumann, *Angew. Chem.*, 1964, **76**, 849.
4. H. Sakurai, *Free Radicals*, ed. J. K. Kochi, Vol. 2, Ch. 25. John Wiley & Sons, New York, 1973.
5. E. J. Kupchik, *Organotin Compounds*, ed. A. K.

Sawyer, Vol. 1, Ch. 2. Marcel Dekker, New York, 1971.
6. D. A. Armitage, *Comprehensive Organometallic Chemistry*, ed. G. Wilkinson, F. G. A. Stone and E. W. Abel, Vol. 2, Ch. 9.1. Pergamon Press, Oxford, 1982.
7. A. G. Davies and P. J. Smith, *Comprehensive Organometallic Chemistry*, ed. G. Wilkinson, F. G. A. Stone and E. W. Abel, Vol. 2, Ch. 9.7. Pergamon Press, Oxford, 1982.
8. L. Kaplan, *J. Chem. Soc., Chem. Commun.*, 1969, 106.
9. P. Riviere, M. R. Baudet and J. Satge, *Comprehensive Organometallic Chemistry*, ed. G. Wilkinson, F. G. A. Stone and E. W. Abel, Vol. 2, Ch. 10.3. Pergamon Press, Oxford 1982.
10. H. Sakurai and K. Mochida, *J. Chem. Soc., Chem. Commun.*, 1971, 1581.
11. H. Sakurai, K. Mochida, A. Hosomi and F. Mita, *J. Organomet. Chem.*, 1972, **38,** 275.
12. H. Sakurai and K. Mochida, *J. Organomet. Chem.*, 1972, **42,** 339.
13. H. Sakurai, K. Mochida and M. Kira, *J. Am. Chem. Soc.*, 1976, **94,** 929.
14. H. Sakurai and K. Mochida, *Bull. Chem. Soc. Jpn*, 1976, **49,** 3703.
15. H. Sakurai, K. Mochida and M. Kira, *J. Organomet. Chem.*, 1977, **124,** 235.
16. H. Schumann and B. Pachaly, *Angew. Chem., Int. Ed.*, 1981, **20,** 1043.
17. Y. Ueno, K. Chino, M. Watanabe, O. Moriya and M. Okawara, *J. Am. Chem. Soc.*, 1982, **104,** 5564.
18. B. L. Miller and J. W. Hershberger, *J. Polymer. Science: Part C: Polymer Lett.*, 1987, **25,** 219.
19. U. Gerigk, M. Gerlach, W. P. Neumann, R. Vieler and V. Weintritt, *Synthesis*, 1990, 448.
20. M. Gerlach, F. Jordens, H. Kuhn, W. P. Neumann and M. Peterseim, *J. Org. Chem.*, 1991, **56,** 5971.
21. G. Ruel, N. K. The, G. Dumartin, B. Delmond and M. Pereyre, *J. Organomet. Chem.*, 1993, **444,** C18.

Pergamon

PII: S0277-5387(96)00504-9

Polyhedron Vol. 16, No. 11, pp. 1771–1774, 1997
© 1997 Elsevier Science Ltd
All rights reserved. Printed in Great Britain
0277-5387/97 $17.00+0.00

Mono- and dinuclear copper(II) complexes of a Schiff base ligand, 4′,5′-bis(salicylideneimino)benzo-15-crown-5

Serdar Karaböcek[a]* and Nevin Karaböcek[b]

Departments of [a]Chemistry and [b]Science Education, Karadeniz Technical University, Trabzon, Turkey

(Received 30 April 1996; accepted 16 October 1996)

Abstract—Mono- and dinuclear copper(II) complexes with a tetradentate Schiff base, 4′,5′-bis(salicylideneimino)benzo-15-crown-5, ($SALH_2$) have been prepared and characterized by elemental analyses, magnetic moments, IR, UV/VIS, and ESR spectral studies. The elemental analyses, stoichiometry and the spectroscopic data of the complexes indicate that the copper(II) ions are coordinated by the dianion of the ligand. IR spectra show that the ligand acts in a tetradentate manner and coordinates throught (C=N) and (C—O) groups. The geometry of the metal chelates is discussed with the help of magnetic and spectroscopic measurements. © 1997 Elsevier Science Ltd. All rights reserved.

Keywords: Schiff base; crown ether; copper complexes; mononuclear; dinuclear; metallobiosites.

Numerous copper-containing proteins utilize molecular oxygen in respiratory and biosynthetic functions. The best studied copper proteins, hemocyanin and tyrosinase, serve, respectively, in O_2 transport and in activating O_2 for the oxidation of tyrosine. Many excellent papers have been published during the last two decades on the preparation and properties of model copper complexes. Particular attention was devoted to their correlation with the active site of metalloenzymes and metalloproteins containing dinuclear metallocenters in order to elucidate the factors that determine the reversible binding and activation of O_2 in various natural oxygen transport systems and mono- and dioxygenases and to mimic their activity [1–3]. A number of dinuclear complexes based on acylic and linear ligand systems have been prepared and investigated for oxygen uptake [4–6]. Particular interest has been devoted to the synthesis and characterization of homo binuclear compounds. Such metal complexes have been prepared by using an acyclic ligand (Fig. 1(B)) containing a coordination site which can link one metal ion in the inner N_2O_2 [7–9].

In the present study, we have used a Schiff base prepared from salicylaldehyde and 4′,5′-diaminobenzo-15-crown-5. This ligating system provides an additional active site besides conferring on the copper(II) ion a square-planar N_2O_2 environment (Fig. 1) which not only mimics the active site in galactose oxidase [8, 9] but also has a role in molecular magnetism.

EXPERIMENTAL

Preparation of the Schiff base

$SALH_2 \cdot H_2O$, [4′,5′-bis(salicylideneimino)benzo-15-crown-5] was prepared as reported previously [10].

Preparation of [Cu(SAL)$CuCl_2$]

A solution of $CuCl_2 \cdot 2H_2O$ (2 mmol, 340.0 mg) in EtOH was added to the ligand (1 mmol, 506 mg) suspended in 10 cm^3 of EtOH and the mixture was stirred for 2.5 h at room temperature. A brown product was filtered off, washed with EtOH and Et_2O and dried over P_4O_{10}. Found: C, 48.0; H, 4.0; N, 3.9; Cu, 18.5. Calc. for [$C_{28}H_{28}N_2O_7Cl_2Cu_2$]: C, 47.9; H, 4.0; N, 4.0; Cu, 18.1%.

Preparation of [Cu(SAL)$(ClO_4)_2$]

The ligand (1 mmol, 506 mg) suspended in 10 cm^3 EtOH was added to the solution of $Cu(ClO_4)_2 \cdot 6H_2O$

*Author to whom correspondence should be addressed.

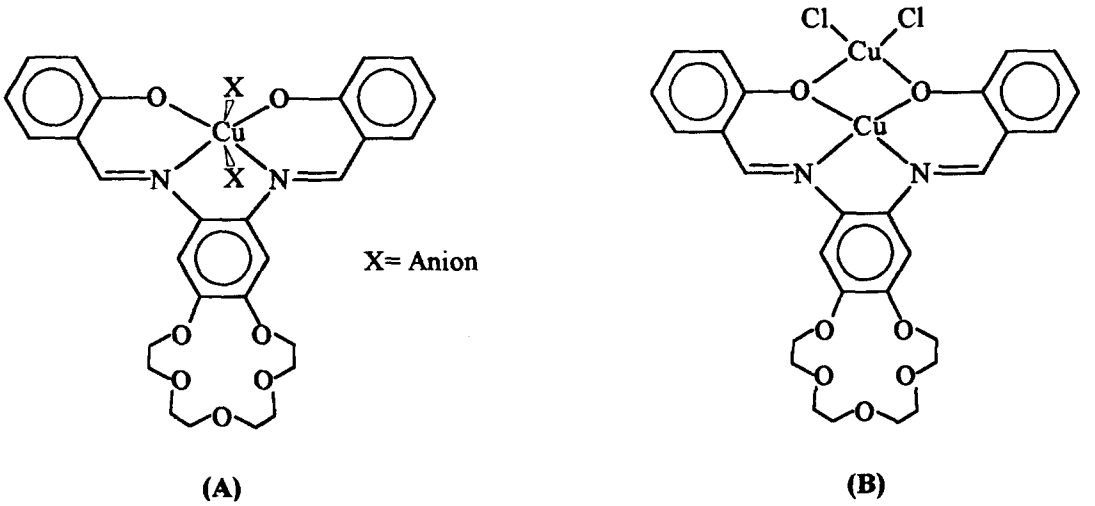


Fig. 1. 4′,5′-bis(salicylideneimino) benzo-15-crown-5. ($SALH_2$)-copper(II) complexes: (A), mono; and (B), binuclear.

(1 mmol, 370.5 mg) in EtOH, and the mixture was stirred for 3 h at room temperature. The brown product was filtered off, washed with EtOH and Et_2O and dried over P_4O_{10}. Found: C, 39.9; H, 3.5; N, 3.4; Cu, 7.5. Calc. for $[C_{28}H_{28}N_2O_{15}Cl_2Cu]$: C, 40.1; H, 3.3; N, 3.3; Cu, 7.6%.

Preparation of $[Cu(SAL)X_2 \cdot Y$ ($X = OAc^-$, $HCOO^-$; $Y = H_2O$)

To a solution of $Cu(ClO_4)_2$ (1.2 mmol, 445 mg), NaOAc/HCOONa as appropriate (1 equiv.) was added and the mixture stirred until dissolved. The ligand (1 mmol, 506 mg) suspended in EtOH was added and the mixture stirred for 3 h at room temperature. The greenish coloured products were filtered, washed with EtOH and Et_2O and dried over P_4O_{10}. $[Cu(SAL)(OAc)_2]$: Found: C, 55.5; H, 5.1; N, 4.1; Cu, 9.1. Calc. for $[C_{32}H_{34}N_2O_{11}Cu]$: C, 56.0; H, 5.0; N, 4.1; Cu, 9.3%. $[Cu(SAL)(HCOO)_2] \cdot H_2O$: Found: C, 53.5; H, 4.8; N, 4.0; Cu, 9.3. Calc. for $[C_{30}H_{32}N_2O_{12}Cu]$: C, 53.3; H, 4.7; N, 4.1; Cu, 9.4%.

Preparation of $[Cu(SAL)(SCN)_2 \cdot H_2O$

To a solution of $CuCl_2 \cdot 2H_2O$ (1.2 mmol, 204.0 mg) in EtOH, a saturated solution of KSCN was added, until no further precipitation of KCl was obtained. This solution was centrifuged and filtrate was added to the ligand (1 mmol, 506 mg) suspended in 10 cm^3 of EtOH, the mixture was stirred for 3 h at room temperature. The deep brown precipitate was filtered and washed with EtOH and Et_2O and dried over P_4O_{10}. Found: C, 57.1; H, 5.5; N, 9.0; Cu, 10.1. Calc. for $[C_{30}H_{30}N_4O_8S_2Cu]$: C, 56.4; H, 4.7; N, 8.8; Cu, 9.9%.

Instrumentation

C, H, N were analysed microanalytically. Copper was estimated spectrophotometrically. Electronic spectra were obtained on a Varian DMS-90 spectrophometer. ESR measurements were made with a Varian model 109 C E-line X-band spectrometer fitted with a quartz Dewar for measurements at liquid nitrogen temperature, IR spectra were obtained on a Perkin–Elmer 598 spectrophotometer in KBr pellets. Room temperature magnetic susceptibility measurements were done on a PAR model 155 vibrating sample magnetometer.

RESULTS AND DISCUSSION

ESR spectroscopy

X-Band ESR studies of the copper(II) complexes were obtained in DMSO. The spectra reveal the presence of less than four components. The broadening of the $g_\perp$ line and splitting is due to the overlap of $g_\parallel$ and $g_\perp$ components, further indicating a lowered site symmetry [11, 12]. The $g_\parallel$ is in the range 2.19–2.22 as observed in mononuclear complexes (Table 1). A clear five-line pattern emerges on the $g_\parallel$ component with ≈ 15 G. Thus the ESR data supports the binding of the tetradentate ligand with two N and two O donor sites to the copper(II) ion, providing a square planar geometry, the other axial sites being occupied by the coordination anion [7]. Figure 2 shows the ESR spectra of the $[Cu(SAL)CuCl_2]$ complex in frozen DMSO. The value of the coupling constant evaluated from the peaks is *ca* 119 G. This value is nearly half of that found for the present mononuclear complexes (Table 1). This situation could arise when two equivalent copper(II) ions are coupled *via* an exchange interaction, in a dinuclear complex.

Table 1. X-Band ESR, electronic spectra and magnetic moment data of $SALH_2$ and its copper(II) complexes

Complexes	Sol.[a] λ_{max} (nm)	μ_{eff}/atom (B.M.)	$g_{\parallel}$	$g_{\perp}$	$A_{\parallel}$	$g_{\parallel}/A_{\parallel}$	$g_{\perp}$ splitting
$SALH_2 \cdot H_2O$	375						
	335						
	265						
$[Cu(SAL)CuCl_2]$	450	1.51					
	325						
$[Cu(SAL)(ClO_4)_2]$	550	2.10	2.19	1.98	200.00	110	114
	415						
	365						
$[Cu(SAL)(OAc)_2]$	580	2.00	2.20	1.96	210.00	104.7	77
	416						
	350						
$[Cu(SAL)(HCOO)_2] \cdot H_2O$	600	2.10	2.22	1.99	230.00	96.5	40
	455						
	415						
$[Cu(SAL)(SCN)_2] \cdot H_2O$	590	1.90	2.20	1.95	200.00	110	77
	410						
	375						

[a]All spectra in DMSO (complexes).

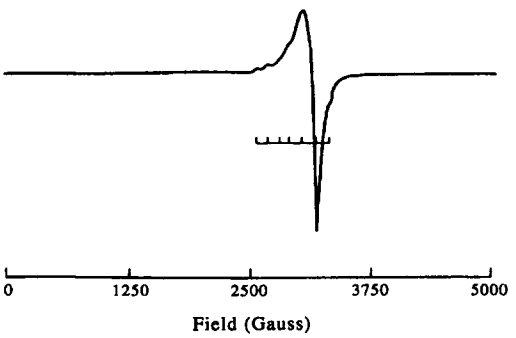


Fig. 2. ESR spectra of frozen DMSO solution of [Cu(SAL)$CuCl_2$].

Magnetic susceptibility

The room temperature solid state magnetic moment data of the copper(II) complexes are reported in Table 1. Mononuclear copper(II) complexes showed normal magnetic moments. The $[Cu(SAL)CuCl_2]$ complex shows μ_{eff} value of 1.51 B.M., indicating an exchange coupled dimeric complex, a structure supported by the ESR study also. The stoichiometry is in keeping with copper(II) complexes reported with similar tetradentate Schiff base ligands [7,13].

Electronic and IR spectroscopy

The ligand was dissolved in MeOH/NaOH and shows characteristic UV–vis spectra of the Schiff base group. The absorption bands are given in Table 1. The electronic spectra of all complexes measured in dimethylsulfoxide showed intense absorptions around 400 nm which are assigned to charge-transfer transition from the $p\pi$ orbitals of the donor atoms to the d orbitals of the metal (Table 1). In the mono copper(II) complexes, d–d transitions were observed around 500–600 nm. The energy of the d–d transition suggests a distorted tetragonal copper(II) complex [14].

In general, the complexes exhibited very similar IR features. This is indirect evidence that the complexes are of similar structures. In the IR spectra of these complexes (OH) stretching vibrations have disappeared and there is no distinct shift in (C=N) stretches after complex formation. The band assigned to ν(C—O) is shifted to higher frequency by 20–25 cm^{-1} in the complexes [15]. The band assigned to ν(C–N) shows a shift of 20–40 cm^{-1} towards a lower frequency. A strong band at *ca* 1600 cm^{-1}, which shifts by 30–50 cm^{-1} towards lower frequency upon coordination is assigned to ν(C=N). The significant shifts in ν(C—N), ν(C—O) and ν(C=N) upon complexation support the concept of coordination of the ligand through the azomethine nitrogen.[10] In the acetate complex sharp bands at 1440 and 1680 cm^{-1} are assigned to the unidentate binding mode of the acetate group. The ν(C=N) stretching frequencies are generally lower for coordinated SCN. This could possibly be due to a sulfur bonded thiocyanate. IR data confirms the binding of the copper(II) by O and N donor groups of the present ligand and supports the tentative structure of the complexes (Fig. 1).

As a conclusion, in the present study, we have demonstrated the preparation of a Schiff base ligand providing N_2O_2 donor array and a crown ether moiety, and its mono- and dinuclear copper complexes. All the spectral data supported a distorted tetragonal

geometry for copper(II) ions. Since such copper complexes have potential use in organic synthesis for the catalysis of a wide range of primary alcohols to the corresponding aldehydes, and may mimic specific types of copper-containing enzymes, their structural and functional identification is necessary for their applications.

Acknowledgements—This work was supported by The Research Fund of Karadeniz Technical University. The authors thank Drs Yasar Gok of Karadeniz Technical University and Fevzi Koksal of Ondokuzmayis University for their criticism and kind support.

REFERENCES

1. K. D. Karlin and J. Zubieta, *Copper Coordination Chemistry and Biochemistry: Biochemical and Inorganic Perspectives*. Adenine Press, Guilderland, N.Y. (1983).
2. D. E. Fenton, U. Casellato, P. A. Vigato and M. Vidali, *Inorg. Chim. Acta* 1984, **95,** 187.
3. D. E. Fenton, U. Casellato, P. A. Vigato and M. Vidali, *Inorg. Chim. Acta* 1982, **62,** 57.
4. N. Kitajima and Y. Morooka, *Chem. Rev.* 1994, **94,** 737.
5. L. Casella and L. Rigoni, *J. Chem. Soc., Chem. Commun.* 1985, 1668.
6. T. Tsumaki, *Bull. Chem. Soc. Jpn.* 1938, **13,** 252.
7. Y. S. Sharma, H. N. Pandey and P. Mathur, *Polyhedron* 1994, **22,** 3111.
8. N. Ito, S. E. W. Phillips, C. Stevens, Z. B. Ogel, M. Y. McPherron, T. N. Keen, K. D. S. Yadov and P. F. Knowles, *Nature* 1991, **350,** 87.
9. N. Ito, S. E. W. Philips, C. Stevens, Z. B. Ogel, M. Y. Mepherron, T. N. Keen, K. D. S. Yadav and P. F. Knowles, *J. Inorg. Bichem.* 1991, **43,** 165.
10. A. Gül, A. İ. Okur, A. Cihan, N. Tan, and Ö. Bekaroğlu, *Synt. React. Inorg. Met.-Org. Chem.* 1986, **16,** 871.
11. V. M. Diebler, M. Eigen and P. Mattheis, *Z. Naturforsch. B: Anorg. Chem. Org. Chem.* 1961, **16B,** 629.
12. (a) U. Weser, E. Bunnenburg, R. Cammack, C. Djerassi, L. Floha, G. Thomas and W. Voelter, *Biochim. Biophys. Acta* 1971, **243,** 203, (b) W. E. Blumberg and Y. Peisach, *J. Biol. Chem.* 1965, **240,** 870.
13. S. J. Gruber, C. M. Harris and E. Sinn, *J. Inorg. Nucl. Chem.* 1968, **30,** 1805.
14. R. Ruiz, J. Sanz, B. Cervera, F. Lloret, M. Julve, C. Bois, J. Faus, and M. C. Munoz, *J. Chem. Soc., Dalton Trans.* 1993, 1623.
15. A. Kushekar and D. D. Khaolkar, *Indian J. Chem.* 1983, **22A,** 6.

Pergamon

PII: S0277-5387(96)00503-7

Polyhedron Vol. 16, No. 11, pp. 1775–1781, 1997
© 1997 Elsevier Science Ltd
All rights reserved. Printed in Great Britain
0277-5387/97 $17.00+0.00

Monodentated, bridged and chelated behaviour of diphosphines towards the fragment CpFe (dppe)$^+$

Carlos Díaz* and Eyleen Araya

Departamento de Química, Facultad de Ciencias, Universidad de Chile, Santiago, Casilla 653, Chile

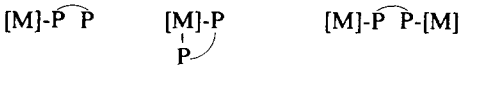
(Received 3 September 1996; accepted 14 October 1996)

Abstract—The reaction of CpFe(dppe)I with $Ph_2P(CH_2)nPPh_2$ ($n = 1$, dppm; $n = 2$, dppe; $n = 3$, dppp; $n = 4$ dppb) in the presence of NH_4PF_6 afforded the novel mononuclear complexes [CpFe(dppe)(η^1-dppm)]PF_6 (1) and [CpFe(dppe)(η^1-dppe)]PF_6(2) when $n = 1$ or 2 or the binuclear [CpFe (dppe)-PPh_2-$(CH_2)_2$ PPh_2-CpFe (dppp)] $(PF_6)_2$ (3) and [CpFe (dppe) $PPh_2(CH)_2PPh_2$-CpFe (dppb)] $(PF_6)_2$ (4) when $n = 3$ or 4. These two bimetallic complexes present two slightly different sites caused by the two different chelate diphosphines linked to the iron atoms and evidenced by ^{31}P-NMR spectroscopy. The two metallic fragments however could not be distinguished by cyclic voltammetry. © 1997 Elsevier Science Ltd. All rights reserved.

Keywords: iron complexes; monodentate diphosphines; chelated diphosphines.

Transition-metal complexes containing diphosphine ligands have been the subject of numerous investigations in recent years, in part because of their potential applications in homogeneous catalysis [1]. The stabilization of organometallic complexes with metals in low oxidation states by tertiary phosphine ligands is widely known [2]. Thus the good donor properties of phosphine ligands together whith their moderately Π-acceptor capacity lead to electron rich organometallic fragments [3–7]. The replacement of carbonyl by diphosphine ligands in $CpM(CO)_2X$ systems, produce variations of *ca* 1.9 V in their oxidation potential [5–7]. The high electron richness of fragments of the type CpFe(P-P) (P-P = tertiary diphosphine) permit the stabilization of alkylidine [8], vinylidene [9] and methylene [10] groups. Recently we have reported the preparation of a series of complexes containing neutral ligands of the type $\{CpFe(dppe)L\}PF_6$ $Cp = \eta^5$-C_5H_5, where dppe = $Ph_2P(CH_2)_2PPh_2$, L = sulfur donor ligand THF, pyridine and $P(n\text{-Bu})_3$ [11–14]. With the phosphine ligand, stable compounds in good yield were obtained. This prompted us to investigate the reaction of CpFe(dppe)I [12] with the series of diphosphines $Ph_2P(CH_2)_nPPh_2$ ($n = 1$–4) about which this paper is concerned.

In general diphosphines can to act toward metal fragments as η^1− monodentate mode of coordination, η^2-chelating mode of coordination as well as μ-bridging mode of coordination.



η^1-mode η^2-mode μ-mode

As have been previously pointed out the chelating tendency decreases as the chain length in $Ph_2P(CH_2)nPPh_2$, increases being greatest for $n = 2$ [2]. This arises from the known stability of the five membered ring chelate. Thus dppe forms numerous stable chelate complexes [11–14; 27,28]. Less common complexes containing dppe as bridge have also been reported [17,18,29,30,32,35]. Unidentate dppe complexes are rare, however some examples have been reported [19,29,31,33–35].

Complexes containing dppp and dppb are more scarce than those with dppm and dppe ligands. With dppp some chelate and bridged complexes have been reported [17–19,22,33–35]. The complex Fe_3Te_2 $(CO)_9$(dppp) containing the η^1-dppp ligand was reported. For dppb, few reports illustrating their chelating and bridging behaviour have appeared [19,22, 23].

Thus, it appears that the mode of coordination of

*Author to whom correspondence should be addressed.

a diphosphine depends on the following three factors: (i) the length of the chain linking the phosphorous atoms; (ii) the steric properties of the fragment [M]; and (iii) the electron richness of the fragment [M].

However, the form in which these three factors influence the mode of coordination of a diphosphine is as yet unclear.

The most studied, dppm, exhibits a great ability to form bridged [2,15–20] binuclear complexes, although the chelate behaviour is also common [2,19,21,22]. Some complexes containing the monodentate dppm have also been reported [2,23–26].

This paper reports an example where the three coordination modes of diphosphines are involved, which are strongly influenced by the steric properties of the fragment CpFe dppe$^+$.

RESULTS AND DISCUSSION

The reaction of CpFe(dppe)I [12] with diphenylphosphinomethane, and with diphenylphinoethane in methanol in the presence of NH_4PF_6 as halide abstractor afforded the brown solids [CpFe(dppe)(η^1-dppm)]PF_6, **1** and [CpFe(dppe)(η^1-dppe)]PF_6, **2** respectively (see scheme, Fig. 1). Structure of the new complexes was established unequivocally by ^{31}P-NMR spectroscopy [23]. The ^{31}P-NMR spectrum of **1** is shown in Fig. 2 and indicates, in addition to the PF_6 signal, three types of phosphorus atoms in the ratio 2:1:1. The doublet at the lowest field is assigned to P_c phosphorus atoms of the chelate dppe ligand (see Table 1).

The doublet nature of this signal arises from their splitting with the P_b phosphorus atom of the monodentate diphosphine ligand. The high-field doublet of triplets corresponds to P_b, the coordinated phosphorus of the monodentate dppm; which is split into a doublet by the uncomplexed P_a and is further split into triplets by the two chemically equivalent atoms P_c of the dppe chelate. The high-field doublet, which has a chemical shift very similar to that of free dppm [15] is assigned to a the uncoordinated phosphorus atom P_a. Similar analysis for **2** gave the ^{31}P-NMR data presented in Table 1.

For comparison, in Table 2 are collected ^{31}P-NMR data for other complexes containing monodentate diphosphine ligands. It is evident that for a given complex [M]-P_bP_a the chemical shift of the coordinated phosphorus atom varies considerably depending on the nature of the metal and of the auxiliary ligands around the metal.

For dppm, δ ^{31}P-NMR values vary from 20–33 ppm for $W(CO)_3$ bipy to 76.4 ppm for the $Fe(CO)_3$ fragment. For a constant metal, δ ^{31}P depends on the withdrawing properties of the auxiliary ligand. Similar tendency is observed for complexes with monodentate dppe. On the other hand the chemical shift for the uncoordinated phosphorus atom is near to the value for the free diphosphines. A characteristic range for unidentate dppm between −22.49 and −29.57 ppm can be viewed from Table 2 while that for unidentate dppe values from −10.49 to −14.1 were observed.

The new complexes were also characterized by elemental analysis, IR, ^{1}H-NMR and UV–visible spectroscopic methods as well as by voltammetric methods.

The ^{1}H-NMR spectra of the complexes **1** and **2** exhibit the characteristic proton signals of the CpFe dppe$^+$ [12,14] moiety; a multiplet between 7–8 ppm corresponding to C_6H_5 group of dppe and dppm, a singlet around 4.5 ppm assigned to a C_5H_5 proton and the methylene protons of dppe and dppm around 1.5 ppm and 2.1–2.7 ppm respectively.

The IR spectra of the complexes **1** and **2** exhibit the expected bands of the CpFedppe moiety [36]. The UV–visible spectra of **1** and **2** shows the lowest absorp-

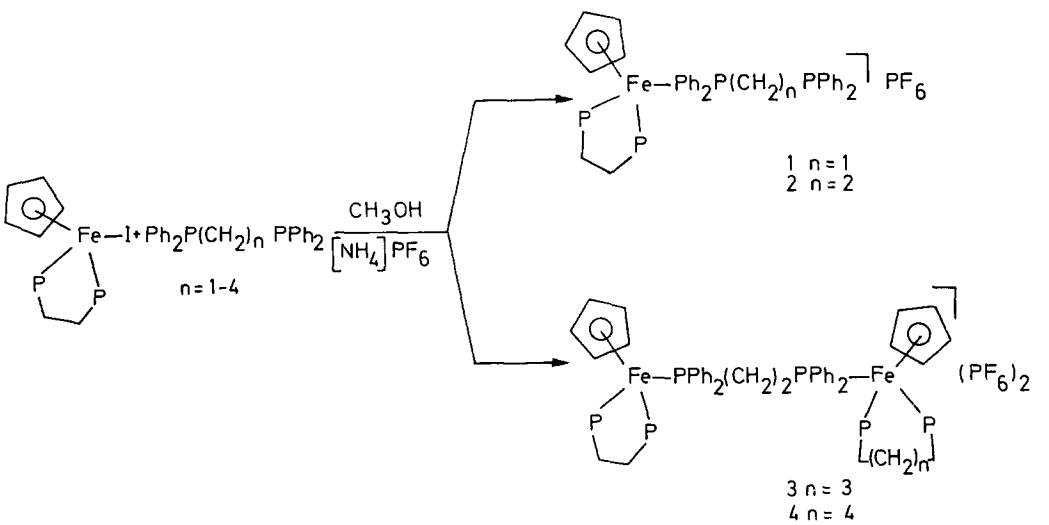


Fig. 1. Schematic representation the reaction of CpFe(dppe)I with diphosphines $Ph_2P(CH_2)_nPPh_2$.

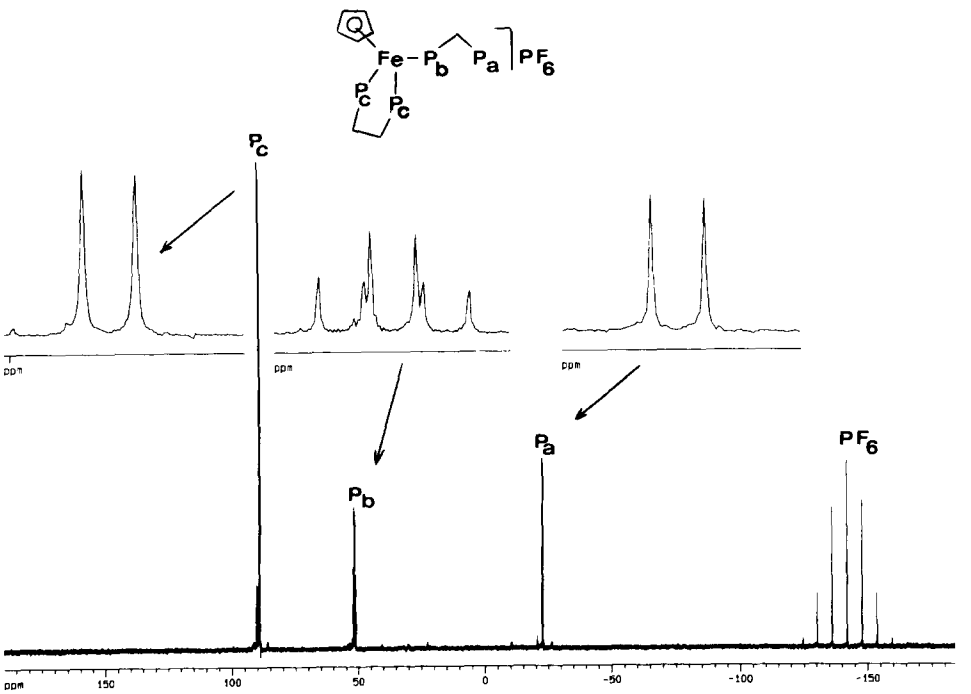


Fig. 2. ^{31}P-NMR spectrum of [CpFe(dppe)η^1-dppm)]PF_6, in CD_2Cl_2 solution at room temperature.

Table 1. ^{31}P-NMR data for the complexes[a]

	Complex					
(a) Mononuclear	$\delta(P_c)$[b]	$\delta(P_b)$[c]	$\delta(P_a)$[b]	(Ja,b)[d]	(Jb,c)	
1	89.29	51.55	−22.85	38.87	44.16	
2	89.78	53.01	−10.49	30.37	44.95	
(b) Binuclear	$\delta(P_c)$[b]	$\delta(P_{c'})$[b]	$\delta(P_b)$[e]	$\delta(P_a)$[e]	(Jb,c)	(Jac')
3	89.46	92.72	48.86	47.86	45,19	45,68
4	89.60	90.87	48.90	48.05	45,43	45,68

[a] In CD_2Cl_2 solution.
[b] Doublet.
[c] Doublet of triplets.
[d] J in Hz.
[e] Triplet.

tion band around 440 nm (see Table 3). This maximum which has been assigned to a *d–d* transition [13] appears in the expected range for [CpFe(dppe)L]$^+$ complexes where L is a phosphorus donor ligand [14].

Using cyclic voltammetry, we observe that the complexes **1** and **2** undergo a single oxidation in CH_2Cl_2. Complex **1** shows a chemically irreversible oxidation due probably to decomposition of the oxidized product. For complex **2** the ratio of anodic to cathodic peak currents is near unity indicating a chemically reversible process. Data are shown in Table 4. The oxidation peak values for complexes **1** and **2** compare well with that of [CpFe(dppe)(*n*-Bu_3P)]PF_6 [14]; (0.77 V).

The reaction of CpFe(dppe)I with diphenylphosphinopropane and with diphenylphosphinobutane in methanol, in the presence of NH_4PF_6 afforded the binuclear complexes [CpFe(dppe)-μ-dppe-Fe(dppp)Cp]$(PF_6)_2$ [3] and [CpFe(dppe)-μ-dppe-Fe(dppb)Cp]$(PF_6)_2$ [4] (see Fig. 1), respectively, the structure of these compounds was also established by ^{31}P-NMR spectroscopy. The ^{31}P-NMR spectrum of 3 (see Fig. 3) consists of two doublets, two triplets and the expected septet signal of PF_6. Consistently with the structure proposed, the signal of the unco-

Table 2. ^{31}P[H]-NMR data for complexes containing monodentate diphosphines

	$^1\delta$P(coord.)	$^1\delta$P(free)	Reference
[CpFe(dppe) (η^1-dppm)]PF_6	51.55	−22.85	This work
[CpFe(dppe) (η^1-dppe)]PF_6	53.01	−10.49	This work
CpFe (CO) (η^1-dppe)H	84.8	−13.5	34
Fe $(CO)_4$ (η^1-dppe)	68.1	−13.1	29
Fe $(CO)_3$ (η^1-dppe)$_2$	76.4	−14.1	29
[Mn $(CO)_3$(bipy)(η^1dppm)]PF_6	45.5	−29.9	26
[Mn $(CO)_2$(bipy)(η^1dppm)$_2$]PF_6	57.5	−28.90	26
Mo $(CO)_3$(η^2-bipy)(η^1-dppm)	27.9	−27.5	25
Mo $(CO)_3$(η^2-phen)(η^1-dppm)	28.7	−27.5	25
fac-Mo$(CO)_3$(η^2-dppm)(η^1-dppm)	30.00	−25.2	23
mer-Mo$(CO)_3$(η^2-dppm)(η^1-dppm)	44.7	−24.3	23
facCr$(CO)_3$(bipy)(η^1-dppm)	45.77	−27.06	41
facMo$(CO)_3$bipy(η^1-dppm)	27.26	−27.93	41
facW$(CO)_3$bipy(η^1-dppm)	20.33	−27.12	41

Table 3. Selected spectral data for complexes

	^{1}H-NMR (CD_2Cl_2)				Visible (CH_2Cl_2) λ^{max}(log ε)
	C_5H_5[a]	C_6H_5[b]	$P(CH_2)_2P$	$P(CH_2)_nP$	
1	4.58	7.6–6.4	1.49	2.76; 2.28	432 (3.05)
2	4.54	7.6–7.0	1.89; 1.4	2.49; 2.13	438 (2.79)
3	4.74	8.0–6.8	2.41–2.70	1.18–1.81; 1.12	442 (2.83)
4	4.57	7.6–7.1	2.49–2.28	2.07; 1.66–1.76; 1.5	443 (2.79)

[a] Singlet signal.
[b] Multiplet signal.

Table 4. Cyclic voltammetric data for complexes

COMPOUND	$E_{1/2}$[a]	E_{p_c}-E_{p_a}
[CpFe(dppe)(η^1-dppm)]PF_6	0.96[b]	—
[CpFe(dppe)(η^1-dppe)]PF_6	0.89	0.06
[CpFe(dppe)μ-dppe-CpFe(dppp)]$(PF_6)_2$	0.88	0.07
[CpFe(dppe)-μ-dppe-CpFe(dppb)]$(PF_6)_2$	0.86	0.05

[a] $E_{1/2} = 1/2[Ep_c + Ep_a]$ *vs* SCE in CH_2Cl_2 solutions; $[NBu_4]PF_6$, 0.1 M used as supporting electrolyte.
[b] Irreversible oxidation, no reduction was observed.

ordinated phosphorus atom is absent. The lowest field doublet at 89.46 ppm is assigned to P_c phosphorus atoms of the chelated dppe ligand, by comparison with the values found for the fragment CpFe(dppe)$^+$ in **1** and **2** (see Table 1). The other doublet is assigned to a phosphorus atom of the chelated dppp ligand linked to the other iron atom. The doublet nature of these two signals arise from their splitting with the phosphorus atom of the bridged dppe. The two triplets at high-field are assigned to the phosphorus atom of the bridged dppe ligand. As expected, the chemical shift values of the phosphorus atom linked to the CpFe(dppe) fragments are very similar (almost identical) for **3** and **4**, while those of the other phosphorus atom exhibit a chemical shift value different for **3** and **4**.

The small but different chemical shift values for the two phosphorus atoms of the bridged dppe indicate that the phosphorus nuclei "see" two slightly different chemical environments arising from the different chelate diphosphines coordinated to the CpFe fragment. Large differences between the chemical shift of the phosphorus atoms of bridged dppe have been found in binuclear systems [30] [$(CO)_5$ M-$PPh_2(CH_2)_2PPh_2$-M′$(CO)_5$] (M, M′ = Cr, Mo and W). Consistently with the proposed structure for **3** and **4** their ^{1}H-NMR spectra exhibit two singlets corresponding to the C_5H_5 proton linked to the different fragments Fe(dppe) and

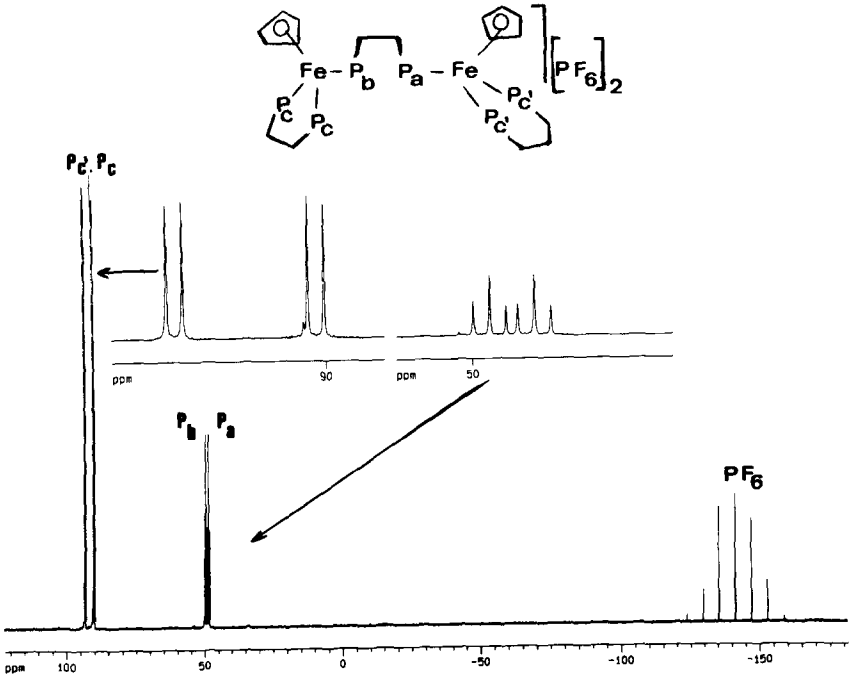


Fig. 3. ^{31}P-NMR spectrum of [CpFe(dppe)-μ-dppe-CpFe(dppp)]$(PF_6)_2$ in CD_2Cl_2 solution at room temperature.

Fe(dppp) in **3** and Fe(dppe) and Fe(dppb) in **4**. The differences between the chemical shift values for C_5H_5 in the different metal environment of each one of the binuclear complexes are comparable to those found in [CpFe(dppe)-CN-CpFe(dppe)]PF_6 [11] and [CpFe(dppe)-C≡C-$(CH_2)_2$-CN-Fe(dppe)Cp]PF_6 [27]. Proton signals for the group C_6H_5 and $P(CH_2)nP$ of the diphosphines were observed normally (see Table 2).

The UV-visible spectra of **3** and **4** exhibit a similar absorption pattern to those of the mononuclear **1** and **2**, which indicate that the environment of the Fe atoms is very similar. In agreement with this the cyclic voltammograms for **3** and **4** exhibit only one oxidation wave as is shown in Table 4. Reversibility parameters indicate a chemical and electrochemical reversible process for the two complexes. The somewhat broad oxidation waves suggest the presence of two oxidation waves with close values of oxidation potential, corresponding to the CpFedppe and CpFe(dppp) (for **3**), CpFe(dppe) and CpFe(dppb) (for **4**) fragments. Alternatively the only oxidation wave observed could be attributed to a two-electron oxidation [37].

The formation of the complexes **3** and **4** containing two different diphosphines chelated to the iron atoms and both with the bridged dppe could be due to the high bridging tendency of the dppe ligand, when the fragments joined by the diphosphine are bulky, as in the CpFe(dppe) [38]. On the other hand the chelating ability of high membered diphosphines $Ph_2P(CH_2)n$ PPh_2 is not unusual [39]. Thus the formation of complexes **3** and **4** involve the opening of the five membered chelate ring Fe(dppe) which is typical behaviour in these type of fragments [34,40].

Notwithstanding the above consideration it surprising that the incoming ligands adopt chelating positions despite giving six- and seven-membered rings (while the ligand becomes bridging) and no formation of the symmetrical complexes [CpFe(L-L)-μ-dppe-FeCp(L-L)]$^+$ has been detected in the product even when excess of the L-L was used.

Until now we have no explanation for this.

EXPERIMENTAL

Infrared spectra were recorded on a FT-Bruker-66 V spectrometer in Nujol. NMR spectra were recorded on a Bruker AMX 300 spectrometer in dichloromethane-d_2 with TMS (H) $\delta = 0.0$ ppm as internal standard or 85% H_3PO_4 and downfield positive to the reference as external standard for the ^{31}P measurements.

UV–visible absorption spectra were recorded using a varian DMS-90 spectrophotometer with 1 cm optical path cuvettes.

Electrochemical measurements were made on a Parc model 370 electrochemistry system, using a three electrode device, employing a carbon glassy working electrode, platinium wire counter electrode and saturated calomel reference electrode.

Solutions were 10^{-3} M in the complex and 0.1 M in $[NBu_4]PF_6$ as supporting electrolyte. Under the same experimental conditions, $E_{1/2}$ for the ferrocene–ferrocenium complex was 0.64 V with peak separations of about 0.060 V (internal standard).

Reactions were carried out under nitrogen using

standard Schlenk-tube techniques. Diethylether and *n*-hexane were dried over sodium and distilled.

$Ph_2P(CH_2)PPh_2$, $Ph_2P(CH_2)_2PPh_2$, $Ph_2P(CH_2)_3PPh_2$, and $Ph_2P(CH_2)_4PPh_2$ were purchased from Aldrich and used without additional purification. CpFe(dppe)I was prepared by a previously reported method [12].

Preparation of the complexes

Synthesis of [CpFe(dppe)(η1-dppm)]PF_6 (**1**)

A solution of CpFe(dppe)I (0.15 g, 0.23 mmol) in CH_3OH (30 cm^3) was stirred with dppm (013 g 0.33 mmol) in the presence of NH_4PF_6 (0.08 g, 0.49 mmol) at room temperature for 20 h. The solvent was removed under reduced pressure and the residue extracted with CH_2Cl_2 and filtered through Celite. Then reduced in volume and *n*-hexane/diethylether 4:1 mixture was added. The maroon powdered precipitate was twice washed with the same mixture and dried under reduced pressure. Yield: 0.14 g (59%). Found: C, 63.2; H, 5.0. Calc. for $C_{56}H_{51}F_6P_5Fe$: C, 64.1; H, 4.9%.

Synthesis of [CpFe(dppe)(η1-dppe)]PF_6 (**2**)

To a solution of CpFe(dppe)I (0.15 g, 0.23 mmol) and $Ph_2P(CH_2)_2PPh_2$ (0.14 g, 0.35 mmol) in CH_3OH (30 cm^3) was added NH_4PF_6 (0.08 g, 0.49 mmol). The mixture was stirred for 20 h at room temperature. After evaporation of the solvent the solid residue was extracted with CH_2Cl_2 (20 cm^3) and the solution filtered through Celite. Then solvent was partially evaporated under reduced pressure and then diethylether was added. The maroon solid precipitate was twice washed with ether and dried. Yield: 0.14 g (57%). Found: C, 64.2; H, 5.1. Calc. for $C_{57}H_{53}F_6P_5Fe$: C, 64.4; H, 5.0%.

Synthesis of [CpFe(dppe)-μ-dppe-CpFe(dppp)]$(PF_6)_2$ (**3**)

A stirred solution of CpFe(dppe)I (0.15 g, 0.23 mmol) in CH_3OH (30 cm^3) was treated with $Ph_2P(CH_2)_3PPh_2$ (0.14 g, 0.34 mmol) in the presence of NH_4PF_6 (0.08 g, 0.49 mmol) at room temperature. After 20 h the reaction mixture was evaporated to dryness. The residue was dissolved in a minimum amount of CH_2Cl_2 and filtered through Celite. The solution was concentrated to a *ca* 5 cm^3 and then diethylether was added. The orange precipitate was washed twice with the same solvent and dried *in vacuo*. Yield: 0.13 g (50%). Found: C, 61.7; H, 5.2. Calc. for $C_{89}H_{84}F_{12}P_8Fe_2$: C, 62.4; H, 4.8%.

Synthesis of [*CpFe(dppe)-μ-dppe-CpFe(dppb)*]$(PF_6)_2$ (**4**)

A mixture of CpFe(dppe)I (0.15 g, 0.23 mmol) and $Ph_2P(CH_2)_4PPh_2$ (0.15 g, 0.35 mmol) in the presence of NH_4PF_6 (0.08 g, 0.49 mmol) were stirred in CH_3OH (30 cm^3) at room temperature for 20 h. After this the solvent was removed *in vacuo* and the solid residue extracted with CH_2Cl_2, filtered through Celite and the solution concentrated to *ca* 10 cm^3. After this $(C_2H_5)_2O$ was added and the orange solid washed with the same solvent. The resultant solid was dried under reduced pressure. Yield: 0.18 g (73%). Found: C, 63.2; H, 5.0. Calc. for $C_{90}H_{86}F_{12}P_8Fe_2$: C, 61.6; H, 4.9%.

Acknowledgement—We are grateful to the FONDECYT Project 1959305 for financial support.

REFERENCES

1. A. L. Balch, *Homogeneous Catalysis with Metal Phosphine Complexes*. (Edited by L. H. Pignolet) Ch. 5. Plenum, New York (1983).
2. B. Chaudret, B. Delavaux and R. Poilblanc. *Coord. Chem. Rev.* 1988, **86,** 191.
3. N. G. Connelly and W. E. Geiger. *Adv. in Organomet. Chem.* 1984, **23,** 1.
4. N. G. Connelly, M. P. Gamasa, J. Gimeno, C. Lapinte, E. Lastra, J. P. Maher, N. Le Narvor, A. L. Rieger and P. H. Rieger. *J. Chem. Soc., Dalton Trans.* 1993, 2575.
5. P. M. Treichel, L. D. Rosenhein and M. S. Schmidt. *Inorg. Chem.* 1983, **22,** 3960.
6. P. M. Treichel and D. A. Komar. *J. Organomet. Chem.* 1991, **206,** 77.
7. W. N. Rogers, J. A. Page and M. C. Baird. *Inorg. Chem.* 1981, **20,** 3521.
8. M. P. Gamasa, J. Gimeno, E. Lastra, M. Lanfranchini and A. Tiripicchio. *J. Organomet. Chem.* 1991, **405,** 333.
9. M. P. Gamasa, J. Gimeno, E. Lastra, B. M. Martín, A. Anillo, A. Tiripicchio. *Organometallics* 1992, **11,** 1373.
10. M. Brookhart, J. R. Tucker, T. C. Flood and J. Jansen. *J. Am. Chem. Soc.* 1980, **102,** 1203.
11. G. Barrado, G. A. Carriedo, C. Díaz and V. Riera. *Inorg. Chem.* 1991, **30,** 4416.
12. C. Díaz and R. Latorre. *Bol. Soc. Chil. Quím.* 1992, **37,** 211.
13. C. Díaz, N. Yutronic and B. Weiss. *Polyhedron* 1993, **12,** 1403.
14. C. Díaz and A. Arancibia. *Polyhedron* 1994, **13,** 117.
15. G. B. Jacobsen, B. L. Shaw and M. Thornton-Pett, *J. Chem. Soc., Dalton Trans.* 1987, 1509 and references therein.
16. G. B. Jacobsen, B. L. Shaw and M. Thornton-Pett, *J. Chem. Soc., Dalton Trans.* 1987, 1489 and references therein.
17. M. L. Brown, J. L. Cramer, J. A. Fergunson, T. J. Mayer and N. Winterton, *J. Am. Chem. Soc.* 1972, **94,** 8707.

18. R. J. Haines and A. L. Du Preez., *Inorg. Chem.* 1972, **11,** 330.
19. A. R. Sanger. *J. Chem. Soc., Chem. Comm.* 1975, 893.
20. J. W. Benson, E. A. Keiter and R. L. Keiter. *J. Organomet. Chem.* 1995, **495,** 77.
21. A. Mishra and U. C. Agarwala, *Inorg. Chim. Acta*, 1990, **170,** 209.
22. C. H. Lindsay, L. S. Benner and L. Balch. *Inorg. Chem.* 1980, **19,** 3505.
23. E. E. Isaacs and W. A. G. Graham. *Inorg. Chem.* 1975, **14,** 2560.
24. M. Canno, J. A. Campo, V. Pérez-Garcia, E. Gutierrez-Puebla and C. Alvarez-Ibarra. *J. Organomet. Chem.* 1990, **382,** 397.
25. M. Canno, J. A. Campo, P. Ovejero and J. V. Heras. *Inorg. Chim. Acta.* 1990, **170,** 139.
26. G. A. Carriedo, M. Carmen Crespo, C. Díaz and V. Riera. *J. Organomet. Chem.* 1990, **397,** 309.
27. G. A. Carriedo, A. Arancibia, C. Díaz, N. Yutronic, E. P. Carreño and S. Garcia-Granda. *J. Organomet. Chem.* 1996, **508,** 23.
28. C. Díaz and C. Leal and N. Yutronic. *J. Organomet. Chem.* 1996, **516,** 59.
29. R. L. Keiter, A. L. Rheingold, J. J. Hamerski and Ch. K. Castle. *Organometallics* 1983, **2,** 1635.
30. R. L. Keiter, S. P. Kaiser, N. L. Hansen, J. W. Brodack and L. W. Cary. *Inorg. Chem.* 1981, **20,** 283.
31. R. L. Keiter, Y. Y. Sun, J. W. Brodack and L. W. Cary. *J. Am. Chem. Soc.* 1979, **101,** 2638.
32. Z. Özer, S. Özkar and H. Ö. Pamuk. *Z. Naturforsch.* 1993, **48b,** 37.
33. P. E. Garrau. *Chem. Rev.* 1981, **81,** 229.
34. S. G. Davies, J. Hibberd and S. J. Simpson. *J. Chem. Soc., Chem. Comm.* 1982, 1404.
35. D. A. Lesch and T. B. Rauchfuss. *Organometallics* 1982, **1,** 499.
36. M. M. Campos, C. Díaz, K. Figueroa, L. Padilla, N. Lara and G. Díaz. *Vib. Spectroscopy* 1994, **7,** 61.
37. Several electrochemical studies have showed that the binuclear complexes containing identical (or similar) noninteracting metal centers exhibit a single oxidation (reduction) wave, although with two electron transfer, in the overall reaction. See e.g. J. B. Flanagan, Sh. Margel, A. J. Bard and F. C. Anson, *J. Am. Chem. Soc.* 1978, **100,** 4248; F. A. Ammar and J. M. Saveant, *Electroanal. Chem. Interf. Electrochem.* 1973, **47,** 215.
38. P. E. Riley, Ch. E. Capshew, R. Pettit and R. E. Davis, *Inorg. Chem.* 1978, **17,** 408; D. H. Hill, M. Parvez and A. Sen, *Acta Cryst.* 1990, **C46,** 133.
39. Ch. Ueng and J. L. Hwang, *Inorg. Chim. Acta* 1994, **218,** 9.
40. M. V. Baker, L. D. Field and T. W. Hambley. *Inorg. Chem.* 1988, **27,** 2872.
41. T. S. Andy Hor and Sh.-Mai Chee. *J. Orgnomet. Chem.* 1987, **331,** 23.

Pergamon

PII: S0277-5387(96)00502-5

Polyhedron Vol. 16, No. 11, pp. 1783–1786, 1997
© 1997 Elsevier Science Ltd
All rights reserved. Printed in Great Britain
0277-5387/97 $17.00+0.00

X-ray crystallographic characterization of a zinc(II) complex with a 14-membered tetraaza macrocycle, 3,14-dimethyl-2,6,13,17-tetraazatricyclo[14,4,$0^{1.18}$,$0^{7.12}$]docosane

Ki-Young Choi,[a]* Il-Hwan Suh[b] and Ju Chang Kim[c]

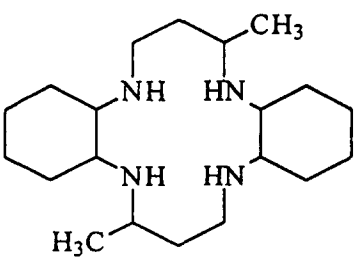
[a]Department of Chemistry Mokwon University Taejeon 301-729, Korea; [b]Department of Physics Chungnam National University Taejeon 305-764, Korea; [c]Department of Chemistry Bukyong National University Pusan 608-737, Korea

(Received 27 August 1996; accepted 14 October 1996)

Abstract—The zinc(II) complex of the tetraaza macrocyclic ligand 3,14-dimethyl-2,6,13,17-tetraazatricyclo[14,4,$0^{1.18}$,$0^{7.12}$]docosane(**L**), $[Zn(L)(H_2O)_2](Cl)_2$ (**1**) and its structural characterization is reported. The zinc(II) ion adopts a tetragonally elongated octahedral geometry with an average Zn—N distance of 2.099(2) Å and a Zn—O distance of 2.388(3) Å. © 1997 Elsevier Science Ltd. All rights reserved.

Keywords: zinc(II) complex; 14-membered tetraaza macrocycle.

Zinc(II) complexes of macrocyclic polyamines have been of great interest due to their importance as models of zinc-containing enzymes such as carbonic anhydrases, carboxypeptidases, glyoxalase I, etc. [1–5]. For mononuclear complexes of macrocyclic polyamines, Zn^{II}-triamines [6–8] and Zn^{II}-tetraamines [9,10] have been the most widely studied models due to their similarity in structural, thermodynamic, and kinetic properties with carbonic anhydrases. The coordination environments around Zn^{II} ions in those complexes are usually a distorted tetrahedron or a square pyramid with one water molecule bound to Zn^{II} ions in which the pK_a values (H_2O) lie 7.3–9.8 [2,11,12]. Since the zinc bound water molecule plays a fundamental role in the catalytic mechanism and the pK_a value of water in that complex appears to be dependent on the chelate ligands, we were quite interested in the synthesis of Zn^{II} complex with modified tetraamine macrocycle, 3,14-dimethyl-2,6,13,17-tetraazatricyclo[14,4,$0^{1.18}$, $0^{7.12}$]docosane(**L**). Interestingly enough, the crystal structure of this complex indicates that the Zn^{II} ion adopts an axially elongated octahedral environment with two *trans* water molecules and four equatorial nitrogens from the macrocycle. This result contrasts with other reports in which they assumed or determined that the Zn^{II} ions with related macrocycles take only one water molecule [1,2,6]. In this study we describe the synthesis and structure of this interesting diaquo Zn^{II} tetraamine macrocycle.



L

EXPERIMENTAL

General

All solvents were reagent grade and purified as described elsewhere prior to use [13]. Distilled water was used for all reactions. $ZnCl_2$, 1,2-diaminocyclohexane, methyl vinyl ketone, perchloric acid, and $NaBH_4$ were purchased from Aldrich Chemical

*Author to whom correspondence should be addressed.

Co. and used without further purification. Infrared spectra of solid complexes were recorded on a Perkin–Elmer Paragon 1000 FT-IR spectrophotometer between 4000 and 400 cm^{-1} as Nujol mulls on KBr plates. ^1H and ^{13}C NMR spectra were recorded at room temperature on a Bruker WP 300 spectrometer. Elemental analyses were performed by Korea Research Institute of Chemical Technology, Taejeon, Korea.

Preparation of neutral ligand (**L**)

The ligand **L** was prepared according to previously published procedures [14,15]. IR (Nujol, cm^{-1}): 3289(νNH), 1359, 1313, 1268, 1248, 1216, 1159, 1137, 1083, 1054, 1019, 913, 871, 837, 808, 766, 721, 621, 566, 502. MS(EI) Calc. (Found) m/z: 336(336) $[M]^+$. Calc. (Found) for $C_{20}H_{40}N_4$: C, 71.4 (71.6); H, 12.0 (12.0); N, 16.6 (16.8)%.

Preparation of $[Zn(\mathbf{L})(H_2O)_2](Cl)_2$ (**1**)

A methanol solution of **L**(200 mg, 0.59 mmol) and $ZnCl_2$(80 mg, 0.59 mmol) was heated at reflux for 2 h. The solution was allowed to cool to room temperature and was then filtered. The filtrate was evaporated to dryness. The product was redissolved in a minimum amount of water. After the solution was allowed to stand at room temperature over a period of several days, white crystals formed. Recrystallization from water/acetonitrile (1 : 1), filtration, washing with diethyl ether, and drying *in vacuo* produced a white solid (236 mg, 79% based on **L**). IR (Nujol, cm^{-1}): 3336(νOH), 3249(νOH), 3153(νNH), 3105(νNH), 1643(νHOH), 1309, 1280, 1176, 1099, 1011, 993, 968, 906, 800, 666. Calc. (Found) for $ZnC_{20}H_{44}N_4O_2Cl_2$: C, 47.2 (47.3); H, 8.7 (8.6); N, 11.0 (11.1)%. ^{13}C NMR ($CDCl_3$): δ 59.8, 56.4 (cyclohexane ring carbon), 47.6, 40.3, 34.2 (N—C—C—C—N), 29.6, 29.1, 24.4, 24.3 (cyclohexane ring carbon), 14.9 (—CH_3). ^1H NMR ($CDCl_3$): δ 1.41 (d, 6H, —CH_3), 2.23 (s, 4H, H_2O).

X-ray structural determination

Suitable crystals of **1** were grown by slow evaporation of aqueous solutions at room temperature. A colorless crystal of **1** of dimensions 0.50 × 0.36 × 0.20 mm was selected for diffraction study. Crystals were unprotected from the atmosphere. Data were collected on an automated Enraf-Nonius CAD-4 diffractometer with Mo-K_α radiation ($\lambda = 0.71069$ Å) employing ω-2θ scan mode at 293 K. The unit cell parameters and orientation matrix were obtained by the least squares fit of 25 reflections. Crystallographic data and refinement details are presented in Table 1. The intensity data were reduced using Lorentz and polarization corrections but no absorption correction was applied. After the reduction step all calculations were performed using the NRCVAX PC software package [16]. Trial models for the structures were obtained from phase sets generated from the SOLVER multistation software of NRCVAX. All non hydrogen atoms were placed with a combination of difference Fourier and least squares calculations. Methyl group hydrogen atoms were located from difference Fourier maps, other hydrogen atoms were placed in calculated positions. Anisotropic thermal parameters were used for all non hydrogen atoms and isotropic thermal parameters were used with the hydrogen atoms. Hydrogen atom positions were fixed during the least squares process. Selected interatomic distances and angles for **1** are listed in Table 2. Full crystallographic details, atomic coordinates, interatomic distances and angles, hydrogen atom coordinates and anisotropic displacement parameters for **1** have been deposited with the editor as supplementary material. Structure factor tables may be obtained directly from the authors.

RESULTS AND DISCUSSION

The reaction of **L** with equimolar amount of $ZnCl_2$ yielded colorless **1**. In common with Zn^{II} complexes of most saturated polyaza macrocyclic ligands, **1** in crystalline solids was stable to air indefinitely. The ^1H NMR spectrum of **1** was complicated by sets of several unresolved multiplets over a range of 1.0–3.5 ppm. Proton decoupled ^{13}C NMR spectrum of this compound clearly shows ten resolved singlets indicating that the complex contains ten different kinds of carbon atoms. **1** was soluble in water, nitromethane, dimethylforamide, and chloroform. The infrared spectrum of **1** contains characteristic ligand bands in addition

Table 1. Crystallographic data for $[Zn(\mathbf{L})(H_2O)_2](Cl)_2$ (**1**)

Formula	$ZnC_{20}H_{44}N_4O_2Cl_2$
Formula weight	508.884
Space group	$P2_1/c$ (No. 14)
a (Å)	9.0155(6)
b (Å)	18.6976(14)
c (Å)	7.7448(20)
β (Å)	110.155(9)
V (Å^3)	1225.5(3)
T (K)	293
d(calcd) (g cm^{-3})	1.379
Z	2
λ (Mo K_α)(Å)	0.71069
μ (cm^{-1})	1.379
R^a	0.029
$R_w{}^b$	0.031

[a] $R = \Sigma(F_o - F_c)/\Sigma(F_o)$.
[b] $R_w = [\Sigma w(F_o - F_c)^2/\Sigma(wF_o^2)]^{1/2}$.

Table 2. Selected interatomic distances (Å) and angles (°) for $[Zn(\mathbf{L})(H_2O)_2](Cl)_2$ (**1**)

Zn—N(1)	2.084(2)	Zn—N(2)	2.113(2)
Zn—O	2.388(3)	N(1)—C(6)	1.484(4)
N(1)—C(7)	1.477(4)	N(2)—C(1)	1.487(4)
C(1)—C(6)	1.532(4)	C(7)—C(8)	1.532(5)
C(8)—C(9)	1.532(5)	C(9)—C(10)	1.508(5)
O—Zn—O^i	180.0	O—Zn—N(1)	90.7(1)
O—Zn—N(1)^i	89.3(1)	O—Zn—N(2)	85.8(1)
O—Zn—N(2)^i	94.2(1)	N(1)—Zn—N(1)^i	180.0
N(1)—Zn—N(2)	83.6(1)	N(1)—Zn—N(2)^i	96.4(1)
Zn—N(2)—C(1)	107.4(2)	Zn—N(2)—C(9)^i	119.7(2)

Symmetry code: (i) $-x, -y, -z$

to the bands due to coordinated water molecules. Absorptions at 3336 cm^{-1} and 3249 cm^{-1} were assignable to antisymmetric and symmetric OH stretchings, and a band at 1643 cm^{-1} was assigned to HOH bending vibration of coordinated water [17]. The bands originated from water disappear upon heating **1** to 100°C for several hours *in vacuo*. Such a behavior is consistent with the loss of molecules of water in the complex.

Structure of **1**

Figure 1 shows the structure of **1** determined by single crystal X-ray crystallography. This is also the first report on the Zn^{II} complex of **L** studied by X-ray crystallography. Most of the related macrocyclic polyamines and their derivatives were earlier reported to form a five-coordinate Zn^{II} complexes with an aquo ligand. However, their solid state structures determined by X-ray crystal structure analysis are scarce [2–12]. The crystal structure of **1** consists of $[Zn(\mathbf{L})(H_2O)_2]^{2+}$ complex cation and two Cl^- anions. The coordination environment around Zn^{II} ion shows an axially elongated octahedron with two oxygen atoms of water molecules and four nitrogen atoms of the macrocyclic ligand. An inversion center exists on the central Zn^{II} ion. The structure of **1** is very similar to that of $[Cu(\mathbf{L})(H_2O)_2](Cl)_2$ which was described

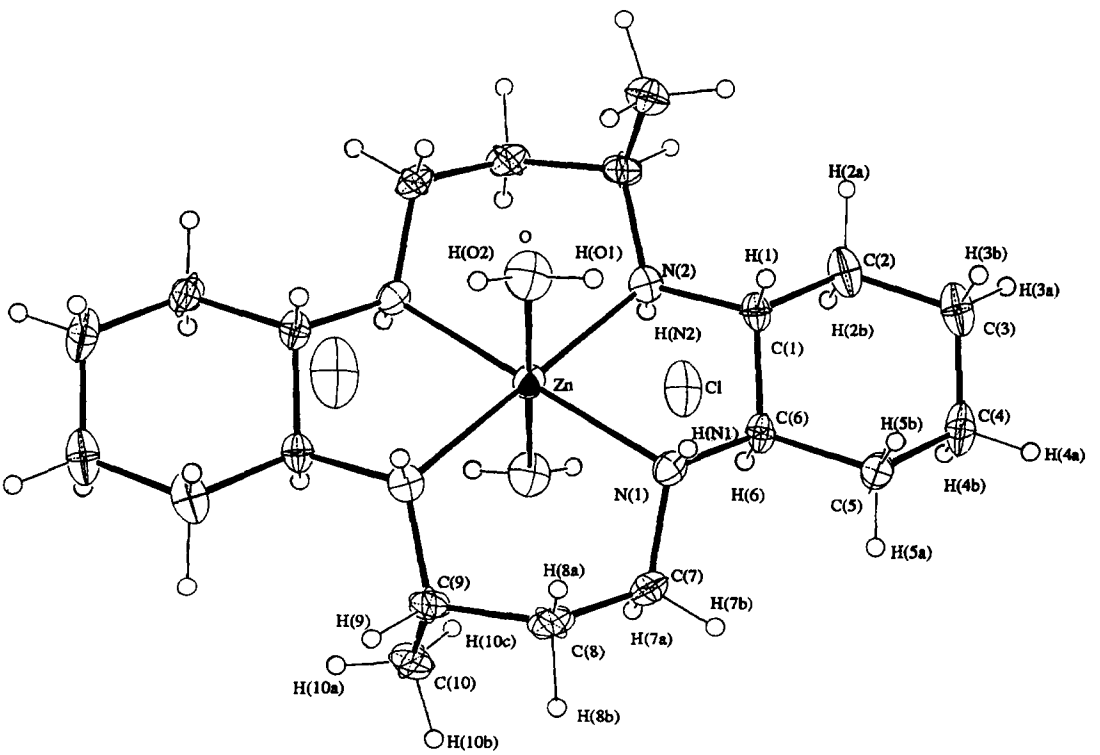


Fig. 1. ORTEP drawing of **1** with atom-labeling scheme.

Table 3. Hydrogen-bond parameters (Å,) for $[Zn(L)(H_2O)_2](Cl)_2$ (**1**)

D—H···A	D—H	H···A	D···A	D—A···A
N(1)—HN(1)···Cl'	0.085(4) Å	2.59(4) Å	3.418(3) Å	167(3)°
N(2)—HN(2)···Cl	0.80(3) Å	2.71(3) Å	3.500(3) Å	170(3)°
O—HO(2)···Cl	0.78(4) Å	2.38(4) Å	3.122(3) Å	159(4)°
O—HO(1)···Cl'	0.83(5) Å	2.31(5) Å	3.115(3) Å	163(4)°

Symmetry code: (i) $-x, -y, -1-z$

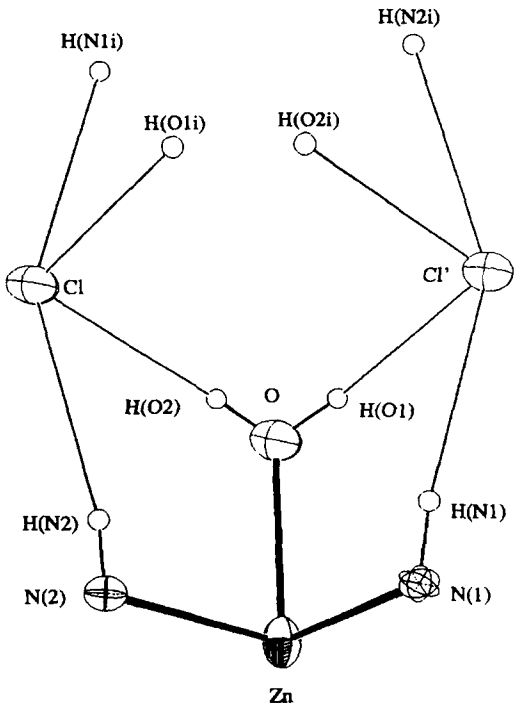


Fig. 2. Hydrogen-bond system of **1**.

recently by us [18]. The ligand skeleton of the complex contains two cyclohexane rings and two gauche five-membered and two chair six-membered chelate rings with most stable trans-III conformation. The bond distances of Zn—N in this complex are 2.084 (2) Å and 2.113 (2) Å, which are comparable to those found in $Zn(O_2COCH_3)([14]aneN_4)(ClO_4)$ (2.111 (3) Å and 2.088(3) Å) [9]. The determined distance of 2.388(3) Å is, to our best knowledge, the longest reported in a complex of this type. The average Zn—O (O = terminal aquo) distance is 2.090 ± 0.061 Å determined for 56 structures [19]. The longer Zn—O bond distance may be explained by the four hydrogen bonding chelate rings consisted of chlorides, water molecules, secondary amines of macrocycle, and the central Zn^{II} ion (Table 3 and Fig. 2). Under this situation, the coordination of the water molecules to the central Zn^{II} ion seems to be stabilized although the Zn—O bond distance is longer [20].

Acknowledgements—This work was supported by the research fund of Mokwon University (1996). J. C. K. acknowledges the Bukyong National University of Technology for providing partial financial support.

REFERENCES

1. P. Woolley, *Nature* 1975, **258,** 677.
2. E. Kimura and T. Koike, *Comments Inorg. Chem.* 1991, **11,** 285.
3. X. Zhang and R. van Eldik, *Inorg. Chem.* 1995, **34,** 5606.
4. P. Chaudhuri, C. Stockheim, K. Wieghardt, W. Deck, R. Gregorzik, H. Vahrenkamp, B. Nuber and J. Weiss, *Inorg. Chem.* 1992, **31,** 1451.
5. L. Garcia-Iniguez, L. Powers, B. Chance, S. Sellin, B. Mannervick and A. S. Mildvan, *Biochemistry* 1984, **23,** 685.
6. E. Kimura, T. Shiota, T. Koike, M. Shiro and M. Kodama, *J. Am. Chem. Soc.* 1990, **112,** 5805.
7. E. Kimura, I. Nakamura, T. Koike, M. Shionoya, Y. Kodama, T. Ikeda and M. Shiro, *J. Am. Chem. Soc.* 1994, **116,** 4764.
8. X. Zhang, R. van Eldik, T. Koike and E. Kimura, *Inorg. Chem.* 1993, **32,** 5749.
9. M. Kato and T. Ito, *Inorg. Chem.* 1985, **24,** 509.
10. P. R. Norman, *Inorg. Chim. Acta* 1987, **130,** 1.
11. E. Kimura, M. Shionoya, A. Hoshino, T. Ikeda and Y. Yadama, *J. Am. Chem. Soc.* 1992, **114,** 10134.
12. E. Kimura, *Tetrahedron* 1992, **48,** 6175.
13. D. D. Perrin, W. L. F. Armarego and D. R. Perrin, *Purification of Laboratory Chemicals*, 2nd edn. Pergamon Press, New York (1985).
14. S.-G. Kang, J. K. Kweon and S.-K. Jung, *Bull. Kor. Chem. Soc.* 1991, **12,** 483.
15. R. W. Hay and G. A. Lawrence, *J. Chem. Soc., Dalton Trans.* 1975, 1466.
16. E. J. Gabe, Y. L. Page, J. P. Charland, F. L. Lee and P. S. White, *J. Appl. Cryst.* 1989, **22,** 384.
17. K. Nakamoto, *Infrared and Raman Spectra of Inorganic and Coordination Compounds*, 4th edn. pp. 227–229. John Wiley & Sons, New York (1986).
18. K. Y. Choi, J. C. Kim, W. P. Jensen, I.-H. Suh and S.-S. Choi, *Acta Cryst., Sect.* C52, 1996, 2166.
19. A. G. Orpen, L. Brammer, F. H. Allen, O. Kennard, D. G. Watson and R. Taylor, *J. Chem. Soc., Dalton Trans.*, 1989, S1.
20. A similar hydrogen-bond system has just appeared in *trans*-$[Ni(OH_2)_2(cyclam)]Cl_2 \cdot 4H_2O$. K. Mochizuki and T. Kondo, *Inorg. Chem.* 1995, **34,** 6241.

Pergamon

PII: S0277-5387(96)00501-3

Polyhedron Vol. 16, No. 11, pp. 1787–1792, 1997
© 1997 Elsevier Science Ltd
All rights reserved. Printed in Great Britain
0277-5387/97 $17.00+0.00

Crystal structure and spectral properties of a new type of polymeric complex with 18-membered macrocycles $[Nd(C_{16}H_{18}S_2O_2)_2(NO_3)_3]_n$

Ruo-Hua Zhang,[a]* Bao-Qing Ma,[a] Xian-He Bu,[a] Hong-Gen Wang[b] and Xin-Kan Yao[b]

[a]Department of Chemistry, Nankai University, Tianjin 300071, P. R. China; [b]Centre Laboratory, Nankai University, Tianjin 300071, P. R. China

(Received 19 August 1996; accepted 14 October 1996)

Abstract—The neodymium nitrate complex with 1,4-bis(phenylsulfinyl)butane(bphsb)$[Ln(bphsb)_2(NO_3)_3]_n$ has been synthesized and characterized. The X-ray crystal structure determination of the complex indicates that bphsb and neodymium(III) ion form a polymeric chain involving 18-membered macrocycles, each macrocycle comprising two neodymium(III) ions. The adjacent metal centres are linked by the bridging ligand. Each neodymium ion is ten-coordinated and the coordination geometry is a distorted 4,4-bicapped square antiprism. The IR and absorption spectra of solid and solution for the complex were also studied. © 1997 Elsevier Science Ltd. All rights reserved.

Keywords: neodymium; 1,4-bis(phenylsulfinyl)butane; crystal structure; complex of polymeric chain; 18-membered macrocycle; absorption spectrum.

Synthesis and characterization of lanthanide polynuclear complexes are important for developing the nature and applications of lanthanide metal–metal interaction in lasers, light-conversion molecular devices and paramagnetic contrast enhancing agents in magnetic resonance imaging [1–3].

Appropriate choice of metal and polydentate ligand is the key in forming polynuclear complexes. It is noticed that the number and types of atoms between the bridging units and the nature of terminal group of polydentate ligand which are important in preparing lanthanide polynuclear complexes. We chose 1,4-bis(phenylsulfinyl)butane (bphsb) as bridging ligand containing two phenyl terminal groups and having a separation of six atoms between coordinated atoms in order to obtain a polynuclear complex. A polynuclear europium(III) complex has been prepared by reaction of $Eu(NO_3)_3$ and bphsb [4]. It is shown that this ligand is the preferred bridging ligand for forming polynuclear complexes. We report here the results of synthesis, crystal structure and spectroscopic studies of a novel homopolynuclear neodymium complex of 1,4-bis(phenylsulfinyl)butane with a polymeric chain involving 18-membered macrocycles.

EXPERIMENTAL

Synthesis of complex $[Nd(bphsb)_2(NO_3)_3]_n$

1 mmol of hydrated neodymium nitrate dissolved in 10 cm^3 of anhydrous methanol was dehydrated by the addition of 2 cm^3 triethylorthoformate. The solution was added dropwise to 4 cm^3 anhydrous methanol solution of ligand (bphsb, 3 mmol). The mixture was stirred at 70–80°C for 6 h. Small precipitate was filtered, the filtrate was allowed to evaporate slowly at room temperature, and after a week, reddish single crystals were obtained. Found: C, 39.8; H, 4.2; N, 4.0. Calc. for $C_{32}H_{36}N_3S_4O_{13}Nd$: C, 40.7; H, 3.8; N, 4.4%.

*Author to whom correspondence should be addressed.

Physical measurements

The IR spectrum of the complex in the 4000–400 cm^{-1} range (as KBr pellets) was recorded on a WHF-30 model spectrometer. Conductivity of the complex in the methanol solution (10^{-3} mol dm^{-3}) was measured at room temperature using a DDS-11A conductometer. Thermal analysis in air was carried out on a PCT-1 analyzer. Electronic spectrum of the methanol solution of the complex was recorded in the 190–325 nm range and solid and solution spectra in the 800–350 nm range were also measured at room temperature on a Shimadzu UV-240 spectrophotometer.

The X-ray data collection was performed at 299 ± 1 K on an Enraf-Nonius CAD4 diffractometer with graphite-monochromated Mo-K_α radiation (=0.071073 nm) in ω-2θ scan mode. Reflections were collected in the range of $2 \leqslant \theta \leqslant 23°$. An empirical absorption correction was applied. The crystal structure was solved by direct methods (MULTAN82). The final refinement was by the full-matrix least squares method. All the calculations were carried out on a PDP11/44 and IBM-486 computer using a SDP-PLUS program system.

Crystallographic data for the title complex is listed in Table 1.

RESULTS AND DISCUSSION

The complex has the stoichiometry [Nd(bphsb)$_2$(NO$_3$)$_3$]. The electrical conductance values ($\sim$0 s mol^{-1} cm^2) of the complex in methanol indicate that the complex behaves as a non-electrolyte. The complex is air stable at room temperature. Thermal analysis of the complex shows that decomposition started above 215°C. In the IR spectrum of the complex, the S=O band is shifted to lower frequencies (986 cm^{-1}) than that for the free ligand (1039.8 cm^{-1}), which indicate coordination through the oxygen of the S=O moieties of the bphsb. The IR spectral data also show that absorption peaks of bidentate coordinated nitrate ions (C_{2v}) present at 1458($\nu_1(A_1)$), 1334($\nu_4(B_1)$), 1020($\nu_2(A_1)$), 820($\nu_3(A_1)$), 740 cm^{-1} ($\nu_5(B_1)$) and 1774($\nu_2 + \nu_5$), 1746 cm^{-1} ($\nu_2 + \nu_6$) [5].

Table 1. Selected crystallographic data for the complex

Formula	$C_{64}H_{72}N_6O_{26}S_8Nd_2$
Formula wt	1886.30
Crystal system	monoclinic
Space group	$P2_1/n$
Cell constants	
a (nm)	1.8211(9)
b (nm)	2.2444(4)
c (nm)	1.8479(5)
β (°)	97.65(3)
V (nm^3)	7.486(4)
Z	4
$D_{calc.}$ (g cm^{-3})	1.674
Crystal size (mm)	0.3 × 0.3 × 0.35
F(000)	3816
μ_{calc} (mm^{-1})	1.671
Radiation	Mo-K_α (λ = 0.071073 nm)
Total reflections	11093
Independent reflections	8806
Observed reflections	5565 [$I \geqslant 3\sigma(I)$]
R	0.051
Rw	0.057
T (K)	299 ± 1

Description of the crystal structure

Selected bond lengths and angles are listed in Tables 2 and 3. A table of atomic coordinates and equivalent isotropic displacement coefficients and structure factors are included as supplementary material.

Single crystal structure analysis shows the complex to have the stoichiometry [Nd(bphsb)$_2$(NO$_3$)$_3$)] and to be polymeric structure (Figs 1 and 2). Each neodymium centre is ten-coordinated and is bound to one oxygen atom of each of four bphsb ligands and three bidentate nitrates. The Nd—O distances lie in two groups, those to the sulfoxide oxygen atoms in the range 0.2416–0.2503 nm and those to nitrate oxygens in the range 0.2548–0.2620 nm. The coordinated geometry is best described as a 4,4-bicapped square antiprism with O(1), O(8), O(13), O(31), O(4), O(2), O(22), O(32), forming the vertices with bi-capped by O(12) and O(21) for Nd(1) (Fig. 3).

Adjacent neodymium centers are linked *via* oxygens of bphsb ligands which form a chain linked system of a polymeric molecule. The bphsb ligands perform a bridging function. Each chain system comprises 18-membered macrocyclic rings, each containing two neodymium(III) ions. In each chain system, the arrangement of the 18-membered macrocyclic rings is ordered (Fig. 2).

The stoichiometry and structure of the crystal products obtained from the methanol solution of bphsb for neodymium(III) and europium(III) nitrate are not the same. The neodymium(III) ion afforded the complex [Nd(bphsb)$_2$(NO$_3$)$_3$]$_n$, molar ratio (M : L) = 1 : 2, but europium(III) ion gave the compound of stoichiometry [Eu(bphsb)$_{1.5}$(NO$_3$)$_3$]$_n$ [4], molar ratio

Table 2. Selected bond lengths (nm)

Nd(1)—O(1)	0.2445(10)	Nd(2)—O(3)	0.2419(15)
Nd(1)—O(2)	0.2432(10)	Nd(2)—O(5)	0.2485(10)
Nd(1)—O(4)	0.2416(15)	Nd(2)—O(6)	0.2440(11)
Nd(1)—O(8)	0.2503(14)	Nd(2)—O(7)	0.2489(16)
Nd(1)—O(12)	0.2548(13)	Nd(2)—O(42)	0.2572(10)
Nd(1)—O(13)	0.2609(11)	Nd(2)—O(43)	0.2595(11)
Nd(1)—O(21)	0.2617(12)	Nd(2)—O(51)	0.2665(13)
Nd(1)—O(22)	0.2569(11)	Nd(2)—O(53)	0.2544(12)
Nd(1)—O(31)	0.2595(14)	Nd(2)—O(61)	0.2579(13)
Nd(1)—O(32)	0.2620(11)	Nd(2)—O(62)	0.2616(11)

Table 3. Selected bond angles (°)

O(1)—Nd(1)—O(2)	138.3(4)	O(8)—Nd(1)—N(1)	69.3(4)
O(1)—Nd(1)—O(4)	72.4(4)	O(12)—Nd(1)—N(1)	24.6(4)
O(2)—Nd(1)—O(4)	80.9(4)	O(13)—Nd(1)—N(1)	24.0(3)
O(1)—Nd(1)—O(8)	76.5(4)	O(21)—Nd(1)—N(1)	128.8(4)
O(2)—Nd(1)—O(8)	70.7(4)	O(22)—Nd(1)—N(1)	81.2(3)
O(4)—Nd(1)—O(8)	87.2(5)	O(31)—Nd(1)—N(1)	72.8(4)
O(1)—Nd(1)—O(12)	70.7(4)	O(32)—Nd(1)—N(1)	120.4(3)
O(2)—Nd(1)—O(12)	118.5(4)	O(1)—Nd(1)—N(2)	146.1(4)
O(4)—Nd(1)—O(12)	139.9(5)	O(2)—Nd(1)—N(2)	66.7(3)
O(8)—Nd(1)—O(12)	69.6(5)	O(4)—Nd(1)—N(2)	96.3(4)
O(1)—Nd(1)—O(13)	117.9(4)	O(8)—Nd(1)—N(2)	136.0(3)
O(2)—Nd(1)—O(13)	75.5(4)	O(12)—Nd(1)—N(2)	123.3(4)
O(4)—Nd(1)—O(13)	152.7(4)	O(13)—Nd(1)—N(2)	87.0(3)
O(8)—Nd(1)—O(13)	72.1(4)	O(21)—Nd(1)—N(2)	23.5(4)
O(12)—Nd(1)—O(13)	48.6(4)	O(22)—Nd(1)—N(2)	24.6(3)
O(1)—Nd(1)—O(21)	130.5(4)	O(31)—Nd(1)—N(2)	82.4(4)
O(2)—Nd(1)—O(21)	66.6(4)	O(32)—Nd(1)—N(2)	73.8(3)
O(4)—Nd(1)—O(21)	72.9(4)	N(1)—Nd(1)—N(2)	105.4(3)
O(8)—Nd(1)—O(21)	135.0(4)	O(3)—Nd(2)—O(5)	71.8(4)
O(12)—Nd(1)—O(21)	145.7(5)	O(3)—Nd(2)—O(6)	80.4(4)
O(13)—Nd(1)—O(21)	109.2(4)	O(5)—Nd(2)—O(6)	140.0(4)
O(1)—Nd(1)—O(22)	147.6(4)	O(3)—Nd(2)—O(7)	82.0(5)
O(2)—Nd(1)—O(22)	73.9(4)	O(5)—Nd(2)—O(7)	77.8(4)
O(4)—Nd(1)—O(22)	120.9(4)	O(6)—Nd(2)—O(7)	70.2(4)
O(8)—Nd(1)—O(22)	129.8(4)	O(3)—Nd(2)—O(42)	137.1(4)
O(12)—Nd(1)—O(22)	98.9(4)	O(5)—Nd(2)—O(42)	70.6(4)
O(13)—Nd(1)—O(22)	65.3(4)	O(6)—Nd(2)—O(42)	117.9(4)
O(21)—Nd(1)—O(22)	48.0(4)	O(7)—Nd(2)—O(42)	70.5(4)
O(1)—Nd(1)—O(31)	77.8(4)	O(3)—Nd(2)—O(43)	152.5(4)
O(2)—Nd(1)—O(31)	143.8(4)	O(5)—Nd(2)—O(43)	117.2(3)
O(4)—Nd(1)—O(31)	122.3(5)	O(6)—Nd(2)—O(43)	77.4(4)
O(8)—Nd(1)—O(31)	131.6(4)	O(7)—Nd(2)—O(43)	75.3(4)
O(12)—Nd(1)—O(31)	63.4(5)	O(42)—Nd(2)—O(43)	47.1(3)
O(13)—Nd(1)—O(31)	85.0(4)	O(3)—Nd(2)—O(51)	74.9(4)
O(21)—Nd(1)—O(31)	92.4(4)	O(5)—Nd(2)—O(51)	128.3(4)
O(22)—Nd(1)—O(31)	70.3(4)	O(6)—Nd(2)—O(51)	67.7(4)
O(1)—Nd(1)—O(32)	72.5(4)	O(7)—Nd(2)—O(51)	134.6(4)
O(2)—Nd(1)—O(32)	131.4(4)	O(42)—Nd(2)—O(51)	146.9(4)
O(4)—Nd(1)—O(32)	76.3(4)	O(43)—Nd(2)—O(51)	110.7(4)
O(8)—Nd(1)—O(32)	148.1(4)	O(3)—Nd(2)—O(53)	123.0(4)
O(12)—Nd(1)—O(32)	106.3(4)	O(5)—Nd(2)—O(53)	146.3(4)
O(13)—Nd(1)—O(32)	130.1(3)	O(6)—Nd(2)—O(53)	73.4(4)
O(21)—Nd(1)—O(32)	65.8(4)	O(7)—Nd(2)—O(53)	130.8(5)
O(22)—Nd(1)—O(32)	81.9(4)	O(42)—Nd(2)—O(53)	99.8(4)
O(31)—Nd(1)—O(32)	47.7(4)	O(43)—Nd(2)—O(53)	65.2(4)
O(1)—Nd(1)—N(1)	94.7(3)	O(51)—Nd(2)—O(53)	48.5(4)
O(2)—Nd(1)—N(1)	97.0(3)	O(3)—Nd(2)—O(61)	124.1(5)
O(4)—Nd(1)—N(1)	155.5(4)	O(5)—Nd(2)—O(61)	75.6(4)
		O(51)—Nd(2)—O(62)	64.6(4)
O(6)—Nd(2)—O(61)	144.3(4)	O(53)—Nd(2)—O(62)	82.4(4)
O(7)—Nd(2)—O(61)	132.8(4)	O(61)—Nd(2)—O(62)	48.1(4)
O(42)—Nd(2)—O(61)	64.1(4)	O(3)—Nd(2)—N(4)	153.5(4)
O(43)—Nd(2)—O(61)	83.2(4)	O(5)—Nd(2)—N(4)	94.3(3)
O(51)—Nd(2)—O(61)	92.3(4)	O(6)—Nd(2)—N(4)	98.4(4)
O(53)—Nd(2)—O(61)	71.3(4)	O(7)—Nd(2)—N(4)	72.8(4)
O(3)—Nd(2)—O(62)	78.5(5)	O(42)—Nd(2)—N(4)	23.8(3)
O(5)—Nd(2)—O(62)	70.7(3)	O(43)—Nd(2)—N(4)	23.4(3)
O(6)—Nd(2)—O(62)	131.3(4)	O(51)—Nd(2)—N(4)	129.4(4)
O(7)—Nd(2)—O(62)	146.8(4)	O(53)—Nd(2)—N(4)	81.0(3)
O(42)—Nd(2)—O(62)	107.4(4)	O(61)—Nd(2)—N(4)	71.1(4)
O(43)—Nd(2)—O(62)	128.8(3)	O(62)—Nd(2)—N(4)	119.1(3)

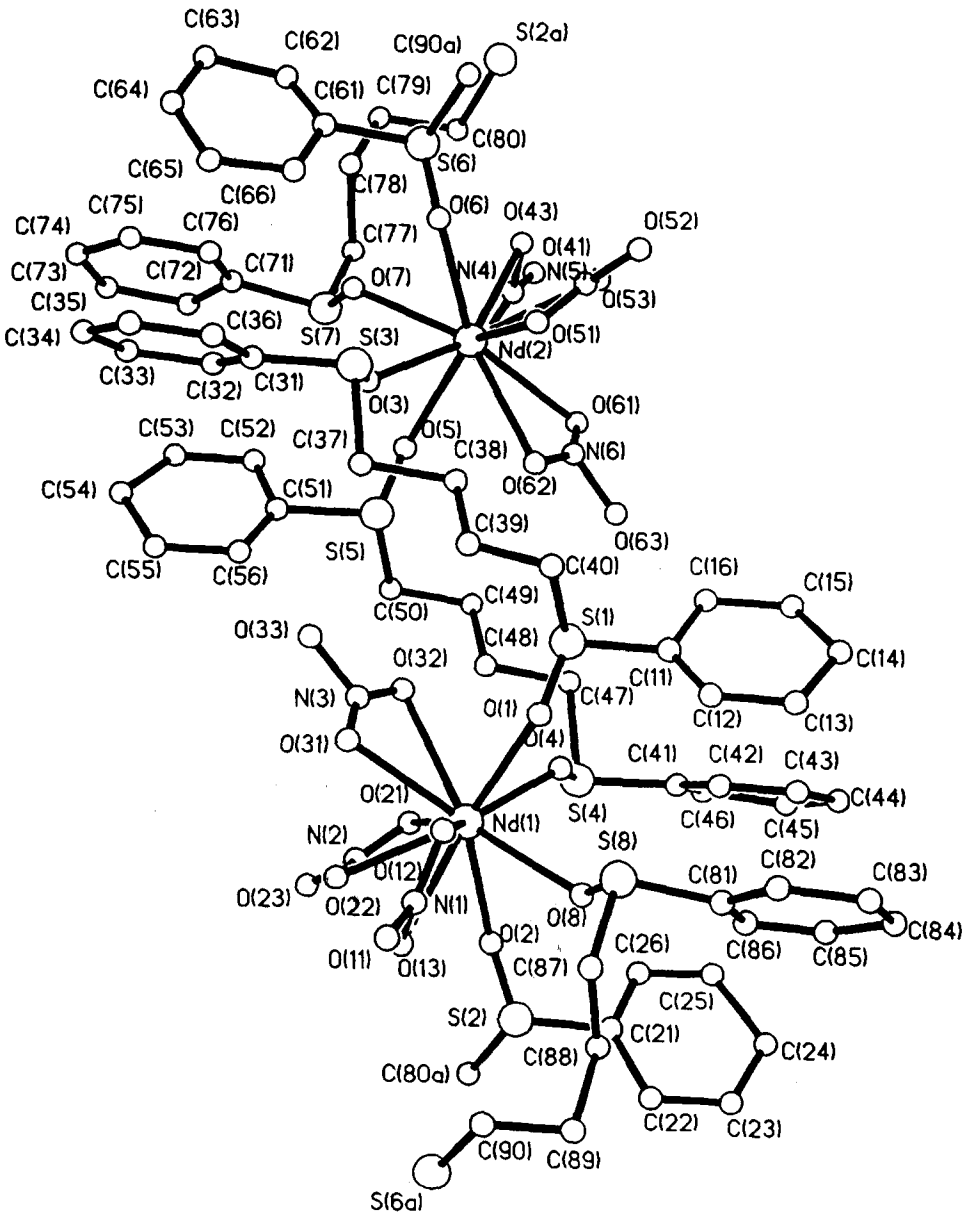


Fig. 1. The ORTEP stereoview of $Nd_2(bphsb)_4(NO_3)_6$ with hydrogen atoms omitted (35% probability thermal ellipsoids).

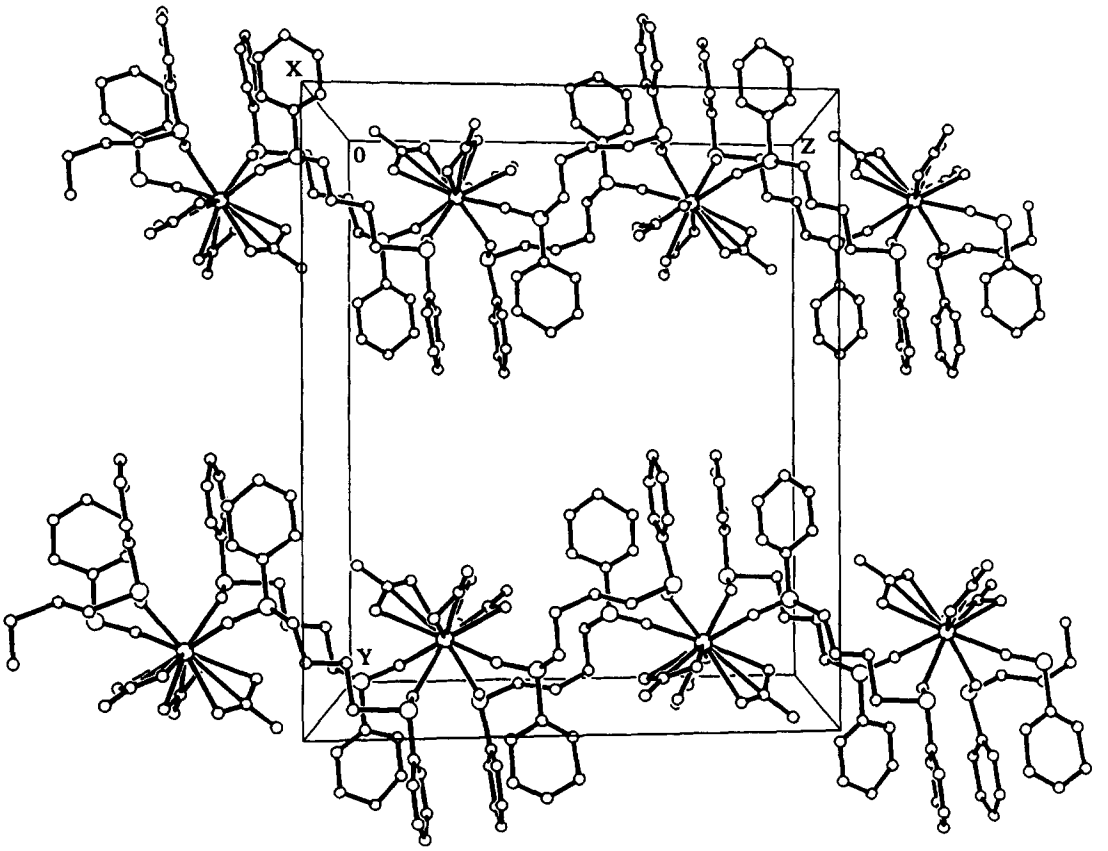


Fig. 2. Part of the polymeric chains of the complex showing the 18-membered rings.

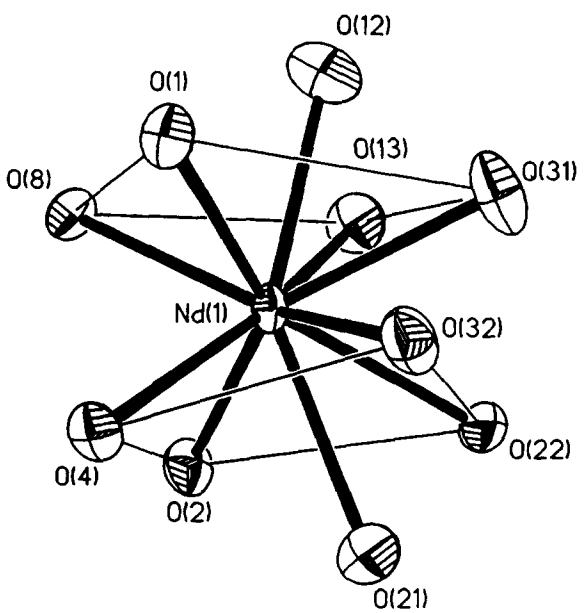


Fig. 3. The coordination around each Nd atom.

(M : L) = 1 : 1.5. These results may be due to the size of the lanthanide ion influencing complex type and structure, the europium polynuclear complex [Eu(bphsb)$_{1.5}$(NO$_3$)$_3$]$_n$ is a supramolecular compound with a framework structure [4].

Spectral properties

The absorption spectra of the methanol solution and solid for the complex were examined. The absorption spectra of solution and solid in the visible region show *f–f* transitions. Tentative assignments and strengths for the bands are given in Table 4. The average values of Sinha's parameter (δ) [6] for solution and solid case suggest a very weak covalent character for the metal–ligand bonding.

The absorption spectrum of solution in the range 190–330 nm shows that n–π^* transition (212 nm) of S=O of bphsb and π–π^* transitions (239 and 270 nm) of phenyl of bphsb.

Table 4. Electronic spectral data of the title complex

Ground $^4I_{9/2}$	Nd^{3+}_{aquo}	λ_{max} (nm) Solution ($P \times 10^{-6}$)	Solid
$^4F_{5/2}$	793.8	794.4(8.65)	794.8
$^4F_{7/2}$	739.8		738.9
$^4S_{3/2}$	731.4	736.5(9.19)	733.0
$^4F_{9/2}$	679.2	673.5(0.58)	674.4
$^4G_{5/2}$, $^2G_{7/2}$	573.9	577.8(23.17)	580.6
$^4G_{7/2}$	520.2	522.1(4.55)	521.9
$^4G_{9/2}$	510.6	508.8(3.94)	509.4
β		0.9996	0.9991
$b^{1/2}$		0.0128	0.0202
δ		0.040	0.090

REFERENCES

1. C. Piguet, J.-C. G. Bünzli, G. Bernardinelli, G. Hopfgartner and F. Williams, *J. Am. Chem. Soc.* 1993, **115,** 8197.
2. M. Latva, H. Takalo, K. Simberg and J. Kankare, *J. Chem. Soc., Perkin Trans.* 1995, 995.
3. I. A. Kahwa, S. Folkes, D. J. Williams, S. V. Ley, C. A. O'Manhoney and G. L. Mcpherson, *J. Chem. Soc., Chem. Commun.* 1989, 1531.
4. R.-H. Zhang, B.-Q. Ma, X.-H. Bu, H.-G. Wang, X.-K. Yao, *Polyhedron* (in press).
5. M. R. Rosenthal, *J. Chem. Educ.* 1973, **50,** 331; R. J. Foster and D. G. Hendriker, *Inorg. Chim. Acta* 1972, **6,** 371.
6. S. P. Sinha, *Spectrochim. Acta* 1966, **22,** 57.

Pergamon

PII: S0277-5387(96)00500-1

Polyhedron Vol. 16, No. 11, pp. 1793–1802, 1997
© 1997 Elsevier Science Ltd
All rights reserved. Printed in Great Britain
0277-5387/97 $17.00+0.00

Novel pentacoordinated ruthenium(II) complexes with a NNS chelating ligand: synthesis, characterization and electrochemical studies

Mosarraf Hossain, Shyamal Kumar Chattopadhyay† and Saktiprosad Ghosh*

Department of Inorganic Chemistry, Indian Association for the Cultivation of Science, Calcutta 700 032, India.

(Received 29 May 1996; accepted 14 October 1996)

Abstract—The NNS chelating donor *N*-2-mercaptophenyl-(2′-pyridyl)methylenimine (PabtH) reacted with $Ru(PPh_3)_3Cl_2$ to give a series of ruthenium(II) complexes Ru(Pabt) $(PPh_3)X$ {X = Cl(**1**), Br(**3**)}, Ru(Pabt) $(PPh_3)_2Cl$ (**2**), [Ru(Pabt) $(PPh_3)L]ClO_4$ {L = 1-Meimz (**2a**), 2-Meimz (**1c**)}, [Ru(Pabt) (PPh_3) $(L')_2]ClO_4$ {L′ = 1-Meimz (**1a**), imz (**1b**), H_2O (**1f**)} and [Ru(Pabt) (PPh_3) (L-L)]ClO_4 {L-L = bpy (**1d**), Phen (**1e**); bpy = 2, 2′-bipyridine, Phen = 1,10-phenanthroline}. They have been characterized using IR, UV–vis, {^1H and ^{31}P} NMR, EPR, magnetic susceptibility at room temperature, measurement of molecular weight, molecular conductance in solution and elemental analysis. The stabilisation of the pentacoordinated 16-electron complexes (**1, 3, 1c** and **2a**) is attributed to $p\pi$ donation by the sulfur atom of the ligand Pabt. Square pyramidal structure is proposed for these pentacoordinated complexes. Electron transfer behaviour of all the complexes has been explored by cyclic voltammetry in CH_2Cl_2 and CH_3CN using TEAP as the supporting electrolyte. The five-coordinated complexes display cathodically shifted oxidation waves in CH_2Cl_2, when TEACl was used as supporting electrolyte. Linear correlation of electrochemical data in terms of Lever's electrochemical parameter E_L and the energy of metal to ligand charge transfer band has been attempted. © 1997 Elsevier Science Ltd. All rights reserved.

Keywords: pentacoordination; ruthenium(II) complexes; mixed ligand complexes; NNS-ligand; chemical reactivity; electrochemical studies.

The chemistry of nitrogen–sulfur chelating ligands has witnessed phenomenal growth during the last decade. This was stimulated particularly by the discovery of the occurrence of similar donor environment in the prosthetic groups of several oxidoreductases [1,2]. However, one of the metal ions that has received little attention in such studies is ruthenium, probably because of its non-availability in biological systems. The relatively small amount of work so far carried out on ruthenium complexes involving such ligands indicate that they exhibit very interesting redox, electronic and structural characteristics [3–9]. It is also well known that chelating nitrogen–sulfur donors can stabilise complexes of unusual oxidation states [10–15] and uncommon coordination numbers of metal ions [13–16]. Such complexes are also known to participate in diverse redox reactions [17–19], sometimes even forming complete electrochemical series [17]. In this chemical milieu, the chemistry of ruthenium ligated to nitrogen–sulfur chelating ligands promises to be quite fascinating. This paper reports the synthesis and reactivity of ruthenium complexes of the NNS chelating ligand N-2-mercaptophenyl (2′-pyridyl) methylenimine (PabtH), which affords a few ruthenium complexes with unusual coordination number. Exploration of the redox behaviour of the ruthenium complexes of PabtH itself and those in which other coligands are present in the first coordination sphere of the ruthenium centre receives appropriate attention in this work.

*Author to whom all correspondence should be addressed.
†Permanent address: Department of Chemistry, Bengal Engineering College (Deemed University), Howrah 711 103, West Bengal, India.

EXPERIMENTAL

Physical measurement

Carbon, hydrogen and nitrogen analyses were performed in a Perkin–Elmer 240 C,H,N analyser and halogens were estimated by the reported method.[20] IR spectra were recorded with a Perkin-Elmer 783 Spectrophotometer using the KBr and polythene powder wafer techniques. Thermogravimetric (TG) and differential thermal analysis (DTA) were done in a Shimadzu DT-30 thermal analyser. Electronic spectra of the compounds were taken on a Shimadzu Model UV-2100 UV–vis recording spectrophotometer. Electrical conductance data in solution were collected using a Philips PR-9500 conductivity bridge fitted with a dip-type cell calibrated with 0.02 M KCl solution. Static susceptibility measurements at room temperature were made with the help of a Princeton Applied Research Model 155 vibrating-sample magnetometer using $Hg[Co(SCN)_4]$ as the calibrant. Molecular weight in CH_2Cl_2 was determined by KNAUER model Vapor Pressure Osmometer connected to a Recorder (type 11.15) using benzil as the calibrant. Proton NMR spectra were recorded on a Varian XL100 FT-NMR spectrometer using TMS as internal indicator. $\{^{31}P\}$NMR spectrum was recorded in $CDCl_3$ using 85% H_3PO_4 as external reference. Electron spin resonance spectra were recorded on a Varian E4 X-band EPR spectrometer, using diphenylpicrylhydrazyl (dpph) as an internal field marker. Electrochemical studies were done with the help of a PAR Model 370-4 electrochemistry system, 174A polarographic analyser, 175 universal programmer, RE 0074 X-Y recorder at 298 K. All these experiments were carried out under dry nitrogen. A planar Beckman model 39273 platinum-inlay working electrode, a platinum-wire auxiliary electrode and a saturated calomel electrode (SCE) as the reference electrode were used in the three-electrode configuration. The saturated calomel electrode (SCE) was separated from the sample compartment by a salt bridge connected by glass frit filled with the solvent (0.1 M supporting electrolyte) for the measurement. Under these experimental conditions the ferricenium–ferrocene couple was located at 0.42 V. In controlled potential electrolysis, a platinum mesh was used as working electrode and the auxiliary electrode was separated from the solution by a sintered glass disk.

Chemicals

$RuCl_3$ was obtained from Arora-Matthey Limited. 2-(2-Pyridyl)benzothiazoline (PabtH) [15], $Ru(PPh_3)_3Cl_2$ and $Ru(PPh_3)_3Br_2$ were prepared using the published procedure [21,22]. All other chemicals used for preparative work were of reagent grade and were used without further purification. Reagent grade solvents were dried and distilled by the usual methods [23]. Tetraethylammonium perchlorate (TEAP) was prepared from tetraethylammonium bromide (Fluka AG) by following a standard procedure [24]. All reactions were performed under dry nitrogen.

Preparation of $Ru(Pabt)(PPh_3)Cl$ (**1**) *and* $Ru(Pabt)(PPh_3)_2Cl$ (**2**). Solid $Ru(PPh_3)_3Cl_2$ [120 mg, 0.125 mmol] in 20 cm^3 benzene was refluxed with a benzene (5 cm^3) solution of 2-(2-pyridyl) benzothiazoline [54 mg, 0.25 mmol] for 2 h. A brown complex **1** separated from hot solution. The mixture was cooled and filtered under nitrogen. The residue was washed several times with degassed benzene and dried over fused $CaCl_2$. Yield 63 mg (82%).

The volume of the filtrate was reduced to one-third in a rota-evaporator, excess of degassed ether was added to it and the mixture was allowed to settle (5 min). Compound **2** separated out and was filtered, washed thrice with degassed ether and dried *in vacuo*. Yield 10 mg (9%).

When the above reaction was carried out in benzene using (1 : 1) molar ratio of the reactants, compound **1** separated out from the hot solution, being the only product in this reaction. When the reaction was carried out in CH_2Cl_2 using 1 : 1 molar ratio of reactants, the compound **1** had to be precipitated by the addition of excess degassed ether.

Preparation of $Ru(Pabt)(PPh_3)Br$ (**3**). This complex was prepared by a method similar to that of complex **1** using $Ru(PPh_3)_3Br_2$ as the starting material. Yield 70 mg (85%).

Preparation of $[Ru(Pabt)(PPh_3)(1\text{-}Meimz)_2]ClO_4 \cdot 1.5CH_2Cl_2$ (**1a**). ***Warning***: Perchlorate salts of metal complexes are potentially explosive [25]. To a stirred solution of $Ru(Pabt)(PPh_3)Cl$ (**1**) [1 mmol] in 40 ml dichloromethane, excess [~100 mmol] 1-methylimidazole (1-Meimz) was added and the mixture was stirred at room temperature for 24 h. The volume was then reduced to 10 cm^3 in a rotaevaporator. To this concentrated solution, excess petroleum ether (60–80 °C) was added and the mixture was allowed to settle [10 min] in a refrigerator. When an oily product settled down, the supernatant liquid was decanted off, the oily compound was dissolved in acetone and excess ether was added. The separated oily product was again dissolved in methanol and excess degassed aqueous solution of $LiClO_4$ was added to it. A granular compound precipitated out. It was filtered, washed thoroughly with degassed water and dried over fused $CaCl_2$. The compound was recrystallised from degassed CH_2Cl_2. Yield 600 mg (62%).

Preparation of $[Ru(Pabt)(PPh_3)(imz)_2]ClO_4 \cdot 0.5 CH_2Cl_2$ (**1b**), $[Ru(Pabt)(PPh_3)(2\text{-}Meimz)]ClO_4$ (**1C**). ***Warning***: Perchlorate salts of metal complexes are potentially explosive [25]. These two compounds were synthesized and purified by the above procedure using imidazole (imz) and 2-methylimidazole (2-Meimz), respectively, in place of 1-methylimidazole. The complexes **1a, 1b** and **1c** can also be prepared using methanol as the solvent. Yield of **1b** was 495 mg (58%). Yield of **1c** was 360 mg (48%).

Preparation of [Ru(Pabt)(PPh_3)(1-Meimz)]ClO_4 (**2a**). ***Warning***: Perchlorate salts of metal complexes are potentially explosive [25]. This compound was prepared and purified by reacting Ru(Pabt) (PPh_3)$_2$Cl (**2**) with excess 1-methylimidazole following the procedure used for **1a**. Yield 320 mg (42%).

Preparation of [Ru(Pabt)(PPh_3)(bpy)]Cl · 1.5CH_2Cl_2 (**1d**) *and* [Ru(Pabt)(PPh_3)(phen)]Cl · CH_2Cl_2 (**1e**). To a dichloromethane [40 cm^3] solution of Ru(Pabt) (PPh_3) Cl (**1**) [1.0 mmol], a solution of 10 ml of 2,2′-bipyridine (bpy) and 1,10-phenanthroline (phen) [1.05 mmol] was added and the mixture was refluxed for 7 h. The volume of the resultant solution was reduced to 5 cm^3 in a rotaevaporator and excess petroleum ether was added. The precipitated compound was allowed to settle and then filtered. The residue was stirred with ether twice to remove excess 2,2′-bipyridine/1,10-phenanthroline. It was then filtered and dried over fused $CaCl_2$. Both **1d** and **1e** were recrystallised from degassed CH_2Cl_2. Yield of **1d** was 350 mg (39%). Yield of **1e** was 440 mg (49%).

Preparation of [Ru(Pabt)(PPh_3)(H_2O)$_2$]ClO_4 (**1f**). ***Warning***: Perchlorate salts of metal complexes are potentially explosive [25]. To a methanolic solution 50 cm^3 of Ru(Pabt) (PPh_3)Cl (**1**) [0.5 mmol], aqueous silver perchlorate solution [0.6 mmol in 10 cm^3 H_2O] was added with stirring. The mixture was refluxed with stirring for about 1h, cooled and filtered through a sintered bed funnel (G4) to remove AgCl. The volume of the filtrate was reduced to 10 cm^3 and aqueous $LiClO_4$ solution was added in excess. The compound that separated out was filtered, thoroughly washed with water and dried over fused $CaCl_2$. It was recrystallised from CH_2Cl_2. Yield 370 mg (52%).

RESULTS AND DISCUSSION

The ligand PabtH exists in the benzothiazoline form [26] in the free state and is transformed to the corresponding Schiff base in the presence of either a base or a metal ion (Fig. 1). The complexes **1** and **3** of general formula Ru(Pabt)(PPh_3)X [X = Cl, Br respectively] were isolated by the reaction of Ru (PPh_3)$_3$$X_2$ with the ligand in 1 : 2 molar ratio in refluxing benzene and Ru(Pabt) (PPh_3)$_2$Cl (**2**) was isolated from the filtrate of **1**. When the reaction was carried out in benzene using 1 : 1 molar ratio of the reactants, compound **1** separated out from hot benzene as the only product. When Ru(PPh_3)$_3$$Cl_2$ was reacted with one mole of PabtH in refluxing CH_2Cl_2 **1** was obtained as the sole product, while **3** was isolated as the only product when Ru(PPh_3)$_3$$Br_2$ was used. Molecular weight determination in CH_2Cl_2 [Molecular weight of **1**, Exp. = 601, Calc. = 611.79; **3**, Exp. = 639, Calc = 656.19] clearly indicated the monomeric nature of **1** and **3**. The penta-coordinated complex **1** reacted with excess of different N-donor ligands (imidazole, 1-methylimidazole and 2-methylimidazole) producing hexacoordinated complexes [Ru(Pabt) (PPh_3) (B)$_2$]ClO_4 [where B = imz, 1-Meimz] and also the pentacoordinated species [Ru(Pabt) (PPh_3) (2-Meimz)]ClO_4. Moreover, complex **1** reacted with bidentate N—N donor ligands such as 2,2′-bipyridyl or *o*-phenanthroline in 1 : 1 molar ratio to produce hexacoordinated [Ru(Pabt)(PPh_3)(L—L)]Cl type complexes [where L—L = bipy, *o*-phen]. Another pentacoordinated complex [Ru(Pabt)(PPh_3)(1-Meimz)]ClO_4 (**2a**), was obtained by reacting Ru(Pabt) (PPh_3)$_2$Cl (**2**) with excess 1-Meimz in CH_2Cl_2 and subsequent treatment with a concentrated aqueous $LiClO_4$ solution. The aquo complex **1f** was prepared by Cl^- abstraction from Ru(Pabt)(PPh_3)Cl using $AgClO_4$ in methanol solution. For convenience the different synthetic routes for the preparation of various ruthenium complexes are summarised in Equation I. The compounds gave satisfactory analytical results (Table 1) which are in good agreement with the assigned formulation. The formula of compounds **1a**, **1c** and **2a** were also checked by {^{1}H}NMR spectrum using the integration ratio of the methyl proton signal to those of the residual proton signals. The conductance data (Table 1) also supports the proposed formulation of the compounds **1a–1f** and **2a** as 1 : 1 electrolytes [27] with their anion Cl^- or ClO_4^- not participating in coordination. However compound **1**, **2** and **3** are nonelectrolytes and hence contain coordinated halide. This is supported by the presence of the ν(Ru—Cl) bands in their IR spectra (*vide infra*). The diamagnetic nature of all the complexes suggests the presence of the +2 oxidation state of ruthenium. The complexes (**1a–1f, 2a**) are highly soluble in common organic solvents. The complexes **1**, **2** and **3** are moderately soluble in CH_3CN, but fairly soluble in CH_2Cl_2.

Infrared spectroscopy

The ligand PabtH exhibits a strong band at 3190 cm^{-1} due to ν(N—H) vibration [15], which is absent

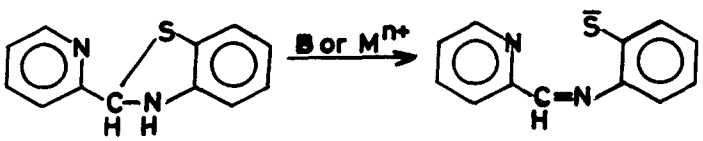


Fig. 1. Metal/base induced conversion of Pabt.

Table 1. Analytical and physical data for the ruthenium complexes

Complex	Colour	Molar Conductance[a] (ohm^{-1} cm^2 mol^{-1})	Analysis Found (Calc.)% X	C	H	N
1. $Ru(Pabt)(PPh_3)Cl$	Brown	81	5.4 (5.8)	58.5 (58.8)	4.0 (3.9)	4.6 (4.6)
2. $Ru(Pabt)(PPh_3)_2Cl$	Violet	79	3.6 (4.1)	65.4 (65.9)	4.4 (4.5)	3.5 (3.2)
3. $Ru(Pabt)(PPh_3)Br$	Brown	74	11.7 (12.2)	54.5 (54.9)	4.2 (4.3)	3.7 (3.7)
1a. $[Ru(Pabt)(PPh_3)(1\text{-Meimz})_2]ClO_4 \cdot 1.5\,CH_2Cl_2$	Violet	145	- -	49.3 (49.0)	3.9 (4.0)	8.4 (8.7)
1b. $[Ru(Pabt)(PPh_3)(imz)_2]ClO_4 \cdot 0.5CH_2Cl_2$	Dark Violet	138	—	51.7 (51.3)	3.9 (3.9)	9.5 (9.8)
1c. $[Ru(Pabt)(PPh_3)(2\text{-Meimz})]ClO_4$	Dark Violet	124	—	53.7 (53.8)	3.9 (4.0)	7.2 (7.4)
1d. $[Ru(Pabt)(PPh_3)(bpy)]Cl \cdot 1.5CH_2Cl_2$	Violet	132	3.6 (4.0)	55.5 (55.6)	3.7 (3.9)	6.0 (6.2)
1e. $[Ru(Pabt)(PPh_3)(Phen)]Cl \cdot CH_2Cl_2$	Dark Violet	118	3.8 (4.1)	58.5 (58.8)	4.0 (3.9)	6.6 (6.4)
1f. $[Ru(Pabt)(PPh_3)(H_2O)_2]ClO_4$	Dark Violet	127	—	51.0 (50.6)	3.8 (3.9)	4.2 (3.9)
2a. $[Ru(Pabt)(PPh_3)(1\text{-Meimz})]ClO_4$	Violet	128	—	54.2 (53.8)	4.1 (4.0)	7.6 (7.4)

[a] = MeCN, X = Cl or Br

in the complexes **1, 2** and **3**. This strongly suggests that the ligand is present in its Schiff base form, in which it is known [26] to act as a monoanionic tridentate ligand coordinating through pyridine N, imine N and thiolato S. In the spectra of the mixed ligand complexes **1a–1e** and **2a,** there seems to be extensive mixing between the bands of the main ligand (Pabt) and those of the coligand bases. This makes precise assignment of the individual vibrations to definite vibrational modes very difficult. However, absence of any band at 2400–2500 cm^{-1} due to ν(S—H) in all these complexes indicates that the ligand is coordinated to the metal through the thiolato sulfur [28]. A medium intensity band at 1585 cm^{-1} assigned to ν(CN) vibration in the ligand is red shifted by $\sim$40 cm^{-1} in the complexes due to coordination [9,29] of the azomethine nitrogen to the Ru^{II} centre. The ν(CS) band present at 750 cm^{-1} in the ligand is lowered by $\sim$5 cm^{-1} on complexation and indicates M—S bond formation [30]. The pyridine ring vibration at 620 cm^{-1} and 420 cm^{-1} are blue shifted by *ca* 10 cm^{-1} because of the coordination through the pyridine ring nitrogen. In addition, the presence of a broad band around 1100 cm^{-1} in the IR spectra of the complexes **1a–1c, 1f** and **2a** indicates that ionic ClO_4^- is present in these complexes [9]. The band at 300 cm^{-1} and 320 cm^{-1} in complexes **1** and **2** respectively can be assigned as ν(Ru—Cl) band [8, 31]. However, we could not detect the ν(Ru—Br) for the compound **3** up to 300 cm^{-1}, which is the detection limit of our instrument.

$\{^1H\}$NMR spectroscopy

The $\{^1H\}$NMR spectra of the ligand PabtH exhibits a signal at 5.12 ppm which is assigned to the N—H proton and is confirmed by D_2O exchange experiment. The complexes **1, 2** and **3** do not exhibit the characteristic N—H proton signal and indicate that in the metal complexes the ligand is present in its deprotonated form of the Schiff base. All the complexes exhibit proton signals in the aromatic region 6.8–7.6 ppm, which cannot be properly assigned due to overlap of corresponding signals of PPh_3 and the ligands. The compound $[Ru(Pabt)(PPh_3)(1\text{-Meimz})_2]ClO_4$ (**1a**) in $CDCl_3$ exhibits two methyl signals of almost equal intensity at 3.51 ppm and 3.66 ppm indicating *cis* disposition of the two coordinated 1-methylimidazoles. The complex **2a** which contains only one 1-Meimz moiety, exhibits two signals of equal intensity (in $CDCl_3$) at 3.50 ppm and 3.63 ppm, whose combined integration corresponds to one methyl proton. This may indicate that two isomers of square pyramidal geometry (*vide infra*) coexists in solution.

Electronic spectroscopy

The electronic spectrum of 2-(2-pyridyl) benzothiazoline consists of three bands at 232, 255 and 310 nm, characteristic of the cyclic form. These may be attributed to the σ–σ^*, π–π^* and n–π^* benzenoid transitions [32]. All the complexes exhibit rich electronic spectra (Table 2) characteristic of the

Table 2. Electronic spectral data for the ruthenium complexes

Complex	Bands λ_{max} (nm) [ε ($dm^3\ mol^{-1}\ cm^{-1}$)] Solvent CH_3CN	Solvent CH_2Cl_2	Nujol mull spectra
1. $Ru(Pabt)(PPh_3)Cl$	523(b)(2012), 466(b)(2468) 343(sh)(10,934), 322(14,150) 276(sh)(12,298), 222(48,224)	522(2878), 355(sh)(8080), 328(sh)(13,343), 276(12,626) 246(sh)(27,090), 233(34,565)	
2. $Ru(Pabt)(PPh_3)_2Cl$	537(sh)(>1844), 453(>3926) 351(sh)(>11,685), 306(>17,111) 276(sh)(>22,035), 226(>69,092)	522(1958), 326(9958) 274(20,021), 230(37,687)	541, 331(sh), 280
3. $Ru(Pabt)(PPh_3)Br$	520(b)(1395), 456(2120) 347(sh)(8594), 321(11,763) 240(25,000)	520(2076), 352(sh)(6939) 332(10,279), 252(sh)(23,336) 230(30,105)	
1a. $[Ru(Pabt)(PPh_3)(1\text{-}Meimz)_2]\ ClO_4 \cdot 1.5CH_2Cl_2$	521(b)(2837), 434(4293) 314(19,353), 275(14,100) 223(56,109)	524(sh)(2621), 442(3654), 318(16,934), 275(sh)(12,595), 232(39,745)	534, 439, 318
1b. $[Ru(Pabt)(PPh_3)(imz)_2]\ ClO_4 \cdot 0.5CH_2Cl_2$	504(b)(3503), 355(sh)(9312), 323(18,777), 275(12,968) 221(57,775)	526(b)(3474), 356(sh)(9069) 328(16,552), 275(sh)(11,715) 231(41,095)	548, 352, 243
1c. $[Ru(Pabt)(PPh_3)(2\text{-}Meimz)]ClO_4$	480(b)(2229), 352(sh)(8077) 318(11,437), 271(sh)(9375), 226(34,854)	493(2946), 356(sh)(8492), 325(12,969), 274(sh)(11,201) 231(30,575)	497, 336, 276(sh)
1d. $[Ru(Pabt)(PPh_3)(bpy)]Cl \cdot 1.5CH_2Cl_2$	502(3909), 362(sh)(12,040) 332(19,702), 307(sh)(17,351) 235(49,646)	503(3601), 353(sh)(10,979) 327(17,313), 298(sh)(14,645) 247(sh)(28,451)230(39,683)	
1e. $[Ru(Pabt)(PPh_3)(phen)]Cl \cdot CH_2Cl_2$	486(b,sh)(3921), 426(b) (4690), 351(sh)(8996), 322(sh)(14,071), 291(sh) (18,065), 265(sh)(39,721), 224(82,173)	497(4210), 427(5152), 355(sh)(9529), 333(sh)(14,088) 319(15,380), 292(sh)(19,759) 268(42,188), 232(67,219)	
1f. $[Ru(Pabt)(PPh_3)(H_2O)_2]ClO_4$	477(b)(2026), 351(sh)(7978) 315(10,873), 273(sh)(11,070) 222(sh)(35,175), 211(43,275)	493(b)(1948), 357(sh)(7431) 322(9968), 274(sh)(10,485), 230(24,537)	490(b) 399, 262(sh)
2a. $[Ru(Pabt)(PPh_3)(1\text{-}Meimz)]ClO_4$	515(b)(2569), 351(sh)(8284) 319(14,103), 273(sh)(11,485) 223(50,319)	532(2632), 357(sh)(6638), 321(12,790), 274(sh)(10,515) 231(36,137)	530, 307(sh), 266

b = broad, sh = shoulder

complexes of Pabt with other metals [15]. However, correct assignment of the bands is difficult without detailed analysis. In the UV-visible region there are generally two bands near 460–550 nm and 350–450 nm regions. The high extinction coefficient of the bands indicate that they are mainly of charge transfer origin. Among them, the lower energy band is probably due to a MLCT transition from the Ru^{II} centre to the Pabt ligand. This is supported by the fact that the plot (Fig. 4(a) and Fig. 4(b)) of $E_{Ru^{III}/Ru^{II}}$ (*vide infra*) *vs* the above MLCT transition expressed in eV gives a straight line, as has been observed for similar systems [5,33]. However, for bipyridine and orthophenanthroline complexes the above assignments are not unambiguous as transitions from Ru^{II} $d\pi$ to π^* of bpy or phen occur in the same region [33]. The band at 220–325 nm region is due to intraligand transitions.

Proposed structure of the complexes

The complexes Ru(Pabt)(PPh_3)X [X = Cl (**1**) and X = Br (**3**)] are five-coordinated and probably square pyramidal. The five-coordinated nature of these complexes is supported by the molecular weight determination of Ru(Pabt) (PPh_3)Cl. TG-DTA traces clearly exhibit the absence of any water or solvent molecule in the complexes. The formation of such five-coordinated square pyramidal complexes is supported by Sellmann's work on a series of complexes of sulfur and nitrogen-sulfur donors. Sellmann reported the reaction of [Ru(PPh_3)$_2$(dttd)] and [Ru(PPh_3)$_2$(bmae)] [where dttd$^{2(-)}$ = 2,3,8,9-dibenzo-1,4,7,10-tetrathiadecane(−2), bmae$^{2(-)}$ = 1,2-bis(2-mercaptoanilino)ethane(−2)] with CO proceeds through the unsaturated 5-coordinated intermediate [3,34]. Moreover, he succeeded in isolating the distorted square pyramidal [Ru(^{bu}bmae)]$_2$ [where ^{bu}bmae$^{2(-)}$ = 1,2-bis(2-mercapto-3,5-di-^{t}butyl-anilino)ethane (2−)] having a vacant coordination site [35]. The formation of stable five-coordinated complexes **1** and **3** and lability of the six-coordinated complex **2** [to form five-coordinated **2a**] is probably due to the stabilisation of five-coordinated 16 electron species through $p\pi$ donation by sulfur as suggested by Sellmann [3,34,35].

It has also been proposed that complexes of five-coordinated d^6 ions are best classified as square-pyramidal [36] which is in agreement with the second-order Jahn–Teller effect [37,38]. This view, taken along with the fact that most of the reported five-coordinated complexes of ruthenium are square pyramidal with varying degree of distortions, has induced us to propose that the five-coordinated complexes reported in this study also possess square pyramidal coordination geometry. As the ligand (Pabt) is planar [25] due to conjugation of all the atoms present, two isomeric arrangements are possible for the square pyramidal geometry (Fig. 2). Among these two possibilities, isomer "**a**" containing PPh_3 in axial position is expected to be more stable, both from steric as well as electronic point of view. The isomer "**b**" may be stabilised from the agostic interaction of H atom from the PPh_3 ligand [39] which is known to stabilise Ru(PPh_3)$_3$Cl$_2$. Formation of **1a, 1b, 1d** and **1e** can then be easily explained by replacement of equatorial X and occupation of the vacant axial position by two N donor atoms of two imidazoles or a bipyridyl/phenanthroline.

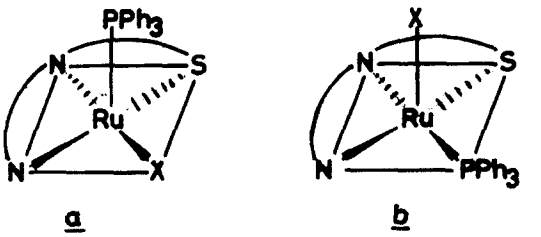


Fig. 2. Two possible isomeric arrangements of Ru(Pabt)(PPh_3)Cl (**1**)

The structure of six-coordinated complexes [Ru(pabt) (PPh_3)$_2$Cl] (**2**) is established by $\{^{31}P\}$NMR spectrum in $CDCl_3$, which exhibits a single sharp peak at 20.2 ppm indicating that the two PPh_3 groups are trans to each other [40]. Thus the square plane is occupied by the ligand Pabt and a chloride (Fig. 3(a)).

The probable structure of the complex [Ru(pabt) (PPh_3)(2-Meimz)]ClO_4 (**1c**) is shown in (Fig. 3(b)). Molecular model shows that the CH_3^- group on the ligated 2-Meimz sterically restricts the access of a second 2-Meimz at the vacant sixth position of Ru.

Cyclic voltammetry. The electron transfer behaviour of all the complexes has been examined in dichloromethane and acetonitrile solvents, containing 0.1 M TEAP using cyclic voltammetric technique (scan rate 200 mV s^{-1}). The results are summarised in Table 3.

The complexes exhibit reversible oxidative responses in the potential range 0.3–1.0 V. The compound **1** exhibits a one electron anodic wave at a $E_{1/2}$ of 0.40 V *vs* SCE in both the solvents which corresponds to the process (**I**).

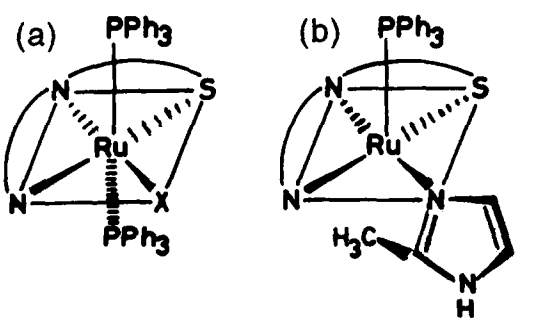


Fig. 3. (a) Possible structure of Ru(Pabt)(PPh_3)$_2$Cl (**2**); (b) Possible structure of [Ru(Pabt)(PPh_3)(2-Meimz)]ClO_4 (**1c**).

Table 3. Cyclic voltammetric results for [a,b] Ru^{II} complexes in 0.1 M TEAP at 298 K

Complex	In CH_2Cl_2 $E_{1/2}$, V[ΔE_p(mV)]	In CH_3CN $E_{1/2}$, V[ΔE_p(mV)]
1. Ru(Pabt) $(PPh_3)Cl$	0.40(70), 0.19(60)[c]	0.40(60), 0.14(75)[c]
2. Ru(Pabt) $(PPh_3)_2Cl$	−0.08(60), 0.65(69)	−0.07(60), 0.62(68)
3. Ru(Pabt) $(PPh_3)Br$	0.44(60), 0.21(50)[c]	E_{pa} = 0.66[d]
1a. [Ru(Pabt) (PPh_3) (1-Meimz)$_2$]$ClO_4 \cdot 1.5\ CH_2Cl_2$	0.75(62)	0.74(81)
1b. [Ru(Pabt) (PPh_3) (imz)$_2$]$ClO_4 \cdot 0.5CH_2Cl_2$	0.76(100)	0.74(63)
1c. Ru(Pabt) (PPh_3) (2-Meimz)]ClO_4	0.85(60), 0.52[c]	1.02(125)
1d. [Ru(Pabt) (PPh_3) (bpy)]$Cl \cdot 1.5CH_2Cl_2$	0.90(70)	0.96(76)
1e. [Ru(Pabt) (PPh_3) (phen)]$Cl \cdot CH_2Cl_2$	1.03(125)	0.98(118)
1f. [Ru(Pabt) (PPh_3) $(H_2O)_2$]ClO_4	E_{pa} = 0.94	1.00(80)
2a. [Ru(Pabt) (PPh_3) (1-Meimz)]ClO_4	0.72(62), 0.31[c]	0.70(75)

[a]Working electrode platinum; reference electrode SCE; $E_{1/2} = 0.5\ (E_{pa} + E_{pc})$; $\Delta E_{pc} = E_{pc} - E_{pa}$, where E_{pa} and E_{pc} are anodic and cathodic peak potentials, respectively.

[b]Supporting electrolyte 0.1 M TEAP, solute concentration $\sim 10^{-3}$ M, scan rate 200 $mV^{-1}s^{-1}$.

[c]Supporting electrolyte TEACl (0.1 M).

[d]Corresponding cathodic wave E_{pc} = 0.45 V.

$$Ru(NNS^-)(PPh_3)Cl \underset{+e}{\overset{-e}{\rightleftharpoons}} [Ru^{III}(NNS^-)(PPh_3)Cl]^+. \quad \textbf{(I)}$$

This assignment is justified by the fact that, when compound **1** is oxidised chemically with iodine in dichloromethane solution, the EPR spectrum of the oxidised species at 77 K is found to be highly anisotropic. It is known that Ru^{III} compounds give rise to highly anisotropic EPR spectra [23]. The g values ($g_1 = 2.12$, $g_2 = 2.29$ and $g_3 = 2.59$), as well as a large separation of 530 G between the lowest and highest field peak indicates that the unpaired electron is predominantly metal centred [41]. So the above oxidation involves a metal based redox orbital. Complex **3**, the bromo analogue of **1**, exhibits a peak at $E_{1/2}$ = 0.44 V in dichloromethane, which is consistent with a reaction similar to the one described by process (**I**). But when compound **3** is scanned in MeCN it reveals an irreversible anodic wave at E_{pa} = 0.66 V. The anodic shift of this peak is probably due to the solvent participation [42].

When the scanning is extended to higher positive potentials, it reveals ill-defined peaks which may be due to ligand oxidation or can be attributed to oxidation of triphenyl phosphine [43].

When the voltammogram of **1** is run in dichloromethane with TEACL as the supporting electrolyte a cathodic shift of the anodic peak is observed (Table 3). The negative shift of the first anodic peak ($E_{1/2}$ = 0.19 V) can be explained considering direct coordination of Cl ion to the metal centre of the coordinatively unsaturated complex, prior to its participation in electrolysis [19]. The involvement of the Cl facilitates the oxidation of the complex by decreasing the overall positive charge of the complex ion [process (**II**)].

$$Ru^{II}(NNS^-)(PPh_3)Cl \underset{-Cl^-}{\overset{+Cl^-}{\rightleftharpoons}} [Ru^{II}(NNS^-)(PPh_3)Cl_2] \underset{+e}{\overset{-e,0.19}{\rightleftharpoons}} Ru^{III}(NNS^-)(PPh_3)Cl. \quad \textbf{(II)}$$

The corresponding bromo complex **3** exhibits similar behaviour. The five coordinated complexes **1c** and **2a** similarly display cathodically shifted oxidation waves in dichloromethane when TEACL used as supporting electrolyte.

The six-coordinated complex **2** displays an anodic wave at 0.63 V. Here, due to the presence of additional PPh_3 in the sixth position, Ru^{III}/Ru^{II} potentials are anodically shifted [44]. This happens because the presence of an extra PPh_3 results in a HOMO with different energy. The reductive couple at −0.08 V of same current height may be due to Ru^{II}/Ru^{I} reduction as reported earlier [45].

As expected, the $E_{1/2}$ values of the cationic complexes (**1a–1f**) and **2a** are more positive compared to the neutral [46] parent complexes **1** and **3**. The one-electron change of the complexes **1d** and **1e** was checked coulometrically [for **1d** n = 0.98 (1.15 V); for **1e** n = 1.03 (1.15 V)]. It is obvious that in all the complexes the oxidation potential values in CH_2Cl_2 are greater than those in MeCN, due to the difference in solvent polarity.

During the cyclic voltammetric study of the complex **1e** in acetonitrile solution using TEAP as the supporting electrolyte, attention was drawn to an interesting observation. Gradual addition of PPh_3 to the solution of the complexes caused an increase in the i_{pa}/i_{pc} value at 0.98 V accompanied by a small anodic shift. This may happen due to the interaction between **1e** or its oxidised species with PPh_3, the latter

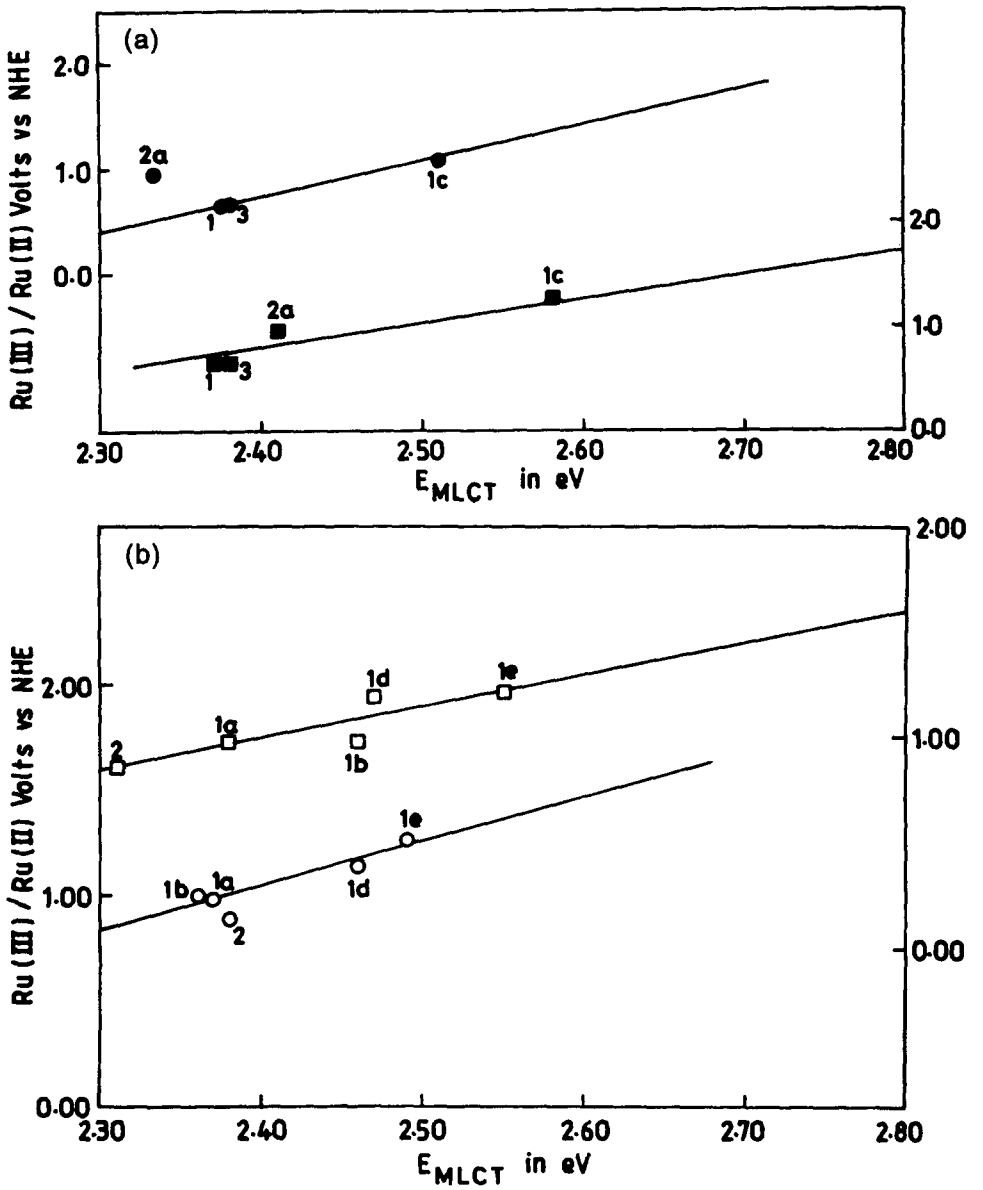


Fig. 4. Plots of observed Ru^{III}/Ru^{II} potentials ($E_{1/2}$) against the energy of the metal-to-ligand charge transfer transition (E_{MLCT}) of (a) six-coordinated complexes: (bottom, open circles) measured in CH_2Cl_2 and referred to left-hand y-axis; (top, open square) measured in CH_3CN and referred to right-hand y-axis. All data are *vs* NHE (1 V *vs* SCE = 1.242 V *vs* NHE); (b) five-coordinated complexes: (top, closed circles) measured in CH_2Cl_2 and referred to left-hand y-axis; (bottom, closed square) measured in CH_3CN and referred to right hand y-axis. All data are *vs* NHE (1 V *vs* SCE = 1.242 V *vs* NHE).

undergoing catalytic oxidation. The complex **1d** also behaves similarly. Similar observations were made in dichloromethane solution. Such observations were recorded previously for electrochemical reduction of molybdenum complexes [47–49].

It is possible to compare the observed $E_{1/2}$ values of Ru^{III}/Ru^{II} couples of the six-coordinated complexes with that calculated according to the linear relation given by Lever in organic solvents, based on his electrochemical ligand parameter E_L [50]. Two least-square lines (Fig. 5) obtained are as follows: dichloromethane: $E_{Ru^{III/II}} = 0.73\,[\Sigma E_L] + 0.30$; acetonitrile: $E_{Ru^{III/II}} = 0.80[\Sigma E_L] + 0.22$.

This linear correlation of $E_{1/2}$ values with ΣE_L parameter suggests that the assignment of $E_{1/2}$ values for Ru^{III}/Ru^{II} couples in these complexes are self-consistent and there are no synergic interactions between the metal and the ligand.

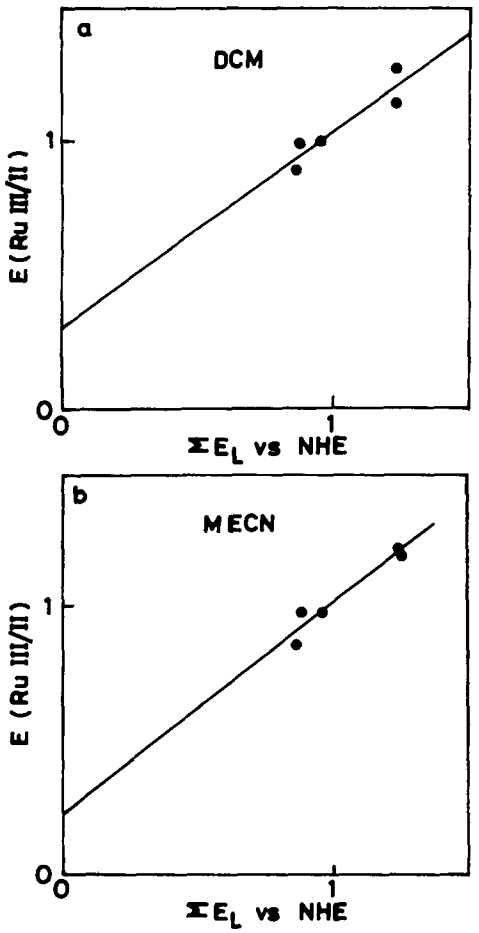


Fig. 5. Plot of observed Ru^{III}/Ru^{II} potentials against ΣE_L of six-coordinated complexes (a) measured in CH_2Cl_2, (b) measured in CH_3CN. All data are *vs* NHE (1 V *vs* SCE = 1.242 V *vs* NHE). Taking $E_{Pabt} = 0.33$, calculated from Lever's equation [50].

REFERENCES

1. P. M. Harisson, *Metalloproteins (part 1), Metal proteins with Redox Roles.* Verlag Chemie, Weinheim, FRG (1985).
2. A. Muller and B. Krebs, *Sulfur, its significance for Chemistry, for the Geo-, Bio-, and Cosmosphere and Technology; Studies in Inorganic Chemistry*, Vol. 5. Elsevier Science Publishers B. V. Amsterdam (1984).
3. D. Sellmann and O. Käppler, *Angew Chem. Int. Ed. Eng.* 1988, **27,** 689.
4. M. A. Greaney, C. L. Coyle, M. A. Harmer, A. Jordan and E. I. Stiefel, *Inorg. Chem.* 1989, **28,** 912.
5. S. R. Fletcher and A. C. Spaski, *J. Chem. Soc., Dalton Trans.* 1972, 635.
6. P. Mura, B. G. Olby and S. D. Robinson, *J. Chem. Soc., Dalton Trans.* 1985, 2101.
7. A. K. Mahapatra, S. Datta, S. Goswami, M. Mukherjee, A. K. Mukherjee and A. Chakravorty, *Inorg. Chem.* 1986, **25,** 1715.
8. S. K. Chattopadhyay and S. Ghosh, *Inorg. Chim. Acta* 1987, **131,** 15.
9. S. K. Chattopadhyay and S. Ghosh, *Inorg. Chim. Acta* 1989, **163,** 245.
10. S. A. Koch, *J. Am. Chem. Soc.* 1983, **105,** 3362.
11. H. J. Kruger and R. H. Holm, *Inorg. Chem.* 1989, **28,** 1148.
12. H. J. Kruger, Gang Peng and R. H. Holm, *Inorg. Chem.* 1991, **30,** 734.
13. A. P. Koley, S. Purohit, S. Ghosh, L. S. Prasad and P. T. Manoharan, *J. Chem. Soc., Dalton Trans.* 1988, 2607.
14. A. P. Koley, S. Purohit, L. S. Prasad, S. Ghosh, and P. T. Manoharan, *Inorg. Chem.* 1992, **31,** 305.
15. A. P. Koley, R. Nirmala, L. S. Prasad, S. Ghosh and P. T. Manoharan, *Inorg. Chem.* 1992, **31,** 1764.
16. D. Sellmann, W. Ludwig, G. Huttner, L. Zsolnai, *J. Organomet. Chem.* 1985, **294,** 199.
17. C. E. Forbes, A. Gold and R. H. Holm. *Inorg. Chem.* 1971, **10,** 2479.
18. S. I. Shupack., E. Billig, R. J. H. Clark, R. Williams and H. B. Gray, *J. Am. Chem. Soc.* 1964, **86,** 4594.
19. S. Purohit, A. P. Koley, L. S. Prasad, P. T. Manoharan and S. Ghosh, *Inorg. Chem.* 1989, **28,** 3735.
20. A. I. Vogel, *Quantitative Inorganic Analysis*, 3rd edn. ELBS, Longman, London (1962).
21. T. A. Stephenson and G. Wilkinson, *J. Inorg. Nucl. Chem.* 1966, **28,** 945.
22. P. S. Hallman, T. A. Stephenson and G. Wilkinson, *Inorg. Synth.* 1970, **12,** 237.
23. G. K. Lahiri, S. Bhattacharya, B. K. Ghosh and A. Chakravorty, *Inorg. Chem.* 1987, **26,** 4324.
24. D. T. Sawyer, J. L. Roberts, *Experimental Electrochemistry for Chemists*, p. 212. Wiley, New York (1974).
25. *Chem. Eng. News* 1983, **61** (Dec. 5) 4.
26. L. F. Lindoy and S. E. Livingstone, *Inorg. Chem.* 1968, **7,** 1149.
27. W. J. Geary, *Coord. Chem. Rev.* 1971, **7,** 81.
28. N. B. Colthup, L. H. Daly and S. E. Wiberley, *Introduction to Infrared and Raman Spectroscopy.* Academic Press, New York (1964).
29. M. J. Campbell, R. Grzeskowiak and R. Thomas, *Spectrochim. Acta* 1976, **32A,** 556.
30. G. J. Sutton, *Aust. J. Chem.* 1963, **16,** 1137.
31. J. D. Gilbert, D. Rose and G. Wilkinson, *J. Chem. Soc., (A)* 1970, 2765.
32. N. Kanoongo, R. V. Singh, J. P. Tandon and R. B. Goyal, *J. Inorg. Biochem.* 1990, **38,** 57.
33. M. Akbar Ali, S. E. Livingstone, *Coord. Chem. Rev.* 1974, **13,** 101.
34. D. Sellmann, U. Reineke, G. Huttner and L. Zsolnai, *J. Organomet. Chem.* 1986, **310,** 83.
35. D. Sellmann, O. Käppler and F. Knoch, *J. Organomet. Chem.* 1989, **367,** 161.
36. P. R. Hoffman and K. G. Caulton, *J. Am. Chem. Soc.* 1975, **97,** 4221.
37. R. G. Pearson, *J. Am. Chem. Soc.* 1969, **91,** 4947.
38. A. R. Rossi and R. Hoffmann, *Inorg. Chem.* 1975, **14,** 365.
39. S. J. LaPlaca and J. A. Ibers, *Inorg. Chem.* 1965, **4,** 778.

40. M. A. M. Queiros and S. D. Robinson, *Inorg. Chem.* 1978, **17,** 310.
41. D. E. Morris, Y. Ohsawa, D. P. Segers, M. K. Dearmond and K. W. Hanck, *Inorg. Chem.* 1984, **23,** 3010.
42. S. H. Wheeler, B. M. Mattson, G. L. Miessler and L. H. Pignolet, *Inorg. Chem.* 1978, **17,** 340.
43. G. Schiavon, S. Zecchin, G. Cogoni and G. Bontempelli, *J. Electroanal. Chem.* 1973, **48,** 425.
44. W. S. Sheldrick and R. Exner, *Inorg. Chim. Acta* 1992, **195,** 1.
45. J. Amarasekera, T. B. Rauchfuss and S. R. Wilson, *Inorg. Chem.* 1987, **26,** 3328.
46. M. J. Root, B. P. Sullivan, T. J. Meyer and E. Deutsch, *Inorg. Chem.* 1985, **24,** 2731.
47. A. F. Isbell, Jr and D. T. Sawyer, *Inorg. Chem.* 1971, **10,** 2449.
48. L. J. De Hayes, H. C. Faulkner, W. H. Doub, Jr and D. T. Sawyer, *Inorg. Chem.* 1975, **14,** 2110.
49. O. A. Rajan and A. Chakravorty, *Inorg. Chem.* 1981, **20,** 660.
50. A. B. P. Lever, *Inorg. Chem.* 1990, **29,** 1271.

Pergamon

PII: S0277-5387(96)00499-8

Polyhedron Vol. 16, No. 11, pp. 1803–1809, 1997
© 1997 Elsevier Science Ltd
All rights reserved. Printed in Great Britain
0277-5387/97 $17.00+0.00

Chemistry of a transition metal cluster substituted carboxylic acid: synthesis and structure of $Cd_2\{(CO)_9Co_3(\mu_3\text{-}CCO_2)\}_4[CH_3(OCH_2CH_2)_4OCH_3]$

Xinjian Lei, Maoyu Shang and Thomas P. Fehlner*

Department of Chemistry and Biochemistry, University of Notre Dame, IN 46556, U.S.A.

(Received 17 June 1996; accepted 9 October 1996)

Abstract—The reaction of the cluster substituted carboxylic acid $[(CO)_9Co_3(\mu_3\text{-}CCO_2H)]$ with $Cd(CH_3CO_2)_2 \cdot H_2O$ in the presence of tetraethylene glycol dimethyl ether(TGM) afforded the binuclear complex $[Cd_2\{(CO)_9Co_3(\mu_3\text{-}CCO_2)\}_4(TGM)]$. The solid state structure shows that the cluster carboxylate ligands act as chelating and asymmetrical bridging ligands, respectively, and the TGM ligand exhibits a conformation not previously observed. The coordination number of each cadmium atom is seven, resulting in a coordination geometry consisting of a distorted trigonal capped square-based polyhedron. © 1997 Elsevier Science Ltd. All rights reserved.

Keywords: cadmium carboxylate; cobalt cluster; polyether ligand.

We are interested in defining the properties of a transition metal cluster as a substituent and have incorporated this interest in a strategy for the synthesis of large cluster arrays. Thus, by using the transition metal cluster substituted carboxylic acid $[(CO)_9Co_3(\mu_3\text{-}CCO_2H)]$ in an exchange reaction with metal acetates, [1,2] in a reaction with metal alkyls,[3–6] and in a reaction with metal alkoxides,[7] a number of compounds with new structure types and unusual properties were isolated. For example, $[Pb\{(CO)_9Co_3(\mu_3\text{-}CCO_2)\}_2]_n$ resulted from the reaction of $Pb(CH_3CO_2)_2 \cdot 3H_2O$ and $(CO)_9Co_3(\mu_3\text{-}CCO_2H)$,[2] $Zn_4O\{(CO)_9Co_3(\mu_3\text{-}CCO_2)\}_6$, from the reaction of $ZnEt_2$ and $(CO)_9Co_3(\mu_3\text{-}CCO_2H)$,[3,6] and $[Ti_6(\mu_3\text{-}O)_4(\mu\text{-}OEt)_4(OEt)_8\{(CO)_9Co_3(\mu_3\text{-}CCO_2)\}_4]$ from the reaction of $Ti(OEt)_4$ with $(CO)_9Co_3(\mu_3\text{-}CCO_2H)$ [7]. In these cases the chemistry is straightforward, i.e. the cluster functions like an organic substituent albeit with different properties. In other cases, the fragile nature of metal clusters yields unexpected products. For example, heating a reaction mixture of $CdMe_2$ and $(CO)_9Co_3(\mu_3\text{-}CCO_2H)$ gave rise to $[\{\mu_3\text{-}Co(CO)_3\}Cd_3\{(CO)_9Co_3(\mu_3\text{-}CCO_2)\}_3(THF)_3]$ [4].

The structural chemistry of cadmium carboxylates is separately of interest because of the various coordination geometries of cadmium and coordination modes of carboxylate groups. The structures of mono cadmium carboxylates are almost all three-dimensional polymeric species with Cd coordination numbers of up to eight and in which the carboxylate groups act in both chelating and bridging modes [8,9]. As noted, the structurally characterized compound isolated from the reaction of $CdMe_2$ with $(CO)_9Co_3(\mu_3\text{-}CCO_2H)$ [4] was not the simple cluster cadmium carboxylate expected, i.e., $Cd\{(CO)_9Co_3(\mu_3\text{-}CCO_2)\}_2 \cdot n\text{-}THF$, and an alternative pathway was investigated. The reaction of $Cd(CH_3CO_2)_2 \cdot H_2O$ and $(CO)_9Co_3(\mu_3\text{-}CCO_2H)$ has now been explored and in this paper we report a cluster cadmium complex $Cd_2\{(CO)_9Co_3(\mu_3\text{-}CCO_2)\}_4[CH_3(OCH_2CH_2)_4OCH_3]$, **1**, which contains asymmetrical bridging and chelating cluster carboxylate ligands, as well as a linear polyether ligand, tetraethylene glycol dimethyl ether (TGM).

*Author to whom correspondence should be addressed.

EXPERIMENTAL

All operations were conducted under dinitrogen using standard Schlenk techniques. Solvents were distilled before use from drying agents under N_2 as described below: sodium benzophenone ketyl for hexane and tetrahydrofuran; P_2O_5 for CH_2Cl_2. $(CO)_9Co_3(\mu_3\text{-}CCO_2H)$ was prepared according to the literature methods [6,10]. $Cd(CH_3CO_2)_2 \cdot H_2O$ and tetraethylene glycol dimethyl ether(TGM) were used directly as received from Aldrich. FT-IR was measured on a Nicolet 205 spectrometer. Elemental analyses were performed by M-H-W Laboratories, Phoenix, AZ.

Synthesis of $Cd_2\{(CO)_9Co_3(\mu_3\text{-}CCO_2)\}_4(TGM)$

In a typical procedure, $Cd(CH_3CO_2)_2 \cdot H_2O$ (0.2 mmol; 0.066 g) and $(CO)_9Co_3(\mu_3\text{-}CCO_2H)$ (0.4 mmol; 0.194 g) were loaded into a 100 cm^3 Schlenk flask equipped with a rubber septum and a magnetic stirring bar. This flask had been evacuated and refilled with dinitrogen several times before 15 cm^3 of THF was added to the flask *via* syringe with rapid stirring. The reaction mixture was stirred for 20 h at room temperature to give a purple solution. THF was removed *in vacuo*. The solid obtained was dissolved in 10 cm^3 of THF and to the solution was added 0.05 cm^3 (0.2 mmol) of TGM. The mixture was stirred for 10 h to give a purple solution and then the THF was removed *in vacuo*. The solid obtained was dissolved in 15 cm^3 of CH_2Cl_2 and the purple solution was layered by hexane. After several days, black block-like crystals appeared on the upper wall of the flask. The yield is 10% based on Co.

Spectroscopic and analytical data for $Cd_2\{(CO)_9Co_3(\mu_3\text{-}CCO_2)\}_4(TGM)$. Found: C, 27.3; H, 1.0. Calc. for $Cd_2Co_{12}O_{49}C_{54}H_{22}$: C, 27.2; H, 0.93%. IR(KBr, cm^{-1}): 2106 m, 2047 vs,br, 1537 m,sh, 1531 m, 1373 m, 1344 w,sh, 1092 w, 782 m, 765 w, 701 m, 552 m, 529 m, 502 v, 407 w.

Crystal structure

A black block-like crystal was mounted on the top of a glass fiber and data were collected on an Enraf-Nonius CAD4 diffractometer equipped with graphite crystal monochromated Mo-K_α radiation at room temperature. The data were corrected for Lorentz and polarization effects, and linear decay. And an empirical absorption correction was also applied. The structure was solved by the MULTAN direct method followed by successive difference Fourier syntheses. Full-matrix least-squares refinements were employed. All non-hydrogen atoms were refined with anisotropic thermal parameters in the final cycle, $R = 0.03678$, $R_w = 0.04314$, and GOF = 1.265 (528 variables refined) for 3466 reflections with $F_0^2 > 3\sigma(F_0^2)$. The detailed crystallographic data are given in Table 1.

RESULTS AND DISCUSSION

Synthetic studies

The reaction of $Cd(CH_3CO_2)_2 \cdot H_2O$ and $[(CO)_9Co_3(\mu_3\text{-}CCO_2H]$ in THF gave rise to a red–brown solid after the THF was removed *in vacuo*. According to the solid state IR (KBr, cm^{-1}: 2107 m, 2041 vs, 1540 w,br, 1363 m, 1334 m,sh, 750 w, 707 w, 550 w, 504 m, 471 w,sh), the product is probably $[Cd\{(CO)_9Co_3(\mu_3\text{-}CCO_2)\}_2 \cdot n\text{THF}]$. However, all attempts to obtain crystals of this product suitable for X-ray diffraction were unsuccessful. In order to satisfy the requirement of a high coordination number with a single ligand, the polydentate ligand $CH_3(OCH_2CH_2)_4OCH_3$ (TGM) was introduced into this system. Compound **1**, $Cd_2\{(CO)_9Co_3(\mu_3\text{-}CCO_2)\}_4[CH_3(OCH_2CH_2)_4OCH_3]$ crystallized very nicely from the solution. The solid state IR exhibits the bands characteristic of the CO ligands of the cluster substituents at 2106, 2047 cm^{-1} and the carboxylate groups at 1537, 1531, 1373, 1344 cm^{-1} which are significantly different from those of the initial product.

Structural studies

There are four molecules in a unit cell and an asymmetric unit consists of one cadmium atom, two cluster ligands, and a half of TGM. As shown in Fig. 1, compound **1** is a binuclear species with a formula $Cd_2\{(CO)_9Co_3(\mu_3\text{-}CCO_2)\}_4[CH_3(OCH_2CH_2)_4OCH_3]$ which is located on a crystallographic two-fold axis. The two-fold axis runs through O1 and the middle of Cd—Cd′. Figure 2 shows the core structure of **1** and selected atomic distances and angles are listed in Table 2. The coordination geometry of each cadmium atom is best described as a distorted trigonal capped square-based polyhedron with four oxygen atoms from the cluster ligands and three from TGM.

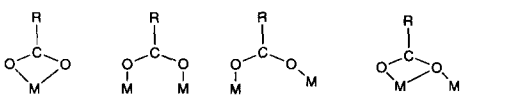
First consider the polyether ligand which is interesting in terms of its conformation. Iwamoto *et al.* [11–15] investigated the effect of the coordination on molecular conformations of the complexes of polyether $RO(CH_2CH_2O)_nR$ with MCl_2(M = Hg, Cd). They found that TGM (tetraethylene glycol dimethyl ether) shows different coordination modes, i.e. either coordinated to one or two metal atoms, which lead to different molecular conformations. In **1** TGM is symmetrically coordinated to two cadmium atoms and is different from those of the known compounds where TGM is coordinated to one metal atom or asymmetrically chelated to two metal centres. As we can see from Table 2, the C—C bonds (1.50 Å) of TGM are comparable to those [15] of the TGM-$CdCl_2$ complex and slightly shorter than a normal single C—C bond (1.54 Å). The C—O bond distances range

Table 1. Crystal data for $Cd_2\{(CO)_9Co_3(\mu_3\text{-}CCO_2)\}_4$ (TGM)

Formula	$C_{54}H_{22}Cd_2Co_{12}O_{49}$
fw	2386.74
F(000)	4632
Crystal dimensions	0.25 × 0.23 × 0.01 (mm)
Mo-K_α radiation	λ = 0.71073 (Å)
Temperature	23(°C)
Space group	$P4_32_12$ (No. 96)
a	13.7836(9) (Å)
c	42.900(4) (Å)
V	8150.5(9) (Å^{-3})
Z	4
Cal. density	1.945 (g cm^3)
μ (Mo-K_α)	29.741 (cm^{-1})
No. of refl. measured	5088 total, 4457 unique
Corrections	Lorentz-polarization linear decay (0.9958–1.1492 on I) empirical absorption (0.8015–0.9971 on I)
Solution	direct methods
Hydrogen atoms	not included
Refinement	full-matrix least-squares
Minimization function	$\Sigma w(\|F_o\| - \|F_c\|)^2$
Least-squares weights	$4F_o^2/\sigma^2(F_o^2) = 1/\sigma^2(F_o)$
Anomalous dispersion	all non-hydrogen atoms
Reflections included	3466 with $F_o^2 > 3.0\sigma(F_o^2)$
Parameters refined	528
Unweighted agreement factor	0.03678
Weighted agreement factor	0.04314
Esd of obs. of unit weight	1.265
Convergence, largest shift	0.03
High peak in final diff. map	0.63 (8) (e Å^{-3})
Low peak in final diff. map	−0.50 (8) (e Å^{-3})

from 1.41 to 1.46 Å, while those [15] of TGM-$CdCl_2$ range from 1.41 to 1.48 Å. The C—O—C angles (111.0 to 119.5°) are larger than the C—C—O angles (104.6 to 109.4°). The largest C(1)—O(1)—C(1)′ angle may be related to the bridging character of the O(1) atom which is coordinated to two cadmium atoms. The three oxygen atoms of TGM are almost co-planar with the Cd atom to which they are coordinated (Table 3). The Cd—O distances range from 2.48 to 2.58 Å and the longest one is to O(1). The torsional angles of TGM are given in Table 4 where it is seen that all C—O bonds are trans (172.3–175.2°) except for the C—O bonds connected to O(1) atom, which have a torsional angle of 86.71°. Thus, the conformation of TGM is totally different from those of the known TGM complexes such as TGM-$HgCl_2$ and TMG-$CdCl_2$ [14,15]. The conformational difference may be connected to the steric effect of the cluster ligands.

Next consider the carboxylate ligands for which a variety of coordination modes are known (Chart 1) [16]. The acetate group acts most frequently as a symmetrical bridging ligand i.e. *syn-syn* mode, such as in copper acetate [17] and basic carboxylates $[M_3O(OAc)_6]^+$(M = Fe, Mn) [18,19]. In some cases the acetate ligand functions not only as a bridging ligand, but also a chelating ligand [9]. However the bidentate chelating mode, as shown in the case of zinc and uranyl acetates,[20,21] is not as common, presumably because the chelate ring is a four-membered one. Asymmetrical bridging, i.e. *anti–syn* mode, is also rare and only a few examples are known, such as $Cu(O_2CH)_2(H_2O)$ and $Cu(O_2CH)_2$(Royal blue) [22,23]. As with the metal acetates, we have observed *syn–syn* bridging cluster carboxylate ligands in most of the cluster derivatives prepared to date [1–7,24].



As shown in Table 5, the coordination modes of the cluster ligands fall into two types: bidentate chelating and *anti–syn* bridging. Hence there are two distinct Cd—O distances, involving both cluster carboxylate groups; Cd—O(11) 2.197 Å, Cd—O(12) 2.287 Å, and Cd—O(21) 2.270 Å, Cd—O(22) 2.417 Å. The Cd—O distances observed in **1** lie in the shorter range of those found in other cadmium acetates, such as CaCd $[OAc]_4 \cdot H_2O$(2.289(7) to 2.677(8) Å) [8] and $Cd(OAc)_2 \cdot H_2O$ [9] (2.294(4) to 2.597(4) Å) in which the acetate groups are both chelating and bridging.

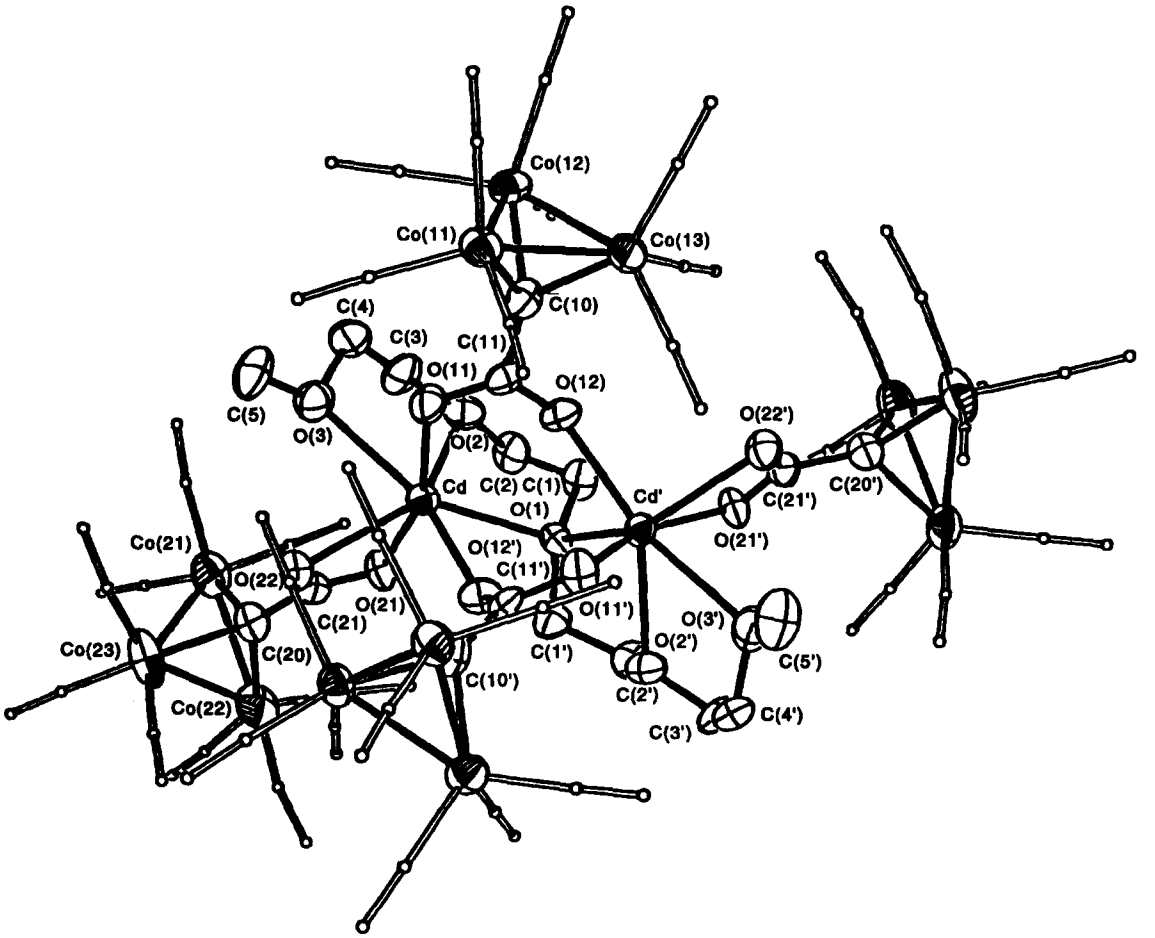


Fig. 1. Molecular structure of $Cd_2\{(CO)_9Co_3(\mu_3\text{-}CCO_2)\}_4[CH_3(OCH_2CH_2)_4OCH_3]$ **1** with thermal ellipsoids drawn at the 40% probability.

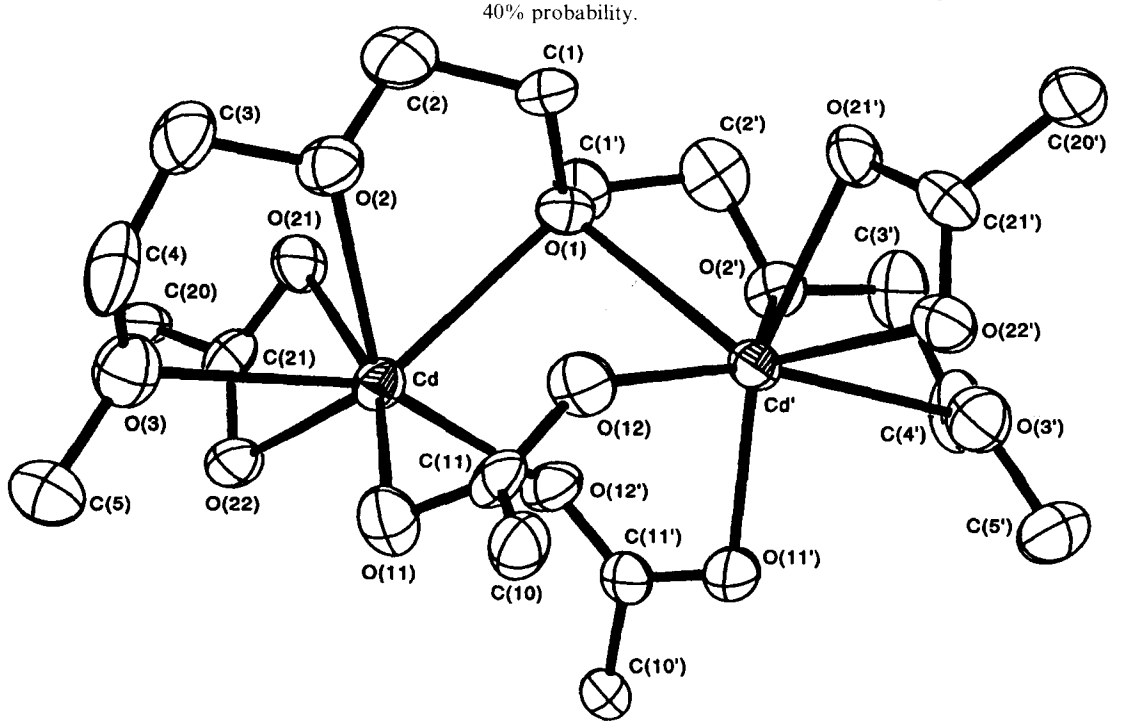


Fig. 2. A view of the core structure of $Cd_2\{(CO)_9Co_3(\mu_3\text{-}CCO_2)\}_4[CH_3(OCH_2CH_2)_4OCH_3]$ **1** with thermal ellipsoids drawn at the 40% probability.

Table 2. Selected interatomic distances (Å) and angles (°) for $Cd_2\{(CO)_9Co_3(\mu_3\text{-}CCO_2)\}_4$ (TGM)

Cd—Cd′	3.741(1)	Co(11)—C(10)	1.90(1)
Cd—O(1)	2.580(3)	Co(12)—C(10)	1.91(1)
Cd—O(2)	2.482(8)	Co(13)—C(10)	1.88(1)
Cd—O(3)	2.54(1)	Co(21)—C(20)	1.92(1)
Cd—O(11)	2.206(8)	Co(22)—C(20)	1.88(1)
Cd—O(12′)	2.289(9)	Co(23)—C(20)	1.85(1)
Cd—O(21)	2.277(8)	O(1)—C(1)	1.44(1)
Cd—O(22)	2.405(9)	O(1)—C(1)	1.44(1)
Co(11)—Co(12)	2.461(3)	O(2)—C(2)	1.42(2)
Co(11)—Co(13)	2.472(3)	O(2)—C(3)	1.37(2)
Co(11)—C(10)	1.90(1)	O(3)—C(4)	1.38(2)
Co(12)—Co(13)	2.452(3)	O(3)—C(5)	1.44(2)
Co(12)—C(10)	1.91(1)	O(11)—C(11)	1.27(1)
Co(13)—C(10)	1.88(1)	O(12)—C(11)	1.23(1)
Co(21)—Co(22)	2.446(3)	O(21)—C(21)	1.27(1)
Co(21)—Co(23)	2.455(3)	O(22)—C(21)	1.26(1)
Co(21)—C(20)	1.92(1)	C(1)—C(2)	1.50(2)
Co(22)—Co(23)	2.434(3)	C(3)—C(4)	1.49(2)
Co(22)—C(20)	1.88(1)	C(10)—C(11)	1.45(1)
Co(23)—C(20)	1.85(1)	C(20)—C(21)	1.46(2)

O(1)—Cd—O(2)	66.9(2)	O(1)—C(1)—C(2)	109.(1)
O(1)—Cd—O(3)	132.1(2)	O(2)—C(2)—C(1)	104.(1)
O(1)—Cd—O(11)	116.2(3)	O(3)—C(4)—C(3)	109.(1)
O(1)—Cd—O(12′)	74.4(2)	O(1)—Cd—O(21)	79.9(2)
O(12′)—Cd—C(21)	101.6(3)	O(1)—Cd—O(22)	128.8(2)
O(21)—Cd—O(22)	56.0(3)	O(1)—Cd—C(21)	105.4(3)
C(4)—O(3)—C(5)	111.(1)	O(2)—Cd—O(3)	66.0(3)
O(2)—Cd—O(11)	96.7(3)	Co(21)—Co(22)—C(20)	50.7(4)
O(2)—Cd—O(12′)	139.5(3)	Co(23)—Co(22)—C(20)	48.8(4)
O(2)—Cd—O(21)	79.3(3)	Co(21)—Co(23)—Co(22)	60.1(1)
O(2)—Cd—O(22)	120.8(3)	Co(21)—Co(23)—C(20)	50.7(4)
O(3)—Cd—O(11)	77.6(3)	Co(22)—Co(23)—C(20)	49.7(4)
O(3)—Cd—O(12′)	153.4(3)	C(1)—O(1)—C(1)	119.8(9)
O(3)—Cd—O(21)	83.6(3)	C(2)—O(2)—C(3)	114.(1)
O(3)—Cd—O(22)	71.8(3)	O(2)—C(3)—C(4)	110.(1)
O(11)—Cd—O(12′)	89.6(3)	Co(11)—C(10)—Co(12)	80.5(4)
O(11)—Cd—O(21)	160.7(3)	Co(11)—C(10)—Co(13)	81.6(5)
O(11)—Cd—O(22)	112.9(3)	Co(11)—C(10)—C(11)	133.6(9)
O(12)—Cd—O(21)	105.8(3)	Co(12)—C(10)—Co(13)	80.7(5)
O(12)—Cd—O(22)	92.6(3)	Co(12)—C(10)—C(11)	129.2(9)
Co(12)—Co(11)—Co(13)	59.61(8)	Co(13)—C(10)—C(11)	131.4(9)
Co(12)—Co(11)—C(10)	49.8(4)	O(11)—C(11)—O(12)	122(1)
Co(13)—Co(11)—C(10)	48.8(4)	O(11)—C(11)—C(10)	118(1)
Co(11)—Co(12)—Co(13)	60.41(8)	O(12)—C(11)—C(10)	120.(1)
Co(11)—Co(12)—C(10)	49.7(4)	Co(21)—C(20)—Co(22)	80.1(5)
Co(13)—Co(12)—C(10)	49.1(4)	Co(21)—C(20)—Co(23)	81.1(5)
Co(11)—Co(13)—Co(12)	59.98(8)	Co(21)—C(20)—C(21)	124.9(8)
Co(11)—Co(13)—C(10)	49.6(4)	Co(22)—C(20)—Co(23)	81.5(5)
Co(12)—Co(13)—C(10)	50.1(4)	Co(22)—C(20)—C(21)	131.5(9)
Co(22)—Co(21)—Co(23)	59.6(1)	Co(23)—C(20)—C(21)	137.2(9)
Co(22)—Co(21)—C(20)	49.1(4)	O(21)—C(21)—O(22)	121.(1)
Co(23)—Co(21)—C(20)	48.2(4)	O(21)—C(21)—C(20)	120.(1)
Co(21)—Co(22)—Co(23)	60.40(9)	O(22)—C(21)—C(20)	119.(1)

Numbers in parentheses are estimated standard deviations in the least significant digits.

Table 3. Least-squares planes for $Cd_2\{(CO)_9Co_3(\mu_3\text{-}CCO_2)\}_4$(TGM)

Plane No.	A	B	C	D	Atom	x	y	z	Distance
1	−0.1705	0.8866	−0.4300	−9.1388			Atoms in Plane		
					Cd	11.9831	11.9988	41.0250	0.093
					O(11)	9.8642	11.5438	41.3870	−0.105
					O(12)	10.4019	12.6235	43.2676	−0.048
					C(11)	9.5433	12.0964	42.5211	−0.048
					C(10)	8.1085	12.1737	42.8835	0.109
							Other Atoms		
					Cd′	11.9988	11.9831	44.7750	−1.537
2	0.8543	0.0794	−0.5137	−9.7715			Atoms in Plane		
					Cd	11.9831	11.9988	41.0250	−0.114
					O(1)	13.2405	13.2405	42.9000	0.096
					O(2)	11.7171	14.4702	40.8965	−0.079
					O(3)	10.8476	12.8115	38.8534	0.096
3	0.5870	0.5631	−0.5816	−24.2370			Atoms in Plane		
					Cd	11.9831	11.9988	41.0250	0.097
					O(21)	13.8992	12.5555	39.9433	−0.085
					O(22)	12.8998	10.7447	39.1733	−0.070
					C(20)	14.6952	11.6273	37.9045	0.111
					C(21)	13.7844	11.5968	39.0746	−0.052

The equation of the plane is of the form: $A^*x + B^*y + C^*z - D = 0$ where A, B, C and D are constants and x, y and z are orthogonalized coordinates.

Table 4. Torsional angles (°) for TGM in $Cd_2\{(CO)_9Co_3(\mu_3 - CCO_2)\}_4$(TGM)

C(5)—O(3)—C(4)—C(3)	−173.92	C(1)—O(1)—C(1′)—C(2′)	86.71
O(3)—C(4)—C(3)—O(2)	−65.72	O(1)—C(1′)—C(2′)—O(2′)	67.44
C(4)—C(3)—O(2)—C(2)	175.22	C(1′)—C(2′)—O(2′)—C(3′)	172.03
C(3)—O(2)—C(2)—C(1)	172.03	C(2′)—O(2′)—C(3′)—C(4′)	175.22
O(2)—C(2)—C(1)—O(1)	67.44	O(2′)—C(3′)—C(4′)—O(3′)	−65.72
C(2)—C(1)—O(1)—C(1′)	86.71	C(3′)—C(4′)—O(3′)—C(5′)	−173.92

Table 5. Comparison of coordination modes and Cd—O distances (Å) of carboxylate groups in **1** and related cadmium carboxylate compounds

Compound	Chelating	*Syn–syn* bridging	*Anti–syn* bridging	Chelating and bridging	Reference
$Cd\{(CO)_9Co_3$	2.270(6)		2.197(6)		This work
$(\mu_3\text{-}CCO_2)\}_4$(TGM)	2.417(6)		2.287(6)		
$\{\mu_3\text{-}(CO)_3Co\}Cd_3\{(CO)_9Co_3$		2.221(7)			4
$(\mu_3\text{-}CCO_2)\}_3(THF)_3$					
$Cd(CH_3CO_2)_2 \cdot 2H_2O$				2.297(4)	9
				2.294(4)	
				2.597(3)	
$Ca[Cd(CH_3CO_2)_4] \cdot 6H_2O$				2.289(7)	8
				2.677(8)	
$[Cd(HOC_6H_4CO_2)_2 \cdot 2H_2O]_2$	2.332(2)			2.271(2)	25
	2.429(1)			2.314(1)	
				2.535(2)	
$[Cd(CF_3CO_2)_2 \cdot PPh_3]_2$		2.266(19)			26

The Cd—O distances (2.197, 2.287 Å) for the chelating cluster ligand are significantly shorter than those of the chelating acetate group (2.304(4), 2.546(4) Å) in $Cd(OAc)_2 \cdot H_2O$. For the *anti–syn* cluster bridging ligands, the Cd—O distance for the oxygen atom occupied *anti*-position (Cd—O(21), 2.270(6) Å) is much shorter than that of oxygen atom occupied *syn*-position (Cd—O(22), 2.417(6) Å). However, both are shorter than those of acetate groups acting as chelating and bridging. As shown in Table 3, the chelating cluster carboxylate group (C(10), C(11), O(11), O(12)) and Cd are coplanar. And the *anti–syn* bridging cluster carboxylate group (C(20), C(21), O(21), O(22)) are also coplanar with Cd while Cd′ is far away from the plane. This is consistent with the *anti*-mode character of the cluster carboxylate ligand. The C—O distances (average 1.27(1) Å) and O—C—O angles (121.7°) for the cluster carboxylate groups are in the normal range found for the acetate compounds.

The Cd···Cd separation (3.741 Å) is comparable to that of $[Cd(HOC_6H_4CO_2)_2 \cdot H_2O]_2$ (3.715 Å) [25] and much longer than those of $[Cd(CF_3CO_2)_2 \cdot PPh_3]_2$(3.452 Å), [26] and TMG-$CdCl_2$ (3.457 Å), [15] which is also bridged by an oxygen atom from TGM. The Cd···Cd distance in **1** is also significantly larger than that (2.98(3) Å) of $\{\mu_3\text{-}Co(CO)_3\}Cd_3\{(CO)_9Co_3(\mu_3\text{-}CCO_2)\}_3(THF)_3$ [4] in which the cluster ligands are in the *syn–syn* coordination mode. As expected the Co—Co distances, as well as the other structural metrics of the cluster ligands in **1** are in the normal range found for the uncoordinated cluster acid [6].

CONCLUSIONS

Cadmium complexes with organic carboxylic acids having monocarboxylate groups, two functional groups, and dicarboxylate groups generally have polymeric structures with coordination numbers of up to eight [9,27–33]. Only a few like $[Cd(HOC_6H_4CO_2)_2 \cdot H_2O]_2$,[25] $[Cd(CF_3CO_2)_2 \cdot PPh_3]_2$,[26] and $[Cd(HOC_6H_4CO_2)_2 \cdot (pyridine)_3]$ [25] are dimeric or monomeric species. The steric bulk of the tricobalt cluster substituted carboxylate ligand leads to complexes having a lower coordination number. We have observed that $[Pb\{(CO)_9Co_3(\mu_3\text{-}CCO_2)\}_2]_n$ has a coordination number of six whereas related organic lead carboxylates have coordination numbers greater than six [2]. Thus, the unusual conformation of TGM and the coordination modes of the cluster carboxylates in **1** are ascribed to the different steric and electronic effects of the cluster substituent relative to organic substituents.

Supplementary data available from the Cambridge Crystallographic Data Centre. Positional parameters and estimated equivalent isotropic thermal parameters, anisotropic thermal parameters, full list of atomic distances and angles.

Acknowledgement—We are grateful for the support of the National Sciences Foundation.

REFERENCES

1. W. Cen, P. Lindenfeld and T. P. Fehlner, *J. Am. Chem. Soc.* 1992, **114,** 5451.
2. X. Lei, M. Shang, A. Patil, E. E. Wolf and T. P. Fehlner, *Inorg. Chem.* 1996, **35,** 3217.
3. W. Cen, K. J. Haller and T. P. Fehlner, *Inorg. Chem.* 1991, **30,** 3120.
4. W. Cen, K. J. Haller and T. P. Fehlner, *Organometallics* 1992, **11,** 3499.
5. W. Cen, K. J. Haller and T. P. Fehlner, *Inorg. Chem.* 1992, **31,** 2672.
6. W. Cen, K. J. Haller and T. P. Fehlner, *Inorg. Chem.* 1993, **32,** 995.
7. X. Lei, M. Shang and T. P. Fehlner, *Organometallics* 1996, **15,** 3779.
8. D. A. Langs and C. R. Hare, *J. Chem. Soc., Chem. Commun.* 1967, 890.
9. W. Harrison and J. Trotter, *J. Chem. Soc., Dalton. Trans.* 1972, 956.
10. D. Seyferth, *Adv. Organomet. Chem.* 1976, **14,** 97.
11. R. Iwamoto, Y. Saito, H. Ishihara and H. Tadokoro, *J. Polym. Sci., Part A*-2 1968, **6,** 1509.
12. M. Yokoyama, H. Ishihara, R. Iwamoto and H. Tadokoro, *Macromolecules* 1969, **2,** 184.
13. R. Iwamoto, *Bull. Chem. Jpn* 1973, **46,** 1118.
14. R. Iwamoto, *Bull. Chem. Jpn* 1973, **46,** 1114.
15. R. Iwamoto and H. Wakano, *J. Am. Chem. Soc.* 1976, **98,** 3764.
16. R. C. Mehrotra and R. Bohra, *Metal Carboxylates.* Academic Press, New York (1983).
17. J. N. V. Niekerk and F. R. L. Schoening, *Acta Cryst.* 1953, **6,** 227.
18. B. N. Figgis and G. B. Robertson, *Nature* 1965, **205,** 694.
19. A. R. E. Baikie, M. B. Hursthouse, D. B. New and P. Thornton, *J. Chem. Soc., Chem. Commun.* 1978, 62.
20. J. N. van Niekerk, F. R. L. Schoening and J. H. Talbot, *Acta Cryst.* 1953, **6,** 720.
21. W. H. Zachariasen and M. A. Plettinger, *Acta Cryst.* 1959, **12,** 526.
22. G. A. Barclay and C. H. L. Kannard, *J. Chem. Soc.* 1961, 3289.
23. M. G. B. Drew, D. E. Edwards and R. Richards, *J. Chem. Soc., Chem. Commun.* 1973, 124.
24. M. A. Bañares, L. Dauphin, X. Lei, W. Cen, M. Shang, E. E. Wolf and T. P. Fehlner, *Chem. Mater.* 1995, **7,** 553.
25. N. G. Charles, E. A. H. Griffith, P. F. Rodesiler and E. L. Amma, *Inorg. Chem.* 1983, **22,** 2717.
26. T. Allman, R. C. Goel, N. K. Jha and A. L. Beauchamp, *Inorg. Chem.* 1984, **23,** 914.
27. M. L. Post and J. Trotter, *J. Chem. Soc., Dalton Trans.* 1974, 285.
28. M. L. Post and J. Trotter, *J. Chem. Soc., Dalton Trans.* 1974, 1922.
29. S. H. Whitlow, *Acta Cryst., Sect. B* 1975, **B31,** 2531.
30. R. J. Flook, H. C. Freeman and M. L. Scudder, *Acta Cryst., Sect. B* 1977, **B33,** 801.
31. A. Hempel, S. E. Hull, R. Ram and M. P. Gupta, *Acta Cryst., Sect. B* 1979, **B35,** 2115.
32. G. Weber, *Acta Cryst., Sect. B* 1980, **B36,** 1947.
33. P. Kauuttila, *Polyhedron* 1984, **3,** 303.

Pergamon

PII: S0277-5387(96)00494-9

Polyhedron Vol. 16, No. 11, pp. 1811–1817, 1997
© 1997 Elsevier Science Ltd
All rights reserved. Printed in Great Britain
0277-5387/97 $17.00+0.00

Diphenylphosphino(phenylthio)methane as a monodentate or bidentate chelate ligand in rhodium, iridium and ruthenium complexes, crystal structure of $[(\eta^5\text{-}C_5Me_5)IrCl(\eta^2\text{-}Ph_2PCH_2SPh\text{—}P,S)]BF_4 \cdot Me_2CO$

Mauricio Valderrama,[a]* Raul Contreras[a] and Daphne Boys[b]

[a]Departamento de Química Inorgánica, Facultad de Química, Pontificia Universidad Católica de Chile, Casilla 306, Santiago-22, Chile; [b]Departamento de Física, Facultad de Ciencias Físicas y Matemáticas, Universidad de Chile, Casilla 487-3, Santiago, Chile

(Received 16 September 1996; accepted 4 October 1996)

Abstract—Reactions of complexes $[\{(\eta^5\text{-}C_5Me_5)MCl_2\}_2]$ (M = Rh, Ir) and $[\{(\eta^6\text{-}MeC_6H_4Pr^i)RuCl_2\}_2]$ with the ligand Ph_2PCH_2SPh in acetone solution led to neutral complexes with the general formula $[(ring)MCl_2(\eta^1\text{-}Ph_2PCH_2SPh\text{—}P)]$ (**1–3**). These compounds react with thallium tetrafluoroborate in acetone solution to yield new cationic complexes in which the ligand is acting in its chelate P,S-donor fashion, $[(ring)MCl(\eta^2\text{-}Ph_2PCH_2SPh\text{—}P,S)]BF_4$ (**4–6**). When the removal of the chloride ligand in complexes **1–3** was carried out in the presence of a stoichiometric amount of Ph_2PCH_2SPh, cationic compounds containing two P-donor monodentate ligands of the type $[(\eta^5\text{-}C_5Me_5)MCl(\eta^1\text{-}Ph_2PCH_2SPh\text{—}P)_2]BF_4$ (**7** and **8**) were obtained. The structure of the iridium derivative $[(\eta^5\text{-}C_5Me_5)IrCl(\eta^2\text{-}Ph_2PCH_2SPh\text{—}P,S)]BF_4 \cdot Me_2CO$ has been determined by single-crystal X-ray diffraction methods. The complex cation contains a C_5Me_5 group occupying three coordination positions of a distorted octahedral iridium centre, a bidentate chelate P,S-bonded ligand and a chloride atom completing the coordination sphere. © 1997 Elsevier Science Ltd. All rights reserved.

Keywords: diphenylphosphino(phenylthio)methane; rhodium; indium; ruthenium.

There is currently much interest in the synthesis of mono- and bimetallic platinum-group metal complexes containing, short-bite, unsymmetrical ligands such as (diphenylarsino)(diphenylphosphino)methane,[1] 2-(diphenylphosphino)pyridine,[2] diphenylphosphino(methylthio)methane,[3] diphenylphosphino(benzylthio)methane [4] and diphenylphosphino(phenylthio)methane [5].

In particular, the P and S donor site ligands are described as monodentate P-donor ligands in Pd^{II}, Pt^{II}, Rh^{I} and Ir^{I} complexes, or as bidentate bridging P,S-donor ligands in bimetallic complexes with similar (Pd—Pd, Pt—Pt, Rh—Rh) or dissimilar (Pd—Rh) metal centres [3–5]. In these compounds the ligands acquire a head-to-tail arrangement and the metal centres are bonded by a metal–metal bond. However, only few examples of complexes with these ligands acting in its chelate bidentate form are reported.

In this paper we describe the preparation of mononuclear neutral complexes of the general formula $[(ring)MCl_2(\eta^1\text{-}Ph_2PCH_2SPh\text{—}P)]$ [(ring)M = $(\eta^5\text{-}C_5Me_5)Rh$ (**1**), $(\eta^5\text{-}C_5Me_5)Ir$ (**2**), $(\eta^6\text{-}p\text{-}MeC_6H_4Pr^i)Ru$ (**3**)] and the related cationic complexes of the types $[(ring)MCl(\eta^2\text{-}Ph_2PCH_2SPh\text{—}P,S)]BF_4$ [(ring)M = $(\eta^5\text{-}C_5Me_5)Rh$ (**4**), $(\eta^5\text{-}C_5Me_5)Ir$ (**5**), $(\eta^6\text{-}p\text{-}MeC_6H_4Pr^i)Ru$ (**6**)] and $[(ring)MCl(\eta^1\text{-}Ph_2PCH_2SPh\text{—}P)_2]BF_4$ [(ring)M = $(\eta^5\text{-}C_5Me_5)Rh$ (**7**), $(\eta^5\text{-}C_5Me_5)Ir$ (**8**)]. The structure of the complex $[(\eta^5\text{-}C_5Me_5)IrCl(\eta^2\text{-}Ph_2PCH_2SPh\text{—}P,S)]BF_4$, determined by single-crystal X-ray diffraction, is also reported.

EXPERIMENTAL

Elemental analyses (C, H and S) were made with a Perkin–Elmer 240C microanalyser. IR spectra were

*Author to whom correspondence should be addressed.

recorded on a Bruker IFS-25 spectrophotometer using KBr pellets. Conductivities were measured in *ca* 5×10^{-4} M acetone solutions using a WTW LF-521 conductimeter. ^1H (200 MHz) and ^{31}P ^1H (81 MHz) NMR spectra were recorded on a Bruker AC-200P spectrometer and the chemical shifts are reported in ppm relative to Me_4Si and 85% H_3PO_4 (positive shifts downfield) in D_2O as internal and external standards, respectively.

All reactions were carried out by Schlenk techniques under purified nitrogen. Reagent-grade solvents were dried, distilled and stored under a nitrogen atmosphere. The starting complexes $[\{(\eta^5\text{-}C_5Me_5)MCl_2\}_2]$ (M = Rh, Ir),[6] $[\{(\eta^6\text{-}MeC_6H_4Pr^i)RuCl_2\}_2]$ [7] and the ligand Ph_2PCH_2SPh [5b] were prepared by published procedures.

Preparation of $[(\eta^5\text{-}C_5Me_5)MCl_2(\eta^1\text{-}Ph_2PCH_2SPh\text{—}P)]$ [M = Rh (**1**), Ir (**2**)]

1: To a suspension of the binuclear complex $[\{(\eta^5\text{-}C_5Me_5)RhCl_2\}_2]$ (124 mg, 0.2 mmol) in acetone (10 cm^3) the ligand Ph_2PCH_2SPh (123 mg, 0.4 mmol) was added with an immediate formation of a red solid. After stirring the mixture for 1 h, the solid complex was filtered off, washed with diethylether and air-dried. The complex was recrystallized from chloroform–diethylether. Yield: 167 mg (68%). Found: C, 56.8; H, 5.7; S, 5.3. Calc. for $C_{29}H_{32}Cl_2PRhS$: C, 56.4; H, 5.2; S, 5.2%.

2: To a solution of the binuclear complex $[\{(\eta^5\text{-}C_5Me_5)IrCl_2\}_2]$ (159 mg, 0.2 mmol) in dichloromethane (15 cm^3) was added the ligand Ph_2PCH_2SPh (123 mg, 0.4 mmol). The colour of the solution changed from orange to yellow. The solution was stirred at room temperature for 1 h and then evaporated to a small volume (3–5 cm^3). The addition of *n*-hexane caused the precipitation of a yellow solid, which was filtered off, washed with *n*-hexane and crystallized from dichloromethane–*n*-hexane. Yield: 240 mg (85%). Found: C, 49.1; H, 4.2; S, 4.7. Calc. for $C_{29}H_{32}Cl_2PIrS$: C, 49.4; H, 4.6; S, 4.7%.

Preparation of $[(\eta^6\text{-}MeC_6H_4Pr^i)RuCl_2(\eta^1\text{-}Ph_2PCH_2SPh\text{—}P)]$ (**3**)

To a solution of complex $[\{(\eta^6\text{-}MeC_6H_4Pr^i)RuCl_2\}_2]$ (122 mg, 0.2 mmol) in dichloromethane (15 cm^3) a stoichiometric amount of the ligand Ph_2PCH_2SPh (123 mg, 0.4 mmol) was added and the mixture was stirred for 1 h. The solution obtained was concentrated and chromatographed on Kieselgel (HF_{254} type 60) using $CHCl_3$: *n*-hexane (2 : 1) as eluent. The solution was evaporated to dryness, the residue extracted with $CHCl_3$, and the complex isolated as red crystals by addition of *n*-hexane. Yield: 215 mg (87%). Found: C, 56.8; H. 4.9; S. 5.1. Calc. for $C_{29}H_{31}Cl_2PRuS$: C, 56.7; H, 5.1; S, 5.2%.

Preparation of $[(\eta^5\text{-}C_5Me_5)MCl(\eta^2\text{-}Ph_2PCH_2SPh\text{—}P,S)]BF_4$ [M = Rh (**4**), Ir (**5**)]

To a solution of complex **1** or **2** (0.15 mmol) in acetone (10 cm^3) was added a stoichiometric amount of $TlBF_4$ (44 mg, 0.15 mmol). The resulting mixture was stirred for 8 h. During this time TlCl was precipitated and the colour of the solution changed from orange (**1**) or yellow (**2**) to pale yellow. The solution was filtered off through Kieselguhr, concentrated to a small volume and the complexes precipitated by addition of diethylether or *n*-hexane. (**4**) Orange crystals from chloroform–diethylether. Yield: 70 mg (69%). Found: C, 51.5; H, 4.3; S, 4.9. Calc. for $C_{29}H_{32}BClF_4PRhS$: C, 52.0; H, 4.8; S, 4.8%. Λ = 131 $cm^2\ mol^{-1}\ ohm^{-1}$. **5**: Yellow crystals from acetone–diethylether–pentane. Yield: 109 mg (96%). Found: C, 46.9; H, 4.5; S, 4.0. Calc. for $C_{29}H_{32}BClF_4PIrS \cdot C_3H_6O$: C, 47.1; H, 4.7; S, 3.9%. Λ = 126 $cm^2\ mol^{-1}\ ohm^{-1}$.

Preparation of $[(\eta^6\text{-}MeC_6H_4Pr^i)RuCl(\eta^2\text{-}Ph_2PCH_2SPh\text{—}P,S)]BF_4$ (**6**)

To a solution of complex **3** (92 mg, 0.15 mmol) in acetone (15 cm^3) was added a stoichiometric amount of $TlBF_4$ (44 mg, 0.15 mmol). After stiring the mixture for 12 h, the TlCl formed was filtered off through Kieselghur and the solution evaporated to a small volume. Careful addition of *n*-hexane gave red–orange crystals. Yield: 70 mg (70%). Found: C, 52.2; H, 4.9; S, 4.7. Calc. for $C_{29}H_{31}BClF_4PRhS$: C, 52.3; H, 4.7; S, 4.8%. Λ = 141 $cm^2\ mol^{-1}\ ohm^{-1}$.

Preparation of $[(\eta^5\text{-}C_5Me_5)MCl(\eta^1\text{-}Ph_2PCH_2SPh\text{—}P)_2]BF_4$ [M = Rh (**7**), Ir (**8**)]

To a solution of 0.1 mmol of complex **1** (62 mg) or **2** (70 mg) in acetone solution (10 cm^3) was added the ligand Ph_2PCH_2SPh (31 mg, 0.1 mmol) and the stoichiometric amount of $AgBF_4$ (195 mg, 0.1 mmol). Solid AgCl was formed and the colour of the solution changed from orange to yellow. After stirring for 24 h the mixture was filtered off, the solution was concentrated to a small volume and the complexes precipitated as yellow solids by careful addition of *n*-hexane. The complexes were filtered, washed with *n*-hexane and dried *in vacuo*. **7**: Yield: 33 mg (36 %). Found: C, 58.3; H, 5.3; S, 6.4. Calc. for $C_{48}H_{49}BClF_4P_2RhS_2$: C, 59.0; H, 5.1; S, 6.6%. **8**: Yield: 48 mg (48 %). Found: C, 53.5; H, 4.8; S, 6.0. Calc. for $C_{48}H_{49}BClF_4P_2IrS_2$: C, 54.1; H, 4.6; S, 6.0%.

Crystal structure of complex **5**

A yellow, parallelepiped-shaped crystal, of approximate dimensions 0.22 × 0.22 × 0.20 mm, obtained from a slow diffusion of diethylether into an acetone

solution of the complex, was selected for structure determination by X-ray diffraction. Intensity data were collected on a Siemens R3m/v diffractometer in $\theta/2\theta$ scan mode, using graphite-monochromated MoK_α radiation ($\lambda = 0.71073$ Å). 4492 reflections collected gave 4272 independent reflections ($R_{int} = 0.0199$), of which 2899 had $I < 2\sigma(I)$. Semi-empirical corrections for absorption, *via* psi-scans, were applied to the intensities.

A summary of the crystal data and relevant refinement parameters are presented in Table 1. The structure was solved by direct methods and refined on F^2 by full-matrix least-squares calculations, using all 4272 reflections. Non-H atoms were refined anisotropically. H atoms were placed at geometrically idealized positions with C—H = 0.96 Å and were allowed to ride over their parent C atoms with the isotropic displacement parameter U_{iso} equal to the equivalent isotropic U_{eq} of the attached C atom. Final $R(F)$ [$I < 2\sigma(I)$] was 0.034. All calculations were performed with the Siemens SHELXTL [8] and SHELXL-93 [9] programs. The absolute structure was determined using SHELXL-93 routine to refine the Flack parameter x which converged to 0.001(9).

Tables of positional and thermal parameters, full list of bond distances and angles, short contacts, least-squares planes with dihedral angles, and listing of observed and calculated structure factors have been deposited with the Editor as supplementary material.

RESULTS AND DISCUSSION

The binuclear complexes $[\{(\eta^5C_5Me_5)MCl_2\}_2]$ (M = Rh, Ir) and $[\{\eta^6\text{-}MeC_6H_4Pr^i)RuCl_2\}_2]$ react with the ligand diphenylphosphino (phenylthio)methane, Ph_2PCH_2SPh, in acetone or dichloromethane solution by cleavage of the chlorine bridges to yield neutral complexes with the ligand acting as a unidentate P-donor ligand, in accord with the general equation:

$$1/2[\{(ring)MCl_2\}_2] + Ph_2PCH_2SPh \longrightarrow [(ring)MCl_2(\eta^1\text{-}Ph_2PCH_2SPh\text{—}P)]$$

where (ring)M = $(\eta^5\text{-}C_5Me_5)$Rh (**1**), $(\eta^5\text{-}C_5Me_5)$Ir (**2**) and $(\eta^6\text{-}p\text{-}MeC_6H_4Pr^i)$Ru (**3**).

The ^{1}H NMR spectra of complexes **1**–**3** exhibit a doublet resonance in the range δ 4.1–4.4 ppm assigned to methylene protons of the ligand together with the expected signals of coordinated rings. Their ^{31}P ^{1}H NMR spectra show a doublet resonance for complex **1** and a singlet resonance for complexes **2** and **3**. In all cases the signals are substantially shifted to low field compared to those of the free ligand (coordination shifts in the range $\Delta\,\delta P = 21$–54 ppm). Relevant NMR chemical shifts and coupling constants are listed in Table 2.

Complexes **1**–**3** slowly react in acetone solution with thallium tetrafluoroborate at room temperature to give non soluble thallium chloride and the corresponding cationic complexes with the ligands acting in their bidentate chelate fashion, according to the general equation:

$$\mathbf{1\text{–}3} + TlBF_4 \longrightarrow [(ring)MCl(\eta^2\text{-}Ph_2PCH_2SPh\text{—}P,S)]BF_4 + TlCl$$

where (ring)M = $(\eta^5\text{-}C_5Me_5)$Rh (**4**), $(\eta^5\text{-}C_5Me_5)$Ir (**5**) and $(\eta^6\text{-}p\text{-}MeC_6H_4Pr^i)$Ru (**6**).

Table 1. Crystallographic data for complex **5**

Empirical formula	$C_{32}H_{38}BClF_4IrOPS$
Formula weight	816.11
Crystal system	Orthorhombic
Space group	$Pna2_1$
Unit cell dimensions	$a = 16.172(4)$ Å, $\alpha = 90.0°$
	$b = 11.782(3)$ Å, $\beta = 90.0°$
	$c = 17.754(4)$ Å, $\gamma = 90.0°$
Volume (Å^3)	3382.8(14)
Z	4
Density (calculated) (Mg m^{-3})	1.602
Absorption coefficient (mm^{-1})	4.181
$F(000)$	1616
θ range for data collection (°)	2.07–28.06
Index ranges	$0 \leqslant h \leqslant 21$, $0 \leqslant k \leqslant 15$, $-23 \leqslant l \leqslant 0$
Absorption correction	Semi-empirical, *via* psi-scans
Maximum and minimum transmission	0.931 and 0.762
Data/restraints/parameters	4272/0/378
Weighting scheme	$1/[\sigma^2(F_o^2) + (0.0356\,P)^2]$, where $P = [\text{Max}(F_o^2,0) + 2F_c^2]/3$
Goodness-of-fit on F^2	0.872
Final R indices [$I > 2\sigma(I)$]	$R(F) = 0.0339$, $wR(F^2) = 0.0641$
R indices (all data)	$R(F) = 0.0648$, $wR(F^2) = 0.0705$
Largest difference peak and hole (e Å^{-3})	1.111 and −0.766

Table 2. NMR chemical shifts (δ ppm) and coupling constants (Hz) of isolated complexes[a]

	^{1}H Ring	CH_2	^{31}P $\{^1H\}$ δP	$\Delta\,\delta P$[b]
1	1.37 (d, C_5Me_5) ^4J(PH) = 3.52	4.42 (d) ^2J(PH) = 3.50	34.29 (d) ^1J(PRh) = 141.3	53.69
2	1.37 (d, C_5Me_5) ^4J(PH) = 2.27	4.45 (d) ^2J(PH) = 4.54	1.68 (s)	21.08
3	0.80 (d, Me, Pr^i) ^3J(HH) = 6.9 1.89 (s, Me) 2.51 (m, CH, Pr^i)	4.17 (d) ^2J(PH) = 3.50	29.52 (s)	48.92
4	1.66 (d, C_5Me_5) ^4J(PH) = 4.40	4.78 (m, H_a) 5.67 (m, H_b)	−2.45 (d) ^1J(PRh) = 120.5	16.95
5	1.72 (d, C_5Me_5) ^4J(PH) = 2.93	5.07 (dd, H_a)[c] ^2J(PH_a) = 10.51 ^2J(HH) = 12.20	−34.14 (s)	−14.74
6	1.03 (d, Me, Pr^i) 1.14 (d, Me, Pr^i) ^3J(HH) = 6.9 1.85 (s, Me) 2.41 (m, CH, Pr^i)	4.89 (dd, H_a) 5.79 (dd, H_b)[d] ^2J(PH_a) = 10.39 ^2J(PH_b) = 8.16 ^2J(HH) = 11.83	−1,72 (s)	17.68
7	1.26 (t, C_5Me_5) ^4J(PH) = 3.60	3.24 (m, 2H) 3.80 (m, 2H)	26.64 (d) ^1J(PRh) = 133.9	46.04
8	1.27 (t, C_5Me_5) ^4J(PH) = 2.30	3.30 (m, 2H) 3.83 (m, 2H)	−10.85 (s)	8.55

[a]Measured in $CDCl_3$ at room temperature. Chemical shifts relative to Me_4Si and H_3PO_4 (85%) in D_2O as standards. s, singlet; d, doublet; dd, doublet of doublets; t, triplet; m, multiplet; br, broad. All complexes show multiplets in the region 7.0–8.0 ppm corresponding to phenyl groups of the ligands.

[b]$\Delta\delta P$ = [δP(monodentate complex)-δP(free ligand)] (free ligand: $\delta P = -19.40$ ppm).

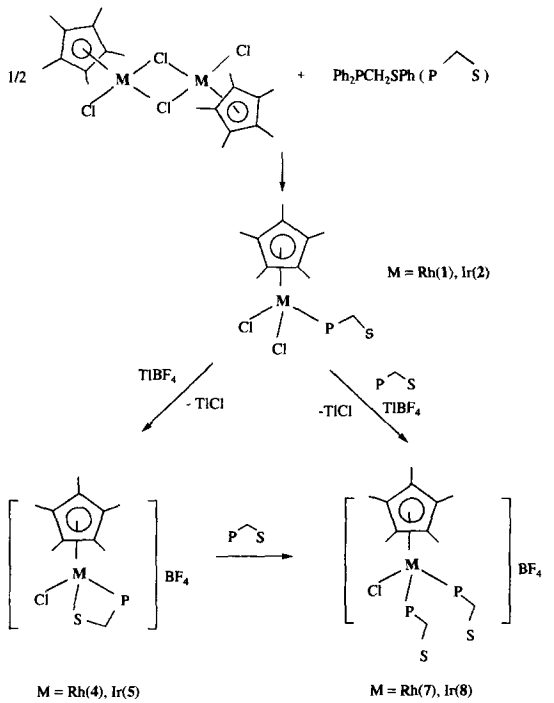
[c]The resonance of the H_b proton is masked by the signals of phenyl rings.

[d]This signal is superposed with those of the ring protons of the *p*-cymene ligand. This assignment was made with the aid of double irradiation techniques.

These cationic complexes were isolated as stable microcrystalline solids and behave as 1 : 1 electrolytes in acetone solution. Their ^{1}H NMR spectra exhibit the expected resonances of the coordinated ring and two resonances which correspond to the non-equivalent protons H_a and H_b. The proton endo to the chlorine atom is labelled H_a and is assigned to the highest field resonance on the basis of results obtained for related complexes containing bis(diphenylphosphine)methane(dppm) or their chalcogenides derivatives as chelate ligands [10]. Complex **5** shows only a doublet of doublets at δ 5.07 ppm for the H_a proton. The H_b proton appears in the range δ 7.0–8.0 ppm and is masked by the phenyl resonances of the ligand. This assignment is based on the NMR results obtained for the similar complex [(η^5-C_5Me_5)IrCl(η^2-$MeSCH_2SMe$—S,S)]BF_4, which shows two doublet resonances for the methylene protons at δ 5.56 (H_a) and 7.28 (H_b) ppm [11]. The ^{1}H NMR spectrum of complex **6** shows two doublets of doublets resonances assigned to H_a and H_b with their corresponding different ^2J(PH) couplings.

The ^{31}P $\{^1H\}$ NMR of complexes **4–6** show a shift of the signals to high field respect to the starting neutral complexes **1–3**, respectively. The large shielding of P atom ($\Delta\delta P$ = 31–37 ppm) is the typical behaviour of a coordinated P atom, which is part of a four-membered chelate ring, where the conformational change produces an increase in their electron density [12]. The decrease in the value of the phosphorus–rhodium coupling constant in complex **4** [^1J(RhP) = 120.5 Hz] with respect to complex **1** [^1J(RhP) = 141.3 Hz] suggests that the formation of the chelate ring causes a decrease of the σ character of the metal–phosphorus bond.

The addition of an excess of the ligand Ph_2PCH_2SPh to an acetone solution of complexes **4** and **5** causes the cleavage of the labile metal–thioether bond to form new cationic complexes in which the ligands are acting in their monodentate P-donor form, [(η^5-C_5Me_5)MCl(η^1-Ph_2PCH_2SPh—P)$_2$]BF_4, where M = Rh (**7**) and Ir (**8**). These compounds have not been isolated as pure samples by this synthethic method and always contain traces of the cor-



Scheme 1

responding starting derivatives. However, the direct reaction of complexes **1** and **2** with a stoichiometric amount of the ligand in the presence of $TlBF_4$ led only to the formation of complexes **7** and **8**, respectively. All these reactions are represented in Scheme 1.

At room temperature (25°C) the ^1H NMR spectra of complexes **7** and **8** exhibit the expected triplet resonance for the permethylated ring and two broad multiplet resonances assigned to different methylene protons. When the temperature is raised to 60°C, these broad signals split in a doublet of multiplets with a $^2J(HH) \simeq 14.5$ Hz. With cooling at −60°C only very broad signals were observed. The $^{31}P\{^1H\}$ NMR spectra at room temperature show a doublet and singlet resonances for complexes **7** and **8**, respectively. The doublet signal shown by complex **7**, centred at δ 26.64 ppm [$^1J(RhP) = 133.9$ Hz], is shifted to high field respect to that of the starting complex **1** [δ 34.29 ppm; $^1J(RhP) = 141.3$ Hz], indicating the existence of π-backbonding from the metal centre to the phosphorus atom. This effect causes a decrease of the σ character of the Rh—P bond and, consequently, a decrease of the phophorus–rhodium coupling.

In order to obtain an unambiguous characterization of complex **5**, an X-ray diffraction study was undertaken. Table 3 lists the relevant bonds distances and angles. Figure 1 shows a perspective ORTEP view of the cation, showing the metal centre with a pseudo-octahedral geometry, commonly referred as "three-legged piano stool" configuration, with the centroid of the pentamethylcyclopentadienyl ligand occupying the centre of three octahedral sites, the diphenylphosphino(phenylthio)methane ligand bonded to the iridium atom through the phosphorus and sulfur atoms and a chloride atom completing the coordination sphere.

The methyl substituents are bent away from the iridium atom and the Ir—C(ring) distances span the range 2.161(7)–2.238(8) Å and compares well with those found in other pentamethylcyclopentadienyl iridium complexes [8b,13].

The Ir—S distance, 2.402(3) Å, is larger than those found in the thioether–iridium(III) complex [IrCl(1,4,8,11-tetrathiocyclotetradecane)]BPh_4 [average: 2.293(4) Å],[14] and is similar to the distances found in the thiolate complex $[Ir(S_2CNEt_2)_3]$ [average: 2.370(2) Å][15] and the phosphine sulfide complex $[(\eta^5\text{-}C_5Me_5)Ir\{PO(OMe)_2\}\{\eta^2\text{-}(SPPh_2)_2CH_2\}]BF_4$ [average: 2.398(2) Å].[8b] The Ir—P distance, 2.303(3) Å, compares well with those found in the phosphine–iridium(III) complexes $[IrH(\eta^1,\eta^3\text{-}C_8H_{12})(dppm)]$ [Ir—P: average 2.288(2) Å][16] and $[IrCl_2(CO)_2(\mu\text{-}CO)(\mu\text{-}dppm)]$ [Ir—P: average 2.330(3) Å] [17]. The Ir—Cl separation, 2.381(2) Å, is similar to those found in related complexes containing the "$(C_5Me_5)Ir$" moiety, as in the mono-

Table 3. Selected bond lengths (Å) and bond angles (°), with e.s.d.s in parentheses

Ir—C(1)	2.229(9)	Ir—P	2.303(3)
Ir—C(2)	2.169(10)	Ir—S	2.402(3)
Ir—C(3)	2.174(9)	Ir—Cl	2.381(2)
Ir—C(4)	2.161(7)	P—C	1.854(9)
Ir—C(5)	2.238(8)	S—C	1.836(10)
P—C(11)	1.819(9)	P—C(21)	1.823(14)
S—C(31)	1.781(10)		
P—Ir—Cl	86.99(9)	S—C—P	96.4(5)
P—Ir—S	71.51(9)	Ir—S—C	91.6(3)
Cl—Ir—S	89.59(9)	Ir—P—C	94.3(3)
Ir—S—C(31)	118.0(4)	Ir—P—C(11)	122.1(3)
Ir—P—C(21)	118.4(4)	C(11)—P—C(21)	105.5(5)

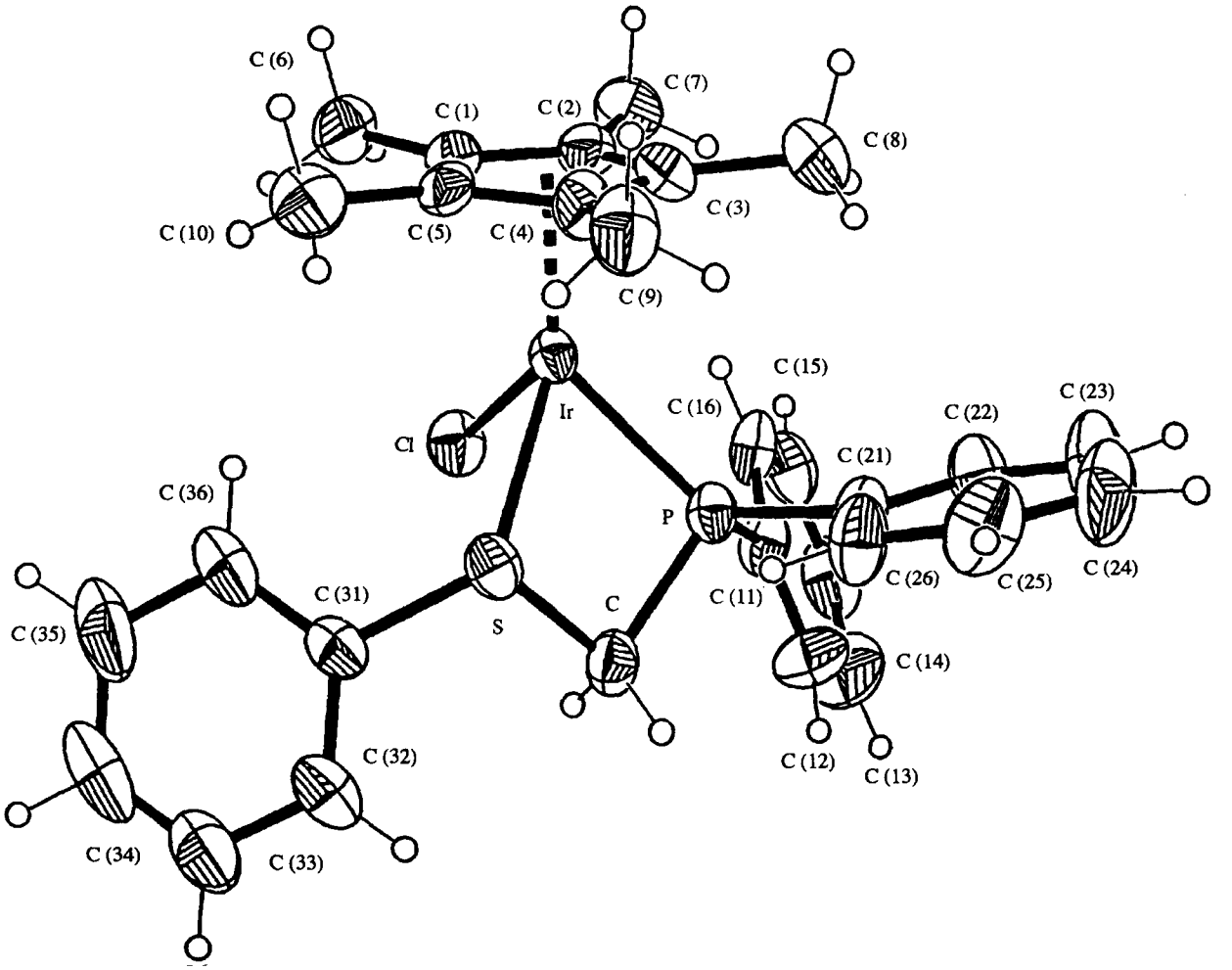


Fig. 1. ORTEP view of the cation in complex **5**, with 40% probability ellipsoids and atom numbering. H atoms are drawn as circles of arbitrary radius.

nuclear complexes $[(\eta^5\text{-}C_5Me_5)IrCl(\text{L-prolinate})]$ [Ir—Cl: 2.417(3) Å] and $[(\eta^5\text{-}C_5Me_5)IrCl(\text{L-histidine})]Cl$ [Ir—Cl: 2.402(5) Å] [18].

The P—C [1.854(9) Å] and S—C [1.836(10) Å] distances in the coordinated chelate ligand are similar to those found in the A-frame complexes containing the related bidentate bridging ligand $Ph_2PCH_2SCH_2Ph$, $[Pd_2Cl_2(\mu\text{-}Ph_2PCH_2SCH_2Ph)]$ [P—C: 1.87(2) and P—S: 1.77(3) Å][4b] and $[Rh_2Cl_4(CO)_2(\mu\text{-}Ph_2PCH_2SCH_2Ph)]$ [P—C: 1.840(5) and P—S: 1.813(3) Å] [4a]. However, the angle P—C—S 96.4(5)°, is smaller than the corresponding angle observed in the ligand of the above mentioned A-frame complexes: P—C—S: 104.2(8) and 108.3(8)°, respectively.

Acknowledgements—We thank the "Fondo de Desarrollo Científico y Tecnológico, Chile" (Grant No 460/93-95), Dirección de Investigación y Postgrado, Pontificia Universidad Católica de Chile (DIPUC) and Fundación Andes for financial support.

REFERENCES

1. (a) A. L. Balch, R. R. Guimererans, J. Linehan, M. M. Olmstead and D. E. Oram, *Organometallics*, 1985, **4,** 1445; (b) P. D. Enlow and C. Woods, *Organometallics*, 1983, **2,** 64.
2. J. P. Farr, F. F. Woods and A. L. Balch, *Inorg. Chem.* 1983, **22,** 3387.
3. (a) G. A. Anderson, *J. Organomet. Chem.* 1989, **368,** 365; (b) G. A. Anderson and R. Kumar, *J. Organomet. Chem.* 1988, **342,** 263; (c) G. A. Anderson and R. Kumar, *Inorg. Chim. Acta*, 1985, **97,** L21.
4. (a) Y. Fuchita, Y. Ohta, K. Hiraki, M. Kawatani and N. Nishiyama. *J. Chem. Soc., Dalton Trans.* 1990, 3767; (b) Y. Fuchita, K. J. Hardcastle, K. Hiraki and M. Kawatani, *Bull. Chem. Soc. Jpn*, 1990, **63,** 1961.
5. (a) A. R. Sanger, *Can. J. Chem.* 1984, **62,** 822; (b) A. R. Sanger, *Can. J. Chem.* 1983, **61,** 2214; (c) A. L. Sanger, C. G. Lobe and J. E. Weiner-Fedorak, *Inorg. Chim. Acta*, 1991, **53,** L123.
6. P. M. Maitlis, *Acc. Chem. Res.* 1978, **11,** 301.

7. M. A. Bennett, T. N. Huang, T. W. Matheson and A. K. Smith, *Inorg. Synth.* 1982, **21,** 74.
8. G. M. Sheldrick, *SHELXTL/PC.* Release 4.2 for Siemens Crystallographic Research System. Siemens Analytical X-Ray Instruments, Inc., Madison, WI, U.S.A., 1991.
9. G. M. Sheldrick, *SHELXL-93. Program for the Refinement of Crystal Structures.* University of Göttingen, Germany, 1993.
10. (a) M. Valderrama, R. Contreras, M. Bascuñan, S. Alegría and D. Boys, *Polyhedron*, 1995, **14,** 2239; (b) M. Valderrama and R. Contreras, *J. Organomet. Chem.* 1996, **513,** 7; (c) S. Muralidharan, J. H. Espenson and S. A. Ross, *Inorg. Chem.* 1986, **25,** 2557; (d) M. P. Brown, J. R. Fisher, R. Puddephatt, and K. R. Seddon, *Inorg. Chem.* 1979, **18,** 2808.
11. M. Valderrama, R. Contreras and D. Boys, Unpublished results.
12. P. E. Garrou, *Chem. Rev.* 1981, **81,** 229.
13. (a) D. Carmona, F. J. Lahoz, L. A. Oro, J. Reyes and M. P. Lamata, *J. Chem. Soc., Dalton Trans.* 1990, 3551; (b) D. Carmona, F. J. Lahoz, L. A. Oro, M. P. Lamata and S. Buzarra, *Organometallics*, 1991, **10,** 3132; (c) M. Valderrama, J. Cuevas, D. Boys, D. Carmona, M. P. Lamata, F. Viguri, R. Atencio, F. J. Lahoz and L. A. Oro, *J. Chem. Soc., Dalton Trans.*, 1996, 2877.
14. A. J. Blake, R. O. Gould, G. Reid and M. Shröder, *J. Organomet. Chem.* 1988, **356,** 389.
15. C. L. Raston and A. H. White, *J. Chem. Soc., Dalton Trans.* 1976, 32.
16. M. Esteruelas, M. Oliván, L. A. Oro, M. Schulz, E. Sola and H. Werner, *Organometallics*, 1992, **11,** 3659.
17. B. R. Sutherland and M. Cowie, *Inorg. Chem.* 1984, **23,** 2324.
18. P. Kramer, K. Polborn, H. Wanjek, I. Zahn and M. Beck, *Chem. Ber.* 1990, **123,** 767.

Pergamon

PII: S0277-5387(96)00493-7

Polyhedron Vol. 16, No. 11, pp. 1819-1824, 1997
© 1997 Elsevier Science Ltd
All rights reserved. Printed in Great Britain
0277-5387/97 $17.00+0.00

The synthesis and X-ray crystal structure of $S{=}CS_2C_2B_{10}H_{10}$

James D. McKinney, Thomas A. Hamor, Christopher J. Jones* and Keith Paxton

School of Chemistry, the University of Birmingham, Edgbaston, Birmingham B15 2TT, U.K.

(Received 12 September 1996; accepted 4 October 1996)

Abstract—The reactions of 1,2-dicarbadodecaborane-1,2-dithiol with tetrachloroethene, oxalyl chloride, phosgene, triphosgene and thiophosgene have been examined and $S{=}CS_2C_2B_{10}H_{10}$ isolated. The crystal structure of $S{=}CS_2C_2B_{10}H_{10}$ reveals a stacked arrangement of the planar $\{S_2C{=}S\}$ moieties present in the molecule, but intermolecular distances are all greater than the van der Waals contact distance, the shortest S···S distance of 3.552(1) Å lying between the singly bonded sulfurs, $S(CB_{10}H_{10}C)\cdots S(CB_{10}H_{10}C)$. © 1997 Elsevier Science Ltd. All rights reserved.

Keywords: dicarbaborane; thione; disulfur heterocycle; crystal structure.

Tetrathiafulvalene, TTF (Fig. 1), has played an important role in the development of new molecular materials, in particular stacked salts exhibiting electrical conductivity [1]. Elaboration of the TTF structure has given rise to a number of TTF analogues including BEDT-TTF [2] and *bis*benzotetrathiafulvalene, **1** (Fig. 1) [3]. Transition metal complexes exemplified by $[Ni(dmit)_2]^{2-}$ $\{dmitH_2 = S{=}CS_2C_2(SH)_2\}$ (Fig. 1) have also been synthesized [4]. Such compounds may be used to prepare new molecular materials and to allow the relationship between molecular structure and bulk properties to be examined in more detail. In order to provide a further example of a compound containing a $\{C_2S_2C{=}\}_2$ core, but in a rather different molecular environment from that found in existing examples of TTF analogues, we have been seeking a synthetic route to the carborane containing TTF analogue $B_{10}H_{10}C_2S_2C{=}CS_2C_2B_{10}H_{10}$, **2** (Fig. 1). This compound contains two sterically bulky 1,2-$C_2B_{10}H_{10}$ cages linked by a tetrathioethene moiety to give a structure incorporating a TTF core, but terminated by carborane cages. There are two features in this structure which distinguish it from other TTF derivatives. Firstly, the steric bulk of the carborane cages would create clefts above and below the $\{S_2C{=}CS_2\}$ moiety into which small planar molecules might fit. Secondly, the electron-withdrawing effects of the carborane cages might be expected to modify the electronic properties of the TTF like centre, increasing its electron affinity compared with TTF itself. In an attempt to make inroads into this area of chemistry we set out to try to synthesize **2**. Since benzene-1,2-dithiol is known to be a precursor for the preparation of **1**,[3] it was hoped that 1,2-dicarbadodecaborane-1,2-dithiol,[5] $3H_2$ (Fig. 1) might undergo similar reactions to afford **2**. A number of synthetic routes for converting **3** to **2** were investigated and these included the reactions of 1,2-dicarbadodecaborane-1,2-dithiol with tetrachloroethylene, oxalyl chloride, triphosgene, phosgene and thiophosgene.

RESULTS AND DISCUSSION

Synthetic studies

In the presence of the organic base $C_{10}H_8(NMe_2)_2$ (**4**, proton sponge), $3H_2$ failed to react with tetrachloroethylene. Only the salt [**4**H][**3**H] was isolated from the reaction mixture. This compound was identified by positive ion fast atom bombardment mass spectrometry {(+)FABMS} and by IR, ^1H and ^{11}B NMR spectroscopy [6]. The reaction between $3H_2$ and oxalyl chloride in the presence of **4** afforded an orange

*Author to whom correspondence should be addressed.

hygroscopic compound. The (+)FABMS spectrum of this product contains an ion envelope based at *m/z* 215, which corresponds to $4H^+$, together with an ion based at *m/z* 403. The negative ion FABMS {(−)FABMS}spectrum contains its highest mass ion cluster at *m/z* 402 which may correspond with the ion $[C_2B_{10}H_{10}(\mu\text{-}S_2)_2C_2B_9H_{10}]^-$ (**5**, Fig. 1). It is possible, therefore, that the positive ion at *m/z* 403 corresponds with the protonated form of this disulfide $[C_2B_{10}H_{10}(\mu\text{-}S_2)_2C_2B_9H_{11}]^+$. The IR spectrum of the product contains a strong IR band assigned to ν_{max}(BH) at 2500 cm^{-1}, showing the presence of the boron cage in addition to bands attributable to aromatic C—H deformations in the region 1400–1600 cm^{-1}. The conductivity of a 10^{-4} mol dm^{-3} solution of the compound in acetonitrile showed that the product was a 1 : 1 electrolyte and elemental analyses for C, H and N are consistent with the formulation $[4H][C_2B_{10}H_{10}(\mu\text{-}S_2)_2C_2B_9H_{10}]$. The failure to produce the expected product **2** in this reaction reflects the difference in reactivity between the carborane cage and the benzene ring.

No reaction between $3H_2$ and phosgene or triphosgene was observed in the presence of **4**. However, the reaction between $[Bu_4N]_2[Zn3_2]$ and phosgene afforded a white crystalline solid. The (−)FABMS of the product contains, as its highest mass species, an ion cluster based at *m/z* 223, which corresponds to the carbonyl species $(C_2B_9H_{10}S_2CO)^-$ (**6**, Fig. 1), whilst the (+)FABMS spectrum contains an ion at *m/z* 242, which corresponds to the Bu_4N^+ cation. A strong IR band assigned to ν_{max}(BH) was observed at *ca* 2550 cm^{-1}, showing the presence of the boron cage. A strong absorption band at 1626 cm^{-1} is also observed in the spectrum and may be due to a carbonyl stretch $\{\nu_{max}(CO)\}$, although this is at a much lower frequency than the 1671 cm^{-1} reported for ν_{max}(CO) in $C_5H_4S_4CO$ (**7**, Fig. 1) [7]. The conductivity of a 10^{-4} mol dm^{-3} solution of the compound in acetonitrile showed that the product was a 1 : 1 electrolyte and elemental analyses for C, H and N are consistent with the formulation $[Bu_4N][C_2B_9H_{10}S_2CO]$.

In the reactions described above, the use of carbonyl compounds with $3H_2$ in the presence of base appears to result in some degradation of the carborane cage to produce *nido*-$C_2B_9H_{11}^-$ derivatives. The oxophilic nature of the boron presumably contributes to this reactivity and so, to circumvent these degradation reactions, $3H_2$ was instead reacted with thiophosgene. This reaction afforded an orange oil from which yellow crystals of compound **8** (Fig. 1) were isolated by sublimation. The IR spectrum of **8** contains a strong IR band assigned to ν_{max}(BH) at 2550 cm^{-1}, showing the presence of the carborane cage. In addition, an

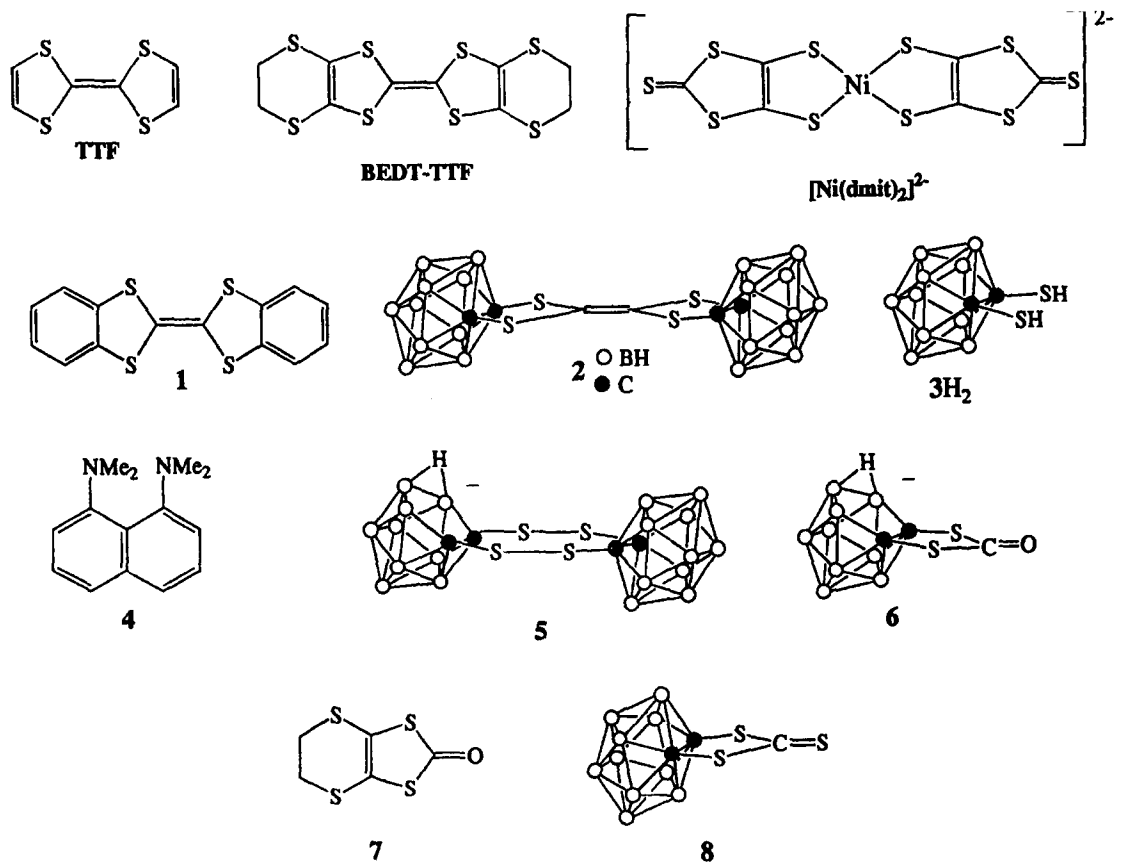


Fig. 1. Structural formulae of TTF, BEDT-TTF, $[Ni(dmit)_2]^{2-}$, **1**, **2**, $3H_2$, **4**, **7** and **8** and proposed structures for **5** and **6**.

intense absorption band is also present at 1091 cm^{-1}, which may be due to ν_{max}(CS); in the thione analogue of **7** ν_{max}(CS) appears at 1065 cm^{-1} [7]. The EI mass spectrum of **8** contains a molecular ion cluster based on m/z 250 with a second ion cluster at m/z 206 attributable to $[M - CS]^+$. The formulation of **8** as $C_2B_{10}H_{10}S_2C{=}S$ was confirmed by the single crystal X-ray diffraction study described below. Coupling of **8** would lead to the TTF analogue $(C_2B_{10}H_{10}S_2C)_2$. However, attempts to effect this coupling using reaction conditions described in published methods for related systems [8] were unsuccessful.

The electrochemical properties of $C_2B_{10}H_{10}S_2C{=}S$ were investigated using cyclic voltammetry. In dichloromethane solution **8** was reduced at a potential of -1.01 V, although the reduction process was both electrochemically and chemically irreversible. No oxidation wave was observed in the potential range 0 to $+1.4$ V. These results clearly demonstrate that **8** is not easily reduced or oxidised and so is not well suited for forming charge-transfer compounds with electron donors or acceptors.

Structural studies

The crystal structure of $C_2B_{10}H_{10}S_2C{=}S$ is shown in Fig. 2 [9]. The molecule has two-fold (C_2) symmetry, atoms S(2) and C(2) lying on the axis, which also passes through the centres of the C(1)—C(1*) and B(4)—B(4*) bonds. The S(2)—C(2) bond length is 1.621(3) Å, which is significantly shorter than the other C—S bonds in the molecule and corresponds in length to a C=S double bond [10,11]. This establishes the formulation of the molecule as a thione, $R_2C{=}S$. The other C—S bond lengths correspond to single bonds with C(1)—S(1) [1.781(2) Å] longer than the bond between S(1) and the sp^2-hybridized C(2) [1.747(2) Å]. Boron–boron and boron–carbon bonds in the cage range from 1.743 to 1.793, mean 1.778(4) Å, and 1.704 to 1.749, mean 1.727(12) Å, respectively. These values are in good agreement with those given by Allen *et al.*,[11] 1.775 Å for B—B and 1.716 Å for B—C in comparable cage structures [11]. The carbon–carbon bond length at 1.632(3) Å is similar to the long C—C lengths commonly found in dicarbadodecaborane structures [mean 1.659(2) Å for 104 structures extracted from the CSD] [12].

The molecules appear to pack in the crystal so that the C=S functions stack one on top of another (Fig. 3) [13]. However, there are no intermolecular contact distances shorter than the sum of the van der Waals radii, so that there is little or no π–π orbital overlap between these moieties. There are no abnormally short intermolecular contact distances. The closest S···S intermolecular contact is between single-bonded sulfurs, S(1)···S(1*), 3.552(1) Å (see Fig. 3).

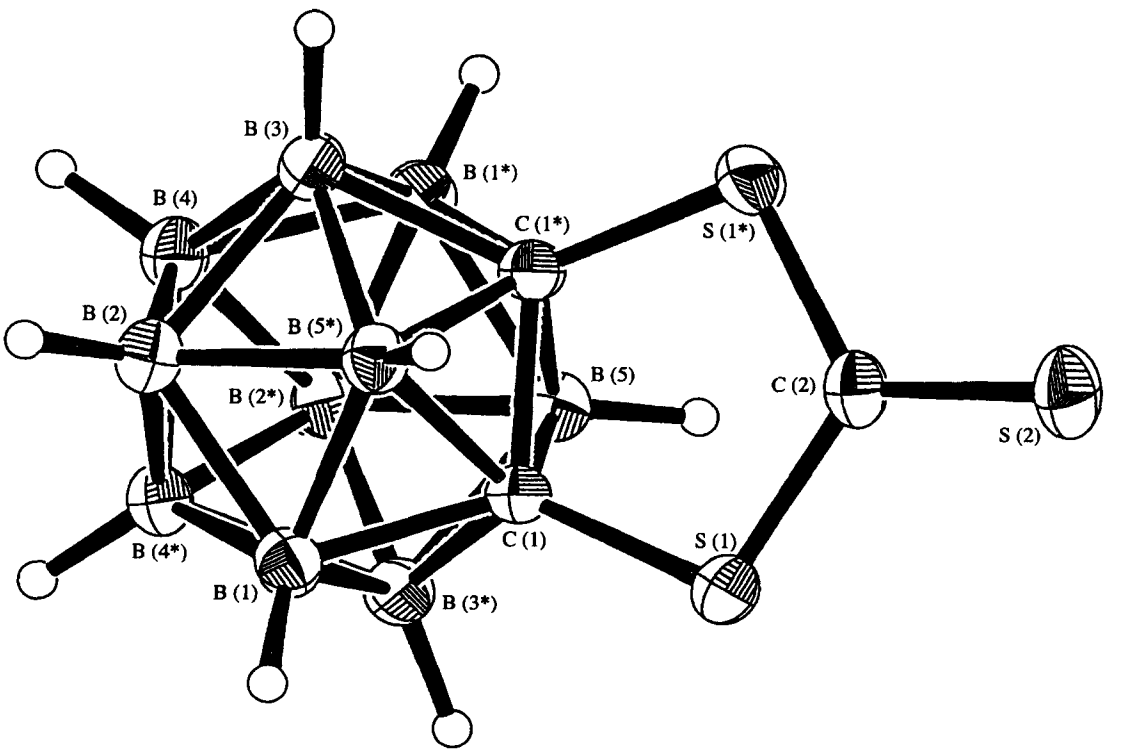


Fig. 2. ORTEP [9] view of the molecule of $C_2B_{10}S_2C{=}S$. Ellipsoids are drawn at the 50% probability level. "Starred" atoms are related to the corresponding unstarred ones by a crystallographic two-fold symmetry axis.

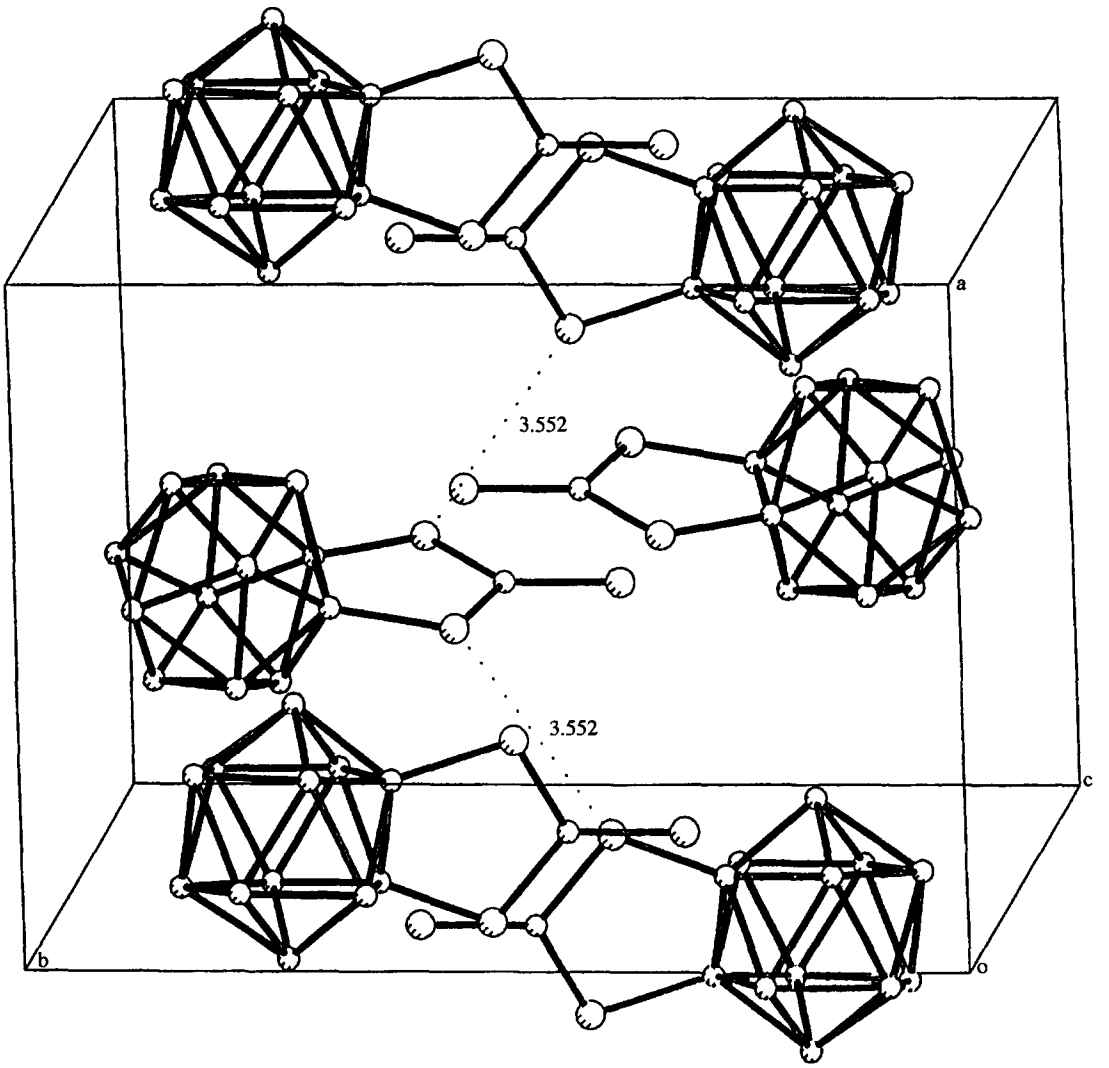


Fig. 3. Packing diagram for $C_2B_{10}S_2C{=}S$ showing the S···S contacts.[13]

EXPERIMENTAL

Synthetic studies

Reaction solvents were purified by distillation under nitrogen from standard drying agents before use. The reagents TTF [14] and $C_2B_{10}H_{10}(SH)_2$.[5] were prepared by literature methods. All commercial chemicals were pre-dried before use, but otherwise were used as received unless otherwise stated. Reactions were carried out under an atmosphere of dry nitrogen. IR spectra were recorded from KBr discs using a Perkin–Elmer 1600 series FT-IR spectrophotometer. ^{11}B NMR spectra were recorded at 87 MHz from dichloromethane and acetonitrile solutions using a Jeol GX270 spectrometer and ^{13}C (25 MHz) NMR spectra were recorded using a Brucker AC300 spectrometer. Mass spectra were recorded using a Kratos RF80 instrument with positive or negative ion fast atom bombardment of a *meta*-nitrobenzyl alcohol (NOBA) matrix. Conductivity measurements were recorded using a PTI 58 digital conductivity meter. Elemental analyses were performed by the Microanalytical Service, School of Chemistry, University of Birmingham or the Microanalytical Service, School of Chemistry, University of Sheffield.

Reaction of $C_2B_{10}H_{10}(SH)_2$ *with oxalyl chloride*

Proton sponge **4** (0.214 g, 1.0 mmol) was dissolved in THF (10 cm^3) and the solution added dropwise to a solution of $C_2B_{10}H_{10}(SH)_2$ (0.100 g, 0.48 mmol) in THF (10 cm^3). After vigorous stirring oxalyl chloride (0.032 g, 0.25 mmol) was added with caution. An immediate colour change from colourless to orange was observed. The solvent was removed *in vacuo* and the product purified by column chromatography using dichloromethane/hexane (50 : 50) as the eluants. The second orange band was collected and the solvent

removed *in vacuo* to yield an amorphous orange solid (0.090 g, 86%). Found: C, 35.3; H 6.5; N, 3.5. $C_{20}H_{40}B_{20}N_2O_2S_4$ requires: C, 35.1; H, 5.9; N, 4.1%. ν_{max} (BH): 2546 cm^{-1}, ^{11}B $\{^1H\}$ (CH_2Cl_2) δ: −18.74, −24.85, −26.12, −29.65 ppm; ^{13}C NMR ($CDCl_3$) δ: 165.2, 142.1, 135.7, 132.7, 126.2, 125.9, 125.1 ($C_{14}H_{19}N_2$), 83.1 ppm ($C_2B_{10}H_{10}(SH)_2$); mass spectrum *m/z* (*I* %): (+)FABMS, 215 (100) $[C_{14}H_{19}N_2]^+$, 200 (9) $[C_{13}H_{16}N_2]^+$, (−)FABMS, 402 (100) $[C_2B_9H_{10}S_4C_2B_{10}H_{10}]^-$. Λ_m 166 Ω^{-1} cm^2 mol^{-1}.

Preparation of $[Bu_4N]_2[Zn^{II}(C_2B_{10}H_{10}S_2)_2]$

$C_2B_{10}H_{10}(SH)_2$ (1.00 g, 4.8 mmol) was dissolved in THF (20 cm^3) and $ZnCl_2$ (0.34 g, 2.5 mmol) was added. The suspension was heated under reflux for 16 h. The solution was allowed to cool to room temperature. $[Bu_4N]Cl$ (1.39 g, 5.0 mmol) was dissolved in deionised water (5 cm^3) and added dropwise with stirring to this solution over a 10 min period. The solution was then stirred for a further hour, the solvent removed *in vacuo* and the residue dissolved in dichloromethane (10 cm^3). Any residual solid was removed by vacuum filtration. The solution was warmed (35°C) and hexane added until the product just started to precipitate. On standing a white microcrystalline solid deposited (2.12 g, 92%). Found: C, 44.8; H, 8.3; N, 4.0. $C_{36}H_{92}N_2S_4B_{20}Zn$ requires: C, 44.9 H, 9.6; N, 2.9%. ν_{max}(BH) 2559s cm^{-1}; ^{11}B $\{^1H\}$ (CH_2Cl_2) δ: −19.42, −25.70, −26.88, −29.00 ppm; mass spectrum *m/z* (I%): (+)FABMS, 242 (100) $[Bu_4N^+]$.

Reaction between $[Bu_4N]_2[Zn^{II}(C_2B_{10}H_{10}S_2)_2]$ *and phosgene*

A solution of phosgene in toluene (1.93 M, 0.17 cm^3) was added to a solution of $[Bu_4N]_2[Zn^{II}(C_2B_{10}H_{10}S_2)_2]$ (0.15 g, 0.16 mmol) in toluene (10 cm^3) and the mixture stirred vigorously for 30 min at room temperature then heated under reflux for a further 2 h. The solvent was removed *in vacuo* to yield a white solid which was collected and recrystallized twice from dichloromethane/hexane to yield large needle-shaped crystals (0.054 g, 78%). Found: C, 48.8; H, 10.0; N, 3.0. $C_{19}H_{46}B_9OS_2$ requires: C, 49.0; H, 10.0; N, 3.0%. ν_{max} (BH) 2538s, ν_{max} (C=O) 1626s cm^{-1}; mass spectrum *m/z* (I%): (+)FABMS, 242 (100) $[Bu_4N]^+$; (−)FABMS, 223 (100) $[C_2B_9H_9S_2CO]^-$, Λ_m 171 Ω^{-1} cm^2 mol^{-1}.

Preparation of $C_2B_{10}S_2C{=}S$ (**8**)

To an ice-cold, nitrogen blanketed solution of $C_2B_{10}H_{10}(SH)_2$ (0.25 g, 1.2 mmol) in THF (25 cm^3), thiophosgene (0.17 g, 1.5 mmol) was added with stirring to this solution over a 10 min period. The mixture was stirred vigorously for 30 min at 0°C, allowed to warm up to room temperature, heated under reflux for 2 h, allowed to cool to room temperature and any solid was removed by vacuum filtration. The filtrate was then evaporated *in vacuo* and the $C_2B_{10}H_{10}S_2C{=}S$ formed was extracted from the orange residue using dry hexane. The hexane solution was filtered under vacuum and the filtrate then evaporated *in vacuo* to yield a yellow solid. Further purification was achieved by sublimation at room temperature *in vacuo* (0.144 g, 48%). Found: C, 18.7; H, 4.7; N, 0.00. $C_3H_{10}B_{10}S_3$ requires: C, 14.4; H, 4.0; N, 0.00%. ν_{max} (BH) 2611s, 2601s, 2589, ν_{max} (C=S) 1092 cm^{-1}; mass spectrum *m/z* (I %): EI, 250 (100) $[M]^+$, 206 (44) $[M - CS]^+$, 173 (41) $[M - CS_2]^+$, 161 (25) $[M - C_2S_2]^+$; Λ_m 0 Ω^{-1} cm^2 mol^{-1}.

Structural studies

1197 independent reflections (θ 3 to 27°), with $I > \sigma(I)$, measured on a Rigaku R-AXIS II area detector diffractometer, were used in the analysis.

Crystal data. $C_3H_{10}B_{10}S_3$, $M_r = 250.4$, orthorhombic, space group *Pcca*, $a = 9.478(5)$, $b = 13.137(7)$, $c = 9.669(6)$ Å, $U = 1204$ $Å^3$, $Z = 4$, $D_c = 1.381$ g cm^{-3}, μ(Mo-K_α) = 0.566 mm^{-1}, $\lambda = 0.71069$ Å.

The structure was determined [15] by direct methods and refined [16] by least-squares using anisotropic thermal parameters for all the non-hydrogen atoms. Hydrogen atoms were located from difference maps and were refined with isotropic temperature factors. Final $R = 0.0352$ for 1069 observed reflections [$I > 2\sigma(I)$] and 0.0464 for all 1197 data. Residual electron density in a final difference map was within the range −0.31 to 0.18 e $Å^{-3}$.

Supplementary material. Atomic coordinates, thermal parameters, full lists of bond lengths and angles, crystal data and refinement details.

Acknowledgement—We are grateful to EPSRC for supporting this work through a studentship (J.D.McK.) and through a grant GR/G44390.

REFERENCES

1. (a) F. Wudl, G. M. Smith and E. F. Hufnagel, *J. Chem. Soc., Chem. Commun.* 1453, 1970; (b) A. F. Garito and A. J. Heeger, *Acc. Chem. Res.* 1974, **7,** 232; (c) Kreif, A., *Tetrahedron*, 1986, **42,** 1209; (d) T. K. Hansen and J. Becher, *Adv. Mat.* 1993, **5,** 288; (e) T. Jørgensen, T. K. Hansen and J. Becher, *Chem. Soc. Rev.* 1994, **23,** 41.
2. (a) T. J. Enge, W. A. Bryden, F. M. Wiygul, D. O. Cowan, T. J. Kistenmacher and A. N. Bloch, *J. Chem. Phys.* 1982, **77,** 3188; (b) A. Bondi, *J. Phys. Chem.* 1964, **68,** 441.
3. (a) W. R. H. Hurtley and S. S. Smiles, *J. Chem. Soc.* 2263, 1926; (b) J. Nakayama, *Synthesis*, 1975, 168; (c) C. A. Brown, R. D. Miller, C. M. Lindsey and K. Smith, *Tetrahedron Lett.* 1984, 991; (d) C. M. Lindsey, K. Smith, C. A. Brown

and K. Betterton-Cruz, *Tetrahedron Lett.* 1984, 995.
4. (a) J. R. Ferraro and J. M. Williams, *Introduction to Synthetic Electrical Conductors*, Academic Press, New York, (1987), pp 1–327. (b) M. Williams, A. J. Schultz, A. E. Underhill and D. M. Watkins, *Extended Linear Chain Compounds*, Vol. 1. Plenum Press, New York, (1982), p. 73.
5. H. D. Smith Jr, C. O. Obenland and S. Papetti, *Inorg. Chem.* 1966, **5,** 1013.
6. The positive ion FABMS contains an ion at *m/z* 215 corresponding with the presence of **4** H^+, whilst the negative ion FABMS contains an ion cluster based at *m/z* 207 corresponding with the anion **3**H^-. The ^{13}C NMR of [**4**H][**3**H] confirms the presence of these two ions and exhibits eight different carbon environments, seven associated with **4**H^+ and a further signal due to **3**H^-. In accord with this the IR spectrum contained characteristic aromatic C—H stretching bands in the region 1400–1600 cm^{-1} attributable to the presence of the cation **4**H^+. The conductivity of a solution of [**4**H][**3**H] in acetonitrile was typical of a 1 : 1 electrolyte.
7. T. K. Hansen, J. Becher, T. Jørgensen, K. S. Varma, R. Khedeker and M. P. Cava, *Org. Synth.* 1996, **73,** 270.
8. (a) T. K. Hansen, T. Jørgensen, P. C. Stein and J. Becher, *J. Org. Chem.* 1992, **57,** 6403; (b) J. Röhrich, P. Wolf, V. Enkelmann and K. Müllen, *Angew. Chem.* 1988, **100,** 1429.
9. C. K. Johnson, *ORTEPII.* Report ORNL-5138. Oak Ridge National Laboratory, Tennessee, U.S.A., 1976.
10. (a) M. Bousseau, L. Valade, J.-P. Legros, P. Cassoux, M. Garbauskas and L. V. Interrante, *J. Am. Chem. Soc.* 1986, **108,** 1908; T. A. James and J. A. McCleverty, *J. Chem. Soc. A*, 1970, 3308.
11. F. H. Allen, O. Kennard, D. G. Watson, L. Brammer, A. G. Orpen and R. Taylor, *J. Chem., Soc. Perkin Trans.* 2, 1987, S1.
12. *CSD.* Cambridge Structural Database (April 1996 release). Cambridge Crystallographic Data Centre, Cambridge CB2 1EZ, U.K., 1996.
13. W. D. S. Motherwell and W. Clegg, *PLUTO* 88. *Program for Plotting Molecular and Crystal Structures.* Cambridge Structural Database System, Users Manual, Part II, Cambridge, 1988 (implemented at the Manchester Computing Centre).
14. F. Wudl and M. L. Kaplan, *J. Org. Chem.* 1974, **39,** 3608.
15. *TeXsan. Single Crystal Analysis Software*, Version 1.6. Molecular Structure Corporation, The Woodlands, TX 77381, U.S.A., 1993.
16. G. M. Sheldrick, *SHELXL*-93. *Program for Crystal Structure Refinement.* University of Gottingen, Germany, 1993.

Pergamon

PII: S0277-5387(96)00487-1

Polyhedron Vol. 16, No. 11, pp. 1825–1829, 1997
© 1997 Published by Elsevier Science Ltd
All rights reserved. Printed in Great Britain
0277-5387/97 $17.00+0.00

Oxovanadium binuclear (IV) Schiff base complexes derived from aroyl hydrazones having subnormal magnetic moments

Sumita. N. Rao,[a] D. D. Mishra,[a] R. C. Maurya[a]* and N. Nageswara Rao[b]

[a]Department of Post Graduate Studies and Research in Chemistry, Rani Durgavati Vishwavidyalaya, Jabalpur 482 001, India; [b]Central Salt & Marine Chemicals Research Institute, Bhavnagar 364 002, India

(Received 25 June 1996; accepted 4 October 1996)

Abstract—Oxovanadium(IV) complexes of aroyl hydrazone Schiff bases, *viz.* salicyloyl, nicotinoyl and benzoyl hydrazones, have been synthesized and characterized by elemental analysis, spectroscopy (IR and UV–vis) methods, magnetic susceptibility, EPR measurements, molar conductance and cyclic voltammetry studies. The room-temperature magnetic moments of the complexes are in the range 0.97–1.03 B.M. and are indicative of the presence of anti-ferromagnetic exchange. A binuclear structure has been proposed for the complexes.
© 1997 Published by Elsevier Science Ltd. All rights reserved.

Keywords: Schiff base complexes; oxovanadium(IV); aroyl hydrazones; magnetic moments.

The oxovanadium(IV) ion, VO^{2+}, is considered to be the most stable oxocation of the first-row transition metal ion [1]. It forms stable anionic, cationic and neutral complexes with various types of ligands. Monomeric and five coordinate oxovanadium(IV) complexes are formed with several bidentate Schiff bases, but dimeric and five- or six-coordinate complexes are formed with tridentate Schiff bases [2–5]. Recently, there has been considerable research interest in the study of the magnetic exchange behaviour of polymetallic oxovanadium (IV) complexes [4]. The dibasic tridentate ligands are expected to give such polymetallic oxovanadium complexes, since these ligands will satisfy the valence as well as the coordination number of the metal ion by forming the polymetallic complexes. It is also known that the coordination complexes of aroylhydrazones act as enzyme inhibitors [6] and are useful due to their pharmacological applications [7–9]. In view of the above, we report the synthesis and characterization of some oxovanadium(IV) complexes of benzoyl, salicyloyl and nicotinoyl hydrazones derived from benzoic acid hydrazide, salicylic acid hydrazide and nicotinic acid hydrazide with 4-benzoyl-3-methyl-1-phenyl-5-pyrazolone (BMPHP) and 4-nitrobenzoyl-3-methyl-1-phenyl-5-pyrazolone (NBMPHP). The complexes were characterized by elemental analysis, molar conductance, spectroscopic methods (IR and UV–vis), magnetic susceptibility, EPR measurements and cyclic voltammetry.

*Author to whom correspondence should be addressed.

EXPERIMENTAL

Synthesis of ligands

4-Benzoyl-3-methyl-1-phenyl-5-pyrazolone (BMPHP) and 4-nitrobenzoyl-3-methyl-1-phenyl-5-pyrazolone (NBMPHP) were prepared according to the reported method [10]. The ligands, BMPHP-BH (**1a**), BMPHP-SH (**2a**), BMPHP-NH (**3a**), NBMPHP-BH (**4a**), NBMPHP-SH (**5a**) and NBMPHP-NH (**6a**) were prepared by a general method in which a 1:1 hot ethanolic solution of BMPHP or NBMPHP and benzoic acid hydrazide (BH), salicylic acid hydrazide (SH) and nicotinic acid hydrazide (NH) were taken and refluxed for 3–4 h. After cooling, the solution was then poured into an excess of distilled water (250 cm^3), whereupon a yellow precipitates of the ligands were obtained from their respective solutions. The precipitate thus obtained

was filtered, washed with water and then dried *in vacuo*. Yield 60–70%.

Synthesis of oxovanadium(IV) *complexes*

Vanadyl sulfate was used as a precursor for the synthesis of oxovanadium(IV) complexes. In a general procedure, the oxovanadium(IV) Schiff base complexes $[V_2O_2(BMPHP\text{-}BH)_2]$ (**1b**), $[V_2O_2(BHPHP\text{-}SH)_2]$ (**2b**), $[V_2O_2(BMPHP\text{-}NH)_2]$ (**3b**), $[V_2O_2(NBMPHP\text{-}BH)_2]$ (**4b**), $[V_2O_2(NBMPHP\text{-}SH)_2]$ (**5b**) and $[V_2O_2(NBMPHP\text{-}NH)_2]$ (**6b**) were prepared by adding a hot methanolic solution of the Schiff base ligand to the hot methanolic solution of vanadyl sulphate in a 2 : 1 ratio, respectively, and the resulting solution was refluxed for 6 h. On cooling the reaction mixture, the precipitates of the complexes were obtained from their respective solutions, which were then filtered, washed with methanol and then dried *in vacuo*. Yield 55–60%.

All the chemicals and solvents used in this study were of analytical reagent grade.

Physical measurements

Microanalyses (C,H,N) of the ligands and complexes were carried out on a Carlo-Erba 1106 elemental analyser. Solution electrical conductivity was measured at 298 K using a Digisun Electronics Conductivity meter. IR spectra were recorded on FTS-40 FT-IR instrument (Bio-Rad, USA) as Nujol mulls/KBr pellets. Electronic spectra were recorded in DMF solution on a Shimadzu UV-160 spectrophotometer. Magnetic susceptibility measurements (Gouy Balance) were made at room temperature using $CuSO_4 \cdot 5H_2O$ as a calibrant. EPR spectra of the samples were recorded as powder samples at room temperature using DPPH as the *g*-marker. Cyclic voltammetry traces of the complexes were recorded on a Princeton Applied Research Model 384B polarographic analyser.

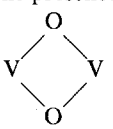
RESULTS AND DISCUSSION

The analytical data and IR data of the ligands are presented in Table 1. In the IR spectra of ligands $\nu_{(O\text{-}H)}$, $\nu_{(N\text{-}H)}$, $\nu_{(C\text{-}O)}$, $\nu_{(C\text{=}N)}$ and $\nu_{(C\text{-}O)}$ appear at 3510, 3360–3300, 1650, 1630–1610 and 1180–1185 cm^{-1}, respectively. The structure of the tridentate Schiff base ligands in general can be written as shown in Scheme. I(a).

Vanadyl sulfate reacts with these tridentate ligands in methanol to give stable VO^{IV} ligand-bridged binuclear complexes **1b–6b**. The analytical and IR data for the complexes **1b–6b** (Table 1) support the given formulation for the complexes. The low molar conductance values (7–10 Ω^{-1} cm^{-1} mol^{-1}) of freshly prepared solutions of the complexes **1b–6b** in acetonitrile solvent showed that they are non electrolytes.

IR spectra

In the IR spectra of the complexes (Table 1), the $\nu_{(v=o)}$ mode [11] was seen in the region 940–960 cm^{-1}. The bands due to $\nu_{(N\text{-}H)}$ and $\nu_{(C\text{-}O)}$ were absent in all the complexes and the presence of bands at 1600 and 1595 cm^{-1} suggests the enolization of the —C=O of the aroyl keto group giving rise to the —C=N—N=C moiety [12]. Of the two bands at 1600 and 1595 cm^{-1}, one may be due to the new $\nu_{(C\text{=}N)}$ and the other may be attributed to the original $\nu_{(C\text{=}N)}$, which has undergone shift to lower wavenumber by 20–25 cm^{-1}, suggesting the coordination of azomethine nitrogen to the metal center. This enolization is further evidenced by the appearance of a new band due to $\nu_{(C\text{-}O)}$, which was observed in the region 1171–1200 cm^{-1} (Table 1). The increase in original pyrazolone based $\nu_{(C\text{-}O)}$ 1210–1215 cm^{-1} compared with the free ligand suggests its coordination to the metal center. This shift of $\nu_{(C\text{-}O)}$ 1180–1210 cm^{-1} by 20–30 cm^{-1} may be due to the presence of



bridge formed by the enolic oxygens [13–15]. In all the complexes the peak due to $\nu_{(O\text{-}H)}$ was absent, indicating the deprotonation of the —OH group. In complexes **2b** and **5b** the peak due to salicyloyl —OH was intact and its $\nu_{(C\text{-}O)}$ did not show any shift compared with the free ligand (1140 cm^{-1}), indicating its nonparticipation in complexation.

Electronic spectra

Usually, the electronic spectra of the square-pyramidal oxovandium(IV) complexes (d^1) are characterized by the presence of three absorption bands corresponding to $d_{xy} \rightarrow d_{xz}$, d_{yz}, $d_{xy} \rightarrow d_{x^2-y^2}$ and $d_{xy} \rightarrow d_{z^2}$ transitions [16]. Similarly, in the electronic spectra of the present complexes three absorption bands were observed in the ranges 13,240–15,300, 18,100–20,000 and 23,200–23,410 cm^{-1}. The second band at 18,100–20,000 cm^{-1} appeared as a shoulder. The band due to LMCT may have merged with the third band (23,200–23,410 cm^{-1}).

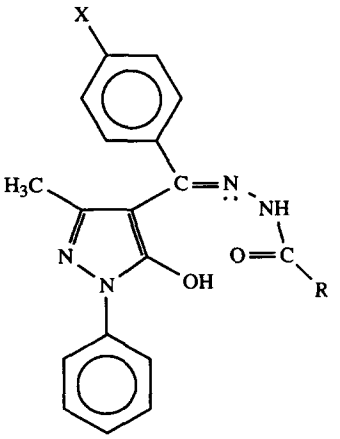
Magnetic measurement

The oxovanadium(IV) ion belongs to the $S = 1/2$ system. The magnetically dilute oxovanadium(IV) complexes usually exhibit magnetic moments close to their spin-only value of 1.73 B.M. The magnetic moments of the present complexes at room temperature were found to be in the range 1.02–1.08 B.M.

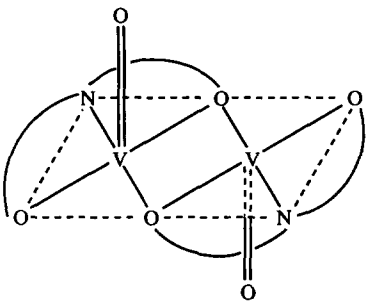
Table 1. Decomposition temperature (T_d), magnetic moments (μ_{eff}), elemental analysis, IR data, EPR parameters and cyclic voltammetry data for the Schiff base ligands (**1a–6a**) and VO^{IV} Schiff base complexes (**1b–6b**)

Ligand/Complex	T_d (°C)	μ_{eff}[a] (B.M)	Elemental Analysis (%)[b]			IR data (cm^{-1})[c]				EPR data			CV data[d]	
			C	H	N	$\nu_{V=O}$	$\nu_{C=N}$	$\nu_{C=O}$	$\nu_{C=O}$	$g_\perp$	$g_\parallel$	g_{av}	$V^{IV,III}$	$V^{IV,V}$
1a BMPHP-BH		—	72.5	4.9	14.3	—	1630	1650	1180					
	100		(72.7)	(5.0)	(14.1)									
1b $[V_2O_2(BMPHP\text{-}BH)_2]$	>250	1.03	62.3	3.9	11.9	958	1610	—	1176	1.98	1.97	1.97	−0.796	+0.85
			(62.4)	(3.9)	(12.1)		1595		1210					
2a BMPHP-SH		—	70.0	4.7	13.5	—	1625	1645	1140					
	155		(69.9)	(4.8)	(13.6)				1185					
2b $[V_2O_2(BMPHP\text{-}SH)_2]$	>250	1.01	61.0	3.9	11.8	958	1600	—	1140	1.96	1.95	1.95	−0.785	+0.85
			(60.4)	(3.7)	(11.7)		1594		1170					
									1200					
3a BMPHP-NH		—	69.4	4.7	17.5	—	1630	1647	1185					
	150		(69.5)	(4.7)	(17.6)									
3b $[V_2O_2(BMPHP\text{-}NH)_2]$	>250	0.98	60.0	3.7	15.2	948	1610	—	1170	1.98	1.97	1.97	−0.648	+0.85
			(59.7)	(3.6)	(15.1)		1597		1197					
4a NBMPHP-BH		—	65.1	4.3	15.7	—	1620	1645	1180					
	110		(65.3)	(4.3)	(15.8)									
4b $[V_2O_2(NBMPHP\text{-}BH)_2]$	>250	1.03	55.5	4.1	13.0	950	1600	—	1170	1.99	1.98	1.98	−0.50	+1.70
			(55.6)	(4.1)	(12.9)		1590		1210					
5a NBMPHP-SH			63.0	4.1	15.3	—	1620	1650	1140					
	152		(63.0)	(4.1)	(15.3)				1182					
5b $[V_2O_2(NBMPHP\text{-}SH)_2]$	>250	1.01	55.2	3.2	13.5	950	1610	—	1140	1.98	1.97	1.97	−0.48	+1.65
			(55.1)	(3.2)	(13.4)		1595		1170					
									1215					
6a NBMPHP-NH			62.5	3.9	19.0	—	1620	1650	1180					
	140		(62.4)	(4.0)	(19.0)									
6b $[V_2O_2(NBMPHP\text{-}NH)_2]$	>250	0.97	54.1	3.7	16.4	960	1600	—	1170	1.98	1.97	1.97	−0.48	+1.65
			(54.2)	(3.5)	(16.5)		1590		1210					

[a] TIP = 50×10^{-6} cgs units, $\mu_{eff} = 2.84\ (\chi_M^{corr}T)^{1/2}$ B. M.
[b] Found (Calcd).
[c] In KBr pellets.
[d] Glassy carbon electrode, CH_3CN solvent, $Bu_4N^+PE_6^-$ supporting electrolyte, Ag/AgCl reference electrode.



(a)



(b)

LIGANDS

1a X = H R = 

2a X = H R = 

3a X = H R = 

4a X = NO_2 R = 

5a X = NO_2 R = 

6a X = NO_2 R = 

Scheme 1

(Table 1), which were significantly lower than the spin-only value. There exist several reports in the literature on oxovanadium(IV) complexes with tridentate Schiff base ligands having subnormal magnetic moments [17]. The low magnetic moments may arise due to the antiferromagnetic spin–spin interation between the neighboring oxovanadium (IV) centers [18].

The EPR spectra of the complexes recorded for polycrystalline solid complexes at room temperature exhibited a weak band at 1600 G due to a spin forbidden $\Delta M_s = \pm 2$ transition [18]. This indicates the presence of triplet state dimeric species. The $g_\perp$ and $g_\parallel$ values for the complexes **1b–6b** are 1.98 + 0.02 and 1.97 ± 0.02, respectively, with $g_{av} = 1.97 \pm 0.02$ (Table 1). The EPR spectra of all the complexes are similar, indicating the similarity in the structure of these complexes.

Cyclic voltammetry

The cyclic voltammograms (scan range +1.3 to −1.8 V *vs* Ag/AgCl) for the complexes **1b–6b** in acetonitrile consist of an irreversible reduction wave in the range −0.48 to −0.796 V (Table 1). This irreversible reduction may be attributed to reduction of V^{IV} to V^{III}. The V^{IV} to V^{V} oxidation in complexes **1b–3b** occurred at +0.85 V (irreversible), whereas for complexes **4b–6b** (with Schiff bases of NBMPHP) the same occurred at +1.65 to +1.70 V. The corresponding Schiff base ligands **4a–6a** did not exhibit any oxidation wave in this region, but showed a reversible redox couple at −0.98 ± 0.03 V. The reduction of V^{IV} in **4b–6b** is relatively easy compared with that in **1b–3b**, whereas its oxidation is apparently difficult in **4b–6b** requiring potentials as high as +1.65 V. Electrochemical measurements of oxovanadium(IV) complexes with tridentate dibasic Schiff base ligands are reported [19] to show oxidation to V^{V} and reduction to V^{III} at +0.98 to +1.26 and −1.08 to −1.50 V *vs* SCE, respectively.

Thus, on the basis of the above discussions, it is evident that the present Schiff base ligands behave as dibasic tridentate ligands which on reaction with VO^{2+} form stable binuclear oxovanadium(IV) com-

plexes bridging through enolic oxygens. The neighboring vanadyl groups participate in spin–spin exchange interaction leading to subnormal magnetic moments. A square-pyramidal geometry is proposed for the binuclear complexes, as shown in Scheme I(b).

Acknowledgments—NSR is grateful to CSIR, New Delhi, for awarding Research Associateship. Authors wish to thank Professor P. Natarajan (Director) and Sophisticated Instrumentation Section, C.S.M.C.R.I, Bhavnagar, for providing analytical facilities.

REFERENCES

1. N. D. Chasteen, *Biological Magnetic Resonance*, Vol. 3. Plenum Press, New York, 1981, p. 54.
2. A. Syamal and L. J. Theriot, *J. Coord. Chem.* 1973, **2,** 193.
3. A. P. Sinsberg, E. Roubek, and H. J. Williams, *Inorg. Chem.* 1966, **5,** 1656.
4. A. Syamal, *Coord. Chem. Rev.* 1975, **16,** 309.
5. U. Casellato, P. Vigato and M. Vidali, *Coord. Chem. Rev.* 1977, **23,** 31.
6. J. C. Craliz, J. C. Rub, D. Willis and J. Edger, *Nature*, 1955, **34,** 176.
7. J. R. Dilworth, *Coord. Chem. Rev.* 1976, **21,** 29.
8. J. R. Merchant and D. S. Clothia, *J. Med. Chem.* 1970, **13,** 335.
9. N. S. Biradar and G. R. Havinale, *Inorg. Chim. Acta*, 1976, **17,** 157.
10. H. C. Arora and G. N. Rao, *Ind. J. Chem., Sect. A*, 1981, **20A,** 539.
11. J. Selbin, *Chem. Rev.* 1965, **65,** 153; *Coord. Chem. Rev.* 1966, **1,** 293.
12. L. E. Sayed and M. F. Iskander, *J. Inorg. Nucl. Chem.* 1971, **33,** 435.
13. E. Sinn and C. M. Harris, *Coord. Chem. Rev.* 1969, **4,** 39.
14. T. Tokii, Y. Muto, M. Kato and H. B. Jonassen, *J. Inorg. Nucl. Chem.* 1972, **34,** 3377.
15. A. Syamal and K. S. Kale, *Ind. J. Chem. Sect. A*, 1981, **20A,** 205.
16. L. G. Vanquickenborne and S. P. McGlynn, *Theoret. Chim. Acta*, 1968, **9,** 390.
17. L. V. Boas and J. C. Pessoa, *Comprehensive Coordination Chemistry*, ed. Sir G. Wilkinson, Vol. 3. Pergamon Press, Oxford 1987, p. 484, and reference therein
18. A. Syamal and K. S. Kale, *Ind. J. Chem., Sect. A*, 1980, **19A,** 486.
19. R. N. Mohanty, V. Chakravorthy and K. C. Dash, *Ind. J. Chem. Sect. A*, 1991, **30A,** 454.

Pergamon

PII: S0277-5387(96)00497-4

Polyhedron Vol. 16, No. 11, pp. 1831–1835, 1997
© 1997 Elsevier Science Ltd
All rights reserved. Printed in Great Britain
0277-5387/97 $17.00+0.00

An efficient synthetic route to tribridged dimolybdenum compounds: synthesis and structural characterization of dichlorotris (μ-*N*,*N*′-diarylformamidinato)-dimolybdenum(II,III), Aryl = phenyl and *p*-tolyl

F. Albert Cotton,[a]* Glenn T. Jordan IV,[a] Carlos A. Murillo,[a*,b] and Jianrui Su[a]

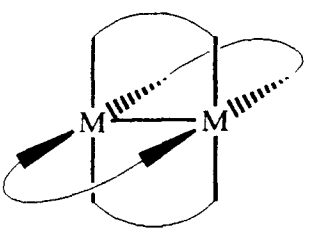
[a]Department of Chemistry and Laboratory for Molecular Structure and Bonding, Texas A&M University, College Station, TX 77843, U.S.A.
[b]Department of Chemistry, University of Costa Rica, Ciudad Universitaria, Costa Rica

(Received 22 August 1996; accepted 2 October 1996)

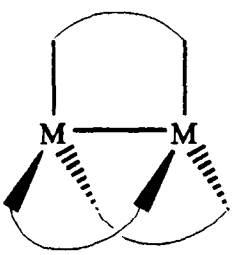
Abstract—A method for the preparation of $Mo_2(DTolF)_3Cl_2$, **I**, $DTolF^- = [N,N'$-di-*p*-tolylformamidinate] and $Mo_2(DPhF)_3Cl_2$, **II**, $DPhF^- = [N,N'$-diphenylformamidinate] from the reaction of the corresponding tetraformamidinate compound with one equivalent of ferrocenium chloride and chlorotrimethylsilane is described. X-ray crystallography shows that the structures of both of these mixed valent compounds are essentially the same. Each structure consists of three bridging amidinate ligands with two chloride ions *trans* to one of the amidinate ligands and the molecule has virtual C_{2v} symmetry. The metal–metal bond lengths are 2.1510(5) Å for **I** and 2.148(1) Å for **II**. © 1997 Elsevier Science Ltd. All rights reserved.

Keywords: dimolybdenum(II,III), tribridged; formamidinato; starting material; crystal structure.

One of the most prevalent motifs in the chemistry of dinuclear transition metal compounds is the so-called tetragonal lantern structure in which two metal centers are bridged by four ligands, such as carboxylates and amidinates [1].



Recently, we prepared a new class of dinuclear compounds in which the dinuclear unit is bridged by three amidinate ligands. These neutral trigonal lantern complexes, known only for Fe [2] and Co [3], possess an idealized D_{3h} symmetry.



We hope to prepare more of the latter using other transition metals. However, we have encountered a lack of potential starting materials. One obvious approach is the reduction of tetraformamidinates containing the M_2^{4+} core with subsequent elimination of one of the bridging groups, but this has not been successful in our hands. Thus, we have decided to seek other methods.

A recent report [4], described the preparation and

*Authors to whom correspondence should be addressed.

structural characterization of $Tc_2(DPhF)_3Cl_2$, which contains three bridging formamidinate groups and a chloride attached to each Tc atom. This type of structural arrangement looks very appealing for the accomplishment of our goal. Unfortunately, the reaction by which it was synthesized yielded a mixture of the tribridged and the tetrabridged species, $Tc_2(DPhF)_4Cl$. In this paper, we report the synthesis and structural characterization of two new dimolybdenum complexes of the type $Mo_2(DArF)_3Cl_2$ prepared by a designed route in good purity and yield.

EXPERIMENTAL

Material and methods

All manipulations were carried out by employing standard Schlenk techniques under nitrogen. Tetrahydrofuran, toluene, diethyl ether, and hexanes were freshly distilled from Na/K benzophenone, and dichloromethane was distilled from CaH_2 prior to use. *N,N'*-Diphenylformamidine (HDPhF) and $(CH_3)_3SiCl$ were purchased from Aldrich and used as received. Chlorotrimethylsilane solutions were freshly prepared in THF prior to use. Ferrocenium chloride was prepared by bubbling Cl_2 through a hexane solution of ferrocene. Di(*p*-tolyl)formamidine (HDTolF) was synthesized by high temperature condensation between toluidine and triethyl orthoformate using a slightly modified published procedure [5]. $Mo_2Cl_4(PPh_2Me)_4$ [6], $Mo_2(DPhF)_4$ and $Mo_2(DTolF)_4$ [7] were prepared as reported. Infrared spectral data were recorded as KBr pellets using a Perkin–Elmer 16PC FT-IR spectrophotometer at 2 cm^{-1} resolution. Electronic absorption spectra were measured on a Cary 17 spectrophotometer. Elemental analyses were performed by Canadian Microanalytical Service, Delta, British Columbia. Single crystal X-ray diffraction studies were done on an Enraf-Nonius FAST diffractometer equipped with an area detector, utilizing the software program MADNES [8].

$Mo_2(DTolF)_3Cl_2$ (**I**)

In a 200 cm^3 round-bottom flask, 0.544 g (0.501 mmol) of $Mo_2(DTolF)_4$ was dissolved in 40 cm^3 of THF and 60 cm^3 of toluene. A ferrocenium chloride solution, prepared by dissolving 0.112 g (0.507 mmol) of $[Cp_2Fe]Cl$ in 20 cm^3 of THF, was added slowly over a 25 min period. The color of the solution changed from bright yellow to dark brown. The resulting solution was stirred for 1 h at room temperature, after which, 0.51 mmol of $(CH_3)_3SiCl$ was added. The solution was refluxed for 2 h. After removal of the solvent, the brown free-flowing powder was washed with several small portions of Et_2O and then several small portions of hot hexanes. The solid was dissolved in 17 cm^3 of CH_2Cl_2 and layered with hexanes to yield a large crop of dark brown crystals (0.241 g, 51.4%) of **I**. Found: C, 57.6; H, 4.9; N, 8.9; Cl, 8.5. Calc. for $Mo_2Cl_2N_6C_{45}H_{45}$: C, 57.9; H, 4.9; N, 9.0; Cl, 7.6%. IR (KBr, cm^{-1}): 3026(w), 2919(w), 2858(w), 1609(w), 1517(s), 1505(vs), 1311(s), 1298(s), 1213(s), 1113(w), 1017(w), 967(w), 936(m), 822(m), 813(m), 499(w), 488(w), 416(m). UV/vis (CH_2Cl_2): λ = 515(sh) nm; 445 nm; 278 nm.

$Mo_2(DPhF)_3Cl_2$ (**II**)

In a 200 cm^3 round-bottom flask, 0.486 g (0.500 mmol) of $Mo_2(DPhF)_4$ was suspended in 40 cm^3 of THF and 40 cm^3 of toluene. Ferrocenium chloride (0.510 mmol) was added slowly from a solid addition tube over a 20 min period. The resulting dark brown solution was stirred for 1 h at room temperature, after which, 0.50 mmol of $(CH_3)_3SiCl$ was added. The solution was refluxed for 1 h and then filtered to remove unreacted $Mo_2(DPhF)_4$. The filtrate was evaporated to dryness, leaving behind a free-flowing brown powder. The solid was washed with several small portions of hexanes and then several small portions of Et_2O. This solid was dissolved in 14 cm^3 of CH_2Cl_2 and layered with hexanes to yield dark brown needles (0.096 g, 23%) of **II**. Found: C, 55.1; H, 4.0; N, 9.8; Cl, 9.6. Calc. for $Mo_2Cl_2N_6C_{39}H_{33}$: C, 55.2; H, 3.9; N, 9.9; Cl, 8.4%. IR (KBr, cm^{-1}): 3059(w), 3033(w), 2931(w), 1592(m) 1583(m), 1517(s), 1487(s), 1306(s), 1212(s) 1027(m), 938(s), 766(m), 755(s), 695(s), 689(s), 530(w), 490(m). UV/vis (CH_2Cl_2): λ = 540(sh) nm; 435 nm; 330(sh) nm; 275 nm.

Structure determination

Crystals of **I**,* grown from slow diffusion of CH_2Cl_2 and hexanes, were examined under a mixed layer of the mother liquor and mineral oil in air. A suitable crystal was mounted on top of quartz fiber with grease and transferred to a goniometer head under a nitrogen flow at −60°C. The cell parameters were obtained from an auto-indexing routine and were refined with 250 strong reflections in the 2θ range of 18.1 to 41.6°.

*The structure of **II** is similar to that of **I**, except that the substituents on the amidinato nitrogen atoms are phenyl groups instead of *p*-tolyl. Because the data set had a low data to parameter ratio, (4.7 : 1 for $I > 2\sigma(I)$) we did not attempt a complete refinement of the structure. However, the chemical composition was clear from the preliminary study. It crystallizes in space group $P2_1/n$ with the following unit cell parameters: a = 18.647(3), b = 15.796(4), c = 24.552(6) Å, β = 90.06(2)°, V = 7231(3) Å^3, and Z = 8. Data were collected at −105°C on an Enraf-Nonius CAD-4 diffractometer with Mo-K_α radiation. The unit cell contains two independent molecules. The Mo(1)—Mo(2) and Mo(3)—Mo(4) bond distances are 2.143(2) and 2.149(2) Å, respectively. Further crystal data and atomic coordinates for **II** have been deposited with the Cambridge Crystallographic Data Center.

Axial lengths and Laue symmetry (2/m) were confirmed by axial photographs. Details for data collection have been fully described elsewhere [9]. Data were corrected for Lorentz and polarization effects, and an absorption correction was applied using the program SORTAV [10]. The structure was solved by direct methods [11] and was refined using SHELXL-93 [12]. All non-hydrogen atoms were refined anisotropically. Details of data collection and refinement are presented in Table 1. Supplementary data have been deposited with the Cambridge Crystallographic Data Centre.

RESULTS AND DISCUSSION

Syntheses

Our first approach to preparing $Mo_2(DTolF)_3Cl_2$ and $Mo_2(DPhF)_3Cl_2$ involved a modification of the procedure used to prepare $Tc_2(DPhF)_3Cl_2$. $Tc_2(DPhF)_3Cl_2$ was synthesized from a one-electron oxidation of $Tc_2Cl_4(PEt_3)_4$ with excess molten formamidine, eq. (1):

$$Tc_2Cl_4(PEt_3)_4 + \text{excess HDPhF} \xrightarrow[-HCl,\ -PEt_3]{140\ ^\circ C} Tc_2(DPhF)_3Cl_2 + Tc_2(DPhF)_4Cl. \quad (1)$$

However, after refluxing a solution of $Mo_2Cl_4(PPh_2Me)_4$ with excess HDPhF in *o*-dichlorobenzene, the only product isolated from the reaction was the yellow tetraformamidinate compound, $Mo_2(DPhF)_4$, in 41% yield, and no oxidation of the dimetal core was observed. This led us to choose an alternative synthetic route that entailed deliberate oxidation of the tetraformamidinate compound followed by replacement of one of the formamidinate ligands by two chloride ions.

The syntheses of **I** and **II** can be summarized by the following two steps (eqs. (2) and (3)).

$$Mo_2(DArF)_4 + [Cp_2Fe]Cl \longrightarrow [Mo_2(DArF)_4]Cl + Cp_2Fe, \quad (2)$$

$$[Mo_2(DArF)_4]Cl + (CH_3)_3SiCl \longrightarrow Mo_2(DArF)_3Cl_2 + \text{"}(CH_3)_3Si\text{-}DArF\text{"}, \quad (3)$$

$$DArF = DTolF^-, DPhF^-.$$

The first step involves oxidation of the dimolybdenum tetraformamidinate by $[Cp_2Fe]Cl$. The oxidation of $Mo_2(DTolF)_4$ to $[Mo_2(DTolF)_4]^+$ has been previously reported using $AgPF_6$ [7]. The advantage of the ferrocenium chloride in this synthesis is two fold: (1) it is an efficient one-electron oxidizing agent, and (2) it provides one equivalent of the chloride ion needed to form the final product. The second equivalent of chloride is furnished by $(CH_3)_3SiCl$ which also aids in removal of one of the formamidinate ligands, driven by the formation of the strong N—Si bond. Since the ferrocene (produced in the first step) does not interfere with the second step, the conversion is easily accomplished as a "one-pot" synthesis.

Both **I** and **II** are dark brown, air-stable solids. However, it is interesting to note the disparity between the yields of **I** and **II**. This can best be explained on the basis of the solubility of the starting materials. If

Table 1. Crystallographic data and structure refinement for $Mo_2(DTolF)_3Cl_2$, **I**

Empirical formula	$C_{45}H_{45}Cl_2N_6Mo_2$
Formula weight	932.65
Space group	$P2_1/n$
a (Å)	16.0435(3)
b (Å)	15.645(1)
c (Å)	17.7437(5)
β (°)	109.272(7)
V (Å^3)	4204.1(3)
Z	4
d_{calc} (g cm^{-3})	1.474
Absorption coefficient (mm^{-1})	0.763
Radiation (monochromated in incident beam)	Mo-K_α(λ_α = 0.71073 Å)
Temperature (°C)	−60(2)
Scan method	ω-scan/area det.
Data collection range, θ(°)	2.60–25.12
Number of unique data, total	6023
Number of parameters refined	496
R indices ($F_0^2 > 2\sigma(F_0^2)$) R_w[a], wR_2[b]	0.052, 0.122
R indices (all data) R_w, wR_2	0.079, 0.133
Quality-of-fit indicator	1.047

[a] $R_1 = [\Sigma w(F_o - F_c)^2/\Sigma wF_o^2]^{1/2}$.

[b] $wR_2 = [\Sigma[w(F_o^2 - F_c^2)^2]/\Sigma w(F_o^2)^2]^{1/2}$, $w = 1/[\sigma^2(F_o^2) + (0.0623P)^2]$, where $P = [\max(F_o^2 \text{ or } 0) + 2(F_c)^2]/3$.

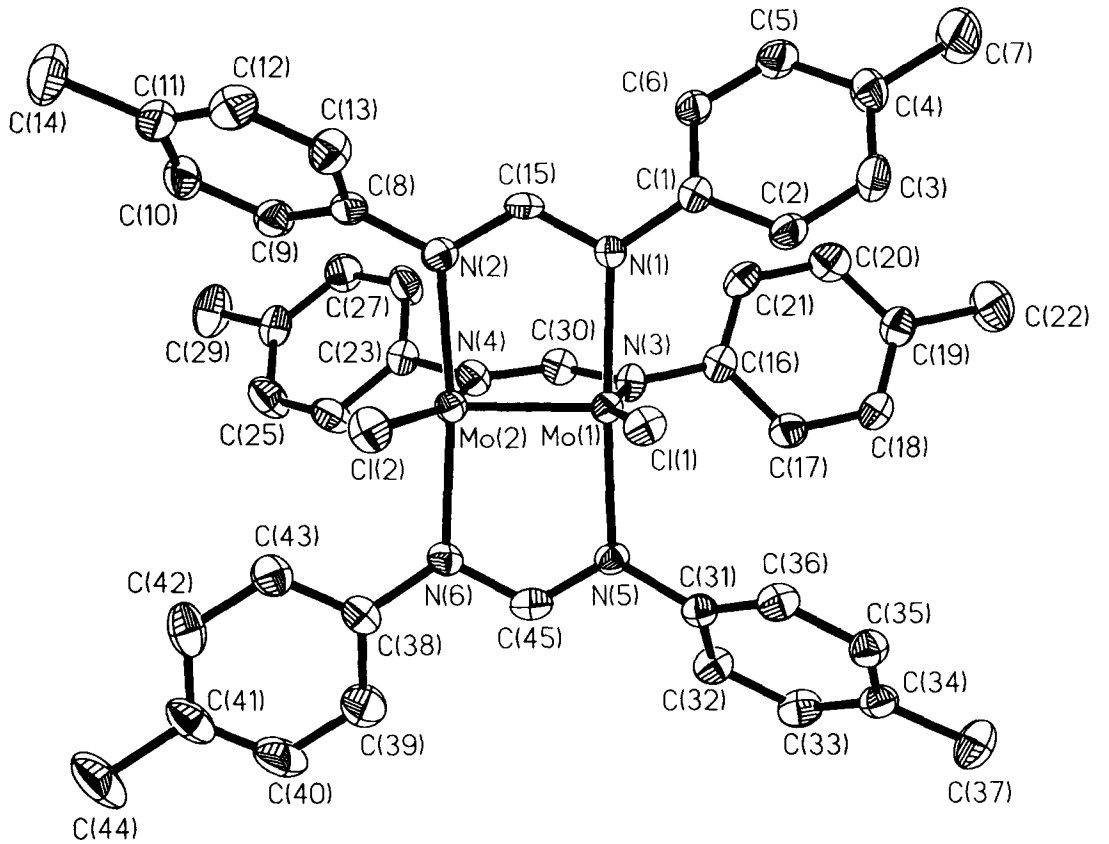


Fig. 1. A drawing of the molecular structure of **I**. Atoms are represented by their 50% probability ellipsoids.

the overall yield of the reaction is determined by the amount of the oxidized intermediate produced in the first step, then the limited solubility of $Mo_2(DPhF)_4$ reduces the concentration of $[Mo_2(DPhF)_4]^+$, and hence the yield of **II**. In fact, even when the $[Cp_2Fe]Cl$ was added slowly to $Mo_2(DPhF)_4$ over a 20 min time period, there was still unreacted starting material present. In contrast, $Mo_2(DTolF)_4$ dissolved completely and the crystalline yield for **I** increased to more than twice that of **II**.

Structural results

The molecular structure of **I** is shown in Fig. 1. There is one independent molecule within the asymmetric unit. The structure features three amidinato ligands bridging the dimetal core in the typical lantern or paddlewheel array. The two *cis* chloride ligands occupy the fourth coordination site on each of the metal atoms. The molecule has approximate C_{2v} symmetry; the C_2 axis bisects the Mo—Mo bond, and passes through the methine carbon, C(30).

Selected bond distances and angles for **I** are presented in Table 2. The Mo(1)—Mo(2) distance is 2.1510(5) Å which is comparable to the Mo—Mo distance of 2.122(3) Å found in $[Mo_2(DTolF)_4]PF_6$ [7]. The chlorine atoms are directed away from each other as evidenced by the N(3)—Mo(1)—Cl(1) and N(4)—Mo(2)—Cl(2) angles of 158.5(1)° and 162.2(1)°, respectively.

Summary

We have described a useful synthetic route for the preparation of dichlorotrisamidinato $Mo_2^{II,III}$ compounds. The structural characterization of these compounds demonstrates the *cis* arrangement of the chloride ligands. Currently, our efforts are directed towards removal of these chloride ligands, through reductive elimination, so as to leave a neutral trigonal lantern complex of molybdenum.

Acknowledgements—We are grateful to the National Science Foundation and the University of Costa Rica for support. We also wish to thank Alex Yokochi for the generous donation of $[Cp_2Fe]Cl$ and Dr L. M. Daniels for crystallographic advice.

Table 2. Selected bond lengths (Å) and angles (°) for $Mo_2(DTolF)_3Cl_2$, **I**

Mo(1)—Mo(2)	2.1510(5)	Mo(2)—N(2)	2.130(4)
Mo(1)—Cl(1)	2.399(1)	Mo(2)—N(4)	2.124(4)
Mo(2)—Cl(2)	2.383(1)	Mo(2)—N(6)	2.160(3)
Mo(1)—N(1)	2.139(3)	N(3)—C(30)	1.324(6)
Mo(1)—N(3)	2.092(4)	N(4)—C(30)	1.339(6)
Mo(1)—N(5)	2.122(3)		

N(3)—Mo(1)—N(1)	85.7(1)	N(4)—Mo(2)—Mo(1)	90.9(1)
N(3)—Mo(1)—N(5)	91.9(1)	N(2)—Mo(2)—Mo(1)	92.3(1)
N(5)—Mo(1)—N(1)	176.3(1)	N(4)—Mo(2)—N(6)	93.1(1)
N(3)—Mo(1)—Mo(2)	93.2(1)	N(2)—Mo(2)—N(6)	173.6(1)
N(5)—Mo(1)—Mo(2)	91.2(1)	Mo(1)—Mo(2)—N(6)	93.28(9)
N(1)—Mo(1)—Mo(2)	91.82(9)	N(4)—Mo(2)—Cl(2)	162.2(1)
N(3)—Mo(1)—Cl(1)	158.5(1)	N(2)—Mo(2)—Cl(2)	85.8(1)
N(5)—Mo(1)—Cl(1)	91.5(1)	Mo(1)—Mo(2)—Cl(2)	106.54(3)
N(1)—Mo(1)—Cl(1)	89.7(1)	N(6)—Mo(2)—Cl(2)	89.5(1)
Mo(2)—Mo(1)—Cl(1)	107.96(3)	N(3)—C(30)—N(4)	119.5(4)
N(4)—Mo(2)—N(2)	90.1(1)		

REFERENCES

1. F. A. Cotton and R. A. Walton, *Multiple Bonds Between Metal Atoms*, 2nd. ed. Oxford University Press, Oxford (1993).
2. (a) F. A. Cotton, L. M. Daniels and C. A. Murillo, *Inorg. Chim. Acta* 1994, **219,** 7; (b) F. A. Cotton, L. M. Daniels, L. R. Falvello, J. H. Matonic, and C. A. Murillo, *Inorg. Chim. Acta*, in press.
3. (a) F. A. Cotton, L. M. Daniels, D. J. Maloney and C. A. Murillo, *Inorg. Chim. Acta* 1996, **249,** 9; (b) F. A. Cotton, L. M. Daniels, D. J. Maloney, J. H. Matonic and C. A. Murillo, *Inorg. Chim. Acta*, in press.
4. F. A. Cotton, S. C. Haefner, and A. P. Sattelberger, *Inorg. Chem.* 1996, **35,** 735.
5. R. M. Roberts, *J. Org. Chem.* 1949, **14,** 277.
6. H. D. Glicksman, A. D. Hamer, T. J. Smith, and R. A. Walton, *Inorg. Chem.* 1976, **15,** 2205.
7. F. A. Cotton, X. Feng, and M. Matusz, *Inorg. Chem.* 1989, **28,** 594.
8. J. Pflugrath, A. Messerschmitt, MADNES, Munich Area Detector (New EEC) System, Version EEC 11/1/89, with enhancements by Enraf-Nonius Corporation, Delft, The Netherlands. A description of MADNES appears in: A. Messerschmitt and J. Pflugrath *J. Appl. Cryst.* 1987, **20,** 306.
9. (a) J. C. Bryan, F. A. Cotton, L. M. Daniels, S. C. Haefner, and A. P. Sattelberger, *Inorg. Chem.* 1995, **34,** 1875; (b) W. R. Scheidt and I. Turowska-Turk, *Inorg. Chem.* 1994, **33,** 1314.
10. R. H. Blessing, *Acta Cryst.* 1995, **A51,** 33.
11. G. M. Sheldrick, in *Crystallographic Computing* 3 (Edited by G. M. Sheldrick, C. Kruger and R. Goddard), pp. 175–189. Oxford University Press, Oxford (1985).
12. G. M. Sheldrick, in *Crystallographic Computing* 6 (edited by H. D. Flack, L. Parkanyi and K. Simon), pp. 111–122. Oxford University Press, Oxford (1993).

Pergamon

PII:S0277-S387(96)00496-2

Polyhedron Vol. 16, No. 11, pp. 1837–1841, 1997
© 1997 Elsevier Science Ltd
All rights reserved. Printed in Great Britain
0277-5387/97 $17.00+0.00

Bis(*N*,*N*′-diphenylformamidine)silver(I) triflate: a three-coordinate silver formamidine compound stabilized by intramolecular hydrogen bonds

Deirdre I. Arnold,[a] F. Albert Cotton,[a]* John H. Matonic[a] and Carlos A. Murillo[b]*

[a]Department of Chemistry and Laboratory for Molecular Structure and Bonding, Texas A & M University, College Station, TX 77843, U.S.A.; [b]Department of Chemistry and Laboratory for Molecular Structure and Bonding, Texas A & M University, College Station, TX 77843, U.S.A.; and Department of Chemistry, University of Costa Rica, Ciudad Universitaria, Costa Rica

(Received 12 August 1996; accepted 2 October 1996)

Abstract—A formally three-coordinate silver(I) complex, $Ag(HDPhF)_2(OSO_2CF_3)$ (**1**), has been prepared from the reaction of $AgSO_3CF_3$ with HDPhF (HDPhF = *N*,*N*′-diphenylformamidine) in toluene and characterized through spectroscopic methods and single-crystal X-ray diffraction studies. The silver atom is bound through one nitrogen atom each to two neutral formamidine ligands and weakly coordinated to the triflate anion through an oxygen atom. The AgN_2O group is practically planar with an N—Ag—N angle of 142.3(2)° and O—Ag—N angles of 122.4(2) and 92.0(1)°. Hydrogen bonding possibly related to the mechanism of formamidine cleavage seen in other complexes occurs between oxygen atoms of the triflate anion and amine hydrogen atoms in **1**. © 1997 Elsevier Science Ltd. All rights reserved.

Keywords: silver; three-coordinate; hydrogen bonding; crystal structure; formamidine complex.

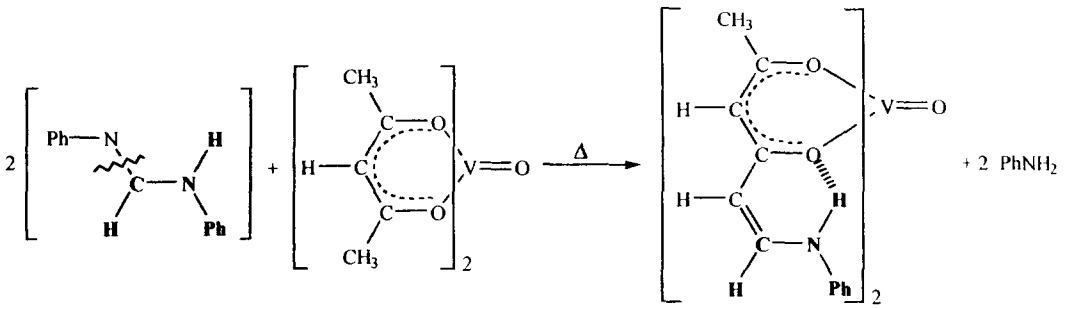
Although formamidinates $[RNC(H)NR]^-$ can bind in a variety of modes [1], we have been interested in them primarily as bridging ligands in dinuclear molecules which contain metal–metal bonds [2]. We have found that one of the best methods for preparing divalent compounds is to react $MCl_2(formamidine)_2$ complexes [3] with methyllithium, which deprotonates the neutral ligands to afford compounds of the type $M_2(formamidinate)_4$ [4].

More recently we have observed that under suitable conditions, formamidines or formamidinate ligands undergo cleavage at a C—N bond. For example, a tantalum compound containing both the RNCH and NR fragments of a formamidinate ligand has been isolated in our laboratory [5]. In other cases, the ligand fragments react further with other ligands attached to the metal ion to produce new species as in the reaction of $VO(acac)_2$ with HDPhF shown in the scheme below [6].

We believe that in many of these reactions the formamidine probably binds to the metal center before undergoing cleavage. For this reason, it is important to study the bonding modes of formamidines in various complexes. As mentioned above, we have synthesized and studied several compounds in which the tetrahedrally coordinated central atom is bound to two halide ions and to two neutral formamidines; however, no other compounds of this type having other coordination geometries have been studied in detail.

While attempting oxidations with silver ions in the presence of formamidines, we observed that coordination can also occur between Ag^+ and HDPhF. It is well known that silver can form a variety of compounds having different coordination numbers. For example, silver in its +1 oxidation state most commonly exhibits twofold linear or fourfold tetrahedral coordination [7], but there are also complexes

*Authors to whom correspondence should be addressed.



Scheme 1.

known in which Ag^I is formally three-coordinate. Among these are $(Me_2NC_6H_4PEt_2)_2AgI$ [7], diphenyl bis(pyrazolyl)borate complexes [8], and mononuclear and dihalide-bridged dinuclear complexes containing tricyclohexylphosphine [9]. In this paper we report the synthesis and characterization of the three-coordinate mononuclear complex $Ag(HDPhF)_2SO_3CF_3$ (**1**) (HDPhF = *N*,*N*′-diphenylformamidine) in which each ligand is bound to Ag^I through one nitrogen atom or an oxygen atom of a weakly coordinated triflate anion.

EXPERIMENTAL

General procedures

The reaction was performed under dry nitrogen, but the solid product was handled in air; measures were taken to protect the reaction mixture and the product from light, however. Toluene and hexanes were freshly distilled under nitrogen from sodium/potassium benzophenone ketyl. *N*,*N*′-diphenylformamidine and silver triflate were purchased from Aldrich Chemical Co.; the HDPhF was washed with warm ethanol and dried under reduced pressure prior to use. The IR spectrum of **1** was obtained on a Perkin Elmer 16 PC FT-IR spectrometer using a KBr matrix. The ^1H NMR spectrum was obtained on a Varian 200XL-E spectrometer in CD_2Cl_2. Elemental analyses were performed by Canadian Microanalytical Services, Ltd.

Preparation

In a typical experiment 0.25 g (9.7×10^{-4} mole) of $AgSO_3CF_3$ and 0.39 g (2.0×10^{-3} mole) of HDPhF were combined in a flask which was then evacuated for about 1 h to remove any residual moisture. About 30 cm^3 of toluene was added, whereupon nearly all of the solid dissolved. The reaction mixture was refluxed for 1 h to afford a clear solution with a slight beige tint. About 50 cm^3 of isomeric hexanes was layered onto the cooled mixture; after a week, colorless crystals had formed and the mixture was placed in a freezer overnight. An additional 20 cm^3 of hexanes was added and the mixture was stirred and replaced in the freezer. The product, a pale beige-colored semicrystalline solid, precipitated and was collected by filtration. The yield was 0.36 g (57.3% based on $AgSO_3CF_3$). IR (cm^{-1}): 2962(w), 1681(s), 1587(s), 1488(s), 1449(w), 1261(s), 1209(m), 1166(m), 1098(m), 1025(s), 987(w), 912(w), 900(w), 805(s), 754(s), 695(s), 652(m), 634(m), 601(w), 575(w), 518(m), 506(m), 431(w). ^1H NMR (ppm): complex multiplets of split peaks centered at 7.20 and 7.35 (phenyl C—H protons), sharp singlet at 8.25 (methine protons). Elemental analysis: Found: C, 49.6; N, 8.6; H, 3.8. Calc: C, 49.9; N, 8.6; H, 3.7%. Single crystals suitable for X-ray diffraction studies were obtained by combining about 40 mg of **1** with 10 cm^3 of toluene, filtering off any undissolved material, layering the solution in a Schlenk tube with 15 cm^3 of hexanes, and placing the tube in a freezer. Needlelike crystals formed within two weeks.

X-ray crystallography

Data were collected on a Rigaku AFC5R diffractometer (Cu-K_α radiation) equipped with a rotating anode at room temperature using procedures described elsewhere [10]. A set of 25 reflections for cell indexing were found using an automated search routine. The cell dimensions and Laue group were confirmed with axial photographs. Data were collected using ω-2θ scans and corrected for Lorentz and polarization effects; an absorption correction based on ψ-scans was applied. The structure was developed using SHELXS-86 and SHELXL-93 [11]. All of the non-hydrogen atoms were found in a direct methods *E*-map; the hydrogen atoms were placed in idealized positions. All of the atoms were refined anisotropically by full-matrix least-squares methods; the refinement on F^2 converged to $R_1 = 0.042$, $wR2 = 0.102$ for $I > 2\sigma(I)$. Other information pertinent to the data collection and structure solution are

given in Table 1. A representation of **1** showing the atom labeling scheme is given in Fig. 1. Selected bond lengths and angles are given in Table 2. Supplementary data have been deposited with the Cambridge Crystallographic Data Centre.*

RESULTS AND DISCUSSION

The reaction between $AgSO_3CF_3$ and HDPhF in toluene produces $Ag(HDPhF)_2SO_3CF_3$ (**1**), a three-coordinate complex in which two neutral formamidine ligands are each bound *via* one nitrogen atom to the silver ion and the triflate anion is bound through an oxygen atom as shown in Fig. 1. The Ag—N distances are 2.179(4) Å and 2.206(4) Å while the Ag—O distance is relatively long at 2.575(4) Å. The N—Ag—N angle is 142.3(2)° and the silver atom is located 0.40 Å out of the plane defined by the oxygen and nitrogen atoms coordinated to the metal atom. The Ag—N distances in **1** are comparable to those found in $Ag(en)ClO_4$ [12] (2.17(1) Å) which exhibits linear twofold coordination, but longer than those found in $[Ag(NH_3)_2]Ag(NO_2)_2$ [13] (2.112(6) and 2.117(6) Å) which also contains linear N—Ag—N units; they are, however, shorter than those found in the planar, three-coordinate complex $Ag(dmp)NO_3$ [14] (dmp = dimethylphenanthroline) (2.283(6) and 2.300(5) Å) and in the nearly tetrahedral complex $Ag(py)_4ClO_4$ [15] (py = pyridine) (2.322(3) Å).

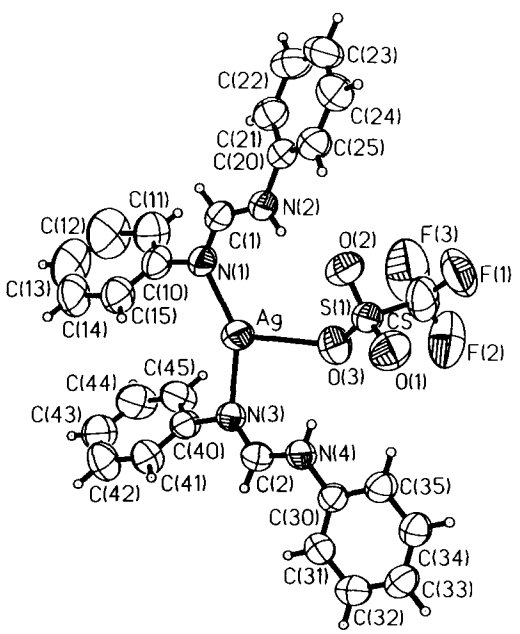


Fig. 1. Thermal ellipsoid plot of $Ag(HDPhF)_2SO_3CF_3$. Atoms are represented by their 50% probability ellipsoids.

*Supplementary material available: Tables of positional parameters, full tables of displacement parameters and molecular dimensions (7 pages).

Threefold coordination is uncommon for Ag^I complexes; consequently, there are few opportunities available for comparison of **1** with known compounds. Bruce and coworkers have reported the structure of $Ag[P(p\text{-}MeC_6H_4)_3][BPh_2(pyrazolyl)_2]$ [8], and while this complex is not strictly analogous to **1**, it displays a similar coordination geometry about the silver atom, which is bound to the pyrazolyl nitrogen atoms at 2.194(4) Å and 2.411(4) Å and to the phosphorus atom at 2.351(1) Å; the larger of the P—Ag—N angles is 160.3(1)°. In this case, as in that of **1**, the silver atom in its +1 oxidation state is bound to two ligands and weakly coordinated to a third; this coordination is relatively weak as born out by the long bond distances, but strong enough to cause significant deviation of the P—Ag—N and N—Ag—N angles from the linearity common to two-coordinate Ag^I complexes.

Our interest in **1** lies primarily in the coordination mode of and the hydrogen bonding exhibited by the neutral formamidine ligands through the N(4)—O(3) and N(2)—O(2) distances of 2.950(6) Å and 2.966(6) Å, respectively. With the hydrogen atoms placed in idealized positions, the H(4A)···O(3) distance is 2.127 Å and the O(2)···H(2A) distance is 2.167 Å; the O(3)—H(4A)—N(4) and O(2)—H(2A)—N(2) angles are 160.0 and 154.3°, respectively. These molecular dimensions are consistent with the presence of hydrogen bonds.

Cleavage of formamidines during reactions with transition metals has been observed in several instances in our laboratories, notably in the reaction between $VO(acac)_2$ and HDPhF with concomitant release of aniline [6]. We believe that hydrogen bonding similar to that exhibited in **1** by the amine hydrogen atoms of the neutral formamidine ligands may play a crucial role in the mechanism by which the ligands are cleaved in other reactions. It is possible that in the reaction between $VO(acac)_2$ and HDPhF, the formamidine initially coordinates to the metal atom at the vacant site opposite to the vanadyl oxygen atom to form a pseudooctahedral intermediate stabilized by hydrogen bonding between the amine hydrogen atom and a coordinated acac oxygen atom. The coordinated HDPhF would then attack the methyl carbon of the acac and subsequently undergo C—N bond cleavage to release aniline and form the new ligand 6-(phenylamino)-2,4-hexanedionate. The pseudooctaheral intermediate would display an O—V—N angle of approximately 90°. One of the formamidines in **1** is coordinated in just such a manner, forming an angle of 92.0(1)° with the silver atom and the coordinated triflate oxygen atom shown in Fig. 2. This fact and the presence of stabilizing intramolecular hydrogen bonding in **1** lends credence to our assumptions regarding the mechanism by which HDPhF is cleaved during its reaction with $VO(acac)_2$. Further investigations into the chemistry of amidine ligands, particularly into their cleavage reactions, are currently underway in our laboratories.

Table 1. Crystal data for $Ag(HDPhF)_2SO_3CF_3$

Formula	$C_{27}H_{24}AgF_3N_4O_3S$
Formula weight	649.43
Space group	$P2_1/c$
a (Å)	15.728(2)
b (Å)	7.406(3)
c (Å)	23.855(2)
α(°)	90
β(°)	98.150(9)
γ(°)	90
V(Å^3)	2751(1)
Z	4
d_{calc}(g cm^{-3})	1.568
Crystal size (mm^3)	$0.30 \times 0.20 \times 0.20$
Absorption coefficient (mm^{-1})	7.084
Data collection instrument	Rigaku AFC5R
Radiation (monochromated in incident beam)	Cu-K$_\alpha$ (λ_α = 1.54184 Å)
Temperature (K)	293(2)
Data collection range, θ(°)	2.84 to 60.10
Number of unique data, total with $F_0^2 > 2\sigma(F_0^2)$	4100
Number of parameters refined	352
R_w[a]	0.042
$wR2$[b]	0.102
Quality-of-fit indicator[c]	1.027

[a] $R_w = [\Sigma w(F_0 - F_c)^2/\Sigma wF_0^2]^{1/2}$.

[b] $wR2 = [\Sigma w(F_0^2 - F_c^2)^2/\Sigma w(F_0^2)^2]^{1/2}$, $w = 1/[\sigma^2(F_0^2) + (0.0468 \times p)^2 + 3.1016 \times p$, $p = [\max(F_0^2 \text{ or } 0) + 2(F_c^2)]/3$.

[c] Quality-of-fit = $[\Sigma w(|F_0^2| - |F_c^2|)^2/(N_{obs} - N_{parameters})]^{1/2}$.

Table 2. Selected bond lengths (Å) and angles (°) for $Ag(HDPhF)_2SO_3CF_3$

Ag—N(1)	2.179(4)	C(1)—N(2)	1.338(6)
Ag—N(3)	2.206(4)	C(2)—N(3)	1.285(6)
Ag—O(3)	2.575(4)	C(2)—N(4)	1.325(6)
C(1)—N(1)	1.288(6)		
N(1)—Ag—N(3)	142.3(2)	N(3)—Ag—O(3)	92.0(1)
N(1)—Ag—O(3)	122.4(2)		

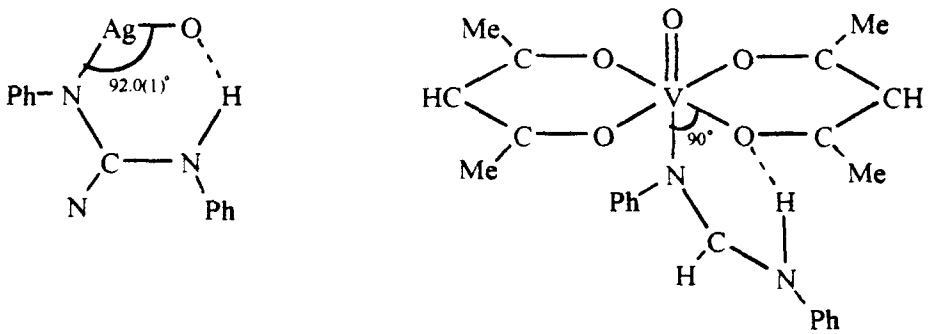


Fig. 2. A schematic representation of one of the hydrogen bonding interactions in $Ag(HDPhF)_2SO_3CF_3$ and a possible interaction in a vanadyl complex requiring a similar geometry.

Acknowledgements—We are grateful to the Vicerrectoría de Investigación U.C.R. (Project 115-87-516) and the Department of Chemistry for support of work at the University of Costa Rica and to the National Science Foundation for support of work at Texas A & M University.

REFERENCES

1. J. Barker and M. Kilner, *Coord. Chem. Rev.* 1994, **133,** 219.
2. F. A. Cotton, L. M. Daniels and C. A. Murillo, *Inorg. Chem.* 1993, **32,** 2881 and references therein.
3. (a) F. A. Cotton, L. M. Daniels, D. J. Maloney, J. H. Matonic and C. A. Murillo, *Polyhedron* 1994, **13,** 815; (b) D. I. Arnold, F. A. Cotton, D. J. Maloney, J. H. Matonic and C. A. Murillo, *Polyhedron*, 1997, **16,** 133.
4. See for example F. A. Cotton, L. M. Daniels, X. Feng, D. J. Maloney, J. H. Matonic and C. A. Murillo, *Inorg. Chim. Acta*, in press.
5. F. A. Cotton, L. M. Daniels, J. H. Matonic, C. A. Murillo and X. Wang, *Polyhedron*, 1997, **16,** 1177.
6. D. I. Arnold, F. A. Cotton, J. H. Matonic and C. A. Murillo, *J. Chem. Soc., Chem. Commun.* 1996, 2113.
7. F. A. Cotton and G. Wilkinson, *Advanced Inorganic Chemistry*, 5th edn., pp. 940–943. Wiley, New York (1988).
8. M. I. Bruce, J. D. Walsh, B. W. Skelton and A. H. White, *J. Chem. Soc., Dalton Trans.* 1981, 956.
9. (a) G. A. Bowmaker, Effendy, P. J. Harvey, P. C. Healy, B. W. Skelton and A. H. White, *J. Chem. Soc., Dalton Trans* 1996, 2449; (b) G. A. Bowmaker, Effendy, P. J. Harvey, P. C. Healy, B. W. Skelton and A. H. White, *J. Chem. Soc., Dalton Trans* 1996, 2459.
10. A. Bino, F. A. Cotton and P. E. Fanwick, *Inorg. Chem.* 1979, **18,** 3558.
11. (a) G. M. Sheldrick, in *Crystallographic Computing* 3 (Edited by G. M. Sheldrick, C. Kruger and R. Goddard), pp. 175–189. Oxford University Press, Oxford (1985); (b) G. M. Sheldrick, in *Crystallographic Computing* 6 (Edited by H. D. Flack, L. Parkanyi and K. Simon), pp. 111–122. Oxford University Press, Oxford (1993).
12. E. Bang, *Acta Chem. Scand. A* 1978, **32,** 555.
13. H. M. Maurer and A. Weiss, *Z. Kristallogr.* 1977, **146,** 227.
14. G. Swarnabala and M. V. Rajasekharan, *Polyhedron* 1996, **15,** 3197.
15. K. Nilsson and Å. Oskarsson, *Acta Chem. Scand. A* 1982, **36,** 605.

Pergamon

PII: S0277-5387(96)00495-0

Polyhedron Vol. 16, No. 11, pp. 1843–1854, 1997
© 1997 Elsevier Science Ltd
All rights reserved. Printed in Great Britain
0277-5387/97 $17.00+0.00

An investigation of P,P′-di(2-ethylhexyl) methanediphosphonic acid and some of its metal complexes†

Albert W. Herlinger,[a]* John R. Ferraro,[b] Renato Chiarizia[b] and E. Philip Horwitz[b]

[a]Department of Chemistry, Loyola University Chicago, Chicago, Illinois, 60626 U.S.A.; [b]Chemistry Division, Argonne National Laboratory, Argonne, Illinois, 60439 U.S.A.

(Received 5 August 1996; accepted 2 October 1996)

Abstract—Copper(II), iron(III), europium(III), thorium(IV) and uranium(VI) complexes of P,P′-di(2-ethylhexyl) methanediphosphonic acid, H_2DEH[MDP], were prepared along with calcium and sodium salts. The compounds were characterized by elemental analysis, infrared spectroscopy, and vapor phase osmometry (VPO). Infrared spectra reveal that the asymmetric, $\nu_{asym}(POO^-)$, and symmetric, $\nu_{sym}(POO^-)$, phosphorus–oxygen stretching modes of the ligand are sensitive to the nature of the metal ion present in the compound. The dramatic variation in $\nu_{asym}(POO^-)$ with metal ion indicates a wide range in strength of the metal–diphosphonate interaction. The shift of both $\nu_{asym}(POO^-)$ and $\nu_{sym}(POO^-)$ to lower energies relative to their values in the sodium salt indicates symmetrical coordination of the phosphonate groups through chelate and/or bridging interactions. The difference $\Delta\nu$ between the POO^- stretching frequencies, $[\nu_{asym}(POO^-)-\nu_{sym}(POO^-)]$, becomes smaller as the ionic potential of the metal ion increases.

H_2DEH[MDP] was found by VPO to be dimeric in toluene at 25°C in the 0.2–0.005 *m* concentration range. Dimerization is achieved through strong intermolecular hydrogen bonding between the phosphoryl and P—OH groups of two H_2DEH[MDP] molecules. Pre-equilibration with water or 1.0 *M* nitric acid does not effect the aggregation of the ligand in toluene. The apparent aggregation numbers measured for H_2DEH[MDP] solutions contacted with aqueous metal ions indicate that the ligand has a tendency to form polynuclear complexes. Aggregation increases with increasing metal ion concentration, deprotonation of the P—OH groups, and the ionic potential of the metal ion. The absence of nitrate ion in these solutions shows that, under high metal loading conditions, cations are extracted from aqueous nitric acid by H_2DEH[MDP] with displacement of hydrogen ions. Ligand band shifts indicate that when excess un-ionized H_2DEH[MDP] is present in solution, the phosphoryl oxygen atoms of the acid participate in the complexation process. © 1997 Elsevier Science Ltd. All rights reserved.

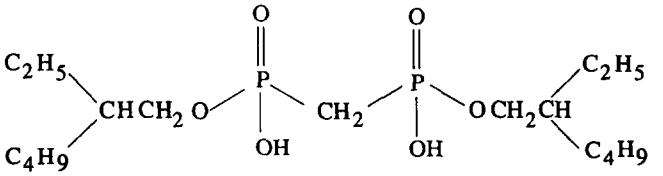
Keywords: alkyl diphosphonic acids; metal complexes; P,P′-di(2-ethylhexyl) methanediphosphonic acid.

Diphosphonic acids have been recognized for a number of years as powerful complexing agents for metal ions [1]. Recent studies have shown that simple diphosphonate ligands form much stronger complexes with lanthanides [2] and actinides [3] than analogous polycarboxylic acid complexants. The strong acidity of the diphosphonic acid group and its ability to chelate metal ions through ionized phosphonic acid groups and P=O groups permits the formation of metal complexes of high stability under very acidic conditions. Since most actinide processing is carried out in acid, this property suggests that suitable diphosphonate ligands have great potential for use in decontamination of nuclear waste streams and the recovery of transuranic elements in the nuclear fuel cycle.

In P,P′-di(2-ethylhexyl) methanediphosphonic acid, two of the four acidic protons of the parent acid have been replaced by alkyl groups to make the

*Author to whom correspondence should be addressed. Visiting Scientist from Department of Chemistry, Loyola University, Chicago.

†Work performed under the auspices of the Office of Basic Energy Sciences, Division of Chemical Sciences, U.S. Department of Energy, under contract number W-31-109-ENG-38.



H_2DEH[MDP]

molecule lipophilic, and therefore, soluble in water immiscible solvents. Thus, H_2DEH[MDP] can be used in solvent extraction and extraction chromatographic procedures. This novel ligand functions in highly acidic media and exhibits an extraordinary selectivity for iron(III) and actinides in all valence states. The remarkable phase separation properties and high distribution ratios of H_2DEH[MDP] led to the development of a new extraction chromatographic resin called Dipex [4]. This resin will find application in procedures for the separation of actinides from complex mixed acidic waste as well as from environmental and biological samples. H_2DEH[MDP] is formally similar to a dicarboxylic acid but little information is available about its fundamental coordination chemistry. Interest in the Dipex resin and the complexation chemistry of alkyl substituted diphosphonic acids prompted this investigation.

The extraction of metal ions at tracer concentration levels by H_2DEH[MDP] was recently investigated in *o*-xylene and found to be quite unusual [5]. The metal extraction reactions written in this study were based on the limited information available in the literature which indicated that H_2DEH[MDP] should be dimeric in *o*-xylene [6–8]. The actual state of aggregation of the ligand in aromatic solvents, however, is not known. Di(2-ethylhexyl) phosphoric acid, HDEHP, is dimeric in benzene [9], but mono(2-ethylhexyl) phosphoric acid, H_2MEHP, the monofunctional analog of H_2DEH[MDP], forms much larger aggregates. H_2MEHP is reported to have an aggregation number as high as 12 in benzene [9,10]. Thus, there is a question as to whether the aggregation behavior of H_2DEH[MDP] is similar to that of dibasic H_2MEHP or if it is limited to the formation of dimeric aggregates like monobasic HDEHP.

Knowledge about the aggregation state of an extraction reagent is necessary to understand its metal extraction chemistry. In our earlier study, the extractant dependencies for Fe^{III}, Am^{III} and U^{VI} were observed to decrease continuously with aqueous phase acidity from a value of about 2 in 5 M HNO_3 to a value of almost zero in 0.1 M acid [5]. The variation in extractant dependency was tentatively attributed to an increase in the aggregation of the ligand which occurs when the ionization of H_2DEH[MDP] increases as a result of being in contact with solutions of low acidity. In the related H_2MEHP-Eu^{III} system, the variation in the extractant dependency was shown to be due to changes in the aggregation state of the organophosphorus acid in different solvents [10]. In *n*-decanol, which depolymerizes the ligand, the extractant dependency is three; in toluene, with an aggregation number for H_2MEHP of 12, the extractant dependency is one.

Thus, the goals of the present study were: 1. To measure the extent of aggregation of H_2DEH[MDP] in an aromatic diluent; 2. to measure the extent of aggregation of metal complexes of H_2DEH[MDP] which tends to polymerize according to extraction data [5]; 3. to characterize the metal–ligand interactions in H_2DEH[MDP] complexes and solution species formed under high metal loading extraction conditions.

EXPERIMENTAL

Materials

Reagent grade $Ca(NO_3)_2 \cdot 4H_2O$, $Cu(NO_3)_2 \cdot 3H_2O$, and $Fe(NO_3)_3 \cdot 9H_2O$ obtained from Mallinckrodt Chemical Co. were used without further purification. Reagent grade $Th(NO_3)_4 \cdot 4H_2O$ from J. T. Baker Chemical Co. and $UO_2(NO_3)_2 \cdot H_2O$ from Fisher Scientific Co. were used as received. Aqueous solutions were prepared using Ultrex reagent nitric acid (J. T. Baker Chemical Co.) and water obtained from a Milli-Q2 purification system. Eu_2O_3 obtained from Apache Chemical Co. was dissolved in nitric acid and used to prepare a Eu^{III} stock solution. The metal ion concentration in this solution was determined to be 0.88 M by titration with EDTA. The stock solution was used to prepare a 0.05 *m* Eu^{III} solution by dilution with 1.0 M HNO_3. "Baker Analyzed" Photrex reagent for spectrophotometry toluene was used without further purification for the VPO measurements. The metal extraction data reported earlier for H_2DEH[MDP] were obtained in *o*-xylene [5]. Toluene was used for the osmometric measurements since the low volatility of *o*-xylene would cause the equilibration time required for each VPO measurement to be excessively long. The aggregation behavior of H_2DEH[MDP] and the metal complexes should be very similar in these two aromatic diluents. Bibenzyl obtained from Aldrich Chemical Co. was recrys-

tallized twice from methanol and dried overnight *in vacuo* at 45°C, m.p. 51.0–52.2°C after recrystallization.

Measurements

Apparent aggregation numbers were measured in toluene by VPO using a Corona Wescan 117 Molecular Weight Apparatus. The temperature was maintained at 25.0 ± 0.1°C by operating two Neslab constant temperature baths in series. The instrument was calibrated using standard toluene solutions of bibenzyl. A plot of measured voltage *vs* bibenzyl molality gave a slope of 10,320 μV/m for an instrument calibration constant. All residual traces of moisture and volatile organic compounds were removed from $H_2DEH[MDP]$ by dissolving the ligand in toluene and evaporating the solvent under reduced pressure at 60°C. The ligand was shown to be 99% pure by potentiometric titration with standard base after this treatment. The solutions used in the osmometric measurements, including those containing metal species, were prepared by quantitative dilution of standard 0.10 m $H_2DEH[MDP]$ solutions. The solvent used for the dilutions and as the reference in the VPO measurements was subjected to conditions similar to those used for the extractions, i.e. pre-equilibration with aqueous nitric acid of the appropriate concentration in the absence of metal ion. The VPO measurements were carried out on solutions in order of increasing concentration. Each data point corresponds to the average of 3–5 voltage measurements.

Metal ions were introduced into the solutions used for the VPO measurements by vortex mixing equal volumes of aqueous and toluene solutions that were ~0.05 m in metal ion and 0.10 m in $H_2DEH[MDP]$, respectively. The resulting mixture was centrifuged to form two layers which were physically separated by pipet. Metal ion analyses of the aqueous phase before and after extraction were performed by the ANL Analytical Chemistry Division using ICP-AES. The concentration of metal ion in the organic phase was determined by mass balance from the difference between the two values. The aqueous Fe^{III}, Eu^{III}, Th^{IV}, and U^{VI} solutions used were 1.0 M in HNO_3 while the aqueous Ca^{II} and Cu^{II} solutions were 0.01 M in HNO_3. In an earlier investigation, $H_2DEH[MDP]$ was shown to be highly effective in the extraction of iron(III) and actinide ions from 1 M HNO_3 [5]. Although Cu^{II} was not included in the initial study, it was assumed that conditions which lead to high extraction of Ca^{II}, i.e. 0.01 M HNO_3, would be required for effective extraction of Cu^{II}.

The molecular weights of the iron and uranyl $H_2DEH[MDP]$ compounds which are soluble in toluene were determined using the Corona Wescan molecular weight apparatus. A 0.045 mmole sample of the compound was dissolved in 3 g of dry toluene for the VPO measurements. The results of these single concentration point determinations indicate that the complexes are highly polymerized in toluene.

Infrared spectra were obtained on a Nicolet 510P PC/IR Fourier Transform Spectrometer operating in the 4800–400 cm^{-1} region. Routine spectra were recorded collecting 32 scans at 4 cm^{-1} resolution. Solid samples were run as KBr pellets and checked as Nujol mulls supported on KBr plates. Spectra in the 650–150 cm^{-1} range were obtained on a Bruker 98 Vacuum FT-IR Interferometer. Solid samples were run as CsI pellets referenced against CsI. These were checked as Nujol mulls supported on polyethylene plates. The spectrum of $H_2DEH[MDP]$ was obtained as a liquid film supported on KBr plates and as a 0.10 m toluene solution in a liquid IR cell with NaCl windows. The solution spectrum was recorded at 2 cm^{-1} resolution after collecting 256 scans. Spectra of the solution samples used in the VPO measurements were also recorded using the liquid cell. Solution spectra were measured with toluene in the cell as the background.

^1H and ^{31}P NMR spectra were recorded in $CDCl_3$ on a 300 MHz General Electric Omega 300 spectrometer. Chemical shifts are relative to internal TMS and external 85% H_3PO_4 for ^1H and ^{31}P spectra, respectively. Melting points were recorded on an Arthur H. Thomas, Hoover capillary melting point apparatus using a calibrated thermometer. Elemental analyses were performed by Galbraith Laboratories, Inc., Knoxville, TN. Metal ion analyses for the metal compounds were performed by the Analytical Chemistry Division of ANL using ICP-AES. Solid samples were weighed into a platinium crucible and ignited in air at 1100°C. The residue was fumed with concentrated H_2SO_4 and made up to the final volume with dilute nitric acid. The relative uncertainty in the metal ion analysis is estimated to be ~5%.

Preparation of compounds

P,P′-di(2-ethylhexyl) methanediphosphonic acid. The title compound was prepared by the reaction of 2 equivalents of 2-ethylhexanol with methane diphosphonic acid in dry tetrahydrofuran following the procedure of Burger and Anderson [11] as described previously [5]. The proton decoupled ^{31}P NMR spectrum shows a single resonance at δ 19.87 ppm. The ^1H NMR spectrum shows peaks at δ 11.27 (s), 3.98 (b, m), 2.44 (t, $J_{P\text{-}H}$ = 21.4 Hz), 1.55 (p, J = 5.7 Hz), 1.27 (m), and 0.88 (m) ppm with relative intensities of 2 : 4 : 2 : 2 : 16 : 12. Titration with standard base gave an equivalent weight of 202.6 ± 2 daltons. Found: C, 50.6; H, 9.9; P, 15.2; O, 24.2; Calc. for $C_{17}H_{38}O_6P_2$; C, 51.0; H, 9.6; P, 15.5; O, 24.0%.

$Na_2(C_{17}H_{36}O_6P_2)$. The sodium salt of $H_2DEH[MDP]$ was obtained by titrating a 0.1673 g (0.4178 mmol) sample of the acid in contact with 10 cm^3 of water with 0.10 M NaOH. After addition of 0.8377 mmol of base, the solution was evaporated to dryness under a stream of nitrogen using low heat.

The resulting residue was dried *in vacuo* at 70°C for 12 h. The infrared spectrum of this white waxy solid indicates that the salt is isolated as a hydrate.

$Fe_2(C_{17}H_{36}O_6P_2)_3$. An iron(III) complex of $H_2DEH[MDP]$ was prepared by shaking a 0.10 *m* toluene solution of $H_2DEH[MDP]$ with an equal volume of a 0.10 *m* aqueous iron(III) nitrate solution that was 1 M in HNO_3. A copious off-white precipitate formed immediately upon contacting the two solutions. The liquids were removed by pipet and the oily residue washed with several portions of water and toluene. The solid was collected by filtration, washed with hexane, and dried *in vacuo* at 60°C to an off-white powder. Yield: 169 mg (0.124 mmol), 61%. Found: C, 46.5; H, 8.3; P, 14.8; Fe, 8.0, O, 22.4; Calc. for $Fe_2C_{51}H_{108}O_{18}P_6$: C, 46.9; H, 8.3; P, 14.2; Fe, 8.5; O, 22.0%. The complex is polymeric in toluene with the molecular weight determined by VPO to be 69,400 daltons.

$Th(C_{17}H_{36}O_6P_2)_2$. A 0.4009 g (1.0011 mmol) sample of $H_2DEH[MDP]$ was exactly neutralized with an equivalent amount of aqueous NaOH. The pH of the resulting solution was adjusted to 6 with nitric acid and slowly added to 0.3737 g (0.6768 mmol) of $Th(NO_3)_4 \cdot 4H_2O$ dissolved in 0.1 M HNO_3. A white precipitate formed almost immediately upon mixing the two solutions. After stirring several minutes at room temperature, the precipitate was collected by filtration, washed with several portions of warm water, ethanol, and pentane, and dried *in vacuo* at 60°C overnight. Yield: 327.7 mg (0.3185 mmol), 63.6%. Found: C, 39.6; H, 7.0; Th, 22.3; Calc. for $ThC_{34}H_{72}O_{12}P_4$: C, 39.7; H, 7.0; Th, 22.5%. The compound is insoluble in water, toluene, hexane, ethanol, and acetone.

$UO_2(C_{17}H_{36}O_6P_2) \cdot 2H_2O$. A 0.2046 g (0.5109 mmol) sample of $H_2DEH[MDP]$ was exactly neutralized with an equivalent amount of aqueous NaOH. The pH of the resulting solution was adjusted to 6 with nitric acid and slowly added to 0.3194 g (0.6360 mmol) of $UO_2(NO_3)_2 \cdot 6H_2O$ dissolved in 0.10 M HNO_3. The yellow precipitate which formed immediately upon mixing the two solutions was stirred for several minutes, collected by filtration, and washed with several portions of warm water and ethanol. Recrystallization from a 50 : 50 v : v pentane–ethanol mixture gave large yellow crystals of a pentane soluble hydrate. The crystals were amorphous and unsuitable for X-ray analysis. The uranyl compound proved to be very difficult to dissolve for analysis by ICP-AES and required two digestion attempts. The relative uncertainty in the metal ion analysis in this case is estimated to be ~10%. Yield: 235.3 mg (0.3428 mmol), 67.1%. Found: C, 30.5; H, 5.6; U, 31.1: Calc. for $UC_{17}H_{40}O_{10}P_2$: C, 29.0; H, 5.7; U, 33.8%. The complex is polymeric in toluene with the molecular weight determined by VPO to be 11,340 daltons.

$Eu_2(C_{17}H_{36}O_6P_2)_3$. A 0.1443 g (0.3604 mmol) sample of $H_2DEH[MDP]$ dissolved in a mixture of 3 cm^3 of toluene and 17 cm^3 of isopropanol was exactly neutralized with an equivalent amount of aqueous NaOH. The nominal pH of the solution was adjusted to 6 with nitric acid and slowly added to 0.0811 g (0.240 mmol) of $Eu(NO_3)_3$ dissolved in water. After stirring the reaction mixture overnight at room temperature, the solvent was removed under a stream of N_2 using low heat. The residue was washed with several portions of hot water, collected by filtration, and dried *in vacuo* at 60°C. Found: C, 41.2; H, 7.3; Eu, 18.8; Calc. for $Eu_2C_{51}H_{108}O_{18}P_6$: C, 40.9; H, 7.3, Eu, 20.3%. The infrared spectrum of this compound indicates that it is initially isolated from solution as a hydrate.

$Ca(C_{17}H_{36}O_6P_2)$. A 0.2717 g (0.6785 mmol) sample of $H_2DEH[MDP]$ was exactly neutralized with an equivalent amount of 0.1000 M NaOH. The pH of the resulting solution was adjusted to 7 with nitric acid and slowly added to 0.1715 g (0.7262 mmol) of $Ca(NO_3)_2 \cdot 4H_2O$ dissolved in water. The flocculent precipitate, which formed immediately upon mixing the two solutions, was isolated by filtration, washed with several portions of hot water and ethanol, and dried *in vacuo* at 65°C. Yield: 214 mg (0.488 mmol), 71.9%. Found: C, 46.7; H, 8.1; Ca, 8.7: Calc. for $CaC_{17}H_{36}O_6P_2$: C, 46.6; H, 8.3; Ca, 9.1%.

$Cu(C_{17}H_{36}O_6P_2)$. A 0.2105 g (0.526 mmol) sample of $H_2DEH[MDP]$ was exactly neutralized with an equivalent amount of aqueous NaOH. The pH of the resulting solution was adjusted to 6 with nitric acid and slowly added to 0.1375 g (0.569 mmol) of $Cu(NO_3)_2 \cdot 5H_2O$ dissolved in 0.001 M HNO_3. The blue precipitate which formed almost immediately upon mixing the two solutions was stirred overnight at room temperature, collected by filtration, washed with several portions of warm water and acetone, and dried *in vacuo* at 70°C. Yield: 101 mg (0.226 mmol), 43.0%. Found C, 44.8; H, 7.8: Calc. for $CuC_{17}H_{36}O_6P_2$: C, 44.2; H, 7.8%. The infrared spectrum of this compound indicates that it is initially isolated from solution as a hydrate.

RESULTS

Osmometry

Figure 1 compares the results of the vapor phase osmometry measurements for $H_2DEH[MDP]$ with those for the monomeric standard bibenzyl. The VPO data indicate that $H_2DEH[MDP]$ is dimeric in toluene at 25°C. These results are similar to those for the di-*n*-octyl [7] and di-*n*-butyl [8] esters of methanediphosphonic acid which are reported to be dimeric in chloroform at room temperature. The linearity of the $H_2DEH[MDP]$ data indicates that the dimerization constant in toluene is sufficiently large so that the ligand is dimeric over the entire concentration range investigated. Partial neutralization of the acid has a significant effect on the apparent aggregation number, η, where η = molecular weight/formula

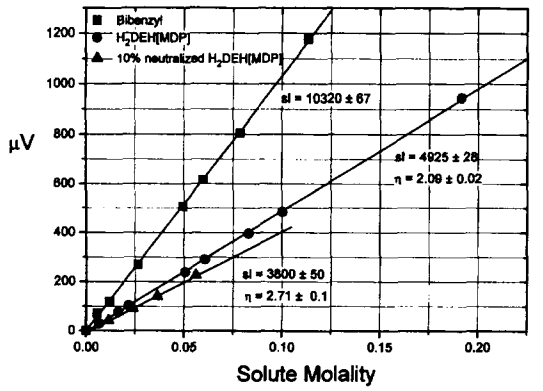


Fig. 1. Osmometric measurements for bibenzyl and $H_2DEH[MDP]$ in toluene at 25°C; sl = slope, η = aggregation number.

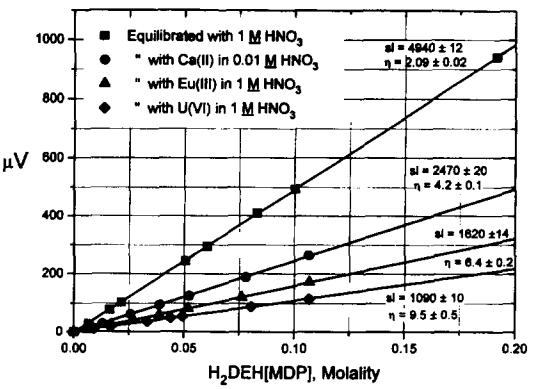


Fig. 3. Osmometric measurements for $H_2DEH[MDP]$ in toluene at 25°C after equilibration with aqueous solutions of Ca^{II}, Eu^{III}, and U^{VI} as described in the Experimental Section; sl = slope, η = aggregation number.

weight = bibenzyl slope/$H_2DEH[MDP]$ slope. Neutralization of approximately 10% of the $H_2DEH[MDP]$ in a sample, for example, resulted in a 35% increase in the calculated η value.

Figure 2 shows the effect of acid and the presence of metal ions on the aggregation of $H_2DEH[MDP]$. Cu^{II} is not extracted by $H_2DEH[MDP]$ from 1.0 M nitric acid and the measured η value is virtually unchanged. Cu^{II} is extracted from 0.01 *M* HNO_3 and the η value calculated for the ligand doubles. Fe^{III} and Th^{IV} are extracted almost quantitatively from 1 M HNO_3. $H_2DEH[MDP]$ solutions containing these metal ions give rise to the highest measured aggregation numbers. Figure 3 shows the results for samples pre-equilibrated with aqueous nitric acid solutions of Ca^{II}, Eu^{III}, and UO_2^{2+}. These metal ions also substantially increase the aggregation of $H_2DEH[MDP]$.

The results of the aggregation measurements are reported in Table 1. Pre-equilibration with water or 1.0 M nitric acid does not effect the aggregation of the ligand. The degree of aggregation, however, increases with increasing metal ion concentration and deprotonation of the P—OH groups. The η values in Table 1

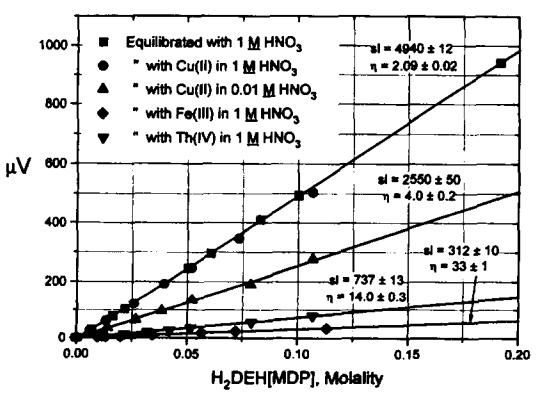


Fig. 2. Osmometric measurements for $H_2DEH[MDP]$ in toluene at 25°C after equilibration with 1 *M* HNO_3 and aqueous solutions of Cu^{II}, Fe^{III}, and Th^{IV} as described in the Experimental Section; sl = slope, η = aggregation number.

Table 1. Apparent aggregation number η for 0.10 *m* $H_2DEH[MDP]$ solutions

Metal ion	molality	[L]:[M]	η
None	—	—	2.09 ± 0.02
Ca^{II}	0.025	4.0	4.2 ± 0.1
Cu^{II}	0.042	2.4	4.0 ± 0.1
Eu^{III}	0.028	3.7	6.4 ± 0.2
U^{VI}	0.067	1.5	9.5 ± 0.5
Th^{IV}	0.040	2.5	14 ± 0.3
Fe^{III}	0.048	2.1	33 ± 1.0

do not correspond to the aggregation numbers for the metal compounds described in the experimental section. Rather, the values represent the average state of aggregation of $H_2DEH[MDP]$ in solutions containing an extracted metal species and more ligand than required for stoichiometric salt formation. The values are roughly proportional to the ionic potential (e/r) of the metal ions and are a qualitative indication of the tendency of metal ions to polymerize $H_2DEH[MDP]$. It is evident from the [L]:[M] ratios and the apparent aggregation numbers that the metal ions investigated, with the exception of Ca^{II}, form polynuclear complexes with $H_2DEH[MDP]$. The molecular weights for the iron and uranyl compounds, which are soluble in toluene, were measured (*vide supra*) and the calculated η values (159 and 17, respectively) verify this observation.

Infrared spectra

$H_2DEH[MDP]$. The infrared spectrum of $H_2DEH[MDP]$ in toluene is shown in Fig. 4. There are no absorption bands in this spectrum which can be attributed to free hydroxyl groups. The three broad bands of medium intensity which are characteristic of the P(O)(OH) group of an alkyl phosphonic acid appear at 2716, 2324, and 1675 cm^{-1}. While there is

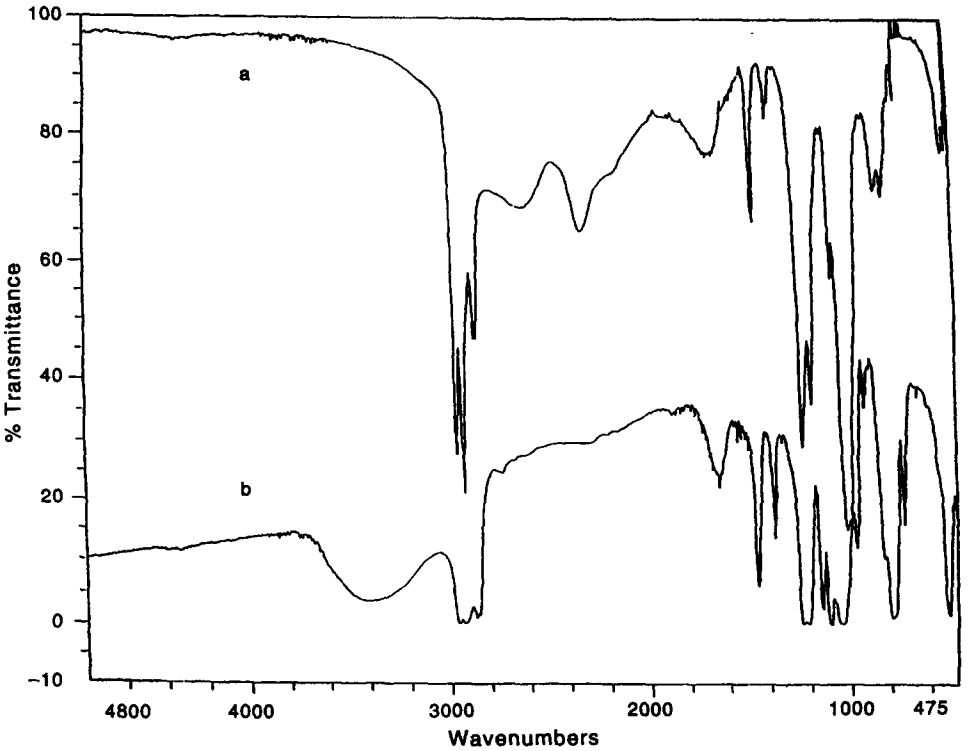


Fig. 4. The infrared spectra of 0.10 *m* H_2DEH[MDP] in toluene (a) and a KBr pellet of Na_2(DEH[MDP]) (b).

some controversy over the assignment of these bands, it is generally agreed that their presence is unequivocal evidence of a strongly hydrogen bonded phosphonic acid [9,10]. These bands disappear upon salt formation as expected. This behavior is similar to that reported earlier for the di-*n*-octyl [7] and di-*n*-butyl [8] esters of methanediphosphonic acid and related organophosphorus acids [14]. The stretching and bending vibrations of the 2-ethylhexyl group appear in the conventional regions characteristic of alkyl groups. The absorption frequencies of these bands are listed in Table 2.

Some of the strongest absorption bands in the spectrum of H_2DEH[MDP] occur in the 950–1250 cm^{-1} region. The frequencies and tentative assignments of the bands in this region are compared with those for 2-ethylhexyl phosphonic acid, H_2[EHP], and mono(2-ethylhexyl) phosphoric acid, H_2MEHP in Table 3. The major bands in this region are typically broad and complex in structure. This suggests that some of the bands may not represent pure vibrational modes and may have components of several vibrations. The thin film spectrum of H_2DEH[MDP], for example, has a single very broad strong band at 1221 cm^{-1} while the higher resolution solution spectrum shows two well resolved bands close to this energy. By comparison with the spectrum of the sodium salt and related organophosphorus acids [12–14] these bands are tentatively assigned as phosphoryl absorptions. The appearance of two bands in this region in the solution spectrum may be due to symmetric and asymmetric stretching motions of the two P=O groups in the molecule, a Fermi resonance, or two different types of hydrogen bonding in the dimer (*vide infra*).

The P—OR stretching vibration in H_2DEH[MDP] occurs as a very strong band in the 1020–1050 cm^{-1} region. There are no bands in this region of the spectrum of H_2[EHP] which has no ester groups. The P—OR band generally appears at somewhat higher energy in the metal compounds than in the free acid. The P—OH stretching vibration for H_2DEH[MDP] is clearly evident as a strong band in the solution spectrum at 1007 cm^{-1}. This band is absent in the spectra for all the metal compounds. The band of medium intensity at 1082 cm^{-1} most likely arises from either C—O bond stretching or deformation of the alkyl chain. This band is too high in energy and too low in intensity to be either a P—OH or P—OR vibration. The absorption bands for the P—OH and P—OR stretching vibrations for a monoester of an alkyl phosphonic acid typically are strong and appear in the characteristic frequency ranges of 990–1029 cm^{-1} and 987–1042 cm^{-1}, respectively [13].

Metal compounds. The absorption frequencies for the metal compounds prepared in this study are listed in Table 2. In all cases, the stretching and bending vibrations of the 2-ethylhexyl group appear at nearly the same frequency as in the free acid. The C—C stretching motion of the alkyl chain gives rise to an absorption band of weak-to-medium intensity at *ca* 975 cm^{-1}. The sodium, copper, europium, and uranyl compounds, as initially isolated, have bands in the

Table 2. Absorption frequencies (cm^{-1}) for H_2DEH[MDP] and its metal compounds[a]

H_2DEH[MDP]	2961(s), 2926(s), 2874(m), 2860(m), 2617(m, br), 2324(m, br), 2162(sh, br), 1675(m, br), 1462(w), 1381(w), 1238(s), 1222(sh), 1190(s), 1157(sh) 1082(m), 1020(vs), 1007(s), 977(sh), 855(w), 816(w), 800(sh), 767(vw), 727(w), 515(w), 498(w)
Na^{I}	3388(vs, br), 3201(sh, br), 2961(s), 2932(s), 2874(m), 2864(m), 1653(w, br), 1464(m), 1379(w), 1246(s), 1219(s, br), 1144(m), 1105(s), 1047(vs, br), 974(w), 930(vw), 838(sh), 801(s), 788(sh), 739(w), 517(s), 473(w), 461(w), 237(w)
Ca^{II}	2961(s), 2932(s), 2875(m), 2862(m), 1461(s), 1381(w), 1203(s), 1170(s), 1102(s), 1045(vs, br), 979(sh), 838(m), 802(w), 760(w), 534(s), 459(w)
Cu^{II}	3434(m, br), 3249(sh, br), 2959(s), 2932(s), 2874(m), 2861(m), 1632(w, br), 1464(w), 1383(w), 1181(vs), 1121(s), 1109(sh), 1085(m), 1059(sh), 1043(s), 1019(sh), 980(m), 854(w), 816(m), 771(sh), 739(w), 554(m), 527(w), 455(w), 420(vw)
Fe^{III}	2961(s), 2932(s), 2874(m), 2861(m), 1466(w), 1381(w), 1136(vs, br), 1096(s, br), 1047(vs), 1040(sh), 979(sh), 857(w), 816(w), 768(w), 727(vw), 550(m), 446(w), 419(vw), 355(vw), 256(w)
Eu^{III}	3428(s, br), 3210(sh), 2961(s), 2932(s), 2874(m), 2861(m), 1636(m), 1466(m), 1383(w), 1171(vs, br), 1107(vs), 1046(vs), 980(sh), 933(sh), 814(m), 775(w), 593(sh), 530(m), 451(w), 175(w)
Th^{IV}	2961(s), 2933(s), 2874(m), 2862(m), 1466(w), 1384(w), 1260(sh), 1156(vs, br), 1099(s), 1043(vs, br), 979(sh), 931(vw), 849(w), 812(m), 770(w), 727(vw), 625(vw), 534(m), 447(w)
U^{VI}	3562(sh), 3450(s, br), 3180(sh), 2961(s), 2932(s), 2875(m), 2862(m), 1636(w, br), 1466(m), 1384(w), 1199(s), 1167(s), 1110(vs), 1054(s), 1039(s), 979(sh), 923(s), 872(sh), 847(sh), 817(m), 771(w), 728(vw), 593(vw), 532(m), 443(w)

[a]Results reported for H_2DEH[MDP] are for a toluene solution spectrum checked against a liquid film spectrum. Results reported for solid salts are for spectra obtained with KBr and CsI disks checked against Nujol mull spectra. vs = very strong, s = strong, m = medium, w = weak, vw = very weak, br = broad, sh = shoulder.

conventional regions characteristic of water of hydration. The uranium compound exhibits additional bands at 923 and 872 cm^{-1} which are ascribed to ν_3 and ν_1 of the uranyl ion, respectively [15].

The frequencies and tentative assignments of the absorption bands in the 950–1250 cm^{-1} region for the metal compounds are listed in Table 4. The highest energy bands in this region are assigned to $\nu_{asym}(POO^-)$ and $\nu_{sym}(POO^-)$, respectively. Ionized organophosphorus compounds containing the PO_2^- group show two absorption bands attributable to the asymmetric and symmetric POO^- stretching vibrations of the anion. The frequency of the asymmetric stretching mode, $\nu_{asym}(POO^-)$, is typically higher than that of the symmetric stretching mode, $\nu_{sym}(POO^-)$. In the spectra of salts of monoesters of alkylphosphonic acids, these bands generally fall within the overall frequency region of 1153–1245 cm^{-1} and 1053–1110 cm^{-1}, respectively [13]. While the energy of both stretching modes in these compounds depends upon the metal ion present, $\nu_{asym}(POO^-)$ is especially sensitive to the nature of the cation. The frequency of the asymmetric stretching mode decreases dramatically as the degree of aggregation induced by the metal ion increases. The decrease in $\nu_{asym}(POO^-)$ may be interpreted to indicate an increase in the strength of the metal–diphosphonate interaction. Of the compounds listed in Table 4, $\nu_{asym}(POO^-)$ appears at the highest energies in the sodium and calcium compounds and at the lowest energy in the iron compound. Thus, the binding of sodium and calcium to the ligand appears to be relatively weak while the other metal ions are bound more strongly to H_2DEH[MDP].

Both the symmetric and asymmetric POO^- stretching frequencies are lower in the metal complexes than in the sodium salt. The decrease observed in $\nu_{asym}(POO^-)$ upon complexation essentially rules out monodentate coordination of the phosphonate

Table 3. Absorption frequencies for dibasic organophosphorus acids in the P—O stretching region

H_2DEH[MDP]	H_2[EHP][a]	H_2MEHP[a]	Tentative assignments
1238 s	1210 s	1175 sh	P=O str
1190 s	1155 s	1145 s	
1082 m			C—O str or alkyl def
1020 vs		1025 vs	P—OR and P—OH str
1007 s	1002 s		P—OH str
977 sh	970 s	950 sh	C—C str

[a]From [14].

Table 4. Absorption bands for the metal compounds in the P–O stretching region

Na^{I}	Ca^{II}	Cu^{II}	Eu^{III}	U^{VI}	Th^{IV}	Fe^{III}	Tentative assignments
1246 s	1203 s	1181 s	1171 s	1199 s	1156 vs	1136 vs	asym POO^- str
1219 s	1170 s			1167 s			
1144 m	1102 s	1121 s	1107 s	1110 vs	1099 s	1096 s	sym POO^- str
1105 s		1085 m					
1047 vs	1045 vs	1043 s	1046 vs	1054 s	1043 vs	1047 vs	P—OR str
				1039 s			
974 w	979 sh	980 m	980 sh	979 sh	979 sh	979 sh	C—C str

groups. Coordination of a single oxygen of a PO_2^- group would result in considerably different P—O bond orders and the asymmetric stretching frequency should increase. Symmetrical coordination of the phosphonate groups through chelate and/or bridging interactions, on the other hand, could reduce the bond order of both P—O bonds by the same amount and both $\nu_{asym}(POO^-)$ and $\nu_{asym}(POO^-)$ should decrease.

The absorptions in the region below 600 cm^{-1} are very similar to those reported earlier for monobasic [16] and dibasic [14] organophosphorus acids. The compounds reported in Table 2 have two bands in the 450–540 cm^{-1} region where the O—P—O and C—P—O deformation modes generally appear [12,13]. The bands are at nearly the same energy in H_2DEH[MDP] and are sensitive to the metal ion present. Upon salt formation, the energy separation between the two bands increases. The energy difference between the bands is smallest in the sodium salt and greatest in the iron complex. Although there is no way to differentiate unambiguously between the two bands based on the available data, it appears on the basis of the frequency shifts that the higher energy band is the O—P—O deformation. Assuming that this assignment is correct, the higher energy of the O—P—O deformation mode in the metal complexes is consistent with increased strength in the metal-ligand interaction.

Metal containing H_2DEH[MDP] *solutions.* The infrared spectra of the metal containing solutions of H_2DEH[MDP] used for the VPO measurements cannot be reproduced simply by adding the spectrum of a metal salt to that of the dimer. The excess ligand in these samples appears to be intimately associated with the metal containing species in solution. In fact, with the exception of the uranium and iron compounds, excess ligand is required to solubilize these otherwise insoluble salts. The spectra resemble that of a single species rather than a physical mixture of the metal salt and the dimer. The spectra of the iron, thorium, and uranyl containing solutions are very similar to those of the corresponding metal complexes. These samples have the highest aggregation numbers and the lowest ligand-to-metal ion concentration ratios. It is clearly evident from the solution stoichiometry, the calculated η values, and the molecular weight of the iron and uranyl salts that these solutions contain polynuclear species.

In spite of the 25–50% excess ligand present in the iron, thorium and uranium containing solutions, there are no obvious absorption bands which correspond to unionized P—OH or uncomplexed P=O groups of the free dimer (see Table 5). The spectra appear to be that of the salt into which the excess H_2DEH[MDP] has been incorporated with complete disruption of the dimer bonding. The spectrum of the iron containing solution is virtually indistinguishable from that of solid Fe_2(DEH[MDP])$_3$, see Fig. 5. The most obvious difference is that the P—O bands are slightly broadened and appear at somewhat higher energy in the solution spectrum. Dilution of the iron sample with 0.1 *m* H_2DEH[MDP] yields a spectrum which becomes progressively more like that of the dimer until the two are virtually indistinguishable at a fourfold dilution. The absorption maxima of the most intense P—O stretching bands at a 1 : 1 dilution occur at 1183 and 1030 cm^{-1}, with band envelopes that are very similar to those observed for the calcium, copper, and europium samples. These changes suggest that the structure of the extractant–metal complex may change with different loading conditions.

The spectra of the calcium, copper, and europium-containing solutions are intermediate between those of the metal compound and the H_2DEH[MDP] dimer. These solutions show the greatest number of absorption bands in the P—O stretching region. The bands are broad, poorly resolved, shifted in energy, and changed in relative intensity compared with the dimer or the metal compound. The observed bands correspond to P—OR and P=O groups as well as ionized and un-ionized P—OH groups (*vide infra*). The frequencies of these bands are somewhat different from the values observed in the spectra of the ligand or the metal salts. The greatest differences occur for europium where the frequency of the highest energy band in the P—O stretching region of the VPO sample is 33 cm^{-1} higher and 34 cm^{-1} lower than the corresponding bands in the spectra of the salt and dimer, respectively. The spectra appear to be those of the partially-ionized dimer in which the hydrogen bonding has been disrupted by the metal ion. The solution stoichiometry and the η values indicate that the copper

Table 5. Absorption bands for the VPO solutions in the P—O stretching region

H_2DEH[MDP]	Ca^{II}	Cu^{II}	Eu^{III}	U^{VI}	Th^{IV}	Fe^{III}
1238 s	1227 vs	1240 m	1204 vs	1202 s	1181 s	1136 vs
1190 s	1193 sh	1196 s		1175 sh	1154 s	
	1177 m	1184 sh	1177 m			
		1167 m	1166 sh			
1082 m	1087 m	1090 m	1096 m	1101 s	1100 s	1100 vs
	1033 s	1034 s	1036 vs	1043 vs	1040 vs	1051 vs
1020 vs	1020 vs	1020 vs	1023 s			
1007 s	1002 sh	1007 sh	1002 sh			
977 sh	975 sh	976 sh	976 sh	980 sh	973 m	980 sh

and europium samples contain binuclear complexes while the calcium sample contains a mononuclear species.

There are a number of features of the solution spectra which indicate that the P=O groups of the excess un-ionized H_2DEH[MDP] in the samples participate in the complexation process. In the thorium solution spectrum, a new band appears in the phosphoryl stretching region at 1181 cm^{-1}. This band is 57 cm^{-1} lower in energy than the highest phosphoryl stretching vibration in the H_2DEH[MDP] dimer. In the europium solution spectrum, the P=O band is shifted 34 cm^{-1} to lower energy. The corresponding band shift is 11 cm^{-1} for the calcium solution. The broadness and frequency shifts of the P—O bands in the uranium and iron containing samples suggest that additional vibrational components are present. Addition of H_2DEH[MDP] to the iron sample progressively shifts the frequency of the most intense band in the P—O stretching region to higher energy. In an equal volume mixture of the iron solution and 0.10 *m* H_2DEH[MDP], the highest energy P—O band is 55 cm^{-1} lower in energy than the phosphoryl stretching vibration of the dimer. Phosphoryl band shifts of this magnitude have been used to establish that the P=O group is the preferred coordination site in neutral bifunctional carbamoyl–phosphoryl extractants [17].

The copper, europium, and uranium-containing solutions show absorption bands at ~3400 cm^{-1} and ~1640 cm^{-1} typical of water coordinated to a metal ion. Coordination of water to a metal ion does not preclude chelation or bridging by the diphosphonate

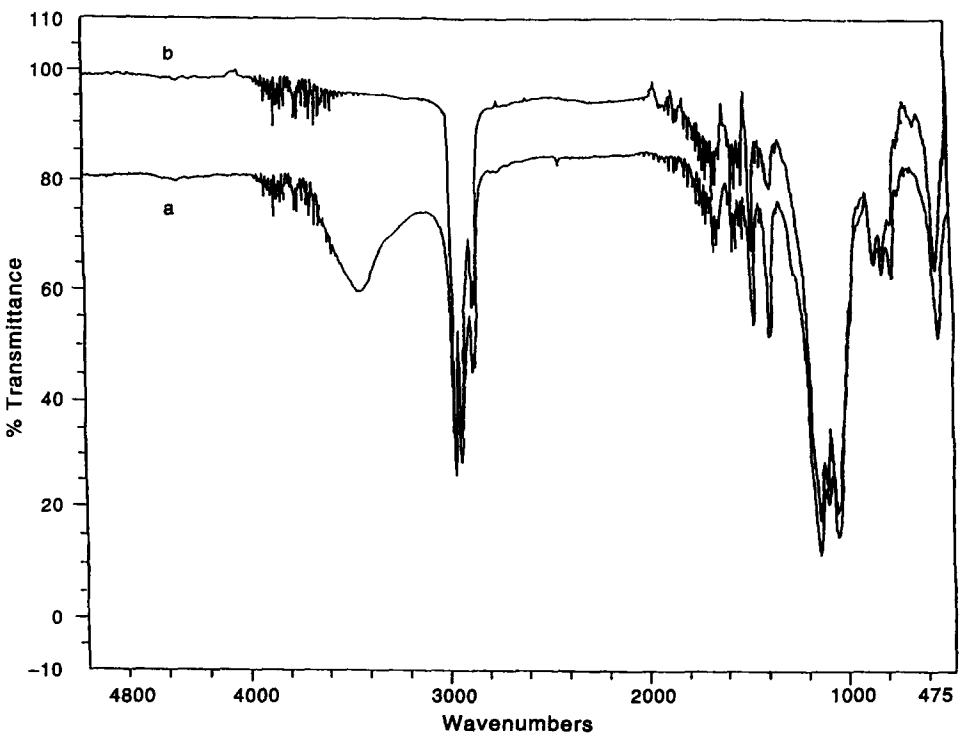


Fig. 5. The infrared spectra of a KBr pellet of solid $Fe_2(DEH[MDP])_3$ (a) and 0.05 *m* Fe^{III} extracted into 0.10 *m* H_2DEH[MDP] in toluene (b).

ligand. Physico-chemical studies and molecular mechanics calculations performed on Eu^{III} complexes of some related diphosphonate ligands show that the complexes exhibit a hemispherical geometry with metal coordinated water molecules occupying space left by the ligand [18].

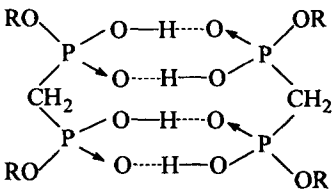
DISCUSSION

Pre-equilibration with water or nitric acid does not affect H_2DEH[MDP] aggregation in toluene. This observation rejects the hypothesis that variations in extractant dependencies with aqueous acidity could be due to changes in ligand aggregation. Ionization of the phosphonic acid groups in the presence of metal ions, however, dramatically increases the aggregation of H_2DEH[MDP]. The linearity of the VPO data and the solution IR spectra suggest that a single solution species may be present, but the aggregation numbers for these samples must be interpreted with caution. The calculated η value represents the average state of aggregation of all solution species present and does not necessarily refer to a single species. For example, the solutions could be physical mixtures of the dimer and highly polymerized metal complexes. While this conclusion was rejected based upon observed ligand band shifts, highly aggregated species like those in the iron system may contain a range of similar but different sized aggregates. Small angle neutron scattering experiments are currently underway to address this possibility.

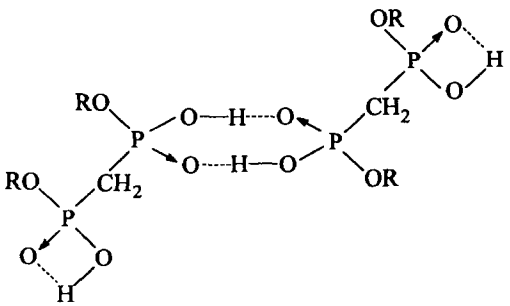
There are no absorption bands in the spectra of the VPO samples that would indicate the presence of nitrate ion. Additionally, the intensities of the P(O)(OH) bands in the 1600–2750 cm^{-1} region are quantitatively reduced as expected based on the stoichiometric amount of metal ion present in solution. The absence of nitrate ion and the diminished intensity of the P(O)(OH) bands indicates that under high metal loading conditions, extraction of metal ions by H_2DEH[MDP] proceeds with the displacement of hydrogen ions. These results are in contrast to those of our earlier extraction study [5] which was carried out under very low metal loading conditions. The extraction data indicated that at very low metal ion concentrations, iron(III) and tetra- and hexavalent actinides are extracted by H_2DEH[MDP] with little or no H^+ ion displacement. The data also indicated that under these conditions, the ligand is coordinated to the metal primarily through the neutral P=O groups. Based on these observations, it appears that metal extraction by H_2DEH[MDP] can occur by different pathways which depend upon reaction conditions. At very low metal ion concentrations, metal extraction apparently proceeds by a solvation process involving the phosphoryl oxygen atoms of the ligand. At high metal ion concentrations, the extraction process changes from solvation to ion exchange with acidic protons of the ligand being displaced by the metal ion.

Thomas has thoroughly discussed the use of frequency ranges, band intensities, and band contours as diagnostic tools for assigning infrared bands in the spectra of organophosphorus compounds [12,13]. Monoesters of alkylphosphonic acids have a band of medium-to-strong intensity in the 1170–1225 cm^{-1} region with a characteristic band shape that arises from the P=O stretching vibration. The band is broadened and reduced in frequency as a result of strong hydrogen bonding to the P—OH group. The P—OH and P—OR groups are both characterized by a strong absorption band at about 1000 cm^{-1}. There is no evidence in molecules with two or more ester groups that the groups interact to give symmetric and asymmetric vibrational bands. In the case of higher normal esters, a second absorption band is usually found between 939–982 cm^{-1} that is assigned to a C—C stretching vibration. Thomas also reports that the P—CH_2—P group gives rise to characteristic symmetric and asymmetric stretching vibrations in the 720–770 cm^{-1} and 780–845 cm^{-1} regions, respectively. All these vibrations are observed in the spectra of the compounds reported in Table 2.

Two possible structures for the H_2DEH[MDP] dimer are shown in Fig. 6. Molecular modeling energy minimization calculations reveal that, as an isolated species, the open hydrogen bonded structure B is significantly more stable than the closed cyclic structure A [19]. The infrared data indicate that strong hydrogen-bonding is responsible for the stability of the dimer. The absorption bands associated with the phosphonic acid functionality of the ligand are broad and



A



B

Fig. 6. Possible structures for the H_2DEH[MDP] dimer.

appear at relatively low frequencies. This behavior is characteristic of O—H groups that are strongly involved in hydrogen bonding to phosphoryl oxygen atoms. The P=O stretching vibrations are also highly perturbed and occur at lower frequencies than normal for a P=O bond [12,13]. The appearance of two phosphoryl stretching bands lends support for structure B since two distinctly different types of hydrogen bonds are present, i.e. intramolecular as well as intermolecular hydrogen bonds.

Under favorable circumstances, ligand band shifts can be used to obtain qualitative information about ligand coordination modes in metal complexes. This approach has been used extensively for carboxylic acids [20,21] which are formally similar to the monoesters of phosphonic acids and the same bonding arguments should apply. In both classes of acids, the X—O bonds of the uncomplexed anion are equivalent. Upon coordination to a metal ion, $\nu_{asym}(XOO^-)$ and $\nu_{sym}(XOO^-)$ of the XO_2^- group should shift to higher or lower frequencies depending on the structure of the metal complex formed. The X—O bonds are no longer equivalent if monodentate coordination occurs. In monodentate carboxylate complexes, $\nu_{asym}(COO^-)$ and $\nu_{sym}(COO^-)$ shift to higher and lower frequencies, respectively. Monodentate coordination of the PO_2^- groups in the diphosphonate complexes reported in Table 4 thus can be ruled out on the basis of the direction of the band shifts.

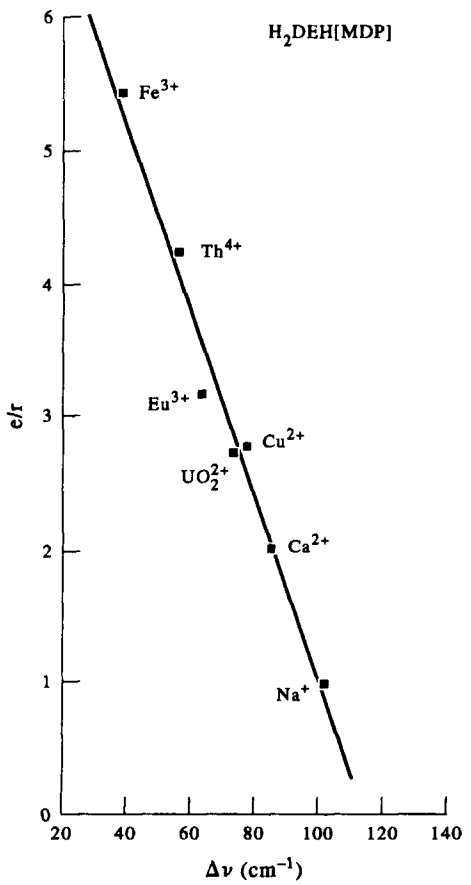


Fig. 7. A plot of the ionic potential of the metal ion, e/r, versus the difference between $\nu_{asym}(POO^-)$ and $\nu_{sym}(POO^-)$, $\Delta\nu$, in H_2DEH[MDP] compounds, where e = ion charge and r = Shannon ionic radius.

Figure 7 shows a plot of the ionic potential (charge/radius) of the metal ion versus the observed frequency difference $\Delta\nu$, $[\nu_{asym}(POO^-) - \nu_{sym}(POO^-)]$, for the H_2DEH[MDP] compounds. The difference between the POO^- stretching frequencies in these diphosphonate compounds becomes smaller as the ionic potential of the metal ion increases. A similar correlation has been observed for ionic complexes of organophosphoric acids of the type $(RO)_2PO(OH)$ [22].

The separation between $\nu_{asym}(COO^-)$ and $\nu_{sym}(COO^-)$ may be used to distinguish between bridging and chelating coordination modes for carboxylate ligands. The difference between these frequencies is considerably larger for a bridged complex than it is for a chelate complex [20, 21]. The $\Delta\nu$ values observed for the H_2DEH[MDP] compounds are much smaller than those reported for carboxylate complexes. The small separations and absence of model complexes of known structure make it difficult to distinguish unambiguously between bridging and chelating coordination modes. Based on ligand geometry and the extensive polymerization of the complexes, it is likely that both coordination modes are utilized so that the metal ions can achieve their preferred coordination numbers.

Acknowledgements—The authors wish to express their gratitude to the Analytical Chemistry Division of ANL for analyses performed, to Paul G. Rickert for preparing the P,P′-di(2-ethylhexyl) methanediphosphonic acid, to Herb Diamond for help with the VPO measurements, and to Ken L. Nash for helpful discussions. One of us (AWH) wishes to thank Loyola University for a research leave of absence and ANL for support under the Faculty Research Leave at Argonne program.

REFERENCES

1. E. N. Rizkalla, *Rev. Inorg. Chem.*, 1983, **5**, 223.
2. K. L. Nash and E. P. Horwitz, *Inorg. Chim. Acta* 1990, **169**, 245.
3. K. L. Nash, *Radiochim. Acta* 1991, **54**, 171.
4. E. P. Horwitz, R. Chiarizia and M. L. Dietz, *A Method for the Chromatographic Separation of Cations from Aqueous Samples*, U. S. Patent granted (1996).
5. R. Chiarizia, E. P. Horwitz, P. G. Rickert, and A. W. Herlinger, *Solvent Extr. Ion Exch.* 1996, **14**, 773.
6. C. Djordjevic and H. Gorican, *J. Inorg. Nucl. Chem.* 1966, **28**, 1451.
7. C. Djordjevic, H. Gorican and S. L. Tan, *J. Inorg. Nucl. Chem.* 1967, **29**, 1505.
8. H. Meider-Gorican, *J. Inorg. Nucl. Chem.* 1971, **33**, 1919.

9. J. R. Ferraro, G. W. Mason and D. F. Peppard, *J. Inorg. Nucl. Chem.* 1961, **22,** 285.
10. G. S. Rao, G. W. Mason and D. F. Peppard, *J. Inorg. Nucl. Chem.* 1966, **28,** 887.
11. A. Burger and J. J. Anderson, *J. Am. Chem. Soc.* 1957, **79,** 3575.
12. L. C. Thomas, in *Analysis of Organic Materials, An International Series of Monographs* (edited by R. Belcher and D. M. W. Anderson) Vol. 7, Academic Press, London, U.K. (1974).
13. L. C. Thomas, *Interpretation of the Infrared Spectra of Organophosphorus Compounds.* Heyden, London, U. K. (1974).
14. J. R. Ferraro, D. F. Peppard and G. W. Mason, *J. Inorg. Nucl. Chem.* 1965, **27,** 2055.
15. J. R. Ferraro and A. Walker, *J. Chem. Phys.* 1966, **45,** 550.
16. J. R. Ferraro, D. F. Peppard and G. W. Mason, *Spectrochim. Acta* 1963, **19,** 811.
17. K. A. Martin, E. P. Horwitz and J. R. Ferraro, *Solvent Extr. Ion Exch.* 1986, **4,** 1149.
18. K. L. Nash, L. F. Rao, and G. R. Choppin, *Inorg. Chem.* 1995, **34,** 2753.
19. K. L. Nash, Private communication (1995).
20. K. Iton and H. J. Bernstein, *Can. J. Chem.* 1956, **34,** 170.
21. G. B. Deacon and R. J. Phillips, *Coord. Chem. Rev.* 1980, **33,** 227.
22. J. R. Ferraro and D. F. Peppard, *Nucl. Sci. Eng.* 1963, **16,** 389.

Pergamon

PII: S0277-5387(96)00492-5

Polyhedron Vol. 16, No. 11, pp. 1855–1861, 1997
© 1997 Elsevier Science Ltd
All rights reserved. Printed in Great Britain
0277-5387/97 $17.00+0.00

Tert-butyl-2,4,6-trimethylphenylphosphine—a chiral secondary phosphine with bulky substituents: synthesis and NMR spectroscopic studies

William McFarlane* and Christian T. Regius

Department of Chemistry, University of Newcastle, Newcastle upon Tyne NE1 7RU, U.K.

(Received 10 September 1996; accepted 30 September 1996)

Abstract—The preparation and characterization of the secondary phosphine Bu^{t}MesPH [Mes = 2,4,6-$(CH_3)_3C_6H_2$—], its precursor Bu^{t}MesPCl, and its chalcogenides Bu^{t}MesP(E)H (E = O, S, Se) are described. Their ^{1}H, ^{13}C and ^{31}P NMR spectra are reported and show that rotation about the P—Mes bond is hindered with $\Delta G\ddagger$ ranging from 56 to 88 kJ mol^{-1}. Two-dimensional proton ROESY spectra indicate a single preferred conformation in solution which is determined by the need to minimize the Bu^t-Mes interaction in all cases.
© 1997 Elsevier Science Ltd. All rights reserved.

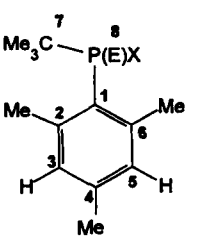
Keywords: secondary phosphine; bulky substituent; chirality; NMR; ROESY; hindered rotation.

Tertiary phosphines with bulky substituents are important for their ability to stabilize unusual metal oxidation states and coordination geometries in their complexes and in this connection those with *tert*-butyl (Bu^t) or 2,4,6-trimethylphenyl (Mes) substituents have been extensively studied [1]. Also of continuing interest in the context of asymmetric synthesis are phosphines, which are chiral at phosphorus, well known examples being *tert*-butylmethylphenylphosphine [2] and (2-aminophenyl)methylphenylphosphine [3].

Less work has been carried out on secondary phosphines in either of these categories, although Mes_2PH [4] and Bu^t_2PH [5] are well characterized, as are the chiral secondary phosphines *tert*-butylphenylphosphine [5] and (2-aminophenyl)phenylphosphine [3]. Normally, in secondary phosphines ready P—H exchange leads to rapid racemization and to our knowledge there is only one report of the successful resolution of a free chiral secondary phosphine, namely, (-)-methyl-mesitylphosphine [6], and even in this case only a diastereomeric form has been isolated. The title secondary phosphine Bu^{t}MesPH (**2**) is therefore of considerable interest and we report here its synthesis and those of its precursor Bu^{t}MesPCl (**1**) and its chalcogenides Bu^{t}MesP(E)H (E = O, S, Se, **3**–**5**) together with one- and two-dimensional ^{1}H, ^{13}C and ^{31}P and dynamic NMR studies, which reveal hindered rotation about the P—Mes bond and the nature of the preferred conformation in solution.

RESULTS

The reaction between 2,4,6-trimethylphenylmagnesiumbromide and Bu^tPCl_2 in 1,2-dimethoxyethane gave Bu^{t}MesPCl (**1**) as an off-white waxy solid; this was then reduced with $LiAlH_4$ in diethylether to **2**, which was isolated as a colourless somewhat air-sensitive liquid. The reaction of **2** with aqueous H_2O_2 gave Bu^{t}MesP(O)H (**3**) and with elemental sulfur and selenium gave Bu^{t}MesP(S)H (**4**) and Bu^{t}MesP(Se)H (**5**), respectively. The identities of **3** and **4** were confirmed by elemental analysis and of



(1) E = lone pair X = Cl
(2) E = lone pair X = H
(3) E = O X = H
(4) E = S X = H
(5) E = Se X = H

*Author to whom correspondence should be addressed.

Table 1. ^{1}H-NMR data for **1–5**[a,b]

Proton	Bu^t(Mes)PCl $CDCl_3$, 233 K	Bu^t(Mes)PH toluene-d_8, 210 K	Bu^t(Mes)PHO toluene-d_8, 248 K	Bu^t(Mes)PHS $CDCl_3$, 295 K	Bu^t(Mes)PHSe $CDCl_3$, 295 K
H-3	6.88	6.73	6.82	6.86	6.96
	(d, 6.1)	(d, 3.2)	(s)	(s)	(s)
H-5	6.91	6.80	6.69	6.81	6.82
	(s)	(s)	(d, 3.2)	(d, 4.1)	(d, 4.2)
Me-2	2.61	2.67	3.08	2.71	2.70
	(s)	(s)	(s)	(s)	(s)
Me-6	2.58	2.32	2.15	2.42	2.41
	(d, 5.7)	(s)	(s)	(s)	(s)
Me-4	2.28	2.18	2.21	2.10	2.20
	(s)	(s)	(s)	(s)	(s)
Me-7	1.19	1.13	1.18	1.20	1.22
	(d, 14.1)	(d, 12.0)	(d, 16.0)	(d, 18.4)	(d, 18.9)
H-8	—	4.26	7.64	7.40	7.06
		(d, 215.8)	(d, 444.0)	(d, 446.7)	(d, 439.0)

[a]Chemical shifts are in ppm ±0.01 ppm. Coupling constants J(^{31}P—H) (in parenthesis) are in Hz ±0.1 Hz.
[b]The designation (s) indicates that any coupling is less than 0.5 Hz.

all five by ^{1}H, ^{13}C and ^{31}P NMR spectroscopy (see Tables 1 and 2).

NMR spectral assignments were confirmed by ^{1}H{^{31}P} decoupling experiments and HMQC [7] and HMBC [8] two-dimensional ^{1}H/^{13}C correlation spectra. For **4** and **5** hindered rotation of the Mes group led to inequivalence of the proton and carbon 2- and 6-methyl and 3- and 5-phenyl resonances at all accessible temperatures (up to 413 K), although there was some line broadening of the 2- and 6-proton methyl res-

Table 2. ^{13}C NMR data for **1–5**[a,b]

Carbon	Bu^t(Mes)PCl, $CDCl_3$, 233 K	Bu^t(Mes)PH, toluene-d_8, 210 K	Bu^t(Mes)PHO toluene-d_8, 248 K	Bu^t(Mes)PHS $CDCl_3$, 295 K	Bu^t(Mes)PHSe $CDCl_3$, 295 K
C-1	127.8	130.3	124.3	122.5	121.0
	(d, 57.9)	(d, 16.4)	(d, 85.5)	(d, 71.0)	(d, 64.0)
C-2	144.5	144.8	141.4	143.9	143.9
	(d, 36.5)	(d, 27.7)	(d, 11.3)	(d, 10.0)	(d, 11.3)
C-6	140.6	142.8	145.9	140.0	139.9
	(s)	(d, 5.0)	(d, 7.5)	(d, 7.5)	(d, 7.0)
C-3	132.1	130.2	132.3	131.9	131.9
	(s)	(s)	(d, 10.1)	(d, 11.3)	(d, 8.8)
C-5	130.0	130.3	130.8	130.2	130.1
	(d, 7.5)	(s)	(d, 10.1)	(d, 10.0)	(d, 5.0)
C-4	144.4	138.5	142.0	141.5	141.6
	(d, 2.5)	(s)	(d, 2.5)	(d, 2.7)	(d, 2.5)
Me-2	24.4	24.3	23.3	23.2	24.0
	(d, 23.1)	(d, 26.4)	(s)	(d, 5.4)	(d, 7.9)
Me-6	24.8	25.9	23.4	23.8	23.6
	(s)	(d, 3.4)	(s)	(d, 8.3)	(d, 6.0)
Me-4	21.4	21.9	23.2	21.0	21.0
	(s)	(s)	(d, 3.2)	(s)	(s)
C-7	38.4	33.0	35.4	36.5	35.4
	(d, 35.3)	(d, 11.8)	(d, 69.2)	(d, 49.7)	(d, 41.5)
Me-7	27.2	31.3	25.2	26.1	26.6
	(d, 18.2)	(d, 12.7)	(s)	(s)	(s)

[a]Chemical shifts are in ppm ±0.1 ppm. Coupling constants J(^{31}P—^{13}C) (in parentheses) are in Hz ±0.1 Hz.
[b]The designation (s) indicates that any coupling is less than 0.5 Hz.

Table 3. Thermodynamic parameters for rotation about the P—Mes bond of **1–4**

	Bu^{t}MesPCl	Bu^{t}MesPH	Bu^{t}MesPHO	Bu^{t}MesPHS
$\Delta H\ddagger$ (kJ mol^{-1})	67.8 ± 3.4	56.6 ± 3.2	65.4 ± 1.8	—
$\Delta S\ddagger$ (J mol^{-1} K^{-1})	30.4 ± 12.6	17.2 ± 12.7	27.6 ± 6.6	—
$\Delta G\ddagger$ (295 K, kJ mol^{-1})	57.8	55.5	57.3	88.1[a]

[a]Estimate based on line-broadening measurements at 393 K and corrected to 295 K on the assumption that $\Delta S\ddagger \sim 25$ J mol^{-1} K^{-1}.

onances of **4** at 393 K in naphthalene which made it possible to derive $\Delta G\ddagger$ for the barrier to rotation. In the cases of **1, 2** and **3** lower barriers to rotation led to separate resonances only at temperatures below ambient and their ^{1}H and ^{13}C parameters are therefore quoted at 233, 210 and 248 K, respectively. The program gNMR [9] was used to simulate the spectra given by the 2,6-methyl and 3,5-ring protons in the temperature ranges of 233–296 for **1**, 223–295 for **2** and 248–330 K for **3** and the resulting thermodynamic parameters from Eyring plots for the barrier to rotation of the Mes group are in Table 3.

Figure 1 shows the fit of calculated and experimental spectra for the 2,6-methyl protons of **2**.

In order to assess the conformational distribution in **1–5** a series of proton rotating frame nuclear Overhauser effect (ROESY [10]) spectra was obtained. These used a spin-locking (mixing) time of 250 ms and in them negative off-diagonal peaks indicate protons that are spatially close. Figure 2 shows a typical spectrum obtained from **2** at 210 K (rotation slow on the NMR timescale). The spectrum also shows some positive off-diagonal peaks due to residual chemical exchange at this temperature associated with the (slow) rotation of the 2,4,6-trimethylphenyl group.

DISCUSSION

The cone angle [11] of **2** can be estimated at 160°, which is significantly larger than those for Ph_3P (145°) and Bu^t_2PH (150°), but smaller than that for Mes^t_2PH (170°). It should be noted, however, that in metal complexes a secondary phosphine may be able to rotate about the P—metal bond into a position which minimizes steric interactions between its bulkier groups and the other substituents of the metal and hence its *effective* cone angle may be considerably smaller than that calculated in the usual way.[11] The pattern of cone angles for Bu^t_2PH, Bu^{t}MesPH and Mes_2PH is paralleled by their $^1J(^{31}P—H)$ coupling constants which are 197, 215.8 and 234 Hz, respectively.

$^1J(^{31}P—H)$ for **2** is thus almost identical to the mean (215.5 Hz) of the other two and this presumably reflects corresponding trends in the phosphorus hybridization and interbond angles at phosphorus. As expected, chalcogenization leads to substantial increases in $^1J(^{31}P—H)$ arising from greater *s*-character for the phosphorus hybrid orbital forming the P—H bond.

In contrast to the foregoing, $\delta(^{31}P)$ for **2** [−49.3 ppm] differs significantly from the mean [−36 ppm] of those for Bu^t_2PH [20 ppm] and Mes_2PH [−92 ppm], whereas group contribution theory [12] would predict close correspondence. On this basis using values of the group contributions σ^P for Bu^t and Mes derived from Bu^t_3P and Mes_3P the predicted ^{31}P chemical shifts of Bu^t_2PH, Bu^{t}MesPH and Mes_2PH are +25, −24 and −72 ppm, respectively, and so it appears that the Mes rather than the *tert*-butyl group is the principal origin of the discrepancy. This may be because restricted rotation about the P—C_{ipso} bond leads to a strong dominance of particular conformers in **2** and indeed in Mes_3P itself. The ^{31}P chemical shifts of compounds **1** and **3–5** are in the expected ranges.

The observation of pairs of resonance signals from the off-axis nuclei of the Mes groups of **1–5** indicates not only that rotation is slow about the P—C_{ipso} carbon bond, but that pyramidal inversion at phosphorus is also slow on the NMR time scale. In secondary phosphines this latter process is catalysed both by bases (*via* R_2P^-) and by acids (*via* $R_2P^+H_2$) and information on energy barriers is sparse. However, in $PhPr^iPH$ $\Delta G\ddagger$ for the inversion exceeds 97.5 kJ mol^{-1} corresponding to a rate of *ca* 6.6 s^{-1} at 413 K, so it seems likely that the $\Delta G\ddagger$ of *ca* 56 kJ mol^{-1} in **2** is associated exclusively with the rotation rather than inversion. In the cases of **3–5** neither base- nor acid-catalysed mechanisms can facilitate inversion and so the observed barriers must relate solely to rotation.

The observed barriers to rotation of the Mes group in these molecules are surprisingly high in view of the small size of the hydrogen substituent on phosphorus and the fact that we find that at temperatures down to 188 K the corresponding process is essentially unhindered in Mes_2PH and $Mes_2P(S)H$. From cone angle considerations Mes is apparently bulkier than Bu^t so the contrary might have been expected. Inspection of molecular models shows that whilst a *rotating* Mes group is indeed considerably bulkier than a *tert*-butyl group, a pair of Mes groups can mesh and rotate concertedly thus reducing their effective combined bulk; however, no such cog-wheel gearing is possible for a Bu^t/Mes pair. It is this that accounts for the

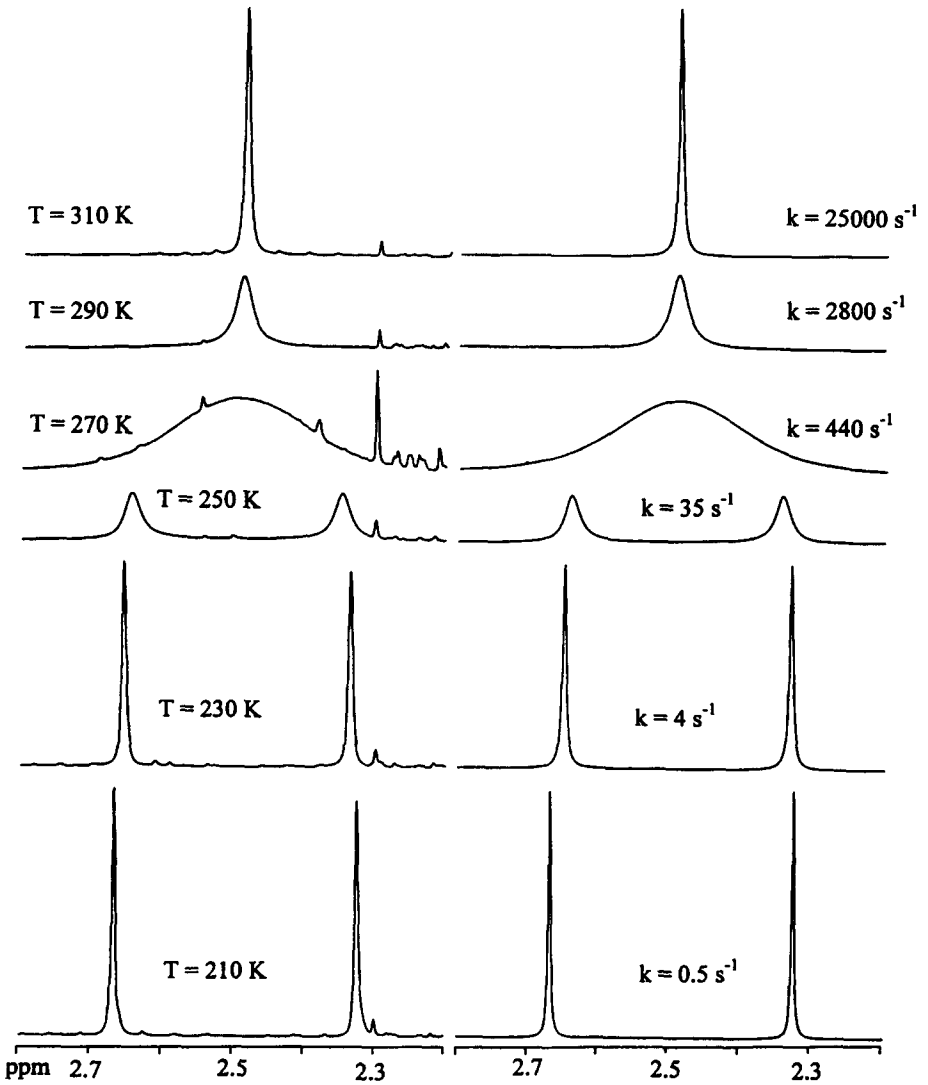
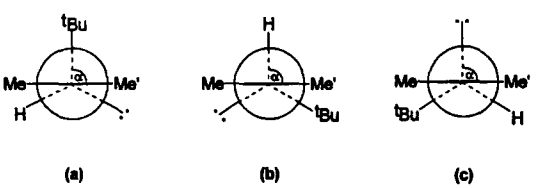


Fig. 1. Experimental (left) and calculated (right) 500 MHz NMR spectra of the aromatic-CH_3 protons of Bu^{t}MesPH in toluene-d_8 for different temperatures and exchange rates.

difference between **2** and Mes_2PH, and also between their corresponding derivatives. Taken together our results provide firm evidence for concerted (cog-wheel) rotation of the Mes groups in Mes_2PH and its derivatives. In the cases of Mes_3P and Mes_3PS such concerted rotation is parity forbidden and in accord with this the value of $\Delta G\ddagger$ for rotation of a Mes group is substantial in these molecules [13].

Projections down the P—C_{ipso} bond of three conformations of one enantiomer of **2**, which minimize interaction between the ortho-methyls of the Mes group and (a) the *tert*-butyl group, (b) the P—hydrogen and (c) the phosphorus lone pair are shown below, where the angle α is expected to be *approximately* 90°.



In view of the large bulk of *tert*-butyl, (a) is likely to be the dominant conformer and this was confirmed by the proton two-dimensional rotating frame nuclear Overhauser (ROESY) experiment performed at 210 K and illustrated in Fig. 2.

At this temperature the rate of rotation (exchange) is *ca* 0.5 s^{-1} and thus the 2- and 6-methyl protons display mutual positive chemical exchange peaks as do the 3- and 5-aromatic protons. Nonetheless, the rate of exchange is sufficiently slow for significant differential N.O.E.s to be observed. The crucial ones are:

(i) *Strong* N.O.E. from P—H to Me at δ 2.32 and

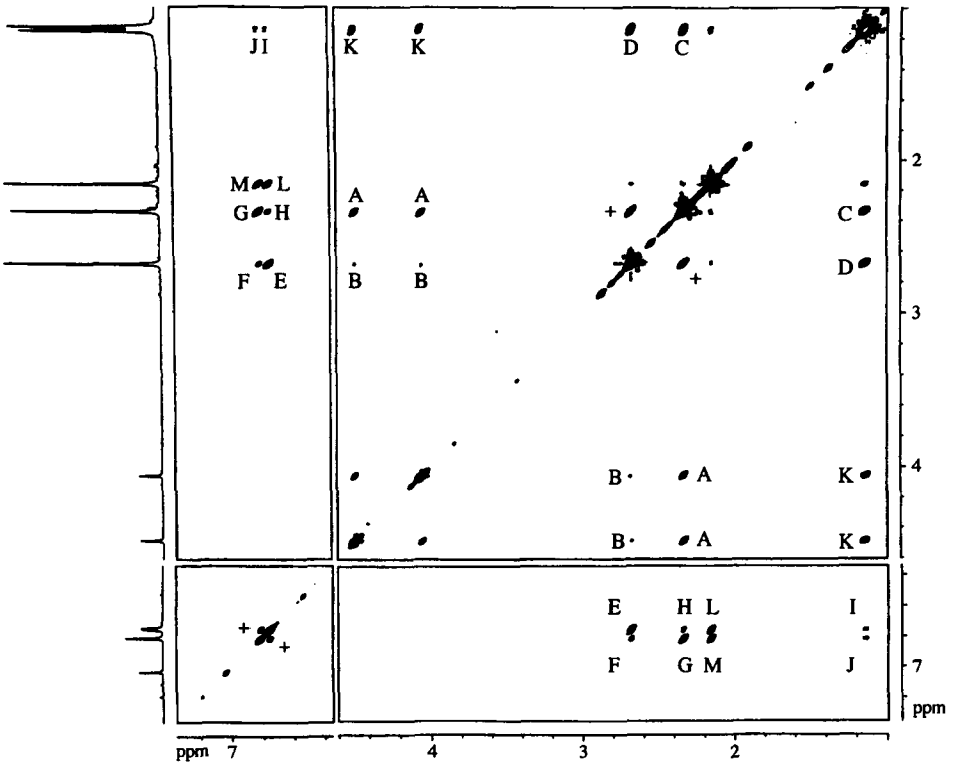


Fig. 2. 500 MHz proton ROESY spectrum of Bu^{t}MesPH in toluene-d_8 at 210 K with spin-locking (mixing) time of 250 ms. Off-diagonal peaks marked + are positive and arise from chemical exchange. The negative off-diagonal peaks referred to in the text are: A: P-H/Me6; B: P-H/Me2; C: Bu^t/Me6; D: Bu^t/Me2; E: Me2/H3; F: Me2/H5; G: Me6/H5; H: Me6/H3; I: Bu^t/H3; J: Bu^t/H5; K: Bu^t/P—H; L: Me4/H3; M: Me4/H5.

a very weak N.O.E. to Me at δ 2.67. This rules out conformer (b).

(ii) Approximately *equally* strong N.O.E.s from Bu^t to Me at δ 2.67 *and* δ 2.32. This is consistent with (a), but not with (b) or (c).

(iii) Strong N.O.E. from Me at δ 2.67 to aromatic H at δ 6.73 and weak to aromatic H at δ 6.80. Strong N.O.E. from Me at δ 2.32 to aromatic H at δ 6.80 and weak to aromatic H at δ 6.73. This gives the relative assignments of the Mes protons.

(iv) Approximately *equally* weak N.O.E.s from both aromatic protons to Bu^t. This is consistent with conformer (a). There are also approximately equally strong N.O.E.s between the aromatic protons and Me4, and between Bu^t and P—H.

We therefore conclude that the dominant conformation of **2** is (a) and that in the numbering scheme position 2 corresponds to Me′ and position 6 to Me. Corresponding ROESY spectra were obtained for **3–5** and confirmed that for each of these the dominant conformation is also (a). Thus for all of these, the positions 2 and 3 are on the side of the Mes ring adjacent to the phosphorus lone pair. In the case of **1** the absence of a proton attached to P prevents any such determination, but it is clear that the dominant conformation is (a) for this species also, in view of the equality of the n.O.es from the Bu^t to each ring methyl group.

There is a clear stereochemical dependence of the P—H and P—C couplings in the Mes groups in these species. Thus, for **2** pathways involving a *ca* 30° dihedral angle between the P-lone pair direction and the Mes plane (i.e. positions 2 and 3) $^4J(^{31}P—H)$, $^2J(^{31}P—^{13}C)$ and $^3J(^{31}P—^{13}C_{Mes})$ are much larger than when the dihedral angle is *ca* 150° (positions 5 and 6). It is likely that this also applies to **1**, although in this case the assignment is not certain. For the P^V derivatives **3–5** only $^4J(^{31}P—H)$ displays such a *marked* stereochemical dependence and is larger for the 150° dihedral angle. The one-bond P—C couplings show the expected dependence on phosphorus oxidation state and hybridization, it being likely that they are negative in **1** and **2** and positive in **3–5**.

The oxide **3** was also modelled using the program QUANTA [14] and in the range 0–180° a plot of energy against the dihedral angle α showed only one minimum, with a barrier height of 62 kJ mol^{-1}. Thus, the modelled minimum structure corresponds to conformer (a) with the angle α close to 90° and no significant predicted contributions from (b) and (c). The calculated barrier height agrees remarkably well with that found experimentally.

It is clear that the large difference in bulk between

tert-butyl and H imposes special conformational constraints upon the Mes group in **2** and its derivatives. This is likely to be an important feature of the complexes of this chiral secondary phosphine ligand in which barrier to rotation of the Mes group could exceed 90 kJ mol^{-1} and this may well facilitate their optical resolution and affect their catalytic behaviour.

EXPERIMENTAL

^1H and ^{13}C NMR spectra were obtained on a Bruker AMX 500 spectrometer at frequencies of 500.13 and 125.75 MHz, respectively, on samples contained in 5 mm o.d. spinning tubes. ^{31}P NMR spectra were recorded on a JEOL FX90Q spectrometer at 36.2 MHz. Chemical shifts are to high frequency of internal t.m.s. for ^1H and ^{13}C, and external 85% H_3PO_4 for ^{31}P. Proton phase-sensitive ROESY spectra were acquired using the sequence 90°–t_1–spinlock–acquire(t_2) with phase cycling by the time-proportional incrementation method. Typically 32 transients were acquired into 1024 data points for each of the 512 values of t_1 and then Fourier transformed into a 1024 × 1024 matrix after weighting in each dimension with a sine-bell function. The spin-locking field had $\gamma B_1/2\pi$ = 5000 Hz.

All materials were handled under dry dinitrogen and diethylether and 1,2-dimethoxyethane were dried over sodium/benzophenone.

Chloro-tert-*butyl*-2,4,6-*trimethylphenylphosphine* (**1**)

MesMgBr (100 cm^3, 0.1 molar in diethylether, ALDRICH) was placed in a three-necked flask. The ether was removed under reduced pressure and replaced by 50 cm^3 of dimethoxyethane. To the resulting stirred yellow suspension Bu^tPCl_2 (15.8 g, 100 mmol) in dimethoxyethane (50 cm^3) was added over 0.5 h. Stirring for 1 h yielded a white suspension. The solvent was removed under reduced pressure and the resulting off-white solid was extracted with *ca* 100 cm^3 of diethylether. The ether was distilled off and the product was distilled at 145°C/0.5 torr (m.p. 34°C, yield 83%), $\delta(^{31}P)$ = 111.0 ppm.

Tert-*butyl*-2,4,6-*trimethylphenylphosphine* (**2**)

A solution of $Bu^tMesPCl$ (20 g, 83 mmol) in diethylether (50 cm^3) was added dropwise to a suspension of $LiAlH_4$ (1.6 g, 42 mmol) in diethylether (50 cm^3) at 0°C. The mixture was stirred for 2 h at 22°C and then filtered. The filtrate was washed with deaerated water (50 cm^3) and the organic layer was dried over magnesium sulfate and the diethylether was removed under reduced pressure. Distillation at 90°C/0.5 torr gave the product (yield 87%) as a colourless air-sensitive oil, $\delta(^{31}P)$ = −49.3 ppm.

Tert-*butyl*-2,4,6-*trimethylphenylphosphineoxide* (**3**)

A solution of Bu^tMesPH (1 g, 0.84 mmol) in dichloromethane (10 cm^3) was stirred vigorously with 5 cm^3 of 5% aqueous H_2O_2 for 1 h. The water layer was removed and the dichloromethane was removed under reduced pressure. The remaining white solid was dissolved in diethylether and recrystallized at −18°C to give **3** as white powder in 87% yield, m.p. 99°C, $\delta(^{31}P)$ = 33.7 ppm. Found: C, 69.3; H, 9.6. $C_{13}H_{21}OP$ requires: C, 69.6; H, 9.4%.

Tert-*butyl*-2,4,6-*trimethylphenylphosphinesulfide* (**4**)

Bu^tMesPH (1 g, 0.84 mmol) in dichloromethane (cm^3) was reacted with elemental sulfur (27 mg, 0.84 mmol; 10 h, 22°C) to give **4** as a white solid after the solvent was removed under reduced pressure. Recrystallization from dichloromethane/methanol yielded **4** as colourless crystals (yield 84%), m.p. 90°C, $\delta(^{31}P)$ = 31.3 ppm. Found: C, 65.0; H, 9.1. $C_{13}H_{21}PS$ requires: C, 64.9; H, 8.8%

Tert-*butyl*-2,4,6-*trimethylphenylphosphineselenide* (**5**)

The corresponding reaction of Bu^tMesPH with elemental selenium gave **5** as off-white crystals, m.p. 93°C (yield 83%), which turned into a yellowish solid in air after 5 h. $\delta(^{31}P)$ = 12.6 ppm, $^1J11(^{77}Se—^{31}P)$ = 703.2 Hz.

Acknowledgements—We thank Dr N.H. Rees for assistance with some spectra and the EPSRC for support.

REFERENCES

1. E. Zeller, A. Schier and H. Schmidbaur, *Z. Naturforsch.* 1994, **49B,** 1243; A. Sladek and H. Schmidbaur, *Z. Naturforsch.*, 1995, **50B,** 859; E. Lindner, A. Nothdurft, R. Fawzi and C. Maichle, *J. Organomet. Chem.* 1992, **435,** 213; J. Bruckmann and C. Krüger, *Acta Cryst.* 1995, **C51,** 1152; T. A. Vanderknaap, F. Bickelhaupt, H. Vanderpoel, G. Vankoten and C. H. Stam, *J. Am. Chem. Soc.* 1982, **104,** 1756; E. C. Alyea, S. A. Dias, G. Ferguson and P. Y. Siew, *Croatica Chem. Acta*, 1984, **57,** 457; W. J. J. Smeets, A. L. Spek, T. Vanderdoes, and F. Bickelhaupt, *Acta Cryst.*, 1987, **C43,** 1838.
2. V. V. Dunina and E. B. Golovan, *Tetrahedron–Asymmetry*, 1995, **6,** 2747, and refs therein.
3. C. E. Barclay, G. Deeble, R. J. Doyle, S. A. Elix, G. Salem, T. L. Jones, S. B. Wild and A. C. Willis, *J. Chem. Soc, Dalton Trans.* 1995, 57.
4. N. A. Rozanel'skaya, A. I. Bokanov and B. I. Stepanov, *J. Gen. Chem. USSR* (*Engl. Transl.*) 1979, **49,** 1732; R. A. Bartlett, M. M. Olmstead, P. P. Power and G. A. Sigel, *Inorg. Chem.* 1987, **26,** 1941.

5. H. Hoffmann and P. Schellenbeck, *Chem. Ber.* 1966, **99,** 1134.
6. A. Bader, M. Pabel and S. B. Wild, *J. Chem. Soc., Chem. Commun.* 1994, 1405.
7. A. Bax, R. H. Griffey and B. L. Hawkins, *J. Magn. Reson.* 1983, **55,** 301.
8. A. Bax and M. F. Summers, *J. Am. Chem. Soc.* 1986, **108,** 2043.
9. P. H. M. Budzelaar, *gNMR NMR Simulation Program.* Version 3.6 for Windows, Cherwell Scientific Publishing, Oxford, 1995.
10. A. Bax and D. G. Lewis, *J. Magn. Reson.* 1985, **63,** 207.
11. C. A. Tolman, *J. Am. Chem. Soc.* 1970, **92,** 2956.
12. S. O. Grim and W. McFarlane, *Nature*, 1965, **208,** 995; S. O. Grim, W. McFarlane and E. F. Davidoff, *J. Org. Chem.* 1967, **32,** 781; L. Maier, *Helv. Chim. Acta*, 1966, **49,** 1718; E. Fluck, and T. Z. Lorenz, *Z. Naturforsch.* 1967, **22B,** 1095.
13. B. I. Stepanov, V. M. Matyuk, A. I. Bokanov and E. N. Karpova, *J. Gen. Chem. U.S.S.R.* (*Engl. Transl.*) 1975, **45,** 2096.
14. QUANTA Version 3.3. Molecular Simulations Inc., Waltham, MA 1992.

Pergamon

PII: S0277-5387(96)00491-3

Polyhedron Vol. 16, No. 11, pp. 1863–1871, 1997
© 1997 Elsevier Science Ltd
All rights reserved. Printed in Great Britain
0277 5387/97 $17.00+0.00

Mono- and dinuclear oxovanadium(IV) compounds containing VO(ONS) basic core: synthesis, structure and spectroscopic properties

Subodh Kanti Dutta,[a] Edward R. T. Tiekink[b] and Muktimoy Chaudhury[a]*

[a]Department of Inorganic Chemistry, Indian Association for the Cultivation of Science, Calcutta 700 032, India; [b]Department of Chemistry, The University of Adelaide, South Australia 5005, Australia

(Received 4 September 1996; accepted 30 September 1996)

Abstract—Reaction of $[VO(acac)_2]$ with *S*-methyl 3-(2-hydroxyphenyl) methylenedithiocarbazate (H_2L^1) and its nitro- (H_2L^2) and bromo derivatives (H_2L^3) as tridentate heterodonor $(ONS)^{2-}$ ligands offers a basic VO(ONS) core. In the presence of bidentate (N,N′) donor ancillary ligands, various mono- and dinuclear oxovanadium(IV) complexes [VOL(2,2′-bipy)] (**1–3**), [VOL(Phen)] (**4, 5**) and [LOV(μ-4,4′-bipy)VOL] (**6–8**) were obtained. The compounds have been characterized by EPR, electronic and FAB mass spectroscopic studies. The X-ray crystal structure of a representative compound [VOL^2(2,2′-bipy)] (**2**) is reported and shows the presence of the tridentate ONS ligand occupying the meridional sites leading to distorted octahedral geometry. The nitrogen donor, occupying an apical position has a *trans*-labilizing influence, resulting in elongation of the V=O terminal bond. Magnetic susceptibility and EPR spectral studies indicate non-interacting nature ($|J| \approx 0$) of the vanadium(IV) unpaired electrons in the dinuclear complexes (**6–8**). © 1997 Elsevier Science Ltd. All rights reserved.

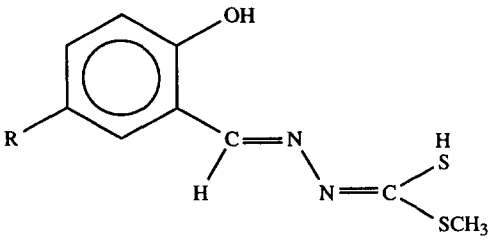
Keywords: oxovanadium(IV) complex; sulfur coordination; crystal structure; EPR; FAB mass spectroscopy.

Recognition of vanadium as an essential trace element [1–4] has generated increasing interest in the structure and function of its complexes found in the living organisms [5,6]. The minimal structures of the vanadium active sites as delineated by EXAFS and other spectroscopic investigations have shown a distinct preference of this metal center for N- and/or O-coordinated environments provided by the histidine imidazole, tyrosine phenolate and carboxylate oxygen of the protein residues [7–10]. In order to gain an insight into how vanadium might function in relatively intricate biomolecules, it is worthwhile to acquire information on the basic coordination chemistry of this element with simple biomimetic ligands. Information level in this area is becoming enriched from the outcome of some recent studies on small molecular complexes with interesting structure and spectroscopic properties. In most of these investigations nitrogen and/or oxygen donor ligands are used to bind the metal center in the oxidation states from +3 to +5 at limited nuclearity range [11–24].

Studies on the coordination chemistry of vanadium in ligand environments containing sulfur unlike those with O/N donor systems, have only started gaining momentum in view of the use of this metal center as catalysts in the oxidation of organic sulfide into sulfoxides [25] and the expected catalytic role of vanadium (IV) in dehydrosulfurization of crude oil,[26] apart from the ambitious goal of modeling the Fe/V cofactor of alternative vanadium nitrogenase [27]. A number of vanadium complexes in complete [28–30] and partial [31–34] sulfur environments, covering a wide nuclearity and oxidation state range have been reported in recent years to meet the above objectives.

For quite some time we have been working on an ambitious project of exploring the reactivity, redox and spectroscopic properties of structurally interesting metal complexes in sulfur-containing ligand environments [35–37]. Herein we report oxovanadium(IV) complexes of some tridentate (ONS) ligands, *viz.* *S*-methyl 3-(5-R-2-hydroxyphenyl)-

*Author to whom correspondence should be addressed.



R	H_2L
H	H_2L^1
NO_2	H_2L^2
Br	H_2L^3

methylenedithiocarbazates [R = H (H_2L^1), NO_2 (H_2L^2) and Br (H_2L^3)], which are of intrinsic interest because of the formation of a basic VOL core having one or more vacant coordination site(s) to potentially bind an ancillary ligand. Alternatively, the available site could be involved in bridging to a second vanadium center, forming a dinuclear complex. In this paper the synthesis of both mono- and dinuclear oxovanadium(IV) complexes of the ligands H_2L^1–H_2L^3 is described. Magnetism, EPR, positive-ion FAB mass and electronic spectroscopic properties of the complexes have been examined and the crystal and molecular structure of a representative complex (**2**) is reported.

EXPERIMENTAL

Materials

Carbon disulfide, hydrazine hydrate (both from E. Merck), methyl iodide (Loba), acetyl acetone (Fluka) and salicylaldehyde (BDH) were freshly distilled before use. Vanadium pentoxide (Loba), 2,2′-bipyridyl, 4,4′-bipyridyl, 1,10-phenanthroline, 5-bromosalicylaldehyde and 5-nitrosalicylaldehyde (all from Aldrich) were used as received. [VO(acac)$_2$] [38] and *S*-methyl dithiocarbazate [39] were prepared following published procedures. Solvents were dried by conventional methods [40] and distilled under nitrogen prior to use. All the reactions were carried out under dry nitrogen.

Preparation of ligands

S-Methyl 3-(2-hydroxyphenyl)methylenedithiocarbazate (H_2L^1). A solution of salicylaldehyde (2.45 g, 20 mmol) in ethyl alcohol (10 cm^3) was added with stirring to a hot solution of *S*-methyl dithiocarbazate (2.44 g, 20 mmol) in the same solvent (60 cm^3). The mixture was heated on a steam bath for 10 min and allowed to cool in the air. Crystalline product (off-white in color) was obtained and recrystallized from ethyl alcohol. Yield: 3.85 g (85%); m.p. 206°C.

The remaining ligands H_2L^2 (m.p. 192°C) and H_2L^3 (m.p. 215°C) were prepared similarly using appropriate derivatives of salicylaldehyde and their purity confirmed by elemental analysis, UV–vis and ^{1}H NMR spectra.

Preparation of complexes

[VOL^1(2,2′-bipy)] (**1**). To a stirred dichloromethane (20 cm^3) solution of [VO(acac)$_2$] (0.40 g, 1.5 mmol) was added a solid sample of the ligand H_2L^1 (0.34 g, 1.5 mmol) and the mixture was heated to reflux for 10 min. The solution turned brown at this stage. A stoichiometric amount of 2,2′-bipyridyl (0.24 g, 1.5 mmol) was then added and the solution was refluxed further for *ca* 30 min. The clear solution was combined with 10 cm^3 of petroleum ether (40–60°C fraction), cooled to room temperature and allowed to stand overnight in the air. Crystals which formed were filtered, washed with Et_2O and dried *in vacuo*. Recrystallization was carried out from CH_2Cl_2/*n*-hexane. Yield: 0.35 g (80 %). Found: C, 50.7; H, 3.5; N, 12.3. Calc. for $C_{19}H_{16}N_4O_2S_2V$: C, 51.0; H, 3.5; N, 12.5%. IR (KBr disc): ν(C=N), 1590s; ν(C—O/phenolate), 1585s; ν(V=O), 960s; ν(C—S), 650m cm^{-1}. μ_{eff}(solid, 25°C), 1.75 μ_B.

[VOL^2(2,2′-bipy)] (**2**). This compound was prepared following the same procedure as described for **1**, using the appropriate tridentate ligand H_2L^2. Yield: 80%. Found: C, 45.8; H, 3.0; N, 14.2. Calc. for $C_{19}H_{15}N_5O_4S_2V$: C, 46.3; H, 3.0; N, 14.2%. IR (KBr disc): ν(C=N), 1590s; ν(C—O/phenolate) 1580s; ν(V=O), 960s; ν(C—S), 660m cm^{-1}. μ_{eff}(solid, 25°C), 1.72 μ_B.

[VOL^3(2,2′-bipy)] (**3**). This compound can be synthesized similarly using H_2L^3 as the tridentate ligand with 75% yield. Found: C, 43.0; H, 2.7; N, 10.5. Calc. for $C_{19}H_{15}N_4O_2S_2BrV$: C, 43.3; H, 2.8; N, 10.6%. IR (KBr disc): ν(C=N), 1590s; ν(C—O/phenolate) 1570s; ν(V=O), 960s; ν(C—S), 650m cm^{-1}. μ_{eff} (solid, 25°C), 1.71 μ_B.

Remaining mononuclear oxovanadium(IV) complexes (**4** and **5**) were prepared following an identical procedure as adopted for **1–3** but using 1,10-phenanthroline as the bidentate ligand.

[VOL^1(phen)] (**4**). Yield: 80%. Found: C, 52.8; H, 3.2; N, 11.8. Calc. for $C_{21}H_{16}N_4O_2S_2V$: C, 53.5; H, 3.4; N, 11.9%. IR (KBr disc): ν(C=N), 1585s; ν(C—O/phenolate) 1570s; ν(V=O), 950s; ν(C—S), 640m cm^{-1}. μ_{eff}(solid, 25°C), 1.74 μ_B.

[VOL^2(phen)] (**5**). Yield: 78%. Found: C, 48.2; H, 2.8; N, 13.3. Calc. for $C_{21}H_{15}N_5O_4S_2V$: C, 48.8; H, 2.9;

N, 13.5%. IR (KBr disc): ν(C=N), 1595s; ν(C—O/phenolate), 1545s; ν(V=O), 950s; ν(C—S), 660m cm^{-1}. μ_{eff} (solid, 25°C), 1.72 μ_B.

[$L^1OV(\mu$-4,4′-bipy)VOL^1] (**6**). To a stirred solution of [$VO(acac)_2$] (0.40 g, 1.5 mmol) in acetonitrile (20 cm^3) was added a stoichiometric amount of the ligand H_2L^1 (0.34 g, 1.5 mmol) in solid form. The resulting mixture was heated to reflux for 10 min when a clear brown solution was obtained. A solid sample of 4,4′-bipyridyl (0.13 g, 0.8 mmol) was then added and the mixture was refluxed again for *ca* 30 min to ensure completion of the reaction. A clear deep green solution obtained at this stage was cooled to room temperature to obtain the microcrystalline product, which was collected by filtration, washed with Et_2O and dried *in vacuo*. The compound has very poor solubilities in most of the common organic solvents except dmf. Several attempts to recrystallize from dmf were unsuccessful. Yield: 0.42 g (58 %). Found: C, 45.2; H, 3.0; N, 11.5. Calc. for $C_{28}H_{24}N_6O_4S_4V_2$: C, 45.5; H, 3.2; N, 11.4%. IR (KBr disc): ν(C=N), 1600s; ν(C—O/phenolate), 1540s; ν(V=O), 990s; ν(C—S), 645m cm^{-1}. μ_{eff} per mol (solid, 25°C), 2.40 μ_B.

The remaining dinuclear compounds (**7** and **8**) were obtained following the same procedure as described for **6** using 4,4′-bipyridyl and the appropriate tridentate ligands.

[$L^2OV(\mu$-4,4′-bipy)VOL^2] (**7**). Yield: 42%. Found: C, 40.2; H, 2.5; N, 13.3. Calc. for $C_{28}H_{22}N_8O_8S_4V_2$: C, 40.5; H, 2.6; N, 13.5%. IR (KBr disc): ν(C=N), 1600s; ν(C—O/phenolate), 1548s; ν(V=O), 980s; ν(C—S), 665m cm^{-1}. μ_{eff} per mol (solid, 25°C), 2.32 μ_B.

[$L^3OV(\mu$-4,4′-bipy)VOL^3] (**8**). Yield: 40%. Found: C, 38.1; H, 2.3; N, 13.5. Calc. for $C_{28}H_{22}N_6O_4S_4Br_2V_2$: C, 37.5; H, 2.4; N, 13.5%. IR (KBr disc): ν(C=N), 1600s; ν(C—O/phenolate), 1580s; ν(V=O), 980s; ν(C—S), 650m cm^{-1}. μ_{eff} per mol (solid, 25°C), 2.38 μ_B.

Physical methods

Details of IR, UV–vis and magnetic measurements have been described elsewhere [36]. X-band EPR spectra in solution at room temperature as well as in the frozen state (77 K) were recorded on a Bruker model ER 220-SRC spectrometer and positive-ion fast atom bombardment (FAB) mass spectra using Kratos MS80RF or VG Pro/Spec Electrospray instruments. Elemental analyses for C, H and N were performed in this laboratory (IACS) with a Perkin–Elmer 2400 analyser.

X-ray crystallography

Intensity data for a brown crystal of **2** (0.10 × 0.24 × 0.37 mm), obtained from CH_3CN solution by slow evaporation, was measured at 293 K on a Rigaku AFC6R diffractometer fitted with graphite monochromatized Mo-K_α radiation, λ = 0.71073 Å; the ω : 2θ scan technique was employed to measure data such that θ_{max} was 25.0°. No decomposition of the crystal occurred during the data collection and only absorption corrected data [41] which satisfied the $I \geq 3.0\sigma(I)$ criterion were used in the subsequent analyses. Relevant crystal data are summarized in Table 1. The structure was solved by direct methods [42] and refined by a full-matrix least-squares procedure based on F [43]. Non-H atoms were refined with anisotropic thermal parameters and H atoms were included in the model at their calculated positions (C—H 0.97 Å). At convergence R = 0.044 and R_w = 0.039 [sigma weights, $1/\sigma^2(F11)$]; final refinement details are collected in Table 1. Scattering factors for all atoms were those incorporated in the TEXAN program.[43] The atom labeling scheme employed is shown in Fig. 1, drawn with the ORTEP [44] program at 30% probability ellipsoid. Selected bond distances and angles are given in Table 2. The TEXAN [43] package, installed on an Iris Indigo workstation, was employed in all calculations.

RESULTS AND DISCUSSION

Refluxing [$VO(acac)_2$] with the tridentate (ONS) ligands (1 : 1 mol ratio) under nitrogen in dichloromethane or acetonitrile yielded oxovanadium(IV) compounds in moderate to high yields (40–80%) in the presence of a Lewis base needed to complete the vacant metal coordination site(s). Thus, mono- (**1**–**5**) and dinuclear oxovanadium(IV) compounds (**6**–**8**) were obtained using 2,2′-bipyridyl, 1,10-phen-

Table 1. Crystal data and refinement details for [VOL^2(2,2′-bipy)] (**2**)

	2
Chemical formula	$C_{19}H_{15}N_5O_4S_2V$
Formula weight (fw)	492.4
Symmetry	Orthorhombic
Space group	*Pccn*
a (Å)	10.216(4)
b (Å)	31.909(4)
c (Å)	12.990(4)
V (Å^3)	4234(1)
Z	8
D_c (g cm^{-3})	1.545
F (000)	2008
μ (cm^{-1})	7.03
Transmission coefficients	0.886–1.044
No. data measured	4250
No. unique data	4250
No. observed data [$I \geq 3.0\sigma(I)$]	1573
R^a	0.044
R_w^b	0.039
Max. residual density (e Å^{-3})	0.22

$^aR = \Sigma(||F_o| - |F_c||)/\Sigma|F_o|$.
$^bR_w = [\Sigma w(||F_o| - |F_c||)^2/\Sigma w|F_o|^2]^{1/2}$.

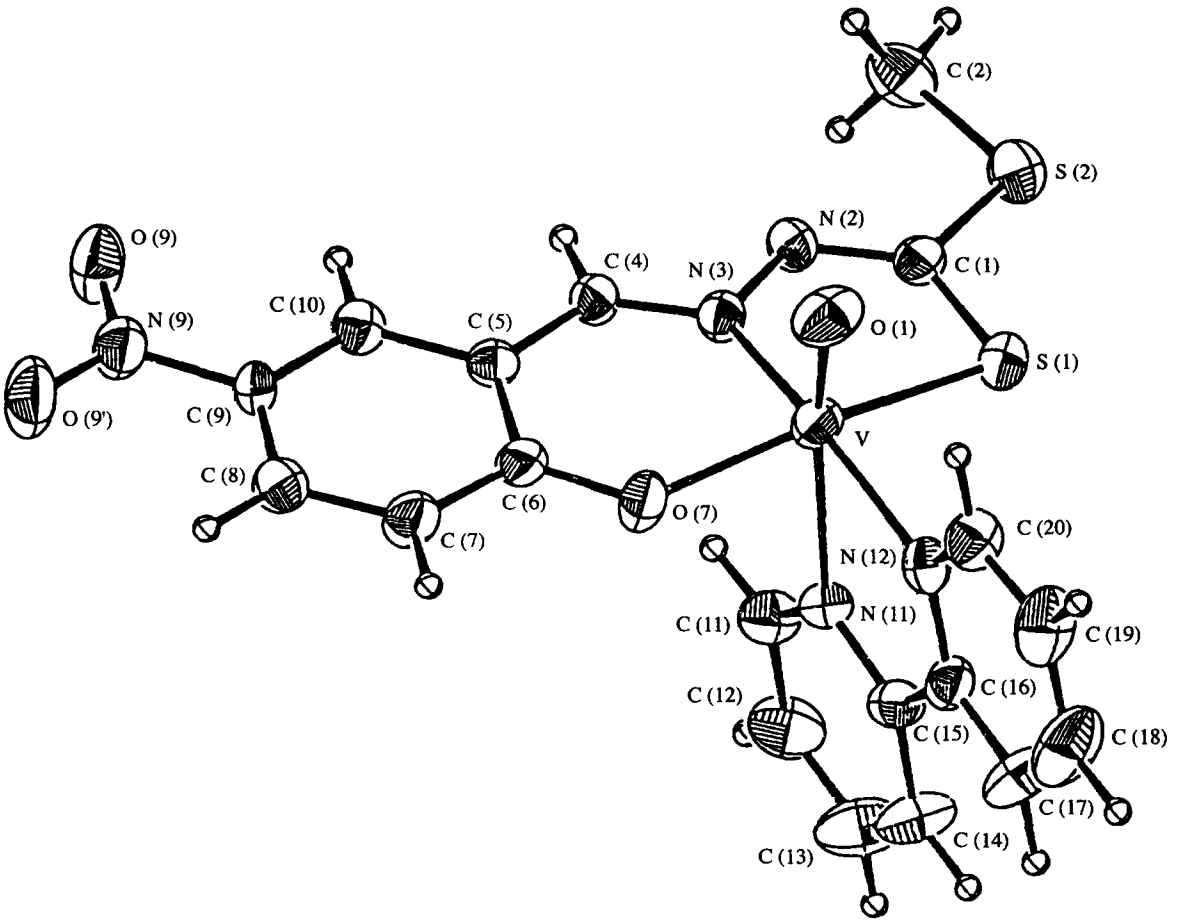


Fig. 1. Molecular structure and crystallographic numbering scheme for [VOL^2(2,2′-bipy)] (**2**).

Table 2. Selected bond distances (Å) and angles ( ) for [VOL^2(2,2′-bipy)] (**2**)

V—S(1)	2.408(2)	V—O(1)	1.590(4)
V—O(7)	1.977(4)	V—N(3)	2.087(4)
V—N(11)	2.305(5)	V—N(12)	2.134(5)
S(1)—C(1)	1.725(6)	S(2)—C(1)	1.733(6)
O(7)—C(6)	1.300(6)	O(9)—N(9)	1.225(6)
O(9′)—N(9)	1.228(6)	N(2)—N(3)	1.405(6)
N(2)—C(1)	1.306(7)	N(3)—C(4)	1.285(6)
N(9)—C(9)	1.445(7)	C(4)—C(5)	1.438(7)
S(1)—V—O(1)	100.0(2)	S(1)—V—O(7)	158.3(1)
S(1)—V—N(3)	80.7(2)	S(1)—V—N(11)	82.4(1)
S(1)—V—N(12)	91.8(1)	O(1)—V—O(7)	100.4(2)
O(1)—V—N(3)	102.0(2)	O(1)—V—N(11)	166.0(2)
O(1)—V—N(12)	94.1(2)	O(7)—V—N(3)	87.7(2)
O(7)—V—N(11)	79.7(2)	O(7)—V—N(12)	94.1(2)
N(3)—V—N(11)	92.0(2)	N(3)—V—N(12)	163.2(2)
N(11)—V—N(12)	72.0(2)	V—S(1)—C(1)	95.5(2)
C(1)—S(2)—C(2′)	102.9(3)	V—O(7)—C(6)	130.2(4)
N(3)—N(2)—C(1)	113.9(5)	V—N(3)—N(2)	121.9(4)
V—N(3)—C(4)	125.6(4)	N(2)—N(3)—C(4)	112.3(5)
S(1)—C(1)—S(2)	114.6(4)	S(1)—C(1)—N(2)	127.2(5)
S(2)—C(1)—N(2)	118.2(5)	N(3)—C(4)—C(5)	125.9(5)

anthroline and 4,4′-bipyridyl as the neutral donors. The mononuclear complexes (**1–5**) are soluble in CH_2Cl_2 and dmf, while their dinuclear counterparts (**6–8**) are only soluble in dmf. All these compounds are air stable in the solid state. In solution also they are fairly stable and undergo slow decomposition only on prolonged standing.

IR spectra of the free ligands have several prominent bands appearing at *ca* 3100, 2960 and 1040 cm^{-1} due to ν(O—H), ν(N—H) and ν(C=S) stretching modes, respectively, which are altogether missing in the complexes. Further screening reveals the appearance of a new band in the complexes at 650 cm^{-1} due to the ν(C—S) stretch. All these indicate (ONS) mode of chelation by the thioenol form of the ligands in the present series of complexes [45]. In addition, the complexes display a strong V=O terminal stretch appearing at 990 cm^{-1} in the pentacoordinated complexes (**6–8**) as against 960 cm^{-1} observed with the octahedral vanadium(IV) complexes (**1–5**), containing a coordinated nitrogen atom *trans* to the terminal oxo group. The results clearly indicate the structural *trans* effect of the coordinated nitrogen atom in the mononuclear complexes (as confirmed by X-ray structure analyses, see later) that leads to weakening of the V=O terminal bond [32].

FAB mass spectra

Positive-ion FAB mass spectra of two representative compounds **4** and **6** have been recorded in *m*-nitrobenzyl alcohol matrix. The spectrum of [VOL^1(phen)] (**4**) features a molecular ion peak (MH^+) at *m/z* 472 together with fragmentation peaks at *m/z* 263 and 247, most likely corresponding to the positive ions $[VO_2(phen)]^+$ and $[VO(phen)]^+$, respectively. The most abundant peak at *m/z* 366 probably corresponds to the fragment $[VO(phen)(—N=N—CSSCH_3)]^+$. The FAB spectrum of [$L^1OV(\mu$-4,4′-bipy)$VOL^1$] (**6**, Fig. 2) contains a molecular ion (MH^+) peak at *m/z* 739, which is much less intense in comparison to many of those due to fragments. Two most intense peaks observed at *m/z* 448 and 292 due to positive ions [VOL^1(4,4′-bipy)H]$^+$ and [VOL^1H]$^+$ signify gradual break down of the molecule.

Description of structure

The molecular structure of **2** is shown in Fig. 1 and important geometric parameters are listed in Table 2. The unit cell is comprised of discrete molecular entities with the closest non-H intermolecular contact of 3.186(8) Å occurring between the O(9′) and C(11″) atoms (symmetry operation: 0.5-*x*, 0.5-*y*, *z*). The V atom in **2** is octahedrally coordinated by the S, O and N donor atoms of the tridentate ligand, the two N atoms of the bipyridyl ligand and the oxo atom; the arrangement of the tridentate ligand is such that it defines the meridion in a distorted octahedral geometry. That both of the five- and six-membered rings which are formed upon coordination of L^2 are almost planar are seen in the magnitude of the V/S(1)/C(1)/N(2), V/O(7)/C(6)/C(5) and V/N(3)/C(4)/C(5) torsion angles of −7.4(6), 14.8(9) and −8.2(9)°, respectively. There is a small disparity in the V—N bond distances involving the 2,2′-bipyridyl ligand, which can be related to the greater *trans* influence of the oxo group on the V—N(11) bond.

Determination of structure of the dinuclear compound was not possible as the complexes (**6–8**) eluded all attempts to grow diffraction quality crystals.

Magnetism and EPR

Oxovanadium(IV) complexes are magnetically straightforward. At room temperature (298 K) the observed values of magnetic moments (Table 3) for the mononuclear complexes (**1–5**) are in the range 1.71–1.75 μ_B, as expected for a simple $S = 1/2$ paramagnet with d_{xy}-based ground state.[46] EPR spectra of these complexes have essentially identical features both in the fluid (CH_2Cl_2/toluene, 1 : 10 v/v at 298 K) as well as in the frozen solution (77 K). At room temperature, a typical spectrum (**2**) shows an eight-line pattern: $\langle g \rangle$, 1.977 and $\langle A \rangle$, 84 × 10^{-4} cm^{-1}, characteristic of an unpaired electron being coupled to a vanadium nuclear spin (^{51}V, 99.76 atom %, $I = 7/2$). In the frozen state, the same solution displays well-resolved axial anisotropy with two sets of eight-line patterns. The corresponding spin-Hamiltonian parameters are $g_\parallel$, 1.956 ($A_\parallel$, 153 × 10^{-4} cm^{-1}) and $g_\perp$, 1.986 ($A_\perp$, 51 × 10^{-4} cm^{-1}) summarized in Table 3. Inspection of these data reveals a close agreement between the spectral parameters obtained at room temperature and in the frozen solution [$\langle g \rangle = 1/3(g_\parallel + 2g_\perp)$; $\langle A \rangle = 1/3(A_\parallel + 2\ A_\perp)$], thus indicating the molecules retaining their structural identity in solution throughout this temperature range. Another interesting feature that deserves mention are the small hyperfine coupling constants (both $A_\parallel$ and $A_\perp$) and relatively large $g_\perp$ values when compared with those for related complexes in N/O donor environments [22, 47]. This indicates moderate π-interaction of sulfur in the present ligand system, leading to increased delocalization of the vanadium unpaired electron [48].

At room temperature the dinuclear vanadium(IV) complexes (**6–8**) exhibit a similar eight-line pattern as observed with the mononuclear complexes (Table 3). A representative spectrum (**8**) is shown in Fig. 3 (inset) which provides an ideal example of a dinuclear vanadium(IV) spectrum with $|J| \approx 0$ [49]. The spectrum in the frozen solution (Fig. 3) has an axial profile with no feature due to "forbidden" $\Delta M_s \pm 2$-triplet singlet transition, appearing in the half-field region [50]. The spin–spin interactions in these compounds are so insignificant that each unpaired electron virtually interacts with only one vanadium center. Mag-

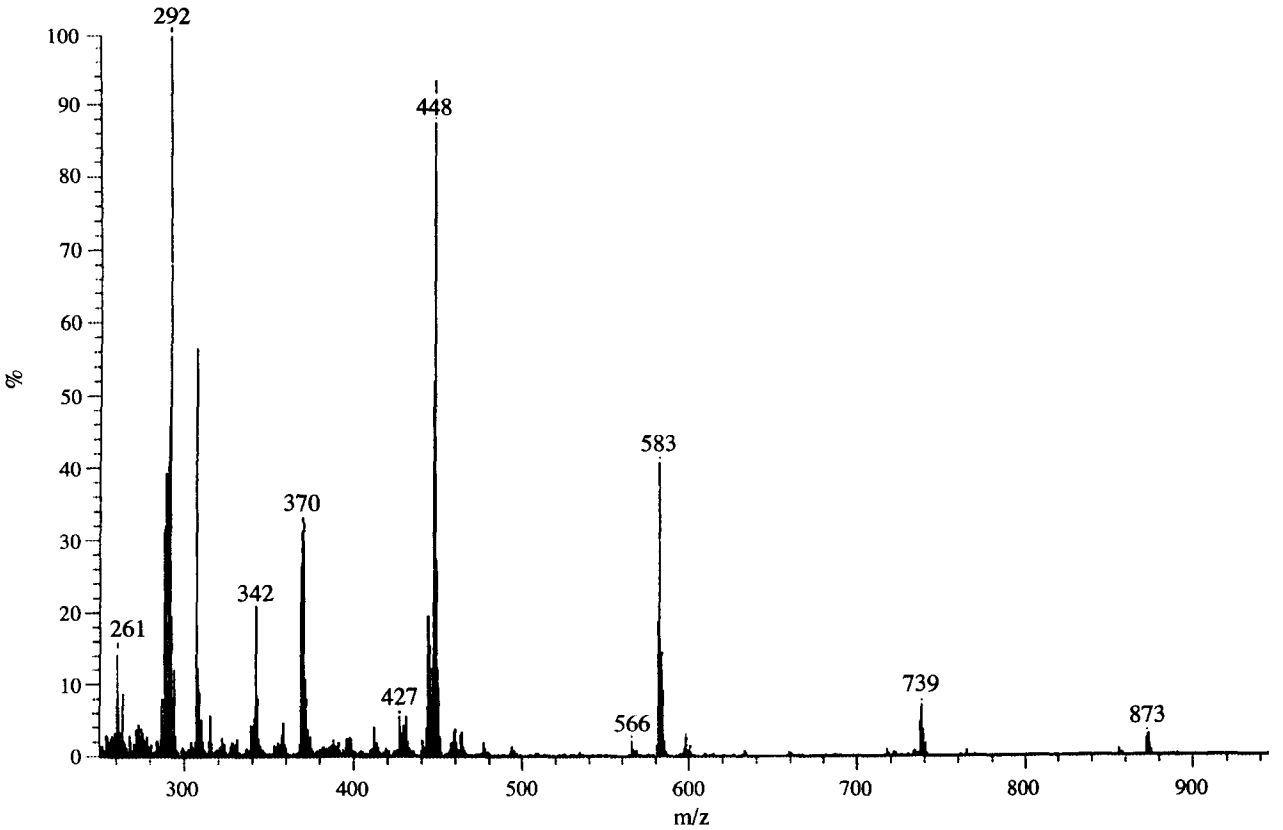


Fig. 2. Positive-ion FAB mass spectrum of [L¹OV(μ-4,4′-bipy)VOL¹] (**6**) in *m*-nitrobenzyl alcohol matrix.

netic moments in the polycrystalline state of these compounds are in the range 2.38–2.42 μ_B per mole, equivalent to *ca* 1.73 μ_B per vanadium(IV) center. The results also speak in favor of the dinuclear vanadium(IV) systems with $|J| \approx 0$ as established from EPR spectroscopy.

Electronic spectra

The electronic spectra of these complexes are summarized in Table 4. The divanadium complexes (**6–8**) in dmf solution show three low intensity (ε, 120–380 $dm^3\ mol^{-1}\ cm^{-1}$) ligand-field transitions, characteristic of vanadyl complexes having C_{4v} symmetry [50]. A representative spectrum (**6**) is shown in Fig. 4(a) along with the absorption manifold (inset) for such complexes based on the Ballhausen and Gray model [51]. Observed bands at 820 nm (ε, 220 $dm^3\ mol^{-1}\ cm^{-1}$), 655 nm (290 $dm^3\ mol^{-1}\ cm^{-1}$) and 546 nm (ε, 380 $dm^3\ mol^{-1}\ cm^{-1}$) are labeled I, II and III corresponding to electronic transitions from d_{xy} to (d_{xz}, d_{yz}), $d_{x^2-y^2}$ and d_{z^2}, respectively.

In mononuclear complexes (**1–5**) bands I and II are poorly resolved and appear under a broad envelope, centered at 720 nm as shown in the Fig. 4(b) for a representative compound (**1**) in CH_2Cl_2. Careful

Table 3. Magnetic moment and spin-Hamiltonian parameters for the complexes

						$\times 10^4/(cm^{-1})$	
	μ_{eff}/μ_B	$\langle g \rangle$	$g_\perp$	$g_\parallel$	$\langle A \rangle$	$A_\parallel$	$A_\perp$
1	1.75	1.975	1.953	1.982	82	154	50
2	1.72	1.977	1.956	1.986	84	153	51
3	1.71	1.980	1.955	1.988	82	153	50
4	1.74	1.974	1.955	1.985	86	155	52
5	1.72	1.974	1.956	1.982	83	152	51
6	2.40	1.980	1.950	1.981	86	157	53
7	2.42	1.982	1.954	1.980	85	156	53
8	2.38	1.979	1.946	1.984	91	161	54

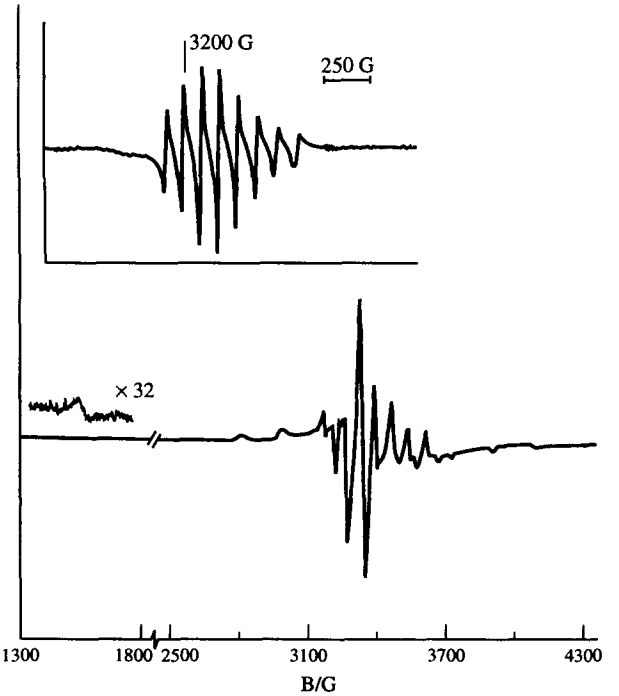


Fig. 3. The X-band EPR spectrum of [$L^3OV(\mu$-4,4′-bipy)VOL^3] (**8**) in frozen solution (dmf/toluene 1 : 10 v/v, 77 K). The inset shows the spectrum of the same solution at room temperature (298 K).

scrutiny (by second derivative plot) of this spectrum reveals the peak positions at *ca* 770 and 695 nm for bands I and II, respectively. Band III is missing and probably masked by the tail of a charge-transfer band appearing in the near-UV region (426 nm, 8100 dm^3 mol^{-1} cm^{-1}). The addition of a sixth donor ligand *trans* to the terminal V=O bond in **1–5** thus exerts a destabilizing force to alter the energetic of orbital manifold (Fig. 4, inset), so that transition to e (d_{xz}, d_{yz}), band I, and $a_1(d_{z^2})$, band III, are blue shifted compared with their dinuclear counterparts (**6–8**).

In addition to the *d–d* bands, the oxovanadium(IV) compounds (**1–8**) also have a strong charge-transfer band in the 440–380 nm region (ε, 7050–43800 dm^3 mol^{-1} cm^{-1}), the position of which is tunable by the substituent X (X = H, NO_2 and Br) in the tridentate ONS ligand (Table 4). We interpret this band as ligand-to-metal charge-transfer (l.m.c.t., $PhO^- \rightarrow V$) in origin. All remaining bands appearing in the UV region are due to ligand internal transitions.

Acknowledgements—We gratefully acknowledge support of this work by the Council of Scientific and Industrial Research, New Delhi, and thank Mr P. R. Ashton (Birmingham University, U.K.) and Dr S. B. Kumar (Universitat de Barcelona, Spain) for their help in recording the FAB mass and EPR spectra, respectively. The Australian Research Council is thanked for the support of the crystallographic facility.

Table 4. Electronic spectral data[a,b] for the complexes

Complex	λ_{max}/nm (ε/dm^3 mol^{-1} cm^{-1})
1	720 (60), 426 (8100), 301 (28,100), 243 (31,200)
2	720 (60), 384 (14,600), 306 (29,900), 241 (28,100)
3	720 (58), 439 (8600), 301 (27,800), 243 (31,600)
4	750 (42), 429 (7050), 350 (6700), 313 (15,200)
5	720 (50), 383 (14,600), 319 (21,100), 298 (21,000)
6	820 (220), 655 (290), 546 (380), 395 (16,100), 282 (42,100)
7	789 (120), 659 (130), 556 (170), 381 (43,800), 216 (54,200)
8	802 (150), 660 (230), 551 (280), 402 (16,000), 345 (20,300)

[a]Spectra of compounds **1–5** recorded in CH_2Cl_2.
[b]Spectra of **6–8** recorded in dmf.

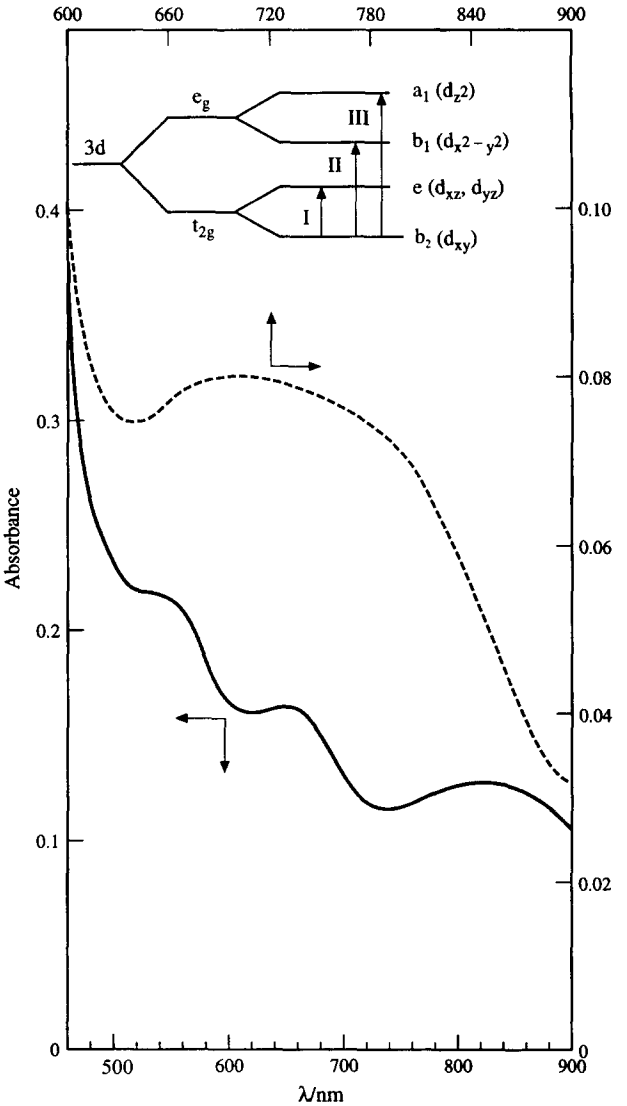


Fig. 4. Visible absorption spectra of (a) [$L^1OV(\mu$-4,4′-bipy)VOL^1] (**6**) (———) in dmf (5.76×10^{-4} mol dm^{-3}) and (b) [VOL^1(2,2′-bipy)] (**1**) (– – –) in CH_2Cl_2 (1.30×10^{-3} mol dm^{-3}) solutions.

REFERENCES

1. N. D. Chasteen, Ed., *Vanadium in Biological Systems*. Kluwer Academic Publishers, Dordrecht, The Netherlands, 1990.
2. R. Wever and K. Kustin, *Adv. Inorg. Chem.* 1990, **35,** 81.
3. D. Rehder, *Angew. Chem., Int. Edn. Engl.* 1991, **30,** 148.
4. A. Butler and C. J. Carrano, *Coord. Chem. Rev.* 1991, **109,** 61.
5. E. M. Armstrong, R. L. Beddoes, L. J. Calviou, J. M. Charnock, D. Collison, N. Ertok, J. H. Naismith and C. D. Garner, *J. Am. Chem. Soc.* 1993, **115,** 807.
6. M. J. Smith, D. Kim, B. Horenstein, K. Nakanishi and K. Kustin, *Acc. Chem. Res.* 1991, **24,** 117.
7. J. M. Arber, E. deBoer, C. D. Garner, S. S. Hasnain and R. Wever, *Biochemistry*, 1989, **28,** 7968.
8. E. deBoer, C. P. Keijzers, A. A. K. Klaasen, E. J. Reijerse, D. Collison, C. D. Garner and R. Wever, *FEBS Lett.* 1988, **235,** 93.
9. A. Butler and H. Eckert, *J. Am. Chem. Soc.* 1989, **111,** 2802.
10. H. Vilter and D. Rehder, *Inorg. Chim. Acta*, 1987, **136,** L7.
11. K. K. Nanda, S. Mohanta, S. Ghosh, M. Mukherjee, M. Helliwell and K. Nag, *Inorg. Chem.* 1995, **34,** 2861.
12. C. J. Carrano, M. Mohan, S. M. Holmes, R. de la Rosa, A. Butler, J. M. Charnock and C. D. Garner, *Inorg. Chem.* 1994, **33,** 646.
13. D. C. Crans and P. K. Shin, *J. Am. Chem. Soc.* 1994, **116,** 1305; D. C. Crans, H. Chen, O. P.

Anderson and M. M. Miller, *J. Am. Chem. Soc.* 1993, **115,** 6769.
14. I. Cavaco, J. C. Pessoa, D. Costa, M. J. Duarte, R. D. Gillard and P. Matias, *J. Chem. Soc., Dalton Trans.* 1994, 149.
15. J. Chakraborty, S. Dutta, A. Dey and A. Chakravorty, *J. Chem. Soc., Dalton Trans.* 1994, 557; J. Chakraborty, S. Dutta, S. K. Chandra, P. Basu and A. Chakravorty, *Inorg. Chem.* 1993, **32,** 4249.
16. T. M. Dewey, J. DuBois and K. N. Raymond, *Inorg. Chem.* 1993, **32,** 1729.
17. M. J. Clague, N. L. Keder and A. Butler, *Inorg. Chem.* 1993, **32,** 4754.
18. V. Vergopoulos, W. Priebsch, M. Fritzsche and D. Rehder, *Inorg. Chem.* 1993, **32,** 1844.
19. C. P. Magill, C. Floriani, A. Chiesi-Villa and C. Rizzoli, *Inorg. Chem.* 1993, **32,** 2729.
20. G. R. Hanson, T. A. Kabanos, A. D. Keramidas, D. Mentzafos and A. Terzis, *Inorg. Chem.* 1992, **31,** 2587; T. A. Kabanos, A. M. Z. Slawin, D. J. Williams and J. D. Woollins, *J. Chem. Soc., Dalton Trans.* 1992, 1423.
21. M. Mohan, S. M. Holmes, R. J. Butcher, J. P. Jasinski and C. J. Carrano, *Inorg. Chem.* 1992, **31,** 2029; S. M. Holmes and C. J. Carrano, *Inorg. Chem.* 1991, **30,** 1231.
22. C. R. Cornman, J. Kampf, M. S. Lah and V. L. Pecoraro, *Inorg. Chem.* 1992, **31,** 2035.
23. A. Hills, D. L. Hughes, G. J. Leigh and J. R. Sanders, *J. Chem. Soc., Dalton Trans.* 1991, **61,** 325.
24. A. R. Bulls, C. G. Pippin, F. E. Hahn and K. N. Raymond, *J. Am. Chem. Soc.* 1990, **112,** 2627; C. L. Simpson and C. G. Pierpont, *Inorg. Chem.* 1992, **31,** 4308; S. G. Brand, N. Edelstein, C. J. Hawkins, G. Shalimoff, M. R. Snow and E. R. T. Tiekink, *Inorg. Chem.* 1990, **29,** 434.
25. K. Nakajima, K. Kojima, M. Kojima and J. Fujita, *Bull. Chem. Soc. Jpn*, 1990, **63,** 2620.
26. T. F. Yen, *The Role of Trace Metals in Petroleum*, Ch. 1. Ann Arbor Science, Ann Arbor, Michigan, 1975.
27. N. Pau, in *Biology and Biochemistry of Nitrogen Fixation*, ed., M. J. Dilworth and A. R. Glenn. Elsevier, Amsterdam, 1991, p. 37.
28. D. D. Heinrich, K. Folting, J. C. Huffman, J. G. Reynolds and G. Christou, *Inorg. Chem.* 1991, **30,** 300.
29. J. K. Money, J. C. Huffman and G. Christou, *J. Am. Chem. Soc.* 1987, **109,** 2210.
30. C. R. Randall and W. H. Armstrong, *J. Chem. Soc., Chem. Commun.* 1988, 986.
31. K. K. Nanda, E. Sinn and A. W. Addision, *Inorg. Chem.* 1996, **35,** 1.
32. J. G. Reynolds, S. C. Sendlinger, A. M. Murray, J. C. Huffman and G. Christou, *Inorg. Chem.* 1995, **34,** 5745, and refs therein.
33. G. Henkel, B. Krebs and W. Schmidt, *Angew. Chem., Int. Ed. Engl.* 1992, **31,** 1367.
34. J. C. Dutton, G. D. Fallon and K. S. Murray, *Inorg. Chem.* 1988, **27,** 34.
35. S. Bhattacharyya, S. B. Kumar, S. K. Dutta, E. R. T. Tiekink and M. Chaudhury, *Inorg. Chem.* 1996, **35,** 1967.
36. S. B. Kumar, S. Bhattacharyya, S. K. Dutta, E. R. T. Tiekink and M. Chaudhury, *J. Chem. Soc., Dalton Trans.* 1995, 2619.
37. S. K. Dutta, S. B. Kumar, S. Bhattacharyya and M. Chaudhury, *J. Chem. Soc., Dalton Trans.* 1994, 97, and refs therein.
38. R. A. Rowe and M. M. Jones, *Inorg. Synth.* 1957, **5,** 113.
39. G. Bahr and G. Schleitzer, *Z. Anorg. Allg. Chem.* 1955, **280,** 161.
40. D. D. Perrin, W. L. F. Armarego and D. R. Perrin, *Purification of Laboratory Chemicals*, 2nd edn. Pergamon Press, Oxford, 1980.
41. N. Walker and D. Stuart, *Acta. Cryst.* 1983, **A39,** 158.
42. G. M. Sheldrick, *SHELXS* 86. *Program for the Automatic Solution of Crystal Structure.* University of Gottingen, Germany, 1986.
43. TEXAN Structure Analysis Software. Molecular Structure Corporation, Houston, Texas, 1992.
44. C. K. Johnson, *ORTEP II.* Report ORNL-5138. Oak Ridge National Laboratory, Oak Ridge, Tennessee, 1976.
45. M. Akbar Ali, D. A. Chowdhury-I and M. Nazim Uddin, *Inorg. Chim. Acta*, 1973, **7,** 179; R. Mukhopadhyay, S. Bhattacharjee and R. Bhattacharyya, *J. Chem. Soc., Dalton Trans.* 1994, 2799.
46. D. Collison, B. Graham, C. D. Garner and F. E. Mabbs, *J. Chem. Soc., Dalton Trans.* 1980, 667.
47. N. D. Chasteen, in *Biological Magnetic Resonance* ed., L. J. Berliner and J. Reuben, Vol. 3. Plenum Press, New York, 1981, p. 53.
48. I. W. Boyd, I. G. Dance, K. S. Murray and A. G. Wedd, *Aust. J. Chem.* 1978, **31,** 279.
49. (a) F. E. Mabbs, *Chem. Soc. Rev.* 1993, 313; (b) M. R. Bond, L. M. Morky, T. Otieno, J. Thompson and C. J. Carrano, *Inorg. Chem.* 1995, **34,** 1894.
50. C. W. Hahn, P. G. Rasmussen and J. C. Bayon, *Inorg. Chem.* 1992, **31,** 1963.
51. J. Selbin, *Chem. Rev.* 1965, **65,** 153.

Pergamon

PII: S0277-5387(96)00489-5

Polyhedron Vol. 16, No. 11, pp. 1873–1876, 1997
© 1997 Elsevier Science Ltd
All rights reserved. Printed in Great Britain
0277-5387/97 $17.00+0.00

Synthesis and crystal structure of a novel oxo-bridged di-iron(III) complex: μ-oxo[chlorotetrakis(thiazole)iron(III)] [trichloro-iron(III)]

Michael James, Hiroyuki Kawaguchi and Kazuyuki Tatsumi*

Department of Chemistry, Faculty of Science, Nagoya University, Furo-cho, Chikusa-ku, Nagoya 464-01, Japan

(Received 30 August 1996; accepted 30 September 1996)

Abstract—The title compound, [ClFe(thiazole)$_4$-O-FeCl$_3$] (**1**) has been synthesized by the hydrolysis of anhydrous FeCl$_3$ in an ethanol–thiazole solvent mixture. Compound **1** consists of a tetrahedrally coordinated OFeCl$_3$ group bridged by the oxo ligand to an Fe(thiazole)$_4$Cl group, wherein the thiazole groups occupy the equatorial positions in an octahedral coordination polyhedron. © 1997 Elsevier Science Ltd. All rights reserved.

Keywords: thiazole; iron; μ-oxo complex.

EXPERIMENTAL

IR spectra were recorded (Nujol mull) in the 300–5200 cm^{-1} range on a Perkin–Elmer FT-IR 2000 spectrophotometer. ^{1}H NMR spectra were recorded on a Varian INOVA-500 spectrometer using DMSO-d_6 as a solvent and the chemical shifts reported in ppm *vs* TMS. Elemental analyses were carried out on a LECO CHNS-900 elemental analyser. Anhydrous FeCl$_2$, FeCl$_3$ and thiazole were obtained from commercial sources and used as received. Ethanol was of A.R. grade and was used both with and without further purification.

Reactions of FeCl$_2$ *and* FeCl$_3$ *with thiazole*

When warm ethanolic (A.R. grade) solutions of FeCl$_2$ (6 mmol, 16 cm^3) and thiazole (12 mmol, 2 cm^3) were mixed with stirring, a yellow–orange powder was immediately precipitated. The precipitate was washed with ether and benzene and dried *in vacuo*. In common with the polymeric species Cu(thiazole)$_2$X$_2$ (X = Cl and Br)[1], the precipitate was insoluble in common organic solvents, but soluble in DMF. IR measurements indicate the presence of thiazole, while elemental analyses suggest a molecular formula Fe(thiazole)$_2$Cl$_2$ (**2**). Attempts to grow single crystals of this compound have thus far been unsuccessful. Found: C, 24.6; H, 2.0; N, 9.4; S, 21.6. Calc. for **2**: C, 24.7; H, 2.0; N, 9.1; S, 21.2%. IR (Nujol): *ν*(ligand) 608(m), 737(m), 808(m), 879(w), 912(w), 1060(w), 1112(w), 1231(w) cm^{-1}.

No precipitate was formed when the analogous reaction was carried out with FeCl$_3$ (4 mmol, 16 cm^3) and thiazole (12 mmol, 2 cm^3). When freshly distilled ethanol was used under dry Ar, a clear yellow–orange solution was obtained. Upon allowing to stand for 24 h in a refrigerator orange polycrystals were formed. IR spectra and elemental analysis of this compound suggest a molecular formula: Fe(thiazole)$_3$Cl$_3$ (**3**). Thus far, recrystallizations of this compound have failed to produce single crystals. Found: C, 26.0; H, 2.1; N, 9.9; S, 23.1. Calc. for **3**: C, 25.9; H, 2.2 N, 10.1; S, 23.0%. IR (Nujol): *ν*(ligand) 609(s), 730(m), 823(s), 876(m), 911(m), 1048(s), 1111(m), 1234(m) cm^{-1}.

When A.R. grade ethanol was used with no further purification, the solution filtered and allowed to stand in air for 2–3 days, orange polycrystals of **3** as well as orange–brown single crystals of the title compound (**1**) were formed. In instances when substantial amounts of water may have been present in the ethanol, product **3** did not crystallize. For both **1** and **3**,

*Author to whom correspondence should be addressed.

IR spectra confirmed the presence of thiazole. Found: C, 23.9; H, 1.9; N, 8.9; S, 20.9. Calc. for **1**: C, 23.6; H, 2.0; N, 9.2; S, 21.0%. IR (Nujol): ν(ligand, cm^{-1}) 319(m), 353(m) 613(m), 747(w), 841(vs-broad), 878(w), 912(m), 1051(s), 1114(w), 1235(w). ^1H NMR (DMSO-d_6) δ (ppm): 7.81 and 8.00 (8H), 9.19 (4H).

Crystal structure determination

Measurements were made on Rigaku AFC7R diffractometer at ambient temperature using monochromated Mo-K_α radiation ($\lambda = 0.71069$ Å). An orange–brown single crystal of **1** was mounted at the top of a glass fibre. Cell constants were obtained by least-squares analysis of 23 strong reflections in the range $29.7 < 2\theta < 30.0°$. Details of crystal data, data collection and structure refinement are summarized in Table 1.

The intensity data were corrected for Lorentz and polarization effects and an empirical absorption correction based on azimuthal scans of several reflections was also applied. The structure of **1** was solved by direct methods and developed by alternating cycles of difference-Fourier syntheses and full-matrix least-squares refinements. The positions of the iron, chlorine, oxygen and nitrogens were determined unequivocally, as were the carbons [C(1), C(2) and C(3)] and sulfur [(S(1)] of one of the thiazole ligands. The remaining three thiazole ligands displayed static disorder between adjacent carbon and sulfur sites, due to 180° rotations about their Fe—N bonds. In these cases the disorder was modeled by refinement of jointly occupied S/C sites. The minority component of these jointly occupied sites is indicated by a primed label, such that the site S/C′ contains a majority of sulfur, while the adjacent C/S′ site is constrained so as to give an equal proportion of carbon. The occupation factors of sulfur atoms were refined only at the S/C′ sites, while the C′ and S′ occupation factors were constrained so as to give fully occupied sites. The non-hydrogen atoms were refined anisotropically, with the exception of the atoms at the disordered sites, which, along with the hydrogen atoms, were refined isotropically. Hydrogen atoms were located using difference-Fourier synthesis. Neutral atom scattering factors were taken from [2] and anomalous dispersion corrections were taken from [3]. Crystallographic calculations were carried out with a teXsan crystallographic software package of Molecular Structure corporation (1985, 1992).

RESULTS AND DISCUSSION

The chemical reactivity of iron(II) chloride with thiazole does not appear to be substantially different to that observed for copper(II) halides. Although the structure of $Fe(thiazole)_2Cl_2$ (**2**) has not been confirmed by X-ray crystallography, its solubility, as well as its elemental analysis and IR spectrum, suggest that it has a similar structure to that of polymeric $Cu(thiazole)_2Cl_2$.[1] While numerous examples of M^{II}-thiazole-halides (M = Co, Ni, Cu, Zn and Pd) [4] have been characterized, analogous compounds based on transition metals of 3+ oxidation state are rare. The compound $Fe(thiazole)_3Cl_3$ (**3**) appears to be moisture-sensitive; not forming when the water content of the ethanol solutions is too high and oxidizing in the presence of air to $Fe_2O(thiazole)_4Cl_4$ (**1**). In this respect, the chemistry of formation of **1** is similar to that of $[Hpy]_2[Fe_2OCl_6]\cdot py$ (py = pyridine)[5].

The compound **1** crystallizes in the monoclinic space group $P2_1/c$ with $a = 9.626(5)$, $b = 15.484(4)$, $c = 15.544(5)$ Å $\beta = 90.58(3)°$, $V = 2316(1)$ Å^3 and $Z = 4$. The crystal structure of **1** is shown in Fig. 1. Selected bond lengths and bond angles are given in Table 2.

Compound **1** is comprised of an —$OFeCl_3$ tetrahedral group that corner-shares its oxygen with an octahedral —$OFe(thiazole)_4Cl$ group, such that the thiazole ligands occupy the equatorial positions and

Table 1. Summary of crystallographic data for **1**

Chemical formula	$Fe_2O(NSC_3H_3)_4Cl_4$	Formula weight	610.023
Crystal system	monoclinic	Space group	$P2_1/c$ (no. 14)
a (Å)	9.626(5)	α ( )	90
b (Å)	15.484(4)	β ( )	90.58(3)
c (Å)	15.544(5)	γ ( )	90
V (Å^3)	2316(1)	Z	4
Crystal size (mm)	0.40 × 0.30 × 0.60	D_c (g cm^{-3})	1.749
Radiation (Å)	0.71069	μ (Mo-K_α) (cm^{-1})	20.83
$2\theta_{max}$ (°)	55.0	No. of reflections	5521
No. of reflections used	3396 ($I > 3\sigma(I)$)	No. of variables	613
$(\Delta/\sigma)_{max}$	0.40	ρ_{max}/ρ_{min} (e Å^{-3})	1.13/−0.90
R^a	0.056	$R_w{}^b$	0.058
GOF^c	2.51		

$^aR = \Sigma \| |F_o| - |F_c| \| / \Sigma |F_o|$.
$^bR_w = [\Sigma w(|F_o| - |F_c|)^2 / \Sigma w |F_o|^2]^{1/2}$.
^{c}GOF $= [\Sigma(|F_o| - |F_c|)^2 / \Sigma(N_{reflns} - N_{params})]^{1/2}$.

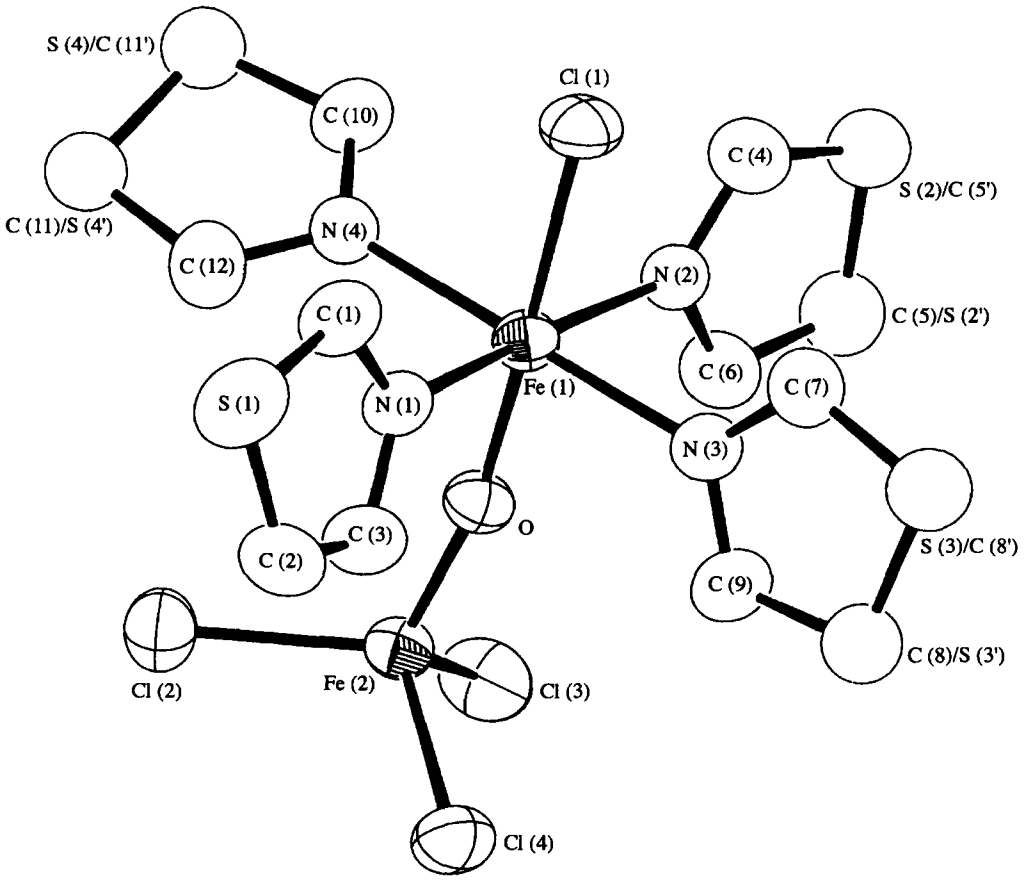


Fig. 1. An ORTEP drawing of $Fe_2O(thiazole)_4Cl_4$ (**1**). All atoms are represented by the thermal ellipsoids at 50% probability. Hydrogen atoms are omitted for clarity.

Table 2. Selected bond lengths (Å) and angles (°) for **1**

Fe(1)—O	1.807(3)	N(1)—C(1)	1.305(7)
Fe(2)—O	1.758(3)	C(1)—S(1)	1.696(6)
Fe(1)—Cl(1)	2.387(2)	S(1)—C(2)	1.699(7)
Fe(2)—Cl(2)	2.224(2)	C(2)—C(3)	1.342(8)
Fe(2)—Cl(3)	2.215(2)	C(3)—N(1)	1.369(7)
Fe(2)—Cl(4)	2.228(2)	N—C_{av}[a]	1.340(8)
Fe(1)—N(1)	2.190(4)	C—S/C'_{av}[a]	1.607(7)
Fe(1)—N(2)	2.179(4)	S/C'—C/S'_{av}[a]	1.738(3)
Fe(1)—N(3)	2.183(5)	C/S'—C_{av}[a]	1.573(7)
Fe(1)—N(4)	2.164(5)		
Fe(1)—O—Fe(2)	169.2(2)	N(1)—C(1)—S(1)	114.6(5)
O—Fe(1)—Cl(1)	178.2(1)	C(1)—S(1)—C(2)	89.7(3)
O—Fe(1)—N_{av}[b]	91.3(2)	S(1)—C(2)—C(3)	110.1(5)
N(1)—Fe(1)—N(3)	86.9(2)	C(2)—C(3)—N(1)	115.3(6)
N(1)—Fe(1)—N(4)	94.5(2)	Fe(1)—N—C_{av}[a]	125.0(4)
N(2)—Fe(1)—N(3)	87.3(2)	C—N(2)—C_{av}[a]	109.8(5)
N(2)—Fe(1)—N(4)	94.5(2)	N(2)—C—S/C_{av}[a]	116.9(5)
Fe(1)—N(1)—C	127.0(4)	C—S/C—C/S_{av}[a]	98.8(3)
Fe(1)—N(1)—C(3)	122.7(4)	Cl—Fe(2)—Cl_{av}	108.5(7)
C(1)—N(1)—C(3)	110.3(5)	O—Fe(2)—Cl_{av}	110.4(1)

[a] Bond length and bond angle averaged over disordered thiazole ligands.
[b] Bond angle averaged over all thiazole ligands.

the oxo and chloro ligands occupy the axial positions. To our knowledge **1** is the first oxo-bridged di-iron complex to show both tetrahedral and octahedral coordination about iron.

The tetrahedral —$OFeCl_3$ fragment of **1** has many structural features in common with complex salts containing the μ-oxo-bis(trichloro-iron(III)) dianion (for a comprehensive review of these complex salts see [6]), including a Fe(2)—O bond length of 1.758(3) Å (Fe—O ~ 1.756 Å) [6] as well as approximately regular tetrahedral bond angles of Cl—Fe(2)—Cl_{av} = 108.5(7) and O—Fe(2)—Cl_{av} = 110.4(1)°. The average Fe(2)—Cl bond length in **1** [2.222(2) Å] is also similar to those found in this family of compounds (2.20–2.23 Å)[6].

The single Fe(1)—Cl(1) bond [2.387(2) Å] in the octahedral fragment of **1** is substantially longer than the Fe—Cl bonds in the tetrahedral fragment, possibly due to a significant *trans*-influence with the bridging oxygen. The oxo link in **1** with a Fe—O—Fe angle of 169.2(2)° is at the upper end of the range of angles (146.5–170.8°) observed in complex salts containing μ-oxo-bis(trichloro-iron(III)) dianions [6].

Nitrogen coordination in oxo-bridged di-iron species is commonly observed *via* phthalocyaninato and porphyrinato ligands [7]. In these compounds, iron shows a tendency towards square-pyramidal coordination, with average apical Fe—O distances of ~1.75 Å and basal Fe—N distances of ~2.08 Å. Pseudo-octahedrally coordinated oxo-bridged di-iron compounds that contain nitrogen-bound ligands are relatively rare. There are, however, examples to be found in complexes containing the $[Fe_2O(phenanthroline)_4(H_2O)_2]^{4+}$ ion[8]. A notable difference between the average Fe—N bond lengths *cis* (~2.15 Å) and *trans* (~2.26 Å) to the oxo ligand is observed for these compounds, again suggesting a significant *trans* influence [8]. The average of the Fe(1)—N bond lengths in **1** [2.178(5) Å] is similar to the distances between Fe and *cis*-N in $[Fe_2O(phenanthroline)_4(H_2O)_2]^{4+}$. In both cases, these distances are indicative of nitrogen bonds to high-spin iron(III); while considerably shorter average Fe—N bond lengths (~1.973 Å) are observed in low-spin complex ions such as $[Fe(phenanthroline)_3]^{3+}$ [9]. The octahedral arrangement about Fe(1) in **1**, with average N—Fe—N angles of 90.8(2)°, average O—Fe(1)—N angles of 91.3(2)° and a O—Fe(1)—Cl angle of 178.2(2)° is substantialy more regular than those found in complex salts containing the $[Fe_2O(phenanthroline)_4(H_2O)_2]^{4+}$ cation [8].

Static disorder between the S site and the site corresponding to C(2) in the ordered thiazole was found to present in three of the four thiazole ligands; this being due to 180° rotations about the Fe—N bonds. Bond lengths and angles observed for the non-disordered thiazole ligand are almost identical to those found for the copper compound $Cu(thiazole)_2Cl_2$ [1]. As one might anticipate, identification of hydrogen positions was only possible for the ordered thiazole ligand and the carbon atoms adjacent to the nitrogen atom in the disordered ligands.

The principal IR absorption bands observed for **1**, **2** and **3** are similar to those of the thiazole ligands found in other metal-thiazole-chlorides such as $M(tz)_2Cl_2$ (M = Co and Cu)[10]. Notably, the broad, very strong peak observed at 841 cm^{-1} in the IR spectra of **1** is not present in the spectra of **2, 3** or the latter polymeric bis-thiazole compounds and may be attributed to an antisymmetric Fe—O—Fe stretching mode [5]. The absorption bands at 353 and 319 cm^{-1}, corresponding to antisymmetric and symmetric $FeCl_3$ stretches, respectively, were found only in the IR spectrum of **1**. Given the absence of these terminal vibrational modes in the IR spectrum of **2**, as well as the elemental analysis of this compound we propose a structure similar to that of the above polymeric species.

The ^1H NMR spectrum of **1**, indicates three relatively broad singlets in the aromatic region centred at 7.81 and 8.00 and 9.19 ppm (the widths at half-height are $\nu_{1/2}$ = 45, 54 and 60 Hz, respectively), each corresponding to four protons per molecule. Free-rotation about the Fe—N bonds in solution at room temperature should give the three chemically distinct hydrogen signals in the ^1H NMR spectrum. It should be noted that the three proton resonances in free thiazole occur at 7.40, 7.94 and 8.86 ppm. This discrepancy with the above observed values, as well as the broad line widths of these singlets is indicative of the presence of paramagnetic high-spin iron(III).

REFERENCES

1. W. E. Estes, D. P. Gavel, W. E. Hatfield and D. J. Hodgson, *Inorg. Chem.* 1978, **17,** 1415.
2. D. T. Cromer and J. T. Waber, *International Tables for X-ray Crystallography*, ed. T. Hahn, Vol. IV, Table 2.2A. Kynoch Press, Birmingham, (1974.)
3. J. A. Ibers and W. C. Hamilton, *Acta. Cryst.* 1964, **17,** 781.
4. M. N. Hughes and K. J. Rutt, *J. Chem. Soc. (A)*, 1970, 3015.
5. M. G. B. Drew, V. McKee and S. M. Nelson, *J. Chem. Soc. Dalton Trans.* 1978, 80.
6. G. Haselhorst, K. Wieghardt, S. Keller and B. Schrader, *Inorg. Chem.* 1993, **32,** 520.
7. B. Cheng, J. D. Hobbs, P. G. Debrunner, J. Erlebacher, J. A. Shelnutt and W. R. Scheidt, *Inorg. Chem.* 1995, **34,** 102.
8. J. E. Plowman, T. M. Loehr, C. K. Schauer and O. P. Anderson, *Inorg. Chem.* 1984, **23,** 3559.
9. J. Baker, L. M. Engelhardt, B. N. Figgis and A. H. White, *J. Chem. Soc. Dalton Trans.* 1975, 530.
10. W. J. Eilbeck, F. Holmes and A. E. Underhill, *J. Chem. Soc. A*, 1967, 757.

Pergamon

PII: S0277-5387(96)00486-X

Polyhedron Vol. 16, No. 11, pp. 1877–1883, 1997
© 1997 Elsevier Science Ltd
All rights reserved. Printed in Great Britain
0277-5387/97 $17.00+0.00

Electrochemical and spectral properties of octakis(hexylthio)-substituted phthalocyanines

Ali Rıza Özkaya,[a] Ayşe Gül Gürek,[b] Ahmet Gül[c] and Özer Bekaroğlu[c]*

[a]Department of Chemistry, Atatürk Faculty of Education, Marmara University, Kadıköy, İstanbul, Turkey; [b]Department of Chemistry, TÜBİTAK Marmara Research Center, PO Box 21, 41470 Gebze, Kocaeli, Turkey; [c]Department of Chemistry, Technical University of İstanbul, Maslak, İstanbul, Turkey

(Received 24 May 1996; accepted 30 September 1996)

Abstract—The redox properties of octakis(hexylthio)-substituted phthalocyanines with 2H, Zn^{II} and Cu^{II} in the phthalocyanine core have been investigated by cyclic voltammetry in dichloromethane and the energies of photo-excitation and oxido-reduction processes have been compared. Two successive one-electron reduction and one-electron oxidation processes were observed for the complexes used in this work. The displacement of two protons in the inner core with metal ion was found to shift the first reduction potential of phthalocyanine ring to more negative values as a result of the π-back donation of the filled d_π of metal ion into the empty *pc*-π^* orbitals. The evaluation of cyclic voltammetry data together with the absorption spectra showed that photo-excitation arises from the orbitals below the HOMO for all the complexes used in this work. © 1997 Elsevier Science Ltd. All rights reserved.

Keywords: phthalocyanines; electrochemistry; cyclic voltammetry; zinc; copper.

The redox properties of phthalocyanines (Pcs) are critically related to most of their industrial applications [1,2]. The aromatic 18 π-electron system of pcs with the usual two negative charges enables oxidation and reduction on the macrocycle before any redox process on the central metal ions such as Ni^{II}, Cu^{II} or Zn^{II}. Here the energies of photo-excitation and oxido-reduction processes can be compared while both are occurring on the highest energy orbitals [3].

A limiting factor for the solution studies on pcs is the insolubility of the parent compound. Peripheral substitution with bulky substituents or the use of donor solvents capable of binding to axial positions of the central metal ion have been two practical ways to overcome this hindrance. In the previous works on macrocycle-substituted pcs we have accomplished the synthesis of very soluble examples in a wide range of organic solvents [4–8]. In addition to novel functionalities such as alkali [4,5] or transition metal [7, 8] ion binding, ion channel formation,[9] enhanced conductivity, [10] etc., the solubility of pc products has been reached up to 10^{-3} mol dm^{-3} level [4,5]. Also recently new soluble derivatives with eight alkylthio substituents have been synthesized through cyclotetramerization of 4,5-bis(hexylthio)phthalonitrile which has been prepared directly from the 4,5-dichloro-compound with hexanethiol [11]. In the present work, the redox properties of these soluble pcs with 2H, Zn^{II} and Cu^{II} in the pc core (H_2htpc, Znhtpc and Cuhtpc, Fig. 1) have been investigated by cyclic voltammetry in dichloromethane (DCM) and the results are evaluated together with their absorption spectra in the visible range.

RESULTS AND DISCUSSION

Cyclic voltammetry data for H_2htpc, Zn(htpc) and Cu(htpc) are shown in Table 1. Voltammetric behaviours of Zn(htpc) and Cuhtpc on the oxidation side are similar to H_2htpc. Figure 2 shows the cyclic voltammogram (CV) of Zn(htpc) on sweeping to positive potentials. All pcs used in this work gave two quasi-reversible one-electron oxidation couples with the peak separations (ΔE_p) of 0.090–0.105 V. The half peak potentials of Zn(htpc) and Cu(htpc) for each oxidation couple had approximately the same values

*Author to whom correspondence should be addressed.

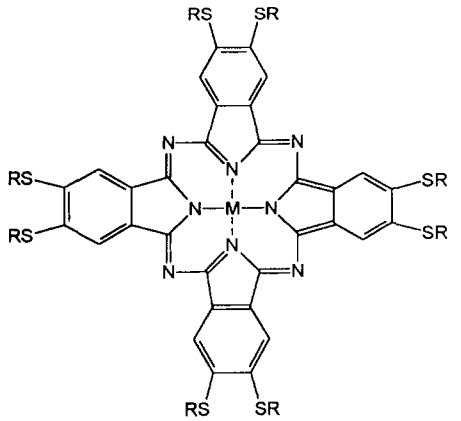


Fig. 1. Octakis (hexylthio)-substituted phthalocyanines [R: C_6H_{13}; M: 2H (H_2htpc), Zn^{II} (Zn(htpc)) or Cu^{II} (Cu(htpc))].

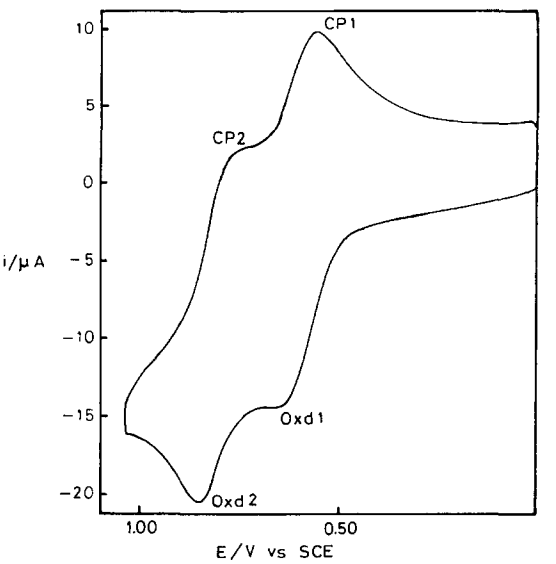


Fig. 2. Cyclic voltammogram of Zn(htpc) (5×10^{-4} M) on sweeping to positive potentials in DCM with $v = 0.050$ V s^{-1}.

as with those of H_2htpc. The similarities in oxidation potentials between these phthalocyanines indicate that both the first and the second oxidation couples are ligand based. Two successive ring oxidations from the non-degenerate $a_{1u}(\pi)$ orbital of the pc ligand are possible in metal phthalocyanine complexes [12]. The potentials shown in Table 1 [0.585–0.805 V vs saturated calomel electrode (SCE)] are in the range reported for pc ligand oxidation [1,13,14] in H_2pc and metal pc complexes, providing an additional support for pc ring oxidation and hence corresponds to the formation of π-cation radical species.

The cyclic voltammetry of Zn(htpc) was reported previously on the glassy carbon electrode in dimethylformamide by Takahashi *et al.* [15]. They reported that the adsorption and irreversible oxidation had been observed on the oxidation side. In our work, voltammetric behaviour of Zn(htpc) on Pt in the oxidation side was found to be considerably different compared with the previous report. The CV of Zn(htpc) displays two quasi-reversible one-electron oxidation peaks with the corresponding two cathodic peaks. The peak current of the first oxidation (Oxd 1 in Fig. 2) was found to be higher than that of the second oxidation (Oxd 2 in Fig. 2) and also the value of i_{pc}/i_{pa} for the first oxidation process is less than unity, suggesting decomposition of the first oxidation product. However, decomposition should be very slow and ineffective with respect to the electron transfer rate since the second oxidation and re-reduction peaks are observed. The controlled-potential electrolysis of Zn(htpc) at 0.7 V and 0.9 V *vs* SCE did not show the adsorption of Zn(htpc) or its oxidation products on

Table 1. Redox potentials of H_2htpc, Znhtpc and Cuhtpc in dichloromethane

Complex	Redox couple	E^a_{pc} or E^a_{pa} $(\Delta e_p)^c$ (V *vs* SCE)	$E^d_{1/2}$ (V *vs* SCE)
	$[H_2htpc(0)]^{2+}/[H_2htpc(1-)]^+$	0.860[b](0.120)	0.800
$H_2htpc(2-)$	$[H_2htpc(1-)]^+/H_2htpc(2-)$	0.650[b](0.100)	0.600
	$H_2htpc(2-)/[H_2htpc(3-)]^-$	−0.700[a]	—
	$[H_2htpc(3-)]^-/[H_2htpc(4-)]^{2-}$	−1.150[a]	—
	$[Zn(htpc)(0)]^{2+}/[Znhtpc(1-)]^+$	0.850[b](0.090)	0.805
Zn(htpc)(2−)	$[Zn(htpc)(1-)]^+/Zn(htpc)(2-)]$	0.645[b](0.090)	0.600
	$[Zn(htpc)(2-)/[Zn(htpc)(3-)]$	−0.830[a](0.080)	−0.790
	$[Zn(htpc)(3-)]^-/[Zn(htpc)(4-)]^{2-}$	−1.150[a](0.100)	−1.100
	$[Cu(htpc)(0)]^{2+}/[Cu(htpc)(1-)]^+$	0.855[b](0.105)	0.800
Cu(htpc)(2−)	$[Cu(htpc)(1-)]^+/Cu(htpc)(2-)$	0.635[b](0.100)	0.585
	$Cu(htpc)(2-)/[Cu(htpc)(3-)]$	—	—
	$[Cu(htpc)(3-)]^-/[Cu(htpc)(4-)]^{2-}$	−1.090[a](0.200)	−0.990

[a]Cathodic peak potential.
[b]Anodic peak potential.
[c]Peak splitting (V) evaluated by $\Delta E_p = (E_{\text{anodic peak}} - E_{\text{cathodic peak}})$.
[d]Half-wave potential estimated by $E_{1/2} = (E_{\text{anodic peak}} + E_{\text{cathodic peak}})/2$.

platinium gauze electrode. The shape of the CV of Zn(htpc) in the oxidation side is also consistent with the absence of adsorption. The difference in the voltammetric behavior of Zn(htpc) in the oxidation side compared with the previous work [15] may be attributed to the use of DCM as the solvent in this work. The potentials of the first oxidation and two reduction processes of Zn(htpc) (Table 1) are in accord with those measured for the analogous compound with octakis(butylthio) substituents.

Voltammetric behaviors of H_2htpc, Zn(htpc) and Cu(htpc) on the reduction side are significantly different from each other. Figures 3 and 4 show the CVs of H_2htpc on sweeping to negative potentials at 0.050 and 0.250 V s^{-1}, respectively. H_2htpc gives two one-electron reduction peaks without the corresponding anodic waves on the reverse sweep at 0.050 V s^{-1}. However, an anodic peak (AP2 in Fig. 4) was observed at the scan rate of 0.250 V s^{-1}, which appears to correspond to the second reduction process. The first reduction process is irreversible since it has no coupled re-oxidation peak. The value of $E_p - E_{p/2}$ for Red1 peak was found to be 0.070 V and $i_{pc}/v^{1/2}$ was constant, suggesting a diffusion controlled one-electron reduction. The absence of the re-oxidation peak for the first reduction process should not indicate that the monoanion of H_2htpc is unoxidizable. In our previous work, [16] the first reduction process of tetra-crown-ether-substituted metal-free phthalocyanine in dimethylsulfoxide displayed the anodic peak on the reverse sweep. Changing the peripheral substituents or the solvents used are not expected to make such a drastic effect on the voltammetric behavior of the pc ring. The absence of the anodic peak for the first reduction process may be attributed to a fast chemical reaction which follows the first electron transfer and produces a reducible but unoxidizable species (EC process). The shape of the Red1 peak is consistent with the EC process. The value of i_{Red2} is considerably higher than that of i_{Red1}, indicating the adsorption of the species produced by the EC process. $i_{Red2}/v^{1/2}$ was found to increase with increasing scan rate providing additional support for the adsorption. The appearance of a re-oxidation peak at 0.250 V s^{-1} indicates that the transfer of the second electron to the metal free complex is also followed by a chemical reaction.

The CV of Zn(htpc) in the reduction side at 0.050 V s^{-1} (Fig. 5) displayed two reduction processes (Red1 and Red2) with coupled re-oxidation peaks, the wave shapes and peak splittings ($\Delta E_p = 0.080$ V for Red1 and $E_p = 0.100$ V for Red2), which indicate reversible and quasi-reversible one-electron transfer processes without coupled chemical reactions. The

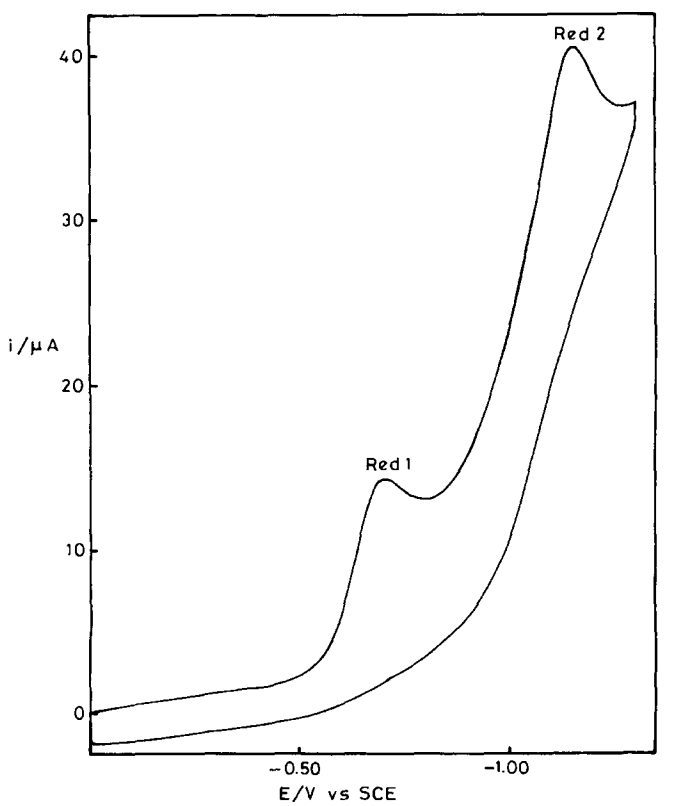


Fig. 3. Cyclic voltammogram of H_2htpc (5×10^{-4} M) on sweeping to negative potentials in DCM with $v = 0.050$ V s^{-1}.

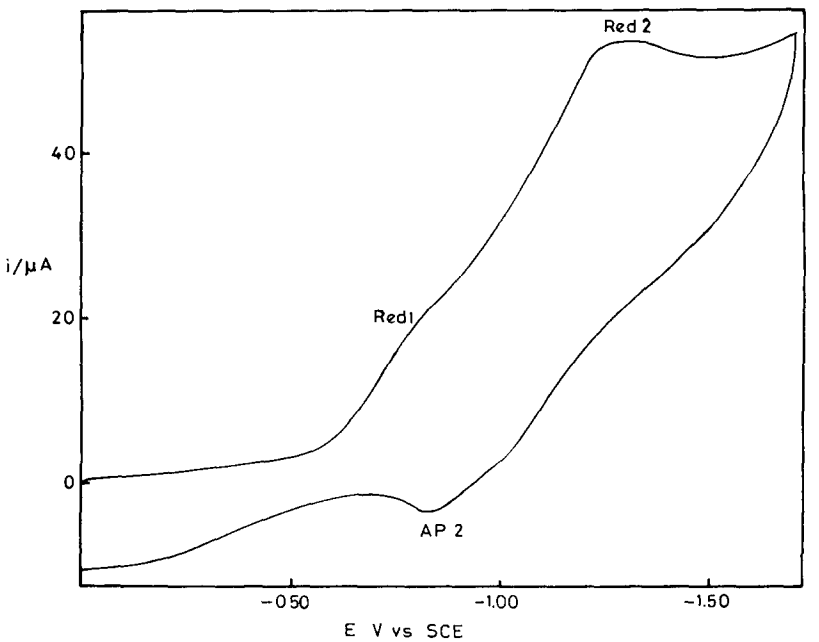


Fig. 4. Cyclic voltammogram of H_2htpc (5×10^{-4} M) on sweeping to negative potentials in DCM with $v = 0.250$ V s^{-1}.

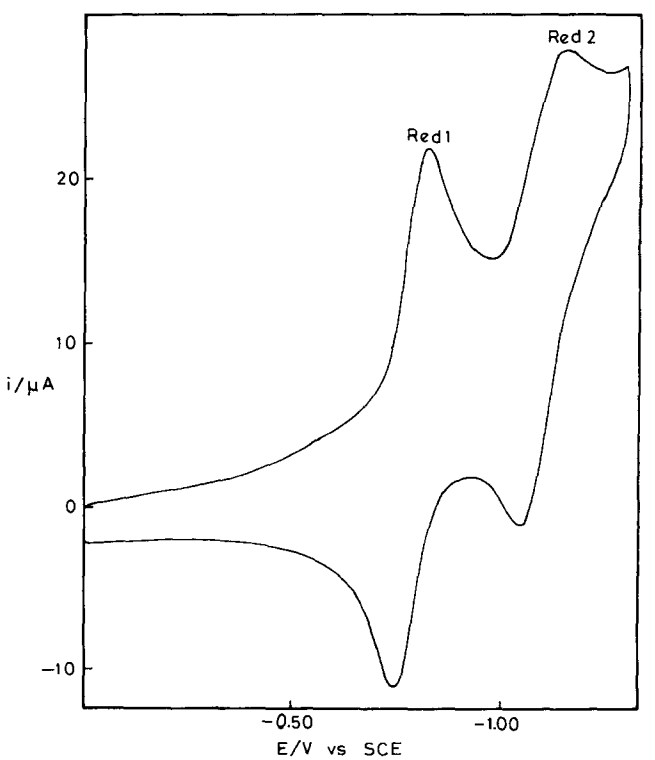


Fig. 5. Cyclic voltammogram of Zn(htpc) (5×10^{-4} M) on sweeping to negative potentials in DCM with $v = 0.050$ V s^{-1}.

half peak potentials for the reduction couples of Zn(htpc) are in accord with those previously reported, [14,15,17–19] the small differences being due to solvent and substituent effects.

The CV of Cu(htpc) (Figs 6 and 7) displayed a reduction peak (Red1,2) on sweeping to negative potentials with two anodic peaks (AP2 and AP1) on the reverse scan. The reduction of Cu(htpc) by controlled-potential electrolysis at the potential of Red1,2 peak afforded a two-electron redox process. However, the appearance of two re-oxidation peaks on the reverse sweep probably suggests that reduction of Cu(htpc) occurs in two successive one-electron steps. The potential difference between the first and the second reduction processes should be considerably small leading to the formation of a composite wave (Red1,2 peak in Fig. 6). The formation of the composite wave may be related to the fact that the singly reduced copper phthalocyanines are known to be unstable compared with the other metal phthalocyanines [20]. While the difference between the peak potentials of AP2 and AP1 is 0.20 V at 0.050 V s^{-1} (Fig. 6), it becomes 0.30 V at 0.250 V s^{-1} (Fig. 7). This voltammetric behaviour indicates that the first reduction process of Cu(htpc) is more irreversible than the second reduction process since the anodic peaks shift to more positive potentials with increasing scan rate. Therefore, two re-oxidation peaks are observed clearly due to the different irreversibility of the first and the second electron transfer processes, whereas only one cathodic peak is observed on sweeping to negative potentials.

Zn(pc) has frequently been selected as a candidate for the investigation of ligand-based redox processes, while the zinc(II) ion exhibits a stable oxidation state during the electrochemical measurements [3,14,15,17,21,22]. The potentials which appeared on the reduction side on the voltammograms of Zn(htpc) and Cu(htpc) are similar to one another. The reduction processes for both Zn(htpc) and Cu(htpc) are thought to be ligand based, as reported for most metal phthalocyanines [3,12,13,21,23].

The displacement of two protons with the zinc(II) ion shifts the first reduction potential of the pc ring to more negative values [−0.70 V for H_2htpc and −0.83 V for Zn(htpc)]. This voltammetric behaviour has been also observed previously with various metal free and metal phthalocyanines [13,20,24] and may be attributed to the increase in the negative charge of the pc ring as a result of the strong coordination of nitrogen atoms to the metal ion. The π-back-donation of the filled d_π of the metal ion into the empty pc-π^*-orbitals and the polarization of the ligand due to the E_g symmetry with the displacement of protons with metal ion was previously reported [25] as providing an additional support for the negative shift in the reduction potential of the pc ring. Although it was not possible to determine the first reduction potential of Cu(htpc) due to the formation of the composite wave, it is clear from the potential of Red1,2 peak that the

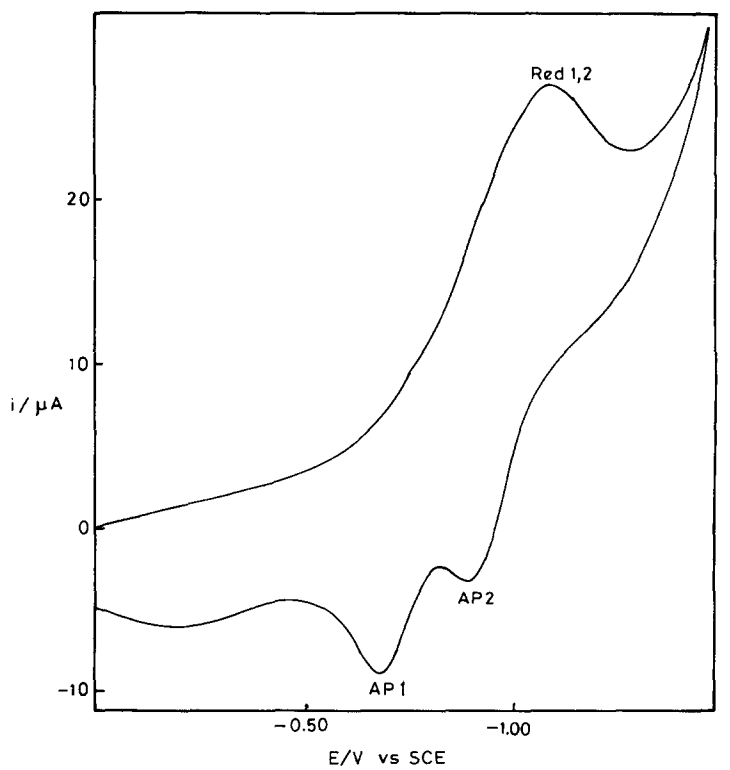


Fig. 6. Cyclic voltammogram of Cu(htpc) (5×10^{-4} M) on sweeping to negative potentials in DCM with $v = 0.050$ V s^{-1}.

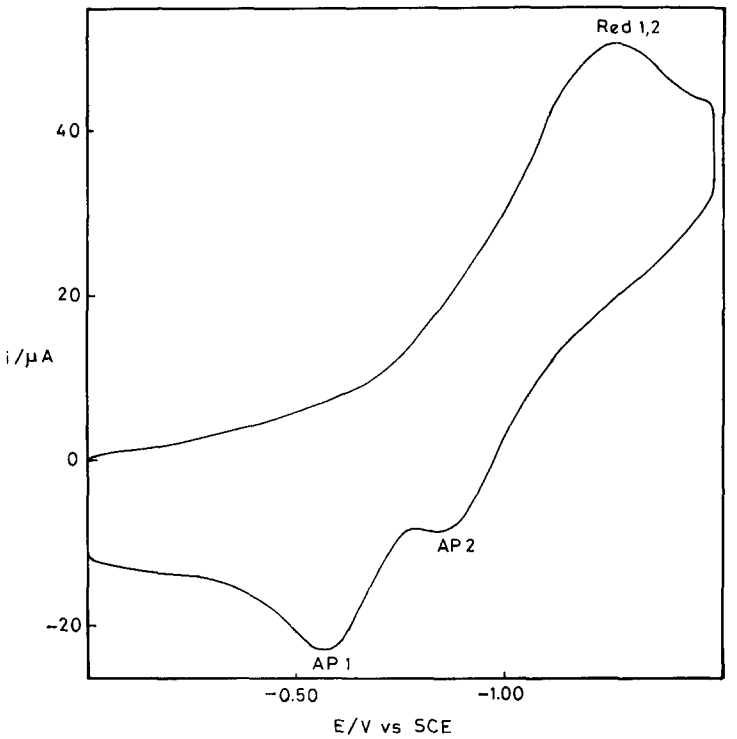


Fig. 7. Cyclic voltammogram of Cu(htpc) (5×10^{-4} M) on sweeping to negative potentials in DCM with $v = 0.250$ V s^{-1}.

first electron transfer to Cuhtpc should occur at a more negative potential with respect to H_2htpc. On the other hand, the presence of metals coordinated to nitrogen atoms of the pc ring did not make an important effect on the oxidation potentials [20]. For all complexes used in this work, the first oxidation and the first reduction can be supposed to involve the highest occupied molecular orbital (HOMO) and the lowest unoccupied molecular orbital (LUMO), respectively. On the other hand, the main peaks of the Q band in the UV–vis spectra of metal free and metal phthalocyanines have been attributed to the electronic transition from the HOMO to the LUMO [$b_{2g} \rightarrow e_g(\pi^*)$ for metal free and $a_{1u}(\pi) \rightarrow e_g(\pi^*)$] for metal phthalocyanines [25,26]. The UV–vis absorption spectra of the complexes used in this work have been reported previously [11]. The main peaks of the Q band in H_2htpc appeared at 740 and 700 nm corresponding to the non-degenerate transitions to the split $e_g(\pi^*)$ LUMO, which splits at the lower symmetry of the D_{2h} H_2htpc species to give two bands labelled Q_x and Q_y, respectively [27–29]. The UV–vis spectra of both Zn(htpc) and Cu(htpc) showed a peak at 710 nm. The difference between the first oxidation and the first reduction potentials [1.35 V for H_2htpc and 1.475 V for Zn(htpc)] do not match the energies of the π–π^* transition visible absorption bands [1.77 and 1.67 eV for H_2htpc and 1.75 eV for Zn(htpc)], indicating that photo-excitation arises from the orbitals below the HOMO for the all phthalocyanines used in this work.

EXPERIMENTAL

Cyclic voltammetry was performed with a Princeton Applied Research (PAR) Model 273 potentiostat, controlled by an external computer. Cyclic voltammograms were collected with the usual three electrode set up and recorded using an X-Y recorder (RE 0091). For cyclic voltammetry, a platinium wire served as a counter electrode and a commercial saturated calomel electrode (SCE) was employed as the reference electrode. The working electrode was a platinium plate, polished with a water suspension of Al_2O_3 before each experiment. The last polishing was done with a particle size of 50 nm. The SCE was separated from the solution by a double bridge containing saturated KCl adjacent to the SCE, and dimethylsulfoxide and carrier adjacent to the solution in order to minimize liquid–liquid junction potentials. Controlled-potential electrolysis was performed at the constant potentials corresponding to the CV peak potentials of the phthalocyanines with the bulk electroylsis of 5×10^{-4} mol dm^{-3} solutions using platinium gauze working and counter electrodes and SCE.

Dichloromethane (DCM), dried over molecular sieves, was used as the solvent in the experiments. Electrochemical grade tetrabutylammonium perchlorate (TBAP) was employed as the supporting electrolyte in a 0.1 mol dm^{-3} concentration.

Acknowledgement—We thank the Research Fund of the Technical University of İstanbul for financial support.

REFERENCES

1. C. C. Leznoff and A. B. P. Lever, eds., *Phthalocyanines: Properties and Applications*, Vol. 3. VCH, Weinheim, 1993.
2. I. B. Hugun, D. Lexa and J. M. Saveant, *J. Am. Chem. Soc.*, 1996, **118,** 1769.
3. D. Wöhrle and V. Schmidt, *J. Chem. Soc., Dalton Trans.*, 1988, 549.
4. V. Ahsen, E. Yilmazer, M. Ertaş and Ö. Bekaroğlu, *J. Chem. Soc., Dalton Trans.*, 1988, 401.
5. V. Ahsen, E. Yilmazer, A. Gürek, A. Gül and Ö. Bekaroğlu, *Helv. Chim. Acta*, 1988, **71,** 1616.
6. E. Musluoğlu, V. Ahsen, A. Gül and Ö. Bekaroğlu, *Chem. Ber.*, 1991, **124,** 2531.
7. A. Gürek, V. Ahsen, A. Gül and Ö. Bekaroğlu, *J. Chem. Soc., Dalton Trans.*, 1991, 3367.
8. M. Koçak, A. İ. Okur and Ö. Bekaroğlu, *J. Chem. Soc. Dalton Trans.*, 1994, 323.
9. C. Sirlin, C. Bosio, J. Simon, V. Ahsen, E. Yilmazer and Ö. Bekaroğlu, *Chem. Phys. Lett.*, 1987, **139,** 362.
10. V. Ahsen, M. Özdemir, Z. Z. Öztürk, A. Gül and Ö. Bekaroğlu, *J. Chem. Res. (S)*, 1995, 348; (M) 2050.
11. A. Gürek and Ö. Bekaroğlu, *J. Chem. Soc. Dalton Trans.*, 1994, 1419.
12. T. Nyokong, *Polyhedron*, 1993, **12,** 375.
13. R. H. Campbell, G. A. Heath, G. T. Hefter and R. C. S. McQueen, *J. Chem. Soc., Chem. Commun.*, 1983, 1123.
14. Y. Fu, G. Fu and A. B. P. Lever, *Inorg. Chem.*, 1994, **33,** 1038.
15. K. Takahashi, M. Kawashima, Y. Tomita and M. Itoh, *Inorg. Chim. Acta*, 1995, **232,** 69.
16. A. R. Özkaya, A. İ. Okur, A. Gül and Ö. Bekaroğlu, *J. Coord. Chem.*, 1994, **33,** 311.
17. T. Nyokong, Z. Gasyna and M. J. Stillman, *Inorg. Chem.*, 1987, **26,** 548.
18. A. B. P. Lever and J. P. Wilshire, *Can. J. Chem.*, 1976, **54,** 2514.
19. A. B. P. Lever and P. C. Minor, *Inorg. Chem.*, 1981, **20,** 4015.
20. L. D. Rolmann and R. T. Iwamoto, *J. Am. Chem. Soc.*, 1968, **90,** 1455.
21. A. Giraudeau, A. Louati, M. Gross, J. J. Andre, J. Simon, C. H. Su and K. M. Kadish, *J. Am. Chem. Soc.*, 1983, **105,** 2917.
22. K. Kasuga, T. Nakao and T. Mihara, *Bull. Chem. Soc. Jpn*, 1991, **64,** 3766.
23. J. T. S. Irvine and B. R. Eggins, *J. Electroanal. Chem.*, 1989, **271,** 161.
24. A. Giraudeau, F. F. Fan and A. J. Bard, *J. Am. Chem. Soc.*, 1980, **102,** 5137.
25. A. Rosa and A. J. Baerends, *Inorg. Chem.*, 1994, **33,** 584.
26. C. C. Leznoff and A. B. P. Lever, eds., *Phthalocyanines: Properties and Applications*, Vol. 1. VCH, Weinheim, 1989.
27. K. A. Martin and M. J. Stillman, *Can. J. Chem.*, 1979, **57,** 1111.
28. M. J. Stillman and A. J. Thomson, *J. Chem. Soc., Faraday Trans.*, 1974, **2,** 790.
29. M. J. Stillman and A. J. Thomson, *J. Chem. Soc., Faraday Trans.*, 1974, **2,** 805.

Pergamon

PII: S0277-S387(96)00485-8

Polyhedron Vol. 16, No. 11, pp. 1885–1888, 1997
© 1997 Elsevier Science Ltd
All rights reserved. Printed in Great Britain
0277–5387/97 $17.00+0.00

Reaction of tetrakis[(3-pyridylmethyl)oxy] *p-tert*-butylcalix(4)arene with $KAuCl_4$ and K_2PtCl_6. New pyridinocalix(4)arene adducts of gold(III) and platinum(IV)

Angela F. Danil de Namor,* Felix J. Sueros Velarde and Mercedes C. Cabaleiro

Laboratory of Thermochemistry, Department of Chemistry, University of Surrey, Guildford, Surrey GU2 5XH, U.K.

(Received 3 April 1996; accepted 30 September 1996)

Abstract—Tetrakis[(3-pyridylmethyl)oxy]*p-tert*-butylcalix(4)arene prepared from *p-tert*-butylcalix(4)arene and 3-chloromethylpyridine under basic conditions was characterized by ^1H and ^{13}C NMR. Protonation constants of this ligand in methanol at 298.15 K derived from potentiometric data are reported. Au^{III} and Pt^{IV} adducts of tetrakis[(3-pyridylmethyl)oxy]*p-tert*-butylcalix(4)arene have been isolated. It is concluded that this calixarene derivative displaces chloride ions from the coordination spheres of the central atoms in $AuCl_4^-$ and $PtCl_6^-$ species, engaging itself in direct interaction with Au^{III} and Pt^{IV}. © 1997 Elsevier Science Ltd. All rights reserved.

Keywords: calixarenes; gold(III) complexes; platinum(IV) complexes; macrocycles; tetrakis [3-pyridylmethyl)oxy]*p-tert*-butylcalix(4)arene; adduct formation.

Calixarene chemistry has been the subject of considerable research in recent years [1,2]. A great deal of the interest generated by these macrocycles is attributed to the possibility of introducing functional groups in the lower or upper rim of these compounds in order to target particular ionic or neutral species. Among lower rim calixarene derivatives so far synthesized are those reported by Bottino and Pappalardo [3] and by Shinkai [4] known as pyridinocalix(n)arenes (n = 4 [3], 6 [3,4], 8 [3,4]). In these compounds, carbon atoms (C-2) next to the nitrogens in the pyridine rings are linked *via* a methylene bridge to the phenolic oxygens of the parent calixarenes. Thus, the cooperative effect of the mixed donor atoms, oxygen and nitrogen enable these ligands to interact not only with transition metals, but also with alkali and lanthanide cations. Our interest in the extraction of precious metals led us to the design of a new pyridinocalix(4)arene: tetrakis[(3-pyridylmethyl)oxy]*p-tert*-butylcalix(4)arene (**1**). The main feature of this novel ligand relative to others previously reported is that the present arrangement facilitates the availability of the pyridyl nitrogens (rather than the phenolic oxygens), which are suitable active centres for coordination with gold(III) and platinum(IV) compounds. This paper reports for the first time investigations based on spectrophotometric (IR and ^1H NMR) of **1** and its interaction with $KAuCl_4$ and K_2PtCl_6 compounds in solution.

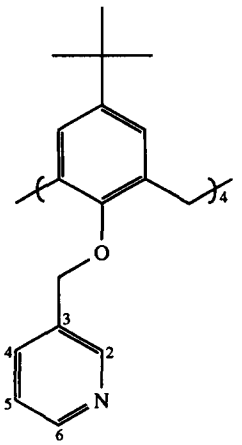
EXPERIMENTAL

Chemicals

p-tert-Butylcalix(4)arene, 3-chloromethyl pyridine, sodium hydride and tetrahydrofuran (HPLC grade) were purchased from Aldrich. *p-tert*-Butylcalix(4)arene was dried over P_2O_5 *in vacuo* at 100°C for at least 12 h before use.

N,N-Dimethylformamide (Fisons, HPLC grade) was stored over molecular sieves (4 Å) before use. Ethyl acetate, dichloromethane, hexane, sodium sulfate, acetonitrile, $KAuCl_4$ and K_2PtCl_6 were purchased from Fisons. Acetonitrile, hexane and meth-

*Author to whom correspondence should be addressed.



1

anol were HPLC grade. For the potentiometric titrations, perchloric acid 70%, redistilled (99.999% grade), purchased from Aldrich was used. Methanol was often used without further purification. However, when the water content tested by Karl Fischer titration was higher than 0.05%, this was removed by refluxing the solvent with magnesium in the presence of iodine (0.5 g I_2/5 g Mg) and distilled. The middle fraction of the distillate was used.

Synthesis of tetrakis [(3-*pyridylmethyl*)*oxy*]p-*tert*-*butylcalix*(4)*arene*

This ligand was prepared by treatment of a THF/DMF solution of *p-tert*-butylcalix(4)arene with 3-chloromethyl pyridine under basic conditions. Details are as follows: sodium hydride (5.158 g, 129 mmol) and *p-tert*-butylcalix(4)arene (2.15 g, 3.85 mmol) were suspended in a mixture of tetrahydrofuran (75 cm^3) and *N*,*N*-dimethylformamide (20 cm^3). The reaction mixture was stirred for 40 min at room temperature and a yellow-greyish suspension was formed. Then, 3-chloromethyl pyridine hydrochloride (7.04 g, 42.9 mmol) was added. The flask containing the mixture was placed in an oil bath and heated at 45°C for a period of 5 h. The course of the reaction was monitored by TLC using hexane : ethyl acetate (4 : 1) and dichloromethane : methanol (9 : 1) mixtures as developing solvents. The solvents were removed under reduced pressure and the organic materials were twice extracted with dichloromethane (100 cm^3). After drying the organic layer with sodium sulphate, the solvent was removed *in vacuo*. The viscous residue was treated with acetonitrile and activated charcoal in order to remove impurities. After filtration and cooling, white crystals were obtained in 56% yield (2.20 g, 2.17 mmol). The compound was recrystallized from acetone. Microanalyses were carried out at the University of Surrey. Found: C, 80.6; H, 7.6; N, 5.5. Calc. for $C_{68}H_{76}N_4O_4$: C, 80.6; H, 7.6; N, 5.5%.

Potentiometric determination of the protonation constants of **1** *in methanol at* 298.15 K

Potentiometric measurements were carried out with an ABU12 Radiometer autoburette interfaced to a microprocessor model Hanna H1 8417 in conjunction with a PHM 82 potentiometer and an Ingold pH combination electrode. All titrations were performed at 298.15 ± 0.10 K in a water-jacketed vessel. Potentiometric data were collected by using an acquisition program and these were recorded as a matrix of time–voltage pairs. Before each measurement, the electrode was calibrated by using a standard solution of perchloric acid (standardized against sodium hydroxide using phenolphalein as indicator) in methanol. For the determination of pK_a values a solution of **1** in methanol was titrated at 298.15 K against a standard solution of perchloric acid. About 110 points were recorded by this titration mode. A Miniquad program was used to analyse the data. All titrations were carried out in triplicate. For the calculation of pK_a values, the autoprotolysis constant of methanol at 298.15 K was considered.

Spectrophotometric studies on the interaction of **1** *with gold*(III) *in methanol*

The interaction of **1** with gold(III) in methanol was studied by spectrophotometry using a Pye Unicam PU8720 UV–vis scanning spectrophotometer. Thus, a methanolic solution of $KAuCl_4$ (2.15×10^{-3} mol dm^{-3}) was titrated against a solution of **1** in methanol (2.55×10^{-3} mol dm^{-3}) over ligand/metal ratio concentrations from 0.12 to 0.95. The absorption spectra was recorded over the 230–500 nm wavelength range.

Isolation of gold(III) *and platinum*(IV) *complexes*

The preparation of gold and platinum complexes was carried out by extraction using mutually saturated solvents. Thus, a solution of the ligand in dichloromethane (0.15 g, 0.15 mmol in 40 cm^3 of solvent) was treated with an aqueous solution of $KAuCl_4$ (0.94 mmol). Thus, for the preparation of the gold complex of **1**, a solution of the ligand (0.15 mmol) in dichloromethane (40 cm^3) was shaken for a few hours with an aqueous solution (40 cm^3) of KCl (1.013 mol dm^{-3}) containing $KAuCl_4$ (0.94 mmol) at 298.15 K (pH = 4.8). Then, the organic layer was dried over Na_2SO_4, filtered and evaporated *in vacuo*. The yellow product was dried over P_2O_5 *in vacuo* (yield 90%) and characterized by elemental analysis. Found: C, 36.8; H, 3.4; N, 2.3. Calc. for $C_{68}H_{76}N_4O_4Au_4Cl_{12}$: C, 36.7; H, 3.4; N, 2.5%. For the preparation of the platinum complex, a solution of the ligand (0.08 mmol) in

dichloromethane (25 cm^3) was shaken for a period of 12 h with an aqueous solution (100 cm^3) of K_2PtCl_6 (0.32 mmol). Before extraction the pH of the aqueous solution was 2.5. After separating the water and organic phases the latter was dried over Na_2SO_4, filtered and evaporated *in vacuo*. The bright yellow product was dried over P_2O_5 *in vacuo* (95% yield) and characterized by elemental analysis. Found C, 57.1; H, 5.4; N, 3.8. Calc. for $C_{68}H_{76}N_4O_4H_2PtCl_6$: C, 57.4; H, 5.5; N, 3.9%. IR measurements were recorded on a Perkin–Elmer 2000 Fourier transform instrument.

RESULTS AND DISCUSSION

^1H *and* ^{13}C *NMR spectra of tetrakis* [(3-*pyridylmethyl*)*oxy*]p-tert-*butylcalix*(4)*arene* (**1**)

The ^1H NMR spectrum of **1** in $CDCl_3$ at 300 K exhibits three sets of resonance centred at δ 8.56 (H-2 and H-6), 7.48 (H-4) and 7.12 ppm (H-5) characteristic of the pyridyl moiety. The spectrum also shows a singlet at δ 4.84 ppm for the methylene groups adjacent to the phenolic oxygens, a pair of doublets at δ 3.96 and 2.80 ppm (J = 12.6 Hz) corresponding to the protons of the methylene bridge and a singlet for the *tert-butyl* groups. These spectral features are compatible with calix(4)arene derivatives in their cone conformation[5]. This is reinforced by a ^{13}C NMR line at δ 31.00 ppm arising from the $ArCH_2Ar$.[6]

Protonation constants

Due to the nature of this ligand (four pyridine moieties) in searching for cation–ligand interactions the affinity of **1** for the proton was investigated in order to select the pH at which any possible metal ion–ligand interaction could be studied without the competitive effect of the proton. Thus, Table 1 lists the protonation constants of **1** in methanol at 298.15 K. These are referred to the following processes where Pyr_4 Calix (4) denotes **1**:

$$Pyr_4Calix(4) + H^+ \xrightarrow{\log K_{p1}} HPyr_4Calix(4)^+ \quad (1)$$

$$HPyr_4Calix(4)^+ + H^+ \xrightarrow{\log K_{p2}} H_2Pyr_4Calix(4)^{2+} \quad (2)$$

$$H_2Pyr_4Calix(4)^{2+} + H^+ \xrightarrow{\log K_{p3}} H_3Pyr_4Calix(4)^{3+} \quad (3)$$

$$H_3Pyr_4Calix(4)^{3+} + H^+ \xrightarrow{\log K_{p4}} H_4Pyr_4Calix(4)^{4+} \quad (4)$$

Table 1. Protonation constants of tetrakis[(3-pyridylmethyl)oxy]*p-tert*-butylcalix(4)arene in methanol at 298.15 K

$\log K_{p1}$	5.71
$\log K_{p2}$	4.52
$\log K_{p3}$	4.12
$\log K_{p4}$	3.59

It is quite clear from the data shown in Table 1 that each pyridine group in the calix(4)arene unit behave quite independently from each other, since the difference in log K_p values for the first and fourth protonation is ~2 log units. The neutral macrocycle is the strongest base and as such it shows the highest proton affinity.

These data can be used to calculate the percentages of the various species as a function of solution pH's. Unlike for acids in their neutral form, the medium effect for the dissociation (or the reverse, association) of cationic acids in the various solvents is very small, since no new charge fields [see eqs (1)–(4)] are originated in the process. Therefore, the data shown in Table 1 provide a good indication about the pH to be chosen to investigate the possible isolation of a gold(III) complex of **1**.

Complexation studies with gold(III) *and platinum*(IV)

As discussed in the experimental section, complexation of gold(III) and $Pyr_4Calix(4)$ was obtained by extracting an aqueous solution of $KAuCl_4$ containing an excess of KCl with an equal volume of a solution of the ligand in dichloromethane.

The UV spectrum of this compound showed that the absorption maximum at 320 nm corresponding to $KAuCl_4$ was shifted to 308 nm in the complex, suggesting that a change in the coordination shell of the metal has occurred. In the IR spectra (KBr) the band arising from the pyridyl group (1578 cm^{-1} for the free ligand) appears at a higher frequency (1609 cm^{-1}), indicating that the pyridyl residues are involved in the complexation. A comparison of ^1H NMR spectrum of the $(AuCl_3)_4Pyr_4Calix(4)$ complex with that of the free ligand revealed that the resonances due to H-2 and H-6 (see structure) move downfield on complexation ($\Delta\delta$ = 0.57 and 0.55 ppm, respectively). A similar pattern of deshielding effects, although more pronounced, was found [7] for the proton resonances of pyridine coordinated to $ZnCl_2$ and to $AlCl_3$ when compared with those of the corresponding protons in the free pyridine molecule ($\Delta\delta$H-2 and H-6 $\geqslant \Delta\delta$ H-4 $\geqslant \Delta\delta$H-3 and H-5).

Attempts to study the interaction of **1** with K_2PtCl_6 under the same pH conditions as those selected for the isolation of the gold(III) complex were hindered by the low solubility of the platinum salt in KCl. Therefore, K_2PtCl_6 aqueous solution (pH 2.7) was extracted by an equal volume of the dichloromethane solution of **1**, following the procedure described in the experimental section. The IR spectrum of this complex showed that the band at 1578 cm^{-1} for the free ligand is replaced by both a residual absorption at the same wavelength and a coordination band at 1609 cm^{-1}. The complex also exhibits a strong maximum at 3420

cm^{-1}, indicating the presence of the NH bonding, although no band between 2500 and 3200 cm^{-1} corresponding to NH^+Cl^- was observed. These facts can be accounted for in terms of a complex species containing both pyridyl coordination and free pyridinium ions. This interpretation is reinforced by inspection of the ^1H NMR spectral changes which occur in the calixarene protons after interaction with the platinum salt. It revealed that whereas the absorptions due to H-4 and H-5 in the free ligand appear as a set of unresolved resonances in the 6.80–7.60 ppm region; in the complex, those centred at δ 8.56 (H-2 and H-6) are replaced by two equally intense signals at δ 9.31 and 8.50 ppm, suggesting the presence of two different types of pyridyl moieties. The shift from δ 8.56 to 9.31 ppm ($\Delta\delta = 0.75$ ppm) experienced by half of the pyridyl protons adjacent to the nitrogen is not very different from that exhibited by the 2 and 6 protons signal of the protonated pyridine ($\Delta\delta = 0.53$ ppm) when compared with the free ligand. Further inspection of the ^1H NMR spectra showed that the resonances due to the methylene protons adjacent to the oxygen (one singlet in the free ligand) appear in the Pt^{IV} complex as two unresolved doublets at $\delta = 4.70$ and 4.59 ppm. Furthermore, three sets of doublets were observed for the $ArCH_2Ar$ protons in the region $\delta = 4.30$–2.73 ppm in an approximate ratio of 2 : 1 : 1 (one set in the free ligand), which reveals the presence of three types of bridge methylene groups and two types of phenoxy methylene protons indicating that the species has lost the symmetry shown by the parent calixarene.

From the above discussion we conclude that this novel ligand displaces chloride ions from the coordination spheres of the central atoms in $AuCl_4^-$ and $PtCl_6^{2-}$ species, engaging itself in direct interaction with Au^{III} and Pt^{IV}. As far as the gold(III) adduct is concerned each of the pyridyl nitrogens participates in the coordination process.

Consequently, four $AuCl_3$ moieties are coordinated per unit of calix(4)arene [eq.(5)].

$$Pyr_4Calix(4) + 4\,KAuCl_4 \xrightarrow{CH_2Cl_2} Au_4Pyr_4Calix(4)Cl_{12} + 4\,KCl \quad (5)$$

As far as Pt^{IV} is concerned, microanalysis data in conjunction with the spectral properties described above lead us to conclude that each calix(4)arene coordinates to one $PtCl_4$ unit by providing two of its pyridyl nitrogens likely to be in proximal positions (two chloride ions are abstracted) to complete the octahedral arrangement required by the central atom, while the remaining pyridine rings in **1** carry protonated nitrogens. The overall process is represented as follows:

$$Pyr_4Calix(4) + K_2PtCl_6 + 2H^+ \xrightarrow{CH_2Cl_2} H_2{}^{2+}Pyr_2PtCl_4Pyr_2Calix(4) + 2\,KCl \quad (6)$$

Given that (a) the solubility of **1** in water is negligible, (b) *via* a pH switching mechanism the free ligand can be recovered from either the gold(III) or indeed the platinum(IV) adducts, this new pyridinocalix(4)arene is a potential extracting agent for the removal of Au^{III} and Pt^{IV} compounds from aqueous solutions. Attempts to isolate suitable crystals for X-ray crystallographic studies in order to investigate the structures of these adducts in the solid state (which may or may not be the same of that in solution) are now in progress.

Acknowledgements—The authors are grateful to the European Union, International Scientific Cooperation for the support given to this project under grant. CI1*-CT92-0055.

REFERENCES

1. *Calixarenes. A, Versatile Class of Macrocyclic Compounds*, ed. J. Vicens and V. Böhmer. Academic Publishers, Dordrecht, 1991.
2. *Calixarenes 50th Anniversary*, Commemorative Volume, ed. J. Vicens, Z. Asfari and J. M. Harrowfield. Kluwer Academic Publishers, Dordrecht, 1994.
3. (a) F. Bottino, L. Giunta and S. Pappalardo, *J. Org. Chem.*, 1989, **54,** 5407; (b) S. Pappalardo, L. Giunta, M. Foti, G. Ferguson, J. Gallagher and B. Kaitner, *J. Org. Chem.*, 1991, **57,** 2611.
4. S. Shinkai, T. Otsuka, K. Araki and T. Matsuda, *Bull. Chem. Soc. Jpn*, 1989, **62,** 4055.
5. C. D. Gutsche, B. Dawan and J. Levine, *Tetrahedron*, 1983, **39,** 409.
6. C. Jaime, J. de Mendoza, P. Prado, P. M. Nieto and C. Sánchez, *J. Org. Chem.*, 1991, **56,** 3372.
7. A. D. Buckingham, *Can. J. Chem.*, 1960, **38,** 300.

Pergamon

PII: S0277-5387(96)00460-3

Polyhedron Vol. 16, No. 11, pp. 1889–1893, 1997
© 1997 Elsevier Science Ltd
All rights reserved. Printed in Great Britain
0277-5387/97 $17.00+0.00

Crystal and molecular structures of bis[2-(2-benzoxazolyl)phenol-*N*]dichloropalladium(II)

Mitsuhiro Ito,[a] Akiko Furuhashi[a]* and Mamoru Shimoi[b]

[a] Department of Chemistry, Aoyama Gakuin University, Morinosato-Aoyama, Atsugi-shi, Kanagawa 243-01, Japan

[b] Department of Chemistry, College of Arts and Sciences, The University of Tokyo, Komaba, Meguro-ku, Tokyo 153, Japan

(Received 4 June 1996; accepted 16 September 1996)

Abstract—The crystal and molecular structure of bis[2-(2-benzoxazolyl)phenol-*N*]dichloropalladium(II), was determined by the single-crystal X-ray diffraction. The palladium atom is at the symmetry centre in a square-planar geometry, where two 2-(2-benzoxazolyl)phenol (Hbxp) molecules are coordinated with their N atoms as unidentate ligands in the *trans* position. © 1997 Elsevier Science Ltd. All rights reserved.

Keywords: palladium(II) complex; 2-(2-benzoxazolyl)phenol; synthesis; X-ray analysis.

2-(2-Benzoxazolyl)phenol (Hbxp) has been known as an analytical chelating reagent for many bivalent metals such as zinc, cadmium and copper. Of these, the structures of the copper(II) and cadmium(II) complexes have already been determined by single-crystal X-ray diffraction [1]. As a result of ongoing work on the synthesis of the complexes of Hbxp, Furuhashi and workers have reported the synthesis and X-ray structure of the iron(III) [2], platinum(II) [3] and platinum(V) [4] complexes. In the iron(III) complex, Hbxp acts as a uninegative ion, bxp^-, coordinating to the metal atom through its benzoxazolyl-N and phenolato-O atoms and forming a chelate ring as reported in the cases of copper(II), cadmium(II) and palladium(II) [1]. In the case of platinum(V), Hbxp not only coordinates as a uninegative bxp^-, but the crystal contains neutral, uncoordinating Hbxp molecules. In the platinum(II) complex, Hbxp acts as a unidentate non-charged Hbxp ligand coordinating through its benzoxazolyl-N atom. Owing to a twisting of the planes of the two Hbxp ligands in the *cis* position of the square-planar Pt^{II}, two kinds of optical isomers could be obtained simultaneously. We have now obtained a new palladium(II) complex of Hbxp, $PdCl_2(Hbxp)_2$, in crystal form, which is different from that reported by Urdy [5]. The crystal and molecular structures were determined by the single-crystal X-ray diffraction technique.

* Author to whom correspondence should be addressed.

EXPERIMENTAL

Synthesis of bis[2-(2-*benzoxazolyl*)*phenol*]*dichloropalladium*(*II*)

A solution of Hbxp (0.55 g) in n-propanol (150 cm^3) was added to a solution of *trans*-bis(benzonitrile)dichloropalladium [6] (0.5 g) in n-propanol (50 cm^3). The mixture was left standing for about 20 days. A light precipitate was removed by shaking and decanting, fresh n-propanol was added and this action was repeated many times until the light precipitate was completely removed, leaving a heavy precipitate. The residual orange–yellow crystals were dried on a porous sheet and in a desiccator over silica gel. Found: C, 52.1; H, 3.1; N, 4.6. Calc. for $C_{26}H_{18}N_2O_4Cl_2Pd$: C, 52.1; H, 3.1; N, 4.7%.

Table 1. Crystal data and refinment details

Chemical formula	$C_{26}H_{18}N_2O_4Cl_2Pd$
Formula weight	599.77
Unit-cell dimensions	$a = 11.718(4)$ Å
	$b = 12.929(4)$ Å
	$c = 17.225(6)$ Å
	$\beta = 98.95(3)°$
Volume of unit cell	2398(1) Å^3
Crystal system	Monoclinic
Space group	$P2_1/a$
Z value	4
Densities	
D_m	1.60 g cm^{-3}
D_x	1.63 g cm^{-3}
Total reflections	7002
R_{int}	0.07
Structure solution	SHELXS-86
Structure refinement	SHELXL-93
Least squares refinement	Full matrix
Function minimized	$\Sigma [w(\lvert F_o \rvert - \lvert F_c \rvert)^2]$
Weight method	$w = (\sigma_c{}^2 + (0.02 \lvert F_o \rvert)^2)^{-1}$
$F(000)$	1199
Reflections used in L. S.	3008
Data reduction cut-off	$\lvert F_o \rvert > 3\sigma(\lvert F_o \rvert)$
R	0.055
R_w	0.063

Crystal structure determination

The crystal used for the X-ray analysis was chosen from the synthesized product, then shaped into a $0.40 \times 0.40 \times 0.45$ mm^3 block. The crystallographic data and some experimental conditions used to obtain the intensity data are given in Table 1. The reflections were collected on a Rigaku AFC-5S automated four-circle diffractometer with the graphite-monochromated Mo-K_α radiation ($\lambda = 0.7107$ Å) [scan speed: 4° min^{-1} (θ)] at the University of Tokyo using the ω–θ scan technique.

Structure determination

The structure of the complex was solved using Patterson and Fourier syntheses. The positional and thermal parameters were refined by the full-matrix, least-squares procedure. At the final stage, all the non-hydrogen atoms were refined anisotropically. All the calculations were carried out with the SHELXS-86 [7] and the SHELXL-93 [8] programs for crystal structure determination.

RESULTS AND DISCUSSION

Selected bond lengths and bond angles for the title complex are given in Tables 2 and 3. Although there are two crystallographically independent complex molecules, each of which is positioned at the centre of symmetry, they are almost identical so only one is shown in Fig. 1, which shows the palladium complex as viewed from above the coordination plane. The complex molecules have the *trans* configuration with two Cl atoms and two Hbxp molecules, which act as neutral unidentate ligands through the N atoms of the oxazolyl rings. The Pd—Cl and Pd—N distances are 2.299 and 2.002 Å, respectively. These values are a little shorter than the values expected from the sum of Shannon's ionic radii [9] (Pd—N = 2.10;

Table 2. Intramolecular bond lengths (Å)

Pd(1)—Cl(1)	2.299(3)	Pd(2)—C1(2)	2.298(3)
Pd(1)—N(1)	2.002(9)	Pd(2)—N(2)	2.026(8)
O(11)—C(101)	1.341(14)	O(21)—C(201)	1.367(15)
O(12)—C(107)	1.358(14)	N(2)—C(207)	1.272(13)
O(12)—C(108)	1.357(14)	N(2)—C(213)	1.399(15)
N(1)—C(107)	1.313(14)	O(22)—C(207)	1.385(13)
N(1)—C(113)	1.421(14)	O(22)—C(208)	1.370(14)
C(101)—C(102)	1.368(17)	C(201)—C(202)	1.374(19)
C(101)—C(106)	1.408(16)	C(201)—C(206)	1.379(16)
C(102)—C(103)	1.402(18)	C(202)—C(203)	1.37(3)
C(103)—C(104)	1.32(2)	C(203)—C(204)	1.37(3)
C(104)—C(105)	1.37(3)	C(204)—C(205)	1.39(2)
C(105)—C(106)	1.372(17)	C(205)—C(206)	1.384(18)
C(106)—C(107)	1.477(18)	C(206)—C(207)	1.492(17)
C(108)—C(109)	1.417(18)	C(208)—C(209)	1.361(17)
C(108)—C(113)	1.379(16)	C(208)—C(213)	1.371(16)
C(109)—C(110)	1.35(3)	C(209)—C(210)	1.391(19)
C(110)—C(111)	1.39(3)	C(210)—C(211)	1.43(2)
C(111)—C(112)	1.41(2)	C(211)—C(212)	1.377(18)
C(112)—C(113)	1.361(16)	C(212)—C(213)	1.382(18)

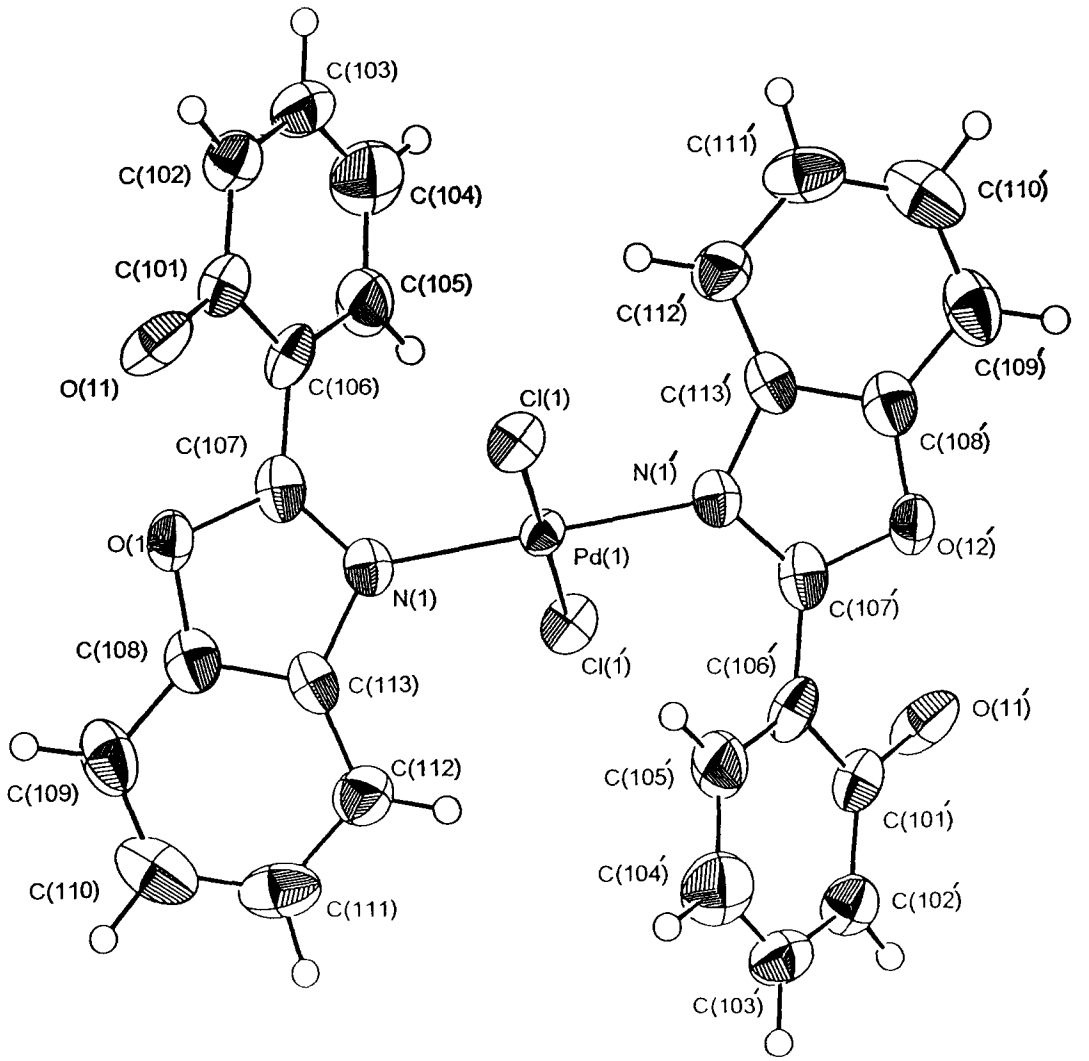


Fig. 1. The structure of one molecule of the complex.

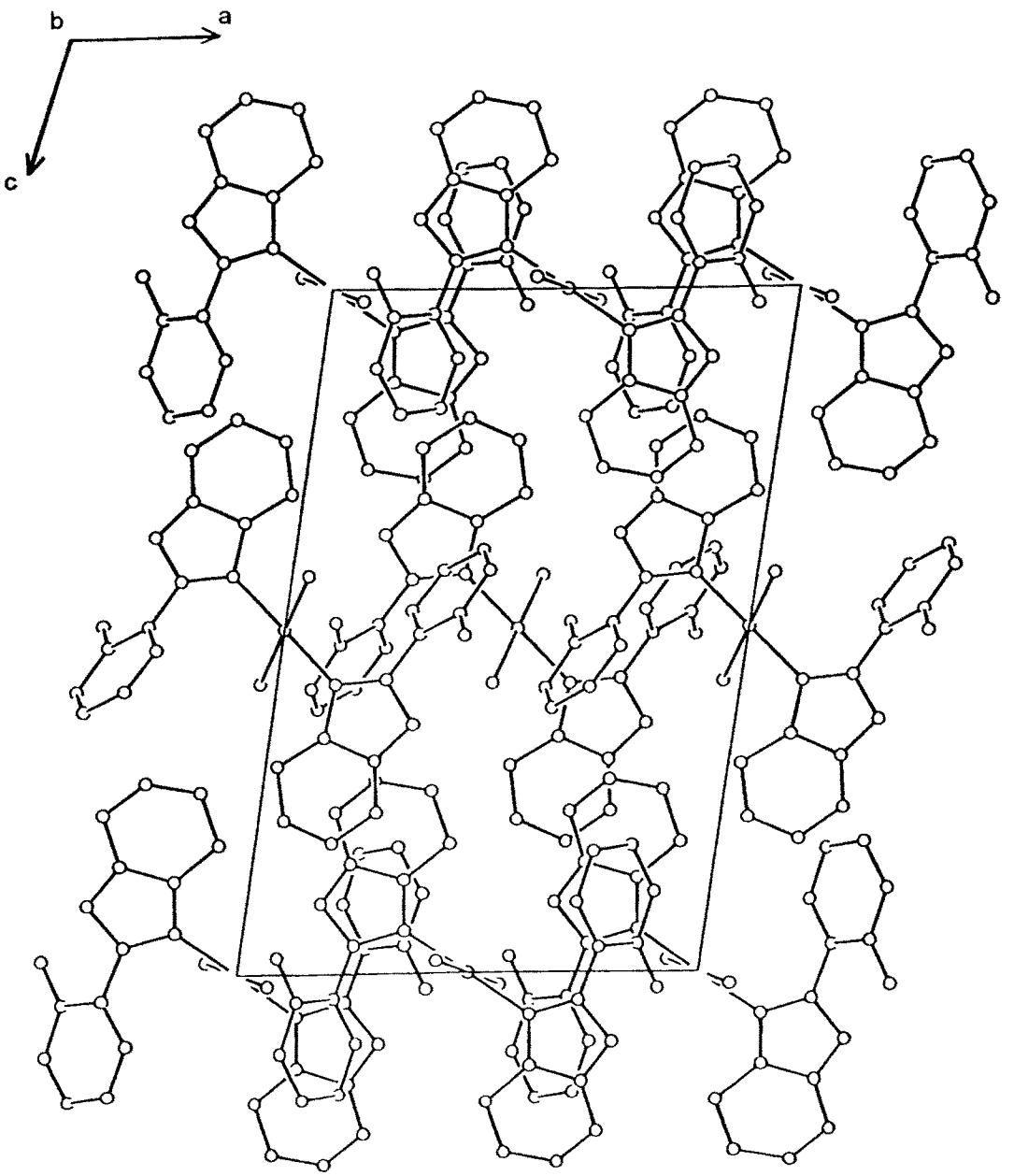


Fig. 2. Projection of the unit cell along the *b*-axis.

Table 3. Intramolecular bond angles (°)

Cl(1)—Pd(1)—N(1)	89.4(3)	Cl(2)—Pd(2)—N(2)	89.0(3)
Pd(1)—N(1)—C(107)	127.7(8)	Pd(2)—N(2)—C(207)	125.2(8)
Pd(1)—N(1)—C(113)	126.7(7)	Pd(2)—N(2)—C(213)	127.1(7)
C(101)—C(102)—C(103)	118.6(11)	C(201)—C(202)—C(203)	119.6(13)
C(102)—C(103)—C(104)	120.7(13)	C(202)—C(203)—C(204)	120.1(14)
C(103)—C(104)—C(105)	122.3(14)	C(203)—C(204)—C(205)	122.3(14)
C(104)—C(105)—C(106)	118.6(12)	C(204)—C(205)—C(206)	116.0(13)
C(101)—C(106)—C(105)	120.2(12)	C(201)—C(206)—C(205)	122.4(12)
C(102)—C(101)—C(106)	119.3(11)	C(202)—C(201)—C(206)	119.4(11)
O(11)—C(101)—C(102)	123.0(10)	O(21)—C(201)—C(202)	121.2(10)
O(11)—C(101)—C(106)	117.7(11)	O(21)—C(201)—C(206)	119.4(11)
C(101)—C(106)—C(107)	119.9(10)	C(201)—C(206)—C(207)	121.5(11)
C(105)—C(106)—C(107)	119.9(10)	C(205)—C(206)—C(207)	116.1(11)
N(1)—C(107)—C(106)	127.1(10)	N(2)—C(207)—C(206)	127.8(10)
O(12)—C(107)—C(106)	118.9(10)	O(22)—C(207)—C(206)	119.0(9)
C(107)—O(12)—C(108)	104.2(9)	C(207)—O(22)—C(208)	103.8(8)
O(12)—C(108)—C(113)	110.8(10)	O(22)—C(208)—C(213)	109.3(10)
N(1)—C(113)—C(108)	105.3(9)	N(2)—C(213)—C(208)	106.3(10)
C(107)—N(1)—C(113)	105.6(9)	C(207)—N(2)—C(213)	107.4(9)
O(12)—C(107)—N(1)	114.0(10)	O(22)—C(207)—N(2)	113.2(10)
O(12)—C(108)—C(109)	128.3(12)	O(22)—C(208)—C(209)	128.0(10)
N(1)—C(113)—C(112)	129.9(10)	N(2)—C(213)—C(212)	129.8(11)
C(109)—C(108)—C(113)	120.8(12)	C(209)—C(208)—C(213)	122.6(11)
C(108)—C(109)—C(110)	115.6(13)	C(208)—C(209)—C(210)	115.3(12)
C(109)—C(110)—C(111)	122.5(13)	C(209)—C(210)—C(211)	122.0(13)
C(110)—C(111)—C(112)	122.6(13)	C(210)—C(211)—C(212)	121.2(13)
C(111)—C(112)—C(113)	113.7(11)	C(211)—C(212)—C(213)	114.9(12)
C(108)—C(113)—C(112)	124.6(11)	C(208)—C(213)—C(212)	123.9(12)

Pd—Cl = 2.45 Å). The two phenol rings are also headed in opposite directions with a little twisting between the plane of the metal atom and the plane of the oxazolyl ring, the dihedral angle between the oxazoryl ring and the phenol ring being 128.90°. Thus, this palladium complex as a whole is in complete symmetry with the palladium atom at the symmetry centre of the complex molecule in a square-planar configuration. This is different from the palladium(II) complex reported by Urdy [5]. He obtained the complex formulated as $Pd(bxp)_2$, the ligand acting as a uninegative bidentate. We have synthesized the complex in a neutral medium which is different from Urdy's method, which used a basic medium.

A projection of the unit cell along the *b*-axis is shown in Fig. 2. The complex molecules are arranged in parallel and are laid along the *a*-axis.

REFERENCES

1. Stenson, P., *Acta Chem. Scand.*, 1969, **23,** 1514.
2. Furuhashi, A., Inayashi, T. and Ouchi, A., *Bull. Chem. Soc. Jpn*, 1987, **60,** 3207.
3. Furuhashi, A., Endo, K., Kondo, Y., Ouchi, A. and Saito, Y., *Croat. Chem. Acta*, 1989, **62,** 141.
4. Furuhashi, A., Ono, I., Ouchi, A. and Yamasaki, A., *Bull. Chem. Soc. Jpn*, 1991, **64,** 149.
5. Urdy, C. E., *Diss. Abstr.*, 1964, **24,** 4015.
6. Inorg. Synth., (ed. G. K. Anderson and E. Grets) 1990, **28,** 60.
7. Sheldrick, G. M., SHELXS-86, Program for Crystal Structure Determination, Univ. of Göttingen, Federal Republic of Germany (1986).
8. Sheldrick, G. M., SHELXS-93, Program for the Refinement of Crystal Structures, Univ. of Göttingen, Germany (1993).
9. Shannon, R. D., *Acta Cryst.*, 1976, **A32,** 751.

Pergamon

PII: S0277-5387(96)00468-8

Polyhedron Vol. 16, No. 11, pp. 1895–1905, 1997
© 1997 Elsevier Science Ltd
All rights reserved. Printed in Great Britain
0277-5387/97 $17.00+0.00

Copper(II) and nickel(II) complexes of 2,3-butanedione bis(N(3)-substituted thiosemicarbazones)

Douglas X. West,[a]* Janeice S. Ives,[a] Gordon A. Bain,[a] Anthony E. Liberta,[a] Jesús Valdés-Martínez,[b] Klaus H. Ebert[b] and Simón Hernández-Ortega[b]

[a]Department of Chemistry, Illinois State University, Normal, IL 61790-4160, USA;
[b]Instituto de Química, Universidad Nacional Autónoma de México, Circuito Exterior, Ciudad Universitaria, Coyoacán 04510, México D.F.

(Received 15 April 1996; accepted 15 September 1996)

Abstract—Copper(II) and nickel(II) complexes of 2,3-butanedione bis(N(3)-methyl-, bis(N(3)-dimethyl-, bis(pyridyl- and bis(hexamethyleneiminylthiosemicarbazone), (H_2Bu3M, H_2Bu3DM, H_2Bupip and H_2Buhexim, respectively) have been prepared and studied spectroscopically. The four thiosemicarbazones have been characterized by their melting points, as well as IR, electronic and NMR (^{1}H, ^{13}C) spectra. The four coordinate copper(II) complexes have been studied by EPR spectroscopy and the copper(II) and nickel(II) complexes by a number of the spectroscopic techniques mentioned above. Upon formation of these complexes, loss of the N(2)H hydrogens occurs and the ligands coordinate to the metal centers as dianionic, tetradentate N_2S_2 ligands. The crystal structures of H_2Bupip and the nickel(II) complex of 2,3-butanedione N3-methyl-phenylthiosemicarbazone, [Ni(Bu3MPh)], have been solved. © 1997 Elsevier Science Ltd. All rights reserved.

Keywords: bis(thiosemicarbazone); copper; nickel; crystal structure.

During the past several years a large number of heterocyclic tridentate NNS [1,2] and ONS [1–3] chelating thiosemicarbazones has been studied extensively. However, a lesser effort has been directed to the synthesis and characterization of metal complexes of tetradentate N_2S_2 bis(N3-substituted thiosemicarbazone) ligands [4,5]. Crystal structure determinations have shown that 1,2-bis(thiosemicarbazones) form square-planar N_2S_2 tetradentate ligands with copper(II) and that sulfurs of adjacent molecules coordinate weakly in the axial positions [6,7]. Due to the antitumor activity of α-diketone and α-ketoaldehyde bis(thiosemicarbazones) [8]as well as their metal complexes [9], a series of copper(II) and nickel(II) complexes of 2,3-butanedione bis(N(3)-substituted thiosemicarbazones) have been prepared; characterization of these complexes includes spectroscopic and physical techniques. The crystal structures of a representative 2,3-butanedione bis(thiosemicarbazone), H_2Bupip, and nickel(II) complex, [Ni(Bu 3MPh)] are included (Figs 1 and 2, respectively).

*Author to whom correspondence should be addressed.

EXPERIMENTAL

N(3)-methylthiosemicarbazide was purchased from Aldrich and used without further purification. N(3)-dimethyl-, piperidyl and hexamethyleneiminylthiosemicarbazide were prepared by the method described by Scovill [10]. The different 2,3-butanedione bis(N(3)-substituted thiosemicarbazones) were prepared by stirring 2,3-butanedione and an excess (greater than 2:1 mol ratio thiosemicarbazide to 2,3-butanedione) of the desired thiosemicarbazide in absolute ethanol with a few drops of H_2SO_4 added to catalyse the reaction. The purity of these bis(thiosemicarbazones) has been confirmed by their ^{1}H and ^{13}C NMR spectra. The metal complexes were prepared with a 2–4 h reflux of an absolute ethanol solution of the bis(thiosemicarbazone) with an equimolar amount of copper(II) or nickel(II) acetate. The volume was reduced on a warm plate (35°C) until sufficient solid was present, filtered with suction, washed to apparent dryness with anhydrous diethyl ether and dried at 35°C. Partial elemental analyses were performed by National Chemical Consulting,

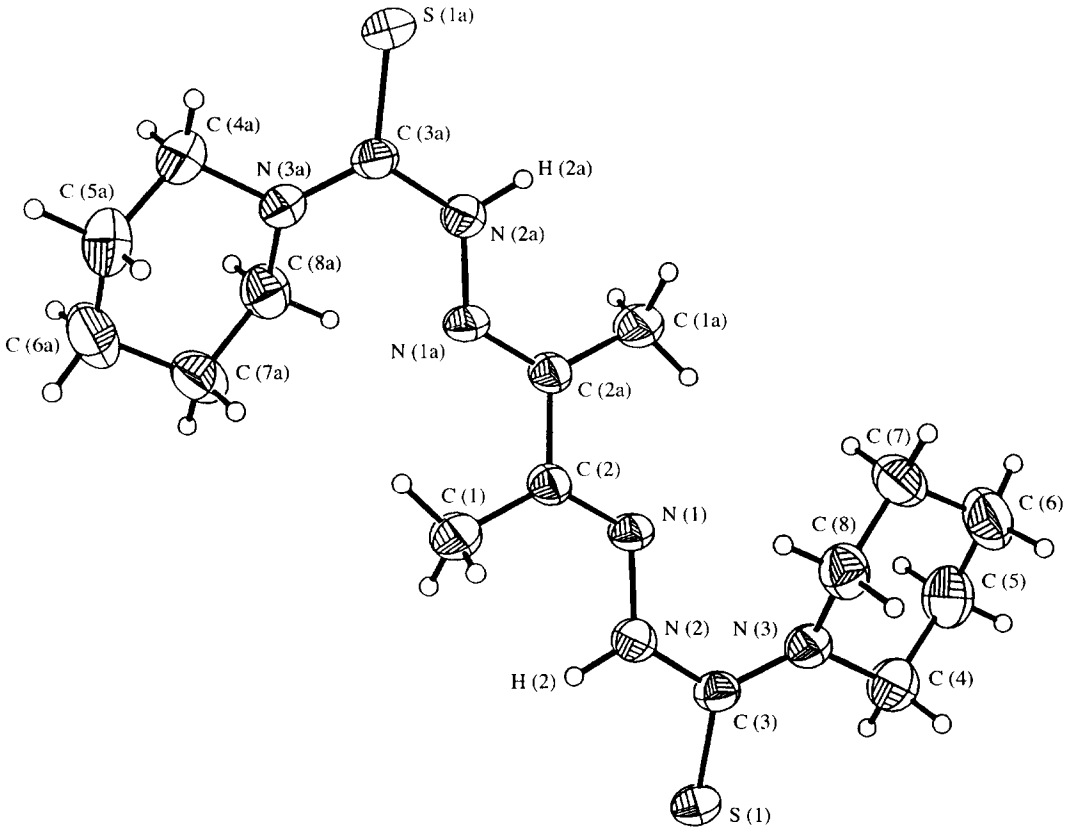


Fig. 1. A perspective view of H_2Bupip.

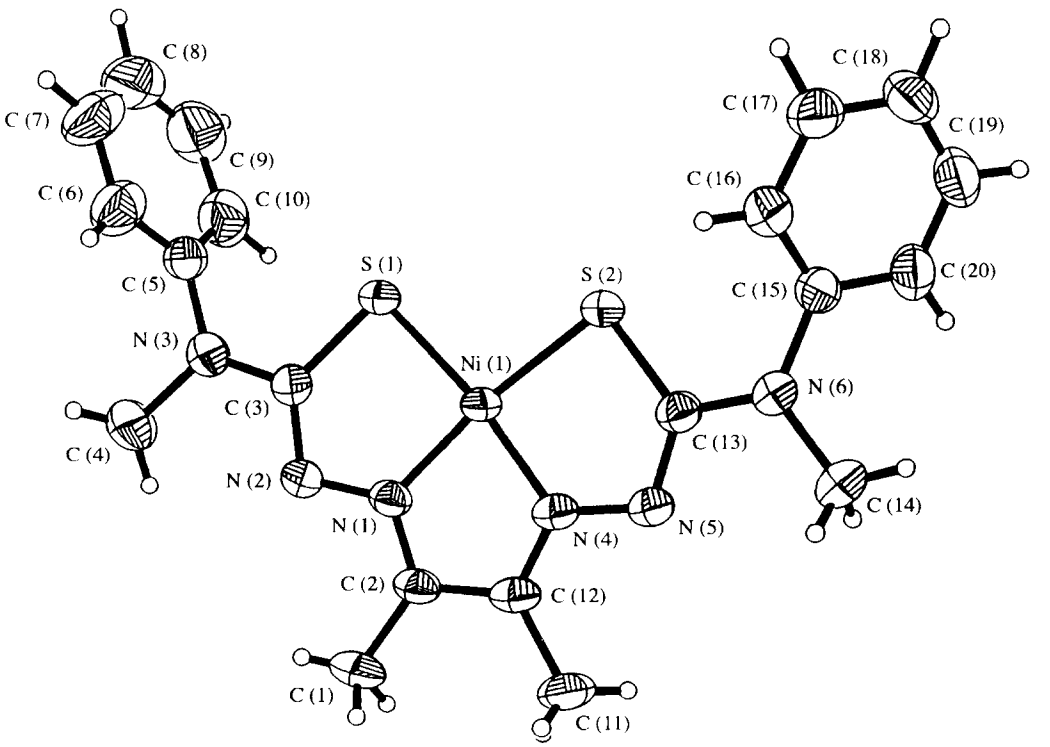


Fig. 2. A perspective view of [Ni(Bu3MPh)].

Inc. of Tenafly, NJ, and the spectral methods and instrumentation were accomplished as follows: molar conductivities were measured with a Beckmann Conductivity Bridge using 10^{-3} M solutions, magnetic susceptibilities were determined with a Johnson–Matthey Magnetic Susceptibility balance, IR spectra were recorded as Nujol mulls between CsI plates using a Perkin–Elmer 760 spectrometer, electronic spectra were acquired as Nujol mulls impregnated on pieces of filter paper and as DMF solutions in conventional quartz 1 cm cells with a Perkin–Elmer 330 spectrometer, EPR spectra were recorded with a Varian E104 spectrometer using a conventional insert Dewar and calibrated with DPPH and NMR spectra were acquired with a Varian 300 MHz Gemini spectrometer using $CDCl_3$ or dimethyl sulfoxide-d_6 as the solvent. Residual chloroform and tetramethylsilane peaks were used as internal references in $CDCl_3$ and DMSO-d_6, respectively.

The crystals of H_2Bupip, [Ni(Bu3MPh)] and [Ni(Buhexim)] (a crystal of this latter compound could not be solved with sufficient accuracy except to show the mode of coordination) were grown by slow diffusion of diethyl ether (−10 C) into chloroform. Data were collected for H_2Bupip on a Nicolet P3/F diffractometer and for [Ni(Bu3MPh)] on a Siemens P4 diffractometer. A yellow laminar of H_2Bupip having dimensions 0.40 × 0.36 × 0.04 mm and a black rectangular crystal of [Ni(Bu3MPh)] having dimensions 0.64 × 0.35 × 0.26 mm were mounted in random orientation on glass fibers. Crystal stability was monitored using three standard reflections every 97 reflections for both compounds. 1181 reflections were collected and 983 unique reflections, 876 ($F > 3\sigma F$) were used in the structure solution and refinement of H_2Bupip; 7462 reflections were collected and 6012 unique reflections, 3342 ($F > 6\sigma F$) were used in structure solution and refinement of [Ni(Bu3MPh)]. Semi-empirical absorption corrections were applied for both crystals. The structures were solved by direct methods [11] and refined by the full-matrix least-squares technique with anisotropic temperature factors for the non-H atoms. The coordinates of the C—H atoms were constrained, the N—H atoms were refined and both assigned a fixed isotropic temperature factor, $U = 0.06$ Å^2. The minimized function was $\Sigma\ w(F_o - F_c)^2$ with, $w = [\sigma^2(F_o) + 0.0016(F_o)^2]^{-1}$ and $w = [\sigma^2(F) + 0.0004F^2$ for H_2Bupip and [Ni(Bu(4)MPh)], respectively. The residual electron density was within −0.35 and 0.25 e Å^{-3} and −0.26 and 0.63 e Å^{-3} for H_2Bupip and [Ni(Bu3MPh)], respectively. Scattering factors were taken from International Tables for X-ray Crystallography (1974, Vol. IV).

RESULTS AND DISCUSSION

Table 1 shows a summary of crystal data and X-ray analysis information for H_2Bupip and [Ni(Bu3MPh)]. Selected interatomic distances are compiled in Table 2 and bond angles in Table 3; the supplementary material contains a complete list of bond distances and angles, the mean plane equations and the hydrogen bonding parameters, as well as a list of the final positional and equivalent isotropic thermal parameters of the non-H atoms for both compounds. Since H_2Bupip is centrosymmetric, its supplementary material is based on one half the molecule. Tables 2 and 3 are arranged to compare the analogous bonds in the two compounds. Perspective views, as well as the numbering system, for H_2Bupip and [Ni(Bu3MPh)] are shown in Figs 1 and 2, respectively, and the packing of the molecules in Figs 3 and 4.

The two thiosemicarbazone moieties of H_2Bupip are located on opposite sides of the four carbon butyl backbone which minimizes their intramolecular interactions. Therefore, no intramolecular hydrogen bonding interactions are available for N(2)H (or N(3)H of H_2Bu3M). The two thiosemicarbazone moieties of the centrosymmetric H_2Bupip are, of course, identical, and the values for only one are listed in Tables 2 and 3, respectively. The C(3)—N(3) bond distance of 1.329(4) Å is considerably shorter than 1.371(4) Å for N(2)—C(3) and the former bond is not much longer than the 1.288(3) Å found for azomethine C(2)—N(1), which is formally a double bond. All three of these C—N bonds are considerably shorter than the single N(3)—C(4) and N(3)—C(8) bonds of the piperidyl ring (i.e. *ca* 1.466 Å). Thus, all three of the C—N bonds of the thiosemicarbazone moiety have significant double bond character (C(2)—N(1) > C(3)—N(3) > C(3)—N(2)).

The bond angles about C(3) show the steric effect of the bulky piperidyl substituent. The S(1)—C(3)—N(3) angle with the piperidyl nitrogen is 124.5(4)° compared with 117.4(4)° for the thiosemicarbazone's S(1)—C(3)—N(2) angle. The thiosemicarbazone moiety, C(2)—N(1)—N(2)—C(3)—N(3)—S(1) has a mean plane deviation of 0.122 Å with N(2) showing the greatest displacement of 0.337(3) Å. The dihedral angle between C(1)—C(2)—N(1)—N(2) and the remainder of the thiosemicarbazone moiety, N(2)—C(3)—N(3)—S(1) is 34.4(1)° due to a twisting of the moiety. The torsion angle of N(1)—N(2)—C(3)—S(1) is 146.1(5)° and is due primarily to the repulsion of S(1) and the piperidyl substituent, as well as weak intermolecular hydrogen bonding between N(2)H and a neighboring molecule's S(1) (Fig. 3).

The two thiosemicarbazone moieties of [Ni(Bu3MPh)] possess some significantly different bond lengths and angles so that values for both are included in Tables 2 and 3. Upon complexation the azomethine bond, C(2)—N(1), although coordinated to Ni^{II} *via* this nitrogen, is only slightly longer in [Ni(Bu3MPh)] than in H_2Bupip. In contrast, on change from a thione to a thiolato function and coordination by the sulfur atom, the S(1)—C(3) and S(2)—C(13) bonds are lengthened by *ca* 0.7 Å. Also, the N(2)—C(3) and

Table 1. Crystallographic data for H_2Bupip and [Ni(Bu3MPh)]

Empirical formula	$C_{16}H_{28}N_6S_2$	$C_{20}H_{22}N_6S_2Ni$
Color; habit	Yellow; laminar	Black, rectangular
Crystal size (mm)	0.40 × 0.36 × 0.04	0.64 × 0.35 × 0.26
Crystal system	Monoclinic	Monoclinic
Space group	$P2_1/c$	$P2_1/n$
Unit-cell dimensions		
a (Å)	10.709(2)	8.07050(10)
b (Å)	9.381(2)	15.6440(10)
c (Å)	10.459(2)	15.829(2)
β (°)	109.55(3)	98.360(0)
Volume (Å^3)	990.1(5)	2134.1(3)
Z	2	4
Formula weight	368.6	469.3
Density (calc.) (Mg m^{-3})	1.236	1.461
Absorption coefficient (mm^{-1})	2.512	1.124
F(000)	396	976
Radiation	Cu-K_α (λ = 1.54178 Å)	Mo-K_α (λ = 0.71073 Å)
Temperature (K)	298	298
Filter	Nickel	Highly oriented graphite crystal
2θ range (°)	3.0–50.0	2.0–60.0
Scan type	$2\theta:\theta$	2θ–ω
Scan and speed (° min^{-1})	Variable; 4.00–29.30 in θ	Variable; 4.00–60.00 in ω
Scan range (°)	2.00 (2θ) $-10 < h < 10$	0.56 (ω) $-1 < h < 12$
Index ranges	$0 < k < 0$ $0 < l < 10$	$1 < k < 22$ $-22 < l < 22$
Absorption correction	Semi-empirical	Semi-empirical
Min./Max. transmission	0.6539/0.9647	0.7875/0.9914
Final R Indices (obs. data) (%)	R = 5.57, wR = 7.86	R = 3.16, wR = 3.78
R Indices (all data) (%)	R = 5.94, wR = 8.02	R = 6.43, wR = 10.11
Goodness-of-fit	1.74	1.02
Largest and mean D/s:	0.000, 0.000	0.746, 0.032
Data-to-parameter ratio	7.7:1	10.0:1

N(5)—C(13) bonds, which formally become double bonds on coordination, are shortened by *ca* 0.5 Å. Other bonds of the thiosemicarbazone moiety, as well as the carbon–carbon bond, C(2)—C(12), between the two azomethine groups, undergo smaller changes on coordination. As expected, the Ni—S bonds are longer than the Ni—N bonds by *ca* 0.3 Å. A crystal of [Ni(Buhexim)] has a similar structure, but we were unable to solve it with sufficient accuracy to comment further.

The bond angles about the nickel(II) center are indicative of the sizes of the donor atoms. The S(1)—Ni(1)—S(2) angle is 102.12(5)°, the S(1)—Ni(1)—N(1) and S(2)—Ni(1)—N(4) angles are 87.3(1) and 87.2(1)°, respectively, and the N(1)—Ni(1)—N(4) angle is 83.3(2)°. The mean plane

Table 2. Bond distances (Å) for H_2Bupip and [Ni(Bu3MPh)]

H_2Bupip		[Ni(Bu(4)MPh)]	
		Ni(1)—S(1), Ni(1)—S(2)	2.157(1), 2.154(1)
		Ni(1)—N(1), Ni(1)—N(4)	1.854(2), 1.847(2)
S(1)—C(3)	1.681(4)	S(1)—C(3), S(2)—C(13)	1.759(3), 1.763(2)
C(1)—C(2)	1.487(4)	C(2)—C(1), C(12)—C(11)	1.490(4), 1.495(4)
C(2)—N(1)	1.288(3)	C(2)—N(1), C(12)—N(4)	1.300(3), 1.295(3)
C(2)—C(2A)	1.471(5)	C(12)—C(11)	1.495(4)
N(1)—N(2)	1.390(4)	N(1)—N(2), N(4)—N(5)	1.374(3), 1.380(3)
N(2)—C(3)	1.371(4)	N(2)—C(3), N(5)—C(13)	1.317(3), 1.320(3)
C(3)—N(3)	1.330(4)	C(3)—N(3), C(13)—N(6)	1.342(4), 1.358(4)
N(3)—C(4)	1.468(4)	N(3)—C(4), N(6)—C(14)	1.471(6), 1.475(4)
N(3)—C(8)	1.464(5)	N(3)—C(5), N(6)—C(15)	1.429(4), 1.427(4)

Table 3. Bond angles (°) for H_2Bupip and [Ni(Bu3MPh)]

H_2Bupip		[Ni(Bu3MPh)]	
		S(1)—Ni(1)—S(2) etc	102.1(1)
		S(1)—Ni(1)—N(1), S(2)—Ni(1)—N(4) etc	87.3(1), 87.2(1)
		N(1)—Ni(1)—N(4)	83.3(1)
		S(1)—Ni(1)—N(4), S(2)—Ni(1)—N(1)	170.6(1), 170.4(1)
		Ni(1)—S(1)—C(3), Ni(1)—S(2)—C(13)	94.3(1), 94.8(1)
		Ni(1)—N(1)—C(2), Ni(1)—N(4)—C(12)	115.5(2), 115.9(2)
		Ni(1)—N(1)—N(2), Ni(1)—N(4)—N(5)	124.2(1), 124.5(2)
C(1)—C(2)—N(1)	125.0(5)	C(1)—C(2)—N(1), C(11)—C(12)—N(4)	124.2(3), 123.8(3)
C(1)—C(2)—C(2A)	120.4(5)	C(1)—C(2)—C(12), C(11)—C(12)—C(2)	123.4(2), 123.6(2)
N(1)—C(2)—C(2A)	114.6(5)	N(1)—C(2)—C(12), N(4)—C(12)—C(2)	112.5(2), 112.6(2)
C(2)—N(1)—N(2)	117.4(4)	C(2)—N(1)—N(2), C(12)—N(4)—N(5)	120.3(2), 119.7(2)
N(1)—N(2)—C(3)	118.7(4)	N(1)—N(2)—C(3), N(4)—N(5)—C(13)	110.1(2), 110.1(2)
S(1)—C(3)—N(2)	117.4(4)	S(1)—C(3)—N(2), S(2)—C(13)—N(5)	124.0(2), 123.3(2)
S(1)—C(3)—N(3)	124.5(4)	S(1)—C(2)—N(3), S(2)—C(13)—N(6)	119.2(2), 120.4(2)
N(2)—C(3)—N(3)	118.0(5)	N(2)—C(3)—N(3), N(5)—C(13)—N(6)	116.8(3), 116.3(2)
C(3)—N(3)—C(4)	121.6(5)	C(3)—N(3)—C(4), C(13)—N(6)—C(14)	119.5(3), 117.7(2)
C(3)—N(3)—C(8)	125.0(5)	C(3)—N(3)—C(5), C(13)—N(6)—C(15)	123.8(3), 124.1(2)
C(4)—N(3)—C(8)	111.5(5)	C(4)—N(3)—C(5), C(14)—N(6)—C(15)	116.5(3), 118.2(3)

deviation of the nickel coordination center, Ni(1)—S(1)—S(2)—N(1)—N(4) is 0.016 Å with N(1) having the greatest displacement of 0.042(2) Å. The three five-membered chelate rings also deviate from planarity as follows: Ni(1)—N(1)—C(2)—C(12)—N(4), Ni(1)—N(1)—N(2)—C(3)—S(1) and Ni(1)—N(4)—N(5)—C(13)—S(2) have mean plane deviations of 0.019, 0.022 and 0.015 Å, respectively. In the first plane, Ni(1)—N(1)—C(2)—C(12)—N(4), the Ni atom is essentially in the plane, the two nitrogens slightly below the plane [0.028(2) Å] and the two carbons slightly above the plane [0.023(3) Å]. The angles between the coordinate plane, Ni(1)—N(1)—S(1)—S(2)—N(4), and the two phenyl rings, C(5)—C(6)—C(7)—C(8)—C(9)—C(10) and C(15)—C(16)—C(17)—C(18)—C(19)—C(20), are 80.1(1) and 50.1(1)°, respectively. Compared with the uncomplexed thiosemicarbazone moiety of H_2Bupip, which has a mean plane deviation of 0.122 Å, the coordinated thiosemicarbazone moieties,

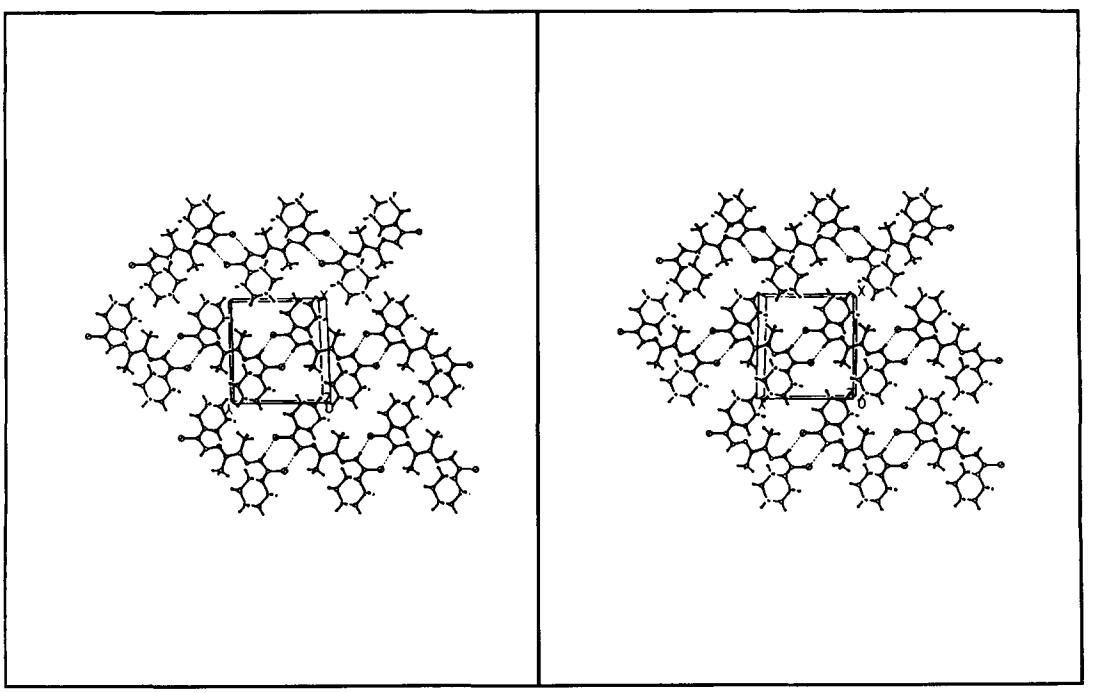


Fig. 3. Packing arrangement for H_2Bupip.

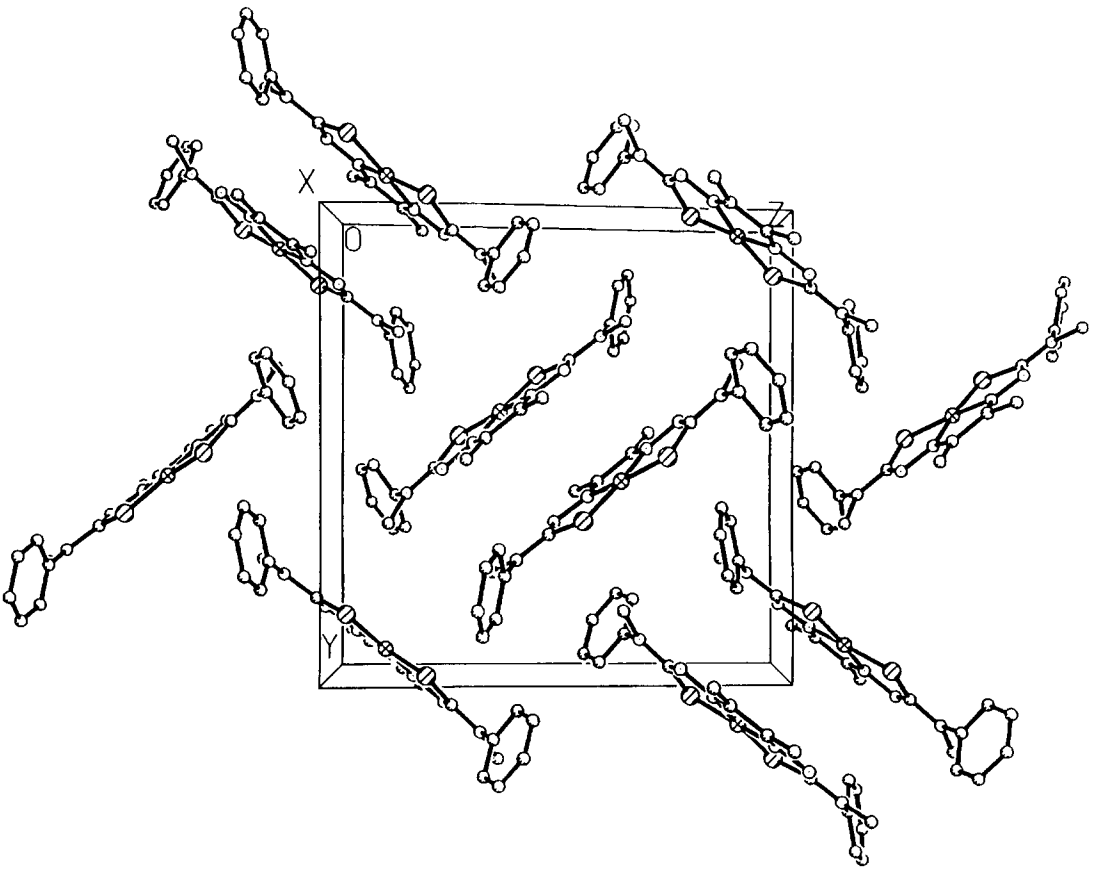


Fig. 4. Packing arrangement for [Ni(Bu3MPh)].

C(2)—N(1)—N(2)—C(3)—S(1)—N(3) and C(12)—N(4)—N(5)—C(13)—S(2)—N(6), are considerably more planar having mean deviations of 0.017 and 0.009 Å, respectively.

In Table 4 selected bond distances and angles are compiled for 2-keto-3-ethoxybutyraldehyde bis(thiosemicarbazone), H_2KTS,[12] a heterocyclic N(3)-substituted thiosemicarbazone [13] and some metal complexes [5,14,15] to compare with the values reported here for H_2Bupip and [Ni(Bu3MPh)]. Comparing the bond distances of H_2KTS to those of H_2Bupip shows that N(1)—N(2), N(2)—C(3) and C(3)—N(3) are shorter for H_2KTS, but the bond angles are similar. In contrast, the bonds in [Ni(BuBzTHZ)], where BuBzTHZ is the dianion of 2,3-butanedione bis(benzylthiohydrazone) are more similar to those of [Ni(Bu3MPh)]. For example, the C(2)—N(1) bond distances are nearly the same and the small changes in the other bond distances in Table 4 for the two complexes probably represent the differences in the two ligands. The structure of HAchexim, 2-acetylpyridine 3-hexamethyleneiminyl-thiosemicarbazone, is the bifurcated form where the hydrogen shifts to the azomethine nitrogen and hydrogen bonds to the pyridyl N and thiol S. A result of this bifurcated hydrogen bonding is that the thiosemicarbazone moiety is conjugated resulting in a bright yellow solid. Even with this drastic change, the bond lengths within the thiosemicarbazone moiety for H_2Bupip and HAchexim are nearly the same. However, the bond angles in the azomethine part of the moiety, which is involved in hydrogen bonding, are considerably different. For example, C(2)—N(1)—N(2) is *ca* 117.4° for H_2Bupip, but 125° for HAchexim and N(1)—N(2)—C(3) is *ca* 119° for H_2Bupip, but 110.8° for HAchexim.

A comparison of the bond distances and angles of the thiosemicarbazone moieties of [Ni(Bu3MPh)] with those of [Cu(KTS)] [6] shows no major differences even though bonding to nickel(II) by thiosemicarbazone moieties is considerably stronger than for copper(II).[15] The M—N bond distances are *ca* 1.850(2) and 1.970(5) Å for [Ni(Bu3MPh)] and [Cu(KTS)], respectively; the M—S bond distances of *ca* 2.155(1) and 2.265(1) Å also show stronger bonding to the nickel(II) center. However, the nickel(II) complex of 2,3-butanedione bis(benzylthiohydrazone),[14] [Ni(BuBzTHZ)], has almost identical Ni—N and Ni—S bond distances of *ca* 1.853(2) and 2.151(1) Å, respectively. Unfortunately, the bond angles for this complex were not reported. [Ni(Pe3DH)]NCS, where Pe3DH is the anion [loss of C(3)*H*] of 2,4-pentanedione bis(thiosemicarbazone), would be expected to be considerably different from the other

Table 4. Comparison of thiosemicarbazone moiety bond distances and angles for H_2Bupip, H_2KTS and some heterocyclic thiosemicarbazones (the estimated standard deviations for these structures are comparable to those shown in Table 2)

Compound	C(2)—N(1)	N(1)—N(2)	N(2)—C(3)	C(3)—S(1)	C(3)—N(3)
Bond distances (Å)					
H_2Bupip	1.288	1.390	1.371	1.682	1.329
H_2KTS[a]	1.292[b] 1.284[c]	1.368[b] 1.375[c]	1.356[b] 1.351[c]	1.684[b] 1.690[c]	1.308[b] 1.312[c]
HAchexim[d]	1.29	1.37	1.36	1.70	1.36
[Ni(Bu3MPh)]	1.300 1.295	1.374 1.380	1.317 1.320	1.759 1.763	1.342 1.358
[Nl(BuBzTHZ)][e]	1.305 1.298	1.386 1.400	1.289 1.301	1.743 1.750	
[Cu(KTS)][f]	1.281	1.357	1.321	1.746	1.341
[Ni(HPe3DH)]NCS[g]	1.333 1.338	1.408 1.393	1.309 1.315	1.687 1.693	1.354 1.344
Bond angles (°)	C(2)—N(1)—N(2)	N(1)—N(2)—C(3)	N(2)—C(3)—S(1)	N(2)—C(3)—N(3)	S(1)—C(3)—N(3)
H_2Bupip	117.4	118.7	117.4	118.0	124.5
H_2KTS[a]	117.4[b] 115.7[c]	119.5[b] 119.4[c]	118.0[b] 118.2[c]	117.8[b] 118.1[c]	124.3[b] 123.8[c]
HAchexim[d]	125	110.8	124.7	112	123.4
[Ni(Bu3MPh)]	120.3	110.1	124.0	116.8	119.2
[Cu(KTS)][f]	120.8	110.9	126.1	116.1	117.8
[Ni(HPe3DH)]NCS[g]	115.0 116.6	117.9 119.9	119.6 118.1	119.1 120.7	121.4 121.2

[a]2-Keto-3-ethoxybutyraldehyde-bis(thiosemicarbazone).[12]
[b]Ketone thiosemicarbazone.
[c]Aldehyde thiosemicarbazone.
[d]2-Acetylpyridine 3-hexamethyleneiminylthiosemicarbazone.[13]
[e]Nickel(II) complex of 2,3-butanedione bis(benzylthiohydrazone).[14]
[f]Copper(II) complex of 3-ethoxy-2-oxobutyraldehyde bis(thiosemicarbazone).[6]
[g]Nickel complex of 2,4-pentanedione bis(thiosemicarbazone).[5]

metal complexes since its thiosemicarbazone moieties do not lose the N(2)*H*s on complexation.[5] Information in Table 4 confirms that the bonds of [Ni(Pe 3DH)]NCS are considerably different from those of [Ni(Bu(4)MPh)], [Ni(BuBzTHZ)] and [Cu(KTS)].

The ^{1}H NMR spectral assignments for the CH_3 functions of the butyl backbone, as well as N(2)*H* and N(3)*H* are listed in Table 5 for the series of 2,3-butanedione N(3)-substituted bis(thiosemicarbazones) along with their diamagnetic nickel(II) complexes. The CH_3 assignments are essentially the same for the various bis(thiosemicarbazones); differences are expected for the spectrum of H_2Bu3M, which was recorded in DMSO-d_6 due to its low solubility in $CDCl_3$. Also, the thiosemicarbazone moiety's N(2)*H* chemical shift is essentially the same (i.e. δ = 8.348–8.422) for the various bis(thiosemicarbazones). These chemical shifts indicate an absence of hydrogen bonding, consistent with the two thiosemicarbazone moieties being on opposite sides of the butyl backbone. N(3)*H* is assigned at δ = 10.200 in the spectrum of H_2Bu3M, indicating hydrogen bonding with DMSO-d_6.

Upon complexation the bis(thiosemicarbazones) are deprotonated and the N(2)*H* signals are absent in the ^{1}H NMR spectra of the nickel(II) complexes. In the spectrum of [Ni(Bu3M)] the N(3)*H* appears at δ = 7.670, indicating hydrogen bonding to the DMSO

Table 5. ^{1}H and ^{13}C NMR spectra of the 2,3-butanedione bis(N(3)-substituted thiosemicarbazones) and their nickel(II) complexes

Compound	N(2)*H*	N(3)*H*	CH_3	*C*H$_3$	*C*=N	*C*=S
H_2Bu3M[a]	8.374	10.200	2.219	11.59	147.90	178.47
H_2Bu3DM[b,c]	8.422	—	2.060			
H_2Bupip[b]	8.336	—	2.043	9.97	146.57	181.86
H_2Buhexim[b]	8.417	—	2.071	10.04	146.80	181.38
[Ni(Bu3M)][a]	—	7.670	1.924	13.73	155.74	176.31
[Ni(Bu3DM)][a]	—	—	1.894		155.53	171.79
[Ni(Buhexim)][a]	—	—	1.872	13.55	154.81	177.51

[a]Recorded in DMSO-d_6.
[b]Recorded in $CDCl_3$.
[c]Not sufficiently soluble to acquire a ^{13}C spectrum.

Table 6. Colors, magnetic susceptibilities and partial elemental analyses of copper(II) and nickel(II) complexes of 2,3-butanedione bis(N(3)-substituted thiosemicarbazones)

Compound	Color	C	H	μ (B.M.)
[Cu(Bu3M)]	Brown	29.5(29.9)	4.3(4.4)	2.4
[Cu(Bu3DM)]	Red–brown	34.4(34.3)	5.3(5.2)	1.6
[Cu(Bupip)]	Red–brown	44.4(44.7)	6.1(6.1)	1.8
[Cu(Buhexim)]	Red–brown	47.1(47.2)	6.6(6.6)	2.0
[Ni(Bu3M)]	Dark green	30.0(30.3)	4.5(4.5)	0.0
[Ni(Bu3DM)]	Brown	34.7(34.8)	5.3(5.3)	0.0
[Ni(Buhexim)]	Dark green	47.7(48.3)	6.7(6.7)	0.0

solvent molecules does not occur in the complex. The thiosemicarbazone moiety arms of a free ligand are on opposite sides of the butyl backbone and, therefore, the N(3)H functions are in a more open environment in H_2Bu3M than in [Ni(Bu3M)]. This steric crowding, as well as electronic effects, may account for the lack of hydrogen bonding by DMSO in the ^{1}H NMR spectrum of [Ni(Bu3M)]. In the nickel(II) complex's spectra the butyl backbone CH_3 peaks are shifted upfield (δ = 1.872–1.918) compared with the uncomplexed thiosemicarbazones due to shielding of the protons *via* π-back-bonding by the metal center into the azomethine π system. Also shown in Table 5 are the ^{13}C resonances showing significant shifts on complexation. *C*=S shifts upfield by 2–4 ppm consistent with the increase in bond distance resulting in a less polar carbon. The C=N bond distance is essentially unchanged on coordination, but *C*=N shifts downfield by 7–9 ppm in the complexes suggesting considerable back donation into the π-electron system by the nickel(II) center.

The colors, partial elemental analyses and magnetic susceptibilities for the isolated metal complexes are shown in Table 6. Most of the complexes are various shades of brown and two of the nickel(II) complexes are dark green. The nickel complexes are diamagnetic indicative of square-planar N_2S_2 tetradentate coordination. The copper(II) complexes are paramagnetic and have magnetic moments close to the theoretical spin only value (1.73 B.M.). Thus, a square-planar N_2S_2 ligation about the copper(II) ion is probable.

The IR spectral assignments most useful for determining the ligand's mode of coordination are listed in Table 7. The shift of ν(C=N) spectral bands of the bis(thiosemicarbazones) from 1550–1578 to 1540–1568 cm^{-1} for the metal complexes indicates the coordination of the azomethine nitrogen. The formation of the complexes and simultaneous loss of the protons from the thiosemicarbazone moieties produces a second carbon–nitrogen double bond, which often complicates this portion of the spectrum. Also, the bands having considerable ν(C=S) character shift from the range 822–843 cm^{-1} in the bis(thiosemicarbazones) to the lower energy range 750–778 cm^{-1} for the metal complexes indicating coordination of the thiolato sulfur atoms. Bands in the 343–375 cm^{-1} region have been assigned to ν(MS) and bands in the 428–465 cm^{-1} region to the ν(MN) supporting the coordination of the ligands as tetradentate N_2S_2 chelating agents [16].

Listed in Table 8 are the band maxima of the solid state and solution (DMF) electronic transitions for the four thiosemicarbazones and their copper(II) and nickel(II) complexes. Omitted from Table 7 are the higher energy $\pi \rightarrow \pi^*$ transitions (*ca* 42,000 cm^{-1}), which are not significantly altered on complex formation. The $n \rightarrow \pi^*$ transitions associated with the azomethine and thioamide functions are found at *ca* 29,000–33,000 and 24,000–29,000 cm^{-1}, respectively, in the solid-state spectra. In solution three bands are observed; the higher energy $n \rightarrow \pi^*$ band appears to have been resolved into two peaks for many of the compounds.

The spectra of the complexes of both metal ions generally show the higher energy band unshifted and a second band at about 29,000 cm^{-1}. This latter band has been assigned by others to a S(σ) $\rightarrow$ Cu^{II} charge transfer band [14]. The spectra of the heavier nickel(II) complexes have a band at a similar energy which we assign to S(σ) $\rightarrow$ Ni(II). The lower energy $n \rightarrow \pi^*$ band in the thiosemicarbazone spectrum is apparently shifted to higher energy in the spectra of the metal complexes and it also contributes to the band in the 29,000 cm^{-1} region. Additional bands in the 20,000–21,000 cm^{-1} region of the spectra of the copper(II) complexes and 22,000–24,000 cm^{-1} for the nickel(II) complexes are due to S(π) $\rightarrow$ M^{II} charge transfer bands [17,18]. Solid-state spectra of the copper(II) complexes, except for [Cu(Bu3M)], have $d \rightarrow d$ bands at *ca* 18,000 and 14,000 cm^{-1}, $^2B_{1g} \rightarrow {}^2E_g$ and $^2B_{1g} \rightarrow {}^2B_{2g}$, respectively, which is consistent with a planar stereochemistry. In DMF solution the number of $d \rightarrow d$ bands is reduced to one and the single band is shifted to higher energy, suggesting weak interaction with the solvent. This shift also shows that solid-state interactions are important for the copper(II) complexes.

As shown by crystal structure determinations of related copper complexes,[6,7] sulfur atoms from adjacent coordination spheres weakly interact in the axial positions of the copper(II) center of each CuN_2S_2 chromophore. The spectra of the nickel(II) complexes do not have bands below 10,000 cm^{-1}, consistent with

Table 7. IR spectra (cm^{-1}) of 2,3-butanedione bis(N(3)-substituted thiosemicarbazones) and their copper(II) and nickel(II) complexes.

Compound	ν(N3—H)	ν(N(2)—H)	ν(C=N)	ν(C=S)	ν(MN)	ν(MS)
H_2Bu3M	3338m	3224m	1550m	809w	—	—
H_2Bu3DM	—	3310m	1575m	795w	—	—
H_2Bupip	—	3190m	1575m	792w	—	—
H_2Buhexim	—	?	1578m	800w	—	—
[Cu(Bu3M)]	3315s	—	1540m	769w	448m	349m
[Cu(Bu3DM)]	—	—	1535sh	770m	421m	342w
[Cu(Bupip)]	—	—	1568m	730sh	445w	368w
[Cu(Buhexim)]	—	—	1522w	750w	421sh	315m
[Ni(Bu3M)]	3332s	—	1564m	769m	441w	339m
[Ni(Bu3DM)]	—	—	1538m	778m	442m	360w
[Ni(Buhexim)]	—	—	1522m	770m	435sh	352w

Table 8. Solid-state and solution (DMF) electronic spectra (cm^{-1}) of 2,3-butanedione bis(N(3)-substituted thiosemicarbazones) and their copper(II) and nickel(II) complexes

Compound	Intraligand and charge transfer	*d–d*		
H_2Bu3M	29,240			
DMF	29,850 28,990 23,810			
H_2Bu3DM	32,260 24,270			
DMF	30,760 24,390 21,280			
H_2Bupip	28,990 26,880			
DMF	32,790 30,120 24,690			
H_2Buhexim	28,570 24,390 20,920			
DMF	31,250 28,170 20,830			
[Cu(Bu3M)]	31,750 28,170 21,280	19,610		
DMF	32,050 29,410 21,050	20,000		
[Cu(Bu3DM)]	30,120 27,470 21,100	18,450	14,660	
DMF	31,250 22,220 20,410	19,050		
[Cu(Bupip)]	30,120 26,880 20,330	18,180	14,180	
DMF	31,250 28,740 20,620	19,310		
[Cu(Buhexim)]	31,250 27,400 20,410	18,350	14,430	
DMF	31,750 29,240 20,620	19,420		
[Ni(Bu3M)]	31,750 25,000 22,220	17,090	15,630	14,330
DMF	31,056 25,000 24,100		15,380	
[Ni(Bu3DM)]	31,750 24,390 21,510	17,240	14,710	
DMF	31,060 29,240 24,390 23,150		14,710	
[Ni(Buhexim)]	29,850 23,810 22,470	17,090	14,930	13,990
DMF	30,300 28,570 24,100 22,730		14,710	

their planar coordination. Like the copper(II) complexes there are two bands in the solid-state spectra assignable to $d \rightarrow d$ transitions. However, the single band occurring in their solution spectra is at considerably lower energy than found for the copper(II) complexes, indicating that interaction with the solvent is considerably stronger for the nickel(II) complexes. That is, the solid-state interaction between neighboring complexes in the nickel(II) compounds must be less than for the copper(II) complexes, but interaction with the DMF solvent molecules appears to be greater for the nickel(II) complexes.

Table 9 contains the solid-state and solution (DMF) EPR parameters for the copper(II) complexes. As would be expected, the values for $g_\perp$ (or $g_\parallel$) are rather low, indicating considerable covalency, a consequence of two sulfur donor atoms in the coordination spheres. Of the complexes studied [Cu(Bu3M)] has the highest value for $g_\perp$, 2.113, while the other three complexes have $g_\perp$ below 2.100 at room temperature. This suggests that the bonding to sulfur is weaker for [Cu(Bu3M)], when there is a N(3)H present, than when hydrocarbon substituents are attached to the thioamide nitrogen, N(3). On cooling to 77 K all values for $g_\perp$ increase, suggesting greater interaction with the sulfur donor atoms of adjacent copper(II) centers at the lower temperature. A small increase in $g_\perp$ ($g_\parallel$) also occurs in the frozen solution

Table 9. EPR spectra the copper(II) complexes of 2,3-butanedione bis(N(3)-substituted thiosemicarbazones)

Compound	Phase	Temperature[a]	$g_{\parallel}$ or g_1	g_2	$g_{\perp}$ or g_3	g_{av} or g_0	$A_{\parallel}$(G)	A_0(G)
[Cu(Bu3M)]	Solid	RT	2.113	2.029	2.026	2.056		
		77 K	2.121	2.032	2.030	2.061		
	DMF	RT				2.064		98
		77 K	2.130		2.026	2.061	184	
[Cu(Bu3DM)]	Solid	RT	2.085	2.033	2.024	2.047		
		77 K	2.107	2.035	2.026	2.056		
	DMF	RT				2.056		89
		77 K	2.114		2.030	2.058	190	
[Cu(Bupip)]	Solid	RT	2.084	2.041	2.027	2.051		
		77 K	2.096	2.042	2.028	2.055		
	DMF	RT				2.056		89
		77 K	2.126		2.034	2.064	194	
[Cu(Buhexim)]	Solid	RT	2.099	2.034	2.024	2.052		
		77 K	2.104	2.034	2.026	2.055		
	DMF	RT				2.058		89
		77 K	2.102		2.022	2.049	195	

[a]RT = room temperature.

spectra, suggesting a weak interaction with solvent molecules, although the increase of 0.01 is considerably less than 0.03–0.04 observed for Cu(NNS)Cl centers [18]. Also, the values of g_0 for the room-temperature solution spectra are not much higher than the room-temperature solid state g_{av}. This is in agreement with the electronic spectra of the copper(II) complexes, which indicated that although there was some interaction with solvent molecules, it is not substantial. The large values for both A_0 and A are consistent with the strong planar bonding that exists in these complexes. A 1% [Cu(Bupip)]/[Ni(Bupip)] solid produces a spectrum with the copper hyperfine lines, and the highest field parallel feature is nicely resolved to show the nitrogen superhyperfine lines ($A_N = 18$ G) in a 1:2:3:2:1 ratio consistent with the coordination of two equivalent nitrogen donor atoms. The perpendicular feature is also resolved, but falls right on the third parallel feature making interpretation difficult.

The covalency parameter, α^2, in frozen DMF equals 0.635, 0.633, 0.659 and 0.629 for [Cu(Bu3M)], [Cu(Bu3DM)], [Cu(Bupip)] and [Cu(Buhexim), respectively, indicating considerable covalency in their bonding. This value is at the lower end of the range 0.63–0.84 proposed [19] for CuN_4, as would be expected with sulfur in place of two nitrogens in the coordination sphere. The Racah parameters, $k_{\parallel}$ and $k_{\perp}$, have values of 0.43, 0.55; 0.42, 0.59 and 0.46, 0.55 for [Cu(Bu3DM)], [Cu(Bupip)] and [Cu(Buhexim)], respectively. These values also show that there is considerable covalent nature [20] in the metal–ligand bonding of these complexes and that in-plane π-bonding is more important than out-of-plane π-bonding.

Each compound of this study was subjected to antifungal testing against *Paecillomyces variotii* at 1000 μg cm^{-3} concentrations with the following results: H_2Bu3M showed no activity, H_2Bu3DM yielded a small inhibition zone of 8.0 mm (6.0 mm = no activity), H_2Bupip gave a large inhibition zone of 32.6 mm and H_2Buhexim, a zone of 21.8 mm. H_2Bupip was active at 100 μg cm^{-3} (zone of inhibition = 25.9). None of the nickel(II) complexes showed any activity, and [Cu(Bupip)] and [Cu(Buhexim)] were inactive. [Cu(Bu3M)] and [Cu(Bu3DM)] showed small zones of 9.1 and 10.1 mm, respectively. Like other thiosemicarbazones tested for antifungal activity, the substituent attached at N(3) plays a significant role in the compounds activity [21]. Also, the copper(II) complexes, which are often more active than the uncomplexed thiosemicarbazone [22,23], are less active in this series of compounds.

Acknowledgments—Acknowledgment is made to the Donors of the Petroleum Research Fund, administered by the American Chemical Society, and the Camille and Henry Dreyfus Foundation for the partial support of this research. J. V.-M. thanks Universidad Nacional Autonoma de México PAPIIT Program (IN1038393) and Consejo Nacional de Ciencia y Tecnologia (3920-E). We thank one of the referees for calling our attention to an important reference.

REFERENCES

1. D. X. West, S. B. Padhye, and P. B. Sonawane, *Structure and Bonding*, 1991, **76,** 1.
2. D. X. West, A. E. Liberta, S. B. Padhye, R. C. Chikate, P. B. Sonawane, A. S. Kumbhar, and R. G. Yerande, *Coord. Chem. Rev.*, 1993, **123,** 49.
3. D. X. West, S. B. Padhye, P. B. Sonawane, and R. C. Chikate, *Asian J. Chem. Rev.*, 1990, **1,** 125.
4. K. Dey and D. Bandyopadhyay, *Trans Met. Chem.*, 1991, **16,** 267.
5. V. M. Leovac, V. I. Cesljevic, G. Argay, A. Kál-

mán, and B. Ribár, *J. Coord. Chem.*, 1995, **34,** 357.
6. M. R. Taylor, J. P. Glusker, E. J. Gabe, and J. Minkin, *Bioinorg. Chem.*, 1974, **3,** 189.
7. E. John, P. E. Fanwick, A. T. McKenzie, J. G. Stowell, and M. A. Green, *Nucl. Med. Biol.*, 1989, **16,** 791.
8. H. G. Petering, H. H. Buskirk, and G. E. Underwood, *Cancer Res.*, 1964, **24,** 367.
9. G. J. Van Giessen, J. A. Crim, D. H. Petering, and H. G. Petering, *J. Natl. Cancer Inst.*, 1973, **51,** 139.
10. J. P. Scovill, *Phosphorus, Sulfur and Silicon*, 1991, **60,** 15.
11. Siemens, SHELEXTL-PC™, Release 4.1. Siemens Crystallographic Research Systems, Siemens Analytical X-Ray Instruments, 1990.
12. E. J. Gabe, M. R. Taylor, J. P. Glusker, J. A. Minkins, and A. L. Patterson, *Acta Cryst.* 1969, **B25,** 1620.
13. D. X. West, G. A. Bain, R. J. Butcher, J. P. Jasinski, Y. Li, R. Y. Pozdniakiv, J. Valdés-Martínez, R. A. Toscano, and S. Hernández-Ortega, *Polyhedron*, 1996, **15,** 665.
14. F. Hansen and S. Larsen, *Acta Chem. Scand.*, 1977, **A31,** 825.
15. D. X. West, H. Gebremedhin, R. J. Butcher, J. P. Jasinski, and A. E. Liberta, *Polyhedron*, 1993, **12,** 2489.
16. M. A. Ali, C. M. Haroon, M. Nazimuddin, S. M. M. Majumbder, M. T. H. Tarafder, and M. A. Khair, *Trans Met. Chem.*, 1992, **17,** 133.
17. J. M. Downes, J. Whelan, and B. Bosnich, *Inorg. Chem.*, 1981, **20,** 1081.
18. M. Mikurya, H. Okama, and S. Kida, *Bull. Chem. Soc. Japan*, 1980, **53,** 2871.
19. E. W. Ainscough, A. G. Binghan, A. M. Brodie, J. M. Husbands, and J. E. Plowman, *J. Chem. Soc., Dalton Trans.*, 1981, 1701.
20. B. J. Hathaway, *Structure and Bonding*, Vol. 4. Springer-Verlag, Berlin, 1973, p. 60.
21. A. E. Liberta, and D. X. West, *Biometals*, 1992, **5,** 121.
22. D. X. West, C. S. Carlson, C. P. Galloway, A. E. Liberta, and C. R. Daniel, *Trans Met. Chem.*, 1990, **15,** 91.
23. D. X. West, D. L. Huffman, J. S. Saleda, and A. E. Liberta, *Trans Met. Chem.*, 1991, **16,** 565.

Pergamon

PII: S0277-5387(96)00467-6

Polyhedron Vol. 16, No. 11, pp. 1907–1919, 1997
© 1997 Elsevier Science Ltd
All rights reserved. Printed in Great Britain
0277-5387/97 $17.00+0.00

Interaction of β-diketones with La^{III}, Eu^{III} and Y^{III} complexes of the six-nitrogen-donor macrocyclic ligand $C_{22}H_{26}N_6$ and crystal structure of $[Eu(CH_3COO)\{(C_6H_5CO)_2CH\}(C_{22}H_{26}N_6)](CH_3COO)\cdot 6(H_2O)$

F. Benetollo,[a] G. Bombieri,[b] K. K. Fonda[c] and L. M. Vallarino[c]*

[a]I.C.T.M.A., C.N.R., Corso Stati Uniti 4, Padova 35100, Italy; [b]Istituto di Chimica Farmaceutica, Universita' di Milano, Milano, Italy; [c]Department of Chemistry, Virginia Commonwealth University, Richmond VA 23284, U.S.A.

(*Received* 26 *February* 1996; *accepted* 15 *September* 1996)

Abstract—The interaction of several β-diketones [pentane-2,4-dione, 1,3-diphenylpropane-1,3-dione, 1,1,1-trifluoro-4(2-thienyl)butane-2,4-dione] and their sodium salts with complexes of the type $[ML(CH_3COO)_2]X\cdot n(H_2O)$, where M is La^{III}, Eu^{III} or Y^{III}, L is the macrocyclic ligand $C_{22}H_{26}N_6$, X is Cl^- or CH_3COO^- and n is 4–9, was investigated in solution by NMR and luminescence spectroscopy. A number of crystalline $\{ML\}$-(β-diketonate) complexes were isolated and characterized; the structure of one member of the series, $[EuL(CH_3COO)\{(C_6H_5CO)_2CH\}](CH_3COO)\cdot 6(H_2O)$, was established by X-ray crystallography. The structure is ionic; the 10-coordinate Eu^{III} is bonded to the six nitrogens of the macrocyclic ligand, two oxygens of a bidentate acetate and two oxygens of the chelating β-diketonate. The coordinated acetate and the β-diketonate are situated on opposite sides of the $\{EuL\}$ macrocycle; an uncoordinated acetate provides charge neutrality.
© 1997 Elsevier Science Ltd. All rights reserved.

Keywords: lanthanides; macrocycles; β-diketones; luminescence.

The structures and properties of the lanthanide(III) complexes of the formula $[ML(OAc)_2]X\cdot nH_2O$, where M is a trivalent lanthanide, AcO is acetate, L is the six-nitrogen-donor macrocyclic ligand $C_{22}H_{26}N_6$ (Fig. 1), X is chloride or acetate and n is 4–9, have been extensively investigated [1–10]. The Eu^{III} complex, which exhibits long-lived, UV-excited luminescence in aqueous solution at room temperature,[3] has attracted considerable attention as a prototype of a new class of luminescent markers for cytology and immunology [12,13]. It was also reported that the luminescence of the $[EuL(Ac)_2]^+$ macrocyclic entity can be considerably enhanced by substitution of the acetates with other counterion ligands [8]. These results suggested that a study of the interaction between β-diketonates and the $\{ML\}$ macrocycles could be especially interesting, since β-diketonates are

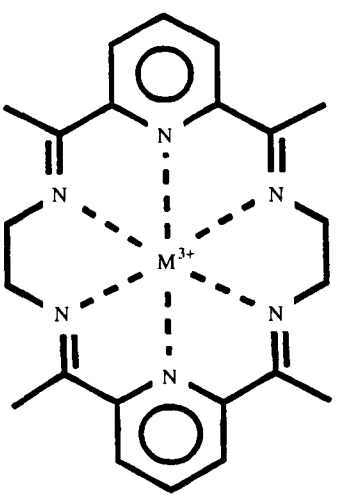


Fig. 1. Schematic formula of the $\{ML\} = \{M(C_2H_{26}N_6\}^+$ macrocyclic moiety.

*Author to whom correspondence should be addressed.

known to form very stable complexes with the lanthanide(III) ions [14(a–c)] and their Eu^{III} complexes are highly luminescent [15].

The lanthanides selected for this study were Eu^{III}, for its luminescence, and La^{III} because it is diamagnetic and allows reliable assignments of NMR spectra. The lanthanide-like Y^{III} was also investigated because its ionic radius and coordination properties closely resemble those of Eu^{III}. The β-diketones selected were 1,1,1-trifluoro-4(2-thienyl)butane-2,4-dione and 1,3-diphenylpropane-1,3-dione, the anions of which are known to form highly stable [14(b,d)] and luminescent [15] complexes with the free Eu^{III} ion; pentane-2,4-dione was also investigated because the structures [16] and stabilities [14(a–c)] of its complexes with lanthanide(III) ions are well established.

EXPERIMENTAL

Materials and procedures

Pentane-2,4-dione (acetylacetone, HACAC), 1,3-diphenylpropane-1,3-dione (dibenzoylmethane, HDBM) and 1,1,1-trifluoro-4(2-thienyl)butane-2,4-dione (thenoyltrifluoroacetone, HTTFA), from Aldrich Chemical Co., were distilled or recrystallized before use. Sodium pentane-2,4-dionate, NaACAC, and sodium 1,3-diphenylpropane-1,3-dionate, NaDBM, were prepared from the diketones and sodium metal (1 : 1 mol ratio) in anhydrous ethanol, followed by evaporation to dryness under reduced pressure and recrystallization from methanol/diethyl ether. The macrocyclic complexes $[ML(OAc)_2]Cl\cdot 4(H_2O)$ and $[ML(OAc)_2]Ac\cdot 9(H_2O)$ were prepared as previously described [1,8]. Deuterated and spectrograde solvents (Aldrich) were used as received. Microanalyses were performed by Atlantic Microlabs, Atlanta, GA (for C, H, N) and Galbraith Laboratories, Knoxville, TN (for S, Cl).

NMR spectra. Experiments were carried out with a GE QE-300 spectrometer at ambient temperature (24–26°C). Chemical shifts (as δ for ^1H spectra) are reported in ppm; coupling constants, J, are given in Hz; other abbreviations are specified in Table 1. Proton spectra were referenced to tetramethylsilane (TMS, 0.00) or to the residual proton signal of the solvent: $CHCl_3$, 7.26(1); CD_3OD, 3.30(5); deuterodimethylsulfoxide, DMSO-d_6, 2.49(5). ^{13}C spectra were referenced to the solvent signal: $CDCl_3$, 77.0(3); CD_3OD, 49.0(7); DMSO-d_6, 39.5(7). Assignments of ^{13}C spectra were confirmed by attached proton test (APT) and heteronuclear correlation (HETCOR) experiments. For the paramagnetic Eu^{III} complexes, both proton and ^{13}C chemical shifts varied slightly with sample concentration and moisture content; integrations were within ±10% of expected values.

IR spectra. Spectra were obtained on a Perkin–Elmer Model 1600 FT instrument (4000–500 cm^{-1}). Samples were examined as KBr pellets and as mulls in hexachlorobutadiene (4000–1800 and 1500–1300 cm^{-1}, on NaCl disks) and Nujol (1800–1500 and 1300–400 cm^{-1}, on KBr disks); no difference was observed between the two sets of spectra in KBr and those in mulls. Absorption frequencies are reported in cm^{-1}; abbreviations: s = strong, m = medium, w = weak, br = broad, v = very; an asterisk indicates an absorption only partly resolved from an adjacent stronger peak.

Absorption, emission and excitation spectra. UV–vis absorption spectra (230–600 nm) were recorded on a Shimadzu 265 UV–vis spectrophotometer. Excitation spectra (230–550 nm) and emission spectra (550–710 nm) of the {EuL}-(β-diketonate) complexes were recorded on a SLM 8000 spectrofluorimeter, using methanol solutions.

Syntheses of solid complexes

The complexes were prepared by the general procedures outlined below; all were obtained as hydrates. Different samples of the same complex, although identical in every other respect, occasionally contained different amounts of lattice water; in such cases, formulae and microanalyses (Table 2) are reported only for one hydrate. All solid complexes were stable to air and moisture at room temperature; they gradually lost water when heated between 35 and 110°C, but rapidly rehydrated upon cooling in a moist atmosphere. Complexes containing chloride and acetate counterions were very soluble in chloroform, methanol, ethanol and other polar organic solvents; they were insoluble in diethyl ether, hydrocarbons and water. Complexes containing perchlorate counterions were sparingly soluble in dimethylsulfoxide and dimethylformamide; they were insoluble in other common solvents and water. In the following, the abbreviations ACAC, DBM and TTFA indicate the mono-negative anions of the corresponding diketones.

(1) *Reaction of HDBM with* $[ML(OAc)_2]X\cdot n(H_2O)$, *where* M = La^{III}, Eu^{III} *or* Y^{III}, X = Cl *or* OAc *and* n = 4 or 9. The complex (2×10^{-4} mol) was dissolved in methanol (5 cm^3), solid HDBM was added and the mixture was warmed with stirring at *ca* 50°C until all HDBM had dissolved. The resulting pale yellow solution was cooled and diluted with diethyl ether until a slight persistent cloudiness formed. The mixture was gravity filtered, discarding the solid; the clear solution was further diluted with diethyl ether to a persistent milky cloudiness and stored in a freezer. A small amount of a pale yellow solid formed after several days; it was filtered off, washed with diethyl ether and dried at 60°C in air. Additional fractions of yellow crystals were similarly obtained by successive dilutions of the clear filtrate with diethyl ether, followed by prolonged cooling in a freezer. Each fraction was examined for homogeneity with a microscope and characterized by IR and ^1H NMR spectra. Various HDBM-to-{ML} mole ratios

Table 1. Proton NMR spectra of {ML}-(β-diketonate) complexes[a]

Complex (solvent)	Macrocycle CH_3	Macrocycle CH_2	Macrocycle py	Phenyl	β-Diketonate DBM CH		Acetate CH_3
$LaL(DBM)(OAc)_2 \cdot 2(H_2O)(CD_3OD)$	2.59 s	4.08 s	8.20[b]	7.24–7.43 m	6.49 s		1.79 s
$LaL(DBM)(OAc)_2 \cdot 2(H_2O)(CDCl_3)$	2.63 s	4.12 s	8.16 β-H[c] 8.31 γ-H[c] $J = 7.7$	8.00–7.52 m	6.89 s		1.68 s
$YL(DBM)(OAc)Cl \cdot 5.5(H_2O)(CD_3OD)$	2.55 s	3.99 m	8.18–8.22 m	7.23–7.44 m	6.66 s		1.54 s
$YL(DBM)(OAc)Cl \cdot 5.5(H_2O)(CDCl_3)$	2.51 s	[d]	7.98 β-H[c] 8.13 γ-H[c] $J = 7.7$	7.23–7.40 m	6.66 s		1.54 s
$EuL(DBM)(OAc)Cl \cdot 5.5(H_2O)(CD_3OD)$	6.16 s	3.42, 4.17	4.96 β-H d 7.53 γ-H t $J = 7.9$	6.71–6.71 m	[e]		[e]
$EuL(DBM)_2(ClO_4) \cdot H_2O(CD_3OD)$	7.69 s	5.02, 5.04	7.71 β-H d 8.01 γ-H t $J = 7.8$	6.56–7.73 m	[e]		[e]
				TTFA Thiophene ring			
				CH(3)	CH(4)	CH(5)	CH
$LaL(TTFA)_2Cl \cdot 2(H_2O) \cdot 0.25(C_4H_{10}O)[f](CDCl_3)$	2.61 s	4.02 s	8.12 β-H[c] 8.28 γ-H[c] $J = 8.0$	7.33 d $J_{3-4} = 3.6$	6.95 dd $J_{4-5} = 4.8$ $J_{3-4} = 3.6$	7.41 d $J_{4-5} = 4.8$	5.94 s
$YL(TTFA)_2Cl \cdot H_2O\ (CDCl_3)$	2.54 s	3.94 s	8.04 β-H[c] 8.21 γ-H[c] $J = 8.3$	7.30 d $J_{3-4} = 3.0$	6.96 dd $J_{4-5} = 5.0$ $J_{3-4} = 3.0$	7.40 d $J_{4-5} = 5.0$	5.95 s
$YL(TTFA)_2Cl \cdot H_2O\ (CD_3OD)$	2.54 s	3.99 s	8.14 β-H[c] 8.18 γ-H[c] $J = 8.0$	7.43 d $J_{3-4} = 3.9$	6.98 dd $J_{4-5} = 4.8$ $J_{3-4} = 3.9$	7.52 d $J_{4-5} = 4.8$	6.03 s
				ACAC			
				CH_3		CH	
$YL(ACAC)(OAc)(Cl_x, OH_{1-x}) \cdot n(H_2O)$ $(CDCl_3)$	2.51 s	3.96 m, br 4.16 m, br	8.02 β-H[c] 8.33 γ-H[c] $J = 7.8$	1.16 s		[e]	1.77 s
$EuL(ACAC)(Cl_x, OH_{1-x})_2 \cdot n(H_2O)\ (CDCl_3)$	7.13 s	3.96 m, br 4.06 m, br	8.49 β-H[c] 8.89 γ-H[c] $J = 7.5$	−2.04 s		[e]	1.77 s

[a]Chemical shifts δ are given in ppm: coupling constants J are in Hz; all integrations as expected. Abbreviations: s = singlet, d = doublet, dd = doublet of doublets, t = triplet, m = multiplet.
[b]Signal broadened at base by ill-resolved side-peaks.
[c]Calculated from A_2B spin pattern.
[d]Complex pattern, see discussion.
[e]Signal was not observed.
[f]Also: diethyl ether signals at 1.30 t and 3.40 q.

Table 2. Analytical data of complexes

Complex	C% Found	C% Calc.	H% Found	H% Calc.	N% Found	N% Calc.
EuL(DBM)(OAc)Cl·5.5(H_2O)-$C_{39}H_{51}O_{9.5}N_6Eu$	49.57	49.66	5.42	5.45	8.86	8.91
YL(DBM)(OAc)Cl·5.5(H_2O)$C_{39}H_{51}O_{9.5}N_6Y$	52.21	52.22	5.78	5.84	9.55	9.55
LaL(DBM)$(OAc)_2$·2(H_2O)$C_{41}H_{47}O_8N_6La$	55.28	55.28	5.32	5.32	9.43	9.44
EuL(DBM)$(OAc)_2$·9(H_2O)$C_{41}H_{61}O_{15}N_6Eu$	47.38	47.81	5.55	5.96	8.16	8.16
EuL$(DBM)_2(ClO_4)$·H_2O $C_{52}H_{50}O_9N_6ClEu$	57.04	57.28	4.67	4.62	7.82	7.71
LaL$(TTFA)_2$Cl·2(H_2O)·0.25($C_4H_{10}O$)[a] $C_{39}H_{40.5}F_6O_{6.25}S_2N_6ClLa$	44.68	44.78	3.75	3.90	8.02	8.04
EuL$(TTFA)_2$Cl·2(H_2O)$C_{38}H_{38}F_6S_2N_6ClEu$[b]	43.83	43.88	3.71	3.68	8.14	8.08
YL$(TTFA)_2$Cl·H_2O $C_{38}H_{36}F_6O_5S_2N_6ClY$[c]	47.81	47.58	3.59	3.78	8.73	8.76

[a]Diethyl ether confirmed by ^1H NMR spectrum.
[b]Also: S: found, 6.06; calc. 6.16 and Cl: found, 3.48; calc. 3.41%.
[c]Also: S: found, 6.74; calc. 6.69 and Cl: found, 3.02; calc. 3.70%.

were used: 1:1 and 2:1 for {LaL} and {YL}; 1:1, 2:1, 3:1, 4:1 and 5:1 for {EuL}.

All fractions from the 1:1 ratio experiments, as well as the first fractions from the higher ratio experiments, were mixtures (white and yellow crystals) consisting of the parent complex (40–60%) and of a species with a 1:1 DBM-to-{ML} ratio. Subsequent fractions from experiments with 2:1 or higher HDBM-to-{ML} ratios appeared homogeneous (yellow plates or prisms) and a few consisted only of the 1:1 DBM-to-{ML} complex. Fractions that contained the residual parent complex (10–20%) were further treated with an excess of HDBM until pure 1:1 DBM-to-{ML} complexes were obtained (formulae given below); the total yields of 1:1 DBM-to-{ML} complexes ranged from 30 to 50% in different experiments. No species with a DBM-to-{ML} ratio higher than 1:1 was observed in these experiments.

IR absorptions and selected assignments. EuL(DBM)(OAc)Cl·5.5(H_2O) and YL(DBM)(OAc)Cl·5.5(H_2O): 3425 s, br, ν(OH), water; 3072 vvw; 2919 w; 2849 vvw*; 1643 m, ν(C=N), imine; 1590 m-s, ν(C=N), pyridine and ν(C--O/C--C), DBM; 1549 s, ν(COO)asym., Ac; 1519 s; 1472 w*; 1449 m; 1384 s, ν(C--O/C--C), DBM and ν(COO)sym., Ac; 1302 w; 1249 vw; 1220 vw*; 1198 m-w; 1155 vvw; 1126 vvw; 1067 m-w; 1020 vvw*; 1002 m-w; 932 w; 814 m; 767 vw*; 720 m; 691 vvw*; 673 vvw*; 644 vvw; 597 w; 515 w. LaL(DBM)$(Ac)_2$·2(H_2O) and EuL(DBM)$(Ac)_2$·9(H_2O) had nearly identical spectra, except that the absorptions at 1554 and 1400 cm^{-1} were more intense and broader.

NMR Spectra. LaL(DBM)$(OAc)_2$·2(H_2O), EuL(DBM)(OAc)Cl·5.5(H_2O) and YL(DBM)(Ac)Cl·5.5(H_2O): Proton spectra, Table 1. LaL(DBM)$(OAc)_2$·2(H_2O): ^{13}C NMR spectrum (CD_3OD), 16.35 (CH_3, macrocycle), 24.08 (CH_3, Ac), 53.99 (CH_2), 127.22 (β-C, pyridine), 127.78, 129.20, 131.88 (phenyl), 142.24 (γ-C, pyridine), 156.51 (α-C, pyridine), 170.56 (C=N). The signals of the —COO (acetate), CH (DBM) and C--O (DBM) were not observed.

(2) *Reaction of* NaDBM *with* [ML$(OAc)_2$]Cl·4(H_2O), *where* M = La^{III}, Eu^{III} *and* Y^{III}. The complex (2×10^{-4} mol) and NaDBM were placed in chloroform (10 cm^3) and warmed to *ca* 50°C until all NaDBM had dissolved and a yellow solution containing a small amount of a white semi-gelatinous solid had formed. The mixture was cooled and gravity filtered, discarding the solid. The subsequent procedure was similar to that described for the reaction with HDBM. The following NaDBM-to-{ML} ratios were used: 1:1 and 2:1 for {LaL} and {YL}, 1:1, 2:1 and 3:1 for {EuL}. The 1:1 experiments gave cream-colored powdery products with 1:1 DBM-to-{ML} ratio, identical to those obtained with HDBM (yields, 60–70%). Higher DBM-to-{ML} ratios gave orange–yellow powdery products (yields, 55–60%), which were found to contain (source of evidence in parentheses): no acetate (IR, ^1H NMR spectra), no chloride (chemical analysis), water and/or hydroxide (IR spectra), {ML}:DBM ratios ranging from 1.9 to 2.3 (^1H NMR spectra) and no other organic species (^1H NMR spectra). These products did not give C,N,H microanalyses corresponding to well-defined stoichiometries; they were considered to be mixtures in which the +3 ionic charge of the {ML} moiety was balanced by a combination of DBM and OH^- counterions, present in non-integral ratios. A sample with DBM-to-{EuL} ratio = 2.3 was treated with excess $NaClO_4$ in methanol. Tiny bright yellow crystals of EuL$(DBM)_2(ClO_4)$·H_2O separated slowly from solution at room temperature; they were filtered off, washed with methanol and dried at 60°C.

IR absorptions and selected assignments. 3432 m-w, br, ν(OH), water; 3056 w; 3926 w; 1644 m, ν(C=N), imine; 1597 s, ν(C=N), pyridine and ν(C--O/C--C), DBM; 1554 s; 1515 s; 1478 m; 1456 m; 1398 vs, ν(C--O/C--C), DBM; 1308 w; 1288 w; 1247 vw; 1218 vw; 1194 w; 1151 vw; 1092 s, $\nu(ClO_4)$asymm.;

1023 vw; 1003 vw; 940 vvw; 813 w; 723 m; 692 w; 622 w; 519 vw.

^1H NMR spectrum (*DMSO*-d_6). Table 1.

(3) *Reaction of* HTTFA *with* $[ML(OAc)_2]Cl \cdot 4(H_2O)$, *where* M = La^{III}, Eu^{III} *and* Y^{III}. The reaction was carried out as described for HDBM; the HTTFA-to-{ML} ratios employed were 1 : 1, 2 : 1 and 3 : 1. Several fractions were isolated in each experiment; no further treatment with HTTFA was performed. Fractions obtained from 1 : 1 and 3 : 1 experiments were mixtures from which no single complex was isolated. Fractions obtained from 2 : 1 experiments (total yields 80–85%) appeared homogeneous under a microscope (small almond-coloured platelets or needles) and consisted of single species with a 2 : 1 TTFA-to-{ML} ratio.

IR absorptions and selected assignments. $LaL(TTFA)_2Cl \cdot 2.5(H_2O) \cdot 0.25(C_4H_{10}O)$, $EuL(TTFA)_2Cl \cdot 2(H_2O)$ and $YL(TTFA)_2Cl \cdot H_2O$: 3417 m, br, ν(OH), water; 3070 vw; 2929 vvw; 1645 m*, ν(C=N), imine; 1610 vvs; 1595 sh, ν(C=N) pyridine; 1534 s; 1508 w*; 1500 m-w; 1467 w*; 1458 m-w; 1412 s; 1376 m;1351 m; 1306 vvs; 1292 sh; 1245 m-w; 1229 m-w; 1186 m; 1137 s; 1184 vvw*; 1060 w; 1006 w; 934 w; 859 vw; 815 w; 784 m; 746 w; 715 w; 678 w; 639 m-w; 578 m-w.

NMR spectra. The proton spectra of $LaL(TTFA)_2(OAc)_{0.5}Cl_{0.5} \cdot 2.5(H_2O)$ and $YL(TTFA)_2Cl \cdot H_2O$ are given in Table 1; the spectrum of $EuL(TTFA)_2Cl \cdot 2(H_2O)$ was not assigned. ^{13}C NMR spectrum of $LaL(TTFA)_2(Ac)_{0.5}Cl_{0.5} \cdot 2.5(H_2O)$ ($CDCl_3$): 16.52 (CH_3, macrocycle), 52.49 (CH_2), 90.67 (CH, TTFA, unconfirmed assignment), 125.8 (β-C, pyridine), 128.30, 128.55, 131.97 (thienyl), 140.78 (γ-C, pyridine), 154.94 (α-C, pyridine), 168.14 (C=N), 179.91 (C--O, TTFA or COO, Ac; unconfirmed assignment). The signal of the CH_3, Ac was not observed.

(4) *Reaction of* HACAC *and* NaACAC *with* $[ML(OAc)_2]Cl \cdot 4(H_2O)$, *where* M = La^{III}, Eu^{III} *and* Y^{III}. The reaction with HACAC was carried out as described for HDBM, except that a large excess of the diketone was used (1 cm^3 of HACAC for 2×10^{-4} mol of complex) and the mixture was refluxed for 1 h and then allowed to stand at room temperature for several hours before addition of diethyl ether. All fractions isolated in each experiment (colourless powders) were mixtures consisting of the parent complex and minor quantities of a species with a 1 : 1 ACAC-to-{ML} ratio. Repeated treatment with excess HACAC resulted in a gradual increase of the 1 : 1 ACAC-to-{ML} species, but no product completely free from the parent complex was isolated.

The reaction with NaACAC was carried out as described for NaDBM, using 1 : 1, 2 : 1 and 3 : 1 Na ACAC-to-{ML} ratios. All reactions gave mixtures (colourless powders) from which several samples were isolated by fractional crystallization and were identified by IR and ^1H NMR spectra (approximate yields in parentheses are relative to the $[ML(Ac)_2]Cl \cdot n(H_2O)$ parent complex). The 1 : 1 reaction gave: (1) unreacted NaACAC, (2) the parent complex (40–60%) and (3) the same 1 : 1 ACAC-to-{ML} complex observed for HACAC (10%), containing a small amount of parent complex. The 1 : 2 and 1 : 3 reactions gave: (1) a very small quantity of a $M(ACAC)_3(H_2O)_n$ complex, identified by comparison with an authentic sample; (2) a {ML} species containing no ACAC or acetate (10–20%); (3) a species with 1 : 1 ACAC-to-{ML} ratio (20%), containing a small amount of parent complex. For Y^{III} and Eu^{III}, repeated recrystallization of fraction (3) from methanol/diethyl ether gave small samples (5%) with 1 : 1 ACAC-to-{ML} ratios and free of parent complex. These species contained chloride (chemical analysis) as well as hydroxide (IR spectra) and were considered to be mixtures in which the cationic charges of the $\{YL(ACAC)(Ac)\}^+$ and $\{EuL(ACAC)\}^{2+}$ moieties were balanced by chloride and hydroxide ions, present in non-stoichiometric ratios.

IR absorptions and selected assignments. YL(ACAC) (Ac) $(Cl_x,OH_{1-x}) \cdot n(H_2O)$: 3470–3400 m, vbr and 3200 sh, ν (OH), water and OH^-); 3073 vw; 3007 vw; 2965 vw; 2911 vw; 1644 m, ν(C=N), imine; 1592 vvs, ν(C---11-O/C---C), ACAC and ν(C=N), pyridine; 1560 s*, ν(COO) asymm., Ac; 1513 s; 1441 s; 1398–1991 s, br, ν(C---O/C---C), ACAC and ν(COO) symm., Ac; 1295 w; 1265 m-w; 1250 m-w; 1195 m; 1155 vw; 1125 vw; 1067 vw; 1006 m; 934 vw; 916 w; 818 w; 815 w; 743 m; 712 vw; 671 m-w; 592 vw. The spectrum of the Eu^{III} complex was nearly identical, except for differences in the relative intensities of the absorptions in the 1660–1380 cm^{-1} region.

NMR spectra. YL(ACAC) (Ac) $(Cl_x,OH_{1-x}) \cdot n(H_2O)$: Proton spectrum in Table 1. ^{13}C NMR spectrum ($CDCl_3$): 15.88 (CH_3, macrocycle); 23.9, 26.93 (CH_3, ACAC and Ac; not individually assigned); 52.50 (CH_2); 124.47 (β-C, pyridine); 140.75 (γ-C pyridine); 153.24 (α-C pyridine); 165.37 (C=N). The signals from COO, Ac and from CH and C---, ACAC were not observed. EuL(ACAC) $(Cl_x,OH_{1-x})_2 \cdot n(H_2O)$: Proton spectrum in Table 1. ^{13}C NMR spectrum ($CDCl_3$, assignments not confirmed by HETCOR): −21.13 (CH_3, ACAC); −12.79 (CH_3 macrocycle); 62.21 (CH_2); 108.29 (β-C pyridine); 145.15 (α-C pyridine), 149.58 (γ-C pyridine); 164.67 (C=N); 180.81 (C---O, ACAC). The signal from CH, ACAC was not observed.

"NMR titrations and scrambling" experiments

$[EuL(OAc)_2]Cl \cdot 4(H_2O)$ was "titrated" with β-diketones or sodium β-diketonates as follows: The proton spectrum of the titrating ligand alone (0.03 M in CD_3OD) was recorded first; an equimolar amount of the solid "parent complex", $[EuL(OAc)_2]Cl \cdot 4(H_2O)$, was added and the spectrum was recorded again. Further equimolar aliquots of (solid or liquid) ligand were then added stepwise, recording

the spectrum after each addition. The spectrum of each "titration step" was assigned by comparison with the spectra of the titrant, of the parent complex and of the respective [EuL(β-diketonate) (OAc)]$^+$ complex; the approximate ratio of the two complexes was estimated from the integrated intensities of suitable signals. The initial spectrum of the diketone also gave the percentage of enol form present in solution: 80–84% for HACAC and over 90% for both HDBM and HTTFA, in agreement with the literature.[14(a)] The following results were obtained: (1) HACAC/[EuL(OAc)$_2$]$^+$ ratios, 1:1, 2:1, 3:1, 4:1, 5:1; corresponding [EuL(ACAC) (Ac)]$^+$/[EuL(Ac)$_2$]$^+$ ratios, 0.3:1, 0.6:1, 0.8:1, 1.2:1, 1.7:1. (2) NaACAC/[EuL(OAc)$_2$]$^+$ ratio, 1:1; [EuL(ACAC)(OAc)]$^+$/[EuL(Ac)$_2$]$^+$ ratio, 1:1; at higher titrant/macrocycle ratios gradual decomposition of the {EuL} moiety occurred. (3) HDBM/[EuL(OAc)$_2$]$^+$ ratios, 1:1, 2:1, 3:1; corresponding [EuL(DBM) (Ac)]$^+$/[EuL(OAc)$_2$]$^+$ ratios, 2:1, 7:1, 13:1; higher titrant/macrocycle ratios were prevented by insufficient solubility of HDBM. (4) NaDBM/[EuL(OAc)$_2$]$^+$ ratio, 1:1; [EuL(DBM)(OAc)]$^+$/[EuL(Ac)$_2$]$^+$ ratio, 2:1; at higher titrant/macrocycle ratios, severe broadening of signals occurred. (5) HTTFA/[EuL(OAc)$_2$]$^+$ ratios, 1:1, 2:1; corresponding [EuL(TTFA)(OAc)]$^+$/[EuL(OAc)$_2$]$^+$ ratios, 0.7:1, 5:1; at higher titrant/macrocycle ratios, complete OAc-by-TTFA replacement occurred but signals were severely broadened.

Proton NMR spectra were recorded for YL(TTFA)$_2$Cl·H$_2$O (1.3×10^{-2} M in CD_3OD) in the presence of HTTFA, with HTTFA/{YL(TTFA)$_2$}$^+$ mol ratios = 1:1, 2:1 and 3:1. Each spectrum showed the signals of the {YL(TTFA)$_2$}$^+$ moiety and of (uncoordinated) HTTFA in the expected ratio and unchanged relative to the parent species. In contrast, the signals of the coordinated TTFA, although unshifted, became progressively broader as the HTTFA concentration increased. The spectrum of the 3:1 solution was monitored over a period of 1 week; no change was observed.

Anion exchange reaction were studied as follows: Spectra were recorded separately for EuL(DBM)(OAc)Cl·5.5(H$_2$O) and YL(OAc)$_2$Cl·4(H$_2$O), each dissolved in $CDCl_3$. The two solutions were mixed (1:1 mol ratio) and the spectrum of the mixture was recorded immediately. The procedure was repeated using YL(DBM)(OAc)Cl·5.5(H$_2$O) and EuL(OAc)$_2$Cl·4(H$_2$O). In both experiments, the spectrum of the mixture showed the presence of {YL(OAc)$_2$}, {YL(DBM) (OAc)}, {EuL(OAc)$_2$} and {EuL(DBM) (OAc)}; the intensity ratio for the —CH_3— (macrocycle) signals of {YL(DBM) (OAc)} and {YL(OAc)$_2$}, which occur in a region free from other signals, was approximately 1:1.

Absorption, emission and excitation spectra

All {ML}-(β-diketonate) complexes (1×10^{-4} M in methanol) had two broad absorptions with maxima at *ca* 250 nm ($\varepsilon = 3.8$–3.9×10^4) and *ca* 295 nm ($\varepsilon = 1.4$–2.0×10^4); in addition, the {ML}-DBM complexes absorbed at *ca* 365 nm ($\varepsilon = 1.7 \times 10^4$) and the (ML}-TTFA complexes absorbed at *ca* 347 nm ($\varepsilon = 2.9 \times 10^4$). For each {ML}-diketonate complex, the absorption spectrum essentially consisted of the superimposed spectra of [ML(OAc)$_2$]Cl·4((H$_2$O) [3] and of the respective [M(β-diketonate)$_3$(H$_2$O)$_n$] complex [16]. No appreciable differences were observed among the absorption spectra of different {ML} entities containing the same β-diketonate.

The excitation spectra of the {EuL}-(βdiketonate) complexes, obtained by monitoring the $^5D_0 \rightarrow {}^7F_2$ Eu^{III} emission at 618 nm, matched the respective absorption spectra in the 290–400 nm region, except that the 365 and 347 nm excitation bands of {Eu}-DBM and {EuL}-TTFA, respectively, had much higher relative intensities than the corresponding absorption bands. No Eu^{III} emission was observed for irradiation into the 250 nm absorption.

The emission spectra of the {Eu}-(β-diketonate) complexes were very similar, in regard to patterns and energies, to the spectrum of [EuL(OAc)$_2$]Cl·4(H$_2$O),[3] but differed in intensities. Under comparable experimental conditions, and taking the [EuL(OAc)$_2$]Cl·4(H$_2$O) as unit reference, the emission intensities of the {EuL}-(β-diketonate) complexes varied approximately as follows: {Eu}-ACAC, 1.5; {Eu}-DBM, 5; {EuL}-TTFA, 50.

The emission intensities of methanol solutions containing 2×10^{-4} M [EuL(OAc)$_2$]Cl·4(H$_2$O) and increasing mole ratios (0.0–4.0, by 0.5 increments) of the β-diketone or sodium β-diketonate were measured under comparable instrumental conditions. With HACAC, only minor enhancement of the emission intensity was observed at all ratios; with NaACAC, the emission intensity nearly doubled at NaACAC-to-{EuL} = 0.5:1, then decreased at higher ratios. With HDBM, the intensity gradually increased to about three times its initial value for HDBM-to-{EuL} = 2.5 and 3.0, then decreased slightly; with NaDBM, an approximate four-fold increase was achieved for 1.5 and 2.0 ratios, followed by a sharp decrease at higher ratios. With HTTFA, the intensity gradually increased to approximately 30 times its initial value for HTTFA-to-{EuL]} = 3.0, then remained constant.

Crystal data for [EuL(DBM) (OAc)](OAc)·6H$_2$O = $EuC_{41}H_{55}O_{12}N_6$. $M_r = 975.89$, monoclinic, space group $P2_{1/c}$, $a = 13.787(4)$, $b = 10.055(3)$, $c = 32.408(5)$ Å, $\beta = 101.88(3)^\circ$, $V = 4396(2)$ Å^3, $Z = 4$, $D_x = 1.47$ Mg m^{-3}, λ = (Mo-K_α) = 0.71069 Å, μ(Mo-K_α) = 1.49 mm^{-1}, $F(000) = 2008$, $T = 293$ K.

A prismatic yellow crystal of dimensions 0.40 × 0.52 × 0.30 mm was centred on a four-circle Philips PW1100 (Febo System) diffractometer with graphite-monochromated (Mo-K_α) radiation (λ = 0.71069 Å). The orientation matrix and preliminary unit-cell dimensions were determined from 30 reflections found by mounting the crystal at random, vary-

ing the orientation angles χ and ϕ over a range of 120°, with $7 \leqslant \theta \leqslant 9°$. For the determination of precise lattice parameters, 40 strong reflections with $10 \leqslant \theta \leqslant 13°$ were considered; integrated intensities for *hkl* reflections ($h = \pm 17$; $k = 0 \rightarrow 12$, $l = 0 \rightarrow 42$) were measured in the interval $\theta = 2$–28°, using $\theta/2\theta$ scans. Three standard reflections, 4,0,2; −3,1,8 and −2,1,10, were collected every 200 reflections. There were no significant fluctuations of intensities other than those expected from Poisson statistics. The intensity data were corrected for Lorentz–polarization effects and for absorption, as described by North *et al.* [17]. No correction was made for extinction.

The structure was solved by heavy atoms methods [18]. Refinement was carried out by full-matrix least-squares; the function minimized was $\Sigma w(F_o^2 - F_c^2)^2$, with weighting scheme $w = 1/[\sigma^2(F_o^2) + (0.0132P)^2 + 8.54P]$, where $P = \max(F_o^2 + 2F_c^2)/3$. All non-hydrogen atoms were refined with anisotropic thermal parameters. The H atoms were located from difference-Fourier maps and refined isotropically, except for those belonging to the methyl groups which were placed in calculated positions with fixed, isotropic thermal parameters (1.2 U_{equiv} of the parent carbon atom). For a total of 665 parameters, $wR' = [\Sigma w(F_o^2 - F_c^2)^2/\Sigma w(F_o^2)^2]^{1/2} = 0.077$, $S = 1.186$ and conventional $R = 0.0257$, based on F values of 7302 reflections having $F_o^2 \geqslant 3\sigma(F_o^2)$. Scattering factors were taken from.[19] Structure refinement and final geometrical calculations were carried out with SHELXL-93 [20] and PARST [21] programs, drawings were produced using ORTEPII [22]. Supplementary material is available from the author on request.

RESULTS AND DISCUSSION

Synthesis of the complexes

The results obtained in the reactions between the $[ML(OAc)_2]X \cdot n(H_2O)$ complexes and the β-diketones (HACAC, HDBM or HTTFA) were quite similar for M = La^{III}, Eu^{III} or Y^{III} and depended primarily on the β-diketone and on the mole ratio of the reactants. With HTTFA at 2:1 or higher (β-diketone)-to-{ML} ratios, the acetates present in the parent complex were both readily replaced by TTFA anions; cream-coloured crystalline complexes of formulae $[LaL(TTFA)_2]Cl \cdot 2(H_2O) \cdot 0.25(C_4H_{10}O)$, $[EuL(TTFA)_2]Cl \cdot 2(H_2O)$ and $[YL(TTFA)_2]Cl \cdot (H_2O)$ were obtained in high yields. With HDBM, only one acetate was replaced by a DBM anion even after repeated treatment with a large excess of the β-diketone; the resulting pale yellow crystalline complexes had formulae $[EuL(DBM)(OAc)]Cl \cdot 5.5(H_2O)$, $[YL(DBM)(OAc)]Cl \cdot 5.5(H_2O)$, $[LaL(DBM)(OAc)](OAc) \cdot 2(H_2O)$, $[EuL(DBM)(OAc)](OAc) \cdot 6(H_2O)$ and $[EuL(DBM)(OAc)](OAc) \cdot 9(H_2O)$. When NaDBM was used as reactant, both acetates of the parent complex were replaced; a di-substituted Eu^{III}-DBM complex was isolated as the perchlorate salt, $[EuL(DBM)_2](ClO_4) \cdot (H_2O)$ (bright yellow tiny crystals). Finally, reaction with HACAC in large excess produced 1:1 {ML}-(ACAC) species, but always contaminated by appreciable quantities of the parent complex. With NaACAC, mixtures of mono-substituted complexes with compositions corresponding to $YL(ACAC)(OAc)(Cl_x,OH_{1-x}) \cdot n(H_2O)$ and $EuL(ACAC)Cl_x(OH)_{2-x} \cdot n(H_2O)$ were isolated in low yields; minor quantities of the non-macrocyclic $[M(ACAC_3] \cdot n(H_2O)$ complexes were also formed.

The acid strengths of the three β-diketones in anhydrous methanol, which was the solvent used for the above reactions, may be expected to vary in the order: HDBM ≪ HTTFA ⩽ HACAC ≪ HAc. For the corresponding β-diketonates, the tendency to coordinate with the {LaL}, {EuL} and {YL} entities may be expected to vary in the order: OAc ≪ ACAC < TTFA ⩽ DBM. Although these trends are based on literature data [14(a–c)] obtained under conditions very different from those of the present work, they do provide some rationalization of the results reported above. The HTTFA is more effective than HDBM in replacing the acetates of $[ML(OAc)_2]^+$ chiefly because its acid form has a much greater tendency to deprotonate; this factor overrides the slightly lower affinity of TTFA for the M^{III} ions. Conversely, HACAC, although comparable to HTTFA in acidity, produces a less coordinating conjugate anion and is less effective as a reagent in acetate-replacement reactions.

For acetate-replacement reactions carried out with sodium β-diketonates, the outcome should depend primarily on the affinity of the β-diketonate for the M^{III} ions; these reactions, however, are complicated by the high concentration of OH^- ions that results from the hydrolysis of β-diketonate in the presence of traces of moisture. An example is the base-catalysed hydrolysis of the {ML} macrocycles, which takes place to some extent in the presence of NaACAC and results in the release of the metal ions and formation of their tris-acetylacetonates.

Crystal structure of $[EuL(DBM)(OAc)](OAc) \cdot 6(H_2O)$

The complex is ionic. The structure of the cationic coordination entity is illustrated in Fig. 2; selected bond lengths and angles are listed in Table 3. The Eu^{III} ion is 10-coordinate and the ligand environment consists of the six nitrogen atoms of the macrocycle and of four oxygen atoms, two from a chelating β-diketonate and two from a chelating acetate. The exocyclic acetate and β-diketonate ligands are situated on opposite sides of the macrocycle, with the four oxygen donor atoms in a slightly distorted tetrahedral arrangement. A non-coordinated acetate provides charge neutrality and the clathrated water molecules

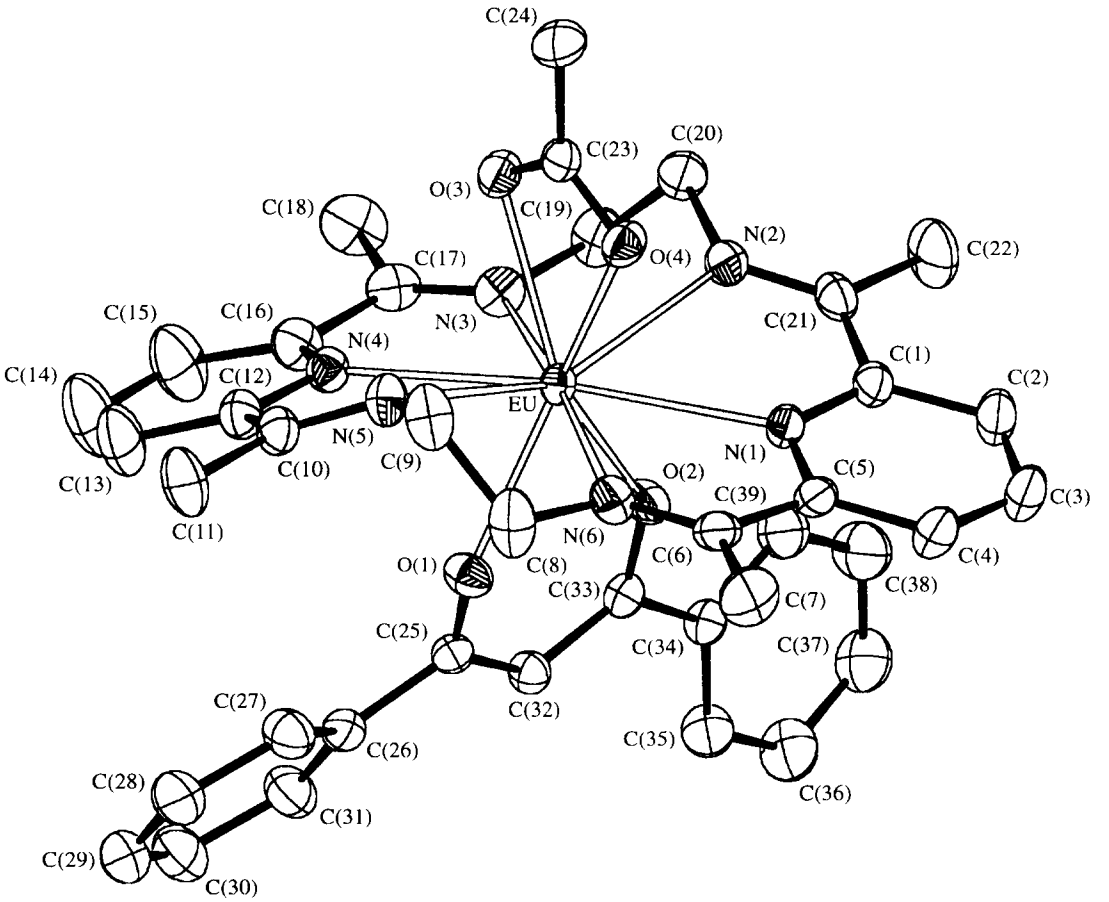


Fig. 2. ORTEP view of the complex cation $[EuL(DBM)(Ac)]^+$. (Ellipsoids are at 40% probability.)

(six per complex unit) form a network of hydrogen bonds that extends throughout the crystal and involves the ionic acetate (Fig. 3 and Table 4) with relatively strong interactions (H---O $\simeq$ 1.8 Å), as well as the coordinated acetate with weaker interactions (H---O $\simeq$ 2.6 Å).

The Eu-macrocycle moiety has the "folded butterfly" conformation typical for complexes of the $C_{22}H_{26}N_6$ ligand and consists of two quasi-planar "wings" that contain the pyridine rings and are hinged at the —CH_2—CH_2— side chains with an interplanar angle of 144.21(8)°. The β-diketonate ligand is situated on the concave side of the macrocycle, with its two phenyl rings rotated by 140.5(2)° relative to one another. The chelation plane of the β-diketonate, aligned with the fold line of the macrocycle, is tilted toward one of the macrocycle wings and forms an angle of 56.0(1)° with it; the angle with the other wing is 88.4(1)°. In the wing closer to the β-diketonate, the deviations of the atoms from the best mean-plane range from −0.0155(4) to 0.106(4) Å; deviations from planarity in the other wing range from −0.094(4) to 0.084(4) Å.

A comparison of $[EuL(DBM)(OAc)](OAc)\cdot 6H_2O$ with $[EuL(OAc)_2](OAc)\cdot 9(H_2O)$ [8] and $[EuL(OAc)_2]Cl\cdot 4(H_2O)$ [5] shows similarities as well as differences. In each complex the exocyclic anionic ligands are staggered and their chelation planes are nearly perpendicular to one another {in $[EuL(DBM)(OAc)]^+$ the O—C—O plane of the acetate and the O=C—CH—C=O plane of the β-diketonate form an angle of 89.0(2)°}. However, the "wings" of the macrocycle are more open when the bulkier β-diketonate is present on the concave side; the macrocycle fold-angle increases from 122.50(7)° in $[Eu(OAc)_2L](OAc)\cdot 9(H_2O)$ [8] and 132.37(6)11° in $[EuL(OAc)_2]Cl\cdot 4(H_2O)$ [5] to 144.21(8)° in $[EuL(DBM)(OAc)](OAc)\cdot 6(H_2O)$. The two Eu—O(acetate) bond lengths in $[EuL(DBM)(OAc)]^+$ are identical to one another [Eu—O(3) 2.506(3); Eu—O(4) 2.508(3) Å] and similar to those found in the $[EuL(OAc)_2]^+$ complexes; the two Eu—O (diketonate) bond lengths are also very close to one another [Eu—O(1) 2.376(3), Eu—O(2) 2.394(3) Å]. Consistent with the partial double bond character of metal-(β-diketonate) coordination, the Eu—O (diketonate) bonds are appreciably shorter than the Eu—O(acetate) bonds; this shortening of the Eu—O bonds on the β-diketonate side of the macrocycle is accompanied by a lengthening of the Eu—N bonds of $[EuL(DBM)(OAc)]^+$ relative to $[EuL(OAc)_2]^+$. As in the latter, however, the Eu—N distances of

Table 3. Selected bond lengths (Å) and angles (°)

Eu—N(1)	2.660(3)	Eu—N(2)	2.623(3)
Eu—N(3)	2.687(4)	Eu—N(4)	2.683(3)
Eu—N(5)	2.628(4)	Eu—N(6)	2.655(4)
Eu—O(1)	2.377(3)	Eu—O(2)	2.394(3)
Eu—O(3)	2.507(3)	Eu—O(4)	2.507(3)
N(1)—C(1)	1.345(5)	N(1)—C(5)	1.350(6)
N(2)—C(20)	1.468(6)	N(2)—C(21)	1.274(5)
N(3)—C(17)	1.275(6)	N(3)—C(19)	1.467(6)
N(4)—C(12)	1.342(5)	N(4)—C(16)	1.345(6)
N(5)—C(9)	1.457(7)	N(5)—C(10)	1.270(5)
N(6)—C(6)	1.275(5)	N(6)—C(8)	1.471(6)
O(1)—C(25)	1.266(5)	O(2)—C(33)	1.258(5)
O(3)—C(23)	1.259(6)	O(4)—C(23)	1.270(5)
C(1)—C(21)	1.492(6)	C(5)—C(6)	1.491(6)
C(6)—C(7)	1.502(7)	C(8)—C(9)	1.499(8)
C(16)—C(17)	1.487(6)	C(17)—C(18)	1.510(8)
C(19)—C(20)	1.508(8)	C(21)—C(22)	1.508(7)
C(23)—C(24)	1.497(6)	C(25)—C(26)	1.506(5)
C(25)—C(32)	1.405(6)	C(32)—C(33)	1.401(5)
C(33)—C(34)	1.513(6)	O(5)—C(40)	1.246(9)
O(6)—C(40)	1.258(9)	C(40)—C(41)	1.51(1)

O(3)—Eu—O(4)	52.0(1)	O(1)—Eu—O(2)	69.2(1)
N(5)—Eu—N(6)	64.2(1)	N(4)—Eu—N(5)	59.5(1)
N(3)—Eu—N(4)	59.6(1)	N(2)—Eu—N(3)	64.3(1)
N(1)—Eu—N(6)	60.1(1)	N(1)—Eu—N(2)	60.4(1)
C(17)—N(3)—C(19)	120.2(4)	C(12)—N(4)—C(16)	118.5(4)
C(9)—N(5)—C(10)	119.2(4)	C(6)—N(6)—C(8)	119.3(4)
N(1)—C(1)—C(21)	116.6(4)	N(1)—C(5)—C(6)	116.5(4)
N(6)—C(6)—C(5)	116.4(4)	N(6)—C(8)—C(9)	109.7(4)
N(5)—C(9)—C(8)	108.6(4)	N(5)—C(10)—C(12)	115.9(4)
N(4)—C(12)—C(10)	115.9(4)	N(4)—C(16)—C(17)	115.9(4)
N(3)—C(17)—C(16)	116.9(4)	N(3)—C(19)—C(20)	110.1(4)
N(2)—C(20)—C(19)	109.4(4)	N(2)—C(21)—C(1)	116.1(4)
Eu—O(1)—C(25)	136.5(3)	Eu—O(2)—C(33)	138.4(3)
Eu—C(23)—O(4)	60.4(2)	Eu—C(23)—O(3)	60.4(2)
O(3)—C(23)—C(24)	119.8(4)	O(1)—C(25)—C(32)	124.2(4)
O(1)—C(25)—C(26)	115.9(3)	C(26)—C(25)—C(32)	119.9(3)
C(25)—C(32)—C(33)	122.4(4)	O(2)—C(33)—C(32)	124.3(4)
C(32)—C(33)—C(34)	119.7(3)	O(2)—C(33)—C(34)	116.0(3)
O(5)—C(40)—O(6)	124.3(7)	O(6)—C(40)—C(41)	118.4(6)
O(5)—C(40)—C(41)	117.3(6)		

$[EuL(DBM)(OAc)]^+$ fall into three equal pairs [Eu—N(imine 2,5) 2.624(3), Eu—N(pyridine) 2.656(4) and Eu—N (imine 4,5) 2.685(4) Å]. The corresponding Eu—N distances (all in Å) for $[EuL(OAc)_2](OAc)\cdot 9(H_2O)$ [8] are 2.570(2), 2.604(3) and 2.642(3); those of $[EuL(OAc)_2]Cl\cdot 4(H_2O)$ [5] are 2.607(3), 2.638(3) and 2.658(3).

The ring puckering analysis of the six-nitrogen system of $[EuL(DBM)(OAc)]^+$ shows a boat conformation with puckering constants $Q = 0.950(4)$ Å, $\theta = 90.2(2)°$ and $\phi = 58.8(2)°$; in contrast, the ring conformation of $[Eu(OAc)_2L](OAc)\cdot 9(H_2O)$ [8] is slightly twisted and that of $[EuL(OAc)_2]Cl\cdot 4(H_2O)$ [5] is of the twist-boat type. This comparison provides further evidence of the high flexibility of the $C_{22}H_{26}N_6$ macrocyclic ligand, which can adjust its conformation to the requirements of exocyclic ligands, external counterions and lattice water molecules.

NMR spectra

The ^1H NMR spectra of the complexes are summarized in Table 1. For each complex, the spectrum consists of the superimposed patterns of the lanthanide-macrocycle [5] and of the lanthanide-coordinated β-diketonate,[16] confirming that the {ML} species retain their integrity in solution and the β-diketonates exhibit their usual bidentate chelating coordination. However, the spectra of the {EuL}-(β-diketonate) and {YL}-(β-diketonate) complexes present a unique feature, in that the CH_2 groups of the

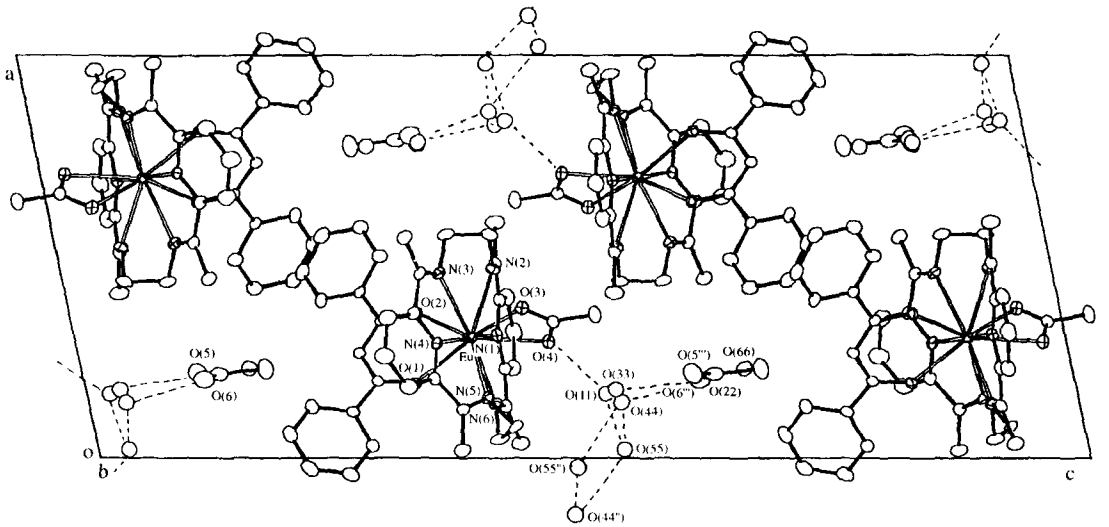


Fig. 3. Crystal packing of [EuL(DBM)Ac)](Ac)·6(H_2O), including anions and water molecules, and showing hydrogen bond interactions.

macrocycle di-imine side-chains, =N—CH_2—CH_2—N=, give rise to two distinct signals in a 1 : 1 ratio, instead of the sharp singlet observed for the same macrocycles when coordinated to other anionic ligands. [In contrast, the spectrum of the {LaL}-(β-diketonate) shows the usual CH_2 singlet.] In the {ML}-(β-diketonate) complexes of Eu^{III} and Y^{III}, therefore, the four CH_2 groups are no longer equivalent but constitute two distinct pairs; in turn, this means that the symmetry of the macrocycle, usually attained through a rapid interconversion of different conformers, is substantially reduced by coordination of the β-diketonate ligand(s). The effect is far more marked in $CDCl_3$ than in more ionizing solvents such as CD_3OD or DMSO-d_6 and is most likely related to the high stability and/or inertness of the β-diketonate ligands when coordinated to the (relatively) small Eu^{III} and Y^{III} ions.

The CH_2 region in the ^1H NMR spectrum of {YL}(DBM)(OAc)Cl·5.5(H_2O) in $CDCl_3$ is shown in Fig. 4, together with a Newman projection along the —CH_2—CH_2— side chains and a coupling scheme consistent with the observed splitting pattern. The observed vicinal coupling constants ($J_{AC} = J_{BD} = 12$, $J_{AD} = J_{BC} = 6$ Hz) suggest a nearly eclipsed arrangement in which the H_A—C—C—H_D angle is quite similar to the H_B—C—C—H_C angle. (In a staggered conformation, J_{BC} would be about 10 Hz and J_{AD} would be only 2 Hz.) The proposed scheme is qualitatively consistent with the Karplus correlation, which

Table 4. Hydrogen bond interactions[a]

Donor	Distance (Å)	Acceptor	H → Acceptor (Å)		Angle (°)
O(11)	2.774(6)	O(4)	H(110)	2.62(11)	95(8)
O(11)	2.933(9)	O(22)	H(110)	2.65(10)	106(9)
O(11)	2.788(8)	O(55)	H(110)	2.64(9)	94(8)
O(22)	3.070(9)	O(66)	H(220)	2.72(8)	115(7)
O(44)	2.894(8)	O(55)	H(441)	2.34(6)	118(5)
O(55)	2.788(8)	O(11)	H(551)	2.53(6)	96(4)
O(55)	2.894(8)	O(44)	H(551)	2.33(6)	119(5)
O(66)	3.070(9)	O(22)	H(660)	2.19(4)	170(4)
O(11)	2.752(9)	$O(33)^{i}$	H(111)	2.27(6)	128(6)
O(55)	2.832(8)	$O(44)^{ii}$	H(550)	1.96(4)	133(4)
O(22)	2.833(8)	$O(5)^{iii}$	H(221)	1.84(7)	164(6)
O(44)	2.788(8)	$O(6)^{iv}$	H(440)	1.71(7)	148(5)
O(44)	2.788(8)	$O(6)^{iv}$	H(441)	2.63(6)	90(4)
O(66)	2.904(6)	$O(6)^{iv}$	H(661)	2.24(5)	133(4)

Key of symmetry: (i) x, $1 - y$, z; (ii) $-x$, $1 - y$, $1 - z$; (iii) x, $0.5 - y$, $0.5 + z$; (iv) x, $1.5 - y$, $0.5 + z$.
[a]The water oxygens are identified by two equal digits.

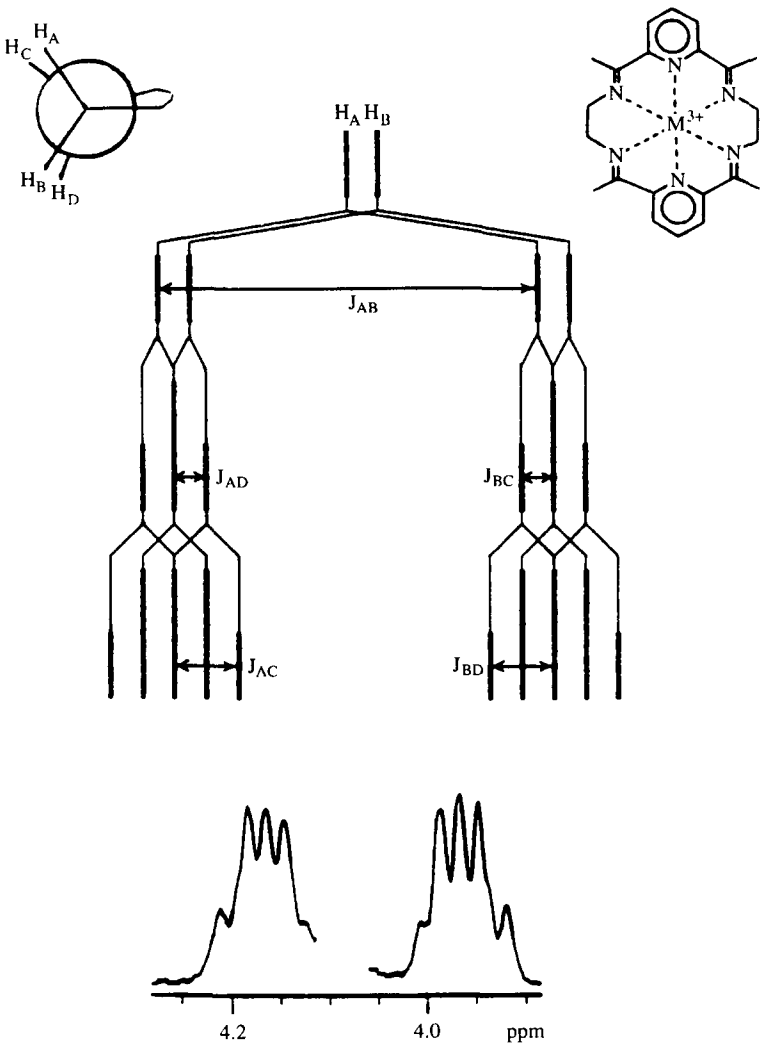


Fig. 4. Proton NMR spectrum of $[YL(DBM)(Ac)](Ac) \cdot 5.5(H_2O)$ in $CDCl_3$ solution: —CH_2 signals and coupling scheme. The chemical shifts of H_A and H_C are very close, as are those of H_B and H_D; accordingly, H_C and H_D have been omitted from the scheme for simplicity.

predicts a J value of 8 Hz for a dihedral angle near 0° and a J value of 4 Hz for a dihedral angle near 120°.

Proton NMR spectra were obtained for series of solutions containing the same concentration of $[ML(OAc)_2]Cl \cdot 4(H_2O)$ and increasing mole ratios of β-diketone. In each case the amount of {ML}-(β-diketonate) relative to residual $[ML(OAc)_2]^+$ increased with the amount of added β-diketone, but the extent of increase differed greatly for the three β-diketones and varied in the order HTTFA ≫ HDBM ≫ HACAC. These spectra also showed the presence of both coordinated β-diketonate and free β-diketone, but of only one kind of acetate. Similar results were obtained when increasing amounts of HTTFA were added to a solution of the pre-formed $[YL(TTFA)_2]Cl \cdot H_2O$ complex, although the signals of coordinated TTFA were severely broadened.

Different results were obtained when NaACAC or NaDBM were used as "titrants". At 1 : 1 (β-diketonate)-to-{ML} ratio, signals of both the {ML}-(β-diketonate) and the residual parent complex were present, but only the signals of coordinated β-diketonate were observed. At higher (β-diketonate)-to-{ML} ratios, replacement of coordinated acetate by β-diketonate appeared to be complete but reliable assignments were prevented by severe broadening of the signals and, for NaACAC, by gradual decomposition of the {ML} entity.

In the "anion scrambling" experiments, the spectra of chloroform solutions obtained by mixing in a 1 : 1 mole ratio $\{EuL(OAc)_2\}$ and {YL(DBM)(OAc)} or

{YL(OAc)$_2$} and {YL(DBM)(OAc)} showed the presence of the four macrocyclic species resulting from an approximately even redistribution of the DBM and OAc anions.

The results of the "NMR titrations and scrambling" experiments indicate that in the [ML(β-diketonate)(OAc)]$^+$ species the exchange between coordinated and free β-diketonate is fast on the NMR time scale and so is the exchange between coordinated and free acetates. In contrast, the exchange of β-diketonate between different {ML} entities, although it reaches equilibrium within the short time required for the NMR experiment, is slow on the NMR timescale and so is the exchange between coordinated β-diketonate and free β-diketone, which involves ionization of the diketone-enol.

Luminescence of the Eu^{III} *complexes*

The {EuL}-(β-diketonate) complexes investigated in this work exhibit enhanced luminescence relative to [EuL(OAc)$_2$]Cl·4(H$_2$O), without significant changes in the patterns and energies of the emission spectra; this shows that the coordination symmetry of the emitting Eu^{III} is essentially unchanged, in agreement with the structure established by X-ray crystallography for [EuL(DBM)(OAc)](OAc)·6(H$_2$O). In contrast, the absorption spectra of the {EuL}-(β-diketonate) complexes differ markedly from the absorption spectrum of [EuL(OAc)$_2$]Cl·4(H$_2$O),[3] as they consist of the superimposed patterns of the {EuL} entity and of the Eu-bound β-diketonate;[16] when the latter absorb intensely in the 340–370 nm region, which is best suited for energy transfer to the Eu^{III} ion, their contribution to the excitation process becomes dominant. Thus, irradiation into the 365 nm absorption of the {Eu}-DBM species results in an emission intensity approximately five times higher than that of [EuL(OAc)$_2$]Cl·4(H$_2$O) [3] and a nearly 50-fold enhancement occurs for irradiation into the 355 nm absorption of {Eu}-TTFA (Fig. 5); only a minor enhancement (less than two-fold) occurs instead when the {Eu}-ACAC complex is irradiated into its β-diketonate absorption at *ca* 300 nm. The luminescence of the {EuL}-DBM and {Eu}-TTFA complexes, therefore, must be due primarily to the efficient antenna role of the respective β-diketonates; the protection from vibrational deactivation provided by the bulky and hydrophobic substituents (phenyl, thienyl and trifluoromethyl groups) also undoubtedly contributes to the enhanced luminescence.

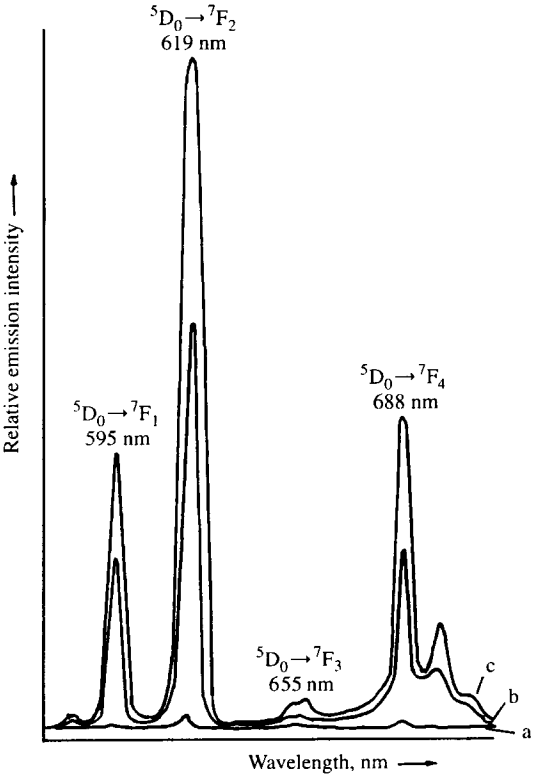


Fig. 5. Emission spectra: (a) [EuL(Ac)$_2$]Cl·4(H$_2$O), $\lambda_{excit.}$ = 310 nm; (b) HTTFA and [EuL(Ac)$_2$]Cl·4(H$_2$O) in 2.5:1 mol ratio, $\lambda_{excit.}$ = 355 nm; (c) [EuL(TTFA)$_2$]Cl·2(H$_2$O), $\lambda_{excit.}$ = 355 nm. (Methanol solutions, 1×10^{-4} M Eu^{III}; identical instrumental settings.)

CONCLUSIONS

The results of this study show that the reaction of β-diketones or β-diketonates with the lanthanide(III) macrocyclic complexes [ML(OAc)$_2$L]$^+$ results solely in anion metathesis. The β-diketonates replace either one or both acetates of the original complex, depending on the nature of the diketonate and the reaction conditions, but do not abstract the lanthanide from the uncharged macrocyclic ligand. Since β-diketonates have a very strong affinity for the lanthanide(III) ions, this behaviour confirms the unique resistance of the {ML} systems to metal release under the influence of strongly competing ligands—an essential property if any of these complexes is to be used as a bio-marker.

The crystallographic analysis of [EuL(DBM)(OAc)](OAc)·6(H$_2$O) has shown that in the solid {ML}-(β-diketonate) complexes the β-diketonates behave as usual as bidentate chelating ligands and that the metal-macrocycles retain their usual folded configuration. In solution, the {ML}-(β-diketonate) complexes remain undissociated and the {ML} entities of Eu^{III} and Y^{III} no longer exhibit the conformational fluxionality that characterizes their complexes with other anionic ligands. Also, in {ML}-(β-diketonate) complexes the coordinated β-diketonates do not exchange rapidly, at least not on the NMR time scale, with "free" β-diketones; this inertness contrasts with the rapid exchange observed for other anionic organic ligands previously studied in association with the {ML} species.

Finally, TTFA was found to be an extremely effective luminescence-enhancing ligand the {EuL}

moiety. This enhancement, which is another important factor in the development of Eu macrocycles as luminescent bio-markers, appears to result chiefly from the "antenna role" of the TTFA chelate, which absorb light in a spectral region suitable for efficient energy transfer to the Eu^{III} centre. Furthermore, the stability/inertness of the TTFA-{ML} coordination, as well as the bulk and hydrophobicity of the thienyl and trifluoromethyl groups of TTFA, provide increased protection of the excited Eu^{III} from vibrational deactivation by solvent molecules.

REFERENCES

1. L. De Cola, D. L. Smailes and L. M. Vallarino, *Inorg. Chem.*, 1986, **25,** 1729.
2. G. Bombieri, F. Benetollo, A. Polo, L. De Cola, D. L. Smailes and L. M. Vallarino, *Inorg. Chem.*, 1986, **25,** 1127.
3. N. Sabbatini, L. De Cola and L. M. Vallarino, *J. Phys. Chem.*, 1987, **91,** 4681.
4. F. Benetollo, A. Polo, L. De Cola, W. T. Hawkins, G. Bombieri and L. M. Vallarino, *Polyhedron*, 1989, **8,** 2157.
5. F. Benetollo, A. Polo, G. Bombieri, K. K. Fonda and L. M. Vallarino, *Polyhedron*, 1990, **9,** 1411.
6. G. Bombieri, F. Benetollo, A. Polo, K. K. Fonda and L. M. Vallarino, *Polyhedron*, 1991, **10,** 1385.
7. K. K. Fonda, J. Kroll, D. D. Shillady and L. M. Vallarino, in *Charge and Field Effects in Biosystems*-3, ed. M. J. Allen, S. F. Cleary, A. E. Sowers, and D. D. Shillady. Birkhauser, Boston (U.S.A.) 1991, p. 411.
8. K. K. Fonda, D. L. Smailes, L. M. Vallarino, G. Bombieri, F. Benetollo, A. Polo and L. De Cola, *Polyhedron*, 1993, **12,** 549.
9. F. Benetollo, G. Bombieri, P. Gilli, P. M. Harlow, A. Polo and L. M. Vallarino, *Polyhedron*, 1995, **14,** 2255.
10. J. D. Ayala, G. Bombieri, F. Benetollo, P. Gilli and L. M. Vallarino, *J. Chem. Crystallography*, 1995, **125**.
11. R. C. Leif and L. M. Vallarino, in *Cell Separation Science and Technology*, D. H. Kompala, P. Todd Eds.; ACS Symposium Series Vol. 464, American Chemical Society, Washington DC, 1991, p. 41.
12. L. M. Vallarino and R. C. Leif, U.S. Patent No. 5,373,093, 1994.
13. R. C. Leif, P. M. Harlow, and L. M. Vallarino, *Proc. SPIE-Int. Soc. Opt. Eng.* 1994, **2136**, 255.
14. (a) *Stability Constants of Metal-Ion Complexes*, Special Publication No. 17, Section II: *Organic Ligands*. The Chemical Society, London, 1964; (b) *Stability Constants Supplement No.* 1, Special Publication No. 25, Part II: *Organic Including Macromolecule Ligands*. The Chemical Society, London, 1971; (c) *IUPAC Stability Constants of Metal-Ion Complexes*, Part B, *Organic Ligands*. Pergamon Press, New York, 1979.
15. G. A. Crosby, *Mol. Cryst.* 1966, **1,** 37.
16. R. C. Mehrotra, B. Bohra, and D. P. Gaur, *Metal, β-Diketonates and Allied Derivatives*. Academic Press, New York, 1978.
17. A. C. T. North, D. C. Philips, and F. S. Mathews, *Acta Cryst. A* 1968, **24,** 351.
18. G. M. Sheldrick, *SHELX*-86, *Crystallographic Computing* 3, ed. G. M. Sheldrick, C. Kruger and R. Goddard. Oxford University Press, England, 1985.
19. *International Tables for X-ray Crystallography*, 2nd edn., Vol. 4. Kynoch Press, Birmingham, England, 1974, p. 101.
20. (a) G. M. Sheldrick, *Acta Cryst.* 1990, **A46,** 467; (b) G. M. Sheldrick, Z. Dauter, K. S. Wilson, H. Hope and L. C. Sieker, *Acta Cryst.* 1993, **D49,** 18.
21. M. Nardelli, *Computing Chem.* 1983, **7,** 95.
22. C. K. Johnson, *ORTEP II*, Report ORNL-5138. Oak Ridge National Laboratory, Oak Ridge, TN, 1976.

Pergamon

PII: S0277-5387(96)00447-0

Polyhedron Vol. 16, No. 11, pp. 1921–1923, 1997
© 1997 Elsevier Science Ltd
All rights reserved. Printed in Great Britain
0277-5387/97 $17.00+0.00

Base hydrolysis of acetonitrile coordinated to a ruthenium(II) polypyridine complex

Florencia Fagalde, Noemí D. Lis de Katz and Néstor E. Katz*

Instituto de Química Física, Facultad de Bioquímica, Química y Farmacia, Universidad Nacional de Tucumán, Ayacucho 491, (4000) San Miguel de Tucumán, Argentina

(Received 25 June 1996; accepted 3 September 1996)

Abstract—On coordination to $Ru(terpy)(bipy)^{2+}$ (terpy = 2,2′:6′,2″-terpyridine, bipy = 2,2′-bipyridine), acetonitrile is converted to acetamide in aqueous basic solution, through hydroxide attack with a catalytic factor of *ca* 3×10^3 ($k_{OH} = 4.6\times10^{-3}$ M^{-1} s^{-1}). This is a remarkable effect for a d^6 transition metal in the (II) oxidation state, and can be ascribed to π backbonding from the metal to the polypyridyl ligands, which makes the ruthenium(II) centre more electropositive than ruthenium(II) in the $Ru(NH_3)_5^{2+}$ moiety. The final hydrolysis product is the $[Ru(terpy)(bipy)(OH)]^+$ complex, since amides, being poor π-acceptor ligands, are rapidly released from the coordination sphere of ruthenium(II). © 1997 Elsevier Science Ltd. All rights reserved.

Keywords: base hydrolysis; acetonitrile complexes; ruthenium(II); polypyridine; catalysis; π-backbonding.

The hydrolysis of nitrile groups catalysed by transition metal complexes has been extensively studied in aqueous solutions, in part because of the connection to enzymatic proteolytic reactions [1]. Large metal-promoted acceleration of the rate of basic nitrile hydrolysis has been observed, especially when the metal is trivalent. Thus, $Co^{III}(NH_3)_5$ enhances the rate of acetonitrile conversion into acetamide [2] by a factor of *ca* 10^6, while $Ru^{III}(NH_3)_5$ has a catalytic factor of *ca* 10^8, over the free ligand value [3]. In contrast, $Ru^{II}(NH_3)_5$ has little or almost no effect on this rate [3], a result attributed to π backbonding from ruthenium(II) into the nitrile group, which increases the electron density at the nitrile C atom and thus makes it less susceptible to nucleophilic attack by hydroxide ion. We have been interested in the general properties of mono- and di-nuclear complexes derived from the $Ru^{II}(terpy)(bipy)$ group (terpy = 2,2′:6′,2″-terpyridine; bipy = 2,2′-bipyridine) [4]. In a recent paper [5], we reported a nitrile hydrolysis reaction induced by oxidation of the dinuclear complex $[(terpy)(bipy)Ru^{II}(4\text{-}CNpy)Ru^{II}(NH_3)_5]^{4+}$ (4-CNpy = 4-cyanopyridine). There, we attributed the observed rate enhancement to an inductive effect of the $Ru^{II}(terpy)(bipy)$ moiety acting as a remote substituent. Now, we wish to report on a rate increase owing to an electronic effect caused by direct coordination of a nitrile group to $Ru^{II}(terpy)(bipy)$, the catalytic factor being remarkable for a divalent transition metal complex.

EXPERIMENTAL

Syntheses

The previously reported PF_6^- salt of the $[Ru(terpy)(bipy)(NCCH_3)]^{2+}$ ion was prepared by a modified technique [6]. A solution of 83 mg of $[Ru(terpy)(bipy)(Cl)](PF_6)$, prepared as described in ref. [7], dissolved in 30 cm^3 of MeCN/ethylene glycol (2:1 v/v) was refluxed for 2 h. Then, the solution was rotoevaporated to 8 cm^3, cooled and sorbed on to a neutral alumina column, previously equilibrated with MeCN/toluene (1:2 v/v). MeCN/toluene was used as an eluent, followed by pure MeCN. The last fraction was collected and the solvent was removed by evaporation. The solid residue was dissolved in 10 cm^3 of water and then 1 g of NH_4PF_6 was added. The red-orange precipitate was filtered off, washed with cold water and diethyl ether and dried *in vacuo* over P_4O_{10}. It was recrystallized from acetone/ether. Yield: 75 mg (74%). The Br^- salt of the ion $[Ru(terpy)(bipy)(NCCH_3)]^{2+}$ was obtained by dissolving 50 mg of the PF_6^- salt in 5 cm^3 of acetone and adding 1 g of $Bu_4^nN^+Br^-$

* Author to whom correspondence should be addressed.

NBr in 3 cm^3 of Me_2CO. The precipitate was collected by filtration, washed with cold acetone and dried *in vacuo* over P_4O_{10}. Yield: 34 mg (81%).

Materials, instrumentation and techniques

All chemicals were reagent grade and used as received. Triply distilled water was used for all kinetic determinations.

pH measurements were carried out with a precision of ± 0.05 pH units, using a Luftman–Reliance II pH meter. UV–visible spectra were run with a Shimadzu UV-160A spectrophotometer, equipped with a thermostatted cell compartment.

Stock solutions of NaOH were prepared at the desired total concentrations. A fresh solution of $[Ru(terpy)(bipy)(NCCH_3)]^{2+}$ in water was used for each set of experiments. Absorbance *vs* time data were recorded at a value of $\lambda = 453$ nm (maximum of the initial complex). Duplicate or triplicate runs were made at each value of pH and temperature. Rate constants were obtained by least-squares fits of $\ln(A_t - A_\infty)$ *vs* time t, which were linear up to three half-lives. The estimated error in the base hydrolysis rate constant k_{OH} is $\pm 5\%$.

RESULTS AND DISCUSSION

Figure 1 shows consecutive spectra obtained at pH = 12.5 and $T = 25.0$°C of an aqueous solution of $[Ru(terpy)(bipy)(NCCH_3)]^{2+}$ ($C = 4.4 \times 10^{-5}$ M). The metal-to-ligand charge transfer (MLCT) absorption band at $\lambda_{max} = 454$ nm (same value in MeCN) [6] is shifted to higher wavelengths, reaching a value of $\lambda_{max} = 500$ nm after 1 day. Isosbestic points are observed at 470 and 390 nm. These changes are indicative of an hydrolysis process followed by aquation; *i.e.* a reaction of the coordinated ligand followed by a substitution process. The observed final peak value is coincident with that of the $[Ru(terpy)(bipy)(OH)]^+$ ion [8]. To confirm the identity of the product, one drop of 6 N HCl was added to this last solution. As shown in Fig. 2, a value of $\lambda_{max} = 475$ nm obtains, which agrees very well with the already reported value for the $[Ru(terpy)(bipy)(OH_2)]^{2+}$ ion [8].

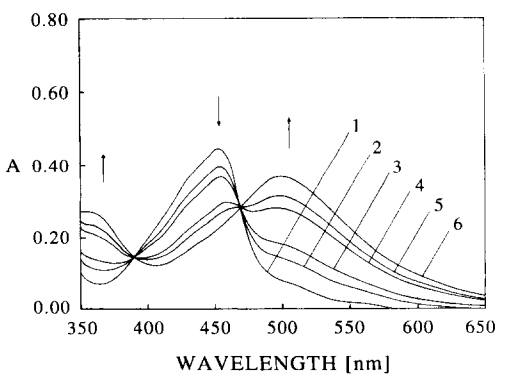


Fig. 1. Spectra obtained after adding 0.05 M NaOH to an aqueous solution of $[Ru(terpy)(bipy)(NCCH_3)]^{2+}$, $C = 4.4 \times 10^{-5}$ M, at $T = 25.0$°C. Approximate times of reaction are: 1) 0 h; 2) 1 h, 3) 2 h; 4) 6 h; 5) 8 h; 6) 24 h.

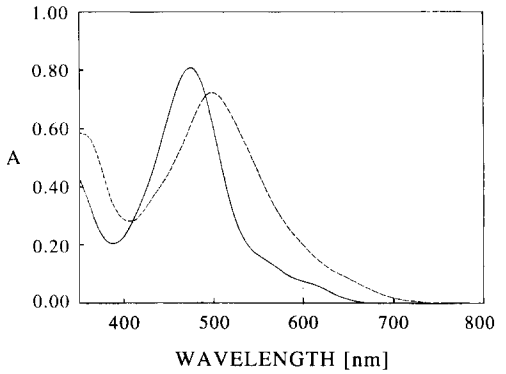


Fig. 2. Absorption spectra of the hydrolysed products of the complex $[Ru(terpy)(bipy)(NCCH_3)]^{2+}$ at pH = 11.9 (– – –) and at pH = 0 (——), $C = 7.0 \times 10^{-5}$ M.

The value obtained for $k_{obs} = 4.7 \times 10^{-4}$ s^{-1} at pH = 13.0 ($\mu = 0.1$ M) is several orders of magnitude higher than that of the expected rate constant for a ligand substitution process [9]. Thus, after adding excess pyrazine (pz) to the $[Ru(terpy)(bipy)(NCCH_3)]^{2+}$ ion at pH = 5.0, no evidence of formation of $[Ru(terpy)(bipy)(pz)]^{2+}$ ($\lambda_{max} = 428$ nm) [4] was obtained after several days. On the other hand, the acetamide ligand was aquated very rapidly, since, as usually found in Ru^{II} complexes [10], amides are poor π-acceptor ligands and are thus rapidly released from the coordination sphere of Ru^{II}.

As shown in Table 1, the observed first-order rate constants k_{obs} for the hydrolysis process vary linearly with $[OH^-]$. From the rate law $k_{obs} = k_{OH}[OH^-]$, a value of $k_{OH} = 4.6 \times 10^{-3}$ M^{-1} s^{-1} was calculated, which can be compared with other metal-catalysed hydrolysis second-order rate constants for acetonitrile, as shown in Table 2. The value obtained for the complex studied in this work is intermediate between those of the acetonitrile complexes of $Ru^{II}(NH_3)_5$ and $Co^{III}(NH_3)_5$. The catalytic factor is *ca* 3×10^3 over the free ligand value. This effect is quite remarkable for a d^6 transition metal in the (II) oxidation state and can

Table 1. k_{obs} for the hydrolysis of coordinated CH_3CN in $[Ru(terpy)(bipy)(NCCH_3)]^{2+}$ at different hydroxide concentrations (25.0°C)

$[OH^-]$, M	k_{obs} s^{-1}
1.80×10^{-3}	2.64×10^{-5}
1.05×10^{-2}	4.64×10^{-5}
2.09×10^{-2}	1.42×10^{-4}
3.98×10^{-2}	2.77×10^{-4}
1.00×10^{-1}	4.68×10^{-4}

Table 2. Base-catalysed hydrolysis of acetonitrile complexes at 25.0°C

Nitrile	k_{OH}, $M^{-1} s^{-1}$	Reference
CH_3CN	1.60×10^{-6}	3
$[(NH_3)_5Ru(NCCH_3)]^{2+}$	$<6 \times 10^{-5}$	3
$[(terpy)(bipy)Ru(NCCH_3)]^{2+}$	4.6×10^{-3}	This work
$[(NH_3)_5Co(NCCH_3)]^{3+}$	3.40	3
$[(NH_3)_5Ru(NCCH_3)]^{3+}$	2.2×10^{2}	3

be ascribed to π backbonding from the metal to the polypyridyl ligands, which makes the Ru^{II} centre more electropositive than the Ru^{II} centre in the $Ru^{II}(NH_3)_5$ moiety. The ability of Ru^{II} to promote the hydrolysis of a nitrile group when coordinated to π-acceptor ligands was previously detected in a work [11] on the stability of aqueous solutions of $[Ru(bipy)_2(4\text{-}CNpy)_2]^{2+}$.

The values of k_{OH} as a function of temperature are shown in Table 3. The variation of $\ln(k_{OH}/T)$ with $(1/T)$ is displayed in Fig. 3. From Eyring's rate equation [12], values of $\Delta H^{\#} = (74 \pm 4)$ kJ mol^{-1} and $\Delta S^{\#} = (-42 \pm 12)$ J mol^{-1} K^{-1} are determined, which compare reasonably well with other nitrile hydrolysis activation parameters. For example, values of $\Delta H^{\#} = 63.2$ kJ mol^{-1} and $\Delta S^{\#} = -84$ J mol^{-1} K^{-1} have been obtained for the base-catalysed reaction of 2-cyano-1,10-phenthroline [13]. These values indicate the operation of an associative process.

Table 3. Temperature dependence of the second-order rate constant k_{OH} for the hydrolysis of coordinated CH_3CN in$[Ru(terpy)(bipy)(NCCH_3)]^{2+}$

T, °C	k_{OH}, $M^{-1} s^{-1}$
17.0	1.95×10^{-3}
20.0	2.30×10^{-3}
25.0	4.68×10^{-3}
30.0	7.54×10^{-3}
35.0	1.23×10^{-2}
40.0	1.84×10^{-2}

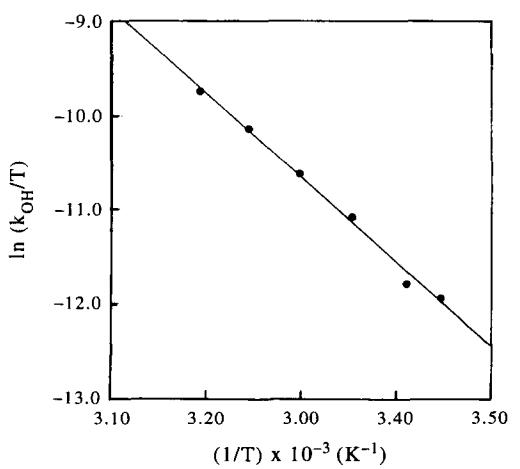


Fig. 3. Eyring plots for base hydrolysis of [Ru(terpy)(bipy)$(NCCH_3)]^{2+}$ in aqueous solutions.

By following the arguments already pointed out by Deutsch *et al.* [14], we can anticipate that the orbitals of $Ru(terpy)(bipy)^{2+}$ are not as basic as those of $Ru(NH_3)_5^{2+}$, because of the presence of the π electron-accepting polypyridyl ligands. Therefore, the Ru^{II} centre in $Ru(terpy)(bipy)^{2+}$ is capable of stabilizing a bimolecular reaction mechanism, either in the H_2O_2 oxidation of a chalcogenoether [14], or in the hydroxide attack on a nitrile group, as reported here. Work in progress in our laboratory will address the extent of the catalytic action of the $Ru(terpy)(bipy)^{2+}$ moiety on the hydrolysis rate of other nitrile derivatives.

Acknowledgements—We are grateful to Consejo Nacional de Investigaciones Cientificas y Técnicas (CONICET, Argentina), Consejo de Investigaciones de la Universidad Nacional de Tucumán (CIUNT, Argentina) and Consejo de Ciencia y Técnica de la Provincia de Tucumán (COCYTUC, Argentina) for financial help. F.F. thanks CONICET for a postgraduate fellowship. N.E.K. is a Member of the Research Career (CONICET).

REFERENCES

1. Belokon, Y. N., Tararov, V. Y., Savel'eva, T. E., Vitt, S. V., Paskonova, E. A., Dotdayev, S. C., Borisov, Y. A., Struchkov, Y. T., Batasanov, A. S. and Belikov, V. M., *Inorg. Chem.*, 1988, **27,** 4046.
2. Buckingham, D. A., Keene, F. R. and Sargeson, A. M., *J. Am. Chem. Soc.*, 1973, **95,** 5649.
3. Zanella, A. W. and Ford, P. C., *Inorg. Chem.*, 1975, **14,** 42.
4. Fagalde, F. and Katz, N. E., *Polyhedron*, 1995, **14,** 1213.
5. Lis de Katz, N. D., Fagalde, F. and Katz, N. E., *Polyhedron*, 1995, **14,** 3111.
6. Hecker, C. R., Fanwick, P. E. and McMillin, D. R., *Inorg. Chem.*, 1991, **30,** 659.
7. Ware, D. C., Lay, P. A., Taube, H., *Inorg. Synth.*, 1986, **24,** 300.
8. Davies, N. R. and Mullins, T. L., *Aust. J. Chem.*, 1967, **20,** 657.
9. Davies, N. R. and Mullins, T. L., *Aust. J. Chem.*, 1968, **21,** 915.
10. Naal, Z., Tfouni, E. and Benedetti, A. V., *Polyhedron*, 1994, **13,** 133.
11. Katz, N. E., Creutz, C. and Sutin, N., *Inorg. Chem.*, 1988, **27,** 1687.
12. Wilkins, R. G., *Kinetic and Mechanism of Reactions of Transition Metal Complexes*, 2nd edn. VCH, Weinheim, 1991, p. 88.
13. Breslow, R., Fairweather, R. and Keana, J., *J. Am. Chem. Soc.*, 1967, **89,** 2135.
14. Root, M. J. and Deutsch, E., *Inorg. Chem.*, 1985, **24,** 1464.

Pergamon

PII: S0277-5387(96)00446-9

Polyhedron Vol. 16, No. 11, pp. 1925–1930, 1997
© 1997 Elsevier Science Ltd
All rights reserved. Printed in Great Britain
0277-5387/97 $17.00+0.00

Studies of nickel(II) complexes of 3-hydroxyiminobutanone thiosemicarbazone and 3-hydroxyiminobutanone (4-phenyl thiosemicarbazone). Crystal structure of bis(3-hydroxyiminobutanone (4-phenyl thiosemicarbazone) nickel(II) nitrate, monohydrate, $[Ni(C_{11}H_{14}N_4OS)_2](NO_3)_2 \cdot H_2O$

Shyamal Kumar Chattopadhyay,[a] Debashish Chattopadhyay,[b] Tapati Banerjee,[b] Reiko Kuroda[c] and Saktiprosad Ghosh[d]*

[a] Department of Chemistry, B.E. College (Deemed University), Howrah 711103, India

[b] Crystallography and Molecular Biology Division, Saha Institute of Nuclear Physics, Block AF, Sector I, Bidhannagar, Calcutta 700064, India

[c] Department of Chemistry, College of Arts and Science, Tokyo University, Komaba, Meguro, Tokyo 153, Japan

[d] Department of Inorganic Chemistry, Indian Association for the Cultivation of Science, Calcutta 700032, India

(Received 31 January 1996; accepted 30 August 1996)

Abstract—Nickel(II) complexes of two tridentate N.N.S-chelating ligands, 3-hydroxyiminobutanonethiosemicarbazone (L_1H_2) and 3-hydroxyiminobutanone (4-phenylthiosemicarbazone) (LH_2), have been synthesized and characterized by elemental analysis, IR, UV–vis spectroscopy and cyclic voltammetric studies. The structure of $Ni(LH_2)_2(NO_3)_2 \cdot H_2O$ has been determined by single-crystal X-ray diffraction. Nickel(II) is in a distorted octahedral N_4S_2 donor environment; one of the nitrate groups exhibits partial disorder.
© 1997 Elsevier Science Ltd. All rights reserved.

Keywords: nickel(II) complexes; hydroxyiminobutanonethiosemicarbazone; X-ray structure; spectroscopic studies; cyclic voltammetry.

The chemistry of divalent and trivalent nickel complexes with nitrogen–sulfur donor ligands has received much attention [1–11] particularly since the discovery [10–12] that a number of dehydrogenases contain nickel at their active sites, surrounded by more than one thiolate ligand, as well as one or two nitrogen donors. Nickel(II) is also used as a spectroscopic probe in metal replacement studies of other metalloenzyme systems [13–17]. Although a variety of nitrogen–sulfur donors have been investigated, thiosemicarbazides and thiosemicarbazones have received inadequate attention. We have been studying complexes of thiosemicarbazides and thiosemicarbazones [19–25] of a number of metal ions for the past few years. The emphasis has been on the synthesis of new compounds, the characterization by different physicochemical methods, exploration of their chemical reactivity and biological activity (such as antibacterial and antitumour properties) and determination of structures of key members of this series of complexes by X-ray crystallography, with the final objective of

* Author to whom all correspondence should be addressed.

arriving at a fruitful structure–activity correlation. In this paper we report our studies on the ligational behavior of 3-hydroxyiminobutanonethiosemicarbazone (L_1H_2) and its 4-phenyl derivative (LH_2) towards nickel(II). The X-ray crystal structure of one of the nickel compounds, $Ni(LH_2)_2(NO_3)_2 \cdot H_2O$, is also reported. The ligand 3-hydroxyiminobutanonethiosemicarbazone is known to be effective against vaccina infection in mice, probably acting through chelation of some essential metal ions [26,27]. It is also known [19] that the antibacterial activity of the ligand decreases on introduction of a phenyl ring at the hydrazinic end of the thiosemicarbazide moiety. However, a proper understanding of the actual mechanism of action requires detailed knowledge of the ligational behaviour of the thiosemicarbazone and structural features of its metal complexes. The present work is an attempt to contribute to research in this direction.

Table 1. Analytical data[a] of the complexes

Complex	Analysis (%)		
	C	H	N
$Ni(TSCDAMO)_2Cl_2 \cdot 2H_2O$	23.5 (23.3)	4.5 (4.7)	22.0 (21.8)
$Ni(TSCDAMO)_2Br_2 \cdot 2H_2O$	19.9 (19.9)	4.1 (4.0)	18.5 (18.6)
$Ni(TSCDAMO)_2(NO_3)_2 \cdot H_2O$	22.1 (21.9)	4.1 (4.0)	20.3 (20.4)
$Ni(4PhTSCDAMO)_2Cl_2 \cdot 2H_2O$	39.4 (39.6)	4.6 (4.8)	16.9 (16.8)
$Ni(4PhTSCDAMO)_2Br_2 \cdot 2H_2O$	35.2 (35.0)	4.4 (4.2)	14.6 (14.8)
$Ni(4PhTSCDAMO)_2(NO_3)_2 \cdot H_2O$	37.9 (37.7)	4.2 (4.3)	20.0 (20.0)

[a] Calculated values in parentheses.

EXPERIMENTAL

Chemicals

$NiCl_2 \cdot 6H_2O$, $NiBr_2 \cdot 6H_2O$ and $Ni(NO_3)_2 \cdot 6H_2O$ were obtained from Merck (India). The ligands 3-hydroxyiminobutanonethiosemicarbazone (TSCDAMO) and 3-hydroxyiminobutanone(4-phenylthiosemicarbazone) (4PhTSCDAMO) were prepared by reported methods [18,19]. All other chemicals were of reagent grade and were used without further purification.

Preparation

The metal complexes were prepared by reacting an aqueous solution (15 cm^3) of 1 mmole of the appropriate nickel salt, with an alcoholic solution (30 cm^3) of 2 mmole of the ligand for 2 h. The pH of the solution was adjusted to between 2–3 by addition of the appropriate acid ($HCl/HBr/HNO_3$). The resultant brown solution was allowed to evaporate at room temperature where upon dark brown crystalline compounds separated out. The crystals were collected by filtration, washed successively with cold ethanol and water and dried over fused calcium chloride.

The different instrumental techniques used for characterization of the compounds have been described in our earlier paper [28]. Analytical data are presented in Table 1.

Crystallography

Crystal data. $C_{22}H_{30}N_{10}O_9S_2Ni$, $M = 701.4$, triclinic, space group $P\bar{1}$ $a = 14.983(2)$, $b = 13.202(2)$, $c = 8.193(1)$Å, $\alpha = 91.54(1)^\circ$, $\beta = 77.38(1)^\circ$, $\gamma = 100.58(4)^\circ$, $U = 1554.4$ Å^3 (unit-cell parameters were calculated from least-squares fitting of 2θ angles of 25 selected strong reflections): λ(Mo-$K\alpha$) = 0.71073 Å, $D_M = 1.51$ g cm^{-3}, $Z = 2$, $D_c = 1.498$ g cm^{-3}, brown crystals $0.21 \times 0.25 \times 0.18$ mm^3, μ(Mo-$K\alpha$) = 0.816 mm^{-1}, $F(000) = 728$.

Data collection and processing. A total of 9458 reflections were collected (of which 7390 were unique) on a Rigaku AFC6 diffractometer at 298 K using graphite-monochromated Mo-$K\alpha$ radiation by ω–2θ mode, with $2\theta_{max}$ of 70° and a scan speed of 4° min^{-1}. Crystal stability was monitored by recording three check reflections at intervals of every 100 measurements. No significant variation in the intensity of these monitoring reflections was observed. Reorientation checking was done where $|w_{cal} - w_{obs}| > 0.2$. The time allowed for background count was constant (7 s). Intensities were corrected for Lorentz and polarization effects, but not for absorption.

Structure analysis and refinement. The structure was solved by Patterson and heavy-atom methods. Full-matrix least-squares refinement of the positional and isotropic thermal parameters of the non-hydrogen atoms resulted in a residual index of 0.17. Thermal parameters of two oxygen atoms O(5) and O(6), belonging to the nitrate group 2 were significantly high. Refinement was then carried out with anisotropic thermal parameters. The thermal parameters of the above-mentioned two atoms were very high at the end of the first cycle. An electron density map computed at this state indicated that there may be partial disorder in this region of the molecule. In subsequent refinement, the atoms of this nitrate group were kept fixed with final isotropic thermal parameters. Refinement of the remaining non-hydrogen atoms with anisotropic thermal parameters converged to the R value to 0.12. Twenty-two hydrogen atoms were located from successive difference electron density maps. Seven hydrogen atoms were placed at calculated positions. The positional and isotropic thermal parameters ($U = 0.05$ Å^2) of all the hydrogen atoms were kept fixed in the last two cycles of refine-

ment. The final R value was 0.097 with 4756 observed reflections $[I > 2.5\sigma(I)]$, $R_w = 0.106$, $w = [\sigma^2|F_o| + 0.033|F_o|^2]^{-1}$. The maximum value of shift/e.s.d. was 0.20 in the last cycle. The maximum residual electron density in a final difference electron density map was 2.4 eÅ^{-3}, lying close to the disordered nitrate group. Patterson synthesis and refinement were carried out using SHELX 76 [29]. Atomic scattering factors were taken from *International Tables for X-ray Crystallography* [30].

RESULTS AND DISCUSSION

Description of crystal structure

The ORTEP plot of one asymmetric unit is shown in Fig. 1, along with the atom-numbering scheme. The asymmetric unit consists of a nickel atom, coordinated by two molecules of the ligand (H_2L); two nitrate ions and a molecule of water remain uncoordinated. For the sake of convenience of discussion these two molecules of the ligand are designated as ligand A and ligand B and the individual atoms in the ligand are identified with suffix A and B where necessary. Selected bond distances and bond angles are listed in Table 2.

Each of the ligand molecules acts in a tridentate manner coordinating through the thione sulfur, the imine nitrogen and oxime nitrogen. The nickel atom is in a distorted octahedral environment, with each ligand occupying a meridional plane, which favours extensive delocalization of the electron cloud. The best description of the geometry around nickel is obtained when $S(1)_A$, $N(4)_B$, $N(4)_A$ and $S(1)_B$ are considered to form a square plane and $N(3)_A$ and $N(3)_B$ act as axial ligands. Angles generated at the Ni^{II} centre by the chelating donor points (N and S) differ slightly in the two coordinating ligands (Table 2). It appears that the angles at the Ni^{II} centre in the chelate rings are controlled to some extent by the ligand geometry.

Nickel–sulfur and nickel–nitrogen bond distances

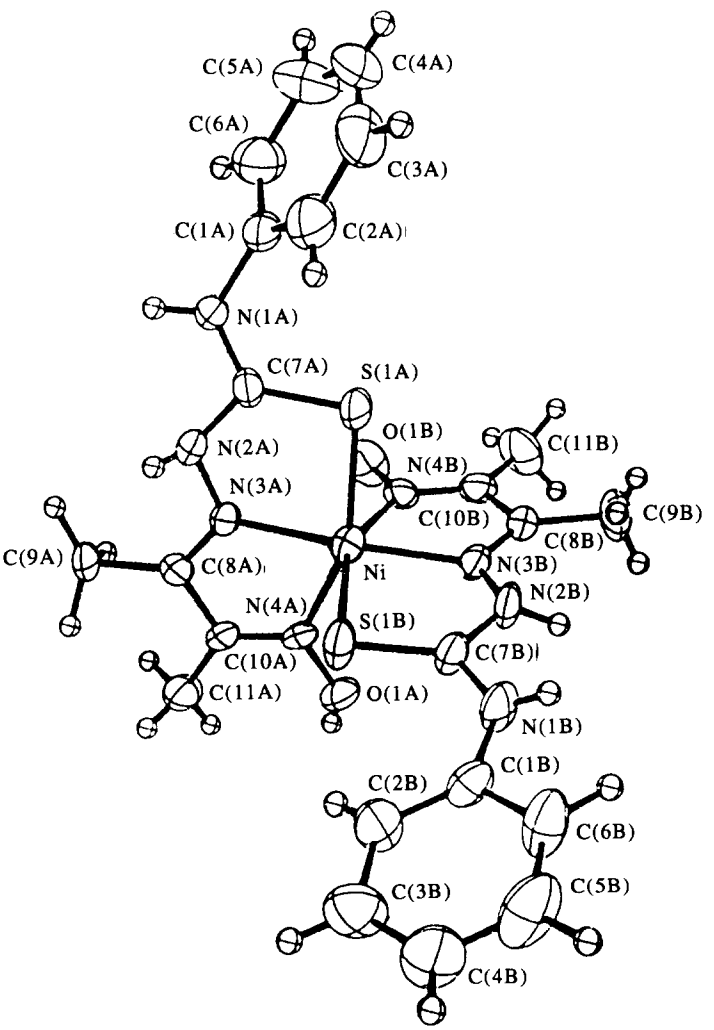


Fig. 1. Atom-labelling scheme for bis[3-hydroxyiminobutanone(4-phenylthiosemicarbazone)] nickel(II) nitrate monohydrate.

Table 2. Bond distances (Å) and angles (°) with estimated standard deviations in parentheses

Ni—S_A	2.373(2)	Ni—S_B	2.417(3)
Ni—$N(3)_A$	2.001(6)	Ni—$N(3)_B$	2.013(7)
Ni—$N(4)_A$	2.062(6)	Ni—$N(4)_B$	2.110(7)
	Ligand A		*Ligand B*
S—C(7)	1.680(9)		1.663(9)
O(1)—N(4)	1.405(0)		1.369(9)
N(2)—N(3)	1.381(8)		1.347(9)
N(3)—C(8)	1.298(9)		1.28(1)
N(4)—C(10)	1.30(1)		1.29(1)
S_A—Ni—$N(3)_A$	82.9(2)	S_B—Ni—$N(3)_B$	82.0(2)
S_A—Ni—$N(4)_A$	157.5(2)	S_B—Ni—$N(4)_B$	156.2(2)
$N(3)_A$—Ni—$N(4)_A$	75.8(2)	$N(3)_B$—Ni—$N(4)_B$	76.1(3)
$N(3)_A$—Ni—$N(4)_B$	107.1(2)	$N(3)_B$—Ni—$N(4)_A$	111.0(2)
S_A—Ni—$N(3)_B$	90.6(2)	S_B—Ni—$N(3)_A$	95.7(2)
S_A—Ni—$N(4)_B$	09.6(2)	S_B—Ni—$N(4)_A$	89.4(2)
$N(3)_B$—Ni—$N(3)_A$	172.7(2)	S_B—Ni—S_A	99.8(1)
$N(4)_A$—Ni—$N(4)_B$	90.0(3)		
	Ligand A		*Ligand B*
N(1)—C(7)—N(2)	114.1(7)		111.0(7)
S—C(7)—N(2)	122.1(6)		121.6(6)
S—C(7)—N(1)	123.8(6)		127.4(6)
N(3)—C(8)—C(10)	113.8(7)		113.9(7)
N(3)—C(8)—C(9)	125.3(7)		125.6(7)
C(9)—C(8)—C(10)	120.9(7)		121.5(7)
N(4)—C(10)—C(8)	112.6(6)		114.8(7)
C(8)—C(10)—C(11)	122.4(7)		119.8(8)
N(4)—C(10)—C(11)	125.0(7)		125.4(9)

are comparable to those in the nickel(II) complexes of 1-formylisoquinolinethiosemicarbazone [31] and 1-formylpyridinethiosemicarbazone [32].

As expected [32], the sulfur and imine nitrogen atoms in both molecules of the ligand are in the *cis* conformation with respect to the C(7)—N(2) bonds. The two donor nitrogen atoms, N(3) and N(4), in A and B also lie *cis* to each other. The hydrogen atoms attached to the oxime oxygen atoms could not be located.

The phenyl rings in ligands A and B are almost planar, while the thiosemicarbazide chains deviated from planarity. The dispositions of the phenyl rings with respect to the thiosemicarbazide moiety are different in the two molecules of the ligand. The dihedral angle between the mean planes of the phenyl ring and that calculated with S, C(7), N(2) and N(3) are 114.8(3)° and 18.5(2)° in A and B, respectively. The atoms N(3), C(8), C(10) and N(4), which form a five-membered ring with nickel, are almost planar in both ligand molecules.

Table 3. Selected torsion angles (°) with estimated standard deviations in parentheses

	Ligand A	Ligand B
C(1)—N(1)—C(7)—S	6(1)	9(1)
C(7)—N(1)—C(1)—C(2)	−66(1)	10(1)
N(3)—N(2)—C(7)—S	−10.8(4)	−10(1)
N(3)—N(2)—C(7)—N(1)	171.4(6)	171.3(7)
O(1)—N(4)—C(10)—C(8)	−179.4(6)	−177.9(6)
N(3)—C(8)—C(10)—N(4)	3.5(9)	5(1)
N(3)—C(8)—C(10)—C(11)	−178.3(7)	−176.2(8)

The crystal structure is stabilized by ionic interaction, van der Waals forces and a network of hydrogen bonds involving the water molecules, the nitrate ions and the donor atoms from the ligand molecules (Fig. 2). All the hydrogen atoms available for forming hydrogen bonds are involved in hydrogen bonding. Each of the hydrogen atoms bonded to $N(1)_A$, $N(2)_A$ and $N(1)_B$ and one of the hydrogen atoms, H(82), of the water molecule participate in formation of one hydrogen bond. The other hydrogen atom of the water molecule accepts three hydrogen bonds. Figure 2 shows a view of the crystal packing.

IR spectra

The IR spectrum of the complex recorded in a KBr disk exhibited a broad bond spanning the 3400–3100 cm^{-1} region, probably arising from the overlap of the ν_{OH} modes of the lattice water with the ν_{NH} and ν_{OH} modes of the ligand. the $\nu_{C=N}$ (imine) band observed at 1590 cm^{-1} in the free ligand was shifted towards

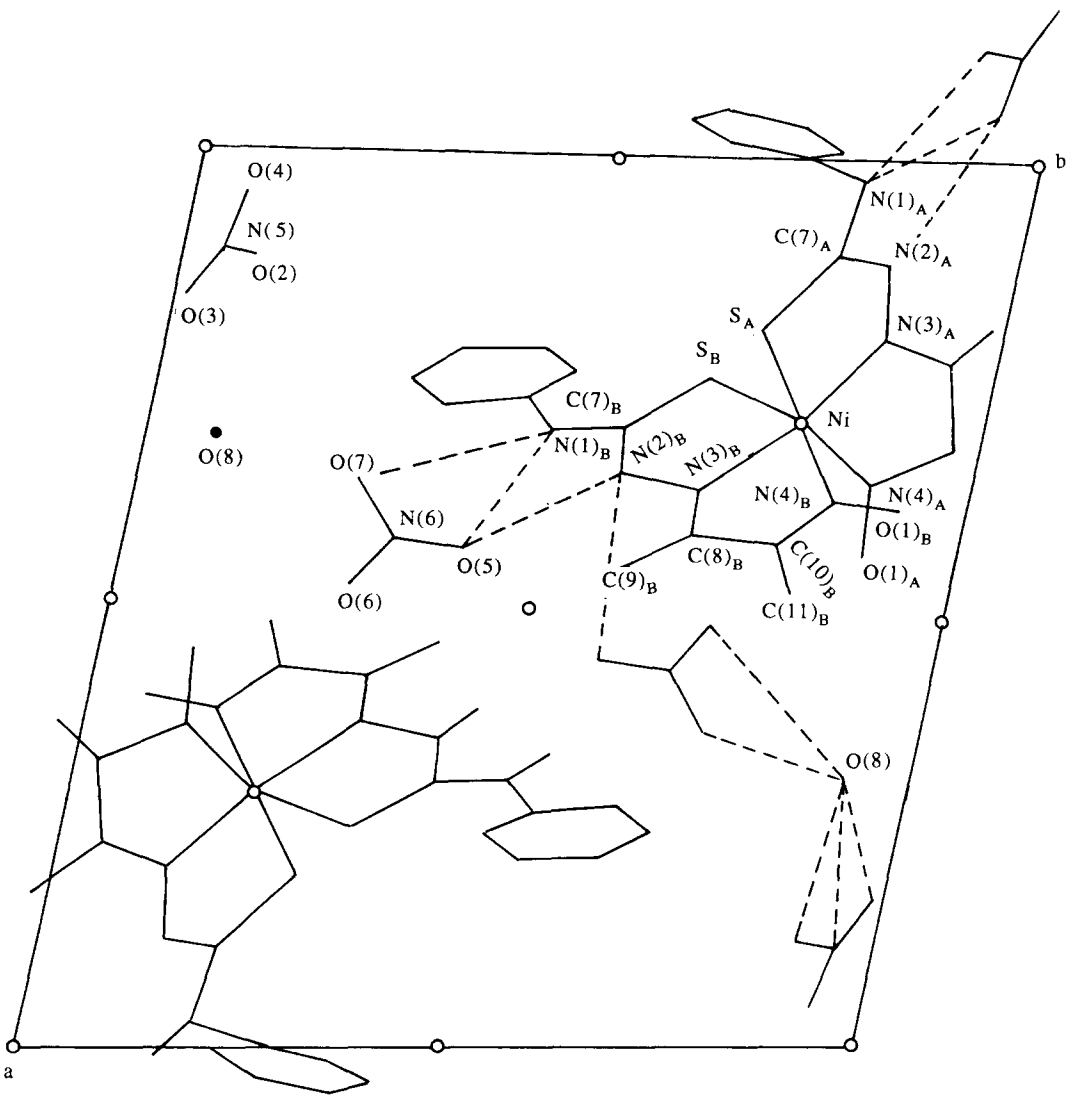


Fig. 2. The crystal structure of bis[3-hydroxyiminobutanone(4-phenylthiosemicarbazone)] nickel(II) nitrate, monohydrate.

lower wavenumber by 10–15 cm^{-1}, indicating involvement of the imine nitrogen, N(3), in coordination [22–24]. Participation of the oxime nitrogen N(4), in coordination was indicated by a positive shift of 20 cm^{-1} of the ligand $\nu_{C=N}$ (oxime) mode at 1440 cm^{-1}, as well as a hypsochromic shift of 30 cm^{-1} of the $\nu_{N=O}$ mode around 1010 cm^{-1}. The ν_{CS} mode of the ligand at 750 cm^{+1} is lowered by 10–15 cm^{-1}, indicating participation of the thione sulfur in coordination [22–24].

Magnetic moment and electronic spectra

The magnetic moment, measured at 303 K, was found to be in the range 2.95–3.20 B.M. which is quite normal for octahedral Ni^{II} complexes.

The electronic spectra of the complexes recorded in alcohol and Nujol mull, exhibit two bands of comparable intensity ($\varepsilon \sim 100$) at 990 and 800 nm. The band around 800 nm is broad and seems to be made up of two overlapping bands. The band around 990 nm is assigned to the $^3A_2 \rightarrow {}^3T_2$ (ν_1) transition and that around 800 nm to overlapping of the spin-allowed transition $^3A_2 \rightarrow {}^3T_1$ (ν_2) with the spin-forbidden transition $^3A_2 \rightarrow {}^1E$ [33]. Another band of comparable intensity at 550 nm is observed in the mull spectrum. This may arise because of splitting of the ν_2 band in the low symmetry ligand field present in the complex [33]. The ν_3 band is masked by the high intensity charge transfer bands at 450 and 350 nm in Nujol, which shift to 390 and 300 nm, respectively, in ethanol solution. The first CT band is probably a MLCT transition, whereas the second CT band is probably a result of an intraligand transition. From the spectra

the crystal field splitting (10 Dq) produced by two TSCDAMO/4PhTSCDAMO ligands around the Ni^{+2} centre is found to be 10,100 cm^{-1}. This may be compared with the 10Dq value obtained for the $Ni(TSC)_3^{+2}$ complex [34] of 10,000 cm^{-1}.

Cyclic voltammetry

On an initial positive scan all the complexes exhibit an irreversible oxidation around 0.95–1 V. The free ligands and their zinc complexes, however, do not undergo oxidation up to 1.2 V. This strongly suggests that the above anodic peak is owing to Ni^{II}/Ni^{III} oxidation. As mentioned earlier, the Ni^{II} complex is in a distorted octahedral environment. After oxidation, the resultant Ni^{III} complex, being a d^7 species, would undergo Jahn–Teller distortion which would result in a severe strain on the octahedral complex, ultimately leading to dissociation of the ligand from the complex. This may explain the irreversible nature of the complex.

On cathodic scan the TSCDAMO complexes exhibit four reductions at −0.65 (irreversible), −1.13 (irreversible), −1.375 (reversible, $\Delta E = 100$ mV) and −1.61 V (quasi-reversible, $\Delta E = 120$ mV). It is well known [35] that oximes undergo reduction in $2e^-$ steps. In the first step a ketimine is formed, which is then reduced to amine. In the present case the first two peaks at −0.65 and −1.13 V are assigned to the reduction of the oxime part of the ligand. The other two cathodic couples at −1.375 and −1.61 V are assigned to the reduction of the imine part of the thiosemicarbazone moiety. For 4PhTSCDAMO complexes a similar behavior is observed, except that there is a slight cathodic shift of the reductive couples; moreover, the 1st, 3rd and the 4th couples are irreversible in this case, while the 2nd couple behaves reversibly.

REFERENCES

1. Kruger, H. J. and Holm. R. H., *Inorg. Chem.*, 1989, **28,** 1148.
2. Kruger, H. J. and Holm, R. H., *Inorg. Chem.*, 1987, **26,** 3645.
3. Kumar, M., Day, R. O., Colpas, G. J. and Maroney, M. J., *J. Am. Chem. Soc.*, 1989, **111,** 5974.
4. Colpas, G. J., Kumar, M., Day, R. O. and Maroney, M. J., *Inorg. Chem.*, 1990, **29,** 4779.
5. Turner, M. A., Driessen, W. L. and Reedijk, J., *Inorg. Chem.*, 1990, **29,** 3331.
6. Rosenfield, S. G., Wong, M. L. Y., Stephen, D. W. and Mascharak, P. K., *Inorg. Chem.*, 1987, **26,** 4119.
7. Rosenfield, S. G., Armstrong, W. H. and Mascharak, P. K., *Inorg. Chem.*, 1986, **26,** 3014.
8. Baidya, N., Olmstead, M. M. and Mascharak, P. K., *J. Am. Chem. Soc.*, 1992, **114,** 9666.
9. Choudhury, S. B., Ray, D. and Chakravorty, A., *Inorg. Chem.*, 1990, **29,** 4603.
10. Lu, Z., White, C., Rheingold, A. L. and Crabtree, R. H., *Inorg. Chem.*, 1993, **32,** 3991.
11. Mandal, S., Bharadraj, P. K., Zhose, Z. and Mak, T. C. W., *Polyhedron*, 1995, **14,** 919.
12. J. R. Lancaster, Jr., (ed.), *The Bioinorganic Chemistry of Nickel.* VCH Publishers, New York, 1988.
13. Cammack, R., Patil, D. S., Hatchikian, E. C., Fernande, V. M., *Biochem. Biophys. Acta*, 1987, **98,** 912.
14. Tennent, D. L. and McMillin, R. D., *J. Am. Chem. Soc.*, 1979, **101,** 2307.
15. Lum, V. and Gray, H. B., *Isr. J. Chem.*, 1981, **21,** 23.
16. Engeseth, H. R., McMillin, D. R. and Ulrich, E. L., *Inorg. Chim. Acta*, 1982, **67,** 145.
17. Blaszak, J. A., Ulrich, E. L., Markley, J. L. and McMillin, D. R., *Biochemistry*, 1981, **21,** 6253.
18. Nandi, A. K., Chaudhuri, S., Mazumder, S. K. and Ghosh, S., *Acta Cryst.*, 1984, **C40,** 1193.
19. Nandi, A. K., Sheldrick, W. S. and Ghosh, S., *Acta Cryst.*, 1986, **C42,** 1570.
20. Bregant, F., Pacor, S., Ghosh, S., Chattopadhyay, S. K. and Sava, G., *Anticancer Res.*, 1993, **13,** 1007.
21. Chattopadhyay, D., Mazumder, S. K., Lowe, P., Schwalbe, C. H., Chattopadhyay, S. K. and Ghosh, S., *J. Chem. Soc., Dalton Trans.*, 1991, 2121.
22. Chattopadhyay, S. K., Hussain, M., Ghosh, S. and Guha, A. K., *Trans. Met. Chem.*, 1990, **15,** 473.
23. Chattopadhyay, S. K. and Ghosh, S., *Inorg. Chim. Acta*, 1987, **131,** 15.
24. Chattopadhyay, S. K. and Ghosh, S., *Inorg. Chim. Acta*, 1989, **163,** 245.
25. Nandi, A. K., Chaudhuri, S., Mazumdar, S. K. and Ghosh, S., *Inorg. Chim. Acta*, 1984, **92,** 235.
26. Thompson, R. L., Davis, J., Russel, F. B. and Hutchings, G. H., *Proc. Soc. Expt. Bio. Met.*, 1953, **84,** 496.
27. Terrin, D. D., *Topics Curr. Chem.*, 1976, **64,** 181.
28. Chattopadhyay, S. K., Mak, T. C. W., Luo, B., Thompson, L. K., Rana, A. and Ghosh, S., *Polyhedron*, 1995, **14,** 3661.
29. Sheldrick, G. M., *SHELX* 76, *Program for Crystal Structure Determination*, University of Cambridge, Cambridge, 1976.
30. *International Tables for X-ray Crystallography*, Vol. 4. Kynoch Press, Birmingham, 1974.
31. Mathew, M. and Palenik, G. J., *J. Am. Chem. Soc.*, 1973, **91,** 6310,
32. Campbell, M. J. M., *Coord. Chem. Rev.*, 1975, **15,** 279.
33. Lever, A. B. P., *Inorganic Electronic Spectroscopy*, 2nd edn. Elsevier, Amsterdam, 1984, pp. 507–520.
34. Jorgenson, C. K., *J. Inorg. Nucl. Chem.*, 1962, **24,** 1571.
35. Lund, H., *Acta Chem. Scand.*, 1964, **18,** 563.

Pergamon

PII: S0277-5387(96)00445-7

Polyhedron Vol. 16, No. 11, pp. 1931–1935, 1997
© 1997 Elsevier Science Ltd
All rights reserved. Printed in Great Britain
0277-5387/97 $17.00+0.00

Complexes of nickel(II), palladium(II) and platinum(II) with 2,6-bis(mercaptomethyl)pyridine

V. E. Márquez[a]* and J. R. Anacona[b]

[a]Departamento de Química Aplicada, Instituto Universitario de Technología, Apartado Postal 255, Cumaná, Venezuela

[b]Departmento de Química, Universidad de Oriente, Apartado Postal 208, Cumaná, Venezuela

(Received 8 January 1996; accepted 30 August 1996)

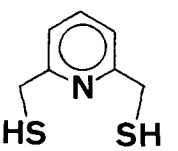
Abstract—2,6-Bis(mercaptomethyl)pyridine (H_2L) and its binuclear nickel(II), palladium(II) and platinum(II) complexes, containing the dianion as a bridging ligand, were prepared and characterized by physicochemical and spectroscopic data. Square-planar geometries are proposed for these divalent metal complexes. Cyclic voltammetry of Ni_2L_2 in DMSO shows a reversible one-electron reduction wave at -1.48 V *vs* a $Ag/AgBF_4$ reference electrode. Quantitative reduction of this complex by controlled potential electrolysis at -1.80 V yielded the corresponding Ni^I product as shown by ESR spectroscopy. © 1997 Elsevier Science Ltd. All rights reserved.

Keywords: pyridine derivative; binuclear metal complexes.

Interest in the synthesis, magnetic, spectroscopic and electrochemical properties of bridged polynuclear complexes has risen considerably in recent years because of their importance in the understanding of the mechanism of magnetic interactions between metal ions [1,2].

The behaviour of the mercaptide ion as a donor in transition metal complexes has not been subjected to such detailed study as a number of other donor groups. This arises, in part, because the mercapto group often gives metal ion derivatives that are extremely insoluble, bridged or even polymeric. Furthermore these substances are easily oxidized. These properties greatly complicate the characterization of mercapto complexes. However, the theoretical interest and biological importance of mercaptans means that elucidation of the manner of interaction of this functional group with metal ions is of great interest [3].

One of the most distinguishing properties associated with the mercaptide group is its ability to react readily with many metals to form complexes containing sulfur bridges and, in order to investigate the characteristics of the mercaptide complexes further, particularly the bridging and reactivity of coordinated sulfur atoms, the present work was undertaken. The ligand studied, H_2L = 2,6-bis(mercaptomethyl) pyridine (**1**), is similar to 2-(2-mercaptoethyl)pyridine and β-mercaptoetylamine in its donor atoms, but differs in stereochemistry and type of nitrogen atom and in the size of the chelate ring it may form.



(1)

EXPERIMENTAL

Materials

Published methods were used to prepare 2,6-bis(bromomethyl)pyridine [4], and 2,6-bis(mercaptomethyl)pyridine [5–7]. Solvents used for synthetic and spectroscopic work were distilled over appropriate drying agents prior to use. All other

* Author to whom correspondence should be addressed.

chemicals were of analytical grade, available commercially. Unless otherwise stated the reactions were carried out under dry dinitrogen, but the final work-up was performed in air.

Physical measurements

The IR spectra were recorded on a Perkin–Elmer model 983 spectrophotometer using KBr or CsBr disks. The spectra were calibrated against the 1603 cm^{-1} band of polystyrene. Mass spectra were obtained from A.E.I. MS9, MS12 or MS30 spectrometers at 70 eV. Measurements of *d–d* transitions in the visible and near-IR region were taken with a Cary recording spectrophotometer model 17D, while a Pye Unicam PU8800 spectrophotometer was used for recording the visible and UV spectra. Conductance measurements were made using a Wayne Kerr universal bridge. The conductivity cell was calibrated with aqueous KCl. The electrochemical measurements were made on a Princeton Applied Research (PAR) electrochemistry system, model 170. All readings were taken using three potentiostatic systems and are quoted referenced to an external silver/silver(I) pseudo-reference electrode with tetra-*n*-butylammonium tetrafluoroborate (0.1 M) as supporting electrolyte. Magnetic moments were recorded on a John Matthey magnetic susceptibility balance model MSB1. Microanalyses were performed by the Cambridge University Microanalytical Department. ESR spectra were measured on a Varian E109 model spectrophotometer (*X*-band).

Preparation of bis[2,6-*bis*(*mercaptomethyl*)*pyridino*] *dinickel*(II)

Method I. Nickel sulfate hexahydrate (6 g, 22.8 mmol) was dissolved in concentrated ammonia solution ($d = 0.880$ g cm^{-3}, 20 cm^3) and water (75 cm^3). To this solution was added, with stirring, 2,6-bis (mercaptomethyl)pyridine (1.98 g, 11.6 mmol) dissolved in methanol (15 cm^3). A light brown precipitate was formed immediately. The solid was separated by filtration and dried *in vacuo* over sulfuric acid. Yield 2.23 g, 85.5%

Method II. Nickel chloride hexahydrate (1.19 g, 5 mmol) was dissolved in absolute ethanol (50 cm^3). To this solution was added slowly, with stirring, 2,6-bis(mercaptomethyl)pyridine (0.86 g, 5 mmol) in absolute ethanol (13 cm^3). A light brown precipitate was formed immediately and separated by filtration, washed with absolute ethanol, and diethyl ether and then dried *in vacuo* over sulfuric acid. Yield 0.95 g, 82.6%.

Preparation of bis[2,6-*bis*(*mercaptomethyl*)*pyridino*] *dipalladium*(II)

Potassium chloride (0.3 g, 4 mmol) and palladium chloride (0.3 g, 1.7 mmol) were dissolved in water (50 cm^3) and concentrated ammonium hydroxide (17 cm^3). Upon stirring and warming all the solid had dissolved. To this solution was added, with stirring, 2,6-bis(mercaptomethyl)pyridine (0.4 g, 2.3 mmol) dissolved in water (2.5 cm^3) and 30 drops of concentrated hydrochloric acid. An orange precipitate was formed immediately. Stirring was continued for 10 minutes, then the solution was filtered and the orange solid washed with water, methanol and diethyl ether and dried *in vacuo* over sulfuric acid. Yield 0.58 g, 90%.

Preparation of bis[2,6-*bis*(*mercaptomethyl*)*pyridino*] *diplatinum*(II)

Platinum chloride (0.3 g, 1.1 mmol) and potassium chloride (0.3 g, 4 mmol) were dissolved in water (17 cm^3) and concentrated ammonium hydroxide (10 cm^3). Upon stirring and warming all the platinum chloride had dissolved. To this solution was added, with stirring, 2,6-bis(mercaptomethyl)pyridine (0.2 g, 1.2 mmol) dissolved in methanol (10 cm^3). A pale yellow precipitate formed at once. The mixture was warmed, with stirring, for 1 h and then filtered. The pale yellow solid was washed with water, methanol and diethyl ether and dried *in vacuo* over sulfuric acid. Yield 0.54 g, 87%.

RESULTS AND DISCUSSION

The ligand 2,6-bis(mercaptomethyl)pyridine was prepared from a mixture of 2,6-bis(bromomethyl) pyridine with thiourea and reacted with nickel(II), palladium(II) and platinum(II) salts to form, preferentially, binuclear metal complexes. The complexes were all amorphous precipitates. In strongly ammoniacal solution or in neutral methanolic solution, complexes of stoichiometry M_2L_2 were formed. The analytical data supporting the stoichiometry of these complexes are given in Table 1 together with the molar conductivity values. The complexes are believed to be dimeric. Their solubilities are quite low but after heating and prolonged shaking they can be dissolved to a small extent in DMSO, DMF, CH_2Cl_2, chloroform or nitromethane. The palladium(II) and platinum(II) complexes proved to be very insoluble in both polar and non-polar solvents. The conductivity measurement of the Ni_2L_2 complex in DMSO, DMF and nitromethane shows that it is a non-electrolyte (Table 1).

Transition metal ions tend to expand their coordination number if an electron donor group is available. Treatment of planar four-coordinate complexes with pyridine usually results in expansion of the coordination number to six [8]. However, the reaction of pyridine with Ni_2L_2, Pd_2L_2 or Pt_2L_2 failed to produce such a derivative and the starting materials were recovered unchanged.

The pertinent IR absorption bands of these com-

Table 1. Physical and analytical data[a] for the 2,6-bis(mercaptomethyl)pyridine complexes

Compound	Colour	Analysis (%)			Λ^b (S cm^2 mol^{-1})
		C	H	N	
H_2L	Light transparent	49.3 (49.1)	5.3 (5.3)	8.2 (8.2)	
Ni_2L_2	Brown	36.8 (36.8)	3.0 (3.1)	6.1 (6.1)	4, 5,[c] 7[d]
Pd_2L_2	Orange	30.2 (30.4)	2.6 (2.6)	5.0 (5.1)	
Pt_2L_2	Light yellow	23.1 (23.0)	1.6 (1.9)	3.7 (3.9)	

[a] Calculated values are given in parentheses.
[b] In DMSO.
[c] In acetonitrile.

plexes are reported in Table 2 and are all consistent with the absence of the band associated with the S—H stretching vibrational mode (2250 cm^{-1}). The spectra of these complexes show similarities to one another and exhibit four characteristic bands in the 1600—1400 cm^{-1} region attributable to the pyridine ring. The presence of ν(M—S) and ν(M—N) at *ca* 350 and 420 cm^{-1}, respectively, support coordination by the ligand [9].

The mass spectra of the nickel(II), palladium(II) and platinum(II) complexes showed two principal peaks: one corresponding to the dimeric molecular weight and the other one corresponding to a half molecular weight owing to formation of the monomer. The mass spectrum of the nickel(II) complex exhibited the highest mass peaks centred around m/z 456; this corresponds to a dimeric formulation, Ni_2L_2, which has an expected m/z 454 based on ^{58}Ni and ^{32}S. In the same way, Pd_2L_2 and Pt_2L_2 complexes display no mass peaks above the band of isotopic peaks centred around m/z 550 and 728, respectively, which correspond to expected molecular weights based on ^{106}Pd and ^{195}Pt isotopes.

Magnetic moment measurements of the Ni_2L_2, Pd_2L_2 and Pt_2L_2 complexes show that they are diamagnetic, suggesting that they have square-planar structures. They are low-spin d^8 transition metals without unpaired electrons. The electronic spectrum of Ni_2L_2 was recorded in DMSO, DMF, methanol and acetonitrile and two peak bands at 17,510 and 23,750 cm^{-1} appeared clearly resolved and they were assigned to $^1A_{1g} \rightarrow {}^1A_{2g}$ and $^1A_{1g} \rightarrow {}^1B_{1g}$ transitions, respectively, in a square-planar geometry [10]. The diamagnetic nature of the complexes supports the above geometry. The electronic spectrum of Ni_2L_2 also displays bands above 30,000 cm^{-1} which can be assigned to the S → M charge transfer and L → L* transitions of the dinegative ligand, consistent with other sulfur ligands [10,11].

Based on physicochemical and spectroscopic data a possible sulfur-bridged dimeric structure may be assumed for the divalent square-planar complexes (Fig. 1). These complexes are analogous to the 2-(2-mercaptoethyl)pyridine and β-mercaptoethylamine complexes described previously [12].

Electrochemistry and ESR spectrum of the Ni_2L_2 *complex*

The cyclic voltammetry of the nickel(II) complex was investigated in DMSO as solvent with 0.1 M in tetra-n-butylammonium tetrafluoroborate as supporting electrolyte. The complex dissolved freely in DMSO to yield a deep brown solution. Figure 2 shows a voltammogram for the nickel(II) complex indicating that the compound underwent a fully reversible one-electron reduction at −1.48 V *vs* Ag/$AgBF_4$ reference electrode. Cyclic voltammetry at a scan rate 100 mV s^{-1} showed a peak separation ($E_{pc} - E_{pa}$) of 70 mV and with the ratio of the peak cathodic and anodic currents being nearly 1.0, suggesting that the electrode

Table 2. Infrared bands (cm^{-1}) and assignments

Compound	S—H (str)	Pyridine ring bands				M—S	M—py
H_2L	2250	1588	1572	1452	1421		
Ni_2L_2		1598	1559	1458	1422	350	430
Pd_2L_2		1594	1565	1459	1404	355	430
Pt_2L_2		1586	1568	1459	1408	360	400

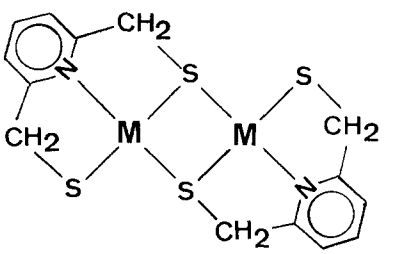


Fig. 1. Proposed structure for M_2L_2 complexes, M = Ni^{II}, Pd^{II} or Pt^{II}.

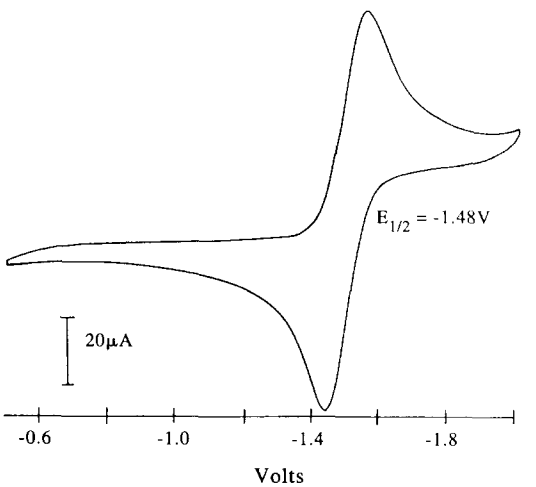


Fig. 2. The cyclic voltammogram of Ni_2L_2 in DMSO solution. Scan rate 100 mV s^{-1}.

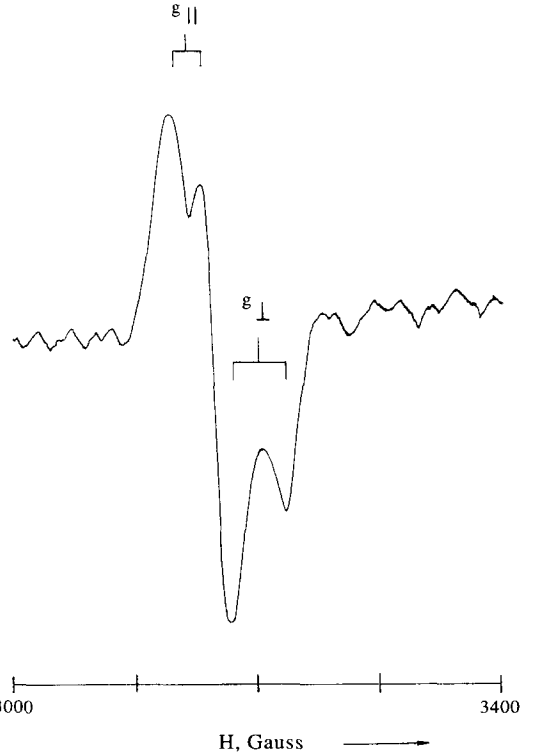


Fig. 3. ESR spectrum of the electrogenerated nickel(I) complex in DMSO at 77 K.

reactions approach Nernstian behaviour. The high negative reduction potential nickel(II) → nickel(I) shows that the metal ion is highly stabilized by the strong sigma-donor properties, which overcomes the π-acceptor properties of the ligand [13]. The nickel(I) was generated and characterized using controlled potential electrolysis and ESR techniques, respectively.

One cannot distinguish between an authentic Ni^{I} species and Ni^{II}-stabilized ligand radical species on the basis of magnetic moment measurements alone. An advantage of ESR studies is that one can in fact distinguish between the two possibilities. The ESR measurements for the one-electron reduction product show an axially symmetric spectrum with $g_{\perp} < g_{\parallel}$ suggesting a d^9, Ni^{I} configuration, i.e. $(e_g)^4(a_{1g})^2(b_{2g})^2(b_{1g})^1$. An isotropic ESR spectrum with no hyperfine splitting and a g value very nearly equal to the free electron value (2.0023) should be expected in the case of a Ni^{II}-stabilized ligand radical species. The reduction of the Ni^{II} complex in DMSO with supporting electrolyte was carried out by the controlled potential technique at −1.80 V under a constant stream of argon. The colour of the initial solution slowly changed from brown to black. The ESR spectrum of this solution as a DMSO glass at 77 K showed two g values in accord with previous ESR results of this d^9 species with similar ligands [14]. The g values, $g_{\parallel} = 2.091$ and $g_{\perp} = 2.051$, are consistent with the presence of a $S = \frac{1}{2}$ complex ligated by groups with δ-donor properties [15,16]. The hyperfine coupling patterns owing to ^{61}Ni nuclear spin $I = \frac{3}{2}$ (1.19% natural abundance) could not be completely resolved, probably as a result of the influence of the supporting electrolyte. This phenomenon, whereby added salts improve the resolution, has been noted by other authors [17]. The ESR spectrum of the Ni^{I} complex at 77 K can be seen in Fig. 3. In the absence of information such as the nickel hyperfine coupling constant, it is not possible to estimate the extent of delocalization of the unpaired electron on to the ligand [18].

Attempts to characterize further the nickel(I) complex were unsuccessful. The dark brown electrolysed solution at −1.80 V was transferred by syringe to a Schlenk tube and the nickel(I) species was isolated as an oil by the addition of dry, oxygen-free diethyl ether followed by evaporation under reduced pressure. The oil remaining could not be crystallized on trituration with a little cold MeOH.

Acknowledgements—V.E.M. thanks to Prof. Lord Lewis and Dr E. Constable for many useful suggestions and encouragement.

REFERENCES

1. Willet, R. D., Gatteshi, D. and Kahn, O., *Magnetic Structural Correlation in Exchange-Coupled Systems*, NATO ASI series. Reidel, Dordrecht, The Netherlands, 1985, p. 523.
2. Li, X., Hang, Z., Liao, D., Van, S., Li, Y. and Wang, G., *Polyhedron*, 1990, **13,** 99.
3. Livingstone, S. E., *J. Chem. Soc.*, 1956, 437.
4. Baker, W. O., Buggle, K. M., McOmie, J. F. W. and Watkin, D. A. M., *J. Chem. Soc.*, 1958, 3594.
5. Bristol-Myers Co., US Patent 3 290 319/1966; *Chem. Abstr.*, 1967, **66,** 115609K.
6. Banyu Pharmaceutical Co., Ltd, Japanese Patent, 7 217 778/1972; *Chem. Abstr.*, 1972, **77,** 151979S.
7. Márquez, V. E., Ph.D. Thesis, University of Cambridge, Cambridge, 1988.
8. Jicha, D. C. and Busch, D. H., *Inorg. Chem.*, 1962, **1,** 872.
9. Nakamoto, K., *Infrared Spectra of Inorganic and Coordination Compounds*, 2nd edn., Wiley-Interscience, New York, 1970.
10. Maki, G., *J. Chem. Phys.*, 1958, **28,** 651; 1958, **29,** 162, 1129.
11. Ali, M. A., Haroon, C. M., Nazimuddin, M., Majumder, S. M. M. H., Tarafder, M. T. H. and Khair, M. A., *Trans. Met. Chem.*, 1992, **17,** 133.
12. Jicha, D. C. and Busch, D. H., *Inorg. Chem.*, 1962, **1,** 878, 884; J. H. Mason, *J. Chem. Soc.*, 1952, 146.
13. Constable, E. C., Lewis, J., Liptrot, M. C., Raithby, P. R. and Schröder, M., *Polyhedron*, 1983, **2,** 301.
14. Lewis, J. and Schröder, M., *J. Chem. Soc., Dalton Trans.*, 1982, 1085.
15. Borefield, E. K., Krost, D. A., Edwards, D. S., Van Derneer, D. G., Trytko, R L. and O'Rear, S. P., *J. Am. Chem. Soc.*, 1981, **103,** 6219.
16. Bowmaker, G. A., Boyd, P. D. W. and Campbell, G. K., *Inorg. Chem.*, 1983, **22,** 1208.
17. Cockle, S., Hill, H. A. D., Ridsdale, S. and Williams, R. J. P., *J. Chem. Soc., Dalton Trans.*, 1972, 297.
18. Camus, J., Meghea, A. and Anacona, J. R., *Polyhedron*, 1996, **15,** 2953.

Pergamon

PII: S0277-5387(96)00430-5

Polyhedron Vol. 16, No. 11, pp. 1937–1943, 1997
© 1997 Elsevier Science Ltd
All rights reserved. Printed in Great Britain
0277-5387/97 $17.00+0.00

Photogeneration and characterization of Group 6 metal carbonyl derivatives on alumina

I. M. Baibich,[a]* J. H. Z. Dos Santos,[a] F. C. Stedile,[a] V. E. Santarosa[a] and I. J. R. Baumvol[b]

[a] Instituto de Química, Universidade Federal do Rio Grande do Sul, 91540-000 Porto Alegre, Brazil

[b] Instituto de Física, Universidade Federal do Rio Grande do Sul, 91540-000 Porto Alegre, Brazil

(Received 5 July 1996; accepted 22 August 1996)

Abstract—The photochemically-induced CO substitution reactions of $[M(CO)_6]$ (M = Cr, Mo, W) have been investigated in the presence of triphenylphosphine (PPh_3) and γ-alumina. The metal loading was determined by Rutherford backscattering spectrometry (RBS) and the generated species were analysed by Fourier transform IR spectroscopy (FT-IR) and ^{13}C NMR spectroscopy. The metal loading on the alumina surface was seen to increase with the irradiation time reaching 0.6, 0.8 and 3.4% for Cr, W and Mo, respectively. The ligand cone angle plays an important role in the case of Cr, where only the *trans* disubstituted species was found on the alumina surface. However, it is less important for the two other metals, where the *cis* compound was formed preferentially and the electronic *cis*-labilization factor seems more important. After grafting, only the disubstituted species was seen to remain on alumina evidencing a stronger interaction with the support than in the case of the monosubstituted and the hexacarbonyl compounds. © 1997 Elsevier Science Ltd. All rights reserved.

Keywords: metal carbonyl derivatives; alumina; Group 6 metals; substitution reactions; characterization.

Transition metal carbonyls anchored on various inorganic supports, such as alumina, zeolite and silica, have been intensively studied due to their catalytic properties. Their behavior is of particular interest as precursors that lead by decomposition to highly dispersed metals on the support surface and to low-valence metal catalysts without reduction treatments. These catalysts can be several times more active, in reactions such as metathesis of alkenes, hydrogenation of CO or alkenes, than their analogous supported metal oxides systems that have higher valences [1].

Group 6 metal carbonyls anchored on inorganic oxides have been extensively studied since the pioneering researches of Burwell *et al.* [2] and Smith *et al.* [3] on the decarbonylation and catalytic properties of $[Mo(CO)_6]$ and its derivatives subcarbonyl species immobilized on the Al_2O_3 surface. In particular, chromium(VI) compounds supported on silica are among the most used and studied catalyst systems in petrochemistry. Among them, the Philips catalyst Cr/SiO_2 is largely employed for the low-pressure polymerization of ethylene. This supported catalyst can be achieved by several routes, such as deposition of $[Cr(CO)_6]$, followed by thermal treatment, among others [4].

Supported molybdenum systems can act as catalysts for hydrogenation, hydrotreating, metathesis, isomerization and hydrogenolysis reactions. The surface structure of thermally reduced catalysts (a reduction step is necessary in order to activate such systems) has often three or four Mo oxidation states, depending on the reduction temperature. A more recent application for immobilized molybdenum systems is the attempt to replace the expensive rhodium in the three-way catalysts that contain supported platinum, palladium and rhodium, which are widely used in automobile exhaust converters. The Pd–Mo interaction in such systems was very recently proposed to be achieved *via* the immobilization of either a bimetallic cluster $[Pd_2Mo_2(Cp)_2(CO)_6(PPh_3)_2]$ or the organometallic precursors $[PdCl_2(PhCN)_2]$ and $[Mo(CO)_6]$ on MgO [5]. The supported tungsten compound applications

* Author to whom correspondence should be addressed.

resemble those of molybdenum. In particular, it is worth mentioning the activity of $[W(CO)_6]$ in propene metathesis, when anchored on Al_2O_3, SiO_2, ZrO_2 and ThO_2.

Besides their catalytic activity, the hexacarbonyl complexes of Cr, Mo and W have been suggested to be viable precursors to film growth due to their high vapor pressures and their photolability in the UV region [6]. Thus, continuous wave visible [7] and excimer lasers [8] have been mentioned to deposit conformal metal films for microelectronic applications.

In order to combine the catalytic activity of the Group 6 metal carbonyls with their intrinsic photosensitivity we have chosen a convenient route to obtain a metallic deposit on alumina, in the presence of triphenylphosphine and activated by UV radiation. In a previous work [9] the photochemically induced CO substitution reactions of $[Cr(CO)_6]$ with the tertiary group 15 of ligands (LPh_3, where L = P, As or Sb, Ph = phenyl), in the presence of γ-alumina was demonstrated to induce the exclusive generation of the [*trans*-$Cr(CO)_4(PPh_3)_2$] species on the support surface. Upon descending the group series, a neat reduction in the stereospecificity of the species being immobilized on the support was observed. This difference was attributed to the concomitant decrease in the cone angle [10] and, therefore, to the steric effect of the ligand L.

In the present work the metal loading on alumina surface from Group 6 metal carbonyls and their derivatives by photochemical activation was investigated by Rutherford backscattering spectrometry (RBS), Fourier-transform IR spectroscopy (FT-IR) and ^{13}C NMR spectroscopy. The metal loading dependence on the irradiation time was followed by RBS, while by FT-IR and ^{13}C NMR the chemical species present in the decanted solution and on alumina, as well as those extracted from the support were identified.

EXPERIMENTAL

Materials

The starting materials $[Cr(CO)_6]$, $[Mo(CO)_6]$, $[W(CO)_6]$ and PPh_3 were purchased from Aldrich Chemical Co. The Al_2O_3 (Oxyde C, 90 $m^2\ g^{-1}$) provided by Degussa was treated at 723 K in air for 3 h and then *in vacuo* for 1 h. The solvents (purum grade) were deoxygenated and dried with Na. Gaseous Ar and N_2 were purified by passage over BASF catalyst and through molecular sieves.

Primary sample preparation

All the experiments were performed under inert atmosphere using the Schlenk technique. Metal carbonyls were supported on alumina by mixing the pretreated support (400 mg) and a pentane solution of the metal hexacarbonyls (40 cm^3, 2% M) at room temperature for 30 min under stirring.

Photochemical reactions

The photochemical reactions were performed under an inert atmosphere using a Philips HPL-N (125 W) UV lamp fitted into a Pyrex cold finger. The minimum transmitted UV wavelength was limited by the Pyrex glass to 220 nm. In a typical photochemically induced CO substitution reaction $[Cr(CO)_6]/\gamma$-Al_2O_3 and PPh_3 were added to pentane. The resulting slurry was placed inside the photochemical reactor. The solutions were irradiated up to 360 min, but samples of the solution and of the solid phase were withdrawn at regular intervals to be analysed.

Fourier-transform IR spectroscopy (FT-IR)

Transmission FT-IR spectra were recorded at room temperature on a FT Mattson 3020 spectrometer (2 cm^{-1} resolution). The study was restricted to the mid-IR region (4000–1100 cm^{-1}) due to strong bulk absorption of alumina in the low wavenumber region. The solution was analysed with a pair of matched NaCl solution cells (0.10 mm pathlengths), while the solid phases were analysed as Nujol mulls. These solid samples were analysed as withdrawn from the reactor and after they were washed with pentane. The spectra were calibrated against the 1601.4 cm^{-1} band of a standard polystyrene film.

^{13}C NMR spectroscopy

The ^{13}C NMR spectra were obtained in $CDCl_3$ solution in a Varian Gemini VXR 200 MHz instrument and externally referred to TMS. The spectra were recorded after 20,000 scans at room temperature. The pulse width was 45° and a pulse delay of 1.5 s was used. The relaxing agent $[Cr(acac)_3]$ was added in all samples to overcome the long T_1 relaxation time of the carbonyl resonance. The species on the alumina surface were extracted with CH_2Cl_2 or THF prior to measurement.

Rutherford backscattering spectrometry (RBS)

The principle of RBS is to place a sample in the pathway of a monoenergetic ion beam originating from an ion accelerator and to detect the particles that are elastically scattered in the coulombic field of the sample atomic nuclei. The most common incident beam is $^4He^+$ and the detector (normally a surface barrier detector is used to detect the scattered particles) is usually place at 165° with respect to the incidence direction of the beam, characterizing a backscattering geometry (see the scheme sketched in the

top of Fig. 1). The energy of the scattered particles depends, among other factors [11], on the incidence energy, on the atomic mass of the atoms involved and on the depth in the sample where the scattering event occurred. In the RBS spectra shown in Fig. 1 the energy of the scattered particles is proportional to the channel number. In the present work the samples were homogeneous tablets made from a randomly oriented alumina powder after washing with pentane, with the organometallic compound supported on the surface of the grains. The samples' depth homogeneity is revealed by the plateaus in the Al and Mo signals in the spectra of Fig. 1: when an incident particle penetrates the sample it loses kinetic energy by interactions with the electrons of the medium before and after being scattered by energy by interactions with the electrons of the medium before and after being scattered by the nuclei. The kinetic energy that is lost depends on the composition of the sample and on the length of the trajectory (or depth) of the incident ion in the material. Each RBS spectrum shown in Fig. 1 can be decomposed in the Mo, Al and O signals, giving rectangular-shaped individual contributions, which added up constitute the experimental spectrum. Since the height of the signal corresponding to a certain element is proportional to the density of that element in the sample, the Mo/Al ratio, for example, can be calculated from the ratio of the two signal heights (Mo to Al). The RBS spectra of the present work were obtained using α-particle beams with energies of 0.8 and 2.0 MeV. The incidence direction was perpendicular to the sample surface and detection angle was 165° with respect to the direction of the beam.

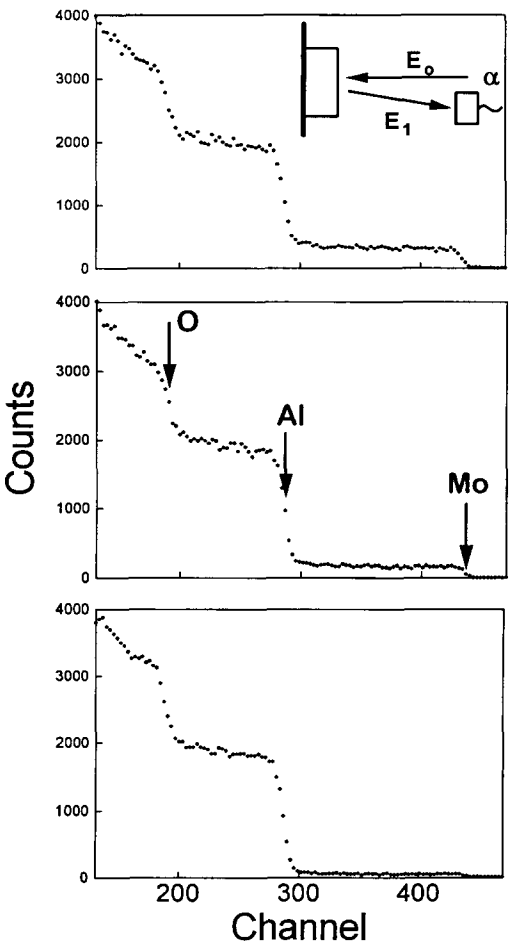


Fig. 1. Rutherford backscattering spectra obtained from samples of $[Mo(CO)_6]$ whose pentane solution together with PPh_3 and Al_2O_3 was irradiated with UV light. These spectra correspond, from bottom to top, to samples withdrawn after 1, 4 and 6 h of irradiation. The energy of the incident α-particle beam was 2.0 MeV. The incidence angle was 0° with the sample normal and the detection angle was 165° with respect to the incidence direction of the beam. A scheme of this geometry, also showing the sample and the detector, is sketched in the top of the figure. The arrows in the second spectrum indicate the outermost position of the corresponding elements in the samples.

RESULTS AND DISCUSSION

RBS results

RBS was used throughout this work to determine the metal loading on the alumina surface before and after photochemical activation. Figure 1 shows the RBS spectra corresponding to some steps of the reactions induced by UV light in the case of irradiating a $[Mo(CO)_6]$ pentane solution, PPh_3 and Al_2O_3, from which the Mo/Al_2O_3 atomic ratios could be calculated. It is noticeable that the increase of the irradiation time (from bottom to top of Fig. 1) increases the height of the Mo signal while maintaining the Al and O signals at a constant level, indicating a growth of the Mo loading on the alumina surface. The dependence of metal loading on irradiation time from 0 to 6 h is summarized in Fig. 2 for the three metals. The ever increasing behavior of Mo loading on alumina with the reaction time contrasts with the saturating behavior of Cr and W. In these two last cases, a surface saturation about 0.8% for W and 0.6% for Cr is reached. In fact, in a preliminary study [12] of the first steps, these trends were already evidenced. The present work confirms those trends for much longer UV irradiation times.

FT-IR results

Figure 3 represents the IR transmission spectra of $[Cr(CO)_6]/\gamma$-Al_2O_3 and PPh_3 reaction restricted to the ν(CO) region of the products. The top figure corresponds to spectra of chromium carbonyl derivatives in the solution, withdrawn from the reactor, after stopping stirring and letting alumina to decant; the bottom figure shows spectra corresponding to the derivatives supported on alumina. The solution spectra (Fig. 3, top) show a strong band at 1987 cm^{-1} (T_{1u} mode of $[Cr(CO)_6]$). The low-intensity band situated

at 1965 cm^{-1}, which is more visible in the spectrum that corresponds to the nonirradiated sample, is attributed to the isotopic effect pertinent to ^{13}CO. A band at 1945 cm^{-1} corresponding to the $E+A_1^2$ axial modes of C_{4v} pentacarbonyl species $[Cr(CO)_5PPh_3]$, appears mainly in the irradiated spectrum. The A_1^1 radial mode is also present at 2063 cm^{-1} in this spectrum.

In the solid phase (Fig. 3, bottom) the presence of $[Cr(CO)_5L]$ adsorbed on alumina surface can be observed by the presence of the bands at 2061 and 1937 cm^{-1}. The shift of the bands to low energy, compared with the same species in solution, especially of the $E+A_1$ mode, reflects the interaction of the metal carbonyls with the support: the Al^{3+} Lewis acid sites weakens the CO bond. The [*trans*-$Cr(CO)_4(PPh_3)_2$] species was evidenced by the band at 1879 cm^{-1} (E_u mode of D_{4h} symmetry). These spectra confirm our previous results [9] with this system. When the solid obtained in such conditions is washed with pentane, only the [*trans*-$Cr(CO)_4(PPh_3)_2$] species remains on the surface, the monosubstituted species being completely washed out. This fact suggests that the disubstituted species have a stronger interaction with the solid surface than the other species. The weak band at 1984 cm^{-1} shows the presence of traces of $[Cr(CO)_6]$ remaining after irradiation.

The solution phase IR spectra corresponding to the reaction with molybdenum (Fig. 4, top) show a behavior similar to the chromium one. The T_{1u} $[Mo(CO)_6]$ band at 1989 cm^{-1} and that of the monosubstituted C_{4v} species (1950 cm^{-1}, $E+A_1^2$ axial modes) appear. The alumina surface spectra (Fig 4, bottom) exhibit a more complex pattern, when compared with Cr, revealing the presence of several adsorbed species (see Table 1): traces of $[Mo(CO)_6]$ immobilized species (1986 cm^{-1}) are present plus the C_{4v} monosubstituted species (2071 cm^{-1}, A_1^1; 1947 cm^{-1}, $E+A_1^2$). Furthermore, the band centered to 1887 cm^{-1} and the shoulder around 1915 cm^{-1}, together with band centered at 2020 cm^{-1} (A_1^1) suggest

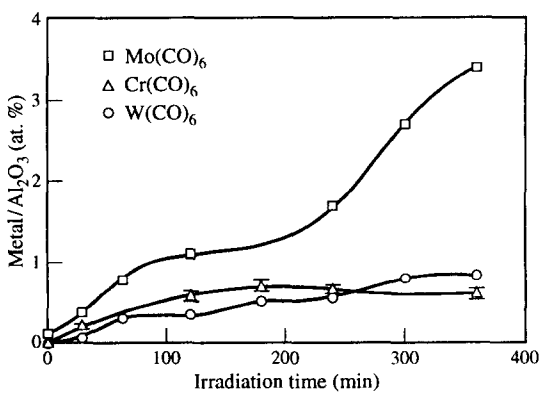


Fig. 2. Metal loadings on the γ-alumina surface, obtained from the RBS spectra, as a function of the irradiation time for the organometallic precursors: (□) $[Mo(CO)_6]$ (△) $[Cr(CO)_6]$ (○) $[W(CO)_6]$. The isotherms were obtained at room temperature. Typical statistical error bars associated with the Rutherford backscattering technique are given for the case of Cr coverage results. The lines are not fittings, they are used to guide the eyes.

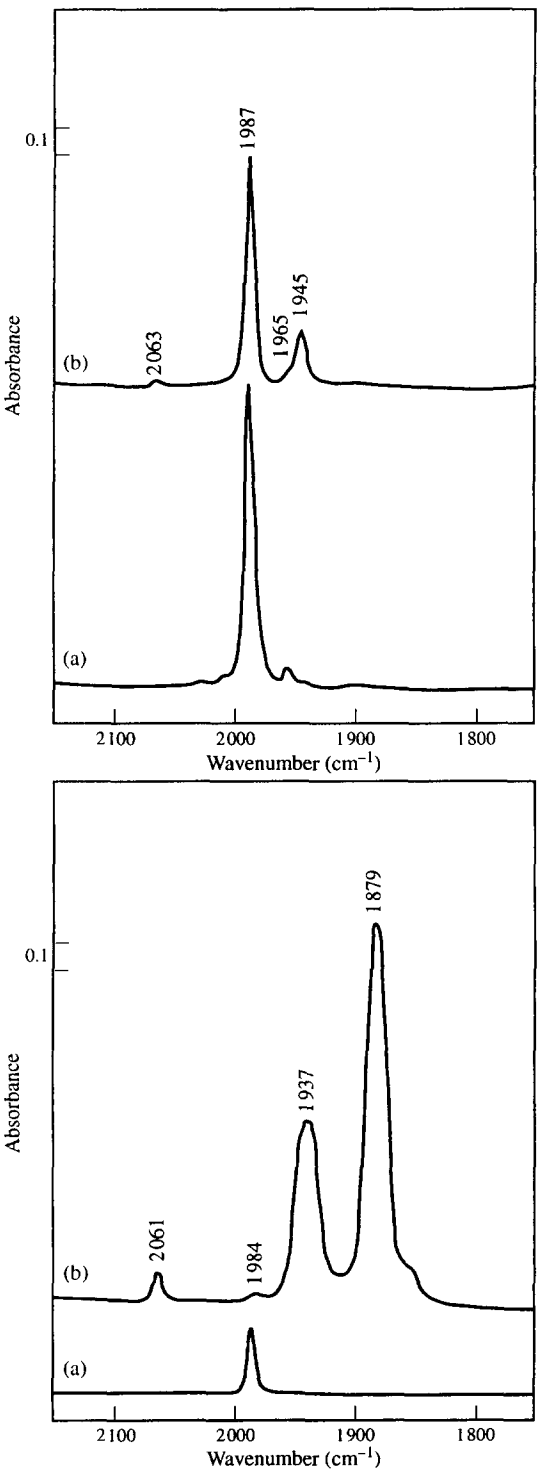


Fig. 3. IR spectra in the ν(CO) region of the products of the photochemically induced reaction of $[Cr(CO)_6]$ supported on Al_2O_3 with PPh_3 in pentane: top—solution phase, bottom—solid phase in nujol; (a) zero time, (b) 120 min.

the presence of [*cis*-$Mo(CO)_4(PPh_3)_2$] in analogy with similar compounds [13]. The strong band at 1901 cm^{-1} can be assigned to the E_u mode of the disubstituted *trans* species. After successive pentane washings, the support IR spectrum shows the presence of mainly the disubstituted species.

The [$W(CO)_6$] reaction spectra for both the solution and the solid phase show a similar behavior to that of Mo (Table 1). In solution, the presence of the hexacarbonyl and the monosubstituted pentacarbonyl species are observed and on the alumina surface the *cis* disubstituted species is confirmed besides [$W(CO)_5L$] and traces of the hexacarbonyl. There is no evidence for the *trans* disubstituted species ($\sim$1900 cm^{-1}). As in the preceding cases, after pentane washing only the disubstituted species remain on the support. Once again, these results suggest that the disubstituted species interact more strongly with the support than the monosubstituted and hexacarbonyl ones.

The same photochemical reactions in the absence of phosphine lead to the same general features in the IR spectra. However, after pentane washings no subcarbonyl species remain on alumina.

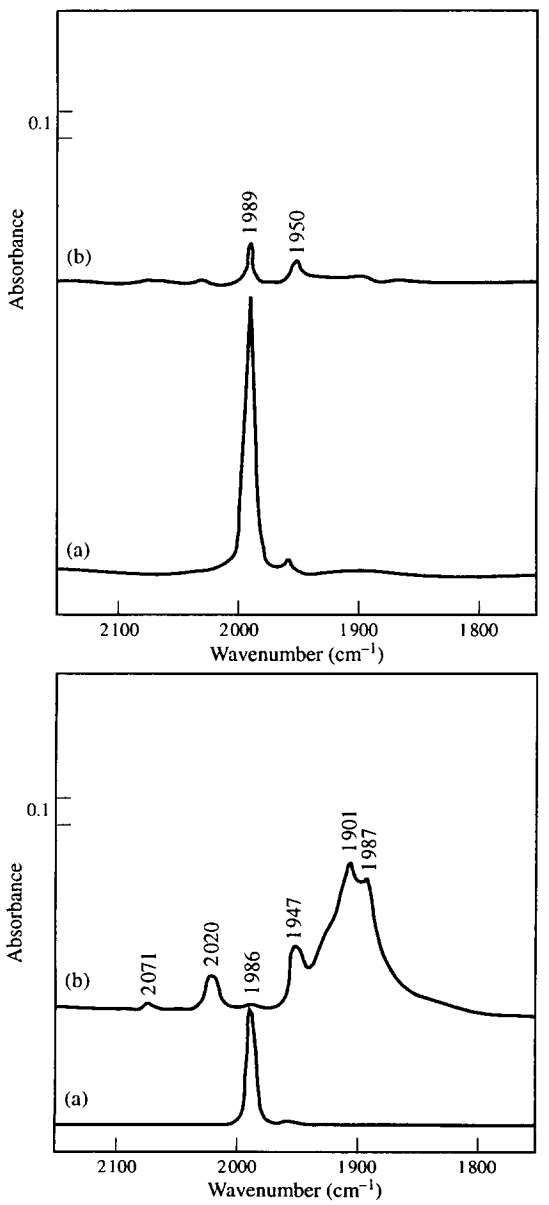


Fig. 4. IR spectra in the ν(CO) region of the products of the photochemically induced reactions of [$Mo(CO)_6$] supported on Al_2O_3 with PPh_3 in pentane: top—solution, bottom—solid phase in nujol; (a) zero time, (b) 120 min.

NMR results

^{13}C NMR spectra of the species generated in solution and anchored on alumina were obtained, giving the following result: the spectrum of the species generated in solution evidences the presence of [$Mo(CO)_6$] (200.8 ppm), the sextets due to Mo^{95} and Mo^{97} both with $I = 5/2$, and [$Mo(CO)_5L$] with *cis* CO chemical shifts appearing as a doublet around 205.5 ppm ($J_{^{13}C\text{-}M^{31}P} \approx 9.0$ Hz) and the δ_{CO}^{trans} around 210.1 ppm ($J_{^{13}C\text{-}M^{31}P} \approx 23.0$ Hz) in agreement with the data in the literature [14]. The spectrum of the species generated in the solid phase evidences the presence of [$Mo(CO)_5L$] (the doublet around 206.2 ppm corresponding to δ_{CO}^{cis}). The doublet attributed to the *trans* monosubstituted species is underneath one of the triplets of the *cis* disubstituted species around 215.4 ppm, (the other triplet appears at 210.4 ppm), ($J_{^{13}C\text{-}M^{31}P} \approx 8.0$ Hz). (On the other hand, the *trans*-disubstituted compound shows one triplet around 211.9 ppm, $J_{^{13}C\text{-}M^{31}P} \approx 9.0$ Hz.) The amount of this compound is seen to be smaller than the one of the *cis* species. The bands integration shows roughly a *trans*:*cis* ratio of 1:3, confirming the suspect of the existence of the *trans* species in the IR spectra, but in a smaller amount compared with the *cis* species.

DISCUSSION

In solution and in the presence of very weak coordination solvents, the generation of [$Mo(CO)_5$(solvent)] transients takes place [15]. In the presence of nucleophiles, such as phosphines and pyridine, the [$Mo(CO)_5$(solvent)] species undergo rapid thermal or photochemical substitution to produce [$Mo(CO)_5L$] and further reaction leads to the disubstituted species. In the present work, the photodissociations of [$Mo(CO)_6$] (M = Cr, Mo, W) in the presence of alumina and triphenylphosphine followed different trends, depending on the metal. From the analyses of the IR spectra, one sees that no metal remains on the support for zero irradiation time after pentane washings, evidencing a weak interaction between the precursor and the alumina surface. It is worth mentioning here that although no carbonyl species were detected by IR, the RBS measurements indicate that *ca* 0.01% in the case of Cr and W, and a relative higher

Table 1. IR frequencies in the CO stretching region of $M(CO)_6$ carbonyls and their derivatives

Complex	Symmetry	Type	ν(CO) (cm^{-1})
$Cr(CO)_6$	O_h	I	1987vs (T_{1u})
	O_h	II	1984m (T_{1u})
$Cr(CO)_5L$	C_{4v}	I	2063vw (A_1^2), 1945w ($E+A_1^1$)
	C_{4v}	II	2061vw (A_1^2), 1937vs ($E+A_1^1$)
trans-$Cr(CO)_4L_2$	D_{4h}	II	1879vs (E_u)
$Mo(CO)_6$	O_h	I	1989vs (T_{1u})
	O_h	II	1986vs (T_{1u})
$Mo(CO)_5L$	C_{4v}	I	1950m ($E+A_1^1$)
	C_{4v}	II	2071vw (A_1^2), 1947vs ($E+A_1^1$)
trans-$Mo(CO)_4L_2$	D_{4h}	II	1901vs (E_u)
cis-$Mo(CO)_4L_2$	C_{2v}	II	2020m (A_1), 1915sh (B_1), 1887s (B_2)
$W(CO)_6$	O_h	I	1983vs (T_{1u})
	O_h	II	1980vs (T_{1u})
$W(CO)_5L$	C_{4v}	I	1944s ($E+A_1^1$)
	C_{4v}	II	2070vw (A_1^2), 1939vs ($E+A_1^1$)
cis-$W(CO)_4L_2$	C_{2v}	II	2016w (A_1), 1919w (B_1), 1894s (A_1), (1875)sh (B_1)

L = PPh_3; I: solution; II: alumina.

value of 0.1% in the case of Mo, remain anchored on the support. Although the different information provided by each technique (IR detects the ν(CO) associated to $[Mo(CO)_x]$ species, while RBS measures the metal coverage of the surface no matter its chemical environment), the total metal loading determined by RBS after washing must come necessarily from a small amount of $[Mo(CO)_6]$ not removed from the support, since the total decarbonylation and production of a bare metal or metal oxide at room temperature without any activation is unlikely. This evidences the greater sensitivity of the RBS technique when compared with IR under the present experimental conditions.

From the adsorption isotherms (Fig. 2), it is noticeable that Mo presents the steepest slope. These metal loadings come exclusively from the subcarbonyl species generated photochemically in the presence of phosphine. The higher metal loading for Mo confirms the phosphine substitution reaction tendency of such metal carbonyl, when compared with the two others [16,17]. The photolability tendency of Group 6 is Mo > Cr > W. So, based on the determination of the metal loadings by RBS, one can say that under the present experimental conditions $[Mo(CO)_6]$ has the most remarkable photolability. The relative easy formation of $[Mo(CO)_4]$ and $[Mo(CO)_3]$ by photolysis of $[Mo(CO)_6]$ in low-temperature matrices compared with Cr and W is also mentioned in the literature [18].

Besides the photolability inherent to each parent metal carbonyl, it is observed that the photogenerated surface species depend on the metal atom size. For Cr, the ligand cone angle directed the substitution reaction to produce only the *trans* disubstituted species on the alumina surface. It is worth mentioning that $[Cr(CO)_6]$ derivatives present, whenever it is allowed, *cis–trans* isomerism [19]. In this case, however, no evidence for *cis* species was found. As the metal atom size increases, the *cis* compounds were formed preferentially, accompanied with some *trans* species generation, according to IR and NMR data for molybdenum. For these larger atoms, the ligand cone angle has almost no influence on the products and a mixture of disubstituted compounds is generated on the alumina surface.

Conclusions

The photochemical reactions of the Group 6 metal carbonyls with triphenylphosphine and the alumina surface showed different behaviors depending on the M—CO bond strength and on the atomic size of the metal. The metal loading on the alumina surface was found to be $[Cr(CO)_6] < [W(CO)_6] < [Mo(CO)_6]$. For chromium, the cone angle of the ligand directed the reaction to produce only the *trans* disubstituted species on the alumina surface. No evidence for the *cis* species was found from the IR spectra. On the other hand, for the larger metals molybdenum and tungsten, the *cis* compound was formed preferentially, although the observed presence of the *trans* species in the case of Mo in a smaller ratio is noted. In these two later cases, the ligand cone angle does not seem to influence very much the kind of the originated products. After grafting, only the disubstituted species remain on alumina evidencing a stronger interaction with the support than in the case of the monosubstituted, and the hexacarbonyl compounds.

Acknowledgments—This work was partially supported by CNPq, FINEP, CAPES and FAPERGS.

REFERENCES

1. Howe, R. F., *Tailored Metal Catalysts*. Reidel Publishers, New York, 1986, p. 141. See also Gates, B. C., Guczi, L. and Knözinger, H., *Metal Clusters in Catalysis*. Elsevier, Amsterdam, 1986.
2. Burwell, R. L., Haller, G. L., Taylor, K. C. and Read, J. F., *Adv. Catal.* 1969, **20,** 1.
3. Smith, J., Howe, R. F. and Whan, D. A., *J. Catal.* 1974, **34,** 191.
4. Collucia, S., Marchese, L., Martra, G., Spoto, G., Zecchina, A. and Louis, C., *J. Mol. Catal.* 1990, **60,** 71.
5. Kawi, S., Alexeev, O., Shelef, M. and Gates, B. C., *J. Phys. Chem.* 1995, **99,** 6926.
6. Geoffroy, G. L. and Wrighton, M. S., *Organometallic Photochemistry*. Academic Press, New York, 1979.
7. Houle, F. A., and Yeh, L., *J. Phys. Chem.* 1992, **96,** 2691. See also Houle, F. A. and Singmaster, K. A., *J. Phys. Chem.* 1992, **96,** 10425.
8. Tyndall, G. W. and Jackson, R. L., *J. Phys. Chem.* 1991, **95,** 687.
9. Baibich, I. M. and Dos Santos, J. H. Z., *Can. J. Appl. Spectrosc.* 1994, **95,** 4596.
10. Tolman, C. A., *J. Am. Chem. Soc.* 1970, **92,** 2956.
11. Chu, W. K., Mayer, J. W. and Nicolet, M. A., *Backscattering Spectrometry*. Academic Press, New York, 1963. See also Green, P. F. and Doyle, B. L., in *New Characterization Techniques for Thin Polymer Films*. ed. H.-M. Tong and L. T. Nguyen, John Wiley and Sons, New York, 1990, p. 139.
12. Baibich, I. M., Stedile, F. C., Baumvol, I. R. J., Dos Santos, J. H. Z. and Santarosa, V. E., *Phys. Stat. Sol.* 1995, **192,** 519.
13. Bodner, G. M., *Inorg. Chem.* 1975, **14,** 2694.
14. Bodner, G. M., May. M. P. and McKinney, L. E., *Inorg. Chem.* 1980, **19,** 1951.
15. Walsh, E. F., Popov, V. K., George, M. W. and Poliakoff, M. J., *J. Phys. Chem.* 1995, **99,** 12016.
16. Ishikawa, Y., Brown, C. E., Hackett, P. A. and Rayner, D. M., *J. Phys. Chem.* 1987, **91,** 3945.
17. Zecchina, A., Platero, E. E. and Arean, C. A., *Inorg. Chem.* 1988, **27,** 102.
18. Perutz, R. N. and Turner, J. J., *J. Am. Chem. Soc.* 1975, **97,** 4800.
19. Grobe, J. and Zimmermann, H. Z., *Naturforsch.* 1981, **36b,** 482.

Pergamon

PII: S0277-5387(96)00403-2

Polyhedron Vol. 16, No. 11, pp. 1945–1956, 1997
© 1997 Elsevier Science Ltd
All rights reserved. Printed in Great Britain
0277-5387/97 $17.00+0.00

Substitution of chloride in $[PtCl_2(PEt_3)_2]$ by the chiral anionic ligand $[Mo(CO)_5(PPhH)]^-$ to give mixed platinum–molybdenum compounds and a $^{31}P\{^1H\}$ NMR analysis of their fluxionality. X-ray crystal structure of $[PtCl(PEt_3)_2(\mu\text{-}PPhH)\{Mo(CO)_5\}]$ and *trans*-$[Pt(PEt_3)_2(\mu\text{-}PPH)_2\{Mo(CO)_5\}_2]$

Antony J. Deeming,* Bruce R. Cockerton and Simon Doherty†

Department of Chemistry, University College London, 20 Gordon Street, London WC1H 0AJ, U.K.

(Received 18 July, 1996; accepted 12 August 1996)

Abstract—Deprotonation of the primary phosphine complex $[Mo(CO)_5(PPhH_2)]$ generated $[Mo(CO)_5(PPhH)]^-$, a chiral anionic ligand which reacted readily with *cis*- or *trans*-$[PtCl_2(PEt_3)_2]$ *via* facile nucleophilic substitution of one or both chloride ligands to afford *trans*-$[PtCl(PEt_3)_2(\mu\text{-}PPhH)\{Mo(CO)_5\}]$ (**1**) and *cis*- and *trans*-$[Pt(PEt_3)_2(\mu\text{-}PPhH)_2\{Mo(CO)_5\}_2]$ (**2**), respectively. These are rare examples of heterometallic complexes containing primary phosphido bridges. Compound **1** can be described either as the square-planar Pt^{II} complex with the anionic ligand $PPhH\{Mo(CO)_5\}^-$ or as the Pt-Mo phosphido-bridged dimer *trans*-$[PtCl(PEt_3)_2(\mu\text{-}PPhH)\{Mo(CO)_5\}]$. As a phosphido-bridged heterobimetallic **1** possesses an exceptionally large Pt—P—Mo angle [120.9(1)°] reflecting the long Pt—Mo nonbonding interaction (4.5 Å). Compound **2** can correspondingly be described either as a phosphido-bridged $PtMo_2$ trimer or a square-planar arrangement of two neutral PEt_3 and two anionic $PPhH\{Mo(CO)_5\}$ ligands at Pt. The low-temperature $^{31}P\{^1H\}$ NMR spectrum of **1** showed several ABXY spin systems together with their associated ABXYM (M = ^{195}Pt) counterparts and variable-temperature studies revealed the dynamic interconversion of several rotametric isomers arising from restricted rotation about the Pt—Pμ bond. The $^{31}P\{^1H\}$ NMR spectrum of *trans*-**2** shows its two possible *RR*/*SS* and *meso* diastereoisomers, the latter existing in clearly identifiable rotameric forms which interconvert slowly at −75°C. We note very different values between ^2J(P—P) and $^1J(^{195}Pt—P)$ for the anionic ligands $[PPhH\{Mo(CO)_5\}]^-$ and PEt_3, unattributable to bond length variation but which must reflect reduced *s*-orbital contribution to the Pt—P bond of the anionic phosphines $PPhH\{Mo(CO)_5\}$.© 1997 Elsevier Science Ltd. All rights reserved.

Keywords: platinum; molybdenum; bridging PHPh; X-ray structures.

There has been an explosive growth in the synthesis, characterization and reactivity of heterometallic complexes, many of which comprise metals with very different electronic and coordinative properties [1]. Stephan's review article in 1989 highlighted the large number of heterobimetallics supported by a variety of different bridging ligands [2]. The desire to develop these early–late heterobimetallics has been driven by the belief that they should react with substrates in a cooperative manner [3]. Although there are few examples of successful cooperativity between electron-poor early transition metals and electron-rich transition metal centres, there have been several noteworthy approaches towards achieving this goal. Recent reports by Bergman [4] and Braunstein [5] serve to highlight the value of designed synthesis to achieve participation from each metal. Bergman's elegant syn-

* Author to whom correspondence should be addressed.
† Present address: Department of Chemistry, University of Newcastle, Newcastle-upon-Tyne NE1 7RU, U.K.

thesis and reactivity studies with an imido-bridged zirconium–iridium heterometallic clearly demonstrates a cooperativity in its reactions with both polar and non-polar X—H bonds. In contrast, Braunstein and co-workers have shown that the reactivity of iron–platinum heterometallics depends markedly on the nature of the bridging ligand. Following a recent highlight by Herberhold and Jin [6] focusing on heterometallics with polar metal–metal bonds, Chisholm *et al.* [7] suggested that the reactivity anticipated for such early–late heterometallics could be achieved by asymmetric homometallic complexes with polar W—W bonds (W^{VI}—W^{II}) with the metals in vastly different coordination environments.

Although heterobimetallics with various bridging ligands [8] have been prepared the predominant use of the phosphido ligand (PR_2) [9] can be attributed to: (i) the ease of synthesis via the bridge-assisted method [10], (ii) stabilization of the metal–atom framework during chemical transformation [11] and (iii) the presence of a ^{31}P nucleus which is useful for probing solution-state structures and fluxionality [12]. However, several recently reported transformations involving phosphido ligands set limits on their use for framework-stabilizing since they do not invariably behave as innocent bridging ligands [13]. Of the many phosphido-bridged heterometallic complexes reported, most contain two bridging ligands and Baker *et al.* [14] recently surveyed the area of diphosphido-bridged ELHB compounds up to 1990. However, current efforts have focused on the preparation of singly-bridged μ-phosphido binuclear complexes without metal–metal bonds [15] with large M—P—M′ angles. Particularly noteworthy are $[Cp_2M(H)(\mu\text{-}PR_2)M'(CO)_5]$ (M = Mo, W; M′ = Cr, Mo, W) and $[CpFe(CO)_2(\mu\text{-}PR_2)W(CO)_4L]$ (L = PMe_3, CH_3CN) prepared by the groups of Kubicki [15a] and Shyu, respectively [15c].

The synthesis of μ-PR_2 Pt—M (M = Mo, W) heterometallics continues to be of considerable scientific interest despite their limited applications. Geoffroy and co-workers have reported a number of such complexes dominated by M—M′ bonding interactions [16] and later Powell demonstrated that oxidative addition of the P—H bond of secondary phosphine complexes to zero-valent platinum centres is an efficient route to heterobimetallics, including $[(CO)_4M(\mu\text{-}PR_2)(\mu\text{-}H)Pt(PPh_3)_2]$ [M = Mo, W] [17]. The catalytic activity of diphenylphosphido-bridged heterometallics have been evaluated by Mathieu [18] and there have been studies on metal-assisted substitutions *via* M—M bond formation [19].

This report follows our discovery of some unusual structural and spectroscopic characteristics of chiral MoPt heterometallics bridged by the primary phosphido ligand PPhH. We have recently reported [20] that nucleophilic substitution of chloride in $[PtCl_2(dppe)]$ by the chiral anionic ligand $[Mo(CO)_5(PPhH)]^-$ affords the phosphido-bridged Mo_2Pt trimer $[Pt(\mu\text{-}PPhH)_2\{Mo(CO)_5\}_2(dppe)]$ (**3**). The $^{31}P\{^1H\}$ NMR spectra of **3** are quite remarkable, highlighting this technique in elucidation of structure and of solution-state fluxional processes. We report the synthesis, spectroscopic and structural characterization of the heterometallic complexes *trans*-$[PtCl(PEt_3)_2(\mu\text{-}PPhH)\{Mo(CO)_5\}]$ (**1**) and *cis*- and *trans*-$[Pt(PEt_3)_2(\mu\text{-}PPhH)_2\{Mo(CO)_5\}_2]$ (**2**), each containing chiral primary phosphido bridges.

EXPERIMENTAL

General consideration

Standard double manifold vacuum-line techniques were used for all chemical manipulations and all reactions were performed under dry nitrogen. All solvents were dried prior to use, hexane and tetrahydrofuran over sodium/benzophenone and dichloromethane over P_2O_5. Reactions were monitored by IR spectroscopy and TLC (Baker flex, silica gel 1B-F). Products were purified by column chromatography (330 × 30 mm) with silica gel (70–230 mesh) or TLC on silica gel plates (20 × 20 cm, Merck, TLC grade, Aldrich Chemical Co.). Solution IR spectra were recorded on a Perkin–Elmer 983 spectrometer using calcium fluoride cells. ^1H NMR spectra were recorded on Varian VXR400 or XL200 spectrometers and all ^{31}P NMR spectra were recorded on a Varian VXR400 instrument at 162.0 MHz and referenced to external 85% H_3PO_4. Elemental analysis were carried out in the Analytical Laboratory at University College London. All chemicals except where stated were used as obtained from commercial sources and the starting materials $[PtCl_2(PEt_3)_2]$ [21] and $[Mo(CO)_5(PPhH_2)]$ [22] were prepared as reported.

Reaction of $[Mo(CO)_5(PPhH)]^-$ *with* cis-$[PtCl_2(PEt_3)_2]$

A solution of $[Mo(CO)_5(PPhH_2)]$ (0.1264 g, 0.4 mmol) in dry THF (50 cm^3) was treated with the base DBU (0.160 cm^3, 1.1 mmol). The reaction mixture was stirred for 10 min and a solution of $[PtCl_2(PEt_3)_2]$ (0.090 g, 0.18 mmol) in THF (5 cm^3) was added dropwise. After stirring for a further 20 min, the solvent was removed under reduced pressure to leave a brown–orange oil, which was dissolved in a minimum of dichloromethane and chromatographed on silica gel plates. Elution with dichloromethane/*n*-hexane (2/3, v/v) afforded three well-separated bands. The fastest band gave *trans*-$[Pt(PEt_3)_2(\mu\text{-}PPhH)_2\{Mo(CO)_5\}_2]$ (**2**), which was crystallized from dichloromethane/ethanol and vacuum-dried to afford colourless crystal of **2** (0.025 g, 24%). IR [ν(CO), cm^{-1}, C_6H_{14}]: 2061 (w), 1938 (s), 1924 (sh). Found: C, 33.6; H, 4.3; P, 11.8. Calc. for $C_{34}H_{42}Mo_2O_{10}P_4Pt$ (mol.wt = 1121.61): C, 36.3; H, 3.7; P, 11.1%. The second minor bad was identified spectroscopically as *cis*-$[Pt(PEt_3)_2(\mu\text{-}PPhH)_2\{Mo(CO)_5\}_2]$ (**2**) and crys-

Table 1. $^{31}P^1H$ NMR data for the phosphido-bridged heterometallic complexes $[PtCl(PEt_3)_2(\mu\text{-}PPhH)\{Mo(CO)_5\}]$ (**1**) and *trans*-$[Pt(PEt_3)_2(\mu\text{-}PPhH)_2\{Mo(CO)_5\}_2]$ (**2**)

Compound	δ^a	Assignment	$J(PP)^{trans}$ (Hz)	$J(PP)^{cis}$ (Hz)	$J(^{195}Pt—P)$ (Hz)
$PtCl(PEt_3)_2(\mu\text{-}PPhH)\{Mo(CO)_5\}$	+10.5	PEt_3	—	—	2465.2
Room temperature	−66.4	*P*PhH	—	25.5	2078.0
$[PtCl(PEt_3)_2(\mu\text{-}PPhH)\{Mo(CO)_5\}]^b$	+9.0	PEt_3	366.0	17.3	2526.4
Major rotamer A^1B^1X	+14.1	PEt_3	366.0	9.6	2413.0
	−66.5	*P*PhH	—	17.3, 9.6	2135.0
$[PtCl(PEt_3)_2(\mu\text{-}PPhH)\{Mo(CO)_5\}]^b$	+8.6	PEt_3	376.0	15.0	—
Minor rotamer A^2B^2X	+13.7	PEt_3	376.0	9.0	—
	−67.0	*P*PhH	—	15.0, 9.0	2179.6
$[PtCl(PEt_3)_2(\mu\text{-}PPhH)\{Mo(CO)_5\}]^b$	+8.4	PEt_3	376.0	15.4	—
Minor rotamer A^3B^3X	+13.6	PEt_3	376.0	9.6	—
	−67.2	*P*PhH	—	15.0, 9.6	—
$[PtCl(PEt_3)_2(\mu\text{-}PPhH)_2\{Mo(CO)_5\}_2]$	+44.7	PEt_3	200.0	−15.0	2277.7
cis isomer	+5.7	*P*PhH	200.0	−15.0	1400.6
$[PtCl(PEt_3)_2(\mu\text{-}PPhH)_2\{Mo(CO)_5\}_2]$	+0.7	PEt_3	—	13.6	2512.0
trans minor diastereoisomer A'^3	−71.4	*P*PhH	—	13.6	1110.0
$[PtCl(PEt_3)_2(\mu\text{-}PPhH)_2\{Mo(CO)_5\}_2]^c$	+1.2	PEt_3	—	—	2512.0
trans major diastereoisomer	−68.5	*P*PhH	—	12.7	1146.0
$[PtCl(PEt_3)_2(\mu\text{-}PPhH)_2\{Mo(CO)_5\}_2]^b$	+1.8	PEt_3	—	14.8	2459.0
Major diastereoisomer rotamer A^2	−67.8	*P*PhH	—	16.4	1127.0
$[PtCl(PEt_3)_2(\mu\text{-}PPhH)_2\{Mo(CO)_5\}_2]^b$	+5.8	PEt_3	340.0	16.6	2401.0
Major diastereoisomer rotamer	−2.4	PEt_3	340.0	8.8	2592.0
A'^1 and B^1	−72.0	*P*PhH	—	12.8	1136.0

[a] Recorded in $CDCl_3$ at 162 MHz with chemical shifts referenced to external 85% H_3PO_4.
[b] Recorded CD_2Cl_2 at −80° C.
[c] Recorded in $CDCl_3$ at room temperature.

tallization form dichloromethane/ethanol gave colourless crystals of *cis*-**2** (0.010 g, 9.7%). IR [ν(CO), cm^{-1}, C_6H_{14}]: 2063 (w), 1935 (s), 1929 (sh). The final band to elute was identified as *trans*-$[PtCl(PEt_3)_2(\mu\text{-}PPhH)\{Mo(CO)_5\}]$ (**1**). Crystallization from dichloromethane/ethanol drying *in vacuo* afforded colourless crystalline **1** (0.017 g, 16.5%). IR [ν(CO), cm^{-1}, C_6H_{14}]: 2057 (w), 1928 (s), 1901 (sh). Found: C, 34.0; H, 4.4; Cl, 5.2. Calc. $C_{23}H_{36}ClMoO_5P_3Pt$ (mol.wt = 811.98): C, 33.7; H, 3.9; Cl, 4.4%.

X-ray structure analysis of **1** *and* trans-**2**

Colourless crystals of **1** and *trans*-**2** were grown from dichloromethane/ethanol at room temperature. A suitable crystal of each was glued to a glass fibre using epoxy resin and mounted on a goniometer head. Unit-cell parameters were obtained from least-squares refinement of 30 orientation reflections in the range $10 < 2\theta < 30°$ for **1** and 26 orientation reflections in the range $6 < 2\theta < 27°$ for **2**, selected from a rotation photograph.

Collection and reduction of intensity data. Details of the intensity data collection parameters for **1** and *trans*-**2** are presented in Table 2. The intensity data for both **1** and **2** were collected at 294 K on a Nicolet R3v/m automatic four-circle diffractometer using graphite monochromated Mo-K_α ($\lambda = 0.71073$ Å) radiation with the diffractometer operating in the ω–2θ scan mode. Three standard reflections monitored every 100 measurements showed no significant deviations during the data collection. Empirical absorption corrections for **1** and *trans*-**2** were made by the Ψ-scan method (maximum and minimum transmission factors were 0.950 and 0.511 for **1** and 0.966 and 0.636 for *trans*-**2**). Reflections were considered observed when $I_0 > 3\sigma(I_0)$.

Solution and refinement of the intensity data. The structures were solved by direct methods, followed by full-matrix least-squares refinement of positional and thermal parameters and subsequent conversion to anisotropic coefficients for all non-hydrogen atoms. All hydrogen atoms except those bonded directly to P were included in idealized positions and allowed to ride on carbon atoms with C—H distances fixed at 0.86 Å and isotropic thermal parameters at 0.08 $Å^2$. The function minimized in the least-squares calculations was $\Sigma w(|F_o| - |F_c|)^2$. The weighted R value is defined as $Rw = [\Sigma w(|F_o| - |F_c|)^2/\Sigma w|F_o|^2]^{1/2}$. All calculations were performed on a MicroVax II computer running SHELXTL PLUS (G. M. Sheldrick, Package for crystal structure determination, University of Göttingen, 1986). Further details are available as supplementary material (atomic coordinates, bond distances, bond angles, anisotropic thermal parameters and hydrogen atom positions) deposited at

Table 2. Crystal and intensity data for $[PtCl(PEt_3)_2(\mu\text{-}PPhH)\{Mo(CO)_5\}]$ (**1**) and *trans*-$[Pt(PEt_3)_2(\mu\text{-}PPhH)_2\{Mo(CO)_5\}_2]$ (**2**)

	1	*trans*-**2**
Formula	$C_{23}H_{36}ClMoO_5P_3Pt$	$C_{34}H_{42}Mo_2O_{10}P_4Pt$
fw	811.98	1121.61
Crystal size (mm)	$0.16\times0.20\times0.30$	$0.34\times0.15\times0.08$
Space group	$P2_1/n$	$P2_1/a$
a (Å)	11.159(4)	20.027(9)
b (Å)	24.57(1)	10.465(4)
c (Å)	11.897(4)	20.774(9)
β (°)	106.61(3)	103.00(3)
V (Å^3)	3125(2)	4242(2)
Z	4	4
D_{calc} (g cm^{-3})	1.73	1.76
Radiation, λ (Å)	Mo, 0.71073	Mo, 0.71073
Temperature (°C)	17	18
μ(Mo-K_α) (cm^{-1})	51.8	40.9
Total data	5905	8086
Unique data	5459	7411
Reflections used	3575	4135
Parameters	307	463
R^a	0.0458	0.0850
R_w^b	0.0500	0.0679
Weight *w* in weighting scheme	$1/[\sigma^2(F)+0.00186F^2]$	$1/[\sigma^2(F)+0.000247F^2]$
Goodness of fit	1.099	1.587
Max shift/e.s.d.	0.006	0.005
Residual density (e Å^{-3})	0.96	1.8

$^a R = \Sigma[|F_o|-|F_c|]/\Sigma|F_o|$.
$^b R_w = [\Sigma w(|F_o|-|F_c|)^2/\Sigma w|F_o|^2]^{1/2}$.

the Cambridge Crystallographic Data Centre. Observed and calculated structure factors are available from the authors on request. Tables 3 and 4 contain an appropriate selection of bond lengths and angles for these molecules.

RESULTS AND DISCUSSION

Reaction of the chiral anion $[Mo(CO)_5(PPPhH)]^-$ with *cis*-$[PtCl_2(PEt_3)_2]$ proceeds rapidly at room temperature to afford, after chromatographic work-up, a mixture of $[PtCl(PEt_3)(\mu\text{-}PPhH)\{Mo(CO)_5\}]$ (**1**) and *cis*- and *trans*-$[Pt(PEt_3)_2(\mu\text{-}PPhH)_2\{Mo(CO)_5\}_2]$ (**2**) complexes containing primary phosphido bridges.

Table 3. Selected interatomic bond distances (Å) and angles (°) for $[PtCl(PEt_3)_2(\mu\text{-}PPhH)\{Mo(CO)_5\}]$ (**1**)

Pt—Pt(1)	2.288(3)	Mo—C(1)	1.972(16)
Pt—P(2)	2.327(3)	Mo—C(2)	2.052(15)
Pt—P(3)	2.325(4)	Mo—C(3)	2.051(12)
Pt—Cl	2.384(4)	Mo—C(4)	2.065(17)
Mo—P(1)	2.601(3)	Mo—C(5)	2.053(11)
P(1)—Pt—P(2)	95.6(1)	P(2)—Pt—Cl	83.3(1)
P(1)—Pt—P(3)	93.8(1)	P(3)—Pt—Cl	87.4(1)
P(2)—Pt—P(3)	169.9(1)	P(1)—Pt—Cl	177.5(1)
Pt—P(1)—Mo	120.9(1)		

Table 4. Selected interatomic bond distances (Å) and angles (°) for *trans*-$[Pt(PEt_3)_2(\mu\text{-}PPhH)_2\{Mo(CO)_5\}_2]$ (**2**)

Pt(1)—P(1)	2.407(5)	Mo(1)—P(1)	2.644(5)
Pt(1)—P(2)	2.340(6)	Mo(2)—P(2)	2.648(5)
Pt(2)—P(3)	2.397(4)	Mo(1)—C(20)	2.064(22)
Pt(2)—P(4)	2.333(6)	Mo(1)—C(21)	2.069(24)
Mo(1)—C(22)	2.048(23)	Mo(1)—C(23)	2.027(25)
Mo(1)—C(24)	1.981(23)	Mo(2)—C(50)	2.089(23)
Mo(2)—C(51)	2.061(21)	Mo(2)—C(52)	2.040(25)
Mo(2)—C(53)	2.077(24)	Mo(2)—C(54)	1.968(20)
P(1)—Pt(1)—P(2)	87.3(2)	P(3)—Pt(2)—P(4a)	87.4(2)
P(2)—Pt(1)—P(1a)	92.7(2)	Mo(1)—P(1)—Pt(1)	126.1(2)
P(3)—Pt(2)—P(4)	92.6(2)	Mo(2)—P(3)—Pt(2)	130.0(2)

Elemental analytical data for **1** was insufficient to distinguish between $[PtCl(PEt_3)(\mu\text{-}PPhH)\{Mo(CO)_5\}]$ and $[Pt(PEt_3)_2(\mu\text{-}PPhH)_2\{Mo(CO)_5\}_2]\cdot CH_2Cl_2$. However, $^{31}P\{^1H\}$ NMR spectroscopy confirmed its structure as well as giving considerable insight into a fluxional process in solution. The $^{31}P\{^1H\}$ NMR spectrum of **1** contains two distinct types of resonance. Our assignment of the high-field triplet

resonance ($\delta = -66.0$ ppm) to the bridging phosphido ligand was confirmed by its large one-bond phosphorus–hydrogen coupling constant [$^1J(P\mu—H) = 287$ Hz] consistent with previous observations [22]. Note that a high-field chemical shift (δ +50 to −200 ppm) for a phosphido bridge indicates the presence of a metal–metal bond, while low-field resonances (δ +50 to 300 ppm) imply non-bonded metal atoms [12]. An exchange-broadened low-field resonance [$\delta = +11.5$ ppm], although uninformative, confirmed the presence of PEt_3 ligands. The room-temperature triplet phosphido resonance [$^2J(PEt_3$-$P\mu) = 25.0$ Hz] is consistent with the presence of two PEt_3 ligands *cis* to the anionic phosphine $[PPhH\{Mo(CO)_5\}]^-$. The low-temperature $^{31}P^1H$ NMR spectrum of **1** (CD_2Cl_2, −75°C) several rotational isomers in slow exchange (*vide infra*). Also, the PEt_3 ligands each couple to ^{195}Pt with different $^1J(^{195}Pt—PEt_3)$ values (2413 and 2526 Hz), although these are in the range expected for mutually *trans* tertiary phosphines [23]. $^1J(^{195}Pt—P\mu)$ (2078 Hz) is lower than expected for a phosphorus donor *trans* to a chloride, based on the value for PEt_3 *trans* to chloride in *cis*-$[PtCl_2(PEt_3)_2]$ [$^1J(^{195}Pt—PEt_3) = 3500$ Hz] [23]. We have previously noted a similar low value for $^1J(^{195}Pt—P\mu)$ for coordinated $[PPhH\{Mo(CO)_5\}]^-$, consistent with lower *s*-orbital contribution to the Pt-phosphido bond compared with Pt-phosphine bonds of similar length. The values of $^2J(PEt_3—PEt_3)$ (366 Hz) and $^1J(^{195}Pt—PEt_3)$ (2413 and 2526 Hz) for **1** are close to those expected for complexes containing *trans*-tertiary phosphines [23,24] indicating that there is, if any, only a weak dependence on the nature of the *cis* ligand. Note that $^2J(P—P)$ values for *trans*-phosphines are typically an order of magnitude greater than those of their *cis* counterparts [24].

Two products analysing as $[Pt(PEt_3)_2(\mu\text{-}PPhH)_2\{Mo(CO)_5\}_2]$ (**2**) were isolated from the reaction of *cis*-$[PtCl_2(PEt_3)_2]$ with $[PPhH\{Mo(CO)_5\}]^-$ and $^{31}P\{^1H\}$ NMR spectroscopy was used to identify these as *cis*-**2** and *trans*-**2**. Both isomers are formed from pure *cis* or a mixture of *cis*- and *trans*-$[PtCl_2(PEt_3)_2]$. One striking characteristic of the $^{31}P\{^1H\}$ NMR spectrum of *cis*-**2** is that $^2J(PEt_3—P\mu)$ (200 Hz) is lower than expected for *trans* tertiary phosphines [24], but large enough to confirm the presence of a PEt_3 *trans* to $[PPhH\{Mo(CO)_5\}]^-$. We have recently reported [20] similar spectroscopic characteristics for $[Pt(\mu\text{-}PPhH)_2\{Mo(CO)_5\}_2(dppe)]$ (**3**) in which $^2J(Pdppe—P\mu)$ for $[PPhH\{Mo(CO)_5\}]^-$ *trans* to dppe was 213.0 Hz. The reduced $^2J(P—P\mu)$ values in *cis*-**2** and in **3** are also paralleled by lower $^1J(^{105}Pt—P\mu)$ coupling constants [$^1J(^{195}Pt—PEt_3) = 2277.7$ Hz and $^1J(^{195}Pt—P\mu) = 1400.6$ Hz for *cis*-**2** and $^1J(^{195}Pt$-dppe) = 2323.0 Hz and $^1J(^{195}Pt—P\mu) = 1450.0$ Hz for **3**] emphasizing the unusual spectroscopic characteristics associated with the $[PPhH\{Mo(CO)_5\}]^-$ ligand. The close structural and spectroscopic similarities of *cis*-**2** and **3** are further highlighted by their distinctive non-first-order AA′XX′ spin systems. Each set of resonances for **2** results from the superposition of two spin systems, an AA′XX′ corresponding to isotopomers with no ^{195}Pt and an AA′XX′M spin system for the ^{195}Pt isotopomer. Figure 1 shows the $^{31}P\{^1H\}$ NMR spectrum of *cis*-**2** together with an accurate computer simulation of its AA′XX′ region. This simulation was obtained by fixing the *trans* coupling constants at +200 Hz, measured directly from the spectrum, and varying the *cis* coupling constant which refined at $^2J(PEt_3—P\mu) = -15$ Hz. We [25] and others [26] have previously noted that *cis* and *trans*-$^2J(P—P)$ coupling constants are of opposite sign in the sign-simulated $^{31}P\{^1H\}$ spectra of complexes containing four coplanar phosphorus donor ligands. The most notable differences between the $^{31}P\{^1H\}$ NMR spectra of *cis*-**2** and **3** is the absence of line broadening and the observation of only a single diastereoisomer for *cis*-**2**.

The $^{31}P\{^1H\}$ spectral characteristics of *trans*-**2** are markedly different to those of *cis*-**2** and consistent with *trans*-PEt_3 ligands. Its room-temperature $^{31}P\{^1H\}$ NMR spectrum contains two sets of resonances, signals for PEt_3 ($\delta = +0.7$, 1.2 ppm) as well as high-field signals ($\delta = -71.4$, −68.5 ppm) for a phosphido ligand bridging non-bonded metal atoms [13,17a–c]. The most striking spectral feature of *trans*-**2** is that the PEt_3 resonance of the minor diastereoisomer is a sharp triplet resonances flanked by ^{195}Pt satellites, while that of the major diastereoisomer appears as a broad featureless resonance. The value of $^1J(^{195}Pt—PEt_3)$ for the minor diastereoisomer (2512 Hz) is similar to that in *trans*-$[PtCl_2(PEt_3)_2]$ [23] and supports a *trans* arrangement of these ligands. The lower $^1J(^{195}Pt—P\mu)$ coupling constant (1146.0 Hz) confirms our previous observation of reduced $^1J(^{195}Pt—P\mu)$ and $^2J(P—P\mu)$ values associated the $[PPhH\{Mo(CO)_5\}]^-$ ligand. Specifically, $^1J(^{195}Pt—P\mu)$ is approximately 50% that of $^1J(^{195}Pt—PR_3)$ in complexes with similar bond lengths. The value of $^{31}P^1H$ NMR spectra in studying Pt-phosphido complexes has been noted [27]. For instance, several characteristics of the recently reported phosphido-bridged complex $[(HBut_2P)_2Pt(\mu\text{-}H)(\mu\text{-}PBut_2)Pt(H)(PBut_2H)][BF_4]$ [27a] parallel features of the $^{31}P\{^1H\}$ NMR spectrum of *cis*- and *trans*-**2** including reduced values of $^1J(^{195}Pt—P\mu)$ and $^2J(P—P\mu)$.

Finally, *trans*-**2** contains two chiral primary phosphido bridges and, as with **3**, we assign the two sets of $^{31}P\{^1H\}$ NMR resonances to the *meso* and *racemic* diastereoisomers.

X-ray structures of trans-$[PtCl(PEt_3)_2(\mu\text{-}PPhH)\{Mo(CO)_5\}]$ (**1**) *and* trans-$[Pt(PEt_3)_2(\mu\text{-}PPhH)_2\{Mo(CO)_5\}_2]$ (**2**)

The unusual $^{31}P\{^1H\}$ NMR spectroscopic characteristics associated with **1** and **2** together with the presence of rare examples of chiral phosphido bridges has prompted single-crystal X-ray structural studies.

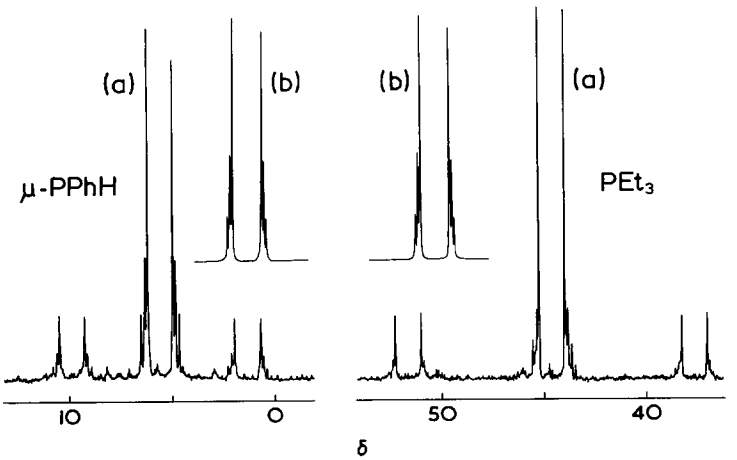


Fig. 1. $^{31}P\{^1H\}$ NMR spectra of *cis*-$[Pt(PEt_3)_2(\mu\text{-}PPhH)_2\{Mo(CO)_5\}_2]$ (**2**) in $CDCl_3$ (a) together with an accurate spin simulation, (b) illustrating the non first-order AA'XX' nature of its spin system.

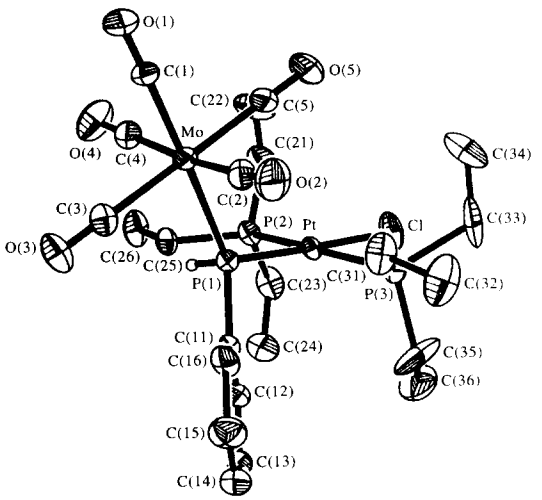


Fig. 2. Perspective ORTEP view of the molecular structure of *trans*-$[PtCl(PEt_3)_2(\mu\text{-}PPhH)\{Mo(CO)_5\}]$ (**1**) showing the square-planar coordination geometry at platinum.

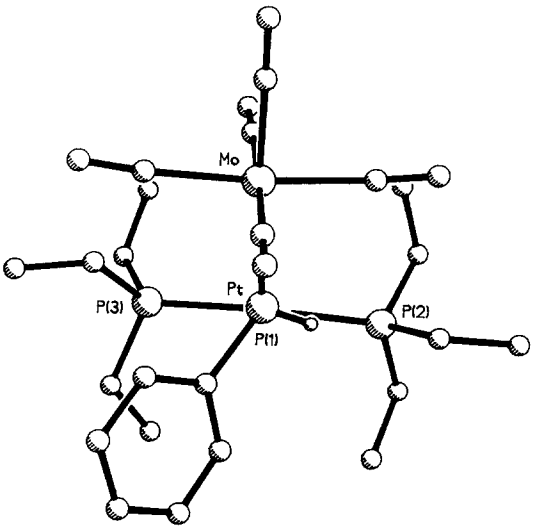


Fig. 3. View down the P(1)—Pt—Cl axis of $[PtCl(PEt_3)_2(\mu\text{-}PPhH)\{Mo(CO)_5\}]$ (**1**) showing the conformation about the Pt—$PPhHMo(CO)_5$ bond.

(a) Trans-**1**. The molecular structure of **1** in Fig. 2 unequivocally identifies it as *trans*-$[PtCl(PEt_3)_2(\mu\text{-}PPhH)\{Mo(CO)_5\}]$ (**1**), a μ-PPhH-bridged Mo—Pt dimer. Selected bond lengths and bond angles in Table 3. An alternative projection (Fig. 3) illustrates the PtP_3Cl planar arrangement of ligands, which successfully accounts for its unusual $^{31}P\{^1H\}$ NMR spectroscopic characteristics (*vide infra*).

The crystal structure of **1** reveals that only a single chloride ligand has been substituted by $[PPhH\{Mo(CO)_5\}]^-$ resulting in a Pt^{II} coordination sphere comprised of one chloride, one $[PPhH\{Mo(CO)_5\}]^-$ and two PEt_3 ligands. The geometry about the platinum centre is essentially square planar [Cl—Pt—P(1) = 177.5(1) and P(1)—Pt—P(2) = 169.9(1)°] with the larger angles of P(1)—Pt—P(2) = 95.6(1) and P(1)—Pt—P(3) = 93.8(1)° compared with P(2)—Pt—Cl = 83.3(1) and P(3)—Pt—Cl = 87.4(1)°, reflecting a greater steric demand of the anionic phosphine over chloride. The Pt—P(1)—Mo angle of 120.9(1)° is comparable to those recently reported for $[Pt(\mu\text{-}PPhH)_2\{Mo(CO)_5\}_2(dppe)]$ [21] and $[Cp_2W(H)(\mu\text{-}PPh_2)W(CO)_5]$ [15], rare examples of singly bridged heterometallics without metal–metal bonds. The Pt—Mo non-bonded distance in **2** [Pt—Mo = 4.255 Å], one of the longest to be reported, is responsible for the high-field shifted $^{31}P\{^1H\}$ NMR signal of the phosphido ligand [13,17]. The platinum-phosphido bond in **1** is considerably shorter [Pt—P(1) = 2.288(3) Å] than those in **3** [Pt—P_{av} = 2.362(3) Å], which presumably reflects the smaller *trans* influence of the chloride ligand compared with dppe. However, the value of $^1J(^{195}Pt—P\mu)$ is too low and the bond too long for $[PPhH\{Mo(CO)_5\}]^-$ to be treated as a "simple" phos-

phine [for example in *trans*-$PtCl_2(PEt_3)_2$, Pt—P = 2.258(4) Å]. Finally, the geometry about molybdenum is octahedral with a molybdenum–phosphorus distance [Mo—P(1) = 2.601(3) Å] greater than in $[Mo(CO)_5(PMe_3)]$ (2.5082 Å) [28], possibly reflecting the greater steric requirements of $[PPhH\{Mo(CO)_5\}]^-$. However, the axial carbonyl bond length [Mo—C(1) = 1.972(1) Å] is characteristic of a Mo—C bond *trans* to a phosphino donor while the equatorial Mo—C bond lengths are unexceptional. Compound **1** can thus be described either as (i) a square-planar Pt^{II} with three phosphorus donor ligands and one chloride or (ii) a rare example of a primary phosphido-bridged Mo—Pt heterobimetallic containing an exceptionally large Mo—P—Pt bond angle.

(b) Trans-**2**. The molecular structure of *trans*-**2** is shown in Figs 4 and 5 with a selection of bond lengths and angles in Table 4. *trans*-**2** crystallizes in the monoclinic space group $P2_1/a$ with two independent molecules in the asymmetric unit and with platinum located on an inversion centre. The projection of *trans*-**2** in Fig. 4 clearly identifies it as a trinuclear phosphido ligand compound, whilst that in Fig. 5 emphasises its alternative description as a square-planar Pt^{II} complex containing two *trans*-PEt_3 and two *trans*-$[PPhH\{Mo(CO)_5\}]^-$ ligands. Notable features include the exceptionally large Pt—P—Mo angles [Mo(1)—P(1)—Pt(1) = 126.1(2) and Mo(2)—P(3)—Pt(2) = 130.0(2)°], the largest phosphido bridging angles to be reported, as well as long Pt—Mo non-bonded distances [Pt(1)—Mo(1) = 4.504(2) and Pt(2)—Mo(2) = 4.573(2) Å]. The asymmetric bridging mode of the phosphido ligand in **2** [Pt(1)—P(1) = 2.407(5), Pt(2)—P(3) = 2.397(4) and Mo(1)—P(1) = 2.644(5), Mo(2)—P(3) = 2.648(5) Å] is a common feature of heterometallic phosphido-bridged complexes. These platinum–phosphido bond lengths are among the longest reported, far greater than that in **1** reflecting the stronger *trans* influence of $[PPhH\{Mo(CO)_5\}]^-$ compared with chloride. As for **1** the axial Mo—CO bonds are substantially longer than their equatorial counterparts supporting the significant *trans* influence associated with the μ-PPhH group.

Although **2** contains a PtP_4 planar arrangement of ligands, it adopts a staggered conformation of *trans*

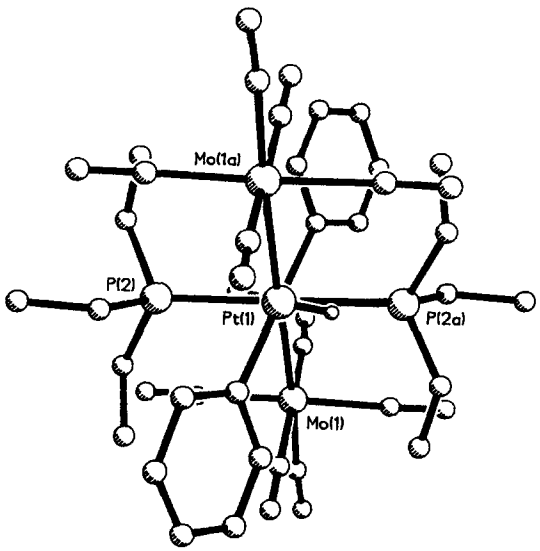


Fig. 5. A projection down the P(1)—Pt(1)—P(1a) axis of *trans*-$[Pt(PEt_3)_2(\mu\text{-}PPhH)_2\{Mo(CO)_5\}_2]$ (**2**) showing the staggered nature of the *trans* ligands and the disposition of the substituents at phosphorus with respect to this plane.

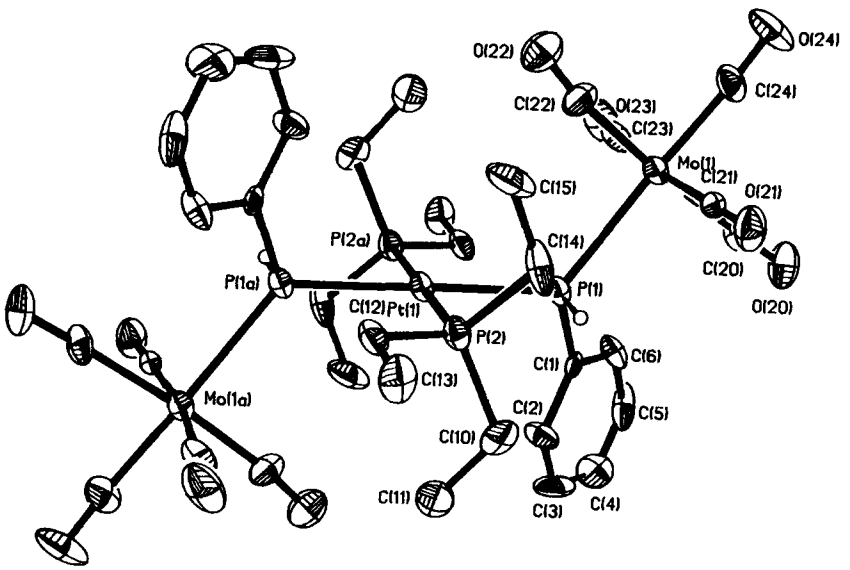


Fig. 4. Perspective ORTEP view of the molecular structure of one independent molecule of *trans*-$[Pt(PEt_3)_2(\mu\text{-}PPhH)_2\{Mo(CO)_5\}_2]$ (**2**) showing the square-planar coordination at platinum which lies at a centre of symmetry.

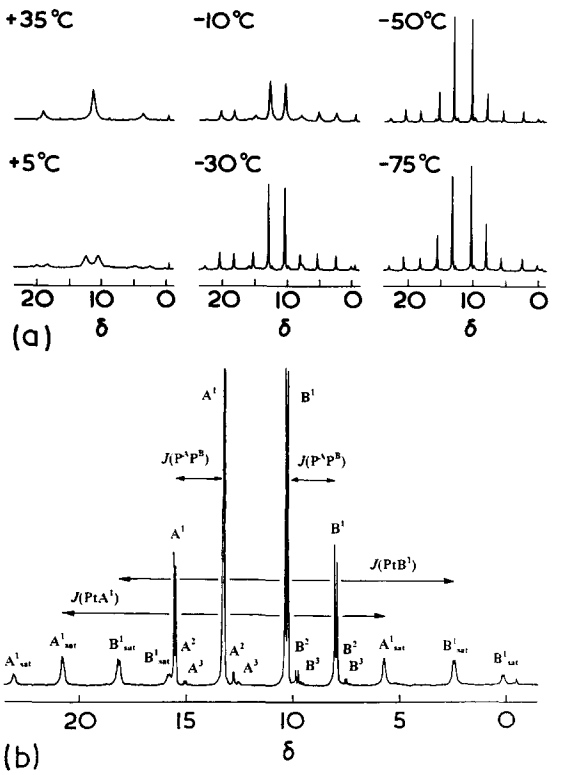


Fig. 6. (a) Variable-temperature $^{31}P^{1}H$ NMR spectra of $[PtCl(PEt_3)_2(\mu\text{-}PPhH)_2\{Mo(CO)_5\}]$ (**1**) in the PEt_3 region (AB part of ABX spectrum, plus ^{195}Pt satellites) showing the broadening and collapse of signals for three rotational isomers. (b) $^{31}P^{1}H$ NMR spectra of **1** (CD_2Cl_2, −75°C), major ABX (A^1B^1) and minor (A^2B^2 and A^3B^3) rotational isomers and assignment of the $^1J(^{195}Pt—PEt_3)$ and $^2J(P^{A^1}P^{B^1})$ coupling constants for the major isomer. The ^{195}Pt satellites for the minor isomers were not detected, although the main signals are qualitatively equivalent to those of the major isomer.

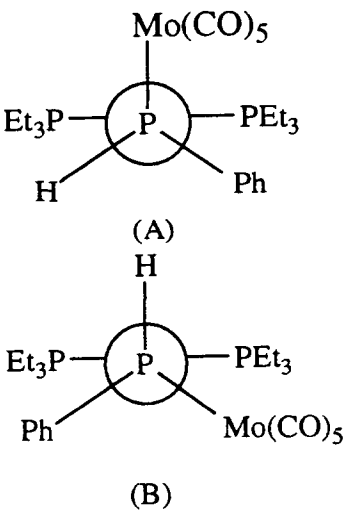
ligands with the bulky $[Mo(CO)_5]$ substituents in an *anti* arrangement, presumably the sterically least demanding conformation. This contrasts with our recent characterization of several square-planar complexes, each of which contains four phosphorus donor ligands with substituents on *trans* ligands eclipsed [29]. Compound **2** is only the second example of a phosphido-bridged heterometallic trimer with the four unique substituents attached to the phosphido ligand, Ph, H, Mo and Pt. Therefore, both *meso* and *racemic* forms are expected, however, the crystal for which the structure was determined was that of the *meso* stereoisomer, *RS*-$[Pt(PEt_3)_2(\mu\text{-}PPhH)_2\{Mo(CO)_5\}_2]$.

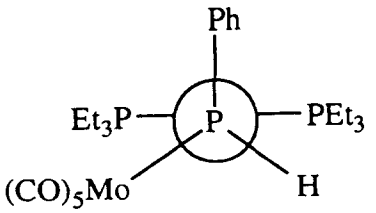
Rotational isomers of trans-**1** *and* trans-**2**: *a variable-temperature* $^{31}P\{^1H\}$ *NMR study*

Relatively high rotation barriers in octahedral metal complexes containing four coplanar phosphines are common [25,29a]. However, we recently found evidence for rotational isomers of $[Pt(\mu\text{-}PPhH)_2\{Mo(CO)_5\}_2(dppe)]$ (**3**), a molecule containing two neutral and two anionic phosphines. Line broadening in the $^{31}P\{^1H\}$ NMR spectra of **1** and *trans*-**2** prompted us to undertake a variable-temperature study, which also revealed that rotational isomers of these molecules could be observed and that their interconversion is slow at −80°C.

(a) Trans-**1**. A representative set of $^{31}P^{1}H$ NMR spectra for **1**, in the PEt_3 region, is shown in Fig. 6(a) together with our assignment of the low temperature limiting spectrum (−75°C) in Fig. 6(b).

The room-temperature spectrum of **1** contains a sharp high-field triplet resonance [δ −66.4, $^1J(^{195}Pt—P\mu)$ = 2078 Hz] for the phosphido bridge and an exchange broadened resonance (δ = +10.5 ppm) corresponding to the PEt_3 ligands. The low-temperature $^{31}P^{1}H$ NMR spectrum of **1** unequivocally established the presence of three isomers, a dominant one (94%) characterized by an AB quartet [δ +9.0(B^1), +14.1 (A^1)] together with low concentrations of two others (A^2B^2 and A^3B^3, 5 and 1%, respectively), each with similar spectroscopic features. The diastereotopic PEt_3 ligands couple to the bridging phosphido with different $^2J(PEt_3—P\mu)$ values [$^2J(PP)$ = 17.3 Hz (B^1) and $^2J(PP)$ = 9.6 Hz (A^1)] and flanked by ^{195}Pt satellites also of different magnitude [$^1J(^{195}Pt—P^{A^1})$ = 2413.0 Hz and $^1J(^{195}Pt—P^{B^1})$ = 2526.4 Hz], although both values are in the range expected for *trans*-PEt_3 ligands [22]. Figure 6(b) also identifies the two low concentration species, each with a similar AB quartet resonance flanked by ^{195}Pt satellites [δ +8.6 (B^2), +13.7 (A^2) and +8.4 (B^3), 13.6 (A^3)] again with different values of $^2J(PEt_3—P\mu)$ [$^2J(P\mu—P^{A^2})$ = 9.0, $^2J(P\mu—P^{B^2})$ = 15.0, $^2J(P\mu—P^{A^3})$ = 9.6, $^2J(P\mu—P^{B^3})$ = 15.4 Hz]. These three sets of resonances have been assigned to three conformational isomers each with an ABX spin system. We believe that the predominant ABX (A_1B_1) at low temperature belongs to rotamer (A), the sterically least hindered conformer and that found in the crystal. Rotamers (B) and (C) with the bulky $[Mo(CO)_5]$ substituents in closer proximity to the PEt_3 are sterically more demanding and much less populated. At higher temperatures rapid rotation about the





(C)

Pt—Pμ bond interconverts these rotamers to afford the exchange broadened spectrum illustrated in Fig. 6(a) (+35°C).

(b) Trans-**2**. The room-temperature $^{31}P\{^1H\}$ NMR spectrum of **2** contains two sets of resonances, each with signals in the phosphido and PEt_3 regions consistent with the two possible non-interconverting diastereoisomeric forms. While the resonances belonging to the minor diastereoisomer are sharp those corresponding to the major stereoisomer are broad and featureless. A representative set of $^{31}P\{^1H\}$ NMR spectra are illustrated in Fig. 7(a) with our assignment of the low-temperature limiting spectrum in the PEt_3 region, shown in Fig. 7(b). The low-temperature limiting spectrum of *trans*-**2** [Fig. 7(b)] consists of three sets of resonances in significant abundance, two belonging to the major (*meso*) diastereoisomer [an A triplet of an $(AX)_2$ spin system at δ +1.8 (A'^2) and the AB part of an ABXY pattern at δ +5.8 and −2.4 for A'^1 and B'^1, respectively] and the other, another A triplet of an $(AX)_2$ system, to the minor (*rac*) diastereoisomer [δ +0.7 (A'^3)]. These isomers have been designated $A'^1B'^1$, A'^2 and A'^3 to distinguish them from those associated with **1** shown in Fig. 6. Fractional crystallization of *trans*-**2** provided sufficient sample to confirm, by $^{31}P\{^1H\}$ NMR spectroscopy, that the exchange broadened resonance corresponds to the *meso* stereoisomer, for which the crystal structure was determined. Once separated by crystallization, there is no conversion of the *meso* into the *rac* stereoisomer.

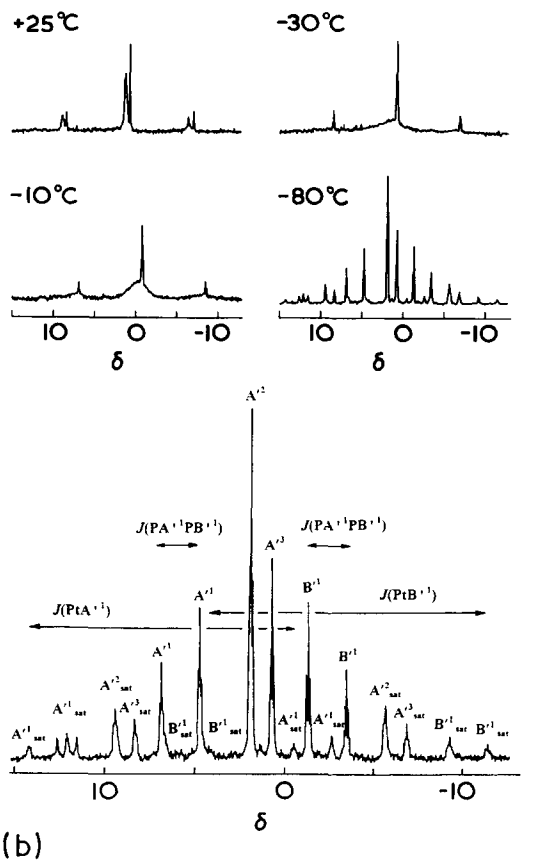
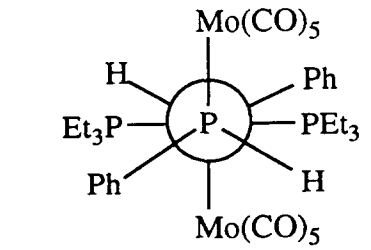
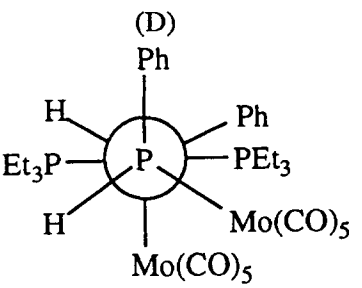
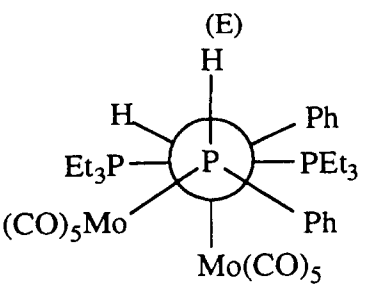


Fig. 7. (a) Variable-temperature $^{31}P^1H$ NMR spectra of a diastereomeric mixture of *trans*-$[Pt(PEt_3)_2(\mu\text{-}PPhH)_2\{Mo(CO)_5\}_2]$ (**2**) in the PEt_3 region. (b) $^{31}P^1H$ NMR spectrum of *trans*-**2** (CD_2Cl_2, −80°C), major ($A'^1B'^1$) and (A'^2) and minor (A'^3) diastereoisomers illustrating their $^1J(^{195}Pt—PEt_3)$ and $^2J(PEt_3—P\mu)$ coupling constants.







(F)

The *meso*-stereoisomer contains pairs of staggered *trans*-phosphines for which there should exist three possible rotamers, (D)–(F). However, only one of these, rotamer (D), contains magnetically equivalent PEt_3 ligands which must therefore correspond to the triplet resonance at δ +0.7, while either rotamer (E) or (F) could give rise to the ABXY pattern. Above −80°C these resonances start to broaden and at

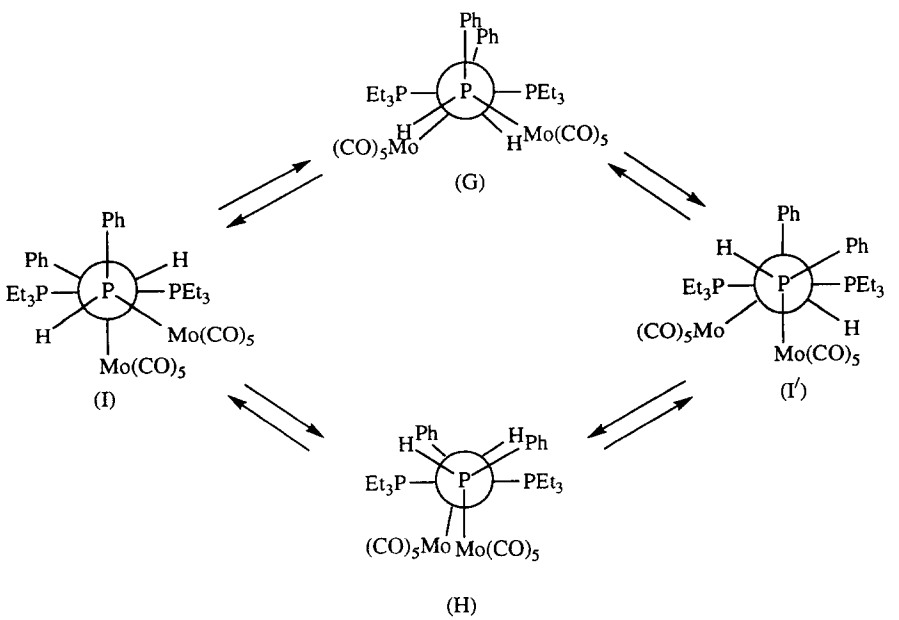
+35°C rotamers (D), (E) or (F) exchange *via* rotation about their Pt—Pμ bonds.

In contrast the $^{31}P\{^1H\}$ NMR spectrum of the minor *RR/SS* diastereoisomer is unchanged over the temperature range +25 to −80°C. The observed A_2X_2 pattern is not consistent with any one static staggered rotamer since the PEt_3 ligands are necessarily non-equivalent. However, its spectra could be rationalized in terms of one of the eclipsed rotamers (G) or (H). An alternative view is that the lowest energy rotamer is the staggered form (I), which is in rapid equilibrium with its enantiomer (I′) by the mechanism shown in Scheme 1, which leads to PEt_3 exchange. However, why should the equilibrium in Scheme 1 be very fast even at −80°C, whereas the equilibria between (D) and (E) or (F) are much slower? Although the projections shown are reminiscent of ethane-type conformations, the dominant steric interactions are between *cis* ligands and not between the mutually *trans*-PPhH$\{Mo(CO)_5\}$ groups. Thus, the barrier to rotation is a consequence of the movement of the H, $Mo(CO)_5$ or Ph substituents past the *cis*-PEt_3 ligands. In the equilibria in Scheme 1, the Ph and $Mo(CO)_5$ groups do not migrate from one side of the Pt coordination plane to the other and only the H substituents are required to migrate past the PEt_3 ligands. Hence, the energy barriers for these rotational equilibria are much lower than for the interconversion of (D) with (E) or (F), which requires the Ph or $Mo(CO)_5$ substituents to slide past the PEt_3 ligands. On this model, equilibria in Scheme 1 must be fast enough for coalescence temperatures to be well below −80°C. In spite of these arguments we have no experimental evidence to discriminate between (G), (H) and (I).

The fluxionality of **1** and **2** is best understood by considering them as square-planar Pt^{II} complexes with PtP_3Cl and PtP_4 arrangements of ligands. Some time ago we reported detailed variable-temperature $^{31}P\{^1H\}$ NMR studies of the tetrakisphosphine complexes $[IrCl_2(PMe_2Ph)_3L][ClO_4]$ (L = PMe_3, PMe_2Ph, $PMePh_2$) [25,29a] which revealed the existence of rotameric forms that interconvert slowly at −50°C. It appeared that a general requirement for the occurrence of these rotamers was the presence of four coplanar phosphines. More recently we revealed that line broadening effects in the $^{31}P\{^1H\}$ NMR spectrum of $[Pt(\mu\text{-}PPhH)_4\{Mo(CO)_5\}_2(dppe)$ (**3**) resulted from restricted rotation about the Pt—Pμ bond generating rotational isomers. The similarity between $[Pt(\mu\text{-}PPhH)_2\{Mo(CO)_5\}_2(dppe)]$ (**3**) and $[PtCl(PEt_3)_2(\mu\text{-}PPhH)\{Mo(CO)_5\}]$ (**1**) and *trans*-$[Pt(PEt_3)_2(\mu\text{-}PPhH)_2\{Mo(CO)_5\}_2]$ (**2**) suggests they too may have accessible rotameric forms. For **1** this results in population of the sterically least demanding rotamer (A) with only very low concentrations of less favourable (B) and (C), while restricted rotation at the Pt—Pμ bonds in *meso*-**2** gives rise to rotamers (D) and one of either (E) or (F). In contrast *RR/SS*-**2** is either the conformationally rigid eclipsed rotamer (G) or (H) or the highly dynamic staggered rotamer (I).

Correlation of $^1J(^{195}Pt—P)$ *and* Pt—P *bond lengths*

Correlation between $^1J(^{195}Pt—P)$ and Pt—P bond lengths in platinum(II) phosphine complexes, a parameter sensitive to the *s*-orbital character of the Pt—P bond, has been the focus of several investigations [17,22]. Powell reports a close correlation between the $^1J(^{195}Pt—P\mu)$ and platinum phosphorus distances for several heterometallic complexes and our observations for complexes **1**–**2** support this, provided



Scheme 1.

ligands of the same type are compared, that is we have to distinguish between tertiary and anionic phosphines in order to obtain credible correlations. Powell has also suggested that the decreasing values of $^1J(^{195}Pt—P)$ with increasing bond length reflect a change in *s*-orbital overlap in the platinum–phosphorus bond [17b,c]. We too have observed a similar trend with $^1J(^{195}Pt—P\mu) = 2135$ Hz *trans* to chloride in **1** [Pt—P = 2.288(3) Å] and $^1J(^{195}Pt—P\mu) = 1450$ Hz *trans* in dppe in $[Pt(\mu\text{-}PPhH)_2\{Mo(CO)_5\}_2(dppe)]$ (**3**) [Pt—P = 2.361(3) Å]. Thus, the values of $^1J(^{195}Pt—P)$ for tertiary phosphines do reflect the Pt—P distances as do those of $^1J(^{195}Pt—P\mu)$ for $[PPhH\{Mo(CO)_5\}]^-$, which are, in general, considerably lower than their tertiary phosphine counterparts of similar bond length. An examination of the $^1J(^{195}Pt—P\mu)$ values in **1** and *cis*-**2** (i.e. 2135 Hz and 1400.6 Hz for **1** and **2**, respectively) illustrates the effect of the *trans* ligand on this parameter, clearly demonstrating that ligands with a strong *trans* influence lead to reduced $^1J(^{195}Pt—P\mu)$ values and that these are considerably lower than their tertiary phosphine counterparts with similar *trans* ligands. These reduced $^1J(^{195}Pt—P\mu)$ values are illustrated by comparing $[PtCl(PEt_3)_2(\mu\text{-}PPhH)\{Mo(CO)_5\}]$ (**1**) with *cis*-$[PtCl_2(PEt_3)_2]$ for which $^1J(^{195}Pt—P\mu) = 2135$ Hz and $^1J(^{195}Pt—PEt_3) = 3500$ Hz in the absence of significant *cis* effects.

Conclusions

While the synthetic approach described here extends the utility of the bridge-assisted approach for constructing heterometallic complexes, the thrust of our effort has been the structural and spectroscopic characterization of rare examples of heterometallic complexes bridged by chiral primary phosphido bridges. The heterometallic complexes *trans*-$[PtCl(PEt_3)_2(\mu\text{-}PPhH)\{Mo(CO)_5\}]$ (**1**) and *cis*- and *trans*-$[Pt(PEt_3)_2(\mu\text{-}PPhH)_2\{Mo(CO)_5\}_2$ (**2**) have been prepared by the nucleophilic substitution of chloride in *cis*-$[PtCl_2(PEt_3)_2]$ by the chiral anion $[PPhH\{Mo(CO)_5\}]^-$. Information contained in their $^{31}P\{^1H\}$ NMR spectra has provided insight into the nature of their accessible rotational isomers. The exchange broadened $^{31}P\{^1H\}$ NMR spectra of **1** and *trans*-**2** have been explained in terms of the presence of several rotameric forms which interconvert by rotation about their Pt—Pμ bonds, an interpretation supported by similar observations for $[Pt(\mu\text{-}PPhH)_2\{Mo(CO)_5\}_2(dppe)]$ (**3**). *cis*-**2** with PEt_3 *trans* to $[PPhH\{Mo(CO)_5\}]^-$ is characterized by reduced values of $^2J(PEt_3—P\mu)$ (200 Hz) and $^1J(^{195}Pt—P\mu)$ (1400.6 Hz) compared with values reported for mutually *trans* neutral phosphines for which values close to 300 Hz and 2500 Hz would have been expected. These reduced Pt—P and P—P coupling constants are consistent with a lower *s*-orbital contribution to the Pt—P bond for the anion $[PPhH\{Mo(CO)_5\}]^-$ compared with their tertiary phosphine counterparts. We conclude that the spectroscopic characteristics of **1** and *cis*- and *trans*-**2** can most aptly be accounted for by considering them as square-planar Pt^{II} complexes containing phosphorus donor ligands rather than μ-PPhH bridged heterometallics. Finally, the P—H functionalities of the primary phosphido bridges in **1** and **2** are sites of additional reactivity not available to their μ-PR_2 (R = alkyl or aryl) bridged counterparts, thus, complexes of this type allow new developments in heterobimetallic reactivity.

Supplementary material available. Further details for **1** and *trans*-**2** are available as supplementary material (atomic coordinates, anisotropic thermal parameters, bond distances and bond angles, hydrogen-atom coordinates) deposited at the Cambridge Crystallographic Centre. Structure factors are available from the author upon request.

Acknowledgements—We thank the SERC for research studentships (for S.D. and B.R.C.) and for funds for the purchase of a diffractometer.

REFERENCES

1. For an account of the bridge assisted method see: Roberts, D. A. and Geoffroy, G. L., in *Comprehensive Organometallic Chemistry*, Ch. 40, ed. G. Wilkinson, F. G. A. Stone and E. Abel. Pergamon Press, Oxford, 1982.
2. Stephan, D. W., *Coord. Chem. Rev.* 1989, **95,** 41.
3. For a selection of recent references see: (a) Hostetler, M. J., Butts, M. D. and Bergman, R. G., *Organometallics* 1993, **12,** 62; (b) Butts, M. D. and Bergman, R. G., *Organometallics* 1994, **13,** 1699; (c) Braunstein, P., Knorr, M. and Stahrfeldt, T., *J. Chem. Soc., Chem. Commun.* 1994, 1913; (d) Hirpo, W., Curtis, M. D. and Kampf, J. W., *Organometallics* 1994, **13,** 3360; (e) Moldes, I., Delavauxnicot, B., Lugan, N. and Mathieu, R., *Inorg. Chem.* 1994, **33,** 3510; (f) Cernerud, M., Warnmark, K. and Moberg, C., *Tetrahedron Lett.* 1994, **35,** 5473; (g) Casey, C. P., Wang, Y., Tanke, R. S., Hazin, P. N. and Rutter, E. W., *New J. Chem.* 1994, **18,** 43; (h) Akita, M., Ishii, N., Takabuchi, A., Tanaka, M. and Morooka, Y., *Organometallics* 1994, **13,** 258; (i) He, Z., Nefedov, S., Lugan, N., Neibecker, D. and Mathieu, R., *Organometallics* 1993, **12,** 3837; (j) Michos, D., Luo, X.-L. and Crabtree, R. H., *Inorg. Chem.* 1993, **32,** 2118.
4. Baranger, A. M. and Bergman, R. G., *J. Am. Chem. Soc.* 1994, **116,** 3822; (b) Baranger, A. M., Hollander, F. L. and Bergman, R. G., *J. Am. Chem. Soc.* 1993, **115,** 7890; (c) Hostetler, J., Butts, M. D. and Bergman, R. G., *J. Am. Chem. Soc.* 1993, **115,** 2743.
5. Knorr, M., Braunstein, P., Decian, A. and Fischer, J., *Organometallics*, 1995, **14,** 1302; (b) Braunstein, P., Knorr, M., Hirle, B., Reinhard, G. and Schubert, U., *Angew. Chem., Int. Ed. Engl.* 1992, **31,** 1583.

6. Herberhold, M. and Jin, G., *Angew. Chem., Int. Ed. Engl.* 1994, **33,** 964.
7. Chisholm, M. H., Kramer, K. S. and Streib, W. E., *Angew. Chem., Int. Ed. Engl.* 1995, **34,** 891.
8. Adams, R. D. in *The Chemistry of Metal Cluster Complexes*, ed. D. F. Shriver, H. D. Kaesz, R. D. Adams, VCH Publisher, Inc., New York, 1990 pp. 121. For some recent examples see: (a) Mathur, P., Sekar, P., Satyanarayana, C. V. V. and Mahon, M. F., *Organometallics* 1995, **14,** 2115; (b) Carmona, D., Ferrer, J., Mendoza, A., Lahoz, F. J., Oro, L. A., Viguri, F. and Reyes, J., *Organometallics* 1995, **14,** 2066; (c) Wang, L.-S. and Cowie, M., *Organometallics*, 1995, **14,** 2374; (d) Jones, C. M. and Doherty, N. M., *Polyhedron*, 1995, **14,** 81; (e) Bartlone, A. F., Chetcuti, M., Navarro, R. and Shang, M. Y., *Inorg. Chem.* 1995, **34,** 980.
9. (a) Oudet, P., Kubicki, M. M. and Moise, C., *Organometallics* 1994, **13,** 4278; (b) Shyu, S.-G., Wu, W.-J., Wen, Y.-S., Peng, S.-M. and Lee, G.-H., *J. Organomet. Chem.* 1995, **489,** 113; (c) Shyu, S.-G., Lin, P.-J. and Wen, Y.-S., *J. Organomet. Chem.* 1993, **443,** 115; (d) Shyu, S.-G., Hsu, J.-Y. and Wen, Y.-S., *J. Organomet. Chem.* 1993, **453,** 97; (e) Baker, R. T., Tulip, T. M. and Wreford, S. S., *Inorg. Chem.* 1985, **24,** 1379.
10. Rosenberg, S., Mahoney, W. S., Hayes, J. M., Geoffroy, G. L. and Rheingold, A. L., *Organometallics* 1986, **5,** 1065.
11. (a) Carty, A. J., MacLaughlin, S. A. and Taylor, N. J., *J. Organomet. Chem.* 1981, **204,** C27; (b) Lugan, N., Bonnet, J.-J. and Ibers, J. A., *Organometallics*, 1988, **7,** 1538; (c) Corrigan, J. F., Doherty, S., Taylor, N. J., Carty, A. J., Boroni, E. and Tiripicchio, A., *J. Organomet. Chem.* 1993, **462,** C24; (d) Corrigan, J. F., Di-Nardo, M., Doherty, S., Hogarth, G., Sun, Y., Taylor, N. J. and Carty, A. J., *Organometallics* 1994; **13,** 3572; (e) Lugan, N., Fabre, P.-L., de Montauzon, D., Lavigne, G., Bonnet, J.-J., Saillard, J.-Y. and Halet, J.-F., *Inorg. Chem.* 1993, **32,** 1363, and refs therein.
12. (a) Carty, A. J., MacLaughlin, S. A. and Nucciarone, D., in *Phosphorus-31 NMR Spectroscopy in Stereochemical Analysis: Organic Compounds and Metal Complexes*, ed. J. B. Verkade, L. D. Quinn. VCH, Deerfield Beach, FL, 1987, p. 539; (b) Carty, A. J., *Adv. Chem. Ser.* 1982, **196,** 163.
13. (a) Corrigan, J. F., Doherty, S., Taylor, N. J. and Carty, A. J., *J. Am. Chem. Soc.* 1992, **114,** 7557; (b) Corrigan, J. F., Doherty, S., Taylor, N. J. and Carty, A. J., *Organometallics* 1993, **12,** 993; (c) Corrigan, J. F., Di-Nardo, M., Doherty, S. and Carty, A. J., *J. Cluster Sci.* 1992, **3,** 313; (d) Lugan, N., Lavigne, G., Bonnet, J.-J., Reau, R., Neibecker, D. and Tkatchenko, I., *J. Am. Chem. Soc.* 1988, **110,** 5369; (e) Etienne, M., Mathieu, R. and Lugan, N., *Organometallics* 1993, **12,** 140; (f) Adams, H., Bailey, N. A., Blenkiron, P. and Morris, M. J., *J. Organomet. Chem.* 1993, **460,** 73; (f) Blenkiron, P., Lavender, M. H. and Morris, M., *J. Organomet. Chem.* 1992, **426,** C28; (g) Manojlovic-Muir, L., Mays, M. J., Muir, K. W. and Woulfe, K. W., *J. Chem. Soc., Dalton Trans.* 1992, 1531.
14. Baker, R. T., Fultz, W. C., Marder, T. B. and Williams, I. D., *Organometallics* 1990, **9,** 2357.
15. (a) Barre, C., Boudot, P., Kubicki, M. M. and Moise, C., *Inorg. Chem.* 1995, **34,** 284; (b) Lin, J.-A.-T., Yeh, A.-C., Chou, Y.-C., Tsai, T.-Y.-R. and Wen, Y.-S., *J. Organomet. Chem.* 1995, **486,** 147; (c) Shyu, S.-G., Hsu, J.-Y., Lin, P.-J., Wu, W.-J., Peng, S.-M., Lee, G.-H. and Wen, Y.-S., *Organometallics* 1994, **13,** 1699.
16. (a) Mercer, W. C., Geoffroy, G. L. and Rheingold, A. L., *Organometallics* 1985, **4,** 1418; (b) Morrison, E., Harley, A. D., Marcelli, M. A., Geoffroy, G. L., Rheingold, A. L. and Fultz, W. C., *Organometallics* 1984, **3,** 1407; (c) Mercer, W. C., Whittle, R. R., Burkhardt, E. W. and Geoffroy, G. L., *Organometallics* 1985, **4,** 68; (d) Shulman, P. M., Burkhardt, E. D., Lindquist, E. G., Pilato, R. S., Geoffroy, G. L. and Rheingold, A. L., *Organometallics* 1987, **6,** 101.
17. (a) Powell, J., Gregg, M. R. and Sawyer, J. F., *Inorg. Chem.* 1989, **28,** 4451; (b) Powell, J., Sawyer, J. F. and Stainer, M. V. R., *Inorg. Chem.* 1989, **28,** 4461; (c) Powell, J., Fuchs, E., Gregg, M. R., Phillips, J. and Stainer, M. V. R., *Organometallics* 1990, **9,** 387.
18. He, Z., Lugan, N., Neibecker, D., Mathieu, R. and Bonnet, J.-J., *J. Organomet. Chem.* 1992, **426,** 247.
19. Shyu, S.-G., Lin, P.-J., Lin, K.-J., Chang, M.-C. and Wen, Y.-S., *Organometallics*, 1995, **14,** 2253.
20. Deeming, A. J. and Doherty, S., *Polyhedron*, 1995, **15,** 1175.
21. (a) Chatt, J. and Wilkins, R. G., *J. Chem. Soc.* 1952, 273; (b) Goggin, P. L. and Goodfellow, R. J., *J. Chem. Soc(A)*, 1966, 1462.
22. Deeming, A. J., Doherty, S. and Powell, N. I., *Inorg. Chim. Acta*, 1992, **198–200,** 469.
23. (a) Mather, G. G., Pidcock, A. and Rapsey, G. J. N., *J. Chem. Soc., Dalton Trans.* 1973, 2095; (b) Pidcock, A., *Adv. Chem. Ser.* 1982, **196,** 1.
24. Pregosin, P. S. and Kunz, R. W., *NMR: Basic Princ. Prog.* 1979, 16.
25. Deeming, A. J., Doherty, S., Marshall, J. E. and Powell, N. I., *J. Chem. Soc., Chem. Commun.* 1989, 1351.
26. (a) Baacke, M., Hietkamp, S., Morton, S. and Stelzer, O., *Chem. Ber.* 1981, **114,** 3691; (b) Baacke, M., Stelzer, O. and Wray, V., *Chem. Ber.* 1980, **113,** 1356; (c) Baacke, M., Hietkamp, S., Morton, S. and Stelzer, O., *Chem. Ber.* 1982, **115,** 1389.
27. (a) Leoni, P., Manetti, S. and Pasquali, M., *Inorg. Chem.* 1995, **34,** 749; (b) Blum, T., Braunstein, P., Tiripicchio, A. and Tiripicchio-Camellini, M., *Organometallics*, 1989, **8,** 2504; (c) Siedle, A. R., Newmark, R. and Gleason, W. B., *J. Am. Chem. Soc.* 1986, **108,** 757.
28. Davies, M. S., Aroney, M. J., Buys, I. E., Hambley, T. W. and Calvert, J. L., *Inorg. Chem.* 1995, **34,** 330.
29. (a) Deeming, A. J., Doherty, S. and Marshall, J. E., *Polyhedron*, 1991, **10,** 1857; (b) Deeming, A. J., Doherty, S., Marshall, J. E., Powell, J. L. and Senior, A. M., *J. Chem. Soc., Dalton Trans.* 1992, 1093.

Pergamon

PII: S0277-5387(96)00397-X

Polyhedron Vol. 16, No. 11, pp. 1957–1962, 1997
© 1997 Elsevier Science Ltd
All rights reserved. Printed in Great Britain
0277-5387/97 $17.00+0.00

Syntheses, structures and spectroscopic properties of $[Ag(dppm)(O_2CCH_2Ph)]_2$ and $[Ag_2(dppm)_3](NO_3)_2 \cdot 3H_2O$

Maochun Hong,[a]* Daxu Wu,[a] Hanqin Liu,[a] Thomas C. W. Mak,[b]* Zhongyong Zhou,[b] Dedong Wu[b] and Songling Li[b]

[a] State Key Laboratory of Structure Chemistry, Fujian Institute of Research on the Structure of Matter, Fuzhou, Fujian 350002, P.R. China

[b] Department of Chemistry, The Chinese University of Hong Kong, Shaitin, New Territories, Hong Kong

(Received 25 April 1996; accepted 6 August 1996)

Abstract—The reaction of $[Ag(dppm)(NO_3)]_2$ with sodium phenylacetate and dppm in THF at room temperature gave rise to the silver complexes $[Ag(dppm)(O_2CCH_2Ph)]_2$ (**1**) and $[Ag_2(dppm)_3](NO_3)_2$ (**2**), respectively. Their crystal structures have been determined by single crystal X-ray diffraction analysis. Complex **1** is binuclear with a silver–silver separation of 3.080 Å and bridged by two dppm ligands. The cation in complex **2** possesses a Ag_2P_6 core with Ag—Ag distance of 2.987 Å and the silver atoms are each coordinated by three phosphorus atoms in an ideal trigonal-planar environment. Their IR, Raman, ^1H and ^{31}P NMR spectroscopic properties are also reported. © 1997 Elsevier Science Ltd. All rights reserved.

Keywords: Silver(I) complexes; dinuclear; synthesis; crystal structure; Raman spectra; NMR spectra.

Bis(diphenylphosphino)methane (dppm) complexes containing the $M_2(dppm)_2$ structural unit have been intensively investigated [1–7]. A key feature in the chemistry of this class of the complexes is the relatively stable and nearly planar M_2P_4 framework and two silver atoms are connected by a pair of bridging dppm ligands. The stable M_2P_4 framework places much of the burden for any structural adjustment on the substrate species themselves and on any additional ligand present. This feature is presumably one of the chief reasons for their unusual bonding, reactivity and catalytic properties. There are many examples of binuclear complexes with the formula of $M_2(dppm)_2X_2$ (M = Ag, Au, Pd and Pt; X = univalent anion) [1–7]. To our knowledge, for complexes with $M_2(dppm)_3$ fragment, only $Pd(dppm)_3$ [8] and $Pt_2(dppm)_3$ [9] have been structurally characterized. Recently, we started our investigation on the syntheses of polynuclear silver cluster compounds containing mixed phosphine and carboxylate ligands and obtained a series of silver(I) complexes. In this paper, we report the syntheses and structural characterization along with the spectroscopic properties of two silver(I) complexes with mixed bis(diphenylphosphino)methane and phenylacetate ligands, namely $[Ag(dppm)(O_2CCH_2Ph)]_2$ (**1**) and $[Ag_2(dppm)_3](NO_3)_2$ (**2**), in which the dppm ligand bridges two silver atoms to form the dimers with Ag_2P_4 core in **1** and Ag_2P_6 core in **2**.

EXPERIMENTAL

All manipulations were carried out under N_2 unless otherwise indicated. $[Ag(dppm)(NO_3)]_2$ was prepared according to literature methods [2]. NaO_2CCH_2Ph was prepared by the stoichiometric neutral reaction of HO_2CCH_2Ph with NaOH in H_2O/EtOH. Dppm was purchased from Fluka. Elemental analyses were performed by the Analytical Chemistry Group of this institute.

Instrumentation

^1H and ^{31}P NMR spectra were recorded on a Varian Unity-500 spectrometer. $CDCl_3$ was used as solvent,

* Author to whom correspondence should be addressed.

and TMS and 85% H_3PO_4 as standards. IR and Raman spectra were measured on a Niclet Magna 750 spectrophotometer and on a Niclet 910FT spectrophotometer, respectively.

Synthesis of $[Ag(dppm)(O_2CCH_2Ph)]_2$ (**1**)

NaO_2CCH_2Ph (0.40 g, 0.25 mmol) and $[Ag(dppm)(NO_3)]_2$ (2.80 g, 0.25 mmol) were mixed in THF (30 cm^3) under ambient conditions. The reaction solution was stirred overnight and the resulting white precipitate was filtered. The solution upon evaporation in air yielded colorless air- and light-stable prismatic crystals (1.92 g, 61%). The complex is very soluble in CH_2Cl_2, soluble in THF or CH_3CN and insoluble in alcohol, DMF or DMSO. Found: C, 63.4; H, 4.8; Ag, 17.0; P, 10.0. Calc. for $C_{66}H_{58}O_4P_4Ag_2$: C, 63.2; H, 4.7; Ag, 17.2; P, 9.9%. IR (KBr, cm^{-1}): 410 m, 440 s, 473 s, 4785, 507 m, 518 m, 571 s, 615 m. Raman (KBr, cm^{-1}): 143 m, 167 m, 219 w, 272 w, 360 w. ^1H NMR (ppm, TMS as standard): 3.52, 3.75, 7.17, 7.25, 7.40. ^{31}P NMR (ppm, 85% H_3PO_4 as standard): 5.74 (doublet, $J = 218$ Hz) and 4.61 (doublet, $J = 239$ Hz).

Synthesis of $[Ag_2(dppm)_3](NO_3)_2 \cdot 3H_2O$ (**2**$\cdot 3H_2O$)

$[Ag(dppm)(NO_3)]_2$ (2.80 g, 0.25 mmol) and dppm (1.82 g, 0.50 mmol) were mixed in THF and MeOH (30 cm^3, v:v = 2:1) under ambient conditions. The reaction solution was stirred overnight and then filtered. The filtrate was kept in 4°C for 2 weeks to yield colorless air- and light-stable prismatic crystals of **2**$\cdot 3H_2O$ (1.48 g, 39%). The complex is soluble in THF or CH_3CN and slightly soluble in alcohol, DMF or DMSO. Found: C, 58.6; H, 4.5; N, 1.9; Ag, 14.2; P, 11.8. Calc. For $C_{75}H_{72}N_2O_9P_6Ag_2$: C, 58.2; H, 4.7; N, 1.8; Ag, 14.0; P, 12.0%. IR (KBr, cm^{-1}): 417 m, 446 s, 473 s, 515 m, 518 m. Raman (KBr, cm^{-1}): 137 m, 197 w, 227 m, 254 w, 351 w. ^1H NMR (ppm, TMS as standard): 3.53, 7.14, 7.37. ^{31}P NMR (ppm, 85% H_3PO_4 as standard): 2.32.

X-ray crystal structural determination

The colorless prismatic crystals of complex **1** and **2**$\cdot 3H_2O$ suitable for single-crystal X-ray diffraction analysis were grown by slow diffusion of hexane into the sample solution in THF. All data were measured on an MSC/Rigaku RAXIS-II imaging plate diffractometer. Determination of the crystal class, orientation matrix and cell dimensions were performed according to established procedures. All data processing was performed on a 486 PC computer using the SHELXTL-PLUS system. Analytical expressions of neutral-atom scattering factors were employed and anomalous corrections were incorporated. Both struc-

Table 1. Crystallographic data for **1** and **2**$\cdot 3H_2O$

	1	**2**$\cdot 3H_2O$
Formula	$C_{66}H_{58}O_4P_4Ag_2$	$C_{75}H_{72}N_2O_9P_6Ag_2$
Fw	1254.80	1546.97
Crystal system	Monoclinic	Hexagonal
Space group	$P2_1/c$	$P6_3/m$
a (Å)	11.267(2)	14.448(2)
b (Å)	23.361(5)	
c (Å)	10.900(2)	21.071(4)
β (°)	99.36(3)	
V (Å^3)	2830.8(14)	3810.0(20)
Z	2	2
d_{calc} (g cm^{-1})	1.472	1.341
Crystal size	$0.20 \times 0.25 \times 0.30$	$0.20 \times 0.25 \times 0.35$
T (K)	291	291
μ (mm^{-1})	0.854	0.689
F (000)	1280	1584
λ/Å (Mo-$K\alpha$)	0.71073	0.71073
Total data collected	14000	7343
Total unique data	5434	2997
No. of observed reflections [$F_0 > 4\sigma(F_0)$]	4785	1485
No. of variables	344	143
Weight	$[\sigma^2(F) + 0.005F^2]^{-1}$	$[\sigma^2(F) + 0.005F^2]^{-1}$
$R(F_0)^a$	0.040	0.094
$R_w(F_0)^b$	0.046	0.099
Largest residue (e Å^{-3})	0.65	1.27
Mean shift (Δ/σ)	0.01	0.06

[a] $R = \Sigma||F_0| - |F_0|/\Sigma|F_0|$.
[b] $R_w = [\Sigma(w|F_0| - |F_c|)^2/\Sigma w|F_0|^2]^{1/2}$.

tures were solved with the Patterson superposition method. The positions of all hydrogen atoms were generated geometrically (C—H bond fixed at 0.96 Å), assigned isotropic thermal parameters and allowed to ride on their respective parent C atoms. For complex **1**, the refinement of all non hydrogen atoms with anisotropic temperature factors and all hydrogens with isotropic temperature factors led to convergence; for compiles **2**·3H$_2$O, the refinement of all non hydrogen atoms of cation with anisotropic temperature factors and all atoms of hydrogen, anion and solvent molecules with isotropic temperature factors led to convergence. Owing to the high disorder of NO_3^-, the R values for complex **2**·3H$_2$O are higher. Crystallographic data for **1** and **2**·3H$_2$O are listed in Table 1 and selected bond distances and angles in Table 2.

RESULTS AND DISCUSSION

Syntheses

The reaction of [Ag(dppm)(NO$_3$)]$_2$ with 2 equiv. of sodium phenylacetate in THF at room temperature gave rise to the binuclear silver complex [Ag(dppm)(O$_2$CCH$_2$Ph)]$_2$ (**1**),

$$[Ag(dppm)(NO_3)]_2 + 2NaO_2CCH_2Ph = [Ag(dppm)(O_2CCH_2PH)]_2 + 2NaNO_3$$

while the reaction of [Ag(dppm)(NO$_3$)]$_2$ with 2 equiv. (one-fold excess) of dppm in THF and MeOH at room temperature gave rise to another binuclear silver complex **2**.

$$[Ag_2(dppm)(NO_3)]_2 + dppm(excess) = [Ag(dppm)_3](NO_3)_2$$

Clearly, complex **1** was prepared by the simple ligand substitution reaction, however, complex **2** might be obtained from the addition reaction of dppm to complex of [Ag(dppm)(NO$_3$)]$_2$.

Spectroscopic properties

Both complex **1** and **2**·3H$_2$O have been characterized by IR, Raman, ^{1}H and ^{31}P NMR spectra. The ^{31}P NMR spectra of the complex **1** shows two resonance peaks at 5.74 [doublet, $J(^{107,109}Ag—^{31}P) = 218$ Hz] and 4.61 [doublet, $J(^{107,109}Ag—^{31}P) = 239$ Hz], which is downfield of the signal of the respective free ligand and indicates that

Table 2. Selected bond lengths (Å) and angles (°)

[Ag(dppm)(O$_2$CCH$_2$Ph)]$_2$

Ag(1)—Ag(1a)	3.080(1)	Ag(1)—O(1)	2.328(3)
Ag(1)—P(1)	2.429(1)		
Ag(1)—P(2a)	2.438(1)		
O(1)—C(1)	1.251(4)	O(2)—C(1)	1.233(4)
C(1)—C(2)	1.518(6)	C(2)—C(3)	1.506(6)
P(1)—C(9)	1.834(3)	P(1)—C(10)	1.825(3)
P(1)—C(16)	1.838(3)	P(2)—C(9)	1.833(3)
P(2)—C(22)	1.822(3)	P(2)—C(28)	1.821(3)
P(2)—Ag(1a)	2.438(1)		
O(1)—Ag(1)—P(1)	107.4(1)	O(1)—Ag(1)—Ag(1a)	129.9(1)
P(1)—Ag(1)—Ag(1a)	93.7(1)	O(1)—Ag(1)—P(2a)	100.3(1)
P(1)—Ag(1)—P(2a)	149.2(1)	Ag(1a)—Ag(1)—P(2a)	78.2(1)
Ag(1)—O(1)—C(1)	115.5(2)	O(1)—C(1)—O(2)	125.9(3)
O(1)—C(1)—C(2)	118.9(3)	O(2)—C(1)—C(2)	115.2(3)
Ag(1)—P(1)—C(9)	109.7(1)	Ag(1)—P(1)—C(10)	117.0(1)
Ag(1)—P(1)—C(16)	114.7(1)	P(1)—C(9)—P(2)	110.3(2)

[Ag$_2$(dppm)$_3$](NO$_3$)$_2$·3H$_2$O

Ag(1)—Ag(1a)	2.987(2)	Ag(1)—P(1)	2.483(5)
Ag(1)—P(1a)	2.482(4)	Ag(1)—P(1b)	2.482(4)
P(1)—C(1)	1.918(14)	P(1)—C(7)	1.809(14)
P(1)—C(13)	1.771(15)		
P(1)—Ag(1)—Ag(1a)	90.7(1)	P(1)—Ag(1)—P(1a)	120.0(1)
Ag(1a)—Ag(1)—P(1a)	90.7(1)	P(1)—Ag(1)—P(1b)	120.0(1)
Ag(1a)—Ag(1)—P(1b)	90.7(1)	P(1a)—Ag(1)—P(1b)	120.0(1)
Ag(1)—P(1)—C(1)	118.0(6)	Ag(1)—P(1)—C(7)	111.6(6)
Ag(1)—P(1)—C(13)	111.5(8)	P(1)—C(13)—P(1c)	118.9(17)

there are two different ^{31}P spin systems, while that of complex **2** appears as a broad single resonance peak at 2.32, which may be due to the weak interaction of $^{107,109}Ag$—^{31}P and cannot be resolved at room temperature. The shielding is less pronounced for **1** compared with that for **2**.

^1H NMR spectra of complex **1** and **2** in CD_2Cl_2 at ambient temperature exhibit phenyl resonances in the range of 7.14–7.40 ppm and the methylene resonance as a broad unresolved multiplet with the chemical shifts of 3.52–3.75 ppm. The proton chemical shifts of both complex **1** and **2** are similar to the respective free ligands.

The Raman spectra of lower frequency region show that complex **1** has absorption peaks at 360, 272, 219, 167 and 143 cm^{-1} and complex **2** at 351, 254, 227, 197 and 137 cm^{-1}. Using assignments made for $[M_2(dppm)_2X_2]$ and $[M_2(dppm)_3]$ (M = Pd, Pt; X = Cl, Br) [13], the following assignment can be deduced: for complex **1**, $\nu_{(Ag\text{-}P)}$, 360 cm^{-1}; $\delta_{(C\text{-}P\text{-}C)}$ 272 cm^{-1}; $\delta_{(P\text{-}Ag\text{-})}$, 219 and 167 cm^{-1}, for complex **2**, $\nu_{(Ag\text{-}P)}$, 351 cm^{-1}; $\delta_{(C\text{-}P\text{-}C)}$ 254 cm^{-1}; $\delta_{(P\text{-}Ag\text{-}P)}$, 227 and 197 cm^{-1}.

The 400–4000 cm^{-1} region of IR spectra for both complexes is the diphosphine and phenylacetate ligand fingerprints and very little changes are observed upon complexation with silver atoms.

Structure description

Both complexes have been unequivocally characterized by single-crystal X-ray analysis. The molecular structure of **1**, which possesses a crystallographic centrosymmetry, $\bar{1}$, is depicted in Fig. 1. The structure consists of a neutral dimmeric molecular unit with two silver atoms bridged by a pair of bridging dppm ligands to give an eight-membered $Ag_2P_4C_2$ ring, similar to the structure of $[Ag(dppm)(NO_3)]_2$ [2]. In addition, each silver atom is coordinated by one oxygen atom from a terminal phenylacetate group. Therefore, each silver atom is in a highly distorted $AgOP_2$ trigonal planar coordinated environment.

Complex **2** is composed of a discrete cation, $[Ag_2(dppm)_3]^{2+}$ with crystallographic $6/m$ symmetry, two nitrate anions NO^{3-} and three H_2O molecules. The cation structure is very similar to that of palladium(0) and platinum (0) complexes of $[Pd_2(dppm)_3$ [8] and $[Pt_2(dppm)_3]$ [9]. The structure is a dimer with two silver atoms bridged by three dppm ligands. The geometry of each silver atom is exactly in an ideal trigonal planar environment. The cation structure with thermal vibration ellipsoids and the adopted number scheme is shown in an ORTEP drawing (Fig. 2).

The Ag—P bond distance in complex **2** is 2.482(4) Å,

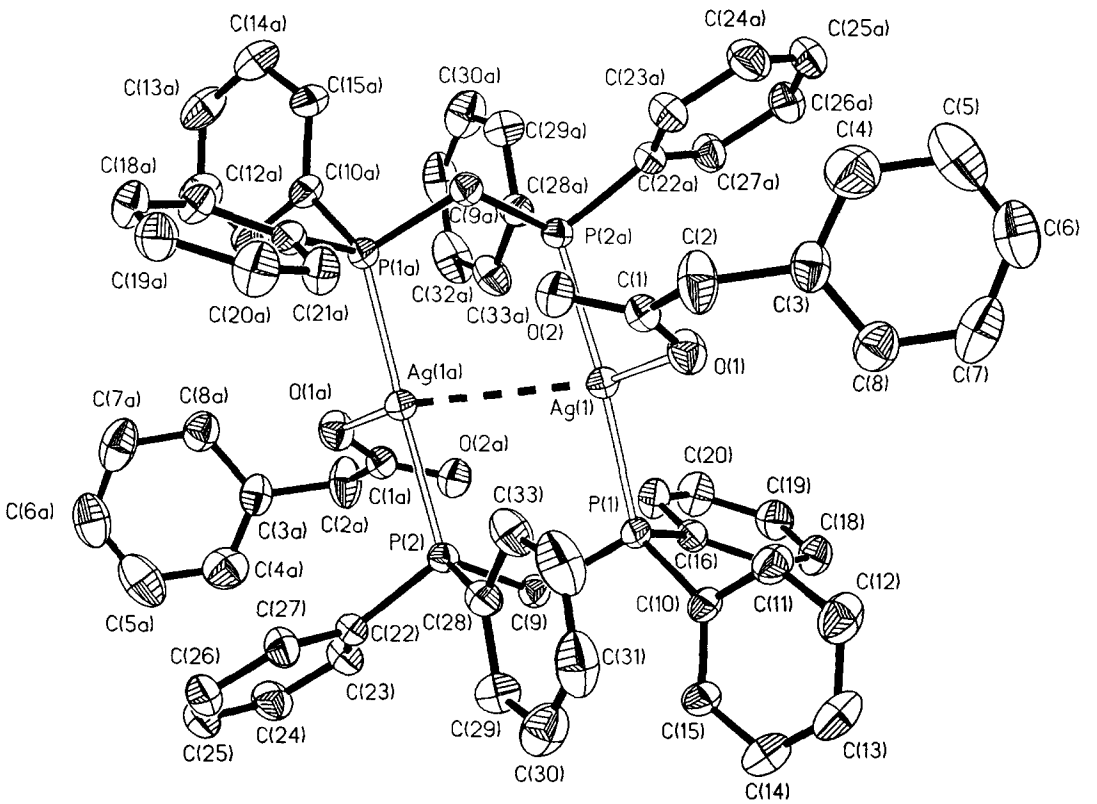


Fig. 1. Perspective view of complex **1**. Hydrogen atoms are omitted and 30% probability ellipsoids are displayed.

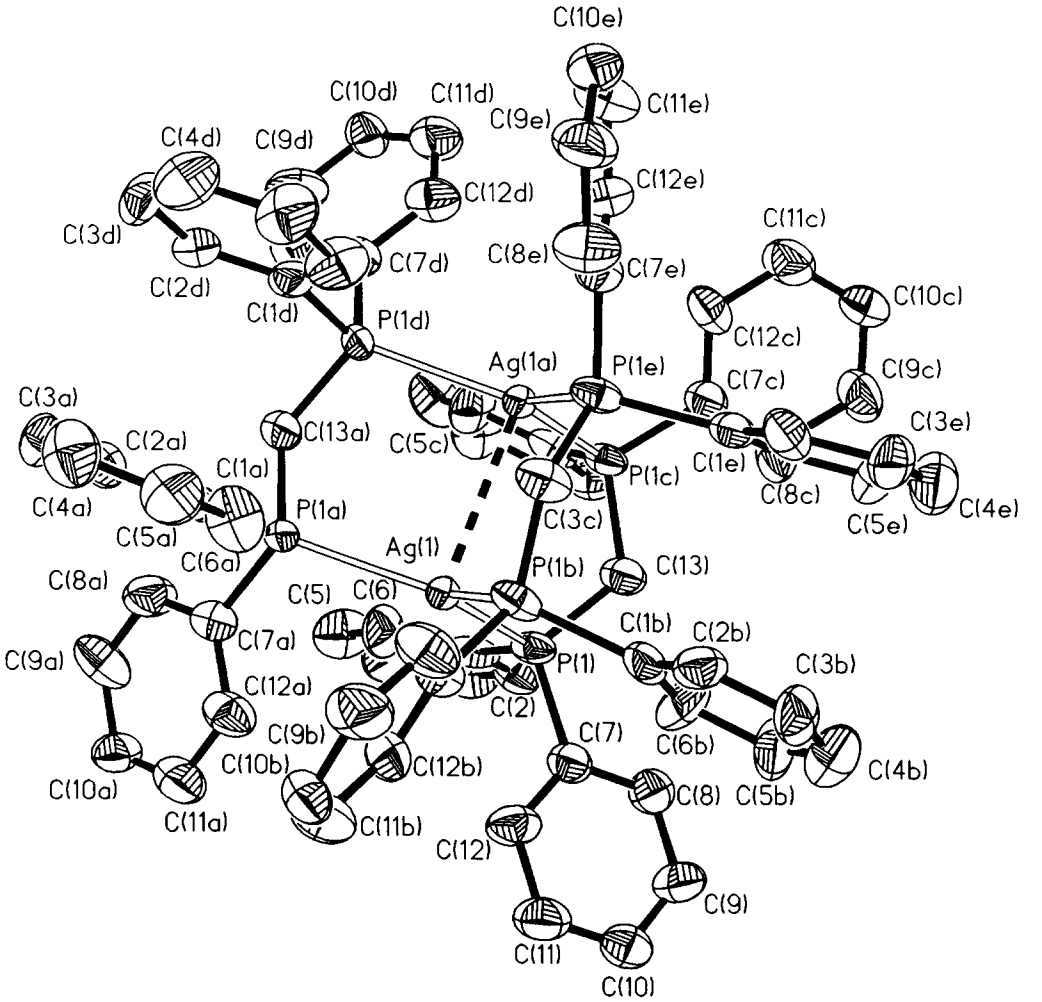


Fig. 2. Perspective view of $[Ag_2(dppm)_3]^{2+}$ in complex **2**. Hydrogen atoms are omitted and 30% probability ellipsoids are displayed.

which is significantly longer than the distance of 2.434(5) Å in complex **1** and those found in silver(I)–dppm complexes of [Ag(dppm)(O$_2$CCH$_2$Ph)]$_2$ [2.434(5) Å], [Ag(dppm)(NO$_3$)]$_2$ [2.426(2) Å] [2] and is slightly longer than those found in silver(I)–triphenylphosphine complexes of [Ph$_3$PAgI]$_4$ [2.455(5) Å][10], [(Ph$_3$P)$_2$Ag(NCS)]$_2$ [2.455(3) Å] [11]. The observed Ag—O distance of 2.328(3) Å in **1** is much shorter than the distances of 2.418(5) Å and 2.689(6) Å found in [Ag(dppm)(NO$_3$)]$_2$ [2]. The Ag···Ag distance of 3.080(1) Å in **1** is significantly longer than that of 2.987(2) Å in **2** and comparable to Ag$_2$(dppm)$_2$(NO$_3$)$_2$ 3.085(1) Å [2], but shorter than the sum of the van der Waals radius (3.4 Å) of the silver atom [12].

The P—Ag—P bond angles of 149.2° in the complex **1** is significantly larger than the corresponding P—Ag—P angle of 138.3(1)° found in [Ag(dppm)(NO$_3$)]$_2$ and 133.69(9)° in [Ag(dmpm)Br]$_2$ [13] [dmpm = bis(dimethylphosphino)methane]. This value is essentially intermediate between 180° (linear structure) and 120° (ideal trigonal planar structure). The average P—Ag—O bond angle of 103.8° is comparable to that observed in [Ag(dppm)(NO$_3$)]$_2$ [2]. The Ag(1a)···Ag(1)—P(1) and Ag(1a)···Ag(1)—P(2) are 93.7(1) and 78.2(1)°, respectively, while the bond angle of Ag(1a)···Ag(1)—O(1) is 129.9(1)°, clearly indicating the nonlinearity of the Ag···Ag—O$_2$C— arrangement. All P—Ag—P bond angles in complex **2** are exactly 120°, indicating the coordination geometry of each silver atom is an ideal trigonal planar. The comparison of M—M and M—P distances as well as P—M—P angles in selected binuclear palladium, platinum and silver complexes are listed in Table 3.

The NO$_3$ group shows apparent disorder, but the atom positions correspond to trigonal coordination of nitrogen atom with slightly short bond (1.29 Å). The O—N—O angles deviate from 120° by an average of 10°.

Acknowledgements—The authors gratefully acknowledge the

Table 3. Comparison of M—M and M—P distances as well as P—M—P angles in selected dinuclear palladium, platinum and silver complexes

Complex	M—M (Å)	M—P (Å)	P—M—P (°)	Reference
$[Pd(dppm)X]_2$[a]	2.652	2.278	linear	[5]
$[Pd_2(dppm)_3]$	2.959	2.310	119.93	[8]
$[Pt_2(dppm)_3]$	3.023	2.266	120.0	[9]
$[Ag(dppm)NO_3]_2$	3.085	2.423	138.3	[2]
$[Ag(dppm)(pa)]_2$[b]	3.080	2.434	149.2	This work
$[Ag(dmpm)Br]_2$[c]	3.041	2.434	133.69	[13]
$[Ag_2(dppm)_3](NO_3)_2$	2.987	2.482	120.0	This work

[a] X = Cl.
[b] pa = pheneylacetate.
[c] dmpm = bis(dimethylphosphine)methane.

National Natural Science Foundation of China and Fong Shing Cotton Mill (Hong Kong Ltd) for financial support.

REFERENCES

1. Neo, S. P., Zhou, Z. Y., Mak, T. C. W. and Hor, T. S. A., *Inorg. Chem.* 1995, **34,** 520.
2. Ho, D. M. and Bau, R., *Inorg. Chem.* 1983, **22,** 4073.
3. van der Ploeg, A. F. M. J., van Koten, G. and Spek, A. L., *Inorg. Chem.* 1979, **18,** 1052.
4. van der Ploeg, A. F. M. J., van Koten, G. and Spek, A. L., *Inorg. Chim. Acta*, 1981, **51,** 225.
5. Brown, M. P., Puddephatt, R. J., Rashidi, M., Manojlokic-Muir, L., Muir, K. W., Solomun, T. and Seddon, K. R., *Inorg. Chim. Acta*, 1977, **23,** L33.
6. Brown, M. P., Puddephatt, R. J., Rashidi, M. and Seddon, K. R., *J. Chem. Soc., Dalton Trans.* 1978, 1540.
7. Benner, L. S. and Balch, A. L., *J. Am. Chem. Soc.* 1978, **100,** 6099.
8. Kirss, R. U. and Eisenberg, R., *Inorg. Chem.* 1989, **28,** 3372.
9. Manojlokic-Muir, L., Muir, K. W., Grossel, M. C. and Brown, M. P., *J. Chem. Soc., Dalton Trans.*, 1986, 1955.
10. Teo, B. K. and Calabresi, J. C., *Inorg. Chem.* 1976, **15,** 10.
11. Howatson, J. and Morosin, B., *Cryst. Struct. Commun.* 1973, **2,** 51.
12. Bondi, A. J., *Phys. Chem.* 1964, **68,** 441.
13. Perreault, D., Drouin, M., Michel, A., Miskowski, V. M., Schaefer, W. P. and Harvey, P. D., *Inorg. Chem.* 1992, **31,** 695.

Pergamon

PII: S0277-5387(96)00533-5

Polyhedron Vol. 16, No. 12, pp. 1963–1970, 1997
© 1997 Elsevier Science Ltd
All rights reserved. Printed in Great Britain
0277-5387/97 $17.00+0.00

Neutral and cationic monocarbonyl derivatives of palladium(II). X-ray crystal structure of $[Pd(8\text{-mq})(CO)(SPPh_3)]ClO_4$

Irene Ara, Juan Forniés,* Rafael Navarro, Violeta Sicilia and Esteban P. Urriolabeitia

Departamento de Química Inorgánica, Instituto de Ciencia de Materiales de Aragón, Universidad de Zaragoza-C. S. I. C., 50009 Zaragoza, Spain

(Received 23 September 1996; accepted 30 October 1996)

Abstract—Carbonylation of $[Pd(8\text{-mq})(OCMe_2)_x]ClO_4$ (8-mq = 8-quinolylmethyl-C,N) in CH_2Cl_2/Me_2CO at low temperature gave $[Pd(8\text{-mq})(OClO_3)(CO)]$. Reactions of $[Pd(8\text{-mq})(OClO_3)(CO)]$ with anionic (Cl^-, Br^-, I^-) or neutral ($SPPh_3$, $SPMe_2Ph$) nucleophiles in a 1 : 1 molar ratio resulted in the displacement of the weakly coordinated $OClO_3^-$ group and the formation of the corresponding neutral $[Pd(8\text{-mq})(X)(CO)]$ (X = Cl, Br, I) or cationic $[Pd(8\text{-mq})(CO)L]ClO_4$ (L = $SPPh_3$, $SPMe_2Ph$) carbonyl complexes. The cationic complexes, $[Pd(8\text{-mq})(CO)L]ClO_4$, were synthesized by the reaction of $[Pd(8\text{-mq})(OClO_3)(SPPh_3)]$ or $[Pd(8\text{-mq})(\mu\text{-}SPMe_2Ph)]_2(ClO_4)_2$ with CO. The X-ray structure of a cationic palladium carbonyl derivative, $[Pd(8\text{-mq})(CO)(SPPh_3)]ClO_4$, is reported. © 1997 Elsevier Science Ltd. All rights reserved.

Keywords: carbonyl; palladium; cationic; cyclometallated.

Palladium compounds have been used as catalysts in some of the most important homogeneous catalytic processes involving CO [1]. Insertion of CO in a Pd—C σ-bond is an elementary step which should occur through intermediates in which the coordinated carbonyl and organic groups are located in the *cis* position [2]. This ability to form acyl derivatives adds to the general tendency of Pd^{II} compounds to be reduced to lower oxidation states by carbon monoxide and to the lability of the Pd—CO bond, justifying the small number of organocarbonylpalladium(II) complexes that have been reported and characterized [3]. Most of them have been structurally studied on the basis of spectroscopic data (mainly IR) and only very recently have the crystal structures of seven such compounds: $[PdX_3(CO)]^-$ (X = Cl, Br) [4], $[PPh_3(CH_2Ph)][Pd(C_6H_3Me\text{-}2,NO_2\text{-}6)Cl_2(CO)]$ [5], $[Pd(\eta^3\text{-}C_4H_7)(SnCl_3)(CO)]$ [6], [2-(CO)-2-(PPh_3)-*closo*-2,1-$PdTeB_{10}H_9(PPh_3)]BF_4$ [7], [*cis*-$Pd(SO_3F)_2(CO)_2$] [8] and [(phen)Pd $(C(O)CH_3)(CO)]$ $Ar'_4B \cdot CH_2Cl_2$ [9], been reported.

The main synthetic routes for the preparation of palladium carbonyls involve the displacement of weakly coordinated ligands by CO [9,10]. Working on C,N-cyclometallated compounds of Pd^{II}, we have prepared several complexes with this kind of ligand: $[Pd(8\text{-mq})(NCMe)_2]ClO_4$ [11], $[Pd(8\text{-mq})(OClO_3)(SPPh_3)]$ [12], $[Pd(8\text{-mq})(\mu\text{-}SPMe_2Ph)]_2(ClO_4)_2$ and $[Pd(8\text{-mq})(OCMe)_x]^+$ (*in situ*), and we have found that they are very good precursors for the preparation of new carbonyl complexes of Pd^{II}.

Herein we report the synthesis and characterization of some cationic and neutral thermally stable carbonylpalladium(II) complexes, as well as the molecular structure of one of the cationic derivatives, $[Pd(8\text{-mq})(CO)(SPPh_3)]ClO_4$.

EXPERIMENTAL

General procedures

Infrared spectra were recorded on a Perkin–Elmer 883 IR spectrometer using Nujol mulls between polyethylene plates. NMR spectra were recorded on a Varian Unity-300 or a Bruker ARX-300 spectrometer in $CDCl_3$ or acetone-d_6, using the solvent signal as an

*Author to whom correspondence should be addressed.

internal standard for ^1H and ^{13}C $\{^1H\}$, and H_3PO_4 (85%) as external reference for ^{31}P $\{^1H\}$. Elemental analyses were performed on a Perkin–Elmer 240-B microanalyser. Molar conductivity measurements were performed on a Philips P.W. 9509 digital conductimeter in approximately 5×10^{-4} M acetone solutions. [Pd(8-mq)($OClO_3$)($SPPh_3$)] [12] and [Pd(8-mq)(μ-Cl)]$_2$ [13] were prepared by literature methods.

[Pd(8-mq)(μ-I)]$_2$

[Pd(8-mq)(μ-Cl)]$_2$ (0.200 g, 0.352 mmol) and $AgClO_4$ (0.146 g, 0.704 mmol) were stirred in acetone (20 cm^3) for 1 h, and then the AgCl formed was filtered off. NBu_4I (0.260 g, 0.704 mmol) was added to the resulting solution giving rise to the precipitation of a yellow solid, which was separated by filtration, washed with acetone and vacuum dried (0.212 g, 80% yield). Found: C, 32.0; H, 1.8; N, 3.5. Calc. for $C_{20}H_{16}I_2N_2Pd_2$: C, 32.0; H, 2.2; N, 3.7%. IR (Nujol, cm^{-1}): 8-mq 1591 m, 1581 s, 1506 vs, 1071 s, 1052 vs, 816 vs, 776 vs, 751 vs, 666 m.

[Pd(8-mq)(μ-$SPMe_2Ph$)]$_2$(ClO_4)$_2$

[Pd(8-mq)(μ-Cl)]$_2$ (0.120 g, 0.211 mmol) and $AgClO_4$ (0.087 g, 0.422 mmol) were stirred in THF (20 cm^3) for 30 min and then the AgCl formed was filtered off. $SPMe_2Ph$ (0.72 g, 0.422 mmol) was added to the resulting solution and the mixture was stirred for 30 min. Following this, the solvent was concentrated to *ca* 5 cm^3 and the precipitated yellow solid was separated by filtration (0.197 g, 90% yield). Found: C, 41.9; H, 3.7; N, 2.9. Calc. for $C_{36}H_{38}Cl_2N_2O_8P_2Pd_2S_2$: C, 41.7; H, 3.7; N, 2.7%. Molar conductivity (S cm^2 mol^{-1}): 291. IR (Nujol, cm^{-1}): 8-mq 1598 w, 1500 vs, 832 s, 782 m, 778 m, 758 s; $SPMe_2Ph$ 950 s, 912 vs, 745 vs, 688 s, 518 s, 523 s [ν(P—S)]; ClO_4^- 1100 vs, 620 s. ^{31}P $\{^1H\}$ NMR: δ 41.99 (s).

[Pd(8-mq)($OClO_3$)(CO)] (**1**)

[Pd(8-mq)(μ-Cl)]$_2$ (0.200 g, 0.352 mmol) and $AgClO_4$ (0.146 g, 0.704 mmol) were stirred in acetone (20 cm^3) for 30 min, and the AgCl formed was filtered off. The solution was evaporated to *ca* 2 cm^3, then 5 cm^3 of CH_2Cl_2 was added and carbon monoxide was gently bubbled through the resulting pale yellow suspension at −60°C for 10 min. Addition of diethyl ether (25 cm^3) to the suspension afforded a white solid, which was filtered off and dried *in vacuo*. **1** (0.238 g, 90% yield). Found: C, 34.8; H, 1.8; N, 3.6. Calc. for $C_{11}H_8ClNO_5Pd$ (**1**): C, 35.1; H, 2.1; N, 3.7%. Molar conductivity (S cm^2 mol^{-1}): 156. IR (Nujol, cm^{-1}): 8-mq: 1596 w, 1514 vs, 825 s, 788 m, 768 s; $OClO_3^-$ 1144 vs, 1025 vs, 908 vs, 624 s, 612 m; ν(CO) 2140 vs.

[Pd(8-mq)X(CO)] [X = Cl (**2a**), Br (**2b**), I (**2c**)].

X = Cl (**2a**). (a) *Method* 1. To a suspension of [Pd(8-mq)($OClO_3$)(CO)] (**1**) (0.175 g, 0.465 mmol) in CH_2Cl_2 (20 cm^3) was added an equimolar amount of [$PBzPh_3$]Cl (0.180 g, 0.465 mmol) at room temperature. The mixture was stirred for 3 min and filtered to remove a small amount of suspended solid. The addition of cold Pr^{i}OH (80 cm^3, −30°C) to the resulting solution rendered a white solid which was identified by IR spectroscopy as **2a**, with a small amount of [Pd(8-mq)(μ-Cl)]$_2$ as an impurity.

(b) *Method* 2. CO was gently bubbled through a suspension of [Pd(8-mq)(μ-Cl)]$_2$ (0.420 g, 0.739 mmol) in 12 cm^3 of CH_2Cl_2 at −30°C for 15 min. After filtration, the resulting solution was added to cold n-hexane (90 cm^3, −30°C) affording a white solid which was filtered off and dried *in vacuo*. **2a**, (0.16 g, 35% yield). Found: C, 42.1; H, 2.2; N, 4.3. Calc. for $C_{11}H_8ClNOPd$: C, 42.3; H, 2.6; N, 4.5%. IR (Nujol, cm^{-1}): 8-mq 1593 w, 1509 vs, 826 s, 787 s, 768 s, 694 m; ν(Pd—Cl) 290 m; ν(CO) 2112 vs (solid), 2121 (CH_2Cl_2 solution). ^1H NMR (proton labelling is shown in Fig. 1): δ 9.48 (d, H1, $^3J_{1\text{-}2}$ = 5.04 Hz), 8.38 (d, H3, $^3J_{3\text{-}2}$ = 8.30 Hz), 7.72 (d, H6, $^3J_{5\text{-}6}$ = 7.90 Hz), 7.65 (d, H4, $^3J_{4\text{-}5}$ = 7.1 Hz), 7.58 (pt, H5), 7.54 (dd, H2), 3.89 (s, -CH_2-Pd). ^{13}C NMR: δ 151.83, 150.59, 144.24, 139.66, 130.05, 129.11, 128.57, 124.88, 121.67 (C_9H_6N), 30.14 (-CH_2-Pd); 176.98 (CO).

X = Br (**2b**). To a suspension of [Pd(8-mq)($OClO_3$)(CO)] (**1**) (0.049 g, 0.131 mmol) in CH_2Cl_2 (10 cm^3) an equimolar amount of NBu_4Br (0.042 g, 0.131 mmol) was added. The mixture was stirred at room temperature for 5 min and filtered to remove a small amount of suspended solid. The resulting solution was added to cold ^{i}PrOH (60 cm^3, −30°C) giving rise to pure **2b** (0.023 g, 50% yield). Found: C, 37.1; H, 2.2; N, 3.9. Calc. for $C_{11}H_8BrNOPd$: C, 37.1; H, 2.3; N, 3.9%. IR (Nujol, cm^{-1}): 8-mq 1593 w, 1510 vs, 823 s, 776 s, 764 m, 689 m; ν(CO) 2108 vs (solid), 2117 (CH_2Cl_2 solution). ^1H NMR: δ 9.67 (dd, H1, $^3J_{1\text{-}2}$ = 5.09 Hz, $^4J_{1\text{-}3}$ = 1.42 Hz), 8.38 (dd, H3, $^3J_{3\text{-}2}$ = 8.32 Hz), 7.73 (dd, H6, $^3J_{5\text{-}6}$ = 7.80 Hz, $^4J_{4\text{-}6}$ = 1.09 Hz), 7.66 (dd, H4, $^3J_{4\text{-}5}$ = 7.1 Hz), 7.59 (pseudo t, H5), 7.55 (dd, H2), 3.99 (s, -CH_2-Pd). ^{13}C

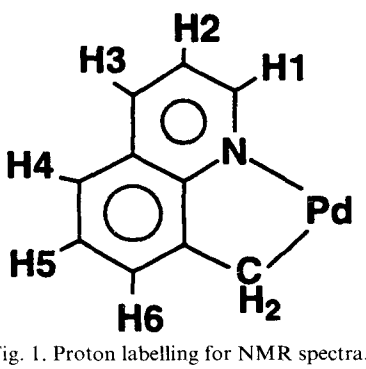


Fig. 1. Proton labelling for NMR spectra.

NMR δ: 152.24, 151.86, 144.29, 139.61, 130.17, 129.23, 128.60, 125.00, 121.99 (C_9H_6N), 32.52 (-CH_2-Pd); 177.65 (CO).

X = *I* (**2c**). (a) *Method* 1. To a suspension of [Pd(8-mq)($OClO_3$)(CO)] (**1**) (0.135 g, 0.360 mmol) in CH_2Cl_2 (10 cm^3) an equimolar amount of PMe_3PhI (0.100 g, 0.360 mmol) was added at room temperature. The mixture was stirred for 5 min and filtered to remove a small amount of suspended solid. Addition of Pr^{i}OH (50 cm^3) to the resulting solution afforded a yellow solid which was separated by filtration and vacuum dried. The solid was identified by IR spectroscopy as **2c** with a small amount of [Pd(8-mq)(μ-I)]$_2$ as an impurity.

(b) *Method* 2. CO was gently bubbled through a suspension of [Pd(8-mq)(μ-I)]$_2$. (0.150 g, 0.200 mmol) in 20 cm^3 of CH_2Cl_2 at -5°C for 30 min. After filtration of the suspended solid the resulting solution was added to cold *n*-hexane (80 cm^3, -30°C) affording **2c** (yield 0.10 g, 62%). Found: C, 32.6; H, 1.9; N, 3.4. Calc. for $C_{11}H_8INOPd$: C, 32.7; H, 2.0; N, 3.5%. IR (Nujol, cm^{-1}): 8-mq 1592 w, 1510 vs, 822 s, 774 vs, 761 m, 682 m; ν(CO): 2103 vs (solid), 2110 (CH_2Cl_2 solution). ^{1}H NMR: δ 9.89 (dd, H1, $^3J_{1\text{-}2}$ = 5.04 Hz, $^4J_{1\text{-}3}$ = 1.30 Hz), 8.35 (dd, H3, $^3J_{3\text{-}2}$ = 8.32 Hz), 7.71 (dd, H6, $^3J_{5\text{-}6}$ = 7.85 Hz, $^4J_{4\text{-}6}$ = 1.0 Hz), 7.64 (dd, H4, $^3J_{4\text{-}5}$ = 7.1 Hz), 7.60 (pseudo t, H5), 7.49 (dd, H2), 4.08 (s, -CH_2-Pd). ^{13}C NMR: δ 151.82, 151.15, 144.64, 139.34, 130.36, 129.40, 128.76, 125.08, 122.44 (C_9H_6N), 35.92 (-CH_2-Pd); 179.22 (CO).

[Pd(8-mq)(CO)($SPPh_3$)]ClO_4 (**3a**)

(a) *Method* 1. $SPPh_3$ (0.109 g, 0.372 mmol) was added to a CH_2Cl_2 suspension (5 cm^3) of **1** (0.14 g, 0.372 mmol) to give a pale yellow solution. The mixture was stirred for 2 min at room temperature and then 15 cm^3 of n-hexane was added. The resulting pale yellow precipitate was filtered off and dried *in vacuo* to give **3a**, (0.200 g, 80% yield).

(b) *Method* 2. Carbon monoxide was gently bubbled through a CH_2Cl_2 (1.5 cm^3) solution of [Pd(8-mq)($OClO_3$)($SPPh_3$)] (0.143 g, 0.223 mmol) for 5 min at -30°C. Addition of n-hexane (20 cm^3) rendered a pale yellow precipitate, **3a** (0.105 g, 70% yield). Found: C, 51.7; H, 3.1; N, 2.1. Calc. for $C_{29}H_{23}ClNO_5PPdS$: C, 52.0; H, 3.5; N, 2.1%. Molar conductivity (S cm^2 mol^{-1}): 150. IR (Nujol, cm^{-1}): 8-mq 1585 w, 1510 vs, 826 s, 788 m, 769 m, 699 s; $SPPh_3$ 758 m, 752 m, 699 s, 690 s, 600 s [ν(P-S)], 511 s; ClO_4^- 1100 vs, 620 s; ν(CO): 2115 vs (solid), 2118 (CH_2Cl_2 soiution). ^{31}P {^{1}H} NMR: δ 45.65 (s). ^{1}H NMR: δ 8.81 (m, H1), 8.41 (d, H3, $^3J_{3\text{-}2}$ = 7.93 Hz), 7-8 (m, H2, H4, H5, H6, $SPPh_3$), 3.98 (s, -CH_2-Pd). ^{13}C NMR: δ 151.09, 150.47, 142.59, 140.69, 130.14, 129.20, 128.91, 125.76, 122.34 (C_9H_6N), 36.57 (-CH_2-Pd); 176.26 (CO).

[Pd(8-mq)(CO)($SPMe_2Ph$)]ClO_4 (**3b**)

(a) *Method* 1. $SPMe_2Ph$ (0.104 g, 0.614 mmol) was added to a CH_2Cl_2 suspension (20 cm^3) of **1** (0.231 g, 0.614 mmol) and the mixture was stirred at room temperature for 5 min. After filtration of the suspended solid, cold Et_2O (100 cm^3, -10°C) was added to the resulting solution giving rise to **3b** (0.110 g, 33% yield).

(b) *Method* 2. Carbon monoxide was bubbled through a suspension of [Pd(8-mq)(μ-$SPMe_2Ph$)]$_2$(ClO_4)$_2$ (0.150 g, 0.145 mmol) in 2 cm^3 of CH_2Cl_2 at -10°C for 10 min. The resulting white solid was isolated by filtration and dried *in vacuo*, **3b** (0.118 g, 75% yield). Found: C, 41.5; H, 3.7; N, 2.7. Calc. for $C_{19}H_{19}ClNO_5PPdS$: C, 41.8; H, 3.5; N, 2.6%. Molar conductivity (S cm^2 mol^{-1}): 172. IR (Nujol, cm^{-1}): 8-mq 1592 w, 1510 vs, 831 s, 789 m, 777 s, 691 s; $SPMe_2Ph$ 958 s, 929 vs, 754 s, 733 s, 563 s [ν(P-S)]; ClO_4^- 1100 vs, 620 s; ν(CO) 2113 vs (solid). ^{31}P {^{1}H} NMR: δ 43.16 (s). ^{1}H NMR: δ 9.52 (m, H1), 8.41 (m, H3), 8.1–7.5 [m, H2, H4, H5, H6, C_6H_5 ($SPMe_2Ph$)], 3.92 (s, -CH_2-Pd), 2.93 [d, $^2J_{P\text{-}H}$ = 15 Hz, Me ($SPMe_2Ph$)]. The low solubility of **3b** prevented ^{13}C {^{1}H} NMR measurements.

Crystallographic studies

Suitable single crystals for X-ray structure determination of [Pd(8-mq)(CO)($SPPh_3$)]ClO_4 (**3a**) were obtained by slow diffusion of a diethyl ether layer into a solution of **3a** (8 mg) in $CHCl_3$ (4 cm^3) at 5°C.

Crystal data. $C_{29}H_{23}ClNO_5PPdS$, yellow, prismatic, M = 670.36, triclinic, space group P-1, a = 10.767(2), b = 10.843(1), c = 14.263(2) Å, α = 85.31(1), β = 73.04(1), γ = 61.40(1)°, V = 1395.1(3) Å^3, Z = 2, D_c = 1.596 g cm^{-3}, λ = 0.71073 Å, T = 200(2) K, crystal size = 0.40 × 0.34 × 0.22 mm, μ(Mo-K_α) = 0.933 mm^{-1}, F(000) = 676.

Data collection and processing. Siemens P4 automated four-circle diffractometer equipped with an Oxford Cryosystems low-temperature device, graphite-monochomated Mo-K_α radiation, ω–θ scan technique, 4650 independent reflections collected in two shells ($2\theta < 40°$, $50°$; $0 \leqslant h \leqslant 12$, $-11 \leqslant k \leqslant 12$, $-15 \leqslant l \leqslant 16$), of which 4492 were used in all calculations, three check reflections measured at regular intervals showed no intensity decay. An empirical absorption correction based on psi scans was applied (transmission factors = 0.995 and 0.871).

Structure analysis and refinement. The position of the palladium atom was determined from the Patterson map. The remaining atoms were located in successive difference Fourier syntheses and refined by full-matrix least squares on F^2. All non-hydrogen atoms were refined with anisotropic displacement parameters. H atoms were added at calculated positions with a common isotropic thermal parameter. At final convergence $R[F \geqslant 4\sigma(F)]$ = 0.0302, $wR(F^2$, all data) = 0.0772, $S(F^2)$ = 1.029 for 353 parameters, $w^{-1} = [\sigma^2(F_o^2) + (0.0385\ P)^2 + 1.53\ P]$, $P = 1/3$ [max $(F_o^2, 0) + 2F_c^2$], largest difference peak and hole = 0.996 and -0.560 e/Å^3. All calculations were

performed on a local area VAX cluster (VAX/VMS V5.5) with the Siemens SHELXTL PLUS and SHELXL 93 software packages [14,15].

RESULTS AND DISCUSSION

All the carbonylpalladium complexes described in this paper have been obtained as indicated in Scheme I.

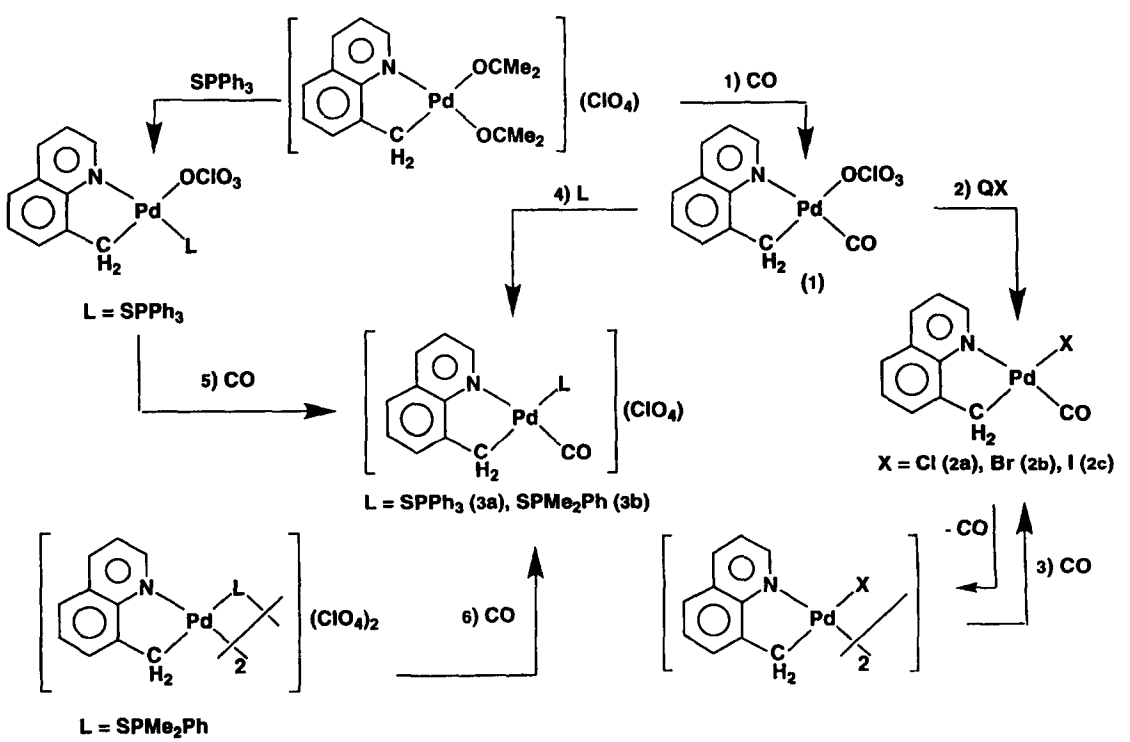
Synthesis and characterization of [Pd(8-mq)($OClO_3$)(CO)] (**1**)

When CO is bubbled through a suspension which contains the solvento species [Pd(8-mq)($OCMe_2$)$_x$]ClO_4 in CH_2Cl_2/Me_2CO (5:2) at −60 °C [Scheme I, (**1**)], the neutral monocarbonyl complex [Pd(8-mq)($OClO_3$)(CO)] (**1**) precipitates. It is important to point out that, although CO is able to displace $OClO_3$ in other palladium complexes (M—$OClO_3$) to produce the corresponding cationic carbonyl derivatives [M—CO]ClO_4 [10a], in this case the neutral monocarbonyl complex is obtained instead of the cationic bis(carbonyl) complex [Pd(8-mq)$(CO)_2$]ClO_4 which could be expected. Compound **1** is a stable solid at room temperature and can be stored at 5 °C for long periods. Compound **1** is only slightly soluble in dichloromethane at room temperature and its solution decomposes very quickly rendering palladium metal. Decomposition can be partially prevented by working at low temperature; however, the solubility of this complex is very low under these conditions which prevents conductivity or NMR studies in solution.

The IR spectrum of **1** shows (see Experimental): (a) characteristic absorptions due to the $OClO_3^-$ ligand [16]; (b) a strong absorption at 2140 cm^{-1} due to ν(CO), which suggests that only one isomer is formed in the reaction. Taking into account the *trans* disposition of the $OClO_3^-$ anion to the C donor atom of the C,N-groups observed in complexes such as [Pd(C_6H_4-N = N-C_6H_5-C,N)($OClO_3$)($SPPh_3$)] [12] and [Pd(8-mq)($OClO_3$)($SPPh_3$)] [12,17], we think that **1** has the structure depicted in Scheme I, in concert with the value of ν(CO) observed for a carbonyl group *trans* to a N donor atom in palladium carbonyl complexes [9,10b,18]. Since the carbonyl complex **1** is slightly stable in solution, we decided to explore its reactivity towards some neutral or anionic ligands (in a 1:1 molar ratio only) in order to establish whether the Pd—CO or Pd—$OClO_3$ is the more inert bond in the presence of nucleophiles.

Reactivity of [Pd(8-mq)($OClO_3$)(CO)] (**1**) *towards anionic ligands. Synthesis of* [Pd(8-mq)X(CO)] (X = Cl, Br, I)

In reactions between [Pd(8-mq)($OClO_3$)(CO)] (**1**) and the halides (X^- = Cl^-, Br^-, I^-) in a 1:1 molar ratio the substitution of the perchlorate anion by the corresponding halides, which are better coordinating ligands, takes place giving rise to [Pd(8-mq)X(CO)] [X = Cl (**2a**), Br (**2b**), I (**2c**)] with small impurities of



Scheme I.

the respective dinuclear compounds $[Pd(8\text{-mq})(\mu\text{-X})]_2$ according to Scheme I (2). The latter seems to be formed by the intermolecular substitution of the CO by the halide. Pure samples of complexes **2a,** and **2c** have also been prepared by bubbling CO through suspensions of the dinuclear complexes $[Pd(8\text{-mq})(\mu\text{-X})]_2$(X = Cl, I) [Scheme I, (3)] [19]. Complexes **2a, b, c** are stable in the solid state at 5 °C for several months, but, at room temperature, their CH_2Cl_2 solutions lose CO slowly, giving rise to the dinuclear derivatives $[Pd(8\text{-mq})(\mu\text{-X})]_2$.

Complexes **2a, b, c** have been characterized by elemental analysis, IR and NMR (^1H, ^{13}C) spectra. The IR spectra in CH_2Cl_2 solution show only one absorption assignable to ν(CO) at 2121 (**2a**), 2117 (**2b**) and 2110 (**2c**) cm^{-1}, respectively, indicating that only one isomer is present in each case. The sequence observed for ν(CO) absorptions in **2a–2c** is similar to that observed in the complexes $[PdX_3(CO)]^-$ [4], $[Pd(C_6H_4\text{-}C(R) = N\text{-}OH)X(CO)]$ [20] and $[Pt(CO)LX_2]$ (X = Cl, Br, I; L = CO, py, aniline) [21] and can be explained by the different electronegativity of the halogens (Cl > Br > I). Moreover, a higher ν(CO) in $[Pd(8\text{-mq})(OClO_3)(CO)]$ (**1**) is also a consequence of the lower nucleophilic character of the $OClO_3^-$ ligand with respect to the X^- halides. The observed values of ν(CO) in **2a–2c** suggest that the CO ligand is *trans* to the N atom of the 8-mq group [18]. In addition, the ν(Pd—Cl) for complex **2a** is in the range observed in palladium chloro complexes with *trans* alkyl or phenyl groups [22]. The structure proposed for complexes **2a, b, c** (Scheme I) is that observed in other complexes of stoichiometry [Pd(CN)XL] (C N = azobenzene-2,*C*,*N*; *N*,*N*-dimethylbenzylamine-2,*C*,*N*; 2-methoxy-3,*N*,*N*-dimethylaminopropyl; X = Cl, Br; L = py, PEt_3, PPh_3) obtained by cleavage of the halide-bridged system of the corresponding binuclear $[Pd(C\ N)(\mu\text{-X})]_2$ (X = Cl, Br) with neutral ligands (L) [23], and indicates that the substitution process [Scheme I (2)] takes place with stereoretention. The ^1H NMR spectra of **2a, b, c** show, in each case, six resonances corresponding to the six chemically inequivalent aromatic protons and a singlet resonance which is due to the methylene protons of the Pd—CH_2 group (see Experimental). The $^{13}C\{^1H\}$ NMR spectra show the expected resonances for all the carbon atoms present in the different molecules, including the CO ligand. It is noteworthy that the moderate stability of these carbonyl complexes at a low temperature (−5 °C) allows a $^{13}C\{^1H\}$ NMR study to be made, which is very unusual for Pd^{II} carbonyl complexes [9].

Reactions of $[Pd(8\text{-mq})(OClO_3)(CO)]$ (**1**) *with* SPR_3. *Synthesis of* $[Pd(8\text{-mq})(CO)L]ClO_4$ [L = $SPPh_3$ (**3a**), $SPMe_2Ph$ (**3b**)]

$[Pd(8\text{-mq})(OClO_3)(CO)]$ (**1**) reacts with the neutral ligands $SPPh_3$ and $SPMe_2Ph$ (monodentate ligands which are able to act as bridging ligands) in a 1 : 1 molar ratio giving rise to $[Pd(8\text{-mq})(CO)L]ClO_4$ [L = $SPPh_3$ (**3a**), $SPMe_2Ph$ (**3b**)], as is indicated in Scheme I (4). Both complexes are thermally stable and decompose between 130 and 140 °C. They have been isolated and fully characterized by elemental analysis, IR and NMR spectroscopy.

The structure of **3a** and **3b** (Scheme I) has been proposed on the basis of these data and confirmed by an X-ray study on **3a**. The IR spectra of these complexes show: (a) absorptions due to the SPR_3 ligands. The absorption due to ν(P—S) appears in both cases at lower frequencies than in the corresponding free ligand [$\Delta\nu$(P—S) = 36 cm^{-1} (**3a**), 20 cm^{-1} (**3b**)]. This small decrease indicates that, in both cases, the SPR_3 ligands act as terminal ligands [12]. (b) One absorption attributable to ν(CO) at *ca* 2120 cm^{-1} confirms the presence of the CO ligand in the complex. (c) Two absorptions at 1100 and 620 cm^{-1}, which are typical of the uncoordinated ClO_4^-(Td) anion [16]. The ^1H NMR spectra of **3a, b** show the resonances for all the groups that were expected to be present in the molecule, although the presence of phenyl groups in $SPPh_3$ and $SPMe_2Ph$ precludes any unambiguous assignment of the aromatic resonances. The $^{31}P\{^1H\}$ NMR spectra show only one singlet and the $^{13}C\{^1H\}$ NMR spectrum of **3a** shows the expected resonances for the cyclometallated group (8-mq) and the terminal CO ligand [9]. All these data confirm that the reactions take place with the substitution of the $OClO_3^-$ ligand by L (L: $SPPh_3$, $SPMe_2Ph$) and that only one of the two possible isomers is formed in both cases. The molecular structure of **3a,** which has been established by an X-ray diffraction study is discussed in detail below, indicates that the CO ligand is *trans* to the N atom (as in all the aforementioned complexes) of the 8-mq; i.e. that the substitution reaction of $OClO_3^-$ by the L ligands on complex **1** [Scheme I (4)] occurred regiospecifically.

Complexes **3a** and **3b** can also be prepared by reacting CO with other starting materials. Thus, **3a** is obtained when CO is bubbled through a dichloromethane solution of $[Pd(8\text{-mq})(OClO_3)(SPPh_3)]$ [Scheme I (5)]. Given the structure of the starting complex $[Pd(8\text{-mq})(OClO_3)(SPPh_3)]$ (which has been unequivocally established by a ^1H–^1H NOESY experiment [17]), in which the $OClO_3^-$ group is *trans* to the σ Pd—C bond and the structure of **3a,** the substitution reaction of $OClO_3^-$ by CO takes place with isomerization and this isomerization process has to occur very quickly since, when the reaction is monitored in CH_2Cl_2 solution by IR spectroscopy, no other isomers are detected. Isomerization processes have been observed previously, i.e. for *trans*-$[PtX_2(CO)L]$ (X = Cl, L = PBu_3, PEt_3, PMe_2Ph, $PMePh_2$, PPh_3, $AsMePh_2$, $AsPh_3$; X = Br, L = PMe_2Ph) [24a], which isomerize to *cis*-$[PtX_2(CO)L]$, the *trans* to *cis* isomerization being dramatically catalyzed by carbon monoxide. The proposed mechanism for CO-catalyzed isomerizations is that of pseudorotation pro-

cesses involving five-coordinate intermediates [24b]. Complex **3b** can also be prepared by carbonylation of the binuclear $[Pd(8\text{-mq})(\mu\text{-SPMe}_2Ph]_2$ [Scheme I (6)] which takes place with cleavage of the bridging system to produce only one isomer.

Molecular structure of $[Pd(8\text{-mq})(CO)(SPPh_3)](ClO_4)$ **(3a)**

The molecular structure of the cationic carbonyl palladium complex $[Pd(8\text{-mq})(CO)(SPPh_3)](ClO_4)$ (**3a**) has been determined by single crystal X-ray diffraction. A drawing of the structure is presented in Fig. 2 and relevant bond distances and bond angles are shown in Table 1.

As can be seen, the cation shows a slightly distorted square-planar geometry around the palladium centre with C(1) and C(2) atoms 0.154(6) Å and 0.126(5) Å away, respectively, from the best least-squares plane defined by the C(1), C(2), N(1), Pd(1) and S(1) atoms. The angle between the normal to this plane and the C(1)—O(1) vector is 95.5(3)° and the Pd—C—O angle is 177.7(4)°. The Pd—C(1) bond length [1.894(4) Å)] is within the range of distances observed in the neutral complex $[Pd(\eta^3\text{-}C_4H_7)(SnCl_3)(CO)]$ [1.947(11) Å] [6] or the cationic $[(phen)Pd(C(O)CH_3)(CO)]Ar'_4B\cdot CH_2Cl_2$ [1.922(11) Å] [9] and the anionic species $[Pd(C_6H_3Me\text{-}2,NO_2\text{-}6)Cl_2(CO)]^-$ [1.853(10) Å] [5], and is shorter than that observed in the cationic derivative [2-(CO)-2-(PPh_3)-*closo*-2,1-$PdTeB_{10}H_9(PPh_3)]^+$ [2.003(9) Å] [7]. Bond distances and angles corresponding to the $PdC_{10}H_8N$ metallocycle are similar to those observed in other complexes involving the 8-mq ligand [25]. The best least-squares planes defined by the $C_{10}H_8N$ ligand and the palladium coordination plane are not coplanar, but rather their dihedral angle is 20.28(5)°. The Pd—S(1) distance, 2.453(1) Å, is longer than that observed in

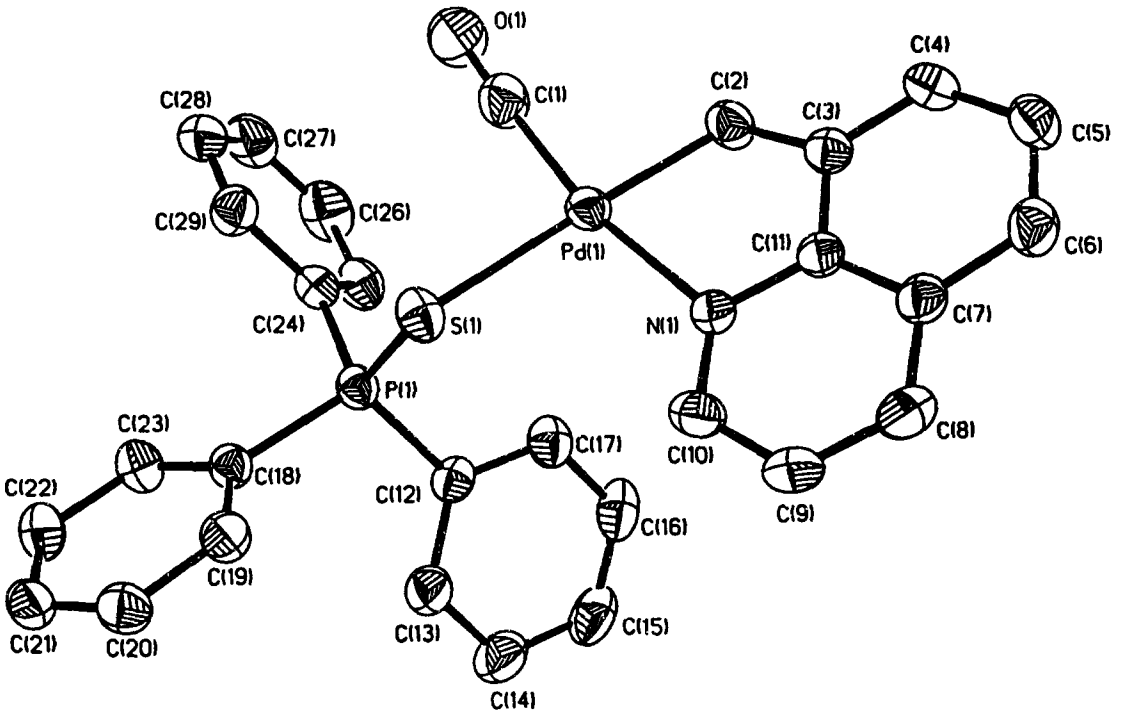


Fig. 2. Molecular structure of the cation $[Pd(8\text{-mq})(CO)(SPPh_3)]^+$ showing the atom numbering scheme. The thermal ellipsoids are drawn at the 50% probability level.

Table 1. Selected bond lengths (Å) and angles (°) for complex $[Pd(8\text{-mq})(CO)(SPPh_3)]ClO_4$ (**3a**)

Pd(1)—C(1)	1.894(4)	Pd(1)—C(2)	2.062(3)
Pd(1)—N(1)	2.084(3)	Pd(1)—S(1)	2.453(1)
C(1)—O(1)	1.123(4)		
C(1)—Pd(1)—C(2)	87.7(2)	C(2)—Pd(1)—N(1)	82.44(12)
N(1)—Pd(1)—S(1)	93.96(7)	C(1)—Pd(1)—S(1)	95.65(12)
O(1)—C(1)—Pd(1)	177.7(4)		

[Pd(az)($OClO_3$)($SPPh_3$)] (az: azobencene-2,C,N) [2.326(1) Å] [12] where the S atom is *trans* to a Pd—N bond, in accord with the greater *trans* influence of a C σ-bonded ligand than a Pd—N-bonded one.

CONCLUSIONS

The synthesis of the neutral [Pd(8-mq)($OClO_3$)(CO)] (**1**), which is moderately stable, allows us to study its reaction with different neutral (SPR_3) or anionic (X^-) ligands. In such processes, the Pd—CO bond is preserved and cationic and neutral carbonyl derivatives of palladium are obtained. However, the usual lability of the Pd—CO bond is also observed in these complexes since intermolecular substitution reactions involving CO displacement take place in their dichloromethane solutions. In spite of this fact $^{13}C\{^1H\}$ NMR data have been obtained for all sufficiently soluble complexes. The δC(CO) value is, in all cases, close to 177 ppm, a similar value to the corresponding resonance found in [(phen)Pd(C(O)CH_3)(CO)]$Ar'_4B \cdot CH_2Cl_2$ [9].

Supplementary material—Tables of atomic coordinates, bond lengths and angles, anisotropic displacement parameters, H-atom coordinates and observed and calculated structure factors, have been deposited at the Cambridge Crystallographic Data Centre.

Acknowledgement—We thank the Dirección General de Investigación Científica y Técnica (Spain) for financial support (Project PB92-0364).

REFERENCES

1. (a) Cotton, F. A. and Wilkinson, G., *Advanced Inorganic Chemistry*. Wiley, New York, 1980; (b) Falbe, J. *New Synthesis with Carbon Monoxide*. Springer-Verlag, Berlin, Heidelberg, New York, 1980; (c) Heck, R. F., *Palladium Reagents in Organic Synthesis*. Academic Press, New York, 1987.
2. Tóth, I. Elsevier, C. J., *Journal of the American Chemical Society*, 1993, **115,** 10388 and references therein.
3. (a) Maitlis, P. M., Espinet, P. and Russell, M. J. H., *Comprehensive Organometallic Chemistry*, Vol. 6. Pergamon, London, 1982, p 279; (b) Usón, R., Forniés, J., Tomás, M. and Menjón, B., *Organometallics*, 1985, **4,** 1912.
4. Andreini, B. P., Belli Dell'Amico, D., Calderazzo, F. and Venturi, M. G., *Journal of Organometallic Chemistry*, 1988, **354,** 369.
5. Vicente, J., Arcas, A. and Borrachero, M. V., *Organometallics*, 1991, **10,** 3873.
6. Grassi, M., Meille, S. V., Musco, A., Pontellini, R. and Sironi, A., *Journal of the Chemical Society, Dalton Transactions*, 1989, 615.
7. Sheehan, J. P., Spalding, T. R., Ferguson, G., Gallagher, J. F., Kaitner, B. and Kennedy, J. D., *Journal of the Chemical Society, Dalton Transactions*, 1993, 35.
8. Wang, C. Q., Willner, H., Bodenbinder, M., Batchelor, R. J., Einstein, F. W. B. and Aubke, F. *Inorganic Chemistry*, 1994, **33,** 3521.
9. Rix, F. C., Brookhart, M. and White, P. S., *Journal of the American Chemical Society*, 1996, **118,** 4746.
10. (a) Usón, R., Forniés, J. and Martínez, F., *Journal of Organometallic Chemistry*, 1976, **112,** 105; (b) Cinellu, M. A., Gladiali, S. and Minghetti, G. *Journal of Organometallic Chemistry*, 1989, **363,** 401. (c) Majima, T. and Kurosawa, H., *Journal of Organometallic Chemistry*, 1977, **134,** C45.
11. Forniés, J., Navarro, R. and Sicilia, V. *Polyhedron*, 1988, **7,** 2659.
12. Forniés, J., Navarro, R., Sicilia, V. and Tomás, M. *Inorganica Chimica Acta*, 1990, **168,** 201.
13. Deeming, A. C. and Rothwell, J. *Journal of Organometallic Chemistry*, 1981, **205,** 117.
14. SHELXTL-PLUS, *Software Package for the Determination of Crystal Structures*, Release 4.0; Siemens Analytical X-ray Instruments, Inc., Madison, WI, 1990.
15. Sheldrick, G. M., SHELXL 93, *FORTRAN* 77 *Program for the Refinement of Crystal Structures from Diffraction Data*, University of Göttingen, 1993.
16. Hathaway, B. J. and Underhill, A. E., *Journal of the Chemical Society*, 1961, 3091.
17. The ^1H–^1H 2D NOESY experiment was performed on compound [Pd(8-mq)($OClO_3$)($SPPh_3$)] at a measuring frequency of 300.13 MHz. The mixing time was 400 ms and the data were acquired into a 512 × 1024 matrix, then transformed into 1024 × 1024 points using a sine window in each dimension. Selective irradiation of the methylene CH_2—Pd resonance produces a clear NOE enhancement at the resonances because of the H_6 proton (see Fig. 1) of the 8-mq ligand and the *ortho*-H protons of the $SPPh_3$ ligand (see Scheme I). This last fact suggests the proximity of the interacting nuclei (i.e. the CH_2 group and the $SPPh_3$ ligand) and, consequently, the *cis* coordination of the $SPPh_3$ ligand relative to the CH_2—Pd bond.
18. Pfeffer, M., Grandjean, D. and Le Borgne, G., *Inorganic Chemistry*, 1981, **20,** 4426.
19. The [Pd(8-mq)Cl(CO)] complex has been previously prepared from [Pd(8-mq)(μ-Cl)]$_2$ and CO [21]. The authors reported that ν(CO) for [Pd(8-mq)Cl(CO)] in a KBr pellet appears at 2108 cm^{-1}, at the same frequency observed by us for [Pd(8-mq)Br(CO)] (**3b**), probably because, in KBr, there was a substitution of Cl by Br.
20. Onoue, H., Nakagawa, K. and Moritani, I., *Journal of Organometallic Chemistry*, 1972, **35,** 217.
21. Irving, R. J. and Magnusson, E. A., *Journal of the Chemical Society*, 1958, 2283.
22. (a) Coates, G. E. and Parkin, C., *Journal of the Chemical Society*, 1963, 421; (b) During, I. R., Mitchell, B. R., Sink, D. W., Willis, J. N. and Wilson, A. S., *Spectrochimica Acta*, 1967, **23,** 1121.
23. Crociani, B., Boschi, T., Pietropaolo, R. and

Belluco, U., *Journal of the Chemical Society (A)*, 1970, 531.

24. (a) Anderson, G. K. and Cross, R. J., *Journal of the Chemical Society, Dalton Transactions*, 1980, 1988. (b) Anderson, G. K. and Cross, R. J., *Chemical Society Reviews*, 1984, **13,** 185.
25. (a) Forniés, J., Navarro, R., Sicilia, V., Martínez, F. and Welch, A. J., *Journal of Organometallic Chemistry*, 1991, **408,** 425; (b) Forniés, J., Navarro, R., Sicilia, V. and Tomás, M., *Inorganic Chemistry*, 1993, **32,** 3675.

Pergamon

PII: S0277-5387(96)00532-3

Polyhedron Vol. 16, No. 12, pp. 1971–1977, 1997
© 1997 Elsevier Science Ltd
All rights reserved. Printed in Great Britain
0277-5387/97 $17.00+0.00

Synthesis and crystal structure of Ni^{II} complexes containing the NiS_2P_2 chromophore

A. Manohar,[a] V. Venkatachalam,[a] K. Ramalingam,[a] U. Casellato[b]* and R. Graziani[c]

[a]Department of Chemistry, Annamalai University, Annamalainagar-608002, India

[b]ICTIMA, CNR Corso Stati Uniti 4-35100 Padova, Italy

[c]Dipartimento di Chimica Inorganica, Università di Padova, Italy

(Received 20 September 1996; accepted 30 October 1996)

Abstract—The nickel(II) complexes $[Ni(nmedtc)(PPh_3)_2]ClO_4$ (**1**) and $[Ni(nmedtc)dppe]BPh_4 \cdot CH_2Cl_2$ (**2**) [nmedtc = *N*-methyl,*N*-ethanoldithiocarbamate, dppe = 1,2-bis(diphenylphosphino)ethane] were prepared and characterized by electronic and IR spectra, and their structures determined by X-ray crystallography. In both complexes the NiS_2P_2 chromophore is planar and the thioureide C—N has double bond character. Hydrogen bond interaction is observed in 1 between the ethanolic group and the perchlorate anion. Electronic and IR spectra confirm the planarity of the chromophores in both complexes and the contribution of the thioureide form in the molecular structure. © 1997 Elsevier Science Ltd. All rights reserved.

Keywords: nickel; complexes; synthesis; structure.

Group VIII dithiolates containing planar MS_4 chromophores show variable behaviour in their reactions with Lewis bases [1,2]. Soft Pd^{II} and Pt^{II} dithiolates react preferably with soft phosphines to give planar MS_2P_2 chromophores [3,4], but chromophores with square-pyramidal geometry have also been observed in solution for these metals. Detailed structural studies on a variety of MS_2P_2 chromophores have been made [5,6]. Unlike its congeners, Ni^{II} is a borderline acceptor. Ni^{II} complexes of dithiocarbamates are typically planar and contain the NiS_4 chromophore. They react preferably with soft Lewis bases such as phosphines, rather than with hard bases such as NH_3 or pyridine. The symbiotically induced softness and the electronic effects of the substituents on the dithiocarbamate ligands were found to be important in this respect [7,8]. With ligands such as PR_3 or dppe they form planar and diamagnetic complexes [9–11] containing the NiS_2P_2 chromophore. Mixed complexes of the type $[Ni(S_2CNR_2)X(PR_3)]$ were obtained by reacting NiX_2 with dithiocarbamate and PR_3 [12]. Complexes of the type $[Ni(dtc)Cl(PPh_3)]$ and $[Ni(dtc)(PPh_3)_2]ClO_4$ {dtc = $[S_2CN(C_2H_5)_2]^-$, $[S_2CNH(C_2H_4OH)]^-$, $[[S_2CN(C_2H_4OH)_2]$, $[S_2CN(C_5H_{10})]^-$} have also been prepared [13,14].

In order to see the influence of an electronegative substituent such as $-C_2H_4OH$, and of free and chelated phosphines, on the NiS_2P_2 chromophore and on the thioureide C—N bond, we report here the synthesis and structural characterization of two new complexes, $[NiL(PPh_3)]ClO_4$ (**1**), and $[NiL(dppe)]BPh_4 \cdot CH_2Cl_2$ (**2**), where L is the ligand *N*-methyl,*N*-ethanoldithiocarbamate (nmedtc) and dppe = 1,2-bis (diphenylphosphino)ethane.

EXPERIMENTAL

All reagents and solvents employed were commercially available high-grade purity materials (E-Merck) and were used as supplied.

Physical measurements

IR spectra were recorded on Jasco IR-700 spectrophotometer (range 4000–400 cm^{-1}) as KBr pellets. The UV–vis spectra were recorded in $CHCl_3$ solution

*Author to whom correspondence should be addressed.

on the Jasco UVIDEC double-beam spectrophotometer.

Preparation of complexes

Bis(triphenylphosphine)(N-methyl,N-ethanoldithiocarbamato) nickel(II) perchlorate, [Ni(nmedtc)(PPh_3)]ClO_4 (**1**). A mixture of Ni(nmedtc)$_2$ [15] (358 mg, 1 mmol), PPh_3 (520 mg, 2 mmol) $NiCl_2 \cdot 6H_2O$ (120 mg, 0.5 mmol) and $NaClO_4$ (125 mg, 1 mmol) was refluxed for about 3 h in a methanol/dichloromethane solvent mixture (50 cm^3), then concentrated to *ca* 25 cm^3, and allowed to settle for 2 days. The precipitated purple-red compound was filtered off and dried over anhydrous calcium chloride. Well-formed crystals were obtained by recrystallization from a dichloromethane/methanol solution (yield 70%, m.p. 160°C).

[1,2-*Bis(diphenylphosphino*-K,P,P′)*ethane*]-(N-*methyl*,N-*ethanoldithiocarbamato)nickel(II)tetraphenylborate dichloromethane solvate*, [Ni(nmedtc)(dppe)]$BPh_4 \cdot CH_2Cl_2$ (**2**). A mixture of Ni(nmedtc)$_2$ (358 mg, 1 mmol), dppe (400 mg, 1 mmol) and $NaClO_4$(125 mg, 1 mmol) was refluxed in a methanol/dichloromethane solvent mixture (50 cm^3) for about 3 h, concentrated to 25 cm^3 and then allowed to settle for 2 days. The orange–yellow solid separated from the solution was filtered off and dried over anhydrous calcium chloride. Well-formed crystals were obtained by recrystallization from a methanol/dichloromethane solvent mixture (yield 70%, m.p. 165°C).

X-ray crystallography

Details of the crystal data, data collection and refinement parameters for **1** and **2** are summarized in Table 1. Intensity data were collected at ambient temperature (295 K) on a Philips four-circle diffractometer using graphite-monochromated Mo-K_α radiation (λ = 0.71069 Å). Of the 52 non-hydrogen atoms of complex **1**, 16 atoms were refined anisotropically while the phenyl groups were refined isotropically. Bond lengths and bond angles are given in Tables 2 and 3.

RESULTS AND DISCUSSION

IR spectra show ν(C—N) bands at 1550 cm^{-1} for **1** and 1529 cm^{-1} for **2**. The shift in ν(C—N) values to higher wavenumber compared with the parent Ni(nmedtc)$_2$ complex is attributed to the mesomeric drift of electrons from the dithiocarbamate moiety towards the metal. The ν(C—S) bands around 997 cm^{-1}, without any splitting, indicate that the dithiocarbamate ligand is chelated [16]. The electronic absorption spectrum of **1** shows bands at 400, 460, 550 and 570 nm. The strong band at 400 nm can be attributed to metal-to-ligand charge transfer [13], other bands being due to *d–d* transitions: $d_{yz} \rightarrow d_{xy}$ (460 nm), $d_{xz} \rightarrow d_{xy}$ (550 nm) and $d_{x^2-y^2} \rightarrow d_{xy}$ (570 nm). Similar transitions were reported for [Ni(dedtc)(PPh_3)$_2$]$^+$, based on a single crystal polarized spectral study [13,17]. Two absorption bands at 450 and 480 nm in **2** are due to *d–d* transitions.

Structure analysis

The structure of **1**, along with the numbering scheme, is shown in Fig. 1. The crystal contains discrete mononuclear [Ni(nmedtc)(PPh_3)$_2$]$^+$ units which have no significant intermolecular contacts. Four formula units are present in the unit cell. The Ni, S(1), S(2), P(1) and P(2) atoms are coplanar [deviations (Å) from the mean S_2P_2 plane are: S(1) +0.51, S(2) −0.156, P(2) +0.126, P(1) −0.120]. The planarity of the molecule is in keeping with the observed diamagnetism of the complex. Severe distortions with respect to the idealized square-planar geometry are observed in coordination angles: the small S—Ni—S chelation angle [78.4(1)°] is determined by the geometry of the chelate ligand, while the opposite P—Ni—P angle [102.9(1)°] is rather large, probably owing to the high hindrance of the tripenylphosphine groups.

The bidentate ligand, which is essentially planar [apart from the C(4) and O(1) atoms], is inclined by 24.4° with respect to the coordination plane. The Ni—S, as well as the S—C, bond distances are chemically equivalent, showing that the negative charge of the bidentate ligand is equally distributed over the two donor atoms. Moreover, the short C(1)—N distance of 1.31(1) Å, which has double bond character, indicates that the electron density is delocalized over the entire S_2CN moiety. This is supported by the circumstance that the two S—C—N angles are generally greater than the S—C—S one. The O(1)···O(5) contact distance of 2.746(9) Å strongly suggests the presence of a hydrogen bond between the ligand oxygen and the perchlorate anion. Structural details of the dithiocarbamate ligand are normal and comparable with those observed in other compounds [18]. Attempts to obtain suitable crystals of the parent Ni(nmedtc)$_2$ complex in order to carry out a comparative study were unsuccessful.

It is noteworthy that the phenyl groups C(17)–C(22) bonded to P(1), and C(23)–C(28) bonded to P(2), are roughly parallel (the dihedral angle between the two planes is 19.1°) and that the distance of 3.82 Å calculated between the centroids of the two hexagonal rings is compatible with a graphite-type interaction.

Complex **2** is monomeric, with four molecules per unit cell. The structure of **2**, along with the numbering scheme used, is shown in Fig. 2. The molecule is approximately planar, in keeping with the observed diamagnetism [deviations (Å) from the mean S_2P_2 plane are: S(1) +0.042, S(2) −0.45, P(2) +0.042,

Table 1. Crystal and intensity data

Compound	**1**	**2**
Empirical formula	$C_{40}H_{38}ClNO_5P_2S_2Ni$	$C_{55}H_{54}BNOP_2S_2Cl_2Ni$
Formula weight	833	1010.3
Crystal dimensions (mm)	0.30 × 0.20 × 0.25	0.30 × 0.25 × 0.30
Crystal system	Monoclinic	Monoclinic
Space group	$P\,2_1/n$	$P\,2_1/c$
a (Å)	11.729(5)	9.559(5)
b (Å)	20.697(6)	14.652(6)
c (Å)	15.918(6)	37.080(7)
β (°)	94.44(5)	91.08(5)
V (Å^3)	3852.6(2)	5192(2)
Z	4	4
D_c (g cm ^{3})	1.44	1.26
μ (cm^{-1})	7.6	6.1
$F(000)$	1728	2112.0
θ_{max} (°)	27	28
Scan mode, scan speed (° min^{-1})	$\theta/2\theta$, 2	$\theta/2\theta$, 2
Index range	$-14 < h < 13$	$-12 < h < 11$
	$0 < k < 26$	$0 < k < 18$
	$0 < l < 17$	$0 < l < 46$
Independent reflections	2942	3939
Observed reflections $F > 4\sigma$ (F)	2892	3860
Number of parameters refined	217	482
Final R (conventional)	0.032	0.074

Table 2. Bond distances (Å) and angles (°) for $[NiL(PPh_3)_2](ClO_4)$

Ni—P(1)	2.215(2)	S(1)—C(1)	1.736(9)
Ni—P(2)	2.242(3)	S(2)—C(1)	1.73(1)
Ni—S(1)	2.213(3)	C(1)—N(1)	1.31(1)
Ni—S(2)	2.230(2)	N(1)—C(2)	1.49(1)
P(1)—C(5)	1.818(6)	N(1)—C(3)	1.48(1)
P(1)—C(11)	1.839(6)	C(3)—C(4)	1.56(2)
P(1)—C(17)	1.824(6)	C(4)—O(1)	1.45(2)
P(2)—C(23)	1.837(6)	Cl—O(2)	1.40(1)
P(2)—C(29)	1.837(6)	Cl—O(3)	1.39(1)
P(2)—C(35)	1.838(6)	Cl—O(4)	1.38(1)
		Cl—O(5)	1.445(9)
Possible hydrogen bond:		O(1)···O(5)	2.746(9)
P(1)—Ni—P(2)	102.9(1)	Ni—S(1)—C(1)	85.2(3)
S(1)—Ni—S(2)	78.4(1)	Ni—S(2)—C(1)	84.7(3)
P(1)—Ni—S(1)	92.4(1)	S(1)—C(1)—S(2)	108.1(5)
P(2)—Ni—(S(2)	87.02(9)	S(1)—C(1)—N(1)	125.2(7)
P(1)—Ni—S(2)	169.6(1)	S(2)—C(1)—N(1)	126.7(7)
P(2)—Ni—S(1)	161.8(1)	C(1)—N(1)—C(2)	120.3(8)
Ni—P(1)—C(5)	115.1(2)	C(1)—N(1)—C(3)	121.3(8)
Ni—P(1)—C(11)	116.9(2)	C(2)—N(1)—C(3)	118.3(8)
Ni—P(1)—C(17)	111.4(2)	N(1)—C(3)—C(4)	112.0(9)
Ni—P(2)—C(23)	125.8(2)	C(3)—C(4)—O(1)	109(1)
Ni—P(2)—C(29)	107.8(2)	O(2)—Cl—O(3)	106.4(7)
Ni—P(2)—C(35)	110.9(2)	O(2)—Cl—O(4)	110.0(8)
C(5)—P(1)—C(11)	99.2(3)	O(2)—Cl—O(5)	105.9(6)
C(5)—P(1)—C(17)	109.6(3)	O(3)—Cl—O(4)	113.7(7)
C(11)—P(1)—C(17)	103.5(3)	O(3)—Cl—O(5)	108.8(6)
C(23)—P(2)—C(29)	104.4(3)	O(4)—Cl—O(5)	111.8(7)
C(23)—P(2)—C(35)	100.3(2)		
C(29)—P(2)—C(35)	106.2(3)		

Table 3. Selected bond distances (Å) and angles (°) for [NiL (dppe)] $(BPh_4)\cdot CH_2Cl_2$

Ni(1)—P(2)	2.163(3)	Ni(1)—S(1)	2.218(3)
Ni(1)—P(1)	2.175(3)	Ni(1)—S(2)	2.195(4)
P(2)—C(18)	1.82(1)	P(2)—C(19)	1.80(1)
P(2)—C(25)	1.79(1)	S(1)—C(1)	1.74(1)
P(1)—C(5)	1.81(1)	P(1)—C(11)	1.80(1)
P(1)—C(17)	1.84(1)	S(2)—C(1)	1.71(1)
C(1)—N(1)	1.28(2)	N(1)—C(2)	1.48(2)
N(1)—C(4)	1.50(1)	C(2)—C(3)	1.45(2)
C(17)—C(18)	1.54(2)	C(3)—O(1)	1.53(2)
B(1)—C(37)	1.71(2)	B(1)—C(31)	1.68(2)
B(1)—C(49)	1.68(2)	B(1)—C(43)	1.71(2)
C(55)—Cl(2)	1.76(2)	C(55)—Cl(1)	1.65(2)

P(1)—Ni(1)—S(2)	175.3(1)	S(1)—Ni(1)—S(2)	79.4(1)
S(1)—Ni(1)—P(1)	100.0(1)	P(2)—Ni(1)—S(2)	94.0(1)
P(2)—NI(1)—P(1)	86.6(1)	P(2)—Ni(1)—S(1)	173.4(1)
Ni(1)—P(2)—C(25)	111.5(3)	Ni(1)—P(2)—C(19)	114.8(3)
Ni(1)—P(2)—C(18)	109.7(4)	C(19)—P(2)—C(25)	106.5(4)
C(18)—P(2)—C(25)	105.6(5)	C(18)—P(2)—C(19)	108.4(5)
Ni(1)—S(1)—C(1)	84.7(4)	Ni(1)—P(1)—C(17)	108.2(4)
Ni(1)—P(1)—C(11)	109.7(3)	Ni(1)—P(1)—C(5)	121.1(3)
C(11)—P(1)—C(17)	104.4(5)	C(5)—P(1)—C(17)	107.1(4)
C(5)—P(1)—C(11)	105.2(4)	Ni(1)—S(2)—C(1)	86.1(4)
S(1)—C(1)—S(2)	109.5(7)	S(2)—C(1)—N(1)	124(1)
S(1)—C(1)—N(1)	126(1)	C(1)—N(1)—C(4)	123(1)
C(1)—N(1)—C(2)	122(1)	C(2)—N(1)—C(4)	111(1)
N(1)—C(2)—C(3)	110(1)	C(2)—C(3)—O(1)	111(1)
P(1)—C(17)—C(18)	106.5(7)	P(2)—C(18)—C(17)	106.2(8)
C(37)—B(1)—C(49)	107.9(8)	C(43)—B(1)—C(49)	113(1)
C(31)—B(1)—C(49)	112(1)	C(37)—B(1)—C(43)	107(1)
C(31)—B(1)—C(37)	109(1)	C(31)—B(1)—C(43)	108(1)
Cl(1)—C(55)—Cl(2)	118(1)		

P(1) −0.040]. The two carbon atoms of the aliphatic chain between the P atoms are alternatively displaced from the coordination plane by +0.363 [C(17)] and −0.374 Å [C(18)]. The Ni—S, as well as the S—C, bond distances are comparable, showing that the negative charge of the dithiocarbamate ligand is equally distributed over the two donor atoms, as found in **1**. In addition, the short C(1)—N distance of 1.28(2) Å indicates that the electron density is delocalized over the S_2CN moiety and that this bond is double in character. Also, in this compound, the two S—C—N angles are generally greater than the S—C—S ones. One molecule of CH_2Cl_2, which was used as solvent in the preparation of the compound, is present as clathrate in the crystal packing.

Comparison of $[Ni(nmedtc)(dppe)]^+$ with the corresponding $[Ni(nmedtc)(PPh_3)_2]^+$ cation shows that bond lengths and angles compare well in the dithiocarbamato ligands. In particular the S—Ni—S chelation angles [79.4 *vs* 78.4°] and the Ni—S—C angles [mean value 85° in both compounds] are very similar, irrespective of the fact that the CNS_2 plane in $[Ni(nmedtc)(dppe)]BPh_4\cdot CH_2Cl_2$ is inclined by only 8.1° with respect to the coordination plane, while the corresponding dihedral angle is 24.4° in $[Ni(nmedtc)(PPh_3)_2]ClO_4$. On the other hand, a significant difference is observed in the P—Ni—P angles that are subtended by the dppe bidentate ligand, being about 16° smaller than those found in $[Ni(nmedtc)(PPh_3)_2]^+$, where the PPh_3 groups have a higher steric hindrance. Thus, the P—Ni—P angle seems to be greatly influenced by the bulkiness of the phosphorus substitutents.

The Ni—P distances are similar to those reported earlier in [1,2-bis(diisopropylphosphinoethane]carbenenickel(0) [14] [2.175(3) and 2.163(2)Å]. Bond parameters in a series of different bisdithiocarbamates and phosphine-substituted planar nickel complexes are given in Table 4. It is noteworthy that in all the dppe complexes the Ni—P distances are shorter and the P—Ni—P angles are smaller when compared with the corresponding values observed in the PPh_3 complexes.

The structural parameters of the complexes are clearly unaffected by the presence of the alcoholic substituent on the dithiocarbamate ligand. However, the properties of this substituent have been found to influence the reactivity of similar complexes in solution [8].

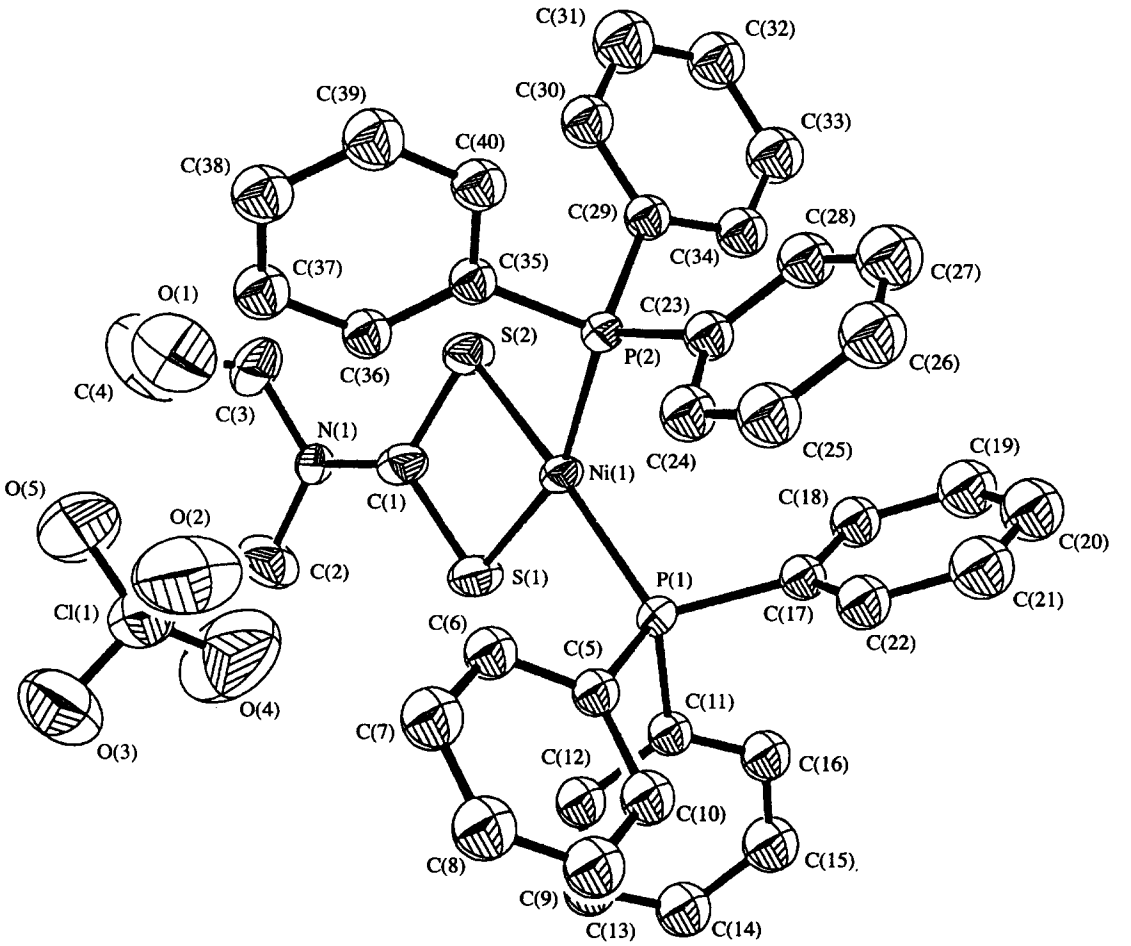


Fig. 1. The crystal structure of $[NiL(PPh_3)_2](ClO_4)$, (**1**).

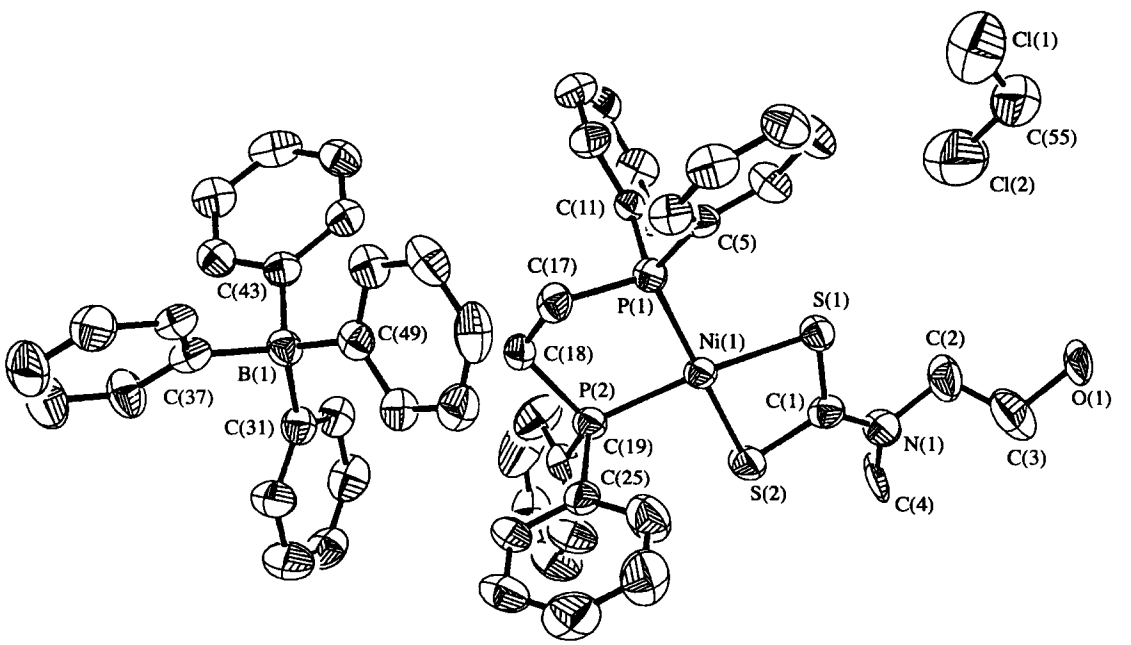


Fig. 2. The crystal structure of $[NiL(dppe)](BPh_4) \cdot CH_2Cl_2$, (**2**).

Table 4. Comparison of bond parameters for NiS_4 and NiS_2P_2 chromophores, lengths in Å, angles in °

Complex	Ni—S(1)	Ni—S(2)	Ni—P(1)	Ni—P(2)	C—N	P(1)—Ni—P(2)	S—Ni—S	Reference
$Ni(dedtc)_2$	2.195(2)	2.207(2)	—	—	1.33(1)	—	—	21
$[Ni(dedtc)(PPh_3)_2]^+$	2.190(2)	2.239(2)	2.200(2)	2.230(3)	1.307(1)	99.7(1)	78.2(1)	13*
$Ni(deadtc)_2$	2.209(1)	2.193(1)	—	—	1.319(5)	—	79.3(1)	19*
$[Ni(padtc)(PPh_3)_2]^+$	2.228(3)	2.199(3)	2.205(3)	2.225(3)	1.307(10)	99.7(1)	78.5(1)	18*
$[Ni(padtc)(dppe)]^+$	2.200(2)	2.204(2)	2.182(2)	2.170(2)	1.323(7)	86.7(1)	79.6(1)	18
$Ni(dipdtc)_2$	2.183(3)	2.182(3)	—	—	1.307(4)	—	79.6(1)	16
$[Ni(dipdtc)(PPh_3)_2]^+$	2.209(3)	2.201(3)	2.215(2)	2.224(3)	1.321(1)	99.4(1)	77.7(1)	20*
$[Ni(dipdtc)(dppe)]^+$	2.194(2)	2.196(2)	2.165(2)	2.160(2)	1.316(8)	87.3(1)	79.0(1)	20
$[Ni(nmedtc)(PPh_3)_2]^+$	2.213(3)	2.230(2)	2.215(2)	2.242(3)	1.31(1)	102.9(1)	78.4(1)	this work
$[Ni(nmedtc)(dppe)]^+$	2.218(3)	2.195(4)	2.175(3)	2.163(3)	1.28(2)	86.6(1)	79.4(1)	this work

$dedtc^-$ = diethyldithiocarbamate; $deadtc^-$ = 2,2′-iminodiethanoldithiocarbamate; $padtc^-$ = *N*,*N*′-(iminodiethylene)bisphthalimidedithiocarbamate; $dipdtc^-$ = diisopropyldithiocarbamate.
*Reported from our laboratory.

REFERENCES

1. Chakravorty, A., *Progress in Inorganic Chemistry*, 1966, **7,** 83.
2. Fackler, Jr., J. P. and Seidel, W. C. *Inorganic Chemistry*, 1969, **8,** 1631.
3. Lin, I. J. B., Chen, H. W. and Fackler, Jr., J. P., *Inorganic Chemistry*, 1978, **17,** 394.
4. Alison, J. M. C. and Stephenson, T. A., *Journal of the Chemical Society, Dalton Transaction*, 1973, 254.
5. Fackler, Jr., J. P., Thompson, L. D., Lin, I. J. B., Stephenson, T. A., Gould, R. O., Alison, J. M. C. and Fraser, A. J. F., *Inorganic Chemistry*, 1982, **21,** 2397.
6. Anderson, D. M., Ebsworth, E. A. V., Stephenson, T. A. and Walkingshaw, M. D., *Journal of the Chemical Society, Dalton Transaction*, 1982, 2343.
7. Jorgensen, C. K., *Inorganic Chemistry*, 1964, **3,** 1201.
8. Ramalingam, K., Aravamudan, G. and Venkatachalam, V., *Bulletin of the Chemical Society of Japan*, 1993, **66,** 1554.
9. McCleverty, J. A. and Morrizon, N. J., *Journal of the Chemical Society, Dalton Transaction*, 1976, 541.
10. Lachenal, D., *Inorganic and Nuclear Chemistry Letters*, 1975, **11,** 101.
11. Burns, R. P., McCullough, F. P. and McAuliffe, C. A., *Advances in Inorganic Chemistry and Radiochemistry*, 1980, **23,** 211.
12. Maxfield, P. L., *Inorganic and Nuclear Chemistry Letters*, 1970, **6,** 693.
13. Ramalingam, K., Aravamudan, G. and Seshasayee, M., *Inorganica Chimica Acta*, 1987, **128,** 231.
14. Akilan, R., Sivakumar, K., Venkatachalam, V., Ramalingam, K., Chinnakali, K. and Fun, H. K., *Acta Crystallographica*, 1995, **C51,** 368.
15. Newman, P. W. G. and White, A. H., *Journal of the Chemical Society, Dalton Transaction*, 1972, 2239.
16. Hadjikostas, C. C., Katsovlos, G. A., Sigalas, M. P. and Tsipis, C. A., *Inorganica Chimica Acta*, 1989, **163,** 173.
17. Rajasekaran, M. V., Chandramouli, G. V. R. and Manoharan, P. T., *Chemistry Physics Letters*, 1989, **162,** 110.
18. Venkatachalam, V., Ramalingam, K., Bocelli, G. and Andrea, C., *Inorganica Chimica Acta*, communicated.
19. Ramalingam, K., Aravamudan, G., Seshasayee, M. and Subramanyam, Ch, *Acta Crystallographica*, 1984, **C40,** 965.
20. Venkatachalam, V., Ramalingam, K., Mak, T. C. W. and Bao-Sheng, Luo, *Polyhedron*, 1996, **15,** 1295.
21. Bonamico, M., Dessy, G., Mariani, C., Vaciago, A. and Zambonelli, L., *Acta Crystallographica*, 1965, **C19,** 619.

Pergamon

PII: S0277-5387(96)00527-X

Polyhedron Vol. 16, No. 12, pp. 1979–1981, 1997
© 1997 Elsevier Science Ltd
All rights reserved. Printed in Great Britain
0277-5387/97 $17.00+0.00

Photoreduction of molecular nitrogen using the complex $[ReH_5(dppe)(PPh_3)]$

Jan O. Dzięgielewski,* Romualda Gil-Bortnowska, Janusz Mrzigod and Barbara Machura

Department of Inorganic and Radiation Chemistry, Institute of Chemistry, Silesian University, Szkolna 9, 40-006 Katowice, Poland

(Received 29 July 1996; accepted 29 October 1996)

Abstract—A Re^V hydrido complex with bis-1,2-(diphenylphosphine)ethane and triphenylphosphine was employed for the photochemically induced fixation and reduction of dinitrogen. Tetrahydrofuran/cyclohexane (1 : 1) solutions, acidified and non-acidified, were examined in the UV radiation field. © 1997 Elsevier Science Ltd. All rights reserved.

Keywords: dinitrogen reduction; photochemistry; catalytic complexes.

One of the most important agricultural problems is "nitrogen hunger", i.e. the lack of nitrogen compounds (needed for protein synthesis) in the soil. Atmospheric dinitrogen, as the most stable diatomic molecule, can be used only by plants living in a symbiosis with bacteria, which activate dinitrogen *in vivo*. In other cases the lack of nitrogen compounds must be supplemented by fertilisers. Industrial production of ammonia using molecular nitrogen requires expensive catalysts and techniques. Chemists have been searching for a long time for a chemical equivalent of *nitrogenase*, a bacterial enzyme allowing chemical reactions of dinitrogen at room temperature and under atmospheric pressure. In our investigations we examined initially the hydrido complexes of molybdenum and tungsten, which, under conditions of pure chemical reduction, give low yields of hydrazine and ammonia, but activated by electromagnetic radiation (γ or UV) become effective catalysts of this process [1–10].

Given the possibility of dinitrogen fixation and reduction in the UV radiation field using a pentahydrido rhenium(V) complex with triphenylphosphine [11], we have examined the usefulness of the $[ReH_5(dppe)(PPh_3)]$ complex for this reaction {dppe = bis-1,2-(diphenylphosphine)ethane, diphos}. This complex should be more effective than the one examined earlier because of the presence of the bidentate phosphine in its coordination sphere. Its higher stability compared with hydrido complexes of tungsten with phosphines is shown, for instance, in a higher value for the force constant of the M—H bond: $f' = 2.167$mdyn Å^{-1} for $[ReH_5(dppe)(PPh_3)]$, while in the case of a tungsten complex with ethyldiphenylphosphine $f' = 1.99$mdyn Å^{-1} (for vibrations of analogous symmetry). The higher stability of hydrido rhenium complexes with water-soluble phosphines may facilitate reduction of dinitrogen in aqueous solutions under homogeneous conditions, whereas tungsten complexes with such phosphines under such conditions decompose, forming tungsten blues.

EXPERIMENTAL

Diphos was synthesised from triphenylphosphine by the standard method [12]. Triphenylphosphine and other reagents were of analytical grade. $[ReH_5(dppe)(PPh_3)]$ was obtained using a literature method [13].

Samples of 10 cm^3 with concentrations of the complex of 1×10^{-3}, 5×10^{-3} and 1×10^{-2} mol dm^{-3}, saturated with a mixture of deoxygenated nitrogen and hydrogen (1 : 3), were irradiated in a cylindrical quartz vessel (diameter 2.5 cm). A tetrahydrofuran/cyclohexane (1 : 1) mixture was used as solvent; the cyclohexane was added in order to minimise C_4H_8O insertion into the rhenium coordination

*Author to whom correspondence should be addressed.

sphere. The gases were bubbled through the vessel at 15 $cm^3\ min^{-1}$ (N_2) and 45 $cm^3\ min^{-1}$ (H_2), which ensured vigorous stirring of the solution. A 100 W Blak-Ray B-100A UV lamp with a blue filter (blocking the visible part of the spectrum) was used to eliminate H_2 and to convert the hydride complex into the unsaturated intermediate compound. In order to maintain constant concentrations, the gases were passed through washers and after their saturation by the solvent they were introduced into the irradiated solution of the rhenium complex. Two series of measurements for each concentration were carried out in acidified and non-acidified solutions. The concentration of sulfuric acid in the sample was 0.1 M. In each of the above cases the irradiation periods were in the range 1–60 min. With times shorter than 4 min, no measurable amounts of molecular nitrogen reduction products were found. The reduced nitrogen reaction products were absorbed from the waste gases in a washer with an aqueous solution of sulfuric acid (*ca* 0.1 mol dm^{-3}).

The light intensity of the lamp was 5.55×10^{13} eV $cm^{-2}\ s^{-1}$. Hydrazine and ammonia were determined by spectrophotometrical methods as described previously [1–4,14]. The concentrations of dinitrogen reduction products were measured both in the irradiated solution and in the sulfuric acid washer.

RESULTS AND DISCUSSION

Curves of ammonia and hydrazine formation are presented in Figs 1 and 2, respectively, showing the dependencies of product molecule numbers *vs* irradiation dose (the courses or the functions were obtained by computer optimisation). These plots present the summarised values of the product's molecule numbers (measured both in irradiated solution and in the washer).

Table 1 presents a comparison of the catalytic efficiencies of the rhenium and tungsten complexes examined. The numbers of cycles have been calculated as in previous papers [1–11].

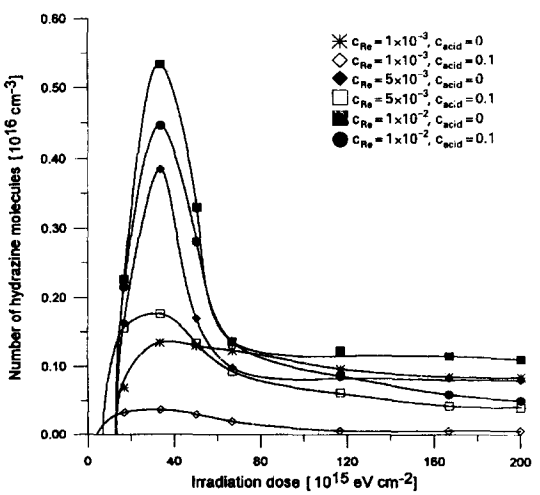


Fig. 1. Formation of hydrazine *vs* irradiation dose in UV-irradiated solutions, solvent: THF–*c*-C_6H_{12} (1 : 1) mixture.

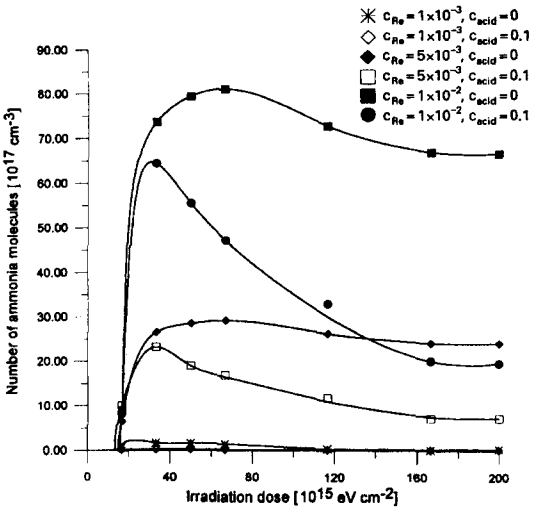


Fig. 2. Formation of ammonia *vs* irradiation dose in UV-irradiated solutions, solvent: THF–*c*-C_6H_{12} (1 : 1) mixture.

The curves obtained do not differ in shape from the dependencies ascertained earlier for tungsten complexes in γ or UV radiation fields. The curves of hydrazine formation show an induction period and a maximum. The induction period is connected to a lack of measurable amounts of dinitrogen complex and consequently a lack of hydrazine for the shortest irradiation times (the lowest doses), while the maximum results from the further reduction of N_2H_4 to ammonia at higher doses of electromagnetic radiation. On the other hand, the induction period in the ammonia formation curves results from the fact that, to make the hydrazine reduction possible, a higher concentration of hydrazine complex is needed. Such a concentration occurs in the range of higher doses. The maxima in ammonia formation curves (less distinct, however, than for tungsten complexes under similar conditions) results from further NH_3 reactions in the sample under irradiation.

As shown by the data in Table 1, the photochemical reduction of molecular nitrogen using rhenium complexes is a cyclic process. Acid addition lowers the catalytic efficiency, owing to lower stability of the $[ReH(N_2)_2(dppe)(PPh_3)]$ complex in acidic solution, compared with $[ReH_5(dppe)(PPh_3)]$.

As for hydrazine, the effect of acid proved to be less distinct than for ammonia. This is in accordance with the assumption that hydrazine forms by reaction with hydrogen atoms in the systems examined.

Based on the above, and on the data from earlier experiments, it can be stated that the mechanism of dinitrogen fixation and reduction using the $[ReH_5(dppe)(PPh_3)]$ complex is analogous to that of the hydrido tungsten complexes with phosphines (both in γ and for UV irradiated fields).

Table 1. Comparison of catalytic efficiencies of rhenium and tungsten hydrido–phosphine complexes (all concentration in mol dm^{-3})

Complex	Complex concentration	Number of cycles at maximum ammonia yield (number of NH_3 moles per 1 mole of Re^V complex)	
		$c_{acid} = 0$	$c_{acid} = 0.1$
$[ReH_5(dppe)(PPh_3)]$	1×10^{-3}	0.90	0.16
$[ReH_5(dppe)(PPh_3)]$	5×10^{-3}	2.91	2.32
$[ReH_5(dppe)(PPh_3)]$	1×10^{-2}	4.05	3.22
$[ReH_5(PPh_3)_3]^a$	1×10^{-2}	2.71	1.80
$[WH_4(dppe)_2]^b$	1×10^{-2}	5.00	4.00

[a]According to ref. 11.
[b]According to ref. 19.

At the first stage hydrogen elimination under the influence of radiation occurs [15–17] and an unsaturated intermediate product forms. Next, the intermediate product is able to coordinate gas molecules present in the sample [16], which under experimental conditions means not only regeneration of the initial complex (with H_2), but also formation of a dinitrogen complex. The last compound is reduced by hydrogen atoms to the hydrazine complex (the possibility of H atom transfer from Re—H groups to other ligands has also been ascertained in other processes [18]). The hydrazine complex formed can undergo decomposition, giving hydrazine (and regenerating unsaturated intermediate product). However, in the range of higher doses of radiation the concentration of the hydrazine complex exceeds the concentration of the dis-dinitrogen complex and increases the probability of further coordinated hydrazine reduction (in comparison with the probability of Re—N_2 group reduction). As a result of coordinated hydrazine reduction by hydrido ions coming from Re—H groups, NH_3 is formed and its induction period results from the reactions proposed above.

Lower yields of photoreduction products and lower catalytic efficiencies in the case of rhenium complexes may result from the fact that as these are more stable than the analogous tungsten complexes, the M—H bond (as shown by force constant comparison) reduces the ease of formation of the unsaturated intermediate product. At irradiation times longer than 60 minutes the decomposition of the catalyst usually occurs (in a γ radiation field the examined complexes are stabilised by the presence of high concentrations of reducing agents, such as solvated electrons and free radicals). Application of rhenium complexes containing phosphines more strongly bonded to the central ion should give higher yields of molecular nitrogen reduction products.

REFERENCES

1. Dzięgielewski, J. O. and Małecki, J., *Polyhedron*, 1991, **10**, 2827.
2. Dzięgielewski, J. O., Gil-Bortnowska, R. and Mrzigod, J., *Polish Journal of Chemistry*, 1993, **67**, 391.
3. Dzięgielewski, J. O., Jeżowska-Trzebiatowska, B., Gil-Bortnowska, R. and Grzybek, R., *Polyhedron*, 1986, **5**, 833.
4. Dzięgielewski, J. O., Małecki, J. and Grzybek, R., *Polyhedron*, 1991, **10**, 1007.
5. Dzięgielewski, J. O., Grzybek, R. and Gil-Bortnowska, R., *Journal of Radioanalytical and Nuclear Chemistry*, 1989, **132**, 115.
6. Dzięgielewski, J. O. and Grzybek, R., *Polyhedron*, 1990, **9**, 645.
7. Dzięgielewski, J. O. and Małecki, J. G., *Polish Journal of Chemistry*, 1993, **67**, 397.
8. Dzięgielewski, J. O. and Grzybek, R., *Journal of Radioanalytical and Nuclear Chemistry*, 1989, **132**, 115.
9. Dzięgielewski, J. O., Gil-Bortnowska, R. and Mrzigod, J., *Journal of Radioanalytical and Nuclear Chemistry*, 1992, **163**, 325.
10. Dzięgielewski, J. O., Małecki, J. G. and Grzybek, R., *Polyhedron*, 1994, **13**, 241.
11. Dzięgielewski, J. O., Gil-Bortnowska, R., Mrzigod, J. and Machura, B., *Polish Journal of Chemistry*, 1996.
12. Bianco, V. D. and Doronzo, S., *Inorganic Synthesis*, 1976, **16**, 157.
13. Carr, S. W., Fowles, E. H., Fontaine, X. L. R. and Shaw, B. L., *Journal of the Chemical Society, Dalton Transactions*, 1990, 573.
14. Dzięgielewski, J. O. and Małecki, J., *Polyhedron*, 1992, **11**, 2383.
15. Roberts, D. A., Geoffroy, G. L., and Bradley, M. G., *Journal of Organometallic Chemistry*, 1980, **198**, C75.
16. Bradley, M. G., Roberts, D. A. and Geoffroy, G. L., *Journal of the American Chemical Society*, 1981, **103**, 379.
17. Chatt, J. and Coffey, R. S., *Coordination Chemistry Review*, 1985, **65**, 45.
18. Slater, S. G., Lusk, R., Schumann, B. F. and Darensbourg, M., *Organometallics*, 1982, **1**, 1662.
19. Dzięgielewski, J. O., Gil-Bortnowska, R., Mrzigod, J. and Małecki, J. G., *Polyhedron*, 1995, **14**, 1375.

Pergamon

PII: S0277-5387(96)00529-3

Polyhedron Vol. 16, No. 12, pp. 1983–1991, 1997
© 1997 Published by Elsevier Science Ltd
All rights reserved. Printed in Great Britain
0277-5387/97 $17.00+0.00

Reactivity of 1,3,5-trithiacyclohexane and 1,3,5-triselenacyclohexane towards molecular diiodine. Crystal structures of the diiodine adducts

Massimiliano Arca,[a] Franco Cristiani,[a] Francesco A. Devillanova,[a] Alessandra Garau,[a] Francesco Isaia,[a] Vito Lippolis,[a] Gaetano Verani[a]* and Francesco Demartin[b]

[a]Dipartimento di Chimica e Tecnologie Inorganiche e Metallorganiche, University of Cagliari, Via Ospedale 72, 09124 Cagliari, Italy; [b]Dipartimento di Chimica Strutturale e Stereochimica Inorganica, University of Milano, Via G. Venezian 21, 20133 Milano, Italy

(Received 7 August 1996; accepted 28 October 1996)

Abstract—The reactions between I_2 and the donors (D) 1,3,5-trithiacyclohexane (**1**) and 1,3,5-triselenacyclohexane (**2**), in methylene chloride and hot benzene respectively (1 : 1 I_2 : D molar ratio) give the solid adducts $\mathbf{1}\cdot I_2$ (**I**) and $\mathbf{2}\cdot I_2$ (**II**) whose structures have been solved by X-ray diffraction. The use of an excess of diiodine up to the molar ratio 2 : 1 always gives **II** from **2**, and $\mathbf{1}\cdot 2I_2$ (**III**) from **1**. Compound **I** consists of polymeric chains in which each diiodine bridges between different **1** molecules, while **II** consists of discrete molecular units. The Raman ν(I—I) frequency and I—I bond distance in **I** fits well with the previously found linear correlation. This correlation suggests two different I—I bond distances for **III**. The comparison of the FT-IR and FT-Raman spectra for **II** is consistent with the three-body model for Se—I—I. The association constant between **1** and I_2 in methylene chloride has been also studied both by UV–visible and ^{13}C NMR spectroscopy, giving K values at 21°C in good agreement. © 1997 Published by Elsevier Science Ltd.

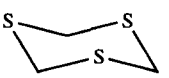
Keywords: 1,3,5-trithiacyclohexane; 1,3,5-triselenacyclohexane; diiodine adducts; crystal structure; formation constants.

Compounds containing sulfur/selenium donor atoms (D) react with molecular diiodine to give, in low polarity solvents, molecular charge-transfer (CT) complexes [1], $D\cdot I_2$, according to equilibrium (1):

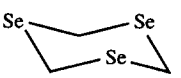
$$D + I_2 \rightleftharpoons D\cdot I_2 \qquad (1)$$

The strength of the S/Se···I_2 interaction in solution can be assessed by evaluating the formation constant (K) and enthalpy of Eq. (1) by UV–vis spectroscopy. However, Raman and ^{13}C NMR spectroscopy can also give information on this interaction. While 1 : 1 adducts are the products usually identified in solution for I_2/D molar ratios higher than one, different and unpredictable solid compounds can be obtained [2–6] from the solutions of D and I_2. In many instances X-ray crystal structure determination has been proved essential to characterization of the solid products. However, when this is not possible, Raman spectroscopy on solid samples becomes useful to hypothesize structural features [7–11].

Here, attention is focused on the solid adducts obtained by reacting 1,3,5-trithiacyclohexane (**1**) and 1,3,5-triselenacyclohexane (**2**) with I_2, and on the study of equilibrium (1) in dichloromethane solution using **1** as donor, since the high insolubility of **2** in low polar solvents has precluded an analogous study.



(1)



(2)

*Author to whom correspondence should be addressed. E-mail address: verani@vaxcal.unica.it. Fax number: +70-6758670.

The use of **1** and **2** as ligands has been very limited. For **1**, the literature only reports the X-ray structure of a dimeric silver complex [12] and a study in solution [13] on its interaction with π- and σ-acceptors, including molecular diiodine, whereas the coordinative chemistry of **2** has not been explored yet.

On the other hand, in the past decade, thio- and seleno-macrocyclic ethers have been the subject of great interest because of their peculiar coordinating abilities towards both transition and non-transition metal ions [14] and, very recently, towards halides [15–17]. Molecules **1** and **2** present three donor centres and, as mesocycles, can be considered prototypes of thio- and seleno-macrocycles in their interaction with diiodine.

EXPERIMENTAL

Materials

1,3,5-Trithiacyclohexane (**1**) was purchased from Aldrich and purified several times by recrystallization. 1,3,5-Triselenacyclohexane (**2**) was prepared according to the literature [18] and purified by sublimation.

Preparation of compounds **1** · I_2 **(I),** **2** · I_2 **(II)** *and* **1** · $2I_2$ **(III)**

Compounds **I** and **II** were obtained as black crystals with metallic lustre; for **I**, a dichloromethane solution containing **1** and diiodine in a 1 : 1 molar ratio was allowed to stand in air at room temperature until the formation of crystals. For **II**, a mixture of **2** and diiodine (1 : 1 molar ratio) and benzene (100 cm^3 per 100 mg of **2**) was heated in a sealed tube at 80°C until dissolution of **2**. Well-shaped crystals of **II** were formed when the reaction mixture was allowed to cool to room temperature and stand for several days in air. Found (Calc.) for $C_3H_6S_3I_2$; **I**: C, 9.1 (9.1); H, 1.6 (1.5). Found (Calc.) for $C_3H_6Se_3I_2$; **II**: C, 6.8 (6.8); H, 1.1 (1.1%). By standing a mixture of **1** and diiodine (1 : 2 molar ratio) in dichloromethane for several days, a black powder of **III** was obtained. Found (Calc.) for $C_3H_6S_3I_4$; **III**: C, 5.7 (5.5); H, 1.0 (0.9%).

FT-IR and FT-Raman spectra

The FT-IR spectra were recorded as polyethylene pellets (400–50 cm^{-1}) using a Bruker IFS55 fourier transform infrared spectrometer. The FT-Raman spectra (resolution $\pm$ 4 cm^{-1}) were recorded on a Bruker RFS100 Fourier transform Raman spectrometer (400–50 cm^{-1}) operating with an excitation frequency of 1064 nm (Nd–YAG laser). The power level of the laser source was 300 mW. Detection of the signal was made with an indium–gallium–arsenide detector operating at room temperature. The samples were packed as powder into a suitable cell and then fitted into the compartment designed for use with a 180° scattering geometry. No sample decomposition was observed during the experiment.

Spectrophotometric measurements

Spectrophotometric measurements in CH_2Cl_2 solutions were carried out on a Varian model Cary 5 UV–vis NIR spectrophotometer with a temperature controller and connected with an IBM PS 2 type 8513. The spectra of 13 different solutions were recorded in the range 300–500 nm at 15, 20, 25, 30 and 35°C. The choice of concentrations of the reagents was made according to the criteria outlined in ref. [19] and widely discussed in previous papers [1]. However, in all solutions, the concentration of **1** was always kept higher than that of diiodine in order to avoid the formation of adducts other than 1 : 1. Data analysis was carried out with a program based on a non-linear least-squares method [20] optimizing the absorbance values at six different wavelengths for each temperature value. The ΔH have been obtained as mean values of the slopes of the straight lines of $\ln(K \cdot \varepsilon)$ versus $1/T$ obtained at six different wavelengths: $\Delta H = (\Sigma \Delta H_i/\sigma_i)/\Sigma 1/\sigma_i$, $\sigma = [(N\text{-}1)\Sigma\sigma_i^2/(N \cdot n \cdot (N \cdot n\text{-}1))]^{1/2}$, where N and n are the numbers of the different temperatures and wavelengths, respectively.

^{13}C *NMR measurements*

The ^{13}C NMR spectra were recorded at 21°C on a Varian VXR 300 FT-NMR spectrometer, operating at 75.4 MHz frequency. $CDCl_3$ (77.00 ppm) was employed as the external reference. Several CH_2Cl_2 solutions having a $[I_2]^0/[\mathbf{1}]^0$ molar ratio ranging from 0.28 to 8.00 were recorded. The ^{13}C chemical shifts recorded were: δ 35.925, 36.021, 36.116, 36.192, 36.345, 36.440, 36.630, 36.780, 36.878 for solutions having $[\mathbf{1}]^0 = 2.5 \times 10^{-2}$ M (for the last solution $[\mathbf{1}]^0$ was 2.0×10^{-2} M) and $[I_2]^0/[\mathbf{1}]^0 = 0.28$, 0.56, 0.84, 1.12, 1.68, 2.24, 3.36, 5.16, 7.99, respectively.

X-ray crystal structure determination

Details of the data collection and refinement of the structures are reported in Table 1. Crystals of compounds **I** and **II** were mounted on a glass fibre in random orientation. Preliminary examination and data collection were performed with graphite-monochromatized Mo-K_α radiation (0.71073Å) on an Enraf–Nonius CAD4 computer-controlled kappa-axis diffractometer. Cell constants and an orientation matrix for data collection were obtained from least-squares refinement, using the setting angles of 25 reflections. The data were collected at room temperature using a scan rate variable of 2–20° min^{-1} (in ω). Three representative reflections were measured every hour to check the stability of the crystals under

Table 1. Crystallographic data

Compound	I	II
Formula	$C_3H_6I_2S_3$	$C_3H_6I_2Se_3$
Formula weight	392.08	532.77
Crystal system	Monoclinic	Triclinic
Space group	$P2_1/m$ (No. 11)	$P\bar{1}$ (No. 2)
a (Å)	4.427(2)	6.343(4)
b (Å)	16.744(4)	8.946(6)
c (Å)	6.650(2)	9.712(5)
α (°)	90	76.17(5)
β (°)	103.55(3)	74.74(5)
γ (°)	90	75.94(5)
V (Å^3)	479.2(3)	506.7(6)
Z	2	2
$F(000)$	356	464
$D_{calc.}$ (g cm^{-3})	2.717	3.492
Crystal dimensions (mm)	0.10 × 0.12 × 0.45	0.10 × 0.15 × 0.25
μ (Mo-K_α) (cm^{-1})	70.5	167.5
Transmission factors	0.73–1.00	0.49–1.00
Scan mode	ω	ω
ω-scan width (°)	$1.00 + 0.35 \tan\theta$	$1.00 + 0.35 \tan\theta$
θ-range (°)	3–25	3–28
Octants of reciprocal space explored	$+h, +k, \pm l$	$\pm h, +k, \pm l$
Measured reflections	984	2623
Unique refl. with $I > 3\sigma(I)$	800	1939
Final R and R_w indices[a]	0.023, 0.034	0.029, 0.042
No. of variables	41	74
GOF[b]	1.459	1.257

[a] $R = [\Sigma(F_0 - k\|F_c\|)/\Sigma F_0]$; $R_w = [\Sigma w(F_0 - k\|F_c\|)^2/\Sigma w F_0^2]^{1/2}$.
[b] $\text{GOF} = [\Sigma w(F_0 - k\|F_c\|)^2/(N_{\text{observations}} - N_{\text{variables}})]^{1/2}$.

X-ray exposure; these measurements revealed a decay of the scattering power of the crystal which amounts to 27% and 5% for **I** and **II**, respectively. Lorentz polarization and a linear correction for decay were applied to the intensities. An empirical absorption correction based on a series of psi-scans was also applied to the data. The structure was solved using direct methods (MULTAN). The remaining atoms were located in succeeding difference Fourier syntheses. The structure was refined in full-matrix least squares where the function minimized was $\Sigma w(|F_0| - |Fc|)^2$. All the hydrogen atoms were introduced in the structure model at calculated positions (C—H 0.95 Å) and were unrefined. Scattering factors were taken from Cromer and Waber [21]. Anomalous dispersion effects were included in Fc; the values for f' and f'' were those of Cromer [22]. All calculations were performed on a 80486/33 computer using Personal SDP software [23]. Selected interatomic distances and angles for **I** and **II**, respectively, are shown in Table 2. The crystallographic data have been deposited at the Cambridge Crystallographic Data Centre (CCDC).

RESULTS AND DISCUSSION

The reaction between 1,3,5-trithiacyclohexane (**1**, in methylene chloride), and 1,3,5-triselenacyclohexane (**2**, in hot benzene) with molecular diiodine in a 1 : 1 molar ratio gave the solid adducts **1**·I_2 (**I**) and **1**·I_2 (**II**). The use of an excess of diiodine up to molar ratio of 2 : 1 always gave **II** with **2**, and **1**·$2I_2$ (**III**) with **1**. Only **I** and **II** were obtained as crystals suitable for X-ray investigation.

X-ray crystal structures of **I** *and* **II**

The different nature of **I** and **II** is shown from their crystal packings as shown in Figs 1 and 2.

Compound **I** consists of polymeric chains extending along [010] in which each diiodine molecule acts as a bridge in a zig-zag pattern between different 1,3,5-trithiacyclohexane molecules. The S···I interchain contacts range from 4.096(1) to 4.335(1)Å, with an I···I contact of 4.427(1)Å. Compound **II** contains discrete molecular units, **2**·I_2, weakly interacting with each other, with I···I and Se···I intermolecular contacts of 4.243(1)Å and 3.764(1)Å respectively. In both cases the rings are in the chair conformation and the diiodine molecules are bonded equatorially to the sulfur in **I** and to the selenium in **II**, to give almost linear S—I—I and Se—I—I moieties [169.04(2)° and 179.31(2)°]. The adducts with diiodine and interhalogens of similar six-membered ring systems having S/Se heteroatoms such as 1,4-dithiacyclohexane [24],

Table 2. Selected interatomic distances (Å) and angles (°) for **I** and **II**

Compound **I***			
I—I[e]	2.754(1)	I···I[b]	4.427(1)
I—S(1)	3.169(1)	I···S(1)[b]	4.335(1)
S(1)—C(1)	1.806(3)	I···S(1)[c]	4.096(1)
S(1)—C(2)	1.801(3)	I···S(2)[d]	4.220(1)
S(2)—C(2)	1.803(3)		
I[e]—I···S(1)	169.04(2)	C(1)—S(1)—C(2)	98.4(2)
I···S(1)—C(1)	95.1(1)	C(2)—S(2)—C(2)[a]	98.2(2)
I···S(1)—C(2)	120.4(1)	S(1)—C(1)—S(1)[a]	113.9(2)
		S(1)—C(2)—S(2)	113.8(2)
Compound **II**†			
I(1)—I(2)	2.944(1)	I(1)···I(2)[a]	4.306(1)
I(1)—Se(1)	2.734(1)	I(1)···I(2)[b]	4.243(1)
Se(1)—C(1)	1.963(5)	I(1)···Se(1)[c]	4.445(1)
Se(1)—C(3)	1.965(5)	I(1)···Se(2)[c]	4.335(1)
Se(2)—C(1)	1.924(5)	I(2)···Se(1)[c]	3.764(1)
Se(2)—C(2)	1.932(5)	I(2)···Se(2)[d]	4.120(1)
Se(3)—C(2)	1.937(5)	I(2)···Se(2)[e]	3.950(1)
Se(3)—C(3)	1.910(5)	I(2)···Se(3)[f]	4.478(1)
		I(2)···Se(3)[g]	3.890(1)
I(2)—I(1)—Se(1)	179.31(2)	C(2)—Se(3)—C(3)	96.0(2)
I(1)—Se(1)—C(1)	100.8(1)	Se(1)—C(1)—Se(2)	112.7(2)
I(1)—Se(1)—C(3)	96.7(1)	Se(2)—C(2)—Se(3)	117.4(2)
C(1)—Se(1)—C(3)	96.2(2)	Se(1)—C(3)—Se(3)	111.5(2)
C(1)—Se(2)—C(2)	96.7(2)		

*Symmetry codes: a = $x, \frac{1}{2} - y, z$; b = $x - 1, y, z$; c = $1 - x, 1 - y, 1 - z$; d = $x - 1, y, z - 1$; e = $-x, 1 - y, -z$.

†Symmetry codes: a = $1 + x, y, z$; b = $-x, 1 - y, -z$; c = $x - 1, y, z$; d = $x - 1, y - 1, z$; e = $1 - x, 1 - y, -z$; f = $x, y - 1, z$; g = $-x, 1 - y, 1 - z$.

1,4-diselenacyclohexane [25] and 1-oxa-4-selenacyclohexane [26], are characterized by the halogen and interhalogen molecules always being bonded equatorially to the sulfur and axially to the selenium, with the exception of 1-selena-4-thiacyclohexane bis(diiodine) [27], where the two diiodine molecules are equatorial. Since molecular crowding is practically the same in all systems, no rationalization was given for this. As expected on the basis of the diversity of sulfur and selenium as donors the Se—I bond distance [2.734(1)Å] is shorter than S—I [3.169(1)Å] and the I—I bond length in **II** [2.944(1)Å] is longer than that in **I** [2.754(1)Å]. The values of these distances fit very well the reported hyperbolic correlations *d*(S—I) *vs* *d*(I—I) and *d*(Se—I) *vs* *d*(I—I) [3,28]. However, the S—I distance is longer than those observed in the adducts $([9]aneS_3)_2 \cdot 4I_2$ [15,16] and $[9]aneS_3 \cdot 3I_2$ [16] ([9]aneS$_3$ = 1,4,7-trithiacyclononane) and is one of the longest of all the reported sulfur adducts [3,25]. Compound **I** is the first case of a polymeric structure for diiodine adducts with a mesocycle molecule containing S/Se. This trend, however, has been observed for macrocycle molecules. [9]aneS$_3$ [15,16] reacts with diiodine to yield two crystalline adducts, the monomeric species $[9]aneS_3 \cdot 3I_2$ and the dimeric $([9]aneS_3)_2 \cdot 4I_2$; only for the latter do the dimeric units form an infinite three-dimensional network through I···I and S···I contacts. [12]aneS$_4$ [29] ([12]aneS$_4$ = 1,4,7,10-tetrathiocyclododecane) with diiodine gives a polymeric adduct $[([12]aneS_4 \cdot I_2)_\infty]$, in which a diiodine molecule bridges symmetrically between two macrocyclic molecules.

Vibrational spectra of **I**, **II** *and* **III**

Since the I—I stretching vibration is Raman active, FT-Raman spectroscopy is useful in studying the I—I bond in the adducts. Previous studies [2,3,5,6,10,11] have shown differences in the vibrational spectra between the adducts of sulfur and selenium, since selenium binds diiodine more strongly than sulfur. In the S···I—I system, although slightly perturbed, the diiodine molecule still retains its identity, whereas the same does not happen in the Se—I—I system, and a three-body model should be used for its description. In the case of weak or medium-weak adducts (I—I bond order > 0.6) [10], the lengthening of the I—I bond induces a downward shift in the ν(I—I) Raman band, which can be roughly correlated to the *d*(I—I)

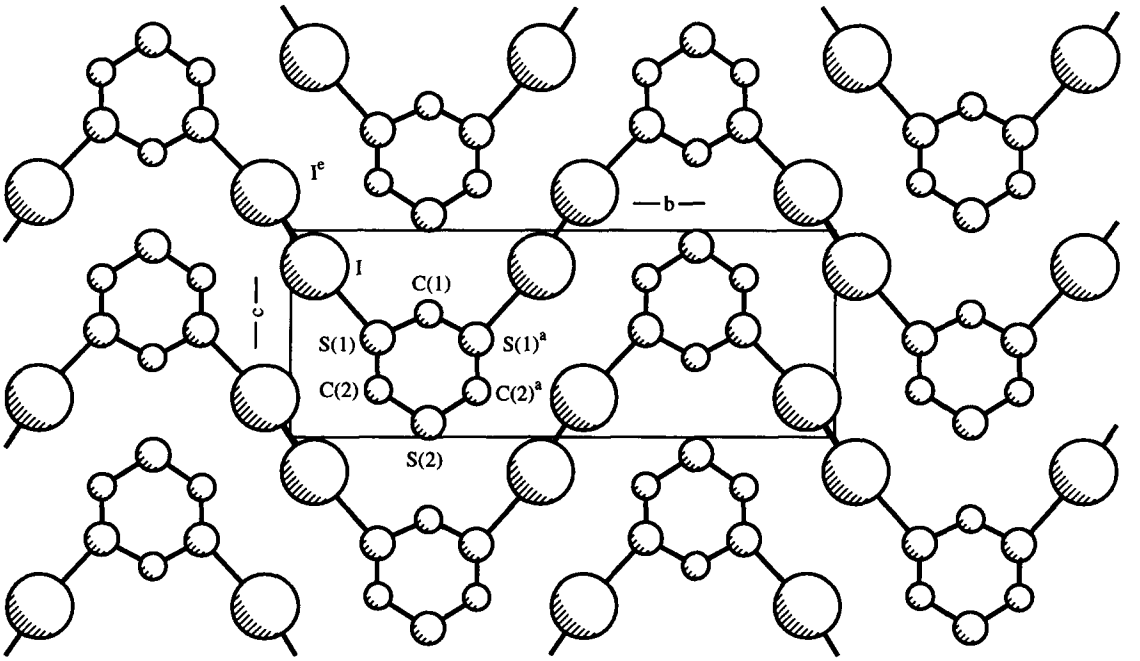


Fig. 1. Crystal packing of **I**.

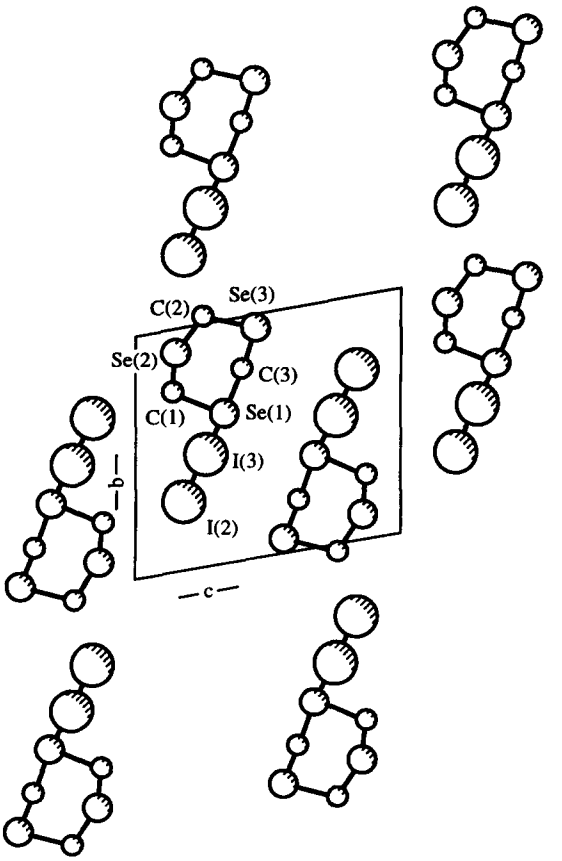


Fig. 2. Crystal packing of **II**.

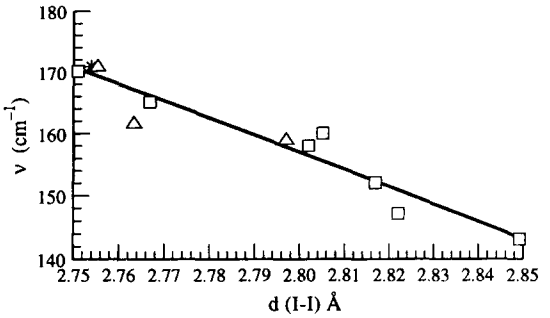


Fig. 3. Linear correlation ($r = 0.984$) between ν(I—I) Raman stretching vibrations and the d(I—I) bond distances in several structurally characterized adducts (ref. 10, squares; ref. 16 triangles; *, this work).

bond distance [10] as shown in Fig. 3 for several structurally characterized adducts.

The data related to **I** [d(I—I) = 2.754 Å and ν(I—I) = 171 cm^{-1}] match the correlation fairly well. The adduct **1**·$2I_2$ (**III**) shows two Raman bands at 177 and 163 cm^{-1}, indicating the presence of two differently perturbed I_2 molecules. From Fig. 3, d(I—I) bond distances of 2.737 and 2.777 Å can be predicted for the two I_2 molecules. This situation is close to that found in ([9]aneS_3)$_2$·$4I_2$ [16], where two Raman peaks at 159 and 171 cm^{-1} agree well with the two types of d(I—I) bond distances [2.792(1), 2.781(1), 2.818(1) Å terminal diiodine (mean value 2.797Å) and 2.755(1)Å bridged diiodine]. In the case of [9]aneS_3·$3I_2$, [16] only one Raman peak has been observed, at 162 cm^{-1}, in accord with the close three d(I—I) distances verified in the structure [2.772(1), 2.786(2), 2.751(2)Å (mean value 2.7636Å)]. On the other hand, 1,4-dithiacyclohexanebis(diiodine) shows two Raman peaks at 162 and 153 cm^{-1}, which should be correlated with two significantly different d(I—I) distances. On the contrary, only one d(I—I) distance [2.787(2)Å] is reported [22a] but the R factor of 0.18 clearly shows that this structure should be reconsidered.

In Fig. 4 the FT-Raman and the FT-IR spectra of **II** are shown superimposed within the range 250–50 cm^{-1}. The Raman spectrum exhibits four main bands at 88, 111, 167 and 220 cm^{-1}. The first three bands can be assigned to δ, ν_s and ν_{as} modes, respectively. As expected for the Se—I—I three-body system, the FT-IR spectrum shows roughly the same bands at 88, 125 (broad) and 165 cm^{-1}.

Association constant of **I** *obtained by UV–vis and* ^{13}C *NMR techniques*

The reaction between molecular diiodine and **1** has been studied in dichloromethane solutions; the presence of an isosbestic point, kept also in excess of I_2, justifies the use of a 1 : 1 model in the data treatment of the equilibrium (1). In Table 3 the association constants evaluated for six wavelengths, their molar

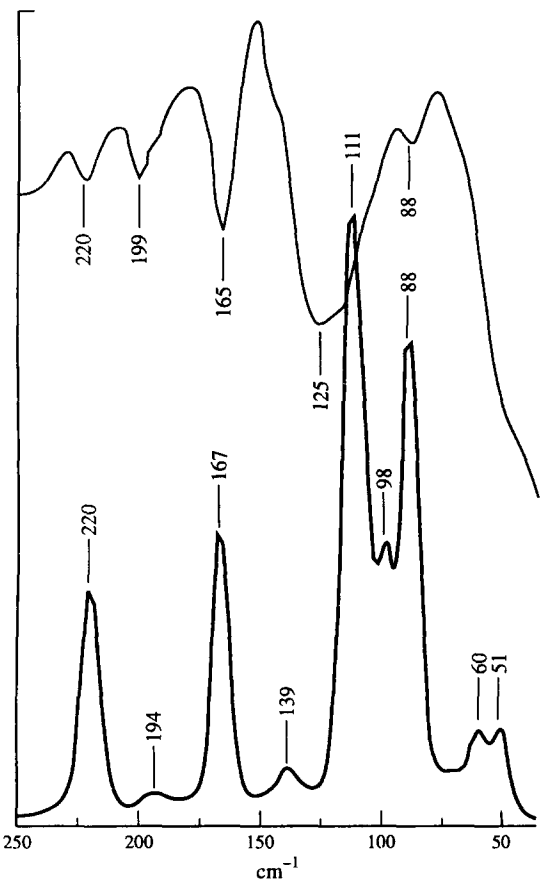


Fig. 4. Superimposed FT-Raman and FT-IR spectra of **II**.

extinction coefficients, the ranges of saturation fraction and the sum of the square deviations are reported. Although the experimental conditions were the best possible [16] the independence of the calculated K and ε values, and consequently the Arrhenius plot, were not satisfactory. To calculate a more reliable ΔH value, the plot of $\ln(K \cdot \varepsilon)$ versus $1/T$ has been adopted (see footnote to Table 3). The association constants and the ΔH values of **I** have been reported in the literature [13] [K 31.2 ± 2.0 dm^3 mol^{-1} at 25°C and −20.8 ± 0.3 kJ mol^{-1}]. However, they were obtained using the Benesi–Hildebrand and Scott equations, whereas our data [K 13 ± 0.7 dm^3 mol^{-1} at 25°C and −26.38 ± 0.04 kJ·mol^{-1}], obtained by a non-least-squares method, are based on an accurate choice of the reagent concentrations.

In order to have an independent method to determine the K value, we also used the ^{13}C NMR technique, by measuring the ^{13}C signal for mixtures of **1** with increasing amounts of diiodine (see Fig. 5a).

As a consequence of equilibrium (1), the ^{13}C chemical shift δ can be correlated to the concentrations of free [**1**] and bonded **1** ([**1**·I_2]) by Eq. (2) [7]:

$$\delta = \delta_1^0[\mathbf{1}]/[\mathbf{1}]^0 + \delta_{1\text{-}I_2}^0[\mathbf{1}\cdot I_2]/[\mathbf{1}]^0 \qquad (2)$$

where $[\mathbf{1}]^0$ is the analytical concentration of **1** while

Table 3. Molar extinction coefficients (ε) at the wavelengths (λ) used for the calculation, association constants (K), ranges of the saturation fraction (s) and sum of the squared deviations (χ^2) for **I** with I_2. (Standard deviation in parentheses)

T (°C)	λ (nm)	ε (dm^3 mol^{-1} cm^{-1})	K (dm^3 mol^{-1})	s[a]	χ^2
15	340	18520(70)	21(0.5)	0.024 ÷ 0.33	0.01
	330	26130(100)			
	320	32460(130)			
	310	34240(110)			
	300	29800(190)			
	290	21370(240)			
20	340	19280(80)	16(0.5)	0.019 ÷ 0.28	0.01
	330	27000(120)			
	320	33460(150)			
	310	35380(140)			
	300	30940(230)			
	290	22410(290)			
25	340	19700(140)	13(0.7)	0.016 ÷ 0.25	0.02
	330	27330(180)			
	320	33800(200)			
	310	35870(220)			
	300	31520(330)			
	290	23030(380)			
30	340	20020(200)	11(0.8)	0.013 ÷ 0.21	0.02
	330	27580(230)			
	320	34090(270)			
	310	36230(310)			
	300	32110(410)			
	290	23650(480)			
35	340	21420(140)	9(0.6)	0.010 ÷ 0.18	0.01
	330	29310(200)			
	320	36090(250)			
	310	38430(270)			
	300	34030(310)			
	290	25320(370)			

$\Delta H = -26.38 \pm 0.04$ kJ mol^{-1} and r[b] = 1.000

[a]The saturation fraction (s) is defined as the ratio between the concentration of the adduct and the analytical concentration of the donor.

[b]Correlation coefficient of the plots $\ln(K \cdot \varepsilon)$ *vs* $1/T^0$ obtained for the six wavelengths.

$\delta_1{}^0$and $\delta^0_{1\cdot I_2}$ represent the ^{13}C chemical shift values of pure **1** (35.84 ppm in CH_2Cl_2) and **1** · I_2, respectively. Considering the mass concentration equations and the expression for K it is possible to fit the experimental δ values as a function of K by using a Gauss–Newton iterative cycle [30]. A K value of 12.8 ± 0.1 dm^3 mol^{-1} with $\Sigma r^2 = 0.0178$, where r represents the difference between the observed and the calculated values, is obtained. The calculated values are represented in Fig. 5a and the correspondence with the experimental data is fairly good. The absence of an equilibrium leading to the adduct **1** · $2I_2$ can easily be proved by combining Eq. (2) with the relation $[\mathbf{1}]^0 = [\mathbf{1} \cdot I_2] + [\mathbf{1}]$ to give Eq. (3):

$$(\delta - \delta_1^0)[\mathbf{1}]^0 = (\delta^0_{1\cdot I_2} - \delta_1^0)[\mathbf{1} \cdot I_2] \qquad (3)$$

Hence, by plotting $(\delta - \delta_1^0)[\mathbf{1}]^0$ versus $[\mathbf{1} \cdot I_2]$, calculated from the K value previously obtained, a straight line crossing the origin should be obtained only if the 1 : 1 adduct is formed, and deviation from linearity should be due to 1 : 2 adduct formation. In Fig. 5b this plot is shown and the 1 : 1 model seems to be fully verified up to a $[I_2]^0/[[\mathbf{1}]^0$ ratio of eight ($r = 0.998$), with a $\delta^0_{1\cdot I_2}$ value of 37.48 ppm calculated from the slope of the straight line (Fig. 5b). Whenever the NMR technique requires reagent concentrations ten times higher than those required for the UV–vis technique, by interpolating the K value at 21°C from the data obtained spectrophotometrically, a value of 15.8 dm^3 mol^{-1}, close to 12.8 dm^3 mol^{-1} measured by the NMR technique, is obtained. This fact further supports the reliability of our UV–vis K data with respect to those previously reported [13].

If the value of K for equilibrium (1) at 25°C is compared with that reported for [9]aneS_3 [169(4) dm^3

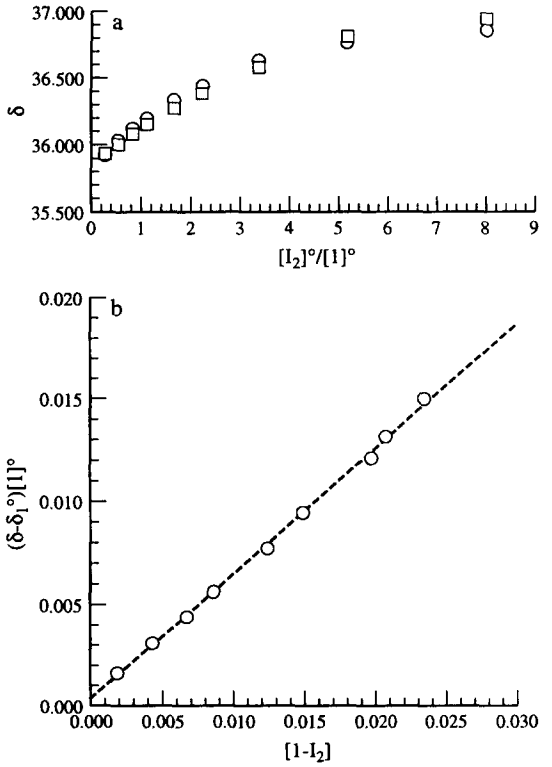


Fig. 5. (a) ^{13}C chemical shifts as a function of increasing amounts of diiodine (circles, experimental; squares, calculated data). (b) Plot of $(\delta - \delta_1{}^0)$ $[\mathbf{1}]^0$ *vs* $[\mathbf{1} \cdot I_2]$ ($r = 0.998$).

mol^{-1}], it can be seen that the sulfur is a better donor in [9]aneS$_3$ [14] than in **1**, perhaps as a consequence of a stronger inductive effect owing to the two CH_2 groups in [9]aneS$_3$.

Acknowledgements—We thank the "Comitato Nazionale per le Scienze Chimiche" of CNR of Rome for financial support (bilateral project).

REFERENCES

1. Cristiani, F., Devillanova, F. A., Diaz, A., Isaia, F. and Verani, G., *Heteroatom Chemistry*, 1990, **1,** 363, and refs therein.
2. Cristiani, F., Demartin, F., Devillanova, F. A., Isaia, F., Saba, G. and Verani, G., *Journal of the Chemical Society, Dalton Transactions*, 1992, 3553 and refs therein.
3. Cristiani, F., Demartin, F., Devillanova, F. A., Isaia, F., Lippolis, V. and Verani, G., *Inorganic Chemistry*, 1994, **33,** 6315 and refs therein.
4. Cristiani, F., Demartin, F., Devillanova, F. A., Isaia, F., Lippolis, V. and Verani, G., *Polyhedron*, 1995, **14,** 2937.
5. Bigoli, F., Deplano, P., Devillanova, F. A., Lippolis, V., Mercuri, M. L., Pellinghelli, M. A., Trogu, E. F., *Gazzetta Chimica Italiana*, 1994, **124,** 445.
6. Demartin, F., Deplano, P., Devillanova, F. A., Isaia, F., Lippolis, V. and Verani, G., *Inorganic Chemistry*, 1993, **32,** 3694 and refs therein.
7. Cristiani, F., Devillanova, F. A., Garau, A., Isaia, F., Lippolis, V. and Verani, G., *Heteroatom Chemistry*, 1994, **5,** 421.
8. Ferraro, J. R. and Williams, J., in *Practical Fourier Transform Infrared Spectroscopy* ed. Ferraro, J. R. and Krishnan, K. Academic Press, New York, 1990.
9. (a) Marks, T. J. and Kalina, D. W., in *Extended Linear Chain Compounds*, Vol. 2, ed. Miller, J. S., Plenum Press, New York, 1982; (b) Teitebaum, R. C., Ruby, S. L. and Marks, T. J., *Journal of the American Chemical Society*, 1980, **102,** 3322 and refs therein; (c) Diel, B. N., Inabe, T. J., Lyding, W., Schoch, K. F., Kannewurf Jr., C. R. and Marks, T. J., *Journal of the American Chemical Society*, 1983, **105,** 1551.
10. Deplano, P., Devillanova, F. A., Ferraro, J. R., Isaia, F., Lippolis, V. and Mercuri, M. L., *Applied Spectroscopy*, 1992, **46,** 1625.
11. Deplano, P., Devillanova, F. A., Ferraro, J. R., Mercuri, M. L., Lippolis, V. and Trogu, E. F., *Applied Spectroscopy*, 1994, **48,** 1236.
12. Edema, J. J. H., Buter, J., van Bolhuis, F., Meetsma, A., Kellogg, R. M., Kooijman, H. and Spek, A. L., *Inorganica Chimica Acta*, 1993, **207,** 263.
13. Hamed, M. M. A., Mohamed, M. B. and Mahmoud, M. R., *Bulletin of the Chemical Society of Japan*, 1994, **67,** 2006.
14. (a) Blake, A. J. and Schröder, M., *Advances in Inorganic Chemistry*, 1990, **35,** 1; (b) Hope, E. G. and Levason, W., *Coordination Chemistry Review*, 1993, **122,** 109; (c) Champness, N. R., Kelly, P. F., Levason, W., Reid, G., Slawin, A. M. Z. and Williams, D. J., *Inorganic Chemistry*, 1995, **34,** 651 and refs therein; (d) Willey, G. R., Lakin, M. T., Ravindran, M., Alcock, N. W., *Journal of the Chemical Society, Chemical Communications*, 1991, 271; (e) Willey, G. R., Lakin, M. T., Alcock, N. W., *Journal of the Chemical Society, Dalton Transactions*, 1992, 591.
15. Blake, A. J., Gould, R. O., Radek, C. and Schröder, M., *Journal of the Chemical Society, Chemical Communications*, 1993, 1191.
16. Cristiani, F., Devillanova, F. A., Isaia, F., Lippolis, V., Verani, G. and Demartin, F., *Heteroatom Chemistry*, 1993, **4,** 571.
17. Blake, A. J., Cristiani, F., Devillanova, F. A., Garau, A., Gilby, L., Gould, R. O., Isaia, F., Lippolis, V., Parsons, S., Radek, C. and Schröder, M., *Journal of the Chemical Society, Dalton Transactions*, in press.
18. Mortillaro, L., Credali, L., Mammi, M. and Valle, G., *Journal of the Chemical Society*, 1965, 137.
19. (a) Carta, G., Crisponi, G. and Nurchi, V., *Tetrahedron*, 1981, **37,** 2115; (b) Carta, G. and Crisponi, G., *Journal of the Chemical Society, Perkin Transactions II*, 1982, 53.
20. Crisponi, G. and Nurchi, V., *Journal of Chemical Education*, 1989, **66,** 54.
21. Cromer, D. T. and Waber, J. T., *International Tables for X-Ray Crystallography*, Vol. IV Table 2.2B. The Kynoch Press, Birmingham, England, 1974.

22. Cromer, D. T., *International Tables for X-Ray Crystallography*, Vol. IV Table 2.3.1. The Kynoch Press, Birmingham, England, 1974.
23. (a) Frenz, B., *Computers in Physics*, 1988, **3,** 42; (b) Frenz, B., *Crystallographic Computing* 5. Oxford University Press, (1991). Ch. 11, p. 126–135.
24. (a) Chao, G. Y. and McCullough, J. D., *Acta Crystallograph*, 1960, **13,** 727; (b) Knobler, C., Baker, C., Hope, H. and McCullough, J. D., *Inorganic Chemistry*, 1971, **10,** 697.
25. Chao, G. Y. and McCullough, J. D., *Acta Crystallograph*, 1961, **14,** 940.
26. (a) Maddox, H. and McCullough, J. D., *Inorganic Chemistry*, 1966, **5,** 522; (b) Knobler, C. and McCullough, J. D., *Inorganic Chemistry*, 1968, **7,** 365.
27. Hope, H. and McCullough, J. D., *Acta Crystallograph*, 1962, **15,** 806.
28. Herbstein, F. H. and Schwotzer, W., *Journal of the American Chemical Society*, 1984, **106,** 2367.
29. Durrant, M. C., Hughes, D. L., Richard, R. L., Baker, P. K. and Harris, S. D., *Acta Crystallograph*, 1995, **C 51**, 697.
30. Carta, G., Crisponi, G. and Lai, A., *Journal of Magnetic Resonance*, 1982, **48,** 341.

Pergamon

PII: S0277-5387(96)00526-8

Polyhedron Vol. 16, No. 12, pp. 1993–1998, 1997
© 1997 Elsevier Science Ltd
All rights reserved. Printed in Great Britain
0277–5387/97 $17.00+0.00

Binding sites of *cis*-$Ru^{II}Cl_2(DMSO)_4$ to mononucleotides: ^1H and ^{31}P NMR evidence

Yan-Ni Tian,[a] Pin Yang,[b]* Qing-Shan Li[b] and Mao-Lin Guo[b] and Ming-Gen Zhao[c]

[a]State Key Laboratory of Coordination Chemistry, Nanjing University, Nanjing 210093, P. R. China; [b]Institute of Molecular Science, Shanxi University, Taiyuan 030006, P. R. China; [c]Xin Zhou Normal College, Xin Zhou 034000, P. R. China

(Received 30 July 1996; accepted 28 October 1996)

Abstract—The binding modes of *cis*-$Ru^{II}Cl_2(DMSO)_3(DMSO)$ (*cis*-RDT, three out of the four DMSO's are S-bonded to the Ru, while the last one is O-bonded) with 5′-GMP and 5′-AMP in aqueous solution at physiological pH value were investigated by high-resolution ^1H and ^{31}P NMR. A ^1H NMR recognition probe, [*trans*-$en_2Os(\eta\text{-}H_2)](CF_3SO_3)_2$, was used in order to verify further the results. 5′-GMP with *cis*-RDT formed two products, clearly indicating that the guanine N_7 and phosphate group bind to Ru^{II} and form a chelate to the metal center; but binding of 5′-AMP to *cis*-RDT may only occur *via* the phosphate group. © 1997 Elsevier Science Ltd. All rights reserved.

Keywords: antitumor compound; ruthenium complex; mononucleotides; binding mode; NMR recognition probe; NMR spectra.

Among the various anticancer metal compounds, ruthenium complexes have shown good antitumor activity [1–3] and a remarkably low toxicity [4], which makes them interesting for possible clinical use [5]. After the discovery of the mutagenic properties [6] and good antineoplastic activity [4] of *cis*-RDT, which suggested that one target of the complex *in vivo* is DNA, many efforts have been made to understand its mechanism of action and to investigate its binding sites to DNA [7]. Despite the success observed with the change of the CD spectrum of poly(dGdC) and poly(dAdT) with *cis*-RDT [8], the binding sites suggested, N_7 of guanine and N_7 of adenine, are only a deduction.

In this paper we present the reaction of *cis*-RDT with 5′-GMP and 5′-AMP in aqueous solution under physiological conditions using the NMR method. In contrast to previous investigations [9,10], we have demonstrated that 5′-GMP can coordinate to the initially achiral *cis*-RDT antitumor agent to form, predominantly, two isomers which have an opposite chirality at Ru^{II}. In a diastereomeric pair of isomers the nucleotide chelates to Ru by N_7 and a phosphate oxygen. We have also demonstrated that 5′-AMP can coordinate to *cis*-RDT through the phosphate group, but the binding of 5′-AMP's N_7 with *cis*-RDT was not observed.

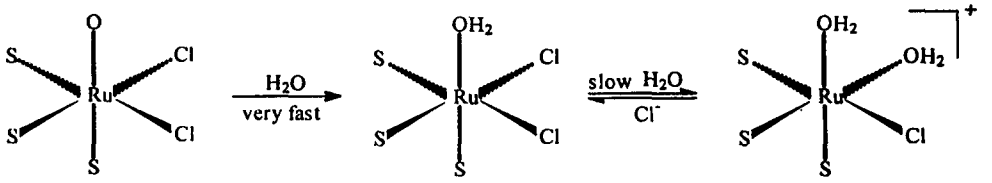
EXPERIMENTAL

cis-RDT was synthesized as already reported [11] and recrystallized from a DMSO/acetone mixture.

The nucleotides, adenosine-5′-monophosphate (AMP), guanosine-5′-monophosphate (GMP) and 2′-deoxyguanosine-5′-monophosphate (dGMP) were purchased from Sigma Chemical Company, purified by precipitation from an aqueous solution and purity was verified with ^1H and ^{31}P NMR spectroscopy. The probe, [*trans*-$en_2Os(\eta\text{-}H_2)](CF_3SO_3)_2$, was a generous gift from Professor Henry Taube and Dr Zeiwei Li, Stanford University, CA, and its purity was checked by ^1H NMR spectroscopy.

Proton and phosphorus NMR were recorded on a VXR-300 MHz NMR spectrometer in D_2O, proton chemical shifts are referenced to DSS as internal standard, and phosphorus chemical shifts are referenced to 85% H_3PO_4 as external standard. The probe, *cis*-RDT and the mononucleotide were mixed as 1 : 1 : 1

*Author to whom correspondence should be addressed.



Scheme 1.

(each 0.01 mol L^{-1}, pD 7.0) in oxygen-free D_2O. D_2O was thoroughly saturated with nitrogen before use. pH measurements were carried out with an American Scientific pH 1 meter and a Wilmad combination pH electrode. All reported pD values in D_2O are corrected pH readings (pD = pH + 0.44).

RESULTS AND DISCUSSION

The octahedral complex *cis*-RDT dissolved in water shows the dissociation mechanism reported [8] in Scheme 1.

As shown above, *cis*-RDT, once dissolved in water, immediately releases the O-bonded dimethyl sulfoxide molecule, this step is followed by the slow dissociation of a Cl^- anion to give the cationic species.

The NMR spectroscopic data for *cis*-RDT with 5′-GMP and 5′-AMP are shown in Table 1.

When *cis*-RDT (0.01 mol L^{-1}) was incubated with 5′-GMP in a 1 : 1 molar ratio in D_2O at 25 °C, examination of reaction mixtures by ^1H NMR (Fig. 1c) revealed two new major species (**I** and **II**) after 12 h at pD7.0; species **I** and **II** exist in nearly equal amounts and 5′-GMP is nearly all consumed. These suggest that the ratio of 5′-GMP to Ru in the products is 1 : 1. The downfield position of the H_8 signals, δ 8.00 for **I** and 8.20 for **II**, and the downfield position of the H_1, resonance of the sugar, δ 5.78 for **I** and δ 5.97 for **II**, suggests N_7 coordination [12].

The ^{31}P NMR spectrum also reveals consumption of the 5′-GMP, but, more importantly, an unusually far downfield position of the two signals (δ11.29 for **I** and 12.90 for **II**) establishes phosphate group coordination [10,13] (Fig. 1d). The above results are very similar to those for 5′-GMP with *trans*-RDT. A comparison of *cis*-RDT–5′-GMP with *trans*-RDT–5′-GMP is shown in Table 2, and suggests that **I** and **II** are chelate complexes with the N_7 and phosphate group of 5′-GMP bound to the same Ru^{II} center, and that the two species are diastereomers with the same Ru coordination environment, differing primarily in the orientation of the chelate moiety, as shown in Scheme 2.

When *cis*-RDT (0.01 mol L^{-1}) was incubated with 5′-AMP under the same conditions as 5′-GMP, an upfield shift of *ca* 0.1 ppm for H_8 and *ca* 1.7 ppm for ^{31}P signals, but almost unchanged H_2 signals, were observed (Table 1). Protonation of the base function of a nucleotide should cause a downfield shift of the nucleobase proton signals, whilst protonation on the phosphate group should cause an upfield shift of the nucleobase proton signals [14]. Also, diamagnetic metallation of a nucleoside produces effects quite similar to protonation [15]. So, the slight upfield shift of H_8 could be a consequence of the direct phosphate coordination to ruthenium.

In order to further examine the sites of *cis*-RDT at 5′-GMP and 5′-AMP, we used [*trans*-$en_2Os(\eta$-$H_2)]^{2+}$ (Scheme 3) as a ^1H NMR recognition probe. The probe, as previously demonstrated [16], binds readily to a variety of biomolecules such as nucleotides, with its sixth ligand, L, substituted by these biomolecules, which results in the direct coordination of Os^{II} to the donor atoms (such as N, O) of the biomolecules. In each case the binding leads to a characteristic ^1H NMR spectrum for the dihydrogen unit that appears in a spectral window in the range $\delta = 0$ to -20.

When 5′-dGMP was added to a solution of the probe in D_2O at 25°C each solute at 0.01 mol L^{-1}, the phosphate oxygen and N_7 of dGMP both coordinated to the probe, the former being dynamically preferred, and the interaction was complete in 10 min. The equilibrium quotient (K) for the formation of Os^{II}–RPO_4 (dGMP) is 3×10^2, while the latter is thermodynamically preferred, the binding of Os^{II}–N_7(dGMP) is complete in 24 h, and the value of K is

Table 1. NMR spectroscopic data (ppm) for *cis*-RDT with 5′-GMP and 5′-AMP (pD 7.0)

Compound	H_8	H_2	P
5′-GMP	7.97		3.14
5′-GMP–*cis*-RDT	8.20, 8.00		12.90, 11.29
5′-AMP	8.39	8.02	3.76
5′-AMP–*cis*-RDT	8.29	8.04	2.06

*^1H chemical shift *vs* DSS and ^{31}P chemical shift *vs* 85% H_3PO_4.

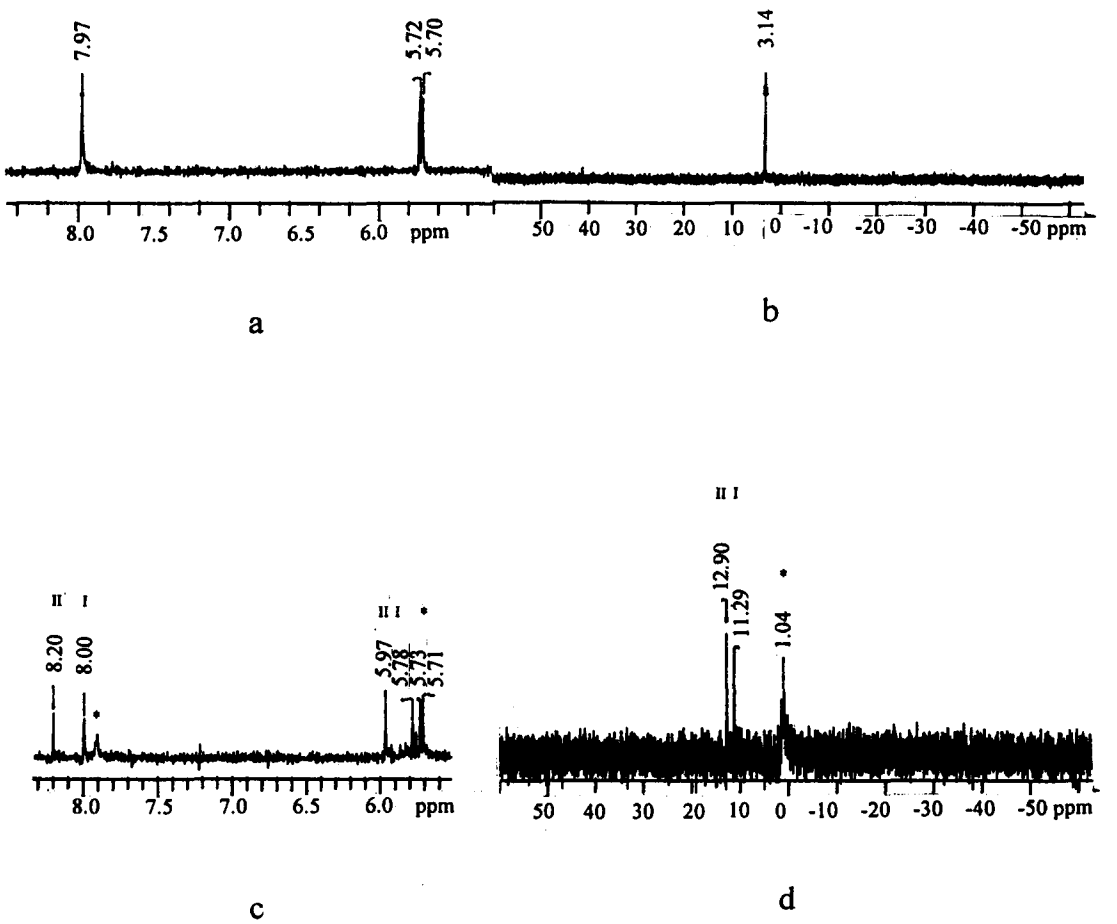
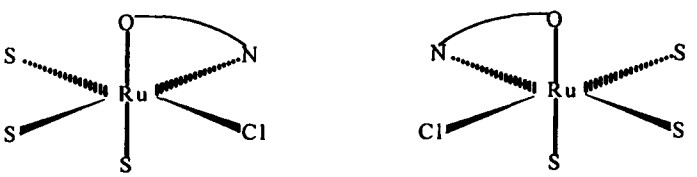


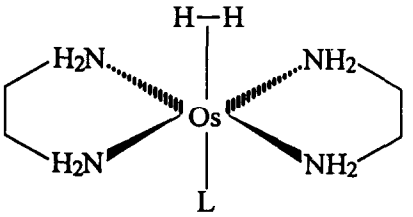
Fig. 1. 2′-Guanosine-5′-monophosphate (5′-GMP) with *cis*-RDT in D_2O as monitored by 300 MHz ^1H and ^{31}P NMR spectroscopy. Asterisk(*) represent signals of free 5′-GMP. (a) ^1H NMR of free 5′-GMP. (b) ^{31}P NMR of free 5′-GMP. (c) ^1H NMR of 5′-GMP–*cis*-RDT. (d) ^{31}P NMR of 5′-GMP–*cis*-RDT.

Table 2. A comparison of NMR chemical shift data (ppm) for *cis*-RDT and *trans*-RDT with 5′-GMP

Compound	H_8	P	Ref.
cis-RDT–5′-GMP	8.20, 8.00	12.90, 11.29	This work
trans-RDT–5′-GMP	8.43, 8.31	9.69, 8.21	9



Scheme 2.



Scheme 3.

2.9×10^3. Figure 2 clearly shows the reaction process. The peaks at δ −13.38 and −13.76 grow in 10 min. The second peak is due to phosphate oxygen binding. Meanwhile, a peak at δ −9.93, already discernible after 10 min (Fig 2a), continues to grow at the expense of the others. This peak is assigned to the N_7 binding. There is a competing reaction between D_2O binding, phosphate binding and N_7 binding, which is not in complete equilibrium in 10 min. The affinity of Os^{II} for the D_2O and phosphate is not high and the conversion from D_2O binding and phosphate binding to N_7 binding is almost complete after 24 h (Fig. 2b). Usually the binding of an antitumor metallic agent to dGMP is also *via* N_7 or the phosphate group of dGMP; therefore, if an antitumor metal agent is added to the probe–dGMP binary system, it will compete for these binding sites of dGMP with the probe, and the characteristic peaks due to binding of the probe with phosphate or N_7 of dGMP will change. According to these changes, the binding sites of the antitumor metal complexes to dGMP can be determined.

When dGMP, *cis*-RDT and the probe were mixed at the same time at 25 °C, both of the peaks due to the phosphate binding and N_7 binding diminished obviously in their intensity after 10 min (Fig. 2c) compared with those of the dGMP–probe binary system. After 24 h the peaks for D_2O binding were still present, indicating that N_7 binding of *cis*-RDT has restrained the conversion from D_2O binding to N_7 binding of the

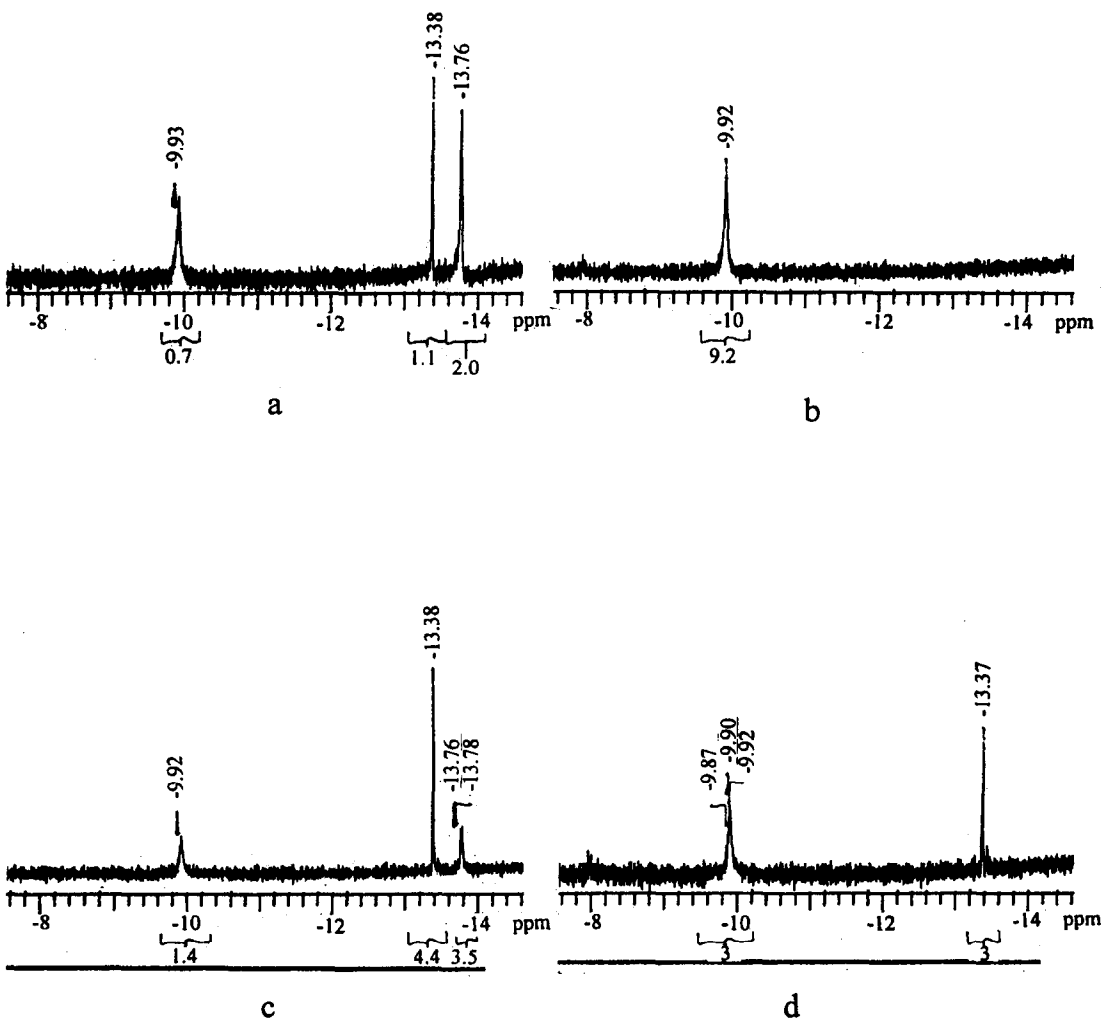


Fig. 2. ^1H NMR spectra (300 MHz) of 5′-dGMP mixed system. (a) Probe with dGMP after 10 min. (b) Probe with dGMP after 24 h. (c) Probe, dGMP and *cis*-RDT after 10 min. (d) Probe, dGMP and *cis*-RDT after 24 h.

probe (Fig. 2d). This result provides further evidence of N_7 and phosphate group coordination.

The interaction process between the probe and AMP is shown in Fig. 3a and b. Because the K value for the formation of Os^{II}–PO_4–AMP is 1.9×10^2, much higher than the corresponding K for the formation of Os^{II}–N_7–AMP, which is 1.2×10 [16], the dominant signal in the AMP–probe system is that of phosphate binding, which appears at δ −13.77, while the signal for N_7 binding is too weak to be observed. It can be seen from Fig. 3c that *cis*-RDT mixed into the AMP–probe system results in the loss of the peak at δ −13.77 after 10 min in contrast to the AMP–probe binary system. After 24 h, the peak due to the phosphate binding has disappeared completely (Fig. 3d). These results suggest that *cis*-RDT can bind to AMP *via* the phosphate oxygen.

^{31}P NMR is a commonly used method to investigate the direct coordination of metal ions to mononucleotides *via* phosphate group [17]. In particular, the case of direct binding leads to a large ^{31}P NMR shift. However, in some cases, the binding of metal ions to phosphate group of mononucleotides, owing to the possible conformation changes or H bond changes in the mononucleotides caused by metal ions, only leads to a small ^{31}P NMR shift (less than 1 ppm) [8,19]. It is difficult to determine which form mentioned above should be responsible for so little ^{31}P NMR changes

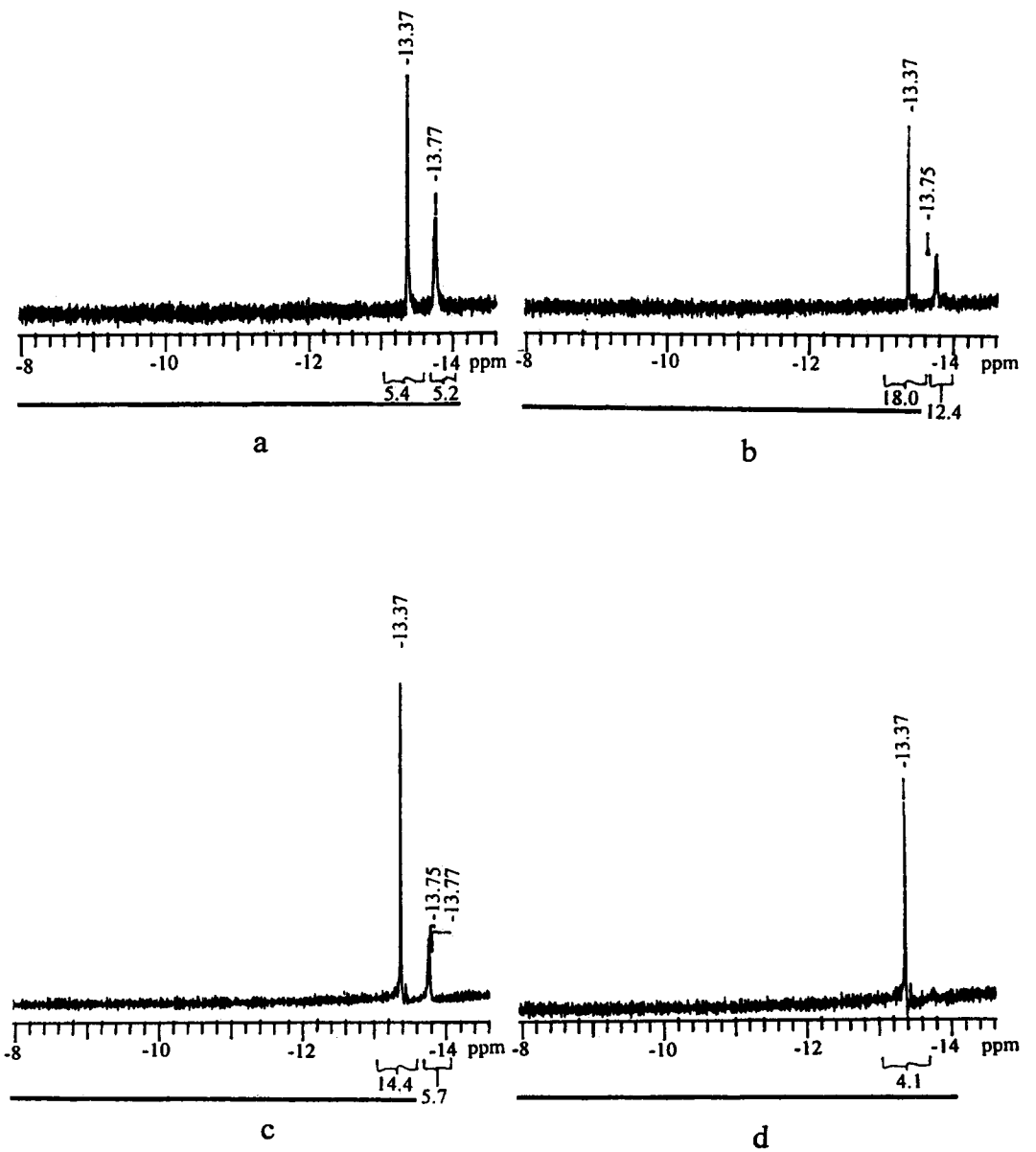


Fig. 3. ^1H NMR spectra (300 MHz) of 5′-AMP mixed system. (a) Probe with AMP after 10 min. (b) Probe with AMP after 24 h. (c) Probe, AMP and *cis*-RDT after 10 min. (d) Probe, AMP and *cis*-RDT after 24 h.

in the case of *cis*-RDT with 5′-AMP, whereas, as demonstrated above, it is easy to distinguish the direct coordination *via* phosphate group using the probe.

As discussed above, the binding mode of *cis*-RDT to AMP is different from that of *cis*-RDT to GMP. The coordination sites are both the phosphate group and N_7 between *cis*-RDT and GMP, but the coordination sites between *cis*-RDT and AMP may be only the phosphate group.

Acknowledgements—The financial support of the National Natural Science Foundation of China and the National Research Laboratories of Natural and Biomimetic Drugs are gratefully acknowledged. We wish to thank Professor Henry Taube and Dr Zaiwei Li for their generous gift of the probe.

REFERENCES

1. Clarke, M. J., *Metal Ions in Biological Systems*, 1980, **11,** 231.
2. Clarke, M. J., in *Inorganic Chemistry in Biology and Medicine*, ACS Symposium Series, Vol. 190, ed. A. E. Martell, American, Chemical Society, Washington, D.C. (1980), p. 157.
3. Sava, G., Giraldi, T., Mestroni, G. and Zassinovich, G., *Chemistry of Biological Interactions*, 1983, **45,** 1.
4. Sava, G., Zorzet, S., Giraldi, T., Mestroni, G. and Zassinovich, G., *European Journal of Cancer and Clinical Oncology*, 1984, **20,** 841.
5. Garzon, F. T., Berger, M. R., Keppler, B. K. and Schmahl, D., *Cancer Chemotherapy and Pharmacology*, 1987, **19,** 347.
6. Monti-Bragadin, C., Giacca, M., Dolzani, L. and Tamaro, M., *Inorganica Chimica Acta*, 1987, **137,** 31.
7. Mestroni, G., Alessio, E., Calligaris, M., Attia, W. M., Quadrifoglio, F., Cauci, S., Sava, G., *et al.*, *Progress in Clinical and Biochemical Medicine*, 1989, **10,** 71.
8. Cauci, S., Alessio, E. and Giovanni, M., *Inorganica Chimica Acta*, 1987, **137,** 19.
9. Alessio, E., Xu, Y. H., Cauci, S., Mestroni, G., Quadrifoglio, F., Viglino, P. and Marzilli, L. G., *Journal of the American Chemical Society*, 1989, **111,** 7068.
10. Reily, M. D. and Marzilli, L. G., *Journal of the American Chemical Society*, 1986, **108,** 8299.
11. Evans, I. P., Spencer, A. and Wilkinson, G., *Journal of the Chemical Society, Dalton Transactions*, 1973, 204.
12. Millre, S. K. and Marzilli, L. G., *Inorganic Chemistry*, 1985, **24,** 2421.
13. Reily, M. D., Hambley, T. W. and Marzilli, L. G., *Journal of the American Chemical Society*, 1988, **110,** 2999.
14. Martin, R. B., *Accounts of Chemical Research*, 1985, **18,** 32.
15. Nelson, D. J., Yeagle, P. L., Miller, T. L. and Martin, R. B., *Bioinorganic Chemistry*, 1976, **5,** 353.
16. Li, Z. W. and Taube, H., *Science*, 1992, **256,** 210.
17. Gorenstein, D. C., in *Phosphorus ^{31}P NMR Principles and Application*. Academic Press, Orlando, FL, 1984, p. 7.
18. Marzilli, L. G., Reily, M. D., Mcmurray, C. T. and Wilson, W. D., *FEBS*, 1984, **176,** 384.
19. Toney, J. H., Brock, C. P. and Mark, J., *Journal of the American Chemical Society*, 1986, **108,** 7163.

Pergamon

PII: S0277-5387(96)00519-0

Polyhedron Vol. 16, No. 12, pp. 1999–2004, 1997
© 1997 Elsevier Science Ltd
All rights reserved. Printed in Great Britain
0277-5387/97 $17.00+0.00

Crystal structure of copper(II) pivaloyltrifluoracetonate adducts with *o*-phenanthroline and 2,2′-dipyridyl

O. Yu. Gorbenko,[a] S. I. Troyanov,[a]* A. Meetsma[b] and A. A. Bosak[c]

[a]Chemistry Department, Moscow State University, 119899 Moscow, Russia; [b]Chemistry Department, Groningen University, Nijenborgh 4, 9747 Groningen, The Netherlands; [c]High School of Material Science, Moscow State University, 119899 Moscow, Russia

(Received 23 September 1996; accepted 21 October 1996)

Abstract—The crystal structure of $Cu(pta)_2 \cdot Phen$ has been determined. The phenanthroline ligand occupies a position in the equatorial plane of the tetragonally distorted octahedron with equal Cu—N distances and equivalent β-diketonate-anions. $Cu(pta)_2 \cdot 2,2'$-Dipy is isostructural to $Cu(pta)_2 \cdot Phen$. The volatility of adducts decreases in the sequence $Cu(thd)_2 \cdot Phen$, $Cu(pta)_2 \cdot Phen$ and $Cu(hfa)_2 \cdot Phen$ changing inversely to that of the β-diketonates. The variation of packing mode caused by the difference of the molecular structure is considered to be responsible for the effect. The changes of the electronic spectra of copper(II) β-diketonates caused by adduct formation are discussed. © 1997 Elsevier Science Ltd. All rights reserved.

Keywords: copper(II) beta-diketonates; adducts; crystal structure; electronic spectra; volatility.

Copper(II) β-diketonates are well known volatile compounds widely applied as precursors for MOCVD of metallic copper as well as copper-containing oxides [1,2]. The formation of adducts with neutral donor ligands allows us to modify the properties of metal β-diketonates [3,4]. Unexpectedly, there is a lack of information about sublimation characteristics and their correlation to the structure for copper(II) β-diketonate adducts.

There are three possible positions for donor atoms of a neutral bidentate ligand Q in $CuL_2 \cdot Q$ (L is a β-diketonate-anion) with tetragonally distorted octahedral Cu^{II} system (Fig. 1): (a) *trans*-coordination leading to the chain structure like $Cu(acac)_2 \cdot 4,4'$-Dipy[5–7], where acac = acetylacetonate, Dipy- = dipyridyl, (b) *cis*-coordination in the equatorial plane resulting in equal Cu—N distances and equivalent β-diketonate-anions in $Cu(hfa)_2 \cdot 2,2'$-Dipy [8] (hfa = hexafluoracetylacetonate), (c) *cis*-coordination not in the equatorial plane with non-equivalent β-diketonate-anions due to Jahn–Teller distortion. $Cu(thd)_2 \cdot Phen$ (thd = 2,2,6,6-tetramethylheptan-3,5-dionate, Phen = *o*-phenanthroline) is the only example of coordination of type (c) for $CuL_2 \cdot Q$ [9]. The complex of type (c) possesses the lowest symmetry of Cu coordination environment due to both Jahn–Teller distortion and rigidity of ligands.

In the complexes of type (b) and (c) only one of 3 bidentate chelate ligands can place both its donor atoms in the equatorial plane. For π-donating ligand this position is the most preferable [10] so the competition of ligands for such a position could be expected. The complex would be stable if one of the competitive configurations is markedly preferable. If no configuration is preferable then both (b) and (c) structures would be unstable and rearrange to other

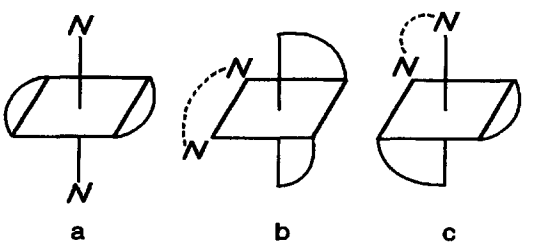


Fig. 1. Possible positions for donor atoms in $CuL_2 \cdot Q$ with tetragonally distorted octahedral Cu^{II} system.

*Author to whom correspondence should be addressed.

coordination modes in the presence of other ligands [11].

Phen or 2,2′-Dipy occupies *cis*-positions in the equatorial plane in tetragonally distorted octahedral Cu-complexes if other ligands are weaker donors like hfa. On the contrary, stronger donor (thd^-) substitutes Phen in *cis*-position of the equatorial plane ($Cu(thd)_2 \cdot Phen$).

Thus, $Cu(pta)_2 \cdot Q$ (pta = pivaloyltrifluoracetonate) is an interesting object for investigation because the competition for the equatorial plane takes place among three pairs of donor atoms: O of the pivaloyl group of β-diketonate, O of the trifluoracetyl group of β-diketonate and N of the neutral donor ligand.

EXPERIMENTAL

Synthetic procedures

$Cu(thd)_2$ and $Cu(pta)_2$ were synthesized by the reaction of stoichiometric amounts of aqueous solution of $Cu(CH_3COO)_2 \cdot H_2O$ and β-diketone and purified by vacuum sublimation at 160 and 130°C, respectively.

To prepare $Cu(hfa)_2$, an equivalent quantity of Hhfa was added to the ethanol suspension of $Cu(CH_3COO)_2 \cdot H_2O$. Then light-green crystals $Cu(hfa)_2 \cdot 2H_2O$ were precipitated from green solution by adding the excess of water. $Cu(hfa)_2$ was obtained by dehydration of $Cu(hfa)_2 \cdot 2H_2O$ during the vacuum sublimation (70–80°C).

$Cu(thd)_2 \cdot Phen$. The solution of unhydrous Phen (5 mmole) and $Cu(thd)_2$ (5 mmole) in 35 cm^3 of dry benzene was prepared. Then benzene was evaporated under aspiration. The green precipitate formed was purified by vacuum sublimation (130°C).

The same synthetic procedure was carried out with $Cu(thd)_2$ and 2,2′-Dipy. No new copper compounds were detected in the solid phase by powder XRD. After vacuum sublimation of the solid residue only $Cu(thd)_2$ and Dipy has been condensed separately due to the temperature gradient in the tube. The same result was obtained even after 3 h stirring of the benzene solution of $Cu(thd)_2$ and 2,2′-Dipy.

$Cu(hfa)_2 \cdot Phen$, $Cu(hfa)_2 \cdot 2,2'$-Dipy, $Cu(pta)_2 \cdot Phen$, $Cu(pta)_2 \cdot 2,2'$-Dipy were synthesised by adding the solid unhydrous N-donor containing ligand (2 mmole) to solutions of β-diketonates (2 mmole) in dry benzene (10 cm^3) and stirring for 30 min. Green precipitates were separated from the solution. About 1 g portions of the adducts were sublimated in vacuum (0.01 torr) without appreciable destruction. Sublimation rate was approximately equal at the temperature 220–240°C, 220–220°C, 180–200°C and 160–180°C, respectively for $Cu(hfa)_2 \cdot Phen$, $Cu(hfa)_2 \cdot 2,2'$-Dipy, $Cu(pta)_2 \cdot Phen$ and $Cu(pta)_2 \cdot 2,2'$-Dipy.

Crystal structure determination

Needle-like single crystals of $Cu(pta)_2 \cdot Phen$ and $Cu(pta)_2 \cdot 2,2'$-Dipy were grown by slow cooling of hot benzene solutions. A crystal of $Cu(pta)_2 \cdot Phen$ had approximate dimensions 0.2 × 0.2 × 0.4 mm. The data were collected on a CAD-4 (Enraf Nonius) diffractometer using Mo-K_α radiation with a graphite monochromator (ω-2θ scan method, θ range 1.7–26.0°). The crystallographic calculations were performed using the SHELXS-86 and SHELXL-93 program packages [12]. The structure was solved using a combination of direct and difference Fourier methods and refined by the full-matrix least-squares technique with anisotropic thermal parameters for all non-hydrogen atoms. The CF_3 and *tert*-Bu groups were found to be disordered in two positions around their C—C axes with the occupancies 0.67 (CF_3) and 0.60 (*tert*-Bu) for the more abundant components. The positions of the hydrogen atoms were calculated at idealized positions and refined in riding mode. Crystal data and structure refinement parameters for $Cu(pta)_2 \cdot Phen$ are given in Table 1. Selected bond lengths and angles are listed in Table 2. $Cu(pta)_2 \cdot 2,2'$-Dipy single crystals were of lower quality. The measurement and the structure determination revealed the same space group and the ligands arrangement around the Cu atom. The structural data are not presented due to too high R_1 value (0.11), However, we believe that both Phen and 2,2′-Dipy adducts are isostructural (Table 1).

Powder diffraction measurement (θ-2θ scan) was performed with DRON-3M diffractometer using Co-K_α radiation in the range of 2θ 6–50°. The comparison of the diffraction patterns $Cu(pta)_2 \cdot Phen$ and $Cu(pta)_2 \cdot 2,2'$-Dipy as well as $Cu(hfa)_2 \cdot Phen$ and $Cu(pta)_2 \cdot 2,2'$-Dipy allows us to conclude that the compounds in the pairs are isostructural.

Electronic spectroscopy

Electronic spectra were measured with absorption spectrofotometer KFK-3 in the range 12,500–25,000 cm^{-1} using a 1 cm cuvette. Benzene was used as a solvent. Components were mixed to achieve total concentration 0.01 mol/l, but solutions of $Cu(pta)_2 \cdot Phen$ and $Cu(hfa)_2 \cdot Phen$ were already saturated under such conditions with about half of the adduct weight being dissolved.

RESULTS AND DISCUSSION

The molecular structure of $Cu(pta)_2 \cdot Phen$ is shown in Fig. 2. $Cu(pta)_2 \cdot Phen$ belongs to the type (b) like $Cu(hfa)_2 \cdot 2,2'$-Dipy [8]. Many structural features, for instance, the position of Cu (and neutral donor ligand) on a twofold axis as well as bond lengths in the CuO_4N_2 distorted octahedron are similar for both complexes. The twofold axis requires the Cu—N bonds to be equal (2.029 Å). There are also two pairs of Cu—O bonds: Cu—O(1) 2.246 Å, Cu—O(2) 1.970 Å. The corresponding bond lengths for $Cu(hfa)_2 \cdot 2,2'$-Dipy are: Cu—N 1.998 Å, Cu—O(1) 2.296 Å,

Table 1. Crystal data for $Cu(pta)_2 \cdot Q$ and the details of structure refinement for $Cu(pta)_2 \cdot Phen$

Q	Phen	2,2′-Dipy
Formula	$C_{28}H_{28}CuF_6N_2O_4$	$C_{26}H_{28}CuF_6N_2O_4$
Formula weight	634.08	610.05
Crystal system	Monoclinic	Monoclinic
Space group	*I*2/*a*	*I*2/*a*
a (Å)	10.111(1)	9.698(2)
b (Å)	17.008(2)	16.944(2)
c (Å)	17.038(3)	17.240(2)
β (°)	97.12(1)	93.01(1)
V (Å^3)	2907.4(7)	2829.0(9)
Z	4	4
D_c (g cm^3)	1.449	1.432
μ (cm^{-1})	8.25	
Radiation, Mo-K_α, λ (Å)	0.71073	
Reflections measured	2866	
Unique reflections	2855 [*R*(int) = 0.0361]	
Data/restraints/parameters	2556/28/248	
Goodness-of-fit on F^2	1.052	
wR_2 (on F^2)	0.1146	
R_1 [$I > 2\sigma(I)$]	0.0546	
Largest diff. peak and hole (e/Å^3)	0.33 and −0.24	

Table 2. Selected bond lengths (Å) and angles (°) for $Cu(pta)_2 \cdot Phen$

Cu—O(1)	2.246(3)	O(1)—Cu—O(1a)	168.19(9)
Cu—O(2)	1.970(3)	O(2)—Cu—O(2a)	95.16(11)
Cu—N	2.029(3)	O(2)—Cu—O(1)	85.54(11)
O(1)—C(2)	1.247(4)	O(2)—Cu—O(1a)	86.50(11)
O(2)—C(4)	1.248(4)	N—Cu—O(1)	96.18(11)
N—C(9)	1.322(4)	N—Cu—O(1a)	92.79(10)
N—C(13)	1.360(4)	O(2)—Cu—N	91.86(11)
C(1)—F(1)	1.284(15)	O(2)—Cu—N(a)	172.67(11)
C(1)—F(2)	1.328(15)	N—Cu—N(a)	81.22(12)
C(1)—F(3)	1.289(12)	C(2)—O(1)—Cu	117.8(2)
C(1)—F(11)*	1.26(2)	C(4)—O(2)—Cu	131.0(3)
C(1)—F(21)*	1.30(2)	C(9)—N—Cu	129.5(2)
C(1)—F(31)*	1.31(2)	C(13)—N—Cu	112.8(2)
C(1)—C(2)	1.534(7)	C(9)—N—C(13)	117.7(3)
C(2)—C(3)	1.386(5)	O(1)—C(2)—C(1)	113.6(4)
C(3)—C(4)	1.387(6)	O(1)—C(2)—C(3)	130.0(4)
C(4)—C(5)	1.534(5)	O(2)—C(4)—C(3)	123.9(4)
C(5)—C(6)	1.486(14)	O(2)—C(4)—C(5)	115.8(4)
C(5)—C(7)	1.542(18)	C(4)—C(3)—C(2)	124.9(4)
C(5)—C(8)	1.483(14)		
C(5)—C(61)**	1.49(2)		
C(5)—C(71)**	1.51(3)		
C(5)—C(81)**	1.50(3)		

Symmetry transformation used to generate equivalent atoms (a): $-x + 1/2, y, -z$

*The distances in the minor component of disordered CF_3 group.

**The distances in the minor component of disordered *tert*-Bu group.

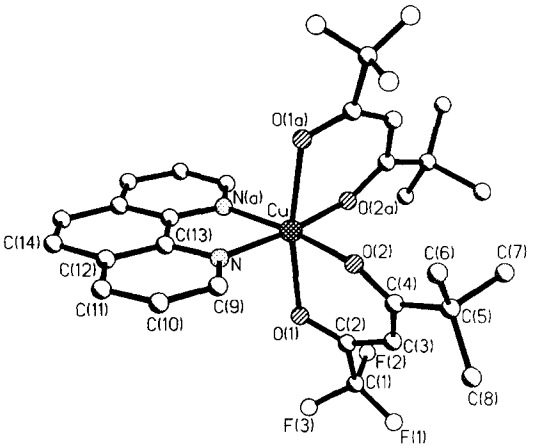


Fig. 2. Molecular structure of $Cu(pta)_2 \cdot Phen$.

Cu—O(2) 1.967 Å. The small elongation of Cu—N bond correlates to the change of β-diketone acidity (Hhfa is a stronger acid than Hpta), which is generally reciprocal to the donor ability of β-diketonate ligand.

Oxygen atoms of the pivaloyl group of β-diketonates occupy positions in the equatorial plane and oxygen atoms of the trifluoracetyl groups are pushed out to the apical positions. The result is in agreement with the relative donor ability of carbonyl groups taking into account the opposite inductive effects of *tert*-Bu and CF_3 groups.

It is noteworthy that both C—O bond lengths are nearly the same in contrast to $Cu(hfa)_2 \cdot 2,2'$-Dipy, where the C—O bonds are significantly different*. The difference could be expected considering the change of Cu—O bond lengths: the shorter Cu—O bond corresponds to the longer C—O bond. Evidently in the case of pta-complexes, the effect is compensated by the inductive effect of the groups attached to the chelate ring. The same is valid for C—C bonds in the chelate ring: they are different in $Cu(hfa)_2 \cdot 2,2'$-Dipy**, but nearly equal in the pta-complexes. Thus nearly symmetrical π-system occurs in the chelate ring of pta.

Due to the rigidity of ligands the bond angles in the CuO_4N_2 polyhedron deviate from those of the tetragonally stretched octahedron. Nevertheless, the distortion is smaller as compared to that in $Cu(thd)_2 \cdot Phen$ (type(c)). Phen or 2,2′-Dipy requires N—Cu—N angle markedly lower than 90°. As a result the O—Cu—O angle in the equatorial plane is more than 90°. The Cu—O bonds directed to the apical oxygen atoms deviate from the normal to the equatorial plane by 6°. The latter effect is probably due to repulsion from the π-electron system of Phen. Thus the molecule would possess a dipole directed along the twofold axis because of the displacement of CF_3 groups to one side of the molecule.

*1.261 and 1.218 Å.
**1.385 and 1.433 Å.

The dipole interaction probably plays an important role in the packing of $CuL_2 \cdot Q$ molecules in the crystal. The packing of $Cu(pta)_2 \cdot Phen$ molecules, shown in Fig. 3(a), consists of separate layers. In each layer the dipoles of the neighbouring molecules are antiparallel and the attraction of dipoles is maximal. The packing of molecules in the crystal of $Cu(thd)_2 \cdot Phen$ is quite different (Fig. 3(b)). Interaction of aromatic systems of Phen ligands from the neighbouring molecules determines the packing in the structure. For low symmetrical $Cu(thd)_2 \cdot Phen$ the mutual antiparallel orientation of dipoles is less probable.

The packing mode correlates with the volatility of the adducts. Even qualitative estimation by sublimation temperature at the same pressure (0.01 torr) given in the experimental part supports this viewpoint. The sublimation temperature increases in the order $Cu(thd)_2 \cdot Phen < Cu(pta)_2 \cdot Phen < Cu(hfa)_2 \cdot Phen$ significantly. The sequence is opposite to the sequence of the volatility of copper(II) β-diketonates [13,14]. In the latter case the oxygen atoms of the β-diketonates form a rectangle around the copper atom and the whole molecule is planar [15]. The volatility is determined by interaction of peripheral groups of ligands, the repulsion of fluorinated groups being stronger than that of alkyl groups. The lower sublimation temperature of 2,2′-Dipy adducts than Phen adducts may be caused by the change in the molecule dipole due to lower repulsion between the π-electron

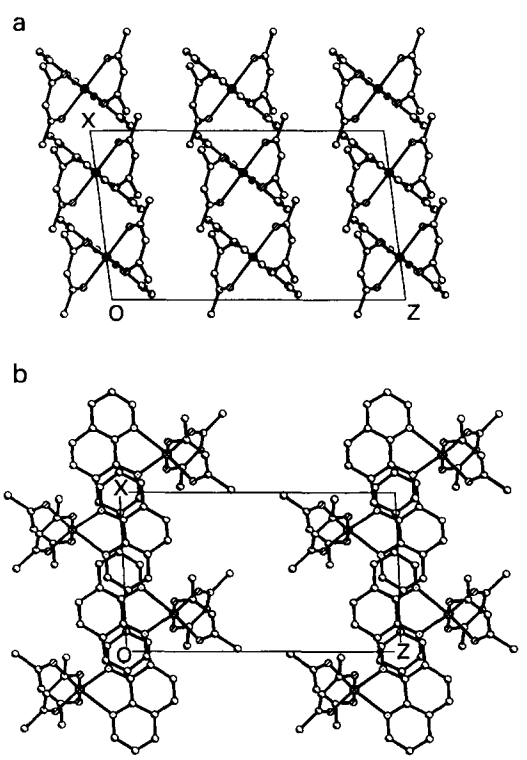


Fig. 3. Molecular packing of copper(II) β-diketonates adducts: $Cu(pta)_2 \cdot Phen$ (a), $Cu(thd)_2 \cdot Phen$ (b). F atoms and Me groups are omitted for clarity.

Table 3. Electronic spectra of copper(II) β-diketonates and their adducts with Phen and 2,2′-Dipy in benzene solutions

Compound	Chromophore-effective group of symmetry	$d_{xz},d_{yz} \rightarrow d_{xy}$ transition, $\times 10^{-3}$ (cm^{-1})	d_{z^2}, $d_{x^2-y^2} \rightarrow d_{xy}$ transition, $\times 10^{-3}$ (cm^{-1})	Charge transfer band
$Cu(hfa)_2$	O_4-D_{2h}	17.5	14.5	—
$Cu(pta)_2$	O_4-D_{2h}	17.9	14.4	—
$Cu(thd)_2$	O_4-D_{2h}	18.6	14.5	—
$Cu(hfa)_2 \cdot$ Phen	O_4N_2-C_{2v}	13.4	infra red	22.3
$Cu(hfa)_2 \cdot$ 2,2′-Dipy	O_4N_2-C_{2v}	13.5	infra red	22.5
$Cu(pta)_2 \cdot$ Phen	O_4N_2-C_{2v}	12.9	infra red	22.8
$Cu(pta)_2 \cdot$ 2,2′-Dipy	O_4N_2-C_{2v}	13.3	infra red	22.2
$Cu(thd)_2 \cdot$ Phen	O_4N_2-C_1	18.7	14.4	—

system of the neutral ligand and the apical oxygen. But details of molecular structure to support the idea are missing.

The results obtained should be taken into account in the flash and aerosol MOCVD [16,17] of complex copper oxides, like high T_c superconductors. If Phen is added to stabilize β-diketonates of some other metals, the ligand exchange can influence the volatility of the copper precursor.

Electronic spectra are known to be very similar for various copper(II) β-diketonates [18]. A broad band visible envelope can be resolved into Gaussian components. The procedure for the spectrum of a solution [19,20] results in two Gaussian bands centered nearby 18,000 and 15,000 cm^{-1}. Our data (Table 3) are in agreement with the results: the spectra are similar for complexes with both fluorinated and unfluorinated, symmetric and asymmetric ligands.

Polarized spectra of single crystals [19,21] of copper(II) β-diketonates revealed three *d–d* absorption bands at 18,000, 15,000 and 14,000 cm^{-1}. The effective spectroscopic symmetry of the chromophore O_4 is close to D_{2h} even for asymmetrical β-diketonate like benzoylacetonate [21]. For correct assignment of the bands it is necessary to define the molecular coordinate system. The preferable choice of the coordinate frame is as follows: *z* axis is normal to the rectangular chromophore group O_4, *x*,*y* axes are along the auxiliary C_2 axes. The highest *d*-orbital is σ-antibonding d_{xy}. As d_{xz} and d_{yz} states are almost degenerate for the group D_{2h}, $d_{xz} \rightarrow d_{xy}$ and $d_{yz} \rightarrow d_{xy}$ transitions give one band at 18,000 cm^{-1}. The bands at the lower energies are $d_{z^2} \rightarrow d_{xy}$ and $d_{x^2-y^2} \rightarrow d_{xy}$ [21].

In the adduct of type (b) chromophore O_4N_2 has effective symmetry C_{2v}. The coordinate frame is modified so that the *x* axis is parallel to the C_2 axis. The only adduct studied previously is $Cu(hfa)_2 \cdot$ 2,2′-Dipy [22] (a range from 8000 to 18,000 cm^{-1} only was inspected). The $d_{z^2} \rightarrow d_{xy}$ transition was found to be shifted to the infra-red (9500 cm^{-1}). It is quite understandable taking into account that apical donors destabilize the d_{z^2} orbital. Other transitions form a wide band at about 14,000 cm^{-1}.

Similar spectra were observed for all adducts of type (b) studied (Table 3). These data allow us also to conclude that (1) d_{xz} and d_{yz} orbitals are still almost degenerate; (2) 2,2′-Dipy and Phen produce approximately the same ligand field; (3) change of hfa for pta has minor influence on the band energies. The $d_{z^2} \rightarrow d_{xy}$ transition in the infra-red could not be measured in our work.

Additionally the more intense band was observed at 22,000–23,000 cm^{-1} for adducts of type (b). Strong absorption at the energies higher than 24,000 cm^{-1} is typical for all complexes studied and originates through charge transfer from β-diketonate, but only adducts of type (b) reveal the extra band. As the position of a neutral bidentate ligand in the equatorial plane is necessary for the appearance of the band we can assign the absorption to the charge transfer from this ligand.

The electronic spectrum of $Cu(thd)_2 \cdot$ Phen is difficult to predict because of the low molecular symmetry. The observed absorption spectrum is very similar to that of $Cu(thd)_2$ or $Cu(thd)_2$ and 2,2′-Dipy (1 : 1) benzene solutions. Thus, the formation of adduct of type (b), but not of type (c), can be easily registered by electronic spectroscopy of the benzene solutions.

CONCLUSIONS

As can be seen from Table 4 the occurrence of $CuL_2 \cdot Q$ structure depends on the nature of β-diketonate ligand. Decrease of HL acidity results in the change of the preferable coordination type. The competition of ligands for the place in the equatorial plane of tetragonally stretched octahedral coordination sphere of Cu^{II} is a dominating factor for their arrangement. We have found that some $CuL_2 \cdot Q$, including $Cu(hfa)_2 \cdot$ Phen, $Cu(hfa)_2 \cdot$ 2,2′-Dipy, $Cu(pta)_2 \cdot$ Phen, $Cu(pta)_2 \cdot$ 2,2′-Dipy, are able to evaporate congruently in vacuum. Nevertheless $Cu(thd)_2 \cdot$ Phen (structure type (c)) has a lower sublimation temperature than the complexes of structure type (b) in spite of the presence of the fluorinated β-diketonate ligands.

Acknowledgements—The work was partly supported by Volkswagen Foundation grant N I/69341.

Table 4. Coordination types for adducts $CuL_2 \cdot Q$ (notations according to Fig. 1)

Ligand	hfa	pta	acac	thd
Phen	(b)	(b)	unstable	(c)
2,2′-Dipy	(b)	(b)	unstable	unstable

REFERENCES

1. P. Doppelt and T. H. Baum, *MRS Bull.* 1994, **19,** N8, 41.
2. T. Ozawa, *Thermochimica Acta* 1991, **174,** 185.
3. K. Timmer, C. I. M. A. Spee, A. Mackor, H. A. Meinema, A. L. Spek and P. van der Sluis, *Inorg. Chim. Acta* 1991, **190,** 109.
4. B. C. Richards, S. L. Cook, D. L. Pinch and G. W. Andrews, *J. de Phys. IV* 1995, **5,** C5, 407.
5. R. C. E. Belford, D. E. Fenton and M. R. Truter, *J. Chem. Soc., Dalton. Trans.* 1972, 2208.
6. Yuanzhi Xu and Shu Shi, *Acta Chim. Sin.* 1986, **44,** 336.
7. R. C. E. Belford, D. E. Fenton and M. R. Truter, *J. Chem. Soc., Dalton. Trans.* 1974, 17.
8. M. V. Veidis, G. H. Schreiber, T. E. Gough and G. J. Palenik, *J. Am. Chem. Soc.* 1969, **91,** 1859.
9. S. I. Troyanov, O. Yu. Gorbenko and A. A. Bosak, *Polyhedron* 1997, **16,** 1595.
10. J. A. Pretorius and J. C. A. Boeyens, *J. Inorg. Nucl. Chem.* 1978, **40,** 407.
11. S. I. Troyanov, A. N. Grigor'ev, A. A. Drozdov and L. I. Martynenko, *Zh. Neorg. Khim.* 1992, **37,** 107 (*Russ. J. Inorg. Chem.* 1992, **37,** 57).
12. G. M. Sheldrick, SHELXS-*Acta Crystallogr.* 1990, **A46,** 467; SHELXL93. *Program for crystal structure refinement.* University of Göttingen (1993).
13. I. K. Igumenov, Yu. V. Chumachenko and S. V. Zemskov, *Problems of Chemistry and Applications of Metal β-Diketonates*, 100. Nauka, Moscow (1982).
14. I. K. Igumenov, Yu. V. Chumachenko and S. V. Zemskov, *The Structure, Properties and Application of Metal β-Diketonates*, 105. Nauka, Moscow (1978).
15. L. M. Shkol'nikova and M. A. Porai-Koshitz, *Itogi Nauki i Techniki*, 1982, **16,** 117.
16. O. Yu. Gorbenko, V. N. Fuflyigin, Yu. Yu. Erokhin, I. E. Graboy, A. R. Kaul, Yu. D. Tretyakov, G. Wahl and L. Klippe, *J. Mater. Chem.* 1994, **4,** 1585.
17. S. V. Samoylenkov, O. Yu. Gorbenko, I. E. Graboy, A. R. Kaul and Yu. D. Tretyakov, *J. Mater. Chem.* 1996, **6,** 623.
18. A. B. P. Lever, *Inorganic Electronic Spectroscopy*, 2nd ed., 553. Elsevier, Amsterdam (1984).
19. J. Ferguson, *J. Chem. Phys.* 1961, **34,** 1609.
20. R. L. Belford, M. Calvin and G. Belford, *J. Chem. Phys.* 1957, **26,** 1165.
21. M. A. Hitchman and R. L. Belford, *Inorg. Chem.* 1971, **10,** 984.
22. R. J. Dudley and B. J. Hathaway, *J. Chem. Soc. (A)* 1970, 2794.